Single Crystal Electron Spin Resonance Spectra of Magnetically Dilute Copper(II) Ion in Some Five-coordinate Adducts of Zinc(II) β-Diketonate Complexes

Seizo MISUMI, Toshiyuki ISOBE, and Kuniyoshi SUGIYAMA
Inorganic Chemistry Laboratory, Faculty of Science, Kyushu University, Fukuoka 812
(Received July 3, 1973)

The single crystal ESR spectra of some five-coordinate adducts of copper(II)-doped zinc(II) β-diketonate complexes [Cu/Zn(acac)$_2$H$_2$O], [Cu/Zn(acac)$_2$γ-pic], [Cu/Zn(bzac)$_2$MeOH], and [Cu/Zn(bzac)$_2$py] (acac= acetylacetone anion, bzac=benzoylacetone anion, py=pyridine, γ-pic=γ-picoline, MeOH=methanol) were measured at room temperature. The principal values of the g tensor and A tensor of ^{63}Cu were calculated. The single crystal g-values of all the adducts suggested a $d_{x^2-y^2}$ ground state for the approximately square-based pyramidal structure, and were found to be consistent with crystallographic data. In the single crystals of [Cu/Zn-(acac)$_2$H$_2$O] and [Cu/Zn(bzac)$_2$py], two magnetic centers were determined, this being the first time for them to have been found by ESR study.

A survey of well-known five-coordinate complexes shows the possibility of their being square pyramidal (SP) and trigonal bipyramidal (TBP). Most of them contain two bidentate ligands and one unidentate ligand. A central metal atom in the square pyramidal structure suggests two types of structure according to the coordination site of the unidentate ligand, one with a unidentate ligand in the apical position (SP-1) and the other in the basal plane (SP-2). The square-based pyramidal stereochemistry occurs much more frequently than the trigonal bipyramidal.

Bis-(*o*-hydroxyacetophenonato)γ-picoline copper(II)[1] and bis-(acetylacetonato)quinoline copper(II)[2] were reported to be of SP-1 structure, and bis-(acetylacetonato)4-aminopyridine copper(II)[3] of SP-2 structure by means of X-ray crystallography. The crystal structure of monoaquobis-(acetylacetonato) zinc(II) [Zn(acac)$_2$H$_2$O] has been determined by a three-dimensional X-ray crystal-structure analysis.[4,5] Lippert and Truter[4] reported that zinc atom is five-coordinated with the bonds arranged in a trigonal bipyramid. On the other hand, Montgomery and Lingafelter[5] confirmed that the structure is made up of discrete molecules, containing five-coordinate zinc-(II) with an intermediate coordination configuration between tetragonal pyramidal and trigonal bipyramidal.

The powder ESR spectra of the adduct complexes of SP-1 structure, such as [Cu(acac)$_2$quinoline], [Cu-(acac)$_2$γ-pic],[6] and [Cu(bzac)$_2$py],[7] show an axial pattern with $g_\parallel > g_\perp$ and the ground state is suggested to be $d_{x^2-y^2}$.[8] [Cu(acac)$_2$4-aminopyridine], which forms a typical SP-2 complex, gives typical rhombic pattern (neither rhombic nor axial) of the powder ESR spectrum and the ground state is also suggested to be $d_{x^2-y^2}$. In TBP complexes, the d_{z^2} ground state is usually observed, indicating that $g_\perp$ is greater than $g_\parallel$.

In this work, the single crystals of four five-coordinate adducts of copper(II)-doped zinc(II) β-diketonate complexes were prepared and their structures were estimated by comparing the single crystal ESR spectra with crystallographic data.

Experimental

Preparation. The single crystal of the five-coordinate adducts of copper(II)-doped (1 mol%) zinc(II) β-diketonate complexes was prepared by the method of Graddon and Weeden,[9,10] except that Zn(ClO$_4$)$_2$·6H$_2$O was used as the starting material.

Measurements. Single crystal ESR spectra were taken on a JEOL/JES-ME-3X spectrometer at room temperature. Calibration was made with a DPPH (g=2.0036). All the single crystal ESR spectra were recorded on a holder similar to that used by Hathaway and Billing,[11] except that it was made of silica rod. As the single crystal of all the adducts decomposed easily on exposure to air, it was coated with silicone grease throughout the measurements. The crystal was rotated about three orthogonal axes and the spectra were obtained in each rotation.[12-15]

Results and Discussion

For all the complexes, well-resolved ^{63}Cu hyperfine structures were observed in the magnetically dilute single crystal ESR spectra, in which the first and last lines are partly split due to the presence of the ^{65}Cu isotope.[16] The ESR spectra of [Cu/Zn(acac)$_2$γ-pic] and [Cu/Zn(bzac)$_2$MeOH] gave four hyperfine absorption lines. However, those of [Cu/Zn(acac)$_2$H$_2$O] and [Cu/Zn(bzac)$_2$py] gave eight lines, suggesting that there are two magnetic sites per unit cell. The single crystal ESR spectra at room temperature, shown in Figs. 1 and 2, exhibit strong Zeeman and hyperfine-

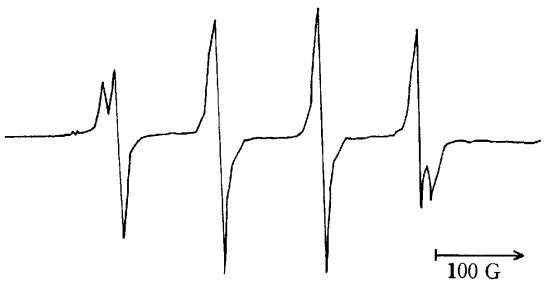

Fig. 1. ESR spectrum of [Cu(bzac)$_2$MeOH] in a [Zn-(bzac)$_2$MeOH] single crystal at room temperature.

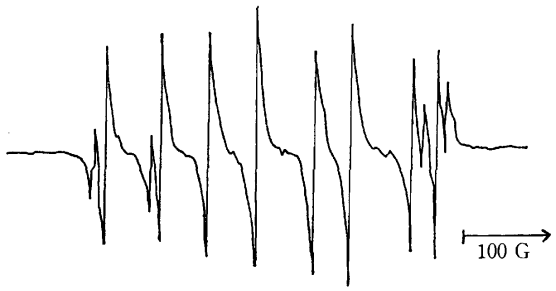

Fig. 2. ESR spectrum of $[Cu(acac)_2H_2O]$ in a $[Zn(acac)_2H_2O]$ single crystal at room temperature.

interaction anisotropies. Plots of the peak position as a function of the angle are shown in Figs. 3—5. The principal g- and A-values determined by the method of Schonland,[17] given in Table 1, are in agreement within experimental error with the approximate data obtained from powder ESR measurements.

a) *[Cu/Zn(acac)$_2\gamma$-pic] and [Cu/Zn(bzac)$_2$MeOH].* These two adduct complexes yield non-axial ESR spectra (neither axial nor rhombic) with $g_1 \sim g_2 < g_3$ and $A_1 < A_2 \ll A_3$, which suggests a characteristic square pyramidal symmetry indicating $d_{x^2-y^2}$ ground state. Thus the complexes are estimated to be of SP-1 structure *i.e.*, a γ-picoline or a MeOH molecule lies at the apical position of the square pyramidal structure. The ESR spectra of $[Cu/Zn(acac)_2\gamma\text{-pic}]$ at room temperature gave no superhyperfine interaction with a nitrogen atom of γ-picoline at the apical position of the square pyramidal structure.

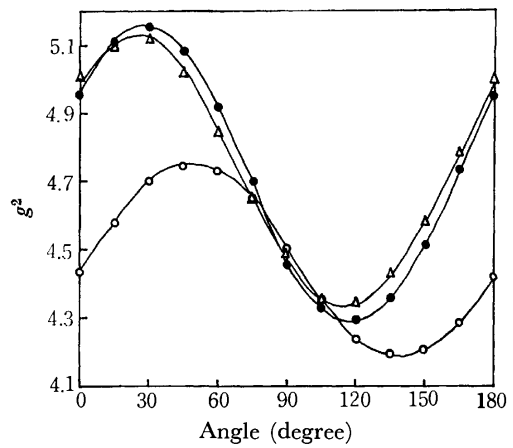

Fig. 3. Angular variations of g-value for $[Cu(bzac)_2MeOH]$ in a $[Zn(bzac)_2MeOH]$ single crystal at room temperature (ESR spectra were recorded about every 15° in the three perpendicular planes. △: 1·2-plane, ○: 2·3-plane and ●: 1·3-plane).

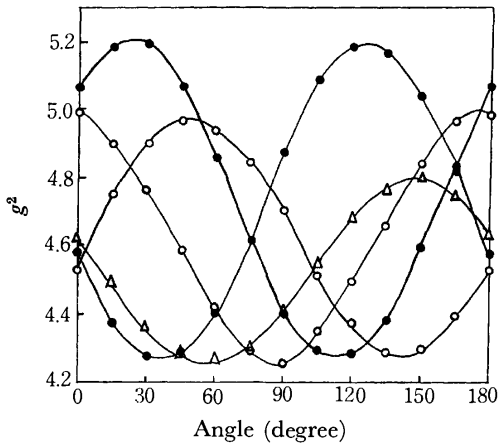

Fig. 4. Angular variations of g-value for $[Cu(acac)_2H_2O]$ in a $[Zn(acac)_2H_2O]$ single crystal at room temperature (ESR spectra were recorded about every 15° in the three perpendicular planes. There are two units of this complex per unit cell. △: 1·2-plane, ○: 2·3-plane and ●: 1·3-plane).

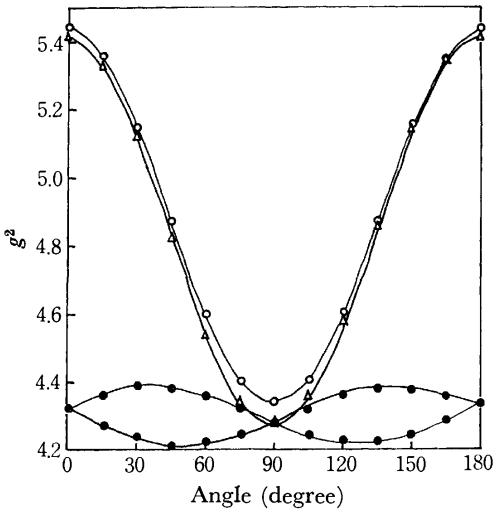

Fig. 5. Angular variations of g-value for $[Cu(bzac)_2py]$ in a $[Zn(bzac)_2py]$ single crystal at room temperature. (ESR spectra were recorded about every 15° in the three perpendicular planes. There are two units of this complex per unit cell. △: 1·2-plane, ○: 2·3-plane and ●: 1·3-plane).

b) *[Cu/Zn(acac)$_2H_2O$].* Lippert and Truter[4] showed that this adduct complex forms a distorted

Table 1. Single crystal g- and A-values for five-coordinate adducts

Adduct		g_1	g_2	g_3	A_1 (G)	A_2 (G)	A_3 (G)
$[Cu/Zn(acac)_2H_2O]$[a]	I	2.060	2.071	2.316	21.2	38.1	153.4
	II	2.065	2.073	2.317	20.3	37.0	152.6
$[Cu/Zn(acac)_2\gamma\text{-pic}]$		2.058	2.076	2.312	12.0	52.0	150.6
$[Cu/Zn(bzac)_2MeOH]$		2.045	2.094	2.312	26.8	37.2	139.9
$[Cu/Zn(bzac)_2py]$[a]	I	2.055	2.094	2.330	29.4	38.9	123.8
	II	2.053	2.095	2.330	27.9	40.0	123.8

a) There are two units of this complex per unit cell.

TBP structure, whereas Montgomery and Lingafelter[5] reported it to be an intermediate configuration between SP-1 and TBP by X-ray measurements. A significant difference might be seen in the ESR spectra. Usually a $d_{x^2-y^2}$ ground state with $g_1 \sim g_2 < g_3$ is expected for SP-1 structure and a d_{z^2} ground state with $g_1 \sim g_2 > g_3$ for TBP structure. As shown in Table 1, the principal g-values for this adduct complex show $g_1 \sim g_2 < g_3$. Thus it does not seem to be of effective TBP symmetry. For $[Zn(acac)_2H_2O]$, the distorted square-based pyramidal structure or an intermediate configuration between SP-1 and TBP, rather than the distorted TBP, could be proposed. There are two magnetic sites per unit cell, two units being symmetric in 1·2-plane but not symmetric in 1·3- and 2·3-planes, as shown in Fig. 4. The crystal is monoclinic, and the 3-axis lies approximately parallel to the crystal needle axis, b. This is in line with the fact that the unit cell possesses the two-fold screw axis, as was expected from X-ray analysis.[4]

c) *[Cu/Zn(bzac)$_2$py]*. It was found that there are two magnetic sites of $[Zn(bzac)_2py]$ per unit cell from single crystal ESR spectra (Fig. 5). Measurement by the X-ray method has not yet been carried out, $[Cu/Zn(bzac)_2py]$ shows principal g-values with $g_1 \sim g_2 < g_3$. This indicates the ground state to be $d_{x^2-y^2}$ which would favor the square pyramidal coordination. Thus, it seems that a pyridine molecule lies in the apical position in the square pyramidal structure. The ^{14}N superhyperfine structure of a pyridine molecule was not resolved in these ESR spectra, nor in those of $[Cu/Zn(acac)_2\gamma\text{-pic}]$.

Financial support by the Ministry of Education for part of this work is gratefully acknowledged.

References

1) V. F. Duckworth and N. C. Stephenson, *Acta Crystallogr.*, **B25**, 2245 (1969).
2) S. Ooi and Q. Fernando, *Chem. Commun.*, **1967**, 532.
3) G. W. Bushnell, *Can. J. Chem.*, **49**, 555 (1971).
4) E. L. Lippert and M. R. Truter, *J. Chem. Soc.*, **1960**, 4996.
5) H. Montgomery and E. C. Lingafelter, *Acta Crystallogr.*, **16**, 748 (1963).
6) D. P. Graddon and E. C. Watton, *J. Inorg. Nucl. Chem.*, **21**, 49 (1961).
7) H. Yokoi, M. Sai, and T. Isobe, This Bulletin, **43**, 1078 (1970).
8) H. Elliott, B. J. Hathaway, and R. C. Slade, *J. Chem. Soc., A*, **1966**, 1443.
9) D. P. Graddon and D. G. Weeden, *Aust. J. Chem.*, **16**, 980 (1963).
10) D. P. Graddon and D. G. Weeden, *ibid.*, **17**, 607 (1964).
11) B. J. Hathaway and D. E. Billing, *Coord. Chem. Rev.*, **5**, 143 (1970).
12) B. J. Hathaway, D. E. Billing, R. J. Dudley, R. J. Fereday, and A. A. G. Tomlinson, *J. Chem. Soc., A*, **1970**, 806.
13) M. V. Veidis, G. H. Schreiber, T. E. Gough, and G. J. Palenik, *J. Amer. Chem. Soc.*, **91**, 1859 (1969).
14) B. B. Wayland and M. D. Wisniewski, *Chem. Commun.*, **1971**, 1025.
15) C. J. Ballhausen, "An Introduction to Ligand Field Theory", McGraw-Hill, New York (1962).
16) J. G. M. van Rens, C. P. Keijzers, and H. van Willigen, *J. Chem. Phys.*, **52**, 2858 (1970).
17) D. S. Schonland, *Proc. Phys. Soc.*, **73**, 788 (1959).

An ESR Study of Methylamino Radicals Photoproduced on the Porous Vycor Glass Surface

Keiichiro HATANO,* Norio SHIMAMOTO,** Takashi KATSU, and Yuzaburo FUJITA***

Faculty of Pharmaceutical Sciences, The University of Tokyo, Hongo, Bunkyo-ku, Tokyo 113

(Received July 9, 1973)

The photochemical decomposition of methylamines adsorbed on the surface of the porous Vycor glass was studied at 77 K by the ESR method, and the ESR spectra of the methylamino radicals, CH_3NH, CH_3ND, CD_3NH, CD_3ND, CH_2DNH, and CH_2DND, were observed as primary radicals from variously-deuterated methylamines upon irradiation with the light of a low-pressure mercury lamp. This result shows that the primary process is preferentially a rupture of the N–H or N–D bond of methylamine. These spectra were characterized by an apparent quenching of the *N*-hyperfine splitting resulting from large hyperfine anisotropy, and by nearly isotropic proton hyperfine splittings in both methyl and amino groups. The hyperfine splitting constants of the N, H, and D nuclei of each radical were determined, and consequently a D-substitution effect on the β-proton hf splitting in the methyl group was found. The characteristics of the ESR spectra were discussed in relation to the adsorbed state of the methylamino radical on the porous Vycor glass surface.

It has generally been accepted that the CH_3, NH_2, CH_3NH, CH_2NH_2, and H radicals are produced in the primary processes of the photochemical decomposition of methylamine in the gas and liquid phases.[1] Among these radicals, the CH_3, NH_2, and H radicals have been studied extensively, and their ESR spectra have been unambiguously defined in various matrices and adsorbed states.[2] However, those of the CH_3NH[3] and CH_2NH_2[4] radicals have only been obtained as poorly-resolved spectra in randomly-oriented states; especially, the anisotropic hyperfine interaction of the ^{14}N-nucleus in the methylamino radical has not yet been studied extensively.[5]

As has been reported previously, simple molecules adsorbed on the surface of the porous Vycor glass (PVG) are photolyzed efficiently with the light of a low-pressure mercury lamp at room temperature and 77 K into simple radicals, which exhibit well-resolved hf splittings.[6] For example, the NH_2 radical, which is the simplest *N*-centered radical, has been photoproduced from NH_3 molecules adsorbed on the PVG surface and stabilized on the surface at 77 K.[7] Under appropriate conditions, well-resolved anisotropic hf splittings of ^{14}N have been clearly observed; from them one can deduce the adsorbed state of the radicals on the surface. A similar effect is expected to be observed in the case of the CH_3NH radical, which may be formed by the photolysis of the methylamine adsorbed on the PVG surface. The primary object of this work was to identify radical species generated by the primary photolysis of methylamine. For this purpose, variously deuterated methylamines were utilized as adsorbates. As a result, the dominant radical species produced by the photolysis of methylamines was identified conclusively as of the CH_3NH type, and at the same time valuable information on the interaction between the radical and the surface of the PVG was obtained.

In this report, the ESR findings on the photochemical decomposition of methylamines in the adsorbed state and on the analysis of the ESR spectra of the radical species will be presented.

Experimental

Materials. Two commercial reagents, CH_3NH_2 in an aqueous solution (Wako Junyaku, GR) and $CD_3NH_2 \cdot HCl$ (Merck, GR), were used without further purification. $CH_2DNH_2 \cdot HCl$, a special product of Merck, was kindly offered by Professor Masamichi Tsuboi and Dr. Keietsu Tamagake in this faculty.

Gaseous methylamine was prepared by adding an aqueous solution of methylamine or methylamine hydrochloride to a concentrated potassium hydroxide solution, and dried by passing it through a column packed with potassium hydroxide tablets.

The deuteration of the NH_2 group in methylamine was carried out in the usual manner, D_2O and KOD being used in place of H_2O and KOH.

Procedures. PVG rods (Corning code No. 7930; 4 mm in diameter; 2 cm in length; surface area 75 m^2/sample) were used in all the experiments. The PVG rod was dipped in conc. HNO_3 for a day and then in distilled water for several days. After several repetitions of this procedure, the PVG rod was dried in air at 100 °C and then preheated in air at 500 °C. After the retreatment of the PVG rod with oxygen and evacuation for several hours at 550—600 °C in a quartz sample tube attached to a conventional high-vacuum system, a specified amount of methylamine was introduced into the sample tube at room temperature. The sample tube was then gradually cooled from room temperature to that of liquid nitrogen in order to secure the homogeneous adsorption of methylamine on the PVG surface; it was subsequently submitted to the irradiation and the ESR measurement.

The sample tube was irradiated at 77 K with the light of a low-pressure mercury lamp (UL2-2HQ, 200 W, Ushio Electric Inc.) without any filter, after which the sample tube was immediately transferred into a Dewar vessel inserted in the cavity.

The ESR spectra were recorded at 77 K with a JEOL P-10 spectrometer (X-band, 100 kHz field modulation) equipped with a Dewar insert and a temperature-controlling apparatus.

Results and Discussion

Photoproduced Radical Species. The ESR spectra

* Present address: Faculty of Pharmaceutical Sciences, Nagoya City University, Mizuho-ku, Nagoya.

** Present address: Central Research Division, Takeda Chemical Industries, Ltd., Higashiyodogawa-ku, Osaka.

*** To whom inquiries should be addressed.

of the photoproduced radicals did not practically alter with the change in the amount adsorbed in the range from the monolayer to less than 1/10 of the monolayer. Figures 1, 2, 3, 4, 5, and 6 show some typical ESR spectra of radicals trapped on the surface of PVG at 77 K by the photolysis of CH_3NH_2, CH_3ND_2, CD_3NH_2, CD_3ND_2, CH_2DNH_2, and CH_2DND_2 respectively. Since the free radicals produced from the variously-deuterated methylamines seem to have a common structure, it is appropriate to analyze the ESR spectrum of the simplest one.

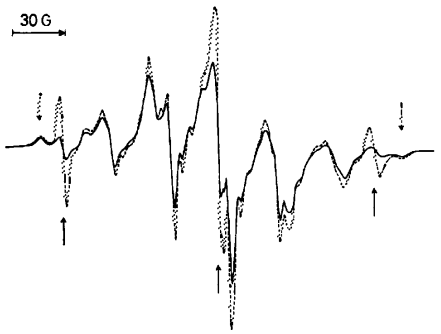

Fig. 1. ESR spectrum of CH_3NH radical on PVG.
Solid line: irradiated for 3 min.
Dotted line: irradiated for 10 min.
Arrows: ←—, CH_2=N radical; ←—, hump

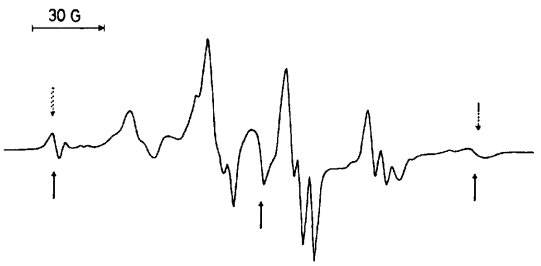

Fig. 2. ESR spectrum of CH_3ND radical on PVG.
Arrows: ←—, CH_2=N radical; ←—, hump

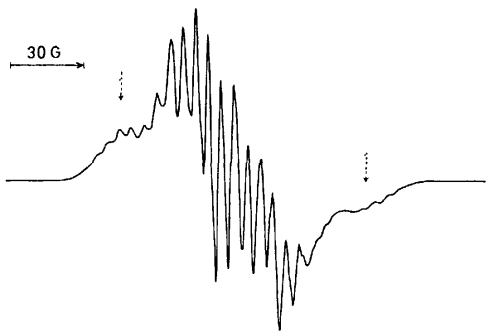

Fig. 3. ESR spectrum of CD_3NH radical on PVG.
Arrows: hump

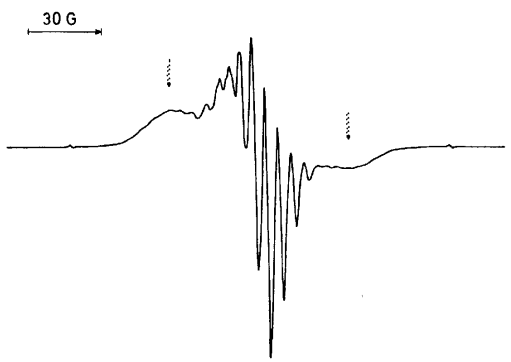

Fig. 4. ESR spectrum of CD_3ND radical on PVG.
Arrows: hump

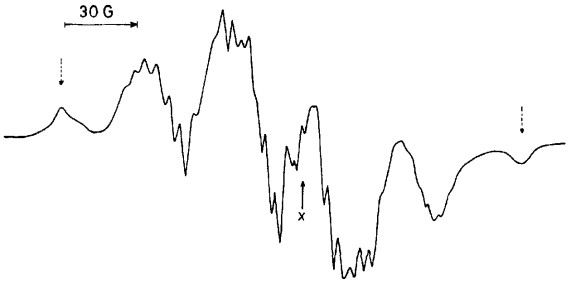

Fig. 5. ESR spectrum of CH_2DNH radical on PVG.
Arrows: ←—x, defect signal; ←—, hump

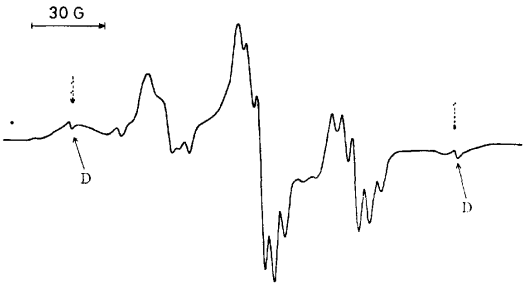

Fig. 6. ESR spectrum of CH_2DND radical on PVG.
Arrows: ←—D, D atom; ←—, hump

In Fig. 2, the spectrum consists of a quartet, whose component splits into a triplet in the higher magnetic field, and of two humps which are on the outer sides of the quartet. Furthermore, besides these lines, there is observed a triplet which is denoted with arrows in the figure. Since this triplet becomes more distinct than the other lines upon prolonged irradiation, it can be attributed to a different radical species from that of the main quartet and humps. A similar distinctive effect of prolonged irradiation on the spectral pattern was also observed in the case of CH_3NH_2, as is shown in Fig. 1.

As to the spectrum of the quartet with a triplet, it can easily be interpreted that the quartet with the splitting of 34 G and the approximate intensity ratio of 1 : 3 : 3 : 1 arises from the hf interaction with three equivalent proton nuclei and its triplet component with one deuteron nucleus, taking account of its approximate intensity ratio of 1 : 1 : 1 and its splitting of 4 G. Moreover, considering that this radical is generated by the photolysis of CH_3ND_2, it can unambiguously be assigned to the CH_3ND radical. The absence of the hf splitting due to the ^{14}N nucleus can reasonably be explained by the fact that the ^{14}N-hf splitting in the NH_2 radical is obscured by a large anisotropy, as has been reported recently by many workers.[8] This interpretation is supported by the existence of outer humps in the spectrum. The present assignment of the radical species is confirmed by mutual and comparative analyses of the spectra in Figs. 1—6,

making use of the theoretical ratio of $a^H/a^D=6.5$. For example, the spectrum in Fig. 1 can be understood to consist of 5 main lines, which arise from the three protons in the methyl group and from one proton in the amino group of the CH_3NH radical; the latter is approximately equivalent with the former. The observed a^H/a^D ratio between the CH_3NH and CH_3ND radicals, 5.5, is close to the theoretical one.

Thus, all the spectra in Figs. 3, 4, 5, and 6 can be identified as those of CD_3NH, CD_3ND, CH_2DNH, and CH_2DND radicals respectively.

TABLE 1. HYPERFINE COUPLING PARAMETERS OF METHYLAMINO RADICALS (G)

Species	a^H_{CH}	a^D_{CD}	a^H_{NH}	a^D_{ND}	$a^N_\perp$	$a^N_\parallel$
CH_3NH	34		22		~0	~40
CH_3ND	34			4	~0	~40
CD_3NH		5	22		~0	~40
CD_3ND		5		5	~0	~40
CH_2DNH	37	4	22		~0	~40
CH_2DND	37	4		4	~0	~40

Observed $a^H/a^D=5\sim8$ (theor.; 6.5)
a^N; estimated from the position of the humps.

The ESR parameters of these radicals are listed in Table 1. The values of the anisotropic hf splitting constants of the ^{14}N nucleus are estimated approximately from the positions of the humps, assuming an axial symmetry in the ^{14}N hf tensors.

The extra triplet lines, growing on prolonged irradiation, may be assigned to the methyleneimino radical, $H_2C=N$,[9] judging from the extraordinary large hf splitting constant of ~87 G. Together with these two radicals, the spectrum of the H or D atom was observed to be small in intensity, in accordance with the poor trapping efficiency for hydrogen atoms on the PVG surface.[11] The ESR spectra of other radicals, such as CH_3 and NH_2, were hardly observed under irradiation for several minutes by means of the light of a low-pressure mercury lamp.

From the above results, the primary process of the photochemical decomposition of methylamine on the surface of PVG can be described as:

$$CH_3NH_2 \xrightarrow{h\nu} CH_3NH + H.$$

The methyleneimino radical may secondarily be produced from the methylamino radical by means of the light of a low-pressure mercury lamp;

$$CH_3NH \xrightarrow{h\nu'} H_2C=N + H_2.$$

However, this process does not seem to be a very efficient one, since the signal intensity of this radical is much smaller than that of the methylamino radical, regardless of the prolonged irradiation.

For comparison, the photolysis of the dimethylamine-d_1 ($(CH_3)_2ND$) adsorbed on the surface of the PVG was carried out under the same conditions. The result is shown in Fig. 7. Although the methyl radical is slightly perceptible in the spectrum, as is indicated by

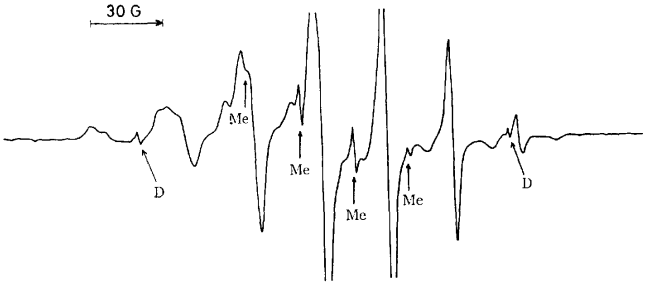

Fig. 7. ESR spectrum of $(CH_3)_2N$ radical on PVG.
Arrows: Me, CH_3 radical; D, D atom

the arrows in the figure, its signal intensity is very small compared with that of the $(CH_3)_2N$ radical. Therefore, the primary photochemical process is considered to be the rupture of the N–D bond, as in the case of monomethylamine, and the possibility of the C–N bond scission seems to be negligibly small. This was further supported by the finding that the $H_2C=N$ radical, which might secondarily be produced from the CH_3NH radical, was not observed, not even on prolonged irradiation.

It may be worthwhile to refer here to the important role of the PVG in the photodecomposition of methylamine. Since gaseous methylamine is essentially transparent above 240 nm, and since the PVG is opaque below 220 nm, it seems that the quantity of light quanta limited in a narrow range of wavelengths between 220 and 240 nm are not sufficient for the photodecomposition of methylamine as far as the direct absorption of photons by the methylamine molecule is concerned. Really, the efficiency of the photodecomposition of methylamine, as deduced from the signal intensities of the photoproduced radicals, is considerable. Therefore, the methylamino radicals are considered to be produced from methylamines not by the photochemical direct process, but by a photosensitized process resulting from some metal impurities in the PVG, analogously to our previous findings on the photosensitized decompositions of hydrocarbons and hydrogen molecules on the surface of the PVG coated with transition-metal oxides.[10,11]

Anisotropic ^{14}N-hf Splitting of the Methylamino Radical. As was described in the previous section, the hf interaction of ^{14}N is expected to have a large anisotropy. The angular-dependent hf values of $a_\perp^N\sim0$ and $a_\parallel^N\sim$ 40 G were estimated on due basis of the anisotropic spectral patterns of the radicals and the findings on the NH_2 radical.[8] Because of this anisotropy, the linewidth of the lines due to $m_I^N=\pm1$ is expected to be spread over about 40 G, so that the $m_I^N=\pm1$ lines are obscured. As a result, only the isotropic proton lines are observed as sharp lines, while the $m_I^N=\pm1$ lines are recognized as humps on both sides of the proton lines. This is the reason why the hf splitting due to ^{14}N is apparently quenched in all the spectra of the methylamino radicals observed in this study.

On the other hand, the linewidth of each line is too broad compared with the difference in the g tensors, $\Delta g=g_\perp-g_\parallel$, for the precise value of Δg to be decided.

However, a linewidth alternation with a change in the proton quantum numbers is clearly observable in most spectra. For example, in the case of the CD_3ND radical (Fig. 4), the hf splittings due to the D nucleus are much more distinct in the higher magnetic field. This phenomenon in the linewidth shows the simultaneous existence of small anisotropies in both g and hf tensors.[12] Therefore, the magnitude of the anisotropies in g and hf tensors is considered to be as small as the order of the linewidth of the spectra.

Isotope Effect of D-Substitution in the Methyl Group on the β-Proton Hf Splitting. As is shown in Table 1, the substitution of a D atom in the methyl group of the methylamino radical causes an abnormal increase in the β-proton hfs constant over than the value expected from that of the undeuterated radical; that is, it increases from the value of $a^{H}_{CH_3}=34$ G in the CH_3NH (or CH_3ND) to that of $a^{H}_{CH_2D}=37$ G in the CH_2DNH (or CH_2DND) radical. This rather large isotope effect can not be explained by that observed in deuterated methyl radicals, which has been extensively investigated by many workers from both experimental and theoretical aspects.[13] The latter isotope effect has now been established to be attributable to the change in the s-character of the carbon 2pπ-orbital occupied by an unpaired electron due to the change in the out-of-plane vibration, and the magnitude of this effect has been shown to be quite small; moreover, the effect due to the D-substitution is in the negative direction. Therefore, it seems that the isotope effect in the β-position is different from that in the α-position. This may be quite natural considering that the origin of the hf splitting of the β-proton can be explained by the hypercojugation mechanism, while that of the α-proton can be explained by the spin-polarization mechanism.

As is well known, the hf splitting of the β-proton is given by a relation such as:

$$a_{\beta}^{H} = B + A\cos^2\theta$$

where B and A are constants, and θ, the dihedral angle between the 2pπ-orbital and the C–H bond in the methyl group. For a rapidly-rotating methyl group in the methylamino radical, neglecting B compared with the second term, the $\cos^2\theta$ in the second term is averaged to 1/2, thus leading to this equation: $a_{\beta}^{H}=1/2A$. As long as the isotropic free rotation of the methyl group is assumed, the ratio between the hfs constants of H and D in the methyl group of the CH_2DNH (or CH_2DND) radical should also coincide with the theoretical one. However, this is not the case. This rather large deviation may be explained by the following postulation;[14] the internal rotation of the methyl group resulting from asymmetric substitution with a deuterium atom is no longer isotropic, and an anisotropic averaging may occur over internal rotation, with a preferential orientation of the 2pπ-orbital coplanar with the C–H bond in the methyl group of the β-substituted methylamino radical.

The same isotope effect has recently been observed more distinctively in a complete set of deuterated ethyl radicals, which have been produced by the trapping of hydrogen atoms with ethylene molecules preadsorbed on the surface of the PVG coated with vanadium oxide, which acts as a photosensitizer for the dissociation of hydrogen molecules with the light of a wavelength longer than 350 nm.[11]

According to the above explanation, it is necessary also that $a^{D}_{CH_2D}$ be smaller than $a^{D}_{CD_3}$. Unfortunately, however, the experimental accuracy is not sufficient to ascertain this point because of the rather large linewidth of the adsorbed radicals.

Rotational State of the Methylamino Radical on the PVG Surface. As has been described above, the methylamino radicals trapped on the surface of the PVG have the following characteristics:

(1) Little anisotropy is observed in the methyl-proton hf splitting.

(2) The anisotropy in the nitrogen-proton hf is relatively larger than that of the methyl-proton, judging from the linewidth difference between the CH_3ND and CH_2DNH radicals.

(3) The anisotropy in the ^{14}N hf splitting is quite large, and the values of $a_{\parallel}^{N}\sim40$ and $a_{\perp}^{N}\sim0$ G were estimated.

From (1), the rotation of the methyl group around the axis of the C–N bond is inferred to be rapid enough, and the methyl group is judged to be free from interaction with the surface of the PVG. The (2) and (3) show that the NH group interacts strongly with the surface, and that it rotates approximately around the axis of the 2pπ-orbital of nitrogen. The rotation around the 2pπ-axis may be explained by the fact that the value of $a_{\parallel}^{N}\sim40$ G for the methylamino radical is very close to that of $a_{\parallel}^{N}=\sim38$ G for the NH_2 radical, which is the principal value for the direction of the 2pπ-orbital of the nitrogen of the NH_2 radical.[7,8]

The authors are indebted to Professor Masamichi Tsuboi and Dr. Keietsu Tamagake for their kind offer of the precious reagent $CH_2DNH_2\cdot HCl$.

References

1) J. G. Calvert and J. N. Pitts, Jr., "Photochemistry," John Wiley & Sons, Inc. (1966).

2) P. W. Atkins and M. C. R. Symons, "The Structure of Inorganic Radicals," Elsevier Pub. Co. (1967).

3) S. G. Hadley and D. H. Volman, *J. Amer. Chem. Soc.*, **89**, 1053 (1967).

4) G. V. Pukhal'skaya, A. G. Kotov, and S. Ya Pshezhetskii, *Dokl. Akad. Nauk SSSR*, **171**, 1380 (1966).

5) D. Cordischi and R. Di Blasi, *Can. J. Chem.*, **47**, 2601 (1969).

6) J. Turkevich and Y. Fujita, *Science*, **152**, 1619 (1966); N. Shimamoto, Y. Fujita, and T. Kwan, This Bulletin, **43**, 580 (1970).

7) Y. Fujita, N. Shimamoto, K. Hatano, and T. Kwan, Preprint, 10th Symposium on Electron Spin Resonance, Osaka, Japan, 1971; munuscript is in preparation.

8) O. I. Brotikovskii, G. M. Zhidmirov, V. B. Kazanskii, A. I. Mashchenko, and B. N. Shelimov, *Kinet. Katal.*, **12**, 700 (1971); E. F. Vansant and J. H. Lunsford, *J. Phys. Chem.*, **76**, 2716 (1972).

9) F. J. Adrian, E. L. Cochran, and V. A. Bowers, *Advan. Chem. Ser.*, **36**, 50 (1962); S. A. Marshall, A. R. Reinberg, R. A. Serwey, and J. A. Hoges, *Mol. Phys.*, **8**, 223 (1964).
10) Y. Fujita, K. Hatano, M. Yanagita, T. Katsu, M. Sato, and T. Kwan, This Bulletin, **44**, 2884 (1971).
11) T. Katsu, M. Sato, and Y. Fujita, *J. Phys. Chem.*, **76**, 2637 (1972).
12) A. Carrington and A. D. McLachlan, "Introduction to Magnetic Resonance," Harper & Row. (1967).
13) R. W. Fessenden, *J. Phys. Chem.*, **71**, 74 (1967).
14) R. W. Fessenden and R. H. Schuler, *J. Chem. Phys.*, **39**, 2147 (1963).

The Phenanthrene/Anthracene–Picric Acid System

Shigeo KOIZUMI* and Yoshio MATSUNAGA**

Department of Chemistry, Faculty of Science, Hokkaido University, Sapporo 060

(Received July 17, 1973)

The phase relations in the phenanthrene/anthracene–picric acid system have been determined by calorimetry and X-ray diffraction. Four series of solid solutions occur in this system: the terminal solid solutions P and A, which are based on the parent picrate lattices, and the I and II solutions, which are based on the incongruently-melting ternary compounds. A eutectic is observed at about 47 mol% anthracene and at 124 °C. Enantiotropic transitions appear at about 76, 103, and 120 °C in the I solid solution and at about 80, 103, and 120 °C in the II solid solution. The Gibbs energy of formation from the solid component compounds has been estimated as −2.04, −1.67, −1.21, and −0.68 kcal/mol for the stable forms at the room temperature of the phenanthrene picrate, the I solid solution (at 34.58 mol% anthracene), the II solid solution (at 58.96 mol%), and the anthracene picrate respectively. The two transitions in the phenanthrene picrate have been shown to be easily detectable by recording the electrical resistivity as a function of the temperature.

The mutual solid solubility in many pairs of molecular complexes has been examined by Rheinboldt and Senise and by Lower;[1,2] however, no determination of the phase boundaries in the solids has been reported except for phenanthrene/anthracene–*s*-trinitrobenzene. In connection with our finding of the marked effects of impurities on an enantiotropic transition at 77 °C in phenanthrene picrate,[3,4] we have determined the phase diagram of the phenanthrene/carbazole–picric acid system. As part of our general interest in the physical properties of solid molecular complexes, we decided to study further the phase diagram of a binary system with phenanthrene picrate as one component. The system chosen was phenanthrene/anthracene–picric acid because a comparison of it with the phenanthrene/anthracene–*s*-trinitrobenzene system studied by Lower seemed to be interesting.

Experimental

Materials. Phenanthrene, Eastman white label, was purified according to the method reported by Feldman *et al.*[5] and then zone-refined. Pure anthracene was obtained by the reduction of anthraquinone prepared starting from benzene and phthalic anhydride. Picric acid, Wako special reagent, was twice recrystallized from ethanol. The picrate of the former hydrocarbon was crystallized from methanol and that of the latter, from carbon tetrachloride, as has been described by Kofler.[6] They were mixed together in various ratios and then fused in a small test tube by heating in an oil-bath for a short time. The melt was well shaken and then rapidly cooled. Finally the samples were kept at room temperature for various periods of time. Over forty samples were prepared for the examinations.

Measurements. Calorimetric curves up to the thaw points were recorded on a Rigaku Denki differential scanning calorimeter, Model 8001 SL/C, at a heating rate of 3 °C/min. The heats of transitions were estimated by comparing the peak areas with that for the transition in hexamethylbenzene, which is known to take place at 110.6 °C with ΔH=0.422 kcal/mol.[7] The melting points were visually measured with a magnifying lens and a polarizer. X-Ray measurements on powdered samples were made with a Toshiba recording diffractometer, Model ADG-301, with filtered copper radiation. In order to examine the powder pattern at various temperatures, the sample was mounted on an aluminum plate with a 20 W heater attached to the other side. The temperature of the plate was controlled with the aid of an autotransformer and was monitored by means of a copper-constantan thermocouple.

The approximate values of the Gibbs energy of formation at 25 °C from the solid-component compounds (ΔG_f, kcal/mol) were determined from the $\Delta G_f = RT \cdot \ln(c_2/c_1)$ relation, where c_1 (mol/l) is the concentration of undissociated picric acid in the saturated aqueous solution of picric acid and where c_2 is its concentration in equilibrium with a solid complex and solid hydrocarbon.[8] The assumption is made that the solutions are sufficiently dilute for the activities to be proportional to the concentrations. The total concentrations of picric acid (C, mol/l) in these solutions were measured by the spectrophotometric method and also by the gravimetric method.

The electrical resistivity of the hydrocarbon picrates was measured on pressed pellets by the two-probe method. The pellet and its holder were accommodated in a brass cylinder and were slowly heated with an electric furnace. During this process, the temperature of the holder was recorded on the X-axis of a Yokogawa X–Y recorder, Type 3078, and the current was amplified by a Keithley 3010 operational amplifier on the Y-axis.

Results and Discussion

Phase Diagram. If only the thaw-point-melting-point method of Rheinboldt was employed,[9] one would conclude that this system is of the V type in the Roozeboom classification of two-component solid solutions,[10] as are the phenanthrene/anthracene–*s*-trinitrobenzene and phenanthrene/carbazole–picric acid systems.[2,4] The eutectic is located at about 47 mol% anthracene and at 124 °C. Actually, the phase relations in this "immiscibility region", extending from about 20 to 80 mol% anthracene, are not at all simple. The appearance of two solid solutions is shown by X-ray diffraction patterns distinctly different from those of the terminal solid solutions. Although peritectics cannot be located in Fig. 1, these two solid solutions based on new ternary molecular complexes appear to melt incongruently. Therefore, the whole diagram is a combination of two diagrams of the IV type and

* Present address: Fuji Photo-Film Co., Minami-ashigara, Kanagawa.

** To whom inquiries may be addressed.

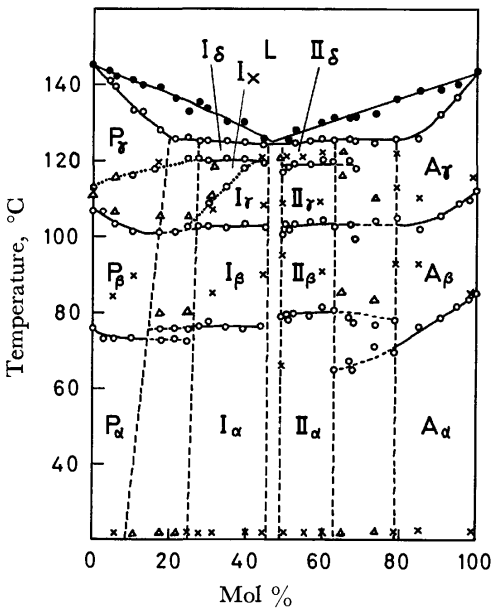

Fig. 1. The phenanthrene/anthracene–picric acid phase diagram: × single phase by X-ray diffraction, △ two phases by X-ray diffraction.

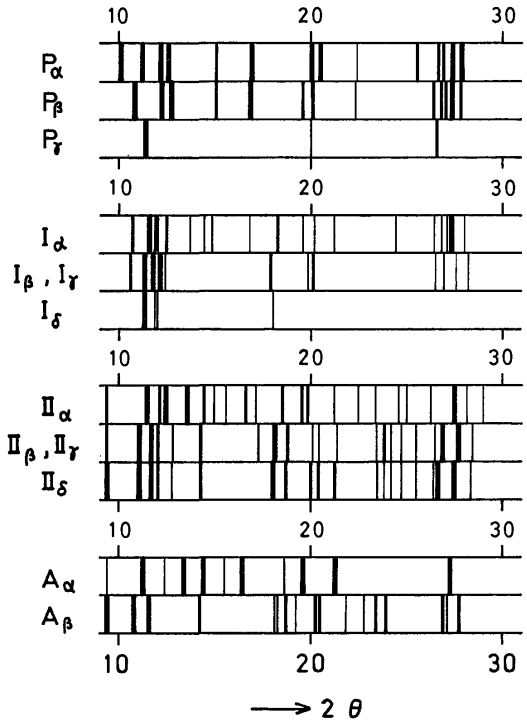

Fig. 2. X-Ray diffraction patterns of the phenanthrene/anthracene–picric acid system: the solid solution I at 31.18 mol % anthracene, the solid solution II at 58.86 mol %.

one of the V type in the Roozeboom classification. The solid solutions, I and II, may be regarded as non-stoichiometric compounds.

As was described in our earlier notes,[3,4] two enantiotropic transitions are observed in the P solid solution. The three phases, denoted as P_α, P_β, and P_γ in Fig. 1, can be well distinguished from each other by the X-ray method (see Fig. 2). It must be noted that the pattern given by the P_γ phase is very simple. The change from P_β to P_α is slow, and it becomes slower upon the addition of anthracene picrate;[3] therefore, the P_α phase can be observed up to only 4 mol% with the samples annealed for one week instead of 9 mol%, as is indicated in Fig. 1. After the same period of storage, the samples in the composition range from 4 to 6.5 mol% were shown by X-ray examination to be mixtures of P_α and P_β and only the P_β phase was found between 6.5 and 12 mol%. These observations are in reasonable agreement with the results of calorimetry reported previously.[3] The anthracene-rich solid solution P is metastable. The samples in the composition range from 9 to 12 mol% became mixtures of the P_α and I_α phases upon standing for five months. The P_β phase is gradually transformed into P_γ upon heating when the anthracene picrate is added. The dotted curve indicates the upper limit of the temperature range given by the point of return to the base line of the calorimetric curve. The temperature-dependence of the X-ray diffraction pattern also shows the coexistence of the P_β and P_γ phases over a wide temperature range.

The I solid solution, examined within one week after melting, exhibits only an enantiotropic transition near 120 °C. After the samples have been left at room temperature for three months, the I_α phase, extending from about 25 to 45 mol% anthracene, appears. Upon heating, two more well-separated endothermic peaks are observed at about 76 and 103 °C (see Fig. 1). Although the enthalpy changes at these transitions are comparable, the I_γ phase cannot be distinguished from I_β by X-ray diffraction. In addition, one or two extra peak(s) partially overlapped with the one near 120 °C are detectable below 40 mol% anthracene. The dotted curve in this composition range was drawn on the basis of the point of departure from the base line of the calorimetric curve. The X-ray diffraction also shows that the solid solution above this boundary is heterogeneous. The phase(s) appearing in this region could not be clarified; therefore, the region is denoted as I_x in the diagram. The absence of the transitions from I_α to I_β and from I_β to I_γ, the temperatures of which are close to those of the transitions from P_α to P_β and from P_β to P_γ, in newly-prepared samples can be considered as additional evidence of the appearance of the I solid solution. The range of the solid solution embraces such simple compositions as 2:5, 1:2, 2:3, and 3:4. For the present, there is no *a priori* reason for preferring any one of the possible compositions.

The II solid solution extends from about 49 to 63 mol% anthracene after storage for several months. Upon heating, three transitions, the temperatures of which are essentially the same as those in the I solid solution, are observed by the calorimetric method. The enthalpy change at the transition from II_β to II_γ is small, and these two phases are not distinguishable from each other by X-ray diffraction. Nevertheless, the recovery of the II_β phase from the II_γ phase is so slow that II_γ and II_δ are the only phases observable if the sample is examined within a day after melting. Qualitatively speaking, the behavior of the II solid

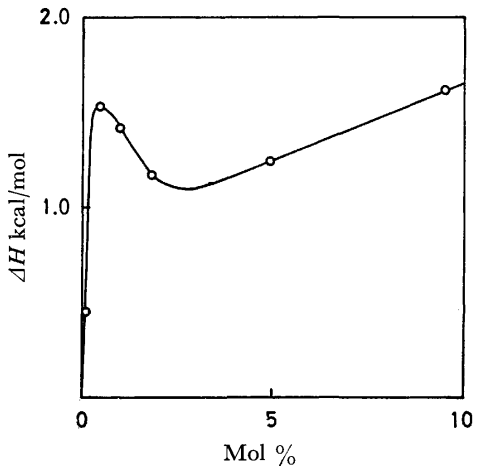

Fig. 3. Heat of the transition from A_β to A_γ plotted against the amount of added phenanthrene picrate.

solution is similar to that of the I solid solution. However, it must be noted that the diffraction patterns observed with the former solid solution are more complicated than those observed with the latter. Possible simple compositions included in the range of solid solution are 1:1, 5:4, 4:4, 3:2, and so forth.

The limit of the solubility of phenanthrene picrate into anthracene picrate is about 20 mol%. Although only one transition (at 85 °C) is seen in pure anthracene picrate, an additional transition detectable only by the calorimetric method appears in this terminal solid solution. Even the addition of as little as 0.1 mol% of phenanthrene picrate is enough to induce a sizable peak. The amount of the heat of this new transition is plotted against the composition in Fig. 3. The enthalpy and entropy of the transition both reach their maximum values at 0.5 mol% phenanthrene, and then reach their shallow minima around 3 mol%. The transition temperature and the amount of the enthalpy and entropy changes for representative samples of the four series of solid solutions are summarized in Table 1.

Gibbs Energy of Formation. The concentration of

Table 1. Transition temperatures and enthalpy and entropy changes of the representative samples in the phenanthrene/anthracene–picric acid system

Sample		Transitions		
		$\alpha\rightarrow\beta$	$\beta\rightarrow\gamma$	$\gamma\rightarrow\delta$
Phenanthrene picrate	T (°C)	77	106	—
	ΔH(kcal/mol)	1.10	3.10	—
	ΔS(e.u.)	3.1	8.2	—
Solid solution I	T (°C)	76	103	120
(at 31.18 mol%)	ΔH(kcal/mol)	0.66	0.76	0.88
	ΔS(e.u.)	1.9	2.0	2.3
Solid solution II	T (°C)	80	103	119
(at 59.86 mol%)	ΔH(kcal/mol)	2.39	0.06	0.72
	ΔS(e.u.)	6.8	0.16	1.8
Anthracene picrate	T (°C)	85	112[a]	—
	ΔH(kcal/mol)	3.50	1.53[a]	—
	ΔS(e.u.)	9.8	4.4[a]	—

a) With 0.5 mol% of phenanthrene picrate.

Table 2. Stabilities of solid hydrocarbon picrates at 25°C

Compound	C(mol/l)	$-\Delta G_f$ (kcal/mol) This work	$-\Delta G_f$ (kcal/mol) Literature[a]
Naphthalene picrate	0.00656	2.10	2.05,[8] 2.08[13] 2.07,[14] (2.08)[16]
Phenanthrene picrate	0.00797	2.04	(2.41)[16]
Phase I_α (at 34.58 mol%)	0.0116	1.67	—
Phase II_α (at 58.96 mol%)	0.0174	1.21	—
Anthracene picrate	0.0283	0.68	(0.84)[16]
Picric acid	0.0573	—	—

a) The values in parentheses are for the corresponding *s*-trinitrobenzene complexes.

picric acid (C) in equilibrium with the solid hydrocarbon picrates and the Gibbs energies of formation (ΔG_f) from their parent solids are collected in Table 2. As naphthalene picrate is the only hydrocarbon picrate for which the Gibbs energy of formation is available in the literature, this picrate was included in our measurements for the sake of comparison. The concentrations given here were spectrophotometrically measured and were in reasonable agreement with those obtained by the evaporation of the solutions to dryness—*e.g.*, 0.0572 mol/l for picric acid and 0.0173 mol/l for the II solid solution. The dissociation constant of picric acid in an aqueous solution is required in order to calculate the concentration of undissociated acid. Four values ranging from 0.196 to 0.60, have been compiled by Kortüm *et al.*[11] Of these, the compilers have considered the value of 0.381 by Halban and Seiler to be most reliable.[12] However, the Gibbs energy of the formation of naphthalene picrate calculated with this constant, −2.44 kcal/mol, is appreciably larger than the value of −2.05 kcal/mol at 20 °C reported by Brönsted,[8] the value of −2.08 kcal/mol at 3 °C reported by Brown from cryoscopic measurements in nitrobenzene,[13] and also the value of −2.07 kcal/mol at 25 °C reported by Bell and Fendley from direct electrometric measurements.[14] On the other hand, the constant determined by Dippy *et al.* gives a value of 2.10 kcal/mol, which is in fair agreement with the above-mentioned literature values. Consequently, the energies in Table 2 were calculated using the latter value, that is, 0.196.[15]

Hammick and Hutchison have determined the Gibbs energies of formation for ten hydrocarbon-*s*-trinitrobenzene complexes and have noted that the value for the naphthalene complex is very close to that of the corresponding picrate.[16] On the basis of the data of this pair only, they have concluded that there is no very great difference in the stabilities of the solid picrates and the corresponding *s*-trinitrobenzene complexes. Our results are in accordance with their conclusion. However, it may be noted that the relative stabilities are not parallel in these two series. Such an inversion of the relative stabilities of naphthalene and phenanthrene has also been found in the *s*-tri-

nitrobenzene and the trinitrotoluene complexes studied by Hammick and Hutchison.

The values of the Gibbs energy of formation listed in Table 2 indicate that the I_α phase is more stable by 0.10 kcal/mol, while the II_α phase is less stable by 0.03 kcal/mol, than mixtures of the parent picrates. Although the latter difference is within the limits of our experimental error, strictly speaking, the comparison must be made with mixtures of the P_α phase containing about 9 mol% anthracene and the A_α phase containing about 20 mol% phenanthrene. As these solid solutions are, to some extent, more stable than the pure picrates, it is almost certain that the II_α phase is metastable. So far, though, we have not succeeded in the crystallization of the I and II solid solutions from solutions. The possibility that the I solid solution disappears if the samples are stored for a sufficiently long time cannot be completely eliminated.

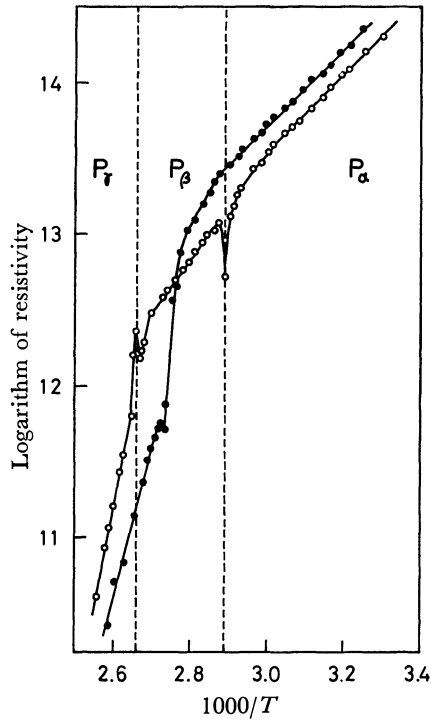

Fig. 4. Electrical resistivity of compressed phenanthrene picrate: ○ ascending temperature, ●: descending temperature.

Electrical Resistivity. The logarithm of the resistivity of the phenanthrene picrate, recorded at ascending and descending temperatures, is plotted against the reciprocal temperature in Fig. 4. In the former process, not only the changes in the slope but also the minima were observed at the transition temperatures. The minimum at the transition from P_α to P_β is deep and sharp, while that from P_β to P_γ is shallow and broad. The activation energy for semiconduction tends to be large in the high-temperature phase. The resistivity at 25 °C is in the order of 10^{14} ohm cm. This value is appreciably smaller than that reported for the corresponding *s*-trinitrobenzene complex. Kuroda *et al.* have measured the temperature-dependence of the resistivity of the *s*-trinitrobenzene complex in a range from room temperature to a little below the melting point; they obtained 7×10^{18} ohm cm for the resistivity at 15 °C and 1.24 eV for the activation energy.[17] The latter quantity in the picrate is smaller by a factor of approximately two in the P_α and P_β phases and larger almost by the same factor in the P_γ phase. The presence of an enantiotropic transition located 15 °C below the melting point has been reported in the phenanthrene–*s*-trinitrobenzene complex by Kofler.[6] Nevertheless, no anomaly in the resistivity due to this transition has been noted by Kuroda *et al.* The appearance of a sharp resistivity minimum at the transition point has been found in Würster's blue perchlorate by Pott and Kommandeur.[18] Contrary to our case, this phenomenon could be observed only on crystals, not in compressed polycrystalline samples. As is shown in Fig. 4, there is a large hysteresis in the high-temperature region. A delayed transition from P_γ to P_β could be detected by the resistivity measurements. Moreover, the activation energies observed in the cooling process are little smaller than those observed in the heating process.

Although a gradual change in slope in the resistivity curves was observed near the transition temperature(s) in the anthracene picrate and in that doped with phenanthrene picrate (1 mol%) upon an increase in the temperature, no resistivity minimum at the transition temperature(s) was detected with these samples. Again, the resistivity at 25 °C is in the order of 10^{14} ohm cm, which is about one-hundredth of the resistivity of the anthracene–*s*-trinitrobenzene reported by Kuroda *et al.* Such a large difference is in marked contrast to the observations made by Labes *et al.* that the resistivity of coronene–picric acid is of the order of 10^{12} ohm cm, while that of the corresponding *s*-trinitrobenzene complex is 10^{13} ohm cm at room temperature.[19]

The authors wish to express their thanks to Professor Toshio Yokokawa for letting them use the X-ray diffractometer.

References

1) H. Rheinboldt and P. Senise, *Bols. faculdade filosofia, cienc. letras. Univ. São Paulo*, **14**, *Quimica* No. 1, 3 (1942), through *Chem. Abstr.*, **40**, 2049 (1946).
2) S. K. Lower, *Mol. Cryst. Liq. Cryst.*, **5**, 363 (1969).
3) Y. Matsunaga, This Bulletin, **44**, 2868 (1971).
4) S. Koizumi and Y. Matsunaga, *ibid.*, **46**, 1875 (1973).
5) J. Feldman, P. Pantages, and M. Orchin, *J. Amer. Chem. Soc.*, **73**, 4341 (1951).
6) A. Kofler, *Z. Elektrochem.*, **50**, 200 (1944).
7) M. E. Spaght, S. B. Thomas, and G. S. Parks, *J. Phys. Chem.*, **36**, 882 (1932).
8) J. N. Brönsted, *Z. Phys. Chem.*, **78**, 284 (1912).
9) H. Rheinboldt, *J. Prakt. Chem.*, (2) **111**, 242 (1925).
10) H. W. B. Roozeboom, *Z. Phys. Chem.*, **30**, 385 (1899).
11) G. Kortüm, W. Vogel, and K. Andrussow, "Dissociation Constants of Organic Acids in Aqueous Solution", Butterworths, London (1961), p. 453.
12) H. v. Halban and M. Seiler, *Helv. Chim. Acta*, **21**, 385 (1938).
13) F. S. Brown, *J. Chem. Soc.*, **1925**, 345.
14) R. P. Bell and J. A. Fendley, *Trans. Faraday Soc.*, **45**,

121 (1949).
15) J. F. J. Dippy, S. R. C. Hughes, and J. W. Laxton, *J. Chem. Soc.*, **1956**, 2995.
16) D. L. Hammick and H. P. Hutchison, *ibid.*, **1955**, 89.
17) H. Kuroda, K. Yoshihara, and H. Akamatu, This Bulletin, **35**, 1604 (1962).
18) G. T. Pott and J. Kommandeur, *J. Chem. Phys.*, **47**, 395 (1967).
19) M. M. Labes, R. Sehr, and M. Bose, *ibid.*, **33**, 868 (1960).

The ESR of the Fast-rotating $-CH_2$ of the Radical Formed by the Photolysis of CH_2I_2 on Silica Gel

Kazuo SHIMOKOSHI

Department of Chemistry, Tokyo Institute of Technology, Ohokayama, Meguro-ku, Tokyo 152

(Received July 26, 1973)

The electron spin resonance spectra have been measured for the radical formed by the photolysis of methylene iodide adsorbed on silica gel. The spectra were anisotropic and were attributed to the radical of the $\equiv Si-O-CH_2$ form by an analysis of the hyperfine splittings due to two protons, taking into consideration the photochemical processes on the silica gel surface. From a line-shape analysis of the observed spectrum, the following anisotropic hyperfine interaction parameters for the protons and g-value have been obtained:

$$\mathbf{A}_{//} = 28.5 \pm 0.5\text{G}, \quad \mathbf{A}_{\perp} = 18.8 \pm 0.5\text{G}, \quad g = 2.0030 \pm 0.0005.$$

It has been concluded from the analysis of the spectra that the hyperfine structure observed with axially-symmetric tensors is a result of the fast internal rotation of the methylene group of the radical.

The effects of the internal motion of radicals on the ESR spectrum have been reported by many authors. The reorientation of terminal methylene has been found in the CH_2COO^- radical, formed by the irradiation of glycine,[1] triglycinesulphate,[2] zinc acetate, and sodium acetate.[3] Of these, CH_2COO^- in zinc acetate has been studied extensively by Hayes *et al.*[4] and by Ohigashi and Kurita,[5] who have studied the temperature dependence of the hyperfine pattern in the light of the internal rotation of the methylene group. Lefebvre and Maruani[6] have theoretically shown the effect of the fast-rotating methylene group on the spectrum of randomly-oriented radicals in solids, in particular the case of CH_2COOH, by means of computer simulation. More recently, McDowell, Raghunathan and Shimokoshi[7] have reported this effect in the interpretation of the anisotropic spectrum of an ethyl radical trapped in an argon matrix at 4.2 K, taking into consideration the free rotation of the methylene group in the radical.

On the other hand, the surface properties of silica gel have been the subject of much research. ESR investigations of the radicals formed on the surface have also provided detailed information about the surface properties, together with the mechanism of the radical formation. Recently, Melamund *et al.*[8] have observed the radical ($\equiv Si-O-CH_2$) formed by the photolysis of methylated Vycor glass and have discussed the mechanism of the formation of the radical. However, they did not give the anisotropic hyperfine coupling of the protons based on the internal rotation of the methylene group. This paper will report the results of our ESR studies of the fast-rotating methylene group of the radical formed by the photolysis of CH_2I_2 on silica gel.

Experimental

Silica gel (SILICAR TLC-7GF) was introduced into a 3 mm *i.d.* quartz tube and pretreated at various temperatures (200—900 °C) for 2—12 hr in a vacuum. Methylene iodide obtained from the Eastman Co., Ltd., was purified by vacuum distillation before use. After the pretreatment, the silica gel was brought into contact with various amounts of methylene iodide at room temperature. In order to obtain a high concentration on the surface, methylene iodide was condensed by cooling the samples to 77 K.

In addition to this procedure, the pretreated silica gel was exposed to a small amount of water vapor (0.1—2.0 Torr) before the contact of methylene iodide. Remarkable effects were thus observed in the case of the samples pretreated at temperatures higher than 600 °C.

After sealing off the tube, the samples were cooled in a liquid nitrogen Dewar, placed in an X-band cavity of a JES 3 BSX spectrometer, and irradiated by means of a low-pressure mercury lamp which emitted the 2537 and 1849 Å wavelengths. For purposes of comparison, samples which had never been exposed to methylene iodide were irradiated under the same conditions as those used for the methylene iodide samples.

Results and Discussion

After irradiation for several minutes, the samples turned brown and the ESR spectra were observed. The spectrum shown in Fig. 1 is typical; it was obtained at 77 K by the irradiation of samples pretreated at 400 °C or lower for 2—6 hr. When the samples pretreated at 700 °C or higher for 2—12 hr, the spectra obtained by the irradiation were complicated and very different from that shown in Fig. 1. However, the

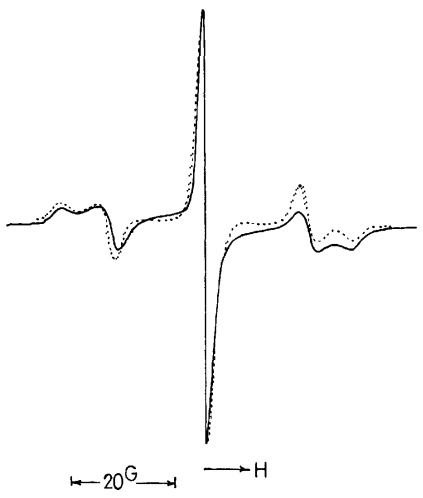

Fig. 1. The spectrum (full line) obtained by the photolysis of CH_2I_2 on silica gel at 77 K. The broken line shows calculated spectrum with the ESR parameters of $\mathbf{A}_{//}=28.5$ G, $\mathbf{A}_{\perp}=18.8$ G and $g=2.0030$.

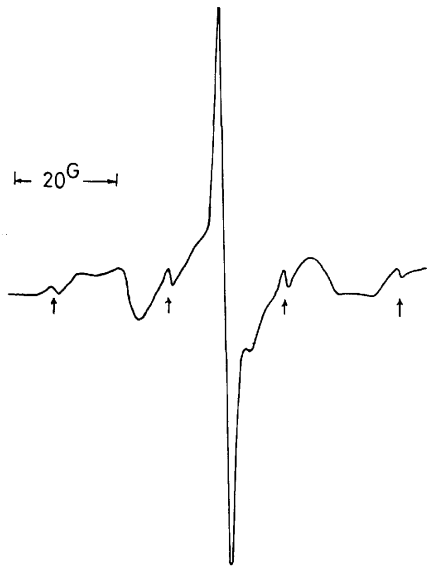

Fig. 2. The spectrum obtained by the photolysis of condensed CH_2I_2 on silica gel at 77 K. Arrows show the lines due to methyl radical.

same spectrum as that of Fig. 1 appeared again with much less intensity upon the irradiation of the samples treated at 700 °C when a small amount of water vapor was admitted onto the samples before they adsorbed the methylene iodide. The spectrum shown in Fig. 2 was obtained by the irradiation of concentrated methylene iodide on silica gel pretreated at 400 °C. Obviously, the spectrum is identical with that shown in Fig. 1 except that weak signals due to the methyl radical are present. This spectrum disappeared when the samples were warmed to 150 K. The irradiation of silica gel under the same conditions as in the case of methylene iodide samples showed very weak signals. The absorption lines due to the hydrogen atom and an asymmetric line near $g=2$, which is also seen in Figs. 1 and 2 with much less intensity than the other lines, were observed upon further irradiation.

Methylene iodide has absorption maxima at 2890, 2490, and 2120 Å.[9] Gregory and Style[10] have done the photolysis of this compound at 3100 Å mainly and have thus produced methylene, although they were not certain whether the primary process was

$$CH_2I_2 + h\nu \longrightarrow CH_2I + I \quad (1)$$

followed by

$$CH_2I \longrightarrow CH_2 + I \quad (2)$$

or a direct process;

$$CH_2I_2 + h\nu \longrightarrow CH_2 + I_2(2I) \quad (3)$$

The primary process in the vacuum ultraviolet photolysis has been studied by Style and Ward,[11] who suggested that the irradiation with 1250—2000 Å excites the fluorescence spectrum of iodine. They concluded that the process was as follows:

$$CH_2I_2 + h\nu \longrightarrow CH_2 + I_2^* \quad (4)$$

Therefore, it is likely that methylene is formed primarily in the present system by photolysis.

It is also of interest to observe the ESR spectrum of the free methylene radical formed in the present system. The methylene radical is triplet in its ground state; its ESR spectrum has been observed by Bernheim *et al.*[12] and by Wasserman *et al.*,[13] who have reported the values of spin-spin interaction as $D=0.7$—$0.9\ cm^{-1}$ and $E\cong 0.03\ cm^{-1}$. However, no spectrum could be detected up to 10000 G in the present experiments except for that shown in Figs. 1 and 2. If the motion of the radical is random and rapid enough to average out such a large spin-spin interaction, it may be possible to observe the spectrum of the radical in the near $g=2$ region. In this case, however, the spectrum is expected to be rather isotropic in its hyperfine structure, unlike the spectrum shown in Fig. 1, even though the hyperfine splittings due to the protons of free methylene are comparable to that measured from the observed spectrum.*1 Further, a preferential rotation of the radical around any axis may not cancel out the fine structure in the spectra of the randomly oriented powder specimens. Therefore, the spectrum shown in Fig. 1 could not be identified with that of the free methylene radical.

In the identification of the spectrum, a possibility of another radical, CH_2I, which may be formed by Process (1), may be excluded, because there seems to be no evidence for any further splitting or line-broadening due to a magnetic iodine nucleus ($\mathbf{I}=5/2, 7/2$).

The observed spectrum of Fig. 1 is very similar to that of $\equiv Si-O-CH_2$ reported by Melamud *et al.*,[8] who obtained the radical by the photolysis of methylated Vycor glass. Therefore, although the radicals on Vycor glass were more stable and although the line-shape of the outer components was slightly different from the present one, the radical species observed in the present experiments may also be $\equiv Si-O-CH_2$ formed by processes on the silica gel surface subsequent to the photolysis, as will be discussed later.

It may readily be seen in Fig. 1 that the spectrum consists of three lines, *i.e.*, the intense, symmetrical, and sharp line in the center and two other asymmetric lines, suggesting the presence of two equivalent protons with axially-symmetric hyperfine tensors. The spectrum was then simulated with the aid of a HITAC 8700 computer, using a Fortran IV program that solved the spin Hamiltonian:

$$H = \beta \mathbf{H}\tilde{g}\mathbf{S} + \mathbf{I}\tilde{A}\mathbf{S}$$

to the second order in hyperfine interaction with a good approximation for the present purposes.[6] The best-fitting spectrum (shown in Fig. 1) was thus obtained, assuming an isotropic g value ($g=2.0030$) and

*1 Acording to a recent calculation by T. A. Claxton (*Trans. Faraday Soc.*, **66**, 1537, 1540 (1970)), the isotropic hyperfine splitting due to a proton in the NH radical, which has two unpaired electrons, is about twice that in the single unpaired electron radical, NH_2. However, the values of the spin-spin interaction (D, E)[12,13] reported predict the bent structure for the free methylene radical. This may reduce the isotropic hyperfine coupling of the protons, because in the bent structure s-p hybridization is positive; it may therefore cancel out the negative contribution of the π-electron to the hyperfine couplings.[13]

TABLE 1. ESR PARAMETERS of Si–O–CH_2

	Observed	Calculated by Eq. (7)[a]
g	2.0030	
$\mathbf{A}_{//}$	28.5±0.5 G	−27.4 G
$\mathbf{A}_{\perp}$	18.8±0.5 G	−18.4 G
$\mathbf{A}_{iso}$	22.0±0.5 G	−21.1 G

a) In the case of CH_2COOH produced in a single crystal of $CH_2(COOH)_2$ two α protons were not equivalent because of its different crystalline environment. Therefore, the averaged values were used.

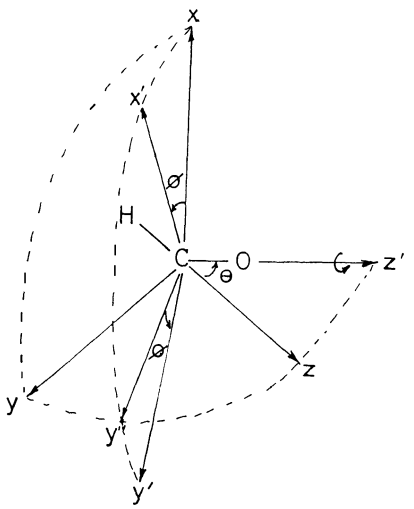

Fig. 3. Coordinate systems chosen for the transformation of hyperfine tensors from the principal system to the rotating system.

equal values of the hyperfine tensor ($\mathbf{A}_{\perp}$=18.8 G and $\mathbf{A}_{//}$=28.5 G) for both protons, with a gaussian linewidth of 3 G. The parameters obtained in this way are listed in Table 1, where $\mathbf{A}_{iso}$ was determined assuming that $\mathbf{A}_{\perp}$ and $\mathbf{A}_{//}$ have the same sign.

The sharpness and the symmetricity of the central line show that when the two proton spins are antiparallel, the hyperfine anisotropy is cancelled out. This means that the two protons are magnetically equivalent and that the $-CH_2$ group reorients sufficiently rapidly for the hyperfine interaction by the protons to be averaged out over all the orientations of the $-CH_2$.

The averaged hyperfine coupling tensors can be obtained by first transforming from the principal-axis system to a coordinate system in which the rotation axis lies along the C–O bond, and then by rotating about this axis, as is shown in Fig. 3. The transformation is performed according to the following unitary relation;

$$\mathbf{A}_r = \mathbf{U}\mathbf{A}^0\mathbf{U}^{-1} \tag{5}$$

where $\mathbf{A}_r$ is the tensor for the rotating coordinate system and where U is the transformation matrix, which can be expressed by the angles, θ and ϕ, associated with the transformation between the two reference frames;

$$\mathbf{U} = \begin{pmatrix} \cos\phi & -\sin\phi & 0 \\ \cos\theta\sin\phi & \cos\theta\cos\phi & -\sin\theta \\ \sin\theta\sin\phi & \sin\theta\cos\phi & \cos\theta \end{pmatrix} \tag{6}$$

One can obtain the following simple expressions for the tensor in the rotating system, as have been previously derived by the present author;[7]

$$\langle \mathbf{A}^r_{x'x'} \rangle_{av} = \langle \mathbf{A}^r_{y'y'} \rangle_{av} = 1/2(\mathbf{A}^0_{xx} + \mathbf{A}^0_{yy}\cos^2\theta + \mathbf{A}^0_{zz}\sin^2\theta)$$
$$\langle \mathbf{A}^r_{z'z'} \rangle_{av} = \mathbf{A}^0_{yy}\sin^2\theta + \mathbf{A}^0_{zz}\cos^2\theta$$
$$\langle \mathbf{A}^r_{x'y'} \rangle_{av} = \langle \mathbf{A}^r_{y'z'} \rangle_{av} = \langle \mathbf{A}^r_{x'z'} \rangle_{av} = 0 \tag{7}$$

where z' is the rotation axis and where θ is the angle between the z axis in the principal system and the rotation axis. Apparently, these equations give the axially-symmetric tensor corresponding to the hyperfine coupling in the fast-rotating system, with

$$\langle \mathbf{A}^r_{z'z'} \rangle_{av} = \mathbf{A}_{//} \text{ and } \langle \mathbf{A}^r_{x'x'} \rangle_{av} = \mathbf{A}_{\perp}.$$

It was not possible to obtain the principal values from the observed parameters and from those given by Eq. (7), for, in the present experiment, the spectrum of non-rotating $-CH_2$ could not be obtained. However, this type of radical may have a relatively narrow range of principal values whose principal axes are parallel to the C–H bond, perpendicular to the CH_2 plane, and parallel to the direction perpendicular to them. Therefore, using the values obtained for CH_2COOH trapped in irradiated single crystals of $CH_2(COOH)_2$[14] and using Eq. (7), the rotationally-averaged values were obtained; they are listed in the second column of Table 1, where the HCH angle was assumed to be 120°.

According to the above discussion, the spectrum can be well explained in terms of the ≡Si–O–CH_2 radical formed on the silica gel. Therefore, it is of interest to consider the processes occurring on the surface. It has now been established by infrared studies[15] that silica gel surfaces may possess both a "free" hydroxyl group and an "interacting" hydroxyl group, depending on their mutual distances. By dehydration at temperatures lower than 400 °C, the adsorbed water and part of the terminal hydroxyl group are eliminated to form both monomeric (free) and dimeric (interacting) surface hydroxyl groups, but most of the surface silanols remain. This process occurs reversibly; it can be shown as follows:

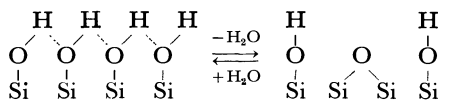

(8)

It has been established that evacuation at temperatures higher than 400 °C gives rise to an irreversible loss of surface hydroxyl groups, especially of interacting hydroxyl groups.[15] This effect of the pretreatment upon the nature of the silica gel surface suggests the participation of the surface hydroxyl groups in the formation of the radical; this fact can be used in interpreting the observation of the spectrum shown in Fig. 1 upon the photolysis of the samples pretreated at lower temperatures and by admitting water vapor onto the silica gel pretreated at higher temperatures before the photolysis. Therefore, a possible mechanism for the formation of the radical is as follows:

A) methylene iodide photolized by 2537 or 1849 Å gives CH_2 and 2I and/or an excited iodine molecule, I_2*; these iodine species then abstract hydrogen

from the surface silanol to make it possible to form the $\equiv Si-O-CH_2$ radical through recombination, or

B) the recombination of CH_2 and the surface siloxy which was produced independently by the photolysis of the surface silanol.

Since the formation of atomic hydrogen from silica gel without methylene iodide was much less efficient than that of $-CH_2$ from methylene iodide, A) is more likely in this case.

The formation of CH_3 by the photolysis of condensed methylene iodide is possibly due to the abstraction of hydrogen from methylene iodide or to that of the surface silanol by the CH_2 formed primarily.

In conclusion, the photolysis of methylene iodide on the silica gel, which has surface hydroxyl groups, gives rise to the formation of the radical $-CH_2$ chemically bonded to the silica gel surface. The ESR spectrum of this radical observed at 77 K shows the anisotropic hyperfine structure to be expected from the axially-symmetric hyperfine interaction of two equivalent protons. The observed hyperfine splittings due to two protons can be reasonably explained by taking into consideration the free rotation of the methylene group.

The author wishes to thank Professor C. A. McDowell of The University of British Columbia for his interest in this work. Part of the present work has been done during the author's staying at The University of British Columbia.

References

1) J. R. Morton, *J. Amer. Chem. Soc.*, **86**, 2325 (1964).
2) T. Kato and R. Abe, *J. Phys. Soc. Japan*, **29**, 389 (1970).
3) W. M. Tolles, L. P. Crowford, and J. L. Valenti, *J. Chem. Phys.*, **49**, 4745 (1968).
4) R. G. Hayes, D. J. Steible, W. M. Tolles, and J. W. Hunt, *ibid.*, **53**, 4466 (1970).
5) H. Ohigashi and Y. Kurita, This Bulletin, **41**, 275 (1968).
6) Rlefebvre and J. Maruani, *J. Chem. Phys.*, **42**, 1480 (1965).
7) C. A. McDowell, P. Raghunathan, and K. Shimokoshi, *ibid.*, **58**, 114 (1973).
8) E. Melamud, M. G. Reisner, and U. Garbatski, *J. Phys. Chem.*, **77**, 1023 (1973).
9) M. Ito, P. C. Kuang, and E. M. Kosower, *Trans. Faraday Soc.*, **57**, 1661 (1961).
10) R. A. Gregory and D. W. G. Style, *ibid.*, **32**, 124 (1936).
11) D. W. G. Style and J. C. Ward, *J. Chem. Soc.*, **1952**, 2125.
12) R. A. Bernheim, H. W. Bernard, P. S. Wang, L. S. Wood, and P. S. Skell, *ibid.*, **53**, 1280 (1970).
13) E. Wasserman, W. A. Yager, and V. J. Kuck, *Chem. Phys. Lett.*, **7**, 409 (1970).
14) A. Horsefield, J. R. Morton, and D. H. Whiffen, *Mol. Phys.*, **4**, 327 (1961).
15) L. H. Little, "Infrared Spectra of Adsorbed Species" Academic Press (1966), pp. 257—267.

The Crystal and Molecular Structure of Bicyclomycin, a New Antibiotic

Yoji TOKUMA, Shigetaka KODA, Toshio MIYOSHI, and Yukiyoshi MORIMOTO
Research Laboratories, Fujisawa Pharmaceutical Co., Ltd., Higashiyodogawa-ku, Osaka 532
(Received August 27, 1973)

The molecular structure of a new antibiotic, Bicyclomycin ($C_{12}H_{18}O_7N_2$), has been elucidated by X-ray diffraction analysis. Bicyclomycin crystallizes from aqueous solution in two forms, an orthorhombic and a monoclinic systems. The crystal data for the former are $a=11.72$, $b=12.72$, $c=8.80$ Å and the space group $P2_12_12_1$, while those for the latter are $a=10.27$, $b=10.91$, $c=6.67$ Å, $\beta=101.4°$, and the space group $P2_1$. The crystal structure of the former was solved by the direct method and refined by least-squares method to a final R factor of 0.07 for 1623 reflections. The established structure is

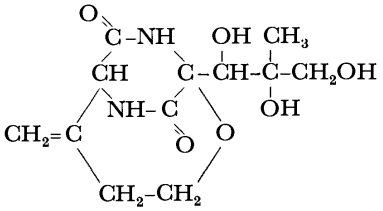

The diketopiperazine ring is folded into a boat form. The conformations of the side chain are all *gauche* or nearly so. All the oxygen and nitrogen atoms participate in two intramolecular and four intermolecular hydrogen bonds.

A new antibiotic Bicyclomycin was obtained from the culture filtrate of *Streptomyces sapporonensis* which was isolated from a soil sample collected at Sapporo City. Bicyclomycin has an antibacterial activity against Gram-negative bacteria and exhibits no cross resistance to major antibiotics for human use.[1] Chemical and spectroscopic investigations[2] suggested several functional groups in the molecule, but the precise stereochemistry of the structure remained to be unknown. X-Ray diffraction study was thus undertaken to establish the whole structure of the molecule.

Experimental

Bicyclomycin crystallizes from aqueous solution in two forms, colorless prisms and plates. Oscillation and Weissenberg photographs uniquely identified the space groups as $P2_12_12_1$ for the former and $P2_1$ for the latter. The unit cell dimensions were determined by the least-squares calculation using the high angle spots of Cu$K\alpha_1$ and Cu$K\alpha_2$ on zero-layer Weissenberg photographs superimposed by the Al wire patterns for calibration. The densities were measured by a floatation method in a chloroform–carbon tetrachloride mixture for the orthorhombic crystal and a benzene–carbon tetrachloride mixture for the monoclinic one, respectively. Crystal data were summarized in Table 1. The intensity data for the orthorhombic modification were collected from the multiple-film equi-inclination Weissenberg photographs for the layer lines 0 to 8 on the a axis and 0 to 6 on the c axis, respectively using the Ni-filtered Cu$K\alpha$ radiation. The intensities were estimated visually by comparison with a calibrated film strip. Corrections were made for Lorentz and polarization factors and spot sizes. A total of 1623 intensities was recorded, but 74 of these were too weak to be measured. Structure factor magnitudes $|F|$ and normalized structure factor magnitudes $|E|$ were derived by the Wilson's method. The values of the statistical average, $\langle|E|\rangle$ and $\langle|E|^2-1\rangle$, were 0.867 and 0.778, respectively, as compared with 0.886 and 0.736, the theoretical values for noncentrosymmetric space groups.

Table 1. Crystal data

Crystal system	orthorhombic	monoclinic
Molecular formula	$C_{12}H_{18}O_7N_2$	$C_{12}H_{18}O_7N_2\cdot H_2O$
Unit cell constants	$a=11.72(1)$Å	$a=10.27(1)$Å
	$b=12.72(1)$	$b=10.91(1)$
	$c=8.80(1)$	$c=6.67(1)$
		$\beta=101.4(1)°$
V	1312 Å^3	732 Å^3
D_m	1.54	1.46
D_c	1.53 g/cm^3	1.45 g/cm^3
Z	4	2
Absent spectra	$h00$ when h is odd,	$0k0$ when k is odd.
	$0k0$ when k is odd,	
	$00l$ when l is odd.	
Space group	$P2_12_12_1$	$P2_1$

Structure Determination

The structure of Bicyclomycin was solved using the symbolic addition technique applied to noncentrosymmetric structures.[3] The Eq. (1) was used to define 30 phases ($|E|\geq1.5$) in terms of initial set of phases listed in Table 2. From multiple indications, it soon became obvious that $2b\simeq0$, $2c\simeq\pi$, and $2p\simeq\pi$. As for the value a, there were no confirmative indications.

$$\varphi_{\boldsymbol{h}} \simeq \langle\varphi_{\boldsymbol{k}}+\varphi_{\boldsymbol{h}-\boldsymbol{k}}\rangle_{\boldsymbol{k}r} \quad (1)$$

Thus, various combinations of symbolic phases for

Table 2. Initial set of phases

Reflection	Phase	$\|E\|$
0 3 7	$\pi/2$	2.56
0 9 4	$\pi/2$	2.73
5 0 8	0	3.29
4 2 10	a	2.67
5 10 4	b	2.69
10 4 1	c	2.78
4 5 8	p	2.57

the use of the tangent formula were assigned as follows:

$$a = \pi/6, 3\pi/6, 5\pi/6, -\pi/6, -3\pi/6, -5\pi/6$$
$$b = 0, \pi$$
$$c = \pi/2, -\pi/2$$
$$p = \pi/2, -\pi/2.$$

For each of the 48 sets with 185 phases ($|E| \geq 1.50$), six cycles of tangent refinement were carried out. Only four sets of them converged characteristically at lowest R' index,[3] defined by

$$R' = \frac{\sum_{kr} ||E_h|_{obs} - |E_h|_{calc}|}{\sum_{kr} |E_h|_{obs}} \quad . \quad (2)$$

Further eight cycles of tangent refinement for each of these four sets of 391 phases ($|E| \geq 1.20$) converged at the same R' index of 0.26.

Three dimensional E-maps with 391 terms were then calculated for these sets. The 21 largest peaks appeared on the respective four E-maps; each of them was found to give the same molecular structure. There was only one unique set, however, to which the other three were related by a mirror symmetry or by a translation. Assuming all the atoms to be nitrogen atom, structure factor calculation based on these 21 atoms gave an R factor of 0.25 for all reflections, and the corresponding Fourier synthesis showed no spurious peaks. All the 21 non-hydrogen atoms were assigned to 12 carbon, 7 oxygen and 2 nitrogen atoms, respectively on the basis of this Fourier map and the partial structure known from chemical and spectroscopic investigations.[2]

The atomic coordinates and isotropic thermal parameters for the 21 atoms were refined by block-diagonal least-squares method for four cycles. The function minimized was $\sum w(|F_o| - |F_c|)^2$. Then, anisotropic temperature factors for all non-hydrogen atoms were introduced, and two more cycles of refinement reduced the R factor to 0.09. A difference map calculated at this stage revealed all the 18 hydrogen atoms. Setting the isotropic temperature factor of each hydrogen atom

Table 3. The fractional atomic coordinates and their estimated standard deviations in parentheses

Atom	x	y	z
C(1)	0.1686(3)	0.2872(3)	0.2093(4)
C(2)	0.2539(3)	0.2885(3)	0.3436(4)
C(4)	0.3899(3)	0.3824(3)	0.1740(4)
C(6)	0.2563(3)	0.5317(3)	0.2167(5)
C(7)	0.1437(4)	0.4891(4)	0.1549(5)
C(8)	0.0988(3)	0.3887(4)	0.2235(4)
C(10)	0.3371(3)	0.3203(3)	0.0399(4)
C(13)	0.5216(3)	0.3802(3)	0.1637(4)
C(15)	0.5869(3)	0.4369(3)	0.2948(4)
C(17)	0.7150(4)	0.4338(4)	0.2601(6)
C(18)	0.5495(4)	0.5514(3)	0.3199(5)
C(20)	0.0006(4)	0.3870(5)	0.3001(6)
N(3)	0.3527(3)	0.3412(3)	0.3188(3)
N(9)	0.2323(3)	0.2819(3)	0.0654(3)
O(5)	0.3575(2)	0.4898(2)	0.1452(3)
O(11)	0.1035(3)	0.1967(3)	0.2230(4)
O(12)	0.2311(3)	0.2516(3)	0.4675(3)
O(14)	0.5587(2)	0.2740(2)	0.1537(3)
O(16)	0.5610(3)	0.3868(3)	0.4359(3)
O(19)	0.5455(4)	0.6134(3)	0.1831(4)
O(21)	0.3845(3)	0.3150(3)	−0.0840(3)

Table 4. The anisotropic temperature factors[a] and their estimated standard deviations in parentheses (multiplied by 10^4)

Atom	B_{11}	B_{22}	B_{33}	B_{12}	B_{13}	B_{23}
C(1)	24(2)	36(3)	15(4)	−24(4)	−10(6)	− 5(6)
C(2)	21(2)	34(2)	19(4)	− 5(4)	10(6)	12(5)
C(4)	16(2)	20(2)	7(3)	3(4)	3(5)	2(5)
C(6)	24(2)	26(2)	33(4)	23(4)	−12(6)	− 6(5)
C(7)	27(3)	40(3)	31(4)	22(5)	−30(7)	6(6)
C(8)	22(2)	42(3)	18(4)	3(4)	−14(6)	−17(6)
C(10)	22(2)	22(2)	8(4)	16(4)	− 3(6)	7(5)
C(13)	15(2)	16(2)	19(4)	1(3)	14(6)	− 5(5)
C(15)	16(2)	26(2)	24(4)	− 1(4)	3(6)	− 7(5)
C(17)	17(2)	52(3)	79(6)	−12(5)	3(7)	−15(8)
C(18)	40(3)	24(2)	58(5)	− 3(5)	−13(8)	−18(6)
C(20)	31(3)	71(4)	92(7)	−10(6)	34(9)	−58(10)
N(3)	17(2)	26(2)	8(3)	− 3(3)	− 6(5)	5(4)
N(9)	28(2)	33(2)	5(3)	− 7(4)	−22(5)	−24(5)
O(5)	22(2)	21(2)	34(3)	13(3)	8(5)	13(4)
O(11)	28(2)	44(2)	71(4)	−34(4)	−13(5)	11(5)
O(12)	41(2)	62(2)	18(3)	−42(4)	0(5)	35(5)
O(14)	27(2)	17(1)	44(3)	11(3)	23(5)	− 8(4)
O(16)	25(2)	40(2)	28(3)	8(3)	−16(5)	17(4)
O(19)	60(3)	22(2)	84(5)	−14(4)	27(7)	12(5)
O(21)	31(2)	49(2)	10(3)	10(4)	8(5)	−12(4)

a) The aniostropic temperature factor is in the form: $\exp\{-(B_{11}h^2+B_{22}k^2+B_{33}l^2+B_{12}hk+B_{13}hl+B_{23}kl)\}$.

Table 5. The fractional atomic coordinates for hydrogen atoms and their X–H bond lengths (X=C, N, or O)

Atom	Bonded to	x	y	z	X–H (Å)
H(1)	N(3)	0.405	0.353	0.395	0.92
H(2)	C(6)	0.258	0.605	0.192	0.96
H(3)	C(6)	0.255	0.520	0.327	0.98
H(4)	C(7)	0.156	0.472	0.049	0.96
H(5)	C(7)	0.081	0.550	0.171	1.08
H(6)	N(9)	0.191	0.266	−0.009	0.84
H(7)	O(11)	0.034	0.209	0.157	1.01
H(8)	C(13)	0.536	0.412	0.071	0.93
H(9)	O(14)	0.522	0.238	0.214	0.82
H(10)	O(16)	0.612	0.343	0.467	0.86
H(11)	C(17)	0.753	0.484	0.341	1.06
H(12)	C(17)	0.733	0.344	0.243	1.17
H(13)	C(17)	0.730	0.464	0.166	0.93
H(14)	C(18)	0.614	0.587	0.392	1.09
H(15)	C(18)	0.473	0.554	0.384	1.06
H(16)	O(19)	0.469	0.587	0.136	1.05
H(17)	C(20)	−0.043	0.459	0.314	1.05
H(18)	C(20)	−0.028	0.326	0.338	0.91

The mean standard deviation in atomic coordinates is 0.08 Å, and that of the distance X–H is 0.09 Å.

equal to 3.0 Å^2, four more cycles of least-squares refinement brought the R factor down to 0.07, the positions of all the hydrogen atoms being converged satisfactorily. The maximum shift of the non-hydrogen atom coordinates became less than the estimated standard deviations; their mean value for C, N, and O was 0.004 Å (0.003~0.007 Å). The weighting scheme adopted in the final least-squares calculation was:

$$w = 0.4 \quad \text{for } |F_0| < 2.0$$

$$w = 1.0 \quad \text{for } 2.0 \leq |F_0| < 10.0$$

$$w = 10.0/|F_0| \quad \text{for } |F_0| \geq 10.0.$$

The scattering factors for H, C, N, and O were taken from International Tables for X-ray Crystallography.[4] The final atomic coordinates and thermal parameters for non-hydrogen atoms are given in Tables 3 and 4, and those for hydrogen atoms in Table 5. The observed and calculated structure factors are given in Table 6.

Most of the computer programs used were in the UNICS.[5] Tangent refinement was performed with the program TANG, written by T. Ashida. All the programs were modified by the authors to allow calculations on middle size of computer, HITAC 8400 at Nippon Business Consultant and Fujisawa Pharmaceutical Co., Ltds.

TABLE 6. THE OBSERVED AND CALCULATED STRUCTURE FACTORS

L FO FC	L FO FC	L FO FC	L FO FC	L FO FC	L FO FC	L FO FC	L FO FC	L FO FC
H=K= 0 0	3 245 272	10 126 125	9 43 40	0 31 46	7 145 134	5 274 264	1 64 68	H=K= 5 5
4 50 35	4 136 128	H=K= 5 1	10 42 48	1 200 185	8 101 100	6 84 76	2 251 266	0 19 1
6 326 339	5 185 192	0 889 957	11 88 95	2 263 287	9 42 52	7 299 332	3 100 102	1 280 263
8 474 487	6 139 141	1 310 299	H=K= 1 2	3 189 221	10 189 164	8 201 222	4 181 190	2 118 110
10 157 170	H=K= 10 0	2 302 276	0 507 559	4 154 154	H=K= 5 3	9 34 43	5 111 115	3 286 280
H=K= 1 0	0 304 316	3 241 212	1 504 551	5 185 189	0 253 252	10 143 145	6 138 137	4 131 140
1 839 738	1 23 12	4 257 247	2 702 756	6 82 76	1 174 150	H=K= 1 4	H=K= 10 4	5 135 120
2 402 410	2 96 105	5 185 180	3 191 187	H=K= 10 2	2 123 122	0 622 639	0 287 286	6 104 92
3 336 343	3 0 16	6 276 301	4 317 330	0 23 16	3 298 279	1 280 289	1 401 414	7 280 303
4 243 237	4 227 224	7 109 89	5 170 180	1 88 100	4 221 217	2 254 229	2 135 155	8 149 145
5 455 479	5 0 20	8 185 171	6 99 99	2 127 138	5 255 256	3 413 416	3 132 146	9 83 77
6 266 281	6 226 253	9 31 36	7 206 193	3 191 222	6 107 91	4 251 259	4 218 201	10 22 29
7 411 428	H=K= 11 0	10 143 131	8 227 232	4 118 121	7 134 134	5 194 183	5 84 82	H=K= 6 5
8 198 210	1 336 318	H=K= 6 1	9 107 119	5 70 77	8 192 195	6 100 82	6 138 130	0 62 53
9 0 24	2 88 87	0 535 558	10 119 104	6 53 55	9 49 43	7 287 278	H=K= 11 4	1 107 102
10 139 128	3 192 205	1 476 454	11 73 72	H=K= 11 2	10 121 117	8 115 114	0 62 57	2 150 151
11 125 132	4 198 214	2 341 346	H=K= 2 2	0 49 33	H=K= 6 5	9 106 105	1 71 71	3 202 197
H=K= 2 0	5 96 92	3 203 190	0 364 385	1 41 37	0 167 151	10 41 55	2 106 94	4 238 254
0 99 94	6 68 64	4 200 185	1 75 75	2 113 127	1 243 218	H=K= 2 4	3 77 75	5 206 215
1 372 390	H=K= 12 0	5 119 108	2 509 513	3 153 164	2 123 113	1 266 253	4 125 133	6 94 93
2 484 477	0 78 91	6 88 78	3 588 607	4 178 189	3 127 122	2 370 347	5 190 189	7 113 110
3 541 530	1 0 20	7 181 179	4 119 109	5 102 108	4 202 189	3 107 104	6 159 149	8 152 132
4 348 341	2 44 56	8 162 177	5 290 271	6 89 69	5 131 133	4 108 95	H=K= 12 4	9 169 145
5 391 399	3 88 86	9 0 14	6 127 141	H=K= 12 2	6 134 132	5 219 208	0 63 64	H=K= 7 5
6 158 169	4 124 123	10 97 79	7 0 13	0 77 88	7 180 210	6 78 65	1 80 84	0 232 216
7 45 17	5 72 65	H=K= 7 1	8 209 220	1 132 150	8 99 92	7 96 91	2 86 77	1 119 113
8 119 120	6 0 5	0 400 395	9 53 58	2 0 12	9 42 51	8 202 208	3 32 36	2 224 220
9 106 115	H=K= 13 0	1 278 274	10 25 33	3 114 116	10 95 92	9 100 114	4 62 60	3 252 270
10 95 101	1 31 42	2 170 154	11 30 38	4 145 139	H=K= 7 3	10 175 156	5 128 104	4 197 191
11 32 42	2 25 25	3 87 66	H=K= 3 2	5 70 62	0 142 138	H=K= 3 4	6 28 28	5 157 165
H=K= 3 0	3 0 18	4 137 117	0 497 609	6 71 75	1 185 173	0 50 46	H=K= 13 4	6 56 73
1 263 252	4 101 95	5 42 36	1 454 477	H=K= 13 2	2 280 292	1 166 160	0 82 89	7 59 60
2 185 196	5 36 39	6 96 105	2 497 510	0 0 7	3 226 211	2 267 249	1 66 71	8 180 154
3 187 175	H=K= 14 0	7 115 113	3 148 136	1 27 27	4 281 271	3 227 212	2 0 19	9 95 82
4 202 172	0 23 25	8 169 130	4 47 52	2 108 121	5 140 122	4 158 151	3 95 82	H=K= 8 5
5 73 62	1 44 46	9 178 142	5 104 89	3 0 1	6 162 153	5 252 248	4 73 65	0 147 154
6 201 207	2 34 36	H=K= 8 1	6 164 169	4 59 48	7 113 115	6 80 83	H=K= 14 4	1 149 145
7 0 10	3 80 75	0 347 330	7 214 203	5 103 104	8 47 50	7 186 187	0 36 39	2 167 156
8 138 132	4 54 53	1 75 70	8 110 107	H=K= 14 2	9 85 68	8 182 193	1 75 73	3 262 297
9 85 93	H=K= 0 1	2 159 148	9 25 7	0 168 158	H=K= 8 3	9 69 72	2 76 76	4 44 52
10 132 134	1 342 325	3 129 118	10 213 220	1 103 98	0 101 89	10 45 49	3 43 48	5 112 118
11 58 69	2 324 290	4 238 240	H=K= 4 2	2 77 70	1 240 229	H=K= 4 4	H=K= 0 5	6 49 43
H=K= 4 0	3 230 220	5 211 227	0 154 145	3 47 49	2 390 433	0 168 152	1 71 67	7 179 172
1 10 5	4 311 330	6 60 64	1 219 205	H=K= 0 3	3 197 204	1 423 424	2 133 106	8 0 18
2 194 167	5 152 155	7 205 206	2 402 398	1 312 309	4 239 243	2 208 201	3 354 356	H=K= 9 5
3 142 118	6 132 161	8 80 72	3 192 178	2 429 414	5 132 125	3 144 131	4 285 295	0 398 375
4 158 152	7 163 159	9 26 24	4 284 279	3 266 267	6 53 58	4 264 270	5 76 71	1 127 128
5 110 113	8 223 228	H=K= 9 1	5 163 147	4 15 17	7 147 126	5 139 116	6 36 48	2 212 228
6 52 45	9 35 33	0 307 296	6 270 301	5 80 69	8 45 44	6 112 103	7 95 92	3 66 66
7 233 232	10 54 78	1 133 136	7 196 187	6 135 147	9 140 121	7 81 80	8 81 76	4 253 240
8 0 4	11 52 53	2 130 132	8 67 75	7 439 422	H=K= 9 3	8 136 129	9 135 142	5 74 75
9 51 50	H=K= 1 1	3 138 137	9 93 86	8 79 70	0 106 106	9 125 116	10 97 103	6 141 136
10 111 106	1 625 666	4 119 112	10 245 231	9 81 86	1 36 43	10 32 32	H=K= 1 5	H=K= 10 5
H=K= 5 0	2 108 99	5 52 52	H=K= 5 2	10 40 46	2 255 246	H=K= 5 4	0 792 846	0 65 61
1 131 129	3 256 257	6 71 67	0 420 439	11 39 34	3 108 108	0 355 350	1 389 354	1 131 132
2 412 359	4 276 274	H=K= 10 1	1 42 53	H=K= 1 3	4 44 36	1 120 119	2 328 320	2 192 212
3 203 180	5 154 146	0 16 12	2 66 54	0 293 294	5 0 16	2 346 342	3 458 465	3 262 275
4 343 340	6 277 286	1 88 88	3 69 61	1 529 546	6 72 68	3 76 81	4 149 149	4 56 50
5 150 137	7 412 377	2 161 165	4 172 161	2 230 225	H=K= 10 3	4 68 66	5 221 219	5 163 174
6 186 189	8 325 326	3 100 105	5 111 19	3 354 356	0 28 30	5 73 66	6 35 29	6 133 109
7 236 246	9 81 86	4 115 124	6 233 250	4 137 123	1 47 54	6 193 191	7 128 128	H=K= 11 5
8 414 429	10 43 51	5 66 67	7 182 171	5 419 447	2 194 209	7 30 14	8 114 118	0 212 228
9 93 92	11 52 52	6 0 4	8 184 182	6 102 83	3 133 129	8 197 184	9 102 99	1 0 17
10 144 142	H=K= 2 1	H=K= 11 1	9 76 59	7 79 76	4 152 161	9 101 88	10 125 112	2 169 166
H=K= 6 0	0 262 270	0 86 104	10 180 196	8 191 186	5 34 42	10 34 40	H=K= 2 5	3 0 22
0 530 540	1 394 390	1 50 49	H=K= 6 2	9 79 87	6 113 103	H=K= 6 4	0 529 549	4 132 132
1 219 204	2 439 427	2 113 122	0 217 231	10 93 83	H=K= 11 3	0 157 151	1 407 389	5 47 51
2 91 65	3 275 267	3 93 97	1 178 179	11 73 74	0 23 17	1 139 133	2 203 182	6 108 95
3 288 276	4 355 323	4 56 52	2 249 226	H=K= 2 3	1 77 86	2 50 51	3 208 204	H=K= 12 5
4 186 174	5 268 244	5 36 29	3 125 131	0 241 229	2 60 66	3 121 112	4 65 69	0 139 138
5 194 193	6 188 203	6 67 55	4 285 280	1 320 338	3 75 77	4 46 48	5 211 213	1 98 64
6 211 212	7 297 298	H=K= 12 1	5 113 108	2 347 340	4 87 85	5 237 264	6 160 159	2 86 79
7 172 150	8 161 162	0 54 52	6 112 112	3 371 366	5 96 97	6 109 113	7 0 25	3 93 96
8 61 64	9 106 114	1 27 36	7 110 109	4 517 495	6 113 103	7 64 60	8 123 135	4 48 42
9 149 124	10 49 52	2 207 205	8 144 143	5 102 91	H=K= 12 3	8 79 70	9 89 98	5 77 66
10 0 13	11 0 15	3 115 113	9 76 66	6 286 295	0 85 95	9 99 89	10 29 38	H=K= 13 5
H=K= 7 0	H=K= 3 1	4 106 105	10 196 208	7 234 230	1 0 12	H=K= 7 4	H=K= 3 5	0 48 50
1 265 256	0 328 339	5 72 68	H=K= 7 2	8 127 119	2 36 27	0 218 211	0 160 155	1 21 21
2 125 99	1 50 42	6 92 81	0 0 0	9 78 73	3 64 52	1 32 30	1 250 213	2 30 35
3 178 166	2 415 417	H=K= 13 1	1 123 110	10 0 16	4 150 135	2 179 173	2 348 334	3 0 11
4 426 456	3 879 932	0 70 73	2 127 108	H=K= 3 3	5 137 128	3 218 208	3 106 102	4 35 36
5 0 10	4 444 410	1 137 150	3 129 128	0 299 284	6 82 87	4 235 289	4 187 190	H=K= 14 5
6 98 92	5 236 230	2 35 32	4 86 76	1 657 687	H=K= 13 3	5 293 324	5 53 52	0 103 101
7 96 77	6 52 42	3 63 61	5 247 260	2 116 113	0 103 101	6 134 127	6 66 53	1 95 107
8 116 91	7 145 137	4 152 149	6 199 185	3 534 537	1 153 166	7 33 29	7 177 185	H=K= 0 6
9 142 123	8 232 236	5 62 71	7 114 112	4 122 114	2 72 63	8 164 134	8 83 92	0 132 114
H=K= 8 0	9 36 37	H=K= 14 1	8 48 51	5 244 232	3 119 125	9 26 31	9 36 40	1 133 126
0 346 343	10 108 104	0 118 109	9 89 65	6 124 118	4 70 81	H=K= 8 4	10 78 69	2 90 29
1 117 107	11 126 141	1 66 74	H=K= 8 2	7 214 195	5 122 144	0 110 117	H=K= 4 5	3 115 115
2 113 104	H=K= 4 1	2 63 60	0 31 25	8 72 74	H=K= 14 3	1 126 120	0 248 237	4 221 230
3 238 242	0 210 222	3 82 79	1 114 112	9 72 80	0 69 70	2 191 189	1 300 269	5 173 170
4 80 45	1 599 594	4 80 87	2 179 182	10 212 194	1 46 46	3 213 235	2 116 101	6 53 25
5 186 188	2 196 172	H=K= 0 2	3 171 165	H=K= 4 3	2 194 191	4 158 167	3 114 110	7 45 40
6 53 50	3 185 159	2 652 704	4 266 280	0 20 20	3 148 118	5 28 35	4 240 224	8 55 41
7 0 15	4 189 168	3 16 6	5 237 244	1 140 134	H=K= 0 4	6 115 103	5 201 200	9 151 157
8 0 14	5 204 192	4 168 161	6 117 114	2 561 596	0 123 120	7 69 56	6 229 258	10 0 22
9 59 49	6 135 129	5 77 51	7 179 178	3 260 246	1 33 39	8 51 50	7 135 126	H=K= 15 6
H=K= 9 0	7 233 219	6 143 124	8 108 92	4 133 120	2 262 247	9 137 145	8 301 330	0 214 213
1 318 298	8 170 173	7 293 291	9 0 3	5 32 15	3 175 162	H=K= 9 4	9 136 136	1 304 273
2 97 91	9 129 129	8 122 131	H=K= 9 2	6 224 232	4 113 117	0 22 32	10 29 41	2 303 288

L FO FC
H=K= 5 5
3 201 211
4 122 104
5 171 158
6 80 72
7 81 80
8 256 267
9 72 77
10 155 154
H=K= 2 6
0 278 242
1 361 330
2 383 367
3 172 173
4 154 153
5 223 207
6 130 133
7 115 108
8 89 87
9 0 22
10 200 206
H=K= 3 6
0 0 19
1 319 295
2 153 143
3 167 145
4 158 146
5 109 112
6 196 212
7 231 235
8 90 99
9 126 111
H=K= 4 6
0 634 665
1 120 117
2 242 228
3 167 141
4 100 97
5 87 92
6 88 89
7 80 88
8 204 189
9 27 36
10 135 162
H=K= 5 6
0 283 259
1 325 329
2 130 108
3 346 347
4 123 119
5 172 172
6 112 112
7 87 80
8 31 22
9 90 84
H=K= 6 6
0 422 409
1 117 114
2 177 186
3 240 200
4 106 95
5 225 231
6 172 184
7 96 93
8 108 94
9 52 53
H=K= 7 6
0 50 36
1 248 246
2 282 289
3 174 182
4 28 26
5 201 219
6 122 123
7 80 73
8 89 81
9 75 80
H=K= 8 6
0 266 265
1 244 244
2 140 141
3 180 188
4 175 180
5 58 65
6 119 114
7 34 31
8 157 152
H=K= 9 6
0 87 91
1 89 86
2 171 174
3 35 39
4 139 144
5 72 70
6 169 164
H=K= 10 6
0 123 131
1 206 210
2 124 136
3 44 43

Table 6. Continued.

L	FO	FC	L	FO	FC	L	FO	FC	L	FO	FC	L	FO	FC	L	FO	FC	L	FO	FC	L	FO	FC	L	FO	FC
H,K= 10 6			2	111	95	H,K= 1 8			0	27	22	0	145	156	1	144	135	2	36	45	0	62	45	H,K= 10 12			1	96	95
4	67	65	3	129	137	0	38	19	1	0	21	1	168	142	2	53	36	3	146	149	1	51	49	0	59	44	2	94	85
5	160	149	4	160	174	1	241	218	2	114	115	2	102	97	3	73	70	4	29	34	2	57	66	1	44	55	3	62	56
6	105	83	5	56	62	2	121	115	3	68	61	3	56	53	4	119	119	5	113	131	3	53	60	H,K= 0 13			4	111	115
H,K= 11 6			6	117	121	3	161	164	4	69	67	4	120	130	5	136	153	6	22	25	H,K= 11 11			1	8	11	5	25	27
0	133	137	7	136	117	4	88	95	5	89	84	5	148	166	6	81	90	7	0	4	0	37	39	2	16	33	H,K= 3 14		
1	46	52	8	48	57	5	154	157	6	83	86	6	93	97	7	100	92	8	135	141	H,K= 0 12			3	0	0	0	11	23
2	90	83	9	88	67	6	209	228	H,K= 10 8			7	0	17	8	0	2	H,K= 1 11			0	221	233	4	161	172	1	62	56
3	73	70	H,K= 6 7			7	259	276	0	120	118	8	99	98	H,K= 3 10			0	75	63	1	132	138	5	80	76	2	0	10
4	118	109	0	120	108	8	0	18	1	21	22	H,K= 6 9			0	267	246	1	188	175	2	186	197	6	113	116	3	37	37
5	98	81	1	31	34	9	38	48	2	0	14	0	84	86	1	116	112	2	40	36	3	93	92	H,K= 1 13			4	107	113
6	67	65	2	41	42	H,K= 2 8			3	42	55	1	149	142	2	44	42	3	80	91	4	0	7	0	11	11	5	52	53
H,K= 12 6			3	138	128	0	202	196	4	127	121	2	65	66	3	104	99	4	134	139	5	21	28	1	31	31	H,K= 4 14		
0	0	0	4	200	215	1	87	84	5	88	88	3	166	178	4	98	101	5	62	65	6	24	19	2	53	52	0	11	15
1	41	44	5	135	134	2	155	150	6	70	66	4	63	60	5	125	135	6	91	95	7	69	55	3	123	110	1	110	94
2	132	132	6	179	207	3	69	61	H,K= 11 8			5	68	81	6	49	45	7	110	109	H,K= 1 12			4	69	70	2	92	88
3	83	79	7	64	58	4	61	62	0	30	22	6	137	153	7	0	13	8	91	87	0	0	11	5	115	118	3	31	26
4	41	35	8	149	141	5	97	100	1	49	52	7	101	82	8	65	57	H,K= 2 11			1	129	127	6	66	64	4	0	13
5	49	49	9	89	88	6	55	54	2	73	60	8	73	71	H,K= 4 10			0	75	80	2	132	144	H,K= 2 13			H,K= 5 14		
H,K= 13 6			H,K= 7 7			7	81	83	3	31	31	H,K= 7 9			0	172	184	1	167	172	3	87	89	0	198	163	0	46	36
0	0	9	0	55	64	8	67	60	4	60	49	0	271	279	1	101	103	2	44	51	4	0	7	1	11	16	1	77	66
1	113	110	1	232	226	9	42	48	5	42	49	1	58	61	2	38	30	3	82	85	5	99	95	2	41	39	2	74	61
2	68	69	2	186	200	H,K= 3 8			H,K= 12 8			2	54	62	3	165	180	4	60	67	6	176	183	3	116	110	3	9	17
3	59	70	3	137	128	0	317	289	0	43	46	3	138	137	4	150	140	5	0	21	7	162	139	4	25	21	4	63	70
H,K= 0 7			4	172	178	1	67	64	1	121	116	4	44	45	5	128	116	6	98	97	H,K= 2 12			5	0	4	H,K= 6 14		
1	433	423	5	90	88	2	70	66	2	19	20	5	74	71	6	125	128	7	125	137	0	144	150	6	57	44	0	9	10
2	184	171	6	57	52	3	28	26	3	79	76	6	149	142	7	122	110	8	132	129	1	70	66	H,K= 3 13			1	55	44
3	222	227	7	178	164	4	297	329	H,K= 13 8			7	104	71	8	89	79	H,K= 3 11			2	119	124	0	49	50	2	45	48
4	294	293	8	86	74	5	99	89	0	73	78	H,K= 8 9			H,K= 5 10			0	267	276	3	46	44	1	112	110	3	30	31
5	93	91	H,K= 8 7			6	57	54	1	112	139	0	31	29	0	66	66	1	185	197	4	72	68	2	111	102	H,K= 7 14		
6	38	43	0	134	138	7	117	106	H,K= 0 9			1	181	199	1	47	57	2	51	48	5	94	98	3	0	12	0	27	27
7	94	90	1	11	25	8	80	79	1	140	149	2	58	59	2	203	204	3	176	185	6	111	99	4	40	42	1	0	11
8	66	59	2	186	206	9	116	110	2	535	540	3	70	64	3	276	317	4	113	105	7	25	32	5	78	73	2	24	27
9	75	75	3	74	70	H,K= 4 8			3	190	188	4	183	189	4	313	345	5	0	10	H,K= 3 12			6	50	56	H,K= 8 15		
10	51	53	4	109	117	0	206	186	4	427	489	5	81	77	5	143	151	6	54	59	0	103	113	H,K= 4 13			1	10	22
H,K= 1 7			5	88	94	1	277	263	5	55	67	6	25	18	6	23	30	7	22	28	1	233	240	0	54	52	2	36	44
0	238	190	6	146	150	2	104	110	6	58	58	7	143	171	7	163	151	H,K= 4 11			2	43	37	1	122	124	3	32	30
1	80	75	7	74	57	3	228	235	7	255	253	H,K= 9 9			8	66	72	0	11	23	3	124	125	2	26	29	4	39	44
2	342	323	8	113	107	4	145	143	8	35	35	0	34	31	H,K= 6 10			1	117	113	4	64	64	3	30	28	H,K= 1 15		
3	118	112	H,K= 9 7			5	130	136	9	93	84	1	0	11	0	28	21	2	91	93	5	13	21	4	40	35	0	47	55
4	140	145	0	46	48	6	121	138	H,K= 1 9			2	113	122	1	116	119	3	298	325	6	0	18	5	97	100	1	50	46
5	180	178	1	128	123	7	96	97	0	236	213	3	104	107	2	151	137	4	0	21	H,K= 4 12			6	39	51	2	63	61
6	117	121	2	210	236	8	133	121	1	123	107	4	143	129	3	191	202	5	214	234	0	180	178	H,K= 5 13			3	54	53
7	60	60	3	73	65	9	35	33	2	219	218	5	46	45	4	53	61	6	96	93	1	68	73	0	12	9	4	105	121
8	74	75	4	75	78	H,K= 5 8			3	472	494	6	91	88	5	70	64	7	61	59	2	73	69	1	98	86	H,K= 2 15		
9	72	67	5	119	127	0	141	138	4	108	101	H,K= 10 9			6	40	82	H,K= 5 11			3	72	75	2	123	118	0	72	69
10	76	73	6	193	193	1	166	161	5	247	253	0	56	52	7	77	69	0	72	61	4	136	136	3	62	60	1	0	12
H,K= 2 7			H,K= 10 7			2	268	276	6	40	39	1	31	31	H,K= 7 10			1	32	27	5	26	32	4	55	53	2	0	19
0	346	321	0	15	19	3	167	165	7	152	154	2	86	84	0	33	33	2	104	110	6	114	111	5	32	36	3	21	21
1	352	318	1	103	106	4	268	273	8	42	40	3	60	57	1	33	30	3	48	56	7	45	48	H,K= 6 13			4	30	38
2	255	247	2	41	45	5	126	128	9	124	117	4	131	122	2	52	49	4	0	4	H,K= 5 12			0	11	19	H,K= 3 15		
3	154	155	3	85	86	6	31	30	H,K= 2 9			5	72	75	3	59	60	5	28	22	0	0	2	1	70	74	0	34	35
4	82	78	4	41	44	7	133	124	0	97	80	H,K= 11 9			4	75	79	6	53	51	1	49	50	2	47	48	1	96	82
5	135	136	5	120	104	8	141	128	1	153	150	0	71	63	5	13	19	7	20	12	2	0	10	3	86	80	2	23	28
6	186	196	6	147	133	H,K= 6 8			2	303	290	1	38	41	6	72	62	H,K= 6 11			3	40	44	4	92	89	3	78	77
7	201	221	H,K= 11 7			0	72	69	3	48	45	2	0	13	7	120	108	0	11	24	4	151	163	5	38	47	H,K= 4 15		
8	125	117	0	14	13	1	220	198	4	267	283	3	83	86	H,K= 8 10			1	84	98	5	24	15	H,K= 7 13			0	37	22
9	94	90	1	64	71	2	214	225	5	115	125	4	109	112	0	86	100	2	126	142	6	70	67	0	184	155	1	97	89
10	68	77	2	43	39	3	261	335	6	77	81	H,K= 12 9			1	82	86	3	127	127	H,K= 6 12			1	97	86	2	98	91
H,K= 3 7			3	139	142	4	112	107	7	105	107	0	30	24	2	145	100	4	125	130	0	166	165	2	114	98	3	66	71
0	537	521	4	112	98	5	186	194	8	162	143	1	56	61	3	56	32	5	50	48	1	149	146	3	96	86	H,K= 5 15		
1	121	125	5	76	70	6	78	78	9	17	17	2	77	92	4	97	89	6	11	22	2	117	107	H,K= 8 13			0	16	6
2	224	206	H,K= 12 7			7	152	141	H,K= 3 9			H,K= 0 10			5	86	77	H,K= 7 11			3	60	61	0	24	25	1	100	95
3	73	66	0	108	106	8	57	48	0	247	241	0	517	509	6	59	55	0	143	142	4	39	38	1	160	153	2	81	90
4	119	120	1	132	134	H,K= 7 8			1	164	140	1	243	239	H,K= 9 10			1	119	128	5	67	58	2	70	60	H,K= 0 16		
5	113	121	2	59	53	0	216	210	2	135	137	2	83	72	8	0	103	2	147	141	6	25	23	3	96	110	0	106	92
6	173	192	3	88	74	1	126	116	3	125	126	3	207	231	1	55	54	3	0	13	H,K= 7 12			H,K= 9 13			1	20	0
7	80	91	4	0	4	2	218	235	4	133	95	4	104	104	2	25	32	4	12	24	0	95	90	0	105	118	2	0	4
8	95	101	H,K= 13 7			3	99	94	5	121	131	5	168	186	3	34	22	5	46	44	1	104	102	H,K= 0 14			H,K= 1 16		
9	134	118	0	157	148	4	120	125	6	50	54	6	13	20	4	22	24	6	95	97	2	111	101	0	56	71	0	0	1
H,K= 4 7			1	97	99	5	43	35	7	54	56	7	35	44	5	129	133	H,K= 8 11			3	31	30	1	86	94	1	67	55
0	37	33	2	70	76	6	83	77	8	131	117	8	0	17	H,K= 10 10			0	112	111	4	10	16	2	61	55	2	68	83
1	111	98	3	29	32	7	51	57	9	72	76	H,K= 1 10			0	21	21	1	125	129	5	69	61	3	59	36	H,K= 2 16		
2	142	138	H,K= 0 8			8	99	85	H,K= 4 9			0	54	34	1	42	49	2	47	39	H,K= 8 12			4	77	76	0	127	118
3	75	58	0	249	231	H,K= 8 8			0	30	37	1	151	153	2	80	67	3	35	33	0	28	21	5	82	84	1	113	115
4	145	132	1	223	216	0	64	63	1	83	85	2	137	143	3	105	98	4	82	75	1	49	49	H,K= 1 14					
5	238	246	2	18	20	1	97	97	2	174	180	3	192	179	4	94	82	5	29	27	2	91	81	0	7	10			
6	91	83	3	0	30	2	86	85	3	75	71	4	166	171	H,K= 11 10			H,K= 9 11			3	69	69	1	17	11			
7	54	51	4	188	212	3	55	55	4	248	264	5	53	59	0	25	24	0	49	42	4	62	49	2	38	33			
8	0	15	5	95	91	4	12	14	5	75	78	6	135	144	1	55	44	1	107	99	H,K= 9 12			3	34	32			
9	42	38	6	248	289	5	97	91	6	26	22	7	35	34	2	42	45	2	68	59	0	23	27	4	53	52			
H,K= 5 7			7	0	18	6	155	161	7	77	76	8	94	85	3	45	45	3	139	129	1	23	26	5	60	62			
0	195	178	8	22	30	7	120	108	8	25	23	H,K= 12 10			H,K= 0 11			4	101	97	2	85	83	H,K= 2 14					
1	197	175	9	62	51	H,K= 9 8			H,K= 5 9			0	109	104	1	124	125	H,K= 10 11			3	86	86	0	120	111			

Results and Discussion

The configuration of the Bicyclomycin molecule can be seen in Fig. 1. The bond distances and angles of the non-hydrogen atoms are shown in Fig. 2. The mean estimated standard deviations are 0.006 Å and 0.3° for bond distances and angles, respectively. The bond lengths involving the hydrogen atoms are listed in Table 5.

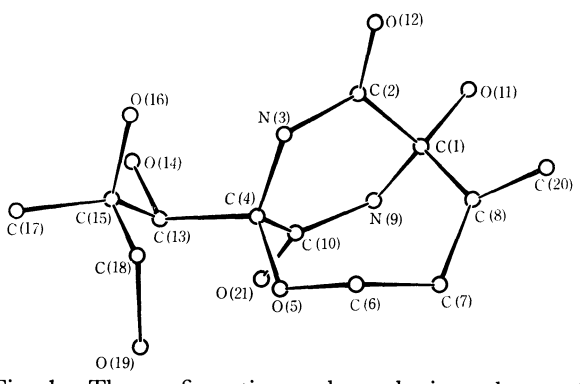

Fig. 1. The configuration and numbering scheme of Bicyclomycin molecule.

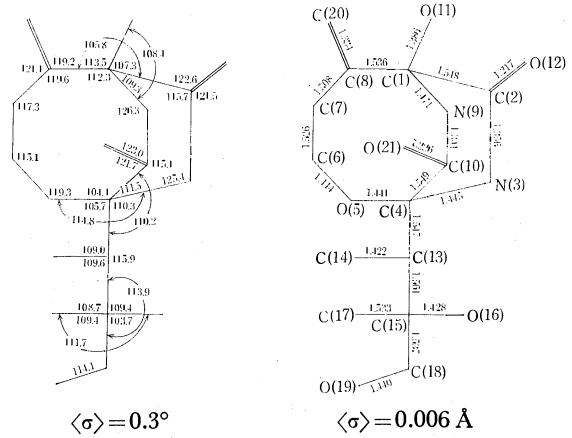

Fig. 2. Bond distances and angles.

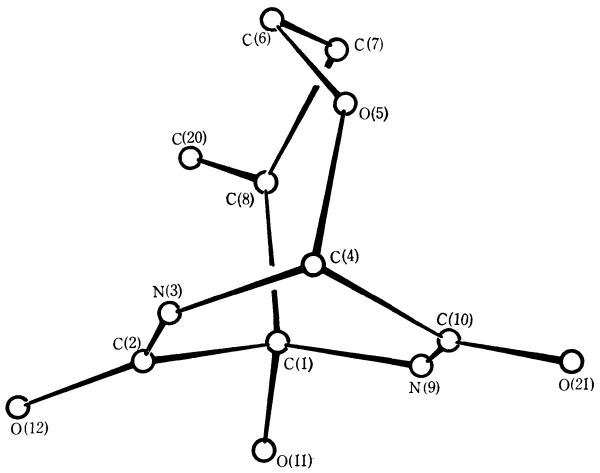

Fig. 3. A part of the molecule showing the cage type of ring system.

The diketopiperazine ring is folded into a boat conformation. Bridging the axial bonds of C(1) and C(4) in the ring, four atoms, O(5), C(6), C(7), and C(8), constitute the two eight-membered rings together with ⩾C–CO–NH–C⩽ moieties of the six-membered ring and thus establish the cage type of ring system. These features are shown in Fig. 3. There exists an approximate two fold axis going through the center of the diketopiperazine ring and the middle point of the C(6)–C(7) bond.

Atoms C(1), C(2), N(3), and O(12) are coplanar within 0.03 Å (amide plane I) and those C(1), C(4), N(9), C(10), and O(21) are also coplanar within 0.03 Å (amide plane II). The dihedral angle between amide plane I and II is 144°. The moiety, C(1), C(8), C(7), and C(20) involving the methylene group, displays the good planarity (methylene plane). The equations of the best planes and the deviations of respective atoms from the planes are listed in Table 7.

The distances, C(2)–N(3) (1.36 Å) and C(10)–N(9) (1.34 Å) significantly shorter than that of C–N single

Table 7. Some of the least-squares planes and the deviation of atoms from the planes (Å)

1) Amide plane I			
$0.4088X-0.8604Y-0.3045Z=-2.888$			
C(1)	−0.008	O(12)	0.011
C(2)	0.026	C(4)*	0.105
N(3)	−0.010	H(1)*	−0.09
2) Amide plane II			
$0.4286X-0.8493Y+0.3084Z=-1.690$			
C(1)	0.002	C(10)	0.031
C(4)	−0.010	O(21)	−0.010
N(9)	−0.011	H(6)*	−0.25
3) Methylene plane			
$0.4823X+0.2134Y+0.8496Z=3.295$			
C(1)	−0.003	C(20)	−0.004
C(7)	−0.003	H(17)*	−0.06
C(8)	0.010	H(18)*	0.04

In the above equations, X, Y, and Z are the rectangular coordinates in Å unit.
Asterisks indicate atoms not included in the calculation of the plane.

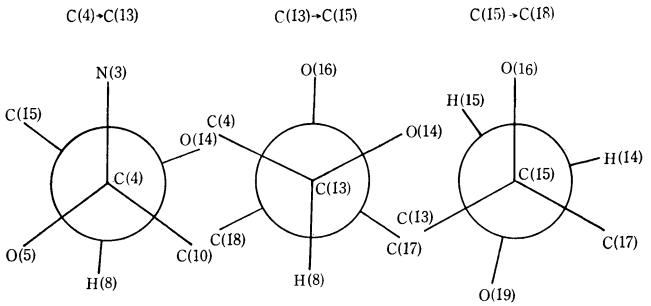

Fig. 4. Newman projections about C(4)–C(13), C(13)–C(15), and C(15)–C(18) bonds.

bond length (1.47 Å), indicate some double bond character; similar shortening of the bond length has been reported in diketopiperazine[6] and in many peptides.[7] The distance C(1)–O(11) (1.39 Å) seems to be shorter than that of the corresponding single bond length.

The conformation of the side chain is presented by the Newman projections down the C(4)–C(13), C(13)–C(15), and C(15)–C(18) bonds. As shown in Fig. 4,

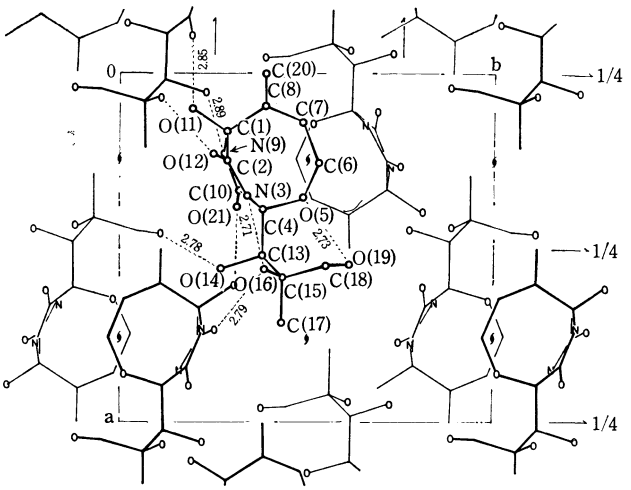

Fig. 5. The crystal structure viewed along the c axis. The hydrogen bonds are indicated by dashed lines.

Table 8. Inter- and intramolecular hydrogen bonds (D–H···A)

Donor	H	Acceptor	D···A (Å)	H···A (Å)	D–H···A (°)
I) Intermolecular					
N(9)	H(6)	$O(14)^{I}$	2.89	2.07	166
O(11)	H(7)	$O(21)^{I}$	2.85	1.89	156
O(14)	H(9)	$O(19)^{II}$	2.78	1.99	161
O(16)	H(10)	$O(12)^{III}$	2.79	1.93	178
II) Intramolecular					
N(3)	H(1)	O(16)	2.71	1.91	144
O(19)	H(16)	O(5)	2.73	1.80	146

Roman numerals as superscripts denote the following transformations relative to the reference molecule at x, y, z:

I	$-1/2+x$,	$1/2-y$,	$-z$,
II	$1-x$,	$-1/2+y$,	$1/2-z$,
III	$1/2+x$,	$1/2-y$,	$1-z$,

all the conformations are *gauche* or nearly so.

All the oxygen and nitrogen atoms in the molecule participate in two intramolecular and four intermolecular hydrogen bonds. Two oxygen atoms, O(16) and O(19), in the side chain participate in intramolecular hydrogen bonds, N(3)–H(1)···O(16) and O(19)–H(16)···O(5). These hydrogen bonds are of particular contribution to retain the molecular frameworks.

The crystal structure viewed along the *c* axis is shown in Fig. 5. The hydrogen bonds are indicated by dashed lines and detailed features of these hydrogen bonds are listed in Table 8.

The authors are indebted to Professor Masao Kakudo and Dr. Tamaichi Ashida, Institute for Protein Research, Osaka University, for discussions and suggestions in the progress of this work and for permitting us to use original program, TANG.

References

1) T. Miyoshi, N. Miyairi, H. Aoki, M. Kohsaka, H. Sakai, and H. Imanaka, *J. Antibiotics*, **25**, 569 (1972).

2) T. Kamiya, S. Maeno, M. Hashimoto, and Y. Mine, *ibid.*, **25**, 576 (1972).

3) J. Karle and I. L. Karle, *Acta Crystallogr.*, **21**, 849 (1966).

4) "International Tables for X-ray Crystallography," Vol. III, Kynoch Press, Birmingham (1962), p. 202.

5) "Universal Crystallographic Computation Program System (UNICS)," ed. by T. Sakurai, The Crystallographic Society of Japan, Tokyo (1967).

6) R. Degeilh and R. E. Marsh, *Acta Crystallogr.*, **12**, 1007 (1959).

7) R. E. Marsh and J. Donohue, "Advances in Protein Chemistry," Vol. 22, ed. by C. B. Anfinsen, Jr., M. L. Anson, J. T. Edsall, and F. M. Richards, Academic Press, New York and London (1967), p. 235.

Fluorescence Depolarization Study of Hydrogen Bonded 1-Anthrol

Sanyo HAMAI and Hiroshi KOKUBUN

Department of Chemistry, Faculty of Science, Tohoku University, Aoba, Aramaki, Sendai 980

(Received September 17, 1973)

Rotaional depolarization of 1-anthrol fluorescence was studied in liquid paraffin. The molecular volume of 1-anthrol becomes large when it forms a hydrogen bonded complex. The molecular volume of the complex depends on the concentration of acceptor as well as the kind of acceptor. The molecular volume obtained by extrapolation to nil acceptor concentration increases with increasing size of acceptor molecule and is appreciably larger for amines than for ethers. The emitting species in the case of amines is 1-anthrolate ion pair whose strong dipolar nature may cause further interaction with excess amine molecules. It is probable that more than one molecule of amine participate in the rotating unit, leading to a large molecular volume. The rotational relaxation time was evaluated and found to depend on acceptor concentration. Two competitive effects occur by the increase in acceptor concentration, one shortening the relaxation time because of reduction of viscosity, and the other lengthening it because of molecular volume enlargement.

Fluorescence from the viscous solution is more or less polarized. The degree of polarization P depends on viscosity η and temperature T. For linearly polarized excitation light, the degree of polarization is given by the following equation derived by Perrin[1] assuming a spherical molecular shape of fluorescent solute.

$$\frac{1}{P}-\frac{1}{3}=\left(\frac{1}{P_0}-\frac{1}{3}\right)\left(1+\frac{kT}{V\eta}\tau\right) \quad (1)$$

where P_0, V, and τ stand for the limiting polarization, the molecular volume, and the mean fluorescence lifetime respectively.

From the measurements of the degree of polarization as a function of T/η aided by the lifetime determination, it is possible to obtain the molecular volume as well as the rotational relaxation time ρ, which is defined as $\rho=3V\eta/kT$. Depolarization studies have been made so far mostly in alcoholic solutions such as glycerol and cyclohexanol.[2] However, a molecular volume obtained from these highly associative solutions involves the solvated shell and becomes extremely large in some cases.[2] In order to minimize the solvation effect, liquid paraffin was employed as a viscous solvent. Since liquid paraffin consists of mainly alkyl naphthenes, the interaction between solute and solvent is expected to be small enough to prevent the solvation shell formation.

As a fluorescent solute, 1-anthrol (1-A) was selected. The molecular volumes, the rotational relaxation times and the activation energies of rotational motion were determined for the liquid paraffin solutions of 1-A containing various kinds of proton acceptor.

Experimental

Apparatus and Procedure. Absorption spectra were measured with a Hitachi EPS-3T spectrophotometer. Fluorescence polarization measurements were made with an apparatus similar to that of Weber.[3] A Polacoat PL-40 polarizing plate and a Polaroid KN-36 were employed as polarizer and analyzer, respectively. A sheet of pergament paper as a depolarizer was placed in front of a photomultiplier. Excitation light was obtained by combining a Xe arc lamp and a Hitachi G-3 grating monochromator. 0–0 absorption band was excited in every case.

Fluorescence lifetime was measured with a phase fluorometer similar to that described elsewhere.[4] Fluorescence spectra were recorded on a modified Hitachi EPU spectrophotometer equipped with an EMI 9558QB photomultiplier. Excitation light source was the same type as in the polarization measurements. The spectral calibration factors of this photometer were obtained by the method of Lippert *et al.*[5]

Viscosity was measured with an Ostwald viscometer.

Material. Scintillator grade anthracene was employed. 1-A was synthesized and recrystallized 5 times from a water–ethanol mixture.[6] Triethylamine (Wako G.R.) was dried with calcium chloride or alumina, and fractionally distilled under reduced pressure. *N,N*-Dimethylbenzylamine (Tokyo Kasei G.R.) was passed through a column of activated alumina.

Ethyl ether, *n*-butyl ether, *n*-hexyl ether, and *p*-dioxane (Wako G.R.) were distilled over sodium wire. Benzyl ether (Wako G.R.) was distilled over sodium wire under reduced pressure.

Liquid paraffin (Merck) was treated with columns of silica gel until the optical density for the 1 cm path around 270—280 nm became less than 0.02. Glycerol was distilled under reduced pressure. *n*-Hexane was purified by the standard method.

Results and Discussion

Molecular Volume. Absorption and fluorescence spectra of 1-A in liquid paraffin are given in Fig. 1.

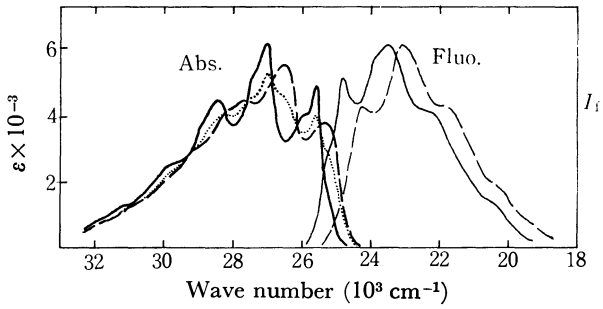

Fig. 1. Absorption and fluorescence spectra of 1-A in liquid paraffin.
Absorptoin; [1-A]$=1.41\times10^{-4}$M
——: [ethyl ether]$=0.0$ M, ----: [ethyl ether]$=9.62\times10^{-2}$M, — —: [ethyl ether]$=4.81\times10^{-1}$M
Fluorescence;
——: 1-A, — —: hydrogen bonded 1-A with ethyl ether.

The mirror image relationship between absorption and fluorescence spectra is rather poor. The excitation spectra at several points in the fluorescence band agree well with absorption spectrum. Thus, the observed fluorescence is intrinsic for 1-A and not an artifact such as impurity. $1/P$ *vs.* T/η plots for 1-A and for anthracene are shown in Fig. 2 for the sake of comparison. T/η varied with temperature. The solute concentrations were sufficiently low to prevent undesirable depolarizing effects such as reabsorption and concentration quenching.

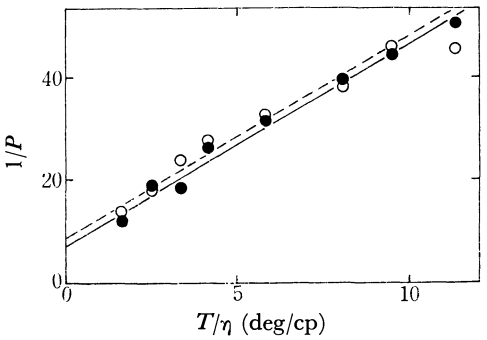

Fig. 2. Perrin plots for anthracene (--○--) and 1-A (—●—) in liquid paraffin.

Fluorescence lifetimes of anthracene and 1-A were determined respectively as 5.1 and 6.9 ns. They did not change within the experimental error in the temperature range studied. The molecular volume of anthracene was thus found to be 138 Å^3. This value corresponds to the radius of 3.21 Å assumed to be a sphere. Assuming one half of the length of the long axis, 4.6 Å, for the radius we obtain the volume 408 Å^3. The experimental value is much smaller and is close to the value of 120 Å^3 estimated for a prolate shape.

The molecular volume of 1-A was found to be 172 Å^3 which corresponds to the radius 3.43 Å. It may be due to volume expansion by the substituent that the molecular volume is larger for 1-A than for anthracene. Rather small molecular volumes obtained suggest that there is no participation of the solvation shell in the solute–liquid paraffin system.

1-A forms a hydrogen bonded complex with many acceptors. The absorption spectrum of 1-A in liquid paraffin containing various amount of ethyl ether is shown in Fig. 1. A similar result to that of Suzuki and Baba was obtained.[7] At ether concentration higher than ~0.5 M, the complexing seems to be almost complete in the ground state. The fluorescence spectrum of this solution is less structured than that of free 1-A as shown in Fig. 1. Beyond ether concentration of ~0.2 M, the fluorescence spectrum becomes a single component which is attributed to the hydrogen bonded 1-A. 1-A becomes a stronger hydrogen bond donor upon excitation to the first singlet excited state as expected from the spectral shifts by hydrogen bond formation. For other ethers absorption and fluorescence spectra are similar to the case of ethyl ether except for slight changes in shape and band positions.

Depolarization studies for hydrogen bonded 1-A were performed in liquid paraffin containing various amounts

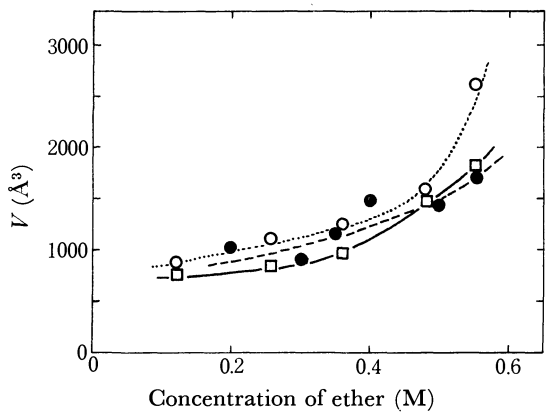

Fig. 3. Change of the molecular volume for various concentrations of ether.
—□—: *n*-butyl ether, ---○---: *n*-hexyl ether,
--●--: benzyl ether.

of ether. Linear $1/P$ *vs.* T/η plots were obtained for all the solutions studied. Fluorescence lifetimes of hydrogen bonded 1-A with ethers were found to be 14—15 ns and did not differ appreciably from each other. It was found that the molecular volume increased with the increase of acceptor concentration. As a typical example, Fig. 3 shows the molecular volume changes as a function of ether concentration. The increase of the molecular volume might be attributed to the formation of the solvation shell around the hydrogen bonded 1-A by excess ether molecules. This view is supported by the fact that the fluorescence spectrum changes in shape slightly at higher acceptor concentration in the case of benzyl ether. Solvent effect on the fluorescence spectrum of hydrogen bonded complex was found in the case of acridone–acetic acid in benzene.[8]

An empirical equation which fits the dependence of molecular volume on the concentration of ether added at a given temperature was found to be:

$$V = V_0 + A\frac{[C]^2}{\eta}$$

where V_0 is the molecular volume of the hydrogen bonded complex free from the solvation and [C] the ether concentration. V *vs.* $[C]^2/\eta$ plots for several

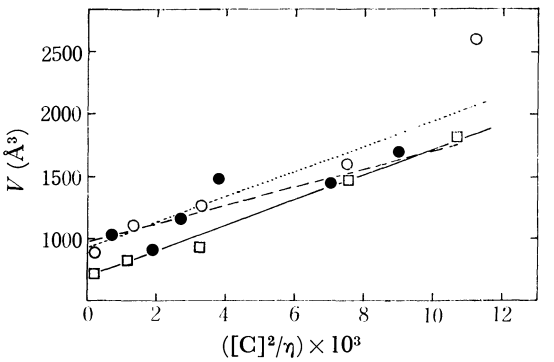

Fig. 4. Plots according to the empirical formula at 15 °C: $V = V_0 + A \cdot [C]^2/\eta$.
—□—: *n*-butyl ether, ---○---: *n*-hexyl ether,
--●--: benzyl ether.
[C] is the concentration of ether.

TABLE 1.

Proton acceptor	V_0 (A^3)
Ethyl ether	~200
p-Dioxane	~500
n-Butyl ether	700
n-Hexyl ether	920
Benzyl ether	960
Triethylamine	1720
N,N-Dimethylbenzylamine	2300

ethers are shown in Fig. 4. The V_0 values thus obtained are summarized in Table 1. There is a clear tendency for the molecular volume to increase with the increase in size of acceptor molecule.

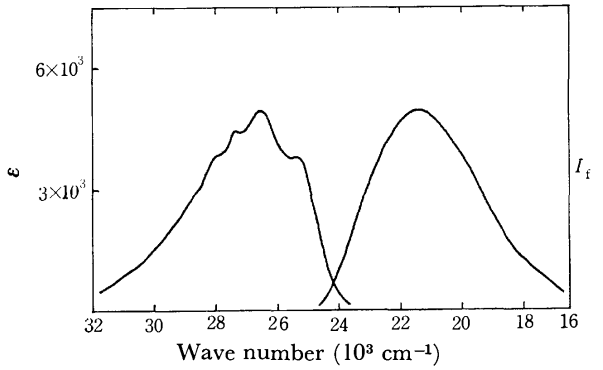

Fig. 5. Absorption and fluorescence spectra of 1-A in glycerol–water (9:1).

As a different kind of solvent, a glycerol–water mixture (9:1) was employed. Absorption and fluorescence spectra in this solution are shown in Fig. 5. Due to hydrogen bonding and strong solvent effects, structures in the spectra are considerably blurred, the spectrum showing no structure particularly for fluorescence.

The molecular volume of 1-A was obtained from the slope of Perrin's plot and the measured lifetime of 18.6 ns as 688 Å^3. This volume is considerably larger than the molecular volume of free 1-A in liquid paraffin, but smaller than that of hydrogen bonded 1-A with some larger ethers. This might suggest that the solvated shell of 1-A water–glycerol mixture is smaller than that expected from the highly associative nature of solvent. However, the evaluation of molecular volume is not based on the 'micro' viscosity, but on the measured 'macro' viscosity. Furthermore, the shape of rotating unit may differ for liquid paraffin and glycerol–water. A straightforward comparison of the results obtained for different solvents may lead to an erroneous conclusion.

Triethylamine and *N,N*-dimethylbenzylamine were employed as stronger proton acceptors than ethers. The absorption spectrum in liquid paraffin containing various amounts of triethylamine is shown in Fig. 6. At 0.4 M of amine concentration, the hydrogen bond formation seems almost complete. Absorption maxima of hydrogen bonded complex lie in a slightly smaller wavenumber compared to the case of ethers. In contrast to absorption, the fluorescence spectrum

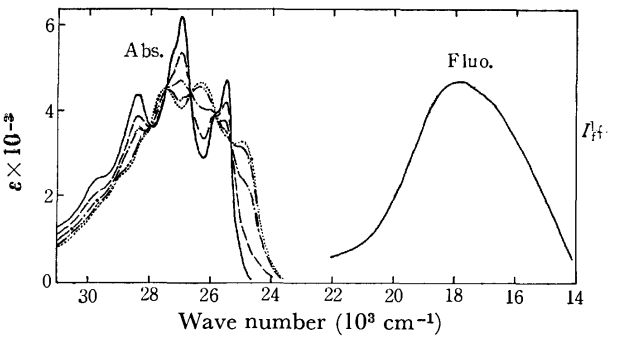

Fig. 6. Absorption and fluorescence spectra of hydrogen bonded 1-A with triethylamine.
Absorption spectra: [1-A]=1.33×10^{-4}M
——: [triethylamine]=0.0 M, — —: [triethylamine]=3.56×10^{-3}M, — · —: [triethylamine]=1.43×10^{-2}M, —·· —: [triethylamine]=3.56×10^{-2}M, ------: [triethylamine]=7.17×10^{-1}M.

changes drastically, being almost structureless and shifting to a smaller wavenumber to a great extent. Fluorescence maxima lie at 17900 and 17500 cm^{-1} for triethylamine and *N,N*-dimethylbenzylamine, respectively, which are smaller by 3600 and 4000 cm^{-1} than those in the glycerol–water mixture. The fluorescence spectrum resembles that of aqueous alkaline solution of 1-A in which maximum lies at 15000 cm^{-1}. We thus concluded that in the 1-A–amine–liquid paraffin system the usual hydrogen bond is formed between 1-A and amine in the ground state, while proton transfer occurs through the hydrogen bond in the excited state. On account of a low dielectric constant of liquid paraffin, 1-A–amine complex can exist as a hydrogen bonded ion pair. The difference in fluorescence maxima of liquid paraffin and aqueous alkaline solutions might be due to the solvent effects resulting from a very large difference in the dielectric nature.

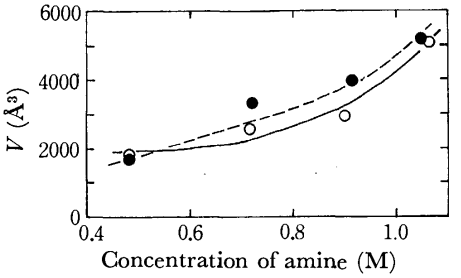

Fig. 7. Change of the molecular volume for various concentrations of amine.
—○—: triethylamine, --●--: *N,N*-dimethylbenzylamine.

Molecuar volumes obtained for the system containing amines depend also on the amine concentration (Fig. 7). The same empirical formula as that for ether fits the results. The V_0 values for triethylamine and benzylamine are given in Table 1. The molecular volume for benzylamine is considerably larger than that for triethylamine reflecting the larger size of benzylamine. However, the molecular volume for triethylamine is considerably large as compared with that for ethers such as butyl , hexyl-, and benzyl ether which

have larger molecular size than that of triethylamine. The most significant difference between amines and ethers is that the fluorescent molecule exists as a hydrogen bonded ion pair. The highly dipolar species may further interact with excess amine molecules which have a large dipole moment. Thus, there is a possibility that even at an amine concentration lower than 0.4 M more than one molecule of amine take part in the rotating fluorescent unit by forming an amine-shared ion pair or some other kind of aggregate. This may be the reason why V_0 for the amine system is appreciably large compared with that for the ether one.

Due to the short lifetime of the amine complex, the degree of polarization is relatively large. Consequently, viscosity can be varied in a wide range by adding less viscous *n*-hexane instead of varying the temperature. The molecular volume of the amine complex was proportional to the concentration of *n*-hexane added. At a given temperature, viscosity was inversely proportional to *n*-hexane concentration up to at least 4×10^{-2} M. The molecular volume, therefore, was proportional to the reciprocal of viscosity. The reason for such a relation is not clear. The difference between 'macro' and 'micro' viscosity is a possible explanation.

Rotational Relaxation Time. Rotational relaxation times in various solutions were evaluated. For anthracene in liquid paraffin, ρ is 5.2 ns at 22 °C. The rotational relaxation time of benzophenone in benzene at room temperature determined by the dielectric relaxation method is 18.7 ps. Viscosity of benzene at 20 °C is 0.65 cp, which is ~1/100 of liquid paraffin. Hence, the relaxation time in liquid paraffin should be several ns. The ρ value obtained by fluorescence depolarization method gave the same order of magnitude as that obtained by other methods.

Temperature dependence of ρ is given by

$$\rho = \rho_0 \exp(E_{rot}/kT)$$

where E_{rot} is the activation energy of rotational relaxation. The values of E_{rot} for various solutions were 11—14 kcal/mol. These values correspond to the activation energy of viscous flow of each solution as expected.

The rotational relaxation time of hydrogen bonded 1-A is given in Fig. 8 as a function of acceptor concentration. In the case of ethers, a minimum value of ρ appears at certain ether concentration. At low acceptor concentration, the molecular volume is small but viscosity is large enough to give a greater ρ value.

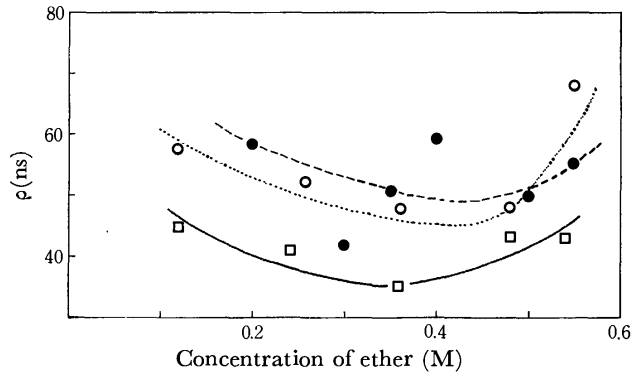

Fig. 8. Relationship of the rotational relaxation time to the concentration of ether at 12 °C.
—□—: *n*-butyl ether, ---○---: *n*-hexyl ether, --●--: benzyl ether.

With increasing acceptor concentration, viscosity decreases to give shorter ρ value. Further increase of acceptor concentration gives rise to a prominent increase in molecular volume reducing the viscosity. However, the trend for volume expansion to lengthen ρ overcomes that to shorten ρ by viscosity change, giving longer ρ as a whole. In the case of amines, the presence of minimum is not clear because of scattering of data.

H. K. wishes to thank the Mitsubishi Foundation for financial support.

References

1) F. Perrin, *J. Phys. Radium*, **7**, 390 (1926). F. Perrin, *Ann. Phys.*, **12**, 169 (1929).
2) N. D. Zhevandrov and V. P. Nikolaev, *Soviet Phys. Doklady*, **2**, 175 (1958). A. M. Sarzhevskii, *Opt. Spectr.*, **10**, 326 (1961). R. K. Bauer and K. I. Rudik, *Acta Phys. Pol.*, **35**, 259 (1969). R. K. Bauer, *Z. Naturforschg.*, **18a**, 718 (1963). R. K. Bauer, *Acta Phys. Pol.*, **33**, 441 (1968).
3) G. Weber, *J. Opt. Soc. Amer.*, **46**, 962 (1956).
4) A. Müller, R. Lumry, and H. Kokubun, *Rev. Sci. Instr.*, **36**, 1214 (1965).
5) E. Lippert, W. Nägele, I. Seibold-Blankenstein, U. Staiger, and W. Voss, *Z. Anal. Chem.*, **170**, 1 (1959).
6) P. Ferrero and A. Conzetti, *Helv. Chim. Acta*, **11**, 1152 (1928). R. E. Schmidt, *Ber.*, **37**, 66 (1904).
7) S. Suzuki and H. Baba, *J. Chem. Phys.*, **38**, 349 (1963). H. Baba and S. Suzuki, This Bulletin, **35**, 683 (1962).
8) H. Kokubun, *Z. Phys. Chem.* (Frankfurt), **17**, 281 (1958).

Formation of Alkyl Radicals by Photoionization of Alcohol Radicals Trapped in Glassy Matrices

Masaru SHIOTANI and Claude CHACHATY

Faculty of Engineering, Hokkaido University, Sapporo 060
Service de Chimie Physique, Centre d'Etudes Nucleaires de SACLAY, B.P. n° 2 (91)-Gif-sur-Yvette, France

(Received October 30, 1972)

Experiments were carried out in order to elucidate the formation mechanism of $C_2H_5\cdot$ radicals formed by the UV irradiation ($250<\lambda<350$ nm) of $CH_3\dot{C}HOH$ radicals. The kinetics of the formation of the $C_2H_5\cdot$ radical was examined by means of ESR in neutral, acidic, and alkaline ethanol glasses at 77 K. The initial rate of the formation of $C_2H_5\cdot$ was nearly independent of the concentration of added acid (H_2SO_4), but it decreased sharply with that of added NaOH. Moreover, the limiting yield of $C_2H_5\cdot$ decreased with the concentrations of both the acid and the base. Our experimental results suggest that the $C_2H_5\cdot$ radicals are formed by this reaction:

$$C_2H_5OH_2^+ + e^- \longrightarrow C_2H_5\cdot + H_2O$$

The $C_2H_5OH_2^+$ ion and the electron result from the photoionization of $CH_3\dot{C}HOH$ radicals according to these reactions:

$$CH_3\dot{C}HOH \xrightarrow{h\nu} (CH_3CHOH)^+ + e^-$$
$$(CH_3CHOH)^+ + C_2H_5OH \longrightarrow CH_3CHO + C_2H_5OH_2^+$$

The free radicals produced by the abstraction of α hydrogen atoms from aliphatic alcohols have an absorption band between 200 and 350 nm.[1,2] Under irradiation in this wavelength range, $R\dot{C}HOH$ radicals are photolyzed, giving rise to $R\cdot$ and/or $RCH_2\cdot$ alkyl radicals.[3-6] The mechanism of the formation of $RCH_2\cdot$ radicals has not yet been definitely established, however.

By the photolysis of the $CH_3\dot{C}HOH$ radical (generated by the γ-irradiation of ethanol and trapped in the glassy state), which has been the most extensively studied,[3-6] both $\dot{C}H_3$ and $\dot{C}_2H_5$[3,5] are produced. The former disappears quickly upon hydrogen abstraction, whereas $C_2H_5\cdot$ reaches a stationary concentration. Moreover, it has been calculated[7] and confirmed experimentally[8] that $CH_3\dot{C}HOH$ trapped in polar solids may be photoionized in the near UV region, since its ionization potential is lowered from 7 eV in the gas phase to 2.5 eV in the solid state (2.5 eV corresponds to 495 nm).

The present work has been designed to show, using the example of $CH_3\dot{C}HOH$, that the photolytic formation of $RCH_2\cdot$ from $R\dot{C}HOH$ radicals trapped in glassy alcohols is a consequence of the photoionization rather than of the reaction of excited hydroxyalkyl radicals on the substrate, as has been suggested.[9]

Experimental

The ethanol was purified by fractional distillation. Neutral, acidic, and alkaline samples of ethanol containing 5% of water were degassed in "spectrosil" silica tubes and then γ-irradiated at 77 K in the glassy state, using a ^{60}Co source and a dose of 8×10^{19} eV ml^{-1}.

After irradiation, the samples were bleached by visible light to remove the trapped electrons. The ESR spectra were then recorded with a "STRAND Labs" 601 BX Spectrometer operating at 9.3 GHz. The concentration of radicals was determined by double integration and by comparison with a reference sample of pure glassy ethanol, taking $G(CH_3\dot{C}HOH)=8$[6] after bleaching. The UV irradiation was carried out by focusing the output of a 500 W mercury arc (Phillips SP. 500) onto the sample placed in a liquid-nitrogen Dewar vessel located in the cavity. Two intensities of illumination were used: 10^{17} quanta cm^{-3} s^{-1} and 2×10^{16} quanta cm^{-3} s^{-1} ($250\text{ nm}<\lambda<400$ nm).

Results and Discussion

The rate of the formation and the limiting yield of $C_2H_5\cdot$ from UV-irradiated $CH_3\dot{C}HOH$ produced by γ irradiation have been studied in neutral ethanol, as well as in acidic and alkaline media, as a function of the concentrations of the added H_2SO_4 and NaOH.

During photolysis the overall concentration of radicals ($CH_3\dot{C}HOH$ and $C_2H_5\cdot$) was determined by integration, as has been indicated previously.

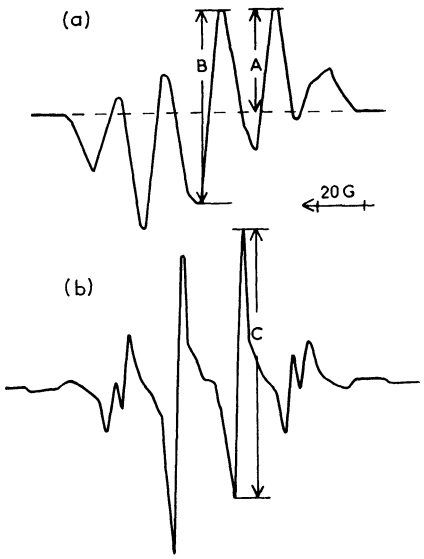

Fig. 1. a) ESR spectrum of $CH_3\dot{C}HOH$ radical observed at 77 K after γ irradiation of pure C_2H_5OH and subsequent bleaching to trapped electrones.
b) Spectrum of $C_2H_5\cdot$ observed at 77 K after UV photolysis of $CH_3\dot{C}HOH$.

The relative concentration of radicals was determined by measureing the amplitude of Bands A and B for $CH_3\dot{C}HOH$ (Fig. 1a) and of Band C for $C_2H_5\cdot$ (Fig. 1b). These amplitudes were correlated with the true concentration of radicals by calibration with the spectra of both radicals obtained separately, and then integrated.

The variations in the concentrations of the $CH_3\dot{C}HOH$ and $C_2H_5\cdot$ radicals with the time of UV irradiation are represented in Figs. 2 and 3.

In the case of neutral ethanol, the signal amplitude of $CH_3\dot{C}HOH$ falls to an undetectable level after 5 to 15 min of illumination, the rate of decrease depending on the UV-light intensity, while the concentration of $C_2H_5\cdot$ passes through a maximum and decays slowly by recombination after the complete consumption of $CH_3\dot{C}HOH$. The logarithmic plot of $CH_3\dot{C}HOH$ against the time of illumination is linear the slope being pro ortional to the intensity of UV irradiation, indicating a first-order decay of this radical (Fig. 4). This means that the optical density of the $CH_3\dot{C}HOH$ radical may be very small. Under the same conditions, the rate of the formation of $C_2H_5\cdot$ and its limiting

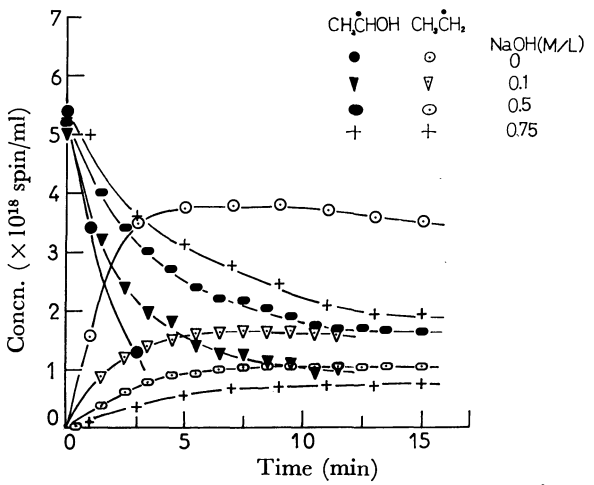

Fig. 2. Variation of the concentration of $CH_3\dot{C}HOH$ and $C_2H_5\cdot$ radicals in the course of UV photolysis ($I=2\times10^{16}$ quanta $cm^{-3}s^{-1}$): neutral and alkaline matrices.

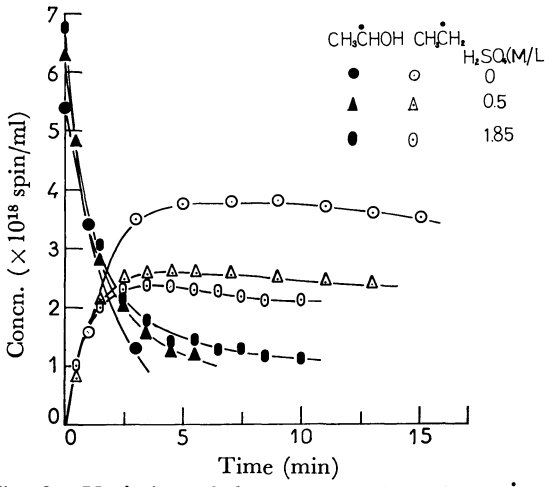

Fig. 3. Variation of the concentration of $CH_3\dot{C}HOH$ and $C_2H_5\cdot$ radicals in the course of UV photolysis ($I=2\times10^{16}$ quanta $cm^{-3}s^{-1}$): neutral and acidic matrices.

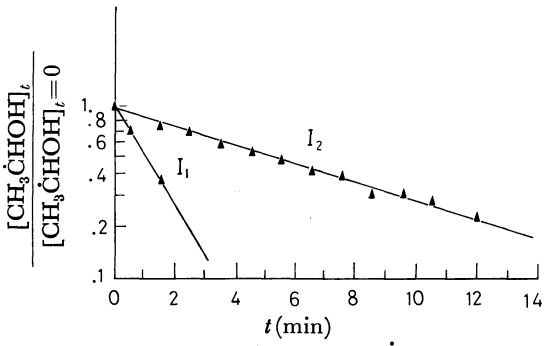

Fig. 4. Logarithmic plot of $[CH_3\dot{C}HOH]_t$ *versus* UV irradiation time, $[CH_3\dot{C}HOH]_t=0$ being the initial concentration. $I=10^{17}$ quanta cm^{-3} s^{-1}, $I_2=2\times10^{16}$ quanta cm^{-3} s^{-1}.

yield are drastically reduced as the concentration of NaOH is increased (Fig. 2). On the other hand, the initial rate of the formation of $C_2H_5\cdot$ is about the same in acidic and neutral media, while its limiting yield is lowered by the presence of H_2SO_4.

In order to interpret these results, which are summarized in Figs. 5 and 6, the reaction scheme proposed in a previous paper[8] by one of the present authors has been somewhat modified as follows.

The photoionization of $CH_3\dot{C}HOH$ and the consecutive ion-molecule reactions are:

$$CH_3\dot{C}HOH \xrightarrow{h\nu} (CH_3CHOH)^+ + e^- \quad (1)$$

$$(CH_3CHOH)^+ + C_2H_5OH \longrightarrow C_2H_5OH_2^+ + CH_3CHO \quad (2)$$

An increase in the concentration of $CH_3\dot{C}HO$ has actually been observed in the course of the photolysis of $CH_3\dot{C}HOH$.[9]

The released electron can participate in the competitive reactions:

$$e^- + 2C_2H_5OH \longrightarrow CH_3\dot{C}HOH + C_2H_5O^- + H_2$$

and/or

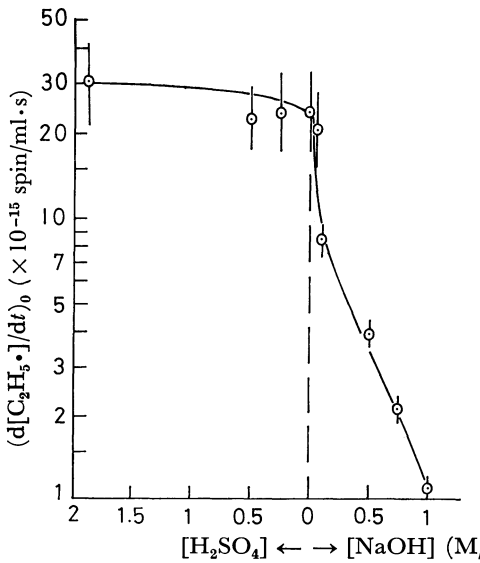

Fig. 5. Initial rate of formation of $C_2H_5\cdot$ as a function of H_2SO_4 and NaOH concentrations.

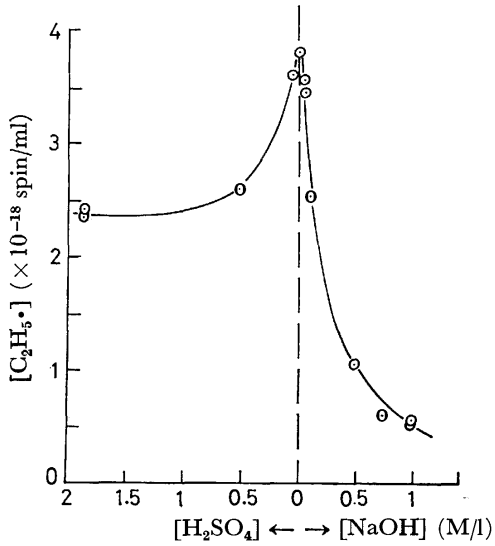

Fig. 6. Maximum yield of $C_2H_5\cdot$ as a function of H_2SO_4 and NaOH concentrations.

$$\left\{\begin{array}{l} e^- + C_2H_5OH \longrightarrow C_2H_5O^- + H\cdot \\ H\cdot + C_2H_5OH \longrightarrow CH_3\dot{C}HOH + H_2 \end{array}\right. \quad (3)$$

$$e^- + C_2H_5OH_2^+ \longrightarrow H_2O + C_2H_5\cdot \quad (4)$$

Reaction (3) is supported by the experimental finding that the $CH_3\dot{C}HOH$ radicals are formed by the decay of electrons formed when alkali metals are added to C_2H_5OH glass at 77 K,[10] while Reaction (4) has been suggested by Yoshida *et al.*[11] However, in the present case, the rate of Reaction (4) is most likely larger than that of Reaction (3).

A reaction similar to (4) has been proposed by Symons *et al.*[12] to account for the formation of methyl and isopropyl radicals in γ-irradiated solutions of methanol and isopropanol in glassy acidic ice. It may be pointed out that Reaction (4) is energetically favourable, the electron affinity of H_2O^+ being markedly larger than the C–O bond energy (12.6 eV against 4 eV[13]).

In the alkaline matrix, the $C_2H_5OH_2^+$ ions, precursors of $C_2H_5\cdot$, are scavenged by an excess of $C_2H_5O^-$ and/or OH^- ions:

$$C_2H_5O^- + C_2H_5OH_2^+ \longrightarrow 2C_2H_5OH$$

and/or (5)

$$OH^- + C_2H_5OH_2^+ \longrightarrow C_2H_5OH + H_2O$$

$CH_3\dot{C}HOH$ being regenerated by Reaction (3). The failure to observe the ESR spectrum of the solvated electron, even in the alkaline medium may be attributed to its high quantum yield of untrapping by UV light.[2]

It could be expected that, in the acidic matrix, the contribution of Reaction (4) would be enhanced by the increase in the concentration of $C_2H_5OH_2^+$. The decay in the yield of $C_2H_5\cdot$ as the concentration of H_2SO_4 is increased suggests that the electrons released by Reaction (1) are partially scavenged by HSO_4^-, producing $CH_3\dot{C}HOH$ radicals according to these reactions:

$$e^- + HSO_4^- \longrightarrow SO_4^{2-} + H\cdot \quad (6)$$

$$H\cdot + C_2H_5OH \longrightarrow CH_3\dot{C}HOH + H_2 \quad (7)$$

The hypothesis of an ionic contribution to the near-UV photolysis of hydroxyalkyl radials, trapped in glassy alcohols, seems, therefore, supported by the effect of added acids and bases presented here.

References

1) R. S. Alger, T. H. Anderson, and L. A. Weeb, *J. Chem. Phys.*, **30**, 695 (1959).
2) A. Bernas, D. Grand, and C. Chachaty, *Chem. Commun.*, **1970**, 1667.
3) (a) B. N. Shelimov, N. B. Fok, and V. V. Voevodskii, *Kinet. Katal.*, **5**, 539 (1963). (b) B. N. Shelimov, N. B. Fok, and V. V. Voevodskii, *ibid.*, **5**, 1008 (1964).
4) (a) R. H. Johnsen, *J. Phys. Chem.*, **65**, 2144 (1961). (b) R. H. Johnsen, *ibid.*, **67**, 681 (1963).
5) C. Chachaty and E. Hayon, *J. Chim. Phys.*, **61**, 1115, (1964).
6) C. Chachaty, Dr. Sc. Thesis, Univ. de PARIS, (1968), C.E.A. Report R 3537 (1969).
7) Ye. I. Finkelshtein, *Visokomol. Soyed., A*, **9**, 70 (1967).
8) C. Chachaty, A. Forchioni, and J. Desalos, *C. R. Acad. Sci. Paris, C*, **270**, 449 (1970).
9) H. S. Judeikis and S. Siegel, *J. Chem. Phys.*, **43**, 3625 (1965).
10) J. E. Bennett, B. Mile, and A. Thomas, *J. Chem. Soc. Ser., A*, **1967**, 1399.
11) H. Yoshida, M. Irie, O. Shimada, and K. Hayashi, *J. Phys. Chem.*, **76**, 3747 (1972).
12) D. R. G. Brimage, J. D. P. Cassel, J. H. Sharp, and M. C. R. Symons, *J. Chem. Soc., Ser. A*, **1969**, 2619.
13) Y. I. Venenyev, L. V. Gurvich, V. N. Kondratiev, V. A. Medvedev, and Ye. L. Frankevich, "Bond Energies, Ionization Potentials and Electron Affinities," Edward Arnold Publisher, London (1966).

The Radiophoto-luminescence of γ-Irradiated Hydrocarbon Glasses at 77 K

Hideo YAMAZAKI, Koichi OKA, Masabumi SATO, and Shoji SHIDA
Laboratory Physical Chemistry, Tokyo Institute of Technology, Meguro-ku, Tokyo 152
(Received March 9, 1973)

The radiophoto-luminescence (RPL) from γ-irradiated hydrocarbon glasses, *i.e.*, 3-methylhexane, methylcyclohexane, and ethylcyclohexane, containing small amounts of various aromatics (1,3,5-trimethylbenzene, biphenyl, naphthalene, and 1,4-diazine) is investigated at 77 K by infrared-light irradiation. The spectra of the RPL consist of the fluorescence and phosphorescence of the guest aromatic molecule, and the ratio of the phosphorescence to the fluorescence intensity is larger than that in the photoexcitation, indicating the existence of another path to the triplet state. The RPL is quenched by the addition of N_2O, but it is not much affected by that of NH_3. A possible mechanism for the RPL is considered, and its analysis is given.

In the primary process of the radiation chemistry of hydrocarbons, the mechanism of neutralization is not quite understood because of the rapidity of the process. The rigid-solvent method has been used to slow down the reaction rate and to facilitate the measurements. The radiation energy stored in a rigid matrix can be liberated by means of several methods; elevation of temperature[1,2] (radiothermo-luminescence), irradiation by infrared light[3-6] (radiophoto-luminescence, RPL), and application of an electric field.[7-10] The control of the luminescence intensity is easiest in RPL, and the relaxation time of emission can be measured from the response time of the luminescence by intermittent irradiation of infrared light, so the RPL is used in this study. Hamill *et al.*[3,4] have measured the RPL from biphenyl in a 3-methylpentane solution and obtained a rather diffused spectrum of the phosphorescence of biphenyl by rapid scanning with an oscilloscope. Magat *et al.*[5,6] studied the RPL spectrum of biphenyl and its excitation spectrum in a methylcyclohexane solution. In their measurement of the excitation spectrum, a filter was used to pass through the whole wavelength of the phosphorescence. A more precise experiment is necessary, however, to obtain detailed information.

Experimental

Hydrocarbon samples purchased from Merck, Aldrich Chemical, and the Phillips Co. were passed through an activated silica gel column and then outgassed by the freeze-pump method and stored with a sodium mirror. The biphenyl and naphthalene were purified by the zone-melting method. The 1,4-diazine and 1,3,5-trimethylbenzene (Merck and Tokyo Kasei Co.) were used without further purification. The sample tubes used were made of high-purity quartz or of molybdenum glass; the dimension of diameters are 5 and 10 mm. After degassing *in vacuo*, the samples were irradiated by γ-rays from ^{60}Co with total doses of 10^4—10^5 r at 77 K in darkness. The spectra of RPL were measured with a Hitachi MPF-2A fluorometer, the intensity of emission was standardized by using the data of emission from β-naphthol in photoexcitation.[11] The sample was irradiated by diffracting infrared light of the zeroth order through a grating from a light source of a 150 W Xe-lamp equipped with Toshiba IR-D1A and VB-46 filters. The average intensity of emission was used to obtain a spectrum by repeating the forward and backward scanning, since the intensity of emission decreased slowly as the concentration of trapped electrons decreased.

Results and Discussion

The RPL spectra of 3-methylhexane, methylcyclohexane, and ethylcyclohexane (3-MHX, MCHX, and ECHX) showed a weak and broad spectrum with a maximum at about 420 nm; the response time of the emission by the infrared light was several seconds, so it is likely that the emission is due to the transition of a different spin multiplicity. Such a diffuse emission spectrum was also observed in the RTL and RPL of 3-methylpentane.[12,13] The low-lying electronic states of saturated hydrocarbons have been observed by Hamill in a solid matrix with the energy-loss spectrum[14] of electrons and with the emission spectrum upon electron impact.[15,16] When small amounts of aromatic hydrocarbons (10—100 ppm) were added to these solvents, distinct fluorescence and phosphorescence of aromatic hydrocarbons were observed. Figure 1 shows the relaxation of the phosphorescence at 465 nm from biphenyl in 3-MHX due to the intermittent irradiation of infrared light. The relaxation time is determined by the lifetime of the phosphorescence, and the intensity of the emission decreases slowly as the concentration of trapped electrons in the matrix decreases. Figures 2—4 show the emission (solid curves) of fluorescence and phosphorescence with reference to those (dotted curves) of the photoexcitation in the ultraviolet region. In these figures the maximum values of the intensities of the fluorescence for both cases were standardized as unity. No appreciable difference in the spectrum was observed with the change

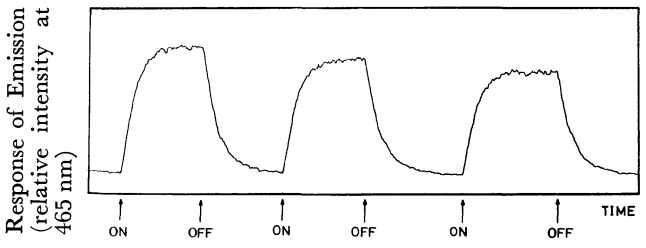

Fig. 1. Response of the emission at 465 nm from biphenyl in 3-MHX at 77 K by the intermittent irradiation of infrared light. The interval between "on" and "off" is 30 s in the time scale.

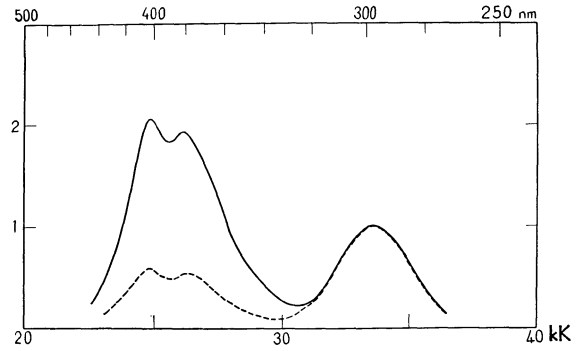

Fig. 2. RPL (full curve) and photoexcited emission (dotted curve) from 1,3,5-trimethylbenzene in 3-MHX at 77 K.

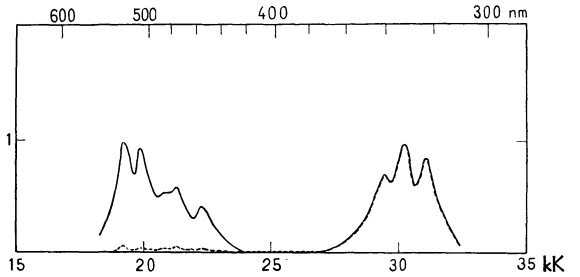

Fig. 3. RPL (full curve) and photoexcited emission (dotted curve) from naphthalene in 3-MHX at 77 K.

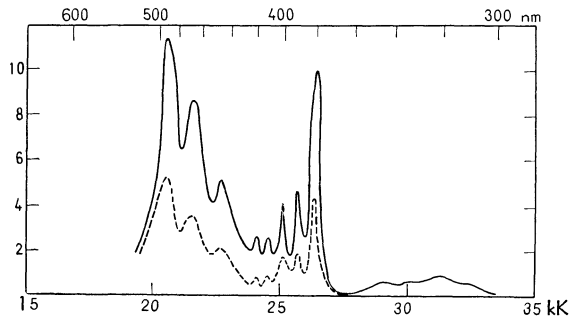

Fig. 4. RPL (full curve) and photoexcited emission (dotted curve) from the one-to-one mixture of 1,4-diazine and biphenyl in 3-MHX at 77 K.

in the solvents (3-MHX, MCHX, and ECHX). The ratio of the intensity of the phosphorescence to the fluorescence was larger in the case of RPL than in that of photoexcitation as observed by a number of authors.[12,17,18] The ratio of the phosphorescence and fluorescence depends on the sample. A very large relative intensity of phosphorescence was observed in a naphthalene solution, as is shown in Fig. 3. The proportion of phosphorescence in the total emission gradually changed upon prolonged irradiation by infrared light. The dilute solution of a one-to-one mixture of two aromatic compounds generally showed the phosphorescence of each component with a certain ratio of intensity; *e.g.*, the ratio of the intensity of the phosphorescence of a one-to-one mixture of 1,4-diazine and biphenyl in 3-MHX was about 1 : 4 (Fig. 4). The ratio of the intensities of the component fluorescences from such a solution depended on the concentration, since the ratio was much perturbed by the energy-transfer process. The RPL was quenched by the addition of an electron scavenger such as N_2O, as was observed in the emission due to a recombination process after photoionization,[19-21] but it was not much affected by the addition of NH_3, which was used as a positive-charge scavenger in the liquid phase.

The emission process must be followed by the excitation of aromatic compounds. The production of the excited states of aromatic compounds is expressed by the following scheme:

$$e_t^- \xrightarrow{h\nu} e_m^- \quad (1)$$

$$RH^+ + e_m^- \longrightarrow RH^* \quad (2)$$

$$RH^* + RH \longrightarrow RH + RH^* \quad (3)$$

$$RH^* \longrightarrow RH + h\nu \quad (4)$$

$$RH^* + A \longrightarrow RH + A^* \quad (5)$$

where e_t^- and e_m^- are the trapped and mobilized electrons and where RH and A refer to the hydrocarbon and aromatic molecules. By the absorption of infrared light, the trapped electrons are mobilized by means of Reaction (1).

$$RH^+ + A^- \longrightarrow RH + A^* \quad (6)$$

$$A^+ + A^- \longrightarrow A^* + A \quad (7)$$

$$A^+ + e_m^- \longrightarrow A^* \quad (8)$$

$$A^* \longrightarrow A + h\nu' \quad (9)$$

The geminate and random recombination can produce RH* by means of Reaction (2), and the energy migration may take place in solid hydrocarbon, as is expressed by Reaction (3). In the absence of an aromatic compound, a weak emission at 420 nm was detectable; this may be attributed to Reaction (4). In the presence of aromatic additives, the excited states of the aromatic molecule, A*, can be produced by the energy-transfer reaction (5), the ionic neutralizations (6) and (7), and the recombination of A^+ with an electron by means of Reaction (8).

Three types of direct excitations of aromatic molecule are considered, namely, the excitation by the reaction between A^+ and an electron (8), that by A^- and RH^+ (6), and that by A^+ and A^- (7). From the experimental results that the mobilities of A^-, A^+, and RH^+ are not large and that the excitation spectrum of the RPL is similar to the absorption spectrum of a trapped electron,[5] the process involving the transport of these species (A^-, A^+, and RH^+) can be ignored. The neutralization between A^+ and an electron is not important under the present condition of a low concentration (10—100 ppm) of A, because A^+ can be detected only at high concentrations of aromatic additives in hydrocarbon matrices. Therefore, the indirect excitation by the energy transfer from RH* produced by the neutralization between RH^+ and electron is most probable in forming A*. Such an energy transfer from the excited states of paraffins to additives was observed by the measurement of the emission[16] and by the method of product analysis[22,23] in the vacuum ultraviolet photolysis of liquid paraffins. This explanation is consistent with the experimental result that the RPL is quenched by the addition of an electron scavenger and not much affected by the addition of a positive-charge scavenger.

Apart from the detailed mechanism of the excitation, the aromatic molecule can be excited to the singlet- or triplet-excited state by the liberation of a trapped electron. The process can be symbolically written by Reactions (10) and (11). Therefore, the emission process from the transition of these excited states is described by the following reactions:

$$A \dashrightarrow A^*(\text{singlet}) \qquad k_s \qquad (10)$$

$$A \dashrightarrow A^*(\text{triplet}) \qquad k_t \qquad (11)$$

$$A^*(\text{singlet}) \longrightarrow A + h\nu_f \qquad k_f \qquad (9')$$

$$A^*(\text{triplet}) \longrightarrow A + h\nu_p \qquad k_p \qquad (9'')$$

$$A^*(\text{singlet}) \longrightarrow A^*(\text{triplet}) \qquad k_{isc} \qquad (12)$$

$$A^*(\text{singlet}) \longrightarrow A \text{ or products} \qquad \sum k_x \qquad (13)$$

$$A^*(\text{triplet}) \longrightarrow A \text{ or products} \qquad \sum k_y \qquad (14)$$

where k_s, k_t, k_f, k_p, k_{isc}, $\sum k_x$, and $\sum k_y$ are the rate constants for the production of the singlet state and for the triplet state, for the emission of fluorescence and of phosphorescence for the intersystem crossing, for reactions from the singlet state and for reactions from the triplet state respectively.

From Reactions (9'), (9''), (10)—(14), the intensity ratio between the fluorescence and the phosphorescence (F/P value) in the electron-recombination process can be evaluated by:

$$\sigma_e \equiv (F/P)_e = \frac{k_f k_s (k_p + \sum k_y)}{(k_s k_{isc} + k_t k_f + k_t k_{isc} + k_t \sum k_x) k_p} \qquad [1]$$

In the photoexcitation by the first singlet-excited state, the F/P value is given by:

$$\sigma_h \equiv (F/P)_h = \frac{k_f (k_p + \sum k_y)}{k_{isc} k_p} \qquad [2]$$

The ratio of the initial distribution of the singlet state to the triplet state of the aromatic molecule is given by:

$$\rho = (k_s/k_t) = \frac{\sigma_e \sigma_h k_p/(k_p + \sum k_y) + \sigma_e + \sigma_e \sum k_x/k_{isc}}{\sigma_h - \sigma_e} \qquad [3]$$

Under the conditions of $\sum k_x = 0$ and $\sum k_y = 0$, the F/P values, σ_e and σ_h, are reduced to:

$$\sigma_e = \frac{k_f (k_s/k_t)}{k_{isc}(k_s/k_t) + k_f + k_{isc}} \qquad [4]$$

and:

$$\sigma_h = k_f/k_{isc} \qquad [5]$$

Then, the singlet-triplet ratio is expressed by:

$$\rho = k_s/k_t = (\sigma_h \sigma_e + \sigma_e)/(\sigma_h - \sigma_e) \qquad [6]$$

In Eq. [3] the increase in $\sum k_x$ may cause the increase in ρ, but the increase in $\sum k_y$ may cause the decrease in ρ. If both the values $\sum k_x$ and $\sum k_y$ increase from zero in Eq. [3], the value of ρ will not change much from the value of ρ given by Eq. [6]. Thus, Eq. [6] is still a plausible approximation for the small values of $\sum k_x$ and $\sum k_y$. For example, the values of ρ calculated from the spectra (Figs. 2 and 3) and assuming Eq. [6] are 0.93 and 1.0 for 1,3,5-trimethylbenzene and naphthalene respectively in 3-MHX. These results indicate that the values of k_t and k_s are almost equal. However, the value of k_t would be expected to be three times larger than that of k_s if the triplet and singlet states are produced by random recombination with the spin conservation. The departure from the statistical value in the ρ value may be another evidence of indirect excitation. Recently Tsubomura *et al.*[24] found that the F/P value was 0.7—0.8 for the photothermoluminescence of *N,N,N',N'*-tetramethyl-*p*-phenylene diamine in various matrices and that the F/P value was approximately equal to the ratio of the production of singlet and triplet states, therefore, the simple spin conservation rule does not hold in their case, either.

The authors wish to thank Professor Hiroshi Tsubomura, Drs. Naoto Yamamoto and Yoshihiro Nakato of Osaka University for reading the preliminary manuscript of this paper and for their helpfull discussions.

References

1) B. Brocklehurst, R. D. Russell, and M. I. Savadatti, *Trans. Faraday Soc.*, **62**, 1129 (1966).
2) M. Burton, M. Dillon, and R. Rein, *J. Chem. Phys.*, **41**, 2228 (1964).
3) D. W. Skelly and W. H. Hamill, *ibid.*, **43**, 3497 (1965); **44**, 2891 (1966).
4) W. H. Hamill, "Ion Radicals," E. T. Kaiser, and L. Keran, ed., John Wiley, New York (1968), p. 383.
5) A. Deroulede, F. Keiffer, and M. Magat, *Advan. Chem. Ser.*, **82**, 401 (1968).
6) M. Magat, "Progress and Problems in Contemporary Radiation Chemistry," Prague (1971), p. 423.
7) A. C. Albrecht, *ibid.*, p. 331.
8) G. H. Johnson, W. M. McCain, and A. C. Albrecht, *J. Chem. Phys.*, **43**, 2911 (1965).
9) J. Bullot and A. C. Albrecht, *Acta Phys. Polon.*, **34**, 691 (1968).
10) J. Bullot and A. C. Albrecht, *J. Chem. Phys.*, **51**, 2220 (1969).
11) E. Lippert, W. Nägele, I. Seibold-Blankenstein, V. Staiger, and W. Voss, *Z. Anal. Chem.*, **170**, 1 (1959).
12) K. Funabashi, C. Hebert, and J. L. Magee, *J. Phys. Chem.*, **75**, 3221 (1971).
13) P. B. Merkel and W. H. Hamill, *J. Chem. Phys.*, **53**, 3414 (1970).
14) L. M. Hunter, D. Lewis, and W. H. Hamill, *ibid.*, **52**, 1733 (1970).
15) P. B. Merkel and W. H. Hamill, *ibid.*, **54**, 1695 (1971).
16) F. Hirayama and S. Lipsky, *ibid.*, **51**, 3616 (1969).
17) D. S. Klinger, J. D. Laposa, and A. C. Albrecht, *ibid.*, **48**, 4326 (1968).
18) N. Yamamoto, Y. Nakato, and H. Tsubomura, This Bulletin, **39**, 2603 (1966).
19) K. Yoshinaga, N. Yamamoto, M. Ozaki, and H. Tsubomura, *Nippon Kagaku Zasshi*, **92**, 124 (1971).
20) K. Yoshinaga, N. Yamamoto, and H. Tsubomura, *J. Luminescence*, **4**, 417 (1971).
21) K. D. Cadogan and A. C. Albrecht, *J. Phys. Chem.*, **72**, 929 (1968).
22) H. A. Holroyd, *Adv. Chem. Ser.*, **82**, 488 (1968).
23) V. I. Pitchoozhkin, H. Yamazaki, and S. Shida, This Bulletin, **46**, 67 (1973).
24) K. Yoshinaga, N. Yamamoto, and H. Tsubomura, *J. Luminescence*, **6**, 179 (1973).

A Molecular Orbital Study on the Effects of Excess Charges at the Donor and Acceptor Atoms on the Hydrogen Bond

Akira IGAWA and Hideo FUKUTOME
Department of Physics, Kyoto University, Kyoto 606
(Received April 6, 1973)

Effects of the excess charges at the donor and acceptor atoms on the properties of the hydrogen bond were studied in a simple three-center four-electron model for a hydrogen bond system using CNDO/2 type molecular orbital calculation. It was shown that three types of hydrogen bonds, normal, proton transferred and abnormal, are possible according to the value of the excess charges. The dependence of the hydrogen bond distance, proton equilibrium distance, frequency of proton stretching vibration and hydrogen bond energy on the excess charges were calculated for the normal type hydrogen bond. The correlations between these quantities obtained by changing the amounts of the excess charges are in good agreement with the experimental results, suggesting that the excess charges at the donor and acceptor atoms primarily determine the correlation. The potential of proton movement at the equilibrium hydrogen bond distance is shown not to have double minima for any value of the excess charges, indicating that the excess charges are not essential for producing a double well potential.

Many theoretical works have been carried out on the hydrogen bond (HB) which can be classified into two categories, those based on the simplified three-center four-electron model using the valence bond (VB)[1-3] or the molecular orbital (MO)[4,5] method and those on the calculations for total HB systems using the non-empirical[7-9] or the semi-empirical[6] MO method. The early works belong to the former category, but the main trend in recent works seems to be in the latter one. Morokuma and Pedersen[7] and Kollman and Allen,[8] from their non-empirical calculation for total HB systems, emphasized that electron reorganization within them is important, and the simple three-center model has nothing to do with the explanation of the properties of the HB. Their criticism is sound as far as the original simple three-center model is concerned. However, they seem to underestimate the usefulness of a suitably modified three-center model in explaining the properties of the HB. The three-center model can be modified to incorporate some effects of the residual part of the HB system into its parameters. Such modifications of the three-center model were studied for the HB in ice with positive and negative defect,[4] the HB coupled with π electron system[5] and the HB with donor and acceptor atoms of varying net charges.[3]

We have studied the effects of the excess charges at donor and acceptor atoms on the properties of the HB by means of the three-center model and semi-empirical MO calculation. Change in the net charges at the donor and acceptor atoms is considered to be one of the most important factors of the residual part of the HB system which would strongly affect the properties of the HB. The model was studied by Hasegawa *et al.*[3] with use of the VB method. However, their calculation was not extensive enough to confirm the importance of the change of the net charges at the donor and acceptor atoms. We have shown that this model can satisfactorily explain the empirical correlations between the HB distance, proton equilibrium position, frequency of proton stretching vibration and HB energy. A comparison of the calculations for this model and those for total HB systems provides a quantitative estimation of the dynamical effects of the residual part of HB system which cannot be renormalized into the effect of the net charges of the donor and acceptor atoms.

Model and Method of Calculation

We take the three-center four-electron model of the HB system (Fig. 1) and consider the case in which donor A, acceptor B and proton H are arranged linearly, both A and B being oxygen atoms. The HB MO is constructed from the three atomic orbitals (AO), the 1s AO of H and the two AO's, one from A and the other from B each extending toward H. The hybridization of the AO's of A and B is assumed and fixed to be sp^3. Four electrons, two from B and one from A and one from H, enter into the HB MO. The electrons in the other hybridized AO's of A and B are treated as the source of external charges, and they are not constrained to be the integers 5 and 4 respectively. The excess charges at A and B are denoted by $\delta_A e$ and $\delta_B e$ respectively. The 1s cores of A and B are treated as the points with charge of 6e. In the following, we use the term "the core of A or B" meaning that it represents the 1s core and the electrons in the hybridized AO's at A or B not involved in the HB MO.

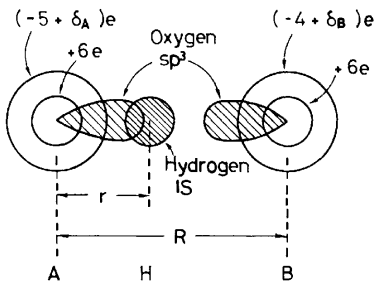

Fig. 1. Three-center four-electron model of hydrogen bond with excess charges.

The HB MO was calculated by CNDO/2 approximation.[10] To obtain consistency with CNDO/2 approximation, the core-core interaction between A and B should be estimated by

$$E_{cc} = \frac{(6e)^2}{R} + \gamma_{AB}\{(5-\delta_A)(4-\delta_B)-6(5-\delta_A)-6(4-\delta_B)\}, \quad (1)$$

and the electron-core interactions by

$$V_{iA} = (1+\delta_A)\gamma_{iA}$$
$$V_{iB} = (2+\delta_B)\gamma_{iB} \quad (2)$$

where i is either A, B, or H. The values of the ionization potential 24.39 eV and electron affinity 6.11 eV were used for the sp^3 AO's involved in HB MO after Hinze and Jaffé.[11]

Calculations were carried out for the mesh of R and r with a 0.1 Å interval and that of δ_A and δ_B in the range from -1.0 to 1.0 with a 0.2 interval. The equilibrium distance R_e of A–B and r_e of A–H, the potential energy E_{eq} and the stretching frequency ν_s of proton at the equilibrium position of proton were calculated by an interpolation of the four mesh points of R and r around the energy minimum. The HB energy ΔE_e at the equilibrium position of A, B, and H was calculated by

$$\Delta E_e = \left(E_{eq}+\frac{1}{2}h\nu_s\right)^{\delta_A,\,\delta_B}_{R=R_e} - \left(E_{eq}+\frac{1}{2}h\nu_s\right)^{\delta_A,\,\delta_B}_{R=\infty}, \quad (3)$$

taking into account the zero point energy of proton motion since the frequency shift due to it is not negligible when δ_A or δ_B is large.

Results

Three Types of Hydrogen Bonds in Relation to the Excess Charges at the Donor and Acceptor Atoms. The dependence of ΔE_e on δ_A and δ_B is shown in Table 1. We see that an attractive HB occurs in the region of δ_A and δ_B with opposite signs. The region may be divided into regions I, II, and III (Fig. 2). When δ_A and δ_B satisfy the relation

$$\delta_A = \delta_B + 1, \quad (4)$$

we see from Eqs. (1) and (2) that the cores of A and B are equivalent and the system becomes symmetric, *viz.*, the potential curve of proton is always symmetric for any value of R. For two points in regions I and II which are mirror images of each other with respect to the straight line (4), the potential curves of proton for the two systems are mirror images of each other for any value of R.

Table 1. Dependence of E_e (eV) on the excess charges δ_A and δ_B

Symbol + denotes the repulsive HB without equilibrium R.

δ_A \ δ_B	1.0	0.8	0.6	0.4	0.2	0.0	0.2	0.4	0.6	0.8	1.0
1.0	-17.41	-13.78	-10.39	-7.28	-4.44	-1.91	+	+	+	+	+
0.8	-14.31	-11.43	-8.46	-5.78	-3.41	-1.35	+	+	+	+	+
0.6	-11.95	-9.11	-6.59	-4.40	-2.51	-0.92	+	+	+	+	+
0.4	-9.20	-6.85	-4.84	-3.14	-1.74	-0.58	+	+	+	+	+
0.2	-6.54	-4.72	-3.23	-2.04	-1.09	-0.35	+	+	+	+	+
0.0	-4.28	-2.76	-1.79	-1.07	-0.56	-0.20	+	+	+	+	+
-0.2	-1.75	-1.00	-0.53	-0.26	-0.13	-0.10	-0.13	-0.20	-0.28	-0.37	-0.47
-0.4	+	+	+	+	+	-0.05	-0.32	-0.60	-0.90	-1.22	-1.55
-0.6	+	+	+	+	+	-0.02	-0.51	-1.02	-1.56	-2.12	-2.70
-0.8	+	+	+	+	+	+	-0.71	-1.45	-2.24	-3.06	-3.91
-1.0	+	+	+	+	+	+	-0.90	-1.89	-2.93	-4.01	-5.15

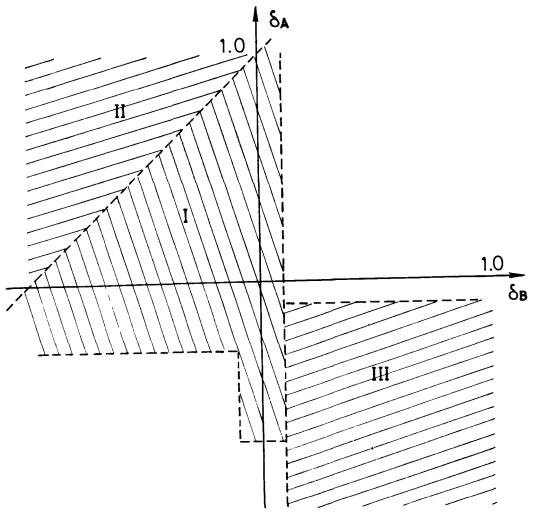

Fig. 2. Three regions of attractive HB.
I: normal HB, II: proton transferred HB, III: abnormal HB.

Region I corresponds to the normal HB in the form of $A^{\delta+}$–H---$B^{\delta'-}$ where the equilibrium position of H is on the side of A. Region II corresponds to the HB in

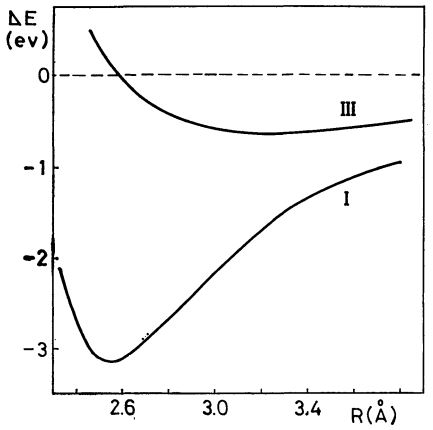

Fig. 3 (a).

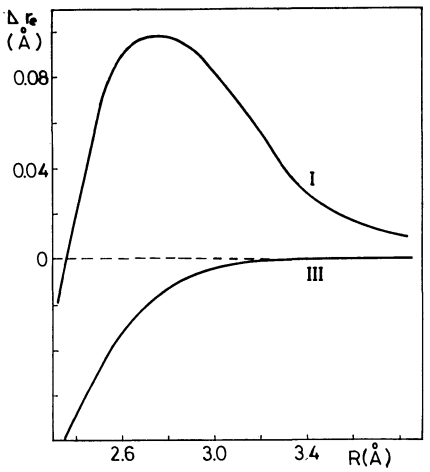

Fig. 3 (b).

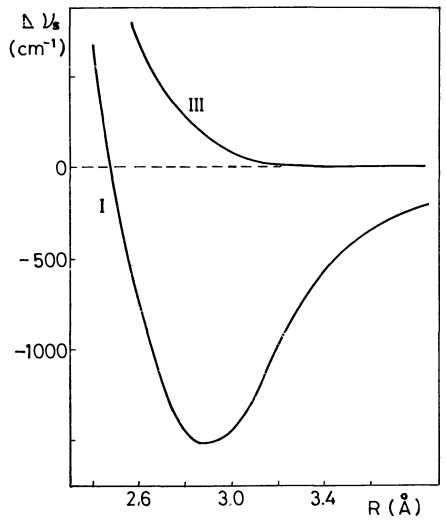

Fig. 3 (c).

Fig. 3. Dependences of the hydrogen bond energy ΔE(a), the shift of proton equilibrium distance Δr_e (b) and the shift of frequency of stretching vibration of proton $\Delta\nu_s$ (c) on the A–B distance R. Typical cases are represented;
I($\delta_A=0.4$, $\delta_B=-0.4$) and III ($\delta_A=-0.4$, $\delta_B=0.4$).

the form of $A^{\delta+}$---H–$B^{\delta'-}$ in which the effect of the excess charge is so strong that the equilibrium position of H is shifted toward the side of B, namely, the HB of proton transferred state. The HB in the region III is of the form $A^{\delta-}$–H---$B^{\delta'+}$ and abnormal. The R dependence of ΔE, Δr_e and $\Delta\nu_s$ for typical systems in regions I and III is shown in Fig. 3, where ΔE, Δr_e and $\Delta\nu_s$ are respectively the HB energy and the shifts of r_e, ν_s being due to HB at A–B distance R. For the HB system in region I, $\Delta r_e>0$ and $\Delta\nu_s<0$ at $R=R_e$ exhibit the normal character of HB (Fig. 3). Distance R giving the maximal Δr_e and $\Delta\nu_s$ coincides with R_e in a weak HB with a small ΔE_e, while Δr_e and $\Delta\nu_s$ at R_e tend to be somewhat smaller than their maximal values in a strong HB with large ΔE_e. This seems to be the effect of compression of R_e in the strong HB.

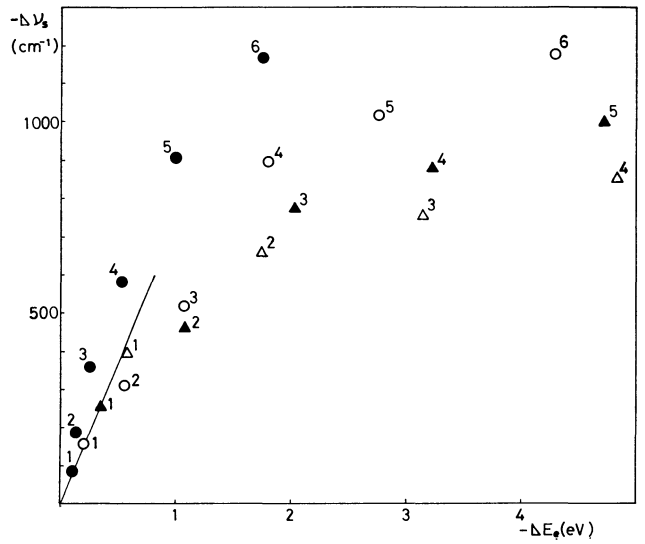

Fig. 4 (a).

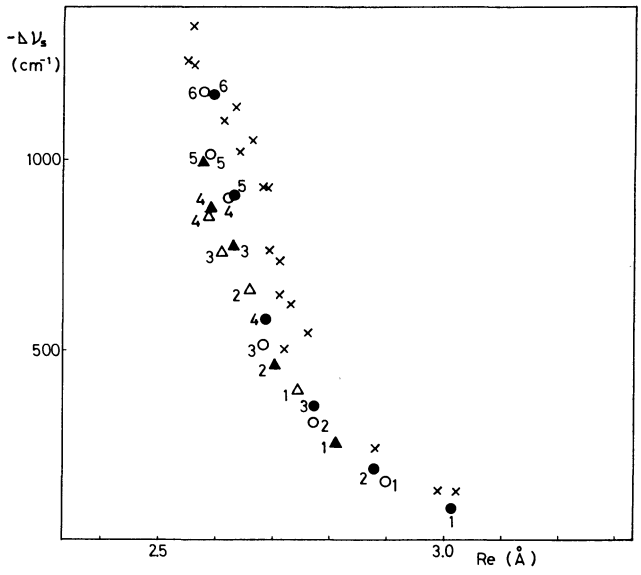

Fig. 4 (b).

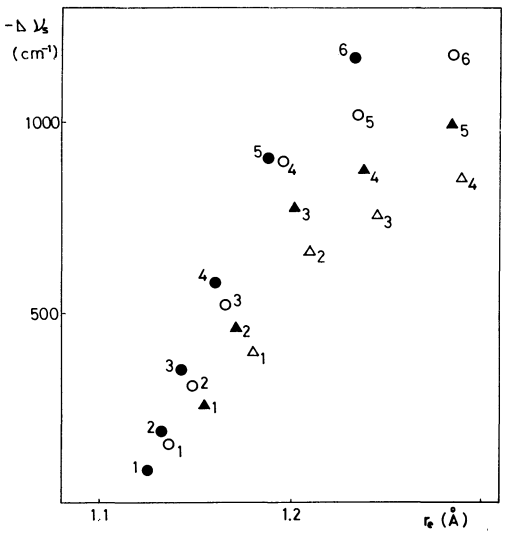

Fig. 4 (c).

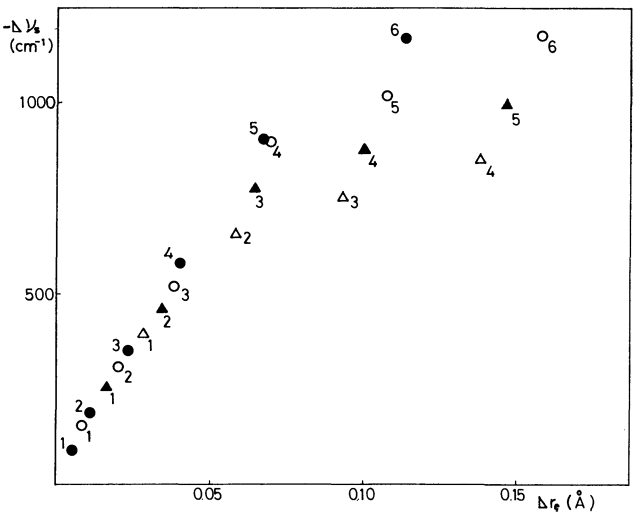

Fig. 4 (d).

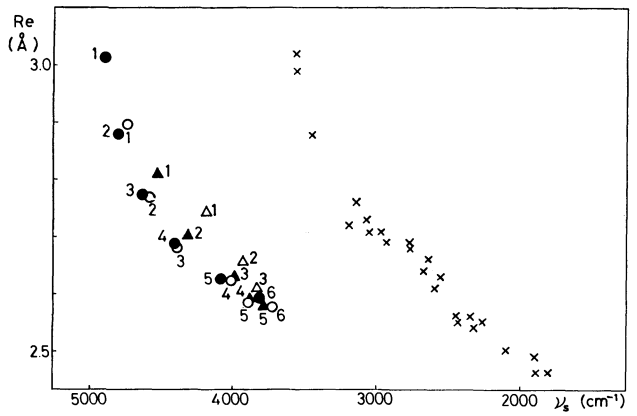

Fig. 4 (e).

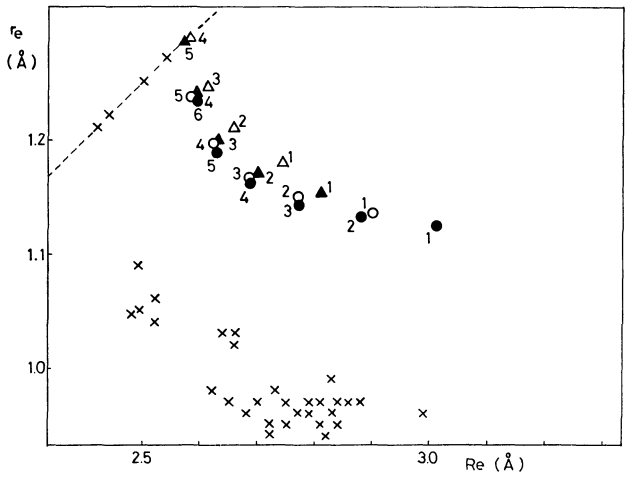

Fig. 4 (f).

Fig. 4. Correlations between the hydrogen bond distance R_e, the proton equilibrium position r_e, the shift Δr_e of r_e due to formation of HB, the frequency of proton stretching vibration ν_s, the shift $\Delta\nu_s$ of ν_s and hydrogen bond energy ΔE_e. The correlations shown are those between $-\Delta E_e$ and $-\Delta\nu_s$ (a), R_e and $-\Delta\nu_s$ (b), r_e and $-\Delta\nu_s$ (c), Δr_e and $-\Delta\nu_s$ (d), ν_s and R_e (e) and between R_e and r_e (f).

The values of the excess charges δ_A and δ_B are discriminated by the following symbols;
$\delta_A=-0.2$(●), 0(○), 0.2(▲), 0.4(△).
$\delta_B=0$(1), -0.2(2), -0.4(3), -0.6(4), -0.8(5), $-1.$(6).

The solid line in (a) is the experimental curve given by Badger and Bauer[13] for water and alcohol.

The points x in (b) and (e) are the experimental points compiled by Nakamoto *et al.*[14] for O–H---O bonds and those in (f) are the data compiled by Hamilton and Ibers[15] for O–H···O bonds in solid.

The dashed line in (f) represents the case of symmetric HB with $r_e=R_e/2$.

On the other hand, for the HB system in region III, we have $\Delta r_e<0$ and $\Delta\nu_s>0$ at $R=R_e$ exhibiting an abnormal character in contrast to the normal HB.

Correlation between the Hydrogen Bond Distance, Proton Equilibrium Position, Frequency of Proton Stretching Vibration and Hydrogen Bond Energy. We may obtain the theoretical correlation between R_e, r_e, Δr_e, ν_s, $\Delta\nu_s$ and ΔE_e for the normal HB by adjusting δ_A and δ_B within region I. The results are shown in Fig. 4. The theoretical correlation plots including r_e or ν_s are shifted toward larger values of r_e and ν_s (Figs. 4e and f). However, when we subtract the constant amounts of 0.2 Å and 1300 cm^{-1} from r_e and ν_s respectively, the theoretical correlation plots overlap the observed ones. Apart from these constant deviations of r_e and ν_s, agreement of the theoretical correlation plots with the observed ones is good. The deviation of theoretical values of r_e and ν_s in a larger direction than the observed ones is already present in the isolated A–H system and seems to be due to a failure of the CNDO/2 method to give a correct potential for the covalent bond.

In some of the observed correlation plots, the experimental points exhibit a considerable scattering (Figs. 4b, e, and f). However, if the experimental points are selected in such a way that either one of the acid or base is fixed and the other changed, then the correlation plot, which exhibits considerable scattering when both acid and base are arbitrarily changed, becomes a smooth one. This behavior is also reproduced in the present calculation. When either one of δ_A or δ_B is fixed and the other changed, then the theoretical correlation plot becomes a smooth one, but

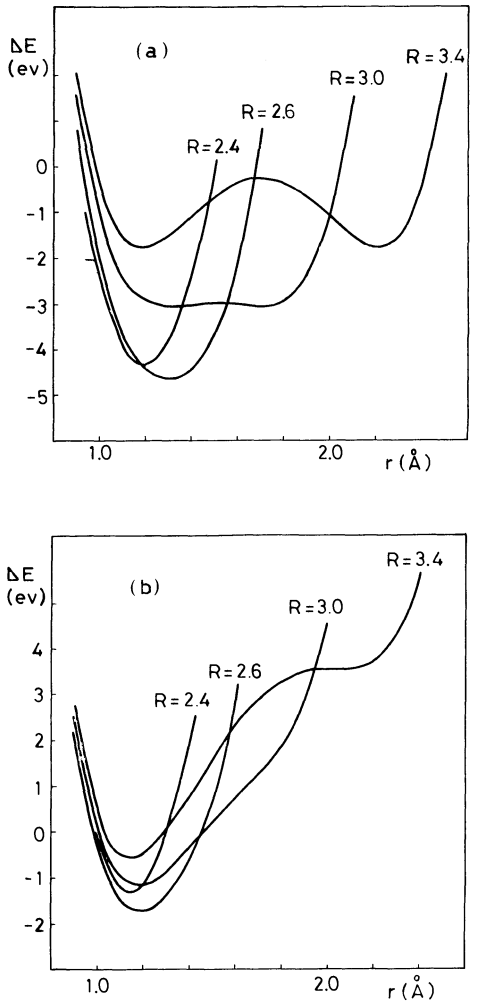

Fig. 5. The proton potential curves at various AB distances R.
(a) The symmetric system with $\delta_A=0.2$, $\delta_B=-0.8$
(b) The asymmetric system with $\delta_A=0.0$, $\delta_B=-0.6$

the correlation plots with different values of the fixed δ are not identical, and each of the theoretical correlation exhibits a spread (Fig. 4).

The good agreement between the theoretical correlation plots and the experimental ones strongly suggests that the correlation plots are primarily determined by the excess charges at the donor and acceptor atoms.

Potential Shape for Proton Movement. Many studies have been carried out concerning the potential shape for proton movement in the HB system, particularly the existence or non-existence of double minima. Hardly any MO calculations carried out so far on total systems with a single HB between oxygens led to a double well potential at theoretical R_e although it may be obtained at larger R. Clementi[9] emphasized in his non-empirical calculations that a coupling between more than two HB's would be a necessary requisite for the second minimum to occur. Nevertheless, the factors principally responsible for occurrence of double minima do not seem to have been determined.

The present model does not give a double well potential at R_e for all values of δ_A and δ_B. If δ_A and δ_B are close to the symmetric system satisfying Eq. (4), then a double well potential appears at slightly larger R than R_e (Fig. 5a). For the system in region I, the minimum of the potential well is on the side near A, but for that in region II it is on the side near B. If the asymmetry of the system becomes large, the R where the double well potential appears shifts toward much larger R than R_e (Fig. 5b). Thus, the excess charges at the donor and acceptor atoms are not the essential factor to produce a double well potential although the excess charges with the signs $\delta_A>0$ and $\delta_B<0$ stabilize the configuration A···H–B and facilitate occurrence of the second minimum.

Mechanism of the Effect of Excess Charges on the Hydrogen Bond and Proton Transfer. We now consider the mechanism of how the excess charges with the signs $\delta_A>0$ and $\delta_B<0$ enhance HB and proton transfer. As represented in the scheme $A\text{–}H+B\rightarrow A^{\delta-}\text{–}H\cdots B^{\delta+}$, formation of the HB leads to an increase in the electron density at A and a decrease at B. This change in the electron density is due to an increase of the lone pair electron density at A by transfer of the lone pair electrons at B to the antibonding orbital of A–H as seen from the HB MO (Fig. 6b). Let $E_l(z)$ and $E_s(z)$ respectively be the energies of the lone pair in A^- or

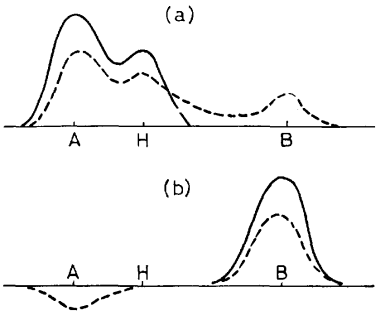

Fig. 6. A change in molecular orbitals induced by HB. Isolated state (——) and hydrogen bonding state (----). Bonding orbital (a) and lone pair orbital (b).

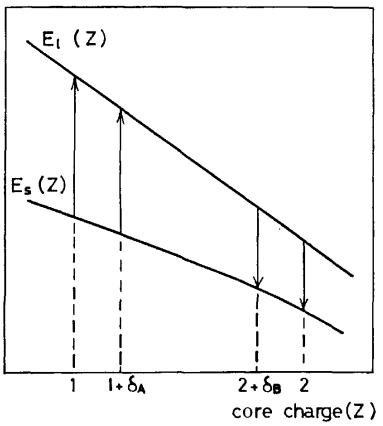

Fig. 7. Dependences of the lone pair energy E_l and the single bond energy E_s on the core charge.

B and the single bond A–H or $H\text{–}B^+$ regarded as the functions of the core charge z. We show their z dependence in Fig. 7. The energy loss by the process $A\text{–}H\rightarrow A^-$ may be related to $E_l(1+\delta_A)-E_s(1+\delta_A)$. Since the effect of the core charge is greater for the lone pair electrons than those in the single bond, a greater change is induced in $E_l(1+\delta_A)$ than in $E_s(1+\delta_A)$ by an increase in δ_A. Thus it follows that $E_l(1)-E_s(1)>E_l(1+\delta_A)-E_s(1+\delta_A)$ for $\delta_A>0$ (Fig. 7). This means that the energy loss accompanied by the process $A\text{–}H\rightarrow A^-$ is smaller for $\delta_A>0$ than for $\delta_A=0$, and the HB and proton transfer are made easier by the excess charge $\delta_A>0$.

As site B, HB formation leads to a decrease of the lone pair density and to an increase of electrons in the single bond $H\text{–}B^+$. The energy gain by the process $B\rightarrow H\text{–}B^+$ may be related to $E_l(2+\delta_B)-E_s(2+\delta_B)$. As seen in Fig. 7, $E_l(2+\delta_B)-E_s(2+\delta_B)>E_l(2)-E_s(2)$ for $\delta_B<0$. This means that the lenergy gain accompanied by the process $B\rightarrow H\text{–}B^+$ is greater for $\delta_B<0$ than $\delta_B=0$, and HB and proton transfer are enhanced by the excess charge $\delta_B<0$. As both processes occur in the HB, the quantity

$$\Delta(\delta_A,\delta_B)=\{E_l(1+\delta_A)-E_s(1+\delta_A)\}-\{E_l(2+\delta_B)-E_s(2+\delta_B)\}$$

may well be related to the power of the HB. Since there is an approximately linear correlation between ΔE_e and Δ (Fig. 8), a very simplified picture of the HB regarded as a combined process of $A\text{–}H\rightarrow A^-$ and $B\rightarrow H\text{–}B^+$ might explain the dependence of HB strength on the excess charges, though it might fail to explain more detailed properties of the HB. The functional dependence of $\Delta(\delta_A,\delta_B)$ on δ_A and δ_B is similar to ΔE_e when either one of δ_A or δ_B is changed, but it leads to a different ordering of HB energy from that of MO calculation when both δ_A and δ_B are changed. For instance, $\Delta(\delta_A=0,\ \delta_B=-0.2)>\Delta(\delta_A=0.2,\ \delta_B=0)$ although the MO calculation leads to $\Delta E_e(\delta_A=0,\ \delta_B=-0.2)<\Delta E_e(\delta_A=0.2,\ \delta_B=0)$. A similar correlation between ΔE_e and Δ is obtained for the calculation on the total HB systems.[12]

In the process of proton transfer, $A\text{–}H\rightarrow A^-$ and $B\rightarrow H\text{–}B^+$ occur to a greater extent than in the normal

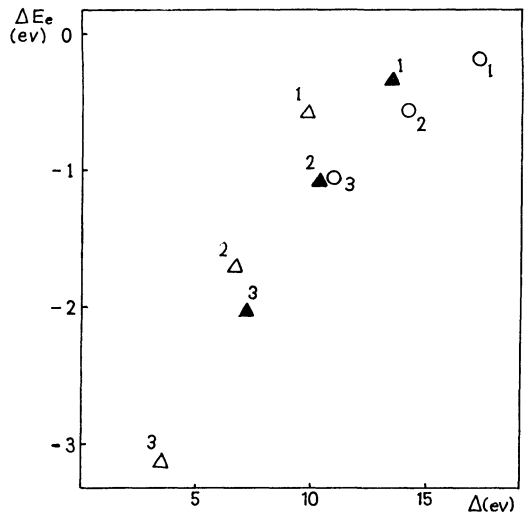

Fig. 8. Correlation between ΔE_e and Δ.
δ_A and δ_B for each point are discriminated by the same symbols as Fig. 4.

HB. Thus, the above interpretation for the effect of the excess charges is more applicable to the systems in region II.

Discussion

In contrast to our result, Hasegawa *et al.*[3] obtained a double well potential in their VB calculation with changing orbital exponents using a similar model to ours. They calculated the potential at an R near the experimental one without confirming whether it was close to the theoretical equilibrium distance or not. However, even if the R they chose was the one deviated from the theoretical R_e, the extent of the appearance of the double minima was more enhanced than that in the present result. Thus, either the electron correlation or the change of the orbital exponent, which are not taken into consideration in the present MO calculation, might be important for producing the double well potential.

In the present model the amounts of excess charges δ_A and δ_B are fixed parameters, but in a real hydrogen bond system they may be changed by the dynamic polarization of the molecules caused by HB formation. It seems possible that the dynamic polarization affects the HB dominantly through a change of the excess charges at the donor and acceptor atoms. The present model may be utilized as a reference system to evaluate validity of such mechanism. If the dynamic polarization affects the HB mainly through a change of the excess charges, the correlation plots between the quantities such as R_e, r_e *etc.* obtained for the system with the effect of dynamic polarization should be almost the same as those obtained for the present model. A good agreement of the theoretical correlation plots in the present model with the experimental ones offers indirect support for such a mechanism.

The shape of the proton potential, in contrast to the correlation curves, is affected by the change of the excess charges due to dynamic polarization. It is of interest to see how the proton potential is affected by dynamic polarization.

References

1) C. A. Coulson and U. Danielson, *Ark. Fys.*, **8**, 239, 245 (1954).
2) H. Tsubomura, This Bulletin, **27**, 445 (1954).
3) M. Hasegawa, K. Daiyasu, and S. Yomosa, *J. Phys. Soc. Japan*, **27**, 999 (1969); **28**, 1304 (1970).
4) M. Weissmann and N. V. Cohan, *J. Chem. Phys.*, **43**, 119, 124 (1965).
5) R. Rein and F. E. Harris, *ibid.*, **41**, 3393 (1964); **42**, 2177 (1965).
6) A. S. N. Murthy and C. N. R. Rao, *J. Mol. Struct.*, **6**, 253 (1970).
7) K. Morokuma and L. Pedersen, *J. Chem. Phys.*, **48**, 3275 (1968).
8) P. A. Kollman and L. C. Allen, *ibid.*, **51**, 3286 (1969); *J. Amer. Chem. Soc.*, **92**, 753, 1601 (1970).
9) E. Clementi, *J. Chem. Phys.*, **46**, 3851 (1967); **54**, 508 (1971).
10) J. A. Pople, *ibid.*, **43**, S129, S136 (1965); **44**, 3289 (1966).
11) J. Hinze and H. H. Jaffé, *J. Amer. Chem. Soc.*, **84**, 540 (1962).
12) P. Schuster, *Theoret. Chim. Acta*, **19**, 212 (1970).
13) R. M. Badger and S. H. Bauer, *J. Chem. Phys.*, **5**, 839 (1937).
14) K. Nakamoto, M. Margoshes, and R. E. Rundle, *J. Amer. Chem. Soc.*, **77**, 6480 (1955).
15) W. C. Hamilton and J. A. Ibers, "Hydrogen Bonding in Solid," W. A. Benjamine Inc., New York (1968), p. 259.

The INDO and CNDO/2 SCF LCAO MO Calculation of Intermolecular Forces and Their Pairwise Additivity

Masao HASHIMOTO and Taro ISOBE

The Chemical Research Institute of Non-Aqueous Solutions, Tohoku University, Katahira, Sendai 980

(Received June 28, 1973)

The assumption of pairwise additivity of the intermolecular forces was examined within a CNDO/2-Clementi approximation. It was found that the deviation from the pairwise additivity, defined as the difference between the three-body interaction and the sum of the two-body interaction energies in the system of three neighboring molecules in a crystal, was small enough to be neglected as compared with the lattice energy. The CNDO/2-Clementi method, in which the overlap integrals are calculated by using the Clementi AO's, was found to be more useful than the usual CNDO/2 method, in which the overlap integrals are calculated by means of Slater AO's. The discrepancy in the calculated interaction energies from the experimental ones in the form of the heat of sublimation was found to be quite large for CO. This discrepancy becomes small, though, if the centers of the molecules are displaced away from the origin and along the nonintersecting threefold axes of the unit cell; the crystal structure belongs not to the Pa3 space group, but to the $P2_13$ space group. From a comparison of the CNDO/2-Clementi results and the results of the exp-6 potential superimposed on the quadrupole-quadrupole interaction potential, it was found that the former is superior to the latter in anticipating the conformation of the $(CO_2)_2$ dimer.

In a previous paper[1] (designated **I** henceforth), we calculated the intermolecular forces between closed-shell molecules in the ground-state, treating the dimer system as if it were one molecule and using the difference between the total energy of this system and that of the monomeric molecules. The total energies were calculated with the CNDO/2 SCF LCAO MO (completely neglecting the differential overlaps in self-consistent field molecular orbital approximated by a linear combination of atomic orbitals) method by using the Clementi AO's (we will designate this by "CNDO/2-Clementi method" henceforth).

In **I**, the calculated interaction energy was compared with the experimental one in the form of the lattice energy by assuming a pairwise additivity of the intermolecular forces. This assumption is justified if the deviation from the pairwise additivity is relatively small. However, no examination for the pairwise additivity was made in **I**.

In the present paper, we will calculate the interaction energy among three molecules treating them as if they were one molecule. The deviation from the pairwise additivity will, then, be obtained as the difference between the three-body interaction energy and the sum of the two-body interaction energies. We will compare the interaction energy obtained by using the Slater AO's and that obtained by using Clementi AO's. This comparison was made in **I** only for ethylene. Furthermore, the INDO (with an intermediate neglect of the differential overlaps) and CNDO/2 results will be compared.

The substances treated in this paper and their crystal data are summarized in Table 1.

Table 1. Crystal structural data

Crystal	Space group	Lattice onstant	Literature
α-N_2	T_h^6-Pa3	$a=5.667$	2)
CO_2	T_h^6-Pa3	$a=5.883$	3)
High temperature form C_2H_2	T_h^6-Pa3	$a=6.14$	4)
α-N_2O	T_h^6-Pa3	$a=5.72$	5)
α-CO	T_h^6-Pa3	$a=5.63$	6)
Low temperature form HCN	C_{2v}^{20}-Imm2	$a=4.13$ $b=4.85$ $c=4.34$	7)
C_2H_4	C_{2h}^5-$P2_1/n$	$a=4.87$ $b=6.46$ $c=4.14$ $\beta=90.0°$	8)
α-F_2	C_{2h}^3-C2/m	$a=5.50$ $b=3.28$ $c=10.01$ $\beta=134.66°$	31)

Theoretical

In this section, we will supplement the theoretical part of **I**.

INDO Parametrization. The F matrix in INDO is as follows:

$$F_{rr} = U_{rr} + \frac{1}{2}P_{rr}\gamma_{AA} + \sum_{s(\neq r)}^{(A)} P_{ss}\left[(rr/ss) - \frac{1}{2}(rs/rs)\right] + \sum_{B(\neq A)} (P_{BB} - Z_B)\gamma_{AB} \quad (r, s \in A) \tag{1}$$

$$F_{rs} = P_{rs}\left[(3/2)(rs/rs) - \frac{1}{2}(rr/ss)\right] \quad (r \neq s,\ r, s \in A)$$

$$F_{rs} = \frac{1}{2}S_{rs}(\beta_A + \beta_B) - \frac{1}{2}P_{rs}\gamma_{AB} \quad (r \neq s,\ r \in A,\ s \in B)$$

The integrals appearing in (1) are expressed as follows:

$$\begin{aligned} (ss/ss) &= (ss/xx) = F^0 = \gamma_{AA} \\ (xx/xx) &= F^0 + (4/25)F^2 \\ (xx/yy) &= F^0 - (2/25)F^2 \\ (xs/xs) &= (1/3)G^1 \\ (xy/xy) &= (3/25)F^2, \text{ etc.,} \end{aligned} \tag{2}$$

where s, x, y, *etc.* are 2s, $2p_x$, $2p_y$, and so on; F^2 and G^1 are semiempirical parameters given by Pople *et al.*[9] F^0 is calculated theoretically by using the Slater AO's.[10] The bonding parameters β's, were parametrized as usual.[9]

The overlap integrals, S_{rs}, were calculated by using both Slater AO's and Clementi AO's (see **I**); they are compared in part in Tables 2 and 3.

Table 2. Comparison of overlap integrals calculated by using Clementi AO's and Slater AO's (1s and 2s)

Å r(C···H)	S_{rs} Slater AO	S_{rs} Clementi AO
1.0500	0.5414	0.5277
1.0631	0.5340	0.5210
1.0800	0.5245	0.5123
2.0998	0.1301	0.1387
2.2500	0.1019	0.1105
3.2760	0.0165	0.0205
3.3700	0.0138	0.0174
3.4568	0.0117	0.0150
4.7506	0.0009	0.0015
4.9623	0.0006	0.0010
5.3803	0.0002	0.0005
5.6882	0.0001	0.0003
6.7276	0.0	0.0

Table 3. Comparison of overlap integrals calculated by using Clementi AO's and Slater AO's (2s and 2s)

Å r(C···C)	S_{rs} Slater AO	S_{rs} Clementi AO
1.2000	0.5114	0.5250
1.3400	0.4368	0.4511
3.8523	0.0051	0.0084
3.9248	0.0043	0.0073
4.1274	0.0028	0.0051
4.3391	0.0017	0.0034
4.6301	0.0014	0.0020
4.8471	0.0005	0.0013
5.6300	0.0001	0.0003
6.1400	0.0000	0.0001
6.8196	—	0.0000

In this series of papers, one- and two-center electron repulsion integrals, γ_{AA} and γ_{AB}, are always calculated by using the Slater AO's. There is no clear *rationale* for this. However, the final results using the γ_{AA} and γ_{AB}, which were calculated with the Clementi AO's, did not seem to be superior to those calculated with the Slater AO's.

Deviation from Pairwise Additivity. In the previous paper, we calculated the lattice energy taking the summation of the pair interaction energies over the 1st and the 2nd neighboring pairs in a crystal, and assuming the pairwise additivity of the intermolecular forces. This assumption is, however, not strictly justified. Several authors[11-15] have approached the problem of the non-additive part of molecular interactions in $(He)_3$ using an SCF LCAO MO approximation. Novaro and Beltran-Lopez[15] have indicated that the three-body effect, which is considered to be the main part of the deviation from the pairwise additivity in many particle systems, can be quite large at smaller distances, but wanes quickly when approaching the region of the $(He)_2$ van der Waals well.

The three-body effects, or the deviation from the pairwise additivity, is defined as follows:

$$D = U_{abc} - (U_{ab} + U_{bc} + U_{ca}) \quad (3)$$

where:

$$U_{abc} = E(M_a, M_b, M_c) - [E(M_a) + E(M_b) + E(M_c)] \quad (4)$$

and

$$U_{ab} = E(M_a, M_b) - [E(M_a) + E(M_b)], \text{ etc.} \quad (5)$$

In Eqs. (4) and (5), the E's are the sums of the total electronic and Coulombic repulsion energies between the cores (see **I**).

Results and Discussion

In Figs. 1 and 2, D, the deviation from the pairwise additivity, is plotted against the intermolecular distances, R, keeping the relative orientations of the molecules fixed to those in real crystals. These figures show that, D at R_0, which is the intermolecular distance in a real crystal, can be neglected in comparison with the lattice energy (see Table 4). The assumption of the pairwise additivity in **I** is thus satisfied approximately.

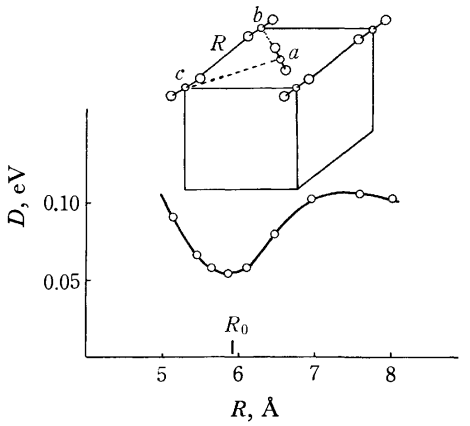

Fig. 1. Deviation from the pairwise additivity of intermolecular force of CO_2 by CNDO/2-Clementi method.

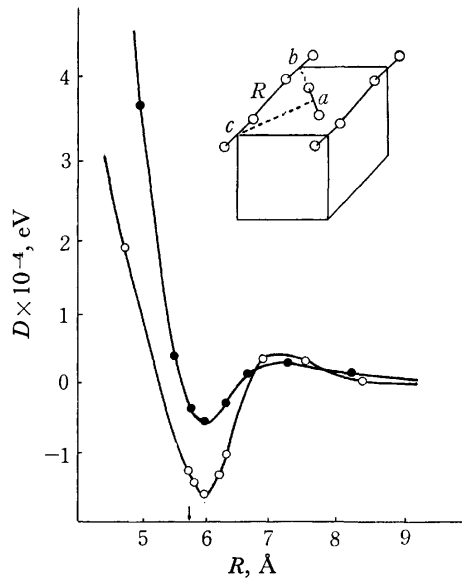

Fig. 2. Deviation from the pairwise additivity of intermolecular force of N_2 by CNDO/2-Clementi method. (●) with the space group Pa3, (○) $P2_13$.

Table 4. Calculated and experimental heat of sublimation of crystals, in electron volts, error ±0.00025

	$1/2\sum U_{ab}$				
	CNDO/2		INDO		Obsd
	Slater	Clementi	Slater	Clementi	
HCN	−0.09612	−0.51174	−0.10355	−0.59502	−0.39727[24]
CO	−0.02808	−0.55290	+0.00750	−0.71835	−0.08617[25]
N_2O	−0.09502	−0.17718	−0.16406	—	−0.25153[26]
CO_2	−0.04971	−0.28465	−0.08034	−0.38247	−0.28621[27]
N_2	−0.00105	−0.06480	−0.00246	−0.08205	−0.07164[28]
C_2H_2	−0.01584	−0.24834	−0.01992	−0.16101	−0.23851[29]
C_2H_4	−0.01715	−0.11360	−0.01697	−0.13868	−0.18213[30]
F_2	−0.00088	−0.07882	−0.00099	−0.09134	−0.08066[32]

In Table 4, the calculated heats of sublimation (a half of the lattice energy) are compared with the experimental ones. These calculated values were obtained by taking the summation of (5) over the nearest and the 2nd-nearest neighbor molecules in the crystals. The contribution of the higher neighbors is small enough to be neglected (see **I**). The 3rd column of Table 4 shows the CNDO/2-Clementi results obtained by using the Clementi AO's to calculate the overlap integrals. The 5th column shows the corresponding INDO-Clementi resulst. The 2nd and 4th columns show those for usual CNDO/2 and INDO calculations. From this Table we can see that the best agreement between the calculated and the observed interaction energies is obtained when the calculation is done by using the Clementi AO's. We can also see that the INDO results are not so superior to the CNDO/2 results as is generally expected.

The deviation of the calculated heat of sublimation from the experimental one in CO becomes small if we assume that the molecules in the crystal are displaced from the approximate centers of inversion and, hence, if we assume that the resultant space group is not Pa3, but $P2_13$. Defining the displacement from the centrosymmetric positions by δ, as is shown in Fig. 3, we calculated the δ-dependency of the heat of the sublimation of α-CO crystals. $\delta=0.0$ Å corresponds to the Pa3 space group. The results are shown in Table 5. We can see that the Pa3 space group is not preferable in explaining the heat of the sublimation of

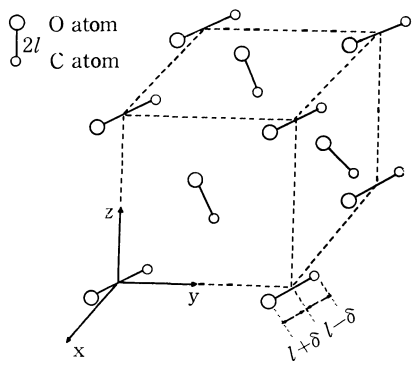

Fig. 3. Definition of displacement δ from centrosymmetric positions of the structure with space group Pa3.

Table 5. Dependency of heat of sublimation upon the deviation from Pa3 structure

δ deviation from Pa3, Å	$1/2\sum U_{ab}$ by CNDO/2–Clementi, eV	
	CO	N_2
−0.25	−0.11669	—
−0.20	−0.13428	—
−0.17	—	−0.06336
−0.15	−0.15246	−0.06624
−0.10	−0.50166	−0.07386
−0.05	−0.19380	−0.05904
0.0	−0.55290	−0.06480
+0.05	−0.24258	−0.09162
+0.10	−0.26946	−0.10056
+0.15	−0.64942	−0.10998
+0.20	−0.34674	−0.09900

the α-CO crystal. Thus, the crystal structure of α-CO may belong to the $P2_13$ space group. This situation is somewhat analogous to that with the α-N_2 crystal, for which the space group might be $P2_13$, according to recent far-IR absorption spectral data.[16] In order to check this, we calculated the δ-dependency of the α-N_2 crystal (see Table 5). It may be seen that the agreement with the experimental heat of sublimation is best when $\delta=-0.1$ Å. X-Ray diffraction study of α-N_2 by Lipscomb *et al.*[17] has given this δ-value as from −0.1 to −0.2 Å. By the way, the deviation from the pairwise additivity of α-N_2 is small, even with the $P2_13$ space group, compared with the heat of sublimation, as may be seen from Curve (b) of Fig. 2 ($\delta=-0.1$ Å). Thus, evidence has been reported both for [16–18] and against [19] the $P2_13$ space group for α-N_2 in experiments; our calculations support $P2_13$.

Thus, the CNDO/2-Clementi method for the calculation of the intermolecular forces is quite useful, as may be seen from Table 4, if we use the Clementi AO's to calculate the overlap integrals. Moreover, this method is more rigorous from the theoretical point of view than is the usual method,[20] in which intermolecular forces are divided into three parts (exchange repulsion, dispersion, and electrostatic interaction forces) and calculated separately in terms of each different method. The CNDO/2-Clementi method unifies these forces and reduces the unknown errors due to the above

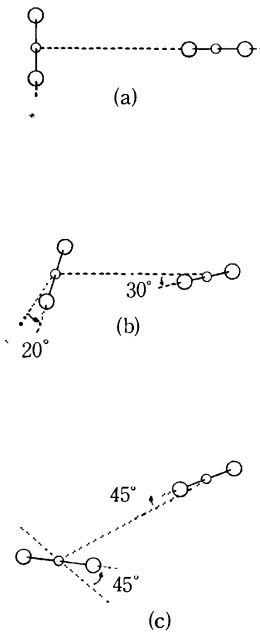

Fig. 4. Typical configurations of two CO_2 molecules separated by distance 4.1 Å.

division of intermolecular forces.

Now let us examine the reliability of the present method. This has been discussed partially in **I**; we would now like to add the following facts.

Figure 4 shows three typical configurations of two CO_2 molecules, separated by an R_0 distance of 4.1 Å. The interaction energies calculated by the present method are −0.17135, −0.08876, and −0.06419 eV for Configurations (a), (b), and (c) respectively. We can see that the (a) configuration, that is, the T-configuration, is the most stable one; this corresponds to the experimental results of Welsh *et al.*[21] They found that the two components of the (ν_1, $2\nu_2$) Fermi doublet of gaseous CO_2 show a complex structure in a long-absorption pathlength at a low temperature. They analyzed this absorption and interpreted it in terms of the rotation and vibration of $(CO_2)_2$ dimers held in a locked T-position at an intermolecular distance of 4.1 Å.

For comparison, we have done this configuration calculation by using the non-bonded-atom-atom pair interaction potential superimposed on the quadrupole-quadrupole interaction potential. This is shown by the following equation:

$$V(R,\theta,\theta',\phi,\phi') = V_{\exp-6} + V_{Q-Q} \tag{6}$$

$$V_{\exp-6} = \sum_j [a_j \exp(-b_j r_j)/r_j^{d_j} - c_j/r_j^6] \tag{7}$$

$$\begin{aligned} V_{Q-Q} = 3Q^2\{&1-5(\sin^2\phi\sin^2\theta+\sin^2\phi'\sin^2\theta') \\ &-15\sin^2\phi\sin^2\theta\sin^2\phi'\sin^2\theta' \\ &+2[4\sin\phi\sin\theta\sin\phi'\sin\theta' \\ &-(1-\sin^2\phi\sin^2\theta)^{1/2}(1-\sin^2\phi'\sin^2\theta')^{1/2} \\ &\times\cos(\theta-\theta')]^2\}/4R^5 \end{aligned} \tag{8}$$

Table 6. Parameters in Eq. (7), in kcal/mol and Å units

j	$a_j\times10^5$	b_j	c_j	d_j
C···C	3.012	0.0	327.0	12.0
C···O	1.785	2.304	202.2	6.0
O···O	1.057	4.608	125.10	0.0

In Eq. (7), the summation over j is taken over all the pairs of atoms between two molecules. The four parameters, a_j, b_j, c_j, and d_j, were derived from the Table of Liquori *et al.*[22] (Table 6). In Eq. (8), Q is a molecular quadrupole moment and is 4.3×10^{-26} cm^2 esu for CO_2 molecule;[23] the relative orientation $(\theta,\theta',\phi,\phi')$ of the two molecules is defined as is shown in Fig. 5.

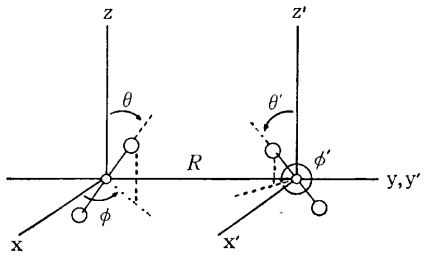

Fig. 5. Geometrical representation of two CO_2 molecules in interaction.

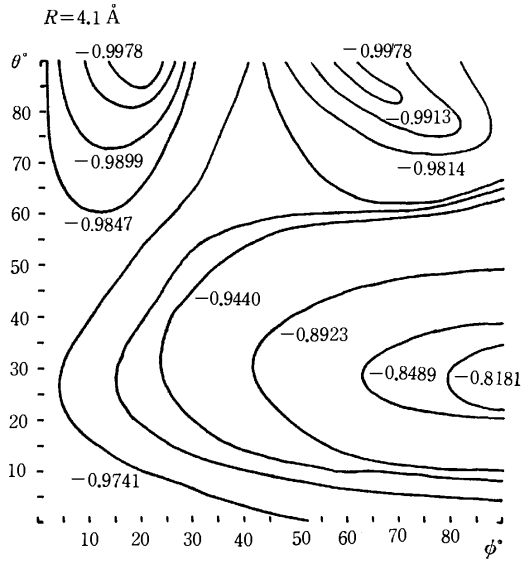

Fig. 6. θ-ϕ energy surface between two CO_2 molecules. The values in the figure are the minimum with regard to θ' and ϕ'. (in kcal/mol unit)

In Fig. 6, the θ–ϕ dependency of the interaction energy (6) is indicated, in which each point, $P(\theta,\phi)$, corresponds to the most stable configuration with regard to the θ' and ϕ' values. From Fig. 6, we found that the most stable configuration at R_0=4.1 Å is the one indicated in Fig. 4(b); this is somewhat different from the experimental findings.

Thus, the present CNDO/2 method is superior to a method using such a potential as (6).

In conclusion, the CNDO/2-Clementi method is useful in calculating the interaction energy between such molecules, as is indicated in Table 1.

We are now proceeding to calculate the interaction energy of more complex molecules by the same method. The results will be reported elsewhere.

All the computing in the present paper was done at the Computer Center of Tohoku University using the NEAC-2200 model 700 and its TSS.

References

1) M. Hashimoto and T. Isobe, This Bulletin, **46**, 2581 (1973).
2) B. C. Kohin, *J. Chem. Phys.*, **33**, 883 (1960).
3) T. Kihara, *Adv. Chem. Phys.*, **5**, 147 (1963).
4) T. Sugawara and E. Kanda, *Sci. Rept. Res. Inst., Tohoku Univ. Ser.*, **A4**, 607 (1952).
5) W. C. Hamilton and M. Petrie, *J. Phys. Chem.*, **65**, 1453 (1961).
6) L. Jansen, A. Michels, and J. M. Lupton, *Physica*, **20**, 1235 (1954).
7) A. I. M. Rae, *Mol. Phys.*, **16**, 257 (1969).
8) S. M. Blumenfeld, S. P. Reddy, and H. L. Welsh, *Canad. J. Phys.*, **48**, 513 (1970).
9) J. A. Pople and D. L. Beveridge, "Approximate Molecular Orbital Theory," McGraw-Hill (1970).
10) C. C. J. Roothaan, *J. Chem. Phys.*, **19**, 1445 (1951).
11) P. Rosen, *ibid.*, **21**, 1007 (1953).
12) A. Shostak, *ibid.*, **23**, 1808 (1955).
13) R. Block, R. Roel, and G. T. Maten, *Chem. Phys. Lett.*, **11**, 425 (1971).
14) R. F. W. Bader, O. A. Navaro, and V. Beltran-Lopez, *ibid.*, **8**, 568 (1971).
15) O. A. Navaro and V. Beltran-Lopez, *J. Chem. Phys.*, **56**, 815 (1972).
16) E. J. Wachtel, *ibid.*, **57**, 5620 (1972).
17) T. H. Jordan, H. W. Smith, W. E. Streib, and W. N. Lipscomb, *ibid.*, **41**, 756 (1964).
18) J. R. Brookman, M. M. McEnaan, and J. A. Scott, *Phys. Rev.*, **B4**, 3661 (1971).
19) A. F. Schuch and R. L. Mills, *J. Chem. Phys.*, **52**, 6000 (1970).
20) See for example, M. Hashimoto, M. Hashimoto, and T. Isobe, This Bulletin, **44**, 649 (1971).
21) L. Mannik, J. S. Stryland, and H. L. Welsh, *Can. J. Phys.*, **49**, 3056 (1971).
22) P. de Santis, E. Giglio, A. M. Liquori, and A. Ripamonti, *J. Polym. Sci.*, **A1**, 1383 (1963).
23) A. D. King, *J. Chem. Phys.*, **51**, 1262 (1969).
24) W. F. Giauque and R. A. Ruehrwein, *J. Amer. Chem. Soc.*, **61**, 2626 (1939); see also literature (7).
25) J. O. Clayton and W. F. Giauque, *ibid.*, **54**, 2610 (1932); see also literature (6).
26) R. W. Blue and W. F. Giauque, *ibid.*, **57**, 991 (1935).
27) W. F. Giauque and C. J. Egan, *J. Chem. Phys.*, **5**, 45 (1937).
28) See literature (2).
29) D. McIntosh, *J. Phys. Chem.*, **11**, 306 (1907).
30) C. J. Egan and J. D. Kemp, *J. Amer. Chem. Soc.*, **59**, 1264 (1937).
31) L. Meyer, C. S. Barret, and S. C. Greer, *J. Chem. Phys.*, **49**, 1902 (1968).
32) J. H. Hu, D. White, and H. L. Johnston, *J. Amer. Chem. Soc.*, **75**, 5642 (1953).

An ENDOR Study of the Relaxation Behavior of the Nuclei in Several Semiquinone Anion Radicals[1]

Yashige KOTAKE and Keiji KUWATA

Department of Chemistry, Faculty of Science, Osaka University, Toyonaka, Osaka 560

(Received July 20, 1973)

The ENDOR intensities of several semiquinone anion radicals were measured at various temperatures. The optimum temperature for the ENDOR intensity of protons in a radical was interpreted on the basis of their characteristic ways of relaxation. The electron nuclear dipolar (END) mechanism could be applied very well in most cases. However, in the case of protons whose END terms are very small this interaction might not explain the optimum temperature. Possible substitute mechanisms were discussed.

The ENDOR signal intensity depends on both the electron and nuclear relaxation times. As the temperature of a system changes, these relaxation times change in their characteristic ways, and this causes the temperature dependence of the intensity of the ENDOR signal. When the nuclei in a radical have their own relaxation paths of different temperature dependences, their ENDOR lines show a characteristic temperature dependence. Therefore, the ENDOR intensity is not an intrinsic parameter of the free radical. For this reason, ENDOR has a limitation as an analytical tool.

The investigation into the relaxation behavior which affects the ENDOR intensity is essential in providing fundamental knowledge for the assignment of the ENDOR spectra. Moreover, by the analysis of the temperature dependence, especially of the optimum temperature at which the strongest ENDOR line appears, we can find the relaxation mechanism of a nucleus relating to its position and its surroundings in a radical.

Freed[2,3] has developed a theory of the ENDOR enhancement on the basis of the equation of motion for the density matrix of a system and has obtained qualitative agreement with Hyde's experimental results.[4] He has explained the characteristic optimum temperature for each nucleus in terms of the electron nuclear dipolar (END) interaction being the dominant cause of the nuclear spin relaxation process in the liquid phase. In this process, a nucleus which has larger dipolar *hf* interaction with an electron spin must have a higher optimum temperature.

Allendoerfer and Maki[5] have made a unique study of the optimum conditions for the ENDOR enhancement in the tri-*t*-butyl phenoxyl radical in the liquid phase. However, no other detailed study of the optimum temperature for the ENDOR enhancement has yet been done; thus, it is not clear whether or not the END interaction is a common process in the nuclear relaxation in solution ENDOR. Especially in the case of protons which have a small END term, like the *t*-butyl protons, the END interaction seems to be inefficient in explaining the optimum temperature.

In the present study, using some semiquinone anions as probes in an ENDOR study, the END interaction was proved to be the dominant cause of proton relaxation when the anisotropic *hf* interaction between a proton and an electron spin is of a considerable magnitude. Also, the temperature dependence of the ENDOR intensity for the protons with small anisotropic *hf* coupling was proved not to be explainable in terms of the END interaction, and other nuclear relaxation mechanisms which may explain the ENDOR intensity were discussed.

Experimental

Though the measurement of the temperature dependence of the ENDOR intensity is useful for the investigation of the relaxation phenomena in a radical, its quantitative measurement involves some experimental difficulties. These difficulties arise for the following reasons.

1. Change in the radical concentration by a chemical equilibrium.

This causes not only a change in the intensity itself, but also many incidental effects. Upon the change in the concentration, the rate of Heisenberg spin exchange varies according as this equation:[6]

$$\omega_{HE} = 4\pi Da[R] \quad (1)$$

where D is the translational diffusion coefficient, a is the molecular radius, and [R] is the radical concentration. ω_{HE} lowers with the decrease in the temperature and affects the ENDOR enhancement factor.[2]

2. Change in the spin-lattice relaxation time of the electron.

The viscosity of the solvent accordingly varies with the temperature. There are many electron-relaxation processes which are viscosity-dependent, *e.g.*, the relaxation *via g*- and *hf*-tensor anisotropy and that *via* spin-rotational interaction. Therefore, the saturation factor of an ESR line changes with the temperature and the degree of saturation changes when the microwave power level is kept fixed during the measurements.

Freed's theory shows[2] that the Heisenberg exchange process diminishes the percentage of the enhancement of an ESR line by the ENDOR effect, but does not affect the optimum temperature, this has been confirmed by the experimental results of Hyde.[4] Thus, the exchange process does not move the optimum temperature for the ENDOR intensity. These facts show that, by suitable arrangements, *e.g.*, the dilution and the calibration of the ENDOR intensity by its ESR intensity, the first experimental difficulty can be removed.

The incident microwave power which gives the strongest ENDOR signal shifts as the temperature changes, but in the case of the semiquinone anion the shift is within the range of several db of microwave power. The measurement of the temperature dependency was done without changing the incident microwave power fed into the cavity. This may cause an error of the measurement of the optimum temperature.

The quinones used were of a guaranteed grade, and their anion radicals were produced by dissolving them into an alcohol which was in contact with the sodium metal. The solution was degassed thoroughly and then transferred into

a glass sample tube 4 mm in o.d.

All the radicals formed were assigned to the primary radicals of the semiquinone anions on the basis of their ESR spectra. In the case of 2,5-dimethyl benzoquinone, the concentration of sodium ethylate was kept low in order to avoid further reaction.[7,8]

The ENDOR spectra were observed at various temperatures by controlling the flow of the chilled nitrogen passing through the sample. The ENDOR spectrometer was based upon an ordinary ESR spectrometer with a 200 Hz field modulation. The RF power supply delivered a maximum output of peak 600 watts of sinusoidally amplitude-modulated power, and the modulation frequency was variable from 5 to 15 kHz. The field lock[4] obtained by observing the ESR signal of DPPH was partly used.

Results

The features of the ENDOR signals of the 2,5-di-*t*-butyl-*p*-benzosemiquinone (DBQ) anion at various temperatures are shown in Fig. 1. This radical has two ring protons with a 6.13 MHz isotropic *hf* coupling and eighteen *t*-butyl protons with a 0.19 MHz isotropic *hf* coupling. The temperature dependences of the intensities of these lines in methanol, ethanol, and 2-propanol solution are shown in Figs. 2a and 3a, while the plots *versus* η/T, where η is the viscosity of the solvent, are shown in Figs. 2b and 3b. The intensity plotted on the ordinate was an integrated intensity because there was considerable variation in the ENDOR linewidths. In the case of the lines for the *t*-butyl group especially, two lines were very close to each other; these overlapping two lines were integrated together.

The η/T dependences of the intensity of the ENDOR line in the 2,5-dimethyl-*p*-benzosemiquinone (DMQ) anion and the 9,10-anthrasemiquinone (ANQ) anion in ethanol were also measured by the same procedure; they are shown in Figs. 4 and 5.

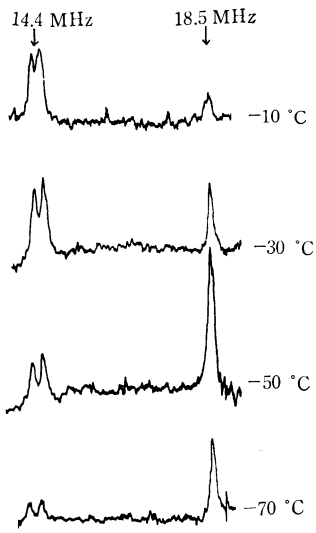

Fig. 1. The ENDOR spectra of 2,5-di-*t*-butyl-*p*-benzosemiquinone anion radical in ethanol at various temperatures.

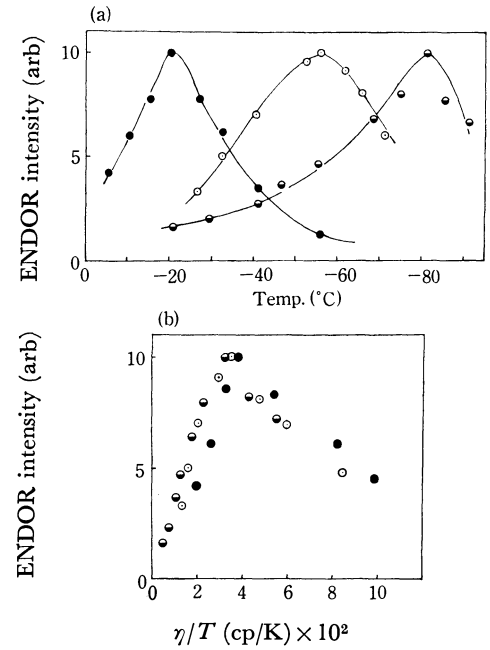

Fig. 2. The temperature (a) and η/T (b) dependences of ENDOR intensity of ring protons in 2,5-di-*t*-butyl-*p*-benzosemiquinone anion, ◒ in methanol, ⊙ in ethanol, ● in 2-propanol.

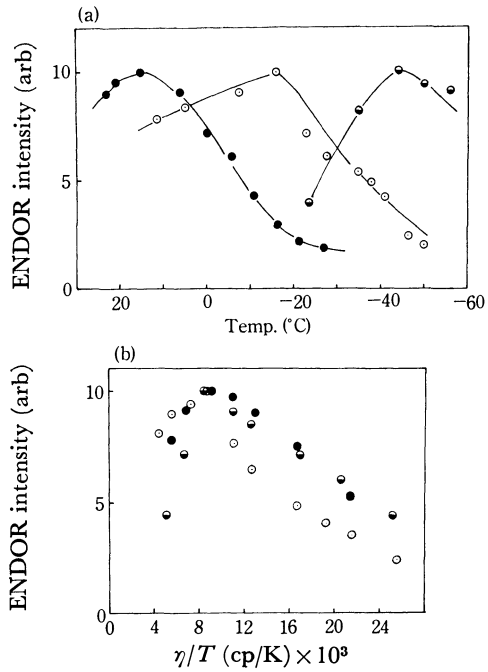

Fig. 3. The temperature (a) and η/T (b) dependence of ENDOR intensity of *t*-butyl protons in 2,5-di-*t*-butyl-*p*-benzosemiquinone anion, ◒ in methanol, ⊙ in ethanol, ● in 2-propanol.

Discussion

In an organic radical, *g*- and *hf*-anisotropy play dominant roles in the electron-spin relaxation. In this situation the assumption of a simple exponential correlation function with a correlation time of τ_R leads to the transition probability of the electron spin

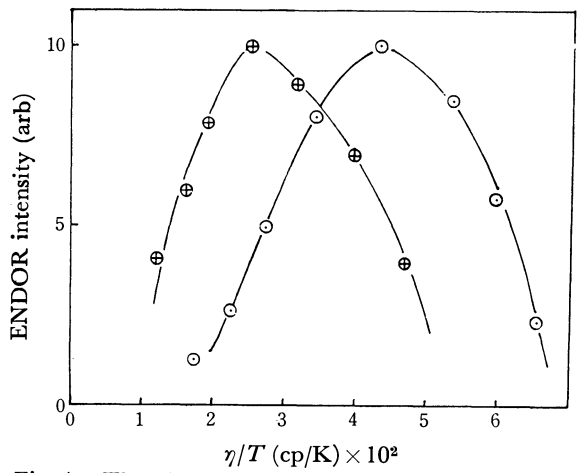

Fig. 4. The η/T dependence of ENDOR intensity of 2,5-dimethyl-*p*-benzosemiquinone anion radical in ethanol, ⊕ ring proton, ⊙ methyl proton.

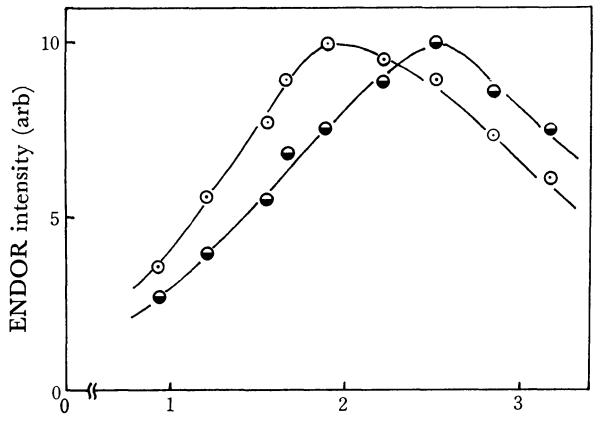

Fig. 5. The η/T dependence of ENDOR intensity of 9, 10-anthrasemiquinone anion radical in ethanol, ◒ 1-proton, ⊙ 2-proton.

W_e, which is identical with $1/T_{el}$ as:

$$W_e \propto \tau_R/(1+\omega_e^2\tau_R^2) \quad (2)$$

where ω_e is the Larmor frequency of the electron spin.

At high temperatures spin-rotational relaxation occurs by the fluctuating field caused by a molecular tumbling motion, but the deviation of the g values of semiquinone anions from the free electron g value is too small to cause spin-rotational relaxation.[9]

On the other hand, the nuclei in a radical are in the special situation because of the large magnetic dipole moment of an electron spin very close to them. Thus, the magnetic relaxation behavior of the nuclei may be very different from that in a diamagnetic molecule.

The nuclear transition probability for a radical is decided mainly by the electron-nuclear dipolar (END) interaction fluctuating by the Brownian motion of the molecule, because other nuclear relaxation processes, *e.g.*, nuclear dipole-dipole interaction, chemical shift anisotropy, and nuclear spin-rotational interaction, are comparatively small and may be neglected when the anisotropic *hf* interaction is of a considerable magnitude.

In a fluctuating END interaction, the nuclear transition probability can be written as:

$$W_n^{END} \propto \tau_R/(1+\omega_n^2\tau_R^2) \quad (3)$$

where ω_n is the Larmor frequency of the nucleus. When we adopt the Stokes-Einstein model, the isotropic rotational correlation time is given by:

$$\tau_R = 4\pi\eta a^3/3kT \quad (4)$$

where η is the viscosity of the solvent and a is the molecular radius. A schematic figure of the η/T dependence of W_e and W_n is shown in Fig. 6. Under ordinary experimental conditions in the liquid phase,

$$\omega_e^2\tau_R^2 \gg 1 \quad (5)$$

and

$$\omega_n^2\tau_R^2 \ll 1 \quad (6)$$

Under these conditions, W_e slows down when the sample is cooled, while, on the contrary, W_n becomes larger.

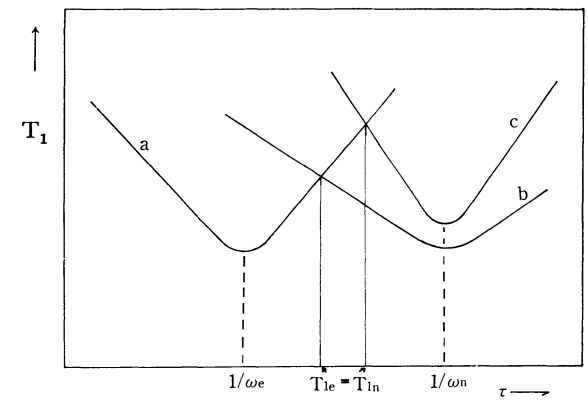

Fig. 6. The schematic figure of the τ dependence of T_{1e} and T_{1n}.
a: T_{1e}, b: T_{1n} with smaller END term, c: T_{1n} with larger END term.

In the temperature range where Eqs. (5) and (6) hold, W_e can be written as:[2]

$$W_e = A(1/\tau_R) \quad (7)$$

where A is the constant relating to the magnitude of the g and hf anisotropy. Moreover, W_n^{END} can be written as:[1]

$$W_n^{END} = B\tau_R \quad (8)$$

where B is the constant which is related to the magnitude of the anisotropic hf interaction.

Thus, the ratio of the two transition probabilities becomes:

$$b = \frac{W_n^{END}}{W_e} = (B/A)\tau_R^2 \quad (9)$$

The optimum conditions for the observation of the ENDOR signal are realized when the two transition probabilities become almost comparable,[2,3] that is, when:

$$b \sim 1 \quad (10)$$

The optimum η/T of an ENDOR line is decided by B/A and when a radical has two groups of protons, the ratio of the optimum η/T's becomes:

$$\frac{(\eta/T)_1}{(\eta/T)_2} = \left(\frac{B_2}{B_1}\right)^{1/2} \quad (11)$$

Thus, the ENDOR line of protons in a radical which have larger END terms has a smaller optimum η/T, *i.e.*, a higher temperature. This situation is shown schematically in Fig. 6.

ANQ Anion. In order to confirm the results described above, the ANQ anion radical in ethanol was studied. The ENDOR spectrum of this radical shows simple features because there are only two groups of equivalent protons; their isotropic *hf* coupling constants are $a_1=1.50$ MHz and $a_2=2.73$ MHz.

The magnitude of the B constant is proportional to the square of the END terms. The contribution of the END terms to the magnitude of B may be assumed to be proportional to $<1/r^3>_{av}^2$, where r is the distance between the proton and the unpaired electron and where $<\ >_{av}$ denotes the averaged value over the unpaired electron distribution. The END terms of the ring protons are approximately proportional to the spin density of adjacent carbon atoms if the cross contribution from the spin density on other carbon atoms is neglected. According to the McConnell relationship between the spin density on a carbon atom and the Fermi contact term of a proton,[10]

$$\rho_i = \frac{a_i}{Q} \tag{12}$$

where ρ_i is the spin density on the i-th carbon atom, a_i is the isotropic *hf* coupling constant of the proton bonded to the i-th carbon atom, and where Q is a constant peculiar to the radical.

The results of the above discussion lead to this equation:

$$B_i \propto <1/r^3>_{av}^2 \propto \rho_i^2 \propto a_i^2 \tag{13}$$

Thus,

$$\frac{(\eta/T)_1}{(\eta/T)_2} = \frac{a_2}{a_1} \tag{14}$$

In the ANQ radical, the ratio of the optimum η/T's between the protons of Positions 1 and 2 is estimated to be:

$$\left[\frac{(\eta/T)_1}{(\eta/T)_2}\right]_{ANQ} = 1.8 \tag{15}$$

The ratio of the η/T's which give the maxima in Fig. 5 is *ca.* 1.3. The coincidence between the theory and the experiment is fairly good and shows that the dominant mechanism of the relaxation of nuclear spins at Positions 1 and 2 in the ANQ anion is the END mechanism.

DMQ Anion. Figure 4 shows the η/T dependence of the ENDOR intensity for the ring ($a_1=5.24$ MHz) and the methyl protons ($a_2=6.47$ MHz) in the DMQ anion. Even though the isotropic *hf* coupling constant is larger than the ring protons, the optimum η/T of the methyl protons is larger than that of the ring protons.

According to Eq. (14), this result seems to conflict with the theoretical prediction of the optimum η/T. In the ANQ anion both protons are ring protons, and the electronic structures around them are very similar, whereas in the DMQ anion the comparison is made between the ring and methyl protons.

Generally, the *hf* anisotropy of the methyl proton is small compared to that of the ring proton, as has been shown by single crystal studies. The results for the DMQ anion can be interpreted in terms of the small END interaction of the methyl protons in spite of the large isotropic *hf* interaction.

The assumption of the END mechanism enables us to estimate the amount of the END term of the methyl protons. From Fig. 4, the ratio of the optimum η/T's for the methyl and ring protons is 1.8: 1. By a simple calculation, the $g_e\beta_e g_N\beta_N <1/r^3>_{av}$. of the methyl protons was estimated to be 2 MHz.

There is another plausible interpretation which has been proposed by Atherton and Day for the β-proton in the 2,6-di-*t*-butyl-4-cyclohexyl phenoxyl radical.[11] They proposed the fluctuation of the isotropic *hf* coupling of the β-proton as a cause of the nuclear relaxation. They made use of the difference in selection rules for the relaxation *via* the END interaction and isotropic *hf* modulation in explaining the dependence of the ENDOR intensity on the sitting ESR line of the magnetic field during the ENDOR measurement. However, there is still a quantitative uncertainty concerning the rotational correlation time of a substituent and the amount of the END interaction which has the same selection rule (S^+I^- and S^-I^+) as the isotropic *hf* modulation.

In the case of DMQ anion there was no apparent change in the relative signal intensity upon a change in the sitting point of the ESR spectra during the ENDOR measurements. No other experimental result which can be the evidence for the isotropic modulation mechanism was found in the present study.

DBQ Anion. The ring protons of the DBQ anion showed the most intense ENDOR signal at $\eta/T=3.5\times10^{-2}$ cp/K (Fig. 2). The optimum temperatures are very different for the three solvents, *i.e.*, methanol, ethanol, and 2-propanol, but the curves almost coincide with each other in the η/T plot. This shows all the relaxation processes relating to the ENDOR intensity are η/T-dependent in the present system.

The optimum η/T for the *t*-butyl protons is much smaller than that of the ring protons. This result could not be interpreted by the nuclear relaxation mechanism caused by END interaction, because the *t*-butyl protons which have the isotropic *hf* coupling of 0.19 MHz are not thought to have a larger END interaction than the ring protons, which have a 6.13 MHz isotropic *hf* coupling. In fact, in the liquid crystal phase the shift of the *t*-butyl *hf* coupling in the 2,4,6-tri-*t*-butylphenoxyl radical is negligibly small.[12]

On the basis of the difference in the magnitudes of the END interactions of two types of protons in the DBQ anion, we can predict a larger optimum η/T for the *t*-butyl protons than that of the ring protons by applying the END mechanism. The experimental results show, however, that the *t*-butyl protons have a much smaller optimum η/T than the ring protons. The same tendency was found in the experimental results of the ENDOR of the 2,4,6-tri-*t*-butylphenoxyl radical.[5]

The transition probability of electron spin[13] may

show the η/T dependence, which is characteristic of the relaxation by the g and hf anisotropy even at room temperature, because the difference in the components of the g-tensor from the free electron g-value is small enough for us to neglect the contribution of the electron spin-rotation to W_e. The normal situation of the electron-spin relaxation as discussed above suggests that the nuclear relaxation is effective in determining the optimum η/T for the t-butyl protons.

The fact that the optimum η/T for the t-butyl protons is much smaller than that of the ring protons shows the existence of a nuclear relaxation mechanism which is effective when η/T becomes small. Some of the mechanisms described below may become effective in determining the optimum conditions:

1. Nuclear Spin-rotational Relaxation: When the nuclear spin-rotational interaction is effective, W_n increases with an increase in the temperature (decreasing η/T).[14] As a result, the η/T where W_e and W_n become comparable shifts to a lower value. However, in order to get a W_n as high as W_e the spin-rotational constant should be as large as 1 MHz, which is exceptionally large.

2. Isotropic Modulation: When this mechanism is dominant for the ENDOR enhancement, the enhancement factor is expressed by W_{x2}/W_e,[2,3] where W_{x2} is the nonsecular $(+-\longleftrightarrow-+)$ transition probability. The effective correlation time for the t-butyl substituent is smaller than that of the electron spin and W_{x2} has a maximum at a slightly larger η/T value than the point where $\omega_e\tau_R\sim1$. The enhancement factor reaches its maximum at the η/T where W_{x2} is at its maximum; this η/T possibly has a smaller value than that of the optimum η/T for the ring proton. The modulation amplitude of *hfs* for the t-butyl protons may be small because the absolute value of its *hf* coupling constant is very small.

3. The Violation of the $\omega_e\tau_R\gg1$ Condition: At high temperatures $\omega_e\tau_R\gg1$ condition is not always valid. When $\omega_e\tau_R<1$, there is a temperature where $W_e\sim W_n$. The measurement of T_1 and T_2 showed, however, that even at 25 °C T_1 was longer than T_2. By the rough estimation of τ_R at the optimum η/T for the t-butyl protons, it becomes 2×10^{-9} s, much larger than $1/\omega_e$ (2×10^{-11} s).

In the present stage of this study, the lack of quantitative data prevents a detailed determination of the ENDOR mechanism of the t-butyl protons. The first and the second mechanism may, however, explain the optimum temperature to some extent. We also cannot discard such intermolecular mechanism as the intermolecular dipolar mechanism or the modulation of the intermolecular contact interaction by molecular motion.

Partial support by the Takeda Science Foundation is gratefully acknowledged.

References

1) This work was presented at the 11th symposium on ESR spectroscopy (Kanazawa), Nov., 1972.
2) J. H. Freed, *J. Phys. Chem.*, **72**, 49 (1967).
3) J. H. Freed, *J. Chem. Phys.*, **43**, 2312 (1965).
4) J. S. Hyde, *ibid.*, **43**, 1806 (1965).
5) R. D. Allendoerfer and A. H. Maki, *J. Mag. Resonance*, **3**, 296 (1970).
6) D. Kivelson, *J. Chem. Phys.*, **27**, 1094 (1960).
7) N. M. Atherton and J. Blackhurst, *J. Chem. Soc. Faraday II*, **68**, 470 (1972).
8) Y. Kotake and K. Kuwata, This Bulletin, **45**, 2663 (1972).
9) For example, tetrachlorosemiquinone (chloranil) anion sodium salt has $g_{//}=2.0087$ and $g_{\perp}=2.0050$.
10) H. M. McConnell and D. B. Chestnut, *J. Chem. Phys.*, **27**, 984 (1957).
11) N. M. Atherton and B. Day, *Chem. Phys. Lett.*, **15**, 428 (1972).
12) K. P. Dinse, R. Biehl, K. Möbius, and H. Haustein, *ibid.*, **12**, 399 (1971).
13) We measured the T_1 and T_2 of the electron spin in DBQ in ethanol by the stationary saturation method. The ESR lines of this radical consist of inhomogeneously broadened lines, so that we analyzed the saturation curve following Castner's method (T. G. Castner, Jr., *Phys. Rev.*, **115**, 1506 (1959). The results of the analysis are $T_1=4\times10^{-5}$ s, and $T_2=2.2\times10^{-7}$ s at -50 °C and $T_1=6\times10^{-7}$ s and $T_2=2.2\times10^{-7}$ s at 25 °C.
14) For example, H. S. Gutowsky, I. J. Lawrenson, and K. Shimomura, *Phys. Rev. Lett.*, **6**, 349 (1961).

X-Ray Photoelectron Spectroscopy of EDTA

Tooru YOSHIDA and Shigemasa SAWADA

Osaka Prefectural Industrial Research Institute, Enokojima, Nishi-ku, Osaka 550

(Received August 3, 1973)

The binding energies of N(1s) in ethylenediaminetetraacetic acid (EDTA) and its related compounds were measured by means of a photoelectron spectrometer, and the molecular structures of EDTA were discussed. Two kinds of peaks were observed in the N(1s) spectra of EDTA and its related compounds, with binding energies of about 401 and 399 eV. In EDTA-4H, the heights of the two peaks were almost equal, while in its sodium salts the peak height with the higher binding energy decreased as the number of carboxylate groups in the molecule increased. In EDTA-4Na, only a single peak with a low binding energy was observed. In EDTP-4H and GEDTA-4H, the spectra showed two peaks with different heights. The binding energy values of the main peaks of simple amino acids, such as glycine and alanine, were about 401 eV. From the above results, it can be deduced that there are two kinds of N atoms, $=N^{+}H-$ and $=N-$ types, in an EDTA molecule.

Ethylenediaminetetraacetic acid (EDTA) is widely used as a chemical reagent because of its ability to form stable and soluble chelate complexes with metal ions. Since the complex stability is partly related to the proton affinity of the acid, a clear idea of the structure of the acid could lead to a better understanding of the metal-complex formation.

EDTA is a compound belonging to the group of amino acids including glycine or alanine, and it may take a zwitterion structure even in the solid state. However, the results obtained from the IR spectra do not always give the obvious conclusion. Chapman[1] concluded that the tendency to form a zwitterion in both EDTA-4H and EDTA-2Na·$2H_2O$ is less than in simple mono-amino acid, while Nakamoto *et al.*[2] reported that EDTA-2Na·$2H_2O$ is almost zwitterionic.

The exact crystal structure of EDTA-4H was determined by Cotrait[3] by X-ray analysis. According to his conclusions, two of the four carboxyl groups are used to make intermolecular hydrogen bonds with neighboring molecules, while the remaining two are bonded to the nitrogen atoms intramolecularly.

Recently a new technique of X-ray photoelectron spectroscopy called ESCA has been developed; this method is a very useful tool for learning new aspects of the natures of chemical bonds. A detailed description of the ESCA method has been published by Siegbahn *et al.*[4]

Experimental

The X-ray photoelectron spectra were measured on an AEI ES100 spectrometer under the control of a DS100/32 computer data processing system. Al-Kα (1486.6 eV) and Mg-Kα (1253.6 eV) X-ray lines were used as the excitation sources. The abscissa of the chart is the binding energy (BE), while the ordinate is the relative intensity of each peak.

All the compounds measured are given in Table 1. They were all commercially available, were of an analytical grade, and were used without further purification. The samples were ground to powder, dusted onto a double-backed adhesive tape or pressed on a copper mesh, and set inside the measuring chamber. The measurements were then run at room temperature under a vacuum of about 10^{-6} Torr.

Results

1s Spectra of Carbon. Figure 1 shows the spectrum of the C(1s) of EDTA-4H. Two peaks with the different binding energies shown by the broken lines in the figure were obtained by a curve resolution. The

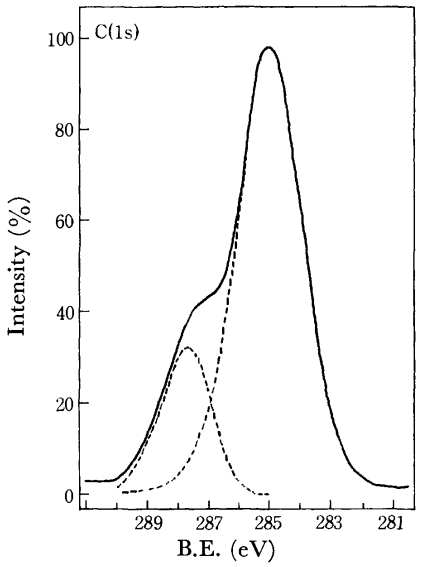

Fig. 1. C(1s) electron spectrum of EDTA-4H.

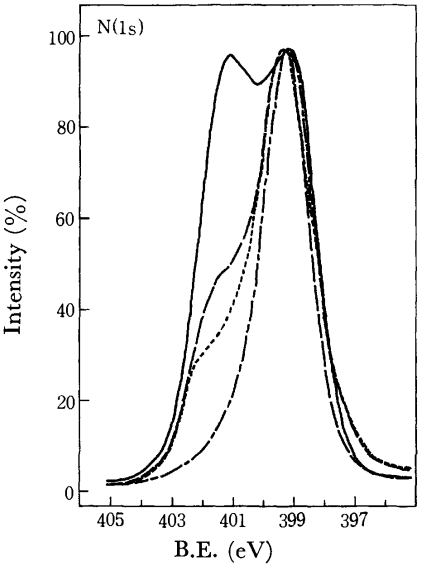

Fig. 2. N(1s) electron spectra
——: EDTA-4H, – – –: EDTA-2Na
·····: EDTA-3Na, —·—: EDTA-4Na

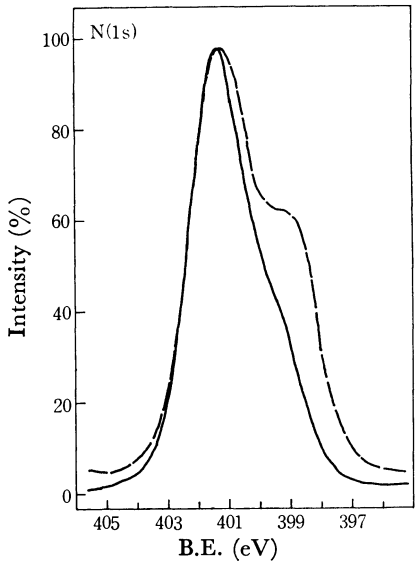

Fig. 3. N(1s) electron spectra.
——: EDTP-4H, ——: GEDTA-4H

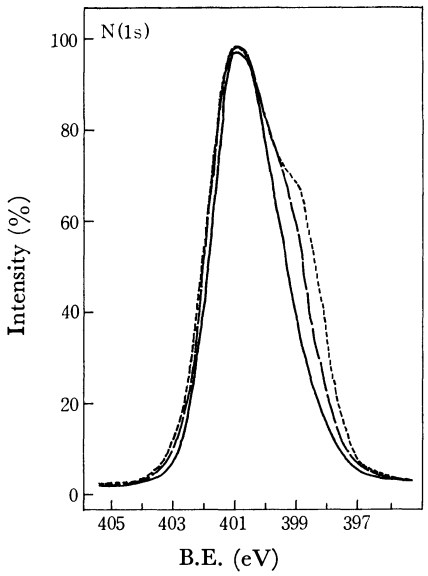

Fig. 4. N(1s) electron spectra.
——: AA, ——: γ-AB, ----: NTA

C(1s) spectra of the other compounds also give profiles similar to that of EDTA-4H. The taller peak (the right-hand one of the two) was used as the energy standard throughout the present experiments.

The differences in binding energy between the two peaks of EDTA-4H and EDTA-4Na were 2.7 and 3.1 eV respectively.

1s Spectra of Nitrogen. In Figs. 2, 3, 4, and 5, the N(1s) spectra of some EDTA derivatives and mono-amino acids are given. EDTA-4H and EDTA-2Na·2H_2O show two peaks very clearly, while EDTA-4Na shows a well-defined single peak. The other compounds show spectra with a shoulder or an asymmetric broad profile which suggests the existence of two peaks.

Table 1. N(1s) binding energy valufs

Compounds		N(1s) B.E. (eV)	
Ethylenediaminetetraacetic acid (EDTA-4H)	$HOOCH_2C\diagdown\ \ \diagup CH_2COOH$ $N(CH_2)_2N$ $HOOCH_2C\diagup\ \ \diagdown CH_2COOH$	401.3 (1)	399.1 (1)
Disodium ethylenediaminetetraacetate (EDTA-2Na)		401.4 (2)	399.3 (5)
Trisodium ethylenediaminetetraacetate (EDTA-3Na)		401.4 (1)	399.3 (3)
Tetrasodium ethylenediaminetetraacetate (EDTA-4Na)			399.2
Ethylenediaminetetrapropionic acid (EDTP-4H)	$HOOC(H_2C)_2\diagdown\ \ \diagup (CH_2)_2COOH$ $N(CH_2)_2N$ $HOOC(H_2C)_2\diagup\ \ \diagdown (CH_2)_2COOH$	401.4 (3)	399.3 (1)
Glycoletherdiaminetetraacetic acid (GEDTA-4H)	$HOOCH_2C\diagdown\ \ \diagup CH_2COOH$ $N(CH_2)_2O(CH_2)_2O(CH_2)_2N$ $HOOCH_2C\diagup\ \ \diagdown CH_2COOH$	401.3 (2)	399.1 (1)
Disodium ethylenediaminetetraacetate dihydrate (EDTA-2Na·2H_2O)		401.4 (2)	399.3 (3)
Tetrasodium ethylenediaminetetraacetate dihydrate (EDTA-4Na·2H_2O)			399.2
Zinc disodium ethylenediaminetetraacetate (EDTA-Zn)			399.5
Aminoacetic acid (AA)	H_2NCH_2COOH	400.8 (5)	398.9 (1)
Iminodiacetic acid (IDA)	$HN\langle^{CH_2COOH}_{CH_2COOH}$	400.9 (3)	399.1 (1)
Nitrilotriacetic acid (NTA)	$N-CH_2COOH$	400.9 (2)	398.9 (1)
β-Aminopropionic acid (β-AP)	$H_2N(CH_2)_2COOH$	400.9 (4)	399.1 (1)
γ-Aminobutyric acid (γ-AB)	$H_2N(CH_2)_3COOH$	401.0 (3)	399.0 (1)

The numbers in parentheses are the relative intensities roughly determined from the two peaks.

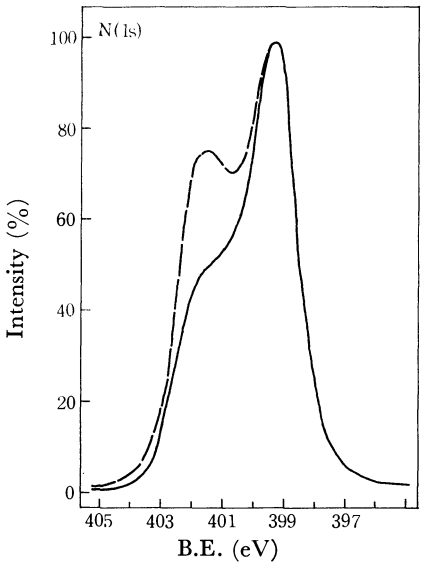

Fig. 5. N(1s) electron spectra.
——: EDTA-2Na, ——: EDTA-2Na·$2H_2O$

The measured values for the N(1s) binding energy are listed in Table 1. The numbers in parentheses indicate the relative intensities roughly determined from the two peaks.

Discussion

C(1s) Signal. There are two kinds of carbons, $-CH_2-$ and $-CO-$, in EDTA distinguishable by the ESCA method. As the O atom has a higher electronegativity than the H atom, the electron density on the C atom in $-CO-$ is lower than that in $-CH_2-$. Accordingly, the C(1s) signal of $-CO-$ must have a higher binding energy than that of the $-CH_2-$. The fact that the binding-energy difference between these two kinds of carbons in EDTA-4H is about 0.4 eV lower than that in EDTA-4Na may be explained as follows; the electron density on the C atom in $-CO-$ in the former is higher than that in the latter because of the presence of an intermolecular hydrogen bond in the former, so the binding energy of the C atom in $-CO-$ in the former is lower than that in the latter.

As many precise discussions[5] based on some theoretical calculations have been reported with regard to this difference in binding energy, which is called a chemical shift, no further discussion will be given here. The binding energy value of C(1s) of $-CH_2-$ is taken to be 285.0 eV.

N(1s) Signals. Figure 2 shows the existence of two different states of the nitrogen atom in EDTA. From the binding energy values of the major peaks of N(1s) observed in simple amino acids, such as AA, IDA, NTA, β-AP, and γ-AB, it may be concluded that the higher binding energy peak of the two in EDTA can be assigned to the N atom with the $-\overset{+}{N}H-$ structure. The value of this binding energy is about 401 eV. Hence, the remaining peak, with a lower binding energy, can be assigned to the ordinary N atom, which has the $=N-$ structure. The binding energy value of the remaining peak is about 399 eV, almost coincident with that of the single peak of EDTA-4Na, in which the zwitterion structure can not exist.

According to the analysis of the X-ray diffraction patterns, EDTA-4H belongs to the $C_{2/c}$ space group and has a symmetry center at the middle point of $=NCH_2CH_2N=$. Two of the four carboxylic H atoms have a shorter distance to the N atom than the other two, suggesting protonation or hydrogen bonding. On the contrary, the ESCA spectrum shows that, in a crystalline state, the two N atoms in an EDTA-4H molecule are not equivalent in electronic charge.

As for the series of the Na salts of EDTA, the spectra also show the existence of two kinds of nitrogen and a trend for the peak height of the protonated $=\overset{+}{N}H-$ group to decrease as the number of the carboxylate group in the molecule increases. The decrease in the number of carboxyl groups in a molecule will reduce the possibility of protonation to the N atom.

As is shown in Fig. 5, crystal water in EDTA-2Na seems to have a particular effect on the ESCA spectrum of N(1s), but it does not in EDTA-4Na. Assuming that the hydrated Na salt conforms the same spatial molecular arrangement as that[6] of the hydrated K or Rb salt, it may be considered that H atoms from crystal water are preferably used to make an intermolecular hydrogen bond, while the two H atoms of the carboxyl group serve to make an intramolecular hydrogen bond with their own nitrogen atom. Therefore, in EDTA-2Na·$2H_2O$ the opportunity to make a charged amino group will increase.

EDTP-4H and GEDTA-4H have chemical structures similar to that of EDTA-4H, but give different ESCA spectra; that is, the $=\overset{+}{N}H-$ peak is dominant over the $=N-$ peak. This may be explained as follows: in EDTP-4H, the distance between the two N atoms is the same as in EDTA-4H, but the side-chain is longer. Therefore, ring formation is easier than in EDTA-4H. In GEDTA-4H, the side-chain is the same as in EDTA-4H, but the N-to-N distance is longer, so the repulsion of the developed positive charge on each nitrogen atom is less than in EDTA-4H.

On the basis of the results obtained here, it may be considered that there are at least two factors affecting the appearance of two peaks on the ESCA spectrum of EDTA-4H. One is steric hindrance, which makes it hard to build up a five-membered ring, and the other is charge repulsion, which prevents too much density of the positive charge at the center of a molecule.

The N(1s) spectrum of the EDTA-Zn chelate showed a single peak with a binding energy falling between those of the protonated and the unprotonated N(1s) of EDTA-4H. Detailed discussions of this and other EDTA-metal chelates will be published elesewhere.

All of the N(1s) spectra in the simple amino acids examined are more or less doublets. Although no clear explanation of this can be given here, it may be conceived that the steric environment around the N atom in AA, IDA, and NTA will reduce the chance for the H atom to attach to the N atom.

The authors wish to thank Drs. Kyoozo Nakajima and Masao Wakae for their helpful comments and

discussions. In addition, they wish to thank Dr. Takanobu Hamaguchi for his aid in performing this experiment.

Reference

1) D. Chapman, *J. Chem. Soc.*, **1955**, 1766.
2) K. Nakamoto, Y. Morimoto, and A. E. Martell, *J. Amer. Chem. Soc.*, **85**, 309 (1963).
3) M. Cotrait, *Acta Crystallogr., B*, **28**, 781 (1972).
4) K. Siegbahn, C. Nordling, A. Fahlman, R. Nordberg, K. Hamrin, J. Hedman, G. Johansson, T. Bergmark, S. E. Karlsson, I. Lindgren, and B. Lindberg, "ESCA Atomic, Molecular and Solid State Structure Studied by Means of Electron Spectroscopy," Almqvist and Wiksells AB, Uppsala (1967).
5) a) T. D. Thomas, *J. Amer. Chem. Soc.*, **92**, 4184 (1970). b) D. N. Hendrickson, J. M. Hollander, and W. L. Jolly, *Inorg. Chem.*, **9**, 612 (1970). c) H. Kato, K. Ishida, H. Nakatsuji, and T. Yonezawa, This Bulletin, **44**, 2587 (1971).
6) M. Cotrait, *Acta Crystallogr., B*, **26**, 1152 (1970).

An Investigation of the Gas-Solid Interface Reaction on the Surface of Ag and Ag_2S

Masayuki KATSUMOTO, Kazuo FUEKI, and Takashi MUKAIBO

Department of Industrial Chemistry, Faculty of Engineering, The University of Tokyo, Hongo, Bunkyo-ku, Tokyo 113

(Received July 9, 1973)

In order to elucidate the mechanism of the redox reaction at the gas-solid interface, the isotopic exchange between H_2S and D_2 on Ag and Ag_2S has been studied in the temperature range from 410 to 521 °C. The transfer of isotopic species between "hydrogen sulfide" [1] and "hydrogen" [1] was found to proceed by means of the reaction:

$$\text{"}H_2S\text{"}^{1)} \underset{k_1'}{\overset{k_1}{\rightleftharpoons}} \text{"}H_2\text{"}^{1)} + S(ad)$$

on both surfaces. From the analysis of the kinetic data, the redox reaction rate constants, k_1 and k_1', were determined as a function of the sulfur activity. It was found that k_1 is inversely proportional to the sulfur activity, whereas k_1' is independent of it. The mechanism of the reaction on the surfaces of Ag and Ag_2S is discussed.

In previous works, the authors and their co-workers have kinetically studied the H_2S–D_2 exchange reaction on Cu_2S(p-type semiconductor),[2] β-$Fe_{1-x}S$(metallic conductor),[3] MoS_2(intrinsic semiconductor), and MnS-(p-type semiconductor)[4] in order to elucidate the mechanism of the redox reaction at the gas-solid interface. It was found that the activation energies and the dependence of the rate constants of the surface reaction on the sulfur activity are nearly the same for all these sulfides. Except in the case of Cu_2S, these results can not be explained by the theory proposed by Kobayashi and Wagner.[5] The mechanism proposed by the authors is that the rate-determining reaction is that between adsorbed sulfur atoms and gaseous molecules.[4]

The present work aims to study the redox reaction on Ag and Ag_2S(n-type semiconductor). Since the adsorption of sulfur atoms on Ag in "H_2S"–"H_2" gas mixtures, obeying a Langmuir-type adsorption isotherm, has already been reported,[6] one can confirm the validity of the theory proposed by the authors.

As the sulfur activity in the presence of both Ag and Ag_2S is 1/3.3~1/3.7 in the temperature range from 400 to 520 °C,[7] one can examine the H_2S–D_2 exchange reaction on Ag if the sulfur activity is smaller than 1/3.3~1/3.7. The sulfur activity, a_s, is defined as the pressure ratio of "hydrogen sulfide" to "hydrogen".

Experimental

Isotopic Exchange Study. The apparatus, the method of the purification of gases, and the experimental procedure were essentially the same as in previous works.[2-4] The samples were prepared as follows.

a) Ag sample: Silver powder of 99.9% purity was treated in "hydrogen" at 570 °C for 1 hour. The surface area of the powder was 2.86×10^3 cm^2 g^{-1}.

b) Ag_2S sample: Silver powder, treated as above, was sulfurized with a "H_2S"–"H_2" gas mixture at 570 °C until the sulfurization was completed. The surface area of the sulfide was 4.76×10^3 cm^2 g^{-1}.

Prior to the isotopic exchange run, the sample was equilibrated with the "H_2S"–"H_2" gas mixture, the sulfur activity of which was the same as that of the H_2S–D_2 gas mixture to be used. Therefore, the sulfur activity, a_s, was kept constant throughout the isotopic exchange run, irrespective of the change in the concentration of the isotopic species.

Results and Discussion

Isotopic Exchange Reaction. Figures 1 and 2 show the change in x_{H_2}, x_{HD}, and x_{D_2}, the mole fractions of

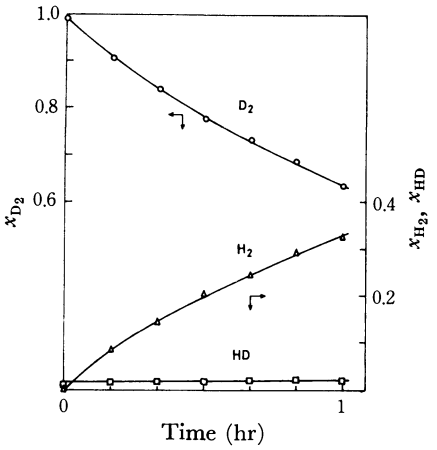

Fig. 1. Change in x_{H_2}, x_{HD}, and x_{D_2} with time. (Ag_2S, 446 °C, $P^\circ_{H_2S}$=278 mmHg, $P^\circ_{D_2}$=27.8 mmHg, a_s=10)

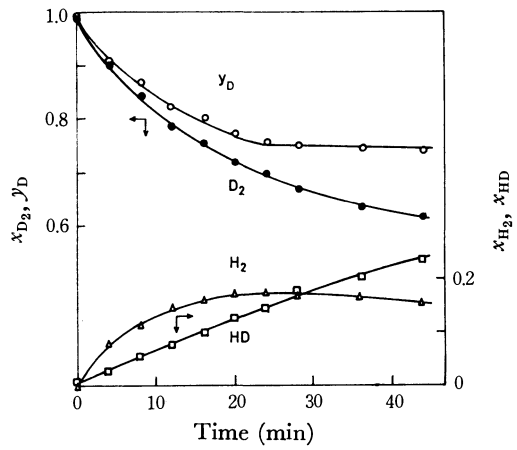

Fig. 2. Change in x_{H_2}, x_{HD}, and y_D with time. (Ag_2S, 480 °C, $P^\circ_{H_2S}$=27.3 mmHg, $P^\circ_{D_2}$=81.7 mmHg, a_s=1/3)

H_2, HD, and D_2 respectively, at different sulfur activities in the presence of Ag_2S. The higher range of a_S, x_{HD} remains unchanged, whereas x_{H_2} increases and x_{D_2} decreases. Thus, it may be concluded that the isotopic exchange occurs as follows:

$$H_2S + D_2 = D_2S + H_2 \quad (1)$$

This means that "H_2S" is directly converted to "H_2" by means of the reaction:

$$\text{"}H_2S\text{"} = \text{"}H_2\text{"} + S(ad) \quad (2)$$

where S(ad) represents the sulfur atom adsorbed on the surface. Reaction (2) is characterized as a redox reaction.

At $a_S=1/3$, the HD formation becomes remarkable. However, the fraction of D in "hydrogen", $y_D(=x_{D_2}+1/2x_{HD})$, reaches its isotopic equilibrium value, 0.75, at the time corresponding to the maximum of x_{H_2} (Fig. 2) and then remains constant. This fact suggests that the HD formation takes place mainly by virtue of these steps:

$$H_2S = H_2 + S(ad) \quad (2')$$

$$H_2 + D_2 = 2HD \quad (3)$$

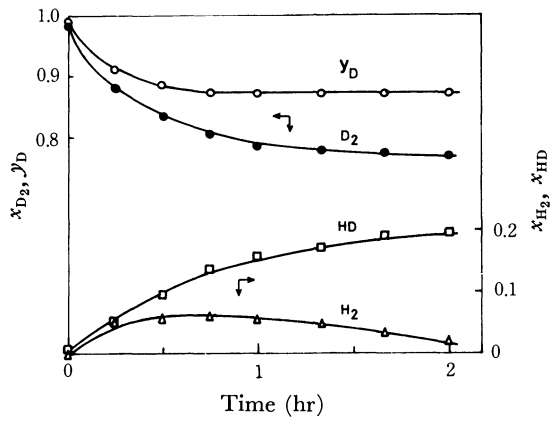

Fig. 3. Change in x_{H_2}, x_{HD}, x_{D_2}, and y_D with time. (Ag, 480 °C, $P^\circ_{H_2S}=14.8$ mmHg, $P^\circ_{D_2}=114.3$ mmHg, $a_S=1/7.7$)

Figure 3 shows the change in x_{H_2}, x_{HD}, x_{D_2}, and y_D at $a_S=1/7.7$ in the presence of Ag. The time variation of these quantities is essentially the same as in the case of Ag_2S. That is, y_D reaches its isotopic equilibrium value, 0.885, at the time corresponding to the maximum of x_{H_2}, and then it remains unchanged. Therefore, it may be concluded that the exchange reaction in the presence of Ag also proceeds *via* the (2')—(3) steps.

One can determine k_i and k_i', the rate constants of the sulfurization and reduction of Reaction (2) respectively, by the method proposed in the previous paper.[3] Figure 4 give the plots of $\log k_i$ and $\log k_i'$ against $\log a_S$. The plots are linear. The slopes are summarized in Table 1.

Therefore, the rate equation of Reaction (2) on the surfaces of Ag and Ag_2S is expressed in the form:

$$v = kP_{\text{"}H_2S\text{"}}a_S^{-1} - k'P_{\text{"}H_2\text{"}} \quad (4)$$

The Arrhenius plots of k_i at $a_S=1/5$ for Ag and that at $a_S=1$ for Ag_2S are given in Fig. 5. The activation

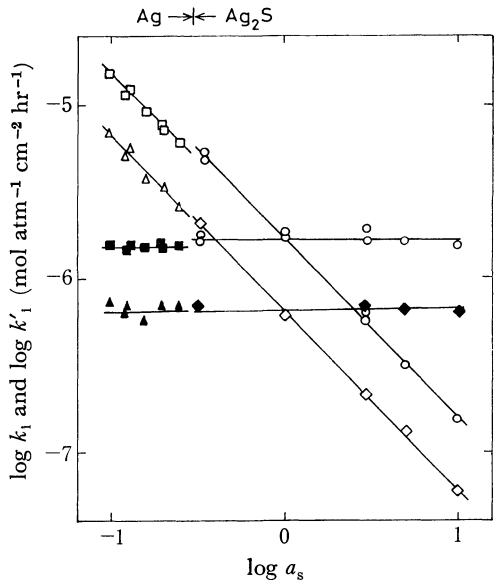

Fig. 4. Plots of $\log k_i$ and $\log k_i'$ against $\log a_S$.
Ag {□ k_i, 480 °C △ k_i, 446 °C
■ k_i' ▲ k_i'
Ag_2S {○ k_i, 480 °C ◇ k_i, 446 °C
● k_i' ◆ k_i'

Table 1. Values of $(\partial \log k_i/\partial \log a_S)$ and $(\partial \log k'_i/\partial \log a_S)$

Sample	Temperature (°C)	$(\partial \log k_i/\partial \log a_S)$	$(\partial \log k'_i/\partial \log a_S)$
Ag	480	−1.01	−0.01
	446	−1.06	−0.06
Ag_2S	480	−1.03	−0.03
	446	−1.05	−0.05

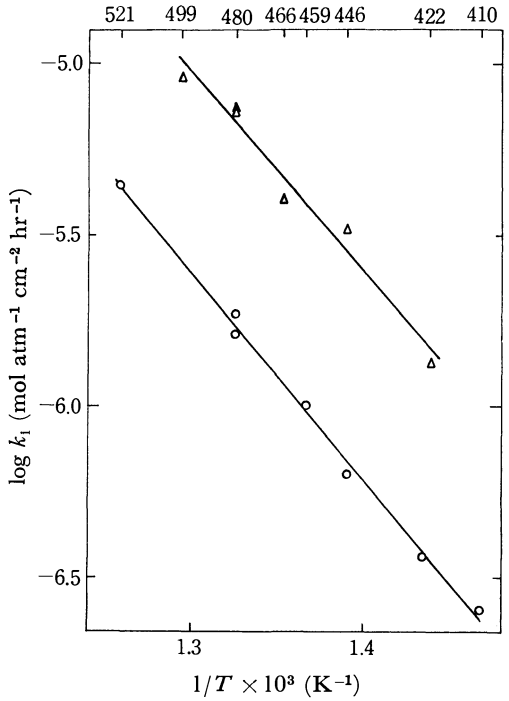

Fig. 5. Arrhenius plots for k_i at $a_S=1$ (Ag_2S) and at $a_S=1/5$ (Ag)
○ Ag_2S, △ Ag

Calorimetric Study of Glassy State. IX. Thermodynamic Properties of Stannous Chloride Dihydrate and Dideuterate Crystals*

Takasuke MATSUO, Masaharu OGUNI, Hiroshi SUGA, and Syûzô SEKI
Department of Chemistry, Faculty of Science, Osaka University, Toyonaka, Osaka 560

Appendix: High Temperature Entropy Calculation

John F. NAGLE
Department of Physics, Carnegie-Mellon University, Pittsburgh, Penn. 15213 USA

(Received September 27, 1973)

The heat capacity of $SnCl_2 \cdot 2H_2O$ and $SnCl_2 \cdot 2D_2O$ crystals, substances with layer structure, was measured from 13 to 300 K. Anomalies due to ordering of the hydrogen (deuterium) position were observed at $T_c(H_2O) = 217.94$ K and at $T_c(D_2O) = 234.47 \pm 0.05$ K. The total entropy change of the transition was estimated to be 4.6 J K^{-1} mol^{-1} for both compounds. An exact calculation of the high temperature entropy based on the two-dimensional lattice model gave 3.13 J K^{-1} mol^{-1}. The critical indices $\alpha_\pm$ of the divergent heat capacity anomalies are as follows: $\alpha_+(H_2O) = 0.53$, $\alpha_-(H_2O) = 0.48$, $\alpha_+(D_2O) = 0.57$, $\alpha_-(D_2O) = 0.54$. Another heat capacity anomaly was found at 140—160 K where the heat capacity values depended on the thermal history of the specimen. The enthalpy relaxation observed at the temperature region was analysed by use of the first-order rate equation, giving the activation enthalpies $\Delta H_a(H_2O) = 49.9$ kJ mol^{-1} and $\Delta H_a(D_2O) = 49.8$ kJ mol^{-1}. The concept of long-range-ordered glassy state was introduced for description of the non-equilibrium state of the present substances below 140 K. A general consideration of the relation between molecular relaxation and phase change in terms of the Deborah number is presented.

Stannous chloride dihydrate has a layer structure in which double layers of the stannous chloride molecules are sandwiched between the hydrogen-bonded networks of the water molecules.[1,2] A phase transition was found in this substance and its deuterate analogue by use of dielectric, nuclear magnetic resonance and electric conductivity measurements,[3] and was attributed to the order-disorder change of the hydrogen positions in the network. Since thermodynamic properties are of special interest in connection with the two-dimensional nature of the crystal structure, we measured the heat capacity of the hydrate and deuterate from 13 to 300 K. Both compounds exhibited sharp heat capacity peak at the transition point. In addition, an unexpected thermal relaxation phenomenon was observed at a lower temperature and could be interpreted quantitatively as caused by a slow ordering process of the hydrogen position. The phenomenon is interesting in connection with the recently proposed concept of the glassy crystalline state.[4]

Experimental

Sample Preparation. Commercially available stannous chloride dihydrate of the highest purity was molten in an air-tight flask (melting point: 40 °C), and cooled slowly in a temperature-controlled water bath. When about half of the material was crystallized, the remaining melt was discarded. The crystal was kept in a closed vessel before use. The water content of the crystal was determined from the weight loss accompanying the dehydration to the anhydrous salt. It was found to be 15.97% in an excellent agreement with the stoichiometric value, 15.96%. Spectrometric analysis of the specimen taken from the calorimeter cell after completion of the measurement showed that impurity ions in the crystal were copper, iron, nickel and calcium, each less than 10 ppm.

Before the above method of fractional melting was found to be successful, recrystallization from the saturated aqueous solution was attempted. The water content of the crystal obtained by this method was consistently higher than the ideal value by 0.2 to 0.3%. Heat capacity of the crystal containing the excess water was also measured from 13 to 300 K, though the main body of the experimental data refers to the crystal obtained by the improved method. Qualitative behaviors of the differently prepared crystals were similar to each other as will be described below.

The deuterate was prepared from the purified hydrate by the similar method as follows. The hydrate was first dehydrated to the stoichiometric anhydrous salt, to which an appropriate quantity of 99.75% heavy water and a small amount of deuterochloric acid were added. The mixture was heated to 45 °C, and when a clear solution was obtained, it was cooled slowly. The crystallization began at about 41 °C. The procedure taken thereafter was similar to that for the hydrate.

Calorimetric Apparatus. The calorimetric system used was the same one described elsewhere,[5] with minor modifications. The hand-set type of the potentiometer formerly used for the electric energy measurement was replaced with a digital voltmeter (Hewlett Packard model 3462 A) and the clock, with a digital time interval counter (Takeda Riken Model TR-5766 U/6). The cryostat, temperature measureing apparatus and the adiabatic control circuit remained unaltered. The overall accuracy of the measurement is believed to be about 1% at 20 K and better than 0.3% above 50 K.

Sample Handling. In order to avoid efflorescence and deliquescence of the specimen, the crystal was handled in a glove box in which the humidity was adjusted to the dissociation pressure of the crystal by placing in the box a quantity of the partially dehydrated crystal. Similar precaution was taken for the deuterate by using the crude deuterate material. The sample crystals were crushed to 2—3 mm in the linear dimension and loaded in the calorimeter cell. The loaded cell, with the gas-filling tube open, was cooled to liquid nitrogen temperature in a glass vessel. The glass vessel was evacuated,

* A brief account of the present paper was published in *Proc. Japan Acad.*, **48**, 237 (1972).

flushed twice, and filled with one atm of helium gas. After being allowed to warm up to the room temperature, the cell was taken out of the glass vessel and the filling tube was sealed promptly with low melting solder. The sample weight was 97.507 g and 92.949 g for the hydrate and the deuterate, respectively.

Calorimetric Procedure. As was stated above the heat capacity was measured first on a sample containing excess water. The calorimeter was first cooled to the liquid nitrogen temperature, at which the first series of measurement was commenced. At temperature around 150 K, a marked upward temperature drift was observed. At about 162 K, it changed to downward drift, indicating a slow equilibration in the calorimeter. An appreciable cooling was observed for more than 45 min after turning off the calorimeter heater, compared to the typical equilibration time of 6—7 min. The heat capacity curve exhibited a step-like anomaly at this temperature. The heat capacity value could not be defined precisely in this temperature region, because it depended on the annealing condition of the sample and on the time spent in the measurement. Another anomaly was found at around 218 K which corresponds to the phase transition temperature reported by Kiriyama.[3] The equilibration time did not change appreciably around the transition point. At still higher temperature a broad hump was found, which could be attributed to the eutectic melting due to the presence of the excess water. The cell was dismantled from the cryostat and the excess water was carefully removed. Subsequent measurement showed the broad hump was absent, though the first two anomalies remained unaffected. Since the relaxational anomaly mentioned above was quite unexpected, it was suspected that it might be caused by impurity in the sample crystal. The extremely pure crystal was prepared as was mentioned above. The measurement on the improved specimen yielded the same result in regard to the relaxational and the lambda anomalies. Therefore it was concluded that the first two anomalies are intrinsic properties of the crystal. Since different cooling history of the sample was found to cause change in the behavior of the crystal, a detailed measurement was attempted which enabled a quantitative analysis of the hysteretic phenomenon under controlled condition. The procedure was as follows. The calorimeter was cooled through the anomalous region as rapidly as possible to 133 K, at which temperature a series of measurement was started in the usual intermittent heating mode with the temperature step of 1—1.5 K. At 138.1 K a significant heat evolution began. The temperature rose linearly with time, indicating that the relaxational effect involved is a slow process. After following the temperature drift for 30 min, the temperature was raised by about 1 K by introducing the electric energy in the calorimeter and again the temperature rise was followed for 30 min. The same procedure was repeated to above 160 K. The rate of the spontaneous temperature rise reached its maximum at 149.5 K, above which it decreased rapidly, reaching null approximately at 154 K. Above 154 K, the temperature drift after turning-off of the heater current was endothermic and non-linear in time. The linear exothermic drift rate at the lower temperatures is plotted in Fig. 1 as a function of the temperature. A similar behavior was observed in the deuterate crystal. As is

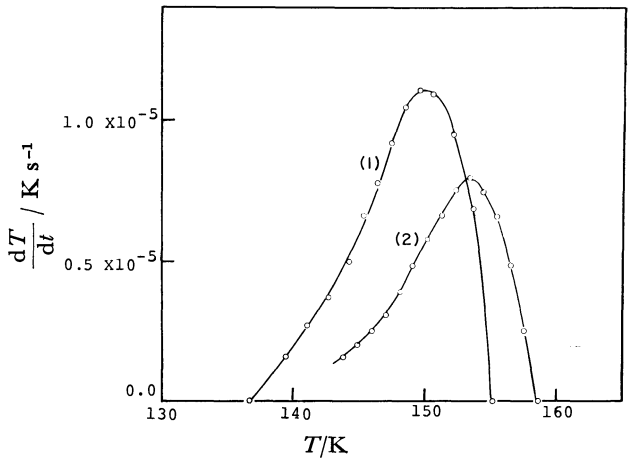

Fig. 1. Rate of spontaneous temperature rise of the calorimeter loaded with (1) $SnCl_2 \cdot 2H_2O$ and (2) $SnCl_2 \cdot 2D_2O$.

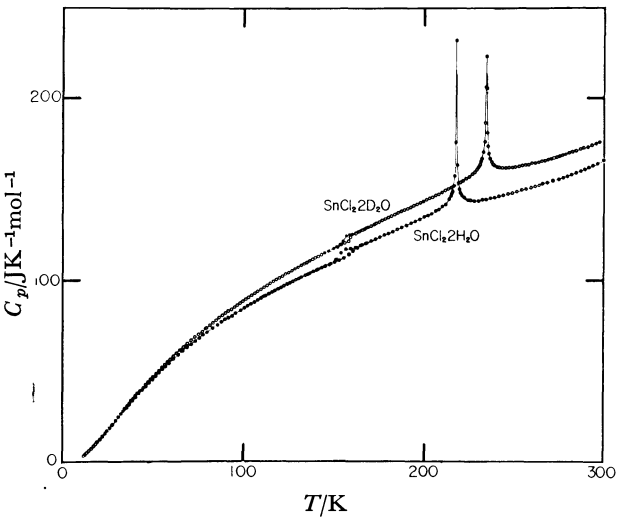

Fig. 2. Heat capacity of $SnCl_2 \cdot 2H_2O$ and $SnCl_2 \cdot 2D_2O$ crystals.

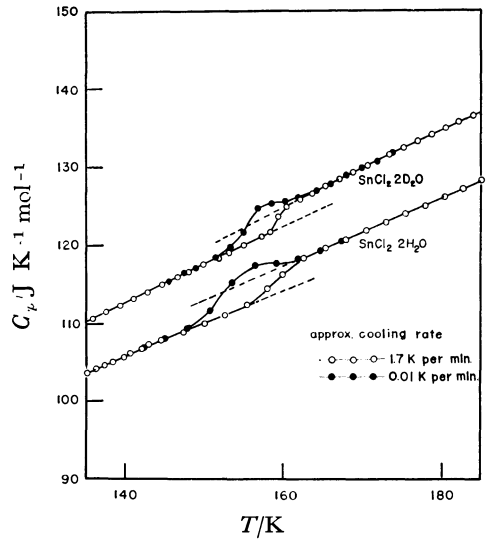

Fig. 3. Heat capacity of $SnCl_2 \cdot 2H_2O$ and $SnCl_2 \cdot 2D_2O$ around their "glass transition" temperatures. Because of spontaneous heat evolution and other non-equilibrium phenomenon, some arbitrariness is necessarily introduced to the observed values. The effect of different sample prehistory is indicated by the open and closed circles in the plot. Measurement after rapid cooling (1.7 K per min) gave the smaller values (open circles), and after slow cooling (0.01 K per min), the larger value (closed circles) in the temperature region 150—163 K.

TABLE 2. HEAT CAPACITY OF $SnCl_2 \cdot 2D_2O$

T/K	C_p/J K^{-1} mol^{-1}	T/K	C_p/J K^{-1} mol^{-1}	T/K	C_p/J K^{-1} mol^{-1}	T/K	C_p/J K^{-1} mol^{-1}
241.75	162.82	112.71	98.17	220.10	154.74	238.0153	165.13
243.58	162.74	114.41	99.20	221.62	155.61	238.1902	164.75
245.41	162.59	116.09	100.23	223.28	156.82	238.3657	164.51
247.24	162.64	117.76	101.24	225.02	157.90	238.5407	164.14
249.07	162.88	119.41	102.23	226.77	159.37	238.7162	164.35
250.90	163.04	121.09	103.25	228.22	160.77	238.8916	163.83
252.72	163.46	122.85	104.23	229.23	161.69	239.0670	164.39
254.54	164.03	124.61	105.17	229.80	163.00	239.2425	163.82
256.37	164.47	126.37	106.26			239.4283	163.77
258.17	164.63	128.10	107.25	226.5014	158.89	239.5937	164.18
259.97	165.36	129.82	108.22	227.1171	159.64	239.7693	163.39
261.78	165.34	131.53	109.15	227.6538	159.83	239.9450	163.87
263.58	165.79	133.22	110.07	228.1974	160.36	240.2086	163.54
265.38	166.34	134.58	110.84	228.7389	161.20	240.5605	163.16
267.18	166.59	136.26	111.69	229.2787	161.63	240.9710	163.40
268.96	167.28	137.88	112.55	229.7203	162.38	241.4400	163.33
270.77	167.76	139.43	113.38	229.9785	162.79	241.9019	163.06
272.60	168.43	141.04	114.22	230.1502	163.12		
		142.76	115.01	230.3219	162.92	141.10	114.23
288.34	173.62	144.52	115.93	230.4936	163.35	142.16	114.44
290.61	174.26	146.25	116.78	230.6648	164.09	143.22	115.31
292.88	175.20	147.97	117.65	230.8358	164.04	144.30	115.88
295.15	176.11	149.67	118.49	231.0067	164.47	145.37	116.51
297.40	177.27	151.39	119.45	231.1774	164.57	146.43	116.94
		153.14	120.79	231.3478	165.27	147.50	117.60
227.79	160.23	154.89	122.58	231.5177	165.68	148.56	118.11
229.74	162.63	156.61	125.57	231.6874	166.03	149.62	118.47
231.67	166.53	158.30	126.29	231.8567	166.82	150.68	119.21
233.51	182.51	159.97	126.52	232.0256	166.84	151.74	119.32
235.28	185.22	161.68	127.17	232.1967	167.74	152.81	119.87
237.11	166.99	163.44	127.65	232.3695	168.36	153.86	120.51
239.01	164.43	165.19	128.58	232.5419	169.12	154.92	120.97
240.93	163.49	166.92	129.40	232.7162	170.22	155.96	121.53
		168.68	130.31	232.8924	171.30	156.99	122.05
273.87	169.43	170.45	131.07	233.0684	171.79	158.02	122.67
275.78	169.86	172.24	131.88	233.2437	173.39	159.02	124.90
277.68	170.49	173.29	132.40	233.4173	175.12	160.27	125.93
279.57	171.17	175.03	133.25	233.5893	177.65	162.00	126.84
281.47	171.84	176.77	134.09	233.7591	181.26	163.97	127.97
283.35	172.49	178.50	134.91	233.9234	187.72	165.92	128.86
285.23	173.04	180.22	135.72	234.0884	192.73	167.86	129.96
287.10	173.79	181.92	136.53	234.2453	207.30	169.79	130.89
		183.66	137.38	234.3985	223.19	171.70	131.56
79.34	74.87	185.41	138.19	234.5443	223.92	173.61	132.63
81.14	76.36	187.16	138.98	234.6973	206.45		
82.91	77.79	188.90	139.77	234.8599	190.82	11.90	3.89
84.64	79.18	190.63	140.55	235.0301	182.36	12.87	4.49
86.35	80.57	192.35	141.35	235.2049	177.45	13.81	5.63
88.06	81.87	194.06	142.22	235.3824	174.69	14.73	6.58
89.74	83.08	195.80	142.96	235.5619	172.69	15.69	7.55
91.39	84.21	197.55	143.84	235.7400	171.18	16.69	8.69
93.02	85.32	199.30	144.45	235.9159	170.42	17.66	9.70
94.62	86.38	201.04	145.44	236.0924	169.39	18.56	10.84
96.22	87.51	202.78	146.15	236.2697	168.54	19.68	11.93
97.82	88.23	204.50	146.92	236.4474	168.07	20.62	13.16
99.40	89.63	206.24	147.82	236.6228	167.43	21.47	14.12
100.96	90.68	208.01	148.48	236.7959	167.07	22.42	15.30
102.51	91.70	209.78	149.43	236.9693	167.06	23.55	16.68
104.17	92.73	211.53	150.35	237.1430	166.07	24.69	18.07
105.91	93.93	213.28	151.17	237.3171	166.19	25.74	19.31
107.63	94.99	215.01	152.09	237.4912	165.94	26.79	20.70
109.34	96.08	216.74	152.85	237.6757	165.20	27.85	21.99
111.02	97.09	218.49	153.83	237.8405	165.29	29.13	23.53

Table 2. (Continued)

T/K	C_p/J K^{-1} mol^{-1}	T/K	C_p/J K^{-1} mol^{-1}	T/K	C_p/J K^{-1} mol^{-1}	T/K	C_p/J K^{-1} mol^{-1}
30.60	25.35	61.12	59.00	230.5518	164.24	235.3367	175.76
31.95	27.08	62.98	60.81	230.7832	164.68	235.5574	173.17
33.22	28.64	64.78	62.50	231.0143	164.73	235.7800	171.59
34.43	29.99	66.78	64.28	231.2451	165.20	236.0037	170.59
35.57	31.50	68.96	66.14	231.4752	166.05	236.2286	169.39
36.79	32.94	71.07	67.94	231.7044	166.31	236.4546	168.46
37.96	34.30	73.13	69.69	231.9329	167.38	236.6809	168.40
39.07	35.59	75.13	71.35	232.1605	168.32	236.9077	167.31
40.25	36.96	77.07	72.98	232.3871	169.06	237.1352	166.79
41.38	38.26	78.98	74.55	232.6129	169.90	237.3635	166.60
42.71	39.83	80.84	76.13	232.8377	171.04	237.5913	165.63
44.24	41.42	82.66	77.62	233.0612	172.64	237.8201	165.64
45.70	43.08			233.2831	174.40	238.0490	165.37
47.10	44.58	74.78	71.09	233.5032	176.81	238.2780	165.34
48.44	46.14	77.46	73.54	233.7200	181.24	237.5073	164.68
49.86	47.62	80.25	75.62	233.9324	186.90	238.7369	164.82
51.48	49.32			234.1378	198.64	238.9665	164.53
53.19	51.07	229.4506	162.03	234.3319	217.24	239.1961	164.85
54.83	52.75	229.6621	162.76	234.5167	225.71	239.4257	164.57
56.42	54.32	229.8823	162.81	234.7053	206.22	239.6554	164.68
57.95	55.86	230.1015	163.41	234.9073	188.27	239.8857	163.01
59.44	57.35	230.3234	163.43	235.1193	180.63		

shown in the figure the anomaly occurred in the deuterate at somewhat higher temperature. An analysis of the observed effect will be given in the later section.

After measuring the heat capacity for the entire temperature region, the transition region was investigated in more detail. The temperature increment for one step of measurement was 0.007—0.23 K, compared to 1—3 K for the normal region. The observed heat capacity was 10 times as large as the normal heat capacity at the peak, but no latent heat was observed.

Experimental Results. The heat capacity curves for the entire temperature region are shown in Fig. 2. The numerical values are given in Tables I and II. The lambda peaks at 218 K and 235 K are nearly symmetrical in shape with respect to the respective peak temperature. In Fig. 3, the anomalies around 150 K are represented in an expanded scale. The open circles correspond to the quenched sample and the filled circles to the annealed. Similar curves for the deuterate are also shown in the figure. As was stated earlier, the *endo-* and *exo-*thermic effects made it difficult to determine unambiguously the heat capacity around the temperature. The values plotted in the figure are those calculated by employing the temperatures extrapolated to the mid-point of the heat-on period in case of the linear exothermic drifts. In the endothermic case, the temperatures observed at 30 minutes after the heat input interval were taken as the final temperatures. This convention of the data reduction is arbitrarily adopted.

General feature of the heat capacity curve and the enthalpy relaxation observed around this temperature are quite similar to those reported in a number of glass forming substances including the glassy crystals.[4] However, the heat capacity jump (2—3 J K^{-1}mol^{-1}) is considerably smaller than is usual in a glassy crystal (30—50 J K^{-1}mol^{-1}). Absence of any effects attributable to crystallization is also in clear contrast to the typical behavior of the glassy state formed by low molecular-weight substances. As will be discussed later in more detail, the newly found non-equilibrium state may be regarded as a new type of glassy states in which incompletely long-range-ordered proton (or deuteron) configuration is frozen in the immobile state.

Discussion

The Relaxational Anomaly. In order to derive physically informative parameters from the heat evolution rate observed around 150 K, the heat evolution rate given in Fig. 1 was integrated numerically with time, to give the enthalpy-temperature relation shown in Fig. 4, where the configurational enthalpy was separated from the rest by taking the low temperature

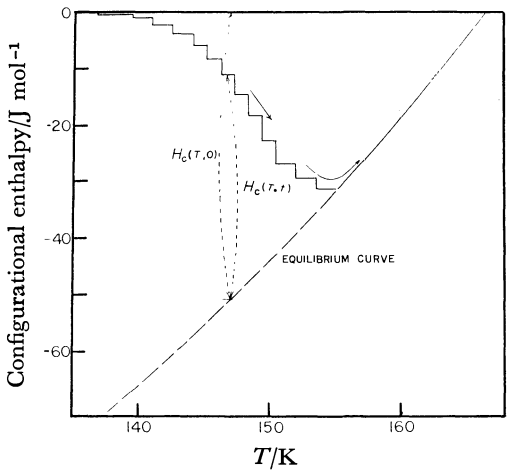

Fig. 4. Temperature-configurational enthalpy relation of $SnCl_2 \cdot 2H_2O$ crystal around its "glass transition" temperature. The arrows indicate the path followed by the crystal in this particular measurement. $H_c(T_0,)$ and $H_c(T,t)$ is the variables in the rate equation given in the text. The equilibrium curve below 155 K is calculated from the extrapolated configurational heat capacity.

heat capacity as the back-ground contribution. The reference temperature was chosen arbitrarily as T_0= 166.50 K for the hydrate. The equilibrium curve was calculated by integrating numerically the difference between the extrapolated high temperature heat capacity and the low temperature one. The zig-zag chain in Fig. 4 is the path whicn the configurational enthalpy followed as the crystal was warmed after rapid cooling. A similar zig-zag curve was obtained for the deuterate. Decrease of the enthalpy with increasing temperature indicates, of course, that the process is not a thermodynamically equilibrium one. Moreover, the enthalpy-temperature relation shown by the curve is not a unique representation of the property of the crystal, but depends on the thermal history of the crystal, particularily on the cooling rate and the time spent on the measurement. The nearly horizontal segments in the curve correspond to the heat-on period, while the nearly vertical segments to the drift period. From the observed drift rates, the relaxation time was evaluated as follows. If an exponential law is assumed for the approach to the equilibrium configuration, the rate law can be written as follows:

$$\frac{dH(T,t)}{dt} = -\frac{H(T,t)}{\tau} \quad (1)$$

where $H(T,t)$ is the configurational enthalpy referred to the equilibrium value at temperature T and time t and τ the relaxation time. The left-hand side of Eq. (1) is related to the temperature drift rate dT/dt by the equation:

$$\frac{dH(T,t)}{dt} = -C\frac{dT}{dt}, \quad (2)$$

where C is the heat capacity of the cell containing the sample crystal. Combining the Eqs. (1) and (2), one obtains:

$$\tau = \frac{H(T,t)}{C\frac{dT}{dt}} \quad (3)$$

By taking $H(T,t)$ from Fig. 4 and C and dT/dt from the experimental values, the relaxation time could be evaluated as a function of temperature. The heat capacity C is not defined around this temperature but the fraction of the ambiguous portion is small compared with the total heat capactiy. The calculated τ is affected little by the ambiguity in the estimation of the heat capacity value. The relaxation time thus evaluated is shown in Fig. 5 as an Arrhenius plot. It is remarkable that the drift rate *vs.* temperature curves in Fig. 1 could be reduced to the straight lines in Fig. 5. The lines were least-square-fitted to a linear equation from which the activation energies were estimated to be 49.88±0.33 and 49.78±0.23 kJ mol^{-1} for the hydrate and the deuterate, respectively. The frequency factors evaluated are $(1.92\pm0.6)\times10^{13}$ and $(0.5\pm0.2)\times10^{13}$ Hz. The derived activation energies are significantly smaller than that obtained by Kiriyama from the temperature dependence of the DC conductivity (17 kcal mol$^{-1}\cong$71 kJ mol^{-1}). This may simply mean that the mechanisms involved in the two dissipative processes are different from each other. The DC conduction is caused by transportation of the ionic species in the crystal. On the other hand, the enthalpy relaxation can proceed without involving ionic species, so that the two activation energies should not necessarily be equal to each other. The activation energy, 49.8 kJ mol^{-1}, is twice as large as the typical hydrogen bond energy of O–H···O system. Molecular interpretation of this value seems to be complicated as is explained in the following.

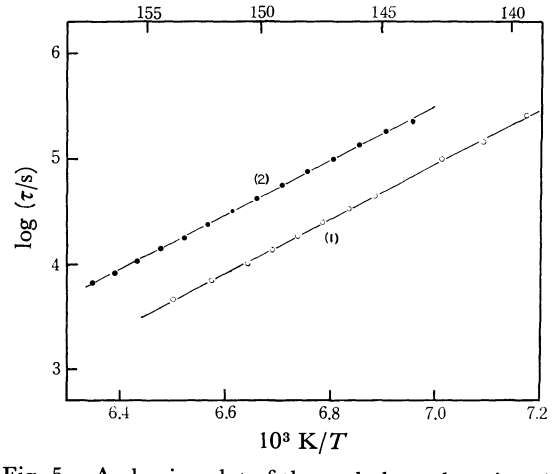

Fig. 5. Arrhenius plot of the enthalpy relaxation time τ of (1) $SnCl_2\cdot2H_2O$ and (2) $SnCl_2\cdot2D_2O$.

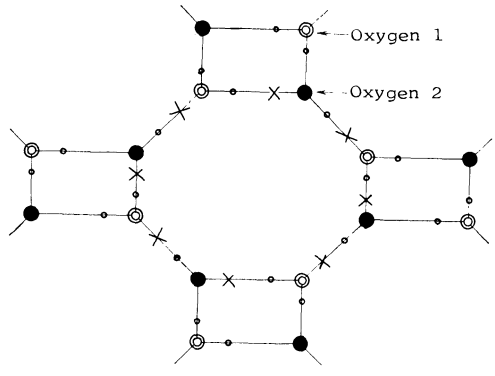

Fig. 6. Schematic diagram of the hydrogen bond network of $SnCl_2\cdot2H_2O$ and $SnCl_2\cdot2D_2O$. Oxygens 1 indicated by the double circles have two mobile hydrogen (or deuterium) atoms, while Oxygens 2 indicated by the closed circles have one mobile hydrogen and one immobile hydrogen. The latter not shown in the figure is hydrogen bonded to the chlorine atom. The small circles indicate the perfectly ordered hydrogen positions. The set of the eight crosses is the smallest unit by which the network deviates from the perfect order if the ice condition is imposed.

The hydrogen position determined by neutron diffraction[2] is described schematically in Fig. 6. This corresponds to the perfectly ordered situation, which could never be attained in the usual experimental time scale. But as is revealed in the configurational entropy diagram (Fig. 7) constructed by integrating the extrapolated anomalous heat capacity curve, the residual disorder retained in the real crystal is so small that the hydrogen position given by the diffrac-

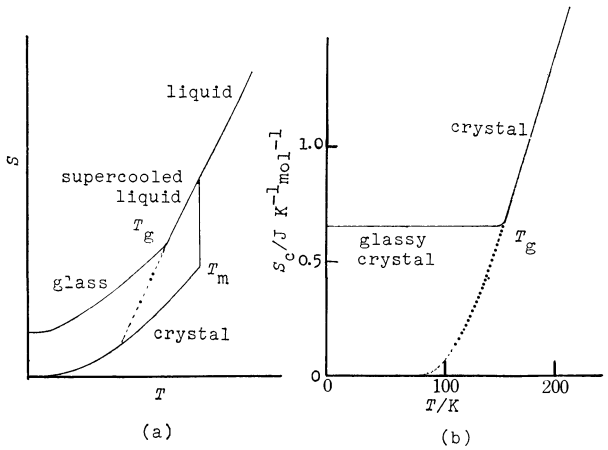

Fig. 7. Entropy of the glass-forming systems.
(a) Entropy of a typical substance forming a crystal, liquid and glass.
(b) Configurational entropy of $SnCl_2 \cdot 2H_2O$ crysatl retaining a small residual entropy (~ 0.65 J K^{-1} mol^{-1}). The broken portion of the curve is calculated from the extrapolated configurational heat capacity.

tion method and the weight assigned to each position are essentially those of the perfectly ordered crystal. Now, careful examination of this figure shows that if the ice condition is to be satisfied the smallest unit that can deviate from the perfect order is the eight-membered ring. The crosses in the figure indicate the position which the hydrogen atoms occupy in the locally disordered state. If this disordered state tries to approach the perfect order, the eight hydrogen atoms had to move in unison, so that the activation energy would be eight times as large as is needed to break one hydrogen bond, or 25 kJ mol$^{-1} \times 8 = 200$ kJ mol^{-1}. This is about four times as large as the experimental value. This seems to mean that some defect mechanism has to be invoked. Possibly, Bjerrum defects (D and L) take part in the reorientation process causing change of the order parameter.

It should be added here that the residual entropy indicated in Fig. 7 is an apparent one, since it is not based on equilibrium measurements but was simply calculated from the extrapolated heat capacity data. But it is believed to be close to the correct value because the structural data indicate that the crystal retains no other disorder than that of the hydrogen position.

In closing the discussion of the relaxational anomaly, relation of the present observation to the widely observed glass transitions is discussed. In addition to the widely-known polymeric glass-forming materials, a number of substances composed of relatively simple molecules were found to form glassy states.[4] The glassy states are classified into the glassy liquids, glassy crystals and glassy liquid crystals according to the type of disorder that is brought into the non-equilibrium state. In the first both the molecular position and molecular orientation are at random and do not possess long range periodicity. In the second the position is regular but the random orientation of the molecules is frozen in, and in the third, the positional disorder is retained, while the molecular orientation is in the ordered state. In stannous chloride dihydrate, the heavy atom positions are ordered and the hydrogen positions are nearly ordered, as is suggested by the entropy diagram (Fig. 7). It is, therefore, appropriate to classify it into a new type of glassy crystal in which the frozen-in degree of freedom has a long range order. Although there have not been examples of this kind reported so far, there seems to be nothing unnatural in the concept of the long-range-ordered glassy state. An important qualitative consequence is that a substance in this non-equilibrium state will not be induced to crystallize; only the long range order develops further without any discontinuous change of the crystal symmetry or other properties of the substance. This is one of the reasons why the relaxational effect could be investigated in detail to enable evaluation of the activation energy precisely.

Origin of the variety of the glassy states mentioned above can be traced back to the relation of the transition temperature and the temperature dependence of the molecular relaxation time. Here, the transition temperature means the temperature at which a long range order begins to develop in the (high-temperature) disordered degree of freedom of the substance. Temperature dependence of the order parameter is different from substance to substance. It may develop abruptly as in the first-order transitions (*e.g.* crystallization or transitions from plastic to non-plastic crystals). More gradual changes are typically observed in lambda anomalies in a number of order-disorder transitions. The molecular relaxation time, on the other hand, depends primarily on the barrier height which the molecules have to overcome if they are to reorient or to be redistributed in the substance. It increases generally rapidly with decreasing temperature, sometimes accompanied by a discontinuous change at transition temperatures. The ratio of the relaxation time to the experimental observation time is called the Deborah number[6] by Rheologists. By using the concept of Deborah number, the glassy state can conveniently be classified, together with other equilibrium and non-equilibrium states.

If the Deborah number of a substance is already large at high enough temperatures as compared to the hypothetical transition temperature, no relaxational effects will be observed thermally. This may be the case of CO, NO, or N_2O crystals. These crystals have residual entropies at 0 K[7] and are not known to exhibit thermal relaxation. In ice and heavy ice, for which the residual entropy has been discussed long, a small relaxational anomaly was recently discovered calorimetrically.[8,9] The temperatures at which the anomaly occurs are 95 and 105 K for the ordinary ice and heavy ice, respectively. It was proposed that the Deborah number happens to approach unity at the temperatures where the short range order of the proton configuration in the ice crystals begins to develop.

Next, if the Deborah number becomes unity at the temperature where the long range order is present but not complete, the relaxational effect will again be observed. This is what happens in the present case

of stannous chloride dihydrate. Finally if the ordering is already completed before the Deborah number approaches unity, no relaxational phenomena will be observed. This is the case for a number of substances for which the third law of thermodynamics is verified experimentally.

The variety of experimental observations could thus be classified according to the relative magnitude of the (in some cases, hypothetical) transition temperature and the temperature at which calorimetric Deborah number becomes unity.

The Phase Transition. The gradual anomaly at 218 K is due to the order-disorder transition of the hydrogen position. A similar anomaly occurs at 235 K in the deuterate. Structurally these are antiferroelectric to paraelectric transitions, as was shown by Kiriyama by use of magnetic resonance, X ray and neutron diffraction methods.[2] Although the heat capacity peak at 218 K is relatively narrow the outskirt region is extended over a wide temperature range. In fact, according to the interpretation of the relaxational anomaly discussed in the last section, the anomalous contribution is appreciable even at 150 K. The total entropy change is, therefore, difficult to estimate with certainty. In order to minimize arbitrariness, heat capacity of barium chloride dihydrate[10] was compared with the present heat capacity curve. This crystal has a similar layer structure and, moreover, its molecular weight is very close to that of stannous chloride dihydrate. Since barium chloride dihydrate does not show heat capacity anomaly below room temperature, it was expected to serve as a reference material. The heat capacity is a smooth function of temperature, and slightly smaller than that of stannous chloride dihydrate at 260 K. The normal heat capacity of stannous chloride dihydrate was assumed by joining the $BaCl_2 \cdot 2H_2O$ value at 260 K and the $SnCl_2 \cdot 2H_2O$ value at 150 K with a smooth curve. The anomalous part above 260 K was assumed to follow the T^{-2} law, as is expected for any interacting systems by a high temperature expansion. The low temperature contribution which could not be measured because of the long relaxation time was calculated from the extrapolated heat capacity curve. The total entropy change thus estimated is 4.6 J K^{-1} mol^{-1}, for the both crystals. Rigorous theoretical value given in the appendix is 3.13 J K^{-1} mol^{-1}. It is probable that the high temperature contribution to the estimated experimental value might be too large and also that other degrees of freedom than the hydrogen configuration would be contributing significantly to the observed transition entropy. Since the base line determination introduces a large uncertaintyin to the experimental value, detailed discussion of these values would be difficult at present.

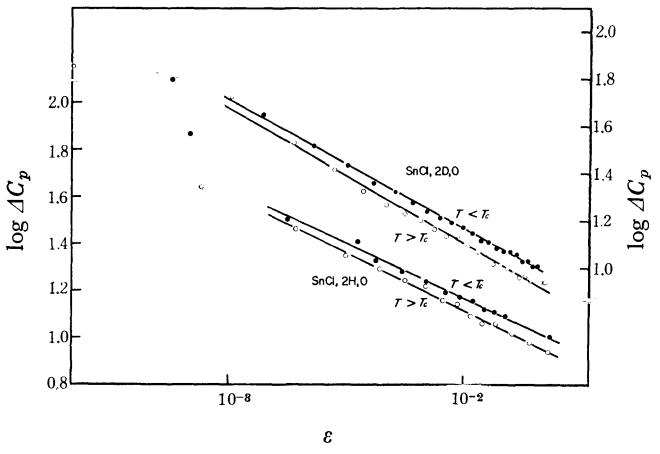

Fig. 8. Logarithmic plot of the anomalous part of the heat capacity of $SnCl_2 \cdot 2H_2O$ and $SnCl_2 \cdot 2D_2O$.

In the vicinity of the lambda transition the heat capacity diverges as is shown in Fig. 2. There has been discussion on the types of the singularity of the heat capacity curves at ferroelectric transitions. For the antiferroelectrics, there seems to be relatively fewer examples. It has been conjectured that the effect of domain formation and of finite crystal size would affect the critical behavior of the ferroelectric crystals. Such effects will be absent or at least relatively unimportant in antiferroelectrics. It is hoped that the present crystal would provide an ideal system to study the critical behaviors on. The anomalous heat capacity is plotted in Fig. 8 in a logarithmic scale, which, at least for $\varepsilon = |(T - T_c)/T_c| > 10^{-3}$, is linear, indicating that

$$\Delta C = A_{\pm} |(T - T_c)/T_c|^{-\alpha_{\pm}}$$

where $\alpha_{\pm}$ are given in Table 3. Attempts were made to fit the data to

$$\Delta C = A_{\pm} \ln |(T - T_c)/T_c|$$

But no good fits were obtained. Any possible change of the normal heat capacity does not alter the conclusion. It should be added that the calorimeter used was not entirely suitable for the high resolution measurement, so that the important region of $\varepsilon < 10^{-3}$ was missed. A high resolution calorimeter capable of the temperature resolution smaller than 10^{-5} K was constructed. Heat capacity measurement with the new apparatus was performed on a single crystal of $SnCl_2 \cdot 2H_2O$ in the close vicinity of the critical temperature. The result will be reported soon in a separate publication.

Table 3.

	$SnCl_2 \cdot 2H_2O$	$SnCl_2 \cdot 2D_2O$
T_c/K	217.94 ±0.05	234.47±0.05
α_+	0.534±0.021	0.574±0.010
α_-	0.478±0.010	0.544±0.010

The error bounds assigned to the α values refer to the scattering of the data about the linear plot. If the ambiguity in the estimation of the normal heat capacity is taken into account, they will be somewhat larger.

Finally, the thermal behavior of the present crystal is compared with that of other hydrate crystals. Copper formate tetrahydrate and its deuterate analogue have a similar layer structure, in which the water molecules form a hydrogen-bonded network.[11-14] The

† T. Matsuo, H. Suga, and S. Seki, unpublished work.

Kiriyama and Hideko Kiriyama for the fruitful discussion on the crystal structure and for making their unpublished structural data available to them. Contributions of the former students at the laboratory, Mr. Yasushi Miyoshi, now at Sanyo Electric Co. and Mr. Koji Kitamura, now at Kyoto University, were substantial at the early stage of the experiment, to whom the authors are grateful.

References

1) B. Kamenar and D. Grdenic, *J. Chem. Soc.*, **1961**, 3957.
2) H. Kiriyama, K. Kitahama, O. Nakamura, and R. Kiriyama, This Bulletin, **46**, 1389 (1973); *Acta Crystallogr.*, **A28**, S240 (1972).
3) H. Kiriyama and R. Kiriyama, *J. Phys. Soc. Japan*, **28**, Suppl., 114 (1970).
4) K. Adachi, H. Suga, and S. Seki, This Bulletin, **41**, 1073 (1968); **43**, 1916 (1970); **44**, 78 (1971).
5) T. Matsuo, H. Suga, and S. Seki, *J. Phys. Soc. Japan*, **30**, 785 (1971).
6) M. Reiner, *Physics Today*, **17**, (1), 62 (1964).
7) J. Wilks, The Third Law of thermodynamics," Oxford University Press, London and New York (1967).
8) O. Haida, T. Matsuo, H. Suga, and S. Seki, *Proc. Japan Acad.*, **48**, 489 (1972).
9) O. Haida, H. Suga, and S. Seki, *Proc. Japan Acad.*, **49**, 191 (1973).
10) O. L. I. Brown, W. V. Smith, and W. M. Latimer, *J. Amer. Chem. Soc.*, **58**, 1758 (1936).
11) R. Kiriyama, H. Ibamoto, and K. Matsuo, *Acta Crystallogr.*, **7**, 482 (1954).
12) K. Okada, M. I. Kay, D. T. Cromer, and I. Almodovar, *J. Chem. Phys.*, **44**, 1648 (1966).
13) K. C. Turberfield, *Solid State Commun.*, **5**, 887 (1967).
14) M. I. Kay and R. Kleinberg, *Ferroelectrics*, **4**, 147 (1972).
15) T. Matsuo, M. Oguni, H. Suga, and S. Seki, *Proc. Japan Acad.*, **49**, 196 (1973).
16) R. Kiriyama, H. Kiriyama, T. Wada, N. Niizeki, and H. Hirabayashi, *J. Phys. Soc. Japan*, **19**, 540 (1964).
17) J. C. Taylor, M. H. Mueller, and R. H. Hitterman, *Acta Crystallogr.*, **A26**, 559 (1970).
18) e.g., R. J. Birgeneau, H. J. Guggenheim, and G. Shirane, *Phys. Rev. Lett.*, **22**, 720 (1969); R. J. Birgeneau, J. Skalyo, and G. Shirane, *Phys. Rev.*, **B3**, 1736 (1971).
19) P. W. Kasteleijn, *J. Math. Phys.*, **4**, 287 (1963).
20) A review of this method is given by E. W. Montroll, in "Applied Combinatorial Mathematics," ed. by E. F. Beckenbach, Wiley, New York (1964), Chap. 4.
21) L. Onsager, *Phys. Rev.*, **65**, 117 (1944). See especially equation (7.5) in the Appendix.

Molecular Structure of Formamide as Studied by Gas Electron Diffraction

Mitsuo KITANO and Kozo KUCHITSU

Department of Chemistry, Faculty of Science, The University of Tokyo, Hongo, Bunkyo-ku, Tokyo 113

(Received September 10, 1973)

The structure of formamide $HCONH_2$ has been determined by gas electron diffraction. The rotational constants determined in previous microwave studies have also been used for determining the hydrogen parameters. From a joint least-squares analysis of the diffraction intensity and the rotational constants, where the out-of-plane vibrations are treated as finite-amplitude motions in the corrections for vibrational effects, the following r_g bond distances and r_z angles have been derived: C–N = 1.368±0.003 Å, C=O = 1.212±0.003 Å, ∠N–C=O = 125.0±0.4°, N–H(average) = 1.027±0.006 Å, C–H = 1.125±0.012 Å, ∠C–N–H(*cis* to C=O) = 118.7±1.0°, and ∠C–N–H (*trans* to C=O) = 119.7±1.0°, where the uncertainties represent estimated limits of experimental error. The C–N bond is about 0.07 Å longer, whereas the C=O bond is about 0.04 Å shorter, in the free molecule than in the crystal studied by X-ray diffraction. The C–N and C=O bonds are about 0.01 Å or more shorter, and the N–C=O angle is about 3° larger than the corresponding parameters in acetamide and *N*-methylacetamide.

The primary purpose of the present study is to determine the skeletal structure of formamide as accurately as possible, since neither spectroscopic nor diffraction studies have yet afforded a structure accurate enough to enable a critical comparison with analogous amide structures determined in the vapor and crystal phases. Particularly, a comparison of the skeletal structure of formamide with those of acetamide[1] and *N*-methylacetamide[2] determined in our preceding studies is intended in order to appraise the effect of methyl substitutions on simple amide structures. The r_g distances and r_z angles[3,4] should provide more consistent and suitable measures for this comparison than the r_s parameters, since the skeletal r_s parameters in formamide determined by microwave studies[5–7] suffer from appreciable uncertainties in the carbon coordinates, and no r_s structures are yet available for other amides.

On the other hand, the rotational constants of formamide determined by microwave spectroscopy[5–8] for the normal and deuterated species supply valuable information on the positions of the hydrogen atoms, particularly on the planarity of the molecule and the potential function in regard to the NH_2 wagging motion,[7] which is hard to determine precisely by the diffraction experiment.[4] Therefore, the diffraction intensity measured in the present study has been merged with the rotational constants in a least-squares analysis. Because of the relatively low frequencies of the out-of-plane vibrations, a finite-amplitude treatment[9] instead of the conventional treatment based on infinitesimal vibrational amplitudes[3] has been made for the vibrational corrections in the comparison of the diffraction and spectroscopic observables.

Experimental

A commercial guaranteed reagent was heated to about 160 °C by a high-temperature nozzle,[10] and diffraction photographs were taken with 40 kV electrons at camera distances of 112.30 mm (short) and 246.86 mm (long).[11] The scale factors of the diffraction patterns were calibrated to within 0.1% with reference to the r_a (C=O) distance of carbon dioxide (1.1646 Å).[11] The densities of four plates taken at each

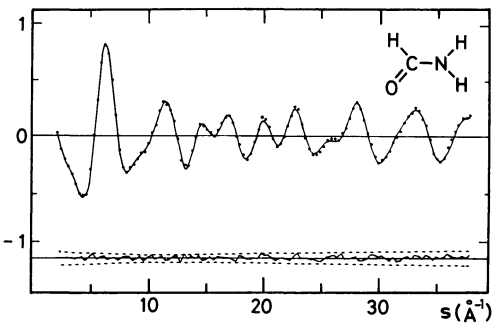

Fig. 1. Experimental and theoretical molecular intensities for formamide. Typical observed $sM(s)$ values are shown in dots, and the best-fit theoretical is shown in the solid curve. The indices of resolution for long and short camera-distances are 0.752 and 0.912, respectively. The lower solid and broken curves represent the residuals and the error limits in the $sM(s)$ to a fractional error of 1×10^{-3} of the original photocurrent,[12] respectively.

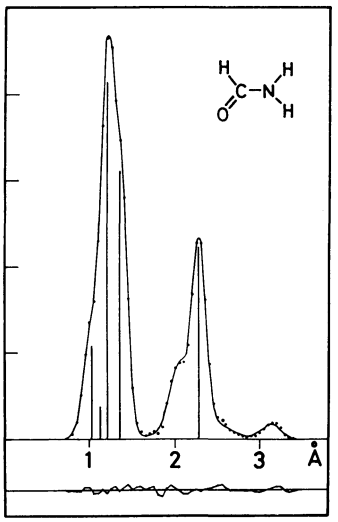

Fig. 2. Experimental (dots) and theoretical radial distribution curves for formamide. The lower curve represents residuals. Vertical bars correspond to principal internuclear distances. A damping factor, $\exp(-0.0016\ s^2)$, is used.

camera distance were measured by a digital microphotometer.[12] Other experimental procedures have been described elsewhere.[11,13]

Molecular intensities were obtained in the ranges of s= 2.2—15.7 Å^{-1} and 9.4—37.7 Å^{-1} from the long and short camera-distance data, respectively.[14] They agreed with each other in the overlapping region within experimental error of about 0.03 in the absolute $sM(s)$ scale, and hence were joined at s=12.7 Å^{-1} (Fig. 1). A hand-drawn background was adjusted to get the radial distribution curve shown in Fig. 2. Most calculations were carried out on a HITAC 5020E and 8700/8800 in the Computer Center of the University of Tokyo.

Analysis of Electron Diffraction Data

The skeletal parameters, r_g(C–N), r_g(C=O), and ϕ_α(N–C=O), and the average r_g(N–H) distance were determined by a least-squares analysis of the molecular intensity with a uniform empirical weight function.[15] The molecule was assumed to be planar in equilibrium,[7] and the r_α(C–H) distance and all the ϕ_α angles involving the hydrogen atoms were fixed to the corresponding r_s-values.[7] The mean amplitudes and the vibrational corrections (r_a-r_α)[3,16] were calculated by the use of an approximate set of the modified Urey-Bradley force constants for the in-plane vibrations shown in Table 1; they were taken from those reported by Suzuki[17]

Table 1. Approximate in-plane force constants for formamide[a] (in md/Å)

	I	II		I	II
K(N–H)	6.58	5.80	H(H–C=O)	0.20	0.20
K(C–H)	3.50	3.74	H(N–C=O)	0.14	0.34
K(C=O)	9.00	8.80	F(H···H)	0	0
K(C–N)	6.15	6.15	F(H···C)	0.41	0.46
H(H–N–H)	0.45	0.40	F(H···N)	0.70	0.70
H(H–N–C)	0.18	0.32	F(H···O)	0.92	0.92
H(H–C–N)	0.24	0.18	F(O···N)	1.50	1.50

a) See Ref. 17 for definitions of the modified Urey-Bradley force constants, K, H, and F.
I: Present estimates, II: Estimated by Suzuki, Ref. 17.

and adjusted slightly to reproduce the vibrational frequencies observed recently by King[18] in the gas phase. For the NH_2 rocking frequency, however, that assigned tentatively by King (602 cm^{-1}) seems to be unlikely, since the calculated value (about 958 cm^{-1}) deviated significantly from it and it was impossible to reporduce the former value by a reasonable adjustment of the force constants. A further spectroscopic work, particularly on the deuteride vapors, is necessary to make a decisive assignment.

In calculations of the vibrational corrections, the contributions from the out-of-plane vibrations were excluded, since their amplitudes cannot be treated as infinitesimal[9] (see next section). All but the skeletal mean amplitudes were fixed to the calculated values listed in Table 2. The asymmetry parameters κ for the bonded C–H and N–H distances were assumed to be 1.8×10^{-5} Å^3, and the rest of the κ parameters were ignored.[19]

The structural parameters and the mean amplitudes

Table 2. Mean amplitudes and vibrational corrections for formamide[a] (in 10^{-4} Å)

	l	r_a-r_α		l	r_a-r_α
C=O	394	4	N···H_a	981	−11
C–N	427	2	O···H_a	923	9
C–H_a	800	1	O···H_c	1402	40
N–H	715	30	O···H_t	923	83
N···O	563	−17	H_a···H_c	1196	55
C···H_c	1001	−18	H_a···H_t	1634	64
C···H_t	982	−21	H_c···H_t	1151	20

a) Calculated at 160 °C. The aldehyde hydrogen atom is denoted as H_a. The amide hydrogen atoms which are *trans* and *cis* to the C=O bond are denoted as H_t and H_c, respectively.

Table 3. Structural parameters for formamide[a]

	ED[b]		ED+MW[c]		MW[d]
	r_g	r_α	r_g	r_z	r_s
C=O	1.211(4)	1.209	1.212(3)	1.210	1.219(12)
C–N	1.367(4)	1.365	1.368(3)	1.366_5	1.352(12)
N–H_{av}	1.021(9)	1.013	1.027(6)	1.018_5	1.002(3)
C–H_a	1.12 fix	1.115	1.125(12)	1.119	1.098(10)
∠N–C=O		124.9(5)		125.0(4)	124.7(3)
∠C–N–H_c		118.5 fix		118.7(10)	118.5(5)
∠C–N–H_t		120.0 fix		119.7(10)	120.0(5)
∠H_a–C–N		112.7 fix		112.7 fix	112.7(20)
l(C=O)[e]	0.043(3)		0.043(3)		
l(C–N)	0.050(4)		0.050(4)		
k_l[f]	0.75 (2)		0.75 (2)		
k_s	0.91 (5)		0.91 (5)		

a) Distances in Å and angles in degrees. The numbers in parentheses represent uncertainties attached to the last significant figures. For definitions of r_g, r_α, r_z, and r_s, see Ref. 3.
b) Structures based on the analysis of electron-diffraction intensity with estimated limits of error.
c) Structures based on the analysis of electron-diffraction intensity and rotational constants, with estimated limits of error. The r_z structure derived in this procedure is sometimes denoted as r_{av}.[22]
d) The r_s structure determined by Hirota *et al.* by microwave spectroscopy. Ref. 7.
e) Mean amplitudes with estimated limits of error.
f) Indices of resolution for diffraction intensities taken with the long (l) and short (s) camera-distances.

derived from the least-squares analysis are listed in Table 3. The quoted limits of error were estimated as 2.5 times the random errors plus systematic errors.[20,21]

Joint Analysis of Diffraction Intensity and Rotational Constants

A further analysis was made by the use of the observed rotational constants for the normal and four deuterated species for the ground vibrational state[6] for testing the accuracy of the diffraction parameters and for refinement of the hydrogen parameters.[22] The analysis was

based on the rotational constants A_z, B_z, and C_z (hereafter represented, as a set, by B_z) corresponding to a hypothetical set of the planar nuclear positions averaged over the in-plane vibrations.

The B_z constants were estimated in the following steps of eliminating the effect of in-plane and out-of-plane vibrations.

From the spectroscopic side, the B_z constants were obtained from the corresponding B_0 constants by making the following corrections:[23]

$$B_z = B_0 + \Delta B_{\text{electronic}} + \Delta B_{\text{centrifugal}} + \Delta B_{\text{Coriolis}} + \sum_s \Delta B_s + \sum_t \Delta B_t \quad (1)$$

where the electronic corrections were estimated by Oka's formulation[24] from the molecular g-values observed by Flygare and Benson,[25] and the centrifugal corrections[24] were ignored. The Coriolis corrections and the vibrational corrections for the in-plane modes were calculated in a conventional way by the use of the force constants given in Table 1 as[3,23]

$$\Delta B_{\text{Coriolis}} = -4B_e^2 \sum_s \omega_s \sum_{s'} (\zeta_{ss'}^{(\alpha)})^2/(\omega_s^2 - \omega_{s'}^2) \quad (2)$$

and

$$\Delta B_s = -(B_e^2/\omega_s)[3A_{ss}^{(\alpha\alpha)} - 4\sum_{s'}(\zeta_{ss'}^{(\alpha)})^2] \quad (3)$$

where Nielsen's notations[26] are followed. Individual in-plane and out-of-plane modes are represented by s and t, respectively, and s' includes all s and t. The vibrational corrections for the out-of-plane motions were approximated on the assumption that the NH_2 wagging, torsion and C–H out-of-plane bending motions were independent of one another,

$$\sum_t \Delta B_t \cong \Delta B_{\text{wag}} + \Delta B_{\text{torsion}} + \Delta B_{\text{bend}} \quad (4)$$

The correction for the wagging motion followed the calculation by Hirota *et al.*,[7]

$$\Delta B_{\text{wag}} = -B_1\langle\tau^2\rangle_0 - B_2\langle\tau^4\rangle_0 \quad (5)$$

where the coefficients B_1, B_2 and the average values of the NH_2 wagging displacement τ for the ground state are given in their paper. The corrections for the torsion and the C–H bending motion were estimated in a similar way. A two-fold harmonic potential for the torsion with V_2=20 kcal/mol[27] and the C–H bending frequency[18] of 1050 cm^{-1} were assumed, and only quadratic averages of the displacements were taken into account. The correction terms are listed in Table 4. The inertia defects calculated from the present B_z do not vanish exactly, as mentioned by Hirota *et al.*,[7] but they fall within the limits of uncertainty in the correction terms estimated above (-0.04 ± 0.10 amu. Å^2 for all the isotopic species).

From the diffraction side, the r_g parameters were related to the r_a parameters by making conventional shrinkage corrections[3] for the in-plane contributions, and for the nonbonded distances which vary with the out-of-plane vibrations, classical averages over the motions based on a rigid frame, analogous to Karle's shrinkage correction for internal rotation,[28] were made[9] by the use of the mean displacements used in the spectroscopic corrections. Then the r_a parameters were assumed to be equal to the corresponding r_z parameters, since the frequencies of the in-plane vibrations are so high that thermal effects are unimportant.[3,29]

Table 4. Corrections for rotational constants,[a] B_z-B_0 (in 10^{-5} cm^{-1})

		ΔB_1	ΔB_2	ΔB_3	ΔB_4	ΔB_5	ΔB_6
$HCONH_2$	A	−38	2549	994	−1099	−170	199
	B	−1	81	41	122	−15	−9
	C	0	47	−29	137	15	10
$DCONH_2$	A	−28	1542	606	−627	−95	131
	B	−1	86	43	122	−17	−8
	C	0	47	−32	126	14	8
c-HCONHD[b]	A	−32	1981	659	−699	−33	157
	B	1	83	43	150	−20	−9
	C	0	46	−30	164	10	9
t-HCONHD[c]	A	−37	2763	834	−1797	−295	182
	B	1	78	31	148	−8	−7
	C	0	44	−29	156	15	8
$HCOND_2$	A	−31	2110	548	−1103	−144	143
	B	1	79	33	164	−14	−8
	C	0	43	−30	172	13	8

a) ΔB_1: electronic, ΔB_2: Coriolis, Eq. (2), ΔB_3: in-plane vibrational, Eq. (3), ΔB_4: NH_2 wagging, Eq. (5), ΔB_5: torsion, ΔB_6: C–H out-of-plane bending. See text.
b) The deuterium atom is *cis* to the C=O bond.
c) The deuterium atom is *trans* to the C=O bond.

The relative statistical weights assigned to the rotational constants were such that their standard errors were approximately equal to their estimated uncertainties.[20] They were taken by a trial and error procedure as 1×10^2, 2×10^5, and 1×10^6 for A_z, B_z, and C_z, respectively, for all the isotopic species, whereas a unit weight was assigned to each molecular intensity of electron diffraction from s=6.3 to 26.7 Å^{-1} taken at unit q ($10\ s/\pi$) intervals.

All the independent structural parameters were varied except that the r_z(N–H) distances were set equal to each other and that the ϕ_z(H–C–N) angle was fixed to 112.7°, the r_s angle reported by Hirota *et al.*[7] As for the mean amplitudes, all but the bonded C–N and C=O amplitudes were fixed to the calculated values given in Table 2. The isotopic differences for the r_z(N–H)$-r_z$(N–D) and r_z(C–H)$-r_z$(C–D) distances were initially estimated by use of an approximate formula,[22,29]

$$r_z(\text{H}) - r_z(\text{D}) \cong \frac{3}{2}a_3[\langle\Delta z^2\rangle_0(\text{H}) - \langle\Delta z^2\rangle_0(\text{D})] - [\langle\Delta x^2\rangle_0(\text{H}) - \langle\Delta x^2\rangle_0(\text{D})]/2r_z \quad (6)$$

where the anharmonicity parameters a_3 for N–H and C–H were assumed to be[30] 2.19 Å^{-1} and 1.98 Å^{-1}, respectively, and the in-plane relative displacements of the nuclei parallel and perpendicular to the equilibrium bond axes, Δz and Δx, respectively, were taken into account. In line with the finite-amplitude treatment mentioned above, contributions from the out-of-plane displacements, Δy, were not included in the calculation. The isotopic differences were estimated to be 0.003_2 and 0.002_0 Å, respectively, for N–H and C–H. (A conventional treatment including the out-of-plane contributions resulted in -0.004_8 and 0.000_6 Å, respec-

Table 7. Comparison of skeletal bond distances in the gas and crystal phases (in Å)

	C=O		C–N		Ref.	
	gas (r_g)	cryst.[a]	gas (r_g)	cryst.	gas	cryst.
$HCONH_2$	1.212(3)	1.255(13)	1.368(3)	1.300(13)	b	31
CH_3CONH_2	1.220(3)	1.260(11)	1.380(4)	1.334(17)	1	32
$CH_3CONHCH_3$	1.225(3)	1.236(12)	1.386(4)	1.290(13)	2	33
	C=O		C–O		Ref.	
	gas(r_a)	cryst.	gas(r_a)	cryst.	gas	cryst.
HCOOH	1.217(3)	1.23 (3)	1.361(3)	1.26 (3)	34	35
CH_3COOH	1.214(3)	1.220(6)	1.364(3)	1.318(7)	36	37

a) Bond lengths in molecules in the crystal phase studied by X-ray diffraction.
b) Present study.

Table 8. Comparison of carbon valence angles[a]

	∠N-C=O	Ref.		∠C-C=O	Ref.		∠C-C=C	Ref.
$HCONH_2$	125.0(4)	b	$HCOCH_3$	124.2(5)	38, 39	$CH_3CH=CH_2$	124.3(4)	9
CH_3CONH_2	122.0(5)	1	CH_3COCH_3	122.0(2)	40	$(CH_3)_2C=CH_2$	122.2(2)	42
$CH_3CONHCH_3$	121.8(4)	2	$CH_3COCH_2CH_3$	121.3(7)	41			

a) The r_z structures. Numbers in parentheses represent estimated limits of experimental error in 0.1 degrees.
b) Present study.

in Table 7 and also in Table 8, where observed carbon valence angles formed by a single bond and a double bond are listed. The methyl substitutions in formamide forming acetamide and *N*-methylacetamide increase the C–N and C=O bond lengths simultaneously by about 0.01 Å or more and decrease the N–C=O angle by about 3°. Analogous trends are observed in the acetaldehyde[38,39]–acetone[40]–methyl ethyl ketone[41] system and in the propene[9]–isobutene[42] system. These systematic trends conform to those observed in many more methyl-substituted compounds collected by Jacob *et al.*,[43] who accounted for the trends consistently in terms of the influence of interactions among nonbonded atoms.

The $r_g(N–H_{av})$ and $r_g(C–H_a)$ distances listed in Table 3 (ED+MW) are essentially equal to, respectively, the r_g(N–H) distance in NH_3 (1.030±0.002 Å)[44] and the r_g(C–H) distances in a number of aldehydes (1.13 Å).[4]

The authors are indebted to Professor Eizi Hirota of Kyushu University for his supply of numerical data prior to publication and for his helpful discussions.

References

1) M. Kitano and K. Kuchitsu, This Bulletin, **46**, 3048 (1973).
2) M. Kitano, T. Fukuyama, and K. Kuchitsu, *ibid.*, **46**, 384 (1973).
3) K. Kuchitsu and S. J. Cyvin, "Molecular Structures and Vibrations," ed. by S. J. Cyvin, Chapter 12, Elsevier, Amsterdam (1972).
4) K. Kuchitsu, MTP International Review of Science, Physical Chemistry Series One, Vol. 2, ed. by G. Allen, Chapter 6, Medical and Technical Publishing Co. Ltd., Oxford (1972).
5) R. J. Kurland and E. B. Wilson, Jr., *J. Chem. Phys.*, **27**, 585 (1957).
6) C. C. Costain and J. M. Dowling, *ibid.*, **32**, 158 (1960).
7) E. Hirota, R. Sugisaki, C. J. Nielsen, and G. O. Sørensen, *J. Mol. Spectrosc.*, in press.
8) W. H. Kirchhoff and D. R. Johnson, *ibid.*, **45**, 159 (1973).
9) I. Tokue, T. Fukuyama, and K. Kuchitsu, *J. Mol. Structure*, **17**, 207 (1973).
10) A. Yokozeki and K. Kuchitsu, *ibid.*, **44**, 72 (1971).
11) Y. Murata, K. Kuchitsu, and M. Kimura, *Jap. J. Appl. Phys.*, **7**, 591 (1970).
12) Y. Morino, K. Kuchitsu, and T. Fukuyama, This Bulletin, **40**, 423 (1967).
13) M. Tanimoto, K. Kuchitsu, and Y. Morino, *ibid.*, **43**, 2776 (1970).
14) Numerical experimental data of the leveled total intensity and the background have been deposited with the Chemical Society of Japan. (Document No. 7401).
15) Y. Morino, K. Kuchitsu, and Y. Murata, *Acta Crystallogr.*, **18**, 549 (1965).
16) K. Kuchitsu and S. Konaka, *J. Chem. Phys.*, **45**, 4342 (1966).
17) I. Suzuki, This Bulletin, **33**, 1359 (1960).
18) S. T. King, *J. Phys. Chem.*, **75**, 405 (1971). The authors are grateful to Dr. S. T. King and Dr. I. Suzuki for their helpful comments on the force field of formamide.
19) K. Kuchitsu, This Bulletin, **40**, 505 (1967).
20) K. Kuchitsu, T. Fukuyama, and Y. Morino, *J. Mol. Structure*, **1**, 463 (1968).
21) K. Kuchitsu, "Molecular Structures and Vibrations," ed. by S. J. Cyvin, Chapter 10, Elsevier, Amsterdam (1972).
22) K. Kuchitsu, T. Fukuyama, and Y. Morino, *J. Mol. Structure*, **4**, 41 (1969).
23) T. Oka and Y. Morino, *J. Mol. Specrtosc.*, **6**, 472 (1961).
24) T. Oka, *J. Phys. Soc. Jap.*, **15**, 2274 (1960).
25) W. H. Flygare and R. C. Benson, *Mol. Phys.*, **20**, 1225 (1971), Table 4.
26) H. H. Nielsen, *Rev. Mod. Phys.*, **23**, 90 (1951).
27) A. Warshel, M. Levitt, and S. Lifson, *J. Mol. Spectrosc.*, **33**, 84 (1970).
28) J. Karle, *J. Chem. Phys.*, **22**, 1246 (1954).
29) K. Kuchitsu, *ibid*, **49**, 4456 (1968).

30) K. Kuchitsu and Y. Morino, This Bulletin, **38**, 805 (1965).
31) J. Ladell and B. Post, *Acta Crystallogr.*, **7**, 559 (1954).
32) W. C. Hamilton, *ibid.*, **18** 866 (1965).
33) J. L. Katz and B. Post, *ibid.*, **13**, 624 (1960).
34) A. Almenningen, O. Bastiansen, and T. Motzfeldt, *Acta Chem. Scand.*, **23**, 2848 (1969).
35) F. Holtzberg, B. Post, and I. Fankuchen, *Acta Crystallogr.*, **6**, 127 (1953).
36) J. L. Derissen, *J. Mol. Structure*, **7**, 67 (1971).
37) I. Nahringbauer, *Acta Chem. Scand.*, **24**, 453 (1970).
38) C. Kato, S. Konaka, T. Iijima, and M. Kimura, This Bulletin, **42**, 2148 (1969).
39) T. Iijima and S. Tsuchiya, *J. Mol. Spectrosc.*, **44**, 88 (1972).
40) T. Iijima, *ibid.*, **45**, 3526 (1972).
41) M. Abe, K. Kuchitsu, and T. Shimanouchi, *J. Mol. Structure*, **4**, 245 (1969).
42) I. Tokue, T. Fukuyama, and K. Kuchitsu, *ibid.*, in press.
43) E. J. Jacob, H. B. Thompson, and L. S. Bartell, *J. Chem. Phys.*, **47**, 3736 (1967).
44) K. Kuchitsu, J. P. Guillory, and L. S. Bartell, *ibid.*, **49**, 2488 (1968).

Rotational Isomerism in Methyl-*d*-amine

Keietsu TAMAGAKE and Masamichi TSUBOI

Faculty of Pharmaceutical Sciences, University of Tokyo, Bunkyo-ku, Tokyo 113

(Received August 1, 1973)

Infrared absorption spectra of methyl-*d*-amine and methyl-*d*-amine-d_2 have been observed in their gaseous states. For each of seven vibrations of the former and seven vibrations of the latter, two Q-branch peaks are observed assignable to *trans* and *gauche* forms of the molecule. In the microwave absorption spectrum of methyl-*d*-amine 60 lines assignable to the *trans* form (whose rotational constants are $A=86085$, $B=20546$, and $C=20475$ MHz) and 140 lines assignable to the *gauche* form ($A=86512$, $B=21243$, and $C=19911$ MHz) are found. Every *trans* line shows an inversion doubling which is considered to reach an observable amount only through a *trans-gauche* mixing of the vibration-rotation wavefunctions. This *trans-gauche* mixing should in turn depend upon the energy difference ΔE_{TG} between the ground vibration-rotation levels of the *trans* and *gauche* forms. On the basis of the observed amount of the inversion splitting, ΔE_{TG} has been determined to be 6.7 ± 0.4 cm^{-1}. The ΔE_{TG} value has then been refined by observing an accidental degeneracy of the *trans* and *gauche* energy levels, so that $\Delta E_{TG}=7.06\pm0.03$ cm^{-1}.

For the normal methylamine (CH_3NH_2) molecule, there are three equivalent equilibrium positions of the methyl group in the internal rotation with respect to the amino group. On substituting one of the methyl hydrogens by deuterium (*i.e.*, on going from CH_3NH_2 to CH_2DNH_2), the threefold symmetry of the torsion Hamiltonian is removed. The three potential minima are not equivalent any more; one of them corresponds to the *trans* and the other two *gauche* conformations (see Fig. 1). It should be remembered, however, that the intramolecular potential itself is not affected by an isotopic substitution. Thus, the shape of the potential function is exactly equal in the vicinity of the *trans* conformation to that in the vicinity of the *gauche* conformation even in the methyl-*d*-amine molecule. In addition, the reduced moment of inertia of the torsional oscillation would not greatly different in the *trans* form from that in the *gauche* form. Therefore, at first thought, one might guess that the energy difference between the torsional levels of *trans* and *gauche* forms would be very small and a pronounced mixing between the wavefunctions of these forms may take place so that no appreciable rotational isomerism can be observed.

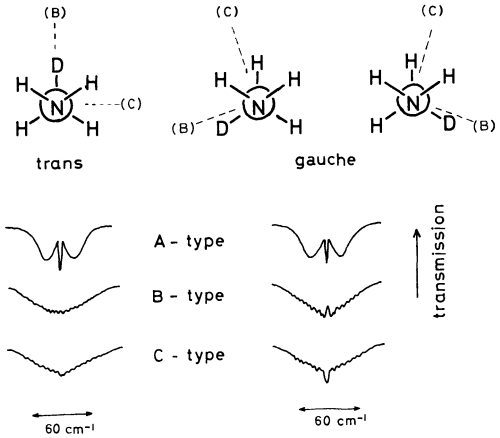

Fig. 1. Three equilibrium positions of the CH_2D group in the internal rotation with respect to the NH_2 group of the CH_2DNH_2 molecule. Of the three principal axes of inertia, A-axis is nearly along the C–N bond, while B- and C-axes are directed as shown in this figure. The band envelope of each of the A-, B-, and C-type bands expected with the resolving power 3 cm^{-1} of CH_2DNH_2 is also given on the basis of a calculation made by Ueda and Shimanouchi (*J. Mol. Spectroscopy*, **28**, 350 (1968)).

Actually, however, our analysis[1] of the far-infrared absorption spectrum of CH_2DNH_2 indicated that, in the ground torsional state ($n=0$) and in the first excited state ($n=1$), there are well-defined *trans* and *gauche* rotational isomers. Such a lack of mixing was attributed mostly to the situation that the mode of coupling of the torsional oscillation with other vibrations is different in the *trans* and *gauche* forms. Only in the higher excited states ($n\geqq2$), a pronounced mixing was found to take place between the *trans* and *gauche* torsional wavefunctions. In the present paper, we report our examination on how this isomerism appears in the infrared and microwave absorption spectra. From an analysis of the microwave spectrum, the energy difference of the rotational isomers in the vibrational ground state has been determined. This will also be reported below.

Infrared Absorption Spectra

Infrared absorption spectra of methyl-*d*-amine (CH_2DNH_2) and methyl-*d*-amine-d_2 (CH_2DND_2) have been observed in their gaseous states.

The sample of CH_2DNH_2 gas used is the same as what was used in our previous work.[1] The sample was placed in a gas cell, with two KBr windows, a pathlength of 10 cm, and potassium hydroxide as a desiccant. CH_2DND_2 gas was obtained by adding D_2O solution of methyl-*d*-ammonium-d_3-chloride (CH_2DND_3Cl) on solid sodium deuteroxide (NaOD). Here, CH_2DND_3Cl was prepared by dissolving methyl-*d*-ammonium chloride into D_2O, by removing the solvent in vacuum, and by repeating this procedure several times. Before introducing the CH_2DND_2 sample in a gas cell (10 cm^{-1}), D_2O gas was filled in the cell several times so that the absorbed gas on the cell wall was completely deuterated. As a desiccant, metallic sodium was placed in the cell.

Infrared absorption measurements were made in the

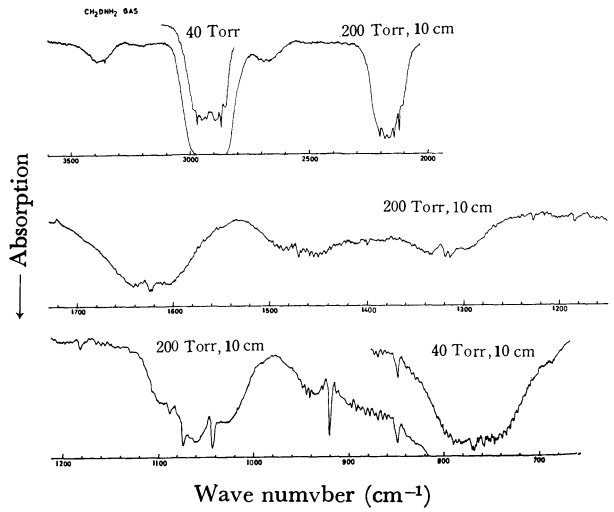

Fig. 2. Infrared absorption spectrum of CH_2DNH_2 (gas).

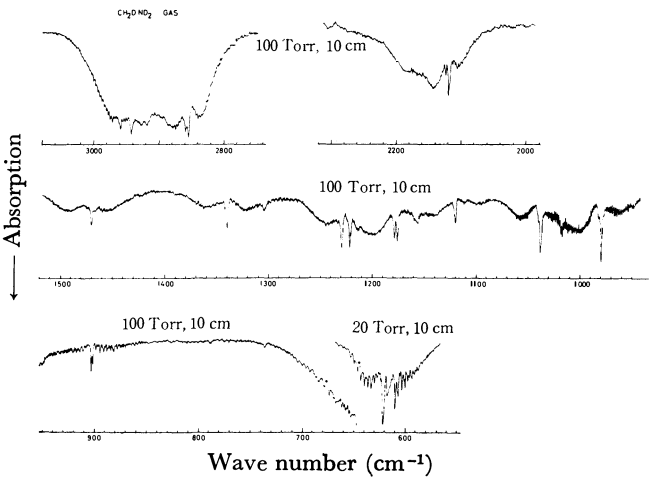

Fig. 3. Infrared absorption spectrum of CH_2DND_2 (gas).

4000—400 cm^{-1} region by the use of a Perkin-Elmer 621 spectrophotometer. The results are shown in Figs. 2 and 3.

A Normal Coordinate Treatment

In an attempt to obtain a guide in our interpretation of the infrared spectra, we have made a calculation of the vibrational frequencies and normal modes of vibration of *trans* and *gauche* forms of CH_2DNH_2 and CH_2DND_2 molecules. The relation between the force constants and the vibrational frequencies is given by the secular equation

$$|\mathbf{GF}-\mathbf{E}\lambda| = 0 \qquad (1)$$

where **G** is the inverse kinetic energy matrix, **F** the potential energy matrix, **E** the unit matrix, and λ is equal to $4\pi^2c^2\nu^2$, c being the light velocity, N the Avogadro number, and ν the vibrational wave number. As the basis of the **G** and **F** matrices, we choose a set of symmetry coordinates S defined in our previous paper on the five isotopic species of methylamine.[2] The set of normal coordinates **Q** is given as

$$\mathbf{S} = \mathbf{L}_S\mathbf{Q} \qquad (2)$$

In our treatment we chose the local symmetry force field.[3] The values of force constants, *i.e.* the **F** matrix elements are assumed as shown in Table 1, for all of the four molecules, CH_2DNH_2 (*trans*), CH_2DNH_2 (*gauche*), CH_2DND_2 (*trans*), and CH_2DND_2 (*gauche*). This set of force constants explains reasonably well the vibrational spectra of CH_3NH_2, CH_3ND_2, CD_3NH_2, CD_3ND_2, and $CH_3{}^{15}NH_2$,[2] and we did not attempt any further adjustment of the force constant values this time. The calculation was made by a HITAC 5020E at the Computer Centre of the University of Tokyo, by the use of programs written by Professor T. Shimanouchi and his collaborators.[4] The calculated fre-

TABLE 1. ASSUMED VALUES[a] OF THE F-MATRIX ELEMENTS

	S_1	S_2	S_3	S_4	S_5	S_6	S_7	S_8	S_9
S_1 NH_2 sym. str.	6.444								
S_2 Methyl sym.str.	0	4.616							
S_3 Methyl deg. str. (A′)[b]	0	0	4.739						
S_4 CN str.	0.443	0.826	0	5.123					
S_5 NH_2 scissor.	0.076	0	0	−0.230	0.661				
S_6 NH_2 wag.	0.289	0	0	0.304	−0.197	0.566			
S_7 Methyl deg. def. (A′)[b]	0	0	−0.093	0	0.030	0	0.567		
S_8 Methyl sym. def.	0	0.093	0	0.499	−0.023	−0.037	0	0.642	
S_9 Methyl rock (A′)[b]	0	0	0.317	0	0.030	−0.024	−0.057	0	0.789

	S_{10}	S_{11}	S_{12}	S_{23}	S_{14}	S_{15}
S_{10} NH_2 antisym. str.	6.385					
S_{11} Methyl deg. str. (A″)[b]	0	4.739				
S_{12} NH_2 twist.	0.192	0	1.101			
S_{13} Methyl deg. def. (A″)[b]	0	−0.093	0.074	0.567		
S_{14} Methyl rock. (A″)[b]	0	0.317	−0.185	−0.057	0.789	
S_{15} Torsion	0	0	0	0	0	0.048

a) Unit: mdyn/Å for stretch-stretch elements, mdyn/rad for stretch-deform elements, and mdyn·Å/rad² for deform-deform elements.

b) A′ and A″ mean the vibrational modes which would be symmetric and antisymmetric, respectively, with respect to the symmetry plane of the molecule if CH_2D group were ordinary CH_3 group.

quencies are given in Table 2 with approximate statements of the vibrational modes which were derived from the calculated $\mathbf{L}_S$ matrix elements and potential energy distribution.

Ferquency Differences of the *trans* and *gauche* Forms

Some of the observed frequencies assignable to the calculated frequencies are listed also in Table 2.

Table 2. Calculated and observed frequencies (in cm^{-1}) of CH_2DNH_2 and CH_2DND_2 in their gaseous states

Mode	Calculated		Observed
	trans	*gauche*	
CH_2DNH_2			
NH_2 antisym. str.	3427	3427	3395
NH_2 sym. str.	3361	3361	3355
CH_2 antisym. str.	2961	2961	2967, 2927
CH_2 sym. str.	2873	2872	2873, 2868
CD str.	2126	2128	2143, 2118
NH_2 scissor.	1624	1624	1623
CH_2 scissor.	1461	1460	1469
NH_2 tiwst.	1423	1423	——
CH_2 wag.	1333	1336	1319, 1313
CH_2 twist	1278	1279	1227
CN str.	1059	1046	1073, 1042
CH_2 rock. (out-of-pl.)[a]	1055	1088	1187, 1087
CD in-pl. def.	938	879	921, 849
NH_2 wag.	744	779	768, 756
torsion	256	255	~250
CH_2DND_2			
CH_2 antisym. str.	2961	2961	2960, 2943
CH_2 sym. str.	2873	2873	2860, 2855
ND_2antisym. str.	2526	2526	2575, 2557
ND_2 sym. str.	2423	2424	2478, 2469
CD str.	2125	2126	2124, 2119.5
CH_2 scissor.	1460	1459	1471
CH_2 wag.	1335	1338	1340
CH_2 twist.	1279	1279	1213
ND_2 scissor.	1219	1230	1230, 1223
ND_2 twist.	1059	1054	——
CH_2 rock. (out-of-pl.)[a]	1049	1079	——
CN str.	1025	999	1038, 979.5
CD in-pl. def.	900	870	903, 901
ND_2 wag.	585	601	622, 610
torsion	207	207	——

a) "In-pl." means symmetric with respect to the symmetry plane of the CH_2D group, and "out-of-pl." means antisymmetric with respect to this plane.

For each of the CH_2 wagging, CN stretching, NCD bending (along the direction parallel to the symmetry plane of the CH_2D group), and NH_2 wagging vibrations a sharp Q-branch peak is expected both for *trans* and *gauche* forms (see Fig. 1). The calculation indicates that the frequencies of *trans* and *gauche* forms should be appreciably different for each of these vibrations. In fact for each of these vibrations two sharp Q-branch peaks are observed, one of which may be assigned to the *trans* form and the other to the *gauche* form. Likewise, for each of the ND_2 scissoring, C–N stretching, NCD bending, and ND_2 wagging vibrations of CH_2D-ND_2, two bands are observed as are expected from the normal coordinate treatment.

Two bands are also observed for each of the CH_2 antisymmetric stretching, CH_2 symmetric stretching and CD stretching vibrations of both of the CH_2DNH_2 and CH_2DND_2. In our present calculation, the frequency of each of these vibrations does not come out to be different in the *trans* form from that in the *gauche* form. Obviously this is because the assumed values of **F**-matrix elements are not proper. Thus, an equal value was assigned to the diagonal elements $F(S_3, S_3)$ and $F(S_{11}, S_{11})$, and the off-diagonal element $F(S_2, S_3)$ was arbitrarily set at zero. The CH stretching frequencies depend almost only upon the **F**-matrix elements $F(S_2, S_2)$, $F(S_3, S_3)$, $F(S_{11}, S_{11})$ and $F(S_2, S_3)$. The normal methylamine CH_3NH_2 molecule gives only three observed CH frequencies (CH_3 symmetric stretching, and two CH_3 "degenerate" stretching frequencies), and therefore it has not been possible so far to fix the values of the four **F**-matrix elements.[2] While, CH_2D-NH_2 molecule gives four CH frequencies (*i.e.*, CH_2 symmetric stretching frequencies of *trans* and *gauche* forms and CH_2 antisymmetric stretching frequencies of *trans* and *gauche* forms). Therefore, if the assignments of these observed frequencies to the *trans* and *gauche* forms are fixed (by an analysis of the rotational-structures, for example), then the four **F**-matrix elements should be almost uniquely determined. This should lead us to an interesting piece of information on how one of the CH bonds in methylamine molecule is chemically different from the other two.

Microwave Spectrum

Microwave absorption spectrum of CH_2DNH_2 in its gaseous state was observed by the use of an instrument constructed by Professor Y. Morino, Professor E. Hirota, and their collaborators in the Department of Chemistry, Faculty of Science, here in the University, through their kindness. Assingments of rotational transitions to the observed lines were made by examining the Stark effect and also by some double-resonance experiments. On the basis of the molecular parameters of the so-called r_0-structures (effective structures at vibrational ground state and at $J=0$ and $K=0$) of CH_3NH_2

Table 3. Rotational constants of CH_2DNH_2 (in cm^{-1})

		Calculated[a]	Observed[b]
trans	A	2.86332	2.871396
	B	0.685775	0.685339
	C	0.684532	0.682969
gauche	A	2.885705	2.890871
	B	0.708859	0.708660
	C	0.663108	0.664078

a) On the basis of the r_0-structure of CH_3NH_2 determined by Takagi and Kojima.[5]
b) See text.

and CH_3ND_2 molecules determined by Takagi and Kojima,[5] the rotational constants A, B, and C are calculated for *trans* and *gauche* forms as shown in Table 3. Absorption lines of the *trans* and *gauche* forms are actually found nearly at the frequencies predicted from these values of the rotational constants. They are 34 Q-branch lines ($\Delta J=0$) and 26 P- and R-branch lines ($\Delta J=\pm 1$) of the *trans* form, and 72 Q-branch lines and 68 P- and R-branch lines of the *gauche* forms. All of the *trans*-form lines are explained by considering that every transition expected for a rigid-rotor splits into two components because of the inversion. On the other hand, all of the *gauche*-form lines are explained by considering that every transition expected for a rigid-rotor splits into four components because of the inversion and internal-rotation. After taking an average of the frequencies of these split lines the rotational constants of the *trans*- and *gauche*-form molecules are derived as given in the last column of Table 3.

The results of our microwave study on this molecule will be detailed elsewhere. Only an outline of our work on the energy difference ΔE_{TG} between the *trans*- and *gauche*-forms will be reported below.

ΔE_{TG} from Inversion Splitting

By means of the microwave spectroscopy, we can determine the positions of the energy levels of the *trans* form with respect to one another and those of the *gauche* form with respect to one another. It is not usually easy, on the other hand, to determine the positions of the *trans* levels with respect to the *gauche* levels, because there are no transitions allowed between the *trans* and *gauche* levels (unless there is a strong *trans-gauche* mixing). In the present particular case, however, the *trans-gauche* energy difference ΔE_{TG} at $J=0$, $K=0$ can be estimated from the amounts of the inversion splitting of the *trans* levels.

In addition to the internal-rotation, the methylamine molecule experiences another large-scale internal motion, *i.e.*, the inversion of the amino group. Thus, the molecule in question has a two-dimensional six-minimum potential, which is schematically shown in Fig. 4. The inversion splitting of the *trans* form is considered to be caused by a resonance of the energy levels in the two equivalent *trans* valleys in this potential map. If the wavefunction of a vibration-rotation level were completely localized in each of these valleys, however, the amount of the inversion splitting should be negligibly small, because the two *trans* valleys are situated far away from each other (Fig. 4). While, if an appreciable amount of mixing of the *trans* and *gauche* states takes place, an appreciable amount of the inversion splitting of the so-called "*trans*" level (which now involves a small contribution from the *gauche* state) may occur. As has been shown by Itoh,[6] by Kivelson and Lide,[7] and by Tsuboi *et al.*,[8] the inversion splitting of the amino group in the molecule with the rotational quantum number K should be given as

$$E^a - E^s = (-1)^K(E^- - E^+)\int_0^{2\pi} \phi_{\tau K}(x)^* \phi_{\tau K}(x+\pi)\mathrm{d}x, \quad (3)$$

where $E^- - E^+$ is the hypothetical inversion splitting when the coupling were absent between the inversion and internal-rotation, and $\phi_{\tau K}(x)$ is the internal-rotation eigenfunction for the vibration-rotation state now in question. This $\phi_{\tau K}(x)$ is not a completely localized function but an eigenfunction of a proper internal-rotation Hamiltonian. The subscript τ is for distinguishing three internal-rotation sublevels of the $n=0$ state. The value of the overlap integral in the right side of Eq. (3) for the "*trans*" form should be sensitive to how much mixing takes place of the *trans* and *gauche* states, and hence to the amount of ΔE_{TG}. The integral can be estimated on the basis of a theory of asymmetric internal rotor developed in our previous paper.[1] It comes out as a periodic function of K (rotational quantum number). Therefore, the inversion splitting of the $K+1 \leftarrow K$ transition frequency should also be a periodic function of K. In Fig. 5, the amounts of inversion splitting actually observed in the microwave absorption lines of $K+1 \leftarrow K$ transitions are plotted against K. The observed values are reproduced by an empirical formula

$$E^a - E^s = 81.85 \sin\left[51°41' \times \left(K+\frac{1}{2}\right)\right] \text{ MHz} \quad (4)$$

The observed set of values is found to be in a good

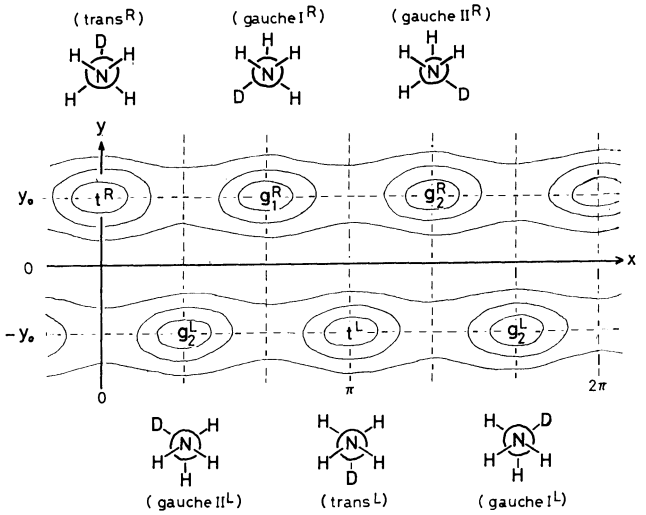

Fig. 4. A schematic drawing of the two-dimensional six-minimum potential function of the CH_2DNH_2 molecule. x: internal rotation. y: inversion.

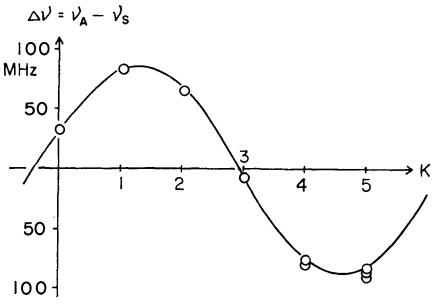

Fig. 5. The amount of inversion splitting, ν_a—ν_s, of the absorption lines of the $K+1 \leftarrow K$ transitions plotted against K. o: observed. ——: calculated by equation (4).

agreement with the calculated set (on Eq. (3)) if ΔE_{TG} is assumed to be 6.7 cm^{-1}. The ambiguity of this value is ± 0.4 cm^{-1} here.

ΔE_{TG} from a *trans-gauche* Accidental Degeneracy

The ΔE_{TG} value (6.7 cm^{-1}) just estimated happens to be close to the value (6.6 cm^{-1}) of $3[A-(B+C)/2]$ of this molecule. Therefore, the $K=1$ levels of the *trans* form should be situated close to the $K=2$ levels of the *gauche* form (see Fig. 6), and an interaction may be

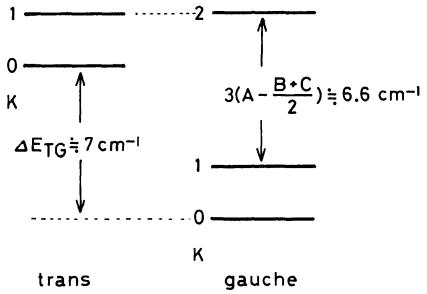

Fig. 6. Accidental degeneracy of the *trans* ($K=1$) and *gauche* ($K=2$) levels.

expected between one of such *trans* levels and a *gauche* level with the same J-value. In fact, an anomaly in the observed frequency of the *trans* form has been found for $K=1\leftarrow 0$ and $J=10\leftarrow 10$ transition (see Fig. 7). This fact is interpreted by considering that the ($K=1$, $J=10$) level of the *trans* form is accidentally coincident with the ($K=2$, $J=10$) level of the *gauche* form. On the basis of this interpretation the difference (ΔE_{TG}) between the ($K=0$, $J=0$) levels of the *trans* and *gauche* forms is determined to be 7.06 ± 0.03 cm^{-1}. This is probably the first example of the energy difference precisely determined of rotational isomers caused by an isotopic substitution.

We wish to express our deep appreciation to Professor Yonezo Morino, Professor Eiji Hirota, and Professor Takehiko Tanaka for their kindness in allowing us to use their microwave instrument, for their kind instruction and valuable discussions.

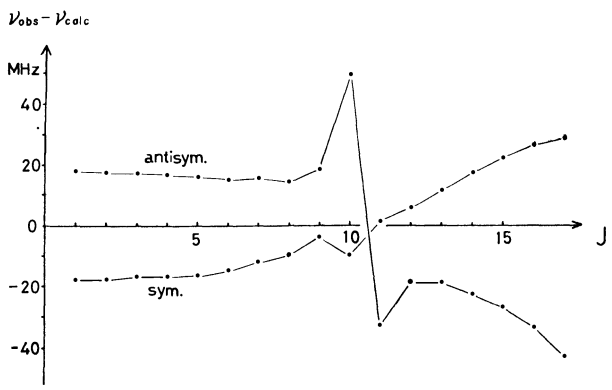

Fig. 7. $\nu_{obs}-\nu_{calc}$ plotted against J. Here ν_{obs} are the observed frequencies (MHz) of the Q-branch lines ($J_{1,J-1}\leftarrow J_{0,J}$) of the trans form. ν_{calc} are the frequencies calculated on the assumption that the molecule is a rigid rotor with the ratotional constants given in Table 3. For every ($K=1\leftarrow 0$, $J=J\leftarrow J$) transition two absorption lines are observed, and they are considered to be caused by the inversion of the amino group.

References

1) K. Tamagake, M. Tsuboi, and A. Y. Hirakawa, *J. Chem. Phys.*, **51**, 2592 (1969).
2) A. Y. Hirakawa, M. Tsuboi, and T. Shimanouchi, *ibid.*, **57**, 1236 (1972).
3) T. Shimanouchi, "Physical Chemistry," Vol. 4, ed. by D. Henderson, Academic Press, New York (1970), p. 233.
4) T. Shimanouchi, "Computer Programs for Normal Coordinate Treatment of Polyatomic Molecules," Department of Chemistry, University of Tokyo, July, 1968.
5) K. Takagi and T. Kojima, *J. Phys. Soc. Japan*, **30**, 1145 (1971).
6) T. Itoh, *ibid.*, **11**, 264 (1956).
7) D. Kivelson and D. R. Lide, Jr., *J. Chem. Phys.*, **27**, 353 (1957).
8) M. Tsuboi, A. Y. Hirakawa, T. Ino, T. Sasaki, and K. Tamagake, *ibid.*, **41**, 2721 (1964).

Resonance Raman Spectra of Acid-Base Indicators. I. *p*-Aminoazobenzene Derivatives

Katsunosuke MACHIDA, Bak-Kwang KIM, Yutaka SAITO, Kyoko IGARASHI, and Toyozo UNO

Faculty of Pharmaceutical Sciences, Kyoto University, Sakyo-ku, Kyoto 606

(Received July 17, 1973)

Resonance Raman spectra between 1800 and 1000 cm^{-1} of methyl orange and a few other *p*-aminoazobenzene-type acid-base indicators have been investigated at various pH, and a marked spectral change has been observed on the transformation between the acid and the base forms of these indicators. The characteristic Raman frequencies have been assigned by referring to the spectra of related compounds and the deuteration effects. The spectra of the acid form are well elucidated on the basis of the quinoid-type structure.

The color change of acid-base indicators is generally understood as a consequence of the change in molecular structures accompanying various redistributions of electrons on the transformation between the indicator acids and their conjugate bases. Spectroscopic evidence, however, has rarely been obtained for details of such a structure change of indicators. The visible and ultraviolet spectra should reflect the electron redistributions directly, but they are too simple in most cases to afford sufficient information on the complicated structure of indicator molecules. The infrared and ordinary Raman spectra may be informative, but their application is severely restricted by the solvents and the concentrations with which indicators are practically used. These difficulties are expected to be overcome by the recently developed technique of the laser-excited resonance Raman spectra, which seem to be very promising to inquire into the molecular structure of indicators in dilute aqueous solutions. Most of the acid-base indicators show absorption maxima in the spectral region around 500 nm, where two intense excitation lines, 488.0 and 514.5 nm, are available from the Ar^+ laser, and rigorous resonances with high sensitivities are expected even at very low concentrations.

The resonance Raman spectrum of methyl orange in the neutral aqueous solution has been reported by Hacker[1] and Carey *et al.*[2] and several bands attributable to the azobenzene structure postulated for the base form have been identified. For any acid-base indicator, however, the pH dependence of the Raman spectrum does not seem to have been investigated. In this paper we report the resonance Raman spectra of methyl orange and a few other *p*-aminoazobenzene type indicators at various pH. The structures of the acid and the base forms of these indicators are discussed by referring to the spectra of related compounds and deuteration effects.

Experimental

Materials. The azobenzene derivatives listed with the abbreviations in Table 1 and two other reference compounds, quinone dioxime and diazoaminobenzene, were obtained from commercial sources, and were recrystallized several times from water or ethanol. *O*-Deuterated quinone dioxime and *N*-deuterated diazoaminobenzene were prepared by the usual exchange reaction with ethanol-*d*.

Measurements. The Raman spectra between 1800 and 1000 cm^{-1} were recorded on a JEOL S-1 laser Raman spectrophotometer with the excitation lines 488.0 nm and 514.5 nm of a Coherent 52G Ar^+ laser (2 W). The spectral slitwidth was 12 cm^{-1} and 14 cm^{-1} for the 514.5 nm and the 488.0 nm excitations, respectively. The measurements were made for solid samples of quinone dioxime and its *O*-deuterated compound and for the solutions of the other compounds in various solvents. Each sample was sealed in a 1 mm capillary tube. The pH of the aqueous solutions was adjusted by using 0.1M HCl, 0.1M NaOH and the phthalate buffers.[5] When the desired solubility was not attained with water alone, suitable amounts of ethanol or acetone-d_6 were added to the solvents. At the concentrations adopted presently, acetone-d_6 shows no interfering Raman band in the region between 1650 and 1100 cm^{-1}, but shows a weak band at 1690 cm^{-1} which may be used as an internal standard. For the measurements of the deuterated compounds, the stock solution of 1M DCl was prepared by mixing the calculated amounts of 20% DCl (Merck) and heavy water in a 1 ml syringe, and was reserved in a sealed ampule. Similarly, 1M NaOD in heavy water was prepared from 40% NaOD (Merck). These solutions were diluted with heavy water to the desired concentration before use.

TABLE 1. STRUCTURE 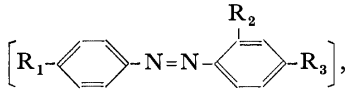 , ABSORPTION MAXIMUM AND COLOR-CHANGE INTERVAL

Compound	Abbr.	Structure			Absorption Maximum (nm)		Color-change interval (pH)
		R_1	R_2	R_3	Basic form	Acidic form	
Methyl orange	MO	$N(CH_3)_2$	H	SO_3Na	464	508	3.1—4.4[3]
Methyl red	MR	$N(CH_3)_2$	COOH	H	430	512	4.2—6.3[3]
Methyl yellow	MY	$N(CH_3)_2$	H	H	440	512	2.9—4.0[3]
p-Aminoazobenzene	AAB	NH_2	H	H	383	503	1.9—3.3[3]
Tropaeolin OO	TOO	NHC_6H_5	H	SO_3Na	447	530	1.3—3.0[4]
Azobenzene	AB	H	H	H	446	—	—

Fig. 1. Resonance Raman spectra of MO: (a) 1×10^{-4} M in 0.1M HCl (solid line) and in 0.1M DCl (broken line), 514.5 nm; (b) 2×10^{-4} M in water, 488.0 nm; (c) 2×10^{-4} M in the phthalate buffer (pH 3.4), 488.0 nm.

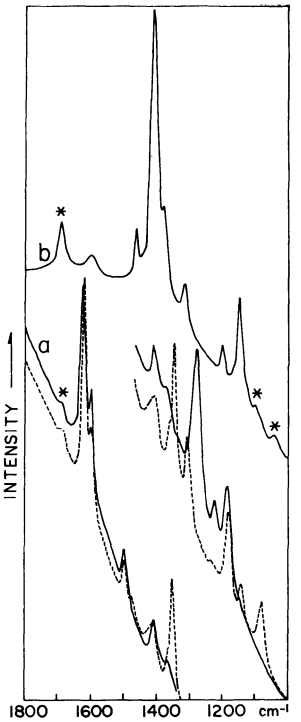

Fig. 3. Resonance Raman spectra of MY: (a) 1×10^{-4} M in a 1:4 mixture of acetone-d_6 and 0.1M HCl (solid line) and in a 1:4 mixture of acetone-d_6 and 0.1M DCl (broken line), 514.5 nm; (b) 2×10^{-4} M in a 1:4 mixture of acetone-d_6 and water, 488.0 nm.

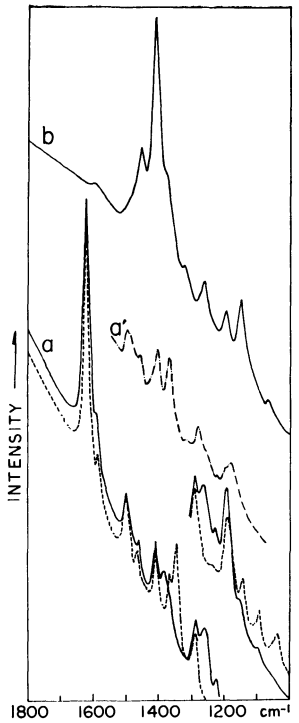

Fig. 2. Resonance Raman spectra of MR: (a) 1×10^{-4} M in 0.1M HCl (solid line) and in 0.1M DCl (broken line), 514.5 nm; (a') 1×10^{-4} M in a 1:3 mixture of ethanol and the phthalate buffer (pH 4), 514.5 nm; (b) 2×10^{-4} M in 0.1M NaOH, 488.0 nm.

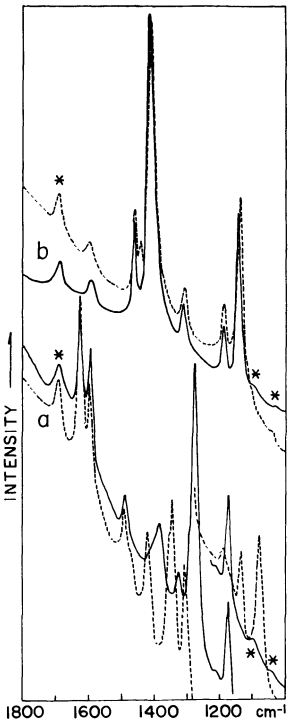

Fig. 4. Resonance Raman spectra of AAB: (a) 5×10^{-4} M in a 1:4 mixture of acetone-d_6 and 0.1M HCl (solid line) and in a 1:4 mixture of acetone-d_6 and 0.1M DCl (broken line), 488.0 nm; (b) 5×10^{-3} M in a 1:4 mixture of acetone-d_6 and water (solid line) and in a 1:4 mixture of acetone-d_6 and heavy water (broken line), 488.0 nm.

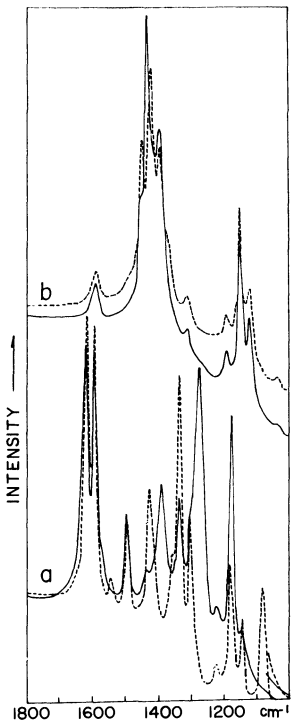

Fig. 5. Resonance Raman spectra of TOO: (a) 1×10^{-4} M in 0.1M HCl (solid line) and in 0.1M DCl (broken line), 514.5 nm; (b) 5×10^{-4} M in water (solid line) and in heavy water (broken line), 488.0 nm.

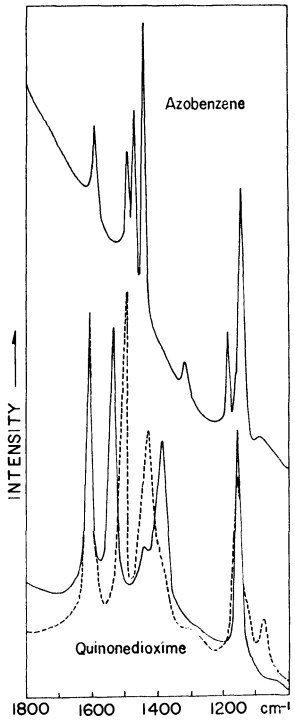

Fig. 6. Resonance Raman spectrum (488.0 nm) of azobenzene in methanol-d_6 (1×10^{-2} M) and Raman spectra (514.5 nm) of solid sample of quinone dioxime (solid line) and its *O*-deuterated compound (broken line).

The concentration dependence of the Raman intensities was briefly surveyed for MO between 1×10^{-7} M and 1×10^{-3} M, and the optimum concentration was found to be about 1×10^{-4} M for the acid form excited by the 514.5 nm and the 488.0 nm lines and about 3×10^{-4} M for the base form excited by the 488.0 nm line. For the base form, a little higher concentration (about 1×10^{-3} M) was found suitable when the 514.5 nm line was used. The change in the relative intensities of Raman bands on changing the excitation wavelength from 488.0 nm to 514.5 nm was not appreciable and was left out of detailed examination. At the concentrations investigated, no detectable spectral change due to the thermal effect or the decomposition was observed on the prolonged exposure of the samples to the excitation beam. The representative Raman spectra are shown in Figs. 1—6.

The electronic spectra between 380 and 600 nm were recorded on a Shimadzu W-40 spectrophotometer for the same solutions of the indicators as those used for the Raman measurement by using a cell of 1 mm path length. The absorption maxima obtained are given in Table 1. They are essentially the same as those in literatures. The electronic spectra of the indicators in the deuterated solutions, either acidic or basic, were identical with those for the corresponding undeuterated solvents. The infrared spectra of solid samples of diazoaminobenzene and its *N*-deuterated compound were recorded on a JASCO DS-301 infrared spectrophotometer for Nujol or hexachlorobutadiene mulls (Fig. 7).

Results and Discussion

The yellowish color of any *p*-aminoazobenzene type indicator in a neutral or a basic solution changes to a reddish color when the solution is acidified to a pH below the color-change interval of the indicator. This color change has been attributed to a change of the molecular structure from an azo-type to a quinoid-type with the protonation to the azo group as shown in

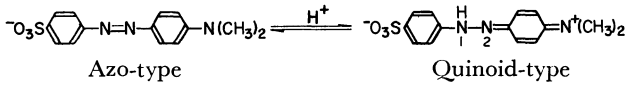

Azo-type Quinoid-type

Chart 1

Chart 1.[3,6] Such a structure change is expected to give rise to a marked change in the resonance Raman spectra, in which the band intensity is often enhanced for the group vibrations participating in the resonant electronic transition. Previously, Hacker investigated the resonance Raman spectra of a number of azo compounds among which MO in water and MR, AAB, and AB in methanol and CCl_4 were included.[1] The presently recorded spectra for the neutral to alkaline solutions of these compounds are essentially the same as Hacker's result, except the N=N stretching frequency ($\nu_{N=N}$) of MR, for which the present value is about 40 cm^{-1} lower than Hacker's value. Table 2 summarizes the characteristic Raman frequencies of the base form identified by referring to the previous works on the vibrational spectra of azobenzene derivatives.[1,7] By the revision of $\nu_{N=N}$ of MR, a correlation between $\nu_{N=N}$ and the nature of the *p*-substituent was revealed. If we take the $\nu_{N=N}$ of MO to be the mean value of the doublet frequencies 1395 and 1420 cm^{-1}, the substituents arranged in the decreasing order of $\nu_{N=N}$,

$$H- > C_6H_5NH- > NH_2- > (CH_3)_2N-$$

follow well the order that both the electron donating effect and the pH of the color-change interval (Table 1) increase.

Table 2. Observed frequencies (cm^{-1}) and assignments for the base form

MO	MR	MY	AAB($\Delta\nu$)	TOO($\Delta\nu$)	AB	Assignment
1600 w	1600 vw	1600 w	1600 (0) w	1591 (0) w	1598 m	Benzene ring
1450 w	1460 m	1465 m	1468 (1) m	1455 (0) sh	1475 s	Benzene ring
1420, 1395 vs	1412 vs	1415 vs	1420 (3) vs	1437 (12) vs	1444 vs	N=N str.
1320 w	1325 vw	1320 w	1317 (0) w	1315 (1) w	1318 w	Benzene ring
1200 w	1195 w	1198 w	1193 (0) w	1195 (1) w	1187 m	Benzene ring
1155 m	1150 m	1150 m	1147 (4) m	1150 (1) m	1147 vs	Ph–N str.

$\Delta\nu = \nu$ (in the ordinary solvent) $-\nu$(in the deuterated solvent)

The deuteration of the solvent gives no change in the resonance Raman spectra of the base form of MO, MR, and MY as expected from the azo structure of these indicators containing no active hydrogen. The base form of TOO and AAB in the deuterated solvent gives essentially the same spectra as those in the undeuterated solvent, but the $\nu_{N=N}$ of these compounds are affected a little on the deuteration of the NH or NH_2 group, suggesting a slight coupling of this vibration with the ND or ND_2 deformation vibrations (Figs. 4 and 5).

The resonance Raman spectrum of MO in the 0.1M HCl solution is completely different from that in the neutral solution as shown in Fig. 1. When the pH is adjusted close to the pK_a of MO (3.4 at 25 °C),[8] an intermediate spectral feature between the acid and the base forms is observed in accord with the color change in the visible region (Fig. 1c). The acid form shows no strong Raman band assignable to the N=N stretching vibration near 1420 cm^{-1}, but shows a very strong Raman band at 1624 cm^{-1}, which may be assigned to a stretching vibration of the ring C=C bonds of the quinoid structure. This frequency, however, is appreciably lower than the C=C symmetric stretching frequency of *p*-quinone (1667 cm^{-1} [9,10]), and it is desirable to clarify how far the latter may diminish on replacing both the C=O groups by the C=N– groups. Since the Raman spectra of quinonediimine-like compounds were not found in literatures, we examined the Raman spectra of quinone dioxime and its *O*-deuterated compound, regarding them as the simplest reference compounds. As shown in Fig. 6, quinone dioxime exhibits two strong Raman bands at 1617 and 1544 cm^{-1} assignable to the symmetric C=C and C=N stretching vibrations, respectively. The low-frequency shift of the latter on the *O*-deuteration is quite analogous to the case of the C=N stretching band in the infrared spectrum of quinone monoxime reported by Hadži.[11] Based on this result, the characteristic 1624 cm^{-1} band of MO can be assigned to the C=C stretching vibration. The absence of any strong band assignable to the C=N stretching vibration in the resonance Raman spectrum of MO may be due to the difference either in the substituents on the nitrogen atoms between MO and quinone dioxime or in the sensitivity to the resonance enhancement between the C=C and the C=N stretching vibrations.

The quinoid structure shown in Chart 1 has an active hydrogen atom attached on N_1. If the acid form of MO takes such a structure, the deuteration of this hydrogen by a simple exchange reaction may give rise to a change in the resonance Raman spectrum. In agreement with this expectation, MO in 0.1M DCl shows a much different spectrum from that in 0.1M HCl in the region between 1400 and 1000 cm^{-1} (Fig. 2). In order to clarify the difference in the vibrational frequencies between the Ph–NH–N= and the Ph–ND–N= groups, we examined the effect of the *N*-deuteration on the infrared spectrum of diazoaminobenzene, C_6H_5–NH–N=N–C_6H_5. For this compound, reliable assignments of the Ph–NH–N= group frequencies have been made on the basis of a detailed analysis of various N^{15} isotope shifts in the infrared spectra,[7] but the vibrational spectra of the *N*-deuterated diazoaminobenzene have not yet been reported. Unfortunately, the Raman spectra of diazoaminobenzene could not be recorded because of a very strong fluorescence. According to Kübler *et al.*,[7] the infrared bands at 1520 and 1248 cm^{-1} of diazoaminobenzene arise from the N–H deformation and the Ph–N stretching vibrations, respectively. As shown in Fig. 7, both these bands disappear on the *N*-deuteration, and new bands arising possibly from a coupling which may involve the Ph–N stretching and the N–D deformation vibrations are observed at 1364, 1105, and 1068 cm^{-1} for diazoaminobenzene-*d*. Correspondingly, the resonance Raman band at 1272 cm^{-1} of the acid form of MO is replaced by three bands at 1338, 1145, and 1076 cm^{-1} on changing the solvent from 0.1M HCl to 0.1M DCl. This result is a strong support to the presence of a Ph–NH–N= group in the acid form of MO.

The resonance Raman spectra of MR and MY show marked changes analogous to the case of MO

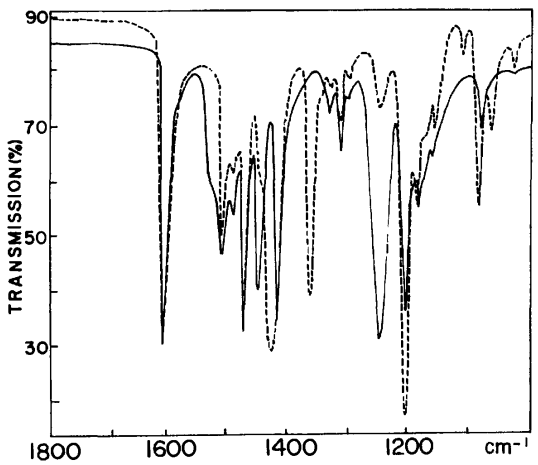

Fig. 7. Infrared spectra of diazoaminobenzene (solid line) and its *N*-deuterated compound (broken line).

not only on the color change from the base form to the acid form but also on the deuteration of the latter. Besides the strongest C=C stretching band around 1620 cm^{-1} and the deuteration sensitive Ph–N stretching band around 1270 cm^{-1}, four bands around 1600, 1500, 1380, and 1180 cm^{-1} are commonly observed for the undeuterated acid forms of MO, MR, and MY. The 1600 and 1500 cm^{-1} bands, which persist in the 0.1M DCl solution, may be assigned to the benzene ring vibrations. The origin of the 1380 cm^{-1} band, which is very weak but is clearly recognized from its disappearance on the *N*-deuteration, is not obvious at this stage. A possible interpretation of this band will be given later. The 1180 cm^{-1} band seems to be the counterpart of the infrared band at 1202 cm^{-1} of diazoaminobenzene due to the N–N stretching vibration,[7] since no effect of the *N*-deuteration is observed in either case. For the quinoid structure of MR, an acid-base equilibrium was suggested from the pH gradient thin layer chromatography.[12] We accordingly measured the resonance Raman spectrum of the acid form of MR at various pH's below the color change interval, and observed a little spectral change around 1400 and 1200 cm^{-1} accompanying the pH change (Fig. 2). This result supports the existence of the equilibrium shown in Chart 2, since the coupled vibrations of the C–O stretching and the OH deformation vibrations of the COOH group[13] and the symmetric stretching vibration of the CO_2^- group[14] are expected to give Raman bands around these frequencies.

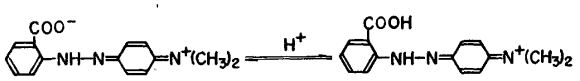

Chart 2

The acid forms of TOO and AAB show similar resonance Raman spectra to that of MO. On changing the solvent from 0.1M HCl to 0.1M DCl, the spectra of these compounds change complicatedly as shown in Figs. 4 and 5, but the characteristic features of the spectral change observed for MO, MR, and MY are recognized also for these compounds. Both TOO and AAB show a band around 1390 cm^{-1} which is replaced by a band around 1430 cm^{-1} on going to the 0.1M DCl solution. The disappearance of the 1390 cm^{-1} band on the *N*-deuteration suggests a common nature between this band and the weak 1380 cm^{-1} band of MO, MR, and MY mentioned above. The high-frequency shift of the latter seems to be obscured by the overlap of a band near 1410 cm^{-1} attributable to the N–CH_3 group. For quinone dioxime, an analogous shift of a Ramanb and from 1391 cm^{-1} to 1439 cm^{-1} is observed on the *O*-deuteration. Probably, this band of quinone dioxime corresponds to the b_{1g} C–C stretching band of *p*-quinone[9] and the 1390 cm^{-1} band of TOO and AAB as well as the 1380 cm^{-1} band of MO, MR, and MY may be interpreted on the same basis. The proposed assignments of the resonance Raman bands of the acid form are summarized in Table 3.

According to the present assignment, the quinoid ring C–C stretching frequency for each of the undeuterated and the deuterated acid form increases in almost the same order as the $\nu_{N=N}$ of the base form. This trend is reasonable since both the azo N=N and the quinoid ring C–C bond orders increase on the increase of the azo-type character of the conjugate system, and the electron donation from the amino-nitrogen to the ring opposes this change. For the suructure of the acid form, a resonance hybrid between the quinoid-type and the protonated azo-type has been postulated, the latter being pictured as the azo-type with a hydrogenated and positively charged nitrogen,[15,16] *p*-$(CH_3)_2N$–C_6H_4–N=N$^+$H–C_6H_4–SO_3^-. The resonance Raman spectra of the acid form as revealed in this work indicate that the quinoid-type is much predominant over the azo-type in this resonance, if any. As suggested by the behavior of the C–C stretching frequency, however, the contribution of the azo-type is not entirely excluded at present. More knowledge on the vibrations of both the quinoid- and azo-type structures seems to be necessary to deal with this hybridization quantitatively.

We wish to thank Professor H. Tanaka for helpful discussions and for the use of the W-40 spectrophotometer.

References

1) H. Hacker, *Spectrochim. Acta*, **21**, 1989 (1965).
2) P. R. Carey, H. Schneider, and H. J. Bernstein, *Biochem. Biophys. Res. Commun.*, **47**, 588 (1972).
3) I. M. Kolthoff, "Acid-Base Indicators," The Macmillan Co., New York (1937).
4) F. M. Cray and G. M. Westrip, *Trans. Faraday Soc.*, **21**,

TABLE 3. OBSERVED FREQUENCIES (cm^{-1}) OF THE ACID FORM IN THE ORDINARY AND DEUTERATED SOLVENTS AND ASSIGNMENTS

MO		MR		MY		AAB		TOO		Assignments
ord.	deut.	ord.	deut.	ord.	deut.	ord.	deut.	ord.	deut.	
1624 s	1620 s	1623 vs	1621 vs	1623 vs	1620 vs	1630 s	1628 s	1624 vs	1617 vs	C=C str.
1601 sh	1600 sh	1595 sh	1585 vw	1599 m	1595 m	1598 m	1600 m	1594 vs	1593 vs	Benzene ring
1502 m	1500 m	1499 m	1496 m	1499 w	1499 w	1495 m	1495 m	1499 m	1497 m	Benzene ring
1370 sh	1411 m	1385 w	1410 m	1370 vw	1410 w	1386 m	1421 m	1396 m	1430 m	C–C str.[a]
1272 m	1338 m	1288 w	1348 m	1282 s	1350 m	1280 vs	1347 s	1279 vs	1337 s	Ph–N str.
1183 m	1183 m	1190 m	1190 m	1184 m	1184 m	1177 m	1195 w	1178 m	1182 m	N–N str.
—	1145 w	—	1145 w	—	1145 w	—	1140 m	—	1146 w	?
—	1076 w	—	1095 w	—	1084 m	—	1083 s	—	1084 w	?

a) Tentative assignment

326 (1926).
5) L. Meites, "Handbook of Analytical Chemistry," McGraw-Hill Co., New York (1963), Section 11.
6) C. A. Peters and B. C. Redmon, *J. Chem. Educ.*, **17**, 525 (1940).
7) R. Kübler, W. Lüttke, and S. Weckherin, *Z. Electrochem.*, **64**, 650 (1960).
8) L. Meites, "Handbook of Analytical Chemistry," McGraw-Hill Co., New York (1963), Section 3.
9) H. Stammereich and T. T. Sans, *J. Chem. Phys.*, **42**, 920 (1964).
10) E. D. Becker, E. C. Harney, and T. Anno, *J. Chem. Phys.*, **42**, 942 (1964).
11) D. Hadži, *J. Chem. Soc.*, **1956**, 2725.
12) E. Stahl and R. Dumont, *J. Chromat. Sci.*, **7**, 517 (1969).
13) F. Gonzales-Sanchez, *Spectrochim. Acta*, **12**, 17 (1958).
14) J. H. S. Green, W. Kynaston, and A. S. Lindsey, *ibid.*, **17**, 486 (1961).
15) E. Sawicki, *J. Org. Chem.*, **21**, 605 (1956); **22**, 1084 (1957).
16) C. F. Hiskey and T. A. Downey, *J. Phys. Chem.*, **58**, 835 (1954).

Dielectric Relaxation and Molecular Structure. VIII. Dielectric Relaxation of Alkyl Acetates in Benzene Solution

Yoshinori KOGA, Hiroaki TAKAHASHI, and Keniti HIGASI

School of Science and Engineering, Waseda University, Shinjuku, Tokyo 160

(Received October 1, 1973)

Dielectric constants and losses at the microwave frequency of 96.52 GHz have been measured at 25 °C for methyl, ethyl, *n*-butyl, isobutyl, *s*-butyl, *t*-butyl, *n*-amyl, isoamyl, *n*-hexyl, and *n*-octyl acetates in benzene solutions. Static dielectric constants, refractive indices and densities have also been measured. The effective mean relaxation times of normal alkyl acetates increase with increasing chain length of the alkyl radical, eventually approaching a steady value. The distribution parameters α of all these molecules seem to have appreciable values which may be due to various segment orientations by internal rotation.

According to Wheland[1] the esters of carboxylic acids provide an example with which there appears to be little, if any, freedom of rotation about the bond that links the carbon atom of the carbonyl group to the oxygen atom of the alkoxyl group. If this C–O bond has no freedom of rotation at all, the molecule will have only two planar configurations I (*trans*) and II (*cis*).

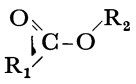

I (*trans*)

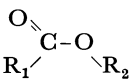

II (*cis*)

From this viewpoint Marsden and Sutton[2] reached a conclusion from dipole moment measurements that the *trans* form (I) would be more stable than the *cis* form (II).

Williams, Owen, and Sheridan[3] studied the molecular configuration of methyl acetate, *i.e.* $R_1=R_2=CH_3$ by means of microwave spectroscopy and showed that it has the *trans* planar configuration. And methyl and ethyl formates were also shown by microwave spectroscopy[4,5] to exist only in the *trans* planar form. On the other hand Karpovitch[6] suggested the existence of two isomers I and II based on his results of ultrasonic absorption measurements. By use of various spectroscopic methods Ōki and Nakanishi[7] examined the possibility of having two isomers and found that the *cis* conformation, which is very much stabilized in some special cases, does not exist in a great majority of alkyl acetates.

The results of electron diffraction are puzzling because O'Gorman, Shand, and Shomaker[8] showed that the structures of methyl acetate and methyl formate are not perfectly *trans* planar but slightly twisted, that is, the R_2–O bond makes an average dihedral angle 25° with the O=C–R_1 plane of the molecule. They suggested as one of the possibilities that a rather wide oscillation occurs about the completely planar *trans* configuration for these molecules.

The present work was undertaken in order to make a systematic study of dielectric behavior of alkyl acetates in solution and also to examine the aspect of internal motion in these molecules. The molecules examined are ten alkyl acetates, *i.e.* $R_1=CH_3$ and $R_2=C_nH_{2n+1}$, $n=1, 2\cdots8$.

Experimental

All compounds used in this study were obtained from commercial sources. Further, they were purified by distillation after drying over Molecular Sieve 4A for 24 hours. The apparatus and the experimental technique for dielectric measurements of the free-space method at 100 GHz employed in this work were described in a previous paper.[9] Static dielectric constants at 1 MHz were measured by the heterodyne beat method and refractive indices for sodium D-line were measured with use of a Pulfrich refractometer.

Results

The values of the so-called "slopes" a_0, a', a'', a_D, and b obtained in this experiment for alkyl acetates in benzene solutions are shown in Table 1. The definition of these slopes is given by Eqs. (1) and (2). The dielectric constants ε' and losses ε'' of the dilute solutions are linear functions of the concentration (weight fraction w_2) of the solute.

Table 1. Slopes a', a'' obtained at 96.52 GHz in benzene (25 °C) and a_0, a_D and b

Substance	a_0	a'	a''	a_D	b
Methyl acetate	3.989	1.227	1.321	−0.412	−0.055
Ethyl acetate	3.722	0.757	0.972	−0.410	−0.018
n-Butyl acetate	2.963	0.449	0.563	−0.352	−0.002
Isobutyl acetate	2.951	0.466	0.589	−0.336	0.017
s-Butyl acetate	2.942	0.287	0.460	−0.370	0.021
t-Butyl acetate	3.122	0.264	0.632	−0.363	0.022
n-Amyl acetate	2.648	0.348	0.493	−0.312	0.009
Isoamyl acetate	2.606	0.351	0.470	−0.337	0.019
n-Hexyl acetate	2.347	0.331	0.416	−0.301	0.017
n-Octyl acetate	1.909	0.202	0.311	−0.270	0.024

$$\varepsilon' = \varepsilon_1' + a'w_2$$
$$\varepsilon'' = a''w_2 \qquad (1)$$

in which subscripts 1 and 2 refer to the pure solvent and to the solute, respectively. Similarly, the static dielectric constants, ε_0, the infinite dielectric constants (the dielectric constants at high-frequency limit), ε_∞, the square of refractive indices, n_D, (for the sodium D-line), and the specific volumes, v, are also assumed to be linear with the concentration.

$$\varepsilon_0 = \varepsilon_{10} + a_0 w_2, \quad \varepsilon_\infty = \varepsilon_{1\infty} + a_\infty w_2$$
$$n_D^2 = n_{1D}^2 + a_D w_2, \quad v = v_1 + b w_2 \tag{2}$$

The total molar polarization ${}_\infty P_2$, the distortion polarization P_A+P_E, the molecular refraction R_D and the dipole moment μ together with the literature values are recorded in Table 2. The total molar polarization of the solute at infinite dilution ($w_2 \to 0$) was obtained from the Halverstadt-Kumler equation.[10]

Table 2. Total molar polarizations ${}_\infty P_2$, molecular refraction R_D, and dipole moments μ of alkyl acetates in benzene at 25 °C with the literature values

Substance	${}_\infty P_2$ [cm³]	R_D [cm³]	μ [a)] [D]	μ (lit[b)]) [D]
Methyl acetate	79.6	17.8	1.72	1.77
Ethyl acetate	91.2	22.2	1.82	1.83
n-Butyl acetate	104.3	31.1	1.87	1.87
Isobutyl acetate	104.7	32.1	1.86	1.89
s-Butyl acetate	104.6	31.5	1.87	—
t-Butyl acetate	108.6	31.7	1.92	1.93 (22 °C)
n-Amyl acetate	109.6	36.3	1.87	1.93
Isoamyl acetate	108.9	36.0	1.86	1.8
n-Hexyl acetate	113.5	40.8	1.86	—
n-Octyl acetate	121.8	50.0	1.84	—

a) $\mu = 0.0128\sqrt{({}_\infty P_2 - 1.05R_D)T}$

b) A. L. McClellan, "Tables of Experimental Dipole Moments," W. H. Freeman and Co., San Francisco and London (1963).

$${}_\infty P_2 \simeq M_2\left\{\frac{3a_0v_1}{(\varepsilon_{10}+2)^2} + (v_1+b)\frac{\varepsilon_{10}-1}{\varepsilon_{10}+2}\right\} \tag{3}$$

in which M_2 is the molecular weight of the solute. The distortion polarization P_A+P_E is obtained by using a_∞ and $\varepsilon_{1\infty}$ instead of a_0 and ε_{10} in Eq. (3), respectively.[11]

$$P_A + P_E \simeq M_2\left\{\frac{3a_\infty v_1}{(\varepsilon_{1\infty}+2)^2} + (v_1+b)\frac{\varepsilon_{1\infty}-1}{\varepsilon_{1\infty}+2}\right\} \tag{4}$$

Similarly, the molecular refraction for the D-line is given by

$$R_D \simeq M_2\left\{\frac{3a_D v_1}{(n_{1D}^2+2)^2} + (v_1+b)\frac{n_{1D}^2-1}{n_{1D}^2+2}\right\} \tag{5}$$

The dielectric relaxation times $\tau(1)$, $\tau(2)$, and τ_0 and the distribution parameter α are shown in Table 3. The relaxation times $\tau(1)$ and $\tau(2)$ were calculated from the following equations[12]

$$\tau = \frac{1}{\omega}\frac{a''}{a'-a_\infty} \equiv \tau(1) \tag{6}$$

$$\tau = \frac{1}{\omega}\frac{a_0-a'}{a''} \equiv \tau(2) \tag{7}$$

on the assumption of a single Debye relaxation. On the other hand, if the system is not of the single relaxation but of the multi-relaxation times which follow Cole-Cole's[13] rule, Eq. (8) will become valid instead.

$$a^* = a' - ja'' = a_\infty + \frac{a_0-a_\infty}{1+(j\omega\tau_0)^{1-\alpha}} \tag{8}$$

The probable relaxation time τ_0 and the distribution parameter α are estimated by measurements of a' and a'' at a single frequency.[14]

$$\tau_0 = \frac{1}{\omega}\left\{\frac{A^2+B^2}{C^2}\right\}^{(1-\alpha)/2} \tag{9}$$

$$1-\alpha = \frac{2}{\pi}\tan^{-1}\left(\frac{A}{B}\right) \tag{10}$$

where

$$A = a''(a_0-a_\infty)$$
$$B = (a_0-a')(a'-a_\infty) - a''^2 \tag{11}$$
$$C = (a'-a_\infty) + a''^2$$

The term a_∞ which we find in Eqs. (6) and (11) may be estimated in the following way. Assuming the familiar assumption of $P_A+P_E \simeq 1.05R_D$ for the dipole moment work to be valid, we shall obtain probable but tentative values of a_∞ from Eqs. (4) and (5). That is,

$$a_\infty = \frac{(\varepsilon_1'+2)^2}{3v_1}\left\{\frac{1.05R_D}{M_2} - (v_1+b)\frac{\varepsilon_1'-1}{\varepsilon_1'+2}\right\} \tag{12}$$

where $\varepsilon_{1\infty} \simeq \varepsilon_1'$ for non-polar solvent is assumed. The probable relaxation time τ_0 is found to be nearly equal to the geometrical mean, $\sqrt{\tau(1)\tau(2)}$, of $\tau(1)$ and $\tau(2)$. (See Table 3.)

Table 3. Dielectric relaxation times $\tau(1)$, $\tau(2)$ and τ_0 and distribution parameters α and a_∞ obtained from Eq. (12) on the assumption of $P_A+P_E \simeq 1.05\ R_D$

Substance	a_∞	$\tau(1)$ [ps]	$\tau(2)$ [ps]	$\sqrt{\tau(1)\tau(2)}$ [ps]	τ_0 [ps]	α
Methyl acetate	−0.382	1.4	3.5	2.2	2.1	0.28
Ethyl acetate	−0.377	1.4	5.0	2.7	2.7	0.35
n-Butyl acetate	−0.315	1.2	7.4	3.0	2.8	0.46
Isobutyl acetate	−0.296	1.3	7.0	3.0	2.9	0.43
s-Butyl acetate	−0.334	1.2	9.5	3.4	3.1	0.49
t-Butyl acetate	−0.325	1.8	7.5	3.6	3.7	0.34
n-Amyl acetate	−0.272	1.3	7.7	3.2	3.0	0.44
Isoamyl acetate	−0.296	1.2	7.9	3.1	2.9	0.47
n-Hexyl acetate	−0.260	1.2	8.0	3.0	2.8	0.48
n-Octyl acetate	−0.228	1.2	9.1	3.3	3.0	0.49

Discussion

Among the observed dipole moments of ten alkyl acetates in benzene solutions recorded in Table 2, those for *s*-butyl acetate (1.87 D), *n*-hexyl acetate (1.86 D) and *n*-octyl acetate (1.84 D) are new values; and all the moments (1.72—1.92 D) are in good agreement with literature values.

The dielectric relaxation time of methyl acetate in benzene has been given by Krishna[15] to be 2.2 ps at 28 °C, by Cripwell and Sutherland[16] 3.73 ps at 18.5 °C and Whiffen and Thompson[17] 3.1 ps at 19 °C. The average relaxation time of methyl acetate τ_0 obtained in this study is 2.1 ps, which is near to Krishna's value. The observed relaxation time for ethyl acetate $\tau_0 = 2.7$ ps in benzene solution is smaller than 4.4 ps in liquid at 20 °C by Smyth *et al.*[18]

Three relaxation times, $\tau(1)$, $\tau(2)$, and τ_0 of normal alkyl acetates are plotted against the carbon number

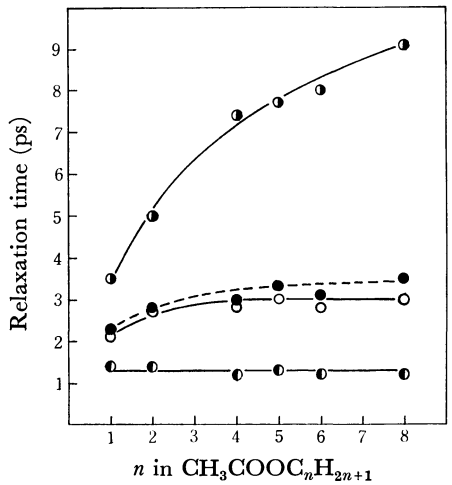

Fig. 1. The dependence of the relaxation times $\tau(1)$, $\tau(2)$, τ_0 and τ_0' upon the carbon number (n) of the alkyl radical (R_2) in normal alkyl acetates.
◐: $\tau(1)$, ◑: $\tau(2)$, ○: τ_0, ●: τ_0'.

(n) of the alkyl radical, R_2. (See Fig. 1.) The increase in the carbon number (n) of the alkyl radical is accompanied with a large increase in $\tau(2)$ while it gives little effect upon $\tau(1)$. The most probable relaxation time τ_0 from the Cole-Cole equation based on the assumption $P_A+P_E\simeq 1.05\,R_D$ are also plotted in Fig. 1. For the sake of comparison the values τ_0' calculated on $P_A+P_E\simeq 1.10\,R_D$ are shown in the same figure by a broken line—the latter relaxation times are denoted by τ_0' in order to distinguish from τ_0 based on $P_A+P_E\simeq 1.05\,R_D$. Both τ_0 and τ_0' values increase with increasing chain length of the alkyl radical and eventually approach steady values of 3.0 and 3.5 ps, respectively. The above tendency, if it is true, could be explained by supposing that with long alkyl chains the dipole can rotate more or less freely without much affecting the other end of the chain to which it is attached.

According to the analysis[19] of the systems with two Debye dispersions, $\tau(1)$ obtained at a very high frequency *e.g.* 100 GHz is slightly larger than the shorter relaxation time, while $\tau(2)$ is a weighted mean of the two relaxation times and then the longer relaxation time becomes important. Although the present system seems to have more than two dispersions, the above results can be used in a qualitative manner. It is striking to notice that $\tau(1)$ for all the alkyl acetates have values between 1.2—1.4 ps which correspond to the relaxation time for a very small rotating unit. Contrary to $\tau(1)$, the other average relaxation time $\tau(2)$ regularly increases with increasing chain length, which may suggest that molecular rotation as a whole could occur to a certain extent. As shown before the probable relaxation time τ_0 approximates a geometrical average of $\tau(1)$ and $\tau(2)$ and its distribution parameter α increases with increasing chain length (see Table 3).

The free energy of activation ΔF^* can be calculated from the relaxation time τ by the following equation

$$\Delta F^* = 2.303RT\log\frac{kT\tau}{h} \qquad (13)$$

Table 4. Free energy of activation ΔF^* and heat of activation ΔH^* on the assumption of $\tau=\tau_0$ and $\Delta S^*=-1$ e.u.

Substance	ΔF^* (kcal/mol)	ΔH^* (kcal/mol)
Methyl acetate	1.52	1.22
Ethyl acetate	1.66	1.36
n-Butyl acetate	1.69	1.39
Isobutyl acetate	1.70	1.40
s-Butyl acetate	1.76	1.46
t-Butyl acetate	1.85	1.55
n-Amyl acetate	1.74	1.44
Isoamyl acetate	1.71	1.41
n-Hexyl acetate	1.70	1.40
n-Octyl acetate	1.73	1.43

where R is the gas constant and T is the absolute temperature and k, h are Boltzmann and Planck constants. Assuming τ is equal to τ_0, ΔF^* are estimated to have 1.5—1.9 kcal/mol for all the alkyl acetates. (See Table 4.)

The heat of activation is given by

$$\Delta H^* = \Delta F^* + T\Delta S^* \qquad (14)$$

The values ΔH^* recorded in Table 4 are obtained from ΔF^* on a very tentative assumption[20] $\Delta S^*=-1$ e.u. for all the acetates—it will be expected that ΔS^* will increase with increasing chain length, thus ΔH^* will become much larger. If $\tau(1)$ is used instead of τ_0, ΔF^* would become 1.2—1.3 kcal/mol and $\Delta H^*=0.9$—1.0 kcal/mol.

The observed dipole moments of alkyl acetates are 1.72—1.92 D, which are between those calculated for the *trans* 1.64 D and the *cis* 3.51 D. Consequently we may infer that the *cis* configuration is not completely ruled out but there are a small amount (3—10%) of the *cis* isomers present. Smyth[21] favored a view that a wide oscillation occurs about the *trans* position. From this viewpoint it is found that the average twisted configuration out of the *trans* position would have a dihedral angle 20—38°. Lastly there is the remaining possibility that the *trans* planar configuration alone exists with the observed polarity.[2]

From the probable dielectric relaxation times τ_0 and the distribution parameters α obtained in this work, we shall be able to say that all the alkyl acetates have multiple relaxation times and they have flexible and nonrigid configurations. The small value $\tau(1)=1.2$—1.4 ps suggests a small unit of rotation or a very small barrier for the rotating polar group. Estimated values of both ΔF^* and ΔH^* (using τ_0) are also small in magnitude compared with the size of the molecule.

In the present work a_∞ is very tentatively estimated on the assumption of $P_A+P_E\simeq 1.05\ R_D$. Alternatively, if the assumption of single Debye dispersion is valid, we can calculate a_∞ from[9]

$$a_\infty = a_G = a' - \frac{(a'')^2}{a_0-a'} \qquad (15)$$

and if Eq. (15) is used in acetates, we shall find both $\tau(1)$ and τ_0 to be equal to $\tau(2)$ and hence $\alpha=0$. However, the use of $a_\infty=a_G$ would result in a considerably

large atomic polarization which is inconsistent with experimental data. It seems that Eq. (15) is invalid and the dielectric system of acetates in benzene has multi-relaxation times.

We thank Professor Mansel Davies, the University College of Wales, for his interest in this work and also for correcting errors of English in this manuscript. We are also grateful to Toray Science Foundation for financial aids.

References

1) G. W. Wheland, "Resonance in Organic Chemistry," John Wiley, New York (1955), p. 235.
2) R. J. B. Marsden and L. E. Sutton, *J. Chem. Soc.*, **1936**, 1383.
3) G. Williams, N. L. Owen, and J. Sheridan, *Trans. Faraday Soc.*, **67**, 922 (1971).
4) R. F. Curl, *J. Chem. Phys.*, **30**, 1529 (1959).
5) J. M. Riveros and E. B. Wilson, Jr., *ibid.*, **46**, 4605 (1967).
6) J. Karpovitch, *ibid.*, **22**, 1767 (1954).
7) M. Ōki and H. Nakanishi, This Bulletin, **44**, 3144 (1971); **43**, 2558 (1970).
8) J. M. O'Gorman, W. Shand, Jr., and V. Schomaker, *J. Amer. Chem. Soc.*, **72**, 4222 (1950).
9) K. Chitoku, K. Higasi, M. Nakamura, Y. Koga, and H. Takahashi, This Bulletin, **44**, 992 (1971).
10) I. F. Halverstadt and W. D. Kumler, *J. Amer. Chem. Soc.*, **64**, 2988 (1942).
11) Y. Koga, H. Takahashi, and K. Higasi, This Bulletin, **46**, 3359 (1973).
12) K. Higasi, and O. Kiyohara *Bull. Res. Inst. Appl. Elect.*, **18**, 24 (1966).
13) K. S. Cole and R. H. Cole, *J. Chem. Phys.*, **9**, 341 (1941).
14) K. Higasi, This Bulletin, **39**, 2157 (1966).
15) K. V. Gopal Krishna, *Trans. Faraday Soc.*, **53**, 767 (1957).
16) F. J. Cripwell, G. B. B. M. Sutherland, *ibid.*, **42A**, 149 (1946).
17) D. H. Whiffen and H. W. Thompson, *ibid.*, **42A**, 114 (1946).
18) A. J. Curtis, P. L. McGeer, G. B. Rathmann, and C. P. Smyth, *J. Amer. Chem. Soc.*, **74**, 644 (1952).
19) K. Higasi, Y. Koga, and M. Nakamura, This Bulletin, **44**, 988 (1971).
20) K. Higasi, "Dielectric Relaxation and Molecular Structure," *Monogr. Res. Inst. Appl. Elect.*, Hokkaido Univ. Sapporo (1961), No. 9, pp. 9—16.
21) C. P. Smyth, "Dielectric Behavior and Structures," McGraw-Hill Book Company, New York (1955), pp. 303—311.

Theoretical Considerations of Lower Excited States of *trans*-Polyene Carbaldehydes. I. Electronic Structure and Oscillator Strength of π-π^* Transition

Kozo INUZUKA and Ralph S. BECKER*

Tokyo Electrical Engineering College, Kanda, Chiyoda-ku, Tokyo 101

**Department of Chemistry, University of Houston, Houston, Texas 77004, U.S.A.*

(Received July 9, 1973)

The lower n,π^* and π,π^* excited state energies of four *trans*-polyenecarbaldehydes, acrolein, 2,4-pentadienal, 2,4,6-heptatrienal, and 2,4,6,8-nonatetraenal, were calculated within the framework of the conventional P-P-P SCF-MO-CI method and then discussed. Also, the oscillator strength for the π-π^* transition was obtained in terms of the dipole length and the dipole velocity.

So far systematic studies of the electronic properties of polyenecarbaldehydes have been relatively rare. Among them, only two compounds, acrolein,[1-4] which is a fundamental molecule of this series, and retinal[5-10] which corresponds to 2,4,6,8,10-dodecapentaenal in the skeletal structure of the π-electron system, have been well studied both experimentally and theoretically in terms of their electronic properties. The purpose of this investigation was to study theoretically the properties of the lower electronic states of certain *trans*-polyenecarbaldehydes, that is, acrolein, 2,4-pentadienal, 2,4,6-heptatrienal, and 2,4,6,8-nonatetraenal. In this series we want to discuss the following three subjects from a theoretical point of view; (i) the electronic structure of the lower n,π^* and π,π^* states of *trans*-polyenecarbaldehydes and their oscillator strengths for π-π^* transition, (ii) their emission spectra, and (iii) their triplet-triplet transition and oscillator strength.

In this investigation the lower n,π^* and π,π^* excited-state energies of four *trans*-polyenecarbaldehydes were calculated within the framework of the conventional P–P–P SCF–MO–CI method[11,12] and then discussed. Also, their oscillator strengths for the π-π^* transition were obtained in terms of the dipole length and the dipole velocity.[13-15] These results were then compared with the experimental values.

Method of Calculation

Electronic Structure. The following numerical values[16] were assumed for the skeletal structure of the four polyenecarbaldehydes in the present paper: 1.36 Å for the carbon double bond, 1.46 Å for the single bond, and 1.22 Å for the carbonyl group. Moreover, the value of 120° was assigned to the ∠CCC and ∠CCO bond angles. *Only the trans and planar skeletal structures were taken into account.*

All the calculations were carried out within the framework of the general semi-empirical SCF-MO-CI method,[11,12] and the Pariser-Parr approximation[11] was used for the π-electron repulsion integrals, with Z_c= 3.25 and Z_o=4.55. All the penetration terms were neglected. The resonance integral for the nearest neighbor carbon atom was treated as a parameter, and the values of −2.50 and −2.30 eV were used for the carbon double and single bonds respectively. The resonance integral value for the carbonyl group was obtained by means of Kon's equation,[17] and the value of −2.67 eV was used for all the polyenecarbaldehydes. The n,π^* and π,π^* state energies were calculated including all singly-excited configurations.

On the other hand, Sidman[18] carried out n,π^* state energy calculations for the several carbonyl molecules within the framework of the P-P-P SCF-MO-CI method. He assumed that the energy of the *n*-orbital of the carbonyl molecule is constant, and −10.50 eV was assigned to the *n*-orbital energy of carbonyl molecule. In this paper, the *n*-orbital on the oxygen atom is assumed to be a 2pπ atomic orbital,[19] and its energy, ε_n, was calculated by means of the following equation:[19,20]

$$\varepsilon_n = U_n + \sum_{\mu \neq o}(P_{\mu\mu}-1)\gamma_{\mu n} + (P_{oo}-1)(\gamma_{no}-\delta_{no}/2) \quad (1)$$

The two one-center integrals concerning the oxygen atom, γ_{no} and δ_{no}, represent $\langle n_o\pi_o|r_{12}^{-1}|n_o\pi_o\rangle$ and $\langle n_o\pi_o|r_{12}^{-1}|\pi_o n_o\rangle$ respectively. The value of 12.865 eV[18] was used for the former integral, while the value of 0.903 eV[21] was assigned to the latter one. The $\gamma_{\mu n}$ is a two-center atomic repulsion integral between the π-electron of the carbon atom, μ, and the *n*-electron of the oxygen atom. The $\gamma_{\mu n}$ was calculated by means of the usual Pariser-Parr approximation.[11] U_n is treated as a parameter for the *n*-electron orbital energy. The calculated n,π^* singlet state energy of acrolein was adjusted to the corresponding observed value for acrolein by means of parameter, U_n, and the value of −15.25 eV was assigned to it. In a previous paper,[19] the value of −14.75 eV[22] was used for U_n, but this value brought about a lower value in the n,π^* singlet-state energy than the value observed in the case of the P–P approximation.

Oscillator Strength of the π-π^* Electronic Transition. A. Transition Density: In MO theory, the transition probability is related to the transition density, ρ. In the absence of degeneracy, the transition density for an allowed singlet absorption from a closed-shell ground state to an upper state is given by:

$$\rho = \sqrt{2}\,\phi_i\phi_j \quad (2)$$

where ϕ_i and ϕ_j are the molecular orbitals concerning an electron excitation. Expressing the molecular orbitals as linear combinations of atomic orbitals:

$$\phi_j = \sum_t c_{tj}\chi_t \quad (3)$$

one gets the transition density matrix, ρ, in the atomic

orbital basis with elements:

$$\rho_{st} = \sqrt{2}\, c_{st} c_{tj} \tag{4}$$

The transition moment becomes:

$$M = \sum_s \sum_t \rho_{st} m_{st} \quad \text{where } m_{st} = \langle \chi_s | r | \chi_t \rangle. \tag{5}$$

In an analogous manner, the transition gradient is:

$$D = \sum_s \sum_t \rho_{st} d_{st} \quad \text{where } d_{st} = \langle \chi_s | \text{grad} | \chi_t \rangle. \tag{6}$$

The oscillator strengths, f_1 and f_2, are given by Eqs. (7) and (8):

$$f_1 = 1.085 \times 10^{11} \nu M^2 \tag{7}$$

$$f_2 = 1.465 \times 10^5 D^2/\nu \tag{8}$$

where ν is in wave number and where the integral is expressed in atomic units. In the present calculation, the f_1 oscillator strength is represented in terms of the conventional dipole length assuming a zero-differential overlap.

B. Transition Gradient Integral: In Cartesian coordinates in terms of the unit vectors, **i**, **j**, and **k**, the transition gradient integral between 2pπ atomic orbitals, a and b, is expressed by Eq. (9):

$$\langle a | \sum_j \nabla_j | b \rangle = (\mathbf{i} \cos x_{ab} + \mathbf{j} \cos y_{ab} + \mathbf{k} \cos z_{ab}) V_{ab} \tag{9}$$

where $\cos x_{ab}$ is the direction cosine of the directed line connecting the atom a to the atom b with respect to the x axis. Similarly for y and z, V_{ab} is the absolute value of the $\langle x_a | \nabla | x_b \rangle$. The only component which contributes to the integral, V_{ab}, is the one directly along the bond from the atom a to the atom b, because of the symmetry of the 2pπ atomic orbital, the value of the intergral remains unchanged by reflection in the plane perpendicular to the orbital axis.

Let the molecule lie on the y z plane and let the 2pπ atomic orbital be along the x-axis. Then, the 2pπ atomic orbital of the q atom is:

$$\chi_q = (\mu_q^5/\pi)^{1/2} r \exp(-\mu_q r) \sin\theta \cos\phi \tag{10}$$

The μ_q corresponds to the Slater-μ-value of the orbital exponent of the q atom. In the present calculation, the values of 1.625 and 2.275 were used as the Slater-μ-values for the carbon and oxygen atoms respectively. The z axis is taken directly along the bond from the a atom to the b atom. The z component of the gradient primitive integral is:

$$V_{ab} = \langle \chi_a | \partial/\partial Z | \chi_b \rangle \tag{11}$$

Then,

$$V_{ab} = -\mu_b \langle \chi_a | z/r | \chi_b \rangle \tag{12}$$

The integral (12) was transformed into elliptical coordinates[23] after the substitution of the atomic orbital (10); it was evaluated as follows:

$$V_{ab} = -\mu_b (R/2)^5 (\mu_a \mu_b)^{5/2} \{(B_1 - B_3)(A_4 - 2A_2 + A_0) + (B_4 - 2B_2 + B_0)(A_1 - A_3)\} \tag{13}$$

In the case of $t=0$, Eq. (12) may be simplified as follows:

$$V_{ab} = -\mu_b (p/5)(1 + p + p^2/3) \exp(-p) \tag{14}$$

where

$$p = (1/2)(\mu_a + \mu_b) R/a_0, \quad t = (\mu_a - \mu_b)/(\mu_a + \mu_b) \tag{15}$$

R is the bond distance between the a and b atoms, and a_0 is the Bohr radius (0.529 Å).

Results and Discussion

The calculated results of the π,π^* state energy and the oscillator strength of the present polyenecarbaldehydes are shown in Table 1, along with their calculated n,π^* state energies. The calculated values for the lowest singlet and triplet states are plotted in Fig. 1. The calculated n-π^* transition energies for the

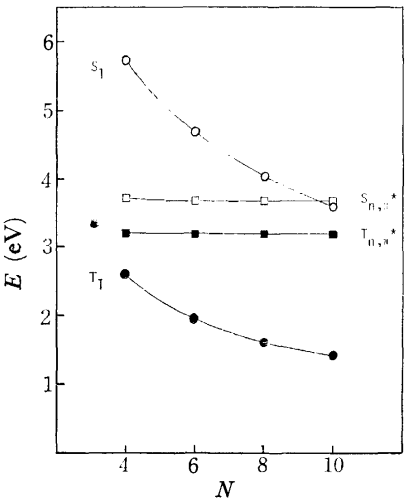

Fig. 1. Calculated lowest n,π^* and π,π^* state energies of *trans*-polyene aldehydes. N corresponds to the number of atom in the conjugated system of polyene aldehyde.

four *trans*-polyenecarbaldehydes from acrolein to 2,4,6,8-nonatetraenal are almost all the same. The present theoretical calculation suggests that the n,π^* singlet state is lower than the π,π^* singlet state from *trans*-acrolein to *trans*-2,4,6-heptatrienal, while the former state of *trans*-2,4,6,8-nonatetraenal is higher than its latter state. However, from the experimental fact about retinals,[7] the n,π^* singlet state of *trans*-2,4,6,8-nonatetraenal may be still lower than its π,π^* state. Judging from the experimental results[7] and the fact that the π-electronic structure of retinal is not exactly the same as that of the corresponding polyenecarbaldehyde because of the difference in the molecular structure between retinal and dodecapentaenal, the relative order of the n,π^* and π,π^* singlet states of dodecapentaenal may be critical. The n,π^* singlet state of a polyenecarbaldehyde larger than dodecapentaenal should be higher than its π,π^* singlet state.

On the other hand, all the calculated n,π^* triplet states of the present molecules are higher than their π,π^* triplet states, though the experimental result for acrolein shows that the n,π^* triplet state, 3.01 eV,[4,24] is lower than the π,π^* triplet state, 3.05 eV.[3] The energy difference in acrolein between the n,π^* singlet and triplet states is about 0.7 and 0.5 eV in the experimental and theoretical values respectively. The energy difference between the two states depends on the one-center integral, $\langle n_O \pi_O | r_{12}^{-1} | \pi_O n_O \rangle$; the value of 0.903 eV[21] was assigned to that. To improve the present difference, a larger one-center integral value may be better. Plotnikov[25] used the value of 1.26 eV for this

Table 1. Calculated n,π^* and π,π^* singlet and triplet state energies of *trans*-polyenecarbaldehydes (in eV)

Molecule	Sym.	Singlet					Triplet	
		E_{calcd}	E_{obsd}	f_1	f_2	f_{obsd}	E_{calcd}	E_{obsd}
Acrolein								
1	A′	5.746	5.96[a]	0.852	0.427		2.630	3.05[b]
2	A′	7.351		0.063	0.018		4.187	
3	A′	8.006		0.048	0.016		7.572	
1	A″	3.720	3.71[a]				3.207	3.01[c]
2,4-Pentadienal								
1	A′	4.685	4.60[d]	1.285	0.576	0.58[d]	1.957	
2	A′	6.603		0.012	0.012		3.419	
3	A′	6.671		0.053	0.010		4.273	
1	A″	3.694	3.50[d]				3.190	
2,4,6-Heptatrienal								
1	A′	4.039	4.06[e]	1.688	0.708	0.86[e]	1.616	2.2[f]
2	A′	5.836		0.060	0.013	0.14	2.778	
3	A′	5.939		0.004	0.013		3.778	
1	A″	3.693					3.193	
2,4,6,8-Nonatetraenal								
1	A′	3.609	3.65[d]	2.055	0.821		1.423	1.9[f]
2	A′	5.298		0.049	0.019		2.336	
3	A′	5.401		0.012	0.018		3.264	
1	A″	3.694					3.197	

a) See Ref. 2. b) See Ref. 3. c) See Ref. 4. d) See Ref. 29. This f number corresponds to that of 2,4-hexadienal which was calculated from the data in Ref. 29. e) See Ref. 30. f) See Ref. 26.

integral in his calculation. The calculated n,π^* triplet states of the other molecules are higher than their π,π^* triplet states. This result seems reasonable in view of experimental results on acrolein and the n,π^* and π,π^* singlet-triplet energy separation.

Judging from the present results, the lowest triplet state of polyenecarbaldehyde may be said to be of the π,π^* character, but not of the n,π^* character except for the case of acrolein. The slope of the n,π^* state energy curves in Fig. 1 is nearly flat compared with that of the π,π^* state energy curves. This result suggests that the lowest n,π^* triplet state may also be higher than the lowest π,π^* singlet state from the polyenecarbaldehyde larger than nonatetraenal. The calculated π,π^* triplet state energies of the present molecules are not in good agreement with the observed values.[26] The energy difference between the calculated and observed values is within the range of about 0.5 eV. The theoretical values are lower than the experimental values.[26] A similar result was reported by Forster[27] in the triplet-state calculation of polyene by the SCF-MO method using the Mataga-Nishimoto approximation.[28] In his case, the calculated values range from 1.43 to 0.98 eV as the carbon chain varies from C_4 to C_{22}. We also have obtained the similar result that SCF-MO calculation using the Mataga-Nishimoto approximation gives lower values than the values calculated by means of the Pariser-Parr integral with respect to the triplet state of polyenecarbaldehyde. Figure 1 shows that the singlet-triplet splitting of polyenecarbaldehyde decreases in the n,π^* and π,π^* states as the number of the atom in the conjugated system increases.

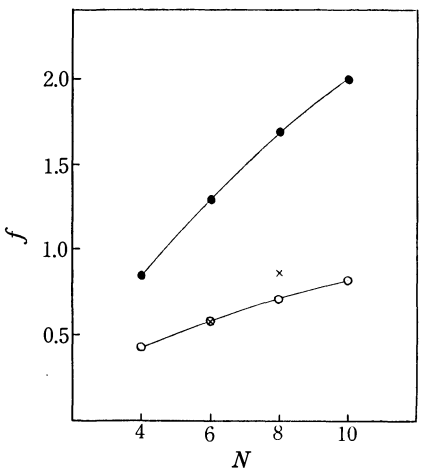

Fig. 2. Oscillator strength of the lowest π-π^* transition of *trans*-polyene aldehydes.
● corresponds to f_1, ○ to f_2, and × to f_{obsd}

The oscillator strengths, f_1, f_2, and f_{obsd}, are plotted in Fig. 2. The oscillator strengths calculated by means of Eq. (7) are larger than the observed values, and they increase rapidly as the number of the atom, N, increases. The ratio of f_1 to f_{obsd} is about 2.

On the other hand, the oscillator strengths calculated by means of Eq. (8) are smaller than the observed values, but the agreement between them is much better. The ratio of f_2 to f_{obsd} ranges from 0.8 to 1. The trend of the f_2 curve is closer to that of f_{obsd} than the trend of the f_1 curve in Fig. 2. Comparison with the

both theoretical results suggests that the dipole-velocity treatment is better than the dipole-length method in the molecular orbital calculation of conjugated molecules as long as the point charge approximation is adopted to the calculation of the oscillator strength.

This work was supported by grants from the Tokyo Electrical Engineering College (T. E. E. C.) Research Fund and from the Robert A. Welch Foundation. One of authors (K. I.) especially wishes to acknowledge the assistance of the staff of the T. E. E. C. Computing Center in the present work. He would also like to thank the referee his kind opinions and suggestions.

References

1) R. S. Becker, K. Inuzuka, and J. King, *J. Chem. Phys.*, **52**, 5164 (1970).
2) K. Inuzuka, This Bulletin, **34**, 6, 729 (1961).
3) J. M. Hollas, *Specrtochim. Acta*, **19**, 1425 (1963).
4) J. C. D. Brand and D. G. Williamson, *Discuss. Faraday Soc.*, **35**, 184 (1963).
5) K. Inuzuka and R. S. Becker, *Nature*, **219**, 383 (1968).
6) R. S. Becker, K. Inuzuka, and D. E. Balke, *J. Amer. Chem. Soc.*, **93**, 38 (1971).
7) R. S. Becker, K. Inuzuka, J. King, and D. E. Balke, *ibid.*, **93**, 43 (1971).
8) D. E. Balke and R. S. Becker, *ibid.*, **89**, 5061 (1967).
9) D. E. Balke and R. S. Becker, *ibid.*, **90**, 6710 (1968).
10) J. R. Wiesenfeld and E. W. Abrahamson, *Photochem. Photobiol.*, **8**, 487 (1968).
11) R. Pariser and R. G. Parr, *J. Chem. Phys.*, **21**, 466, 767 (1953).
12) J. A. Pople, *Trans. Faraday Soc.*, **49**, 1375 (1953).
13) D. P. Chong, *Mol. Phys.*, **14**, 275 (1968).
14) C. P. Yue and D. P. Chong, *ibid.*, **14**, 487 (1968).
15) A. J. McHugh and M. Gouterman, *Theoret. Chim. Acta*, **13**, 249 (1969).
16) H. Mackle and L. E. Sutton, *Trans. Faraday Soc.*, **47**, 691 (1951).
17) H. Kon, This Bulletin, **28**, 275 (1955).
18) J. W. Sidman, *J. Chem. Phys.*, **27**, 429 (1957).
19) K. Inuzuka and R. S. Becker, *ibid.*, **45**, 1557 (1972).
20) P. Lindner, R. Manne, and O. Martensson, *Theoret. Chim. Acta*, **5**, 406 (1966).
21) J. M. Parks and R. G. Parr, *J. Chem. Phys.*, **32**, 1657 (1960).
22) H. A. Skinner and H. O. Pritchard, *Trans. Faraday Soc.*, **49**, 1254 (1953).
23) R. S. Mulliken, C. A. Rieke, D. Orloff, and H. Orloff, *J. Chem. Phys.*, **17**, 1248 (1949).
24) W. H. Eberhard and H. Renner, *J. Mol. Spectrosc.*, **6**, 483 (1961).
25) V. G. Plotnikov, *Opt. Spectrosc.*, **20**, 217 (1966).
26) D. F. Evans, *J. Chem. Soc.*, **1960**, 1735.
27) L. S. Forster, *Theoret. Chim. Acta*, **5**, 81 (1966).
28) N. Mataga and K. Nishimoto. *Z. Phys. Chem.*, **13**, 140 (1957).
29) E. R. Blout and M. Fields, *J. Amer. Chem. Soc.*, **70**, 189 (1948).
30) H. Hosoya, J. Tanaka, and S. Nagakura, *Tetrahedron*, **18**, 859 (1962).

Interaction between Carbon Dioxide and the Zinc Oxide Surface

Tetsuo MORIMOTO and Kunimitsu MORISHIGE

Department of Chemistry, Faculty of Science, Okayama University, Tsushima, Okayama 700

(Received May 1, 1973)

The adsorption of carbon dioxide has been measured at 25 °C on zinc oxide surfaces with different amounts of preadsorbed carbon dioxide. As a result, it has been found that carbon dioxide molecules are chemisorbed more weakly to zinc oxide surfaces than water; the desorbability of carbon dioxide is almost complete upon evacuation at temperatures higher than 300 °C, whereas upon evacuation at 25 °C 80% of the carbon dioxide remains on the surface. Also, the adsorption isotherms of carbon dioxide have been obtained at 25 °C on differently-hydroxylated surfaces of zinc oxide. On such surfaces, the adsorption amount of carbon dioxide decreases linearly with an increase in the amount of surface hydroxyl groups. This suggests that most of the carbon dioxide is adsorbed strongly on the vacant sites formed by dehydroxylation, and not on the surface hydroxyl groups.

Recently, it has been reported that surface hydroxyl groups react with carbon dioxide to form bicarbonate species on a variety of metal oxides.[1-5] Especially, Boehm has applied the adsorption measurement of carbon dioxide to the titration of basic hydroxyl groups on η-Al_2O_3.[2] On the other hand, Taylor and Amberg[6] and Hockey *et al.*[7] have discovered, from IR studies, that absorption bands due to surface hydroxyl groups on zinc oxide are not disturbed by the chemisorption of carbon dioxide. It would probably be difficult to ascertain the formation of bicarbonate species on zinc oxide surfaces from such IR spectra, since the perturbation in the surface hydroxyl region due to bicarbonate formation is very small.

Consequently, it seems that it would be interesting to examine the adsorption of carbon dioxide on zinc oxide in connection with the population of surface hydroxyl groups. Hitherto, though many authors have measured the adsorption isotherms of carbon dioxide on zinc oxide, most of them have been concerned with the measurements to obtain isosteric heats of adsorption at elevated temperatures.[8-11] Very recently, it has been found[12,13] that surface hydroxyl groups on zinc oxide can be removed by degassing at rather higher temperatures, and that a two-dimensional condensation of water occurs on such hydroxylated surfaces. In relation to these problems, the measurements of the adsorption of various gases on well-defined zinc oxide surfaces are desirable.

This work will deal with the interaction between carbon dioxide and zinc oxide surfaces covered with controlled amounts of preadsorbed carbon dioxide or surface hydroxyl groups, on the basis of the adsorption measurements of carbon dioxide at room temperature.

Experimental

Materials. Zinc oxide was prepared by burning zinc metal in air in our laboratory. The purity of the zinc metal used was, according to the maker's assay, 0.01% Pb, 0.002% Cu, 0.005% Cd and Fe, 0.00005% As, and traces of S and P. X-ray analysis showed that the zinc oxide thus prepared was highly crystalline. Carbon dioxide gas from dry ice was purified by trapping and degassing at the temperature of liquid nitrogen and by following to sublimation at the temperature of the dry ice-ethanol mixture.

Adsorption of Carbon Dioxide. The adsorption of carbon dioxide was measured volumetrically by means of a conventional adsorption apparatus equipped with an oil manometer. Prior to the adsorption measurements, a zinc oxide sample of *ca.* 6 g was degassed at 600 °C under a reduced pressure of 10^{-5} Torr for 30hr in order to remove the chemisorbed water and carbon dioxide.

The adsorption isotherm of carbon dioxide was first measured at 25 °C on a fresh surface of a sample degassed at 600 °C. After this, the sample was degassed for 4 hr at 25 °C and was then applied to the second adsorption isotherm at 25 °C. By increasing the degassing temperatures, the adsorption isotherms on the surfaces with partially-preadsorbed carbon dioxide were obtained at 25 °C by using the same sample.

In order to examine the influence of surface hydroxyl groups upon the adsorption of carbon dioxide, the sample was degassed for 30 hr at 600 °C and was then exposed to the saturated water vapor over night at room temperature. This sample was again degassed for 4hr at different temperatures (100, 300, 350, and 400 °C) to prepare differently-hydroxylated surfaces. On these surfaces, the adsorption of carbon dioxide was measured at 25 °C.

Measurement of the Water Content. The surface water content was measured by the successive-ignition-loss method on a sample which had been pretreated at 600 °C, exposed to the saturated water vapor overnight at room temperature, and degassed for 4 hr at 30 °C in a vacuum of 10^{-5} Torr in order to remove the physisorbed water. A small amount of carbon dioxide expelled from the sample together with the water vapor was removed from the mixture by evacuating the mixture in a condensed state at −78 °C.[14]

Measurement of the Surface Area. The surface area of zinc oxide was measured by the BET method with nitrogen as an adsorbate. The specific surface area of the sample evacuated at 600 °C for 30 hr was 3.5 m^2/g.

Results and Discussion

The adsorption amount of carbon dioxide at 300 °C on the zinc oxide evacuated at 600 °C for 30 hr changes with the time, as is shown in Fig. 1. It can be seen from Fig. 1 that the initial fast adsorption is followed by a slow process for every dose of carbon dioxide, and that the slow adsorption increases linearly with the time and that its rate is proportional to the pressure. The adsorption at the initial stage is too rapid to pursue accurately by means of an oil manometer, and it largely finishes within a few minutes. The same trend also appears in adsorption experiments at different temperatures, but the lower the adsorption temperature, the shorter the time required for the attainment of

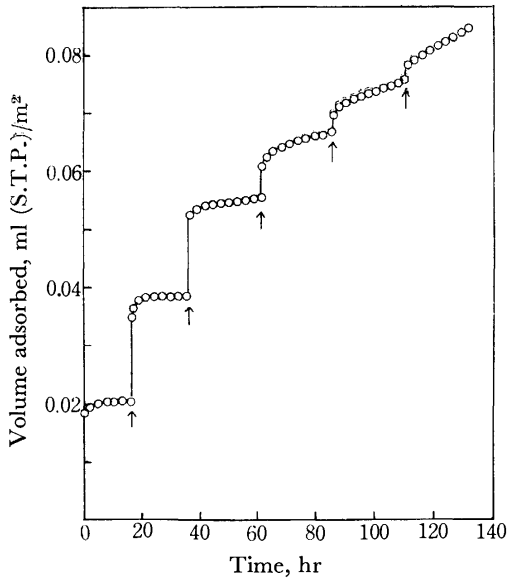

Fig. 1. Change in the amount of adsorbed CO_2 with time; arrows indicate admissions of small amount of CO_2.

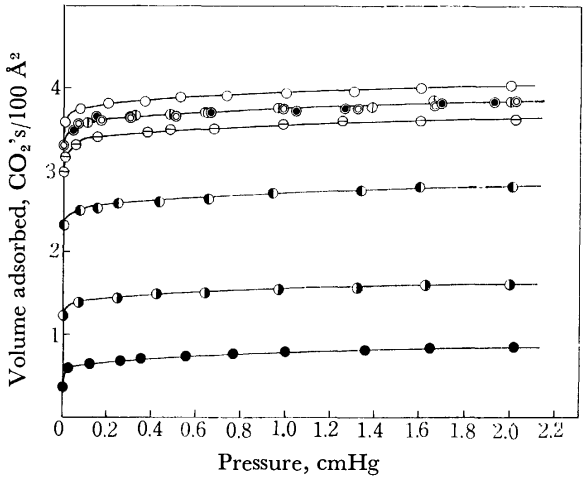

Fig. 2. Adsorption isotherms (25 °C) of CO_2 on ZnO pretreated at various temperatures. ○: after initial degassing at 600, ●: after degassing at 25, ◑: 100, ◐: 200, ⊖: 300, ◎: 400, ⊙: 500, ⓘ: 600 °C.

the adsorption equilibrium. Thus, it follows that the adsorption measurements based on the pressure reading within one or two hours after every dose of carbon dioxide should refer only to the fast adsorption.

Figure 2 is an example of the adsorption isotherms of carbon dioxide obtained at 25 °C over various surfaces with preadsorbed carbon dioxide; the ordinate is expressed in the number of carbon dioxide molecules adsorbed per 100 Å² of the surface. The isotherm obtained on a fresh surface degassed at 600 °C is much higher than that obtained on a sample degassed at 25 °C after the first adsorption experiment. The amount of carbon dioxide adsorbed on the surfaces with preadsorbed carbon dioxide increases with the evacuating temperature, and approaches that on the fresh surface when the surfaces are evacuated above 300 °C. All the adsorption data thus obtained can be

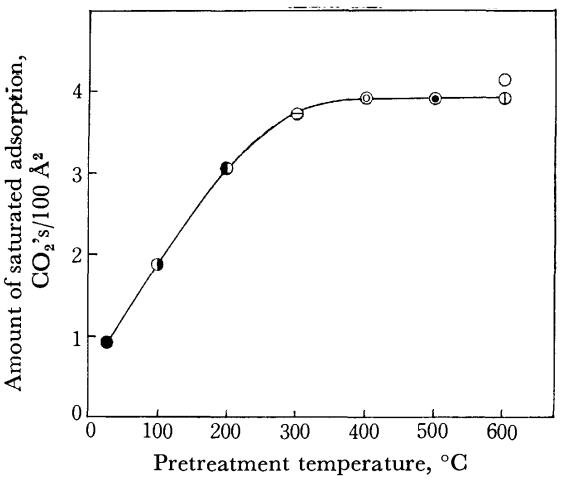

Fig. 3. Dependence of the amount of adsorbed CO_2 at 25 °C upon degassing temperature, ○: after initial degassing at 600, ●: after degassing at 25, ◑: 100, ◐: 200, ⊖: 300, ◎: 400, ⊙: 500, ⓘ: 600 °C.

expressed approximately by the Langmuir equation, which makes it possible to calculate the saturated values of adsorbed carbon dioxide, as is shown in Fig. 3. It may be seen clearly from Fig. 3 that the higher the degassing temperature before the second adsorption, the larger the second adsorption amount of carbon dioxide; the amount of adsorption on the zinc oxide degassed at 300 °C is approximately equal to that on the zinc oxide degassed at 600 °C. In other words, the carbon dioxide adsorbed on zinc oxide is almost completely desorbed at temperatures higher than 300 °C, while about 20% of the adsorbed carbon dioxide can be removed by evacuation at 25 °C.

Infrared studies performed by Taylor and Amberg[6] point out that the adsorption of carbon dioxide on zinc oxide at room temperature can be classified into three types of adsorption: physisorption, and weak and strong chemisorption, and that the former two are desorbable by degassing at room temperature. Therefore, the 80% of the carbon dioxide remaining on zinc oxide surfaces may be the strong chemisorption of Taylor's classification.

Table 1. Water content of zinc oxide (OH's/100 Å²)

Treatment	Initial 600 °C[a]	After hydration[b]	Temperature (°C) 100	200	300	350	400	500
Water content	0.34	9.13	8.82	7.17	7.00	4.86	2.63	1.53

a) Degassed at 600 °C for 30 hr.
b) Exposed to the saturated water vapor overnight at room temperature, and then degassed at 30 °C for 4 hr.

The water content of zinc oxide is given in Table 1, which is the number of surface hydroxyl groups remaining on 100 Å² of the surfaces pretreated at the temperatures indicated. It is known that only a small amount of the surface hydroxyl groups on zinc oxide can be desorbed by evacuation up to 300 °C, while most of them can be removed at temperatures ranging

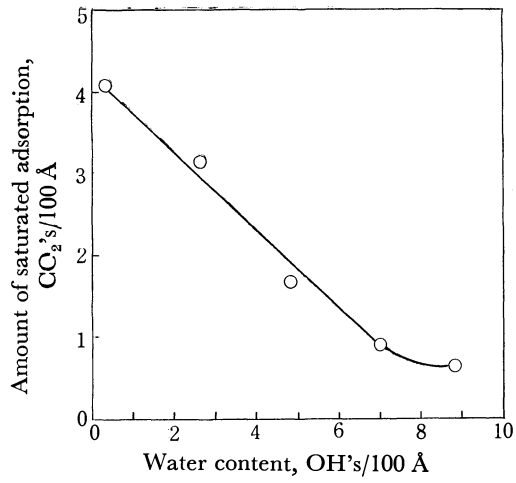

Fig. 4. Relation between amount of adsorbed CO_2 and water content on ZnO.

from 300 to 400 °C.[13] On the other hand, a large part of the strongly-adsorbed carbon dioxide can be removed by evacuating up to 300 °C, as may be seen from Fig. 3. This indicates that water is chemisorbed more strongly than carbon dioxide on the surface of zinc oxide. The adsorption isotherms of carbon dioxide, which were of the same type as those shown in Fig. 2, were also obtained at 25 °C on such differently-hydroxylated zinc oxides as are listed in Table 1. The amounts of the saturated adsorption of carbon dioxide computed from the isotherms are plotted against the water content in Fig. 4. It can be seen from Fig. 4 that the amounts of adsorbed carbon dioxide decrease linearly with an increase in the amount of the remaining surface hydroxyl groups. This suggests that carbon dioxide can be chemisorbed on the vacant sites free from hydroxyl groups; accordingly, under the conditions studied at least most of the chemisorbed carbon dioxide is not combined with the surface hydroxyl groups to form bicarbonate species, contrary to the results reported for the other systems of metal oxide-carbon dioxide.[1-5]

The authors wish to express their thanks to Dr. Mahiko Nagao for his kind advice during this study.

References

1) A. Zecchina, S. Coluccia, E. Guglielminotti, and G. Ghiotti, *J. Phys. Chem.*, **75**, 2790 (1971).
2) H. P. Boehm, *Discuss. Faraday Soc.*, **52**, 264 (1971).
3) Ya. M. Grigor'ev, D. V. Pozdnyakov, V. N. Fillimonov, *Zh. Fiz. Khim.*, **46**, 316 (1972).
4) J. V. Evans, T. L. Whateley, *Trans. Faraday Soc.*, **63**, 2679 (1967).
5) N. N. Parkyns, *J. Phys. Chem.*, **75**, 526 (1971).
6) J. H. Taylor and C. H. Amberg, *Can. J. Chem.*, **39**, 535 (1961).
7) K. Atherton, G. Newbold, and J. A. Hockey, *Discuss. Faraday Soc.*, **52**, 33 (1971).
8) Y. Kubokawa and O. Toyama, This Bulletin, **35**, 1407 (1962).
9) R. J. Kokes and R. Glemza, *J. Phys. Chem.*, **69**, 17 (1965).
10) P. M. G. Hart and F. Sebba, *Trans. Faraday Soc.*, **56**, 557 (1960).
11) T. Kwan, T. Kinuyama, and Y. Fujita, *J. Res. Inst. Catalysis, Hokkaido Univ.*, **3**, 31 (1953).
12) M. Nagao, *J. Phys. Chem.*, **75** 3822 (1971).
13) T. Morimoto, M. Nagao, and F. Tokuda, This Bulletin, **41**, 1533 (1968).
14) T. Morimoto, M. Nagao, and F. Tokuda, *J. Phys. Chem.*, **73**, 243 (1969).

Emission Spectra of Carbon Disulfide, Hydrogen Sulfide, and Thiols by Controlled Electron Impact

Minoru TOYODA, Teiichiro OGAWA, and Nobuhiko ISHIBASHI
Faculty of Engineering, Kyushu University, Hakozaki, Fukuoka 812
(Received May 22, 1973)

The emission spectra in the 200—600 nm region produced by the controlled electron impact method were investigated in the vapor phase on hydrogen sulfide, carbon disulfide, methanethiol, and ethanethiol at low pressures. The photoemissions were observed and assigned for an excited parent molecule, molecular ions, and fragments, such as CS_2, CS_2^+, H_2S^+, H, CH, CS, and HS^+. The intensities of the photoemission of most of the species were found to increase linearly with both the electron beam current and the gas pressure, and these species were concluded to be produced in some one-electron unimolecular processes.

The formation of excited molecules and excited molecular ions and their emission spectra have been investigated by a number of methods for excitation, such as by photons, flames, or electric discharges.[1] Although these methods are useful for chemical analyses, secondary reactions induce difficulties in a detailed analysis of the mechanism of fragmentation and excitation processes of the species concerned. A crossed-beam technique, in which the molecular vapor is excited by a controlled electron source, has been employed in recent years to overcome the above difficulties.[2] Since the gas pressure can be kept very low in the controlled electron impact method, the effect of molecular collisions is greatly reduced and, consequently, the bands of the primarily excited species appear with relatively high intensity. It is, therefore, possible to observe primary reactions more accurately; this may lead not only to the elucidation of the fragmentation processes of the parent molecule, but also to the information about the collision phenomena.

The emission spectra of aromatic molecules by controlled electron impact have been reported by the present authors.[3] Those of CS_2 and H_2S have been measured by Smith[4] and by Horani *et al.*[5,6] respectively, and the bands of CS ($A^1\Pi$—$X^1\Sigma^+$), CS_2^+ ($\tilde{B}^2\Sigma_u^+$—$\tilde{X}^2\Pi_g$), HS^+ ($A^3\Pi$—$X^3\Sigma^-$), and H_2S^+ (A^2A_1—$\tilde{X}^2B_1$) have been observed and assigned. In the present paper, the emission spectra of carbon disulfide, hydrogen sulfide, methanethiol, and ethanethiol under excitation by a controlled electron beam will be presented, and the mechanism of the excitation will be discussed in relation to the intensity measurements.

Experimental

The experimental method used in the present work has been described in detail in the previous papers.[3,7] The electrons from a heated tungsten filament were accelerated and introduced into the collision chamber through a slit (2×15 mm). The energies of the electrons were externally controlled from 15 to 300 eV. The sample gas was jetted through a nozzle (0.1 mm in diameter) and collided with the electron beam. The pressure during the operation, as measured with a Penning gauge, was of the order of 10^{-4} mmHg, though the density of the gas in the middle of the molecular jet was higher. The photoemission produced by collisions between electrons and molecules was measured photoelectrically with either a Jarrell Ash JE-25 or a JASCO CT-50 monochromator.

The H_2S was obtained from the Takachiho Chemical Ind., while the D_2S was prepared from FeS and D_2SO_4. The HDS[8] was prepared from FeS and a 1:1 mixture of H_2SO_4 and D_2O. The methanethiol was purchased from the Matheson Co., and the CS_2 and the ethanethiol, from the Wako Pure Chemical Ind. The samples were frozen and degassed repeatedly before use.

Results and Discussion

Carbon Disulfide. A typical emission spectrum of carbon disulfide in the 220—320 nm region is shown in Fig. 1. The impact energy was 100 eV with the electron beam current of 100 μA. The spectrum is in good agreement with the published one; the bands around 260 nm are assigned to CS ($A^1\Pi$—$X^1\Sigma^+$) and the most intense bands at 282 and 285 nm to CS_2^+ ($\tilde{B}^2\Sigma_u^+$—$\tilde{X}^2\Pi_g$).[4]

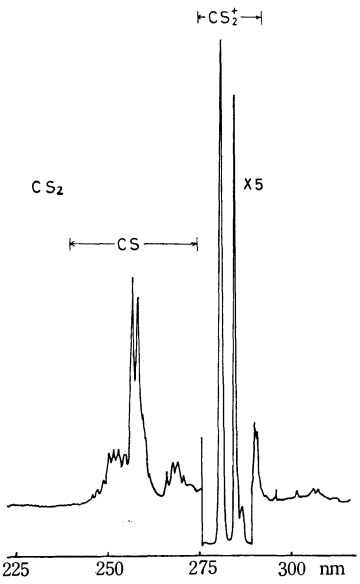

Fig. 1. Emission spectrum obtained from CS_2 excited by 100 eV electrons in the region of 220—320 nm. Beam current, 100 μA.

A typical spectrum of carbon disulfide in the 300—650 nm region is shown in Fig. 2. There seem to be two emission systems in this region, judging from the different intensity ratios for various impact energies. The first one is a continuous band extending from 340 to 640 nm. The second one, which is superimposed

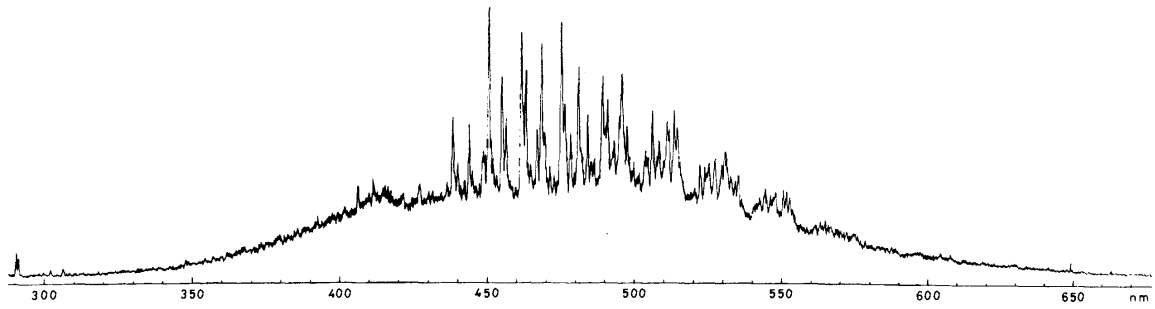

Fig. 2. Emission spectrum obtained from CS_2 excited by 200 eV electrons in the region of 300—650 nm. Beam current, 250 μA.

on the first one, is much sharper, shows a vibrational structure, and disappears much more rapidly than the other at lower impact energies. The intensities of the photoemission of these bands were determined for various currents of the incident electrons and were found to be proportional to the electron beam current, as is shown in Fig. 3.

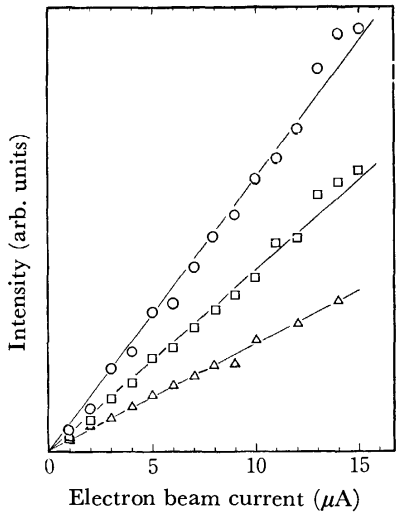

Fig. 3. Dependence of photoemission intensities of CS_2 (△), CS_2^+ (A–X transition) (○) and CS_2^+ (B–X transition measured in the second order) (□) from CS_2 on electron beam current. Electron energy was 200 eV.

The first band system in the 300—650 nm region is similar to the one observed in the discharge[9] and has been assigned to the CS_2 fluorescence. Arnold and Kimbel proposed a three-body recombination mechanism for this emission. In the present study, however, the pressure in the collision chamber is so low ($<10^{-2}$ mmHg) that the intermolecular collision seems to be negligible. An alternative suggestion as to the mechanism for the emission of CS_2* in the present research would be a direct excitation of CS_2;

$$CS_2 \xrightarrow{e} CS_2^* \longrightarrow CS_2 + h\nu$$

The linearity of the emission intensity to the electron beam current supports this mechanism. Furthermore, the finding that the intensity of this band relative to that of CS_2^+ at 282 nm did not vary with the pressure supports the above conclusion.

The second band system has complicated vibrational structures; the apparent intensity of the 449 nm band

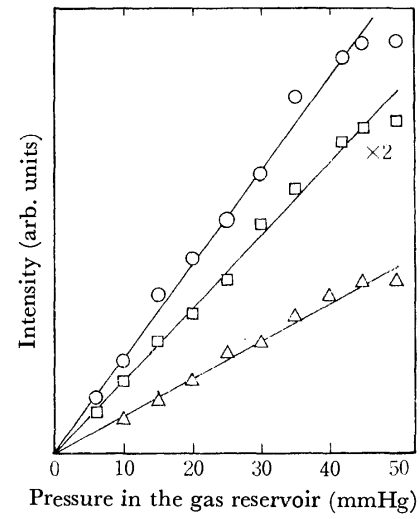

Fig. 4. Dependence of photoemission intensities of CS (△), CS_2^+ (A–X transition) (○) and CS_2^+ (B–X transition) (□) on gas pressure in the gas reservoir. Electron energy was 300 eV and beam current, 20 μA.

(the strongest one in this region) is about 1/10 of that of the 282 nm band of CS_2^+ (the quantum efficiency was not calibrated). The emission intensities of these bands are also proportional to the electron beam current and to the gas pressure, as are shown in Figs. 3 and 4 respectively. These facts suggest that the emitting species are produced directly from the parent molecules, as are those of the first band. The emission spectra of a mixture of CS_2 and H_2 was measured by this method as well as that of CS_2 and H_2S. The spectra were superpositions of the bands of the two parent molecules. These bands also appeared in the spectrum of methanethiol; in this case the intensity ratio between the band at 449 nm and that at 282 nm (CS_2^+) is about 1/10 as it is in the case of carbon disulfide, though the intensity of CS_2^+ from methanethiol is much smaller than that of CS. Among the possible photoemitting species of these bands, such as CS_2, CS, C, S or their ions, the complicated appearance of the band and related data in the literature[1,10] make it possbile to exclude the atomic species. If they were CS or CS^+, they should appear in the cases of thiols and methyl phenyl sulfide with much higher intensities. Furthermore, the A–X transition of the CS radical is in the region of 240—290 nm,[1] which is not coincident with that of the second bands. The adiabatic and the vertical transition energies of CS_2^+ to the first excited

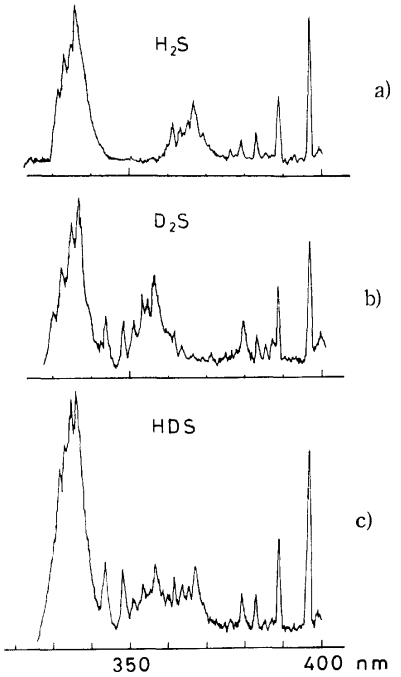

Fig. 5. Emission spectra obtained from H_2S (a), D_2S (b) and HDS[8] (c) excited by 200 eV electrons. Beam current, 500 μA.

state were determined to be 2.63 eV (472 nm) and 2.77 eV (448 nm).[11] The latter coincides with the position of the strongest band in the present spectrum. These results suggest that this second band can be assigned to CS_2^+ ($A^2\Pi_u$—$\tilde{X}^2\Pi_g$).

Hydrogen Sulfide. Some typical emission spectra of H_2S, D_2S, and HDS[8] in the region of 330—400 nm are shown in Fig. 5. The impact voltage was 200 V and the electron beam current was 500 μA in these measurements. The sharp lines at 486, 434, 410, 397, and 389 nm, which have been observed for all the molecules containing the hydrogen atom, are assigned to the hydrogen Balmer series. There are two intense bands at about 336 nm and at about 366 nm in the spectrum of H_2S; the latter seems to shift toward the shorter wavelength side, at about 357 nm, in the spectrum of D_2S. The spectrum of HDS may be regarded as a superposition of those of H_2S and D_2S. This finding suggests that these bands are related to a diatomic molecule containing both a hydrogen and a sulfur atom. This is confirmed by the facts that these bands also appeared in the spectra of methanethiol, ethanethiol, and benzenethiol, whereas they did not appear in CS_2, H_2, methyl phenyl sulfide or thiophene, which have no H–S bond; they may not form such species as HS since two-body collisions are infrequent at the pressure of $10^{-2\sim-3}$ mmHg. The A–X transition of the HS radical was observed below 324 nm[1] and seems to be undetectable in the emission because of predissociation.[12] Thus these bands can be assigned to the A–X transition of HS^+ and DS^+ radicals, as Horani *et al.* indicated.[5] The separations between successive bands of HS^+ and DS^+ are estimated to be 2470 ± 100 cm^{-1} and 1790 ± 100 cm^{-1} respectively. The former value is slightly smaller than that between

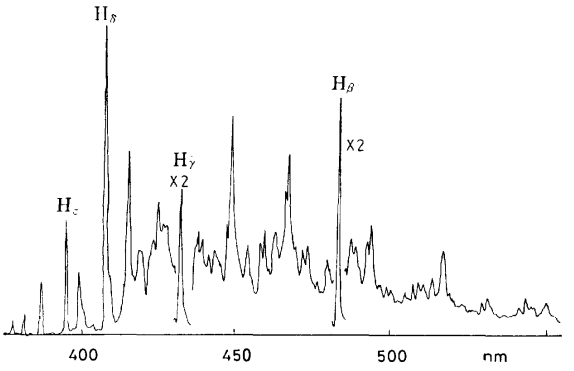

Fig. 6. Emission spectrum obtained from H_2S excited by 200 eV electrons in the region of 400—550 nm. Beam current, 500 μA.

successive bands of the HS radical in the ground state, 2582 cm^{-1}.[13] The difference in the separation between HS^+ and DS^+ may be interpreted as an isotopic shift; this finding also confirms the above assignment.

There are a number of prominent bands in the 400—550 nm region, as is shown in Fig. 6. These bands, except for the hydrogen Balmer series, were not observed in other molecules, such as methanethiol, ethanethiol, hydrocarbons, carbon disulfide, and thiophene. The observed spectrum of a mixture of CS_2 and H_2S was simply a superposition of the spectra of the parent molecules. This finding also suggests that the excited species come directly from the parent molecule, and the band can be assigned to H_2S^+, as did the previous authors.[6]

A number of MO calculations[14] on this molecule have been reported. If Koopmans' theorem holds in this molecule, the energy difference between the ground and the first excited states of H_2S^+ is estimated to be about 2.7 eV (459 nm). The adiabatic and the vertical transition energies between $^2A_1$—$^2B_1$ were determined to be 2.28 eV (544 nm) and 2.77 eV (448 nm) respectively in photoelectron spectroscopy.[11] The latter value

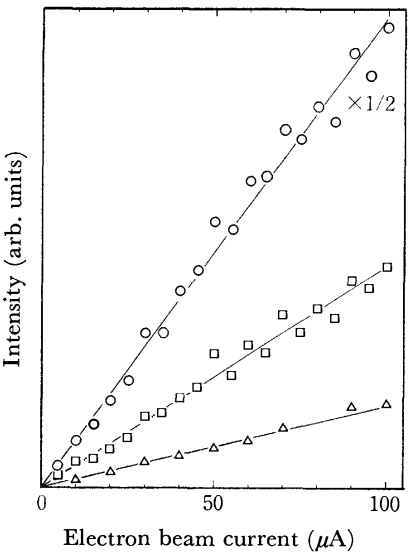

Fig. 7. Dependence of photoemission intensities of HS^+ (○), H (□) and H_2S^+ (△) on electron beam current. Electron energy was 200 eV.

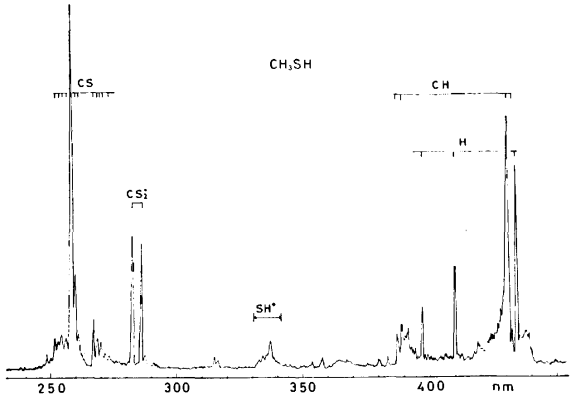

Fig. 8. Emission spectrum obtained from methanethiol excited by 200 eV electrons. Beam current, 400 μA.

is in good agreement with the strongest band of the H_2S^+ in the present work.

The intensities of the photoemission of H, HS^+, and H_2S^+ from H_2S for various electron beam currents are shown in Fig. 7. The linearity also holds for ethanethiol and proves that these species are excited in single-electron processes.

Thiols. A typical emission spectrum of methanethiol was observed by electron impact at 200 eV and a beam current of 1 mA, as is shown in Fig. 8. The spectrum of ethanethiol was similar to that of methanethiol except for the relative intensites of the fragments. The Balmer series of hydrogen is also the most prominent. The emission bands at 431 and 387 nm were assigned to the (0,0) bands of the CH radical in the $A^2\Delta$—$X^2\Pi$ and $B^2\Sigma^-$—$X^2\Pi$ transitions respectively. The bands at 282 and 285 nm were assigned to the CS_2^+ ion and the bands around 260 nm to the CS radical, as in the case of CS_2. In this case, however, the bands of CS are much more intense than those of CS_2^+ which would not be formed by a simple collision between an electron and a CH_3SH molecule.

The authors wish to thank Professor Tomoo Oyama for the use of his CT-50 monochromator and Mr. Masaharu Tsuji for his discussion.

References

1) R. W. B. Pearse and A. G. Gaydon, "The Identification of Molecular Spectra", Chapman and Hall, London (1965)
2) T. Horie, M. Otsuka, and T. Nagura, *J. Phys. Soc. Japan*, **12**, 1099 (1957); S. Tsurubuchi, T. Iwai, and T. Horie, *ibid.*, **34**, 166 (1973).
3) T. Ogawa, M. Tsuji, M. Toyoda, and N. Ishibashi, *Chem. Lett.*, **1972**, 233, 1157; This Bulletin, **46**, 1063, 2637 (1973).
4) W. H. Smith, *J. Quant. Spectrosc. Radiat. Transfer*, **9**, 1191 (1967).
5) M. Horani, S. Leach, and J. Rostas, *J. Mol. Spectrosc.*, **23**, 115 (1967).
6) R. N. Dixon, G. Guxbury, M. Horani, and J. Rostas, *Mol. Phys.*, **22**, 997 (1971).
7) T. Ogawa, M. Toyoda, M. Tsuji, and N. Ishibashi, *Technology Repts. Kyushu Univ.*, **45**, 427 (1972).
8) An equilibrium mixture of H_2S, D_2S, and HDS.
9) S. J. Arnold, and G. H. Kimbel *Can. J. Chem.*, **49**, 4110 (1971).
10) A. N. Zaidel', V. K. Prokof'ev, S. M. Raiskii, V. A. Slavnyi, and E. Ya. Shreider, "Tables of Spectral Lines", Pergamon Press, New York (1970).
11) D. W. Turner, C. Baker, A. D. Baker, and C. R. Brundle "Molecular Photoelectron Spectroscopy", John Wiley & Sons, London (1970).
12) A. G. Gaydon, "Dissociation Energies and Spectra of Diatomic Molecules", Dover Pub., New York (1950).
13) D. A. Ramsey, *J. Chem. Phys.*, **20**, 1920 (1952).
14) B. Roos and P. Siegbahn, *Theoret. Chim. Acta*, **21**, 368 (1971); R. Moccia, *J. Chem. Phys.*, **40**, 2186 (1964); D. G. Carroll, A. T. Armstrong, and S. P. McGlynn, *J. Chem. Phys.*, **44**, 1865 (1966).

The Electronic States of 2,5-Dibromo-3,6-dichloro-1,4-benzoquinone and Its Anion Radical as Studied by Means of Their Infrared Spectra

Yôichi IIDA

Department of Chemistry, Faculty of Science, Hokkaido University, Sapporo 060

(Received June 30, 1973)

The infrared spectra (400—4000 cm^{-1}) of neutral 2,5-dibromo-3,6-dichloro-1,4-benzoquinone and its anion radical were measured in order to observe the appreciable frequency differences between their corresponding bands. The vibrational assignments were made and the simple Urey-Bradley force fields were determined for both the neutral 2,5-dibromo-3,6-dichloro-1,4-benzoquinone and its anion radical. The differences in the molecular and electronic structures between these two molecules were investigated on the basis of these experimental and theoretical results. The half-occupied molecular orbital of the anion radical was found to belong to the b_g irreducible representation.

The infrared spectrum of an ion radical is known to be appreciably different from that of its neutral molecule.[1-13] The spectrum difference seems to be attributable to the difference in their intramolecular force fields. Thus far, however, few attempts have been made to study such differences quantitatively.[8,12,13] In previous papers,[8,13] we examined the infrared spectra of *p*-chloranil (*p*-QCl_4), *p*-bromanil (*p*-QBr_4), and their anion radicals (see Fig. 1). For the neutral molecule and its anion radical, the fundamental frequencies were assigned and the simple Urey-Bradley force fields (UBFF's) were determined in order to explain the appreciable frequency differences between their corresponding bands.

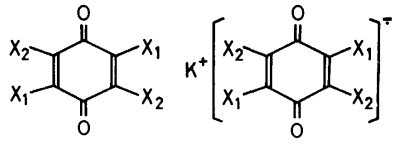

(a); $X_1 = X_2 = Cl$
(b); $X_1 = X_2 = Br$
(c); $X_1 = Br$, $X_2 = Cl$

Fig. 1. The halogen-substituted *p*-benzoquinones and their anion radical salts with potassium cations; (a) *p*-chloranil, (b) *p*-bromanil and (c) 2,5-dibromo-3,6-dichloro-1,4-benzoquinone.

The present paper will describe the infrared spectra (400—4000 cm^{-1}) of neutral 2,5-dibromo-3,6-dichloro-1,4-benzoquinone (*p*-QBr_2Cl_2) and its anion radical (see Fig. 1). For these molecules, we also observed the appreciable frequency shifts between their corresponding bands. The normal coordinate treatments were carried out for the in-plane vibrations by using the simple UBFF's in order to make the vibrational assignments and in order to clarify the difference in the force constants between these molecules. It was shown that the force constants of *p*-QBr_2Cl_2 and its anion radical could be transferred from those of *p*-QX_4 (X=Cl or Br) and its anion radical respectively, as estimated in previous papers.[8,13] In this respect, it will be interesting to compare the effect of the symmetry degradation of *p*-QBr_2Cl_2 and its anion radical with that of the D_{2h} point group of *p*-QX_4 (X=Cl or Br) and its anion radical. The electronic states of the neutral *p*-QBr_2Cl_2 and its anion radical will also be discussed on the basis of these experimental and theoretical investigations. We shall examine how the extra electron on the anion radical causes the differences in the molecular and electronic structures between the neutral *p*-QBr_2Cl_2 and its anion radical.

Experimental

Materials. The neutral *p*-QBr_2Cl_2 was synthesized by the bromination of 2,5-dichloro-1,4-benzoquinone. It was purified by recrystallization from benzene or glacial acetic acid. Its anion radical salt with the potassium cation (K^+ *p*-$QBr_2Cl_2^-$) was prepared according to the method of Torrey and Hunter.[14]

Measurements. The infrared spectra of these solid compounds were measured as Nujol mulls in the range from 400 to 4000 cm^{-1} using a JASCO IR-G infrared spectrophotometer. Alternative measurements in the regions where the absorption due to Nujol appears were made using hexachlorobutadiene mulls. The spectra obtained for these compounds are reproduced in Fig. 2. Since the counter cation of the salt is a simple alkali metal cation, the observed spectrum of K^+ *p*-$QBr_2Cl_2^-$ in the 400—4000 cm^{-1} region is probably due to that of the *p*-QBr_2Cl_2 anion radical itself. The values of the absorption peaks observed for the neutral *p*-QBr_2Cl_2 and its anion radical are listed in Table 1.

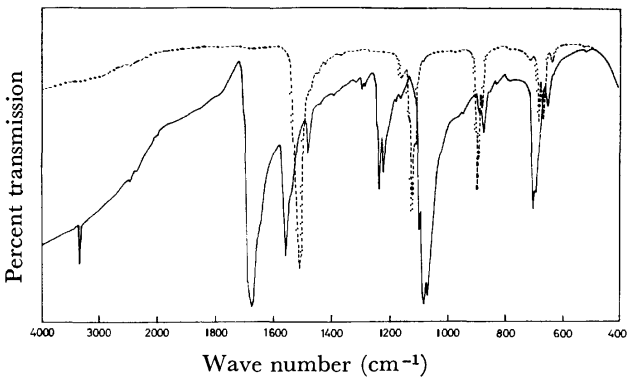

Fig. 2. The infrared spectra of 2,5-dibromo-3,6-dichloro-1,4-benzoquinone and its anion radical salt with potassium cation.
——: 2,5-dibromo-3,6-dichloro-1,4-benzoquinone
------: K^+ 2,5-dibromo-3,6-dichloro-1,4-benzoquinone$^-$

TABLE 1. THE OBSERVED AND CALCULATED FREQUENCIES (cm^{-1}) FOR IN-PLANE FUNDAMENTAL VIBRATIONS OF THE NEUTRAL p-QBr_2Cl_2 AND ITS ANION RADICAL[a)]

Species		The neutral p-QBr_2Cl_2		Its anion radical	
		Obsd	Calcd	Obsd	Calcd
A_g	ν_1		1698		1433
	ν_2		1551		1604
	ν_3		1294		1348
	ν_4		930		930
	ν_5		840		831
	ν_6		740		741
	ν_7		471		476
	ν_8		311		313
	ν_9		281		281
	ν_{10}		201		203
	ν_{11}		125		126
B_u	ν_{12}	1675 (s)	1674	1514 (s)	1503
	ν_{13}	1560 (s)	1565	1535 (sh)	1537
	ν_{14}	1237 (s) 1223 (m)	1223	—	1263
		1099 (s)		1136 (sh)	
	ν_{15}	1083 (s)	1087	1124 (s)	1111
		1070 (s)		1115 (sh)	
	ν_{16}	890 (w) 877 (m)	892	898 (s) 884 (m)	886
	ν_{17}	708 (s) 697 (s)	696	689 (m) 672 (m)	671
	ν_{18}	—	400	—	397
	ν_{19}	—	338	—	335
	ν_{20}	—	182	—	183
	ν_{21}	—	121	—	122

a) s; strong, m; medium, w; weak, sh; shoulder.

Normal Coordinate Treatment for In-Plane Vibrations

In the infrared spectra of neutral p-QBr_2Cl_2 and its anion radical, we have observed appreciable frequency differences between their corresponding bands. For example, the C=O stretching mode of 1675 cm^{-1} in the neutral p-QBr_2Cl_2 is found to be considerably red-shifted to 1514 cm^{-1} in the anion radical. Since only the intramolecular vibrations are expected to appear in the region from 400 to 4000 cm^{-1}, we attributed the observed spectrum difference between the neutral p-QBr_2Cl_2 and its anion radical to the difference in their intramolecular force fields. The effect of crystal fields upon the vibrational frequencies is small in comparison with that of the intramolecular force fields. Therefore, to a first approximation, the contribution of the crystal fields to the spectra of p-QBr_2Cl_2 and its anion radical was ignored in the present investigation.

The vibrational spectra of p-QBr_2Cl_2 and its anion radical were then treated under the molecular point group, C_{2h}, and were analyzed by using the normal coordinate treatment. The molecular and crystal structures of the neutral p-QBr_2Cl_2 have not yet been ascertained, although those of p-QCl_4 were determined by Chu, Jeffrey, and Sakurai.[15] It was assumed that the p-QBr_2Cl_2 molecule was planar. By referring to the molecular structure of p-QCl_4, the equilibrium bond lengths of p-QBr_2Cl_2 were taken as $l(C{=}O)=1.195$ Å, $l(C{=}C)=1.342$, $l(C_1{-}C_2)=l(C_3{-}C_4)=1.477$, $l(C{-}Br)=1.89$, and $l(C{-}Cl)=1.714$, while the bond angles were taken as $\angle(O{=}C_1{-}C_2)=\angle(O{=}C_4{-}C_3)=121°22'$, $\angle(C{-}C{-}Br)=\angle(C{-}C{-}Cl)=116°15'$, and $\angle(C{=}C{-}Br)=\angle(C{=}C{-}Cl)=122°23'$ (see Fig. 1). Since the structure of K^+ p-$QBr_2Cl_2^-$ has not yet been determined, it was assumed that the molecular structure of the anion radical was almost identical with that of the neutral p-QBr_2Cl_2. This assumption meant that the $\boldsymbol{G}$ matrix calculated for p-QBr_2Cl_2 was also used for its anion radical (see below).

By taking the molecular C_{2h} point group into consideration, thirty normal modes of fundamental vibrations for p-QBr_2Cl_2 or its anion radical are reduced to the symmetry species:

$$\Gamma = 11A_g(R) + 10B_u(IR) + 4B_g(R) + 5A_u(IR), \quad (1)$$

where the first two are the in-plane vibrations, and the rest, the out-of-plane vibrations. The signs of (R) and (IR) indicate the Raman and infrared active modes respectively. In connection with the number and species of the fundamentals for p-QX_4 (X=Cl or Br) and its anion radical, the correlation diagram between the C_{2h} and D_{2h} point groups is given in Table 2.

TABLE 2. THE CORRELATION DIAGRAM BETWEEN THE C_{2h} POINT GROUP OF p-QBr_2Cl_2 OR ITS ANION RADICAL AND THE D_{2h} POINT GROUP OF p-QX_4, (X=Cl OR Br), OR ITS ANION RADICAL[a)]

C_{2h}	D_{2h}
A_g (11)	A_g (6)
	B_{1g} (5)
B_g (4)	B_{2g} (1)
	B_{3g} (3)
A_u (5)	A_u (2)
	B_{1u} (3)
B_u (10)	B_{2u} (5)
	B_{3u} (5)

a) The number in parentheses indicates that of the fundamental vibrations.

Wilson's $\boldsymbol{GF}$ matrix method was applied to p-QBr_2Cl_2 and its anion radical.[16] We calculated only the in-plane vibrations, because no out-of-plane vibration is expected to appear in the region now under consideration. A simple UBFF was employed as the potential function. Note that the numbering of the carbon atoms in p-QBr_2Cl_2 or its anion radical is taken as 2,5-dibromo-3,6-dichloro-1,4-benzoquinone. Therefore, six bond-stretching ($K(C{=}O)$, $K(C{=}C)$, $K(C_1{-}C_2)$, $K(C_3{-}C_4)$, $K(C{-}Br)$, and $K(C{-}Cl)$), nine angle-bending ($H(O{=}C_1{-}C_2)$, $H(O{=}C_4{-}C_3)$, $H(C{-}C{-}Br)$, $H(C{-}C{-}Cl)$, $H(C{=}C{-}Br)$, $H(C{=}C{-}Cl)$, $H(C{-}C{-}C)$, $H(C_1{-}C_2{=}C_3)$, and $H(C_2{=}C_3{-}C_4)$) and nine non-bonded repulsion force constants ($F(O{=}C_1{-}C_2)$, $F(O{=}C_4{-}C_3)$, $F(C{-}C{-}Br)$, $F(C{-}C{-}Cl)$, $F(C{=}C{-}Br)$, $F(C{=}C{-}Cl)$, $F(C{-}C{-}C)$, $F(C_1{-}$

C_2=C_3), and $F(C_2=C_3-C_4)$) were necessary.

The trial force constants for the neutral *p*-QBr_2Cl_2 were transferred from the values for the neutral *p*-QX_4 (X=Cl or Br), while those for the *p*-QBr_2Cl_2 anion radical were transferred from the values for the *p*-QX_4 anion radical (X=Cl or Br).[8,13] For either the neutral *p*-QBr_2Cl_2 or its anion radical, it seems that $K(C_1-C_2)\approx K(C_3-C_4)$, $H(O=C_1-C_2)\approx H(O=C_4-C_3)$, $H(C_1-C_2=C_3)\approx H(C_2=C_3-C_4)$, $F(O=C_1-C_2)\approx F(O=C_4-C_3)$, and $F(C_1-C_2=C_3)\approx F(C_2=C_3-C_4)$. Refinements of the force constants were then carried out by the trial-and-error method, making use of the Jacobian matrix. In order to adjust the calculated frequencies to the observed fundamental frequencies, we paid much attention to the bond-stretching force constants, because the observed fundamental frequencies of the infrared spectra are almost all due to the bond-stretching modes. The final sets of force constants thus obtained for the neutral *p*-QBr_2Cl_2 and its anion radical are given in Table 3, while the frequencies calculated with these constants are in Table 1 compared with the observed values. In both of these molecules, the calculated vaues of the fundamental vibrations were found to agree well with the observed values, except for the following two points, which remain to be elucidated:

(1) In addition to the fundamental vibrations, shoulders or extra absorptions appear in both the neutral *p*-QBr_2Cl_2 and its anion radical. Some of them may arise from the splitting of the fundamental vibrations through the factor-group splitting.

(2) The calculated 1263 cm^{-1} band in the anion radical cannot be assigned to any of the observed bands, presumably because of its weak intensity.

Table 3. Some of the force constants estimated for the neutral *p*-QBr_2Cl_2, *p*-QCl_4 and *p*-QBr_4 molecules and their anion radicals (md/Å)[a]

Force constant	Neutral molecule			Anion radical		
	p-QBr_2Cl_2	*p*-QCl_4[b]	*p*-QBr_4[c]	*p*-QBr_2Cl_2	*p*-QCl_4[b]	*p*-QBr_4[c]
K(C=O)	9.62	9.7	9.62	7.10	7.3	7.10
K(C=C)	6.67	6.6	6.67	6.26	6.1	6.26
$K(C_2-C_1)$	2.96	3.0	2.96	3.33	3.5	3.33
$K(C_3-C_4)$	2.96	3.0	2.96	3.33	3.5	3.33
K(C-Br)	2.63	—	2.63	2.17	—	2.17
K(C-Cl)	2.67	2.67	—	2.45	2.67	—

a) The values of the bending and non-bonded repulsion force constants for the neutral *p*-QBr_2Cl_2 were transferred from those for the neutral *p*-QCl_4 and *p*-QBr_4, while the values for the *p*-QBr_2Cl_2 anion radical, from those for the *p*-QCl_4 and *p*-QBr_4 anion radicals. See Refs. 8 and 13.
b) Ref. 8.
c) Ref. 13.

Discussion

Comparison with the Results of p-QX_4 *(X=Cl or Br) and Its Anion Radical.* Since the observations of the fundamental frequencies are limited to the infrared spectra, we suspect that the sets of the force constants presented in Table 3 are not the best ones for either the neutral *p*-QBr_2Cl_2 or its anion radical. However, the stretching force constants are still meaningful, for the observed fundamental frequencies are almost all due to the bond-stretching modes. Therefore, below, we will discuss only the difference in the stretching force constants between the neutral *p*-QBr_2Cl_2 and its anion radical. From Table 3, we can easily see that an extra electron on the *p*-QBr_2Cl_2 anion radical markedly causes a decrease in the K(C=O), K(C=C), K(C-Br), and K(C-Cl) values and an increase in the $K(C_1-C_2)$ and $K(C_3-C_4)$ values. Regardless of the symmetry degradation, this situation is very similar to that of the bond-stretching force constant difference between *p*-QX_4 (X=Cl or Br) and its anion radical reported in previous papers.[8,13] Table 3 clearly shows that the force constants of the neutral *p*-QBr_2Cl_2 are transferable from those of the neutral *p*-QCl_4 and *p*-QBr_4, and that the force constants of the anion radical of *p*-QBr_2Cl_2 are transferable from those of the *p*-QCl_4 and *p*-QBr_4 anion radicals. We can further see that, in spite of the symmetry degradation, the force constants of the benzoquinone system of the neutral *p*-QBr_2Cl_2 or its anion radical are scarcely affected by exchanging the chlorine substituents for the bromine substituents. This fact means that the carbon atoms bonded to the chlorine and bromine substituents are practically identical, and that the molecular structure and the force field for the benzoquinone system of the neutral *p*-QBr_2Cl_2 or its anion radical are very similar to those of the neutral *p*-QX_4 (X=Cl or Br) or its anion radical respectively.[8,13]

Although the previous paper stated that the extra electron on the *p*-QCl_4 anion radical did not decrease the K(C-Cl) value,[8] this description is no longer adequate. More accurate assignments of the fundamental frequencies of *p*-QCl_4 and its anion radical show a decrease in the K(C-Cl) value in the anion radical[17]; this situation seems to be analogous to that of *p*-QBr_2Cl_2 and its anion radical.

The Electronic States of p-QBr_2Cl_2 *and Its Anion Radical.* The electronic state of the neutral *p*-QBr_2Cl_2 differs from that of its anion radical, since the extra electron on the anion radical causes a marked decrease in the K(C=O), K(C=C), K(C-Br), and K(C-Cl) values and an increase in the $K(C_1-C_2)$ and $K(C_3-C_4)$ values. In this section, we shall investigate the electronic states of the neutral *p*-QBr_2Cl_2 and its anion radical by using the difference in their force constants.

It is well known that the stretching force constant, $K(12)$, of a bond (12) in a conjugated system is greatly affected by its bond order, $p(12)$. According to Coulson and Longuet-Higgins,[18] $K(12)$ can be expressed by:

$$K(12) = \{(1-p(12))K_s+p(12)K_d\} + \left\{\frac{K_sK_d(s-d)}{K_s(1-p(12))+K_dp(12)}\right\}^2 \frac{\pi(1212)}{2}, \quad (2)$$

where K_s and K_d are the force constants associated with pure single and double bonds respectively; $\pi(1212)$ is the self-polarizability of the bond (12), and s and d

are the bond lengths of pure single and double bonds respectively.

In a homopolar carbon-carbon bond, the second term involving the self-polarizability may be small.[19] In this case, the stretching force constant, $K(12)$, is predominantly determined by the bond order, $p(12)$. An empirical relationship between $K(12)$ and $p(12)$ has been given in a previous paper,[8] where several standard points of $K(12)$ and $p(12)$ were connected smoothly. This relationship enables us to evaluate the bond orders of the C=C, C_1–C_2, and C_3–C_4 bonds for p-QBr_2Cl_2 and its anion radical. From the values of $K(C=C)$, $K(C_1–C_2)$, and $K(C_3–C_4)$ in the infrared spectra, the $p(C=C)$, $p(C_1–C_2)$, and $p(C_3–C_4)$ values for the neutral p-QBr_2Cl_2 were thus estimated to be 0.88, 0.27, and 0.27 respectively, while those for its anion radical were estimated to be 0.82, 0.36, and 0.36 respectively. Therefore, the extra electron on the p-QBr_2Cl_2 anion radical was found to cause a decrease in $p(C=C)$ by 0.06 and an increase in $p(C_1–C_2)$ and $p(C_3–C_4)$ by 0.09.

On the other hand, let us examine the heteropolar C=O bond. If we take, in Eq. (2), the $K_s=5.0$ md/Å and $K_d=10.7$ md/Å values proposed by Bratoz and Besnainou,[20] and if we neglect the contribution of the self-polarizability to $K(C=O)$, those C=O stretching force constants for p-QBr_2Cl_2 and its anion radical give the values of $p(C=O)$ as 0.81 and 0.37 respectively. Therefore, the extra electron on the p-QBr_2Cl_2 anion radical definitely decreases the $p(C=O)$ values.

The values for the bond orders of the benzoquinone system of the neutral p-QBr_2Cl_2 and its anion radical were found to coincide well with those of the neutral p-QX_4 (X=Cl or Br) and its anion radical respectively.[21] We can further see that, for either of the neutral p-QBr_2Cl_2 or its anion radical, the $p(C_1–C_2)$ value is practically equal to the $p(C_3–C_4)$ value. For the molecular D_{2h} point group, the half-occupied molecular orbital in the p-QX_4 anion radical (X=Cl or Br) has been reported to belong to the b_{3g} irreducible representation.[8,13] The half-occupied molecular orbital of the p-QBr_2Cl_2 anion radical should belong to the b_g irreducible representation, since the point group of the anion radical is degraded into C_{2h}. This symmetry consideration of the half-occupied molecular orbital of the p-QBr_2Cl_2 anion radical is strongly supported by the fact that the extra electron on the anion radical causes a decrease in the $p(C=C)$ and $p(C=O)$ values and an increase in the $p(C_1–C_2)$ and $p(C_3–C_4)$ values compared to the values of the neutral p-QBr_2Cl_2. The electronic states of the benzoquinone system of the neutral p-QBr_2Cl_2 and its anion radical, although their point groups are degraded into C_{2h}, seem to be very similar to those of the neutral p-QX_4 (X=Cl or Br) and its anion radical respectively, which were reported in previous papers.[8,13]

As for the C–Cl and C–Br bonds, although the description of $K(C–X)$ *versus* $p(C–X)$ (X=Cl or Br) for the neutral p-QBr_2Cl_2 and its anion radical is not so simple, the extra electron on the p-QBr_2Cl_2 anion radical causes a decrease in $K(C–Cl)$ and $K(C–Br)$, which will definitely lead to a decrease in $p(C–Cl)$ and $p(C–Br)$. However, the estimation of $p(C–Cl)$ and $p(C–Br)$ by the molecular orbital method is rather complicated, for there are some difficulties in taking appropriate parameters for the Cl and Br atomic orbitals.

Some Information on the Molecular Structures of p-QBr_2Cl_2 *and Its Anion Radical.* There is a well-known relation between the bond order, $p(12)$, and the bond length, $l(12)$, of a carbon–carbon bond (12); it was first derived by Coulson.[19,22] By using this relationship, the $p(C=C)$, $p(C_1–C_2)$, and $p(C_3–C_4)$ values estimated from the infrared spectra give $l(C=C)$, $l(C_1–C_2)$, and $l(C_3–C_4)$ respectively. The $l(C=C)$, $l(C_1–C_2)$, and $l(C_3–C_4)$ values for the neutral p-QBr_2Cl_2 were thus estimated to be 1.35_6, 1.47_5, and 1.47_5 Å, respectively, while those for its anion radical were estimated to be 1.36_8, 1.45_6, and 1.45_6 Å, respectively. The values of the neutral p-QBr_2Cl_2 are in good agreement with those of $l(C=C)=1.342$ Å, $l(C_1–C_2)=l(C_3–C_4)=1.477$ respectively, which were employed in the previous calculation. We can further see that the extra electron on the anion radical may cause an increase of 0.01 Å in $l(C=C)$ and a decrease of 0.02 Å in $l(C_1–C_2)$ and $l(C_3–C_4)$ compared to the values of p-QBr_2Cl_2. However, no observation of the molecular structure has yet been made for the anion radical.

As for the relation between the stretching force constant and the bond length of a C=O bond, Badger proposed the following equation:[23]

$$K(C=O) = 1.86/\{l(C=O)-0.68\}^3, \qquad (3)$$

where K and l are in md/Å and Å units respectively. For p-QBr_2Cl_2 and its anion radical, the values of $l(C=O)$ derived from their force constants by Eq. (3) are 1.26 Å and 1.32 respectively. The former value is rather larger than the observed value of 1.195 Å. We may expect that the C=O bond length of the p-QBr_2Cl_2 anion radical is longer than that of its neutral molecule by 0.06 Å; however, no experimental result is available at present.

Although we have no information on the relation between the stretching force constant and the bond lenght for the C–Cl and C–Br bonds, the extra electron on the p-QBr_2Cl_2 anion radical probably causes the difference in $l(C–Cl)$ and $l(C–Br)$ between p-QBr_2Cl_2 and its anion radical.

Concluding Remarks

In the present work, the difference in the vibrational spectra between the neutral p-QBr_2Cl_2 and its anion radical was interpreted in terms of the difference in their intramolecular force fields. On the other hand, the crystal-field effect may make some contribution to the frequency shifts in these vibrational spectra. Indeed, certain vibrational frequencies of the p-QBr_2Cl_2 anion radical salts will be influenced by the species of the counter cation. However, in a first approximation, this contribution can be neglected in comparison with that of the intramolecular force fields.

Rigorously speaking, the $\boldsymbol{G}$ matrix for the anion radical is not identical with that for the neutral p-QBr_2Cl_2, since the molecular structure of the anion radical

will be slightly different from that of the neutral p-QBr_2Cl_2. The difference in their $\boldsymbol{G}$ matrices may make some contribution to the frequency difference. However, this contribution is negligibly small for the bands due to the bond-stretching modes.

The set of force constants presented in Table 3 cannot be regarded as a unique solution, since the observations for the fundamental frequencies are limited to the infrared spectra. In this sense, it is quite desirable to measure the Raman spectra of p-QBr_2Cl_2 and its anion radical. We consider, however, that the set of force constants presented here is reliable enough for studying the difference in the stretching force constants between the neutral p-QBr_2Cl_2 and its anion radical.

References

1) Y. Matsunaga, *Can. J. Chem.*, **38**, 1172 (1960).
2) Y. Matsunaga, *Helv. Phys. Acta*, **36**, 800 (1963).
3) Y. Matsunaga, *J. Chem. Phys.*, **41**, 1609 (1963).
4) M. Kinoshita and H. Akamatu, *Nature*, **207**, 291 (1965).
5) J. Stanley, D. Smith, B. Latimer, and J. P. Devlin, *J. Phys. Chem.*, **70**, 2011 (1966).
6) Y. Matsunaga, *Nippon Kagaku Zasshi*, **89**, 905 (1968).
7) Y. Iida, *J. Phys. Soc. Japan*, **27**, 1371 (1969).
8) Y. Iida, This Bulletin, **43**, 345 (1970).
9) Y. Iida, *ibid.*, **44**, 1271 (1971).
10) J. C. Moore, D. Smith, Y. Youhne, and J. P. Devlin, *J. Phys. Chem.*, **75**, 325 (1971).
11) I. N. Juchnovski and I. G. Binev, *Chem. Phys. Lett.*, **12**, 40 (1971).
12) Y. Iida, This Bulletin, **46**, 423 (1973).
13) Y. Iida, *ibid.*, **46**, 2955 (1973).
14) H. A. Torrey and W. H. Hunter, *J. Amer. Chem. Soc.*, **34**, 702 (1912).
15) S. Chu, G. A. Jeffrey, and T. Sakurai, *Acta Crystallogr.*, **15**, 661 (1962).
16) E. B. Wilson, Jr., *J. Chem. Phys.*, **7**, 1047 (1939); **9**, 76. (1941).
17) Y. Iida, This Bulletin, to be published.
18) C. A. Coulson and H. C. Longuet-Higgins, *Proc. Roy. Soc. Ser. A*, **193**, 456 (1948).
19) A. Streitwieser, Jr., "Molecular Orbital Theory," John Wiley & Sons, New York and London (1961).
20) S. Bratoz and M. S. Besnainou, *J. Chem. Phys.*, **34**, 1142 (1961).
21) By using the relationship between $K(12)$ and $p(12)$, the values of the bond orders for the neutral p-QCl_4 have been reported to be $p(C{=}C)=0.87$, $p(C{-}C)=0.27$, and $p(C{=}O)=0.82$, while those for its anion radical, $p(C{=}C)=0.79$, $p(C{-}C)=0.37$ and $p(C{=}O)=0.40$. On the other hand, the values for the neutral p-QBr_4 were $p(C{=}C)=0.88$, $p(C{-}C)=0.27$ and $p(C{=}O)=0.81$, while those for its anion radical, $p(C{=}C)=0.82$, $p(C{-}C)=0.36$ and $p(C{=}O)=0.37$. See Refs. 8 and 13.
22) C. A. Coulson, *Proc. Roy. Soc. Ser. A*, **169**, 413 (1939).
23) R. M. Badger, *J. Chem. Phys.*, **3**, 710 (1935); see also J. A. Ladd, W. J. Orville-Thomas, and B. C. Cox, *Spectrochim. Acta*, **20**, 1771 (1964).

The Chemistry of Protactinium. X. A Study of the Effect of Chromium(II) on the Solvent Extraction of Protactinium(IV), Using *N*-Benzoyl-*N*-phenylhydroxylamine, Tri-*n*-octylamine and Thenoyltrifluoroacetone as the Extractants

Isamu KAWASUJI and Shin SUZUKI

The Research Institute for Iron, Steel and Other Metals, Tohoku University, Katahira 2-Chome, Sendai 980

(Received May 25, 1973)

Cr(II) has been used for reducing protactinium in microquantities to the tetravalent state and for protecting it from re-oxidation. However, the effect of Cr(II) on the extraction behavior of Pa(IV) has not been taken into account by all of the previous investigators. On the basis of the above facts, the influence of Cr(II) on the extraction of Pa(IV) was studied by using such extractants as BPHA, TTA, and TOA. In every case, the distribution ratio of Pa(IV) decreased with an increase in the concentration of Cr(II) in the aqueous phase. One of the most reliable explanations for the phenomena is the possibility that a multi-nuclear complex between Pa(IV) and Cr(II) or Cr(III) is formed. However, the effect of Cr(II) on the absorption spectra of Pa(IV) could not be found, and many more experiments will be necessary to explain the effect of Cr(II) on the extraction behavior of Pa(IV).

Guillaumont[1] investigated the behavior of Pa(IV) in a perchlorate solution by means of the TTA-benzene extraction method and showed that Pa^{4+} was gradually hydrolyzed to $Pa(OH)_3^+$ in the pH range from −0.3 to 3.0 at the ionic strength of 3. The same author[2] also studied the chloro-, sulfato-, and fluoro-complexes in aqueous solutions and calculated their stability constants. Muxart and Arapaki[3] pointed out in their TOA-xylene extraction study that Pa(IV) formed an anionic ion in a sulfuric acid solution. Mitsuji[4] investigated the behavior of Pa(IV) in perchloric, hydrochloric, and sulfuric acid solutions by means of TTA-benzene extraction in the pH range from 0.5 to 1.1, and suggested that $Pa(OH)_2^{2+}$ and $Pa(SO_4)(OH)^+$ were the most probable ionic species in perchlorate and chloride solutions and in the sulfate solution respectively.

In these experiments, Pa(V) was reduced to Pa(IV) by means of a liquid zinc amalgam in the presence of about 10^{-2} M Cr(III). Protactinium in microquantitites can not be reduced only by the liquid zinc amalgam method, even in an argon atmosphere, because the contact between protactinium and amalgam is not sufficient and because the Pa(IV) reduced is affected by any traces of oxygen which might remain in the solution. The role of Cr(III) is considered to be that the Cr(II) formed by the liquid zinc amalgam reduction mediates the reduction of Pa(V) and protects Pa(IV) from re-oxidation. In view of the above facts, Cr(III) has generally been used as a carrier for reduction in studies of the aqueous chemistry of Pa(IV).

Mitsuji[5] reported that Pa(V) in the concentration range down to tracer level was readily reduced with a liquid zinc amalgam in the presence of more than 10^{-4} M of Cr(III), and that the co-precipitation with thorium fluoride was an excellent method for identifying the oxidation state of protactinium in a tracer concentration. It is very useful that the performance of the reduction of Pa(V) can be checked by the color change of the solution from green (Cr(III)) to light blue (Cr(II)). However, since the molar extinction coefficient of Cr(II) is only about 5 at its characteristic peak of 720 nm, about 10^{-2} M Cr(III) has been generally used in previous reports.[1-4] Therefore, a fairly large amount of Cr(II) is always present in a solution of Pa(IV). Nevertheless, the influence of Cr(II) on the extraction behavior of Pa(IV) has not been taken into account in all of the experiments described above.

Guillaumont[6] investigated the behavior of Pa(IV) in the perchlorate solution in detail by means of the TTA-benzene extraction method, and pointed out that TTA extracted not only Pa(IV), but also Cr(II). Therefore, the correction for the concentration of TTA, which chelates with Cr(II), was carried out, and it was found that the change in the distribution ratio of Pa(IV) was within the limits of experimental error for chromium concentration from 10^{-3} M to 10^{-1} M.

The purpose of the present study is to investigate the effect of the co-existence of Cr(II) on the extraction behavior of Pa(IV), using-*N*-benzoyl-*N*-phenylhydroxylamine (BPHA), tri-*n*-octylamine (TOA), or thenoyltrifluoroacetone (TTA) as an extractant.

BPHA is a weak acid ($pK_a=8.15$[7]) and has been widely used as a gravimetric or spectrophotometric reagent. Recently, it has also been used as an extracting agent for separation or purification; it is inclined to form chelate compounds with various metal ions, such as Ti(IV), Zr(IV), Hf(IV), Ta(V), Pa(V), and Pu(IV), but the extraction behavior of Pa(IV) or Cr(II) with BPHA has not yet been investigated. In this investigation we studied the BPHA extraction of Pa(IV) and Cr(II) in detail.

TTA[1,2,4] and TOA[3] have been widely used as extractants and also to investigate the behavior of Pa(IV). Taking account of the previously-reported information, we could define the experimental conditions without further study.

Experimental

Reagents. The ^{231}Pa was purified by the method reported previously[8], and its radiochemical purity was certified by α-ray and γ-ray spectroscopy. The concentration of protactinium in the ^{231}Pa solution was determined by gravimetry as Pa_2O_5 and by means of the absolute α-counting method. These two results agreed well within the limits of

experimental error, so we can confirm that there was no contamination by non-radioactive impurities. The ^{233}Pa was prepared by the method reported by Suzuki and Inoue[8].

The extraction behavior of Cr(II) and Cr(III) was examined using ^{51}Cr as a tracer. ^{51}Cr was obtained as a chemical form of Na_2CrO_4 and was reduced to the divalent state with a liquid zinc amalgam after adding some carriers of Cr(III). Cr(II) was readily oxidized to Cr(III) by exposure to air. After two cycles of reduction and oxidation, the Cr(III) thus prepared was used in this experiment. The radiochemical purity of ^{51}Cr was certified by γ-ray spectroscopy. The water used was purified by distillation, followed by ion-exchange treatment. The TTA, BPHA, TOA, and other reagents used in this experiment were of the highest purity.

Apparatus. Both the reduction and the extraction of protactinium were carried out in the reduction apparatus described in the previous report.[9] For the solvent-extraction procedure, an Iwaki universal mechanical shaker, Model V-S, was used. The α- and γ-ray spectra were measured with an Osaka-Denpa gridded ionization chamber and with a 1 3/4 in$\times$1 in NaI(Tl) detector respectively, coupled with a Toshiba 800-channel pulse-height analyzer. A Hitachi Model SP-3 well-type NaI(Tl) scintillation probe coupled with a Kobe Kogyo Model SA-250 scaler was used for the γ-activity measurements. For measuring the absorption spectrum, a Hitachi Model EPS-3 recording spectrophotometer and a 1 cm quartz cell were used.

Procedure. Ten milliliters of a perchlorate or a sulfate solution which included 10^{-7}M Pa(V) and a definite amount of Cr(III) were introduced into a reduction apparatus and thoroughly deoxygenated by bubbling with argon gas which had passed through a dilute sulfuric acid solution of ammonium metavanadate. By shaking the reduction apparatus for about 15 min, protactinium and chromium were reduced with a freshly-prepared liquid zinc amalgam. After the amalgam had been excluded from the apparatus, 10 ml of a TTA-benzene, BPHA-benzene, or TOA-xylene mixture was introduced. Then the solvent extraction was carried out with a mechanical shaker until the equilibrium was established. After the two phases had been completely separated, an aliquot of each phase was placed in a polyethylene test tube and its γ-radioactivity was counted. The distribution ratio (D) was calculated by the usual equation:

$$D = \frac{\gamma\text{-activity per ml of the organic phase}}{\gamma\text{-activity per ml of the aqueous phase}} \quad (1)$$

The ionic strength was kept constant by the use of $LiClO_4$, if needed. All the experiments were carried out in an argon atmosphere at room temperature, 17—20 °C.

Results

The Stability of Pa(IV). After protactinium is once reduced to the tetravalent state, it is fairly stable in an oxygen-free atmosphere. For example, the re-oxidation rate of Pa(IV) in a hydrochloric acid solution is 8% per 15 hr,[9] and Pa(IV) is more stable in a sulfuric acid solution.

The oxidation-reduction potential of the Pa(IV)–Pa(V) has been reported to be -0.29 ± 0.03 V,[10] and that of Cr(II)–Cr(III), -0.40 V.[11] It was known from two reasons to be described below that Cr(II), which had been expected to be less stable than Pa(IV), was stable in both the aqueous and organic phases for 6 hr after the BPHA-benzene extraction was carried out. One of the reasons for this is that, if Cr(II),

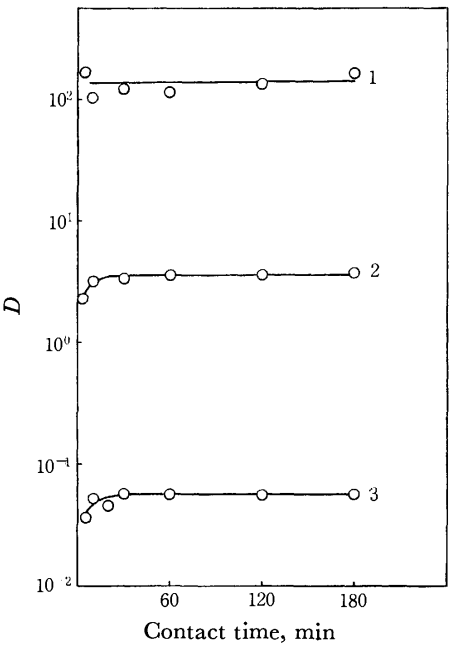

Fig. 1. Effect of contact time on distribution ratio of Pa.
Aq. phase: 0.125 M H_2SO_4, 6.22×10^{-3} M [Cr], 1: Pa(V), 2,3: Pa(IV)
Org. phase: 1,2: 0.05 M BPHA-benzene, 3: 0.03 M BPHA-benzene

which is extracted with BPHA from a weak acid solution as will be described below, is re-oxidized to Cr (III), it should not be extracted with BPHA from an acid solution; another is that the aqueous phase still shows the light-blue color of Cr(II) after the two phases are separated. For the same reason, it was found that Cr(II) was also stable in both the phases during the TTA-benzene extraction and in the aqueous phase during the TOA-xylene extraction, by which Cr(II) was not extracted. Moreover, the distribution ratio of Pa(IV) with BPHA reaches a nearly constant value within 30 min, as is clearly shown in Fig. 1. It should be noted that there is a wide difference in the distribution ratio between Pa(IV) and Pa(V); for instance, the distribution ratio of Pa(V) under the same conditions as those of Pa(IV) is about two orders greater than that of Pa(IV),[12] as is shown in Fig. 1. For these reasons, it may be concluded that Pa(IV) is very stable during the solvent extraction in both the aqueous and organic phases.

BPHA Extraction. The Effect of the Contact Time: From the results shown in Fig. 1, a 1-hr shaking was done in the case of the BPHA extraction of Pa(IV).

The Relation between the Distribution Ratio and the BPHA Concentration: The log-log plot of the distribution ratio of Pa(IV) in a sulfate solution and the concentration of BPHA shows a good linearity, with a slope of about 4; this value is independent of the concentration of Cr(II), as is shown in Fig. 2.

The BPHA Extraction of Cr(II): Cr(II) is also extracted with BPHA from an acid solution when the acid concentration is lower than 0.1 M, as is shown in Fig. 3. As is shown in Fig. 4, the log-log plot of the distribution ratio of Cr(II) and the concentration

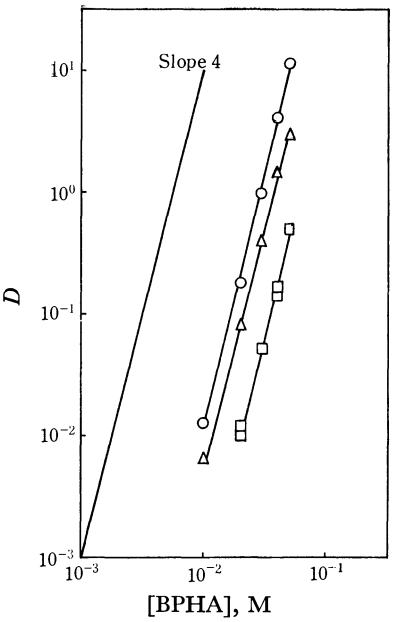

Fig. 2. Dependence of distribution ratio of Pa(IV) on BPHA concentration in benzene.
○: I=2 (adding $LiClO_4$), 1.7×10^{-2} M [Cr(II)], 0.159 M H_2SO_4, △: I=2 (adding Na_2SO_4), 1.7×10^{-3} M [Cr(II)], 0.159 M H_2SO_4, □: I=2 (adding Na_2SO_4), 8.5×10^{-3} M [Cr(II)], 0.159 M H_2SO_4.

of BPHA shows a linear relationship, with a slope of about 2. This means that one atom of Cr(II) chelates with two molecules of BPHA, and that its chelating compound is extracted into the benzene phase, the color of which is green. The concentration of BPHA can be corrected by Eq. (2), but it is not necessary when the acid concentration is higher than 0.1 M. Cr(III) was not extracted with BPHA-benzene under the same conditions as Cr(II).

The Influence of the Cr(II) Concentration on the BPHA Extraction of Pa(IV): As is shown in Fig. 5, the log-log plot of the distribution ratio of Pa(IV) and the concentration of Cr(II) shows a good linearity, and the distribution ratio of Pa(IV) decreases with an increase in the concentration of Cr(II).

TTA Extraction. *TTA Extraction of Cr(II)*: Cr(II) is extracted from a perchlorate or a sulfate solution with TTA-benzene. The log-log plot of the

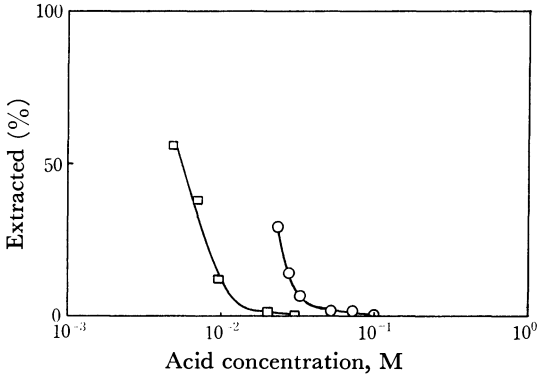

Fig. 3. Extraction of Cr(II) with 0.05 M BPHA-benzene from H_2SO_4 and $HClO_4$ solution.
○: $HClO_4$ solution, □: H_2SO_4 solution.

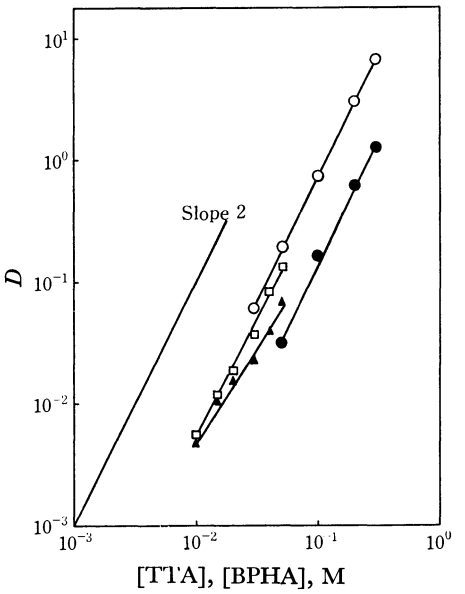

Fig. 4. Dependence of distribution ratio of Cr(II) on TTA and BPHA concentration in benzene.
Org. phase: ○,●: TTA-benzene, ▲,□: BPHA-benzene
Aq. phase: I=2, ○: 0.5 M $HClO_4$, 4.4×10^{-3} M [Cr (II)], ●: 0.5 M H_2SO_4, 6.8×10^{-3} M [Cr(II)], ▲: 0.033 M $HClO_4$, 2.2×10^{-3} M [Cr(II)], □: 0.01 M H_2SO_4, 4.6×10^{-3} M [Cr(II)].

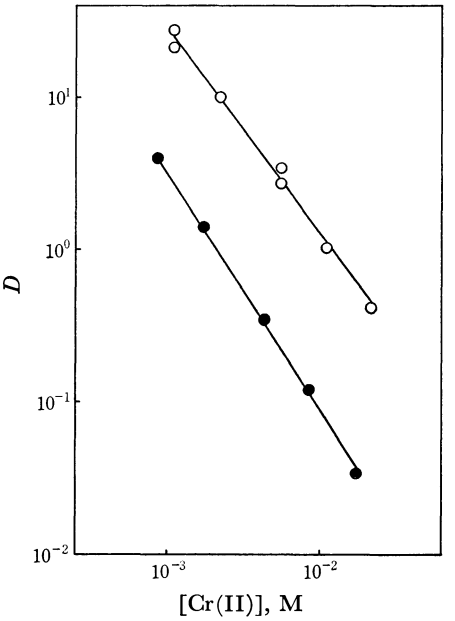

Fig. 5. Influence of Cr(II) concentration on extraction of Pa(IV) with BPHA.
Org. phase: ○: 0.01 M BPHA-benzene, ●: 0.03 M BPHA-benzene
Aq. phase: ●: I=2, 0.5 M H_2SO_4, ○: I=2, 0.5 M $HClO_4$.

distribution ratio of Cr(II) and the concentration of TTA shows a linear relation, with a slope of about 2, as is shown in Fig. 4. This means that one atom of Cr(II) chelates with two molecules of TTA, and that its chelating compound is extracted into the benzene phase, the color of which is yellow. On the other

hand, Cr(III) is not extracted under the same conditions.

The correction to the concentration of the TTA-benzene solution resulting from the co-existence of Cr(II) can be made by means of Eq. (2):

$$[HA]_e = [HA]_i - \frac{2D}{1+D}[Cr(II)]_i \quad (2)$$

where

$[HA]_e$=effective TTA or BPHA concentration in equilibrium

$[HA]_i$=initial TTA or BPHA concentration

$[Cr(II)]_i$=initial Cr(II) concentration

D=distribution ratio of Cr(II)

It is well known that one atom of Pa(IV) chelates with four molecules of TTA.[1,4,6] Consequently, we can correct the distribution ratio of Pa(IV) on the basis of these values.

The Influence of the Concentration of Cr(II) on the Extraction of Pa(IV) with TTA: Taking account of previous information,[4,6] the contact time of 30 min was chosen. The log-log plot of the distribution ratio of Pa(IV) and the concentration of Cr(II) is shown in Fig. 6. The distribution ratio of Pa(IV) decreases with an increase in the concentration of Cr(II).

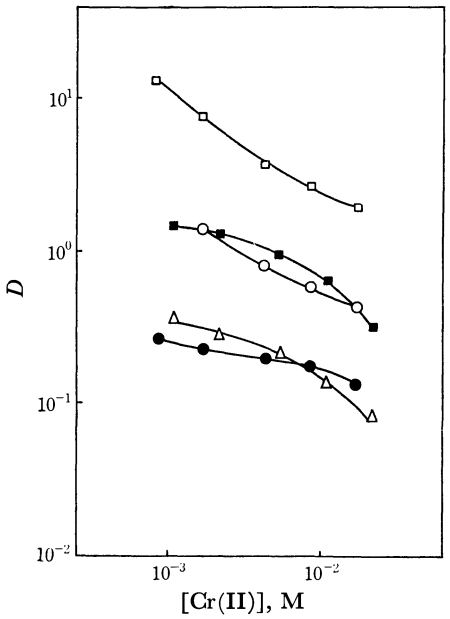

Fig. 6. Influence of Cr(II) concentration on extraction of Pa(IV) with TTA and TOA.
Org. phase: ●: 0.3 M TTA-benzene, ■,△: 0.1 M TTA-benzene, □,○: 5 v/v% TOA-xylene
Aq. phase: ●: I=2, 0.5 M H_2SO_4, ■: I=2, 0.5 M $HClO_4$, △: I=2, 1.0 M $HClO_4$, □: 0.236 M H_2SO_4, ○: 0.516 M H_2SO_4.

TOA Extraction. From the results of the previous paper,[3] the contact time of 30 min was chosen. As an anionic species of Pa(IV) is extracted with TOA, we investigated it only in a sulfuric acid solution, in which Pa(IV) was expected to form an anionic complex. The extraction of Pa(IV) from 0.263 and 0.516 M sulfuric acid solutions with 5 v/v % TOA-xylene was carried out; the log-log plot of the distribution ratio of Pa(IV) and the concentration of Cr(II) is shown in Fig. 6. The distribution ratio of Pa(IV) decreases as the concentration of Cr(II) increases, much as in the above results for the BPHA and TTA extractions. Under the same conditions, Cr(II) and Cr(III) were not extracted at all.

Discussion

Chromium(II) has been used in the investigation of the aqueous chemistry of Pa(IV) in microquantities, and protactinium exists quantitatively in the tetravalent state in the presence of more than 10^{-4} M of Cr(II). However, there is no particular information about the influence of Cr(II) on the study of Pa(IV). The present authors, therefore, investigated the effect of Cr(II) on the extraction behavior of Pa(IV). The relations between the concentration of Cr(II) and the distribution ratio of Pa(IV) were examined by the use of such extractants as BPHA, TTA, and TOA, and it was found that the distribution ratio of Pa(IV) decreases with an increase in the concentration of Cr(II) in every case. It is considered that one of the causes leading to these results may be the re-oxidation of Pa(IV). However, Pa(IV) is fairly stable in an oxygen-free atmosphere. From the above experiments, it was found that Cr(II), which is less stable than Pa(IV), is sufficiently stable in both aqueous and organic phases after extraction. Moreover, in the BPHA extraction, if Pa(IV) is re-oxidized the apparent distribution ratio of Pa(IV) should be increased with an increase in the contact time, because Pa(V) has a larger distribution ratio than Pa(IV). The distribution ratio, however, becomes constant after about 30 min, as is shown in Fig. 1. In the TTA extraction, the distribution ratio must be increased because Pa(IV) has a larger distribution ratio than Pa(V),[13] but Fig. 6 shows the reverse of this, contrary to expectation. For these reasons, it is clear that protactinium is quantitatively in the tetravalent state during the extraction.

It is considered that one of the most reliable explanations of the results shown in Figs. 5 and 6 is the possibility that a multi-nuclear complex between Pa(IV) and Cr(II) or Cr(III) is formed. There is some previously-reported information on the Cr(III)–Np(V) complex[14] and Cr(III)–U(IV) complex[15] which is confirmed by the spectrophotometric measurement of the solution. The present authors also tried to measure the absorption spectra of Pa(IV), but could not find any influence of Cr(II) on it. However, it does not necessarily follow that the possibility of the Cr(II)–Pa(IV) complex cannot be denied, because the formation of a multinuclear complex does not always cause a change in the absorption spectrum. The influence of Pa(IV) on the absorption spectrum of Cr(II) could not be found because of its small molar extinction coefficient.

Much more investigations will be necessary to explain the direct interaction between Pa(IV) and Cr(II) completely.

References

1) R. Guillaumont, *C. R. Acad. Sci. Paris*, **260**, 1416 (1965).
2) R. Guillaumont, *ibid.*, **260**, 4738 (1965).
3) R. Muxart and H. Arapaki, *Bull. Soc. Chim. Fr.*, **1963**, 888.
4) T. Mitsuji, This Bulletin, **41**, 115 (1968).
5) T. Mitsuji, *ibid.*, **40**, 2822 (1967).
6) R. Guillaumont, *Bull. Soc. Chim. Fr.*, **1968**, 162.
7) D. Dyrssen, *Acta Chem. Scand.*, **10**, 353 (1956).
8) S. Suzuki and Y. Inoue, This Bulletin, **39**, 490 (1966).
9) T. Mitsuji, *ibid.*, **40**, 2091 (1967).
10) M. Haïssinsky snd E. Pluchet, *J. Chem. Phys.*, **59**, 608 (1962).
11) G. S. Forbes and H. W. Richter, *J. Amer. Chem. Soc.*, **39**, 1140 (1917).
12) E. S. Palshin, B. F. Myasoedov, and Yu. P. Novikov, *Zh. Analit. Khim.*, **18**, 657 (1963).
13) G. Bouissières and J. Vernois, *C. R. Acad. Sci. Paris.*, **244**, 2508 (1957).
14) J. C. Sullivan, *J. Amer. Chem. Soc.*, **84**, 4256 (1962).
15) T. W. Newton and F. B. Baker, *Inorg. Chem.*, **1**, 368 (1962).

The Preparation and Characterization of Bis[2-(2-pyridyl)-imidazole]iron(II) Complexes

Yoshihiro SASAKI and Tsunenobu SHIGEMATSU
Institute for Chemical Research, Kyoto University, Uji, Kyoto 611
(Received June 21, 1973)

Bis[2-(2-pyridyl)imidazole]iron(II) complexes, $Fe(PI)_2X_2$ ($X=Cl^-$, Br^-, NCS^-, N_3^-, and CN^-), were prepared and characterized on the basis of their infrared and Mössbauer spectra and their magnetic data. In $Fe(PI)_2(NCS)_2$, the NCS^- groups are N-bonded and are in a *cis* position. $Fe(PI)_2(CN)_2H_2O$ also has a *cis* configuration about the CN^- ligands. Except for $Fe(PI)_2(CN)_2H_2O$, the magnetic moments of the complexes lie in the 4.94—5.27 B.M. range. $Fe(PI)_2(CN)_2H_2O$ is a diamagnetic compound.

In the series of bis(1,10-phenanthroline)iron(II) complexes, $Fe(phen)_2X_2$, four types of compounds may be classified on the basis of their magnetic properties: (i) if the X ligand gives rise to a weak ligand field, the ground state is $^5T_2$[1]; (ii) if X affords a strong field, the complex is diamagnetic[1]; (iii) if X is F^-, 1/2 mal^{2-}, and 1/2 ox^{2-}, a spin triplet ground state is produced[2,3]; (iv) if $X=NCS^-$ or $NCSe^-$, a transition between the $^5T_2$ and $^1A_1$ ground states is observed at $T_c=174$ and 232 K.[4] In $Fe(bipy)_2(NCS)_2$, such a second-order transition at 216 K has also been reported.[5]

2-(2-Pyridyl)imidazole, possessing the characteristic of α-diimine, gives rise to a slightly weaker ligand field than does 2,2'-bipyridyl in nickel(II) complexes.[6,7] Certain tris[2-(2-pyridyl)imidazole]iron(II) complexes exhibit anomalous magnetic behavior indicative of the $^5T_2$–$^1A_1$ crossover.[8,9]

We have prepared bis[2-(2-pyridyl)imidazole]iron(II) complexes $Fe(PI)_2X_2$ ($X=Cl^-$, Br^-, NCS^-, N_3^-, and CN^-) and investigated their physical properties by means of infrared spectroscopy, Mössbauer-effect, and magnetic-susceptibility measurements; we will report our results here.

Experimental

2-(2-Pyridyl)imidazole was prepared by using a procedure similar to that described by Chiswell, *et al.*[10]

Preparation of Complexes. All the preparations were carried out in a nitrogen atmosphere using air-free water, acetone, and 3-methyl-1-butanol. All the complexes were dried *in vacuo* over silica gel at room temperature.

(a) Dichlorobis[2-(2-pyridyl)imidazole]iron(II), $Fe(PI)_2Cl_2$. The complex was prepared by suspending $Fe(II)(PI)_3Cl_2$-H_2O in 3-methyl-1-butanol and by then refluxing the mixture for 6 hrs. The orange crystals were washed by 3-methyl-1-butanol and were not recrystallized.

(b) Dibromobis[2-(2-pyridyl)imidazole]iron(II), $Fe(PI)_2Br_2$. 2-(2-Pyridyl)imidazole dissolved in acetone was added to a ferrous bromide solution prepared by mixing ferrous sulfate heptahydrate and barium bromide dihydrate solutions. When acetone was added to the filtered solution, orange crystals were precipitated.

(c) Dithiocyanatobis[2-(2-pyridyl)imidazole]iron(II), $Fe(PI)_2$-$(NCS)_2$. A concentrated aqueous solution of NaSCN was added to a mixed solution of $FeCl_24H_2O$ and 2-(2-pyridyl)-imidazole. The orange precipitate was washed with an ice-cold acetone-water mixture.

(d) Dicyanobis[2-(2-pyridyl)imidazole]iron(II) Monohydrate, $Fe(PI)_2(CN)_2H_2O$. A concentrated aqueous solution of KCN was added to a filtered solution of $FeCl_24H_2O$ and 2-(2-pyridyl)imidazole. After the acetone has been removed by using an evaporator, reddish-brown crystals were precipitated. One mole of H_2O per mole of the resulting compound was determined by the weight loss at 95 °C over P_2O_5.

(e) Diazidobis[2-(2-pyridyl)imidazole]iron(II), $Fe(PI)_2$-$(N_3)_2$. A concentrated aqueous solution of NaN_3 was added to the filtered starting solution, and the wine-red crystals thus precipitated were washed by water.

The analytical results of these complexes are given in Table 1. The quantitative determination of N in $Fe(PI)_2(N_3)_2$ met with difficulties.

Infrared Spectra. The infrared spectra were measured in Nujol mull with a Perkin-Elmer 521 spectrophotometer.

Magnetic Measurements. The magnetic susceptibilities were measured with a torsion-balance magnetometer. All the measurements were made at two different field strengths; no field dependence of the magnetic susceptibility was observed. The molar susceptibilities were corrected for diamagnetism, the following corrections: Fe^{2+}, −13; H_2O, −13; Cl^-, −23.4; Br^-, −34.6; NCS^-, −31.0; CN^-, −13; N_3^-, −13.7; 2-(2-pyridyl)imidazole, −82 (in units of 10^{-6} cgs/mol). The effective magnetic moment, μ_{eff}, was obtained from the $\mu_{eff}=2.828\sqrt{\chi_{M'}T}$ relation, $\chi_{M'}$ being the fully corrected molar susceptibility, and T, the temperature in K.

Mössbauer Effect Measurements. The Mössbauer spectra were obtained with a scanning velocity spectrometer in the time mode. The radiation source was ^{57}Co diffused in a copper foil and kept at room temperature during all the

Table 1. Analytical results (amounts in %)

Complex	C		H		N		Fe	
	Found	Calcd	Found	Calcd	Found	Calcd	Found	Calcd
$Fe(PI)_2Cl_2$	45.78	46.07	3.42	3.38	19.59	20.15	12.66	13.39
$Fe(PI)_2Br_2$	37.97	37.98	2.80	2.97	16.45	16.61	10.81	11.04
$Fe(PI)_2(NCS)_2$	46.74	46.76	2.83	3.05	23.69	24.24	11.46	12.08
$Fe(PI)_2(CN)_2H_2O$	51.46	51.94	3.66	3.88	26.33	26.93	13.11	13.42
$Fe(PI)_2(N_3)_2$	44.45	44.66	3.17	3.28	37.46	39.08	12.29	12.98

measurements. The velocity scale was calibrated with metallic iron, and the velocity was determined to an accuracy of ± 0.04 mm/s.

Results and Discussion

Infrared Spectra. The frequencies of the band maxima of the X ligands in the $Fe(PI)_2X_2$ complexes (X=NCS^-, CN^-, and N_3^-) are listed in Table 2. Since the absorption bands due to the 2-(2-pyridyl)-imidazole of these complexes change little from those of $Fe(PI)_2Cl_2$ and $Fe(PI)_2Br_2$, it is easy to assign the bands due to the X ligands.

Table 2. Infra-red frequencies of ligands X in $Fe(PI)_2X_2$ complexes (in cm^{-1})

Complex	Frequencies of band maxima	Assignment
$Fe(PI)_2(NCS)_2$	2071 vs, 2083 vs	C–N stretching
	975 s	C–S stretching
	460 m	N–C–S bending
$Fe(PI)_2(CN)_2H_2O$	2043 vs, 2051 vs	C–N stretching
$Fe(PI)_2(N_3)_2$	2037 vs, 2056 vs	N–N stretching

The thiocyanate group has three fundamental frequencies, *i.e.*, ν_1 (C–N stretching), ν_2 (N–C–S bending), and ν_3 (C–S stretching). Since thiocyanate is a bifunctional ligand, the positions of ν_1, ν_2, and ν_3 depend on whether this group is attached to the metal ion through N or through S. In $Fe(PI)_2(NCS)_2$, ν_1, ν_2, and ν_3 are in the range characteristic of N-bonded thiocyanate.[11-13] A splitting of the C–N stretching mode is observed. A *cis* configuration has been reported for both $Fe(phen)_2(NCS)_2$ and $Fe(bipy)_2(NCS)_2$, which exhibit splittings of the C–N stretching band of 12 and 10 cm^{-1} respectively[4,5] as well as for $Fe(phen)_2(CN)_2$, where the C–N stretching shows two peaks at 2075 and 2062 cm^{-1}.[14] In $Fe(PI)_2(NCS)_2$, the splitting of the C–N stretching mode is, therefore, taken as an indication of a *cis* configuration about the thiocyanate ligands. In $Fe(PI)_2(CN)_2H_2O$, the splitting of the C–N stretching mode is also observed. Therefore, this complex may have a *cis* configuration about the cyano ligands. Though $Fe(PI)_2(CN)_2H_2O$ is a low-spin compound, as will be described later, the absorption bands due to 2-(2-pyridyl)imidazole are similar to those of other complexes.

Magnetic Data. The results of magnetic-susceptibility measurements of polycrystalline samples between 77.2 and 283.0 K are compiled in Table 3. Except for $Fe(PI)_2(CN)_2H_2O$, the magnetic moments of the present complexes are characteristic of an iron(II) ion in a $^5T_2$ ground state. Within the temperature range of 77.2—283.0 K, the susceptibilities follow the Curie-Weiss law, $\chi_M'=C/(T-\Theta)$. The resulting values of the Weiss constant are included in Table 3. The magnetic moment observed in $Fe(PI)_2(CN)_2H_2O$ is indicative of a $^1A_1$ ground state of iron(II).

Mössbauer Spectra. The Mössbauer parameters are listed in Table 4. Some typical spectra of $Fe(PI)_2(N_3)_2$ are shown in Fig. 1. It was impossible to

Table 3. Magnetic data of $Fe(PI)_2X_2$ complexes

Compound	Temp. (K)	$10^6\chi_M'$ (cgs/mol)	μ_{eff} (B.M.)	Θ (K)
$Fe(PI)_2Cl_2$	77.2	39600	4.94	−7
	103.8	29879	4.98	
	141.3	22250	5.01	
	190.2	16836	5.06	
	236.5	13636	5.08	
	283.0	11545	5.11	
$Fe(PI)_2Br_2$	77.2	41502	5.06	−9
	103.8	31217	5.09	
	141.3	23503	5.15	
	190.2	17894	5.22	
	236.5	14504	5.24	
	283.0	12284	5.27	
$Fe(PI)_2(NCS)_2$	77.2	39725	4.95	−7
	103.8	30169	5.00	
	141.3	22326	5.02	
	190.2	16917	5.07	
	236.5	13762	5.10	
	283.0	11598	5.12	
$Fe(PI)_2(N_3)_2$	77.2	41535	5.06	−6
	103.8	31455	5.11	
	141.3	23502	5.15	
	190.2	17901	5.22	
	236.5	14317	5.20	
	283.0	12077	5.23	
$Fe(PI)_2(CN)_2H_2O$	77.2	279	0.42	—
	103.8	256	0.46	
	141.3	238	0.52	
	190.2	224	0.58	
	236.5	218	0.64	
	283.0	212	0.69	

Table 4. Mössbauer parameters δ^{IS} and ΔE_Q (in mm/s)

Compound	Temp. (K)	δ^{IS} (mm/s)	ΔE_Q (mm/s)
$Fe(PI)_2Cl_2$	298	1.03	2.64
	77.2	1.14	3.04
$Fe(PI)_2Br_2$	298	—	—
	110	1.27	3.05
$Fe(PI)_2(NCS)_2$	298	1.01	2.65
	77.2	1.09	2.94
$Fe(PI)_2(N_3)_2$	298	1.01	1.25
	77.2	1.15	2.24
$Fe(PI)_2(CN)_2H_2O$	298	0.21	0.11
	77.2	0.32	0.18

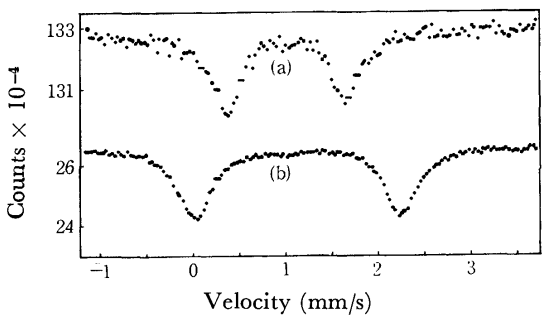

Fig. 1. Mössbauer spectra of $Fe(PI)_2(N_3)_2$.
a: 298 K b: 77.2 K

observe the Mössbauer effect of $Fe(PI)_2Br_2$ at 298 K. The parameters of $Fe(PI)_2X_2$ ($X=Cl^-$, Br^-, NCS^-, and N_3^-) are in the range characteristic of a Fe^{2+} ion in a high-spin form.[15] The spectra of $Fe(PI)_2(N_3)_2$ show marked features in the magnitude and the temperature dependency of the quadrupole splitting. In addition, the spectrum at 298 K exhibits a difference in the peak intensity of the doublet lines. The variation with the temperature predicts that there is an anisotropic recoilless fraction in this complex. On the other hand, the parameters of $Fe(PI)_2(CN)_2H_2O$ are characteristic of an iron(II) ion in a low-spin form.

The bis[2-(2-pyridyl)imidazole]iron(II) complexes, $Fe(PI)_2X_2$, may be classified into three groups on the basis of their magnetic properties: (i) if $X=Cl^-$, Br^-, NCS^-, and N_3^-, $Fe(PI)_2X_2$ is a high-spin compound; (ii) $Fe(PI)_2(CN)_2H_2O$ is a diamagnetic complex; (iii) $[Fe(PI)_3]^{2+}$ complexes in which X=1/2[2-(2-pyridyl)-imidazole] exhibit a spin equilibrium between $^1A_1$ and $^5T_2$ states.[8,9] The tris(1,10-phenanthroline)iron(II) and tris(2,2'-bipyridyl)iron(II) complexes are diamagnetic compounds, and $Fe(phen)_2(NCS)_2$ and $Fe(bipy)_2(NCS)_2$ have an anomalous magnetic property due to a $^1A_1$ and $^5T_2$ crossover.[4,5] Such a change in the spin state from ligand to ligand indicates that 2-(2-pyridyl)-imidazole gives rise to a weaker ligand field than do 1,10-phenanthroline and 2,2'-bipyridyl in iron(II) complexes.

The authors wish to thank Dr. T. Shinjo and Mr. T. Matsuzawa for permitting to use the equipment for the Mössbauer and magnetic measurements respectively.

References

1) K. Madeja and E. König, *J. Inorg. Nucl. Chem.*, **25**, 377 (1963).
2) E. König and K. Madeja, *J. Amer. Chem. Soc.*, **88**, 4528 (1966).
3) E. König and K. Madeja, *Inorg. Chem.*, **7**, 1848 (1968).
4) E. König and K. Madeja, *ibid.*, **6**, 48 (1967).
5) E. König, K. Madeja, and K. J. Watson, *J. Amer. Chem. Soc.*, **90**, 1146 (1968).
6) W. J. Eilbeck and F. Holmes, *J. Chem. Soc., A*, **1967**, 1777.
7) R. J. Dosser and A. E. Underhill, *ibid.*, **1972**, 611.
8) D. M. L. Goodgame and A. A. S. C. Machado, *Inorg. Chem.*, **8**, 2031 (1969).
9) R. L. Dosser, W. J. Eilbeck, A. E. Underhill, P. R. Edwards, and C. E. Johnson, *J. Chem. Soc., A*, **1969**, 810.
10) B. Chiswell, F. Lions, and B. S. Morris, *Inorg. Chem.*, **3**, 110 (1964).
11) P. C. H. Mitchell and R. J. P. Williams, *J. Chem. Soc.*, **1960**, 1912.
12) J. Lewis, R. S. Nyholm, and P. W. Smith, *ibid.*, **1961**, 4590.
13) F. A. Cotten, D. M. L. Goodgame, M. Goodgame, and T. E. Haas, *Inorg. Chem.*, **1**, 565 (1962).
14) A. A. Schilt, *ibid.*, **3**, 1323 (1964).
15) J. F. Duncan and R. M. Golding, *Quart. Rev.*, **19**, 36 (1965).

Acid Dissociation Constants of Some Histidine-containing Peptides and Formation Constants of Their Metal Complexes

Akira YOKOYAMA, Hiroji AIBA, and Hisashi TANAKA
Faculty of Pharmaceutical Sciences, Kyoto University, Yoshida, Sakyo-ku, Kyoto 606
(Received June 18, 1973)

Glycyl-L-histidine, L-histidylglycine, glycylglycyl-L-histidine, glycyl-L-histidylglycine, and L-histidylglycylglycine were synthesized by the carbobenzoxy azide procedure. The acid dissociation constants of these peptides and their related compounds were determined from the potentiometric titration curves of 0.01 M solutions at 21 °C. The dissociation of one ionization group is greatly influenced by the charge on the other groups. The formation constants of metal complexes of L-histidylglycine, L-histidylglycylglycine, and L-3-benzylhistidine were calculated by the least-squares method from the titration curves of the solution containing the ligand (0.01 M) and metal in the molar ratio 2: 1, assuming the formation of 1: 1 and 2: 1 normal complexes (ML^+ and ML_2), and the results were compared with those of L-histidine-metal complexes. For any metal ion, the order of formation constants was found to be histidine≈3-benzylhistidine>histidylglycine>histidylglycylglycine, in agreement with that of the basicity of amino and imidazole groups. In these metal complexes, metal ion is considered to bind through amino, imidazole, and carboxyl or carbonyl groups of histidine residue.

Histidine residue of the protein molecule plays a particularly important role in the interaction with metal ion, due to the presence of three coordinating groups, but detailed studies on the complex formation of the peptides with metal ions as a model system of the protein-metal interaction have been mostly confined to a limited number of simple peptides not containing histidine residue. Recently, however, some valuable information has been given on the complex formation of histidine-containing peptides.[1-5] Because of its significance in the study of protein-metal interaction, we have undertaken an extensive study on the complex formation of various histidine-containing peptides in order to obtain more information. This paper deals with the syntheses and the acid dissociation constants of glycyl-L-histidine, L-histidylglycine, glycylglycyl-L-histidine, glycyl-L-histidylglycine, and L-histidylglycylglycine (abbreviated as H–Gly–His–OH, H–His–Gly–OH, H–Gly–Gly–His–OH, H–Gly–His–Gly–OH, and H–His–Gly–Gly–OH, respectively) and the formation constants of some metal complexes of these peptides.

Experimental

Syntheses. *L-Histidylglycine*: H–His–Gly–OH was synthesized according to the method given by Photaki *et al.*,[6] with some modifications.

Carbobenzoxyglycyl-L-histidine Methyl Ester (Z–Gly–His–OCH_3): To a solution of 0.02 mol of carbobenzoxyglycine hydrazide[7] in 20 ml of 2 M hydrochloric acid and 100 ml of *N,N*-dimethylformamide (DMF) was added a cold concentrated aqueous solution of 0.02 mol of sodium nitrite under cooling with an ice-bath. After 30 min, 0.02 mol of L-histidine methyl ester dihydrochloride was added and the solution was neutralized with triethylamine. The solution was then allowed to stand under cooling for 24 hr. The solvent was evaporated and the residue was dissolved in water. The pH of the solution was adjusted to 8—9 with the addition of 1 M sodium hydroxide, and the resulting precipitate was collected and washed with water; yield 80%.

Carbobenzoxyglycyl-L-histidine (Z–Gly–His–OH): To a solution of 0.01 mol of Z–Gly–His–OCH_3 in 20 ml of methanol was added 10 ml of 1 M sodium hydroxide. After 30 min the solution was neutralized by the addition of 1 M hydrochloric acid and evaporated to dryness. The residue was dissolved in methanol. After removing the insoluble material, the solution was allowed to stand. The crystals of Z–Gly–His–OH precipitated within about 30 min. After 1 hr, the product was collected and used in the subsequent procedure without further purification; yield 95%.

Glycyl-L-histidine: To a solution of 0.005 mol of Z–Gly–His–OH in 20 ml of methanol, 10 ml of water and 1 ml of glacial acetic acid was added 100 mg of 10% Pd/C, and hydrogen was bubbled for 3 hr. The catalyst was removed by filtration. The filtrate was concentrated and applied to a column of Dowex 50-X2, H-form. Water was passed until no chlorine ion was detected in the effluent. H–Gly–His–OH was eluted with 1 M ammonium hydroxide and the effluent was concentrated to dryness. Dehydrated ethanol was added and evaporated. The procedure was repeated to obtain H–Gly–His–OH as amorphous powder; yield 95%.

Carbobenzoxyglycylglycyl-L-histidine Methyl Ester (Z–Gly–Gly–His–OCH_3), Carbobenzoxyglycyl-L-histidylglycine Ethyl Ester (Z–Gly–His–Gly–OC_2H_5), and Carbobenzoxy-L-histidylglycylglycine Ethyl Ester (Z–His–Gly–Gly–OC_2H_5): These peptides were prepared in the same way as in the syntheses of Z–Gly–His–OCH_3, from carbobenzoxydipeptide hydrazides[7] with amino acid ester hydrochlorides; yield 80%.

Carbobenzoxyglycylglycyl-L-histidine (Z–Gly–Gly–His–OH) and Carbobenzoxyglycyl-L-histidylglycine (Z–Gly–His–Gly–OH): To a solution of 0.01 mol of carbobenzoxytripeptide ester in 20 ml of DMF was added 10 ml of 1 M sodium hydroxide. After 30 min the solution containing carbobenzoxytripeptide was neutralized with 1 M hydrochloric acid and used in the subsequent procedure.

Glycylglycyl-L-histidine and Glycyl-L-histidylglycine: These peptides were prepared from the solutions of carbobenzoxytripeptides in the same way as in the synthesis of H–Gly–His–OH; yield 90%.

L-Histidylglycylglycine Ethyl Ester (H–His–Gly–Gly–OC_2H_5): To a solution of 0.005 mol of Z–His–Gly–Gly–OC_2H_5 in 50 ml of DMF was added 100 mg of 10% Pd/C, and hydrogen was bubbled for 3 hr. The catalyst was removed and the solution containing H–His–Gly–Gly–OC_2H_5 was used in the subsequent reaction.

L-Histidylglycylglycine: To a solution of H–His–Gly–Gly–OC_2H_5 was added 5 ml of 1 M sodium hydroxide. After 1 hr, the solution was neutralized with 1 M hydrochloric acid and concentrated. NaCl was removed in the same way

TABLE 1. HISTIDINE-CONTAINING PEPTIDES AND THEIR DERIVATIVES

Compound	Molecular formula	Mol. wt.	Mp, °C	Anal. Calcd % C	Calcd % H	Calcd % N	Found % C	Found % H	Found % N
Z-Gly-His-OH[a]	$C_{16}H_{18}O_5N_4 \cdot 1\frac{1}{3}H_2O$	370.37	(b)	51.88	5.63	15.13	51.75	5.76	14.94
Z-His-Gly-OH	$C_{16}H_{18}O_5N_4$	346.34	232	55.48	5.24	16.18	55.22	5.40	16.13
H-Gly-His-OH	$C_8H_{12}O_3N_4 \cdot H_2O \cdot \frac{1}{3}C_2H_5OH$	245.59	(c)	42.38	6.58	22.82	42.75	6.34	22.79
H-His-Gly-OH	$C_8H_{12}O_3N_4$	212.21	201	45.28	5.70	26.40	45.29	5.71	26.69
Z-Gly-His-$NHNH_2$	$C_{16}H_{20}O_4N_6$	360.37	146	53.32	5.59	23.32	53.43	5.58	22.80
Z-His-Gly-$NHNH_2$	$C_{16}H_{20}O_4N_6$	360.37	116	53.32	5.59	23.32	53.38	5.59	23.20
Z-Gly-Gly-$NHNH_2$	$C_{12}H_{16}O_4N_4$	280.28	160	51.42	5.75	19.99	51.53	5.64	19.71
Z-Gly-Gly-His-OCH_3	$C_{19}H_{23}O_6N_5 \cdot \frac{1}{2}H_2O$	426.42	(b)	53.51	5.68	16.42	53.46	5.77	16.31
Z-Gly-His-Gly-OC_2H_5	$C_{20}H_{25}O_6N_5$	431.44	173	55.67	5.84	16.23	55.84	5.83	16.45
Z-His-Gly-Gly-OC_2H_5	$C_{20}H_{25}O_6N_5$	431.44	182	55.67	5.84	16.23	55.92	6.06	16.13
H-Gly-Gly-His-OH	$C_{10}H_{15}O_4N_5 \cdot 1\frac{1}{3}H_2O$	293.28	(c)	40.95	6.05	23.87	41.28	5.95	23.47
H-Gly-His-Gly-OH	$C_{10}H_{15}O_4N_5 \cdot \frac{1}{2}H_2O$	278.27	224	43.15	5.81	25.17	43.23	5.94	25.47
H-His-Gly-Gly-OH	$C_{10}H_{15}O_4N_5 \cdot \frac{1}{2}H_2O$	278.27	205	43.15	5.81	25.17	43.13	5.90	25.17

a) Sample desalted by Dowex 50-X2.
b) Not determined.
c) Hygroscopic.

as in the case of H-Gly-His-OH; yield 90%.

Other Materials. L-3-Benzylhistidine (3-Bzl-His-OH) (from Peptide Institute, Protein Research Foundation) and commercial ligands and metal salts were used. Metal ion solutions prepared from metal chlorides or metal sulfate were standardized with EDTA.

Potentiometric Titration. Potentiometric titration was carried out with a Radiometer Titrator TTT 1 and a Titrigraph according to the prescription given by Albert and Serjeant.[8] A solution (10 ml) containing a ligand (10^{-2}M) and hydrochloric acid (0—2.0×10^{-2} M), or a ligand (10^{-3} M), hydrochloric acid (1.0—2.0×10^{-3} M) and a metal ion (0.5×10^{-3} M) was titrated with 0.1 M potassium hydroxide. During the course of titration, the temperature was maintained at 21 °C and a stream of CO_2 free nitrogen was passed through the titration vessel.

Results and Discussion

Syntheses. Histidine-containing peptides were synthesized by the carbobenzoxy azide method.[6,7] A slight modification was necessary in some cases. In the synthesis of H-His-Gly-Gly-OH, catalytic reduction was carried out prior to the hydrolysis of Z-His-Gly-Gly-OC_2H_5, because a side reaction took place in the hydrolysis. The analytical data of the peptides synthesized are shown in Table 1, together with their melting points. The results of the electrophoresis and thin layer chromatography confirmed the purity of these peptides.

Acid Dissociation Constants. The potentiometric titration curves for histidine-containing peptides and their related compounds are shown in Figs. 1 and 2. Acid dissociation corresponding to three coordinating groups, namely amino, imidazole, and carboxyl groups, are observed in all these ligands. The equilibria in the dissociation are expressed as follows.

$$LH_3^{2+} \rightleftharpoons LH_2^+ + H^+$$
$$K_{COOH} = [LH_2^+][H^+]/[LH_3^{2+}] \quad (1)$$

$$LH_2^+ \rightleftharpoons LH + H^+$$
$$K_{Im} = [LH][H^+]/[LH_2^+] \quad (2)$$

$$LH \rightleftharpoons L^- + H^+$$
$$K_{NH_2} = [L^-][H^+]/[LH] \quad (3)$$

The values of K_{Im} and K_{NH_2} were calculated simultaneously as shown below, since the acid dissociations of amino and imidazole groups overlap in most of the ligands. In the range where a value, which represents moles of KOH added per mole of completely protonated ligand, is between 1 and 3, total concentration of the ligand and the electroneutrality are expressed by

$$[L]_T = [LH_2^+] + [LH] + [L^-] \quad (4)$$

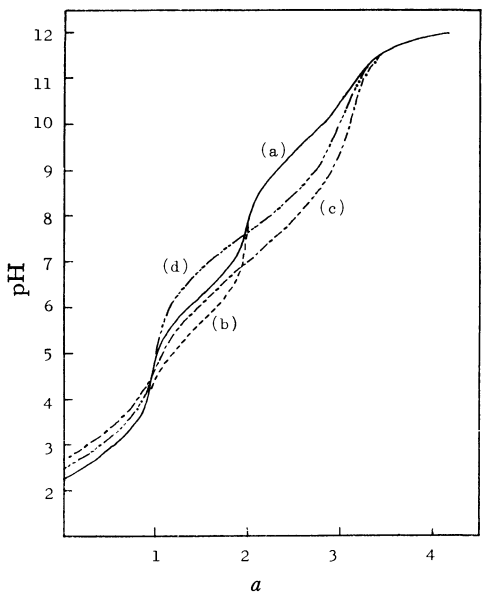

Fig. 1. Titration curves of histidine-containing dipeptides and related compounds;
(a) histidine·HCl+HCl, (b) 3-Bzl-His-OH+2HCl, (c) H-His-Gly-OH+2HCl, (d) H-Gly-His-OH+2HCl; ligand concentration: 10^{-2} M.

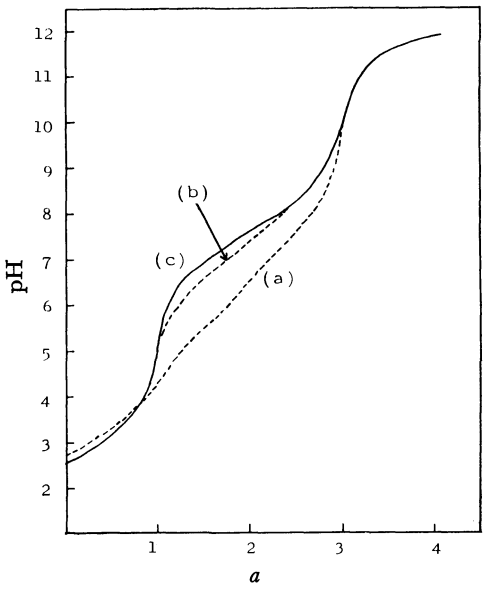

Fig. 2. Titration curves of histidine-containing tripeptides;
(a) H–His–Gly–Gly–OH+2HCl, (b) H–His–Gly–OH +2HCl, (c) H–Gly–Gly–His–OH+2HCl; ligand concentration: 10^{-2} M.

$$[LH_2^+] + [H^+] + [K^+] = [OH^-] + [Cl^-] + [L^-]. \quad (5)$$

From Eqs. (2)~(5), we obtain

$$[H^+]([L]_T - P)/P = K_{Im} + ([L]_T + P)K_{Im}K_{NH_3}/P[H^+] \quad (6)$$

where $[L]_T$=total concentration of ligand
$[L^-]$=concentration of completely deprotonated ligand
$[LH]$=concentration of monoprotonated ligand
$[LH_2^+]$=concentration of diprotonated ligand
$[LH_3^{2+}]$=concentration of triprotonated ligand
$P=[L^-]([H^+]^2/K_{Im}K_{NH_3}-1)$.

The values of K_{Im} and K_{NH_3} were calculated by the least-squares treatment of Eq. (6). The constants of L-histidine methyl ester (H–His–OCH_3) were similarly calculated. The values of K_{COOH} were calculated by the usual method. The results are shown in Table 2.

The value of pK_{COOH} increases in the order histidine ≈3-Bzl–His–OH < H–Gly–His–OH < H–Gly–Gly–His–OH < H–His–Gly–OH < H–His–Gly–Gly–OH ≈ H–Gly–His–Gly–OH. This indicates that the dissociation of the carboxyl group is greatly influenced by the electrostatic effect[9] of the positive charges on amino and imidazole groups. The basicity of the imidazole group decreases in the order H–Gly–Gly–His–OH > H–Gly–His–OH > H–Gly–His–Gly–OH > histidine > H–His–Gly–OH > 3-Bzl–His–OH > H–His–Gly–Gly–OH. This order agrees with that expected from the electrostatic effect of the amino and the carboxyl groups, except for the case of 3-Bzl–His–OH, *viz.*, the basicity of the imidazole group is strengthened by the negative charge but weakened by the positive charge. A weaker basicity of the imidazole group of 3-Bzl–His–OH than expected is explicable in terms of the decrease of the electron-delocalization in the imidazole ring. Similarly, it seems that the values of pK_{NH_3} are mainly governed by the electrostatic effect based on the carboxyl and

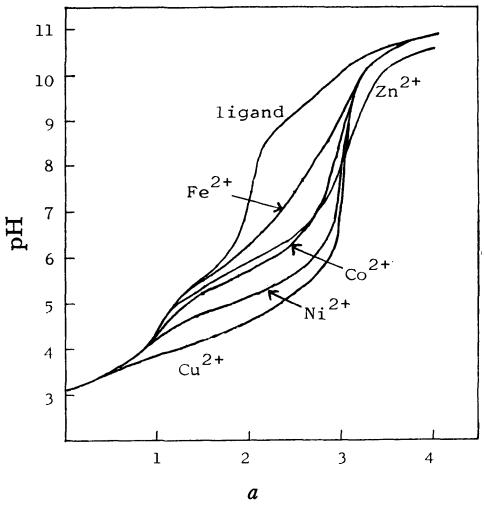

Fig. 3. Titration curves of 3-Bzl–His–OH in the presence of metal ion; ligand (10^{-3}M) to metal ratio=2: 1.

TABLE 2. ACID DISSOCIATION CONSTANTS OF HISTIDINE-CONTAINING PEPTIDES AND ITS RELATED COMPOUNDS AT 21 °C CALCULATED FROM THE TITRATION CURVES OF 0.01 M SOLUTIONS

	Present study			Results of other workers		
	pK_{COOH}	pK_{Im}	pK_{NH_3}	pK_{COOH}	pK_{Im}	pK_{NH_3}
Histidine	2.22	6.17	9.28	1.82[b]	6.00[b]	9.16[b]
3-Bzl–His–OH	2.25	5.59	9.26			
H–His–Gly–OH	2.94	6.01	7.87	2.96[c]	5.58[c]	7.50[c]
H–Gly–His–OH	2.75	6.85	8.33	2.66[c]	6.77[c]	8.24[c]
H–His–Gly–Gly–OH	3.17	5.52	7.62			
H–Gly–His–Gly–OH	3.19	6.63	8.17	3.26[d]	6.92[d]	7.96[d]
H–Gly–Gly–His–OH	2.84	6.99	8.23	2.84[c]	6.87[c]	8.22[c]
Z–Gly–His–OH[a]	3.33	6.94	—			
Z–His–Gly–OH[a]	3.81	6.82	—			
H–His–OCH_3	—	5.10	7.18	—	5.39[e]	7.37[e]

No activity coefficient corrections were made.
a) Ligand concentration: 10^{-3} M.
b) Ref. 12, Ligand concentration is 0.01 M at the commencement of the titration, 25 °C.
c) Ref. 16, μ=0.16, 25 °C.
d) Ref. 17, μ=1.0, 25 °C.
e) Ref. 14, μ=0.16, 25 °C.

imidazole groups. The higher values of pK_{Im} and pK_{COOH_3} of carbobenzoxy dipeptides, in which amino groups are blocked, than those of corresponding free dipeptides can be accepted in view of the influence of electrostatic effect. The lower values of pK_{Im} and pK_{NH_3} of H–His–OCH_3 than those of histidine are explicable in terms of the absence of the electrostatic effect of the carboxyl group.

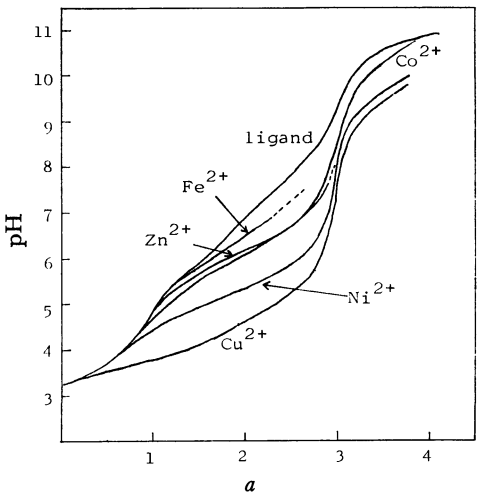

Fig. 4. Titration curves of H–His–Gly–OH in the presence of metal ion; ligand (10^{-3}M) to metal ratio= 2: 1. Dotted lines indicate precipitations.

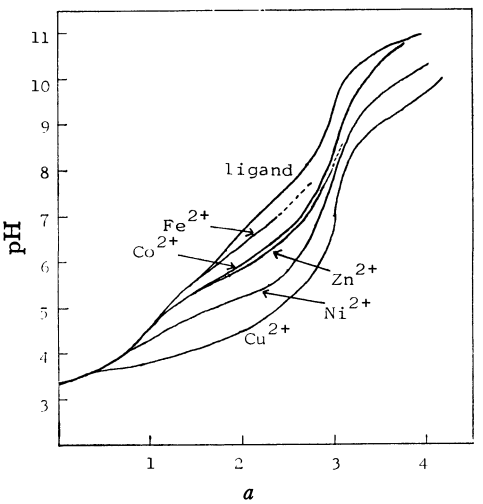

Fig. 5. Titration curves of H–His–Gly–Gly–OH in the presence of metal ion; ligand (10^{-3}M) to metal ratio= 2: 1. Dotted lines indicate precipitations.

Complex Formation of H–His–Gly–OH and H–His–Gly–Gly–OH with Some Transition Metal Ions. The titration curves of the solutions containing H–His–Gly–OH, H–His–Gly–Gly–OH, and 3-Bzl–His–OH and metal ions with the ratio of 2 to 1 are shown in Figs. 3, 4, and 5. They are very similar to those of histidine and metal ions. The inflection of pH was observed at $a=3$, indicating the formation of 2: 1 (ligand to metal) complexes in all cases. The following equilibria are postulated in the complex formation which occurred in the range where a value is between 1 and 3. The formation constants are denoted by K_1 and K_2.

$$M^{2+} + L^- \rightleftarrows ML^+ \quad K_1 = [ML^+]/[M^{2+}][L^-] \quad (7)$$

$$ML^+ + L^- \rightleftarrows ML_2 \quad K_2 = ML_2/[ML^+][L^-] \quad (8)$$

The formation constants were calculated by the least-squares treatment of the equation of Irving and Rossotti.[10,11]

$$\bar{n}/(\bar{n}-1)[L^-] = (2-\bar{n})[L^-]K_1K_2/(\bar{n}-1) - K_1 \quad (9)$$

The calculated values do not vary significantly with pH values in most cases. In the systems H–His–Gly–OH–Fe(II) and H–His–Gly–Gly–OH–Fe(II), only log K_1 was approximately obtained from the formation curves, assuming $\log K_1 = -\log[L^-]$ at $\bar{n}=0.5$, since the precipitation occurred in the course of the titrations and the accurate values were not obtained by least-squares treatment. In the systems 3-Bzl–His–OH–Cu(II) and histidine-Cu(II), the occurrence of complicated complex formation is suggested, since consistent values were not obtained. The results are shown in Table 3. The validity of these constants was approved in most cases, by the coincidence of the experimental and calculated formation curves, obtained from the formation constants determined (Figs. 6, 7, and 8). The results might indicate that the formation of species other than normal complexes can be neglected. In the case of 3-Bzl–His–OH–Cu(II) and histidine-Cu(II) sys-

Table 3. Formation constants of divalent metal complexes of histidine containing peptides and their related compounds at 21 °C obtained from mixtures of ligand (0.001 M) and metal in molar ratio 2:1

No activity coefficient corrections were made.

	Fe(II)		Co(II)		Ni(II)		Cu(II)		Zn(II)	
	$\log K_1$	$\log K_2$	$\log K_1$	$\log K_2$	$\log K_1$	$\log K_2$	$\log K_1$	$\log K_2$	$\log K_1$	$\log K_2$
Histidine	5.39[a]	3.35[a]	6.92[b]	5.52[b]	8.96[b]	6.83[b]	10.56[b]	8.25[b]	6.63[b]	5.63[b]
	5.25	4.44	6.88	5.83	7.89	6.94	10.14[c]	7.49[c]	6.36	5.77
3-Bzl–His–OH	5.65	4.59	6.87	6.17	7.95	7.39	10.17[c]	8.03[c]	6.54	6.00
H–His–Gly–OH	4.20	(e)	5.52	4.23	6.88	5.94	9.13	6.78	4.86	4.68
H–His–Gly–Gly–OH	3.92	(e)	5.09	4.11	6.50	5.73	8.60	6.47	4.93	4.71

a) Ref. 18, $\mu=0.2$, 15 °C.
b) Ref. 12, Ligand concentration is 0.01 M at the commencement of titration, 25 °C.
c) Consistent value could not be obtained.
d) Obtained from formation curve.
e) Not determined.

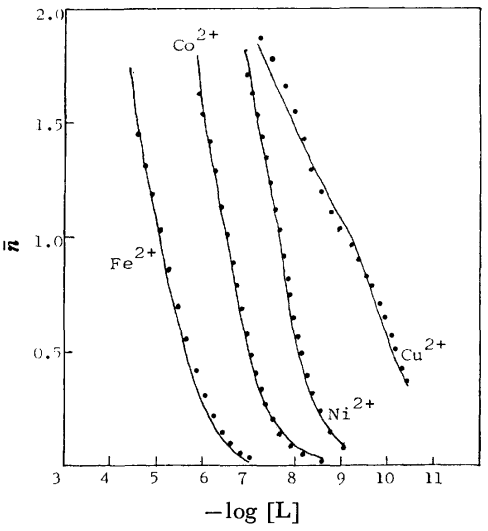

Fig. 6. Formation curves of metal complexes of 3-Bzl-His-OH. The curves were obtained directly from the experimental data. The value of each point was calculated by the use of the values in Table 3.

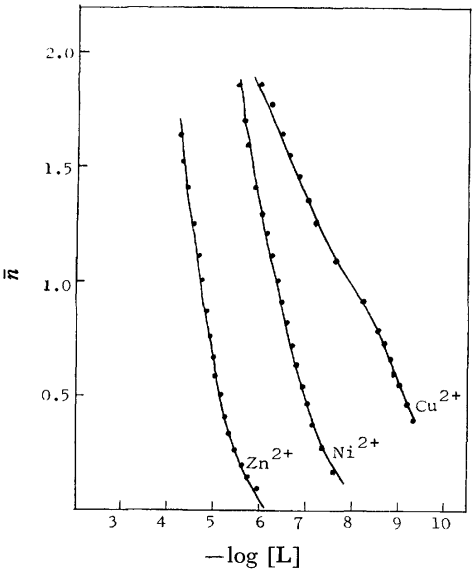

Fig. 7. Formation curves of metal complexes of H-His-Gly-OH.

tems, experimental and calculated formation curves did not coincide. In histidine-Cu(II) system the discrepancy has been explained on the basis of the formation of the protonated complex, in which Cu(II) is assumed to bind to imidazole and carboxyl groups, in addition to the normal complex.[11-14] Accordingly, the formation of a similar protonated complex can possibly be presumed also in 3-Bzl-His-OH-Cu(II) system. In this connection, the coincidence between experimental and calculated formation curves in the systems H-His-Gly-OH-Cu(II) and H-His-Gly-Gly-OH-Cu(II) suggests that the formation of the protonated complex might be neglected in these systems. The low stability of the protonated complex is explained in the light of the structure of these ligands, *viz.*, the existence of imidazole and carboxyl groups with long distance. It is clear from Table 3 that the Irving-

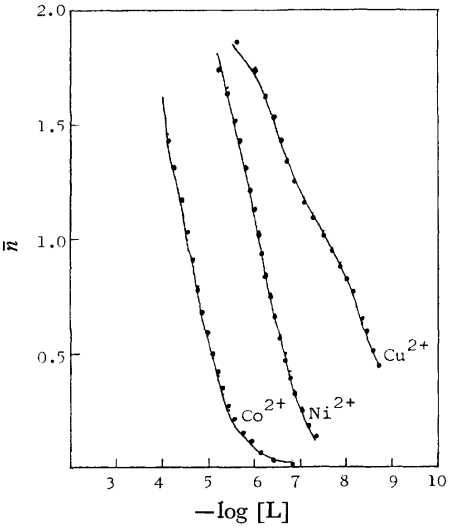

Fig. 8. Formation curves of metal complexes of H-His-Gly-Gly-OH.

Williams' order,[19] Fe(II)<Co(II)<Ni(II)<Cu(II)>Zn(II), is satisfied for all ligands. Further, with any given metal ion, the order of the stability constants with respect to the four ligands is 3-Bzl-His-OH≈histidine>H-His-Gly-OH>H-His-Gly-Gly-OH, agreeing with that of the basicity of amino and imidazole groups. This indicates that metal ions strongly bind to amino and imidazole groups in 3-Bzl-His-OH, H-His-Gly-OH, and H-His-Gly-Gly-OH, as in the case of histidine. The third coordination site may be oxygen atom of carboxyl or carbonyl groups. The probable structures of the 2: 1 complexes, ML_2, may be expressed as **I** and **II**. In the region where *a* value is larger

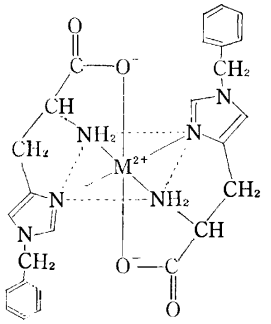

(**I**)

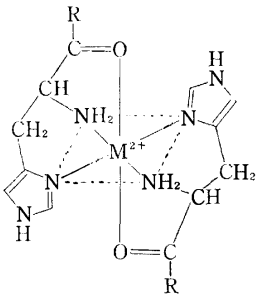

(**II**)

R {NHCH$_2$COO$^-$: H-His-Gly-OH
NHCH$_2$CONHCH$_2$COO$^-$: H-His-Gly-Gly-OH

than 3, additional dissociation of proton from amide group occurs in the systems H-His-Gly-OH and H-His-Gly-Gly-OH with Cu(II) and Ni(II) and the dissociation causes remarkable change in the structure of the complex. Information was briefly given on this point.[5]

The authors wish to express their thanks to the staff of the Kyoto University Computer Center for the use of FACOM 230-60 Computer, and to the members of the Micro Analytical Center of Kyoto University for elemental analysis.

References

1) F. R. N. Gurd and G. F. Bryce, "The Biochemistry of Copper," ed. by J. Peisach, P. Aisen, and W. Blumberg, Academic Press, Inc., New York, (1966), p. 115.
2) J. F. Blount, K. A. Fraser, H. C. Freeman, J. T. Szymanski, and C. H. Wang, *Acta Crystallogr.*, **22**, 396 (1967).
3) P. J. Morris and R. B. Martin, *J. Inorg. Nucl. Chem.*, **33**, 2913 (1971).
4) R. Osterberg and B. Sjoberg. *Chem. Commun.*, **1972**, 983.
5) A. Yokoyama, H. Aiba, and H. Tanaka, *Chem. Lett.*, **1972**, 489.
6) I. Photaki, D. Schaufele, S. Fallab, and H. Erlenmeyer, *Helv. Chim. Acta*, **40**, 187 (1957).
7) B. F. Erlanger and E. Brand, *J. Amer. Chem. Soc.*, **73**, 3508 (1951).
8) A. Albert and E. P. Serjeant, "Ionization Constants of Acids and Bases, ' Chap. 2, Methuen, London, 1962.
9) R. B. Martin, "Introduction to Biophysical Chemistry," Chap. 4, McGraw Hill Book Company, Inc., New York, 1964.
10) H. Irving and F.J.C. Rossotti, *J. Chem. Soc.*, **1953**, 3397.
11) A. Albert and E. P. Serjeant, "Ionization Constants of Acids and Bases," Chap. 9, Methuen, London, 1962.
12) R. Leberman and B. R. Rabin, *Trans. Faraday Soc.*, **55**, 1660 (1959).
13) D. D. Perrin and V. S. Sharma, *J. Chem. Soc., A*, **1967**, 724.
14) J. L. Meyer and J. E. Bauman, Jr., *J. Amer. Chem. Soc.*, **92**, 4210 (1970).
15) D. R. Williams, *J. Chem. Soc. Dalton*, **1972**, 790.
16) G. E. Bryce, R. W. Roeske, and F. R. N. Gurd, *J. Biol. Chem.*, **240**, 3837 (1965).
17) R. Osterberg, *J. Phys. Chem.*, **73**, 2230 (1969).
18) E. V. Raju and H. B. Mather, *J. Inorg. Nucl. Chem.*, **31**, 425 (1969).
19) H. Irving and R. J. P. Williams, *J. Chem. Soc.*, **1953**, 3192.

The Extraction of Tris(1,10-phenanthroline)ruthenium(II). I. Distribution Studies

Takejiro TAKAMATSU

Department of Chemistry, Faculty of Science, Kyoto University, Sakyo-ku, Kyoto 606

(Received June 26, 1973)

Tris(1,10-phenanthroline)Ru(II) was extracted into various organic solvents with several anions, such as the perchlorate ion, the iodide ion, or the thiocyanate ion. The association constants of ion-pairs were successfully determined by analysis of the extraction curves in the solvents with low polarities. It was found that the ion-pairs were extracted mainly as the associated form and that only the first-step dissociation could slightly occur ($<10^{-7}$) in such solvents; furthermore, the degree of association was considerable even in water. Therefore, the distribution ratio of the complex cation must be governed by both the hydration energy of the counter anion and the solubility parameter of the extraction solvent rather than its dielectric property. An abnormal decrease in the distribution ratio was observed when the tetraphenylborate ion was used as the counter anion. This phenomenon can be explained clearly in terms of the hydrotropism which was often encountered in the solution of an electrolyte with a large ion.

In recent years, the ion-pair extraction systems have been widely investigated, mainly out of analytical interest.[1] However, very few theories which can satisfactorily explain its mechanism have yet been developed. Some authors have successfully tried to discuss the extraction mechanism in connection with the dielectric properties of the solvents.[1,2] On the other hand, Freiser[3] suggested the possibility that the regular solution theory could also be applied to the ion-pair distribution with the organic solvent of a low polarity (≤ 10), much as in the case of chelate distribution.[4] Gibson and Weatherburn[5] have tried to discuss the extraction behavior in connection with the hydration energies of the ions.

In this paper, in order to describe one approach to the systematic investigation of the ion-pair extraction system, tris(1,10-phenanthroline)Ru(II), $Ru(II)(phen)_3$ has been chosen as the extractant to be transferred into various organic solvents in the presence of such anions as the perchlorate ion, the iodide ion, the thiocyanate ion, the tetrafluoroborate ion, and the tetraphenylborate ion. The extraction mechanism can be analysed clearly in the $Ru(II)(phen)_3$ system, because $Ru(II)(phen)_3$ is very substitution-inert so that the interference of the free ligand can be neglected. The distribution ratios were discussed as a function of the bulk character of the solvents and of the hydration energies of the anions. The distribution ratios of sodium perchlorate into chloroform, *o*-dichlorobenzene, *etc.*, which could hardly be determined by direct-extraction measurements, can also be determined indirectly by analyses of the extraction curves of $Ru(II)(phen)_3$. In the extraction of $Ru(II)(phen)_3$ with the tetraphenylborate ion, the decrease in the distribution ratio appeared in the region where the concentration of the tetraphenylborate ion was high. This abnormal phenomenon was explained in terms of the hydrotropism advanced by Neuberg[6] in 1916.

In the next paper,[7] the distribution ratio will be discussed in connection with the solubilities by applying the regular solution theory and the electrostatic theory.

Experimental

Reagents. All the reagents were of a reagent-grade purity. The organic solvents were purified mainly by distillation before use. Sodium perchlorate was used as an anhydrous salt after recrystallization. ^{106}Ru (Lot. No. 1210) was supplied by the Japan Radioisotope Association. The radiochemical purity was checked by means of the γ-ray spectrum. The water was distilled twice with an all-quartz distillation apparatus.

Molar absorptivity of $Ru(II)(phen)_3$. The determination of the molar absorptivity of Ru(II) $(phen)_3$ was carried out by using a ruthenium chloride solution (ruthenium content: 0.07392 mg/ml) in a manner almost identical with that of Banks and ÓLaughlin[8] except that 0.5 M KH_2PO_4–Na_2HPO_4 was used to maintain the pH at 6 during the reaction. The calculated molar absorptivity at 448 nm was 18500 liters per mole-cm. In this series of extraction studies, the concentration of Ru(II) $(phen)_3$ was determined from this value.

Preparation of the $^{106}Ru(II)(phen)_3$ Solution. A crude aqueous solution of $^{106}Ru(II)(phen)_3$ was prepared from $^{106}RuCl_3$ (containing as adequate amount of the carrier) as has been described above except that the NaOH–HCl system was used to adjust the pH to 6. After the reacted mixture has been washed several times with chloroform and then with *n*-hexane, the $Ru(II)(phen)_3$ was extracted with the perchlorate ion into 1,2-dichloroethane. This organic phase was evaporated to dryness and then dissolved with a minimum volume of acetonitrile. If any residue was detected, it was filtered out. This filtrate was dried again and then dissolved in a small amount of water. This resulting solution was passed through the anion-exchanger column in order to convert the counter anions to chloride or sulfate. It is recommended that a labelled complex of a high specific activity should be used immediately after preparation, since serious radiation decomposition was noticed; in a sample of 1 μCi/ml, several percent were found to be decomposed within one week.

Extraction Procedure of $Ru(II)(phen)_3$. An appropriate amount of the $^{106}Ru(II)(phen)_3$ solution and various amounts of sodium-salt solutions of different anions, such as the perchlorate ion, the iodide ion, and the thiocyanate ion, were placed in a 50 ml glass centrifuge tube equipped with a ground stopper. After sodium chloride or sodium sulfate has been added to keep the ionic strength constant and after the aqueous phase has been diluted up to 10 ml with water, a 10 ml portion of the organic solvent was added. The two phases were shaken vigorously for 30 min in the thermostat at 25 ° and

then separated by centrifugation. The net distribution ratio was calculated by measureing the γ-radioactivities of both the phases with a single-channel pulse-height analyser (Osaka Denpa Model LA-3T, or Nuclear-Chicago 1185 series).

Theoretical

The ion-pair extraction equilibrium is independent of the salt which is added in the aqueous phase to keep the ionic strength constant except in the very low concentration region of the counter anion, A^-. Therefore, in the extraction of $Ru(II)(phen)_3$ with various anions, the following concentration constants have been defined in the two phases:

$$k_1 = \frac{[MA^+]_a}{[M^{2+}]_a[A^-]_a} \quad (1)$$

$$k_2 = \frac{[MA_2]_a}{[MA^+]_a[A^-]_a} \quad (2)$$

$$K_D = \frac{[MA_2]_o}{[MA_2]_a} \quad (3)$$

$$K_1 = \frac{[MA^+]_o[A^-]_o}{[MA_2]_o} \quad (4)$$

$$K_2 = \frac{[M^{2+}]_o[A^-]_o}{[MA^+]_o} \quad (5)$$

In these expressions, the subscripts a and o refer to the aqueous and organic phases respectively, M^{2+}, to the complex cation $Ru(II)(phen)_3$, and A^-, to the counter anion.

At the distribution equilibrium, the distribution ratio, D, of MA_2 is written as:

$$D = \frac{[M^{2+}]_o+[MA^+]_o+[MA_2]_o}{[M^{2+}]_a+[MA^+]_a+[MA_2]_a} \quad (6)$$

By combining Eqs. (1)—(6), D can be expressed as:

$$D = K_D \times \frac{k_1k_2[A^-]_a^2}{1+k_1[A^-]_a+k_1k_2[A^-]_a^2} \times \frac{K_1K_2+K_1[A^-]_o+[A^-]_o^2}{[A^-]_o^2} \quad (7)$$

In the application of Eq. (7), the following four cases can be assumed:

(i) When the dissociation does not occur at all in the organic phase, Eq. (7) can be simplified to Eq. (8):

$$D = K_D \times \frac{k_1k_2[A^-]_a^2}{1+k_1[A^-]_a+k_1k_2[A^-]_a^2} \quad (8)$$

This equation shows that the D values depend only upon $[A^-]_a$. Therefore, the D values are kept constant, even though the concentration of the complex cations changes.

(ii) When the first-step dissociation occurs alone in the organic phase ($K_2=0$), Eq. (7) can be represented as Eq. (9):

$$D = K_D \times \frac{k_1k_2[A^-]_a^2}{1+k_1[A^-]_a+k_1k_2[A^-]_a^2} \times \frac{K_1+[A^-]_o}{[A^-]_o} \quad (9)$$

The electrical neutrality in the organic phase requires the following equation:

$$[MA^+]_o = [A^-]_o \quad (10)$$

In addition, the total concentration of the extracted species, $(C_M)_o$, is represented by Eq. (11):

$$(C_M)_o = [MA^+]_o + [MA_2]_o \quad (11)$$

By combining Eqs. (4), (10), and (11), the next relation is obtained:

$$[A^-]_o = (\sqrt{K_1^2+4K_1(C_M)_o}-K_1)/2 \quad (12)$$

From Eqs. (9), and (12), we obtain Eq. (13):

$$D = K_D \times \frac{k_1k_2[A^-]_a^2}{1+k_1[A^-]_a+k_1k_2[A^-]_a^2} \times \frac{K_1+\sqrt{K_1^2+4K_1(C_M)_o}+2(C_M)_o}{2(C_M)_o} \quad (13)$$

According to Eq. (13), if $[A^-]_a$ is kept constant, the slope of the plot of log D *vs.* $\log(C_M)_o$ must be -1 in the low $(C_M)_o$ region, must increase with the increase in $(C_M)_o$, and must finally reach 0 in the high $(C_M)_o$ region. In the region where D is independent of the change of $(C_M)_o$, the third term of Eq. (13) becomes 1 and Eq. (13) is simplified to Eq. (8). Equation (8) can be converted into Eq. (14) by using the method of Sillén:[9]

$$(K_D-D)D^{-1}[A^-]_a^2 = k_2^{-1}[A^-]_a + k_1^{-1}k_2^{-1} \quad (14)$$

If K_D is known, k_1 and k_2 can be calculated from the plot of $(K_D-D)D^{-1}[A^-]_a^2$ *vs.* $[A^-]_a$. K_D, here, is experimentally obtained by taking the D value to be equal to K_D in the high $[A^-]_a$ region on the plot of log D *vs.* log $[A^-]_a$, where D becomes constant. If k_1, k_2, and K_D are obtained in this way, K_1 can be estimated from the slope of the plot of D *vs.* $1/(C_M)_o$ in the region where the slope of the plot of log D *vs.* log $(C_M)_o$ becomes -1, because its slope is represented by

$$K_DK_1k_1k_2[A^-]_a^2/(1+k_1[A^-]_a+k_1k_2[A^-]_a^2).$$

(iii) When the first-step dissociation occurs almost completely in the organic phase, that is, when K_1 is very large, Eq. (7) can be written as follows:

$$D = K_D \times \frac{k_1k_2[A^-]_a^2}{1+k_1[A^-]_a+k_1k_2[A^-]_a^2} \times \frac{K_1K_2+K_1[A^-]_o}{[A^-]_o^2} \quad (15)$$

From the electrical neutrality in the organic phase, the following relation can be said to hold:

$$[MA^+]_o + 2[M^{2+}]_o = [A^-]_o \quad (16)$$

Further, $(C_M)_o$ is represented as:

$$(C_M)_o = [MA^+]_o + [M^{2+}]_o \quad (17)$$

By combining Eqs. (5), (16), and (17), the next relation is obtained:

$$[A^-]_o = \{(C_M)_o-K_2+\sqrt{K_2^2+(C_M)_o^2+6K_2(C_M)_o}\}/2 \quad (18)$$

From Eqs. (15), and (18), we obtain:

$$D = K_D \times \frac{k_1k_2[A^-]_a^2}{1+k_1[A^-]_a+k_1k_2[A^-]_a^2} \times \frac{K_1[K_2^2+4K_2(C_M)_o-(C_M)_o^2+\{K_2+(C_M)_o\}\sqrt{K_2^2+(C_M)_o^2+6K_2(C_M)_o}]}{8K_2(C_M)_o^2} \quad (19)$$

According to Eq. (19), if $[A^-]_a$ is kept constant, the slope of the plot of log D *vs.* log $(C_M)_0$ must change from -2 in the low-$(C_M)_0$ region to -1 in the high-$(C_M)_0$ region.

(iv) When the first- and second-step dissociations occur to a considerable extent in the organic phase, from Eq. (7) the slope of the plot of log D *vs.* log $(C_M)_0$ can be assumed to change from -2 in the low-$(C_M)_0$ region to -1 in the intermediate-$(C_M)_0$ region, finally reaching 0 in the high-$(C_M)_0$ region.

In the last two cases, (iii) and (iv), the estimation of the constants by analysis of the extraction curves becomes complicated. Fortunately, however, no such case has been encountered so far, except when a solvent with a relatively high dielectric constant, such as nitrobenzene, has been used.

Results and Discussion

The Extraction of Ru(II)(phen)$_3$ with the Perchlorate Ion into Various Solvents. In Figs. 1 and 2 the relations between log D and log $[ClO_4^-]_a$, with several organic solvents, are shown. In these studies the initial concentration, C_M, of the complex cation in the aqueous phase was fixed at 3.15×10^{-6} M, while the ionic strength in the aqueous phase was controlled either at 0.75 with sodium sulfate or at 0.1 with sodium chloride. The extraction curves represented in Fig. 1 are sigmoidal ones which are encountered in oridnary chelate extraction systems with low formation constants. On the other hand, those in Fig. 2 possess inflection points. This phenomenon will be explained by the distribution of sodium perchlorate. From the extraction curves in Fig. 1, the K_D values can be obtained graphically by taking the D values at the high-$[ClO_4^-]_a$ regions, where the slopes of the plots of log D *vs.* log $[ClO_4^-]_a$ are 0. These values are shown in Table 1. In Figs. 3—8, log D is plotted against log $(C_M)_0$ at the fixed $[ClO_4^-]_i$, where $[ClO_4^-]_i$ shows the initial concentration of the perchlorate ion added to the aqueous phase. As is shown in most of the figures, the slope of the plot of

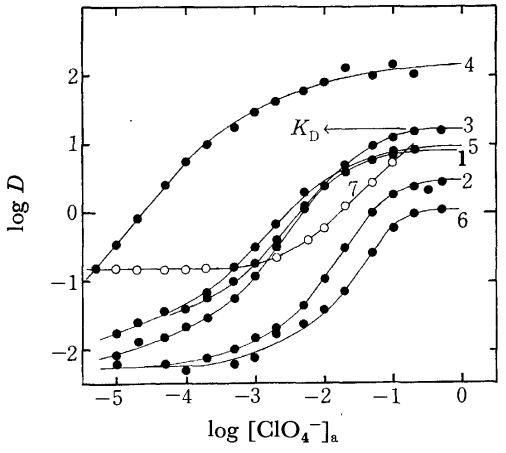

Fig. 1. The extraction of Ru(II)(phen)$_3$ into various solvents. (1) chloroform, (2) chlorobenzene, (3) methyl isobutyl ketone, (4) acetophenone, (5) *o*-dichlorobenzene, (6) *m*-dichlorobenzene, (7) isoamyl-alcohol. (●) I=0.75(Na_2SO_4), (○) I=0.1(NaCl).

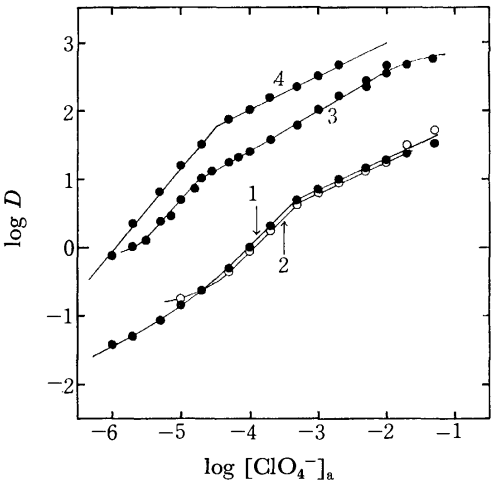

Fig. 2. The extraction of Ru(II)(phen)$_3$ into various solvents. (1) 1,2-dichloroethane, (2) 1,1,2,2-tetrachloroethane, (3) bis(2-chloroethyl) ether, (4) nitrobenzene. I=0.1 (NaCl).

log D *vs.* log $(C_M)_0$ changes from -1 in the low-$(C_M)_0$ region to 0 in the high-$(C_M)_0$ region. This result suggests that, in the solvents with low dielectric constants, the extracted Ru(phen)$_3$(ClO_4)$_2$ dissociates only at the first step. When $[ClO_4^-]_i$ is kept high, D becomes constant independently of the change in $(C_M)_0$. This tendency is observed in all the solvents examined. This phenomenon can be explained by the fact that,

TABLE 1. VARIOUS CONSTANTS OF Ru(phen)$_3$(ClO_4)$_2$

Solvent	K_D	k_1	k_2	K_1	K_2
		(from extraction)			
Chloroform	8.5	2.4×10^2	5.4×10	5.1×10^{-8}	0
Chlorobenzene	3.0	—	—	9.5×10^{-9}	0
MIBK	16.0	—	—	8.5×10^{-9}	0
Acetophenone	200	2.7×10^5	3.1×10^2	8.2×10^{-10}	0
o-Dichlorobenzene	10.0	—	—	3.0×10^{-7}	0
m-Dichlorobenzene	1.3	—	—	3.0×10^{-8}	0
		(from solubility)			
H_2O	—	2.3×10^3	6.7	—	—

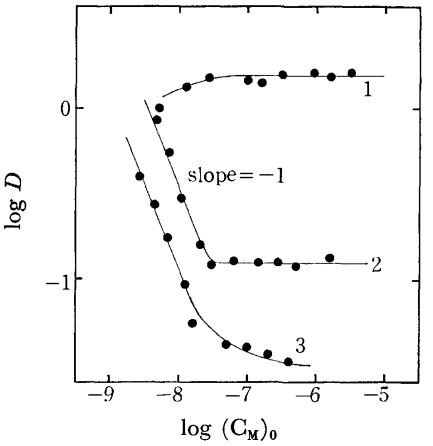

Fig. 3. The relation between log D and log $(C_M)_0$ in chloroform. $[ClO_4^-]_i$: (1) 1×10^{-2}M, (2) 1×10^{-3}M, (3) 1×10^{-4}M. I=0.75 (Na_2SO_4).

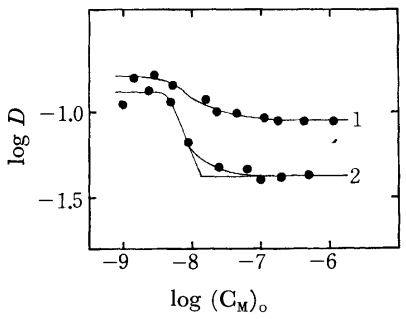

Fig. 4. The relation between log D and log $(C_M)_o$ in chlorobenzene. $[ClO_4^-]_i$: (1) 1×10^{-2}M, (2) 5×10^{-3}M. I=0.75 (Na_2SO_4).

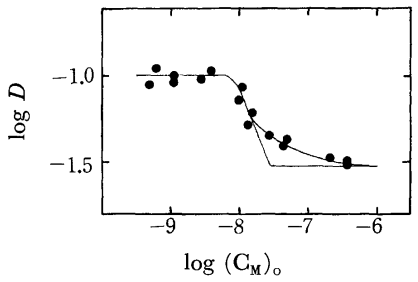

Fig. 5. The relation between log D and log $(C_M)_o$ in m-dichlorobenzene. $[ClO_4^-]_i=1\times10^{-2}$M. I=0.75 (Na_2SO_4).

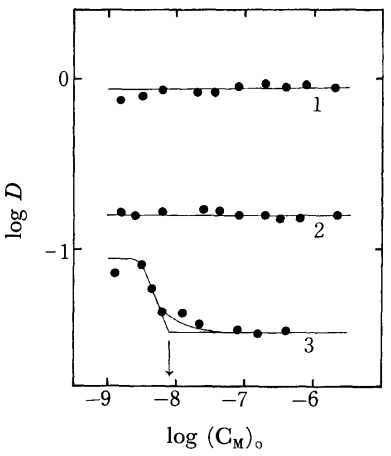

Fig. 6. The relation between log D and log $(C_M)_o$ in MIBK. $[ClO_4^-]_i$: (1) 5×10^{-3}M, (2) 1×10^{-3}M, (3) 1×10^{-4}M. I=0.75 (Na_2SO_4).

in the high-$[ClO_4^-]_i$ region, the $[A^-]_0$ in the third term of Eq. (9) is no longer determined by the dissociation of $Ru(phen)_3(ClO_4)_2$, but by the dissociation of the sodium perchlorate present in the organic phase; the sodium perchlorate in the organic phase begins to act as an anion buffer. This phenomenon can be used in the estimation of the distribution coefficient of sodium perchlorate.

The Determination of the Association and Dissociation Constants. If chloroform is used as the extraction solvent, the third term of Eq. (9) can be taken as 1 in the region where $(C_M)_o$ is more than 10^{-7} M. (See Fig. 3) Therefore, the extraction curve can be analysed according to Eq. (8) in the range where D is

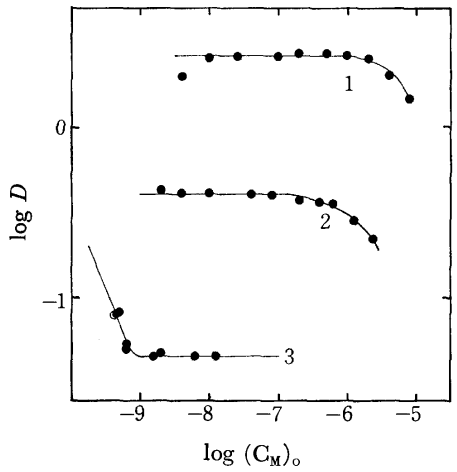

Fig. 7. The relation between log D and log $(C_M)_o$ in acetophenone. $[ClO_4^-]_i$: (1) 5×10^{-5}M, (2) 1×10^{-5} M, (3) 1×10^{-6}M. I=0.75 (Na_2SO_4).

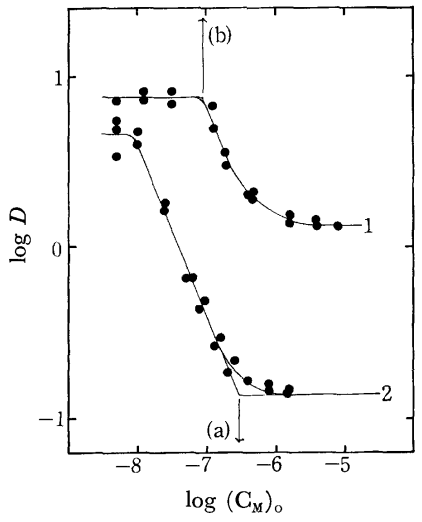

Fig. 8. The relation between log D and log $(C_M)_o$ in o-dichlorobenzene. $[ClO_4^-]_i$: (1) 1×10^{-2}M, (2) 1×10^{-3}M. I=0.75 (Na_2SO_4).

above 3.3×10^{-2}. Figure 9 demonstrates the plot of $(K_D-D)D^{-1}[ClO_4^-]_a^2$ *vs.* $[ClO_4^-]_a$ in that region; it shows a good linearity. k_1 and k_2, as calculated from the slope and the intercept on the $(K_D-D)D^{-1}[ClO_4^-]_a^2$ axis in Fig. 9, are 2.4×10^2 and 54 respectively.

In order to calculate K_1, D was plotted as a function of $1/(C_M)_o$ in the region where the slope of the plot of log D *vs.* log $(C_M)_o$ is -1 in Fig. 3. (See Fig. 10) From the slope of the plot in this figure, the estimation of K_1 can be made by using the k_1 and k_2 values calculated previously. For determining K_1, the slope (1) at 1×10^{-3} M $[ClO_4^-]_i$ was used, since the effect of sodium sulfate, added in the aqueous phase to maintain the ionic strength constant, and other experimental errors are minimized in that region.

Another example is shown in the case of acetophenone. As is shown in Fig. 7, the third term of Eq. (9) could be taken as 1 in the region where $(C_M)_o$ is more than 10^{-7} M, much as in the case of chloroform. Therefore, from the plot of Eq. (14), we can calculate

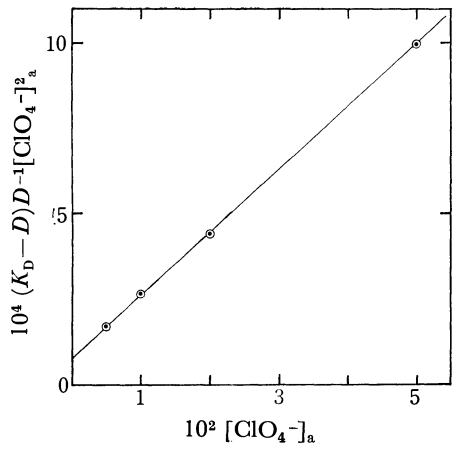

Fig. 9. Linear plot between $(K_D-D)D^{-1}\,[ClO_4^-]^2_a$ and $[ClO_4^-]_a$ in chloroform.
Slope$=k_2^{-1}=1.84\times10^{-2}$, Intercept$=k_1^{-1}k_2^{-1}=7.7\times10^{-5}$.

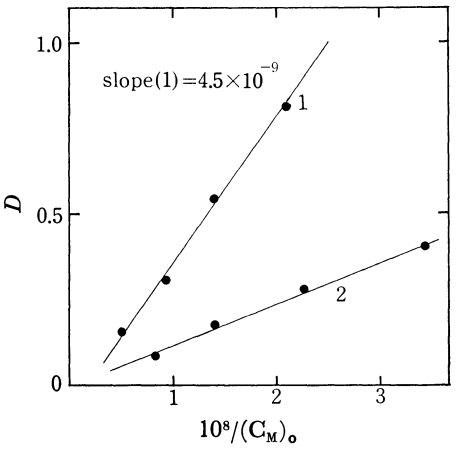

Fig. 10. The relation between D and $1/(C_M)_o$.
$[ClO_4^-]_i$: (1) 1×10^{-3}M, (2) 1×10^{-4}M.

k_1 and k_2. The k_1 and k_2 values thus obtained are 2.7×10^5 and 3.1×10^2 respectively, which are considerably larger than those obtained in the chloroform system. Perhaps this difference is caused by the apparent decrease in the dielectric constant of the aqueous phase, since acetophenone is more soluble in chloroform than water. The ionic equilibrium in the acetophenone phase is governed by sodium perchlorate, which is extracted in a small amount. Therefore, the slope of -1 in the plot of log D *vs.* log $(C_M)_o$ does not appear until $[ClO_4^-]_i$ gets down as low as 1×10^{-6} M under the experimental conditions employed, as is shown in Fig. 7. As can be seen from Curve (3) in Fig. 7, the concentration of the perchlorate ion in the aqueous phase should be constant, because the concentration of the perchlorate ion which is extracted with Ru(II)(phen)$_3$ into the organic phase is negligible. Therefore, the plot of D *vs.* $1/(C_M)_o$ in the region where the slope of the plot of log D *vs.* log $(C_M)_o$ shows -1 can be utilized for the calculation of K_1. The K_1 thus calculated was 8.2×10^{-10}.

In the other solvents the plot of Eq. (14) did not show a good linearity. Therefore, the precise values of k_1 and k_2 in these systems could not be estimated on the basis of the theoretical analysis. Therefore, in such systems K_1 was assumed to be equal to $(C_M)_o$ at the inflection point (for example, point (a) in Fig. 8), which appears between the slope of -1 and 0 in the plot of log D *vs.* log $(C_M)_o$.

As has been shown, in the system where the solvent has a low dielectric constant (<20), the calculation of those constants can be done either by fitting numerical values to the equations or by graphical analysis. On the other hand, in the system where a solvent with a high dielectric constant is used, such analysis becomes impossible, because sodium perchlorate is considerably extracted into the organic phase and, furthermore, K_D can not be estimated from the extraction curves. In addition, to make the k_1 and k_2 values obtained from the extraction studies more reliable, those values were reexamined from the point of view of solubility. The solubility product, K_{sp} in water, which was defined as $K_{sp}=[M^{2+}][ClO_4^-]^2$, was calculated at 1.52×10^{-10} at 25°.

All the constants are summarized in Table 1. From these results, Ru(phen)$_3$(ClO$_4$)$_2$ can be said almost to be associated with the solvents with low dielectric constants. When ketones are the extraction solvents, the K_D values are fairly much larger than those in the other solvents. This can be explained by the tendency of Ru(II)(phen)$_3$ to solvate with ketones, since Ru(II)-(phen)$_3$ has considerable electron affinity because of its double positive charge, although it is a very large cation. The distribution to the solvent with a high dielectric constant (>20) is also promoted by the dissociation in the organic phase. Our data on both the extraction and the solubility show that Ru(phen)$_3$-(ClO$_4$)$_2$ is considerably associated in water. This is contradictory to the conclusion of Yamamoto[1] in a similar study with Fe(phen)$_3$(ClO$_4$)$_2$; they concluded that this ion-pair is completely dissociated in water and in nitrobenzene. In Fig. 1, the distribution ratio into isoamyl alcohol is relatively higher than that into other solvents in the low-$[ClO_4^-]_a$ region. This can be explained by the high solubility of chloride in alcohol; this phenomenon was confirmed by the solubility measurements, which will be reported in the next paper.[7]

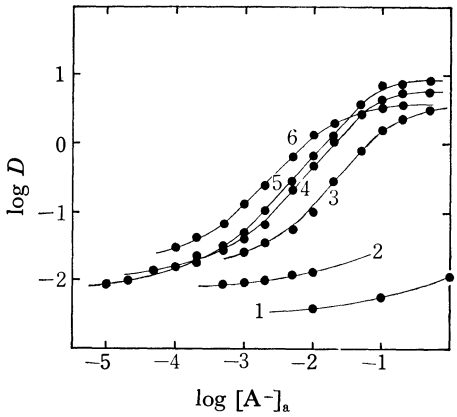

Fig. 11. The extraction of Ru(II)(phen)$_3$ into chloroform with various anions.
(1) Cl^-, (2) NO_3^-, (3) BF_4^-, (4) SCN^-, (5) I^-, (6) IO_4^-. $I=0.75$ (Na_2SO_4).

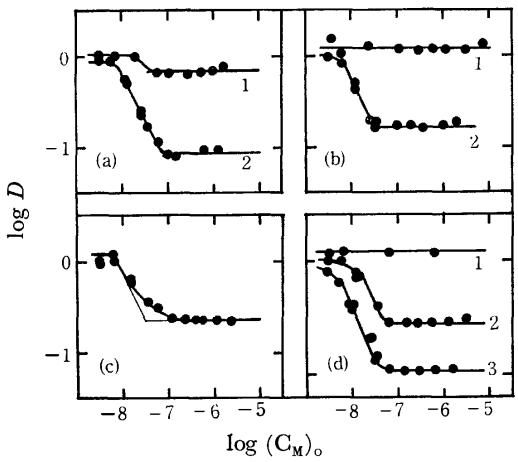

Fig. 12. The extraction of Ru(II)(phen)$_3$ into chloroform with various anions as a function of $(C_M)_o$. (a) with iodide ion: (1) 1×10^{-2}M, (2) 2×10^{-3}M. (b) with thiocyanate ion: (1) 2×10^{-2}M, (2) 5×10^{-3}M. (c) with periodide ion: 2×10^{-3}M. (d) with tetrafluoroborate ion: (1) 5×10^{-2}M, (2) 2×10^{-2}M, (3) 1×10^{-2}M. I=0.75 (Na_2SO_4).

TABLE 2. CONSTANTS OF Ru(phen)$_3$A$_2$ IN CHLOROFORM

Anion	K_D	k_1	k_2
BF_4^-	3.6	4.9×10	8.9
SCN^-	5.7	6.3×10^2	10.5
I^-	9.2	3.8×10^2	9.8
ClO_4^-	8.5	2.4×10^2	54.0
IO_4^-	3.7	2.9×10^3	43.0

Extraction of Ru(II)(phen)$_3$ into Chloroform with Various Anions. Ru(II)(phen)$_3$ was extracted into chloroform with several anions; the relations between log D *vs.* log $[A^-]_a$ are shown in Fig. 11. In Fig. 12, the extraction behavior on changing counter anions is shown by plotting log D as a function of log $(C_M)_o$. The constants, K_D, k_1, and k_2, which were obtained by means of the theoretical analysis described in the previous sections, are summarized in Table 2.

By examining the extraction curves shown in Fig. 12, it becomes obvious that the ion-pairs extracted into chloroform dissociate only at the first step, and that the calculated values of K_1 were present in the $10^{-8}\leq K_1\leq10^{-7}$ region in all the systems. Therefore, these ion-pairs exist mostly as associated molecules in chloroform. The order of extractability as a measure of half-extraction $[A^-]_a$ is as follows: $B(C_6H_5)_4^-\gg IO_4^-\sim ClO_4^->I^->SCN^->BF_4^-\gg NO_3^->Cl^-\sim OH^-\gg SO_4^{2-}$. This sequence suggests that the enthalpy of the hydration of the anion is the major factor determining the distribution ratio, because, in this system, the enthalpy of the hydration of the cation is negligible compared with that of the anion. Strongly hydrated ions, such as SO_4^{2-} and F^-, are scarcely extracted at all. This result is in good agreement with those obtained by Gibson and Weatherburn[5] with the quatenary phosphonium and arsonium, by Biswas and Mandal[10] with surfactant cations, and by Diamond *et al.*[11,12] with ammonium. As is shown in Fig. 11, the great change in the distribution ratio appears between NO_3^- and BF_4^-. This observation also agrees with that obtained by Gibson and Weatherburn;[5] the distribution ratio increases remarkably when the enthalpy of hydration of the anions is below 70—80 kcal/mol. This phenomenon can be explained successfully by the equation derived by Ionin and Kurina,[13] assuming that the distribution ratio is determined solely by changes in the enthalpies of the hydration of the anion. Moreover, as is shown in Table 2, the association constants, k_1 and k_2 increase with the decrease in the enthalpy of the hydration of the anion and with the increase in the size of the anion. It is also noticeable that the ratio of k_1 to k_2 becomes larger with the increase in the size of the anion. This tendency can be understood in terms of the repulsion between the anions which combine with Ru(II)(phen)$_3$. When quite large anions such as ClO_4^- are used, k_1 and k_2 become larger than would be expected from the electrostatic theory. Therefore, the concept of water structure-enforced ion-pairing should be applied.[14]

On the basis of the above discussion, the distribution ratio is mainly determined by both the degree of association of the ion-pair in the aqueous phase and the distribution of the associated ion-pair when the solvent, whose dielectric constant is low and whose solvation power is weak, is used for ion-pair extraction. The former depends on the enthalpy of the hydration of ion, and the latter, on the solubility of the associated ion-pair in the extraction solvent, which might be correlated with the solubility parameter.

It should be mentioned that the above discussion is not applicable to a system with a strong basic or acidic solvent; in such a system the distribution of ion-pairs is influenced not only by the solubility of the associated form, but also by the dissociation due to the ion-solvent interaction in the organic phase.

The Extraction of Ru(II)(phen)$_3$ with the Tetraphenylborate Ion. Ru(II)(phen)$_3$ was extracted into chloroform, ethyl acetate, MIBK, or nitrobenzene with the tetraphenylborate ion. The relations between log D *vs.* log $[B(C_6H_5)_4^-]_i$ in chloroform and MIBK respectively are shown in Figs. 13 and 14. An abnormal

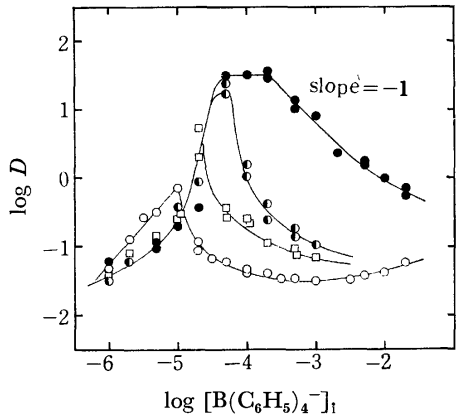

Fig. 13. The extraction of Ru(II)(phen)$_3$ into chloroform as a function of $[B(C_6H_5)_4^-]_i$.
concn of chloride ion in the aqueous phase: (○) in the absence of NaCl, (□) 1×10^{-3}M, (◐) 1×10^{-2}M, (●) 1×10^{-1}M.

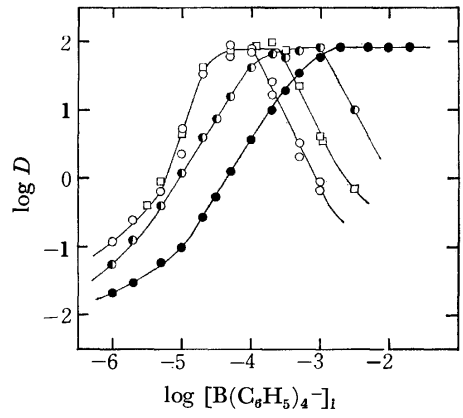

Fig. 14. The extraction of Ru(II)(Phen)$_3$ into MIBK as a function of $[B(C_6H_5)_4^-]_i$.
concn of chloride ion in the aqueous phase: (○) in the absence of NaCl, (□) 1×10^{-3}M, (◐) 1×10^{-2}M, (●) 1×10^{-1}M.

decrease of D at the higher concentrations of sodium tetraphenylborate was more or less observed in every solvent so far examined. Moreover, the extraction behavior is largely dependent upon the concentration of sodium chloride in the aqueous phase. In the extraction, the adsorption of Ru(II)(phen)$_3$ on the wall of the glass tube and on the interface was observed at low concentrations of sodium chloride. Therefore, it seems that the ion-pair is difficult to dissolve in both the phases. Such results have not been observed in the systems with anions other than the tetraphenylborate ion.

In order to compare this abnormal tetraphenylborate system with another anion system, the behavior of sodium tetraphenylborate itself should be considered. For this purpose, its distribution into chloroform or MIBK was examined by using the tracer technique (see Fig. 15); furthermore, its association in both the phases was also measured on the basis of the conductivity by applying the Shedlovsky method[15] (see Table 3).

By correcting for the behavior of sodium tetraphenylborate, it becomes clear that the tetraphenylborate ion possesses a very high extractability compared with the other anions such as ClO_4^- and I^-. This observation can be explained by the facts that the tetraphenylborate ion has a very low enthalpy of hydration and a very hydrophobic structure, and that the ion-pairing with such anions is promoted by the structure-making force of water. Moreover, in the MIBK system, the extraction behavior is influenced greatly in the low $[B(C_6H_5)_4^-]_i$ region by the presence of sodium chloride in the aqueous phase; the decrease is caused by the high distribution of sodium tetraphenylborate into the organic phase because of the addition of sodium chloride. On the other hand, the partition of sodium tetraphenylborate into chloroform is so rare that the extraction curves have not been influenced by the addition of sodium chloride to the aqueous phase, as would be expected. Therefore, its influence on the distribution ratio of Ru(II)(phen)$_3$ must be due to the salting-out effect, which will be described later.

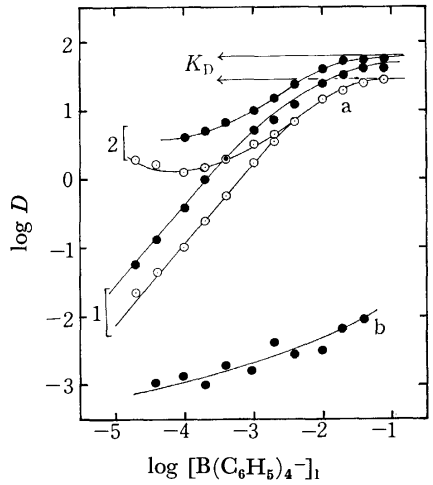

Fig. 15. The extraction of $NaB(C_6H_5)_4$ into chloroform (b) and into MIBK(a). (●) pH is adjusted about 6 by adding $NaHCO_3$, (○) pH is not adjusted. (1) in the absence of NaCl in the aqueous phase, (2) 2×10^{-3} M NaCl is added in the aqueous phase.

TABLE 3. ASSOCIATION CONSTANTS OF SODIUM TETRAPHENYLBORATE AT 25°

Solvent	ε	K(association)
H_2O	78.304	8.46
H_2O saturated with MIBK	76.922	10.92
MIBK	13.11	4.03×10^2 (3.21×10^2)[a]
MIBK saturated with H_2O	14.65	2.55×10^2

a) The value calculated from the Fuoss equation, $K(\text{diss.})=(3000/4\pi a^3N)\exp(-e/a\varepsilon kT)$, $a=7.5$(Å).

It has been described how the distribution of sodium tetraphenylborate into the organic phase influences the extraction curve of Ru(II)(phen)$_3$. However, as far as the abnormal phenomenon is concerned, it can not be explained by this correction. Accordingly, in order to elucidate this phenomenon, the following three possibilities were examined; (1) an anion such as Cl^- or OH^- might be involved in the associated species; this seems probable judging from the fact that the associated ion-pair has a low solubility in the organic phase in spite of its hydrophobicity; (2) this phenomenon might be explained by selecting appropriate values of the constants, k_1, k_2, K_1, and K_2, or (3) the distribution constant of the associated ion-pair might decrease greatly as a result of the change in the bulk properties of both the phases in the high $[B(C_6H_5)_4^-]_i$ region, or as a result of the increased solubility of molecules due to solubilization in a surfactant solution.

The first possibility was examined by the extraction study of $^{36}Cl^-$, which was added in an equivalent amount to Ru(II)(phen)$_3$ in the presence of various concentrations of sodium tetraphenylborate. As a result, no uptake of chloride into the organic phase was observed at all. In addition, the extraction behavior of Ru(II)(phen)$_3$ in the presence of sodium fluoride or sodium sulfate exhibits a pattern similar to that in the presence of sodium chloride in spite of the fact that the hydration energies of the fluoride ion and the sulfate ion are much larger than that of the chloride ion.

Therefore, it is not feasible to consider that the associated ion-pair contains an anion other than the tetraphenylborate ion.

Next, if k_1 and k_2 are very large and if K_1 is much larger than K_2, then the extraction curve will exhibit the pattern shown in Figs. 13 and 14, according to Eq. (9). Although those theoretical conditions could be fulfilled provided the theory of Diamond[14] is applied, $\log K_D$ in this system would then have to become a negative value. This is very improbable, because the $Ru(phen)_3(B(C_6H_5)_4)_2$ has a very hydrophobic property and the K_D values in the systems of the other anions have large positive values.

The last possibility was examined as follows: the solubilities of $Ru(phen)_3(B(C_6H_5)_4)_2$ were measured in two systems; in one system the precipitates of $Ru(phen)_3(B(C_6H_5)_4)_2$ were added to an aqueous sodium tetraphenylborate solution (1% sodium bicarbonate has been added), while in the other system an aqueous sodium tetraphenylborate solution (1% sodium bicarbonate has been added) was added to a $\sim 10^{-6}$ M $Ru(phen)_3Cl_2$ solution. This means that both the crystallization and dissolution processes were cross-checked. As a result, it was found that the presence of sodium chloride (0.01—0.1 M) accelerates the rate of attaining the equilibrium between the precipitate and the solution; therefore, the solubilities have been measured both in the presence and in the absence of sodium chloride. The absorbance or the radioactivity was measured after equilibriating for 2 days' shaking in a thermostat at 25°; sodium tetraphenylborate decomposes after longer standing. The results obtained with the two systems are in good agreement with each other except when sodium chloride was not added; in the absence of sodium chloride, in the latter system equilibrium was not attained completely.

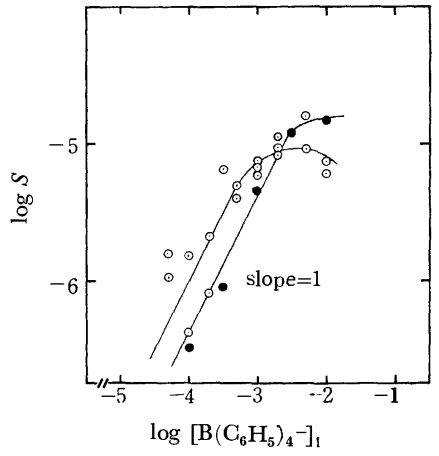

Fig. 16. The solubility of $Ru(phen)_3(B(C_6H_5)_4)_2$ in the sodium tetraphenylborate solution at 25 °C. (○) in the absence of NaCl, (●) 0.1 M NaCl is added.

In Fig. 16, $\log S$ is plotted against $\log [B(C_6H_5)_4^-]_i$. The solubility of $Ru(phen)_3(B(C_6H_5)_4)_2$ increases remarkably with the increase in the concentration of sodium tetraphenylborate, and the slope of the plot of $\log S$ *vs.* $\log [B(C_6H_5)_4^-]_i$ becomes about 1. This phenomenon can be explained on the assumption that the increase in the solubility is due to the formation of a large anion, $[Ru(phen)_3(B(C_6H_5)_4)_3]^-$, which is produced as a result of the addition of one more $B(C_6H_5)_4^-$ to the neutral ion-pair. This assumption seems probable if the concept of water structure-enforced ion-pairing can be extended to this system. $Ru(phen)_3(B(C_6H_5)_4)_2$ and $B(C_6H_5)_4^-$ are alike with respect to their hydrophobic and poorly hydrated character. Therefore, it is much more probable for $Ru(phen)_3(B(C_6H_5)_4)_2$ and $B(C_6H_5)_4^-$ to form one large anion, which causes only one disturbance of the water structure, instead of surviving as two species which produce two disturbances.

Another possible assumption is that the increase in the solubility is to be explained not by the formation of a rigid anion such as $[Ru(phen)_3(B(C_6H_5)_4)_3]^-$, but by a solubilization similar to that with surfactant solutions. However, the micelle formation can not be considered, because the tetraphenylborate ion has no long alkyl chain in its structure and is a spherical ion. Therefore, this solubilization must be a kind of hydrotropism, an idea which was advanced by Neuberg[6] in 1916. Hydrotropism[16] is the general term for the phenomenon in which many nonelectrolytes, mostly polar but including nonpolar ones, are salted in by salts with large ions, such as tetraalkylammonium chloride and sodium *p*-toluenesulfonate.

In order to examine which assumption is more suitable to explain the present system, two additional investigations were performed—paper-electrophoresis and dialysis. The electrophoresis on paper strips (17—46 V/cm, 1—5 hr, 5 mA) revealed that $Ru(II)(phen)_3$ did not migrate at all in the 10^{-2}—10^{-1} M sodium tetraphenylborate solution. The dialysis was carried out by using a cellulose tube which had holes of 15—20(Å) and which was permeable for molecules with molecular weights below 10000—20000. $Ru(II)(phen)_3$ was dialyzed for two days against a 1×10^{-2} M sodium tetraphenylborate solution or against a 1×10^{-2} M sodium chloride solution. However, no $Ru(II)(phen)_3$ was dialyzed into the sodium tetraphenylborate solution, although the dialysis equilibrium was achieved within several hours in the sodium chloride solution.

In addition to the results presented above, the solubilized $Ru(phen)_3(B(C_6H_5)_4)_2$ solution often became colloidal. The addition of excess salts to this solution induced a salting-out effect. Therefore, the latter assumption seems to explain more satisfactorily the phenomenon of the present system, and we believe that $Ru(phen)_3(B(C_6H_5)_4)_2$ is solubilized by forming such an anionic colloid as $[Ru(phen)_3(B(C_6H_5)_4)_2]_n$-$[B(C_6H_5)_4^-]_m$. The actual structure is assumed to be that of aggregated molecules, *i.e.*, $[Ru(phen)_3(B(C_6H_5)_4)_2]_n$ surrounded with $B(C_6H_5)_4^-$. The aggregation numbers, n and m, are expected to be almost equal, because, as is shown in Fig. 16, the slope of the plot of $\log S$ *vs.* $\log [B(C_6H_5)_4^-]_i$ is almost 1.

References

1) Y. Yamamoto, *Bunseki Kagaku*, **21**, 418 (1972).
2) R. L. McDonald and T. H. Hufen, *J. Phys. Chem.*, **74**, 1926 (1970).

3) H. Freiser, *Anal. Chem.*, **41**, 1354 (1969).
4) N. Suzuki, K. Akiba, T. Kanno, and T. Wakabayashi, *J. Inorg. Nucl. Chem.*, **30**, 2521 (1968).
5) N. A. Gibson and D. C. Weatherburn, *Anal. Chim. Acta.*, **58**, 159 (1972).
6) C. Neuberg, *Biochem. Z.*, **76**, 107 (1916).
7) T. Takamatsu, This Bulletin, in press.
8) C. V. Banks and J. W. ÓLaughlin, *Anal. Chem.*, **29**, 1412 (1957).
9) L. G. Sillén, *Acta. Chem. Scand.*, **10**, 186 (1956).
10) H. K. Biswas and B. M. Mandal, *Anal. Chem.*, **44**, 1636 (1972).
11) W. Müller and R. M. Diamond, *J. Phys. Chem.*, **70**, 3469 (1966).
12) J. J. Bucher and R. M. Diamond, *ibid.*, **69**, 1565 (1965).
13) M. V. Ionin and N. V. Kurina, *Tr. Kom. Anal. Khim.*, **14**, 87 (1963).
14) R. M. Diamond, *J. Phys. Chem.*, **67**, 2513 (1963).
15) T. Shedlovsky, *J. Franklin. Inst.*, **225**, 739 (1938).
16) F. A. Long and W. F. McDerit, *Chem. Rev.*, **51**, 119 (1952).

Polarographic Studies of Some Metal(II)-Thiocyanate Complexes in Acetonitrile

Seizo MISUMI, Makoto AIHARA, and Setsuko KINOSHITA

Inorganic Chemistry Laboratory, Faculty of Science, Kyushu University, Fukuoka 812

(Received April 14, 1973)

The formation of thiocyanate complexes of cadmium(II), copper(II), cobalt(II), and iron(II) has been studied in acetonitrile by polarographic, conductometric, and spectrophotometric methods. The values of overall stability constants were found to be; $\log \beta_4 = 19.7$ for $[Cd(SCN)_4]^{2-}$, $\log \beta_2 = 7.6$ for $[Cu(SCN)_2]^-$ and $\log \beta_4 = 15.5$ for $[Co(NCS)_4]^{2-}$. The reaction between copper(II) species and mercury metal was investigated and the electrode reaction was estimated. Kinetic current for cobalt(II)-thiocyanate complex was observed and the rate constant for the dissociation of the complex was obtained. The rate constant of reduction in the iron(II)-thiocyanate system was determined to be 1.9×10^{-3} cm/s by cyclic voltammetry.

In the previous work,[1] cadmium(II), zinc(II), and manganese(II) iodide complexes were studied polarographically in acetonitrile and the overall formation constants of the complexes were evaluated. These values for other halide complexes of cadmium(II) and zinc(II) were determined by potentiometric titration using a saturated metal amalgam indicator electrode.[2]

In this work, the association constant of tetraethylammonium thiocyanate was determined by conductance measurements, and cadmium(II), copper(II), cobalt(II), and iron(II) thiocyanate complexes have been investigated in acetonitrile by polarography, conductometry and spectrophotometry.

Experimental

Materials. Tetraethylammonium thiocyanate (Et_4NSCN) was synthesized by the reaction of tetraethylammonium perchlorate and potassium thiocyanate in ethanol and fractionated by using acetone-ethyl ether mixture.

Found: C, 57.16; H, 10.65; N, 14.76%. Calcd for Et_4NSCN: C, 57.40; H, 10.71; N, 14.87%.

Et_4NClO_4 (TEAP) was used to keep the concentration of Et_4N^+ to be 0.1 M, and Triton X-100 as maximum suppressor. Other reagents were the same as described previously.[1]

Apparatus. Polarographic measurements have been described previously.[1] Conductance measurements were done by a Yokogawa universal bridge using a cathode ray tube as a detector. The cell, which was of the Pyrex cylinder type, had bright platinum electrodes. A Hitachi EPS-2 spectrophotometer was utilized in the spectral studies.

Procedure. A sample solution was prepared by dissolving 0.5 mM metal(II) perchlorate and an appropriate amount of Et_4NSCN in TEAP-acetonitrile and it was introduced into a polarographic or spectrophotometric cell. Conductance was measured at 1 kHz to 20 kHz at 25 ± 0.01 °C and extrapolated to the infinite frequency (R *vs.* f^{-1}).[3] The cell constant was determined by using the Fuoss' equation[4] for the conductance of potassium chloride solution in water. The cell constant was found to be 0.09975 cm^{-1}.

Other procedures were the same as described previously.[1]

Results and Discussion

Determination of the Association Constant of Tetraethylammonium Thiocyanate. The data for Et_4NSCN were analyzed by the Fuoss-Onsager conductance theory.[5] The parameters obtained are as follows; $\Lambda_0 = 198.35$, $\hat{a} = 2.85$ and $K_A = 0$. (refer to the values of $\lambda_0^+ = 85.05$[6] for Et_4N^+ and $\lambda_0^- = 113.4$[7] for SCN^- in acetonitrile) Conductance data for Et_4NSCN in acetonitrile are shown in Table 1. The values of Λ_{calcd} in Table 1 were calculated by the Fuoss-Onsager conductance equation[5] for non-associated electrolyte. Therefore, tetraethylammonium thiocyanate used was assumed to be completely dissociated in the range from 0.5 to 50 mM in acetonitrile.

TABLE 1. CONDUCTANCE DATA FOR TETRAETHYLAMMONIUM THIOCYANATE IN ACETONITRILE

10^4C M	Λ_{obsd} $cm^2/(\Omega \cdot equiv)$	Λ_{calcd} $cm^2/(\Omega \cdot equiv)$	$\Delta\Lambda$ $cm^2/(\Omega \cdot equiv)$
8.181	186.87	186.87	0.00
17.902	181.36	181.37	0.01
28.817	177.03	176.95	−0.08
28.232	173.99	173.88	−0.11
50.983	170.30	170.41	0.11
64.781	167.12	167.27	0.15

Cd(II)–SCN^- System. The electrode reaction of solvated cadmium(II) is reversible and of two-electron reduction and diffusion-controlled. The half-wave potential of the polarographic wave was −0.275 V *vs.* SCE. The wave due to the complexed species appeared by addition of thiocyanate ion. The electrode reaction was the same as that of solvated cadmium(II) and the plot of the difference of the half-wave potential, $\Delta E_{1/2}$ *vs.* $\log [SCN^-]_0$ was found to be linear. The value of number p of ligands attached to Cd(II) was calculated to be 4.2. The value of $\log \beta_4$ was 19.7.

Cu(II)–SCN^- System. The Cu(II)–SCN^- system was investigated in acetonitrile by conductometric titration. When the conductance was plotted against mole ratio $[SCN^-]_t/[Cu(II)]_t$, the distinct inflection points were observed at 1.1 and 4.0, indicating the formation of $[CuSCN]^+$ and $[Cu(SCN)_4]^{2-}$ and other inflection points were ill-defined.

Polarograms of 0.5 mM Cu(II) in the presence of thiocyanate ions are shown in Fig. 1. Cu(II) perchlorate shows double wave. The half-wave potentials of the first and second waves are *ca.* +0.56 and −0.335 V *vs.* SCE. The first wave decreased and new waves (II and III) developed by addition of thiocyanate

i n. The second wave was shifted to more negative potentials (Wave IV) with increasing concentration of thiocyanate ion. The electrode reactions of the first and third waves were found to be two-electron reduction and diffusion-controlled. The electrode reaction of the fourth wave was one electron and of reversible and diffusion-controlled.

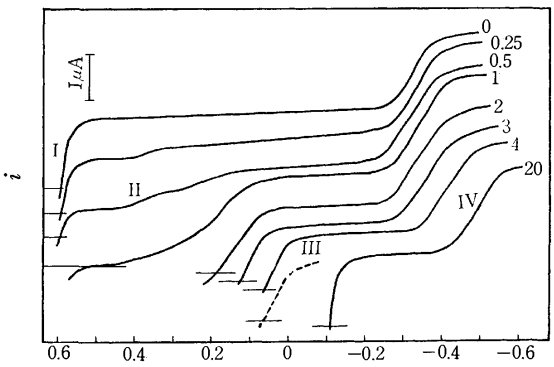

Fig. 1. DC polarograms of acetonitrile solutions containing copper(II)-thiocyanate complexes. Numbers on curves indicate mole ratio, $[SCN^-]_t/[Cu(II)]_t$.

Solvated Cu(II) reacts completely with mercury metal in acetonitrile as follows[8]

$$Cu^{2+}_{solv} + \frac{1}{2}Hg \longrightarrow Cu^{+}_{solv} + \frac{1}{2}Hg^{2+}_{solv} \quad (3)$$

A solution containing Cu(II) and thiocyanate ions was reddish brown in color in acetonitrile. It's color disappeared after a polarograms was recorded at $[SCN^-]_t/[Cu(II)]_t<10$. Even at $[SCN^-]_t/[Cu(II)]_t=50$, decolorization was complete when the solution containing metallic mercury was shaken. The polarograms did not give any changes for the solutions before and after decolorization. Therefore, the following chemical reaction must proceed at the electrode surface before the electrode reaction took place.

$$[Cu(SCN)_4]^{2-} + \frac{1}{2}Hg \longrightarrow [Cu(SCN)_2]^- + \frac{1}{2}[Hg(SCN)_4]^{2-} \quad (4)$$

The electrode reaction for each wave was presumed. The first wave corresponds to the reduction of Hg^{2+}_{solv} formed in solution according to Eq. (3).

$$Hg^{2+}_{solv} + 2e \rightleftarrows Hg(0) \quad (5)$$

This wave decreased with increasing concentration of thiocyanate ion and disappeared at mole ratio $[SCN^-]_t/[Cu(II)]_t=1$. This is caused by complex formation of mercury ion with thiocyanate ion.

The second wave may correspond to the reduction of Hg(II)–SCN^- species, *e.g.* $[Hg(SCN)_3]^-$ *etc.*

The dashed line in Fig. 1 shows the reduction wave of tetrathiocyanato-mercurate(II) in acetonitrile. Therefore, the electrode reaction for the third wave is

$$[Hg(SCN)_4]^{2-} + 2e \rightleftarrows Hg(0) + 4SCN^- \quad (6)$$

The fourth wave was always observed in the presence or the absence of thiocyanate ion. The half-wave potential was shifted to more negative potentials with increasing concentration of thiocyanate ion (Table 2). The electrode reactions of Cu(I) and Cu(I) complex are reversible, of one electron reduction and diffusion-controlled. The plot of $\Delta E_{1/2}$ *vs.* $\log [SCN^-]_0$ was found to be linear and p was calculated to be $2._3$. The value of $\log \beta_2$ was 7.6 for $[Cu(SCN)_2]^-$.

Table 2. Polarographic data for copper(II)-thiocyanate system (The fourth wave)
$[Cu(II)]=0.5$ mM

$[SCN^-]_t$ mM	i_d μA	$E_{1/2}$ V *vs.* SCE
0	1.58	−0.335
5	1.56	−0.465
10	1.56	−0.508
15	1.64	−0.531
20	1.57	−0.556
25	1.60	−0.559

The electrode reactions are expressed as Eqs. (7) and (8) in the absence or the presence of thiocyanate ion, respectively.

$$Cu^{+}_{solv} + e + Hg \rightleftarrows Cu^{\circ}(Hg) \quad (7)$$

$$[Cu(SCN)_2]^- + e + Hg \rightleftarrows Cu^{\circ}(Hg) + 2SCN^- \quad (8)$$

The stability ($\log \beta_2$) of CuX_2^- (X^-: halide and thiocyanate ion) is in the order $Br^-(7.1)<SCN^-(7.6)<Cl^-(10.5)$[9] in acetonitrile.

Co(II)–SCN^- System. Cobalt(II) and thiocyanate ion are known to form $[Co(NCS)]^+$, $[Co(NCS)_3]^-$, and $[Co(NCS)_4]^{2-}$ [10] but the formation constants for these complexes were not yet determined. The cobalt-(II)-thiocyanate complex has an absorption spectrum characterized by maxima at 16000 and 31447 cm^{-1}. The intensity of these bands increases with increasing concentration of thiocyanate ion until $[SCN^-]_t/[Co(II)]_t$ attained to 4. The relation between absorbance for unit concentration of Co(II) at 16000 cm^{-1} *vs.* mole ratio, $[SCN^-]_t/[Co(II)]_t$ is shown in Fig. 2. This indicates the formation of $[Co(NCS)_4]^{2-}$ in acetonitrile. The value of β_4 was calculated by the molar ratio method.[11] From absorbance at 16000 and 31447 cm^{-1}, the values of $\log \beta_4$ (15.6_4 and 15.5_3) were obtained, respectively. (The following spectral data were

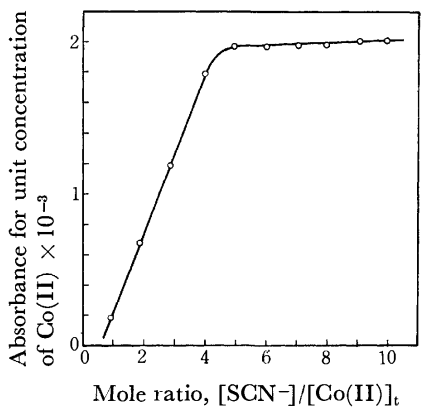

Fig. 2. Absorbance for unit concentration of Co(II) at 16000 cm^{-1} *versus* mole ratio, $[SCN^-]_t/[Co(II)]_t$.

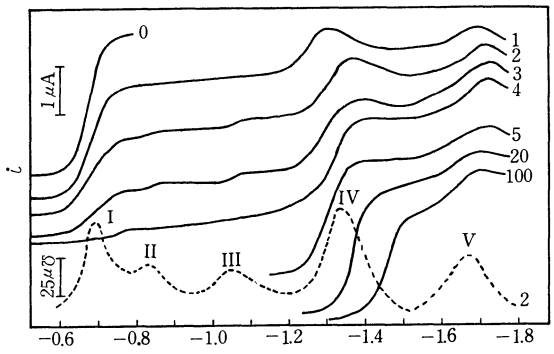

Fig. 3. DC and AC polarograms of cobalt(II)-thiocyanate complexes. Numbers on curves indicate mole ratio, $[SCN^-]_t/[Co(II)]_t$.

used for calculation. E_m=0.994 and E_s=0.890 at 16000 cm^{-1}. E_m=0.762 and E_s=0.678 at 31447 cm^{-1}.) The value of log K_4, 5.2 for $[Co(NCS)_4]^{2-}$ was obtained by assuming that the concentration of $[Co(NCS)]^+$ and $[Co(NCS)_2]$ to be negligible at excess thiocyanate ion.

DC and AC polarograms of 0.5 mM cobalt(II) in the presence of thiocyanate ion are shown in Fig. 3. The electrode reaction of solvated cobalt(II) in acetonitrile is reversible, of two-electron reduction and diffusion-controlled. The original first wave decreased with increasing concentration of thiocyanate ion and the new waves appeared at more negative potentials. The waves in AC polarogram were termed as I, II, III, IV, and V. The waves II and III were ill-defined in DC polarogram. The wave IV had a maximum till $[SCN^-]_t/[Co(II)]_t$=4 but no maximum wave was observed at higher thiocyanate concentrations. The wave V appeared at low concentration of thiocyanate ion. The plots of limiting current and peak admittance *vs.* mole ratio, $[SCN^-]_t/[Co(II)]_t$ are shown in Fig. 4. The wave I which corresponds to the reduction of solvated cobalt(II) disappeared at $[SCN^-]_t/[Co(II)]_t$= 4. The waves II and III may correspond to the reduction of Co(II)–SCN^- species, *e.g.*, $[Co(NCS)]^+$ *etc.*, but the heights of these waves are small because of large stability of $[Co(NCS)_4]^{2-}$. The wave IV increased till $[SCN^-]_t/[Co(II)]_t$=6 and decreased slightly at the above ratio. The wave V was almost constant. The wave IV did not diminish at high excess of thiocyanate ion ($[SCN^-]_t/[Co(II)]_t$=100) as shown in Fig. 3. Therefore, this wave must be due to the species of $[Co(NCS)_4]^{2-}$ and the current was found to be kinetic current. This kinetic current was treated by assumption of the following reaction layer.[12] Consider the reduction of $[Co(NCS)_3]^-$ according to the following reaction

$$Co^{2+}_{solv} + 4SCN^- \rightleftharpoons [Co(NCS)_4]^{2-} \quad (9)$$

$$[Co(NCS)_4]^{2-} \underset{\overleftarrow{k}}{\overset{\vec{k}}{\rightleftharpoons}} [Co(NCS)_3]^- + SCN^- \quad (10)$$

$$[Co(NCS)_3]^- + 2e \rightleftharpoons Co(0) + 3SCN^- \quad (11)$$

The kinetic current, i_k is expressed as follows

$$\frac{i_k}{i_d - i_k} = 0.81 \frac{\vec{k}^{1/2} t^{1/2}}{K_4^{1/2}[SCN^-]_0^{1/2}} \quad (12)$$

where $[SCN^-]_0$ is the concentration of the thiocyanate ion at the electrode surface. $[SCN^-]_0$ was calculated by using $[SCN^-]_0 = [SCN^-]_t - 4\{(i_d - i_k)/i_d\}[Co(NCS)_4^{2-}]_{eq}$. Equation 12 predicts a slope −0.5 for a plot of log $i_k/(i_d - i_k)$ *vs.* log $[SCN^-]_0$. The value of slope was found experimentally to be −0.44 as given in Fig. 5. $\vec{k}$ was calculated to be 1.2×10^4 s^{-1} using log K_4= 5.2 and t=5.88 sec. This indicates that kinetic current due to the fast dissociation of $[Co(NCS)_4]^{2-}$ occurs.

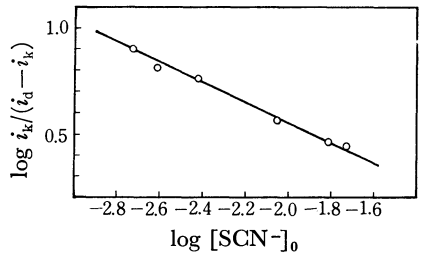

Fig. 5. Log $i_k/(i_d - i_k)$ *versus* log $[SCN^-]_0$ for cobalt(II)-thiocyanate system.

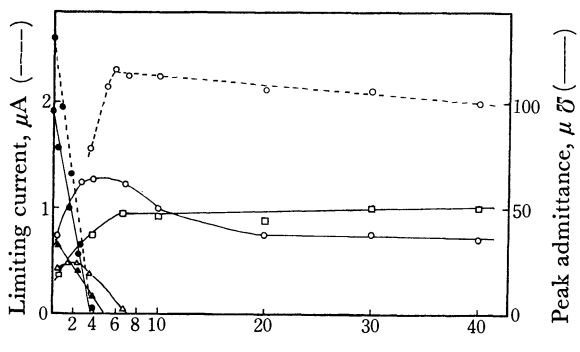

Fig. 4. Limiting current and peak admittance *versus* mole ratio, $[SCN^-]_t/[Co(II)]_t$ for cobalt(II)-thiocyanate system. ●, wave I; ▲, wave II; △, wave III; ○, wave IV; □, wave V.

Fe(II)-SCN^- System. The formation of iron(II)-thiocyanate complexes was investigated by conductometric and spectrophotometric methods.

In conductometric titration curve for Fe(II)–SCN^- system, the inflection point was at $[SCN^-]_t/[Fe(II)]_t$= 1.0 and other points were ill-defined. The thiocyanate complex of iron(II) has an absorption band at 20284 cm^{-1}. The intensity of this band increased until $[SCN^-]_t/[Fe(II)]_t$=3. Above this ratio, this band was shifted to 20619 cm^{-1}. The curves of absorbance for unit concentration of Fe(II) at 20284 and 20619 cm^{-1} *vs.* mole ratio, $[SCN^-]_t/[Fe(II)]_t$ showed the inflection points at $[SCN^-]_t/[Fe(II)]_t$=3 and 4. These indicate the formation of $[Fe(NCS)]^+$, $[Fe(NCS)_3]^-$ and $[Fe(NCS)_4]^{2-}$.

The polarograms of Fe(II)–SCN^- system are shown in Fig. 6. Solvated Fe(II) perchlorate has a single reduction wave with the half-wave potential of −0.995 V *vs.* SCE. The electrode reaction was found to be two-electron reduction and diffusion-controlled. This

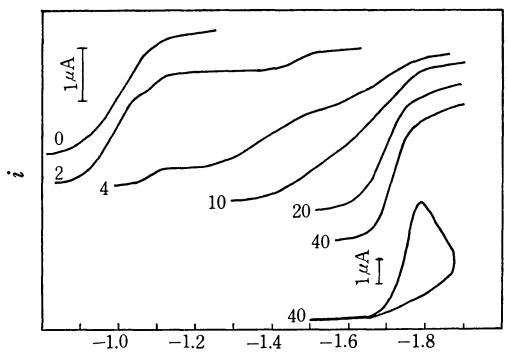

Fig. 6. DC polarograms and cyclic voltammogram of iron(II)-thiocyanate complexes. Number on curves indicate mole ratio, $[SCN^-]_t/[Fe(II)]_t$.

wave decreased with increasing concentration of thiocyanate ion and the new waves appeared at more negative potentials. The wave of complex ion appeared due to the reduction of $[Fe(NCS)_4]^{2-}$ at $[SCN^-]_t/[Fe(II)]_t \geq 20$. The electrode reaction was two-electron reduction and diffusion-controlled.

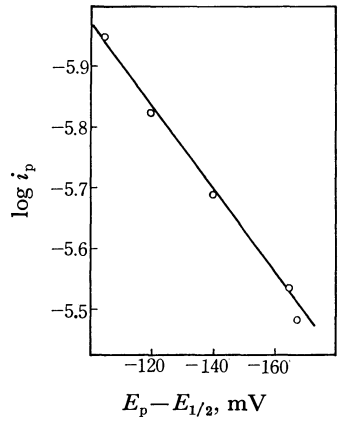

Fig. 7. Determination of the rate constant for solvated iron(II).

The rate constants of the electrode reaction were determined by cyclic voltammetry. Typical cyclic voltammogram (scan rate 0.2 V/s) is shown in Fig. 6. The determination of the rate constants was made by using the method proposed by Matsuda and Ayabe.[13]

The plot of log i_p *vs.* $(E_p-E_{1/2})$ for solvated Fe(II) system is shown in Fig. 7 for example. The value of standard rate constant, k_s was calculated from the point of intersection on ordinate. Polarographic data for Fe(II)–SCN^- system are shown in Table 3. These data indicate that the electrode reactions for solvated Fe(II) and Fe(II)-thiocyanate complex are quasi-reversible.

Table 3. Polarographic data for iron(II)-thiocyanate system

[Fe(II)]=0.5 mM

$[SCN^-]$ mM	i_d μA	$E_{1/2}$ V *vs.* SCE	Slope mV	α	k_s cm/s
0	2.28	−0.995	75	0.39	6.6×10^{-4}
10	2.04	−1.672	59	0.50	9.8×10^{-4}
20	2.02	−1.691	35	0.84	1.9×10^{-3}

The authors are grateful for financial support given by the Ministry of Education for this work.

References

1) S. Misumi and M. Aihara, *Talanta*, **19**, 549 (1972).
2) S. Misumi and M. Aihara, This Bulletin, **46**, 1674 (1973).
3) J. E. Lind, Jr., and R. M. Fuoss, *J. Phys. Chem.*, **65**, 999 (1961).
4) J. E. Lind, Jr., J. J. Zwolenik, and R. M. Fuoss, *J. Amer. Chem. Soc.*, **81**, 1557 (1959).
5) R. M. Fuoss and F. Accascina, "Electrolytic Conductance," Interscience Publishers, New York (1959).
6) D. S. Berns and R. M. Fuoss, *J. Amer. Chem. Soc.*, **82**, 5585 (1960).
7) H. L. Yeager and B. Kratochvil, *J. Phys. Chem.*, **74**, 963 (1970).
8) C. Furlani, L. Sestili, A. Ciana, and F. Garbassi, *Electrochim. Acta*, **12**, 1393 (1967).
9) L. Sestili, C. Furlani, A. Ciana, and F. Garbassi, *ibid.*, **15**, 225 (1970).
10) V. Gutmann and O. Bohunovsky, *Monatsh. Chem.*, **99**, 751 (1968).
11) A. E. Harvey, Jr., and D. L. Manning, *J. Amer. Chem. Soc.*, **72**, 4488 (1950).
12) R. Brdička, "Advances in Polarography," Vol. 2, Longmuir (1960), p. 655.
13) H. Matsuda and Y. Ayabe, *Z. Elektrochem.*, **59**, 494 (1955).

Optical Resolution and Racemization of Tris(acetylacetonato)-germanium(IV) in Organic Solvents

Akira NAGASAWA and Kazuo SAITO

Chemistry Department, Faculty of Science, Tohoku University, Aoba, Aramaki, Sendai 980

(Received September 28, 1973)

The tris(acetylacetonato)germanium(IV) has been resolved by the crystallization of its hydrogen-*R,R*-dibenzoyltartrate in a mixture of acetonitrile, ethanol, and water. The racemization kinetics of perchlorate of the *Δ*-enantiomer has been studied in 1,1,2,2-tetrachloroethane (TCE), nitromethane, acetonitrile (AN), and *N,N*-dimethylformamide, the activation enthalpies ($\Delta H^{\ddagger}$/kcal·mol^{-1}) and the activation entropies ($\Delta S^{\ddagger}$/cal·K^{-1} mol^{-1}) being 27.9, 26.6, 24.3, and 23.3, and +3.7, −1.1, −4.4, and −5.0, respectively. The ligand isotopic exchange is much slower than the racemization under similar conditions. Consideration of acid (in TCE) and base (in AN) catalysis, influence of ionic strength and solvent effect suggests an intra-molecular mechanism *via* an intermediate in which one of the ligands is in unidentate state.

The number of work concerning germanium compounds has been increasing in these decades. However, most of them are related to tetrahedral organometallic compounds, and much less to octahedral and co-ordination compounds. Especially, the dynamic properties of six co-ordinated germanium complexes are almost unknown.[1-3]

Geometrical isomerization and racemization of octahedral complexes with tris-bidentate ligands have been studied by many workers with *β*-diketonato complexes of various metal ions. Most of these reactions in organic solvents are claimed to proceed *via* intra-molecular mechanism.[4] These works centered around chargeless complexes, and those related to univalent cationic complexes are limited to tris(acetylacetonato)-silicon(IV).[5]

We intended to extend the work to those with germanium(IV) analogues. Morgan and Drew[6] first prepared the tris(acetylacetonato)germanium(IV) ion, $[Ge(acac)_3]^+$, and its physical properties are better known than others. We have resolved this complex and studied the racemization kinetics in various organic solvents. The mechanism has been discussed and the lability of this complex compared with those of related compounds.

Experimental

Materials. Preparation of Tris(acetylacetonato)germanium-(IV) Perchlorate: The complex ion $[Ge(acac)_3]^+$ was synthesized as hexachloroantimonate by Cox and co-workers' method.[7] This salt (3.5 g, 5×10^{-3}mol) was dissolved in 30 ml of chloroform–ethanol (3: 1), and mixed with silver perchlorate (1.25 g, 6×10^{-3}mol) in 20 ml chloroform–ethanol (1: 1). Silver chloride was filtered off, and the filtrate was treated with magnesium perchlorate (1.3 g) in 20 ml of chloroform–ethanol (1: 3). Crystals of $[Ge(acac)_3]ClO_4$ obtained on addition of diethyl ether (450 ml) were filtered off, washed with ether, recrystallized from chloroform solution by adding diethyl ether, washed with diethyl ether, and dried *in vacuo*. Yield, 80—87%. Found: C, 38.45; H, 4.64%. Calcd for $C_{15}H_{21}O_{10}ClGe$: C, 38.38; H, 4.51%. Colorless needles melt at 245—251 °C with decomposition. IR spectra in KBr disk and Nujol mull gave the absorption peaks of carbonyl group co-ordinated to metal ions, perchlorate anion, but not of hydroxyl groups. Proton NMR in deuterochloroform has singlet signals at 2.33 and 6.18 ppm (*δ*, TMS), corresponding to six methyls and one methyne, respectively. Figure 1 shows the UV absorption spectrum in acetonitrile. The pattern and the peaks agree with those of $[Ge(acac)_3]^+$ in $[Ge(acac)_3][FeCl_4]$.

Optical Resolution: The complex ion was resolved into optical isomers by the crystallization of its hydrogen-*R,R*-dibenzoyltartrate. Racemic perchlorate (1.6 g, 3.4×10^{-3} mol) was dissolved in 75 ml of acetonitrile–ethanol–water (1: 1: 1), treated with 20 ml of sodium hydrogen dibenzoyltartrate (5.3×10^{-3}mol) in water, the mixture was poured into 130 ml of cold water, and set aside in an ice bath. The colorless needles were filtered off within 30 minutes and dried. The product was recrystallized from acetonitrile–ethanol (1: 1) solution by adding twice volume of water, filtered off and dried *in vacuo*. Found: C, 54.31; H, 4.53%. Calcd for $C_{33}H_{34}O_{14}Ge$: C, 54.40; H, 4.71%. mp 141—143 °C (decompn.). $[\alpha]_{589}$ −656 ° (4.4×10^{-4}M in AN, 20 °C).

This diastereoisomer (1.0 g, 1.4×10^{-3}mol) and magnesium perchlorate (1.0 g, 4.5×10^{-3}mol) were dissolved in 60 ml of

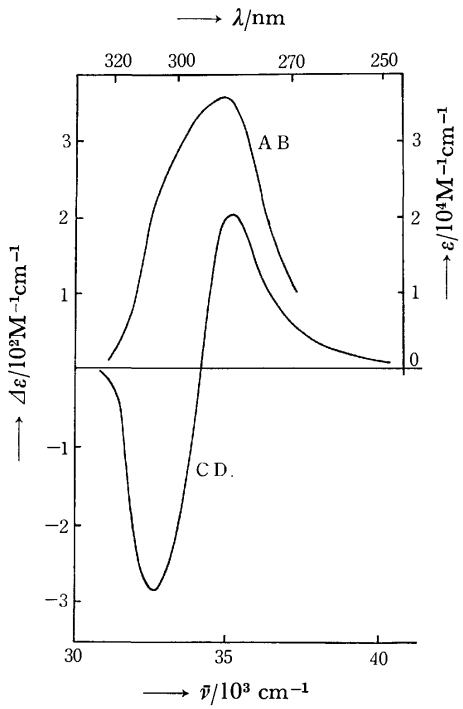

Fig. 1. Ultraviolet absorption (AB) and circular dichroism (CD) spectrum of $(-)_{589}$-$[Ge(acac)_3]^+$ in acetonitrile.

glacial acetic acid, and poured into diethyl ether. The crystals were washed with diethyl ether, recrystallized from chloroform solution with diethyl ether, and dried. The yield was 20% on the basis of racemic perchlorate. Found: C, 38.50; H, 4.63%. Calcd for $C_{15}H_{21}O_{10}ClGe$: C, 38.38; H, 4.51%. $[\alpha]_{589}$ −930° (3.2×10^{-4}M in AN, 20 °C). Circular dichroism (CD) spectrum of the complex is shown in Fig. 1.

Solvents for Kinetic Runs: Acetonitrile (AN) was dried with calcium chloride, refluxed with diphosphorus pentoxide and distilled. This procedure was repeated and the middle fraction was finally distilled. Nitromethane was washed successively with aqueous sodium bicarbonate, sodium bisulfite, 5% sulfuric acid and water. One fourth volume of water was added and refluxed. The mixture was distilled slowly, a large amount of the first fraction was discarded and the oily layer of the middle fraction was again distilled. 1,1,2,2-Tetrachloroethane (TCE) was shaken with several portions of concentrated sulfuric acid until the acid remained colorless, and distilled under reduced pressure. Chloroform was washed with aqueous sodium hydroxide, sulfuric acid and water, and distilled. *N*,*N*-Dimethylformamide (DMF) was dried with anhydrous copper sulfate and distilled under reduced pressure. Dimethyl sulfoxide (DMSO) was dried with activated alumina and distilled under reduced pressure.

The purities of these solvents were checked by gas chromatography, and the water contents titrated by Karl Fischer method.

Other Reagents: Pyridine was recrystallized as perchlorate and dissolved in a small amount of water, treated with solid sodium hydroxide, the pyridine layer decanted and distilled under reduced pressure. Glacial acetic acid was frozen at 5 °C and distilled. Commercially available extra pure sodium perchlorate and magnesium perchlorate were used without purification. Acetylacetone (Hacac) was distilled by the usual method. The labelled acetylacetone (Hacac-^{14}C) was prepared as reported in the literature.[8]

Kinetic Procedure. Racemization: The optically active perchlorate (0.01 g) was dissolved in a given solvent (25 ml) and, whenever necessary, other reagents were mixed. Aliquots of the solution were sealed in small glass test tubes with silicone rubber stoppers. All these procedures were operated in a dry grove box. Several ampoules were prepared, placed in a thermostat (30 to 70 °C±0.1 °C) and picked up one by one at proper intervals. They were cooled in ice water for 30 s, and their optical rotation and UV absorption were measured at room temperature (15—25 °C) at a proper wavelength in the range 310 to 365 nm. (AN, 310—325 nm; chloroform, 316 nm; TCE, DMF, and DMSO, 318 nm; nitromethane, 360—365 nm). The rate constant was calculated by the following equation,

$$k_{obsd} = (1/2t)\ln(\alpha_0/\alpha_t) \quad (1)$$

where α_0 and α_t are the optical rotation at time zero and t, respectively, and t is the lapse of time in second.

Isotopic Exchange: The complex and acetylacetone-^{14}C (10^{-3} M) were dissolved in acetonitrile. Aliquots were sealed in glass tubes, and kept in a thermostat (60 to 80 °C). They were chilled one by one at proper time intervals, the ampoules cut and poured into cold diethyl ether. The precipitated complex was filtered off with a piece of filter paper, washed with diethyl ether, and dried *in vacuo*. The activity of a weighed amount of crystals was counted with a 2π gas flow counter in a current of Q-gas.

Apparatuses. JASCO model ORD/UV-5 was used for the measurement of optical rotation and the recording of CD spectra. JASCO DIP-SL Polarimeter was used for optical rotation measurement at Na-D line. Hitachi 323 Spectrophotometer was used for the recording of absorption spectra, and K53 Gas Chromatograph with TCD for detecting the impurity of the solvents. Aloka FC-1E Counter was used for the β-activity counting of ^{14}C. The water content was measured by the Karl Fischer method. Metrohm E 365 B Konduktoskop and EA 608 bright platinum electrodes were used for the conductance measurement.

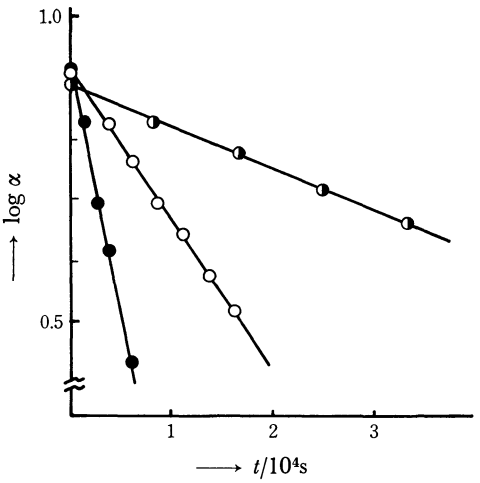

Fig. 2. Change in optical rotation at 312 nm in acetonitrile.
◑ 40 °C, ○ 50 °C, ● 60 °C

Results

The Kinetics of Racemization in Acetonitrile. The changes in optical rotation at 312 nm are illustrated in Fig. 2. The absorbances at 305 and 288 nm showed no change during several half-lives, and the decrease in optical rotation should be due to net racemization of the complex. The rate constant was found to be independent of the complex concentration. Hence the rate formula is expressed as follows:

$$\text{Rate} = k_{obsd}[\text{complex}] \quad (2)$$

The water content of the solution gave no significant effect on the racemization rate in the range from 10^{-2} to 2×10^{-1} M. (Fig. 3). Free acetylacetone (Hacac) and acetic acid gave no catalytic effect on the racemiza-

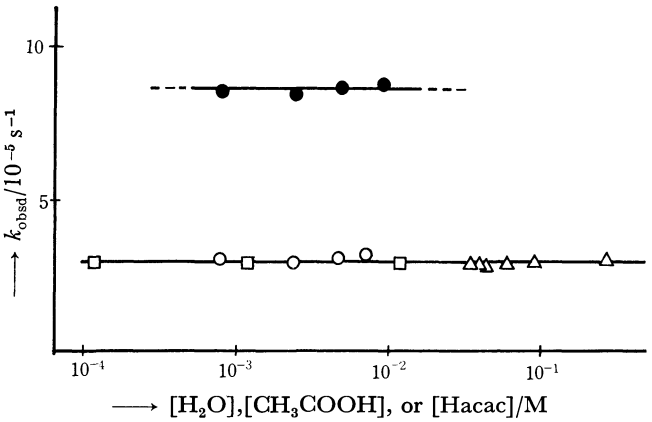

Fig. 3. Influence of water, acid, and ligand concentration upon the racemization rate in acetonitrile.
△ for water at 50 °C, ○ and ● for acetic acid at 50 and 60 °C, respectively, □ for Hacac at 50 °C.

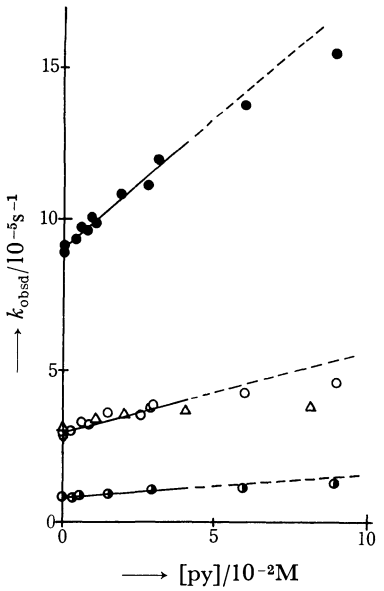

Fig. 4. Influence of pyridine concentration in acetonitrile.
Circles in the absence of $NaClO_4$, ◑ 40 °C, ○ 50 °C, ● 60 °C; △ in 0.124 M $NaClO_4$ at 50 °C.

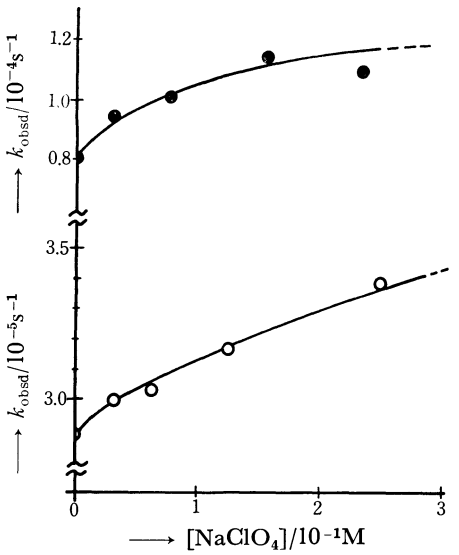

Fig. 5. Salt effect on the racemization rate in acetonitrile.
○ 50 °C, ● 60 °C.

tion rate (Fig. 3) in the ranges from 10^{-5} to 10^{-2} M and from 5×10^{-4} to 10^{-2} M, respectively.

The relationship between pyridine concentration and racemization rate is illustrated in Fig. 4. The diagrams are linear at least up to 4×10^{-2} M of pyridine. The intercepts coincide with the k_{obsd} values in the absence of pyridine. Hence the k_{obsd} is expressed by

$$k_{obsd} = k_1 + k_2[py] \quad (3)$$

The values of k_1 and k_2 at several temperatures and the activation parameters are shown in Table 1.

The values of k_1 and k_2 depend on the concentration of sodium perchlorate. Conductance measurements suggested that sodium perchlorate is a strong, while the complex is a weak electrolyte in AN. Hence the increase in k_{obsd} with the electrolyte concentration seems to be due to ionic strength effect (see Fig. 5).

When the water content was increased to 1 M, UV absorption changes, but no isosbestic point was observed. The decrease in absorbance at 316 nm was in accord with the first-order kinetic formula at 70 °C and the apparent rate constant linearly increases with increase in water concentration up to 8 M. It seems that such a change is due to hydrolysis of the complex, presumably taking place step by step. The rate is so small, ($1\times10^{-4}/M^{-1}s^{-1}$ at 70 °C), however, that it can be ignored when the racemization mechanism is discussed.

Racemization in Other Solvents. No change in absorption of the complex was observed for several half-lives in nitromethane, and for a few half-lives in TCE. The racemization was catalyzed by acetic acid in TCE. The decrease in optical rotation in DMF was accompanied by the change in absorption. The absorption spectrum has an isosbestic point at 279 nm, and this change seems to be due to a reaction giving free acetylacetone. The net racemization was followed by use of the quotient (optical rotation at 316 nm)/(absorbance at 305 nm), and the calculated k_{obsd} values are shown in Table 2. The decrease in optical activity in DMSO and chloroform is mostly due to decomposition of the complex. Intrinsic racemization may be taking place, but it is distinguished with difficulty. The k_{obsd} values and the activation parameters in various solvents are summarized in Table 2.

Ligand Isotopic Exchange in Acetonitrile. No exchange took place within 2000 minutes at 60 °C both in the presence and the absence of pyridine. No exchange was either observed at 80 °C suggesting a negligibly smaller rate of ligand isotopic exchange than the racemization.

Table 1. Rate constants and activation parameters in acetonitrile

t/°C	$[Ge(acac)_3]^+$		$[Si(acac)_3]^+$ [5]	
	$k_1/10^{-5}s^{-1}$	$k_2/10^{-4}M^{-1}s^{-1}$	$k_1/10^{-5}s^{-1}$	$k_2/10^{-4}M^{-1}s^{-1}$
30	—	—	0.263	1.5
40	0.797	0.85	1.08	—
50	2.88	2.7	3.87	—
60	8.85	8.7	13.7	—
ΔH^*/kcal·mol^{-1}	24.3±0.4	23.7±3.0	25.7±0.2	—
ΔS^*/cal·K^{-1}·mol^{-1}	−4.4±1.4	−1.7±9.9	+0.5	—

TABLE 2. RACEMIZATION RATE CONSTANTS AND ACTIVATION PARAMETERS OF $[Ge(acac)_3]^+$ IN VARIOUS ORGANIC SOLVENTS

Solvent	1,1,2,2-Tetrachloroethane	Nitromethane	Acetonitrile	*N*,*N*-Dimethylformamide
$k_{323}/10^{-5}s^{-1}$ a)	0.579	0.420	2.88	10.4
$k_{298}/10^{-7}s^{-1}$ b)	1.39	1.17	11.0	44
ΔH^*/kcal·mol^{-1}	27.9±0.8	26.6±1.0	24.3±0.4	23.3±2.6
ΔS^*/cal·K^{-1}·mol^{-1}	+3.8±2.8	−1.1±3.5	−4.4±1.4	−5.0±8.6
ε c)	8.20	35.9	37.5	36.7
$\mu/10^{-18}$ CGSesu d)	1.71	3.56	3.44	3.86
D.N. e)	(~0)	2.7	14.1	27

a) Observed value at 50 °C.
b) extrapolated value to 25 °C.
c) dielectric constant.
d) dipole moment.
e) Gutmann's donor number.[9]

Discussion

Mechanism of Racemization of Tris(acetylacetonato)germanium(IV). Absence of ligand isotopic exchange and of decomposition clearly indicates that the racemization proceeds *via* an intra-molecular mechanism. Independence of the rate constant on the complex and the ligand concentration also supports such a mechanism.

An intra-molecular mechanism can proceed with or without break of one of the metal-ligand bonds. The former involves an intermediate with a unidentate ligand and the latter that with tris-bidentate ligands. It is difficult, however, to give a direct evidence for distinguishing them, and the discussion should be based on indirect evidences as follows.

The racemization was catalysed by acetic acid in TCE and by pyridine in AN. It is not likely that an acid or a base gives catalytic effect on the twisting of the complex without bond-break. Further, the racemization rate was found to increase with increase in ionic strength. It is likely that increase in ionic strength facilitates the bond break resulting in charge separation.

The values of ΔH^* and ΔS^* are not very different from one another in various solvents (Table 2), and the overall mechanism should not be very different in all of them, although the above observations were mainly made in AN. As Table 2 shows, the dielectric constant and the dipole moment do not seem to play an important role in determining the racemization rate. It seems that the rate increases and ΔH^* decreases with increase in donor number[9] of the solvents. The donor number reflects the ease with which the solvent molecules have interaction with the central metal ion, and its increase would facilitate the break of Ge–O bond of the complex. In those solvents with bigger donor numbers, even decomposition of the complex was observed to produce free acetylacetone.

On the basis of these facts, we propose a racemization mechanism involving an intermediate with a unidentate ligand, as shown in Fig. 6. Such a mechanism can have either the bond break or the succeeding intra-molecular rearrangement as rate-determining step. Although a direct evidence is given with difficulty, we tend to think that the rate-determining step would be the solvent-assisted break of the first metal-ligand bond. If the solvent molecules did not assist the bond break but just occupied the vacant coordination site of the intermediate, or if they gave an indirect effect to ease the break of ionic Ge–O bond, not the donor number but rather the dipole moment or the dielectric constant would be related to the rate and the activation enthalpy of the complex. Further, if the internal rearrangement were the rate determining step, the effect of the solvents would be reversed.

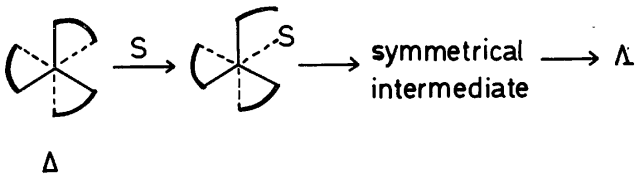

Fig. 6. Plausible reaction mechanism.
(The "symmetrical intermediate" can be either trigonal bipyramid or square pyramid, but its structure is not known from the present experiments.)

Holm and co-workers measured the coalescence of the proton signals of tris-type germanium(IV) complexes of substituted tropolonate in various chlorohydrocarbons by NMR, and discussed the mechanism of intra-molecular geometrical isomerization and racemization.[3] It was suggested that the intramolecular rearrangement proceeds without involving bond-break. They obtained ΔH^* values 12 to 17 kcal/mol and log A 12, which are common with those of other tris-α-diketonato complexes. Our ΔH^* values are significantly larger than theirs and our present racemization is more adequately presumed to have a different rate-determining step from theirs.

Comparison with Related Compounds. Tris(acetylacetonato)germanium(IV) gives very similar absorption and circular dichroism spectra to those of tris(acetylacetonato)silicon(IV). The $(-)_{589}$-isomer of $[Ge(acac)_3]^+$ can be assigned to absolute configuration Δ from comparison of the CD spectrum in the UV π-π^* transition region with that of tris(acetylacetonato)-silicon(IV),[10] whose absolute configuration was supported by the CD spectrum[11] and X-ray crystallography of tris(catecholato)arsenic(V).[12]

The solubility of various salts of $[Ge(acac)_3]^+$ in various organic solvents is also very similar to that of $[Si(acac)_3]^+$ salts.

Table 1 shows the values of rate constants and activation parameters of racemization of $[Si(acac)_3]^+$, too. The ligand isotopic exchange of the silicon complex is also very slow. Its racemization is catalysed by acids in TCE and by bases in AN, and an intramolecular mechanism involving bond-break was proposed. The activation parameters for the germanium and silicon complexes are very near to each other. All these facts are reckoned as to reflect the overall similarity of these two elements.

A number of studies have been published concerning the kinetics of geometrical isomerization and racemization ("site-exchange") of α-[3,13] and β-diketonato[4] complexes of various metal ions. The site exchange is generally understood to proceed intra-molecularly in organic solvents, but various mechanisms have been proposed for their detailed progress. Examination of the references suggests that tris-β-diketonato complexes mostly undergo site exchange with one bond-break, whereas tris-α-diketonato complexes without bond-break. However, the experimental evidence for such a statement is rather indirect, and our present discussion provides more concrete support to the mechanism. Semi-empirical calculation on the basis of structural parameters also supports such a mechanism.[14] Most of these studies were made with chargeless complexes, but the discussion seems to be applicable to cationic complexes with +1 charge, *i.e.* our study with β- and Holm's with α-diketonatogermanium(IV).

The approximate order of overall site-exchange rate for tris-β-diketonato complexes of various metal ions is given below:[4]

$$\text{Fe(III), In(III)}>\text{Mn(III)}>\text{Ga(III)}>\text{Al(III)}>\text{Si(IV)}\gtrsim \text{Ge(IV)}>\text{Co(III)}>\text{Cr(III)}>\text{Ru(III)}\gtrsim\text{Rh(III)} \quad (4)$$

The labilities of silicon(IV) and germanium(IV) complexes are larger than that of cobalt(III) complexes and smaller than those of Family IIIB elements. The activation enthalpies (ΔH^*/kcal·mol^{-1}) involving bond-rupture process for site exchange of cobalt(III)[15] and aluminium(III)[16] are 20 to 30 and 15 to 20, and the log A's 14 to 16 and 13 to 17 respectively. The ΔS^* values are all positive. Although the present silicon and germanium complexes have +1 charge, the activation parameters for racemization are between those of Co(III) and Al(III) complexes. The sequence 4 seems to reflect the order of ease of break of the first metal-ligand bond.

On the other hand, ligand isotopic exchange studies suggested the break of the remaining bond of the unidentate ligand in the intermediate as rate-determining step. The rate of such inter-molecular reactions of octahedral β-diketonato complexes decrease approximately in the order,[5,8,17–19]

$$\text{In(III)}>\text{Ga(III)}>\text{Al(III)}>\text{Co(III)}>\text{Si(IV)},\ \text{Ge(IV)}>\text{Cr(III)} \quad (5)$$

While the major part of this sequence is similar to sequence 4, silicon(IV) and germanium(IV) come next to cobalt(III). Such a difference may be related to the stability of the intermediate with five metal-ligand bonds. These ions with higher positive charge may interact with solvent molecules at the vacant coordination site more significantly to stabilize the intermediate.

The authors thank the Ministry of Education for Grant-in-Aid.

References

1) T. Moeller and N. C. Nielsen, *J. Amer. Chem. Soc.*, **75**, 5106 (1953).
2) E. L. Muetterties and C. M. Wright, *ibid.*, **86**, 5132 (1964); **87**, 21 (1965).
3) S. S. Eaton, G. R. Eaton, R. H. Holm, and E. L. Muetterties, *ibid.*, **95**, 1116 (1973).
4) J. J. Fortman and R. E. Sievers, *Coord. Chem. Rev.*, **6**, 331 (1971).
5) T. Inoue and K. Saito, This Bulletin, **46**, 2417 (1973).
6) G. T. Morgan and H. D. K. Drew, *J. Chem. Soc.*, **125**, 1261 (1924).
7) M. Cox, J. Lewis, and R. S. Nyholm, *J. Chem. Soc., Suppl.* **1964**, 6113.
8) K. Saito and K. Masuda, This Bulletin, **41**, 384 (1968).
9) V. Gutmann, "Coordination Chemistry in Non-Aqueous Solutions," Springer, Wien (1968).
10) E. Larsen, S. F. Mason, and G. H. Searle, *Acta Chem. Scand.*, **20**, 191 (1966).
11) T. Ito, N. Tanaka, I. Hanazaki, and S. Nagakura, *Inorg. Nucl. Chem. Lett.*, **5**, 781 (1969).
12) T. Ito, A. Kobayashi, F. Marumo, and Y. Saito, *ibid.*, **7**, 1097 (1971).
13) S. S. Eaton, J. R. Hutchison, R. H. Holm, and E. L. Muetterties, *J. Amer. Chem. Soc.*, **94**, 6411 (1972).
14) E. I. Stiefel and G. F. Brown, *Inorg. Chem.*, **11**, 434 (1972); E. L. Muetterties and L. J. Guggenberger, *J. Amer. Chem. Soc.*, **94**, 8046 (1972).
15) R. C. Fay and T. S. Piper, *J. Amer. Chem. Soc.*, **84**, 2303 (1962); *Inorg. Chem.*, **3**, 348 (1964). J. G. Gordon, Jr. and R. H. Holm, *J. Amer. Chem. Soc.*, **92**, 5319 (1970). A. Y. Girgis and R. C. Fay, *ibid.*, **92**, 7061 (1970).
16) D. A. Case and T. J. Pinnavaia, *Inorg. Chem.*, **10**, 482 (1971).
17) C. Chatterjee, K. Matsuzawa, and K. Saito, This Bulletin, in press.
18) K. Saito and M. Murakami, *ibid.*, **45**, 2472 (1972).
19) H. Kido and K. Saito, unpublished result.

Copper(II) Complexes of L-Histidylglycine and L-Histidylglycylglycine in Aqueous Solution

Hiroji AIBA, Akira YOKOYAMA, and Hisashi TANAKA
Faculty of Pharmaceutical Sciences, Kyoto University, Yoshida, Sakyo-ku, Kyoto 606
(Received July 30, 1973)

Equilibrium constants were determined in the complex formations of L-histidylgylcine (HG) and L-histidylglycylglycine (HGG) with copper(II) ion in aqueous solution by potentiometric titration, and the structures of the complexes were discussed based on the observations in the titration and infrared and electronic absorption spectra. In the acid region, a cationic chelate, in which copper(II) binds to nitrogen atoms of amino and imidazole groups, is formed. In the neutral region, deprotonation of the peptide amide group occurs to form a dimer, in which four coordination positions of copper(II) are occupied by nitrogen atoms of deprotonated amide and amino groups and an oxygen atom of carboxyl or carbonyl group in one molecule and a nitrogen atom of imidazole group of another molecule. In HGG–Cu(II) system, the dimer is decomposed in the alkaline region with further deprotonation of the second peptide amide group to form an anionic chelate as in the case of the glycylglycylglycine-Cu(II) complex.

The complex formation of some histidine-containing peptides has been studied by various physico-chemical methods,[1-12] based on the importance of the histidyl residue as a binding site with metal ions in protein. However, the experimental results, such as the data on the potentiometric titration, the spectral measurement and X-ray analysis, are not always sufficiently detailed to discuss the behavior of these peptides in the interaction with the metal ions in aqueous solution. The copper(II) complex of L-histidylglycine has been studied by the potentiometric titration[12] and the visible and CD spectra,[5] but the behavior and the structure of the complex in aqueous solution were not interpreted in detail with the experimental results. The complex formation of L-histidylglycylglycine has not been investigated so far.

In the preceding paper,[13] we reported the syntheses and the acid dissociation constants of some histidine-containing peptides, and also the formation constants of some 2:1 (ligand:metal) metal complexes of L-histidylglycine and L-histidylglycylglycine (abbreviated as HG and HGG hereafter). Further, the dimer formation in the reaction of HG and HGG with copper(II) ion was briefly reported.[14] This paper deals with the detailed description of the study and the discussions on the complex formation of these peptides with copper(II) ion in aqueous solution.

Experimental

Materials. The preparations of HG and HGG were described in the preceding paper.[13] All other reagents were commercially obtained.

Potentiometric Titrations. The details of the method and the experimental conditions have been described previously.[13] Titrations were carried out in the solutions (10 ml) containing a ligand (10^{-3}M), HCl (2×10^{-3}M) and $CuCl_2$ (10^{-3}M) with 0.1 M KOH.

Infrared Absorption Spectra. The infrared absorption spectra were recorded on a Koken DS-301 infrared spectrophotometer equipped with sodium chloride prisms. Measurements were made on the D_2O solutions of a ligand with or without copper(II) ion, in a KRS-5 cell. The concentration of the ligand was approximately 0.3 M.

Visible Absorption Spectra. The visible absorption spectra were recorded on a Shimadzu Double 40-R spectrophotometer. Spectral measurements were made on the solutions of a ligand containing copper(II) ion with the concentration ranging from 4×10^{-3}M to 1×10^{-2}M.

Results and Discussion

Potentiometric Titrations. Titration curves for the solutions containing 1:1 molar ratio of copper(II) ion to ligand in the presence of two equivalents of HCl are given in Figs. 1 and 2. Both curves show sharp pH inflections at $a=3$ and $a=4$, where a represents moles of KOH added per mole of the ligand. Another pH inflection is observed at $a=5$ in the HGG–Cu(II) system. The pH inflection at $a=3$ suggests the formation of the 1:1 ligand-copper(II) complex in both systems. Therefore, the following reactions were assumed in the region where a value is between 1 and 3.

$$LH_3^{2+} \rightleftharpoons LH_2^{+} + H^{+}$$

$$K_{COOH} = [LH_2^{+}][H^{+}]/[LH_3^{2+}] \quad (1)$$

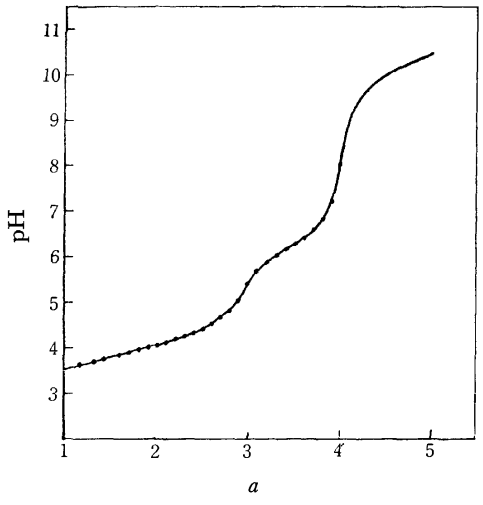

Fig. 1. Titration curve of HG in the presence of equimolar $CuCl_2$ and two equivalents of HCl.
At $a=0$, $[HG]_T=[Cu]_T=10^{-3}$M. The line is experimental curve. The points are the values calculated from equilibrium constants.

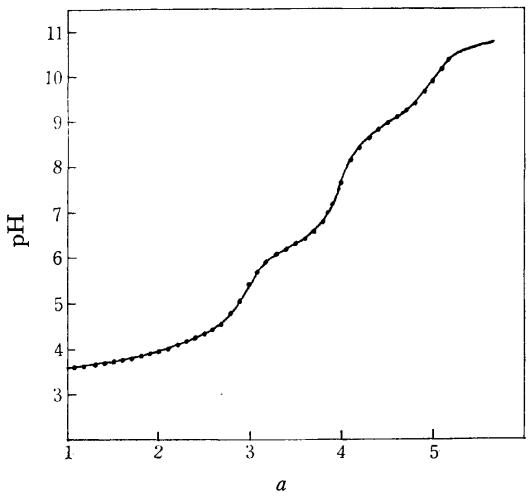

Fig. 2. Titration curve of HGG in the presence of equimolar $CuCl_2$ and two equivalents of HCl.
At $a=0$, $[HGG]_T=[Cu]_T=10^{-3}$M. The line is experimental curve. The points are the values calculated from equlibrium constants.

$$LH_2^+ \rightleftarrows LH + H^+$$
$$K_{Im} = [LH][H^+]/[LH_2^+] \quad (2)$$
$$LH \rightleftarrows L^- + H^+$$
$$K_{NH_2} = [L^-][H^+]/[LH] \quad (3)$$
$$Cu^{2+} + L^- \rightleftarrows CuL^+$$
$$K_1 = [CuL^+]/[Cu^{2+}][L^-] \quad (4)$$

Electroneutrality requires Eq. (5).

$$2[Cu^{2+}] + [CuL^+] + 2[LH_3^{2+}] + [LH_2^+] + [K^+] + [H^+] = [L^-] + [Cl^-] + [OH^-] \quad (5)$$

The total concentrations of copper(II) and the ligand are expressed as Eqs. (6) and (7).

$$[Cu]_T = [Cu^{2+}] + [CuL^+] \quad (6)$$
$$[L]_T = [CuL^+] + [LH_3^{2+}] + [LH_2^+] + [LH] + [L^-] \quad (7)$$

Since copper(II) ion was added as chloride and two equivalents of HCl per ligand were added, the concentration of Cl^- is expressed as Eq. (8).

$$[Cl^-] = 2[Cu]_T + 2[L]_T \quad (8)$$

Equation (9) is derived from these equations.

$$K_1 = \beta(\beta[Cu]_T - \alpha\gamma)/\alpha\gamma^2, \quad (9)$$

where

$$\alpha = 1 + [H^+]/K_{NH_2} + [H^+]^2/K_{Im}K_{NH_2} + [H^+]^3/K_{COOH}K_{Im}K_{NH_2},$$
$$\beta = [H^+]/K_{NH_2} + 2[H^+]^2/K_{Im}K_{NH_2} + 3[H^+]^3/K_{COOH}K_{Im}K_{NH_2},$$
$$\gamma = [Cu]_T + 2[L]_T + [OH^-] - [H^+] - [K^+].$$

The formation constant, K_1, was calculated at each point of the experiments from Eq. (6), based on the data of the titration in the region where a value is between 1 and 3. The results are given in Table 1. Fairly good constant values of $\log K_1$ were obtained with varying a values in each system. These values are in good agreement with those we obtained in the 2:1 systems.[13] In CuL^+, the nitrogen atoms of α-amino and imidazole groups may be bound to the copper atom, as we mentioned previously.[13]

The deprotonation in the region where the a value is between 3 and 4 can not be interpreted by a simple ionization (Table 2). On the other hand, the spectral features of the complexes in the visible region suggested the formation of a polymer (Cu_nX_n) accompanying the

Table 1. $\log K_1$ Calculated according to Eq. (9)

a value	His-Gly-Cu(II) system		His-Gly-Gly-Cu(II) system	
	pH	$\log K_1$	pH	$\log K_1$
1.2	3.67	9.06	3.65	8.64
1.3	3.72	9.04	3.70	8.59
1.4	3.76	9.05	3.74	8.58
1.5	3.81	9.03	3.77	8.60
1.6	3.86	9.01	3.81	8.60
1.7	3.90	9.03	3.85	8.60
1.8	3.95	9.02	3.90	8.58
1.9	4.01	9.00	3.94	8.59
2.0	4.06	9.01	3.98	8.62
2.1	4.11	9.02	4.04	8.59
2.2	4.18	9.00	4.10	8.59
2.3	4.25	9.00	4.16	8.59
2.4	4.32	9.01	4.22	8.62
2.5	4.41	9.01	4.40	8.61
2.6	4.50	9.04	4.52	8.63
2.7	4.63	9.05	4.70	8.65
2.8	4.81	9.06	5.02	8.65
Average	9.03±0.03		8.61±0.04	

Table 2. pK_c^n Calculated according to Eq. (10)

a	His-Gly-Cu(II) system						a	His-Gly-Gly-Cu(II) system					
	pH	pK_c^1	pK_c^2	pK_c^3	pK_c^4	pK_c^5		pH	pK_c^1	pK_c^2	pK_c^3	pK_c^4	pK_c^5
3.1	5.67	6.61	9.53	12.32	15.06	17.77	3.1	5.77	6.72	9.73	12.12	15.46	18.27
3.2	5.83	6.43	9.45	12.35	15.20	18.02	3.2	5.95	6.55	9.69	12.71	15.68	18.62
3.3	5.98	6.35	9.46	12.45	15.39	18.30	3.3	6.09	6.46	9.68	12.78	15.83	18.85
3.4	6.12	6.29	9.48	12.55	15.56	18.54	3.4	6.22	6.40	9.68	12.85	15.96	19.04
3.5	6.23	6.23	9.45	12.54	15.58	18.60	3.5	6.36	6.36	9.71	12.93	16.10	19.25
3.6	6.37	6.19	9.45	12.59	15.68	18.73	3.6	6.47	6.29	9.65	12.89	16.08	19.23
3.7	6.53	6.16	9.46	12.63	15.75	18.84	3.7	6.62	6.25	9.64	12.90	16.11	19.29
3.8	6.73	6.13	9.45	12.64	15.79	18.90	3.8	6.82	6.22	9.63	12.91	16.15	19.35
3.9	7.03	6.08	9.39	12.59	15.73	18.85	3.9	7.10	6.15	9.53	12.80	16.01	19.20

Average value of pK_c^2 between $a=3.2$ and $a=3.8$; His-Gly-Cu(II): 9.46±0.02, His-Gly-Gly-Cu(II): 9.67±0.04.

deprotonation, as shown later. Therefore, the equilibrium constants for the polymer formations were calculated based on Eq. (10), where $L^-=XH^-$.

$$n\mathrm{CuL}^+ \rightleftarrows \mathrm{Cu}_n\mathrm{X}_n + n\mathrm{H}^+$$

$$K_c^n = [\mathrm{Cu}_n\mathrm{X}_n][\mathrm{H}^+]^n/[\mathrm{CuL}^+]^n \qquad (10)$$

Table 2 represents the results of the calculations for pK_c^n, where n is from 1 to 5. The values of pK_c^1 which corresponds to the simple ionization decrease with the increase of the a value, while the values of pK_c^n for the trimer, tetramer, and pentamer increase with the increase of the a value. On the other hand, values of pK_c^2 which are applied to the formation of a dimer remain constant over the wide range. These facts support the presence of a dimer produced by the release of a proton from each CuL^+ complex.

As shown later by visible absorption spectra, further deprotonation in the region where the a value is between 4 and 5 in the HGG–Cu(II) system seems to be accompanied by the formation of an anionic chelate, CuY^-, as well as in the case of glycylglycylglycine.[16] For this deprotonation, the following reaction is assumed, where $YH_2^-=XH^-=L^-$.

$$\mathrm{Cu}_2\mathrm{X}_2 \rightleftarrows 2\mathrm{CuY}^- + 2\mathrm{H}^+$$

$$K_c'^2 = [\mathrm{CuY}^-]^2[\mathrm{H}^+]^2/[\mathrm{Cu}_2\mathrm{X}_2] \qquad (11)$$

The values of $pK_c'^2$ calculated according to Eq. (11) are roughly constant as seen in Table 3. Slight scatter among the values in Table 3 suggests that the deprotonation overlaps to some extent with the preceding deprotonation.

TABLE 3. $pK_c'^2$ CALCULATED ACCORDING TO Eq. (11)

a	pH	$pK_c'^2$
4.1	7.85	20.37
4.2	8.29	20.60
4.3	8.55	20.72
4.4	8.75	20.80
4.5	8.01	20.86
4.6	9.05	20.89
4.7	9.18	20.90
4.8	9.31	20.90
4.9	9.47	20.89

Average value of $pK_c'^2$ between $a=4.4$ and $a=4.9$: 20.87 ± 0.07.

In the reactions mentioned above, the proton is presumed to be liberated from the amide group of the peptide. However, the pH values of the region where the deprotonations occur are rather higher than those in the glycylglycine–Cu(II)[15] and glycylglycylglycine–Cu(II)[16] systems. The difficulty of the deprotonation in HG–Cu(II) and HGG–Cu(II) complexes may be due to the higher stability of the complexes, CuL^+ and Cu_2X_2, because the cleavage and recombination of the coordination bonds are necessary to cause these deprotonations. This structural conversion will be described later. The second deprotonation in the region where the a value is between 4 and 5 is also observed in the HG–Cu(II) system. Since this deprotonation occurs in the high pH region, equilibrium constants could not be determined accurately. The apparent ionization constant, which is the pH value at the half-neutralization point, is 10.00. The proton may be liberated from the imino group of the imidazole ring to give an anionic chelate, $Cu_2Y_2^{2-}$. It has been reported that the deprotonation of imino group occurs at the extremely high pH region in free imidazole and histidine[17] ($pK_a\approx14$). In the HG–Cu(II) complex, it is presumed that the electron-withdrawing effect of Cu(II) which binds to pyridine-type nitrogen of imidazole ring weakens the basicity of imino group.

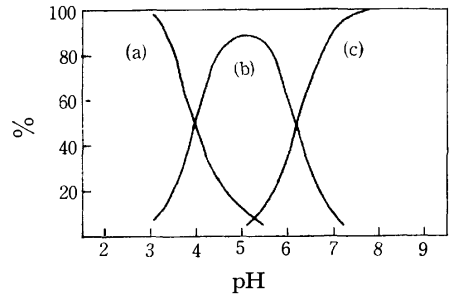

Fig. 3. Distribution of complex species for the 1:1 system of HG and copper(II):
(a) Cu^{2+}, (b) CuL^+, (c) Cu_2X_2.

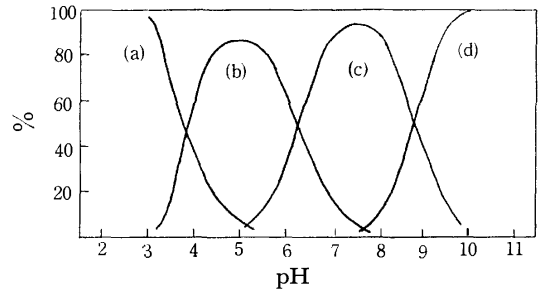

Fig. 4. Distribution of complex species for the 1:1 system of HGG and copper(II):
(a) Cu^{2+}, (b) CuL^+, (c) Cu_2X_2, (d) CuY^-.

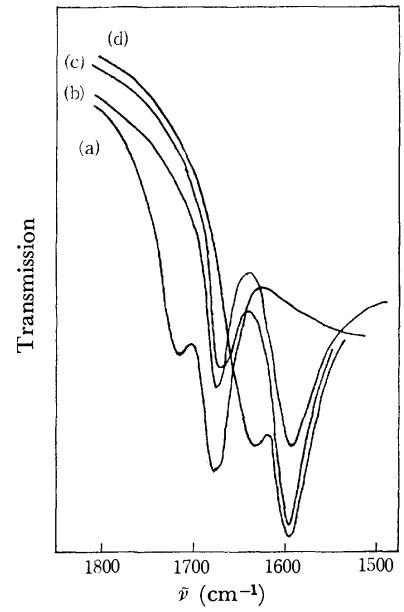

Fig. 5. Infrared spectra of HG in D_2O solutions. $[HG]_T=\sim0.3$ M, (a) HG+2DCl, (b) HG+DCl, (c) HG, (d) HG+NaOD.

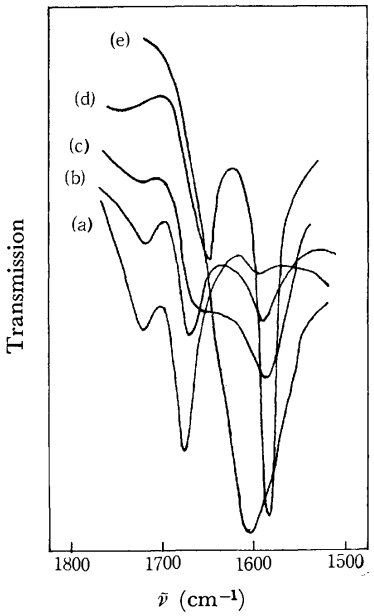

Fig. 6. Infrared spectra of HG–Cu(II) complexes in D_2O solution (1 : 1):
$[HG]_T=[Cu]_T=\sim 0.3$ M, (a) HG+Cu(II)+2DCl, (b) HG+Cu(II)+DCl, (c) HG+Cu(II), (d) HG+Cu(II)+NaOD, (e) HG+Cu(II)+2NaOD.

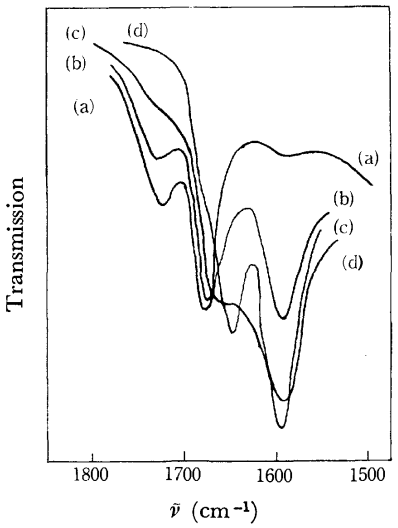

Fig. 7. Infrared spectra of HG–Cu(II) complexes in D_2O solution (2 : 1):
$[HG]_T=\sim 0.3$ M, $[Cu]_T=\sim 0.15$ M,
(a) HG+1/2Cu(II)+2DCl, (b) HG+1/2Cu(II)+ +DCl, (c) HG+1/2Cu(II), (d) HG+1/2Cu(II)+ NaOD.

From the equilibrium constants obtained, the titration curves were re-calculated and they were compared with the experimental curves. Coincidence of both titration curves as seen in Figs. 1 and 2, supports the validity of these constants. Based on the constants, the distribution ratios of various complexes were calculated at various pH. The results shown in Figs. 3 and 4, indicate that main species in the region of pH 5 is a cationic chelate, CuL^+. The distribution ratio for the dimer, Cu_2X_2, increases with the increase of pH and reaches its maximum at the neutral region. In the alkaline region, anionic chelates, $Cu_2Y_2^{2-}$ or CuY^-, are predominant species.

Infrared Absorption Spectra. Infrared absorption spectra of D_2O solutions of HG in the absence and the presence of copper(II) ion were measured in the carbonyl absorption region to provide the information for the copper(II) binding sites. Figure 5 shows the infrared absorption spectra of HG. Figures 6 and 7 show the spectra of the 1 : 1 and 2 : 1 HG–Cu(II) complexes. The carbonyl and carboxylate absorption bands are observed in both spectra. The assignments of these bands were made by reference to those in the infrared absorption spectra of glycine peptides[18] and their Cu(II) complexes.[15,16] The results are given in

Table 4. Carbonyl and carboxylate bands in infrared absorption spectra of HG and its Cu(II) complexes in D_2O solution

System	*a* value	Absorption band cm^{-1} -COOH	-CONH-	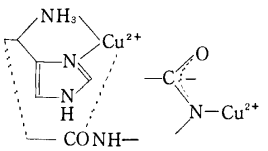	-COO$^-$
HG	0	1720	1680		
	1		1680		1593
	2		1675		1595
	3		1632		1595
HG+Cu(II)	0	1722	1677		1595 (w)
	1	1722	1677	1647 (w)	1595
	2		1670	1647 (sh)	1595
	3			1647	1595
	4			1608	1590 (sh)
HG+½Cu(II)	0	1725	1680		1595 (w)
	1	1725	1680	1647 (w)	1595
	2		1675	1645 (sh)	1595
	3			1645	1595

Table 4. For the convenience of the interpretation of the spectra, a values which are equivalent to those in the titrations are used.

In Fig. 5 two bands assigned to be due to undissociated carboxyl and peptide carbonyl groups respectively are observed at 1720 and 1680 cm^{-1}, in the spectrum before the addition of alkali. In the region where the a is larger than 1, the band of carboxylate appears at 1595 cm^{-1}. The bands at 1675 and 1632 cm^{-1} observed at $a=2$ and $a=3$ respectively, are assigned to the peptide carbonyl group. These shifts of carbonyl band to the lower frequency will be attributed to the deprotonation of imidazole and α-amino groups. The inductive effect of the α-amino group is much stronger than that of imidazole group. The spectral features of HG described above are similar to those of glycylglycine.[18]

In the 1 : 1 HG–Cu(II) system, a new band appears at 1647 cm^{-1} in the region where CuL^+ is predominantly present. This band will be assigned to the peptide carbonyl group in CuL^+. The appearance of the band of carbonyl group at the higher frequency in the complex CuL^+ than in the ligand is worth noticing. In the glycylglycine–Cu(II) system,[15] the band of carbonyl group moves to the lower frequency (1632 $cm^{-1}\rightarrow$ 1625 cm^{-1}). The shift of the carbonyl band may be controlled by two contrastive effects, namely the inductive effect of Cu(II) and the reduction of the bond order of the carbonyl group based on bonding between Cu(II) and carbonyl oxygen. The shift to the higher frequency observed in the HG–Cu(II) system suggests that the latter effect is very weak. This finding is in accord with the conclusion that the peptide carbonyl group does not bind to Cu(II) in the plane. In the 2: 1 HG–Cu(II) system, the same band appears at

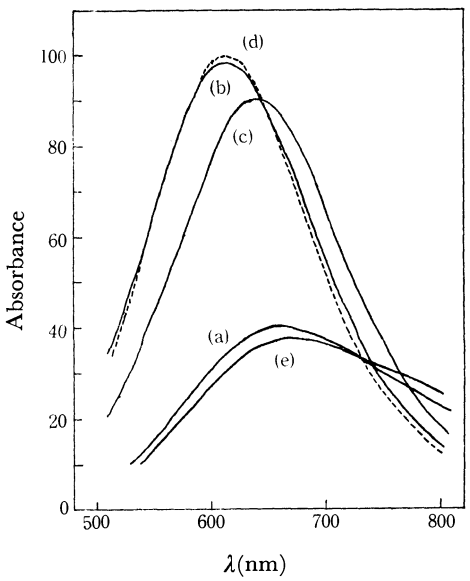

Fig. 8. Electronic spectra of HG–Cu(II) complexes in aqueous solution (1 : 1):
(a) HG+Cu(II)+KOH, (b) HG+Cu(II)+2KOH, (c) GG+Cu(II)+2KOH, (d) GG+Cu(II)+Im+2KOH, (e) His+Cu(II)+KOH.
Absorbance is expressed on a molar copper basis.
GG=glycylglycine, His=L-histidine, Im=imidazole.

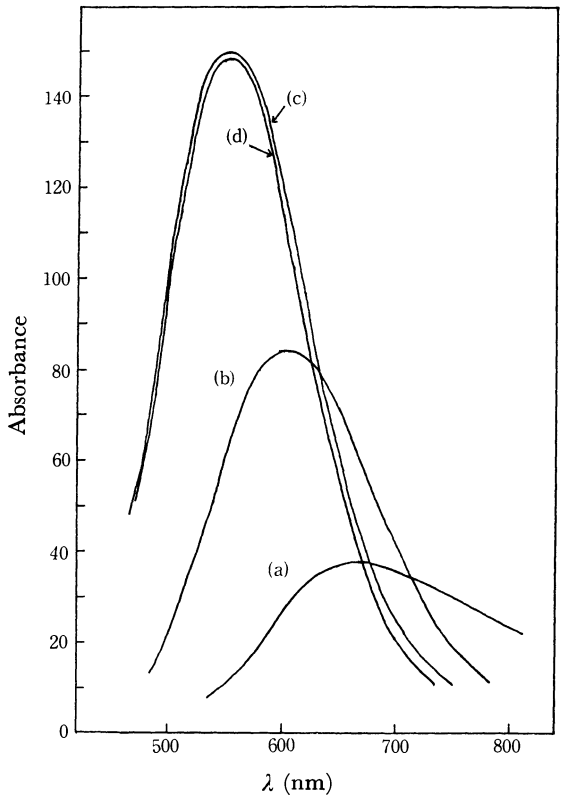

Fig. 9. Electronic spectra of HGG–Cu(II) complexes in aqueous solution (1 : 1):
(a) HGG+Cu(II)+KOH, (b) HGG+Cu(II)+2KOH, (c) HGG+Cu(II)+3KOH, (d) GGG+Cu(II)+3KOH. GGG=glycylglycylglycine.

1645 cm^{-1} in the region where the a value is between 1 and 3 and this band may be attributed to the complexes CuL^+ and CuL_2.

At $a=4$ in the 1 : 1 system, where the dimer, Cu_2X_2, is the predominant species, a new band appears at 1608 cm^{-1} with a shoulder at ~1570 cm^{-1}. The band at 1608 cm^{-1} is assigned to the carbonyl group of the peptide which involves deprotonated peptide nitrogen bound to Cu(II).[15] Accordingly, it is proved that the neutral dimer Cu_2X_2 has metal-peptide nitrogen bonds.

Visible Absorption Spectra. The visible absorption spectra of Cu(II) complexes in solution were studied to provide further evidence for the structures of the species formed in solution. Figures 8 and 9 show the spectra obtained on the solutions of 1 : 1 ligand–Cu(II) systems. For the convenience of the interpretation of the spectra a values which are equivalent to those in the titrations are used. The absorption spectra of the HG–Cu(II) and HGG–Cu(II) systems at $a=3$ are similar to the absorption spectrum of histidine–Cu(II) system. This observation suggests that the coordination structures of these complexes are similar each other. Consequently in this region, HG and HGG seem to bind to copper(II) through the nitrogen atoms of amino and imidazole group, as also presumed from the results of the titrations and infrared spectra. The structure of CuL^+ is given by **I**.

In the HG–Cu(II) system a shift of the absorption maximum to the shorter wavelength with a remarkable

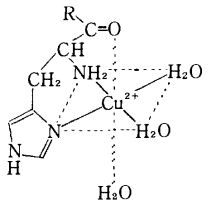

(I)

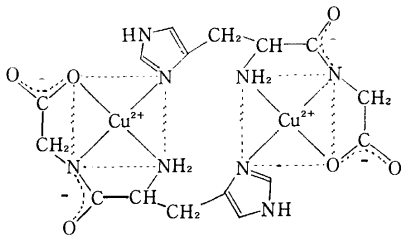

(II)

(I), CuL^+, $R=NHCH_2COO^-$: HG-Cu(II)
$R=NHCH_2CONHCH_2COO^-$: HGG-Cu(II)
(II), Cu_2X_2, HG-Cu(II)

increase of the absorbance was observed when the a value increases from 3 to 4. An absorption maximum appears at 613 nm ($\varepsilon=99$). This spectral change suggests the coordination of the copper(II) to the peptide nitrogen with a displacement of the proton and the formation of a neutral chelate, similar to glycylglycine–Cu(II) complex. However, it is noteworthy that the absorption maximum is observed at the shorter wavelength and the absorbance is larger than that in the case of glycylglycine–Cu(II) system (Fig. 8). These spectral features of HG–Cu(II) complex can be explained in terms of the following assumption. One imidazole group dissociates from the copper(II) with the deprotonation of the peptide amide group and then occupies the fourth coordination position of another copper atom to form a polymer. This structural change is reasonable from the molecular model, because the simultaneous coordination of one copper(II) ion to the nitrogen atoms of amino, imidazole, and deprotonated amide groups in one molecule of peptide are sterically unfavorable. The coordination of the imidazole group of the other molecule to the fourth position will form a somewhat stronger ligand field around copper(II) ion than in the case of the glycylglycine–Cu(II) complex. Consequently, the absorption maximum appears at the shorter wavelength than in glycylglycine–Cu(II) complex. The larger absorbance may be attributed to the steric strain caused by the coordination of the imidazole group. The structural change mentioned above leads to the formation of a polymer through imidazole group. The formation of a dimer is already indicated by the quantitative analysis on the results of the potentiometric titrations. The absorption spectrum of the 1 : 1 : 1 solution of glycylglycine, copper(II) ion and imidazole agrees with that of the HG–Cu(II) system. This agreement suggests the similarity of the coordination structures of both systems and supports the assumption mentioned above strongly.

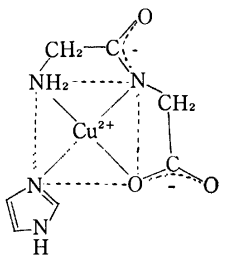

(III), GG-Cu(II)-Im

The structures for the HG–Cu(II) and glycylglycine–Cu(II)–imidazole complexes are given by **II** and **III**. It is interesting that the dimer structure is also proposed in β-alanyl-L-histidine–Cu(II) complex.[1]

In the HGG–Cu(II) system, similar spectral features are observed at $a=4$ (Fig. 9). Therefore, similar dimer complex seems to form in this region, as shown by **IV**.

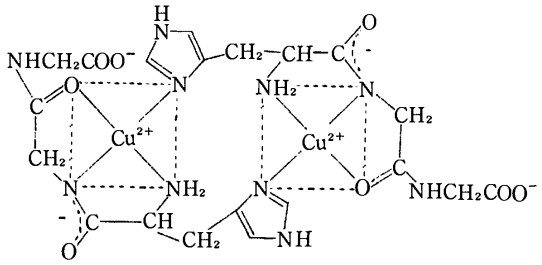

(IV), Cu_2X_2, HGG-Cu(II)

In this system, further shift of the absorption maximum to the shorter wavelength with a remarkable increase of the absorbance is observed where the a value is larger than 4. The spectrum at $a=5$ shows the absorption maximum at 555 nm ($\varepsilon=150$) and is similar to that of the 1 : 1 glycylglycylglycine–Cu(II) system under the same condition. This fact suggests that in this region the dimer is decomposed with the dissociation of the hydrogen of the second peptide amide group to form an anionic chelate, CuY^-, similar to the 1 : 1 glycylglycylglycine–Cu(II) complex.[16] The structure of CuY^- can be represented by **V**.

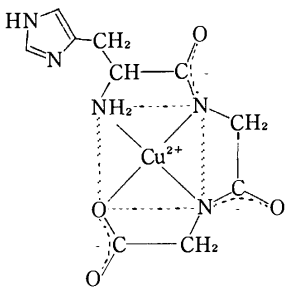

(V), CuY^-, HGG-Cu(II)

The authors wish to express their thanks to Dr. K. Machida, Kyoto University, for his helpful advices in IR measurements, to the staff of the Kyoto University Computer Center for the use of FACOM 203-60 Computer, and to the members of the Micro Analytical Center of Kyoto University for elemental analysis.

References

1) H. C. Freeman and J. T. Szymanski, *Acta Crystallogr.*, **22**, 406 (1967).
2) M. Ihnat and R. Bersohn, *Biochemistry*, **9**, 4555 (1970).
3) G. R. Lenz and A. E. Martell, *ibid.*, **3**, 750 (1964).
4) R. F. Pasternack and K. Kustin, *J. Amer. Chem. Soc.*, **90**, 2295 (1968).
5) J. F. Blount, K. A. Fraser, H. C. Freeman, J. T. Szymanski, and C. H. Wang, *Acta Crystallogr.*, **22**, 396 (1967).
6) P. J. Morris and R. B. Martin, *J. Inorg. Nucl. Chem.*, **33**, 2913 (1971).
7) R. Osterberg, B. Sjöberg, and R. Söderquist, *Chem. Commun.*, **1972**, 983.

8) M. A. Doran and A. E. Martell, *J. Amer. Chem. Soc.*, **86**, 2129 (1964).
9) A. Levitzki, I. Pecht, and A. Berger, *ibid.*, **94**, 6844 (1972).
10) F. R. N. Gurd and G. F. Bryce, "The Biochemistry of Copper," ed. by J. Peisach, P. Aisen, and W. Blumberg, Academic Press, Inc., New York (1966), pp. 115—130.
11) E. W. Wilson, Jr., M. H. Kasperian, and R. B. Martin, *J. Amer. Chem. Soc.*, **92**, 5365 (1970).
12) G. F. Bryce, R. W. Roeske, and F. R. N. Gurd, *J. Biol. Chem.*, **240**, 3837 (1965).
13) A. Yokoyama, H. Aiba, and H. Tanaka, This Bulletin, **47**, 112 (1974).
14) A. Yokoyama, H. Aiba, and H. Tanaka, *Chem. Lett.*, **1972**, 489.
15) M. K. Kim and A. E. Martell, *Biochemistry*, **3**, 1169 (1964).
16) M. K. Kim and A. E. Martell, *J. Amer. Chem. Soc.*, **88**, 914 (1966).
17) G. Yagil, *Tetrahedron*, **23**, 2855 (1969).
18) M. K. Kim and A. E. Martell, *J. Amer. Chem. Soc.*, **85**, 3080 (1963).

The Chlorobromination of Olefins with Antimony (III and V) Chlorides

Sakae UEMURA,* Akira ONOE, and Masaya OKANO
Institute for Chemical Research, Kyoto University, Uji, Kyoto 611
(Received June 5, 1973)

By the reaction of olefins with equimolar mixtures of $SbCl_5$ and Br_2 or LiBr, and of $SbCl_3$ and Br_2, in carbon tetrachloride, various bromochloroalkanes were obtained in good yields. The mixtures of certain metal chlorides of the Lewis acid type (*e.g.*, $FeCl_3$, $SnCl_4$, and $TiCl_4$) and Br_2 could also be used as chlorobrominating agents, but these mixtures were found to be inferior to the $SbCl_5$–Br_2 mixture in product selectivities.

The *in situ* formation of ICl and its addition to olefins, by the use of mixtures consisting of certain metal chlorides (*e.g.*, AgCl, $HgCl_2$, CuCl, *etc.*) and I_2

$$MCl_n + I_2 \longrightarrow MCl_{n-1}I + ICl \quad (1)$$

[Eq. (1)], have been known for a long time.[1] Baird *et al.* have recently found a more efficient system containing $CuCl_2$, in which the oxidation of the iodide anion with the copper(II) salt is involved and a com-

$$2CuCl_2 + I_2 \longrightarrow 2CuCl + 2ICl \quad (2)$$

plete utilization of I_2 is achieved [Eq. (2)].[2] A similar chlorobromination using the $CuCl_2$–Br_2 mixture, however, appears to be less satisfactory in yield and product selectivity.[2b] Though a mixture of bromine and chlorine has also been used as a source of BrCl, the reported yields of bromochloroalkanes are not very high.[3] During the studies of halogenation reactions with $SbCl_5$, we have found convenient new chlorobrominating agents consisting of $SbCl_5$ or $SbCl_3$ and Br_2. When various olefins were treated with these equimolar mixtures in carbon tetrachloride, bromochloroalkanes were obtained in good yields, just as when the mixture of *N*-bromoacetamide and hydrogen chloride was used.[4] This paper will describe some results of mixed halogenations with these metal chloride–halogen mixtures.

Results and Discussion

The reaction of cyclohexene with an equimolar mixture of $SbCl_5$ and Br_2 in carbon tetrachloride was completed at room temperature within a few minutes. Some other metal chlorides which were soluble in carbon tetrachloride were also examined as chloride components under somewhat different reaction conditions. In these reactions, *trans*-1-bromo-2-chlorocyclohexane was generally obtained in good yields, together with smaller amounts of *trans*-1,2-dibromocyclohexane. All the results are given in Table 1a. As can be seen from the table, the $SbCl_5$–Br_2 mixture in carbon tetrachloride was found to be superior to the other ones in yield and in product selectivity. Dichloroethane could be used as an effective solvent, but the use of carbon disulfide resulted in less satisfactory results (compare Runs 1—3 in Table 1a).

When $SbCl_5$ was used as a chloride component, nearly two moles of the bromochloride were formed from one mole of Br_2; hence, the stoichiometry of the reaction is given by Eq. (3).

$$2C_6H_{10} + SbCl_5 + Br_2 \longrightarrow 2C_6H_{10}BrCl + SbCl_3 \quad (3)$$

Here, the generation of two moles of BrCl can be rationalized by assuming the following successive re-

$$SbCl_5 + Br_2 \rightleftharpoons BrCl + SbCl_4Br \quad (4)$$

$$SbCl_4Br \rightleftharpoons BrCl + SbCl_3 \quad (5)$$

actions [Eqs. (4) and (5)]. Since the BrCl formation of the former type is similarly observed for certain metal chlorides (see below), the presumed participation of Eq. (4) may not be unreasonable. The latter reductive dissociation may be anticipated from the favorable reduction potential of Sb(V)[5] and facilitated by the presence of the more electropositive bromine atom in the ligands,[6] but the reverse reaction does not seem to be easy. Thus, the overall reaction [(4)+(5)] would be highly in favor of the BrCl formation. In connection with this a similar observation has been reported in the literature[7] that $SbCl_5$ reacted with I_2 to afford ICl and $SbCl_3$ and that no isolation of $SbCl_4I$ was achieved. Another possibility, that of BrCl formation from Br_2 and Cl_2 (liberated from $SbCl_5$), can be excluded, because Cl_2 generation has not been observed in the chlorination of olefins with $SbCl_5$ under similar reaction conditions.[8]

Though the *in situ* formation of BrCl in this reaction is highly probable, as has been described above, its attacking form is not decisive. The following observation, however, appears to suggest that the attacking entity is the BrCl molecule itself (probably somewhat activated by $SbCl_5$ or $SbCl_3$). In the competitive bromination of benzene and toluene with the $SbCl_5$–Br_2 mixture under the same conditions (in CCl_4 at 25 °C), a considerably high selectivity (k_T/k_B value) was observed;[9] this selectivity was slightly less than that for the attack of the Br_2 molecule itself.

On the other hand, when other metal chlorides of the Lewis acid type, such as $FeCl_3$, $SnCl_4$, and $TiCl_4$, were used as chloride components, nearly one (but not more than one) mole of the mixtures of the bromochloride and dibromide, with the amount of the former being dominant, were obtained from one mole of Br_2 (Runs 4—6 in Table 1a). Further, in the halogenation with the $FeCl_3$–Br_2 mixture, it was confirmed that the reaction was accompanied by almost no reduction of the Fe(III) cation (<10% by iodometry). The oxidations of Br^- with the above metal chlorides (except for $SbCl_5$) were also not observed appreciably (see below). These results seem natural because of the very low reduction potentials of the metal cations. The *in situ* BrCl formation was similarly observed even in the case

Table 1. Chlorobromination and chloroiodination of cyclohexene in carbon tetrachloride
cyclohexene (100 mmol)

Run	Metal chloride mmol	Halogen donor mmol	Solvent ml	Temp. °C	Time min	Products[a] Chlorohalide mmol (yield[b] %; selectivity %)	Other halide mmol
	(a) Chlorobromination						
1	$SbCl_5$ 25	Br_2 25	100	30	5	47.9 (96; 98)	diBr 0.4; diCl 0.6
2	$SbCl_5$ 25	Br_2 25	100[c]	30	5	46.5 (93; 97)	diBr 0.9; diCl 0.5
3	$SbCl_5$ 25	Br_2 25	100[d]	30	5	42.9 (86; 89)	diBr 5.3; diCl 0.1
4	$FeCl_3$ 50	Br_2 25	150	76	10	17.6 (70; 72)	diBr 7.0
5	$SnCl_4$ 50	Br_2 25	100	25	5	21.6 (86; 87)	diBr 3.2
6	$TiCl_4$ 50	Br_2 25	100	5	10	18.8 (75; 75)	diBr 6.2
7	$SbCl_3$ 50	Br_2 25	100	76	10	20.0 (80; 82)	diBr 4.4
8	$SbCl_3$ 52	Br_2 50	100	76	10	31.7 (63; 71)	diBr 13.0
9	$SbCl_5$ 25	LiBr 12.5	150	76	5	6.1 (49; 32)	diCl 12.9
10	$SbCl_5$ 25	LiBr 25	150	76	5	20.3 (81; 95)	diCl 1.2
11	$SbCl_5$ 25	LiBr 37.5	150	76	5	14.1 (56; 94)	diBr 1.0
12	$FeCl_3$ 50	LiBr 50	150	76	60	1.2 (2)	—
	(b) Chloroiodination						
	$SbCl_5$ 25	I_2 25	200	76	10	47.0 (94)[e]	
	$SnCl_4$ 25	I_2 25	100	76	10	23.7 (95)[e]	
	$SbCl_3$ 50	I_2 50	300	76	180	36.8 (74)[e]	
	$SbCl_5$ 25	LiI 27	100	76	10	23.4 (94)[e]	

a) Yields were determined by glc.
b) Based on Eq. 3 for $SbCl_5$–Br_2 couple, Eq. 7 for MCl–Br_2 couple, and Eq. 9 for $SbCl_5$–LiBr couple, respectively.
c) Solvent, dichloroethane.
d) Solvent, carbon disulfide.
e) Isolated yield.

of a low-valence compound, $SbCl_3$ (see Runs 7 and 8). Thus, it seems very likely that BrCl is formed by the

$$MCl_n + Br_2 \rightleftharpoons BrCl + MCl_{n-1}Br \quad (6)$$

halogen exchange reaction [Eq. (6)], though no direct evidence for the formation of the mixed metal halide is available at present. Since it is known that all these metal chlorides have a considerable affinity for Cl^-,[10] this transformation may proceed *via* an ionic adduct intermediate, *e.g.*, $Br^+[FeCl_3Br]^-$. The stoichiometry of the halogenation using the mixtures of these metal chlorides and Br_2 may be expressed by Eq. (7).

$$C_6H_{10} + MCl_n + Br_2 \longrightarrow C_6H_{10}BrCl + MCl_{n-1}Br \quad (7)$$

The formation of the by-product, *trans*-1,2-dibromocyclohexane, can be explained in terms of the attack of Br_2, which is equilibrated [*cf.* Eq. (6)].

Furthermore, when various metal chlorides were mixed with LiBr in carbon tetrachloride and the mixtures (slightly heterogeneous, probably because of the lower solubility of the LiCl formed) were treated with cyclohexene, no significant red-coloration (due to the generation of BrCl) and no, or only a slight, formation of 1-bromo-2-chlorocyclohexane was observed, except only for the case of $SbCl_5$ (see Runs 9—12 in Table 1a). In the $SbCl_5$–LiBr system, the use of an equimolar mixture of both salts was required for the chlorobromination. Perhaps the BrCl[11] may arise from the mixed pentahalide formed by means of Eq. (8) and

$$SbCl_5 + LiBr \rightleftharpoons Li^+[SbCl_5Br^-] \rightleftharpoons LiCl + SbCl_4Br \quad (8)$$

$$SbCl_4Br \rightleftharpoons BrCl + SbCl_3 \quad (5)$$

$$C_6H_{10} + SbCl_5 + LiBr \longrightarrow C_6H_{10}BrCl + SbCl_3 + LiCl \quad (9)$$

the stoichiometry of the reaction may be represented by Eq. (9). Excess $SbCl_5$ caused a considerable formation of *cis*- and *trans*-1,2-dichlorocyclohexanes as by-products,[8] and excess LiBr resulted in contamination with the dibromide [see Eq. (10)]. In addition, the use of KBr instead of LiBr was not successful because of its lower solubility in the solvent.

$$BrCl + LiBr \rightleftharpoons Br_2 + LiCl \quad (10)$$

The method using $SbCl_5$ or $SbCl_3$ as a chloride source was found to be applicable to the chloroiodination of olefins. The data for cyclohexene are given in Table 1b. Though somewhat severe reaction conditions were required as compared to those in the chlorobromination, the yield was satisfactory. Both our results and Baird's data show that, in the chlorobromination, some competitive bromination always occurred, the quantity depending on the combination of metal chlorides and bromine, whereas in the chloroiodination no competitive iodination was observed. Such trends may be reasonably explained by differences in the reactivities between halogens and interhalogens (reported relative rates for the addition to olefins in acetic acid:[12] BrCl: Br_2=400: 1, ICl: I_2=10^5: 1). The use of $SnCl_4$ instead of $SbCl_5$ or $SbCl_3$ was also successful, but the system containing $FeCl_3$ was ineffective.

The chlorobromination of various olefins other than

Table 2. Chlorobromination of various olefins in carbon tetrachloride
olefin (50—100 mmol); halogenating agent A, $SbCl_5$ (25 mmol)+Br_2(25 mmol), B, $SbCl_3$ (50—100 mmol)+Br_2(50 mmol); solvent (100—200 ml)

Olefin	Halogenating agent	Temp. °C	Time min	Product (yield %)[a]	
$C_6H_{13}CH=CH_2$	B	76	10	$C_6H_{13}CHClCH_2Br$(I) $C_6H_{13}CHBrCH_2Cl$(II)	(73)[b,c]
$C_6H_5CH=CH_2$	B	0	10	$C_6H_5CHClCH_2Br$	(87)
trans-$C_6H_5CH=CHC_6H_5$	A	45	10	$C_6H_5CHClCHBrC_6H_5$	(74)[d]
$CH_2=CHOAc$	A	5	10	$CH_2BrCHCl(OAc)$	(79)
trans-$C_6H_5CH=CHCOOEt$	A	76	10	$C_6H_5CHClCHBrCOOEt$	(73)[d]
$CH_2=CHCH_2Cl$	B	76	10	$CH_2ClCHBrCH_2Cl$(I) $CH_2BrCHClCH_2Cl$(II)	(71)[e]
$CH_2=CHCH_2Br$	B	76	10	$CH_2ClCHBrCH_2Br$(I) $CH_2BrCHClCH_2Br$(II)	(83)[e]
cis-CHCl=CHCl	A	76	60	$CHClBrCHCl_2$	(77)
trans-CHCl=CHCl	A	76	60	$CHClBrCHCl_2$	(75)
cis-EtOOCCH=CHCOOEt	A	76	60	EtOOCCHBrCHClCOOEt	(52)[f]
trans-EtOOCCH=CHCOOEt	A	76	60	EtOOCCHBrCHClCOOEt	(66)[d]

a) Isolated yield.
b) I: II=7: 3 (glc, Gorey column (BDS, 90 m)).
c) By-product, dibromide (20%).
d) *erythro*.
e) I: II=*ca.* 7: 3 (IR).
f) *threo*.

cyclohexene was easily achieved by the use of mixtures of $SbCl_5$ or $SbCl_3$ and Br_2. Unsymmetrical olefins, such as 1-octene and allyl chloride or bromide, yielded mixtures of the Markownikov and *anti*-Markownikov adducts. 1-Octene afforded the former adduct predominantly, while the reverse was found for allyl halides. Such an abnormal orientation has also been found in the reaction of allyl halides with HOCl; it can be explained by neighbouring group participation.[13] Styrene, vinyl acetate, and ethyl cinnamate gave only products in accordance with Markownikov's rule, as anticipated on the basis of electronic and steric effects. For certain olefins, the $SbCl_3$–Br_2 mixture would be useful—*e.g.*, the use of $SbCl_5$ resulted in a decrease in the product selectivity in the reaction with 1-octene and a considerable formation of a tarry product in the reaction with styrene.

Experimental

Materials. All the organic starting materials, including the solvents, were distilled before use. Commercial metal halides, Br_2, and I_2 (best grade) were used without further purification.

Reaction of Cyclohexene with Metal Chlorides and Bromine Donors. To a nearly homogeneous solution of a metal chloride (25 or 50 mmol) and Br_2 or LiBr (25 or 50 mmol) in CCl_4 (100 or 150 ml), cyclohexene (100 mmol) was gradually added at the prescribed temperature. After stirring was continued for a definite period, the reaction mixture was treated with water, and the inorganic precipitate thus formed was removed by filtration. The CCl_4 layer was separated from the aqueous one, and the solvent was evaporated. A liquid fraction boiling at 91—95 °C/17 mmHg was collected; it consisted of *trans*-1-bromo-2-chlorocyclohexane and *trans*-1,2-dibromocyclohexane, and occasionally also *cis*- and *trans*-1,2-dichlorocyclohexanes. The structural confirmation of these products was made by a comparison of the NMR spectra with those reported in the literature.[14] The composition of the above fraction was determined by means of the glc analysis [apparatus, Shimadzu 5APTF; columns, PEG 6000 (25%)-Chromosorb W(3m), Silicon D.C. 550 (25%)-Shimalite (3m), and Apiezon L(30%)-Celite (1m); carrier gas, N_2].

Syntheses of Bromochloroalkanes and Chloroiodoalkane. Several examples are given below.

1-Acetoxy-1-chloro-2-bromoethane. Vinyl acetate (8.6 g, 100 mmol) was added drop by drop to a mixture of $SbCl_5$ (7.5 g, 25 mmol) and Br_2 (4.0 g, 25 mmol) in CCl_4 (100 ml) near 5 °C. Stirring was continued for 10 min at that temperature, after which the reaction mixture was worked-up as has been described above. Distillation gave the chlorobromide (8.0 g, 39.4 mmol) in a 79% yield; bp 64—65 °C/10 mmHg. NMR: τ 3.45 (t, 1H), 6.25 (d, 2H), 7.84 (s, 3H).

Found: C, 23.90; H, 3.01; Br, 39.30; Cl, 17.43%. Calcd for $C_4H_6BrClO_2$: C, 23.85; H, 3.00; Br, 39.66; Cl, 17.59%.

Diethyl erythro- *and* threo-*α-Bromo-β-chlorosuccinate.* The procedure was the same as that described for vinyl acetate except that the reaction temperature and time were 76 °C and 60 min respectively. From diethyl fumarate (8.6 g, 50 mmol), the *erythro* isomer of diethyl α-bromo-β-chlorosuccinate was obtained in a 66% yield (based on $SbCl_5$ used); bp 121—122 °C/6 mmHg. NMR: τ 5.30—5.40 (m, 2H), 5.72 (q, J=7.5 Hz, 4H), 8.69 (t, J=7.5 Hz, 6H).

Found: C, 33.09; H, 4.08; Br, 28.12; Cl, 12.47%. Calcd for $C_8H_{12}BrClO_4$: C, 33.42; H, 4.21; Br, 27.79; Cl, 12.33%.

In addition, when this ester (5.0 g, 17.4 mmol) was treated with Zn (10.0 g, 154 mmol) (a reagent for specific *trans*-dehalogenation) in boiling ethanol for 5 hr, only the original fumarate was formed as a product (70%).

In a similar way, the *threo* ester was obtained from diethyl maleate in a 52% yield; bp 123—124 °C/9 mmHg. NMR: τ 5.30 (s, 2H), 5.75 (q, J=7.5 Hz, 4H), 8.70 (t, J=7.5 Hz, 6H).

Found: C, 33.73; H, 4.28; Br, 27.54; Cl, 12.20%. Calcd for $C_8H_{12}BrClO_4$: C, 33.42; H, 4.21; Br, 27.79; Cl, 12.33%.

1-Chloro-1-phenyl-2-bromoethane. To a stirred solution

of $SbCl_3$ (11.4 g, 50 mmol) and Br_2 (8.0 g, 50 mmol) in CCl_4 (200 ml), styrene (10.4 g, 100 mmol) was added, drop by drop so that the temperature remained near 0 °C. After stirring had been continued for an additional 10 min, the reaction mixture was worked-up as before. Distillation afforded the chlorobromide (9.6 g, 43.7 mmol) in an 87% yield; bp 85—86 °C/2 mmHg (lit,[4] 95—99 °C/3.5 mmHg). The structure was confirmed by a comparison of its IR spectrum with that of an authentic sample prepared from styrene, *N*-bromoacetamide, and HCl.[4]

1,2-Dibromo-3-chloropropane (1) and 1,3-Dibromo-2-chloropropane (2). When allyl bromide (12.1 g, 100 mmol) was treated similarly with a CCl_4 solution (100 ml) containing $SbCl_3$ and Br_2 at the refluxing temperature, a mixture of two isomeric dibromomonochloropropanes (**1** and **2**) was obtained in an 83% yield; bp 94—97 °C/26 mmHg. IR: 725 (s), 650 (m), 627 (m), 610 (m), 568 cm^{-1} (s). The ratio of **1** and **2** was determined by comparisons of the IR spectrum with those of mixtures of a known composition; it was found to be *ca.* 7: 3. Here, an authentic sample of **1** was prepared from allyl chloride and bromine (bp 84.5—85 °C/18 mmHg [IR: 725 (s), 650 (m), 568 cm^{-1} (s)]), while the authentic sample of **2** was prepared by the chlorination of 1,3-dibromopropan-2-ol with PCl_5 (bp 84—85 °C/18 mmHg [IR: 722 (m), 623 (s), 609 (s), 568 cm^{-1} (m)]).

Some physical data on the other chlorobromide, which was a new compound are given below.

erythro-*1-Carboethoxy-1-bromo-2-chloro-2-phenylethane.* Bp 116—117 °C/11 mmHg. NMR: τ 2.63 (s, 5H), 4.22 (d, 1H), 5.38 (d, 1H), 5.67 (q, 2H), 8.66 (t, 3H).

Found: C, 45.61; H, 4.12; Br, 27.19; Cl, 12.06%. Calcd for $C_{11}H_{12}BrClO_2$: C, 45.31; H, 4.15; Br, 27.40; Cl, 12.16%.

trans-*1-Chloro-2-iodocyclohexane.* To a boiling CCl_4 solution (200 ml) containing $SbCl_5$ (7.5 g, 25 mmol) and I_2 (6.3 g, 25 mmol), cyclohexene (8.2 g, 100 mmol) was added gradually. After stirring had been continued for an additional 10 min, the reaction mixture was worked-up as before with water. The yield of the chloroiodide (11.5 g, 47.0 mmol) was 94%; bp 49—50 °C/1 mmHg (lit,[2a] 37 °C/0.2 mmHg).

References

1) A brief summary is included in Ref. 2a.

2) (a) W. C. Baird, Jr., J. H. Surridge, and M. Buza, *J. Org. Chem.*, **36**, 2088 (1971). (b) W. C. Baird, Jr., J. H. Surridge, and M. Buza, *ibid.*, **36**, 3324 (1971).

3) *E.g.*, R. E. Buckles, J. L. Forrester, R. L. Burham, and T. W. McGee, *ibid.*, **25**, 24 (1960).

4) R. E. Buckles and J. W. Long, *J. Amer. Chem. Soc.*, **73**, 998 (1951).

5) "Handbook of Chemistry and Physics", 39th ed., ed. by C. D. Hodgman, Chemical Rubber Pub. Co., Cleveland, Ohio (1957—58), p. 1637.

6) The known mixed pentahalides of antimony are limited to only a few chlorofluorides ($SbCl_3F_2$, $SbCl_2F_3$, and $SbCl_4F$). Further, considerable thermal stabilities of SbF_5 and $SbCl_5$ are known, but the existence of $SbBr_5$ is unknown. See F. A. Cotton and G. Wilkinson, "Advanced Inorganic Chemistry", 3rd ed., Interscience, London (1972), p. 376 and 377.

7) A. W. Mellor, "A Comprehensive Treatise on Inorganic and Theoretical Chemistry", vol. 9, Longsman, London (1929), p. 487.

8) S. Uemura, A. Onoe, and M. Okano, This Bulletin, in press.

9) S. Uemura, A. Onoe, and M. Okano, This Bulletin, **47**, 147 (1974).

10) (a) M. Baaz, V. Gutmann, and J. R. Msaaguer, *Monatsh. Chem.*, **92**, 582, 590 (1961). (b) Ref. 6, p. 375.

11) A similar ICl formation from $SbCl_5$ and KI was already reported (see Ref. 7, p. 488).

12) E. P. White and P. W. Robertson, *J. Chem. Soc.*, **1939**, 1509.

13) P. B. D. de la Mare and R. Bolton, "Electrophilic Additions to Unsaturated Systems", Elsevier, Amsterdam (1966), p. 94.

14) H. W. van Dort and Th. J. Sekuur, *Tetrahedron Lett.*, **1963**, 1301.

Aromatic Bromination and Iodination with Mixtures of Antimony(V) Chloride and Halogens

Sakae UEMURA,* Akira ONOE, and Masaya OKANO
Institute for Chemical Research, Kyoto University, Uji, Kyoto 611
(Received June 5, 1973)

Equimolar mixtures of $SbCl_5$ and Br_2 or I_2 were found to be elegant reagents for the halogenation of certain aromatic substrates. In carbon tetrachloride, halogenobenzenes afforded the corresponding bromo- and iodo-derivatives with high *para*-selectivities (more than 95%) in good yields. The bromination of aromatic compounds with deactivating groups, such as ethyl benzoate and nitrobenzene, was simply achieved in 1,2-dichloroethane. Based on competitive halogenation data, the attack of BrCl or ICl (both formed *in situ*) on aromatics has been suggested.

Though aromatic halogenation with elementary halogens has been thoroughly investigated from the synthetic and mechanistic points of view, little is known about the halogenation by means of mixed halogens. The synthetic usage of ICl[1] for aromatic iodination and that of IBr[2] or BrCl (*in situ*)[3] for bromination are discussed in the literature, but the given examples are limited to reactive substrates, such as phenols and aromatic amines. Recently, a new aromatic iodination using copper(II) chloride–iodide donor (*e.g.*, I_2, AlI_3, or $FeI_2 \cdot 4H_2O$) mixtures has been reported by Baird and Surridge,[4] though the formation of ICl as a potent iodinating agent as not definitely stated. In a previous paper,[5] we reported the mixed halogenation of olefins with ICl or BrCl formed *in situ* by the interaction of antimony(V) chloride and halogens. When this system was applied to aromatic substrates in carbon tetrachloride or 1,2-dichloroethane, aryl bromides and iodides were obtained in good yields even from less-reactive aromatics. The present paper will describe some characteristics of this reaction.

Results and Discussion

The treatment of aromatic compounds with equimolar mixtures of $SbCl_5$ and halogens (Br_2 or I_2) in chlorinated solvents afforded the corresponding aryl bromides and iodides with ease. Aromatic compounds bearing an activating group were readily brominated at 25 °C and iodinated at the refluxing temperature, both in carbon tetrachloride, with high yields. In the cases of less-reactive aromatic compounds (*e.g.*, ethyl benzoate and nitrobenzene), the use of a more polar solvent such as 1,2-dichloroethane was revealed to be preferable. In the bromination of acetophenone, three equivalents of $SbCl_5$ (to Br_2) were used, since the formation of a complex with ketone was expected, as in the case of $AlCl_3$ catalyst.[6] All the results are summarized in Table 1.

In these halogenations, more than one (nearly two) moles of aryl halides were generally formed from one mole of the halogenating agent; thus, the reaction appeared to occur in accord with the stoichiometry

$$2ArH + SbCl_5 + X_2 \longrightarrow 2ArX + SbCl_3 + 2HCl \quad (1)$$
$$(X = Br \text{ or } I)$$

shown by Eq. (1). Here, the net oxidation of X^- with $SbCl_5$ is involved, and the complete utilization of halogens is achieved. The $SbCl_5$–LiX mixture was also revealed to be effective as a halogenating agent, but the yields of halogenated compounds were somewhat unsatisfactory [see Runs 16, 17, and 26 in Table 1 and Eq. (2)].

$$ArH + SbCl_5 + LiX \longrightarrow ArX + SbCl_3 + LiCl + HCl \quad (2)$$

As can be seen in Table 1, two marked characteristics noteworthy from the synthetic point of view are found in our halogenation. First, this method may serve as a simple procedure for the bromination of aromatic compounds bearing an electron-withdrawing group. For example, nitrobenzene afforded *m*-bromonitrobenzene in a 63% yield by treating with an equimolar mixture of $SbCl_5$ and Br_2 in 1,2-dichloroethane at 84 °C for 3 hr; ethyl benzoate was similarly brominated (yield, 74%) or iodinated (48%) on refluxing for 3—5 hr in the same solvent. The halogenations of these compounds are usually carried out under drastic conditions; that is, high temperatures and/or stronger electrophilic catalysts are necessary [*e.g.*, for benzoic acid, its ester, and nitrobenzene, the Fe-catalysed bromination (above 140 °C)[7] and the Ag(I) salt-catalysed bromination[8] or iodination[9] (in concentrated HNO_3 or H_2SO_4)]. Further, in the bromination of acetophenone, our method made the preformation of the ketone-Lewis acid complex before bromine addition unnecessary (see Experimental section and compare with the procedure in Reference 6; in CCl_4, yield 86%). Though our iodinating system was found to be more efficient than the $CuCl_2$–iodide system[4] (*e.g.*, for benzene, 76 °C, 0.5 hr, in CCl_4 *vs.* 80 °C, 5 hr, neat), its reactivity did not appear to be high enough. For example, attempts to prepare *m*-iodonitrobenzene and *o*-, *p*-diiodobenzenes were unsuccessful (86 °C, in dichloroethane), and the unreacted aromatics were recovered.

Secondly, this halogenation may provide a convenient method for preparing *p*-dihalogenobenzenes with similar or dissimilar halogen atoms, since the *para*-selectivity of the reaction is quite high. In the bromination of chloro-, bromo-, and fluorobenzenes by a bromine molecule with a Fe- or $AlBr_3$-catalyst, the degree of *para*-substitution has been known to be in the 84—89% range,[10] except only for the Fe-catalysed reaction of fluorobenzene, in which a *para*-selectivity of 98% has been observed.[11] The iodination of

TABLE 1. AROMATIC HALOGENATION BY ANTIMONY(V) CHLORIDE-HALOGEN DONOR COMBINATIONS
$SbCl_5$, 25 mmol; X_2 or LiX 25 mmol; solvent, 100 ml

Run	Substituent in ArH (mmol)	Halogen donor	Solvent	Temp. (°C)	Time (min)	Yield[a] (%)	Isomer distribution of ArX (%)[b]	
							o-	*p*-
	(a) Bromination							
1	CH_3O (100)	Br_2	CCl_4	25	5	86	12	88[c]
2	CH_3O (50)	Br_2	CCl_4	25	5	93	6	94[c]
3	CH_3 (100)	Br_2	CCl_4	25	5	92	38	62[c,d]
4	CH_3 (50)	Br_2	CCl_4	25	5	94	39	61[c]
5	H (50)	Br_2	CCl_4	25	5	88	—	—
6	F (50)	Br_2	CCl_4	76	10	90	1	99
7	Cl (100)	Br_2	CCl_4	76	30	96	8	92
8	Cl (50)	Br_2	CCl_4	76	30	84	4	96
9	Br (100)	Br_2	CCl_4	76	30	91	9	91
10	Br (50)	Br_2	CCl_4	76	30	86	5	95
11	Br (50)	Br_2	$ClCH_2CH_2Cl$	84	30	89	13	87
12	I (50)	Br_2	CCl_4	76	30	88	5	95
13	$COCH_3$	Br_2	CCl_4	35	30	86	only *meta*-	
14	$COOC_2H_5$ (100)	Br_2	$ClCH_2CH_2Cl$	84	180	74	only *meta*-	
15	NO_2 (100)	Br_2	$ClCH_2CH_2Cl$	84	180	63	only *meta*-	
16	CH_3 (100)	LiBr	CCl_4	76	5	75	41	59
17	H (100)	LiBr	CCl_4	76	5	61	—	—
	(b) Iodination							
18	CH_3O (50)	I_2	CCl_4	76	30	75	0	100[c]
19	CH_3 (50)	I_2	CCl_4	76	30	96	58	42[c]
20	H (50)	I_2	CCl_4	76	30	84	—	—
21	F (50)	I_2	CCl_4	76	30	74	2	98
22	Cl (100)	I_2	CCl_4	76	30	70	1	99
23	Br (100)	I_2	CCl_4	76	30	73	0	100
24	Br (50)	I_2	$ClCH_2CH_2Cl$	84	30	62	19	81
25	$COOC_2H_5$ (100)	I_2	$ClCH_2CH_2Cl$	84	300	48	only *meta*-	
26	H	LiI	CCl_4	76	60	22	—	—

a) Isolated yield (based on halogen donor, *cf.* Eqs. 1 and 2).
b) Determined by glc before isolation.
c) Determined also by NMR.
d) No *m*-isomer was formed (confirmed by NMR).
e) No *o*- and *p*-isomers were formed (confirmed by glc).

chloro- and bromo-benzenes with CuI_2–AlI_3 showed *o*/*p* ratios of 18/82 and 0/100 respectively, and the yields were rather low (*ca.* 30%).[4] In contrast to this, the halogenation of halogenobenzenes with $SbCl_5$–X_2 in carbon tetrachloride, where the molar ratio of a halogenobenzene and the halogenating agent was 2:1, showed high selectivities in the *para*-attack (over 95% in bromination and over 98% in iodination). Moreover, the yields were generally good—nearly 85—90% in bromination and 70—75% in iodination. When excess amounts (more than 2 equivalents) of halobenzenes or anisole were used, a decrease in the *para*-selectivity was observed, while in the case of toluene no variation in selectivity was found. Thus, the preferred *para*-substitution might be the result of the coordination between the antimony salt and the hetero atom with lone pairs of electrons in aromatic substrates, which may depress an *ortho*-attack of the halogenating agent for steric reasons.

In order to obtain some information on the attacking species, the competitive halogenations of benzene and toluene were carried out under various conditions. Some data on the relative rate ratio (k_T/k_B) and on the isomer ratio (*o*/*p*) in the halotoluenes formed are shown in Table 2. The k_T/k_B and *o*/*p* ratios for iodination with $SbCl_5$–I_2 in CCl_4 were almost identical with

TABLE 2. COMPETITIVE HALOGENATION
benzene, 250 mmol; toluene, 50 mmol; halogenating agent 12.5 mmol; solvent, 100 ml

Run	Halogenating agent	Solvent	k_T/k_B	*o*/*p* ratio
	(a) Bromination[a]			
1	Br_2+SbCl_5	CCl_4	257	0.69
2	Br_2+SbCl_5	$ClCH_2CH_2Cl$	6.2	1.33
	(b) Iodination[b]			
3	I_2+SbCl_5	CCl_4	105	1.38
4	$ICl+SbCl_5$[c]	CCl_4	107	1.42
5	$ICl+SbCl_3$[c]	CCl_4	160	1.47
6	ICl	CCl_4	248	1.34

a) At 25 °C.
b) At 76 °C.
c) The amount of the catalyst ($SbCl_3$ or $SbCl_5$) was 12.5 mmol.

those for the $SbCl_5$-catalyzed iodination with ICl, while somewhat higher k_T/k_B values were obtained in the $SbCl_3$-catalyzed one. All these k_T/k_B values, however, are of the same order as the reported one (>140, in HOAc) for the $ZnCl_2$-catalyzed iodination with ICl,[12] and they differ greatly from that (2.0, in CH_3CN) for an electrochemical iodination involving the attack of I^+ species.[13] Besides, the obtained k_T/k_B value for the ICl iodination (without catalyst) was considerably higher than those for the catalyzed reactions. Thus, it may be suggested that the formation of ICl *in situ* and the attack of polarized ICl (activated by $SbCl_5$) rather than I^+ are involved in our iodination in CCl_4. As to BrCl, though its formation *in situ* is highly probable, as has been shown previously in the bromochloriantion of olefins using the same halogenating system, a direct confirmation as in the case of ICl was difficult because of the inaccessibility of BrCl in the pure state. In the bromination with $SbCl_5$–Br_2 in CCl_4, however, the observed k_T/k_B and *o*/*p* ratios were similar in magnitude to those (340 and 0.45, respectively) for the uncatalyzed bromination with Br_2 in aqueous HOAc, where the attack of molecular bromine is supposed.[14] On the other hand, when 1,2-dichloroethane was used as a solvent, quite a low k_T/k_B value and a high *o*/*p* ratio were obtained. These values are comparable to those (3.6 and 2.33, respectively) for the $FeCl_3$-catalyzed bromination in CH_3NO_2, where Br^+ is considered to be the attacking species.[15] Thus, the existence of two different attacking species derived from BrCl is feasible, in view of the solvent used; *i.e.*, the attack of polarized BrCl (activated by $SbCl_5$) and Br^+ (probably as an ion-pair). The following facts should be noted here. In the bromination of anisole, the exclusive *para*-substitution has been previously reported in a synthetic procedure (Br_2 bromination in AcOH without catalyst);[16] we confirmed this by glc analysis. On the other hand, our bromination products were contaminated by the *o*-isomer. This can be explained by a higher reactivity of BrCl compared to that of the Br_2 species. In contrast to this, the iodination product was free from the *o*-isomer, as is anticipated from the mild reactivity of ICl.

Experimental

The NMR spectra were determined by means of a Varian A-60 spectrometer in $CDCl_3$, using TMS as the internal standard. Glc analysis was carried out on a Shimadzu 5APTF apparatus, using PEG 6000 (25%)-Chromosorb W (3m) and Apiezon L(30%)-Celite (1m) columns.

Materials. All the organic substrates, including the solvents, were used after distillation, while commercial $SbCl_5$, LiBr, LiI, Br_2, I_2, and ICl of the best grade were used without further purification.

Aromatic Halogenation with $SbCl_5$–Halogen Mixtures. Several examples are given below; they should be synthetically useful.

(a) p-*Dibromobenzene.* To a homogeneous solution of $SbCl_5$ (7.5 g, 25 mmol) and Br_2 (4.0 g, 25 mmol) in CCl_4 (100 ml), bromobenzene (7.9 g, 50 mmol) was added, drop by drop, at 78 °C. Stirring was continued for 30 min. The reaction was accompanied by a considerable evolution of HCl gas, and the dark-red color of the solution disappeared. The reaction mixture was then cooled and treated with water. The inorganic precipitate thus formed was removed by filtration. The organic layer was separated from the aqueous one, and the solvent and unreacted bromobenzene were evaporated. A liquid fraction corresponding to isomeric dibromobenzenes (bp 102—103 °C/22 mmHg) was collected by distillation. The yield was 86% (10.2 g, 43.2 mmol). By a comparison of the retention times on glc with those of authentic samples, the *o*/*p* ratio was found to be 5/95. A single recrystallization from ethanol afforded the pure *p*-isomer; mp 88 °C (lit,[17] 87.3 °C).

(b) m-*Bromoacetophenone.* Acetophenone (6.0 g, 50 mmol) was added to a stirred mixture of $SbCl_5$ (22.5 g, 75 mmol) and Br_2 (4.0 g, 25 mmol) in CCl_4 (100 ml) at 35 °C. After 30 min, the reaction mixture was worked up as has been described above. Subsequent distillation afforded the product (8.6 g, 43.2 mmol) in an 86% yield; bp 92.5—93 °C/4 mmHg (lit,[6] 75—76 °C/0.5 mmHg). NMR: τ 1.98 (m, 4H), 7.49 (s, 3H).

(c) m-*Bromonitrobenzene.* A stirred mixture of $SbCl_5$ (7.5 g, 25 mmol), Br_2 (4.0 g, 25 mmol), and nitrobenzene (12.3 g, 100 mmol) in 1,2-dichloroethane (100 ml) was heated at 84 °C for 3 hr. After the usual work-up procedure, the product was obtained in a 63% yield (6.5 g, 31.6 mmol); bp 136—136.5 °C/22 mmHg (lit,[7b] 117—118 °C/9 mmHg). The absence of the *o*- and *p*-isomers was confirmed by glc analysis.

(d) *Iodobenzene.* To a mixture of $SbCl_5$ (7.5 g, 25 mmol) and I_2 (6.3 g, 25 mmol) in CCl_4 (100 ml), benzene (3.9 g, 50 mmol) was added in small portions at 76 °C. Stirring was then continued for 30 min, after which the reaction mixture was worked-up as before. Distillation afforded iodobenzene in an 84% yield (8.6 g, 42.1 mmol); bp 80—80.5 °C/22 mmHg (lit,[18] 69 °C/15 mmHg).

(e) p-*Bromoiodobenzene.* The procedure was the same as that described for benzene except that the aromatic substrate was used in excess. From bromobenzene (15.7 g, 100 mmol), the corresponding *p*-iodo derivative was obtained in a 73% yield (10.4 g, 36.8 mmol); bp 118.5—119 °C/14 mmHg; mp 92 °C (lit,[19] 92 °C). In addition, glc analysis revealed that no other isomers were formed in this reaction.

(f) *Ethyl* p-*Iodobenzoate.* When ethyl benzoate (15.0 g, 100 mmol) was treated similarly with a 1,2-dichloroethane solution (100 ml) containing $SbCl_5$ and I_2 at the refluxing temperature for 3 hr, the product (5.9 g, 24.1 mmol) was isolated in a 48% yield; bp 93—94 °C/1.5 mmHg (lit,[20] 153.5 °C/14 mmHg).

Competitive Halogenations of Benzene and Toluene. The competitive iodination was carried out as follows; a mixture of benzene (250 mmol) and toluene (50 mmol) was added, drop by drop, to a stirred CCl_4 solution (100 ml) containing $SbCl_5$ (12.5 mmol) and I_2 (12.5 mmol) at 76 °C; the resulting mixture was kept for 30 min at that temperature under stirring. On the other hand, an inverse addition was adopted in the competitive bromination because of its rapid reaction; *i.e.*, a CCl_4 solution (30 ml) of $SbCl_5$ and Br_2 was slowly stirred into a mixture of benzene (250 mmol) and toluene (50 mmol) in CCl_4 (70 ml) at 25 °C, after which the solution was allowed to stand for another 5 min. Both reaction mixtures were then worked up as usual. In both cases, the amounts of halobenzene and isomeric halotoluenes were determined by glc and the *o*/*p* ratio was determined by NMR spectra (the methyl protons of *o*- and *p*-iodotoluene were observed at τ 7.60 and 7.70 respectively, and those of *o*- and *p*-bromotoluene at τ 7.62 and 7.73 respectively).

References

1) For example, (a) "Organic Syntheses," ed. by A. H. Blatt, Coll. Vol. II, p. 196, 343, and 349 (1948). (b) H. R. Frank, P. E. Fanta, and D. S. Tarbell, *J. Amer. Chem. Soc.*, **70**, 2317 (1948).
2) W. Militzer, *ibid.*, **60**, 256 (1938).
3) C. O. Obenland, *J. Chem. Educ.*, **41**, 566 (1964).
4) W. C. Baird, Jr. and J. H. Surridge, *J. Org. Chem.*, **35**, 3436 (1970).
5) S. Uemura, A. Onoe, and M. Okano, This Bulletin, **47**, 143 (1974).
6) "Organic Syntheses", ed. by H. E. Baumgarten, Coll. Vol. V, p. 117 (1973).
7) (a) H. Becker and others, "Organikum", 5 ed., Deutscher Verlag der Wissenschaften, Berlin (1965), p. 298. (b) "Organic Syntheses", ed. by H. Gilman, Coll. Vol. I, p. 123 (1948).
8) D. H. Derbyshire and W. A. Waters, *J. Chem. Soc.*, **1950**, 573.
9) (a) D. H. Derbyshire and W. A. Waters, *ibid.*, **1950**, 3694. (b) I. R. L. Barker and W. A. Waters, *ibid.*, **1952**, 150.
10) L. N. Ferguson, A. Y. Garner, and J. L. Mack, *J. Amer. Chem. Soc.*, **76**, 1250 (1954).
11) G. A. Olah, A. Pavlath, and G. Varsanyi, *J. Chem. Soc.*, **1957**, 1823.
12) R. M. Keefer and L. A. Andrews, *J. Amer. Chem. Soc.*, **78**, 5623 (1956).
13) L. Miller, E. P. Kayawa, and C. B. Campbell, *ibid.*, **92**, 2821 (1970).
14) P. W. Robertson, P. B. D. de la Mare, and B. E. Swedlund, *J. Chem. Soc.*, **1953**, 782.
15) G. A. Olah, S. J. Kuhn, S. H. Flood, and B. A. Hardie, *J. Amer. Chem. Soc.*, **86**, 1039 (1964).
16) D. A. Shirley, "Preparation of Organic Intermediate," John Wiley, New York (1951), p. 31.
17) R. R. Dreisbach and A. A. Martius, *Ind. Eng. Chem.*, **41**, 2875 (1949).
18) H. S. Patterson and D. P. McDonald, *J. Chem. Soc.*, **93**, 943 (1908).
19) F. D. Chattaway, F. L. Garton, and G. D. Parkens, *ibid.*, **125**, 1985 (1924).
20) H. McCombie and H. A. Scarborough, *ibid.*, **107**, 161 (1915).

Studies of Unusual Amino Acids and Their Peptides.[1] V. The Synthesis and the Absolute Configuration of β-(2-Thiazolyl)-β-alanine Present in Bottromycin

Yasuhiko SETO, Kazuhira TORII, Kōichi BORI,* Kenichiro INABATA,**
Shigeru KUWATA, and Hiroshi WATANABE

Laboratory of Chemistry, Faculty of Science, Kōnan University, Okamoto, Higashinada, Kobe 658

(Received June 11, 1973)

In order to obtain an optically-active β-(2-thiazolyl)-β-alanine, *N*-acyl-L-aspartic α-thionamide-β-methyl ester was condensed with diethyl bromoacetal, but the amino acid thus obtained showed no perceptible optical activity. The racemic amino acid, however, could be resolved into its antipodes by treating its phthalyl derivative with brucine. Thus, the (+)-amino acid, a constituent of bottromycin, was isolated in a pure state; it was determined to belong to the L-series by examining its optical behavior. This amino acid was proved to racemize easily under the conditions of the acid hydrolysis of bottromycin.

Bottromycin is a peptidic antibiotic first obtained by Waisvisz and his co-workers[2] from the fermentation broths of *Streptomyces bottropensis*. The chemical structure of this antibiotic was partly determined by the same authors,[3] and later the formula shown in Fig. 1 was proposed by Umezawa and his school.[4]

It differs from other peptidic antibiotics in several respects. In the first place, it is a linear oligopeptide ester, unlike usual peptidic antibiotics such as gramicidin S, tyrocidine or polymixin, which are cyclic oligopeptides containing D-amino acids. Secondly, it contains too many unusual amino acids. Bottromycin A, for instance, contains a total of 6 amino acids, 4 of which are unusual. Thirdly, it contains an iminopeptide bond in the middle of the molecule.

Interest in these differences, especially the relationship between these characteristics and its biological activities,[5] led us to make a synthetic study of this antibiotic.

In the proposed formula, the absolute configurations of the carboxyl-terminal two amino acids had been left undetermined. One of them, β-methylphenylalanine, was recently determined by Arold[6] to belong to the *erythro*-L-series. The other and last amino acid, β-(2-thiazolyl)-β-alanine, has had ambiguities from the beginning: by hydrolyzing the antibiotic with concentrated hydrochloric acid, Waisvisz[3] obtained a sample of this amino acid showing no optical activity. On the other hand, Umezawa and others[7] obtained an optically-active amino acid $[\alpha]_D^{18}$ +9° (*c* 1, water), by hydrolyzing the product produced by treating the antibiotic with acetic anhydride.

As the first step in our work concerning the study of bottromycin, we prepared β-(2-thiazolyl)-β-alanine and resolved it into two antipodes. The racemic form of this amino acid has already been synthesized by Waisvisz; here the same scheme was used. Though an effort was made to improve the yield, and though in effect the step giving (II) from (I) was improved

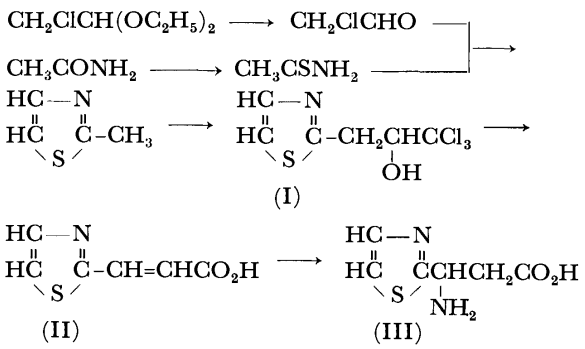

Scheme 1. The scheme of the synthesis of β-(2-thiazolyl)-β-alanine by the method of Waisvisz.

pretty well, on the whole there were too many steps and the overall yield was far from satisfactory. It should be mentioned that, in this series of experiments, we found a noticeable fact. Though the amination of β-(2-thiazolyl)-acrylic acid with hydroxylamine proceeded, the yield (30%) was so poor that in an experiment the hydroxylamine was replaced with ammonia. The yield of the addition product was remarkably enhanced, but it consisted cheifly of α-amino acid (yield, 70%); the desired β-amino acid was obtained only in a trace.

In order to resolve the racemate obtained here,

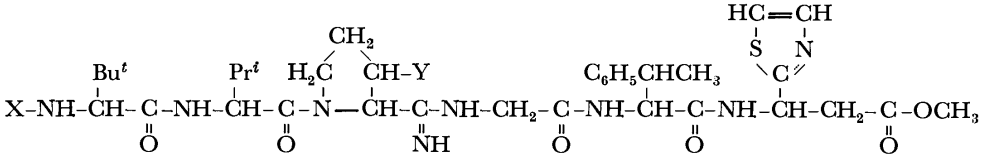

Fig. 1. The structure of bottromycin proposed by Umezawa *et al.* X=pivaloyl or Δ^1-isocaproyl; Y=H or CH_3; Bu^t=*tert*-butyl; Pr^i=isopropyl

* Present address: Daicel, Ltd., Central Research Laboratory, Tsurugaoka 171, Oimachi, Iruma-gun, Saitama-ken.

** Present address: Inabata Perfumery Co., Ltd., Fragrance Laboratory, Tagawadori 6-16, Higashiyodogawa-ku, Osaka.

TABLE 1. SALT FORMATION OF ACYL DERIVATIVES OF β-(2-THIAZOLYL)-β-ALANINE WITH ALKALOIDS IN SOME SOLVENTS

Acyl-group	Quinine		Brucine		Ephedrine
	Acetone	Ethanol	Acetone	Ethanol	Ethanol
Z-	−	−	−	oil	−
Bz-	±	−	−	+	−
Pht-	−	±	+	oil	−
Tos-	−	+	−	−	

Z=benzyloxycarbonyl, Bz=benzoyl, Pht=phthalyl, and Tos=tosyl. +, crystalline salt; ±, amorphous solid; −, no precipitate

benzoyl, tosyl, benzyloxycarbonyl, and phthalyl derivatives were prepared and treated with quinine, brucine, and ephedrine in various solvents; the results are shown in Table 1. As may be seen there, the brucine salt of the phthalyl derivative was proved to be useful for the resolution when fractionally crystallized from a mixture of chloroform and acetone. By this treatment, a less soluble salt, $[\alpha]_D^{25}$ +10.6° (*c* 1, chloroform), and an easily soluble one, $[\alpha]_D^{25}$ −39° (*c* 1, chloroform), were obtained; from the former, the free acid of $[\alpha]_D^{25}$ +33.4° (*c* 1, methanol) was liberated and from the latter, that of $[\alpha]_D^{25}$ −35.4° (*c* 1, methanol). The hydrazinolysis of the (+)-phthalyl amino acid gave β-(2-thiazolyl)-β-alanine with $[\alpha]_D^{17}$ +22.4° (*c* 1, water).

The value of $[\alpha]_D$ of the amino acid isolated here is markedly larger than the one reported by Umezawa and his co-workers,[7] though the signs themselves are equal. This amino acid showed no detectable change in its optical activity when it was left to stand in 6 M hydrochloric acid at room temperature, but after the solution had been heated to reflux for 8 hr no activity was detected. This fact suggests that the optically-inactive β-(2-thiazolyl)-β-alanine obtained by Waisvisz[3] by a prolonged hydrolysis of bottromycin and the amino acid of $[\alpha]_D^{18}$ +9° obtained by Umezawa by a milder treatment from the same source were entirely or partly racemized products.

The susceptibility of this amino acid to racemization is also retained in its derivatives, *i.e.*, the *N*-phthalyl amino acid and its methyl ester, both of which lost their optical activity upon being heated with 6 M hydrochloric acid more easily than the amino acid itself, though no change was observed when they were treated with a sodium bicarbonate solution, when they were passed through a silica gel column, when the amino acid was allowed to stand in 0.1 M sodium hydroxide for 12 days, or when it was refluxed with a large excess of hydrazine hydrate in methanol. That other amino acids containing a thiazole nucleus, found in some antibiotics, also show the same tendency to racemize upon acid treatment has been described in some reports.[8]

Trying to determine the absolute configuration of the optically-active amino acids separated here, we attempted to prepare one of them starting from L-aspartic acid according to Scheme 2.

β-Methyl aspartate was prepared from L-aspartic acid by the thionyl chloride method and was then

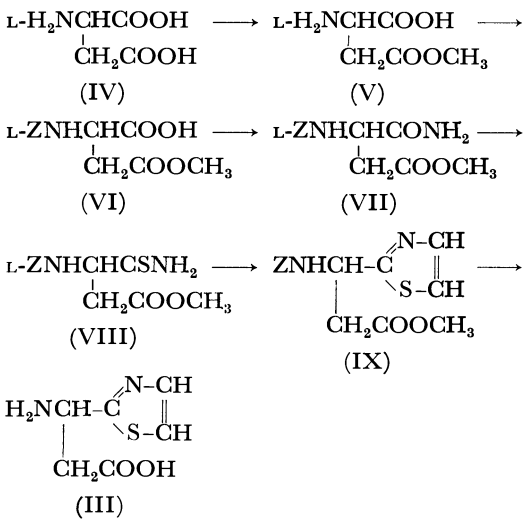

Scheme 2. The scheme of a synthesis of β-(2-thiazolyl)-β-alanine from aspartic acid (a-series). In b-series phthalyl group was used as an amino protecting group in place of benzyloxycarbonyl group (Z).

derived to the benzyloxycarbonyl or phthalyl derivative in the usual way. The amides of these *N*-protected L-aspartic acid β-methyl esters were prepared by the mixed acid anhydride method. The thionamide (VIII) was obtained from the amide (VII) in a good yield of 70—80% by only stirring the amide with phosphorus pentasulfide in dioxane at room temperature. This simple method was also applicable to other *N*-protected amino acid amides, *e.g.*, the amides of benzyloxycarbonylated glycine and L-phenylalanine.

The thionamides thus obtained from the aspartic acid derivatives were proved unstable when they were in contact with silica gel. When these compounds were chromatographed on a thin-layer of Merck silica gel G (ethyl acetate–cyclohexane (1:1)), the sample gave two spots; a major one with a low R_f value, which was identical with that of the desired compound, and a minor one with a high R_f value, which was the same as that of the compound obtained as a by-product in the course of the preparation of the thionamide. The amount of the latter compound increased with the lapse of time after the spotting of the sample. With the benzyloxycarbonyl derivative, after 2 hr, while with the phthalyl derivative, after 15 min, the two spots of the low and high R_f values occupied about the same area; the spot of the low R_f value of the phthalyl derivative disappeared after 2 hr. It is apparent that the compound responsible for the spot of the high R_f value is identical with the by-product of thionamide-synthesis mentioned above, because both the isolated compounds showed no depression of the melting point when mixed. We may conclude that this compound is phthalylamino thionsuccinimide produced by the intramolecular condensation of the thionamide (VIII-b).

Thiazole-ring formation was performed by condensing the thionamide (VIII) with bromoacetaldehyde or, more conveniently, though in a somewhat lower yield, with bromoacetal.

The *N*-phthalyl derivative of β-(2-thiazolyl)-β-alanine methyl ester (IX-b) thus obtained unexpectedly showed

a melting point of 113—115 °C, identical with that of the racemic methyl ester, but quite different from that of the optically-active one (mp 100 °C). The corresponding *N*-benzyloxycarbonyl acid was also identical with the racemic one in melting point, IR spectrum, and thin-layer chromatogram. The optical activities of both the *N*-phthalyl (IX-b) and *N*-benzyloxycarbonyl esters (IX-a) were so obscure that it was difficult to deduce any conclusion concerning their configurations. On the other hand, the methyl ester obtained from the optically-active *N*-phthalyl amino acid by treating it with diazomethane was apparently optically active. From these facts, we could not but conclude that, during the step of cyclization ((VIII)→(IX)), a substantial racemization did occur.

We could not attain the initial aim of determining the absolute configuration of β-(2-thiazolyl)-β-alanine by synthesis, but the synthetic route itself is valuable for a larger scale preparation of this amino acid because the steps are fewer and the total yield is better than those in Waisvisz's method.

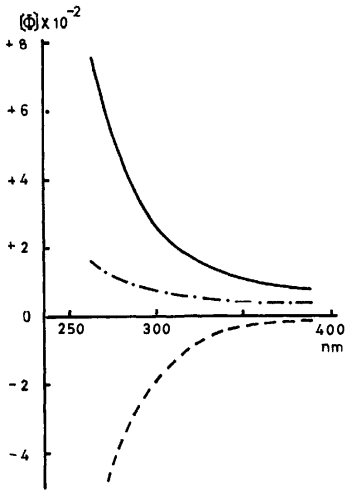

Fig. 2. Optical rotatory dispersion curves of (+)-β-(2-thiazolyl)-β-alanine; *c* 0.377, water, 26 °C.
——: neutral, —•—: acidic, ----: alkaline.

In order to determine the absolute configuration of this β-amino acid, we studied the optical properties of some optically-active β-amino acids, which have been reported previously.[9] When the optical rotatory dispersion (ORD) of (+)-β-(2-thiazolyl)-β-alanine was measured in acidic, neutral, and alkaline media, the value of the optical rotatory power decreased in the order of; neutral>acidic>alkaline (Fig. 2). This suggests that the amino acid belongs to the L-series.[9] The fact that the *N*-dithiocarbamate of this amino acid shows a negative Cotton effect in methanol, especially markedly in the presence of triethylamine, may also support this deduction.[9] Further evidence may be supplied by a comparison of the optical behavior of this amino acid derivative with that of the corresponding one of β-phenyl-β-alanine. (+)-β-(2-Thiazolyl)-β-alanine and L-β-phenyl-β-alanine gave positive ORD curves in water; the *N*-phthalyl derivatives of both the amino acids also gave positive Cotton effects in methanol. According to Freudenberg,[10] this means that both the amino acids have the same configuration. For these reasons, we conclude that the β-(2-thiazolyl)-β-alanine present in bottromycin belongs to the L-series.

Experimental[11]

2-(3',3',3'-Trichloro-2'-hydroxypropyl)-thiazole (I). (I) was synthesized from 2-methylthiazole and chloral; yield, 30%; mp 124—127 °C, lit,[12] mp 126—128 °C.

β-(2-Thiazolyl)-acrylic Acid (II). (II) was obtained by hydrolyzing 43 g of (I) with 87.5 g of potassium hydroxide in 500 ml of methanol at 40 °C for 1 hr and then at 70 °C for 30 min; yield, 26 g (64%); mp 184.5—185.5 °C, lit,[12] mp 187—190 °C.

DL-β-(2-Thiazolyl)-β-alanine (DL-III). This compound was obtained from (II) and hydroxylamine according to the method of Waisvisz; mp 198—199 °C, lit,[3] mp 199—202 °C. Circular paper chromatographies; R_f 0.30 (Solvent A) and 0.29 (Solvent B).

Acyl Derivatives of (DL-III). The following acyl derivatives were prepared by the usual method.

Phthalyl Derivative: Obtained by melting (DL-III) with phthalic anhydride at 150 °C for 40 min; yield, 75%; mp 161—162 °C.

Found: C, 55.58; H, 3.33; N, 9.21%. Calcd for $C_{14}H_{10}N_2O_4S$: C, 55.62; H, 3.33; N, 9.27%.

Benzyloxycarbonyl Derivative: Yield, 63%; mp 122.5—123.5 °C.

Found: C, 55.02; H, 4.56; N, 9.07%. Calcd for $C_{14}H_{14}N_2O_4S$: C, 54.89; H, 4.61; N, 9.14%.

Benzoyl Derivative: Yield, 50%; mp 169—170.5 °C.

Found: C, 56.32; H, 4.42; N, 10.10%. Calcd for $C_{13}H_{12}N_2O_3S$: C, 56.51; H, 4.38; N, 10.14%.

Tosyl Derivative: Yield, 36%; mp 164—165 °C.

Found: C, 47.84; H, 4.16; N, 8.62%. Calcd for $C_{13}H_{14}N_2O_4S_2$: C, 47.84; H, 4.32; N, 8.58%.

An Optical Resolution of DL-Phthalyl-β-(2-thiazolyl)-β-alanine. To a solution of 10.7 g of DL-phthalyl-β-(2-thiazolyl)-β-alanine and 14.0 g of brucine in 100 ml of chloroform, we added 100 ml of acetone; after the mixture had been allowed to stand at room temperature overnight, the separated crystals were collected; yield, 5.4 g; $[\alpha]_D^{22}$ −3.2° (*c* 1, chloroform). After repeated recrystallizations from chloroform–acetone, the optical rotation settled upon $[\alpha]_D^{22}$ +10.6° (*c* 1, chloroform); yield, 4 g. From the mother liquor, the more soluble salt of $[\alpha]_D^{22}$ −39° (*c* 1, chloroform) was obtained; yield, 7 g.

To remove the brucine, the salt was dissolved in hot water; the solution was ice-cooled quickly and then after a small excess of aqueous sodium hydroxide had been added, the freed base was extracted with chloroform. The aqueous layer was acidified to pH 2 with 6 M hydrochloric acid and then concentrated. After ice-cooling, the separated phthalyl derivative was collected. No change in the optical rotation was observed after recrystallization from methanol–water. The properties of the phthalyl-β-(2-thiazolyl)-β-alanine thus obtained were as follows:

From the less soluble brucine salt; $[\alpha]_D^{22}$ +33.4° (*c* 1, methanol), mp 138—140 °C (solidified immediately and melted again at 162—163 °C).

From the easily soluble brucine salt; $[\alpha]_D^{22}$ −35.4° (*c* 1, methanol); the melting point is completely identical with that of the above sample.

Phthalyl-(+)-β-(2-thiazolyl)-β-alanine Methyl Ester. This compound was obtained from the phthalyl-(+)-acid by treating it with diazomethane. Recrystallization from methanol–water gave a sample with a mp of 99—100 °C, $[\alpha]_D^{15}$

+23.5° (*c* 1.065, methanol).

(+)-β-(2-Thiazolyl)-β-alanine. ((+)-III). To a solution of the phthalyl derivative with $[\alpha]_D^{22}$ +33.4° in a small amount of methanol, we added 3 equivalents of hydrazine hydrate and then heated the mixture to reflux for 30 min. After the solvent had been distilled off, the residue was dissolved in water, acidified with acetic acid, and refluxed for 1 hr. The ice-cooled mixture was filtered, the filtrate was evaporated to dryness, and the remaining hydrazine hydrate was thoroughly removed under a high vacuum. By recrystallizing the residue from alcohol, (+)-β-(2-thiazolyl)-β-alanine was obtained as crystals; yield, 55%, mp 203.5—204.5 °C, $[\alpha]_D^{17}$ +22.4° (*c* 1, water). Further recrystallization from water–ethanol had no influence on the value of the specific rotatory power. Circular paper chromatographies; R_f 0.30 (Solvent A) and 0.29 (Solvent B).

Found: C, 41.62; H, 4.69; N, 16.26%. Calcd for $C_6H_8N_2O_2S$: C, 41.85; H, 4.68; N, 16.27%.

Lit,[7] mp 200—201 °C, $[\alpha]_D^{18}$ +9° (*c* 1, water).

((+)-III) in 6 M hydrochloric acid showed no perceptible change in optical rotation in the range of 270—700 nm after 24 hr at room temperature, but after 50 hr a little change was observed. When the solution was refluxed, however, for 1, 2.5, and 8 hr, the optical activity decreased to about 50%, less than 10%, and 0% respectively.

Addition of Ammonia to β-(2-Thiazolyl)-acrylic Acid (II). A solution of 1 g of (II) in 7 ml of 25% aqueous ammonia was heated in a sealed tube at 90 °C for 1 hr and then at 120 °C for a further 40 hr. After the reaction mixture had been treated with charcoal, it was evaporated to dryness and the residue was washed with ethanol. The yield of the crude product (mp 180—184 °C) was 0.79 g (70%). This product consisted of two components, because it gave two ninhydrin positive spots on circular paper chromatography. The major one was brown (R_f 0.26 (Solvent A) and 0.33 (Solvent B)), and the minor one, faint purple (R_f 0.30 (Solvent A) and 0.29 (Solvent B)). The latter was confirmed to be β-(2-thiazolyl)-β-alanine by comparing it with the authentic sample. By recrystallizing the crude product from methanol–water, the major component was obtained in a chromatographically pure state in a good yield, and it coincided with β-(2-thiazolyl)-α-alanine in all respects: mp 202—202.5 °C. Reported value for β-(2-thiazolyl)-α-alanine,[12] mp 197—198 °C. 2,4-Dinitrophenyl derivative, mp 209—210 °C. Lit,[3] mp 203—210 °C. Phthalyl derivative, mp 188.5—189 °C.

Found: C, 55.87; H, 3.42; N, 9.25%. Calcd for $C_{14}H_{10}N_2O_4S$: C, 55.62; H, 3.33; N, 9.27%.

L-Aspartic Acid β-Methyl Ester Hydrochloride (V). This compound was prepared by the method of Brenner;[13] yield, 97%, mp 186—187 °C, $[\alpha]_D^{19}$ +14.4° (*c* 1, ethanol–water (1:3)). Lit,[14] mp 199—200 °C, $[\alpha]_D^{25}$ +14.4° (*c* 1, ethanol–water (1:3)).

Benzyloxycarbonyl-L-aspartic Acid β-Methyl Ester (VI-a). This compound was prepared from (V) and benzyloxycarbonylchloride by the usual method; yield, 82%, mp 91—92 °C, $[\alpha]_D^{26}$ −18.2° (*c* 2.5, pyridine). Lit,[15] mp 97—98 °C, $[\alpha]_D^{25}$ −18.5° (*c* 2.5, pyridine). This product was used for the next reaction without further purification.

Benzyloxycarbonyl-L-aspartic Acid β-Methyl Ester α-Amide (VII-a). To a cold solution of 7.88 g of (VI-a) and 2.83 g of triethylamine in 60 ml of tetrahydrofuran, we added 3.05 g of ethyl chloroformate with ice-cooling over a 7 min period. After stirring for 20 min at −8 °C, 4.20 g (2.5 equivalents) of 28% aqueous ammonia were added; the stirring was continued at −4 °C for a further 40 min and then at room temperature overnight. The mixture was subsequently evaporated under reduced pressure, and the residue was dissolved in ethyl acetate. The extract was washed with water, dried with anhydrous sodium sulfate, and evaporated to yield needle crystals; yield, 5.16 g (66%); mp 118.5—120 °C. After recrystallization from benzene, mp 120—121 °C, $[\alpha]_D^{28}$ +5.3° (*c* 1, acetic acid). ORD; $[\phi]_{270}$ −560°, $[\phi]_{299}$ −280°, $[\phi]_{552}$ 0°, $[\phi]_{650}$ +15° (*c* 2, methanol). Lit,[16] mp 121 °C, $[\alpha]_D^{20}$ +9.0° (acetic acid).

Benzyloxycarbonyl-L-aspartic Acid β-Methyl Ester α-Thionamide (VIII-a). To a solution of 2 g of the amide (VII-a) in 10 ml of dry dioxane, we added 1.74 g of finely powdered phosphorus pentasulfide; stirring was continued for 8 hr at room temperature until the mixture became almost homogeneous. A little residual phosphorus pentasulfide was filtered off, and the filtrate was vigorously stirred into 100 ml of ice-water. The separated pale yellow oil was extracted with ether, and the ether extract was washed with water, dried with anhydrous sodium sulfate, and evaporated to the crude thionamide; yield, 1.81 g (86%); mp 67—87 °C. Recrystallization from tetrahydrofuran–petroleum ether gave crystals, mp 78.5—79.5 °C, $[\alpha]_D^{28}$ −22° (*c* 1, methanol). ORD; $[\phi]_{364}$ −680°, $[\phi]_{378}$ −950°, $[\phi]_{410}$ −470°, $[\phi]_{650}$ −44° (*c* 1, ethanol).

Found: C, 52.97; H, 5.45; N, 9.45%. Calcd for $C_{13}H_{16}N_2O_4S$: C, 52.69; H, 5.44; N, 9.45%.

From the mother liquor of the recrystallization we obtained fine long needles (mp 87—88 °C) which gave a spot with the same R_f value as the thionamide in thin-layer chromatography, but no details were investigated.

Thionamides of Benzyloxycarbonyl-glycine and -L-Phenylalanine. By the same method, both the thionamides were also prepared in good yields.

Benzyloxycarbonyl-glycine Thionamide: mp 146.5—148 °C.

Found: C, 54.18; H, 5.43; N, 12.49%. Calcd for $C_{10}H_{12}N_2O_2S$: C, 53.55; H, 5.39; N, 12.49%.

Benzyloxycarbonyl-L-phenylalanine Thionamide: mp 145—145.5 °C, $[\alpha]_D^{17}$ +13.0° (*c* 0.766, methanol).

Found: C, 64.95; H, 5.97; N, 8.87%. Calcd for $C_{17}H_{18}N_2O_2S$: C, 64.94; H, 5.77; N, 8.91%.

Benzyloxycarbonyl-β-(2-thiazolyl)-β-alanine Methyl Ester (IX-a). A mixture of 20.8 g of (VIII-a) and 80.5 g of diethyl bromoacetal in a vessel equipped with a condenser was kept at 60—65 °C in a water bath under reduced pressure (35 mmHg) for 1.5 hr with occasional shaking. After 20 min, the pale yellow solution began to separate into two layers. The upper layer, consisting of an excess of acetal, was decanted off, after which the orange-coloured lower oil was washed several times with ethyl acetate. After being made alkaline with aqueous sodium bicarbonate, the oil was extracted with ethyl acetate, and the extract was washed with water, dried with anhydrous sodium sulfate, and evaporated to dryness. The yield of the crude ester (mp 62—67 °C (sinter from 59 °C)) was 17.4 g (77%). After recrystallization from ethyl acetate–petroleum ether, the ester melted at 70.5—71.5 °C.

Found: C, 56.20; H, 5.10; N, 8.60%. Calcd for $C_{15}H_{16}N_2O_4S$: C, 56.24; H, 5.03; N, 8.74%.

Benzyloxycarbonyl-β-(2-thiazolyl)-β-alanine (X). This compound was obtained by hydrolyzing the ester (IX-a) with 6 M hydrochloric acid at 70 °C for 1 hr; mp 122—123.5 °C, $[\phi]_{280-700}$ 0° (*c* 2, ethanol). The thin-layer chromatograms, melting points (including mixed melting point), and IR spectrum of this compound were identical with those of the authentic sample prepared according to the Waisvisz method.

Phthalyl-L-aspartic Acid β-Methyl Ester (VI-b). This compound was prepared from (V) using the Nefkens reagent;[17] yield, 80%; mp 130—134 °C. After recrystalliza-

tion from benzene, mp 133.5—134.5 °C, $[\alpha]_D^{16}$ −75.8° (*c* 1, methanol).

Found: C, 56.32; H, 4.04; N, 5.00%. Calcd for $C_{13}H_{11}NO_6$: C, 56.32; H, 4.00; N, 5.05%.

Phthalyl-L-aspartic Acid β-Methyl Ester α-Amide (VII-b). Into a cold solution of 15 g of (VI-b) and 5.4 g of triethylamine in 75 ml of tetrahydrofuran, we vigorously stirred 5.90 g of ethyl chloroformate at −10 °C for 7 min. After additional stirring for 10 min at −10 °C, 5 g (1.5 equivalents) of 28% aqueous ammonia were added; the stirring was then continued at 0 °C for 2 hr and at room temperature for 3 hr. The reaction mixture was evaporated, and the residue was washed with water to give the crude amide; mp 163—166 °C. Recrystallization from ethanol gave 11.5 g (77%) of the amide; mp 167—168 °C. $[\alpha]_D^{19}$ −81° (*c* 1, dimethylformamide). ORD; $[\phi]_{326}$ −2150°, $[\phi]_{330}$ −2430°, $[\phi]_{350}$ −1200°, $[\phi]_{650}$ −80° (*c* 1, dimethylformamide).

Found: C, 56.56; H, 4.50; N, 10.05%. Calcd for $C_{13}H_{12}N_2O_5$: C, 56.52; H, 4.38; N, 10.14%.

In this reaction a small amount of a crystalline by-product was obtained from the mother liquor. After recrystallization from methanol, it melted at 227—228 °C and yielded aspartic acid upon hydrolysis. From this fact and the elemental analysis of this product, the by-product may be concluded to be the phthalylamino succinimide derived from (VII-b) by the removal of the methanol.

Found: C, 58.79; H, 3.34; N, 11.48%. Calcd for $C_{12}H_8N_2O_4$: C, 59.02; H, 3.30; N, 11.47%.

Phthalyl-L-aspartic Acid β-Methyl Ester α-Thionamide (VIII-b). To a solution of 162 g of the amide (VII-b) in 800 ml of dry dioxane, we added 162 g of finely powdered phosphorus pentasulfide. The mixture was stirred at room temperature for 9 hr. Any insoluble material was filtered off, and the residue was washed with dioxane. The combined filtrate and washings were concentrated to about 1/3 in volume and vigorously stirred into ice water. The oil thus separated, which soon solidified, was isolated by filtration, washed with water, dried over calcium chloride under a vacuum, and recrystallized from methanol; yield, 120 g (70%); mp 158—159.5 °C. Prisms (colourless, but once coloured it is difficult to remove the colour). Analytical sample; mp 163.5—164.5 °C, $[\alpha]_D^{17}$ −6.5° (*c* 1, tetrahydrofuran). ORD; $[\phi]_{358}$ −230°, $[\phi]_{383}$ −550°, $[\phi]_{409}$ −260°, $[\phi]_{650}$ −9° (*c* 1, tetrahydrofuran).

Found: C, 53.79; H, 4.19; N, 9.37%. Calcd for $C_{13}H_{12}N_2O_4S$: C, 53.42; H, 4.14; N, 9.58%.

From the mother liquor, a small amount of crystals was isolated as a by-product. It melted at 220—223 °C after recrystallization from methanol. This compound was found to be produced by treating the thionamide (VIII-b) with Merck silica gel G, *e.g.*, by passing the thionamide through the silica gel column. The identity of the two compounds obtained by the two different methods was proved by a comparison of their melting points, IR spectra, and analytical data; from this identity we conclude that the compound is 2-phthalylamino-L-thionsuccinimide. This compound showed a characteristic Cotton effect with a peak at 426 nm and a trough at 382 nm. ORD; $[\phi]_{360}$ −2500°, $[\phi]_{382}$ −2900°, $[\phi]_{406}$ −1500°, $[\phi]_{426}$ −150°, $[\phi]_{470}$ −360°, $[\phi]_{650}$ −100° (*c* 0.5, tetrahydrofuran).

Found: C, 55.06; H, 3.01; N, 10.79%. Calcd for $C_{12}H_8N_2O_3S$: C, 55.38; H, 3.10; N, 10.76%.

Phthalyl-β-(2-thiazolyl)-β-alanine. A solution of 8.9 g of thionamide (VIII-b) and 8.9 g of diethyl bromoacetal in 8 ml of tetrahydrofuran was heated to reflux over a 7 hr period. After the reaction mixture had then been evaporated, the residual oil was washed with petroleum ether to remove the excess of acetal, made alkaline with aqueous sodium bicarbonate, and extracted with ethyl acetate. The extract was washed with water, dried with anhydrous sodium sulfate, and evaporated to the crude ester (IX-b); yield, 7.4 g (77%); mp 106—110 °C. After recrystallization from methanol, the ester melted at 115 °C.

By the hydrolysis of this ester with 6 M hydrochloric acid at 60 °C for 2.5 hr, phthalyl-β-(2-thiazolyl)-β-alanine was obtained; mp 160—161.5 °C. No optical activity was detected in the range of 380—700 nm. A mixed melting point determination with the phthalyl derivative obtained from (DL-III) showed no depression, and the IR spectra of the two compounds were completely identical.

References

1) The previous heading of this series, "Studies of Unnatural Amino Acids and Their Peptides," is altered as above. Previous reports: This Bulletin, **38**, 1461 (1965); **39**, 2473 (1966); **41**, 1634 (1968); **43**, 2874 (1970).

2) J. M. Waisvisz, M. G. van der Hoeven, J. van Peppen, and W. C. M. Zwennis, *J. Amer. Chem. Soc.*, **79**, 4520 (1957).

3) J. M. Waisvisz, M. G. van der Hoeven, and B. te Nijenhuis, *ibid.*, **79**, 4524 (1957).

4) S. Nakamura and H. Umezawa, *J. Antibiotics*, **19**, 10 (1966); S. Nakamura, T. Yajima, Y. C. Lin, and H. Umezawa, *ibid.*, **20**, 1 (1967).

5) Y. C. Lin, T. Kinoshita, and N. Tanaka, *ibid.*, **21**, 471 (1968).

6) H. Arold, M. Eule, and S. Reissmann, *Z. Chem.*, **9**, 447 (1969).

7) S. Nakamura, T. Chikaike, H. Yonehara, and H. Umezawa, *Chem. Pharm. Bull.*, **13**, 599 (1965).

8) D. F. W. Cross, G. W. Kenner, R. C. Sheppard, and C. E. Stehr, *J. Chem. Soc.*, **1963**, 2143; M. Bodanszky, J. T. Sheehan, J. Fried, N. J. Williams, and C. A. Birkhimer, *J. Amer. Chem. Soc.*, **82**, 4747 (1960); B. M. Dean, M. P. V. Mijovic, and J. Walker, *J. Chem. Soc.*, **1961**, 3394.

9) Y. Seto, T. Yamada, K. Niwa, S. Miwa, F. Tanaka, S. Kuwata, and H. Watanabe, *Chem. Lett.*, **1973**, 151; *cf.* K. Balenović, "The Stereochemistry of Naturally Occuring β-Amino Acids," in Amino Acids and Peptides with Antimetabolic Activity, Ciba Found. Symp., J. & A. Churchill, London (1958), p. 5.

10) J. P. Greenstein and M. Winitz, "Chemistry of Amino Acids," Vol. 1, John Wiley & Sons, Inc., New York, N. Y. (1961), p. 99.

11) All the melting points are uncorrected. The optical rotations were measured by means of a Yanagimoto Polarimeter OR-20. ORD curves were recorded on a JASCO ORD/UV-5 spectropolarimeter. Thin-layer chromatographies were performed on Merck silica gel G using *n*-butanol–acetic acid–water (4:1:2 v/v, upper phase) (Solvent A) or pyridine–acetic acid–water (3:12:5 v/v, upper phase) (Solvent B) as the developing solvent. Circular paper chromatographies were performed on Toyo Roshi No. 2.

12) R. G. Jones, E. C. Kornfeld, and K. C. McLaughlin, *J. Amer. Chem. Soc.*, **72**, 4526 (1950).

13) M. Brenner and W. Huber, *Helv. Chim. Acta*, **36**, 1109 (1953).

14) M. C. Khosla, R. R. Smeby, and F. M. Bumpus, *Indian J. Chem.*, **5**, 279 (1967).

15) M. Goodman and F. Boardman, *J. Amer. Chem. Soc.*, **85**, 2483 (1963).

16) M. Bergmann and L. Zervas, *Ber.*, **65**, 1192 (1932).

17) G. H. L. Nefkens, G. I. Tesser, and R. J. F. Nivard, *Recl. Trav. Chim. Pays-Bas*, **79**, 688 (1960).

Kinetics of the Oxidation of Acrolein Initiated by Di-*t*-butyl Diperoxyoxalate

Takao HARA, Yasukazu OHKATSU,* and Tetsuo OSA*

Department of Chemistry, Faculty of Engineering, Yokohama National University, Ohoka, Minami-ku, Yokohama 233

**Department of Industrial Chemistry, Faculty of Engineering, The University of Tokyo, Hongo, Bunkyo-ku, Tokyo 113*

(Received June 14, 1973)

The kinetics of the liquid-phase autoxidation of acrolein were studied using di-*t*-butyl diperoxyoxalate as an initiator. The ratios of the rate constants for the propagation *vs* the termination steps ($k_3k_6^{-1/2}$ and $k_2k_4^{-1/2}$) in the autoxidation mechanism were determined from the empirical rate equation thus obtained. The lower reactivity of acrolein was explained by comparing the ratios with those of saturated aldehydes.

There are only a few articles relating to the liquid-phase oxidation of α,β-unsaturated aldehydes to the corresponding carboxylic acids.[1-5] They refer mainly to the selective formation of the carboxylic acids and do not emphasize the kinetics and mechanisms. The absolute rate constants in the elementary steps of the oxidation or the ratio of the rate constants for the propagation *vs.* the termination steps have not yet been determined. In a series of studies of the liquid-phase oxidation of acrolein, we have mainly clarified the action of the metal-salt catalysts.[6-11]

In this paper, the kinetics of the autoxidation of acrolein initiated by a peroxy ester were studied. It is well known that di-*t*-butyl diperoxyoxalate (DBPO) is decomposed at room temperature in benzene or cumene to yield carbon dioxide and *t*-butoxy radicals.[12] It can be used as a radical initiator to be decomposed quantitatively in the liquid-phase oxidation. The ratios of the rate constants were first determined in the case of acrolein, and the lower reactivity of acrolein discussed in comparison with saturated aldehydes.

Experimental

The DBPO used as an initiator was prepared according to the method in the literature.[12] DBPO was usually stored in *n*-pentane below −25 °C. The crystals were filtered off just before an experiment and were dried *in vacuo* below 0 °C. An accurately-weighed amount of DBPO was used for the oxidation reaction.

The reaction apparatus used was the same as one described previously.[7] Carbon dioxide, evolved in the course of the reaction by the decomposition of DBPO and the reaction intermediates, was eliminated by placing the absorption tube packed with soda lime in a gas recycling system. It was also confirmed that other gaseous compounds did not affect the measurement of the absorbed oxygen. The total volume of the reaction solution was maintained at 75 ml, and the reaction was carried out under an atmospheric pressure by the dilution of the oxygen with nitrogen, if necessary. The partial pressure of oxygen was calculated after revision using the vapor pressure of acrolein.[13] The concentration of oxygen dissolved in a benzene solution under an atmospheric pressure of oxygen is given as 7.73×10^{-3} mol/l.[14] Besides, the stirring speed and the amount of oxygen flow were maintained so as not to have an effect on the reaction rate.[9]

All the peroxide products were estimated by iodometry; we thus obtained each concentration of hydrogen peroxide, hydroperoxides, and the other peroxides.[8,15] The concentration of hydrogen peroxide was below 3×10^{-3} wt% in any feedstock of the reaction solution, measured at the first step of the titration. Peracrylic acid and the peroxide complex (1:1 adduct from peracrylic acid and acrolein) could be completely analyzed at the second and the last steps, as has been reported previously.[8]

The formation rate of radicals by the decomposition of DBPO was measured by the method that Bawn and Mellish,[16] and Hammond *et al.*[17] used for benzoyl peroxide and azobisisobutyronitrile. DBPO was decomposed in benzene in the presence of diphenylpicryl hydrazyl (DPPH). The solution showed an absorption maximum at 520 nm which obeyed Beer's law throughout the range of concentrations used in the present work. The optical densities of the solution were measured at adequate intervals during the reaction by means of a spectrophotometer (Hitachi, ESP-2).

Results and Discussion

The oxidation of acrolein was carried out in benzene at 40 °C. In the absence of an initiator, the absorption of oxygen was not observed for 3 hr; this behavior was different from that of the oxidation of the corre-

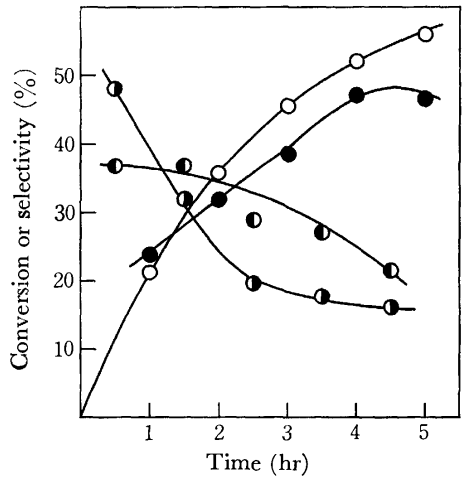

Fig. 1. Products in the oxidation of acrolein initiated by DBPO. Reaction conditions; [acrolein] 3.0 mol/l, [DBPO] 2.2×10^{-2} mol/l, 40 °C, in benzene. ○: conversion of acrolein, ●: selectivity of acrylic acid, ◑: selectivity of peracrylic acid, ◐: selectivity of the peroxide complex. Selectivities are based on consumed acrolein.

sponding saturated aldehydes. Oxygen was absorbed steadily without any induction period after the addition of DBPO. An aspect of the oxidation is illustrated in Fig. 1, with the selectivities of the products based on the acrolein consumed. The reaction intermediates, namely, peracrylic acid and the peroxide complex, remained rather stable at 40 °C, and 42% of the acrolein consumed was converted into these two kinds of peroxides at 4 hr. The formation of insoluble polymers was not observed throughout the oxidation.

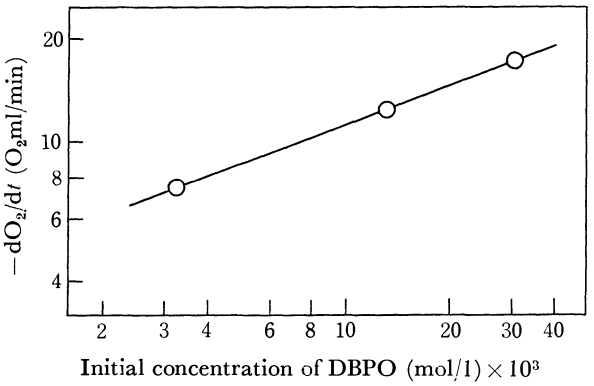

Fig. 2. Effect of DBPO on absorption rate of oxygen. Reaction conditions; [acrolein] 3.0 mol/l, $[O_2]$ 5.1×10^{-3} mol/l, 40 °C, in benzene.

The initial concentration of DBPO showed a half-order dependence on the absorption rate of oxygen (Fig. 2). The orders of the dependence of the initial concentration of acrolein and of the partial pressure of oxygen were also found to be near 0.6 and 0.5 respectively. These results give the following rate equation, as will be discussed in detail below (Table 1):

$$-dO_2/dt = \frac{A[O_2][\text{acrolein}]}{[\text{acrolein}]+B[O_2]} \qquad \text{(I)}$$

where A and B are constants which depend neither on the concentration of acrolein nor on the oxygen pressure. Moreover, the A constant contains a term of the initiation rate, as will be explained below.

Equation (I) can be transformed into Eq. (II):

$$1/-dO_2/dt = 1/A[O_2] + B/A[\text{acrolein}] \qquad \text{(II)}$$

A linear relationship was obtained between $1/-dO_2/dt$ and both $1/[O_2]$ and 1/[acrolein], as is illustrated in Figs. 3 and 4 respectively. The values of A and B could be calculated from the lines of both figures; they accorded well as is shown below:

	A (s^{-1})	B
From Fig. 3	2.8×10^{-2}	6.8×10^{2}
From Fig. 4	2.8×10^{-2}	6.6×10^{2}
Average	2.8×10^{-2}	6.7×10^{2}

The observed absorption rate of oxygen accorded quite well with those calculated by means of the assumed rate Eq. (I) when the values of A and B were taken as $2.8\times 10^{-2}\,s^{-1}$ and 6.7×10^{2} (Table 1).

Assuming that the oxidation proceeds through the autoxidation mechanism shown below, the theoretical rate Eq. (III) may be derived by appling the stationary-state treatment:

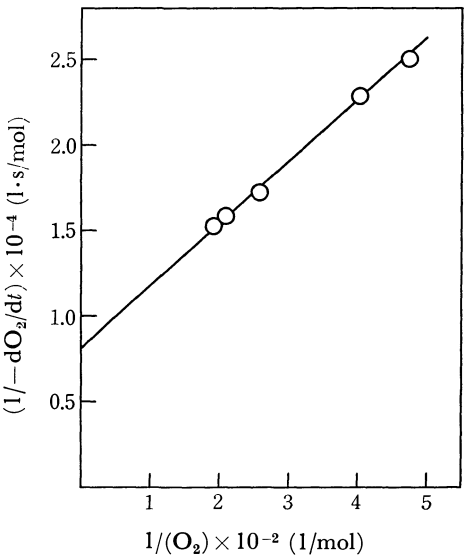

Fig. 3. Effect of oxygen pressure on absorption rate of oxygen. Reaction conditions; [acrolein] 3.0 mol/l, [DBPO] 3.4×10^{-3} mol/l, 40 °C, in benzene. Slope= $1/A=0.35\times 10^{2}$ s, B/A[acrolein]$=0.80\times 10^{4}$ l·s/mol.

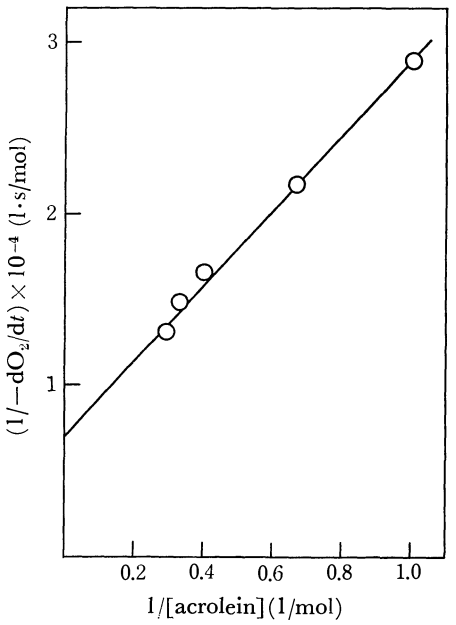

Fig. 4. Effect of acrolein on absorption rate of oxygen. Reaction conditions; $[O_2]$ 5.1×10^{-3} mol/l, [DBPO] 3.4×10^{-3} mol/l, 40 °C, in benzene. Slope$=B/A=$ 2.35×10^{4} s, $1/A[O_2]=0.70\times 10^{4}$ l·s/mol.

$$RH \xrightarrow{R_i} R\cdot \qquad (1)$$

$$R\cdot + O_2 \xrightarrow{k_2} RO_2\cdot \qquad (2)$$

$$RO_2\cdot + RH \xrightarrow{k_3} RO_2H + R\cdot \qquad (3)$$

$$2R\cdot \xrightarrow{k_4} \qquad (4)$$

$$R\cdot + RO_2\cdot \xrightarrow{k_5} \text{non-radical products} \qquad (5)$$

$$2RO_2\cdot \xrightarrow{k_6} \qquad (6)$$

where RH and R_i denote the acrolein molecule and

TABLE 1. EFFECT OF ACROLEIN AND OXYGEN PRESSURE ON ABSORPTION RATE OF OXYGEN

Concn. of acrolein mol/l	Oxygen pressure atm.	Concn. of oxygen mol/l$\times 10^3$	Absorption rate of oxygen mol/l s$\times 10^5$	
			Obsd	Calcd[a]
3.0	0.66	5.1	6.6	6.7
3.0	0.62	4.8	6.5	6.5
3.0	0.50	3.9	6.0	5.8
3.0	0.32	2.5	4.4	4.5
3.0	0.27	2.1	4.1	4.0
3.0	0.22	1.7	3.6	3.5
3.5	0.66	5.1	7.4	7.2
2.5	0.66	5.1	5.9	6.0
1.5	0.66	5.1	4.5	4.3
1.0	0.66	5.1	3.5	3.3

Reaction conditions; [DBPO] 3.4×10^{-3} mol/l, 40 °C, in benzene.

a) Calculated by the Eq. (I), where the values of A and B are 2.8×10^{-2} s^{-1} and 6.7×10^2, respectively.

the rate of initiation respectively.

$$-dO_2/dt = \frac{R_i^{1/2}k_2k_3[RH][O_2]}{k_3k_4^{1/2}[RH]+k_2k_6^{1/2}[O_2]} \qquad (III)$$

The initiation reaction is considered to proceed in the following manner because the absorption rate in the absence of DBPO is negligible:[18]

$$DBPO \xrightarrow{k_{11}} 2t\text{-BuO}\cdot + 2CO_2$$

$$t\text{-BuO}\cdot + RH \xrightarrow{k_{12}} t\text{-BuOH} + R\cdot$$

Accordingly, R_i is given as the following expression and is dependent on neither the concentration of acrolein nor on the oxygen pressure:[18]

$$R_i = 2ek_{11}[DBPO]$$

The coefficient e is the efficiency of the radical initiator. In order to determine the value of ek_{11}, DBPO was decomposed in benzene at 40 °C in the presence of DPPH and the rate of decrease of DPPH was measured. According to Shine *et al.*,[19] if the concentration of peroxide is higher than that of the hydrazyl, the yield of carbon dioxide is not affected by the presence of the hydrazyl. Therefore, the formation rate of *t*-butoxy radicals can be derived from the rate of decrease of DPPH under the present reaction conditions. From Fig. 5 the value of ek_{11} was determined to be 8.5×10^{-5} s^{-1} at 40 °C. Bartlett *et al.* measured the decomposition rate of DBPO in benzene by observing the decline of the absorption of the carbonyl frequency and found that the decomposition occurred through a uni-molecular mechanism.[12] The rate constant of the decomposition at 40 °C can be calculated to be 10.5×10^{-5} s^{-1} from the reported values. The ratio of the two constants may correspond to an e value of 0.81 at 40 °C. Burnett *et al.* also determined the efficiency of azobisisobutyronitrile by DPPH-inhibitor techniques.[21]

Therefore, A and B in Eq. (I) can be expressed by the rate constants of the elementary steps in the following manner, and the ratios of the constants, $k_3k_6^{-1/2}$ and $k_2k_4^{-1/2}$, at 40 °C can be determined in the oxidation of acrolein:

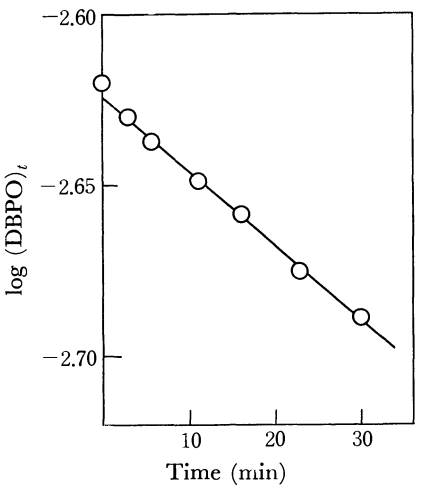

Fig. 5. Formation of *t*-butoxy radicals from the decomposition of DBPO. Reaction conditions; initial concentration of DBPO 2.40×10^{-3} mol/l, initial concentration of DPPH 1.82×10^{-3} mol/l, 40 °C, in benzene. $[DBPO]_t=[DBPO]_0-1/2\ \{[DPPH]_0-[DPPH]_t\}$. $[X]_t$ and $[X]_0$ denote the concentrations of X at $t=t$ and 0, respectively.

$$A = \{2ek_{11}[DBPO]\}^{1/2}k_2k_4^{-1/2},\quad B = k_2k_4^{-1/2}/k_3k_6^{-1/2}$$

$$k_3k_6^{-1/2} = 5.5\times 10^{-2}\ (l^{1/2}\cdot mol^{-1/2}\cdot s^{-1/2})$$

$$k_2k_4^{-1/2} = 3.7\times 10\quad (l^{1/2}\cdot mol^{-1/2}\cdot s^{-1/2})$$

The ratios of the rate constants, $k_3k_6^{-1/2}$, have been reported in many kinds of hydrocarbons; they seem to be dependent both on the property of the hydrogen being abstracted and on the structure and reactivity of the peroxy radicals.[20] In the oxidation of acetaldehyde, $k_3k_6^{-1/2}$ has been reported to be 2.7×10^{-1} $(l^{1/2}\cdot mol^{-1/2}\cdot s^{-1/2})$ at 0 °C.[22] Considering that the activation energies of k_3 and k_6 are 2—4 and 0—2 kcal respectively,[23] the ratio in acetaldehyde may be said to be 10 times larger than that in acrolein.

On the other hand, Zaikov *et al.* found that, in the oxidation of various aldehydes, the values of $k_3k_6^{-1/2}$ differed only slightly from one another because there were compensating changes for the rate constants of propagation and termination,[24] the values of $k_3k_6^{-1/2}$ being substantially constant, independently of the kind of aldehyde. The termination rate constants, k_6, for acrolein and acetaldehyde may depend on the stability of these two kinds of acyloxy radicals formed in the tetroxide homolysis. Considering the more rapid decarboxylation of acetoxy radicals, the constant, k_6, of acrolein may be larger than that of acetaldehyde because of the existence of the conjugated double bond, as has been reported in the case between benzaldehyde and alkanals.[24] The propagation rate constant, k_3, may be discussed in two ways; (1) the reactivity of aldehyde hydrogen, that is, the C–H bond strength and the steric effect, and (2) the reactivity of the attacking acylperoxy radicals. The bond strength is estimated to be 74 kcal for benzaldehyde and 88 kcal for acetaldehyde.[25] The reason why compensating changes are

found between benzaldehyde and alkanals may be mainly attributed to the difference in the bond strength. On the contrary, though the bond strength may be smaller for acrolein than for acetaldehyde because of the resonance stabilization of acryloyl radicals, the value of $k_3k_6^{-1/2}$ in the oxidation of acrolein is smaller than that of acetaldehyde or benzaldehyde. Russell claimed that the polar effect of acylperoxy radicals played an important role in the propagation step:[26]

$$RO_2\cdot + RH \xrightarrow{k_3} [RO_2^-:H\ R^+] \longrightarrow RO_2H + R\cdot$$

Such an intermediate complex will be elucidated in this oxidation. However, there may be two forms of complexes ((1) and (2)) which are stabilized by the existence of the conjugated C=C double bond:

$$CH_2{=}CHCHO + RO_2\cdot \longrightarrow$$

$$\left[O{=}\overset{+}{C}\diagup CH{=}CH_2 \;\cdot\; H{:}\,O_2^-{-}R\right] \longleftrightarrow \left[O{=}C\diagup\!\!\diagup CH{-}C^+H_2 \;\cdot\; H{:}\,O_2^-{-}R\right]$$

(1) (2)

$$\longrightarrow CH_2{=}CH\dot{C}O + RO_2H$$

The (2) complex is considered to be more stabilized than the (1) complex because of its electronic structure, and the (1) complex may produce an acryloyl radical and peracrylic acid faster than the (2) complex. This results in the lower reactivity for the abstraction of the hydrogen of acrolein as compared with that of the other aldehydes, such as acetaldehyde, with only one form of an intermediate complex. Besides, the steric hindrance may arise for acrolein in the abstraction reaction, because the rotation about the C–C single bond is restricted. The proportion of s-*trans* to s-*cis* isomers was reported to be 95:5 at room temperature.[27] As the sum of these effects, it may be possible to consider that k_3 does not compensate for the change of k_6 for acrolein, resulting in the following order with regard to the values of $k_3k_6^{-1/2}$:

$$\text{benzaldehyde} \fallingdotseq \text{acetaldehyde} > \text{acrolein}$$

There are no reports concerning the values of $k_2k_4^{-1/2}$. In the oxidation of saturated aldehydes, the rate-determining step is Step (3) and oxygen reacts with an acyl radical so fast that the absorption rate has no dependence on the oxygen pressure. However, the k_2 constant is considered to be smaller for acrolein because of the resonance stabilization, as has been reported in the case of allyl or benzyl radicals.[28] The ratio of $k_2k_4^{-1/2}$ to $k_3k_6^{-1/2}$ reaches only 670 for acrolein. As the ratios of the concentrations of acrolein to dissolved oxygen are near 10^3 in the present work, the absorption rate has a certain dependence on the oxygen pressure. It has already been reported that a near-first-order dependence on the oxygen pressure can be observed in oxidations catalyzed by various metal salts.[29] Brill and Lister also reported a first-order dependence in the catalyzed oxidation of methacrolein.[2] As the catalyzed oxidation proceeds through the same reaction mechanism except for the initiation step (1), part of the higher dependence on the oxygen pressure may be ascribed to the initiation step; that is, the abstraction of aldehyde hydrogen by a metal ion may be accelerated by the presence of oxygen.

References

1) J. M. Church and L. Lynn, *Ind. Eng. Chem.*, **42**, 768 (1950).
2) W. F. Brill and F. Lister, *J. Org. Chem.*, **26**, 565 (1961).
3) M. I. Farberov and G. N. Kosheli, *Kinet. Katal.*, **6**, 666 (1965).
4) W. F. Brill and F. J. Barone, U.S. 3253025 (1966).
5) G. N. Kosheli and M. I. Farberov, *Zh. Prikl. Khim.*, **39**, 2101 (1966).
6) A. Misono, T. Osa, Y. Ohkatsu, and M. Takeda, *Kogyo Kagaku Zasshi*, **69**, 2129 (1966).
7) Y. Ohkatsu, M. Takeda, T. Hara, T. Osa, and A, Misono, This Bulletin, **40**, 1893 (1967).
8) Y. Ohkatsu, T. Hara, T. Osa, and A. Misono, *ibid.*, **40**, 1413 (1967).
9) Y. Ohkatsu, T. Osa, and A. Misono, *ibid.*, **40**, 2111 (1967).
10) Y. Ohkatsu, T. Osa, and A. Misono, *ibid.*, **40**, 2116 (1967).
11) T. Hara, Y. Ohkatsu, T. Osa, and A. Misono, *Yukagaku*, **20**, 340 (1971).
12) P. D. Bartlett, E. P. Benzing, and R. E. Pincock. *J. Amer. Chem. Soc.*, **82**, 1762 (1960).
13) C. W. Smith, "Acrolein," John Wiley & Sons, New York, N. Y. (1962), p. 17.
14) T. Takeuchi and T. Osa, *Nippon Kagaku Kaishi*, **1972**, 2374.
15) F. P. Greenspan, *Anal. Chem.*, **20**, 1061 (1948).
16) C. E. H. Bawn and S. F. Mellish, *Trans. Faraday Soc.*, **47**, 1261 (1951).
17) G. S. Hammond, J. N. Sen, and C. E. Boozer, *J. Amer. Chem. Soc.*, **77**, 3244 (1955).
18) M. F. R. Mulcahy and I. C. Watt, *Proc. Roy. Soc.*, **216**, 10 (1952).
19) H. J. Shine, J. A. Waters, and D. M. Hoffman, *J. Amer. Chem. Soc.*, **85**, 3613 (1963).
20) K. U. Ingold, New Concepts and Techniques in Oxidation of Hydrocarbons, Amer. Chem. Soc. Mexico Meeting Session of Petrochem. (1967), p. 31.
21) G. M. Burnett, W. S. Dailey, and J. M. Pearson, *Trans. Faraday Soc.*, **61**, 1216 (1965).
22) D. B. Sharp, *J. Amer. Chem. Soc.*, **74**, 1802 (1952).
23) Y. Kamiya, "Organic Peroxides," Kagaku Kogyo Co. (1972), p. 69.
24) G. E. Zaikov, J. A. Howard, and K. U. Ingold, *Can. J. Chem.*, **47**, 3017 (1969).
25) J. A. Kerr, *Chem. Revs.*, **66**, 465 (1966).
26) G. A. Russell, *J. Amer. Chem. Soc.*, **86**, 2357 (1964).
27) C. W. Smith, Ref. 13, p. 24.
28) S. W. Benson, *J. Amer. Chem. Soc.*, **87**, 972 (1965).
29) A. Misono, T. Osa, and Y. Ohkatsu, Advances in Chemistry Series, No. 75, Oxidation of Organic Compounds-I, Amer. Chem. Soc. (1968), p. 120.

Asymmetric Synthesis with Sugar Derivatives. V.[1,2] The Synthesis of α-Hydroxy Acids on Insoluble Polymer Supports

Masajiro KAWANA and Sakae EMOTO

The Institute of Physical and Chemical Research, Wako-shi, Saitama 351

(Received July 2, 1973)

The styrene-2% divinylbenzene copolymer containing 1,2-*O*-cyclohexylidene-5-*O*-trityl-α-D- or -L-xylofuranose (D- or L-**3a**) was prepared. Asymmetric Grignard additions to benzoylformate (**3b**) and pyruvate (**3c**) were carried out using these polymers as chiral ester-components. Enantiomers of α-hydroxy acids, such as atrolactic acid (**4**) and 2-hydroxy-2-phenyl-2-(*p*-tolyl)acetic acid (**5**), were obtained in relatively good synthetic and optical yields, depending on the use of either D- or L-**3a**. The optical yields of **4** for the polymer were higher than those for a low-molecular-weight compound, 1,2-*O*-cyclohexylidene-5-*O*-trityl-α-D-xylofuranose (**8a**). It was shown that the polymer could be used repeatedly.

The application of the method[3] for the synthesis of polypeptides on polymer supports to asymmetric synthesis[4] seems to be very advantageous for the following reasons: (1) the isolation of a desired product from the reaction mixtures is very much simplified; (2) the polymer containing chiral groups which serve as a chiral environment for the asymmetric synthesis can be used repeatedly; and (3) the polymer chain may effect an increase in the stereoselectivities of the reagents.

Recently we have demonstrated[5] that sugar derivatives such as 1,2: 5,6-di-*O*-cyclohexylidene-α-D-glucofuranose can be used effectively as chiral alcohols for the asymmetric synthesis of atrolactic acid (2-hydroxy-2-phenylpropionic acid) (**4**)[6] by Grignard additions to the sugar-esters of benzoylformic acid, and that the increase in the steric bulkiness of a substituent on the C-4 of the furanose ring of gluco- or xylo-furanoside containing a 1,2-*O*-cyclohexylidene or -isopropylidene group causes the optical yield of the acid to increase. Therefore, the use of a cross-linked polystyrene-bound 1,2-*O*-cyclohexylidene-5-*O*-trityl-α-D- or -L-xylofuranose (D- or L-**3a**), which has a bigger substituent on the C-4 of the furanose ring, may be effected to increase the optical yield and provide a convenient method for the asymmetric synthesis.[7] In this paper we would like to report on the asymmetric synthesis of some α-hydroxy acids with insoluble-polymer supports, D- and L-**3a**, and on that with a low-molecular-weight compound, 1,2-*O*-cyclohexylidene-5-*O*-trityl-α-D-xylofuranose (**8a**).[8]

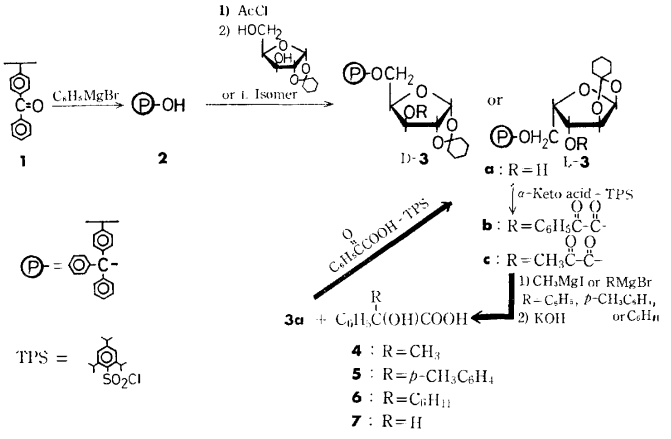

Scheme 1.

Results and Discussion

The polymer (**3a**) was prepared by a procedure similar to that reported earlier.[9] A commercially-available styrene-2% divinylbenzene copolymer (100—200 mesh) was converted into a 21 or 9 mol% benzoylated polymer (**1**) by the use of a limited amount of benzoyl chloride in the presence of aluminum chloride; hereafter, the polymers derived therefrom will be designated as P-21 or -9 respectively. The reaction of **1** with an excess of phenylmagnesium bromide gave a tritylated polymer (**2**) in an almost quantitative yield. On the treatment of **2** with an excess of acetyl chloride, followed by a reaction with 1,2-*O*-cyclohexylidene-α-D-[10] or -L-xylofuranose,[11] D- or L-**3a** was obtained in a 73—87% yield based on the amount of the trityl group in **2**; the remaining chloride was treated with absolute methanol. The hydrolysis of D-**3a** (P-21: 1.0 g) with an acid released ~0.9 mmol of 1,2-*O*-cyclohexylidene-α-D-xylofuranose, this value being very consistent with that calculated from the gain in weight.

The polymer (**3a**) was easily esterified with an excess of benzoylformic acid[12] or pyruvic acid and 2,4,6-triisopropylbenzenesulfonyl chloride (TPS)[13] to give the polymer-bound benzoylformate (**3b**) or the corresponding pyruvate (**3c**) respectively in an almost quantitative yield. In these reactions every 100 styrene units, ~15 and ~7 in P-21 and -9 respectively, were derivatized to the ester functions. The polymers of the P-9 series were much more swelled than those of P-21 in a solvent such as tetrahydrofuran or benzene.

The polymer (**3b** or **c**) thus obtained was subjected to an asymmetric Grignard reaction, which was completed at room temperature. The complete detachment of the acid moiety was effected with a solution of potassium hydroxide at room temperature. The isolated free acids were almost pure, judging from their IR and NMR spectra and from tlc analyses. The results are summarized in Table 1.

From the reaction of D- or L-**3b** (P-21) with methylmagnesium iodide, *R*-(−)- or *S*-(+)-**4**[14] was obtained respectively in a 65% (maximum) optical yield; the synthetic yields, based on the amount of the esters charged on the polymers, were also fairly high (Runs 1 and 5). Similar results were obtained in the case of

Table 2. Repetition of the asymmetric synthesis of *R*-(−)-atrolactic acid (**4**) with the polymer (D-**3b**)[a]

Repet.	Synthetic yield,[b] %	Optical yield,[c] %
1st	70	62
2nd	80	61
3rd	69	55
4th	78	54
5th	78	56
6th	81	58
7th	72	60

a) P-21: see footnote a in Table 1.
b) and c) See the corresponding footnotes in Table 1.

be used for the asymmetric synthesis without any loss of capability.

Although at present a detailed explanation of the steric course of the reaction cannot be offered,[20] some general tendencies of the direction of the attack of the Grignard reagent on the α-keto carbonyl group of the sugar-ester are apparent, as can be seen in Table 1.

Experimental

The melting points are uncorrected. The IR spectra were recorded on a Shimadzu IR-27 instrument in KBr unless otherwise stated. The NMR spectra were obtained using a Model JNM-C-60 HL spectrometer (Japan Electronic Optics Laboratory Co.) with DSS as an internal standard. The chemical shifts are expressed in the δ values. The optical rotations were measured with a Perkin-Elmer Model 141 polarimeter and a 1 dm tube. The elemental analyses were performed by this Institute.

Thin-layer chromatography was accomplished on 2.5×10 cm plates coated with 0.25 mm layers of E. Merck GF-254 silica gel. The following products were detected on these plates: the sugar derivatives, by the use of a methanol–sulfuric acid–*p*-methoxybenzaldehyde (85: 10: 5, v/v) spray, followed by heating; the α-keto and hydroxy acids, under an UV light or by the use of a 0.1% methanolic methyl red spray, followed by heating. The following solvents were used as developers: chloroform or chloroform–methanol (9: 1) for the sugar derivatives; benzene–methanol–acetic acid (45: 8: 4) for the acids.

The polymers were dried over KOH–P_2O_5 at room temperature *in vacuo* overnight unless otherwise stated. The Grignard reagents were prepared by the reactions of magnesium and halides in ether. The crude acids obtained from the asymmetric reactions were identified by comparisons of their IR (in chloroform) and NMR spectra and thin-layer chromatograms with those of analytically-pure racemic samples which had been prepared from the reactions of methyl benzoylformate and Grignard reagents by the standard methods.

A styrene-2% divinylbenzene copolymer was purchased from the Protein Research Foundation (Minoo, Osaka).

The Benzoylated Polymer (1). To a stirred suspension of a styrene-2% divinylbenzene copolymer (100—200 mesh, 20.0 g, 0.19 mol of the phenyl group) in carbon disulfide (200 ml), we added benzoyl chloride (5.6 g, 39.8 mmol) at room temperature, and then added aluminum chloride (5.6 g) at 0—5 °C (bath). The mixture was stirred at 0—5 °C for 1 hr and at room temperature for 16 hr, and then stirred into a mixture of iced water (250 ml) and dioxane (250 ml). After the inorganic materials had been dissolved, the polymer was collected on a glass filter, washed successively with dioxane–water (500 ml, 1: 1), water (1 l), dioxane–water (500 ml, 1: 1), dioxane (400 ml), methanol (250 ml), and ether (500 ml), and then dried to give **1** (P-21). The yield was 24.1 g, which corresponded to 29.4 mmol of the benzoyl group, as judged by the increase in weight. Therefore, 21% of the starting phenyl groups were derivatized to the benzoyl groups. $\nu_{C=O}$, 1655 cm^{-1}.

Under similar conditions, **1** (P-9) was prepared using benzoyl chloride (3.0 g, 21.4 mmol) and aluminum chloride (3.0 g); the yield was 21.8 g (17.3 mmol of the benzoyl group).

The Tritylated Polymer (2). To a stirred suspension of **1** (P-21) (24.0 g, 38.4 mmol of the benzoyl group) in dry tetrahydrofuran (120 ml), we added a solution of phenylmagnesium bromide (78 mmol) in dry tetrahydrofuran (100 ml) at room temperature under a dry nitrogen atmosphere over a period of 30 min. After the completion of the addition, the mixture was stirred at room temperature for 18 hr and then refluxed gently for 6 hr. After the mixture had been cooled, it was stirred into iced 3 M HCl–acetic acid (500 ml, 1: 1). The polymer was collected on a glass filter, washed successively with 3 M HCl–acetic acid (500 ml, 1: 1), water (1 l), tetrahydrofuran–water (500 ml, 1: 1), dioxane–water (500 ml, 1: 1), dioxane (400 ml), methanol (400 ml), and ether (400 ml), and then dried to give **2** (P-21); the yield was 27.0 g (38.5 mmol of the trityl group). There was no carbonyl band detectable at 1655 cm^{-1}, indicating that the reaction had essentially been completed.

Under similar conditions, **2** (P-9) was prepared using **1** (P-9) (43.0 g, 35.3 mmol of the benzoyl group); the yield was 46.0 g, (38.5 mmol of the trityl group).

*The Polymer-bound 1,2-O-Cyclohexylidene-α-*D*- or -*L*-Xylofuranose (*D*- or *L*-3a).* To a suspension of **2** (P-21) (13.0 g, 18.4 mmol of the trityl group) in dry benzene (80 ml), we added acetyl chloride (10 ml), after which the mixture was gently refluxed for 16 hr with stirring. After the mixture had been cooled, the polymer was collected on a glass filter in a dry-box, washed successively with dry benzene (200 ml) and dry ether (200 ml), and then dried. To a suspension of this polymer in a mixture of dry pyridine (15 ml) and dry benzene (80 ml), we then added 1,2-*O*-cyclohexylidene-α-D-[10] or -L-xylofuranose[11] (6.0 g, 26 mmol), after which the mixture was stirred at room temperature under a dry nitrogen atmosphere for 48 hr. In order to decompose the unreacted trityl chloride groups, absolute methanol (5 ml) was added and the mixture was stirred for another 24 hr. The polymer was collected on a glass filter, washed successively with benzene (100 ml), benzene–chloroform (200 ml, 1: 1), chloroform (200 ml), chloroform–tetrahydrofuran (100 ml, 1: 1), tetrahydrofuran (100 ml), tetrahydrofuran–water (100 ml, 1: 1), water (400 ml), water–dioxane (100 ml, 1: 1), dioxane (100 ml), dioxane-methanol (100 ml, 1: 1), methanol (200 ml), methanol–ether (100 ml, 1: 1), and ether (200 ml), and then dried to give **3a**. The yields of D- and L-**3a** (P-21) were 16.1 and 16.4 g, which corresponded to 14.6 and 16.0 mmol of the sugar respectively. Therefore, 80—87% of the trityl groups were converted into the sugar functions.

Under similar conditions, D-**3a** (P-9) was prepared using **2** (P-9) (45.0 g, 37.8 mmol of the trityl group), acetyl chloride (35 ml), and 1,2-*O*-cyclohexylidene-α-D-xylofuranose (31.1 g, 57 mmol); the yield was 50.8 g (27.4 mmol of the sugar).

The Acid Hydrolysis of the Polymer-bound Sugar (D-3a; P-21). Freshly-distilled dioxane was used in this experiment.

To a strirred suspension of D-**3a** (P-20) (1.0 g, 0.91 mmol of the sugar) in dioxane (5 ml), we added dioxane–8 M HCl

(5 ml, 100: 1, v/v) at room temperature under a nitrogen atmosphere over a period of 15 min, after which the mixture was stirred for 24 hr. The polymer was collected on a glass filter, washed successively with dioxane (20 ml), dioxane–water (20 ml, 1: 1), water (5 ml), dioxane–water (10 ml, 1: 1), dioxane (10 ml), methanol (20 ml), and ether (20 ml), and then dried. The weight of the recovered polymer was 807 mg.

The combined filtrate and washings were treated with Dowex-1, X-2 (OH^- form, 5 ml) for 5 min. The ion-exchange resin was removed by filtration and washed with successively with dioxane–water (20 ml, 1: 1) and water (30 ml). The combined filtrate and washings were then concentrated to dryness to give 1,2-*O*-cyclohexylidene-α-D-xylofuranose as a crystal (208 mg, 0.9 mmol), the spectral data of which were almost identical with those of an authentic sample.[10] No free D-xylose was detected by the tlc analysis.

The recovered polymer (747 mg) was further treated with dioxane–12 M HCl (5 ml, 100: 1, v/v) for 48 hr under conditions similar to those described above, thus giving 1.5 mg of 1,2-*O*-cyclohexylidene-α-D-xylofuranose. The IR spectrum of the resulting polymer showed that only a trace of the sugar function remained.

The Polymer-bound Benzoylformate (3b). To a stirred suspension of D-**3a** (P-21) (15.0 g, 14.7 mmol of the sugar) in a mixture of dry benzene (75 ml) and dry pyridine (25 ml), we added benzoylformic acid (3.76 g, 25 mmol), and then we added TPS (7.6 g, 25 mmol) at room temperature under a dry nitrogen atmosphere. After the mixture had been stirred for 5 hr, absolute methanol (2.5 ml) was added; the stirring was then continued for another hour. The polymer was collected on a glass filter, washed successively with pyridine (80 ml), pyridine–iced water (200 ml, 1: 1), water (1 l), dioxane–water (300 ml, 1:1), dioxane (300 ml), dioxane–methanol (300 ml, 1: 1), methanol (200 ml), methanol–ether (200 ml, 1: 1), and ether (200 ml), and dried to give D-**3b** (P-21). The yield was 17.16 g, which corresponded to 16.4 mmol of the ester, as judged by the increase in weight. Therefore, the esterification had been essentially completed. $\nu_{C=O}$, 1740, 1691 cm^{-1}.

Under similar conditions, L-**3b** (P-21) (6.69 g, 5.23 mmol of the ester) and D-**3b** (P-9) (9.67 g, 5.1 mmol of the ester) were prepared starting from L-**3a** (P-21) (6.0 g, 5.88 mmol of the sugar) and D-**3a** (P-9) (9.0 g, 4.9 mmol of the sugar) respectively.

The Polymer-bound Pyruvate (3c). To a stirred suspension of D-**3a** (P-9) (9.0 g, 4.9 mmol of the sugar) in a mixture of dry benzene (60 ml) and dry pyridine (10 ml), we added freshly-distilled pyruvic acid (1.27 g, 14.7 mmol); we then added TPS (4.45 g, 14.7 mmol) at room temperature under a dry nitrogen atmosphere. The mixture was treated in a similar manner to that described for the synthesis of **3b**, giving D-**3c** (P-9). The yield was 9.38 g (5.4 mmol of the ester). $\nu_{C=O}$, 1760 (shoulder), 1734 cm^{-1}.

Analogously, D-**3c** (P-21) (14.98 g, 14.0 mmol of the ester) was prepared starting from D-**3a** (P-21) (14.0 g, 12.6 mmol of the sugar).

1,2-O-Cyclohexylidene-5-O-trityl-α-D-xylofuranose (8a). To a solution of 1,2-*O*-cyclohexylidene-α-D-xylofuranose[10] (23.0 g, 0.1 mol) in dry pyridine (100 ml), we added trityl chloride (32.3 g, 0.12 mol) at room temperature; the mixture was stirred for 1 hr and then allowed to stand at room temperature for 2 days. The mixture was poured into iced water (500 ml), and the undissolved materials were collected by decantation and dissolved in ether (600 ml). The ethereal solution was washed with water (2×100 ml) and dried over magnesium sulfate. The ether was then removed, and the pyridine was distilled by repeated co-evaporation with xylene. The residue was crystallized from benzene–*n*-hexane to afford **8a** (38.7 g, 82%). Further recrystallization gave an analytically pure sample: mp 145—147 °C; $[\alpha]_D^{25}$ −28.3° (*c* 1, EtOH); NMR (DMSO-d_6) 5.11 (d, 1H of the hydroxyl group on C-3).

Found: C, 76.45; H, 6.62%. Calcd for $C_{30}H_{32}O_5$: C, 76.24; H, 6.83%.

3-O-Benzoylformyl-1,2-O-cyclohexylidene-5-O-trityl-α-D-xylofuranose (8b). To a stirred solution of **8a** (4.7 g, 0.01 mol) in a mixture of dry pyridine (10 ml) and dry benzene (20 ml), we added benzoylformic acid (1.65 g, 0.011 mol); then we added TPS (3.34 g, 0.011 mol) at room temperature. After having been stirred for 3 hr, the mixture was stirred into iced water (100 ml) and then extracted with ether (300 ml). The extract was washed with water (2×50 ml) and dried over magnesium sulfate. The ether was then evaporated, and the pyridine was removed by repeated co-evaporation with toluene *in vacuo* to give a syrup, which was subsequently chromatographed on a silica gel column (100 g, 3.5×22 cm) packed with chloroform. Rapid elution (13 ml/min) was effected in order to avoid the decomposition of the product; 25 ml fractions were collected. Fractions 9—12 contained **8b** (3.5 g, 58%) slightly contaminated with impurities. Fractions 13—16 were combined, and the solvent was removed to give analytically pure **8b** (1.3 g, 22%) as a glass after drying over P_2O_5 at 100 °C *in vacuo* for 2 hr: $[\alpha]_D^{25}$ −23.1° (*c* 1, $CHCl_3$); $\nu_{C=O}$, 1740, 1695 cm^{-1}.

Found: C, 75.68; H, 5.92%. Calcd for $C_{38}H_{36}O_7$: C, 75.48; H, 6.00%.

1,2-O-Cyclohexylidene-3-O-pyruvinyl-5-O-trityl-α-D-xylofuranose (8c). To a stirred solution of **8a** (7.1 g, 15 mmol) in a mixture of dry pyridine (20 ml) and dry benzene (30 ml), we added freshly-distilled pyruvic acid (1.94 g, 22 mmol); following the subsequent addition of TPS (6.1 g, 20 mmol) at room temperature, the mixture was treated in a similar manner to that described for the synthesis of **8b**. The resulting syrup was crystallized from *n*-hexane–benzene to afford **8c** (4.5 g, 55%). Recrystallization from the same solvents gave an analytically pure sample: mp 149—152 °C; $[\alpha]_D^{25}$ −46.3° (*c* 1, $CHCl_3$); $\nu_{C=O}$, 1756, 1737 cm^{-1}.

Found: C, 73.20; H, 6.30%. Calcd for $C_{33}H_{34}O_7$: C, 73.04; H, 6.32%.

The Reaction Vessel for the Asymmetric Synthesis on the Polymer. The reaction vessel consisted of a three-necked flask (100 ml) fitted with a 2.5 cm medium-porosity fritted disk filter in the central part of the side of the flask. The tubing was led beyond the disk and sealed to a bore stopcock through which the solvents were removed under suction. A Grignard reagent which had been prepared in another three-necked flask (50 ml) was transferred directly into the above-mentioned flask through a tube fitted with a 1.3 cm rough-porosity fritted disk filter and a stopcock.

Asymmetric Synthesis of Atrolactic Acid (4). Some of the reaction conditions and results are presented in Tables 1 and 2.

(A) Synthesis on the polymer. To a stirred suspension of D- or L-**3b** (3—4 g, 2.1—2.5 mmol of the esters) in dry benzene (20—25 ml) in the reaction vessel, we added a solution of the Grignard reagent (6 mmol) in dry ether (18 ml) under a dry nitrogen atmosphere. After the reaction had been completed, the solvents were removed through the filter. The polymer was washed successively with a solution of ammonium chloride (10 g) in iced water–dioxane (200 ml, 1: 1), water (200 ml), dioxane–water (200 ml, 1: 1), dioxane (100 ml), dioxane–methanol (100 ml, 1: 1), and methanol (100 ml), and then dried over KOH–P_2O_5 at room tem-

perature *in vacuo* for 2—3 hr. The IR spectrum of the polymer showed the absence of the α-keto carbonyl group.

Freshly-distilled tetrahydrofuran was used in the next experiment. The polymer was swelled in tetrahydrofuran (15—25 ml), and then a solution of potassium hydroxide (600 mg, 11 mmol) in a tetrahydrofuran–methanol–water mixture (12 ml, 5: 5: 2) was added at room temperature under a nitrogen atmosphere over a period of 20 min. After the mixture had been stirred for 5 hr, the solvents were filtered; the polymer was then washed successively with tetrahydrofuran–methanol–water (100 ml, 20: 5: 2), water (50 ml), and tetrahydrofuran–water (100 ml). The resulting polymer could be used repeatedly; see (*B*). The combined filtrate and washings were concentrated to *ca.* 7 ml below 50 °C (bath) *in vacuo*. The residue was diluted with water (15 ml), and the undissolved material was removed by filtration through a Celite pad and washed with a small amount of water. The combined filtrate and washings were cooled, acidified with 12 M HCl (2 ml), and extracted with ether (3×100 ml). The ethereal extract was washed with water (10 ml) and dried over magnesium sulfate. The removal of the ether gave a slightly colored crystal, which was decolorized with active charcoal in water (20 ml). The water was removed *in vacuo*, and the crystalline residue was again dissolved in ethanol (15 ml). The solution was filtered through a Celite pad. The removal of the ethanol gave **4** as a colorless crystal, which was then dried over KOH–P_2O_5 at room temperature *in vacuo* for 20 min; yields, 52—308 mg.

(B) Repetition of the reactions. Under the same conditions as are described in (*A*), D-**3b** (P-20) (3.0 g, 2.5 mmol of the ester) was treated in the reaction vessel. The resulting polymer was washed with tetrahydrofuran (100 ml) and then stirred in a mixture of acetic acid–tetrahydrofuran–water (100 ml, 1: 95: 4) at room temperature for 30 min in order to remove the potassium hydroxide remaining in the polymer. After the solvents had been removed, the polymer was washed successively with tetrahydrofuran-water (100 ml, 19: 1), tetrahydrofuran–water (100 ml, 1: 1), tetrahydrofuran–pyridine (50 ml, 49: 1), tetrahydrofuran (100 ml), dioxane–methanol (50 ml, 1: 1), and methanol (100 ml), and then dried.

The polymer was then swelled in benzene (15 ml). To this suspension we added, successively, pyridine (3 ml), benzoylformic acid (750 mg, 5.0 mmol), and TPS (1.5 g, 5.0 mmol), after which the mixture was treated under the conditions described for the synthesis of **3b**. The resulting polymer was again subjected to the Grignard addition, and the subsequent reactions were repeated.

The yields were 288—336 mg. The IR and NMR spectra of **4** from the 1st and 7th runs were identical with those of an analytically pure racemic sample.

(C) Synthesis with low-molecular-weight compounds. **8b** (1.21 g, 2.0 mmol) or **8c** (1.25 g, 2.3 mmol) was treated under the conditions described in (*A*), except for the following conditions: (1) The Grignard adduct was hydrolyzed with a solution of ammonium chloride (10 g) in cold water (100 ml), and the resulting ester was extracted with ether (3×100 ml). The extract was then dried over magnesium sulfate, and the ether was removed. (2) The ester of **4** was completely hydrolyzed in methanol (15 ml) with a solution of potassium hydroxide in a mixture of methanol (6 ml) and water (3 ml). The concentrated reaction mixture was then diluted with water (20 ml) and extracted with chloroform (4×100 ml). The water layer was concentrated to *ca.* 10 ml and acidified. (3) In the case of **8c**, the crude product (**4**) was placed in a solution of sodium bicarbonate (300 mg) in water (15 ml), after which the mixture was extracted with ether (100 ml). The extract was washed with water (5 ml). The combined water layer was then acidified to give **4**.

The yields were 221—226 and 82 mg from **8b** and **c** respectively.

*Asymmetric Synthesis of 2-Hydroxy-2-phenyl-2-(*p*-tolyl)acetic Acid (5).* Some of the reaction conditions and results are listed in Table 1. To a stirred suspension of D-**3b** (P-21) (3.0 g, 2.64 mmol of the ester), L-**3b** (P-21) (3.0 g, 2.34 mmol of the ester), or D-**3b** (P-9) (4.0 g, 2.4 mmol of the ester) in dry benzene (20—25 ml) in the reaction vessel, we added a solution of *p*-tolylmagnesium bromide (6 mmol) in dry ether (18 ml) over a period of 35 min under a dry nitrogen atmosphere. The polymer was treated in a manner similar to that described for the synthesis of **4**, except that after the hydrolysis with potassium hydroxide, the diluted solution with water (15 ml) was decolorized at this stage. The crude **5** was crystallized on standing at room temperature over KOH–P_2O_5 for 1—2 days; the yields were 310—394 mg.

Asymmetric Synthesis of 2-Cyclohexyl-2-hydroxy-2-phenylacetic Acid (6). Some of the reaction conditions and results are listed in the Table 1. To a stirred suspension of D-**3b** (P-21) (4.0 g, 3.8 mmol of the ester) in dry benzene (30 ml) in the reaction vessel, we added a solution of cyclohexylmagnesium bromide (11.4 mmol) in dry ether (25 ml) over a period of 35 min under a dry nitrogen atmosphere. The polymer was treated in a manner similar to that described for the synthesis of **5**, thus yielding the crude product (593 mg) as a syrup. Its NMR spectrum and thin-layer chromatogram showed the presence of **7** (~15%) and small amounts of benzoylformic acid and impurities, besides **6**.

In order to remove these undesirable acids, which were highly soluble in water, a carborundum[21] column (100 mesh, 2.8×19 cm) packed with cold water was used. A crude sample (530 mg) was dissolved in a small amount of ethanol, and the solution was put on the top of the column. After a few ml of water had been eluted, a few ml of cold water was added. The carborundum steeped with the ethanolic solution was stirred with a spatula so that the water-insoluble **6** could be precipitated. The column was then washed with cold water (125 ml), and the **6** was eluted with ethanol. The subsequent evaporation of the solvents gave a syrup, which was then decolorized with active charcoal in aqueous ethanol. The removal of the solvents afforded crystalline **6** (355 mg) after drying over KOH–P_2O_5 at room temperature for 2 days. Although a small amount of **6** was eluted while the column was being washed with water, **6** obtained was free from the water-soluble acids, judging from NMR spectroscopy and tlc analysis.

We wish to thank Dr. Haruo Homma and his staff for the elemental analyses, and Mr. Jun Uzawa and Mrs. Tamiko Chijimatsu for their measurements of the NMR spectra.

References

1) Part IV: M. Kawana and S. Emoto, This Bulletin, **41**, 259 (1968).

2) This work was supported in part by a Research Grant for studies of Life Sciences by this Institute.

3) R. B. Merrifield, *J. Amer. Chem. Soc.*, **85**, 2149 (1963).

4) For reviews, see (a) J. D. Morrison and H. S. Mosher, "Asymmetric Organic Reactions," Prentice-Hall, Englewood Cliffs, N. J. (1971); (b) T. D. Inch, "Advances in Carbohydrate Chemistry and Biochemistry," Vol. 27, ed. by S. Tipson and D. Horton, Academic Press, New York, N. Y. (1972), pp. 191—225.

5) M. Kawana and S. Emoto, This Bulletin, **40**, 2168 (1967).

6) (a) A. McKenzie, *J. Chem. Soc.*, **85**, 1249 (1904); (b) A. McKenzie and G. W. Clough, *ibid.*, **97**, 1016 (1910); (c) V. Prelog, *Helv. Chim. Acta*, **36**, 308 (1953).

7) S. Tsuboyama has reported on the asymmetric synthesis of mandelonitrile by the use of a cross-linked polystyrene-bound methyl D-glucosaminide as a catalyst; This Bulletin, **35**, 1004 (1962).

8) For a preliminary report, see M. Kawana and S. Emoto, *Tetrahedron Lett.*, **1972**, 4855.

9) H. Hayatsu and H. G. Khorana, *J. Amer. Chem. Soc.*, **88**, 3182 (1966); *ibid.*, **89**, 3880 (1967); F. Cramer, R. Helbig, H. Hettler, K. H. Scheit, and H. Seliger, *Angew. Chem.*, **78**, 640 (1966); L. R. Melby and D. R. Strobach, *J. Amer. Chem. Soc.*, **89**, 450 (1967).

10) K. Heyns and J. Lenz, *Chem. Ber.*, **94**, 348 (1961).

11) S. Schuching and G. H. Frye, *J. Org. Chem.*, **30**, 1288 (1965).

12) B. B. Corson, R. A. Dodge, S. A. Harris, and R. K. Hazene, "Organic Syntheses," Coll. Vol. I, p. 241 (1956).

13) T. Neilson and E. S. Werstiuk, *Can. J. Chem.*, **49**, 493 (1971).

14) K. Mislow, *J. Amer. Chem. Soc.*, **73**, 3954 (1951); J. H. Brewster, *ibid.*, **78**, 4061 (1956); J. A. Mills and W. Klyne, "Progress in Stereochemistry," Vol. 1 ed. by W. Klyne, Academic Press, New York, N. Y. (1954), pp. 186—188.

15) For example, see A. Abe and M. Goodman, *J. Polym. Sci., Part A*, **1**, 2193 (1963); R. D. Guthrie, A. D. Jenkins, and J. Stehlicek, *J. Chem. Soc., Ser. C*, **1971**, 2690; F. Ciardelli, P. Salvadori, C. Carlini, and E. Chiellini, *J. Amer. Chem. Soc.*, **94**, 6536 (1972).

16) (a) A. McKenzie and P. D. Ritchie, *J. Chem. Soc.*, **1935**, 153; (b) A. McKenzie and E. W. Christie, *Biochem. Z.* **277**, 426 (1935).

17) T. D. Inch, R. V. Ley, and P. Rich, *J. Chem. Soc., Ser. C*, **1968**, 1693.

18) For reviews, see M. S. Kharasch and O. Reinmuth, "Grignard Reactions of Nonmetallic Substances," Prentice-Hall, Englewood, N. J. (1954), pp. 147—160; Ref. 4a, pp. 177—202.

19) T. D. Inch has described that *R*-(−)-**6** was obtained in a 76% optical yield from the reaction of 1,2: 5,6-di-*O*-isopropylidene-3-*O*-benzoylformyl-α-D-glucofuranose and cyclohexylmagnesium bromide, followed by hydrolysis; *Synthesis*, **1970**, 466.

20) For example, see Ref. 4a, pp. 60—61.

21) The carborundum was washed successively with water, 6 M HCl, water, methanol, chloroform, ethanol, and water before use.

The Reaction of Sulfinic Acids with *N,N*-Dimethylaniline

Shigeru OAE, Osamu YAMADA, and Tetsuya MAEDA

Department of Applied Chemistry, Faculty of Engineering, Osaka City University, Sumiyoshi-ku, Osaka 558

(Received July 13, 1973)

When *N,N*-dimethylaniline was allowed to react with *p*-toluenesulfinic acid, unusual demethylation products, *i.e.*, *p*-(*N,N*-dimethylamino)benzyl *p*-tolyl sulfone and *p*-(*N*-methylamino)benzyl *p*-tolyl sulfone were obtained. *N*-*p*-Toluenesulfonylmethyl-*N*-methylaniline was proposed to be a discrete intermediate, which undergoes intermolecular rearrangement in the presence of acid eventually to afford the above products. Similar results were obtained for the reaction of *N*-methylaniline with *p*-toluenesulfinic acid.

The reaction of benzenesulfinic acid with phenylhydrazine is known to give benzenesulfonyl phenylhydrazide,[1] presumably proceeding *via* a dehydrated intermediate, benzenesulfinyl phenylhydrazide. A similar reaction with aniline has also been suggested to proceed through sulfinamide to give a rearranged product of *p*-aminophenyl phenyl sulfoxide.[2]

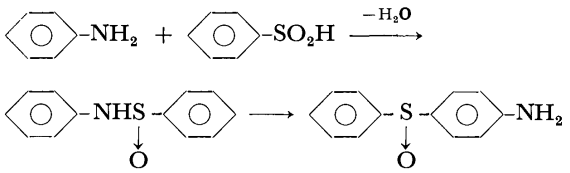

This reaction is an example of sulfinyl migration from neutral nitrogen atom to the *para* position of the aniline ring, although the rearrangement may proceed after protonation of the nitrogen. A few reactions of sulfonyl and sulfonate migration, on the other hand, are known to proceed from the quartenary nitrogen atom. The reactions of azoxybenzene with arenesulfinyl chloride,[3] arenesulfonyl chloride,[4] and with arenesulfonic anhydride[5] are considered to proceed *via* either an intramolecular or intermolecular nucleophilic attack of sulfinate or sulfonate ion on the benzene ring to form the final products.

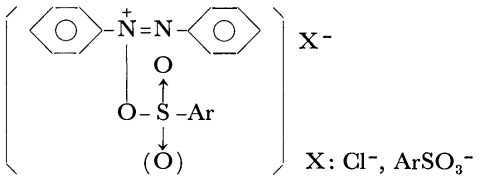

In contrast to the nucleophilic rearrangement of sulfinate or sulfonate groups, electrophilic rearrangements are well known. The rearrangement of benzenesulfinanilide to *p*-aminophenyl phenyl sulfoxide[6] and that of benzenesulfonanilide to *o*-aminophenyl phenyl sulfone[7] in concentrated sulfuric acid are considered to preceed *via* cationic rearrangement of sulfinyl or sulfonyl groups.

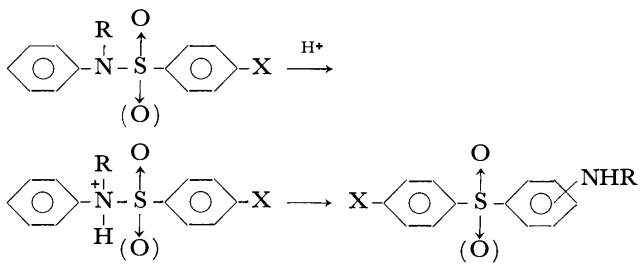

In order to clarify the ambiguity of the sulfinyl and sulfonyl rearrangements, we have reexamined the reaction of aniline with benzenesulfinic acid using *N,N*-dimethylaniline as a substrate. The neutral intermediate, sulfinanilide, can not be formed in this reaction as in the case of aniline. The reaction is expected to give *p*-aminophenyl phenyl sulfone by the nucleophilic attack of the sufinate on the *N,N*-dimethylanilinium ion, analogous to the reaction of azobenzene with benzenesulfinic acid to give *p*-benzenesulfonyl azobenzene.[8] However, we found that the reaction gave complex products, one of which was derived from the demethylation of the *N*-methyl group. In this paper, we deal with the reaction of *N,N*-dimethylaniline with benzenesulfinic acid, referring mainly to the intermediates of the reaction and also some other reactions with the related compounds.

Results and Discussion

N,N-Dimethylaniline was allowed to react with excess *p*-toluenesulfinic acid in refluxing ethanol for 15 hr. *p*-(*N,N*-Dimethylamino)benzyl *p*-tolyl sulfone (Ib) and *p*-(*N*-methylamino)benzyl *p*-tolyl sulfone (IIb) were found to be the major products and *p*-(*N,N*-dimethylamino)phenyl *p*-tolyl sulfoxide (IIIb) a minor product along with the disproportionation products of *p*-toluenesulfinic acid such as *p*-tolyl *p*-toluenethiolsulfonate (IVb), *p,p'*-ditolyl disulfide (Vb) and *p*-toluenesulfonic acid (VIb). Several *p*-substituted benzenesulfinic acids, allowed to react similarly, were found to give the

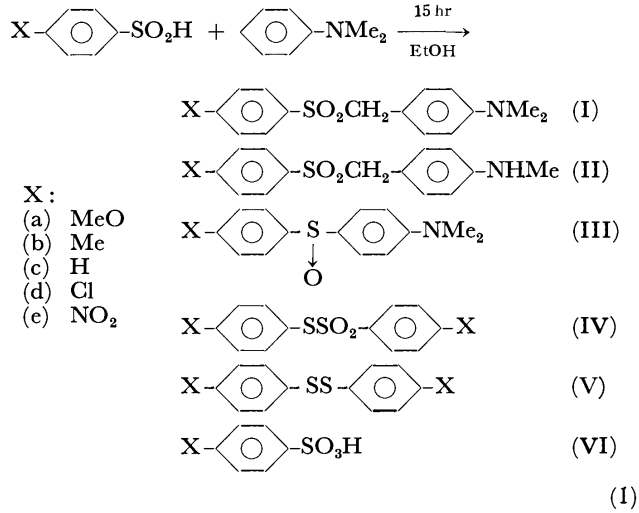

(I)

Table 1. Products of the reaction of *N,N*-dimethylaniline with excess arenesulfinic acid[a)]

X		Solvent	Yield of products (%)		
			I	II	III
a)	MeO	EtOH	32	3.4	3.6
b)	Me	EtOH	22	23	4.7
		CH_3CN	18	18	4
		Benzene	17	10	4.5
c)	H	EtOH	12	39	6
d)	Cl	EtOH	5	18	trace
e)	NO_2	EtOH	11	trace	9

a) Yields were obtained on the basis of the amount of *N,N*-dimethylaniline used.

corresponding products shown in Eq. (1). The yields except for those of the disproportionation products of the sulfinic acid are given in Table 1.

Products IV, V, and VI are considered to be formed by the disproportionation of the sulfinic acid.[9)] This was confirmed by an experiment involving the refluxing of the sulfinic acid alone in ethanol. The mechanism of the disproportionation of the sulfinic acid suggested by Kice *et al.* includes sulfinylsulfone (VII) as the intermediate[10)] which is known to be decomposed by the attack of a nucleophile.[11)]

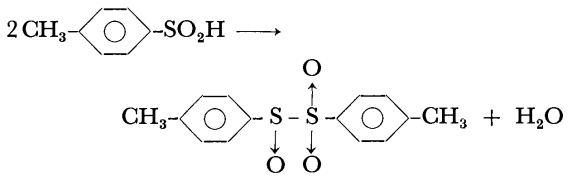

(VIIb)

In the reaction of *N,N*-dimethylaniline with *p*-toluenesulfinic acid, the nucleophilic attack of aniline on the intermediate, VIIb is plausible.

The reaction of *N,N*-dimethylaniline with an equimolar amount of *p*-tolyl *p*-toluenesulfinyl sulfone (VIIb) was carried out. As expected, *p*-(*N,N*-dimethylamino)-benzyl *p*-tolyl sulfone (Ib), *p*-(*N*-methylamino)benzyl *p*-tolyl sulfone (IIb) *p*-(*N,N*-dimethylamino)phenyl *p*-tolyl sulfoxide (IIIb) were obtained as the main products along with disproportionation products of the sulfinic acid as shown in the following.

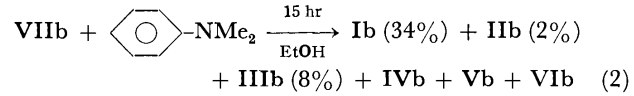

+ IIIb (8%) + IVb + Vb + VIb (2)

As to the mechanism of the reaction of the sulfinyl sulfone with *N,N*-dimethylaniline, the demethylation is considered to proceed through *N*-*p*-toluenesulfonyl-methyl-*N*-methylaniline (VIIIb) as an intermediate as in the case of similar Pummerer[12)] or Polonovski reactions.

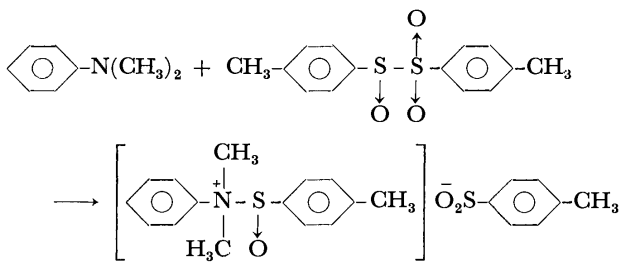

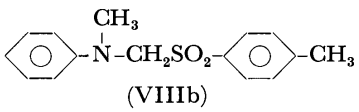

(VIIIb)

Succeeding rearrangements of VIIIb should proceed quite easily in view of the acid-catalyzed rearrangement of *N*-arenesulfenylmethyl *N*-methylaniline (IX).[13)]

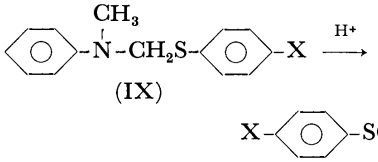

(IX)

N-*p*-Toluenesulfonylmethyl-*N*-methylaniline (VIIIb) was prepared from *p*-toluenesulfinic acid, formaldehyde and *N*-methylaniline and was refluxed in ethanol with a trace amount of *p*-toluenesulfinic acid. *p*-(*N*-Methylamino)benzyl *p*-tolyl sulfone (IIb) was found as the product of the acid-catalyzed rearrangement of VIIIb. The rearrangement of VIIIb with an equimolar amount of *N,N*-dimethylaniline was found to give Ib, IIb, and *N*-methylaniline.

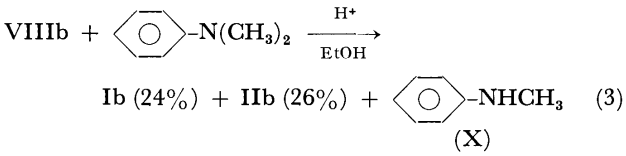

(X)

The formation of Ib and *N*-methylaniline indicates the reaction to be an intermolecular rearrangement of VIIIb to give IIb.

The overall processes of the reaction of *N,N*-dimethylaniline with arenesulfinic acid can thus be written as shown in Scheme 1. In relation to the reaction of *N,N*-dimethylaniline with *p*-toluenesulfinic acid, we examined the reaction of *N,N*-dimethylaniline *N*-oxide with *p*-toluenesulfinic acid. *p*-(*N,N*-Dimethylamino)-phenyl *p*-tolyl sulfone was isolated as follows. The sulfone is presumed to be formed *via* the Bamberger type rearrangement process.[14)]

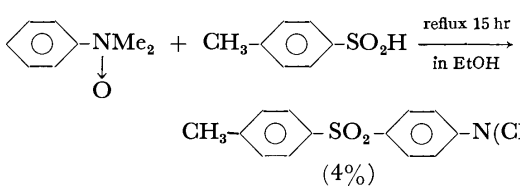

(4%)

We carried out the reaction of *N*-methylaniline with

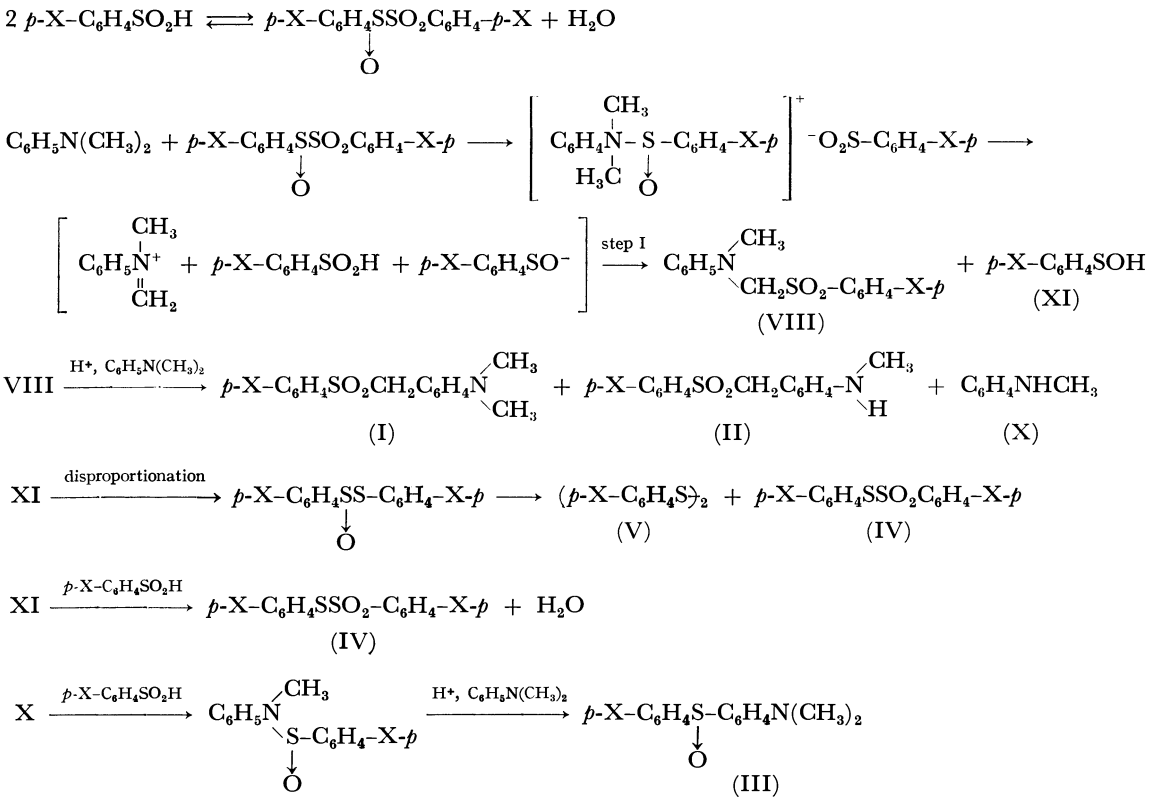

Scheme 1.

p-toluenesulfinic acid under the same conditions and obtained *p*-(*N*-methylamino)phenyl *p*-tolyl sulfoxide and *p*-(*N*-methyl)aminobenzyl *p*-tolyl sulfone as follows.

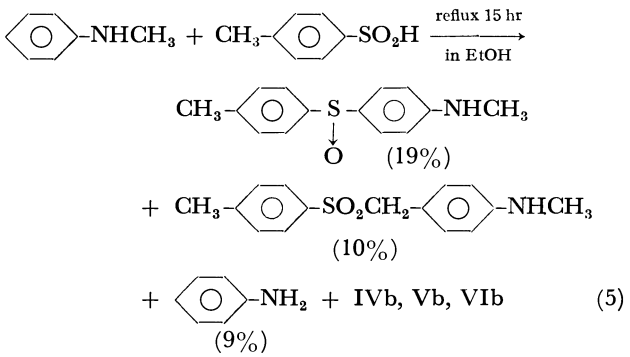

However, *N*,*N*-dimethylbenzylamine and *N*-methylmorpholine did not undergo any demethylation reaction with arenesulfinic acid. This reaction apparently takes place only in the cases of *N*-methyl and *N*,*N*-dimethyl aromatic amines because of the formation of the stabilized anilinium ion formed in the reaction.

Experimental

Materials. *p*-Toluenesulfinic acid was prepared by the reduction of *p*-toluenesulfonyl chloride by the usual method.[15] *p*-Nitrobenzenesulfinic acid was prepared by the alkaline hydrolysis of *p*-nitrobenzenesulfinyl chloride which was synthesized by the oxidative chlorination of *p*,*p*'-dinitrodiphenyl disulfide by bubbling Cl_2 in methylene chloride.[16] Mp *p*-X-C_6H_4-SO_2H: X: OCH_3 97—98 °C, CH_3 85 °C, H 81 °C, Cl 92—93 °C, NO_2 135 °C. *p*-Tolyl *p*-toluenesulfinylsulfone was prepared from *p*-toluenesulfinyl chloride and sodium *p*-toluenesulfinate according to the process given by Bredereck *et al.*[17] *N*,*N*-Dimethylaniline *N*-oxide was prepared by the oxidation of *N*,*N*-dimethylaniline with H_2O_2.[18] *N*-*p*-Toluenesulfonylmethyl-*N*-methylaniline was prepared as follows: Formalin (1.04 g) was added to *p*-toluenesulfinic acid (2.0 g, 0.013 mol) in methanol (3 ml). An equimolar amount of *N*-methylaniline in 15 ml methanol was then added to the reaction mixture with stirring at room temperature. The white crystals precipitated were filtered off and washed with dilute Na_2CO_3. *N*-*p*-Toluenesulfonylmethyl-*N*-methylaniline was obtained. (2.7 g, mp 107—110 °C).

Reaction of N,N-*Dimethylaniline with Arenesulfinic Acid.* A typical run was carried out as follows: *N*,*N*-Dimethylaniline (0.5 g, 0.004 mol) was refluxed with *p*-toluenesulfinic acid (2 g, 0.013 mol) in absolute ethanol (1 ml) for 15 hr. After evaporation of the solvent, the residue was dissolved in $CHCl_3$ and the solution was extracted with water. *p*-Toluenesulfonic acid was obtained from the water layer. The compound was identified by comparison of the *S*-benzyl isothiouronium salt of the acid (mp 181—182 °C) with that of the authentic sample. The $CHCl_3$ layer was dried over Na_2SO_4 and chromatographed on silica gel with $CHCl_3$ as an eluent. *p*-(*N*,*N*-Dimethylamino)benzyl *p*-tolyl sulfone and *p*-(*N*-methyl)aminobenzyl *p*-tolyl sulfone were obtained. The former was identified by comparison of the physical properties with those of the authentic sample[19] and the structure of the latter was confirmed by IR, NMR, and elemental analysis. Found: C, 65.42; H, 6.22; N, 5.08%. Calcd for $C_{15}H_{17}NO_2S$: C, 65.26; H, 6.13; N, 5.01%.

p-(*N*,*N*-Dimethyl)aminophenyl *p*-tolyl sulfoxide was identified by comparison of the physical properties with those of the authentic sample prepared by the methylation of *p*-aminophenyl *p*-tolyl sulfoxide (mp 140—142 °C). Melting points of the products are given in Table 2.

Reaction of N,N-*Dimethylaniline with* p-*Tolyl* p-*Toluenesulfinyl Sulfone.* An ethanol solution of *N*,*N*-dimethylaniline

Table 2. Melting points of the products obtained by the reaction of *N,N*-dimethylaniline with arenesulfinic acids

	X	Products	
		X-C6H4-SO2CH2-C6H4-NMe2	X-C6H4-SO2CH2-C6H4-NHMe
a)	MeO	146—148 °C	
b)	Me	192—193 °C	156—157 °C
c)	H	147 °C	158—159 °C
d)	Cl	158 °C	164—166 °C
e)	NO^2	201 °C	

	X	Products		
		X-C6H4-S(=O)-C6H4-NMe2	X-C6H4-S-SO2-C6H4-X	(X-C6H4-S)2
a)	MeO		44— 45 °C	91— 93 °C
b)	Me	140—141 °C	46 °C	75— 76 °C
c)	H	130 °C	60— 61 °C	45 °C
d)	Cl		70— 71 °C	134—135 °C
e)	NO_2	150—152 °C	180—181 °C	154—155 °C

(0.5 g, 0.004 mol) and an equimolar amount of *p*-tolyl *p*-toluenesulfinyl sulfone was refluxed for 15 hr. Analysis was carried out as described above.

Rearrangement of N-p-*Toluenesulfonylmethyl* N-*Methylaniline in the Presence of Acid.* An ethanol solution of *N*-*p*-Toluenesulfonylmethyl *N*-methylaniline (0.2 g) with a trace amount of *p*-toluenesulfinic acid was refluxed for 15 hr. *p*-(*N*-Methyl)-amino)benzyl *p*-tolyl sulfone (0.14 g) was obtained.

Reaction of N-p-*Toluenesulfonylmethyl* N-*Methylaniline with* N,N-*Dimethylaniline.* An ethanol solution of the title compound (0.5 g, 0.0018 mol) was refluxed for 15 hr with an equimolar amount of *N,N*-dimethylaniline and a trace amount of HCl. *p*-(*N,N*-Dimethylamino)benzyl *p*-tolyl sulfone (0.12 g), *p*-(*N*-methylamino)benzyl *p*-tolyl sulfone (0.13 g) and *N*-methyl- and *N,N*-dimethylanilines were isolated from the reaction mixture by chromatography on silica gel with $CHCl_3$ as an eluent.

Reaction of N,N-*Dimethylaniline* N-*Oxide with* p-*Toluenesulfinic Acid.* An ethanol solution of the *N*-oxide (1 g, 0.007 mol) and the sulfinic acid (3.4 g, 0.0021 mol) was refluxed for 15 hr. *p*-(*N,N*-Dimethylamino)phenyl *p*-tolyl sulfone (0.065 g, mp 212 °C), *p,p'*-ditolyl disulfide (0.037 g), *p*-tolyl *p*-toluenethiolsulfonate (0.30 g) and *p*-toluenesulfonic acid were obtained.

Reaction of N-*Methylaniline with* p-*Toluenesulfinic Acid.* An ethanol solution of *N*-methylaniline (0.5 g, 0.047 mol) and *p*-toluenesulfinic acid (2.2 g, 0.014 mol) was refluxed for 15 hr. *p*-(*N*-Methylamino)benzyl *p*-tolyl sulfone (0.105 g) and *p*-(*N*-methylamino)benzyl *p*-tolyl sulfoxide (0.214 g, mp 146—147 °C) were obtained along with *p,p'*-ditolyl disulfide, *p*-tolyl *p*-toluenethiolsulfonate and *p*-toluenesulfonic acid.

References

1) O. Escales, *Ber.*, **18**, 893 (1885).
2) C. J. M. Stirling, *Int. J. Sulfur. Chem.*, **B**, **6**, 277 (1971).
3) Unpublished results of this laboratory.
4) S. Oae, T. Maeda, S. Kozuka, and M. Nakai, This Bulletin, **44**, 2495 (1971).
5) S. Oae, and T. Maeda, *Tetrahedron*, **28**, 2127 (1972).
6) J. Vonkennel and J. Kimmig, *Chem. Zentr.*, **1953**, 8143.
7) S. Searles and S. Nukina, *Chem. Rev.*, **59**, 1077 (1959).
8) W. Bradley, and J. D. Hammon, *J. Chem. Soc.*, **1962**, 2713.
9) L. Horner and O. H. Basedow, *Ann., Chem.*, **612**, 108 (1958).
10) J. L. Kice, and K. W. Bowers, *J. Amer. Chem. Soc.*, **84**, 605 (1962); J. L. Kice, and K. W. Bowers, *J. Org. Chem.*, **29**, 1162 (1963).
11) J. L. Kice, and G. Guarald, *Tetrahedron Lett.*, **1966**, 6135.
12) R. Pummerer, *Ber.*, **43**, 1041 (1910).
13) G. F. Grillot, and P. T. S. Lau, *J. Org. Chem.*, **30**, 28 (1965).
14) C. K. Ingold, "Structure and Mechanism in Organic Chemistry", 2nd. Ed. Cornell Univ. Press, (1969), pp. 906—909.
15) "Organic Syntheses", Coll. Vol. 1, p. 492 (1941).
16) I. B. Douglass, B. S. Farah, and E. G. Thomas, *J. Org. Chem.*, **26**, 1996 (1961).
17) H. Bredereck, A. Wagner, H. Beck, and R. J. Klein, *Chem. Ber.*, **93**, 2736 (1960).
18) S. Oae, T. Kitao, and Y. Kitaoka, *J. Amer. Chem. Soc.*, **84**, 3366 (1962).
19) E. Bader, *Chem. Ber.*, **88**, 41 (1955).

Studies on Reactions of the *N*-Phosphonium Salts of Pyridines. V. The Preparation of Carboxylic Amides and Esters by Means of the One-electron-transfer Oxidation of Phosphorous Acid and Its Esters in the Presence of Tertiary Amines

Noboru YAMAZAKI and Fukuji HIGASHI

Department of Polymer Science, Tokyo Institute of Technology, Ookayama, Meguro-ku, Tokyo 152

(Received August 7, 1973)

The oxidation of phosphorous acid and its esters with an equimolar amount of mercurous chloride and half an equimolar amount of mercuric chloride was carried out in tertiary amines. On the treatment of the oxidation mixture with carboxylic acids, amines, and alcohols, followed by aminolysis, alcoholysis, or acidolysis, the corresponding carboxylic amides and esters were obtained in good yields, together with a nearly quantitative yield of metallic mercury. The yield was affected by the tertiary amines, the alkyl groups in the dialkyl phosphites, and the steric effect of the carboxylic acids. The reaction was proposed to proceed through the activation of carboxylic acids, amines, and alcohols *via* the *N*-phosphonium salts prepared by the oxidation. The electron-transfer processes involved in the oxidation were discussed on the basis of the yield of the amides obtained. These procedures were successfully extended to the preparation of peptides and active esters of amino acids, using diphenyl phosphite in pyridine.

In previous papers,[1-4] we showed a convenient method for the preparation of carboxylic amides and esters through the activation of carboxyl, amino, and hydroxyl groups by means of the *N*-phosphonium salts of pyridines given by the oxidation of phosphorous acid and its esters with mercuric salts in pyridines.

In these reactions, mercuric salts were used in amounts equimolar with the phosphorous compounds; the amount of liberated mercury after the reactions was nearly quantitative. Obviously, these facts show that the mercuric salts accepted two electrons from the phosphorous compounds, were changed into metallic mercury, and reversely oxidized the phosphorus(III) compounds into the phosphorus(V) compounds. Hence, the reactions can be described as the oxidation by a two-electron transfer:[1]

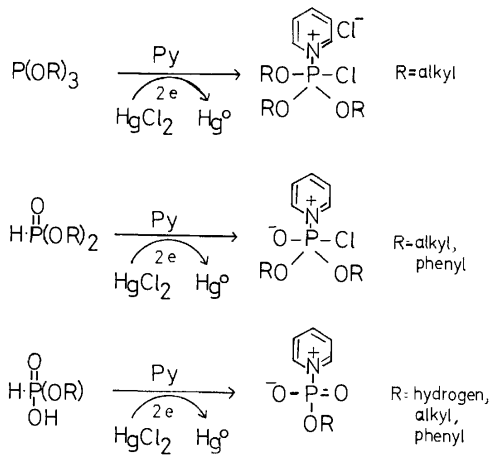

We have also found[5] that the oxidation products prepared from phosphorus compounds with an equimolar amount of mercurous chloride or half an equimolar amount of mercuric chloride in pyridine could cause coupling reactions between carboxylic acids and amines, and alcohols to produce the carboxylic amides and esters. It has been assumed[5] that the phosphorus (III) compounds are oxidized by an one-electron transfer to the corresponding phosphorus(IV) compounds, which then form the corresponding *N*-phosphonium salts of pyridine similar to those obtained by the two-electron-transfer oxidation

This paper will describe in detail the results of the oxidations of phosphorous acid and its esters with mercurous and mercuric chlorides in pyridines, and of application of the process to the syntheses of carboxylic amides and esters. It will also show a successful extension of this procedure to the preparation of peptides and active esters of amino acids.

Results and Discussion

Such as in the two-electron oxidation, phosphorous acid and its esters (25 mmol) was oxidized in refluxing pyridine with an equimolar amount of mercurous chloride (25 mmol) or half an equimolar amount of mercuric chloride (12.5 mmol). When the oxidation mixture (I) thus formed was treated with a carboxylic acid and then with aniline, the corresponding anilide was obtained in the yield shown in Table 1, together with a nearly quantitative yield of metallic mercury (Method A). In Method B, I was refluxed first with aniline and then acidolized with carboxylic acids.

Furthermore, the reaction of I with carboxylic acids and then with alcohols gave the corresponding carboxylic esters (Method C). The esters were also prepared by adding the two components in the reverse order, that is, by the reaction of I initially with alcohols and then with carboxylic acids (Method D). Several anilides and esters thus obtained are listed in Tables 1 and 2.

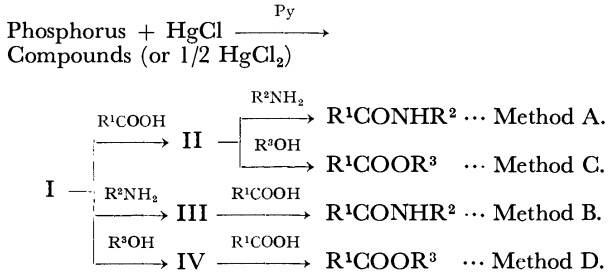

Table 1. Preparation of anilides by means of the one-electron oxidation of phosphorus compounds with mercurous and mercuric chlorides in pyridine

Phosphorus compounds	Yield of anilides obtained (%)			
	Method A		Method B	
	Acetanilide[a]	Pivalanilide	Acetanilide[a]	Pivalanilide
Phosphorous acid	79 (53)	0	61 (66)	9
Monophenyl ester	45 (51)	—	65 (61)	—
Diisopropyl ester	80 (81)	63	85 (93)	58
Triisopropyl ester	50 (48)	—	57 (58)	—

a) Values in the parentheses are those obtained by the oxidation with half an equivalent of mercuric chloride.

Table 2. Preparation of carboxylic esters by means of the one-electron oxidation of phosphorus compounds with mercurous chloride in pyridine

Phosphorus compounds	Carboxylic esters	Yield (%)	
		Method C	Method D
Phosphorous acid	Phenyl acetate	60	65
Diisopropyl ester	*n*-Butyl *n*-butyrate	59	56

There are two possible ways of electron transfer, in principle, in the oxidation of the phosphorus(III) compounds with an equimolar amount of mercurous chloride or with half an equimolar amount of mercuric chloride. One is the one-electron-transfer oxidation of the phosphorus(III) compounds to yield the corresponding phosphorus(IV) compounds, and the other is two-electron transfer to the phosphorus(V) compounds.

The type of oxidation process involved in the oxidation of phosphorus(III) compounds was examined in terms of the yield of the acetanilide obtained (Table 1).

In the case of the oxidation of phosphorus(III) compounds with mercurous chloride, phosphorous acid and its diisopropyl ester gave acetanilide in excellent yields. The yields higher than 50% indicate that mercurous chloride can oxidize one equivalent of the phosphorus compounds by one-electron transfer to yield the corresponding active product (I), which could then condensate one equivalent of acetic acid and aniline to give the anilide in the high yields. The reactions with the monophenyl and triisopropyl esters, which gave yields of nearly 50% or more of acetanilide, possibly support the involvement of the one-electron-transfer oxidation in the reactions.

Similar situations were encountered in the oxidation with half an equivalent of mercuric chloride (Table 1). Especially, the diisopropyl ester gave acetanilide in a surprisingly high yield (93%). It is also the case with the reactions yielding carboxylic esters in yields higher than 50%.

In one-electron-transfer oxidation with mercuric chloride, the oxidation may not proceed step-by-step *via* one-electron oxidation, first with mercuric chloride and then with the resultant mercurous chloride, since mercuric chloride can undergo two-electron oxidation under these conditions. Therefore, the oxidation might take place between two moles of phosphorus(III) compounds and one mole of mercuric chloride *via* an intermediate, as is shown below;

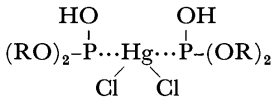

The reaction producing amides by way of one-electron-transfer oxidation with mercurous chloride in pyridine was investigated in detail using phosphorous acid and its diesters. The reaction has been proposed[5] to proceed *via* the quaternary *N*-phosphonium salt of pyridine (I in the scheme), similar to that given by the two-electron oxidation, though the formation of quaternary phosphonium salts has been known only in the reactions of phosphorus(III) compounds with nucleophiles. If the *N*-phosphonium salt has a similar structure, the yield of anilides would be influenced by the alkyl groups of the phosphites, tertiary amines, and carboxylic acids, as in the cases of the two-electron-transfer oxidation.

Table 3. Effect of ester residues of the dialkyl and diphenyl phosphites upon the yield

Diester	Yield of acetanilide (%)
Dimethyl	33
Diethyl	75
Diisopropyl	80
Di-*n*-butyl	72
Diphenyl	79

Table 4. Effect of tertiary amines upon the yield

Tertiary amine	pK_a	Yield of acetanilide[a] (%)
Pyridine	5.23	79 (92)
3-Methylpyridine	5.52	50 (90)
2-Methylpyridine	5.97	39 (64)
4-Methylpyridine	6.02	45 (67)
2,6-Dimethylpyridine	6.99	30 (0)

a) Values in the parentheses are those obtained by two-electron oxidation[2].

The effect of alkyl groups upon the yield of acetanilide in the reactions using several dialkyl and diphenyl phosphites may be in the following order: methyl<ethyl≈*n*-butyl<isopropyl≈phenyl. This was similar to that observed in the reaction by two-electron oxidation. In addition, among the diesters of phos-

phorous acid examined, diphenyl phosphite with electron-attracting phenyl groups was found to be most effective for the reaction at low temperatures and so was used for peptide synthesis, as will be discussed below.

In Table 4 the effect of tertiary amines upon the reaction is compared with that in the two-electron oxidation. An increase in the basicity of amines decreases the yield of acetanilide, as in the latter case. However, the effect is not explicable only by the basicity, because a small difference in pK_a value between pyridine and other pyridine derivatives had an unexpectedly large effect upon the yield. The facts that the yield in 2-methylpyridine was nearly equal to that in 4-methylpyridine, and that even in 2,6-dimethylpyridine acetanilide was obtained in a 30% yield, suggested the presence of a slight steric effect.

The steric effect of carboxylic acids upon the yield was reflected by the yields of pivalanilide, lower than those of acetanilide in both one- and two-electron oxidations.

The proposed reaction mechanism was investigated using diethyl phosphite, since the diester of phosphorous acid proceeded predominantly *via* one-electron-transfer oxidation, as has been discussed above. The salts, I, II, III, and IV, were separated according to previously described procedures,[1-4] though their amounts were not satisfactory.

The IR spectrum of I showed a band at 1630 cm^{-1} due to the $\nu_{C=N^+}$ of the *N*-phosphonium salts of pyridine.[1] II, III, and IV exhibited bands due to the $\nu_{C=O}$ of the acetoxy group, the $\nu_{C=C}$ of the anilino group, and the $\nu_{C=C}$ of the phenoxy group respectively, together with the band due to the $\nu_{C=N^+}$ of the *N*-phosphonium salt.

On the basis of the experimental results obtained, the reaction may be explained by assuming the initial formation of the *N*-phosphonium salt (I) by the one-electron-transfer oxidation of phosphorus compounds. Salt I reacts with carboxylic acids, amines, and alcohols to yield the corresponding products, II, III, and IV. The carboxyl, amino, and alkoxy groups carried by these products are activated enough to be converted into carboxylic amides and esters on further aminolysis, alcoholysis, and acidolysis (see the scheme).

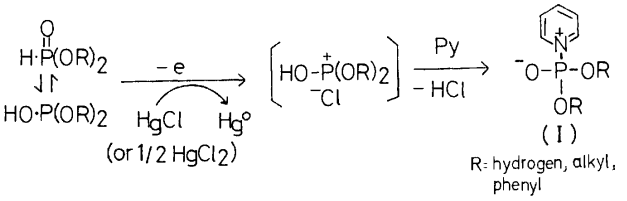

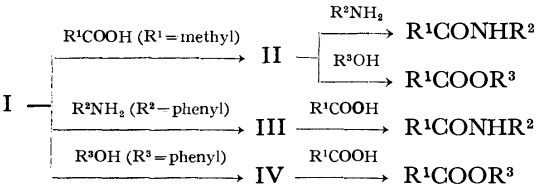

Scheme

As has been discussed above, simple carboxylic amides and esters were synthesized by way of the one-electron-transfer oxidation of the phosphorus compounds with mercurous and mercuric chlorides in pyridines.

Then this method for the preparation of the amides and esters were applied in the syntheses of peptides and active esters of amino acids, using diphenyl phosphite in pyridine. The coupling reactions between carboxyl and amino components, and hydroxyl components were carried out at 45 °C by mixing the reactants with the oxidation product (I) obtained from diphenyl phosphite in order to prevent racemization.

Several peptides and an active ester were obtained in good yields without any detectable racemization within the limits of experimental error (see Table 5).

The presence of the free side chains of glutamic acid, glutamine, and methionine in the carboxyl component, and of tyrosine in the amino component, did not cause any difficulties in the reactions as have been observed in two-electron oxidation.[3] In the case of glutamic acid, the α-carboxyl group was activated in preference to the γ-carboxyl group, yielding the α-peptide in a good yield. Similarly, a peptide of glutamine was obtained without any accompanying side reactions such

Table 5. Preparation of peptides and an active ester by means of the oxidation of diphenyl phosphite with mercurous chloride in pyridine

Peptide and an active ester	Reaction time (hr)	Yield (%)	(Mp °C)	$[\alpha]_D$
Z-Gly-Gly-OEt	12	91[a]	80	
Z-Gly-Gly-OEt	6	92	—	
Z-Gly-Gly-Gly-OEt	6	82	163—164	
Z-Phe-Gly-OEt(L)	6	80	108—109	−17.5° (*c* 5, EtOH)
Z-Phe-Gly-OEt(L)	12	91	—	
Z-Gly-Tyr-OEt(L)	6	77	125—126	+18.9° (*c* 5, EtOH)
Z-Gly-Tyr-OEt(L)	12	91	—	
Z-Met-Gly-OEt(DL)	12	93	72—73	
Z-Glu(NH_2)-Gly-OEt(L)	12	81	166—168	− 6.5° (*c* 1, DMF)
Z-α-Glu-Gly-OEt(L)	6	72	122—123	
Z-Gly-O-C_6H_5-NO_2(*p*)	20	82	128	
Z-Gly-O-C_6H_5-NO_2(*p*)	20	84[a]	—	

a) Half an equivalent of mercuric chloride was used in the place of mercurous chloride.

as nitrile formation. In the reaction of ethyl tyrosinate, with both amino and hydroxyl groups, the amino group was preferably activated to produce the corresponding amide with the glycine.

Experimental

The salts (I, II, III, and IV), carboxylic amides and esters, peptides, and active esters were prepared according to previously reported procedures,[1-4] except for the use of one equivalent of mercurous chloride and half an equivalent of mercuric chloride in the place of one equivalent of mercuric chloride.

References

1) Part I; N. Yamazaki and F. Higashi, This Bulletin, **46**, 1235 (1973).
2) Part II; N. Yamazaki and F. Higashi, *ibid.*, **46**, 1239 (1973).
3) Part III; N. Yamazaki and F. Higashi, *ibid.*, **46**, 3824 (1973).
4) Part IV; N. Yamazaki and F. Higashi, *J. Amer. Chem. Soc.*, submitted for publication.
5) N. Yamazaki and F. Higashi, presented at the 26th Annual Meeting of the Chemical Society of Japan, Tokyo, April, 1972.

Kinetics of the Autoxidation of Substituted Anthranols to Anthraquinones in Buffered Aqueous Dioxane[1]

Yoshiro OGATA, Kazuo NATE, and Mitsuji YAMASHITA

Department of Applied Chemistry, Faculty of Engineering, Nagoya University, Chikusa-ku, Nagoya 464

(Received March 2, 1973)

Autoxidation of 2-substituted anthranols to the corresponding anthraquinones in alkaline buffered aqueous dioxane (2:1 in vol) has been studied kinetically at 35 °C by means of the manometric method. The relative rate constants for the autoxidation of anthranyl oxide ions have been evaluated, in which dissociation of anthrones is taken into account. Application of substituent effect on the one-electron transfer to the oxide ion to the Hammett equation gives an average ρ-value of -1.5, which was little influenced by pH of the solution.

Anthrone is a tautometric compound which exists in most solvents predominantly in a keto form at room temperature, but the equilibrium is shifted much to the enol form at high pH.[2]

Anthranol is easily oxidized to anthraquinone by molecular oxygen in alkaline solutions. In a previous paper,[3] it was reported that the autoxidation rate of anthranol in alkaline buffered aqueous dioxane is expressed as: $v=k[\text{Anthrone}]_T[OH^-]_p$, where p is the partial pressure of oxygen and [ ]$_T$ the stoichiometric concentration. The results suggest a mechanism involving a rate-determining attack to form anthranyl oxide radical, which is rapidly oxidized to give anthraquinone.

The present study was undertaken to obtain further information on the mechanism of reaction, especially with respect to the substituent effect on anthranols. The experiments were carried out in alkaline buffered dioxane–water (2:1 in vol) under the conditions where anthraquinone was the only organic products; the product was confirmed by tlc (See Experimental).

Experimental

Materials. Purification of dioxane and preparation of anthrone were described previously.[3] 2-Methylanthrone[4] was prepared by the Friedel-Crafts condensation of phthalic anhydride and toluene followed by the reduction of formed 2-(4-methylbenzoyl)benzoic acid with zinc and ammonia and then cyclization of 4-methyldiphenylmethane-2′-carboxylic acid with concentrated H_2SO_4. Recrystallization from a mixture of benzene and petroleum ether (3:1 in vol) gave crystals of mp 98.5—99.5 °C (lit,[4] 99.5—100 °C). λ_{max} (log ε) 263 mμ (4.24).

2-Chloroanthrone,[5] 2-methoxyanthrone,[6] and 2-bromoanthrone[4] were prepared similarly by the reaction of 4-chloro, 4-methoxy, and 4-bromodiphenylmethane-2′-carboxylic acid with concentrated H_2SO_4, respectively, and then purified. 2-Chloroanthrone; mp 152—153 °C (lit,[5] mp 155 °C), λ_{max} (log ε) 264 mμ (4.23). 2-Methoxyanthrone; mp 92—93 °C (lit,[6] mp 94—95 °C), λ_{max} (log ε) 267 mμ (4.23). 2-Bromoanthrone; mp 157—158 °C (lit,[4] mp 160 °C), λ_{max} (log ε) 268 mμ (4.27).

2-Substituted anthraquinones[7] were prepared by the cyclization of 2-(4-substituted benzoyl)benzoic acids with fuming H_2SO_4 and recrystallized from ethanol. 2-Methylanthraquinone; mp 178 °C (lit,[5] mp 177—178 °C), λ_{max} (log ε) 255 mμ (4.68). 2-Chloroanthraquinone; mp 214 °C (lit,[8] mp 210 °C), λ_{max} (log ε) 256 mμ (4.67). 2-Methoxyanthraquinone; mp 194—196 °C (lit, mp 194.5 °C,[9a] 196 °C,[9b] 195—197 °C[9c]). 2-Bromoanthraquinone; mp 210—211 °C (lit,[10] mp 205—207 °C). Inorganic reagents were of commercial guaranteed grade.

Kinetic Procedure. The kinetic experiments were carried out by the manometric method.[11]

Reaction Products. The main products of autoxidation of anthranols under kinetic conditions were the corresponding anthraquinones, which were confirmed by tlc and melting points. Chloroform was used as an eluent for the tlc analysis with silica gel.

Hydroxylation of Nitrobenzene During Autoxidation of Anthranol. Nitrobenzene (1 g) was added to a solution of anthranol (10 g) which was treated under the same conditions as those for autoxidation. The resulting nitrophenols were identified and estimated by means of glc employing a Yanagimoto Model GCG 550F gas chromatograph with a flame ionization detector operated with a column of 15% Apiezone L grease using N_2 (15 ml/min) as a carrier with programming attachment (60—180 °C) and H_2 in a flow rate of 30 ml/min. Retention times were as follows: *o*-nitrophenol, 12 min; *m*-isomer, 19.3 min; *p*-isomer, 20.3 min. Authentic nitrophenols were used as reference compounds.

Spectroscopy. UV spectra were measured with an automatic recording spectrophotometer (Shimadzu SV-50A) equipped with quartz cells (light path of 10 mm). NMR spectra were measured with a Japan Electron Optics Laboratory NMR spectrometer C-60HL.

Determination of Dissociation Constant of Anthrones. The pK_a values of anthrones were measured by UV spectrophotometry in water at 25 °C using a H_3BO_3–KCl buffer solution. Determination of pK_a values in aqueous dioxane was unsuccessful, since the pH-meter was not stabilized in the solvent.

Keto-enol Equilibrium Constants. The anthrones–anthranols equilibrium constants were determined by means of NMR spectrometry in $CDCl_3$ at 35 °C,[12] and by iodometry[13,14] of anthranols in dioxane–water (2:1 in vol) according to Bansho *et al.* in the absence of oxygen.[15]

Results and Discussion

Effect of Substituent in Anthranol. The present reaction is of first-order in anthranols with large excess of oxygen and was carried out under vigorous stirring sufficient to avoid the rate-determining dissolution of gaseous oxygen. The observed pseudo-first-order rate constants at various pH were shown in Table 1, where [ ]$_0$ denotes the initial concentration. The k_{obsd} value varies little with different substituent, because it involves equilibrium and rate constants which are affected reversely by a substituent.

Effect of Acidity. The rates were measured at various pH values using H_3BO_3–KCl–NaOH buffer

Table 1. Effect of substituents on the rate of autoxidation of anthranols in $NaOH-H_3BO_3$ KCl buffered aqueous dioxane

Substituent in anthranol	$10^4 k_{obs}$ (s^{-1})			
	pH 10.31	pH 10.78	pH 11.20	pH 11.80
2-CH_3	0.690	2.74	7.64	14.3
H	1.01	3.18	11.7	17.8
2-CH_3O	0.725	2.69	8.95	15.9
2-Cl	0.644	2.26	7.67	14.0
2-Br	0.655	—	6.15	11.7

Initial concentration of anthranols: 1.4×10^{-2} M. Partial pressure of oxygen 600 mmHg at 35 °C.

solutions. A plot of pH *vs.* log k_{obsd} is shown in Fig. 1. where k_{obsd} is a pseudo-first-order rate constant.

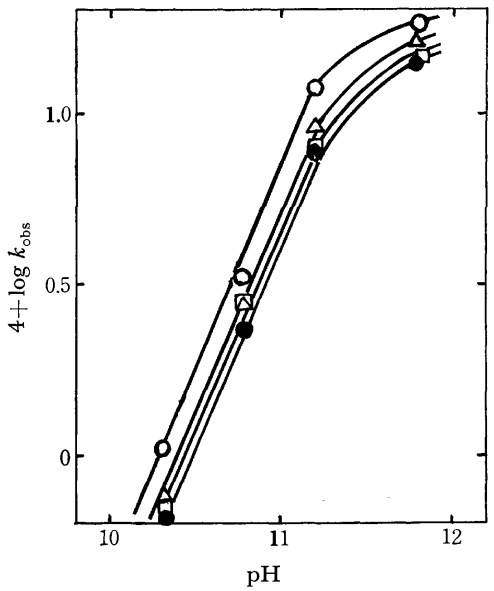

Fig. 1. Effect of pH of solution on the first-order rate constants for the autoxidation of anthranols in dioxane–water (2: 1) in Vol. at 35 °C.
○: H, □: 2-CH_3, △: 2-CH_3O, ●: 2-Cl

We see that straight lines with a slope of nearly unity were obtained at lower pH (pH<11.2), the lines tending to curve slightly at higher pH. This may be explained by the dissociation of anthranol to anthranyl oxide ion.

The pK_a values of anthranols were measured in water. In general, the strengths of acidity and basicity of the weak electrolytes are weakened in going from an aqueous solution to aquo-organic solutions. Hence, the observed pK_a values in the reaction solvent may be a little higher than those in water, and enable us to calculate the extent of ionization of anthranols at the respective pH values. For example, the ionization is over 90% complete when the difference of pH and pK_a is *ca.* unity.

The slope of the lines above pH 12 is much lower than unity (Fig. 1). Thus the dissociation of anthranols to the anions might be almost complete above this pH,

Dissociation Constant of Anthrones. The pK_a values of substituted anthrones containing anthranols were measured by UV spectrophotometry in water at 25 °C. Determination of pK_a values in dioxane–water was unsuccessful, since a pH meter was not stabilized in the aquo-organic solutions. The results are given in Table 2.

Table 2. Equilibrium constants for the dissociation of anthrones in water at 25 °C

Substituent in anthrone	$K_a\times10^{11}$	pK_a
2-CH_3	2.58	10.59
H	5.51	10.26
2-CH_3O	9.14	10.04
2-Cl	13.5	9.87
2-Br	10.7	9.97

A plot of log (K_a^x/K_a^H) *vs.* σ (Hammett's *meta*-value), where K_a^H and K_a^x denote the dissociation constants of unsubstituted and substituted 9-anthrones, respectively, gives an approximate ρ-value of 1.20 (r, 0.885), although the deviation is large. If the *para* σ values are used, the Hammett plot is less satisfactory ($\rho=0.730$, $r=0.578$). The reported ρ value for the dissociation constants of phenols is 2.091.[16]

Keto-Enol Equilibrium. The keto-enol equilibrium constants of anthrones–anthranols could be determined by NMR in $CDCl_3$.[12] However, they could not be determined in aqueous dioxane because of low solubility and the overlap of the peak of enolic proton with that of solvent. Thus, the equilibrium constants in dioxane–water (2: 1 in vol) were measured by iodometry[13,14] of anthranols in a similar way to that of Bansho *et al.*[15] The results are shown in Table 3.

Table 3. Keto-enol equilibrium constants for the reaction of Eq. (1) in dioxane–water (2: 1 in vol) at 35 °C

Substituent in anthranol	2-CH_3	H	2-CH_3O	2-Cl
K_1	0.0988	0.080	0.120	0.227

Effect of Temperature. The first-order rate constants were measured at 25, 35, and 45 °C. The Arrhenius plots giving energies and entropies of activation are given in Table 4.

In general, one-electron transfer reactions have low energy of activation and large negative entropy of

Table 4. Apparent energies and entropies of activation for the autoxidation of anthranols

Substituent in anthranol	$10^4 k_{obs}$ (s^{-1})			E_a (kcal mol^{-1})	$\Delta S^{\neq}$ at 35 °C (e.u.)
	25 °C	35 °C	45 °C		
2-CH_3	6.31	7.64	9.09	3.52	−63.6
H	10.2	11.7	14.0	2.86	−64.7
2-Cl	6.65	7.67	8.72	2.44	−67.1

Initial concentration of anthranols: 1.4×10^{-2} M. Partail pressure of oxygen: 600 mmHg at pH 11.2.

activation.[3,17] This was observed in the present case.

Mechanism. Our data support the following mechanism for the initial steps of autoxidation of substituted anthranols.[3]

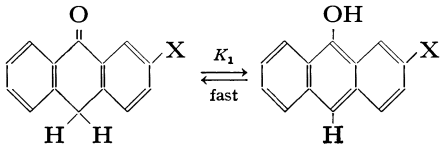

(1)

(Ia) (Ib)

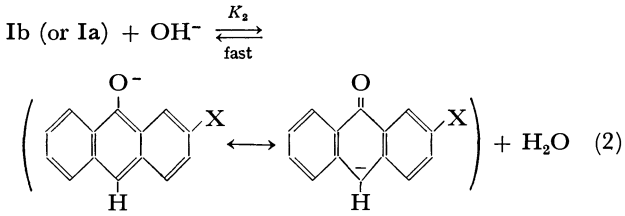

(2)

(II)

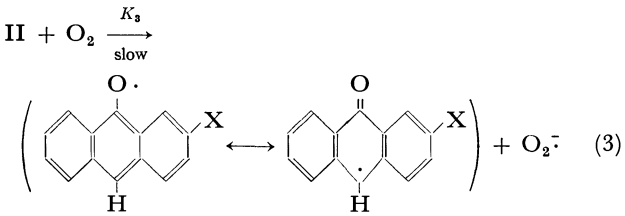

(3)

(III)

The formed anthranyl oxide radical (III) resonates as shown in Eq. (3), leading to the rapid reaction with molecular oxygen to form peroxy radical (IV).

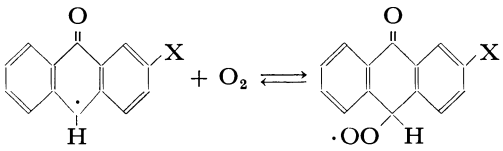

(4)

(III) (IV)

The reactions of carbanions with molecular oxygen to form peroxy radical as an initial step for the autoxilddation were reported.[17,18]

The peroxy radical may be rapidly converted into anthraquinone by expelling the hydroxy radical, which may couple to form hydrogen peroxide.

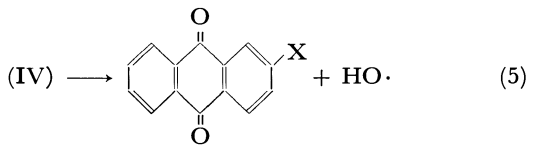

(5)

(V)

$$2HO\cdot \longrightarrow H_2O_2 \qquad (6)$$

Radical HO· may abstract a hydrogen atom from the solvent, but no product derived from the solvent radical could be detected, the chain length of the reaction being very short. Thus the main reaction seems to be the coupling of highly reactive HO· radicals (Eq. (6)).

The formation of H_2O_2 by a bimolecular reaction of IV

$$2\,IV \longrightarrow 2\,V + H_2O_2 \qquad (7)$$

is also conceivable, but the low concentration of IV and the high stability of anthraquinone make Eq. (5) preferable to Eq. (7) as in the case of the conversion of the cyclohexylperoxy radical into cyclohexanone. Another bimolecular reaction of IV, as in the case of the *t*-butylperoxy radical, leading to anthraquinone *via* 10-hydroxy-9-anthrone is less probable because of the necessity of many steps, *i.e.*, three hydrogen abstractions and two electron transfers to molecular oxygen.

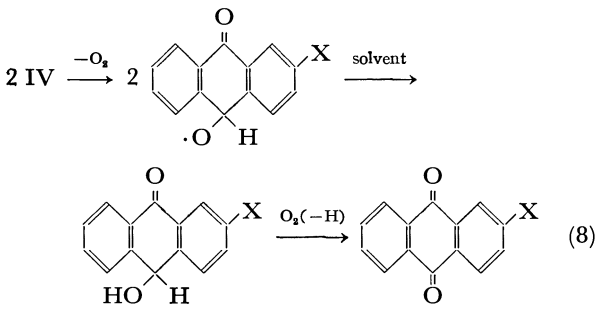

(8)

Alternatively, radical IV may abstract a hydrogen atom from the substrate followed by the dehydration of 10-hydroperoxy-9-anthrone (VI), affording anthraquinone[19] as follows.

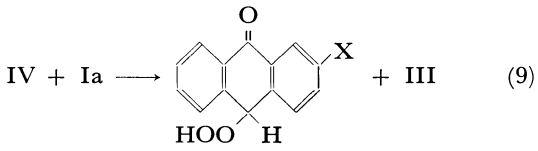

(9)

(VI)

$$VI \longrightarrow V + H_2O \qquad (10)$$

Although hydroperoxide VI was said to be prepared in the case of autoxidation of 10-phenylanthranol and even unsubstituted 9-anthranol,[20] our attempt to prepare VI under the reported conditions gave anthraquinone as the only isolable product. The crude product contained only a few percent peroxidic oxygen, which was detectable by iodometry. Radical initiators and metallic ions had no appreciable influence on the rate and no induction period was observed. Hence, the autoxidation seems to have no radical chain. In view of these facts, the chain mechanism involving Eqs. (4) and (9) is less probable. Hydroperoxide VI, if formed, should decompose rapidly *via* elimination of H_2O, which is unimportant.

Radical III in Eq. (3) might be consumed rapidly to react with peroxy radical IV.

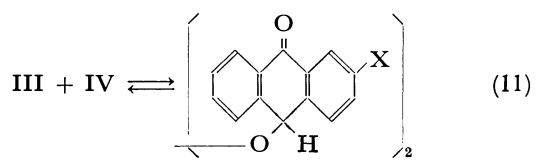

(11)

(VII)

Scheme 11 is unfavorble, since no organic peroxide is detectable in the products and a large steric interaction is expected in peroxide VII.

Equation (5) indicates an intramolecular abstraction of a hydrogen atom by peroxy radicals (IV) to give anthraquinone and a hydroxy radical. Although the hydroxy radical is an energy-rich species, the reaction may occur fairly easily in view of the large heat of formation giving stable anthraquinone; this seems to

act as a driving force to accelerate the reaction.

It has been observed that nitrobenzene is hydroxylated at room temperature by a hydroxy radical produced by a mixture of H_2O_2–Fe(II) (Fenton's reagent).[21] This hydroxylation of nitrobenzene occurs during the autoxidation of anthranol, which supports the presence of hydroxy radical produced by Eq. (5), *i.e.*, glc analysis confirms that *o*-, *m*-, and *p*-nitrophenols were formed in the ratio 30: 35: 35. On the other hand, no nitrophenol was detected on addition of nitrobenzene to the autoxidation mixture of hydroquinone or pyrogallol, where $O_2^{\cdot-}$ and H_2O_2 are formed but no HO· radical.

Radical ion, $O_2^{\cdot-}$, formed in Eq. (3) is easily protonated in an aqueous solution to give hydroperoxy radical, HO_2·, which can then be converted into hydrogen peroxide[11] (Eq. (13)), and/or reacts with anthranol anion (II) (Eq. (14)).

$$O_2^{\cdot-} + H_2O \longrightarrow HO_2\cdot + OH^- \quad (12)$$

$$2HO_2\cdot \longrightarrow H_2O_2 + O_2 \quad (13)$$

$$HO_2\cdot + II \longrightarrow III + HO_2^- \quad (14)$$

The observed concentration of hydrogen peroxide (*ca.* 1—1/5) is less than that expected from the stoichiometry of Eqs. (5) and (6) at partial pressure of oxygen p of 113—620 mmHg and at pH of 10.41—11.60.[2] The change of concentration of hydrogen peroxide in the presence of anthranol in a dioxane–water (2: 1 in vol) buffer at 35 °C under nitrogen (spontaneous decomposition of H_2O_2) was negligible, while that under oxygen at higher pH (11.80), *ca.* 35% increase of the concentration of H_2O_2 after 15 min was observed.

The rate can be determined by Eq. (3) and expressed by the following equation, where p is the partial pressure of oxygen.

$$V = k_3[II]p \quad (15)$$

The measured dissociation constant, K_a, is equal to $[II][H_2O]/([I_a]+[I_b])\times[OH^-]$ or $[II][H_2O]/[I]\text{-}[OH^-]$, where $[I]=[I_a]+[I_b]$; the mechanism leads to the rate law:

$$v = k_3K_a[I]_T p \Big/ \left(\frac{[H_2O]}{K_a[OH^-]}+1\right)$$

$$= \frac{k_3K_a[I]_T[OH^-]p}{K_a[OH^-]+[H_2O]}$$

where $[\ \ ]_T$ denotes stoichiometric (total) concentration. The equation agrees with our results at pH 10.31—11.80 (Table 1).

Our estimation of the K_a value enables us to evaluate the rate constant k_3 for Eq. (3), *i.e.*, one-electron transfer to oxygen molecule from anthranyl oxide ion. The results for substituted anthrones are shown in Fig. 2 and Table 5. Application of the k_3 values for substituted anthranols to the Hammett equation using *meta* σ values gave a rough estimate of ρ-value of -1.5, which was little influenced by pH of the reaction medium (Table 5). The use of *para* σ value gave a poorer Hammett plot.

The one-electron transfer is accelerated by the introduction of electron-releasing groups. In the application of the Hammett rule to radical reactions, which were first attempted by Walling[22] and Swain[23] and reviewed by Otsu *et al.*,[24] fairly large negative ρ-values are sometimes reported in cases such as the reaction of peroxy radicals with phenols, -3.7,[25] autoxidation of phenylhydrazones, -1.7,[26] and autoxidation of phenylhydroxylamines, -1.6.[27] The effect of substituents for reduction of anthraquinones[28] was reported to afford a positive ρ-value of 1.11, which is convincing in view of the reverse of the present reaction (one-electron donation to quinones).

The present autoxidation of anthranols giving a ρ-value of -1.5 supports the mechanism which involves a rate-determining attack of molecular oxygen on anthranyl oxide ion to form anthranyl oxide radical by the one-electron abstraction from anthranyl oxide ion.

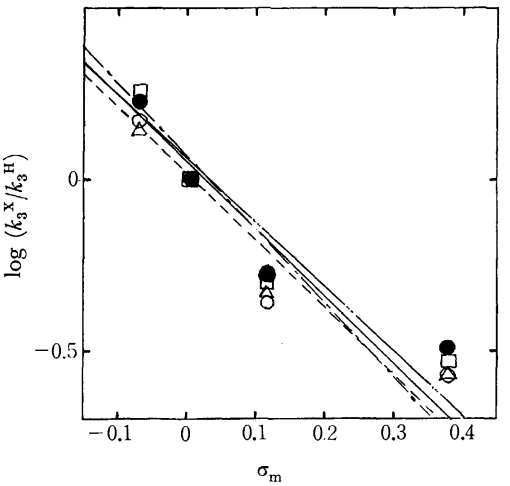

Fig. 2. Plots of σ_m (Hammett) *vs.* log (k_3^X/k_3^H) for the autoxidation of anthranols in alkaline buffered aqueous dioxane at p of 600 mmHg at 35 °C: —○—, pH 10.31; --×--, pH 10.78; -•-△-•-, pH 11.20; and -•••●-•••-, pH 11.80.

Table 5. The ρ-value for one-electron transfer to oxygen molecule from anthranyl oxide ions at various pH values

pH	10.31	10.78	11.20	11.80
$\rho(\sigma)$	−1.41	−1.69	−1.50	−1.42
r	−0.934	−0.946	−0.970	−0.957

References

1) Contribution No. 177.

2) a) H. Baba and T. Takemura, This Bulletin, **37**, 1241 (1964). b) H. Baba and T. Takemura, *Nippon Kagaku Zasshi*, **89**, 629 (1968).

3) Y. Ogata, Y. Kosugi, and K. Nate, *Tetrahedron*, **27**, 2705 (1971).

4) E. D. Bergmann and E. Loewenthal, *Bull. Soc. Chim. Fr.*, **1952**, 66.

5) E. de B. Barnett and J. L. Wiltshire, *J. Chem. Soc.*, **1928**, 1823.

6) F. F. Blicke and O. J. Weinkauff, *J. Amer. Chem. Soc.*, **54**, 1460 (1932).

7) a) C. Norrison, *Ber.*, **19**, 2103 (1886). b) M. Phillips, *Ind. Eng. Chem.*, **17**, 722 (1925). c) M. Hayashi, *J. Chem. Soc.*, **1930**, 1513, 1519. d) C. F. H. Allen, A. C. Bell, A. Bell, and J. V. Allan, *J. Amer. Chem. Soc.*, **62**, 656, 663 (1940).
8) A. Steyermark and J. H. Gardner, *ibid.*, **52**, 4884, 4887 (1930).
9) a) F. F. Blicke and O. J. Weinkauff, *ibid.*, **54**, 1460 (1932). b) R. W. Hardacre and A. D. Perkin, *J. Chem. Soc.*, **1929**, 180.
10) W. H. Carothers, A. M. Collins, and J. E. Kirby, *J. Amer. Chem. Soc.*, **55**, 786 (1933).
11) Y. Ogata, Y. Kosugi, and T. Morimoto, *Tetrahedron*, **24**, 4057 (1968).
12) Our NMR data of K_1: 2-CH_3, 0.351; H, 0.0638; 2-CH_3O, 0.124; 2-Cl, 0.136.
13) K. H. Meyer, *Ann. Chem.*, **379**, 37 (1911).
14) H. Bäckström and H. Beatty, *J. Phys. Chem.*, **35**, 2549 (1930).
15) a) Y. Bansho and K. Nukada, This Bulletin, **33**, 579 (1960). b) K. Nukada and Y. Bansho, *ibid.*, **26**, 454 (1953). c) Y. Bansho and K. Nukada, *Kogyo Kagaku Zasshi*, **63**, 620 (1960).
16) F. G. Bordwell and G. D. Cooper, *J. Amer. Chem. Soc.*, **74**, 1059 (1952).
17) G. A. Russell, A. J. More, and K. Nagpal, *J. Amer. Chem. Soc.*, **84**, 4154 (1962).
18) a) G. A. Russell and G. Kaupp, *ibid.*, **91**, 3851 (1969). b) D. H. R. Barton and D. W. Jones, *J. Chem. Soc.*, **1965**, 3563.
19) a) C. Dufraisse, A. Etienne, and J. Rigaudy, *C. R. Acad. Sci., Paris*, **226**, 1773 (1948). b) J. Rigaudy and C. Dufraisse, *ibid.*, **228**, 253 (1949).
20) C. T. Bedford, *J. Chem. Soc., C*, **1968**, 2514.
21) H. Loebl, G. Stein, and J. Weiss, *ibid.*, **1949**, 2074.
22) C. Walling, E. R. Brigg, K. B. Wolfstirm, and F. R. Mayo, *J. Amer. Chem. Soc.*, **70**, 1537 (1948).
23) C. G. Swain, W. H. Stockmayer, and J. T. Clarke, *ibid.*, **72**, 5426 (1950).
24) T. Otsu and T. Yamamoto, *Yuki Gosei Kagaku Kyokaishi*, **23**, 643 (1965).
25) R. G. Caldwell and J. L. Ihrig, *J. Amer. Chem. Soc.*, **84**, 2878 (1962).
26) K. H. Pausacker, *J. Chem. Soc.*, **1950**, 3478.
27) Y. Ogata, Y. Sawaki, J. Mibae, and T. Morimoto, *J. Amer. Chem. Soc.*, **86**, 3854 (1964).
28) K. Yasukouchi, H. Yamaguchi, Y. Ono, and M. Urabe, *Nippon Kagaku Zasshi*, **88**, 428 (1967); *ibid.*, **88**, 626 (1967).

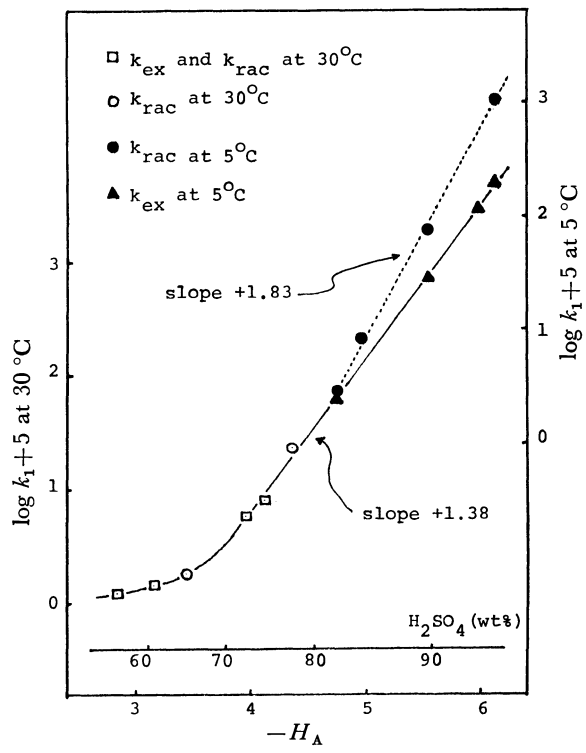

Fig. 1. Correlation between rate constant and acidity function H_A.

that the reaction is of the A-1-like mechanism according to the Zucker-Hammett hypothesis.[19] The energy and entropy of activation for the racemization in 82% acid are found to be 21.8 kcal/mol and −2.68 e.u., respectively (Table 2). The small negative value of entropy of activation also favors the rate-determining A-1-like S–O bond cleavage of sulfoxide.

TABLE 2. ACTIVATION PARAMETERS FOR RACEMIZATION OF (+)-*n*-BUTYL METHYL SULFOXIDE (**1**) IN SULFURIC ACID

H_2SO_4 (wt%)	E_a (kcal/mol)	$\Delta S^{\neq}$ (e.u.)
89.7	17.3	−13.8
82.0	21.8	− 2.68
65.6	21.4	−11.7
56.1	16.7	−28.0

However, above 85% sulfuric acid, the racemization would be caused by both an A-1-like reaction and some other reaction without oxygen exchange. The following possibilities are considered for the racemization without oxygen exchange: 1) formation of an intimate ion pair produced by S–O bond fission of protonated sulfoxide followed by a fast internal return in solvent cage to afford the racemized sulfoxide; 2) a thermal racemization of protonated sulfoxide caused by a pyramidal inversion process; 3) a fast equilibrium of protonated sulfoxide and the corresponding ylide produced by abstraction of α-hydrogen of the protonated sulfoxide.

(1) Intimate ion-pair in solvent cage

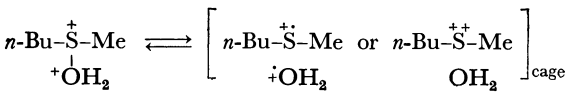

(2) Pyramidal inversion

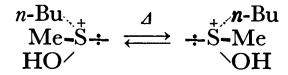

(3) Ylide-ylene intermediate

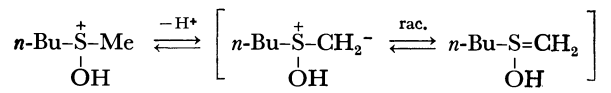

However, since the rate of racemization is so fast in concentrated sulfuric acid of around 95%, in which racemization without oxygen exchange takes place almost predominantly, its mechanism can not be visualized on the basis of kinetic observation alone.

The third possibility may be readily tested by using α-deuterium labeled sulfoxide. When *n*-butyl trideuteriomethyl sulfoxide (**1**—d_3) was dissolved in an excess non-labeled sulfuric acid, no detectable amount of H–D exchange was observed under both normal and drastic reaction conditions (See Experimental). It can thus be ruled out.

It is well known that a pyramidal inversion of an optically active trialkyl substituted sulfonium salt takes place slowly only on being heated around 50 °C,[20-22] while there is no thermal racemization without any oxygen exchange reaction of sulfoxides for both alkyl aryl and diaryl sulfoxides in the concentrated sulfuric acid.[10-12] Therefore the second possibility would not be significant.

Thus, the first possibility seems to be most favorable in view of the fact[23] that a highly concentrated sulfuric acid should have a larger solvent cage effect, because of the higher viscosity and a lower nucleophilicity of water molecules.

In order to clarify the mechanism, we have analyzed the data on the basis of the Φ parameter.[24] This is taken from the slope of the plots of log $[k_1+H_0]$ *vs.* $[H_0+\log[H^+]]$ and is an indication of the change in solvation from the initial to the transition states; namely, if Φ value is larger than 0.58, water is involved as a proton transfer agent in the rate-determining step; in the Φ range 0.22—0.56, water is involved as a nucleophile in the rate-determining step; while if the Φ value is smaller than zero, water is not involved in the rate-determining step.

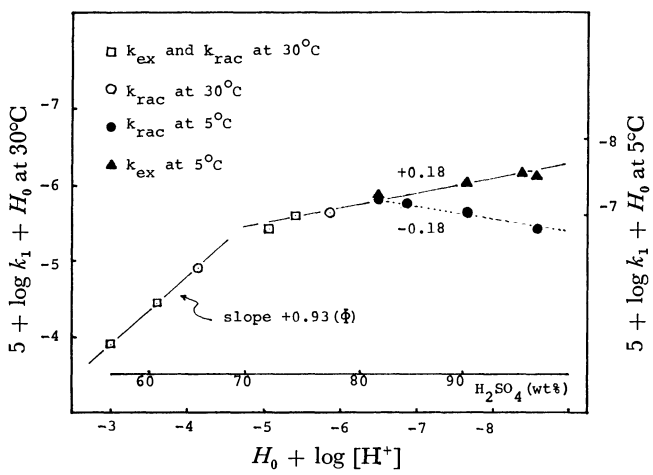

Fig. 2. Bunnett-Olsen plot of rate constant.

The plot, in which straight lines with slopes (Φ values) of +0.93 and +0.18 were obtained for below 70% and above 70% sulfuric acids, respectively, is shown in Fig. 2.

Thus, the oxygen exchange reaction below 70% sulfuric acid would proceed through the rate-determining A-1-like S–O bond cleavage in which water is involved as a proton transfer agent and the solvation in the transition state is markedly high from the data of Φ value. The unity of k_{ex}/k_{rac} and a large negative activation entropy ($\Delta S^{\neq} = -28.0$ e.u.) for racemization in 56.8% sulfuric acid also supported this (Tables 1 and 2). A similar mechanism was proposed in the A-1-like oxygen exchange reaction of sulfoxide with acetic acid and chloroacetic acids,[5] in which acetic acid acts as an acid-catalyst and the solvation is remarkably high at the transition state ($k_{ex}/k_{rac} = 1.01$, $\Delta S^{\neq} = -23.4 \sim -32.9$ e.u.).

An overall scheme for the oxygen exchange and racemization of *n*-butyl methyl sulfoxide (**1**) might be schematically drawn as shown below.

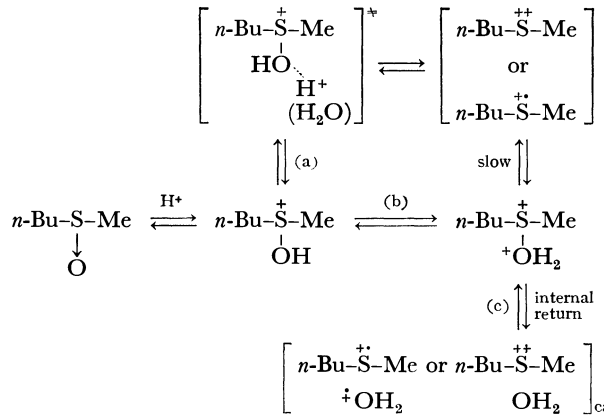

The reaction seems to proceed through path (a) below 70% acid, path (b) above 70% acid and paths (b) and (c) above 85% acid to afford the symmetrical dication ($-\overset{++}{S}-$) or cation radical ($-\overset{+\cdot}{S}-$) intermediate, while the subsequent attack of water should be very fast.

The labile symmetrical intermediate should be detected by the following ^{18}O tracer experiment by quenching the solution of the non-labeled sulfoxide with ^{18}O-enriched water. A small amount of incorporation of ^{18}O into the sulfinyl function of the recovered sulfoxide was observed by quenching the non-labeled sulfuric acid solution containing non-labeled sulfoxide (**1**) with a large amount of cold ^{18}O-labeled water (See Experimental).

Experimental

Materials. *Optically Active (+)n-Butyl Methyl Sulfoxide*, **(+)-1**, was prepared from the reaction of (−)menthyl (−)*n*-butanesulfinate with methylmagnesium iodide in ether according to the method of Andersen.[25] The optically active sulfoxide thus obtained was purified by the method of Mislow *et al.*[26] $[\alpha]_D$ +33.0° (*c* 1.20, $CHCl_3$) (lit,[27] +112° (*c* 1.02, isooctane, 94% optically pure)).

^{18}O-Labeled n-Butyl Methyl Sulfoxide, **1**, was prepared by the oxidation of *n*-butyl methyl sulfide with bromine in the presence of pyridine in acetic acid and $H_2{}^{18}O$, according to the usual procedure.[28] ^{18}O-Content was 1.70 atom %.

n-Butyl Trideuteriomethyl Sulfoxide, **1-d_3**, was prepared by treating *n*-butyl methyl sulfoxide with NaOD–D_2O at 60 °C for 14 hr. The deuterium content was determined by NMR measurement and the D content was found to be above 95%.

Sulfuric Acid. Concentrations of sulfuric acid were determined by titration with a standard alkali solution. H_A values are taken from reported tables[17,18] and H_0 values from the table prepared by Johnson *et al.*[16]

Test for H–D Exchange of Sulfoxide, **1-d_3**, *with Sulfuric Acid.* Deuterium labeled sulfoxide, **1-d_3**, (*ca.* 50 mg) was dissolved in 0.5 ml sulfuric acid and the sulfuric acid solution was introduced into an NMR tube. After being kept standing under three different conditions, *i.e.*, i) 92% sulfuric acid at room temperature for 240 hr; ii) 72.3% acid at room temperature for 50 hr; iii) 56.1% acid at 50 °C for 58 hr, ^1H-NMR spectra of the sulfoxide solution were measured. However, no detectable peak of methyl proton (CH_3SO; 3.3 ppm) appeared.

Trapping of the Dication or Cation Radical Intermediate by Quenching with $H_2{}^{18}O$. Non-labeled sulfoxide (**1**) was dissolved in non-labeled sulfuric acid and kept standing under appropriate conditions and then the sulfuric acid solution was quenched with a large excess of cold $H_2{}^{18}O$. The sulfoxide was recovered according to the procedure described below, and subjected to ^{18}O-analysis. The result is given in Table 3.

Table 3. ^{18}O-Contents of sulfoxide (**1**) recovered by quenching with $H_2{}^{18}O$ [a,b]

H_2SO_4 (wt%)	Time (hr)	Temperature (°C)	^{18}O-Content (atom%)[c]
56.1	24	30	0.204
72.3	1.5	30	0.214
96.8	0.7	25	0.244

a) Sulfoxide: 0.1 mol/l.
b) ^{18}O-Content of water used is 1.67 atom%.
c) Natural abundance: 0.204, accuracy of analysis of mass spectrum: ±0.005 atom%.

Kinetic Procedure. The rates of oxygen exchange and racemization were measured by the following two methods with a Yanagimoto OR-10 type polarimeter and a Hitachi RMU-6E mass spectrometer.

Method A (for Both Oxygen Exchange and Racemization). In order to compare the rate constants, both oxygen exchange and racemization reactions were carried out under identical conditions. An ^{18}O-labeled or optically active sulfoxide was dissolved in a sulfuric acid in such a way as to maintain the concentration of the sulfoxide at just about 0.1 mol/l at a given temperature. Five aliquot portions of the solution were removed from the constant temperature bath at appropriate time intervals and quenched with a large amount of ice-water. The sulfoxide was extracted from the solution with chloroform or dichloromethane by the salting-out technique, and the extract was washed with a 5% aqueous solution of sodium carbonate and water containing salt, and then dried over anhydrous sodium sulfate after which the solvent was distilled off. The resulting sulfoxide was subjected to both ^{18}O-analysis and specific rotation measurement. The ^{18}O-atom % was calculated from the mass peak heights of 44 and 46 according to the method of Samuel.[29]

Method B (for Racemization). A sulfuric acid solution containing an optically active sulfoxide of a set mol was placed in a square cell (5 cm). The rate was measured directly by checking the rotation α of the polarimeter, which

was connected with a constant temperature bath at the desired temperature.

Calculation of Pseudo first-order Rate Constant. For racemization, $\log[\alpha_0]-\log[\alpha_t]=kt/2.303$, where α_0 and α_t are the rotations at times 0 and t, respectively; and for oxygen exchange, $\log[\beta_0-\beta]-\log[\beta_t-\beta]=kt/2.303$, where β_0 and β_t are the atom% of ^{18}O at times 0 and t, respectively, and β is that of natural CO_2.

References

1) Paper 48 on Sulfoxides.
2) a) K. Mislow, T. Simmons, J. T. Melillo, and A. L. Ternay, Jr., *J. Amer. Chem. Soc.*, **86**, 1452 (1964). b) K. Mislow, *Rec. Chem. Progr.*, **28**, 217 (1967).
3) H. Yoshida, T. Numata, and S. Oae, This Bulletin, **44**, 2875 (1971).
4) G. Modena, U. Quintly, and G. Scorrano, *J. Amer. Chem. Soc.*, **94**, 202 (1972).
5) S. Oae, M. Yokoyama, and M. Kise, This Bulletin, **41**, 1221 (1968).
6) N. Kunieda and S. Oae, *ibid.*, **41**, 1025 (1968).
7) a) S. Oae, N. Kunieda, and W. Tagaki, *Chem. & Ind.*, **1965**, 1790. b) N. Kunieda, K. Sakai, and S. Oae, This Bulletin, **42**, 1090 (1969).
8) M. Kise and S. Oae, *ibid.*, **43**, 1416, 1421, 1426, 1804 (1970).
9) S. Oae, T. Kitao, Y. Kitaoka, and S. Kawamura, *ibid.*, **38**, 546 (1965).
10) S. Oae and N. Kunieda, *ibid.*, **41**, 696 (1968).
11) N. Kunieda and S. Oae, *ibid.*, **42**, 1324 (1968).
12) N. Kunieda and S. Oae, *ibid.*, **46**, 1745 (1973).
13) D. Landini, G. Modena, F. Montanari, and G. Scorrano, *J. Amer. Chem. Soc.*, **92**, 7168 (1970).
14) D. Landini, G. Modena, G. Scorrano, and F. Taddei, *ibid.*, **91**, 6703 (1969).
15) G. Scorrano, *Accounts Chem. Res.*, **6**, 132 (1973).
16) C. D. Johnson, A. R. Katritzky, and S. A. Shapiro, *J. Amer. Chem. Soc.*, **91**, 6654 (1969).
17) K. Yates, J. B. Stevens, and A. R. Katritzky, *Can. J. Chem.*, **42**, 1957 (1964).
18) C. D. Johnson, A. R. Katritzky, and N. Shakir, *J. Chem. Soc. B*, **1967**, 1235.
19) M. A. Paul and F. A. Long, *Chem. Rev.*, **57**, 935 (1957); L. Zucker and L. P. Hammett, *J. Amer. Chem. Soc.*, **61**, 2791 (1937).
20) R. Scartazzini and K. Mislow, *Tetrahedron Lett.*, **1967**, 2719.
21) D. Darwish and G. Tourigny, *J. Amer. Chem. Soc.*, **88**, 4303 (1966).
22) D. Darwish, S. H. Hui, and R. Tomilson, *ibid.*, **90**, 5631 (1968).
23) M. Liler, "Reaction Mechanism in Sulfuric Acid and Other Strong Acid Solutions," Academic Press, New York, N.Y. (1971).
24) J. F. Bunnett and F. P. Olsen, *Can. J. Chem.*, **44**, 1899, 1917 (1966).
25) K. K. Andersen, *Tetrahedron Lett.*, **1962**, 93.
26) K. Mislow, M. M. Green, P. Laur, J. T. Melillo, T. Simmons, and A. L. Ternay, Jr., *J. Amer. Chem. Soc.*, **87**, 1958 (1965).
27) J. P. Lockard, C. W. Schroeck, and C. R. Johnson, *Synthesis*, **1973**, 485.
28) S. Oae, Y. Ohnishi, S. Kozuka, and W. Tagaki, This Bulletin, **39**, 364 (1966).
29) D. Samuel, "Oxygenase," ed. by O. Hayaishi, Academic Press, New York, N.Y. (1962), Chapt. 2.

The Heck Reaction of 2-Vinylpyridine

Akira KASAHARA, Taeko IZUMI, Toru TAKEDA, and Hayao IMAMURA*

Department of Applied Chemistry, Faculty of Engineering, Yamagata University, Yonezawa, Yamagata 992
**Research Laboratory of Resources Utilization, Tokyo Institute of Technology, Ookayama, Meguro-ku, Tokyo 152*

(Received August 6, 1973)

In the presence of lithium chloropalladite, 2-vinylpyridine reacted with phenylmercuric chloride to give di-μ-chloro-bis[2-phenyl-2-(α-pyridyl)ethyl]dipalladium(II). Similar complexes were obtained from *p*-tolyl-, *p*-anisyl-, or *m*-nitrophenylmercuric chloride. The σ-bonded structures of these complexes have been confirmed by a study of their absorption and of the NMR spectra.

We wish to report that 2-vinylpyridine (**1**) reacted with arylmercuric chloride in the presence of lithium chloropalladite(II) to give complexes (**2**) containing both a carbon-palladium σ-bond and an aryl group.

Experimental

Materials. All the melting points are uncorrected. The arylmercuric chlorides were prepared by the methods described in the literature: *p*-tolylmercuric chloride,[1] mp 232—233 °C; *p*-anisylmercuric chloride,[2] mp 173—174 °C; *m*-nitrophenylmercuric chloride,[3] mp 218—221 °C. Phenylmercuric chloride (mp 250—251 °C) was obtained from the commercially available phenylmercuric acetate by treating with alcoholic lithium chloride.

*The General Procedure for the Preparation of Di-μ-chloro-bis-[2-aryl-2-(α-pyridyl)ethyl]dipalladium(II) (**2a—d**).* A lithium chloropalladite solution was prepared by stirring 0.42 g (10 mmol) of anhydrous lithium chloride and 1.77 g (10 mmol) of anhydrous palladium chloride overnight at room temperature in 100 ml of acetonitrile. Into the lithium chloropalladite solution, arylmercuric chloride (10 mmol) was then stirred at room temperature for five minutes, after which 1.26 g (12 mmol) of **1** was added in one portion. After the mixture had then been stirred at room temperature for 6 hr, the product was isolated by filtration to remove a precipitated palladium and by distillation under reduced pressure to remove the solvent. The residue was dissolved in chloroform and chromatographed on neutral alumina. The first elution with chloroform and recrystallization from methanol afforded colorless crystals, which were identified as biphenyls (**3a—d**) by a comparison of the IR spectra and by a mixed-melting-point determination with an authentic sample. Further elution with chloroform and recrystallization from chloroform–cyclohexane afforded yellow products (**2a—d**). The results are summarized in Table 1.

*The Preparation of Chloro-[2-aryl-2-(α-pyridyl)ethyl]-pyridine-palladium Complexes (**4a—d**).* A solution of the chloro-bridged palladium complex (**4**) (0.10 g) in methylene chloride was treated with a solution of pyridine (5% excess) in ether. After 10 min, the solvent was removed under reduced pressure; the residue was then recrystallized from benzene–cyclohexane to give pale yellow crystals. The results are summarized in Table 1.

Results and Discussion

In the presence of lithium chloropalladite, **1** reacted with phenylmercuric chloride in acetonitrile to give a yellow crystal, di-μ-chloro-bis[2-phenyl-2-(α-pyridyl)-ethyl]dipalladium(II) (**2a**), accompanied by a small amount of biphenyl (**3a**). Similarly, *p*-tolylmercuric chloride, *p*-anisylmercuric chloride, and *m*-nitrophenylmercuric chloride all reacted with **1** to afford yellow complexes (**2b—d**).

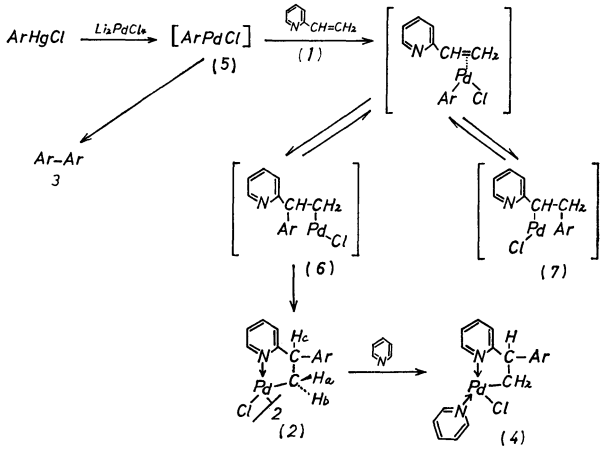

Fig 1.

The mechanism of the formation of **3a—d** as a by-product may involve a coupling reaction of aryl-palladium chloride (**5**), prepared *in situ* from arylmercuric chloride and lithium chloropalladite in acetonitrile. The σ-bonded structure for the yellow complexes (**2a—d**) was supported by the molecular-weight determinations and by the reaction with pyridine to give readily soluble monomeric derivatives (**4a—d**). Moreover, the far-infrared spectra of **2a—d** showed a bridged Pd–Cl stretching absorption at about 290 and 255 cm^{-1}. The NMR spectra of **2a—d** were in agreement with the proposed structures. For example, the NMR spectrum of **2a** consists of four resonances, at σ 3.48, 3.73 (the protons of the *N*-methylene group (H_a and H_b)), 4.55 (the methine proton H_c), and 7.05—8.52 ppm (the protons of the phenyl and pyridyl groups). The nonequivalence of the methylene protons (H_a and H_b) can most easily be explained in terms of a cyclic system in which nitrogen is coordinated to the metal. Similarly, in the NMR spectra of **2a—d**, all the resonances can be satisfactorily accounted for by the presence of the σ-bond and a cyclic system.

Recently, Heck[4] has reported that the arylation of olefin with **5** was stereospecific with internal olefin, giving products consistent with a *cis* addition of the organopalladium reagent to the olefin, followed by a *cis* elimination of a hydridopalladium(II) species. In

TABLE 1. THE HECK REACTION OF 2-VINYLPYRIDINE (**1**)

Arylating agent RC_6H_4HgCl	Product	Yield (%)[a]	Mp °C (lit.)	Found % (Calcd) C	H	N	IR (cm^{-1}) and NMR (δ, ppm) spectra,[b] mol wt (in $CHCl_3$) and pyridine derivative (**4**)
R=H	Biphenyl (**3a**)	15	68—69 (69—70[c])				
	2a (Ar=Phenyl)	28	162—163 (dec.)	48.26 (48.17)	3.78 (3.70)	4.12 (4.31)	IR 750 and 690 (phenyl), 294 and 257 (bridged Pd–Cl stretching). NMR 3.48 (*q*, 1H, H_a or H_b, A or B part of an ABX spin system, J_{AB} =16 Hz, J_{AX}=8 Hz, J_{BX}=1.5 Hz), 3.73 (*q*, 1H, H_b or H_a, B or A part of an ABX spin system), 4.55 (*d-d*, 1H, H_c, X part of an ABX spin system) and 7.05—8.52 (*m*, 9H, phenyl and pyridyl protons). Mol. wt, 637 (648). Pyridine derivative (**4a**), mp 126—128 °C (dec.).
R=*p*-Me	Bi-*p*-tolyl (**3b**)	18	119—120 (120[c])				
	2b (Ar=*p*-Tolyl)	24	148—150 (dec.)	49.66 (49.71)	4.01 (4.14)	4.12 (4.12)	IR 805 (tolyl), 292 and 253 (bridged Pd–Cl stretching). NMR 2.07 (*s*, 3H, CH_3), 3.51 (*q*, 1H, H_a or H_b, A or B part of an ABX spin system, J_{AB}=15 Hz, J_{AX} =7.5 Hz, J_{BX}=1.5 Hz), 3.72 (*q*, 1H, H_b or H_a, B or A part of an ABX spin system), 4.64 (*q*, 1H, H_c, X part of an ABX spin system), and 6.90—8.56 (*m*, 8H, tolyl and pyridyl protons). Mol wt 670 (675). Pyridine derivative (**4b**), mp 128—130 °C (dec.).
R=*p*-MeO	Bi-*p*-anisyl (**3c**)	16	170—171 (170—172[c])				
	2c (Ar=*p*-Anisyl)	30	128—131 (dec.)	47.62 (47.78)	3.85 (3.97)	3.88 (3.96)	IR 808 (anisyl), 292 and 255 (bridged Pd–Cl stretching). NMR 3.50 (*q*, 1H, H_a or H_b, A or B part of an ABX spin system, J_{AB} =15Hz, J_{AX}=8 Hz, J_{BX}=1.5 Hz), 3.67 (*s*, 3H, CH_3O–), 3.73 (*q*, 1H, H_b or H_a, B or A part of an ABX spin system), 4.65 (*q*, 1H, H_c, X part of an ABX spin system), and 6.99—8.55 (*m*, 8H, anisyl and pyridyl protons). Mol wt 698 (707). Pyridine derivative (**4c**), mp 125—127 °C (dec.).
R=*m*-NO_2	3,3′-Dinitrobiphenyl (**3d**)	20	201—203 (198.5—199.5[d])				
	2d (Ar=*m*-Nitrophenyl)	25	145—148 (dec.)	42.22 (42.30)	2.89 (3.00)	7.51 (7.55)	IR 1530 and 1350 (–NO_2), 860 and 805 (*m*-disubstituted aromatic ring), 293 and 255 (bridged Pd–Cl stretching). NMR 3.16—3.45 (*m*, 2H, H_a+H_b), 4.15 (*q*, 1H, H_c), and 6.88—8.87 (*m*, 8H, aromatic and pyridyl protons). Mol wt 722 (738). Pyridine derivative (**4d**), mp 134—136 °C (dec.).

a) Yields are based upon the arylating agent.

b) IR spectra were measured on KBr disks (4000—650 cm^{-1}) or in Nujol mulls mounted on thin polythene windows. NMR spectra were observed by means of a Hitachi R-22 NMR spectrometer at 90 MHz, using TMS as an internal standard. The chemical shifts were followed by the splitting patterns (*s*, singlet; *q*, quartet; *d-d*, double-doublet; *m*, multiplet) and the relative strengths.

c) E. Müller and T. Topel, *Ber.*, **72**, 273 (1939).

d) B. W. Williamson and W. H. Rodebush, *J. Amer. Chem. Soc.*, **63**, 3018 (1941).

the reactions of **1** with **5**, the formation of σ-complexes (**2a**—**d**) suggests that the reaction involves the intermediate formation of an arylpalladium chloride–olefin adduct and favors the formation of the adduct (**6**), where palladium is attached to the terminal methylene carbon, over with the formation of the *anti*-Markovnikov adduct (**7**).

References

1) F. C. Whitemore, F. H. Hamilton, and N. Thurman, "Organic Syntheses," Coll. Vol. I, p. 519 (1941).
2) O. Dimroth, *Ber.*, **35**, 2867 (1902).
3) C. Kapproth and F. Westheimer, *J. Amer. Chem. Soc.*, **72**, 4461 (1950).
4) R. F. Heck, *ibid.*, **91**, 6707 (1969); **93**, 6896 (1971).

Synthesis of Furfuryl and Nitrofurfuryl Derivatives of Adenine and Uracil

Shunzo FUKATSU,* Aiko SAWA,** and Sumio UMEZAWA

Department of Applied Chemistry, Faculty of Engineering, Keio University, Hiyoshi, Yokohama 222

(Received September 19, 1973)

Condensation of 5-nitrofurfuryl iodide with uracil in dimethylformamide in the presence of lithium hydride gave 1-(5′-nitrofurfuryl)uracil. When the iodide was treated with adenine, 3-substituted adenine was mainly obtained, whereas the analogous reaction of benzamidopurine gave 9-substituted adenine. These compounds showed antitumor and broad antibacterial activity. Furfuryl derivatives were also described.

Since the introduction of nitrofurazone (5-nitrofurfural semicarbazone) as an antibacterial agent, many nitrofuran derivatives have been prepared in an effort to increase and to modify activity. Among the derivatives, 5-nitrofurfuryl derivatives of pyrazolopyrimidines have been prepared by Burch[1] and found to possess excellent antibacterial activity. Furthermore, the 5-nitrofurfuryl derivative of a tetrahydropyrimidine compound prepared by Hurst *et al.*[2] has been found to be antiviral but not antibacterial. On the other hand, a series of furfuryl pyrimidines and purines have been prepared by Hull[3] in connection with kinetine which is an adenine derivative and a cell division stimulator.

In the course of an investigation of the synthesis of nucleoside-related compounds, we have recently reported[4] the synthesis of some reversed nucleosides of pyrimidine and purine bases. As a part of this investigation, it seemed of interest to synthesize further nitrofurfuryl and furfuryl analogs in which the furanose structure is replaced by furan. This paper describes the preparation of 9-furfuryl-, 9-(5′-nitrofurfuryl)-, and 3-(5′-nitrofurfuryl)adenine(**1**, **4**, and **5**) and 1-furfuryl- and 1-(5′-nitrofurfuryl)uracil (**2** and **3**).

In the previous paper,[4] the authors have shown that the condensation of terminal iodo-sugars with pyrimidine bases in dimethylformamide smoothly occurred in the presence of lithium hydride or sodium hydride. This reaction was extended in the present synthesis, using furfuryl and 5-nitrofurfuryl iodide.

Furfuryl iodide, which was prepared by the reaction of triphenyl phosphate methiodide with furfuryl alcohol according to the method of Lanauer and Rydon,[5] was, *in situ*, condensed with 6-benzamidopurine (8) in the presence of sodium hydride to afford 6-benzamido-9-furfurylpurine (**7**) in 51% yield. Ammonolysis of the benzamido derivative with methanolic ammonia gave 9-furfuryladenine (**1**) (Scheme 1), which showed a melting point corresponding with that reported for the substance prepared by a entirely different method by Hull.[3] An analogous reaction of furfuryl iodide with uracil (9) in the presence of lithium hydride gave 1-furfuryluracil (**2**).

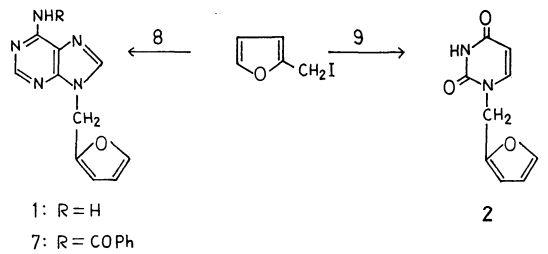

Scheme 1.

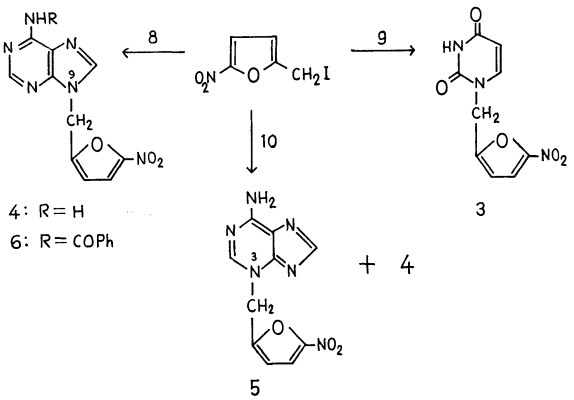

Scheme 2.

Likewise, 5′-nitrofurfuryl derivatives have been prepared from 5-nitrofurfuryl iodide[6] and uracil, adenine (10) and 6-benzamidopurine (Scheme 2).

The condensation of the iodide with uracil in the presence of lithium hydride afforded 1-(5′-nitrofurfuryl)uracil (**3**).

Analogous reaction of the iodide with adenine and 6-benzamidopurine (benzoyladenine) led to different derivatives. It has been found that the reaction using 6-benzamidopurine followed by hydrolysis gave 9-(5′-nitrofurfuryl)adenine (**4**), while the reaction using adenine mainly gave 3-(5′-nitrofurfuryl)adenine (**5**).

3- and 9-subsitutions on adenine and 1-substitution on uracil have been established by comparison of the ultraviolet spectra (Table 1) of the products with substituted adenines and uracils of known structure.[7-10] The structures of the above described products have further been supported by their IR and NMR spectra by reference to the compilations by Jackman[11] and Bhacca *et al.*[12]

In preliminary experiments to assess the biological activity of the above products, it has been observed that the nitrofurfuryl derivatives **3**, **4**, and **5** interestingly showed antitumor activity. All these compounds also

* Present address: Development Laboratories, Meij Seika Kaisha, Ltd., 580 Horikawa-cho, Saiwaiku, Kawasaki 210.

** Present address: Department of Pharmacology, School of Medicine, Keio University, Shinanomachi, Shinjuku-ku, Tokyo 162.

Table 1. Ultraviolet spectral data

3: 1-(5′-nitrofurfuryl)uracil **4**: 9-(5′-nitrofurfuryl)adenine **5**: 3-(5′-nitrofurfuryl)adenine

Solvent	3		4		5	
	max (ε)	min (ε)	max (ε)	min (ε)	max (ε)	min (ε)
0.1N HCl	262 (10300)	230 (5500)	258 (15650)	230 (6720)	276 (17700)	237 (6140)
	318 (10750)	286 (6000)	315 (11700)	286 (6870)	313 (10150)	300 (9240)
water	263 (10300)	233 (5800)	259 (15600)	227 (6250)	276 (15050)	244 (6430)
	318 (10950)	285 (6200)	317 (11700)	284 (5600)	310 (10500)[b]	
0.1N NaOH	225 (14000)	308 (4700)	258 (15100)[a]	226 (5550)[a]	285 (10700)[a]	248 (6230)[a]
			317 (11300)[a]	283 (5100)[a]		

a) pH 9.0; The UV absorption (315 mμ) by the nitrofuran moiety of **3** and **5** disappear, being decomposable by alkali.
b) Shoulder.

showed wide antimicrobial spectra against bacteria and fungi.

Experimental

9-Furfuryladenine (1). A solution of furfuryl alcohol (1.01 g, 10.3 mmol) and methyltriphenoxyphosphonium iodide (5.27 g, 11.6 mmol) in dry ether (15 ml) was stirred at room temperature for 1 hr. To the solution, a solution of 6-benzamidopurine (2.43 g, 10.2 mmol) and sodium hydride (270 mg, 11.3 mmol) in dry dimethylformamide (30 ml) was added and the mixture was heated at 80—83 °C (bath temperature) for 5 hr and evaporated to dryness at 40 °C. The residue was dissolved in chloroform (120 ml) and the solution was washed with two 40 ml portion of water, dried with sodium sulfate, filtered, and evaporated to sirup. The residue (6.4 g) was chromatographed on a short column (2.5×30 cm) of alumina (Merck, acid washed, 110 g) and eluted successively with benzene, benzene–ethyl acetate (1: 1), ethyl acetate, ethyl acetate–methanol (1: 1) and methanol. The condensation product (**7**) was eluted with ethyl acetate–methanol (1: 1), being recognized by ultraviolet absorption. The fractions were combined and evaporated to dryness. The residue was crystallized from ethanol, 1.64 g (51%) of needles of 6-benzamido-9-furfurylpurine (**7**), mp 192.5—193.5 °C, UV: λ_{max}^{MeOH} 331 mμ(ε 15000).

Found: C, 64.05; H, 4.33; N, 21.87%. Calcd for $C_{17}H_{13}N_5O_2$: C, 63.94; H, 4.10; N, 21.93%.

A sample of **7** (1.64 g) was dissolved in 40 ml of methanolic ammonia (saturated at 0 °C) and kept at 0 °C for 16 hr. The solution was evaporated *in vacuo* to dryness. The residue was crystallized from hot water to give 9-furfuryladenine (**1**), 0.48 g (21.5%) of needles, mp 193.5—194 °C (lit,[3] mp 191—192 °C), UV $\lambda_{max}^{0.1N\ HCl}$ 260 mμ (ε 17800), $\lambda_{max}^{H_2O}$ 261 mμ (ε 17700), $\lambda_{max}^{0.1N\ NaOH}$ 261 mμ(ε 18100).

Found: C, 56.30; H, 4.58; N, 31.93%. Calcd for $C_{10}H_9N_5O$: C, 55.81; H, 4.22; N, 32.54%.

1-Furfuryluracil (2). Uracil (0.810 g, 7.2 mmol) and lithium hydride (52 mg, 8.0 mmol) dissolved in 20 ml of dry dimethylformamide by heating to 120—130 °C was added to a solution of triphenyl posphate methiodide (3.61 g, 8.0 mmol) and furfuryl alcohol (0.70 g, 7.2 mmol) in ether (10 ml). After heating at 110—120 °C for 45 min, the solution was evaporated *in vacuo* and the dark sirup was extracted with hot water (40 ml). The extract was evaporated to dryness *in vacuo* and chromatographed over 80 g of silica gel (Mallineckrodt) using benzene–methanol (4: 1) to give crystals of **2**, 0.28 g (20.2%), which was recrystallized from water; colorless needles, mp 117—119 °C.

Found: C, 56.25; H, 4.20; N, 14.58%. Calcd for $C_9H_8N_2O_3$: C, 56.05; H, 4.64; N, 14.51%.

UV: $\lambda_{max}^{0.1N\ HCl}$ 266 mμ (ε 6860), $\lambda_{min}^{0.1N\ HCl}$ 238 mμ (ε 2250), $\lambda_{max}^{H_2O}$ 265 mμ (9800), $\lambda_{min}^{H_2O}$ 240 mμ (ε 2680), $\lambda_{max}^{0.1N\ NaOH}$ 264 mμ (ε 6840), $\lambda_{min}^{0.1N\ NaOH}$ 245 mμ(ε 4600).

1-(5′-Nitrofurfuryl)uracil (3). To a mixture of uracil (1.68 g, 15 mmol) and lithium hydride (0.12 g, 15 mmol) dissolved in dry dimethylformamide (100 ml) by heating to 80 °C, 5-nitrofurfuryl iodide (2.68 g, 10 mmol) was added and stirred at 80 °C for 80 min. The reaction mixture was condensed to 15 ml and filtered. To the filtrate, water (80 ml) was added and the mixture was shaken with benzene (50 ml×2). The benzene layer was evaporated to dryness *in vacuo* to give a dark residue which was chromatographed over silica gel (Mallineckrodt, 70 g) using benzene–methanol (9: 1) as the eluent. The main fractions were evaporated to dryness *in vacuo* to yield 0.447 g (20%) of crude 1-(5′-nitrofurfuryl)uracil. Recrystallization from ethanol or water–ethanol gave pale yellow needles. Mp 209—210 °C (decomp.).

Found: C, 45.74; H, 3.25; N, 17.30%. Calcd for $C_9H_7N_3O_5$: C, 45.57; H, 2.98; N, 17.72%.

IR: ν_{max}^{KBr} 1500, 1360 cm^{-1} (–NO_2). NMR (DMSO-d_6): δ 5.12 (2H singlet, –CH_2–), δ 5.74 (1H doublet, J=8 Hz, H_5), δ 6.90 and 7.74 (1H each doublet, J=4 Hz, H_3' and H_4'), δ 7.85 (1H doublet, J=8 Hz, H_6), δ 11.41 (1H, 3-NH).

9-(5′-Nitrofurfuryl)adenine (4). To a sample of **6** (116 mg) dissolved in hot methanol (40 ml) was added 2 M hydrochloric acid (40 ml) and the mixture was refluxed on boiling water bath for 2 hr. After concentration *in vacuo* to about 27 ml and subsequent washing with ethyl ether (20 ml×3), the solution was further concentrated to give fine needles of 9-(5′-nitrofurfuryl)adenine hydrochloride (82.5 mg, 88%). It decomposed at >216 °C.

Found: C, 40.03; H, 3.69; N, 27.90; Cl, 11.54%. Calcd for $C_{10}H_9N_6O_3Cl$: C, 40.49; H, 3.06; N, 28.32; Cl, 11.95%.

The crystals gave a single spot ($R_f \simeq 0.5$) (tlc with butanol saturated with water). IR: ν_{max}^{KBr} 1700, 1610 (–N=C=), 1510, 1350 (–NO_2), 1235, 1225 cm^{-1} (furan ring).

A sample of the hydrochloride (73.2 mg, 0.25 mmol) was dissolved in a mixture of hot water (45 ml) and methanol (5 ml) and the solution was cooled to room temperature. To the solution, sodium carbonate (14.5 mg, 0.13 mmol) was added to give pale yellow needles of **4** (51.7 mg, 80.5%). It decomposed at >235 °C.

Found: C, 46.66; H, 3.55; N, 32.65%. Calcd for $C_{10}H_8N_6O_3$: C, 46.16; H, 3.10; N, 32.30%.

IR: ν_{max}^{KBr} 1645, 1595 (–N=C=), 1500, 1350 (–NO_2), 1240 cm^{-1} (furan ring). NMR (DMSO-d_6): δ 6.56 (2H, –CH_2–), δ 7.34 (2H, –NH_2), δ 6.90 and 7.70 (each 1H, H_4' and H_3'), δ 8.27 and 8.34 (each 1H, H_2 and H_8).

3-(5′-Nitrofurfuryl)adenine (5). To a mixture of adenine (1.06 g, 8 mmol) and lithium hydride (64 mg, 8 mmol) dis-

solved in dry dimethylformamide (40 ml) by heating to 55 °C, 5-nitrofurfuryl iodide (2.14 g, 8 mmol) was added and the mixture was stirred at 50—55 °C for 2 hr. The mixture was concentrated and the dark residue was chromatographed on a column of silica gel (90 g, Mallineckrodt), being washed with benzene (300 ml) and eluted with ethyl acetate–methanol (4: 1). Evaporation of the initial fractions followed by crystallization from water–methanol gave 9-(5′-nitrofurfuryl)-adenine (**4**), 42.1 mg (2.2%). From the middle fractions, 3-(5′-nitrofurfuryl)adenine (**5**) was obtained, colorless crystals, 344 mg (16.5%), mp 214 °C (decomp.).

Found: C, 46.34; H, 3.31; N, 32.34%. Calcd for $C_{10}H_8N_6O_3$: C, 46.16; H, 3.10; N, 32.30%.

IR: ν_{max}^{KBr} 1495, 1345 cm^{-1} ($-NO_2$). MNR (DMSO-d_6): δ 5.77 (2H, $-CH_2-$), δ 6.99 and 7.68 (each 1H, H_4' and H_3'), δ 7.83 and 8.56 (each 1H, H_8 and H_2), δ 8.19 (2H, $-NH_2$).

6-Benzamido-9-(5′-nitrofurfuryl)purine (**6**). To a mixture of 6-benzamidopurine (2.524 g, 10.6 mmol) and lithium hydride (80 mg, 10.1 mmol) dissolved in dry dimethylformamide (100 ml) by heating to 80 °C, 5-nitrofurfuryl iodide (2.680 g, 10.6 mmol) was added and the mixture was heated at 78—85 °C for 3 hr. The reaction mixture was evaporated to dryness *in vacuo* and the residue was dissolved in methanol (10 ml). The solution was chromatographed on a column of silica gel (200 g, Mallineckrodt, 100 mesh), being washed with benzene (900 ml) and eluted with benzene–methanol (15: 1). The middle fractions gave crude 6-benzamido-9-(5′-nitrofurfuryl)purine (yield 24.6%). Analytical sample was obtained as colorless needles by recrystallization from 2-propanol. Mp 171—172.5 °C.

Found: C, 56.15; H, 3.63; N, 22.88%. Calcd for $C_{17}H_{12}N_6O_4$: C, 56.04; H, 3.32; N, 23.07%.

UV: λ_{max}^{MeOH} 282 mμ(ε 28000). IR: ν_{max}^{KBr} 1695 (C=O), 1500, 1360, 1330 ($-NO_2$), 1240 cm^{-1} (C–O–C). NMR (DMSO-d_6): δ 5.80 (2H, $-CH_2-$), δ 7.00 and 7.7 (H_4' and H_3'), δ 8.69 and 8.84 (each 1H, H_8 and H_2).

Bioassay. It is interesting that compounds **3**, **4**, and **5** showed significant antitumor activity against Yoshida *sarcoma ascites*. The inhibition % of **3**, **4**, and **5** at concentrations 10 mcg/ml and (100 mcg/ml) were 66.3 (83.0), 78.1 (78.7) and 75.7 (83.7) %, respectively. (Control: 6-mercapto-9-β-D-ribofuranosylpurine at 10 mcg/ml and (100 mcg/ml): 49.4 (77.8) %.

Compounds **3**, **4**, **5**, and **6** also showed broad antibacterial and antifungal activity. Their minimum inhibitory concentrations (mcg/ml) were 1.0—7.8 against Gram-positive bacteria tested, 31.2—62.4 against *E. coli* K-12 and 15.6—31.2 against some fungi tested.

References

1) H. A. Burch, *J. Med. Chem.*, **11**, 79 (1968).
2) E. W. Hurst and R. Hull, *J. Med. Pharm. Chem.*, **3**, 215 (1961).
3) R. Hull, *J. Chem. Soc.*, **1958**, 2746.
4) S. Fukatsu, Y. Takeda, and S. Umezawa, This Bulletin, **46**, 3165 (1973).
5) S. R. Landauer and H. N. Rydon, *J. Chem. Soc.*, **1953**, 2224.
6) J. C. Howard and G. Klein, *J. Org. Chem.*, **24**, 255 (1959).
7) N. J. Leonard and T. Fujii, *J. Amer. Chem. Soc.*, **85**, 2026 (1963).
8) N. J. Leonard and J. A. Deyrup, *ibid.*, **84**, 2148 (1962).
9) R. Denayer, A. Cave, and R. Goutarel, *C.R. Acad. Sci., Paris*, **253**, 2004 (1961); R. Denayer, *Bull. Soc. Chim. Fr.*, **1962**, 1358.
10) C. J. Abshire and L. Berlinguet, *Can. J. Chem.*, **42**, 1599 (1964).
11) L. M. Jackman and S. Sternhell, "Application of Nuclear Magnetic Resonance Spectroscopy in Organic Chemistry," Pergamon Press (1961), p. 210.
12) N. S. Bhacca, D. P. Hollis, L. F. Johonson, and E.A. Pier, "High Resolution NMR Spectra Catalog", Vol. 2, Varian Associates (1963).

Photolysis of 2,2-Diethoxy-2,3-dihydrophenalene-1,3-dione

Yoshio Otsuji, Shigeo Wake, Eiichi Maeda, and Eiji Imoto

Department of Applied Chemistry, College of Engineering, University of Osaka Prefecture, Sakai-shi, Osaka 591

(Received August 30, 1973)

Irradiation of 2,2-diethoxy-2,3-dihydrophenalene-1,3-dione (**6**) with a pyrex-filtered high-pressure Hg arc lamp afforded acetaldehyde, 2-ethoxy-3-hydroxyphenalene-1-one (**7**) and bis-2-(2-ethoxy-1,3-dioxo-2,3-dihydro) phenalenyl (**8**). Mechanistic studies revealed that the first step of this photoreaction was a homolytic fission of the C–OC_2H_5 bond to 2-(2-ethoxy-1,3-dioxo-2,3-dihydro)phenalenyl radical (**9**) and ethoxyl radical. This homolytic fission occurred mostly from the triplet and in part from the singlet excited state of **6**. Dimerization of **9** gave **8** and the disproportionation between **9** and ethoxyl radical gave acetaldehyde and **7**. The photochemical behaviors of a variety of triketone derivatives were discussed.

In a separate paper,[1] we have reported that 2,2-dihydroxy-2,3-dihydrophenalene-1,3-dione (**1**) undergoes the redox disproportionation with elimination of CO_2 to 2,3-dihydroxyphenalene-1-one (**2**) and acenaphthene-1,2-dione (**3**) upon irradiation in organic solvents. A key step of this reaction was a rearrangement of **1** to 2-carboxy-2-hydroxyacenaphthene-1-one (**4**) from the singlet excited state of **1** (see Scheme 1).

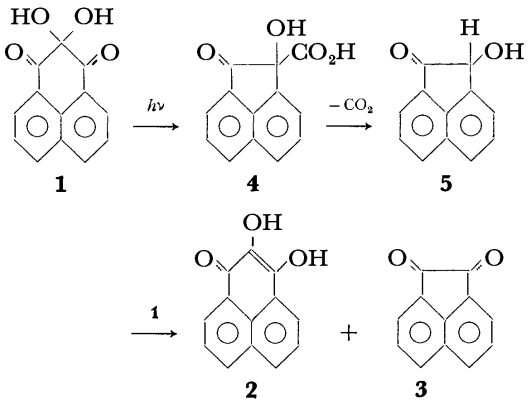

Scheme 1

However, we have previously presented evidence supporting that 2,2-dihydroxy- or 2,2-dialkoxy-1,3-diketones such as alloxan monohydrate,[2] ninhydrin[2] or 5,5-dialkoxybarbituric acids[3] undergo the photoreaction involving an α-cleavage as illustrated in Scheme 2.

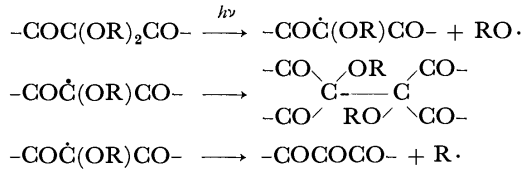

where R represents H or alkyl.

Scheme 2.

These diverse photochemical behaviors of triketone derivatives prompted us to study the photochemistry of 2,2-diethoxy-2,3-dihydrophenalene-1,3-dione (**6**). The specific effect such as an intramolecular hydrogen bonding, which is present between the hydroxyl and carbonyl groups of **1**, is absent in **6**. We observed that **6** undergoes the α-cleavage reaction upon irradiation, but the radical produced behaves differently from those represented in Scheme 2. In this paper, the results so far obtained are summarized and the mechanism of the photoreaction is discussed.

Results

Products. A Pyrex-filtered irradiation of a solution of **6** in benzene with a high-pressure Hg arc lamp under nitrogen at room temperature afforded acetaldehyde, 2-ethoxy-3-hydroxyphenalene-1-one (**7**) and bis-2-(2-ethoxy-1,3-dioxo-2,3-dihydro)phenalenyl (**8**). Acetaldehyde, which distilled out upon passing nitrogen into the reaction mixture, was identified as its 2,4-dinitrophenylhydrazone. The dimer **8** deposited on the bottom of the reaction vessel and it was easily separated from other products by filtration. The unreacted starting material and **7** were satisfactorily separated by a column-chromatography on silica gel.

The structure of **7** was confirmed by the analytical and spectral data. The NMR spectrum ($CDCl_3$) showed a triplet (J=7.5 Hz, 3H) at 1.40 ppm (–CH_2–CH_3), a quartet (J=7.5 Hz, 2H) at 4.42 ppm (–CH_2–CH_3), a broad singlet (1H) at 6.96 ppm (–OH), and the multiplet signal (6H) due to the aromatic protons from 7.28 to 8.47 ppm. The IR spectrum (KBr) exhibited a band at 3520 cm^{-1} due to the hydroxyl group and at 1630 cm^{-1} attributable to the carbonyl group. The mass spectrum displayed prominent peaks at m/e 240 (M^+), 212 (M^+—CO), and 196 (M^+—CH_3–CHO).

In support of the structure assignment of **8**, we observed the molecular weight to be 474 (calcd 478) by the Rast method. The IR spectrum (KBr) indicated a band at 1679 cm^{-1} due to the carbonyl group. The analytical data showed the molecular formula to be $C_{30}H_{22}O_6$.

The same sort of the products was also obtained when irradiation was carried out in acetonitrile and 2-propanol. The isolated yields are shown in Table 1.

A ratio of the yield of the dimer **8** to that of **7** was higher in the non-polar solvent, benzene, than in the polar solvents such as acetonitrile and 2-propanol.

Quantum Yields for the Formation of **7**. The photolysis of **6** was conducted in three solvents in a 1 cm optical cell under anaerobic conditions by irradiation of 313 nm light. As the reaction proceeded, an absorption of 320 nm band due to **6** decayed with

Table 1. Photolyses of **6**

Solvent	Recovered starting material %	Yields of products %[a]	
		7	**8**
C_6H_6[b]	36	21	14
CH_3CN[b]	28	61	1.5
2-PrOH[c]	20	66	5.0

a) The yields are based on the total amount of the starting material initially used.
b) A solution of 200 mg of **6** in 50 ml of the solvent in a quartz vessel was irradiated for 48 hr externally from the outside of the reaction vessel.
c) A solution of 200 mg of **6** in 200 ml of the solvent was irradiated for 6 hr employing an immersion-type apparatus.

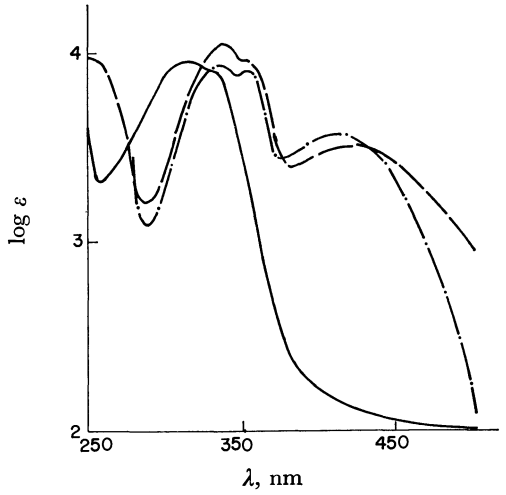

Fig. 1. Absorption spectra of 2,2-diethoxy-2,3-dihydrophenalene-1,3-dione (**6**) and 2-ethoxy-3-hydroxyphenalen-1,-one (**7**)
——, **6** in 2-PrOH; ——, **7** in 2-PrOH; —•—, **7** in C_6H_6 and CH_3CN. The stectra of **6** in C_6H_6 and CH_3CN were almost identical with that in 2-PrOH.

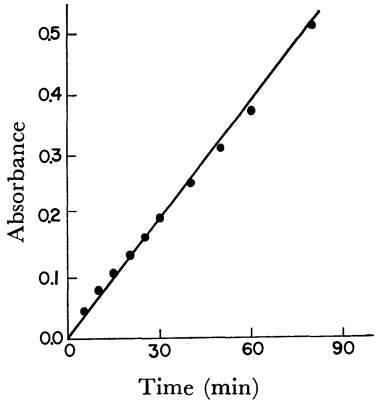

Fig. 2. Rate of appearance of the absorbance of 2-ethoxy-3-hydroxyphenalene-1-one (**7**) at 413 nm upon irradiation of 2,2-diethoxy-2,3-dihydrophenalene-1,3-dione (**6**) in C_6H_6.

appearance of 410—425 nm band due to **7** as shown in Fig. 1. The rates of the formation of **7** were followed by monitoring an appearance of the absorptions at 413 nm in benzene, at 410 nm in acetonitrile, and at 425 nm in 2-propanol. The amounts of **7** formed linearly increased with irradiation time in all solvents until more than 50% of **6** was consumed. In a typical example, the result of the photolysis of **2** in benzene is shown in Fig. 2. The rate data were then converted into the quantum yields by use of the ferric oxalate actinometer. The quantum yields obtained are summarized in Table 2.

Table 2. Quantum yields for the formation of **7** upon irradiation by 313 nm light

Concn. of **6**, M	Solvent	Φ
1.01×10^{-3}	C_6H_6	0.040
1.04×10^{-4}	CH_3CN	0.035
1.00×10^{-3}	CH_3CN	0.046
9.97×10^{-3}	CH_3CN	0.059
1.00×10^{-3}	2-C_3H_7OH	0.043

The results of Table 2 indicate that the quantum yield for the formation of **7** is not so much affected by the concentration of **6** present and not at all by the nature of solvents used.

Stern-Volmer Plots. In order to gain information on the nature of the excited state involved, quenching experiments were carried out. A 1.00×10^{-3} M solution of **6** in benzene was irradiated in the presence of various concentrations (0—0.01 M) of cyclohexadiene, a triplet quencher, and the quantum yield for the formation of **7** was measured as described above. In

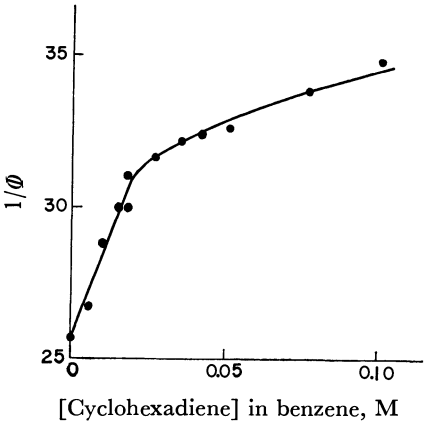

Fig. 3. Stern-Volmer plot for the formation of 2-ethoxy-3-hydroxyphenalene-1-one (**7**) by irradiation of 2,2-diethoxy-2,3-dihydrophenalene-1,3-dione (**6**) in C_6H_6.

Fig. 3, the reciprocals of the quantum yields were plotted against the concentrations of cyclohexadiene added (Stern-Volmer plot). From Fig. 3, it can be seen that the quantum yield for the formation of **7** is reduced strongly by the presence of lower concentrations of cyclohexadiene, but weakly by the presence of higher concentrations of cyclohexadiene. This phenomenon suggests that **7** is formed mostly from a triplet

excited state and in part from a singlet excited state of **6**.[4]

Discussion

A plausible mechanism which explains the results presented earlier is given in Scheme 3. The first step of the photoreaction is a homolytic cleavage of the C–OC_2H_5 bond in **6** to form the radical **9** and the ethoxyl radical. This cleavage reaction occurs mostly from a triplet excited state of **6** and in part from its singlet excited state. The radical **9** dimerizes to form the dimer **8**. On the other hand, the disproportionation between **9** and the ethoxyl radical gives **7** and acetaldehyde. The dimerization reaction is favored in non-polar solvent such as benzene, while the disproportionation reaction is favored in polar solvents such as acetonitrile and 2-propanol. The solvent effect of this sort in radical reactions has frequently been observed.[5]

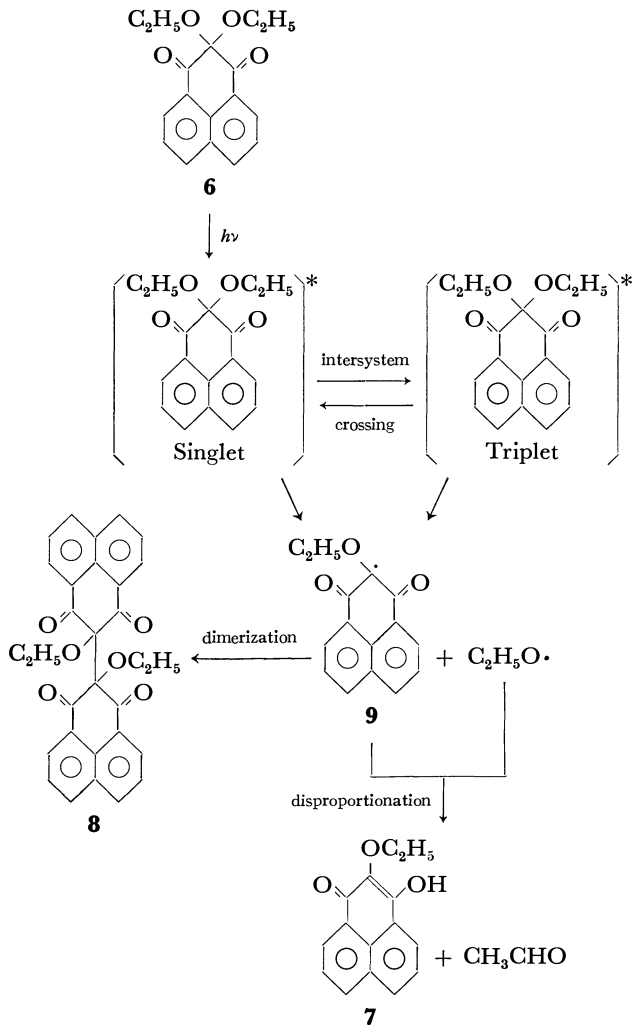

Scheme 3

The formation of **7** and acetaldehyde may also be explained by the other mechanism involving the 1,4-biradical intermediate **10** which can be formed *via* a γ-hydrogen abstraction by the excited carbonyl of **6**; a decomposition of **10** would lead to **7** and acetaldehyde. However, this possibility can be eliminated from the fact that the quantum yield for the formation of **7** was actually independent on the polarity of solvents used as shown in Table 2. If the biradical **10** participates as an intermediate of the photoreaction, then the quantum yield should become higher in the solvents of higher polarity, since the intermediate would be stabilized in polar solvents.[6] However, this was not the case.

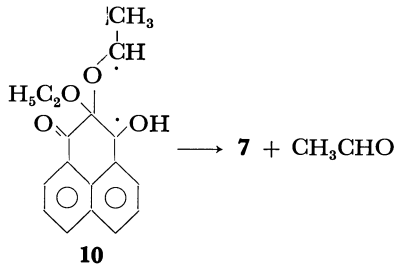

Unfortunately, the systematic understanding on the diversity of the photochemical behaviors of triketone derivatives is not attained at present. However, it would be important to note that the ionic-type reaction of **1** takes place from its singlet excited state,[1] while the α-cleavage reaction of a radical-type as observed in **6** occurs mainly from a triplet excited state of the carbonyl group. An intramolecular hydrogen bonding between the hydroxyl and carbonyl groups of **1**, which was inferred from a broad hydroxyl band centered at 3200 cm^{-1} in the IR spectrum, may contribute at least in part to an exclusive formation of the singlet excited state.

A difference in the reactivity between the 1,3-dioxoradical generated from **6** and that from ninhydrin might be explained in terms of the stability of the radicals. The radical **9** generated from **6** can be stabilized by a conjugation with the vicinal carbonyl groups. In contrast, the radical **11** generated from ninhydrin would gain destabilization rather than stabilization by a conjugation with the vicinal carbonyl groups, since the structure of the type **11a** is of an anti-aromatic character.[7]

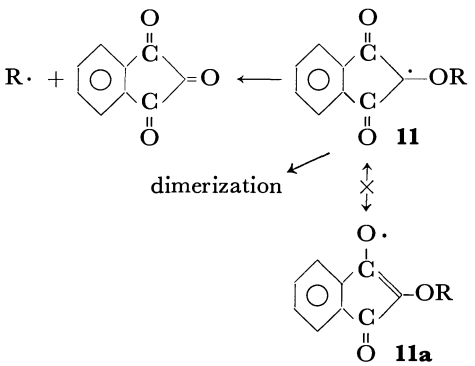

An odd electron in the radical **11** thus become fixed to a greater extent at the 2-position, and hence the radical is forced to undergo dimerization or cleavage reaction to indanetrione and the radical R·. On the other hand, the resonance-stabilized radical **9** undergoes dimerization or disproportionation if other radicals are present in the reaction mixture.

Experimental

All melting points are uncorrected. Electronic absorption spectra were recorded with a Hitachi EPS-3T recording spectrophotometer or a Hitachi Perkin-Elmer 139 spectrophotometer. IR spectra were obtained with a Hitachi 215 infrared spectrophotometer. NMR spectra were obtained on a Hitachi H-60 high resolution NMR spectrometer with tetramethylsilane as an internal standard. Microanalyses were performed with a Hitachi 026 CHN analyzer. Irradiations were carried out with a 100 W Ushio UM-102 high-pressure Hg arc lamp equipped with a Pyrex water-cooling jacket.

Materials. 2,2-Diethoxy-2,3-dihydrophenalene-1,3-dione (**6**) was prepared by the method of Regitz and Adolph[8] and purified by recrystallization from ethanol; mp 137—138 °C (lit,[8] mp 138—139 °C). Cyclohexadiene was prepared by the method of Blomquist and Kwiatek[9] and purified by distillation; bp 79—81 °C (lit,[9] bp 79—81 °C).

Photoreaction of 6. *(a) In Benzene*: A solution of 200 mg (0.704 mmol) of **6** in 50 ml of benzene was placed in a cylindrical quartz vessel. An outlet of the vessel was connected with a vinyl tubing to a flask containing a solution of 2,4-dinitrophenylhydrazine in an aqueous HCl. Nitrogen was introduced into the reactant solution for 30 min and then irradiation was carried out externally from the outside of the vessel at room temperature under bubbling nitrogen in the solution. After irradiation for 8 hr, nitrogen-bubbling was stopped and the outlet of the reaction vessel was sealed with a glass stopper. During this period, red precipitates appeared in the flask containing 2,4-dinitrophenylhydrazine. The precipitates, 20 mg, were separated by filtration. They melted at 146—147 °C and were identical with the authentic sample of 2,4-dinitrophenylhydrazone of acetaldehyde in every respect.

On the other hand, when the irradiation was continued for 48 hr, brown crystals appeared on the bottom of the reaction vessel. They were removed by filtration, and washed thoroughly with dioxane and then with chloroform. The crystals thus obtained were found to be 47 mg (14%) of **8**: mp 236—237 °C (decomp.). Found: C, 75.29; H, 4.65%. Calcd for $C_{30}H_{22}O_6$: C, 75.30; H, 4.63%.

Evaporation of the solvent from the filtrate, which was obtained after removal of **8**, under reduced pressure gave a brown oil. The oil was dissolved in benzene–chloroform (1 : 1) and chromatographed on a silica gel column using the same solvent as an eluent. Evaporation of the first eluent gave 73 mg (36%) of the unreacted starting material as light yellow crystals of mp 134—137 °C, which melted at 138—139 °C after recrystallization from ethanol.

Further elution with benzene–chloroform and evaporation of the eluent gave 35 mg (21%) of **7**. Recrystallization from methanol gave orange crystals: mp 125—126 °C. Found: C, 75.05; H, 4.94%. Calcd for $C_{15}H_{12}O_3$: C, 74.99; H, 5.03%.

(b) In Acetonitrile: A solution 200 mg (0.704 mmol) of **6** in 50 ml of acetonitrile was irradiated for 48 hr as described above. After irradiation, the reaction mixture was worked up in the manner similar to that described above. From the reaction mixture, 5 mg (1.5%) of **8**, 56 mg (28%) of the unreacted starting material and 103 mg (61%) of **7** were obtained. 2,4-Dinitrophenylhydrazone of acetaldehyde was also isolated.

(c) In 2-Propanol: A solution of 200 mg (0.704 mmol) of **6** in 200 ml of 2-propanol was placed in an immersion-type apparatus, and nitrogen was bubbled for 30 min. Irradiation was then carried out in a stream of nitrogen at room temperature for 6 hr. Treatment of the reaction mixture afforded 17 mg (5.0%) of **8**, 41 mg (21%) of the starting material and 111 mg (66%) of **7**. 2,4-Dinitrophenylhydrazone of acetaldehyde was also isolated in this photolysis.

Determination of Quantum Yields. The same apparatus and procedure as those described separately[1] were employed for determination of the quantum yields. The rates of the formation of **7** were followed by monitoring the absorbances at 413 nm in benzene, at 410 nm in acetonitrile and at 425 nm in 2-propanol. In quenching experiments, the rates of the formation of **7** were measured by monitoring the absorbances at the same wavelengths as described above.

References

1) Y. Otsuji, S. Wake, E. Maeda, and E. Imoto, This Bulletin, submitted for publication.
2) Y. Otsuji, S. Wake, and E. Imoto, *Tetrahedron*, **26**, 4139 (1970).
3) Y. Otsuji, S. Wake, and E. Imoto, *ibid.*, **26**, 4293 (1970).
4) T. R. Evans, "Technique of Organic Chemistry," Vol, XIV, ed. by P. A. Leermakers and A. Weissberger, Interscience Publishers, New York, N.Y. (1969), Chapt. IV.
5) P. S. Dixon, A. P. Stefani, and M. Szwac, *J. Amer. Chem. Soc.*, **85**, 2551, 3344 (1963).
6) P. J. Wagner, *ibid.*, **89**, 5897 (1967).
7) P. H. Lacy and D. C. C. Smith, *J. Chem. Soc. C*, **1971**, 41.
8) M. Regitz and H. G. Adolph, *Ann. Chem.*, **723**, 47 (1969).
9) A. T. Blomquist and J. Kwiatek, *J. Amer. Chem. Soc.*, **73**, 2098 (1951).

N-Alkylideneanilines. III.[1] Behavior of *N*-Isopropylideneanilines in Methanol-d_4

Hiizu IWAMURA,* Michiko TSUCHIMOTO,** and Shigeo NISHIMURA**

**Department of Chemistry, Faculty of Science, The University of Tokyo, Hongo, Tokyo 113*

***Department of Industrial Chemistry, Tokyo University of Agriculture and Technology, Koganei, Tokyo 184*

(Received August 6, 1973)

When *N*-isopropylideneanilines are dissolved in methanol-d_4, three types of reactions, exchange of protons in isopropylidene moiety, formation of carbinolamine ethers, and liberation of anilines with formation of acetone dimethyl acetal take place as revealed by NMR spectra of the solutions. The H–D exchange reaction is favored by electron-releasing ring substituents and yet is considerably slower than the rates of the E–Z isomerization of the corresponding imines. The carbinolamine ethers are formed when the substituents are strongly electronegative. Formation of acetone dimethyl acetal occurs additionally with imines carrying halogen atoms as the ring substituents. The competitive reaction mechanism is proposed.

Recently Jennings and Boyd pointed out the intermediacy of enamine tautomers for the E–Z isomerization of imines containing HCC=N moiety.[2] To test the role of this mechanism in the E–Z isomerization of a series of *N*-isopropylideneanilines with various ring substituents, we have examined their rates of H–D exchange reaction by the NMR spectroscopy and found that the above mechanism is not operative in these imines and that they behave quite differently in methanol-d_4, depending on the nature of the ring substituents. Specifically the following three types of reactions were observed for *N*-isopropylideneanilines.

1) Exchange of protons in isopropylidene moiety.
2) Formation of adducts of *N*-isopropylideneanilines with methanol-d_4.
3) Liberation of anilines with formation of acetone dimethyl acetal-d_6.

Experimental

NMR spectra were obtained on a JEOL C-60 HL (Japan Electron Optics Lab. Co., Ltd.) high resolution NMR instrument (60 MHz). *N*-Isopropylideneanilines (0.25 mmol) were dissolved in 0.5 ml of CD_3OD (99.5%). The measurement was carried out at time intervals on the growth and decay of resonance signals by recorder integration (the accuracy of each integration is about ±4%). The chemical shifts were read relative to TMS as the internal reference at 25 °C.

General procedure of the preparation of *N*-isopropylideneanilines:[3] 30 g of molecular sieve 4A were added to a solution of 0.1 mol of acetone and 0.05 mol of aniline in anhydrous ether. The mixture was kept at 10 °C for 9 to 10 days, by renewing the molecular sieve 2—3 times. After removing the molecular sieve by filtration and the solvent by application of a rotary evaporator, the residue was fractionaly distilled.

N-Isopropylidene-*p*-iodoaniline was obtained as a yellow oil (bp 127 °C/8 mmHg, n_D^{25} 1.5732); NMR spectrum ($CDCl_3$, 25 °C): *syn* CH_3, s, 1.80 ppm; *anti* CH_3, s, 2.18 ppm;[4] 2,6 ring protons, d, 6.55 ppm; 3,5 ring protons, d, 7.66 ppm. Found: C, 41.67; H, 3.70; N, 5.37%. Calcd for $C_9H_{10}NI$: C, 41.72; H, 3.89; N, 5.41%.

N-Isopropylidene-*p*-fluoroaniline; a colorless oil (bp 54—56 °C/5 mmHg, n_D^{25} 1.5081; NMR spectrum ($CDCl_3$, 25 °C): *syn* CH_3, s, 1.80 ppm; *anti* CH_3, s, 2.18 ppm;[4] ring protons, centered at 6.88 ppm. Found: C, 71.34; H, 6.53; N, 9.34%. Calcd for $C_9H_{10}NF$: C, 71.50; H, 6.67; N, 9.27%.

N-Isopropylidene-*m*-trifluoromethylaniline: a yellow oil (bp 52 °C/5 mmHg, n_D^{25} 1.4712); NMR spectrum ($CDCl_3$, 25 °C): *syn* CH_3, s, 1.82 ppm; *anti* CH_3, s, 2.20 ppm;[4] 2,6 ring protons, d, 7.01 ppm; 3,4 ring protons, d, 7.42 ppm. Found: C, 59.73; H, 5.02; N, 7.14%. Calcd for $C_{10}H_{10}NF_3$: C, 59.70; H, 5.01; N, 6.96%.

Table 1. Kinetic data of H–D exchange reactions

X in 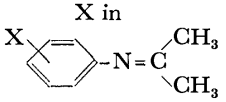	k/sec
p-OCH_3	2.80×10^{-5}
p-CH_3	1.69×10^{-5}
H	6.60×10^{-6}
p-F	3.70×10^{-6}
p-I	2.59×10^{-6}
p-Cl	5.66×10^{-6}
p-Br	5.38×10^{-6}
m-CF_3	1.19×10^{-6}

Results and Discussion

The H–D Exchange Reaction. The isopropylidene methyl protons of *N*-isopropylideneanilines carrying electron-releasing *p*-substituents exchange with deuterium in methanol-d_4 solution at ambient temperature. The rate of the reaction can readily be followed by measuring the decrease of their proton signals or the

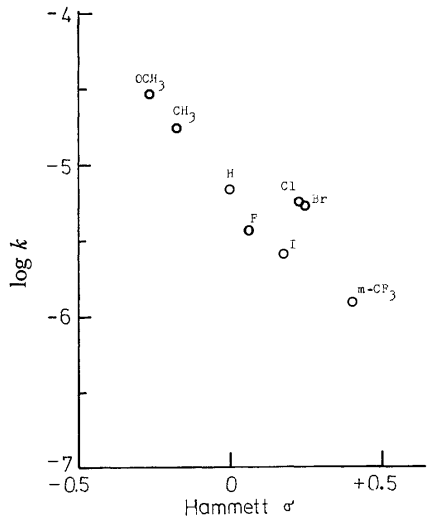

Fig. 1. The Hammett plots of the rates of H–D exchange reaction.

increase of the OH protons[5] due to CD_3OH produced. The pseudo-first-order rate constants for the exchange reaction in a large excess of CD_3OD are calculated and given in Table 1. Note that the rates of exchange increase with increasing electron-donating ability of the substituents. This relation is demonstrated more clearly by the Hammett expression as shown in Fig. 1. The trend indicates that the exchange reaction is nucleophilic and that protonation either to the imines or to the enamines is the rate-determining step. The values for *p*-Cl and *p*-Br deviate from the straight line. This might be due to inaccuracy of the determination of the rates because of the concurrent occurrence of the addition reaction (*vide infra*). In those having more electron-withdrawing substituents than the halogenes, the exchange is not observed to detectable extent and the addition reaction is the exclusive one.

We recall that the rates of E–Z isomerization [$k(s^{-1}) = 4.0\times10^{-2}$ for *m*-CF_3 and 2.5×10^{-3} for *p*-OCH_3 at 25 °C][6] are faster by order of magnitude than the rates of exchange in Table 1 and are subject to reverse substituent effects; the electron-withdrawing groups enhance while the electron-releasing substituents retard the isomerization. It is concluded from these results that formation of enamine is slower and cannot be the contributing mechanism for the E–Z isomerization.

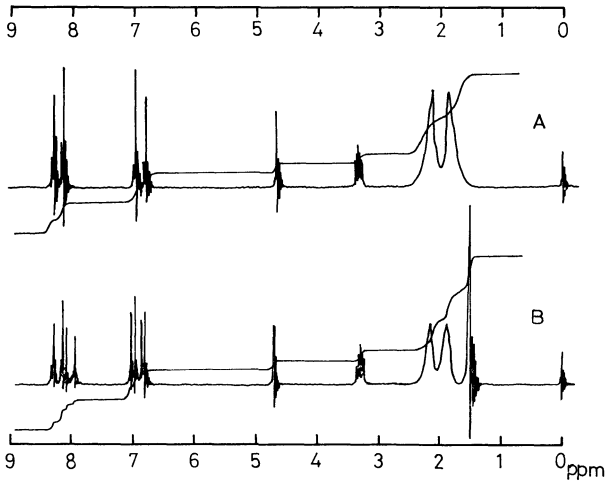

Fig. 2. NMR spectra of *N*-isopropylidene-*p*-nitroaniline (0.25 mmol) in CD_3OD (0.5 ml), 25 °C.
A: At the beginning of the reaction.
B: After 212 min with 32% adduct formation.

The Addition Reaction. When *N*-isopropylidene-*p*-nitroaniline is allowed to stand in CD_3OD, the signals due to the *syn*- and *anti*-methyl protons (δ 1.87 and 2.21) as well as A_2X_2 type aromatic protons (δ 6.93 and 8.23) diminish their intensity with a corresponding increase of a new singlet at δ 1.51, as shown in Fig. 2. The new A_2X_2 type multiplets start to develop in the aromatic region (δ 6.98 and 8.07). No increase in the OH proton signal was detected. The diamagnetic shift of the singlet signal suggests that the carbon atom to which the methyl groups are attached has changed its hybridization from sp^2 to sp^3. The chemical shifts of the aromatic protons are now more like those of *p*-nitroaniline.[7]

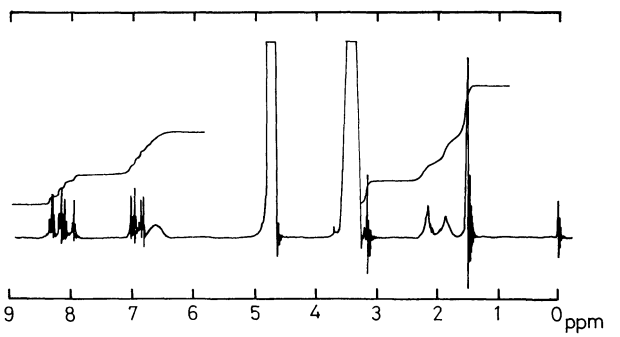

Fig. 3. NMR spectra of *N*-isopropylidene-*p*-nitroaniline (0.25 mmol) in CH_3OH (0.5 ml), 25 °C, taken at 300 min after the start of the reaction. 40% conversion.

While we have not succeeded in isolating the product, these spectral changes can be fully explained in terms of the formation of the adduct of the *N*-isopropylidene-aniline with methanol. The carbinolamine ether structure is further supported by the change in the NMR signals when the *N*-isopropylidene-*p*-nitroaniline is dissolved in CH_3OH (Fig. 3). Thus the additional singlets at δ 6.67 and 3.17 are consistent with the NH and OCH_3 protons in structure

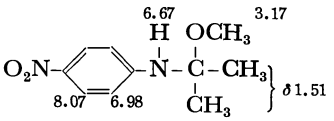

In Table 2 are given the equilibrium constants K_c, which are defined for the addition reactions by equation

$$K_c = X_e/[(a-X_e)(b-X_e)]$$

where *a* and *b* are the stoichiometric molar concentrations of *N*-isopropylideneanilines (2.50×10^{-4}) and CD_3OD (1.09×10^{-2}) and X_e is the molar concentration of the adduct in equilibrium. The pseudo-first-order rate constants for the addition reaction of various substituted *N*-isopropylideneanilines are also calculated

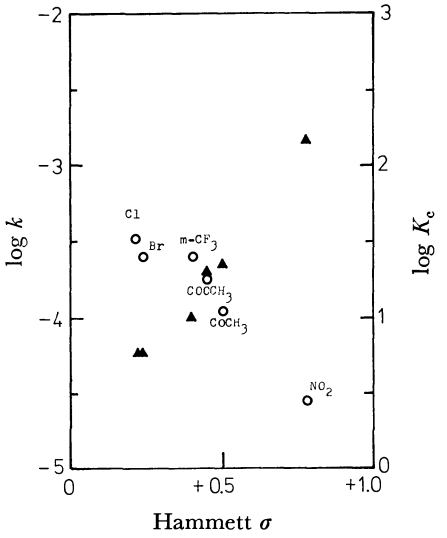

Fig. 4. The Hammett plots of the equilibrium constant K_c and the rate of adduct formation.
(○) for log *k*, (▲) for log K_c.

Table 2. Kinetic data of addition reactions

X in 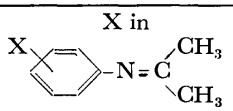	k/sec	X_e/%	X_e/mol	K_c	Time to equiribrium (min)
p-Cl	3.31×10^{-4}	6.1	1.53×10^{-5}	5.97	18
p-Br	2.34×10^{-4}	6.1	1.53×10^{-5}	5.97	14
m-CF_3	2.63×10^{-4}	9.0	2.25×10^{-4}	9.07	25
p-$COOCH_3$	2.29×10^{-4}	17.9	4.48×10^{-5}	20.1	36
p-$COCH_3$	1.41×10^{-4}	19.3	4.83×10^{-5}	22.0	74
p-NO_2	3.20×10^{-5}	61.7	1.54×10^{-4}	1.49×10^{2}	24 hr

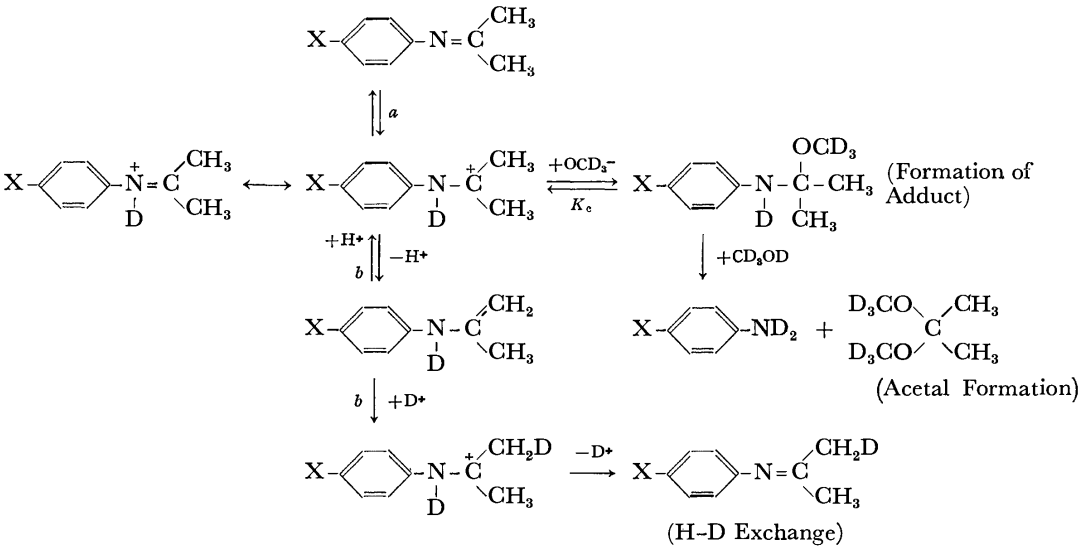

Scheme 1

and shown in the same Table. At 25 °C, the equilibrium is attained for the addition reaction in approximately 20—70 min. Especially *p*-NO_2 compound requires 24 hr before the equilibrium state is obtained. We note that, with increasing electronegativity of the ring substituents, the rate of formation of the adduct decreases, but the equilibrium constant for formation of the adduct increases. The effects of the ring substituents obey the Hammett relationship as shown in Fig. 4.

Relevant to the mechanism is the fact that there is no incorporation of deuterium observed in the methyl groups of the carbinolamine ether adducts.

The Acetal Formation. In the *N*-isopropylideneanilines having *p*-Cl, *p*-Br, *p*-I, and *m*-CF_3, it has been found that the formation of the carbinolamine ether is followed by the slow formation ($k\simeq10^{-6}$—10^{-7}) of acetone dimethyl acetal which is identified by the appearance of the signal at δ 1.30, independent of the ring substituents. The assignment is confirmed by comparison of the chemical shift with that of an authentic sample.[8] The reactions are practically complete in 2 weeks at ambient temperature with *ca.* 11% conversion.

It is of interest that the formation of the acetal is seen only in these *N*-isopropylideneanilines. In those having more electron-releasing substituents the formation of the intermediate adduct is very small, while in those having more electronegative substituents the intermediate adduct seems too stable to undergo further reaction into the acetal.

The Mechanism of the Reaction. As seen from the results described above, the course and rates of the reactions of *N*-isopropylideneanilines in CD_3OD are characteristically dependent on the nature of ring substituents. The reaction scheme and probable mechanisms for the whole reactions are summarized in Scheme 1.[9] Whereas the substituent effects on the rates of H–D exchange and formation of carbinolamine ethers have the same trend, the fact that the latter without H–D exchange has larger rate constants rules out the possibility that protonation or deuteration of the imines (step *a*) is rate-determining step in both cases. Step *a* may well be the rate-determining step for adduct formation, but protonation of enamines (step *b*) is more likely to be slower than step *a* and rate-determining for exchange reactions. The extent of formation of the carbinolamine ethers is governed by the electrophilicity of the conjugate acid of the imines.

References

1) For Part II see: H. Iwamura, M. Tsuchimoto, and S. Nishimura, *Chem. Lett.*, **1972**, 1073.

2) W. B. Jennings and D. R. Boyd, *J. Amer. Chem. Soc.*, **94**, 7187 (1972).

3) M. Tsuchimoto, S. Nishimura, and H. Iwamura,

This Bulletin, **46**, 675 (1973).

4) See Ref. 1 for the signal assignment.

5) Divided by six to obtain the rate constant per proton of the two methyl groups.

6) M. Tsuchimoto, S. Nishimura, and H. Iwamura, The 5th Symposium on Structural Organic Chemistry, October 11, Nagoya (1972), p. 63 of the Proceedings; to be published elsewhere.

7) *p*-Nitroaniline shows the A_2X_2 multiplets at δ 6.60 and 7.97 in methanol-d_4.

8) The *O*-methyl protons which should appear at δ 3.09 cannnot be detected for the reactions in methanol-d_4.

9) For the mechanism of analogous hydrolysis of the imines see: E. H. Cordes and W. P. Jencks, *J. Amer. Chem. Soc.*, **85**, 2843 (1963); E. F. Pratt and M. J. Kamlet, *J. Org. Chem.*, **26**, 4029 (1961); and papers cited therein.

Syntheses and Reactions of Optically Active Polymers. I. Syntheses and Polymerizations of *N*-Vinylbenzyl-L-amino Acid Derivatives

Mitsuaki NARITA and Masayasu AKIYAMA
Tokyo University of Agriculture and Technology, Koganei, Tokyo 184

(Received July 16, 1973)

N-Vinylbenzyl-L-amino acids were synthesized by the reaction of L-amino acids with formylstyrenes and the subsequent reduction of the condensation products with sodium borohydride. The procedure was performed without protection of the various functional groups of amino acids and racemization was not accompanied by the above process. The method is useful for the synthesis of optically active vinyl monomers containing various amino acids with their intact functionality. As a representative L-amino acid, a variety of *N*-vinylbenzyl-L-leucine derivatives such as *N*-methyl-L-leucine, L-leucine ethyl ester, L-leucinol and *N*-formyl-L-leucine ethyl ester were prepared by means of chemical transformation. These optically active monomers of leucine derivatives were polymerized to optically active polymers.

Though considerable attempts were made to carry out asymmetric syntheses using optically active polymers as catalysts or reagents,[1-5] no clear asymmetric courses, as usually seen in the formation of low optically active products, have been established. Steric regulation for asymmetric induction would be better achieved by proper selection of a functional group responsible for the asymmetry in the reaction course.

We previously reported on the use of polymers as chemical reagents in amide group formation.[6] To extend the utility of reagents of this type, we have undertaken the investigation of syntheses and reactions of polymers containing optically active groups.

The groups of our primary concern are those derived from α-amino acids, which contain one asymmetric carbon and various functional groups. Some devices have been worked out for the preparation of synthetic polymers possessing α-amino acid residues. Most polymers were synthesized through polymer reactions by which α-amino acids were introduced into reactive polymers, such as chloromethylated polystyrene[7] polymethacroyl chloride.[8] A few polymers have also been obtained by polymerizations of vinyl monomers containing α-amino acids as shown below.[9-11]

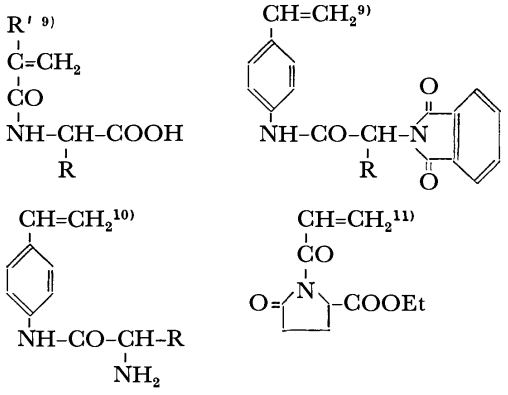

In polymer reactions, undesirable side reactions are sometimes inevitable. As to the monomers hitherto prepared, either amino- or carboxyl-group was transformed into amide for introduction of the vinyl group.

In order to use optically active polymers as chiral components for asymmetric reactions, it is desirable that they are prepared by polymerization of optically active monomers. This paper describes a new convenient synthesis and polymerization of vinyl monomers which contain an optically active α-amino acid moiety.

Results and Discussion

Syntheses of N-*Vinylbenzyl-*L-*amino Acids.* Quitt *et al.*[12] reported a synthetic procedure of *N*-benzyl-L-amino acids, in which L-amino acids were allowed to react with benzaldehyde and be reduced subsequently with sodium borohydride.

This procedure was applied and a variety of *N*-vinylbenzyl-L-amino acids were prepared by the reaction of L-amino acids with *o*- or *p*-formylstyrene according to Scheme 1.

The reaction of sodium salt of L-amino acids, glycine, valine, leucine, tyrosine, histidine and glutamine, was carried out in methanol at room temperature. Intermediate (I') formed was not isolated but was reduced with sodium borohydride under cooling conditions to give *N*-vinylbenzyl-L-amino acids (II or III) as crystals after acidification of the reaction mixture. Vinyl monomers II and III were obtained in good yield without protection of the functional groups. The physical data of the monomers synthesized by the above procedure

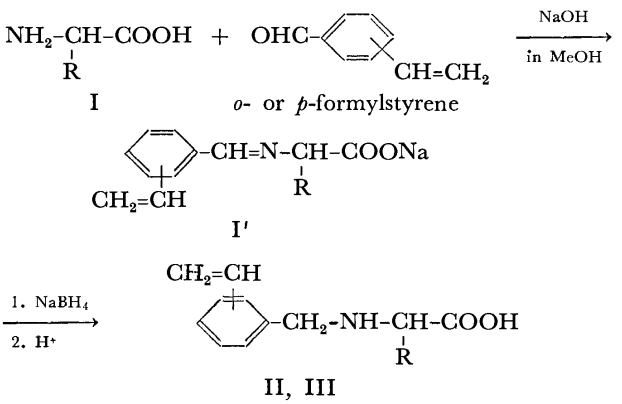

II; *o*-vinyl derivatives, III; *p*-vinyl derivatives
R; IIa=H, IIb=*iso*-Pro, IIc=*iso*-Bu,

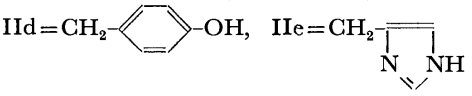

IIf=$CH_2CH_2CONH_2$
IIIa=*iso*-Bu, IIIb=$CH_2CH_2CONH_2$

Scheme 1.

TABLE 1. PHYSICAL DATA OF *N*-VINYLBENZYL-L-AMINO ACIDS

Product (Formula)	Yield (%)	Mp (°C)	Recrystallization Solvent	$[\alpha]_D^{23}$	Anal. (Calcd) (%) C	H	N
IIa ($C_{11}H_{13}O_2N$)	48	202 (dec.)	Water		68.72 (69.09	6.83 6.85	7.39 7.33)
IIb ($C_{14}H_{19}O_2N$)	62	224 (dec.)	Water-DMF[a)]	+39.5[b)]	71.56 (72.07	8.28 8.21	6.20 6.20)
IIc ($C_{15}H_{21}O_2N$)	76	196 (dec.)	Water-Acetic acid	+27.5[b)]	73.28 (72.84	8.76 8.56	5.78 5.66)
IId ($C_{18}H_{19}O_3N$)	83	235 (dec.)	DMF	+ 3.5[c)]	72.01 (72.70	6.51 6.44	4.99 4.71)
IIe ($C_{15}H_{17}O_2N_3$)	66	113 (dec.)	Water	−12.0[b)]	66.37 (66.40	6.54 6.32	15.06 15.49)
IIf ($C_{14}H_{18}O_3N_2$)	58	164 (dec.)	Water	+ 9.5[b)]	64.07 (64.10	7.00 6.92	10.65 10.68)
IIIa ($C_{15}H_{21}O_2N$)	80	208 (dec.)	d)	+11.0[c)]	72.58 (72.84	8.59 8.56	5.46 5.66)
IIIb ($C_{14}H_{18}O_3N_2$)	83	188 (dec.)	Water	+24.0	63.95 (64.10	6.89 6.92	10.54 10.68)

a) DMF; *N*,*N*-dimethylformamide. b) $c=2.0$, in acetic acid. c) $c=2.0$, formic acid. d) The compound was purified by reprecipitation twice from formic acid into water.

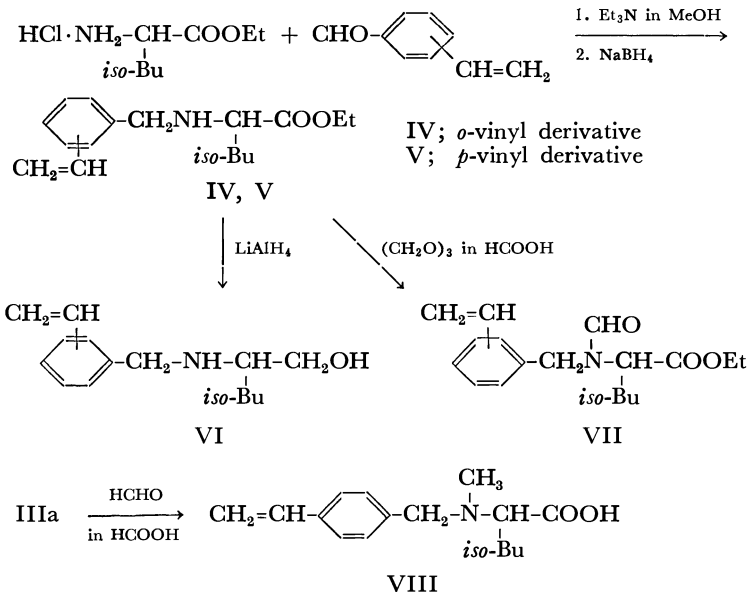

Scheme 2.

are given in Table 1. These amino acid derivatives are optically active and are insoluble in non-polar organic solvents. *o*-Vinyl derivatives are more soluble than *p*-vinyl derivatives in acetic acid, trifluoroacetic acid and formic acid.

Hydrogenolysis of compounds IIb and IIc with palladium-carbon catalyst produced the starting amino acids, L-valine and L-leucine. Optical rotations of the hydrogenolysis products coincided with those of the starting L-amino acids, indicating that the reactions according to Scheme 1 proceed without recemization.

Syntheses of N-*Vinylbenzyl-*L-*leucine Derivatives.* L-Leucine was selected as a representative, and several vinyl monomers carrying the derivatives of this amino acid were prepared according to Scheme 2.

The reaction of L-leucine ethyl ester with formylstyrenes gave *N*-vinylbenzyl-L-leucine ethyl esters IV and V. The reduction of IV with lithium aluminium hydride yielded *N*-*o*-vinylbenzyl-L-leucinol (VI). The reaction of IV with trioxane in formic acid did not give the *N*-methylated product but *N*-formyl-*N*-*o*-vinylbenzyl-L-leucine ethyl ester (VII). *N*-methylation of IIIa was carried out with formalin in formic acid to give *N*-methyl-*N*-*p*-vinyl-benzyl-L-leucine (VIII). The results are summarized in Table 2. The L-leucine derivatives are optically active. Vinyl monomers IV, V, VI and VII are easily soluble in almost all organic solvents, while the *N*-methylated amino acid(VIII) is soluble in acetone, methanol, chloroform and other polar solvents.

Optically active vinyl monomers containing various functional groups derived from α-amino acids were

Table 2. Physical data of *N*-vinylbenzyl-L-leucine derivatives

Product (Formula)	Yield (%)	Bp (Mp) (°C/mmHg)	$[\alpha]_D^{23}$	Anal. (Calcd) (%) C	H	N
IV ($C_{17}H_{25}O_2N$)	66	129—131/0.5	−39.5[a]	74.45 (74.14	9.36 9.15	4.97 5.09)
V ($C_{17}H_{25}O_2N$)	73	153—155/1	−50.5[a]	73.96 (74.14	8.69 9.15	5.01 5.09)
VI ($C_{15}H_{23}ON$)	70	(57—59 °C)	+22.3[a]	77.27 (77.20	10.22 9.94	6.06 6.00)
VII ($C_{18}H_{25}O_3N$)	59	173—177/1	−17.0[a]	71.39 (71.25	8.16 8.31	4.57 4.62)
VIII ($C_{18}H_{27}O_2N$)	73	(158—160 °C)	+48.5[b]	73.56 (73.53	8.86 8.87	5.30 5.36)

a) $c=2.0$, in abs. ethanol. b) $c=2.0$, in acetic acid.

Table 3. Polymerization of *N*-vinylbenzyl-L-leucine derivatives[a]

Monomer	(g)	AIBN (mg)	Solvent	Polymerization Time (hr)	Product	Yield (g)
			Homopolymerization			
IIIa	2.47	82	Formic acid	60	IX	2.52
V	2.74	164	Bulk	40	X	2.24
VIII	2.61	82	Acetic acid	40	XI	2.54
			Copolymerization with Styrene[b]			
IIc	2.47	328	Acetic acid	40	XII	3.66
V	4.11	492	Bulk	40	XIII	8.31
V	2.74	328	Benzene	60	XIV	5.10
VIII	2.61	328	Acetic acid	40	XV	5.64
			Cross-linking Polymerization[c]			
IIc	2.47	328	Acetic acid	20	XVI	5.81
V	5.48	492	Benzene	20	XVII	12.85
VIII	2.61	328	Acetic acid	20	XVIII	6.19

a) Polymerization conditions; solvent 10 ml, temperature 75—80 °C, in sealed tube. b) Mole ratios of initial mixture; leucine derivative: styrene=1 : 3. c) Mole ratios of initial mixture; leucine derivatives : styrene : divinylbenzene=2 : 5 : 1.7.

prepared easily without protection of the functional groups (Schemes 1 and 2).

Polymerization of N-*Vinylbenzyl-*L-*leucine Derivatives.* Homo- and co-polymerizations of *N*-vinylbenzyl-L-leucine derivatives were carried out with the use of azobisisobutyronitrile (AIBN) as an initiator at 75—80 °C. The results are summarized in Tables 3 and 4.

Homopolymerization of IIIa in formic acid gave *N*-formylated homopolymer (IX). Homopolymer of V was gummy and became insoluble after a few weeks. Copolymerization of IIc, V, and VIII with styrene gave the corresponding copolymers, whose compositions coincided with mole ratios of the initial monomer mixtures. The inherent viscosities of copolymers were low, but the infrared absorption bands at 990 and 910 cm^{-1} (–CH=CH_2) disappeared virtually in the IR spectra of the products. The homo- and co-polymers shown in Table 4, are optically active. Cross-linking polymerization of L-leucine derivatives in the presence of divinylbenzene (DVB) was carried out with an AIBN initiator. Cross-linked insoluble polymers were obtained in good yield. Polymers IX and XI are soluble in formic acid, acetic acid, and trifluoroacetic acid and insoluble in other organic solvents. Polymers XII and XV are soluble in formic acid, trifluoroacetic acid, pyridine, and *N*,*N*-dimethylformamide and insoluble in ether and methanol. Polymers XIII and XIV are soluble in almost all organic solvents except methanol and ethanol.

These optically active functional polymers might be useful as adsorbents for the chromatographic resolution of amino acid racemates, or as chiral components for asymmetric syntheses.

Experimental

The melting points were uncorrected. The IR spectra were obtained as potassium bromide disks with a Jasco Model DS-403G grating infrared spectrophotometer. Optical rotations were determined with a Jasco Model ORD/UV-5 optical rotatory dispersion recorder. Formylstyrenes were prepared by Dale's method.[13]

Preparation of N-*vinylbenzyl-*L-*amino Acids.* The following is an example of the general procedure. L-Leucine, 3.93 g (0.03 mol), was dissolved in 30 ml of methanol containing 1.20 g (0.03 mol) of sodium hydroxide and 1.0 ml of water. To this solution was added 4.20 g (0.032 mol) of *o*-formylstyrene with stirring at room temperature. After 1 hr, 5 ml of water containing 0.75 g (0.02 mol) of sodium borohydride was added dropwise below 20 °C by cooling

TABLE 4. PHYSICAL PROPERTIES OF POLY-*N*-VINYLBENZYL-L-LEUCINE DERIVATIVES

Polymer	Softening Temp. (°C)	$[\alpha]_D^{23}$	$[\eta]$ inh	Anal. (Calcd) (%) C	H	N	Mole-% of Amino acid[a]
			Homopolymer				
IX	>300	−20.0[b]	0.77[c]	69.40 (69.79	7.91 7.69	5.20 5.09)[d]	—
X	—	—	—	73.62 (74.14	9.04 9.15	5.32 5.09)	—
XI	>300	+4.2[b]	0.57[c]	72.81 (73.53	8.80 8.87	5.37 5.36)	—
			Copolymer with Styrene				
XII	95—115	−3.1[e]	0.07[f]	82.80 (83.72	7.99 8.05	2.59 2.50)[g]	26.2
XIII	85— 95	−25.0[e]	0.17[f]	83.61 (84.0	8.37 8.36	2.49 2.39)[g]	26.5
XIV	85— 95	−23.6[e]	0.09[f]	83.50 (84.0	8.32 8.36	2.70 2.39)[g]	29.0
XV	160—170	−11.2[e]	0.11[f]	82.63 (83.70	8.21 8.19	2.77 2.44)[g]	29.9
			Cross-linked Copolymer				
XVI	>300	—	—	84.65	8.14	2.92	32.2
XVII	>300	—	—	85.14	8.47	2.27	22.9
XVIII	>300	—	—	85.25	8.34	2.32	24.4

a) Based on nitrogen analysis. b) $c=2.0$, in formic acid. c) $c=0.5$ g/dl, in formic acid. d) calculated for the *N*-formylated polymer ($C_{16}H_{21}O_3N$). e) $c=2.0$, in tetrahydrofuran. f) $c=0.5$ g/dl, in tetrahydrofuran. g) calculated for the initial copolymerization mixture.

with ice-cold water, and the solution was stirred for 1 hr under cooling. The pH was then adjusted to 5—6 with diluted hydrochloric acid. *N-o*-Vinylbenzyl-L-leucine was precipitated as white crystals and filtered and washed with acetone. The yield was 6.8 g (76%). Recrystallization from water-acetic acid gave a pure material, mp 196 °C (dec.).

N-p-Vinylbenzyl-L-leucine was prepared with *p*-formylstyrene instead of *o*-formylstyrene. The other *N*-vinylbenzyl-L-amino acids were similarly obtained by the reactions of L-amino acids with formylstyrenes. The results are summarized in Table 1.

IR absorption bands common to *N-o*-vinylbenzyl-L-amino acids are as follows: (cm^{-1}), 3200 (NH), 3080—3020 (aromatic CH), 1620—1550 (COO^-), 990, 910 (−CH=CH_2), 780 (*o*-substituted benzene), and those for *N-p*-vinylbenzyl-L-amino acids are 3200 (NH), 3080—3030 (aromatic CH), 1620—1550 (COO^{-1}), 990, 910 (−CH=CH_2), 850—800 (*p*-substituted benzene).

Hydrogenolyses of compounds (IIb) and (IIc) (1.0 g) with 10% palladium-carbon catalyst (0.5 g) were carried out in acetic acid (20 ml) at 80 °C and 100 atm for 10 hr. Palladium-carbon was filtered off. Acetic acid was then, evaporated under vacuum, and the residue was recrystallized from water. L-Leucine; yield 0.42 g, mp 293 °C (dec.), $[\alpha]_D^{27}$ −11.0 (*c* 2.0, H_2O). L-Valine; yield 0.37 g, mp 300 °C, $[\alpha]_D^{27}$ +6.3 (*c* 4.8, H_2O).

Preparation of N-*Vinylbenzyl-L-leucine Ethyl Ester.* L-Leucine ethyl ester hydrochloride, 19.5 g (0.10 mol), and triethylamine, 10.2 g (0.10 mol), were dissolved in 100 ml of methanol. *o*-Formylstyrene, 13.5 g (0.10 mol), was added to this solution at room temperature. After stirring for 1 hr, 30 ml of water containing 3.8 g (0.10 mol) of sodium borohydride was added dropwise below 20 °C by cooling with ice-cold water and stirring. The solution was stirred for 1 hr under cooling, and then 20 ml of 5% sodium carbonate solution was added. This solution was extracted three times with 150 ml of ether. The ether solution was dried with sodium sulfate, and concentrated. The residue was distilled in the presence of 0.5 g of cuprous chloride under vacuum to yield 18.2 g (66%) of *N-o*-vinylbenzyl-L-leucine ethyl ester, bp 129—131 °C/0.5 mmHg.

N-p-Vinylbenzyl-L-leucine ethyl ester was similarly obtained, bp 153—155 °C/1 mmHg. The yield was 70%.

IR data (cm^{-1}); 3080, 3070 (aromatic CH), 2980, 2880 (isobutyl), 1720 (COOEt), 1625 (−CH=CH_2), 1450, 1370 (isobutyl), 1170, 1150 (ester), 990, 910 (−CH=CH_2), 825 (*p*-vinyl compound), 775 (*o*-vinyl compound).

Preparation of N-o-*Vinylbenzyl-L-leucinol.* *N-o*-Vinylbenzyl-L-leucine ethyl ester, 16.0 g (0.058 mol), in 70 ml of ether was added dropwise with stirring to lithium aluminium hydride, 3.8 g (0.10 mol) in 80 ml of ether. After the mixture was stirred for 40 min and then diluted with ether, 10 ml of water was added with vigorous stirring. The ether solution was filtered, and the precipitate was washed with ether and with methanol. The washings were combined with the filtrate. The mixture was dried, and concentrated under vacuum to give crystals. Recrystallization from *n*-hexane gave a pure material in 70% (9.4 g) yield, mp 57—59 °C.

IR data (cm^{-1}); 3500 (OH), 3080—3000 (aromatic CH), 2990, 2920, 2880 (isobutyl), 1630 (−CH=CH_2), 1590, 1490, 1450 (benzene ring), 1100—1050 (−C−O−) 990, 910 (−CH=CH_2), 780 (*o*-substituted benzene).

Reaction of N-o-*Vinylbenzyl-L-leucine Ethyl Ester with Trioxane in Formic Acid.* *N-o*-Vinylbenzyl-L-leucine ethyl ester, 8.0 g, and trioxane, 1.0 g, were dissolved in 5 ml of formic acid. The solution was heated at 95—1000 °C for 2 hr, and then concentrated under vacuum. The residue was distilled under vacuum to give *N-o*-vinylbenzyl-*N*-formyl-L-leucine ethyl ester, bp 173—176 °C/1 mmHg. The yield was 5.1 g.

IR data (cm^{-1}); 3080, 3070 (aromatic CH), 2980, 2970 (isobutyl), 1730 (ester), 1670 (amide), 1625 (−CH=CH_2).

Preparation of N-p-*Vinylbenzyl-N-methyl-L-leucine.* *N-p*-Vinylbenzyl-L-leucine, 15.0 g (0.06 mol) was suspended in

the solution of formic acid (12 ml) and 40% formalin (9 ml; *ca.* 0.12 mol) and heated on a water bath for 30 min. *N-p*-Vinylbenzyl-L-leucine was gradually dissolved into the solution with vigorous carbon dioxide evolution. This solution was concentrated under vacuum. Water was added to the residue and then evaporated. The procedure was repeated three times. *N-p*-Vinylbenzyl-*N*-methyl-L-leucine, thus separated, was recrystallized from benzene two times. The yield was 12.2 g, mp 158—160 °C.

IR data (cm^{-1}); 1600 (COO^-), 1370 (CH_3), 990, 910 ($-CH=CH_2$), 845, 825 (*p*-substituted benzene).

Polymerization of N-*Vinylbenzyl-L-leucine Derivatives.* Homo- and co-polymerizations of *N*-vinylbenzyl-L-leucine derivatives were carried out with 5—10 mol% of azobisisobutyronitrile (AIBN) as an initiator at 75—80 °C. The amounts of monomers and solvents used are given in Table 3.

The polymerization tubes were sealed off under vacuum, and heated in a thermostated bath. After polymerization, the polymer solution was poured into a non-solvent and the polymer obtained as precipitates was purified by reprecipitation.

Cross-linked polymers (XVI—XVIII) were similarly prepared by polymerization in the presence of divinylbenzene, purified by washing with benzene and with methanol, respectively, in a Soxhlet extractor for 5 hr.

Non-solvents were acetone for IX, water for X, ether for XI and XV, and methanol for XII, XIII and XIV. Solvents were formic acid for IX and XI, and tetrahydrofuran for X, XII, XIII, XIV and XV.

In the IR spectra of homopolymers, the bands at 990 and 910 cm^{-1} ($-CH=CH_2$) disappeared completely. In the IR spectra of copolymers the bands at 1630, 990 and 910 cm^{-1} ($-CH=CH_2$) disappeared, and those at 1490, 750 and 690 cm^{-1} ($-CH=CH_2$) disappeared, and those at 1490, 750 and 690 cm^{-1} ($-CH_2-CH-C_6H_5$) appeared.

Reference

1) S. Tsuboyama, This Bulletin, **35**, 1004 (1962); **38**, 354 (1965); **39**, 698 (1966).
2) S. Inoue, S. Ohashi, A. Tabata, and T. Tsuruta, *Makromol. Chem.*, **112**, 66 (1968).
3) C. G. Overberger and I. Cho, *J. Polym. Sci., A-1*, **6**, 2741 (1968).
4) M. Hatano, T. Nozawa, and M. Yoneyama, This Bulletin, **43**, 295 (1970).
5) H. Hirai and T. Furuta, *J. Polym. Sci.*, B, **9**, 463 (1971).
6) M. Akiyama, M. Narita, and M. Okawara, *J. Polym. Sci., A-1*, **7**, 1299 (1969); M. Narita, T. Teramoto, and M. Okawara, This Bulletin, **45**, 3149 (1972).
7) C. W. Roberts and D. H. Haigh, *J. Org. Chem.*, **27**, 3375 (1962); V. V. Korshak, S. V. Rogozhin, and V. A. Davankov, U. S. S. R. 176064 (1965).
8) A. G. Inventia, Belg. 621135 (1962); *Chem. Abstr.*, **60**, 661f (1964).
9) N. Nakamura, T. Yamashita, and T. Uemura, *Nippon Kagaku Zasshi*, **88**, 1238 (1970).
10) T. Yamashita, This Bulletin, **45**, 195 (1972).
11) H. Suda, Y. Hosono, Y. Hosokawa, and T. Seto, *Kogyo Kagaku Zasshi*, **73**, 1250 (1970).
12) P. Quitt, J. Hellerbach, and K. Vogler, *Helv. Chim. Acta*, **46**, 327 (1963).
13) W. J. Dale, L. Starr, and C. W. Strobel, *J. Org. Chem.*, **26**, 2225 (1961).

Synthesis of TACK, a New Chloromethyl Ketone Derivative of Arginine[1,2]

Ken INOUYE, Atsushi SASAKI, and Nobuo YOSHIDA

Shionogi Research Laboratory, Shionogi & Co., Ltd., Fukushima-ku, Osaka 553

(Received September 7, 1973)

A synthesis is described of TACK, the chloromethyl ketone derivative of N^{α}-tosyl-L-arginine, in which a crystalline intermediate N^{G}-nitro-TACK is found to be converted into TACK with hydrogen fluoride without appreciable impairment of the chloromethyl ketone moiety.

TLCK is an active site-directed reagent for trypsin, first described by Shaw *et al.*[3] Their initial synthesis involves the hydrolytic removal of a benzyloxycarbonyl group from the N^{ε}-protected derivative to lead to the formation of TLCK in a rather low yield. Recently Shaw and Glover[4] have improved the yield greatly by the use of trifluoroacetic acid[5] in this deprotection step. A trifluoroacetic acid-hydrochloric acid mixture was also used by other authors.[6] For the same purpose we tried to use the hydrogen fluoride treatment[7] in which the treatment was found to cause no detectable damage in the chloromethyl ketone moiety of TLCK, affording the reagent in a good yield.[8] This finding prompted us to extend the use of hydrogen fluoride to the synthesis of N^{α}-tosyl-L-arginine chloromethyl ketone (TACK). The only chloromethyl ketone derivative of arginine ever known is *p*-nitrobenzyloxycarbonyl-L-arginine chloromethyl ketone (Z(NO_2)ACK) which has been prepared by Shaw and Glover.[4] Attempts we have made to obtain TACK are as follows:

$$\text{H-Arg(R)-OH} \xrightarrow{\text{Tos-Cl}} \text{Tos-Arg(R)-OH} \xrightarrow{PCl_5}$$

$$\text{Tos-Arg(R)-Cl} \xrightarrow{CH_2N_2} \text{Tos-Arg(R)-CHN}_2 \xrightarrow{\text{HCl}}$$

$$\text{Tos-Arg(R)-CH}_2\text{Cl} \xrightarrow{\text{HF}} \text{Tos-Arg-CH}_2\text{Cl (TACK)}$$

where R is either a tosyl or a nitro group, which is known to be split with hydrogen fluoride.[7,9] When R=NO_2, the penultimate compound Tos-Arg(NO_2)-CH_2Cl was crystalline and was found to be fairly stable. In the case of R=Tos, however, all the intermediates were amorphous and their purification seemed to be of trouble. In this communication we wish to report our TACK synthesis starting from nitroarginine.

TACK, prepared in the present work, was homogeneous in thin-layer chromatography. The chlorine content of TACK hydrochloride has remained unchanged at least for six months, provided that the preparation has been kept dry and refrigerated. The inhibition studies of enzymes with TACK will be described in a separate communication.[10]

Experimental

All melting points were uncorrected.

N^{α}-p-*Toluenesulfonyl*-N^{G}-*nitro*-L-*arginine (I).* Nitroarginine (5.50 g, 25 mmol) was dissolved in 2M sodium hydroxide (37.5 ml), and sodium carbonate (2.65 g, 25 mmol) and acetone (25 ml) were introduced. To this was then added dropwise a solution of *p*-toluenesulfonyl chloride (7.15 g, 37.5 mmol) in acetone (20 ml) at 0 °C. The mixture was stirred at 0 °C for 3.5 hr. After removal of acetone by evaporation *in vacuo*, the aqueous solution was acidified with 4 M hydrochloric acid. The crystalline precipitates which separated were filtered off, washed with water and dried *in vacuo* (8.16 g, 88%). Recrystallization from methanol–water gave the desired product in pure form; wt, 7.39 g (79%), mp 167—169 °C, $[\alpha]_D^{22}+23.6\pm0.7°$ (*c* 1.0, methanol).

Found: C, 42.05; H, 5.20; N, 18.74; S, 8.75%. Calcd for $C_{13}H_{19}N_5O_6S$: C, 41.82; H, 5.13; N, 18.76; S, 8.59%.

N^{α}-p-*Toluenesulfonyl*-N^{G}-*nitro*-L-*arginyl Diazomethane (III).* A solution of I (0.75 g, 2 mmol) in anhydrous tetrahydrofuran (10 ml) was chilled in an ice-salt bath and to this was added phosphorus pentachloride (0.84 g, 4 mmol) in several portions. The mixture was stirred for 60 min during which the temperature was allowed to rise to 0 °C. Anhydrous ether (80 ml) was then introduced to yield sirupy precipitates. The supernatant solution was removed by decantation and the residue was triturated with ether and dried *in vacuo* over sodium hydroxide pellets at 4 °C to give N^{α}-*p-toluenesulfonyl*-N^{G}-*nitro*-L-*arginyl chloride (II)* as amorphous solid (0.47 g, 60%); IR (Nujol) 1790 cm^{-1}. A small sample was dissolved in methanol and this was subjected to tlc (Silica gel GF, E. Mreck) in methanol–chloroform (2 : 8 by vol) to give a single component which was indistinguishable from the authentic methyl ester of I.

The chloride (II) obtained above was dissolved in anhydrous tetrahydrofuran (10 ml) and to this solution was added an ethereal solution of diazomethane at 0 °C until an yellow color persisted. The reaction mixture was stirred at 0 °C for 60 min, after which time anhydrous ether (80 ml) was introduced. The resulting precipitates were filtered off, washed with ether and dried *in vacuo* to give III; wt, 0.36 g (45%, as based on I used), IR (chloroform) 2145 cm^{-1}, $[\alpha]_D^{22}$ $-51.3\pm1.0°$ (*c* 1.0, methanol). The product was used for the subsequent reaction without further purification.

N^{α}-p-*Toluenesulfonyl*-N^{G}-*nitro*-L-*arginyl Chloromethane (IV).* To a 0.25 g-sample of III was added M hydrogen chloride in acetic acid (10 ml) to cause the reaction to occur with the instant evolution of nitrogen. The mixture was kept at room temperature for 60 min, followed by evaporation *in vacuo* at a bath temperature of 35 °C. The residue was then lyophilized from acetic acid. The resulting crude preparation of IV was submitted to a column of silica-gel (0.05—0.2 mm, E. Merck, 25 g) using a mixture of methanol–chloroform (1 : 9 by vol) as a solvent for elution. Tubes 17—30 (5 g/tube) containing the desired product as a main component (as examined by tlc) were collected and evaporated *in vacuo* to give a sirupy residue which crystallized upon addition of chloroform (0.12 g, 49%). Recrystallization from methanol yielded a pure and odorless preparation of IV in an 86% recovery; mp 165—167 °C decomp., $[\alpha]_D^{24}$ $-23.7\pm0.7°$ (*c* 1.0, dimethylformamide), IR (Nujol) 1745 cm^{-1}.

Found: C, 41.64; H, 5.11; N, 17.34; S, 8.02; Cl, 8.80%. Calcd for $C_{14}H_{20}N_5O_5SCl$: C, 41.43; H, 4.97; N, 17.26; S, 7.90; Cl, 8.74%.

N^{α}-p-*Toluenesulfonyl*-L-*arginyl Chloromethane* (N^{G}-*Tosyl*-L-*arginine Chloromethyl Ketone, TACK) Hydrochloride (V).* Compound IV (0.18 g) and anisole (0.2 ml) were put into a reaction vessel (made of fluorinated polyethylene) and hydrogen

fluoride (*ca.* 5 ml) was introduced into the vessel placed in a dry ice-acetone bath. The mixture was stirred at 0 °C for 30 min. After removal of hydrogen fluoride by evaporation *in vacuo* the residue was dissolved in water and the solution was, after washing with ethyl acetate, passed through a column (0.9×10 cm) of Amberlite CG-400 (acetate form); the column was washed with portions of water. The aqueous solutions were combined and M hydrochloric acid (0.5 ml) was added. Lyophilization of the resulting solution gave the desired TACK hydrochloride; wt, 0.18 g (98%), $[\alpha]_D^{25}$ $-21.2\pm0.6°$ (*c*, 1.0, 0.1 M hydrochloric acid), IR (KBr) 1737 cm^{-1}. Tlc revealed that the product was homogeneous to Sakaguchi reagent (Cellulose F, E. Merck, 1-butanol-acetic acid-water (18 : 2 : 5 by vol)).

Found: C, 40.95; H, 5.66; N, 13.13; S, 7.17; Cl, 17.95%. Calcd for $C_{14}H_{22}N_4O_3SCl\cdot HCl\cdot H_2O$: C, 40.48; H, 5.82; N, 13.49; S, 7.72; Cl, 17.07%.

References

1) Presented at the 44th Annual Meeting of the Japanese Biochemical Society, Sendai, Oct. 1971.

2) Abbreviations used in this work are: TLCK, N^{α}-*p*-toluenesulfonyl-L-lysine chloromethyl ketone, N^{α}-*p*-toluenesulfonyl-L-lysyl chloromethane or L-1-chloro-3-tosylamido-7-aminoheptan-2-one; TACK, N^{α}-*p*-toluenesulfonyl-L-arginine chloromethyl ketone, N^{α}-*p*-toluenesulfonyl-L-arginyl chloromethane or L-1-chloro-3-tosylamido-6-guanidinohexan-2-one; Z, benzyloxycarbonyl; Tos, *p*-toluenesulfonyl or tosyl.

3) E. Shaw, M. Mares-Guia, and W. Cohen, *Biochemistry*, **4**, 2219 (1965).

4) E. Shaw and G. Glover, *Arch. Biochem. Biophys.*, **139**, 298 (1970).

5) F. Weygand and W. Steglich, *Z. Naturforsch.*, **14b**, 472 (1959).

6) F. Sebestyén and J. Samu, *Chem. Ind.* (London), **1970**, 1568.

7) S. Sakakibara and Y. Shimonishi, This Bulletin, **38**, 1412 (1965); S. Sakakibara, Y. Shimonishi, M. Okada, and Y. Kishida, "Peptides," Proceedings of the 8th European Peptide Symposium," ed. by H. C. Beyerman, A. van de Linde, and W. Maasen van den Brink, North-Holland Publishing Co., Amsterdam (1967), p. 44.

8) K. Inouye, A. Sasaki, and N. Yoshida, Unpublished.

9) R. H. Mazur and G. Plume, *Experientia*, **24**, 661 (1968).

10) N. Yoshida, A. Sasaki, and K. Inouye, *Biochem. Biophys. Acta*, **321**, 615 (1973),

The Photo-desulfurization of Crude Naphtha by UV Irradiation

Yoshio BABA

National Research Institute for Pollution and Resources, Kawaguchi, Saitama 332

(Received July 5, 1973)

The photolysis of crude naphtha in the presence of an oxidizing reagent was studied with a view to accomplishing the desulfurization of crude naphtha. The irradiation of crude naphtha consisting of 0.15% sulfur by means of a 200-W high-pressure mercury-vapor lamp, with the aeration of air or oxygen at the flow rates of 5—15 ml/min at 0 °C, resulted in an 80—90% photolysis of the principal mercaptans and sulfides in the crude naphtha within 20 min. The major photo-oxidation products were water-soluble oxygenated sulfur compounds; thus, this process resulted in 67.8% desulfurization when the irradiated naphtha was washed with water. The effects on the photolysis of the molecular weights and the structures of sulfur compounds were also examined with 11 mercaptans and 3 sulfides.

An alkali-sweetening process, *e. g.*, doctor sweetening, Merox process, the Unisol process, is a low-cost process to remove corrosive and malodorous mercaptans and to increase the lead susceptibility of gasoline, but it has several disadvantages: the susceptibility to the oxidation of the mercaptans by alkali solution is markedly influenced by the structural features of mercaptan, and thus the process is not effective for removing *tert*-mercaptans; desulfurization is usually low because sulfides in crude naphtha cannot be removed by this method, and this process produces a malodorous waste liquor.

In this paper a photo-desulfurization of light straight naphtha was studied on the basis of the fact that mercaptans and sulfides can be photolyzed by UV irradiation.

Although many reports on the photolysis of mercaptans and sulfides have been published, most of them have been focused on the reaction mechanism of the photolysis of these sulfur compounds,[1-10] and few works have been undertaken for the purpose of a practical application.[11-12] In related works, Murray[11] studied the photo-oxidation method as a possible means of controlling malodorous waste gases containing mercaptans and sulfides from a kraft pulp mill. In his study of the effects of UV light on the oxidation of methyl mercaptan (MM), dimethyl sulfide (DMS), and dimethyl disulfide (DMDS), Murray was able to demonstrate the photo-oxidation of these compounds at both 2537 and 3600 Å. By monitoring the disappearance of the starting materials, he showed that DMDS undergoes photo-oxidation most rapidly, while DMS was found to be the least reactive. In addition MM exposed to solar radiation was found to disappear with a half-life of approximately 7 days during a period with an average noon temperature of 10 °C.

Bentley[12] has reported that about a 7-hr irradiation of dimethyl sulfide in air with a 200-W high-pressure mercury-vapor lamp caused a more than 91% decomposition of the sulfide.

In this study 11 mercaptans, *i. e.*, ethyl-, *n*-propyl-, isopropyl-, *n*-butyl-, *sec*-butyl-, isobutyl-, *tert*-butyl-, *n*-amyl-, *sec*-isoamyl-, *tert*-amyl-, and *n*-hexyl-mercaptans and 3 sulfides, *i.e.*, diethyl-, di-*n*-butyl-, and diallyl-sulfides, were irradiated with a 100-W low-pressure mercury-vapor lamp at 0 °C to determine the effects of the molecular weights and structures of these sulfur compounds on the photolysis; further experiments were also performed in order to determine the rates of the photo-decomposition and photo-oxidation of important mercaptans and sulfides in crude naphtha by the irradiation of light straight naphtha with a bp 27—95 °C from Iranian heavy by means of a 200-W high-pressure mercury-vapor lamp at the temperatures of 0, 30, 50 °C, and by irradiation in the presence of oxidizing reagents, air, and oxygen at 0 °C.

The results showed that the irradiation of the crude naphtha consisting of 0.15% sulfur by means of a 200-W high-pressure mercury vapor lamp, with the aeration of air or oxygen at the flow rate of 5—15 ml/min and at 0 °C, resulted in an 80—90% photolysis of the major mercaptans and sulfides in the crude naphtha within 20 min; unlike the alkali-sweetening process, no difference in the reactivity of mercaptan due to its structural features has been observed. The principal photo-oxidation products were SO_2, SO_3, and sulfonic acids; the reaction afforded a 67.8% reduction of the total sulfur content in the photo-desulfurized naphtha.

Experimental

1. Materials and Apparatus. The mercaptans and sulfides used to determine the effects of thier molecular weights and structures on the photolysis, and used as the internal standards for the gas chromatography, were analytical-standard reagents (Poly Science Corp.).

The crude naphtha used for the photo-desulfurization study was a light straight naptha (bp 27—95 °C) from Iranian heavy.

The photolysis was conducted in a 200-ml round-bottom, Pyrex flask fitted with a water-cooled lamp housing, a thermometer, and a reflux condenser cooled with ice water.

The light sources were a 100-W low-pressure mercury-vapor lamp, which emits predominantly 2357 Å light, in the runs for determining the effects of the molecular weights and structures on the photolysis of mercaptans and sulfides, and a 200-W high-pressure mercury-vapor lamp with a predominant light of 3650 Å in the runs for the photo-desulfurization of crude naphtha.

Gas chromatography was done by means of Micro Tek Instruments Corp. Model 160 gas chromatograph equipped with a flame photometric detector and a 3 m×3 mm i.d. Teflon analytical column packed with 1,2,3-tris(cyanoethoxy)-propane on Shimalite 25%, 80/100 mesh.

2. Procedure. Each 100-ml portion of *n*-hexane solutions (100 ppm) of mercaptans and sulfides or the crude naphtha was placed in the flask, and the reaction solution

was irradiated with a mercury-vapor lamp at a constant temperature. One ml portions of the sample solution were taken off at discrete periods of irradiation time and mixed with the *n*-propyl sulfide standard solution (prepared by dissolving 10 μl of the sulfide in 5 ml of *n*-hexane and stored in a cooled dark place) to serve as internal standards for the gas chromatography.

The rates of the reaction of mercaptans and sulfides on the photolysis were determined by comparing the peak area of each sulfur compounds to be analyzed with that of the internal standard, calculated by means of a digital integrator; the relative amounts of sulfur compounds in the sample solutions were compared with those in the original solutions.

In the runs to study the effects of the molecular weights and structures of mercaptans and sulfides on the photolysis, the reactions were carried out at 0 °C; in the runs of the photo-desulfurization of the crude naphtha, the reaction temperatures of 0 °C, 30 °C, and 50 °C were used.

The experiments of the photo-oxidation of the crude naphtha were performed at 0 °C; with the aeration of air or oxygen at the flow rates of 5—30 ml/min. In these experiments, corresponding dark reactions under the same reaction conditions except for irradiation were done in order to check the amount of possible mechanical losses or chemical reactions.

The total sulfur contents in the crude and the photo-desulfurized naphtha were determined by the UOP oxygen-hydrogen combustion method (UOP 586—66); the reaction product was washed with distilled water, and a measured aliquot of the water solution was used for determining SO_2 and SO_3 by gravimetric $BaSO_4$ analysis.

The reaction product formed by UV irradiation was identified as higher-molecular-weight sulfides by gas chromatography utilizing a mercaptan-substracting column ($Hg(CN)_2$ 1% on Chromosorb).

Results and Discussion

The studies of the photolysis of organic sulfur compounds indicate that the photolysis of disulfide is initiated through –S–S– fission[1] rather than C–S fission,[2] while in the cases of monosulfides and mercaptans, the reactions are believed to occur through an initial cleavage of the C–S and S–H bonds respectively.[4,12]

In any case, however, the initial photo-decomposed reaction products are thinyl and alkyl radicals; these radicals are considered to produce hydrocarbons, mercaptans, and various sulfides by the following series of recombination reactions:

$$CH_3\cdot + \cdot CH_3 \rightarrow C_2H_6 \quad (1)$$

$$CH_3S\cdot + \cdot CH_3 \rightarrow CH_4 + CH_2{=}S \quad (2)$$

$$CH_3S\cdot + CH_3SCH_2R \rightarrow CH_3SH + CH_2{=}SCH_2R \quad (3)$$

$$CH_3S\cdot + CH_3S\cdot \rightarrow CH_3SSCH_3 \quad (4)$$

$$CH_3S\cdot + CH_2{=}S \rightarrow CH_3SCH_2S \xrightarrow{\cdot CH_3} CH_3SCH_2SCH_3 \quad (5)$$

The reaction becomes complex and produces oxygenated sulfur compounds (*i.e.*, sulfoxides, sulfones, sulfonic acids, SO_2 and SO_3) and oxygenated compounds (*i.e.*, alcohols, carboxylic acids, aldehydes, and esters) when an oxidizing reagent, such as air or oxygen is present in the reaction system.

A possible reaction mechanism for the formation of the oxygenated sulfur compounds, proposed by Bentley,[12] can be briefly described as follows:

$$CH_3S\cdot + O_2 \rightarrow CH_3SOO\cdot \xrightarrow{RH\ (e.g.,H_2O)} CH_3SOOH + R\cdot \quad (6)$$

$$\rightarrow SO_2 + \cdot CH_3 \quad (7)$$

$$CH_3SOOH \xrightarrow{h\nu} CH_3SO\cdot + \cdot OH \quad (8)$$

$$CH_3SO\cdot + RH \longrightarrow CH_3SOH + R\cdot \quad (9)$$

$$3\,CH_3SOOH \longrightarrow CH_3SOOSCH_3 + CH_3SO_3H \quad (10)$$

(1) Effect of the Molecular Weight on the Photolysis of Mercaptans. When the photochemical labilities of five mercaptans with a straight carbon chain (*i.e.*, ethyl-, *n*-propyl-, *n*-butyl-, *n*-amyl-, and *n*-hexyl-mercaptans) are compared, photochemical stability is found to increase with an increase in the carbon number of mercaptans.

As is shown in Fig. 1, with ethyl- and *n*-propyl-

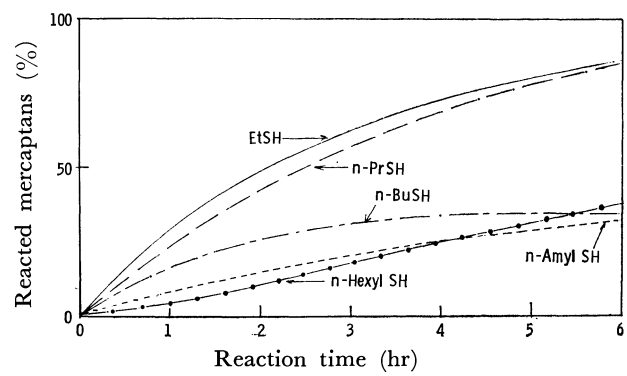

Fig. 1. Effect of molecular weight on photo-decomposition of mercaptans.

mercaptans a 3-hr irradiation of *n*-hexane solutions of these mercaptans at 0 °C with a low-pressure mercury-vapor lamp gave a more than 50% conversion, while with C_4–C_6 straight chain mercaptans the photolysis afforded only a 15—30% conversion under the same reaction conditions. Although a 6-hr irradiation caused an 85% decomposition with C_2 and C_3 mercaptans, C_4–C_6 mercaptans afforded only a 30—40% decomposition.

(2) Effect of the Molecular Structure on the Photolysis of Mercaptans and Sulfides. As the photolysis of mercaptans and sulfides is considered to be initiated through –S–S–, C–S, or S–H fission, the photochemical labilities were compared with *n*-propyl, isopropyl-, *n*-butyl-, *tert*-butyl-, *sec*-butyl, isobutyl, *n*-amyl-, *sec*-isoamyl-, and *tert*-amyl-mercaptane in order to examine the difference in photochemical stability with the structural features of the carbon atom attached to the –S– or –SH group.

In the cases of mercaptans with lower molecular weights, as is shown in Figs. 2 and 3, no difference in photochemical stability due to the change in the molecular structure was observed. With butyl mercaptan isomers, only a slight difference in the photochemical

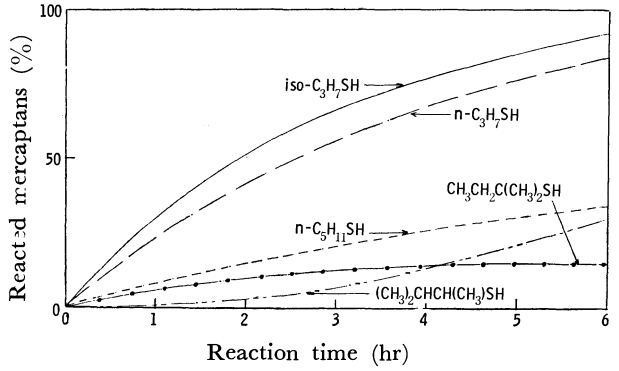

Fig. 2. Effect of molecular structure on photo-decomposition of mercaptans.
(Propyl mercaptans and amyl mercaptans)

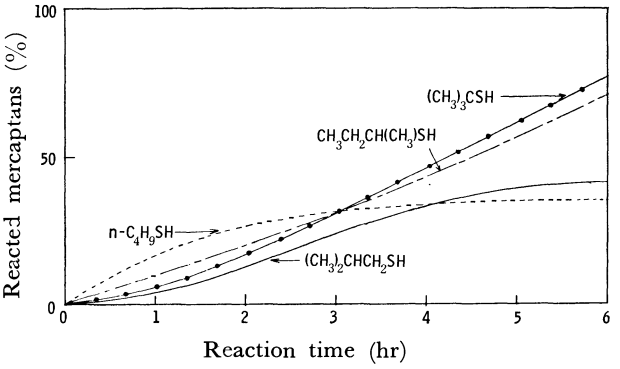

Fig. 3. Effect of molecular structure on photo-decomposition of mercaptans.
(Butyl mercaptans)

stability was observed at the beginning of the irradiation, but after a 6-hr irradiation *n*-butyl- and isobutyl-mercaptans, which have primary carbon atoms, were decomposed by 35—40%, while the irradiation of mercaptans containing secondary or tertiary carbon atoms (*i.e.*, *sec*-butyl- and *tert*-butyl-mercaptans) resulted in a 70—75% conversion.

It is, however, apparent from a comparison of the amyl mercaptan isomers with mercaptans of higher molecular weights, that the structural features of the carbon atoms attached to the –SH group slightly influence the photochemical stability.

Sulfides are more stable upon photolysis than the mercaptans, and Milligan[8] reported that, on the

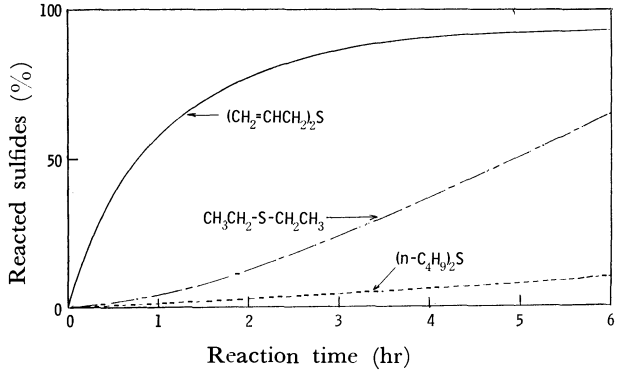

Fig. 4. Effect of molecular structure on photo-decomposition of sulfides.

photolysis of dialkyl polysulfides, no simple correlation of the stability of dialkyl polysulfides with the nature of the alkyl substituents was observed.

However, the presence of an unsaturated linkage in the carbon chain of the sulfide markedly reduces the photochemical stability of the sulfide. This fact can be demonstrated by comparing the rates of the photo-decomposition of three sulfides. As is shown in Fig. 4, a 2-hr irradiation of diethyl sulfide and di-*n*-butyl sulfide resulted in a 5—15% conversion, while diallyl sulfide, a typical unsaturated sulfide, afforded a 75% conversion, which corresponds to that of the photochemical labile mercaptans with lower molecular weights.

(3) Effect of the Reaction Temperature on the Photolysis of Mercaptans and Sulfides in Crude Naphtha. Inaba[4] reported that no temperature effect had been observed on the photolysis of methyl mercaptan in a gaseous phase because of the heat stability of the thinyl radical, formed as an initial photo-decomposition product of mercaptan.

In this study, UV irradiations of the crude naphtha were carried out at 0, 30, and 50 °C in order to examine the effect of the reaction temperature on the photolysis of the principal mercaptans and sulfide (*i.e.*, ethyl-,

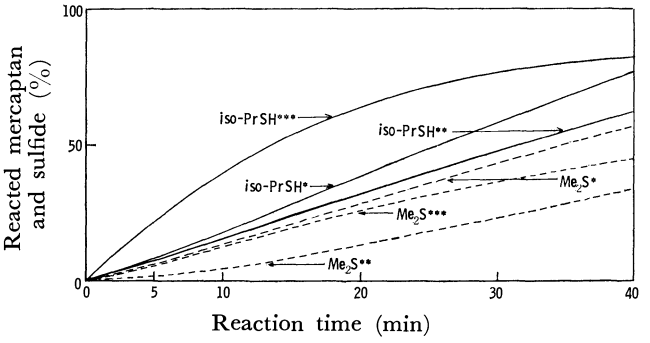

Fig. 5. Effect of reaction temperature on photo-decomposition of mercaptan and sulfide in crude naphtha. (*iso*-PrSH and Me_2S)
* irradiated at 0°C
** irradiated at 30°C
*** irradiated at 50°C

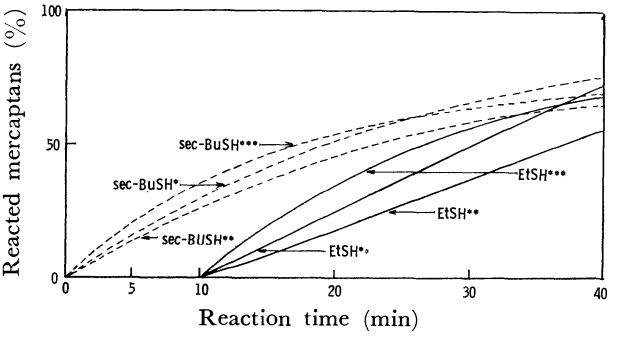

Fig. 6. Effect of reaction temperatures on photo-decomposition of mercaptans in crude naphtha. (EtSH and *sec*-BuSH).
* irradiated at 0°C
** irradiated at 30°C
*** irradiated at 50°C

TABLE 1. PERCENTAGES OF REACTED MERCAPTANS AND SULFIDES IN THE CRUDE NAPHTHA BY UV IRRADIATION UNDER VARIOUS REACTION CONDITIONS

Mercaptans and sulfides	Reaction conditions: Irradiated at 0 °C, Reaction time (min)					Irradiated at 30 °C, Reaction time (min)					Irradiated at 50 °C, Reaction time (min)					Irradiated at 0 °C with aeration (5 ml air/min), Reaction time (min)				
	5	10	20	30	40	5	10	20	30	40	5	10	20	30	40	5	10	20	30	40
Ethyl mercaptan	0	3	32	55	76	0	7	27	53	67	0	1	38	57	71	23	47	80	92	98
Isopropyl mercaptan	10	20	43	58	75	18	27	43	60	70	31	35	59	69	77	40	57	81	91	96
Dimethyl sulfide	3	12	33	42	58	8	8	19	36	44	10	14	26	34	43	31	43	66	77	87
Methyl ethyl sulfide	15	33	68	83	91	19	39	61	78	87	41	56	72	82	90	51	69	90	97	100
sec-Butyl mercaptan	17	30	51	65	73	23	38	47	61	69	33	41	51	59	68	42	55	76	86	93
Isobutyl mercaptan	11	31	53	80	82	37	44	60	69	85	31	48	45	52	71	38	56	74	87	92
Diethyl sulfide	8	33	52	62	69	24	29	50	52	55	14	30	27	53	36	37	52	68	77	82

Mercaptans and sulfides	Reaction conditions: Irradiated at 0 °C with aeration (15 ml air/min), Reaction time (min)					Irradiated at 0°C with aeration (5 ml O_2/min), Reaction time (min)					Irradiated at 0 °C with aeration (15 ml O_2/min), Reaction time (min)					Irradiated at 0 °C with aeration (30 ml O_3/min), Reaction time (min)				
	5	10	20	30	40	5	10	20	30	40	5	10	20	30	40	5	10	20	30	40
Ethyl mercaptan	25	55	90	99	100	24	59	95	100	100	22	60	94	99	100	9	35	81	97	100
Isopropyl mercaptan	33	53	83	97	100	37	57	88	99	100	26	51	84	93	99	17	34	66	88	98
Dimethyl sulfide	27	50	81	96	100	34	56	90	100	100	33	62	94	100	100	18	43	81	98	100
Methyl ethyl sulfide	54	73	100	100	100	48	81	100	100	100	52	72	96	100	100	22	51	88	100	100
sec-Butyl mercaptan	47	62	88	97	100	37	66	89	99	100	41	59	89	98	99	20	44	75	90	98
Isobutyl mercaptan	54	69	100	100	100	44	100	100	100	100	46	64	100	100	100	16	45	65	100	100
Diethyl sulfide	43	64	87	100	100	43	74	95	100	100	51	74	95	100	100	20	52	84	100	100

isopropyl-, and *sec*-butyl-mercaptans and dimethyl sulfide) in the crude naphtha.

As is shown in Figs. 5 and 6, no influence of the reaction temperature was observed with any mercaptan or sulfide.

(4) Effect of an Oxidizing Reagent on the Photo-oxidation of Mercaptans and Sulfides in Crude Naphtha. Bentley[12] obtained CH_3SO_3H (21%) and SO_2+SO_3 (30%) as the principal photo-oxidation products on the photolysis of dimethyl sulfide in air, and he concluded that the presence of air had altered the mode of the photolysis of the sulfide.

In this study, photolysis in the presence of oxidizing reagent, air, and oxygen was undertaken with a view to accomplishing the desulfurization of the crude naphtha rather than to oxidize the mercaptans to the sulfides. As the irradiation was conducted with aeration, the reaction temperature was kept at 0 °C to prevent any possible mechanical losses or chemical reactions.

Figures 7 and 8 compare the rates of the photo-oxidation of several principal mercaptans and sulfides in crude naphtha. The presence of an oxidizing reagent markedly increases the rate of the photo-decomposition of mercaptans and sulfides, but the difference in either the nature or the flow rate of the oxidizing reagents resulted in no practical influence

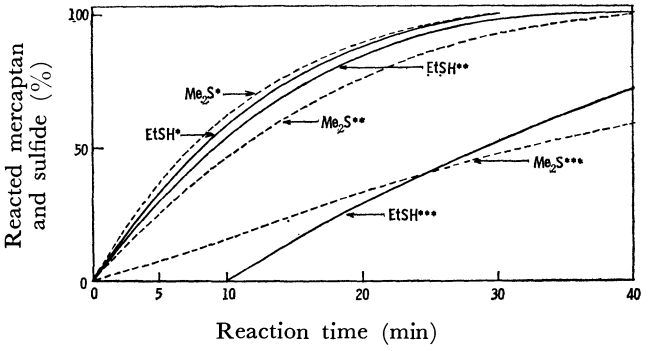

Fig. 7. Effect of oxidizing reagent on photo-decomposition of mercaptans and sulfides in crude naphtha.
* irradiated at 0°C with aeration (15 ml O_2/min)
** irradiated at 0°C with aeration (15 ml air/min)
*** irradiated at 0°C without aeration.

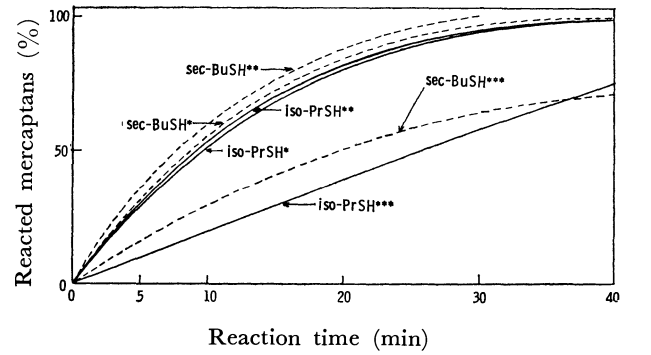

Fig. 8. Effect of oxidizing reagent on photo-decomposition of mercaptans. (*iso*-PrSH and *sec*-BuSH)
* irradiated at 0°C with aeration (15 ml O_2/min)
** irradiated at 0°C with aeration (15 ml air/min)
*** irradiated at 0°C without aeration.

on the rate of the photo-oxidation (cf. Table 1). This suggests that the irradiation of crude naphtha by means of a high-pressure mercury-vapor lamp initiates the S–H and C–S fission of mercaptans and sulfides; thus, the formation of thinyl and alkyl radicals and the subsequent recombination reactions of free radicals (1—5), or the oxidation of these free radicals (6—10), takes place. In the presence of the oxidizing reagents, the oxidation of free radicals might occur in preference to the recombination reactions, but the former would not be accelerated by the presence of an excess of the oxidizing reagent.

The total sulfur content of the photo-desulfurized naphtha, obtained by washing the irradiated naphtha with water after a 40-min irradiation with aeration, decreased by 32.2%, and the sulfur compounds in the oil layer consisted mainly of higher-molecular-weight sulfides produced by the recombination reactions; 67.8% of the original sulfur compounds in the crude naphtha was converted into water-soluble oxygen-containing sulfur compounds, such as SO_2, SO_3, and sulfonic acids.

Unlike the results of the gas-phase photolysis of methyl mercaptan, dimethyl sulfide, and dimethyl disulfide, as reported by Rayner[11] and Haines,[7] or Milligans study[8] of the photolysis of several alkyl polysulfides, in this study no difference was observed in the rates of the photolysis of mrecaptans and sulfides in crude naphtha in either the presence or the absence of an oxidizing reagent.

Conclusion

Although a certain difference was observed in the rates of the photolysis of mercaptans due to their molecular weights and structural features, the UV irradiation of crude naphtha caused a rapid photolysis of the sulfur com ounds in it. This fact indicates the possibility of the practical application of this method for the desulfurization of the crude naphtha.

Thus, the irradiation of crude naphtha consisting of 0.15% sulfur by means of a 200-W high-pressure mercury-vapor lamp, with the aeration of air or oxygen at the flow rate of 5—15 ml/min and at 0 °C, resulted in an 80—90% photolysis of the principal mercaptans and sulfides in the crude naphtha within 20 min.

As the major photo-oxidation products were water-soluble oxygenated sulfur compounds, this process resulted in 67.8% desulfurization of the crude naphtha when the resultant UV irradiated naphtha was washed with water.

References

1) A. J. Parker and N. Kharasch, *Chem. Rev.*, **59**, 583 (1959).
2) J. E. Eager and W. E. Savige, *Photochem. Photobiol.*, **2**, 25 (1963).
3) T. Inaba and H. Ogoro, *Kagyo Kagaku Zasshi*, **72**, 114, 117 (1969).
4) T. Inaba and B. deB Darwent, *J. Phys. Chem.*, **64**, 1431 (1960).
5) T. Ueno and Y. Takezaki, *Bull. Inst. Chem. Res. Kyoto Univ.*, **36**, 19 (1958).

6) P. M. Rao, J. A. Copeck, and A. R. Knight, *Can. J. Chem.*, **45**, 1369 (1967).
7) W. E. Haines, G. L. Cook, and J. S. Ball, *J. Amer. Chem. Soc.*, **78**, 5213 (1956).
8) B. Miligan, D. E. Rivett, and W. E. Savige, *Aust. J. Chem.*, **16**, 1020 (1963).
9) A. Jones, S. Yamashita, and F. P. Lossing, *Can. J. Chem.*, **46**, 833 (1968).
10) L. Horner and J. Dorges, *Tetrahedron Lett.*, **1963**, 757.
11) H. B. Rayner and F. E. Murray, *Pulp Pap. Mag. Can.*, **1970**, **71**, T149.
12) M. D. Bentley, I. B. Douglass, J. A. Lacadle, and D. R. Whittler, *J. Air Pollution Control Assoc.*, **22**, 359 (1972).

Effects of the Wavelength and the Matrix on the Photopolymerization of 2,5-Distyrylpyrazine and Its Related Compounds and on Their Photodepolymerization*

Yasuzo SUZUKI, Takashi TAMAKI, and Masaki HASEGAWA

Research Institute for Polymers and Textiles, Sawatari, Kanagawa-ku, Yokohama 221

(Received November 10, 1972)

The solution photopolymerization of 2,5-distyrylpyrazine (DSP) and its related compounds with the general formula of Ar–CH=CH–Ar′–CH=CH–Ar, where Ar and Ar′ represent aryl and arylene groups respectively, have been investigated. All diolefines were converted in good yields into amorphous oligomers with cyclobutane in the main chain on the exclusive excitation of the monomer molecules, while, in the crystalline state, only DSP and 1,4-bis[β-pyridyl-(2)-vinyl] benzene are known to yield highly crystalline oligomers under the same light. All the oligomers were found to be photodepolymerized to the original monomers in the solution on the excitation of the terminal groups of these oligomers. In consequence, a photoreverse scheme has been demonstrated between the diolefinic monomer and the oligomer, depending on the excitation wavelength. Poly-DSP was photodepolymerized into the monomer in trifluoroacetic acid solution, while amorphous poly-DSP in film was readily photooxidized in the air under sunlight. From the photochemical behavior of DSP, oligo-DSP, and poly-DSP, it was found that chemically the same substance, oligo-DSP, behaved in three ways, photopolymerization, photodepolymerization and no photoreaction, according to the physical state. Such a matrix effect is discussed from the point of view of topochemical reaction.

Various kinds of diolefinic compounds have been known to photopolymerize in the crystalline state into highly crystalline polymers with cyclobutane in the main chain.[1–3] Among a series of diolefinic compounds with the general formula of Ar–CH=CH–Ar′–CH=CH–Ar (where Ar and Ar′ represent aryl and arylene groups respectively), 2,5-distyrylpyrazine(DSP) and 1,4-bis-[β-pyridyl-(2)-vinyl]benzene (P2VB) have been reported to be photopolymerized in the crystalline state.[3] Furthermore, photooligomerization on DSP, P2VB, and other types of diolefinic compounds in the crystalline state has been reported in a preceding paper.[4]

On the other hand, the attempted solution photopolymerization of DSP has been reported in the earlier paper not to produce the polymer.[5] In the present work, it was found that the oligomer of DSP and other related diolefinic compounds were obtained by the irradiation of the light with a wavelength that excites monomer molecule exclusively.

Contrary to the exclusive monomer excitation, all the oligomers obtained were found to be photodepolymerized to the monomer in the solution when terminal groups of these oligomers were excited. In addition, a photooxidative degreadation which is not observed in the solution has been investigated preliminarily on amorphous film of poly-DSP.

In the present paper, the photooligomerization of DSP and related compounds and their photodepolymerization will be described. The results for these diolefinic monomers will be discussed in comparison with the reaction in the crystalline state and with reactivity of the corresponding monoolefines.

Experimental

Preparation of Monomers. DSP,P2VB, and three other monomers, 1,4-bis[β-pyridyl-(3)-vinyl] benzene (P3VB), 1,4-bis[β-pyridyl-(4)-vinyl]benzene(P4VB), and 1,4-distyrylbenzene(DSB), were prepared as has been described in an earlier paper.[3]

Preparation of Oligo-DSP in the Solution. DSP was dissolved in tetrahydrofuran(THF) which had been distilled over calcium hydride. The solution (1.41×10^{-2} mol/l, 50 ml) was irradiated with filtered light of a wavelength longer than 380 mμ for 48 hr at room temperature. The filtered light was produced by using a cut-off filter(Corning. 3—75) on a 500-W xenon lamp. After irradiation, the solvent was removed *in vacuo*; a pale yellow oil was thus obtained. A few milliliters of ethyl alcohol were added to the oil, the mixture was stirred overnight, and the precipitated powder was filtered off, and then dried *in vacuo*. The oligomer structure of the product with cyclobutane and a terminal olefinic double bond was confirmed by NMR and IR spectroscopies. The average molecular weight was about 900 (as determined by vapor-pressure osmometry). The final yield of oligo-DSP was 0.12 g (60%).

Preparation of Other Oligomers in the Solution. The oligomerization of other monomers was carried out in a similar way. However, a 0—51 filter was used in place of the 3—75 filter for the oligomerization of DSP in order to filter out the light shorter than 360 mμ. A mixture of petroleum ether and ethyl ether was used as a precipitant for the oily products. The final yield, the irradiation conditions, and the average molecular weight of the oligomers are summarized in Table 1.

The Attempted Dimerization of Stilbene and 2-Styrylpyridine in the Solution. Stilbene was dissolved in THF which had been distilled over calcium hydride. The solution (2.22×10^{-2} mol/l, 50 ml) was irradiated with filtered light of wavelengths longer than 300 mμ for 48 hr at room temperature. The filtered light was produced by using a cut-off filter(0—54) on a 500-W xenon lamp. After irradiation, the solvent was removed *in vacuo*; an oily product was thus obtained. The oil was dissolved in 0.8 ml of deuterochloroform and then submitted to NMR spectroscopy. Aromatic and vinyl-(*trans*- and *cis*-types) protons and the remaining THF were found in the NMR spectrum. The dimerization of 2-styrylpyridine was attempted under the same reaction conditions as were used in the stilibene. Only a *cis-trans* isomerization reaction was observed by NMR spectroscopy.

Photodepolymerization of the Oligomers. The oligomer

* A part of results were reported in This Bulletin, **43**, 3020 (1970).

was dissolved in chloroform or THF at a suitable concentration for UV measurement. The solution was then irradiated with the monochromatic light from a spectroirradiator(Jasco) equipped with a 2000-W xenon lamp as the light source and a gration monochromater. The reaction was followed by UV spectrometry.

Photodecomposition of Poly-DSP in the Solution and in Amorphous Film. Since crystalline poly-DSP is insoluble in the usual organic solvent, trifluoroacetic acid was used as the solvent of poly-DSP. The trifluoroacetic acid solution of poly-DSP (0.5 mg/40 ml) was irradiated with the light of 300 mμ from the spectroirradiator and the reaction was followed by UV spectrometry.

An amorphous poly-DSP film was made by casting on the glass plate from the trifluoroacetic acid solution. After the solvent had been removed *in vacuo*, the film was washed with triethylamine and then with ethyl alcohol. The poly-DSP film in the glass tube was degassed by means of a vacuum line and replaced by helium gas. After this procedure had been repeated three times, the tube was sealed. The tube was then exposed to sunlight through window glass for 80 days. The film sample thus exposed to the sunlight was subsequently compared with a sample which had been exposed to the sunlight in the air by means of IR spectroscopy. The sample stored in the dark in the air was prepared in a wrapped tube with aluminum foil. After 80 days, the contents were checked by studying the IR spectrum.

Results and Discussion

Solution Photooligomerization of DSP and Related Compounds. Figure 1 shows the UV spectral change in DSP when 0.5 ml of DSP in THF(6.09×10^{-3} mol/l) was irradiated by monochromatic light of 395 mμ. The absorption maximum of DSP at 385 mμ decreased gradually with the irradiation, and finally the absorption spectrum was changed to the f spectrum. This spectrum coincides with that of the oligo-DSP obtained by the photooligomerization of DSP in the crystalline state[4] when the remaining monomer of 19%, which was estimated from the absorption ratio of a and f 385 mμ, is subtracted from the f spectrum; then the concentration of the resulting spectrum was adjusted to the concentration at the spectral measurement of oligo-DSP(g) from the crystalline-state photoreaction. The NMR spectrum of the oligomer through solution photoreaction is shown in Fig. 2. A broad peak at 4.9 ppm due to the aryl cyclobutane[6] and a peak at 7.2—7.9 ppm of aromatic hydrogen-overlapping olefinic hydrogen may be seen in Fig. 2. Furthermore, terminal double bond in the oligomer chain was observed at both 970 and 1630 cm^{-1} in the IR absorption spectrum. From these spectral results, it was concluded that DSP was oligomerized in the solution by means of irradiation with the selected wavelength.

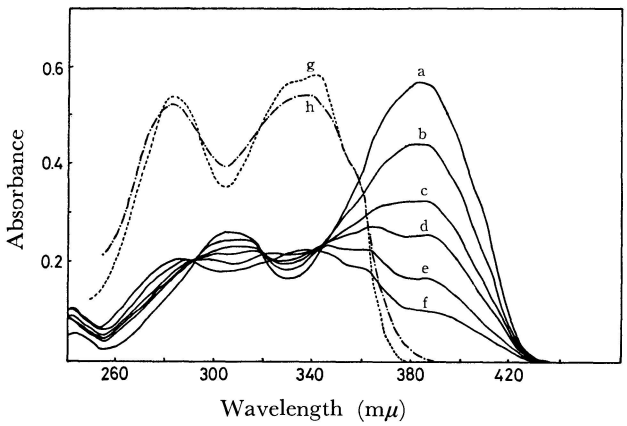

Fig. 1. UV spectral change during the oligomerization of DSP in THF by the irradiation with the light of 395 mμ. a: spectrum of DSP, b—f: after irradiation for 5, 10, 30, 45 and 60 min, respectively, g: oligo-DSP obtained from the crystalline photooligomerization in THF (1.07×10^{-2} g/l), h: spectrum of oligo-DSP estimated from f.

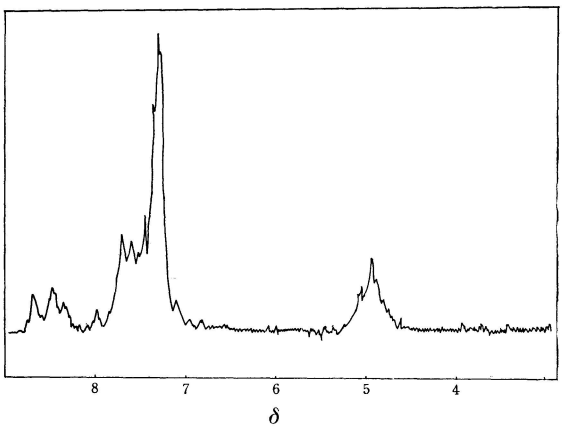

Fig. 2. NMR spectrum of oligo-DSP obtained from solution photooligmerization.

Oligo-DSP was obtained in a 60—80% yield in preparative scale and showed the average molecular weight of 600—900, corresponding to that of the dimer or trimer as is shown in Table 1.

The successful oligomerization of DSP can be explained in terms of two side reaction, the photoreaction of olefinic compound with the solvent[7] and the photocleavage of the resulting cyclobutane in the oligo-DSP, as will be discussed in a later section, being suppressed by interrupting the light shorter than 380 mμ. Another side reaction, the formation of phenanthrene- or azaphenanthrene-type derivatives as photoproducts, can be assumed because of their *cis*-form.[8,9] However, in the present work, such photoproducts were not detected in the oligomerization reaction of any diolefinic compound.

The wavelength of the light for the oligomerization reaction of DSP was chosen from the UV-absorption-spectrum difference between DSP and oligo-DSP. Since the longer-absorption end of oligo-DSP is 380 mμ in the THF solution, an irradiation wavelength longer than 380 mμ excites only DSP, not the terminal olefinic group of the oligomer.

The oligomerization technique of DSP was also extended to other diolefines, P2VB, P3VB, P4VB, and DSB. An irradiation wavelength longer than 360 mμ was decided on for the same reason as in the case of DSP. As a result, all the diolefines examined here gave the same type of oligomers as oligo-DSP, which has a structure with a cyclobutane ring in the main chain. The experimental conditions, the oligomer yield, and their average molecular weights are shown in Table 1.

Table 1. Solution photooligomerization of DSP and its related compounds

Monomers Ar	Monomers Ar'		Irradiated wavelength (mμ)	Reaction time (hr)	Concentration of the monomers in THF (mol/l)	Yield of the oligomer (%)	Molecular weight
	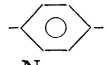	DSB	≥360	48	1.42×10^{-2}	100	634
	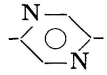	DSP	≥380	48	1.40×10^{-2}	60	900
	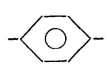	P2VB	≥360	48	1.40×10^{-2}	29	814
	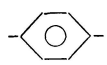	P3VB	≥360	48	1.40×10^{-2}	94	1074
	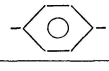	P4VB	≥360	48	1.40×10^{-2}	74	682

The degree of polymerization of the obtained oligomers ranges from 2 to 4, and the yields are relatively high except for the case of oligo-P2VB.

It should be noticed that all the diolefinic compounds attempted were converted to the oligomers, while among this type of compounds only DSP and P2VB are photo-oligomerized or photopolymerized in the crystalline state. These results indicate that the cycloaddition reaction ability on this type of diolefinic compound does not depend on its chemical structure.

A study of the wavelength dependency on the photochemical behavior in solution was carried out for the corresponding to monoolefines, stilbene, and 2-stryl-pyridine for the sake of comparison. However, neither of these two compounds dimerized under experimental condition similar to those of the oligomerization; exclusive excitation of the monoolefines in the highly-concentrated solution suppressed the photocleavage of resulted cyclobutane and isomerization reaction. It can be assumed from the results that, in a solution, the ability of cyclobutane formation of the monoolefines is lower than that of the corresponding diolefines, although the formation of a small amount of a photodimer has been reported in the case of stilbene in benzene by means of long irradiation with an ultraviolet lamp.[6] Although such a difference in reactivity between mono- and di-olefines can not be explained at present, if a unimolecular side reaction, the *cis-trans* isomerization of monoolefines, is presumed to be more striking than that of diolefines, and if cyclobutane is presumed to be produced only from *trans*-olefines, the observed difference in reactivity may be understood.

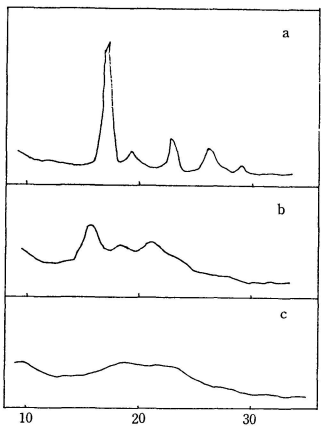

2θ degree

Fig. 3. X-ray diffraction diagrams of oligo-DSP. a: as-polymerized oligomer, b: recrystallized oligomer, c: amorphous oligomer.

One of the most striking features of the step-by-step solution photooligomerization in the present work originates in the monomer structure, in which two reactive double bonds are mutually conjugated through the 1,4-position of an aromatic ring. In such a structure of the monomers, the photocycloaddition step consists of three kinds of addition, as is represented in the case of DSP below:

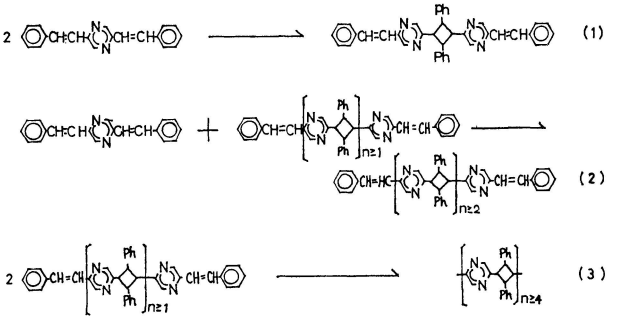

Under the reaction conditions where only the monomer is excited, only Steps(I) and (2) proceed in the solution. Furthermore, these two elementary processes do not proceed after the monomer has been exhausted. The average molecular weight of the oligomers should be determined by the reaction velocity ratio of the two elementary processes, Steps(I) and (2). The actual ratio does not take any extreme values(infinitude or zero), since more of the oligomer mixture than dimer is obtained in the preparative experiment. These are the reasons why all the monomers here can not grow into high polymers in a solution, whereas, for example, bismaleimide derivatives are polymerized by photocycloaddition into high polymers through a step-by-step photoreaction.[10]

Configuration of Oligomers. The oligomers obtained through the solution photooligomerization are distingunished from the oligomers of DSP and P2VB through crystalline-state photooligomerization, which established the following two points. First, the oli-

gomer from the solution is shown to be amorphous by x-ray analysis, as is shown in Fig. 3, while the oligomer obtained through crystalline-state oligomerization shows a high crystallinity. Second, the amorphous oligomers of DSP and P2VB in the solid state do not grow into high polymers on irradiation with the light of 340 mμ, which excites the terminal group of the oligomer.

The first difference suggests that the oligomers obtained through solution photooligomerization consist of mixed structures of cyclobutane units in the oligomers, while the as-polymerized oligomers of DSP are known from the results of x-ray crystal analysis to consist of a single steric configuration of 1,3-*trans*-type cyclobutane.[11,12] However, by NMR analysis, we could not observe the definite differences between these two types of oligomers because of poor spectrum resolution. The second difference in photoreactivity between amorphous and as-polymerized crystalline oligomers suggests that, in the case of the crystalline oligomer, residual terminal olefinic groups face each other in the crystal intermolecularly, but this is not the case with amorphous oligomers of DSP and P2VB.

Photodepolymerization of the Oligomers. In order to study further the photochemical behavior of the oligomers in a solution, a chloroform solution(1 mg/40 ml) of oligomer of DSP, which had been prepared by solution photooligomerization, was irradiated with the monochromatic light of 340 mμ and the reaction was monitored by UV spectroscopy, as is shown in Fig. 4. The peak which appeared at 385 mμ was identified with that of DSP by comparison with the UV spectrum (e in Fig. 4) in chloroform. When oligo-DSP in a chloroform solution (4.85×10^{-3} mol/l) is irradiated with a light longer than 340 mμ, the molecular weight of the oligomer is depressed from the 954 of the original to 475 after irradiation. Accordingly, in the solution unimolecular photodepolymerization reaction is considered to overcome a bimolecular-chain growth reaction(Step (3)), if any. Another type of oligo-DSP obtained through crystalline-state photooligomerization has been confirmed to be photodepolymerized in the solution in the same manner.

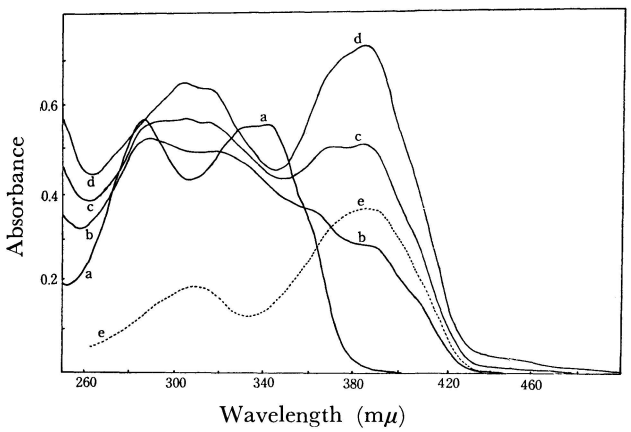

Fig. 4. UV spectral change during the photodepolymerization of oligo-DSP in chloroform by the irradiation with the light of 340 mμ. a: oligo-DSP, b—d: after irradiation for 15, 30 and 60 min, respectively, e: DSP (0.7×10^{-5} mol/l).

Other oligomers, oligo-DSB, -P2VB, -P3VB, and -P4VB, were also found to be photodepolymerized with oligo-DSP in a similar way, as is represented by oligo-DSB in Fig. 5. From these results, it may be concluded that these oligomers are photodepolymerized to the monomers when the terminal groups are excited in the solution. In consequence, a photoreverse scheme has been found between diolefinic monomers and the oligomers, depending on the different excitation wavelength. Such a photodepolymerization reaction results in the irradiation-wavelength effect of the solution oligomerization of these monomers.

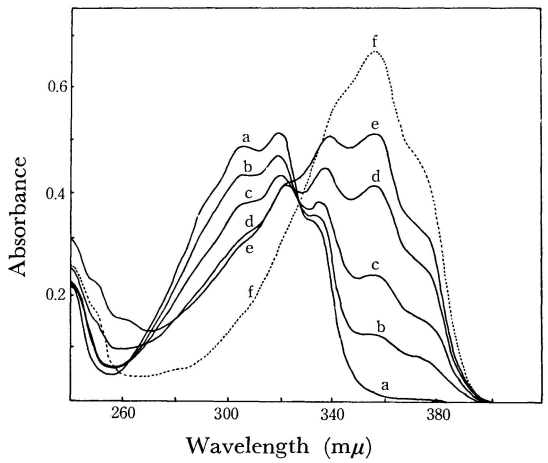

Fig. 5. UV spectral change during the photodepolymerization of oligo-DSB in THF by the irradiation with the light of 277 mμ. a: oligo-DSB, b—e: after irradiation for 1, 3, 12 and 40 min, respectively, f: DSB (1.2×10^{-5} mol/l).

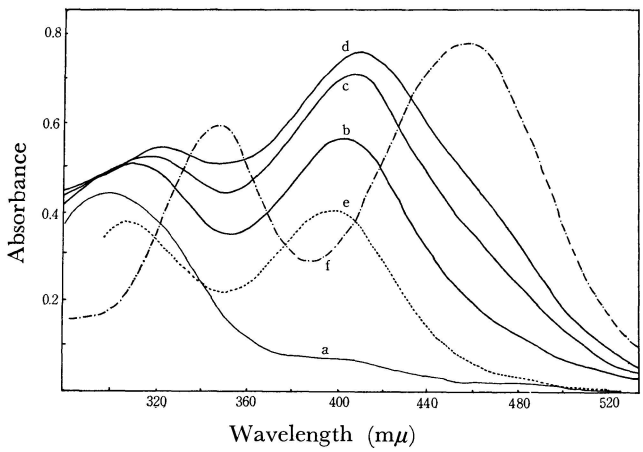

Fig. 6. UV spectral change during the photodepolymerization of poly-DSP in trifluoroacetic acid by the irradiation with the light of 300 mμ. a: poly-DSP, b—d: after irradiation for 20, 120 and 200 sec, respectively, e: oligo-DSP, f: DSP.

Photodegradation of Poly-DSP. In a previous paper, it has been reported that poly-DSP is thermally depolymerized to the monomer in a high yield.[1] In the course of the photochemical study of cyclobutane derivatives, the photodepolymerization of poly-DSP was also examined. Fig. 6 shows the UV spectral

change when the trifluoroacetic acid solution of poly-DSP was irradiated with the light of 300 mμ. In comparision with the spectra of DSP and oligo-DSP in the same solvent, the spectrum obtained was confirmed to be a mixture of the monomer and the oligomer of DSP. From these results, it may be concluded that the photodepolymerization of poly-DSP proceeds at random in the polymer chain under the present experimental conditions.

The photochemical behavior of poly-DSP was also examined in amorphous film. The poly-DSP film did not show any change in IR spectroscopically when the film was stored for eighty days in helium gas in the dark. On the other hand, hydroxy and carbonyl groups appeared vigorously in the IR spectrum when poly-DSP film was stored in the air under the sunlight, as is shown in Fig. 7. Moreover, the photoirradiation of the film by sunlight in helium resulted in little change in the IR spectrum. Although no photoproducts have been isolated from the degrated film, it is obvious that amorphous film of poly-DSP is photooxidized, while the poly-DSP in the solution is mostly photodepolymerized to the monomer. Such an extreme difference in the reactivities between amorphous and solution states of the same polymer is unique in polymeric materials.

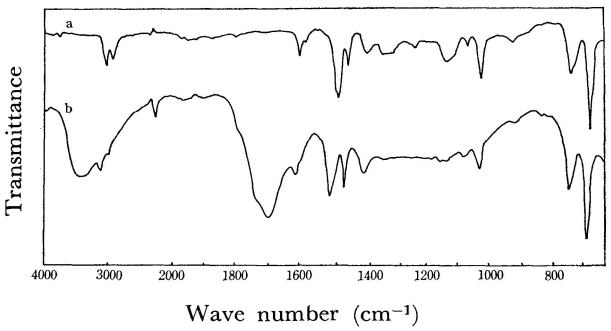

Fig. 7. IR spectra of poly-DSP(a) and the photooxidized poly-DSP(b) in film.

Characteristics of Photopolymerization of DSP. The photochemical interrelationship in DSP, oligo-DSP, and poly-DSP is summarized below:

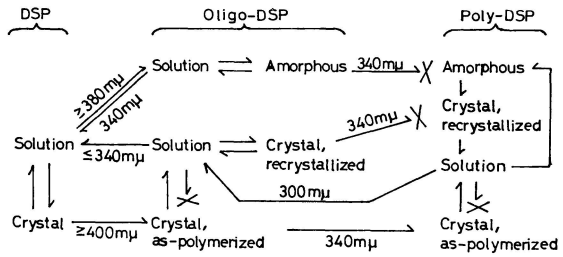

This experiment demonstrates that the DSP molecule in the crystal reacts only with a intermolecularly-facing double bond under the steric control of the crystalline lattice (a topochemical process) to give a thermodynamically metastable polymer (as-polymerized crystalline polymer). As a matter of course, such a metastable polymer crystal can never be reproduced after it has been dissolved, but the thermodynamically-stable polymer crystal with a different form (a recrystallized crystalline polymer) is obtained from a polymer solution.[13]

According to the same explanation, oligo-DSP does not grow further into a high polymer without such topotactic assistance (crystal lattice control) as is presented in the case of the as-polymerized crystalline oligo-DSP. Therefore, the oligo-DSP retains two different reaction paths which are entirely the reverse of each other, cyclobutane formation in the crystalline state and its cleavage in the solution, under the same irradiation light. In other words, the direction of the reaction depends principally on its physical reaction states(matrix effect). Such a matrix effect is also revealed on amorphous and recrystallized oligo-DSP. That is, neither of the oligomers grows into a polymer in the solid state, while both are photodepolymerized to the monomer in a solution. It is interesting that chemically the same substance, the oligomer, behaves in three extremely different ways, photopolymerization, no photoreaction, and photodepolymerization, according to the physical state (in the as-polymerized, amorphous or recrystallized, and solution states). Such a multiplicity of reactivity is clear-cut example of a matrix effect originating in a topochemical process and has been demonstrated for the first time in the organic field.

Reference

1) M. Hasegawa and Y. Suzuki, *J. Polym. Sci., A-1*, **5**, 813 (1967).
2) M. Hasegawa, F. Suzuki, and Y. Suzuki, *ibid.*, **6**, 293 (1968).
3) M. Hasegawa, F. Suzuki, H. Nakanishi, and Y. Suzuki, *ibid.*, **7**, 743 (1969).
4) T. Tamaki, Y. Suzuki, and M. Hasegawa, This Bulletin, **45**, 1988 (1969).
5) H. Nakanishi, Y. Suzuki, F. Suzuki, and M. Hasegawa, *J. Polym. Sci., A-1*, **7**, 753 (1972).
6) H. Shechter, W. J. Link, and G. V. D. Tiers, *J. Amer. Chem. Soc.*, **85**, 1601 (1963).
7) Dov Elad and Raymond D. Youssefyeh, *J. Org. Chem.*, **29**, 2031 (1964).
8) C. S. Wood and F. B. Mallory, *J. Amer. Chem. Soc.*, **86**, 3373 (1964).
9) P. L. Kumler and R. A. Dybas, *J. Org. Chem.*, **35**, 125 (1970).
10) F. C. De Schryver, W. J. Feast, and G. Smets, *J. Polym. Sci., A-1*, **8**, 1939 (1970).
11) H. Nakanishi, M. Hasegawa, and Y. Sasada, *J. Polym. Sci., A-2*, **10**, 1537 (1972).
12) H. Nakanishi, K. Ueno, and M. Hasegawa, *Chem. Lett.*, **1972**, 301.
13) S. Fujishige and M. Hasegawa, *J. Polym. Sci., A-1*, **7**, 2037 (1969).

Total Synthesis of Ferrichrome

Yoshikazu Isowa, Muneki Ohmori, and Hideaki Kurita

Sagami Chemical Research Center, Nishi-ohnuma, Sagamihara, Kanagawa 229

(Received March 31, 1973)

Two different sequence hexapeptides for the synthesis of ferrichrome were prepared using N^{δ}-tosyl-N^{δ}-benzyloxy-L-ornithine by means of *N*-hydroxysuccinimide plus *N,N*-dicyclohexylcarbodiimide or Woodward reagent K method. The linear hexapeptides (XII·HCl and XIX·HCl) were cyclized by excess *N,N*-dicyclohexylcarbodiimide to give cyclo-triglycyltri-N^{δ}-tosyl-N^{δ}-benzyloxy-L-ornithyl (XX). Detosylation, acetylation and successive reductive debenzylation of XX afforded deferri-ferrichrome (XXIV). Addition of ferric iron to XXIV gave ferrichrome, which had the same crystalline form, superimposable infrared and well-agreeing visible spectra and the same value in optical rotation compared with the data in the literature of natural product.

Ferrichrome (I), shown in Fig. 1, is one of a family of iron binding molecules[1] in nature and a representative of siderochrome.[2] It is an extremely powerful and relatively selective chelating agent for ferric iron[3] and it has been assumed this substance acts as a specific iron transport agent, a shuttle necessary for the permeation of the metal through the cellular membrane, or a coenzyme in heme biosynthesis.[4]

Neilands first actually isolated ferrichrome as a crystalline organo-iron pigment from the smut fungus, *Ustilago sphaerogena*, in 1952.[5] Subsequent study on the structure[6] of I showed that it binds a ferric iron mainly through ionic forces and that it is a cyclic hexapeptide built up from three residues of N^{δ}-acetyl-N^{δ}-hydroxy-L-ornithine together with three residues of glycine. The amino acid sequence within the peptide moieties of this naturally occurring ferric trihydroxamate was established by Neilands and collaborators in 1963 as cyclo-triglycyltri-N^{δ}-acetyl-N^{δ}-hydroxy-L-ornithyl.[7] Conformation in solution of I was recently studied by Llinas *et al.*[8]

The chemical synthesis of ferrichrome has been accomplished by Keller-Schierlein and Maurer[9] in 1969 using L-δ-nitronorvaline and glycine. The linear hexapeptide, *t*-butyloxycarbonylglycyltri-L-δ-nitronorvalylglycylglycine methyl ester, was prepared by means of mixed anhydride method using *t*-butyloxycarbonyl group as amino protecting group. The cyclization of the linear hexapeptide was carried out by the *p*-nitrophenyl ester method in pyridine. The reduction of the nitro group to hydroxyamino was accomplished with zinc in aqueous ammonium chloride.

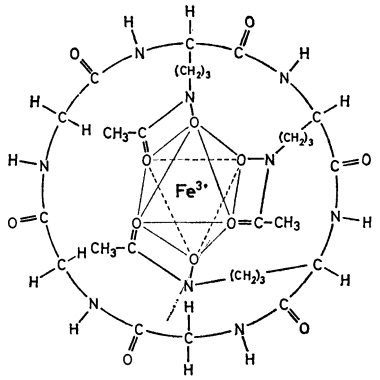

Fig. 1. Structure of ferrichrome (I).

Without isolation of the product, acetylation was carried out with acetic anhydride in pyridine and *O*-acetyl group the removed by treatment of the product with methanolic ammonia. After addition of the ferric chloride, the product, ferrichrome, was purified by countercurrent distribution and crystallized from methanol.

In this paper we also describe the total synthesis of ferrichrome using N^{δ}-tosyl-N^{δ}-benzyloxy-L-ornithine (II), shown in Fig. 2, which has been reported in the paper from our laboratory.[10]

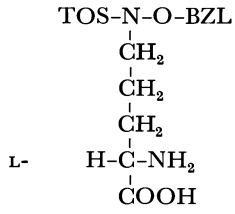

(II)

Fig. 2. N^{δ}-Tosyl-N^{δ}-benzyloxy-L-ornithine: TOS, *p*-toluenesulfonyl; BZL, benzyl.

II has a protected hydroxyamino group at δ-position of L-ornithine and therefore fulfils prerequisites for incorporation into peptides of more complex structures. The linear hexapeptides (XII·HCl and XIX·HCl) were prepared *via* two different routes, shown in Fig. 3 and Fig. 4, in order to ascertain whether or not the protected cyclic peptides obtained from the linear hexapeptides possess the same optical rotatory power. Figure 3 indicates the synthesis of glycyltri-N^{δ}-tosyl-N^{δ}-benzyloxy-L-ornithylglycylglycine hydrochride (XII·HCl), in which glycines are the *N*- and *C*-terminal amino acid residues to remove possible racemization at the step of the cyclization reaction. For a study of the relationship between the optical purity and the coupling method at the preparation of XII·HCl, the linear hexapeptide (XII·HCl) was prepared by a step-by-step elongation using *N*-hydroxysuccinimide plus *N,N*-dicyclohexylcarbodiimide[11] or Woodward reagent K[12] as a coupling reagent. The final product (XII·HCl), obtained by the different coupling methods, possessed the same specific rotation, $-8.1°$ and $-8.2°$ in chloroform each other, and its homogeneity was demonstrated by thin-layer chromatography.

It should be noted that hydroxyamino protecting tosyl and benzyl groups are stable to the reaction conditions employed in the peptide formation and in the deprotection of the α-position. Figure 4 indicates the synthesis of another linear hexapeptide, tri-N^{δ}-tosyl-

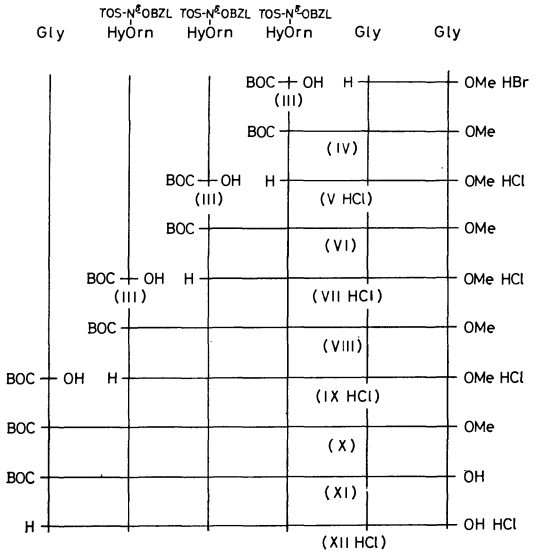

Fig. 3. Synthesis of glycyltri-N^{δ}-tosyl-N^{δ}-benzyloxy-L-ornithylglycylglycine hydrochloride (XII·HCl): HyOrn, N^{δ}-hydroxy-L-ornithine; Gly, glycine; BOC, *t*-butyloxycarbonyl.

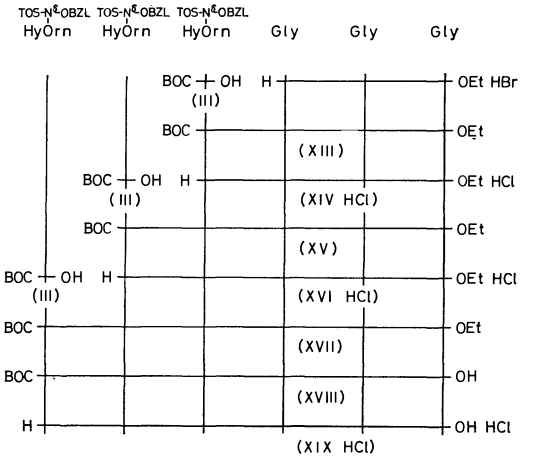

Fig. 4. Synthesis of tri-N^{δ}-tosyl-N^{δ}-benzyloxy-L-ornithyldiglycylglycine hydrochloride (XIX·HCl).

N^{δ}-benzyloxy-L-ornithyldiglycylglycine hydrochloride (XIX·HCl), in which II is *N*-terminal amino acid and glycine is *C*-terminal amino acid. XIX·HCl, prepared by a step-by-step elongation by means of *N*-hydroxysuccinimide plus *N,N*-dicyclohexylcarbodiimide method, possessed the specific rotation, +3.2° in chloroform.

Various methods for the cyclization of the linear hexapeptides (XII·HCl and XIX·HCl) were undertaken. Namely *N,N*-dicyclohexylcarbodiimide, water soluble carbodiimide (*N*-ethyl-*N'*-(3-dimethylaminopropyl)carbodiimide) or *N*-hydroxysuccinimide plus *N,N*-dicyclohexylcarbodiimide method were attempted to cyclize the linear hexapeptides. Since the *N,N*-dicyclohexylcarbodiimide method gave the pure cyclization product in the 41% yield, we describe in detail about the cyclization reaction using *N,N*-dicyclohexylcarbodiimide. The scheme for the cyclization reaction of XII·HCl or XIX·HCl is presented in Fig. 5.

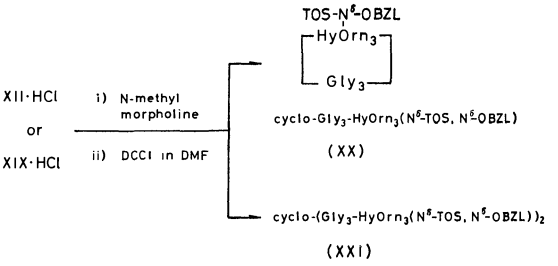

Fig. 5. Cyclization of linear hexapeptide (XII·HCl or XIX·HCl) using *N,N*-dicyclohexylcarbodiimide (DCCI).

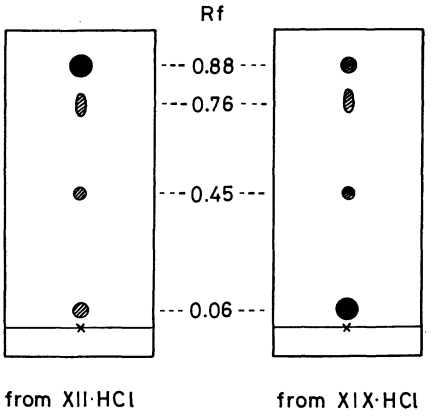

Fig. 6. Thin-layer chromatogram of the crude cyclization products obtained from XII·HCl or XIX·HCl; the R_f value of cyclic hexapeptide is 0.88 and that of dimerization product is 0.06.

The cyclization of XII·HCl using *N,N*-dicyclohexylcarbodiimide in a large amount of dimethylformamide gave a mixture of the desired monomerization product (XX), the dimerization substance (XXI), the unreacted linear hexapeptide (XII) and *N,N*-dicyclohexylurea, which were determined by thin-layer chromatography (Fig.. 6).

The R_f value of 0.06 was proved to be of the dimerization product (XXI), which was demonstrated by the molecular weight determination and elemental analysis, while that of 0.88 was of the desired protected cyclic hexapeptide (XX). The product indicating R_f 0.76 was considered to be a linear hexapeptide (XII) and R_f 0.45 was determined to be of dicyclohexylurea. For the removal of XXI, the reaction mixture was treated with hot methanol. After methanol-insoluble material (XXI) had been filtered off, the methanol solution was evaporated to dryness. Furthermore, for the removal of XII and dicyclohexylurea, the residue thus obtained was dissolved in a mixture of dimethylformamide and water (4 : 1) and passed successively through columns of CG-120 and CG-400; the yield of the crystalline XX from XII·HCl was found to be 41% after recrystallization from methanol. The molecular weight determination demonstrated that the molecular size of this compound was corresponded to that of XX. The cyclization reaction of another linear hexapeptide (XIX·HCl) gave the result indicated in Fig. 6. In this case, the main product, obtained in a *ca.* 40% yield, was found to be

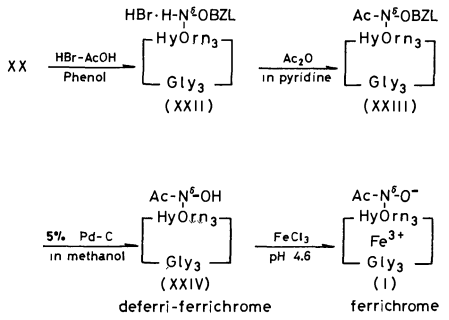

Fig. 7. Transformation of XX to deferri-ferrichrome XXIV and addition of ferric ion to XXIV.

a dimer (XXI). Not more than 7% of the starting material (XIX·HCl) was converted to the cyclic hexapeptide. Since the cyclic hexapeptide, thus obtained, possessed the same specific rotation with that of XX prepared from XII·HCl, the maintenance of optical purity was demonstrated.

The transformation of XX to deferri-ferrichrome (XXIV) and of XXIV to ferrichrome (I) are presented in Fig. 7.

The tosyl group of XX could be removed selectively on treatment with 36% hydrogen bromide in acetic acid in the presence of phenol. However, it was unsuccessful to isolate the detosylated product (XXII·3HBr) in the pure state. The removal of the tosyl group was confirmed by the lacking of the absorptions at 1350 and 1165 cm^{-1} in the infrared spectrum. Experiment in which the crude detosyl-compound was acetylated with acetic anhydride in pyridine, resulted acetyl-derivative (XXIII) in 47% overall conversion (XX to XXIII). On hydrogenation in methanol solution over 5% palladium on charcoal at room temperature under atmospheric pressure for 4 days, XXIII was almost quantitatively converted into XXIV (deferri-ferrichrome), which was ascertained by the comparison with the NMR spectrum obtained from natural product.[13] Figure 8 shows the NMR spectrum of XXIV, in which the characteristic signal of methyl protons in N^{δ}-acetyl group appears at δ 2.61 and the signals of benzyl group are not observable. Figure 9 shows the infrared spectrum of XXIV, in which the removal of the benzyl group is confirmed by the absence of the absorptions at 3025 and 698 cm^{-1}.

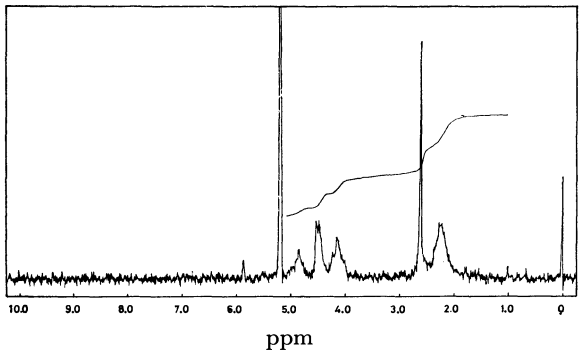

Fig. 8. NMR spectrum of synthetic deferri-ferrichrome (XXIV).

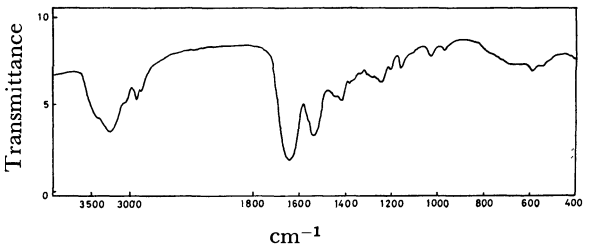

Fig. 9. Infrared spectrum of synthetic deferri-ferrichrome (XXIV).

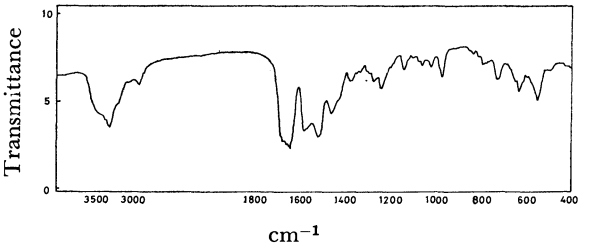

Fig. 10. Infrared spectrum of synthetic ferrichrome (I).

The synthetic ferrichrome (I) was obtained by the reaction of XXIV with three equivalents of ferric chloride in aqueous buffered solution of pH 4.6, at which re-addition of iron to deferri-ferrichrome obtained from naturally occurring ferrichrome was performed by Emery and Neilands.[6b] On recrystallizations from anhydrous methanol, pure synthetic ferrichrome (I) was obtained as long orange needles with the well-agreeing value of elemental analysis. The comparison with the data in the literatures of natural product was made of the melting point, optical rotation and absorptivity in visible absorption; mp 248—251 °C (decomp.) (lit.[5] 240—242 °C (decomp.)), $[\alpha]_D$ +304°± 10° (*c* 0.0425, water) (lit.[9b] +300° (*c* 0.04, water)) and $E_{1cm}^{1\%}$ (428 mμ 39.8 (water) (lit.[5] $E_{1cm}^{1\%}$ (425 mμ) 39.6 (water)). Furthermore, the infrared spectrum of synthetic I, as shown in Fig. 10, corresponded closely to that of natural product described in the literature.[13]

Experimental

All melting points were determined with a Yanagimoto electric micromelting point apparatus unless otherswie indicated and are uncorrected. Optical rotations were measured with a Yanagimoto automatic polarimeter OR-50. The nuclear magnetic resonance spectra were run on a Hitachi Perkin-Elmer R-20 High Resolution NMR spectrometer, using tetramethylsilane as an external or internal standard. Infrared spectra were recorded on a Hitachi G-3 spectrophotometer as KBr disk. Molecular weight was determined by the use of a differential vapor pressure osometer (Hitachi Perkin-Elmer 115 Molecular weight apparatus). The visible spectrum was taken on a Hitachi Recording Spectrophotometer EPS-3. The thin-layer chromatography was carried out on Merck silica gel F_{254} using the solvent system of *n*-butanol–acetic acid–pyridine–water (4 : 1 : 1 : 2 v/v). The paper chromatography was carried out on Toyo Roshi No. 50 using the solvent system of *n*-butanol–acetic acid–water (4 : 1 : 1 v/v).

N$^{\alpha}$-t-*Butyloxycarbonyl*-N$^{\delta}$-*tosyl*-N$^{\delta}$-*benzyloxy*-L-*ornithine (III)*.

This compound was prepared by the procedure described in the previous paper.[15]

N^{α}-t-Butyloxycarbonyl-N^{δ}-tosyl-N^{δ}-benzyloxy-L-ornithylglycylglycine Methyl Ester (IV).[16] *a*): To a stirred solution of *N^{α}-t*-butyloxycarbonyl-*N^{δ}*-tosyl-*N^{δ}*-benzyloxy-L-ornithine (III) (4.92 g, 10 mmol), glycylglycine methyl ester hydrobromide (2.27 g, 10 mmol), *N*-hydroxysuccinimide (2.3 g, 20 mmol) and *N*-methyl morpholine(1.21 ml, 11 mmol) in dimethylformamide (100 ml) was added a solution of dicylcohexylcarbodiimide (2.27 g, 11 mmol) in dimethylformamide (10 ml) at −10 °C. After stirring for 42 hr, the crystalline deposit was removed and the filtrate was evaporated *in vacuo*. The oily residue was dissolved in chloroform (150 ml) and washed successively with water, M sodium bicarbonate, 2 M hydrochloric acid and water. The organic layer was dried over magnesium sulfate and evaporated *in vacuo*. The oily residue was solidified with the aid of petroleum ether; 5.03 g (81%); mp 56—64 °C; $[\alpha]_D$ +6.8° (*c* 1, methanol).

Found: C, 56.35; H, 6.68; N, 8.91%. Calcd for $C_{29}H_{40}N_4O_9S$: C, 56.11; H, 6.50; N, 9.03%.

b): To a stirred suspension of III (9.86 g, 20 mmol) and Woodward reagent K (5.07 g, 20 mmol) in nitromethane (80 ml) was added triethylamine (2.93 ml, 21 mmol) at 5 °C. To the resultant clear solution was added glycylglycine methyl ester hydrobromide (4.5 g, 20 mmol) and triethylamine (2.93 ml, 21 mmol). The mixture was stirred at room temperature for 36 hr and then evaporated *in vacuo*. The oily residue was treated as described above; yield, 8.9 g (72%); mp 61—67 °C; $[\alpha]_D$ +7.0° (*c* 1, methanol).

N^{δ}-Tosyl-N^{δ}-benzyloxy-L-ornithylglycylglycine Methyl Ester Hydrochloride (V·HCl). *i*): To the cold solution of IV-a[17] (5.03 g) in ethyl acetate (20 ml) was added 6 M hydrogen chloride in ethyl acetate (30 ml). After stirring for 2 hr at room temperature, the mixture was evaporated *in vacuo*. The oily residue was crystallized from a small volume of ethyl acetate by addition of ether; yield, 4.30 g (95.5%); mp 108—121 °C; $[\alpha]_D$ +22.3° (*c* 1, ethanol).

Found: C, 51.24; H, 5.97; N, 10.06%. Calcd for $C_{24}H_{33}N_4O_7SCl$: C, 51.67; H, 6.09; N, 9.94%.

ii): The peptide hydrochloride (V·HCl) derived from IV-b[17]; mp 109—120 °C; $[\alpha]_D$ +22.1° (*c* 1, ethanol).

N^{α}-t-Butyloxycarbonyl-N^{δ}-tosyl-N^{δ}-benzyloxy-L-ornithyl-N^{δ}-tosyl-N^{δ}-benzyloxy-L-ornithylglycylglycine Methyl Ester (VI). a): To a stirred colorless solution of III (4.17 g, 8.47 mmol), V·HCl (4.72 g, 8.47 mmol), *N*-hydroxysuccinimide (1.96 g, 17.0 mmol) and *N*-methyl morpholine (1.00 ml, 9.00 mmol) in dimethylformamide (50 ml) was added a solution of dicyclohexylcarbodiimide (1.86 g, 9.00 mmol) in dimethylformamide (10 ml) at −15 °C. After stirring for 45 hr at room temperature, the crystalline deposit was removed by suction and the filterate was evaporated *in vacuo*. The oily residue was dissolved in ethyl acetate (200 ml) and washed successively with water, M sodium bicarbonate, water, 2 M hydrochloric acid and water. The organic layer was dried over anhydrous magnesium sulfate and evaporated *in vacuo*. The residual semi-solid was crystallized from ethyl acetate-ligroin (1 : 1) to give an amorphous powder; yield, 6.9 g (82%); mp 112—120 °C; $[\alpha]_D$ −2.8° (*c* 1, methanol). One more recrystallization from the same solvent raised the mp to 120—123 °C.

Found: C, 57.98; H, 6.10; N, 8.25%. Calcd for $C_{48}H_{62}N_6O_{13}S_2$: C, 57.93; H, 6.28; N, 8.45%.

b): The tetrapeptide ester (VI) was obtained by the same procedure employed for the preparation of IV-b; yield, 72.5 %; mp 118—122 °C; $[\alpha]_D$ −2.7° (*c* 1, methanol).

Di-N^{δ}-tosyl-N^{δ}-benzyloxy-L-ornithylglycylglycine Methyl Ester Hydrochloride (VII·HCl). *i*): Removal of the *t*-butyloxycarbonyl group from VI-a using the same reagent employed for the preparation of V·HCl gave VII·HCl; yield, 93.0%; mp 112—126 °C; $[\alpha]_D$ +16.4° (*c* 1, methanol).

Found: C, 55.22; H, 6.17; N, 8.92%. Calcd for $C_{43}H_{55}N_6O_{11}S_2Cl$: C, 55.44; H, 5.95; N, 9.02%.

ii): The tetrapeptide ester hydrochloride derived from VI-b; mp 110—123 °C; $[\alpha]_D$ +16.0° (*c* 1, methanol).

N^{α}-t-Butyloxycarbonyl-N^{δ}-tosyl-N^{δ}-benzyloxy-L-ornithyldi-N^{δ}-tosyl-N^{δ}-benzoyloxy-L-ornithylglycylglycine Methyl Ester (VIII). *a*): To a stirred colorless solution of III (3.19 g, 6.48 mmol), VII·HCl (6.04 g, 6.48 mmol) and *N*-hydroxysuccinimide 1.50 g, 13.0 mmol) in dimethylformamide (40 ml) was added *N*-methyl morpholine (0.77 ml, 7.0 mmol) at −15 °C. Thereafter dicyclohexlcarbodiimide (1.45 g, 7.0 mmol) in dimethylformamide (10 ml) was added at the same temperature. The mixture was stirred for 48 hr at room temperature. The crystalline deposit was removed and the pale yellow filtrate was evaporated *in vacuo*. The residual semi-solid was triturated several times with water and then the resultant solid was collected by suction. Recrystallization from ethyl acetate-ligroin (3 : 1) gave an amorphous powder; yield, 5.35 g (60.5%); mp 152—154 °C; $[\alpha]_D$ −3.1° (*c* 1, methanol).

Found: C, 58.68; H, 5.92; N, 8.12%. Calcd for $C_{67}H_{84}N_8O_{17}S_3$: C, 58.75; H, 6.18; N, 8.18%.

b) The pentapeptide ester (VIII) was obtained by the same method employed for the preparation of IV-b; yield, 49%; mp 154—156 °C; $[\alpha]_D$ −3.6° (*c* 1, methanol).

Tri-N^{δ}-tosyl-N^{δ}-benzyloxy-L-ornithylglycylglycine Methyl Ester Hydrochloride (IX·HCl). *i*): VIII was converted to the pentapeptide ester hydrochloride (IX·HCl) in the same manner as described above for V·HCl; yield, 91.5%; mp 126—135 °C; $[\alpha]_D$ +5.8° (*c* 1, methanol).

Found: C, 56.52; H, 6.05; N, 8.23%. Calcd for $C_{62}H_{77}N_8O_{15}S_3Cl$: C, 57.02; H, 5.94; N, 8.53%.

ii): IX·HCl from VIII-b by the same procedure employed for the preparation of V·HCl; yield, 96.5%; mp 123—135 °C; $[\alpha]_D$ +4.8° (*c* 1, methanol).

t-Butyloxycarbonylglycyltri-N^{δ}-tosyl-N^{δ}-benzyloxy-L-ornithylglycylglycine Methyl Ester (X). *a*): To a stirred solution of *t*-butyloxycarbonylglycine (0.43 g, 2.45 mmol), IX·HCl (3.2 g, 2.45 mmol) and *N*-hydroxysuccinimide (0.58 g, 5.0 mmol) in dimethylformamide (20 ml) was added *N*-methyl morpholine (0.30 ml, 2.7 mmol) at −15 °C. After stirring for 30 min at the same temperature, dicyclohexylcarbodiimide (0.56 g, 0.70 mmol) in dimethylformamide (5 ml) was added and the reaction mixture was stirred for 48 hr at room temperature. The crystalline deposit was removed and the yellow filtrate was evaporated *in vacuo*. The crude crystalline hexapeptide ester was collected with the aid of water (50 ml), washed successively with water and dried over phosphorus pentoxide under vacuum. Recrystallization from methanol treated with charcoal gave a colorless powder; yield, 3.0 g (86%); mp 170—172 °C; $[\alpha]_D$ +2.4° (*c* 1, chloroform): IR, 1740 cm^{-1} (-COOMe).

Found: C, 57.94; H, 6.11; N, 8.74%. Calcd for $C_{69}H_{87}N_9O_{18}S_3$: C, 58.08; H, 6.15; N, 8.84%.

b): The hexapeptide ester was obtained by the same procedure employed for the preparation of IV-b; mp 168—170 °C (from methanol); $[\alpha]_D$ +2.1° (*c* 1, chloroform).

t-Butyloxycarbonylglycyltri-N^{δ}-tosyl-N^{δ}-benzyloxy-L-ornithyl-glycylglycine (XI). *i*): To a stirred suspension of the hexapeptide methyl ester (X) (2.9 g, 2.0 mmol) in acetone (20 ml) was added M sodium hydroxide (4 ml) at room temperature. After 48 hr, resultant pale yellow clear solution was neutralized with citric acid and then evaporated *in vacuo*. Residual solid was collected with the aid of water and recrystallization from methanol gave a colorless powder; yield, 1.6 g (57%);

mp 138—143 °C; $[\alpha]_D$ +1.4° (*c* 1, chloroform); IR absorption of the ester group in X at 1740 cm^{-1} disappeared.

Found: C, 57.56; H, 5.88; N, 8.66%. Calcd for $C_{68}H_{85}N_9O_{18}S_3$: C, 57.81; H, 6.07; N, 8.92%.

ii): The ester-free hexapeptide derived from X-b; yield, 58%; mp 138—143 °C; $[\alpha]_D$ +1.5° (*c* 1, chloroform).

Glycyltri-N$^\delta$-tosyl-N$^\delta$-benzyloxy-L-ornithylglycylglycine Hydrochloride (XII·HCl). *i*): To a solution of XI-a (1.6 g, 1.1 mmol) in chloroform (30 ml) was added 6 M hydrogen chloride in ethyl acetate (20 ml) under ice cooling. The solution was then allowed to stand at room temperature for 4 hr and evaporated *in vacuo*. Crystalline deposit was collected with the aid of dry ether; yield, 1.4 g (92%); mp 131—138°C; $[\alpha]_D$ −8.1° (*c* 1, chloroform); R_f 0.75 (tlc).

Found: C, 55.94; H, 6.06; N, 9.10%. Calcd for $C_{63}H_{78}N_9O_{16}S_3Cl$: C, 56.09; H, 5.83; N, 9.35%.

ii) The hexapeptide hydrochloride (XII-HCl) derived from XI-b; mp 132—138 °C; $[\alpha]_D$ −8.2° (*c* 1, chloroform); R_f, 0.75 (tlc).

Glycyltri-N$^\delta$-tosyl-N$^\delta$-benzyloxy-L-ornithylglycylglycine (XII). XII was obtained by the treatment of XII·HCl with aqueous ammonia in dimethylformamide. Recrystallization from dimethylformamide-water gave a pure product (XII); mp 212—218 °C; $[\alpha]_D$ −4.2° (*c* 0.5, acetic acid); R_f, 0.76 (tlc).

Found: C, 57.34; H, 5.80; N, 9.30%. Calcd for $C_{63}H_{77}N_9O_{16}S_3$: C, 57.65; H, 5.91; N, 9.61%.

N$^\alpha$-t-Butyloxycarbonyl-N$^\delta$-tosyl-N$^\delta$-benzyloxy-L-ornithyldiglycylglycine Ethyl Ester (XIII). III and diglycylglycine ethyl ester hydrobromide were coupled by the same procedure employed for the preparation of IV-a to give a desired tetrapeptide ester; mp 98—102 °C (from ethyl acetate-ligroin); $[\alpha]_D$ +0.3° (*c* 1, acetic acid).

Found: C, 55.94; H, 6.43; N, 10.19%. Calcd for $C_{32}H_{45}N_5O_{10}S$: C, 55.55; H, 6.56; N, 10.12%.

N$^\delta$-Tosyl-N$^\delta$-benzyloxy-L-ornithyldiglycylglycine Ethyl Ester Hydrochloride (XIV-HCl). Removal of the *t*-butyloxycarbonyl group of XIII was carried out by the same procedure employed for the preparation of V·HCl to give the tetrapeptide ester hydrochloride; mp 115—128 °C; $[\alpha]_D$ +21.7° (*c* 1, methanol).

Found: C, 51.54; H, 5.90; N, 10.89%. Calcd for $C_{27}H_{38}N_5O_8SCl$: C, 51.63; H, 6.10; N, 11.15%.

N$^\alpha$-t-Butyloxycarbonyl-N$^\delta$-tosyl-N$^\delta$-benzyloxy-L-ornithyl-N$^\delta$-tosyl-N$^\delta$-benzyloxy-L-ornithyldiglycylglycine Ethyl Ester (XV). III and XIV·HCl were coupled by the same procedure employed for the preparation of IV-a to give a desired pentapeptide ester; mp 155—157 °C (from methanol); $[\alpha]_D$ −7.4° (*c* 1, acetic acid).

Found: C, 57.50; H, 6.05; N, 9.08%. Calcd for $C_{51}H_{67}N_7O_{14}S_2$: C, 57.45; H, 6.33; N, 9.20%.

Di-N$^\delta$-tosyl-N$^\delta$-benzyloxy-L-ornithyldiglycylglycine Ethyl Ester Hydrochloride (XVI·HCl). XVI·HCl was obtained by the same procedure employed for the preparation of V·HCl; mp 196—201 °C, $[\alpha]_D$ +17.9° (*c* 1, methanol).

Found: C, 54.78; H, 5.82; N, 9.42%. Calcd for $C_{46}H_{60}N_7O_{12}S_2Cl$: C, 55.10; H, 6.03; N, 9.78%.

N$^\alpha$-t-Butyloxycarbonyl-N$^\delta$-tosyl-N$^\delta$-benzyloxy-L-ornithyldi-N$^\delta$-tosyl-N$^\delta$-benzyloxy-L-ornithyldiglycylglycylglycine Ethyl Ester (XVII). III and XVI·HCl were coupled by the same procedure employed for the preparation of IV-a; mp 192—195 °C (from methanol); $[\alpha]_D$ −5.2° (*c* 1, acetic acid).

Found: C, 58.49; H, 6.09; N, 8.67%. Calcd for $C_{70}H_{89}N_9O_{18}S_3$: C, 58.35; H, 6.23; N, 8.75%.

N$^\alpha$-t-Butyloxycarbonyl-N$^\delta$-tosyl-N$^\delta$-benzyloxy-L-ornithyldi-N$^\delta$-tosyl-N$^\delta$-benzyloxy-L-ornithyldiglycylglycine (XVIII). Hydrolysis of the hexapeptide ester (XVIII) in acetone with M sodium hydroxide was carried out by the same method employed for the hydrolysis of X; mp 122—129 °C (from methanol); $[\alpha]_D$ −2.0° (*c* 1, acetic acid).

Found: C, 57.94; H, 6.09; N, 8.87%. Calcd for $C_{68}H_{85}N_9O_{18}S_3$: C, 57.81; H, 6.07; N, 8.92%.

Tri-N$^\delta$-tosyl-N$^\delta$-benzyloxy-L-ornithyldiglycylglycine Hydrochloride (XIX·HCl). XIX·HCl was obtained by the same procedure employed for the preparation of XII·HCl; mp 188—198 °C (from ethanol); $[\alpha]_D$ +3.2° (*c* 1, acetic acid).

Found: C, 56.18; H, 5.98; N, 9.13%. Calcd for $C_{63}H_{78}N_9O_{16}S_3Cl$: C, 56.09; H, 5.83; N, 9.34%.

cyclo-Triglycyltri-N$^\delta$-tosyl-N$^\delta$-benzyloxy-L-ornithyl (XX).

i) From XII·HCl: To a solution of XII·HCl (7.8 g, (5.8 mmol) in dimethylformamide (60 ml), *N*-methyl morpholine (0.66 ml), 6.0 mmol) was added at room temperature. After stirring for 3 hr, the solution was diluted with dimethylformamide to 2 l. The diluted solution of the free base of XII·HCl was added dropwise into a solution of dicyclohexylcarbodiimide (24 g, 115 mmol) in dimethylformamide (4 l) kept at 0—5 °C under stirring over a period of 48 hr. The solution was stirred for another 4 days at room temperature and then evaporated to 200 ml *in vacuo* at 40 °C. To the residual pale yellow solution was added 50% acetic acid (30 ml) under ice cooling to remove an excess of dicyclohexylcarbodiimide as dicyclohexylurea. After 2 hr, crystalline deposit was removed by filtration and the yellow filtrate was evaporated to dryness. Further the residual oil in dimethylformamide (100 ml) was treated wtih 50% acetic acid as described above and this procedure was repeated several times. The oily residue thus obtained was solidified by addition of water. The crude product was collected and dried; yield, 9.15 g. This was dissolved in 1 l of hot methanol and the insoluble substance (550 mg) was removed by filtration. The filtrate was evaporated to dryness and the residue was redissolved in 150 ml of a mixture of dimethylformamide and water (4 : 1). The solution was successively passed through columns (5×20 cm) of CG-120 (H^+ form) and CG-400 (OH^- form). The columns were then washed with the same solvent. The combined effluents were treated with charcoal and evaporated to dryness *in vacuo*. The residue was collected with the aid of water and dried; yield, 5.8 g. Recrystallization of the product from methanol gave the cyclic hexapeptide (XX); yield, 3.1 g (41%); mp 161—167 °C; $[\alpha]_D$ −3.0° (*c* 1, chloroform); R_f 0.88 (tlc); molecular weight, 1308 (calcd 1295) (dimethylformamide as solvent). Ninhydrin reaction was negative. Recrystallization three times from methanol raised the mp to 181—182 °C.

Found: C, 58.43; H, 5.89; N, 9.48%. Calcd for $C_{63}H_{75}N_9O_{15}S_3$: C, 58.45; H, 5.84; N, 9.74%.

Identification of the methanol-insoluble substance as the dimerization reaction product, i.e. cyclo-*(triglycyltri-N$^\delta$-tosyl-N$^\delta$-benzyloxy-L-ornithyl)$_2$.* Recrystallization from acetic acid gave an analytical sample; mp 246—251 °C; R_f 0.06 (tlc); molecular weight, 2603 (calcd 2589) (dimethylformamide as solvent); yield, 550 mg (7.3%).

Found: C, 58.51; H, 5.83; N, 9.98%. Calcd for $(C_{63}H_{75}N_9O_{15}S_3)_2$: C, 58.45; H, 5.84; N, 9.74%.

ii) From XIX·HCl: XIX·HCl was converted to the free base and allowed to cyclize in dimethylformamide using excess dicyclohexylcarbodiimide as a condensing reagent as has been described above; yield, 7%; mp 172—181 °C; $[\alpha]_D$ −2.8° (*c* 1, chloroform). Dimerization product was obtained as main product; yield, 40%; mp 244—250 °C.

cyclo-*Triglycyltri-N$^\delta$-benzyloxy-L-ornithyl Hydrobromide (XXII·3HBr).* To a solution of 36% hydrogen bromide in acetic acid (32 ml) and phenol (4.0 g) in a glass-stoppered bottle, XX (3.0 g, 2.3 mmol) was added. After stirring

for 42 hr at room temperature, the solution was evaporated *in vacuo* at 30 °C. The oily residue was solidified by adding ether. The crude product collected by suction with the aid of ether was dissolved in water (200 ml). After water-insoluble materials were filtered off, the solution was washed three times with ether, treated with charcoal and then evaporated to dryness *in vacuo*. To the residual oil, ethanol was added and evaporated *in vacuo* in order to remove a trace of water. After the residual oil was solidified by the addition of anhydrous ether and collected with the aid of ether, the product (XXII·3HBr) was obtained as a hygroscopic colorless powder. The removal of tosyl group was determined by Infrared absorption spectrum; absorptions at 1350 and 1165 cm^{-1} for tosyl group were absent.

cyclo-*Triglycyltri*-N$^{\delta}$-*acetyl*-N$^{\delta}$-*benzyloxy*-L-*ornithyl* *(XXIII)*. XXII·3HBr was dissolved in a mixture of pyridine (20 ml) and acetic anhydride (1.0 ml) at 5 °C. After stirring for 12 hr at room temperature, the reaction mixture was evaporated to a syrup *in vacuo*. The residue was evaporated twice with water in order to decompose an excess of acetic anhydride. The final residue was taken up in *n*-butanol (150 ml) and the solution was repeatedly washed with water. The organic layer was treated overnight with charcoal and evaporated to dryness *in vacuo*. The residue was triturated with ether to give an amorphous product (XXIII); the over-all yield in the conversion of XX into XXIII was 47%. NMR spectrum (CD_3OD, TMS-internal standard) indicates N^{δ}-acetyl protons at δ 2.04. The signal of *O*-acetyl derivative was not detected in NMR spectrum.

cyclo-*Triglycyltri*-N$^{\delta}$-*acetyl*-N$^{\delta}$-*hydroxy*-L-*ornithyl*; *deferriferrichrome (XXIV)*. A solution of XXIII (1.0 g) in methanol (40 ml) was hydrogenated in the presence of 5% palladium charcoal (2.0 g) for 4 days at room temperature. After the catalyst was filtered off, the filtrate was evaporated *in vacuo* at 25 °C. The residue was triturated with ether to give an amorphous XXIV; the yield of the dried product, 620 mg. NMR spectrum (D_2O, TMS-external standard) indicates N^{δ}-acetyl protons at δ 2.61, β,γ-methylene protons of N^{δ}-hydroxyornithine at δ 2.25, δ-methylene protons of that at δ 4.15, α-methyne proton of that at δ 4.86 and methylene protons of glycine at δ 4.49 respectively, as shown in Fig. 8. The signals of δ 5.87 and 4.53 are those of side bands of water.

Ferrichrome (I). To the colorless solution of XXIV (500 mg) in McIlvain buffer (pH 4.6) (25 ml), M ferric chloride (2.2 ml, ca. three equivalents) was added at room temperature under continuous stirring. On addition of the ferric chloride, the reaction mixture formed a reddish-violet solution. After stirring for an additional 2 hr, the solution was completely saturated with ammonium sulfate. This solution was extracted with benzyl alcohol (600 ml × 2) and the reddish-orange benzyl alcohol layer was washed with water (100 ml × 3). Diethyl ether (3.6 l) was added to the washed benzyl alcohol solution and then the solution extracted with water (200 ml × 3). The combined aqueous extract was shaken with diethyl ether (200 ml × 3) and the ether phase discarded. The fine red aqueous solution was then evaporated to dryness *in vacuo* at 28 °C. The residual product was scratched with acetone (50 ml) and acetone-insoluble substance was collected by suction. The reddish-brown powder obtained was briefly refluxed in anhydrous methanol (120 ml), filtered and the filtrate concentrated slightly on the oil-bath. The ferrichrome (I) began to crystallize at once in long orange needles, whoes paper chromatography gave a single spot (R_f 0.28) using the solvent system of *n*-butanol–acetic acid–water (4 : 1 : 1). The yield was 85 mg; mp 248—251 °C (decomp.) determined with Melting Point Apparatus MP-21 (Yamato Scientific Co., Ltd., open capillary in silicone oil) and uncorrected; $[\alpha]_D$ $+304° \pm 10°$ (*c* 0.0425, water); $E^{1\%}_{1cm}$ (428 mμ) 39.8 in water. For analysis, a part of the product was recrystallized three times from anhydrous methanol.

Found: C, 43.26; H, 5.69; N, 16.72%. Calcd for $C_{27}H_{42}N_9O_{12}Fe$: C, 43.79; H, 5.72; N, 17.02%.

References

1) J. B. Neilands, *Struct. Bond.*, **11**, 145 (1972).
2) a) W. Keller-Schierlein, V. Prelog, and H. Zähner, *Prog. Chem. Org. Nat. Prod.*, **22**, 279 (1964). b) J. B. Neilands, *Struct. Bond.*, **1**, 59 (1966). c) H. Maehr, *Pure Appl. Chem.*, **28**, 603 (1971).
3) G. Anderegg, F. L'Eplattenier, and G. Schwarzenbach, *Helv. Chim. Acta*, **46**, 1409 (1963).
4) a) J. B. Neilands, *Bact. Rev.*, **21**, 101 (1957). b) T. F. Emery, *Advan. Enzymol.*, **35**, 135 (1971).
5) J. B. Neilands, *J. Amer. Chem. Soc.*, **74**, 4846 (1952).
6) a) A. Ehrenberg, *Nature*, **178**, 379 (1956). b) T. F. Emery and J. B. Neilands, *J. Amer. Chem. Soc.*, **82**, 3658 (1960). c) T. F. Emery and J. B. Neilands, *ibid.*, **83**, 1626 (1961).
7) a) S. Rogers, R. A. J. Warren, and J. B. Neilands, *Nature*, **200**, 167 (1963). b) S. Rogers and J. B. Neilands, *Biochemistry*, **3**, 1850 (1964).
8) M. Llinas, M. P. Klein, and J. B. Neilands, *J. Mol. Biol.*, **52**, 399 (1970).
9) a) B. Maurer and W. Keller-Schierlein, *Helv. Chim. Acta*, **52**, 388 (1969). b) W. Keller-Schierlein and B. Maurer, *ibid.*, **52**, 603 (1969).
10) Y. Isowa, T. Takashima, M. Ohmori, H. Kurita, M. Sato, and K. Mori, This Bulletin, **45**, 1461 (1972).
11) a) F. Weygand, D. Hoffman, and E. Wünsch, *Z. Naturforsch.*, **21b**, 426 (1966). b) E. Wünsch and F. Dress, *Chem. Ber.*, **99**, 110 (1966).
12) a) R. B. Woodward, R. A. Olofson, and H. Mayer, *J. Amer. Chem. Soc.*, **83**, 1010 (1961). b) R. B. Woodward, R. A. Olofson, and H. Mayer, *Tetrahedron Suppl.*, **8**, 321 (1966).
13) H. Zähner, W. Keller-Schierlein, R. Hütter, K. Hess-Leisinger, and A. Deer, *Arch. Mikrobiol.*, **45**, 119 (1963).
14) J. A. Garibaldi and J. B. Neilands, *J. Amer. Chem. Soc.*, **77**, 2429 (1955).
15) Y. Isowa, T. Takashima, M. Ohmori, H. Kurita, M. Sato, and K. Mori, This Bulletin, **45**, 1467 (1972).
16) This compound was prepared by two different methods described in the text; a) indicates *N*-hydroxysuccinimide plus *N,N*-dicyclohexylcarbodiimide method and b) indicates Woodward reagent K method. This is repeated in the preparations of VI, VIII and X.
17) The symbol, IV-a, indicates the peptide obtained by the *N*-hydroxysuccinimide plus *N,N*-dicyclohexylcarbodiimide method in the preparation of IV and IV-b indicates that obtained by the Woodward reagent K method. This is to be repeated in the following in order to ascertain whether or not the peptides obtained by the different methods possess the same optical rotation.

Studies of Peptide Antibiotics. XXXI.[1] Syntheses of *iso*-Gramicidin S and *iso*-[2,2′-Lysine]-Gramicidin S[2]

Hideo TAKIGUCHI and Nobuo IZUMIYA*

Department of Chemistry, Faculty of Science, Fukuoka University, Nanakuma, Fukuoka 814
**Laboratory of Biochemistry, Faculty of Science, Kyushu University, Hakozaki, Fukuoka 812*

(Received September 17, 1973)

Structural isomers of gramicidin S and [2,2′-lysine]-gramicidin S, namely *iso*-gramicidin S and *iso*-[2,2′-lysine]-gramicidin S, were prepared to investigate the influence of the ring size for antibacterial activity and conformation of natural gramicidin S. Each isomer involves two peptide bonds between carboxyl group of valine residue and ω-amino group of ornithine or lysine residue. Two isomers showed no antibacterial activity toward several microorganisms. In the experiment of optical rotatory dispersion, two isomers showed similar shaped curves as gramicidin S in a solvent of ethanol. In 6 M urea, the trough of two isomers was moved significantly, whereas that of gramicidin S remained constant.

In studies of relationship between ring size and antibacterial activity of gramicidin S (GS), several analogs have been synthesized.[3] As one analog with a larger ring size than GS, [β-Ala$^{5,5'}$]-GS showed entirely different ORD[4] pattern compared with that of GS and possessed no activity.[5] Recently, two macro-ring analogs of GS, namely sesquiGS and diGS, were synthesized, and the analogs showed similar ORD patterns with GS in a solvent of ethanol and possessed weak activities.[6]

In order to determine further the influence of larger ring size on the activity and the conformation, we have designed the syntheses of *iso*-gramicidin S (*iso*-GS)[7] and *iso*-[2,2′-lysine]-gramicidin S (*iso*-[Lys$^{2,2'}$]-GS) which are the structural isomers of GS and [Lys$^{2,2'}$]-GS, respectively, as shown in Fig. 1. A related analog of GS, [Lys$^{2,2'}$]-GS, was already synthesized, and the analog showed the same ORD curve and antibacterial activity as GS.[8,9]

Among many natural antibiotics with a character of cyclic peptide, it has been reported that several antibiotics involve a peptide bond participating ω-amino group of ornithine or lysine. Tamura and his collaborators reported the structure of aspochracin as *cyclo*-[δ-(−*N*-Me−Val−*N*-Me−Ala)-Orn(α-octatrienoyl)-].[10]

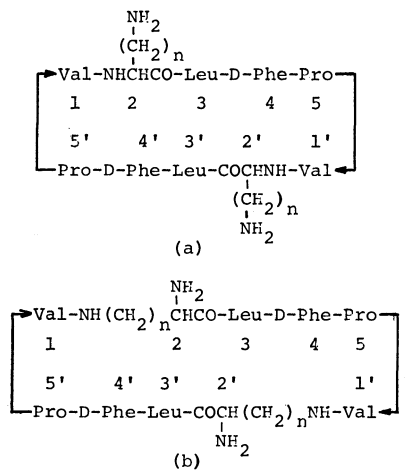

Fig. 1. Structure of gramicidin S (GS) and related peptides.
(a) GS (n=3) and [Lys$^{2,2'}$]-GS (n=4).
(b) *iso*-GS (n=3) *iso*-[Lys$^{2,2'}$]-GS (n=4).

Ressler and her collaborators presented a deduced structure of bacitracin; the antibiotic possesses a cyclic heptapeptide moiety as a partially sequence which involves a peptide bond between α-carboxyl group of asparagine residue and ε-amino group of lysine residue.[11] The present investigation would be worth as a model study to synthesize a natural antibiotic with peptide bond participating ω-amino group of α,ω-diamino acid.

Scheme 1 indicates a route for syntheses of intermediate acylpentapeptide hydrazides (V-A and V-B). Acrylpentapeptide ethyl ester (IV) was prepared without any difficulties by condensation of the azide derived from acyldipeptide hydrazide (III) and a tripeptide ester. The ester (IV) was converted into the

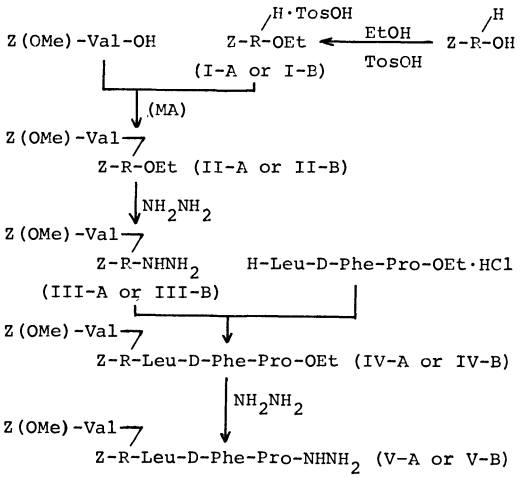

Scheme 1. Syntheses of acylpentapeptide hydrazides. V-A (R=Orn), V-B (R=Lys).

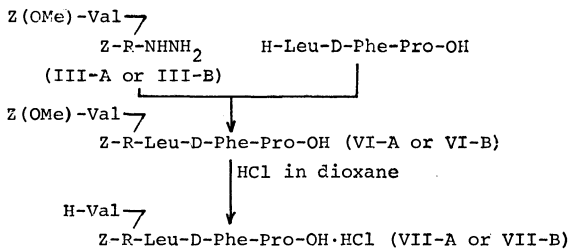

Scheme 2. Syntheses of neutral pentapeptides. VII-A (R=Orn), VII-B (R=Lys).

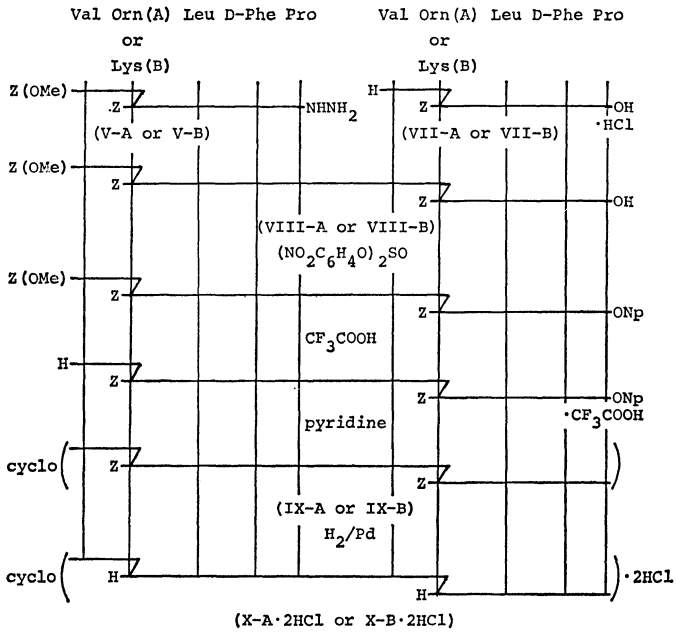

Scheme 3. Syntheses of *iso*-GS (X-A) and *iso*-[Lys$^{2,2'}$]-GS (X-B).

hydrazide (V) by the usual way. Scheme 2 indicates a sequence of reaction employed for the syntheses of another intermediates, namely free pentapeptides (VII-A and VII-B).

Scheme 3 indicates a route for syntheses of the desired cyclic decapeptides (X-A and X-B). The azide derived from Z(OMe)-pentapeptide hydrazide (V) was condensed with a neutral pentapeptide (VII), and the resulting acyldecapeptide acid (VIII) was converted into Z(OMe)-decapeptide *p*-nitrophenyl ester by the action of di-*p*-nitrophenyl sulfite. Its Z(OMe) group was removed with trifluoroacetic acid, and the resulting decapeptide ester trifluoroacetate was treated with pyridine for the cyclization reaction. The reaction mixture yielded a pure Z-substituted cyclic decapeptide (IX-A or IX-B) which was hydrogenated to afford *iso*-GS (X-A) or *iso*-[Lys$^{2,2'}$]-GS (X-B) as a crystalline dihydrochloride. The homogeneity of these cyclic decapeptides was ascertained by paper and thin layer chromatography, paper electrophoresis, and elemental analysis.

The antibacterial activities toward several microorganisms were examined. Both synthetic isomers (X-A and X-B) showed no activity for any of the microorganisms even at 100 μg/ml of the assay medium, whereas minimum concentration of growth inhibition for *Bacillus subtilis* was found to be 1—2 μg/ml with GS as a reference compound.

The ORD curves measured in a solvent of ethanol are shown in Fig. 2-a. The synthetic isomers have similarly shaped curves with a negative trough at 234 nm as GS possesses the same. In 6 M urea solution in 50% ethanol which causes denaturation of some polypeptide, the troughs of two isomers were moved to 225 nm whereas that of GS remained constant (Fig. 2-b). The results indicate that a conformation of the synthetic isomers is unstable, whereas that of GS has the rigid β-pleated sheet structure with four

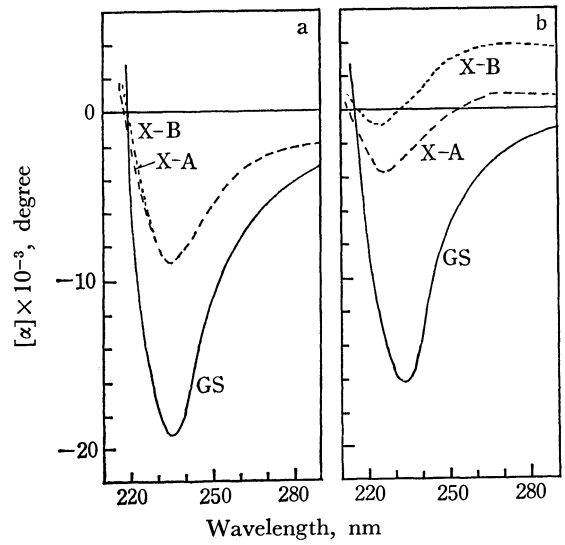

Fig. 2. ORD curves of GS and its isomers.
Solvent: a, ethanol; b, 6 M urea in 50% ethanol.

hydrogen bondings.[3] The isomers may have similar conformation as GS in a mild condition such as a solution in ethanol, but the conformation is transformed in such a urea solution. The fact that the isomers possess no antibacterial activity may be correlated to the unstableness of conformation in a certain medium.

Experimental

All melting points are uncorrected. Prior to analysis, the compounds were dried over phosphorus pentoxide to a constant weight at 80 °C and 2 mmHg except the cyclic peptides (IX-A, IX-B, X-A, and X-B). Thin layer chromatography was carried out on Merck silica gel G with the following solvent system; R_f^1, *n*-butanol-acetic acid-pyridine-water (4 : 1 : 1 : 2, v/v). Paper chromatography was carried out on Toyo Roshi No. 52 with the same solvent, R_f^2 being used.

α-Z-Orn-OEt·TosOH (I-A). This compound was prepared according to the general procedure of Kato *et al.*[12] A solution of α-Z-Orn-OH[13] (6.66 g, 25 mmol) and *p*-toluenesulfonic acid monohydrate (6.09 g, 32 mmol) in a mixture of ethanol (12 ml) and carbon tetrachloride (80 ml) was refluxed, and the water thus liberated was removed as an azeotropic mixture. The reaction mixture was concentrated *in vacuo*, and the residual oil was washed with ether and petroleum ether by decantation. The product was obtained as an oil; yield, 11.7 g (100%); R_f^1 0.77.

α-Z-Lys-OEt·TosOH (I-B). This compound was preparated from α-Z-Lys-OH[14] (5.60 g, 20 mmol) as described above. The product was recrystallized from acetone-ether; yield, 8.84 g (92%); mp 113—115 °C; $[\alpha]_D^{20}$ −7.8° (*c* 2, DMF); R_f^1 0.78.

Found: C, 57.23; H, 6.82; N, 5.77%. Calcd for $C_{23}H_{32}O_7N_2S$: C, 57.48; H, 6.71; N, 5.83%.

δ-[Z(OMe)-Val]-Orn(α-Z)-OEt (II-A). To a solution of Z(OMe)-Val-OH[15] (6.28 g, 22.3 mmol) and TEA (3.12 ml, 22.3 mmol) in tetrahydrofuran (70 ml) at −5 °C, was added isobutyl chloroformate (2.92 ml, 22.3 mmol). After 15 min, to the solution was added a mixture of I-A (10.4 g, 22.3 mmol) and TEA (3.12 ml) in chloroform (70 ml) at 0 °C. The reaction mixture was allowed to stand overnight at room temperature, and evaporated *in vacuo*. The residue was triturated with water and petroleum ether, and the

precipitate was collected by filtration. The product was washed successively with 4% sodium bicarbonate, 10% citric acid, and water. It was recrystallized from methanol-ether-petroleum ether; yield, 9.45 g (76%); mp 155—156 °C; $[\alpha]_D^{30}$ +2.4° (*c* 2, DMF); R_f^1 0.88.

Found: C, 62.83; H, 7.21; N, 7.41%. Calcd for $C_{29}H_{39}O_8N_3$: C, 62.46; H, 7.05; N, 7.54%.

ε-[Z(OMe)-Val]-Lys(α-Z)-OEt (II-B). This compound was obtained from Z(OMe)-Val-OH (4.50 g, 16 mmol) and I-B (7.69 g, 16 mmol) as described above; yield, 7.77 g (85%); mp 148—150 °C; $[\alpha]_D^{20}$ −2.1° (*c* 2, DMF); R_f^1 0.94.

Found: C, 62.72; H, 7.27; N, 7.16%. Calcd for $C_{30}H_{41}O_8N_3$: C, 63.03; H, 7.23; N, 7.35%.

δ-[Z(OMe)-Val]-Orn(α-Z)-NHNH$_2$ (III-A). A solution of II-A (7.81 g, 14 mmol) and hydrazine hydrate (13.6 ml, 280 mmol) in DMF (28 ml) was allowed to stand for 2 days at room temperature. The solution was concentrated *in vacuo* to a small volume. The hydrazide precipitated upon the addition of water (140 ml) was collected by filtration; yield, 5.81 g (76%); mp 162—165 °C; $[\alpha]_D^{31}$ −11.0° (*c* 1, AcOH).

Found: C, 59.40; H, 7.09; N, 13.29%. Calcd for $C_{27}H_{37}O_7N_5$: C, 59.66; H, 6.86; N, 12.88%.

ε-[Z(OMe)-Val]-Lys(α-Z)-NHNH$_2$ (III-B). II-B (5.15 g, 9 mmol) was converted to hydrazide (III-B) as described above; yield, 3.92 g (78%); mp 194—196 °C; $[\alpha]_D^{21}$ −13.2° (*c* 1, AcOH).

Found: C, 60.14; H, 7.32; N, 12.49%. Calcd for $C_{28}H_{39}O_7N_5$: C, 60.31; H, 7.05; N, 12.56%.

δ-[Z(OMe)-Val]-Orn(α-Z)-Leu-D-Phe-Pro-OEt (IV-A). III-A (2.17 g, 4 mmol), in a mixture of glacial acetic acid (48 ml) and N hydrochloric acid (8.8 ml), was treated with N sodium nitrite (4.4 ml) at −5 °C. After 6 min, cold water (200 ml) was added to the mixture. The azide was extracted with ethyl acetate, and the organic layer was washed with 4% sodium bicarbonate and water, and dried over sodium sulfate. The filtered solution was added to a solution of H-Leu-D-Phe-Pro-OEt·HCl[16] (1.76 g, 4 mmol) and TEA (0.56 ml) DMF (20 ml). The mixture was stirred for 3 days at 0 °C and evaporated *in vacuo* to a small volume. The precipitate which formed upon the addition of water was collected, washed with 4% sodium bicarbonate, 10% citric acid, and water, and dried. The product was recrystallized from dioxane-ether-petroleum ether; yield, 2.12 g (58%); mp 118—122 °C; $[\alpha]_D^{30}$ −18.0° (*c* 1, DMF); R_f^1 0.88.

Found: C, 64.01; H, 7.30; N, 9.16%. Calcd for $C_{49}H_{66}O_{11}N_6$: C, 64.31; H, 7.27; N, 9.18%.

ε-[Z(OMe)-Val]-Lys(α-Z)-Leu-D-Phe-Pro-OEt (IV-B). This compound was prepared from III-B (1.67 g, 3 mmol) and H-Leu-D-phe-Pro-OEt·HCl (1.32 g, 3 mmol) as described above; yield, 1.90 g (68%); mp 132—136 °C; $[\alpha]_D^{24}$ −23.6° (*c* 1, DMF); R_f^1 0.96.

Found: C, 64.42; H, 7.30; N, 9.20%. Calcd for $C_{50}H_{63}O_{11}N_6$: C, 64.64; H, 7.38; N, 9.05%.

δ-[Z(OMe)-Val]-Orn(α-Z)-Leu-D-Phe-Pro-NHNH$_2$ (V-A). A solution of IV-A (1.10 g, 1.2 mmol) and hydrazine hydrate (1.2 ml) in DMF (4.5 ml) was allowed to stand for 7 days at room temperature, and evaporated *in vacuo*. The hydrazide which precipitated upon the addition of water (40 ml) was collected and recrystallized from dioxane-ether; yield, 0.873 g (81%); mp 112—115 °C; $[\alpha]_D^{27}$ −31.4° (*c* 1, DMF).

Found: C, 62.24; H, 7.50; N, 12.13%. Calcd for $C_{47}H_{64}O_{10}N_8 \cdot 1/2H_2O$: C, 62.03; H, 7.20; N, 12.31%.

ε-[Z(OMe)-Val]-Lys(α-Z)-Leu-D-Phe-Pro-NHNH$_2$ (V-B). IV-B (1.47 g, 1.58 mmol) was converted to the hydrazide (V-B) as described above; yield, 1.23 g (85%); mp 118—120 °C $[\alpha]_D^{20}$ −28.2° (*c* 1, DMF).

Found: C, 63.25; H, 7.35; N, 12.50%. Calcd for $C_{48}H_{66}O_{10}N_8$: C, 63.00; H, 7.27; N, 12.24%.

δ-[Z(OMe)-Val]-Orn(α-Z)-Leu-D-Phe-Pro-OH (IV-A). III-A (1.63 g, 3 mmol) was converted to the azide as described for the preparation of IV-A. The azide solution in ethyl acetate was added to a solution of H-Leu-D-Phe-Pro-OH[17] (1.13 g, 3 mmol) and TEA (0.42 ml) in DMF (24 ml). The mixture was stirred for 3 days at 0 °C and evaporated *in vacuo*. To the concentrated solution was added 10% citric acid, and the oil separated was extracted with ethyl acetate. The organic layer was washed with 10% citric acid and water, and dried. The filtered solution was evaporated, and the precipitate which formed upon the addition of ether and petroleum ether was collected. It was recrystallized from ethyl acetate-petroleum ether; yield, 1.20 g (45%); mp 112—115 °C; $[\alpha]_D^{27}$ −27.8° (*c* 1, DMF); R_f^1 0.82.

Found: C, 63.34; H, 7.16; N, 9.17%. Calcd for $C_{47}H_{62}O_{11}N_6$: C, 63.64; H, 7.05; N, 9.47%.

ε-[Z(OMe)-Val]-Lys(α-Z)-Leu-D-Phe-Pro-OH (VI-B). This compound was prepared from III-B (1.95 g, 3.5 mmol) and H-Leu-D-Phe-Pro-OH (1.31 g, 3.5 mmol) as described above. The product was recrystallized from methanol-ether-petroleum ether; yield, 2.24 g (71%); mp 126—129 °C; $[\alpha]_D^{25}$ −14.6° (*c* 1, DMF); R_f^1 0.94.

Found: C, 63.53; H, 7.20; N, 9.55%. Calcd for $C_{48}H_{64}O_{11}N_6$: C, 63.98; H, 7.16; N, 9.33%.

δ-(H-Val)-Orn(α-Z)-Leu-D-Phe-Pro-OH·HCl (VII-A). To a solution of VI-A (887 mg, 1 mmol) in dioxane (10 ml), 4.8 N hydrogen chloride in dioxane (6.2 ml) was added at room temperature. After 3 hr, the solution was evaporated to dryness and the product was collected with the aid of ether; yield of a hydroscopic powder, 683 mg (90%); mp 157—164 °C; $[\alpha]_D^{20}$ −12.6° (*c* 1, DMF); R_f^1 0.71.

Found: C, 59.85; H, 7.54; N, 11.37%. Calcd for $C_{38}H_{55}O_8N_6Cl$: C, 60.11; H, 7.30; N, 11.07%.

ε-(H-Val)-Lys(α-Z)-Leu-D-Phe-Pro-OH·HCl (VII-B). VI-B (723 mg, 0.802 mmol) was converted to VII-B as described above; yield of a hygroscopic powder, 564 mg (91%); mp 137—140 °C; $[\alpha]_D^{28}$ +4.0° (*c* 0.5, DMF); R_f^1 0.73.

Found: C, 60.36; H, 7.65; N, 10.98%. Calcd for $C_{39}H_{57}O_8N_6Cl$: C, 60.57; H, 7.43; N, 10.87%.

δ-{δ-[Z(OMe)-Val]-Orn(α-Z)-Leu-D-Phe-Pro-Val}-Orn(α-Z)-Leu-D-Phe-Pro-OH (VIII-A). V-A (808 mg, 0.897 mmol) was converted to corresponding azide as described for the preparation of the azide from III-A. The azide in ethyl acetate was coupled with VII-A (681 mg, 0.897 mmol) in TEA (0.25 ml) and DMF (20 ml) as described for the preparation of VI-A. The product was recrystallized from dioxane-ether-petroleum ether; yield, 871 mg (61%); mp 150—153 °C; $[\alpha]_D^{17}$ −50.0° (*c* 0.5, DMF); R_f^1 0.80.

Found: C, 64.38; H, 7.42; N, 10.56%. Calcd for $C_{85}H_{114}O_{18}N_{12}$: C, 64.13; H, 7.22; N, 10.56%.

ε-{ε-[Z(OMe)-Val]-Lys(α-Z)-Leu-D-Phe-Pro-Val}-Lys(α-Z)-Leu-D-Phe-Pro-OH (VIII-B). This compound was prepared from V-B (641 mg, 0.7 mmol) and VII-B (541 mg, 0.7 mmol) as described above. The product was recrystallized from ethyl acetate-petroleum ether; yield, 952 mg (84%); mp 130—132 °C; $[\alpha]_D^{34}$ −34.6° (*c* 0.5, DMF); R_f^1 0.83.

Found: C, 64.35; H, 7.57; N, 10.63%. Calcd for $C_{87}H_{118}O_{18}N_{12}$: C, 64.51; H, 7.34; N, 10.38%.

cyclo-*{δ-[δ-(-Val)-Orn(α-Z)-Leu-D-Phe-Pro-Val]-Orn(α-Z)-Leu-D-Phe-Pro-} (IX-A).* To a solution of VIII-A

(637 mg, 0.4 mmol) in pyridine (8 ml), di-*p*-nitrophenylsulfite[18] (1.30 g, 4 mmol) was added. The reaction mixture was allowed to stand for 3 days at room temperature. After the solvent had been evaporated, the oily product was triturated with petroleum ether, washed repeatedly with a mixture of ether and petroleum ether (1 : 1) by decantation, and the residual solid was collected. To the solid (the *p*-nitrophenyl ester) were added anisole (0.4 ml) and trifluoroacetic acid (4 ml) at −5 °C. After 30 min, the solution was evaporated at 0 °C, and the residue was triturated with ether. A decapeptide *p*-nitrophenyl ester trifluoroacetate was collected in a cold room, washed with ether, and dried. The trifluoroacetate was dissolved in DMF (10 ml) containing acetic acid (0.4 ml), and the solution added to pyridine (200 ml) which had been kept at 60 °C over a period of 1 hr. The stirring was continued for additional 2 hr. After the solvent had been evaporated, the residue was dissolved in a mixture of methanol (150 ml) and water (50 ml). The solution was passed successively through the columns (2.5 × 12 cm, each) of Dowex 1 (OH^- form) and Dowex 50 (H^+ form). The columns were washed with the same solvent (600 ml), and the effluent was evaporated to dryness. The residual product was collected with the aid of water, and recrystallized from methanol-water; yield, 121 mg (21% from VIII-A); mp 160—163 °C; $[\alpha]_D^{10}$ −68.7° (*c* 0.3, DMF); R_f^1 0.96.

Found: C, 62.86; H, 7.75; N, 11.28%; mol wt, 1420.[19] Calcd for $C_{76}H_{104}O_{14}N_{12}\cdot 2H_2O$: C, 63.14; H, 7.53; N, 11.63%; mol wt, 1446.

cyclo-{*ε*-[*ε*-(−*Val*)−*Lys*(*α*-*Z*)−*Leu*−D-*Phe*−*Pro*−*Val*]−*Lys*(*α*-*Z*)−*Leu*−D−*Phe*−*Pro*−} *(IX-B).* VIII-B (648, 0.4 mmol) was converted to the cyclic diZ-decapeptide (IX-B) as described above; yield, 147 mg (25% from VIII-B); 222—224 °C; $[\alpha]_D^{17}$ −41.3° (*c* 0.3, DMF); R_f^1 0.98.

Found: C, 63.96; H, 7.72; N, 11.40%; mol wt, 1480.[19] Calcd for $C_{78}H_{108}O_{14}N_{12}\cdot 2H_2O$: C, 63.57; H, 7.66; N, 11.40%; mol wt, 1474.

cyclo-{*δ*-[*δ*-(−*Val*)−*Orn*−*Leu*−D-*Phe*−*Pro*−*Val*]−*Orn*−*Leu*−D-*Phe*−*Pro*−}·*2HCl* (iso-*GS Dihydrochloride*) *(X-A·2HCl).* A solution of IX-A (72 mg, 0.05 mmol) in 0.05 M methanolic hydrogen chloride (2.2 ml) was subjected to hydrogenolysis in the presence of palladium black. The filtrate from the catalyst was evaporated to dryness, and the residual solid was collected with the aid of ether; yield of an air-dried product, 44 mg (71%); mp 197—199 °C (decomp.); $[\alpha]_D^{24}$ −77° (*c* 0.2, DMF); R_f^1 0.86 and R_f^2 0.93.

Found: C, 58.02; H, 7.73; N, 13.71%. Calcd for $C_{60}H_{94}O_{10}N_{12}Cl_2\cdot 2H_2O$: C, 57.63; H, 7.90; N, 13.44%.

cyclo-{*ε*-[*ε*-(−*Val*)−*Lys*−*Leu*−D-*Phe*−*Pro*−*Val*] −*Lys*−*Leu*−D-*Phe*−*Pro*}·*2HCl* (iso-[*Lys*$^{2,2'}$]-*GS Dihydrochloride*) *(X-B·2HCl).* IX-B (64 mg, 0.0445 mmol) was converted to X-B-2HCl as described above; yield, 46 mg (78%); mp 201—203 °C (decomp.); $[\alpha]_D^{24}$ −73° (*c* 0.2, DMF); R_f^1 0.85 and R_f^2 0.95.

Found: C, 56.48; H, 8.31; N, 12.61%. Calcd for $C_{62}H_{98}O_{10}N_{12}Cl_2\cdot 4H_2O$: C, 56.65; H, 8.13; N, 12.79%.

Electrophoresis. Electrophoresis on Toyo Roshi No. 50 paper was carried out with a solvent system, formic acid-acetic acid-methanol-water (1 : 3 : 6 : 10, v/v; pH 1.8) for 3 hr at 500 V/30 cm. Figure 3 shows that mobilities of X-A and X-B were comparable with that of GS.

ORD Measurement. The measurements were performed with a Jasco Model ORD/UV 5 spectropolarimeter. Cell of path length 0.2 cm was used and the runs were made at ambient temperature. In Fig. 2 are reported the ORD curves (range 220—300 nm) of the isomers (X-A and X-B) and GS in ethanol or 6 M urea solution in 50% ethanol[20] (*c* 0.1, each).

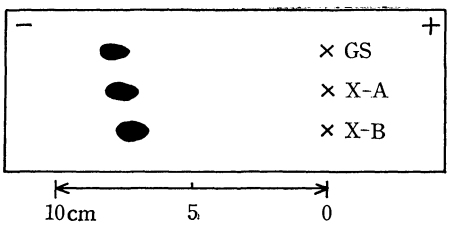

Fig. 3. Paper electrophoresis of GS and its isomers.
GS, gramicidin S; X-A, *iso*-GS; X-B, *iso*-[Lys$^{2,2'}$]-GS.

Microbiological Assays.[21] The microorganisms employed are *Escherichia coli*, *Proteus vulgaris*, *Staphylococcus aureus*, and *Bacillus subtilis*. The minimum amount of the compounds necessary for the complete inhibition of growth was determined by a dilution method in both Bouillon agar medium and synthetic medium. GS was examined as a reference compound. X-A and X-B exhibited no antibacterial activity against the microorganisms tested even at 100 μg/ml, whereas minimum concentration of GS for inhibition were 2—5 μg/ml on *S. aureus* and 1—2 μg/ml on *B. subtilis*.

The authors wish to express their thanks to Drs. T. Kato, M. Waki, and S. Matsuura of Kyushu University for helpful discussions and ORD measurements.

Rerferences

1) Part XXX: H. Sugano, H. Abe, M. Miyoshi, T. Kato, and N. Izumiya, This Bulletin, submitted.

2) Presented at the 28th Annual Meeting of the Chemical Society of Japan, Tokyo, April, 1973.

3) T. Kato and N. Izumiya, "Chemistry and Biochemistry of Amino Acids, Peptides, and Proteins", Vol. 2, ed. by B. Weinstein, Marcel Dekker, New York (1973), in press.

4) Abbreviations: Z, benzyloxycarbonyl; Z(OMe), *p*-methoxybenzyloxycarbonyl; ONp, *p*-nitrophenoxy; MA, mixed anhydride method; TEA, triethylamine; TosOH, *p*-toluenesulfonic acid; DMF, dimethylformamide; ORD, optical rotatory dispersion. Amino acid symbols except D-Phe denote the L-configuration.

5) S. Matsuura, M. Waki, S. Makisumi, and N. Izumiya, This Bulletin, **43**, 1197 (1970).

6) S. Matsuura, M. Waki, T. Kato, and N. Izumiya, *ibid.*, **46**, 977 (1973).

7) An α-isomer (H–Glu–Cys–Gly–OH) of natural glutathione (H–γ-Glu–Cys–Gly–OH) was synthesized and named as *iso*-glutathione [V. du Vigneaud, H. S. Loring, and G. L. Miller, *J. Biol. Chem.*, **118**, 391 (1937)]. In analogy with this case, we introduce the naming of *iso*-GS for X-A in Fig. 1. A structure of *iso*-GS will be described as *cyclo*{*δ*-[*δ*-(−Val)−Orn−Leu−D-Phe−Pro−Val]-Orn−Leu−D-Phe-Pro−}.

8) M. Waki, O. Abe, R. Okawa, T. Kato, S. Makisumi, and N. Izumiya, This Bulletin, **40**, 2904 (1967).

9) T. Kato, M. Waki, S. Matsuura, and N. Izumiya, *J. Biochem.* (Tokyo), **68**, 751 (1970).

10) R. Myokei, A. Sakurai, C. F. Chang, Y. Kodaira, N. Takahashi, and S. Tamura, *Agr. Biol. Chem.*, **33**, 1491 (1969).

11) E. Ratti, C. Lauinger, and C. Ressler, *J. Org. Chem.*, **33**, 1309 (1968).

12) T. Kato, S. Makisumi, M. Ohno, and N. Izumiya, *Nippon Kagaku Zasshi*, **83**, 1151 (1962).

13) E. Schröder, H. S. Petras, and E. Klieger, *Ann. Chem.*, **679**, 221 (1964).
14) B. Benzas and L. Zervas, *J. Amer. Chem. Soc.*, **83**, 719 (1961).
15) T. Kato, M. Kondo, M. Ohno, and N. Izumiya, This Bulletin, **38**, 1202 (1965).
16) M. Waki and N. Izumiya, *ibid.*, **40**, 1687 (1967).
17) N. Mitsuyasu, S. Matsuura, M. Waki, M. Ohno, S. Makisumi, and N. Izumiya, *ibid.*, **43**, 1829 (1970).
18) B. Iselin and R. Schwyzer, *Helv. Chim. Acta*, **43**, 1760 (1960).
19) Molecular weight was determined on a Hitachi Osmometer, type 115, using DMF as a solvent.
20) X-A and X-B are sparingly soluble in 8 M aqueous urea which is an usual solvent for denaturation.
21) We are indebted to the staffs of Takeda Chemical Industries, Ltd. for the assay.

The Allylic Rearrangement of Linalyl Acetate in the Medium of Acetic Acid, Propionic Acid, or Acetic Acid Containing Dioxane or Sulfuric Acid

Kunio KOGAMI and Ju KUMANOTANI

T. Hasegawa Co., Ltd, Nihonbashi, Chuo-ku, Tokyo 103

Engineering Research Institute, Faculty of Engineering, The University of Tokyo, Yayoi, Bunkyo-ku, Tokyo 113

(Received May 9, 1973)

The mechanism of the allylic rearrangement of linalyl acetate in the medium of acetic acid, propionic acid, or acetic acid containing dioxane or sulfuric acid has been investigated. The nature of the carbonium-ion pairs generated from linalyl acetate in low-dielectric-constant solvents or in strong acids, and the behavior of the active intermediate in the transition state were postulated from the kinetic data as well as from the physicochemical properties and distributions of the products.

It has been well known that linalyl acetate (designated as LA), an ester of tertiary monoterpene alcohols, is isomerized through allylic rearrangement. Young and Webb[1] isomerized LA to geranyl acetate in acetic acid (designated as HOAc) containing phosphoric acid (0.1 mol H_3PO_4), and Crabalona[2] to geranyl- and terpinyl acetate, geraniol, terpineol, and terpene hydrocarbons in HOAc containing 5 volume percent of water.

The foregoing studies gave qualitative results, but no quantitative data relating to the mechanism of the rearrangement or to the product distribution are available. In order to clarify the reactivity of LA in non-aqueous solvents containing HOAc, we have investigated rearrangements in the medium of HOAc, propionic acid, and HOAc containing dioxane or sulfuric acid.

The present paper discloses how the rearrangement of LA in the medium of HOAc or HOAc–dioxane has been found to be an S_N1-type solvolytic reaction[3] accompanied by both allylic rearrangement[4] and the common ion effect of the acetate anion.[5] In the case of propionic acid, the rearrangement followed a pseudo-first-order condition. An internal return[6] was postulated from the formation of racemized linalyl propionate *via* an intimate ion pair[7] which had formed among a carbonium ion, an acetate anion, and a propionic acid molecule. A typical acid-catalyzed A1 reaction[8–10] was found in the medium of HOAc containing sulfuric acid.

Experimental

Materials. LA prepared by the acetylation of linalool with ketene[11,12] was supplied by T. Hasegawa Co., Ltd; its purity was analyzed by gas-liquid chromatography (designated as glc and found to be 100%: n_D^{30} 1.4501, d_{30}^{30} 0.9050, bp 88—89 °C/4 mmHg, $[\alpha]_D^{25}$ −7.6° (optical purity 96%). Commercially-available reagents of a chemical pure grade were used in this study. HOAc free from moisture was obtained by the Noyce method[13] (bp 119 °C). Dioxane, which had been refluxed with metallic sodium for 8 hr beforehand, was rectified (bp 101 °C). Sodium acetate was dehydrated by the usual method. *o*-Nitroaniline was recrystallized from ethanol (mp 71 °C).

Measurement of the Acidity Function H_0. The acdity function, H_0, was estimated by spectrophotometry for each medium–LA–HOAc, HOAc–dioxane, and HOAc–sulfuric acid; we then calculated according to the following equation:

$$H_0 = \log (C_B/C_{BH^+}) + pk_a$$

where C_B and C_{BH^+} are the concentrations of the indicator used, *o*-nitroaniline ($pk_a = -0.17$, $\varepsilon = 5000$), and the conjugated acid respectively, both of which values were obtained at 412 mμ.[14] The measurements were carried out at 30 °C, and the density of HOAc was found to be d_{30}^{30} 1.0380.

Estimation of the Reaction Rate. *1) Rearrangement in HOAc*: A mixture (20 ml) of LA and HOAc in a given ratio (10 : 90, 20 : 80 or 30 : 70 vol%) was ampouled in cleaned glass tubes (30 ml) and then dipped at once into an oil bath kept at a desired temperature (80, 100, or 120 °C). At prescribed intervals an ampoule was taken off from the bath and cooled to room temperature with water. The reaction product was poured into 200 ml of ice water, neutralized with a 10% aqueous solution of sodium carbonate, saturated with sodium carbonate, saturated with sodium chloride, and then extracted several times with 100-ml portions of ether. The extracts were then put together and dried over sodium sulfate. An oily matter obtained after the removal of the ether was weighed, and the composition was analyzed by glc using an internal standard method using methyl caprylate. In order to determine the amount of polymeric material present, oily products simultaneously collected from several amouples were distilled *in vacuo* by means of a micro Claisen flask.

The rate constant (k) of the rearrangement was calculated according to the following equation:

$$k = 2.303 \log (a/(a-x))/t$$

where a is the initial concentration of LA and where a–x is the concentration at time t.

2) Rearrangement in the Medium of HOAc Containing Dioxane: A mixture (50 ml) of HOAc and dioxane in a given ratio (90 : 10, 80 : 20, or 70 : 30 vol%) containing 1 ml of LA (0.0046 mol) was ampouled in a glass tube (60 ml) and then placed in a thermostated oil bath at a desired temperature (80, 90, or 100±0.1 °C).

3) Rearrangement in Propionic Acid: LA and propionic acid were ampouled in glass tubes (60 ml) in a given ratio 10 : 90 vol%). The ampoules were kept in a thermostat (100±0.1 °C) for a precribed time.

4) Rearrangement in the Medium of HOAc Containing Sulfuric Acid: A mixture (50 ml) of 90% HOAc and sulfuric acid, the acidity function of which is known,[14] containing 1 ml of LA was put into a 100-ml Erlenmeyer flask. The flask was then closed with a stopper, placed in a thermostat regulated at 0±0.01 °C, and reacted while being stirred with a magnetic stirrer.

Identification of Products. The reaction products, such as LA, *d*-α-terpinyl,[15] neryl- and geranyl acetates, racemized linalool, and linalyl propionates, were separated by distillation with a spinning-band-type column (dia. 6 mm; length 1.5 m) and by preparative gas liquid chromatography

Table 1. Rearrangement of LA in HOAc

Reaction time (min)	T.H. Total	T.H. Comp.	Composition of product (%) LA (a)	TA	NA	GA	Dist. residue	Total yield (%) (b)	LA theor. (a)×(b)	Remarks
		M 8.7								
20	11.0	L 1.3	74.0	4.0	4.0	5.6	1.4	92.1	69.1	Reaction temp.; 80 °C.
		O 0.7								HOAc; 90 vol% (15.57 mol).
		T 0.3								LA; 10 vol% (0.5 mol).
		M 9.7								log C (HOAc) = 1.19
40	12.7	L 1.8	58.4	4.2	4.3	16.2	4.2	90.2	52.6	$H_0 = +1.02$.
		O 0.9								Optical purity $[\alpha]_D^{25}$
		T 0.3								LA (−6.8°); TA (+17°)
		M 10.2								k_1 (mean) = 0.000282 l/s.
60	15.7	L 3.9	42.4	8.5	10.9	18.2	5.0	87.9	37.3	
		O 1.0								
		T 0.6								
		M 10.3								
90	18.1	L 5.6	25.2	10.6	10.9	30.1	5.1	88.2	22.2	
		O 1.0								
		T 1.2								
		M 5.0								
90	7.0	L 1.3	78.0	4.2	4.2	6.2	0.4	90.2	70.2	Reaction temp.; 80 °C
		O 0.6								HOAc: 70 vol% (12.11 mol).
		T 0.1								LA; 30 vol% (1.5 mol).
		M 7.2								log C (HOAc) = 1.08.
180	10.6	L 2.4	68.0	4.2	4.3	11.3	1.6	90.0	61.3	$H_0 = +1.09$.
		O 0.8								Optical purity $[\alpha]_D^{25}$
		T 0.2								LA (−7.0°).
		M 7.9								k_1 (mean) = 0.0000481 l/s.
285	11.6	L 2.5	55.4	4.6	6.4	18.2	3.6	89.1	49.3	
		O 1.0								
		T 0.4								
		M 8.6								
360	12.9	L 2.7	47.5	5.8	7.6	21.2	5.0	88.3	41.9	
		O 1.2								
		T 0.4								
		M 5.6								Reaction temp.; 120 °C.
5	11.2	L 4.6	48.8	3.6	7.8	25.1	3.1	89.2	43.4	HOAc; 90 vol% (15.57 mol).
		O 0.8								LA; 10 vol% (0.5 mol).
		T 0.2								log C (HOAc) = 1.19
		M 6.8								$H_0 = +1.02$.
10	14.6	L 6.6	22.0	10.4	12.8	33.2	7.0	86.8	19.1	Optical purity $[\alpha]_D^{25}$
		O 0.9								LA (−6.4°).
		T 0.3								k_1 (mean) = 0.00257 l/s.
		M 7.0								
20	15.5	L 7.1	8.4	11.8	14.7	40.8	8.8	86.3	7.3	
		O 1.0								
		T 0.4								
		M 7.8								
20	12.0	L 3.8	53.5	5.1	9.5	16.5	3.4	87.8	49.1	Reaction temp.; 120 °C.
		O 0.4								HOAc; 70 vol% (12.11 mol).
		T 0								LA; 30 vol% (1.5 mol).
		M 8.2								log C (HOAc) = 1.08.
40	13.6	L 4.4	28.3	7.3	13.2	30.7	7.0	86.2	24.3	$H_0 = +1.09$.
		O 0.8								Optical purity $[\alpha]_D^{25}$
		T 0.2								LA (−6.9°).
		M 8.6								k_1 (mean) = 0.000589 l/s.
60	15.1	L 5.4	14.1	8.1	15.9	38.6	8.2	86.0	12.1	
		O 0.8								
		T 0.3								

Inscriptions for terpene hydrocarbons (TH): Myrcene-M, limonene-L, ocimene-O, terpinolene-T; for acetate: Linalyl acetate-LA, terpinyl acetate-TA, neryl acetate-NA, geranyl acetate-GA. Product distributions at 100 °C and in 80 vol% of HOAc are abbreviated owing to the same tendency as the others.

according to demand; they were identified by comparing the NMR, IR, and mass spectra with those of an authentic sample.[11,12] Terpene hydrocarbons, such as myrcene, limonene, β-trans-ocimene,[16] and terpinolene, were identified by comparing the mass spectra and the retention times on gas chromatography with those of the authentic samples described in the previous paper.[11,12]

Analyses of Composition. The composition of the rearrangement products of LA obtained in the prescribed medium were analyzed by glc by the internal standard method using methyl caprylate. The calibration curves of components were obtained in the usual way. Thus, LA, for instance, was analyzed within the relative experimental error of ±0.5%, and the other components, within ±1.0% A 2-m stainless steel column (dia. 3 mm) packed with Rac-2R-446 (10 wt%) on Celite 545 sk of 60—80 mesh was used. The operating conditions of the gas chromatograph (Kotaki GU-21): column temperature, 150 °C; flash evaporator, 220 °C; carrier gas, (helium); flow rate, 22 ml/min. In the case of the medium of propionic acid or HOAc containing sulfuric acid, only LA was analyzed by the internal standard method, using methyl caprylate and other components and the area ratio method.

Calculation of the Total Energy of Carbonium Ions. The total energy was calculated for a few typical carbonium ions by Hoffmann's Extended Hückel Molecular Orbital Method.[17] In determining the geometry, the following assumptions were used:

1) *Bond Length*: C–C (1.541 Å), C–C, adjacent to double bond (1.53 Å), C=C (1.337 Å), C–H, monosubstituted (1.101 Å), C–H, disubstituted (1.073 Å), C–H, trisubstituted (1.070 Å), C–H, olefinic (1.071 Å).

2) *Bond Angle*: The bond angle between C=C and C–C is 120 °C; the one between two C–C, 109.5 °C; the one of a charged C atom in the plane sp^2 hybrid structure, 120 °C.

A method of charge iteration was incorporated in the Kikuchi-Konakahara-Ishihara EHMO (Extended Hückel Molecular Orbital) program.[18] For the calculation, a HITAC 5020 computer at the Tokyo University Computer Center was used.

Results and Discussion

Previously we reported that LA prepared by acetylation with acetic anhydride, using sodium acetate or phosphoric acid as a catalyst, is rearranged with ease, and that the rearrangement proceeds from HOAc originating in the acetylation and is accompanied by various by-products as well.[11] The latter fact led us to study the preparation of LA as pure as possible. Thus, it has been found that a method of acetylating linalool with ketene in the presence of phosphoric acid gives neither HOAc nor by-products.[11] In order to reveal the mechanism of rearrangement in LA, the following Reactions (1)—(4) were examined.

Table 2. Rate constants k_1 (1/s) of rearrangement of LA in HOAc

HOAc	80 °C	100 °C	120 °C
90 vol%	2.82×10^{-4}	9.58×10^{-4}	2.57×10^{-3}
80 vol%	1.26×10^{-4}	4.37×10^{-4}	1.45×10^{-3}
70 vol%	4.81×10^{-5}	1.50×10^{-4}	5.89×10^{-4}

Remarks: HOAc 90 vol% (15.57 mol)-LA 10 vol% (0.5 mol)
HOAc 80 vol% (13.84 mol)-LA 20 vol% (1.0 mol)
HOAc 70 vol% (12.11 mol)-LA 30 vol% (1.5 mol)

(1) Rearrangement of LA in HOAc. The results obtained under controlled conditions were as follows. The rates of rearrangement in HOAc were found to be of the first order in any of the concentrations examined on LA (Table 1). The rate contant increased with an increase in both the concentration of HOAc and the reaction temperature (Table 2). Ratios of logarithm of the rate constant against that of the molar concentration of HOAc yield straight lines, with the slope varying from 5.0 to 7.0 (order of solvent participation).[3] This fact proves that the rearrangement of LA in HOAc is an S_N1-type solvolytic reaction. The ionization of LA to carbonium-ion pairs is assumed to result from a solvation due to the formation of hydrogen bonds among a carbonium ion, and an acetate anion and some HOAc molecules. The Arrhenius plots of log k_1 *versus* $1/T$ gave straight lines. The estimated activation energy ranged from 15.00 to 17.20 kcal/mol, and the entropy of activation, from −34.8 to −31.5 e.u. As the concentration of HOAc increases, both the activation energy and the entropy decrease as follows:

HOAc vol%	LA vol%	ΔE kcal/mol	ΔS^* (e.u.) 120 °C	100 °C	80 °C
70	30	17.20	−34.7	−32.4	−31.9
80	20	16.65	−31.9	−31.7	−31.5
90	10	15.00	−34.8	−34.6	−34.6

The results indicate that the carbonium-ion pairs are easily formed in the transition state, and that the formation of a solvent shell due to the surrounding acetic acid molecules diminishes the degree of freedom to react.

The above discussion is based on the apparent kinetical data; however, the product distribution in the rearrangement should be considered as well. The compositions of the rearrangement products were analyzed by glc by the internal standard method using methyl caprylate. The calibration curves of the components,

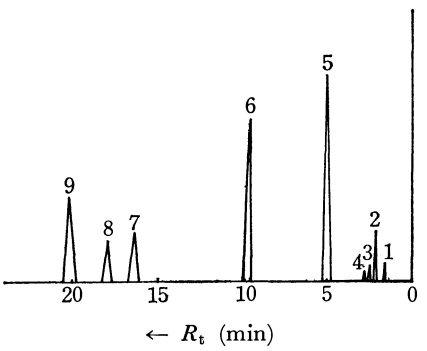

Fig. 1. A typical gas chromatograms of the products in a rearrangement.
1: myrcene, 2: limonene, 3: ocimene, 4: terpinolene, 5: methyl caprylate, 6: LA, 7: terpinylacetate, 8: neryl acetate, 9: geranyl acetate.

such as LA, terpinyl-, neryl-, geranyl acetates and terpene hydrocarbons (the mixture of myrcene, limonene, ocimene and terpinolene was found to have the ratio of 1 : 2 : 1 : 0.2), were obtained by the usual way. All the curves referring to the area ratio against the weight ratio of these compounds to methyl caprylate showed a linear relationship. The products estimated from the gas chromatograms (Fig. 1) were as follows: partially racemized (10—15%) LA, acetates of geranyl, neryl, and the more racemized (65—70%) *d*-α-terpinyl, myrcene, limonene, β-*trans*-ocimene and terpinolene. The degrees of racemization in the LA and terpinyl acetate separated by preparative glc were estimated by the loss of optical purity (Table 1). The partial racemization of LA suggests a much higher stereospecificity for the return from the carbonium-ion pair to LA than for the solvent (HOAc) collapes.[4] On the other hand, the remarkable racemization of terpinyl acetate ($[\alpha]_D^{25}$ of pure acetate, +52.5°) shows a preferential collapse of the terpinyl-carbonium ion with the solvation shell of HOAc.

The amounts of acetates resulting from the allylic rearrangement were found to be in the following order:

geranyl > neryl > linalyl > terpinyl

The acetates of geranyl (*trans*) and neryl (*cis*) were considered to be derived from the primary terpenoid carbonium ion and the *d*-α-terpinyl acetate, from the tertiary terpenoid carbonium ion. The product distribution is proportional to the instability of the following carbonium ions, disclosing that the labile carbonium ions are more reactive:[19]

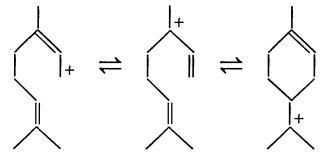

carbonium ion geranyl linalyl terpinyl

As the terpinyl carbonium ion is considered to be the most stable one of the four, the total energies of the other two typical carbonium ions (geranyl and linalyl) were calculated by Hoffmann's EHMO Method (Figs. 2—3). The instability of these carbonium ions was found to be in the following order;

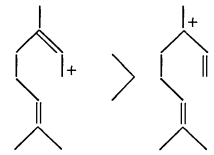

carbonium ion	geranyl	linalyl
eV	−983.724	−984.322

This order well agrees with the results mentioned above.

The acetates of geranyl, neryl, and terpinyl obtained were not further isomerized in HOAc under the same conditions (Table 1, Remarks column). This indicates that; 1) these acetates are directly formed by the alkyl fission of LA *via* carbonium ions, and 2) the rearrangement of LA may be promoted by the delocalization of the tertiary carbonium ions due to the allyl group.

An E_1-type elimination was found to be accompanied

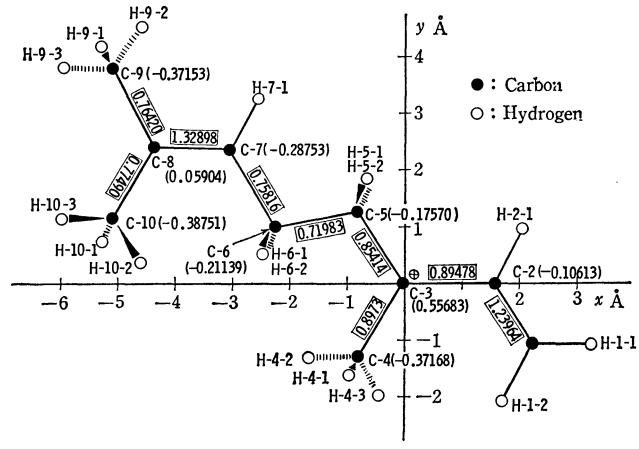

Fig. 2. Calculation on the total energy of a linalyl carbonium ion.
Total energy: −984.3220 eV.
Numerals in ( ) refer to formal charge and those in ▭ to bond population.

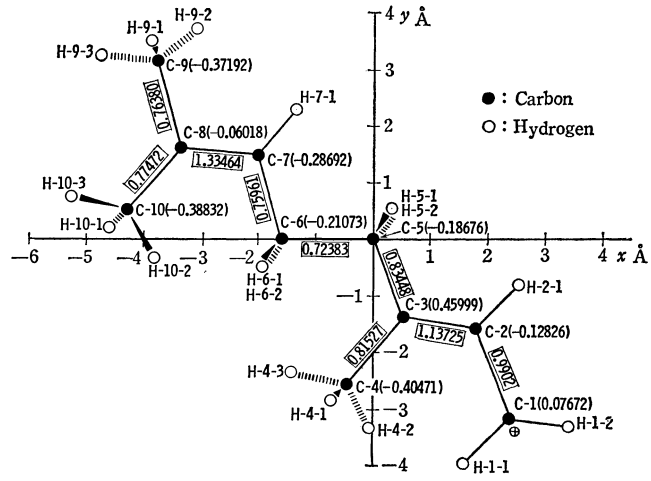

Fig. 3. Calculation on the total energy of a geranyl carbonium ion.
Total energy: −983.7244 eV.

by a S_N1-type solvolytic reaction. The elimination products amounted to as much as 20% of the total. They were terpene hydrocarbons, such as myrcene, limonene, ocimene, and terpinolene, which were also considered to be derived from the above carbonium ions. Even at relatively lower concentrations of HOAc as well as at lower reaction temperatures and in the eary stages of the rearrangement, a great deal of myrcene was found, together with a small amount of limonene, ocimene, and terpinolene. However, the amount of limonene nearly increased with the concentration of HOAc as well as with the advance of the reaction. As a result, the main product under the conditions of an S_N1-type solvolytic reaction was found to be the above-described primary acetates (geranyl and neryl), while the main products of an E_1-type elimination was myrcene. The latter result agrees well with the fact that acetates of geranyl and neryl are broken down to form myrcene in an electron-impact elimination.[12]

For studying the common ion effect charcteristic of the S_N1-type solvolytic reaction, LA was isomerized

Table 3. Rearrangement of LA in the medium of HOAc containing sodium acetate

	Reaction time (hr)	Composition of products (%) TH	LA	TA	NA	GA	Residue	Yield (%)
A	0.5	15.0	54.1	8.8	4.1	15.4	2.6	89.0
	1.0	18.5	45.3	10.8	6.7	14.0	4.7	88.1
			$[\alpha]_D^{25}$ −7.2°					
B	0.5	10.1	76.4	3.4	2.8	6.2	1.1	92.0
	1.0	10.6	74.0	4.5	2.8	6.3	1.8	91.2
			$[\alpha]_D^{25}$ −7.4°					
C	0.5	15.7	52.7	7.4	5.4	15.0	3.8	90.1
	1.0	19.7	30.1	9.3	7.1	27.5	6.5	89.1
			$[\alpha]_D^{25}$ −7.0°					

Remarks: Reaction temperature; 120 °C. A; LA (1.0 mol)-HOAc (3.34 mol)-sodium acetate (0.5 mol). B; LA (1.0 mol)-HOAc (3.34 mol)-sodium acetate (1.5 mol). C; LA (1.0 mol)-HOAc (3.34 mol). Inscriptions for terpene hydrocarbons, TH; for acetates; linalyl acetate, LA; terpinyl acetate, TA; neryl acetate, NA; geranyl acetate, GA.

in the medium of HOAc containing sodium acetate, and was estimated by glc on the basis of the product distribution. The effect seems to suppress the ionization of LA to carbonium ion pairs qualitatively. Table 3 shows the results obtained. The optical purity of LA was almost the same before and after the reaction. It may be postulated that nucleophilic acetate anions dissociated from sodium acetate are attracted to coordinate intimately with the carbonium ion of LA, resulting in the prevention of coordination with the neutral HOAc molecules.

(2) Rearrangement of LA in the Medium of HOAc containing Dioxane. It is well known that a carbonium ion is coordinated from the back with a dioxane molecule.[3] Consequently, dioxane is considered to be a suitable solvent for studying the specific solvation of HOAc. The rearrangement of LA in the medium of HOAc containing dioxane was found to be of the first order with respect to the concentration of LA. The rates constants and the product distributions estimated in the same manner as (1) are summarized in Tables 4 and 5. In the straight lines giving the correlation between the logarithm of the concentration of HOAc and that of the rate constant, the slopes of the lines ranged from 7.3 to 7.5 (the value corresponds to the order of solvent participation).[3] Thus, the rearrangement in this case can be classified as an S_N1-type solvolytic reaction. The plots of the Arrhenius equation relating to log k_1 and $1/T$ gave straight lines. The estimated activation energy changed from −15.41 to −20.63 kcal/mol; however, no linearity was found with the concentration of HOAc as follows:

HOAc vol%	Dioxane vol% (mol. fr.)	ΔE kcal/mol	ΔS^* (e.u.) 100 °C	90 °C	80 °C
45	5 (0.07)	15.41	−34.1	−34.5	−33.7
40	10 (0.14)	20.63	−22.1	−21.7	−21.9
35	15 (0.21)	19.67	−25.7	−26.2	−25.6

LA, 1 vol%, 0.0046 mol.

The value increased nearly parallel with the increase in the molar fraction (up to 0.14) of dioxane, and then decreased. This may be explained in terms of the specific solvation of a polar solvent, HOAc, in the mixed system.[4] In spite of the presence of an actual rearrangement, the well reservation in the optical purity of LA proves that the coordination of dioxane to a carbonium ion eventually occurred from the back alone (Table 4). The entropy of activation, which ranged from −34.5 to −21.7 e.u., also discloses that the solvation of HOAc to a carbonium ion is much stronger than that of dioxane. The smaller effect of dioxane on the solvation in the medium of HOAc containing dioxane resulted also in a product distribution similar to that in the medium of HOAc (Table 4).

(3) Rearrangement of LA in Propionic Acid. There is no available means to prove the reverse reaction, in which a LA molecule returns *via* the carbonium ion or the ion pairs to the original LA in the foregoing system (1)—(2). Thus, the rearrangement of LA in propionic acid was examined. Table 6 gives the results obtained. The kinetics of the rearrangement were found to follow the first-order rate law with respect to the concentration of LA. As products, not only propionates of linalyl, geranyl, neryl, and terpinyl, but also acetates of the same terpene alcohol, were obtained, together with some terpene hydrocarbons. Among the products, only linalyl

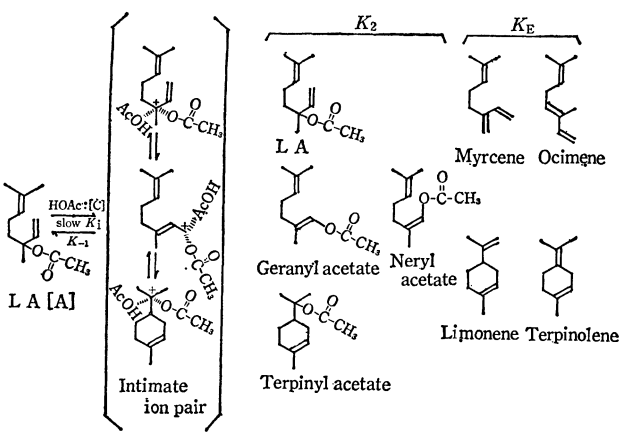

Fig. 4. Postulated mechanism on the rearrangement of LA in HOAc.

Table 4. Rearrangement of LA in the medium of HOAc containing dioxane

Reaction time (min)	TH Total	TH Comp.	LA (a)	TA	NA	GA	Dist. residue	Total yield (%) (b)	LA theor. (a)×(b)	Remarks
		M 1.9								
7	2.1	L 0.1	78.9	4.1	3.5	10.5	1.0	92.3	72.8	Conc.; vol% mol
		O 0.1								HOAc 45 15.57
		T 0								Dioxane 5 1.13
		M 2.2								LA 1 0.0046
14	3.0	L 0.4	58.0	7.1	6.7	22.9	2.3	88.8	51.5	Reaction temp.; 100 °C.
		O 0.4								$H_0=+0.84$. log C (HOAc)
		T 0								$=1.19$.
		M 4.8								Optical purity $[\alpha]_D^{25}$:
21	6.8	L 1.2	41.2	13.4	10.7	24.9	3.0	89.6	36.1	LA (−7.0°); TA (+17.2°).
		O 0.6								k_1 (mean) $=0.000785$ 1/s.
		I 0.2								
		M 1.0								
10	1.2	L 0.1	88.9	1.9	1.9	5.8	0.3	94.1	83.9	Conc.: vol% mol
		O 0.1								HOAc 40 13.84
		T 0								Dioxane 10 2.27
		M 1.2								LA 1 0.0046
20	2.0	L 0.4	79.6	3.6	5.4	8.2	1.0	94.0	74.8	Reaction temp.; 100 °C
		O 0.4								$H_0=+0.96$. log C (HOAc)
		T 0								$=1.14$.
		M 2.6								Optical purity $[\alpha]_D^{25}$:
30	3.9	L 0.7	69.8	5.0	7.0	12.7	1.6	92.2	64.4	LA (−7.2°).
		O 0.5								k_1 (mean) $=0.000260$ 1/s.
		T 0.1								
		M 0.8								
10	1.0	L 0.1	95.9	0.5	1.0	1.3	0.3	94.3	90.4	Conc.: vol% mol
		O 0.1								HOAc 35 12.11
		T 0								Dioxane 15 3.40
		M 3.6								LA 1 0.0046
20	4.3	L 0.4	88.1	1.1	1.6	4.6	0.3	94.4	83.2	Reaction temp.; 100°C.
		O 0.3								$H_0=+1.04$. log C (HOAc)
		T 0								$=1.08$.
		M 5.1								Optical purity $[\alpha]_D^{25}$:
40	6.2	L 0.6	79.9	2.1	3.0	8.2	0.5	90.6	72.2	LA (−7.3°); TA (+18°).
		O 0.5								k_1 (mean) $=0.000150$ 1/s.
		T 0								
		M 9.1								
80	10.9	L 1.0	55.1	4.6	7.8	19.5	2.0	91.0	50.1	
		O 0.6								
		T 0.2								

Inscriptions for terpene hydrocarbons and acetates are the same as those in Table 1.
Product distributions at 80 and 90 °C are abbreviated owing to the same tendency as those at 100 °C.

Table 5. Rearrangement rate constants k_1 (1/s) of LA in the medium of HOAc containing dioxane

Medium						Reaction temperature (°C)		
HOAc		Dioxane		LA				
vol%	mol	vol%	mol	vol%	mol	80	90	100
45	15.57	5	1.13	1	0.0046	2.45×10^{-4}	3.10×10^{-4}	7.85×10^{-4}
40	13.84	10	2.27	1	0.0046	5.48×10^{-5}	1.40×10^{-4}	2.60×10^{-4}
35	12.11	15	3.40	1	0.0046	3.40×10^{-5}	5.64×10^{-5}	1.50×10^{-4}

propionate was found to be racemized. This fact suggests that a leaving-group acetate anion was rather closely associated with a carbonium ion (linalyl) to form an intimate ion pair, and that a selective internal return[6] resulted in the products obtained. This interesting finding reflects the structure of the intimate ion pairs as well as the varieties of the activated intermediate in the transition state.

The same phenomenon can be expected to occur in the rearrangement of LA in the medium of HOAc, because the former system has a dielectric constant and pk_a similar to those in the medium of propionic acid.

Based on the preceding results, the kinetic and mechanism of the rearrangement of LA in HOAc can be postulated to be as follows (Fig. 4):

$$v = k_1(C)^x(A)k_2(C)/(k_{-1}+k_2(C)+k_E)$$

k_{-1} or k_E = very small $\ll k_2(C)$.

$$v = k_1(C)^x(A).$$

TABLE 6. REARRANGEMENT OF LA IN PROPIONIC ACID

Reaction time (min)	TH Total	TH Compos.	LA (a)	Composition of products (%) LP	TA	NA	GA	TP	NP	GP	Yield total (b) (%)	LA theor. (a×b)
45	4.1	M 1.5 L 2.5 O 0.2 T 0	77.3	3.3	0.4	3.4	5.7	0.2	1.5	4.0	94.2	72.9
90	11.4	M 4.4 L 6.5 O 0.3 T 0.2	65.0	3.8	0.7	3.9	6.1	0.5	2.0	4.6	90.0	58.5
180	17.2	M 7.5 L 8.9 O 0.7 T 0.4	40.4	5.9	1.8	6.3	14.1	1.6	4.3	8.1	85.2	35.4

Remarks: Reaction temp; 100 °C. Propionic acid; 90 vol% (12.16 mol). LA; 10 vol% (0.5 mol).
Inscriptions for tepene hydrocarbons-TH; myrcene-M, limonene-L, ocimene-O, terpinolene-T, for acetates; linalyl acetate-LA, terpinyl acetate-TA, neryl acetate-NA, geranyl acetate-GA for propionates; linalyl propionate-LP, terpinyl propionate-TP, neryl-propionate-NP, geranyl propionate-GP. Optical purity $[\overset{25}{D}]$ of the composition of products (180 min); (−7.3), LP (0 °). k_1 (mean) = 0.00010 l/s.

TABLE 7. REARRANGEMENT OF LA IN THE MEDIUM OF HOAc CONTAINING SULFURIC ACID

Reaction time (s)	TH Total	TH Comps.	Composition of products (%) L	LA (a)	T	TA	NA	GA	Yield (%) Total (b)	LA theor. (a)×(b)	Remarks
35	10.6	M 4.0 L′ 5.6 O 0.3 T′ 0.7	9.6	58.9	3.8	5.0	3.2	8.9	92.4	54.4	Reaction temp.; 0 °C. Medium; 90% HOAc-0.8 mol H_2SO_4. H_0; −1.53
60	12.5	M 4.6 L′ 6.3 O 0.6 T′ 1.0	16.7	43.1	5.7	9.1	3.1	9.8	90.4	38.9	LA; 0.0046 mol. Optical purity $[\alpha]_D^{25}$ L (0°). T (+12.9°) k_1 (mean) = 0.01674 l/s.
90	12.8	M 4.7 L′ 6.5 O 0.6 T′ 1.0	26.0	23.8	7.0	15.1	5.3	10.0	90.3	21.9	

Inscriptions for terpene hydrocarbons-TH; myrcene-M, limonene-L′, ocimene-O, terpinolene-T′., for alcohols; linalool-L, terpineol-T, and for acetates; linalyl acetate-LA, terpinyl acetate-TA, neryl acetate-NA, geranyl acetate-GA
Product distributions in 90% HOAc-0.6 mol H_2SO_4 and 90% HOAc-0.4 mol H_2SO_4 are abbreviated owing to the same tendency as the above one.

(4) Rearrangement of LA in the Medium of HOAc Containing Sulfuric Acid, The rearrangement was found to follow the first-order rate law with respect to the concentration of LA. It corresponds to a typical acid-catalyzed A1 reaction, because it shows such a linearity as gives a slope of 1.0 based on the correlation of log k_1 against H_0.[8-10] The following products were obtained: racemized linalool ($[\alpha]_D^{25}$ = 0°), *d*-α-teripneol ($[\alpha]_D^{25}$ = +12.9°), acetates of linalyl, terpinyl, neryl and geranyl, myrcene, limonene, ocimene, and terpinolene (Tables 7, 8, and Fig. 5). The amount of cyclized products, such as terpinyl acetates, terpineol, limonene, and terpinolene, which are considered to be derived *via* a cyclized tertiary carbonium (terpinyl), exceeded that obtained in other solvents. The results agree with the fact that monoterpenoids are readily cyclized in a strong acid.[20,21] No primary terpene alcohols, such as geraniol or nerol, could be found. This proves that the behavior of carbonium ions in a strong acid undoubtedly differs from that in a weak acid, and that a tertiary carbonium ion in a strong acid medium is more stable and reactive than in a weak one.

Lately, Winstein *et al.*[22] reported that the solvolysis of optically-active linalyl *p*-nitrobenzoate in 70% aqueous acetone at 50, 75, and 100 °C was accompanied by a S_N2' reaction to geranyl *p*-nitrobenzoate, neryl *p*-nitrobenzoate, and *d*-α-terpinyl *p*-nitrobenzoate (50—90% optical active, temperature-dependent) as well as terpene hydrocarbons (myrcene, limonene, γ-terpinene, and terpinolene), and that the linalool formed during the solvolysis of the optical active ester was *ca.* 20% active.

However, it might have been expected that the S_N1-type rearrangement of linalyl esters would have been favored over S_N2' reaction because of ability of the intermediates, the carbonium ions, to dissociate favorably in acidic media.

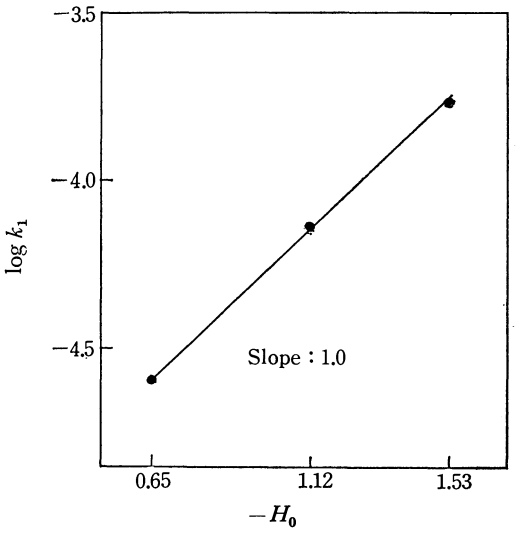

Fig. 5. Effect of the acidity function on the rearrangement rate constant of LA in the medium of HOAc containing sulfuric acid.

Table 8. Rate constants k_1 (1/s) of rearrangement of LA in the medium of HOAc containing sulfuric acid

HOAc-H_2SO_4	H_0	Reaction temperature, 0 °C k_1 (1/s)
90% HOAc-0.8 mol H_2SO_4	−1.53	1.67×10^{-2}
90% HOAc-0.6 mol H_2SO_4	−1.12	7.35×10^{-3}
90% HOAc-0.4 mol H_2SO_4	−0.65	2.45×10^{-3}

The present authors produced racemized linalyl propionate ($[\alpha]_D^{25}=0°$), together with myrcene, ocimene, limonene, and terpinolene, in the rearrangement of LA in propionic acid, and racemized linalool ($[\alpha]_D^{25}=0°$) in that of LA in the medium of HOAc containing sulfuric acid. In addition to these facts, the aforementioned kinetic and product data for the allylic rearrangement of LA in the medium of acetic, propionic acid, or acetic acid containing dioxane or sulfuric acid indicate that intermediate carbonium ions occupy a pivotal position in the rearrangements.

The authors wish to express their gratitude to Mr. Shozo Hasegawa, the president of T. Hasegawa, Co., Ltd. for his permission to publish this paper. One of the authors (Kunio Kogami) would also like to thank Assistant Professor Kazutoshi Yamada, Chiba University, for his guidance in the computer calculation. The authors also wish to thank Professor Kunio Okamoto, Kyoto University, for his valuable suggestions and comments.

References

1) W. G. Young and I. D. Webb, *J. Amer. Chem. Soc.*, **73**, 780 (1951).
2) L. L. Crabalona, *Soap, Perfumery & Cosmetics.*, May, 495 (1960).
3) a) H. E. Zaugg, *J. Amer. Chem. Soc.*, **83**, 837 (1967). b) E. Grunwald, G. Baugham, and G. Kohnstam, *ibid.*, **82**, 5801 (1960). c) C. C. Swain, R. Cardinand, and A. D. Ketlly, *ibid.*, **77**, 934 (1955).
4) a) B. Bensley and G. Khonstam, *J. Chem. Soc.*, **1956**, 287. b) W. G. Young, S. Winstein, and H. L. Goering, *J. Amer. Chem. Soc.*, **73**, 1958 (1951).
5) L. C. Bateman, E. D. Hughes, and C. K. Ingold, *J. Chem. Soc.*, **1940**, 794.
6) S. Winstein and A. H. Fainberg, *J. Amer. Chem. Soc.*, **79**, 5937 (1957).
7) a) S. Winstein and G. C. Robinson, *ibid.*, **80**, 169 (1958). b) S. Winstein, E. Clippinger, A. H. Fainberg, R. Heck, and G. C. Robinson, *ibid.*, **73**, 328 (1956).
8) L. P. Hammett and M. A. Raul, *J. Amer. Chem. Soc.*, **56**, 830 (1934).
9) L. Zucker and L. P. Hammett, *ibid.*, **61**, 2791 (1939).
10) Y. Ogata, M. Okano, and T. Ganke, *ibid.*, **78**, 2962 (1956).
11) K. Kogami, J. Kumanotani, and T. Kuwata, *Perfumery & Essential Oil Record*, Dec., 1 (1967).
12) K. Kogami, T. Konakahara, K. Yamada, and J. Kumanotani, *Kogyo Kagaku Zasshi*, **74**, 2304 (1971).
13) D. S. Noyce and R. Castelfranco, *J. Amer. Chem. Soc.*, **73**, 4482 (1951).
14) Y. Ogata and M. Okano, *ibid.*, **78**, 5423 (1956).
15) V. Prelog and E. Watanabe, *Liebig's Ann. Chem.*, **603**, 1 (1957).
16) Y. R. Naves and F. Bondavalli, *Helv. Chim. Acta*, **48**, 563 (1965).
17) R. Hoffmann, *J. Chem. Phys.*, **39**, 1397 (1963).
18) K. Yamada, S. Ishihara, and H. Iida, *J. Fac. Eng. Chiba. Univ.*, **23**, No. 43, 59 (1971).
19) K. Ohkubo, H, Kitagawa, and H. Sakamoto, *Nippon Kagaku Zasshi*, **92**, 1013 (1971).
20) F. Nerdel, *Naturwissenschaften*, **41**, 119 (1954).
21) S. Winstein, *Experientia, Suppl.*, **11**. 151 (1955).
22) S. Winstein, G. Valkanas, and C. F. Wilcox, Jr., *J. Amer. Chem. Soc.*, **94**, 2286 (1972).

NOTES

BULLETIN OF THE CHEMICAL SOCIETY OF JAPAN, VOL. 47(1), 234—235 (1974)

Comparison of the Catalytic Activities of Metal Oxides for Hydrogen-Deuterium Equilibration and Ortho-Parahydrogen Conversion

Kiyoshi Otsuka and Tominaga Kei

Department of Chemical Engineering, Tokyo Institute of Technology, Ookayama Meguroku, Tokyo 152

(Received April 5, 1972)

Synopsis. The corrected activities, rates divided by square of spin magnetic moment of a metal ion, in ortho-parahydrogen conversion on first series transition metal oxides at 77 K were shown to give a very similar activity pattern to that obtained in hydrogen-deuterium equilibration.

In order to find the relation between catalytic activity and the character of the catalysts, considerable work has been done to examine the activities of the first series transition metal oxides in reactions such as hydrogen-deuterium equilibration,[1] dehydrogenation and disproportionation of cyclohexene,[2] dehydrogenation of propane,[3] hydrogenation of ethylene,[4] isotopic mixing in ethylene[5] and dehydrogenation of cyclohexane.[6] It is noteworthy that a similar activity pattern was obtained in the above reactions.

Systematic studies have not yet been carried out on the activities in ortho-parahydrogen conversion, one of the simplest of catalytic reactions. We thought it of interest to see if an activity pattern similar to that in the above reactions also holds in this conversion. In the present work, we show the activity sequences of the first series transition metal oxides in ortho-parahydrogen conversion at 77 K, and in hydrogen-deuterium equilibration at 178 K.[7]

Experimental

Preparation of Oxides. V_2O_5 was prepared by the decomposition of NH_4VO_3 at 773 K in an oxygen flow. V_2O_3 was obtained by the reduction of V_2O_5 with hydrogen at 873 K. Cr_2O_3, Mn_2O_3, Fe_2O_3, Co_3O_4, NiO, CuO, ZnO, and CdO were prepared by the calcination of the respective hydroxide at 773 K for 5 hr in air. The hydroxide was precipitated with ammonia from the aqueous solution of the corresponding nitrate. Mn_3O_4 was prepared similarly and calcined at 1223 K. FeO was prepared by the reduction of Fe_2O_3 at 1473 K with an equimolar mixture of hydrogen and carbon dioxide. CoO was prepared by the decomposition of Co_3O_4 at 1073 K. SiO_2 and Al_2O_3 were prepared by the calcination of the corresponding hydroxide obtained by the hydrolysis of ethyl-ortho-silicate and that of alminum isopropoxide, respectively. MoO_3 was obtained by the oxidation of ammonium molybdate with the addition of concd. HNO_3. TiO_2 and CrO_3 were obtained from Wako Pure Chemical Industries, Ltd. The oxides, TiO_2 (anatase), V_2O_3, $Cr_2O_3(\alpha)$, Mn_2O_3, Mn_3O_4, $Fe_2O_3(\alpha)$, FeO, Co_3O_4, CoO, NiO, and CuO were confirmed to be well crystallized from X-ray diffraction patterns.

Materials. Hydrogen gas was purified by diffusion through a heated palladium thimble. Deuterium gas (D_2 99.3%, HD 0.7%, Takachiho Chemical Co.) was used without further purification.

Apparatus and Procedure. The reactor attached to the glass-made gas circulation system capable of achieving a vacuum to 10^{-6} Torr was used. The rates of the conversion and the equilibration were measured at temperatures 77—90 K and 77—300 K, respectively, under the total pressure of 100 Torr. Prior to individual runs, the catalyst in the reactor was outgassed at high temperature for more than 4 hr *in vacuo* below 5×10^{-5} Torr. The catalyst thus treated was cooled down to room temperature in herium gas, and the reaction vessel was immersed in a coolant to establish the required temperature for the reaction. The catalyst after being used once for the reaction was substituted by a fresh one before each run.

Results and Discussion

Both the conversion and the equilibration obeyed first order kinetics in the whole temperature range for all the oxides studied. The reaction rate, R_m, was calculated from the first order rate constant k_e to be

$$R_m = k_e N/S \quad \text{molecule}\cdot\text{s}^{-1}\cdot\text{cm}^{-2} \qquad (1)$$

where N is the number of molecules in the reaction system and S the surface area of the catalyst. The rates of conversion at 77 K over paramagnetic oxides and diamagnetic ones are shown in Tables 1 and 2, respectively. The former oxides have magnetic moment due to free spins in their metal ions, but the latter none. The rates of equilibration at 178 K are also shown in Table 3. In the temperature range 77—90 K, the conversion over paramagnetic oxides proceeds rapidly with a small apparent activation energy. However, the equilibration does not take place except over Co_3O_4 in this temperature range. The rates of the conversion over paramagnetic oxides are greater than those over diamagnetic oxides by a factor of $\sim10^3$. This shows that the low-temperature conversion proceeds *via* a paramagnetic mechanism.

Activity Order in the Equilibration and Conversion. The activity order in the equilibration at 178 K is seen from Table 3 to be

$$Co_3O_4 > CoO > NiO > Cr_2O_3 \gg ZnO > V_2O_3,\ Mn_2O_3,\ Mn_3O_4,\ Fe_2O_3,\ FeO,\ CuO.$$

A similar activity sequence was presented in the same reaction[1] and many other different types of reaction.[2-6]

The activity order of the paramagnetic oxides for the conversion at 77 K is seen from Table 1 to be

$$Co_3O_4 > Cr_2O_3 \simeq Mn_3O_4 > CoO > NiO > Fe_2O_3 > V_2O_3 > FeO > Mn_2O_3 > CuO.$$

Table 1. Rates of conversion over paramagnetic oxides

Oxides	Outgassing Temp. (K)	Surface area (m^2/g)	Activation energy at 77—90 K (kcal/mol)	$R_m \times 10^{-14}$ (molecule·$s^{-1}\cdot cm^{-2}$) 77K, 100 Torr
V_2O_3	773	4.85	—	2.01
Cr_2O_3	773	27.4	0.2	13.5
Mn_2O_3	773	28.7	—	0.66
Mn_3O_4	773	1.01	−0.2	13.4
Fe_2O_3	773	29.0	0.2	2.78
FeO	773	0.10	−0.2	1.34
Co_3O_4	773	13.5	0.5	31.9
CoO	773	3.69	—	7.46
NiO	773	16.4	0.2	6.73
CuO	673	1.04	−0.2	0.15

Table 2. Rates of conversion over diamagnetic oxides

Oxides	Outgassing Temp. (K)	Surface area (m^2/g)	Activation energy at 77—90 K (kcal/mol)	$R_m \times 10^{-11}$ (molecule·$s^{-1}\cdot cm^{-2}$) 77K, 100 Torr
TiO_2	773	10.2	−0.2	2.83
V_2O_5	773	4.91	—	6.18
CrO_3	373	4.69	—	0.5
ZnO	673	0.98	−0.2	4.55
Al_2O_3	773	189.0	—	3.12
SiO_2	773	296.0	—	0.5
MoO_3	773	2.20	—	2.46
CdO	673	2.24	—	2.63

Table 3. Rates of equilibration at 178 K

Oxides	Activation energy at 100—300 K (kcal/mol)	$R_m \times 10^{-12}$ (molecule·$s^{-1}\cdot cm^{-2}$) at 178 K
V_2O_5	—	0.00
V_2O_3	—	0.00
Cr_2O_3	6.3	2.00
Mn_3O_4	—	0.00
Fe_2O_3	—	0.00
FeO	—	0.00
Co_3O_4	0.76	1260.00
CoO	—	460.00
NiO	1.7	60.00
CuO	—	0.00
ZnO	5.9	0.03

As in the usual paramagnetic mechanism, the conversion proceeds by the interaction of adsorbed hydrogen molecules with the inhomogeneous magnetic field of a metal ion on the surface. The rate of the conversion can be given by

$$R_m = k \cdot f_a \cdot f_m \cdot n_a \qquad (2)$$

where f_a is a measure of the interaction strength of a catalyst with hydrogen molecule, f_m a measure of the strength of the magnetic field of a metal ion on an oxide, n_a the number of active sites per surface area of an oxide and k the transition probability of hydrogen from para- to ortho-hydrogen or *vice versa*, which is constant over various oxides. It was shown that the probability of the transition depends on the square of the spin magnetic moment of an ion or molecule.[8] The rate of the low temperature conversion on the rare earth metal oxides was confirmed to increase in proportion to the square of the spin magnetic moment of a metal ion in the corresponding metal oxides.[9] Thus, we assume here that f_m can be substituted by μ_M^2 in Eq. (2).[10] The corrected rates of the conversion, *i.e.*, R_m divided by the square of the spin magnetic moment of a metal ion in the corresponding metal oxide, are shown in Fig. 1. The rates of the conversion thus eliminated by the magnetic field contribution give a very similar activity pattern to that obtained in the equilibration.

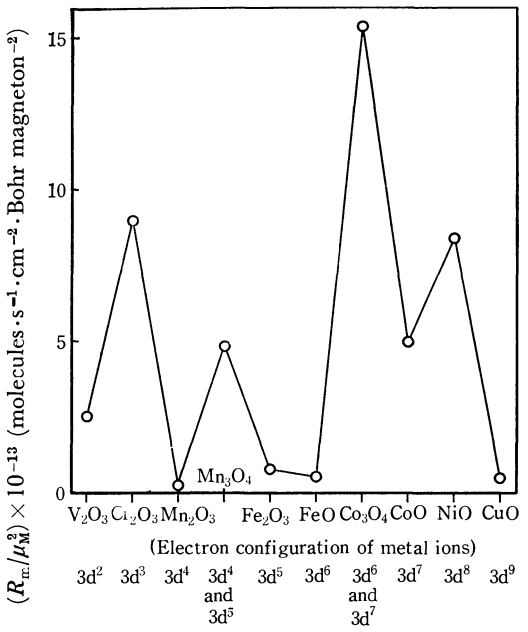

Fig. 1. Comparison of R_m/μ_M^2 for the paramagnetic oxides of the first series transition metal elements.

References

1) D. A. Dowden, N. Mackenzie, and B. M. W. Trapnell, *Proc. Roy. Soc., Ser. A*, **237**, 245 (1956).

2) G. M. Dixon, D. Nicholls, and H. Steiner, "Proc. 3rd Intern. Congr. on Catalysis," Amsterdam, North-Holland Pub. Co. (1965), p. 815.

3) D. A. Dowden, *Endeavour*, **24**, 69 (1965).

4) D. L. Harrison, D. Nicholls, and H. Steiner, *J. Catal.*, **7**, 359 (1967).

5) A. Ozaki, H. Ai, and K. Kimura, Forth Intern. Congr. on Catalysis, Moscow, No. 40 (1968).

6) P. C. Richardson and D. R. Rossington, *J. Catal.*, **14**, 175 (1969).

7) Hereafter, ortho-parahydrogen conversion and hydrogen-deuterium equilibration will be referred to as the conversion and the equilibration, respectively.

8) E. Wigner, *Z. Phys. Chem.*, **B23**, 28 (1933).

9) D. R. Ashmead, D. D. Eley, and R. Rudham, *J. Catal.*, **3**, 280 (1964).

10) The values of spin magnetic moments, μ_M, are given by $\mu_M = \sqrt{n(n+2)}$, where n is the number of free spins of a corresponding metal ion. The value of Co_3O_4 ($Co^{2+}Co_2^{3+}O_4$) or Mn_3O_4 ($Mn^{2+}Mn_2^{3+}O_4$) is given as $\mu_M^2 = (2\mu_{M^{3+}}^2 + \mu_{M^{2+}}^2)/3$.

BULLETIN OF THE CHEMICAL SOCIETY OF JAPAN, VOL. 47(1), 236—237 (1974)

The Decomposition of Nitrous Oxide in the Radiolysis of *n*-Hexane Solutions

Yoshihiko HATANO[1] and José-Luis ABBOUD[2]

Laboratory of Physical Chemistry, Tokyo Institute of Technology, Meguro-ku, Tokyo 152

(Received May 25, 1973)

Synopsis. The effect of the addition of N_2O (10^{-2}—10^{-4} mole fraction) in the radiolysis of liquid *n*-hexane has been examined. The oxygen-containing products such as water and alcohols have been detected. The number of nitrogen molecules produced per an electron scavenged by N_2O exceeds unity even at the lowest concentration.

Nitrous oxide has been widely used as an electron scavenger in radiation chemistry. The mechanism of its decomposition when dissolved in saturated hydrocarbons, however, is not yet fully understood.[3,4]

In this work, the γ-radiolysis of liquid *n*-hexane containing N_2O has been carried out in order to establish the quantitative relationship between the nitrogen yield and the decrease in the hydrogen yield as well as the stoichiometry[4] of the decomposition of N_2O.

Experimental

The *n*-hexane was a Phillips research-grade material. The gas-chromatographic analysis using a dimethylsulfolane column operated at 30 °C showed the main impurities to be methylcyclopentane and 3-methylpentane for a total amount of 0.015%. No unsaturates were detected. The nitrous oxide (>99%), supplied by the Takachiho Shoji Co., was degassed and stored under a vacuum through a −120 °C cold trap.

A given amount (2 or 10 ml) of *n*-hexane was transferred into a tube containing a liquid potassium–sodium alloy freshly distilled *in vacuo*. The tube, fitted with a break-off tip, was stored for one week with frequent shaking. The dried sample was then transferred *in vacuo* into a irradiation cell previously baked and sparkled under a vacuum. The irradiation cells were glass tubes 10 mm in o.d., 7 mm i.d., and 15 mm in o.d., and 12 mm in i.d., with break-off tips. The dead space over the solutions was, at the most, 10% of the total volume.

The samples were irradiated in a ^{60}Co facility at a dose rate of 5.50×10^{19} eV g^{-1} h^{-1}.

After the irradiation, non-condensable gases at the temperature of liquid nitrogen were collected and measured by means of a Toepler pump-gas buret device. The hydrogen was removed by pumping the gaseous mixture into a copper oxide furnace at 250—270 °C. The relative amounts of nitrogen and methane were determined by means of a Hitachi RMU-5 mass spectrometer. The total yield of water and alcohols was determined by the sodium-potassium method.[4,5] The alcohols were identified gas-chromatographically.

Results and Discussion

The sodium-potassium treatment not only dehydrates the *n*-hexane but also eliminates micromolar amounts of CO_2 and O_2, initially dissolved in the *n*-hexane, which may act as electron scavengers.

The radiolysis of pure *n*-hexane at different total doses was undertaken. The dose dependence of the hydrogen yield from pure *n*-hexane closely resembles that reported previously,[6] but the extrapolated initial *G*-value, 5.79 ± 0.05, is the highest ever reported for *n*-hexane and compares well with the recent data on cyclopentane[7] and cyclohexane.[4] This large *G*-value may be due to the removal of the scavengers initially dissolved in *n*-hexane.

TABLE 1. PRODUCT YIELDS IN THE RADIOLYSIS OF *n*-HEXANE SOLUTIONS OF N_2O

Total dose ($\times10^{20}$ eV/g)	Mole fraction of N_2O N_{N_2O}	$G(H_2)$	$G(N_2)$	$G(ROH)$[a]	$\frac{G(ROH)}{G(N_2)}$[a]
6.6	1.50×10^{-2}	2.60	3.8	3.9	1.1
1.1	1.25×10^{-2}	3.03	3.6	3.8	1.1
1.1	8.77×10^{-3}	2.90	3.3	b)	—
6.6	7.26×10^{-3}	2.69	3.6	3.3	0.9
1.1	2.53×10^{-3}	3.93	2.4	2.5	1.0
1.1	1.72×10^{-3}	3.85	2.1	b)	—
1.1	6.71×10^{-4}	4.73	1.4	b)	—
1.1	1.69×10^{-4}	4.90	1.0	0.8	0.8
0.55	7.89×10^{-5}	4.99	0.85	b)	—

a) ROH: oxygen-containing-products,
b) Not measured.

The experimental results on *n*-hexane–N_2O systems are collected in Table 1 as a function of the N_2O mole fraction, N_{N_2O}. The oxygen-containing-products detected here are water and small amounts of 2-hexanol and 3-hexanol. The total *G*-value of alcohols is small, 0.1 at $N_{N_2O}=2\times10^{-3}$. The relative amount of 3-hexanol is *ca.* 50% higher than that of 2-hexanol. The formation of water in this system has already been reported.[8] Alcohols have not yet been detected. As is shown in Table 1, the total yield of the oxygen-containing-products denoted ROH is in good agreement with that of N_2, within the limits of experimental error. This finding shows that the decomposition of N_2O in liquid *n*-hexane finally leads to N_2 and ROH in the ratio of one-to-one. The following possible schemes of ROH formation through ionic processes may be deduced:

$$n\text{-}C_6H_{14} \longrightarrow C_6H_{14}^+ + e^- \quad (1)$$

$$e^- + N_2O \longrightarrow N_2O^- \quad (2)$$

$$N_2O^- + C_6H_{14}^+ \longrightarrow N_2 + OH + C_6H_{13} \quad (3a)$$

$$\searrow\ N_2 + H_2O + C_6H_{12} \quad (3b)$$

$$N_2O^- + n\text{-}C_6H_{14} \longrightarrow N_2 + OH^- + C_6H_{13} \quad (4)$$

$$OH + n\text{-}C_6H_{14} \longrightarrow H_2O + C_6H_{13} \quad (5)$$

$$OH^- + C_6H_{14}^+ \longrightarrow H_2O + C_6H_{13} \quad (6)$$

$$OH + C_6H_{13} \longrightarrow C_6H_{13}OH \quad (7a)$$
$$\searrow C_6H_{12} + H_2O \quad (7b)$$

Since the selective C–H bond scission in both the 2 and 3 positions of *n*-hexane has already been described,[9] the alcohols detected here may be produced *via* Reaction (7a). The above scheme may at least explain the yields of N_2 and ROH arising from the electron scavenging, but not their yields in excess of the expected yield of the electron. The excess yields of N_2 and ROH may be interpreted effectively as:

$$N_2O + X \xrightarrow{n\text{-}C_6H_{14}} N_2 + ROH \quad (8)$$

where X may be intermediates other than N_2O^- or an electron which is captured by N_2O, as is shown in Reaction (2). The intermediate, X, is not determined here, but it must finally lead to the formation of N_2 and ROH again in the ratio of one-to-one. To compare the relative importance of Reactions (2) and (8) as a function of N_{N_2O}, the following attempt has been made.

Let $G(H_2)_0$ be the hydrogen yield in the absence of N_2O corrected for the ionic part of the dose effect on the hydrogen yield.[10] The quantity $\Delta G(H_2)=G(H_2)_0-G(H_2)$ is a measure of the decrease in the hydrogen yield resulting from the interruption of the ion-electron recombination processes by N_2O according to the following reactions:

$$e^- + C_6H_{14}^+ \longrightarrow f'H_2$$
$$e^- + N_2O \longrightarrow N_2O^-$$
$$N_2O^- + C_6H_{14}^+ \longrightarrow f''H_2$$

in which f' and f'' are the efficiencies of hydrogen formation. According to Schuler *et al.*,[11] the efficiency $f'-f''$ for hydrogen formation from *n*-hexane is 0.9. The ratio $\gamma=0.9G(N_2)/\Delta G(H_2)$ is approximately the yield of N_2 formed per electron scavenged. If only the above processes (1)—(7b) were to be taken into account, we should expect the value $\gamma\sim1$. As is shown in Fig. 1, though, the value of γ systematically exceeds 1. This can not be explained solely by Processes (1)—(7b), although this conclusion seems to be less rigorous at very low concentrations because of the large experimental errors. A satisfactory explanation of the excess nitrogen, that is, an intermediate X in Reaction (8), seems to be required.

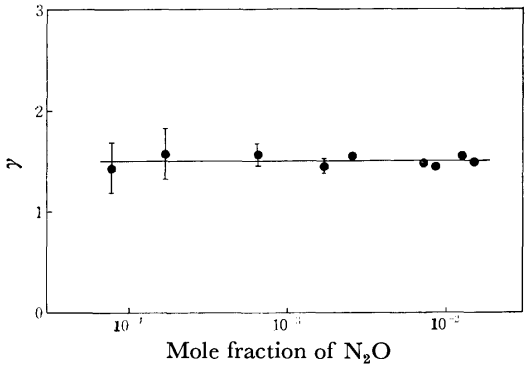

Fig. 1. The ratio γ as a function of the mole fraction of nitrous oxide.

Nitrous oxide appears to be inert towards thermal hydrogen atoms and alkyl radicals. The possibility of a reaction between hydroxyl radical and N_2O is also unlikely.[4] The decomposition of N_2O *via* energy transfer from an excited *n*-hexane molecule does not seem a significant process at least at the lower solute concentrations used here. The same reasoning can be appplied to the proposed[3] secondary reaction between N_2O and its negative ion. If such a reaction had to take place even at the lower concentrations as a significant competing process with Reaction (4), its rate constant would have to be exceedingly high. Among other possibilities deserving further study, the reactions with slow electrons not captured by N_2O or with positive ions may be the most promissing.

This work was supported in part by the Kurata Memorial Foundation. One of the authors (J.L.A.) wishes to thank the Japanese National Commission for the UNESCO for the award of a Postdoctoral Felllowship during the 1971—1972 term.

References

1) To whom the correspondence should be addressed.
2) UNESCO Postdoctoral Fellow. Permanent address: Département de Chimie, Faculté des Sciences, Rabat, Morocco.
3) J. M. Warman, K. D. Asmus, and R. H. Schuler, *Advan. Chem. Ser.*, **82**, 52 (1968).
4) Y. Hatano, K. Takeuchi, and S. Takao, *J. Phys. Chem.*, **77**, 586 (1973).
5) K. Takeuchi, K. Shinsaka, S. Takao, Y. Hatano, and S. Shida, This Bulletin, **44**, 2004 (1971).
6) T. J. Hardwick, *J. Phys. Chem.*, **64**, 1623 (1960).
7) F. Busi and G. R. Freeman, *J. Chem. Phys.*, **46**, 2822 (1967).
8) A. Menger and T. Gäuman, *Helv. Chim. Acta*, **52**, 2129 (1969).
9) K. Shinsaka and S. Shida, This Bulletin, **43**, 3728 (1970); T. Gäuman, "Aspects of Hydrocarbon Radiolysis," Academic Press, (1968), p. 213.
10) Although the precise value of the correction for *n*-hexane has not yet been determined, the values for cyclohexane[11] have been used as an approximation.
11) K. D. Asmus, J. M. Warman, and R. H. Schuler, *J. Phys. Chem.*, **74**, 246 (1970).

BULLETIN OF THE CHEMICAL SOCIETY OF JAPAN, VOL. 47(1), 238—239 (1974)

Photochemical Reaction of Halo-1,3,5-triazines: Photo-triazinylation

Hideo YAMADA, Haruo SHIZUKA, Shizen SEKIGUCHI, and Kohji MATSUI

Department of Chemistry, Gunma University, Kiryu, Gunma 376

(Received July 12, 1973)

Synopsis. Chloro-*s*-triazines or bromo-*s*-triazines containing halogen and/or methoxy substituents in the *s*-triazine nucleus gave the corresponding phenyl-*s*-triazines upon irradiation at 2537 Å in benzene.

It is known that some aryloxy-*s*-triazines rearrange photochemically to give *ortho* or/and *para* hydroxyaryl-*s*-triazines (photo-Fries rearrangement),[1] while aryloxy-*s*-triazines containing an *ortho* amino group give *ortho*-hydroxyarylamino-*s*-triazines on irradiation (photo-Smiles rearrangement);[2] these photochemical reactions are known to occur from the lowest excited singlet states of the corresponding molecules.

Recently, the photochemical reactions of haloarenes have been studied extensively; the photochemical primary processes in halobenzenes involve the fission of the C–Hal bond to give the phenyl radical and the halogen atom.[3] The photolysis of chlorobenzene in the gas phase orginates from the excited singlet state.[4] The photoarylations of aromatic compounds with haloarenes, such as halobenzenes[5-7] and *p*-halophenols,[8,9] proceed *via* a radical process. As for haloheteroaromatics, such as 2-iodothiazole,[10,11] 3-iodothiophen,[12] 3-iodobenzo[*b*]-thiophen,[13] and 3-iodopyridine,[14] similar photochemical reactions take place. However, no photochemical study of halo-*s*-triazine has yet been reported.

In the case of the *s*-triazine derivative, the photo-*s*-triazinylation of aromatic compounds with the halo-*s*-triazines was of interest from two points of view: the influence of the presence of three ring nitrogen atoms and the substituent effect upon the reaction. In addition, the photo-*s*-triazinylation of aromatic compounds with chloro-*s*-triazines will provide a useful and convenient method for the synthesis of aryl-*s*-triazines, since chloro-*s*-triazines containing various substituents in the *s*-triazine nucleus can readily be obtained from cyanuric chloride. This paper will report on the photo-*s*-triazinylation of benzene with halo-*s*-triazines.

Experimental

A low-pressure mercury lamp was used as the 2537 Å radiation source. Table 1 lists the halo-*s*-triazines employed as the starting materials (No. 1—6).

After a long irradiation of benzene solutions of halo-*s*-triazines at 2537 Å, the reaction mixtures were evaporated, after which the photoproducts were separated and purified by column or thin-layer chromatography. The photoproducts were identified by means of elemental analyses, by a study of the IR, UV, and NMR spectra, and by a mixed-melting-point test with an authentic sample in some cases.

Results

In every case, the main product was found to be a phenylated *s*-triazine derivative, showing that the photoarylation of aromatic compound can be carried out using halo-*s*-triazine; Table 1 lists the photoproducts thus obtained (No. 6—9). The photoreaction of halo-*s*-triazines in benzene can be represented by the following general formula:

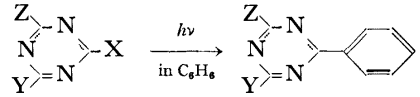

X=-Cl, -Br, Y, Z=-Cl, -Br, $-OCH_3$

Thus, chloro- and bromo-*s*-triazines containing one, two, and three halogen atoms, and halo-*s*-triazines containing methoxyl groups in the *s*-triazine nucleus reacted photochemically with benzene to give the corresponding phenyl-*s*-triazines. However, when a phenyl group or an amino group, such as the *N*-methylanilino- or dimethylamino group, is present in the *s*-triazine nucleus, it was found to be very difficult for the photoreaction of halo-*s*-triazine to take place; therefore, derivatives containing more than two phenyl groups could not be obtained by the photoreaction of dihalo- or trihalo-*s*-triazines with benzene.

Generally, the progresses of these photoreactions were slow compared with those of photo-Fries rearrangements of aryloxy-*s*-triazines or photo-Smiles rearrangements of *O*-*s*-triazinyl-2-aminophenols; for example, the quantum yield for the product formation in the reaction of 2-chloro-4,6-dimethoxy-*s*-triazine with benzene was found to be 0.03 at the concentration of 3×10^{-3} M in benzene. In addition to the photoproducts mentioned above, the formation of hydrogen halide was observed, for example, in the photo-phenyldechlorination of chloro-dimethoxy-*s*-triazine, and the chemical yields of phenylated products in the photoreactions of 2-bromo-4,6-dimethoxy-*s*-triazine, 2-chloro-4,6-dimethoxy-*s*-triazine, 2,4-dichloro-6-methoxy-*s*-triazine, and cyanuric chloride were 21, 22, 20, and 19% respectively, at the concentration of 2×10^{-2} M in benzene at 2537 Å for 24 hr.

The reactive state in the reaction may originate from the excited singlet state of halo-*s*-triazine, judging from the following reasons:

(1) The incident light at 2537 Å is absorbed by benzene (>99%), not by halo-*s*-triazine, under the experimental conditions described above. Therefore, the excited halo-*s*-triazine should be formed by the energy transfer from the excited benzene. The singlet-singlet energy transfer from the excited benzene to halo-*s*-triazine was confirmed by the measurements of the fluorescence quenching of benzene by halo-*s*-tri-

Table 1. Starting materials (halo-*s*-triazines) and photoproducts (phenyl-*s*-triazines)

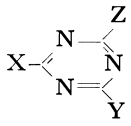

No.	Z	Y	X	Mp (°C)	Anal. (%) Found C	H	N	Br	Calcd C	H	N	Br
1	CH_3O–	CH_3O–	Br–	122—123	27.73	3.16	18.97	—	27.29	2.73	19.10	—
2	CH_3O–	Br–	Br–	155—156	18.29	1.32	15.74	—	17.86	1.12	15.62	—
3	CH_3O–	CH_3O–	Cl–	79—80 (76—77)[a]	—	—	—	—	—	—	—	—
4	CH_3O–	Cl–	Cl–	91—92 (88—90)[a]	—	—	—	—	—	—	—	—
5	Cl–	Cl–	Cl–	145—146 (145.75)[b]	—	—	—	—	—	—	—	—
6	CH_3O–	CH_3O–	C_6H_5–	68—69 (69)[c]	—	—	—	—	—	—	—	—
7	CH_3O–	Br–	C_6H_5–	76—77	45.12	3.45	15.50	30.25	45.15	3.04	15.79	30.03
8	CH_3O–	Cl–	C_6H_5–	75—76	54.12	3.71	18.82	—	54.17	3.61	18.96	—
9	Cl–	Cl–	C_6H_5–	121—122 (120)[d]	—	—	—	—	—	—	—	—

a) J. R. Dudley, J. T. Thurston, F. C. Shaefer, D. Holn Hansen, C. J. Hull, and P. Adams, *J. Amer. Chem. Soc.*, **73**, 2986 (1951).
b) American Cyanamid Co., Cyanuric Chloride, *New Product Bulletin.*
c) Z. N. Pazenko and T. N. Lebedeva, *Ukr. Khim. Zh.*, **30**, 66—68 (1964); *Chem. Abstr.*, **60**, 12014e.
d) R. Hirt, H. Nidecker, and R. Berchtold, *Helv. Chim. Acta*, **33**, 1365 (1950).

azine; the intensity of the fluorescence decreased considerably with an increase in the concentration of halo-*s*-triazine.

(2) Very little effect of dissolved oxygen on the product formation was observed. This fact supports the singlet mechanism in the reaction, although an extremely fast triplet reaction can not be excluded.

When a solution of 2-bromo-4,6-dimethoxy-*s*-triazine in cumene was irradiated, dicumyl was obtained as a photoproduct, while the formation of acetone was observed when it was irradiated in 2-propanol, suggesting that the photoreaction of halo-*s*-triazines proceeded *via* a radical process involving an α-bond dissociation (C–X) into the halogen atom and the *s*-triazinyl radical. The triazinyl radical produced by the dissociation of excited singlet halo-*s*-triazine may attack the benzene molecule to give the final product *via* the intermediate, M. Figure 1 shows the schematic reaction mechanism of the photo-triazinylation of benzene by halo-*s*-triazine at 2537 Å, where B and B* are the ground and the

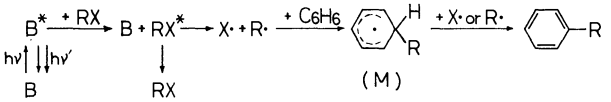

Fig. 1. Schematic reaction mechanism at 2537 Å.

lowest singlet excited states of benzene respectively, where RX and RX* denote the ground and the excited ($^1\pi\pi^*$) singlet states of halo-*s*-triazine respectively, and where X· and R· indicate the ground states of the halogen atom and the *s*-triazinyl radical respectively.

The susbtituent effects on the reaction may suggest that the electronic structures in the excited states of halo-*s*-triazines (the $n\pi^*$ and $\pi\pi^*$ energy levels and the character of the lowest excited state) play an important role in the dissociation of the C–X bond Similar substituent effects were also observed in the case of the photo-Fries rearrangement of *s*-triazine derivatives.[15]

References

1) H. Shizuka, T. Kanai, T. Morita, Y. Ohoto, and K. Matsui, *Tetrahedron*, **27**, 4021 (1971).
2) K. Matsui, N. Maeno, H. Shizuka, and T. Morita, *Tetrahedron Lett.*, **1970**, 1467; H. Shizuka, N. Maeno, and K. Matsui, *Mol. Photochem.*, **4**, 335 (1972).
3) G. Porter and B. Ward, *Proc. Roy. Soc. Ser., A*, **287**, 457 (1965).
4) T. Ichimura and Y. Mori, *J. Chem. Phys.*, **58**, 288 (1973).
5) G. E. Robinson and J. M. Vernon, *J. Chem. Soc., C*, **1971**, 3363.
6) M. A. Chel'tsova and G. I. Nikishin, *Izv. Akad. Nauk. SSSR Ser. Khim.*, **1967**, 456.
7) Pac. Chyongjin, T. Tosa, and H. Sakurai, This Bulletin, **45**, 1169 (1972).
8) K. Omura and T. Matsuura, *Chem. Commun.*, **1969**, 1394.
9) K. Omura and T. Matsuura, *Synthesis*, **1971**, 28.
10) G. Vernin, R. Jauffred, H. J. M. Dou, and J. Metzger, *J. Chem. Soc., B*, **1970**, 1678.
11) G. Vernin, R. Jauffred, C. Ricard, H. J. M. Dou, and J. Metzger, *J. Chem. Soc. Perkin. Trans.*, **II**, **1972**, 1145.
12) G. Martelli, P. Spagnolo, and M. Tiecco, *J. Chem. Soc., B*, **1968**, 901.
13) L. Benati, P. Spagnolo, and M. Tiecco, *ibid.*, **1969**, 472.
14) Hong-Son Ryang and H. Sakurai, *Chem. Commun.*, **1972**, 594.
15) Y. Ohoto, H. Shizuka, and K. Matsui; the details will be published elsewhere.

BULLETIN OF THE CHEMICAL SOCIETY OF JAPAN, VOL. 47(1), 240—241 (1974)

The Photo-Fries Rearrangement of Bis(methoxymethoxy)-phenyl Cinnamates

Jun-ichi ONODERA and Heitaro OBARA

Department of Applied Chemistry, Faculty of Engineering, Yamagata University, Yonezawa 992

(Received August 1, 1973)

Synopsis. The irradiation of bis(methoxymethoxy)-phenyl cinnamates in benzene solution gave 2'-hydroxy-bis-(methoxymethoxy)chalcones in 5.4—7.6% yields and 2',3',4'-, 2',3',5'-, and 2',4',6'-trihydroxychalcone were obtained by the hydrolysis of the resulting chalcones.

In previous papers,[1,2] we have reported the formation of hydroxychalcones by the photo-Fries rearrangement of phenyl cinnamate and hydroxyphenyl cinnamate. Further, we have attempted the photo-irradiation of 2,3- and 3,5-dihydroxyphenyl cinnamate (I and III); however, the isolation of the corresponding trihydroxy-chalcones (X and XII) was very difficult.[3]

In this note we wish to report the photo-Fries rearrangement of dihydroxyphenyl cinnamates protected their hydroxyl groups with methoxymethyl groups.

2,3-,[3] 2,4-, and 3,5-[3] Dihydroxyphenyl cinnamate (I, II, and III) were isolated from the reaction mixture obtained by the acylation of pyrogallol, 1,2,4-trihydroxybenzene, and phloroglucinol with cinnamoyl chloride in pyridine.

The structure of II was confirmed by a comparison of the melting points of the 2,4-dimethoxyphenol obtained by the hydrolysis of the dimethylether of II and its benzoate with those of authentic samples.[4,5]

2,3-, 2,4-, and 3,5-Bis(methoxymethoxy)phenyl cinnamate (IV, V, and VI) were obtained from the corresponding dihydroxyphenyl cinnamate by treatment with sodium amide, followed by that of chloromethyl ether in a tetrahydrofuran–benzene solution; these bis(methoxymethoxy)phenyl cinnamates were then purified by means of silica gel column chromatography.

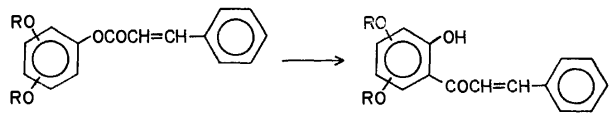

I, IV (2,3-) VII, X (3',4'-)
II, V (2,4-) VIII, XI (3',5'-)
III, VI (3,5-) IX, XII (4',6'-)

I ~ III X ~ XII : R=H IV ~ IX : R=CH_3OCH_2

The irradiation was carried out in a benzene solution under a nitrogen atmosphere and at room temperature using a high-pressure 100 W mercury arc. After irradiation, the benzene was evaporated *in vacuo*, and the residue was chromatographed on a column of silica gel. By the irradiation of IV and VI, 2'-hydroxy-3',4'- and 2'-hydroxy-4',6'-bis(methoxymethoxy)chalcones (VII and IX) were obtained, in 7.6 and 6.0% yields; they were converted into 2',3',4'- and 2',4',6'-trihydroxy-chalcones respectively (X and XII) by heating with methanolic hydrochloric acid. The structures of X and XII were identified by comparing their melting points and IR spectra with those of authentic samples.[6,7]

Similarly, 2'-hydroxy-3',5'-bis(methoxymethoxy)-chalcone (VIII) was obtained in a 6% yield by the irradiation of V; it was then converted into 2',3',5'-trihydroxychalcone (XI) (mp 174—175 °C). The structure of this new chalcone was identified by the elemental analysis and by a study of its UV and IR spectra.

From these results, it may be thought that the protection of the hydroxyl groups of dihydroxyphenyl cinnamate with methoxymethyl group can be used in obtaining trihydroxychalcones by photo-Fries rearrangement.

Experimental

All the melting points are uncorrected.

The 2,3-dihydroxyphenyl cinnamate (I, mp 172—174 °C) and the 3,5-dihydroxyphenyl cinnamate (III, mp 188—189 °C) were prepared according to the method of a previous report.[3]

2,4-Dihydroxyphenyl Cinnamate (II). To a stirred solution of 2.2 g of 1,2,4-trihydroxybenzene in 20 ml of pyridine, there was slowly added 5.2 g of cinnamoyl chloride at 8—12 °C; then the mixture was stirred at 45 °C over a period of about 1 hr. The reaction mixture was then poured into 150 ml of cold 3 M hydrochloric acid and extracted with ethyl acetate; the ethyl acetate layer was washed with water. The ethyl acetate solution was evaporated *in vacuo*, and the residue was chromatographed with benzene–ether (2:1) on a column of silica gel.

From the last elution, II was obtained as light yellow crystals. Yield, 1.2 g (26%); mp 144—145 °C (from benzene). IR (KBr): 3430, 3240 (ν OH) and 1700 cm^{-1} (ν CO). UV: λ_{max}^{EtOH} 283 mμ(log ε=4.44). Found: C, 70.42; H, 4.94%. Calcd for $C_{15}H_{12}O_4$: C, 70.30; H, 4.72%. Dimethyl ether, mp 104—105 °C (colorless prisms from ethanol). NMR ($CDCl_3$): δ 3.80 (-OMe), 6.61, 7.84 (-CH=CH-, J=16.0 Hz). Found: C, 71.66; H, 5.75%. Calcd for $C_{17}H_{16}O_4$: C, 71.82; H, 5.67%.

The hydrolysis of this dimethylether with an aqueous sodium hydroxide solution gave 2,4-dimethoxyphenol (mp 25—27 °C) (lit, mp 28 °C,[4] benzoate, mp 88—89 °C (lit, mp 89 °C[5])).

2,3-Bis(methoxymethoxy)phenyl Cinnamate (IV). To a solution of 1.0 g of I in 10 ml of dry tetrahydrofuran and 30 ml of dry benzene, there was added 2.0 g of sodium amide; after the mixture had then been stirred for 30 min, 3.2 g of monochloromethyl ether was added to the reaction mixture, drop by drop, over a period of about 30 min at room temperature. The reaction mixture was then poured into a cold, dilute, aqueous sodium carbonate solution and extracted with ether. The ether layer was washed with water and dried over anhydrous sodium sulfate. The ether was evapolated

in vacuo, and the resulting crude oil was chromatographed on a column of silica gel. 2,3-Bis(methoxymethoxy)phenyl cinnamate (IV) was obtained as colorless crystals from the second elution with benzene–ether (20: 1). Yield, 0.50 g (37%); mp 75—77 °C (from petroleum ether). IR (KBr): 1730 cm^{-1} (ν CO). NMR ($CDCl_3$): δ 3.49, 3.52 (-OMe), 5.18, 5.12 ($-CH_2-$), 6.67, 7.89 (-CH=CH-, J=16.0 Hz).

3,5-Bis(methoxymethoxy)phenyl Cinnamate (VI). This compound was prepared from III by the method described above. The crude VI was purified by silica-gel-column chromatography with benzene–ethyl acetate (5: 1). Yield, 35%; pale yellow oil. IR ($CHCl_3$): 1725 cm^{-1} (ν CO). NMR ($CDCl_3$): δ 3.44 (-OMe), 5.11 ($-CH_2-$), 6.56, 7.80 (-CH=CH-, J=16.0 Hz).

2,4-Bis(methoxymethoxy)phenyl Cinnamate (V). This compound was prepared from II by the method described above. The crude V was purified by silica-gel-column chromatography with benzene–ethyl acetate (20: 1). Yield, 31%; pale yellow oil. IR (neat): 1730 cm^{-1} (ν CO). NMR ($CDCl_3$): δ 3.44 (-OMe), 5.12 ($-CH_2-$), 7.81, 6.56 (-CH=CH-, J=16.0 Hz).

Irradiation of 2,3-Bis(methoxymethoxy)phenyl Cinnamate (IV). A solution of 500 mg of IV in 300 ml of dry benzene was irradiated under a nitrogen atmosphere at room temperature by means of a high-pressure 100 W mercury arc for 20 hr. After irradiation, the benzene was evapolated *in vacuo*, and the resulting crude mixture was chromatographed on a column of silica gel. 2′-Hydroxy-3′,4′-bis(methoxymethoxy)-chalcone (VII) was obtained as yellow needles from the second elution with petroleum ether–ether (2: 1). Yield, 38 mg (7.6%); mp 95—96 °C (from ligroin). Found: C, 66.26; H, 5.64%. Calcd for $C_{19}H_{20}O_6$: C, 66.27; H, 5.85%. UV: λ_{max}^{EtOH} 336 mμ(log ε=4.47). NMR ($CDCl_3$): δ 3.15, 3.66 (-OMe), 5.22, 5.29 ($-CH_2-$), 7.52, 7.89 (-CH=CH-, J= 16.0 Hz), 13.24 (-OH). A solution of 40 mg of VII in 1.5 ml of methanol containing 0.3 ml of 6 M hydrochloric acid was refluxed for 5 min. After cooling, 2′,3′,4′-trihydroxychalcone (X) was obtained as yellow needles. Yield, 20 mg (67%); mp 164—165 °C (lit, mp 166 °C[6]). The structure of this trihydroxychalcone was identified by comparison with that of an authentic sample.[6]

Irradiation of 3′,5′-Bis(methoxymethoxy)phenyl Cinnamate (VI). A solution of 600 mg of VI in 400 ml of dry benzene was irradiated for 20 hr as has been described above. Subsequent elution with petroleum ether–ether (2: 1) gave 2′-hydroxy-4′,6′-bis(methoxymethoxy)chalcone (IX) as yellow prisms. Yield, 36 mg (6.0%); mp 89—92 °C (from ligroin). Found: C, 66.32; H, 6.01%. Calcd for $C_{19}H_{20}O_6$: C, 66.27; H, 5.85%. NMR ($CDCl_3$): δ 3.49, 3.53 (-OMe), 5.18, 5.29 ($-CH_2-$), 7.76, 7.90 (-CH=CH-, J=16.0 Hz), 13.74 (-OH). The hydrolysis of IX gave 2′,4′,6′-trihydroxychalcone (XII) as yellow needles; mp 176—178 °C (from benzene). The structure of XII was identified by a comparison of its IR spectrum with that of an authentic sample.[7]

Irradiation of 2,4-Bis(methoxymethoxy)phenyl Cinnamate (V). A solution of 820 mg of V in 400 ml of dry benzene was irradiated for 42 hr as has been described above. 2′-Hydroxy-3′,5′-bis(methoxymethoxy)chalcone (VIII) was obtained as orange red crystals from the third elution with benzene–ethyl acetate (20: 1). Yield, 44 mg (5.4%); mp 122—124 °C (from ligroin). Found: C, 66.13; H, 5.98%. Calcd for $C_{19}H_{20}O_6$: C, 66.27; H, 5.85%. UV: λ_{max}^{EtOH} 328 mμ(log ε= 4.40). NMR ($CDCl_3$): δ 3.50, 3.53 (-OMe), 5.12, 5.22 ($-CH_2-$), 7.52, 7.89 (-CH=CH-, J=16.0 Hz), 13.78 (-OH).

2′,3′,5′-Trihydroxychalcone (XI). To a solution of 20 mg of VIII in 0.5 ml of methanol, there was added 0.1 ml of 6 M hydrochloric acid, after which the mixture was boiled for 5—6 min. After cooling, 2 ml of a saturated aqueous sodium chloride solution was added to the mixture, and then the mixture was extracted with ether. The ether layer was dried over anhydrous sodium sulfate, and the ether was evaporated *in vacuo*. The resulting residue was crystalized by the addition of petroleum ether to give 2′,3′,5′-trihydroxychalcone (XI). Yield, 10 mg (65%); mp 174—176 °C (from benzene). Found: C, 70.00; H, 4.68%. Calcd for $C_{15}H_{12}O_4$: C, 70.30; H, 4.72%. UV: λ_{max}^{EtOH} 330 and 440 mμ(log ε= 4.44 and 3.43).

The authors wish to thank Messrs. Hiromichi Hirano, Norio Tanaka, Yasuo Sugawara, and Yutaka Kikuchi for their technical assistances.

References

1) H. Obara and H. Takahashi, This Bulletin, **40**, 1012 (1967).
2) H. Obara, H. Takahashi, and H. Hirano, *ibid.*, **42**, 560 (1969).
3) H. Obara, H. Takahashi, and J. Onodera, *Kogyo Kagaku Zasshi*, **72**, 309 (1969).
4) E. Späth, M. Pailer, and G. Gergely, *Chem. Ber.*, **73**, 795 (1940).
5) H. Bredereck and H. Heckh, *ibid.*, **91**, 1314 (1958).
6) T. E. Ellison, *J. Chem. Soc.*, **1927**, 1720.
7) J. Shinoda and S. Sato, *Yakugaku Zasshi* **48**, 791 (1928).

BULLETIN OF THE CHEMICAL SOCIETY OF JAPAN, VOL. 47(1), 242—243 (1974)

Estimation of Chlorine Content in Single Crystals of Chromium Chalcogenide Spinels by Atomic Absorption Spectrophotometry

Kohei AMETANI

RCA Research Laboratories, Inc., Zushi-machi, Machida-shi, Tokyo 194-02

(Received September 13, 1973)

Synopsis. Analyses using the silver atomic absorption indicated that all the crystals grown by the vapor transport method were contaminated with chlorine. Particularly in crystals containing copper, a large amount of chlorine was incorporated. In crystals with an intended composition $CuCr_2S_3Cl$, the chlorine content was much higher than the expected amount.

Single crystals of chromium chalcogenide spinels such as $CuCr_2S_3Cl$, $CdCr_2S_4$, and $CdCr_2Se_4$, are usually grown by the chemical vapor transport method, using chlorine gas as a transport agent.[1] It is known that the chlorine is incorporated as either a major or minor component in the grown crystals[1,2] and affects the magnetic and electrical properties.[1,3,4] The chlorine content as the major component is commonly determined by Vegard's law comparing the lattice constant of single crystals with that of polycrystals having a known composition.[3] Sleight and Jarrett[4] used a chemical analysis to determine the chlorine content of $CuCr_2S_{4-x}Cl_x(0\leq x\leq 1)$, where the maximum chlorine expected is 11.85 wt%. However, they did not discuss their method of analysis. Similarly, for a chlorine content of less than 0.02 wt% in $CdCr_2Se_4$ crystals, Harbeke and Pinch[5] did not report the details of their chemical analysis. In both cases one must assume that a large number of samples are necessary for the chlorine analysis since the crystals are, at most, 3 mm on edge and weigh only several mg. In the present paper we describe an indirect method, using 10 mg samples, to estimate the chlorine content in some single crystals by atomic absorption spectrophotometry.

The sample is dissolved in nitric acid containing a known amount of silver ions and the chlorine is simultaneously precipitated as AgCl. After filtration, the chlorine content is determined either from the AgCl precipitate dissolved in the ammoniacal solution[6] or the excess silver ions in the filtrate.[7] For the measurement of silver atomic absorption and the precipitation of AgCl, the effects of the constituent elements in the materials are examined.

Experimental

Reagents. (1) Standard chlorine solution: Sodium chloride dried at 110 °C was accurately weighed and dissolved in deionized water. (2) Standard silver solution: Silver nitrate dried at 110 °C was accurately weighed and dissolved in a minimum amount of deionized water, and then diluted with concentrated nitric acid. (3) Other solutions: Metal nitrates and sodium sulfate were dissolved in deionized water and selenium metals were dissolved in nitric acid and then diluted with deionized water. Reagents used were of analytical reagent grade.

Measurement of Silver Atomic Absorption. The silver atomic absorption was measured at 328.1 nm in an acetylene-air flame using a Hitachi Model 208 atomic absorption spectrophotometer and a hollow cathode lamp HLA-3. For the measurement of silver concentrations up to 2 ppm, the nitric acid concentration was adjusted to 0.05 M, taking into account the stability of the dilute silver solution. For this condition, the silver atomic absorption was not affected by 2 ppm Cu^{2+}, Fe^{3+}, and In^{3+}, 3—400 ppm Cr^{3+}, 200—400 ppm Cd^{2+}, 12—1200 ppm SO_4^{2-} and 1000 ppm SeO_3^{2-}. For the measurement from the ammoniacal solution, it was necessary to use at least a 3% ammonia concentration, since the silver atomic absorption remained nearly constant above this concentration.

Precipitation of Silver Chloride. We successfully precipitated more than 10 μg of chlorine as AgCl using a standard chlorine solution. The nitric acid concentration was adjusted to about 1.5 M for this examination. The results suggested that 5 mg of silver was necessary to capture about 1 mg of chlorine and 1 or 0.5 mg of silver was suitable for less than 100 μg of chlorine. Several diverse ions did not interfere with the precipitation of AgCl. Table 1 shows the recovery of chlorine in the presence of diverse ions. The amount of

Table 1. Recovery of chlorine in the presence of diverse ions

Elements[a] added	Cl added	From precipitate		From filtrate	
		Cl found	error	Cl found	error
Cu 2.0 mg	0.500 mg	0.481 mg	−3.8%	0.503 mg	+0.6%
Cr 3.0	1.000	1.000	0	0.985	−1.5
S 3.5	1.500	1.488	−0.8	1.508	+0.5
Cd 3.0 mg	10 μg	9.5 μg	−5.0%	10.8 μg	+8.0%
Cr 3.0	25	24.1	−3.6	26.9	+7.6
	50	51.6	+3.2	51.8	+3.6
S 4.0	100	99.4	−0.6	103.8	+3.8

a) Cu, Cr, and Cd were added as nitrates, and S as sodium sulfate.

added elements was nearly equivalent to the sample weight of 10 mg. The values given on the same line in Table 1 for the precipitate and filtrate were obtained from the same starting solution. The results obtained from both the precipitate and the filtrate are in agreement each other. This indicates that the chlorine can be determined either from the AgCl precipitate dissolved in the ammoniacal solution or the excess silver ions in the filtrate. Considering the simplicity of the experimental procedure, the latter technique seems to be more practical than the former. However, for analyses of the actual samples, both techniques were usually used to attain a satisfactory result as described below.

Analysis of Single Crystals. Ten mg of the sample (usually 5—6 crystals) was dissolved in nitric acid containing excess silver ions of a known quantity and the chlorine was simultaneously precipitated as AgCl to prevent the escape of chlorine from the system during the dissolution.[8] For a sample containing about 1 mg of chlorine, 5 ml of nitric acid containing 1 mg Ag/ml was used, and the solution was then diluted to about 50 ml. However, if the expected chlorine content in the sample was less than 100 μg, 2 ml of nitric acid containing 0.5 or 0.25 mg Ag/ml was used and the solution was then diluted to about 20 ml. The solutions were aged for 30 min over a water bath. After the solution was cooled in ice water, the precipitated AgCl was filtered and washed with six 5 ml portions of cold nitric acid (1: 50), and dissolved in an aqueous ammonia solution. After the dilution of both the ammoniacal solution and the filtrate to an appropriate silver concentration, chlorine was usually determined indirectly from the silver content in both solutions. The results obtained were corrected by the blank test.

Table 2. Results of single crystal analysis

Sample Intended composition	Cl found, wt% From precipitate	From filtrate
$CuCr_2S_3Cl$ (1)	13.2	12.9
$CuCr_2S_3Cl$ (2)	13.8	13.6
$CuCr_2S_3Cl$ (3)	14.1	13.8
$Cu_{0.5}In_{0.5}Cr_2S_4$	2.39—3.56	—
$Fe_{1-x}Cu_xCr_2S_4$ (x=0.4—0.6)	4.52—8.32	—
$FeCr_2S_4$	0.61	—
$CdCr_2S_4$	0.01—0.04	0.01—0.05
$CdCr_2S_4$[a)]	0.004—0.07	0.003—0.07
In-doped $CdCr_2S_4$	0.02—0.04	0.03—0.04
Ag-doped $CdCr_2S_4$	0.08—0.14	—
Cu-doped $CdCr_2S_4$	0.22—0.33	0.22—0.34
$CdCr_2Se_4$	0.03	0.04
In-doped $CdCr_2Se_4$	—	0.05
Ag-doped $CdCr_2Se_4$	0.06—0.15	—
Cu-doped $CdCr_2Se_4$	0.13—0.14	0.14

a) Annealed in vacuum at 500—600 °C for 2—15 days.

The results of the analyses are given in Table 2. The chlorine content determined from both the precipitate and the filtrate are in good agreement each other. In the case of crystals with an intended composition $CuCr_2S_3Cl$, the chlorine content was much higher than the 11.85 wt% expected for the intended composition while Sleight and Jarrett obtained crystals containing a nearly stoichiometric amount of chlorine.[4] In a separate experiment, however, it was found that the sulfur content in our crystals was consistently lower than the stoichiometric amount.[9] Such deviations from the stoichiometric composition would strongly affect the magnetic and electric properties of the crystals.[9] For the other crystals, Table 2 also indicates that all the single crystals grown by the vapor transport method using chlorine gas as a transport agent, were always contaminated with chlorine. Particularly in crystals containing copper, a large amount of chlorine was incorporated.

The author thanks Professor Katsumi Yamamoto of Ibaraki University, Drs. Fumio Okamoto and Yasuo Wada of this laboratories for their helpful suggestions, and Messrs. Katsuhiro Kato and Takao Oka of this laboratories for providing the samples.

References

1) F. Okamoto, T. Takahashi, and Y. Wada, *Oyo Butsuri*, **39**, 471 (1970).
2) H. Schäfer, "Chemical Transport Reactions," Academic Press Inc., New York (1964), Chap. 3, p. 73.
3) K. Miyatani, K. Minematsu, Y. Wada, F. Okamoto, K. Kato, and P. K. Baltzer, *J. Phys. Chem. Solids*, **32**, 1429 (1971).
4) A. W. Sleight and H. S. Jarrett, *ibid.*, **29**, 868 (1968).
5) G. Harbeke and H. Pinch, *Phys. Rev. Lett.*, **17**, 1090 (1966).
6) U. Westerlund-Helmerson, *At. Abs. Newslett.*, **5**, 97 (1966).
7) J. B. Ezell, Jr., *ibid.*, **6**, 84 (1967).
8) I. P. Kalinkin and V. B. Aleslovskii, *Izv. Vyssh. Ucheb. Zaved., Khim. Khim. Tekhnol.*, **6**, 553 (1963).
9) K. Minematsu, K. Miyatani, Y. Wada, and M. Kojima, Presented at the Spring Meeting of the Physical Society of Japan, Proceedings 6a-T-6, 1972, Tokyo.

BULLETIN OF THE CHEMICAL SOCIETY OF JAPAN, VOL. 47(1), 244—245 (1974)

The Structure of the Pechmann Condensation Product of *p*-Orsellinic Acid with Ethyl Acetoacetate

Toshifumi HIRATA and Takayuki SUGA*

Department of Chemistry, Faculty of Science, Hiroshima University, Higashisenda-machi, Hiroshima 730

(Received September 10, 1973)

Synopsis. The product obtained by the Pechmann condensation, followed by the decarboxylation, of *p*-orsellinic acid with ethyl acetoacetate has been established not to be such 4,5-dimethyl-7-hydroxycoumarin as previously reported, but to be 2,5-dimethyl-7-hydroxychromone.

In the course of the structural determination of aloenin,[1] a new bitter glucoside isolated from Aloe species, we carried out the Pechmann condensation of *p*-orsellinic acid (I) with ethyl acetoacetate, followed by the decarboxylation, with a view to obtaining 4,5-dimethyl-7-hydroxycoumarin (II) following the method in a literature.[2] However, all physico-chemical and chemical examinations indicated the product to be 2,5-dimethyl-7-hydroxychromone (III), but not the coumarin. We now wish to describe evidences leading to the chromone structure (III) for the product.

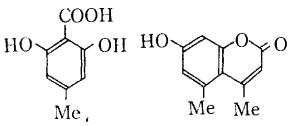

I

II

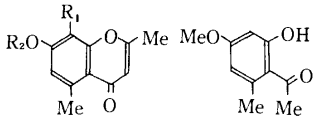

III: $R_1=R_2=H$ V

IV: $R_1=H$, $R_2=Me$

VI: $R_1=COOH$, $R_2=H$

VII: $R_1=COOMe$, $R_2=Me$

VIII: $R_1=H$, $R_2=Ac$

Results and Discussion

We repeated the treatment of *p*-orsellinic acid (I) with ethyl acetoacetate in the presence of sulfuric acid, followed by the decarboxylation, in accordance with Sethna's report[2] and obtained an *O*-heterocyclic compound (III), $C_{11}H_{10}O_3$, whose properties are identical with those reported by Sethna and Shah. The compound exhibited the IR and UV spectra characteristic of a chromone;[3,4] ν_{max} (dioxane) 1663 cm^{-1} (C=O) and λ_{max} (EtOH) 291 nm (log ε 4.08), 250 (4.31), and 241 (4.22). The alkaline degradation of its monomethyl ether (IV) yielded 2-hydroxy-4-methoxy-6-methylacetophenone (V). As the formation of the acetophenone derivative by such a degradation is also characteristic of a chromone,[5] the heterocyclic compound (III) appeared to be 2,5-dimethyl-7-hydroxychromone.

The chromone structure was proved by the mass spectrum, which exhibited a base peak of the parent ion at *m/e* 190 and two significant peaks capable of demonstrating the chromone skeleton at *m/e* 150 and 122. As shown in Scheme 1, the occurrence of the *m/e* 150 peak is caused by the retro-Diels-Alder cleavage, which has not been observed for coumarin derivatives yet,[6,7] with loss of acetylene and retention of the charge on the fragment. The fragment of mass 122 is formed by the sequential loss of a CO molecule from the *m/e* 150 ion. These fragments were completely characterized by high-resolution mass spectrum measurements.

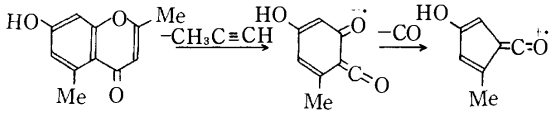

III, *m/e* 190 (M^+) *m/e* 150 *m/e* 122

Scheme 1.

The NMR spectrum of the monomethyl ether (IV) in a deuterochloroform solution showed signals of two methyl (at 2.25 and 2.77 ppm), one methoxy, two aromatic, and one ethylenic protons. The signal at 2.77 ppm was assigned to the C(5)-methyl group, because it is strongly deshielded by the adjacent carbonyl group.[8] This assignment was proved by the benzene-induced downfield shifts[9] ($\Delta\delta=-0.16$ ppm) observed only for the C(5)-methyl group. No such chemical shift and solvent effect in the NMR spectrum can be explained for 4,5-dimethyl-7-hydroxycoumarin (II) proposed previously by Sethna and Shah.[2] Thus, all evidences have established the condensation product (III) to be 2,5-dimethyl-7-hydroxychromone. Such a formation of the chromone is a unique example in the Pechmann condensation in the presence of sulfuric acid, although Simonis and Remmert[10] have described the formation of chromones in the presence of phosphorus pentoxide.

Experimental

The NMR spectra were recorded on a Hitachi Perkin-Elmer R-20 spectrometer. Mass spectral analyses were performed on a Hitachi RMU-7L high-resolution mass spectrometer and a Hitachi RMS-4 mass spectrometer, ionizing at the order of 70 eV.

The Condensation of p-*Orsellinic Acid (I) with Ethyl Acetoacetate.* Following the method in a literature,[2] *p*-orsellinic acid (I) (800 mg; mp 166—167 °C; prepared[11] from orcinol) was stirred with ethyl acetoacetate (640 mg) at 65—70 °C for 4 hr in the presence of sulfuric acid (8.4 ml) and the reaction mixture was poured into water to give a solid product, which then was ground up with a 5% sodium bicarbonate solution. The solution, on acidification, gave 2,5-dimethyl-7-hydroxychromone-8-carboxylic acid (VI) (342 mg): mp 222—225 °C (effervescence); IR (Nujol): 3500—2500 (OH and COOH), 1650 (C=O) and 1580 cm^{-1} (C=C); UV (EtOH): 304 nm (log ε 3.94), 282 (4.03), and 248 (4.41); MS: *m/e* (rel. intensity) 234 (M^+, 64), 216 (94), 190 (18), 188 (18), 160 (100), and 120 (28).

* To whom all inquiries regarding this paper should be addressed.

Found: C, 61.38; H, 4.51%. Calcd for $C_{12}H_{10}O_5$: C, 61.54; H, 4.30%.

The Dimethyl Derivative (VII). The treatment of the acid (VI) with diazomethane as usual gave the dimethyl derivative (VII): mp 147—148 °C; IR (Nujol): 1730 (COOMe), 1650 (C=O), and 1600 cm^{-1} (C=C); NMR ($CDCl_3$): δ 2.30 (s, C(2)-Me), 2.83 (s, C(5)-Me), 3.91 (s, COOMe), 3.94 (s, OMe), 6.01 (s, C(3)-H), and 6.69 ppm (s, C(6)-H); (C_6H_6) δ 1.52 (s, C(2)-Me), 2.97 (s, C(5)-Me), 3.18 (s, COOMe), 3.67 (s, OMe), 5.80 (s, C(3)-H), and 6.19 ppm (s, C(6)-H); MS: *m/e* (rel. intensity) 262 (M^+, 94), 230 (100), and 191 (51).

The Decarboxylation of the Acid (VI). The acid (VI) (100 mg) was maintained at 230 °C for 10 min, melting with the effervescence. The crystalline mass obtained after cooling was crystallized from ethanol to give the heterocyclic compound, 2,5-dimethyl-7-hydroxychromone (III) (48 mg): mp 245 °C (decomp.); IR (Dioxane): 1663 (C=O), 1615 and 1585 (C=C); UV (EtOH), described above; NMR (C_5H_5N): δ 2.06 (s, C(2)-Me) and 2.97 ppm (s, C(5)-Me); MS: *m/e* (rel. intensity) 190 (M^+, 100), 175 (3), 162 (33), 161 (43), 150 (18), and 122 (23); High-resolution MS: *m/e* 190.0636 (calcd for $C_{11}H_{10}O_3$: 190.0630), 162.0654 ($C_{10}H_{10}O_2$: 162.0680), 161.0594 ($C_{10}H_9O_2$: 161.0601), 150.0299 ($C_8H_6O_3$: 150.0316), and 122.0361 ($C_7H_6O_2$: 122.0366).

The Acetyl Derivative (VIII). Mp 117—118 °C; IR (Nujol): 1765, 1659, 1630, and 1615 cm^{-1}; ($CHCl_3$) 1769, 1654, and 1611 cm^{-1}; NMR ($CDCl_3$): δ 2.30 (s, C(2)-Me and OAc), 2.83 (s, C(5)-Me), 6.07 (s, C(3)-H), 6.83 (d, J=2.0 Hz, C(6)-H), and 7.06 ppm (d, J=2.0 Hz, C(8)-H).

The Monomethyl Ether (IV). The treatment of the chromone (III) with diazomethane gave the ether (IV): mp 116—117 °C (recrystallized from ethyl acetate); IR (KBr): 3050, 1655, 1628, 1610, and 1569 cm^{-1}; ($CHCl_3$) 1657, 1612, and 1570 cm^{-1}; NMR ($CDCl_3$): δ 2.25 (s, C(2)-Me), 2.77 (s, C(5)-Me), 3.81 (s, OMe), 5.95 (s, C(3)-H), 6.60 (s, C(6)- and C(8)-H); (C_6H_6) δ 1.64 (s, C(2)-Me), 2.93 (s, C(5)-Me), 3.24 (s, OMe), 5.84 (s, C(3)-H), 6.40 (d, J= 2.5 Hz, C(8)-H), and 6.51 ppm (d, J=2.5 Hz, C(6)-H); MS: *m/e* (rel. intensity) 204 (M^+, 100), 189 (2), 176 (9), 175 (10), 164 (7), and 161 (31).

The Alkaline Degradation of the Monomethyl Ether (IV). The monomethyl ether (IV) (36 mg) was refluxed in a mixture of 50% potassium hydroxide (4 ml) and ethanol (2 ml) for 2 hr in a current of nitrogen. The reaction mixture, after acidification, was extracted with ether and the ether extract was washed with a 5% sodium bicarbonate solution. Removal of the solvent afforded 2-hydroxy-4-methoxy-6-methylacetophenone (V) (25 mg): mp 78.0—78.5 °C (lit,[12] mp 79 °C); IR ($CHCl_3$): 1610 and 1585 cm^{-1}; UV (EtOH): 279 nm (log ε 4.13) and 231 (4.05); NMR ($CDCl_3$): δ 2.53 (s, C(6)-Me), 2.58 (s, $COCH_3$), 3.77 (s, OMe), 6.25 (s, aromatic 2H), and 13.48 ppm (s, phenolic OH); MS: *m/e* (rel. intensity) 180 (M^+, 28) and 165 (100); High-resolution MS: *m/e* 180.0779 (calcd for $C_{10}H_{12}O_3$: 180.0785) and 165.0532 ($C_9H_9O_3$: 165.0550).

Found: C, 66.53; H, 6.58%. Calcd for $C_{10}H_{12}O_3$: C, 66.65; H, 6.71%.

References

1) T. Suga, T. Hirata, and M. Odan, *Chem. Lett.*, **1972**, 547.
2) S. M. Sethna and R. C. Shah, *J. Indian Chem. Soc.*, **17**, 211 (1940).
3) F. M. Dean and D. R. Randell, *J. Chem. Soc.*, **1961**, 798.
4) J. H. Looker and W. W. Hanneman, *J. Org. Chem.*, **27**, 382 (1962).
5) W. Baker, *J. Chem. Soc.*, **1925**, 2349.
6) H. Budzikiewicz, J. I. Brauman, and C. Djerassi, *Tetrahedron*, **21**, 1855 (1965).
7) M. M. Badawi, M. B. E. Fayez, T. A. Brice, and R. I. Reed, *Chem. Ind.* (London), **1966**, 498.
8) C. Bonsall and J. Hill, *J. Chem. Soc., C*, **1967**, 1836.
9) D. H. Williams and N. S. Bhacca, *Tetrahedron*, **21**, 2021 (1965).
10) H. Simonis and P. Remmert, *Chem. Ber.*, **47**, 2229 (1914).
11) A. Robertson and R. Robinson, *J. Chem. Soc.*, **1927**, 2196.
12) K. Hoesch, *Chem. Ber.*, **48**, 1122 (1915).

BULLETIN OF THE CHEMICAL SOCIETY OF JAPAN, VOL. 47(1), 246 (1974)

Double Tridentate Complex of Triquinoyl with Boric Acid

Toshio Goto* and Masanori NAGAO**

Chemical Institute, Faculty of Science, Nagoya University, Nagoya 464

(Received August 25, 1973)

Synopsis. Triquinoyl forms with boric acid a strongly acid double-tridentate complex, dipotassium salt of which is almost insoluble in water. The formation of this complex supports dodecahydroxycyclohexane structure for triquinoyl.

It is well known that some polyol compounds form borate complexes,[1-3] which cause the increased acidity and conductivity of boric acid solutions after the addition of the polyols.[4] There are two types of the borate complexes. One type (**A**), which is usually called as Böeseken complex, is believed to involve *cis*-1,2-diol structures[2] and the borate-polyol reactions forming this type of complexes are usually reversible. Another type is seen in some borate–cyclitol complexes. Cyclitols having three *cis*-1,3,5-hydroxyl groups form complexes by a three-point attachment as in **B**, which are referred to as tridentate complexes.[5,6] The complexes are usually stable and strong acids.[5] *cis*-Phloroglucitol makes tridentate complex (**B**) from its less stable chair form. *cis*-Inositol with three axial hydroxyl groups on the same side of the ring in either chair form, forms by far the firmest complex. Scyllitol in its all equatorial conformation cannot form a tridentate complex and hence forms no borate complex under mild conditions,[5] but under forced conditions it could form a double tridentate complex with borate.[7]

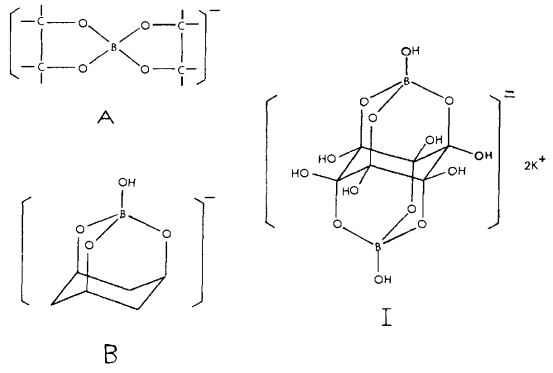

A B I

We found that triquinoyl also forms a stable complex with borate in a 1:2 ratio. When 1 M KCl solution (10 ml) was added to an aqueous 0.5 M boric acid solution (20 ml) of triquinoyl (60 mg) white precipitate appeared immediately, which was collected by centrifugation and washed with water (pH of the supernatant was 2.4). When the borate solution of triquinoyl was slowly titrated with 0.1 M KOH solution two equivalents of KOH per 1 mol of triquinoyl were consumed and crystalline precipitate was formed. The precipitate shows no definite mp, no UV absorption, and apparent pK_a at *ca.* 2.6, and is almost insoluble in water and usual organic solvents, but soluble in conc. HCl; IR spectrum is shown in Fig. 1.

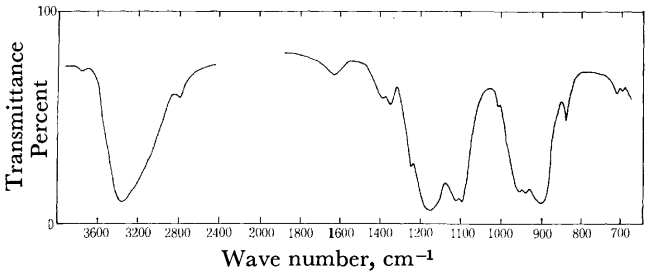

Fig. 1. Infrared spectrum of I.

Found: B, 5.20; K, 19.3%. Calcd for $C_6H_8O_{14}B_2K_2$: B, 5.36; K, 19.35%. The complex is assigned to have the double tridentate structure (**I**) from its elemental analysis, titration equivalent, apparent pK_a, and by analogy from other tridentate complexes.[8]

Böeseken and Meuwissen[9] observed that triquinoyl increases the electronic conductivity of boric acid. They had suggested the structure of triquinoyl as the completely hydrated form, dodecahydroxycyclohexane $[C_6(OH)_{12}\cdot 2H_2O]$, which was later confirmed by IR spectroscopic analysis.[10] The formation of the double tridentate borate complex supports this structure.

References

1) W. Gerrard, *Chem. Ind.* (London), **1966**, 832.
2) J. Böeseken, *Adv. Carbohydrate Chem.*, **4**, 189 (1949).
3) A. B. Foster, *J. Chem. Soc.*, **1953**, 982; A. B. Foster and M. Stacey, *ibid.*, **1955**, 1778.
4) J. J. Fox and A. J. H. Gauge, *ibid.*, **99**, 1075 (1911).
5) S. J. Angyal and D. J. McHugh, *ibid.*, **1957**, 1423.
6) A. B. Foster, *Chem. Ind.* (London), **1953**, 951.
7) A. Weissbach, *J. Org. Chem.*, **23**, 329 (1958).
8) Leuconic acid also forms insoluble barium salt of its borate complex. Alkaline titration indicated 1:1 ratio of leuconic acid and borate. Elemental analysis indicates the composition of $C_5H_6O_{10}BBa_{0.5}\cdot 5$—$6\ H_2O$ (Found: Ba, 17.4; B, 2.64%. Calcd for $C_5H_6O_{10}BBa_{0.5}\cdot 5H_2O$: Ba, 17.36; B, 2.73; for $C_5H_6O_{10}BBa_{0.5}\cdot 6H_2O$: Ba, 16.60; B, 2.62%); removal of water by heating causes gradual decomposition. Polymer structures similar to Böeseken complex **A** may be assumed for this complex.
9) J. Böeseken and J. C. Meuwissen, *Rec. Trav. Chim. Pays-Bas*, **45**, 496 (1926).
10) W. B. Person and D. G. Williams, *J. Phys. Chem.*, **61**, 1017 (1957).

* Present address: Department of Agricultural Chemistry, Nagoya University, Chikusa, Nagoya 464. All correspondences should be addressed to this address.

** Present address: Central Research Laboratories, Ajinomoto Co., Inc., Suzuki-cho, Kawasaki-ku, Kawasaki 210.

BULLETIN OF THE CHEMICAL SOCIETY OF JAPAN, VOL. 47(1), 247—248 (1974)

Vapor-Liquid Equilibrium in the 2-Butanol-Water System and the Effect of Uranyl Nitrate

Norio Yui, Yōichi Kurokawa, and Hiroyuki Ōtsuki

Department of Applied Science, Faculty of Engineering, Tohoku University, Aramaki, Sendai 980

(Received April 13, 1973)

Synopsis. Vapor-liquid equilibrium have been investigated by a modified Randall's method. The activities of solvents showed positive deviation from Raoult's law. There was a sign of salting effect on 2-butanol by addition of uranyl nitrate hexahydrate.

When the solute is non-volatile, the activity of the solvent or the behavior of the solute can be obtained from measurements of the change in the vapor pressure caused by the presence of the solute. Therefore, vapor-liquid equilibrium data for both 2-butanol–water and 2-butanol–water–uranyl nitrate systems have been determined at atmospheric pressure and 25 °C by a modification of Randall's method.

Experimental

Reagents: 2-Butanol and Uranyl Nitrate Hexahydrate. Reagent-grade chemicals were used without further purification. The conductivity water was prepared by the passage of the distilled water through mixed-bed ion-exchange resins.

Procedure. The vapor pressures of the 2-butanol and water system have been determined by a modification of Randall's method, as is shown in Fig. 1.[1,6]

Analysis. The condensates in the high butanol range remaining in a single phase and the aqueous solution containing a large proportion of water were analyzed by means of an Abbe refractometer. Most of the condensates separated into two phases upon standing at room temperature. They were diluted with sufficient *tert*-butyl alcohol to produce a homogeneous solution, and then the solutions were analyzed by gas chromatography.[6]

Results and Discussion

2-Butanol–Water System. The results of the experimental vapor-liquid equilibrium measurements are given in Fig. 2. The experimental value is the mean of two or three runs determined in each experiment. Assuming that the vapor phase obeys the ideal gas law over the complete concentration range, then the activity in the solution is given by $p/p°$. The saturated vapor pressure of a solvent at 25 °C was taken from Ref. 6 ($p°_1$: 23.7, $p°_2$: 17.1 mmHg). Activities are shown in Fig. 3. A positive deviation from Raoult's law, which is represented by the straight line, occurs as predicted. A discontinuous portion of the curve is not realized except in the two-phase region. The activity of the solvent must be the same in the two phases, which are in equilibrium with each other, because the chemical potential of the solvent is the same in each phase. Therefore, the dashed line, which indicates the region of the two phases, parallels the abscissa in the figures. However, in Fig. 3 the axes in water-rich region are magnified so as to be observed easily, and so the discontinuous portion is not shown clearly.

The values are comparable to those of the isomeric butanols.[1,2] Palit has attributed the difference in the solubility of isomeric alcohol in water to the difference in the effects of the hydroxyl group upon electron displacement in the hydrocarbon chain.[3] Paterson reported that the rate of proton exchange increased linearly with the water concentration, and that the τ (s) value for the attachment of the proton in the alcoholic OH group increased in this sequence; n-<

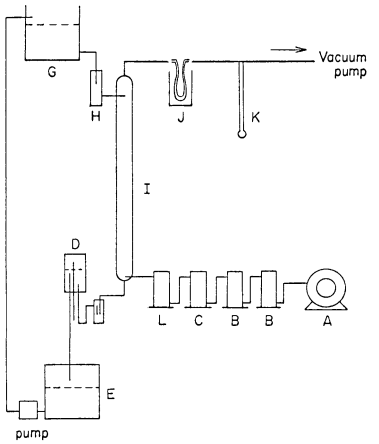

Fig. 1. Apparatus for measuring vapor pressure.
A: wet gas meter, B: $CaCl_2$ tube, C: soda lime tube D, H: flow regulator, E: lower sample tank, G: upper sample tank, I: packing tower, J: trap (Dewar vessel), K: manometer, L: bubbling tube

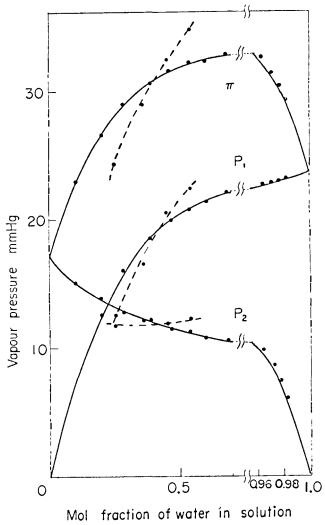

Fig. 2. Partial and total vapor pressures of 2-butanol–water system at 25 °C.
p_1: water, p_2: 2-butanol, slant dotted lines denote the effect of uranyl nitrate on the system of 2-butanol–water

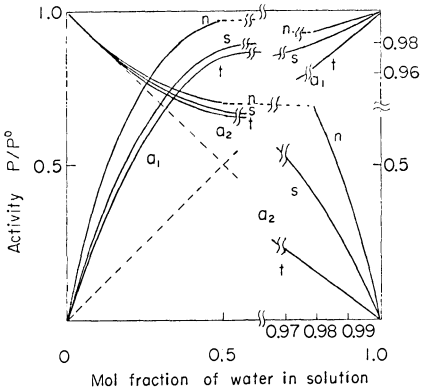

Fig. 3. Activities of components in isomeric butanol–water system at 25 °C. n, s, and t denote *n*-, *sec*-, and *tert*-butanol, respectively

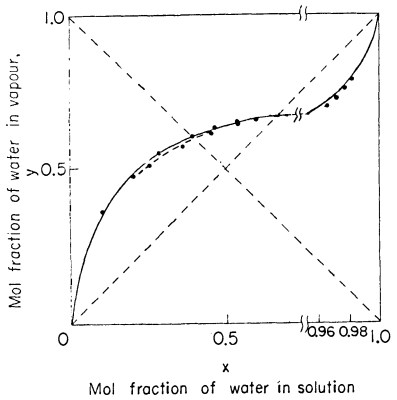

Fig. 4. Vapor-liquid equilibrium (x–y plot)
Solid line: 2-butanol–water
Slant dotted line: 2-butanol–water–uranyl nitrate

iso-<*sec*-<*tert*-butyl alcohol.[4,5] This is the same order as those of the increasing proton-accepting facility and of the deviation from Raoult's law. Positive deviations from Raoult's law are favored differences in the internal pressure or in the molecular-attractive forces, and therefore the activity coefficient, γ, yields much information on the nature of the latter. The increase in γ can bring about a separation into two liquid phases because the two components have their own attractive forces, dissimilar to one another.

The van Laar equation was found to fit the data for the system more closely than the Margules equation, much as in the case of the 1-butanol–water system.[6] The separation of γ into the enthalpy and entropy terms is quite general; they can not be exactly separated. In general, the contribution of the entropy term to γ is larger than that of the enthalpy. Isomeric butanols have almost equal molal volumes. Therefore, the entropy terms may not be so different. Consequently, it seems that the difference in γ of the isomeric butanols must be due to the enthalpy term.

Effect of Uranyl Nitrate on the Vapor-Liquid Equilibrium. The effect of the addition of $UO_2(NO_3)_2 \cdot 6H_2O$ on the 2-butanol–water system was determined, also the behavior of the distribution of the salt in the region of the liquid-liquid distribution was discussed. The addition of a salt to an aqueous solution of a non-electrolyte has a marked effect upon the vapor-liquid equilibrium; may either raise or lower the relative volatility of the non-electrolyte, or in an extreme case, cause the formation of two liquid phases. Various experimental studies of the salt effect on the vapor-liquid equilibrium have been reported.[7] However, these investigations have dealt almost exclusively with the equilibrium either at the boiling point or with a saturated salt concentration. On the other hand, only a few investigations at 25 °C have been performed. The knowledge of the vapor-liquid equilibrium accounts for the behavior of the salt in the range of the two liquid distribution. Each solvent for the liquid sample was determined by means of a refractometer after the salt has been removed by distillation.

The experimental data are shown graphically in Fig. 2 (slant dotted line). The liquid compositions were plotted on a salt-free basis. The addition of uranyl nitrate to the system resulted in an increase in the partial pressures of both water and 2-butanol above *ca.* a 0.5 mol fraction of water, while below that fraction it resulted in a decrease in both. As is shown in Fig. 4, there is a considerable salting-out of 2-butanol. This may be interpreted as being due to a breaking up or a loosening of the interaction between 2-butanol and water molecules. Consequently, the salting-out should largely be due to a preferential attraction between water molecules and uranyl nitrate. Whether uranyl nitrate with a net hydration of six water molecules appears in the butanol phase must depend largely on the competitive strength of the butanol and water molecules with respect to coordination with the uranyl nitrate. However, in this case, 2-butanol may not replace the water molecules as other solvents do.[8] Katzin *et al.* inspected the phase diagram in the region of the liquid-liquid distribution and found that the uranyl nitrate was extracted into the 2-methylpropanol phase with four water molecules coordinated.[6] Considering this result, in the 2-butanol phase it probably takes either $UO_2^{2+}\text{-}(NO_3^-)_2 \cdot (H_2O)_4 \cdot 2H_2O$ form just as in the aqueous phase, or $UO_2^{2+}(NO_3^-)_2 \cdot (H_2O)_4 \cdot x\text{BuOH}$ form and the former joins the water molecules by hydrogen bonding, thus forming the second solvation shell. This can also be suggested on the basis of spectrophotometric measurements with IR and UV.

References

1) M. Randall and H. P. Weber, *J. Phys. Chem.*, **44**, 917 (1940).
2) A. C. Brown and D. J. G. Ives, *J. Chem. Soc.*, **1962**, 1608.
3) S. Palit, *J. Phys. Colloid Chem.*, **51**, 837 (1947).
4) W. G. Paterson, *Can. J. Chem.*, **41**, 2477 (1963).
5) F. Franks and D. J. G. Ives, *Quart. Revs.*, **20**, 1 (1966).
6) H. Otsuki, Y. Kurokawa, and N. Yui, *Tech. Reports Tohoku Univ.*, **38**, 197, 461 (1973).
7) A. L. Thomson and W. F. Furter, *Can. J. Chem. Eng.*, **43**, 356 (1965).
8) L. I. Katzin and J. C. Sullivan, *J. Phys. Colloid Chem.*, **55**, 346 (1951).

The Electrodepositions of Copper and Nickel from Their Trifluoroacetate-Formamide Baths

Tatsuko TAKEI

The Faculty of Engineering, Shinshu University, Wakasato, Nagano 380

(Received March 9, 1973)

The present author has been studying the electrodeposition of metals from non-aqueous solutions of metal trifluoroacetates. In the present study, the properties of the $Cu(CF_3COO)_2$–$HCONH_2$ bath and the $Ni(CF_3COO)_2$–$HCONH_2$ bath, and the mechanism of the electrodeposition of copper and nickel from these baths, were studied. Both $Cu(CF_3COO)_2$ and $Ni(CF_3COO)_2$ were easily dissolved in formamide. The specific conductance of these solutions was high. Satisfactory electrodeposits are obtained from these solutions, with a high current efficiency. The cross-section of the electrodeposits showed a granular structure. The rate of the electrodeposition of copper from the $Cu(CF_3COO)_2$–$HCONH_2$ bath and that of nickel from the $Ni(CF_3COO)_2$–$HCONH_2$ bath were controlled by the charge-transfer reaction at low current densities. The activation overvoltage of the hydrogen-evolution reaction for the electrolysis of the CF_3COOH–$HCONH_2$ bath was higher than that for the electrolysis of the CF_3COOH–H_2O bath.

Menzies *et al.*[1] and Brenner[2,3] pointed out the importance of the study of the electrodeposition of metals from non-aqueous solutions. Studies[2–5] have already been made of various metals.

However, none has thus far been used industrially. In the deposition of metals from non-aqueous solutions, it is hard to find metal salts that are readily soluble in an organic solvent or a solvent which forms a complex ion in a suitable strength with metal ions in the solutions. Moreover, little is known about the properties of the solutions and the mechanism of the electrodeposition of metals.

The present author has been studying the electrodeposition of metals from non-aqueous solvents by the use of metal salts of trifluoroacetic acid. In the present study, examinations were made into the nature of the $Cu(CF_3COO)_2$–$HCONH_2$ bath and that of the $Ni(CF_3COO)_2$–$HCONH_2$ bath, which dissolve $Cu(CF_3COO)_2$ or $Ni(CF_3COO)_2$ respectively, using formamide. Formamide has a high boiling point and a high dielectric constant and readily forms complex ions with metal ions. Electrodeposition was performed in these baths in order to examine the effect of the condition of electrolysis on the current efficiency and on the electrodeposit. The overvoltages were measured by the interrupter method in order to analyze the electrodeposition reactions. Measurements were also made on the hydrogen overvoltage in the formamide bath.

The deposition of copper from the $Cu(CF_3COO)_2$–$HCONH_2$ bath was compared with that of nickel from the $Ni(CF_3COO)_2$–$HCONH_2$ bath.

Experimental

Reagent. *Formamide*: For the measurement of the conductance, the solubility, and the viscosity, guaranteed reagent-grade formamide containing about 0.02% moisture was used. For the electrodeposition and the measurement of the overvoltage, commercial first-grade reagent formamide containing about 0.12% moisture was used.

$Cu(CF_3COO)_2$ and $Ni(CF_3COO)_2$: These substances were prepared by the neutralization method from copper hydroxide and nickel hydroxide with trifluoroacetic acid. The purities of the corresponding products were 99.4 and 99.8% respectively.

Other Chemicals: Phosphoric acid and acetic acid of the first-grade reagent were used. Sulfuric-, nitric-, and hydrochloric acids of a special grade were used.

Measurement of the Solubility. The solubility of $Cu(CF_3COO)_2$ in formamide was measured by the gravimetric determination of copper in a definite amount of a saturated solution obtained by dissolving $Cu(CF_3COO)_2$ in formamide at 20 °C. The gravimetric determination of copper was done by the use of oxine.

Measurement of the Conductance. The electrolytic conductance of $Cu(CF_3COO)_2$–$HCONH_2$ and $Ni(CF_3COO)_2$–$HCONH_2$ solutions was determined by the use of a Yanagimoto electrolytic conductometer MY-7. Before the measurement the solutions to be measured were kept for about an hour at 30, 40, and 50 °C in a thermostat.

Viscosity Measurement. The viscosity of the $Ni(CF_3COO)_2$–$HCONH_2$ solutions was measured by means of an Ostwald viscosimeter at 30.0±0.1 °C.

Density Measurement. The densities of the formamide and $Ni(CF_3COO)_2$–$HCONH_2$ solutions were determined by the use of a Springel densimeter at 30.0±0.1 °C.

Electrodeposition. The electrodeposition was performed by the use of the apparatus shown in Fig. 1. In the case of

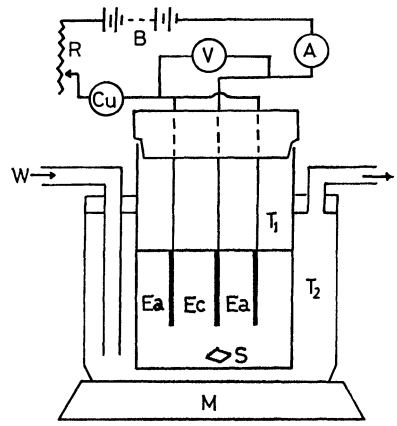

Fig. 1. Apparatus for metal plating.
A: Ammeter, B: Battery, Cu: Copper coulometer, Ea: anode, Ec: cathode, M: Magnetic stirrer, R: Slide rheostat, S: Stirrer, T_1: Electrolysis cell, T_2: Thermostat, V: Voltmeter, W: Water (const. temp.)

copper electrodeposition, two copper plates and one iron plate were used as anode and cathode respectively. For nickel deposition, two nickel plates and one copper plate were used as anode and cathode respectively. These electrodes were pretreated by the usual method as indicated.[6] Nitrogen was passed through formamide for about 30 minutes. A definite amount of the $Cu(CF_3COO)_2$ or $Ni(CF_3COO)_2$ was dissolved in the formamide solution to give a bath used for the electrodeposition. The bath was stirred at a definite rate. The electrodeposition was carried out at a current density of 0.5—15.0 A/dm² at 30—70 °C.

The thickness of the electrodeposited layer was about 5 μ, the thickness being calculated from the amount electricity used for the deposition.

Observation of the Electrodeposited Surface and the Electrodeposited Layer. For these observations, a metallurgical microscope was used.

The specimen with an electrodeposited layer, about 30 μ thick, was mounted in resin and etched.

Analysis of Gases and Electrolytic Solutions. During the electrolysis, a slight evolution of gases from the cathode and the anode was noticed. Therefore, the gases and the electrolytic solution were analyzed by gas-chromatography in order to examine the composition of the gases and the mechanism of the reaction. For the measurement, a gas-chromatograph, Type GCG-220, made by the Yanagimoto Manufacturing Co., Ltd, was used. The packing materials of the column were silicon DC 550 at 53 °C and 100 °C, and active carbon at 33 °C, used for the analysis of the electrolytic solution and of the gas respectively.

Measurement of the Overvoltage. The overvoltage of the copper electrodeposition was measured at 30, 40, and 50 °C for the baths containing 100, 200, and 400 g $Cu(CF_3COO)_2$ per liter respectively. The overvoltage of nickel deposition was measured at 50, 60, and 70 °C for the baths containing 50, 100, 150 g $Ni(CF_3COO)_2$ per liter respectively. The measuement was made by the current-interrupter method, with stirring at a definite rate.

The measurement of the overvoltage of hydrogen evolution was made by the same method as above at 50 °C, in a 0.1 N CF_3COOH–H_2O bath and also in a 0.1 N CF_3COOH–$HCONH_2$ bath.

A platinized-platinum electrode (length, 3 mm; diameter, 0.3 mm) was used as a reference electrode for the measurement of the overvoltage.

A current-interrupter, Type CI-2515, made by the Hokuto Electric Works Co., Ltd., was used.

Results and Discussion

The Properties of Formamide Solutions. Solvolysis: According to Röhler, solvolysis takes place in formamide solutions of copper sulfate and nickel chloride.[7] Therefore, solvolysis can be expected to take place in formamide solutions of $Cu(CF_3COO)_2$ and $Ni(CF_3COO)_2$ by means of the following reaction:

$$M(CF_3COO)_2 + 4HCONH_2 \rightarrow M(HCONH)_2 \cdot 2HCONH_2 + 2CF_3COOH \quad (1)$$

where M represents copper or nickel.

Actually, a light yellow-green precipitate is formed in the $Ni(CF_3COO)_2$–$HCONH_2$ solution by the reaction of $Ni(CF_3COO)_2$ with formamide. This reaction becomes more remarkable with a rise in the bath temperature and with an increase in the $Ni(CF_3COO)_2$ concentration.

When the reaction product was filtered, an almost colorless filtrate was obtained. The gas-chromatographic analysis of this solution showed the presence of CF_3COOH. The precipitate was washed, dried, and then gravimetrically analyzed with dimethyl glyoxime in order to determine the nickel content in the precipitate. The nickel content was about 96.8% of the theoretical amount of Ni in $Ni(HCONH)_2 \cdot 2HCONH_2$. It was found by these results that the reaction shown in Eq. (1) takes place in the $Ni(CF_3COO)_2$–$HCONH_2$ solution.

CF_3COOH was also detected in the $Cu(CF_3COO)_2$–$HCONH_2$ solution. Therefore, it is likely that the reaction shown by Eq. (1) also takes place in this bath.

Solubility. At 20 °C, 182 g $Cu(CF_3COO)_2$ was dissolved in 100 g of formamide. Consequently, the solubility of $Cu(CF_3COO)_2$ in formamide is larger than those in methanol and acetonitrile[8]. The solvolysis takes place very easily in a formamide solution with a high concentration of $Ni(CF_3COO)_2$. Therefore, the solubility of $Ni(CF_3COO)_2$ in formamide could not be determined.

Specific Conductance. Figure 2 shows the specific conductance of the $Cu(CF_3COO)_2$–$HCONH_2$ solution. The specific conductance of the $Cu(CF_3COO)_2$–$HCONH_2$ solution was almost the same as that of the $Ni(CF_3COO)_2$–$HCONH_2$ solution and about 1.5 times that of the $Cu(CF_3COO)_2$–MeOH solution.[8]

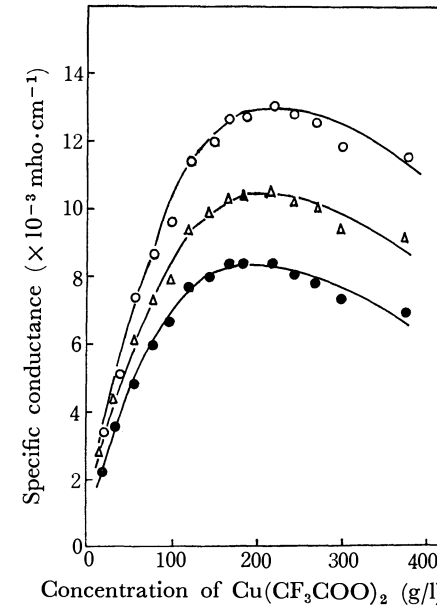

Fig. 2. Specific conductance of $Cu(CF_3COO)_2$–$HCONH_2$ solutions.
-●-: 30 °C, -△-: 40°C, -○-: 50°C

The specific conductance approached a definite value when the $Cu(CF_3COO)_2$ concentration reached about 200 g/l at any temperature. In the solutions containing more than 200 g of $Cu(CF_3COO)_2$, copper trifluoroacetate does not seem to dissociate any more; on the contrary, it seems that the movement of ions in the solutions is interfered with by the presence of non-dissociated salts.

Viscosity. The viscosity of the $Ni(CF_3COO)_2$–

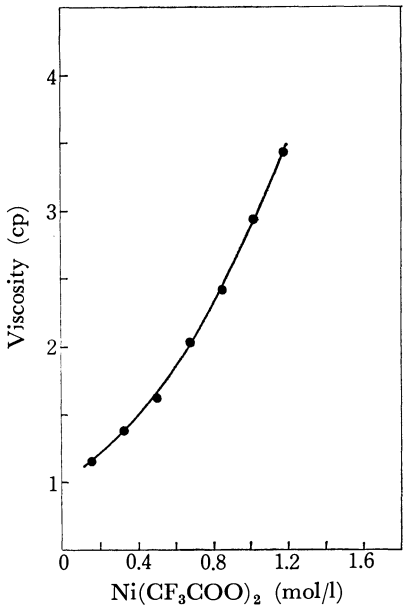

Fig. 3. Relationship between viscosity and concentration of $Ni(CF_3COO)_2$ in $Ni(CF_3COO)_2$–$HCONH_2$ solutions at 30°C.

$HCONH_2$ solution as a function of the concentration of $Ni(CF_3COO)_2$ is shown in Fig. 3. It may be seen in Fig. 3 that the viscosity increases almost linearly with the increase in the $Ni(CF_3COO)_2$ concentration. It thus appears that the viscosity of the $Cu(CF_3COO)_2$–$HCONH_2$ solution increases with the increase in the $Cu(CF_3COO)_2$ concentration, like that of the Ni-$(CF_3COO)_2$–$HCONH_2$ solution.

Electrodeposition. Copper Electrodeposition: Figure 4 shows an example of the current density-current

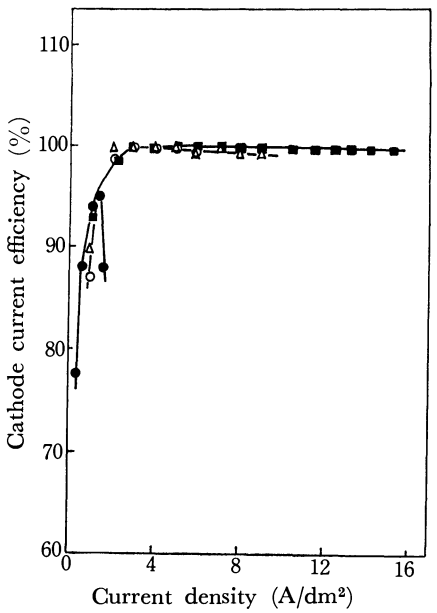

Fig. 4—1. Cathode current efficiency as a function of current density at 40°C.
-●-: $Cu(CF_3COO)_2$ 20 g/$HCONH_2$ 1 l
-○-: $Cu(CF_3COO)_2$ 100 g/$HCONH_2$ 1 l
-△-: $Cu(CF_3COO)_2$ 200 g/$HCONH_2$ 1 l
-■-: $Cu(CF_3COO)_2$ 400 g/$HCONH_2$ 1 l

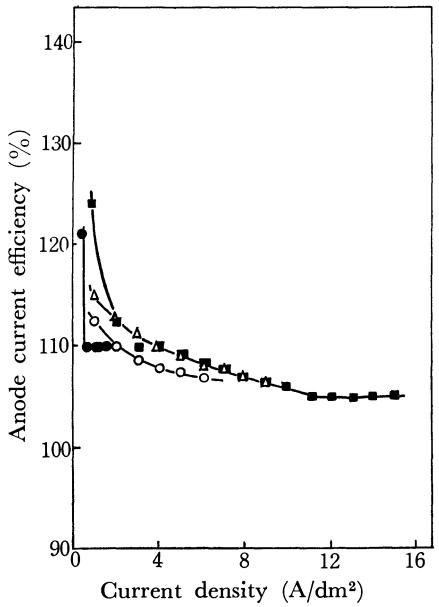

Fig. 4—2. Anode current efficiency as a function of current density at 40 °C.
-●-: $Cu(CF_3COO)_2$ 20 g/$HCONH_2$ 1 l
-○-: $Cu(CF_3COO)_2$ 100 g/$HCONH_2$ 1 l
-△-: $Cu(CF_3COO)_2$ 200 g/$HCONH_2$ 1 l
-■-: $Cu(CF_3COO)_2$ 400 g/$HCONH_2$ 1 l

efficiency curve of copper deposition from the Cu-$(CF_3COO)_2$–$HCONH_2$ bath.

The cathodic current efficiency was close to 100% irrespective of the $Cu(CF_3COO)_2$ concentration. However, the efficiency tends to decrease with the rise in the bath temperature.

It was noticed that a very small amount of hydrogen gas evolved from the cathode during the electrolysis. The lowering of the cathodic current efficiency is attributable to this evolution of hydrogen gas. The evolution of hydrogen gas is attributable to the discharge of hydrogen ions formed by the dissociation of CF_3-COOH, which was itself derived from the reaction shown in Eq. (1).

On the other hand, the anodic current efficiency was found to be more than 100% irrespective of the concentration of $Cu(CF_3COO)_2$ and of the bath temperature. The efficiency even exceeded 110% at a low current density. This efficiency is attributable to the chemical reaction of copper with the CF_3COOH formed by the reaction given by Eq. (1).

No gases evolved from the anode.

Figure 5 shows the current density region in which bright and smooth deposits are obtained. At any temperature, bright and smooth deposits were observed over a wide range of current density when the concentration of $Cu(CF_3COO)_2$ was high.

From the results mentioned above, it was confirmed that bright and smooth deposits of copper are obtained with a high efficiency over a wide region of current density from the $Cu(CF_3COO)_2$ 400 g/l–$HCONH_2$ bath at 40 °C.

Electrodeposition of Nickel: An example of the current density-current efficiency curve for the nickel deposition from $Ni(CF_3COO)_2$–$HCONH_2$ bath is shown

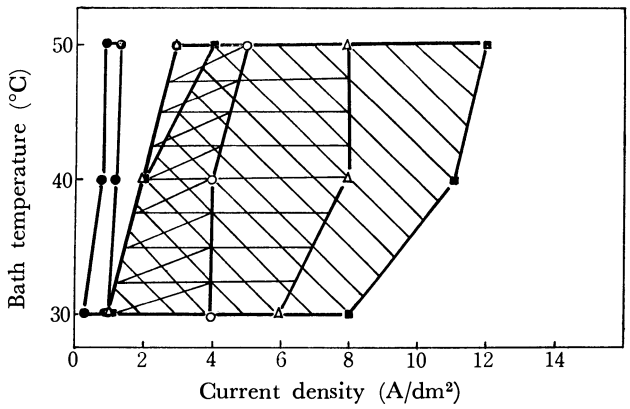

Fig. 5. The range of current density for bright and smooth copper deposit.
●: $Cu(CF_3COO)_2$ 20 g/$HCONH_2$ 1 l
○: $Cu(CF_3COO)_2$ 100 g/$HCONH_2$ 1 l
△: $Cu(CF_3COO)_2$ 200 g/$HCONH_2$ 1 l
■: $Cu(CF_3COO)_2$ 400 g/$HCONH_2$ 1 l

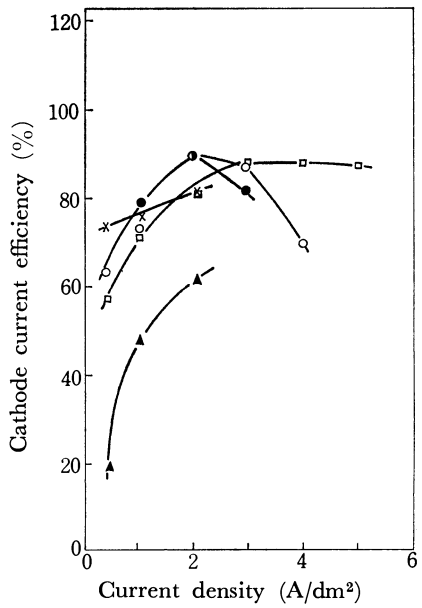

Fig. 6—1. Cathode current efficiency as a function of current density for $Ni(CF_3COO)_2$-$HCONH_2$ baths at 50 °C.
-▲-: $Ni(CF_3COO)_2$ 20 g/$HCONH_2$ 1 l
-□-: $Ni(CF_3COO)_2$ 80 g/$HCONH_2$ 1 l
-○-: $Ni(CF_3COO)_2$ 100 g/$HCONH_2$ 1 l
-✳-: $Ni(CF_3COO)_2$ 150 g/$HCONH_2$ 1 l
-●-: $Ni(CF_3COO)_2$ 200 g/$HCONH_2$ 1 l

in Fig. 6.

With the increase in the $Ni(CF_3COO)_2$ concentration, the cathodic current efficiency increased, but the anodic current efficiency tended to decrease.

When the $Ni(CF_3COO)_2$ concentration was 80—100 g/l, the anodic current efficiency was close to 100% irrespective of the bath temperature. However, the cathodic current efficiency was low at 50 °C and 70 °C when the current density was high. Only at 60 °C was the efficiency about 90% at a high current density.

The discharge of the H^+ formed by the dissociation

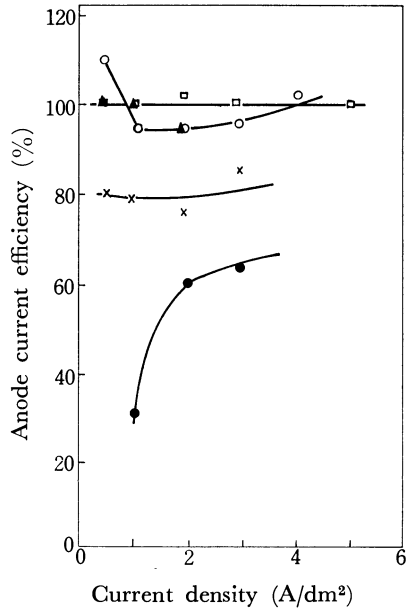

Fig. 6—2. Anode current efficiency as a function of current density for $Ni(CF_3COO)_2$-$HCONH_2$ baths at 50 °C.
-▲-: $Ni(CF_3COO)_2$ 20 g/$HCONH_2$ 1 l
-□-: $Ni(CF_3COO)_2$ 80 g/$HCONH_2$ 1 l
-○-: $Ni(CF_3COO)_2$ 100 g/$HCONH_2$ 1 l
-✳-: $Ni(CF_3COO)_2$ 150 g/$HCONH_2$ 1 l
-●-: $Ni(CF_3COO)_2$ 200 g/$HCONH_2$ 1 l

of CF_3COOH in the bath occurred on the cathode during the electrolysis in the $Ni(CF_3COO)_2$-$HCONH_2$ bath, as in the case of the $Cu(CF_3COO)_2$-$HCONH_2$ bath, resulting in the evolution of a small amount of hydrogen. From the $Ni(CF_3COO)_2$-$HCONH_2$ bath, the evolution of carbon dioxide gas occurred from the anode. However, the amount of carbon dioxide evolved was much smaller than that of the gas evolved from the cathode.

The deposits from the $Ni(CF_3COO)_2$-$HCONH_2$ bath were easily peeled off from the substrate when the $Ni(CF_3COO)_2$ concentration or the bath temperature was low. Table 1 shows the current-density region in which a lustrous and adherent nickel deposit is obtained.

From the results mentioned above, it was confirmed that the conditions which give a lustrous and adherent deposit from the $Ni(CF_3COO)_2$-$HCONH_2$ bath with a high efficiency are: $Ni(CF_3COO)_2$ concentration,

TABLE 1. THE RANGE OF CURRENT DENSITY FOR BRIGHT AND ADHERENT NICKEL DEPOSIT IN $Ni(CF_3COO)_2$-$HCONH_2$ BATH
(unit of current density : A/dm²)

Bath temp. (°C)	$Ni(CF_3COO)_2$ (g/l)			
	80	100	150	200
40	1.0—2.0		0.5—1.0	
50	1.0—2.0	1.0—2.0	0.5—2.0	1.0—2.0
60		0.5—2.0		
70		0.5—4.0		

80—100 g/l; bath temperature, 60 °C; and current density, 0.5—2.0 A/dm².

It will be possible to widen the current-density region which gives satisfactory deposits if the adherence of the deposits to the substrate is improved by the addition of an appropriate additive to the $Ni(CF_3COO)_2$–$HCONH_2$ bath.

Appearance on Deposited Surface and the Structure of the Deposited Layer. An example of the deposited surface and the deposited layer of nickel and copper is shown in Photograph 1. The deposited surfaces of copper and nickel are very smooth and consist of very fine grains when the deposition has been made at a low current density. The grains on the electrodeposited surface of nickel were especially fine. With the increase in the current density, all the deposits tended to show round blocks and cracks.

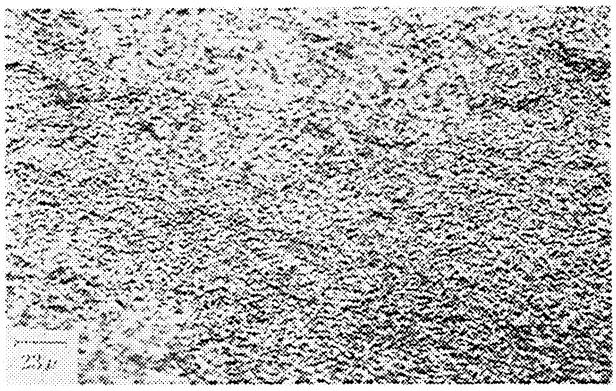

Photo. 1—1. Surface of copper deposit obtained from $Cu(CF_3COO)_2$ (400 g)/$HCONH_2$ (1 l) bath at 11.0 A/dm² at 50 °C.

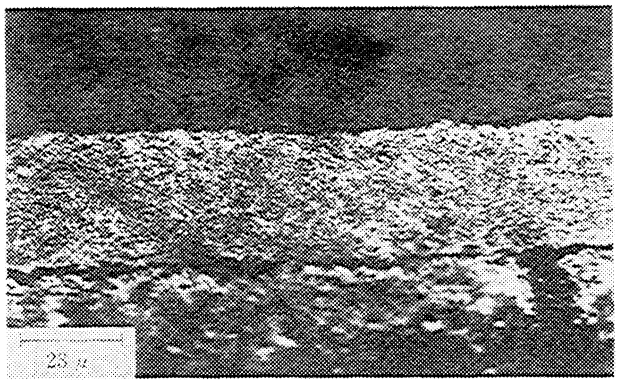

Photo. 1—2. Cross-section of copper deposit obtained from $Cu(CF_3COO)_2$ (400 g)/$HCONH_2$ (1 l) bath at 4.0 A/dm² at 30 °C.

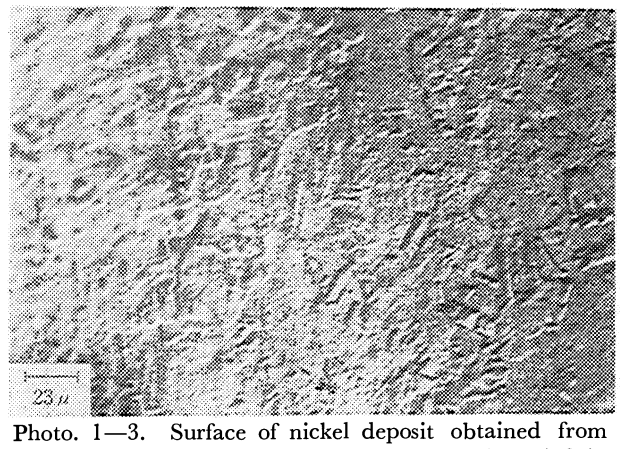

Photo. 1—3. Surface of nickel deposit obtained from $Ni(CF_3COO)_2$ (100 g)/$HCONH_2$ (1 l) bath at 1.0 A/dm² at 60 °C.

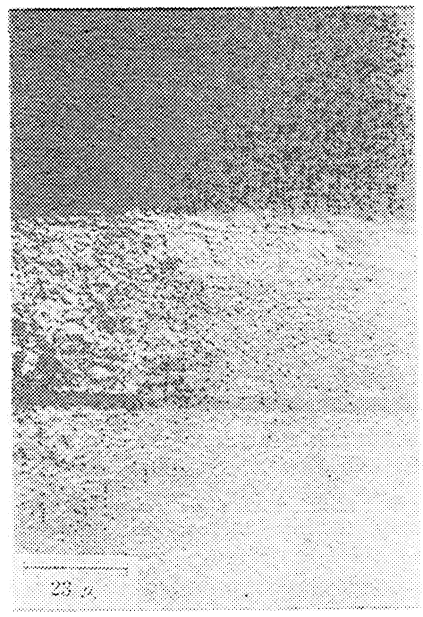

Photo. 1—4. Cross-section of nickel deposit obtained from $Ni(CF_3COO)_2$ (100 g)/$HCONH_2$ (1 l) bath at 1.0 A/dm² at 50 °C.

It was possible to obtain dense deposits when the bath temperature was high.

The structures of the deposits of copper and nickel were granular. The copper- and nickel- ions in the $HCONH_2$ baths form complex ions. The ligands which are adsorbed on the electrode during electrodeposition, suppress any surface diffusion of the adatom and prevent the growth of the nucleus in the vertical direction. Therefore, the frequency of the nucleus formation increases. It appears that the fine grains are produced to form a granular structure.

Activation Overvoltage. From the decay curve of the overvoltage 4 ms after the interruption of the electrolytic current, the resistance polarization was subtracted. The remainder was assumed to be the activation overvoltage.

The Relation between the Current Density (i_c) and the Activation Overvoltage (η_c) of the Electrodeposition of Copper or Nickel: The electrodeposition of metals from the solvated metal complex ions is [11] generally complicated.

This experiment was based upon the thought that the charge-transfer reaction is rate-determining within the range of current density (*i.e.* the Tafel region) with a straight-line relation between the current density and the activation overvoltage. According to the present experiment, the Tafel region was found to be in the range of current density, of 0.7—1.5 A/dm² at a bath temperature of 30 °C, in that of 0.8—2.0 A/dm² at 40 °C, and in that of 0.9—3.5 A/dm² at 50 °C for copper deposition. The ranges of the current density were 0.9—2.3 A/dm² at 50 °C, 0.9—4.4 A/dm² at 60 °C, and 0.9—4.8 A/dm² at 70 °C for nickel

TABLE 2. PARAMETERS OF THE DEPOSITION REACTION OF COPPER FROM $Cu(CF_3COO)_2$-$HCONH_2$ BATH

Concn. of $Cu(CF_3COO)_2$ (mol/l) $\times 10^{-2}$	Bath temp. (°C)	i_{oc} (A/dm²)	α_c	$\alpha_c n$	n	b_c (−V)
35	30	0.44	0.717	0.503	0.704	0.120
	40	0.56	0.773	0.558	0.721	0.112
	50	0.64	0.838	0.765	0.913	0.084
70	30	0.54	0.717	0.524	0.734	0.105
	40	0.63	0.773	0.623	0.806	0.100
	50	0.72	0.838	0.804	0.959	0.080
140	30	0.64	0.717	0.446	0.625	0.135
	40	0.74	0.773	0.578	0.748	0.108
	50	0.80	0.838	0.620	0.741	0.104

TABLE 3. PARAMETERS OF THE DEPOSITION REACTION OF NICKEL FROM $Ni(CF_3COO)_2$-$HCONH_2$ BATH

Concn. of $Ni(CF_3COO)_2$ (mol/l) $\times 10^{-2}$	Bath temp. (°C)	i_{oc} (A/dm²)	α_c	$\alpha_c n$	n	b_c (−V)
17.5	50	0.030	0.520	0.644	1.23	0.100
	60	0.055	0.694	0.604	0.870	0.110
	70	0.070	0.764	0.684	0.895	0.100
35.0	50	0.040	0.520	0.602	1.15	0.107
	60	0.065	0.694	0.651	0.938	0.102
	70	0.080	0.764	0.735	0.962	0.093
52.5	50	0.050	0.520	0.607	1.16	0.106
	60	0.075	0.694	0.651	0.938	0.102
	70	0.090	0.764	0.684	0.895	0.100

deposition.

The Apparent Exchange Current Density (i_{oc}) of the Copper and Nickel Depositions: The apparent exchange current density of copper and nickel depositions was obtained by extrapolating the η_c in the relation of $\eta_c - i_c$ to 0. The apparent exchange current density was thus determined at various temperatures and various salt concentrations. The results are shown in Tables 2 and 3.

The values of the i_{oc} of the copper and nickel depositions tended to increase with the salt concentration in the bath and with the bath temperature.

It was noticed that the i_{oc} of the nickel deposition was smaller than that of the copper deposition.

The Apparent Transfer Coefficient (α_c) and the Apparent Valence (n) of Copper and Nickel Depositions: On the Tafel curves, Eqs. (2) and (3) hold among n, α_c, i_{oc}, the apparent standard rate constant (K_{SR}), and the concentration of Cu^{2+} or Ni^{2+}, C_0 mol/l:

$$i_c = i_{oc} \exp(-\alpha_c F n \eta_c / RT) \quad (2)$$

$$i_{oc} = nFK_{SR}C_0^{(1-\alpha_c)} \quad (3)$$

If the plot of log i_{oc}—log C_0 becomes linear in Eq. (3), its slope is equal to $(1-\alpha_c)$. This relation is shown in Fig. 7 for the deposition of copper from the $Cu(CF_3COO)_2$-$HCONH_2$ bath as an example. Similar results were obtained for the deposition of nickel from the $Ni(CF_3COO)_2$-$HCONH_2$ bath. The relation was approximately linear. Therefore, α_c was determined from the slope. On the other hand, the slopes of the Tafel line are equal to $2.303 \times RT/\alpha_c nF$ as is given by Eq. (2). Therefore, $\alpha_c n$ was determined from this relationship. Tables 2 and 3 show α_c, $\alpha_c n$, n and the slopes of the Tafel lines.

As an average of these results, the following relations were found for copper deposition:

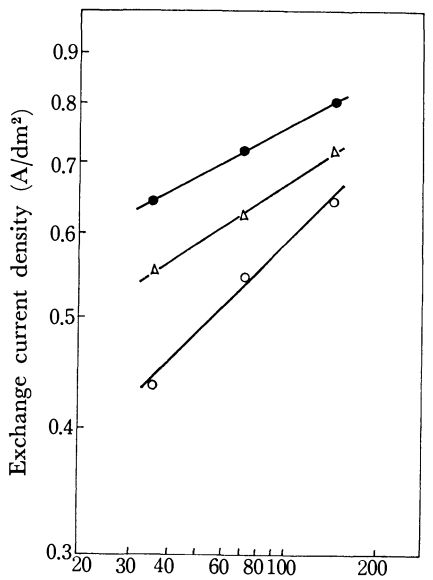

Fig. 7. Relationship between exchange current density and concentration of copper ion.
-○-: 30 °C, -△-: 40 °C, -●-: 50 °C

$\alpha_c = 0.78$ (namely, dlog i_{oc}/dlog $C_0 = 0.22$)

$n = 0.77$

The slope of the Tafel line $(b_c) = -0.113$ V. For nickel deposition:

$\alpha_c = 0.66$ (namely, dlog i_{oc}/dlog $C_0 = 0.34$)

$n = 1.00$

$b_c = -0.102$ V.

Therefore, it may be concluded that the reaction proceeds as is shown in Eqs. (4) and (5) within the

range of 0.7—3.5 A/dm² for copper deposition from the $Cu(CF_3COO)_2$–$HCONH_2$ bath and within that of 0.9—4.8 A/dm² for nickel deposition from the $Ni(CF_3COO)_2$–$HCONH_2$ bath.

$$M^{2+} + e^- \rightarrow M^+ \quad (4)$$

$$M^+ + e^- \rightarrow M \quad (5)$$

where M is Cu or Ni.

It may also be concluded that the reaction of Eq. (4) is rate-determining, because the effect of the potential (current density) on the electrodeposition is relatively slight at low current densities, which give satisfactory deposits.

It seems that the solvation[11] has some effect on the deposition of metals.

The Apparent Activation Energy of Copper and Nickel Depositions: The relation between i_{oc} and the bath temperature (T) is given by the Arrhenius equation. Thus,

$$i_{oc} = K \exp(-E_c/RT) \quad (6)$$

where E_c: the apparent activation energy of the deposition of metals. K: a constant.

Figure 8 shows the relation between the apparent exchange current density and the bath temperature (namely, $\log i_{oc} - 1/T$) for the copper deposition. This relation is approximately shown by a straight line. The same relation also holds for the nickel deposition. The apparent activation energies of the deposition of copper and nickel were determined from the slopes of these curves.

It was thus found that the apparent activation energies were 3.50 kcal/mol, 2.86 kcal/mol, and 2.46 kcal/mol for the deposition of copper from the baths containing 100, 200, and 400 g $Cu(CF_3COO)_2$ per liter respectively. For the deposition of nickel, the activation energies were 8.85 kcal/mol, 8.03 kcal/mol, and 6.31 kcal/mol for the baths containing 50, 100, 150 g $Ni(CF_3COO)_2$ per liter respectively.

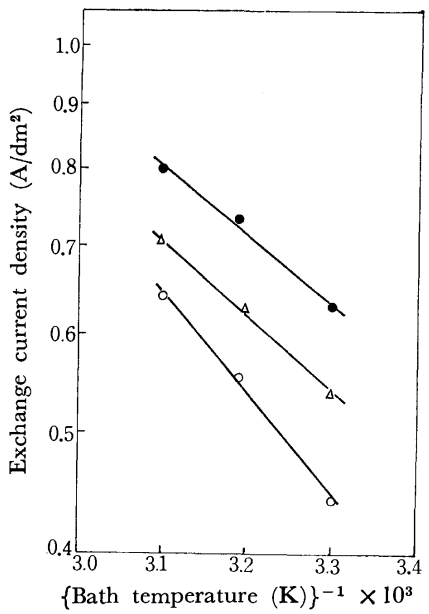

Fig. 8. Relationship between exchange current density and bath temperature.
-●-: concentration of copper ion 140×10^{-2} mol/l
-△-: concentration of copper ion 70×10^{-2} mol/l
-○-: concentration of copper ion 35×10^{-2} mol/l

That is, the activation energy of the copper deposition from the $Cu(CF_3COO)_2$–$HCONH_2$ bath was 2.9 kcal/mol on the average, while that of the nickel deposition from the $Ni(CF_3COO)_2$–$HCONH_2$ bath was 7.7 kcal/mol on the average. In the high-concentration solutions of $Cu(CF_3COO)_2$ or $Ni(CF_3COO)_2$, the true concentration of Cu^{2+} or Ni^{2+} is lower than that of $Cu(CF_3COO)_2$ or $Ni(CF_3COO)_2$. Therefore, it is likely that the true activation energy is larger than those values.

The activation energy of the direct deposition of Cu^{2+} from a copper borofluoride bath is estimated to be about 11—12 kcal/mol.[9] The activation energy as determined by the present study is lower than this value. It may be concluded, in view of the activation energy, that the deposition of copper from the $Cu(CF_3COO)_2$–$HCONH_2$ bath takes place through Cu^+ and that the deposition of nickel takes place through Ni^+.

The Electrodeposition of Metals from a Metal Trifluoroacetate-$HCONH_2$ Bath. It is not sufficient to discuss the deposition of metals from a metal trifluoroacetate–$HCONH_2$ bath from the viewpoint of copper deposition and nickel deposition only. However, the following tendencies were noticed:

(1) Formamide well dissolves metal trifluoroacetate. In this solution, metal-complex ions are formed.

(2) The i_{oc} value of the deposition of metals from a formamide bath is larger than that from an aqueous solution. However, the metals which show large i_{oc} values in aqueous solutions also show large i_{oc} values in formamide baths. Those which show small i_{oc} values in aqueous solutions also show small i_{oc} values in formamide baths.

(3) When the i_{oc} values are large, metals are easily deposited and the deposits are apt to be coarse.[10] In formamide baths, a metal-complex are formed. Therefore, the growth in the perpendicular direction is suppressed, resulting in an increase in the frequency of nucleation. Therefore, a smooth deposited surface with small crystallites is obtained.

(4) In the formamide bath, the i_{oc} values of metal deposition are larger than in aqueous baths. The values of i_{oc} vary little with the kind of metal. It is, therefore, possible to accelerate the deposition of metals, which are hardly deposited at all from aqueous solutions.

Activation Overvoltage of Hydrogen Evolution. When the electrolysis was performed in the CF_3COOH–$HCONH_2$ bath, hydrogen gas evolved from the cathode. However, no gases evolved from the anode.

The activation overvoltage of hydrogen evolution from the CF_3COOH–$HCONH_2$ bath is higher than that from an aqueous solution. Therefore, hardly any evolution of hydrogen takes place in formamide baths because of the activation overvoltage.

The author wishes to express her deep gratitude to Professor Rimpei Kojima for his kind direction and encouragement throughout this work.

References

1) I. A. Menzies, T. Broughton, and V. O. Nwoko, *Trans. Inst. Metal Finishing*, **43**, 9 (1965).
2) A. Brenner, "Advances in Electrochemistry and Electrochemical Engineering" ed. by P. Delahay and C. W. Tobias, Vol. 5, Interscience Pub. (1967) p. 206.
3) D. E. Couch and A. Brenner, *J. Electrochem. Soc.*, **99**, 234 (1952).
4) A. Brenner, *ibid.*, **103**, 652 (1956).
5) H. Connor and A. Brenner, *ibid.*, **103**, 657 (1956).
6) S. Yoshizawa, "Denkikagakuzikkenho", Izumi Shobō (1964), p. 108.
7) H. Röhler, *Z. Electrochem.*, **16**, 419 (1910).
8) T. Takei and R. Kojima, "Nipponkagakukai 19 nenkai Kōenyokōshu", 1ZB, 209 (1966); "Nipponkagakukai 20 nenkai Kōenyokōshu", II, 2C, 204 (1967).
9) Y. Ueno, M. Tsuiki, F. Hine, and S. Yoshizawa, *Denkikagaku*, **32**, 211 (1964).
10) T. Yoshida and N. Nomoto, *ibid.*, **34**, 600 (1966).
11) T. Hayashi, *Kinzokuhyomengijutsu*, **21**, 515 (1970).

The Electrodepositions of Copper and Nickel from Their Trifluoroacetate–*N*,*N*-Dimethylformamide Baths

Tatsuko TAKEI

The Faculty of Engineering, Shinshu University, Wakasato, Nagano 380

(Received August 2, 1973)

This paper will deal with the electrodepositions of copper and nickel from $Cu(CF_3COO)_2$–$HCON(CH_3)_2$, $Cu(CF_3COO)_2$–$HCON(CH_3)_2$–citric acid, $Ni(CF_3COO)_2$–$HCON(CH_3)_2$, and $Ni(CF_3COO)_2$–$HCON(CH_3)_2$–additives baths. The properties of these baths and the mechanism of the electrodeposition of copper from the $Cu(CF_3COO)_2$–$HCON(CH_3)_2$–citric acid bath were studied. The solubility of $Cu(CF_3COO)_2$ in 100 g of $HCON(CH_3)_2$ was 180 g at 20 °C. The specific conductances of the $Cu(CF_3COO)_2$–$HCON(CH_3)_2$ and $Ni(CF_3COO)_2$–$HCON(CH_3)_2$ baths were lower than those of the $Cu(CF_3COO)_2$–$HCONH_2$ and $Ni(CF_3COO)_2$–$HCONH_2$ baths. Cu_2O was electrodeposited at the cathode, while copper was not easily obtained from the $Cu(CF_3COO)_2$–$HCON(CH_3)_2$ bath. By dissolving citric acid in the bath, copper electrodeposition was made easier. Bright and smooth copper deposits were obtained at current densities in the range of 2.0—11.0 A/dm² from the $Cu(CF_3COO)_2$ 500 g/l–$HCON(CH_3)_2$–citric acid 200 g/l bath at 60 °C, the current efficiencies for cathode and anode being about 75% and above 100% respectively. The cross-section of the copper deposits showed that the deposits have a granular structure. The rate of the electrodeposition of copper from the $Cu(CF_3COO)_2$–$HCON(CH_3)_2$–citric acid 200 g/l bath at current densities ranging from 1.0 to 3.5 A/dm² was found to be controlled by the charge-transfer reaction. A black powder nickel deposit was obtained from the $Ni(CF_3COO)_2$–$HCON(CH_3)_2$ bath. By dissolving NH_4Cl, H_3BO_3, sulfamic acid or CCl_3COOH in the bath, adherent bright and smooth nickel deposits were obtained. While the cathode current efficiency was lower in the bath containing sulfamic acid, the anode current efficiency was lower in the bath containing H_3BO_3 or CCl_3COOH. NH_4Cl and $AlCl_3$ have the disadvantage that they are dissolved in $HCON(CH_3)_2$ only with difficulty. Since the bond between the metallic ion and the solvent in the $HCON(CH_3)_2$ bath is stronger than that in the $HCONH_2$ bath, and since dielectric constant of the solvent in the former is lower than that in the latter, metal electrodeposition from the former is more difficult.

Few fundamental data have been reported on the metallic electrodeposition from non-aqueous solutions, in addition, the electrode reaction is not clear in many respects.

The present author previously described[1] the electrodeposition of copper and nickel from the $HCONH_2$ bath, a polar proton solvent.

On the other hand, $HCON(CH_3)_2$ is a polar aprotic solvent; it has a comparatively low melting point and a comparatively high boiling point among the amide solvents. It can be expected that this solvent would also be useful for the electrodeposition of very base metals, because the solvent, lacking in active hydrogen, does not evolve H_2 simultaneously with the metallic electrodeposition from this solution.

The electrodeposition of metal from the $HCON(CH_3)_2$ solution has,. however been investigated only by Baba *et al.*,[2] and the present author cannot find any data fully examining the influence of the electrolysis conditions on the electrodeposit, the mechanism of the electrodeposition reaction, or the properties of the solution.

In the present experiment, the author investigated the properties of the $Cu(CF_3COO)_2$–$HCON(CH_3)_2$ bath and the $Ni(CF_3COO)_2$–$HCON(CH_3)_2$ bath, the electrodepositions of copper and nickel from these baths, and the mechanism of the electrodeposition of copper from the former bath. The author then compared the previously described electrodepositions,[1] of copper and nickel from the $HCONH_2$ bath with those in the present experiment from the $HCON(CH_3)_2$ bath.

Experimental

Reagents. *$HCON(CH_3)_2$*: A reagent grade containing about 0.003% moisture was used.

$Cu(CF_3COO)_2$ and $Ni(CF_3COO)_2$: These were[1] prepared by the neutralization method from $Cu(OH)_2$ and $Ni(OH)_2$ with CF_3COOH.

Other Chemicals: Phosphoric acid and acetic acid of the reagent grade were used. Citric acid (anhydride) and other chemicals of a special grade were used.

Electrodeposition. The electrodepositions of copper and nickel from the $Cu(CF_3COO)_2$–$HCON(CH_3)_2$ and $Ni(CF_3COO)_2$–$HCON(CH_3)_2$ baths, or from these baths with additives, were carried out at a current density of 0.5—14.0 A/dm², using an apparatus already described,[1] at 40—60 °C, while the bath was being stirred at a definite rate.

The thickness of the electrodeposited layer was made about 5 μ, this thickness being calculated from the amount of electricity consumed during the deposition.

Observation of the Electrodeposited Surface and the Electrodeposited Layer. The electrodeposited surfaces and electrodeposited layers were observed by means of a metallurgical microscope. To observe the layers in particular, their thickness was made about 30 μ and they were buried in resin and etched.

Measurement of the Solubility. The solubility of $Cu(CF_3COO)_2$ in $HCON(CH_3)_2$ was obtained by determining quantitatively with oxine (gravimetric method) the copper in a definite amount of a saturated solution of $Cu(CF_3COO)_2$ at 20 °C.

Measurement of the Electrolytic Conductance. The $Cu(CF_3COO)_2$–$HCON(CH_3)_2$, $Cu(CF_3COO)_2$–$HCON(CH_3)_2$–citric acid, and $Ni(CF_3COO)_2$–$HCON(CH_3)_2$ baths were kept at 50 °C for about one hour before the measurement, and

their electrolytic conductance was measured by means of a Yanagimoto electrolytic conductometer Model MY-7.

Measurement of the Ultraviolet Absorption Spectrum. A sample of a 0.10 mol/l $Cu(CF_3COO)_2$–$HCON(CH_3)_2$– 0 to 0.30 mol/l citric acid bath was placed in a quartz cell with a 2-mm light-pass length, and the ultraviolet absorption spectrum was measured by means of Hitachi recording spectrophotometer, Model EPS-3.

Analysis of Gas and Bath. The composition of the gas evolved during the electrolysis of a 100 g/l $Cu(CF_3COO)_2$–$HCON(CH_3)_2$–0 to 200 g/l citric acid bath and the change in the composition of the bath itself were determined by a method previously described.[1)]

Polarography. With a Yanagimoto polarograph, Model PA-102, DC and AC polarograms of a 1.0×10^{-2} mol/l $Cu(CF_3COO)_2$–$HCON(CH_3)_2$–0 to 3.0×10^{-2} mol/l citric acid bath were recorded at 25 °C, using 0.1 M sodium perchlorate as the supporting electrolyte.

Elementary Analysis. Elementary analyses were carried out on the yellowish brown substance produced at theca thode by the electrolysis of a 100 g/l $Cu(CF_3COO)_2$–$HCON(CH_3)_2$ bath and on the precipitate produced after the heating, at about 90 °C for 2 hr, of a 0.1 mol/l $Cu(CF_3COO)_2$–$HCON(CH_3)_2$–0.2 mol/l citric acid bath. H and C were determined by the Pregl method for microanalysis, N, by the Dumas method, and Cu, by the oxine method (gravimetric method).

X-ray Diffraction. The yellowish-brown substance produced at the cathode by the electrolysis of the $Cu(CF_3COO)_2$–$HCON(CH_3)_2$ bath was X-ray diffractometrically determined by means of a Geiger-Flex Model CN2035 manufactured by Rigaku Denki Co. Ltd., using copper as the target.

Measurement of the Overvoltage. The overvoltage of the copper electrodeposition from a $Cu(CF_3COO)_2$–$HCON(CH_3)_2$–200 g/l citric acid bath was measured at 40, 50, and 60 °C by the current interruptor method[1)] for baths containing $Cu(CF_3COO)_2$: 100 g/l (35×10^{-2} mol/l), 150 g/l (52×10^{-2} mol/l), and 200 g/l (70×10^{-2} mol/l) respectively.

Results and Discussion

Electrodeposition. *Nickel Electrodeposition*: Table 1 shows some results obtained on nickel deposition from $Ni(CF_3COO)_2$–$HCON(CH_3)_2$ baths with additives. The additives chosen were such that could dissolve the anode (Ni plate) and/or form a metal complex ion with the metal ion in the bath.

The deposit obtained from the $Ni(CF_3COO)_2$–$HCON(CH_3)_2$ bath was a black powder; bright and smooth nickel deposits were obtained from this bath containing NH_4Cl, $AlCl_3$, H_3BO_3, sulfamic acid, H_3BO_3–NH_4Cl, saccharin–NH_4Cl, CCl_3COOH, hydroxylamine hydrochloride, glycolic acid, H_2SO_4, or phthalic acid. The deposit obtained from the solution containing $AlCl_3$ was particularly bright.

Among these baths, those containing NH_4Cl, H_3BO_3, sulfamic acid, H_3BO_3-NH_4Cl, saccharin-NH_4Cl, or CCl_3COOH gave adherent nickel deposits.

While the cathode current efficiency was lower in the bath containing H_3BO_3 or CCl_3COOH, NH_4Cl and $AlCl_3$ have the disadvantage that they are dissolved in $HCON(CH_3)_2$ only with difficulty.

From these results it is apparent that the nickel electrodeposition from a $Ni(CF_3COO)_2$–$HCON(CH_3)_2$ bath is promoted by adding NH_4Cl, sulfamic acid, H_3BO_3, or CCl_3COOH to the bath. It would improve not only the anode current efficiency but also the adhesion of electrodeposit on the substrate if we could find a chloride highly soluble to $HCON(CH_3)_2$.

Table 1. Electrodeposition of nickel from $Ni(CF_3COO)_2$ 20.0 g/l–$HCON(CH_3)_2$ bath with additives at 40 °C

Additive (g/l)	Current density (A/dm²)	Current efficiency (%)		Deposit
		Cathode	Anode	
No addition	0.5—1.0	56—95	12—65	black
NH_4Cl 4.0	0.5—2.0	28—78	100—110	bright
H_3BO_3 4.0 —22.0	1.0	92—42	31—62	bright
Sulfamic acid 4.0—16.0	1.0	17—9.7	16—18	bright
Citric acid 4.0	0.5—1.0	10—16	5.6—3.1	grey
Tartaric acid 4.0	0.5—1.0	3.6—22	3.6—4.3	grey
LiCl 4.0	0.5—1.0	60—6.3	104—103	black
$AlCl_3$ 4.0	0.5—2.0	59—91	105—107	bright
CCl_3COOH 2.0—6.0	0.5—2.0	65—63	6.7—12	bright
Salicylic acid 2.0	2.0	67	3.0	black
Hydroxylamine Hydrochloride 2.0	0.5—2.0	29—47	14	bright
Oxalic acid 2.0	1.0	49	5.4	bright
Lactic acid 10 ml	2.0—4.0	30—39	20—8.0	black
Glycolic acid 2.0	0.5—1.0	41—63	6.1—4.2	bright
Phthalic acid 2.0	1.0	41	10	bright
H_2SO_4 10 ml	1.0—2.0	27—51	23—23	bright

It appears that, on the anode in the $Ni(CF_3COO)_2$–$HCON(CH_3)_2$ baths containing additives (except chloride), another reaction occurs (such as the electrolysis of the solvent).

It can be concluded that chloride is dissolved in $HCON(CH_3)_2$ with more difficulty than in $HCONH_2$: also, both nickel deposition and anode dissolution are more difficult in a $HCON(CH_3)_2$ bath than in a $HCONH_2$ bath.

Copper Electrodeposition: A bright and smooth copper deposit can be obtained from the $Cu(CF_3COO)_2$–$HCON(CH_3)_2$ bath only if the electrodeposition is carried out in a 20 g/l $Cu(CF_3COO)_2$ concentration at 60 °C for a 1.0 to 3.0 A/dm² current density. Under such electrolysis conditions, the anode current efficiency is about 100%, while the cathode current efficiency is about 75%.

Figure 1 shows an example of the anode and cathode current efficiencies for copper deposition from the $Cu(CF_3COO)_2$–$HCON(CH_3)_2$ bath.

The anode current efficiency was always about 100%, irrespective of the $Cu(CF_3COO)_2$ concentration and the bath temperature. On the other hand, while the cathode current efficiency was also scarcely affected

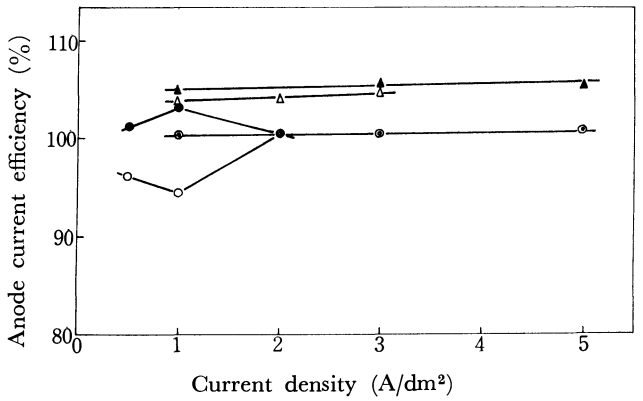

Fig. 1-1. Anode current efficiency as a function of current density for $Cu(CF_3COO)_2$-DMF bath
$Cu(CF_3COO)_2$ 20 g/l, —○—: 40 °C, —●—: 50 °C, —△—: 60 °C
$Cu(CF_3COO)_2$ 100 g/l, —◎—: 40 °C, —▲—: 60 °C

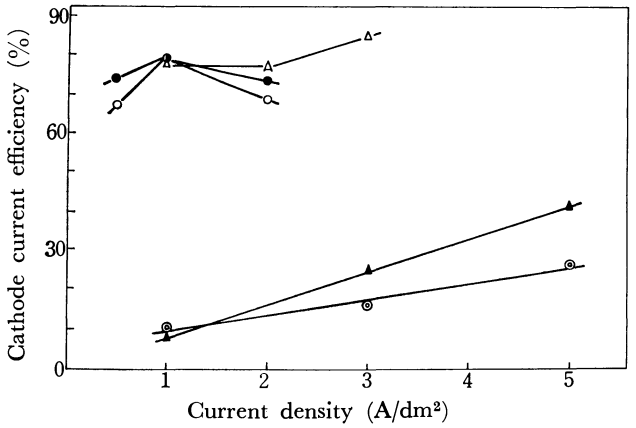

Fig. 1-2. Cathode current efficiency as a function of current density for $Cu(CF_3COO)_2$-DMF bath
$Cu(CF_3COO)_2$ 20 g/l, —○—: 40 °C, —●—: 50 °C, —△—: 60 °C, $Cu(CF_3COO)_2$ 100 g/l, —◎—: 40 °C, —▲—: 60 °C

by the bath temperature, it was decreased down to about 10% at a low current density with an increase in the $Cu(CF_3COO)_2$ concentration.

No gases evolved from the anode and cathode, but during electrolysis a yellowish-brown precipitate was produced at the cathode. Elementary analysis of this precipitate showed C: 6.89%, H: 1.56%, N: 0.88%, and Cu: 55.0%; X-ray diffraction showed that it was mainly composed of Cu_2O.

Moreover, gas chromatographic analysis of the cathode solution proved the existence of $(CF_3CO)_2O$.

Therefore, the following reaction (1) can be said to have occurred at the cathode, resulting in a decrease in the cathode current efficiency:

$$2Cu(CF_3COO)_2 + 2e^- \rightarrow Cu_2O + 2(CF_3CO)_2O + 2CF_3COO^- \quad (1)$$

In view of this fact, it seems that it is difficult for copper electrodeposition to occur from a $Cu(CF_3COO)_2$–$HCON(CH_3)_2$ bath because the copper ion forms a stable complex with $HCON(CH_3)_2$ if the $Cu(CF_3COO)_2$ concentration is high.

The present author has assumed that, if this stable copper complex were broken or if such a substance as forms a more unstable copper complex than the above-mentioned complex were added to the $HCON(CH_3)_2$ bath, it would be possible to facilitate the copper electrodeposition from the bath; the author thus tentatively added citric acid, a complexing agent, to the bath.

Fig. 2 shows an example of the influence of citric acid addition on the anode and cathode current efficiencies. The increased addition of citric acid increases the cathode current efficiency.

While the copper electrodeposition from the $Cu(CF_3COO)_2$–$HCON(CH_3)_2$ bath is difficult because of the strong bond between the copper ion and $HCON(CH_3)_2$, it appears that the addition of citric acid fa-

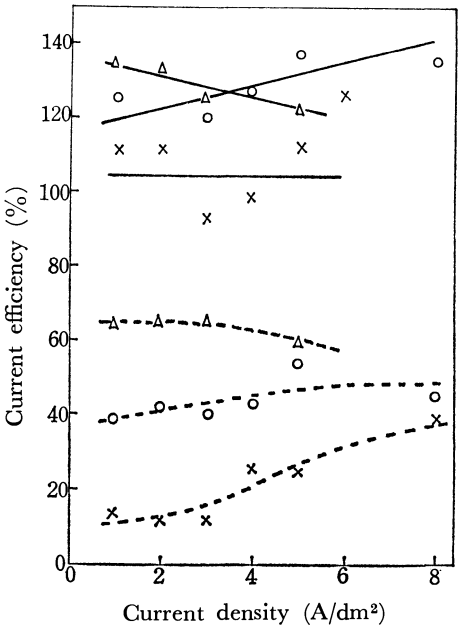

Fig. 2-1. Cathode and anode current efficiencies as a function of current density for $Cu(CF_3COO)_2$ 100 g/l-DMF-citric acid baths at 50 °C
Anode: ——, Cathode: ——,
—×—: citric acid 20 g/l,
—○—: citric acid 100 g/l,
—△—: citric acid 200 g/l

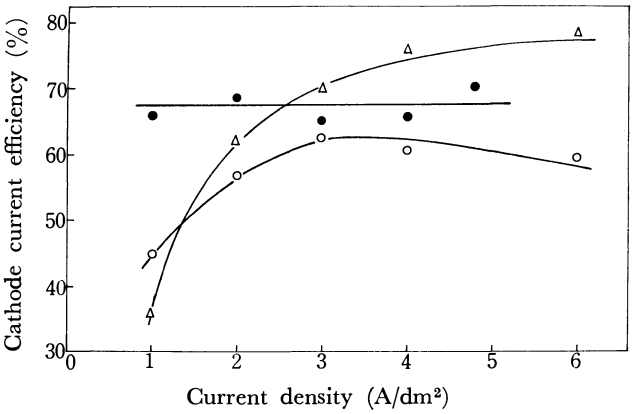

Fig. 2-2. Cathode current efficiency as a function of current density for $Cu(CF_3COO)_2$ 300 g/l-DMF-citric acid 200 g/l bath
—○—: 40 °C, —●—: 50 °C, —△—: 60 °C

cilitates the copper electrodeposition because it alters, as will be described later, the solution's property to weaken the influence of the solvent on the copper ion.

While the anode current efficiency was higher than 100% irrespective of the $Cu(CF_3COO)_2$ concentration and the bath temperature, the cathode current efficiency was affected by the $Cu(CF_3COO)_2$ concentration; it amounted to 75% in 100 to 500 g/l $Cu(CF_3COO)_2$ baths and to 85% in the bath with a $Cu(CF_3COO)_2$ concentration lower than 100 g/l at 60 °C for a high current density.

It seems that the anode current efficiency exceeds 100%, because the anode is also chemically dissolved in the bath's acid (citric acid). The evolution of hydrogen gas from the cathode lowered its current efficiency.

Figure 3 shows the range of current density within which a bright and smooth copper deposit can be obtained from a $Cu(CF_3COO)_2$–$HCON(CH_3)_2$–200 g/l citric acid bath. At each bath temperature, an increase in the $Cu(CF_3COO)_2$ concentration contributes to the tendency for good deposits to be obtained within a wider range of current densities.

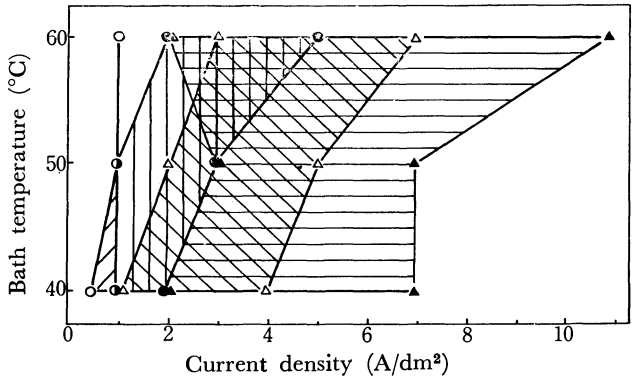

Fig. 3. The range of current density for bright and smooth copper deposit from $Cu(CF_3COO)_2$–DMF–citric acid 200 g/l bath
○: $Cu(CF_3COO)_2$ 20 g/l, ●: $Cu(CF_3COO)_2$ 100 g/l,
△: $Cu(CF_3COO)_2$ 300 g/l, ▲: $Cu(CF_3COO)_2$ 500 g/l

These ranges are remarkably wider than those in the case of the bath without citric acid and are almost equal to those in the case of the formamide bath[1] with the same $Cu(CF_3COO)_2$ concentration.

From the above-mentioned results, it is apparent that the addition of citric acid is effective on the copper electrodeposition from the $Cu(CF_3COO)_2$–$HCON(CH_3)_2$ bath, while the anode-current efficiency in the bath containing citric acid exceeds 100%. The cathode current efficiency reaches a remarkable level of 90% at 50 °C if more than 100 g/l of citric acid is added to a 20 g/l $Cu(CF_3COO)_2$ bath, and it is about 75% at 60 °C if 200 g/l of citric acid is added to a 100—500 g/l $Cu(CF_3COO)_2$ bath. Moreover at 60 °C from a 500 g/l $Cu(CF_3COO)_2$–$HCON(CH_3)_2$–200 g/l citric acid bath, a bright and smooth deposit can be obtained within a current density range of 2.0 to 11.0 A/dm².

Appearance of the Deposited Surface and the Structure of the Deposited Layer. *Nickel Deposit*: A representative nickel deposited surface is shown in Fig. 5. The deposited surfaces obtained from all the baths investigated in the present experiment consist of fine grains; those obtained from the baths containing H_2SO_4, $AlCl_3$, or hydroxylamine hydrochloride consist of very fine grains. A cracked deposited surface is obtained from the bath containing $AlCl_3$ or CCl_3COOH.

Since the deposited surfaces consist of grains, it can be assumed that the deposited layer has a granular structure.

Copper Deposit: Figure 6 shows as an example of the deposited surface and the deposited layer of the copper deposit obtained from the bath containing citric acid.

The deposited surface consists of fine grains, and the deposit becomes more compact for higher concentrations of the copper salt and at high bath temperatures. Moreover, the deposited layers have a granular structure irrespective of the bath temperature, the current density, and the $Cu(CF_3COO)_2$ concentration.

It appears that, since the copper and nickel ions form a complex in the $HCON(CH_3)_2$ bath, the ligands are adsorbed on the electrode during electrodeposition, thus suppressing any surface diffusion of the adatom; the growth in the vertical direction is thus prevented, increasing the frequency of nucleus formation, and fine grains are produced to form a granular structure.

Solubility. In 100 g of $HCON(CH_3)_2$, 180 g of $Cu(CF_3COO)_2$ were dissolved at 20 °C.

After several days, crystals were precipitated in an $Ni(CF_3COO)_2$–$HCON(CH_3)_2$ saturated solution at 20 °C.

The solubility of $HCON(CH_3)_2$ in $Cu(CF_3COO)_2$ is lower than that of $HCONH_2$.

Specific Conductance. Figure 4 shows the specific conductance of the $Cu(CF_3COO)_2$–$HCON(CH_3)_2$ bath. The specific conductance of the $Cu(CF_3COO)_2$–

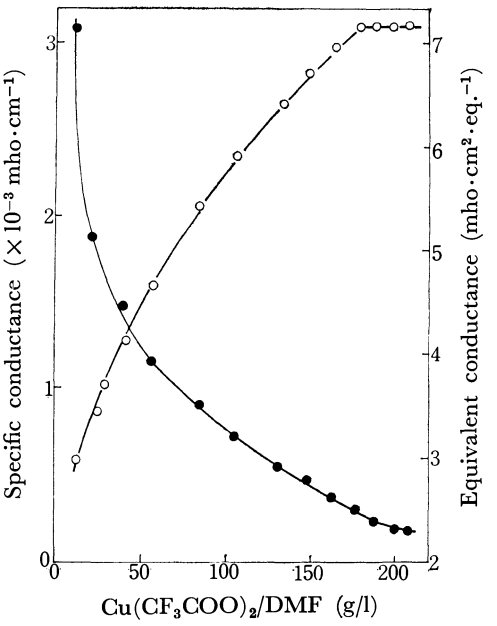

Fig. 4. Specific conductance and equivalent conductance of $Cu(CF_3COO)_2$–DMF solutions at 50 °C
—○—: Specific conductance,
—●—: Equivalent conductance

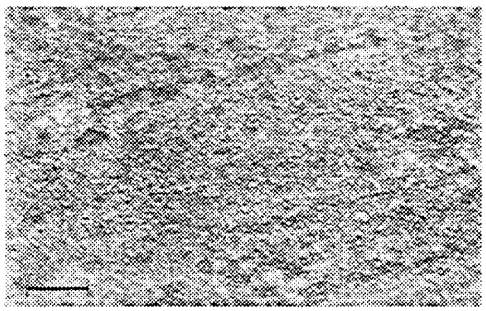

1) No additive bath, at 0.5 A/dm²

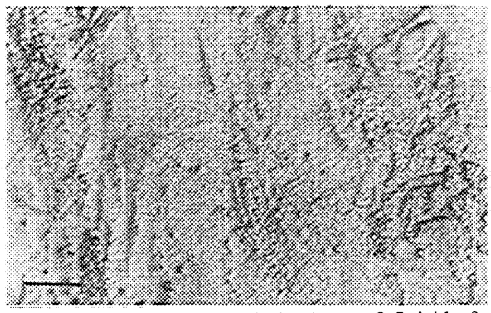

2) NH_4Cl (Saturated) bath, at 0.5 A/dm²

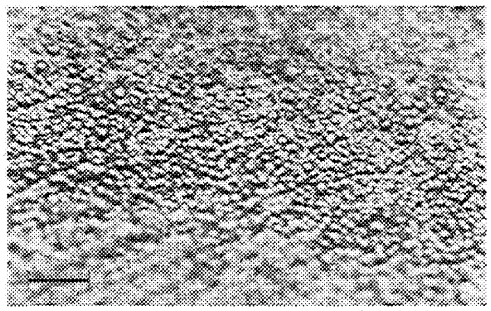

3) H_3BO_3 (22 g/l) bath, at 1.0 A/dm²

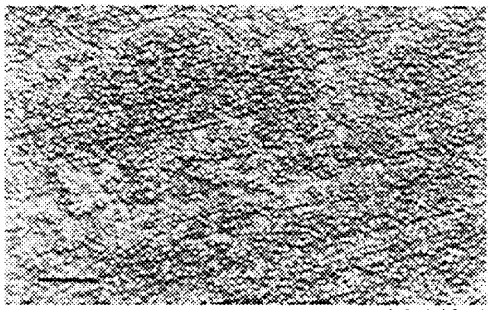

4) Sulfamic acid (4.0 g/l) bath, at 1.0 A/dm²

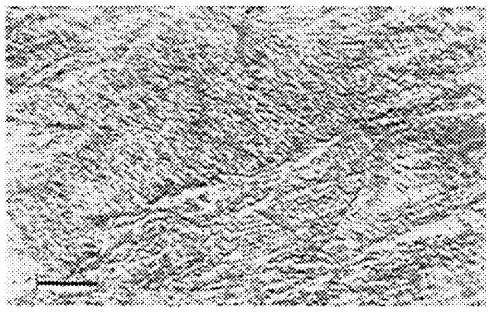

5) Citric acid (4.0 g/l) bath, at 0.5 A/dm²

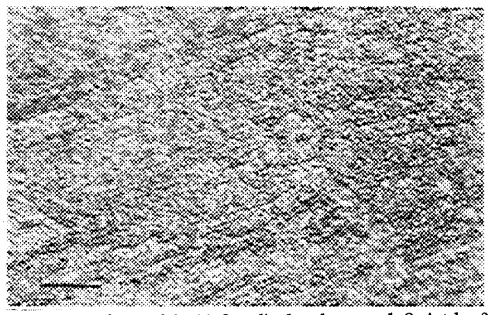

6) Tartaric acid (4.0 g/l) bath, at 1.0 A/dm²

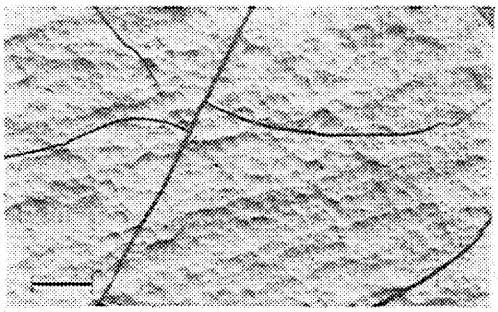

7) $AlCl_3$ (4.0 g/l) bath, at 1.0 A/dm²

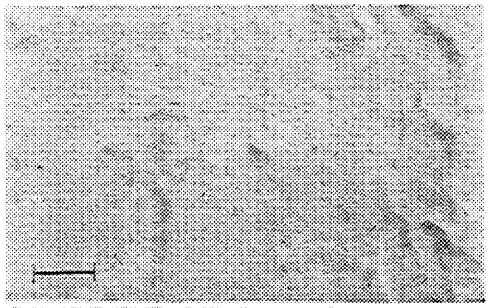

8) Hydroxylamine hydrochloride (2.0 g/l) bath, at 0.5 A/dm²

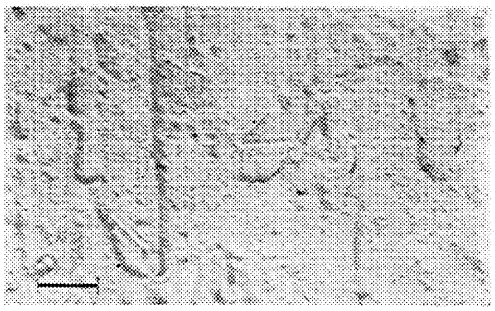

9) H_2SO_4 (10 ml/l) bath, at 1.0 A/dm²

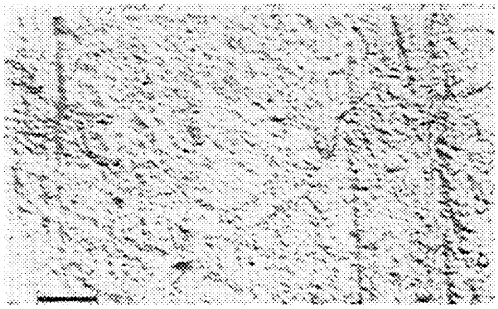

10) CCl_3COOH (6.0 g/l) bath, at 0.5 A/dm²

Fig. 5. Surface of nickel deposit obtained from $Ni(CF_3COO)_2$ 20 g/l-DMF bath with additives at 40 °C (|—| 23 μ).

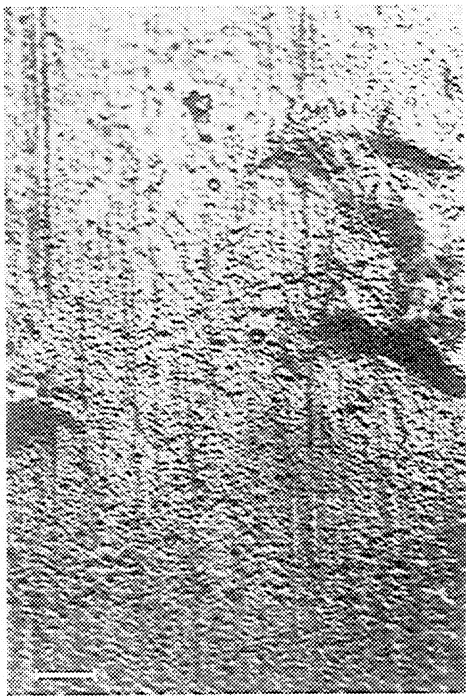

Fig. 6-1. Surface of copper deposit obtained from $Cu(CF_3COO)_2$ 500 g/l-DMF-citric acid 200 g/l bath at 8.0 A/dm² at 40 °C
(|——|: 23 μ).

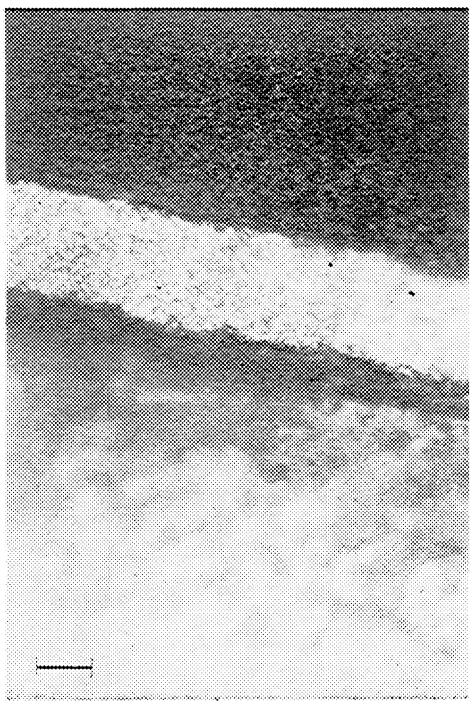

Fig. 6-2. Cross-section of copper deposit obtained from $Cu(CF_3COO)_2$ 300 g/l-DMF-citric acid 200 g/l bath at 2.0 A/dm² at 60 °C
(|——|: 23 μ).

$HCON(CH_3)_2$ bath was almost the same as that of the $Ni(CF_3COO)_2$–$HCON(CH_3)_2$ bath. They are both about 1/4 of those [1] of the $Cu(CF_3COO)_2$–$HCONH_2$ bath and the $Ni(CF_3COO)_2$–$HCONH_2$ bath.

It seems that more viscous $HCONH_2$ bath has a higher electrolytic conductance than the less viscous

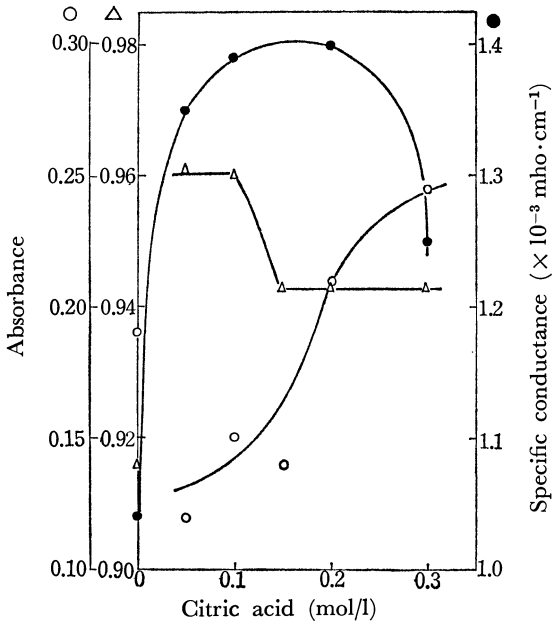

Fig. 7. The properties of $Cu(CF_3COO)_2$ 0.1 mol/l-DMF-citric acid solutions
—○—: absorbance at 1950 mμ
—△—: absorbance at 810 mμ
—●—: specific conductance at 50 °C

$HCON(CH_3)_2$ bath, mainly because the dielectric constant of $HCONH_2$, 110, is about three times that of $HCON(CH_3)_2$, 37.

$Cu(CF_3COO)_2$–$HCON(CH_3)_2$–Citric Acid Solution. Figure 7 shows the specific conductance of a 0.10 mol/l $Cu(CF_3COO)_2$–$HCON(CH_3)_2$– 0 to 0.30 mol/l citric acid bath and the absorbance of its ultraviolet absorption spectrum.

At citric acid concentrations of from 0.1 to 0.2 mol/l the conductance has its maximum, while inflexion points appear at the absorbances of 810 and 1950 mμ. It appears that these inflexion points change the condition of the solution surrounding the copper ion. The present author believes that, in the $Cu(CF_3COO)_2$–$HCON(CH_3)_2$–citric acid bath, coordination perhaps occurs in a ratio of 1 mol of $Cu(CF_3COO)_2$ to 1 mol of citric acid.

Both AC and DC polarograph of 1.0×10^{-2} mol/l $Cu(CF_3COO)_2$–$HCON(CH_3)_2$–0 to 3.0×10^{-2} mol/l citric acid baths show a reduction wave at −0.20 V *vs.* Hg A and −0.36 V *vs.* Hg B of the average half-wave potential. A wave is a clear peak in the AC polarogram, but an ill-defined wave in the DC polarogram.

The following results were obtained by AC polarography. While the wave height of A is increased with an increase in the amount of citric acid added, it becomes constant at amounts more than 2.0×10^{-2} mol/l. On the other hand, the wave height of B is constant, irrespective of the amount of citric acid added. Moreover, the wave heights of A and B coincide with each other for amounts of more than 2.0×10^{-2} mol/l.

It appears that the A wave is a reduction wave corresponding to the valency decrease of the copper–

citric acid complex from 2 to 1, while the B corresponds to the reduction of the latter to copper. Moreover, judging from the wave height, it is apparent that the addition of citric acid is effective for efficient copper electrodeposition in the $Cu(CF_3COO)_2$–$HCON(CH_3)_2$ bath and that the best amount of citric acid to be added is in a ratio of 1 mol of $Cu(CF_3COO)_2$ to more than 2 mol of citric acid rather than in a ratio of 1 mol of $Cu(CF_3COO)_2$ to 1 mol of citric acid, which corresponds to the amount of citric acid necessary for the formation of a copper-citric acid complex. This fact coincides well with the results of electrodeposition.

Activation Overvoltage of Copper Electrodeposition from the $Cu(CF_3COO)_2$–$HCON(CH_3)_2$–Citric Acid Bath. From the decay curve of the overvoltage 4 ms after the interruption of the electrolytic current, the resistance polarization was subtracted. The remainder was assumed to be the activation overvoltage. Figure 8 shows an example of the current density-activation overvoltage relation during the deposition of copper from the $Cu(CF_3COO)_2$–$HCON(CH_3)_2$–citric acid 200 g/l bath. Such ranges of current density as to make

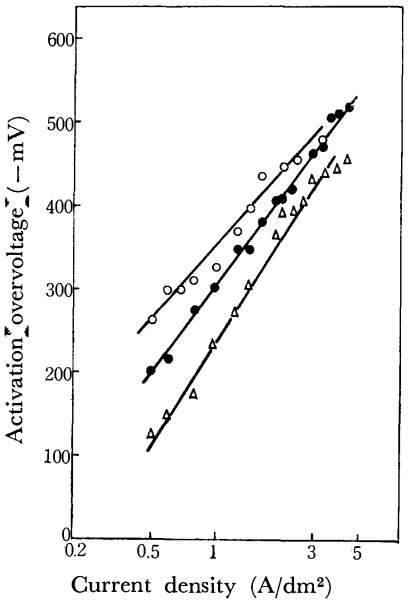

Fig. 8. Current density-activation overvoltage relation during the deposition of copper from $Cu(CF_3COO)_2$ 100 g/l–DMF–citric acid 200 g/l bath
—○—: 40 °C, —●—: 50 °C, —△—: 60 °C

the activation overvoltage, η_c, related to the logarithm of the current density, log i_c, in a direct proportionality are 1.0 to 3.0 A/dm² at a bath temperature of 40 °C, 1.0 to 3.5 A/dm² at 50 °C, and 1.0 to 4.1 A/dm² at 60 °C; it appears that in such ranges of current density Tafer's formula is valid—in other words, the charge-transfer process is rate-determining.

This η_c value is very much larger than that[1] in the $Cu(CF_3COO)_2$–$HCONH_2$ bath.

Table 2 shows the apparent exchange-current density, i_{oc}, the apparent transfer coefficient, α_c, and the apparent valency, n, for copper deposition, all obtained by a method previously described.[1]

While the obtained value of i_{oc} is higher than that[2] obtained by measuring the polarization potential with a potentiometer in a 0.1 M $CuSO_4$–$HCON(CH_3)_2$–0.1 M $NaClO_4$ bath, the former is slightly lower than that[1] obtained from the $Cu(CF_3COO)_2$–$HCONH_2$ bath.

Also, the obtained values of α_c, n and the slope of the Tafel line, b_c, are, in the average, as follows:

$$\alpha_c = 0.20,\ n = 0.960 \text{ and } b_c = -0.336 \text{ V}.$$

Within a range of current density of about 1.0 to 3.5 A/dm², the copper electrodeposition reaction from the $Cu(CF_3COO)_2$–$HCON(CH_3)_2$–200 g/l citric acid bath proceeds as in the following equations:

$$Cu^{2+} + e^- \rightarrow Cu^+ \quad (2)$$

$$Cu^+ + e^- \rightarrow Cu^0 \quad (3)$$

Moreover, it appears that Reaction (2) is rate-determining.

On the assumption of a linear relation between log i_{oc} and the reciprocal of the bath temperature, T, that is, $1/T$, the apparent activation energy, E_c of copper electrodeposition is calculated from the relation's slope; this results in values of 8.45, 8.61, and 9.10 kcal/mol E_c for the baths, the $Cu(CF_3COO)_2$ concentrations of which are 100, 150, and 200 g/l respectively.

Comparison between the Properties of a $Cu(CF_3COO)_2$–$HCONH_2$ or $Ni(CF_3COO)_2$–$HCONH_2$ Bath and a $Cu(CF_3COO)_2$–$HCON(CH_3)_2$ or $Ni(CF_3COO)_2$–$HCON(CH_3)_2$ Bath and between Copper and Nickel Electrodepositions from Those Baths. 1) While solvolysis occurs in the $HCONH_2$ bath, it does not occur in the $HCON(CH_3)_2$ bath. A complex is formed in each bath.

2) Since the bond between the metallic ion and the solvent in the $HCON(CH_3)_2$ bath is stronger than that

Table 2.

$Cu(CF_3COO)_2$ (mol/l) $\times 10^{-2}$	Bath temp. (°C)	i_{oc} (A/dm²)	α_c	$\alpha_c n$	n	b_c (−V)	Current density of linear part (A/dm²)
35	40	0.120	0.194	0.189	0.975	0.330	0.9—2.6
	50	0.170	0.201	0.179	0.890	0.360	0.9—2.8
	60	0.285	0.215	0.168	0.782	0.395	0.9—3.5
52	40	0.162	0.194	0.164	0.850	0.380	1.0—3.0
	50	0.240	0.201	0.172	0.859	0.375	1.1—3.5
	60	0.380	0.215	0.222	1.03	0.300	1.0—4.0
70	40	0.200	0.194	0.223	1.15	0.280	1.2—3.2
	50	0.320	0.201	0.214	1.07	0.300	1.2—4.0
	60	0.490	0.215	0.222	1.03	0.300	1.2—5.0

in the $HCONH_2$ bath, and since the dielectric constant of the solvent in the former is also lower than that in the latter, is difficult to electrodeposit metal and Cu_2O is formed at cathode in the $Cu(CF_3COO)_2$–$HCON(CH_3)_2$ bath.

3) The specific conductance in the $HCON(CH_3)_2$ bath is lower than that in the $HCONH_2$ bath.

4) It is possible to obtain a better copper electrodeposit over a wider range of current density in the $Cu(CF_3COO)_2$–$HCON(CH_3)_2$ bath containing citric acid than in the same bath containing no citric acid. This range almost coincides with that in the $Cu(CF_3COO)_2$–$HCONH_2$ bath.

While it is possible to obtain better nickel electrodeposit in $Ni(CF_3COO)_2$–$HCONH_2$ and $Ni(CF_3COO)_2$ $HCON(CH_3)_2$ baths containing appropriate additives, the range of current density which permits one to obtain a superior electrodeposit in the latter bath is narrower.

The electrodeposit of nickel or copper obtained from the $HCONH_2$ and $HCON(CH_3)_2$ baths has a granular structure.

5) The values of η_c, E_c, and b_c in the copper-electrodeposition reaction from the $Cu(CF_3COO)_2$–$HCON(CH_3)_2$–200 g/l citric acid bath are higher than those in the same reaction from the $Cu(CF_3COO)_2$–$HCONH_2$ bath, while the values of i_{oc} and α_c are lower, so the electrodeposition of copper from the former can be said to be more difficult. On the other hand, the value of n is always about 1 for both the baths.

The author wishes to express her deep gratitude to Professor Rimpei Kojima for his kind direction and encouragement throughout this work.

References

1) T. Takei, This Bulletin, **47**, 249 (1974).
2) N. Baba, Y. Takeuchi, and S. Morisaki, *Denki Kagaku*, **22**, 175 (1971).

Optically-active Vibrations and Elastic Constants of Calcite and Aragonite[1)]

Akio YAMAMOTO, Yuji SHIRO,* and Hiromu MURATA

Department of Chemistry, Faculty of Science, Hiroshima University, Higashisenda-machi, Hiroshima 730

**Shinonome Branch School, Faculty of Education, Hiroshima University, Shinonome-3-chome, Hiroshima 734*

(Received July 23, 1973)

Treatments of the normal coordinate and the elastic constant were undertaken for two calcium carbonate crystals. By the use of the least-squares technique, we obtained sets of the force constants which reproduce satisfactorily both the observed vibrational frequencies and the macroscopic elastic constants. The intermolecular interactions, the elastic strains of the internal coordinates, and the nature of the splitting of the normal frequencies in these crystals were briefly discussed.

The vibrational spectra of molecular crystals and ionic crystals have been studied by many investigators. Some of them have performed normal coordinate analyses, and the force fields of many crystals have been determined. Recently more rigorous treatments of the lattice dynamics, such as those based on the rigid-ion model[2)] or on the shell model,[3)] have been made for relatively simple crystal systems mainly by physicists.[4)] Presumably the impracticability of these treatments arises in part from the difficulties in the reasonable estimation of the potential parameters. The results of these treatments are quite suggestive for the analysis of the crystal vibration in a complex crystal system, though the application of the above models to actual complex crystals is difficult at the present time.

Generally, in contrast to the treatment of isolated free molecules, many restrictions which are characteristic of the solid state make it difficult to determine the force fields from only the vibrational spectra. These restrictions are caused by the experimental limitations, the complicated crystal structures, the strong intra- or inter-molecular interactions, and so on. The short-range interaction, intramolecular or intermolecular, is considered to dominate the crystal vibration and the elastic deformation, at least in molecular crystals or in predominantly covalent crystals. Therefore, it is necessary, for the determination of the force fields in the successional models, to ascertain the fundamental short-range force fields.

The present investigations of the short-range force fields of two calcium carbonates, and of sodium nitrate and sodium nitrite in the low-temperature ferroelectric phase[1)] were undertaken not only in order to check the reasonability of the vibrational force fields, but also to determine those force fields which interpret both the observed vibrational frequencies and the elastic constants.

Methods of Calculation

Crystal Structure. According to the X-ray diffraction analyses,[5,6)] the Bravais unit cells of calcite and aragonite belong to the rhombohedral space group D_{3d}^{6}—$R\bar{3}c$, with Z=2, and the orthorhombic D_{2h}^{16}—Pmcn, with Z=4 respectively. The cell constants are a_{rh}=6.3753 Å and α=46°4.6′ in calcite and a=4.9614 Å, b=7.9671 Å, and c=5.7404 Å in aragonite. Figures 1 and 2 show the structures of calcite and aragonite respectively. The structure of calcite may be regarded as a sodium chloride arrangement

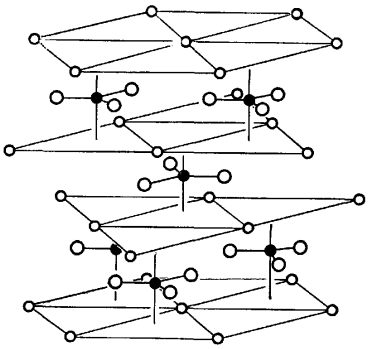

Fig. 1. Crystal structure of calcite.
●: carbon, ○: calcium, ○: oxygen.

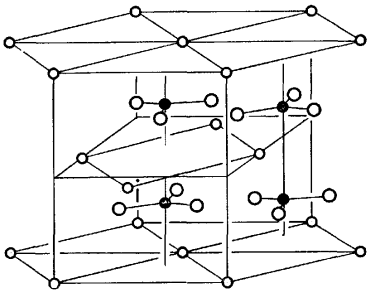

Fig. 2. Crystal structure of aragonite.
●: carbon, ○: calcium, ○: oxygen.

distorted by the introduction of disk-shaped carbonate groups. Each calcium atom is coordinated by six oxygen atoms, each belonging to a different carbonate group, and such oxygen atom is bound to two calcium atoms. On the other hand, the orthorhombic structure of aragonite is related to that of nickel arsenide. Each calcium atom is now surrounded by nine neighbors, each of which is, in its turn, bound to three calcium atoms.

Normal Coordinate Treatment. The application of the *GF*-matrix method[7)] to the analysis of optically-active crystal vibrations was reported previously by Shimanouchi, Tsuboi, and Miyazawa.[8)] The modified Urey-Bradley force field[9)] was applied to the intramolecular vibrations in carbonate groups, the correction terms of which were the bond interaction term, p, for the adjacent C–O bond pairs and the angle interaction term, n, for the adjacent O–C–O angle pairs in a single carbonate group. On the other hand, the central force field, which is based on the two-body interaction, was used for the intermolecular vibrations.

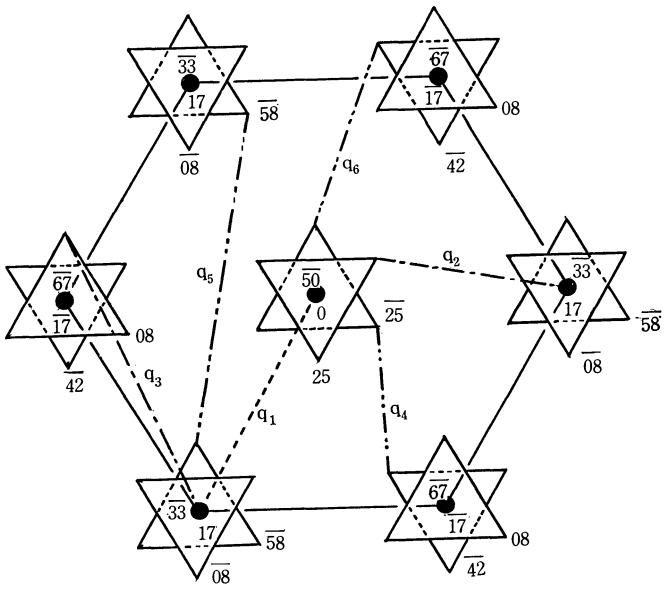

Fig. 3. Short-range interactions in calcite viewed along the z axis of the hexagonal cell. The heights of atoms or carbonate groups are expressed in units of $100/c_0$.
----, calcium···carbon; ———, calcium···oxygen; ————————, oxygen···oxygen.

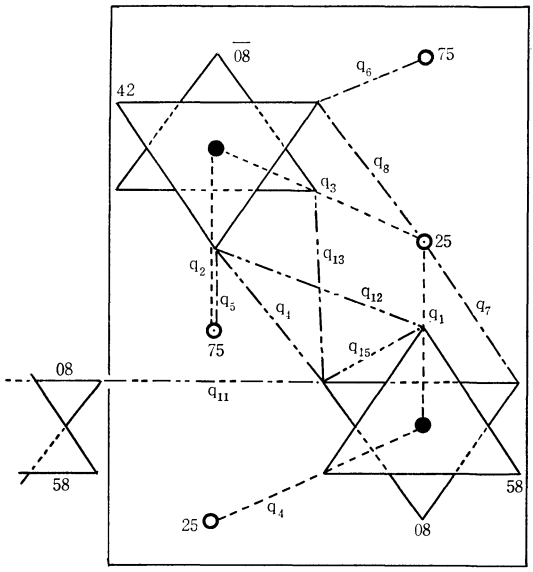

Fig. 4. Short-range interactions in aragonite viewed along the z axis. Other descriptions are the same to Fig. 3.

In this study, only those pairs that lie within 3.5 Å were taken into consideration. As is illustrated in Figs. 3 and 4, there are six different kinds of these pairs in calcite and fifteen in aragonite respectively. The corresponding atomic separations are also listed in Table 3.

In many cases, group theoretical considerations, such as the site-group analysis[10] or the factor-group analysis,[11] have been found to be useful for the analysis of crystal vibrations. The factor-group analysis of these crystals was once performed by Bhagavantam and Venkatarayudu;[11] their results are summarized in Tables 1 and 2. It is obvious from these tables that, of the twenty-seven degrees of freedom for genuine vibrations eight modes are infrared-active, and five, Raman-active, in calcite, and that, of the fifty-seven degrees, twenty-seven are infrared-active, and thirty, Raman-active, in aragonite. The selection rules for the optically-active vibrations are followed under the mutual exclusion rule, since each crystal has a center of symmetry.

TABLE 1. FACTOR-GROUP ANALYSIS OF CALCITE

$D_{3d}{}^6$	E	$2S_6$	$2S_6{}^2$	$S_6{}^3$	$3C_2$	$3\sigma_v$	N_i	T_i	T_i'	R_i'	n_i	IR	Raman
A_{1g}	1	1	1	1	1	1	1	0	0	0	1	f	$\alpha_{xx}=\alpha_{yy}, \alpha_{zz}$
A_{1u}	1	−1	1	−1	1	−1	2	0	1	0	1	f	f
A_{2g}	1	1	1	1	−1	−1	3	0	1	1	1	f	f
A_{2u}	1	−1	1	−1	−1	1	4	1	1	1	1	M_z	f
E_g	2	−1	−1	2	0	0	4	0	1	1	2	f	$\alpha_{xx}=-\alpha_{yy}, \alpha_{xy}, \alpha_{yz}, \alpha_{zx}$
E_u	2	1	−1	−2	0	0	6	1	2	1	2	M_x, M_y	f

f, forbidden; N_i, number of degrees of freedom belonging to the i-th species; T_i, number of over-all translations of Bravais unit cell; T_i', number of translational lattice modes; R_i', number of rotational lattice modes; n_i, number of intramolecular vibrational modes.

TABLE 2. FACTOR-GROUP ANALYSIS OF ARAGONITE

$D_{2h}{}^{16}$	E	$C_2{}^c$	$C_2{}^b$	$C_2{}^a$	i	σ_c	σ_b	σ_a	N_i	T_i	T_i'	R_i'	n_i	IR	Raman
A_{1g}	1	1	1	1	1	1	1	1	9	0	4	1	4	f	$\alpha_{xx}, \alpha_{yy}, \alpha_{zz}$
A_{1u}	1	1	1	1	−1	−1	−1	−1	6	0	2	2	2	f	f
B_{1g}	1	1	−1	−1	1	1	−1	−1	6	0	2	2	2	f	α_{xy}
B_{1u}	1	1	−1	−1	−1	−1	1	1	9	1	3	1	4	M_z	f
B_{2g}	1	−1	1	−1	1	−1	1	−1	6	0	2	2	2	f	α_{zx}
B_{2u}	1	−1	1	−1	−1	1	−1	1	9	1	3	1	4	M_y	f
B_{3g}	1	−1	−1	1	1	−1	−1	1	9	0	4	1	4	f	α_{yz}
B_{3u}	1	−1	−1	1	−1	1	1	−1	6	1	1	2	2	M_x	f

Notations are the same to Table 1.

Table 3. Force constants (mdyn/Å) of calcite and aragonite

Calcite			Aragonite		
Force constant		Distance[a]	Force constant		Distance[a]
K(C-O)	5.520	1.290	K(C-O)	5.669	1.282
H(OCO)[b]	0.340		H(OCO)[b]	0.340	
F(O O)[b]	1.720		H(O O)[b]	1.720	
$\alpha(CO_3)$[c]	0.797		$\alpha(CO_3)$[c]	0.738	
p	0.052		p	−0.125	
n[c]	0.021		n[c]	0.016	
f_1(Ca C)	0.103	3.185	f_1(Ca C)	0.288	2.904
			f_2(Ca C)	0.074	2.937
			f_3(Ca C)	0.030	3.249
			f_4(Ca C)	0.020	3.415
f_2(Ca O)	0.425	2.333	f_5(Ca O)	0.251	2.419
			f_6(Ca O)	0.096	2.445
			f_7(Ca O)	0.040	2.550
			f_8(Ca O)	0.060	2.520
f_3(C O)[b]	0.000	3.392	f_9(Ca O)	0.040	2.653
			f_{10}(C C)	0.123	2.877
			f_{11}(O O)	0.316	2.744
			f_{12}(O O)	0.224	3.065
f_4(O O)	0.080	3.185	f_{13}(O O)	0.132	2.983
f_5(O O)	0.040	3.203	f_{14}(O O)	0.086	3.075
f_6(O O)	0.028	3.392	f_{15}(O O)	0.069	3.149

a) Unit of distances is in Å. b) Fixed force constants.
c) Units of n and α are in mdyn·Å.

Treatment of the Elastic Constant. When a crystal is subjected to homogeneous deformation, the elastic constant of the crystal can be calculated in accordance with the method established by Shiro.[12] The course of the calculation is outlined below. In the first place, by the use of the resulting matrices of the preceding section, *i.e.*, $\boldsymbol{F}_0^{\mathrm{R}}$ and $\boldsymbol{B}_\rho$, and of the external strain matrix, $\boldsymbol{D}$, the (6×6) elastic constant matrix is derived as:

$$\boldsymbol{C}=1/v\tilde{\boldsymbol{H}}\boldsymbol{F}_0^{\mathrm{R}}\boldsymbol{H}, \tag{1}$$

where a tilde denotes a transposed matrix, where v is the unit cell volume, and where

$$\boldsymbol{H}=(\boldsymbol{E}-\boldsymbol{B}_\rho(\tilde{\boldsymbol{B}}_\rho\boldsymbol{F}_0^{\mathrm{R}}\boldsymbol{B}_\rho)^{-1}\tilde{\boldsymbol{B}}_\rho\boldsymbol{F}_0^{\mathrm{R}})\boldsymbol{D}. \tag{2}$$

The Jacobian matrix with respect to the elastic constant, $(\partial C_i/\partial K_h)$, and the contribution of the h-thp otential term to the i-th elastic constant, $(PED)_{ih}$, are also given:

$$J_{ih}^{\mathrm{E}}=(\partial C_i/\partial K_h)=1/v(\tilde{\boldsymbol{H}}\boldsymbol{A}_h\boldsymbol{H})_{ii}, \tag{3}$$

$$(\mathrm{PED})_{ih}=J_{ih}^{\mathrm{E}}K_h/C_i, \tag{4}$$

respectively, where $\boldsymbol{A}_h$ is the coefficient matrix of the k-th term in the potential energy matrix. Furthermore, the change in the internal coordinates due to the elastic stress, $\Delta\boldsymbol{S}$ is calculated as:

$$\Delta\boldsymbol{R}_0=\boldsymbol{H}\boldsymbol{C}^{-1}\Delta\boldsymbol{S}. \tag{5}$$

The change, $\Delta\boldsymbol{R}_0$, is found to be useful for the analysis of the elastic strains.

Refinement of the Force Constant. The Jacobians with respect to the optically-active vibrations, $\boldsymbol{J}^\lambda$, and to the elastic constants, $\boldsymbol{J}^{\mathrm{E}}$, are derived independently from the treatments of the preceding sections. The force constants of the force fields were refined by the least-squares method:

$$\Delta\boldsymbol{K}=(\tilde{\boldsymbol{J}}^\lambda\boldsymbol{W}_\lambda\boldsymbol{J}^\lambda+\tilde{\boldsymbol{J}}^{\mathrm{E}}\boldsymbol{W}_{\mathrm{E}}\boldsymbol{J}^{\mathrm{E}})^{-1}\times(\tilde{\boldsymbol{J}}^\lambda\boldsymbol{W}_\lambda\Delta\lambda+\tilde{\boldsymbol{J}}^{\mathrm{E}}\boldsymbol{W}_{\mathrm{E}}\Delta\boldsymbol{C}), \tag{6}$$

where $\boldsymbol{W}^\lambda$ and $\boldsymbol{W}^{\mathrm{E}}$ are diagonal weight matrices for the observed vibrational frequencies and elastic constants respectively, where $\Delta\lambda$ is a deviation column matrix of the calculated frequencies from the corresponding observed ones, and where $\Delta\boldsymbol{C}$ is that of the elastic constants.

Results and Discussion

Optically-active Vibrations. The vibrational spectra of calcite and aragonite have been reported by several authors.[13–19] However, it seems likely that the observed resonance frequencies will deviate slightly from the corresponding eigenfrequencies[20] when one come to think of the ionic properties of the two crystals. In our normal coordinate treatments, we postulated an equilibrium crystal field, *i.e.*, any dynamical effects are frozen out, since only the short-range interactions were taken into consideration. Consequently, the eigenfrequencies in the idealized equilibrium field should generally deviate from those in the actual dynamical lattices. We have, however, regarded the observed resonance frequencies as the eigenfrequencies without any correction, because the appropriate estimation of the shifts is impracticable, especially for a complex crystal system. Provided that the shifts are brought about through interactions among the vibrating dipoles, the observed frequencies of the g-symmetric vibrations are found to be approximately equal to those in the equilibrium crystal field.[21] Therefore, we have given some priority to the g-symmetric vibrations over the u-symmetric ones in the course of the refinement of the force constants in calcite.

Ramdas'[13] and Tsuboi's data[14] were adopted as the observed frequencies for the intramolecular vibrations of the carbonate groups and for the (intermolecular) lattice vibrations respectively. In the case of aragonite, though few data are available, Couture's data,[13] which were obtained from the depolarization study of Raman scattering, are noteworthy. Hence, only Couture's data were taken as the observed data, the remaining data[16–19] other than Couture's amounted to no more than supplimentary references.

Intramolecular Vibration of the Carbonate Groups: Carbonate groups in calcite occupy a site, the symmetry of which is D_3, while it is C_s in aragonite. Because of the lowering of the site symmetry, more numbers of the optically-active frequencies are to be observed in aragonite than in calcite. The intramolecular vibrations in these crystals may, in principle, be explained in terms of the force field of an isolated free carbonate group, since the observed intramolecular frequencies of these crystals show much similarity. The results on force constants are shown in Table 3. The observed and calculated frequencies in calcite and aragonite are also compared in Tables 4 and 5 respectively. It

TABLE 4. OBSERVED AND CALCULATED FREQUENCIES (cm^{-1}) OF CALCITE

Sym.		Obsd.[a]	Calcd.	Assignment	Sym.		Obsd.[a]	Calcd.	Assignment
A_{1g}	ν_{11}	1086	1086	CO str.	A_{1u}	ν_{41}		1089	CO str.
						ν_{42}		211	Ca trans(z).
A_{2g}	ν_{21}		890	CO_3 out-of-plane def.					
	ν_{22}		287	CO_3 trans(z).	A_{2u}	ν_{51}	885	884	CO_3 out-of-plane def.
	ν_{23}		197	CO_3 rot(z).		ν_{52}	290	334	Ca, CO_3 trans(z).
						ν_{53}	110	120	CO_3 rot(z).
E_g	ν_{31}	1434	1428	CO str.					
	ν_{32}	712	710	OCO def.	E_u	ν_{61}	1484	1428	CO str.
	ν_{33}	284	266	CO_3 rot(x, y).		ν_{62}	706	711	OCO def.
	ν_{34}	156	169	CO_3 trans(x, y).		ν_{63}	320	312	CO_3 rot(x, y).
						ν_{64}	230	224	Ca trans(x, y).
						ν_{65}	110	113	Ca, CO_3 trans(x, y).

a) See Refs. 13 and 14.

TABLE 5. OBSERVED AND CALCULATED FREQUENCIES (cm^{-1}) OF ARAGONITE

Sym.		Obsd.[a]	Calcd.	Assignment	Sym.		Obsd.[b]	Calcd.	Assignment
A_{1g}	ν_{11}	1464	1468	CO str.	A_{1u}	ν_{51}		1456	CO str.
	ν_{12}	1086	1090	CO str.		ν_{52}		685	OCO def.
	ν_{13}	854	853	CO_3 out-of-plane def.		ν_{53}		222	CO_3 rot(y).
	ν_{14}	707	717	OCO def.		ν_{54}		140	Ca, CO_3 trans(x).
	ν_{15}	287	275	CO_3 rot(x).		ν_{55}		105	CO_3 rot(z).
	ν_{16}	191	208	CO_3 trans(y).		ν_{56}		99	Ca trans(x).
	ν_{17}	143	146	Ca, CO_3 trans(z).					
	ν_{18}		121	Ca trans(y).	B_{1u}	ν_{61}		1468	CO str.
	ν_{19}	105	99	Ca trans(z).		ν_{62}	1084	1079	CO str.
						ν_{63}	857	851	CO_3 out-of-plane def.
B_{1g}	ν_{21}	1415	1457	CO str.		ν_{64}	712	708	OCO def.
	ν_{22}	716	717	OCO def.		ν_{65}	294	254	CO_3 rot(x).
	ν_{23}		248	CO_3 rot(y).		ν_{66}	200	185	Ca, CO_3 trans(y).
	ν_{24}		197	CO_3 rot(z).		ν_{67}		152	Ca trans(y), (z).
	ν_{25}	154	138	Ca, CO_3 trans(x).		ν_{68}	114	131	Ca trans(y).
	ν_{26}	114	97	Ca trans(y).					
					B_{2u}	ν_{71}	1480	1467	CO str.
B_{2g}	ν_{31}	1415	1457	CO str.		ν_{72}	1082	1084	CO str.
	ν_{32}	702	711	OCO def.		ν_{73}	877	890	CO_3 out-of-plane def.
	ν_{33}	263	247	CO_3 rot(z).		ν_{74}	706	711	OCO def.
	ν_{34}	250	162	CO_3 rot(y).		ν_{75}	274	272	Ca, CO_3 trans(z).
	ν_{35}	208	147	Ca, CO_3 trans(x).		ν_{76}	200	208	CO_3 rot(x).
	ν_{36}	183	73	Ca, CO_3 trans(x).		ν_{77}		169	Ca, CO_3 trans(y).
						ν_{78}	100	87	Ca, CO_3 trans(z).
B_{3g}	ν_{41}	1466	1470	CO str.					
	ν_{42}	1086	1084	CO str.	B_{3u}	ν_{81}	1480	1456	CO str.
	ν_{43}	854	890	CO_3 out-of-plane def.		ν_{82}	712	691	OCO def.
	ν_{44}	703	718	OCO def.		ν_{83}	274	163	CO_3 rot(y).
	ν_{45}	276	273	CO_3 trans(z).		ν_{84}	200	137	Ca, CO_3 trans(x).
	ν_{46}	222	235	CO_3 trans(y).		ν_{85}	118	123	CO_3 rot(z).
	ν_{47}	193	201	CO_3 rot(x).					
	ν_{48}	113	128	Ca trans(y).					
	ν_{49}	105	117	Ca trans(z).					

a) See Ref. 15. b) See Ref. 11.

is obvious from these tables that the large splittings of the frequencies between g-symmetric and u-symmetric C–O stretching vibrations cannot be explained on the basis of the short-range interaction model. Not only the coupling of the motion of the carbonate groups, but also the interaction between the vibrating dipoles would cause these large splittings. These consideration have been made by Haas and Ketelaar,[21] Decius,[22] and Ishigame *et al.*[23] Their results are quite suggestive, but they give only qualitative explanations for complicated crystal systems. These models will actually be applied in our subsequent papers.

For the observed Raman frequency shifts at 1415 cm^{-1} and around 1460 cm^{-1} in aragonite, there are two ways of interpretation. Krishnan[16] regarded only the shift at 1463 cm^{-1} as the fundamental band and assigned the shift at 1415 cm^{-1} to the overtone band of the fundamental band at 707 cm^{-1} on the basis of his second-order Raman scattering study. On the other hand, Krishnamurti[17] considered all these shifts to be fundamental bands. In this study, we have regarded the shift at 1415 cm^{-1} as the fundamental band, with reference to the spectra of carbonate or nitrate crystals.

Lattice Vibration: Normal coordinate treatments of calcite have been performed by Venkateswarlu and Ramaswamy,[24] Tsuboi,[14] Shiro,[25] and Plihal and Schaack;[26] however, no treatment of aragonite has been reported. Though only the short-range interactions were taken into consideration in both Tsuboi's[14] and Shiro's[25] treatments, their results are satisfactory for at least the factor-group vibrations. Assuming an idealized simpler unit cell which contains only four ions, Plihal and Schaack[26] took the long-range Coulomb interaction of vibrating dipoles and the influence of the electronic polarizability of the component ions as well as the short-range interaction; thus they explained fairly well the observed TO–LO splittings of the optically-active lattice vibrations in the calcite-form crystals. A detailed analysis based on the rigid ion model is now in progress; the results will be published in time.

Therefore, we have determined the short-range fields, which reproduce both the observed vibrational frequencies and the elastic constants, and have also improved the previous treatment.[25] Tables 4 and 5 show the observed and calculated frequencies and the tentative assignments of the observed fundamental bands. The contributions of all the potential terms to the calculated vibrational frequencies are also given in Tables 6 and 7. The results of the calculation imply that certain lattice modes in the same symmetry species are fairly well coupled with each other, but that the couplings between an intramolecular mode and lattice modes are negligibly smal, except for the out-of-plane angle deformation modes in carbonate groups. As is shown in Tables 4 and 5, the calculated frequencies of aragonite agree less well with the observed ones than that of calcite, particularly in the B_{2g} and B_{3u} symmetric vibrations. Our resulting force field for calcite is substantially that obtained by Tsuboi.[14] The interatomic force constants will be discussed briefly in a later section.

Elastic Constants. The elastic constants of these crystals have previously been determined [27,28] and tabulated in the "Landolt-Börnstein Phys. Chem. Tables."[29] However, only a few attempts at theoretical calculation have yet been reported. For example, calculations of the two particular constants were performed by Oke[30,31] on the basis of the electrostatic theory of crystal lattices. We have ourselves calculated the elastic constants by the method described above; the calculated elastic constants are compared

TABLE 6. CONTRIBUTION (%) OF POTENTIAL TERMS TO CALCULATED FREQUENCIES FOR CALCITE

Mode	K	H	F	α	p	n	f_1	f_2	f_3	f_4	f_5	f_6
ν_{11}	50	0	46	0	1	0	0	2	0	0	1	0
ν_{41}	50	0	46	0	1	0	0	2	0	0	1	0
ν_{42}	1	0	1	0	0	0	12	86	0	0	0	0
ν_{21}	0	0	0	96	0	0	2	1	0	1	0	0
ν_{22}	0	0	0	1	0	0	3	70	0	4	8	14
ν_{23}	0	0	0	0	0	0	4	4	0	63	23	6
ν_{51}	0	0	0	97	0	0	2	1	0	1	0	0
ν_{52}	0	0	0	0	0	0	5	88	0	0	5	1
ν_{53}	0	0	0	0	0	0	22	1	0	0	67	9
ν_{31}	85	9	6	0	−1	0	1	0	0	0	0	0
ν_{32}	3	30	59	0	0	−1	1	6	0	1	2	0
ν_{33}	0	0	1	0	0	0	2	64	0	25	0	8
ν_{34}	0	0	0	0	0	0	21	32	0	44	0	4
ν_{61}	85	9	6	0	−1	0	1	0	0	0	0	0
ν_{62}	3	29	58	0	0	−1	1	7	0	0	2	1
ν_{63}	0	1	1	0	0	0	13	81	0	0	0	4
ν_{64}	0	1	3	0	0	0	21	73	0	0	0	2
ν_{64}	0	0	0	0	0	0	43	1	0	0	0	55

Notations are the same to Tables 3 and 4.

TABLE 7. CONTRIBUTION (%) OF POTENTIAL TERMS TO CALCULATED FREQUENCIES FOR ARAGONITE

Mode	K	H	F	α	p	n	f_1	f_2	f_3	f_4	f_5	f_6	f_7	f_8	f_9	f_{10}	f_{11}	f_{12}	f_{13}	f_{14}	f_{15}
ν_{11}	83	8	5	0	2	0	1	0	0	0	0	0	0	0	0	0	0	0	0	0	0
ν_{12}	51	0	46	0	−2	0	0	0	0	0	0	0	0	0	0	0	3	1	0	1	0
ν_{13}	0	0	0	98	0	0	1	0	0	0	0	0	0	0	0	0	0	0	0	0	0
ν_{14}	3	29	58	0	0	−1	1	0	0	0	0	0	0	1	0	0	6	2	0	0	0
ν_{15}	0	0	0	0	0	0	4	0	1	0	30	5	0	2	0	0	0	13	11	2	32
ν_{16}	0	0	0	0	0	0	27	5	0	0	6	0	7	7	1	0	0	24	0	3	19
ν_{17}	0	0	0	0	0	0	20	0	0	3	2	24	6	0	1	0	0	13	5	24	1
ν_{18}	0	0	0	0	0	0	2	0	11	3	32	4	0	3	2	0	0	0	0	2	41
ν_{19}	0	0	0	0	0	0	8	7	1	1	3	19	3	10	3	0	0	28	8	2	7
ν_{21}	84	8	5	0	2	0	0	1	0	0	0	0	0	0	0	0	0	0	0	0	0
ν_{22}	3	30	58	0	0	−1	0	0	0	0	0	0	0	0	1	0	0	4	3	2	0
ν_{23}	0	0	0	0	0	0	0	0	0	0	0	9	0	4	2	0	0	28	14	4	39
ν_{24}	0	0	0	0	0	0	0	3	0	0	0	3	3	0	9	0	0	10	34	2	34
ν_{25}	0	0	1	0	0	0	0	29	0	0	0	1	15	23	7	0	0	9	1	0	14
ν_{26}	0	0	0	0	0	0	0	8	0	15	0	35	0	0	11	0	0	7	9	1	14
ν_{31}	84	8	5	0	2	0	0	1	0	0	0	0	0	0	0	0	0	0	0	0	0
ν_{32}	3	30	59	0	0	−1	0	0	0	0	0	0	0	0	1	0	0	4	3	0	0
ν_{33}	0	0	0	0	0	0	0	2	0	0	0	2	2	3	8	0	0	31	34	8	10
ν_{34}	0	0	1	0	0	0	0	2	0	0	0	12	2	6	1	0	0	9	3	22	41
ν_{35}	0	0	0	0	0	0	0	26	0	5	0	26	2	18	8	0	0	5	1	0	9
ν_{36}	0	1	1	0	0	0	0	5	0	1	0	0	38	0	12	0	0	2	25	6	9
ν_{41}	83	8	5	0	2	0	1	0	0	0	0	0	0	0	0	0	0	0	0	0	0
ν_{42}	51	0	47	0	−2	0	0	0	0	0	0	0	0	0	0	0	3	1	0	0	0
ν_{43}	0	0	0	90	0	0	0	0	0	0	0	0	0	0	0	7	0	0	0	0	1
ν_{44}	3	29	58	0	0	−1	1	0	0	0	0	0	0	1	0	0	6	2	0	0	1
ν_{45}	0	0	0	0	0	0	4	1	1	1	22	4	1	0	0	15	0	0	6	0	44
ν_{46}	0	0	0	0	0	0	12	1	1	0	12	4	2	3	0	2	0	42	7	2	11
ν_{47}	0	0	0	0	0	0	13	0	1	0	10	2	5	0	1	1	0	2	2	38	24
ν_{48}	0	0	0	0	0	0	32	12	0	0	0	1	7	24	0	2	0	5	1	8	6
ν_{49}	0	0	0	0	0	0	0	1	4	4	24	36	0	0	5	3	0	1	6	0	14
ν_{51}	84	8	5	0	2	0	0	1	0	0	0	0	0	0	0	0	0	0	0	0	0
ν_{52}	3	32	63	0	0	−1	0	0	0	0	0	0	0	0	1	0	0	0	0	0	0
ν_{53}	0	0	0	0	0	0	0	0	0	0	0	13	2	2	0	0	0	0	0	9	73
ν_{54}	0	0	0	0	0	0	0	27	0	0	0	3	0	1	31	0	0	0	0	21	16
ν_{55}	0	0	0	0	0	0	0	12	0	0	0	1	13	51	2	0	0	0	0	17	2
ν_{56}	0	0	0	0	0	0	0	5	0	14	0	30	16	0	9	0	0	0	0	8	18
ν_{61}	83	8	5	0	2	0	1	0	0	0	0	0	0	0	0	0	0	0	0	0	0
ν_{62}	52	0	47	0	−2	0	0	0	0	0	0	0	0	0	0	0	3	0	0	0	0
ν_{63}	0	0	0	98	0	0	1	0	0	0	0	0	0	0	0	0	0	0	0	0	0
ν_{64}	3	30	59	0	0	−1	1	0	0	0	0	0	0	1	0	0	5	0	0	0	0
ν_{65}	0	0	0	0	0	0	0	0	0	0	31	0	0	0	2	0	0	0	0	15	51
ν_{66}	0	0	0	0	0	0	42	0	2	0	18	2	11	0	1	0	0	0	0	16	7
ν_{67}	0	0	0	0	0	0	13	1	4	5	18	42	1	1	1	1	0	0	0	0	14
ν_{68}	0	0	0	0	0	0	11	16	3	0	4	3	3	34	0	0	0	0	0	17	8
ν_{71}	83	8	5	0	2	0	1	0	0	0	0	0	0	0	0	0	0	0	0	0	0
ν_{72}	51	0	46	0	−2	0	0	0	0	0	0	0	0	0	0	0	3	0	0	1	0
ν_{73}	0	0	0	90	0	0	0	0	0	0	0	0	0	0	0	7	0	0	0	0	1
ν_{74}	3	30	59	0	0	−1	1	0	0	0	0	0	0	1	0	0	5	0	0	0	1
ν_{75}	0	0	0	0	0	0	3	0	1	0	19	1	1	0	1	16	0	0	0	10	48
ν_{76}	0	0	0	0	0	0	11	2	1	2	33	18	1	7	1	3	0	0	0	0	20
ν_{77}	1	0	0	0	0	0	43	6	1	0	9	4	13	9	2	0	0	0	0	1	12
ν_{78}	0	0	0	0	0	0	0	3	7	6	4	16	0	6	0	0	0	0	0	3	53
ν_{81}	84	8	5	0	2	0	0	1	0	0	0	0	0	0	0	0	0	0	0	0	0
ν_{82}	3	32	62	0	0	−1	0	0	0	0	0	0	0	0	1	0	0	0	0	2	1
ν_{83}	0	0	0	0	0	0	0	12	0	2	0	38	6	0	9	0	0	0	0	7	25
ν_{84}	0	0	0	0	0	0	0	17	0	3	0	0	5	34	3	0	0	0	0	7	30
ν_{85}	0	0	0	0	0	0	0	6	0	1	0	0	11	4	31	0	0	0	0	1	46

Notations are the same to Tables 3 and 5.

Table 8. Observed and calculated elastic constants (10^{10} dyn/cm^2) of calcite and aragonite

D_{3d}^6	Calcite			D_{2h}^{16}	Aragonite		
	Obsd.[a]	Calcd.	Sym.		Obsd.[b]	Calcd.	Sym.
C_{11}	144.0	118.7	A_{1g}, E_g	C_{11}	160.0	165.2	A_{1g}
C_{21}	53.9	49.9	A_{1g}, E_g	C_{21}	37.0	39.1	A_{1g}
C_{31}	51.1	52.8	A_{1g}	C_{22}	89.2	73.4	A_{1g}
C_{33}	84.0	75.5	A_{1g}	C_{31}	1.7	19.8	A_{1g}
C_{41}	−20.5	−20.9	E_g	C_{32}	15.4	24.6	A_{1g}
C_{44}	33.5	33.0	E_g	C_{33}	84.2	89.2	A_{1g}
				C_{44}	41.2	23.2	B_{3g}
				C_{55}	25.6	17.3	B_{2g}
				C_{66}	42.7	24.1	B_{1g}

a) See Ref. 27. b) See Ref. 28.

Table 9. Contribution (%) of potential terms to calculated elastic constants

	Aragonite										Calcite					
	11	21	22	31	32	33	44	55	66		11	21	31	33	41	44
K	2	3	1	1	1	0	0	0	0	K	1	2	1	0	1	0
H	1	−1	0	0	0	0	0	0	0	H	0	−1	0	0	2	1
F	4	1	1	0	0	0	0	0	0	F	2	0	1	0	4	1
α	0	0	0	0	0	0	0	0	0	α	0	0	0	0	0	0
p	0	0	0	0	0	0	0	0	0	p	0	0	0	0	0	0
n	0	0	0	0	0	0	0	0	0	n	0	0	0	0	0	0
f_1	1	5	4	2	2	0	7	0	0	f_1	21	15	16	5	38	26
f_2	5	13	4	12	6	1	4	7	0							
f_3	0	2	2	1	3	0	5	0	0							
f_4	1	3	1	6	3	1	3	9	2							
f_5	0	1	1	5	8	4	4	0	0	f_2	43	75	69	40	43	43
f_6	2	11	7	27	25	8	5	25	4							
f_7	0	2	1	1	1	0	1	1	10							
f_8	1	8	13	5	12	1	10	2	1							
f_9	5	−3	0	6	−1	0	0	6	2	f_3	0	0	0	0	0	0
f_{10}	0	0	0	0	−5	20	0	0	0							
f_{11}	69	−2	0	0	0	0	0	0	0							
f_{12}	0	4	8	−1	−3	0	10	0	16							
f_{13}	5	29	20	2	2	0	0	7	17	f_4	2	−5	5	33	20	23
f_{14}	2	23	28	28	52	9	8	13	37	f_5	26	18	−1	0	−2	0
f_{15}	0	0	7	4	−6	56	42	30	5	f_6	4	−4	9	20	−5	6

Notations are the same to Tables 3 and 8.

with the observed ones in Table 8. It is obvious from these results that a good agreement was obtained for calcite, while only a rough fit was obtained for aragonite. Particularly, the agreement of the elastic constants related to the shear strains, *i.e.*, C_{44}, C_{55}, and C_{66}, is relatively poor in aragonite because of the lack of effective oblique interaction terms compared with those in calcite. The contributions of all the potential terms to the calculated elastic constants are also listed in Table 9. This table shows that the elastic constants have a strong dependence on the following potential terms; f_1, f_2, f_4, and f_5 in calcite, and f_2, f_6, f_8, f_{13}, f_{14}, and f_{15} in aragonite. It is likely that these contributions are partly dependent on the spatial orientation of the internal coordinates. These contributions are considered to be independent of those to the vibrational frequencies, as is shown in Tables 6 and 7; therefore the determination of the interatomic force constants becomes more meaningful.

Interatomic Force Constants. The resulting interatomic force constants are plotted as functions of the interatomic distance in Fig. 5. As this figure illustrates, three steep curves can be drawn through the points of the same pairs, and the distances of their burst upbreaks approximately correspond to the sums of the van der Waals radii or of the Pauling's ionic radii[32] of the constituent atoms, as shown in Fig. 5: $R_{Ca}+R_O=2.39$ Å, $R_{Ca}+R_C=2.69$ Å, and $2R_O=2.80$ Å. Since these interatomic interaction force constants should be derived from the appropriate interatomic potentials, we began to estimate them with simple Lennard-Jones 6-9 type potentials[33] determined for some purely ionic crystals and noble gas crystals; however, we thus obtained unreasonable results except

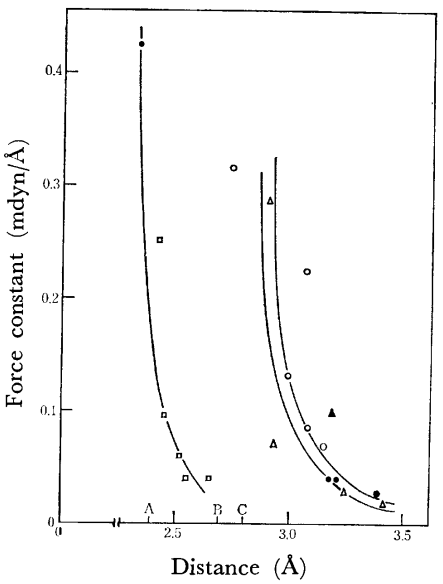

Fig. 5. Interatomic force constants. Closed and open figures indicate those for calcite and aragonite respectively.
△, calcium···carbon; □, calcium···oxygen; ○, oxygen ···oxygen; R_C, van der Waals radius of carbon; R_O, van der Waals radius of oxygen; R_{Ca}, Pauling's ionic radius of calcium.
A: $R_{Ca}+R_O$, B: $R_{Ca}+R_C$, C: R_O

for a few cases. We inevitably chose several trial sets of them which reproduced the observed values as well as possible, and then refined by the least-squares method.[12] As is shown in Fig. 5, some plots were found to deviate from the corresponding curves. This must mainly be because of the uncertainty of the experimental frequencies and/or elastic constants, and the incompleteness of the force fields. The former is considered to have an appreciable influence on the force constants in aragonite, while both the observed frequencies and elastic constants were found to be fairly reliable in calcite. The results listed in Tables 6 and 9 suggest that the force constant, f_1, of calcite contributes particularly to certain lattice modes and to all the elastic constants except C_{33}. If this force constant is reduced to the value on the curve, less agreement will be obtained. Therefore, the large deviation of the closed triangle must arise mainly from the incompleteness of the force field. The incompleteness of the force field can be improved by the rigid ion treatment or by the polarizable ion treatment; these treatments are now in progress. As to the open circles in Fig. 5, f_{11} was found to contribute in particular to C_{11} (see Table 9), and f_{12}, to almost all the lattice modes in aragonite. Therefore, the incompleteness must exert an appreciable influence on the force constants, above all, the force constants which are closely related to the lattice vibrations in aragonite.

The force constants obtained would be useful as the initial values of the force constants in the normal coordinate treatments of similar crystals, though it is meaningless to discuss certain fundamental properties of the solid state on the basis of only these data.

Analysis of Elastic Strain. Table 10 shows the change in the internal coordinates due to unit elastic stress in calcite. We can see from this table that the q_5 coordinate is sensitive to the S_{xx} applied stress, the q_3, q_5, and q_6 coordinates, to the S_{zz} stress, and the q_3, q_4, and q_5 coordinates, to the S_{yz} stress. The internal coordinates of calcite, therefore, can be changed by the applied stress along the direction z. For aragonite, Table 11 suggests that the q_4, q_6, q_{14}, and q_{15} coordinates a strong dependence on the appropriate stresses. As well as in calcite, it seems that calcium atoms in aragonite would be easy to displace in the directions to the adjacent carbonate groups, and that the carbonate would be susceptible to certain deformations along the

Table 10. Change (Å³/mdyn) of internal coordinates due to elastic stress in calcite

Coord.[b]	S_{xx}	S_{yy}	S_{zz}	S_{yz}
CO str.	1	1	0	1
OCO def.[a]	−3	3	0	−2
CO_3 out-of-plane[a]	0	0	0	0
q_1	4	42	−1	−70
q_2	10	16	19	58
q_3	27	−65	121	−156
q_4	−18	−46	144	−109
q_5	142	−26	−72	−110
q_6	−36	−74	121	−64

a) Unit of angle coordinates is in Rad·Å²/mdyn. b) Notations are the same to Fig. 3.

Table 11. Change (Å³/mdyn) of internal coordinates due to elastic stress in aragonite

Coord.[b]	S_{xx}	S_{yy}	S_{zz}	S_{yz}	S_{zx}	S_{xy}
	A_{1g}	A_{1g}	A_{1g}	B_{3g}	B_{2g}	B_{1g}
CO str.	2	0	0	−1	0	−1
	0	1	0	0	0	0
OCO def.[a]	−4	2	0	−1	−1	−9
	5	−3	0	1	0	0
CO_3 out-of-plane[a]	1	1	0	0	0	0
q_1	4	15	1	−27	0	0
q_2	28	21	12	−41	78	5
q_3	−2	42	7	73	0	0
q_4	22	17	32	63	−164	−55
q_5	2	7	19	23	0	0
q_6	12	27	44	41	−124	−35
q_7	9	16	6	−26	−40	88
q_8	−4	70	9	−73	41	−20
q_9	51	−37	19	2	95	41
q_{10}	3	−18	70	−1	0	0
q_{11}	63	−28	4	0	0	0
q_{12}	−3	31	−10	−37	4	47
q_{13}	12	54	−8	−7	−57	62
q_{14}	1	77	40	−54	−95	114
q_{15}	10	−55	91	52	104	23
	11	−32	93	−54	−122	38
	−6	19	89	−116	5	−14

a) Unit of angle coordinates is in Rad·Å²/mdyn.
b) Notations are the same to Fig. 4.

z axis. From these considerations, some information will be gained about the phase transitions between polymorphic crystals, though we cannot reach any definite conclusions on the basis of these data only.

Numerical calculations have been carried out on the TOSBAC 3400 MODEL 41 electronic computer at the Computing Center of Hiroshima University. The authors wish to express their gratitude to Professor Michiro Hayashi of Hiroshima University for his encouragement throughout this work, and also to Mr. Masaru Ohsaku and Mr. Tamaki Utida of Hiroshima University for part of numerical computations and their advisable discussions.

References

1) a) Presented in part at the 26-th Annual Meeting of the Chemical Society of Japan, Fujisawa, April, 1972, and at the Symposium on the Molecular Structure, Sendai, October, 1972; b) to be published.
2) M. Born and K. Huang, "Dynamical Theory of Crystal Lattices," Oxford University Press, London (1954).
3) R. A. Cowley, *Proc. Roy. Soc., Ser. A*, **268**, 121 (1962).
4) See for example, W. Cochran and R. A. Cowley, "Encyclopedia of Physics," **25/2a**, 59 (1963).
5) a) R. W. Wyckoff, *Phys. Rev.*, **16**, 149 (1920); b) D. L. Graf, *Amer. Mineral.*, **46**, 1283 (1961).
6) J. P. R. de Villiers, *ibid.*, **56**, 758 (1971).
7) E. B. Wilson, Jr., *J. Chem. Phys.*, **7**, 1047 (1939).
8) T. Shimanouchi, M. Tsuboi, and T. Miyazawa, *ibid.*, **35**, 1597 (1961).
9) T. Shimanouchi, *Pure Appl. Chem.*, **7**, 131 (1963).
10) a) R. S. Halford, *J. Chem. Phys.*, **14**, 8 (1946); b) H. Winston and R. S. Halford, *ibid.*, **17**, 607 (1949).
11) S. Bhagavantam and T. Ventakarayudu, *Proc. Indian Acad. Sci., Sect. A*, **9**, 224 (1939).
12) Y. Shiro and T. Miyazawa, This Bulletin, **44**, 2371 (1971).
13) A. K. Ramdas, *Proc. Indian Acad. Sci., Sect. A*, **37**, 441 (1953).
14) M. Tsuboi, The International Symposium on Molecular Structure and Spectroscopy, Tokyo, 1962, preprint A305.
15) L. Couture, *C. R. Acad. Sci. Paris.*, **218**, 669 (1944).
16) T. S. Krishnan, *Proc. Indian Acad. Sci., Sect A*, **44**, 96 (1956).
17) D. Krishnamurti, *ibid.*, **51**, 285 (1960).
18) C. E. Weir and E. R. Lippincott, *J. Res. Nat. Bur. Stand., A*, **65**, 173 (1961).
19) W. P. Griffith, *J. Chem. Soc., A*, **1970**, 132.
20) R. Frech and J. C. Decius, *J. Chem. Phys.*, **54**, 2374 (1971).
21) C. Haas and J. A. A. Ketelaar, *Physica*, **22**, 1286 (1956).
22) J. C. Decius, *J. Chem. Phys.*, **49**, 1387 (1968).
23) M. Ishigame, T. Sato, and T. Sakurai, *Phys. Rev.*, **B3**, 4388 (1971).
24) K. Venkateswarlu and K. Ramaswamy, *Ind. J. Pure Appl. Phys.*, **2**, 209 (1964).
25) Y. Shiro, *J. Sci. Hiroshima University, Ser.* **A-II**, **32**, 77 (1968).
26) M. Plihal and G. Schaack, *Phys. Stat. Sol.*, **42**, 485 (1970).
27) D. P. Dandekar, *J. Appl. Phys.*, **32**, 485 (1970).
28) W. Voigt, *Ann. Phys.*(Leipzig), **24**, 290 (1907).
29) K. H. Hellwege Ed., in Landolt-Börnstein Phys. Chem. Tables, new series, Springer-Verlag, Berlin (1966 and 1969), vol. 1.
30) B. V. Oke, *Proc. Indian Acad. Sci.*, **4**, 514 (1936).
31) B. V. Oke, *ibid.*, **4**, 667 (1936).
32) L. Pauling, "The Nature of the Chemical Bond," Cornell University Press, New York (1960), Chap. 13.
33) R. H. Fowler, "Statistical Mechanics," Cambridge University Press, London (1936), Chap. 10.

Studies of the Equilibria between Tetraarylallyl-type Radicals and Their Dimers

Kohji WATANABE, Jun YAMAUCHI, Hiroaki OHYA-NISHIGUCHI* and Yasuo DEGUCHI**

Laboratory of Solid State Chemistry, Institute for Chemical Research, Kyoto University, Uji, Kyoto 611

**Faculty of Science, Kyoto University, Kyoto 606*

***College of Liberal Arts & Science, Kyoto University, Kyoto 606*

(Received August 2, 1973)

Tetraarylallyl-type radicals are stable radicals. In these series, TPA is obtained as radical crystals. However, BDA, BDAA and DDA are obtained as diamagnetic dimerized substances. These are partially dissociated in solution. These can be detected in solution by ESR and optical spectra measurements of these radicals about the equilibrium between the radical monomer and its dimer. The equilibrium constants and the energy of the formation of the dimer are thus determined. The order of the magnitudes of the dimer's formation energies can be explained in terms of the frontier electron densities of the bond-forming positions of radicals.

In a previous paper,[1] hereafter referred as I, we reported that abnormal hyperfine splittings in the ESR spectra of tetraarylallyl-type radicals had been observed, and that the splitting can be explained on the basis of the "twisted allyl" model. Another feature of the tetraarylallyl-type radicals is the existence of an equilibrium between the radical monomer and its diamagnetic dimer in solution.[2-4] $\alpha,\alpha,\gamma,\gamma$-Tetraphenylallyl(TPA) is a stable radical in solution and is also obtained as pure radical crystals.

However, $\alpha,\alpha,\gamma,\gamma$-bisdiphenyleneallyl(BDA), $\alpha,\alpha,\gamma,\gamma$-bisdiphenylene-$\beta$-azoallyl(BDAA), and α,α-diphenyl-γ,γ-diphenyleneallyl(DDA)(Fig. 1) are partially dimerized in solution, as is triphenylmethyl. These substances can be detected in solution by ESR and optical spectra measurements of these radicals about the equilibrium between the radical monomer and its dimer, carried out at various temperatures. The equilibrium constants and the enthalpy of the formation of the dimer are determined. In the following section, some factors for stabilizing the radical will be considered.

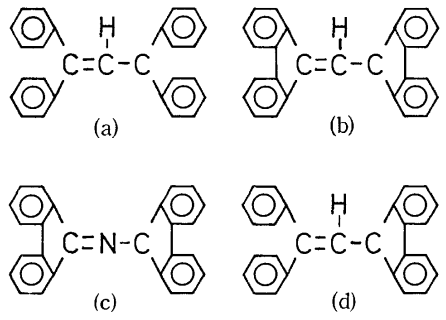

Fig. 1. Tetraarylallyl-type radicals.
(a) TPA (b) BDA (c) BDAA (d) DDA

As is shown in Fig. 1, these radicals resemble one another closely in structure. However, BDA has no degree of free rotation of the four phenyl rings attached to the α and the γ carbons after the partially-hindered DDA, by comparison with the TPA radical which has the degree of free rotation of the four phenyl rings. A comparison of the structures of BDA and DDA shows that DDA has more steric hindrance of phenyl groups than that of BDA. On the other hand, BDAA is an azoallyl which is replaced by a nitrogen at the β-position of the allyl group of BDA. By a comparison of BDA and BDAA, which have the same structures, one can ascertain the influence of the distribution of electron densities. These differences reflect the relative factor of the radical stabilities, which will be discussed in the following section.

Experimental

The samples were prepared following the processes described in Refs. 2, 3, 4 and 5. Their physical constants and the results of the elemental analyses are shown in Table 1.

Table 1. Physical constants and elemental analyses

	Mp[a] (°C)	Obsd / Calcd	C	H	N
TPA		Obsd	92.98	5.58	
		Calcd	93.86	6.14	
BDA	244.5—245.5	Obsd	94.85	5.01	
	245—246[2]	Calcd	95.00	5.00	
BDAA	270.0—271.5	Obsd	90.91	4.97	3.80
	270—272[3]	Calcd	91.62	4.71	3.78
DDA	236.0—237.5	Obsd	94.59	5.38	
	235—237[4]	Calcd	94.42	5.58	

a) Melting points are not corrected.

For the observation of the ESR spectra in solution, the solvents were well purified, dehydrated, and degassed by the usual methods.[6] The ESR signal intensity (I) was measured at various temperatures in the usual way (amplitude of magnetic field modulation: 8 G). The logarithm of the intensity (I) *vs.* the reciprocal of the temperature(T) plot gives directly the association energy of the two radical monomers to the dimer (Fig. 2). Mn^{2+} in MgO was used as the standard for the ESR signal intensity. All the ESR measurements were carried out with an X-band ESR spectrometer, JES-ME3, equipped with a 100 KHz field modulation, while the integration of the signal intensity was carried out by the use of a spectrum computer, EC-5, of the JEOL. Co.

The optical spectra were also measured at various temperatures and at several concentrations with an evacuated quartz cell with a path length of 1 cm, using a MPS-50-type spectrophotometer of the Shimadzu Co. The solvents used were treated in the afore-mentioned way.

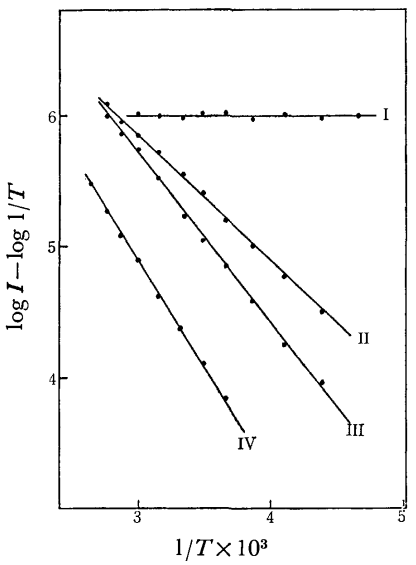

Fig. 2. Temperature dependence of integrated ESR signal intensity (I) TPA (II) BDAA (III) BDA (IV) DDA.

Results and Discussion

The ESR hyperfine structures of TPA, BDA, and BDAA have been reported elsewhere.[1] The ESR hyperfine spectrum of DDA observed in a diluted benzene solution at 60 °C is shown in Fig. 3 with the spectrum reconstructed by the ESR-spectrum computer using the hyperfine coupling constants given in Table 2. Those of the other radicals are also tabulated in Table 2. The values of A_β^H reflect the degree of twisting of the allyl skeleton, because the value of A_β^H is represented by the function of a twisted angle around the bond-axis and the spin densities on the carbons of the allyl skeleton.[1] Furthermore, the fact that the values of the twisted angles around the bond-axis of each allyl skeleton tabulated in Table 2 are in order of BDA→DDA→TPA can be well understood by a comparison with the molecular structure of each.

Now, in order to compare the relative stability among these radicals, each association energy from the two radical monomer to a dimer was determined by measuring the ESR and optical spectra at various temperatures. The equilibrium between a radical monomer (S·) and a dimer (S-S) can be quantitatively explained by the following equations:[9]

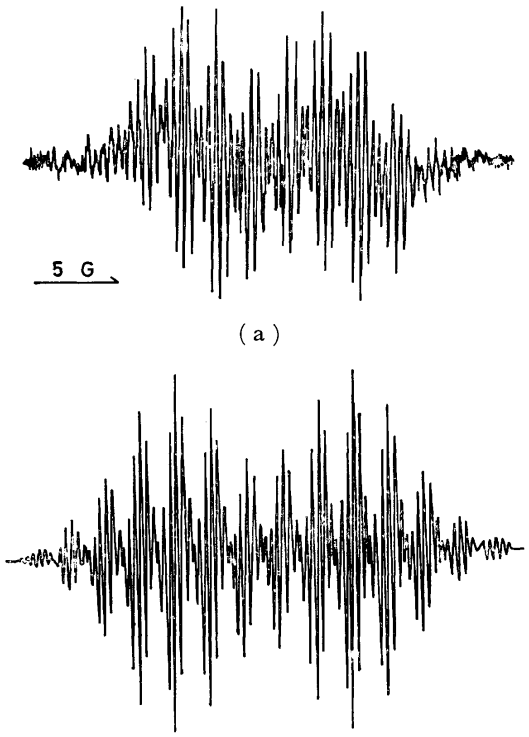

Fig. 3. ESR spectrum of DDA.
(a) Observed spectrum (b) Calculated spectrum

$$2S\cdot \rightleftharpoons S\text{-}S$$
$$K = [S\text{-}S]/[S\cdot]^2, \quad (1)$$

where K is the equilibrium constant expressed by;

$$K = A\exp(-\Delta H/RT), \quad (2)$$

A: proportionality constant
ΔH: association energy
R: gas constant
T: temperature

Hence,

$$\ln K = (-\Delta H/R)(1/T) + \ln A. \quad (3)$$

On the other hand, the intensity of the ESR signal (I) is simply expressed as a function of the radical concentration divided by the temperature, provided that I follows the Curie law in a dilute solution; thus,

$$I = B(1/T)[S\cdot], \quad (4)$$

where B is a proportionality constant. From Eqs. (1)

Table 2. Hyperfine coupling constants of tetraarylallyl-type radicals (in G) and twisted angle of allyl group

	A_β	A_1^H	A_2^H	A_3^H	A_4^H	A_5^H	A_6^H	A_7^H	Twisted angle of allyl group
TPA	8.90[a]	1.95	1.30	0.65					≃26°
BDA	13.4[a]	1.99	1.99	0.46	0.1>				≃37°
(Ref. 7)	13.2[a]	1.92	1.86	0.48	0.36				
(Ref. 8)	13.2[a]	1.89	1.89	0.42	0.06				
BDAA	3.38[b]	1.69	1.69	0.30	0.14				
DDA	9.57[a]	2.45	2.45	2.45	2.45	0.46	0.1>	0.1>	≃32°

a) A_β^H. b) A_β^N.

and (2),

$$I = B(1/T)([\text{S-S}]/K)^{1/2}$$
$$= B(1/T)\{[\text{S-S}]/(A\exp(-\Delta H/RT))\}^{1/2}, \quad (5)$$

Hence,

$$\ln I = 1/2(\Delta H/R)(1/T) + \ln(1/T) + \ln B + 1/2\ln[\text{S-S}] - 1/2\ln A. \quad (6)$$

In the limiting case of a low concentration of the radical monomer, the equilibrium lies so much to the side of the dimer that we finally have:

$$\ln I - \ln(1/T) = 1/2(\Delta H/R)(1/T) + C, \quad (7)$$

where C is a constant which involves $\ln B$, $\ln A$, and $\ln[\text{S-S}]$. The slopes of $\log K$ *vs.* $1/T$(Fig. 4) and $\log I$ *vs.* $1/T$(Fig. 2) enable us to calculate the values of the association energy.

The optical spectra of BDA and BDAA are shown in Figs. 5 and 6, the maximum absorptions being $\lambda_1=750$, $\lambda_2=488(\varepsilon_{max}=2119)$, $\lambda_3=422$ and $\lambda_1=775$, $\lambda_2=466(\varepsilon_{max}=2560)$, $\lambda_3=435$, $\lambda_4=404$, respectively. It may be seen in Figs. 5a(488 nm and 335 nm) and 6a(466 nm and 325 nm) that these dimers dissociate

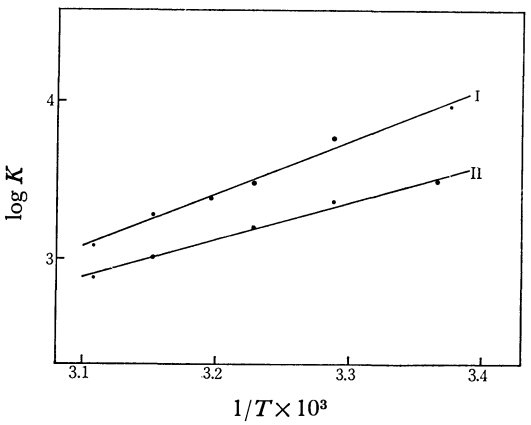

Fig. 4. Temperature dependence of equilibrium constant (I) BDA (II) BDAA.

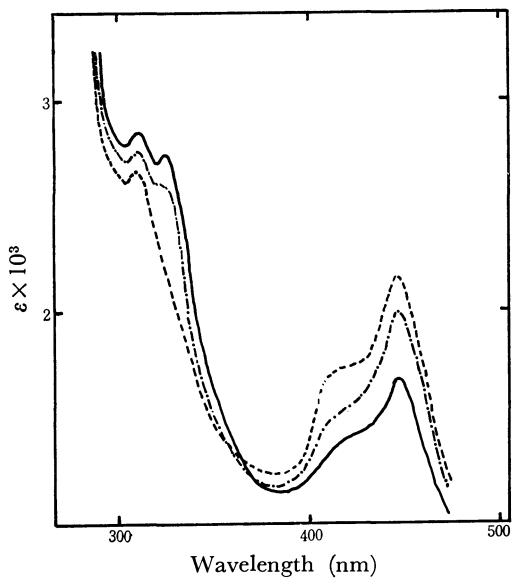

Fig. 5a. Optical spectra of BDA in benzene at 20 °C.
—— 10^{-4} M. —·—·— 10^{-5} M. ---- 10^{-6} M.

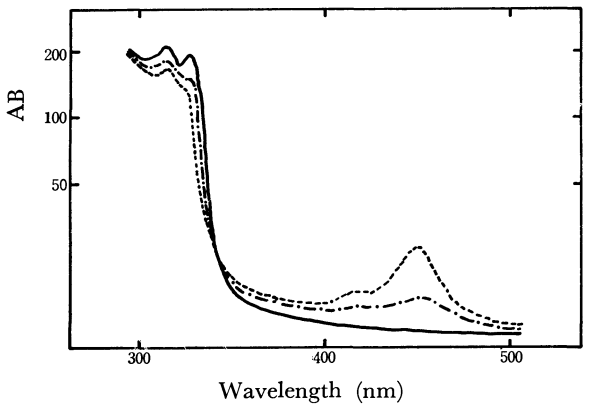

Fig. 5b. Optical spectra of BDA in ether.
---- +20 °C, —·—·— −30 °C, —— −60 °C

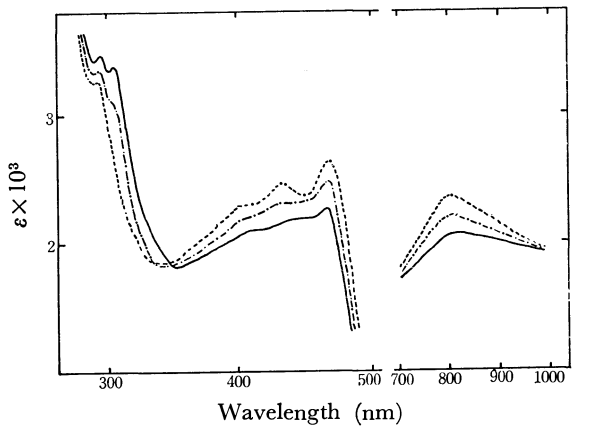

Fig. 6a. Optical spectra of BDAA in benzene at 20 °C.
—— 10^{-4} M. —·—·— 10^{-5} M. ---- 10^{-6} M.

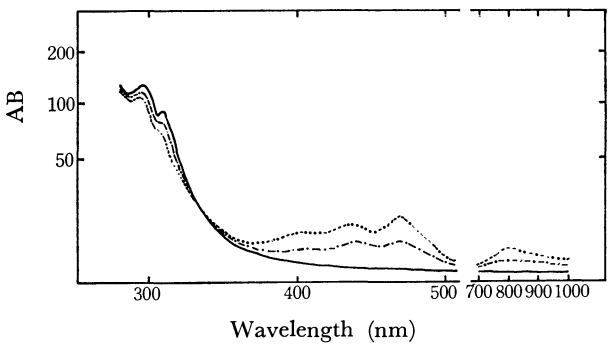

Fig. 6b. Optical spectra of BDAA in ether.
---- +20 °C, —·—·— −30 °C, —— −60 °C

completely into monomers in the concentration of 10^{-6} M. at 20 °C. In this concentration, then, the spectra do not show the temperature dependence explicitly. From the radical concentration obtained from the ε_{max}, the equilibrium constants, K, can be enumerated at each temperature. Log I *vs.* $1/T$ and log K *vs.* $1/T$ are shown in Figs. 2 and 4 respectively, while the association energies thus obtained are tabulated in Table 3. Table 3 shows that TPA is very stable as a radical molecule and that the two values determined by different measuring methods coincide fairly well. Thus, the approximate equations, (3) and (7), have been shown to be correct.

Table 3. Association energy from radicals to dimer (kcal/mol)

	From ESR	From optical spectra
TPA	$\simeq 0$	
BDA	11.9	12.6
(Ref. 2)		($\simeq 13$)
BDAA	8.7	9.2
DDA	14.7	

On the other hand, the reactivity from the radicals to the dimer may be explained by the "frontier electron" theory,[10] where the frontier electron density plays an important role. The frontier electron density of a neutral radical is approximately equal to its odd-electron density. Thus, the odd-electron density in each radical will reflect directly the reactivities of the radicals.

On the other dimerizable radicals, such as triphenylmethyl and phenoxyl, their bond formations do not all occur at the same position. For example, two triphenylmethyls form a bond between the center carbon of one radical and the *para*-position of one phenyl group of the other radical.[11] Of these tetraarylallyl-type radicals, TPA itself is not dimerized, but BDA, BDAA, and DDA are dimerized. According to the IR spectra of these dimerized substances, the bond formation of these dimerized radicals must occur at the α or the γ position of the allyl group.[12]

Table 4 shows the values of the frontier electron densities on the allyl group of each radical, as calculated by the McLachlan method on the basis of the "twisted allyl" model.[1] As has been mentioned above, TPA has never been dimerized in spite of possessing the largest frontier electron density on the possible position of the bond formation in this radical. This fact can be considered as showing that two TPA radicals are difficult of access to each other because of the steric hindrance of the four phenyl rings on the α or the γ position of the allyl group.

On the other hand, since two phenyl groups at one or both ends of the allyl group in DDA, BDA, and BDAA are fixed to each other, these radicals can approach each other and be dimerized in such a manner as to form a bond at the positions with the largest frontier electron densities in the radical molecules. From the values of these densities of the bond-forming position, which are the α or the γ carbon atoms of the allyl groups, one can expect that DDA associates more easily to form a dimer than do BDA and BDAA. This expectation shows a good parallelism to the results of Figs. 2 and 4.

Table 4. Frontier electron densities on allyl group

	α	β	γ	$(\alpha+\gamma)/2$
TPA[a]	+0.318	−0.097	+0.318	+0.318
BDA[b]	+0.260	−0.086	+0.260	+0.260
BDAA[b]	+0.253	−0.051	+0.253	+0.253
DDA[c]	+0.285	−0.067	+0.270	+0.277

a) Each phenyl group is rotated by 30° as that of triphenylmethyl and allyl group is also twisted by 26°. b) Allyl group is twisted by 37°. c) Diphenyl fitt to α position, Phenyl groups are rotated as TPA and allyl group is twisted by 32°.

In general, the stabilization of the radical is mainly affected by the following two factors: the magnitude of the delocalization of an odd-electron, and the magnitude of the steric repulsion around the bond-forming position in the radical molecular frame. For the case of TPA, the latter is the predominant factor, and it is well known to be the predominant factor in the association of the triphenylmethyl derivatives.[13] In the other tetraarylallyl-type radicals, however, the former must be the dominant factor, because the magnitude of the steric repulsion of DDA may be larger than those of BDA and BDAA, judging from the molecular structure of each radical.

On the other hand, the molecular structures of BDA and BDAA are similar except that either a carbon atom or a nitrogen atom occupies the β-position of the allyl group. Then, one may assume that this difference in the occupied atom will not affect the magnitude of steric repulsion, but the magnitude of the delocalization of the odd-electron. In fact, the difference in the magnitudes of the association energy of BDA and of BDAA may be found in Table 3.

It can be concluded that the TPA radical is the most stable radical in these series, since no indication of dimerization has so far been experimentally observed for this radical.

The authors wish to thank Professor Kazuhiko Ishizu, Mr. Osamu Takizawa, and their collaborators for their helpful discussions. They are also indebted to Professors Hideo Takaki and Toshio Takada for their encouragement during this work.

Reference

1) K. Watanabe, J. Yamauchi, H. Ohya-Nishiguchi, Y. Deguchi, and H. Takaki, This Bulletin, **45**, 371 (1972).
2) R. Kuhn, H. Fischer, F. A. Neugebauer, and H. Fischer, *Ann. Chem.*, **654**, 64 (1962).
3) R. Kuhn and F. A. Neugebauer, *Monatsh. Chem.*, **65**, 16 (1964).
4) R. Kuhn and D. Rewicki, *Ann. Chem.*, **690**, 50 (1965).
5) K. Ziegler, *ibid.*, **434**, 34 (1932).
6) Y. Deguchi, This Bulletin, **35**, 910 (1962).
7) R. Kuhn and F. A. Neugebauer, *Manatsh. Chem.*, **95**, 3 (1964).
8) K. H. Hausser, *Z. Naturforsch.*, **14a**, 425 (1959).
9) W. J. Moore, "Physical Chemistry," Chapter VI, Prentice-Hall, Inc., New York, N. Y., (1955).
10) K. Fukui, T. Yonezawa, C. Nagata, and H. Shingu, *J. Chem. Phys.*, **22**, 1433 (1954).
11) H. Lankamp, W. Th. Nauta, and C. MacLean, *Tetrahedron Lett.*, **1968**, 249.
12) To be published.
13) W. Theilacker, H. Schultz, U. Baumgarte, H. -G. Prossler, W. Rhode, F. Thater, and H. Uffmann, *Angew. Chem.*, **69**, 322 (1957).

The Fractionation of Tritiated Water in an Equilibrium between Organic Hydrates and Their Aqueous Solutions

Haruhiko TANAKA*, Tsutomu KADO, and Hisao NEGITA

Department of Chemistry, Faculty of Science, Hiroshima University, Higashisenda-machi, Hiroshima 730

(Received August 6, 1973)

The fractionation of the tritiated water (HTO) was examined during the crystallization of hydrates, such as $(COOH)_2\cdot 2H_2O$, $(COOK)_2\cdot H_2O$, $Cu(HCOO)_2\cdot 4H_2O$, and $Sr(HCOO)_2\cdot 2H_2O$. The dilution of HTO in the organic salts was found to be comparable to that in inorganic salts observed previously. The fractionation of HTO was explained on the basis of an ionic process in an aqueous solution, and the crystal growth mechanism, in a way similar to that described in a previous paper. On the contrary, a considerable dilution was observed for oxalic acid dihydrate. The proton effect on the fractionation in both the ionic and dehydration processes was also discussed.

It has been reported by many workers that the fractionation of deuterated water occurs during the crystallization of various hydrated inorganic salts from aqueous solutions.[1] A similar fractionation of tritiated water (HTO) has been investigated for a number of metal sulfates[2,3] and chlorides[4] by the present authors. It has been found that a dilution of HTO of a few percent occurs in the water of crystallization of these inorganic salts. From these studies, some information has been derived concerning the kinetics of the deposition of the hydration water on the crystal from an aqueous solution.

In order to study the dilution in a more systematic way, it seems worthwhile to determine the separation factor, S, of metal organic salts and to compare it with those of inorganic salts. For this purpose, copper formate tetrahydrate and strontium formate dihydrate have been examined. It may also be quite interesting to examine the fractionation in an organic acid hydrate, *e.g.*, oxalic acid dihydrate, since the acid contains hydrogen atoms besides those of the hydration water. For the estimation of the proton effect in the carboxyl groups on the fractionation, the S value for the hydration water in the metal salt of the acid can properly be used. Potassium oxalate monohydrate has been chosen as the salt in the present study.

Experimental

Strontium formate was prepared by adding strontium carbonate to formic acid. The other samples were obtained from a commercial source and purified by recrystallization. The solvent consisted of twice-distilled water containing a trace of tritiated water (HTO). A large well-developed single crystal of the hydrate was grown from a very slightly supersaturated solution by lowering the temperature gradually within a narrow range. The temperature ranges were 32.5—29.0 °C, 33.0—32.1 °C, 36.3—34.3 °C, and 29.8—28.8 °C for $Sr(HCOO)_2\cdot 2H_2O$, $Cu(HCOO)_2\cdot 4H_2O$, $(COOK)_2\cdot H_2O$, and $(COOH)_2\cdot 2H_2O$ respectively.

Water from both the mother liquid and the hydration water of the single crystal was recovered by dehydrating them *in vacuo* at 45 °C. The β-activity of the dehydrated water was measured with a liquid scintillation counter, a Packard Model 2002 Tri-Carb Scintillation Spectrometer. Besides, the activity due to the tritium in the dihydrate was directly measured by dissolving it in a scintillant in the case of the oxalic acid dihydrate, $(COOH)_2\cdot 2H_2O$. As a scintillant we used a solution composed of toluene, ethylene glycol monomethyl ether, 2,5-diphenyloxazole (PPO), and 1,4-bis-2′-(5′-phenyloxazolyl)benzene (POPOP).

Results and Discussion

The separation factor, S, of HTO for the crystallization of a hydrated salt from an aqueous solution can be given as $S=N_s/N_l$, where N_s and N_l are the mole fractions of HTO in the solid and liquid phases respectively. Table 1 shows the observed fractionation of HTO, together with the average net cpm for 0.1 g of water, which is proportional to the fraction of HTO. We see in copper formate tetrahydrate a very slight dilution of HTO and no practical fractionation, whereas appreciable dilutions are found in the other hydrates, particularly in the oxalic acid dihydrate.

Table 1. The separation factor, S, of HTO for organic hydrates

Crystal	Net cpm of HTO[a]		$S(N_s/N_l)$
	N_s	N_l	
$Sr(HCOO)_2\cdot 2H_2O$	22248±168	23329±157	0.954±0.010
$Cu(HCOO)_2\cdot 4H_2O$	21570±83	21640±91	0.997±0.006
$(COOK)_2\cdot H_2O$	20326±125	20837±92	0.976±0.007
$(COOH)_2\cdot 2H_2O$	25324±152	29278±177	0.865±0.007

a) Averaged for 6—8 measurements with a counter of 35% efficiency.

The HTO Fractionation in the Water of Crystallization. It has been reported that HTO is diluted in the water of crystallization during the crystal growth from a solution if a surface-diffusion mechanism in which the growth unit diffuses over a wide range of the crystal surface before integrating into the kink controls the crystal growth.[2] The R_{HTO}/R_{H_2O} ratio has been approximately derived for the free water on the crystal growth of a hydrated salt *via* surface diffusion:

$$R_{HTO}/R_{H_2O} = (m_{H_2O}/m_{HTO})^{1/2}=0.949, \quad (1)$$

where R_{HTO}/R_{H_2O} is the ratio of integration of HTO into the crystal to that of H_2O and where m_{H_2O}/m_{HTO}

* Present address; Shinonome Branch School, Faculty of Education, Hiroshima University, Shinonome, Hiroshima 734.

is the molecular weight ratio of H_2O to HTO. It can be assumed that minimum S value becomes *ca.* 0.95 when the free water integrates into the crystal from the solution.

In the hydration water of cations in the solution, the fractionation of HTO from the bulk water, if any, has been disregarded in a previous work.[4] Although such a simplification can be justified in the cases of Na^+ and K^+, which exert weak hydration, it may not be justified in the cases of most of the other cations.[5] It seems that HTO should be slightly enriched in the hydration water if the hydration water is held more rigidly in the sphere than in the solvent water itself, as can be seen from the theory of the isotope effect in the exchange reaction.[5,6] Such an ion is frequently referred to as a structure-former. As for the anion, the hydration water can be assumed to exert no considerable effect on the fractionation in the present case. Accordingly, it can be suggested that the more free water molecules and the less hydration water molecules of a structure-former ion there are, in the solution, the more dilution of HTO in the crystal hydrates should result.

In the case of $Sr(HCOO)_2 \cdot 2H_2O$, the hydration water of a Sr^{2+} ion in the solution is taken to become free in order to be integrated into the crystal,[4] since the lifetime of the hydrated cation is extremely short.[7] It can thus be expected that a considerable dilution of HTO occurs for the salt, *i.e.*, the S value becomes close to 0.95.

As for $Cu(HCOO)_2 \cdot 4H_2O$, half of the hydration water of a Cu^{2+} ion in the solution can be assumed to become free to be integrated, because half of the water of crystallization is not coordinated to the Cu^{2+} ion in the crystal.[8] On the other hand, the remaining half, which is coordinated to the cation in the crystal, seems to come from the hydration water in the aqueous solution.

It follows that HTO is diluted in the former according to Eq. (1), whereas a slight enrichment of HTO results in the latter since the Cu^{2+} ion is known to be a structure-former. In these estimations, we assume that no exchange of the proton in the $HCOO^-$ ion with others occurs.[9]

For $(COOK)_2 \cdot H_2O$, the S value can be estimated to be nearly equal to that of $Sr(HCOO)_2 \cdot 2H_2O$, because the lifetime of the hydrated K^+ ion is also very short; *ca.* 10^{-9} s.[7] However, the observed S value was found to be a little larger than the estimated one. The cause of the disagreement is not clear at this stage. A small deviation of the estimated value from the observed value seems to be inevitable, as was the case with a few other salts.[4] It appears, at least qualitatively, that the present treatment is still applicable. The S value for $(COOK)_2 \cdot H_2O$ will help to estimate the value for $(COOH)_2 \cdot 2H_2O$.

It can be seen that, in general, the degree of dilution of HTO in the water of crystallization of the metal organic salts is a few percent or so, comparable to that in the metal inorganic salts. It can thus be suggested that the former dilution can also be explained on the basis of an ionic process in an aqueous solution and the crystal growth mechanism, as is the case with the latter.

The HTO Fractionation in the Oxalic Acid. It is worth noting that a considerable dilution is found to occur in the oxalic acid dihydrate. In order to estimate the fractionation in the carboxyl groups, $(COOH)_2$, we assume that the partial dilution due to the water of crystallization in $(COOH)_2 \cdot 2H_2O$ is nearly equal to be dilution for $(COOK)_2 \cdot H_2O$, 0.976.

The dilution resulting from the others is considered to come from the following three steps: (1) the proton-exchange reaction in an aqueous solution, (2) the proton integration into the crystal from an aqueous solution, and (3) the proton-exchange reaction between $(COOH)_2$ and the hydration water during the course of the vacuum dehydration.

It is well known that deuterium is slightly diluted in the hydronium ion in the exchange reaction:[10]

$$H_2O + H_2DO^+ \rightleftharpoons HDO + H_3O^+. \quad (2)$$

The same process should proceed in the case of tritium, *i. e.*; $H_2O + H_2TO^+ \rightleftharpoons HTO + H_3O^+$.
The HT_2O^+ and T_3O^+ ions can be neglected as a source of tritium, since the mother liquid used contains only a trace of tritium.

For the other species containing hydrogen atoms, $(COOH)_2$ and $C_2O_4H^-$, we can infer that tritium should be diluted, because the bond energy of the hydrogen atoms of H_2O is larger than those of $(COOH)_2$ and $C_2O_4H^-$, as can be seen from the proton level given by Gurney.[11,12] In fact, the dilution of deuterium in $(COOH)_2$ was evidenced by the work of Okazaki and Takemura.[13]

Consequently, tritium should be diluted in all the species in the aqueous solution of oxalic acid. Moreover, these species are subjected to further dilution to a small extent during the integration into the crystal according to the surface-diffusion mechanism. The possible dilution estimated above for the $(COOH)_2$ groups of the crystal can be confirmed by measuring the tritium concentration in the oxalic acid dihydrate, $(COOH)_2 \cdot 2H_2O$.

It is well known that a labeled organic compound containing a weak β-emitter, *e. g.*, tritium, causes a quenching in the liquid scintillation counting. The quenching of the oxalic acid was, therefore, corrected according to the method of Peng.[14] The tritium concentration ratio in the $(COOH)_2 \cdot 2H_2O$ crystal to the mother liquid was thus found to be 0.876 ± 0.009. It can thus be concluded that tritium is diluted in the $(COOH)_2$ groups of the crystal by *ca.* 0.676, assuming the S value of 0.976 for the hydration water, as has been described above.

Tritium Fractionation during the Dehydration. It is generally accepted that hydrogen atoms directly bonded to oxygen atoms are labile and can be exchanged with other hydrogen atoms.[9] In the case of oxalic acid dihydrate, it is likely that there occurs a ready exchange of protons between $(COOH)_2$ and H_2O by mere shifts of protons through the hydrogen bonds in the crystal.[15] The ready exchange under a vacuum dehydration was confirmed using deuterium by Okazaki and Takemura.[13]

In the exchange reaction, the hydrogen isotope effect

can also occur. Okazaki and Takemura reported that deuterium is slightly enriched in the water molecules, as is the case with the aqueous solution of oxalic acid.[13] According to the study, we can assume that tritium is slightly enriched in the water molecules relative to the carboxyl groups during the dehydration. It can be considered qualitatively that the small S value observed for the dehydrated water of $(COOH)_2 \cdot 2H_2O$, 0.865, should result from the fact that the dilution of tritium in the water due to the proton exchange between $(COOH)_2$ and H_2O surpasses the enrichment through the proton exchange during the dehydration.

Although the present discussion is somewhat qualitative, it seems worthwhile to examine the HTO fractionation in the hydrated crystal containing hydrogen atoms other than those of the hydration water, because a very large fractionation may be possible. Such an examination can also contribute to a better understanding of the proton exchange in the solution and/or in the dehydration.

The authors wish to express their thanks to Dr. Osamu Yamamoto for his help in analyzing the activity of tritium.

References

1) R. M. Barrer and A. F. Denny, *J. Chem. Soc.*, **1964**, 4677; M. Johansson and K. E. Holmberg, *Acta Chem. Scand.*, **23**, 765 (1969); K. Heinzinger, *Z. Naturforsch.*, *A*, **24**, 1502 (1969).

2) H. Tanaka and H. Negita, This Bulletin, **43**, 3079 (1970); H. Tanaka, T. Kado, and H. Negita, *ibid.*, **45**, 3342 (1972).

3) H. Tanaka, *ibid.*, **45**, 339 (1972).

4) H. Tanaka, M. Tanga, and H. Negita, *ibid.*, **46**, 1000 (1973).

5) H. Taube, *J. Phys. Chem.*, **58**, 523 (1954).

6) E. K. Thornton and E. R. Thornton, "Isotope Effects in Chemical Reactions," ed. by C. J. Collins and N. S. Bowman, Van Nostrand Reinhold Co., New York (1971), Chap. 4.

7) M. Eigen, *Pure Appl. Chem.*, **6**, 97 (1963).

8) R. Kiriyama, H. Ibamoto, and K. Matsuo, *Acta Crystallogr.*, **7**, 482 (1954).

9) E. A. Evans, "Tritium and Its Compounds," Butterworth & Co. Ltd., London (1966), p. 122.

10) C. G. Swain, R. F. W. Bader, and E. R. Thornton, *Tetrahedron*, **10**, 200 (1960); V. Gold, *Proc. Chem. Soc.*, **1963**, 141.

11) R. W. Gurney, "Ionic Processes in Solution," McGraw-Hill Book Co., Inc., New York (1953), Chap. 7.

12) The hydrogen isotope effect in the present exchange reaction can be explained in terms of the usual theory; see, for example, M. M. Kreevoy, *J. Chem. Educ.*, **41**, 636 (1964) and the references cited therein.

13) N. Okazaki and E. Takemura, This Bulletin, **34**, 977 (1961).

14) C. T. Peng, *Anal. Chem.*, **32**, 1292 (1960).

15) J. M. Robertson and I. Woodward, *J. Chem. Soc.*, **1936**, 1817; J. D. Dunitz and J. M. Robertson, *ibid.*, **1947**, 142.

Spectral Intensities of Some Er^{3+} β-Diketonate Complexes

Toshiyuki Isobe and Seizo Misumi

Inorganic Chemistry Laboratory, Faculty of Science, Kyushu University, Fukuoka 812

(Received August 10, 1973)

The oscillator strengths of the absorption bands of Er^{3+} acetylacetonate, thenoyltrifluoroacetate, and dibenzoylmethide in methanol and dimethylformamide were determined and discussed in terms of the Judd-Ofelt's theory. It was possible to use the Judd-Ofelt parameters for the evaluation of the spectral intensities. The oscillator strength of the hypersensitive transition $^2H_{11/2}\leftarrow{}^4I_{15/2}$ of Er^{3+} complexes, $P(^2H_{11/2})$, was indicated by the $P(^2H_{11/2})\approx\tau_{2\mathrm{comp}}\,\nu_{\mathrm{comp}}\,U(2)/2J+1$ and it is demonstrated that "hypersensitivity" may be explained only by the τ_2 parameter of each complex, originating from the forced electric dipole transition.

The intensities of the solution spectra of the most lanthanoid(III) have been interpreted by the Judd-Ofelt's theory.[1,2] It should be noticed that the oscillator strengths of the certain transitions in lanthanoid(III) complexes are greater than those of the same transitions in the lanthanoid(III) aquo ions. These are known as "hypersensitive transitions"[3] and have hitherto been characterized by the selection rule $\Delta J\leqq 2$ and by relatively larger values of the matrix elements of $U^{(2)}$ in comparison with those of other transitions. However, no satisfactory explanation of hypersensitivity has yet been given. Some possible mechanisms involved in the appearance and the intensity of *f-f* transition have been reported, namely, (a) inhomogeneous dielectric,[3] (b) forced electric dipole transitions,[4] and (c) vibronic mechanism[5]+covalency.[6] In this paper, the Judd-Ofelt's theory was applied to the intensities of the spectra of some erbium(III)[7] β-diketonate complexes[8,9] in methanol and dimethylformamide(DMF).

Theoretical and Calculations

In Judd-Ofelt's theory, the *f-f* transitions (except those involving an allowed magnetic dipole mechanism) are assumed to be forced electric dipole in nature, occurring by the mixing of a higher energy configuration (or configurations) of opposite parity with the $4f^N$ configuration *via* the odd terms in the ligand field. The equation derived for the oscillator strengh (P) of a transition between a ground state ($|f^N\psi_J|$ and an excited state $|f^N\psi'_{J'}\rangle$ of the lanthanoid(III) in solution is given by

$$P=\sum\tau_\lambda\nu U(\lambda)/(2J+1) \qquad (1)$$

$$\lambda=2,\ 4,\ 6$$

$$U(\lambda)=(f^N\psi_J\|U^{(\lambda)}\|f^N\psi'_{J'})^2$$

where ν is the energy of the transition $\psi'_{J'}\leftarrow\psi_J$, *i. e.*, the baricentre of the absorption band in cm^{-1}, $U(\lambda)$ is the reduced matrix elements of the unit tensor operators $U^{(\lambda)}$ concerning the initial and final states of the transition, and the τ_λ vaules are usually treated as empirical parameters in cm. Reduced matrix elements for all the lanthanoids(III) have been published.[10] By using the experimental oscillator strength P_{exp}, ν, and $U(\lambda)$ values in Eq. (1) and carrying out an analysis by least-squares, an optimum set of three parameters, τ_λ, are obtained. The τ_λ parameters were, in turn, used to obtain "calculated oscillator strengths". The root-mean-square (rms) deviations between the calculated and experimental oscillator strengths were also calculated. All calculations were made with a FACOM 230-60 computer of Kyushu University.

Experimental

The absorption measurements were carried out with a Hitachi EPS-2 spectrophotometer and a Jasco ORD/UV-5 recorder by scale expansion. The solvents used were "spec-pure" absolute methanol and DMF. The erbium(III) β-diketonate complexes do not dissociate in these two solvents. The erbium(III) acetylacetonate(AA), thenoyltrifluoroacetonate(TTA), and dibenzoyl methide(DBM) were prepared by using ordinary methods.[11-13] The absorption intensities were determined by measuring the area on the experimental absorption curves with planimeter, and the oscillator strengths were calculated by using the reduced Eq. (2)

$$P_{\mathrm{exp}}=4.318\times10^{-9}\frac{9\eta}{(\eta^2+2)^2}\int\varepsilon(\nu)\mathrm{d}\nu \qquad (2)$$

where η in the refractive index of the solution and $\varepsilon(\nu)$ is the molar extinction coefficient at wave number ν. Refractive indices values of 1.32652 and 1.42817 were used for methanol and DMF, respectively, in calculation. These intensities were reproducible within $\pm0.2\times10^{-6}$ oscillator strength unit.

Results and Discussion

The experimental(P_{exp}) and calculated(P_{calc}) values of oscillator strengths of the absorption bands have been collected in Table 1—3. The τ_λ parameters are given in Table 4. The root-mean-square (rms) deviations obtained are very small in calculating four separated J'-bands ($^4F_{9/2}$, $^4S_{3/2}$, $^2H_{11/2}$, and $^4F_{7/2}$), containing only the hypersensitive $^2H_{11/2}$ band. As far as all four J'-bands are concerned, Judd-Ofelt's theory could be reasonably applied. But, the intensity of another hypersensitive transition $^4G_{11/2}\leftarrow{}^4I_{15/2}$ of Er(III) complex could not be adopted to the experimental oscillator strength, due to UV cut-off caused by intense absorption of the β-diketone ligands except acetylacetone, for calculation of the set of τ_λ parameters.

The results show that the effect of solvent and ligand on spectral intensity of Er(III) is very small for all the bands except for those in the region 18500—20000 cm^{-1}, which are known to be due to the hypersensitive transitions. Figure 1 shows the variation of the τ_λ parameters of Er(III) β-diketonate complexes in meth-

Table 1. Oscillator strengths of the absorption bands of Er^{3+} acetylacetonate

Spectral range (cm^{-1})	S'L'J'	Baricentre (cm^{-1})	ε_{max}	$P\times10^6$ Exptl	$P\times10^6$ Calcd	$P\times10^6$ Exptl-Calcd
(in MeOH)						
14500—16000	$^4F_{9/2}$	15420	2.5	2.26	2.00(2.24)[a]	0.26(0.02)
18000—18850	$^4S_{3/2}$	18665	2.5	0.88	0.72(0.69)[a]	0.16(0.19)
18850—20000	$^2H_{11/2}$	19450	29.5	30.35	55.01(30.35)[a]	−24.66(0)
20000—21200	$^4F_{7/2}$	20600	2.3	2.48	2.54(2.55)[a]	−0.06(−0.07)
21500—23000	$^4F_{5/2}$, $^4F_{3/2}$	22315	1.5	0.11	0.69	−0.58
23800—25100	$^2G_{9/2}$	24660	1.5	1.24	1.01	0.23
25100—26850	$^4G_{11/2}$	26340	98.5	110.17	96.05	14.12
26850—28400	$^4G_{9/2}$, $^2K_{15/2}$, $^2G_{7/2}$	27480	11.5	13.60		
					rms ±14.21(±0.20)	
(in DMF)						
14500—16000	$^4F_{9/2}$	15305	2.0	2.47	2.10(2.42)[a]	0.37(0.05)
18000—18500	$^4S_{3/2}$	18320	2.1	0.68	0.61(0.38)[a]	0.07(0.30)
18500—20000	$^2H_{11/2}$	19130	33.4	32.82	53.62(32.83)[a]	−20.79(0)
20000—21200	$^4F_{7/2}$	20470	1.9	1.74	2.30(1.85)[a]	−0.56(−0.11)
21500—23000	$^4F_{5/2}$, $^4F_{3/2}$	22070	0.8	0.71	0.58	0.13
23800—25100	$^2G_{9/2}$	24500	1.3	1.70	0.89	0.81
25100—26900	$^4G_{11/2}$	26390	92.4	106.99	95.30	11.69
26900—26400	$^4G_{9/2}$, $^2K_{15/2}$, $^2G_{7/2}$	27590	10.3	12.76		
					rms ±11.94(±0.32)	

a) Calculated values based on four J'-bands in parentheses.

Table 2. Oscillator strengths of the absorption bands of Er^{3+} thenoyltrifluoroacetonate

Spectral range (cm^{-1})	S'L'J'	Baricentre (cm^{-1})	ε_{max}	$P\times10^6$ Exptl	$P\times10^6$ Calcd	$P\times10^6$ Exptl-Calcd
(in MeOH)						
14500—16000	$^4F_{9/2}$	15360	4.0	2.37	2.41	−0.04
18000—18700	$^4S_{3/2}$	18525	3.3	0.63	0.89	0.26
18700—20000	$^2H_{11/2}$	19220	46.7	39.40	39.40	0
20000—21200	$^4F_{7/2}$	20585	5.2	3.23	3.12	0.11
					rms ±0.29	
(in DMF)						
14500—16000	$^4F_{9/2}$	15240	1.8	2.98	2.98	0
18000—18550	$^4S_{3/2}$	18320	1.4	0.68	0.68	0
18550—19900	$^2H_{11/2}$	19120	46.0	39.97	39.97	0
19900—21200	$^4F_{7/2}$	20470	3.5	2.82	2.82	0
					rms ±0.003	

Table 3. Oscillator strengths of the absorption bands of Er^{3+} dibenzoylmethide

Spectral range (cm^{-1})	S'L'J'	Baricentre (cm^{-1})	ε_{max}	$P\times10^6$ Exptl	$P\times10^6$ Calcd	$P\times10^6$ Exptl-Calcd
(in MeOH)						
14500—16000	$^4F_{9/2}$	15360	2.5	2.74	2.79	−0.05
18000—18700	$^4S_{3/2}$	18485	2.0	0.73	1.09	−0.36
18700—20000	$^2H_{11/2}$	19240	52.0	48.01	48.01	0
20000—21200	$^4F_{7/2}$	20600	4.2	3.90	3.76	0.14
					rms ±0.39	
(in DMF)						
14500—16000	$^4F_{9/2}$	15270	1.8	2.38	2.34	0.04
18000—18500	$^4S_{3/2}$	18335	2.3	1.19	0.90	0.29
18550—19800	$^2H_{11/2}$	19130	53.0	51.88	51.88	0
19800—21100	$^4F_{7/2}$	20475	4.0	3.06	3.17	−0.11
					rms ±0.31	

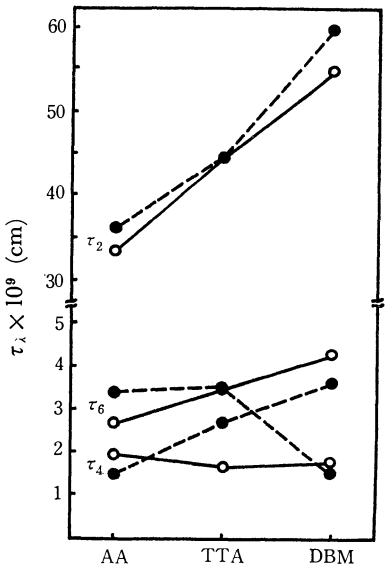

Fig. 1. Plot of the τ_λ parameters for Er(III) β-diketonates; —○— in MeOH, --●-- in DMF.

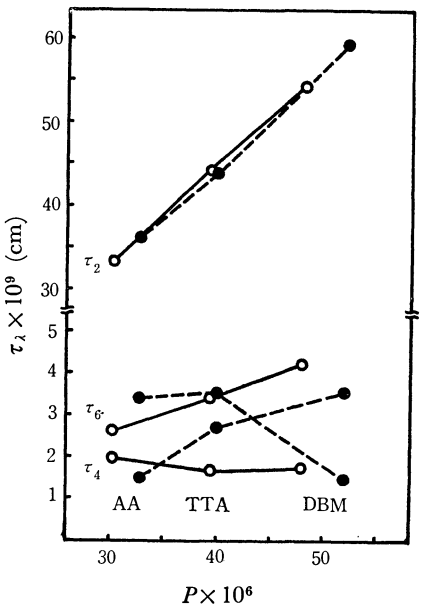

Fig. 2. Plot of the τ_λ parameters *vs.* the oscillator strength of the hypersensitive transition of $^2H_{11/2} \leftarrow {}^4I_{15/2}$ for Er(III) β-diketonates; —○— in MeOH, --●-- in DMF.

Table 4. Values of Judd-Ofelt's parameters for Er(III) β-diketonates in MeOH and DMF

		$\tau_\lambda \times 10^9$ (cm)	
		MeOH	DMF
AA	τ_2	33.55±0.36	36.36±0.59
	τ_4	2.01±0.52	3.43±0.87
	τ_6	2.69±0.30	1.51±0.50
TTA	τ_2	44.60±0.52	44.57±0.01
	τ_4	1.69±0.76	3.51±0.01
	τ_6	3.47±0.43	2.70±0.01
DBM	τ_2	54.46±0.70	59.57±0.57
	τ_4	1.76±1.03	1.50±0.83
	τ_6	4.25±0.59	3.57±0.47
Aquo[14]	τ_2	1.70±0.15	
	τ_4	2.40±0.22	
	τ_6	2.31±0.12	

anol and DMF. The τ_2 parameter in the complex, τ_{2comp}, is the most sensitive to the environment, with marked differences in relative magnitudes of other τ_λ. (Refer to Table 4). The ratios of the experimental intensities (P_{comp}/P_{aquo}) at each J'-band and those of the calculated τ_λ parameters ($\tau_{\lambda comp}/\tau_{\lambda aquo}$) of Er(III) β-diketonate complexes are shown in Table 5. Table 5 seems to indicate that in the case of hypersensitive transition, the increase in the intensity is due to the solvent or ligand, and that it may be correlated with the marked increase in the value of τ_2 parameter.[6-7] This is shown more clearly in Fig. 2, by plotting of τ_λ values of the complexes *vs.* oscillator strength of the hypersensitive band ($^2H_{11/2}$) in the complexes. It may be pointed out that approximately τ_2 value of complex is linear to the intensity of the hypersensitive

Table 5. Values of ratios of the (observed) oscillator strengths and the (calculated) τ_λ parameters of Er(III) complexes to Er(III) aquo ion

Er(III)	S'L'J'	AA		TTA		DBM	
		MeOH	DMF	MeOH	DMF	MeOH	DMF
$\frac{P_{comp}}{P_{aquo}}$	$^4F_{9/2}$	1.00	1.10	1.05	1.32	1.22	1.06
	$^4S_{3/2}$	1.33	1.03	0.95	1.03	1.11	1.80
	$^2H_{11/2}$	10.50	11.36	13.63	13.83	16.61	17.95
	$^4F_{7/2}$	1.09	0.77	1.42	1.24	1.72	1.35
$\frac{\tau_{\lambda comp}}{\tau_{\lambda aquo}}$	λ						
	2	19.74	21.39	26.24	26.22	32.04	35.04
	4	0.84	1.43	0.70	1.46	0.73	0.63
	6	1.16	0.65	1.50	1.17	1.84	1.55
$\frac{P(2)_{comp}}{\sum P(\lambda)_{comp}}$ ($^2H_{11/2}$) $\lambda=2,4,6$		0.96	0.94	0.97	0.95	0.97	0.98

band. The values in the last row of Table 5 are those of

$$\frac{P(2)_{\text{comp}}}{\sum P(\lambda)_{\text{comp}}}, \quad \lambda = 2, 4, 6$$

$$\{P(\lambda) = \tau_\lambda \nu U(\lambda)/2J+1, P = \sum P(\lambda)\} \quad \lambda = 2, 4, 6$$

and this term expresses clearly contribution of τ_2 value to the intensity of the observed hypersensitive band($^2H_{11/2}$). Thus, it is concluded that $P(^2H_{11/2} \leftarrow {}^4I_{15/2})$ is approximately equal to the value of $\tau_{2\text{comp}} \cdot \nu_{\text{comp}} U(2)/2J+1$.

Therefore, this fact seems to support the result that the intensities of hypersensitive transitions are characterized by the magnitude of the τ_2 parameter, in three parameters of the Judd-Ofelt's theory.

The authors wish to thank to Mr. Hideto Yamashita for his kind experimental help.

References

1) B. R. Judd, *Phys. Rev.*, **127**, 750 (1962).
2) G. S. Ofelt, *J. Chem. Phys.*, **37**, 511 (1962).
3) C. K. Jørgensen and B. R. Judd, *Mol. Phys.*, **8**, 281 (1964).
4) B. R. Judd, *J. Chem. Phys.*, **44**, 839 (1966).
5) D. M. Gruen and C. W. DeKock, *ibid.*, **45**, 455 (1966).
6) D. E. Henrie and G. R. Choppin, *ibid.*, **49**, 477 (1968).
7) K. Bukietynska and G. R. Choppin, *ibid.*, **52**, 2875 (1970).
8) P. C. Mehta and S. P. Tandon, *ibid.*, **53**, 414 (1970).
9) S. P. Tandon and P. C. Mehta, *ibid.*, **52**, 4313 (1970).
10) W. T. Carnall, P. R. Fields, and K. Rajnak, *ibid.*, **49**, 4424, 4443, 4447, 4450 (1968).
11) J. G. Stites, C. N. McCarty, and L. L. Quill, *J. Amer. Chem. Soc.*, **70**, 3142 (1968).
12) R. E. Whan and G. A. Crosby, *J. Mol. Spectry*, **8**, 315 (1962).
13) R. G. Charles and R. C. Ohlmann, *J. Inorg, Nucl. Chem.*, **27**, 255 (1965).
14) W. T. Carnall, P. R. Fields, and K. Rajnak, *J. Chem. Phys.*, **49**, 4412 (1968).

Proton Magnetic Resonance in Organic Free Radicals, BDPA–Bz and *p*-Cl-BDPA

Kazuhiro UCHINO,† Jun YAMAUCHI,*†† Hiroaki OHYA-NISHIGUCHI, and Yasuo DEGUCHI**

Department of Chemistry, Faculty of Science, Kyoto University, Kyoto 606

** The Institute for Chemical Research, Kyoto University, Uji 611*

*** College of Liberal Arts and Science, Kyoto University, Kyoto 606*

(Received August 20, 1973)

The proton NMR absorption spectra from 1.3 to 77 K in two organic free radicals, BDPA-Bz and *p*-Cl-BDPA, have been measured on powder samples which undergo a magnetic phase transition from a paramagnetic to an antiferromagnetic state at the temperatures of 1.695 and 3.25 K respectively. The behavior of the NMR absorption spectra associated with the magnetic phase transition has been studied for the first time in the organic free radicals and interpreted in terms of the hyperfine interaction. These results are then compared with those of the TANOL radical, which is a linear antiferromagnet with no magnetic phase transition down to 1.3 K.

Since the original preparation of an organic free radical BDPA (1,3-bisdiphenylene-2-phenyl-allyl) by Koelsch,[1] the magnetic properties of this radical and its derivatives have been studied on powder samples by several authors. For these radicals, especially in the cases of BDPA–Bz (the complex of 1,3-bisdiphenylene-2-phenyl-allyl with benzene) and *p*-Cl-BDPA (1,3-bisdiphenylene-2-[*p*-chloro-phenyl]-allyl), static magnetic susceptibility, magnetic resonance absorption, and specific heat measurements have been carried out.[2–7]

Anderson *et al.*[2] have observed the magnetic susceptibility from the paramagnetic shift, which exhibited a broad maximum at about 6 K. Hamilton and Pake[3] have pointed out the possibility of a long-range magnetic ordering of BDPA–Bz below 1.73 K, judging from the results of the specific heat and ESR measurements. One of the present authors (J.Y.)[4] has measured the magnetic susceptibility and ESR spectra of BDPA–Bz and *p*-Cl-BDPA. A broad maximum in the magnetic susceptibility was observed for both radicals at 5.6 K and a minimum for *p*-Cl-BDPA at 2.8 K; a divergence of the linewidth of the ESR absorption was also observed for BDPA-Bz and *p*-Cl-BDPA at 1.78 and 2.8 K respectively. Recently, Duffy *et al.*[5] have measured the specific heat of BDPA-Bz and observed a sharp peak in the magnetic contribution part at 1.695 K, while Yamauchi *et al.*[6,7] have observed a sharp peak in the magnetic specific heat of *p*-Cl-BDPA at 3.25 K and have also measured the antiferromagnetic resonance spectra below that temperature. Thus, it has become clear that BDPA-Bz and *p*-Cl-BDPA undergo a magnetic phase transition from a paramagnetic to an antiferromagnetic state at the Néel temperatures of 1.695 and 3.25 K respectively.

The behavior associated with the magnetic phase transition of the two BDPA derivatives is as follows: 1) a minimum in the magnetic susceptibility at the Néel temperature, 2) an abrupt increase in the ESR absorption linewidth and in the *g*-value in the vicinity of the Néel temperature, 3) an observation of the antiferromagnetic resonance absorption, and 4) an anomaly in the magnetic specific heat at Néel temperature. The behavior of the NMR absorption spectra associated with the magnetic phase transition, however, has not yet been clarified in organic free radicals. In this paper we would like to demonstrate the behavior associated with both the short-range and the long-range ordering of unpaired electron spins in these radical solids, whose molecular structures are as is shown in Fig. 1.

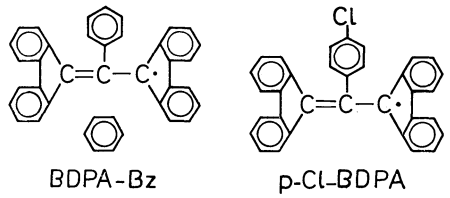

Fig. 1. The molecular structures of the radicals studied.

Experimental

The samples of BDPA-Bz and *p*-Cl-BDPA were prepared according to the procedure of Kuhn and Neugebauer[8] and were recrystallized from a benzene solution. The melting points and the results of the elementary analyses of carbon and hydrogen are in good agreement with those in the literature.

The proton NMR measurements were carried out using Pound-Watkins-type[9] and Robinson-type[10] spectrometers at the oscillation frequency, ν, of 18.0 MHz and at 27.0, 30.0, and 35.0 MHz. During the measurements the oscillation frequency and power level were kept constant. The magnetic field was modulated at 80 Hz, and the phase-sensitive detection was employed following the use of a narrow-band amplifier.

An ordinary cryostat was utilized, and the thermometer, an Allen-Bradley carbon resistor, was calibrated against the vapor pressures of liquid helium, hydrogen, and nitrogen.

Results

The proton NMR spectra of a powder sample of BDPA-Bz at 18.0 MHz are shown in Fig. 2. In addition to the central unshifted line, one more absorption line, shifted to the upper magnetic field and with a relatively small intensity, was observed from the temperature of liquid nitrogen down to about 2 K. The resonance field of the unshifted line corresponded to the magnetic field where the resonance of a free proton occurs at that frequency. The shift of the absorption line which appears at the high field

† Present address: Research Laboratories, Kawasaki Steel Corporation, 1, Kawasaki-cho, Chiba 280.

†† To whom all correspondences should be addressed.

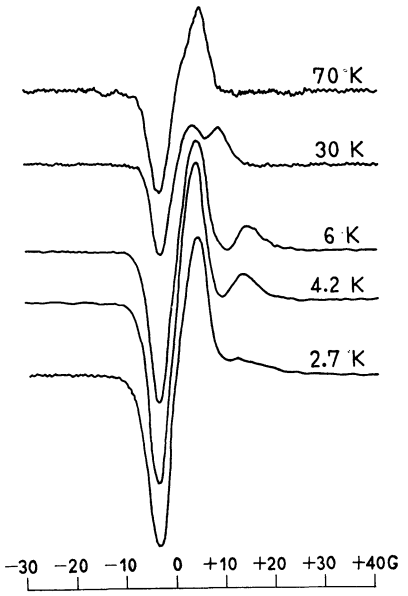

Fig. 2. NMR spectra of BDPA-Bz measured at 18.0 MHz.

is attributed to the paramagnetic shift of some protons attached to the carbon atoms with positive spin densities. The paramagnetic shift can be evaluated from the spacing between the unshifted and shifted absorption lines. Although these two resonance lines are not highly resolved, one may regard the resonance position of the shifted line as the center of the two peaks of the shifted absorption line. Thus, the paramagnetic shift, δH, the peak height of the unshifted line, h, and the half-width between the maximum slopes of the unshifted line, ΔH, were defined as is shown in Fig. 3. As the temperature was lowered to about 2 K, the shifted line became too broad to evaluate the δH, and the peak height of the unshifted line, h, decreased abruptly from 2.2 to 1.5 K, much as in the case of the spectra measured at 30.0 MHz. The curve of Fig. 4 indicates the temperature dependence of h for BDPA-Bz, which is normalized to 100% at 4.2 K.

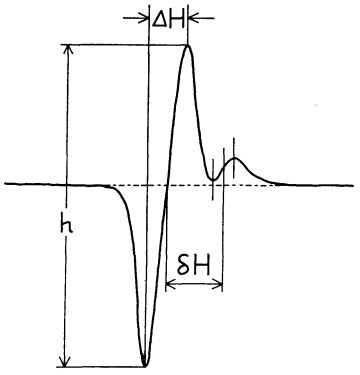

Fig. 3. Definition of δH, h and ΔH in the NMR spectra of the free radicals studied here. The δH stands for the paramagnetic shift to the high field. h and ΔH mean the peak height and the peak-to-peak linewidth of the unshifted absorption line respectively.

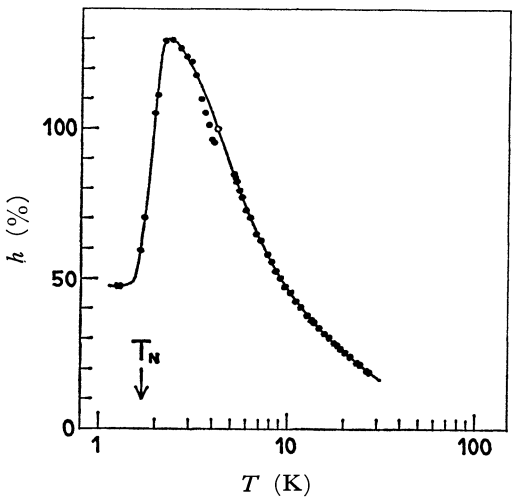

Fig. 4. Peak height of the unshifted line, h, of BDPA-Bz *vs.* temperature measured at 18.0 MHz. h is normalized to 100% at 4.2 K. T_N is the Néel temperature of this radical.

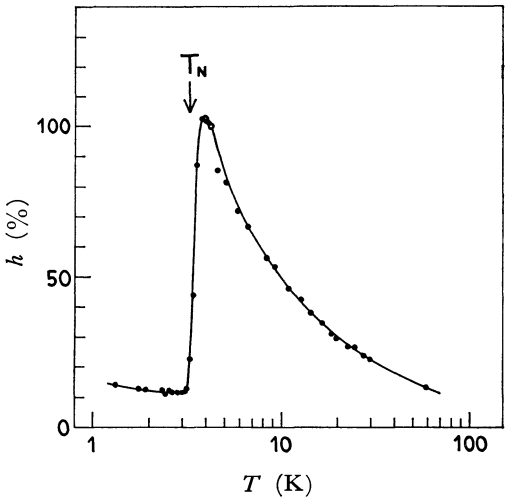

Fig. 5. h of p-Cl-BDPA *vs.* temperature measured at 18.0 MHz.

For the measurements of p-Cl-BDPA, spectra similar to those of BDPA-Bz were obtained except for one or two shifted lines observed above 4 K. The peak height, h, exhibited an abrupt decrease from 3.8 to 3.2 K, as is shown in Fig. 5.

For the sake of comparison, as will be discussed later, the temperature dependence of h for a powder sample of TANOL (2,2,6,6-tetramethyl-4-piperidinol-1-oxyl) was also obtained.

Discussion

Each proton in a radical molecule interacts with an unpaired electron which spreads over a whole molecular framework. In general, the Hamiltonian in the system where such a proton is located in a static magnetic field, H_0, along the z-axis may be given by:

$$\mathcal{H} = \mathcal{H}_{\text{Zeeman}} + \mathcal{H}_{\text{iso}} + \mathcal{H}_{\text{dip}}. \quad (1)$$

Here, $\mathcal{H}_{\text{Zeeman}}$ is the nuclear Zeeman term:

$$\mathcal{H}_{\text{Zeeman}} = -g_N\beta_N H_0 I_z. \quad (2)$$

$\mathcal{H}_{iso}$ and $\mathcal{H}_{dip}$ denote the hyperfine interaction; the former is the isotropic term, and the latter, the anisotropic dipolar term. $\mathcal{H}_{Zeeman}$ decides the free proton resonance field, and $\mathcal{H}_{iso}$ and $\mathcal{H}_{dip}$ contribute to a shift from that field.

Paramagnetic Region. The electron spins fluctuate rapidly as a result of the exchange interaction between the unpaired electrons on neighboring radical molecules. Hence, a small time-averaged local magnetic field acts on a proton.[11] In a powder sample, therefore, the dipolar term does not contribute to the paramagnetic shift, and the isotropic hyperfine term is given by:

$$\mathcal{H}_{iso} = a\boldsymbol{I}_z\langle\delta\boldsymbol{S}_z\rangle. \tag{3}$$

where a is the isotropic hyperfine coupling constant and is proportional to the spin density on the carbon atom adjacent to the proton according to McConnell's relation,[12] and where $\langle\delta\boldsymbol{S}_z\rangle$ denotes the z-component of a time-averaged value of an electron spin which is induced by the external magnetic field, H_0. The relation between $\langle\delta\boldsymbol{S}_z\rangle$ and H_0 is:

$$\chi_M H_0 = -Ng\beta\langle\delta\boldsymbol{S}_z\rangle. \tag{4}$$

where χ_M is the molar static magnetic susceptibility and N, Avogadro number. From Eqs. (2) and (3) the paramagnetic shift, expressed in Gauss, is obtained as:

$$\delta H = \frac{a\langle\delta\boldsymbol{S}_z\rangle}{g_N\beta_N}. \tag{5}$$

From Eq. (4) and the resonance condition ($h\nu = g_N\beta_N H_0$), we obtain:

$$\delta H = \frac{a\chi_M h\nu}{Ng\beta(g_N\beta_N)^2}. \tag{6}$$

Thus, δH is proportional to the hyperfine coupling constant (or the spin density on the adjacent carbon atom), the static magnetic susceptibility, and the resonance frequency.

According to McConnell's relation, a is negative for a proton attached to the carbon atom with a positive spin density. From the results of a simple molecular orbital calculation for BDPA, it is considered that the absorption line shifted to the high field is attributable to eight protons attached to the carbon atoms, with positive spin densities, situated at the 2-, 4-, 9-, and 11-positions on two diphenylene groups in a radical molecule. Since BDPA-Bz is a one-to-one complex of benzene, the absorption intensity ratio of the unshifted line to the shifted line should be 13+6 : 8 (observed 70 : 30). Hence, the line shape of BDPA-Bz in Fig. 3 is valid and also corresponds well with the results by Anderson *et al.* Since the intensity ratio for *p*-Cl-BDPA should be 12 : 8 (observed 60 : 40), the line shape of this radical is also valid.

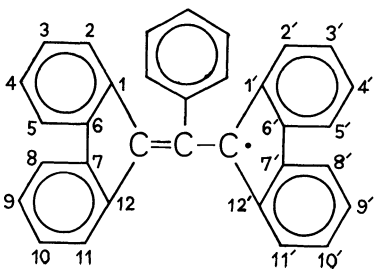

One can recognize the frequency dependence of δH in Fig. 6 and can see quite a good agreement of the temperature dependence curve of δH with that of χ_M as is shown in Fig. 7.

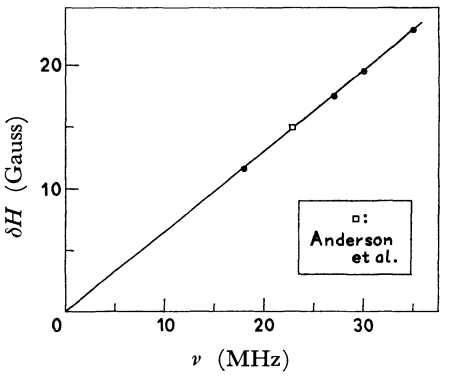

Fig. 6. Paramagnetic shift, δH, of BDPA-Bz *vs.* resonance frequency, ν, measured at 4.2 K. The value by Anderson *et al.* is also plotted for comparison.

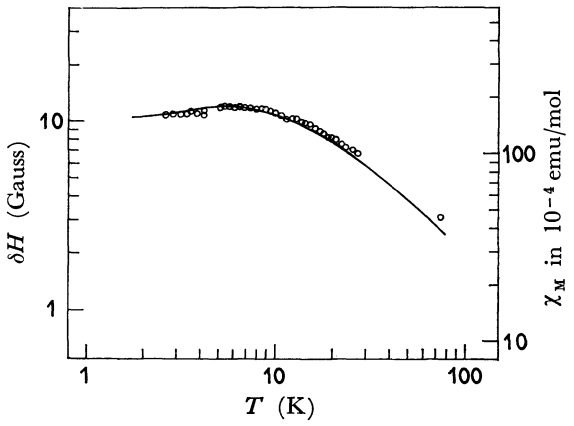

Fig. 7. δH of BDPA-Bz *vs.* temperature. The solid line is the curve of the molar magnetic susceptibility, χ_M, by Yamauchi[4] fitted at the maximum point.

As it is known that the width of the shifted line depends upon $\langle\delta\boldsymbol{S}_z\rangle$,[13] Fig. 2 shows a broadening of that line associated with a rise in the paramagnetic susceptibility.

Critical Region and Antiferromagnetic Region. The electron spins do not fluctuate rapidly any longer. Hence, a spontaneous magnetization of the electron spins occurs and a large time-averaged local field acts on a proton, which is specified as:

$$\mathcal{H}_{iso} = a\boldsymbol{I}_z\langle\boldsymbol{S}_z\rangle. \tag{7}$$

where $\langle\boldsymbol{S}_z\rangle$ denotes the time average of the z-component of the effective spontaneous magnetization of the electron spins which acts on that proton. In the paramagnetic state, $\langle\boldsymbol{S}_z\rangle$ is nonvanishing only in a finite applied field. Though it would be difficult to express $\mathcal{H}_{dip}$ in a simple form for a system where the electron spins are widely delocalized, it can be easily understood that this term also involves $\langle\boldsymbol{S}_z\rangle$. Both the hyperfine terms contribute to the

striking increase in the width of the shifted line shown in Fig. 2. The unshifted line originally consists of the absorption of each proton which is coupled weakly with the unpaired electron (or attached to the carbon atom with a very small spin density). The occurrence of the spontaneous magnetization, therefore, shifts the resonance field of each proton to a point far from the free-proton resonance field.

The temperature dependence of h can be regarded as that of the absorption intensity of the unshifted line, for ΔH does not show a large temperature dependence, as is shown in Fig. 8, and no saturation of the unshifted line[3] was observed. The rapid decrease in h near Néel temperature can, therefore, be ascribed to the long-range ordering of the unpaired electron spins in BDPA-Bz and *p*-Cl-BDPA. In TANOL a short-range ordering occurs, with a maximum susceptibility at 6.5 K,[4,14,15] but a long-range ordering does not occur down to 1.3 K; this radical is believed to be a good linear antiferromagnet.[4] Hence, h (or the absorption intensity) for TANOL is approximately inversely proportional to the temperature, as is shown in Fig. 9, and it may be considered that the absorption intensity is proportional to the "nuclear magnetic susceptibility" in the absence of a long-range ordering. On the other hand, in the presence of a long-range ordering, the absorption intensity of the unshifted line decreases abruptly in the critical temperature region, as is shown for BDPA-Bz and *p*-Cl-BDPA in Figs. 4 and 5 respectively, because of the spontaneous sublattice magnetization, which acts as a large local field on protons through the hyperfine interaction.

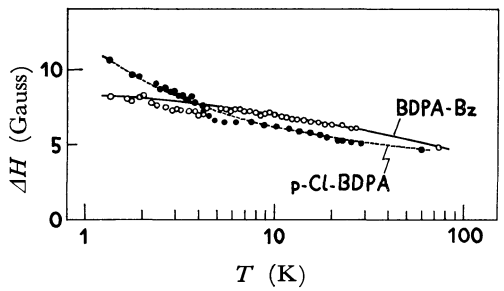

Fig. 8. Linewidth of the unshifted line, ΔH, of BDPA-Bz and *p*-Cl-BDPA *vs.* temperature measured at 18.0 MHz.

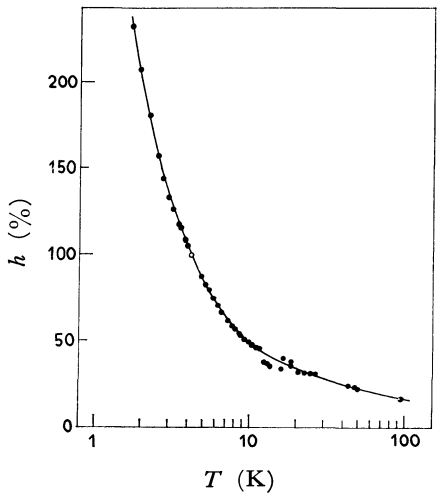

Fig. 9. h of TANOL *vs.* temperature measured at 30.0 MHz.

Thus, the results of the proton NMR measurements are consistent with the other information about the magnetic susceptibility, the ESR, and the specific heat measurements.

The shifted absorption lines in the antiferromagnetic region could not be found for powder samples of the two radicals. It is hoped that the magnetic properties of these radicals will be studied with single crystals in the future.

Conclusion

The proton NMR of the organic free radicals was studied in the paramagnetic and antiferromagnetic regions. The results are consistent with the other information on their magnetic properties; especially, it may be concluded that the intensity of the proton NMR absorption line decreases abruptly in the vicinity of the Néel temperature. This phenomenon illustrates the behavior associated with the long-range magnetic ordering of the two organic free radicals, BDPA-Bz and *p*-Cl-BDPA. Moreover, it may be concluded that the transition temperature in the organic free radicals can be foretold on the basis of the results of the proton NMR measurements of powder samples.

The authors would like to express their sincere thanks to Messrs. Teruaki Fujito and Toshio Yoshioka for their help in the measurements and also to Mr. Kohji Watanabe for his advice on the sample preparation.

Reference

1) C. F. Koelsch, *J. Amer. Chem. Soc.* **54**, 3384 (1932).
2) M. E. Anderson, R. S. Rhodes, and G. E. Pake, *J. Chem. Phys.*, **35**, 1527 (1961).
3) W. O. Hamilton and G. E. Pake, *ibid.*, **39**, 2694 (1963).
4) J. Yamauchi, This Bulletin, **44**, 2301 (1971).
5) W. Duffy, Jr., J. F. Dubach, P. A. Pianetta, J. F. Deck, D. L. Strandburg, and A. R. Miedema, *J. Chem. Phys.*, **56**, 2555 (1972).
6) J. Yamauchi, K. Adachi, and Y. Deguchi, *Chem. Lett.*, 733 (1972); *J. Phys. Soc. Japan*, **35**, 443 (1973).
7) J. Yamauchi, to be published.
8) R. Kuhn and F. A. Neugebauer, *Monatsh. Chem.*, **95**, 3 (1964).
9) G. D. Watkins, Thesis, Harvard University (1952).
10) F. N. H. Robinson, *J. Sci. Instrum.*, **36**, 481 (1959).
11) M. E. Anderson, G. E. Pake, and T. R. Tuttle, *J. Chem. Phys.*, **34**, 1581 (1960).
12) H. M. McConnell, *ibid.*, **24**, 632 (1956).
13) T. H. Brown, D. H. Anderson, and H. S. Gutowsky, *ibid.*, **33**, 720 (1960).
14) Yu. S. Karimov and E. G. Rozantsev, *Soviet Physics-Solid State*, **8**, 2255 (1967).
15) J. Yamauchi, T. Fujito, E. Ando, H. Nishiguchi, and Y. Deguchi, *J. Phys. Soc. Japan*, **25**, 1558 (1968).

Kinetic Studies of the Reaction between Sodium Dodecyl Sulfate and Pinacyanol Chloride

Nobuhide TATSUMOTO, Kunio TAKEDA, Shunji ISSHIKI, and Tatsuya YASUNAGA

Department of Chemistry, Faculty of Science, Hiroshima University, Higashisenda-machi, Hiroshima 730

(Received September 10, 1973)

Below the critical micelle concentration, a kinetic study of the aggregate formation reaction of sodium dodecyl sulfate and pinacyanol chloride was made by means of a stopped-flow system combined with a rapid scanning spectrophotometer. The process involves the following four steps and a precipitate whose composition ratio was dodecyl sulfate : pinacyanol = 1 : 1 was obtained as the final product:

$$\frac{1}{2}D_2 \longleftrightarrow D \underset{S}{\rightleftharpoons} DS \longleftrightarrow DS' \longrightarrow (ppt)$$

where D and S are the dye and detergent molecules respectively. The forward rate constants have been calculated to be 6×10^5 $(M\ s)^{-1}$ for $[S]_0=0.05$—0.1 mM in the second step and 1.2×10^2—3.9×10^{-3} s^{-1} for $[S]_0=$ 0.05—1.0 mM in the third step.

Above the critical micelle concentration (CMC), the color of a mixed solution of sodium dodecyl sulfate (SDS) and pinacyanol chloride is characterized by two absorption bands, α at 615 nm and β at 570 nm.[1] These characteristic absorptions have been attributed to the incorporation of dye into the micelles.[1] In a kinetic study of that incorporation by the stopped-flow method, the absorption at the γ band, 480 nm, which is associated with dye-detergent salt,[1] appeared and reached its maximum within 1 ms. Its absorption gradually decreased with the time, while the absorption at the α band increased. From these results it was nearly proved that the dye is incorporated into micelles through an intermediate, dye-detergent salt. In view of the above considerations, the process of the dye-detergent salt formation should be observed by the stopped-flow method at lower concentrations of SDS. As a preliminary test, the dynamic behavior of the absorption spectrum over a wide range of wavelengths was observed using the stopped-flow system combined with a rapid scanning spectrophotometer. The change in the absorption at the γ band with the time could be observed as expected. Moreover, the absorption at the γ band decreased gradually with the time, while the absorption at 520 nm appeared and subsequently increased. Finally, this new absorption disappeared completely within one or two days.

The purpose of the present investigation is to study the kinetics of the overall reaction in which the salt precipitates after the solutions of pinacyanol chloride and SDS have been mixed below CMC, paying attention to the absorptions at the γ band 520 nm.

Experimental

Materials. The SDS and the pinacyanol chloride were obtained from Nikko Chemicals Co. and Eastmann Organic Chemicals Co. respectively. These reagents were used without further purification. The CMC of SDS was measured to be 7.6, 7.1, and 7.0 mM by the electrical conductivity, surface tension, and viscosity methods respectively, and was measured to be 5.7 mM in 0.02 mM of pinacyanol chloride by the spectral method at 20 °C.

Method. The dynamic spectra were measured by means of a stopped-flow system combined with a rapid scanning spectrophotometer, JASCO, RSP-1D, whose scanning speed was 400 nm/ms. This spectrophotometer, moreover, was also used as a fixed-wavelength monochromator. The dead time of the stopped-flow system was less than 2 ms.[2] All the experiments were performed at 25 °C.

Results and Discussion

The dependence of the static spectrum on the concentration of SDS was measured in a 0.04 mM solution of pinacyanol chloride, and very complex spectra were observed, as can be seen in Fig. 1. In the range of 0.1—3 mM of SDS, the absorption changed with the time, and a precipitate was observed on standing for a long time. Therefore, the measurement was done within one hour after mixing the pinacyanol chloride with the SDS. In the higher concentration range of SDS, no absorption change was observed even after 16 hours.

The stable peaks of absorption due to the incorporation of dye into the micelles were observed at the α and β bands, above the CMC. On the other hand, the quite stable peak of absorption, whose half-life period is greater than 6 hours, associated with the

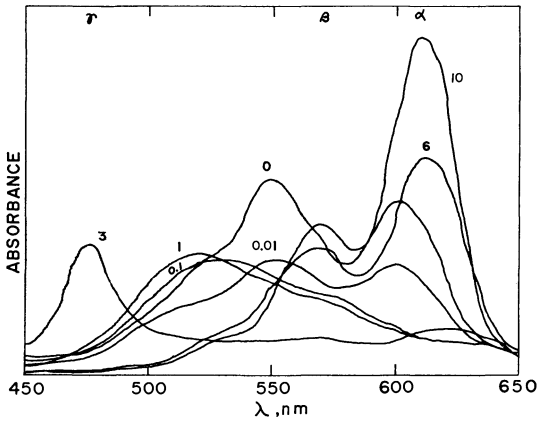

Fig. 1. Change in absorption spectrum with concentration of SDS in 0.04 mM pinacyanol chloride. Numbers in this figure refer to concentration of SDS, mM unit.

dye-detergent salt was observed at the γ band in about 3 mM of SDS. Further, in the lower range (0.1—1 mM) of SDS an unaccountable peak of absorption was observed at 520 nm. Below 0.1 mM of SDS, the characteristic absorptions of pinacyanol chloride were observed at 550 and 600 nm.

In the measurement of the dynamic spectrum, the characteristic absorptions of pinacyanol chloride at 550 and 600 nm in 0.1 mM of SDS decreased with the time, while that at the γ band increased after mixing, as is shown in Fig. 2. Subsequently, the absorption at the γ band gradually decreased with the time, while an unaccountable one at 520 nm appeared and increased. Finally, this absorption at 520 nm disappeared completely and the precipitate settled within one or two days. At a higher concentration, 0.25 mM, of SDS, the absorptions at 550 and 600 nm could not be observed, and that at the γ band reached its maximum within 1 ms after mixing, as is shown in Fig. 3. Subsequently, those at the γ band and 520 nm changed with the time in a manner similar to that in 0.1 mM of SDS. The above results lead us to presume that the species associated with the absorption at 520 nm is produced through the intermediate, the dye-detergent salt. In the meantime, at a lower concentration, 0.025 mM, of SDS, the absorptions at 550 and 600 nm gradually decreased with the time, while the absorption at 520 nm increased after mixing without any appearance of the absorption at the γ band, as can be seen from Fig. 4. These facts indicate that

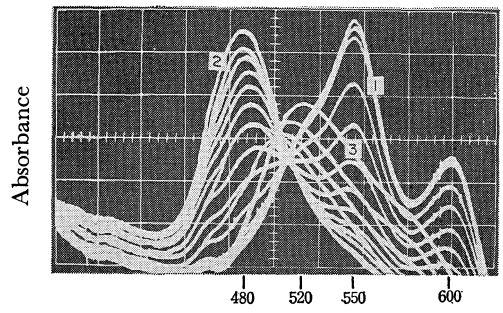

Fig. 2. Change in absorption spectrum with time. $[S]_0=0.1$ mM. $[D]_0=0.04$ mM. Time after mixing, 1 : 1 ms, 2 : 80 ms, 3 : 28 s.

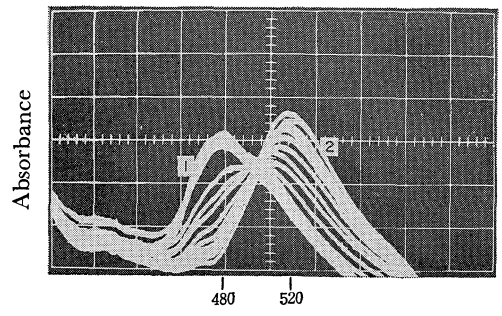

Fig. 3. Change in absoption spectrum with time. $[S]_0=0.25$ mM. $[D]_0=0.04$ mM. Time after mixing, 1 : 1 ms, 2 : 205 s.

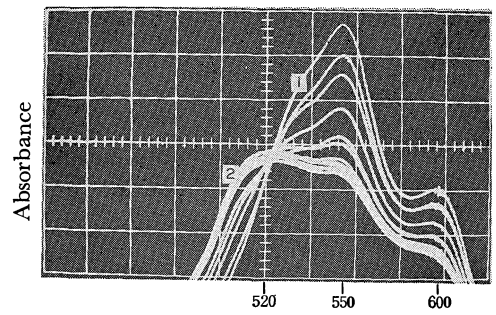

Fig. 4. Change in absorption spectrum with time. $[S]_0=0.025$ mM. $[D]_0=0.04$ mM. Time after mixing, 1 : 50 ms, 2 : 50 s.

the formation rate of dye detergent salt is less than or equal to that of species associated with the absorption at 520 nm.

Then, the changes in the absorptions at the γ band, 520, 550, and 600 nm with the time were measured in further detail at four fixed wavelengths by the stopped-flow method in 0.05 and 0.1 mM of SDS in order to study the overall reaction. The absorbances at 550 and 600 nm changed with the time after the mixing of 0.08 mM of pinacyanol chloride with 0.2 mM of SDS, as is shown in Fig. 5. Here, the dead time was 4 ms, since the mixing-flow time had to be lowered because the sample was a foamy liquid. As can be seen from Fig. 5, the variations in the absorbances at 550 and 600 nm with the time differ from each other in shape. In order to examine the above phenomenon in detail, the concentration dependences of absorptions at 550 and 600 nm were measured in an aqueous solution of dye alone. The plots of the absorbances at both wavelength *vs.* the total concentration of the dye are not linear, as can be seen from Fig. 6.

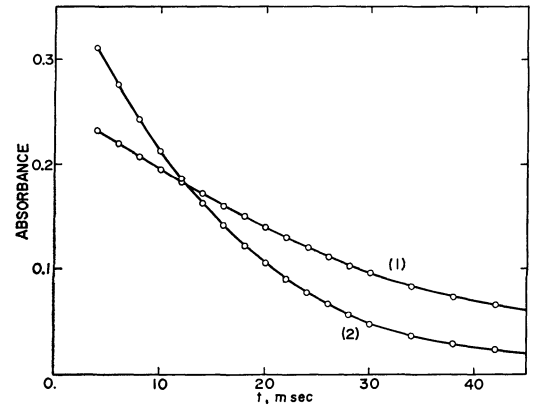

Fig. 5. Changes in absorbance with time. $[S]_0=0.1$ mM. $[D]_0=0.04$ mM. (1) : 550 nm, (2) : 600 nm.

It has been reported that, in a certain range of concentrations, a cationic dye is in equilibrium between the monomer and dimer.[3] Therefore, the following equilibrium for the present system can be assumed:

$$D_2 \rightleftharpoons 2D \qquad (1)$$

where D is the dye molecule. Then, the equilibrium

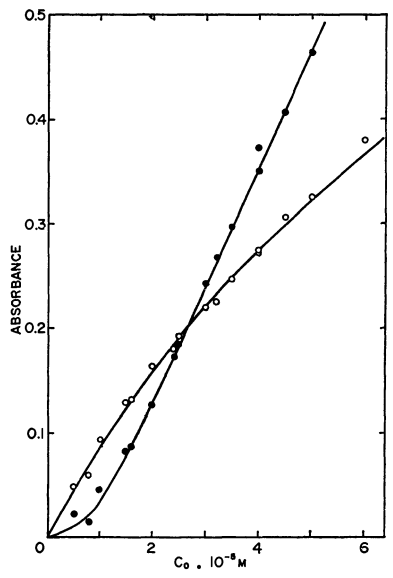

Fig. 6. Changes in absorbance with concentration of pinacyanol chloride. ●: 550 nm, ○: 600 nm.

constant K_1 is given by:

$$K_1 = 2\delta^2 C_0/(1-\delta) \tag{2}$$

where C_0 is the total concentration of dye in the monomer unit and δ, the dissociation degree. On the other hand, the absorbances, A, at the two absorption bands are given by:

$$A_D = \varepsilon_D C_D l = \varepsilon_D(1-\delta)C_0 l/2 \tag{3}$$

$$A_M = \varepsilon_M C_M l = \varepsilon_M \delta C_0 l \tag{4}$$

where ε is the molar absorption coefficient, l, the pass length of the cell, and the subscripts, D and M, refer to the dimer and the monomer respectively. The values of K_1, ε_D, and ε_M were determined so as to obtain the best fit of the data to the theoretical curves calculated by Eqs. (2)—(4). The theoretical curves, which are characterized by $K_1=2\times10^4$ M, $\varepsilon_D=\varepsilon_{550}=3.8\times10^5$ M^{-1} cm^{-1}, and $\varepsilon_M=\varepsilon_{600}=4.5\times10^4$ M^{-1} cm^{-1}, are shown in Fig. 6, along with the experimental data. The good fitting of the experimental and theoretical values indicates that the equilibrium of $D_2 \rightleftharpoons 2D$ is varied for the present system. The kinetic study for this step might be made by the chemical relaxation method.

Assuming that the dye-detergent salt is produced from SDS and the monomer of pinacyanol which is more reactive than the dimer, the formation of salt may be represented by:

$$mD + n_1S \underset{k_{-2}}{\overset{k_2}{\rightleftharpoons}} X \tag{5}$$

where S is the detergent; X, salt; m and n_1, stoichiometric constants, and k_2 and k_{-2}, forward and backward rate constants respectively. Therefore, the formation rate of X is given by:

$$\frac{d[X]}{dt} = k_2[D]^m[S]^{n_1} - k_{-2}[X] \tag{6}$$

$$m[X] = [D]_0 - \left([D]+\frac{1}{2}[D_2]\right) \tag{7}$$

$$[S] = [S]_0 - n_1[X] \tag{8}$$

In an earlier stage of the reaction

$$\frac{d[X]}{dt} = k_2[D]^m[S]^{n_1} \tag{9}$$

and

$$\int_{[X]_i}^{[X]_t} d[X] = k_2 \int_i^t [D]^m[S]^{n_1} dt \tag{10}$$

where i is the dead time. The two integers, m and n_1, were determined so as to obtain the best linear plot of the integration on the left *vs.* that on the right of Eq. (10). In both cases of $[S]_0=0.05$ and 0.1 mM, the assumption of $m=n_1=1$ was sufficient to give the best straight line, whose slope gave $k_2=6\times10^5$ $(M\,s)^{-1}$. Therefore, X can by represented by DS. In practice, the integration on the right was performed by the graphical method. The plot is shown for $[D]_0=0.04$ mM and $[S]_0=0.1$ mM in Fig. 7. The value of k_{-2} can be calculated theoretically from the deviation of the integration on the left-hand side of Eq. (10) from the straight line at the final stage of the reaction, but it could not be determined in practice because the values of [X] were not very accurate there.

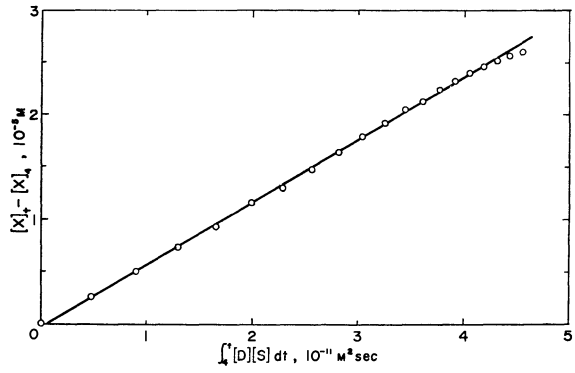

Fig. 7. A plot of $[X]_t-[X]_4$ *vs.* $\int_4^t [D][S]\,dt$. $[S]_0=$ 0.1 mM. $[D]_0=0.04$ mM.

Since the species, Y, associated with the absorption at 520 nm must be produced through the DS associated with that at the γ band, the formation of the former may be represented by:

$$n_2(DS) \underset{}{\overset{k_3}{\rightleftharpoons}} Y \tag{11}$$

where k_3 is a forward rate constant and n_2, a stoichiometric constant. In an earlier stage of the reaction

$$-\frac{d[DS]}{dt} = k_3[DS]^{n_2} \tag{12}$$

$$[DS] = \beta A_\gamma \tag{13}$$

and

$$\log(-dA_\gamma/dt) = \log(k_3\beta^{n_2-1}) + n_2 \log A_\gamma \tag{14}$$

where A_γ is an absorption coefficient at the γ band and β, a constant. All the plots of $\log(-dA_\gamma/dt)$ *vs.* $\log A_\gamma$ were linear, and their slopes, n_2, were nearly equal to unity, as can be seen from Fig. 8. Therefore, the forward process may be described by an equation of a first-order reaction and the product, Y, can be represented by DS′:

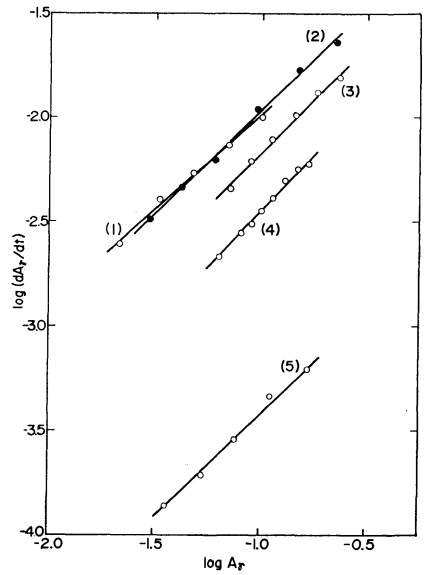

Fig. 8. Plots of $\log(dA_T/dt)$ *vs.* $\log A_T$. $[S]_0=0.05$—1.0 mM. $[D]_0=0.04$ mM. (1) : 0.05 mM, (2) : 0.1 mM, (3) : 0.2 mM, (4) : 0.5 mM, (5) : 1.0 mM.

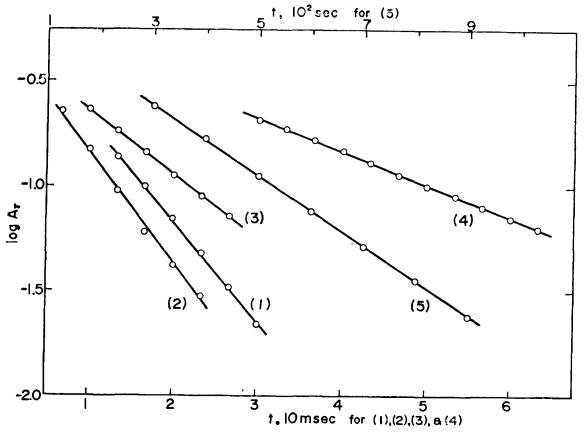

Fig. 9. Changes in $\log A_T$ with time. $[S]_0=0.05$—1.0 mM. $[D]_0=0.04$ mM. (1) : 0.05 mM, (2) : 0.1 mM, (3) : 0.2 mM, (4) : 0.5 mM, (5) : 1.0 mM.

$$DS \xrightarrow{k_3} DS' \tag{15}$$

$$\ln A_T = -k_3 t + \ln A_{T0} \tag{16}$$

The values of k_3 were obtained from the slope of the plots of $\ln A_T$ *vs.* t shown in Fig. 9; they are listed in Table 1.

When the absorption at 520 nm can be observed, as in the case described above, the salt precipitated completely within one or two days. The precipitate was recrystallized from ethanol to form large monoclinic needles, blue-violet in color. Microanalysis gave the results listed in Table 2 for both the recrystallized and unrecrystallized precipitates. Considering that both the analytical values are in good agreement with the theoretical ones calculated by assuming that the ratio of SDS and pinacyanol chloride is unity, the precipitate might be an aggregate of DS′ associated with the absorption at 520 nm:

$$n_3 DS' \rightleftharpoons (DS')_{n_3} \tag{17}$$

where n_3 is a stoichiometric constant. Consequently, the overall reaction may be given by:

$$\frac{1}{2}D_2 \longleftrightarrow D \underset{S}{\overset{}{\rightleftharpoons}} DS \longleftrightarrow DS' \longleftrightarrow \frac{1}{n_3}(DS')_{n_3} \tag{18}$$

Finally, although it should be noted that the forward rate constant in the third process decreases with the concentration of SDS except in 0.1 mM, no definitive conclusion can be drawn on the basis of the above experimental results alone. However, it may be presumed that the stability of DS increases with the concentration of SDS, while that of DS′ increases with the concentration of water. This, moreover, leads us to question whether DS is different from DS′ in the chemical bonding between D and S or is conformational isomers with DS′, which has a steric structure stabilized by a hydrophobic bonding.

Table 1. FORWARD RATE CONSTANTS FOR THE THIRD STEP REACTION

$[S]_0$, mM	k_3, s^{-1}
0.05	1.1×10^2
0.1	1.2×10^2
0.2	7.0×10
0.5	3.6×10
1.0	3.9×10^{-3}

Table 2. MASS RATIO OF ATOMS CONSTITUTING AGGREGATES OF SDS AND PINACYANOL CHLORIDE DETERMINED BY MICROANALYSIS

	N(%)	C(%)	H(%)
Unrecrystallized	4.53	71.81	8.14
Recrystallized	4.47	70.50	8.14
Calculated assuming [S] : [D]=1 : 1	4·28	71.05	8.15

References

1) P. Mukerjee and K. J. Mysels, *J. Amer. Chem. Soc.*, **77**, 2937 (1955).
2) T. Yasunaga, K. Takeda, and S. Harada, *J. Colloid Interfac. Sci.*, **42**, 457 (1973).
3) M. E. Lamm and D. M. Neville, Jr., *J. Phys. Chem.*, **69**, 3872 (1965).

Fluctuation of the Myoglobin Structure

Mamoru NAKANISHI, Masamichi TSUBOI,* and Akira IKEGAMI**

*Faculty of Pharmaceutical Sciences, The University of Tokyo, Hongo, Bunkyo-ku, Tokyo 113

**Department of Physics, Faculty of Science, The University of Tokyo, Hongo, Bunkyo-ku, Tokyo, 113

(Received September 12, 1973)

The kinetics of hydrogen-deuterium exchange in sperm whale metmyoglobin has been followed in aqueous solutions of various pD values (5.6—7.7) and at various temperatures (0—55 °C) by an infrared absorption measurement. At pD=5.6 and at 0 °C, 117 out of the total 148 peptide hydrogen atoms exchange relatively slowly with a rate of an apparent first-order reaction for one hour of the reaction time. This number (117) is almost equal to the sum of the number of peptide NH-groups (108~111) which are found to be involved in hydrogen bonds with the carbonyls of other peptide groups and those (8) which are in hydrogen bonds with oxygen atoms of some sidechains in the myoglobin molecule in the crystalline state. At higher temperatures and/or at higher pD's, however, only 109 peptide NH groups (assignable to those involved in the peptide-peptide hydrogen bonds) are found to exchange relatively slowly. The kinetics of the exchange reactions of these 109 peptide NH groups are explained by assuming that the fluctuation amplitude (*i.e.*, the probability of finding the peptide-peptide hydrogen bonds broken) becomes lower on going from the terminus towards the inner portion in each of the eight α-helices involved in the myoglobin structure.

In our previous works[1-3] it has been shown that a kinetic study of the hydrogen-deuterium exchange reaction of a protein in aqueous solution can provide useful information on the fluctuation of the protein structure. The kinetic data have been connected with the fluctuation of the protein structure through the following two assumptions: (1) The exchange reaction of a peptide NH group is distinctively slow when it is involved in a peptide-peptide hydrogen bonds. (2) The rate constant of such a slow exchange reaction is proportional to the chance of finding the hydrogen bond broken. These assumptions are essentially based upon the reaction scheme proposed by Hvidt[4] many years ago, and by our recent experiments good pieces of evidence have been found for the validity of these assumptions in the case of lysozyme.[1]

In this work myoglobin is the subject of our kinetic measurement. On the hydrogen exchange in myoglobin, Englander and Staley[5] and Abrash[6] made detailed studies. In the former work, special attention was paid to the estimation of the free and hydrogen-bonded peptide NH groups. While, in the latter work the effect of the pH-induced denaturation was intensively examined. Both of the results are interpretable by considering that the assumptions given above are valid. We have extended the hydrogen-exchange measurement into the temperature range of 0 to 55 °C and attempted to discuss a detail of the fluctuation of the structure of this protein in solution.

Experimental

Crystalline sperm whale myoglobin was obtained from Miles-Seravac, Ltd., Maidenhead, Berkshire, England (Batch 57A). The hydrogen-deuterium exchange reaction was followed by infrared absorption measurements according to the method described by Blout, de Lozé and Asadourian.[7] The experimental procedure is the same as given in our previous papers.[1,2,8] The concentration of myoglobin was kept at 3.3%. The solvent was 0.1 M phosphate buffer. The amount of undeuterated peptide group was taken as proportional to the ratio of the absorbance of amide II (at 1550 cm^{-1}) to that of amide I (at 1650 cm^{-1}) bands, A(amide II)/A (amide I). In the absorbance measurements, the baseline for the amide I band was drawn parallel to the 100% transmittance line from the transmittance at 1800 cm^{-1}, and the baseline of the amide II band was taken as the absorption of a solution of the completely deuterated myoglobin. The latter was obtained by keeping the solution of the exchanging protein at pD≒10 and at 45—50 °C for several hours, and then by bringing the pD and temperature of the solution into proper values.

Results and Interpretations

(a) General Features of the Exchange Kinetics. The hydrogen-deuterium exchange reaction was followed for myoglobin in D_2O solutions of pD 5.6, 6.3, 7.0, and 7.7 at 15, 25, 35, 45, and 55 °C. For solution of pD 5.6, the observation was made also at 0 °C and 5 °C. The results are shown in Figs. 1 and 2. As may be seen in these figures, the reaction rate is higher

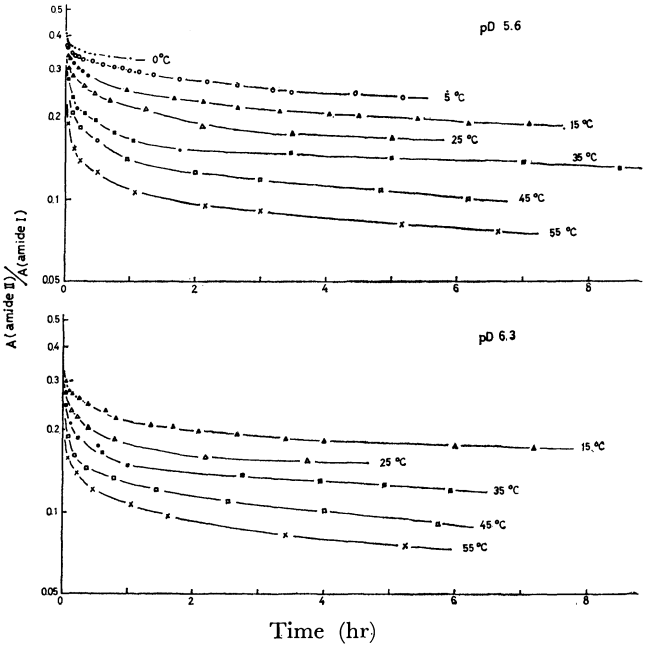

Fig. 1. Semilogarithmic plots of deuterium exchange of myoglobin in D_2O solutions of pD 5.6 (upper) and of pD 6.3 (lower) at various temperatures.

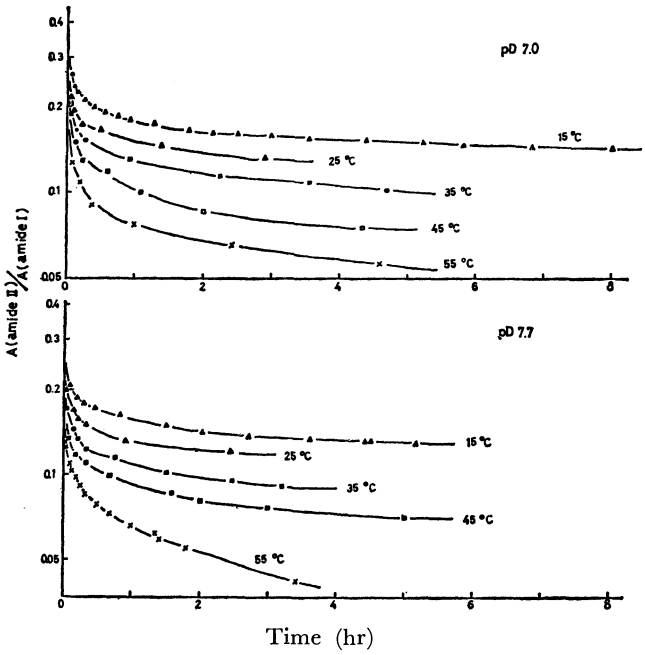

Fig. 2. Semilogarithmic plots of deuterium exchange of myoglobin in D_2O solutions of pD 7.0 (upper) and of pD 7.7 (lower) at various temperatures.

at higher temperatures and in solutions with higher pD's. Under any of these conditions the reaction does not proceed as a simple first-order reaction. This is in contrast to the case of lysozyme,[1,2] where the peptide hydrogen atoms exchange with a rate of an apparent first-order reaction except in an early stage of the reaction. This fact indicates that the peptide NH group in the myoglobin molecule should be classified into a number of categories with different kinetic behaviors from one another.

(b) Measurement of the Free and Hydrogen-bonded Peptide NH Groups. At 0 °C the reaction proceeds so slowly that we can estimate the A(amide II)/A(amide I) value at time zero by an extrapolation (Fig. 3, upper portion). The value is found to be 0.450. This value is equal to what are determined in a less ambiguous for lysozyme[1,2] and α-lactalbumin.[3] The reaction

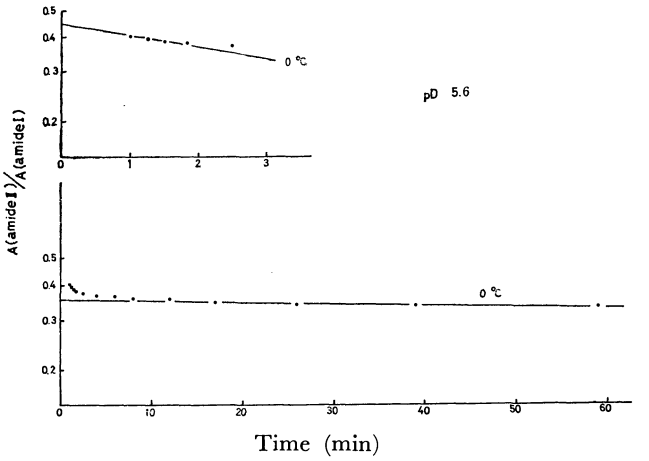

Fig. 3. Semilogarithmic plots of an early stage of the deuterium exchange reaction of myoglobin in a D_2O solution of pD 5.6 at 0 °C.

proceeds rather rapidly in the period of 0 to 10 minutes, and suddenly at about 10 minutes it slows down (see Fig. 3, lower portion). In the period of 17—60 min the exchange proceeds apparently as a simple first-order reaction. The extrapolation of the straight line obtained in the semilogarithmic plots for this stage of the reaction gives an A(amide II)/A(amide I) value of 0.355 at the zero time. This fact indicates that we can divide the peptide NH groups in myoglobin into two main classes; $(0.450-0.355)/0.450=21._0\%$ of them exchange rapidly and the rest $0.355/0.450=79._0\%$ do slowly. Because there are 148 peptide NH groups in the myoglobin molecule, the former corresponds to 31 and the latter 117 in the actual number. According to the crystallographic study of Kendrew *et al.*,[9] 108~111 peptide NH groups in the myoglobin molecule are involved in intramolecular peptide-peptide hydrogen bonds, 8 NH's are involved in intramolecular hydrogen bonds with oxygen atoms in sidechains, and 29—32 are free from such intramolecular hydrogen bonds.[10] Therefore, it is probable that the slowly exchanging 117 peptide NH groups found in our experiment correspond to the $(109+8)\pm2$ peptide NH groups involved in hydrogen bonds in the myoglobin molecule in its crystalline state.

Similar estimation of the free and hydrogen-bonded amides of myoglobin was made by following the tritium exchange by Englander and Staley.[5] Our result is practically equal to theirs. It may be pointed out here, however, that we can extract only the behavior of the peptide NH groups in this protein molecule by the infrared absorption measurement, while in the measurement of ^3H radioactivity one needs to take, in principle, all the exchangeable hydrogen atoms into account.

As may be seen in Fig. 1 (upper), the exchange reaction at 5 °C and at pD=5.6 proceeds as a simple first-order reaction from 18 to 100 minutes. In the semilogarithmic plot, the straight line which corresponds to this part of the reaction intersects the ordinate (A(amide II)/A(amide I)) at 0.330. At 15 °C a straight line in the semilogarithmic plot occurs for the 0~20 minutes period. This also intersects the ordinate at 0.330. This value of A(amide II)/A(amide I) corresponds to 109 peptide NH groups. This is equal to the number of peptides NH groups involved in the peptide-peptide hydrogen bonds. This fact therefore may be interpreted as indicating that, at temperatures higher than 5 °C, only the peptide NH groups involved in the peptide-peptide hydrogen bonds should be classified as the "slowly exchanging peptide NH groups", and those involved in the peptide-sidechain hydrogen bonds are to be classified as the "fast" NH groups. Such an interpretation has been found to be valid for lysozyme[1,2] and for α-chymotrypsin.[11]

(c) Hvidt's "Relaxation Spectra" and the "Fluctuation Amplitude" γ. On the basis of the interpretation just described, we now attempt an analysis of the hydrogen-deuterium exchange reaction with special attention on the 109 peptide NH groups involved in the peptide-peptide hydrogen bonds. For such an analysis, Willumsen[12,13] and Hvidt and Wallevik[14] proposed to display the kinetic data as plots of the number of

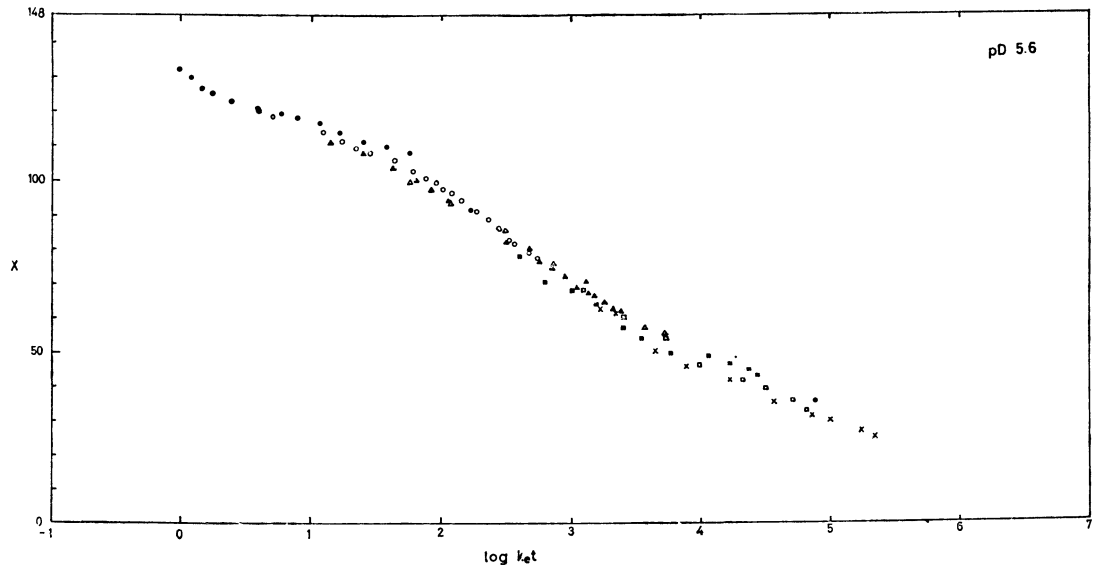

Fig. 4. A re-plotting of the experimental data given in Fig. 1 (upper). X is the number of unexchanged peptide NH groups at time t, and k_e is the rate constant of peptide hydrogen atoms free from hydrogen bonds, calculated according to equation (1). ●, at 0 °C; ○, at 5 °C; ▲, at 15 °C; △, at 25 °C; ■, at 35 °C; □, at 45 °C; and ×, at 55 °C. pD=5.6.

unexchanged peptide hydrogen atoms (X) at a given time (t) *versus* $\log_{10}(k_e t)$, where k_e is the exchange rate constant of solvent-exposed peptide groups. They mentioned such plots as "relaxation spectra". We have re-plotted our kinetic data according this proposal. For k_e at various pD's and temperatures (θ °C), we have adopted, according to Hvidt and Nielsen,[15] the values given by the following formula:

$$k_e = 50(^{0.3-pD} + 10^{pD-6.3})10^{0.05(\theta-20)}\text{min}^{-1} \quad (1)$$

(We have neglected here the primary-structure effects discussed by Molday, Englander and Kallen.[16]) In Fig. 4, an example of the "relaxation spectra" is shown for the peptide NH groups of myoglobin in the solution of pD 5.6; this is obtained by re-plotting the data given in Fig. 1 (upper).

Hvidt and Nielsen[15] showed that most studies of the hydrogen exchange led to the conclusion that the so-called EX_2 reaction mechanism offers the simplest, and the most likely explanation of the slow exchange of the hydrogen-bonded peptide NH groups. Let us consider i-th peptide NH group. The exchange takes place as follows:

$$N_i \underset{k_{2i}}{\overset{k_{1i}}{\rightleftharpoons}} D_i \xrightarrow{k_e} \text{exchange}, \quad (2)$$

where N_i means a state of the i-th NH group involved in a hydrogen-bond and D_i is that after the hydrogen-bond is broken so that it is now ready to exchange with the rate costant k_e. The EX_2 mechanism corresponds to the case of

$$k_e \ll k_2, \quad (3)$$

and in this case X_i (fraction remaining unchanged) is given as

$$X_i = \exp(-\gamma_i k_e t), \quad (4)$$

where

$$\gamma_i = [D_i]/([N_i]+[D_i]) \quad (5)$$

is the probability of finding the particular peptide-peptide hydrogen bond broken so as to be ready to exchange with the rate constant k_e. If the NH group now in question is intrinsically free from hydrogen bond, $\gamma_i \fallingdotseq 1$. While, if it is involved in a peptide-peptide hydrogen bond in the "intact" form of the myoglobin molecule, the γ_i value is very small (in comparison with 1), and such γ_i value may be taken as a measure of the "fluctuation amplitude" of the local structure around the i-th peptide NH group.

Now, according to Eq. (4), the plot of X_i *versus* $\log_{10}(k_e t)$ for a fixed γ_i value should result in a curve whose slope is everywhere independent of the γ_i value, because $dX_i/d\log(k_e t)=2.30X_i \ln X_i$. Therefore, the curves corresponding to different γ values have the same shape but are mutually displaced along the abscissa. The amount of displacement of each curve from that with $\gamma_i=1$ is equal to $-\log_{10}\gamma_i$. The ordinate X in the observed plot such as shown in Fig. 4 should correspond to the sum of X_i at every $\log_{10}(k_e t)$.

$$X = \sum_i \exp(-\gamma_i k_e t) \quad (6)$$

Thus, Hvidt's "relaxation spectrum", *i.e.*, the X *versus* $\log_{10} k_e t$ plot, is considered to be a so-to-say "spectrum" of γ, the probability of finding each NH group free from a hydrogen bond so that it is ready to exchange with the rate constant k_e. In other words, it is a "spectrum" of the amplitude of local fluctuation of the protein structure.

(d) Effects of Temperature and pD *on the Local Fluctuation.* In Fig. 4, observed X *versus* $\log_{10} k_e t$ curves at different temperatures are found to be nearly superposed on one another, although a little more detailed inspection indicates a probably significant tendency that a curve for higher temperature is shifted very slightly towards leftside direction (*i.e.*, towards higher γ value) from a curve for lower temperature. This

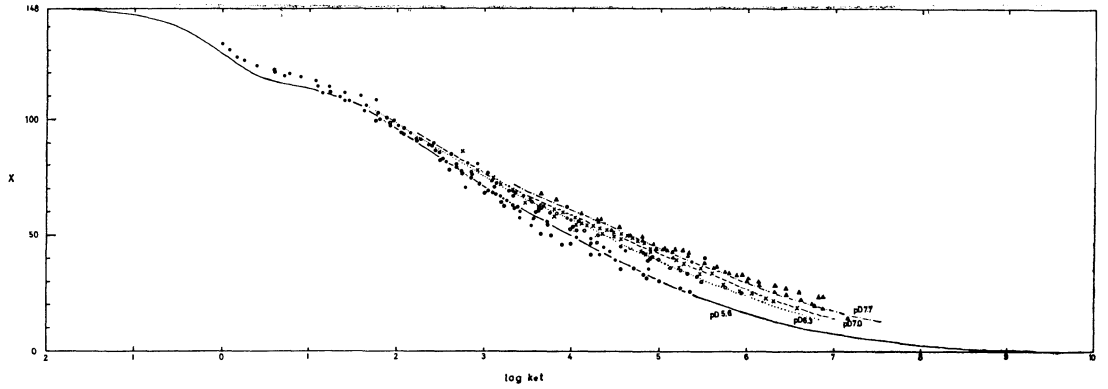

Fig. 5. Observed and calculated "relaxation spectra" of myoglobin. X is the number of unexchanged peptide NH groups at time t. k_e is the rate constant of solvent-exposed peptide hydrogen atoms (free from hydrogen bonds). Points are obtained by re-plotting the experimental data given in Figs. 1 and 2. ●, at pD=5.6 (at various temperatures in the range of 0—55 °C); ○, at pD=6.3; ×, at pD=7.0; ▲, and at pD=7.7. Continuous lines are obtained by calculation on equation (6), and by assigning the γ_i values to the 148 peptide NH groups as shown in Table 1. ——, for pD=5.6; ·····, for pD=6.3; ----, for pD=7.0; and —·—, for pD=7.7.

was found to be the case not only for the plot at pD=5.6 but also for plots at pD=6.3, 7.0, and 7.7. This fact may be taken as indicating that the observed temperature effect on the exchange kinetics is mostly attributable to the temperature effect on k_e, and that γ_i value of every NH group is almost independent of temperature in the range of 0—55 °C, although it becomes very slightly higher on raising the temperature of the solution. This is quite similar to what we found for lysozyme[2] and α-lactalbumin[3] as long as the temperature was kept by 20—25 °C lower than the thermal transition point.

In Fig. 5, we have re-plotted our kinetic data given in Figs. 1 and 2 in the form of X *versus* $\log_{10} k_e t$ curve. On the basis of what has just been stated, no distinction is made here between the points for different temperatures, but different marks are given to points for different pD's. As may be seen in the figure, the "relaxation spectrum" depends slightly but appreciably upon pD. Every γ_i value is considered to become lower as pD of the solution increases from 5.6 to 7.7.

Discussion

The denaturation of sperm whale myoglobin was extensively investigated by Acampora and Hermans[17] as a function of pH and temperature. In Fig. 6, transition temperatures found by them are shown as a function of pH of the solution. The area with hatching corresponds to the native form region. All the place within this region are considered to be similar as far as the optical density and/or optical rotation measurements are concerned. In the manner of fluctuation of the structure, however, there may be a variety even within the native region, and this is just the subject of our study. In this respect, we have examined in the present work the region surrounded by the rectangle in Fig. 6. Within this region, the fluctuation has been found to be greater for lower pH than that for higher pH, while it is almost independent of the temperature of the solution.

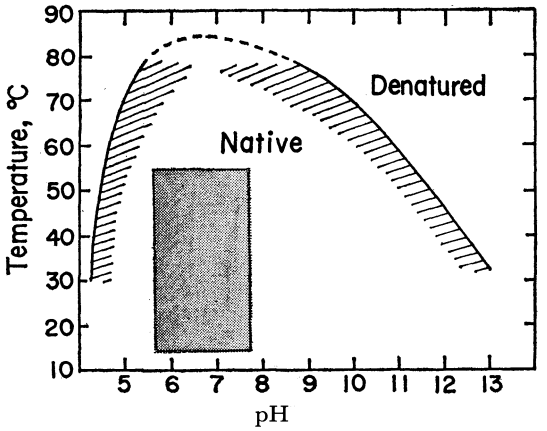

Fig. 6. An equilibrium diagram between the native and denatured forms of myoglobin given by Acampora and Hermans[17]. The rectangular region is what we have examined as to the fluctuation of the structure.

In addition, we have been able to go into some details of the fluctuation of the local structures within the molecule. Some experiments are yet to be designed for determining the rate of hydrogen exchange reaction of every particular NH group, so that the fluctuation amplitude of the structure can be mapped at every exact locus within the molecule. Even by our present study, however, it has been indicated that the map of the local fluctuation is different in myoglobin from that in lysozyme. In the latter, all of the 44 peptide-peptide hydrogen bonds have nearly equal chances of cleavage to one another, while in the former, 109 peptide-peptide hydrogen bonds have various chances, greatly different from one another.

At present, we have no unique solution as for the assignment of each γ_i value to a particular peptide NH group in the molecule. It is not improbable, however, that a peptide NH in a central portion of an α-helix has a lower γ value than that of a peptide NH around the terminal portion of the α-helix. This is just what has often been postulated for explaining various be-

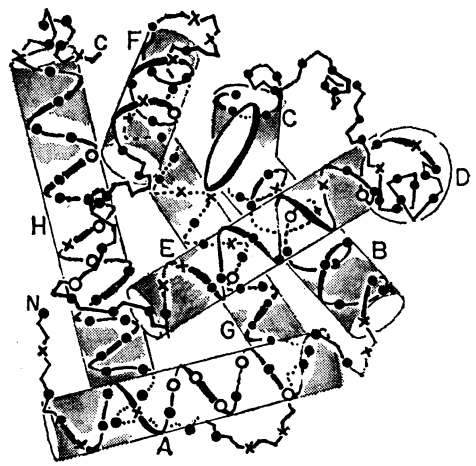

Fig. 7. A schematic drawing of a model of the fluctuation of the myoglobin structure, *i.e.*, a model of the distribution of the γ value in the molecule. γ is the probability of finding each NH···OC hydrogen bond broken, and this is considered to be greater at the terminal portions of each α-helix, and becomes smaller on going towards the central portion. This model is considered to be supported to some extent by a recent neutron diffraction study by Schoenborn.[20] Black and white circles in the figure indicate the deuterated and undeuterated peptide NH groups found by them in a partially deuterated myoglobin crystal. × denotes the absence of any indication for H or D.

haviors of α-helices of synthetic polypeptides.[8,18,19] We found, for example, that the hydrogen-deuterium exchange reaction is slower for longer α-helix of poly-L-glutamic acid.[8] In addition, recent neutron diffraction study of myoglobin by Schoenborn[20] may be taken as supporting the above idea to some extent. By soaking a myoglobin crystal in a solvent with 75% D_2O, they obtained a partially deuterated crystal, and then they located the hydrogen and deuterium atoms in the myoglobin molecule. As may be seen in Fig. 7, the undeuterated peptide groups found by them are mostly located in the central portions of eight α-helices in the molecule.

On the basis of what has just been described, we attempted to construct a tentative model in which the γ value of the peptide NH becomes lower on going from the terminus into the inner portion of each α-helix. The γ value should be proportional to $\exp(-\Delta F_1/kT)$ where ΔF_1 is the effective free energy change caused by the N_i—D_i transition, k the Boltzmann constant, and T the absolute temperature. Let us postulate that the free energy difference ΔF_n for the n-th residue from the terminus is given as

$$\Delta F_n = \Delta F_t + (n-1)\Delta F_s. \quad (7)$$

This is based upon the assumptions that the terminus peptide NH group has the free energy change ΔF_t and that the breaking of every peptide-peptide hydrogen bond in an α-helix takes place always after the next-door peptide-peptide hydrogen bond which is nearer to the terminus has been broken, with an additional free energy change of ΔF_s. After a few trials, we found that the following set of the values for the two parameters fits the observed relaxation spectra: $\Delta F_t=2.86$ and $\Delta F_s=0.82$ kcal/mol at pD=5.6 (25 °C), 3.00 and 0.93 at D=6.3, 3.00 and 0.98 at D=7.0, and 3.13 and 1.02 at pD=7.7. This set of values of ΔF_t and ΔF_s corresponds to a set of γ values given in Fig. 8 and Table 1. The calculated X *versus* $\log_{10}(k_e t)$

Table 1. A proposed set of γ values which fits the observed relaxation spectra

Character of the peptide NH group	$\log_{10}\gamma$ value, assigned at pD= 5.6	6.3	7.0	7.7	Number of the peptide NH groups in the non helical regions	in helix A	B	C	CD	D	E	F	G	GH	H	Total
Free	0	0	0	0	31											
H-bonded with O atoms in side-chains	−1.5	−1.5	−1.5	−1.5	8											
In the terminal residue in an α-helix	−2.1	−2.2	−2.2	−2.3		2	2	2	2	2	2	2	2	1	2	19
In the 2nd residue	−2.7	−2.9	−2.9	−3.0		2	2	1	1	2	2	2	2		2	16
3rd	−3.3	−3.6	−3.7	−3.8		2	2				2	2	2		2	12
4th	−3.9	−4.2	−4.4	−4.5		2	2				2	2	2		2	12
5th	−4.5	−4.9	−5.1	−5.3		2	2				2	2	2		2	12
6th	−5.1	−5.6	−5.8	−6.0		2	2				2	2	2		2	12
7th	−5.7	−6.3	−6.6	−6.8		2	1				2	1	2		2	10
8th	−6.3	−6.9	−7.3	−7.5							2		1		2	5
9th	−6.9	−7.6	−8.0	−8.2							2				2	4
10th	−7.5	−8.3	−8.7	−9.0							1				2	3
11th	−8.1	−9.0	−9·4	−9.7											2	2
12th	−8.7	−9.7	−10.2	−10.5											2	2
				Total	39	14	13	3	3	4	19	13	15	1	24	148

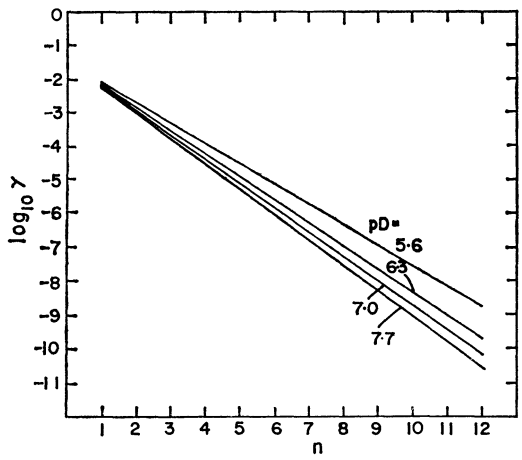

Fig. 8. $\text{Log}_{10}\ \gamma$ values assigned to the peptide NH groups located in the n-th residue from the nearer terminal of the α-helix in the myoglobin structure.

plots on the basis of this set of γ values are shown in Fig. 5 by continuous and broken lines.

References

1) M. Nakanishi, M. Tsuboi, and A. Ikegami, *J. Mol. Biol.*, **70**, 351 (1972).
2) M. Nakanishi, M. Tsuboi, and A. Ikegami, *ibid.*, **75**, 673 (1973).
3) H. Takesada, M. Nakanishi, and M. Tsuboi, *ibid.*, **77**, 605 (1973).
4) A. Hvidt, *Compt. Rend. Trav. Lab. Carlsberg*, **34**, 299 (1964).
5) S. W. Englander and R. Staley, *J. Mol. Biol.*, **45**, 277 (1969).
6) H. I. Abrash, *Compt. Rend. Trav. Lab. Carlsberg*, **37**, 107 (1970).
7) E. R. Blout, C. de Lozé, and A. Asadourian, *J. Amer. Chem. Soc.*, **83**, 1895 (1961).
8) M. Nakanishi, M. Tsuboi, A. Ikegami, and M. Kanehisa, *J. Mol. Biol.*, **64**, 363 (1972).
9) J. C. Kendrew, R. E. Dickerson, B. E. Strandberg, R. G. Hart, D. R. Davies, D. C. Phillips, and V. C. Shore, *Nature*, **185**, 422 (1960).
10) H. C. Watson, "Progress in Stereochemistry," Vol. 4, ed. by M. M. Harris and B. J. Aylett, Butterwood, London (1969), p. 299.
11) M. Nakanishi and M. Tsuboi, to be published.
12) L. Willumsen, *Biochim. Biophys. Acta*, **126**, 382 (1966).
13) L. Willumsen, *Compt. Rend. Trav. Lab. Carlsberg*, **38**, 223 (1971).
14) A. Hvidt and K. Wallevik, *J. Biol. Chem.*, **247**, 1530 (1972).
15) A. Hvidt and S. O. Nielsen, *Adv. Protein Chem*, **21**, 287 (1966).
16) R. S. Molday, S. W. Englander, and R. G. Kallen, *Biochemistry*, **11**, 150 (1972).
17) G. Acampora and J. Hermans, *J. Amer. Chem. Soc.*, **89**, 1543 (1967).
18) R. L. Snipp, W. G. Miller, and R. E. Nylund, *ibid.*, **87**, 3547 (1965).
19) B. H. Zimm and J. K. Bragg, *J. Chem. Phys.*, **31**, 526 (1959).
20) B. P. Schoenborn, *Cold Spr. Har. Symp. Quant. Biol.*, **36**, 569 (1971).

Molecular Structures of Hydrogen Cyanide and Acetonitrile as Studied by Gas Electron Diffraction

Ken-ichi KARAKIDA, Tsutomu FUKUYAMA, and Kozo KUCHITSU

Department of Chemistry, Faculty of Science, The University of Tokyo, Bunkyo-ku, Tokyo 113

(Received October 27, 1973)

The structures of HCN and CH_3CN have been determined by gas electron diffraction for a critical comparison between diffraction and spectroscopic data. For HCN, the r_g(C≡N), determined by gas electron diffraction, 1.158±0.003 Å, is consistent within the estimated limit of experimental error with that calculated from the spectroscopic r_e structure and the harmonic and anharmonic force constants by a perturbation procedure, 1.158_8 Å. For CH_3CN, electron diffraction intensities have been analyzed jointly with the rotational constants for the normal and three deuterated species determined by microwave spectroscopy by Kessler *et al.* and Thomas *et al.* The isotopic difference in the average C–H distance, $\delta r = r_{av}$(C–H) − r_{av}(C–D), has also been treated as one of the independent parameters. The analysis has led to the following structure: r_g(C≡N) = 1.159±0.002 Å, r_g(C–C) = 1.468±0.002 Å, r_g(C–H) = 1.107±0.004 Å, ∠C–C–H (r_{av}) = 109.7±0.2° and δr = 0.001±0.002 Å.

The purpose of the present determination of the r_g structures of hydrogen cyanide and acetonitrile is twofold. First, a comparison of the structures is made with those of analogous molecules with conjugated multiple bonds in pursuit of a systematic variation in the C–C and C≡N bond lengths with environment.[1,2] Second, a comparison is made of the structures determined by electron diffraction (ED) with those determined by spectroscopic (SP) methods, since these molecules are suitable examples for a critical check of SP and ED structures.

For HCN the equilibrium (r_e) structure[3] and the potential constants (up to the quartic)[4] have been determined by infrared spectroscopy with such precision that the r_g structure can be calculated purely from spectroscopic data by a perturbation procedure.[5] A comparison of ED and SP structures should then afford a direct test of the experimental accuracy and the theory of ED[5-7] on which our method is founded. Our attention has primarily been called to the C≡N distance, since the accuracy of the C–H distance determined by ED is not sufficient for such a critical comparison. Similar studies have already been made for a number of molecules, for which r_e structures and potential constants are well known by spectroscopy (diatomics, CO_2, CS_2, NH_3, CH_4, *etc.*), and in all cases the structures are reported to be fully consistent.[2] However, there still remain unsolved problems important for the application of the method to more complicated systems. For instance, for diacetylene[8] the bond lengths, mean amplitudes and rotational constants derived from ED appeared to be slightly different from those determined by SP, and the small discrepancies were tentatively ascribed to a cubic potential term representing bending-stretching interactions.

Furthermore, the hydrogen-deuterium isotope effect on the average structure is another important problem, which has by no means been settled, for a combined analysis of ED and SP measurements. Acetonitrile was selected in this study because of its simplicity, high symmetry, well-defined quadratic force field, and the absence of low frequency motions such as internal rotation.

The ED structure of CH_3CN was reported to be[9] r(C–C) = 1.54±0.02 Å and r(C≡N) = 1.16±0.02 Å, or[10] r(C–C) = 1.49±0.03 Å and r(C≡N) = 1.16±0.03 Å, where the C–H distance and CCH angle were assumed. The r_0 structure was determined from ten rotational constants for eight isotopic species determined by microwave spectroscopy.[11-14] Besides the C–H, C≡N, C–C distances and CCH angle, r_0(C–D) and the CCD angle were taken as independent parameters.[14] The isotope effects on the r_0 structure were: r_0(C–H) − r_0(C–D) = 0.0048 Å and ∠CCH − ∠CCD = 0.1°. The isotopic rotational constants were used by Costain[15] and Matsumura *et al.*[16] to determine the r_s structure by Kraitchman's equations. The r_s and r_0 structures are compared with the r_g structure determined in the present analysis in a later section.

Experimental

A sample of hydrogen cyanide (bp 26 °C) was prepared by adding sulfuric acid to sodium cyanide. The vessel was filled with dry nitrogen and the product was trapped in ice-cold water. The crude product containing water was purified by passing it through a tube heated to about 40 °C packed with calcium chloride. Acetonitrile was obtained from a commercial source (purity 96%, bp 81 °C) and used after distillation. The infrared spectra of HCN gas and CH_3CN liquid showed no band that could be assgined to impurities.

Electron diffraction photographs were taken with an apparatus equipped with an r^3-sector[17] at camera lengths of 107.8 and 243.2 mm. The electron wavelength was about 0.06 Å. The sample gases were maintained in thermal equilibrium with their liquid phase at 0 °C for HCN and at room temperature for CH_3CN. The pressures of the samples were about 250 and 70 Torr for HCN and CH_3CN, respectively. The exposure time for the shorter camera length was about 40 s for each sample, while that for the longer camera length was about one-third of that. Other experimental details are described elsewhere.[17,18]

The scale factor was calibrated with reference to the r_a(C=O) distance (1.164_6 Å) of carbon dioxide measured with the identical camera geometry. The accelerating voltage was monitored during photographic exposures. The observed r_a(C=O) distance and its standard deviation were 1.1649±0.0004 Å. Besides this calibration, the r_a(N≡N) of nitrogen (theoretical, 1.100_7 Å[19]) was also measured, and it was confirmed that carbon dioxide and nitrogen gave consistent scale factors.

Observed molecular intensities covering the range s = 3.5—37.7 Å^{-1} were used in the analysis. The data taken with

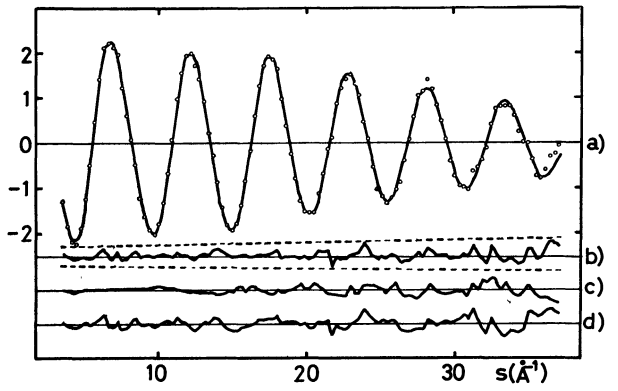

Fig. 1. a) Experimental and best-fit molecular intensities for HCN shown in dots and solid curves, respectively.

b) Experimental minus best-fit theoretical. The broken curve represents the estimated limit of random error in the molecular intensity (corresponding to a relative error of 1×10^{-3} in the original photocurrent).

c) Typical difference between two molecular intensity data used in the analysis illustrating the degree of reproducibility.

d) The observed minus theoretical molecular intensity calculated from spectroscopic parameters.

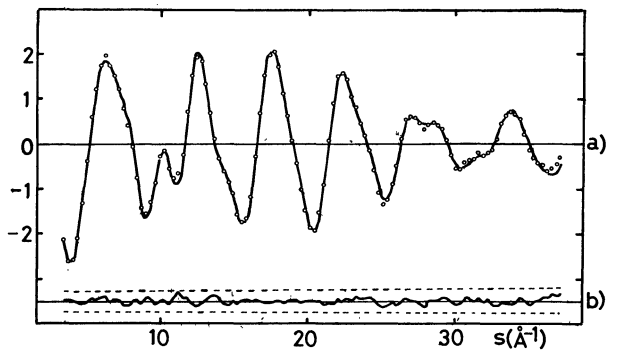

Fig. 2. a) Experimental and best-fit molecular intensities for CH_3CN shown in dots and solid curves, respectively.

b) See caption b) of Fig. 1.

the short and long camera lengths were linked at $s=13.8$ and 11.9 Å^{-1} for HCN and CH_3CN, respectively.[20] The elastic and inelastic scattering factors and the phase shifts were taken from the tables prepared by Bonham *et al.*[21] The molecular intensities are illustrated in Figs. 1 and 2 for HCN and CH_3CN, respectively, and the corresponding radial distribution curves are given in Figs. 3 and 4. For a representation of the reproducibility of the molecular intensity data, a difference between two intensities for HCN selected arbitrarily is shown in Fig. 1 (c). The level of random scatter is similar to that of the residuals (observed minus calculated intensities) derived from a least-squares analysis.

Analysis and Discussion

HCN. A linear equilibrium structure was assumed. A least-squares analysis was carried out with an empirical diagonal weight matrix.[22] The asymmetry parameters κ[19] for the C–H and C≡N bonds

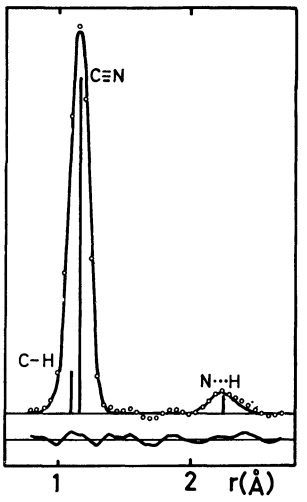

Fig. 3. Experimental (dots) and theoretical radial distribution curves for HCN. The lower curve represents residuals. Vertical bars correspond to internuclear distances. A damping factor, $\exp(-0.0016\,s^2)$, was used.

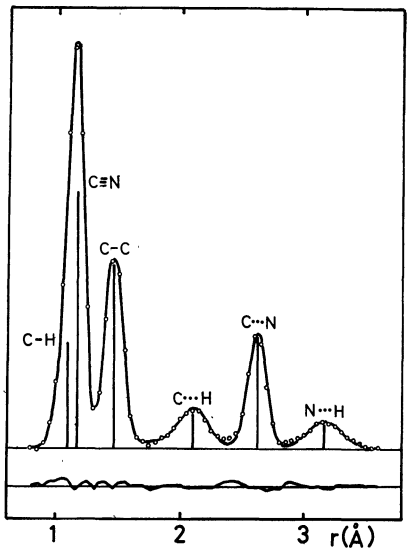

Fig. 4. Experimental and theoretical radial distribution curves for CH_3CN. See captions of Fig. 3.

TABLE 1. MOLECULAR PARAMETERS FOR HCN[a] (in Å units)

	C≡N	C-H	N---H
r_g(ED)[b]	1.158±0.003	1.10±0.02	2.24±0.02
r_g(SP)[c]	1.158_8	1.083_6	2.226_0
l_{obsd}[b]	0.039±0.003	0.07±0.03	0.08±0.02
l_{calcd}[c]	0.034_6	0.075_8	0.079_1
d[d]	0.0002	0.0174	0.0047

a) Uncertainties are estimated limits of error. b) Mean amplitudes, l_m defined in Ref. 19, derived from the present analysis of electron diffraction intensities. They are estimated to be equal to l_e within the quoted experimental error. c) Calculated values, l_e, based on spectroscopic r_e distances, harmonic and anharmonic force constants. d) Shrinkage corrections, r_a-r_α.

Table 2. Error matrix for HCN[a]

	k_1[b]	k_2[c]	l(C-H)	l(N--H)	l(C≡N)	r(C-H)	r(C≡N)
k_1	134						
k_2	171	332					
l(C-H)	125	199	165				
l(N--H)	35	42	31	97			
l(C≡N)	34	65	41	8	14		
r(C-H)	−13	−63	52	−13	11	74	
r(C≡N)	−35	−54	−48	−9	−12	−21	15

a) Units ($\times 10^{-4}$) for the distances are Å, those for the indices are dimensionless. b) Index of resolution for the long-camera region, 0.87±0.03. c) Index of resolution for the short-camera region, 0.98±0.05.

were estimated to be 1.7×10^{-5} and 0.5×10^{-6} Å^3 from the anharmonicity parameter a_3 for the diatomic molecules CH and CN,[23] 1.98 and 2.27 Å^{-1}, respectively. The κ parameter for the nonbonded N–H pair was ignored. The vibrational corrections for the shrinkage effect[24] and the mean amplitudes of vibration ($d=r_a-r_\alpha$ and l_{calcd}, listed in Table 1) were calculated from the force constants.[4] The most probable r_g distances and mean amplitudes are shown in Table 1 with their limits of error estimated from random and systematic uncertainties.[25] The error in the r_g(C≡N) distance originates mainly from the standard deviation in the least-squares analysis (0.0015 Å), and the uncertainties in the scale factor and in the shrinkage corrections (about 0.0006 Å and 0.0003 Å, respectively) are relatively unimportant. A slight discrepancy between the observed and calculated l(C≡N) may be ascribed to a systematic error in the observed mean amplitude due to extraneous scattering observed in large scattering angles. However, the r_g(C≡N) distance is not influenced significantly by this extraneous scattering. A typical error matrix is given in Table 2.

In order to compare the r_g structure with the r_e structure determined by infrared spectroscopy, the values of $r_g-r_e=\langle\Delta r\rangle$ were calculated by use of the anharmonic force constants[4] and perturbation theory.[5,26,27] Mean values of the internal coordinates are calculated from those of the normal coordinates (Table 3). Then thermal averages were taken with the Boltzmann factors, and corrections for centrifugal distortion[28] were included. In the present case, however, the normal frequencies are so high that the temperature corrections are negligible. The results are compared in Table 4 with those estimated by a diatomic approximation,[6,23] $\langle\Delta r\rangle=(3/2)a_3\langle\Delta r^2\rangle$. The $\langle\Delta r\rangle$ values calculated by perturbation theory are estimated to be accurate to about 0.0001 Å, and hence, the diatomic approximation is valid to the order of 0.002 Å (see Table 4). The r_g structure calculated from the spectroscopic equilibrium structure are compared in Table 1 with those determined by electron diffraction. They are consistent with each other within the experimental error of the latter. This situation is illustrated in Fig. 1 (d) as a difference curve between the observed molecular intensity and that calculated from the spectroscopic parameters. The fluctuations of the difference curve are random and similar in magnitude to those of the least-squares residuals.

Table 3. Mean values of the normal coordinates for HCN[a]

$\langle Q_1\rangle$	0.00988	$\langle Q_1Q_2^2\rangle$	0.00032
$\langle Q_3\rangle$	−0.00638	$\langle Q_3Q_2^2\rangle$	−0.00088
$\langle Q_1^2\rangle$	0.00801	$\langle Q_1^2Q_2^2\rangle$	0.00039
$\langle Q_2^2\rangle$	0.04851	$\langle Q_3^2Q_2^2\rangle$	0.00025
$\langle Q_3^2\rangle$	0.00525	$\langle Q_2^4\rangle$	0.00471

a) The normal coordinates are in (amu)$^{1/2}$Å.

Table 4. Mean displacements for HCN[a] (at 300 K)

	C N	C-H	N--H
$\langle\Delta r\rangle_{calcd}$[b]	0.0057	0.0177	0.0070
$\langle\Delta r\rangle_{approx}$[c]	0.0040	0.0170	—

a) $\langle\Delta r\rangle$: in Å units. b) Calculated by perturbation theory. c) Calculated by a diatomic approximation, $\langle\Delta r\rangle=(3/2)a_3\langle\Delta r^2\rangle$, with a_3 assumed to be 1.98 Å^{-1} and 2.27 Å^{-1} for C-H and C≡N, respectively.

CH_3CN. The equilibrium structure was assumed to have C_{3v} symmetry. The κ parameters were estimated to be 1.9×10^{-5}, 2.0×10^{-6} and 0.5×10^{-6} Å^3 for C–H, C–C and C≡N, respectively.[19]

The most probable r_α^0 distances and angle obtained from a least-squares analysis are shown in Table 5 with estimated uncertainties.[25] The most probable

Table 5. Average structures of CH_3CN[a] (in Å units)

	r_α^0[b]	r_{av}[c]	r_z[d]
C-C	1.464±0.002	1.465±0.002	1.45_9±0.01_5
C N	1.154±0.002	1.153±0.002	1.15_9±0.01_5
C-H	1.102±0.015	1.095±0.004	1.10_0±0.02
∠CCH	110.1±0.8°	109.7±0.2°	109.7±0.4°
δr[e]	—	0.001±0.002	(0.002±0.005)

a) Uncertainties are estimated limits of error. b) Derived from electron diffraction data. c) Derived from electron diffraction intensities plus rotational constants for the normal species and three deuterated species. d) Derived from twelve rotational constants. The difference, δr, in the r_z(C-H) distance with isotopic substitution (H to D) was assumed to be 0.002±0.005Å and those in the r_z(C-H), r_z(C-C) and r_z(C≡N) distances with isotopic substitutions (^{12}C to ^{13}C and ^{14}N to ^{15}N) were assumed to be 0±0.0003Å. The secondary isotopic differences in the C-C and C≡N distances in CH_3CN and CD_3CN were ignored. e) Isotopic difference in the C-H bond length, r(C-H)-r(C-D).

Table 8. Rotational constants for CH_3CN[a] (in cm^{-1})

		0[b]	z[c]	av[d]
CH_3CN	B	0.306840	0.30662 (2)	0.30664 (5)
CH_2DCN	B	0.292175 (2)	0.29190 (2)	0.29192 (3)
	C	0.287149 (2)	0.28699 (2)	0.28698 (5)
CHD_2CN	B	0.277527 (2)	0.27727 (2)	0.27728 (3)
	C	0.272336 (2)	0.27218 (2)	0.27216 (4)
CD_3CN	B	0.262112	0.26192 (2)	0.26190 (3)

a) Uncertainties attached to the last significant digits are given in parentheses. b) Observed rotational constants (B_0 and C_0) taken from Refs. 11 and 14. Uncertainties for CH_3CN and CD_3CN were not given. c) Average rotational constants calculated from B_0 and C_0 with corrections for vibrational effects. The limits of error are estimated from the uncertainties in the quadratic force constants used for calculating the corrections. d) Best-fit rotational constants corresponding to the r_{av} structure listed in Table 5, derived from a combined analysis of electron-diffraction and microwave data. Uncertainties represent 2.5 times the estimated standard deviations.

Table 9. Comparison of r_g, r_s and r_0 structures for CH_3CN (in Å units)

	r_g[a]	r_s[b]	r_0[c]
C-C	1.468±0.002	1.4584	1.4582
C N	1.159±0.002	1.1571	1.1572
C-H	1.107±0.004	1.1036	1.1120
∠CCH	109.7±0.2°[d]	109.45°	109.67°
r(CH)-r(CD)	0.001±0.002[e]	0.0022	0.0048
∠CCH-∠CCD	(0±0.1°)[e,f]	0.10°	0.08°

a) Derived from the r_{av} structure determined in the present study. b) Refs. 15, 16. No estimates of uncertainties are given. c) Ref. 14. No estimates of uncertainties are given. d) r_{av} structure. e) Isotopic differences based on the r_{av} structure. f) Assumed value.

to vary δr as one of the parameters. Hence, a major part of the uncertainties resulting from the assumptions about unknown isotopic differences are eliminated, and the precision of these parameters is thereby improved by nearly an order of magnitude.

The r_g structure derived from the r_{av} structure determined in the present study is compared with the r_s[15,16] and r_0 structures[14] in Table 9.* Particularly significant is the discrepancy of about 0.01 Å observed in the r_g(C–C) and $r_s(r_0)$(C–C) distances. The r_g(C≡N) and r_g(C–C) bond distances in acrylonitrile,[35] cyanogen,[36] acetonitrile and hydrogen cyanide are compared in Table 10. The r_g(C≡N) in acrylonitrile is longer than those in the other molecules. The r_g(C–C) in acetonitrile is significantly longer than those in acrylonitrile and cyanogen.

* **Note added in proof**: A more precise r_0 structure of acetonitrile has recently been determined: J. L. Duncan, D. C. McKean, and N. D. Michie, *J. Mol. Structure*, **23** (1974), in press.

Table 10. Comparison of C≡N and C-C distances in analogous molecules (in Å units)

	r_g(C≡N)	r_g(C-C)
CH_2=CH-C≡N[a]	1.167±0.004	1.438±0.003
N≡C-C≡N[b]	1.163±0.002	1.393±0.002
H_3C-C≡N[c]	1.159±0.002	1.468±0.002
H-C≡N[c]	1.158±0.003	—

a) Ref. 35. b) Ref. 36. c) Present study.

The authors wish to thank Professor Robert K. Bohn for his helpful comments on the manuscript and Mr. Masaaki Sugié, Mr. Ichiro Minami and Mr. Takeo Kishimoto for their technical help in the experiment and analysis.

References

1) Y. Morino, K. Kuchitsu, T. Fukuyama, and M. Tanimoto, *Acta Crystallogr.*, **A 25**, S 127 (1969).
2) K. Kuchitsu, "Gas Electron Diffraction," MTP International Review of Science, A Biennial Series, Physical Chemistry, Vol. 2, Chapter 6, G. Allen, Ed., Medical and Technical Publishing, Co., Oxford (1972).
3) D. H. Rank, G. Skorinko, D. P. Eastman, and T. A. Wiggins, *J. Opt. Soc. Amer.*, **50**, 421 (1960).
4) T. Nakagawa and Y. Morino, This Bulletin, **42**, 2212 (1969).
5) K. Kuchitsu and L. S. Bartell, *J. Chem. Phys.*, **35**, 2460 (1962).
6) L. S. Bartell, *ibid.*, **23**, 1219 (1955).
7) Y. Morino, K. Kuchitsu, and T. Oka, *ibid.*, **36**, 1108 (1962).
8) M. Tanimoto, K. Kuchitsu, and Y. Morino, This Bulletin, **44**, 386 (1971).
9) L. O. Brockway, *J. Amer. Chem. Soc.*, **58**, 2516 (1936).
10) L. Pauling, H. D. Springall, and K. J. Palmer, *ibid.*, **61**, 927 (1939).
11) M. Kessler, H. Ring, R. Trambarulo, and W. Gordy, *Phys. Rev.*, **79**, 54 (1950).
12) D. K. Coles, W. E. Good, and R. H. Hughes, *ibid.*, **79**, 224 (1950).
13) R. Trambarulo and W. Gordy, *ibid.*, **79**, 224 (1950).
14) L. F. Thomas, E. I. Sherrad, and J. Sheridan, *Trans. Faraday Soc.*, **51**, 619 (1955).
15) C. C. Costain, *J. Chem. Phys.*, **29**, 864 (1958).
16) C. Matsumura, E. Hirota, T. Oka, and Y. Morino, *J. Mol. Spectrosc.*, **9**, 366 (1962).
17) Y. Murata, K. Kuchitsu, and M. Kimura, *Jap. J. Appl. Phys.*, **9**, 591 (1970).
18) M. Tanimoto, K. Kuchitsu, and Y. Morino, This Bulletin, **43**, 2776 (1970).
19) K. Kuchitsu, *ibid.*, **40**, 498 (1967).
20) Numerical experimental data of the leveled total intensity have been deposited with the Chemical Society of Japan (Document No. 7405).
21) L. Schäfer, A. C. Yates, and R. A. Bonham, *J. Chem. Phys.*, **55**, 3055 (1971).
22) Y. Morino, K. Kuchitsu, and Y. Murata, *Acta Crystallogr.*, **18**, 549 (1965).
23) K. Kuchitsu and Y. Morino, This Bulletin, **38**, 805 (1965).
24) K. Kuchitsu and S. J. Cyvin, "Molecular Structures and Vibrations," ed. by S. J. Cyvin, Chapter 12, Elsevier, Amsterdam (1972).

25) K. Kuchitsu, "Molecular Structures and Vibrations," ed. by S. J. Cyvin, Chapter 10, Elsevier, Amsterdam (1972).
26) Y. Morino and T. Iijima, This Bulletin, **35**, 1661 (1962).
27) K. Kuchitsu, *ibid.*, **40**, 505 (1967).
28) M. Toyama, T. Oka, and Y. Morino, *J. Mol. Spectrosc.*, **13**, 193 (1964).
29) I. Nakagawa and T. Shimanouchi, *Spectrochim. Acta*, **18**, 513 (1962).
30) V. W. Laurie and D. R. Herschbach, *J. Chem. Phys.*, **37**, 1687 (1962).
31) W. J. Lafferty, D. R. Lide, and R. A. Toth, *ibid.*, **43**, 2063 (1965).
32) K. Kuchitsu, T. Fukuyama, and Y. Morino, *J. Mol. Structure*, **4**, 41 (1969).
33) L. S. Bartell and H. K. Higginbotham, *J. Chem. Phys.*, **42**, 851 (1965).
34) R. H. Schwendeman and J. D. Kelly, *ibid.*, **42**, 1132 (1965).
35) T. Fukuyama and K. Kuchitsu, *J. Mol. Structure*, **5**, 131 (1970).
36) Y. Morino, K. Kuchitsu, Y. Hori, and M. Tanimoto, This Bulletin, **41**, 2349 (1968).

Determination of the Number of Hydrogen-Bonds in a Protein Molecule

Mamoru NAKANISHI and Masamichi TSUBOI

Faculty of Pharmaceutical Sciences, University of Tokyo, Hongo, Bunkyo-ku, Tokyo 113

(Received October 27, 1973)

By means of an infrared-spectroscopic observation of the hydrogen-exchange reaction, the number of peptide-peptide hydrogen-bonds involved in a given protein molecule in its aqueous solution can be determined.

Every globular protein is considered to involve a proper set of intra-molecular hydrogen-bonds in its native form, both in its crystalline state and in its aqueous solution. Such a proper set of the hydrogen-bonds seems to keep a proper rigidity and at the same time a proper flexibility of the protein molecule, both of which are essential for playing its biological role.

We propose here a simple and reliable method of determining the number of the peptide-peptide hydrogen bonds in a given protein molecule in its aqueous solution. The method is based on a hypothesis, which is supported by our recent experiments,[1-3] that the slowly exchanging peptide hydrogen atoms are assignable to those involved in such hydrogen bonds. Similar but slightly different hypotheses on the slowly exchanging hydrogen atoms in proteins seem to have for long been kept in minds by a number of investigators.[4-7] Until recently, however, they were not used for obtaining useful pieces of information of the protein structure. A tritium-gel filtration study recently made by Englander and Staley[8] demonstrated, for example, that the amount of slowly exchanging hydrogens found in myoglobin matched the known number of hydrogen-bonded amides.[9] While, in the measurement of ^3H radioactivity, one needs to take, in principle, all the exchangeable hydrogen atoms in the protein molecule in question into account, we can extract only the behavior of the peptide NH groups by an absorption measurement.[5] This is what we propose here to adopt.

The proposed method is as follows. Dissolve, at time zero, a protein into D_2O in 2~3% in concentration, and place the solution into a sealed cell with CaF_2 windows and of 50 μ in optical path length. Measure the time-dependent decrease in the ratio of the peak intensity of amide II band around 1540 cm^{-1} to that of amide I band at about 1650 cm^{-1} (A(amide II)/A(amide I)) (see Fig. 1). In the intensity measurements, the baseline for the amide I band is drawn parallel to the 100% transmittance line from the transmittance at 1800 cm^{-1}, and the baseline of the amide II band is taken as the absorption of a solution of the completely deuterated protein. Com lete deuteration is achieved by heating the solution of the exchanging protein to a proper temperature, or by elevating the pH of the solution to 10 or so. Figure 2 illustrates a set of semilogarithmic plots of such a hydrogen→deuterium exchange reaction. The protein here is bovine pancreatic α-chymotrypsin. As may be seen in the Figure, two kinds of peptide hydrogen atoms are readily found: those which exchange quickly and those which do slowly. At 25 °C and at a proper pH, the exchange reaction of the former usually completes within three hours or so and that of the latter usually takes place

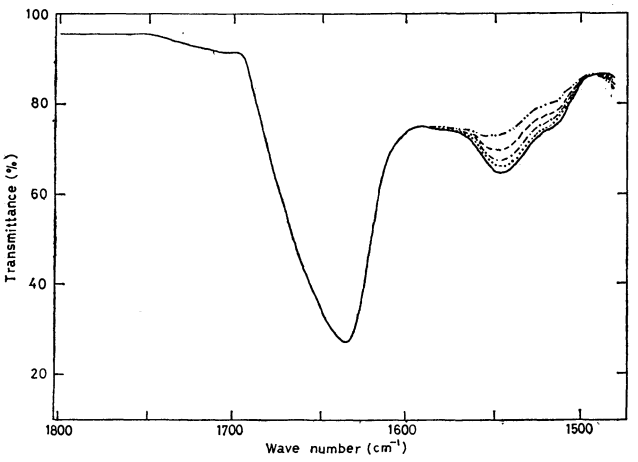

Fig. 1. Infrared absorption curves of bovine pancreatic α-chymotrypsin in D_2O solution of pH 3.5 at 35°C. —— 10 min, ····· 19 min, —·—·— 55 min, ——— 170 min, —···—··— 20 hr.

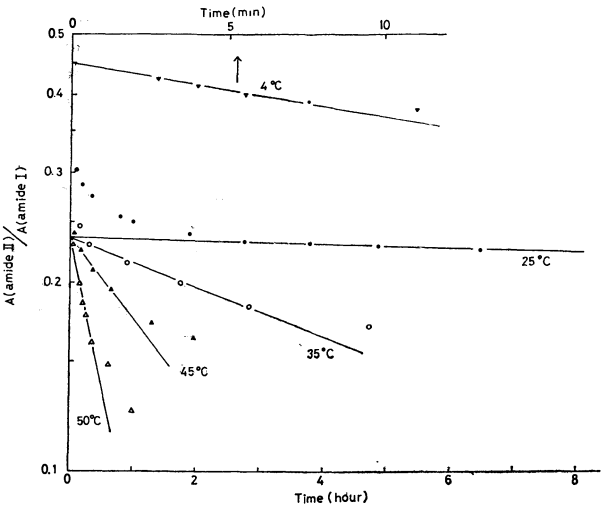

Fig. 2. Semilogarithmic plots of hydrogen → deuterium exchange reaction of bovine pancreatic α-chymotrypsin in D_2O solutions of pH 3.5 at various temperatures.

for one day or so. The semilogarithmic plot corresponding to the latter forms usually a straight line at least for first several hours or at least for first several points of measurement. Extend, then, this straight line till the ordinate axis and find the ordinate value for slowly exchanging peptide NH groups at time zero. Repeat similar kinetic measurements at different temperatures (from 10 °C to denaturation temperature, for example), at different pH's (from 4 to 8, for example), and/or with different concentrations of a denaturation agent (LiCl, for example, from 0

TABLE 1. DETERMINATION OF THE NUMBER OF PEPTIDE-PEPTIDE HYDROGEN-BONDS IN PROTEIN MOLECULES

Protein	Intensity ratio Amide II/Amide I at time zero		Ratio of NH···OC / total peptide NH's (a_i/a_t)	Total peptide NH's (N_t)	Peptide NH's involved in peptide-peptide hydrogen bonds	
	Total peptides (a_t)	Slowly exchanging peptides (a_i)			Hydrogen exchange experiment (N_i)	Found in X-ray analysis
Lysozyme	0.450	0.155[1,2]b)	34.4%	126[10]b)	44[1,2]	44[18]
Myoglobin	0.450	0.335[3]	74.4	148[11]	109[3]	108[9]
α-Chymotrypsin	0.450	0.235	52.2	229[12]	120	121[19]
Bovine pancreatic trypsin inhibitor	(0.450)a)	0.170	37.8	53[13]	20	20[20]
Concanavalin A	(0.450)a)	0.175	38.9	226[14]	88	(86)c)
α-Lactalbumin	0.450	0.130	28.9	120[15]	35	
Soy-bean trypsin inhibitor (Kunitz)	(0.450)a)	0.220	48.9	170[16]	83	
Streptomyces subtilisin inhibitor (17)	(0.450)a)	0.140	31.1	104[17]	33	

a) The a_t value was not determined for this protein. The value was assumed to be 0.450. b) The numbers in these parentheses indicate references. c) Counted on the basis of the description of Edelman *et al.* in the Ref. 14.

to 8 M). It is essential to confirm that the straight lines corresponding to the slowly exchanging hydrogen atoms converge into the same point on the ordinate axis (see Fig. 2). Record the ordinate value of this point as $[\text{A(amide II)/A(amide I)}]_i=a_i$ (given in the third column of Table 1). Next, the A(amide II)/A(amide I) value for the total peptide NH groups of this protein is to be determined. This is done by following very slow hydrogen→deuterium exchange reaction of the protein at pH=3 and/or at a low temperature (0~5 °C). Obtain the ordinate value at time zero by an extrapolation (see Fig. 2), and let it be $[\text{A(amide II)/A(amide I)}]_t=a_t$. For every protein so far examined, the a_t value has been found to be 0.450 (the second column of Table 1). From the result of amino acid analysis of the protein in question, find the total number N_t of peptide NH groups in the molecule. Then, $N_i=N_t(a_i/a_t)$ is considered to be equal to the number of peptide NH groups involved in peptide-peptide (NH···O=C) hydrogen bonds.

The method has been tested for five proteins, for which X-ray crystallographic analyses have been made. The results are shown in Table 1. As may be seen here the N_i values obtained by the proposed method are in accord with the numbers of peptide-peptide hydrogen bonds found by the X-ray analyses within ±1. The method has also been applied to bovine α-lactalbumine, soy-bean trypsin inhibitor (Kunitz), and Streptomyces subtilisin inhibitor. The N_i value found here (respectively 35, 83, and 33) are considered to be predicted numbers of peptide-peptide hydrogen bonds in these proteins.

The method involves an assumption that the contributions of various undeuterated peptide groups in the protein molecule to the A(amide II)/A(amide I) value are equal. This assumption is justified to some extent by our finding[21] that the intensity ratio now in question is practically independent of the helix content for poly-L-glutamic acid in an aqueous system. The assumption is all indirectly supported by our test for five proteins already mentioned.

It is well known that the position of the amide II band is slightly different for different polypeptide conformations (at 1535 cm^{-1} for the random conformation, at 1546 cm^{-1} for the α-helix, and at 1530 cm^{-1} for the β-structure). The amide I band also appears at different frequencies according to the conformations[22] (between 1650 and 1655 cm^{-1} for random, at 1650 cm^{-1} for the α-helix, and at 1630 cm^{-1} for the β structure; for a deuterated polypeptide each of three frequencies is lower than what is given here by about 10 cm^{-1}). In principle, therefore, integrated intensities of the I and II bands should always be measured at each time to determine the number of peptide groups remained undeuterated. Sometimes, this is certainly found to be necessary. Quite often, however, the band widths of both amide I and II do not appreciably all over the reaction time (see Fig. 1, for example). In such a case, a simple measurement of the peak intensities can give an accurate enough kinetic data.

One of the merits of this method is its simplicity. In addition, the reliability of this method is rather easily judged by examining how good is the convergence of the several straight lines corresponding to the kinetic measurements of the slowly exchanging peptide NH groups under several different conditions (in temperature, pH, and/or LiCl concentration).

The peptide NH groups involved in the peptide-sidechain hydrogen-bonds (instead of the peptide-peptide hydrogen bonds) seem to escape completely to be counted in the proposed method.[1,3] By a proper adjustment of the pH and temperature of the solution, however, the number of the peptide NH groups in this category may also be determined by a similar kinetic method.[3] Sometimes, a further classification of the peptide-peptide hydrogen bonds may also be made by a kinetic study by means of an infrared absorption measurement similar to what is described above.

We thank Dr. A. Ikegami for discussions.

Reference

1) M. Nakanishi, M. Tsuboi, and A. Ikegami, *J. Mol. Biol.*, **70**, 351 (1972).
2) M. Nakanishi, M. Tsuboi, and A. Ikegami, *ibid.*, **75**, 673 (1973).
3) M. Nakanishi, M. Tsuboi, and A. Ikegami, This Bulletin, to be published.
4) K. Linderstrøm-Lang, *Chem. Soc. Spec. Publ.*, **2**, 1 (1955).
5) E. R. Blout, C. de Loze, and A. Asadourian, *J. Amer. Chem. Soc.*, **83**, 1895 (1961).
6) A. Hvidt and S. O. Nielsen, *Advanc. Protein Chem.*, **21**, 287 (1966).
7) S. W. Englander, N. W. Downer, and H. Teitelbaum, *Ann. Rev. Biochem.*, **41**, 903 (1972).
8) S. W. Englander and R. Staley, *J. Mol. Biol.*, **45**, 277 (1969).
9) J. C. Kendrew, R. E. Dickerson, B. E. Strandberg, R. G. Hart, D. R. Davies, D. C. Phillips, and V. C. Shore, *Nature*, **185**, 422 (1960); H. C. Watson, "Progress in Stereochemistry," M. M. Harris and B. J. Aylett, Ed. Butterwood, London (1969), Vol. 4, pp. 299—333.
10) R. E. Canfield, *J. Biol. Chem.*, **238**, 2698 (1963).
11) A. B. Edmundson, *Nature*, **205**, 883 (1965).
12) B. S. Hartley, *ibid.*, **201**, 1284 (1964).
13) B. Kassell and M. Laskowski, *Biochem. Biophys. Res. Commun.*, **20**, 463 (1965).
14) G. M. Edelmann, B. A. Cunningham, G. N. Reeke, J. W. Becker, M. J. Waxdal, and J. L. Wang, *Proc. Nat. Acad. Sci. U.S.*, **69**, 2580 (1972).
15) K. Brew, T. C. Vanaman, and R. L. Hill, *J. Biol. Chem.*, **242**, 3747 (1967).
16) T. Koide and T. Ikenaka, *Eur. J. Biochem.*, **34**, 417 (1973).
17) S. Murao and S. Sato, *Agr. Biol. Chem.*, **36**, 160 (1972); T. Ikenaka, personal communication.
18) C. C. F. Blake, D. F. Koenig, G. A. Mair, A. C. T. North, D. C. Phillips, and V. R. Sarma, *Nature*, **206**, 757 (1965); D. C. Phillips, *Scientific American*, **215**, 78 (1966).
19) J. J. Birktoft and D. M. Blow, *J. Mol. Biol.*, **68**, 187 (1972).
20) R. Huber, D. Kukla, A. Rühlmann, and W. Steigemann, *Cold Spr. Har. Symp. Quant. Biol.*, **36**, 141 (1971).
21) M. Nakanishi, M. Tsuboi. A. Ikegami, and M. Kanehisa, *J. Mol. Biol.*, **64**, 363 (1972).
22) T. Miyazawa and E. R. Blout, *J. Amer. Chem. Soc.*, **83**, 712 (1961).

The Kinetics and Mechanisms of the Reactions of Nitric and Nitrous Acids with Hexaaquochromium(II) Ions

Hiroshi OGINO, Keiichi TSUKAHARA, and Nobuyuki TANAKA

Department of Chemistry, Faculty of Science, Tohoku University, Aoba, Aramaki, Sendai 980

(Received August 23, 1973)

Stoichiometric and kinetic investigations of reactions of the nitric and nitrous acids with hexaaquochromium(II) ions have been carried out in acidic media. The stoichiometries of these reactions found in this work were consistent with the mechanisms proposed by Swaddle,[1] in which one mole of nitric acid reacts with four moles of chromium(II) and one mole of nitrous acid reacts with two moles of chromium(II). For the former reaction, it was found that the two-electron reduction of nitric acid by chromium(II) is rate-determining and that the rate constant was 2.2×10^{2} M^{-1} s^{-1} at 25 °C and at an ionic strength of 1.0 ($NaClO_4$). For the latter reaction, it was found that the one-electron reduction of nitrous acid by chromium(II) is rate-determining and that the rate constant was 4.5×10^{3} M^{-1} s^{-1} at 25 °C and at an ionic strength of 1.0 ($NaClO_4$). The rates of the reactions of chromium (II) with anionic species of the parent acids, NO_3^- and NO_2^-, were too slow to be detected under the present experimental conditions.

Ardon and Herman[2] demonstrated that the reaction products of nitrate with hexaaquochromium(II), Cr^{2+}, in acidic media were $Cr(NO)(H_2O)_5^{2+}$, $Cr(H_2O)_6^{3+}$ and $(H_2O)_4Cr(OH)_2Cr(H_2O)_4^{4+}$ and succeeded in isolating a nitrosyl complex, $[Cr(NO)(H_2O)_5]SO_4$. Swaddle[1] suggested, on the basis of the product ratios, that the reduction of the nitrate ion by Cr^{2+} in an acidic solution proceeds through the following reaction paths:

$$Cr^{2+} + NO_3^- + 2H^+ \longrightarrow Cr(IV) + NO_2^- + H_2O \quad (1)$$

$$Cr(IV) + Cr^{2+} \xrightarrow{H_2O} (H_2O)_4Cr(OH)_2Cr(H_2O)_4^{4+} \quad (2)$$

$$Cr^{2+} + NO_2^- + 2H^+ \xrightarrow{H_2O} Cr(H_2O)_6^{3+} + NO + H_2O \quad (3)$$

$$Cr^{2+} + NO \xrightarrow{H_2O} Cr(NO)(H_2O)_5^{2+} \quad (4)$$

Mori *et al.*[3] prepared several salts of $[Cr(NO)(NH_3)_5]^{2+}$ by the reaction of chromium(II) in an ammoniacal solution with sodium nitrite or nitrate. The chloride salt was prepared also by Griffith by the reaction of chromium(II) with NO in liquid ammonia.[4] In early works[2,3] on nitrosyl chromium complexes, the formulation Cr(III)–(NO^-) has been used. Later it was reported,[4,5] however, that the formulation Cr(I)–(NO^+) was more feasible.

In order to ascertain the kinetic and mechanistic details of these interesting reactions, the reactions of nitrate and nitrite with chromium(II) in acidic media have been dealt with in this study.

Experimental

Reagents. All the solutions were prepared with redistilled water. The acidic solution of hexaaquochromium(III) perchlorate was prepared by the reduction of sodium dichromate in perchloric acid with hydrogen peroxide. The chromium(II) perchlorate solutions were prepared by the reduction of hexaaquochromium(III) perchlorate with a zinc amalgam under an atmosphere of nitrogen. The chromium(II) solutions thus obtained contained known amounts of sodium perchlorate and perchloric acid. The concentration of the hydrogen ion was determined by the method reported in the literature.[6,7] A sodium perchlorate solution was prepared by the neutralization of sodium bicarbonate of a primary standard reagent grade with perchloric acid. All the other chemicals were of an analytical reagent grade and were used without further purification.

Kinetic Measurements and Apparatus. For the reaction of nitrate with Cr^{2+}, kinetic measurements were carried out by a conventional method similar to that reported previously.[8] The change in the absorbance with the time was followed at 422 nm with a Hitachi EPS-3 pen-recording spectrophotometer. Solutions containing $NaNO_3$, $NaClO_4$ and $HClO_4$ were added to the optical cell, which was then sealed with a serum cap. After the solution had been purged with nitrogen gas, chromium(II) was added with a syringe.

As the rate of the reaction of HNO_2 with Cr^{2+} was too fast to be measured by a conventional method, the stopped-flow method was employed by the use of a Hitachi EPS-2 rapid-scanning spectrophotometer which was equipped with two syringes as reactant containers. One of the syringes was filled with a deoxygenated $NaNO_2$ solution, and the other, with a solution containing Cr^{2+}, $NaClO_4$ and $HClO_4$. The change in the transmittance at 443 nm was recorded on a storage-type oscilloscope (Hitachi V-018 Memoriscope) as a function of time after the mixing of the two reactant solutions.

In the kinetic measurements, the temperature was controlled at 25 °C and the ionic strength was adjusted to 1.0 with sodium perchlorate.

Product Analyses. The chromium species in the reaction products were separated by SP-Sephadex C-25 (Pharmacia, Sweden) column chromatography. The column used was 2.5 cm^2 in cross-section and 4 cm in height. The separation of the products with the Sephadex column was much more convenient than that with Dowex 50W used by previous workers.[1,2]

After the completion of the reaction between nitrate and Cr^{2+}, the reaction mixture was passed through the column. When the initial concentration of Cr^{2+} was smaller than that of nitrate, the chromium species were adsorbed in three bands···brown at the bottom, bluish-violet in the middle, and green at the top. The brown-colored species was eluted with a 0.1 M $HClO_4$–0.1 M $NaClO_4$ solution and was identified as $Cr(NO)(H_2O)_5^{2+}$ ($CrNO^{2+}$) spectrophotometrically. The bluish-violet species was eluted with a 0.1 M $HClO_4$–0.5 M $NaClO_4$ solution and was identified as $Cr(H_2O)_6^{3+}$ (Cr^{3+}). The green species was eluted with a 0.1 M $HClO_4$–0.9 M $NaClO_4$ solution and was identified as $(H_2O)_4Cr(OH)_2$–$Cr(H_2O)_4^{4+}$ ($Cr(OH)_2Cr^{4+}$). When the initial concentration of Cr^{2+} exceeded that of nitrate, the column gave four bands···of brown, bluish-violet and two kinds of green··· from the bottom to the top of the column. The lower three

products were identified as $CrNO^{2+}$, Cr^{3+}, and $Cr(OH)_2Cr^{4+}$ respectively. The uppermost green species was considered to be produced by the reaction between $CrNO^{2+}$ and Cr^{2+}. Sephadex column chromatography revealed that this green species moves slightly slower than $Cr(OH)_2Cr^{4+}$. This species has not been identified, but the spectrum shows absorption maxima at 584 nm and 422 nm which are very close to those of $Cr(OH)_2Cr^{4+}$.[9]

In the nitrous acid system, the chromium species produced during the reaction were adsorbed on the Sephadex column in two bands···an upper bluish-violet band and a lower brown band, unless the initial concentration of nitrous acid was smaller than that of Cr^{2+}. The brown species was eluted with a 0.1 M $HClO_4$–0.1 M $NaClO_4$ solution and was identified as $CrNO^{2+}$. The bluish-violet species was eluted with a 0.1 M $HClO_4$–0.5 M $NaClO_4$ solution and was identified as Cr^{3+}. Under these experimental conditions the formation of $Cr(OH)_2Cr^{4+}$ was not observed. The chromium content in each effluent was determined spectrophotometrically as CrO_4^{2-} after oxidation with alkaline peroxide.

Results

Reaction of $CrNO^{2+}$ with Cr^{2+}. Stoichiometric and kinetic studies of this reaction were reported by Armor and Buchbinder very recently.[10] According to their results, the stoichiometry is:

$$4Cr^{2+} + 2CrNO^{2+} + 6H_2O + 2H^+ \longrightarrow 3Cr(OH)_2Cr^{4+} + 2NH_3OH^+ \quad (5)$$

The present authors have also investigated the reaction between $CrNO^{2+}$ and Cr^{2+} and found that the rates of the reaction were in agreement with those reported by Armor and Buchbinder. However, a green species which is different from $Cr(OH)_2Cr^{4+}$ and which can not be expected from the stoichiometry of Eq. (5) was found in this work. From the chromatographic behavior described in the Experimental section, the positive charge of this species seems not to be smaller than 4. Further extensive work has not been made of this system, however.

Reaction of Nitrate with Cr^{2+}. The results of the product analyses are summarized in Table 1. If the initial concentration of nitrate is higher than that of Cr^{2+}, nitrate is found to react with four equivalents of Cr^{2+} to produce $CrNO^{2+}$, Cr^{3+}, and $Cr(OH)_2Cr^{4+}$ in the ratio of 1 : 1 : 1. The overall reaction of nitrate with Cr^{2+} is expressed by Eq. (6), which is the same as that reported by Swaddle:[1]

$$NO_3^- + 4Cr^{2+} + 2H^+ \longrightarrow CrNO^{2+} + Cr^{3+} + Cr(OH)_2Cr^{4+} \quad (6)$$

When the initial concentration of nitrate is smaller than that of Cr^{2+}, the yield of $CrNO^{2+}$ is much lower than those of Cr^{3+} and $Cr(OH)_2Cr^{4+}$, as is shown in Table 1. This can be understood in view of the fact that there is a slow reaction between the $CrNO^{2+}$ produced by Reaction (6) and the Cr^{2+} remaining in excess.

The kinetics for the reaction of nitrate with Cr^{2+} were studied under second-order conditions. If it is assumed that the rate equation (7) is valid for this system:

$$\text{Rate} = k[NO_3^-][Cr^{2+}] \quad (7)$$

Eq. (8) is then derived:

$$\log \frac{4\varepsilon_{app}[NO_3^-]_0 - D_t}{D_\infty - D_t} = \frac{4[NO_3^-]_0 - [Cr^{2+}]_0}{4\times 2.303} kt + \log \frac{4[NO_3^-]_0}{[Cr^{2+}]_0} \quad (8)$$

where $[NO_3^-]_0$ and $[Cr^{2+}]_0$ indicate the initial concentrations of nitrate and Cr^{2+} respectively. D_t is the absorbance measured at time t, and D_∞ is the final absorbance. The symbol, ε_{app}, is the apparent extinction coefficient of the products at 422 nm, which was determined from the absorbance after the completion of the reaction. The plots of the left-hand side of Eq. (8) *vs.* t gave a good linear relation for three half-lives. The second-order rate constant, k, was determined from the slope of this straight line. The kinetic results under the experimental condition of nitrate in excess of Cr^{2+} are given in Table 2. The rate constants were independent of the initial concentrations of both nitrate and Cr^{2+} at a given hydrogen-ion concentration. Therefore, the reaction is strictly second-order. Under the condition of Cr^{2+} in excess of nitrate, the second-order rate constants are very different from the values given Table 2. This can be attributed to the fact that the $CrNO^{2+}$ produced reacts further with the Cr^{2+} remaining in the solution. The observed second-order rate constants were considerably dependent on the hydrogen-ion concentrations, as is shown in Table 2. This dependency can be explained by considering the following mechanism:

$$HNO_3 \overset{K_a}{\rightleftharpoons} H^+ + NO_3^- \quad (9)$$

Table 1. Products of the reaction of HNO_3 with Cr^{2+} [a]

Initial concentrations of reactants		Products					
					Ratios		
$[Cr^{2+}]_0$/mM	$[NO_3^-]_0$/mM	$[CrNO^{2+}]$/mM	$[Cr^{3+}]$/mM	$[Cr_2(OH)_2^{4+}]$/mM	$[CrNO^{2+}]$	$[Cr^{3+}]$	$[Cr_2(OH)_2^{4+}]$
15.7	4.00	1.98	3.71	5.32	0.53	1.00	1.43[b]
15.7	16.0	3.50	4.52	4.20	0.77	1.00	0.93
15.7	32.0	3.53	4.22	4.10	0.84	1.00	0.97
15.7	50.0	3.93	4.42	4.25	0.89	1.00	0.96

a) The experiments were made under the following conditions: $[H^+]=0.207$ M, at 25 °C and at an ionic strength of 1.0 ($NaClO_4$). b) In this case, two green species (see Experimental) were observed and were collected together.

Table 2. Rate constants of the reaction between HNO_3 and Cr^{2+} at 25 °C and at an ionic strength of 1.0

$[Cr^{2+}]_0$/mM	$[NO_3^-]_0$/mM	$[H^+]$/M	k/($M^{-1}\,s^{-1}$)
5.03	32.0	0.204	2.73
7.86	32.0	0.199	2.71
10.1	32.0	0.197	2.61
15.7	16.0	0.207	2.61
15.7	18.0	0.207	2.70
15.7	20.0	0.207	2.71
15.7	22.0	0.207	2.96
15.7	24.0	0.207	2.77
15.7	26.0	0.207	2.71
15.7	28.0	0.207	2.85
15.7	30.0	0.207	2.84
15.7	32.0	0.207	2.71
15.7	20.0	0.110	1.66
15.7	20.0	0.301	4.06
15.7	20.0	0.395	5.49
15.7	20.0	0.512	7.05
15.7	20.0	0.599	8.65

$$NO_3^- + Cr^{2+} \xrightarrow{k_1} \text{products} \quad (10)$$

$$HNO_3 + Cr^{2+} \xrightarrow{k_2} \text{products} \quad (11)$$

On the basis of this mechanism, the following rate law was derived:

$$\text{Rate} = \frac{k_1 + k_2 K_a^{-1}[H^+]}{1 + K_a^{-1}[H^+]}[NO_3^-]_T[Cr^{2+}] \quad (12)$$

where

$$[NO_3^-]_T = [NO_3^-] + [HNO_3]$$

$$K_a = \frac{[H^+][NO_3^-]}{[HNO_3]}$$

Many values for the dissociation constant, K_a, of nitric acid have been reported.[11,12] They are in good agreement with each other, almost all of the values ranging from 15 to 34 M at 25 °C and at an ionic strength of zero. Of them, the value of 15.4 which was revised by Davis and de Bruin[13] was used for the analysis of the rate constants without any correction of the ionic strength. The plots of $k(1+K_a^{-1}[H^+])$ *vs.* $[H^+]$ show a linear relation, which is given in Fig. 1. The value of the intercept is practically zero. This means that the contribution of Reaction (10) is negligible and that the whole reaction proceeds almost entirely through the path represented by Eq. (11). The rate constant, k_2, is $2.2\times10^2\ M^{-1}\,s^{-1}$, and the value of k_1 is less than $0.2\ M^{-1}\,s^{-1}$.

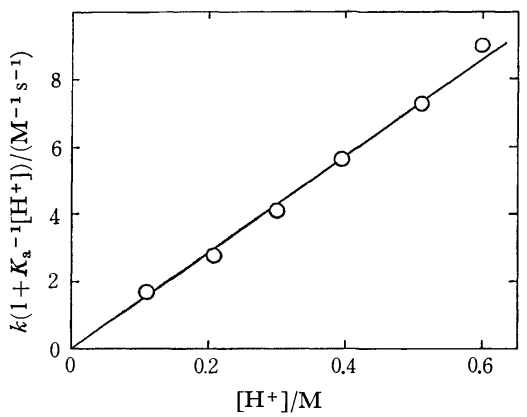

Fig. 1. The plots of $k(1+K_a^{-1}[H^+])$ *vs.* $[H^+]$ at 25 °C. and at an ionic strength of 1.0.

Reaction of Nitrous Acid with Cr^{2+}. Nitrous acid was found to react with two equivalents of Cr^{2+} to produce $CrNO^{2+}$ and Cr^{3+} in the ratio of 1 : 1 under the condition of a higher concentration of nitrous acid than of Cr^{2+}. Therefore, the overall reaction of nitrous acid with Cr^{2+} is as follows:

$$HNO_2 + 2Cr^{2+} + H^+ \longrightarrow CrNO^{2+} + Cr^{3+} + H_2O \quad (13)$$

In order to avoid the interference of the reaction between $CrNO^{2+}$ and Cr^{2+}, the kinetics of the reaction of nitrous acid with Cr^{2+} were studied under the condition that the concentration of nitrous acid exceeded that of Cr^{2+}. When the second-order rate equation:

$$\text{Rate} = k[HNO_2][Cr^{2+}] \quad (14)$$

holds in this case, Eq. (15) is derived:

$$\log\frac{2\varepsilon_{app}[HNO_2]_0 - D_t}{D_\infty - D_t} = \frac{2[HNO_2]_0 - [Cr^{2+}]_0}{2\times2.303}kt + \log\frac{2[HNO_2]_0}{[Cr^{2+}]_0} \quad (15)$$

where $[HNO_2]_0$ and $[Cr^{2+}]_0$ are the initial concentrations of HNO_2 and Cr^{2+} respectively. The symbol, ε_{app} is the apparent extinction coefficient of the products at 443 nm. The plots of the left-hand side of Eq. (15) *vs.* t gave a good linear relation for three half-lives. The second-order rate constant, k, was obtained from the slopes of the plots. The results are given in Table 3. The rate was independent of the hydrogen-ion concentration. The pK_a value of nitrous acid has been reported to be 2.8.[11,12] HNO_2 is the predominant species under the present experimental conditions where the hydrogen-ion concentrations were varied from 0.10 to 0.65 M. Therefore, the mechanism of the reaction can be expressed as:

$$HNO_2 + Cr^{2+} \xrightarrow{k} Cr^{3+} + NO + OH^- \quad (16)$$

$$Cr^{2+} + NO \xrightarrow{\text{fast}} CrNO^{2+} \quad (17)$$

The second-order rate constant, k, was determined to be $(4.5\pm0.3)\times10^3\ M^{-1}\,s^{-1}$. The analysis of the data given in Table 3 revealed that the rate constant of NO_2^- with Cr^{2+} was less than $5\times10^4\ M^{-1}\,s^{-1}$.

Table 3. Rate constants of the reaction between HNO_2 and Cr^{2+} at 25 °C and at an ionic strength of 1.0

$[Cr^{2+}]_0$/mM	$[HNO_2]_0$/mM	$[H^+]$/M	k/($10^3\ M^{-1}\,s^{-1}$)
4.4	6.0	0.10	4.1
4.4	6.0	0.30	4.7
4.3	6.0	0.50	4.9
5.8	6.0	0.65	4.4

Discussion

It is known that the reactions of Cr^{2+} with Tl(III) and O_2 produce $Cr(OH)_2Cr^{4+}$.[9] In the Tl(III) system, the following mechanism has been proposed:

$$Cr^{2+} + Tl(III) \longrightarrow Cr(IV) + Tl(I)$$

$$Cr(IV) + Cr^{2+} \longrightarrow Cr(OH)_2Cr^{4+}$$

A kinetic study of the reaction of molecular oxygen with Cr^{2+} showed that the reaction rate is of the second-order in Cr^{2+} and of the first-order in O_2.[14] From these results, the formation of a μ-peroxo dimer was suggested. In the reaction of HNO_3 with Cr^{2+}, however, the reaction rate is of the first-order in both reactants. Product analysis revealed that $CrNO^{2+}$, Cr^{3+}, and $Cr(OH)_2Cr^{4+}$ were produced in the ratio of 1 : 1 : 1. In the reaction of HNO_2 with Cr^{2+}, only $CrNO^{2+}$ and Cr^{3+} were produced, in the ratio of 1 : 1. Therefore, it is considered that $Cr(OH)_2Cr^{4+}$ is produced in the first step of the reaction between HNO_3 and Cr^{2+}. The experimental results lead to the conclusion that the mechanism expressed by Eqs. (1) to (4) is effective in the reaction between HNO_3 and Cr^{2+} when the contribution of the reaction between $CrNO^{2+}$ and Cr^{2+} is negligibly small.

Table 4 summarizes the rate constants obtained or estimated in this work. It is interesting to note that Cr^{2+} reacts with HNO_3 but not the NO_3^- ion, which is the predominant species under the present experimental conditions. Swaddle reported that $[Co(NO_3)(NH_3)_5]^{2+}$ was reduced by Cr^{2+}.[1] Thirty-three percent of the reaction proceeds through the reduction of the central cobalt(III) ion to the cobalt(II) ion, while the remaining sixty-seven percent of the reaction proceeds through the reduction of the coordinated nitrato ligand instead of the central cobalt(III) ion. Therefore, when the NO_3^- ion is bound to the proton or is coordinated to the pentaamminecobalt(III) ion, which is a Lewis acid, the reduction of nitrate by Cr^{2+} is accelerated.

Table 4. Rate constants of the reactions of Cr^{2+} with some reactants obtained in this work at 25 °C and at an ionic strength of 1.0 ($NaClO_4$)

Reactant	Rate constant/(M^{-1} s^{-1})
HNO_3	2.2×10^2
NO_3^-	<0.2
HNO_2	$(4.5\pm0.3)\times10^3$
NO_2^-	$<5\times10^4$
NO	$>4.5\times10^3$

It was found in this work that the rates of the reactions of Cr^{2+} with HNO_3, HNO_2, and NO are in the following order: $HNO_3<HNO_2<NO$.

The authors wish to thank Professor Kahei Takase in this department for allowing us to use a rapid-scanning spectrophotometer. They also wish to thank the Ministry of Education for the financial support granted for this research.

References

1) T. W. Swaddle, *J. Amer. Chem. Soc.*, **89**, 4338 (1967).
2) M. Ardon and J. I. Herman, *J. Chem. Soc.*, **1962**, 507.
3) M. Mori, S. Ueshiba, and S. Kawaguchi, This Bulletin, **36**, 796 (1963).
4) W. P. Griffith, *J. Chem. Soc.*, **1963**, 3286.
5) I. Bernal, S. D. Robinson, L. S. Meriwether, and G. Wilkinson, *Chem. Commun.*, **1965**, 571.
6) E. L. King and J. A. Neptune, *J. Amer. Chem. Soc.*, **77**, 3186 (1955).
7) K. D. Kopple and R. R. Miller, *Inorg. Chem.*, **2**, 1204 (1963).
8) H. Ogino and N. Tanaka, This Bulletin, **41**, 1622 (1968).
9) M. Ardon and R. A. Plane, *J. Amer. Chem. Soc.*, **81**, 3197 (1959).
10) J. N. Armor and M. Buchbinder, *Inorg. Chem.*, **12**, 1086 (1973).
11) A. E. Martell and L. G. Sillén, "Stability Constants," The Chemical Society, London (1964).
12) A. E. Martell and L. G. Sillén, "Stability Constants, Supplement No. 1," The Chemical Society, London (1971).
13) W. Davis, Jr. and H. J. de Bruin, *J. Inorg. Nucl. Chem.*, **26**, 1069 (1964).
14) R. W. Kolaczkowski and R. A. Plane, *Inorg. Chem.*, **3**, 322 (1964).

Factors Affecting the Line-width of Nitrogen Superhyperfine Structure in the ESR Spectra of Copper(II) Complexes

Yasuomi NONAKA, Tadashi TOKII* and Sigeo KIDA

Department of Chemistry, Faculty of Science, Kyushu University, Hakozaki, Higashi-ku, Fukuoka 812
**Department of Chemistry, Saga University, Saga 840*

(Received August, 13, 1973)

ESR spectra were measured for several series of copper(II) complexes in an attempt to find the best-observable condition for ^{14}N-superhyperfine structure. It was demonstrated that in addition to the temperature and the dilution factors the line-width of ^{14}N-superhyperfine structure is broadened out by the following factors; 1) deviation from square planar configuration around a copper ion, *i. e.*, deformation to elongated octahedron or square pyramid due to weak bonding along the tetragonal axis and/or distortion of coplanality of the coordination bond effected by some steric condition, and 2) the presence of protons that can couple with an unpaired electron and ^{14}N-nuclei.

Although variable informations of coordination bonds are obtainable from an observation of ^{14}N-superhyperfine structure (=^{14}N-shfs) in ESR spectra of copper(II) complexes, there are known rather few examples which give ESR spectra with well-resolved ^{14}N-shfs useful for the discussion of nature of coordination bond. In this study, therefore, it was attempted to investigate under what condition ^{14}N-shfs is observed with a good resolution.

It has been known that broadening of ESR line-width is effected mainly by 1) spin-lattice interaction and 2) spin-spin interaction.[1] Since the spin-orbit coupling plays an essential role at the mechanism, 1), the spin-lattice relaxation time depends very markedly on the energy separation between the ground state and the first excited state capable of coupling with the ground state *via* spin-orbit interaction.[2] Among the various symmetries of copper(II) complexes, the separation between the ground and the first excited states is largest for a square planar complex. Accordingly, deformation of square planar structure to eleongated octahedron, square pyramid or flattered tetrahedron should cause broadening of ESR line-width.

For the mechanism, 2), there are two kinds of spin-spin interactions, that is, intermolecular interaction between paramagnetic ions and interaction between an unpaired electron and nuclear spins. The effect due to the former interaction can be reduced by diluting a sample in diamagnetic host lattice or solvent. The latter interaction sometimes gives a hyperfine or superhyperfine structure with many sharp lines, but when there are so many nuclear spins to interact with an electron spin and line-width are not narrow enough to separate each line, the lines are superposed on each other, making the line-width of the original spectrum broader. Therefore, the effect of ligand protons may play an important role for the resolution of ^{14}N-shfs of copper(II) complexes.

Among the various factors on which ESR line-width is dependent, the two effects, *i. e.*, the effect of deviation from square planar configuration around copper ion and the effect of protons in the ligand capable of coupling with an electron spin, are mainly investigated in the present study.

Experimental

Bis(*N*-alkylsalicylaldiminato)copper(II),[3] bis(*N*,*N*-dialkylglycinato)copper(II),[4] sodium bis(*N*,*N'*-dialkyloxamidato)-cuprate(II),[5] *N*,*N'*-bis(2-aminoethyl)malonamidatocopper-(II),[6] bis(2-hydroxyacetophenone)ethylenediiminatocopper-(II)[7] and bis(salicylaldehyde)ethylenediiminatocopper(II)[7] were prepared according to the methods described in the literatures.

The ESR spectra were measured with a JEOL ESR-apparatus model JES-ME-3X at 130 K and at room temperature using the X-band, DPPH being used as a standard marker.

Absorption and reflectance spectra in the visible region were measured with Hitachi EPS-2 and EPS-3T spectrophotometers, respectively.

Abbreviations of the compounds are tabulated in Table 1.

TABLE 1. THE COMPOUNDS AND THE ABBREVIATIONS

Compound	Abbreviation
Bis(*N*-methylsalicylaldiminato)copper(II)	Cu $msaln_2$
Bis(*N*-ethylsalicylaldiminato)copper(II)	Cu $esaln_2$
Bis(*N*-iso-propylsalicylaldiminato)copper(II)	Cu $psaln_2$
Bis(*N*-tert-butylsalicylaldiminato)copper(II)	Cu $bsaln_2$
Bis(glycinato)copper(II)	Cu gly_2
Bis(*N*,*N*-dimethylglycinato)copper(II)	Cu $dmgly_2$
Bis(*N*,*N*-diethylglycinato)copper(II)	Cu $degly_2$
Bis(*N*,*N*-di-*n*-propylglycinato)copper(II)	Cu $dpgly_2$
N,*N'*-Bis(2-aminoethyl)malonamidato-copper(II)	Cu malen
Sodium bis(oxamidato)cuprate(II)	Cu oxd_2
Sodium bis(*N*,*N'*-dimethyloxamidato)-cuprate(II)	Cu $dmoxd_2$
Sodium bis(*N*,*N'*-diethyloxamidato)cuprate(II)	Cu $deoxd_2$
Bis(2-hydroxyacetophenone)ethylene-diiminatocopper(II)	Cu oapen
Bis(salicylaldehyde)ethylenediiminato-copper(II)	Cu salen

Results and Discussion

Spin-Hamiltonian parameters were obtained from the observed spectra according to the methods of Kneubühl[8] and Sands[9] and are listed in Table 2.

TABLE 2. ESR PARAMETERS AND PEAKS OF ELECTRONIC SPECTRA

Compound	Solvent	g_0	$g_\parallel$	$g_\perp$	A_0	$A_\parallel$	$A_\perp$	A_0^N	$1/2(A_\parallel^N+A_\perp^N)$	$A_\perp^N$	ν_{max} (mμ)
					($\times 10^4$ cm^{-1})						
Cu msaln$_2$	TCE[1]	2.110	2.225	2.053	71.8	171.6	21.9	—	—	—	—
Cu esaln$_2$	TCE	2.113	2.220	2.060	70.3	161.1	24.9	—	—	—	—
Cu psaln$_2$	TCE	2.121	2.229	2.067	62.8	164.9	11.8	—	—	—	—
Cu bsaln$_2$	TCE	—	2.273	—	—	119.3	—	—	—	—	—
Cu gly$_2$	W+E[2]	2.120	2.232	2.065	61.2	152.1	15.8	—	—	—	630
Cu dmgly$_2$	W+E	2.117	2.217	2.067	63.1	157.7	15.8	10.4	—	—	598
Cu degly$_2$	W+E	2.113	2.220	2.060	70.5	161.3	25.0	9.3	—	—	590
Cu dpgly$_2$	W+E	2.111	2.219	2.057	74.2	163.2	29.7	7.4	—	—	583
Cu malen	D_2O	2.090	—	—	83.1	—	—	—	—	11.5	—
	M[3]	2.086	—	—	84.9	—	—	—	—	—	—
Cu oxd$_2$	Ni[4]	—	2.168	—	—	189.1	—	13.0	—	—	520[5]
Cu dmoxd$_2$	Ni	—	2.202	—	—	166.9	—	11.9	—	—	560[5]
Cu deoxd$_2$	Ni	—	2.201	—	—	148.4	—	—	—	—	605[5]
Cu oapen	TCE	2.097	2.198	2.047	85.0	188.1	33.5	13.1	10.9	11.9	555
Cu salen	TCE	2.092	2.173	2.052	82.6	182.5	34.7	—	—	—	570

1) 1,1,2,2-tetrachloroethane, 2) water+ethanol (1 : 1), 3) methanol, 4) corresponding nickel(II) complex, 5) reflectance spectrum

The spectra of a series of bis(*N*-alkylsalicylaldiminato)copper(II), (where, alkyl=methyl, ethyl, *i*-propyl, and *t*-butyl) are shown in Fig. 1. For the methyl homologue ^{14}N-shfs was observed in a perpendicular component of the spectra, though the resolution was rather poor. With the increase of bulkiness of the alkyl group ^{14}N-shfs becomes unresolved as seen in Fig. 1. This is compatible with the trend[10] that the increase of the size of a substituent on the imine nitrogen sterically effects a distortion of the planar configuration around the copper ion. On the contrary to the above results, as shown in Fig. 2, the resolution of ^{14}N-shfs becomes better with the increase of bulkiness of alkyl group for the series of bis(*N*,*N*-dialkylglycinato)copper(II), (where, alkyl=H, methyl, ethyl, and *n*-propyl). Since in these compounds the alkyl groups block the axial coordination sphere from the attack of solvent molecules, the increase of the size of alkyl group reduces the axial perturbation, effecting a good resolution of the ESR line-width. As shown in Table 2, frequency of visible absorption band increases with the increasing order of bulkiness of alkyl groups *i.e.*, H<CH_3<C_2H_5<*n*-C_3H_7. This fact is supporting the above discussion, since it is well known that d-d band of a copper complex shifts to higher frequency with the change from elongated octahedron to square planar configuration.

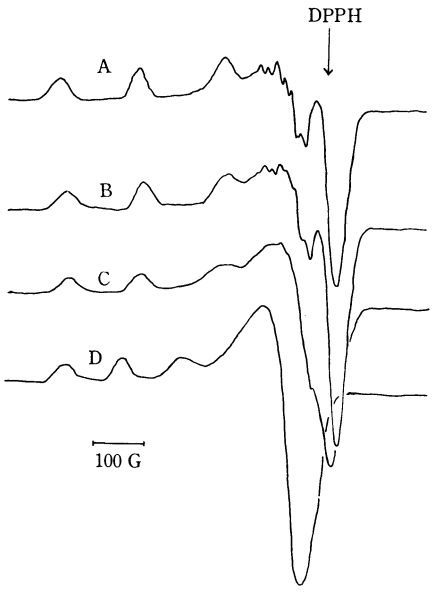

Fig. 1. ESR spectra of bis(*N*-alkylsalicylaldiminato)-copper(II) in 1,1,2,2-tetrachloroethane at room temperature
A: methyl, B: ethyl, C: *i*-propyl, D: *t*-butyl

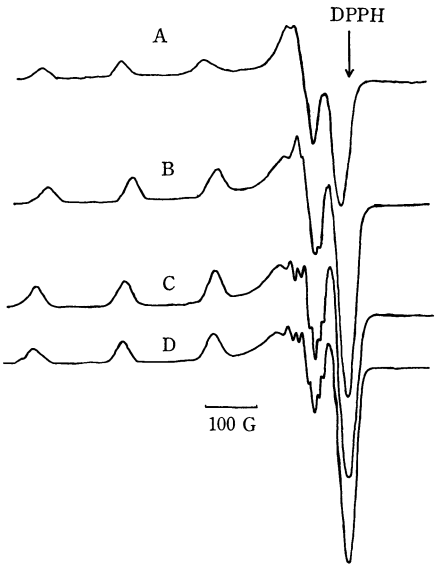

Fig. 2. ESR spectra of bis(*N*,*N*-dialkylglycinato)-copper(II) in water-ethanol (1 : 1) at 133 K
A: H, B: methyl, C: ethyl, D: *n*-propyl

In the series of bis(*N*,*N'*-dialkyloxamidato)copper(II) complexes, frequency of visible band of powder reflectance spectrum decreases with the increase of bulkiness of alkyl group, *i.e.*, $H > CH_3 > C_2H_5$, (*cf.* Table 2), quite reverse to the bis(*N*,*N*-dialkylglycinato)copper(II) series. This fact implies that in this case the alkyl groups function as to twist the planar configuration around the copper ion by steric hindrance.

Accordingly, one might expect that the resolution of ^{14}N-shfs becomes poor with the increase of the size of the substituent. This is true for the methyl and the ethyl derivatives, as obviously seen in Fig. 3. However, the oxamidato complex shows much poorer

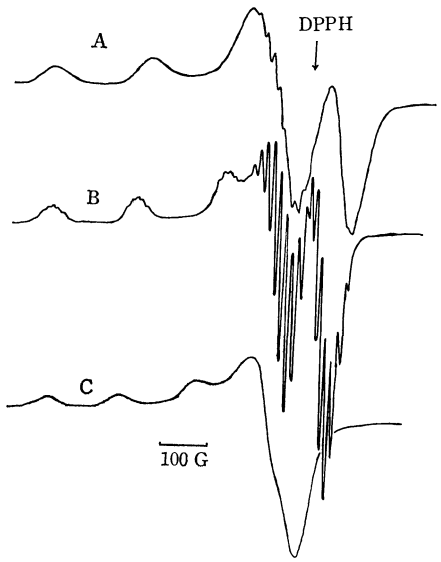

Fig. 3. ESR spectra of sodium bis(*N*,*N'*-dialkyloxamidato)cuprate(II) doped in the corresponding nickel(II) complexes at 130 K
A: H, B: methyl, C: ethyl

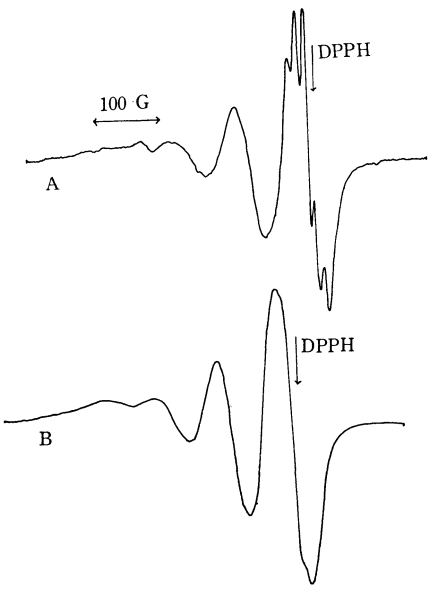

Fig. 4. ESR spectra of bis(salicylaldehyde)ethylenediiminatocopper(II) (B) and its methyl derivative (A) in 1,1,2,2-tetrachloroethane at room temperature.

^{14}N-shfs than the methyl derivative (Fig. 3). This rather complex result seems to be only interpretable in terms of the line-broadening effect of protons on nitrogen atoms of oxamide, *i. e.*, further coupling with the hydrogen nucleus tends to increase the number of ESR lines,[11] but line-width is not so sharp as to separate each line, and as a result, smoothening out the original ^{14}N-shfs.

A similar effect is seen in bis(salicylaldehyde)ethylenediminatocopper(II) (=[Cu salen]) and its methyl derivative (=[Cu oapen]). As evidently seen in Fig. 4, the ^{14}N-shfs was much better resolved in the methyl homologue than that in [Cu salen]. This is also attributed to the line-broadening effect of methine protons which are very close to the C═N═Cu π-bond system.

The effect of protons on ^{14}N-shfs is clearly elucidated by comparison of the spectra of *N*,*N'*-bis(2-aminoethyl)-malonamidatocopper(II) (= [Cu malen]) in methanol and D_2O. As shown in Fig. 5, ^{14}N-shfs was observed in D_2O solution,[12] but hardly observable in methanol solution. This is because the spin-spin interaction between electron and nucleus is much weaker for $^2H(\mu_I=0.857)$ compared to that for ^1H $(\mu_I=2.793)$ and therefore, ^{14}N-shfs of [Cu malen] was observed only in D_2O, where the amino hydrogens are substituted with deuterium.

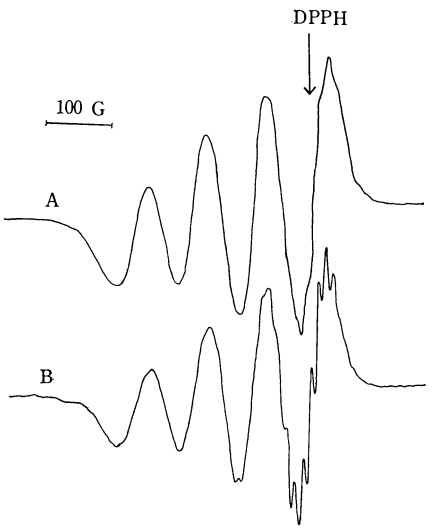

Fig. 5. ESR spectra of *N*,*N'*-bis(2-aminoethyl)malonamidatocopper(II) in methanol (A) and in D_2O (B) at room temperature.

All the above facts support our initial assumption that a deviation from square planar configuration and a presence of protons to couple with an unpaired electron spin are both important factors for the interference of observation of well-resolved ^{14}N-shfs.

References

1) K. D. Bowers and J. Owen, *Reports on Progress in Physics*, **18**, 304 (1955).
2) C. J. Ballhausen, "Introduction to Ligand Field Theory," McGraw-Hill, New York (1962), p. 133.
3) S. Yamada and H. Nishikawa, This Bulletin, **36**,

755 (1963). L. Sacconi, M. Ciampolini, F. Maggio, and G. Del Re, *J. Amer. Chem. Soc.*, **82**, 815 (1960).

4) for example, C. P. Nash and W. P. Schaefer, *J. Amer. Chem. Soc.*, **91**, 1319 (1969). R. E. Bowman and H. H. Stroud, *J. Chem. Soc.*, **1950**, 1342. R. Willstäffer, *Ber.*, **35**, 584 (1902).

5) for example, *Liebigs Ann. Chem.*, **76**, 334, 324 (1850). M. M. Rising, J. S. Hicks and G. A. Moerke, *J. Biol. Chem.*, **89**, 1 (1930).

6) H. Ojima and K. Yamada, *Nippon Kagaku Zasshi*, **91**, 49 (1970).

7) R. H. Holm, G. W. Everett and A. Chakravorty, *Prog. Inorg. Chem.*, **7**, 83 (1965).

8) F. K. Kneubühl, *J. Chem. Phys.*, **33**, 1074 (1960).

9) R. H. Sands, *Phys. Rev.*, **99**, 1222 (1955).

10) for example, P. L. Orioli and L. Sacconi, *J. Amer. Chem. Soc.*, **88**, 277 (1966). T. P. Cheeseman, D. Hall and T. N. Waters, *J. Chem. Soc. (A)*, **1966**, 685.

11) A. H. Maki and B. R. McGarvey, *J. Chem. Phys.*, **29**, 35 (1958).

12) A. K. Wiesema and J. J. Windle, *J. Phys. Chem.*, **68**, 2316 (1964).

Methylene Analogs of Cyclobutenedione. VIII.[1] The Oxidation of 1-Halo- and 1,2-Dihalo-3,4-bis(diphenylmethylene)cyclobut-1-enes

Fumio TODA, Fumio MONDEN, and (in part) Mitsuru OHI

Department of Industrial Chemistry, Faculty of Engineering, Ehime University, Matsuyama 790

(Received July 26, 1973)

The ether peroxide-catalyzed oxidation of 1-chloro- (X) and 1,2-dichloro-3,4-bis(diphenylmethylene)cyclobut-1-enes (V) afforded two ring-opened products, XI and VI respectively. However, neither X nor V was oxidized by photooxidation. By the photooxidation, 1-bromo- (XVI) and 1,2-dibromo-3,4-bis(diphenylmethylene)cyclobut-1-enes (II) were converted to cyclobutanones, XIII and I respectively. Although II was inert to the peroxide-catalyzed oxidation, XVI was oxidized by this procedure. Nevertheless, the main product of the latter reaction was the cyclobutanone (XIII). The mechanisms of these reactions were described.

We have previously reported[2] a photooxidation of 1,2-dibromo-3,4-bis(diphenylmethylene)cyclobut-1-ene (II) in benzene affording 2,2-dibromo-3,4-bis(diphenylmethylene)cyclobutane-1-one (I) in a 78% yield. It was found, however, that the dichloro-analog of II (V) was inert to the photooxidation and did not afford the dichloro-analog of I (IV). On the other hand, V was oxidized in ether containing its peroxide to afford 2,3-bis(diphenylmethylene)succinoyl chloride (VI), while the ether peroxide-catalyzed oxidation of II did not afford any product, II being recovered (Scheme 1).

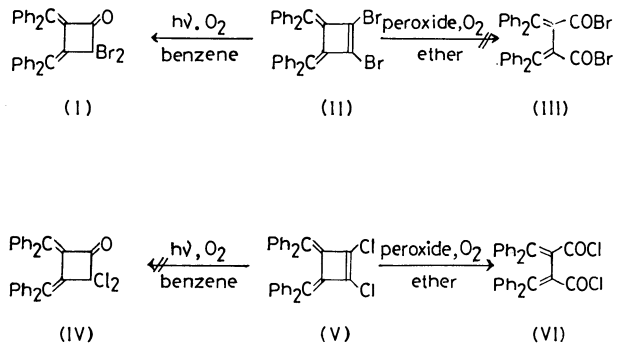

Scheme 1.

These facts suggest that the behavior in response to oxidation reactions varies with the halogen bonded to the 1,2-positions of 3,4-bis(diphenylmethylene)cyclobut-1-ene (XXII). The study was extended to the oxidations of 1-monohalo derivatives of XXII and the Br-Cl-analog (XIX).

The stirring of a solution of V in commercial ether under an oxygen atmosphere at room temperature for 3 hr afforded VI in a 62% yield. The structure of VI was determined by studying its reactions with methanol and with water, which afforded dimethyl 2,3-bis(diphenylmethylene)succinate (VII) and 3,4-bis(diphenylmethylene)succinic anhydride (IX) respectively. Finally VI was identified by a comparison of its spectral data with those of an authentic sample prepared by the reaction of 2,3-bis(diphenylmethylene)succinic acid (VIII) with $SOCl_2$ (Scheme 2).

Although X was inert to the photooxidation in benzene, it underwent the peroxide-catalyzed oxidation; 5-methoxy-3,4-bis(diphenylmethylene)-γ-butyrolactone (XV) (33%) was isolated after the treatment of the

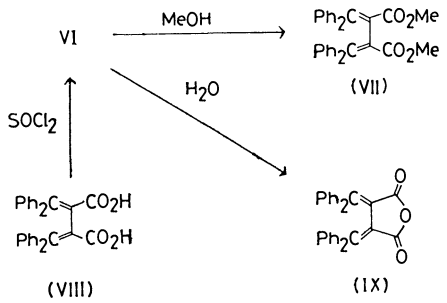

Scheme 2.

reaction mixture with MeOH. The structure of XV was identified by a comparison of its spectral data with those of an authentic sample prepared by the oxidation of 2-methoxy-3,4-bis(diphenylmethylene)-cyclobutane-1-one (XIV) with H_2O_2 in AcOH. The formation of XV can be interpreted in terms of an intramolecular esterification of the hemiacetal (XII) produced by the reaction of the oxidation product (XI) with MeOH (Scheme 3).

The photooxidation of XVI afforded 2-bromo-3,4-bis(diphenylmethylene)cyclobutane-1-one (XIII) in an 81% yield. XVI was also oxidized by the peroxide-

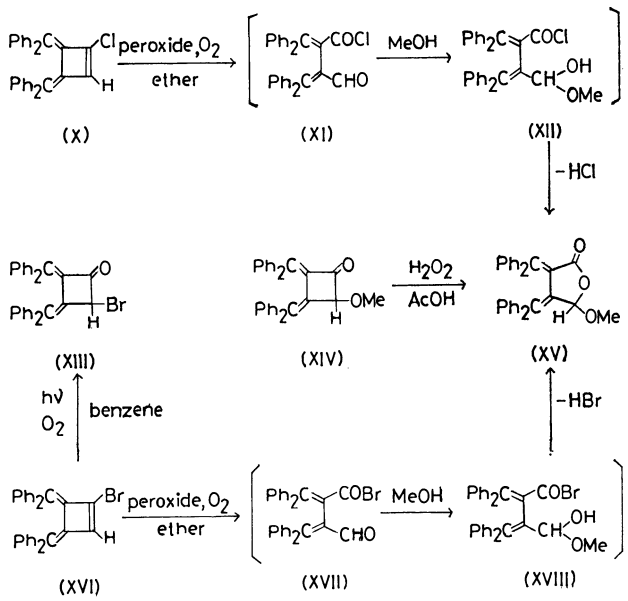

Scheme 3.

catalyzed method to afford, after treatment with MeOH, XIII and XV in 48 and 15% yields respectively. Since the same result was obtained when the oxidation was carried out in the dark, the pathway of the formation of XIII may not be a photochemical one. The mechanism of the formation of XV is probably the same as that of the conversion of X to XV (Scheme 3).

The chloro-derivatives (V and X) were oxidized by the peroxide-catalyzed procedure, but not photochemically. On the contrary, the bromo-derivative (II) was oxidized by the photochemical procedure, but not by the peroxide-catalyzed one. This rule, however, was not applicable to the peroxide-catalyzed oxidation of XVI, even though the main product (XIII) was the same as the photooxidation product of XVI.

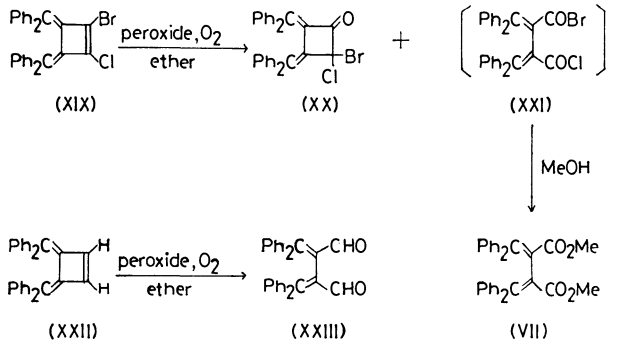

Scheme 4.

The photooxidation of XIX[1] afforded only a resinous material. The peroxide-catalyzed oxidation of XIX afforded, after treatment with MeOH, 2-bromo-2-chloro-3,4-bis(diphenylmethylene)cyclobutane-1-one (XX) and VII in 24 and 12% yields respectively. The acid halide (XXI) may be an initial oxidation product and a precursor of VII (Scheme 4). The peroxide-catalyzed oxidation of XXII in ether afforded 2,3-bis(diphenylmethylene)butanedial (XXIII) in a quantitative yield, whereas the photooxidation of XXII in benzene did not afford any product, XXII being recovered.[3]

Both the photochemical and peroxide-catalyzed oxidations are undoubtedly radical reactions, because they were inhibited by hydroquinone. Nevertheless, the type of oxidation reaction differs widely depending on

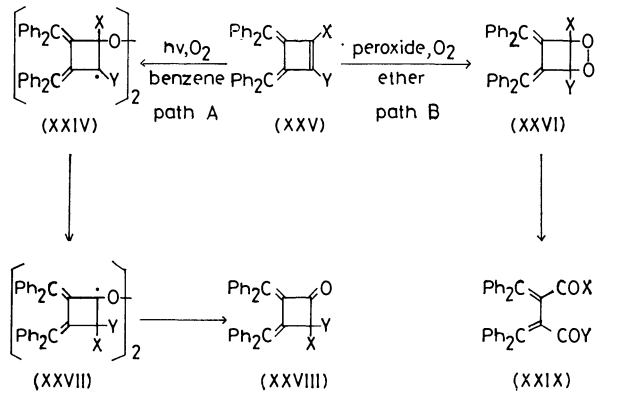

Scheme 5.

whether the halogen bonded to the cyclobutene is Br or Cl. The reason for the difference is not clear, but one plausible interpretation is as follows: the photooxidation proceeds *via* Path A, which includes a 1,2-shift of the halogen atom (X·) in the intermediate (XXIV) initially produced by an intermolecular oxygenation of XXV. The ketonization of XXVII affords XXVIII. The peroxide-catalyzed oxidation proceeds *via* Path B, which includes the ketonization of XXVI initially produced by an intramolecular oxygenation of XXV (Scheme 5). It is understandable that only the cyclobutenes containing Br can be oxidized to cyclobutanone derivatives, because the elimination of the Br atom from a radical species is easier than that of the Cl atom.[4] The formation of XX, which was not contaminated with its dibromo-(I) and/or dichloro-analog (IV), in the oxidation of XIX suggests that the 1,2-shift of X· is an intramolecular one. Because it has been established that 1,2-shifts of hydrogen do not occur to any detectable extent during the lifetime of radicals,[4] the oxidation reaction of XXII to afford XXIII, but not any cyclobutanone derivative, is also understandable. An intermediate similar to XXVI has been postulated for the reaction of tetraphenylcyclobutadiene with oxygen to afford dibenzoyl-*cis*-stilbene.[5]

Experimental

All the melting points are uncorrected. Photooxidation was carried out at room temperature under an oxygen atmosphere in purified dry benzene, using 100-W high-pressure mercury lamp (Riko Kagaku Sangyo Co.). Peroxide-catalyzed oxidation was carried out at room temperature under an oxygen atmosphere in commercial ether. The IR, UV, and NMR spectra were measured in Nujol mull, $CHCl_3$, and $CDCl_3$ respectively.

Peroxide-catalyzed Oxidation of V. A solution of V (0.2 g) in ether (30 ml) was stirred under an oxygen atmosphere at room temperature for 3 hr. The recrystallization from dry AcOEt of the crystals formed when the reaction mixture was allowed to stand for 10 hr afforded VI as pale yellow prisms; 0.133 g (62%); mp 164—165 °C. IR: 1790 and 1770 (C=O) and 1540 cm^{-1} (C=C); λ_{max}: 356 (14000), 306 (13000), and 249 nm (ε, 20000); NMR: 2.8 τ (m, Ph).

Found: C, 74.88; H, 4.09%. Calcd for $C_{30}H_{20}O_2Cl_2$: C, 75.00; H, 4.17%.

Reactions of VI with MeOH and H_2O. A solution of VI (0.1 g) in MeOH (30 ml) was heated under reflux for 1 hr. The subsequent evaporation of the solvent left crude crystals. Recrystallization from AcOEt afforded VII as yellow needles; 0.095 g (97%); mp 233—234 °C (lit,[6] mp 233—234 °C).

A solution of VI (0.1 g) in wet THF (5 ml) was heated under reflux for 1 hr. Recrystallization from AcOEt of the crude crystals obtained by the evaporation of the solvent afforded IX as red rhombs; 0.08 g (90%); mp 230 °C (lit,[2] mp 230 °C).

Preparation of an Authentic Sample of VI. A mixture of VIII (1 g) and $SOCl_2$ (5 ml) was heated at 70 °C for 5 hr. The residue left after the evaporation of the excess $SOCl_2$ was recrystallized from dry AcOEt to afford VI; 0.42 g (38%); mp 164—165 °C.

Peroxide-catalyzed Oxidation of X. A solution of X (0.49 g) in ether (50 ml) was stirred under an oxygen atmosphere at room temperature for 3 hr. The oily material left by the

evaporation of the solvent was crystallized by the addition of MeOH. Recrystallization from AcOEt afforded XV as orange prisms; 0.17 g (33%); mp 212.5—214 °C. IR: 1770 (C=O), 1550 (C=C), and 1080 cm^{-1} (MeO-); λ_{max}: 380 (9600) and 258 nm (ε, 21600); NMR: 3.0 (m, Ph, 20 H), 4.7 (s, CH, 1H), and 6.5 τ (s, OCH_3, 3H).

Found: C, 83.63; H, 5.30%. Calcd for $C_{31}H_{24}O_3$: C, 83.76; H, 5.40%.

Preparation of an Authentic Sample of XV. A solution of XIV[2] (0.1 g) and 30% H_2O_2 (0.4 ml) in AcOH (40 ml) was heated at 60 °C for 7 hr. The subsequent evaporation of the solvent left crude crystals. Recrystallization from AcOEt afforded XV; 0.047 g (45%); mp 212.5—214 °C.

Photooxydation of XVI. A solution of XVI (1 g) in benzene (100 ml) was irradiated under an oxygen atmosphere at room temperature for 3 hr. The subsequent evaporation of the solvent left crude crystals. Recrystallization from AcOEt afforded XIII as orange red hexagonals; 0.84 g (81%); mp 202—203 °C (lit,[2] mp 202—203 °C).

Peroxide-catalyzed Oxidation of XVI. A solution of XVI (0.193 g) in ether (30 ml) was stirred for 3 hr under the same conditions as were used for X. The subsequent evaporation of the solvent left crude oil. Treatment with a small amount of MeOH afforded a mixture of orange red and orange crystals, which were then separated mechanically. The recrystallization of the former from AcOEt afforded XIII; 0.085 g (48%). The recrystallization of the latter from AcOEt afforded XV; 0.027 g (15%).

Peroxide-catalyzed Oxidation of XIX. A solution of XIX (1 g) in ether (100 ml) was stirred for 5 hr under the same conditions as were used for X. The subsequent evaporation of the solvent left an oil, which was crystallized by the addition of a small amount of MeOH to afford a mixture of red prisms and yellow prisms. They were separated mechanically. The recrystallization of the red prisms from AcOEt afforded XX; 0.248 g (24%); mp 169.5—171 °C. IR: 1775 (C=O) and 1540 cm^{-1} (C=C); λ_{max}: 463 (15600), 344 (9200), and 273 nm (ε, 20200).

Found: C, 70.68; H, 3.63%. Calcd for $C_{30}H_{20}OBrCl$: C, 70.40; H, 3.94%.

The recrystallization of the yellow prisms from AcOEt afforded VII; 0.119 g (12%).

Peroxide-catalyzed Oxidation of XXII. A solution of XXII (1 g) in ether (100 ml) was stirred for 3 hr under the same conditions as were used for X. The subsequent evaporation of the solvent left crude crystals. Recrystallization from AcOEt afforded XXIII as pale yellow rhombs; 1.08 g (100%); mp 208.5 °C (lit,[3] mp 208.5 °C). The spectral data were identical with those recorded for XXIII.[3]

References

1) Part VII: F. Toda, H. Nakaoka, K. Yuwane, and E. Todo, This Bulletin, **46**, 1737 (1973).

2) F. Toda and K. Akagi, *Tetrahedron*, **27**, 2801 (1971).

3) In a preliminary communication (F. Toda, M. Higashi, and K. Akagi, *Chem. Commun.*, **1969**, 1219.), we have reported that XXII was oxidized into XXIII photochemically. This oxidation reaction, however, should be corrected to read "by a peroxide-catalyzed process."

4) C. Walling, "Molecular Rearrangements," Vol. 1, ed. by P. de Mayo, Interscience Publishers, New York (1963), Chap. 7.

5) H. H. Freedman, *J. Amer. Chem. Soc.*, **83**, 2194, 2195, (1961).

6) F. Toda, and J. Fujita, This Bulletin, **45**, 1928 (1972).

Photocycloaddition of Thiocarbonyl Compounds to Multiple Bonds. X. Photocycloaddition of *O*-Alkyl Thiobenzoates to Olefins

Atsuyoshi OHNO, Tamotsu KOIZUMI, and Yutaka AKASAKI

Sagami Chemical Research Center, Nishiohnuma, Sagamihara-shi, Kanagawa 229

(Received September 10, 1973)

Photochemical reactions of *O*-ethyl and *O*-methyl thiobenzoates with various olefins have been studied. Some olefins afford ketones, others yield thietanes, and in some cases both products are obtained. Thiobenzoate *O*-esters in the n,π^* triplet state are the reacting species. The mechanism of the reaction has been elucidated: photocycloaddition of a thioester to an olefin results in the formation of a thietane. Photosensitized decomposition of the thietane yields an α,β-unsaturated ether, which is converted to a ketone by general acid-catalyzed hydrolysis.

Photochemistry of carbonyl compounds has been received intensive attention for many decades. In contrast, the photochemical behavior of thiocarbonyl compounds has generated little interest. Although several groups have recently published in this area, almost all the studies dealt with aromatic and alicyclic thioketones.[1-7]

This study was initiated to determine the substituent effects on either the reactivity of photo-excited thiocarbonyl compounds or the transient intermediates in photocycloaddition to olefins, and to synthesize multifunctional compounds that may have synthetic utility.

Results and Discussion

Products. The reaction of *O*-alkyl thiobenzoates (**1**) with some olefins afforded ketone, **3** or **4** or both (Eq. 1), whereas with other olefins thietane derivative, **5** or **6** or both, or **7** or **8** or both, were obtained (Eq. 2). In some cases ketones and thietanes were obtained.

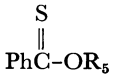

1a: R=Et
1b: R=Me

TABLE 1. DESIGNATION OF COMPOUNDS, **2**—**8**[a]

Designation	R_1	R_2	R_3	R_4
a	$PhCH_2$	H	H	H
b	$PhCH_2$	H	H	CH_3
c	$PhCH_2$	H	CH_3	CH_3
d	$CH_3\backslash CH(Ph)/$	H	H	H
e	*n*-C_3H_7	H	H	H
f	C_2H_5	H	H	CH_3
g	*n*-C_3H_7	CH_3	H	H
h	C_2H_5	H	CH_3	CH_3
i	$CH_3\backslash CH(C_2H_5)/$	H	H	H
j	Ph	H	H	CH_3
k	Ph	H	H	C_2H_5
l	Ph	H	H	$CH_3\backslash CH/CH_3$
m	Ph	CH_3	H	H

a) Stereoisomerism is not represented.

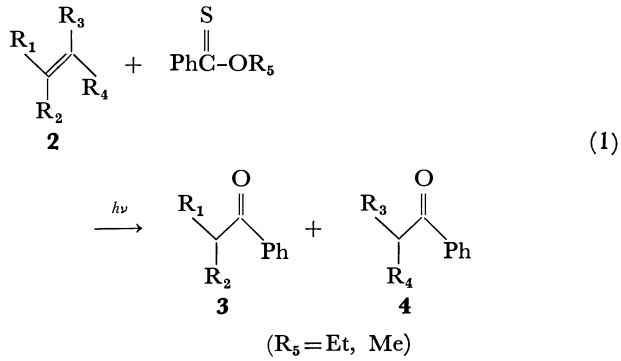

(1)

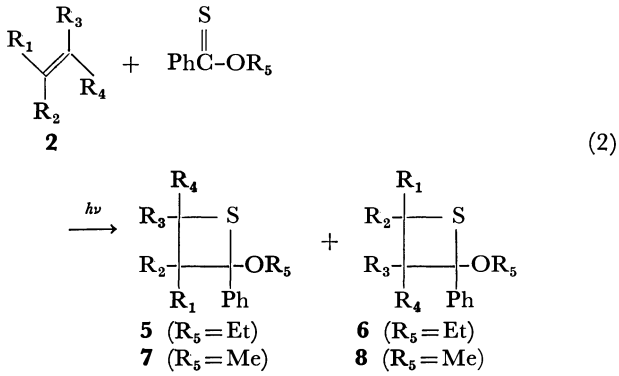

(2)

The unified designation used for compounds **2**—**8** is shown in Table 1 and the reactions are summarized in Tables 2 and 3.

Generally, the reaction mixture was subjected to column chromatography on silica gel and the yield of the isolated products were calculated from their weights. When the reaction mixture was analyzed by vpc before it was subjected to the column chromatography, the yields of ketones were surprisingly lower than those determined after column chromatography, as shown by parenthesized numbers in Tables 2 and 3. However, the vpc analysis indicated that the deficit of ketones was compensated by the presence of corresponding amounts of α,β-unsaturated ethers, **9** or **10** or both, or **11** or **12** or both.

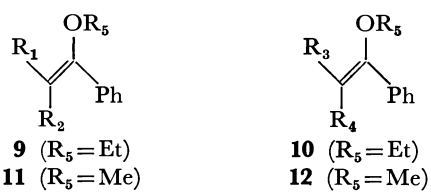

(R_i's are those defined in Table 1)

Table 2. The photoreaction of **1a** with olefins[a]

Run	Olefin, g	**1a**, mg	Irrad. time, day	Product and yield, %[b]			
1	**2a**, 2.78	500	11	**3a** 100 (9)			
2	**2b**, 2.66	561	13	**3b** 85			
3	**2c**, 2.38	469	12	**3c** 25			**6c** 65
4	**2d**, 3.09	603	23	**3d** 40			
5	**2e**, 2.51	497	9	**3e** 62 (19)	**4e** — (4)		
6	**2f**, 2.25	442	11	**3f** 28) (11)	**4f** 28 (11)		
7	**2g**, 3.19	617	12	**3g** 84 (5)	**4g** — (trace)	**5g** 8	**6g** 4
8	**2h**, 3.16	535	3			**5h** 33	**6h** 53
9	**2i**, 2.53	676	34	**3i** 29			
10	**2j**, 2.85	574	5			**5j** 62	**6j** 19
11	**2k**, 2.52	479	6		**4k** — (trace)	**5k** 53	**6k** 19
12	**2l**, 1.01	202	16		**4l** 64	**5l** 48	**6l** 16
13	**2m**, 2.52	557	22	**3m** 72		**5m** 26	

a) The reaction mixture contains 2 ml of benzene in addition to **1** and **2**. b) Isolated yields. Numbers in parentheses are yields determined by vpc. See text for details.

Table 3. The photoreaction of **1b**, with olefins[a]

Run	Olefin, g	**1b**, mg	Irrad. time, day	Product and yield, %			
14	**2a**, 2.59	508	12	**3a** 100			
15	**2b**, 3.09	593	17	**3b** 52	**4b** — (20)		
16	**2c**, 3.14	769	12	**3c** 20			**8c** 48
17	**2e**, 2.26	407	10	**3e** 25 (7)	**4e** — (trace)		
18	**2f**, 2.97	557	9	**3f** 14 (8)	**4f** 18 (5)		
19	**2g**, 2.55	510	16	**3g** 40 (8)	**4g** — (trace)	**7g** 12	**8g** 5
20	**2h**, 2.99	549	6			**7h** 26	**8h** 37
21	**2j**, 2.44	524	8	**3j** 18	**4j** —	**7j** 52	
22	**2k**, 3.17	620	4	**3k** 7	**4k** — (trace)	**7k** 64	

a) See footnotes in Table 2.

Some of these ethers were isolated by subjecting the reaction mixture to column chromatography on neutral alumina. This surprising observation was explained when an authentic sample of the ether was quantitatively converted into the corresponding ketone by the treatment with silica gel—apparently an effective catalyst for this transformation.

Reacting Species. *O*-alkyl thiobenzoates have absorption maxima at around 290 nm ($\varepsilon \approx 12000$) and 420 nm ($\varepsilon \approx 120$) that are attributable to π,π^* and n,π^* transitions, respectively.[8] Excitation at either transition was found to bring about the reaction.

As shown in Fig. 1, when a mixture of *cis*- or *trans*-2-pentene and **1a** in *n*-dodecane was photo-irradiated, *cis-trans* isomerization of the olefin took place and the thermodynamically equilibrated composition of 75% *trans*- and 25% *cis*-2-pentene[9-11] was asymptotically attained.

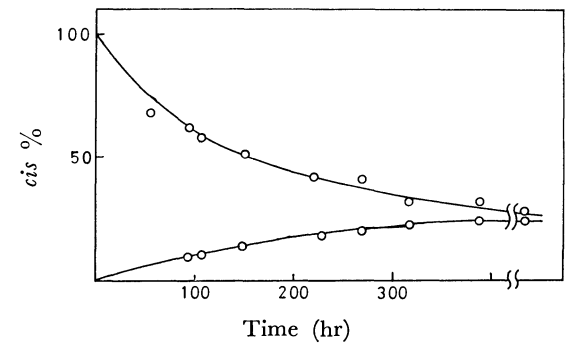

Fig. 1. Photo-initiated isomerizations of *cis*- and *trans*-2-pentene in the presence of *O*-ethyl thiobenzoate.

It is known that thiobenzophenone in the n,π^* triplet state behaves like a thiyl radical, *i. e.*, it attacks an olefin reversibly.[3a] The reactivities of benzophenone in the n,π^* triplet state and an alkoxy radical have also been compared.[12] The *cis-trans* isomerization of 2-pentene reported here suggests that photo-activated **1** is also in the n,π^* triplet state.

Further evidence of the multiplicity of the excited state responsible for the reaction was obtained from the photosensitized reaction of **1a** (E_T=57—58 kcal/mol)[13] with allylbenzene in the presence of Michler's ketone (λ_{max}=370 nm, ε=31000, E_T=62 kcal/mol).[14] Under the condition that more than 99% of the irradiated light was absorbed by Michler's ketone, the reaction was found to proceed similarly to that effected by direct photo-irradiation. However, quantitative observations were precluded by the fact that the quantum yield of the reaction is too low to be measured accurately (as is recognized from the reaction time). The observed effect of the photosensitizer together with the physico-chemical data on thiobenzoate *O*-esters[13] provide additional support for the electronic configuration and state of the reacting **1**.

Since the lowest triplet energies of simple alkenes (74—82 kcal/mol)[15] and substituted styrenes (60—70 kcal/mol)[16] are higher than that[13] of **1**, it is not necessary to take into account the energy transfer from **1** to olefins.

Mechanism of the Reaction. As discussed above,

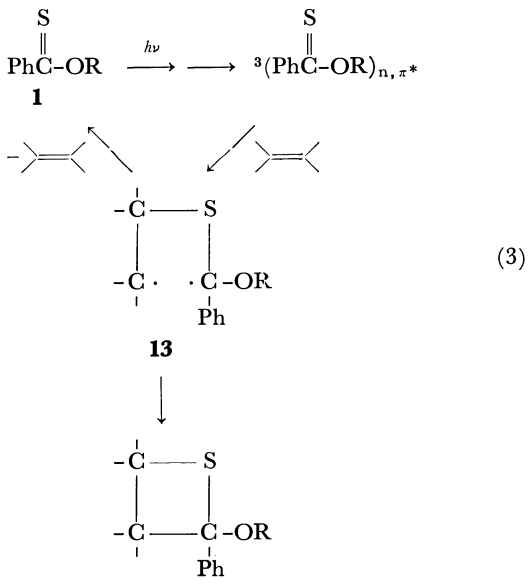

(3)

there is strong indication to propose that the reaction initiated by the attack of **1** in the *n,π* triplet state* on an olefin yielding a composite biradical **13** (Eq. (3)), which may regenerate ground-state **1** and the olefin, or cyclize into a thietane.[17]

The product distribution reveals that the attack of photo-excited **1** on an olefin takes place so as to form the more stable radical. However, when the olefin has a bulky substituent, attack on the less-hindered side is favored (Runs 3, 8, 12, 16, and 20). This observation is consistent with the general trend found in the chemistry of thiyl radicals.[18] In this connection, it is noteworthy that photo-excited **1** reacts with equal facility with tri-, di- or mono-substituted olefins, whereas the addition of thiyl radicals to tri-substituted olefins (compared to di- and mono-substituted olefins) proceeds slower and with increasing amounts of side products.[18]

In the reaction of thiobenzophenone with alkenes the **13**-type biradical, formed as an intermediate, reacted with another molecule of thiobenzophenone giving **14**, then **15**.[3a] This reaction occurred with thiobenzophenone because it is a powerful scavenger of free radicals.[19] In contrast, since **1** has no tendency to react with free radicals,[20] the reactions described here do not afford 1,4-dithiane derivatives.

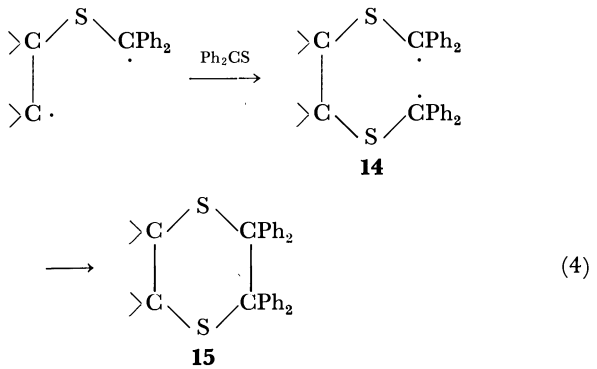

(4)

Again, in the reaction of thiobenzophenone a 1,3-dithiane is the proposed precursor of a thietane.[4b] Although we do not have proof that a 1,3-dithiane derivative is intermediary in the formation of a thietane, it should be noted that 2,4-diphenyl-2,4-diethoxy-1,3 dithiadecalin was obtained in 27% yield by the reaction of **1a** with cyclohexene.[21]

Unsubstituted and alkyl-substituted thietanes are known to be photolyzed into olefins.[22-24] However, there is no evidence for the photochemical transformation of alkoxythietanes into corresponding α,β-unsaturated ethers. Therefore, we studied the photolysis of an alkoxythietane (**7g**) as a controlled experiment. When a benzene solution of **7g** was irradiated with light from a high-pressure mercury lamp (315 and 366 nm), the majority of the products was tarry polymer. The vpc analysis showed that the yield of the ketone, **3g**, was only 7% and the ether, **11g**, was absent. On the other hand, in the presence of a large excess (about 9 equivalents) of **1b**, yields of **3g** and **11g** were improved to 59 and 16.5%, respectively. The present result reveals that α,β-unsaturated ethers are afforded by photosensitized decomposition of alkoxythietanes (Eq. (5)), although detailed mechanism is not known.

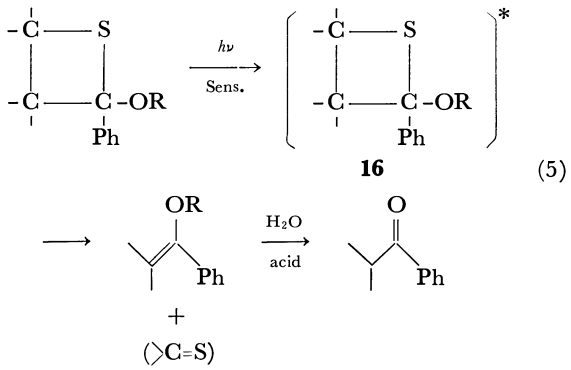

(5)

The fact that irradiation with wavelengths longer than 390 nm is effective in producing the ether (*e.g.*, **2a**+**1a**→**9a**) also supports the idea that the decomposition of the thietane is a photosensitized process. Based on the results reported by Barton and co-workers,[13] **16** is supposed to be in the triplet state. Photochemical reactions of alkoxy- and hydroxyoxetanes leading to the formation of an α,β-unsaturated ether and a ketone, respectively, have also been proposed.[25,26]

As described above, it is confirmed that the α,β-unsaturated ether is easily hydrolyzed into corresponding ketone in the presence of an acid like silica gel or hydrogen chloride.[27]

Experimental

Materials. As previously reported,[28] *O*-alkyl thiobenzoates (**1**) were prepared from the corresponding orthoesters[29] or imido ethers.[30,31] Olefins **2c** and **2l** were prepared according to Klages.[32] A mixture of **2b** and **2d**, obtained by the reaction of phenylmagnesium bromide and 1-chloro-2-butene,[33] was fractionally distilled by a Podbielniak Model 3475 apparatus yielding **2b** and **2d** of 70 and 90% purities, respectively. Other olefins were commercially available. An α,β-unsaturated ether, **11g** (a mixture of *cis*- and *trans*-isomers), was synthesized by refluxing a mixture of α-methylvalerophenone (1.7 g), trimethyl orthoformate (2.4 g), and *p*-toluenesulfonic acid (5 mg) in absolute methanol (8 ml) for 4 hr, followed by fractional distillation under a reduced

TABLE 4. NMR SPECTRAL DATA FOR THIETANES, **5**—**8**[a)]

Compd	Ring-H	Alkoxy-H	Phenyl-H	Other H
6c	3.90 (d-d, J=6, 9)	1.21 (t, J=7) 2.88 (d-q, J=9, 7) 3.47 (d-q, J=9, 7)	6.80—7.40 (m)	0.85 (s, 3H) 1.16 (s, 3H) 2.65 (d-d, 1H, J=9, 13) 2.86 (d-d, 1H, J=6, 13)
8c	3.89 (d-d, J=6, 9)	2.98 (s)	7.02—7.36 (m)	0.86 (s, 3H) 1.14 (s, 3H) 2.66 (d-d, 1H, J=9, 14) 2.87 (d-d, 1H, J=6, 14)
5g	2.31 (d, J=8) 3.18 (d, J=8)	1.20 (t, J=7) 2.88 (d-q, J=9, 7) 3.48 (d-q, J=9, 7)	7.00—7.60 (m)	0.86 (s, 3H) 1.10—2.00 (m, 4H)
6g	2.52 (d, J=9) 2.96 (d, J=9)	1.18 (t, J=7) 2.80 (d-q, J=9, 7) 3.30 (d-q, J=9, 7)	7.00—7.60 (m)	0.94 (s, 3H) 1.10—2.00 (m, 4H)
7g	3.14 (d, J=9) 3.28 (d, J=9)	3.04 (s)	7.10—7.45 (m)	0.86 (s, 3H) 0.93 (t, 3H, J=8) 1.10—1.80 (m, 4H)
8g	2.50 (d, J=9) 2.95 (d, J=9)	3.04 (s)	7.10—7.45 (m)	0.95 (t, 3H, J=8) 1.21 (s, 3H) 1.40—2.10 (m, 4H)
5h	2.60 (t, J=8)	1.15 (t, J=7) 2.86 (d-q,, J=9.7) 3.48 (d-q, J=9, 7)	7.04—7.50 (m)	0.82 (s, 3H) 0.93 (t, H, J=7) 1.19 (s, 3H) 1.60—2.04 (m, 2H)
6h	3.50 (t, J=9)	1.16 (t, J=7) 2.83 (d-q, J=9, 7) 3.40 (d-q, J=9, 7)	7.00—7.50 (m)	0.72 (s, 3H) 0.89 (t, 3H, J=7) 1.19 (s, 3H) 1.50 (d-q, 2H, J=9, 7)
7h	2.62 (t, J=8)	2.97 (s)	7.05—7.40 (m)	0.81 (s, H) 0.92 (t, 3H, J=7) 1.15 (s, 3H) 1.90 (d-q, 2H, J=8, 7)
8h	3.59 (d-d, J=6, 10)	3.02 (s)	7.08—7.66 (m)	0.74 (s, 3H) 0.88 (t, 3H, J=7) 1.18 (s, 3H) 1.35—1.70 (m, 2H)
5j	3.78 (d, J=9) 4.28 (d-q, J=6, 9)	1.15 (t, J=7) 2.98 (d-q, J=9, 7) 3.60 (d-q, J=9, 7)	7.21 (s) 7.24 (s)	1.40 (d, 3H, J=6)
6j	3.57 (d-q, J=6, 8) 4.25 (d, J=8)	1.20 (t, J=8) 2.95 (d-q, J=10, 8) 3.32 (d-q, J=10, 8)	6.66—7.20 (m) 7.20—7.70 (m)	1.55 (d, 3H, J=6)
7j	3.83 (d, J=9) 4.28 (d-q, J=9, 6)	3.09 (s)	7.20 (s) 7.25 (s)	1.39 (d, 3H, J=6)
5k	3.85 (d, J=6) 4.00 (d-t, J=9, 6)	1.08 (t, J=6) 3.02 (d-q, J=8, 6) 4.04 (d-q, J=8.6)	7.20 (s) 7.22 (s)	0.88 (t, 3H, J=6) 1.60—2.00 (m, 2H)
6k	3.39 (d-t, J=8, 6) 4.25 (d, J=8)	1.16 (t, J=7) 2.65—3.02 (m)	6.68—7.50 (m)	0.91 (t, H, J=6) 1.50—2.05 (m, 2H)
7k	3.82 (d, J=10) 4.11 (d-d-d, J=10, 8, 6)	3.05 (s)	7.14 (s) 7.20 (s)	0.87 (t, 3H, J=7) 1.74 (m, 1H)
5l	3.78—4.17 (m)	1.10 (t, J=7) 2.93 (d-q, J=9, 7) 3.56 (d-q, J=9, 7)	7.16 (s) 7.20 (s)	0.65 (d, 3H, J=7) 0.96 (d, 3H, J=7) 1.65—1.98 (m, 1H)
6l	3.20 (t, J=8) 4.30 (d, J=8)	1.15 (t, J=7) 2.92 (d-q, J=9, 7) 3.28 (d-q, J=9, 7)	6.70—8.00 (m)	0.77 (d, 3H, J=7) 0.97 (d, 3H, J=7) 1.85—2.16 (m, 1H)
5m	2.58 (d, J=8) 4.12 (d-d, J=1, 8)	1.03 (t, J=7) 2.98 (d-q, J=9, 7) 3.46 (d-q, J=9, 7)	7.10—7.43 (m)	1.37 (d, 3H, J=1)

a) Chemical shifts are expressed by δ from TMS in CCl_4 and coupling constants, J, have the unit of Hz.

pressure: bp 85 °C/2 Torr; NMR (δ from TMS, CCl_4) 0.60—1.75 (m), 1.57 (s), 1.71 (s), 1.75—2.35 (m), 3.19 (s), and 7.20 (s); IR 3070—3000, 2900—2800, 1440, 1135, 1070, 770, and 700 cm^{-1}.

Found: C, 81.90; H, 9.31%. Calcd for $C_{13}H_{18}O$: C, 82.06; H, 9.54%.

Purities of materials were confirmed by NMR, IR, and vpc.

General Procedure. Reaction solutions were prepared in a dry box under an atmosphere of CO_2 by placing 0.5 g of **1**, 2.5 g of **2** and 2 ml of benzene in a Pyrex vessel.[34] Photoreactions were carried out by external irradiation method with a 400 W high-pressure mercury lamp (Toshiba H-400P) at a temperature of running water. Some reactions were carried out with a Toshiba UV-39 filter (transparent for >390 nm), and it was found that application of the filter did not alter the product distribution.

Photo-irradiation was continued until **1** disappeared completely. At the end of the reaction, products were analyzed directly by vpc (Hitachi K-53, TCD or FID, 20% XF-1150, 1 m, 140 °C for thietanes and **1**; 20% XF-1150, 1 m, 120 °C for alkyl aryl ketones and corresponding ethers; 5% XF-1150, 1 m, 140 °C for aralkyl aryl ketones and corresponding ethers) or, after evaporation of benzene and excess olefin, by column chromatography on silica gel with appropriate compositions of *n*-hexane-benzene mixtures.

cis-trans *Isomerization of 2-Pentene (**2f**).* A mixture of *trans*-2-pentene (578.4 mg, 8.26 mmol) and **1a** (1.0104 g, 6.09 mmol) in *n*-dodecane was irradiated. At an appropriate interval, aliquots were taken out from the mixture with a syringe and compositions of isomers were analyzed by vpc (40% $AgNO_3$/PEG, 1 m, room temperature). Similar experiments were also done with the *cis*-isomer. Results are shown in Fig. 1.

*Photosensitized Reaction of O-Ethyl Thiobenzoate (**1a**) with Allylbenzene (**2a**).* A mixture of **1a** (100.6 mg, 0.606 mmol), **2a** (495.2 mg, 4.20 mmol), and Michler's ketone (164.0 mg, 0.612 mmol) in acetonitrile (15 ml) was irradiated. A filter solution of aqueous 2,3-dihydro-5,7-dimethyl-1,4-diazepine perchlorate[35] (400 mg/l) was circulated through the outer shell of the reaction vessel. Under the condition, more than 99% of the irradiated light (366, 405/408, and 436 nm)[36] was absorbed by Michler's ketone. After 9 days, when no **1a** remained, the reaction mixture was worked-up and subjected to column chromatography on silica gel and the ketone, **3a**, was isolated in quantitative yield.

*Photolysis of 2-Methoxy-2-phenyl-3-methyl-3-propylthietane (**7g**).* A solution composed of **7g** (40 mg, 0.169 mmol) and **1a** (226.7 mg, 1.49 mmol) in 4 ml of benzene was irradiated for 13 days until **7g** had disappeared completely. The

Table 5. IR spectral data for thietanes, **5**—**8**

Compd	Absorption, cm^{-1}
6c	3050, 3020, 2960, 2900, 2850, 1600, 1490, 1445, 1380, 1360, 1250, 1225, 1110, 1070, 1030, 915, 880, 860, 830, 800, 755, 745, 730, 700, 675, 610, 505
8c	8050, 2020, 2975, 2930, 2860, 2820, 1600, 1495, 1470, 1450, 1390, 1370, 1320, 1255, 1235, 1185, 1155, 1130, 1090, 1080, 1030, 1020, 965, 950, 915, 870, 830, 805, 760, 710, 700, 680, 670, 620, 560, 510
5g and **6g**	3050, 3010, 2960, 2920, 2850, 1600, 1480, 1445, 1390, 1375, 1310, 1270, 1250, 1210, 1170, 1160, 1150, 1115, 1090, 1070, 1030, 970, 920, 910, 885, 855, 825, 805, 750, 700, 675, 635, 625, 500
7g and **8g**	3040, 3005, 2940, 2920, 2860, 2810, 1600, 1490, 1470, 1445, 1380, 1315, 1280, 1255, 1230, 1190, 1175, 1145, 1090, 1080, 1035, 1005, 980, 960, 920, 905, 860, 810, 780, 755, 675, 635, 550, 500
5h and **6h**	3050, 3010, 2950, 2900, 2865, 1600, 1490, 1460, 1445, 1380, 1360, 1310, 1300, 1270, 1235, 1175, 1140, 1120, 1085, 1075, 1030, 970, 940, 920, 885, 850, 820, 755, 705, 685, 665, 600, 520
7h and **8h**	3050, 3020, 2950, 2810, 1600, 1490, 1460, 1450, 1385, 1365, 1315, 1300, 1270, 1240, 1190, 1180, 1140, 1115, 1085, 1035, 1005, 950, 940, 915, 870, 855, 820, 755, 700, 675, 665, 600, 550
5j and **6j**	3050, 3010, 2960, 2900, 2875, 1600, 1495, 1450, 1390, 1375, 1280, 1270, 1220, 1205, 1170, 1160, 1130, 1100, 1080, 1065, 1055, 1035, 980, 945, 920, 900, 870, 825, 780, 760, 705, 665, 615, 505
7j	3050, 3025, 2950, 2925, 2820, 1600, 1495, 1450, 1380, 1285, 1270, 1220, 1170, 1110, 1080, 1070, 1040, 1030, 1015, 955, 870, 820, 785, 755, 705, 660, 610, 510,
5k and **6k**	3030, 3000, 2950, 2910, 2850, 1600, 1490, 1450, 1445, 1390, 1335, 1310, 1275, 1240, 1200, 1175, 1155, 1120, 1090, 1075, 1030, 975, 930, 915, 900, 865, 830, 780, 765, 755, 700, 660, 610, 570, 515
7k	3050, 3020, 2950, 2925, 2870, 2820, 1600, 1495, 1450, 1380, 1310, 1280, 1245, 1205, 1190, 1180, 1160, 1110, 1080, 1040, 1030, 960, 945, 910, 870, 830, 790, 775, 755, 705, 660, 610, 560, 505
5l and **6l**	3040, 3010, 2950, 2910, 2850, 1600, 1490, 1445, 1385, 1370, 1310, 1275, 1245, 1215, 1175, 1175, 1160, 1120, 1095, 1075, 1050, 1030, 980, 920, 890, 825, 815, 780, 760, 700, 660, 610, 570, 525
5m	3020, 3000, 2950, 2910, 2850, 1600, 1490, 1445, 1390, 1370, 1310, 1270, 1230, 1200, 1175, 1155, 1125, 1085, 1070, 1030, 965, 920, 900, 880, 855, 800, 760, 740, 715, 700, 670, 630, 590, 555

Table 6. Mass spectral data for thietanes, 5—8[a]

Compd	Intensity, %								
	M^+	$(1)^+$	$(1+H)^+$	$(2)^+$	$(9 \text{ or } 11)^+$	$(10 \text{ or } 12)^+$	$PhC{\equiv}S^+$	$PhCHS^+$	$PhC{\equiv}O^+$
6c[b]	0.3	21	51	26	0	7	12	18	66
8c	0.2	33	100	41	0	16	21	10	12
7g[c]	1.0	100	25	0	7	0	30	19	15
6h	0.4	64	80	7	0	18	34	58	100
8h	1.9	66	100	13	0	16	35	20	14
5j	1.1	13	21	100	9	0	12	14	46
6j	1.2	12	18	100	0	8	27	17	74
7j	0.1	28	5	100	7	0	35	7	78
5k[d]	0.2	17	68	100	54	0	14	15	98
6k	0.2	12	46	100	0	6	24	17	79
7k	0.2	14	19	100	9	0	16	5	19
5l	0.2	55	7	100	5	0	14	13	55
6l[e]	0.1	5	15	29	0	4	42	7	100
5m	1.8	93	14	44	19	0	29	48	100

a) Important peaks are selected. b) **2c**$-H=100\%$. c) **11g**$-C_2H_5=42\%$. d) **2k**$-CH_3\cdot=53\%$. e) $M^+-EtOH=77\%$.

Table 7. Elemental analyses of thietanes

Compd	Molecular formula	Calcd (%)			Found (%)		
		C	H	S	C	H	S
6c	$C_{20}H_{24}OS$	76.88	7.74	10.26	76.89	7.70	10.07
8c[a]	$C_{19}H_{22}OS$	76.47	7.43	10.74	76.73	7.67	10.71
5h	$C_{15}H_{22}OS$	71.95	8.86	12.81	72.20	8.96	12.80
7h	$C_{14}H_{20}OS$	71.14	8.53	13.56	71.20	8.58	13.72
7k	$C_{18}H_{20}OS$	76.01	7.09	11.27	75.54	6.89	11.29

a) Molecular Weight: Calcd for $C_{19}H_{22}OS$; 298. Found; 300.7.

vpc analysis of the reaction mixture showed that **3g** and **11g** were afforded in 59 and 16.5% yields, respectively. However, in the absence of **1a**, the reaction afforded large amount of tarry polymer and the yield of **3g** was only 7% after 21 days. Although aliquots were analyzed by vpc every day, no indication was obtained for the formation of **11g** from this reaction solution.

*Hydrolysis of 1-Methoxy-1-phenyl-2-methyl-1-pentene (**11g**).* A CCl_4 solution (5 ml) of **11g** (190 mg, 1 mmol) containing catalytic amount of silica gel was stirred at room temperature and aliquots were analyzed by vpc. After 2 weeks almost all **11g** was converted into **3g**. When a drop of hydrochloric acid was added to the solution in place of silica gel, the ether transformed into the ketone within a day. Furthermore, a solution of **11g** in benzene was passed through a column of silica gel and the ketone, **3g**, was obtained in quantitative yield. However, a column of neutral alumina did not catalyze this transformation.

Characterization of Products. Ketones and ethers were identified by comparing their NMR, IR spectra, and vpc with those of authentic samples. All thietanes described here are new compounds. Their NMR, IR, and mass spectral data are summarized in Tables 4, 5, and 6, respectively. Since the thietanes are unstable oily materials,[37] most efforts to purify them were not successful and only limited numbers of compounds gave satisfactory results on elemental analyses (Table 7).

Structures of thietanes were determined by NMR: a ring proton bound to a carbon adjacent to the sulfur appears more down-field than that of the other isomer.[3a] Mass spectra provided another support for the structures. Photochemical conversion of **7g** into **3g** and **11g** also confirmed the structure of this thietane.

References

1) E. T. Kaiser and T. F. Wulfers, *J. Amer. Chem. Soc.*, **86**, 1897 (1964).
2) K. Yamada, M. Yoshioka, and N. Sugiyama, *J. Org. Chem.*, **33**, 1240 (1968).
3) a) A. Ohno, Y. Ohnishi, and G. Tsuchihashi, *J. Amer. Chem. Soc.*, **91**, 5038 (1969) and references cited therein; b) A. Ohno, T. Koizumi, and Y. Ohnishi, This Bulletin, **44**, 2511 (1971); c) N. Kito and A. Ohno, *Chem. Commun.*, **1971**, 1338; d) A. Ohno and N. Kito, *Int. J. Sulfur Chem., A*, **1**, 26 (1971).
4) a) D. R. Kemp, A. H. Lawrence, C. C. Liao, R. O. Loutfy, P. de Mayo, A. A. Nicholson, and S. Paszyc, *23rd Interntl. Congress, Pure Appl. Chem.*, Vol. 1, 367 (1971); b) P. de Mayo and A. A. Nicholson, *Israel J. Chem.*, **20**, 341 (1972); c) C. C. Liao and P. de Mayo, *Chem. Commun.*, **1971**, 1525; d) D. R. Kemp and P. de Mayo, *ibid.*, **1972**, 233; e) D. S. L. Blackwell and P. de Mayo, *ibid.*, **1973**, 130.
5) H. J. T. Bos, H. Schinkel, and Th. C. M. Wijsman, *Tetrahedron Lett.*, **1971**, 3905.
6) a) H. Gotthardt, *Chem. Ber.*, **105**, 2008 (1972); b) H. Gotthardt, *Tetrahedron Lett.*, **1973**, 1221.
7) G. Oster, L. Citarel, and M. Goodman, *J. Amer. Chem. Soc.*, **84**, 703 (1962).
8) A. Ohno, T. Koizumi, Y. Ohnishi, and G. Tsuchihashi, This Bulletin, **42**, 3556 (1969).
9) G. C. Bond and M. Hellier, *J. Catal.*, **4**, 1 (1965).

10) H. Mauras, *Bull. Soc. Chim. Fr.*, **1956**, 1642.
11) J. E. Kilpatrick, E. J. Prosen, K. S. Pitzer, and F. D. Rossini, *J. Res. Natl. Bur. Stand.*, **36**, 559 (1946).
12) C. Walling and M. J. Gibian, *J. Amer. Chem. Soc.*, **87**, 3361 (1965).
13) D. H. R. Barton, M. Bolton, P. D. Magnus, P. J. West, G. Porter, and J. Wirz, *Chem. Commun.*, **1972**, 632.
14) G. N. Lewis and M. Kasha, *J. Amer. Chem. Soc.*, **66**, 2100 (1944).
15) N. J. Turro, "Energy Transfer and Organic Photochemistry," ed. by P. A. Leermakers and A. Weissberger, Interscience Publishers, New York, N. Y. (1969), p 144.
16) a) R. A. Caldwell, G. W. Sovocool, and R. J. Peresie, *J. Amer. Chem. Soc.*, **95**, 1496 (1973); b) D. F. Evans, *J. Chem. Soc.*, **1957**, 1351.
17) A. Ohno, T. Koizumi, and Y. Akasaki, *Tetrahedron Lett.*, **1972**, 4993.
18) R. M. Kellogg, "Methods in Free Radical Chemistry," Vol. 2, ed. by E. S. Huyser, Dekker, Inc., New York, N. Y. (1969), pp 17—22.
19) G. Tsuchihashi, M. Yamauchi, and A. Ohno, This Bulletin, **43**, 968 (1970).
20) The radical-capturing powers of thiocarbonyl compounds decrease linearly as their n,π^* transition energies are increased; 4th Symposium on Organosulfur Chemistry, Gifu Feb. 1970, pp 8—11.
21) A. Ohno, *Int. J. Sulfur Chem., B*, **6**, 183 (1971).
22) W. E. Haines, G. L. Cook, and J. S. Ball, *J. Amer. Chem. Soc.*, **78**, 5213 (1956).
23) E. Block, *Quart. Reports Sulfur Chem.*, **4**, 263 (1969).
24) D. R. Dice and R. R. Steer, *Chem. Commun.*, **1973**, 106.
25) H. Nozaki, I. Otani, R. Noyori, and M. Kawanishi, *Tetrahedron*, **24**, 2183 (1968).
26) T. S. Cantrell, *J. Amer. Chem. Soc.*, **95**, 2714 (1973).
27) S. D. Brynes and L. R. Fedor, *ibid.*, **94**, 7016 (1972).
28) A. Ohno, T. Koizumi, Y. Ohnishi, and G. Tsuchihashi, *Org. Mass Spectry.*, **3**, 261 (1970).
29) A. Ohno, T. Koizumi, and G. Tsuchihashi, *Tetrahedron Lett.*, **1968**, 2083.
30) M. Matsui, *Mem. Coll. Sci. Eng. Kyoto*, **1**, 285 (1908); **3**, 247 (1912).
31) Y. Sakurada, *ibid.*, **9**, 237 (1926); **10**, 79 (1926).
32) A. Klages, *Ber.*, **37**, 2301 (1904).
33) K. W. Wilson, J. D. Roberts, and W. G. Young, *J. Amer. Chem. Soc.*, **71**, 2019 (1949).
34) A. Ohno, Y. Ohnishi, M. Fukuyama, and G. Tsuchihashi, *ibid.*, **90**, 7038 (1968).
35) G. Schwarzenbach and K. Lutz, *Helv. Chim. Acta*, **23**, 1139 (1940).
36) A. Schönberg, "Preparative Organic Photochemistry," Springer-Verlag New York Inc., New York, N. Y. (1968), p. 488.
37) They decompose gradually into tarry polymers even in a refrigerator. Thietanes **6g**, **8g**, **5h**, and **7h** are contaminated by the other isomers, respectively.

The Structure-Taste Relationships of the Dipeptide Esters Composed of L-Aspartic Acid and β-Hydroxy Amino Acids

Yasuo ARIYOSHI, Naohiko YASUDA, and Tetsuo YAMATANI

Central Research Laboratories, Ajinomoto Co., Inc., Suzuki-cho, Kawasaki-ku, Kawasaki 210

(Received August 6, 1973)

In order to evaluate the contribution of a hydroxyl group to the degree of sweetness of aspartyl dipeptides, we have synthesized a number of α-L-aspartyl dipeptides, such as the esters of α-L-aspartyl-L-hydroxynorleucine (**16** and **17**), -*O*-acyl-L-serine (**18**—**21**), -D-serine (**22**—**28**), -D-threonine (**30**—**36**), and -D-allothreonine (**37**—**43**); their sweetness potencies were compared with those of the corresponding dipeptides without a hydroxyl group. It has been found that a hydroxyl group makes a major contribution to the sweetness of the α-L-aspartyl dipeptide esters. The introduction of a hydroxyl group into the L–L peptides gave compounds with reduced potency. However, no such regularity was observed in the L–D peptides; the esters of α-L-aspartyl-D-serine (**22**—**28**) and -D-threonine (**30**—**36**) were sweeter than the corresponding esters of α-L-aspartyl-D-alanine and -D-α-amino-*n*-butyric acid respectively, while the esters of α-L-aspartyl-D-allothreonine (**37**—**43**) were less sweet than the corresponding esters of α-L-aspartyl-D-α-amino-*n*-butyric acid. The enzymatic resolution of *N*-acetyl-*erythro*- and -*threo*-β-hydroxy-DL-norleucine is also described.

The pronounced sucrose-like sweetness of α-L-aspartyl-L-phenylalanine methyl ester (APM) was reported by Mazur *et al.*[1] At that time, L-aspartic acid seemed to be necessary for sweetness, but the phenylalanine part could be modified considerably.[1,2] A number of sweet dipeptide esters related to APM have been synthesized by several groups,[3] according to the generalization made by Mazur *et al.*[1,2] Recently, however, Briggs and Murley described that the aspartic acid part could be replaced by amino malonic acid without losing its sweetness.[4] Furthermore, Lapidus and Sweeney reported that an *N*-protected APM, *N*-trifluoroacetyl-L-aspartyl-L-phenylalanine methyl ester, was 120 times as sweet as sucrose,[5] though the free amino group of L-aspartic acid had been considered to be necessary for sweetness.[1]

APM appears attractive as a low-calorie sweetener, but it is somewhat unstable in an aqueous solution, in which APM spontaneously cyclizes to cyclo-L-aspartyl-L-phenylalanyl, which lacks sweetness. In order to obtain more stable sweeteners than APM and, in particular, to draw on for more definite structure-taste relationships of aspartyl dipeptides, we synthesized a number of aspartyl dipeptide derivatives, including D-amino acids and L- and D-hydroxy amino acids, and tasted them.

During the replacement of the phenylalanine part of APM by other amino acids, it was found that α-L-aspartyl-L-norvaline methyl ester (**1**) was somewhat sweet, about 4 times sucrose, while α-L-aspartyl-L-α-amino-*n*-butyric acid methyl ester (**2**) was devoid of sweetness. Mazur *et al.* reported that the methyl esters of α-L-aspartyl-L-valine, -L-leucine, and -L-isoleucine were bitter.[1] The results show that, in the cases of the aspartyl dipeptides with the L–L configuration, L-norvaline seems to be the smallest amino acid to give a sweet derivative; they also show that the substitution of a methyl group for a hydrogen on the β- or γ-carbon of the amino acid results in a bitter taste (Table 2). A similar relationship was found to hold for the methyl esters of α-L-aspartyl-*O*-acyl-L-threonine, -*O*-acyl-L-allothreonine, and -D-alanylsarcosine (*vide post*). α-L-Aspartyl-β-alanine methyl ester (**6**) and -β-alanine *i*-propyl ester (**7**) lacking an asymmetric carbon were sweet, about equal to sucrose and 7 times sucrose respectively. α-L-Aspartyl-DL-β-amino-*n*-butyric acid methyl ester (**4**) and -γ-amino-*n*-butyric acid methyl ester (**5**) were similar in potency to sucrose. α-L-Aspartyl-L-lysine methyl ester (**8**) was bitter, while α-L-aspartyl-N^{ε}-acetyl-L-lysine methyl ester (**9**) as well as α-L-aspartyl-N^{δ}-acetyl-L-ornithine methyl ester (**10**) was sweet, about equal to sucrose. α-L-Aspartyl-DL-(α-methyl)phenylalanine methyl ester (**11**) and -DL-(α-methyl)glutamic acid dimethyl ester (**12**) were sweet, 5 times sucrose and 8 times sucrose respectively. The results show that the α-hydrogen is not necessary for sweetness, but can be replaced by a methyl group without losing sweetness. α-L-Aspartyl-D-alanylglycine methyl ester (**13**), a tripeptide, was 3 times as sweet as sucrose, and the replacement of the glycine by sarcosine resulted in a bitter taste. They are reasonable results if the D-alanylglycine methyl ester is considered as approximately equivalent to an L-2-amino-alkane such as L-2-amino-octane,[2] and if the replacement of the glycine by sarcosine is also considered as approximately equivalent to the introduction of a methyl group into the γ-position of alkyl amines (*e.g.*, L-1,3-dimethylbutylamine[2]) or amino acids (*e.g.*, L-Leu-OMe in Table 2). Therefore, the former is sweet and the latter is bitter. No compound sweeter than APM was found. The results are summarized in Table 1.

At the present time, the phenomenon of a sweet taste seems best explained by the hydrogen bond between receptor site of the "sweet-sensitive protein" and the sweet unit of the chemical compound. Therefore, we are interested in the contribution of a hydroxyl group to the degree of sweetness, since there has been no systematic and thorough study of the evaluation of a hydroxyl group, though the introduction of hetero-atoms, including a hydroxyl group, resulted in the diminution of the potency.[1,2] In order to evaluate the contribution of a hydroxyl group, we intended to introduce a hydroxyl group into the β-position of the norleucine of α-L-aspartyl-L-norleucine methyl ester (**15**) with a sweetness potency of 45 times sucrose. When *erythro*- and *threo*-β-hydroxy-L-norleucine were substituted for the norleucine, the sweetness fell off

Table 1. Taste of aspartyl peptides (α-L-Asp-X)

	X[a]	Taste[b]
1	L-Nva-OMe	4
2	L-Abu-OMe	tasteless
3	D-Abu-OMe	16
4	DL-β-Abu-OMe	+
5	γ-Abu-OMe	+
6	β-Ala-OMe	+
7	β-Ala-OPr^i	7
8	L-Lys-OMe	bitter
9	L-Lys(Ac)-OMe	+
10	L-Orn(Ac)-OMe	+
11	DL-(α-Me)Phe-OMe	5
12	DL-(α-Me)Glu-$(OMe)_2$	8
13	D-Ala-Gly-OMe	3
14	D-Ala-Sar-OMe	bitter

a) Abbreviations according to IUPAC-IUB Commission on Biochemical Nomenclature, *Arch. Biochim. Biophys.*, **150**, 1 (1972). b) Number times sweeter than sucrose. In addition, + = 1—2 times sucrose (5% sucrose level).

rapidly; α-L-aspartyl-*erythro*-β-hydroxy-L-norleucine methyl ester (**16**) was 18 times as sweet as sucrose, and the corresponding *threo*-isomer (**17**) was 7 times sucrose (Table 3). It seems to be true that the introduction of a hydroxyl group into a dipeptide with the L–L configuration results in a diminution in the potency.

Next, we synthesized the esters of α-L-aspartyl-*O*-acyl-L-serine (**18**—**21**). α-L-Aspartyl-*O*-acetyl-L-serine methyl ester (**18**), as well as the *O*-*n*-propionyl (**19**), *O*-*n*-butyroyl (**20**), and *O*-*i*-butyroyl (**21**) analogs, was sweet (Table 3). From an examination of a model, this is a reasonable result if the *O*-acylated part is considered as approximately equivalent to the *n*-butyl part of norleucine of **15** (Table 3). The replacement of the methyl ester group by the ethyl ester gave compounds with reduced potency; α-L-aspartyl-*O*-acetyl-L-serine ethyl ester was slightly sweet, about equal to sucrose, the *O*-*n*-butyroyl analog was 10 times as sweet as sucrose, and the *O*-*i*-butyroyl analog was 3 times sucrose. The replacement of the serine by L-threonine or by L-allothreonine resulted in bitter compounds; the methyl esters of α-L-aspartyl-*O*-acyl-L-threonine and -*O*-acyl-L-allothreonine (acyl: *n*-butyroyl and *i*-butyroyl) were bitter (Table 2). These results support the idea that the substitution of a methyl group for a hydrogen on the β-carbon of amino acids may result in a bitter substance (Table 2 and see also Ref. 1).

In order to find out more information about hydroxyl function, α-L-aspartyl-D-serine esters (**22**—**28**) were synthesized. α-L-Aspartyl-D-serine methyl ester (**22**), as well as the ethyl (**23**), *n*-propyl (**24**), *i*-propyl (**25**), *n*-butyl (**26**), *i*-butyl (**27**), and cyclohexyl (**28**) esters, was found to have an intensely sweet taste (Table 3). It was surprising to us that α-L-aspartyl-D-serine esters, in spite of having a hydroxyl group, were sweeter than α-L-aspartyl-D-alanine esters[3g] without a hydroxyl group; *e.g.*, α-L-aspartyl-D-serine *n*-propyl ester (**24**) was 320 times as sweet as sucrose, while the corresponding α-L-aspartyl-D-alanine *n*-propyl ester (**29**) was 125 times sucrose. The increased sweetness of the peptides

Table 2. Taste of α-L-aspartyl peptides and amides (α-L-Asp-X)

X: Symbol[a]	X: Structure	Taste[b]
L-Nva-OMe (**1**)	$HNCH(COOCH_3)CH_2CH_2CH_3$	4
L-Leu-OMe	$HNCH(COOCH_3)CH_2CH(CH_3)_2$	bitter[2]
L-Ile-OMe	$HNCH(COOCH_3)CH(CH_3)CH_2CH_3$	bitter[2]
D-Ala-Gly-OMe (**13**)	$HNCH(CH_3)CONHCH_2COOCH_3$	3
D-Ala-Sar-OMe (**14**)	$HNCH(CH_3)CON(CH_3)CH_2COOCH_3$	bitter
L-2-Amino-octane	$NHCH(CH_3)CH_2CH_2CH_2CH_2CH_2CH_3$	10[2]
L-Ser-OMe (**21**)	$HNCH(COPr^i)CH_2OCOCH(CH_3)_2$	50
L-Thr-OMe	$HNCH(COPr^i)CH(CH_3)OCOCH(CH_3)_2$	bitter
D-Ser-OPr^n (**24**)	$HNCH(CH_2OH)COOCH_2CH_2CH_3$	320
D-Ala-OPr^n (**29**)	$HNCH(CH_3)COOCH_2CH_2CH_3$	125
L-Amphetamine	$HNCH(CH_3)CH_2C_6H_5$	50[2]
L-1-Hydroxymethyl-2-phenylethyl-amine	$HNCH(CH_2OH)CH_2C_6H_5$	1—2[2]
D-Thr-OPr^n (**32**)	$HN-C(CH_3)(H)-C(H)(COOCH_2CH_2CH_3)$	150
D-aThr-OPr^n (**39**)	$HN-C(CH_3)(OH)-C(H)(COOCH_2CH_2CH_3)$	40
D-Abu-OPr^n (**44**)	$HNCH(CH_2CH_3)COOCH_2CH_2CH_3$	95

a) See Table I for abbreviations. b) Number times sweeter than sucrose (5% sucrose level).

(**22**—**28**) would not have been predicted from the previous results, since the replacement of the amino acids or amines by those with a hydroxyl group always resulted in the diminution of the potency;[1,2] *e.g.*, α-L-aspartyl-L-amphetamine is 50 times as sweet as sucrose, while α-L-aspartyl-1-hydroxymethyl-2-phenylethylamine is only 1—2 times sucrose in sweetness[2] (Table 2).

This finding led us to synthesize the esters of α-L-aspartyl-D-threonine (**30**—**36**) and -D-allothreonine (**37**—**43**). It was found that they all have an intensely sweet taste (Table 3). It is very interesting to note that the esters of α-L-aspartyl-D-threonine (**30**—**36**) were sweeter than the esters of α-L-aspartyl-D-α-amino-*n*-butyric acid,[3g] which lacks a hyrdoxyl group of the D-threonine, as in the case of the esters of α-L-aspartyl-D-serine and -D-alanine. The replacement of the D-threonine by D-allothreonine resulted in a significant diminution of the potency; *e.g.*, α-L-aspartyl-D-α-amino-*n*-butyric acid *n*-propyl ester (**44**) was 95 times as sweet as sucrose, α-L-aspartyl-D-threonine *n*-propyl ester (**32**) was 150 times sucrose, and α-L-aspartyl-D-allothreonine *n*-propyl ester (**39**) was 40 times sucrose. With an increase in the size of the ester, the potency increased peaking at the chain length of three carbons, such as the *n*-propyl and *i*-butyl esters (Table 3). It is also of interest to note that the configurational change in the hydroxyl group results in a change in the potency, as is shown in Table 3 (**16** and **17**, and **30**—**36** and **37**—**43**). In the cases of the peptides with the L-D configuration, the *threo*-isomers were sweeter than the corresponding *erythro*-isomers, in contrast to the cases of the L-L peptides. In the cases of the L-L peptides, the *erythro*-isomers were sweeter than the corresponding *threo*-isomers, as has been described in the case of α-L-aspartyl-β-hydroxy-L-norleucine methyl ester (**16** and **17**). The results (Table 3) indicate that the introduc-

Table 3. Sweetness values of aspartyl dipeptide esters

	Compound[a]	Mp (°C)	Sweetness value[b]	Formula	Calcd %			Found %		
					C	H	N	C	H	N
15	α-L-Asp-L-Nle-OMe	148—149	45	$C_{11}H_{20}O_5N_2\cdot 1/2H_2O$	49.06	7.86	10.40	49.59	7.60	10.50
16	α-L-Asp-L-*e*-HyNle-OMe	172—173	18	$C_{11}H_{20}O_6N_2O\cdot H_2O$	44.89	7.54	9.52	45.08	7.61	9.51
17	α-L-Asp-L-*t*-HyNle-OMe	167—168	7	$C_{11}H_{20}O_6N_2O\cdot H_2O$	44.89	7.54	9.52	44.76	7.61	9.66
18	α-L-Asp-L-Ser-OMe $COCH_3$ |	88—89.5	10	$C_{10}H_{16}O_7N_2\cdot 1/2H_2O$	42.10	6.01	9.82	41.72	5.82	9.76
19	α-L-Asp-L-Ser-OMe $COCH_2CH_3$ |	86—87	40	$C_{11}H_{18}O_7N_2\cdot 1/2H_2O$	44.14	6.40	9.36	44.24	6.32	9.24
20	α-L-Asp-L Ser-OMe $COCH_2CH_2CH_3$ |	102—103	30	$C_{12}H_{20}O_7N_2\cdot 1/2H_2O$	46.00	6.76	8.94	45.72	6.59	8.81
21	α-L-Asp-L-Ser-OMe $COCH(CH_3)_2$ |	116—116.5	50	$C_{12}H_{20}O_7N_2\cdot 1/2H_2O$	46.00	6.76	8.94	45.96	6.62	9.07
22	α-L-Asp-D-Ser-OMe	183—184	45	$C_8H_{14}O_6N_2$	41.02	6.03	11.96	40.74	5.96	11.86
23	α-L-Asp-D-Ser-OEt	193—194	115	$C_9H_{16}O_6N_2$	43.54	6.50	11.29	43.46	6.41	11.26
24	α-L-Asp-D-Ser-OPr^n	194—195	320	$C_{10}H_{18}O_6N_2$	45.79	6.92	10.68	45.42	6.83	10.68
25	α-L-Asp-D-Ser-OPr^i	198—199	120	$C_{10}H_{18}O_6N_2$	45.79	6.92	10.68	45.59	6.78	10.66
26	α-L-Asp-D-Ser-OBu^n	192—193	70	$C_{11}H_{20}O_6N_2$	47.82	7.30	10.14	47.56	7.21	10.05
27	α-L-Asp-D-Ser-OBu^i	188—189	200	$C_{11}H_{20}O_6N_2$	47.82	7.30	10.14	47.63	7.22	10.30
28	α-L-Asp-D-Ser-OC_6H_{11}	198—199	60	$C_{13}H_{22}O_6N_2\cdot 1/2H_2O$	50.15	7.45	9.00	50.10	7.13	8.97
29	α-L-Asp-D-Ala-OPr^n	143—144	125	$C_{10}H_{18}O_5N_2\cdot H_2O$	45.44	7.63	10.60	45.39	7.38	10.66
30	α-L-Asp-D-Thr-OMe	158—159	25	$C_9H_{16}O_6N_2\cdot H_2O$	40.60	6.81	10.52	40.45	6.63	10.14
31	α-L-Asp-D-Thr-OEt	160—161	110	$C_{10}H_{18}O_6N_2\cdot 3/2H_2O$	41.51	7.32	9.68	41.34	6.79	9.62
32	α-L-Asp-D-Thr-OPr^n	155—156	150	$C_{11}H_{20}O_6N_2$	47.82	7.30	10.14	47.96	7.25	10.33
33	α-L-Asp-D-Thr-OPr^i	84—85	105	$C_{11}H_{20}O_6N_2\cdot 3/2H_2O$	43.56	7.64	9.24	43.42	7.65	9.29
34	α-L-Asp-D-Thr-OBu^n	82—83	30	$C_{12}H_{22}O_6N_2\cdot H_2O$	46.74	7.85	9.09	46.50	7.43	9.05
35	α-L-Asp-D-Thr-OBu^i	142—143	110	$C_{12}H_{22}O_6N_2$	49.64	7.64	9.65	49.89	7.42	9.58
36	α-L-Asp-D-Thr-OC_6H_{11}	180—181	30	$C_{14}H_{24}O_6N_2\cdot 1/2H_2O$	51.68	7.75	8.61	51.31	7.58	8.60
37	α-L-Asp-D-aThr-OMe	181—182	7	$C_9H_{16}O_6N_2$	43.54	6.50	11.29	43.37	6.30	11.40
38	α-L-Asp-D-aThr-OEt	181—182	6	$C_{10}H_{18}O_6N_2$	45.79	6.92	10.68	45.91	6.70	10.77
39	α-L-Asp-D-aThr-OPr^n	176—177	40	$C_{11}H_{20}O_6N_2$	47.82	7.30	10.14	47.86	7.12	9.98
40	α-L-Asp-D-aThr-OPr^i	182—183	10	$C_{11}H_{20}O_6N_2$	47.82	7.30	10.14	47.91	7.03	10.26
41	α-L-Asp-D-aThr-OBu^n	173—174	20	$C_{12}H_{22}O_6N_2$	49.64	7.64	9.65	49.51	7.35	9.66
42	α-L-Asp-D-aThr-OBu^i	183—184	27	$C_{12}H_{22}O_6N_2$	49.64	7.64	9.65	49.65	7.44	9.61
43	α-L-Asp-D-aThr-OC_6H_{11}	198—199	22	$C_{14}H_{24}O_6N_2$	53.15	7.65	8.86	53.18	7.36	8.89
44	α-L-Asp-D-Abu-OPr^n	85—86.5	95	$C_{11}H_{20}O_5N_2\cdot H_2O$	47.47	7.97	10.07	47.26	7.74	9.97

a) See Table 1 for abbreviations. b) Number times sweeter than sucrose (5% sucrose level).

tion of a hydroxyl group into the L–D peptides does not always result in a diminution of their potencies, but sometimes increase their potencies, in contrast to the cases of the L–L peptides. In the cases of the L–L peptides, the potencies always decreased when a hydroxyl group was introduced, as has been described above and as has been reported by Mazur *et al.*[1,2] The contribution of a hydroxyl group to the L–D peptides seems to differ significantly from that to the L–L peptides. These results would appear to hold considerable promise for clarifying the interaction between the receptor site and the sweet unit. More detailed studies concerning this problem are now in progress.

Experimental

All the melting points are uncorrected. The optical rotations were measured with a visual polarimeter. All the compounds reported here were homogeneous on thin-layer chromatography on silica. Spots were detected first by the ninhydrin method and then by the starch-iodide method, as modified by one of us.[6] The acylated NH groups, if any, can be detected at the 0.1—0.25 μg level after chromatography by the latter method.

Starting Materials. L- and D-α-Amino-*n*-butyric acid, L-norvaline, L-norleucine, D-serine, and D-allothreonine were obtained without any difficulty *via* the L-directed asymmetric hydrolytic action of the mold acylase on their *N*-acetyl racemates by the usual procedure.[7] L-α-Amino-*n*-butyric acid: $[\alpha]_D^{21}$ +20.5° (*c* 2, 5 M HCl). lit,[7] $[\alpha]_D^{25}$ +20.6° (*c* 2, 5 M HCl). D-α-Amino-*n*-butyric acid: $[\alpha]_D^{21}$ −20.5° (*c* 2, 5 M HCl). lit,[7] $[\alpha]_D^{25}$ −20.7° (c 2, 5 M HCl). L-Norvaline: $[\alpha]_D^{26}$ +24.3° (*c* 2, 5 M HCl). lit,[7] $[\alpha]_D^{25}$ +24.9° (*c* 2, 5 M HCl). L-Norleucine: $[\alpha]_D^{25}$ +24.0° (*c* 1, 6 M HCl). lit,[8] $[\alpha]_D^{23}$ +23.3° (*c* 4.15, 6 M HCl). D-Serine: $[\alpha]_D^{19}$ −15.8° (*c* 2, 6 M HCl). lit,[7] $[\alpha]_D^{25}$ −15.0° (*c* 2, 5 M HCl). D-Allothreonine: $[\alpha]_D^{26}$ −9.6° (*c* 4, water). lit,[7] $[\alpha]_D^{25}$ −9.6° (*c* 4, water). D-Threonine, which had been resolved by the preferential crystallization, was left over from a previous investigation.[9] $[\alpha]_D^{29}$ +28.7° (*c* 2, water). lit,[7] $[\alpha]_D^{25}$ +28.5° (c 2, water). *threo*- and *erythro*-β-Hydroxy-L-norleucine: β-Hydroxynorleucine was resolved *via* the asymmetric synthetic action of papain on *N*-benzoyl-β-methoxynorleucine by Adams and Niemann.[10] We will now describe a more convenient method of resolving the two diastereoisomeric racemates of β-hydroxynorleucine *via* the L-directed asymmetric hydrolytic action of a mold acylase on their *N*-acetyl derivatives. β-Hydroxynorleucine was prepared by the condensation of copper glycinate with *n*-butyraldehyde according to the method described by Mix[11] and was then separated into the two diastereoisomeric racemates through their tetrachlorophthalic acid salts according to the method previously reported by one of the present authors.[12] *N*-Acetyl-*threo*- and -*erythro*-β-hydroxy-DL-norleucine were obtained by the usual acetylation of *threo*- and *erythro*-β-hydroxy-DL-norleucine with acetic anhydride. *N*-Acetyl-*threo*-β-hydroxy-DL-norleucine: yield, 82%; mp 149—150.5 °C (decomp.). Found: C, 50.86; H, 8.08; N, 7.40%. Calcd for $C_8H_{15}O_4N$: C, 50.78; H, 7.99; N, 7.40%. *N*-Acetyl-*erythro*-β-hydroxy-DL-norleucine: yield, 82%; mp 137—138 °C. Found: C, 50.97; H, 8.02; N, 7.35%. The optical resolution of *N*-acetyl-*threo*- and -*erythro*-β-hydroxy-DL-norleucine was not easily accomplished because the rate of the hydrolysis was found to be considerably lower than those observed with other amino acids, such as norvaline and serine.

Incubation with Enzyme. A solution of *N*-acetyl-*threo*-β-hydroxy-DL-norleucine (18.4 g) in water (1800 ml) was adjusted to pH 7.0 with an aqueous sodium hydroxide solution. To the solution, there were then added cobaltous chloride hexahydrate (0.43 g) and the mold acylase (0.36 g).[13] The solution was incubated at 38 °C for 8 days. During the incubation, an additional acylase (0.18 g) was added every other day to the solution.

Isolation of threo-*β-Hydroxy-*D*-norleucine.* In order to separate the free L-amino acid and *N*-acetyl-D-amino acid, the solution was passed through a column (3×50 cm) of Diaion SK 1B[14] (H-form) and the column was washed with water. The fractions containing the *N*-acetyl-D-amino acid were combined and concentrated *in vacuo* to dryness. The residue was dissolved in water and decolorized with charcoal. The solution was concentrated *in vacuo* until the crystals appeared. After storage in a refrigerator overnight, the crystals of *N*-acetyl-*threo*-β-hydroxy-D-norleucine thus formed were collected by filtration; yield, 8.3 g (89%); mp 136—138 °C. Found: C, 50.85; H, 7.95; N, 7.40%.

A solution of *N*-acetyl-*threo*-β-hydroxy-D-norleucine (8.3 g) in 3 M hydrochloric acid (83 ml) was heated under reflux for 6 hr and then concentrated *in vacuo* to dryness. The residue was dissolved in water, and the solution was adjusted to pH 6.0 with an aqueous sodium hydroxide solution and poured onto a column (3×50 cm) of Diaion SK 1B (H-form). The column was washed with water, and then the D-amino acid was eluted with 1.5 M ammonium hydroxide. The eluate was concentrated *in vacuo* to a small volume, and then a sufficient amount of ethanol was added to the concentrate to give 5.7 g (88%) of crystals (*threo*-β-hydroxy-D-norleucine), which were subsequently recrystallized from water–ethanol; yield, 4.8 g (74%); mp 222—224 °C (decomp.); $[\alpha]_D^{25}$ −4.8° (*c* 2, water) and −18.5° (*c* 2, 5 M HCl); $[M]_D^{25}$ −7.0° (*c* 2, water) and −27.2° (*c* 2, 5 M HCl). lit,[10] mp 185—188 °C (decomp.); $[\alpha]_D^{25}$ −4.6° (*c* 3.50, water) and −18.5° (*c* 2.28, 6.03 M HCl). Found: C, 49.40; H, 8.79; N, 9.44%. Calcd for $C_6H_{13}O_3N$: C, 48.96; H, 8.90; N, 9.52%.

Isolation of threo-*β-Hydroxy-*L*-norleucine.* The column, adsorbing the free L-amino acid, was washed with water (200 ml) to remove completely the trace amount of the *N*-acetyl-D-amino acid from the column. The L-amino acid was eluted with 1.5 M ammonium hydroxide. The eluate was concentrated *in vacuo* to a small volume, and then a sufficient amount of ethanol was added to the concentrate to give 5.8 g (89%) of the L-amino acid, which was subsequently recrystallized from water–ethanol; yield, 5.0 g (70%); mp 222—223 °C (decomp.); $[\alpha]_D^{25}$ +4.5° (*c* 2, water) and +18.5° (*c* 2, 5 M HCl); $[M]_D^{25}$ +6.6° (*c* 2, water) and +27.7° (*c* 2, 5 M HCl). lit,[10] mp 184—188 °C (decomp.); $[\alpha]_D^{25}$ +4.6° (*c* 3.46, water) and +18.6° (*c* 2.42, 6.07 M HCl). lit,[15] $[M]_D^{25}$ 6.8° (*c* 2, water) and +27.4° (*c* 2, 5 M HCl). Found: C, 48.80; H, 8.63; N, 9.40%.

The resolution of the racemic *erythro*-isomer was carried out by the manner described in the resolution of the racemic *threo*-isomer, except that the *N*-acetyl-D-amino acid was obtained as an oil; it was subjected to acid hydrolysis without further purification.

erythro-β-Hydroxy-D-norleucine: yield, 76%; mp 241—242 °C (decomp.); $[\alpha]_D^{25}$ +2.3° (*c* 2, water) and −28.3° (*c* 2, 5 M HCl); $[M]_D^{25}$ +3.4° (*c* 2, water) and −41.6° (*c* 2, 5 M HCl). lit,[10] mp 198—202 °C (decomp.); $[\alpha]_D^{26}$ +2.0° (*c* 8.81, water) and $[\alpha]_D^{25}$ −27.4° (*c* 2.63, 6.07 M HCl). Found: C, 48.99; H, 8.72; N, 9.57%.

erythro-β-Hydroxy-L-norleucine: yield, 89%; mp 240.5—241.5 °C (decomp.); $[\alpha]_D^{25}$ −2.3° (*c* 2, water) and +28.3°

(*c* 2, 5 M HCl); $[M]_D^{25}$ −3.4° (*c* 2, water) and +41.6° (*c* 2, 5 M HCl). lit,[10] mp 203—205 °C (decomp.); $[\alpha]_D^{22}$ −2.0° (*c* 5.87, water) and $[\alpha]_D^{25}$ +27.1° (*c* 2.47, 6.07 M HCl). lit,[15] $[M]_D^{25}$ −2.9° (*c* 2, water) and +39.9° (*c* 2, 5 M HCl). Found: C, 48.96; H, 8.63; N, 9.45%.

Hydrochlorides of Amino Acid Esters. In a typical procedure (D-serine *i*-propyl ester hydrochloride), into a suspension of D-serine (10.5 g) in *i*-propyl alcohol (200 ml) was bubbled dry hydrogen chloride gas without external cooling. After the crystals had gone into solution, the reaction mixture was boiled under reflux for 5 hr and then concentrated *in vacuo*. Benzene (100 ml) was added to the residue; the solution was then evaporated *in vacuo* to remove the trace amount of water, and then the esterification procedure was repeated. The reaction mixture was concentrated *in vacuo* to give the crude ester, which was recrystallized from *i*-propyl alcohol–ether; yield, 13.7 g (75%); mp 145—146 °C.

The other amino acids were esterified with an appropriate alcohol by the same procedure, and the resulting hydrochlorides of amino acid esters were recrystallized from the appropriate alcohol and ether. When *n*-butanol, *i*-butyl alcohol and cyclohexanol were employed, the reaction temperature was maintained at 100 °C.

*α-L-Aspartyl-O-acyl-L-serine Esters (**18**—**21**).* In a typical procedure (**21** in Table 3), β-benzyl-*N*-carbobenzoxy-L-aspartyl-L-serine methyl ester[16] (4.6 g) was dissolved in pyridine (50 ml) and cooled in an ice bath, and then *i*-butyric anhydride (3.2 g) was stirred in. After stirring for 3 hr at room temperature, the reaction mixture was stirred into 500 ml of water containing ice flakes. The crystals thus formed were collected by filtration and washed with 0.7 M hydrochloric acid and then water; yield, 5.1 g (98%). Recrystallization from ethyl acetate–petroleum ether gave 4.7 g (91%) of β-benzyl-*N*-carbobenzoxy-L-aspartyl-*O*-*i*-butyroyl-L-serine methyl ester; mp 95—96 °C. Found: C, 61.58; H, 6.16; N, 5.31%. Calcd for $C_{27}H_{32}O_9N_2$: C, 61.35; H, 6.10; N, 5.30%.

A solution of the dipeptide derivative (4.0 g) in 90% methanol (50 ml) was hydrogenated in the presence of 5% palladium on charcoal (0.4 g) for 5 hr. After the removal of the catalyst by filtration, the filtrate was concentrated *in vacuo* to give a crystalline residue. Recrystallization from aqueous methanol gave 1.3 g (54%) of α-L-aspartyl-*O*-*i*-butyroyl-L-serine methyl ester.

The results are shown in Table 3.

*The Esters of α-L-Aspartyl-*erythro- *and* -threo-*β-hydroxy-L-norleucine (**16** and **17**), -D-serine (**22**—**28**), -D-threonine (**30**—**36**), and -D-allothreonine (**37**—**43**).* In a typical procedure (**25** in Table 3), β-benzyl-*N*-carbobenzoxy-L-aspartate[17] (7.2 g) was dissolved in chloroform (50 ml) and cooled in an ice bath, and then *N,N'*-dicyclohexylcarbodiimide (4.3 g) was added. After 20 mins' stirring in the ice bath, a solution of *i*-propyl D-serinate hydrochloride (4.0 g) and triethylamine (2.3 g) in chloroform (50 ml) was added to the reaction mixture. After stirring for 6 hr at room temperature, a few drops of acetic acid were added to the reaction mixture. After the removal of *N,N'*-dicyclohexylurea by filtration, the filtrate was concentrated *in vacuo*. The residue was dissolved in ethyl acetate and washed successively with 1 M hydrochloric acid, a 5% sodium bicarbonate solution, and water, and finally dried over sodium sulfate. After filtration, the filtrate was concentrated *in vacuo* to give 7.6 g (78%) of β-benzyl-*N*-carbobenzoxy-L-aspartyl-D-serine *i*-propyl ester; mp 80.5—81.5 °C. Found: C, 61.35; H, 6.16; N, 5.65%. Calcd for $C_{25}H_{30}O_8N_2$: C, 61.71; H, 6.22; N, 5.76%.

A solution of the protected dipeptide derivative (5.0 g) in 75% acetic acid (100 ml) was hydrogenated in the presence of 5% palladium on charcoal (0.5 g) at room temperature for 5 hr. After the removal of the catalyst by filtration, the filtrate was concentrated *in vacuo* to give crystals, which were subsequently recrystallized from aqueous methanol; yield, 2.2 g (82%). Recrystallization from water gave 1.5 g of α-L-aspartyl-D-serine *i*-propyl ester.

The results are shown in Table 3.

Sweetness Evaluation. The sweetness values of the dipeptide derivatives were organoleptically determined by panel evaluation, with ten to fifteen people per panel, in our Foodstuff Development Laboratory. In a series of tests with aqueous solutions, samples of the peptides and samples of various levels of sucrose (3—8%) were compared for relative sweetness. The tests were carried out at concentrations higher than threshold in order to provide a comparison at a practical level. In a typical comparison test, an aqueous solution of α-L-aspartyl-D-serine *n*-propyl ester containing 0.02% was rated in between a 6.08 and a 7.00% sucrose solution, putting it in the 305—350 sweetness range. Therefore, the compound was assumed about 320 times as sweet as sucrose.

The results are shown in Tables 1, 2, and 3.

The authors wish to express their thanks to Mr. Fusayoshi Kakizaki and Miss Yuki Nakakouji for their skillful technical assistances and to Miss Sachiko Suzuki and Miss Harue Yamada for their evaluations of sweetness.

References

1) R. H. Mazur, J. M. Schlatter, and A. H. Goldkamp, *J. Amer. Chem. Soc.*, **91**, 2684 (1969).
2) R. H. Mazur, A. H. Goldkamp, P. A. James, and J. M. Schlatter, *J. Med. Chem.*, **13**, 1217 (1970).
3) a) J. M. Schlatter, Ger. Offen. 1936159 (1970); b) T. Sheehan, *ibid.*, 2054545 (1971); c) N. Nakajima, H. Aoki, M. Fujino, O. Nishimura, and M. Wakimasu, *ibid.*, 2141771 (1972); d) N. Nakajima, H. Aoki, M. Fujino, O. Nishimura, M. Wakimasu, and M. Mano, *ibid.*, 2160042 (1972); e) J. J. Dahlmans and W. H. J. Boesten, Neth. Appl. 7012897, 7012898, and 7012899; f) R. H. Mazur, A. H. Goldkamp, and J. M. Schlatter, Japan. 7339 (1972); g) R. H. Mazur, J. M. Schlatter, and J. Myron, Fr. Addn. 2114657 (1973); h) Y. Fujimoto, Japan. 8829 (1973).
4) M. T. Briggs and J. S. Murley, Brit. 1299265 (1972).
5) M. Lapidus and M. Sweeney, *J. Med. Chem.*, **16**, 163 (1973).
6) Y. Ariyoshi, N. Sato, H. Zenda, and K. Adachi, This Bulletin, **44**, 2558 (1971).
7) S. M. Birnbaum, L. Levintow, R. B. Kingsley, and J. P. Greenstein, *J. Biol. Chem.*, **194**, 455 (1952).
8) J. P. Greenstein, J. B. Gilbert, and P. J. Fodor, *ibid.*, **182**, 451 (1950).
9) K. Itoh, T. Akashi, and S. Tatsumi, Japan. 17710 (1961).
10) R. T. Adams and C. Niemann, *J. Amer. Chem. Soc.*, **73**, 4260 (1951).
11) H. Mix, *Z. Physiol. Chem.*, **327**, 41 (1961).
12) Y. Ariyoshi and N. Sato, This Bulletin, **44**, 3435 (1971).
13) The acylase was furnished by Amano Seiyaku Co., Nagoya.
14) A strong cation-exchange resin with sulfonic acid functional groups from Mitsubishi Chem. Ind. Ltd.
15) J. P. Greenstein and M. Winitz, "Chemistry of Amino Acids," Vol. 3, John Wiley & Sons, Inc. New York, N. Y. (1961), p. 2608.
16) R. W. Hanson and H. N. Rydon, *J. Chem. Soc.*, **1964**, 836.
17) L. Benoiton, *Can. J. Chem.*, **40**, 570 (1962).

The Photochemical and the Thermal Reaction of Dimethyl *trans*-Spiro[2.6]nona-4,6,8-triene-1,2-dicarboxylate[1]

Katsuhiro SAITO, Takashi TODA, and Toshio MUKAI

Department of Chemistry, Faculty of Science, Tohoku University, Aoba, Aramaki, Sendai 980

(Received August 13, 1973)

The irradiation of dimethyl *trans*-spiro[2.6]nona-4,6,8-trien-1,2-dicarboxylate (I) with a low-pressure mercury lamp afforded two tricyclic valence isomers (II and III). Upon heating, II and III were converted into dimethyl *trans*-indan-1,2-dicarboxylate (IV), which was also obtained by the thermolysis of I. In order to elucidate the reaction mechanism for the formation of IV from I, we studied the thermal reaction using a deuterium-labelled compound (V).

Dimethyl *trans*-spiro[2.6]nona-4,6,8-trien-1,2-dicarboxylate (I)[2,3] is an interesting unsaturated cyclic compound; it possesses both a cycloheptatriene and a cyclopropane ring, like the spiro system. Therefore, it seems that it would be interesting to study the thermal photochemical reactions of I to distinguish whether such a compound behaves as a spiro compound,[3-8] as a cyclopropane derivative, or as a cycloheptatriene derivative. It has already been reported by Jones and Ennis[3] and by our group[2] that I, when heated over 150 °C, easily rearranged to dimethyl *trans*-indan-1,2-dicarboxylate (IV). On the other hand, however, no photochemical study of I has ever been reported. We investigated the photoreaction of I and found that I exhibited the photochemical valence isomerization characteristic of the cycloheptatriene moiety.[9-14] In addition, the reaction mechanism of the thermolysis of I leading to IV was studied using a deuterized spiro compound (V). In this paper, we wish to report the results obtained concerning the photoreaction and the reaction mechanism of the thermolysis of I.

The irradiation of I, which has an absorption maximum at 263 nm (log ε, 3.52) and a tailing around 350 nm (log ε, ca 2.5), using a high-pressure mercury lamp, did not cause any photoreaction, but resulted in the recovery of I in a quantitative yield. The benzophenone-sensitized photoreaction of I also resulted in the recovery of I. On the other hand, when the irradiation of I was carried out in a quartz vessel using a low pressure mercury lamp, a crystalline material (II) (mp 105.5 °C), and an oily substance (III) were obtained in 23 and 22% yields respectively. When methanol, ether and *n*-hexane were used as the solvents, no solvent effect was observed. Under these irradiation conditions, no interconversion between II and III was detected; this fact indicated that II and III were the primary photoproducts.

The two products, II and III, have the same molecular formula, $C_{13}H_{14}O_4$, and the same molecular ion peak (M^+, 234) in their mass spectra. In addition, they possess almost the same spectral properties: IR ($CHCl_3$), 1720, 1440, 1340, and 1160 cm^{-1}; UV (methanol), 225 nm (log ε, 3.39). Their NMR spectra are shown in Table 1, while the coupling constants as determined by the double and triple resonance techniques are shown in Table 2. These data support the idea that II and III are isomers of I, and that they are stereoisomers with relation to each other. In addition, the chemical shifts and coupling constant of the H_c–H_h protons of II and III are similar to those of the corresponding protons of the bicyclo[3.2.0]hept-2,5-diene derivatives.[10-14] The H_a and H_b protons are assigned to the cyclopropane protons which are located in the *trans*-configuration on the basis of the chemical shifts, which are coincident with those of the cyclopropane protons of I, and the coupling constant (5.5 Hz).[15] Thus, the structure shown in Fig. 1 are proposed for II and III.

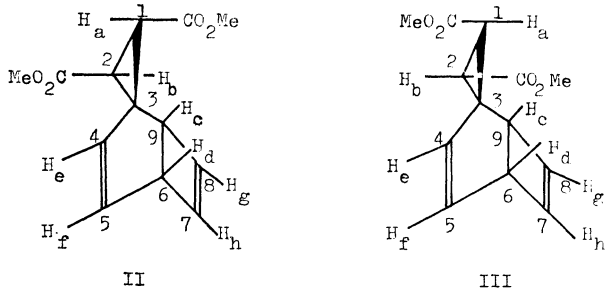

Fig. 1.

The configuration of the two ester groups of II and III could be deduced from the chemical shifts of their H_c and H_g values. The signals of the H_c of II appear at a higher field than those of the H_c of III, and the signals of the H_g of II come at a lower field than those of the H_g of III, while the chemical shifts of the other hydrogens of II and III do not differ very much from each other. By an investigation of the Dreiding models of II and III, the ester group at C_1 of II is found to be closer to H_c; also the H_g of III is closer to the ester group at C_2. Furthermore, by the repulsion between the ester group at C_1 and the cyclopropane protons, the conformation in which the sp^2 plane of the ester carbonyl group is set over to H_c is the most stable form of II; also, for the same reason, in the case of III H_g is

TABLE 1. CHEMICAL SHIFTS OF II AND III (δ ppm) (100 MHz, in $CDCl_3$)

	H_a	H_b	H_c	Ester Me	H_d	H_e	H_f	H_g	H_h
II	2.45	2.57	3.19	3.64, 3.66	3.73	5.61	5.97	6.16	6.40
III	2.43	2.54	3.36	3.67, 3.69	3.80	5.56	6.05	5.78	6.39

Table 2. Coupling constants of II and III (Hz)

	J_{ab}	J_{cd}	J_{df}	J_{dh}	J_{ef}	J_{gh}	J_{ce}
II	5.5	3.5	2.5	~1	5.5	3.0	~1
III	5.5	3.5	2.5	~1	5.3	3.0	1.0

covered by the sp^2 plane of the ester group at C_2. Thus, considering the anisotropic effect of the ester groups, the differences in the chemical shifts of H_c and H_g in II and III can be reasonably explained by those models.

The results obtained above make it clear that the irradiation of I did not undergo a reaction involving the cyclopropane ring; instead, the cycloheptatriene ring dominated its photoreaction. The fact that this photoreaction was not sensitized by benzophenone is compatible with the fact that the photovalence isomerization of the cycloheptatriene derivatives proceeds *via* singlet excited states.[11,12] In addition, it should be noted that both ring-closure products, II and III, were formed in almost the same yield, the yields being 22 and 23% respectively. This seems to prove that the ester groups located near the reaction center do not have any effect on the photochemical ring closure of I, either stereochemically or electronically.

The photoproducts, II and III, were fairly stable to heat, and they were recovered when the thermolysis was attempted by a flow method by heating about 350 °C. Above 400 °C, however, both II and III gave the same pyrolyzate, dimethyl *trans*-indan-1,2-dicarboxylate (IV), in good yields. Since I is transformed thermally to IV under less severe pyrolyzing conditions (about 150 °C), it is most probable that II and III, upon heating, are converted first into I by the ring opening and are then rearranged to IV (Scheme 1).

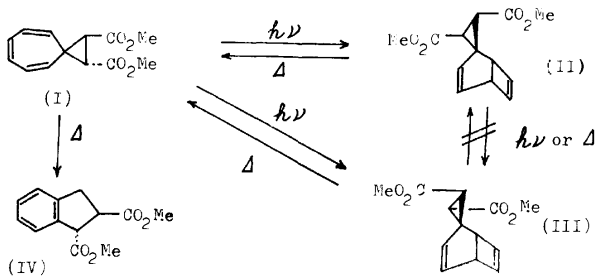

Scheme 1.

Previously, Mukai, Nakazawa, and Isobe suggested the possibility of two reaction paths for the rearrangement of I to IV.[2] Recently, Jones and Ennis also investigated this rearrangement; they pointed out that the rate of the rearrangement depended on the nature of the solvents, and proposed an ionic mechanism resembling the mechanism of Mukai *et al.*[3] Therefore, the following two mechanisms (A and B shown in Scheme 2) are proposed for the rearrangement of I to IV. In order to investigate the adequacy of the mechanisms, A and B, we did the same thermolysis using a dideuterized spiro compound (V), which had been synthesized by the addition reaction of dideuterized dimethyl maleate with cycloheptatrienylidene.[2,3]

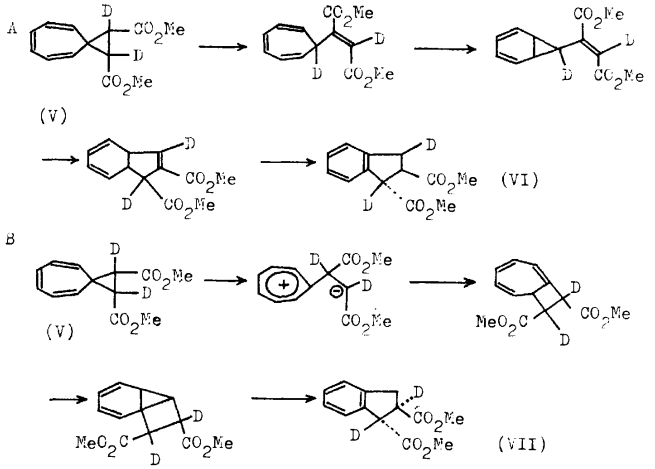

Scheme 2.

As Scheme 2 exhibits, if the reaction proceeds *via* Mechanism A, dimethyl *trans*-1,3-dideuteroindan-1,2-dicarboxylate (VI) will be formed, whereas if Mechanism B occurs, 1,2-dideuteroindane derivative (VII) is formed. On the basis of the NMR spectral data, the indane derivative obtained here found to be VII, not VI. That is, in the NMR spectrum of IV, the methylene protons at the C_3-position and the two methine protons at the C_1- and C_2-positions show their signals at δ 3.1, 3.9 and 4.6 respectively, whereas the indane derivative obtained from V exhibits peaks of the methylene protons at δ 3.1, but does not show any peak ascribed to the methine protons. These results fit VII and confirm that the thermal rearrangement of I proceeds *via* Mechanism B.

Experimental[16]

Photoreaction of I. A solution of I (1.50 g) in *n*-hexane (1.5 l) was irradiated with a low-pressure mercury lamp (Rayonet 2537 Å) in a quartz vessel for 44 hr under a nitrogen atmosphere. After the removal of the resinous substances (100 mg), a yellow oily product (1.4 g) was obtained and subsequently chromatographed on alumina (50 g). A crystalline product (A)(400 mg) was eluted with petroleum ether–benzene (4 : 1); 261 mg of an oily product (B) with petroleum ether–benzene (7 : 3); 174 mg of the starting substance with benzene, and 475 mg of a tarry material with methanol. The crystalline product (A) was found to contain II (60%) and III (40%) by vpc analysis (20% Ucon 50 LB; Chromosorb W; temp. 150 °C). In the same way, the oily product (B) was found to contain II, III, and the starting material in percentages of 18, 42, and 40% respectively. The total yields of II and III were 287 mg and 270 mg (23 and 22%) respectively. Both products were purified by recrystallization from methanol and by distillation. II, mp 104.5—105.5 °C. Found: C, 66.43; H, 6.09%. Calcd for $C_{13}H_{14}O_4$: C, 66.65; H, 6.02%. IR(KBr); 1720, 1440, 1340, and 1160 cm^{-1}. Mass; M^+, 234 at 70 eV. III, oil bp 105 °C/1 mm Hg. Found: C, 66.51; H, 5.92%. Calcd for $C_{13}H_{14}O_4$; C, 66.65; H, 6.02%. IR ($CHCl_3$); 1720, 1440, 1340, and 1160 cm^{-1}. Mass; M^+, 234 at 70 eV.

Thermal Rearrangement of II and III. We attempted to pyrolyze a solution of II (34 mg) in benzene (20 ml) by passing it under a nitrogen stream (30 ml/min) through a quartz tube (9 mm × 45 cm) preheated at 350 °C which

contained quartz pieces. After the removal of the solvent, a white crystalline product was obtained. NMR and vpc studies of the obtained product showed that the crystalline product contained IV and the starting substances in 2.6 and 97.4% yield respectively.

The pyrolysis at a higher temperature (420 °C) resulted in the formation of IV and the recovery of II in 82% and 18% yields respectively. The NMR spectrum and the retention time of the vpc of IV were in accordance with those of an authentic sample of dimethyl *trans*-indan-1,2-dicarboxylate.[2]

By the same procedure at 400 °C, III gave IV in an 80% yield, accompanied by the recovery of III in a 20% yield.

Preparation and Thermal Rearrangement of Dimethyl trans-*1,2-dideuterospiro[2.6]nona-4,6,8-trien-1,2-dicarboxylate (V).* V was formed from the addition reaction of dimethyl dideuteromaleate with troponetosylhydrazone sodium salt by the methods of Jones and Ennis[3] and Mukai *et al.*[2] The thermolysis of V was carried out under the same conditions as were used by Mukai *et al.*[2] Mass; M^+, 236 at 70 eV.

References

1) Organic Photochemistry, XXXII. For the preceeding paper, see H. Tsuruta, T. Kumagai, and T. Mukai, *Chem. Lett.*, **1973**, 933. Presented at the General Local Meeting of the Tohoku District of the Chemical Society of Japan, at Akita, Oct. 1971.

2) T. Mukai, T. Nakazawa, and K. Isobe, *Tetrahedron Lett.*, **1968**, 565.

3) W. M. Jones and C. L. Ennis, *J. Amer. Chem. Soc.*, **91**, 6391 (1969).

4) T. Toda, K. Saito, and T. Mukai, *Tetrahedron Lett.*, **1972**, 1981.

5) M. Jones and E. W. Petrillo, *ibid.*, **1969**, 3953.

6) H. Durr and B. Ruge, *Angew. Chem. Int. Ed. Eng.*, **11**, 225 (1972).

7) D. Rewicki and C. Tuchscherer, *ibid.*, **11**, 44 (1972).

8) Y. Yamamoto, S. Murahashi, and I. Moritani, *Tetrahedron Lett.*, **1973**, 589.

9) R. Srinivasan, *J. Amer. Chem. Soc.*, **84**, 3432 (1962).

10) D. M. Gale, W. J. Middleton, and C. G. Krespan, *ibid.*, **87**, 657 (1965).

11) G. W. Borden, O. L. Chapman, R. Swindell, and T. Tezuka, *J. Amer. Chem. Soc.*, **89**, 2979 (1967).

12) T. Toda, M. Nitta, and T. Mukai, *Tetrahedron Lett.* **1969**, 4401.

13) W. G. Dauben and R. L. Cargill, *Tetrahedron*, **12**, 186 (1961).

14) L. B. Jones and V. K. Jones, *J. Amer. Chem. Soc.*, **89**, 1880 (1967).

15) J. D. Graham and M. T. Rogers, *ibid.*, **84**, 2249 (1962).

16) All mp were uncorrected. NMR spectra were measured by Varian-HA-100 spectrometer, and referred to TMS as an internal standard.

The Formation of Substituted Quinazolines from Substituted Indoles by the Sensitized Photo-oxygenation in the Presence of Ammonium Acetate[1]

Koko MAEDA,* Tamako MISHIMA,* and Taro HAYASHI**

*Department of Chemistry, Faculty of Science, Ochanomizu University, Otsuka, Bunkyo-ku, Tokyo 112

**The Institute of Physical and Chemical Research, Wako-shi, Saitama 351

(Received August 14, 1973)

2,4-Di- and 2,4,6-trisubstituted quinazolines (II) were prepared from 2,3-di- and 2,3,5-trisubstituted indoles (I) respectively by the sensitized photo-oxygenation in aqueous methanol in the presence of ammonium acetate or by fusion with ammonium acetate after the photo-oxygenation. Chemical evidences that II was produced *via* the hydroperoxide (III) of the indole and then the dicarbonyl compound (IV) were provided.

In our previous paper[2] we reported that 2,4,6-triaryl-*s*-triazines were produced from 2,4,5-triarylimidazoles by the sensitized photo-oxygenation in methanol in the presence of ammonium acetate and the reaction proceeded *via* the hydroperoxides which afforded the triazines by the reaction with ammonium acetate. Although the formation of 2,4-dioxo-1,2,3,4-tetrahydroquinazoline from indole and that of 2-phenyl-4-oxo-3,4-dihydroquinazoline from 2-phenylindole, similar to that of triaryl-*s*-triazine from triarylimidazole, on irradiation with sunlight in ethanol in the presence of oxygen and ammonia have been reported,[3] no investigations have been carried out similar reactions for 2,3-di- and 2,3,5-trisubstituted indoles. The present paper deals with the formation of 2,4-di- and 2,4,6-trisubstituted quinazolines from the corresponding 2,3-di- and 2,3,5-trisubstituted indoles by sensitized photo-oxygenation in the presence of ammonium acetate and the reaction mechanism of the ring enlargement.

Results and Discussion

Indoles (Ia, Ib, Ic, Id listed in Table 1) were transformed to quinazolines (IIa, IIb, IIc, IId) respectively by sensitized photo-oxygenation in aqueous methanol in the presence of ammonium acetate. The reaction was carried out at room temperature and completed by boiling the methanolic solution. The procedure was similar to that for the formation of trisubstituted triazines from trisubstituted imidazoles.[2] The time-course of the ring enlargement was followed by UV spectrum and thin layer chromatography. The spectrum and chromatogram changed with the formation of the quinazoline (II) *via* the hydroperoxide (III) and the dicarbonyl compound (IV). Indoles (Ie and If) which have phenyl groups at the 2- and 3-positions did not give quinazolines by the same procedure as that for Ia—Id. These quinazolines (IIe and IIf), however, were obtained by fusion of the solid residue after removal of the solvent from the reaction mixture of the sensitized photo-oxygenation of Ie and If, with ammonium acetate at about 180 °C, respectively.

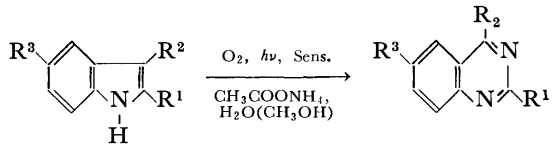

(I) (II)

When about 20 vol% of water was added into methanol, the reaction rate from I to II was increased because of the acceleration of the formation of IV from III. The short reaction time was convenient to avoid a formation of fair amounts of brown oily products by prolonged heating of the reaction mixture in a methanolic solution containing trace amounts of water after the formation of III from I. The yields and melting points of II are shown in Table 1. Ethanol, *n*-propyl alcohol and acetone which contained water were also usable as the solvent.

Table 1. 2,4-Di- and 2,4,6-trisubstituted quinazolines (II) from 2,3-di- and 2,3,5-trisubstituted indoles (I)

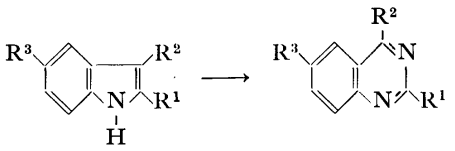

(I) (II)

R¹	R²	R³		II	Mp °C	Yield %[a]
CH_3	CH_3	CH_3	Ia →	IIa	54— 55	67
CH_3	CH_3	Cl	Ib	IIb	108—109.5	72
CH_3	CH_3	OCH_3	Ic	IIc	109—110	44
C_6H_5	CH_3	H	Id	IId	85— 87 (90)[4,5]	65
C_6H_5	C_6H_5	H	Ie	IIe	118—119 (119—120)[6,7]	70
C_6H_5	C_6H_5	CH_3	If	IIf	177—179 (177)[7]	53

a) In methanol containing 20 vol% of water. Reaction conditions are shown in the experimental part.

It was reported[8,9] that several substituted indoles including Ia, Ib and Ic exhibited chemiluminescence on oxidation in basic solutions and the mechanism of the chemiluminescence reaction involved the primary formation of radicals of the indoles and then oxygenation of the radicals to hydroperoxides by molecular oxygen. The mechanism of the chemiluminescence is similar to that of imidazole derivatives.[10] Similarities between indoles and imidazoles in both ring enlargement reaction and mechanism of chemiluminescence reaction suggested that in the ring enlargement reaction of the indole (I) hydroperoxides are also intermediates. Hydroperoxides (IIIa—IIIf in Table 2) (2,3-di- and 2,3,5-trisubstituted-3-hydroperoxy-

indolenins) were prepared to examine the reaction with ammonium acetate in aqueous methanol. Hydroperoxides (IIIa—IIId) were prepared by autoxidation or by sensitized photo-oxygenation of indoles (Ia—Id) whereas IIIe and IIIf were obtained only by sensitized photo-oxygenation of Ie and If. Hydroperoxide (IIIf) was also obtained by reaction of If and singlet oxygen prepared from hydrogen peroxide and sodium hypochlorite.[11] These facts suggested that singlet oxygen was probably involved in oxygenation of Ie and If.

N-Methyl-2,3-diphenylindole which did not transform to a quinazoline derivative by the same procedure as that for Ie and If did not give a hydroperoxide by the sensitized photo-oxygenation. This result shows that hydrogen on nitrogen of the indole (I) is necessary for the oxygenation and also for the ring enlargement.

Table 2. Hydroperoxides of 2,3-di- and 2,3,5-trisubstituted indoles (III)

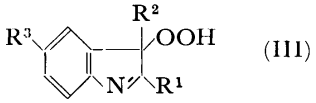

(III)

	R^1	R^2	R^3	Mp (°C)	Yield (%) A	Yield (%) B
IIIa	CH_3	CH_3	CH_3	111.5—112.5 (111.5)[12]	76	88
IIIb	CH_3	CH_3	Cl	112—113	60	89
IIIc	CH_3	CH_3	OCH_3	108—109 (109)[13]	59	
IIId	C_6H_5	CH_3	H	146—148 (148—152)[14]	82	
IIIe	C_6H_5	C_6H_5	H	157—158		85
IIIf	C_6H_5	C_6H_5	CH_3	175—176		70

A: Autoxidation, B: Sensitized photo-oxygenation

By treatment of IIIa, IIIb and IIId with ammonium acetate in aqueous methanol at room temperature or under reflux IIa, IIb and IId were produced respectively (Table 3). Hydroperoxides IIIe and IIIf did not give the corresponding quinazolines by the same procedure, but produced dicarbonyl compounds, 2-benzamidobenzophenone (IVe) and 2-benzamido-5-methylbenzophenone (IVf) as shown in Table 4, respectively, which were transformed to IIe and IIf by fusion with ammonium acetate at about 180 °C. The method of preparation of quinazoline derivatives from dicarbonyl compounds (VI, R^1, R^2, R^3: H, alkyl, aryl) by heating with ammonia in ethanol under pressure or fusion with ammonium acetate is known as Bischler's method.[6,15] When the sensitized photo-oxygenation of Ia and Id in aqueous methanol containing ammonium acetate was stopped before the reaction was completed, dicarbonyl compounds IVa and IVd (Table 4) were isolated with a small amount of IIa and IId, respectively. These facts suggested that dicarbonyl compound (IV) was probably formed from the hydroperoxide (III) and then transformed to the quinazoline (II) by ring closure with ammonia. In order to confirm this reaction process, IIIa, IIIb, IIId, IIIe and IIIf were heated in aqueous methanol and IVa, IVb, IVd, IVe and IVf (Table 4) were obtained. Water was necessary for the transformation of the hydroperoxides to the dicarbonyl compounds. The reaction rate was accelerated with increasing amounts of water in methanol and was very fast on boiling in water. The need of water in methanol for the ring enlargement of the indole (I) to the quinazoline (II) is considered to be associated with the formation of the dicarbonyl compound (IV) by hydrolytic reaction of hydroperoxide (III).

Table 4. Dicarbonyl compounds (IV) from hydroperoxides (III)

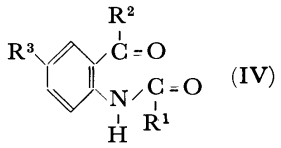

(IV)

	R^1	R^2	R^3	Mp °C	Yield (%)
IVa	CH_3	CH_3	CH_3	123—124 (123—124)[16]	84
IVb	CH_3	CH_3	Cl	133—134 (134—134.5)[12]	70
IVd	C_6H_5	CH_3	H	93.5— 95 (98)[14]	76
IVe	C_6H_5	C_6H_5	H	81— 82 (80.5)[13]	64
IVf	C_6H_5	C_6H_5	CH_3	114—116 (114—117)[16]	92

As shown in Table 5, IIa, IIb and IId were obtained by treating IVa, IVb and IVd, respectively, with ammonium acetate in methanol or aqueous methanol at room temperature or under boiling, whereas IIe and IIf which were not obtained by the same procedure were obtained by fusion of IVe and IVf with ammonium acetate at about 180 °C. Quinazolines (IIa, IIb and IId) were also obtained by fusion of IVa, IVb and IVd with ammonium acetate.

From these results the mechanism of the ring enlargement reaction of 2,3-di- and 2,3,5-trisubstituted in-

Table 3. Yields of quinazolines (II) from hydroperoxides (III)

III		II	Yield (%)
IIIa	→	IIa	60
IIIb		IIb	62
IIId		IId	86
IIIe		IIe	60
IIIf		IIf	55

Table 5. Yields of quinazolines (II) from dicarbonyl compounds (IV)

IV		II	Yield (%)
IVa	→	IIa	86
IVb		IIb	88
IVd		IId	89
IVe		IIc	69
IVf		IIf	70

doles (I) to 2,4-di- and 2,4,6-trisubstituted quinazolines (II) by sensitized photo-oxygenation in the presence of ammonium acetate is concluded to be shown by the following scheme:

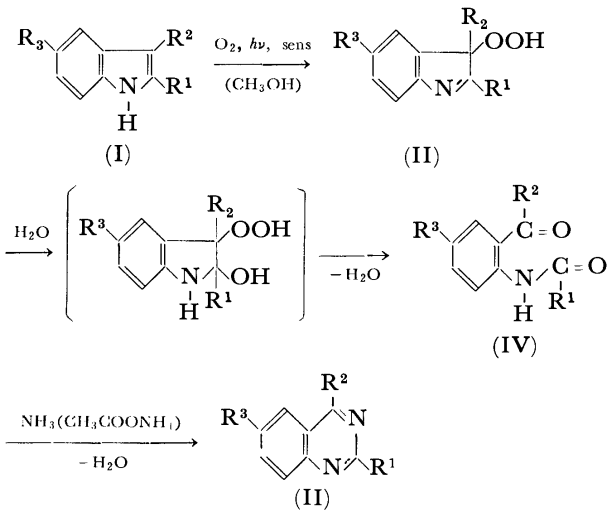

In the transformation of triphenylimidazole to triphenyl-*s*-triazine the carbonyl compound, *N*,*N'*-dibenzoylbenzamidine, did not give the triazine by the reaction with ammonium acetate in a methanolic solution and even by fusion with ammonium acetate at about 180 °C. These results seem to show that the process of the ring enlargement of substituted indoles differs in part from that of substituted imidazoles.

Experimental

All the melting points are uncorrected. The IR spectra were obtained in a JASCO IR-G spectrophotometer. The UV spectra were measured by a Hitachi 124 spectrophotometer.

Preparation of Substituted Indole (I). All the indoles examined were prepared by the method described in the literatures.[14,17,18,19]

2,3,5-Trimethylindole (Ia)[17]: Colorless plates (from ethanol-water), mp 118—119 °C. Found: C, 82.91; H, 8.23; N, 8.58%. Calcd for $C_{11}H_{13}N$: C, 82.97; H, 8.23; N, 8.80%.

2,3-Dimethyl-5-chloroindole (Ib)[17]: Colorless plates with luster (from benzene), mp 142—144 °C. Found: C, 66.94; H, 5.56; N, 7.86; Cl, 19.64%. Calcd for $C_{10}H_{10}NCl$: C, 66.86; H, 5.61; N, 7.80; Cl, 19.73%.

2,3-Dimethyl-5-methoxyindole (Ic)[17]: Colorless needles (from ethanol and then from petroleum ether), mp 104—106 °C. Found: C, 75.76; H, 7.43; N, 8.05%. Calcd for $C_{11}H_{13}NO$: C, 75.48; H, 7.48; N, 7.99%.

2-Phenyl-3-methylindole (Id)[14]: Pale brown prisms (from benzene), mp 88—90 °C. Found: C, 87.28; H, 6.51; N, 6.71%. Calcd for $C_{15}H_{13}N$: C, 86.92; H, 6.32; N, 6.76%.

2,3-Diphenylindole (Ie)[18]: Colorless prisms (from benzene ligroin), mp 123.5—124 °C. Found: C, 89.33; H, 5.64; N, 5.11%. Calcd for $C_{20}H_{15}N$: C, 89.19; H, 5.61; N, 5.20%.

2,3-Diphenyl-5-methylindole (If)[18]: Colorless needles (from acetone-ligroin), mp 158—159 °C. Found: C, 89.10; H, 6.06; N, 5.00%. Calcd for $C_{21}H_{17}N$: C, 89.01; H, 6.05; N, 4.94%.

N-Methyl-2,3-diphenylindole: Colorless needles (from acetic acid), mp 135—136 °C (137 °C[19]). Found: C, 88.99; H, 6.06; N, 4.82%. Calcd for $C_{21}H_{17}N$: C, 89.01; H, 6.05; N, 4.94%. This compound did not give a hydroperoxide and also a quinazoline derivative by the same procedure as those for the other indoles.

Formation of the Quinazoline (II) by Sensitized Photo-oxygenation of the Indole (I) in the Presence of Ammonium Acetate. General Procedure. An aqueous methanolic solution (containing 20 vol% of water) of indoles (Ia, Ib, Ic, Id) which contained ammonium acetate and methylene blue as a sensitizer was irradiated with two incandescent lamps (300 W) for 1—10 hr under bubbling oxygen at room temperature or was refluxed for 1 hr after the irradiation. The solvent was removed under reduced pressure and the residue was extracted with ether. The ether extracts were washed with aqueous sodium carbonate and with water for removing methylene blue and dried over sodium sulfate. Quinazolines IIe and IIf were formed by fusion of the products obtained by sensitized photo-oxygenation with ammonium acetate at about 180 °C.

2,4,6-Trimethylquinazoline (IIa): Ammonium acetate (5 g) was added to the aqueous methanolic solution (300 ml) of Ia (600 mg). The mixture was irradiated for 10 hr at room temperature or for about 1 hr and then refluxed for 1 hr. The brown residue after removal of ether from ether extract was chromatographed on an alumina column with benzene and *n*-hexane (1 : 1). The elute was evaporated and the remaining product was recrystallized from petroleum ether. Colorless prisms. Found: C, 76.72; H, 7.05; N, 16.30%. Calcd for $C_{11}H_{12}N_2$: C, 76.70; H, 7.02; N, 16.28%. λ_{max}^{EtOH} nm (ε): 227 (1.56×10^4), 259 (1.0×10^3), 315 (7.0×10^2). IR(KBr): 1625, 1570, 1560, 1510, 1498, 880, 827 cm^{-1}.

2,4-Dimethyl-6-chloroquinazoline (IIb): Ammonium acetate (5 g) was added to the aqueous methanolic solution (300 ml) of Ib (500 mg) and the resulting solution was irradiated for 7 hr. The product obtained by removal of the solvent from ether extract was recrystallized from ethanol. Colorless needles. Found: C, 62.38; H, 4.89; N, 14.51; Cl, 17.69%. Calcd for $C_{10}H_9N_2Cl$: C, 62.33; H, 4.71; N, 14.55; Cl, 18.41%. λ_{max}^{EtOH} nm (ε): 227 (9.1×10^3), 256 (2.2×10^3), 315 (1.4×10^3). IR(KBr): 1570, 1550, 1480, 865, 835, 805, 670 cm^{-1}.

2,4-Dimethyl-6-methoxyquinazoline (IIc): The aqueous methanol solution (300 ml) of Ic (600 mg) was treated by the same procedure as that in the case of formation of IIa. IIc was obtained as colorless needles by recrystallization from a mixture of ether and acetone. Found: C, 69.82; H, 6.42; N, 14.89%. Calcd for $C_{11}H_{12}N_2O$: C, 70.18; H, 6.43; N, 14.89%. λ_{max}^{EtOH} nm (ε): 232 (2.1×10^4), 247 (2.6×10^3), 256 (2.3×10^3), 318 (1.9×10^3), 335 (1.9×10^3). IR(KBr): 1625, 1572, 1560, 1500, 845, 835 cm^{-1}.

2-Phenyl-4-methylquinazoline (IId): The aqueous methanol solution (200 ml) of Id (200 mg) was treated by the same procedure as that in the case of formation of IIa. IId was obtained as colorless plates by recrystallization from ethanol. Found: C, 81.58; H, 5.49; N, 12.33%. Calcd for $C_{15}H_{12}N_2$: C, 81.79; H, 5.49; N, 12.72%. λ_{max}^{EtOH} nm (ε): 260 (2.9×10^4), 280 (1.0×10^4), 317 (3.4×10^3). IR(KBr): 1620, 1575, 1500, 1495, 780, 750, 704 cm^{-1}.

IId was also prepared by using acetone containing 20 vol % of water with 40% yield.

2,4-Diphenylquinazoline (IIe): Ammonium acetate (5 g) was added to the aqueous solution (300 ml) of Ie (500 mg) and the resulting solution was irradiated for 1 hr and then refluxed for 1 hr. The residue obtained by removal of the solvent

was heated at 180 °C for 1.5 hr and then extracted with ether. The residue obtained by evaporation of the solvent was recrystallized from ethanol. Colorless prisms. Found: C, 85.00; H, 5.05; N, 9.81%. Calcd for $C_{20}H_{14}N_2$: C, 85.07; H, 5.00; N, 9.93%. λ_{max}^{EtOH} nm (ε): 224 (1.36×10^4), 248 (1.27×10^4), 3.08 (9.6×10^3). IR(KBr): 1615, 1560, 1539, 1489, 770, 750, 695 cm^{-1}.

IIe was also obtained in *n*-propyl alcohol containing 20 vol% of water. The alcoholic solution of Ie (200 mg in 200 ml) was irradiated for 5 hr in the presence of methylene blue as a sensitizer under a stream of oxygen. After the solvent was removed from the solution, ammonium acetate (5 g) was added to the residue. The mixture was heated at 180 °C for 1.5 hr and IIe was obtained with 67% yield by the same procedure as that in the methanolic solution.

2,4-Diphenyl-6-methylquinazoline (IIf): The aqueous methanol solution (300 ml) of If (500 mg) was treated by the same procedure as that in the case of formation of IIe. IIf was obtained as colorless prisms by recrystallization from ethanol. Found: C, 85.02; H, 5.50; N, 9.41%. Calcd for $C_{21}H_{16}N_2$: C, 85.11; H, 5.44; N, 9.45%. λ_{max}^{EtOH} nm (ε): 266 (1.37×10^4), 335 (1.3×10^3), 352 (1.3×10^3). IR-(KBr): 1624, 1560, 1540, 1492, 840, 790, 770, 705 cm^{-1}.

IIf was also obtained with 55% yield in *n*-propyl alcohol containing 20 vol% of water.

Preparation of the Hydroperoxide (III). The hydroperoxide (III) was prepared by autoxidation (Method A)[12,13] or by sensitized photo-oxygenation (Method B). The yields and melting points of III are shown in Table 2.

Method A: A trace amount of benzoyl peroxide was added to a warm solution of indole (I) (200—300 mg in 60—80 ml of petroleum ether). Crystalline hydroperoxide began to deposit from the solution after about 1 hr. The solution was left to stand for 4 hr in a refrigerator, and the crystalline hydroperoxide was obtained. These hydroperoxides liberated iodine from potassium iodide and showed an IR absorption at near 2800 cm^{-1} due to a stretching vibration of -OOH.

Method B: A methanolic solution of the indole (I) was irradiated with two incandescent lamps (300 W) in the presence of methylene blue as a sensitizer under oxygen stream at 5—10 °C for 1 hr. The residue obtained by removing the solvent was extracted with ether. The ether solution was washed with water to remove methylene blue. The solution was dried over sodium sulfate. Crude hydroperoxide obtained by removing the solvent under reduced pressure. Although it was reported[13] that indole derivatives having phenyl group at the 3-position resist to the action of oxygen, IIIe and IIIf were obtained by sensitized photo-oxygenation.

IIIa, IIIe and IIIf were also obtained in ethanol.

2,3,5-Trimethyl-3-hydroperoxyindolenin (IIIa): Colorless prisms (from ethyl acetate-petroleum ether). Found: C, 69.07; H, 6.81; N, 7.32%. Calcd for $C_{11}H_{13}NO_2$: C, 69.09; H, 6.85; N, 7.32%. λ_{max}^{EtOH} nm (ε): 217 (2.57×10^4), 222 (2.68×10^4), 261 (6.0×10^3).

2,3-Dimethyl-5-Chloro-3-hydroperoxyindolenin (IIIb): Colorless needles (from ethyl acetate-petroleum ether). Found: C, 56.93; H, 4.79; N, 6.41; Cl, 17.44%. Calcd for $C_{10}H_{10}NO_2Cl$: C, 56.75; H, 4.76; N, 6.62; Cl, 16.75%. λ_{max}^{EtOH} nm (ε): 216(1.14×10^4), 219 (1.18×10^4), 261 (3.2×10^3).

2,3-Dimethyl-5-methoxy-3-hydroperoxyindolenin (IIIc): Pale gray prisms (from ethyl acetate-petroleum ether). Found: C, 63.92; H, 6.30; N, 6.81%. Calcd for $C_{11}H_{13}NO_3$: C, 63.76; H, 6.32; N, 6.76%. λ_{max}^{EtOH} nm (ε): 232 (1.13×10^4), 277 (4.4×10^3), 311 (2.4×10^3).

2-Phenyl-3-methyl-3-hydroperoxyindolenin (IIId): Colorless needles (from ethyl acetate-petroleum ether). Found: C, 74.93; H, 5.53; N, 5.77%. Calcd for $C_{15}H_{13}NO_2$: C, 75.30; H, 5.48; N, 5.85%. λ_{max}^{EtOH} nm (ε): 238 (1.3×10^4), 245 (1.2×10^4), 314 (1.0×10^4).

2,3-Diphenyl-3-hydroperoxindolenin (IIIe): Colorless prisms (from acetone-ligroin). Found: C, 79.72; H, 5.08; N, 4.53%. Calcd for $C_{20}H_{15}NO_2$: C, 79.72; H, 5.02; N, 4.65%. λ_{max}^{EtOH} nm (ε): 222 (9.0×10^3), 250 (8.7×10^3), 317 (6.13×10^3).

2,3-Diphenyl-5-methyl-3-hydroperoxyindolenin (IIIf): Colorless prisms (from acetone-ligroin). Found: C, 79.88; H, 5.50; N, 4.36%. Calcd for $C_{21}H_{17}NO_2$: C, 79.98; H, 5.43; N, 4.44%. λ_{max}^{EtOH} nm (ε): 254 (5.6×10^3), 330 (4.0×10^3).

The hydroperoxide (IIIf) was also obtained by reaction of If with singlet oxygen which was produced by the method of Foote and Wexler.[11] To a methanolic solution (180 ml) of If (1.08 g) hydrogen peroxide (30%, 20 ml) was added. The solution was stirred in nitrogen atmosphere at about 10 °C, and 150 ml of 0.3 M sodium hypochlorite solution was added in 90 min. After the solution was left to stand for 1 hr at 0—5 °C, the solution was diluted with water and extracted with ether. The ether solution was dried over sodium sulfate. Yellowish oil remained by removing ether under reduced pressure was recrystallized from a mixture of ether and ethyl acetate.

Influence of an Amount of Water in Methanol for the Reaction Rate from IIIa to IVa. When a solution of IIIa (100 mg in 40 ml) in dehydrated methanol was allowed to stand for 20 hr and then refluxed for 5 hr, no change was observed by UV spectrum and thin layer chromatogram. In a methanolic solution containing about 1% of water, IIIa was changed to IVa in part by refluxing the solution for 8 hr. In an aqueous methanolic solution containing 20 vol% of water, IIIa was changed to IVa by refluxing for 0.5 hr. In boiling water, the change of IIIa to IVa came to an end in a few minutes.

Preparation of the Dicarbonyl Compound (IV). A methanolic solution (containing 20 vol% of water) (40 ml) of the hydroperoxide (III) (100 mg) was heated on a water bath for 0.5 hr. The solvent was removed under reduced pressure and the brown oily residue was recrystallized from *n*-hexane (in the case of IVa) or ethanol (in the cases of IVb, IVd, IVe, IVf). Their analytical values were satisfactory for the formulas corresponding to the dicarbonyl compounds. The yields and melting points are shown in Table 4.

The authors wish to express their gratitude to Professor Michio Shiota of Ochanomizu University and Dr. Hiroshi Midorikawa of the Institute of Physical and Chemical Research for their kind advice and encouragement in the course of this investigation.

References

1) Presented in part at the 27th Annual Meeting of the Chemical Society of Japan, Nagoya, October, 1972.
2) K. Maeda and T. Hayashi, This Bulletin, **44**, 533 (1971).
3) S. Capuano and L. Giammanco, *Gazz. Chim. Ital.*, **86**, 126 (1956).
4) A. Kövende and M. Kirz, *Chem. Ber.*, **98**, 1094 (1965).
5) M. T. Boegert and F. P. Nabenhauel, *J. Amer. Chem. Soc.*, **46**, 1932 (1924).
6) A. Bischler and D. Barad, *Ber.*, **25**, 3080 (1892).
7) H. Meerwein, P. Laash, R. Mersch, and J. Nentwig, *Chem. Ber.*, **89**, 224 (1956).
8) G. E. Philbrook, J. B. Ayers, J. F. Garst, and J. R. Totter, *Photochem. Photobiol.*, **4**, 869 (1965).
9) N. Sugiyama, M. Akutagawa, T. Gasha, Y. Saiga,

and H. Yamamoto, This Bulletin, **40**, 347 (1967).
10) E. H. White and M. J. D. Harding, *Pthotochem. Photobiol.*, **4**, 1129 (1965).
11) C. S. Foote and S. Wexler, *J. Amer. Chem. Soc.*, **86**, 3879 (1964); C. S. Foote, S. Wexler, W. Ando, and R. Higgins, *ibid.*, **90**, 975 (1968).
12) N. Sugiyama, H. Akutagawa, and H. Yamamoto, This Bulletin, **41**, 936 (1968).
13) R. J. S. Beer, T. Donavanik and A. Robertson, *J. Chem. Soc.*, **1954**, 4139.
14) B. Witkop and J. B. Patrick, *J. Amer. Chem. Soc.*, **74**, 3861 (1952).
15) A. Bischler and F. J. Howell, *Ber.*, **26**, 1384 (1893).
16) D. W. Ockenden and K. Schofield, *J. Chem. Soc.*, **1935**, 612.
17) D. W. Ockenden and K. Schofield, *ibid.*, **1957**, 3175.
18) E. R. Japp and T. S. Murray, *ibid.*, **65**, 889 (1894).
19) M. B. Richards, *ibid.*, **97**, 977 (1910).

proposal[5] regarding the ring opening of the aziridinium compound. The process for the formation of aziridinium bromide (**B**) probably involves the initial attack of diazomethane at the higher electrophilic carbimino position of the iminium bromide, and the subsequent ring closure to the aziridinium bromide (**B**), as is shown in Chart 3. It seems likely that this aziridinium bromide (**B**) is very unstable because of its highly strained structure, and that ring opening takes place spontaneously by the fission of the 1,3-bond to give carbonium ion (**C**), which may then afford a bromide (**D**). Since the presence of the nitrogen atom (at the 4-position) apparently effects the dissociation of the bromide (**D**) to the carbonium ion (**C**), the bromide (**D**) must be in equilibrium with the carbonium ion (**C**); therefore, the ethanolysis of the carbonium ion (**C**) results in the formation of **14**.

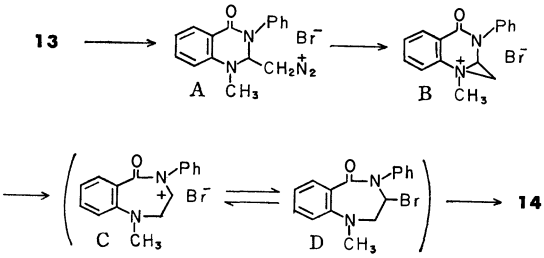

Chart 3.

Treatment of **13** with phenyldiazomethane in EtOH at room temperature afforded a product possessing the benzodiazepine ring system in a moderate yield. The structure was identified as 1-methyl-2,4-diphenyl-3-ethoxy-1,4-benzodiazepin-5(*H*)-one (**16**) on the basis of the elemental analysis and the spectral data, though the stereochemistry of compound **16** remained unclarified. The UV spectrum [maximum at 226 nm (ε 33400), 265 (sh), 334 (4300)] corresponded closely to the data for **14**. The NMR spectrum showed the signals of an ethoxy group in the usual region, a methyl singlet at δ 2.77, and an AB quartet at δ 4.85 and 5.08 (J=6 Hz) assignable to the methine protons in the seven membered ring.

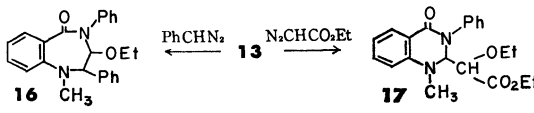

Chart 4.

Reaction of **13** with ethyl diazoacetate in EtOH did not occur even under reflux. On the other hand, reaction with ethyl diazoacetate in the presence of $CuSO_4$ at 65—70 °C gave an oily product which was shown to be homogeneous by the criteria of the glc and tlc. It has been established[9] that the $CuSO_4$-catalyzed decomposition of ethyl diazoacetate results in the formation of the carbene-copper complex, which then reacts with olefins to give cyclopropanes, but which does not undergo insertion into carbon-hydrogen bonds. Therefore, a carbene addition to the $>C=\overset{+}{N}<$ bond may be considered in the present case, though to our knowledge, no addition of a carbene at the positively-charged double bond is yet known. The planar structure of the product was shown to be 1-methyl-2-(1-ethoxy-1-ethoxycarbonylmethyl)-3-phenyl-4-oxo-1,2,3,4-tetrahydroquinazoline (**17**) by the spectral data. The mass spectrum showed a molecular ion peak (*m/e* 368) and a base peak (*m/e* 237) which must have arisen by the loss of the substituent at the 2-position. It has been reported by Bogentoft and Danielsson[10] that this type of cleavage is a main pathway in the mass fragmentation of 4-oxo-1,2,3,4-tetrahydroquinazolines. The structural assignment was also supported by the UV spectrum. The spectrum [maximum at 228 nm (ε 31000), 251 (sh), 354 (3000)] was similar to those of 4-oxo-1,2,3,4-tetrahydroquinazoline compounds and was distinctly different from those of benzodiazepines **14** and **16**. The two singlets due to the *N*-methyl groups in the NMR spectrum of **17** suggested that the product consisted of a 21 : 13 mixture of two isomers. Since no change in the signal pattern was observed at elevated temperatures, the product **17** must be a mixture of diastereoisomers. No further study on the separation of the isomers was attempted.

To evaluate the synthetic utility of this ring expansion reaction, the extension to the synthesis of the 1-dialkylaminoalkyl derivatives of 1,4-benzodiazepine is now in progress.

Experimental

Melting points are uncorrected and were determined on a Yamato apparatus MP-1. The NMR spectra were determined on a Hitachi Perkin-Elmer R-20A instrument (Me_4Si). Mass spectra were measured on a Hitachi RMS-4 spectrometer. IR spectra were determined on a Shimadzu IR-27G spectrometer, and UV spectra on a Hitachi EPS-2U spectrometer.

2-(N-methylbromoacetamido)benzanilide (8). To a stirred solution of 2-(*N*-methylamino)benzanilide (**7**) (4.52 g, 0.02 mol) and pyridine (2.4 g, 0.03 mol) in benzene (120 ml) was added dropwise bromoacetylbromide (2.4 g, 0.022 mol) at room temperature, and the mixture was stirred for 1 hr. The solvent was evaporated under reduced pressure and the residue was dissolved in $CHCl_3$. The chloroform layer was washed with H_2O, dried (Na_2SO_4), and concentrated to dryness. The residual oil was triturated with a mixture of *i*-Pr_2O-EtOH (1 : 1) to afford an almost pure crystalline product (5.8 g, 83%), mp 185—187 °C. An analytical sample was obtained as colorless needles by recrystallization from EtOH; mp 185—187 °C. Found: C, 55.43; H, 4.35; N, 7.72%. Calcd for $C_{16}H_{15}O_2N_2Br$: C, 55.34; H, 4.35; N, 8.07%.

1-Methyl-2-bromomethyl-3-phenyl-4-oxo-3,4-dihydroquinazolinium Perchlorate (9). A solution of **8** (5.0 g) and an excess of 60% $HClO_4$ in EtOH was refluxed for 3 min and the precipitates were collected by filtration and washed with EtOH to give pure **9** (5.6 g, 90.3%); mp 251—253 °C (decomp.). IR ν_{max}^{Nujol} cm^{-1}: 1723, 1625, 1594, 1563, 1490. Found: C, 44.96; H, 3.29; N, 6.30%. Calcd for $C_{16}H_{14}O_5N_2BrCl$: C, 44.72; H, 3.28; N, 6.52%.

1-Methyl-2-bromomethyl-3-phenyl-4-oxo-1,2,3,4-tetrahedroquinazoline (10). To a suspension of **9** (5.0 g, 0.012 mol) in EtOH (200 ml) was added dropwise a solution of $NaBH_4$ (0.46 g, 0.012 mol) in EtOH (20 ml) at 0—5 °C over a 1.5-hr period. The mixture was then concentrated under reduced pressure, and the residue was dissolved in $CHCl_3$.

The chloroform layer was washed with H_2O, dried (Na_2SO_4), and concentrated under reduced pressure. The residue was crystallized by trituration with *i*-Pr_2O and the crystals were collected by filtration to give crude **10** (3.4 g, 88.4%); mp 108—110 °C. Recrystallization from *i*-PrOH gave a pure sample as colorless prisms (3.1 g, 80.0%); mp 108—110 °C. UV λ_{max}^{EtOH} nm ($\varepsilon \times 10^{-3}$): 229 (33.2), 252 (sh), 356 (2.9). NMR ($CDCl_3$) δ: 3.25 (3H, s), 3.53 (1H, d.d, J=11 Hz, J=5 Hz), 3.76 (1H, d.d, J=11 Hz, J=7 Hz), 5.17 (1H, d.d, J=7 Hz, J=5 Hz), 6.15—7.65 (3H, m), 7.37 (5H, s), 8.00 (1H, d.d, J=8 Hz, J=2 Hz). Found: C, 57.99; H, 4.63; N, 8.38%. Calcd for $C_{16}H_{15}ON_2Br$: C, 58.01; H, 4.56; N, 8.45%.

Reaction of ***10*** *with* $AgClO_4$ *in EtOH.* A mixture of **10** (0.5 g 0.0015 mol), $AgClO_4$ (0.31 g, 0.0015 mol), and EtOH (30 ml) was stirred at room temperature for 1.5 hr and at 50—60 °C for 8 hr. The insoluble solid that had formed was then filtered off, and the filtrate was concentrated under reduced pressure. The residue was dissolved in $CHCl_3$ and the solution was washed with aqueous 5% K_2CO_3 solution, dried (K_2CO_3), and concentrated. The residual oil was chromatographed on silica gel (20 g, solvent $CHCl_3$) to give 2-[*N*-methyl-*N*-(1,2-diethoxyethyl)amino]benzanilide (**11**) as an oil (0.3 g, 58.5%). NMR ($CDCl_3$) δ: 1.08 6H, t, J=7 Hz), 2.80 (3H, s), 3.29 (2H, d, J=6 Hz), 3.49 (2H, q, J=7 Hz), 3.55 (2H, q, J=7 Hz), 4.60 (1H, t, J=6 Hz), 7.0—8.3 (9H, m), 11.25 (1H, br.s). Mass *m/e*: 324 (M^+). Found: C, 70.10; H, 7.58; N, 8.44%. Calcd for $C_{20}H_{16}N_2O_3$: C, 70.15; H, 7.65; N, 8.18%.

*2-(N-methylformamido)benzanilide (****12****).* To a mixture of formic acid (20 g) and acetic anhydride (5.0 g) was added 2-(*N*-methylamino)benzanilide (**7**, 10 g) and the reaction mixture was stirred at room temperature for 4 hr. The solution was poured into H_2O and extracted with $CHCl_3$. The chloroform layer was washed, dried (Na_2SO_4), and concentrated. The residual oil was triturated with Et_2O and the solid was collected by filtration to give almost pure **12** (10.0 g, 88.9%), mp 141—142 °C. Recrystallization from benzene gave a pure sample as colorless prisms, mp 141—142 °C. NMR ($CDCl_3$) δ: 3.12 and 3.24 (3H, two singlets in a ratio of 17 : 11), 6.9—7.75 (9H, m), 8.04 and 8.09 (1H, two singlets in the same ratio), 8.73 (1H, br.s). Found: C, 70.63; H, 5.63; N, 10.76%. Calcd for $C_{15}H_{14}O_2N_2$: C, 70.85; H, 5.55; N, 11.02%.

*1-Methyl-3-phenyl-4-oxo-3,4-dihydroquinazolinium Bromide (****13****).* To a solution of **12** (10 g) in EtOH (50 ml) was added an excess of 47% HBr and the solvent was evaporated. The residue was triturated with EtOH to afford crude **13**; mp 222—223 °C (decomp.). Recrystallization from EtOH gave a pure sample (10.5 g, 84.0%); mp 225—227 °C (decomp.). IR ν_{max}^{Nujol} cm^{-1}: 1745, 1730, 1715, 1660, 1600, 1569, 1490. Found: C, 56.43; H, 4.16; N, 8.62%. Calcd for $C_{15}H_{13}ON_2Br$: C, 56.79; H, 4.13; N, 8.83%.

*1-Methyl-3-ethoxy-4-phenyl-1,2,3,4-tetrahydro-1,4-benzodiazepin-5(H)-one (****14****). A)*: To a solution of **13** (1.9 g, 0.006 mol) in EtOH (100 ml) was added dropwise a solution of CH_2N_2 in Et_2O (freshly prepared from 12.9 g of *p*-TsN(NO)-CH_3) at 0—5 °C during 1 hr and the mixture was stirred for 4 hr at the same temperature. After standing overnight, the solvent was evaporated and the residue was poured into aqueous K_2CO_3 solution. The oil was extracted with $CHCl_3$ and the chloroform layer was washed with H_2O, dried (K_2CO_3) and concentrated to dryness. The residue was crystallized by trituration with *i*-Pr_2O and the crystals were collected by filtration to give almost pure **14** (1.2 g, 67.6%); mp 86—88 °C. Recrystallization from *i*-Pr_2O gave a pure sample as colorless prisms; mp 89—90 °C. UV λ_{max}^{EtOH} nm ($\varepsilon \times 10^{-3}$): 225 (24.3), 262 (sh), 352 (2.0). NMR ($CDCl_3$) δ: 0.90 (3H, t, J=7 Hz), 2.90 (3H, s), 3.15—3.85 (4H, m), 4.97 (1H, t, J=5 Hz), 6.8—7.8 (4H, m), 7.36 (5H, s). Found: C, 72.55; H, 6.95; N, 9.38%. Calcd for $C_{18}H_{20}O_2N_2$: C, 72.95; H, 6.80; N, 9.45%.

B): A mixture of 3-ethoxy-4-phenyl-1,2,3,4-tetrahydro-1,4-benzodiazepin-5(*H*)-one[1] (**15**, 5.65 g, 0.02 mol), 37% HCHO (2.5 g, 0.03 mol) and EtOH (200 ml) was warmed at 50—60 °C for 1 hr. The mixture was then hydrogenated with 5% Pd/C (2.5 g) under 2.5 kg/cm². The theoretical volume of H_2 was absorbed in 4 hr on warming. The catalyst was filtered off and the filtrate was concentrated under reduced pressure. The residue was triturated with *i*-Pr_2O and the crystals were collected by filtration to give almost pure **14** (4.9 g, 82.4%); mp 87—88 °C. The product was identical with the sample (**14**) obtained from **13**.

*1-Methyl-2,4-diphenyl-3-ethoxy-1,2,3,4-tetrahydro-1,4-benzodiazepin-5(H)-one (****16****).* To a stirred suspension of **13** (1.0 g) was added dropwise a solution of $PhCHN_2$ in Et_2O [freshly prepared from *N*-nitroso-*N*-benzyl-*p*-toluenesulfonamide (5.8 g) by the method of Oberberger[11]] at room temperature during 1 hr. Stirring was continued overnight. The solvent was evaporated and the residue was poured into 5% aqueous K_2CO_3 solution. The oil was extracted with $CHCl_3$ and the extract was washed with H_2O, dried (K_2CO_3), and concentrated under reduced pressure. This residue was chromatographed on silica gel (100 g, solvent $CHCl_3$) to give a crystalline product **16** (350 mg, 29.8%); mp 182—184 °C (decomp.). Recrystallization from EtOH gave a pure sample colorless prisms (300 mg); mp 184—186 °C (decomp.). UV λ_{max}^{EtOH} nm ($\varepsilon \times 10^{-3}$): 226 (33.4), 265 (sh), 334 (4.3). NMR ($CDCl_3$) δ: 0.81 (3H, t, J=7 Hz), 2.77 (3H, s), 3.05—3.85 (2H, m), 4.85 (1H, d, J=6 Hz), 5.08 (1H, d, J=6 Hz), 6.8—7.85 (14H, m). Found: C, 77.43; H, 6.65; N, 7.69%. Calcd for $C_{23}H_{22}O_2N_2$: C, 77.39; H, 6.50; N, 7.52%.

*1-Methyl-2-(1-ethoxy-1-ethoxycarbonylmethyl)-3-phenyl-4-oxo-1,2,3,4-tetrahydroquinazoline (****17****).* To a stirred suspension of **13** (3.0 g) and $CuSO_4$ (0.6 g) in EtOH (100 ml) was added dropwise a solution of $N_2CHCOOEt$ (3.0 g) in EtOH (50 ml) at 70—75 °C during 3 hr. The insoluble solid was filtered off and the filtrate was concentrated under reduced pressure. The residue was shown by tlc to be a mixture of a major product and three minor products. This residue was chromatographed on silica gel (180 g, solvent $CHCl_3$) to give an oil (600 mg) which was shown to be homogeneous by the criteria of the glc and tlc. IR ν_{max}^{neat} cm^{-1}: 1740, 1660, 1619, 1498. UV λ_{max}^{EtOH} nm ($\varepsilon \times 10^{-3}$): 228 (31.0), 251 (sh), 354 (3.0). NMR (CCl_4) δ: 1.01, 1.10 (6H, two triplets in a ratio of 21 : 13, J=7 Hz), 3.06, 3.13 (3H, two singlets in the same ratio), 3.2—4.3 (5H, m), 5.24, 5.26 (1H, two doublets, J=5 Hz), 6.45—8.05 (9H, m). Mass *m/e*: 368 (M^+), 237 (base peak). Found: C, 65.62; H, 6.54; N, 7.06%. Calcd for $C_{21}H_{24}O_4N_2 \cdot H_2O$: C, 65.27; H, 6.78; N, 7.25%.

We wish to express our gratitude to Mr. T. Takayanagi, Senior Managing Director of our Company, Dr. I. Chibata, Director of our Laboratory, Dr. K. Okumura and Dr. M. Miyoshi for their encouragement. Thanks are due to the members of the analytical center for elemental analyses.

References

1) Part IV: Y. Yamada, T. Oine, and I. Inoue, *Chem. Pharm. Bull.*, in press, "Reaction of 2-Chloromethyl-3-aryl-4-oxo-1,2,3,4-tetrahydroquinazolines."

2) Unpublished data.

3) a) K. Okumura, T. Oine, Y. Yamada, G. Hayashi, and M. Nakama, *J. Med. Chem.*, **11**, 348 (1968). b) K. Okumura, Y. Yamada, T. Oine, J. Tani, T. Ochiai, and I. Inoue, *ibid.*, **15**, 518 (1972).

4) K. Okumura, T. Oine, Y. Yamada, G. Hayashi, M. Nakama, and T. Nose, *ibid.*, **11**, 788 (1968).

5) P. E. Fanta, "Heterocyclic Compounds with Three and Four Membered Ring," Vol. 19, Part 1, ed. by A. Weisberger, Interscience Publisher Inc., New York (1964), p. 548.

6) D. R. Crist and N. J. Leonard, *Angew. Chem. Int. Ed. Engl.*, **8**, 962 (1969).

7) H. O. Bernhard and V. Snieckus, *Tetrahedron.*, **27**, 2091 (1971).

8) N. J. Leonard and J. V. Paukstelis, *J. Org. Chem.*, **30**, 821 (1965).

9) W. Kirmse "Carbene Chemistry," ed. by A. T. Blomquist and H. Wasserman, Organic Chemistry Vol. 1, 2nd Ed., Academic Press Inc., New York (1971), p. 85.

10) C. Bogentoft and B. Danielsson, *J. Hetero. Chem.*, **9**, 193 (1972).

11) C. G. Overberger and J. P. Anselme, *J. Org. Chem.*, **28**, 592 (1963).

Reaction of 1-Methyl-4-phenylquinazolinium Salts with Diazomethane

Yoshihisa YAMADA, Toyonari OINE, and Ichizo INOUE

Research Laboratory of Applied Biochemistry, Tanabe Seiyaku Co., Ltd., Kashima-cho, Higashiyodogawa-ku, Osaka 532

(Received August 17, 1973)

For the synthesis of 5-phenyl-1,4-benzodiazepines, reaction of quinazolinium salts with diazomethane was studied. In the course of the study, it was found by NMR spectroscopy that the starting materials (**2**) reacted even with a slight amount of water present in the solvent to give hydrates **5**. Treatment of **2c** with diazomethane at 10 °C under absolute anhydrous conditions gave quinazoline **8c** and benzodiazepines **9** and **10c** in about the same ratio. In the reactions at lower temperatures, the distribution of the products varied markedly, and the ring expansion product **10c** was obtained in an improved yield. The mechanism for the formation of **8**, **9**, and **10** was discussed.

Within the past decade the synthesis of the 1,4-benzodiazepines has attracted considerable attention since the advent of chlorodiazepoxide and diazepam as tranquilizers,[1] and a number of synthetic approaches[2] to 1,4-benzodiazepine derivatives have been developed. In a previous paper,[3] we have reported that reaction of 1-methyl-3-phenyl-4-oxo-3,4-dihydroquinazolinium bromide with diazomethane in ethanol gave 1-methyl-3-ethoxy-4-phenyl-1,2,3,4-tetrahydro-1,4-benzodiazepin-5*H*-one. We considered that this ring expansion reaction could become a new approach to the preparation of 5-phenyl-1,4-benzodiazepine derivatives from 1-methyl-4-phenylquinazolinium salts (**2**). We present results concerning the ring-expansion reaction of **2** with diazomethane.

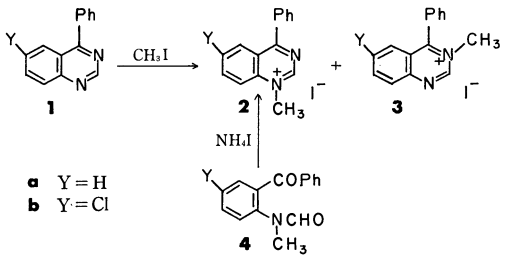

Chart 1.

The starting material, 1-methyl-4-phenylquinazolinium iodide (**2a**), has already been reported by Ott and Denzer.[4] They have observed that treatment of 4-phenylquinazoline (**1a**) with methyl iodide gave a mixture of the 1-methiodide (**2a**) and the 3-methiodide (**3a**) in a 7 : 1 ratio,[5] and that the two methiodides could not be separated by the usual purification technique because of their very similar physical properties. We reexamined the reaction thereby and found that the 1-methiodide could be easily isolated by washing with chloroform. The NMR spectrum of the product in DMSO-d_6 showed a couple of singlet at δ 3.80 and 4.60 (an intensity ratio of 1 : 10) assignable to two different *N*-methyl protons. The presence of the two *N*-methyl signals suggested an incomplete purification. However, since another set of two singlets (at δ 3.08 and 4.14[6]) observed in the spectrum of the original mixture has disappeared, we considered that one of the singlets might be due to the *N*-methyl protons of a contaminant. To ascertain this point, an unequivocal preparation of the 1-methiodide (**2a**) was attempted. Thermal cyclization of 2-(*N*-methylformamido)benzophenone (**4a**) with NH_4I in ethanol gave a product, albeit in a very low yield (4.3%), which showed an NMR spectrum identical with that of the purified 1-methiodide (**2a**) obtained according to Ott's procedure. Consequently, we concluded that the purified 1-methiodide (**2a**) was free from the 3-isomer and that, accordingly, one of the singlets was attributable to the *N*-methyl protons of the contaminant.

Quarternization of 4-phenyl-6-chloroquinazoline (**1b**) with methyl iodide also gave a mixture of a 1- and a 3-methiodide. The purified 1-methiodide (**2b**) exhibited a similar spectral pattern in its NMR spectrum. A presumption that the contaminant was the hydrated form of the 1-methiodide (**2b**) was proved by NMR spectroscopy (see Fig. 1 a, b, c). The hydration reaction of **2b** in DMSO-d_6 was carried out in an NMR sample tube. With an increase in the quantity of the additive water, the intensity of the

Fig. 1. NMR spectral change on hydration of **2b**.
- a The spectrum of **2b** (0.2 mmol) in DMSO-d_6 (0.6 ml).
- b The spectrum of **2b** (0.2 mmol) in DMSO-d_6 (0.6 ml) containing H_2O (0.056 mmol).
- c The spectrum of **2b** (0.2 mmol) in DMSO-d_6 (0.6 ml) containing H_2O (0.224 mmol).
- d The spectrum of **2b** (0.2 mmol) in DMSO-d_6 (0.6 ml) containing D_2O (0.1 ml).

singlet at δ 4.60 varied inversely; on the contrary, the methyl signal at δ 3.78 increased. Simultaneously, the signal at δ 10.20 assignable to $>\overset{+}{N}=CH-$ decreased an intensity in the same ratio, followed with enhancement of the signal at δ 8.91. The other important spectral feature was the disappearance of the doublet at δ 8.43 (J=2 Hz) corresponding to the aromatic proton on the 5-position in **2b** and the appearance of a new doublet at δ 7.05 (J=2 Hz). These high-field shifts was probably caused by the remission of the strong positive charge on the quinazolinium ring and the anisotropic effect of the benzene ring on the sp^3-C(4) formed upon hydration. Preferential occurrence of hydration at C(4) was supported by the absence of the coupling[7] between the hydroxy proton (δ 8.22) and the methine proton (δ 8.91) in the NMR spectrum in DMSO-d_6. The position of hydration may also be explained by a mechanistic consideration of the same type of reaction.[8] The methiodides (**2a-b**) were converted to 1-methyl-4-hydroxy-4-phenyl-1,4-dihydroquinazoline (**6**) and 1-methyl-4-hydroxy-4-phenyl-6-chloro-1,4-dihydroquinazoline (**7**) respectively under mild alkaline conditions. This conversion was found to be reversible. Thus, treatment of **6** and **7** with excess HBr afforded the corresponding quinazolinium bromides (**2c-d**) in a high yield.

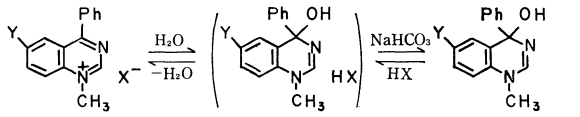

2 a Y=H X=I **5** **6** Y=H
b Y=Cl X=I **7** Y=Cl
c Y=H X=Br
d Y=Cl X=Br

Chart 2.

Reaction of **2a-d** with diazomethane was carried out under absolute anhydrous conditions, because the nucleophilic attack of diazomethane to form an aziridinium compound can take place only at the imminium carbon.[9] Treatment of **2c** with diazomethane in anhydrous CH_2Cl_2 at 10 °C gave three major products in about the same ratio. The first product was characterized as a picrate; the structure was chemically confirmed as 1-methyl-2-bromomethyl-4-phenyl-1,2-dihydroquinazoline (**8c**) by hydrogenation with Raney nickel. The NMR spectrum of the hydrogenation product was consistent with 1,2-dimethyl-4-phenyl-1,2-dihydroquinazoline (**11**), exhibiting a doublet at δ 1.46 (J=6 Hz) assignable to the methyl group at the 2-position and an absence of any signals attributable to methylene protons. Two other products, 1-methyl-3-ethoxy-5-phenyl-2,3-dihydro-1*H*-1,4-benzodiazepine (**9**) and 1-methyl-3-bromomethyl-5-phenyl-2,3-dihydro-1*H*-1,4-benzodiazepine (**10c**) were isolated from the mother liquor by column chromatography. The structure of **9** was established by the presence of the characteristic absorption of 4-phenyl-2,3-dihydro-1*H*-1,4-benzodiazepine[10] at 242 nm (ε 22000) and at 346 (1700) in the UV spectrum and by the signal of an ethoxy group in the NMR spectrum. The structure of **10c** was tentatively assigned on the basis of the spectral data. The UV spectrum [242.5 nm (ε 23000) and 346 (2900)] corresponded to the datum for **9**. The bromomethyl group was indicated by the molecular ion peak (*m/e* 330 and 328) and the base peak (*m/e* 249) in the mass spectrum, and by a multiplet at δ 3.4—3.9 which overlapped with the endocyclic methylene and methine protons in the NMR spectrum. There remained a little ambiguity as to the position of the bromomethyl group.

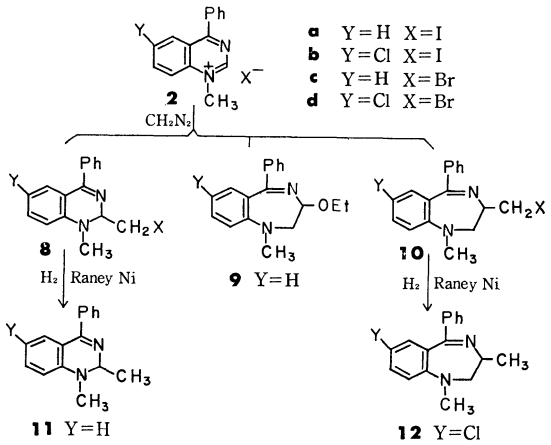

a Y=H X=I
b Y=Cl X=I
c Y=H X=Br
d Y=Cl X=Br

Chart 3.

Since the results of the preliminary reaction presented about was not necessarily satisfactory for our present purposes because of the low yield and the multiple product formation, we attempted to improve the reaction by changing the factors (the anion species, the

Table 1. Products in reaction of **2** with CH_2N_2

Exp. No	Y	X	Solv.	Temp. °C	Yield %		
					8	**9**	**10**
1	H	I	THF	10	69.4[a]		*[b]
2	H	Br	CH_2Cl_2	10	28.3[a]	13.1	11.0
3	H	Br	CH_2Cl_2	−20	*		74.2[c]
4	Cl	I	CH_2Cl_2	−35	24.5		46.6
5	Cl	Br	CH_2Cl_2	−45	*		55.3
6	H[d]	ClO_4	CH_2Cl_2	r. t.	—[e]	—	—

a) As the picrate. b) The tlc showed the presence of the compounds. However, since it seemed that the yields were very low, isolation was not attempted. c) As the picrolonate. d) 207—208 °C (decomp.). e) Nil.

substituent on the benzene ring, and the reaction conditions). Thus, the reactions of the quinazolinium salts (**2a–d**) with diazomethane were examined under various conditions. The results are shown in Table 1.

The reaction of 6-chloroquinazolinium iodide (**2b**) with diazomethane at −30——40 °C gave 1-methyl-2-iodomethyl-4-phenyl-6-chloro-1,2-dihydroquinazoline (**8b**) and 1-methyl-3-iodomethyl-5-phenyl-7-chloro-2,3-dihydro-1*H*-1,4-benzodiazepine (**10b**) in a ratio of about 1 : 2. The structure of **10b** was confirmed by its chemical transformation to a known compound, 1,3-dimethyl-5-phenyl-7-chloro-2,3-dihydro-1*H*-1,4 benzodiazepine (**12**).[11] Hydrogenation of **10b** with Raney nickel afforded **12** in a good yield. These results gave conclusive evidence for the tentative assignment of the structure of **10c**.

The change of the halide ion in the quinazolinium salt did not affect the product ratio. However, the reaction at low temperature showed a tendency to increase markedly the ratio of 3-halomethylbenzodiazepine. We will now attempt to explain the formation of **8**, **9**, and **10** (Chart 4). The process probably involves an initial attack of diazomethane to give an adduct (**A**) and a subsequent ring closure to the aziridinium halide (**B**). According to Crist and Leonard,[12] two pathways, a solvolysis-type reaction at the more substituted ring carbon and a nucleophilic displacement at the less hindered, less substituted ring carbon, are possible for the ring opening of an aziridinium compound. The product (**8**) would then be obtained by SN2-like ring opening with the halide ion at the less hindered methylene. However, an alternate route involving the displacement of the diazo group in (**A**) with the halide ion might be considered.

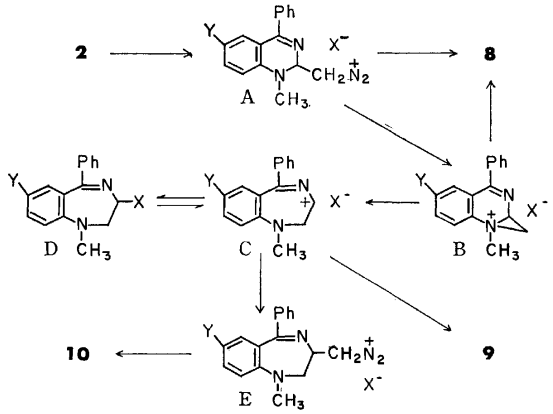

Chart 4.

The ring enlargement to **9** would be due to an *S*N1-type reaction of the most stable carbonium ion, which could arise *via* the ionic cleavage of the aziridinium intermediate (**B**), with the ethanol present in the ethereal diazomethane solution.[13] It seems that the formation of **10** was due to the participation of two equivalents of diazomethane. Bernhard and Snieckus[14] reported the formation of a benzazocine in addition to a seven-membered ring product in the reaction of 3,4-dihydro-2-methylisoquinolinium perchlorate with diazomethane. They explained the benzazocine formation by the second addition of diazomethane to the benzazepinium compound, which could arise from the aziridinium compound. However, the formation of our compound (**10**) could not be explained by their mechanism. Therefore, a different machanism must be operative in our case. Our failure to isolate the aziridinium compound (**B**) suggested that the intermediate (**B**) would be very unstable due to its own nature to afford smoothly the resonance-stabilized carbonium ion (**C**). This carbonium ion would react competitively with diazomethane and with the halide ion to give the adduct (**E**) and the halide (**D**) respectively. However, in view of the allylic nature of the C(3), the halide (**D**) would be amenable to equilibrium with the carbonium ion. Ultimately, the product (**10**) which could be formed *via* the displacement of the diazo group with the halide ion would become an end product.

The reaction of quinazolinium perchlorate with diazomethane was also attempted; however, it resulted only in the recovery of the starting material.

Experimental

Melting points are uncorrected and were determined on a Yamato apparatus, MP-1. The NMR spectra were determined on a Hitachi Perkin-Elmer R-20A instrument (Me_4Si). Mass spectra were measured on a Hitachi RMS-4 spectrometer. IR spectra were determined on a Shimadzu IR-27G spectrometer, and UV spectra, on a Hitachi EPS-2U spectrometer.

1-Methyl-4-phenyl-quinazolinium Iodide (2a). A): A mixture of 4-phenylquinazoline (**1**, 20.0 g) and methyl iodide (50 ml) was refluxed for 6 hr. The precipitates that had formed were collected by filtration and washed with Et_2O to give a crude product (21.0 g); mp 175—177 °C. In the NMR spectrum (DMSO-d_6), four singlets attributable to four different methyls (at δ 3.08, 3.80, 4.14, and 4.60) were observed.[6] The crude product was washed with $CHCl_3$ (300 ml) to give pure **2a** as an orange powder (15.5 g, 44.3%); mp 196—198 °C. IR ν_{max}^{Nujol} cm^{-1}: 1610, 1590, 1520. NMR (DMSO-d_6) δ: 3.80 and 4.60 (3H, two singlets in the ratio of 1 : 10), 7.0—8.7 (9H, m), 8.86 and 10.15 (1H, two singlets in the ratio of 1 : 10). Found: C, 51.85; H, 3.77; N, 7.74%. Calcd for $C_{15}H_{13}N_2I$: C, 51.74; H, 3.76; N, 8.05%.

B): A mixture of 2-(*N*-methylformamido)benzophenone (**4a**, 0.5 g), NH_4I (0.5 g), and EtOH (10 ml) was heated in a sealed tube at 150—160 °C for 10 hr. The mixture was then concentrated to dryness, and the residue was triturated with AcOEt to give a crystalline material. The crystals were extracted with CH_2Cl_2 and the extract was concentrated. The residue was triturated with AcOEt to give **2a** (30 mg, 4.3%). The NMR spectrum of this compound was identical with that of **2a** prepared by Method A.

C): A mixture of 1-methyl-4-hydroxy-4-phenyl-1,4-dihydroquinazoline (**6**, 0.2 g), an excess of 57% HI (*ca.* 0.2 ml) and *i*-PrOH (10 ml) was warmed until it became a clear solution. After cooling, the precipitates were collected by filtration to give almost pure **2a** as orange leaflets (0.25 g, 89%); mp 195—197 °C (decomp.). The NMR spectrum and IR spectrum of this compound were identical with those of **2a**.

1-Methyl-4-phenyl-6-chloroquinazolinium Iodide (2b). A): A mixture of 4-phenyl-6-chloroquinazoline (**1b**, 11.0 g) and methyl iodide (30 ml) was heated in a sealed tube at 100—110 °C for 20 hr. The precipitates were collected by filtration and washed with Et_2O to give a crude product

(15.8 g, 97.7%); mp 204—205 °C (decomp.). NMR (DMSO-d_6) δ: 3.10 and 4.17 (two singlets, N^3-CH_3), 4.63 (s, N^1-CH_3) (3H, the ratio of 3 : 7),[15] 7.0—8.75 (8H, m), 8.99 and 9.95 (two singlets), 10.20 (s), (1H, the ratio of 3 : 7). This product was recrystallized from a mixture of DMF (100 ml) and AcOEt (50 ml) to give pure **2b** as dark red leaflets (8.6 g, 49.4%); mp 211—213 °C (decomp.). IR ν_{max}^{Nujol} cm^{-1}: 1595, 1590, 1521. NMR: The spectrum is shown in Fig. 1. Found: C, 47.06; H, 3.10; N, 7.34%. Calcd for $C_{15}H_{12}N_2ClI$: C, 47.08; H, 3.17; N, 7.32%.

B): A mixture of 2-(*N*-methylformamido)-5-chlorobenzophenone (**4b**, 2.0 g), NH_4I (4.0 g), and EtOH (30 ml) was heated in a sealed tube at 150 °C overnight. The mixture was then concentrated to dryness, and the residue was triturated with AcOEt. The solid was collected by filtration and extracted with CH_2Cl_2 (100 ml). The extract was concentrated to give a crystalline residue (200 mg). A mixture of the residue (100 mg), three drops of 47% HI, and *i*-PrOH (5 ml) was warmed to give a clear solution. After cooling, the crystals which had formed were collected by filtration to give pure **2b** as red leaflets (50 mg, 3.5%); mp 212—213 °C (decomp.). The NMR spectrum of this compound was identical with that of **2b** prepared by Method A. **4b** (1.1 g, 55%) was recovered from the AcOEt filtrate.

*1-Methyl-4-hydroxy-4-phenyl-1,4-dihydroquinazoline (**6**).* To a suspension of **2a** (1.0 g) in H_2O (20 ml) was added $NaHCO_3$ (1.5 g), and the mixture was stirred at room temperature for 1 hr. The crystals were collected by filtration to give almost pure **6** (0.65 g, 95%); mp 135—136 °C (decomp.). Recrystallization from DMF-EtOH gave an analytical sample colorless leaflets; mp 141—143 °C (decomp.). IR ν_{max}^{Nujol} cm^{-1}: 1640, 1600, 1570. NMR (DMSO-d_6) δ: 3.30 (3H, s), 6.22 (1H, br.s), 6.8—7.55 (10H, m). Found: C, 75.65; H, 5.92; N, 11.82%. Calcd for $C_{15}H_{14}ON_2$: C, 75.60; H, 5.92; N, 11.76%.

*1-Methyl-4-hydroxy-4-phenyl-6-chloro-1,4-dihydroquinazoline (**7**).* To a suspension of **2b** (9.0 g) in H_2O (200 ml) was added a small excess of 5% $NaHCO_3$ solution, and the mixture was stirred overnight. The crystals were collected by filtration to give almost pure **7** (6.0 g, 98%); mp 170—172 °C. Recrystallization from dioxane gave a pure sample as colorless leaflets; mp 176—178 °C (decomp.). IR ν_{max}^{Nujol} cm^{-1}: 1640, 1600, 1570, 1513. NMR (DMSO-d_6) δ: 3.31 (3H, s), 6.6—7.6 (10H, m). Found: C, 65.93; H, 4.88; N, 10.26%. Calcd for $C_{15}H_{13}ON_2Cl$: C, 66.05; H, 4.80; N, 10.27%.

*1-Methyl-4-phenylquinazolinium Bromide (**2c**).* **2c** (2.7 g, 78.0%) was prepared from **6** (4.0 g) and excess 47% HBr (8 ml) in *i*-PrOH. Recrystallization from DMF–AcOEt gave an analytical sample as pale yellow leaflets; mp 243—244 °C (decomp.). IR ν_{max}^{Nujol} cm^{-1}: 1610, 1590, 1520. NMR (DMSO-d_6) δ: 3.81, 4.65 (3H, two singlets), 7.35—8.75 (9H, m), 8.97, 10.27 (1H, two singlets). Found: C, 59.80; H, 4.42; N, 9.07%. Calcd for $C_{15}H_{13}N_2Br$: C, 59.81; H, 4.35; N, 9.30%.

*1-Methyl-4-phenyl-6-chloroquinazolinium Bromide (**2d**).* To a suspension of **7** (5.0 g) in *i*-PrOH (50 ml) was added an excess of 25% HBr/AcOH (*ca.* 30 ml) and the mixture was warmed until it became clear. After cooling, the yellow leaflets which had precipitated were collected by filtration and washed with *i*-PrOH (5.0 g, 81.2%); mp 230—231 °C (decomp.). IR ν_{max}^{Nujol} cm^{-1}: 1596, 1528, 1486. NMR (DMSO-d_6) δ: 3.82, 4.67 (3H, two singlets), 7.0—8.8 (8H, m), 9.06, 10.31, (1H, two singltes). Found: C, 53.45; H, 3.64; N, 8.12%. Calcd for $C_{15}H_{12}N_2BrCl$: C, 53.67; H, 3.60; N, 8.34%.

*Reactions of Quinazolinium Salts (**2a—d**) with CH_2N_2.* *1)*: To a stirred suspension of **2a** (1.05 g) in THF (100 ml) was added dropwise a freshly-prepared ethereal solution of CH_2N_2 (from 4 g of *p*-TsN(NO)CH_3) at 10 °C over a 1-hr period. After standing for 15 min, the mixture was concentrated to dryness and the residual oil was crystallized as a picrate (1.2 g, 69.4%); mp 162—164 °C. Recrystallization from a mixture of DMF and EtOH gave 1-methyl-2-iodomethyl-4-phenyl-1,2-dihydroquinazoline (**8a**) picrate as dark red prisms; mp 163—165 °C. NMR (DMSO-d_6) δ: 3.33 (3H, s), 3.45—3.75 (2H, m), 5.79 (1H, d.d, J=10 Hz, J=6 Hz), 6.8—8.0 (9H, m), 8.62 (2H, s). Found: C, 44.53; H, 3.21; N, 11.82%. Calcd for $C_{22}H_{18}O_7N_5I$: C, 44.68; H, 3.07; N, 11.84%.

2): To a stirred suspension of **2c** (0.9 g) in CH_2Cl_2 (100 ml) was added a freshly-prepared ethereal solution of CH_2N_2 (from 6.0 g of *p*-TsN(NO)CH_3) at 10 °C over a 1-hr period. After standing for 1 hr, the mixture was washed with aqueous 5% $NaHCO_3$ solution, dried (Na_2SO_4) and concentrated to dryness. The residual oil was crystallized as a picrate (0.3 g, 28.3%), mp 130—132 °C (decomp.). A pure sample of 1-methyl-2-bromomethyl-4-phenylquinazoline (**8c**) picrate was obtained as red prisms by recrystallization from EtOH; mp 133—135 °C (decomp.). Found: C, 49.75; H, 3.52; N, 13.48%. Calcd for $C_{22}H_{18}O_6N_5Br$: C, 50.01; H, 3.43; N, 13.25%.

The mother liquor from the crystallization of the picrate was concentrated, and the residue was poured into aqueous 5% LiOH solution. The oil was extracted with benzene, and the benzene layer was dried (K_2CO_3) and concentrated to dryness. Tlc of the residual oil indicated the presence of two major products. This was chromatographed on silica gel (30 g, solvent $CHCl_3$–EtOH, 200 : 1). The first fraction (110 mg, 11.0%) was crystallized from *n*-hexane. Recrystallization from petroleum ether gave 1-methyl-3-bromomethyl-5-phenyl-2,3-dihydro-1*H*-1,4-benzodiazepine (**10c**) as colorless prisms, mp 81—83 °C. IR ν_{max}^{Nujol} cm^{-1}: 1614, 1595, 1580, 1563, 1492. UV λ_{max}^{EtOH} nm ($\varepsilon\times10^{-3}$): 242 (23.0), 346 (2.9). NMR ($CDCl_3$) δ: 2.79 (3H, s), 3.4—3.9 (5H, m), 6.9—7.75 (9H, m). Mass *m/e*: 330, 328 (M^+), 249 (M^+-81, M^+-79). Found: C, 61.85; H, 5.34; N, 8.53%. Calcd for $C_{17}H_{17}N_2Br$: C, 62.01; H, 5.21; N, 8.51%.

The second fraction (110 mg, 13.1%) was crystallized from petroleum ether; subsequent recrystallization from petroleum ether gave 1-methyl-3-ethoxy-5-phenyl-2,3-dihydro-1*H*-1,4-benzodiazepine (**9**) as colorless prisms; mp 90—92 °C. IR ν_{max}^{Nujol} cm^{-1}: 1603, 1595, 1564. UV λ_{max}^{EtOH} nm ($\varepsilon\times10^{-3}$): 242 (22.0), 346 (1.7). NMR ($CDCl_3$) δ: 1.29 (3H, t, J=7 Hz), 2.80 (3H, s), 3.25—4.3 (4H, m), 4.73 (1H, q, J=5 Hz), 6.9—7.8 (1H, m). Mass *m/e*: 280 (M^+). Found: C, 76.89; H, 7.11; N, 9.88%. Calcd for $C_{18}H_{20}ON_2$: C, 77.11; H, 7.19; N, 9.99%.

3): The reaction of **2c** (18 g) with CH_2N_2 in CH_2Cl_2 (200 ml) was carried out at −18—−20 °C to obtain **10c** picrolonate (2.7 g, 74%); mp 128—131 °C (decomp.). The crystals were dissolved in $CHCl_3$ and passed through alumina (50 g). The product was identified as **10c**.

4): 1-Methyl-3-iodomethyl-5-phenyl-7-chloro-2,3-dihydro-1*H*-1,4-benzodiazepine (**10b**, 500 mg) was obtained from **2b** (1.0 g) as colorless prisms (*i*-PrOH); mp 145—147 °C. Yield, 46.6%. IR ν_{max}^{Nujol} cm^{-1}: 1615, 1595, 1555, 1490. UV λ_{max}^{EtOH} nm ($\varepsilon\times10^{-3}$): 233 (26.0), 250 (21.0), 358 (1.2). NMR ($CDCl_3$) δ: 2.77 (3H, s), 3.2—3.9 (5H, m), 6.8—7.8 (8H, m). Mass *m/e*: 410 (M^+), 283 (M^+-127). Found: C, 49.55; H, 3.99; N, 6.72%. Calcd for $C_{17}H_{16}N_2ClI$: C, 49.72; H, 3.93; N, 6.82%.

From the mother liquor, 1-methyl-2-iodomethyl-4-phenyl-7-chloro-1,2-dihydroquinazoline (**8b**) picrate (400 mg) was obtained as dark red prisms (DMF–EtOH); mp

156—158 °C. Yield, 24.5%. NMR (DMSO-d_6) δ: 3.30 (3H, s), 3.45—3.95 (2H, m), 5.65—5.95 (1H, m), 7.0—8.0 (9H, m), 8.60 (2H, s). Found: C, 41.95; H, 2.52; N, 11.30%. Calcd for $C_{22}H_{17}O_7N_5ClI$: C, 42.23; H, 2.74; N, 11.19%.

5): 1-Methyl-3-bromomethyl-5-phenyl-7-chloro-3,4-dihydro-1*H*-1,4-benzodiazepine (**10d**, 600 mg) was obtained from **2d** (1.0 g) as colorless prisms (Et_2O-*n*-hexane); mp 140—142 °C. Yield, 55.3%. IR ν_{max}^{Nujol} cm^{-1}: 1615, 1575, 1555, 1490. UV λ_{max}^{EtOH} nm ($\varepsilon \times 10^{-3}$): 233 (26.0), 250 (24.0), 358 (1.0). NMR ($CDCl_3$) δ: 2.78 (3H, s), 3.35—4.0 (5H, m), 6.8—7.8 (8H, m). Mass *m/e*: 364, 362 (M^+), 283 (M^+-81, M^+-79). Found: C, 55.98; H, 4.49; N, 7.68%. Calcd for $C_{17}H_{16}N_2BrCl$: C, 56.14; H, 4.43; N, 7.70%.

*Reduction of 1-Methyl-2-iodomethyl-4-phenyl-1,2-dihydroquinazoline (**8a**) with Raney Ni.* A mixture of **8a** picrate (0.5 g) and aqueous 5% LiOH solution (10 ml) was extracted with benzene and the extract was dried (K_2CO_3). The solution was hydrogenated with 2 ml of Raney Ni under 2.5 kg/cm² (30 min). The catalyst was removed by filtration and the filtrate was washed with aqueous 5% $NaHCO_3$ solution, dried (Na_2SO_4) and concentrated under reduced pressure. The residue was crystallized from EtOH as a picrate and recrystallization from EtOH gave 1,2-dimethyl-4-phenyl-1,2-dihydroquinazoline (**11**) picrate as red needles (0.2 g, 50%); mp 160—163 °C (decomp.). NMR (DMSO-d_6) δ: 1.46 (3H, d, J=6 Hz), 3.20 (3H, s), 5.61 (1H, q, J=6 Hz), 6.75—8.0 (9H, m), 8.60 (2H, s). Found: C, 56.30; H, 4.20; N, 14.78%. Calcd for $C_{22}H_{19}O_7N_5$: C, 56.77; H, 4.12; N, 15.05%.

*Reduction of 1-Methyl-3-iodomethyl-5-phenyl-7-chloro-2,3-dihydro-1H-1,4-benzodiazepine (**10b**) with Raney Ni.* A mixture of **10b** (1.8 g), KOH (300 mg), and EtOH (50 ml) was hydrogenated with 1.5 ml of Raney Ni under 2.5 kg/cm². The catalyst was removed by filtration, and the filtrate was concentrated to dryness. The residue was dissolved in $CHCl_3$, and the solution was washed with H_2O, dried (K_2CO_3), and concentrated. The residue was crystallized from *n*-hexane, and the crystals were collected by filtration. Recrystallization from ether-*n*-hexane gave pure 1,3-dimethyl-5-phenyl-7-chloro-2,3-dihydro-1*H*-1,4-benzodiazepine (**12**, 0.5 g, 40.5%); mp 101—102 °C. IR ν_{max}^{Nujol} cm^{-1}: 1607, 1570, 1490. UV λ_{max}^{EtOH} nm ($\varepsilon \times 10^{-3}$): 231 (23.9), 250 (20.3), 356 (1.1). NMR ($CDCl_3$) δ: 1.42 (3H, d, J=6 Hz), 2.75 (3H, s), 3.4—4.0 (3H, m), 6.75—7.75 (8H, m). Found: C, 71.97; H, 6.06; N, 9.77%. Calcd for $C_{17}H_{17}N_2Cl$: C, 71.69; H, 6.02; N, 9.84%. The IR spectrum of this compound was identical with that of the authentic sample.[11,12] Treatment of the mother liquor from crystallization of crude **12** with MeOH/HCl gave **12**·HCl (0.5 g, 35.5%); mp 231—232 °C. Found: C, 63.88; H, 5.67; N, 8.47%. Calcd for $C_{17}H_{18}N_2Cl_2$: C, 63.55; H, 5.65; N, 8.72%.

Reduction of 1-Methyl-3-bromomethyl-5-phenyl-7-chloro-2,3-dihydro-1H-1,4-benzodiazepine with Raney Ni. **10d** was hydrogenated in the same way, and the product was identified as **12**.

We are indebted to Dr. R. I. Fryer for kindly providing us with the sample. We wish to express our gratitude to Mr. T. Takayanagi, Senior Managing Director of our Company, Dr. I. Chibata, Director of our Laboratory, Dr. K. Okumura and Dr. M. Miyoshi for their encouragement. Thanks are due to the members of the analytical center for elemental analyses.

References

1) a) G. Zbinder and L. O. Randall, "Advances in Pharmacology," Vol. 5, ed. by S. Grattini and P. A. Shore, Academic Press New York (1967), p. 213. b) L. H. Sternbach, L. O. Randall, R. Banziger, and H. Lehr, "Drug Affecting the Central Nervous System," Vol. 2, ed. by A. Burger, Marcel Dekker New York (1968) p. 237.

2) a) L. H. Sternbach, *Angew. Chem. Int. Ed. Eng.*, **10**, 34 (1971). b) S. Inaba, K. Ishizumi, K. Mori, and H. Tamamoto, *Chem. Pharm. Bull.* (Tokyo), **19**, 722 (1971). c) T. Miyadera, A. Terada, M. Fukunaga, Y. Kawano, T. Kamioka, C. Tamura, H. Takagi, and R. Tachikawa, *J. Med. Chem.*, **14**, 520 (1971).

3) Y. Yamada, T. Oine, and I. Inoue, This Bulletin, in the preceding paper, "4-Oxo-1,2,3,4-tetrahydroquinazolines V. Ring Expansion Reaction of 1-Methyl-3-phenyl-4-oxo-3,4-dihydroquinazolinium Bromide with Diazoalkanes."

4) H. Ott and M. Denzer, *J. Org. Chem.*, **33**, 4263 (1968).

5) On our experiment, the ratio of two isomers was shown to be *ca.* 7 : 3 by NMR spectroscopy.

6) A singlet at δ 4.14 may be assigned to N-CH_3 in 3-methiodide (**3a**) and another singlet at δ 3.08 to N-CH_3 in **3a**·hydrate.

7) R. M. Silverstein and G. C. Bassler, "Spectrometric Identification of Organic Compounds," 2nd Ed., John Wiley & Sons, New York, (1967), p. 122.

8) W. A. F. Armergo, "Advances in Heterocyclic Chemistry," Vol. 1, ed. by A. R. Katritzky, Academic Press. Inc., New York and London (1963), p. 253.

9) a) G. Opitz and A. Griesinger, *Ann. Chem.*, **665**, 102 (1963). b) B. Göber, S. Pfeifer, V. Hanus, and G. Engelhardt, *Arch. Pharm. Wienheim*, **301**, 763 (1968).

10) The UV spectrum of 4-phenyl-2,3-dihydro-1*H*-1,4-benzodiazepine which was prepared by the method of Wünsch* showed the absorption at 242 nm (ε 22000) and 346 (1900). *K. H. Wünsch, H. Dettmann, and S. Schönberg, *Chem. Ber.*, **102**, 3891 (1969).

11) A. Walser, G. Silverman, R. I. Fryer, and L. H. Sternbach, *J. Org. Chem.*, **36**, 1248 (1971). The authentic sample was kindly provided by Dr. R. I. Fryer.

12) D. R. Crist and N. J. Leonard, *Angew. Chem. Int. Ed. Eng.*, **8**, 962 (1969).

13) T. J. Boer and H. J. Backer, "Organic Syntheses," Coll. Vol. IV, p. 250 (1963).

14) H. O. Bernhard and V. Snieckus, *Tetrahydron*, **27**, 2091 (1971).

15) The value indicates the integral ratio of the 3- to the 1-methiodide. The signals at δ 4.17 and 3.10 may be assigned to the N-CH_3 in **3b** and **3b**-hydrate, respectively.

The Oxidation of 1,3-Butadienes with Nitric Acid into 2,5-Dihydrofurans

Fumio Toda and Eishiro Todo

Department of Industrial Chemistry, Faculty of Engineering, Ehime University, Matsuyama 790

(Received September 17, 1973)

The oxidation of 3,4-bis(diphenylmethylene)-succinic anhydride (I), -1-benzylsuccinimide (VI), and -γ-butyrolactone (VIII) with nitric acid afforded the corresponding 2,5-dihydrofuran derivatives, III, VII, and IX respectively. The same oxidation of 3,4-bis(diphenylmethylene)cyclobutane-1,2-dione (XI) afforded 3,4-bis(diphenylhydroxymethyl)cyclobut-3-ene-1,2-dione (XIII), probably *via* the bicyclic cyclobutenedione intermediate (XII).

No one-step oxidation of buta-1,3-diene into dihydrofuran has yet been reported. We have now performed the oxidation of the buta-1,3-diene group of I, VI, VIII, and XI with HNO_3 into dihydrofuran.

When a solution of 3,4-bis(diphenylmethylene)succinic anhydride (I)[1] and concd HNO_3 in MeCN was heated under reflux for 10 min, 6,6,8,8-tetraphenyl-2,7-dioxabicyclo[3.3.0]oct-4-ene-1,3-dione (III) was obtained in an 89% yield. The structure of III was identified by the decarboxylation of the 2,2,5,5-tetraphenyl-3,4-dicarboxy-2,5-dihydrofuran (IV) initially produced by the hydrolysis of III; this afforded 2,2,5,5-tetraphenyl-2,5-dihydrofuran (V).[2] The same treatment of 3,4-bis(diphenylmethylene)-1-benzylsuccinimide (VI)[3] and -γ-lactone (VIII)[4] afforded 6,6,8,8-tetraphenyl-2-benzyl-2-aza-7-oxabicyclo[3.3.0]oct-4-ene-1,3-dione (VII) (85%) and 6,6,8,8-tetraphenyl-2,7-dioxabicyclo[3.3.0]oct-4-en-1-one (IX) (51%) respectively.

However, 2,3-bis(diphenylmethylene)-butane-1,4-dial (Xa), -succinic acid (Xb), and its dimethyl ester (Xc) were not oxidized with concd HNO_3. This shows that a fixed s-*cis* configuration of the buta-1,3-diene moiety is essential for the oxidation. Since I was not oxidized with concd $HClO_4$, HBF_4, and H_2SO_4, concd HNO_3 may be a characteristic reagent for the oxidation reaction. A possible pathway of the oxidation of I is illustrated in Scheme 1, *i. e.*, the elimination of HNO_2 from the II initially formed by the 1,4-addition of HNO_3 to the enone group of I.

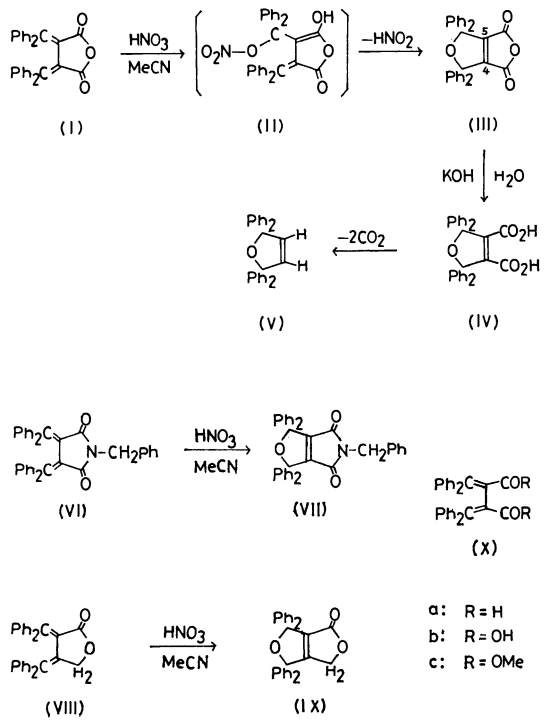

Scheme 1.

The same treatment of 3,4-bis(diphenylmethylene)-cyclobutane-1,2-dione (XI) with concd HNO_3 in MeCN afforded I and 3,4-bis(diphenylhydroxymethyl)cyclobut-3-ene-1,2-dione (XIII)[5] in 37 and 17% yields respectively. Since the oxidation of XI with 30% H_2O_2 or with concd $HClO_4$ to afford I has been reported,[1] I may be produced by a similar Baeyer-Villiger-type oxidation of XI. When the reaction of XI with concd HNO_3 was carried out in a non-poalr solvent such as CCl_4, this Baeyer-Villiger oxidation was inhibited, and XIII was obtained in a 64% yield as the sole isolable product. A possible precursor of XIII is the bicyclic cyclobutenedione (XII), which can be produced by the oxidation of XI *via* a pathway similar to that described for the formation of III.

In order to prove the intermediacy of XII, XI was allowed to react with concd HNO_3 in MeOH, in the expectation of isolating 3-diphenylhydroxymethyl-4-diphenylmethoxymethylcyclobut-3-ene-1,2-dione (XV). The reaction, however, afforded only 2,2-dimethoxy-3,4-bis(diphenylmethylene)cyclobutan-1-one (XIVb),[1] no XV. Nevertheless, when MeOH was added to a reaction mixture of XI, concd HNO_3, and CCl_4, soon the green color of XI disappeared and XV was isolated in a 54% yield. Since XIII did not react with MeOH in the presence of concd HNO_3 at an elevated temperature, the possibility that XIII is a precursor of XV can be ruled out. A plausible pathway of the formation of XV is an acid-catalyzed methanolysis of XII (Scheme 2). Unfortunately, however, all attempts to isolate XII failed.

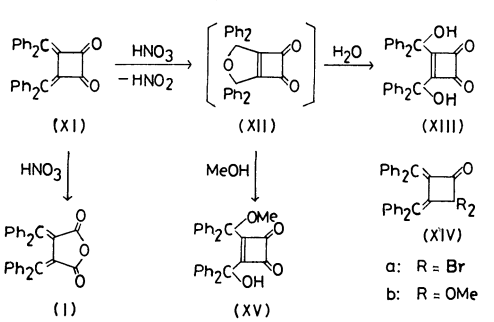

Scheme 2.

The reaction of 2,2-dibromo-3,4-bis(diphenylmethylene)cyclobutan-1-one (XIVa) with concd HNO_3 in MeCN for 2 min afforded I in a 52% yield. The same treatment of XIVb as for XIVa for 2 min afforded XI in a 45% yield.

Experimental

All the melting points were uncorrected. The IR, UV, and NMR spectra were measured in Nujol mull, $CHCl_3$, and $CDCl_3$ respectively, unless otherwise noted. The mass spectra were measured with an ionization energy of 75 eV.

Oxidation of I. A solution of I (1.2 g) and concd HNO_3 (0.8 ml) in MeCN (100 ml) was heated under reflux for 10 min. Crude crystals left by the evaporation of the solvent were recrystallized from MeCN to afford III as colorless needles; 1.0 g (89%); mp 196—197 °C. IR: 1850 and 1780 (C=O), 1670 (C=C), and 1020 cm^{-1} (C–O–C); λ_{max}: 264 (ε, 4700) and 280 nm (4700); NMR: 2.78 τ (s, Ph); MS: *m/e* (rel intensity) 444 (M^+, 30), 323 (100), 289 (80), and 218 (55).

Found: C, 79.81; H, 4.68%. Calcd for $C_{30}H_{20}O_4$: C, 81.06; H, 4.54%.

Hydrolysis of III. A solution of III (0.19 g) and KOH (0.2 g) in MeOH (30 ml) was heated under reflux for 2 hr. The crude crystals which had been separated out by the addition of dil HCl to the reaction mixture were recrystallized from MeCN to afford IV as colorless needles; 0.16 g (74%); mp 204—205 °C. IR: 1740 and 1720 (unsplit doublet, C=O), 1650 (C=C), and 1030 cm^{-1} (C–O–C); λ_{max}^{EtOH}: 240 sh (ε, 10500), 258 sh (5100), and 216 sh nm (3700). MS: *m/e* (rel intensity) 323 (100) and 218 (40).

Found: C, 77.69; H, 4.78%. Calcd for $C_{30}H_{22}O_5$: C, 77.91; H, 4.80%.

Decarboxylation of IV. A mixture of IV (0.104 g), Cu-powder (0.05 g) and quinoline (3 ml) was heated under reflux for 4 hr. The cooled reaction mixture was then diluted with ether (100 ml). The ethereal solution was washed successively with dil HCl and water, and then dried over anhydrous Na_2SO_4. The crude crystals left after the evaporation of the solvent were recrystallized from MeCN to afford V as colorless needles; 0.012 g (14%); mp 179—181 °C (lit,[2] mp 180—183 °C). IR: 1010 cm^{-1} (C–O–C); λ_{max}: 250 sh (ε, 900), 253 (1100), 260 (1200), and 266 nm (1000); NMR: 2.82 (s, Ph, 20H) and 3.52 τ (s, =CH, 2H).

Oxidation of VI. VI (0.1 g) was treated with concd HNO_3 (0.08 ml) in MeCN (10 ml) under the same conditions as were used for I. The crude crystals left by the evaporation of the solvent were recrystallized from MeCN to afford VII as colorless needles; 0.087 g (85%); mp 178—179 °C. IR: 1775 and 1715 (C=O), 1435 (CH_2), and 1010 cm^{-1} (C–O–C); λ_{max}: 252 (ε, 14200) and 295 sh nm (5100); NMR: 2.4—3.2 (m, Ph, 25H) and 5.29 τ (s, CH_2, 2H).

Found: C, 83.15; H, 4.83%. Calcd for $C_{37}H_{27}O_3N$: C, 83.28; H, 5.10%.

Oxidation of VIII. VIII (0.1 g) was treated with concd HNO_3 (0.08 ml) in MeCN (10 ml) under the same conditions as were used for I. The crude crystals left after the evaporation of the solvent were recrystallized from MeCN to afford IX as colorless needles; 0.053 g (51%); mp 227—228 °C. IR: 1770 (C=O), 1675 (C=C), and 1010 cm^{-1} (C–O–C); λ_{max}: 260 sh (ε, 4100), 263 sh (3100), and 270 sh nm (1800); NMR: 2.3—3.2 (m, Ph, 20H) and 4.95 τ (s, CH_2, 2H).

Found: C, 83.55; H, 4.95%. Calcd for $C_{30}H_{22}O_3$: C, 83.70; H, 5.15%.

Oxidation of XI in MeCN. XI (0.1 g) was allowed to react with concd HNO_3 (0.05 ml) in MeCN (20 ml) under the same conditions as were used for I. The evaporation of the solvent gave a mixture of red and colorless crystals. The subsequent recrystallization of this mixture from AcOEt afforded I as red rhombs; 0.038 g (37%); mp 230 °C (lit,[1] mp 230 °C). The AcOEt solution left after the separation of I was evaporated to dryness, and the residue was recrystallized from MeOH to afford XIII as colorless prisms; 0.018 g (17%); mp 205—206 °C (lit,[5] mp 205—206 °C). The IR spectra of I and XIII were identical with those of the authentic samples.

Oxidation of XI in CCl_4. XI (0.1 g) was oxidized with concd HNO_3 (0.05 ml) in CCl_4 (20 ml) by the procedure used for MeCN. The crude crystals left by the evaporation of the solvent were recrystallized from MeOH to afford XIII; 0.069 g (64%).

Oxidation of XI in CCl_4. XI (0.1 g) was oxidized with concd HNO_3 (0.05 ml) in CCl_4 (20 ml) by the procedure used for MeCN. The crude crystals left by the evaporation of the solvent were recrystallized from MeOH to afford XIII; 0.069 g (64%).

Isolation of XV. A solution of XI (0.1 g) and concd HNO_3 (0.07 ml) in CCl_4 (20 ml) was heated under reflux until the green color of XI almost disappeared (*ca.* 7 min). MeOH (10 ml) was then immediately added to the reaction mixture, and it was heated under reflux for 5 min. The crude crystals left by the evaporation of the solvent were recrystallized from MeOH to afford XV as colorless needles; 0.06 g (54%); mp 138—140 °C. IR: 3580 and 3300 (OH), 1790 sh and 1780 (C=O), 1560 (C=C), and 1070 cm^{-1} (C–O–C); λ_{max}^{EtOH}: 241 sh (ε, 13500) and 274 sh nm (6500); NMR: 2.70 (s, Ph, 20H), 3.22 (s, OH, 1H), and 7.04 τ (s, OCH_3, 3H).

Reaction of XI with Concd HNO_3 in MeOH, A solution of XI (0.1 g) and concd HNO_3 (0.07 ml) in MeOH (20 ml) heated under reflux for 2 hr. The crude crystals left by the evaporation of the solvent were recrystallized from AcOEt to afford XIVb as orange red needles; 0.074 g (67%); mp 191—192 °C (lit,[1] mp 191—192 °C). The IR spectrum was identical with that previously-recorded for XIVb.[1]

Reaction of XIVa with Concd HNO_3. A solution of XIVa (0.1 g) and concd HNO_3 (0.04 ml) in MeCN (15 ml) was heated under reflux for 2 min. The crude crystals left by the evaporation of the solvent were recrystallized from AcOEt to afford I as red rhombs; 0.04 g (52%).

Reaction of XIVb with Concd HNO_3. When XIVb (0.1 g) was treated with concd HNO_3 (0.04 ml) in MeCN (15 ml) for 2 min by the procedure used for XIVa, XI was obtained as green prisms; 0.04 g (45%); mp 206—207 °C (lit,[1] mp 206—207 °C). The IR spectrum was identical with that previously-recorded for XI.[1]

References

1) F. Toda and K. Akagi, *Tetrahedron*, **27**, 2801 (1971).
2) R. E. Lutz and C. L. Dickerson, *J. Org. Chem.*, **27**, 2040 (1962).
3) F. Toda, H. Nakaoka, K. Yuwane, and E. Todo, This Bulletin, **46**, 1737 (1973).
4) F. Toda and N. Ooi, *ibid.*, **45**, 1820 (1972).
5) F. Toda and N. Ooi, *ibid.*, **46**, 1733 (1973).

Total Synthesis of Natural Acetylenic Analogues of Isorenieratene and Renieratene[1]

Tetsuji IKE,[2] Junji INANAGA, Akio NAKANO, Nobuhisa OKUKADO, and Masaru YAMAGUCHI

Department of Chemistry, Faculty of Science, Kyushu University, Higashi-ku, Fukuoka 812

(Received September 19, 1973)

The total synthesis of two natural acetylenic aromatic carotenoids, 7,8-didehydroisorenieratene (**1**) and 7,8-didehydrorenieratene (**2**), was carried out. Although the condensations involving C_{15}-acetylenic ylids (derived from the phosphonium salts **7**, and **8**) as the intermediates gave only 9-*cis* isomers of **1** and **2**, low-temperature condensations of C_{25}-hexaene yield (derived from **19** and **28**) with C_{15}-acetylenic aldehyde (**12a**) led to all-*trans* **1** and **2**, which were identical with natural specimens.

It has recently been shown that two minor carotenoid constituents, mp 194—194.5 °C and mp 204—205 °C, isolated from a sea sponge "*Reniera japonica*" ("*Halichondria japonica*") have the acetylenic aromatic structures of **1** and **2**,[3] which correspond to those of the 7,8-didehydro derivatives of isorenieratene[4] and renieratene[5] respectively. The present work has been

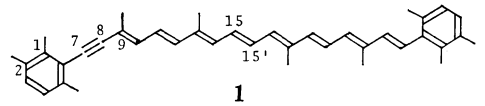

1

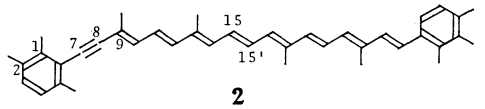

2

undertaken to verify these structures by synthesis. Analogous syntheses have already been done on several alicyclic acetylenic carotenoids by Weedon.[6] In the present work, a similar construction principle, $C_{15}+C_{10}\rightarrow C_{25}$, $C_{25}+C_{15}\rightarrow C_{40}$, has been used.

Results and Discussion

Synthesis of 7,8-Didehydroisorenieratene (1). The first synthesis, which led to the 9-*cis* isomer (**22**) of **1**, was started with 2,3,6-trimethylbenzoic acid,[7] which was converted into the acetylenic alcohol (**5**) through **3** and **4**. The treatment of **5** with triphenylphosphonium bromide gave a sole product, which was later proved to be the *cis* salt (**7**) by comparing its NMR spectrum with that of **8** to be described below. The condensation of the ylid from **7** with the C_{10}-dialdehyde

3 R:$COCH_3$
4 R:C≡CH
5 R:C≡CCCH=CH_2 (with H_3C OH)
6 R:C≡CCOCH$_3$

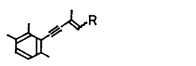

7 R:$CH_2\overset{+}{P}Ph_3\bar{B}r$(2-cis)
8 R:$CH_2\overset{+}{P}Ph_3\bar{B}r$(2-trans)
9a R:CO_2H(2-trans)
9b R:CO_2H(2-cis)
10a R:CH_2OH(2-trans)
10b R:CH_2OH(2-cis)
11a R:CH_2Br(2-trans)
11b R:CH_2Br(2-cis)
12a R:CHO(2-trans)
12b R:CHO(2-cis)

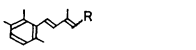

13a R:$CO_2C_2H_5$(2-trans)
13b R:$CO_2C_2H_5$(2-cis)
14a R:CO_2H(2-trans)
14b R:CO_2H(2-cis)
15 R:CH_2OH(2-trans)
16 R:$CH_2\overset{+}{P}Ph_3\bar{B}r$(2-trans)

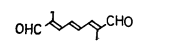

17

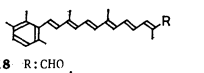

18 R:CHO
19 R:$CH_2\overset{+}{P}Ph_3\bar{B}r$

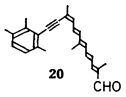

20

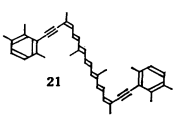

21

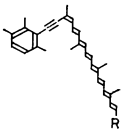

22 R:2,3,6-$(CH_3)_3C_6H_2$
23 R:2,3,4-$(CH_3)_3C_6H_2$

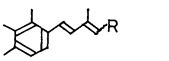

24a R:CO_2CH_3(2-trans)
24b R:CO_2CH_3(2-cis)
25 R:CH_2OH(2-trans)
26 R:$CH_2\overset{+}{P}Ph_3\bar{B}r$(2-trans)

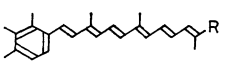

27 R:CHO
28 R:$CH_2\overset{+}{P}Ph_3\bar{B}r$

(**17**)[8] afforded the acetylenic aldehyde (**20**) as the major product (25% yield), besides 9,9′-di-*cis*-7,7′,8,8′-tetradehydroisorenieratene (**21**). The condensation of 2,3,6-trimethylbenzalacetone with ethoxycarbonylmethylenetriphenylphosphorane gave, after saponification, a mixture of the *trans* (**14a**) and the *cis* acid[9] (**14b**) (3 : 1), which were then separated by fractional crystallization. The *trans* acid (**14a**) was converted into the phosphonium bromide (**16**) *via* the corresponding alcohol (**15**). The Wittig reaction of the ylid of **16** with the C_{25}-acetylenic aldehyde (**20**) gave the 9-*cis*-didehydroisorenieratene (**22**) as reddish-orange needles in a 51% yield.

The pigment (**22**) thus obtained exhibited λ_{max} at wavelength locations about 8 nm shorter than those of **1**, and showed a distinct *cis*-peak at 356 nm (Fig. 1).

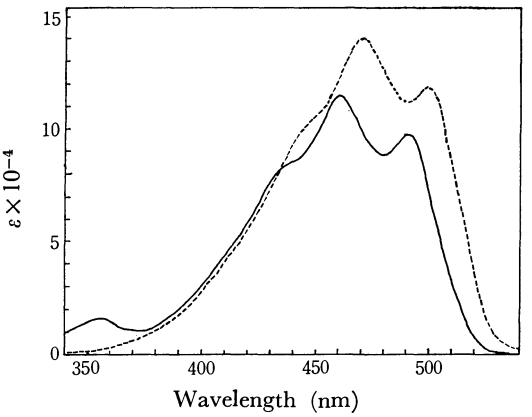

Fig. 1. Absorption spectra of **1** (natural, mp 194—194.5 °C, ——) and its 9-*cis* isomer (**22**, ——) in benzene.

On isomerization (iodine and light[10]), however, both the pigments gave the same absorption curve, which was essentially identical with that of **22**. This means that the 9-*cis* isomer (**22**) is the most stable one among the stereoisomers, including all-*trans* **1**, and that **22** is the major constituent of the equilibrium mixture, which is to be expected in view of the small steric

requirement of the triple bond.

B. C. L. Weedon reported that *trans*-[5-(4-hydroxy-2,2,6-trimethyl-6-cyclohexen-1-yl)-3-methyl-2-penten-4-ynyl]-triphenylphosphonium salt gave an all-*trans* Wittig condensation product when the reaction was conducted in the dark.[6b] In our second synthesis, therefore, *trans*-C_{15}-phosphonium salt (**8**) was prepared in the hope that its configuration would be retained during the condensation, thus leading to the predominant formation of **1**.

A mixture of the *trans* and the *cis* ester (1 : 3), prepared from **4** through **6**, was saponified and separated by fractional crystallization into the corresponding acids (**9a** and **9b**). In contrast to the fact that the base treatment of the ester mixture did not change the isomeric ratio, the *cis* acid seemed to be less stable than the *trans* isomer in an alkaline medium, and the former was converted into the latter by heating with an aqueous-methanolic potassium hydroxide solution. The *trans* acid (**9a**) was converted into the *trans* phosphonium salt (**8**) by the usual procedures. The condensation of the ylid from **8** with the all-*trans* C_{25}-aldehyde (**18**), prepared by the condensation of **16** with C_{10}-dialdehyde (**17**), proceeded smoothly under various reaction conditions, but the product was always predominantly the 9-*cis* isomer (**22**), even when the reaction was run in the dark. The isolation of the *trans* pigment (**1**) was practically impossible, though a very faint zone corresponding to **1** was observed on the chromatographic column.

In order to circumvent the lability of the 2-double bond in the ylid, a reversed combination of ylid and aldehyde was then undertaken. The *trans* C_{15}-aldehyde (**12a**), obtained by the manganese dioxide oxidation of **10a**, seemed to be stable, at least at room temperature, for several days. When **12a** was condensed with C_{25}-ylid (prepared from **19**) at room temperature, however, the predominant product was again **22**. When the reaction was run at a low temperature, on the other hand, the yield of the condensation product was very low, though the product contained a substantial amount of **1**, which could be purified and which was proved to be identical with a natural specimen in every respect.

*Synthesis of 7,8-Didehydrorenieratene (**2**).* 9-*cis*-7,8-Didehydrorenieratene (**23**) was synthesized by a route analogous to that of the first synthesis of **1**. The absorption maxima of the isomer were about 8 nm shorter than those of natural **2**, but both the pigments gave the same absorption curve after isomerization. The all-*trans* **2** was also synthesized in a way corresponding to that used for all-*trans* **1**; it was identical with the natural specimen in every detail examined.

Experimental

All the Wittig condensations were carried out under an atmosphere of nitrogen. The phosphonium salts were dried under a vacuum for several hours just before use. Anhydrous sodium sulfate was used for drying the solutions. The melting or boiling points were uncorrected. Unless otherwise mentioned, the IR spectra were taken in potassium bromide pellets. The NMR spectra were taken in a deuterochloroform solution. Benzene solutions were used for the UV determination.

*2,3,6-Trimethylacetophenone (**3**).* It was prepared from 2,3,6-trimethylbenzoyl chloride (prepared from 2,3,6-trimethylbenzoic acid and thionyl chloride by heating at 60 °C for 12 hr; bp 80—81 °C/6 mmHg) and methyl magnesium iodide in a way similar to that reported for 2,4,6-trimethylacetophenone.[11] A colorless oil;[12] bp 99—101 °C/6 mmHg, IR (liquid film) 1690 cm^{-1}.

2,3,6-Trimethyl-α-chlorostyrene. The method for the synthesis of 2,4,6-trimethyl-α-chlorostyrene[13] was modified because of the very low yield of the product (less than 10%). To a mixture of **3** (30 g) and phosphorus pentachloride (50 g) in benzene (50 ml), we added a portion (10 ml) of a solution of collidine (25 g) in dry benzene (50 ml). After the mixture had been heated at 80 °C for 24 hr with occasional additions of the remainder of the collidine solution, it was cooled and poured into ice water. The organic layer was worked up in a usual way. A colorless liquid (21 g); bp 68—70 °C/5 mmHg; IR (liquid film) 1630, 888 cm^{-1}.

*2,3,6-Trimethylphenylacetylene (**4**).* 2,3,6-Trimethyl-α-chlorostyrene (18 g) was heated (160—180 °C) with sodium amide (12 g) in mineral oil (30 ml) for 3 hr, after which the crude product was fractionally distilled. A fragrant mobile liquid[12] (9.4 g); bp 54—55 °C/5 mmHg. IR (liquid film) 3295, 2090 cm^{-1}.

*3-Methyl-1-(2,3,6-trimethylphenyl)-4-penten-1-yn-3-ol (**5**).* The magnesium derivative was prepared from **4** (5.7 g), isopropyl magnesium bromide (0.04 mol), and a catalytic amount of cuprous chloride in ether (50 ml) in the usual way. A solution of methyl vinyl ketone (2.8 g) in dry ether (20 ml) was stirred into this over a period of 1 hr at room temperature. After refluxing for 3 hr, the reaction mixture was poured into cold water and treated with saturated aqueous ammonium chloride. The organic layer was then washed, dried, and distilled. A viscous oil[12] (3 g); bp 86—87 °C/0.024 mmHg; IR(liquid film) 3370, 2220, 925 cm^{-1}.

*[3-Methyl-5-(2,3,6-trimethylphenyl)-*cis*-2-penten-4-yn-1-yl]triphenylphosphonium Bromide (**7**).* A solution of **5** (1.09 g) and triphenylphosphonium bromide (1.71 g) in dichloromethane (25 ml) was stirred for 20 hr at room temperature. The subsequent evaporation of the solvent gave a solid, which was recrystallized from dichloromethane-ethyl acetate. Colorless needles[12] (2.4 g); mp 211—212 °C; NMR δ 1.97 (3H, d, J=6.0 Hz; 3-methyl).

*2,7,11-Trimethyl-13-(2,3,6-trimethylphenyl)-2,4,6,8,*cis*-10-tridecapentaen-12-yn-1-al (**20**) and 9,9'-Di-*cis*-7,7',8,8'-tetradehydroisorenieratene (**21**).* To a stirred suspension of **7** (0.432 g) in dry ether, we added an ethereal phenyl lithium solution (0.2 mol, 4 ml); the mixture was stirred for 1 hr at room temperature, and then a dichloromethane-ether mixture (2 : 1, 3 ml) was added. The resulting deep red solution of the ylid was added, drop by drop, to a solution of the C_{10}-dial[8] (**17**, 0.256 g) in dichloromethane (20 ml). The mixture was refluxed with stirring for 3 hr, poured into water, and extracted with ether. The extract was dried and evaporated. The reddish-brown residue was chromatographed on neutral alumina [Merck, deactivated by the addition of water (5%)] with a benzene-petroleum benzine mixture (1 : 19) as a developer; this gave two main zones; i) a reddish-orange zone (upper) and ii) a yellow zone (lower). The elute (benzene-methanol, 9 : 1) of i) gave a crude product (63 mg) on evaporation; this product was recrystallized from dichloromethane-methanol. Orange needles[12] (**20**); mp 129—130 °C; λ_{max} 421 nm ($\varepsilon=5.96\times10^4$); IR 1660, 1605 cm^{-1}; NMR δ 9.69 (1H, s; 1-proton).

The elute of ii) gave crude **21** (14 mg), which, on recrystal-

lization, gave red thick plates;[12] mp 174—175 °C; λ_{max} 462 nm ($\varepsilon=10.1\times10^4$); IR 2920, 1455, 1435, 1365, 970, 960, 800 cm^{-1}; NMR δ 1.96 (6H, s), 2.09 (6H, s), 2.25 (6H, s), 2.44 (12H, s), 5.9—6.9 (14H, m).

Ethyl 3-Methyl-5-(2,3,6-trimethylphenyl)-trans-*2*, trans-*4-pentadienoate (**13a**) and Its 2*-cis *Isomer (**13b**).* A mixture of 4-(2,3,6-trimethylphenyl)-3-buten-2-one[14] (3.3 g, bp 127—132 °C/6 mmHg) and ethoxycarbonylmethylenetriphenylphosphorane (7.0 g) was heated at 150 °C for 4 hr with stirring. After cooling, the mixture was extracted with petroleum ether. The extract was then distilled to give a mixture of *trans* and *cis* esters (**13a** : **13b**=3 : 1, NMR) as a colorless oil (3.4 g); bp 156—160 °C/1 mmHg.

3-Methyl-5-(2,3,6-trimethylphenyl)-trans-*2*, trans-*4-pentadienoic Acid (**14a**) and Its 2*-cis *Isomer (**14b**).* A mixture of the above esters (6.7 g) and a 40% aqueous potassium hydroxide solution (10 ml) was stirred at 110 °C for 4 hr, washed with ether, acidified, and extracted with ether. The extract was then dried and evaporated to give a white crystalline solid (5.7 g, *trans* : *cis*=3 : 1), which was separated by fractional crystallization from ethyl acetate. The *trans* acid[12] (**14a**): mp 170—172 °C[9]; IR 2940, 1670, 1600 cm^{-1}; NMR δ 5.85 (1H, s; 2-proton), 6.26 and 7.07 (2H, ABq, J=16.3 Hz; 4,5-protons).

Methyl ester (diazomethane), mp 42 °C.

The *cis* acid[12] (**14b**): mp 173—174 °C,[9] colorless needles; NMR δ 5.76 (1H, broad s; 2-proton), 7.01 and 7.76 (2H, ABq, J=16.7 Hz; 4,5-protons).

*3-Methyl-5-(2,3,6-trimethylphenyl)-2,4-pentadien-1-ol (**15**).* To a cold (0 °C) suspension of lithium aluminium hydride (93.7 mg) in dry ether (15 ml), we added a solution of the methyl ester of **14a** (547 mg) in ether (5 ml) over a 15-min period, after which the mixture was stirred for 20 min at room temperature. After working-up in the usual way, the product was distilled to give an oil (**15**, 387 mg); bp 140—145 °C/0.9 mmHg; NMR δ 4.32(2H, d, J=6.9 Hz; 1,1-protons). This oil was employed for the next step without further purification.

*[3-Methyl-5-(2,3,6-trimethylphenyl)-2,4-pentadien-1-yl]triphenylphosphonium Bromide (**16**).* A mixture of **15** (232 mg), triphenylphosphonium bromide (377 mg), and dichloromethane (3 ml) was stirred at room temperature for 48 hr. The solvent was then removed, and the residue was washed with dry ether. A glass-like white solid (540 mg); NMR δ 4.83 (2H, dd, J=8.0, J=14.2 Hz; 1,1-protons).

*9-cis-7,8-Didehydroisorenieratene (**22**).* To a solution of the ylid of **16** (65 mg), prepared in a way similar to that described in **20**, we added a solution of **20** (10.4 mg) in dry dichloromethane (7 ml). After refluxing for 4 hr, the reaction mixture was treated in the usual way and the product was chromatographed on alumina (containing 5% water) from a benzene-petroleum benzine (1 : 9) solution. The residue (8 mg, 51%) of the elute of the main orange zone gave, on recrystallization from dichloromethane-methanol, reddish-orange needles[12] (**22**); mp 173 °C; λ_{max} 491.5, 462 ($\varepsilon=11.6\times10^4$), (435), 356 nm; IR 3040, 2920, 1590, 1560, 1460, 1440, 1380, 1368, 1035, 1000, 965, 960, 810, 795 cm^{-1}; NMR δ 1.96 (6H, s), 2.08 (6H, s), 2.28 (12H, s), 2.48 (6H, s), 6.1—7.2 (16H, m).

Both **22** and the natural pigment (mp 194—194.5 °C) were isomerized with iodine under diffused daylight in benzene for 1 hr.[10] They gave the same UV curves, with maxima at 490.5, 462, (435), and 357 nm.

4-(2,3,6-Trimethylphenyl)-3-butyn-2-ol. Acetaldehyde (3.0 g) was treated at 0 °C with a solution of the Grignard reagent prepared from **4** (4.0 g, 28 mmol), isopropyl magnesium bromide (30 mmol), and a catalytic amount of cuprous chloride in ether (40 ml). After working-up in the usual manner, the distillation of the product gave colorless crystals[12] (3.3 g); bp 125 °C/1 mmHg, mp 42—44 °C.

*4-(2,3,6-Trimethylphenyl)-3-butyn-2-one (**6**).* A mixture of the above acetylenic alcohol (13 g) and active manganese dioxide[15] (50 g) in dry dichloromethane (100 ml) was stirred overnight at room temperature, after which the reaction mixture was filtered through celite. The evaporation residue (12.5 g) of the filtrate was purified by sublimation; mp 39—40 °C.[12]

3-Methyl-5-(2,3,6-trimethylphenyl)-trans-*2-penten-4-ynoic Acid (**9a**) and Its 2*-cis *Isomer (**9b**).* The condensation reaction and the separation of isomeric acid after hydrolysis were carried out in a manner similar to those used for **13a**, **13b**, **14a**, and **14b**. The ratio of the *trans* and *cis* esters in the mixture was 1 : 3 (NMR). The *trans* acid[12] (**9a**): mp 158—159 °C, colorless prisms; IR 2190, 1680, 1600 cm^{-1}; NMR δ 6.18(1H, q, J=1.6 Hz; 2-proton). Methyl ester (diazomethane); mp 45—46 °C.

The *cis* acid[12] (**9b**): mp 163.5—165.5 °C, white needles; NMR δ 6.03 (1H, q, J=1.5 Hz; 2-proton). Methyl ester (diazomethane); mp 67—68 °C.

*Isomerization of **9b**.* A mixture of the *cis* acid (**9b**, 400 mg), potassium hydroxide (5 g), methanol (2.5 ml), and water (2.5 ml) was stirred at 80 °C for 2 days. After the methanol had been removed, the reddish-brown solution was washed with ether and then acidified with aqueous hydrochloric acid to give a solid (200 mg), which was proved to be the *trans* acid (**9a**) from its NMR spectrum. No *cis* acid was recovered.

3-Methyl-5-(2,3,6-trimethylphenyl)-trans-*2-penten-4-yn-1-ol (**10a**) and Its 2*-cis *Isomer (**10b**).* To a cold (0 °C) suspension of aluminium hydride, prepared from lithium aluminium hydride (11.4 mg) and aluminium chloride (13.3 mg) in dry ether (5 ml), we added a solution of the methyl ester of **9a** (48.4 mg) in ether (5 ml); the mixture was then stirred for 1 hr at room temperature. The reaction mixture was then worked-up in the usual way. A colorless oil (**10a**, 33.3 mg); IR (liquid film) 3350, 2190, 1625 cm^{-1}; NMR δ 6.08 (1H, qt, J=1.7 Hz, J=6.8 Hz; 2-proton). This oil was used for the next step without purification, since the distillation of the alcohol caused a partial isomerization to the *cis* isomer.

The *cis* alcohol (**10b**) was also obtained from the corresponding *cis* ester as a solid[12]: mp 73—75 °C; NMR δ 5.90(1H, qt, J=1.2 Hz, J=6.8 Hz; 2-proton).

3-Methyl-5-(2,3,6-trimethylphenyl)-trans-*2-penten-4-yn-1-yl Bromide (**11a**) and Its 2*-cis *Isomer (**11b**).* To a solution of **10a** (33.3 mg) in ether (6 ml) containing a catalytic amount of pyridine, we added phosphorus tribromide (25 mg), after which the mixture was stirred for 1 hr at room temperature. The reaction mixture was washed with a 5% aqueous sodium hydroxide solution and water, dried, and evaporated to give a viscous oil (32.3 mg); IR (liquid film) 2190, 1450, 1195, 800 cm^{-1}; NMR δ 6.66 (1H, qt, J=1.4 Hz, J=8.6 Hz; 2-proton). It was used for the next step without purification, since distillation caused partial isomerization.

The *cis* bromide (**11b**) was also obtained from **10b** as a viscous oil;[12] bp 80 °C (bath)/5—6 mmHg; NMR δ 5.97 (1H, qt, J=2.0 Hz, J=8.0 Hz).

[3-Methyl-5-(2,3,6-trimethylphenyl)-trans-*2-penten-4-yn-1-yl]triphenylphosphonium Bromide (**8**).* To a solution of **11a** (22.4 mg) in ether (2 ml), we added triphenylphosphine (21.3 mg), after which the mixture was stirred for 14 hr at room temperature. The precipitate was recrystallized from dichloromethane-carbon tetrachloride to give the *trans* salt

(**8**, 25.1 mg); mp 196—199 °C (decomp.); NMR δ 1.65 (3H, d, J=4.4 Hz; 3-methyl).

*2,7,11-Trimethyl-13-(2,3,6-trimethylphenyl)trideca-2,4,6,8,10,12-hexaen-1-al (**18**).* The operations were similar to those described in **20**. The condensation of **16** (540 mg) with the C_{10}-dial (**17**, 450 mg) gave all-*trans* C_{25}-aldehyde (**18**, 8 mg) as reddish-orange needles;[12] mp 126 °C; λ_{max} 426 nm (ε=6.90×10^4); IR 2920, 1655, 1610, 1595, 1550, 1355, 1210, 1185, 970, 960, 810 cm^{-1}; NMR δ 9.52(1H, s; 1-proton).

A mixture of **13a** and **13b** (1.082 g) gave a mixture of *cis* and *trans* **18** (197 mg) in a similar way. This was isomerized by iodine and light in benzene for 3 hr and purified by alumina chromatography and recrystallization to give a further amount of *trans* **18** (134 mg).

*Wittig Reaction of **18** with the Ylid from **8**.* 1) The condensation was carried out in a way similar to that used for the synthesis of **22**. Starting with **8** (58 mg), the main product (6.2 mg) was obtained as reddish-orange needles; it was completely identical with **22**. The elute of the faint orange zone, which moved just above the main orange zone of **22**, gave λ_{max} 500, 470, and 442 nm, values which were very similar to those of **1**,[3] but the amount was too small to be worked out further.

The following three experiments also gave the *cis* pigment (**22**) almost exclusively:

2) Base, sodium methylsulfinylmethide: solvent, benzene–DMSO(1 : 11): 1 hr at room temperature and 2 hr at 35—45 °C.

3) Base, sodium methoxide: solvent, methanol–pyridine (5 : 2): 1 hr at room temperature and 2 hr at 35—45 °C.

4) Base, sodium methoxide: solvent, methanol: 20 hr at room temperature in the dark.[6b]

2,7,11-Trimethyl-13-(2,3,6-trimethylphenyl)-2,4,6,8,10,12-tridecahexaen-1-ol. To a cold (0 °C) suspension of aluminium hydride prepared from lithium aluminium hydride (38 mg) and aluminium chloride (42 mg) in dry ether (30 ml), we added a solution of **18** (116 mg) in dry benzene (10 ml), and the subsequent mixture was stirred for 30 min. The mixture was then treated in the usual way to give a canary yellow solid (114 mg); mp 106—107 °C; λ_{max} 404, 387, 366 nm; IR 3400, 1080, 970 cm^{-1}; NMR δ 4.09 (2H, s; 1,1-protons).

*[2,7,11-Trimethyl-13-(2,3,6-trimethylphenyl)-2,4,6,8,10,12-tridecahexaen-1-yl]triphenylphosphonium Bromide (**19**).* A mixture of the above C_{25}-alcohol (14 mg), triphenylphosphonium bromide (14 mg), and dry dichloromethane (10 ml) was stirred at room temperature for 72 hr under nitrogen in the dark. After the removal of the solvent, the resulting solid (**19**) was dried under a vacuum.

*3-Methyl-5-(2,3,6-trimethylphenyl)-*trans*-2-penten-4-yn-1-al (**12a**) and Its 2-*cis* Isomer (**12b**).* A mixture of **10a** (214 mg), active manganese dioxide[15] (2 g), and dry dichloromethane (10 ml) was stirred at 0 °C for 1 hr, after which the reaction mixture was filtered quickly. The filtrate was then evaporated to dryness at 0 °C to give a solid (214 mg); mp 67 (sinter)—77 °C; λ_{max} 337, 327 nm; IR 2180, 1660, 1595, 853 cm^{-1}; NMR δ 6.32 (1H, qd, J=1.2 Hz, J=8.0 Hz; 2-proton), 10.8 (1H, d, J=8.0 Hz; 1-proton). This was stored in a refrigerator under nitrogen and used without further purification. On sublimation at 60 °C, most of the aldehyde changed into its *cis* isomer (**12b**). In solution in deuterochloroform for NMR measurement, it also changed completely into the *cis* isomer within 12 hr. In the crystalline state, however, it seemed to be stable for more than a week at room temperature.

The *cis* aldehyde (**12b**) was obtained from **10b** and purified by sublimation: mp 89—91 °C;[12] λ_{max} 323 nm; NMR δ 6.19(1H, qd, J=1.6 Hz, J=8.1 Hz; 2-proton), 10.20 (1H, d, J=8.1 Hz; 1-proton).

*7,8-Didehydroisorenieratene (**1**).* A solution of the ylid was prepared from **19** (60 mg) in a way similar to that described in **20**. A solution of **12a** (30 mg) in dichloromethane (2 ml) was added to this on cooling at −78 °C. The mixture was stirred at −78 °C for 3 hr, then at −20 °C for 20 hr, at 0 °C for 4 hr, and at room temperature for 1 hr. Cold water was added to the deep red mixture. The product was extracted with ether, washed with water, dried, and evaporated below 40 °C. The dark red residue was chromatographed on alumina (5% water) with a benzene–petroleum benzine (1 : 9) mixture, thus giving two main zones: a reddish-orange zone (upper) and an orange zone (lower). The upper zone gave, after rechromatography on alumina, crude **1**, which was then recrystallized three times from a dichloromethane–methanol mixture. Red needles (**1**, 0.3 mg, 1% based on the C_{25}-alcohol); mp 196 °C, undepressed by admixture with a natural specimen. A mixed chromatography of the synthetic and the natural pigment showed no separation. The spectral properties (UV, NMR, and mass) were also identical with those reported previously.[3]

In an experiment carried out at room temperature, the product was essentially **22**. A very small amount of **1** was also observed on the column.

All the 2,3,4-trimethylphenyl derivatives necessary for the synthesis of **2** or its *cis* isomer (**23**) were prepared in essentially the same manners as were used for the corresponding compounds described in the syntheses of **1** or **22**.

*Methyl 3-Methyl-5-(2,3,4-trimethylphenyl)-*trans*-2,*trans*-4-pentadienoate (**24a**) and Its 2-*cis* Isomer (**24b**).* 4-(2,3,4-Trimethylphenyl)-3-buten-2-one[16] (4.5 g) was condensed with ethoxycarbonylmethylenetriphenylphosphorane to give a mixture of 2-*trans* and 2-*cis* isomers of the ethyl ester (1 : 1) (6.2 g, bp 100 °C (bath)/5 mmHg). The ester mixture was then saponified, and the acids (5.5 g) were separated by fractional crystallization.

The *trans* acid[12] (mp 214—215 °C) was treated with diazomethane to give the methyl ester (**24a**). Colorless prisms;[12] mp 84—86 °C; bp 80 °C (bath)/4—5 mmHg; IR 1710 cm^{-1}; NMR δ 5.87 (1H, s; 2-proton).

The *cis* acid,[12] mp 183—186 °C. Methyl ester (**24b**): mp 57—59 °C; NMR δ 5.71 (1H, broad s; 2-proton).

*3-Methyl-5-(2,3,4-trimethylphenyl)-2,4-pentadien-1-ol (**25**).* Aluminium hydride reduction of **24a** (531 mg) gave the *trans* alcohol (**25**) (442 mg); mp 56.5—58.5 °C; IR 3370, 1625 cm^{-1}.

*[3-Methyl-5-(2,3,4-trimethylphenyl)-2,4-pentadien-1-yl]triphenylphosphonium Bromide (**26**).* This was obtained from **25** (442 mg) and triphenylphosphonium bromide (700 mg): a glassy solid (900 mg); NMR (90 Mc) δ 4.86 (2H, dd, J=8.5 Hz, J=16.0 Hz; 1,1-protons).

*9-cis-7,8-Didehydrorenieratene (**23**).* The condensation of the ylid from **26** (630 mg) with **20** (10 mg) gave **23** as deep red needles (6.9 mg); mp 170.5 °C; λ_{max} 503.5, 472.5 (ε=11.0×10^4), (445), 369, (353) nm; IR 3030, 2915, 1477, 1460, 1440, 1361, 960, 800 cm^{-1}; NMR δ 1.95(6H, s), 2.05 (6H, s), 2.25 (12H, s), 2.45 (6H, broad s), 6.20—7.50 (16H, m). Mass (*m/e*) 526 (M), 434, 420, 393, 328, 133. Found: C, 90.27[17]; H, 8.87%. Calcd for $C_{40}H_{46}$: C, 91.20; H, 8.80%. The natural pigment (**2**) (mp 204—205 °C) and **23** were isomerized with iodine and light in benzene for 1 hr. Both the isomerized solutions gave the same UV curve, with maxima at 501, 470.5, (444), 370, and (354) nm. From the lower part of the chromatogram, a pigment which melted at 164—164.5 °C was obtained besides **23**; red needles [λ_{max} 498, 467, (439), 372, (354) nm]. It was considered to be

9,11′-di-*cis*-7,8-didehydrorenieratene from the mode of its formation.

*2,7,11-Trimethyl-13-(2,3,4-trimethylphenyl)-2,4,6,8,10,12-tridecahexaen-1-al (**27**).* The condensation of **26** (1 g) and the C_{10}-dial (**17**, 900 mg) gave **27** as red needles (23 mg); mp 161—162 °C; λ_{max} 444 nm ($\varepsilon=6.9\times10^4$); IR 3050, 2925, 1665, 1615, 1540, 1190, 970, 965 cm^{-1}; NMR δ 9.46 (1H, s; 1-proton). Mass (m/e) 346(M), 278, 262, 219, 210, 133, 29. Found: C, 85.86[17]; H, 8.69%. Calcd for $C_{25}H_{30}O$: C, 86.65; H, 8.73%.

From the reaction mixture, the 8-*cis* isomer of **27** was also obtained as red needles; mp 141—142 °C; λ_{max} 440 nm.

*[2,7,11-Trimethyl-13-(2,3,4-trimethylphenyl)-2,4,6,8,10,12-tridecahexaen-1-yl]triphenylphosphonium Bromide (**28**).* The aluminium hydride reduction of **27** (46.8 mg) gave the corresponding alcohol as a canary-yellow solid (46 mg). The crude alcohol [mp 116—126 °C; λ_{max} 432, 409, 389 nm; IR 3350, 1025, 1015, 965 cm^{-1}] (23 mg) was converted into the phosphonium salt (**28**) with triphenylphosphonium bromide (23 mg); this crude salt was used without purification.

*7,8-Didehydrorenieratene (**2**).* The condensation of the ylid of **28** (44 mg) with **12a** (20 mg) was carried out under a low temperature in the way described in the recipe for **1**. The crude product was chromatographed on 5% aqueous alumina with a benzene-petroleum benzine (1 : 4) mixture. After rechromatography and recrystallization (dichloromethane-methanol), **2** was obtained as purplish-red needles (0.05 mg); mp 205—206 °C, undepressed by admixture with a natural specimen. A mixed chromatography of the synthetic and the natural pigment showed no separation. The spectral properties (UV and mass) also agreed with those reported previously.[3]

References

1) Presented in part at the 16th Symposium on The Chemistry of Natural Products, Osaka, October, 1972.

2) Present address: Yoshitomi Pharmaceutical Industries, Ltd., Yoshitomi, Chikujo-gun, Fukuoka 871.

3) T. Hamasaki, N. Okukado, and M. Yamaguchi, This Bulletin, **46**, 1884 (1973).

4) M. Yamaguchi, *ibid.*, **31**, 51 (1958).

5) M. Yamaguchi, *ibid.*, **31**, 739 (1958).

6) a) B. C. L. Weedon, *Pure Appl. Chem.*, **20**, 531 (1969). b) B. C. L. Weedon, Brit. 1173063 (1969); *Chem. Abstr.*, **72**, 67148j (1970).

7) H. A. Smith and J. A. Stanfield, *J. Amer. Chem. Soc.*, **71**, 81 (1949).

8) O. Isler, M. Montavon, R. Rüegg, and P. Zeller, Swiss 321106 (1957); *Chem. Abstr.*, **51**, 18001e (1957).

9) One isomer (mp 172—174 °C) of the acids has been reported (G. Lowe, F. G. Torto, and B. C. L. Weedon, *J. Chem. Soc.*, **1958**, 1855), but it is not clear from the data whether it corresponds to the *cis* or to the *trans* isomer.

10) L. Zechmeister, *Fortschr. Chem. Org. Naturstoffe*, **18**, 223 (1960).

11) R. C. Fuson and J. Corse, *J. Amer. Chem. Soc.*, **60**, 2063 (1938).

12) The compounds isolated in a pure form were analysed for carbon and hydrogen. The results of the analyses agreed with the calculated values within $\pm0.43\%$ or less.

13) T. H. Vaughn and J. A. Nieuwland, *J. Amer. Chem. Soc.*, **56**, 1207 (1934).

14) M. Yamaguchi, This Bulletin, **32**, 1171 (1959).

15) J. Attenburrow, A. F. B. Cameron, J. H. Chapman, R. M. Evans, B. A. Hems, A. B. A. Jansen, and T. Walker, *J. Chem. Soc.*, **1952**, 1094.

16) M. Yamaguchi, This Bulletin, **33**, 1560 (1960).

17) Because the amount available for elementary analysis was too small, a larger deviation from the calculated value was recorded for the carbon content.

Fundamental Studies on Palladium Catalysts. IX. Characteristics of Hydrogen Sorption and Hydrogenation Activity of Supported Palladium Catalysts[1)]

Tsunekichi YAMABE, Katsuhiro SHIRONO, Masaru UEHARA, and Sadao SUZUKI

Research Laboratory of Resources Utilization, Tokyo Institute of Technology, Ookayama, Meguro-ku, Tokyo 152

(Received February 27, 1973)

The sorption of hydrogen and the hydrogenation of ethylene on palladium/silica-alumina catalysts with palladium contents of 0.58—4.5 wt% were investigated. It was found that V_x (the amount of molecularly-adsorbed hydrogen) and V_z (that of dissociatively-adsorbed hydrogen) increase, while V_y (that of dissolved hydrogen) decreases, with the increase in the specific surface area of palladium, and that the saturated value of V_z is proportional to the amount of chemisorbed carbon monoxide. It was also shown that the increase in the palladium content results in a growth of the palladium crystallites, their number staying approximately constant. The rate of ethylene hydrogenation was found to be first-order with respect to hydrogen and zero-order with respect to ethylene over the temperature range of −20—20 °C. The activity was proportional to the surface area of palladium, and the activation energy was almost constant for these catalysts.

It has previously been demonstrated[2)] that the equilibrium amount of hydrogen in the first ascending part of the sorption isotherm is expressed by the sum of the amounts of two hydrogen species, that is, molecularly-adsorbed hydrogen and dissolved hydrogen in the case of palladium-black with a surface area of less than 15 m^2/g. However, another species of dissociated hydrogen strongly adsorbed on palladium has been revealed as a result of an investigation[1,3)] using supported catalysts with a large surface area of palladium (>100 m^2/g).

In this investigation, we have studied the effects of the specific surface area of palladium on the equilibrium amount of each hydrogen species and on the hydrogenation of ethylene.

Experimental

Materials and Catalyst Preparation. The palladium/silica-alumina catalyst was prepared by immersing silica-alumina (Neobead D from the Mizusawa Industrial Chemicals, Ltd.) in a hydrochloric acid solution of $PdCl_2$ for a few weeks at room temperature until the solution became almost colorless. The catalyst, after having been washed with ion-exchanged water, was dried by evacuating it in the reaction cell and then reduced with hydrogen at 200 °C for 2 hr. Before each run, the catalyst was evacuated for 10 hr at 200 °C to arrive at a residual pressure of less than 1×10^{-4} Torr. The palladium-black/silica-alumina mixed catalyst was prepared by the Willstätter method[4)] in the presence of silica-alumina, followed by the same pretreatment as in the case of the supported catalyst. The palladium content was determined by the EDTA titration method. The hydrogen was purified by passage through a palladium thimble. The ethylene contained less than 0.3% methane and a trace amount of ethane as impurities. The purity of the carbon monoxide used for the determination of the palladium surface area was more than 99.8%.

Apparatus and Procedure. Our measurements of the sorption isotherms and the desorption rate were carried out in a conventional static-sorption apparatus incorporating a rotary MacLeod gauge, as has been described in Ref. (3). The catalytic activity was estimated by measuring the rate of ethylene hydrogenation in a batch recirculation system. The amounts of ethylene and ethane were monitored by the measurement of the pressure change in the total gas and checked by a chromatographic analysis of the gas mixture at appropriate intervals.

Results

Relation between the Specific Surface Area of Palladium S and the Amount of Each Type of Hydrogen. As has already been indicated in a previous paper,[1)] the amount of dissociatively-adsorbed hydrogen, V_z, is expressed as follows:

$$V_z = b_3\sqrt{K_3P}/(1+\sqrt{K_3P}) \quad (1)$$

where b_3, K_3 and P represent the site number per atom of palladium (H/Pd), the equilibrium constant, and the equilibrium hydrogen pressure respectively. The assumption that the dissociated hydrogen atoms combine with exposed palladium atoms in the ratio of 1 to 1 makes it possible to calculate the specific surface area of palladium S (m^2/g-Pd) from the b_3 values. Thus, S is determined by assuming that the number of palladium atoms per square meter is 1.2×10^{19}; this is the mean value for the crystallographic planes (100), (110), and (111).

$$S = 472b_3 \quad (2)$$

On the other hand, Scholten and his co-workers have proposed a method of determining the surface area of supported palladium from the chemisorbed amount of carbon monoxide.[5)] Therefore, we have also examined the adsorption of carbon monoxide on a series

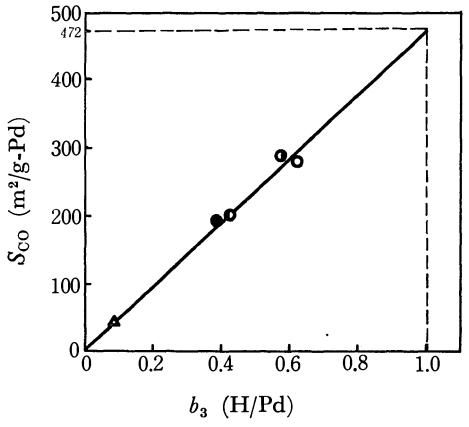

Fig. 1. Relation between S_{CO} and b_3.
Pd content (wt%); ●: 4.5, ◐: 2.1, ◑: 0.81, ○: 0.58
△: Pd-black/silica-alumina mixed catalyst

TABLE 1. RESULTS FOR DISSOCIATIVELY-ADSORBED HYDROGEN

Pd content (wt%)	b_3 (H/Pd)	Temperature (°C)	$\sqrt{K_3}$ $(\text{Torr})^{-1/2}$	Heat of Adsorption (kcal/mol)	k_3' $(\text{H/Pd}\cdot\text{min})^{-1}$	Activation energy for desorption (kcal/mol)
0.81	0.571	0	35.0	7.5	3.82×10^{-4}	8.7
		20	23.0		9.50×10^{-4}	
		35	16.3		2.22×10^{-3}	
2.1	0.424	0	34.7	7.5	3.75×10^{-4}	8.7
		20	22.7		1.03×10^{-3}	
		35	15.9		2.25×10^{-3}	

of catalysts at 20 °C and calculated the S values according to their procedure. The relation between b_3 and S obtained by means of carbon monoxide chemisorption (S_{CO}) is presented in Fig. 1; it suggests the validity of Eq. (2). In Fig. 1, we also show the results obtained with a palladium-black/silica-alumina mixed catalyst, assuming that the amount of residual hydrogen after 1 hr's evacuation at 20 °C is equal to b_3. In addition, we calculated the heat of dissociative adsorption from the temperature dependency of K_3; we thus obtained approximately 7.5 kcal/mol (see Table 1).

Then we have investigated the desorption process of hydrogen taken up at 20 °C, 100 Torr according to the procedure described in Ref. 1. We first determined V_z; then we estimated the amount of molecularly-adsorbed hydrogen, V_x, and that of hydrogen dissolved in the lattice, V_y, assuming that the molecularly-adsorbed hydrogen had just been desorbed by the 30-second's evacuation to the residual pressure of 1×10^{-1}—8×10^{-2}, and that the dissolved hydrogen is not desorbed under the above conditions. The relation between V_x and b_3 (or S) as well as V_y and b_3 (or S) is illustrated in Fig. 2. It is demonstrated in Fig. 2 that V_x increases proportionally, while V_y decreases, with the increase in S.

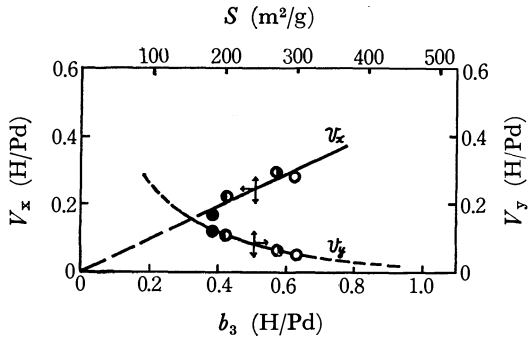

Fig. 2. Relation between (V_x, V_y) and (b_3, S) at 20 °C, 100 Torr.
Pd content (wt%); ●: 4.5, ◐: 2.1, ◑: 0.81, ○: 0.58

In addition, it was found that values of k_3' (the desorption rate constant of dissociatively-adsorbed hydrogen) for the catalysts with the palladium contents of 0.81 wt% and 2.1 wt% were almost identical and that the activation energies calculated from the temperature dependency of k_3' were about 8.7 kcal/mol in both cases (see Table 1).

Hydrogenation of Ethylene. The hydrogenation of ethylene was studied over the temperature range from −20 °C to 20 °C. The circulation velocity of the reactant gas does not influence the kinetics under the standard conditions: the initial pressures of hydrogen and ethylene are around 25 Torr, and no diluent is used. Since the activity was found to decrease slightly with the progress of the reaction, a fresh catalyst was used for each run. The reaction rate, R, was proved to be as follows:

$$R=kP_hP_e^0 \quad (3)$$

where k is the rate constant and where P_h and P_e denote the partial pressures of hydrogen and ethylene respectively. The rate constants[6] per gram of palladium in the catalyst were calculated; they are plotted against b_3 and against S_{co} in Fig. 3. The linear relationship indicates that the hydrogenation activity is proportional to the specific surface area of palladium. The activation energies were about 2.5 kcal/mol for all the catalysts used.

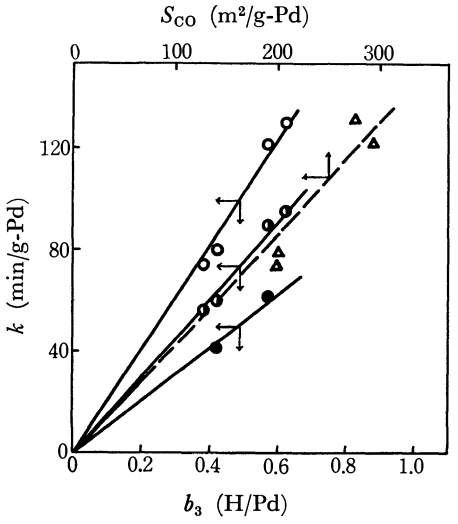

Fig. 3. Relation between k and (b_3, S_{CO}).
Temperature (°C); ○, △: 20, ◑: 0, ●: −20

Discussion

As for dissociatively-adsorbed hydrogen, the validity of the assumption that the hydrogen atoms combine strongly with the palladium atoms exposed in 1-to-1 ratio is supported by Fig. 1. Since b_3 can be easily determined by means of Eq. (1), Eq. (2) may be thought to be very convenient for the estimation of the palladium surface area. In Scholten's method, the modes

of the binding of carbon monoxide on palladium, namely, linear type and bridged type, must be considered in contrast to the method described above, in which only one hydrogen species is concerned. Furthermore, Dorling and Moss have reported[7] that the ratio of linear bonding to bridge bonding varies according to the metal crystallite size in the case of platinum/silica catalysts, so the surface area calculated from b_3 may be thought to be more precise than that determined by means of carbon monoxide chemisorption. This can be seen from Fig. 3, which illustrates better the linearity in the plot of k *vs.* b_3 than in that of k *vs.* S_{co}.

The dependency of V_x on S is similar to the results in Ref. 2. At present, we may suppose that the two surface species are adsorbed on different sites of the palladium, but the situation has not yet been ascertained in detail.

V_y decreases with an increase in S, probably because the number of sites in the lattice decreases with a decrease in the crystallite size of the palladium. In the case of $b_3=1.0$, it can be expected that each palladium atom is exposed to gaseous hydrogen and V_y becomes zero. Thus, b_3 means not only the total site number of the Langmuir isotherm, but also the proportion of palladium atoms exposed.

It may be concluded from the above results that the main role of the support is to disperse palladium, and that the spillover phenomenon reported by Boudart[8] in supported platinum catalysts does not take place in this system.

The increase in the palladium content resulted in a reduction of S, thus suggesting the growth of palladium crystallites. We have examined the relation between the total surface area of palladium per unit of weight of the support, S_t, and its weight, W, by plotting S_t *vs.* $W^{2/3}$ in Fig. 4. The linear relationship shows that the number of crystallites per gram of support is unchanged, irrespective of the palladium content. If the palladium crystallites are regarded as spheres, the number of crystallites per gram of support is calculated to be approximately 3.7×10^{17}; the diameter of the crystallites is considered to change over the range from 10 Å to 30 Å.

It may be concluded from the results obtained by ethylene hydrogenation that all sites are of the same quality in these catalysts, and that their difference in number per unit weight of palladium is reflected in the difference in catalytic activity. However, further

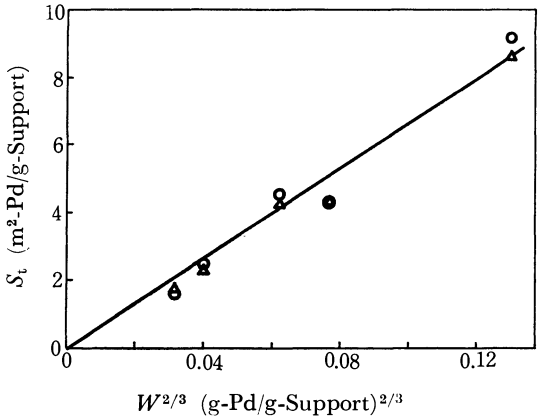

Fig. 4. S_t *vs.* $W^{2/3}$.
S_t: Determined by CO and H_2 adsorption
○: CO, △: H_2

research employing the catalysts with palladium crystallites larger than 30 Å is needed to characterize the catalytic behavior. The results of the present study give no information about the active species of hydrogen, because both V_x and V_z are proportional to S. Nevertheless, the b_3 value appears to be a useful parameter for the activity as long as the reaction in question is "facile". Which of the two surface species of hydrogen contributes to ethylene hydrogenation is an interesting subject for further study.

References

1) Part VIII: T. Yamabe, K. Shirono, M. Uehara, and S. Suzuki, *Nippon Kagaku Kaishi*, **1973**, 1264.
2) For example, S. Suzuki and T. Suzuki, *Nippon Kagaku Zasshi*, **82**, 647 (1961).
3) For example, M. Uehara, T. Yamabe, and S. Suzuki, *Kogyo Kagaku Zasshi*, **73**, 252 (1970).
4) R. Willstätter and E. Waldschmidt-Leitz, *Ber.*, **54**, 113 (1921).
5) J. J. F. Scholten and A. Van. Montfoort, *J. Catal.*, **1**, 85 (1962).
6) They were obtained by averaging the results of several runs. The decrease in pressure by 1 Torr at 20 °C in the apparatus means that the reacted amount is 5.5×10^{-5} mol.
7) T. A. Dorling and R. L. Moss, *J. Catal.*, **7**, 378 (1967).
8) For example, M. Boudart, A. W. Aldag, and M. A. Vannice, *ibid.*, **18**, 46 (1970).

New Photochemical Reactions of 9-ω-Bromoacetylanthracene. I

Tamotsu MATSUMOTO, Masanori SATO, and Satoshi HIRAYAMA

Faculty of Textile Science, Kyoto Technical University, Matsugasaki, Sakyo-ku, Kyoto 606

(Received April 9, 1973)

New photochemical reactions were found on 9-ω-bromoacetylanthracene. The main photo-products were 1-aceanthrenone and 9-bromoanthracene. Their formation was not appreciably affected by the presence of oxygen. Other products such as anthracene, 9-acetylanthracene and anthraquinone were also detected and their yields greatly depended on the reaction conditions. From the low temperature experiments, it was made clear that 9-bromoanthracene and 1-aceanthrenone were formed *via* different mechanisms. A rather stable intermediate, which was not a radical but presumably an intramolecular adduct, was detected spectroscopically. 1-Aceanthrenone was formed from the intermediate both photochemically and thermally with liberation of hydrogen bromide. In the absence of oxygen both the thermal and photochemical reactions of the intermediate yielded almost the same amount of 1-aceanthrenone. The reaction mechanisms were considered in reference to the photochemical reactions of 9-nitroanthracene and sodium 9-anthroate. The relation between these reactions and the radiationless transition processes of carbonyl derivatives of anthracene was also discussed.

Anthracene and its derivatives which have been studied extensively are known to undergo a wide variety of photochemical reactions.[1—4] In most cases, however, they are simple and detailed investigations have been made into their primary photochemical and photophysical processes. It has been made clear that with the anthracene derivatives the radiationless transition processes which sometimes profoundly affect primary photochemical processes are entirely different from those of other organic compounds. The difference is believed to originate from the fairly large energy gap between the lowest excited singlet and the lowest triplet states of these compounds.[5,6]

Recently the substituent effect on the radiationless transition processes has been investigated, valuable results being obtained.[7,8] A detailed investigation we have made of the carbonyl derivatives of anthracene has revealed the existence of interesting relations between the position of a substituent, photochemical reactivity, fluorescent property and the life-times of their triplet state.[9] As regards the fluorescent property, these derivatives are unusual. A typical compound is 9-acetylanthracene (9-CH_3CO-A),[9,10] which is non-fluorescent in various solvents and becomes fluorescent only at temperatures near 77 K. This phenomenon was interpreted in terms of the temperature effect on the intersystem crossing process of $S_{\pi\pi^*} \rightsquigarrow T_{n\pi^*}$.[9,10]

The intersystem crossing process of 9-CH_3CO-A is expected to be perturbed by certain substituents.[11] In order to see what occurs when a hydrogen atom of the acetyl group of 9-CH_3CO-A is substituted by a bromine atom, 9-ω-bromoacetylanthracene (9-CH_2BrCO-A) was synthesized. In contrast to 9-CH_3CO-A, 9-CH_2BrCO-A underwent quite remarkable intramolecular reactions. These new photochemical reactions seem to be useful for clarifying the intramolecular energy dissipation processes of carbonyl derivatives of anthracene and are reported herewith.

Experimental

9-CH_2BrCO-A was synthesized from 9-CH_3CO-A.[13] Commercial solvents of guaranteed grade were used for photochemical reactions without further purification. For spectroscopic measurements, solvents of spectrograde supplied by Nakarai Chemical Co. Ltd. were used.

Absorption spectra were recorded on a Hitachi Spectrophotometer Model 124. The relative yields of the photoproducts were determined spectrophotometrically. Fluorescence and excitation spectra were recorded on a Shimadzu Corrected Recording Spectrofluorophotometer Model RF 502. Fluorescence spectra at low temperature were measured with a modified Beckmann type spectrophotometer equipped with an EMI 9558 QB photomultiplier.

An Ushio 500 W high-pressure mercury-arc lamp was used as an irradiation source. To isolate suitable excitation lines Toshiba glass filter UV-DIB (isolated lines: 313, 334 and 366 nm) or UV-39 (isolated lines: 366 nm and longer ones) was used with a solution filter containing distilled water. A reaction cell was either an ordinary optical cell of 1×1 cm or a cylindrical cell of 3 cm diameter and 3 cm length, each of which was made of quartz and had a side arm for evacuation. Solutions were degassed by repeating freeze-pump-thaw cycles with an oil diffusion pump. When degassing was not necessary, an ordinary optical rectangular cell of 1×1 cm with a ground-glass joint was used.

Irradiation at dry ice-ethanol temperatures (−74——80 °C) was carried out in a Pyrex cylindrical cell of 1.2 cm diameter, which was dipped into a transparent Dewar vessel containing dry ice-ethanol mixture.

Preparative photolysis was carried out in an Ushio photochemical reaction vessel Model UM 103B. A 100 W medium-pressure mercury-arc lamp was immersed in a water-cooled jacket made of Pyrex glass, the outside of which was surrounded by a window glass pipe of 1 mm thickness. Cyclohexane solution of 9-CH_2BrCO-A (*ca.* 1 g/300 ml) was irradiated at 7—10 °C[14] for about 4 hr by bubbling nitrogen gas gently through the solution. After the reaction the solvent was evaporated with a rotary evaporator. The residue was then dissolved in an appropriate amount of ethanol and was allowed to stand for a while to complete the reaction. The solvent was again evaporated and the residue was separated by column chromatography on silica gel. Elution with benzene gave 9-bromoanthracene (9-Br-A) and *ca.* 300 mg of crude 1-aceanthrenone as main photo-products. The latter was identified by means of IR, NMR, mass spectra and elemental analysis. The UV absorption spectrum of photochemically synthesized 1-aceanthrenone agreed with that of the authentic sample synthesized chemically.[15] Recrystallization from acetone and then twice from benzene gave pure 1-aceanthrenone, for which the molar extinction coefficient

was determined.

Electric conductivity measurements were made on a Yanagimoto Conductivity Outfit Model MY-7.

Result

The UV absorption spectrum of 9-CH_2BrCO-A is similar to that of 9-CH_3CO-A, but shifts to the red *ca.* 2 nm and is slightly broader. As regards fluorescence, 9-CH_2BrCO-A also resembles 9-CH_3CO-A,[10] which is non-fluorescent at room temperature and becomes fluorescent at temperatures near 77 K. In spite of these similarities, both compounds differ completely in their photo-reactivity. Only 9-CH_2BrCO-A undergoes photochemical intramolecular reactions, yielding mainly 1-aceanthrenone and 9-Br-A.

Irradiation at Room Temperature. The change in absorption spectra when the aerated cyclohexane solution of 9-CH_2BrCO-A was irradiated at room temperature through the filter UV-39 for about 20 min is shown in Fig. 1. The absorption band assignable to the p-band of anthracene disappears with irradiation and a large new band appears at about 315 nm (curve b). This band is attributed to the intermediate, which reacts both thermally and photochemically to give 1-aceanthrenone. At least two separate reactions seemed to proceed at different rates in cyclohexane so that no isosbestic point was observed.[16] The absorption spectrum (curve c) was observed after standing the solution showing the absorption spectrum b for about 40 hr without irradiation at room temperature. The absorption spectrum with a band maximum at 414 nm is due to 1-aceanthrenone.

The rate of decrease of the intermediate and that of increase of 1-aceanthrenone were obtained by measuring the changes in the optical densities at 315 nm and 414 nm, respectively. Both rates were found to follow the same first order equation with the opposite sign. This means that the intermediate at 315 nm turns unimolecularly into 1-aceanthrenone. It was also ascertained that the rate of the reaction was accelerated as temperature increased. The half life of the intermediate was of the order of several hours in cyclohexane.

Similar experiments were carried out in the deaerated solutions. Almost the same results as those in the presence of oxygen were obtained.

These photochemical reactions did not show any appreciable concentration dependence in the range 5×10^{-6}—2×10^{-4} M in cyclohexane, proceeding likewise in various solvents. Thus the main photochemical reactions of 9-CH_2BrCO-A are considered to be intramolecular.

The stable intermediate observed in cyclohexane could not be detected in alcoholic solutions at 30—35 °C because of its instability. The result obtained in the ethanol solution by irradiation through the filter UV-39 is shown in Fig. 2. There is no absorption attributable to the intermediate. Instead, the isosbestic points are seen at 322 nm and 392 nm, indicating that the final products are formed simultaneously with irradiation.[16]

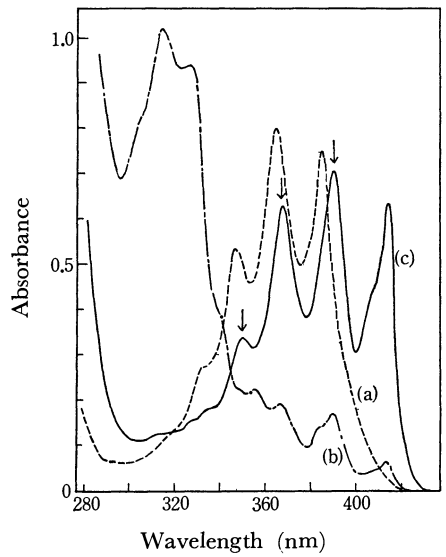

Fig. 1. Change in the absorption spectra of the aerated cyclohexane solution of 9-CH_2BrCO-A caused by irradiation.
(a) ——: 9-CH_2BrCO-A (1.0×10^{-4} M)
(b) ——: the spectrum of the intermediate obtained after 20 min irradiation through the filter UV-39.
(c) ——: final products obtained by the dark reaction of the intermediate (see the text).
The arrows indicate that the absorptions at these wavelength are partly due to 9-Br-A.

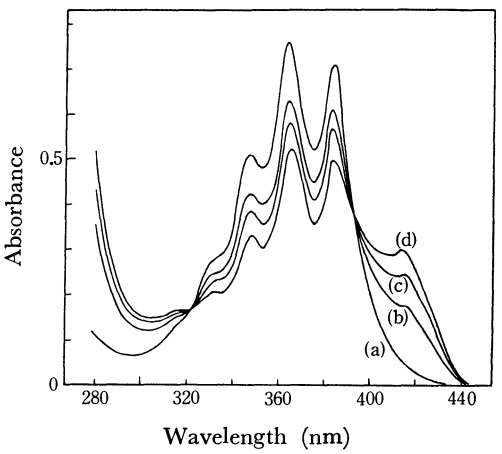

Fig. 2. Change in the absorption spectra of the aerated ethanol solution of 9-CH_2BrCO-A caused by irradiation.
(a) reactant, (b) after 5 min, (c) after 10 min, (d) after 25 min (final products).
The solution was irradiated through the filter UV-39 at 30—35 °C. No absorption attributable to the intermediate is observable and the isosbestic points are seen at 322 nm and 392 nm.

The absorption spectra of 1-aceanthrenone in cyclohexane and in ethanol are shown in Fig. 3. A comparison of the absorption spectrum in cyclohexane with that given in Fig. 1 shows that the increment of the absorption indicated by the arrows is due to 9-Br-A. The yield of each compound can thus be easily calculated from its molar extinction coefficient. The values obtained in this way are given in Table 1.

Table 1. Yields of photo products

Reaction conditions[a]			Yield (%)		Other products[b]
Solvent	Temperature	Presence of oxygen	1-Aceanthrenone	9-Br-A	
Cyclohexane	Room temp.	Yes	71	9	anthraquinone (UV) (425 nm)
Cyclohexane	Room temp.	No	77	11	9-CH_3CO-A (UV, IR) anthracene (Fl, Ex)
Ethanol	Room temp.	Yes	52	14	9,10 di-Br-A (UV) anthraquinone (UV)[c] (387 nm, 425 nm)
Ethanol	Dry ice-ethanol temp.	Yes	58	32	anthraquinone (UV)
Ethanol	Dry ice-ethanol temp.	No	59	36	9-CH_3CO-A (UV) anthracene (Fl, Ex)

a) The yields were obtained in the reactions of dilute solutions (*ca.* 10^{-4} M).
b) Method of detection is given in parentheses in abbreviated form; Fl: fluorescence spectrum, Ex: excitation spectrum. The longest wavelengths of the absorption spectra observed in cyclohexane after separation by column chromatography are also given in parentheses.
c) Prolonged irradiation of a more concentrated solution gave anthraquinone and 9,10-di-Br-A in high yields.

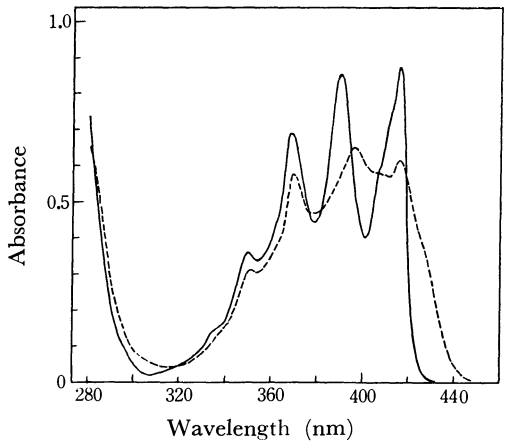

Fig. 3. Absorption spectra of 1-aceanthrenone (1.0×10^{-4} M) in cyclohexane (——) and in ethanol (----).

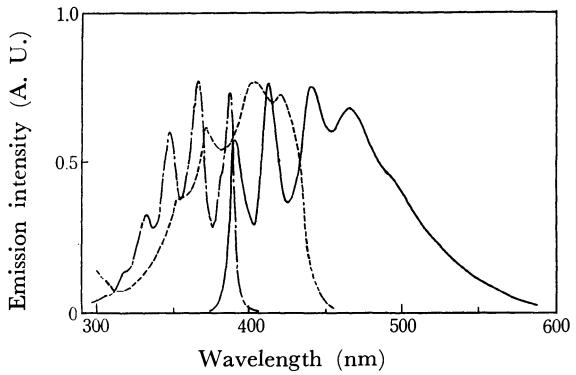

Fig. 4. Fluorescence and excitation spectra of the photoproducts in ethanol. The solution shows the absorption spectrum represented by Fig. 2d.
——: fluorescence spectrum,
– – –: excitation spectrum observed at 412 nm,
----: excitation spectrum observed at 500 nm.
The emission at the shorter wavelength region is not due to 9-Br-A.[17]

The fluorescence and excitation spectra of the solution having the absorption spectrum shown in Fig. 2d are given in Fig. 4. The emission band at the longer wavelength is due to 1-aceanthrenone, judging from the excitation spectrum. The component at the shorter wavelength is not assignable to 9-Br-A and is due to some other unidentified product.[17] The absorption spectrum of this compound overlaps that of 9-Br-A. The yields were thus determined spectrophotometrically after separation by column chromatography.

Irradiation at Dry Ice-Ethanol Temperatures. When the degassed *n*-hexane solution of 9-CH_2BrCO-A was irradiated through the filter UV-39 at dry ice-ethanol temperatures, the absorption spectrum given by curve a in Fig. 5 was obtained. *n*-Hexane was used because of high freezing point of cyclohexane. At these temperatures the reaction of the intermediate to form 1-aceanthrenone is completely retarded. Thus no absorption can be seen at 414 nm (curve a, Fig. 5). There is a small absorption peak at 388 nm where 9-Br-A shows absorption. After temperature was raised to room temperature and the reaction was completed, the yield of 9-Br-A was determined from the difference of the absorbances at 388 nm and at 414 nm. The yield of 9-Br-A obtained in this way agreed well with that gained before temperature was raised. This fact makes it clear that 9-Br-A is not formed by a thermal reaction after irradiation and that only 1-aceanthrenone is formed from the intermediate.

When the solution at the state shown by curve a (Fig. 5) was irradiated further through the filter UV-DIB, photochemical reactions occurred as indicated by curves b-f, the final state being shown by curve f. As seen from the absorption spectrum, 1-aceanthrenone was produced. In the absence of oxygen, the yields obtained by the photochemical and thermal reactions of the intermediate were almost the same. In the presence of oxygen, however, the yield for the former procedure was lower than that for the latter by about 60%. The irradiation of the intermediate seems to produce other compounds than 1-aceanthrenone.

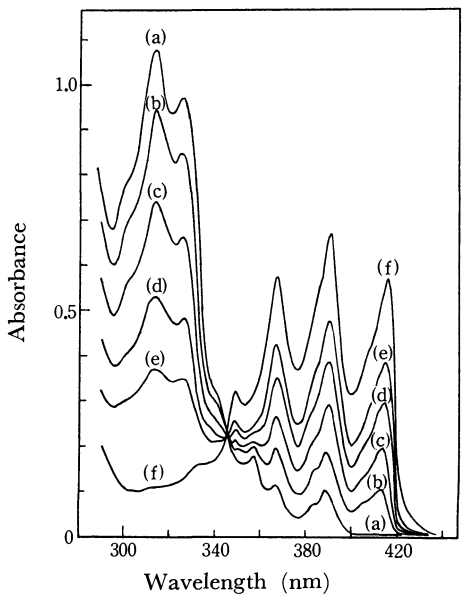

Fig. 5. Photochemical reactions of the intermediate in the degassed *n*-hexane solution.
(a) before the second irradiation, (b) after 30 s (c) after 90 s, (d) after 180 s, (e) after 300 s, (f) final products
Curve a was observed after 30 min irradiation through the filter UV-39 at dry ice-ethanol temperatures. The second irradiation was carried out through the filter UV-DIB at room temperature. The absorption spectrum f did not change by further irradiation.

Their compositions are not identified.

Even in ethanol it was confirmed that the intermediate could exist stably at temperatures as low as dry ice-ethanol temperature in the following way. After sufficient irradiation of the ethanol solution of 9-CH_2BrCO-A at dry ice-ethanol temperatures through the filter UV-39, the reaction cell was dipped into a transparent Dewar vessel containing liquid nitrogen and the fluorescence spectra were measured. The only emissive species was 9-Br-A. When temperature was raised to room temperature, a new fluorescence band due to 1-aceanthrenone appeared. This indicates that the intermediate can exist stably at low temperatures and only 1-aceanthrenone is formed from the intermediate.

Miscellaneous. Measurements of electric conductivity enabled us to elucidate the intermediate. The cyclohexane solution of 9-CH_2BrCO-A (*ca.* 10^{-3} M) which had been irradiated through the filter UV-39 and enriched with the intermediate was shaken well with distilled water. This operation did not appreciably affect the stability of the intermediate. The water layer was separated and its electric conductivity was measured. After this, the aqueous solution was again combined with the cyclohexane layer. The above operation was repeated several times at certain time intervals. The electric conductivity of the water layer was found to increase as the intermediate decreased by the thermal reaction. This shows that the reaction of the intermediate to form 1-aceanthrenone is accompanied by the elimination of a certain molecule which can dissociate into ions. Hydrogen bromide is the most probable candidate, judging from the structures of the reactant and the product and from the reaction mechanisms.

On the irradiation of a completely degassed solution of 9-CH_2BrCO-A, an appreciable amount of 9-CH_3CO-A and a small amount of anthracene were formed as minor photo-products. In an aerated solution, anthraquinone was formed instead of these two compounds. The formation of other minor photo-products depends on reaction conditions. A detailed description is given in Table 1.

1-Aceanthrenone was rather photo-stable in cyclohexane, but in ethanol its absorption spectrum gradually changed with irradiation. The products in this reaction were not identified.

Heating an *o*-dichlorobenzene solution of 9-CH_2BrCO-A to *ca.* 135 °C for 2 hr was unsuccessful to produce 9-Br-A or 1-aceanthrenone, for no UV absorption change was observed.

A preliminary experiment on 9-ω-chloroacetylanthracene showed that it underwent photochemical reactions analogous to those of 9-CH_2BrCO-A.

Discussion

If we neglect the photodimerization of 9-CH_2BrCO-A in the low concentration range 5×10^{-6}—2×10^{-4} M, the photochemical reaction mechanisms of 9-CH_2BrCO-A can be given as shown in Fig. 6. The reactions are noteworthy particularly as regards the following three points: (i) The main photochemical reactions proceed in various solvents in the presence or in the absence of oxygen, *i. e.*, paths (1), (2) and (3) do not seem to be affected greatly by the presence of oxygen. In contrast, oxygen completely suppresses path (4). (ii) With an appropriate choice of excitation wavelength and reaction temperature, the reaction intermediate can be produced stably and can be detected by its UV absorption spectrum. The intermediate gives 1-aceanthrenone by either the dark reaction or the photochemical reaction. (iii) It can be shown that 9-Br-A and 1-aceanthrenone are produced *via* two different processes.

The structure of the intermediate (Fig. 6) has been

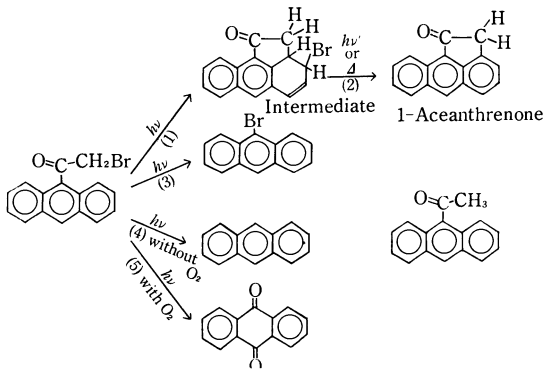

Fig. 6. Mechanisms of the photochemical reactions of 9-CH_2BrCO-A. Only the identified products are shown. For further detailed descriptions on the other products, see Table 1.

proposed on the basis of the following: The intermediate eliminates a hydrogen bromide in path (2). The absorption spectrum of the intermediate can be most reasonably interpreted by assigning it to a derivative of naphthalene. The intermediate has a long half life at room temperature in cyclohexane and shows no ESR signal. Thus it is probably not a free radical. The solvent itself is not involved in the formation of the intermediate.

The thermal and photochemical reaction mechanisms of the intermediate could be reconciled by considering the photochemical reaction of the intermediate to occur at vibrationally excited states, *i. e.*, vibrational excess energy supplied by direct photo-excitation or by a succeeding radiationless transition process would facilitate the liberation of a hydrogen bromide molecule. The structure of the intermediate we proposed seems to be pertinent to this interpretation.

The primary process of the photochemical reactions of 9-nitroanthracene (9-NO_2-A) and sodium 9-anthroate (9-COONa-A) to produce anthraquinone in the presence of oxygen is analogous to that of 9-CH_2BrCO-A. For 9-NO_2-A and 9-COONa-A, the most relevant primary process is considered to be not the dissociation and recombination of the substituent but the intramolecular rearrangement at the $n\pi^*$ states.[18-20] In the ground states of these compounds the plane containing the three atoms of each substituent makes almost a right angle to the anthracene ring[21,22] owing to the steric hindrance by *peri* hydrogen atoms. Thus, in the $n\pi^*$ excited state populated either by direct photo-excitation or by intersystem crossing process, an unpaired electron in the n-orbital of the oxygen atom can just interact attractively with an electron in the p-orbital of the carbon atom at 9-position. As a result, the intramolecular photochemical reactions take place. Experimental evidence for the above supposition, however, has not yet been obtained.

If we take into account the structure of 9-CH_3CO-A, the substituent of 9-CH_2BrCO-A can be considered to be perpendicular to the anthracene ring[9] in the ground state. Although we have no experimental evidence at present with regard to the nature of reactive excited states, a change in the electronic state of the anthracene ring or the carbonyl group on photo-excitation seems to make the lone pair of electrons of the bromine atom interact with a p-orbital electron of the carbon atom at 9- or 2-position. As a result, 9-Br-A or the intermediate will be formed. In the case of 9-NO_2-A and 9-COONa-A, rotation of the substituents on excitation is not taken into account. An unpaired n-orbital electron of these compounds interacts with a p-orbital electron solely at 9-position. In this respect 9-CH_2BrCO-A differs from these compounds. Considering its reaction products, the interactions both at 9- and 2-positions should exist. This leads to the occurrence of rotation of the substituent on photo-excitation.

A change in interaction between a substituent and an anthracene ring caused by photo-excitation has been proposed by Werner and Hercules[23,24] in the case of 9-anthroic acid. They attributed its abnormally large Stokes shift of the fluorescence to the conformational change in the excited state, where the carbonyl group rotates into a co-planar configuration, forming a hydrogen bond with a hydrogen atom at a *peri* position. The photochemical formation of 1-aceanthrenone would verify the existence of such interaction.

Thus it is expected that the relative yield of 9-Br-A and 1-aceanthrenone would be affected by the kind of solvent, viscosity and temperature, which would influence the ease of the rotation of the substituent on photo-excitation. The values cited in Table 1 seem to indicate such a tendency.

It is worthwhile to consider the relation between these new photochemical reactions of 9-CH_2BrCO-A and its relaxation processes of excitation energy.[9,10,12]

With regard to the reactive excited state of 9-CH_2BrCO-A, one possible candidate is the singlet $\pi\pi^*$ state where the change in the π-electron density at 9- or 2-position causes the attractive interaction between the bromine atom and the carbon atom at 9- or 2-position, leading to the bond formation between them. If this is the case, only the existence of a bromine atom is indispensable for the progress of similar intramolecular photochemical reactions and it may be unnecessary for a substituent to have a carbonyl group.

Another possibility is to relate these photochemical reactions to the characteristic radiationless transitions of carbonyl derivatives of anthracene. The non-fluorescent property of the majority of these compounds reflects the existence of the efficient intersystem crossing process of $S_{\pi\pi^*} \rightsquigarrow T_{n\pi^*}$.[9,10,12] 9-$CH_2$BrCO-A is expected to behave as 9-CH_3CO-A and thus the effective intersystem crossing process of $S_{\pi\pi^*} \rightsquigarrow T_{n\pi^*}$ is thought to be working also in this molecule. If this is the case, photo-excitation will mainly produce the triplet $n\pi^*$ state and some highly vibrationally excited states which are produced from the triplet state by radiationless transitions. In the triplet $n\pi^*$ state, excitation is localized to the carbonyl group, so in the vibrationally excited states formed from that state, the excess vibrational energy would be localized also to the bromoacetyl group. In the triplet $n\pi^*$ state itself or in the vibrationally excited state, the bromoacetyl group is supposed to interact strongly with the anthracene ring, or the excess vibrational energy would aid in breaking the C–C and C–Br bonds. As a result, the photochemical reactions including the C–C and C–Br bond rupture are considered to proceed. In the sense that the occurence of the efficient $S_{n\pi^*} \rightsquigarrow T_{n\pi^*}$ intersystem crossing results in the activation of the bromoacetyl group, the photochemical reactions of 9-CH_2BrCO-A is correlated to non-fluorescent property of carbonyl derivatives of anthracene.

Of the two possibilities, the latter is more interesting, since it takes into consideration the role of the carbonyl group and can interpret more reasonably the production of anthracene and 9-CH_3CO-A. However, neither has experimental evidence at present.

References

1) A. Schönberg, "Preparative Organic Photochemistry," Springer-Verlag New York Inc. (1968).

2) S. Kusuhara and R. Hardwick, *J. Chem. Phys.*, **41**,

2386 (1964).
3) J. Osugi, S. Kusuhara, and S. Hirayama, *Rev. Phys. Chem. Jap.*, **37**, 94 (1967).
4) I. Fujihara, M. Okushima, S. Hirayama, S. Kusuhara, and J. Osugi, This Bulletin, **44**, 3495 (1971).
5) E. Bowen and J. Sahu, *J. Phys. Chem.*, **63**, 4 (1959).
6) E. C. Lim, J. D. Laposa, and J. M. H. Yu, *J. Mol. Spectry.*, **19**, 412 (1966).
7) B. R. Henry and J. L. Charlton, *J. Amer. Chem. Soc.*, **95**, 2782 (1973).
8) D. S. Klinger and A. C. Albrecht, *J. Chem. Phys.*, **53**, 4059 (1970).
9) S. Hirayama, *Rev. Phys. Chem. Jap.*, **42**, 49 (1972).
10) T. Matsumoto, M. Sato, and S. Hirayama, *Chem. Phys. Lett.*, **13**, 13 (1972).
11) In the case of 9-benzoylanthracene a distinct substituent effect on the intersystem crossing process has been noted.[12]
12) T. Matsumoto, M. Sato, and S. Hirayama, *Chem. Phys. Lett.*, **18**, 563 (1973).
13) E. L. May and E. Mosetting, *J. Amer. Chem. Soc.*, **70**, 686 (1948).
14) Low temperatures which retarded the thermal reaction (Fig. 6) were preferred because of the low absorptivity of the intermediate (Fig. 1) at the excitation wavelength.
15) "Beilsteins Handbuch der Organischen Chemie," E. III 7, p. 2627 (1968).
16) G. Quinkert, *Angew. Chem. Intern. Ed. Engl.*, **11**, 1072 (1972).
17) Fluorescence of 9-Br-A is rather weak and its o-o band appears at 393 nm.
18) O. L. Chapman, A. A. Griswold, E. Hoganson, G. Lenz, and J. W. Reasoner, *Pur. Appl. Chem.*, **9**, 585 (1964).
19) O. L. Chapamn, D. C. Heckert, J. W. Reasoner, and S. P. Thackaberry, *J. Amer. Chem. Soc.*, **88**, 5550 (1966).
20) A. W. Bradshaw and O. L. Chapman, *ibid.*, **89**, 2372 (1967).
21) J. Trotter, *Acta Cryst.*, **12** 237, 922 (1959).
22) A. S. Cherkasov and K. G. Voldikina, *Izvest. Akad. Nauk SSSR, Ser. Fizicheskaja*, **27**, 628 (1963).
23) T. C. Werner and D. M. Hercules, *J. Phys. Chem.*, **73**, 2005 (1969).
24) T. C. Werner and D. M. Hercules, *ibid.*, **74**, 1030 (1970).

Phase Diagrams of YCl_3–KCl, YCl_3–NaCl, and YCl_3–KCl·NaCl Systems, and Densities of Their Molten Mixtures

Junichi Mochinaga and Kyozan Irisawa

Department of Synthetic Chemistry, Faculty of Engineering, Chiba University, Yayoi-cho, Chiba 280

(Received June 7, 1973)

YCl_3 has been prepared with Y_2O_3 and NH_4Cl, and the optimum conditions for chlorination have been determined. The YCl_3 salt obtained was purified to a pure YCl_3 crystal by sublimation. Phase diagrams of binary YCl_3–KCl and YCl_3–NaCl system, and liquidus curve diagram of quasi-binary YCl_3–KCl·NaCl system have been determined with the use of the purified YCl_3 crystal. Densities of YCl_3 and the mixtures in molten state were measured dilatometrically, and represented by empirical formulas as a function of temperature. From the results thermal expansion coefficients and molar expansibilities of the molten YCl_3 and the molar volumes of molten mixtures were calculated.

YCl_3 can be prepared by heating a mixture of Y_2O_3 and NH_4Cl:

$$Y_2O_3 + 6NH_4Cl = 2YCl_3 + 6NH_3 + 3H_2O \quad (1)$$

Since the product contains H_2O owing to the hygroscopic property of YCl_3, if the reaction temperature is too high, yttrium oxychloride is produced by the reaction of YCl_3 and H_2O, thus reducing the yield of YCl_3. In the present experiment the optimum conditions for the chlorination were determined. The YCl_3 salt was purified to a pure YCl_3 crystal by sublimation. This was used for the determination of phase diagrams and the measurement of densities of the YCl_3 and the mixture systems in molten state. Measurements of melting and transition points were carried out by differential thermal analysis. The dilatometer method was used in the measurements of densities.

Experimental

Preparation of YCl_3. A mixture of Y_2O_3 and NH_4Cl in a glass test tube of standard size was heated for a certain time in an electric furnace. The yields of YCl_3 were determined by chemical analysis of reaction products obtained under various conditions of temperature, time, and mixing ratio of Y_2O_3 and NH_4Cl. When the reaction product is treated with water purified by ion-exchange resins, YCl_3 only is dissolved in the water, but not yttrium oxychloride and Y_2O_3. The precipitate obtained by filtration of the solution was separately dissolved in the hot dilute hydrochloric acid. The amounts of Y^{+3} ions contained in both solutions were determined by the titration with EDTA solution. The yield of YCl_3 can be obtained by

$$\eta = [A/(A+B)] \times 100 \quad (\%)$$

where A is the amount of YCl_3 contained in the filtrate, and B the amount of YCl_3 contained in the solution from the filter cake. The Y_2O_3 used as starting material was 99.9% in purity (Shin-Etsu Chem. Ind. Co. Ltd., Japan: Found: Tb_4O_7, <0.003; Dy_2O_3, 0.030; Fe, 0.0003; Cu, 0.00002%). NH_4Cl(A.R. grade) was dried at about 120 °C for several hours.

Purification of YCl_3. Purification of YCl_3 is necessary since it still contains a small amount of water and NH_4Cl. Purification was carried out by sublimation in a vacuum.

Differential Thermal Analysis. Measurements were carried out from the cooling curve of the molten sample in demoistured argon gas, α-Al_2O_3 powder being used as a reference material. The cooling rates were 15 °C/min at 800 °C and 13 °C/min at 500 °C.

Measurements of Densities. The densities of the liquid chlorides were measured dilatometrically with a transparent silica dilatometer. The meniscus of molten salt was read with a cathetometer. This method was checked by measuring the densities of KCl and NaCl, the result being in good agreement with the data in literature.[1]

Results and Discussion

Preparation of YCl_3. The high yield of YCl_3 in the chlorination of Y_2O_3 makes it necessary to add an excess amount of NH_4Cl as compared with the theoretical amount in Eq. (1). The dependence of reaction time for the yield of YCl_3 at 300 °C is shown in Fig. 1, in which the curves a, b, and c are the results for the reactions with the mixtures of 1.32, 1.72, and 2.13 times the theoretical amount of NH_4Cl in Eq. (1), respectively. For curve a (1.32 times theoretical amount of NH_4Cl), the yield of YCl_3 was less than about 70%, but in the others very high yields were obtained. In cases where a more excess amount of NH_4Cl was contained the reaction rates were greater.

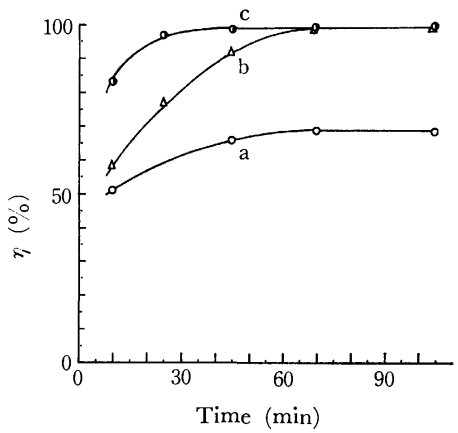

Fig. 1. Dependences of reaction time for the yield of YCl_3 at 300 °C; a: reaction of mixture containing 1.32 times of NH_4Cl, b: 1.72 times, c: 2.13 times.

The dependence of reaction temperature for the yield of YCl_3 in the reaction with 1.72 times the theoretical amount of NH_4Cl is shown in Fig. 2, in which the curves A, B, C, D, and E are the results for the reactions at 200, 250, 300, 350, and 400 °C, respectively. In the reaction at 200 °C, YCl_3 was not formed. The reactions at 350 and 400 °C proceeded rapidly,

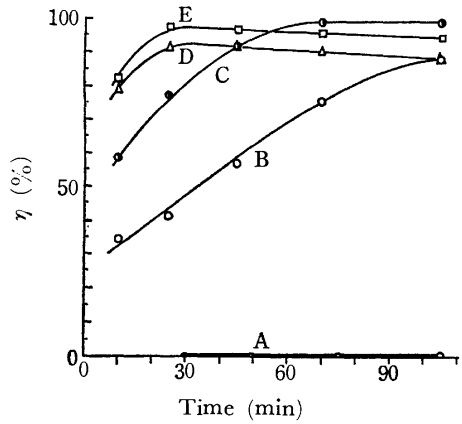

Fig. 2. Dependences of reaction temperature for the yield of YCl_3 in reactions of mixtures containing 1.72 times of NH_4Cl; A: reaction at 200 °C, B: 250 °C, C: 300 °C, D: 350 °C, E: 400 °C.

but the yields of YCl_3 decreased a little after a longer reaction time than 30 min. The tendency might indicate that the yttrium oxychloride was produced from YCl_3 and H_2O in the reaction product due to the high reaction temperature. This was also anticipated by Wendlandt[2] from the results of thermal analysis for YCl_3 containing H_2O.

It is preferable to carry out the reaction under the following optimum conditions for the chlorination of Y_2O_3 with NH_4Cl: reaction temperature 300 °C; addition to Y_2O_3 of 1.7 times or more the theoretical amount of NH_4Cl in Eq. (1); reaction time 70 min or more.

Purification of YCl_3. The maximum yield of YCl_3 crystal in sublimation, obtained when the sublimation temperature was 950—1050 °C, was about 50% after 7 hours. The purified YCl_3 crystal was completely soluble in water, the atomic ratio of Y and Cl being 1 : 3.01. The mp of this crystal was 714 and 717 °C in cooling and heating measurements, respectively, by DTA analysis. The contents of metallic impurities in this crystal are given in Table 1.

Table 1. Contents of metallic impurities in YCl_3 crystal[a]

Element	Content (ppm)	Element	Content (ppm)
La	5	Yb	< 1
Ce	<30	Lu	<10
Pr	<10	Mg	< 1
Nd	<10	Al	< 5
Sm	<10	Si	50
Eu	< 1	V	< 5
Gd	<10	Mn	< 1
Tb	< 5	Fe	5
Dy	60	Ni	< 5
Ho	<10	Cu	< 1
Er	< 5	Sn	< 5
Tm	< 5		

a) Method of analysis: Spectrographic; M. Sato, H. Matsui, and T. Matsubara, *Bunseki Kagaku*, **20**, 215 (1971).

Phase Diagram. Phase diagrams of YCl_3–KCl, YCl_3–NaCl systems and the liquids curve diagram of quasi-binary YCl_3–KCl·NaCl system are shown in Figs. 3, 4, and 5, respectively. In the YCl_3–KCl system, two intermediate compounds ($3YCl_3$·KCl and YCl_3·3KCl), one peritectic point(552 °C, 74 mol% YCl_3), 2 eutectic points(435 °C, 44 mol% YCl_3 and 685 °C, 15 mol% YCl_3), and a polymorphic transition point(367 °C) in solid range between the intermediate compounds were observed.

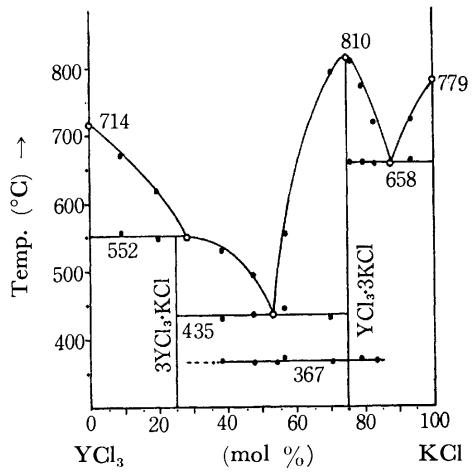

Fig. 3. Phase diagram of YCl_3-KCl system.

This is in fairly good agreement with the diagram given by Korshunov and Drobot,[3] but not with that by Su and Ch'iu.[4] In the YCl_3–NaCl system, one intermediate compound (YCl_3·3NaCl), one peritectic point (556 °C, 33 mol% YCl_3), and one eutectic point (389 °C, 50 mol% YCl_3) were observed. In this system, the intermediate compound NaCl·$9YCl_3$ reported by Su and Ch'iu[4] was not observed.

We see in Fig. 5 that the YCl_3–KCl·NaCl system has 2 minimum points (409 °C, 57 mol% YCl_3 and 600 °C, 86 mol% YCl_3), and one maximum point (632 °C, 76 mol% YCl_3).

Density of Molten YCl_3. The measurement of density of the molten YCl_3 was performed in the range

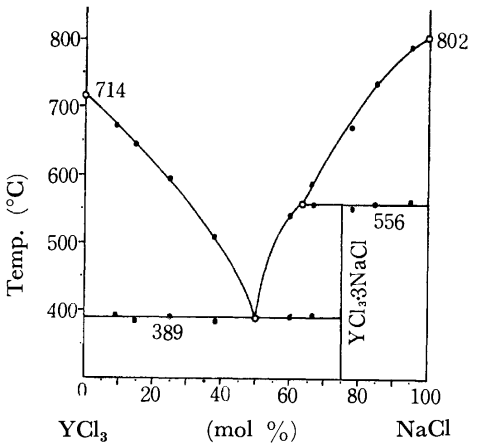

Fig. 4. Phase diagram of YCl_3-NaCl system.

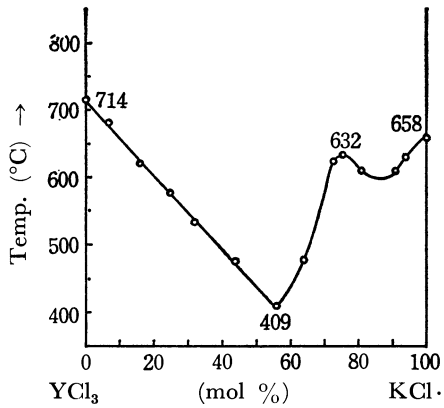

Fig. 5. Liquidus curve diagram of YCl_3-KCl·NaCl (e.m.) system.

809—1005 °C with the use of the method of least squares. The following empirical formula was obtained as a function of temperature;

$$d = 2.9226 - 4.594\times10^{-4}\,t,$$

where d is the density of molten YCl_3 in g/cm³, and t the temperature in °C. Since the density change of the molten salt with temperature is linear, the density of the molten YCl_3 at a mp of 714 °C could be calculated by extrapolation. The density of the molten YCl_3 at mp is 2.595 g/cm³. The volume change of YCl_3 on melting, calculated from the density data at room temperature (2.61 g/cm³), since the thermal expansion of the solid is much smaller than that of the liquid, was +0.594% for the solid volume. This is much smaller than the given values of $PrCl_3$, $NdCl_3$, and $GdCl_3$.[5]

Coefficients of Thermal Expansion of Molten YCl_3.
The expansivity and molar expansibility of molten YCl_3 under atmospheric pressure were calculated by combining the formula with the equation

$$\alpha = -(1/d)(\partial d/\partial t)_p \qquad (2)$$

where α is the expansivity in /°C under the pressure p. The molar expansibility is equal to αV, where V is the molar volume of molten YCl_3. The values of the expansivity and molar expansibility are given in Table 2.

TABLE 2. EXPANSIVITY AND MOLAR EXPANSIBILITY OF MOLTEN YCl_3

Temp. (°C)	Expansivity (/°C)	Molar expansibility (cm³/mol °C)
750	1.782×10^{-4}	1.350×10^{-2}
800	1.798×10^{-4}	1.374×10^{-2}
850	1.814×10^{-4}	1.399×10^{-2}
900	1.831×10^{-4}	1.425×10^{-2}
950	1.848×10^{-4}	1.451×10^{-2}
1000	1.865×10^{-4}	1.479×10^{-2}

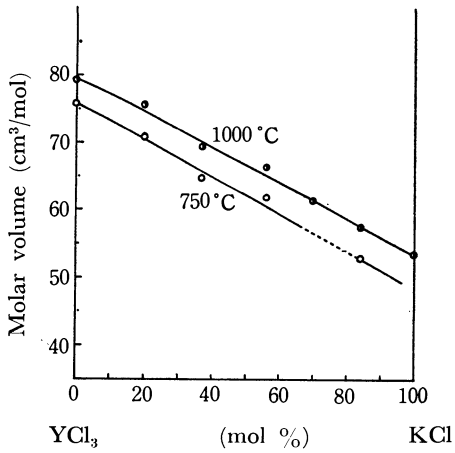

Fig. 6. Molar volume isotherm of molten YCl_3-KCl system.

TABLE 3. EMPIRICAL FORMULAS OF DENSITIES FOR MOLTEN MIXTURES

(a) YCl_3-KCl system

Component (mol %)		Density (d: g/cm²; t: °C)	Temp. range (°C)
YCl_3	KCl	$d=a+bt$	
80.2	19.8	$d=2.8914-6.312\times10^{-4}t$	800—1003
63.2	36.8	$d=2.7995-6.199\times10^{-4}t$	819— 990
44.4	55.6	$d=2.4823-5.594\times10^{-4}t$	800—1000
29.9	70.1	$d=2.3586-5.540\times10^{-4}t$	881— 999
15.8	84.2	$d=2.2017-5.790\times10^{-4}t$	800—1000

(b) YCl_3-NaCl system

Component (mol %)		Density (d: g/cm³; t: °C)	Temp. range (°C)
YCl_3	NaCl	$d=a+bt$	
85.0	15.0	$d=2.8784-4.515\times10^{-4}t$	812— 999
69.8	30.2	$d=2.8663-6.219\times10^{-4}t$	798—1002
59.1	40.9	$d=2.7659-5.398\times10^{-4}t$	807—1005
44.2	55.8	$d=2.5862-5.367\times10^{-4}t$	797— 997
28.1	71.9	$d=2.4230-5.264\times10^{-4}t$	807— 990
14.9	85.1	$d=2.2897-5.501\times10^{-4}t$	797— 960

(c) YCl_3-KCl·NaCl system

Component (mol%)			Density (d: g/cm³; t: °C)	Temp. range (°C)
YCl_3	KCl	NaCl	$d=a+bt$	
83.8	8.1	8.1	$d=2.8932-5.835\times10^{-4}t$	806— 932
69.2	15.4	15.4	$d=2.7918-6.142\times10^{-4}t$	809— 985
49.9	25.05	25.05	$d=2.6089-6.038\times10^{-4}t$	803— 980
27.8	36.1	36.1	$d=2.3457-5.294\times10^{-4}t$	805— 950
16.3	41.85	41·85	$d=2.2729-5.907\times10^{-4}t$	820— 995
0.0	50.0	50.0	$d=1.8865-5.470\times10^{-4}t$	815—1000

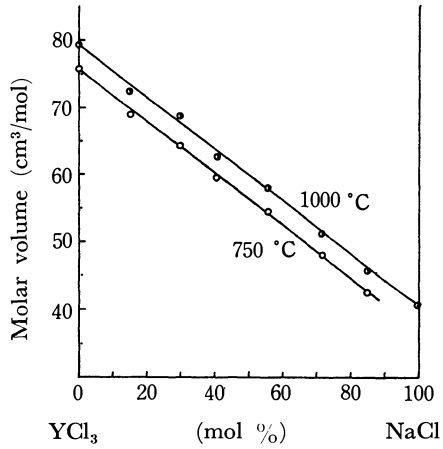

Fig. 7. Molar volume isotherm of molten YCl_3-NaCl system.

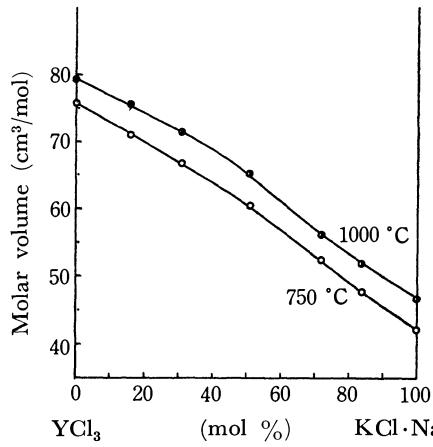

Fig. 8. Molar volume isotherm of molten YCl_3-KCl·NaCl (e.m.) system.

Densities of the Molten Mixtures. The densities of molten mixtures were measured for the various compositions in YCl_3-KCl, YCl_3-NaCl, and YCl_3-KCl·NaCl systems. The density data were treated then by the method of least-squares and represented by the empirical formulas as functions of temperature. The formulas are given in Table 3.

Molar Volume Isotherms. From the formulas in Table 3, the molar volumes of the molten mixtures were calculated by the following equation.

$$V_{mix} = \sum (X_i M_i)/d_{mix},$$

where V_{mix} is the molar volume of molten mixture in cm^3/mol, X_i the mole fraction of component i in the mixture, M_i the molecular weight of the component i in the mixture in g/mol, and d_{mix} the observed density of the molten mixture in g/cm^3. The molar volume isotherms of three molten mixture systems are shown in Figs. 6, 7, and 8.

The authors wish to thank Mr. Matsuji Sato, Shin-Etsu Chem. Ind. Co., for assistance in the analysis of materials.

References

1) E. R. Van Artsdalen and I. S. Yaffe, *J. Phys. Chem.*, **59**, 118 (1955).
2) W. W. Wendlandt, *J. Inorg. Nucl. Chem.*, **5**, 118 (1957).
3) B. G. Korshunov and D. V. Drobot, *Zh. Neorg. Khim.*, **9**, 222 (1964).
4) Mien-Ts'eng Su and Ping-I Ch'iu, *K'o Hsueh T'ung Pao*, **17**, 72 (1966), *Chem. Abstr.*, **67**, 76638t (1967).
5) K. Cho, K. Irisawa, J. Mochinaga, and T. Kuroda, *Electrochim. Acta*, **17**, 1821 (1972).

Formation of Charge-transfer Complexes by Solid State Reaction; Electronic Spectra and Relative Reactivity

Hiroyasu SATO and Tamiharu YASUNIWA

College of Liberal Arts, Kagoshima University, Kamoike, Kagoshima 890

(Received July 13, 1973)

Formation of charge-transfer complexes by solid state reaction was studied for 16 donors and 10 acceptors. The relative reactivity of 160 pairs was determined by the presence or absence of the charge-transfer band on grinding the component pairs of the same concentration (diluted with sodium chloride) for the same length of time. Equilibrium was not reached within the grinding time. This relative reactivity was compared with and found to have a parallel relationship with the relative ease of formation of the charge-transfer complex on evaporating a mixture of the solutions of components, indicating that the relative reactivity is related to an apparent equilibrium established on the grain surface. Relative reactivity was found to be largely dependent on molecular size and geometry. Smaller molecules were more reactive. For molecules with the same number of rings, those with compact structure were more reactive. Most of the new bands given by the reaction were CT bands of microcrystals. They were very broad. A fairly good linear relationship was found between the transition energies of the CT bands and the ionization potentials of the donors or the electron affinities of the acceptors.

A considerable amount of information has been accumulated on the equilibria of charge-transfer (CT) complexes in solutions, but very little is known about those in solid phase. Hammick and Hutchison[1] discussed the free energy of formation of solid CT complexes (from the solid components) from their solubility measurements of trinitrobenzene- or trinitrotoluene-aromatic hydrocarbon systems. Suzuki and Seki[2] calculated the heats of formation of crystalline CT complexes (from the crystalline components) on the basis of their measurements of heat of solution for trinitrobenzene-aromatic hydrocarbon systems. They noted that the relative magnitudes of the thermodynamic data differ from those in solutions. Braun and Kortüm[3] studied CT equilibria of some trinitrobenzene complexes formed by solid state reaction by means of diffuse reflection spectra (DRS). However, very little is known about the relative ease of CT complex formation by solid state reaction. We have carried out a qualitative study of relative reactivity choosing 16 donors and 10 acceptors.

Experimental

Materials. The chemicals used are given in the following with their abbreviations and code numbers or symbols. Donors: (a) *N,N,N′,N′*-tetramethyl-*p*-phenylenediamine (TMPD), (b) hexamethylbenzene, (c) 1,2,4,5-tetramethylbenzene, (d) 1,5-dimethylnaphthalene, (e) naphthalene, (f) *N,N,N′,N′*-tetramethylbenzidine, (g) diphenyl, (h) phenanthrene, (i) anthracene, (j) *p*-terphenyl, (k) pyrene, (l) triphenylene, (m) chrysene, (n) tetracene, (o) *p*-quaterphenyl, (p) perylene. Acceptors: (**1**) tetracyanoethylene (TCNE), (**2**) 7,7,8,8-tetracyano-*p*-quinodimethane (TCNQ), (**3**) 1,2-dichloro-4,5-dicyano-*p*-benzoquinone (DDQ), (**4**) *p*-chloranil, (**5**) 2,5-dichloro-*p*-benzoquinone, (**6**) *p*-benzoquinone, (**7**) α-naphthoquinone, (**8**) anthraquinone, (**9**) pyromellitic anhydride (PMDA), (**10**) tetrachlorophthalic anhydride (TCPA) All of these were commercial products. G.R. reagents (c, d, f, k, l, m, o, p, **4**, **5**, **6**, and **10**) were used without further purification. The others were purified by vacuum sublimation or recrystallization.

Procedure. *(I) Grinding Two Components Only (a preliminary test)*: Appropriate amounts (*ca.* 10 mg each) of two components were ground on a glass plate with a stainless spatula. The formation of CT complexes was monitored visually by color. In some cases (*e.g.* a-**1**, a-**3**) colored products appeared immediately after mixing (before any grinding) the two components together. In most cases (*e.g.* a-**4**), a few seconds of grinding was necessary for obtaining the colored products. In some cases (*e.g.* i-**4**), no color of CT complexes appeared even on prolonged grinding.[4]

(II) Grinding Two Components with NaCl: The measurement of DRS was carried out to follow the CT complex formation.[5] In order to obtain good DRS by minimizing the effect of total reflection, it is necessary to disperse the sample in a white non-absorbing material used as a standard substance, which should neither react with the sample nor affect the CT equilibria. Braun and Kortüm[3] measured DRS of some CT complexes in sodium chloride, which was found not to cause dissociation of the complexes. Thus, sodium chloride was used as the white standard substance. Two components (10^{-4} mol each) and 5 g of sodium chloride were ground together manually in a porcelain mortar, 7.5 cm in diameter, for 30 s at room temperature. Sodium chloride was dried at 150 °C for 2 hours and stored in a desiccator.[6] Another 5 g of sodium chloride, ground in the same manner, was used as a reference. Measurement of DRS was then made quickly on a Shimadzu MPS-50 recording spectrophotometer with a reflection attachment. When a new DRS band or bands appeared, the measurement was repeated for some time to follow the spectral change after the sample was set in the reflection attachment. Values for $-\log R$ were measured rather than those for R. (For the definition of R, see footnote 7.) A very slight change in the spectra can thus be detected. The values for $f(R)$ in the Kubelka-Munk formula[7] were calculated from the measured values for $(-\log R)$, since the $f(R)$ value is proportional to absorbance on the assumption that the scattering coefficient is independent of wavelength. The value $-\log R=0.01$ was detectable in this measurement. This corresponds to $f(R)=2.65\times10^{-4}$. If no new band appeared, another sample was ground for 300 s at room temperature.[8]

(III) Evaporating the Mixture of Dichloromethane Solutions of Each Component: Dichloromethane solutions (10^{-2} mol/l) of a donor and an acceptor were prepared separately. Dichloromethane (Wako, G.R. reagent) was used without further purification. An aliquot (0.1 ml) of the donor solution and that (0.1 ml) of the acceptor solution were mixed. The resulting mixture was then evaporated on a glass plate at room temperature. For sparingly soluble compounds (*i.e.* **9**, **10**, n, o, and p) solutions of smaller concentration were

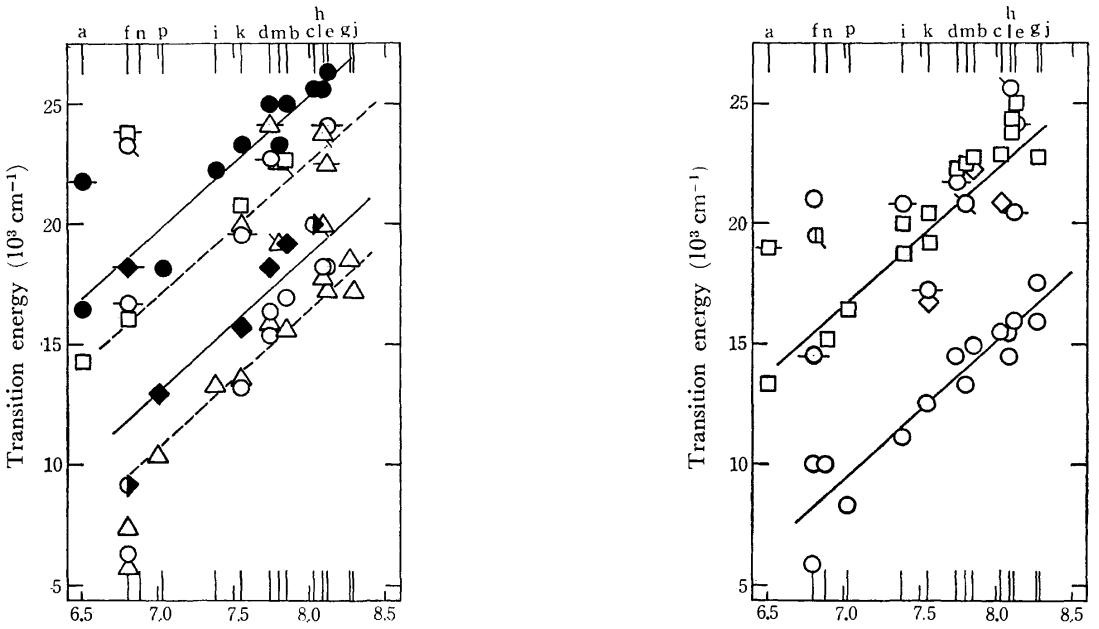

Fig. 1. Transition energies of observed new bands *vs.* ionization potential of donors.[25] The symbols of donors are shown on the upper abscissa.
Acceptors: (a) ○ 1, △ 2, ◆ 4, □ 6, ● 10.
(b) ○ 3, ◇ 5, □ 9.
A short line (horizontal) shows that the band can be assigned to the second CT band.[26] A short oblique line shows that the assignment of the band is uncertain. Such a band was considered as due to "the other product" in the text. Long straight lines in the figure show the approximate linear relationship of the CT transition energies *vs* ionization potentials of the donors. For TMPD complexes, only those bands which can be assigned to outer-complexes are given. For TCNE complexes, those bands attributable to the 1,1,2,3,3-pentacyanopropenide ion are not given.

prepared. An aliquot including 10^{-6} mol of substance was used in one experiment. Whether the solid residue is mostly (a) a CT complex, or (b) a mixture of donor and acceptor crystals, was judged from the color of the residue after evaporation.

Results

Nature of the Product. The positions of observed new DRS bands are shown in Figs. 1 and 2. Most of these bands can be considered as CT bands of minute crystals of CT complex, since their positions essentially coincide with the data of 15 crystalline CT complexes,[9-17] and solution data.[18-20] A few remarks are given here.

(i) TMPD Complexes (Figs. 1 and 2.): For a-**1**, the spectrum of the ion-pair was obtained with a CT band at 850 nm. For a-**3**, the CT band at 800 nm decreased in intensity, with an increase in intensity of the ion-pair bands (at 400, 573, and 625 nm). For a-**2**, **4**, and **5**, the presence of a band in the near infrared can be related to the inner-complex nature of the complexes.[14,17] For a-**9** and a-**10**, the bands can be attributed to outer complexes (Fig. 1a, b.). For a-**6**, the band was very broad. The presence of an apparent peak at 620 nm and a broad shoulder at 1100 nm would be associated with an inner-complex (Fig. 2), while a smaller peak at *ca.* 700 nm indicates

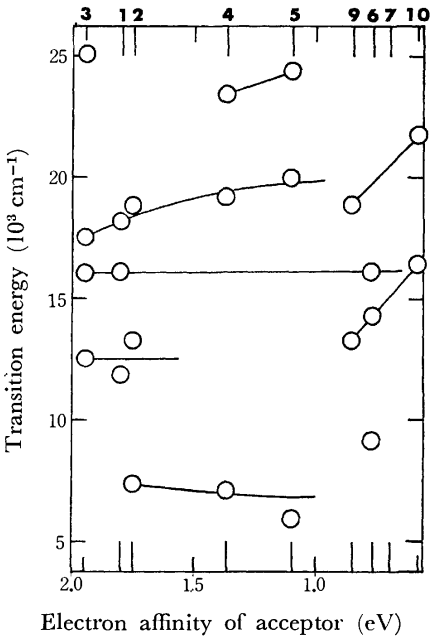

Fig. 2. Transition energy of observed new bands *vs.* electron affinity of acceptors,[27] for the TMPD-acceptor system. The code numbers of acceptors are shown on the abscissa.

TABLE 1. RELATIVE REACTIVITY IN SOLID STATE REACTION

Acceptor	Donor															
	a	b	c	d	e	f	g	h	i	j	k	l	m	n	o	p
1	A	A	A	A	A	B	—	A	—	—	A	—	—	—	—	—
2	A	A	—	A	A	A	A	D	A	A	A	B	D	—	—	A
3	A	A	A	A	A	A	A	B	A	—	A	A	B	A	—	A
4	A	A	A	A	—	A	—	—	—	—	A	—	—	—	—	A
5	A	A	A	—	—	—	—	—	—	—	A	—	—	—	—	—
6	A	A	—	—	—	(A)	—	—	—	—	A	—	—	—	—	—
7	—	—	—	—	—	—	—	—	—	—	—	—	—	—	—	—
8	—	—	—	—	—	—	—	—	—	—	—	—	—	—	—	—
9	A	A	A	A	A	D	(A)	A	A	—	A	A	(A)	(A)	—	A
10	A	A	A	A	A	—	—	A	A	—	A	A	A	—	—	A

that an outer complex is also present (Fig. 1a).

(ii) N,N,N′,N′-*Tetramethylbenzidine Complexes (Fig. 1)*: Most of the observed bands are found near those of single crystals.[13,16] Additional bands in the case of f-**3** (near 500 and 1000 nm) would be related to the cation of the donor, considering that benzidine cation has absorption bands near 450, 760, and 850 nm.[21,22] It is striking that no complex formation was found for f-**4** or f-**5** while the corresponding benzidine complexes were formed under the same conditions. Crystals of these two complexes can be formed by mixing the solutions of the components (experiment III, *cf.* Ref. 13.). These findings can be attributed to the smaller rate of complex formation due to the steric hindrance of the dimethylamino-groups.

Relative Reactivity in the Solid State. The results are summarized in Table 1. Symbols A, B, C, and D are given for those pairs which gave DRS bands not attributable to either parent molecule on 30 s grinding. The symbols A, B, C, and D denote new DRS bands as follows. (A) the CT complex only, (B) the CT complex with a small amount of another product, (C) a small amount of the CT complex and more of an other product, and (D) an other product only. The distinction was made on the criteria of CT bands given above. The symbols in parentheses are given for the pairs which gave such DRS bands not on 30 s grinding but on 300 s grinding. Those which gave no new DRS bands on 300 s grinding are denoted by the symbol — . The relative reactivity in experiment (I) showed similar features to the result given here, though comparison is possible only when the resulting CT complexes are colored, thus confirming that the presence of NaCl did not cause any change in, at least qualitatively, the relative reactivity of CT complex formation. Pairs C and D are excluded from the following discussion of relative reactivity.

Change in f(R) with Time. Although fast reaction was observed during the process of grinding, a very slow reaction continued to take place after grinding was stopped, for most component pairs studied. This is shown in Fig. 3, **k-4** being taken as an example.

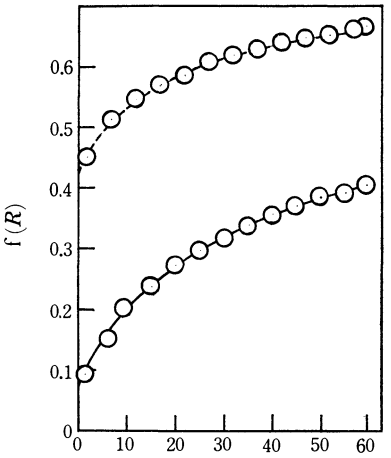

Fig. 3. The change of f(*R*) after grinding is ceased in the measurement of pyrene-*p*-chloranil (at 655 nm).
—— grinding for 30 s.
---- grinding for 300 s.

Time $t=0$ on the abscissa shows the time when the grinding (30 or 300 s) was stopped. Values for f(*R*) are plotted on the ordinate. The value of $[f(R)]_{t=0}$ corresponds to the total amount of the complex given in the process of grinding. Concentration-time curves could not be obtained due to the lack of information concerning (1) whether or not only one type of CT complex contributes, and (2) the molar extinction coefficient. Very few data are available so far on the molar extinction coefficients of solid CT complexes. When grinding was done for a longer time (*i.e.* 300 s), $[f(R)]_{t=0}$ became larger. Thus, the reaction is far from complete by grinding for 30 s. The leveling-off in the f(*R*)-*t* curve is only an apparent one. Only the region near the grain surface seems to have attained equilibrium. To bring the reaction completely up to true equilibrium, much more time will be needed. For a few component pairs, f(*R*) decreases with time because of a further reaction *via* the CT complex. This

TABLE 2. APPEARANCE OF COLORED PRODUCT ON EVAPORATING MIXTURE OF DICHLOROMETHANE SOLUTION

Acceptor	Donor															
	a	b	c	d	e	f	g	h	i	j	k	l	m	n	o	p
1	+	+	−	+	−	+	−	+	−	−	+	+	−	−	−	+
2	+	+	−	+	−	+	+	+	+	+	+	+	+	+	−	+
3	+	+	+	+	+	+	+	+	+	−	+	+	+	+	−	+
4	+	+	+	+		+			−		+	−	−	−	−	+
5	+	+		−		+			−		+			−		−
6	+					+					+			−		−
7	−					+					+			−		−
8						+										
9	+					+			+		+			−		+
10	+					+								−		+

is the case for a-**1**, a-**3**, a-**5**, j-**1**, and k-**1**.

Evaporating the Dichloromethane Solution. The results are given in Table 2, in which the symbol + denotes the appearance of a new color. The color obtained for each pair was in line with that obtained in the solid state reaction with a few exceptions. The symbol − denotes only the color of parent compounds shown by the remaining solid. Since judgement was made only from color change, none can be made when little color change is expected on CT complex formation, *i.e.*, when the CT complex to be obtained (if any) for the given pair is either colorless or in a very close color to that of parent compounds (*i.e.* $\lambda_{CT}<500$ nm). No symbol is given in the Table for these cases.

Discussion

Shape and Position of CT Bands. Most of the new bands can be considered as CT bands of microcrystals. In crystal, the single band in solution splits into several bands, each of which has a peculiar polarization *vs.* crystal axes. In the microcrystalline sample, these bands are amalgamated into a very broad band. Most of the CT bands were very broad, making it sometimes very difficult to find absorption maxima. Nevertheless, a fairly good linear relationship was found between transition energy and ionization potential of the donor (I_D) or the electron affinity of the acceptor (E_A), in most of the cases (Figs. 1 and 2).

Relative Reactivity. The observed difference in chemical reactivity can be interpreted as resulting, mainly from the difference in (i) chemical equilibria or (ii) reaction rates. An important factor in the former is the difference in lattice energy, while in the latter it is the molecular diffusion through the grain boundary. The "relative reactivity" in this study is judged by whether or not the CT band is found on grinding for 30 (or 300) s. The reaction does not proceed to equilibrium for most of the component pairs. Experiment (III) was carried out to see what the relative order of chemical equilibria is like. The chemical equilibrium between complex and component molecules is established in the dichloromethane solution. On evaporating, crystals of DADA··· and/or DD··· plus AA··· were formed. The crystals thus obtained should give information on the equilibrium in solid phase, when the process of crystallization is assumed to be slow enough to establish the equilibrium. The assumption seems to be valid in this experiment. There is generally a good parallelism between the solid state reactivity and the formation of the CT complexes in evaporating the dichloromethane solution (Tables 1 and 2). This shows that an apparent (false) equilibrium was established on the grain surface. This is not the true equilibrium, since a slow reaction (probably by slow diffusion through the grain boundary) still continues.

The relative reactivity should be interpreted in terms of molecular and/or crystal structure (Table 1). Taking the molecular structure into consideration, we make the following qualitative conclusions. (1) The reactivity depends largely on molecular size and structure (Table 1). Smaller molecules are more reactive. (2) For the molecules with the same number of rings, those with compact structure are more reactive (*i.e.* h>i>j, k>l>m>n>o).
(3) For the molecules with similar molecular size and structure, the pairs which have smaller I_D-E_A values are more reactive.

The importance of molecular geometry in determining molecular properties in solid phase is sometimes mentioned. Matsunaga[23] has found the "size and shape effect" in the ionic character of solid molecular compounds. Such an effect will play an important role also in the chemical reactivity in solid phase. The higher selectivity in chemical reaction might thus be expected in solid state rather than in solution.

The observed order of reactivity in solid phase are not in line with that of equilibrium constants in fluid solution. Similar findings are also reported by Hammick and Hutchison,[1] and by Suzuki and Seki[2] for

trinitrobenzene or trinitrotoluene complexes. For h-**4** and i-**4**, the former has greater reactivity in solid phase, though the equilibrium constant in fluid solution[24] is in the reverse order. This is also the case for k-**4** and l-**4**.

The origin of such a difference in reactivity cannot be understood only by means of molecular structure. The difference in crystal structure (space group and dimension of unit cell) undoubtedly plays an important role. In the solid state reaction in the system of mixed microcrystals, the reformation of the crystal on the grain boundary should occur during the course of reaction. If the crystal structure of the resulting CT complex is similar to that of at least one of the component molecules, the reformation will occur with a smaller activation energy. In order to confirm this hypothesis, however, the crystal data are necessary for the CT complex and for the parent molecules. Very few data of CT complexes are available at present to make such a discussion.

Thanks are due to Miss Yumiko Masumitsu and Mr. Shun-ichi Horai for their assistance in the measurement.

References

1) D. L. Hammick and H. P. Hutchison, *J. Chem. Soc.*, **1955**, 89.
2) K. Suzuki and S. Seki, This Bulletin, **28**, 417 (1955).
3) W. Braun and G. Kortüm, *Z. Phys. Chem.* (Frankfurt present to am Main), **61**, 167 (1968).
4) A similar phenomenon was observed when the evaporated films of these components were prepared on glass plates and the compounds were pressed together. For i-**4**, the pressed plates showed only the absorption of components for days.
5) In Experiment (I), the absorption spectrum of the product could be measured by pressing it between two glass plates only when the product was very intensely colored (*e.g.* a-**1**). The positions of bands thus obtained were essentially in accordance with those given from DRS in Experiment (II).
6) This was taken as the standard procedure. Drying conditions gave no significant change on the qualitative feature of DRS in the visible region, except for TCNE complexes, for which a band attributable to 1,1,2,3,3-pentacyanopropenide ion appeared.
7) The Kubelka-Munk equation is given as
$$f(R)=(1-R)^2/2R=k/s$$
where R is the relative diffuse reflectance of the sample referred to a non-absorbing standard substance (NaCl in this work), k is the absorption coefficient of the sample given by Lambert's law
$$I=I_0\exp(-kl),$$
s being the scattering coefficient: P. Kubelka and F. Munk, *Z. Techn. Phys.*, **12**, 593 (1931).
8) Although quantitative reproducibility in $f(R)$ by this manual procedure was rather poor (by a factor of 1.2—1.4), qualitative reproducibility, *i.e.* whether or not the new band appears, was good.
9) H. Kuroda, I. Ikemoto, and H. Akamatu, This Bulletin, **39**, 1842 (1966).
10) H. Kuroda, T. Kunii, S. Hiroma, and H. Akamatu, *J. Mol. Spectrosc.*, **22**, 60 (1967).
11) H. Kuroda, S. Hiroma, and H. Akamatu, This Bulletin, **41**, 2855 (1968).
12) T. Amano, H. Kuroda, and H. Akamatu, *ibid.*, **41**, **83** (1968).
13) *Idem, ibid.*, **42**, 671 (1969).
14) Y. Sato, M. Kinoshita, M. Sano and H. Akamatu, *ibid.*, **43**, 2370 (1970).
15) T. Ohta, H. Kuroda, and T. Kunii, *Theor. Chim. Acta*, **19**, 167 (1970).
16) Y. Matsunaga, and G. Saito, This Bulletin, **44**, 958 (1971).
17) T. Nogami, K. Yoshihara, and S. Nagakura, *ibid.*, **45**, 122 (1972).
18) G. Briegleb, "Electronen-Donator-Acceptor-Komplexe," Springer, Berlin (1961).
19) R. Foster, and T. J. Thomson, *Trans. Faraday Soc.*, **58**, 860 (1962).
20) J. Aihara, M. Tsuda, and H. Inokuchi, This Bulletin, **40**, 2460 (1967); **42**, 1824 (1969); **43**, 2439 (1970).
21) E. I. Kotov, and A. Terenin, *Dokl. Akad. Nauk SSSR*, **124**, 865 (1959).
22) Y. Matsunaga, This Bulletin, **45**, 770 (1972).
23) Y. Matsunaga, *ibid.*, **42**, 2490 (1969).
24) Ref. 18, p. 112ff.
25) Ionization potentials are taken from: J. B. Birks, "Photophysics of Aromatic Molecules," Wiley-Interscience, New York (1970), Table 9.5. The ionization potential of a was assumed to be 6.5 eV after Briegleb (Ref. 18, p. 183). That of f was assumed to be 6.8 eV after Y. Matsunaga and G. Saito (Ref. 16).
26) Assignment to the second CT band was made according to Ref. 9, 13, 16, and 20 (for k-**1**, f-**4** and f-**6**, f-**1**, and d-**1**, respectively); compare the spacing between the band in question and the first CT band for a pair with that between the first and second CT bands for another pair composed of the same donor and a different acceptor, when both bands are reported for the latter pair and when the second CT band is associated with the second highest molecular orbital of the donor (for d-**2**, d-**3**. f-**3**, k-**2**, k-**3**); compare with d-**1**—d-**3** (for e-**1**—e-**3**). The band at 20800 cm^{-1} for i-**3** was assigned to the second CT band since the difference in transition energy of this band and that of the first CT band is close to the difference of the first and second ionization potentials of π-electron system in anthracene (P.A. Clark, F. Brogli and E. Heilbronner, *Helv. Chim. Acta*, **55**, 1415 (1972); See also, J. Aihara and H. Inokuchi, *Chem. Lett.*, **1973**, 421). For a-**9** and a-**10**, the bands at 18900 and 21700 cm^{-1}, respectively, were tentatively assigned to the second CT bands from the relationship shown in Fig. 2.
27) Electron affinities are taken from; G. Briegleb, *Angew., Chem.*, **76**, 326 (1964).

The Crystal and Molecular Structure of Tris(π-cyclopentadienyl nickel)tertiary-butylammonium

Nagao KAMIJYO and Tokunosuké WATANABÉ*

Government Industrial Research Institute, Osaka, Midorigaoka, Ikeda, Osaka 563

** Faculty of Science, Kwansei Gakuin University, Nishinomiya 665*

(Received July, 30, 1973)

The crystal structure of tris(π-cyclopentadienylnickel)tertiary-butylammonium, t-$C_4H_9N(\pi$-$C_5H_5Ni)_3$, has been determined from single crystal X-ray diffractometer data. The space group is C2/c and the lattice constants are $a=28.40$ Å, $b=9.16$ Å, $c=15.28$ Å, $\beta=100°30'$, and $Z=8$. The refinement was carried out using block-diagonal least-squares calculation including anisotropic temperature factors for the three nickel atoms. The final R index for 1620 reflections is 0.138. The molecule is of approximately a trigonal pyramidal structure with an apical nitrogen atom on a triangle of the nickel atoms. The interatomic distances are 2.33—2.39 Å for nickel to nickel, 1.93—1.98 Å for nickel to nitrogen. The distances between a nickel atom and a centroid of a cyclopentadienyl ring are 1.74—1.81 Å. The three cyclopentadienyl rings are inclined to the nickel triangle plane at 68°—69°.

Tris(π-cyclopentadienylnickel)tertiary-butylammonium, t-$C_4H_9N(\pi$-$C_5H_5Ni)_3$, synthesized by a reaction of $(t$-$C_4H_9N)_2S$ with $(\pi$-$C_5H_5)_2Ni$ or with $(\pi$-$C_5H_5Ni(CO))_2$ in heptane solution, is reported to be paramagnetic (1.68 B.M., $g=2.035$).[1] IR, UV, and EPR spectra suggest that the molecule has a pyramidal structure with an apical nitrogen atom on a triangle of the nickel atoms.[1]

We have carried out a crystallographic study of the title substance in order to confirm the suggested structure, special attention being paid to the Ni-Ni distances because of their bondings including one unpaired electron.

Experimental

Crystals obtained from a heptane solution[1] were blue-black irregular platelets. Some effort was required for selecting a suitable specimen, and a platelet $0.4\times0.4\times0.2$ mm was used. Weissenberg photographs showed the crystal to be monoclinic and the systematically absent reflections, hkl for $h+k=2n+1$ and $h0l$ for $l=2n+1$, indicated the space group to be Cc or C2/c. The space group was assumed to C2/c on the evidence of a centric distribution of the three-dimensional intensities.[2] The unit cell dimensions were measured on a Hilger and Watts linear diffractometer using Mo$K\alpha$ radiation ($\lambda=0.7107$ Å). Intensity data were collected with a linear diffractometer using monochromatic Mo$K\alpha$ radiation. The crystal was oriented about the b-axis, ten layers being recorded. There were 2170 independent reflections, of which 550 with $\sin\theta/\lambda\geq0.59$ Å^{-1} were too weak to be observed and were neglected for the structure determination. The intensity data were corrected for Lorentz and polarization factors and placed on an approximately absolute scale by Wilson's method. The crystal data are as follows.

Tris(π-cyclopentadienylnickel)tertiary-butylammonium; t-$C_4H_9N(\pi$-$C_5H_5Ni)_3$; MW=442.1.

Monoclinic: Space group C_{2h}^6—C2/c; $a=28.40\pm0.03$ Å, $b=9.16\pm0.02$ Å, $c=15.28\pm0.02$ Å, $\beta=100°30'\pm10'$; $Z=8$. $D_x=1.48$ g·cm^{-3}, $D_m=1.5$ g·cm^{-3} (flotation method).

The linear absorption coefficient of the substance is 28.0 cm^{-1} for Mo$K\alpha$ radiation. Thus the absorption parameter μR_{max} was 0.6, and no correction for absorption was made.

† $P(U,V,W)=\sum\sum\sum|F(hkl)|^2(1-\exp(-Q\sin^2\theta/\lambda^2))^2\cos(2\pi(hU+kV+lW))$ with $Q=30$.[3]

Determination of the Structure

Appoximate positional parameters of the three Ni atoms were determined from a modified three-dimensional Patternson function.† From a Fourier synthesis calculated with all terms phased by the Ni atoms, twelve out of the twenty non-hydrogen light atoms of the whole molecule were located. Ten of these twelve atoms were easily assigned to the carbon atoms of two cyclopentadienyl rings, and the remaining two were inferred to two carbon atoms of the t-butyl group. Further Fourier syntheses did not reveal the remaining light atoms. The coordinates of eight atoms were assumed with the use of conventional bond distances and angles. By repeating diagonal least-squares refinement with isotropic temperature factors and Fourier syntheses, all the positions of non-hydrogen atoms were obtained. Several cycles of block-diagonal least-squares refinement, minimizing the function $\sum w(k|F_o|-|F_c|)^2$, were carried out with anisotropic temperature factors for the nickel atoms and isotropic ones for all the remaining non-hydrogen atoms. A weighting scheme, $w=1$ if $F_o\geq14.0$, otherwise $w=0.2$, was used. The R index for 1620 reflections ceased to decrease at 13.8%. The final positional and temperature parameters are shown in Tables 1 and 2. The atomic numbering system is shown in Fig. 1. The temperature factors of the carbon atoms of the cyclopentadienyl groups and of the end-members of the t-butyl group are considerably large, especially for C(2), C(3), C(4), C(15), C(16), C(17), C(18) and C(19). The atomic scattering factors were taken from the International Tables for X-ray Crystallography,[5] the contribution of hydrogen atoms being disregarded. Anomalous dispersion corrections of the scattering factors were not made.

The initial solution of the structure and preliminary refinement were made with the program written by one of us (N.K.). The final refinement was performed with the program HBLS-IV[4] written by Dr. T. Ashida for HITAC-5020E computer. The table of the observed and calculated structure factors is preserved by The Chemical Society of Japan. (Document No. 7402).

TABLE 1. THE FINAL FRACTIONAL ATOMIC COORDINATES, ISOTROPIC TEMPERATURE FACTORS AND THEIR STANDARD DEVIATIONS

	x/a	y/b	z/c	B(Å^3)	$\sigma(x)$	$\sigma(y)$	$\sigma(z)$	σB(Å^2)
Ni(1)	−0.1672	0.2152	−0.1071	*	0.003 Å	0.004 Å	0.003 Å	*
Ni(2)	−0.1383	0.4479	−0.0513	*	0.004	0.004	0.003	*
Ni(3)	−0.1121	0.2295	0.0262	*	0.005	0.005	0.004	*
N	−0.1021	0.2921	−0.0929	5.7	0.030	0.033	0.030	0.7
C(1)	−0.0650	0.2850	−0.1170	2.0	0.012	0.013	0.012	0.2
C(2)	−0.0238	0.3504	−0.0965	11.0	0.045	0.049	0.045	1.3
C(3)	−0.0512	0.1278	−0.1452	14.0	0.052	0.056	0.053	1.5
C(4)	−0.0724	0.3413	−0.2101	10.0	0.041	0.045	0.041	1.1
C(5)	−0.2110	0.0241	−0.1097	8.2	0.035	0.038	0.035	0.9
C(6)	−0.2403	0.1402	−0.1099	7.3	0.032	0.035	0.032	0.8
C(7)	−0.2290	0.2202	−0.1874	10.3	0.041	0.044	0.041	1.1
C(8)	−0.2095	0.1440	−0.2659	7.5	0.033	0.036	0.033	0.8
C(9)	−0.1893	0.0283	−0.1853	8.3	0.035	0.038	0.035	0.9
C(10)	−0.1978	0.5920	−0.0551	8.2	0.035	0.038	0.035	0.9
C(11)	−0.1680	0.6057	0.0271	8.5	0.036	0.038	0.036	0.9
C(12)	−0.1188	0.6517	0.0108	7.8	0.034	0.036	0.034	0.8
C(13)	−0.1222	0.6680	−0.0810	10.0	0.041	0.044	0.041	1.1
C(14)	−0.1689	0.6469	−0.1161	8.9	0.037	0.040	0.037	1.0
C(15)	−0.0894	0.0243	0.0888	12.1	0.048	0.053	0.048	1.4
C(16)	−0.1326	0.0805	0.1225	13.0	0.050	0.055	0.051	1.5
C(17)	−0.1210	0.2215	0.1531	12.0	0.047	0.052	0.048	1.4
C(18)	−0.0653	0.2601	0.1549	11.3	0.046	0.050	0.047	1.3
C(19)	−0.0522	0.1214	0.1198	12.2	0.061	0.066	0.061	2.0

* See Table 2.

TABLE 2. TEMPERATURE FACTORS OF THE NICKEL ATOMS

The temperature factors are expressed in the form of $\exp\{-(B_{11}h^2+B_{22}k^2+B_{33}l^2+B_{12}hk+B_{23}kl+B_{13}hl)\}$ with standard deviations in parentheses.

	B_{11}	B_{22}	B_{33}	B_{12}	B_{23}	B_{13}
Ni(1)	0.0015(0)	0.0172(5)	0.0040(2)	−0.0002(0)	−0.0018(2)	0.0008(4)
Ni(2)	0.0015(2)	0.0159(3)	0.0039(1)	0.0001(0)	0.0007(2)	0.0005(1)
Ni(3)	0.0025(0)	0.0253(7)	0.0063(1)	0.0014(3)	−0.0013(1)	0.0018(3)

Description of the Structure and Discussion

The molecular structure is shown in Fig. 1. The three nickel atoms almost form an equilateral triangle. The *t*-butylamine group is situated perpendicularly to this triangle and the three cyclopentadienyl groups are disposed symmetrically. The molecule thus takes approximately a trigonal pyramidal structure with a symmetry C_{3v}–3m. The suggested structure for this molecule by IR, UV, and EPR studies[1] has now been confirmed.

The bond distances and bond angles associated with the nickel atoms are given in Table 3. Not much can be said about the C–C and C–N bond distances and the corresponding bond angles, since the temperature factors of the carbon atoms are large. The cyclopentadienyl groups are essentially planar, the mean deviations of atoms from the least-squares planes of these rings being 0.07, 0.04 and 0.05 Å. The average distance of the C–C bonds in the rings is 1.46 Å, though the maximum deviation amounts to 0.15 Å. The three cyclopentadienyl planes are inclined to the Ni_3 plane by amounts 68°—69° as measured from the opposite direction of the *t*-butyl group. The distances between nickel atoms and centroid of cyclopentadienyl rings are 1.81, 1.80 and 1.74 Å. The

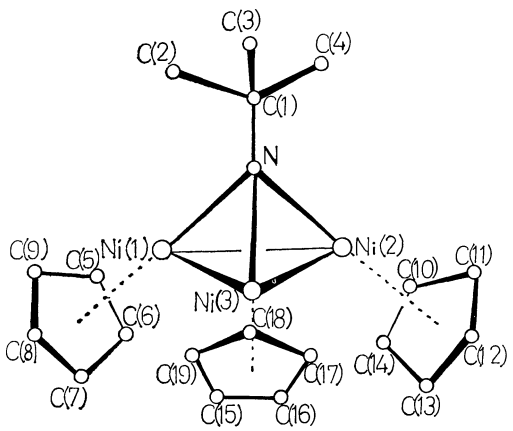

Fig. 1. Schematic representation of the molecule and the atomic numbering system.

TABLE 3. BOND DISTANCES AND BOND ANGLES (IN Å AND DEGREES)
Figures in parentheses are the standard deviations.

Ni(1)—Ni(2)	2.386(5)	Ni(2)—C(10)	2.14(4)	Ni(1)—Ni(2)—Ni(3)	59.1(4)
Ni(2)—Ni(3)	2.374(7)	Ni(2)—C(11)	2.15(4)	Ni(2)—Ni(3)—Ni(1)	60.9(4)
Ni(3)—Ni(1)	2.334(7)	Ni(2)—C(12)	2.12(4)	Ni(3)—Ni(1)—Ni(2)	60.0(4)
		Ni(2)—C(13)	2.13(3)		
average	2.364	Ni(2)—C(14)	2.18(3)	average	60.0
Ni(1)—N	1.95(2)			Ni(1)—N—Ni(2)	75.7(8)
Ni(2)—N	1.93(2)	average	2.14	Ni(2)—N—Ni(3)	74.8(9)
Ni(3)—N	1.98(3)			Ni(3)—N—Ni(1)	72.9(9)
		Ni(3)—C(15)	2.16(5)		
average	1.96	Ni(3)—C(16)	2.16(4)	average	74.5
		Ni(3)—C(17)	2.00(4)		
Ni(1)—C(5)	2.14(4)	Ni(3)—C(18)	2.18(4)	N—Ni(1)—Ni(2)	51.8(8)
Ni(1)—C(6)	2.18(4)	Ni(3)—C(19)	2.25(4)	N—Ni(2)—Ni(1)	52.5(9)
Ni(1)—C(7)	1.95(4)			N—Ni(2)—Ni(3)	53.4(9)
Ni(1)—C(8)	2.59(4)	average	2.15	N—Ni(3)—Ni(2)	51.8(8)
Ni(1)—C(9)	2.12(4)			N—Ni(3)—Ni(1)	53.1(9)
				N—Ni(1)—Ni(3)	54.0(9)
average	2.20			average	52.8

perpendicular distance between the apical nitrogen atom and the nickel triangle is 1.40 Å. The distance of the N–C bond is 1.18(4) Å and the mean angle N–C(1)–C is 118°(3), the numbers in parentheses being the standard deviations. The three end-carbon atoms of the t-butyl group lie almost parallel to the Ni_3 cluster plane. The Ni–N bond roughly makes a tetrahedral angle with the bonds of nickel-to-cyclopentadienyl ring. This situation is in contrast to the cases of the three congeneric complexes, $(C_5H_5Ni)_3(CO)_2$,[7] $(C_5H_5Co)_3S_2$[8] and $(C_5H_5Ni)_3S_2$,[6] where the cyclopentadienyl rings are at right angles to the metallic cluster plane. The mean value of the metal-metal distances, 2.364 Å, found in the present analysis can be compared to the value 2.39 Å, reported for $(C_5H_5Ni)_3(CO)_2$, but is considerably shorter than the values reported for $(C_5H_5Ni)_3S_2$, 2.801 Å, and for $(C_5H_5Co)_3S_2$, 2.691 Å.

A simple M.O. scheme of the metal-metal bondings based upon Cotton-Haas' calculation[9] about the $(Re_3Cl_{12})^{3-}$ ion can be used to account for the Ni–Ni distances of these compounds. Each nickel atom is bonded to the nitrogen atoms as well as to a cyclopentadienyl ring through four electron pair bonds tetrahedrally, 4s $4p^3$. The nickel-to-nickel bonding can be interpreted in terms of the interactions of the electrons. One of the five d-orbitals for each nickel atom may act as non-bonding and the remaining twelve orbitals of the three nickel atoms may form six bonding and six anti-bonding orbitals. There are 49 electrons available for the formation of the molecule; 30 from the three nickel atoms, 15 from the three cyclopentadienyl groups and 4 from the nitrogen atom. Twenty-four of these are used for the bondings for Ni-N's and Ni-cyclopentadienyl groups. Six of these enter the non-bonding orbitals. Thus the remaining 19 electrons interact between the Ni–Ni bondings. Twelve of these will occupy the bonding orbitals and seven the anti-bonding levels giving the molecule the paramagnetic character. The electronic configuration of the nickel-nickel interaction in this complex is, therefore, close to that of $(C_5H_5Ni)_3(CO)_2$ which also has 19 electrons in the nickel-nickel orbitals. With this crude scheme one may understand the close resemblance of the intermetallic distances of these two complexes. The congeneric complexes, $(C_5H_5Ni)_3S_2$ and $(C_5H_5Co)_3S_2$, have much longer intermetallic distances, having four more electrons and one more electron respectively, in the anti-bonding orbitals. The Ni–N interatomic distances as observed in the present compound, 1.93, 1.95 and 1.98 Å, are considerably longer than the sum of the covalent radii of N and Ni atoms, 1.85 Å. In $(CH_3N)_2Fe_3(CO)_9$[10] and $((C_6H_5)_2CNN)_2Fe_3(CO)_9$[11] also, the metal-nitrogen distances 1.93 and 1.95 Å are greater than the sum of the covalent radii, 1.87 Å. The mean distances between a nickel atom and the five carbon atoms of a cyclopentadienyl group are 2.20, 2.14 and 2.15 Å, which can be compared with the value 2.20 Å, reported for nickelocene.[12]

The molecular arrangement in the crystal, projected along the b-axis, is shown in Fig. 2. There are no special short intermolecular contacts in the crystal.

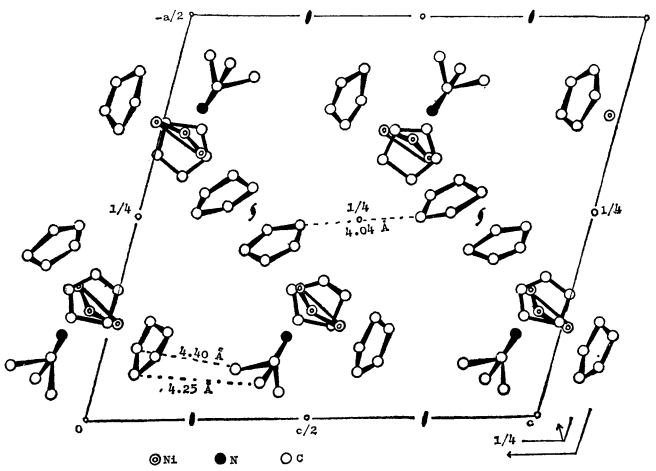

Fig. 2. Projection of the crystal structure along the b-axis (b-axis upwards).

We are indebted to Prof. S. Otsuka, Osaka University, for his interest in this work and for the supply of the sample. We are also indebted to Takeda Chemical Industries Ltd. for use of the Hilger and Watts linear diffractometer. We thank Dr. K. Ogawa and Mrs. H. Tamura, Osaka University, for their discussions.

References

1) S. Otsuka, A. Nakamura, and T. Yoshida, *Inorg. Chem.*, **7**, 261 (1968).
2) E. R. Howells, D. C. Phillips, and D. Rogers, *Acta Crystallogr.*, **3**, 210 (1950).
3) T. Watanabé and Y. Takaki, *Japan. J. Appl. Phys.*, **3**, 783 (1964).
4) T. Ashida, HBLS-IV, "Universal Crystallographic Computation Program System," Crystallographic Society of Japan, Tokyo (1967).
5) "International Tables for X-ray Crystallography," Vol. III, 2nd ed., International Union of Crystallography, Kynoch Press, Birmingham (1962), p. 269.
6) H. Vahrenkamp, V. A. Uchtman, and L. F. Dahl, *J. Amer. Chem. Soc.*, **90**, 3272 (1968).
7) O. S. Mills, A. A. Hock, and G. Robinson, "Advances in Chemistry of Coordination Compounds," ed. by S. Kirschner, Macmillan, New York (1961), p. 640.
8) N. Kamijyo and T. Watanabé, The 23rd Symposium on Coordination Chemistry, Kyushu, Oct. 1973.
9) F. A. Cotton and T. E. Haas, *Inorg. Chem.*, **3**, 10 (1964).
10) R. J. Doedens, *ibid.*, **8**, 570 (1969).
11) P. E. Baikie and O. S. Mills, *Chem. Commun.*, **1967**, 1228.
12) L. Pauling, "The Nature of the Chemical Bond," 3rd ed., Cornell Univ. Press, New York (1960), p. 388.

Semi-empirical SCF-MO Studies of Pd(II)- and Hg(II)-Ethylene Complexes, the Oxymercuration and the Wacker Reaction

Shigeyoshi SAKAKI, Hiroshi KATO,* Hiroyoshi KANAI, and Kimio TARAMA
Department of Hydrocarbon Chemistry, Faculty of Engineering, Kyoto University, Sakyo-ku, Kyoto 606
**Department of General Education, Nagoya University, Chikusa-ku, Nagoya 464*

(Received August 6, 1973)

Using the modified CNDO MO method, the electronic structures of Pd(II)- and Hg(II)-ethylene complexes have been studied successfully. Our MO calculations have shown that the nucleophilic attack of OH^- on ethylene was accelerated by Pd(II) and Hg(II), and that the acceleration by Hg(II) was larger than that by Pd(II), these results agree well with those of the experiments. The *cis*-attack of OH^- in the oxymercuration has also been discussed by the use of the results obtained by the MO calculations. The mechanism of the *cis*-type four-center addition of OH^- to ethylene in the Wacker reaction, which was supposed by Henry and Jira *et al.* in spite of any direct evidence, has been supported by the MO calculations. Our calculations have been able to explain the Markovnikoff rule in the Wacker reaction and in the oxymercuration of propylene.

A number of reactions of nucleophilic attack on olefins coordinated to a metal ion are well known.[1-3] Complex formation reduces the electron density between the carbon atoms of double bond, rendering the double bond more susceptible to nucleophilic attack. This must be the first requisite for the catalytic ability of transition metal ions in nucleophilic reactions. It is, therefore, interesting from the viewpoint of catalytic chemistry to investigate the electronic structures of olefins coordinated to transition-metal ions. There have, though, been few MO studies[4,5] of such transition-metal olefin complexes supposed to be intermediates in catalytic reactions.

The Wacker reaction[1-3] and the oxymercuration[6,7] are known as nucleophilic reactions onto a coordinated olefin; in them Pd(II)- and Hg(II)-olefin complexes are considered to be reaction intermediates. We carried out MO calculations of Pd(II)- and Hg(II)-olefin complexes in order to investigate the electronic structures of the coordinated olefins and discussed the catalytic activities of Pd(II) and Hg(II). Also, using the MO method, we studied whether the *cis*-addition occurs in the oxymercuration, or whether the *trans*-addition does, and whether or not the *cis*-addition of OH^- in the Wacker reaction is a reasonable mechanism; these problems have never been discussed theoretically. Since some work[8,9] using the Iterative Extended Hückel MO method has been done to investigate the catalytic reactions, it is also our object to examine the possibility of applying the more accurate semi-empirical SCF-MO method to studies in the field of catalytic chemistry.

Calculation and Models

Calculation. All the valence orbitals, including the 5d-atomic orbitals of the Hg atom, were considered explicitly. The modified CNDO-type approximation was used; the Hartree-Fock matrix elements have been given in our previous papers.[10] The resonance integral, H_{rs} $(r \neq s)$, was calculated according to the Wolfsberg-Hermholz approximation:[11]

$$H_{rs} = -kS_{rs}(I_r+I_s) \quad (1)^{12}$$

In order to determine the value of k, the MO's of ethylene, propylene, methane, carbon monoxide, and formaldehyde were calculated using various values of k. That is, as to the MO energies of ethylene and the ionization potentials of these compounds, the best-fitting value of k was 0.40.[13] Hereafter, the value of k will be taken as 0.40 for all s and p orbitals. For the AO pair including the d-orbital, the value of k was determined to be equal to 0.50, thus the calculated first and second d-d transitions of $PdCl_4^{-2}$ coincide with the experimental results, as is shown in Table 1.

TABLE 1. THE FIRST AND SECOND d-d TRANSITION ENERGIES OF $PdCl_4^{-2}$

k	0.55	0.50	Obsd	
$^1A_{2g}$	2.62 (eV)	2.54 (eV)	2.62 (eV)[a]	2.48 (eV)[b]
^1E_g	3.40	3.44		2.80

a) Ref. 15. b) Ref. 16.

The values of the ionization potentials, I_r, and the one-center Coulomb repulsion integrals, γ_{rr}, of ligand atoms were taken from Jaffé *et al.*,[16] while those values of the Pd atom were taken from Di Sipio *et al.*[17] Since those values of the Hg atom were not given in the paper of Di Sipio *et al.*, the values of I_r were taken from Bach's paper[18] and those of γ_{rr} were estimated as follows;

$$\gamma_{rr}(6)_{\text{semi-emp}}/\gamma_{rr}(5)_{\text{semi-emp}} = \gamma_{rr}(6)_{\text{nonemp}}/\gamma_{rr}(5)_{\text{nonemp}} \quad (2)$$

where $\gamma_{rr}(5)$ and $\gamma_{rr}(6)$ represent the one-center Coulomb repulsion integrals of a fifth-row element and a sixth-row element, which belong to the same group in the periodic table, respectively. The subscripts "semi-emp" and "nonemp" indicate the semi-empirical value and the nonempirical value of γ_{rr} respectively. $\gamma_{rr}(N)_{\text{nonemp}}$ $(N=5$ or $6)$ was calculated using Clementi's AO,[19] and $\gamma_{rr}(5)_{\text{semi-emp}}$ was taken from Di Sipio's paper.[17] Then the γ_{rr} (6) values used in this work were obtained from the values of $\gamma_{rr}(6)_{\text{semi-emp}}$ by applying the least-squares method and by imposing the restrictive condition[17] that the values of $\gamma_{rr}(6)$ varied linearly with the atomic number. In order to calculate the overlap integrals, a single Slater-type orbital[19,20] was used for all the s- and p-orbitals; the

Table 2. Orbital exponent (ζ_r), valence state ionization potential (I_r), and one-center Coulomb repulsion integral (γ_{rr}) of Pd and Hg atoms

Atom	AO	ζ_r[a]	C[b]	I_r	γ_{rr}
Pd	4d	5.983	0.5264	8.17 (eV)[c]	13.87 (eV)[c]
		2.613	0.6373		
	5s	2.190		7.07	7.46
	5p	2.190		3.30	6.22
Hg	5d	6.436	0.6667	15.66 (eV)[d]	13.53 (eV)[e]
		3.032	0.5401		
	6s	2.649		10.44	7.40
	6p	2.649		5.00	6.31

a) The double-ζ form AO's are used only for d orbitals (Ref. 21). b) Because we neglect the contribution of the 3d orbital in the case of the Pd atom and the contributions of the 3d and 4d orbitals in the case of the Hg atom, the 4d orbital of the Pd atom and the 5d orbital of the Hg atom are renormalized in this work. c) Ref. 17. d) Ref. 18. e) The estimated values.

double-ζ-form orbital[21] was used only for the d-orbitals of metal atoms. The values of the AO exponents, ζ_r, I_r and γ_{rr} of the Pd and Hg atoms are listed in Table 2.

We discussed the bond strength in terms of E_{AB},[22-24] the contribution of the interaction between A and B atoms to the total energy; it is written, using the approximations used in this work, as follows;

$$E_{AB} = E_{AB}^{(1)} + E_{AB}^{(2)} + E_{AB}^{(3)} \quad (3)^{12}$$

$$E_{AB}^{(1)} = 2\sum_r^A \sum_s^B P_{rs}H_{rs} \quad (4)^{12}$$

$$E_{AB}^{(2)} = -0.5\sum_r^A \sum_s^B P_{rs}^2(rr|ss) \quad (5)^{12}$$

$$E_{AB}^{(3)} = \sum_r^A \sum_s^B (N_r - P_{rr})(N_s - P_{ss})(rr|ss) \quad (6)^{12}$$

where $\sum^A$ represents the summation on the A atom.

Geometries of Pd(II)- and Hg(II)-Olefin Complexes. Because of the lack of knowledge of the accurate configurations of these compounds, the configurations of the olefin moieties in these complexes were assumed to be the same as those of the corresponding free olefins.[25] The distances between the metal atom and the center of the double bond were fixed as 2.31 Å for Pd(II) Complexes[25] and as 2.34 Å for the Hg(II) complexes.[4] The metal-olefin coordination bond was assumed to intercept the double bond perpendicularly at its center. The coordinate systems for these complexes are given in Fig. 1.

Models for the Oxymercuration and the Wacker Reaction. In the oxymercuration, both *cis*- and *trans*-addition products were formed from the strained olefins, such as norbornene and bicyclo-[2,2,2]-oct-2-ene,[7,26-29] although only a *trans*-addition product was formed from nonstrained olefins.[6] Therefore, it is meaningful to shed some light on the course of the addition using an MO method. Since mercurinium ions have been postulated as intermediates in oxymercurations of olefins,[6,30] we assumed both *cis*- and *trans*-oxymercurials were derived from a common mercurinium ion, and calculated the MO's of the models for *cis*- and *trans*-addition (cf. Fig. 2). In order to ascertain the effects of reactants and ligands, we calculated the MO's of reaction systems, such as $Hg(C_2H_4)^{+2}\leftarrow OH^-$, $HgCl(C_2H_4)^{+}\leftarrow OH^-$, $HgCl(C_3H_6)^{+}\leftarrow OH^-$, $HgCl(cis\text{-}2\text{-}C_4H_8)^{+}\leftarrow OH^-$, and $HgCl(trans\text{-}2\text{-}C_4H_8)^{+}\leftarrow OH^-$, in which OH^- was assumed to approach olefin in the *trans* position of Hg(II) (see Fig. 3.), since the *trans*-oxymercurials were formed in general.

In the case of the Wacker reaction, an oxypalladate intermediate has not been observed. However, its existence has been postulated on the basis of kinetic studies[31-35] and the step of its formation from Pd(II)-olefin complex has been considered to be the rate-

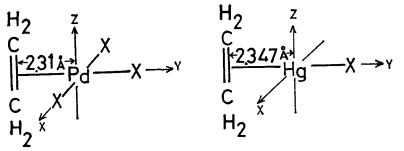

Fig. 1. The coordinate systems of Pd(II)- and Hg(II)-ethylene complexes.
X=F, Cl, Br
Pd-F: 1.88 Å[a], Pd-Cl: 2.23 Å[b], Pd-Br: 2.35 Å[a]
Hg-F: 1.84 Å[b], Hg-Cl: 2.29 Å[b], Hg-Br: 2.41 Å[b]
a) The estimated value. b) Ref. 25.

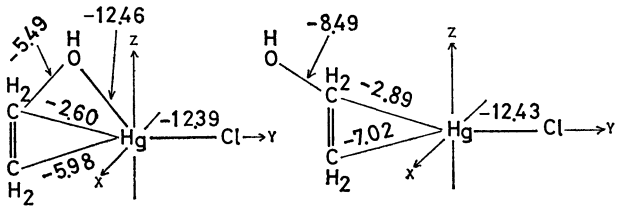

Fig. 2. The values of E_{AB}[a] in the *cis*- and *trans*-addition of oxymercuration.
a) eV unit, b) The relative position of OH^- to ethylene is the same as that of *cis*-addition system. C-O=1.72 Å and Hg-O (in *cis*-configuration)=2.03 Å. c) $E_{total}=-2164.3$ eV. d) $E_{total}=-2159.8$ eV.

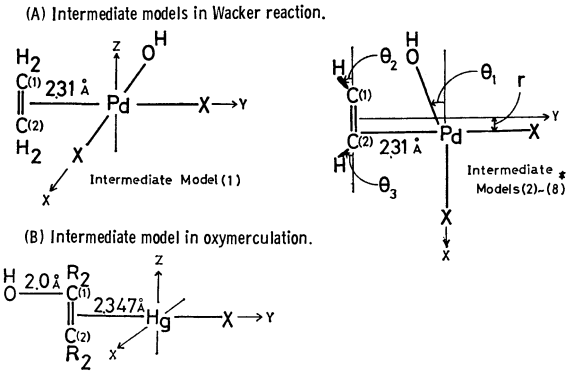

Fig. 3. Intermediate models of Wacker reaction and oxymercuration.
* z-axis is perpendicular to the plane of this figure.
Intermediate Model **2**; $r=0.0$ Å, $\theta_1=0°$, $\theta_2=0°$, $\theta_3=0°$; Model **3**; $r=0.0$ Å, $\theta_1=15°$, $\theta_2=0°$, $\theta_3=0°$; Model **4**; $r=0.0$ Å, $\theta_1=30°$, $\theta_2=0°$, $\theta_3=0°$; Model **5**; $r=0.3$ Å, $\theta_1=30°$, $\theta_2=0°$, $\theta_3=0°$; Model **6**; $r=0.3$ Å, $\theta_1=30°$, $\theta_2=7.5°$, $\theta_3=0°$; Model **7**; $r=0.3$ Å, $\theta_1=30°$, $\theta_2=15°$, $\theta_3=0°$; Model **8**; $r=0.3$ Å, $\theta_1=30°$, $\theta_2=15°$ $\theta_3=7.5°$. Pd-O 1.92 Å

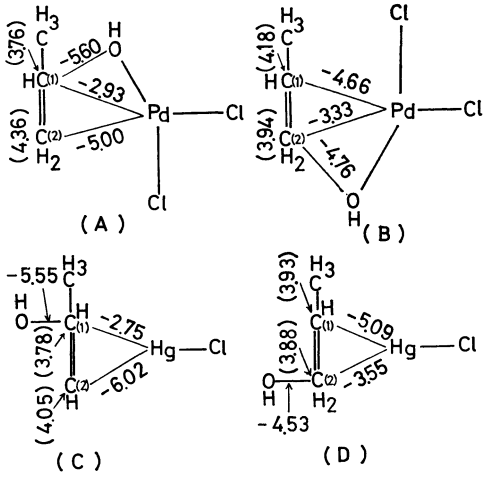

Fig. 4. The values* of E_{AB} and electron densities in Wacker reaction and oxymercuration of propylene. in parenthesis; electron density on atom. *) eV unit. Configurations A and B are the same as the intermediate model **4** in Fig. 3. Configurations C and D are the same as the intermediate model for oxymercuration in Fig. 3.

determining step. The models for these intermediates are shown in Fig. 3.

In order to investigate the selectivity in the Wacker reaction[34] and the oxymercuration,[6] we carried out the MO calculation of the models described in Fig. 4.

Results and Discussion

Pd(II)- and Hg(II)-ethylene Complexes. The electron densities, the π-bond order, P_π,[37] the π^*-bond order, P_{π^*},[37] the quantities of transferred electrons from ethylene to metal-ligand part, ΔQ, are shown in Table 3. The electron densities on the Pd and Hg atoms increase with the decrease in the electron negativity of the halogen atom, except in the case of $HgCl(C_2H_4)^+$ or $HgBr(C_2H_4)^+$. The electron density on the C atom is decreased by the coordination as follows; free ethylene>ethylene coordinated to Pd(II)>ethylene coordinated to Hg(II). It is notable that this decreasing order agrees with the increasing reactivity for the nucleophile; *i.e.*, the nucleophilic attack of OH^- in the Wacker reaction slowly proceeds,[31–35] and that in the oxymercuration proceeds very fast,[38] while the reaction can not occur in the absence of Pd(II) and Hg(II).

Table 3. The electronic structures of Pd(II)- and Hg(II)-ethylene complexes

Compound	Electron density: Metal *d*	Metal *sp*	Carbon	P_π[a]	P_{π^*}[b]	ΔQ[c]
C_2H_4			4.133	1.000	0.0	0.0
$PdF_3(C_2H_4)^-$	8.076	1.418	4.083	0.884	−0.009	0.240
$PdCl_3(C_2H_4)^-$	8.015	2.014	4.080	0.870	−0.012	0.252
$PdBr_3(C_2H_4)^-$	7.975	2.164	4.078	0.864	−0.013	0.259
$Hg(C_2H_4)^{2+}$	9.983	0.751	3.974	0.654	−0.002	0.734
$HgF(C_2H_4)^+$	9.931	1.010	4.050	0.806	−0.003	0.429
$HgCl(C_2H_4)^+$	9.942	1.282	4.044	0.807	−0.003	0.426
$HgBr(C_2H_4)^+$	9.944	1.376	4.045	0.813	−0.003	0.414

a) π-Bond order of the C=C double bond. b) See the footnote (37). c) The quantity of transferred electron from olefin to metal.

Table 4. The coordination bond orders of Pd(II)- and Hg(II)-ethylene complexes

Compound	π-acceptor $P_{d\pi-\pi^*}$[a]	σ-donor $P_{d\sigma-\pi}$	$P_{s-\pi}$	$P_{p\sigma-\pi}$
$PdF_3(C_2H_4)^-$	0.131	0.235	0.256	0.282
$PdCl_3(C_2H_4)^-$	0.144	0.267	0.232	0.310
$PdBr_3(C_2H_4)^-$	0.147	0.273	0.229	0.319
$Hg(C_2H_4)^{2+}$	0.062	0.088	0.630	0.201
$HgF(C_2H_4)^+$	0.072	0.115	0.439	0.294
$HgCl(C_2H_4)^+$	0.060	0.110	0.327	0.259
$HgBr(C_2H_4)^+$	0.074	0.104	0.370	0.344

a) $P_{d\pi-\pi^*}$ represents the bond order matrix element between d_π orbital of metal and π^*-MO of ethylene, and the others such as $P_{d\sigma-\pi}$, *etc.*, represent similar bond order matrix elements.

The values of ΔQ in the Hg(II)-complexes are larger than those in the Pd(II)-complexes, while the values of P_π and P_{π^*} are smaller than those in the Pd(II)-complexes. The coordination bond orders are shown in Table 4. The π-acceptor bond orders, $P_{d\pi-\pi^*}$, in the Pd(II)-complexes are greater than those in the Hg(II)-complexes; this agrees with the larger values of P_{π^*} in the Pd(II)-complexes relative to those values in the Hg(II)-complexes. While in Pd(II)-complexes the contributions of the d-orbitals are remarkably large, their contributions are very small in the Hg(II)-complexes, in which the 6s and 6p orbitals of Hg(II) mainly contribute to the coordination bond. The small contribution of the 5d atomic orbitals of Hg(II) is considered to be due to the $5d^{10}$ configuration of Hg(II) as well as Ag(I)-ethylene complexes.[10b,39]

The Oxymercuration. The results are given in Fig. 2. It may be seen from a comparison of the total energy that the *cis*-attack system is more stable than the *trans*-attack system. The absolute value of E_{C-O} in the *cis*-attack system is smaller than that in the *trans*-attack system, probably because of the interaction of the O atom with the Hg atom in the *cis*-attack system, while there is no interaction between the O and Hg atoms in the *trans*-attack system. On the other hand, the bonding interaction between the O and Hg atoms contributes to the larger stabilization of the *cis*-attack system, suggesting that the mercurinium ion is stabilized by the coordination of the nucleophile. Our results agree with the mechanism proposed by Bach *et al.*:[29] (a) if the concentration of the nucleophile is sufficient, or if the solvent coordinates to Hg(II) to interfere with the coordination of the nucleophile, the *trans*-attack may occur, since the nucleophile in the *trans*-position interacts with the C atom of olefin more strongly than that in the *cis*-position; and (b) the mercurinium ion which is formed from a strained olefin, such as norbornene, is relatively short-lived and is

TABLE 5. THE NUCLEOPHILIC ATTACK OF OH^- TO OLEFIN COORDINATED TO Hg(II)

Reaction system	Electron density			E_{C-O}[b]	$E_{C-O}^{(1)}$	$E_{C-O}^{(2)}$	$E_{C-O}^{(3)}$	$E_{Hg-C(1)}$	$E_{Hg-C(2)}$
	Metal	C(1)[a]	C(2)						
$C_2H_4 \leftarrow OH^-$		3.914	4.290	−3.013	−1.961	−0.479	−0.572		
$Hg(C_2H_4)^{2+} \leftarrow OH^-$	11.599	3.944	3.836	−5.427	−3.548	−1.672	−0.207	−2.540	−3.870
$HgCl(C_2H_4)^+ \leftarrow OH^-$	11.506	3.894	4.013	−4.936	−3.051	−1.277	−0.607	−3.157	−5.788
$PdCl_3(C_2H_4)^- \leftarrow OH^-$ [c]	10.114	3.851	4.105	−3.832	−2.243	−0.617	−0.972	−2.206	−5.254
$HgCl(trans\text{-}2\text{-}C_4H_8)^+ \leftarrow OH^-$	11.586	3.807	3.910	−5.169	−2.935	−1.081	−1.153	−3.193	−5.319
$HgCl(cis\text{-}2\text{-}C_4H_8)^+ \leftarrow OH^-$	11.588	3.806	3.907	−5.172	−2.931	−1.078	−1.163	−3.192	−5.310

a) See Fig. 3—c. b) The E_{AB} value of bond C(1)-O (eV unit). c) The relative position of OH^- to ethylene is the same as that in $Hg(C_2H_4)^{2+} \leftarrow OH^-$ system.

likely to react with the intimate nucleophile coordinated the mercurinium ion nearest to the olefin, since there is a remarkable bonding interaction between the C and O atoms, though this interaction is weak relative to that in the *trans*-attack system. In this case, the *cis*-attack may occur preferably.

The calculated results of the models in Fig. 3 are given in Table 5, together with the results on the interaction of OH^- with free ethylene and on the interaction of OH^- with the ethylene coordinated to the $PdCl_3^-$ anion.[40] The values of E_{C-O}[41] are negative in all cases, suggesting a bonding interaction between the C atom of ethylene and the O atom of OH^-. The absolute values of E_{C-O} increase in the following order; free ethylene$<PdCl_3(C_2H_4)^-<HgCl(C_2H_4)^+<Hg(C_2H_4)^{+2}$. Those results suggest that the nucleophilic attack of OH^- on ethylene is accelerated by Pd(II) and Hg(II), and that the acceleration by Hg(II) is larger than that by Pd(II), which agrees well with the catalytic behaviour of Hg(II)[38] and Pd(II).[35] Compared with the absolute values of $E_{C-O}^{(1)}$, $E_{C-O}^{(2)}$, and $E_{C-O}^{(3)}$ in $C_2H_4 \rightarrow OH^-$ system, those of $E_{C-O}^{(1)}$ and $E_{C-O}^{(3)}$ are largely increased in the $PdCl_3(C_2H_4)^- \leftarrow OH^-$ system, and the values of $E_{C-O}^{(1)}$ and $E_{C-O}^{(2)}$ are also increased in the $Hg(C_2H_4)^{+2} \leftarrow OH^-$ and $HgCl(C_2H_4)^+ \leftarrow OH^-$ systems. Since $E_{AB}^{(1)}$ and $E_{AB}^{(2)}$ indicate approximately the contribution of covalent interaction to the total energy, the existence of Hg(II) and Pd(II) may cause an increase in the covalent bonding ability of ethylene with OH^-. From the results that the electron density on the C atom in ethylene complexes decreases in the following order; free ethylene $> PdX_3(C_2H_4)^- > HgX(C_2H_4)^+ > Hg(C_2H_4)^{+2}$, the absolute values of $E_{C-O}^{(3)}$ can be effected to this order, since $E_{C-O}^{(3)}$ represents approximately the electrostatic energy and since the O atom has a negative charge. However, the absolute values of $E_{C-O}^{(3)}$ increase in the following order: $Hg(C_2H_4)^{+2} \leftarrow OH^- < C_2H_4 \leftarrow OH^- < HgCl(C_2H_4)^+ \leftarrow OH^- < PdCl_3(C_2H_4)^- \leftarrow OH^-$; this trend disagrees with the decreasing trend of electron density on the ethylene carbon atom in the Hg(II)- and Pd(II)-ethylene complexes. This disagreement is a result of the difference in the polarization of the ethylene part between the Pd(II)- and Hg(II)-systems (see Table 5). The π-acceptor bond contributes to the coordination bond in the Pd(II)-ethylene complex, while it scarcely contributes in the Hg(II)-ethylene complex. Therefore, the electron transfer shown in Scheme 1 is more feasible in Pd(II)-complexes than in Hg(II)-complexes, which leads to a higher polarization, a smaller electron density on the C(1) atom, and a larger absolute value of $E_{C-O}^{(3)}$ in the Pd(II)-complexes than in the Hg(II)-complexes. Therefore, the trend of $E_{C-O}^{(3)}$ the is not same as that of the electron density of the C atom in the Pd(II)- and Hg(II)-complexes. That is, the high catalytic activity of Hg(II) is not due to the electrostatic energy, while it is probably important in the long-range interaction.

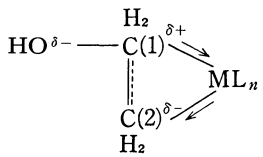

Scheme 1

In the above Scheme, M and L represent a metal and ligand respectively and "→" indicates the direction of electron transfer.

The absolute value of $E_{C-O}^{(3)}$ in the $HgCl(2\text{-}C_4H_8)^+$ system is remarkably large, probably because of the larger positive charge on the olefinic carbon atom of butene coordinated to Hg(II).[42] In these cases, the polarization is small.

When the mercurinium ion has an anion ligand, the absolute value of E_{C-O} is smaller than that of the system containing no anion ligand.

The absolute values of E_{C-O} for various reactants increase in the following order (Table 5, 8); C(β) atom of $CH_3CH{=}CH_2 < C_2H_4 < trans\text{-}2\text{-}C_4H_8 < cis\text{-}2\text{-}C_4H_8 <$ C(α) atom of $CH_3CH{=}CH_2$ in $HgCl(olefin)^+ \leftarrow OH^-$ system. The rate constants for the oxymercuration have been reported to increase in the following order;[38] $trans\text{-}2\text{-}C_4H_8 < C_2H_4 < cis\text{-}2\text{-}C_4H_8 < CH_3CH{=}CH_2$. Our results do not agree with this order. However, it has been shown by our calculation that the reactivity of *cis*-2-C_4H_8 is higher than that of *trans*-2-C_4H_8.

The results given in Table 5 reveal the following aspect of the structure of the intermediate in the oxymercuration; (1) The electron density on the C(1) atom is larger than that on the C(2) atom except in the case of $Hg(C_2H_4)^{+2} \leftarrow OH^-$. (2) The absolute value of $E_{Hg-C(1)}$ is larger than that of $E_{Hg-C(2)}$. These situations are shown in the following Scheme, which agrees well with the situation usually assumed.[7]

TABLE 6. THE ELECTRONIC STRUCTURES OF INTERMEDIATE MODELS[a] IN WACKER REACTION

Intermediate			1	2	3	4	5
E_{total}[b]	F		−2581.5	−2581.5	−2582.7	−2583.0	−2593.7
	Cl		−2234.5	−2234.5	−2235.7	−2234.2	−2235.7
	Br		−2125.7	−2125.8	−2126.9	−2127.3	−2129.4
Electron density on Pd	F		9.563	9.562	9.541	9.537	9.518
	Cl		9.890	9.882	9.871	9.894	9.933
	Br		9.968	9.956	9.949	9.965	10.015
Electron density on Pd	F	C(1)	4.084	4.085	4.027	3.890	3.358
		C(2)	4.084	4.086	4.147	4.325	4.403
	Cl	C(1)	4.081	4.084	4.026	3.884	3.808
		C(2)	4.081	4.085	4.147	4.323	4.406
	Br	C(1)	4.077	4.079	4.022	3.883	3.808
		C(2)	4.077	4.085	4.146	4.323	4.400
$E_{C(1)-O}$[b]	F		0.346	0.379	−0.245	−5.321	−16.083
	Cl		0.327	0.378	−0.225	−5.212	−11.217
	Br		0.249	0.302	−0.229	−5.266	−11.330
F	$E_{Pd-C(1)}$[b]		−3.935	−3.922	−3.536	−2.818	−0.027
	$E_{Pd-C(1)}$		−3.935	−3.960	−4.203	−5.251	−6.713
Cl	$E_{Pd-C(1)}$		−3.901	−3.910	−3.670	−3.055	−1.935
	$E_{Pd-C(1)}$		−3.901	−3.876	−3.979	−4.668	−6.377
Br	$E_{Pd-C(1)}$		−3.873	−3.860	−3.549	−3.097	−2.007
	$E_{Pd-C(2)}$		−3.873	−3.894	−3.971	−4.592	−6.277
E_{Pd-O}[b]	F		−16.928	−16.859	−15.492	−15.246	−13.653
	Cl		−15.493	−15.451	−15.224	−13.848	−12.335
	Br		−15.266	−15.235	−14.978	−13.717	−10.324
P_π[c]	F		0.888	0.888	0.878	0.730	0.527
	Cl		0.878	0.878	0.873	0.727	0.513
	Br		0.873	0.871	0.867	0.722	0.504

a) See Fig. 3. b) eV unit. c) π-Bond order of the C=C double bond.

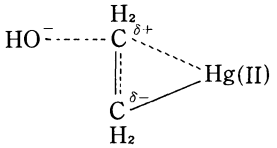

Scheme 2

In the above Scheme, "——" and "----" represent the strong interaction and the weak one respectively.

Wacker Reaction. The calculated results on intermediate models **1**—**5** are given in Table 6. From the intermediate **1** to the intermediate **5**, the values of E_{total} and E_{C-O} decrease gradually; this shows the increases in the stability of the intermediate models and in the strength of the C(1)–O bond. These results suggest that this reaction model is reasonable for the Wacker reaction. The electron densities on the Pd and C(1) atoms decrease in the course of this, while that of the C(2) atom increases. From the above results, ethylene can be said to be polarized by the approach of OH^-. Proceeding from the intermediate **1** to the intermediate **5**, the absolute values of $E_{Pd-C(1)}$, E_{Pd-O}, and P_π decrease, whereas that of $E_{Pd-C(2)}$ increases; *i.e.*, the bonds of C(1)–O and Pd–C(2) become stronger, although the bonds of Pd–C(1), Pd–O, and C–C become weaker, relative to those of the **1** intermediate. These results, pictured in Scheme 3, agree with the *cis*-type four-center reaction speculated by Henry[32] and Jira *et al.*[33] (see Scheme 4.)

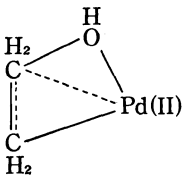

Scheme 3

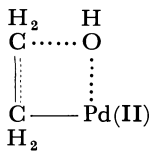

Scheme 4

The results for the intermediate models **5**—**8** (Fig. 3) are given in Table 7. The bending of protons about C(1) makes the total energy more negative, suggesting that the system is more stabilized and that the C(1) atom changes from sp^2 to sp^3. Also, this bending brings about decreases in the absolute values of $E_{Pd-C(1)}$ and

TABLE 7. THE *cis*-BENDING OF PROTONS OF INTERMEDIATES[a] IN THE WACKER REACTION OF $PdCl_2(C_2H_4)OH$

Intemediate	5	6	7	8
E_{total}[b]	−2235.7	−2235.7	−2238.6	−2235.2
$E_{C(1)-O}$[b]	−11.22	−12.59	−13.68	−13.89
$E_{Pd-C(1)}$[b]	−1.94	−1.87	−1.83	−1.74
$E_{Pb-C(2)}$[b]	−6.38	−6.43	−6.14	−6.87
E_{Pd-O}[b]	−12.34	−12.26	−11.92	−12.00
P_π	0.513	0.491	0.475	0.443

a) See Fig. 3. b) eV unit.

P_π and increases in the absolute values of $E_{C(1)-O}$ and $E_{Pd-C(1)}$, which reveal that the reaction more proceeds from the intermediate **5**. However, the bending of the C(2)–H bond destabilizes the system, whereas the absolute values of $E_{C(1)-O}$ and $E_{Pd-C(2)}$ are increased and those of $E_{Pd-C(1)}$ and P_π are decreased. Therefore, any *cis*-bending of the protons about the C(2) atom hardly occurs. These results are considered to be due to the polarization of ethylene, which is expected to be enhanced by the π-acceptor bond with Pd(II), as has been shown in Scheme 1; the C(2) atom should have sp^2 character to obtain the electron through the π-acceptor bond, leading to no *cis*-bending of its proton.

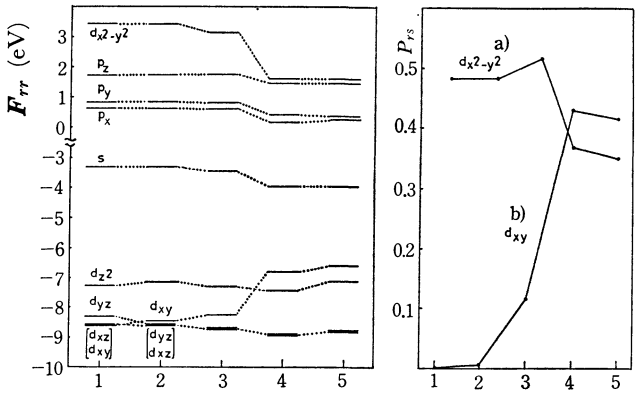

Fig. 5. The changes of values of F_{rr} and bond order. a) The sum of bond orders between $d_{x^2-y^2}$ of Pd atom and s, p_x, p_y orbitals of O atom. b) The sum of bond orders between d_{xy} of Pd atom and s, p_x, p_y orbitals of O atom.

Then, the changes from the intermediate **1** to the intermediate **5** were investigated in detail. The values of the Fock-matrix elements, F_{rr}, are shown in Fig. 5-A, together with the sum of the values of the density matrix elements between the $d_{x^2-y^2}$ orbital of the Pd atom and the s, p_x and p_y orbitals of the O atom, and those between the d_{xy} orbital and the s, p_x, and p_y orbitals of these atoms (Fig. 5-B). There is a remarkable increase in the value of $F_{d_{xy}d_{xy}}$ and a decrease in the value of $F_{d_{x^2-y^2}d_{x^2-y^2}}$, while there are few changes in the other F_{rr}. These remarkable changes are due to the moving of OH^- in the xy plane and suggest the change in the Pd–O bonding character. As is shown in Fig. 3-B, the contribution of the d_{xy} orbital to the Pd-O bond increases, although that of $d_{x^2-y^2}$ decreases in the reaction course. In other words, OH^- attacks the C(1) atom, interacting with the d_{xy} orbital, as has been proposed by Cossee *et al.*[9,43]

Markovnikoff Rule in These Reactions. We calculated the MO's of the models for the nucleophilic attack on propylene; the results are given in Fig. 4 and Table 8. In both the Pd(II)- and Hg(II)-systems, attack on the C(1) atom gives a lower total energy than the attack on the C(2) atom, which reveals that the former attack is superior to the latter attack. Also,

Table 8. Nucleophilic attack of OH^- to propylene

State[a]	$PdCl_2(OH)(C_3H_6)^-$		$HgCl(C_3H_6)^+ \leftarrow OH^-$	
	A	B	C	D
E_{total}[b]	−2426.6	−2426.3	−2353.0	−2352.6
E_{C-O}[b]	−5.596	−4.756	−5.545	−4.528
$E_{C-O}^{(1)}$[b]	−3.674	−3.793	−3.063	−2.923
$E_{C-O}^{(2)}$[b]	−0.618	−0.660	−1.175	−1.185
$E_{C-O}^{(3)}$[b]	−1.305	−0.303	−1.307	−0.420
P_π	0.669	0.718	0.531	0.535

a) See Fig. 4. b) eV unit.

the absolute values of $E_{C(1)-O}$ of models [A] and [C] are greater than those of models [B] and [D]. It is obvious from Table 8 that this difference is a result of the difference of $E_{C-O}^{(3)}$, suggesting that this selectivity is determined by the electrostatic energy. The carbon atom attacked by OH^- is positively charged in both Pd(II)- and Hg(II)-systems(see Tables 5 and 6 and Fig. 4), and the propylene is polarized by the hyperconjugation of the methyl group, as follows,

$$CH_3\text{-}\overset{\delta+}{C}H=\overset{\delta-}{C}H_2$$

Scheme 5

Therefore, the attack on the C(α) atom is superior to the attack on the C(β) atom, since the former attack causes the same polarization, while the latter attack causes an inverse polarization.

As has been described above, the semi-empirical SCF-MO method using the modified CNDO approximation gives fruitful results; this encourages us to apply this method to studies of the other catalytic reactions.

The calculations were carried out by means of the FACOM 230—60 Computer in the Data Processing Center at Kyoto University.

The authors are grateful to Dr. Hideyuki Konishi for his help with these calculations. They also wish to thank Professor Dr. Katsuhiko Ichikawa for his instructive suggestions.

References

1) F. R. Hartly, *Chem. Phys.*, **69**, 799 (1969).
2) J. Tsuji, *Adv. Org. Chem.*, **6**, 109 (1969).
3) E. W. Stern, "Transition Metals in Homogeneous Catalysis," ed. by G. N. Schrauzer, Marcel Dekker Inc., New York (1971), p. 93.
4) R. D. Bach and H. F. Henneike, *J. Amer. Chem. Soc.*, **92**, 5589 (1970).
5) H. F. Henneike, *ibid.*, **94**, 5945 (1972).
6) W. Kitching, *Organometal. Chem. Rev.*, **3**, 61 (1968).
7) T. G. Trayler, *Accounts Chem. Res.*, **2**, 152 (1969).
8) J. W. Begley and F. Pennella, *J. Catal.*, **8**, 203 (1967).
9) R. Cossee, P. Ros and J. H. Schachtschneider, "Proceedings of Fourth International Congress on Catalysis," Moscow, 1968, p. 207.
10) a) S. Sakaki and H. Kato, This Bulletin, **46**, 2227 (1973). b) S. Sakaki, *Theor. Chim. Acta*, **30**, 159 (1973).
11) M. Wolfsberg and L. Hermholz, *J. Chem. Phys.*, **20**, 837 (1952).

12) For the notations in these equations, see Ref. 10.
13) In the case of π–π^* transition energy of ethylene, the best fit value of k is 0.45.
14) A. J. McCaffery, P. N. Schatz, and P. J. Stephens, *J. Amer. Chem. Soc.*, **90**, 5730 (1968).
15) P. Day, A. F. Orchard, A. J. Thomson, and R. J. P. Williams, *J. Chem. Phys.*, **42**, 1973 (1965).
16) J. Hinze and H. H. Jaffé, *J. Amer. Chem. Soc.*, **84**, 540 (1961); *J. Phys. Chem.*, **67**, 1504 (1963). The value of γ_{rr} is obtained by Pariser's approximation using data of these paper.
17) L. Di Sipio, E. Tondello, G. De Michelis, and L. Oleari, *Chem. Phys. Lett.*, **11**, 287 (1971).
18) R. D. Bach, *J. Amer. Chem. Soc.*, **91**, 1771 (1969).
19) E. Clementi, D. L. Raimondi, and W. P. Reinhart, *J. Chem. Phys.*, **47**, 1300 (1967).
20) E. Clementi and D. L. Raimondi, *ibid.*, **38**, 2686 (1963).
21) H. Basch and H. B. Gray, *Theor. Chim. Acta*, **4**, 367 (1966).
22) J. A. Pople, D. P. Santry, and G. A. Segal, *J. Chem. Phys.*, **43**, s129 (1965).
23) M. S. Gordon, *J. Amer. Chem. Soc.*, **91**, 3122 (1969).
24) S. E. Ehrenson and S. Seltzer, *Theor. Chim. Acta*, **20**, 17 (1971).
25) "Tables of Interactomic Distances and Configuration in Molecules and Ions," ed. by L. E. Sutton, The Chemical Society, London (1957).
26) T. G. Traylor and A. W. Baker, *Tetrahedron Lett.*, **1959**, 14.
27) T. G. Traylor, *J. Amer. Chem. Soc.*, **86**, 244 (1964).
28) T. T. Tidwell and T. G. Traylor, *J. Org. Chem.*, **33**, 2614 (1968).
29) R. D. Bach and R. F. Richter, *J. Amer. Chem. Soc.*, **94**, 4747 (1972).
30) G. A. Olah and P. R. Clifford, *ibid.*, **93**, 1261, 2320, (1971).
31) P. M. Henry, *ibid.*, **86**, 3246 (1964).
32) P. M. Henry, *ibid.*, **88**, 1595 (1966).
33) R. Jira, J. Sedlmeier, and J. Schmidt, *Ann. Chem.*, **693**, 99 (1966).
34) T. Dozono and T. Shiba, *Bull. Japan Petrol. Inst.*, **5**, 8 (1963).
35) P. M. Henry, *J. Amer. Chem. Soc.*, **94**, 4437 (1972).
36) W. Hafner, R. Jira, J. Sedlmeier, and J. Schmidt, *Chem. Ber.*, **75**, 1575 (1962).
37) Although in the complex the notations π and π^* MO of olefin lose their physical meanings, we use these terminologies in the local sense of olefin part for simplicity. These terms, $\boldsymbol{P}_\pi$ and $\boldsymbol{P}_{\pi^*}$, are defined as follows;

$$\boldsymbol{P}_\pi = 2\sum_{\pi}^{\text{occ}} C_{\pi^1 p_y} C_{\pi^2 p_y}$$

$$\boldsymbol{P}_{\pi^*} = 2\sum_{\pi^*}^{\text{occ}} C_{\pi^{*1} p_y} C_{\pi^{*2} p_y}$$

where $C_{\pi^1 p_y}$ and $C_{\pi^{*1} p_y}$ represent the MO coefficients of p_y orbital on C(1) atom in π-MO and π^*-MO respectively.
38) J. Halpern and H. B. Tinker, *J. Amer. Chem. Soc.*, **89**, 6427 (1967).
39) H. Basch, *J. Chem. Phys.*, **56**, 441 (1972).
40) Although OH^- is considered to attack to ethylene as shown in Fig. 3, the *trans*-attack model is calculated in this case for comparison with the oxymercuration.
41) These $\boldsymbol{E}_{C-O}$ and $\boldsymbol{E}_{C-O}{}^{(1)}$ *etc.*, represent the value of $\boldsymbol{E}_{AB}$ and $\boldsymbol{E}_{AB}{}^{(1)}$ *etc.*, of bond C(1)–O, respectively (in eV unit and see Fig. 3).
42) In Hg(II)-complexes, the unsaturated C atom of 2-C_4H_8 has a smaller electron density than that of C_2H_4; *i.e.*, 3.993 in $HgCl(cis\text{-}2\text{-}C_4H_8)^+$, 3.995 in $HgCl(trans\text{-}2\text{-}C_4H_8)^+$ and 4.048 in $HgCl(C_2H_4)^+$.
43) P. Cossee, *Rec. Trav. Chim. Pays-Bas*, **85**, 1151 (1966).

Viscosity *B* Coefficients for Some Homologous Series of Organic Electrolytes in Aqueons Solutions. The Effect of Ionic Groups

Kunio TAMAKI, Yōko ŌHARA, Hisashi KURACHI, Mitsuru AKIYAMA, and Hirokazu ODAKI

Department of Chemistry, Yokohama City University, Kanazawa-ku, Yokohama 236

(Received September 19, 1973)

The viscosity *B* coefficients for the three homologous series of sodium alkane carboxylates (acetate to butyrate), sodium *n*-alkyl sulfonates (methyl to hexyl), and *n*-alkylammonium chlorides (methyl to hexyl) in aqueous solutions at 25 °C have been determined. The *B* values increase linearly with the number of carbon atoms in the alkyl chains for each homologous series studied in this work, as well as for a homologous series of *n*-alkyl sulfate ions previously studied. In the case of the three kinds of organic anions with the same alkyl groups, the *B* values increase in the order: $-COO^- \gg -SO_3^- > -OSO_3^-$. The ion-solvent interaction effect, as estimated by the combination of the *B* values with the molal volume at an infinite dilution for ions, is positive for each carboxylate ion; however, it is negative for the lower alkyl sulfonate, alkyl sulfate and alkylammonium ions. From these facts, $-COO^-$ may be classified as an "electrostrictive structure-maker," whereas, $-SO_3^-$, $-OSO_3^-$, and $-NH_3^+$ are "electrostrictive structure-breakers." In this connection, the reported specific interactions of these ionic parts with simple counter-ions on the activity coefficients of organic electrolytes, the counter-ion binding of polyelectrolytes, and the effect of counter-ions on the critical micelle concentrations of long-chain electrolytes are briefly discussed on the basis of the change in water structure induced by both cations and anions in water.

A series of measurements of viscosity *B* coefficients for organic electrolytes in aqueous solutions has been performed in this laboratory in order to elucidate the behavior of organic ions in water. In a previous paper,[1] the results for a homologous series of sodium *n*-alkyl sulfates were reported. This paper will describe the experimental results for the three homologous series of sodium alkane carboxylates, sodium *n*-alkyl sulfonates, and *n*-alkylammonium chloride.

The behavior of ions in water has generally been attributed to the structural change in water upon the introduction of ions into water.[2] In solutions of electrolytes with large ions, such as K^+, Cl^-, and Br^- ions, these ions will decrease the extent of intermolecular hydrogen-bonding of water in the vicinity of ions; thus, they are "electrostrictive structure-breakers."[2] On the other hand, in solutions of salts with small ions, such as Li^+, Na^+, and F^- ions, these ions will promote the water structure in the vicinity of ions; thus, they are "electrostrictive structure-makers."[2] As a third possibility, nonpolar groups are "hydrophobic structure-makers"[2] in water; that is, the water molecules will form "icebergs" around nonpolar molecules or groups in water.[3] As amphiphilic organic ions generally consist of both nonpolar and ionic parts, the behavior of these organic ions in water may be interpreted approximately by the balance of two different modes of interaction, namely, hydrophobic hydration due to nonpolar parts and electrostrictive hydration due to ionic parts. The main object of this paper is to discuss the role of ionic parts on the structural influence in water on the basis of the experimental results of the effect of ionic groups on the viscosity *B* coefficients.

Experimental

Sodium acetate and *n*-butyrate were from Wako Pure Chemical Industries, and all the other organic substances were from Tokyo Kasei Kogyo Co. Sodium propionate and *n*-butyrate were recrystallized from ethanol. All the sodium carboxylates were dried at 100 °C. Sodium methyl and ethyl sulfonates were prepared by the neutralization of the corresponding sulfonic acids with a 2 M solution of sodium hydroxide, and then the water was evaporated to dryness. The sodium salts were twice recrystallized from ethanol-water solutions (80% for methyl salt and 90% for ethyl salt). The other sodium alkyl sulfonates were synthesized by a modification[4] of Strecker method. The *n*-alkyl bromides were added, drop by drop, to the saturated solutions of sodium sulfite at 100 °C, and then the mixtures were dried in air. The sodium salts were extracted with ethanol and were further twice purified by recrystallizing them from ethanol. All the products of sodium alkyl sulfonates were dried *in vacuo* at 100 °C. All the *n*-alkylammonium chlorides except pentyl salt were recrystallized from suitable solvents—*i.e.*, ethanol for methyl salt and an ethanol-benzene solution for the other salts. Pentylammonium chloride was prepared by the neutralization of pentylamine with gaseous hydrogen chloride in benzene; the salt thus prepicitated was recrystallized from an ethanol-benzene solution. All the alkylammonium chlorides were dried in a vacuum desiccator. Water was obtained by redistillation from an alkaline permanganate solutions.

The viscosities were measured at 25 °C by a method similar to that described in a previous paper.[1] Ubbelohde-type viscosimeters with flow times for water of 800—1200 s were used. The densities were measured in Ostwald pycnometers.

Results and Discussion

The B Values for the Organic Ions. The viscosity of aqueous electrolyte solutions can be expressed by the Jone-Dole equation:[5]

$$\eta = \eta_0(1 + AC^{1/2} + BC) \quad (1)$$

where η and η_0 are the viscosity of the solution and of the water respectively; C, the concentration (molarity); A, the constant relating to the ion-ion interaction, and B, the viscosity B coefficient. The viscosity B coefficients can be obtained as slopes of $(\eta/\eta_0 - 1)/C^{1/2}$ *versus* $C^{1/2}$ plots. In this work generally, the viscosity measurements were made at five different concentrations up to about 0.15 M for each salt; the B values thus obtained are summarized in Table 1. The B value for sodium acetate is slightly higher than that reported by Padova.[6] The B values for sodium hexanoate[7] and octanoate[8] calculated from the re-

Table 1. Viscosity *B* coefficients for electrolytes at 25°C (in l/mol)

i	R_iCOONa		R_iSO_3Na	R_iNH_3Cl
1	0.343	0.331[a]	0.213	0.040
2	0.425		0.301	0.125
3	0.505		0.391	0.214
4			0.471	0.290
5		0.680[b]	0.551	0.360
6			0.637	0.422
7		0.862[c]		

a) Ref. 6. b) Calculated from the data in Ref. 7. c) Calculated from the data in Ref. 8.

sults published by Campbell *et al.* are included in Table 1.

The viscosity *B* coefficients of electrolytes are considered to be determined by adding the individual contribution of the solute constituent ions.[9] Adopting the convention of Gurney[9] that the ionic *B* values for K^+ and Cl^- ions are equal, the ionic *B* values for Na^+ and Cl^- ions become 0.086 and −0.007 respectively.[10] The ionic viscosity *B* coefficients, B_{ion}, for the series of alkane carboxylate, alkyl sulfonate, and alkylammonium ions thus calculated are listed in Table 2. The *B* values for the alkylammonium ions are in fairly good agreement with those calculated from the results for alkylammonium bromides by Desnoyers, Arel and Leduc,[11] assuming that the B_{ion} value for Br^- ion[10] is −0.032. The data for a series of alkyl sulfate ions reported in the previous paper[1] are included in Table 2.

The *B* values for homologous electrolytes are found to increase with the chain length. Fig. 1 shows the relationship between the B_{ion} values of the organic ions and the number of carbon atoms in the alkyl chains. It can be seen in Fig. 1 that the linear relation between the B_{ion} values and the number of carbon atoms holds for each series of homologous electrolytes and that the slopes are nearly equal. If the role of the interaction of the organic ion with water could be separated into the effect of the nonpolar part and that of the ionic part, nearly the same strength of interaction for the nonpolar alkyl group with water could be anticipated for all the homologous organic electrolytes. If this assumption is valid, the difference in the B_{ion} values for the organic ions with the same alkyl groups may be attributed to the interaction of the ionic parts

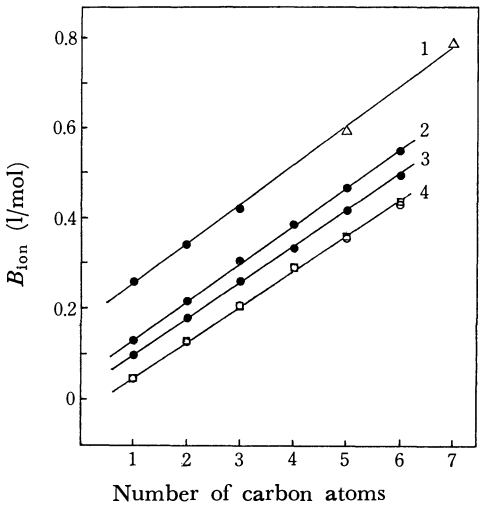

Fig. 1. Plots of viscosity *B* coefficients for organic ions against number of carbon atoms in the alkyl group. 1: alkane carboxylate ions, 2: alkyl sulfonate ions, 3: alkyl sulfate ions, 4: alkylammonium ions, ●, ○: present work, △: Refs 8 and 9, □ Ref. 11.

with water. As is evident in Fig. 1, the B_{ion} values for the four types of homologous organic ions with the same alkyl groups are larger in the order: alkane carboxylate ions≫alkyl sulfonate ions>alkyl sulfate ions>alkylammonium ions. However, there remains some uncertainty as to the comparison of the absolute B_{ion} values between the alkylammonium cations and the three other kinds of the organic anions, because the values depend on the convention used in splitting the *B* values for an electrolyte into the individual values of a cation and an anion. Nevertheless, in the case of the three kinds of organic anions, *i.e.*, alkane carboxylate, alkyl sulfonate, and alkyl sulfate ions, the above sequence of the B_{ion} values is independent of the convention adopted.

The Behavior of $-COO^-$, $-SO_3^-$ and $-OSO_3^-$ in Water. The viscosity *B* coefficient has been interpreted in terms of the size of the solute or the ion (Einstein effect) and in terms of the solute or ion-solvent interaction.[9,10] For a comparison of the size of the solutes, the partial molal volumes at an infinite dilution of the electrolytes in water, $\overline{V}°$, are listed in Table 3. The data for alkane carboxylates,[12,13,14] and some for sulfonates[14] and sulfates[15] are cited from the literature. Because of the incompleteness of data in the liter-

Table 2. Ionic viscosity *B* coefficients at 25°C (in l/mol)

i	R_iCOO^-		$R_iSO_3^-$	$R_iOSO_3^-$	$R_iNH_3^+$	
1	0.257	0.245[a]	0.127	0.102[d]	0.047	0.048[e]
2	0.339		0.215	0.179[d]	0.132	0.141[e]
3	0.419		0.305	0.262[d]	0.221	0.222[e]
4			0.385	0.337[d]	0.297	0.298[e]
5		0.594[b]	0.465	0.418[d]	0.368	0.373[e]
6			0.551	0.496[d]	0.429	0.446[e]
7		0.776[c]				

a) Ref. 6. b) Ref. 7. c) Ref. 8. d) Ref. 1. e) Calculated from the data in Ref. 11 assuming that the *B* value of bromide ion is −0.032.

Table 3. Partial molal volume of electrolytes at infinite dilution at 25°C (in cm^3/mol)

i	R_iCOONa			R_iSO_3Na		R_iOSO_3Na		R_iNH_3Cl	
1	38.75[a]	39.23[b]	39.31[c]	54.7	53.88[c]	63.4		54.5	
2	52.82[a]		53.71[c]	68.9	71.56[c]	81.3	81.1[d]	71.3	71.23[c]
3	68.41[a]	69.19[b]	69.32[c]	85.1		96.8		87.5	
4				101.0		113.5	111.7[d]	103.6	
5			100.58[c]	117.2		128.5		119.8	
6				133.1		145.3	141.3[d]	133.2	135.26[c]

a) Ref. 12. b) Ref. 13. c) Ref. 14. d) Ref. 15.

Table 4. Estimation of the ion-solvent interaction effects

i	R_iCOO^-			$R_iSO_3^-$			$R_iOSO_3^-$			$R_iNH_3^+$		
	B_{ion} (l/mol)	$\overline{V}°_{ion}$ (cm^3/mol)	Δ (l/mol)	B_{ion} (l/mol)	$\overline{V}°_{ion}$ (cm^3/mol)	Δ (l/mol)	B_{ion} (l/mol)	$\overline{V}°_{ion}$ (cm^3/mol)	Δ (l/mol)	B_{ion} (l/mol)	$\overline{V}°_{ion}$ (cm^3/mol)	Δ (l/mol)
1	0.257	45.9	0.142	0.127	61.3	−0.026	0.102	70.0	−0.073	0.047	31.3	−0.031
2	0.339	60.3	0.188	0.215	75.5	0.026	0.179	87.9	−0.041	0.132	48.0	0.012
3	0.419	75.9	0.229	0.305	91.7	0.076	0.262	103.4	0.004	0.221	64.3	0.060
4				0.385	107.6	0.116	0.337	120.1	0.037	0.297	80.4	0.096
5	0.594	107.2	0.326	0.465	123.8	0.156	0.418	135.1	0.080	0.368	96.6	0.126
6				0.551	139.7	0.202	0.496	151.9	0.116	0.429	110.0	0.154

ature, the $\overline{V}°$ values for alkyl sulfonates and sulfates are calculated from the present density data by the use of the standard procedure.[16] Our density measurements are not very accurate, as they were for the calculation of the viscosity. However, these volume data are still instructive for the following discussion. The $\overline{V}°$ values of electrolytes are also composed of the sum of the contributions from both cations and anions. Unfortunately, there has been some controversy about the absolute values of ions, $\overline{V}°_{ion}$.[16] If we use −5.4 cm^3/mol as the $\overline{V}°_{ion}$ value of H^+ ion at 25 °C, recommended by Millero,[16] the $\overline{V}°_{ion}$ values of Na^+ and Cl^- ions become −6.6 and 12.4 cm^3/mol respectively.[16] The $\overline{V}°_{ion}$ values thus calculated are listed in Table 4. Figure 2 represents an approximate linear relation between the B_{ion} values and the $\overline{V}°_{ion}$ values. A similar relation has frequently been reported.[11,15,17]

The viscosity of a dilute suspension of spherical colloids is given by the Einstein equation:[18]

$$\eta = \eta_0(1+2.5\phi) \quad (2)$$

where ϕ is the volume fraction of colloids. Though the coefficient of 2.5 in Eq. (2) becomes slightly varied in the case of elongated solutes,[19] an approximate attempt assuming the spherical form will be made in this paper. For the solution, the B coefficient can be related to $\overline{V}°$ expressed in cm^3/mol:

$$B = 0.0025\,\overline{V}° \quad (3)$$

Thus, the contribution from the Einstein effect in the B_{ion} values is equal to $0.0025\,\overline{V}°_{ion}$. Desnoyers and Perron[20] showed that the values, $B-0.0025\,\overline{V}°$, is a measure of the solute-solvent interation. Similarly, the ion-solvent interaction effect, Δ, for organic ions can be derived by the equation:[20]

$$\Delta = B_{ion} - 0.0025\,\overline{V}°_{ion} \quad (4)$$

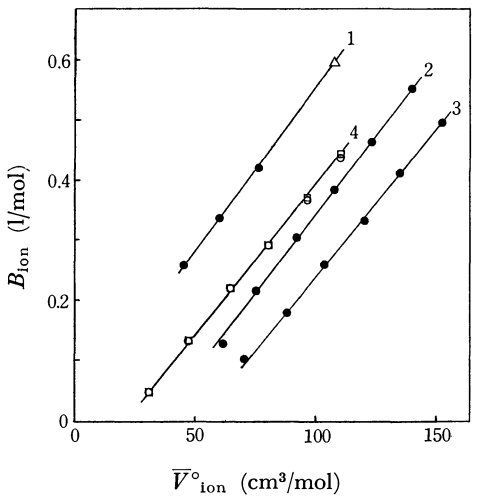

Fig. 2. Plots of viscosity B coefficients for organic ions against molal volumes for ions at infinite dilution.
1: alkane carboxylate ions, 2: alkyl sulfonate ions, 3: alkyl sulfate ions, 4: alkylammonium ions, ●, ○ present work, △: Ref. 8, □: Ref. 11.

It may be noted that the Δ values are of a semi-quantitative nature, because the absolute values of Δ depend on the two conventions adopted for splitting the B values and the $\overline{V}°$ values into the respective ionic B_{ion} and $\overline{V}°_{ion}$ values.

As is indicated in Table 4, the Δ values are positive for all the carboxylate ions. Further, it has been reported that alkane carboxylic acids have rather small B values, those for acetic, propionic, and butyric acids being 0.117, 0.190, and 0.250 respectively.[21] The large difference in the B values between carboxylic acids and carboxylate ions may be interpreted in terms of the strong tendency of the carboxylate anion to

orientate the water molecules around the ions.[9] Therefore, it may be concluded that the $-COO^-$ ionic part acts as an "electrostrictive structure-maker" in the water phase.

On the other hand, the $-SO_3^-$ ionic part and the $-OSO_3^-$ ionic part have quite small B values. With the lower members of sulfonates and sulfates, the Δ values are negative, as is shown in Table 4. Therefore, it may be assumed that these two anionic parts are "electrostrictive structure-breakers" in water. The structure-breaking properties of sulfonate ions have been discussed by Uedaira and Uedaira[22] on the basis of their conductivity measurements, and by Katayama *et al.*[23] on the basis of their partial molal measurements.

The Behavior of $-NH_3^+$ in Water. The $\overline{V}^\circ$ values for alkylammonium chlorides and the $\overline{V}^\circ_{ion}$ values for alkylammonium ions are listed in Tables 3 and 4 respectively. Table 4 indicates a negative Δ value for methylammonium ion. From this fact, the $-NH_3^+$ ionic part is considered to be an "electrostrictive structure-breaker." This is probably supported by the fact that simple ammonium ion has a net structure-breaking effect.[9]

Specific Interactions of the $-COO^-$, $-SO_3^-$, $-OSO_3^-$ and $-NH_3^+$ Ionic Parts with Other Simple Counter-ions. There are several phenomena which indicate the characteristic behavior of the $-COO^-$, $-SO_3^-$, $-OSO_3^-$ and $-NH_3^+$ ionic parts in water, particularly with regard to the interaction of these ionic parts with other simple counter-ions. The mean ionic activity coefficients, γ, for the alkali metal salts of acetic acid for a given concentration decrease in the order: $Li^+<Na^+<K^+$.[24] On the other hand, the γ values for the salts of *p*-toluensulfonic acid[24] as well as the salts of methyl and ethyl sulfonic acids[25] in dilute solutions increase in the order: $Li^+>Na^+>K^+$. The variation in the order of the ionic activity coefficients has been discussed by Gurney[9] and by Frank.[26] The theory of Gurney and Frank implies that an anion and a cation with similar structural influences—both being structure-makers or both structure-breakers—will attract each other, whereas if an anion and a cation have different structural tendencies, they will repel each other. Among the cations, Li^+ is a strong, and Na^+, a weak structure-maker, while K^+, slightly structure-breaking. As has been explained above, the $-COO^-$ ionic part is believed to be a structure-maker, while the $-SO_3^-$ ionic part, a structure-breaker. Therefore, the lithium salt of carboxylic acid, a "maker-maker" salt, and the potassium salt of sulfonic acid, a "breaker-breaker" salt, will give lower-lying activity coefficient *versus* concentration curves because of the tendency toward more attraction between cations and anions. At the opposite extreme, the potassium salt of carboxylic acid, a "breaker-maker" salt, and the lithium salt of sulfonic acid, a "maker-breaker" salt, will give higher-lying curves because of the greater escaping tendency between cations and anions. Steigman and Dobrow[27] also discussed the ionic activity coefficients along the same lines.

With polyelectrolytes, the counter-ions are bound to poly-ions because of the strong electrostatic potential of poly-ions.[28] This phenomenon is called "counter-ion binding". There are characteristic sequences of simple counter-ions with regard to the degree of binding to the poly-ions. In the case of the alkali metal salts of polyacrylic acid, the degree of binding decreases with the size of the counter-ion: $Li^+>Na^+>K^+$.[29] With polyvinyl- and polystyrenesulfonates, on the other hand, the degree of binding increases with the size of the ion: $Li^+<Na^+<K^+$.[24] This characteristic feature may also be interpreted in terms of the structural influences by ions in water. In the case of the "like-like" combinations in the structural influences of both cations and anions, such as lithium polyacrylate and potassium polyvinyl- and polystyrenesulfonates, cations and anions will attract each other more. Conversely, in the case of the incompatible combinations in the structural influences of cations and anions, such as potassium polyacrylate and lithium polyvinyl- and polystyrene-sulfonates, the resultant phenomenon will result in a stronger repulsive force.

The amphiphilic salts containing an alkyl group, higher than octyl, have a tendency to form micelles in aqueous solutions. The critical micelle concentration (CMC) is a measure of the solute-solvent interaction. The CMC value depends mainly on the oleophilic group. However, there are some specific effects of ionic species. In the case of the alkali metal salts of dodecyl sulfuric acid, the CMC values decrease with size of the cations: $Li^+>Na^+>K^+$.[30] In the case of the alkali metal salts of long-chain carboxylic acid, the CMC values are in the order: $Li^+<Na^+<K^+$.[31] Further, the CMC values for dodecylammonium halides are in the order: $I^-<Br^-<Cl^-$.[32] In view of the structural influences in water induced by both cations and anions, the degree of counter-ion binding at the surface of ionic micelles will be in the order of $Li^+<Na^+<K^+$ in the case of the alkali metal salts of dodecyl sulfuric acid, whereas the order will be reversed in the case of the alkali metal salts of alkane carboxylic acid: further, it will be in the order of $I^->Br^->Cl^-$ in the case of dodecylammonium halides. With increased binding of counter-ions the contribution of the electric free energy in the micelle formation per monomer will be reduced, thus resulting in the easier formation of the aggregates at lower concentrations.

References

1) K. Tamaki, Y. Ōhara, and Y. Isomura, This Bulletin, **46**, 1551 (1973).
2) M. J. Blandamer, *Quart. Rev.*, **24**, 169 (1970).
3) H. S. Frank and M. J. Evans, *J. Chem. Phys.*, **13**, 507 (1945).
4) S. Zuffanti, *J. Amer. Chem. Soc.*, **62**, 1044 (1940).
5) G. Jones and M. Dole, *ibid.*, **51**, 1950 (1929).
6) J. Padova, *J. Chem. Phys.*, **38**, 2635 (1963).
7) A. N. Campbell and J. T. Friesen, *Can. J. Chem.*, **38**, 1939 (1960).
8) A. N. Campbell, E. M. Kartzmark, and G. R. Lakshminarayanan, *ibid.*, **40**, 839 (1962).
9) R. W. Gurney, "Ionic Processes in Solution," McGraw-Hill, New York (1953).
10) R. H. Stokes and R. Mills, "Viscosity of Electrolytes

and Related Properties," Pergamon, Oxford (1965).
11) J. E. Desnoyers, M. Arel, and P-A. Leduc, *Can. J. Chem.*, **47**, 547 (1969).
12) G. M. Watson and W. A. Felsing, *J. Amer. Chem. Soc.*, **63**, 410 (1941).
13) E. J. King, *J. Phys. Chem.*, **73**, 1220 (1969).
14) M. Sakurai, This Bulletin, **46**, 1596 (1973).
15) M. Tanaka, S. Kaneshina, W. Nishimoto, and H. Takabatake, *ibid.*, **46**, 364 (1973).
16) F. J. Millero, *Chem. Rev.*, **71**, 147 (1971).
17) B. R. Breslau and I. F. Miller, *J. Phys. Chem.*, **74**, 1056 (1970).
18) A. Einstein, *Ann. Phys.*, **19**, 289 (1906), **34**, 591 (1911).
19) T. T. Herkovits and T. M. Kelly, *J. Phys. Chem.*, **77**, 381 (1973).
20) J. E. Desnoyers and G. Perron, *J. Solution Chem.*, **1**, 199 (1972).
21) J. A. Rupley, *J. Phys. Chem.*, **68**, 2002 (1964).
22) H. Uedaira and H. Uedaira, This Bulletin, **37**, 1885 (1964).
23) A. Katayama, T. Matsuura, H. Kuroki, and K. Konishi, *Sen-i Gakkaishi*, **21**, 598 (1965).
24) R. A. Robinson and R. H. Stokes, "Electrolyte Solutions," Butterworths, London (1968).
25) H. P. Gregor, M. Rothenberg, and N. Fine, *J. Phys. Chem.*, **67**, 1110 (1963).
26) H. S. Frank, *ibid.*, **67**, 1554 (1963); *Z. Phys. Chem.* (Leipzig), **228**, 364 (1965).
27) J. Steigman and J. Dobrow, *J. Phys. Chem.*, **72**, 3424 (1968).
28) S. A. Rice and M. Nagasawa, "Polyelectrolyte Solutions," Academic Press, London and New York (1961).
29) K. Tamaki, M. Ozaki, M. Ogiwara, and I. Takemura, *Nippon Kagaku Zasshi*, **88**, 711 (1967).
30) K. Meguro, T. Kondo, O. Yoda, T. Ino, and N. Ooba, *ibid.*, **77**, 1236 (1956).
31) K. Meguro and T. Kondo, *Yukagaku*, **9**, 346 (1960).
32) K. Meguro and T. Kondo, *Nippon Kagaku Zasshi*, **80**, 818 (1959).

Electron-transfer Kinetics of Transition-metal Complexes in Lower Oxidation States. Part II.[1] The Electrochemical Electron-transfer Rate of the $Cr(bipy)_3^+/Cr(bipy)_3$ System as Measured by the Galvanostatic Double-pulse Method[2]

Tetsuo SAJI and Shigeru AOYAGUI

Faculty of Engineering, Tokyo Institute of Technology, Ohokayama, Meguro-ku, Tokyo 152

(Received August 10, 1973)

The kinetic parameters of the electron-transfer reaction, $Cr(bipy)_3^+ + e \rightleftharpoons Cr(bipy)_3$, were measured by the galvanostatic double-pulse method at a dropping mercury electrode in *N*,*N*-dimethylformamide. The apparent and the corrected standard rate constants were 1.0 ± 0.2 and 0.3 cm s^{-1} respectively, and the transfer coefficient was 0.6 ± 0.1 at 25 °C. These rate constants were discussed in comparison with the corresponding homogeneous rate constant on the basis of the theoretical equation of Marcus. They were quite inconsistent with the value, 10^3 cm s^{-1}, predicted from the corresponding homogeneous rate constant.

The polarograms of $Cr(bipy)_3^+$ and $Cr(bipy)_3$ exhibited three waves with half-wave potentials of -0.21, -0.65 and -1.19 V *vs.* a cationic glass electrode. The diffusion coefficients of these complexes, as determined polarographically, were identical: 3.2×10^{-6} cm^2 s^{-1} at 25 °C.

The theory of Marcus has been successfully applied to a number of electron-transfer reactions[3,4] in order to make the theoretical predictions of (1) the rate constants for the homogeneous and the electrochemical electron-transfer reactions, (2) the transfer coefficients for them, and (3) the correlation between the rate constants for the homogeneous electron-exchange reaction, $A^z + A^{z-n} \rightleftharpoons A^{z-n} + A^z$, and the corresponding electrochemical electron-transfer reaction, $A^z + ne \rightleftharpoons A^{z-n}$. Here, z is the number of the ionic charge, and n, the number of electrons transferred. This paper is concerned with the third aspect: the rate constants of these two types for the $Cr(bipy)_3^+/Cr(bipy)_3$ system are compared and discussed in the light of the theory of Marcus.

According to this theory, the homogeneous electron-exchange rate constant, k_{ex}, is related to the corresponding electrochemical electron-transfer rate constant, k_{el}, by the following simple relationship:[5]

$$(k_{ex}/Z_{hom})^{1/2} = k_{el}/Z_{el} \quad (1)$$

where Z_{hom} is the hypothetical collision number of two uncharged species in a solution when they have a unit concentration, and where Z_{el} is the collision number of an uncharged species with a unit area of the electrode when it has a unit concentration. An electron-transfer reaction with which this relationship is to be tested must have such a large rate constant that the rates of other possible coupled processes, *e.g.*, the bond-rupture, bond-formation, and atom-transfer processes, can be neglected, as this theory is based on the assumption that the reaction proceeds through an outer-sphere mechanism. With the Z values of 10^{11} M^{-1} s^{-1} for Z_{hom} and 10^4 cm s^{-1} for Z_{el}, the (1) relation holds fairly well in the reactions with a rather small rate constant,[5-7] *e.g.*, V^{3+}/V^{2+}, Eu^{3+}/Eu^{2+}, Tl^{3+}/Tl^+, and $Co(phen)_3^{3+}/Co(phen)_3^{2+}$, but it is insufficient in those with a large rate constant,[5] *e.g.*, Fe^{3+}/Fe^{2+}, $Fe(CN)_6^{4-}/Fe(CN)_6^{3-}$, and MnO_4^{2-}/MnO_4^-. According to recent investigations, however, it is quite probable that the reactions of aquo-complexes proceed through a mechanism other than the outer-sphere mechanism.[8] The reaction of $Co(phen)_3^{3+}$-$(t_{2g}^6)/Co(phen)_3^{2+}(t_{2g}^5 e_g^2)$ is also inappropriate for the present purposes, because the two reactants are in different spin states.[8] Consequently, the excellent agreement between the theoretical prediction and experimental results found for these reactions cannot be a support for the validity of Eq. (1) Unfortunately, there are not many homogeneous electron-exchange reactions that have been confirmed to proceed through an outer-sphere mechanism, and even the concept of outer- and inner-sphere mechanisms has never been established in electrochemical electron-transfer reactions. Therefore, we recommend a system with a sufficiently large homogeneous electron-exchange rate constant for testing Eq. (1), for the same reasons as were discussed in a previous paper treating the potential dependence of the transfer coefficient.[9]

Generally an electron-exchange reaction is very fast if it satisfies the following two conditions:[8] (1) the reactants have "conducting" unsaturated ligands, such as cyanide, phenanthroline, bipyridine, and cyclopentadienyl, that is, the reactants are characterized by a highly delocalized π-electron distribution, and (2) the reactants are a pair of complexes differing by one in the number of electrons in the lower orbitals not used in ligand bondings. The electron-exchange reaction between $Fe(phen)_3^{3+}(t_{2g}^5)$ and $Fe(phen)_3^{2+}$-(t_{2g}^6) is a reaction satisfying these conditions; its second-order rate constant[10] is larger than 3×10^7 M^{-1} s^{-1} and some 10^7 times as large as that of the $Co(phen)_3^{3+}/Co(phen)_3^{2+}$ system.[6,7]

It should be borne in mind that Eq. (1) has been derived by neglecting the contribution to the activation free energy from the free energy required to bring the reactant(s) and the product(s) to the positions where electron-transfer takes place. This contribution is referred to as a "work term" in the Marcus theory. The work term may reasonably be neglected in a homogeneous electron-exchange reaction where one of the reactants is uncharged. Our choice of the $Cr(bipy)_3^+(t_{2g}^5)/Cr(bipy)_2(t_{2g}^6)$ system is based partly on this reasoning and partly on its electronic configuration, which is analogous to that of the $Fe(phen)_3^{3+}/Fe(phen)_3^{2+}$ system, thus promising a large electron-transfer rate

constant. Recently we have measured the rate constant of the homogeneous electron-transfer reaction between $Cr(bipy)_3^{+}$ and $Cr(bipy)_3$ in *N,N*-dimethylformamide (DMF) by the electron spin resonance method using the line-broadening procedure.[1] The observed second-order rate constant was 1.5×10^9 M^{-1} s^{-1} at 25 °C. This was in good agreement with the rate constant calculated non-empirically according to the theory of Marcus, with the inner-sphere reorganization energy neglected. Furthermore, the oxidation-reduction potential of the $Cr(bipy)_3^{+}/Cr(bipy)_3$ system is negative *vs.* the oxidation potential of mercury, so the Frumkin correction can be applied, if necessary, to this system. According to Eq. (1), the predicted value for the standard rate constant of this system should be larger than 10^3 cm s^{-1}, beyond the upper limit accessible by existing techniques. In this experiment measurements are made by the galvanostatic double-pulse method; the standard rate constant obtainable by this method is 10 cm s^{-1} at most.

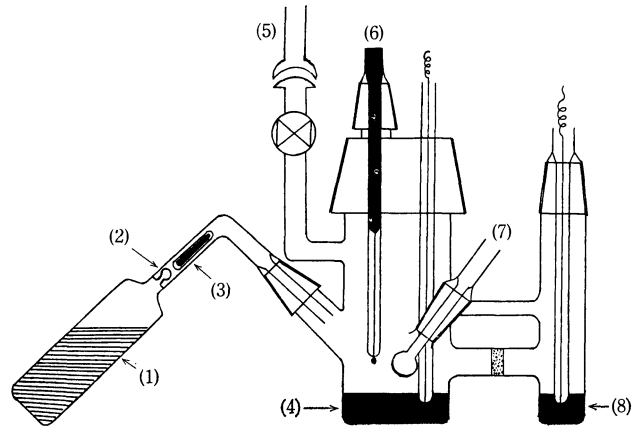

Fig. 1. Electrolysis cell: (1) electrolytic soln, (2) breakable seal, (3) hammer, (4) mercury pool A, (5) joint to vacuum line and inlet for nitrogen gas, (6) working electrode, (7) cationic glass electrode, (8) mercury pool B.

Experimental

Complexes. Both complexes, tris-(2,2′-bipyridine)-chromium(I) perchlorate and tris-(2,2′-bipyridine)-chromium (0), are very sensitive to oxygen. They were prepared and handled in a vacuum or in a nitrogen atmosphere. The preparation and analysis of these complexes were described in a previous paper.[1]

Reagents. Lithium perchlorate (Yoneyama Chemical Industries) and DMF(Wako Pure Chemical Industries) were used as the supporting electrolyte and the solvent, respectively. The former was recrystallized from an oxygen-free aqueous solution under a nitrogen atmosphere and then dried *in vacuo*. The latter was purified in a way described previously.[1]

Solutions. The $Cr(bipy)_3ClO_4$ and $Cr(bipy)_3$ solutions were prepared by dissolving the required amounts of lithium perchlorate and one of the complexes in DMF so that their concentrations might be 0.5 M and of the order of 10^{-3} M with respect to the supporting electrolyte and the complexes. The solutions were then stored in evacuated glass ampoules fitted with breakable-seals. The solution ampoule was connected with the cell *via* a tapered joint. Each aliquot was about 25 ml. All operations in preparing the solutions were performed *in vacuo*, with the subsidiary use of nitrogen. The electrolytic solution used in the double-pulse measurement must contain both the oxidant and the reductant.[11] It was prepared within the cell by the partial electrolytic reduction of a $Cr(bipy)_3ClO_4$ solution at a controlled potential. The concentrations of both species were determined polarographically.

Cell. The Pyrex-glass electrolysis cell shown in Fig. 1 was used. After the cell had been evacuated, nitrogen gas was introduced into it until an atmospheric pressure was reached. The electrolytic solution was then transferred into the cell through the broken breakable-seal by the appropriate rotation of the ampoule around the tapered joint. A cation-permiable glass electrode (CGE) served as a reference electrode in the polarographic measurements and controlled potential electrolyses. Its e.m.f. was −50 mV *vs.* SCE, as measured by the use of a conventional agar bridge; this was sufficiently reproducible within the limits of accuracy of this experiment, *i.e.*, 2 mV. The cell was evacuated easily and completely by the use of this reference electrode. Besides the CGE, a dropping mercury electrode (DME) and two mercury pool electrodes were fitted in the cell. The DME, the CGE, and the mercury pool electrode, A, were used in the polarographic measurements. The apparent area of the mercury pool A was about 10 cm^2. The two mercury electrodes, A and B, served as the working and the couter electrodes respectively in the controlled potential electrolyses. The compartment of the latter electrode was separated by a fritted glass from that of the former electrode. The progress of the controlled potential electrolysis was followed polarographically. A controlled current double-pulse was applied between the DME and the mercury pool electrode A.

Procedure and Devices. A controlled current double-pulse was applied to each drop of DME 3.0 s after the birth of the drop. The controlled current double-pulse generator equipped with an ohmic-drop compensating unit,[13] the synchronizing and timing circuit for DME,[14] and the potentiostat[15] which were used in this experiment have all been described elsewhere. Measurements were made at room temperature maintained at 25 °C.

Results and Discussion

A typical polarogram taken in a 0.3 mM solution of $Cr(bipy)_3$ is shown in Fig. 2. It exhibits three oxidation waves, with half-wave potentials of −0.21, −0.65, and −1.19 V *vs.* CGE respectively. The waves at −0.65 and −1.19 V are reversible, and their wave-heights are identical when corrected for the drop area. Two oxidation waves and a reduction wave with half-wave potentials of −0.20, −0.64, and −1.17 V *vs.* CGE appeared in a polarogram taken in a 0.5 mM solution of $Cr(bipy)_3^{+}$. After the $Cr(bipy)_3^{+}$ had been reduced completely to $Cr(bipy)_3$ by the controlled-potential electrolysis at −1.5 V, the polarogram was exactly the same as that of $Cr(bipy)_3$. On the basis of these experimental results and the proportionality between the wave-height and the concentration of $Cr(bipy)_3ClO_4$, the half-wave potential of −1.19 V *vs.* CGE can be assigned to the following redox system:

$$Cr(bipy)_3^{+} + e \rightleftharpoons Cr(bipy)_3 \qquad (2)$$

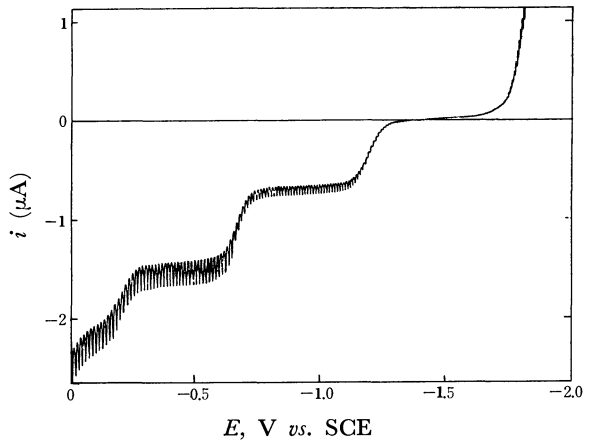

Fig. 2. Polarogram of 0.3 mM $Cr(Bipy)_3$ in a DMF soln containing 0.5 M $LiClO_4$.

There have been several polarograms of $Cr(bipy)_3^{3+}$ reported.[16] They were measured in solvents other than DMF, but in these polarograms one can find a wave corresponding to each wave in Fig. 2.

The diffusion coefficients of $Cr(bipy)_3^+$ and $Cr(bipy)_3$ were identical; they were determined to be 3.2×10^{-6} $cm^2\,s^{-1}$ at 25 °C.

The results obtained by the galvanostatic double-pulse measurement were analyzed according to the following equation:

$$\log(I_0/nFC_O) = \log k_s + \alpha\log(C_R/C_O) \qquad (3)$$

where I_0 is the exchange current density; k_s, the standard rate constant; α, the transfer coefficient, and the C's, the concentrations of the oxidant, O, and the reductant, R. An experimental plot in accordance with Eq. (3) is shown in Fig. 3. The standard rate constant and the transfer coefficient were determined to be 1.0 ± 0.2 cm s^{-1} and 0.6 ± 0.1 respectively. Such a large apparent standard rate constant approaching 1 cm s^{-1} has rarely been reported for the electrochemical electron-transfer reactions of transition-metal complexes.

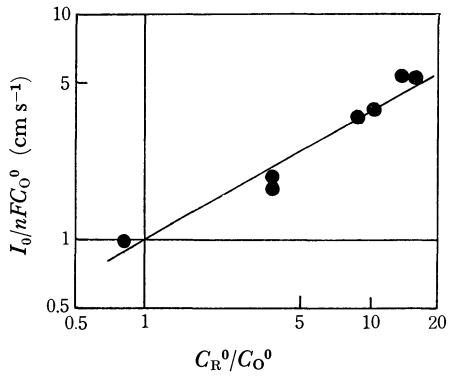

Fig. 3. Plot of $\log(I_0/nFC_O^0)$ *vs.* $\log(C_R^0/C_O^0)$.

Thus, we have found that the rate constants for the homogeneous and the electrochemical electron-transfer reactions of the $Cr(bipy)_3^+/Cr(bipy)_3$ system are both sufficiently large; this system is now considered to be appropriate for testing Eq. (1). Its electrochemical rate constant, however, is quite inconsistent with the value predicted by Eq. (1), *i.e.*, 10^3 cm s^{-1}.

Table 1. The observed, the corrected and the calculated rate constants for the $Cr(bipy)_3^+/Cr(bipy)_3$ system at 25°C

k_{el} (cm s^{-1})		
Observed	Corrected	Calculated
1.0 ± 0.2	0.3	10^3

If the positions occupied by the reactant and the product in their respective activated complexes are located within the diffuse double-layer, the work term for $Cr(bipy)_3^+$ in the electrochemical reaction should not be neglected, whereas this term may reasonably be neglected in the homogeneous electron-transfer of this system. These positions are referred to as the sites of the pre-electrode. The electrical potential at the pre-electrode site must be known in order for the work term to be evaluated. However, this is rather a difficult task. Assuming that the double-layer structure is of the Gouy-Chapman type and that both pre-electrode sites are located on the outer Helmholtz plane, the work term correction can be made according to the Frumkin procedure. Although the validity of the latter assumption is not quite certain, a Frumkin correction is applied as a trial to the electrochemical rate constant obtained above.

The data of the ϕ_2-potential in a DMF solution of lithium perchlorate are not available, but the electrocapillary curves for several electrolytes in this solvent have been reported.[17] The extent of the specific adsorption of perchlorate ions may be seen to be the least of all the anions studied. The electrocapillary curves were analyzed on the assumption that neither the anions nor the cations were specifically adsorbed on the electrode. The ϕ_2-potential at -1.19 V *vs.* CGE was obtained as -76 mV. The corrected standard rate constant was 0.3 cm s^{-1}. The corrected rate constant does not agree with the predicted value better than the apparent rate constant.

The original theory of Marcus regarding the electrochemical reaction does not state anything explicitly about the location of pre-electrode sites. The experimental results show, though, that the corrected rate constant cannot be larger than the observed one, wherever the pre-electrode site is located. Consequently, it is evident that Eq. (1) cannot hold unless the apparent electrochemical rate constant is immeasurably large. The same situation can be expected for a system satisfying the following conditions: (1) the number of electrons transferred is one; (2) k_{ex} is larger than 10^8 $M^{-1}\,s^{-1}$; (3) either species of the system is positively (or negatively) charged, or both species are, and (4) the standard electrode potential is negative (positive) *vs.* the zero-charge potential. Equation (1) has been applied exclusively to systems these conditions are not satisfied.

References

1) Part I: T. Saji and S. Aoyagui, This Bulletin, **46**, 2101 (1973).

2) Presented at the 17th Symposium on Polarography and Electroanalytical Chemistry, Fukuoka, Oct., 1971.

3) R. A. Marcus, *Ann. Rev. Phys. Chem.*, **15**, 155 (1964) and papers cited therein.
4) M. E. Peover and J. S. Powell, *J. Electroanal. Chem.*, **20**, 427 (1969).
5) R. A. Marcus, *J. Phys. Chem.*, **67**, 853 (1963).
6) H. Bartelt, *Electrochim. Acta*, **16**, 629 (1971).
7) B. R. Baker, F. Basolo, and H. M. Neuman, *J. Phys. Chem.*, **63**, 371 (1959).
8) F. Basolo and R. G. Pearson, "Mechanisms of Inorganic Reactions," 2nd ed., John Wiley & Sons Inc., New York, N. Y. (1967), Chap. 6.
9) K. Suga, H. Mizota, Y. Kanzaki, and S. Aoyagui, *J. Electroanal. Chem.*, **41**, 313 (1973).
10) D. W. Larsen and A. C. Wahl, *J. Chem. Phys.*, **43**, 3765 (1965).
11) After this investigation was made, a new galvanostatic double-pulse set-up has been proposed.[12] It requires only either the oxidant or the reductant to be contained in the bulk of solution.
12) H. Mizota, H. Matsuda, Y. Kanzaki, and S. Aoyagui, *J. Electroanal. Chem.*, **45**, 385 (1973).
13) M. Kogoma and S. Aoyagui, *ibid.*, **34**, 123 (1972).
14) T. Rohko, M. Kogoma, and S. Aoyagui, *ibid.*, **38**, 45 (1972).
15) Y. Kanzaki and S. Aoyagui, *ibid.*, **36**, 297 (1972).
16) A. A. Vlcek, *Nature*, **189**, 393 (1961). Y. Sato and N. Tanaka, This Bulletin, **42**, 1021 (1969).
17) V. D. Bezuglyi and L. A. Korshikov, *Elektrokhimiya*, **3**, 390 (1967).

Polymerization of Vinyl Compounds with Hydridodinitrogentris(triphenylphosphine)cobalt(I)

Yoichiro KUBO, Akio YAMAMOTO, and Sakuji IKEDA

Research Laboratory of Resources Utilization, Tokyo Institute of Technology, O-okayama, Meguro, Tokyo 152

(Received March 14, 1973)

The kinetics of polymerization of vinyl compounds (acrylonitrile, methacrylonitrile, and methyl methacrylate) with hydridodinitrogentris(triphenylphosphine)cobalt(I), $CoH(N_2)(PPh_3)_3$ **1** (PPh_3: triphenylphosphine) was studied. By comparison with previous studies on the decomposition of **1** in the presence of vinyl compound a polymerization mechanism involving slow initiation followed by rapid propagation and unimolecular termination was proposed. The effects of concentration of monomer and of added triphenylphosphine on the molecular weight of the polymer were studied. The result of copolymerization was explained by the competitive coordination between the monomers involved. Poly(methyl methacrylate)s obtained by **1** in bulk and the solvent were all rich syndiotactic fraction.

Many investigations on the mechanisms of coordination polymerization by Ziegler type mixed catalysts have been made. However, a clear understanding of the polymerization mechanism by kinetic approaches[1] has been hindered by the complexity and instability of the mixed catalyst systems. By studying the polymerization kinetics with an isolated transition metal complex capable of initiating the polymerization, more information on the mechanism with Ziegler type catalysts might be expected. Employment of isolated transition metal complexes will make it possible to discover new catalysts so far unavailable with the mixed systems, where the reaction of the monomer with a catalyst component often invalidates the catalyst system. Examples of successful polymerization of vinyl monomers with Ziegler type catalysts, previously considered unpolymerizable, are increasing.[2] Recently some isolated transition metal allyls[3] and alkyls[4] have been reported to initiate the vinyl polymerization, detailed kinetic studies being made. Transition metal hydrides are also expected to initiate it, but few studies using the isolated transition metal hydrides have been made so far. We have continued our studies[5] on the reactions of hydridodinitrogentris(triphenylphosphine)-cobalt(I) $CoH(N_2)(PPh_3)_3$[6] and $CoH(CO)(PPh_3)_3$ with olefins, and report in this paper the vinyl polymerization with $CoH(N_2)(PPh_3)_3$ together with information obtained on the polymerization kinetics.

Results and Discussion

Kinetics of Polymerization. The polymerization conditions, polymer yields, and molecular weights of polymers obtained with $CoH(N_2)(PPh_3)_3$ are summarized in Table 1. For cases where the olefins were not polymerized and olefin-coordinated complexes were obtained, the compositions of the complexes are included in the table. The synthesis and characterization of the olefin-coordinated cobalt complexes have been reported.[7] It was confirmed that triphenylphosphine alone does not initiate the polymerization. Nitrogen was released from $CoH(N_2)(PPh_3)_3$ with the polymerization of the vinyl monomers, but no hydrogen was evolved.

Figure 1 shows a typical time-conversion curve in the polymerization of methacrylonitrile by $CoH(N_2)(PPh_3)_3$. Polymerization starts after an induction period of about 2 minutes and the conversion approaches a certain maximum value with time. The induction period does not change with the concentra-

TABLE 1. REACTIVITIES AND POLYMERIZATION ACTIVITIES OF $CoH(N_2)(PPh_3)_3$ TOWARD SUBSTITUTED OLEFINS

Monomer	*e* value	Time	Polymer Yield	Mol. wt.	Complex Isolated
Tetracyanoethylene		1 hr	0	—	$CoH(TCNE)_3(PPh_3)_2$
Maleic anhydride	2.25	2 hr	0	—	$CoH(MAh)_x(PPh_3)_y$
Acryl amide	1.30	2 hr	0	—	$CoH(AcAm)_3$
Methacryl amide		6 hr	0	—	$CoH(MeAcAm)_3$
Acrylonitrile	1.20	3 days	11%	2.00×10^4	
Methacrylonitrile	0.81	5 min	59%	3.63×10^5[a]	
Acrolein	0.73	1 hr	70%	—	
Methyl vinyl ketone	0.69	1 day	a few %	low mol. wt	
Methyl acrylate	0.60	2 hr	0	—	oily product
Methyl methacrylate	0.40	23 hr	20%	6.68×10^4	
Vinyl acetate	−0.22	3 hr	0	—	$CoH(VAc)_2$
Styrene	−0.80	3 hr	0	—	$Co(St)[P(C_6H_4)(C_6H_5)_2](PPh_3)_2$
Isobutyl vinyl ether	−1.77	2 days	0	—	$CoH(IBVE)_2$

Reaction temp: room temperature; −20°C for acrolein and methyl vinyl ketone. a) Poly(methacrylonitrile) produced by $CoH(N_2)(PPh_3)_3$ was soluble in acetone.

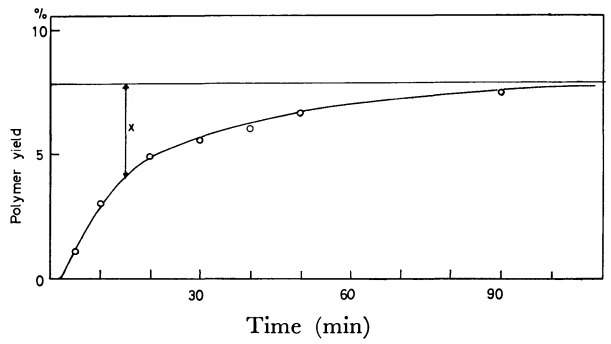

Fig. 1. Time-conversion curve of the polymerization of methacrylonitrile with $CoH(N_2)(PPh_3)_3$ at 25 °C. Yield against time. Methacrylonitrile, 10 ml; toluene, 20 ml; $CoH(N_2)(PPh_3)_3$, 2.28×10^{-3} mol/l.

tions of free triphenylphosphine and of $CoH(N_2)(PPh_3)_3$. The reason for the presence of the induction period remains unexplained. Since the polymer yield is low, concentration of methacrylonitrile can be regarded as constant during the course of polymerization.

The molecular weight of the polymer is independent of time and conversion having a value of 1.5×10^5. The reactions of $CoH(N_2)(PPh_3)_3$ with olefins are of first order in the concentration of $CoH(N_2)(PPh_3)_3$ under the conditions where the olefin concentrations can be regarded invariant,[5] and can be expressed as follows.

$$R_{N_2} = -d[CoH(N_2)(PPh_3)_3]/dt = k_{N_2}[CoH(N_2)(PPh_3)_3] \quad (1)$$

where R_{N_2} denotes the rate of change of $CoH(N_2)(PPh_3)_3$ under nitrogen. Thus, the concentration of $CoH(N_2)(PPh_3)_3$ decreases with time in the presence of an olefin and should markedly decrease in the time scale shown in Fig. 1. It can be concluded that the molecular weight of the polymer is independent also of the concentration of $CoH(N_2)(PPh_3)_3$. This is supported by experimental results showing the invariance of the molecular weights of the polymers with varying initiator concentrations over a three-fold range. Since the molecular weights of the polymers obtained at different conversions are almost constant, the yield of the polymer can be regarded as proportional to the number of polymer chains produced. This suggests that the polymerization process of the vinyl monomer consists of a slow initiation step followed by rapid propagation and termination steps as in the polymerization with dialkylbis(dipyridyl)iron[4] or dihydridotetrakis(triphenylphosphine)ruthenium.[8] Features common to the polymerization by the transition metal complexes are the strong inhibition effects of ligands. As was done previously[4] the logarithm of the value x(=the maximum yield (Y_∞)—the yield at time t(Y_t)) is plotted against time. Except for the induction period the straight lines having the slope $\bar{k}$ are obtained indicating the relationship

$$\log(Y_\infty - Y_t) = -\bar{k}t + \text{const.} \quad (2)$$

The change of slope $\bar{k}$ against the methacrylonitrile concentration is plotted in Fig. 2. The value $\bar{k}$ increases with the increase in methacrylonitrile concentration,

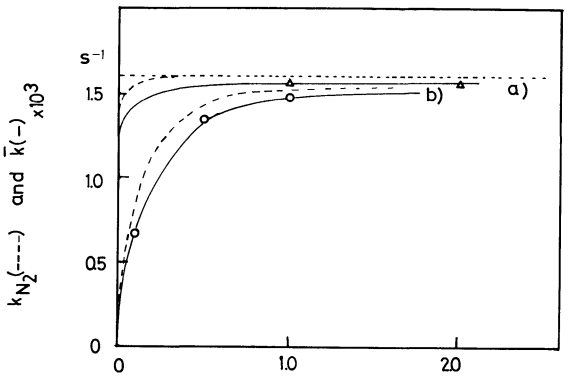

Fig. 2. Plots of pseudo-first-order rate constants, k_{N_2} and $\bar{k}$, against the concentration of methacrylonitrile, a) in the absence of triphenylphosphine; b) Concentration of triphenylphosphine, 8.50×10^{-2} mol/l. Solvent: toluene; $CoH(H_2)(PPh_3)_3$, 3.40×10^{-3} mol/l. Polymerization temperature: 25 °C.
k_{N_2} (·····): pseudo-first-order rate constants obtained by a spectroscopic method.[5]
$\bar{k}$ (——): pseudo-first-order rate constants obtained from the time-conversion curve.

approaching a limiting value of $1.60\times10^{-3}\,s^{-1}$. We proposed the following mechanism of the decomposition of the cobalt complex.[5]

$$CoH(N_2)(PPh_3)_3 \underset{k_{-1}}{\overset{k_1}{\rightleftharpoons}} CoH(N_2)(PPh_3)_2 + PPh_3$$
$$\Big\| \begin{matrix} k_{-2} \uparrow \\ \downarrow k_2 + \text{olefin} \end{matrix}$$
$$CoH(N_2)(\text{olefin})(PPh_3)_2$$
$$\Big\| \begin{matrix} k_{-3} \uparrow \\ \downarrow k_3 \end{matrix}$$
$$CoH(\text{olefin})(PPh_3)_3 + N_2$$
$$\Big\downarrow k_4$$
$$\text{decompsition} \quad (3)$$

The pseudo-first-order rate constant k_{N_2} in Eq. (1) can be expressed as follows.

$$\frac{1}{k_{N_2}} = \frac{1}{k_1} + \frac{k_{-1}}{k_1 k_2 k_3}\frac{[PPh_3]}{[\text{olefin}]}\left\{(k_{-2}+k_{-3}) + \frac{k_{-2}k_{-3}}{k_4}[N_2]\right\} \quad (4)$$

The limiting value of $\bar{k}$, $1.60\times10^{-3}\,s^{-1}$ in Fig. 2 is in agreement with the k_1 value corresponding to the rate constant for the dissociation of a triphenylphosphine ligand from the cobalt complex. The whole feature of the curves (Fig. 2) obtained from the time-conversion curves agrees with the decomposition pattern of $CoH(N_2)(PPh_3)_3$. The results suggest a relationship between the decomposition rate of the cobalt complex and the polymerization rate. If we assume that the cobalt complex initiates the polymerization with initiator effeciency f by insertion of one monomer into the Co–H bond followed by insertion of monomers into the Co–C bonds, and that the growth of the polymers is terminated spontaneously after reaching a certain degree of polymerization $\overline{DP}$, which is constant, the polymerization rate can be expressed as follows:

$$R_p = \frac{d[Y]}{dt} = f \cdot \overline{DP} \cdot \left\{ - \frac{d[CoH(N_2)(PPh_3)_3]}{dt} \right\} \quad (5)$$

Substituting Eq. (1) into Eq. (5), we have

$$\log (Y_\infty - Y_t) = -k_{N_2} t + \log \{ f \cdot \overline{DP} \cdot [CoH(N_2)(PPh_3)_3]_0 \} \quad (6)$$

where $[CoH(N_2)(PPh_3)_3]_0$ is the initial concentration of the cobalt complex. Equation (6) is identical in form with Eq. (2). There is a reasonable agreement between $\bar{k}$ derived from the time-conversion curve, and k_{N_2} rate constant of the decomposition of $CoH(N_2)(PPh_3)_3$ measured by the spectroscopic method (Fig. 2). The results support our assumption that the initiation process, which probably proceeds *via* the insertion of the monomer into the Co–H bond, is the rate-determining step followed by rapid propagation and termination process by which the complex is eventually destroyed.

Table 2. Effects of concentration of added triphenylphosphine on the molecular weight of poly(methacrylonitrile)

$[PPh_3]$ mmol	Yield %	Mol. wt.
0	60	5.71×10^5
1.29	50	2.65×10^5
6.85	30	5.79×10^4
43.8	0	—

Polymerization time, 1 day; Temp., 25°C
[MAN]: 2.00 mol/l; $[CoH(N_2)(PPh_3)_3]$: 0.34 mmol/l

The yield and molecular weight of the polymer are affected by the monomer concentration, the concentration of the added triphenylphosphine and the solvent. The polymer yields and the decrease in molecular weight by the increase of the concentration of the added triphenylphosphine are given in Table 2. If we assume the initiation process to be formulated in Eq. (3) involving the dissociation of triphenylphosphine from $CoH(N_2)(PPh_3)_3$, the inhibition effect of triphenylphosphine can be readily explained. The effects of monomer concentration and the added triphenylphosphine on the molecular weight of the polymer can be explained by assuming a competitive coordination between the monomer, the solvent and the ligand toward the growing polymer chain end with a cobalt-carbon bond as in the polymerization with the alkyliron complex.[4] When the growing polymer end is coordinated by a monomer molecule, the monomer can be inserted between the metal-carbon bond with a certain probability, whereas the coordination of the solvent and the triphenylphosphine may cause the termination of the polymer growth with different probabilities. The effect of solvent is particularly marked in the polymerization of a monomer, such as methyl methacrylate, having a weaker coordinating ability toward the complex. The polymerization of methyl methacrylate, given in Table 3, is retarded in solution, being severely hindered in solvents of stronger coordinating power, such as tetrahydrofuran and dimethylformamide.

Table 3. Effects of solvents on the yield of poly(methyl methacrylate)

MMA	Solvent	Time	Yield %
8 ml	none	1 day	17
5 ml	Toluene	7 days	5
5 ml	Benzene	7 days	0.2
5 ml	Tetrahydrofuran	7 days	trace
5 ml	Dimethylformamide	7 days	trace

$[CoH(N_2)(PPh_3)_3]$: 4—5 mmol/l 25°C

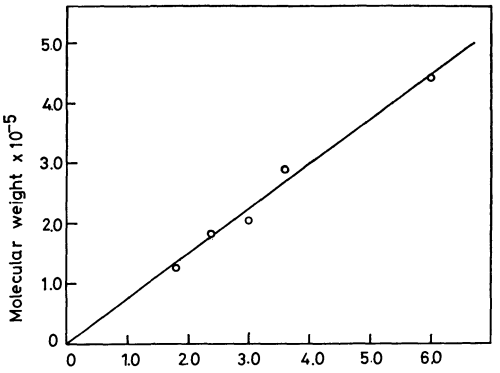

Fig. 3. The effect of concentration of methacrylonitrile on the molecular weight of poly(methacrylonitrile).

The molecular weight of poly(methacrylonitrile) increases linearly with increasing monomer concentration(Fig. 3). This supports our assumption that the coordination of the monomer to the complex with a growing polymer chain leads to the insertion of the monomer between the M–C bond. If we assume the following propagation and termination reactions

$$R_p = k_p[M][C^*]$$
$$R_t = k_t[C^*],$$

where [C*] represents the concentration of the catalyst with a growing polymer chain, the degree of polymerization of the polymer can be given by

$$\overline{DP} = (k_p/k_t)[M],$$

in agreement with the experimental result.

We showed that at least a part of the termination process takes place by hydrogen abstraction from the

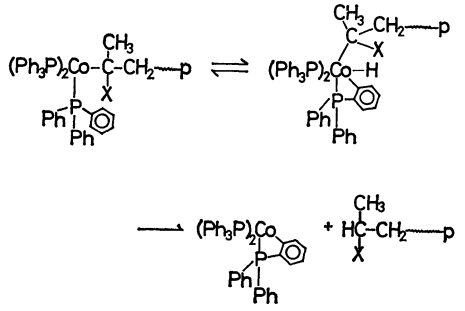

X=CN for methacrylonitrile
$COOCH_3$ for methyl methacrylate
Termination mechanism

Scheme 1.

β-position of the polymer chain bonded to the metal with the polymer end bearing the substituents.[9] If a similar β-hydrogen abstraction takes place also in this case, it would regenerate an active cobalt hydride species to initiate the polymerization again. That the initiator efficiency is lower than unity is not compatible with such a chain transfer mechanism. A possible termination mechanism is the one which involves the participation of ortho hydrogens of the triphenylphosphine ligand (Scheme 1).

The formation of a cobalt complex $Co(styrene)(C_6H_4PPH_2)(PPh_3)_2$,[8] in which cobalt is bonded with an *ortho* carbon of the triphenylphosphine ligand in the reaction of $CoH(N_2)(PPh_3)_3$ with styrene, supports the feasibility of the above mechanism.

TABLE 4. STEREOREGULARITY OF POLY(METHYL METHACRYLATE)

No.	Solvent	Triad[a]			Pm[b]
		mm	mr	rr	
1	—	10	25	65	0.23
2	Toluene	9	32	59	0.27
3	DMF	3	24	73	0.15

a) Triad tacticities: mm, isotactic; mr, heterotactic; rr, syndiotactic; peak areas determined by NMR spectra measured in nitromethane at 120°. b) Probability of *meso* placement; Average values calculated from triad are shown. Catalyst: $CoH(N_2)(PPh_3)_3$ at room temparature.

It was observed that the stereoregularity of poly(methyl methacrylate) obtained by the alkyl iron complex is affected by solvents, an acetone-soluble polymer rich in syndiotactic fraction, and an acetone-insoluble stereoblock type polymer being obtained.[10] The methyl methacrylate polymers obtained by the cobalt complex in toluene, dimethyl formamide and in the absence of solvent were soluble in acetone. The triad tacticities determined by NMR spectroscopy are given in Table 4. The polymers are all rich in syndiotactic fraction. The polymerization process appears to obey the Bernoulli trial with the probability of *meso* placement Pm[11] ranging from 0.15 to 0.27 depending on the solvent employed. The main factor in determining the stereoregularity of the polymer may be the mutual electrostatic and steric interactions between the substituents of the coordinating monomer and those of the polymer end attached to cobalt.

In order to obtain further information on the propagation mechanism, the copolymerization of methyl methacrylate (M_1) with methacrylonitrile (M_2) was studied. The results indicate that the copolymerization curve differs distinctly from that of free radical polymerization,[12] being somewhat similar to that of anionic polymerization.[13] The copolymer produced by the present catalyst, however, contains more methacrylonitrile units than those obtained by the conventional anionic initiators. The monomer reactivity ratios determined by an intersection method[14] for the copolymerization by $CoH(N_2)(PPh_3)_3$ were 0.20 ± 0.05 (r_1), 7.50 ± 0.40 (r_2), and $r_1 \times r_2 = 1.5\pm0.5$. A preferential introduction of methacrylonitrile to methyl methacrylate into the copolymer may be caused by the stronger coordinating ability of methacrylonitrile than methyl methacrylate in the compeptitive coordination of the monomers toward the complex with the growing polymer chain.[4]

In conclusion, the overall feature of the polymerization of vinyl monomers with the cobalt hydride complex is quite similar to that with the alkyliron[4] and ruthenium hydride[8] complexes: (i) the rate-determining initiation process involves the dissociation of the ligand for making a coordination site available toward the incoming monomer which enters into the metal–hydrogen or metal–carbon bond; (ii) the compeptitive coordination process is important in regulating the molecular weight and copolymer composition; (iii) the termination process is probably a spontaneous unimolecular process without involving a chain transfer process.

Experimental

General. Hydridodinitrogentris(triphenylphosphine)-cobalt was prepared as reported.[6] Monomers and solvents were purified by the usual methods and stored under nitrogen.

Polymerization. Polymerization was mostly carried out in a sealed ampoule in which the catalyst, monomer and solvent were transferred in a nitrogen stream or by a trap-to-trap distillation *in vacuo*. The ampoule was opened after the set time of polymerization and the content was poured into acidic methanol. The polymer was filtered, washed with methanol and dried. Kinetic study was carried out with a Schlenk type flask in a thermostatted water bath, the monomer being added with a pipette into the Schlenk type flask containing the catalyst solution. The yield was measured by weighing the polymer obtained after a set interval.

Copolymerization Experiment. Compositions of the copolymers between methyl methacrylate and methacrylonitrile were determined from the microanalysis of carbon, hydrogen and nitrogen.

Molecular Weight. The molecular weights of polymers were measured by a viscocity method using the following equations: for poly(methyl methacrylate),[15] $[\eta]=3.80\times10^{-5}M^{0.79}$; for poly(acrylonitrile),[16] $[\eta]=1.66\times10^{-4}M^{0.8}$; for poly(methacrylonitrile),[17] $[\eta]=9.55\times10^{-4}M^{0.56}$.

NMR Spectra. Proton magnetic resonance spectra of poly(methyl methacrylate) were obtained at 100 °C with a JEOL PS-100 Spectrometer at 100 MHz by using the sample solutions in nitromethane (*ca.* 10% W/V) containing a few per cent of tetramethylsilane as an internal standard.

References

1) L. Reich and A. Schindler, "Polymerization by Organometallic Compounds," Interscience Publishers, New York (1966); T. Keii, "Kinetics of Ziegler-Natta Polymerization," Kodansha Ltd., Tokyo (1971).

2) For example a) S. Inoue, T. Tsuruta, and J. Furukawa, *Makromol. Chem.*, **49**, 13 (1961); (b) N. Ashikari, *Kobunshi Kagaku*, **19**, 728 (1962); c) W. Baker, *J. Polym. Sci.*, **42**, 528 (1969); d) Von K. H. Reichert, J. Berthold, and V. Dornow, *Makromol. Chem.*, **121**, 258 (1969); e) Y. Suzuki and M. Saito, *J. Polym. Sci.*, *A*-1, **9**, 3639 (1971). f) H. Abe, K. Imai, and M. Matsumoto, *Polym. Lett.*, **3**, 1053 (1965);

J. Polym. Sci., C, **No. 23**, 469 (1968); g) A. B. Deshapnde, R. V. Subramanian, and S. L. Kapur, *J. Polym. Sci.*, **4**, 1799 (1966); h) L. C. Anand, S. S. Dixit, and S. L. Kapur, *J. Polym. Sci., A*-1, **6**, 909 (1968); i) S. L. Kapur, 23th IUPAC, Macromolecular Preprints 129, Boston, USA (1971).

3) D. G. H. Ballard, W. H. Jones, and T. Medinger, *J. Chem. Soc., B*, **1968**, 1168, 1176; D. G. H. Ballard, E. Jones, T. Medinger, and J. P. Pioli, *Makromol. Chem.*, **148**, 175 (1972); D. G. H. Ballard and J. Dawkins, *ibid.*, **148**, 195 (1972).

4) T. Yamamoto, A. Yamamoto, and S. Ikeda, This Bulletin, **45**, 1104, 1111 (1972).

5) Y. Kubo, A. Yamamoto, and S. Ikeda, *J. Organometal. Chem.* **60**, 165 (1973).

6) A. Yamamoto, S. Kitazume, L. S. Pu, and S. Ikeda, *J. Amer. Chem. Soc.*, **93**, 371 (1971).

7) Y. Kubo, A. Yamamoto, and S. Ikeda, *J. Organometal.* Chem. **59**, 353 (1973).

8) S. Komiya, A. Yamamoto, and S. Ikeda, Presented at the 20th Symposium of the Society of Polymer Science, Japan, Nov. 4—6, 1971, Tokyo.

9) T. Yamamoto, A. Yamamoto, and S. Ikeda, *Polym. Lett.*, **9**, 281 (1971).

10) A. Yamamoto, T. Shimizu, and S. Ikeda, *Polym. J.* (Tokyo), **1**, 171 (1971).

11) H. L. Frich, C. L. Mallows, and F. A. Bovey, *J. Chem. Phys.*, **45**, 1565 (1966).

12) R. M. Joshi and S. L. Kapur, *J. Sci. Ind. Res.* (India), **16B**, 379 (1957).

13) F. M. Lewis and F. R. Mayo, *J. Amer. Chem. Soc.*, **67**, 1701 (1945).

14) F. R. Mayo and F. M. Lewis, *ibid.*, **66**, 2050 (1944).

15) J. Y. Chine, L. H. Shin, and K. I. Shin, *Acta Chim. Sinica*, **23**, 213 (1957).

16) J. Bisshops, *J. Polym. Sci.*, **17**, 81 (1955).

17) N. Fuhrman and R. B. Besrobian, *J. Amer. Chem. Soc.*, **76**, 5281 (1954).

Tri(hetero)substituted Carbonium Ions. VII.[1] Effect of the Ring System on the Ambident Reactivity of Cyclic Dithiocarbamidium Ions[2]

Takeshi NAKAI, Kazuhisa HIRATANI, and Makoto OKAWARA

Reserach Laboratory of Resources Utilization, Tokyo Institute of Technology, Ookayama, Meguro, Tokyo 152

(Received June 20, 1973)

In order to study the effect of structure on the ambident reactivity of cyclic dithiocarbamidium ions, two *endo*-iminium type cations, 2-methylthio-3-methyl-4,5-dihydrothiazolium ion (**5**) and 2,3,5,6-tetrahydrothiazolo-[2,3-*b*]-thiazolium ion (**6**) were prepared. Their electrophilic reactivities were studied and compared with those of the *exo*-iminium type cations, 2-dimethylamino-1,3-dithiolan-2-ylium ion (**1**) and its ring analogues. 3-Dimethylamino-2,4-benzodithiepan-3-ylium ion (**7**) was prepared and its ambident reactivity was studied. Examination of the products obtained from their reactions with various nucleophiles revealed that the three cation have two reactive sites, *i.e.*, the central (sp^2) carbon (site *a*) and the *S*-methylene (or *S*-methyl) (sp^3) carbon atoms (site *b*). Significant differences in the electrophilic behavior of the *endo*- and *exo*-iminium type cations were observed. They were discussed in terms of the structures as estimated from the spectra. Kinetic experiments showed that the reactivities at site *a* of these cations with hydroxide ion, relative to that of **1**, are 22.5 (**5**): 16.6 (**6**): 27.2 (**7**), and at site *b* with *N*,*N*-dimethyldithiocarbamate ion are 3.3 : 282 : $>10^4$. The reactivity order suggests that the reactivities at the two sites, especially at site *b*, are very sensitive to a change in the ring system of the cations.

In previous papers of this series,[3–6] the electrophilic behaviors of various dithiocarbamidium ions[7] including 2-dimethylamino-1,3-dithiolan-2-ylium ion (**1**), its ring analogues (**2** and **3**), and an open-chain analogue (**4**) were reported. It was shown that (a) the carbonium ions have two reactive sites, *a* and *b* in the formula shown below, (b) the reaction course is determined by both the nature of the attacking reagent employed and the structure of the cation and (c) the electrophilic reactivities at both sites depend markedly upon the the ring-size of the cation.

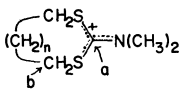

1: $n=0$
2: $n=1$
3: $n=2$

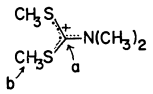

4

In order to obtain further information on the relationship between the structure and reactivity of dithiocarbamidium ions, the electrophilic behavior of 2-methylthio-3-methyl-4,5-dihydrothiazolium ion (**5**) and 2,3,5,6-tetrahydrothiazolo[2.3-*b*]thiazolium ion (**6**) has been investigated and compared with that of cation **1** having the same ring-size as **5** (and **6**). While the cyclic cations such as **1** and **2** are tentatively classified as *exo*-iminium type, **5** and **6** can be classified as *endo*-iminium type. The electrophilic reactivity of another *exo*-iminium type cation, 3-dimethylamino-2,4-benzodithiepan-3-ylium ion (**7**), was studied and compared with that of monocyclic **3** having the same ring-size as **7**.

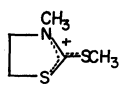

5

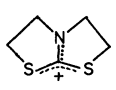

6

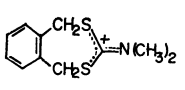

7

Results

Preparation of Carbonium Salts. Cations **5** and **6** were obtained as the iodide (**5a**)[8] and the chloride (**6a**)[9] by the methods in literature. Perchlorate (**5b**) was prepared by methylation of 3-methylthiazolidine-2-thione with dimethyl sulfate followed by treatment with sodium perchlorate. Treatment of **6a** with sodium perchlorate gave perchlorate (**6b**). Cation **7** was obtained as perchlorate by the reaction of *o*-xylylene dibromide with sodium *N*,*N*-dimethyldithiocarbamate followed by treatment with sodium perchlorate. Even under equimolar conditions, the disubstituted product, *o*-xylylene bis(dithiocarbamate) (**8**), was formed in considerable yields together with **7** and the product ratio varied with the solvent used. This suggests that, as in the reactions of 1,2-dichloroethane and 1,3-dichloropropane with the dithiocarbamate anion,[3,5,10] neighboring-group participation of the dithiocarbamate function accelerates the second substitution process, **9**→**8**, through the intermediacy of the isolated anchimeric cation (**7**), as illustrated below.

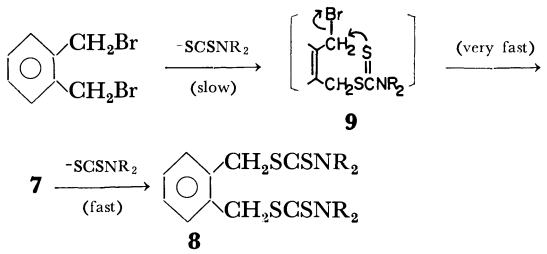

All carbonium salts thus obtained were identified by means of NMR spectroscopy and elemental analyses. The spectral data for the cations are given in Table 1 together with those for **1** and **3** as references.

Reactions with Various Nucleophiles. In order to demonstrate the ambident character of the cations, the reactions of **5** and **6** with a variety of nucleophiles were studied. The products thus obtained are given in Table 2. They were identified by IR, NMR and UV spectroscopy and/or comparison of their physical properties with those of authentic samples (see Experimental). All the products except for **10**, **11**, and the 2-imino-thiazolidines are known compounds,

Table 1. Melting points and spectral data of the carbonium salts

Cation	Mp, °C (counter anion)	UV[a] λ_{max}, mμ	NMR,[b] δ ppm -SCH_2-	-NCH_2-	Others
5	132—135 (I^-)[c] d) (ClO_4^-)	252	3.82(t)	4.55(t)	NCH_3 3.55(s) SCH_3 2.94(s)
6	93—95 (Cl^-)[e] 158—159 (ClO_4^-)	257	4.18(s)[f]		
1[g]		249	3.61(s)		NCH_3 4.08(s)
7	205—207 (ClO_4^-)	267	5.10(s)		NCH_3 2.95—3.10(m) Aromatic 7.7—7.9(m)
3[h]		275	3.47		NCH_3 3.61(s)

a) In water; the molar extinction coefficients (ε) were about 10^4 for all carbonium salts. b) In $(CD_3)_2SO$; multiplicity: s=singlet, t=triplet, and m=multiplet. c) Reported mp 132—135°C: ref. 8. d) The perchlorate was so hygroscopic that mp could not be measured. e) Reported mp 95°C: ref. 9. f) In D_2O: ref. 9. g) Taken from ref. 3. h) Taken from ref. 5.

Table 2. Reactions of the cations with nucleophiles

Nucleophile	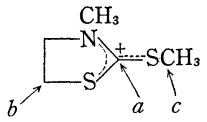 (5)	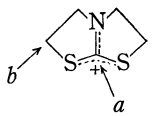 (6)	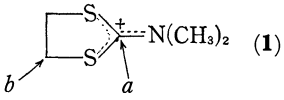 (1)
	Product (Attacking site)	Product (Attacking site)	(Attacking site)
-OH	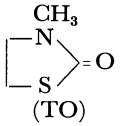 (TO) (*a*)	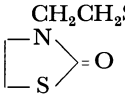 (*a*)	(*a*)
$-OCH_3$	TO (*a*)		(*a*)
-CN	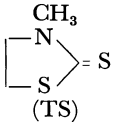 (TS) (*c*)	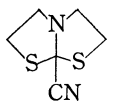 (**10**) (*a*)	(*a*)
H_2NR	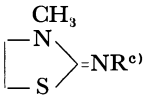 (*a*)		(*a*)
-SR		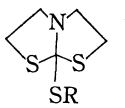 b)d) (*a*)	(*b*)
$-SCSN(CH_3)_2$	TS + $CH_3SCN(CH_3)$ (*c*)	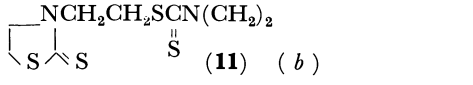 (**11**) (*b*)	(*b*)
$N(C_2H_5)_3$	TS + $[CH_3\overset{+}{N}Et_3]$ (*c*)	An unidentified product[e]	f)

a) Ref. 4. b) Ref. 9. c) R=phenyl and $NHSO_2C_6H_4CH_3(p)$. d) R= 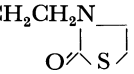 e) In very poor yield; bp 86—89°C/0.3 mmHg. f) A proton abstraction reaction was observed: ref. 4.

The NMR spectrum of **10** showed only one slightly split singlet signal at δ 3.77 (Fig. 1) and the IR spectrum an absorption band at 2200 cm^{-1} due to the cyano group. The NMR spectrum of **11**, on the other hand, showed several signals which were assigned as shown in Fig. 1 through comparison with spectra of 3-methylthiazolidine-2-thione and methyl *N*,*N*-dimethyldithiocarbamate. The structure of **11** was further confirmed by the identity of its UV spectrum with that of an equimolar mixture of the two references.

It was found that **7** reacted with hydroxide and *N*,*N*-dimethyldithiocarbamate ions to yield *o*-mercaptomethylbenzyl thiolcarbamate (**12**) and the bis(dithiocarbamate) (**8**), respectively. The formation of **12** and **8** is best explained as a result of the attack of the nucleophile on the central carbon and on the *S*-methylene carbon, respectively.

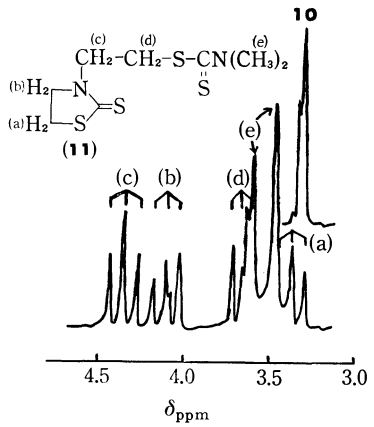

Fig. 1. NMR spectra of **10** and **11** ($CDCl_3$).

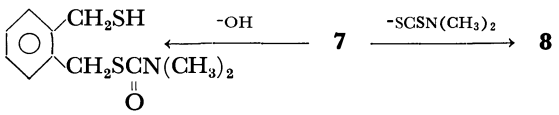

12

Kinetic Studies. The reaction at site *a* is kinetically controlled (mode A) whereas the reaction at site *b* or *c* is thermodynamically controlled (mode B).[3,4] In order to estimate the reactivity of modes A and B of the cation, the rates of reactions of the carbonium perchlorates with hydroxide and *N,N*-dimethyldithiocarbamate ions were measured, according to the procedures previously reported.[5]

The reaction of the cation with hydroxide ion was carried out in buffer solutions at 30 °C under pseudo-first-order conditions. Plots of the observed pseudo-first-order rate constants (k_{obs}) against the hydroxide concentrations were linear in the pH ranges studied for the cations (Fig. 2). The values of the second-order rate constants (k_a) for the reactions with hydroxide ion were obtained from the slopes of the straight lines obtained. The reaction of the cation with the dithiocarbamate ion was studied in dimethylformamide (DMF) at 30 °C. The values of the second-order rate constants (k_b) for the reaction with the dithiocarbamate ion were obtained from the slopes of the second-order rate plots (Fig. 3). The reaction of **7** with the anion

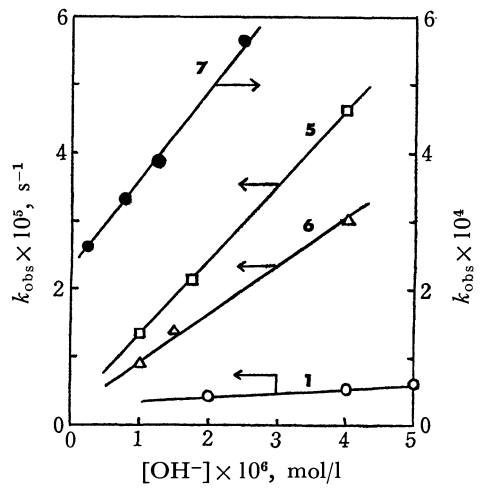

Fig. 2. Plots of k_{obs} *vs.* [OH$^-$]

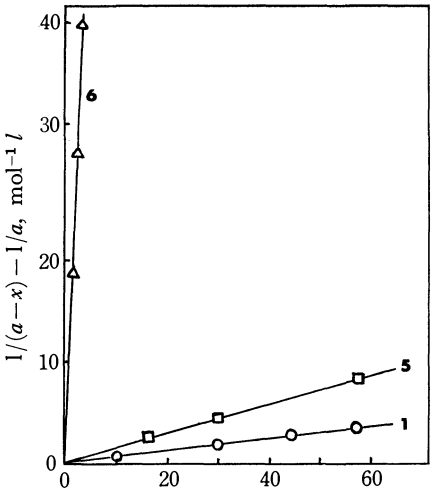

Fig. 3. Second-order rate plots for the reaction of the dithiocarbamate ion.

TABLE 3. RELATIVE REACTIVITIES OF MODE A AND B FOR THE CARBONIUM IONS (30°C)

Cation	Mode A Rel. k_a	Mode B[a] Rel. k_b
1[b]	1.0[c]	1.0[d]
5	22.5	3.3[e]
6	17.6	282
7	27.2	Very fast ($>10^4$)[f]
3	32.5	23.8

a) Unless otherwise stated, the reaction proceeded at site *b*. b) Ref. 5. c) $k_a=5.1\times10^{-1}$ M^{-1} s^{-1}. d) $k_b=1.30\times10^{-3}$ M^{-1} s^{-1}. e) At site *c*. f) See text.

was too fast to be measured by the present method. The value of k_b for **7** was found to be at least 10 M^{-1} s^{-1}. Table 3 shows the relative values of k_a and k_b for the cations.

Discussion

Spectra and Relative Stabilities of the Carbonium Ions. The extent of stabilization of tri(hetero)carbonium ions depends upon the electron-donating power of the hetero-substituents directly adjoining the electron-deficient carbon atom. However, for the series of cyclic dithiocarbamidium ions we studied the extent of stabilization is expected to depend upon other structural factors, *e.g.*, the ring-size and the ring system, which enhance or diminish the internal dissipation of the positive charge.

On the other hand, it has been established[11] that the relative stability of a series of open-chain tri(hetero)-carbonium ions is linearly correlated with the transition energy ($1/\lambda_{max}$) in the electronic spectra; *the more stabilized the tri(hetero)carbonium ion, the shorter (higher energies) the wavelengths to which the maximum absorption band (λ_{max}) shifts.*[12] The linear correlation has not only been confirmed by simple HMO calculation[11] but also accepted experimentally for a series of cyclic dithiocarbamidium ions of *exo*-iminium type.[5,13]

Thus, the UV spectral data (Table 1) indicate that the stability of **5** (*endo*-iminium) is comparable to that of **1** (*exo*-iminium) and that both cations are more stabilized than open-chain **4** (λ_{max} 276 mμ[5]) presumably due to the more developed 1,3-overlapping in the ring system. The former is of particular interest since it could be expected that **5** is more stabilized than **1** if the formal ring-closures leading to the *endo*- (**5**) and *exo*-iminium type (**1**) increase the conjugative (stabilizing) effect of a combination of the nitrogen and sulfur atoms and of the two sulfur atoms in each ring *by the same factor*.[14] This would imply that participation of the nonbonding electron pair on the nitrogen in **5** is less fully involved in the 1,3-overlap seemingly due to twisting of the axis of symmetry of the nitrogen p orbital out of parallel with that of the vacant pπ orbital of the sp^2 carbon.

Another interesting fact obtained from UV spectral comparison is that bicyclic **6** is less stable than **1** and **5**. This suggests that the contribution to stabilization from the iminium structure (**6'**) is to a greater extent reduced by steric requirement presumably due to a larger twisting of the nitrogen p orbital described above, thus making the contribution from the sulfonium structure (**6''**) relatively more favored.[15] This is supported by the unusual observation that the NMR spectrum of **6** showed only singlet at δ 4.18, indicating that the *N*-methylene protons of **6** are more shielded than those of **5** (δ 4.55) while the *S*-methylene protons of **6** (δ 4.18) are much more deshielded than those of **5** (δ 3.82) and **1** (δ 3.61). The spectral observation also indicates a structure with all eight skeletal atoms nearly in one plane for **6**.[15]

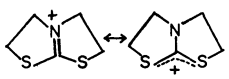

6' **6''**

Comparison of λ_{max} between the two seven-membered cations shows that **7** is more stabilized than **3**; this suggests that the seven-membered ring of **7** is undoubtedly constrained to a near-planar configuration by the fused benzene ring, so that the 1,3-overlap in **7** is more effective.

It can be said that the stabilities of the cyclic dithiocarbamidium ions depend markedly not only on the ring-size but also on the ring system, and decrease in the order: **1**≈**5**>**6**>**2**>**7**>**3**≈**4**.

Effect of Ring System on the Ambident Reactivity

The stability of the tri(hetero)carbonium ion plays an important role in determining both the reaction course and the dual reactivities at the two sites.[4,5]

Let us discuss the effect of the ring system on the course of reaction of the cations with nucleophiles. An examination of the structures of the products given in Table 2 shows that the cations have two electrophilic sites and that the course of reaction with nucleophiles follows the selectivity rule[4]; hard bases, *e.g.*, OH^-, react at site *a* (mode A) while soft bases, *e.g.*, R_2NCSS^-, and bulky bases react at site *b* or *c* (mode B). However, the following significant differences in the reaction course of the *endo*- and *exo*-iminium types were observed: (a) the *endo*-iminium **5** directs the attack of CN^- to site *c* (mode B) while the *exo*-iminium **1** (and **6**) directs it to site *a* (mode A); (b) the bicyclic *endo*-iminium **6** directs the attack of RS^- to site *a* while **1** directs it to site *b*.

Case (a) is not well understood at the present stage. A possible factor responsible for the difference might be steric hindrance by the *N*-methyl of **5** arising from twisting of the nitrogen to attack CN^- at site *a*.

Case (b), on the other hand, is essentially the same as in the course of reaction with RS^- observed between **1** and open-chain **4** which has been best explained in terms of the difference in stability between **1** and **4**.[6] Thus, a similar argument is possible.

The major factor deciding the reaction course is the energy gap between the cation and its kinetically controlled (mode A) product.[4,16] In view of the fact that **6** is less stable than **1**, the energy gap between **6** and its mode A product (**13**) might be larger than that between **1** and its mode A product (**14**) since the process from **6** to **13** would result in the release of energy of both charge neutralization and twisting (ring strain) while the process from **1** to **14** would result in the release of only charge neutralization. As

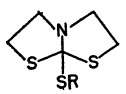

13

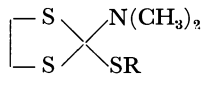

14

a result, the position of the equilibrium in Eq. 1 shifts to the right leading to the formation of the kinetic adduct (**13**), whereas that in Eq. (2) shifts to the left leading to the formation of the thermodynamically stable product (**15**) *via* mode B.

$$\mathbf{6} + RS^- \rightleftharpoons \mathbf{13} \quad (1)$$

$$\mathbf{1} + RS^- \rightleftharpoons \mathbf{14} \quad (2)$$

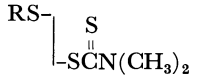

15

Let us now discuss the effect of ring system on the reactivities of both modes of the cations on the basis of the kinetic data given in Table 3. Figure 4 shows plots of the relative reactivities of mode B against those of mode A for the cations of *endo*- and *exo*-iminium types.

It has been suggested[5,16] that the reactivity of modes A and B depends, respectively, upon the energy gap between the cation and the kinetic adduct (the carbinol in this case) and between the cation and the transition state. If the energy contents of the carbinols for mode A and of the transition states for mode B were nearly constant, irrespective of changes in structures of the cations, that is, the rates of reactions were determined solely or at least favorably by the stability of the cations themselves, the rates of reactions of both modes would increase with a decrease in stability of the cation. This is the case for a series of the cations of *exo*-iminium type (Fig. 4). Thus, in view of the stability order of the cations, a similar argument is possible in explaining the observation qualitatively that

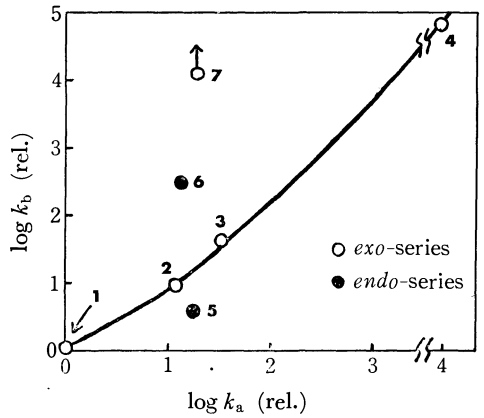

Fig. 4. Plots of log k_b *vs.* log k_a.

the k_a-value for **6** is larger than that for **1** and that the k_a-value for **7** is smaller than that for **3**.

It is obvious, however, that the stability order cannot account for the following observations; (a) mode A reactivity of **5** is larger than that of **1**, (b) mode B reactivity of **6** is much higher than not only that of **1**, but that of the six-membered **2** although **2** is less stable than **6**, and (c) mode B reactivity of **7** is much larger than that of **3** even though **7** is more stable than **3**. Thus, we should consider the unusual observations which are connected purely with the effect of ring system on the reactivity.

Observation (a) cannot be explained at the present stage. The higher reactivity of mode B of **6**, compared with that of the less stable cation **2**, indicates that **6** should represent the transition state of lower energy, *i.e.*, $\Delta F_B^{\neq}$ for **6** $<\Delta F_B^{\neq}$ for **2** in the schematic energy profile (Fig. 5). In view of the structural aspects for **6** it seems that the following factors are operative in activating the reaction center (site *b*); a more favorable contribution to stabilization from the sulfonium structure (**6″**) by steric requirement and a relief of the ring strain. Similarly, the higher reactivity of **7** indicates that $\Delta F_B^{\neq}$ for **7** is smaller than that for **3** in the energy profile even though the energy level for **7** is lower than that for **3**. It appears that the enhanced reactivity of **7** can be ascribed to two factors; the constrained near-planar configuration and the electronic effect of the fused benzene nucleus on the benzylic carbon atom.

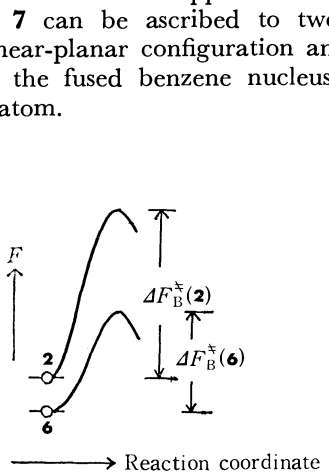

Fig. 5. Schematic ene gy profiles for mode B.

Experimental

General. Melting and boiling points are uncorrected. IR and UV spectra were recorded with Hitachi EPI-S2 and EPS-2 spectrometers. NMR spectra were obtained with a Japan Electron Optics C-100 spectrometer. Chemical shifts are reported in terms of δ ppm downfield from tetramethylsilane as an internal standard.

Materials. 3-Methylthiazolidine-2-thione was obtained in 65% yield from *N*-methylethanol amine and carbon disulfide by a modification of the method reported previously.[8] Bis(β-chloroethyl)amine hydrochloride and *o*-xylylene dibromide were prepared according to the procedure in literature.[9,17] Commercial reagents and solvents were used after purification by standard methods.

*2-Methylthio-3-methyl-4,5-dihydrothiazolium Salts (**5**).* 3-Methylthiazolidine-2-thione (7.5 g) was dissolved in 6.3 ml of methyl iodide. The mixture was heated at 40 °C for 30 min giving precipitates of the carbonium iodide (**5a**) quantitatively. Recrystallization of the precipitates from ethanol gave yellowish crystals; mp 132—135 °C (lit,[8] 132—135 °C).

Perchlorate (**5b**) was obtained as follows. 3-Methylthiazolidine-2-thione (2.7 g) was dissolved in 2.5 g of dimethyl sulfate. A vigorous exothermic reaction occurred when the mixture was heated up to 60 °C. The reaction temperature was kept below 100 °C. After the exothermic reaction was over, the mixture was stirred at 90 °C for 30 min. The mixture was poured into a saturated aqueous solution of sodium perchlorate giving 5.0 g (85%) of a pale yellowish precipitate, which was washed several times with ether and dried over phosphorous pentoxide *in vacuo*. The precipitate was so hygroscopic that its mp could not be determined. The structure of the salt was confirmed by its NMR spectrum (Table 1).

*2,3,5,6-Tetrahydrothiazolo[2.3-b]thiazolium Salts (**6**).* Carbonium chloride (**6a**) was prepared by the method in literature.[9] Bis(β-chloroethyl)amine hydrochloride (7.14 g) was dissolved in a solution of pyridine (10 ml) and water (4 ml). Carbon disulfide (2.4 ml) was added dropwise into the mixture with stirring for one hour; the mixture was kept below 10 °C. The white turbid solution thus formed was stirred at room temperature for 45 min, and warmed at 40 °C for 20 min. The reaction mixture was cooled in an ice box giving 7.9 g (90%) of a colorless precipitate. The precipitate was then dissolved in a minimum amount of water and reprecipitated by addition of ethanol giving colorless crystals; mp 93—95 °C (lit.,[9] 95 °C).

Treatment of **6a** with saturated aqueous solution of sodium perchlorate gave a colorless precipitate; mp 158—159 °C (recrystallized from acetonitrile).

Found: C, 24.40; H, 3.26; N, 5.70%. Calcd for $C_5H_8ClNO_4S_2$: C, 24.57; H, 3.36; N, 5.61%.

*3-Dimethylamino-2,4-benzodithiepan-3-ylium Perchlorate (**7**).* *o*-Xylylene dibromide (5.3 g) was added to a suspension of sodium *N,N*-dimethyldithiocarbamate (3.6 g) in 50 ml of dioxane. The mixture was stirred at 60 °C for 5 hr, then poured onto cold water (*ca.* 150 ml) giving 2.0 g of a white precipitate of *o*-xylylene bis(dithiocarbamate) (**8**); mp 124.5—125.5 °C (recrystallized from benzene); UV (EtOH): λ_{max} 250 and 275.5 mμ. The IR spectrum showed several absorption bands due to –S–CS–N<.

Found: C, 48.84; H, 5.86; N, 8.14%. Calcd for $C_{14}H_{20}N_2S_4$: C, 48.79; H, 5.85; N, 8.13%.

The filtrate was extracted with benzene and the aqueous solution was treated with an excess of sodium perchlorate giving 2.5 g (40%) of a white precipitate. Recrystalliza-

tion of the precipitate from ethanol and benzene gave colorless needles (**7**); mp 205—207 °C (dec.).

Found: C, 41.13; H, 4.24; N, 4.46%. Calcd for $C_{11}H_{14}ClNO_4S_2$: C, 40.80; H, 4.36; N, 4.33%.

Reaction of ***5a*** *with Sodium Methoxide.* **5a** (2.9 g) and sodium methoxide (1.1 g) were added to 25 ml of dioxane. The mixture was stirred at 100 °C for 3 hr and then poured into water. The mixture was extracted with ether. The ethereal layer was dried over anhydrous sodium sulfate, and the solvent evaporated *in vacuo*. Distillation of the residue gave 0.70 g (70%) of 3-methylthiazolidine-2-one; bp 85—87 °C/0.3 mmHg (lit,[18] 84—85 °C/0.2 mmHg); IR (neat): 1665 cm^{-1} (C=O). The IR spectrum of the product was in agreement with that of an authentic sample.

Hydrolysis of ***5a***. **5a** (0.02 mol) was dissolved in 20 ml of water. The mixture was heated at 60 °C for 3 hr and then extracted with ether. The ethereal solution was dried over anhydrous sodium sulfate and the solvent evaporated, giving 1.0 g of a yellowish oily residue. The IR spectrum of the residue was essentially the same as that of 3-methylthiazolidine-2-thione.

Reaction of ***5a*** *with Aniline.* **5a** (0.01 mol) and aniline (0.01 mol) were dissolved in 40 ml of acetic acid. The mixture was heated at 100 °C for 1 hr. The solvent was removed under reduced pressure giving a solidified residue. Recrystallization of the residue from acetonitrile gave crystals of the hydroiodide of 2-phenylimino-3-methylthiazolidine in 58% yield; mp 215—220 °C.

Found: N, 8.60%. Calcd for $C_{10}H_{13}IN_2S$: N, 8.75%.

An aqueous solution of the hydroiodide was treated with sodium methoxide giving the precipitate of 2-phenylimino-3-methylthiazolidine; mp 90—92 °C (recrystallized from methanol); IR (KBr): 1610 cm^{-1} (C=N).

Found: C, 61.97; H, 6.49; N, 14.63%. Calcd for $C_{10}H_{12}N_2S$: C, 62.48; H, 6.29; N, 14.58%.

Reaction of ***5a*** *with Tosylhyrdazine.* Tosylhydrazine (3.7 g) was suspended in a solution of **5a** (0.02 mol) in 40 ml of ethanol. The suspension was stirred at 55—60 °C for 4 hr. The reaction mixture turned into a clear solution. The resulting mixture was cooled in an ice box giving 2.7 g (62%) of a precipitate of the hydrazone. Recrystallization of the precipitate from ethanol gave colorless needles; mp 215 °C (dec.); IR (KBr): 1590 cm^{-1} (C=N).

Found: C, 46.08; H, 5.29; N, 15.06%. Calcd for $C_{11}H_{15}N_3O_2S_2$: C, 46.31; H, 5.30; N, 14.73%.

Reaction of ***5a*** with Triethylamine. **5a** (0.01 mol) was dissolved in a solution of triethylamine (1.0 g) in 20 ml of DMSO. The mixture was heated at 80 °C for 4 hr and then poured onto cold water giving 0.70 g (52%) of the precipitate of 3-methylthiazolidine-2-thione. The IR and UV spectra of the product were in agreement with those of an authentic sample.

Reaction of ***5a*** *with Sodium* N,N-*Dimethyldithiocarbamate.* **5a** (0.01 mol) was dissolved in a solution of sodium dimethyldithiocarbamate (3.0 g, 0.015 mol) in 40 ml of DMF. The reaction mixture was heated at 70 °C for 5 hr and then poured onto cold water. The mixture was extracted with benzene. The benzene layer was dried over anhydrous sodium sulfate and the solvent evaporated *in vacuo* giving a half-solid residue (1.3 g). Thin layer chromatography (tlc) was applied to separation and identification of the residue. The chromatogram was developed over silica gel (G. E. Merck Ag., Darmstadt) by dipping the top end of the glass plate in anhydrous ether. The plate was then exposed to iodine vapor showing two spots which were found to be those of methyl *N,N*-dimethyldithiocarbamate (R_f=0.98) and 3-methylthiazolidine-2-thione (R_f=0.46). The result was confirmed by UV spectroscopy.

Reaction of ***6b*** *with Sodium Cyanide.* **6b** (5.4 g, 0.02 mol) and sodium cyanide (1.0 g) were dissolved in 30 ml of DMF. The mixture was heated at 50—60 °C for 6 hr giving the precipitate of sodium perchlorate which was then filtered off. The filtrate was concentrated under reduced pressure and cooled in an ice box giving 3.2 g (93%) of a pale yellowish precipitate. Recrystallization of the solid from ethanol gave colorless crystals (**10**): mp 72—73 °C; IR (KBr): 2260 cm^{-1}(C≡N); NMR ($CDCl_3$): δ 3.37.

Found: C, 42.62; H, 4.61; N, 16.44%. Calcd for $C_6H_8N_2S_2$: C, 41.86; H, 4.68; N, 16.28%.

Reaction of ***6b*** *with Sodium* N,N-*Dimethyldithiocarbamate.* **6b** (5.4 g) and sodium *N,N*-dimethyldithiocarbamate (3.6 g) were dissolved in 20 ml of DMF. The mixture was heated at 60 °C for 2 hr, then poured onto cold water giving 4.4 g (83%) of a white precipitate. Recrystallization of the precipitate from ethanol and acetonitrile gave colorless needles (**11**); mp 142—143 °C. The IR spectrum of the product showed several absorption bands due to -S-CS-N<. The UV spectrum was in agreement with that of an equimolar mixture of methyl *N,N*-dimethyldithiocarbamate and 3-methylthiazolidine-2-thione.

Found: C, 36.28; H, 5.22; N, 10.18%. Calcd for $C_8H_{14}N_2S_4$: C, 36.10; H, 5.26; N, 10.52%.

The reaction of **6b** (0.01 mol) with sodium *N,N*-diethyldithiocarbamate (0.01 mol) carried out as in the case of sodium *N,N*-dimethyldithiocarbamate gave *N*-(*β*-*N'*,*N'*-diethyldithiocarbamoyl)ethylthiazolidine-2-thione in 80% yield; mp 74—75 °C (recrystallized from ethanol).

Found: C, 40.74; H, 6.21%. Calcd for $C_{10}H_{18}N_2S_4$: C, 40.81; H, 6.17%.

Hydrolysis of ***7***. Perchlorate **7**(0.01 mol) was dissolved in 10 ml of water. The mixture was heated at 60 °C for 3 hr and then extracted with benzene. The benzene layer was dried over anhydrous sodium sulfate and the solvent evaporated *in vacuo* giving a small amount of a yellowish oil; IR (neat): 1650 cm^{-1}(C=O). The oil discolored an aqueous solution of iodine and gave the mercury mercaptide on treatment with mercuric chloride indicating the presence of the mercapto group.

Reaction of ***7*** *with Sodium* N,N-*Dimethyldithiocarbamate.* **7** (0.3 g) and sodium dimethyldithiocarbamate (0.5 g) were dissolved in 20 ml of DMF. The mixture was stirred at 60 °C for 30 min and then poured onto cold water giving 0.35 g (98%) of a white precipitate. The product was identical with *o*-xylylene bis(dithiocarbamate) (**8**).

Kinetic Measurements. Hydrolyses (Mode A). The equipment and procedures were the same as those employed previously.[5] The rates of hydrolyses of the carbonium perchlorates were spectrometrically measured at 30 °C by following the disappearance of the cation. Pseudo-first-order rate constants (k_{obs}) were calculated from the plots of 2.303 log $(OD)_0/(OD)_t$ *vs.* time. The plots of k_{obs} against [OH^-] for the cations were linear in the pH range 7.5—9.0. The second-order rate constant (k_a) for reaction with hydroxide ion was calculated from the slopes of plots of k_{obs} *vs.* [OH^-] (Fig. 2).

Reactions with Sodium N,N-*Dimethyldithiocarbamate (Mode B).* The procedures were the same as those employed previously.[3,5] The rates of reactions with the dithiocarbamate anion were measured at 30 °C by following the disappearance of the anion. All reactions were carried out in DMF under equimolar conditions. At various time intervals the dithiocarbamate ion was gravimetrically determined from the quantity of the nickel chelate precipitated by treatment of the aqueous solution of the sample with an excess of a sa-

turated aqueous solution of nickel chloride. The second-order rate constants (k_b) were calculated from the slopes of plots of $1/a-x$ *vs.* time (Fig. 3).

References

1) Part VI: T. Nakai and M. Okawara, This Bulletin, **43**, 3882 (1970).
2) A part of this work was presented at the 19th Symposium on Organic Reaction Mechanisms, Yamagata, 14, October, 1968. This work was supported in part by a grant from the Ministry of Education.
3) T. Nakai, Y. Ueno, and M. Okawara, *Tetrahedron Lett.*, **1967**, 3831; This Bulletin, **43**, 156 (1970).
4) T. Nakai and M. Okawara, *ibid.*, **1967**, 3835; This Bulletin, **43**, 1864 (1970).
5) T. Nakai, Y. Ueno, and M. Okawara, *ibid.*, **43**, 3175 (1970).
6) T. Nakai and M. Okawara, *ibid.*, **43**, 3528 (1970).
7) According to the carbonium ion nomenclature, the cations are also termed bis(alkylthio)-dialkylamino-carbonium ions.
8) J. W. Batty and B. C. Weedon, *J. Chem. Soc.*, **1949**, 786.
9) S. Seto and Y. Ikegami, This Bulletin, **36**, 730 (1963).
10) T. Nakai, H. Kawaoka, and M. Okawara, *ibid.*, **42**, 508 (1969).
11) T. Nakai, K. Hiratani, and M. Okawara, *ibid.*, **43**, 3016 (1970).
12) The spectral trend suggests that the heterosubstituents stabilize the ground state more than the excited state. A similar trend has been reported for the alkyl substitution on alkenylcarbonium ions: G. A. Olah, C. U. Pittman, Jr., and M. C. R. Symons, "Carbonium Ions," Vol. 1, G. A. Olah and R. v. R. Schleyer, Edit., Interscience Publ., New York, 1968, Chapter 5.
13) T. Nakai and M. Okawara, presented at the 3rd Symposium on Organic Sulfur Chemistry, Tokyo, 8, February, 1969.
14) Note that dialkylamino groups are generally much more electron-donative than alkylthio groups.
15) This fact has been confirmed by vibrational (IR and Raman) spectroscopy.[9]
16) S. Hünig. *Angew. Chem. Int. Ed. Engl.*, **3**, 548 (1964).
17) E. F. M. Stephenson, "Organic Syntheses", Coll. Vol. 4, 984 (1963).
18) Y. Ueno, T. Nakai, and M. Okawara, This Bulletin, **43**, 168 (1970).

Synthetic Studies by the Use of Carbonates. I. The Nucleophilic Substitution Reaction of Ethylene Carbonate with Amine Hydrohalides

Teruo YOSHINO, Shigeru INABA, Hajime KOMURA, and Yoshiharu ISHIDO

Department of Chemistry, Faculty of Science, Tokyo Institute of Technology, O-okayama, Meguro, Tokyo 152

(Received July 25, 1973)

The reaction of ethylene carbonate with various amine hydrohalides gave the corresponding quaternary ammonium salts of β-hydroxyethylamines in good yields.

The nucleophilic substitution reactions of ethylene carbonate(**1**) with metal halides, such as potassium fluoride, lithium chloride, and sodium bromide, accompanied by the evolution of carbon dioxide gas, have been shown to give the corresponding ethylene halohydrins, and the reaction with potassium iodide has been shown to give ethylene oxide exclusively.[1] In view of these facts, the present authors attempted the reaction of **1** by ammonium halides and various amine hydrohalides. The results thus obtained will be described in this paper.

Results and Discussion

On the basis of the idea that the application of ammonium halides to the reaction of **1** in place of the above metal halides may bring about the formation of ethylene halohydrins(**2**), with a concomitant evolution of ammonia and carbon dioxide gas, ammonium bromide(**3**) was allowed to react with three moles of **1** at 145 °C. This reaction, however, afforded no ethylene bromohydrin, but only tri-(**4**) and tetra-β-hydroxyethylammonium bromides(**5**) in 54 and 45% (raw sirup) yields (Scheme 1). The structural assignment of **5** was accomplished by converting it into the corresponding perchlorate of the tetra-*O*-acetate.

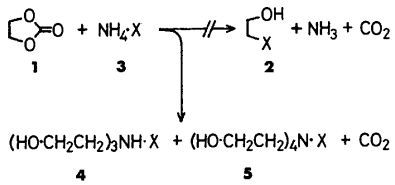

Scheme 1

In addition, the reactions of an equimolar portion and two moles of **1** with **3** afforded **4** in 28 and 36% yields, besides the recovered **3** in 13 and 5% yields, respectively; no formation of *N*-mono-, -di-, and -tetra-β-hydroxyethylammonium bromides could be detected. Ammonium chloride and iodide also provided no halohydrin, but only unseparable mixtures of the corresponding tri- and tetra-β-hydroxyethylammonium halides, in reactions with **1**. Accordingly, such a comparative investigation of the reaction of **1** with these ammonium halides was abandoned. These results, however, led us to the assumptions regarding the reaction that halohydrins and ammonia are generated in the initial stage of the reaction, and that they react with each other successively to afford the products described above.

On the basis of these results, various amine hydrohalides were allowed to react with **1**, assuming that this reaction might be a general method for the preparation of β-hydroxyethylamine hydrohalides. Prior to the extention, the difference in the reactivity arising from the nature of halide ions was examined by heating an equimolar mixture of **1** and triethylamine hydrohalides (**6**) at 145 °C (Scheme 2). Volumes of the concomitantly-evolved gas were measured with a gas buret at room temperature under atmospheric pressure. In the cases of **6** (X=Br and I), the evolution of *ca.* 95% of the theoretical amount of carbon dioxide gas was observed within 1 hr; a steady state was thus obtained. In the case of **6**(X=Cl), on the other hand, the volume of evolved gas reached *ca.* 130% of the theoretical yield in the reaction with an equimolar **1**.[2] Such an unusual phenomenon may coincide with the exceedingly lowered yield (5%) of triethyl-β-hydroxyethylammonium halide(**7**) (X=Cl) in contrast with those of **7**(X=Br, 90%; X=I, 91% yield). In these experiments, the bromide (**7**, X=Br) was proved to be more easily crystallized from ethanol than the chloride and the iodide. Consequently, amine hydrobromides were used in the following experiments. The results thus obtained are summarized in Table 1, while the UV absorption spectral data of aromatic amine derivatives are listed in Table 2. The hydrobromides of tertiary amines, such as trimethylamine, pyridine, 2-(**8**), 4-aminopyridine(**9**), quinoline, 8-quinolinol, and nicotinamide(**10**), gave the corresponding mono-β-hydroxyethylammonium bromides in good yields. Moreover, the hydrobromides of primary and secondary amines, such as ethylamine, cyclohexylamine, and morpholine hydrobromides, afforded the corresponding mono-β-hydroxyethylammonium bromides selectively; this was in contrast with the corresponding free amines, which have well been known to afford the corresponding β-hydroxyethylcarbamates[3] selectively in reactions with **1**. The structural assignments of these products were accomplished on the basis of their UV and NMR spectral data. The structures of **11** and **12**, which were obtained from the reaction of **1** with **8**, and with **9**, were examined, since **8** and **9** have

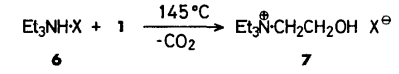

Scheme 2

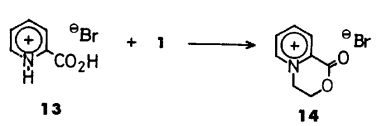

Scheme 3

Table 1. Nucleophilic substitution reaction of ethylene carbonate with various amine hydrobromides[a]

Hydrobromide of	Molar ratio, **1**/Salt	Reaction temp., °C	Period, min	Product[b] Mp, °C[c] (bp/mmHg)	Yield, %
Ethylamine	1.1	140—150	60	(148/15)[d]	32
Cyclohexylamine	1.1	150	60	124—126	70
Morpholine	1.1	155—160	90	(61—63/0.5)[d]	60
Trimethylamine	1.1	140—145	40	230	74
Pyridine	1.5	140—145	50	104—105	81
2-Aminopyridine	1.1	130—135	85	129—131.5	79
4-Aminopyridine	1.1	140—145	70	130—131	99
Quinoline	2.0	145	25	139—139.5	71
8-Quinolinol	2.5	145	45	182.5—183.5	71
Nicotinamide	2.5	155	20	153—154	100
Picolinic acid	2.0	150	15	225	61
Nicotinic acid	5.0	150	40	90—91	87

a) All the reactions were carried out by the use of 10 mmol of the hydrobromides. b) Products are β-hydroxyethylammonium bromides. c) All the melting points are uncorrected. d) These compounds were isolated as free amines.

Table 2. Ultraviolet absorption spectral data of *N*-β-hydroxyethylammonium bromides[a]

Bromide	λ_{max}, nm[b]		$\lambda_{shoulder}$, nm[b]	
N-β-Hydroxyethylpyridinium	260 (4500)		254 (3400),	266 (3400)
$N_{(1)}$-β-Hydroxyethyl-2-aminopyridinium (**11**)[d]	232 (7700),	302 (5700)	251 (220)	
$N_{(1)}$-β-Hydroxyethyl-4-aminopyridinium (**12**)	269 (21000)		—	
N-β-Hydroxyethylquinolinium	316 (12500),	236[d] (54000)	258[c] (280)	
N-β-Hydroxyethyl-8-quinolinolium	256 (35400),	363 (150)	275 (2950)	
$N_{(1)}$-β-Hydroxyethylpicolinolactononium (**14**)	265 (7700)		259 (6550),	271 (6900)
$N_{(1)}$-β-Hydroxyethylnicotinamidium (**17**)	265 (3800)		259 (3100),	272 (3200)
$N_{(1)}$-β-Hydroxyethylnicotinate (**18**)[e]	265 (4300)		258 (3400),	272 (3900)
$N_{(1)}$-β-Hydroxyethylnicotinium (**19**)	266 (3800)		260 (3150),	272 (3200)

a) All the spectra were taken in distilled water. b) Numbers in parentheses are molar extinction coefficient (ε). c) The data are of the minimum absorption. d) In the vicinity of this peak, fine structures were observed at 235, 235.5, 237, and 238.5 nm. d) *cf.* Gol'farb, O. N. Setkina, and Y. L. Danyushevskii, *Zh. Obshch. Khim.*, **18**, 124 (1948); *Chem. Abstr.*, **38**, 4137 (1949). e) This is not bromide but inner salt.

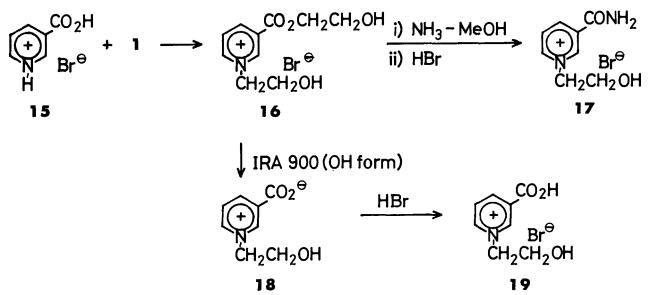

Scheme 4

two potential sites susceptible to the β-hydroxyethylation. Compound **11** was identified with the product of the reaction of **8** with ethylene bromohydrin,[4] and an apparent difference (*ca.* 4.5 Hz) between the $\equiv\overset{+}{N}-CH_2-$ NMR signals of **11** (δ 4.32 ppm) and $N_{(1)}$-β-hydroxyethyl-2-aminopyridinium chloride[5] (δ 3.57 ppm) in their chemical shifts was observed. The esterification of **11** with acetic anhydride–trifluoroboron diethyl etherate afforded the corresponding mono-*O*-acetate. Thus, the structure of **11** was identified as $N_{(1)}$-β-hydroxyethyl-2-aminopyridinium bromide. The structure of **12**($\equiv\overset{+}{N}-CH_2-$ NMR signal: δ 4.32 ppm) was similarly concluded to be $N_{(1)}$-β-hydroxyethyl-4-aminopyridinium bromide. On the other hand, picolinic acid hydrobromide(**13**) and nicotinic acid hydrobromide(**15**) gave $N_{(1)}$-β-hydroxyethylpicolinolactononium bromide(**14**) [IR 1735 cm^{-1} (six-membered

lactone)] and β-hydroxyethyl $N_{(1)}$-β-hydroxyethylnicotinium bromide(**16**) respectively. The treatment of **16** with methanolic ammonia, followed by treatment with aqueous hydrobromic acid, gave $N_{(1)}$-β-hydroxyethylnicotiamidium bromide(**17**), which was identical with the product from the reaction of **1** with **10**; its treatment with Amberlite IRA-900 (OH form) and then with aqueous hydrobromic acid gave $N_{(1)}$-β-hydroxyethylnicotinium bromide(**19**) *via* the zwitter ion, *i.e.*, $N_{(1)}$-β-hydroxyethylnicotinate(**18**).

It can thus be stated, in view of the above results, that this reaction is synthetically advantageous from the following standpoints: 1) The corresponding mono-*N*-β-hydroxyethylated ammonium halides can be prepared in a fairly good yield without regard to whether the amine is aliphatic or aromatic, in contrast with the reactions of **1** with free amines.[3] 2) The process of the reaction can easily be checked by measuring the volume of the carbon dioxide gas evolved in the course of the reaction; this is easier than the procedures involving the reaction of free amines with ethylene halohydrins or those with ethylene oxide in the presence of hydrogen halides or perchloric acid.[6]

The reaction can be assumed to proceed *via* a two-step mechanism; *i.e.*, the first step may be induced by the nucleophilic attack of the halide ion on the methylene carbon atom of **1** to afford an ethylene halohydrin, accompanied by the evolution of carbon dioxide gas; subsequently the resultant amine may attack the methylene carbon, to which the halogen atom is linked, to afford mono-*N*-β-hydroxyethylated ammonium halide, as is shown in Scheme 5.[7]

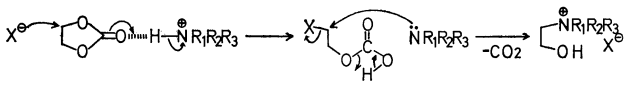

Scheme 5

Experimental

All the melting points are uncorrected. The IR spectra were determined in potassium bromide disks or neat liquid on a Hitachi EPI-S2 spectrophotometer. The NMR spectra were taken with a Varian T-60 spectrometer, in deuterium oxide as the solvent; the chemical shifts were recorded in δ values relative to sodium 2,2-dimethyl-2-silapentanesulfonate (DSS) as the internal standard, unless otherwise noticed.

*Reaction of Ethylene Carbonate(**1**) with Ammonium Bromide (**3**).* A mixture of **1**(2.7 g, 30 mmol) and **3**(0.9 g, 10 mmol) was heated at 145 °C for *ca.* 1.5 hr until the evolution of carbon dioxide gas has ceased. After the mixture had cooled to room temperature, acetone(30 ml) was added to the mixture. The resultant crystals were filtered and recrystallized from ethanol to give triethanolaminehydrobromide[tri-β-(hydroxyethyl)ammonium bromide](**4**) (2.3 g, 54% yield). Mp 187—189 °C. Found: C, 31.44; H, 6.82; N, 6.18%. Calcd for $C_6H_{16}O_3NBr$: C, 31.31; H, 7.00; N, 6.08%. NMR: δ 3.50 (6H, $-CH_2-\overset{+}{N}\equiv$) and 3.99 (6H, $-CH_2-O-$) ppm.

The evaporation of the above filtrate *in vacuo* gave the raw sirup of tetra-β-hydroxyethylammonium bromide(1.1 g, 45% yield). The sirup(2.7 g, *ca.* 10 mmol) was then treated with 1 M sodium ethoxide solution(10 ml), and the mixture was concentrated *in vacuo* to dryness. The residue was treated with anhydrous ethanol(10 ml), and the resultant crystals of sodium bromide were removed by filtration. The solution was neutralized with a 60% aqueous perchloric acid solution and then concentrated *in vacuo* to afford a sirup(1.9 g); this sirup was treated with acetic anhydride(8 ml) in the presence of trifluoroboron diethyl etherate(5 drops) at room temperature and then stirred with methanol(50 ml) for 2 hr, with evaporations *in vacuo* repeated 3 times after the addition of each 20-ml portion of benzene-ethanol(1 : 1 v/v), to give a sirup. The sirup was crystallized in a refrigerator, and the crude crystals were recrystallized from ethanol to give tetra-β-acetoxyethylammonium perchlorate. Mp 103.5—105.5 °C. Found: C, 41.87; H, 6.07; N, 3.21%. Calcd for $C_{16}H_{28}O_{12}NCl$: C, 41.60; H, 6.11; N, 3.03%. NMR-(DMSO-d_6, DSS): δ 2.10(12H, -OAc), 4.00(8H, $-CH_2-\overset{+}{N}\equiv$) and 4.60 (8H, $-CH_2-O-$) ppm.

On the utilization of an equimolar amount and 2 mol of **1** to **3**, tetra-β-hydroxyethylammonium bromide was not obtained, but tri-β-hydroxyethylammonium bromide was obtained in 28 and 36% yields respectively. Moreover, 13 and 5% recoveries of **3** were observed in these two cases.

*Reaction of **1** with Triethylamine Hydrohalides(**6**). The Measurement of the Velocity of Carbon Dioxide Gas Evolution.* The

The reaction vessel used for the measurements was a three-necked, 100-ml, round-bottomed flask fitted with an air-tight stirrer and an Allihn condenser. The top of the condenser was attached to a gas buret. The flask, containing **1**(1.76 g, 20 mmol) and triethylamine hydrohalides (**6**)(20 mmol), was immersed in a constant-temperature bath held at 145±0.2 °C. For the isolation of the products, the reaction mixtures were treated with dried acetone(50 ml); the resulting crystals were filtered and recrystallized from ethanol to give the corresponding triethyl-β-hydroxyethylammonium halides.

The Chloride was obtained as an equimolar mixture with triethylamine hydrochloride; its yield was calculated as 5% by means of the NMR spectrum of the mixture. NMR: δ 1.28 (9H, 3Me), 3.29(6H, $CH_3-CH_2-\overset{+}{N}\equiv$), and 3.38(2H, $HOCH_2-CH_2-\overset{+}{N}\equiv$), and 3.94(2H, $-O-CH_2-$) ppm.

The Bromide: Mp>230 °C. Found: C, 42.74; H, 8.82; N, 6.46%. Calcd for $C_8H_{20}ONBr$: C, 42.48; H, 8.82; N, 6.19%. NMR: δ 1.27(9H, 3Me), 3.29(6H, $CH_3-CH_2-\overset{+}{N}\equiv$), 3.38(2H, $HOCH_2-CH_2-\overset{+}{N}\equiv$), and 3.94(2H, $-CH_2-O-$) ppm.

The Iodide: Mp>230 °C. Found: C, 33.68; H, 7.26; N, 5.03%. Calcd for $C_8H_{20}ONI\cdot 1/2H_2O$: C, 34.05; H, 7.14; N, 4.96%. NMR: δ 1.28(9H, 3Me), 3.40(6H, $CH_3-CH_2-\overset{+}{N}\equiv$), 3.37(2H, $HOCH_2-CH_2-\overset{+}{N}\equiv$), and 3.98(2H, $-CH_2-O-$) ppm.

*Reaction of **1** with Ethylamine Hydrobromide.* Compound **1**(2.7 g, 30 mmol) and ethylamine hydrobromide(3.7 g, 30 mmol) were heated together for 1 hr at 155—160 °C to evolve carbon dioxide gas almost quantitatively. After cooling, the mixture was treated with acetone(30 ml); the resulting crystals were then filtered and recrystallized from ethanol–acetone to give ethyl-β-hydroxyethylammonium bromide(1.7 g, 32% yield). Mp 40—45 °C(hygroscopic). Found: C, 28.34; H, 7.15; N, 8.13%. Calcd for C_4H_{12}-ONBr: C, 28.25; H, 7.11; N, 8.23%. NMR: δ 1.32-(3H, Me), 3.08(2H, $-CH_2-\overset{+}{N}\equiv$), 3.35(2H, $HOCH_2-CH_2-\overset{+}{N}\equiv$), and 3.90(2H, $-CH_2-O-$) ppm. The concentration of the mother liquor of the recrystallization gave a sirup(2.0 g) which was deduced to be a carbamate from its IR spectrum (1688 cm^{-1}).

*Reaction of **1** with Cyclohexylamine Hydrobromide.* The reaction of **1**(2.0 g, 22 mmol) with cyclohexylamine hydro-

bromide(3.6 g, 20 mmol) was carried out in a manner similar to that described above to give cyclohexyl-β-hydroxyethylammonium bromide(3.1 g; 70% yield). Mp 124—126 °C. Found: C, 43.09; H, 9.93; N, 6.5%. Calcd for $C_8H_{18}ONBr$: C, 42.87; H, 9.99; N, 6.25%. NMR: δ 1.2—2.1 (10H, m, ring proton), 3.21(2H, $HOCH_2$-CH_2-$\overset{+}{N}\equiv$), and 3.88 (2H, -CH_2-O-) ppm.

Reaction of ***1*** *with Morpholine Hydrobromide.* Compound **1**(4.8 g, 55 mmol) and morpholine hydrobromide(8.4 g, 50 mmol) were heated together at 155—160 °C for about 1.5 hr. After cooling, ethanol(50 ml) was added to the mixture, and the resulting mixture was treated with a 1 M methanolic sodium methoxide solution to remove the hydrobromic acid. The solvent was vaporated *in vacuo*, and the residue was treated with acetone(80 ml) to remove the sodium bromide by filtration. After the evaporation of the solvent *in vacuo*, the resultant sirup was distilled to give *N*-β-hydroxyethylmorpholine(4.1 g, 61% yield). Bp 61—63 °C/0.5 mmHg. Found: C, 54.64; H, 9.93; N, 10.69%. Calcd for $C_6H_{13}O_2N$: C, 54.94; H, 9.99; N, 10.68%. NMR-($CDCl_3$-TMS): δ 2.51—2.56(6H, -CH_2-$\overset{+}{N}\equiv$) and 3.67-(6H, -CH_2-O-) ppm.

Reaction of ***1*** *with Pyridine Hydrobromide.* Compound **1**(2.7 g, 30 mmol) and pyridine hydrobromide(3.3 g, 20 mmol) were heated together for 50 min at 140—145 °C. After cooling, ethanol(40 ml) was added to the mixture, it was treated with active charcoal, and acetone(50 ml) was added. The resulting crystals were filtered and found to be pure enough for elemental analysis. The yield of *N*-β-hydroxyethylpyridinium bromide was 3.3 g(81%). Mp 104—105 °C. Found: C, 40.81; H, 4.91; N, 6.41%. Calcd for $C_7H_{10}ONBr$: C, 41.19; H, 4.94; N, 6.86%. NMR: δ 4.17 (2H, -CH_2-O-), 4.86(2H, -CH_2-$\overset{+}{N}\equiv$), 8.23(2H, H_β), 8.70 (1H, H_γ), and 9.00(2H, H_α) ppm. UV: $\lambda_{max}^{H_2O}$ 260 nm(ε 4500) and $\lambda_{shoulder}^{H_2O}$ 254 and 266 nm(ε 3400 and 3400 respectively).

Reaction of ***1*** *with Hydrobromides of Trimethylamine, 2-(****8****), 4-Aminopyridine(****9****), Quinoline, 8-Quinolinol, and Nicotinamide (****10****).* These reactions were carried out in almost the same way as has been described in the preceding reactions.

N-β-*Hydroxyethyltrimethylammonium Bromide*: The crystals resulting from the addition of acetone to the ethanolic solution of the resulting reaction mixture were recrystallized from ethanol to give a product(4.1 g, 74% yield). Mp >230 °C. Found: C, 32.71; H, 7.76; N, 7.64%. Calcd for $C_5H_{13}ONBr$: C, 32.62; H, 7.66; N, 7.61%. NMR: δ 3.25(8H, 3Me), 3.53(2H, -CH_2-$\overset{+}{N}\equiv$), and 4.05(2H, -CH_2-O-) ppm.

$N_{(1)}$-β-*Hydroxyethyl-2-aminopyridinium Bromide (****11****)*: The crystals obtained in the way described in the preceding experiment were recrystallized from ethanol to give the product(1.8 g; 79% yield). Mp 129—131.5 °C. Found: C, 38.48; H, 5.36; N, 13.10%. Calcd for $C_7H_{11}ON_2Br$: C, 38.37; H, 5.06; N, 12.78%. NMR: δ 4.05(2H, -CH_2-O-), 4.32(2H, -CH_2-$\overset{+}{N}\equiv$), and 6.8—8.1(4H, m, ring protons) ppm. UV: $\lambda_{max}^{H_2O}$ 232 and 302 nm (ε 7700 and 5700 respectively), and $\lambda_{min}^{H_2O}$ 251 nm (ε 220).

$N_{(1)}$-β-*Hydroxyethyl-4-aminopyridinium Bromide (****12****)*; The crystals obtained in the same way were recrystallized from ethanol to give a product(2.3 g; 99% yield). Mp 130—131 °C. Found: C, 38.60; H, 4.78; N, 13.10%. Calcd for $C_7H_{11}ON_2Br$: C, 38.37; H, 5.06; N, 12.78%. NMR: δ 4.00(2H, -CH_2-O-), 4.32(2H, -CH_2-$\overset{+}{N}\equiv$), 6.92(2H, H_β), and 8.06(2H, H_α) ppm. UV: $\lambda_{max}^{H_2O}$ 269 nm (ε 21000).

Acetylation of ***11*** *and* ***12***: Compounds **11** and **12**(920 mg, 4 mmol) were treated with acetic anhydride(3 ml) and trifluoroboron diethyl etherate(3 drops) respectively at room temperature overnight. After the addition of methanol (50 ml), the mixture was stirred for 3 hr at room temperature and the solvent was evaporated *in vacuo* to dryness. The resultant crystals were recrystallized from ethanol to give colorless crystals.

$N_{(1)}$-β-*Acetoxyethyl-2-aminopyridinium Bromide*: Yield, 1.14 g(81%). Mp 164—166 °C. Found: C, 41.55; H, 5.18; N, 10.58%. Calcd for $C_9H_{13}O_2N_2Br$: C, 41.45; H, 5.02; N, 10.73%. NMR: δ 2.17(3H, -OAc), 4.61(2H, -CH_2-OAc), 4.70(2H, -CH_2-$\overset{+}{N}_{(1)}\equiv$), 6.9—8.1(4H, m, ring protons) ppm.

$N_{(1)}$-β-*Acetoxyethyl-4-aminopyridinium Bromide*: Yield, 0.63 g(67%). Mp 208—209 °C. Found: C, 41.41; H, 4.91; N, 10.87%. Calcd for $C_8H_{13}O_2N_2Br$: C, 41.45; H, 5.02; N, 10.73%. NMR: δ 2.30(3H, -OAc), 4.03(2H, -CH_2-OAc), 4.58(2H, -CH_2-$N_{(1)}\equiv$), 8.10(2H, H_β), and 8.60(2H, H_α) ppm.

N-β-*Hydroxyethylquinolinium Bromide.* The crystals obtained in the same way as in the reaction of **1** with pyridinium bromide were recrystallized from acetonitrile-acetone to give a product(2.24 g; 71% yield). Mp 139—139.5 °C. Found: C, 51.30; H, 4.52; N, 5.31%. NMR: δ 4.38(2H, -CH_2-O-), 5.38(2H, -CH_2-$\overset{+}{N}\equiv$), 7.9—8.7(5H, m, ring protons), 9.28(1H, H-4), and 9.59(1H, H-2) ppm. UV: $\lambda_{max}^{H_2O}$ 236 and 316 nm(ε 54000 and 12500 respectively) and $\lambda_{min}^{H_2O}$ 258 nm(ε 280).

N-β-*Hydroxyethyl-8-quinolinolium Bromide.* The crystals obtained as in the above cases were recrystallized from ethanol-acetone to give a product(3.90 g; 73% yield). Mp 182.5—183.5 °C. Found: C, 48.99; H, 4.54; N, 5.26%. Calcd for $C_{11}H_{12}O_2NBr$: C, 48.90; H, 4.48; N, 5.19%. NMR: δ 4.30(2H, -CH_2-O-), 5.53(2H, -CH_2-$\overset{+}{N}\equiv$), 7.4—8.2(4H, m, ring protons), 9.03(1H, H-4), and 9.15(1H, H-2) ppm. UV: $\lambda_{max}^{H_2O}$ 256 nm(ε 35400), $\lambda_{shoulder}^{H_2O}$ 275 nm(ε 2950), and $\lambda_{min}^{H_2O}$ 363 nm(ε 150).

$N_{(1)}$-β-*Hydroxyethylnicotinamidium Bromide (****17****)*. The crystal obtained in the same way as above were recrystallized from ethanol to give a product(4.9 g; 100% yield). Mp 153—154 °C. Found: C, 38.78; H, 4.40; N, 11.60%. Calcd for $C_8H_{11}O_2N_2Br$: C, 39.04; H, 4.10; N, 11.40%. NMR: δ 4.17(2H, -CH_2-O-), 4.90(2H, -CH_2-$\overset{+}{N}\equiv$), 8.30(1H, H-5), 9.00(1H, H-6), and 9.39(1H, H-2) ppm. UV: $\lambda_{max}^{H_2O}$ 265 nm(ε 3800), $\lambda_{shoulder}^{H_2O}$ 259 and 272 nm(ε 3100 and 3200 respectively).

Reaction of ***1*** *with Picolinic Acid Hydrobromide (****13****).* Compound **1**(1.8 g, 20 mmol) and picolinic acid hydrobromide (2.04 g, 20 mmol) were heated together at 152 °C for 40 min, after which the mixture was treated with acetone-ethanol (1 : 3 v/v, 100 ml). The filtration of the resultant yellow granular crystals gave *N*-β-hydroxyethylpicolinolactononium bromide(2.8 g; 61% yield), which was analytically pure enough. Mp 225 °C. Found: C, 42.06; H, 3.68; N, 6.20%. Calcd for $C_8H_8NO_2Br$: C, 41.77; H, 3.50; N, 6.09%. NMR: δ 5.15(4H, -CH_2-), 8.3—9.0 (3H, ring protons), and 9.15(1H, H-6) ppm. IR: 1735 cm^{-1} (six-membered lactone). UV: $\lambda_{max}^{H_2O}$ 265 nm (ε 7700), $\lambda_{shoulder}^{H_2O}$ 259 and 272 nm (ε 3100 and 3200 respectively).

Reaction of ***1*** *with Nicotinic Acid Hydrobromide (****15****).* Compound **1**(8.8 g, 100 ml) and nicotinic acid hydrobromide (**15**)(4.2 g, 20 mmol) were heated together at 150 °C for 40 min. The resultant red-brown sirup was treated with dioxane-ethanol(1 : 1 v/v, 80 ml) to give colorless crystals of β-hydroxyethyl *N*-β-hydroxyethylnicotinatonium bromide (**16**) (5.07 g, 87% yield). Found: C, 40.97; H, 5.21;

N, 4.69%. Calcd for $C_{10}H_{14}O_4NBr$: C, 41.40; H, 4.83; N, 4.80%. NMR: δ 4.00 and 4.14(2H and 2H respectively, $-CH_2OH$), 4.60(2H, $-CH_2-O-CO-$), 4.88(2H, $-CH_2-\overset{+}{N}\equiv$), 8.29(1H, H-5), 9.11(1H, H-2) ppm.

Treatment of ***16*** *with Methanolic Ammonia.* Compound **16**(290 mg) was treated with methanolic ammonia saturated at 0 °C(50 ml) in a stoppered flask in a refrigerator overnight. The subsequent evaporation of the solvent *in vacuo* gave orange scaly crystals (290 mg); the residue was dissolved in ethanol (30 ml) followed by treatment with 10% aqueous hydrobromic acid, with the pH adjusted at about 5. After the evaporation of the solvent *in vacuo*, the residue was dissolved in ethanol (30 ml), treated with active charcoal, and then filtered. To the filtrate, we added *n*-hexane until the turbidity was noticed; the mixture was then allowed to stand in a refrigerator. The resultant scaly crystals were filtered to afford $N_{(1)}$-β-hydroxyethylnicotinamidium bromide(250 mg; 100% yield). Mp 153—154 °C. The product was identified with **17** by examining the mixed melting point.

Treatment of ***16*** *with Amberlite IRA-900.* Compound **16** (1.0 g) was treated with Amberlite IRA-900(OH form, 20 ml) in methanol(100 ml) under stirring overnight; the resin was then filtered and the solvent was evaporated to about 30 ml to give pale yellow crystals of $N_{(1)}$-β-hydroxyethylnicotinate (**18**) (0.4 g, 72% yield). Mp 230—231 °C. Found: C, 57.58; H, 5.87; N, 8.68%. Calcd for $C_8H_9O_2N$: C, 57.48; H, 5.43; N, 8.38%. NMR δ 4.19(2H, $-CH_2-O-$), 4.80(2H, $-CH_2-\overset{+}{N}\equiv$), 8.14(1H, H-5), 8.90(1H, H-4), and 9.19(1H, H-2) ppm.

Treatment of ***18*** *with Aqueous Hydrobromic Acid.* Compound **18**(167 mg) was dissolved in methanol (30 ml); the mixture was treated with 10% aqueous hydrobromic acid, with the pH adjusted at about 5 by the use of a pH test paper. After the evaporation of the solvent, the residue was recrystallized from ethanol to give $N_{(1)}$-β-hydroxyethylnicotinium bromide (**19**) (140 mg, 57% yield). Mp 107—109 °C. Found: C, 38.44; H, 3.94; N, 5.87%. Calcd for $C_8H_{10}O_3NBr$: C, 38.73; H, 4.06; N, 5.64%. NMR: δ 4.16(2H, $-CH_2-O-$), 4.89(2H, $-CH_2-\overset{+}{N}\equiv$), 8.29(1H, H-5), 9.10(1H, H-4), 9.12(1H, H-6), and 9.47(1H, H-2) ppm. UV: $\lambda_{max}^{H_2O}$ 266 nm(ε 3800) and $\lambda_{shoulder}^{H_2O}$ 260 and 272 nm(ε 3150 and 3200 respectively).

The authors wish to thank to the members of the Laboratory of Elemental Analysis, Department of Chemistry, Tokyo Institute of Technology, for the elemental analyses. They are also grateful to the Ministry of Education, for a Scientific Research Grant-in-Aid, and to the Kurata Foundation for a grant.

References

1) E. D. Bergmann and I. Shahak, *J. Chem. Soc.*, **1966**, 899.

2) The unusual increment in gas evolution may be due to ethylene oxide, which was formed by triethylamine-catalyzed elimination reaction of hydrogen chloride from resulting ethylene chlorohydrin. Actually, ethylene oxide was detected as the bisulfate addition compound when the evolved gas was passed into a sodium bisulfate solution [W. M. Lauer and A. Hill, *J. Amer. Chem. Soc.*, **58**, 1873 (1936)]. In addition, the elimination reaction was followed by heating triethylamine and ethylene chlorohydrin at refluxing point, giving **7** (33%) and triethyamine hydrochloride (20%).

3) H. Najer, P. Chabrier, and R. Giudicelli, *Bull. Chim. Soc. Fr.*, **1954**, 1142; R. Delaby, A. Sekira, P. Chabrier, and P. Piganial, *ibid.*, **1951**, 392.

4) It is well known that alkylation reaction takes place on the ring nitrogen of aminopyridine in the reaction with alkyl halides. *Cf.* A. E. Tschitschibabin and E. D. Ossertrowa, *Chem. Ber.*, **58**, 1708 (1925).

5) N. Weiner and I. A. Kaye, *J. Org. Chem.*, **14**, 868 (1949); The δ values of $-CH_2-\overset{+}{N}\equiv$ NMR signals are little affected by the variation of the counteranion of alkyl ammonium halides as observed in the series of *N*-β-hydroxyethylammonium halides(See the experimental part).

6) A. M. Eastham, *J. Chem. Soc.*, **1956**, 1936; A. M. Eastham, B. deB. Darwent, and P. E. Beanbien, *Can. J. Chem.*, **29**, 575 (1951); A. M. Eastham and B. deB. Darwent, *ibid.*, **29**, 585 (1951); T. Yamamoto, S. Tsunoda, and T. Nanba, *Yukagaku*, **11**, 298, 369, 464 (1962),

7) Kinetic study of this reaction is now in progress in our laboratory, and will be reported elsewhere.

Substituent Effects on the ^{13}C and ^{1}H Chemical Shifts of 1-Phenyl-1,3-butadiene and Phenylallene

Tadashi Okuyama, Kunisuke Izawa, and Takayuki Fueno

Department of Chemistry, Faculty of Engineering Science, Osaka University, Toyonaka, Osaka 560

(Received, August 6, 1973)

CMR and PMR spectra of *trans*-1-phenyl-1,3-butadiene (PBD) and phenylallene (PA) and their ring-substituted derivatives (*p*-CH_3, *m*-CH_3, *p*-Cl, and *m*-Cl) have been measured. The chemical shifts of side-chain carbons and protons were treated with a Hammett-type relationship. The carbon chemical shifts of the side chain gave alternately opposite sign of ρ values while those of PA showed little dependence on the ring substitution. The ^{1}H chemical shifts showed behavior different from that of the ^{13}C shifts. The mode of electron polarization along the side-chain of PBD and PA was discussed to interpret the observations.

It is well known that the efficiency of a C=C double bond in transmitting electronic effects is greater than that of a saturated CH_2 group.[1] The π-bond polarization may contribute to the greater transmission efficiency of double bond. Kajimoto and Fueno[2] have recently found that the alternation of substituent effects on the ^{13}C chemical shifts occurs along the conjugated framework of 1-substituted 1,3-butadienes. The electronic effects are transmitted mainly through successive π-bond polarization.

$$X \leftarrow \overset{\delta-}{C}=\overset{\delta+}{C}-\overset{\delta\delta-}{C}=\overset{\delta\delta+}{C}$$

However, because of direct substitution at the 1-carbon' additional factors may have contributed to the chemical shifts of unsaturated carbons. To avoid this complexity, we have measured CMR spectra of ring-substituted 1-phenyl-1,3-butadienes.

On the other hand, opposite polarization of π-electrons in the orthogonal p-orbitals of the acetylenic bond has recently been considered in an attempt to interpret the substituent effects on the ^{13}C chemical shift of 1-phenylpropyne.[3] In this connection, it is interesting to examine the mode of bond polarization of allene which has cumulative orthogonal π-bonds. Thus, we have measured CMR spectra of some ring-substituted phenylallenes.

Proton chemical shifts have also been measured for the sake of comparison.

Results

The ^{13}C NMR spectra of *trans*-1-phenyl-1,3-butadiene (PBD) and phenylallene (PA) and their derivatives were measured as a neat liquid or a 50% solution in carbon disulfide. The observed signals were assigned by comparison with the partially proton-decoupled spectra and by the aid of the additivity rule[4] in the same way as described previously.[2,3] The chemical shifts of side-chain carbons are listed in Tables 1 and 2 for PBD's and PA's, respectively, in ppm downfield from tetramethylsilane.

Proton spectra were recorded with a 10% solution in carbon tetrachloride at the frequency of 100 MHz. The assignment of signals was accomplished through the analysis of their mode of coupling. The ^{1}H chemical shifts assigned are included in Tables 1 and 2.

Discussion

Butadiene System. Figure 1 shows plots of the chemical shifts of various side-chain carbons of PBD's against Hammett's σ values. It clearly exhibits that the sign of slope changes alternately from the α- to δ-carbon. That is, ρ values for the α- and γ-carbons are negative while those for the β- and δ-carbons are positive as are given in Table 1. These results apparently show the alternation of polar effects in the conjugated system. An electron-donating group on the phenyl ring increases the electron densities at the β- and δ-carbons (unfield shift) while it does decrease the electron densities at the α- and γ-carbons (downfield shift) of PBD.

Another interesting finding is that the ρ values are essentially equal for the β- and δ-carbons, 5.07 and 4.74. That is, the attenuation factor of C=C double bond in transmitting the substituent effects is close to unity (0.93) in the conjugated system. These ρ values are comparable with the value for the β-carbon of

Table 1. Chemical shifts[a] of side-chain carbons and protons of substituted *trans*-1-phenyl-1,3-butadienes

Substituent	α-C	β-C	γ-C	δ-C	γ-H	δ-H (*cis*)	δ-H (*trans*)
p-CH_3	134.0	128.5	137.4	116.2	6.310	5.207	5.061
m-CH_3	133.0	128.8	137.3	116.6	6.390	5.208	5.075
H	133.0	129.3	137.3	117.3	6.401	5.237	5.092
p-Cl	131.4	130.0	136.9	118.2	6.388	5.266	5.138
m-Cl	130.8	131.4	136.9	118.7	6.380	5.259	5.142
ρ[b]	−5.80	5.07	−1.04	4.74		0.113	0.162
s[c]	0.49	0.65	0.17	0.24		0.029	0.019
r[d]	0.990	0.976	0.963	0.996		0.913	0.980

a) In ppm from TMS. b) In ppm/σ. c) Standard deviation of ρ. d) Correlation coefficient.

TABLE 2. CHEMICAL SHIFTS[a] OF SIDE-CHAIN CARBONS AND PROTONS OF SUBSTITUTED PHENYLALLENES

Substituent	α-C	β-C	γ-C	α-H	γ-H
p-CH_3	95.7	210.7	79.9	6.031	5.044
m-CH_3				6.025	5.058
H	95.4	210.2	79.8	6.069	5.064
p-Cl	94.5	210.2	80.2	6.035	5.092
m-Cl	94.6	210.2	80.3	6.033	5.130
ρ[b]	−2.33	−0.80	0.88		0.151
s[c]	0.57	0.47	0.32		0.016
r[d]	0.944	0.769	0.890		0.984

a) In ppm from TMS. b) In ppm/σ. c) Standard deviation of ρ. d) Correlation coefficiemt.

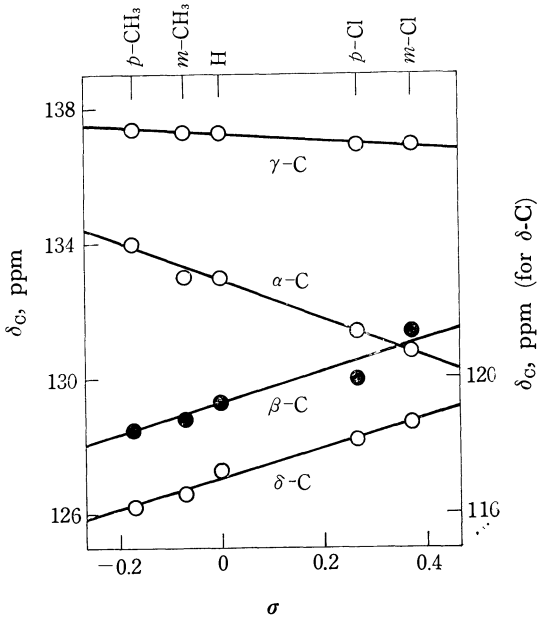

Fig. 1. Hammett-type plots of the ^{13}C chemical shifts of the side-chain carbons of *trans*-1-phenyl-1,3-butadienes.

styrene (4.73).[5]

As for the PMR data, a fairly good linear correlation was obtained between the *trans*-δ-proton chemical shifts and Hammett's σ values with $\rho = 0.162$ ppm/σ. The sign is the same as that for the δ-carbon shift. The attenuation factor of the $C_\gamma = C_\delta$ bond is, however, *ca.* 0.5; the ρ value for the *trans*-β-proton shift of styrene is 0.335.[6]

The different efficiencies of the carbon chain in transmitting the substituent effects on the ^{13}C and ^{1}H chemical shifts contradict the earlier suggestion that ^{1}H shift mainly reflects the electron density of the attached carbon.[7] The ^{13}C shift was concluded on a sound basis to be determined predominantly by the electron density on the carbon atom of question.[8] Therefore, it is very likely that some other factors contribute to the determination of ^{1}H shift. Kajimoto and Fueno[9] pointed out that ^{1}H chemical shift is influenced by electron densities on both the hydrogen atom in question and the carbon atom directly bonded to it and that they very often show different dependence on a structural perturbation. This type of anomaly between ^{13}C and ^{1}H chemical shifts is becoming apparent as CMR data are accumulated.

Allenic System. The chemical shifts of side-chain carbons of PA's summarized in Table 2 show little dependency on the ring substitution. The ρ values were calculated and included in Table 2. The ρ values for the α-, β-, and γ-carbons are negative, nearly zero, and slightly positive, respectively.

These observations might be explained by considering the polarization of π-electrons like

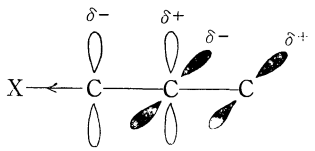

The opposite sign of ρ values between the α- and γ-carbons is understandable by this polarization. The net change in the electron density at the β-carbon would be very small owing to the cancellation of contributions from two orthogonal p-orbitals. This could be a reason for the low ρ value for the β-carbon shift.

On the other hand, chemical shifts of the γ-protons of PA show a fairly good linear correlation with Hammett's σ values. The ρ value is not very small (0.151 ppm/σ), being comparable with that for the δ-proton of PBD.

This distinctive difference between ^{13}C and ^{1}H shifts at the γ-position of PA seems to suggest that some special mechanism of electron polarization is operative in the side-chain bonds of PA. One possible explanation is a hyperconjugative model like

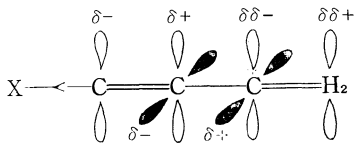

That is, electrons in the orbitals parallel to α-β π-orbitals are alternately polarized like conjugated diene, using the pseudo π-orbital of the γ-hydrogens. This may also explain the small ρ value for the γ-carbon shift. The hyperconjugative interaction may be effective because of the rigid structure of allene with favorable orientation of the γ-hydrogens.

Experimental

Materials. Preparations of *trans*-1-phenyl-1,3-butadiene (PBD) and phenylallene (PA) and their ring-substituted derivatives were described previously.[10,11]

NMR Measurements. The CMR spectra of a neat liquid of PBD derivatives and of a 50% solution in CS_2 of PA derivatives were recorded at 24 °C on a JEOL C-60 HL spectrometer with a 15.09 MHz RF unit as described previously.[2,3]

The PMR spectra were obtained on a JNM 4H-100 spectrometer at room temperature (~22 °C). A 10% solution of a sample in CCl_4 was used for the measurement. TMS was used as internal standard.

The authors wish to thank Messrs. Y. Terawaki and H. Okuda for recording the spectra.

References

1) H. H. Jaffé, *Chem. Rev.*, **53**, 191 (1935).
2) O. Kajimoto and T. Fueno, *Tetrahedron Lett.*, **1972**, 3329.
3) K. Izawa, T. Okuyama, and T. Fueno, This Bulletin, **46**, 2881 (1973).
4) G. B. Savitsky, P. D. Ellis, K. Namikawa, and G. E. Maciel, *J. Chem. Phys.*, **49**, 2395 (1968).
5) K. S. Dhami and J. B. Stothers, *Can. J. Chem.*, **43**, 519 (1965).
6) T. Fueno, O. Kajimoto, K. Izawa, and M. Masago, This Bulletin, **46**, 1418 (1973).
7) J. I. Musher, *J. Chem. Phys.*, **40**, 2399 (1964).
8) M. Karplus and J. A. Pople, *ibid.*, **38**, 2803 (1963).
9) O. Kajimoto and T. Fueno, *Chem. Lett.*, **1972**, 103.
10) K. Izawa, T. Okuyama, T. Sakagami, and T. Fueno, *J. Amer. Chem. Soc.*, **95**, 6752 (1973).
11) T. Okuyama, K. Izawa, and T. Fueno, *ibid.*, **95**, 6749 (1973).

Codimerization of Ethylene and Styrene Catalyzed by Bis(triphenylphosphine)-σ-Arylnickel(II) Halide–Trifluoroboron Etherate

Noboru KAWATA, Ken-ichi MARUYA, Tsutomu MIZOROKI, and Atsumu OZAKI

Research Laboratory of Resources Utilization, Tokyo Institute of Technology, Ookayama, Meguro-ku, Tokyo 152

(Received November 15, 1972)

The codimerization of styrene with ethylene was studied using the catalyst system composed of bis(triphenylphosphine)σ- aryl(bromo)nickel(II) and trifluoroboron etherate in methylene dichloride. The codimerization takes place readily at 0 °C under atmospheric pressure to give 3-phenyl-1-butene selectively. The reaction scheme was discussed on the basis of the product distribution during the course of reaction and its kinetics.

Many catalyst systems have been reported for dimerization of olefins and dienes since transition metal complexes, especially the VIII subgroup, were found to have a significant effect on selective dimerization. Attention has been paid to the active species of the catalyst, which is accepted to be a hydro metal complex. Its activity and selectivity, however, depend considerably on its metal and ligands (including solvent) as well as the olefin specified. During the course of our study on the activity and selectivity of the catalyst composed of nickel(II) compound and a Lewis acid for the ethylene dimerization, it was found that the bis(triphenylphosphine)σ-arylnickel(II) halide–trifluoroboron etherate catalyst system significantly enhanced the rate of ethylene dimerization to give butene selectively.[1] This catalyst system is less active for the dimerization of propylene or its codimerization with ethylene, but highly active and selective for the codimerization of styrene with ethylene.[2]

Rhodium(II) chloride[3] and palladium(II) chloride[4,5] catalyze the codimerization of ethylene and styrene even in the absence of Lewis acid. The former gives 2-phenyl-2-butene under a high pressure of ethylene(100 atm) and the latter 1-phenyl-butenes. Codimerization of styrene with ethylene was studied with two nickel complexes as the catalyst, one consisting of nickel diacetylacetonate, trialkylaluminium and trialkylphosphite, which gave cyclic oligomers of ethylene and styrene and only a small amount of their codimer,[6] and the other consisting of tetrakis(trichlorophosphine)-nickel, aluminium bromide and butyl lithium, which gave a mixture of 3-phenyl-1-butene, 2-phenyl-2-butene and 2-phenyl-1-butene.[7] The present catalyst system, however, gives 3-phenyl-1-butene selectively without being accompanied by 1-phenyl-butenes. This paper deals with the mechanism of the selective formation of 3-phenyl-1-butene.

Experimental

Materials. Dibromobis(triphenylphosphine)nickel(II)[8] and bis(triphenylphosphine)σ-aryl(bromo)nickel(II)[9] were prepared according to the methods given in literature. The results of elemental analysis of the carbon and hydrogen of these nickel complexes were as follows; bis(triphenylphosphine)dibromonickel(II) (Calcd: C, 58.2; H, 4.1%. Found: C, 58.2; H, 4.0%), bis(triphenylphosphine)-1-naphthyl-(bromo)nickel(II) (Calcd. C, 69.9; H, 4.7. Found: C, 69.9; H, 4.5%), bis(triphenylphosphine)-*o*-tolyl(bromo)-nickel(II) (Calcd: C, 68.5; H, 4.9%. Found: C, 67.1; H, 4.6%) and bis(triphenylphosphine)mesityl(bromo)nickel(II) (Calcd: C, 69.1; H, 5.3%. Found: C, 69.1; H, 4.7%). Commercial styrene, α- and ω-methyl styrene, ω-bromo styrene and *o*-, *m*-, and *p*-chlorostyrenes were dried under nitrogen with a molecular sieve before use. *o*-, *m*-, and *p*-Methyl styrene were prepared according to the literature[10] and purified by vacuum distillation. Small amounts of air and water in commercial ethylene were separated by means of a liquid nitrogen trap. Benzene and diethyl ether were well dried with metallic sodium before being purified by distillation, while methylene dichloride was dried with the molecular sieve. Trifluoroboron etherate was also purified by distillating its diethyl ether solution under nitrogen.

Procedure. All experiments were operated under nitrogen atmosphere. To a well dried methylene dichloride solution of bis(triphenylphosphine)σ-aryl(bromo)nickel(II) in a two necked flask(50 ml in vol.) were added trifluoroboron etherate, followed by adding a given amount of styrene. The nitrogen gas in the flask was evacuated at the temperature of liquid nitrogen, and the flask was kept in an ice-water bath before introducing ethylene gas at 0 °C with vigorous stirring. The gaseous pressure inside the flask was kept constant(±1 cmHg) during the course of reaction by adjusting the supply of ethylene with a fine needle valve. After a specified period of time, the reaction was terminated by adding an aqueous sodium hydroxide solution(1 M, 5 ml). Volatile substances such as ethylene, butenes and the solvent had been transferred to another flask by means of a liquid nitrogen trap before non-volatile materials were well extracted with *n*-hexane. They were quantitatively determined by a gaschromatography equipped with an FID detector.

Identification and Analysis. A VZ-7 column (4 mmφ, 8 m) was used at room temperature with nitrogen as a carrier gas for the quantitative dtermination of butenes. A DC-550 column (4 mmφ, 4 m) was used at 120 °C for the styrene-ethylene codimers. Most products were isolated by preparative gas-chromatography to be identified by NMR spectroscopy. Some of them were also checked by IR and mass spectroscopy when necessary.

3-phenyl-1-butene (CH_3– 8.70τ(d) 3H, –CH– 6.60τ(qui) 1H, CH_2=CH– 4.96τ and 4.00τ(m) 3H, and C_6H_5– 2.74τ(m) 5H): *trans*-2-phenyl-2-butene (CH_3– 8.54τ(s) 3H, CH_3–CH= 8.12τ(d) 3H, –CH= 4.48τ(m) 1H, and C_6H_5– 2.79(m) 5H): *cis*-2-phenyl-2-butene (CH_3– 8.16τ(s) 3H, CH_3–CH– 8.40τ(d) 3H, –CH= 4.23τ(m) 1H, and C_6H_5– 2.77τ(m) 5H). These phenyl butenes were all hydrogenated with Raney nickel catalyst to give 2-phenyl butane (CH_3–CH_2– 9.22τ(t) 3H, –CH_2– 8.45τ(qui) 2H, –CH– 7.50τ(m) 1H, CH_3–CH– 8.82 (d) 3H, and C_6H_5– 2.78τ(m) 5H). 3-methyl-3-phenyl-1-pentene (CH_3–CH_2– 9.30τ(t) 3H, –CH_2– 8.32τ(qua) 2H, CH_3–C– 8.75τ(s) 3H, CH_2–CH– 5.0 and 3.95τ(m) 3H, and C_6H_5–, 2.70 (m) 5H), the parent peak of its mass spectrum being 160: 3-(*p*-chlorophenyl)-1-butene (CH_3– 8.73τ(d) 3H, –CH– 6.63 (qiu) 1H, CH_2=CH– 5.00 and 4.14(m) 3H,

TABLE 1. EFFECT OF σ-ARYL LIGAND

No.	Cat.	Styrene consumed (mmol)	3-Phenyl-1-butene formed (mmol)	Select. (%)	Butenes
1	(Mesityl)NiBr($P\phi_3$)$_2$	13.4	11.6	91	trace
2	(1-Naphthyl)Nibr($P\phi_3$)$_2$	12.9	10.2	80	trace
3	(o-Tolyl)NiBr($P\phi_3$)$_2$	12.7	7.2	56	trace
4	$NiBr_2(P\phi_3)_2$	3.6	0	0	no detect
5	None	1.6	0	0	no detect

(σ-aryl)NiBr($P\phi_3$)$_2$, 1 mmol; $BF_3\cdot OEt_2$, 1 mmol; styrene employed, 174 mmol (2 ml); CH_2Cl_2, 30 ml; $P_{C_2H_4}$ 45—50 cmHg; temp. 0°C; time, 15 min.

and Cl–C_6H_4– 2.92τ(m) 4H): 2,3-diphenyl-1-butene (CH_3– 8.83τ(d) 3H, –CH– 6.50τ(qua) 1H, CH_2=C– 3.65τ(s) 2H, and C_6H_5– 2.77τ(m) 10H). The other products were estimated by the relative retention time on their gas chromatograms.

Results

Effect of σ-aryl Ligand: A methylene dichloride solution (30 ml) of bis(triphenylphosphine)σ-aryl(bromo)-nickel(II) (1.0 mmol), trifluoroboron etherate (1.0 mmol) and styrene (17.4 mmol) was treated at 0 °C with ethylene under about 70 cmHg for 15 min. The results are given in Table 1. Bis(triphenylphosphine)-σ-aryl(bromo)nickel(II) (No. 1,2,3) is highly active for codimerization to give 3-phenyl-1-butene selectively. In this case, small amounts of butenes were formed, while only trace amounts of isomers of 3-phenyl-1-butene were detected. Bis(triphenylphosphine)dibromonickel(II) (No. 4) has no activity for the codimerization, where the consumption of some amount of styrene seems to be caused by its polymerization with trifluoroboron etherate. The selectivity to 3-phenyl-1-butene decreases in the order, mesityl> naphthyl>o-tolyl.

Figure 1 shows the variation in the amounts of products during the codimerization of styrene with ethylene under the specified conditions. The results were ob-

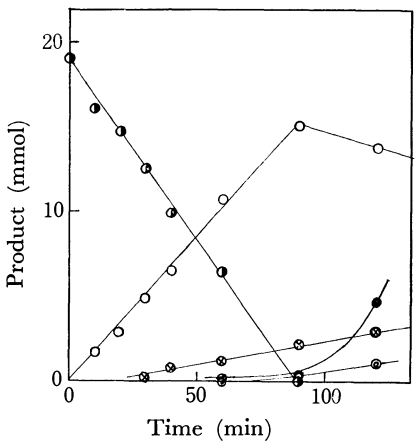

Fig. 1. Product distribution during the course of codimerization.
(1-naphthyl)NiBr($P\phi_3$)$_2$, 0.5 mmol; $BF_3\cdot OEt_2$, 0.5 mmol; styrene 19.1 mmol; CH_2Cl_2, 30 ml; $P_{C_2H_5}$, 50 cmHg; temp. 0°C. ◑: styrene, ○: 3-phenyl-1-butene, ⊗: 3-methyl-3-phenyl-1-pentene, ◎: 2-phenyl-2-butene, ●: butenes.

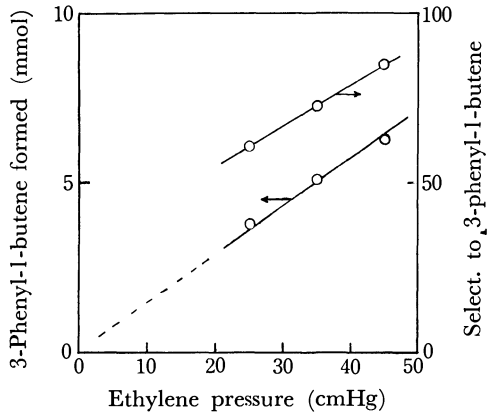

Fig. 2. Effect of ethylene pressure on the rate of codimerization; (1-naphthyl)NiBr($P\phi_3$)$_2$, 0.5 mmol; $BF_3\cdot OEt_2$, 0.5 mmol; styrene, 19.1 mmol; CH_2Cl_2, 30 ml; temp. 0°C; time. 30 min.

tained from repeated runs of the codimerization under the same conditions. It is shown that the reaction rate is independent of the concentration of styrene and that practically no dimerization of ethylene takes place until most of the styrene is consumed. It is to be noted that the ethylene dimerization as well as isomerization of 1-butene formed is accelerated when most of the styrene is consumed, and also that 3-methyl-3-phenyl-1-pentene given by the reaction of ethylene with 2-phenyl-2-butene formed from the isomerization of 3-phenyl-1-butene, is gradually formed during the course of codimerization. The effect of ethylene pressure was examined on the amount of 3-phenyl-1-butene formed. The amount is plotted against the partial pressure of ethylene in Fig. 2, where the vapour pressure of methylene dichloride is 15 cmHg at 0 °C. The amount of 3-phenyl-1-butene increases linearly with the partial pressure of ethylene, indicating that the reaction rate is first order in ethylene

Effect of Concentration of Catalyst Components: The effect of trifluoroboron etherate was examined on the rate of codimerization under a constant pressure(partial pressure of ethylene, 35 mmHg), where the amount of bis(triphenylphosphine)-1-naphthyl(bromo)nickel(II) was kept constant (0.5 mmol). The rate can be shown by the amount of 3-phenyl-1-butene formed for a specific period of reaction time, since the rate is independent of the amount of styrene(Fig. 1). The amount of 3-phenyl-1-butene (mmol) formed for 15 min. is plotted against the mole ratio, trifluoroboron etherate to the nickel complex(Fig. 3). The result at the mole ratio 2.5 was estimated from the amount

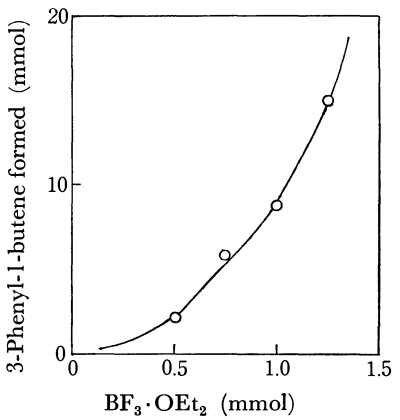

Fig. 3. Effect of the amount of $BF_3 \cdot OEt_2$. (1-naphthyl)NiBr($P\phi_3$)$_2$, 0.5 mmol; styrene, 19.1 mmol; CH_2Cl_2, 30 ml; $P_{C_2H_4}$, 35 cmHg; temp. 0°C; time 15 min.

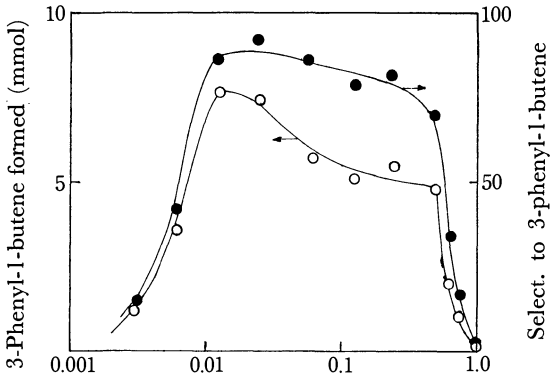

Fig. 4. Effect of the amount of (1-naphthyl)NiBr($P\phi_3$)$_2$ $BF_3 \cdot OEt$, 0.5 mmol; Styrene, 19.1 mmol; $P_{C_2H_4}$, 35 cmHg; CH_2Cl_2, 30 ml; temp. 0°C; time 30 min.

of 3-phenyl-1-butene formed for 10 min., since the reaction rate was too rapid. The rate seems to increase approximately in the second order with respect to the mole ratio of trifluoroboron etherate to bis(triphenylphosphine)-1-naphthyl (bromo) nickel (II). In this case, the amount of butene formed was less than 1% based on that of ethylene consumed. The effect of the amount of bis(triphenylphosphine)-1-naphthyl(bromo)nickel(II) on the codimerization rate and the selectivity to 3-phenyl-1-butene is shown in Fig. 4, where the amount of trifluoroboron etherate is kept constant (0.5 mmol). The rate increases with the amount of nickel complex and reaches maximum at about 0.0125 mmol (the mole ratio of $BF_3 \cdot OEt_2$/Ni-complex=40). Above the maximum, it gradually decreases in the range 0.02~0.5 mmol, within which the selectivity of 3-phenyl-1-butene is fairly high, while the rate rapidly decreases with increasing the amount of nickel complex more than 0.5 mmol (the mole ratio, less than 1).

Codimerization with Styrene Derivatives: The codimerization of ethylene with styrene catalyzed by the present catalyst system was extended to the codimerization with styrene derivatives such as *o*-, *m*-, and *p*-methylstyrene, *o*-, *m*-, and *p*-chlorostyrene, α- and ω-methylstyrene and ω-bromostyrene. The results are summarized in Table 2. *o*-, *m*-, and *p*-Methyl styrenes are also codimerized with ethylene to give the corresponding 2-(chloro- or methyl-phenyl)butenes under the conditions given in Table 2. There is no significant difference between methylstyrene and chlorostyrene in their conversion, while the selectivity of their codimers depends considerably on the position of chloro or methyl substituted on the phenyl. The selectivity increases on the order *ortho*<*meta*<*para* in methyl styrene as well as in chlorostyrene. On the other hand, α- and ω-methyl styrene are less reactive and a considerable amount of ethylene is consumed in the formation of butene (Table 2). No codimer was detected from the reaction of vinyl chloride with ethylene in the presence of this catalyst system. ω-Bromostyrene, however, gave a small amount of its codimers with ethylene consisting of two isomers, both in nearly the same amount.

Discussion

Course of Codimerization of Styrene with Ethylene. It was reported in a previous paper that the active species of the present catalyst system is a nickel hydride complex fromed from dissociative addition of ethylene to σ-aryl nickel(II) compound.[11] This has been clarified by the dimerization of deuteroethylene and its isotopic mixing with ethylene catalyzed by the present catalyst system.[12] From the product distribution of C_2H_4-C_3H_6 codimerization catalyzed by the present catalyst

Table 2. Codimerization of styrene derivatives with ethylene

Styrene derivatives (mmol)	Styrene consumed (mmol)	Codimer formed (mmol)	Select. to codimer (%)	Butenes (mmol)
p-Methylstyrene (15.2)	5.8	4.3	75	0.04
m-Methylstyrene (15.5)	6.0	4.3	72	0.05
o-Methylstyrene (15.1)	2.7	0.6	22	0.03
p-Chlorostyrene (15.1)	5.0	4.9	98	0.12
m-Chlorostyrene (15.0)	5.9	3.1	53	0.19
o-Chlorostyrene (15.0)	5.0	0.7	14	0.16
α-Methylstyrene (15.4)	1.4	0.9	67	7.3
ω-Methylstyrene (15.4)	2.4	1.7	70	2.1
ω-Bromostyrene (15.5)	1.5	0.4	26	0.31

(1-naphthyl)NiBr($P\phi_3$)$_2$, 0.5 mmol; $BF_3 \cdot OEt_2$, 0.5 mmol; CH_2Cl_2, 30 ml; $P_{C_2H_4}$, 35 cmHg; temp. 0° C; time, 30 min.

system, the nickel hydride is considered to be catalytically recycled in the course of the reaction and the reductive coupling processes of the intermediate nickel complexes can be excluded.[13] Thus selcetive formation of 3-phenyl-1-butene can also be understood in terms of the nickel hydride. Styrene reacts with the nickel hydride (Ni–H) to give σ-(1-phenylethyl)nickel intermediate(II), followed by the insertion of ethylene-(III) and elimination of its β-hydrogen to give 3-phenyl-1-butene and regenerate Ni-H. It has not been clarified whether the nickel hydride is formed by dissociative addition of ethylene or styrene.

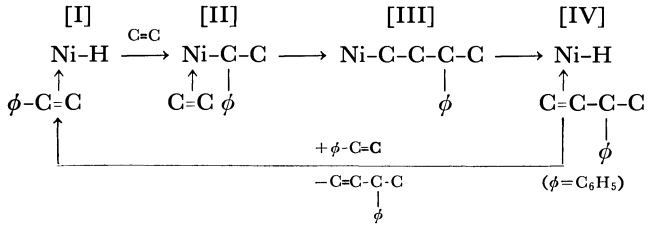

In this scheme, 3-phenyl-1-butene should be readily replaced by styrene, because the codimerization rate is independent of the concentration of styrene. This is consistent with the fact that only a trace amount of butenes and 2-phenyl-2-butene is formed before most of the styrene is consumed(Fig. 1). This might be one reason for 3-phenyl-1-butene being selectively formed. The sterically most crowded complex, [mesityl]Ni($P\phi_3$)$_2$Br, gives the highest selectivity of codimerization (Table 1). This suggests that the aryl ligand remains on the nickel atom. Homodimerization of styrene and its codimerization with its derivatives are probably affected by a steric hindrance of the aryl ligand of the nickel complex. Styrene derivatives having a chloro or methyl substituent on the phenyl also give their codimers fairly selectively, except for *o*-chloro and *o*-methylstyrene (Table 2). Chloro and methyl substituents on the ortho position of phenyl seems to exhibit a sterically unfavorable effect for the reaction with ethylene. On the other hand, a considerable amount of butene is formed in the case of codimerization with α- or ω-methylstyrene. This suggests that the coordination of styrene is weakened by the methyl group.

It should be noted here that 3-phenyl-3-methyl-1-pentene is gradually accumulated during the course of codimerization of ethylene with styrene(Fig. 1). No other path can be considered for the formation of this product than the codimerization of ethylene with 2-phenyl-2-butene. This means that 2-phenyl-2-butene, once it is formed, is also readily codimerized with ethylene, though the isomerization rate of 3-phenyl-1-butene into 2-phenyl-2-butene is very small. However, the difference in their reactivities between 2-phenyl-2-butene and α-(or ω-)methylstyrene remains to be clarified(Table 2).

Role of Trifluoroboron Etherate: In the previous paper[12] dealing with ethylene dimerization catalyzed by present catalyst system, two functions of trifluoroboron etherate were discussed, its contribution as a ligand, where trifluoroboron is in contact with the nickel complex through the bromide ligand, and its removal of

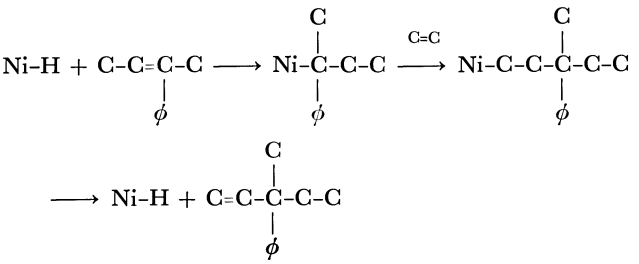

the triphenylphosphine coordinated to the nickel complex to offer a vacant site avairable for the coordination ethylene. It can thus be expected that the codimerization rate increases approximately in the second order with respect to the amount of trifluoroboron etherate as shown in Fig. 3. However, the result shown in Fig. 4 is not obtained only by these two functions. Side reactions of styrene should be taken into account. Preliminary experiments showed that styrene is readily oligomerized in the absence of ethylene by this catalyst system and the oligomerization is highly accelerated by increasing the amount of trifluoroboron etherate, which probably gives rise to a cationic polymerization of styrene. This might be the reason why the selectivity to 3-phenyl-1-butene based on the amount of styrene consumed decreases in the presence of a large amount of trifluoroboron etherate. On the other hand, a decrease in its amount would be more disadvantageous the coordination of ethylene than that of ethylene. This is consistent with the decrease in selectivity to 3-phenyl-1-butene with the decrease in partial pressure of ethylene(Fig. 2). Accordingly, the selectivity to the codimer becomes low again when the amount of trifluoroboron etherate added is less than that of the nickel complex. We thus see why the present catalyst system is active and selective for the codimerization of styrene with ethylene over a range of mole ratio of trifluoroboron etherate to the nickel complex (Fig. 4).

References

1) K. Maruya, T. Mizoroki, and A. Ozaki, This Bulletin, **43**, 3630 (1970).
2) N. Kawata, K. Maruya, T. Mizoroki, and A. Ozaki, *ibid.*, **44**, 3217 (1971).
3) T. Alderson, E. L. Jenner, and R. V. Lindsey Jr., *J. Amer. Chem. Soc.*, **87**, 5638 (1965).
4) K. Kawamoto, A. Tatani, T. Imanaka, and S. Teranishi, This Bulletin, **43**, 2512 (1970); *ibid.*, 44, 1236 (1971).
5) M. G. Barlow, M. J. Beyant, R. N. Hasezeldine, and A. G. Mackie, *J. Organometal. Chem.*, **21**, 215 (1970).
6) H. Muller, D. Wittenberg, H. Seibt, and E. Scharf, *Angew. Chem. Int. Ed. Engl.*, **4**, 327 (1965).
7) C. Dixson, E. W. Duck, and D. K. Jenkins, *Organometal. Chem. Syn.*, **1**, 77 (1970/1971).
8) L. M. Vernanzi, *J. Chem. Soc.*, **1968**, 719.
9) J. Chatt and B. L. Show, *ibid.*, **1960**, 1718.
10) E. C. Horning(Editor in Chief), Organic Syntheses, Vol. 3, 204 (1965).
11) K. Maruya, T. Kuroki, T. Mizoroki, and A. Ozaki, This Bulletin, **44**, 2002 (1971).
12) K. Maruya, T. Mizoroki, and A. Ozaki, *ibid.*, **45**, 2255 (1972).
13) K. Maruya, T. Mizoroki, and A. Ozaki, *ibid.*, **46**, 993 (1973).

8,5′-*O*-Cyclonucleosides of Tubercidin

Kentaro ANZAI and Masanao MATSUI

The Institute of Physical and Chemical Research, Wako-shi, Saitama 351

(Received June 21, 1973)

On treatment with NBS, 2′,3′-*O*-benzylidenetubercidin (**1**) and its isopropylidene analogue (**6**) afforded the 8,5′-*O*-cyclonucleosides **2** and **7** respectively. Catalytic hydrogenation of **2** and **7** afforded the dehalogenated compounds, **9** and **12**.

Conversion of tubercidin[1] to 5′-deoxytubercidin[2] has already been accomplished by the present authors, and 3′-deoxytubercidin has also been synthesized by Robins and his coworkers.[3] We wish to report here the reaction of NBS with 2′,3′-*O*-benzylidenetubercidin (**1**). This work was initially attempted to obtain the 2′(or 3′)-bromo derivative of 3′(or 2′)-*O*-benzoyltubercidin, which might be used as an intermediate in the synthesis of 2′(or 3′)-deoxytubercidin. Ponpipom and Hanessian have already succeeded[4] in the conversion of 2′,3′-*O*-benzylideneuridine into 3′-*O*-benzoyl-5, 2′-dibromo-2′-deoxyuridine; analogously, we carried out the reaction on **1**.

2′,3′-*O*-Benzylidenetubercidin (**1**), shown to be a diastereomeric mixture by a study of its NMR spectrum, was treated with 1.5 equivalent mol of NBS in a mixture of carbon tetrachloride and tetrachloroethane (1 : 1) under reflux. The reaction seemed to proceed with serious decomposition, and from the reaction mixture two products were isolated in low yields. The minor one was identified as 7-bromo-2′,3′-*O*-benzylidenetubercidin (**5**), obtained as a mixture of diastereomers.

The main product, which was obtained in a 36% yield, was identified as 8,5′-*O*-anhydro-7-bromo-8-hydroxy-2′,3′-*O*-benzylidenetubercidin (**2**). Though the isolated sample showed a single spot on tlc, it was found to be a diastereomeric mixture as shown by the NMR spectrum; we succeeded in obtaining one diastereomer by careful crystallization.

The molecular formula, $C_{18}H_{15}N_4O_4Br$, suggested that the substitution with two bromine atoms, followed by the loss of one mole of hydrogen bromide, afforded the product. In the IR spectrum no absorption was observed in the range of 1660—2900 cm^{-1}, showing that it was not a benzoyl ester as had first been expected. Moreover, it was stable in *n*-propanol–1 M NaOH (4 : 1) on prolonged heating; thus, the benzoyl-ester structure is also unlikely. The NMR spectrum exhibited signals of the ABX type assignable to two hydrogens at C–5′ (δ 4.04 and δ 4.54, $J_{gem}=12$ Hz, $J_{4',5'a}=1$ Hz, $J_{4',5'b}=2$ Hz), showing that it was a cyclonucleoside. A signal corresponding to a hydrogen at C–8 in the starting material was lacking. The mass spectrum showed the parent peaks at *m/e* 432 ($C_{18}H_{15}N_4O_4{}^{81}Br$) and *m/e* 430 ($C_{18}H_{15}N_4O_4{}^{79}Br$) as well as four intense peaks corresponding to the ion species, **3b** (*m/e* 230), **4b** (*m/e* 229), **3a** (*m/e* 228) and **4a** (*m/e* 227).

Catalytic reduction of **2** afforded the dehalogenated compound **9**. The mass spectrum of **9** showed the parent peak at *m/e* 352 as well as two intense peaks at *m/e* 150 and *m/e* 149 corresponding to the ion species **10** and **11**.

2′,3′-*O*-Isopropylidenetubercidin (**6**) similarly reacted with NBS to give 8,5′-*O*-anhydro-7-bromo-8-hydroxy-2′,3′-*O*-isopropylidenetubercidin (**7**). When the reaction was carried out at room temperature in a mixture of acetone and methylene chloride (1 : 1), with the molar ratio of NBS to **6** being 1.1, the product was a gummy material, from which **7** was isolated in a 7% yield. The formation of 7-bromo-2′,3′-*O*-isopropylidenetubercidin was also observed, though it was difficult to purify (See Exp). A few further attempts to improve the yield of **7** were made (See Exp.), but we now feel that it is a fruitless work.

The reaction path to give **7** may involve the dibromide **14** and the 3,5′-*O*-cyclonucleoside **15** as the intermediates (Scheme 1). In connection with this mechanism, conversion of adenine 3*N*-oxide and their xanthine and guanine analogues into the 8-oxygenated purines in acetic anhydride has been reported.[5] However, another possible path, which does not involve **15**, can not be excluded (Scheme 2).

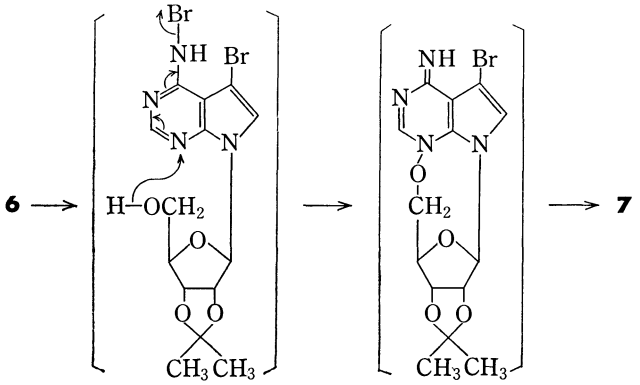

14 **15**

Scheme 1

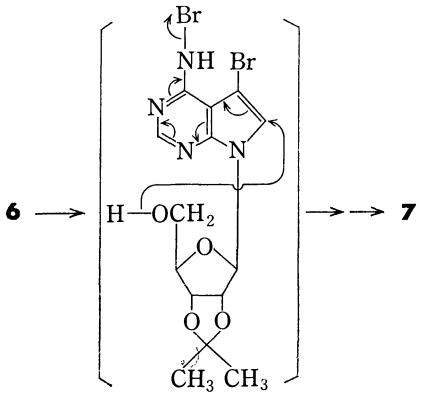

14

Scheme 2

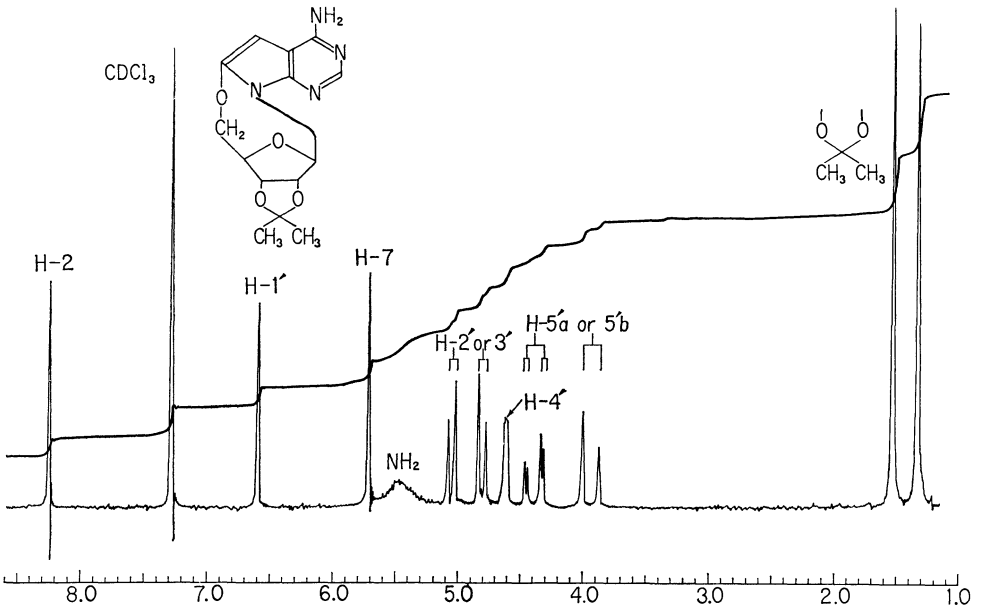

Fig. 1. The NMR spectrum of 8,5′-O-anhydro-2′,3′-O-isopropylidenetubercidin (**12**): 100 MHz, $CDCl_3$.

Catalytic reduction of **7** afforded the dehalogenated compound **12**, the structure of which was also supported by its NMR spectrum (Fig. 1).

Treatment of **12** with excess *p*-toluoyl chloride afforded the di-*p*-toluoyl derivative, **13**, the NMR spectrum of which exhibited a six-proton singlet at δ 2.32 corresponding to two methyls of *p*-toluoyl groups and a pair of four-proton doublets at δ 7.24 and δ 7.67 (J=8 Hz), supporting the N^6,N^6-diacyl structure[6] in **13**.

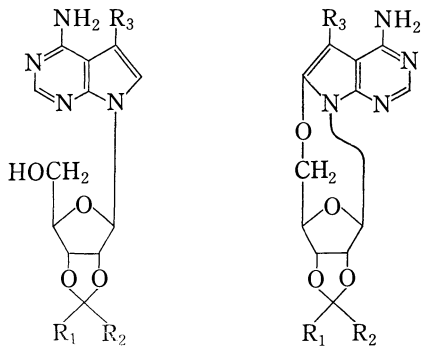

1, R_1=H, R_2=C_6H_5, R_3=H
2, R_1=H, R_2=C_6H_5, R_3=Br
5, R_1=H, R_2=C_6H_5, R_3=Br
7, R_1=CH_3, R_2=CH_3, R_3=Br
6, R_1, R_2=CH_3, R_3=H
9, R_1=H, R_2=C_6H_5, R_3=H
8, R_1, R_2=CH_3, R_3=Br
12, R_1=CH_3, R_2=CH_3, R_3=H

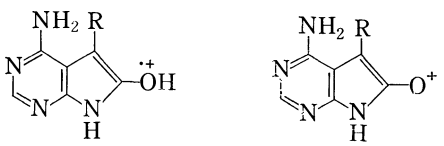

3a, R=^{79}Br
3b, R=^{81}Br
10, R=H

4a, R=^{79}Br
4b, R=^{81}Br
11, R=H

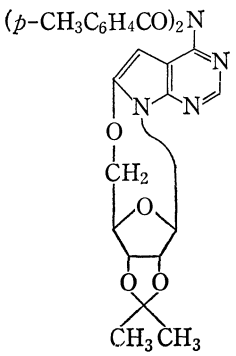

13

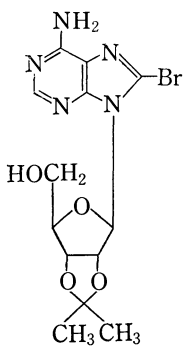

17

When 2′,3′-*O*-isopropylideneadenosine[7] (**16**) was treated with NBS under analogous conditions, the only product, which was isolated in a low yield, was 8-bromo-2′,3′-*O*-isopropylideneadenosine (**17**).

Experimental

*Reaction of NBS with 2′,3′-O-Benzylidenetubercidin (**1**).* NBS (700 mg, 3.94 mmol) and 2′,3′-*O*-benzylidenetubercidin (1) (700 mg, 2.68 mmol) were dissolved in a mixture of carbon tetrachloride and tetrachloroethane (1 : 1) (100 ml), and then $BaCO_3$ (500 mg) was added. The solution was refluxed for 2 hr. After cooling, $(NH_4)_2SO_4$ (1 g) was added, and the solution was stirred for 1 hr. It was then washed with an aqueous solution of sodium bicarbonate and concentrated to dryness. Tlc showed that the residue contained three UV-absorbing compounds; they were separated by silica gel chromatography. The least polar compound was eluted with a mixture of benzene and ethyl acetate (1 : 1); it was thus obtained as a crystalline powder from ethyl acetate and *n*-hexane; yield, 412 mg (36%); mp 201—203 °C. NMR (100 MHz, $CDCl_3$) suggested that it was a 1 : 1 mixture of diastereomers of 8,5′-*O*-anhydro-7-bromo-8-hydroxy-

2′,3′-*O*-benzylidenetubercidin (**2**); δ 5.84 and 6.22 (two s, $C_6H_5CH\langle$), 6.79 and 6.82 (two s, H-1′), 8.23 and 8.25 (two s, H-2). Mass *m/e*: 432.0245 (M^+, $C_{18}H_{15}N_4O_4$ ^{81}Br gives 432.0256), 430 (M^+, $C_{18}H_{15}N_4O_4$ ^{79}Br), 360 and 358 (M^+–OCH_2CHO), 326 and 324 (M^+ –C_6H_5CHO), 283 and 281 (M^+ –C_6H_5CHO–CH_2CHO), 230 (**3b**) (observed 229.9648, $C_6H_5N_4O^{81}Br$ gives 229.9626), 229 (**4b**), 228 (**3a**), 227 (**4a**), 202 (**4b**-*HCN*), 200 (**4a**-*HCN*).

Found: C, 50.24; H, 3.50; N, 13.22; Br, 18.41%. Calcd for $C_{18}H_{15}N_4O_4Br$: C, 50.13; H, 3.51; N, 12.99; Br, 18.53%.

One of the diastereomers was separated as crystals from benzene at room temperature; mp 197—199 °C(dec), $\lambda_{max}^{H_2O}$ 280 nm (ε 12300), $[\alpha]_D^{24}$ −1.5 (*c* 1.5, $CHCl_3$); NMR (100 MHz, $CDCl_3$) δ: 4.04 (dd, 1H, H-5′$_a$, J_{gem}=12 Hz, $J_{4',5'a}$= 1 Hz), 4.54 (dd, 1H, H-5′$_b$, J_{gem}=12 Hz, $J_{4',5'b}$=2 Hz), 4.81 (broad, 1H, H-4′), 4.90 and 5.15 (two d, 2H, H-2′ and H-3′, $J_{=2',3'}$=5.5 Hz), 5.84 (s, 1H, $C_6H_5CH\langle$), 5.95 (broad s, 2H, NH_2, disappeared on the addition of D_2O), 6.79 (s, 1H, H-1′), 8.23 (s, 1H, H-2).

Found: C, 53.94; H, 3.86; N, 12.06; Br, 17.10%. Calcd for $C_{18}H_{15}N_4O_4Br$ 1/2 C_6H_6: C, 53.63; H, 3.86; N, 11.92; Br 16.99%.

Next, a compound, which was identified as 7-bromo-2′,3′-*O*-benzylidenetubercidin (**5**), was eluted from the column using ethyl acetate as the developing solvent; it was obtained as a syrup by partial precipitation from ethyl acetate and *n*-hexane; yield, 226 mg; λ_{max}^{MeOH} 282 nm (ε 11000), M^+ 434 ($C_{18}H_{17}N_4O_4{}^{81}Br$) and 432($C_{18}H_{17}N_4O_4{}^{79}Br$).

Found: C, 49.19; H, 3.82; N, 12.53%. Calcd for $C_{18}H_{17}O_4N_4Br\cdot 1/2H_2O$: C, 48.88; H, 4.10; N, 12.67%.

The most polar compound eluted from the column with a mixture of ethyl acetate and methanol (9 : 1) was found to be the starting material.

*Reaction of NBS with 2′,3′-O-Isopropylidenetubercidin (**6**).* NBS (3.1 g, 17.4 mmol) and 2′,3′-*O*-isopropylidenetubercidin (**6**) (4.8 g, 15.6 mmol) were dissolved in a mixture of acetone and methylene dichloride (1 : 1) (200 ml); after the solution had been stirred at room temperature overnight, it was poured into a cold solution of sodium bicarbonate. The products were extracted with chloroform, and the organic phase was washed with an aqueous solution of sodium thiosulfate and then with water. Two main UV absorbing spots were shown on tlc, and each corresponding compound was separated on a silica gel column. 8,5′-*O*-anhydro-7-bromo-8-hydroxy-2′,3′-*O*-isopropylidenetubercidin (**7**) was first eluted from the column, using ethyl acetate as the developing solvent; yield, 389 mg. An analytical sample was obtained on crystallizing it first from benzene and then from ethanol and water; mp 215—218 °C (dec), λ_{max}^{MeOH} 280 nm (ε 12000), $[\alpha]_D^{23}$ +87.0 (*c* 1 : 1 $CHCl_3$); NMR (100 MHz, $CDCl_3$) δ: 1.37 and 1.57 (two s, 6H, two isopropylidene methyls), 4.03 (dd, 1H, H-5′$_a$, J_{gem}=13 Hz, $J_{3',5'a}$=1 Hz), 4.52 (dd, 1H, H-5′$_b$, J_{gem}=13 Hz, $J_{4',5'b}$=2 Hz), 4.66 (broad, 1H, H-4′), 4.82 and 5.19 (two d, 1H, H-2′ and H-3′, $H_{2',3'}$= 5 Hz), 5.76 (broad s, 1H, NH_2), 6.63 (s, 1H, H-1′), 8.24 (s, 1H, H-2); Mass *m/e*: 384 ($C_{14}H_{15}N_4O_4{}^{81}Br$) and 382 ($C_{14}H_{15}N_4O_4{}^{79}Br$) ($M^+$), 230 (**3b**), 229 (**4b**), 228 (**3a**), 227 (**3b**).

Found: C, 43.84; H, 3.79; N, 14.66; Br, 20.85%. Calcd for $C_{14}H_{15}N_4O_4Br$: C, 43.88; H, 3.95; N, 14.62; Br, 20.85%.

The more polar compound was eluted from the column with a mixture of ethyl acetate and methanol (9 : 1); the subsequent evaporation of the solvent afforded 712 mg of a syrup. The mass spectrum suggested that the product was 7-bromo-2′,3′-*O*-isopropylidenetubercidin (**8**), showing the parent peaks at 386 ($C_{14}H_{17}N_4O_4{}^{81}Br$) and 384 ($C_{14}H_{17}N_4O_4{}^{79}Br$). However, attempts to obtain an analytically pure sample by repeated precipitation from benzene and *n*-hexane were unsuccessful, possibly because of the contamination of the unreacted starting material, which showed an R_f value close to that of **8** on tlc.

When a 4.28 g portion of **6** (14.0 mmol) was treated with 2.0 g of NBS (10.6 mmol) under comparable conditions, 550 mg of **7** and 1.37 g of the starting material were obtained.

The molar ratio of NBS to **6** was then increased to 2.5, and the reaction was carried out in a mixture of carbon tetrachloride and tetrachloroethane (1 : 1) under reflux. In this case, a serious decomposition seemed to proceed and the reaction mixture darkened markedly. No UV absorbing spot could be detected on tlc.

*8,5′-O-Anhydro-8-hydroxy-2′,3′-O-benzylidenetubercidin (**9**).* One diastereomer of **2** (350 mg), obtained in the crystalline state, was catalytically hydrogenated over 10% Pd-C(50 mg) in a mixture of ethanol (50 ml) and 10% CH_3COONa (3 ml) for 3 hr. After the catalyst had been removed by filtration through a Celite pad the ethanol was evaporated. The product was extracted with ethyl acetate and was crystallized from ethyl acetate and carbon tetrachloride; yield, 270 mg, mp 227—228 °C (dec) λ_{max}^{MeOH} 272 nm (ε 16400), $[\alpha]_D^{24}$ −48.7 (*c*, 1.3 $CHCl_3$); Mass *m/e*: 352 (M^+), 150 (**10**), 149 (**11**); ($CDCl_3$, 100 MHz) δ: 4.02 (dd, 1H, H-5′$_a$, J_{gem}=12 Hz, $J_{4',5'a}$=1 Hz), 4.48 (dd, 1H, H-5′$_b$, J_{gem}= 12 Hz, $J_{4',5'b}$=2 Hz), 4.81 (broad, 1H, H-4′), 4.94 and 5.15 (two d, 2H, H-2′ and H-3′, $J_{2',3'}$=6 Hz), 5.86 (s, 2H, C_6H_5-$CH\langle$ and H-7), 6.80 (s, 1H, H-1′), 8.26 (s, 1H, H-2). The assignement of a two-proton singlet at δ 5.86 to a benzylidene methine proton and H-7 was confirmed by the spectrum in CD_3COCD_3, which exhibited two one-proton singlets at δ 5.92 and δ 6.06.

Found: C, 61.37; H, 4.58; N, 15.57%. Calcd for $C_{18}H_{16}N_4O_4$: C, 61.36; H, 4.58; N, 15.90%.

*8-5′-O-Anhydro-8-hydroxy-2′,3′-O-isopropylidenetubercidin (**12**).* Compound **7** (500 mg) was catalytically hydrogenated over 10% Pd-C (100 mg) for 4 hr in a mixture of ethanol (50 ml) and 10% CH_3COONa (2 ml). The reaction mixture was then filtered through a Celite pad, and the ethanol was evaporated. The product was extracted with chloroform and was thus obtained as a powder from benzene and *n*-hexane; yield, 350 mg; mp 107—113 °C, λ_{max}^{MeOH} 272 nm (ε 13900); $[\alpha]_D^{23}$ +86.0 (*c* 0.6 $CHCl_3$); Mass m/e: 304 (M^+), 150 (**10**), 149 (**11**); NMR (100 MHz, $CDCl_3$) δ: 1.36 and 1.56 (two s, 6H, two isopropylidene methyls), 3.96 (broad d, 1H, H-5′$_a$, J_{gem}=13 Hz), 4.40 (dd, 1H, H-5′$_b$, $J_{=gem}$ 13 Hz, $J_{4',5'b}$=2 Hz), 4.62(broad, 1H, H-4′), 4.82 and 5.04 (two d, 2H, H-2′ and H-3′, $J_{2',3'}$=5 Hz), 5.46 (broad s 2H, $-NH_2$, disappeared on the addition of D_2O), 5.72 (s, 1H, H-7), 6.60(s, 1H, H-1′), 8.26 (s, 1H, H-2).

Found: C, 54.45; H, 5.26; N, 17.91%. Calcd for $C_{14}H_{16}N_4O_4\cdot 1/2H_2O$: C, 53.84; H, 5.17; N, 17.94%.

*8-5′-O-Anhydro-8-hydroxy-N^6,N^6-p-toluoyl-2′,3′-O-isopropylidenetubercidin (**13**).* Into a stirred solution of **12** (152 mg) in pyridine (20 ml), *p*-toluoyl chloride (0.5 ml) was added at 0 °C, after which the solution was left in a refrigerator overnight. The reaction mixture was then poured into an ice-cooled solution of sodium bicarbonate, and the product was extracted with chloroform. After evaporation of the solvent to dryness, the residue was washed with a small amount of hot ethyl acetate; it was obtained as a powder; yield, 190 mg; mp 273—273.5 °C (dec); λ_{max}^{MeOH} nm (ε): 305 (12500) 253 (28000); Mass *m/e*: 540 (M^+), 512 (M^+-CO), 484 (M^+-2CO), 421 (M^+-$CH_3C_6H_4CO$), 393 (M^+-$CH_3C_6H_4CO$-CO); NMR (100 MHz, DMSO-*d*) δ: 1.31 and 1.50 (two s, 6H, two isopropylidene methyls), 2.32 (s, 6H, 2*p*-$CH_3C_6H_4$-CO), 5.80 (s, 1H, H-7), 6.42 (s, 1H, H-1′), 7.24 and 7.67 (two d, 8H, 2*p*-$CH_3C_6H_4CO$, J=8 Hz), 8.48 (s, 1H, H-2).

Found: C, 66.34; H, 5.19; N, 9.98%. Calcd for $C_{30}H_{28}N_4O_6$: C, 66.65; H, 5.22; N, 10.37%.

*8-Bromo-2',3'-O-isopropylideneadenosine (**17**).* A solution of 2',3'-O-isopropylideneadenosine (**16**) (1.6 g, 5.2 mmol), NBS (2 g, 11.2 mmol), and $CaCO_3$ (1 g) in acetone (50 ml) was stirred overnight at room temperature and then poured into a cold solution of sodium bicarbonate. The chloroform extract was washed with an aqueous solution of sodium thiosulfate and then with water.

Silica gel chromatography on developing with a mixture of ethyl acetate and methanol (9 : 1) afforded two compounds, the more polar one being the starting material (720 mg). The less polar one, identified as **17**, was crystallized from ethyl acetate; yield, 267 mg; mp 229 °C; λ_{max}^{MeOH} 264 nm (ε 18900); $[\alpha]_D^{23}$ −37.0 (*c* 1.1 DMSO); Mass *m/e*: 387 (M^+, $C_{13}H_{14}N_5O_4{}^{81}Br$), 385 ($M^+$, $C_{13}H_{14}N_4O_5{}^{79}Br$), 214 and 212 (base peak, base moiety of **17**): NMR (100 MHz, DMSO-*d*) δ: 1.34 and 1.56 (two s, 6H, two isopropylidene methyls), 3.50 (m, 2H, H-5'), 4.18 (m, 1H, H-4'), 5.04 (q, 1H, H-3', $J_{3',4'}$=3 Hz, $J_{2',3'}$=6 Hz), 5.67 (q, 1H, H-2', $J_{2',3'}$=6 Hz, $J_{1',2'}$=3 Hz), 6.04 (d, 1H, H-1', $J_{1',2'}$=3 Hz), 7.55 (broad s, 2H, NH_2) 8.16 (s, 1H, H-2).

Found: C, 40.44; H, 4.18; N, 18.57; Br, 20.61%. Calcd for $C_{13}H_{14}N_5O_4Br$: C, 40.43; H, 4.18; N, 18.14; Br, 20.69%.

Under altered conditions, the yield of **17** was not improved; *e.g.*, when **16** (5.47 g) was treated with NBS (3.5 g) in a mixture of tetrachloroethane (75 ml) and carbon tetrachloride (25 ml) in the presence of $CaCO_3$ (5 g) under reflux for 4 hr, the yield of **17** was 257 mg, and 1.13 g of **16** was recovered. An extended reaction time or the use of an increased amount of NBS resulted in a darkening of the reaction mixture and a decreased yield of **17**.

References

1) K. Anzai, G. Nakamura and S. Suzuki, *J. Antibiot.* (Tokyo), *Ser. A*, **10**, 201 (1957); S. Suzuki and S. Marumo, *ibid.*, *Ser A*, **13**, 136 (1960): *ibid.*, *Ser. A*, **14**, 34 (1961); Y. Mizuno, M. Ikehara, K. A. Watanabe, S. Suzaki, and T. Itoh, *J. Org. Chem.*, **28**, 3329 (1963).

2) K. Anzai and M. Matsui, This Bulletin, **46**, 618 (1973).

3) M. J. Robins, J. R. McCarthy, JR., R. A. Jones and Mengel, *Can. J. Chem.*, **51**, 1313 (1973).

4) M. M. Ponpipom and S. Hanessian, *Can. J. Chem.*, **50**, 246, 253 (1972).

5) U. Wölcke, W. Pfleiderer, T. J. Delia and G. B. Brown, *J. Org. Chem.*, **34**, 981 (1969); U. Wölcke, N. J. M. Birdsall, and G. B. Brown, *Tetrahedron Lett.*, **10**, 785 (1969); N. J. M. Birdsall, J. C. Lee and U. Wölcke, Tetrahedron, **27**, 5961 (1971); N. J. M. Birdsall, U. Wolcke, T. C. Lee and G. B. Brown, *ibid.*, **27**, 5969 (1971); N. J. M. Birdsall, J. C. Parham, U. Wölcke and G. B. Brown, *ibid.*, **28**, 3 (1972).

6) K. Anzai and M. Matsui, This Bulletin, **46**, 3228 (1973).

7) J. Baddiley, *J. Chem. Soc.*, **1951**, 1348.

Effect of pH on the Circular Dichroism(CD)-sensitive Transitions of Some Lanthanoid(III) Complexes and "Pseudo CD-sensitive Transitions" of Europium(III) and Terbium(III) Complexes

Seizo MISUMI, Toshiyuki ISOBE, and Haruko FURUTA

Inorganic Chemistry Laboratory, Faculty of Science, Kyushu University, Fukuoka 812

(Received May 23, 1973)

The effect of pH on the CD-sensitive transitions of lanthanoid(III) complexes with *l*-propylenediaminetetraacetic acid(*l*-PDTA) and L-ethylenediaminedisuccinic acid(L-EDDS) was studied. The relation between the cross-over pH where the CD pattern changes or sign of CD reverses and the number of 4f-electrons in lanthanoid(III) complexes with L-EDDS showed a tetrad curve. A strong evidence for coordination of hydroxide ions was suggested. "Pseudo CD-sensitive bands" in the spectra of the complexes of europium(III) and terbium(III) which do not obey the selection rule $\Delta J \leq 1$ were found, and the mechanisms of these transitions were elucidated.

The circular dichroism (CD)-sensitive band has been observed on the J'-band of magnetic dipole character for some lanthanoid(III) complexes with optically active ligands. The experimental result was in accordance with the theory proposed previously.[1,2] It was observed that intensities and patterns of CD-sensitive bands of lanthanoid(III) complexes vary remarkably with pH of solutions, especially with high pH's. This phenomenon in the lanthanoid(III) complexes with *l*-PDTA or L-EDDS was studied in detail. The work has revealed some new information on the coordination bonds of the lanthanoid(III) complexes.

The pseudo CD-sensitive bands in the spectra of europium(III) and terbium(III) complexes were found and the mechanism of these bands which do not obey the selection rule $\Delta J \leq 1$, was discussed.

Experimental

Materials. All lanthanoid(III) perchlorates were prepared by dissolving lanthanoid oxides of 99.9% purity in perchloric acid and their concentrations were standardized by EDTA titration using xylenol orange as an indicator. *l*-PDTA was synthesized by Dwyer's method[3] and L-EDDS by the method of Neal and Rose[4] from 1,2-dibromoethane and L-aspartic acid, respectively. The sample solution was prepared by mixing lanthanoid(III) perchlorate with the ligand at 1 : 1 mole ratio (practically 10% excess of the ligand for *l*-PDTA and 5% excess for L-EDDS). The final concentration of lanthanoid(III) in complex was made to be 0.1 mol/l. The pH of the solution of *l*-PDTA complex was adjusted by 5 M NaOH and that of L-EDDS complex by aqueous ammonia. H[Pr(L-EDDS)]·$2H_2O$ and H[Dy(L-EDDS)]·$2H_2O$ were prepared by Moeller's method[5] and CD spectra of these complexes were measured at various pH values.

Measurements. Absorption and CD spectra of the complexes were measured with a JASCO model ORD/UV-5 optical rotatory dispersion recorder with a CD attachment, a 10 mm cell, at room temperature. It was found more convenient to use a 50 mm cell for H[Pr(L-EDDS)]·$2H_2O$ and H[Dy(L-EDDS)]·$2H_2O$ at various pH values in aqueous solutions. A Hitachi-Horiba model F-5 pH meter was used for pH measurements.

Results

The CD spectra of lanthanoid(III) complexes with *l*-PDTA and L-EDDS were measured at various pH values in aqueous solutions. In a strongly alkaline region, it was found that the patterns of CD-sensitive bands of these complexes vary remarkably with increasing pH value. The changes in the patterns and

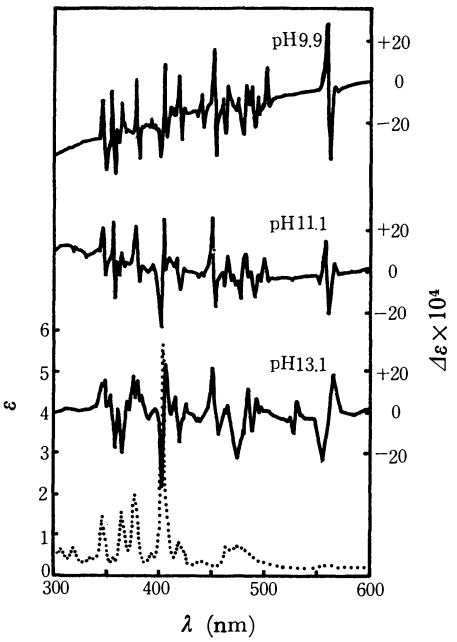

Fig. 1. Alterations of CD spectra for Sm(III)-*l*-PDTA complex: ——, CD spectra ($\Delta\varepsilon$); ·····, absorption spectrum.

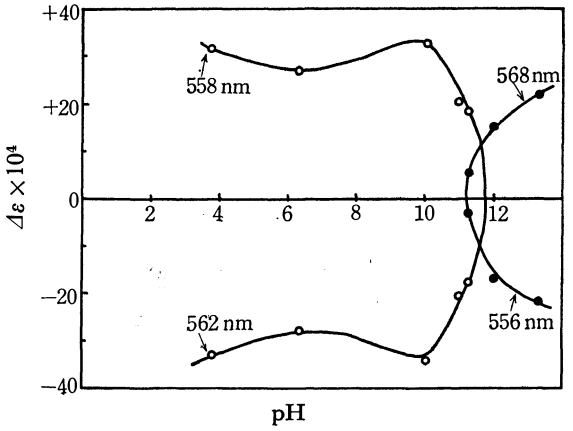

Fig. 2. Plot of $\Delta\varepsilon$ for CD components of the $^4G_{5/2} \leftarrow {}^6H_{5/2}$ transition of Sm(III)-*l*-PDTA complex *vs.* pH.

intensities of the CD spectra of samarium(III) complexes with *l*-PDTA are shown in Fig. 1. The pH values plotted against $\Delta\varepsilon(=\varepsilon_l-\varepsilon_r)$ for CD components of $^4G_{5/2}\leftarrow{}^6H_{5/2}$ transition are shown in Fig. 2. The same features were observed also in the case of the Eu(III), Dy(III), Ho(III), Er(III), and Tm(III) complexes with *l*-PDTA. In order to confirm the phenomena observed for lanthanoid(III) complexes with *l*-PDTA, the CD spectra of Pr(III), Nd(III), Sm(III), Eu(III), Gd(III), Tb(III), Dy(III), Ho(III), Er(III), and Tm (III) complexes with L-EDDS were recorded more precisely by using the chart scales of 4 or 2 nm /cm. The following CD-sensitive and other transitions of the lanthanoid(III) complexes with L-EDDS were studied: Pr(III) complex, $^3P_2\leftarrow{}^3H_4$; Nd(III) complex, $^4G_{9/2}\leftarrow{}^4I_{9/2}$; Sm(III) complex, $^4H_{5/2}\leftarrow{}^6H_{5/2}$; Eu(III) complex, $^5D_0\leftarrow{}^7F_1$ and $^5G_2\leftarrow{}^7F_1$; Gd(III) complex, hardly any change observed in CD spectra in the pH range 9~11.5; Tb(III) complex, $^5G_6\leftarrow{}^7F_6$; Dy(III) complex, $^4I_{15/2}\leftarrow{}^6H_{15/2}$; Ho(III) complex, $^3K_8\leftarrow{}^5I_8$; Er(III) complex, $^2K_{15/2}\leftarrow{}^4I_{15/2}$; and Tm(III) complex, $(^3F_3, {}^3F_2)\leftarrow{}^3H_6$. A few examples are shown in Figs. 3(a) and 3(b). Similar features were observed for the other lanthanoid(III) complexes with L-EDDS. The cross-over pH values, where intensity of CD spectrum of L-EDDS complex changes suddenly, are plotted against the number of 4f-electrons (Fig. 4).

The CD spectra of H[Pr(L-EDDS)]·$2H_2O$ and H[Dy(L-EDDS)]·$2H_2O$ in aqueous solutions coin-

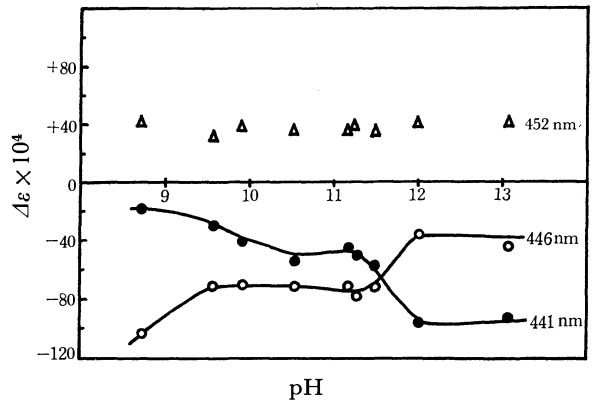

Fig. 3(a). Plot of $\Delta\varepsilon$ for CD components of the $^3P_2\leftarrow{}^3H_4$ transition of Pr(III)-L-EDDS complex *vs.* pH.

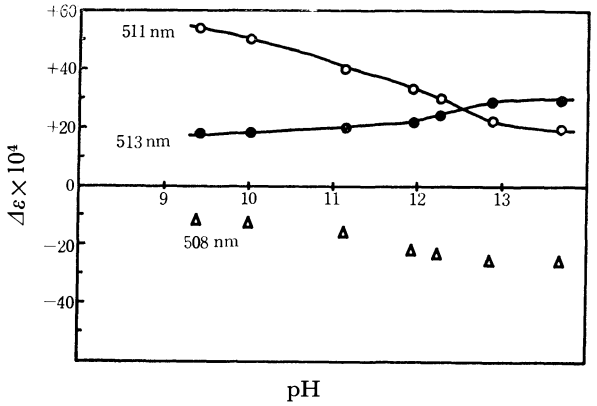

Fig. 3(b). Plot of $\Delta\varepsilon$ for CD components of the $^4G_{9/2}\leftarrow{}^4I_{9/2}$ transition of Nd(III)-L-EDDS complex *vs.* pH.

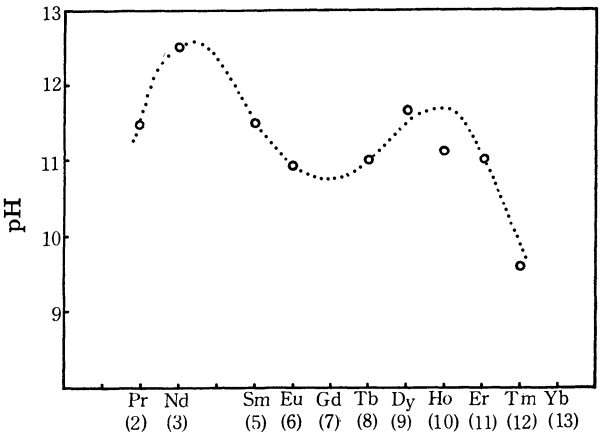

Fig. 4. Relation between the cross-over pH and the number of 4f-electrons for L-EDDS complexes of lanthanoids(III).

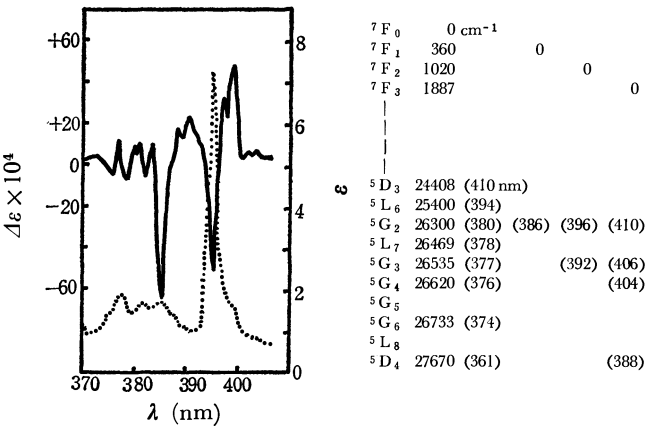

Fig. 5. Absorption and CD spectra of Eu(III)-L-EDDS complex at pH 11.02, 370—400 nm spectral region, and diagrams of the tentatively assigned energy levels: ——, CD spectrum ($\Delta\varepsilon$); ……, absorption spectrum.

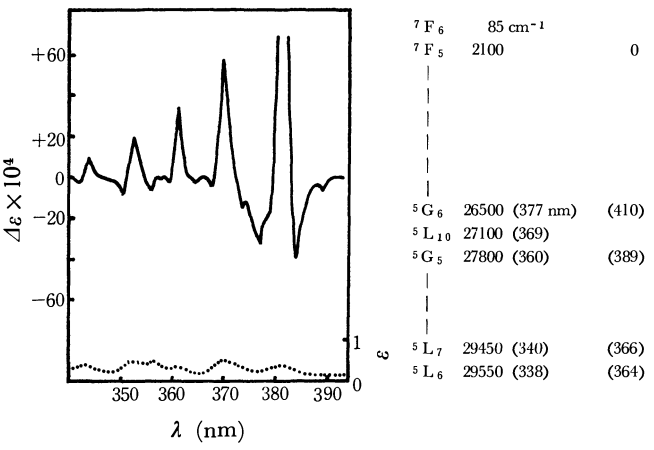

Fig. 6. Absorption and CD spectra of Tb(III)-L-EDDS complex at pH 11.3, 350—390 nm spectral region, and diagrams of the tentatively assigned energy levels: ——, CD spectrum ($\Delta\varepsilon$); ……, absorption spectrum.

cide with those at neutral pH region in the mixed solutions of the lanthanoids(III) and L-EDDS. By increasing the pH of these solutions, similar changes of patterns took place, but they were not so remarkable as those of a mixed solution of lanthanoids(III) and L-EDDS.

Similar to the band (660 nm) of Tm(III) complex with *l*-PDTA,[2] other bands of the same kind which do not obey the selection rule $\Delta J \leq 1$, were also observed in europium(III) and terbium(III) complexes with L-EDDS. We will call these bands "pseudo CD-sensitive bands". The excited levels of such newly located "pseudo CD-sensitive transitions" are the group of bands at 386, 388, 392, and 410 nm of Eu(III) complex and a band at ~370 nm of Tb(III) complex (Figs. 5 and 6).

Discussion

We have reconfirmed that the "CD-sensitive bands",[2] where magnetic dipole transitions are allowed, always show marked intense bands. In Fig. 4, the cross-over pH values where CD pattern changes or sign of CD reverses, are plotted against the number of 4f-electrons. The curve shows a tetrad-type curve. In view of the coordination number of the lanthanoid(III) ion, *l*-PDTA or L-EDDS chelates may be possibly coordinated by hydroxide ions in strongly alkaline solutions.

According to Condon,[6] the rotational strength $\mathbf{R}_{ab}$ is determined by $\mathbf{R}_{ab}=(e^2/2mC)\mathbf{I}_m\langle a\mathbf{Q}b\rangle\langle b\mathbf{L}a\rangle$, where a and b are the wave functions of states a and b of the molecule or ion, $e\langle a\mathbf{Q}b\rangle$ and $e/2mC\cdot\langle b\mathbf{L}a\rangle$ are the induced electric and magnetic moments, respectively, of an electronic transition $b\leftarrow a$, and $\mathbf{I}_m$ is the imaginary part of the scalar product of these two moments. In general, a more simplified and practical expression of the rotational strength is $\mathbf{R}_{ab}=\rho\mu\cos\theta$, where ρ and μ are the real electric and magnetic dipole moments of the transition, respectively, and θ is the angle between the directions of the two moments. Thus, the following interpretation is acceptable for the changes of CD spectra. Coordination of hydroxide ions at the innersphere might perturb the surroundings of the lanthanoid(III) ion, and the magnitude and direction of induced electric dipole moment are forced to change, the intensity and sign of CD changing remarkably at a certain high pH. However, other methods such as pH titration and absorption spectrum could not detect the variation owing to low sensitivity. This was successfully found by means of the "CD-sensitive band". Thus, the variation was examined all over the bands again and "pseudo CD-sensitive bands" in the spectra of the complexes of Eu(III) and Tb(III), not obeying the selection rule $\Delta J \leq 1$, were found. The α $(=\Delta\varepsilon/\varepsilon)$ values of their dissymmetry ratio were estimated to be in the order of 10^{-2}. The phenomena could be elucidated by taking into consideration, transitions not only from the ground state, but also those from some higher excited states (Figs. 5 and 6). For Eu(III) complex, transitions from the first excited state $^7F_1$ and the second excited state $^7F_2$ have been reported.[7] The corresponding "pseudo CD-sensitive transition" of $^5G_2\leftarrow{}^6F_1$ and $^5G_2\leftarrow{}^7F_2$ of Eu(III) complex could be observed at 386 and 396 nm, respectively. The former band could immediately be assigned to the transition $^5G_2\leftarrow{}^7F_1$ on the basis of CD intensity and dissymmetry ratio. However, for the latter band, by overlapping of the band of a transition of $^5L_6\leftarrow{}^7F_0$ at 394 nm, the value of α remains in the order of 10^{-3}. A similar consideration accounted for the intensity of the CD band at 392 nm, superimposed on a band arising from the transition of $^5G_3\leftarrow{}^7F_2$.

By assuming that a transition from the third excited state $^7F_3$ takes place, the intensities of the CD components of the transition $^5G_2\leftarrow{}^7F_3$ for 410 nm and the transition $^5D_4\leftarrow{}^7F_3$ for 388 nm could be explained as due to the "pseudo CD-sensitive transition".

The unexpected intense CD bands at 370 nm of Tb(III) complex could be explained similarly by assuming the corresponding transition from the first excited state, ~2.1 kK higher than the ground level, *i.e.* the transition $^5L_6\leftarrow{}^7F_5$. It is impossible to do more accurate work on account of lack of detailed information on these mechanisms in atomic spectroscopy. However, the CD-sensitivity seems to be easily contained in the formal mechanism already developed for CD intensity of the lanthanoid(III) complex with optically active ligand in solution. It is difficult to study this phenomenon in aqueous solution at a low temperature. Though there is no experimental evidence of this mechanism, it is supposed that the origin of the "pseudo CD-sensitivity" in some europium(III) and terbium(III) complexes lies in the transition from some higher excited levels, satisfying the selection rule $\Delta J \leq 1$.

Financial support was given for this research by the Ministry of Education.

References

1) S. Misumi, S. Kida, and T. Isobe, *Spectrochim. Acta*, **24A**, 271 (1968).
2) S. Misumi, S. Kida, T. Isobe, Y. Nishida, and H. Furuta, This Bulletin, **42**, 3433 (1969).
3) F. P. Dwyer, F. L. Garvan, and A. Shulman, *J. Amer. Chem. Soc.*, **81**, 290 (1959); F. P. Dwyer and F. L. Garvan, *ibid.*, **81**, 2955 (1959).
4) J. A. Neal and N. J. Rose, *Inorg. Chem.*, **7**, 2405 (1968).
5) T. Moeller, F. A. J. Moss, and R. H. Marshall, *J. Amer. Chem. Soc.*, **77**, 3182 (1955).
6) E. U. Condon, *Rev. Mod. Phys.*, **9**, 423 (1937).
7) W. T. Carnall, P. R. Fields, and K. Rajnak, *J. Chem. Phys.*, **49**, 4450 (1968).

Dehydration of Secondary Alcohols Catalyzed by Solid Acids

Tsutomu YAMAGUCHI and Kozo TANABE

Department of Chemistry, Faculty of Science, Hokkaido University, Sapporo 060

(Received June 29, 1973)

In order to examine the correlation between the acidic properties of catalysts and their activity or selectivity and to elucidate the reaction mechanism, dehydration reactions of 4-methyl-2-pentanol and 2-butanol over Al_2O_3, SiO_2, SiO_2–Al_2O_3, ZnS, $NiSO_4$, $Al_2(SO_4)_3$ or Al_2O_3 poisoned with basic compounds were carried out at 80—250 °C by means of the conventional flow method or a thermal desorption method. The following results were obtained. 1) Both Brönsted and Lewis acids are active, the latter being so to a greater extent. 2) Even relatively weak acid catalysts of acid strength $H_0=4.8$—6.8 are active, the catalytic activity being correlated with the number of effective acid sites. 3) The selectivity of 4-methyl-1-pentene/4-methyl-2-pentene and 4-methyl-*cis*-2-pentene/4-methyl-*trans*-2-pentene is lower for Brönsted acids than for Lewis acids and higher for weaker Lewis acid strengths. 4) The composition of butene isomers varies greatly with changes in desorption temperature and the amount of adsorbed 2-butanol in the case of Al_2O_3, but not much for SiO_2–Al_2O_3. 5) The ratios of *cis*-2-butene/*trans*-2-butene and 1-butene/2-butene over Al_2O_3 are remarkably increased by poisoning with pyridine. A reaction mechanism including a new reaction path has been proposed.

The dehydration of secondary alcohols is found to be useful for investigating the properties of catalysts since the selectivity of the catalysts is indicated by the formation of 1-olefins, *cis*-2-olefins and *trans*-2-olefins and the ratios of 1-olefins/2-olefins and *cis*-2-olefins/*trans*-2-olefins.

The dehydration of alcohols is known to be catalyzed by solid acids[1] and it has been pointed out that the basic properties of some solid acids play an important role in dehydration reactions.[2-4] Some problems concerning the effective acid strength of catalysts[5,6] and the nature of reaction intermediates[7] have also been studied. However, the catalysts used for the dehydration of secondary alcohols are limited to several kinds, including alumina. No systematic work has been done on the correlation between acidic properties (the amount, strength and type —Brönsted or Lewis— of the acid sites) of catalyst surfaces and catalytic activity or selectivity.

In the present work, we examined the correlation by employing aluminum sulfate,[8] nickel sulfate,[8] zinc sulfide,[9] silica[10] and silica-alumina[10] in addition to alumina as catalysts whose acidic nature is fairly well understood. From the secondary alcohols, 4-methyl-2-pentanol was selected because of the importance of its main product, 4-methyl-1-pentene, as a synthetic material in surface active agents and perfumes. 2-Butanol was used as another secondary alcohol since it is the simplest secondary alcohol and is suitable for thermal desorption experiments which provide data on dehydration with a known amount of adsorbed alcohol without being accompanied by the isomerization of product olefins.

The dehydration mechanism of secondary alcohols and the catalytic action of solid acids are discussed in the light of the observed results.

Experimental

Catalysts and Reagents. Three kinds of alumina were used. Al_2O_3-I (Kishida Chemicals and Co. Ltd.) was calcined in air at 500 °C for 3 hr (specific surface area: 382 m^2/g). Al_2O_3-II was prepared by the hydrolysis of aluminum isopropoxide and calcination in air at 800 °C for 3 hr. Al_2O_3-III, an alkali-poisoned catalyst, was prepared by immersing Al_2O_3-I in NaOH solution for 24 hr, drying at 120 °C for 24 hr and calcining in air at 500 °C for 3 hr. For thermal desorption experiments, Al_2O_3-I was evacuated at 450 °C for 3 hr. For poisoning experiments, pyridine was adsorbed on the catalyst in a vacuum system. Silica (Kishida Chemicals and Co., Ltd.) was calcined in air at 720 °C for 2.5 hr. Silica-alumina (Shokubai Kasei Co., 25% Al_2O_3, specific surface area: 514 m^2/g) used for thermal desorption experiments was calcined in a vacuum at 450 °C for 3 hr. Nickel and aluminum sulfate catalysts were prepared by heating guaranteed reagents of the heptahydrate (Kanto Chemical Co.) and the octadeca-hydrate(Wako Pure Chemical Industries) respectively in air at various temperatures for 3 hr. The 16—24 mesh powders were stored in sealed ampoules. Zinc sulfide (guaranteed reagent of Kanto Chemical Co.) was calcined in air at 400 °C for 2.5 hr.

4-Methyl-2-pentanol (Tokyo Kasei Kogyo Co.) was purified by fractional distillation. 2-Butanol (guaranteed reagent of Wako Pure Chemical Industries) was distilled over sodium metal and dehydrated and degassed by repeated freeze-thaw cycles after distillation over Molecular Sieve 3A *in vacuo*.

Measurement of Catalyst Acidity. The acid amounts at various strengths for the catalysts were measured by titrating with *n*-butylamine[10,11] using various indicators; benzalacetophenone ($pK_a=-5.6$), dicinnamalacetone (−3.0), benzeneazodiphenylamine(+1.5), *p*-dimethylaminoazobenzene (+3.3), methyl red (+4.8) and neutral red (+6.8).

Reactions and Thermal Desorption. The dehydration of 4-methyl-2-pentanol was carried out by the conventional flow method using nitrogen as carrier gas at temperatures 150—200 °C. The alcohol vapor, whose pressure (25 mmHg) was kept constant in an alcohol saturator, was passed together with nitrogen through a reaction tube containing 1—2 g of catalyst. In order to prevent the condensation of alcohol and its products, the necessary parts of the apparatus were heated by resistance wires. The reaction products were collected in a liquid nitrogen trap and analyzed by gas chromatography. A one meter column of 30% TCP on Kacelite was used for the analysis of olefins and unreacted alcohol, and a 10 m column of Silicone DC-550/Bentone 34/Celite 545 for that of olefins alone. Catalytic activity was obtained from the linear plot of conversion percentage against contact time (W/F, W: catalyst weight, F: flow rate of alcohol).

The thermal desorption experiments of 2-butanol were carried out with a vacuum apparatus in the following way. After alcohol was introduced over 100—200 mg of evacuated catalyst at room temperature, the gas phase and weakly adsorbed alcohol were removed by condensation in a liquid

Table 1. Acid amounts and strengths of various catalysts

Catalysts	Acid amount (mmol g^{-1}) at various pK_a's					
	−5.6	−3.0	+1.5	+3.3	+4.8	+6.8
Al_2O_3-I	+	+	0.665	0.765	0.753	0.850
Al_2O_3-II				0	0.052	2.40
SiO_2	0	0.041	0.052	0.091	0.101	0.204
ZnS		0	0.054	0.10	0.173	0.322
$Al_2(SO_4)_3$-250[a]	0	0.040	0.332	0.348	0.353	0.456
-300[a]	0	0.126	0.357	0.399	0.454	0.694
-350[a]	0	0.124	0.313	0.388	0.421[b]	0.565
-400[a]	0	0.106	0.287	0.342	0.324[b]	0.467
-500[a]	0	0.026	0.135	0.127	0.133[b]	0.261

a) Calcination temperature (°C). b) pK_a = +4.0.

nitrogen trap, and the amount of irreversibly adsorbed alcohol at room temperature was measured as follows. The temperature of the system was elevated and the system kept at this temperature for 1.5 hr. All the species desorbed by the temperature elevation were collected in a liquid nitrogen trap and dried over Molecular Sieve 3A. The amount of each constituent was determined from the total pressure and gas chromatography analysis (1 m column of TCP for the analysis of alcohol-olefins and 5 m of VZ-7 for olefins).

The dehydration of 2-butanol over poisoned catalysts was carried out at 180 °C with a closed circulation apparatus. The initial pressure of alcohol was 12.5±0.3 mmHg. The catalysts were poisoned with pyridine or ammonia in a vacuum apparatus equipped with Tefron greaseless stopcocks. The amount of poisoning was estimated from the values obtained under the same condition as in the following adsorption-desorption experiments. Pyridine or ammonia was adsorbed at 100 °C for 1 hr on 30 mg of Al_2O_3-I which had been calcined *in vacuo* at 500 °C for 5 hr. After the catalyst was evacuated at 100 °C, the amount of adsorbed pyridine or ammonia was obtained by measuring the increase in catalyst weight with a microbalance (sensitivity: 3.4—3.5 mm/mg). The catalyst temperature was then elevated and the amount of pyridine or ammonia remaining on the catalyst was determined from its weight.

Results

Dehydration of 4-Methyl-2-pentanol. The reaction products were only olefins; 4-methyl-1-pentene, 4-methyl-*cis*-2-pentene and 4-methyl-*trans*-2-pentene.

Acidity and Activity of Catalysts: The acid amounts at various strengths of Al_2O_3-I, Al_2O_3-II, SiO_2, ZnS, $NiSO_4$ and $Al_2(SO_4)_3$ are shown in Table 1 and Fig. 1 and their catalytic activities for dehydration are shown in Table 2 and Fig. 1.

The acid strength of Al_2O_3-II was very weak, but its activity fairly high. This is considered to be due to the large number of acid sites having acid strength H_0=4.8—6.8. On the other hand, SiO_2, which has much stronger acid sites H_0=−3, showed relatively low activity. This is partly due to the small total acid amount (only 0.20 mmol/g at $H_0 \leqq +6.8$) and partly due to the fact that the acid sites on SiO_2 are of Brönsted type whose activity is less than that of Lewis type sites. The smaller activity of ZnS than that of Al_2O_3-II is also explained by the smaller total acid amount. In the case of metal sulfates calcined at various tem-

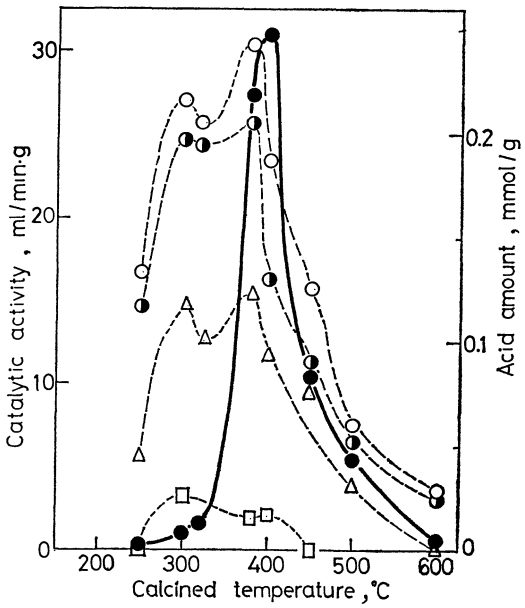

Fig. 1. Acidity and catalytic activity of $NiSO_4$ calcined at various temperatures. Solid line; catalytic activity for dehydration of 4-methyl-2-pentanol. Broken line; acid amount: (○) pK_a=6.8, (◑) pK_a=4.8, (△) pK_a =1.5, (□) pK_a=−3.0.

Table 2. Catalytic activities of various catalysts

Catalysts	Reaction temp. (°C)	Activity (ml g^{-1} min^{-1})
Al_2O_3-I	170	35
	186	80
Al_2O_3-II	170	55
	186	—
ZnS	170	1.0
	198	5.5
SiO_2	167	1.9
$Al_2(SO_4)_3$-250[a]	150	25
-300[a]	150	77
-350[a]	150	81
-400[a]	150	17
-500[a]	150	4.5

a) Calcination temperature (°C).

peratures, the activities were roughly correlated with total acid amount as seen in Fig. 1 and Tables 1 and 2. The activity of Al_2O_3-III decreased with increasing sodium hydroxide, but the catalyst poisoned with 1.75 mmol/g of NaOH which has no acid sites of $H_0 = +3.3$ did not completely lose activity.

These results indicate that the acidic properties of the catalysts are an important factor in activity, and even weak acid sites are active in the dehydration of 4-methyl-2-pentanol. This is in good agreement with the result observed by Misono *et al.*[5] that weak acid sites on silica-alumina poisoned with pyridine were active for the dehydration of tertiary butanol.

The number of acid sites on $NiSO_4$ calcined at 300 °C was large, but activity was very low (Fig. 1). However, the acid amount gives the sum of the amount of Brönsted and Lewis acid sites. According to the infrared study of pyridine adsorbed on nickel sulfate,[12] the maximum amount of Brönsted acid is observed on the sulfate calcined at 250—300 °C, and that of Lewis acid on the sulfate calcined at 400 °C. Since the Lewis acidity change caused by calcination is similar to the activity change, Lewis acid sites are believed to be more active than Brönsted acid sites of the same acid strength.

Since it is known by infrared study that a Lewis acid site can be converted into a Brönsted acid site in the presence of a water molecule,[13] the effect of water formed by the dehydration reaction on the type of acid site should be taken into consideration. However, a comparison of activity and acidity in Fig. 1 shows that the Lewis acid sites which might interact with water molecules differ entirely from the Brönsted acid sites originally present on the catalyst. The same kind of difference was also found for the vapor phase hydrolysis of methylene chloride catalyzed by various solid acid.[14] Matsuzaki *et al.*[15] showed that the acid strength of silica-alumina does not change with the adsorption of water when the temperature of adsorption is high. If a conversion of Lewis sites into Brönsted sites occurred, the acid strength should have changed. These facts indicate that Lewis sites are not converted into Brönsted sites at high temperatures, or that Lewis sites, even if they interact with water molecules, are distinguished from the original Brönsted sites.

Acidity and Selectivity of Catalysts: The ratios of 4-methyl-1-pentene/4-methyl-2-pentene (abbreviated as 1-P/2-P) and 4-methyl-*cis*-2-pentene/4-methyl-*trans*-2-pentene (*cis*-P/*trans*-P) for each catalyst are shown in Table 3. The 1-P/2-P ratio decreased in the order Al_2O_3-II > Al_2O_3-I > ZnS > $NiSO_4$ > $Al_2(SO_4)_3$ > SiO_2. In the case of Al_2O_3-III, the ratio increased with an increase in the amount of NaOH added as shown in Fig. 2. The lowest ratios were found for SiO_2, a well-known Brönsted acid,[16] while the higher ratios were found mainly for Lewis acids such as Al_2O_3-II, Al_2O_3-I, ZnS and $NiSO_4$ calcined at 400 °C. The selectivity of the latter catalysts changed with the Lewis acid strength and the basic properties. The Al_2O_3 catalysts which have basicity[10,17] together with Lewis acidity showed a high selectivity. Among aluminas, Al_2O_3-II which has the weakest acid strength showed the highest selectivity. An intermediate selectivity was found for

TABLE 3. SELECTIVITY OF VARIOUS CATALYSTS

Catalysts	Reaction temp. (°C)	1-P/2-P	*cis*-P/*trans*-P
Al_2O_3-I	150	0.58	3.2
	170	0.49	2.9
Al_2O_3-II	150	1.14	—
	170	0.58	5.5
$NiSO_4$-400[a]	150	0.28	1.2
$Al_2(SO_4)_3$−350[b]	150	0.23	1.0
SiO_2	190	0.23	0.35
ZnS	198	0.41	0.83
equilibrium[c]	170	0.12	0.72

a) Calcined at 400 °C. b) Calcined at 350 °C. c) J. E. Kilpatrick, E. J. Prosen, K. S. Pitzer, and F. E. Rossini, *J. Res. Nat. Bur. Stand.*, **36**, 559 (1946).

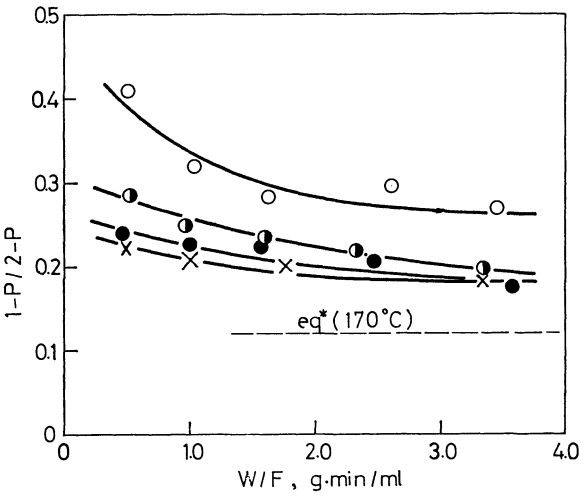

Fig. 2. Poisoning effect of NaOH on selectivity (1-P/2-P).
Reaction temperature: 150 °C, Amount of NaOH on Al_2O_3-III (mmol g^{-1}): (×) 0, (●) 0.12, (◑) 0.2, (○) 0.45.
* Thermodynamic equilibrium composition: J. E. Kilpatrick, E. J. Prosen, K. S. Pitzer, and F. D. Rossini, *J. Res. Nat. Bur. Stand.*, **36**, 559 (1946).

metal sulfate and ZnS which have no basicity,[9] a higher selectivity being observed with the weaker Lewis acid strength. In Al_2O_3-III catalysts, the selectivity became higher as the strong acid sites were poisoned with sodium hydroxide (Fig. 2).

The selectivity for *cis*-P/*trans*-P was similar to that for 1-P/2-P.

Dehydration of 2-Butanol. The reaction products were 1-butene, *cis*-2-butene and *trans*-2-butene.

The changes in the ratios of 1-butene (abbreviated 1-B/2-B) and *cis*-2-butene/*trans*-2-butene (*cis*-B/*trans*-B) with the rise in desorption temperature for Al_2O_3 are shown in Fig. 3. The ratio 1-B/2-B was almost the same as that in equilibrium independent of the amount of adsorbed alcohol above 150 °C, but was higher below 150 °C and increased with increasing amount of adsorbed alcohol (Fig. 3(a)). The ratio *cis*-B/*trans*-B was almost the same as the equilibrium ratio when the amount adsorbed was 0.354 mmol/g, but increased an increase of the amount adsorbed, a higher increase

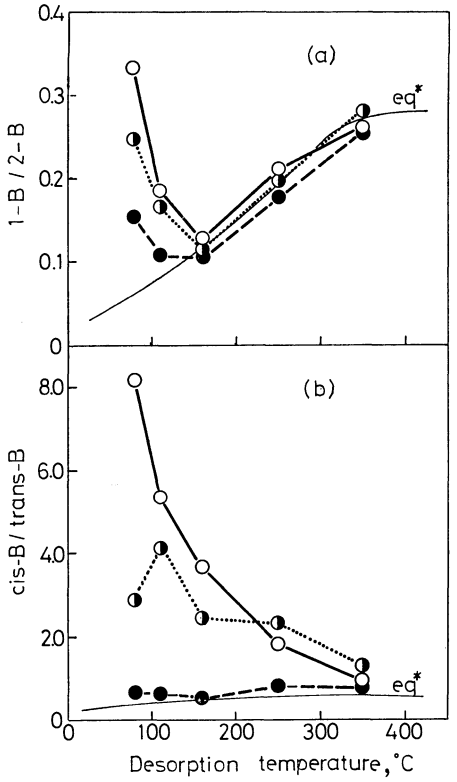

Fig. 3. Changes in 1-B/2-B and *cis*-B/*trans*-B with change in desorption temperature over Al_2O_3-I. Amount of adsorbed 2-butanol (mmol g^{-1}); (○) 1.106 (◑) 0.700, (●) 0.354.
* Thermodynamic equilibrium composition.

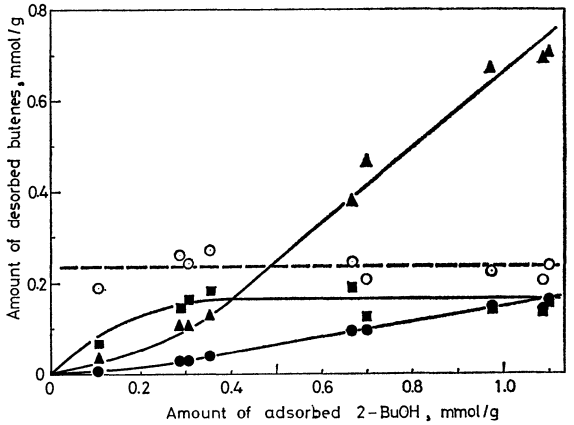

Fig. 4. Amounts of butenes desorbed up to 350 °C *vs.* amount of 2-butanol adsorbed on Al_2O_3-I: (●) 1-B, (▲) *cis*-B, (■) *trans*-B, (○) ratio of 1-B/*cis*-B.

being observed at the lower desorption temperature (Fig. 3 (b)). In Fig. 4, the amount of each butene isomer desorbed up to 350 °C is plotted against the amount of adsorbed alcohol in the case of Al_2O_3. The amount of *trans*-2-butene formed was almost constant independent of the amount of adsorbed alcohol, while that of 1-butene and *cis*-2-butene increased with the amount of adsorbed alcohol. In the case of SiO_2–Al_2O_3 catalyst, both ratios were very close to the equilibrium ratio independent of the amount of adsorbed alcohol, except that a higher *cis*-B/*trans*-B

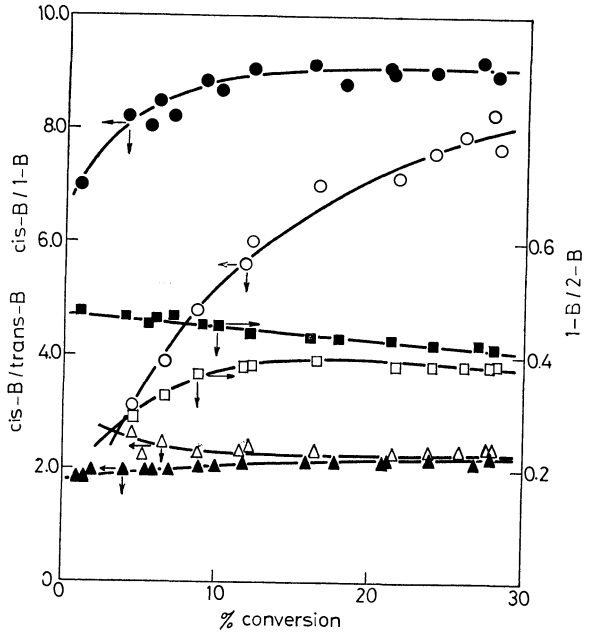

Fig. 5. Poisoning effect of pyridine on dehydration of 2-butanol.
Reaction temperature: 180 °C, Al_2O_3-I without poisoning, (○) *cis*-B/*trans*-B, (□) 1-B/2-B, (△) *cis*-B/1-B. Al_2O_3-I poisoned with 0.11 mmol g^{-1} pyridine, (●) *cis*-B/*trans*-B, (■) 1-B/2-B, (▲) *cis*-B/1-B.

ratio was observed below 160 °C.

The fact that SiO_2–Al_2O_3 which has only high acid strength gives low selectivity, while Al_2O_3 which has different acid strengths gives different kinds of selectivity, depending on the amount of adsorbed alcohol, is discussed later.

The effect of pyridine poisoning on the dehydration of 2-butanol over an alumina catalyst is shown in Fig. 5, where the ratios of butene isomers formed are plotted against the % conversion of 2-butanol. The ratios of *cis*/*trans* and 1-B/2-B over the poisoned catalyst were high compared to the unpoisoned ones at low % conversion. The ratios for the two catalysts approached the same value as the % conversion increased, while the ratio of *cis*/1-B over both catalysts was almost the same and remained nearly constant. Since no isomerization takes place under the present reaction conditions,[18] the results indicate that the formation of *trans*-2-butene was strongly retarded by the poisoning of the catalyst with pyridine. The poisoning effect of ammonia on selectivity was similar to that of pyridine, but the degree of retardation for the formation of *trans*-2-butene was lower. In the case of pure alumina, the ratios were approximately equal to the equilibrium value at low % conversions, but increased with increasing % conversion (Fig. 5). These phenomena are believed to be due to *trans* isomer formation being retarded by poisoning with water molecules formed by the dehydration reaction.

Discussion

The reaction mechanism is discussed in the light of the observed catalyst selectivity. The following

two are well-known mechanisms of olefin formation from alcohol; one includes oxonium ion and carbonium ion as reaction intermediates[19] (type El mechanism) represented by Scheme (A), and the other is an acid-base concerted mechanism[2] (type E2 mechanism), represented by Scheme (B), taking the dehydration of 2-butanol as an example.

$$C_4H_9OH \xrightarrow{H^+} C_4H_9OH_2^+ \xrightarrow{-H_2O} C_4H_9^+ \xrightarrow{-H^+} C_4H_8 \quad (A)$$

$$C_4H_9OH \xrightarrow{-H^+,\ -OH^-} C_4H_8 \quad (B)$$

Scheme (A) includes an alkoxonium ion $C_4H_9OH_2^+$ and carbonium ion $C_4H_9^+$ and the reaction is catalyzed only by Brönsted acid. In Scheme (B), the fissions of C–O and C–H bonds of alcohol occur simultaneously to eliminate a hydroxyl ion and a proton. The latter is effectively catalyzed by solid catalysts such as Al_2O_3 which has both Lewis acidity and basicity.

All the results can not be fully explained only by the above two mechanisms. In particular, it is difficult to explain the effect of Lewis acid strength on catalyst selectivity. We therefore propose a dehydration mechanism of secondary alcohols shown in Fig. 6, which presents a new route for the formation of carbonium ion from alcohol on a Lewis acid catalyst.

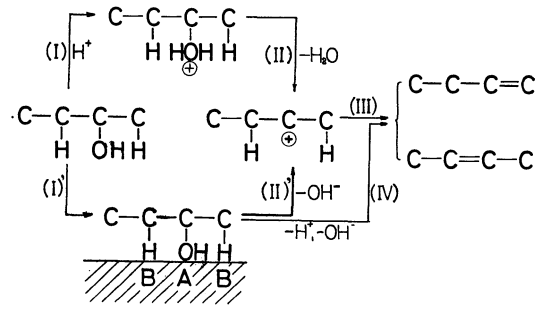

Fig. 6. Reaction paths of dehydration of secondary alcohols.
A: Lewis acid site, B: basic site.

The reaction path (I)-(II)-(III) is an alkoxonium-carbonium ion mechanism catalyzed by Brönsted acid. The dehydration of secondary alcohols over SiO_2 proceeds by this path. Since carbonium ion is formed in this case, the ratio 1-B/2-B tends to approach the equilibrium value. The ratio *cis*-B/*trans*-B also tends to approach the equilibrium value because of free rotation about the C–C bond. The observed selectivity of SiO_2 showed this tendency.

The reaction path (I)'-(IV) is a concerted mechanism, where H^+ and OH^- are eliminated simultaneously for either *cis*-elimination (Fig. 6) or *trans*-elimination. In this case, high ratios of 1-B/2-B and *cis*-B/*trans*-B are usually observed.[2]

A third reaction path (I)'-(II)'-(III) consists of adsorption of alcohol on Lewis acid sites A, the formation of carbonium ion by elimination of OH^- and the formation of an olefin by the elimination of a proton. This mechanism is possible when the Lewis acid strength is so high that the C–O bond is easily broken. Since a carbonium ion is formed as in the case of a Brönsted acid catalyst, both ratios 1-B/2-B and *cis*-B/*trans*-B approach the equilibrium values. Thus the stronger the Lewis acidity, the larger the possibility of reaction path (II)' and the lower the selectivity for 1-olefin and *cis*-2-olefin. On the other hand, as the strength of the Lewis acid becomes weaker, the fission of the C–O bond becomes harder and comparable to that of C–H bond. Thus, the probability that the dehydration proceeds *via* path (IV) becomes large and the selectivity for 1-olefin and *cis*-2-olefin increases. In the case of Al_2O_3, the formation of an alkoxide from an alcohol molecule and an aluminum atom on the surface has been reported,[7,20] but does not affect the conclusion of the above discussion concerning selectivity and reaction mechanism.

Now let us discuss the observed selectivity of various catalysts. Since the acid strength of Al_2O_3-I is higher than that of Al_2O_3-II, the probability that the dehydration proceeds *via* path (II)' becomes larger in Al_2O_3-I and hence the ratios of 1-olefin/2-olefin and *cis*-2-olefin/*trans*-2-olefin over Al_2O_3-I are higher than those of Al_2O_3-II (Table 3). However, since both Al_2O_3-I and Al_2O_3-II have basic properties as well as acidic properties, the probability of the concerted mechanism (IV) over alumina is large and the selectivity is higher than that of SiO_2 over which the dehydration takes place only *via* path (I)-(II)-(III). The selectivity of $Al_2(SO_4)_3$ is low compared with that of $NiSO_4$, because of the higher acid strength of $Al_2(SO_4)_3$. However, since both metal sulfates have no basic properties, the selectivity is low compared with Al_2O_3. Zinc sulfide which has no basicity,[9] but weak acidity (Table 1) shows an intermediate selectivity between Al_2O_3 and sulfates. The decrease in selectivity with increase of the amount of NaOH poisoning over Al_2O_3 is interpreted by assuming that path (IV) is favored over path (II)', because the acid strength is weakened by the poisoning.

In thermal desorption experiments, the fact that the ratio of desorbed butenes is close to the equilibrium value over SiO_2–Al_2O_3, but deviates from the equilibrium value over Al_2O_3 at low temperatures or for large amounts of adsorbed alcohol, is also explained by the scheme shown in Fig. 6. Reaction paths (I)'-(II)'-(III) and (I)-(II)-(III) are favored over SiO_2–Al_2O_3, since the catalyst has high acid strength and contains Brönsted acid sites.[10] In the case of Al_2O_3, the path (I)'-(IV) becomes preferred due to the concerted action of acid sites of weaker Lewis acid strength and basic sites. However, the high selectivity is lowered at higher temperatures, since the C–O bond is more readily broken so that path (II)' is favored. The high selectivity also decreases with decreasing amounts of adsorbed alcohol, since the fraction of adsorbed alcohol reacting with strong acid sites becomes large and path (II)' is thus also favored. The participation of basic sites on Al_2O_3 in the dehydration of secondary alcohols was verified by experimental results in which the isotope effects of the β-hydrogen of 2-propanol[21] and 2-butanol[4] were 4.1 and 2.3 at 160 °C, respectively.

The high ratios 1-B/2-B and *cis*/*trans* observed with Al_2O_3 poisoned with pyridine are explained by the disappearance or the weakening of strong acid sites with pyridine.

References

1) M. E. Winfield, "Catalysis," Vol. 7, ed. by P. H. Emmett, Reinfold, New York (1960), p. 93.
2) H. Pines and J. Manassen, "Advances in Catalysis," Vol. 16, Academic Press, New York (1966), p. 49.
3) T. Tomatsu, T. Yoneda, and H. Ohtsuka, *Yukagaku*, **17**, 237 (1968).
4) H. Knözinger and A. Scheglila, *J. Catal.*, **17**, 252 (1970).
5) M. Misono, Y. Saito, and Y. Yoneda, "Proc. 3rd Intern. Congr. Catalysis," Amsterdam, 1964, **1**, 408.
6) V. A. Dzisko, M. Kolovertnova, T. S. Vinnikova, and Yu. O. Bulgakova, *Kinet. Katal.*, **7**, 655 (1966).
7) For secondary alcohol, D. Treibmann and A. Simon, *Ber. Bunsenges. Phys. Chem.*, **70**, 562 (1966); H. Könzinger, H. Bühl, and E. Ress, *J. Catal.* **12**, 121 (1969); Y. Soma, T. Onishi, and K. Tamaru, *Trans. Faraday Soc.*, **65**, 2215 (1969).
8) K. Tanabe and T. Takeshita, "Advances in Catalysis," Vol. 17, Academic Press, New York (1967), p. 315.
9) K. Tanabe and T. Yamaguchi, *J. Res. Inst. Catal. Hokkaido Univ.*, **11**, 179 (1964).
10) For example, K. Tanabe, "Solid Acids and Bases," Kodansha, Tokyo (1970), p. 61.
11) O. Johnson, *J. Phys. Chem.*, **59**, 827 (1955).
12) H. Hattori, S. Miyashita and K. Tanabe, This Bulletin, **44**, 893 (1971).
13) E. P. Parry, *J. Catal.*, **2**, 371 (1963).
14) T. Yamaguchi and K. Tanabe, "Proc. 4th Intern. Congr. Catalysis," Moscow, 1968, **2**, 410.
15) I. Matsuzaki, M. Nitta, and K. Tanabe, *J. Res. Inst. Catal. Hokkaido Univ.*, **17**, 46 (1969).
16) T. Shirasaki, M. Okada, T. Mizutori, K. Hayakawa, and S. Hashi, *Nippon Kagaku Zasshi*, **85**, 722 (1964).
17) G. M. Schwab and H. Kral, "Proc. 3rd Intern. Congr. Catalysis," Amsterdam, 1964, **1**, 433.
18) It was ascertained by a competition reaction between the dehydration of 2-propanol and the isomerization of 1-butene that isomerization does not occur during dehydration.
19) W. S. Brey, Jr. and K. A. Krieger, *J. Amer. Chem. Soc.*, **71**, 3637 (1949).
20) R. G. Greenler, *J. Chem. Phys.*, **37**, 2094 (1962); A. A. Babushkin and A. V. Urarov, *Dokl. Akad. Nauk SSSR*, **110**, 581 (1956); R. O. Kagel, *J. Phys. Chem.*, **71**, 844 (1967); H. Arai, Y. Saito, and Y. Yoneda, *J. Catal.*, **10**, 128 (1968); This Bulletin, **40**, 731 (1967).
21) T. Yamaguchi and K. Tanabe, *Nippon Kagaku Kaishi*, **1973**, 240.

The Proton Magnetic Resonance in the DPPH–Benzene Complex

Toshio Yoshioka, Hiroaki Ohya-Nishiguchi, and Yasuo Deguchi*

Department of Chemistry, Faculty of Science, Kyoto University, Sakyo-ku, Kyoto 606
**College of Liberal Arts and Science, Kyoto University, Kyoto 606*

(Received July 23, 1973)

The proton magnetic resonance in single crystals of the DPPH-benzene complex has been measured around three Cartesian axes. All the spectra are highly complex, but some lines are clearly identified around all axes. The principal values of their anisotropic hyperfine tensors have been evaluated, in addition to the isotropic hyperfine coupling constants. In the crystalline state, the unpaired electron-spin distributions of one phenyl group is almost twice as large as that of the other phenyl group, as is to be expected from the crystal structure. Besides, the unpaired electron-spin delocalization is larger in the crystalline state than that in solution, particularly on the picryl group and on one phenyl group.

In the proton NMR spectra of some organic free radicals in polycrystalline states, some lines have been shifted from the free-proton position because of the exchange-narrowed hyperfine interaction.[1-5]

Anderson *et al.* have observed the proton resonance of a polycrystalline sample of the 1 : 1 DPPH–benzene complex at 4.2 K.[3] By deuterium substitution, the large central component and the largest downfield-shifted component were attributed to the benzene protons and to the picryl group protons respectively, but the other three components were not identified. Moreover, they reported that the single crystal spectrum is highly complex, containing as many as 15 resolvable peaks in certain orientations.

On the other hand, the ESR spectra of DPPH in mixed organic solvents have been measured, and the high resolution of the Electron-Nuclear Double Resonance (ENDOR) technique has been utilized to obtained precise values for the twelve proton hyperfine couplings of DPPH in a mineral oil solution.[6,7,8] Those results indicate that the unpaired electron-spin distributions of the two phenyl groups are equal in solution.

Recentyl the crystal structure of the 1 : 1 DPPH–benzene complex has been determined by Williams.[9] He reported that the molecular configuration around the α-nitrogen is approximately trigonal planar, with the phenyl groups twisted at angles of 49 and 22°. From his results, the unpaired electron-spin distribution of the two phenyl groups can be expected to be different in the crystalline state. In order to obtain more information about the unpaired electron-spin distribution in the crystalline state and the contribution of the anisotropic hyperfine interaction to the proton resonance shift, we have measured the NMR of protons in the DPPH–benzene complex single crystal around three Cartesian axes at 4.2 K, employing a higher frequency of 40.0 MHz. We have evaluated the principal values of the anisotropic hyperfine tensors for the identified lines. The single crystal and polycrystalline NMR data show that the unpaired electron-spin distribution of one phenyl group is almost twice as large as that of the other phenyl group.

Experimental

α,α-Diphenyl-β-picryl hydrazyl (DPPH) was prepared by the oxidation of commercially-obtained α,α-diphenyl-β-picryl hydrazine ($DPPH_2$) with PbO_2 and was recrystallized several times from a benzene solution. The single crystals of the DPPH–benzene complex used in the measurements was grown by the slow evaporation of the solvent from the benzene solution and had the dimensions of $10\times5\times4$ mm^3.

An x, y, z Cartesian axis system was defined for convenience from its shape. The x-axis was selected parallel to the long edge, and the z-axis, normal to the metallic lustrous face containing the long edge. All the NMR measurements were carried out using a Robinson-type spectrometer[10] at 40.0 MHz, with an 80-Hz field modulation and a field sweep. The angular dependence of the NMR spectra was obtained by rotating the magnet around the x, y, and z axes, with the magnet set perpendicular to the magnetic-field direction.

Results and Discussion

The 4.2 K proton resonance spectrum of a polycrystalline DPPH-benzene complex agrees well with the results reported by Anderson *et al.*,[3] as is shown in Fig. 1(a). Figs. 1(b) and (c) present relatively well-resolved spectra of the single crystal of the DPPH–benzene complex in a certain orientation, measured at 4.2 K and 1.5 K respectively. The angular dependences around the x, y, and z axes measured at 4.2 K are shown in Figs. 2(a), (b) and (c) respectively. The crystal structure obtained by Williams shows that

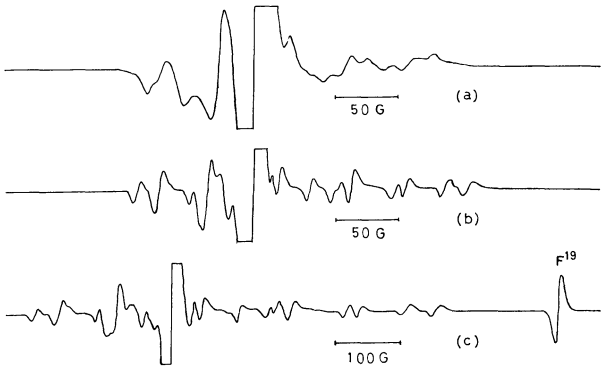

Fig. 1. Proton magnetic resonance absorption derivative curves (a) of the polycrystalline DPPH-benzene complex at 40.0 MHz, 4.2 K, (b), (c) of the single crystal of DPPH-benzene complex at 40.0 MHz, 4.2 K and 1.5 K. The static magnetic field is lying in the xy-plane and makes an angle 20° with the x-axis.

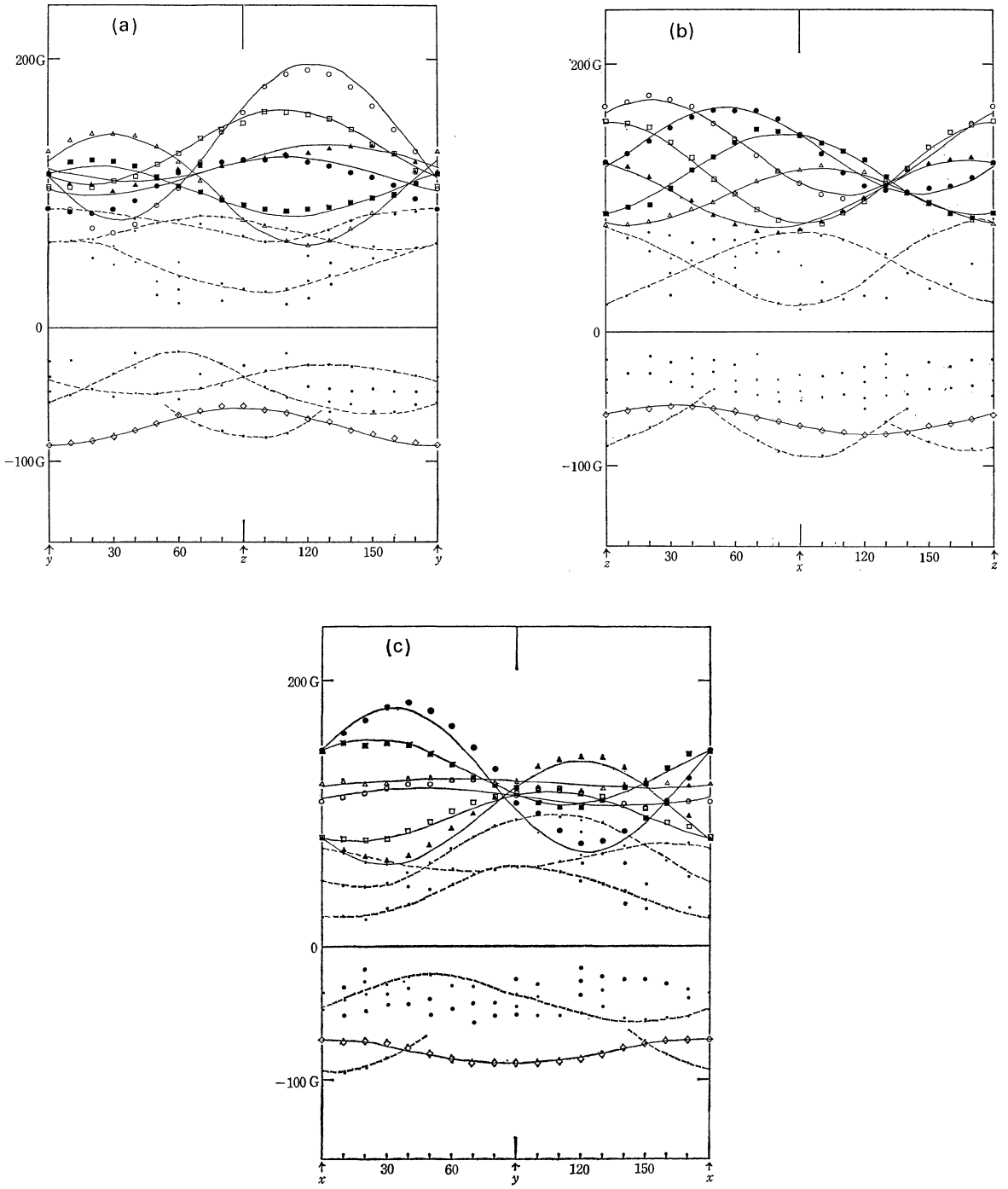

Fig. 2. Angular variation of NMR spectral line positions (a) around the x-axis, (b) around the y-axis, (c) around the z-axis.
The solid curve is the angular variation calculated by the least-square method.
—○— No. **1**, —●— No. **2**, —□— No. **3**, —■— No. **4**, —△— No. **5**, —▲— No. **6**, —◇— No. **7**

there are two DPPH molecules with unequivalent orientations in the crystal unit cell.[9] If the spectrum of the single crystal is completely resolved, 24 lines will be observed at most because of the anisotropic hyperfine interaction, except for the unshifted benzene proton lines. Around any axis we could identify six upfield-shifted lines and one downfield-shifted line, whose intensity is twice as strong as the others. In addition, two downfield-shifted lines can be partially identified around some axes.

The spin Hamiltonian for a free radical in which one proton interacts with one unpaired electron is:

$$\mathscr{H} = -g_N\beta_N\mathbf{H}\cdot\mathbf{I} + \mathbf{S}\cdot\mathbf{T}\cdot\mathbf{I}$$

in which the hyperfine term, $\mathbf{S}\cdot\mathbf{T}\cdot\mathbf{I}$, consists of an isotropic part, $a_H\mathbf{S}\cdot\mathbf{I}$, arising from the Fermi contact interaction and an anisotropic part, $\mathbf{S}\cdot\mathbf{D}\cdot\mathbf{I}$, due to the electron-nuclear dipolar interaction. Here, $\mathbf{T}$, a_H, and $\mathbf{D}$ are the total coupling tensor, the isotropic hyperfine coupling constant, and the traceless dipolar

coupling tensor respectively. The other symbols are used with their conventional significances. If the electron-spin relaxation, T_e, satisfies the condition of $|a_H T_e| \ll 1$, $\mathbf{S}=(\langle S_\alpha\rangle, 0, 0)$, which leads to the following equation: $\chi H=-g\beta\langle S_\alpha\rangle$. Here, $\langle S_\alpha\rangle$ is the α component of a vector **S** (parallel to the magnetic field, **H**) and χ is the static magnetic susceptibility per molecule, formulated by $\chi=g^2\beta^2S(S+1)/3k(T-\theta)$, provided that it obeys the Curie-Weiss law. The other symbols have their usual significances. To first order, therefore, the nuclear resonance signal shifts from the free-proton position to the high field by this amount:

$$\Delta H = -(\chi H/g\beta g_N\beta_N)T_{\alpha\alpha}$$

where $T_{\alpha\alpha}$ is the $\alpha\alpha$ component of the total tensor, **T**.

We reported in the previous paper[11] that, at 4.2 K, the static magnetic susceptibility per molecule of the DPPH–benzene complex obeys the Curie-Weiss law, with the Weiss constant $\theta=-0.5$ K. Although the anisotropy of the ESR g-value becomes larger as the temperature is lowered, it can be neglected in comparison with the magnitude of the anisotropic hyperfine interaction.[12] Consequently, from the angular variation of $T_{\alpha\alpha}$ around three Cartesian axes, it is possible to determine **T**. The tensor components with respect to the xyz-system were determined by the least-square method. Then, the **T**-tensor was diagonalized to obtain the principal values. The isotropic hyperfine coupling constant and the principal values, A, B, and C, of the anisotropic tensor, **D**, for each identified lines are summarized in Table 1, together with the direction cosines of the tensor. The isotropic hyperfine coupling constants of the six lines resemble each other and agree approximately with those obtained from the polycrystalline NMR spectrum, as will be shown afterwards. Using the results for the α-proton tensor in $CH(COOH)_2$,[13] we expect the anisotropic principal values to be $+1.35$, -0.03 and -1.32 for $a_H=-2.60$, and to be -0.84, $+0.02$ and $+0.82$ for $a_H=+1.62$. Those values do not agree well with the measured values listed in Table 1, especially in the case of the latter. Probably the anisotropic term does not depend only upon the spin density on the carbon atom adjacent to the proton, but also upon those on the second-nearest carbon atoms and the nitrogen atoms. Such an effect is serious in the case of the latter, for the positive spin densities on the second-nearest carbon atoms are larger than the negative ones on the carbon atom adjacent to the proton, as will be shown afterwards.[14] The direction of the principal hyperfine axes deviates considerably from that of the

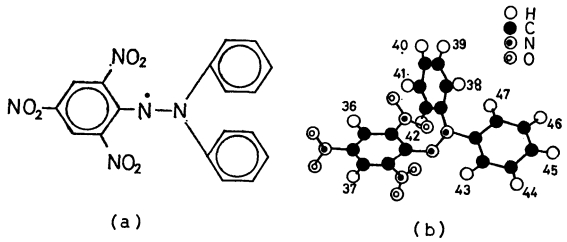

Fig. 3. (a) Molecular structure of DPPH (b) the shape of the DPPH molecule in the DPPH-benzene crystal. Williams' notation is used for the protons.

Table 1. Isotropic hyperfine constants, the principal values and the direction cosines of anisotropic hyperfine tensors

No.	a_H (Gauss)		Principal values (Gauss)	Direction cosines x	y	z
1	-2.86 ± 0.11	A	$+1.28\pm0.11$	-0.427	0.735	0.527
		B	$+0.28\pm0.11$	0.884	0.461	0.074
		C	-1.56 ± 0.11	0.188	-0.497	0.847
2	-2.75 ± 0.14	A	$+1.40\pm0.14$	-0.554	0.743	0.375
		B	-0.04 ± 0.14	-0.073	-0.493	0.867
		C	-1.36 ± 0.14	0.829	0.453	0.327
3	-2.59 ± 0.06	A	$+0.84\pm0.06$	0.956	0.283	0.031
		B	$+0.17\pm0.06$	-0.276	0.898	0.343
		C	-1.01 ± 0.06	0.069	-0.338	0.939
4	-2.58 ± 0.06	A	$+0.74\pm0.06$	-0.005	-0.390	0.921
		B	$+0.15\pm0.06$	-0.463	0.817	0.344
		C	-0.89 ± 0.06	0.886	0.425	0.185
5	-2.42 ± 0.07	A	$+1.09\pm0.07$	0.116	-0.488	0.865
		B	-0.27 ± 0.07	0.992	0.094	-0.080
		C	-0.82 ± 0.07	-0.042	0.868	0.495
6	-2.41 ± 0.09	A	$+1.12\pm0.09$	0.838	0.495	0.230
		B	-0.39 ± 0.09	-0.401	0.272	0.876
		C	-0.73 ± 0.09	-0.370	0.825	-0.427
7	$+1.62\pm0.03$	A	-0.40 ± 0.03	0.520	0.000	0.854
		B	$+0.07\pm0.03$	0.854	-0.016	-0.520
		C	$+0.33\pm0.03$	0.014	1.000	-0.008

α-proton tensor. This cannot be explained by the experimental error. The relation between the directions of the principal hyperfine axes and the molecular structure was not discussed in this paper. Figs. 3(a) and (b) present the molecular structure of DPPH and the shape of the DPPH molecule in the DPPH–benzene crystal respectively. Williams' notation is used for the protons.

Now let us assign the proton resonance signals to the protons of the DPPH molecule. As there are two DPPH molecules with unequivalent orientations in the crystal unit cell, the six upfield-shifted lines are reduced to three for one molecule. In considering the theoretical results, we can expect the isotropic hyperfine coupling constants of two *ortho* protons to be approximately equal to that of one *para* proton.[2,15] Therefore, the three lines are attributable to two *ortho* protons and one *para* proton of the phenyl group twisted at an angle of 22°. These protons correspond to the largest upfield-shifted component in the polycrystalline spectrum. The downfield-shifted lines are assigned to *meta* protons of the picryl group, as has been determined by Anderson *et al.*[3] Another upfield-shifted component in the polycrystalline spectrum is probably due to two *ortho* protons and one *para* proton of the phenyl group twisted at an angle of 49°, and the other two downfield-shifted components (partially resolved), to the *meta* protons of two phenyl groups.

On the basis of the assignment of the polycrystalline NMR spectrum, the isotropic hyperfine coupling constants have been evaluated. The results are tabulated, together with the ESR[7] and ENDOR[8] results of DPPH in the solution state, in Table 2. The results in Table 2 indicate that the unpaired electron-spin distribution of one phenyl group is almost twice as large as that of the other phenyl group in the crystalline state. Further, in spite of the nonplanarity of the hydrazyl skeleton, the unpaired electron-spin delocalization is larger in the crystalline state than in solution, particularly on the picryl group and on one of the two phenyl groups. This fact may be related to the high stabilization of this radical in the crystalline state, in addition to the steric hindrance of the *o*-nitro groups reported by Williams.[9] In the case of a solution, a DPPH molecule may undergo dynamical changes in the hydrazyl skeleton and in the twist angle of the rings.

Table 2. Isotropic hyperfine constants obtained by the NMR spectra in the crystalline state, the ESR spectra and the ENDOR spectra in solutions

Notation of proton	a_H-NMR[a] (Gauss)	a_H-ESR[b] (Gauss)	a_H-ENDOR[c] (Gauss)
H 36, 37	+1.6	0.377	1.0
H 44, 46	+1.1	0.754	0.67, 0.75
H 39, 41	+0.6	0.754	0.67, 0.75
H 38, 40, 42	−1.5	1.885	2.0, 1.9
H 43, 45, 47	−2.6	1.885	2.0, 1.9

a) This work, b) Ref. 7, c) Ref. 8

The authors wish to express their thanks to Dr. Yoshitami Ajiro and Mr. Teruaki Fujito for their technical advice, and also to Mr. Osamu Takizawa for his cooperation in utilizing the computers at the Data Processing Center of Kyoto University.

References

1) H. S. Gutowsky, H. Kusumoto, T. H. Brown, and D. H. Anderson, *J. Chem. Phys.*, **30**, 860 (1959).
2) T. H. Brown, D. H. Anderson, and H. S. Gutowsky, *ibid.*, **33**, 720 (1960).
3) M. E. Anderson, G. E. Pake, and T. R. Tuttle, *ibid.*, **33**, 1581 (1960).
4) M. E. Anderson, R. S. Rhodes, and G. E. Pake, *ibid.*, **35**, 1527 (1961).
5) A. Kawamori and K. Suzuki, *Mol. Phys.*, **8**, 95 (1964).
6) Y. Deguchi, *J. Chem. Phys.*, **32**, 1584 (1960).
7) Z. Haniotis and Hs. H. Gunthard, *Helv. Chim. Acta*, **51**, 561 (1968).
8) N. S. Dalal, D. E. Kennedy, and C. A. McDowell, private communication.
9) D. E. Williams, *J. Amer. Chem. Soc.*, **89**, 4280 (1967).
10) F. N. H. Robinson, *J. Sci. Instrum.*, **36**, 481 (1959).
11) T. Fujito, T. Enoki, H. Ohya-Nishiguchi, and Y. Deguchi, *Chem. Lett.*, **1972**, 557.
12) H. Ohya-Nishiguchi *et al.*, to be published.
13) H. M. McConnell, C. Heller, T. Cole, and R. W. Fessenden, *J. Amer. Chem. Soc.*, **82**, 766 (1960).
14) C. Heller and T. Cole, *J. Chem. Phys.*, **37**, 243 (1962).
15) V. A. Gubanov, V. I. Koriakov, and A. K. Chirkov, *J. Mag. Reson.*, **9**, 263 (1973).

Pressure Effect on the Absorption Spectra of Iron Compounds

Yoji HARA, Ichimin SHIROTANI, Nobuko SAKAI, Saburo NAGAKURA, and Shigeru MINOMURA

The Institute for Solid State Physics, The University of Tokyo, Roppongi, Minato-ku, Tokyo 106

(Received September 1, 1973)

The effect of pressures up to 50 kbar has been measured on the absorption spectra in five ferric compounds, two ferrous compounds, and one mixed valence compound. In six compounds, but not in basic ferric acetate and soluble prussian blue, we observed pressure-induced bands which were assigned to the d-d transition of the converted Fe(II) for the ferric compounds and to the spin-forbidden d-d transition for the ferrous compounds. The absorption spectra for single crystals of potassium ferri- and ferrocyanide were studied at hydrostatic pressures up to 5 kbar. The band-peak intensity decreased with an increase in the pressure in both cases. The charge-transfer band from Fe(II) to Fe(III) of soluble prussian blue showed a blue shift (69 cm^{-1}/kb) at hydrostatic pressures up to 7.2 kbar.

A great deal of knowledge on the pressure-induced electronic transitions of iron compounds has been accumulated from measurements of the Mössbauer effect and of optical absorptions. Drickamer *et al.*[1] first observed that electronic transitions involving the reduction of ferric ions or the spin flip of ferrous ions are induced with various iron compounds by applying a wide range of pressures.

The reduction or spin flip initially increases with the increase in the pressure and exhibits a reversible process, sometimes with hysteresis. This behavior can be explained in terms of such basic effects of the pressure on the electronic structures as the increasing overlap and the relative displacement between adjacent electronic orbitals. In this paper, we wish to present data on the effects of pressures up to 50 kbar on the absorption spectra of some ferric, ferrous, and mixed-valence iron compounds.

The changes in the oxidation states of ferric and ferrous ions with pressure are discussed in connection with the results of the Mössbauer effect reported by Drickamer *et al.*

Experimental

The ferric and ferrous compounds used in this experiment were all of a commercially-available, reagent-grade quality. The absorption spectra were measured as a function of the pressure. The pressures were generated by means of an intensifier using a white gasoline medium up to 8 kbar and a high-pressure optical bomb using a NaCl medium up to 50 kbar.[2] The optical measurements were performed with a Shimadzu double-beam spectrometer and also with a Bausch-Lomb grating spectrometer.

The materials studied are listed in Table 1.

TABLE 1. MATERIALS STUDIED

Compounds	
Potassium ferricyanide	$K_3Fe(CN)_6$
Potassium ferrocyanide	$K_4Fe(CN)_6$
Ferric phosphate hydrate	$FePO_4 \cdot nH_2O$
Basic ferric acetate	$Fe_3(CH_3CO_2)_6(OH)_2 \cdot CH_3CO_2 \cdot H_2O$
Ferric citrate	$Fe(C_6H_5O_7) \cdot 3H_2O$
Ferric chloride	$FeCl_3$
Ferrous chloride hydrate	$FeCl_2 \cdot nH_2O$
Soluble prussian blue	$KFeFe(CN)_6$

Results and Discussion

Potassium Ferricyanide. Potassium ferricyanide and ferrocyanide are low-spin complexes. Figure 1 shows the pressure effect on the absorption spectra with a single crystal of potassium ferricyanide at hydrostatic pressures up to 4.5 kbar. Basu *et al.* assigned the broad band to the charge transfer from a ligand to the central metal ion.[3] The absorption intensity decreases with the increase in the pressure. This behavior was reproducible. Gardiner *et al.* have examined the visible spectrum of a $K_3Fe(CN)_6$ (potassium ferricyanide) solution in water under hydrostatic pressures up to 2 kbar.[4] They found no measureable change (>1/2%) in the absorbance.

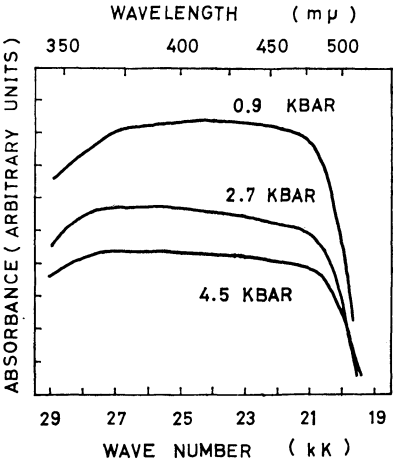

Fig. 1. Absorption spectra of a single crystal of potassium ferricyanide at various hydrostatic pressures.

In our experiment, however, a decrease of about 25% in the band peak intensity was observed upon a change from 0.9 kbar to 4.5 kbar. The decrease was over twice as much as that expected from the Mössbauer data of Champion and Drickamer.[5] This discrepancy may be interpreted as showing the remarkable dependence of the reduction on the samples. Therefore, in the first place, a reduction of the central $Fe(CN)_6^{3-}$ seems to be closely related to the direct interaction with the surrounding K^+ ions and $Fe(CN)_6^{3-}$. In the second place, the reduction can be explained in terms of the influence of the lattice distortion introduced by a kind of increasing local deformation with pressure near vacancies or dislocations in the

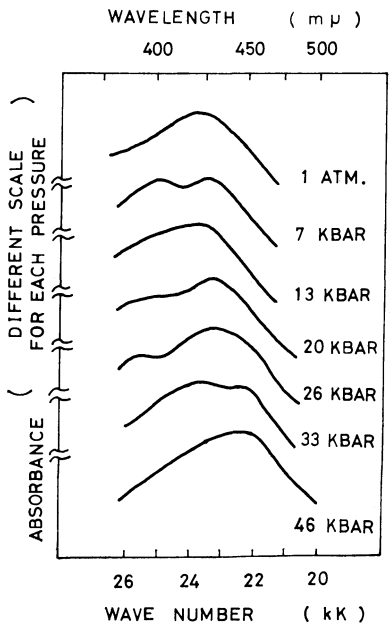

Fig. 2. Absorption spectra of polycrystalline potassium ferricyanide at various pressures.

crystal. The relationship between the reduction and the shearing stress of the sample has already been pointed out.[4,6] The absorption spectrum of a polycrystalline $K_3Fe(CN)_6$ sample diluted with NaCl was measured up to 46 kbar under quasi-hydrostatic pressure. The results are shown in Fig. 2. When the pressure was released, the original spectrum was obtained again. The band at 23.8 kK was assigned to the charge transfer from (CN^-) to the central Fe(III).[7] The intensity of the peak was found to decrease gradually up to 33 kbar, but was found to increase a little at 39 kbar. At 7 kbar, a doublet band appeared. The pressure-induced band at 25 kK exhibited a shift to the higher frequencies (blue shift) of about 500 cm^{-1} at 26 kbar, decreasing in intensity with pressure. By 33 kbar this band has been almost swamped by the lower energy bands. Another pressure-induced band was observed around 22.5 kK at 20 kbar; it was found to swamp the charge-transfer band at 46 kbar, increasing in intensity. These two pressure-induced bands seem to be due to the converted Fe(II).

Potassium Ferrocyanide. Figure 3 shows the pressure effect on the absorption spectra of a single crystal of potassium ferrocyanide at hydrostatic pressures up to 4.5 kbar. In an octahedral environment, the five d orbitals of the metal split into a threefold degenerated t_{2g} level and a doubly-degenerated e_g with the t_{2g} lying lowest.

In a low-spin case such as ferrocyanide, the six d electrons are in the t_{2g} orbital, with their spins paired; this is the ground state $^1A_{1g}$. The spectral assignment $K_4Fe(CN)_6$ in an aqueous solution shows that the band can be assigned to the expected d-d transition, $^1A_{1g} \rightarrow {}^1T_{1g}$.[8] The absorption peak showed a definite blue shift with an increase in the pressure, at the rate of 83 cm^{-1}/kb. The band-peak intensity decreased about 28% upon the pressure change from 0.9 kbar to 4.5 kbar.

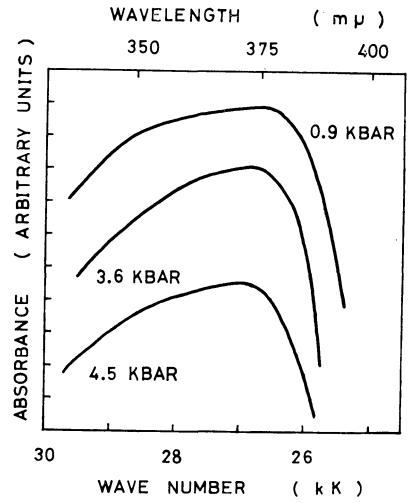

Fig. 3. Absorption spectra of a single crystal of potassium ferrocyanide at various hydrostatic pressures.

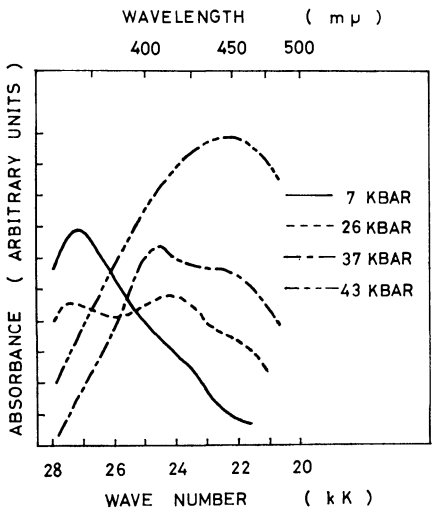

Fig. 4. Absorption spectra of polycrystalline potassium ferrocyanide at various pressures.

The blue shift and the decrease in the intensity continue at higher pressures, as is illustrated in Fig. 4, where the fade-out of the band is exhibited at 37 kbar. A reasonable explanation for the decrease from 2.7 kbar to 4.5 kbar in the absorbance around 27 kK of the single crystal $K_3Fe(CN)_6$, as is illustrated in Fig. 1, presents itself when one considers the decrease in the band intensity due to the converted Fe(II), as is shown in Fig. 3.

The pressure effect on the absorption spectra at quasi-hydrostatic pressures up to 50 kbar was measured. The results are shown in Fig. 4. The band around 24 kK at 7 kbar which appears as a shoulder showed a blue shift, about 500 cm^{-1} in 37 kbar, increasing in intensity drastically with pressure. At 26 kbar, another pressure-induced band was observed around 22 kK. This band also exhibited a blue shift, increasing in intensity drastically with pressure. This behavior was reproducible. The electronic spectrum of $Fe(CN)_6^{4-}$ shows a very weak band at 23.7 kK; this band can be assigned to the first spin-forbidden transition, $^1A_{1g} \rightarrow {}^3T_{1g}$.[8] Thus, the band at 21~26 kK which increased in intensity drastically

seem to be related to this transition. We obtained samples after 50 kbar and measured their infrared with a KBr pellet. No reasonable spectral change in the Fe(II)–C stretching frequency was observed.

Ferric Phosphate Hydrate. The absorption spectra of ferric phosphate hydrate at various pressures are given in Fig. 5. The spectra at 1 atmosphere and 6.3 kbar were measured with a KBr pellet under hydrostatic pressures. When the spectrum at 6.3 kbar was compared with that at 1 atmosphere, a swelling around 24 kK due to a pressure-induced band was found. The band peak at 1 atmosphere showed a red shift, about -700 cm^{-1} at 38 kbar. In 13 kbar a definite pressure-induced band around 24 kK was observed. This band increased in intensity relatively with that at higher wave numbers, exhibiting a slight shift. The spectra were reversible with some hysteresis. The electronic spectrum of ferrous phosphate, $Fe_3(PO_4)_2$, shows a band at about 23 kK at 1 atmosphere. This band corresponds to the pressure-induced band in ferric phosphate hydrate.

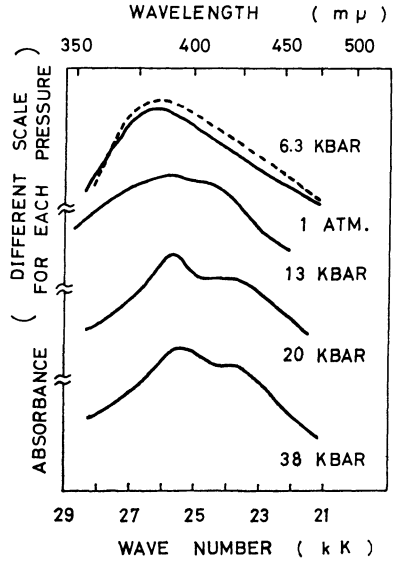

Fig. 5. Absorption spectra of polycrystalline ferric phosphate hydrate at various pressures; The spectra at 1 ATM. and 6.3 KBAR are at hydrostatic pressures.

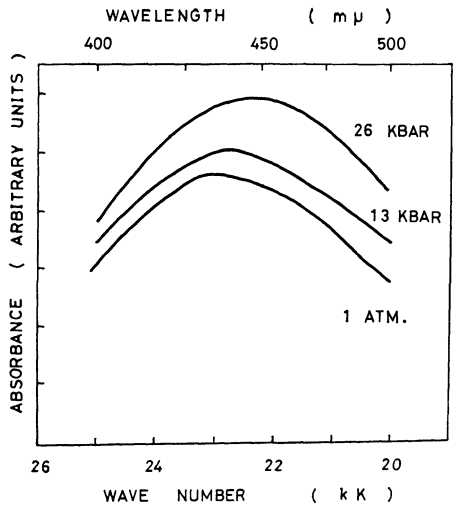

Fig. 6. Absorption spectra of polycrystalline basic ferric acetate at various pressures.

Basic Ferric Acetate. Figure 6 shows the absorption spectra measured with basic ferric acetate at various pressures up to 26 kbar. The measurement of the Mössbauer by Drickamer *et al.* showed evidence of only a trace of any reduction up to 150 kbar.[9,10] The band peak showed a red shift of -1100 cm^{-1} in 26 kbar, increasing in peak intensity about 30%. Basic ferric acetate is a tri-nuclear complex of ferric ions which are joined with each other by a strong linkage of the ($CH_3CO_2^-$) ions.[11]

Therefore, it may be inferred that the complex is difficult either to distort and to reduce because of less influence of a vacany and/or a dislocation.

Ferric Citrate. Figure 7 shows the effect of the hydrostatic pressure on the absorption spectra of ferric citrate with the KBr pellet. The band-peak intensity decreased by about 17% upon the pressure change from 0.9 to 5.4 kbar. This behavior was reproducible. The band shift may be small. According to the experiment which was carried out under quasi-hydrostatic pressures up to 26 kbar, this band shows a red shift, at the rate of -15 cm^{-1}/kb. At about 21.5 kK, a pressure-induced band was observed at 7 kbar, showing a blue shift, at the rate of 37 cm^{-1}/kb up to 26 kbar.

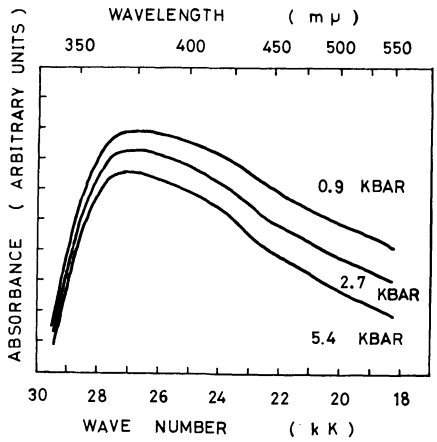

Fig. 7. Absorption spectra of polycrystalline ferric citrate at various hydrostatic pressures.

Ferric Chloride. The pressure effect on the absorption spectra of ferric chloride up to 46 kbar is illustrated in Fig. 8. The absorbance of the peak maximum decreased about 30% up to 46 kbar. The maximum of the broad band is 22.6 kK at 1 atomosphere. Pressure-induced bands were observed around 24.1 and 22 kK in 13 kbar. Judging from the results for ferrous chloride hydrate, these two bands should be assigned to the spin-forbidden bands of Fe(II). The peak around 23 kK due to Fe(III) was left. The band at 24.1 kK was swamped by the lower-energy bands by 20 kbar but was found to appear again at 39 kbar. The shift was approximately 200 cm^{-1} up to 39 kbar. The maximum absorption irregularly exhibited a red shift of about -800 cm^{-1} from 26 to 33 kbar; this is too great to be ascribed to the normal absorption due to Fe(III). A possible explanation of the irregular shift is that a pressure- induced band around 22 kK increases

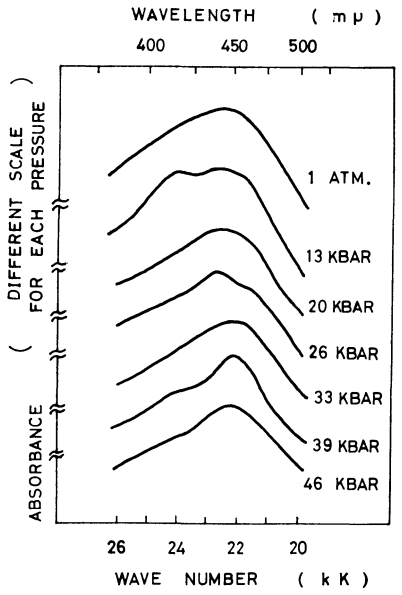

Fig. 8. Absorption spectra of polycrystalline ferric chloride at various pressures.

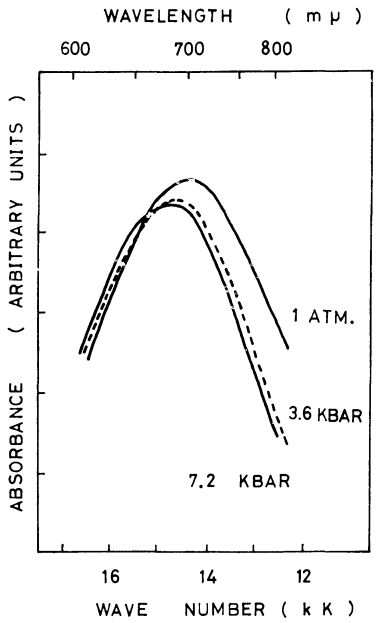

Fig. 10. Absorption spectra of polycrystalline soluble prussian blue at various hydrostatic pressures.

in intensity relative to the band which corresponds to Fe(III), located around 23 kK.

Ferrous Chloride Hydrate. Four d electrons are in the t_{2g} orbital and two are in the e_g orbital, which is the ground state $^5T_{2g}$. The two spin-forbidden d-d bands, $^5T_{2g} \rightarrow {}^3T_{1g}$ and $^5T_{2g} \rightarrow {}^3T_{2g}$, may be expected in the visible region. Figure 9 shows the pressure effect on the absorption spectra of ferrous chloride hydrate up to 36 kbar. No band was found in the 21~25 kK region of the spectrum at 1 atm. At 7 kbar, pressure-induced bands were observed, increasing in intensities drastically with pressure. The shifts of the two bands from 13 to 36 kbar were small. The spin-forbidden bands generally show a slight shift upon pressure.[12] Therefore, these new pressure-induced bands should be assigned to the expected d-d spin-forbidden transition.

Soluble Prussian Blue. The absorption spectra of polycrystalline soluble prussian blue at hydrostatic pressure are shown in Fig. 10. The structure of prussian blue has been elucidated by Robin.[13] A low-spin Fe(II) is coordinated to the carbon, and a high-spin Fe(III) to the nitrogen. The intermetallic charge-transfer band from the Fe(II) to the Fe(III) site assigned to $t_{2g}(\pi) \rightarrow t_{2g}(\pi)$ appears at 14.3 kK for the soluble prussian blue. The band exhibited a shift to higher frequencies of about 69 cm^{-1}/kb with pressure.

The absorbance at the band decreased by about 5% up to 7.2 kbar. This value is almost the same as that (about 5%) extrapolated from the result for $Fe[Fe(CN)_6]_3$ given by Mössbauer measurements by Drickamer *et al.*[14] who measured the transference of an electron from a low-spin Fe(II) site to a high-spin Fe(III) site at low pressure. The decrease in the absorbance at high pressure might be related to results of the Mössbauer spectra.

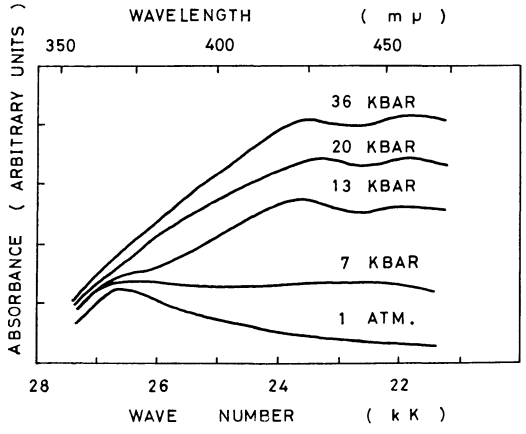

Fig. 9. Absorption spectra of polycrystalline ferrous chloride hydrate at various pressures.

References

1) H. G. Drickamer and C. W. Frank, "Electronic Transitions and the High Pressure Chemistry and Physics of Solids," Chapman and Hall, London (1973).
2) R. A. Fitch, T. E. Slykhouse, and H. G. Drickamer, *J. Opt. Soc. Amer.*, **74**, 1015 (1957).
3) G. Basu and R. L. Belford, *J. Chem. Phys.*, **37**, 1933 (1962).
4) R. G. Gardiner, S. D. Hamann, and M. Linton, *Aust. J. Chem.*, **23**, 2369 (1970).
5) A. R. Champion and H. G. Drickamer, *J. Chem. Phys.*, **47**, 2591 (1967).
6) H. A. Larsen and H. G. Drickamer, *J. Phys. Chem.*, **61**, 1249 (1957).
7) C. S. Naiman, *J. Chem. Phys.*, **35**, 323 (1961).
8) H. B. Gray and N. A. Beach, *J. Amer. Chem. Soc.*, **85**, 2922 (1963).
9) A.R. Champion, R.W. Vaughan, and H.G. Drickamer, *J. Chem. Phys.* **47**, 2583 (1967).
10) S. C. Fung, G. K. Lewis, and H. G. Drickamer, *Proc. Nat. Acad. Sci. U.S.*, **61**, 813 (1968).
11) M. B. Robin and P. Day, "Advances in Inorganic and Radiochemistry," Acad. Press, Vol. 10, p. 294 (1967).
12) B. A. Baldwin and H. W. Offen, *J. Chem. Phys.*, **46**, 4509 (1967).
13) M. B. Robin, *Inorg. Chem.*, **1**, 337 (1962).
14) S. C. Fung and H. G. Drickamer, *J. Chem. Phys.*, **51**, 4353 (1969).

Polarized Absorption Spectra of the Hydroquinone and 1,4-Dimethoxybenzene Crystals in the Near and Vacuum Ultraviolet Regions

Koji KAYA,*,*1 Kiyokazu FUKE,** and Saburo NAGAKURA*,**

*The Institute of Physical and Chemical Research, Wako, Saitama 351

**The Institute for Solid State Physics, The University of Tokyo, Roppongi, Minato, Tokyo 106

(Received September 10, 1973)

We measured the polarized absorption spectra of the γ-hydroquinone and 1,4-dimethoxybenzene crystals in the wave number region between 30000 cm^{-1} and 65000 cm^{-1}. The dichroic ratios determined for the spectra of both crystals show that the bands at ~290 nm and at ~220 nm are polarized parallel with the short and long molecular axes, respectively; these support the assignment that they correspond to the L_b and L_a bands of benzene, respectively. The dichroic ratios and intensities determined for the bands in the vacuum ultraviolet region show that they do not simply correspond to the $B_{a,b}$ bands of benzene and that mixing among appropriate excited states occurs in both crystals.

The measurements of polarized electronic absorption spectra have played an important role in the studies of the electronic structures of molecules and molecular crystals.[1–5] Most of the studies made hitherto have, however, been concerned with polarized spectra in the wavelength regions longer than 250 nm; polarized absorption measurements in the vacuum ultraviolet region are rather scanty because of their experimental difficulties.[6]

In the present study, we have extended the polarized absorption measurements of single crystals to the vacuum ultraviolet region and have studied the electronic structures of the γ-hydroquinone and 1,4-dimethoxybenzene crystals from both theoretical and experimental points of view.

Experimental

Commercially-available (G. R. Grade) hydroquinone and 1,4-dimethoxybenzene were purified by repeated recrystallizations from water and by repeated sublimations in a vacuum, respectively. Single crystals used for the polarized absorption measurements were prepared by sublimation.

Polarized absorption spectra in the wave number region from 30000 cm^{-1} to 65000 cm^{-1} were measured by a vacuum ultraviolet microspectrophotometer constructed in our laboratory, the details of which were described in a previous paper.[7] Sample crystals were sandwiched between two quartz plates (optically flat) and were then put on the stage of the microscope of the spectrophotometer. The polarized absorption measurements were made along the b and c axes on the (100) surface and along the a and b axes on the (001) surface for the γ-hydroquinone and the 1,4-dimethoxybenzene crystals, respectively. The crystal surfaces were determined by comparing the crystal habits observed with the help of an orthonoscope with the crystal structure data obtained by Maartmann-Moe[8] and by Goodwin *et al.*[9] We could not measure the absorption at wavelengths shorter than 180 nm for the 1,4-dimethoxybenzene crystal because of the quick sublimation of the sample due to temperature elevation by the irradiation of the vacuum ultraviolet light.

The absorption spectrum of hydroquinone in the gaseous state was measured by the spectrophotometer used for the polarized absorption measurement, a microscope attached to the instrument being replaced by a gas cell.

*1 Present address: Department of Chemistry, Faculty of Science, Tohoku University, Aramaki, Sendai.

Results and Discussion

Absorption Spectrum of Gaseous Hydroquinone and the Band Assignment. An absorption spectrum measured with gaseous hydroquinone is shown in Fig. 1. It consists of three bands with maxima at 34600, 45200, and 53300 cm^{-1}. Judging from their positions and intensities, they correspond to the $^1B_{2u} \leftarrow {}^1A_{1g}$ (L_b), $^1B_{1u} \leftarrow {}^1A_{1g}$ (L_a), and $^1E_{1u} \leftarrow {}^1A_{1g}$ ($B_{a,b}$) transition bands of benzene, respectively. In order to certify these assignments, the π-electron structure of hydroquinone was calculated by the Pariser-Parr-Pople SCF MO method[10] including the configuration interaction. The calculated and observed transition energies and oscillator strengths are given in Table 1. The calculated wave functions and polarizations are also shown in this table. The wave functions of the respective excited states show that the above-mentioned assignments are correct.

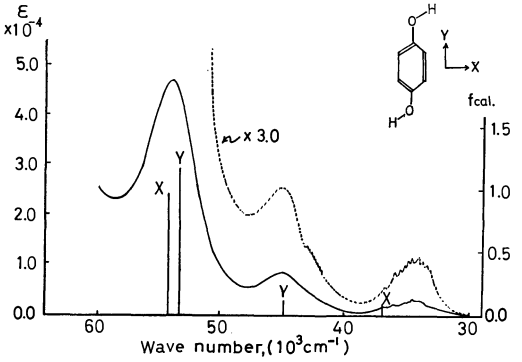

Fig. 1. The absorption spectrum of hydroquinone in the gaseous state. The vertical lines show the band positions and oscillator strengths calculated by the Pariser-Parr-Pople method: x and y indicate the polarization directions.

Polarized Absorption of the γ-Hydroquinone Crystal. The polarized absorption spectrum of the γ-hydroquinone crystal (monoclinic ($P2_1/c$)) is shown in Fig. 2. The projection of the four molecules within a unit cell of the crystal on the (100) face is shown in Fig. 3. Maartmann-Moe[8] reported that hydroquinone crystallizes in the γ-form upon sublimation.

Table 1. Observed and theoretical transition energies (ΔE) and oscillator strengths (f) of hydroquinone

Band	Experimental		Theoretical		Polarization	Configurations mainly contributed to each state[b]
	$\Delta E(\times 10^3\ cm^{-1})$	f[a]	$\Delta E(\times 10^3\ cm^{-1})$	f		
	34.6	0.040	36.9	0.092	x	$0.879\phi(5\rightarrow6)$, $-0.476\phi(4\rightarrow7)$
	45.2	0.097	44.8	0.130	y	$0.863\phi(5\rightarrow7)$, $0.503\phi(4\rightarrow6)$
	53.3	1.330	53.3	1.222	y	$-0.503\phi(5\rightarrow7)$, $0.864\phi(4\rightarrow6)$
			54.2	0.970	x	$0.477\phi(5\rightarrow6)$, $0.879\phi(4\rightarrow7)$

a) The f values of the first and second bands were obtained from the absorption spectrum in cyclohexane. Concerning the third band, f was obtained from the absorption spectrum in gas phase, the molar extinction coefficient (ε) of which was normalized by the absorption spectrum in cyclohexane.

b) $\phi(i\rightarrow j)$ represents the electron configuration in which one electron is excited from the i-th MO to the j-th MO. The coefficient of each configuration is that in the state wave function. ϕ_4, ϕ_5, ϕ_6, and ϕ_7 are as follows:

	a_1	a_2	a_3	a_4	a_5	a_6	a_7	a_8
ϕ_4		0.500	0.500		−0.500	−0.500		
ϕ_5	−0.497	−0.301	0.301	0.497	0.301	−0.301	0.269	−0.269
ϕ_6		0.500	−0.500		0.500	−0.500		
ϕ_7	0.576	−0.265	−0.265	0.576	−0.265	−0.265	−0.167	−0.167

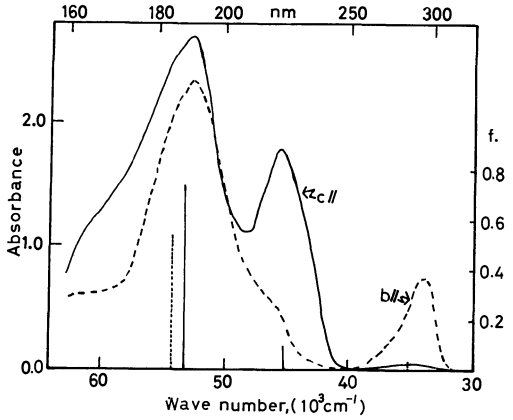

Fig. 2. The polarized absorption spectrum observed with the γ-hydroquinone crystal. The vertical full and broken lines show the absorption intensities estimated for the c- and b-polarized bands by the aid of the oriented gas model, respectively.

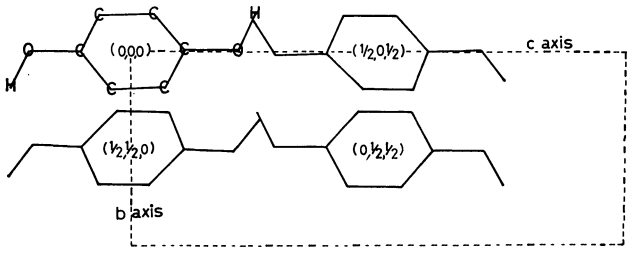

Fig. 3. Projection of the four site molecules on the bc plane of the γ-hydroquinone crystal.

As is clearly seen in Fig. 2, the polarized absorption spectrum of the γ-hydroquinone crystal has four peaks at 34500, 45500, 52000, and 60600 cm^{-1}. The dichroic ratios (D_b/D_c) are 20 : 1 and 1 : 4 for the first and the second bands, respectively, D_b and D_c being the absorbancies observed for each band along the b and c crystal axes, respectively. From the dichroic ratio observed with the crystal and from the orientations of the four site molecules in a unit cell, the molecular dichroic ratio, D_x/D_y, was obtained for the bands at 34500 and 45500 cm^{-1} as shown in Table 2. Here,

Table 2. The dichroic ratios observed for the first and second bands of γ-hydroquinone and 1,4-dimethoxybenzene

	γ-Hydroquinone	
	$D_b : D_c$	$D_x : D_y$
290 nm band	20 : 1	1 : 0
220 nm band	1 : 4	1 : 2.6
	1,4-Dimethoxybenzene	
	$D_b : D_a$	$D_x : D_y$
295 nm band	2 : 1	3 : 1
220 nm band	5 : 1	1 : 8

the x and the y axes are taken to be perpendicular and parallel to the molecular axis connecting the two oxygen atoms on the molecular plane.

Table 2 shows that the band of the crystal at 34500 cm^{-1} is polarized parallel with the x molecular axis and thus corresponds to the 34600 cm^{-1} band of the molecule in the gaseous state, which is expected from theoretical considerations to be polarized in the x-direction. The 45500 cm^{-1} band of the γ-hydroquinone crystal is polarized almost parallel with the y molecular axis; it corresponds to the 45200 cm^{-1} band of the molecule.

Let us turn to polarized absorption bands in the vacuum ultraviolet region. The spectra of the crystal polarized parallel with the b and c crystal axes show the intense absorption peaks at 52000 cm^{-1} and also have shoulders at around 60600 cm^{-1}.[11] As is seen in Fig. 3, the molecular x axis of each molecule in the crystal is almost parallel with the b crystal axis and the y molecular axis with the c crystal axis. Therefore, it is reasonable to assign the b-polarized band at 52000 cm^{-1} of the crystal to the x-polarized component of the intense absorption band of the molecule at 53300 cm^{-1}. The c-polarized absorption of the crystal with a peak at 52000 cm^{-1} can be assigned to the y-polarized absorption of the molecule, which is thought, from theoretical considerations, to overlap with the x-polarized component.

The intensities of the bands polarized parallel with the b and c crystal axes can be obtained on the as-

sumption of the oriented gas model from the experimental values of the oscillator strengths given in Table 1.[12] The results are shown by the vertical lines in Fig. 2. From this figure, it is seen that the polarized absorption spectra observed with the γ-hydroquinone crystal can be explained qualitatively by the oriented gas model. From the quantitative point of view, however, the observed intensity ratios of the 52000 cm^{-1} bands to the first and second bands are much smaller than those to be expected from the oriented gas model. For instance, the intensity ratio of the c axis polarized bands at 52000 cm^{-1} and at 45500 cm^{-1} is observed at 2 : 1 taking the integrated intensities; in case of the oriented gas model, the corresponding value is 7.5 : 1. This discrepancy is beyond the limitations of experimental error and may be due to the fact that the 53300 cm^{-1} band of the molecule in the gaseous state decreases its intensity in the crystalline state because of the intensity borrowing.

In the case of strong coupling, the intensity borrowing among the different excited states of the molecule may occur through the configuration interaction; consequently, the dichroic ratios of the crystal become different from those of the free molecule. Organic molecular crystals have many excited states including a continuous state (excitation from the valence band to the conduction band), so the intensity-borrowing effect may be significant for the exciton bands in this region. Tanaka and Tanaka[13] explained the spectrum of the anthracene crystal by considering the interaction among different exciton configurations. The observed decrease in the intensity of 52000 cm^{-1} bands polarized along the b and c axes of the γ-hydroquinone crystal may be due to the above-mentioned effect.

1,4-Dimethoxybenzene. The crystal of 1,4-dimethoxybenzene is orthorhombic (Pbca) and contains four molecules per unit cell. The polarized absorption spectrum was measured with the (001) plane of the single crystal prepared by sublimation; the results are shown in Fig. 4. The projection of the four molecules within a unit cell of the crystal on the (001) plane is shown in

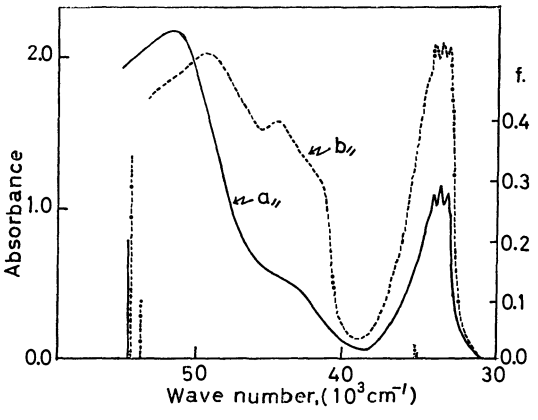

Fig. 4. The polarized absorption spectrum observed with the 1,4-dimethoxybenzene crystal. The vertical full and broken lines show the absorption intensities estimated for the a- and b-polarized bands by the aid of the oriented gas model, respectively.

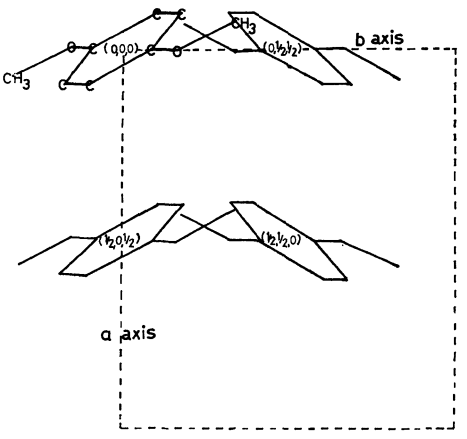

Fig. 5. Projection of the four site molecules on the ab plane of the 1,4-dimethoxybenzene crystal.

Fig. 5. The first and second bands at 295 nm and at 220 nm are polarized along the x and y axes, respectively, as is seen in Table 2. This result which is consistent with that by Albercht and Simpson[14] shows that the 295 nm and 220 nm bands correspond to the L_b and L_a bands of benzene.

In addition to the above-mentioned bands, we succeeded in observing the two absorption peaks at 49500 c n^{-1} and 51800 cm^{-1} polarized along the b and a axes, respectively. From the crystal structure data and the assumption of the oriented gas model, we can expect that the components polarized parallel with the a and b axes are 0.5 and 13.0 percent for the y-axis polarized band, respectively, and that they are 30.0 and 61.4 percent for the x-axis polarized one, respectively. Furthermore, the absorption intensities are almost equal for the bands polarized parallel with the x and y axes. Therefore, the two absorption peaks at 49500 cm^{-1} and 51800 cm^{-1} polarized along the b and a axes, respectively, are interpreted to correspond to the x-polarized band (B_b band for benzene), which is expected to show the Davydov splitting in the crystal. The splitting was calculated for the x-polarized transition by taking the dipole-dipole interaction between molecules within a sphere with a radius of 50 Å. The theoretical result that the a-axis spectrum shifts to higher frequencies than the b-axis one is consistent with the observation. The calculated value of the splitting, 480 cm^{-1} is, however, smaller than the observed value, 2300 cm^{-1}.

A small shoulder at 52200 cm^{-1} in the b axis spectrum may be assigned to the y-polarized transition band (the B_a band of benzene).

The relative intensities of the bands observed with the 1,4-dimethoxybenzene crystal are abnormal compared with those of the free molecule. This may be explained in terms of the interaction among various configurations in the crystals, as was done in the case of the γ-hydroquinone crystal.

Our thanks are due to Professor Ryumyo Onaka, Tokyo University of Education, for his kind suggestions and discussions regarding the design of the vacuum ultraviolet monochromator. We are also indebted to

Mr. Masaki Noma and Mr. Ichiro Sawamura, Olympus Optical Co., Ltd., for their kind help in constructing the reflection-type microscope used for the vacuum ultraviolet absorption measurements.

References

1) D. S. McClure and O. Schnepp, *J. Chem. Phys.*, **23**, 1575 (1955); D. S. McClure, "Solid State Physics," Vol. VIII, ed. by F. Seitz, Academic Press, London (1959), p. 1.
2) W. T. Simpson and D. L. Peterson, *J. Chem. Phys.*, **26**, 588 (1957).
3) R. Silbey, J. Jortner, and S. A. Rice, *ibid.*, **42**, 1515 (1965).
4) J. Tanaka and M. Shibata, This Bulletin, **41**, 34 (1968).
5) H. Hosoya, J. Tanaka, and S. Nagakura, *ibid.*, **33**, 850 (1960).
6) L. E. Lyons and G. C. Morris, *J. Chem. Soc.*, **1959**, 1551.
7) K. Kaya and S. Nagakura, *J. Mol. Spectrosc.*, **44**, 279 (1972).
8) K. Maartmann-Moe, *Acta Crystallogr.*, **21**, 979 (1966).
9) T. H. Goodwin, M. Przybylska, and J. M. Robertson, *ibid.*, **3**, 297 (1950).
10) R. Pariser and R. G. Parr, *J. Chem. Phys.*, **21**, 466, 767 (1953); J. A. Pople, *Trans. Faraday Soc.*, **49**, 1375 (1953).
11) Shoulders at ~170 nm in the b- and c-axis polarized spectra of the γ-hydroquinone crystal are reproducible for the repeated measurements and their existence is conclusive.
12) It is necessary for this estimation to divide the oscillator strength of the 53300 cm^{-1} band into two components polarized along the x- and y-molecular axes. In actuality, we divided the observed oscillator strengths, 1.330, into two parts proportional to the theoretical values, 1.222 and 0.970, calculated for the y- and x-polarized bands.
13) M. Tanaka and J. Tanaka, *Mol. Phys.*, **16**, 1 (1969).
14) A. C. Albrecht and W. T. Simpson, *J. Chem. Phys.*, **23**, 1480 (1955).

Organic Charge Transfer Salts. II.[1] Emission Spectrum of an Organic Charge Transfer Salt, 2,4,6-Triphenylthiopyrylium-1,1,3,3-tetracyanopropenide

Toshiaki TAMAMURA, Masaaki YOKOYAMA, Shigekazu KUSABAYASHI,* and Hiroshi MIKAWA

Department of Applied Chemistry, Faculty of Engineering, Osaka University, Yamadakami, Suita, Osaka 565

(Received September 3, 1973)

The emission spectrum of an organic charge transfer salt, 2,4,6-triphenylthiopyrylium-1,1,3,3-tetracyanopropenide, was studied in solutions of various solvents as well as in the solid state. A charge transfer fluorescence was observed both in the solid state and in non-polar rigid solution at 77 K, but not in fluid solution. In rigid solution, as the polarity of solvent increases, the charge transfer fluorescence shows a blue shift of its maximum wavelength and a remarkable decrease in intensity, the phosphorescence of a dissociated cation appearing predominantly. The strong dependence of the emission spectrum on the solvent polarity was explained in terms of the dissociation of the salt and the insufficient reorientation of solvent molecules around the salt in the excited charge transfer state.

An organic salt in which a charge-transfer (CT) interaction is present between an anion and a cation, which we have called an organic CT salt, has a predominantly ionic ground state and an excited state consisting of two neutral radical species. A report was given[2] on the CT absorption spectra of some new organic salts consisting of a pyrylium or thiopyrylium cation and a polycyanoacid anion(Fig. 1). The CT absorption spectra of these salts in solution were found to be very solvent sensitive due to two factors. With an increase in solvent polarity (i) the intensity of the CT band decreases by the dissociation of the salt into component ions, and (ii) the CT absorption peak shows a remarkable blue shift, which can be explained by Kosower's theorem.[3-5]

Although extensive studies have been carried out on the absorption spectra of organic CT salts,[2-11] few have been made on the emission spectra.[12] It seems that the solvent effect on the emission spectrum has not yet been elucidated in a wide range of solvent polarity. Of the salts we prepared, 2,4,6-triphenylthiopyrylium (TPT, Fig. 1 (2))-1,1,3,3-tetracyanopropenide (TCP, Fig. 1 (5)) is fairly soluble in various solvents including non-polar ones such as toluene or 1,4-dioxane, and with this we could investigate the solvent effect of the emission spectrum of an organic CT salt in detail. In addition to the temperature dependence of the absorption spectrum of TPT-TCP, we have also examined the emission spectrum of this salt in the solid state and in solutions of various solvents. TPT-TCP in the solid state shows exclusively a CT fluorescence, the emission from the component ion being completely quenched. This is the first example of the CT fluorescence of an organic CT salt in a crystalline solid state. In rigid solution of non-polar solvent at 77 K, the salt also shows a CT fluorescence. The CT fluorescence at 77 K shows a remarkable solvent effect both in intensity and energy. These solvent effects should be understood in terms of the dissociation of the salt in rigid solution and the relaxation behavior of solvent molecules around the CT excited state. In contrast to the case of a rigid solution, TPT-TCP does not show a CT fluorescence when dissolved in fluid solution irrespective of the solvent.

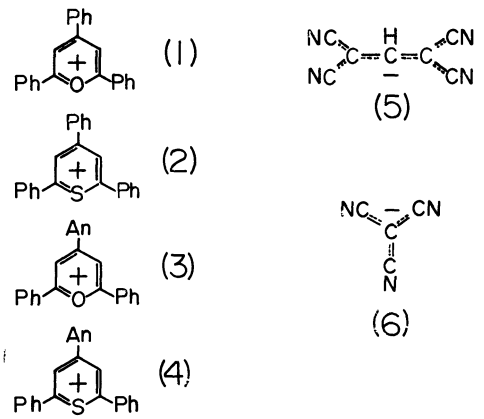

Fig. 1. (1) 2,4,6-triphenylpyrylium (TPP) cation, (2) 2,4,6-triphenylthiopyrylium (TPT) cation, (3) 4-anisyl-2,6-diphenylpyrylium (ADPP) cation, (4) 4-anisyl-2,6-diphenylthiopyrylium (ADPT) cation, (5) 1,1,3,3-tetracyanopropenide (TCP) anion, (6) tricyanomethanide (TCM) anion.

Experimental

The preparation of TPT-TCP and other salts used here have been reported.[2] For the measurement of the emission spectrum in the solid state, the microcrystalline sample was sealed in a pyrex tube (2 mm diameter) under vacuum. Each sample in solution having an appropriate concentration was degassed and sealed in a pyrex tube. All solvents used were purified according to the usual purification method.[13] Emission spectra were recorded on a Hitachi model MPF-3 spectrophotofluorometer equipped with a Xe excitation lamp and an R-446 photomultiplier tube, delayed emissions being measured with a delayed emission accessory including a cylindrical chopper to eliminate prompt emission. The spectra obtained were not corrected both for the excitation source and for the photomultiplier response. Phosphorescence lifetimes were estimated from the decay curves on an oscilloscope. Fluorescence lifetimes were measured by the pulse method with an N_2 gas laser excitation (337 nm, 5 nsec half-width). Absorption spectra were measured with a Hitachi EPS-3 UV spectrophotometer or a Cary model 14 spectrophotometer.

* Present address: Department of Chemical Engineering, Faculty of Engineering, Yamaguchi University, Ube, Yamaguchi.

Results and Discussion

Absorption Spectrum. The absorption spectrum of TPT-TCP in a chloroform solution and the diffuse reflectance spectrum of the salt in the solid state are shown in Figs. 2a and 2b, respectively. These spectra are compared with sodium-TCP and TPT-perchlorate salts in methanol solution and TPT-perchlorate salt in the solid state. The absorption spectrum of TPT-TCP in solution consists mainly of three bands with the maximum wavelength at 350, 390 and 595 nm (Fig. 2a). The 350 and 390 nm bands correspond to the sum of the absorptions of TCP anion and TPT cation, and are assigned to the locally excited (LE) absorption bands of the component ions of the salt. Another absorption band at 595 nm is assigned to an interionic CT band, since it does not appear either in sodium-TCP or TPT-perchlorate salts where a CT interaction is absent between the cation and the anion. In the solid state, the corresponding CT absorption band is observed near 540 nm (Fig. 2b).

In order to understand the low temperature emission spectrum, the absorption spectrum was studied at low temperatures. The CT band shows a considerable blue shift as the temperature is lowered. The absorption spectra of TPT-TCP in 2-methyltetrahydrofuran (2MTHF)-toluene (9 : 1) solution at various temperatures are shown in Fig. 3. At 77 K, the LE bands of the component ions become sharp, but show no shift in maximum wavelength as compared with that at room temperature. The CT absorption maximum, however, shows a blue shift of 45 nm at 227 K and 120 nm at 77 K from the position of this band at room temperature. A consiberable decrease in absorbance of the CT band occurs together with the blue shift. Such a shift was observed in dichloromethane solutions of some alkylpyridinium-halide salts by Brinen *et al.*,[12] but they did not discuss the reason for this. We conclude that the blue shift is due to the increase of solvent polarity at low temperatures.

The maximum wavelength (λ_{max}) and the apparent molar extinction coefficients (ε_{app}) of the CT band of TPT-TCP in various solvents *at room temperature* are given in Table 1. With the increase of solvent polarity, the CT band shows a remarkable blue shift of λ_{max} and a decrease in ε_{app}. Since the energy of the CT band maximum shows a linear dependence on the

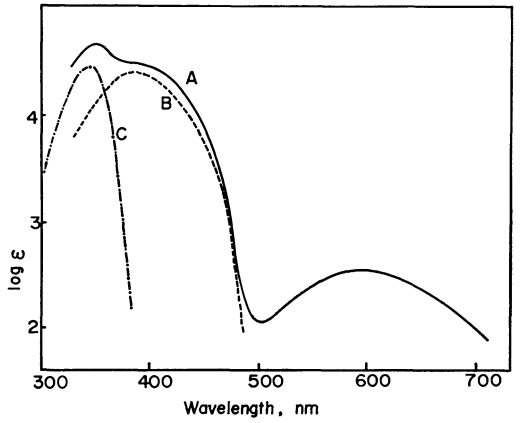

Fig. 2(a). Absorption spectra of TPT-TCP salt in chloroform solution and of its component ions.
(A) TPT-TCP in $CHCl_3$, (B) TPT-perchlorate in CH_3OH, (C) sodium-TCP in CH_3OH.

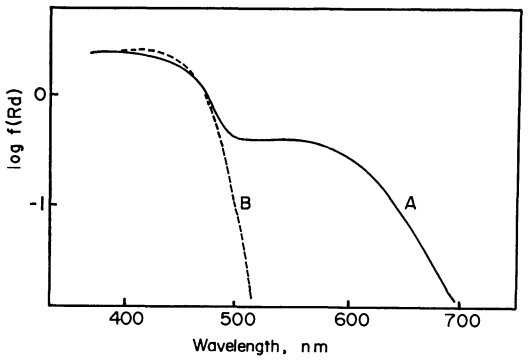

Fig. 2(b). Diffuse reflectance spectra of TPT-TCP and TPT-perchlorate salts in the solid state.
(A) TPT-TCP, (B) TPT-perchlorate.

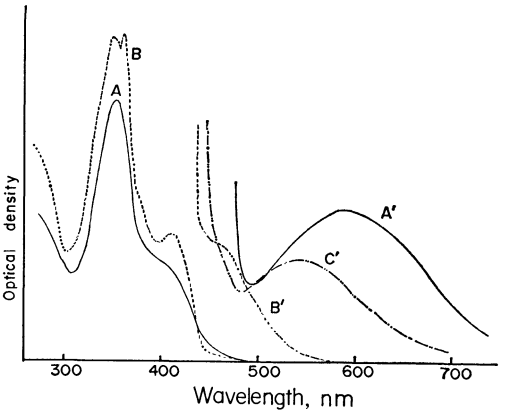

Fig. 3. Absorption spectra of TPT-TCP salt in 2MTHF-toluene (9 : 1) solution at various temperatures.
(A) 4.0×10^{-5} mol/l, room temperature, (A') 2.0×10^{-3} mol/l, room temperature, (B) 4.0×10^{-5} mol/l, 77 K, (B') 2.0×10^{-3} mol/l, 77 K, (C') 2.0×10^{-3} mol/l, 223 K.

Table 1. Solvent effect of the CT absorption band of TPT-TCP at room temperature

Solvent	D	Z-value (kcal/mol)	λ_{max} (nm)	ε_{app}
1,4-Dioxane	2.21	58.3	635	550
Toluene	2.38	55.4	660	525
Chloroform	4.70	63.2	595	370
Ethyl acetate	6.03	57.6	583	240
Acetic acid	6.15	79.2	510	180
2MTHF	7.0	65.0	585	220
Dichloromethane	8.9	64.2	575	100
1,2-Dichloroethane	10.37	62.7	568	70
Benzyl alcohol	13.6	—	—[a]	—
Isopropyl alcohol	16.3	76.3	—[a]	—

a) The CT absorption band did not appear appreciably in this solvent.

Z-value of the solvent, or the empirical parameter of the solvent polarity,[3-5] the shift can be explained on the basis of Kosower's theorem. On the other hand, the decrease in ε_{app} is caused by the dissociation of an ion-pair, $D^-A^+ \rightarrow D^- + A^+$, where D^-A^+ is an ion-pair and D^- and A^+ are dissociated component ions. ε_{app} is more closely related to the dielectric constant (D) of solvent than to the Z-value (Table 1). The CT absorption peak is not conspicuous in the solvents with $D>10$ at room temperature, probably due to the almost complete dissociation of the ion-pair. Thus, the temperature dependence of the CT band shown in Fig. 3 can be understood phenomenologically in terms of the change in the solvent polarity with temperature.

It is known that the polarity of solvent increases with the lowering of temperature because of the enhanced orientation of the solvent dipole. Furutsuka *et al.* reported that the value of D of 2MTHF at 298, 223, just above the glass transition temperature (108 K), and below 108 K are 7.0, 9.0, 18.0, and 3.5, respectively.[14] Thus, the dielectric constant increases with the lowering of temperature down to the glass transition temperature. Even near the glass transition temperature of 2MTHF–toluene (9 : 1), the solvent molecules around the salt are expected to be in a well-oriented state. Although the D value of solvent is very small below glass transition temperature, the local solvent orientation around the salt may be kept even in the frozen state. The Z-value of the solvent, therefore, may increase with the lowering of temperature, and may not decrease even in a glass. From the result shown in Fig. 3, the Z-value of 2MTHF–toluene (9 : 1) at room temperature, 223, and 77 K can be estimated to be about 64, 72, and 88 kcal/mol. Thus the blue shift and the decrease of absorbance of the CT band can be accounted for by the increase of solvent polarity in a low temperature region.

Emission Spectrum in the Cyrstalline State. Although sodium–TCP gives no emission, TPT–perchlorate salt shows an emission both in solution and in the solid state. The emission and excitation spectra of TPT–TCP and TPT–perchlorate salts in the solid state at room temperature are given in Fig. 4. The emission of the perchlorate salt in the solid state is also found in fluid solution. This is assigned to the fluorescence of TPT cation by its lifetime in solution (a few ns), the mirror image relationship between the absorption and emission bands of the cation, and the excitation spectrum which approximately agrees with the absorption spectrum.

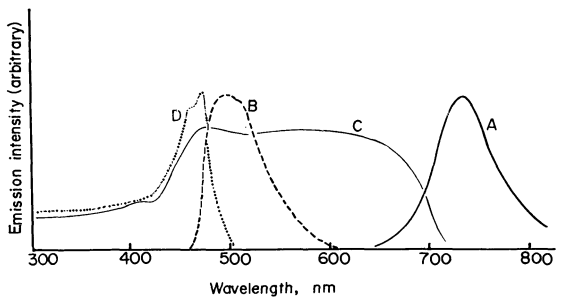

Fig. 4. Emission spectra of TPT-TCP and TPT-perchlorate salts in the crystalline state.
(A) emission spectrum of TPT-TCP, (B) emission spectrum of TPT-perchlorate, (C) excitation spectrum of the emission of TPT-TCP at 740 nm, (D) excitation spectrum of the emission of TPT-perchlorate at 500 nm.

In TPT–TCP in the solid state, the fluorescence of TPT cation was not found, and a new emission was observed at 740 nm which can be assigned to an interionic CT fluorescence for the following reasons: (i) the mirror image relationship with CT absorption holds, (ii) the emission can be found by irradiation not only in the LE band but also in the CT absorption band, (iii) the lifetime is much shorter than 100 μsec. The excitation spectrum of the emission (Fig. 4) does not coincide with the diffuse reflectance spectrum in Fig. 2b. This might be due to the insufficient transmission of the incident light into the microcrystalline sample.

The above assignment is confirmed by the fact that such an emission band is also found in the solid state of other organic CT salts (Fig. 1). The maximum wavelengths of the CT absorption and CT fluorescence bands of these salts are given in Table 2. An approximately parallel relationship is found between the energies of the absorption and emission bands. Thus, when a CT interaction is present, the fluorescence of the component ion is completely quenched and a CT fluorescence is observed in the solid state.

TABLE 2. MAXIMA OF THE CT FLUORESCENCE (λ^F_{max}) AND THE CT ABSORPTION BAND (λ^A_{max}) IN THE SOLID STATE

Salts	λ^F_{max} (nm)	λ^A_{max} (nm)
TPP-TCP	725	565
TPT-TCP	740	540
ADPP-TCP	640	530 (S)
ADPT-TCP	710	560 (S)
TPP-TCM	680	530
TPT-TCM	620	520 (S)
ADPP-TCM	670	520 (S)

(S): shoulder

Emission Spectrum in Fluid Solution. The emission spectrum of TPT–TCP in fluid solution was measured at room temperature in various solvents in various concentrations. In all cases, the fluorescence of TPT cation was observed, but not CT fluorescence. The intensity of the fluorescence of the cation was very sensitive to the solvent polarity, becoming weak with the decrease of the solvent polarity (Fig. 5). This suggests that the fluorescence of the cation is emitted only from the free TPT cation present in solution, and that the amount of the free cation produced by the dissociation of the ion-pair becomes small in a less polar solvent. This is supported by the fact that the excitation spectrum of this emission agrees with the absorption of TPT cation.

Thus, in fluid solution TPT–TCP shows only the fluorescence of the free TPT cation and no emission from the undissociated ion-pair. This is in sharp contrast to the observation of the CT fluoerscence of

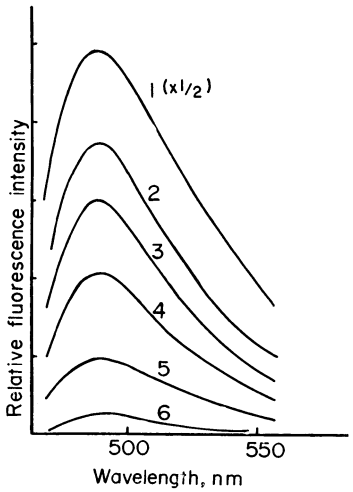

Fig. 5. Solvent effect of the emission spectrum of TPT-TCP salt in fluid solution at room temperature. (1) 2MTHF-C_2H_5OH (2 : 1), (2) 2MTHF, (3) 2MTHF-toluene (9.8 : 0.2), (4) 2MTHF-toluene (9.5 : 0.5), (5) 2MTHF-toluene (8 : 2), (6) 1,4-dioxane.

TPT-TCP in the solid state. In fluid solution the CT excited energy can be deactivated without radiation because of the interionic CT interaction.[15] Similarly, an ordinary molecular CT complex does not show a CT fluorescence even in non-polar solvents except for a few rare cases. This could be understood in terms of an extremely low transition probability of a CT complex in fluid solution.[16–18]

It should be noted that with TPT-TCP the following case is also conceivable: A CT fluorescence emitted near the IR region could not be observed because of the limitation of the spectrofluorometer in the wavelength region longer than 800 nm. In *s*-tetracyanobenzene-polymethylbenzene complexes in which a CT fluorescence can be found in fluid solution, the Stokes shift of the CT transition at room temperature is 8000—12000 cm^{-1}, which is much larger than that in rigid solution at 77 K (4500—8300 cm^{-1}).[17,18] In TPT-TCP the Stokes shift in 2MTHF-toluene (9 : 1) rigid solution at 77 K is estimated to be 4200 cm^{-1}. If the Stokes shift at room temperature were greater than 6000 cm^{-1} as in tetracyanobenzene complexes, the CT fluorescence would have its maximum above 800 nm, which could not be detected by our apparatus.

Emission Spectrum in Rigid Solution at 77 K. The emission spectrum of TPT-TCP in rigid solution is also affected by the nature of the solvent. In a polar solvent, methanol-ethanol(1 : 1), it is essentially the same as that of TPT-perchlorate under the same conditions (Fig. 6). The emission band at 460 nm is the fluorescence of the cation. An emission band at 540 nm is assigned to the phosphorescence of TPT cation, since it is found as a delayed emission of the perchlorate salt at 77 K, its lifetime being about 30 ms. Since in this solvent TPT-TCP dissociates completely into two component ions, the two emissions originate from the free TPT cation present in rigid solution.

The emission spectra of TPT-TCP in a less polar 2MTHF-toluene (9 : 1) solution are shown in Fig. 7.

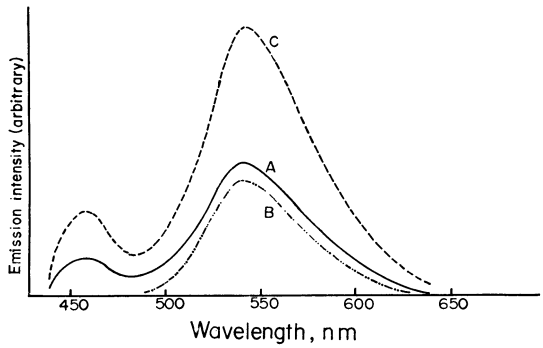

Fig. 6. Emission spectra of TPT-TCP and TPT-perchlorate salts in CH_3OH-C_2H_5OH (1 : 1) rigid solution at 77 K.
(A) total emission of TPT-TCP at 77 K, (B) delayed emission of TPT-TCP, (C) total emission of TPT-perchlorate.

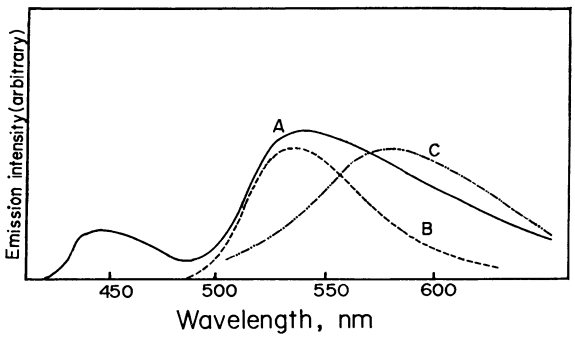

Fig. 7. Emission spectrum of TPT-TCP salt in 2MTHF-toluene (9 : 1) solution at 77 K.
(A) total emission by excitation at 420 nm, (B) delayed emission by excitation at 420 nm, (C) total emission by excitation at 470 nm.

In the case of the excitation of the LE band of the cation, the emission band at 540 nm becomes broad with a new emission around 600 nm. On the excitation of the CT band in rigid solution (at 470 nm), only the new emission was observed at 585 nm. The band can be assigned to the interionic CT fluorescence of TPT-TCP for the following reasons; (i) the lifetime is about 170 ns, (ii) a mirror image relationship holds between this emission band and the CT absorption band shown in Fig. 3, (iii) the Stokes shift of this transition, about 4200 cm^{-1}, is comparable with that of ordinary molecular CT complexes in rigid solution.[19]

The relative intensities of the three emission bands, the fluorescence and phosphorescence of the cation and the CT fluorescence, are very sensitive to solvent polarity. The total emission spectra of TPT-TCP by 420 nm excitation are shown in Fig. 8 for various compositions of 2MTHF-toluene solvent system. In a more polar solvent the phosphorescence of the cation is predominant over the CT fluorescence, while in a less polar solvent the CT fluorescence predominates. The relative intensity of the phosphorescence of the cation is plotted against the solvent composition in Fig. 9. The intensity of the phosphorescence is reduced strikingly with the addition of toluene, its lifetime remaining almost unchanged. Upon direct excitation of the CT absorption band, no phosphores-

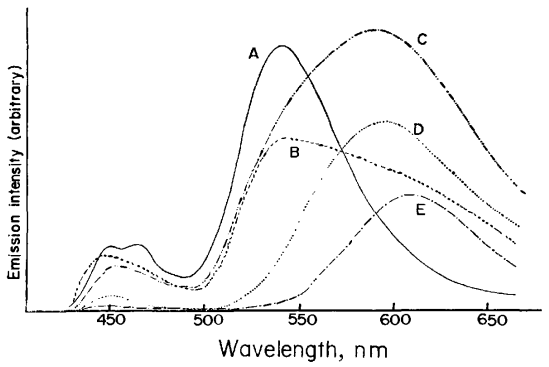

Fig. 8. Emission spectra of TPT-TCP salt in various compositions of 2MTHF-toluene solvent system at 77 K by excitation at 420 nm.
(A) 2MTHF, (B) 2MTHF-toluene (9 : 1), (C) 2MTHF-toluene (8 : 2), (D) 2MTHF-toluene (6.5 : 3.5), (E) 2MTHF-toluene (2 : 8).

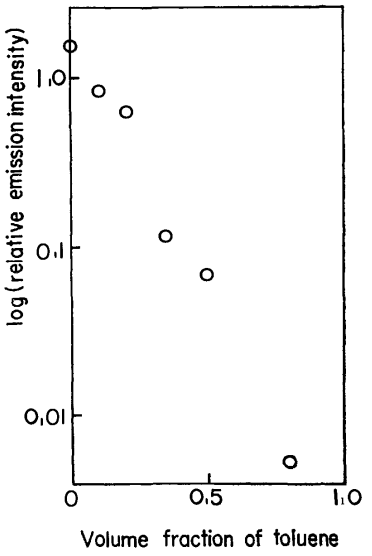

Fig. 9. Relative phosphorescence intensity of TPT cation against the solvent composition of 2MTHF-toluene.

cence of the cation be can observed. This indicates that even in a non-polar solvent the phosphorescence of the cation is emitted only from the dissociated free cation. Thus the dependence of the emission spectrum on the solvent polarity shown in Fig. 8 can be accounted for by the variation of the relative amount of the free TPT cation due to dissociation. This shows that the solvent polarity similar to that of 2MTHF-toluene (9 : 1) is required for the dissociation of the salt in rigid solution. This appears to correspond to the fact that in solution at room temperature the salt dissociates almost completely into two component ions in the solvent with $D>10$.

In the case of some molecular CT complexes, phosphorescence emission often occurs from the lowest CT triplet state which is generated by the intersystem-crossing *via* the CT singlet excited state. CT phosphorescence in particular which is similar to that of the component molecule, is observed in some complexes such as *s*-tetracyanobenzene–naphthalene complex.[20] In TPT-TCP, however, this is not possible since the energy of the phosphorescence is much higher than that of the CT fluorescence.

The solvent polarity is a very important factor in determining the emission spectrum of the interionic CT salt, the degree of dissociation of the salt being primarily determined by this factor. The solvent polarity also has an effect on the maximum wavelength and the lifetime of the CT fluorescence. The maximum wavelengths and lifetimes of the CT fluorescence, and the maximum wavelengths of the CT absorption in various solvents are listed in Table 3. Accurate determination of the maximum of the CT fluorescence is difficult with the excitation in the LE bands, since both the CT fluorescence and the phosphorescence of the cation are observed simultaneously. Thus, the maximum wavelengths given in Table 3 were determined by the excitation of the CT absorption band. The fluorescence lifetimes, however, were measured on the excitation at 337 nm of an N_2 gas laser.

TABLE 3. MAXIMUM WAVELENGTH (λ^{F}_{max}) AND LIFETIME (τ_F) OF CT FLUORESCENCE AT 77 K AND MAXIMUM WAVELENGTH (λ^{A}_{max}) OF THE CT ABSORPTION BAND IN VARIOUS SOLVENTS

Solvent	λ^{F}_{max} [a] (nm)	τ_F [b] (ns)	λ^{A}_{max} at 70 K (nm)	λ^{A}_{max} at 293 K (nm)
2MTHF	585	150	460(S) [c]	585
2MTHF-toluene (9 : 1)	585	170	470	590
2MTHF-toluene (8 : 2)	590	240	—	595
2MTHF-toluene (6.5 : 3.5)	596	290	—	603
2MTHF-toluene (5 : 5)	600	—	—	625
2MTHF-toluene (2 : 8)	610	330	—	635
1,4-Dioxane [d]	635	—	—	635

a) By CT absorption band excitation at 470 nm at 77 K. b) By N_2 gas laser excitation at 337 nm at 77 K. c) Shoulder. d) In a cloudy solid at 77 K.

The increase of solvent polarity causes a blue shift of the CT fluorescence. Its amount is comparable with that of the CT absorption maximum resulting from the increase of the solvent polarity in solution at room temperature. A CT fluorescence of organic CT salts in rigid solution has been reported by Brinen *et al.* on some alkylpyridinium–halide salts.[12] They observed the CT fluorescence of the salts in three solvents, *i.e.*, water, methanol–ethanol (1 : 4), and dichloromethane, and found no solvent effect on the energy of the CT fluorescence. Thus, our result is quite different from that for alkylpyridinium salts.

As a CT salt has an ionic ground state, an ion-pair is strongly solvated in the ground state. Even in Franck-Condon state, the salt is still strongly solvated, despite the fact that the components of the salt are neutral in the excited state. Brinen *et al.* suggested that the solvent-solute reorientation occurs during the relaxation of the excited state from the Franck-Condon state to a fluorescent CT state even in rigid solution. However, Kobayashi *et al.* have shown that in *s*-tetracyanobenzene complexes this kind of reorientation

does not occur sufficiently during the relaxation in rigid solution at 77 K.[18] Our present observation of the blue shift of the CT fluorescence also suggests that the reorientation of the solvent molecules is insufficient at 77 K, and that the salt in the CT fluorescent state is still solvated in a similar fashion to that in the ground state. If the CT fluorescence of this salt could be observed in fluid solution, the energy would remain constant independent of the solvent polarity, since the reorientation of the solvent molecules would occur sufficiently in fluid solution.

The lifetime of the CT fluorescence becomes long with the decrease of solvent polarity. The increase of lifetime may be caused by the decrease of the radiative transition probability or the decrease of the radiationless transition probability of the excited ion-pair. If the emission probability decreases, the quantum efficiency of the CT fluorescence would show a considerable decrease corresponding to the increase of the fluorescence lifetime. Although the quantum efficiency of the CT fluorescence cannot be determined, since the concentration of the undissociating ion-pair in rigid solution is unknown, such a decrease of intensity of the CT fluorescence was not observed. This suggests that the dependence of the fluorescence lifetime is attributable to the decrease of the radiationless transition probability of the excited ion-pair in a less polar solvent.

References

1) Part III of this series, T. Tamamura, H. Yasuba, K. Okamoto, T. Imai, S. Kusabayashi, and H. Mikawa, This Bulletin, **47**, 448 (1974).
2) H. Yasuba, T. Imai, K. Okamoto, S. Kusabayashi, and H. Mikawa, This Bulletin, **43**, 3101 (1970).
3) E. M. Kosower, *J. Amer. Chem. Soc.*, **80**, 3253, 3261 (1958).
4) E. M. Kosower and G. S. Wu, *ibid.*, **83**, 3142 (1961).
5) E. M. Kosower, G. S. Wu, and T. S. Sorensen, *ibid.*, **83**, 3147 (1961).
6) E. M. Kosower, *ibid.*, **77**, 3883 (1955).
7) E. M. Kosower, J. A. Skorcz, W. M. Schwarz, and J. W. Pattor, *ibid.*, **82**, 2188 (1960).
8) S. F. Mason, *J. Chem. Soc.*, 2437 (1960).
9) E. L. Goff and R. B. Laccount, *J. Amer. Chem. Soc.*, **85**, 1354 (1963).
10) A. T. Balaban, M. Mocanu, and Z. Simon, *Tetrahedron*, **20**, 119 (1964).
11) S. Sakanoue, T. Tamamura, S. Kusabayashi, H. Mikawa, N. Kasai, M. Kakudo, and H. Kuroda, This Bulletin, **42**, 2407 (1969).
12) J. S. Brinen, J. G. Koren, H. O. Olmsteaed, and R. C. Hirt, *J. Phys. Chem.*, **69**, 3791 (1965).
13) J. A. Riddich and E. E. Troops, *Jr.*, "Technique of Organic Chemistry," Vol. 7, Organic Solvents, Interscience Publishers, Inc., New York (1955).
14) T. Furutsuka, T. Imura, K. Kawabe, and T. Kojima, *Technology Reports of the Osaka University*, **24** (1973), in press.
15) T. G. Beaumont and K. M. C. Davis, *J. Chem. Soc.*, (B), 456 (1970).
16) J. Prochorow and R. Sieogoczyński, *Chem. Phys. Lett.*, **3**, 635 (1969).
17) N. Mataga and Y. Murata, *J. Amer. Chem. Soc.*, **91**, 3144 (1969).
18) T. Kobayashi, K. Yoshihara, and S. Nagakura, This Bulletin, **44**, 2603 (1971).
19) J. Czekalla, G. Briegleb, and W. Herr, *Z. Electrochem.*, **63**, 712 (1959).
20) S. Iwata, J. Tanaka, and S. Nagakura, *J. Chem. Phys.*, **47**, 2203 (1967).

Organic Charge Transfer Salts. III.[1] Photoconductive and Magnetic Properties of Organic Charge Transfer Salts

Toshiaki TAMAMURA, Hiroshi YASUBA,* Kenichi OKAMOTO,** Tatsuro IMAI,*** Shigekazu KUSABAYASHI,** and Hiroshi MIKAWA

Department of Applied Chemistry, Faculty of Engineering, Osaka University, Yamadakami, Suita, Osaka 565

(Received September 17, 1973)

The photoconductive and semiconductive properties of some organic charge-transfer (CT) salts consisting of a pyrylium or thiopyrylium cation and a polycyanoacid anion were investigated in single crystals. The salts are poor semiconductors with a resistivity of $10^{10}-10^{12}$ ohm·cm at room temperature, but show relatively large photoconduction when irradiated with monochromatized light in the interionic CT absorption band. There is a strong possibility that the photocarrier is intrinsic in nature, being generated spontaneously from the excited CT state. A weak ESR signal observed originally in these salts increased on the CT band or near IR excitation. From the relationship between the darkcarriers, photocarriers, paramagnetic species and the excited CT state, a mechanism of electrical conduction is proposed in which the carrier generation by the CT interaction and the carrier migration by trapping conduction are involved.

Organic charge-transfer (CT) salts are a class of ionic compounds consisting of organic cation and anion, having CT interaction between the component ions. In order to elucidate the role of the interionic CT interaction in them, we have studied the physical properties[1,2] of new organic CT salts consisting of a pyrylium or thiopyrylium cation and a polycyanoacid anion (Fig. 1). We have investigated the photoconductive and semiconductive properties as well as the magnetic properties.

Although photoconduction has been found in several weak molecular CT complexes having low dark conductivity,[3-6] the photocarrier generation in most cases has been considered to be extrinsic in nature, an intrinsic carrier generation not being proved in any of the cases. With weak molecular CT complexes, Akamatu and Kuroda discussed the relationship between the conduction state and the excited CT state.[3] They suggested that a difference of energy equivalent to that necessary for the separation of the excited CT state into free ions, that is, the separation of a D^+A^- ion-radical pair into two charge carriers might prevent the intrinsic carrier generation. However, in the case of an interionic CT salt, the excited CT state might consist of two neutral radical species, D·A·, and the carrier separation from the CT state would be easier than in the case of a weak molecular CT complex. Thus, in an organic CT salt, the possibility of intrinsic carrier generation by the CT excitation is expected.

Actually, all the CT salts studied showed a photocurrent about ten times larger than the dark current on irradiation at the CT absorption band. A weak ESR signal, which seems to originate from the charge carriers in the dark conduction, was enhanced on the CT and near IR excitations. From the results obtained on the electrical and magnetic properties, we will discuss the mechanism of electrical conduction and the possibility of the intrinsic carrier generation in organic CT salts.

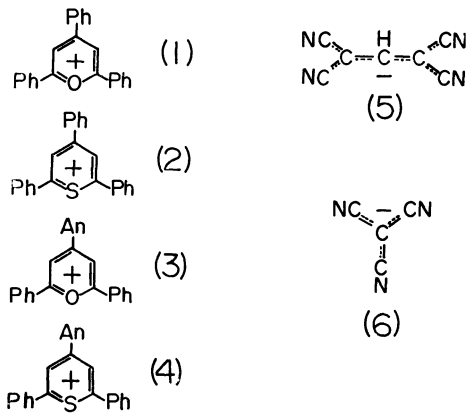

Fig. 1. (1) 2,4,6-triphenylpyrylium (TPP) cation, (2) 2,4,6-triphenylthiopyrylium (TPT) cation, (3) 4-anisyl-2,6-diphenylpyrylium (ADPP) cation, (4) 4-anisyl-2,6-diphenylthiopyrylium (ADPT) cation, (5) 1,1,3,3-tetracyanopropenide (TCP) anion, (6) tricyanomethanide (TCM) anion.

Experimental

Materials. Crystals of the organic CT salts(Fig. 1) were prepared as described previously.[2] The salt was purified by recrystallization at least three times. Vacuum sublimation or zone refining could not be used because of decomposition of the salt. Single crystals of the CT salts, dimensions about $2\times1\times0.5$ mm, were grown from methanol–water (4 : 1) or methanol solution. However, except for TPT-perchlorate, single crystals of the perchlorate salts of other cations could not be obtained.

Conductivity Measurement. The apparatus for the measurement of the dark- and photo-conduction is shown in Fig. 2. The DC conductivity was measured with a Takeda-Riken vibrating reed electrometer, type TR-81. Temperature was controlled by passing cold nitrogen gas or heated air around a single crystal sample, and was monitored with a thermocouple. The light from a 500 W Xe lamp, arc current 20 A, was monochromatized with a monochromator. The energy distribution and the absolute light intensity of the Xe lamp were shown previously.[7] In order to investigate

* Present address: Wireless Research Laboratories, Matsushita Electric Industrial Co. Ltd., Kadoma, Osaka

** Present address; Department of Chemical Engineering, Faculty of Engineering, Yamaguchi University, Ube, Yamaguchi

*** Present address; Nippon Paint Co. Ltd., Shinagawa-ku, Tokyo

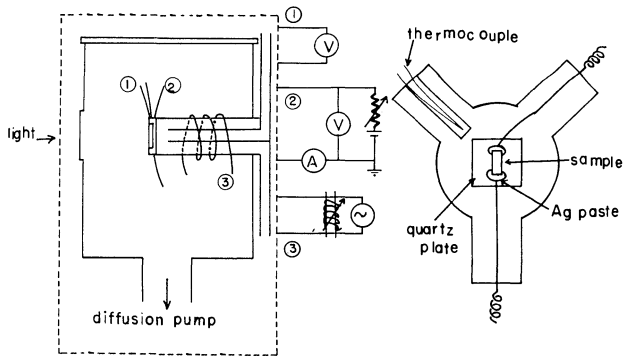

Fig. 2. Apparatus for the conductivity measurements.

the light intensity dependence of the photocurrent, neutral filters of known transmittance were inserted between a sample and a monochromator. A single crystal was placed on a quartz plate with Ag paste, which was used as electrodes (Fig. 2). In the case of TPP-perchlorate, a compressed pellet of powder crystals was used. The voltage-current characteristics were ohmic in all samples up to 200 V applied voltage, no photovoltaic current being observed when no voltage was applied. This indicates that the choice of electrode is adequate, and carrier injection from or to the Ag paste electrode is negligible. All conductivity measurements were performed both in dry air at one atmosphere and in a vacuum at 10^{-4}—10^{-5} mmHg.

ESR Measurement. The electron spin resonance measurement was carried out with an X band, JES-ME2X type spectrometer (Japan Electron Optics Laboratory Co. Ltd.) with a double mode cavity. A microcrystalline sample was packed in a quartz tube in air and in a vacuum at 10^{-2} mmHg. The concentration of unpaired spins of a salt was estimated by comparing its intensity with that of a DPPH sample. DPPH(Wako, pure grade) was purified by repeated recrystallizations from CS_2 or petroleum ether (a fraction of bp< 40 °C) solutions. The benzene solution or the powder sample dispersed in KCl (Merck, ultra pure grade, dried over 2 days at 200 °C in vacuum) was used as a reference substance of known concentration of unpaired spins. Temperature was varied by passing cold nitrogen gas or heated air into the cavity, and was monitored with a thermocouple attached around a sample tube in the cavity. The *g*-value of the unpaired spins in a salt was determined from the *g*-value of Mn^{2+} in a MgO sample.[8] For the measurement of photo-ESR absorption, a 500 W Xe lamp of 20 A was used. The spectral dependence of photo-ESR absorption was roughly estimated by combining several color glass filters of known transmittance at various wavelengths, since the light from a monochromator was too weak for observation of ESR absorption change.

Results

Dark Conductivity and Photoconductivity. The organic CT salts are semiconducting with resistivity in the range 10^{10}—10^{12} ohm·cm at room temperature. On irradiation with a visible light, a photocurrent of *ca.* 10 times greater magnitude than the dark current was observed.

The light intensity dependence of the photocurrent obeyed $i_{ph}=a\cdot L^n$, where L is the incident light intensity, a and n are the constants. This relation is given in Fig. 3 and the results in Table 1. The value of n appears to be independent of the presence of air, being

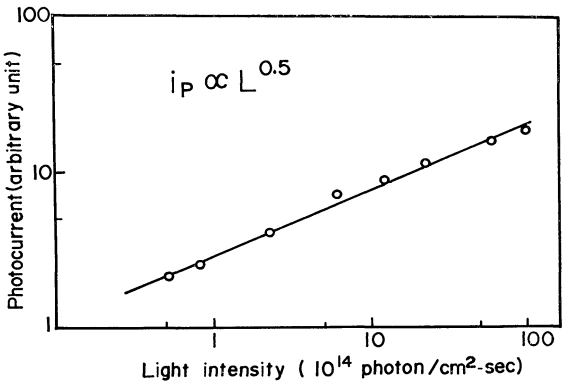

Fig. 3. Light intensity dependence of photocurrent at 650 nm of TPT-TCP salt.

Table 1. Light intensity dependence of photocurrent of organic CT salts

Salts	n in $i_{ph}=a\cdot L^n$		λ_{ex} (nm)[a]
	in vacuum	in air	
TPP-TCP	0.5	0.5	600
TPT-TCP	0.6	0.5	650
TPP-TCM	0.6	0.8	600
TPT-TCM	0.7	0.7	650
ADPP-TCP	—	0.6	600
ADPT-TCP	—	0.5	600
ADPP-TCM	—	0.5	600
TPT-ClO_4	0.4	0.4	500

a) wavelength of illuminating light.

0.5 for all salts.

The spectral dependence of the photoconduction is shown in Figs. 4 (a—d) for several salts, together with the corresponding absorption spectra. Large absorption bands near 400 nm are the locally excited (LE) bands of the component ions.[2] A relatively weak and broad absorption band observed near 550 nm in each CT salt but not in the corresponding perchlorate salt of the cation is assigned to the interionic

Table 2. Specific resistivity (ρ_d) in the dark at room temperature, photoconduction maximum wavelengths (λ_{max}^{ph}) and absorption maximum wavelengths (λ_{max}^{ab}) of organic CT salts

Salts	ρ_d (ohm·cm)	λ_{max}^{ph} (nm)	λ_{max}^{ab} (nm) CT band[a]	LE band[b]
TPP-TCP	10^{11}	640, 500	565	410
TPT-TCP	10^{11}	640, 500	540	390
TPP-TCM	10^{10}	580	530	410
TPT-TCM	10^{11}	600	520(S)[d]	390
ADPP-TCP	10^{12}	580, 520	530(S)	435
ADPT-TCP	10^{10}	620, 520	560(S)	430
ADPP-TCM	10^{11}	630, 520	520(S)	435
TPP-ClO_4[c]	10^{12}	500	—	410
TPT-ClO_4	10^{12}	500	—	390

a) measured by diffuse reflectance spectrum in solid state. b) the lowest LE band of the cation in absorption spectrum in CH_3OH solution. c) measured in a compressed pellet of powder crystals. d) shoulder.

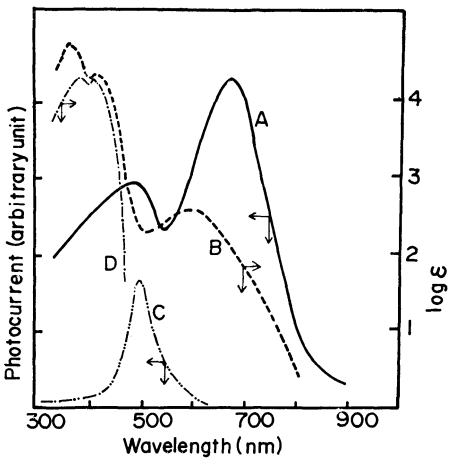

Fig. 4a. Spectral dependence of photocurrent and absorption spectra of TPP-TCP and TPP-perchlorate salts.
(A) photoconduction spectrum of TPP-TCP, (B) absorption spectrum of TPP-TCP in $CHCl_3$ solution, (C) photoconduction spectrum of TPP-ClO_4, (D) absorption spectrum of TPP-ClO_4 in CH_3OH solution.

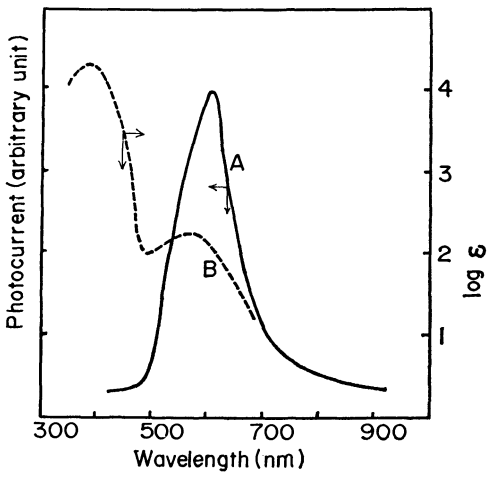

Fig. 4b. Spectral dependence of photocurrent and absorption spectrum of TPP-TCM salt.
(A) photoconduction spectrum, (B) absorption spectrum in $CHCl_3$ solution.

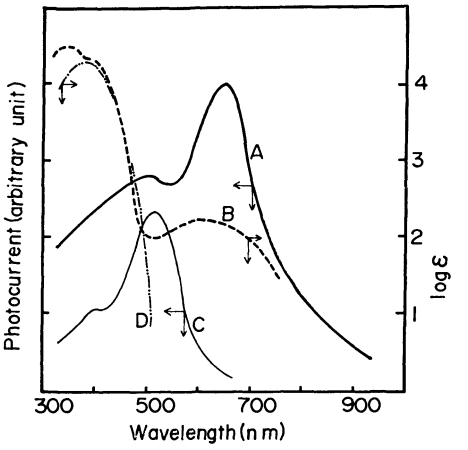

Fig. 4c. Spectral dependence of photocurrent and absorption spectra of TPT-TCP and TPT-perchlorate salts.
(A) photoconduction spectrum of TPT-TCP, (B) absorption spectrum of TPT-TCP in $CHCl_3$ solution, (C) photoconduction spectrum of TPT-ClO_4, (D) absorption spectrum of TPT-ClO_4 in CH_3OH solution.

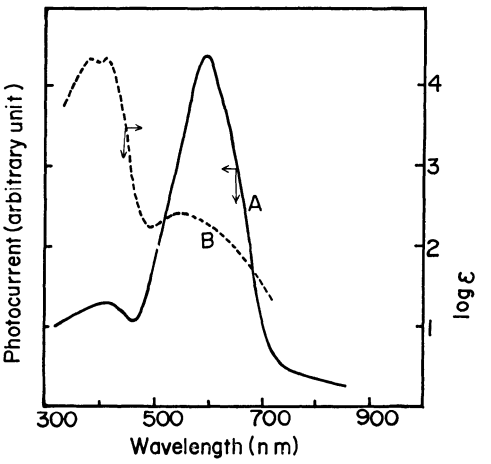

Fig. 4d. Spectral dependence of photocurrent and absorption spectrum of TPT-TCM salt.
(A) photoconduction spectrum, (B) absorption spectrum in $CHCl_3$ solution.

CT absorption band. Each photoconduction spectrum is normalized to the light intensity at 360 nm. The resistivity in the dark, and the maximum wavelengths of the photoconduction and the absorption are summarized in Table 2. A large photoconduction peak was observed in all CT salts in the long wavelength side of the CT absorption band (Fig. 4 and Table 2). In TPP-TCP (Fig. 4a) and TPT-TCP (Fig. 4c), another smaller photoconduction peak was observed at the absorption edge of the LE band of the cation. However, it was not seen clearly in TPP-TCM (Fig. 4b) and TPT-TCM (Fig. 4d), perhaps because it was hidden by the large peak. In TPP-ClO_4 and TPT-ClO_4, in which CT interaction is absent between the cation and the anion, only the small peak was found. This indicates that the large photoconduction peak is due to the excitation at the CT band, and the small one to the local excitation of the cation. A relatively small photocurrent was observed when a CT salt was illuminated with a light in the near IR region (800—1100 nm). This may be due to the presence of the deep traps of charge carriers. The spectral dependence curve was reproducible in repeated measurements, and did not depend on the sample of single crystals. The effect of air on the photoconduction spectra was very small.

A typical time response curve of the photocurrent is given in Fig. 5 for TPT-TCP salt. Upon excitation in the CT band (650 nm), the photocurrent increased immediately and rapidly reached a steady state value. When the excitation was removed, the photocurrent decayed rapidly with a considerably long tail, approaching the initial value of the dark current. This suggests that the photoconduction by CT excitation is not strongly limited by charge carrier traps, although shallow traps are present in the crystal. The excita-

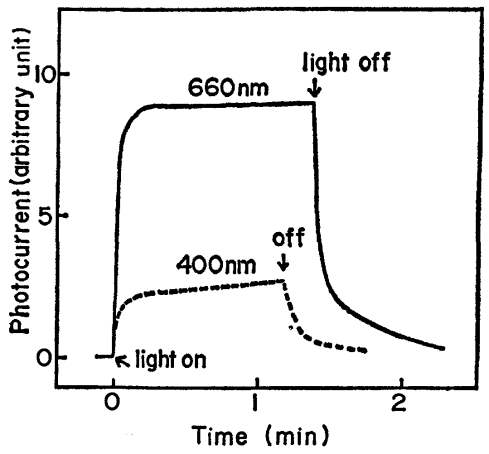

Fig. 5. Time response curves of photocurrent of TPT-TCP salt in vacuum at room temperature.

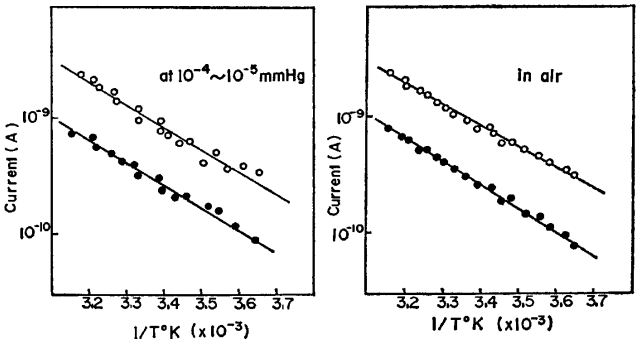

Fig. 6. Temperature dependence of dark current and photocurrent at 650 nm of TPT-TCP salt in vacuum and in air.
—●— dark current, —○— photocurrent.

Table 3. Activation energies of dark and photoconductivities of organic CT salts

Salts	E_{ad} (eV) in vacuum	E_{ad} (eV) in air	E_{aph} (eV) in vacuum	E_{aph} (eV) in air	λ_{ex}[a] (nm)
TPP-TCP	0.6	0.5	0.6	0.6	600
			0.6	0.5	1000
TPT-TCP	0.4	0.4	0.45	0.4	650
			0.5	0.5	1000
TPT-TCM	0.9	0.8	0.8	0.7	600
ADPP-TCP	—	0.45	—	0.45	600
ADPT-TCP	—	0.6	—	0.6	600
ADPP-TCM	—	0.45	—	0.35	600
TPT-ClO_4	1.2	0.9	1.2	0.9	500
			1.2	0.9	1000

a) wavelength of illuminating light.

tion at 450 nm caused a slightly slower response of the photocurrent.

The temperature dependence of the dark conduction and photoconduction was investigated between 273—323 K. Both for dark- and photocurrents, $i = i_0\exp(-E_a/kT)$ holds. A typical result is given in Fig. 6 for TPT-TCP salt both in vacuum and in air. The activation energy E_a of the photocurrent, 0.45 eV in vacuum and 0.4 eV in air, is approximately the same as that of the dark current, 0.4 eV both in vacuum and in air. The photocurrent at 1000 nm had also essentially the same activation energy 0.5 eV as the photocurrent at 650 nm. The other salts gave essentially the same results (Table 3).

ESR Absorption. A weak ESR signal observed initially in perchlorate salts of TPP and TPT cations disappeared by recrystallization of the salts. Therefore, all CT salts were prepared carefully from the corresponding perchlorate salt which gave no ESR signal. Even when prepared in this way, CT salts showed a single broad ESR absorption band which showed no marked change by further recrystallizations. This indicates that the absorption is not due to impurities. As an illustration, the ESR signal of TPT-TCP salt is given in Fig. 7. The *g*-values and the total spin concentrations of the CT salts are listed in Table 4. As the value of spin concentration changed to some extent with the crystal, average values are listed. The total spin concentrations 10^{15}—10^{16} spins/gram are much smaller than those observed in many strong molecular CT complexes,[9,10] and almost the same as those measured in weak molecular complexes.[11] These ESR signals seem to arise from the defects in the crystal. Upon illumination with a visible light, intensity of an ESR signal increased slightly but the *g*-value showed no shift (Fig. 7). The ratio of the ESR intensity on excitation with a white light to that in the dark is listed in Table 4. No ESR absorption was observed when the perchlorate salts of the cation and

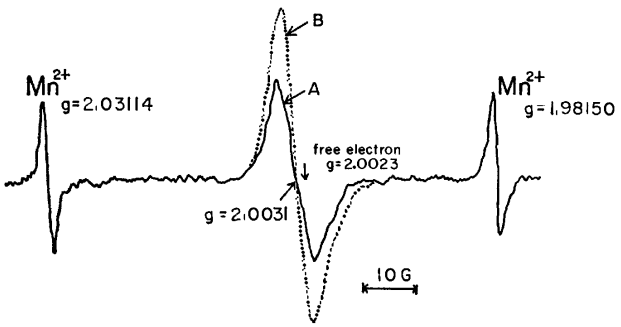

Fig. 7. ESR absorption spectra of TPT-TCP salt in vacuum at room temperature.
—— in the dark, ---- on illumination with a white light.

Table 4. *g*-Values, total spin concentration ([S]) and the ratio (R) of ESR intensity on illumination with a white light to that in the dark of organic CT salts

Salts	*g*-Value	[S] (spins/gram)	R
TPP-TCP	2.00270	1×10^{15}	1.3
TPT-TCP	2.00310	2×10^{15}	1.8
TPP-TCM	2.00295	1×10^{16}	1.3
TPT-TCM	2.00380	5×10^{15}	1.4
ADPT-TCP	2.00530	2×10^{15}	1.5
ADPP-TCM	2.00480	1×10^{15}	1.35

alkali metal salts of the anion were irradiated. The lights in the CT band region and in the near IR region (500—1200 nm) were effective on increasing the ESR signal, while those of shorter than 450 nm were ineffective.

The photoresponse curve of an ESR signal of TPT–TCP salt is given as an example, in Fig. 8. The curve at room temperature showed a fairly rapid rise and decay, and was similar to that of the photocurrent shown in Fig. 5. No significant difference in ESR absorption was found between that in vacuum and in air. The spectral response, time response and the effect of air of the photo-ESR absorption suggest a close relationship between the photo-induced paramagnetism and the photoconduction of the CT salts.

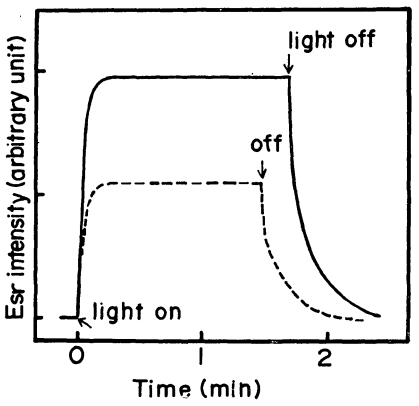

Fig. 8. Time response curves of photo-ESR absorption of TPT-TCP salt in vacuum at room temperature. —— on illumination at 500—1200 nm, ---- on illumination at 500—700 nm.

The temperature dependence of an ESR absorption in the dark and on irradiation was investigated in the range 213—323 K. The total spin concentration and the *g*-value of an ESR signal in the dark showed no significant change when temperature was lowered, indicating that the amount and nature of the paramagnetic species which existed originally in the material are independent of the temperature. The photo-ESR absorption showed a gradual decrease in its spin concentration with the decrease of temperature, activation energy being slightly negative (<0.2 eV). Thus, both the paramagnetic species induced by light and those originally present in the crystal in the dark are not produced by the thermal activation process.

Discussion

General Feature of the Electrical Conduction. *(i) All CT salts show a larger photoconduction peak at the long wavelength side of the interionic CT absorption band, and the photoconduction is almost unaffected by the presence of air*: This photoconduction is much larger than that observed in the perchlorate salt of the corresponding cation. A good reproducibility of the photoconduction was observed during the course of repeated measurements. Even when measured on different single crystals, the behavior of the photoconduction remained almost unchanged. This suggests that the observed conduction in this region is intrinsic and the photoexcitation of the interionic CT band contributes to the photoconduction.

Charge carriers seem to be generated in the bulk rather than on the surface of a crystal. Carrier generation in the bulk can account for the CT absorption peak not coinciding with the photocurrent peak; the number of photons reaching the bulk of a crystal are larger at the edge of the absorption band than at the absorption peak. The photocurrent, which is insensitive to the presence of air, also supports bulk carrier generation.

(ii) All CT salts show a smaller photoconduction in the near IR region of 800—1100 nm, which is also insensitive to the presence of air: This suggests the presence of deep traps at 1.0—1.4 eV below the conduction level. As the value is considerably larger than the observed activation energy, the dark current cannot be caused by the thermally activated carrier generation from these deep traps.

(iii) When excited in a LE band of the cation, the photoconduction does not appear significantly: This may be due to the fact that the photon is absorbed mostly on the surface of a crystal. However, the photon in the absorption edge of the LE band can reach the bulk of a crystal, and produce the photocarrier as in the case of CT band excitation as follows,

$$(D^{-}A^{+}) \xrightarrow{h\nu} (D^{-}A^{+*}) \longrightarrow (D\cdot A\cdot)^{*} \longrightarrow (D\cdot + A\cdot)$$

ground state — locally excited state — excited CT state — photocarriers

(iv) The photocurrent in the CT absorption region is proportional to about the 0.5 power of the incident light intensity: As the photocunduction in this region seems to be intrinsic, one photon absorption produces two charge carriers. However, if the carriers disappear with recombination between electrons and holes during migration, the concentration of the carrier would be proportional to the 0.5 power of the light intensity. Thus the photoconduction in our system may be recombination limited.

(v) Both dark conductivity and photoconductivity in the CT absorption and near IR regions have the same activation energy: As can be seen in Table 3, the most striking results obtained for the electrical properties of organic CT salts is that the values of activation energy for dark conduction and photoconduction are the same without any exception with respect to the six CT salts investigated. The property seems to be general with this kind of organic salts, and is basically important for framing up the conduction mechanism in the salts as in the following.

Mechanism of the Electrical Conduction in Organic CT Salts. The property mentioned above reminds us that a "trapping conduction mechanism" is the simplest model for explaining the agreement of the values of the activation energy of dark conduction and photoconduction. The trapping conduction model is shown schematically with TPT–TCP salt in Fig. 9 as an example. The TPT–TCP crystal has trapped carriers 0.4 eV below the conduction level which are thermally

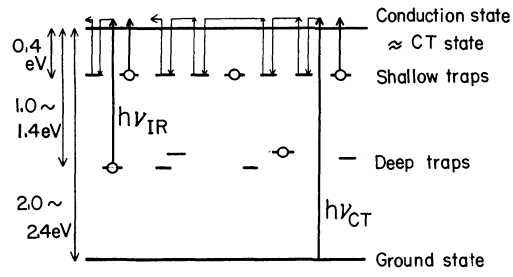

Fig. 9. Trapping conduction model with TPT-TCP salt.

excited up to conduction level in the dark, and the carriers generated in this way migrate through the crystal repeating the trapping and detrapping processes. Thus, the activation energy in dark conduction should be 0.4 eV, the depth of the trap levels below the conduction level, being the energy required for the trapping conduction.

In the case of photoconduction, the photocarriers are spontaneously generated in the conduction level by the absorption of light in the CT band, since the energy level of the conduction state is approximately equal to that of the excited CT state. The photocarriers thus generated migrate by the trapping conduction mechanism. In this mechanism, no activation energy is required for the carrier generation, and the activation energy of 0.4 eV as observed should be consumed in the carrier migration process. Thus, both for dark conduction and photoconduction the same amount, 0.4 eV, of activation energy is required. Photocarriers generated from the deep trap levels by near IR illumination also require the same activation energy 0.4 eV for their migration.

In our present model, only electron carriers are considered. As the molecular size of the acceptor cation is considerably larger than that of the donor anion, the acceptor radical A·, *i.e.*, electron, might contribute predominantly to the photocurrent. Molecular arrangement in the crystal supports this view.[12]

Photoconduction and Paramagnetic Species. An investigation of the ESR of the salts revealed that (a) CT salts showed a temperature independent ESR absorption even in the dark, (b) the perchlorate salts in which CT ineraction is absent gave no ESR signal, (c) the total spin concentration was of the order 10^{15}—10^{16} spins/gram, the amount changing considerably measured on different samples, (d) photo-illumination increased the ESR signal, the photo-ESR absorption showing a similar time response and spectral response with photocurrent, and (e) the temperature dependence of the photo-ESR absorption showed a slightly negative activation energy, the signal increasing with the lowering of temperature, and the time response curve of the phot-ESR absorption showed considerably longer rise and decay at lower temperatures.

The temperature independent ESR signal in the dark may be due to the charge carriers trapped in shallow traps (Fig. 9). These trapped carriers may be generated from crystal defects by CT interaction, because of (b) and (c). Photocarriers and the paramagnetic species of the photo-ESR may be the same (d), as can be seen in Fig. 9. The slightly negative activation energy of the photo-ESR (e) may be understood by the decrease of the recombination of the paramagnetic species with the lowering of temperature. Actually, the time response curve of the photo-ESR absorption shows considerably longer rise and decay at lower temperatures. Since paramagnetic species and the charge carriers are the same, the behavior of the photo-ESR signal is in line with the recombination limited photoconductivity, a photocurrent being proportional to the 0.5 power of the light intensity.

In the case of strong molecular CT complexes, such as perylene-iodine complex, a good coincidence between the values of the activation energy of dark current and of unpaired spin concentration was observed. This was used for proof that the paramagnetic species observed in the ESR spectroscopy were identical with the carriers.[9] This kind of coincidence is not necessary in our system, since the thermal activation process in the dark conduction is the carrier migration process. If the carrier concentration in the dark is equal to the spin concentration, about 10^{15} electrons/gram, the mobility of the carrier is estimated to be 10^{-5}—10^{-6} cm^2/volt·sec from the relation $i=Ne\mu$, where N is carrier concentration, e electric charge and μ mobility. The value seems to be very small as compared with the observed mobilities of organic compounds.[13] However, taking account of the fact that a fairly large energy is required for the carrier migration, and that the photoconduction is recombination limited, this small value of mobility is conceivable.

Another Mechanism of the Electrical Conduction. Although the above mechanism can account for the results of the electrical and magnetic properties of the organic CT salts, it should be noted that other mechanisms are possible for both carrier generation and migration. At first, charge carriers can be generated by the interaction between crystal imperfections and CT excitons migrating in a crystal. In this case, the carrier generation is extrinsic. This mechanism is the same as that suggested by Akamatu and Kuroda for the photoconduction of pyrene complexes.[3] Both mechanisms can explain the spectral, temperature and light intensity dependences of the photocurrent, but from the fact that the behavior of the photoconduction shows a good reproducibility when measured on several samples of single crystals, we consider the former mechanism, that is, the intrinsic carrier generation, to be plausible.

With weak molecular CT complexes, Akamatu and Kuroda suggested that the energy equivalent to the difference of the energy between the conduction level and the CT exciton level is required for the separation of a D^+A^- ion-radical pair. In this case, CT excitons cannot be separated spontaneously into charge carriers. However, in interionic CT salts, the interaction between two neutral radical species, D·A·, in the excited CT state may be small and consequently an energy required for the charge separation is smaller than that in the case of molecular CT complexes, and the photocarriers can be generated from the excited CT state with a very small thermal energy compared with the activation energy for the migration. Thus, the energy level of the conduction state can be approximately

equal to that of the excited CT state, and the intrinsic charge carrier generation seems to be possible in organic CT salts.

A hopping mechanism may be possible for the carrier migration process, instead of the trapping conduction. In this case, the charge carrier migrates from an ion to another with an activation energy 0.4—0.8 eV. This value seems to be fairly large for the activation energy for hopping conduction. However, these two mechanisms, *i.e.*, trapping conduction and hopping conduction, can explain the experimental results, and the latter possibility cannot be excluded.

References

1) Part II of this series, T. Tamamura, M. Yokoyama, S. Kusabayashi, and H. Mikawa, This Bulletin, **47**, 442 (1974).
2) H. Yasuba, T. Imai, K. Okamoto, S. Kusabayashi and H. Mikawa, This Bulletin, **43**, 3101 (1970).
3) H. Akamatu and H. Kuroda, *J. Chem. Phys.*, **39**, 3364 (1963).
4) H. Kokado, H. Hasegawa, and W. G. Schneider, *Can. J. Chem.*, **42**, 1084 (1964).
5) M. C. Tobin and D. P. Spitzer, *J. Chem. Phys.*, **42**, 3654 (1965).
6) C. K. Prout, R. J. P. Williams, and J. D. Wright, *J. Chem. Soc.* (A), 747 (1966).
7) T. Sano, K. Okamoto, S. Kusabayashi, and H. Mikawa, This Bulletin, **42**, 2505 (1969).
8) D. R. Kearns and M. Calvin, *J. Amer. Chem. Soc.*, **83**, 2110 (1961).
9) J. Kommandeur and F. R. Hall, *J. Chem. Phys.*, **34**, 129 (1961).
10) D. B. Chesnut and W. D. Phillips, *ibid.*, **35**, 1002 (1961).
11) J. W. Eastman, G. M. Andros, and M. Clavin, *ibid.*, **36**, 1197 (1962).
12) unpublished data.
13) F. Gutmann and L. E. Lyons, "Organic Semiconductors," John Wiley & Sons, Inc., New York (1967).

Heterocyclic Azomethine Compounds and Their Reduction Products as Analytical Reagents. II. The Reaction of 1-Picolylideneamino-2-naphthol with Zinc(II)

Makoto OTOMO, Kiyoshi FUKUI, and Kazunobu KODAMA

Department of Synthetic Chemistry, Nagoya Institute of Technology, Showa-ku, Nagoya 466

(Received May 15, 1973)

The acid dissociation constants of 1-picolylideneamino-2-naphthol in aqueous dioxane media of various concentrations and the stability constant of the zinc(II) chelate in a 50 v/v% aqueous dioxane medium were determined potentiometrically at 25 °C and $\mu=0.1$. The acid dissociation constants, pK_{a_1}, pK_{a_2}, and pK_{a_3}, at the zero dioxane mole fraction, evaluated by means of a least-squares treatment of the experimental data, are 3.1_6, 4.3_1, and 10.3_1 respectively. The overall stability constant of the zinc chelate was calculated be to $\log\beta_2=12.7_9$. 1-Picolylideneamino-2-naphthol can be used as a sensitive reagent for the extractive spectrophotometric determination of zinc. The zinc chelate extracted into chloroform has an absorption maximum at 520 nm. The bathochromic shift is as large as 120 nm. The color system obeys Beer's law over a concentration range up to 2×10^{-5} M. The molar absorptivity is 4.5×10^4 l/mol·cm at 520 nm.

In a preceding paper,[1] the acid dissociation constants of picolinaldehyde 2-hydroxyanil and some of its derivatives and their reactions with metal ions have been reported. The applicability of these compounds as sensitive reagents for the extractive spectrophotometric determinations of certain divalent-metal ions has also been pointed out. There has, however, been no reported characterization of metal complexes derived from the Schiff bases of 1-amino-2-naphthol or any of its ring-substitution products. In the present work, the chelate formation between 1-picolylideneamino-2-naphthol, a new heterocyclic azomethine compound, and zinc(II) and its application to the extractive spectrophotometric determination of traces of zinc are investigated. Of the divalent-metal chelates with this reagent which can be extracted into chloroform, the zinc chelate has the largest molar absorptivity.

Experimental

Materials and Apparatus. 1-Picolylideneamino-2-naphthol is synthesized as follows. A suspension of 1-amino-2-naphthol (0.05 mol)(purified by Kurzer's method[2]) in benzene(300 ml) is refluxed with freshly-distilled picolinaldehyde (0.055 mol) for a period of 15 min. The resulting crude product is recrystallized from a mixture of methanol and benzene (1 : 1) to obtain yellow fine crystals (4 g, 33%); mp 186—187 °C (with decomposition); IR (KBr): 1627 cm^{-1} (-CH=N-). Found: C, 77.49; H, 4.64; N, 11.26%. Calcd for $C_{16}H_{12}ON_2$: C, 77.40; H, 4.87; N, 11.28%.

A 1×10^{-4} M solution of the reagent in chloroform and a 1×10^{-2} M stock solution of zinc perchlorate are used for the spectrophotometric study. An Iwaki model KM mechanical shaker is used for the shaking.

All the other reagents and apparatus used have been reported previously.[1]

Potentiometric Titrations. As the reagent and the zinc chelate are insoluble in water, the titration is carried out in an aqueous dioxane medium. The experimental conditions and the method for the determination of the acid dissociation constants have been described previously.[1] For the determination of the stability constant, a 50 v/v% dioxane solution containing the ligand (2.5×10^{-3} M), sodium perchlorate (0.1 M), and zinc perchlorate (1.25×10^{-3} M) is titrated with a 0.1850 M sodium hydroxide solution at 25± 0.1 °C.

Standard Procedure for the Zinc Determination. An aliquot of a zinc solution is transferred into a 50-ml separatory funnel along with a 5 ml of a 1 M sodium perchlorate solution and 2 ml of a 1 M tris(hydroxymethyl)aminomethane-hydrochloric acid buffer solution (pH 8.5). The solution is diluted to 10 ml with water and then shaken for 1 min with 10 ml of the reagent solution. The absorbance of the chloroform extract is then measured at 520 nm against the reagent blank.

Results and Discussion

Acid Dissociation Constants. The potentiometric titration curves of the monosodium salt of 1-picolylideneamino-2-naphthol with perchloric acid show that this reagent behaves as a tribasic acid, the equations used to calculate the acid dissociation constants being:

$$\frac{(1-R)[H^+]}{R-2} = \frac{R[H^+]}{R-2}\cdot\frac{1}{K_{a1}} + K_{a2} \quad (1)$$

$$\frac{2-R}{R[H^+]^2} = \frac{R-1}{R[H^+]}\cdot\frac{1}{K_{a2}} + \frac{1}{K_{a1}K_{a2}} \quad (2)$$

and:

$$K_{a3} = \frac{(R-2)[H^+]}{3-R} \quad (3)$$

where $R=\{(3-a)C_A+[H^+]-[OH^-]\}/C_A$, and where C_A is the total concentration of the ligand, and a, the degree of neutralization. The pK_a values of the ligand acid in aqueous dioxane media of various concentrations are given in Table 1. The values of pK_{a1} and pK_{a2} are attributed to the removal of protons from the azomethine and the pyridine nitrogens respectively, whilst that of pK_{a3} is attributed to the dissociation of the naphtholic proton. The values of pK_{a1} and pK_{a2} decrease, and that of pK_{a3} increases, with an

TABLE 1. ACID DISSOCIATION CONSTANTS OF 1-PICOLYLIDENEAMINO-2-NAPHTHOL IN AQUEOUS DIOXANE MEDIA
$\mu=0.1$, 25°C

Mole fraction of dioxane	pK_{a1}	pK_{a2}	pK_{a3}
0	3.1_6	4.3_1	10.3_1
0.1122(37.5 v/v%)	3.0_5	4.2_4	10.7_5
0.1739(50 v/v%)	2.9_5	4.1_7	11.4_0
0.2598(62.5 v/v%)	2.8_6	4.0_9	11.5_3
0.3872(75 v/v%)	2.7_4	4.0_3	12.2_8

increase in the mole fraction of dioxane. On plotting each pK_a value against the mole fraction of dioxane, an approximately linear relationship is obtained in every case. The value of pK_a's at the zero dioxane mole fraction, evaluated by a least-squares treatment of the experimental data, are also included in Table 1.

The pK_{a3} value for 1-picolylideneamino-2-naphthol in the 50 v/v% dioxane medium is lower by 0.9 log unit than the pK_{OH} value for PAN[3] under the same conditions. Contrary to this observation, it has been found that the pK_{a3} values for picolinaldehyde 2-hydroxyanil and its methyl and chloro derivatives are somewhat higher than those for the corresponding azo dyes.[1,4] These results may be explained according to Hadzi's observation[5] that *o*-hydroxyazonaphthols exist as azo-hydrazo tautomers, whereas *o*-hydroxyazophenols are true azo compounds.

Stability Constant of the Zinc Chelate. The results of the continuous variation method show that zinc reacts with the reagent in a neutral to a slightly basic medium to form a 1 : 2 metal-to-ligand chelate easily extractable into chloroform. Therefore, the potentiometric titration is carried out in the molar ratio of 1 : 2.

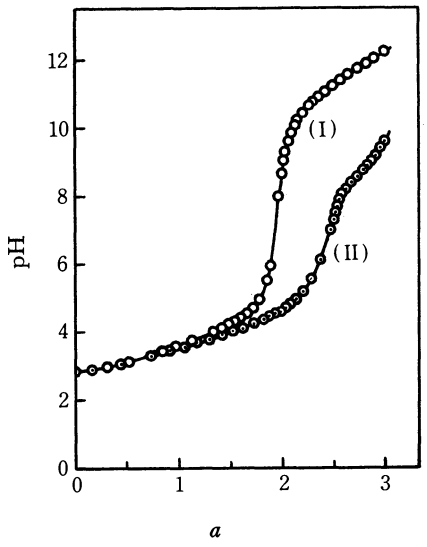

Fig. 1. Potentiometric titration curves of 1-picolylideneamino-2-naphthol and its zinc chelate in 50 v/v% aqueous dioxane, $\mu=0.1$, 25 °C; abscissa a represents moles of alkali added per mole of ligand (tribasic acid).
(I): Ligand, 2.50×10^{-3} M.
(II): Ligand, 2.50×10^{-3} M; Zn, 1.25×10^{-3} M

The titration curves of the reagent in a 50 v/v% dioxane medium in both the presence and absence of zinc are shown in Fig. 1. The pH inflection at $a=2.5$ in the former case suggests that the formation reactions of the 1 : 1 chelate, ZnL^+, and the 1 : 2 chelate, ZnL_2, proceed predominantly below and above $a=2.5$ respectively. The successive stability constants can be obtained from the following relationships[6]:

$$L=\frac{K_{a2}K_{a3}(3C_A+[OH^-]-[Na^+]-[H^+])}{2[H^+]^2+[H^+]K_{a2}} \quad (4)$$

$$\bar{n}=\frac{C_A-(K_{a2}K_{a3}+[H^+]K_{a2}+[H^+]^2)L/K_{a2}K_{a3}}{C_M} \quad (5)$$

where C_A and C_M are the total concentrations of the ligand and of zinc respectively. The values of $\bar{n}$ and L at each point of the titration curve are calculated from Eqs. (4) and (5). From these data, the formation curve is then plotted, a symmetrical pattern being followed. The successive stability constants are estimated from the values of pL at $\bar{n}=0.5$ and $\bar{n}=1.5$ to be 7.6_0 for $\log K_1$ and 5.1_9 for $\log K_2$, by means of the equations given by Schrøder.[7] These values are considerably lower than those for the zinc-PAN chelate ($\log K_1=11.2$, $\log K_2=10.52$[3]) and the zinc-picolinaldehyde 2-hydroxyanil chelate ($\log K_1=10.8$, $\log K_2=8.0$[4]), but higher than those for the zinc chelates of salicylidene-2-aminopyridine ($\log K_1=5.8$, $\log K_2=4.3$[4]) and *o*-aminophenol ($\log K_1=5.99$, $\log K_2=4.96$[8]). 1-Picolylideneamino-2-naphthol, therefore, acts as a terdentate ligand toward zinc to form two five-membered chelate rings. This consideration is supported by the spectral properties of the other divalent-metal chelates with the reagent in chloroform, as will be shown below.

Extractive Spectrophotometric Determination of Zinc. As has already been shown above, the 1 : 2 zinc-1-picolylideneamino-2-naphthol chelate is readily extracted into organic solvents, such as chloroform, 1,2-dichloroethane, *o*-dichlorobenzene, and nitrobenzene, to give a reddish-violet color. Chloroform is chosen because the largest absorbance is obtained in it. The color system obeys Beer's law. It is, therefore, tested for the extractive spectrophotometric determination of traces of zinc. However it is not possible to obtain the distribution coefficients of the reagent and the zinc chelate because of their low stability.

Absorption Spectra: The absorption spectra of the reagent and its zinc chelate in chloroform are shown in Fig. 2, the absorption maximum of the zinc chelate against the reagent blank being found at 520 nm. It may be noted that the bathochromic shift observed on chelation with the reagent is about 120 nm, much larger than that observed with PAN, *i.e.*, 80 nm. This is an advantage in the spectrophotometric determination of metals.

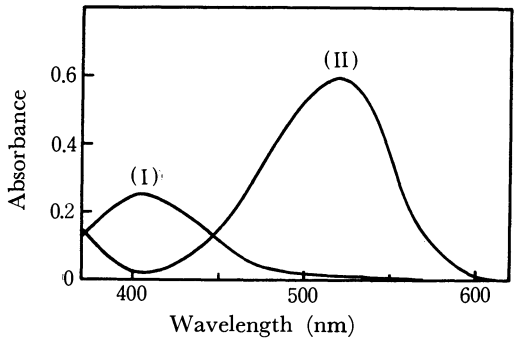

Fig. 2. Visible absorption spectra of 1-picolylideneamino 2-naphthol and its zinc chelate in chloroform.
(I): Reagent, 5.0×10^{-5} M; reference, $CHCl_3$.
(II): Zn, 1.30×10^{-5} M (8.5 μg); reagent, 2.0×10^{-4} M; pH, 8.5; reference, reagent blank.

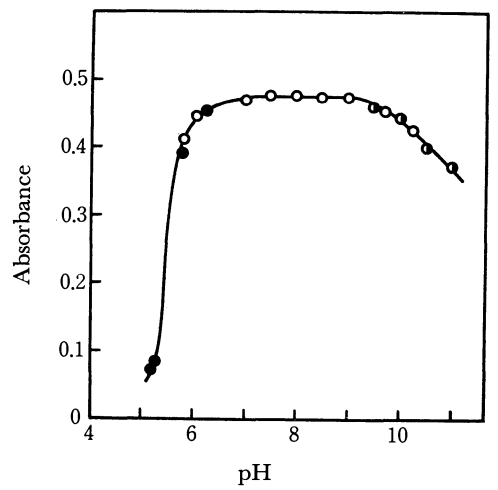

Fig. 3. Effect of pH.
Zn, 1.07×10^{-5} M (7.0 μg); reagent, 2.0×10^{-4} M; reference, reagent blank; ●, hexamethylenetetramine-HCl buffer; ○, tris(hydroxymethyl)aminomethane-HCl buffer; ◑, ammonia-ammonium chloride buffer.

Effect of pH: The absorbance of the organic phase is measured as a function of the pH of the aqueous phase, the results being shown in Fig. 3. At any pH examined, the absorption maximum of the chloroform extract is found at 520 nm, indicating that only one species is extracted. The zinc chelate is extracted above pH 5. The absorbance of the extract is at its maximum at pH 7.5—9.0

Color Stability and Effect of the Shaking Time: The zinc chelate is not very stable in either the aqueous or the organic phase. The absorbance of the chloroform extract decreases by 4.0% per 30 min for 7.3 μg of zinc. The absorbance is thus measured within 5 min after extraction. The maximum absorbance is obtained when a zinc solution is shaken with a chloroform solution of the reagent for 45 s to 2 min at pH 8.5.

Effect of the Reagent Concentration: About a 10-fold excess of the reagent is enough to obtain a constant absorbance.

Beer's Law and Sensitivity: Beer's law is obeyed over the concentration range up to 2×10^{-5} M (13 μg of zinc in 10 ml). At 520 nm, the molar absorptivity is 4.5×10^{4}. The spectrophotometric sensitivity is estimated to be 1.5×10^{-3} μg of zinc per cm^2, corresponding to log $I_0/I=0.001$. The sensitivity of the present method is much higher than that of the methods using zincon (molar absorptivity, $\varepsilon=1.9\times10^{4}$ at 610 nm[9]) or xylenol orange ($\varepsilon=2.74\times10^{4}$ at 550 nm[10]); however, it is lower than those with PAN ($\varepsilon=5.6\times10^{4}$ at 550 nm[11]), 5-chloro-PAN ($\varepsilon=8.4\times10^{4}$ at 564 nm[12]), or dithizone ($\varepsilon=9.6\times10^{4}$ at 532 nm[13]).

Reactions with Other Divalent-metal Ions. 1-Picolylideneamino-2-naphthol reacts with many divalent-metal ions in a neutral or slightly basic medium to form extractable colored chelates. The cobalt(II) chelate, however, changes in color from reddish-violet to brown during the course of extraction with chloroform at pH 8.5, giving a precipitate on the interface. This is probably due to the oxidation of the cobalt(II) chelate to the cobalt(III). In addition, magnesium(II) gives an orange red color to the organic phase during the course of extraction at pH 11, but the color fades away in a moment.

Table 2. Spectral properties of the metal chelates extracted into chloroform

Metal	Absorption maximum (nm)	Molar absorptivity $\times10^{-4}$ (l/mol·cm)	pH
Cd(II)	524	3.6	9.8[b]
Co(II)	523	partly precipitated	8.5
Cu(II)	540	1.5	7.4[b]
Fe(II)[a]	520	0.7	8.5[b]
Hg(II)	530	3.5	6.3[b]
Mn(II)[a]	523	3.7	9.8[b]
Ni(II)	537	3.5	8.5[b]
Pb(II)	520	1.5	9.8[b]
UO_2(II)	510	0.4	6.0
Zn(II)	520	4.5	8.5

a) in the presence of NH_2OH. b) pH value at which the maximum absorbance is obtained.

Table 2 summarizes the spectral properties of several divalent-metal chelates with this reagent extracted into chloroform. The spectrum of each chelate shows a broad, intense band well separated from that of the reagent, the shift being larger than 100 nm. The results tabulated in Table 2 imply that 1-picolylideneamino-2-naphthol can also be used as a sensitive reagent for the extractive spectrophotometric determination of cadmium(II) and manganese(II).

The disadvanatge of the present reagent is that its solution and chelates are not very stable. As it is much more sensitive for cadmium(II), manganese (II), and zinc(II) than copper(II), though, a further search for more stable analogs is in progress.

We are grateful to The Asahi Glass Foundation for Contribution to Industrial Technology for its financial support.

References

1) Part I: M. Otomo, and K. Kodama, This Bulletin, **46**, 2421 (1973).
2) F. Kurzer, *J. Chem. Soc.*, **1949**, 3434.
3) A. Corsini, I. Mai-Ling Yih, Q. Fernando, and H. Freiser, *Anal. Chem.*, **34**, 1090 (1962).
4) W. J. Geary, G. Nickless, and F. H. Pollard, *Anal. Chim. Acta*, **26**, 575 (1962); *ibid.*, **27**, 71 (1962).
5) D. Hadzi, *J. Chem. Soc.*, **1956**, 2143.
6) A. Young and T. R. Sweet, *J. Amer. Chem. Soc.*, **80**, 800 (1966).
7) K. H. Schrøder, *Acta. Chem. Scand.*, **20**, 1401 (1966).
8) R. G. Charles and H. Freiser, *J. Amer. Chem. Soc.*, **74**, 1385 (1952).
9) R. M. Rush and J. H. Yoe, *Anal. Chem.*, **26**, 1345 (1954).
10) T. V. Gurkina and A. H. Igoshin, *Zh. Analit. Khim.*, **20**, 778 (1965).
11) S. Shibata, *Bunseki Kagaku*, **21**, 551 (1972).
12) J. E. Going and P. T. Pflaum, *Anal. Chem.*, **40**, 1098 (1970).
13) S. Ashizawa, *Bunseki Kagaku*, **10**, 350 (1951).

Transition-metal Complexes of Pyrrole Pigments. IX.[1,2] Divalent and Trivalent Iron Chelates of Dipyrromethenes

Yukito MURAKAMI, Yoshihisa MATSUDA, Kazunori SAKATA, and Kenji HARADA

Department of Organic Synthesis, Faculty of Engineering, Kyushu University, Hakozaki, Higashi-ku, Fukuoka 812

(Received August 10, 1973)

The iron chelates of polymethyl-substituted dipyrromethenes were prepared. The ferrous ion was found to form complexes having a ligand to metal ratio of 2 : 1 with 5,5′-substituted dipyrromethenes, 3,3′,5,5′-tetramethyl- and 3,3′,4,4′,5,5′-hexamethyl-dipyrromethene. On the other hand, the ferric ion gave a complex having a 3 : 1 molar ratio of ligand to metal with a 5,5′-unsubstituted ligand, 3,3′,4-trimethyldipyrromethene. The complexes were studied by means of visible and IR spectroscopy as well as by magnetic susceptibility measurements. The iron(II) chelates were confirmed to be of high spin type with distorted tetrahedral structure (D_2), while the iron(III) chelate demonstrated a low spin character with hexacoordination. The strong ligand-field bands of the latter complex was ascribed to the trigonally distorted octahedral coordination (D_3) along with a high covalent nature of metal-ligand bonds.

In connection with metal complexes of macrocyclic pyrrole pigments which occur naturally and play an eminent role in biochemical catalysis, we have investigated metal complexes of synthetic pyrrole pigments of open chain structure from the viewpoint of coordination stereochemistry.[2-9] These pyrrole derivatives include dipyrromethenes and biladienes with various substituents. We clarified that substituent groups placed at the 5 and 5′ positions of dipyrromethenes in the divalent transition-metal complexes yielded a significant steric hindrance among the substituents in the same complex, so that no planar complexes were obtained even with copper(II) and nickel(II) having a good tendency of planar coordination.

For a transition metal in a highly stabilized trivalent state, however, a hexacoordinated bisdipyrromethene complex with an additional anionic ligand can be obtained. This was exemplified by the characterization of acetatobis(3,3′,5,5′-tetramethyldipyrromethenato)chromium(III).[2] The chromium complex undergoes a significant distortion along the C_2-axis due to the steric effect of the 5,5′-substituents. In contrast to the chromium system, the valency state of iron is more susceptible to the ligand-field effect as judged from its oxidation-reduction potential. In the present work, we have undertaken to elucidate the correlation between the valency state of iron in a complex and the nature of the 5,5′-substituents placed in the ligands with the use of 3,3′,4-trimethyl- (**1**), 3,3′,5,5′-tetramethyl- (**2**), and 3,3′,4,4′,5,5′-hexamethyl-dipyrromethene (**3**) as bidentate ligands.

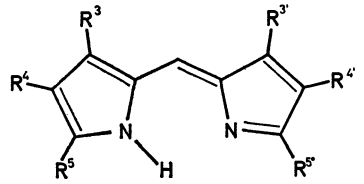

1: $R^3=R^{3'}=R^4=CH_3$, $R^{4'}=R^5=R^{5'}=H$
2: $R^3=R^{3'}=R^5=R^{5'}=CH_3$, $R^4=R^{4'}=H$
3; $R^3=R^{3'}=R^4=R^{4'}=R^5=R^{5'}=CH_3$

Experimental

Ligands. *3,3′,4-Trimethyldipyrromethene hydrochloride*: A mixture of 3-methyl-2-formylpyrrole[10] (0.41 g), 3,4-dimethylpyrrole[10] (0.36 g), and dry ethyl ether (60 ml) was added dropwise to 40 ml of dry ethyl ether placed in a reaction flask under nitrogen atmosphere. The hydrogen chloride gas diluted with dry nitrogen was bubbled through the reaction mixture while the addition was continued for 20 min at an ice-sodium chloride temperature. Dry HCl gas was continuously introduced into the mixture until precipitation of the orange solid no longer took place. The precipitates were recovered by filtration and washed with 50 ml of dry ether. Recrystallization from acetone-chloroform gave reddish orange crystals; yield 0.70 g (82%). UV($CHCl_3$): 280 sh (ε 1150), 286 (ε 1180), 306 (ε 884), 378 (ε 6680), 460 sh (ε 63100), and 468 nm (ε 72200). IR(KBr disk): 1621 cm^{-1}(pyrrole skeletal). NMR(CF_3CO_2H, TMS): δ 2.19 (3H, s, 4-C$\underline{H}_3$), 2.44, 2.53 (6H, each s, 3-C$\underline{H}_3$ and 3′-C$\underline{H}_3$), 6.61 (1H, br.s, 4′-$\underline{H}$), 7.77 (2H, s, 5-$\underline{H}$ and 5′-$\underline{H}$), and 7.84 (1H, s, -C$\underline{H}$=).

Found: C, 64.74; H, 6.88; N, 12.32%. Calcd for $C_{12}H_{15}N_2Cl$: C, 64.71; H, 6.79; N, 12.58%.

The synthesis of 3,3′,5,5′-tetramethyl- and 3,3′,4,4′,5,5′-hexamethyl-dipyrromethene has been described.[3]

Tris(3,3′,4-trimethyldipyrromethenato)iron(III). An aqueous solution (3 ml) containing ferric chloride hexahydrate (0.36 g) was added to a mixture of 3,3′,4-trimethyldipyrromethene hydrochloride (0.60 g) and methanol (180 ml). Crystalline precipitates of dark green luster were obtained from the dark reddish reaction mixture upon dropwise addition of aqueous ammonia (28%, 10 ml) with stirring. After being allowed to stand for 1 hr in a freezer, the crystalline solid was recovered and recrystallized from acetone as dark green crystals; yield 0.43 g (77%).

Found: C, 70.34; H, 6.54; N, 14.13%. Calcd for $C_{36}H_{39}N_6Fe$: C, 70.69; H, 6.44; N, 13.74%.

Bis(3,3′,5,5′-tetramethyldipyrromethenato)iron(II). Aqueous ammonia (28%, 10 ml) was added dropwise into a mixture of the hydrated ferrous chloride (1.2 g) dissolved in 30 ml of water and 3,3′,5,5′-tetramethyldipyrromethene (free base, 1.0 g) in 130 ml of ethanol. A crystalline solid of green luster was recovered after the reaction mixture had been allowed to stand for sometime in a freezer. Recrystallization from *n*-hexane gave green crystals; yield 0.58 g (51%).

Found: C, 68.79; H, 6.65; N, 12.24%. Calcd for $C_{26}H_{30}N_4Fe$: C, 68.72; H, 6.66; N, 12.33%.

Bis(3,3′,4,4′,5,5′-hexamethyldipyrromethenato)iron(II) A crystalline solid was obtained from 3,3′,4,4′,5,5′-hexamethyldipyrromethene (free base, 0.50 g) and the hydrated ferrous chloride (0.50 g) in a manner similar to the above iron(II) complex. Recrystallization from *n*-hexane–benzene gave green crystals; yield 0.45 g (82%).

Found: C, 70.33; H, 7.39; N, 10.92%. Calcd for $C_{30}H_{38}N_4Fe$: C, 70.58; H, 7.50; N, 10.98%.

Physical Measurements. Electronic spectra covering the 250—2000 nm region were recorded on a Hitachi EPS-2 spectrophotometer for chloroform solutions at room temperature. Infrared spectra were measured with a JASCO DS-403G spectrophotometer by a Nujol mull technique. Magnetic susceptibility measurements of solid powdered samples were carried out with Gouy balance. Calibrations were made with use of fresh distilled water and cupric sulfate pentahydrate, while diamagnetic corrections were performed by using Pascal's constants.

Results and Discussion

The reactions of ferrous chloride with dipyrromethene ligands **2** and **3** resulted in the formation of the corresponding iron(II) complexes having a 2 : 1 ligand to metal ratio (bis-complex), while a ferric salt reacted with ligand **1** to give the 3 : 1 dipyrromethene-iron(III) complex (tris-complex). In the latter reaction, ferrous chloride was also utilized in place of the ferric salt to afford the same complex. On the other hand, the reactions of ferric chloride with ligands **2** and **3** failed to give any characteristic metal complex. For the dipyrromethene-iron chelate system, the trivalent iron state appears to be electronically more stable than the divalent state due to the chelate effect, unless other factors such as steric effect come into play. The absence of bulky substituent groups at the 5,5'-positions in one dipyrromethene ligand resulted in the formation of a tris-complex. When methyl groups are substituted at these positions, a significant steric interaction was generated among these substituents of different ligand molecules in the same complex to such an extent that the formation of a tris-complex is completely inhibited. This effect favors the formation of a neutral divalent iron complex, bis-complex.

A hexacoordinated chromium(III) complex was obtained with ligand **2** accompanied with acetate group as an additional anionic ligand.[2] Judging from the standard reduction potentials −0.41 and 0.77 V for chromium(III) and iron(III), respectively,[11] the trivalent state of chromium in a complex is intrinsically more stable than that of iron. The sterically crowded structure of hexacoordinated chromium(III) complex was relaxed by adopting the acetate ion as the third ligand.

The plausible structures for bis- and tri-complexes

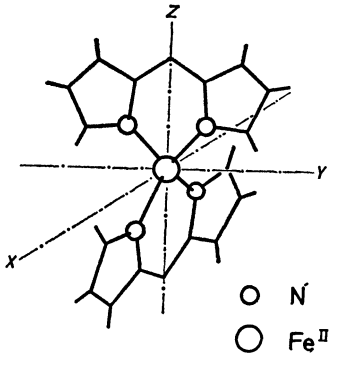

4

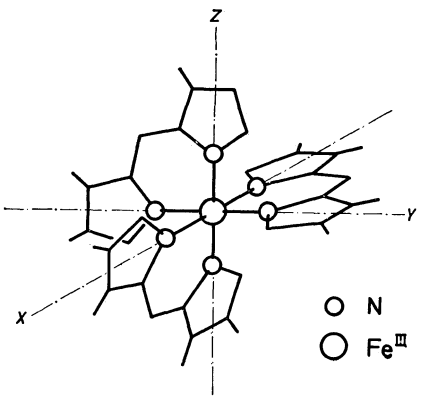

5

are illustrated schematically by **4** and **5**, respectively. A discussion will be made on the basis of these structures.

Electronic Spectra. The electronic absorption spectra for the three iron complexes are shown in Fig. 1, covering the 250—2000 nm region. The absorption bands lying above 20000 cm^{-1} are attributed to charge transfer transitions from metal to ligand and $\pi \rightarrow \pi^*$ transitions within a ligand molecule. The ligand-field bands are observed in a region lying below 18000 cm^{-1} (Figs. 2 and 3) for tris(3,3',4-trimethyldipyrromethenato)iron(III) and bis(3,3',4,4',5,5'-hexamethyldipyrromethenato)iron(II), respectively.

The coordination site symmetry for the tris-complex can be O_h with some minor trigonal distortion, if any. It is rather difficult to presume the spin state of iron(III) on the basis of spectral behavior alone. This is due to the fact that the ligand-field energy for the high spin state is frequently comparable to

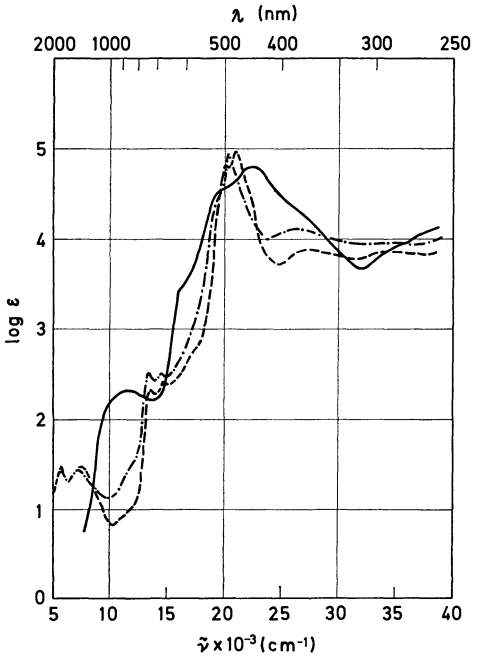

Fig. 1. Electronic absorption spectra of iron chelates in chloroform at room temperature: ——, tris-complex I; ----, bis-complex II; .—.—, bis-complex III. Refer to the footnote of Table 1 for abbreviations.

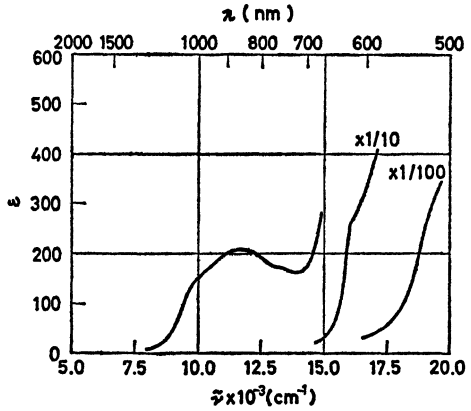

Fig. 2. Ligand-field spectrum for tris(3,3′,4-trimethyldipyrromethenato)iron(III) in chloroform at room temperature. Numbers in this figure (1/10 and 1/100) refer to the reduction factor of the absorption intensity.

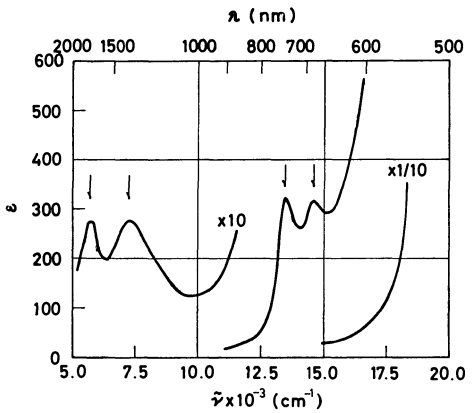

Fig. 3. Ligand-field spectrum for bis(3,3′,4,4′,5,5′-hexamethyldipyrromethenato)iron(II) in chloroform at room temperature. Numbers in this figure refer to the reduction (1/10) and enlarging (10) factors of the absorption intensity.

that for the low spin, and thermal equilibrium between these two states can be expected consequently. On the basis of the below-mentioned magnetic data, the energy level scheme for low spin state[12-14] (Fig. 4) is adopted here for the elucidation of the spectrum.[15] The ground state is $^2T_{2g}(t_{2g}^5, {}^2I)$ and can be split into $^2A_1$ and ^2E states under D_3 coordination symmetry. The spin-allowed excited levels with $t_{2g}^4e_g$ configuration are classified into three groups on the basis of the magnitude of energy separation: $^2A_{2g}$, $^2T_{1g}$, $^2T_{2g}(^2I)$; $^2E_g(^2I)$; and higher excited levels. The assignments of ligand-field bands with self-consistency are listed in Table 1. In spite of the satisfactory assignments of these bands, their absorption intensity is apparently too strong for the ordinary O_h coordination symmetry. The causes for this might be given as follows: a) distortion from O_h to D_3 to release the steric strain generated within a complex molecule; and b) d-p orbital mixing through strong covalent interaction between ligand and metal. Both *Dq* and *B* values were evaluated as shown in Table 1. The Racah parameter (*B*) for the complex is much smaller than the free ion value (~1300 cm^{-1}), indicating a strong

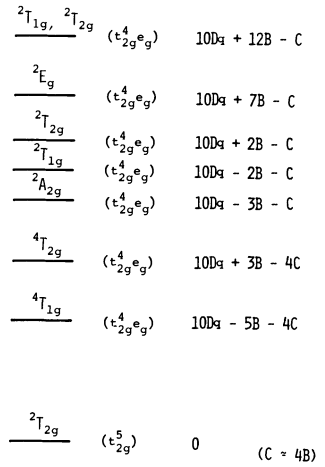

Fig. 4. The energy level scheme with configuration interaction for a low spin d^5 ion under O_h coordination symmetry.

TABLE 1. LIGAND-FIELD BANDS FOR DIPYRROMETHENE-IRON CHELATES AND THEIR ASSIGNMENTS[a]

Chelate[b]	Ligand-field band, cm^{-1} (ε)	Symmetry	Assignment
I[c]	10000 sh (150)	O_h	$^2A_{2g} \leftarrow {}^2T_{2g}$
	11700 (208)		$^2T_{1g} \leftarrow {}^2T_{2g}$
	13200 sh (174)		$^2T_{2g} \leftarrow {}^2T_{2g}$
	16400 sh (2960)		$^2E_g \leftarrow {}^2T_{2g}$
II	5700 (26.0)	D_2	$^5B_2, {}^5B_3 \leftarrow {}^5A_{(1)}, {}^5A_{(2)}$
	7350 (29.4)		
	13600 (209)		$^5B_1 \leftarrow {}^5A_{(1)}, {}^5A_{(2)}$
	14700 (245)		
III	5680 (27.0)	D_2	$^5B_2, {}^5B_3 \leftarrow {}^5A_{(1)}, {}^5A_{(2)}$
	7250 (27.6)		
	13500 (318)		$^5B_1 \leftarrow {}^5A_{(1)}, {}^5A_{(2)}$
	14500 (314)		

a) Measured in chloroform at room temperature. b) I, tris(3,3′,4-trimethyldipyrromethenato)iron(III); II, bis(3,3′,5,5′-tetramethyldipyrromethenato)iron(II); III, bis(3,3′,4,4′,5,5′-hexamethyldipyrromethenato)iron(II). c) Evaluated *Dq* and *B* values under O_h are 1440 and 600 cm^{-1}, respectively.

nephelauxetic effect.

Cobalt(II) complexes with substituted dipyrromethenes exhibit distortion from regular tetrahedral coordination toward planar to an extent that the 5,5′-substituents do not generate any detectable steric effect within a complex molecule.[6] The covalent nature of the coordinate bond may cause a tendency for a tetracoordinated complex to distort toward planar geometry. A similar state of affairs can be expected in the present case, and the bis-complex may assume tetrahedral coordination along with some minor distortion toward planar geometry. Thus, the D_2 local symmetry around iron(II) is tentatively assigned to these complexes. The distortion may arise partly from the skeletal structure of ligand molecule. As has been found for bisdipyrromethenato-copper(II) and -nickel(II) by X-ray diffraction measurements,[16,17] the N-

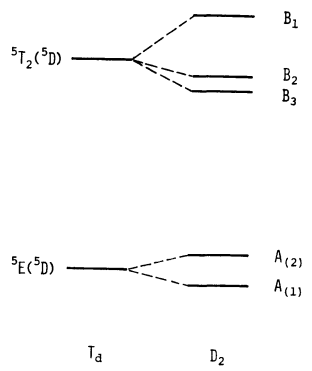

Fig. 5. The energy level schemes of direct concern for a high spin d^6 ion under T_d and D_2 symmetries.

M–N angle within a chelate ring is slightly smaller than the tetrahedral angle. This gives rise to the distortion toward two-fold axial symmetry. The energy level schemes for $T_d(^5D)$ and $D_2(^5D)$ are illustrated in Fig. 5. The possibility of being in the low spin state was excluded on the basis of the fact that the ligand field generated by the present ligands is not strong enough to make spin-pairing for d^6 ion under tetrahedral symmetry as in the case for the corresponding cobalt(II) complexes.[6] This was approved by the magnetic susceptibility measurements described in the following.

If the magnitude of energy separation between $A_{(1)}$ and $A_{(2)}$ levels does not differ widely from that of the thermal energy at the temperature of measurement, a thermal pumping effect which provides some population in $A_{(2)}$ level can be expected. This effect may give two groups of ligand-field bands, each consisting of two absorption peaks with a smaller separation; $B_1 \leftarrow A_{(1)}$, $A_{(2)}$ and B_2, $B_3 \leftarrow A_{(1)}$, $A_{(2)}$. These assignments for the present bis-complexes are summarized in Table 1. A higher energy band in each group, attributable to the transition from $A_{(1)}$ level, shows a greater broadness relative to the lower one (Fig. 3). This is most likely due to vibronic coupling with the vibrational levels of larger energy separation for $A_{(1)}$ level, providing wider phonon wings.

Vibrational Spectra. The IR absorption spectra for the iron chelates, covering the 1500—1700 cm^{-1} region, are shown in Fig. 6. A strong band appearing in the 1600 cm^{-1} range is assigned to the skeletal stretching mode of the pyrrole rings.[3,6,8,9] A slight shift of this band to lower energy is observed for each ligand upon metal-coordination.

In the far-infrared region 700—200 cm^{-1}, the bis-complexes showed absorption peaks of medium intensity in the 400—350 cm^{-1} range in a manner similar to those observed for the cobalt(II), nickel(II), and copper(II) chelates of some dipyrromethenes.[3] This band can be associated with the metal-ligand (M–N) stretching mode since the corresponding band for each free ligand is absent: 388 cm^{-1} for bis(3,3′,5,5′-tetramethyldipyrromethenato)iron(II) and 368 cm^{-1} for bis(3,3′,4,4′,5,5′-hexamethyldipyrromethenato)iron-(II). On the other hand, we failed to assign such a vibrational mode to the tris-complex.

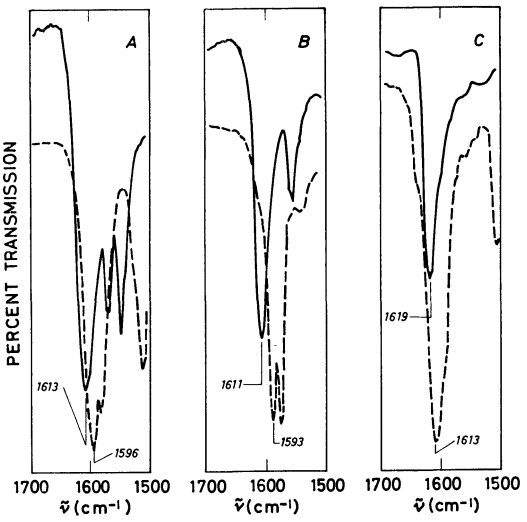

Fig. 6. Infrared spectra of iron chelates (----) and dipyrromethene free base (——) by a Nujol mull technique: A, 3,3′,5,5′-tetramethyldipyrromethene and its iron(II) chelate; B, 3,3′,4,4′,5,5′-hexamethyldipyrromethene and its iron(II) chelate; C, 3,3′,4-trimethyldipyrromethene and its iron(III) chelate. Number refers to the skeletal vibrational mode of the pyrrole rings.

Magnetic Susceptibilities. The results of magnetic susceptibility measurements are listed in Table 2. It became obvious that the tris-complex holds a spin-paired d^5 system, even though μ_{eff} value is no doubt larger than the spin-only value. The effective magnetic moments for some low-spin iron(III) complexes formed with cyano, ethylenediamine,[13] tertiary arsine,[14] and substituted xanthates[18] were found to lie in a 2.2—2.5 range at ordinary temperature. However, there remains some ambiguity as to whether thermal population on the high spin state is still allowed. Further study on the behavior of magnetic susceptibility with variation of temperature is required for clarification of this state of affairs. The bis-complexes apparently

Table 2. Molar magnetic susceptibilities (χ_M) and magnetic moments (μ_{eff}) for dipyrromethene-iron chelates at room temperature

Chelate[a]	Electronic configuration	Temp, °K	$10^6 \times \chi_M$, CGS	$10^6 \times \chi_M^{cor}$, CGS	μ_{eff}, BM	$[4S(S+1)]^{1/2}$	No. of unpaired electrons
I	d^5	297—298	2132—2176	2479—2523	2.43—2.45	1.73	1
II	d^6	297	10670—11520	10930—11770	5.10—5.20	4.90	4
III	d^6	299	10250—10430	10550—10730	5.03—5.07	4.90	4

a) See Table 1, footnote b) for abbreviations.

hold a high spin state. The effective magnetic moments are slightly larger than the spin-only value. This difference may arise from the incomplete quenching of orbital angular momentum.

The authors acknowledge partial support of this work by the Asahi Glass Foundation for the Contribution to Industrial Technology.

References

1) Contribution No. 316 from this Department.
2) Part VIII: Y. Murakami, Y. Matsuda, and K. Iiyama, *Chem. Lett.*, **1972**, 1069.
3) Y. Murakami and K. Sakata, *Inorg. Chim. Acta*, **2**, 273 (1968).
4) Y. Murakami, Y. Kohno, and Y. Matsuda, *ibid.*, **3**, 671 (1969).
5) Y. Murakami, Y. Matsuda, and Y. Kanaoka, This Bulletin, **44**, 409 (1971).
6) Y. Murakami, Y. Matsuda, and K. Sakata, *Inorg. Chem.*, **10**, 1728 (1971).
7) Y. Murakami, Y. Matsuda, and K. Sakata, *ibid.*, **10**, 1734 (1971).
8) Y. Murakami, Y. Matsuda, K. Sakata, and A. E. Martell, *J. Chem. Soc., Dalton*, **1973**, 1729.
9) Y. Murakami, Y. Matsuda, and S. Kobayashi, *ibid.*, **1973**, 1734.
10) G. M. Badger, R. L. N. Harris, and R. A. Jones, *Aust. J. Chem.*, **17**, 1022 (1964).
11) L. Meites, H. C. Thomas, and R. P. Bauman, "Advanced Analytical Chemistry," McGraw-Hill Bock Co., Inc., New York (1958), p. 409.
12) C. S. Naiman, *J. Chem. Phys.*, **35**, 323 (1961).
13) G. A. Renovitch and W. A. Baker, Jr., *J. Amer. Chem. Soc.*, **90**, 3585 (1968).
14) R. D. Feltham and W. Silverthorn, *Inorg. Chem.*, **9**, 1207 (1970).
15) The ferric complex was assumed to be in a spin-free state due to the absence of its magnetic susceptibility data at the time this study was initiated: Y. Murakami, Y. Matsuda, and K. Harada, *Asahi Garasu Kogyo Gijutsu Shoreikai Kenkyu Hokoku* (published by the Asahi Glass Foundation for the Contribution to Industrial Technology), **18**, 203 (1971).
16) M. Elder and B. R. Penfold, *J. Chem. Soc., Ser. A*, **1969**, 2556.
17) F. A. Cotton, B. G. DeBoer, and J. R. Pipal, *Inorg. Chem.*, **9**, 783 (1970).
18) A. H. Ewald, R. L. Martin, E. Sinn, and A. H. White, *ibid.*, **8**, 1837 (1969).

Asymmetric Reactions. IX. On the Catalytic Hydrogenation of Olefinic Compounds with Bis(dimethylglyoximato)cobalt(II)-base Complex[1]

Seiji TAKEUCHI, Yoshiaki OHGO, and Juji YOSHIMURA

Laboratory of Chemistry of Natural Products, Faculty of Science, Tokyo Institute of Technology, Ookayama, Meguro-ku, Tokyo 152

(Received June 28, 1973)

Examination of the catalytic hydrogenation of twenty-one olefinic compounds with bis(dimethylglyoximato)-cobalt(II)-pyridine complex indicates that all $H_2C{=}C\langle^{Y}_{Y}$ type olefinic compounds having an electron-withdrawing and a weakly electron-donating substituent are reducible. Isolation and further hydrogenation of the alkyl complexes in the case of $H_2C{=}C\langle^{Y}_{Y}$ type olefinic compounds, and deuterogenation of α-phenylacrylophenone support the view that α-alkyl complexes are the intermediates in hydrogenation. It is concluded that the electron-withdrawing effect accelerates both the first (alkyl complex formation) and the second (reductive-cleavage of alkyl moiety) steps, while steric compression prevents the first step and accelerates the second step. The reaction mechanism is discussed.

Schrauzer and Windgassen reported that bis(dimethylglyoximato)cobalt(II)-base, $Co^{II}(DMG)_2B$, catalyzes the reductive methylation of amines and thiols with formaldehyde under hydrogen atmosphere,[2] and that the formation of substituted alkyl and alkenylcobaloximes from $Co^{II}(DMG)_2B$ and alkenes or alkines is sometimes followed by reductive cleavage of the alkyl moieties as a side reaction.[3] We have extended the hydrogenation to the homogeneous catalytic hydrogenation of reactive olefinic compounds, α-diketones, α-ketocarboxylic acid esters and unsaturated compounds carrying N=N or N=O double bond[4] and also to their asymmetric hydrogenation with the use of Co^{II}-$(DMG)_2$-quinine complex.[5] We have examined the electronic and steric effects of the substituents of olefinic compounds on their hydrogenation and on the nature of intermediate alkyl complexes, since they are important for making clear the mechanism of the asymmetric hydrogenation.

Results and Discussion

The reaction of the reduced cobaloximes with olefinic compounds having an electron-withdrawing substituent gives α-alkyl complexes (α-ACs) in nearly neutral medium and β-one in alkaline solution, the actually reacting species being considered to be the hydridocobaloxime; $HCo(DMG)_2B$, and cobaloxime(I); $[Co^{I}(DMG)_2B]^-$, respectively.[3] In order to clarify the limitation of the catalytic hydrogenation of olefinic compounds with $Co^{II}(DMG)_2$-pyridine, various substrates were hydrogenated in a slightly alkaline methanol or ethanol under the atmospheric pressure of hydrogen at room temperature. The results are summarized in Table 1, together with the previous ones.[4]

It is apparent that; 1) monosubstituted ethylene compounds (**1**—**3**) are scarcely hydrogenated; 2) α,α-disubstituted compounds (**5**—**11**) ($H_2C{=}C\langle^{Y}_{Y}$), having an electron-withdrawing group (X: $COOCH_3$, COPh, CN) and a weakly electron-donating group (Y: CH_3, Phenyl, NHCOR, CH_2COOCH_3), are commonly hydrogenated very smoothly, but not α,β-disubstituted compounds (**12**—**14**) except for **15** in which both the substitutents are electron-withdrawing; 3) only trisubstituted ethylene compounds having two electron-withdrawing groups (**20**—**21**) are slowly hydrogenated.

The results indicate that the reactivity of olefinic compounds is controlled by electronic and steric effects of substituents. However, the interrelation between these effects and the reactivity is still ambiguous. The slow but successful hydrogenation of **15**, **20**, and **21** may be attributed to the electron deficiency of the ethylenic bond due to the substituents, but the large difference between compounds **5**—**11** and **12**—**14** seems to depend only on the position of both electron-withdrawing and donating substituents. For more detailed discussion, it is necessary to isolate alkyl complexes, and examine their reducibility. Acrylonitrile (**1**), methyl acrylate (**2**) and styrene (**3**) gave the same results as those by Schrauzer and Windgassen[3] (Table 2). They stated that no product was obtained in the reaction of methacrylonitrile (**5**) with reduced cobaloxime under alkaline conditions.[3] We have isolated the corresponding α-AC both under neutral and alkaline conditions.

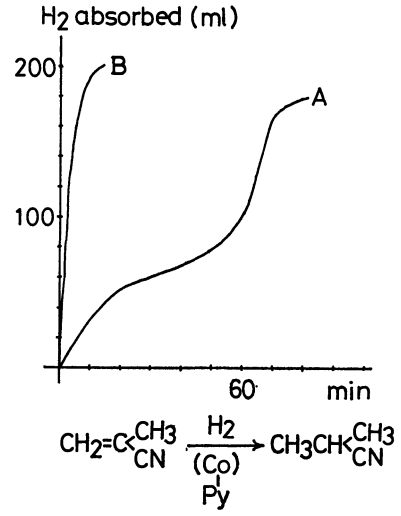

Fig. 1. Hydrogen absorption in the hydrogenation of methacrylonitrile under weakly (A) and strongly (B) alkaline conditions.
Conditions: substrate 7.5 mmol, S/Co=1.9; NaOH/Co=2.8 (A), 3.7 (B).

Table 1. Catalytic hydrogenation of various olefinic compounds with $Co^{II}(DMG)_2$-pyridine

No.	Substrates	S/Co[a]	Reaction[b] time	Products (yield)
1	$CH_2=CHCN$	1	—	—[c]
2	$CH_2=CHCO_2CH_3$	1	—	—[c]
3	$CH_2=CHPh$	4	—	—[c]
4	$CH_2=C(Ph)CH_3$	5	3 day	Recovered
5	$CH_2=C(CN)CH_3$	3.5	4.3 hr	$CH_3CH(CH_3)CN$ (87%)
6	$CH_2=C(CH_3)CO_2CH_3$	10	2 hr	$CH_3CH(CH_3)CO_2CH_3$ (98.5%)
7	$CH_2=C(Ph)CO_2CH_3$	1	1 hr	$CH_3CH(Ph)CO_2CH_3$ (69%)
8	$CH_2=C(CO_2CH_3)CH_2CO_2CH_3$	4	1 hr	$CH_3CH(CH_2CO_2CH_3)CO_2CH_3$ (100%)
9	$CH_2=C(CO_2CH_3)NHAc$	7	30 min	$CH_3CH(NHAc)CO_2CH_3$ (42%)[d]
10	$CH_2=C(CO_2CH_3)NHCOBzl$	3.5	17 min	$CH_3CH(NHCOBzl)CO_2CH_3$ (70%)
11	$CH_2=C(Ph)COPh$	2	15 min	$CH_3CH(Ph)COPh$ (80%)
12	$CH_3CH=CHCO_2CH_3$	10	4 days	Recovered
13	$PhCH=CHCO_2CH_3$	2	4 days	Recovered
14	$PhCH=CHCOCH_3$	7	4 days	Recovered
15	$EtO_2CCH=CHCO_2Et$	4	3 days	$EtO_2CCH_2CH_2CO_2Et$ (69%)
16	$CH_3CH=C(CH_3)CO_2CH_3$	3	1 day	Recovered
17	$PhCH=C(NHBz)CO_2CH_3$	1	1 day	Recovered
18	$PhCH=C(NHC_6H_{11})CO_2CH_3$	1	1 day	Recovered
19	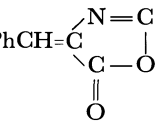	1	2 days	$PhCH_2CH(NHBz)CO_2CH_3$ (7.3%) and **17**
20	$PhCH=C(CN)CO_2Et$	10	8 hr	$PhCH_2CH(CN)CO_2Et$ (80%)
21	*t*-$BuCH=C(Ac)CO_2Et$	3	24 hr	*t*-$BuCH_2CH(Ac)CO_2Et$

a) S/Co; molar ratio of substrate (S) to catalyst (Co). b) Time required for the absorption of theoretical amount of hydrogen. c) Molecular hydrogen was consumed only for formation of the alkyl complex. d) As the hydrogenated material was soluble in water, the yield was lowered.

Table 2. Isolation of alkyl complexes and hydrogenation of α-alkyl complexes

No.	Substrate	Alkyl complex (AC)[a]		Hydrogenation	Alkyl group in α-AC	Autocatalyzed[c] Hydrogenation	Catalytic Hydrogenation[d]
		Neutral	Alkaline				
1	$CH_2=CHCN$	α-AC	β-AC	None	$-CH(CN)CH_3$	None	Fast
2	$CH_2=CHCO_2CH_3$	α-AC	β-AC	None	$-CH(CH_3)CO_2CH_3$	Slow	Fast
3	$CH_2=CHPh$	α-AC	α-AC	None	$-CH(Ph)CH_3$	None	None
5	$CH_2=C(CH_3)CN$	α-AC	α-AC	Relatively slow	$-C(CH_3)(CN)CH_3$	Fast	Very fast
11	$CH_2=C(Ph)COPh$	—	(α-AC)[b]	Very fast	$-C(Ph)(COPh)CH_3$	—	—

a) For example, α- and β-AC of acrylonitrile imply $CH_3(CN)CHCo(DMG)_2$-pyridine and $CNCH_2CH_2Co(DMG)_2$-pyridine, respectively. b) The structure was deduced from the result of deuterogenation. c) Hydrogenation only with molecular hydrogen. d) Hydrogenation with $Co^{II}(DMG)_2$-pyridine and molecular hydrogen in slightly alkaline methanol solution.

Hydrogenation of **5** under weakly alkaline conditions proceeds stepwise, while under strongly alkaline conditions very smoothly (Fig. 1). The presence of α-AC was easily proved by the NMR spectrum, and the α-AC was isolated by concentrating the reaction mixture after the reaction had been interrupted at the first stage when a half-equimolar amount of hydrogen was absorbed. In the case of dimethyl itaconate (**8**) under alkaline conditions, a small amount of β-AC was obtained, and the yield was increased to 30% under strongly alkaline conditions by use of a large excess of imidazole as the axial base.

All β-AC described above could not be hydrogenated even in the presence of excess $Co^{II}(DMG)_2B$ or palladium-charcoal. Both the results with β-AC and **5** strongly indicate that the α-AC is the actual intermediate in the hydrogenation. Since AC could not be detected in all other cases in which the hydrogenation proceeded very fast, deuterogenation of α-phenylacrylphenone (**11**) under deuterium atmosphere in slightly alkaline methanol-d_1 was examined. The ratio of deuterium on β-carbon to that on α-carbon of the corresponding saturated product was determined by NMR spectrum to be about 2.3. This also indicates that the deuterogenation of **11** proceeds *via* α-AC, as in a similar reaction with pentacyanocobaltate.[6] Thus, it is con-

cluded that α-ACs are formed in both neutral and alkaline solution in the cases of $H_2C{=}C\langle^{Y}_{Y}$ type olefinic compounds.

Autocatalytic and catalytic hydrogenation of thus isolated α-ACs was examined (Table 2). Hydrogenation in the absence of catalyst (autocatalytic hydrogenation) of α-AC from **5** proceeded relatively fast, while that of α-AC from **2** slowly. α-ACs from **5**, **1**, and **2** were hydrogenated much faster in the presence of Co^{II}-$(DMG)_2B$ than in the absence of the catalyst. The results show that their reactivity is in the order **5**>**2**>**1**>**3**, indicating that the bulkiness (steric compression including DMG ring) of substituents causes the sequence of the former three. The remarkable stability of α-AC from **3**, inspite of the greater bulkiness of phenyl group than that of methoxycarbonyl group or cyano group, suggests that the electron-withdrawing effect of substituents plays a more decisive role than the steric one. Thus, it can be concluded that both the electron-withdrawing effect and steric compression of substituents accelerate the second step (reductive cleavage) of the hydrogenation, the former playing a more important role.

On the other hand, compounds **4**, **12**—**14**, and **16**—**18** gave neither the saturated product nor the corresponding α-AC. If we compare these compounds with **1**—**3**, **5**—**11**, **20**—**21**, respectively, in structure, we realize the higher electron density of the former. **20** and **21** were hydrogenated more slowly than **5**—**11**, though they have two electron-withdrawing substituents. If they undergo hydrogenation via α-ACs, the α-ACs from **20** and **21** would be more unstable than those of **5**—**11**. Thus, the slow rate may be attributed to the steric hindrance in the formation of α-ACs. It can be considered that the electron-withdrawing effect of substituents accelerates the formation of alkyl complex, and the steric compression of substituents prevents it and the electron-withdrawing effect should overcome the steric hindrance to give α-AC.

It is thus concluded that the electron-withdrawing effect accelerates both the first (alkyl complex formation) and the second (reductive cleavage of the alkyl moiety) steps, while steric compression prevents the first step and accelerates the second step as shown schematically in Fig. 2.

In the first stage, electronic effect (E) and steric effect (S) make $\Delta G_1^{\neq}$ smaller by lowering the free energy of transition state and greater by elevating it, respectively. In the second stage, though it is not evident how E and S affect the transition state, both E and S make $\Delta G_2^{\neq}$ lower by elevating the potential energy of alkyl complex.

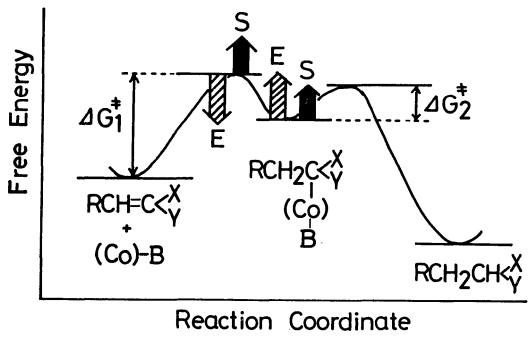

Fig. 2. Schematic presentation of electronic (E) and steric (S) effects of substituents on the hydrogenation.

Nonreactivity of **1**—**2** and **3** would be explained by the absence of steric and electronic acceleration in the second step, respectively, while that of **4** or **12**—**14** by the insufficient electronic acceleration, in the first step. In the hydrogenation of $H_2C{=}C\langle^{X}_{Y}$ type olefinic compounds both electron-withdrawing and steric compression effects of the substituents tend to lower the activation energy of both the two steps, leading to smooth hydrogenation.

On the mechanism of the hydrogenation, Schrauzer and Windgassen stated that the reductive cleavage is apparently catalyzed by cobaloxime(I), which exists in equilibrium with hydridocobaloxime.[3] It is thus understandable that the rate of hydrogenation of olefinic compounds is faster in alkaline solution than in neutral solution as in the case of **5**.

When **5** reacts predominantly with the hydridocobaloxime to form relatively stable α-AC[7] the equilibrium may shift to the hydridocobaloxime, and the concentration of cobaloxime(I), which acts as a reductant of the α-AC, becomes smaller. However, when the alkalinity of the solution becomes higher, the equilibrium shifts to cobaloxime(I) and the rate of of the formation of α-AC decrease, and consequently, the reductive cleavage of the α-AC by cobaloxime(I) will become effective. The mechanism of the hydrogenation is shown in Fig. 3.

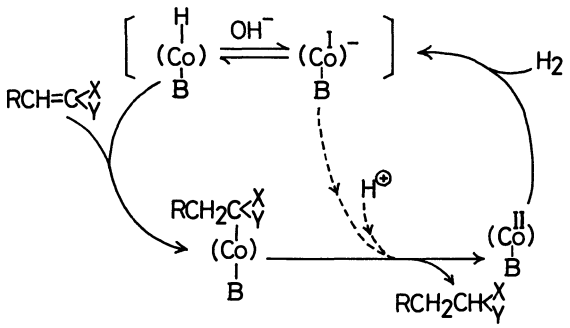

Fig. 3.

Experimental

Catalytic Hydrogenation of Various Olefinic Compounds in the Presence of Pyridino Bis(dimethylglyoximato)cobalt(II). Dimethylglyoxime (0.48 g, 4 mmol) was added to a solution of $CoCl_2 \cdot 6H_2O$ (0.5 g, 2 mmol) in methanol or ethanol, and the mixture was stirred under nitrogen atmosphere for a few min. Aqueous sodium hydroxide (1 ml of 4.87 M, 4.9 mmol), pyridine (0.16 g, 2 mmol) and a substrate (1-10 equivalent to cobalt) were successively added. The flask was purged with hydrogen gas and the solution was then stirred under the atmospheric pressure of hydrogen at room temperature. After absorption of the theoretical amount of hydrogen, the reaction mixture was diluted with water and extracted with ether or methylene chloride. The organic layer was washed with water, dried over anhydrous sodium

sulfate, and concentrated to give the corresponding product which was purified and confirmed by IR and NMR spectra.

Hydrogenation in neutral solution was carried out in a similar way, except for the use of cobaltous acetate in place of cobaltous chloride and sodium hydroxide.

Isolation of α-Cyanoisopropylcobaloxime. Methacrylonitrile (0.25 g, 3.7 mmol) was added to a solution of $CoCl_2 \cdot 6H_2O$ (0.5 g, 2 mmol), dimethylglyoxime (0.48 g, 4 mmol) in aqueous sodium hydroxide (1 ml of 4.87 M solution) and pyridine (0.16 g, 2 mmol). The resulted solution was shaken under hydrogen atmosphere until *ca.* 19 ml (0.9 mmol) of hydrogen was absorbed (6 min). The solvent was then removed *in vacuo* to give crude α-cyanoisopropylcobaloxime (0.9 g). The crude complex showed a sharp absorption of cyano-group at 2200 cm^{-1} in IR spectrum, and characteristic methyl-proton signals (isopropyl; δ 0.7, singlet, 6H; DMG; δ 2.0, singlet, 12H) in NMR spectrum. The complex could not be recrystallized, because it decomposed in ether or chloroform to give black complex whose IR spectrum showed no absorption of CN and alkyl groups. The complex was obtained even when 1.2 ml of aqueous sodium hydroxide (4.87 M solution) was used. Smooth hydrogenation occurred when 1.5 ml of aqueous sodium hydroxide (4.87 M solution) was used.

Deuterogenation of α-Phenylacrylophenone. A solution of anhydrous cobaltous chloride (0.27 g, 2 mmol), dimethylglyoxime (0.48 g, 4 mmol), and α-phenylacrylophenone (2.8 g, 13.5 mmol) in 3.82 M sodium deuteroxide in dideuterium oxide (1.38 ml, 4.7 mmol of NaOD), pyridine (0.16 g, 2 mmol), and methanol-d_1 (30 ml) was shaken under deuterium atmosphere until 289 ml (13 mmol) of D_2 was absorbed 58 min). The reaction mixture was concentrated *in vacuo*, and the residue was extracted with ether. The ether extract was washed with water, dried over anhydrous magnesium sulfate, and evaporated to give an oily product (2.4 g). The crude product was purified by vacuum distillation (124—126 °C/1 mmHg), and the main fraction (1.9 g) crystallized (mp 38.5—41 °C) on standing. NMR spectra of the crude and purified products showed relatively broad signals of α- and β-protons at δ 4.66 and δ 1.50, respectively. The ratio of integration of the signals of phenyl proton, α- and β-proton was 10 : 0.14 : 1.12 in the crude product and 10 : 0.15 : 1.07 in the purified product. The ratio of deuterium distribution in β-carbon to α-carbon was estimated to be 2.5 (crude) and 2.3 (purified), respectively.

Reductive Cleavage of Various Alkyl Complexes. a) Catalytic Cleavage. Catalytic cleavage was carried out in a similar manner to that for hydrogenation of olefinic compounds, except for the use of alkyl complexes instead of olefinic compounds as substrate. α-Phenylethylcobaloxime was recovered quantitatively after reaction for 4 days. α-Cyanoethylcobaloxime and α-methoxycarbonylethylcobaloxime underwent reductive cleavage within 1 hr to give propionitrile and methylpropionate, respectively. *b) Autocatalytic Cleavage.* α-Methoxycarbonylethylcobaloxime underwent reductive cleavage even in the absence of the catalyst when it was dissolved in methanol and stirred under hydrogen atmosphere at room temperature for 1 day. β-Alkyl complexes underwent no reductive cleavage.

β-Alkyl Complex from Dimethyl Itaconate. Dimethyl Itaconate (2.5 g, 1.6 mmol) was added to a catalyst solution (in MeOH) prepared from $CoCl_2 \cdot 6H_2O$ (2.5 g, 10 mmol), dimethylglyoxime (2.45 g, 20 mmol), aqueous sodium hydroxide (10 ml of 4.67 M solution, 47 mmol) and imidazole (4.22 g, 62 mmol), and the resulting solution was shaken under hydrogen atmosphere. After absorption of *ca.* 274 ml (12 mmol) of hydrogen within 26 min, the reaction mixture was poured into water and extracted with methylene chloride. The extract was washed with water, dried over calcium chloride, and concentrated to give an oily product which crystallized by scratching. The crude alkyl complex (1.7 g, 34%) was purified by recrystallization from methanol. Yellow crystals, mp 166 °C (167—168 °C dec.). Spectral data showed typical absorptions for β-alkyl complex; *i. e.*, characteristic absorption of ester (1720—1730 cm^{-1}) in IR and broad doublet signal at δ 2.45 (Co–CH_2; 2H) and broad multiplet (–CH–) and doublet (–CH_2CO–) at δ 2.3—1.9 (3H) in NMR spectrum.

Found: C, 42.29; H, 5.97; N, 16.49%. Calcd for $C_{18}H_{29}N_6O_8Co$: C, 41.87; H, 5.62; N, 16.28%.

When the amount of aqueous hydroxide and imidazole was decreased to about half (5 ml, 24 mmol) and one fourth (0.7 g, 10 mmol), respectively, the formation of alkyl complex was negligible.

The authors are indebted to Mr. H. Matsumoto for the NMR measurements, and members of the Laboratory of Organic Analysis for the microanalyses.

References

1) Part VIII. This Bulletin, **46**, 1892 (1973).

2) G. N. Schrauzer, *Accounts Chem. Res.*, **1**, 97 (1968); G. N. Schrauzer and R. J. Windgassen, *Nature*, **214**, 492 (1967).

3) G. N. Schrauzer and R. J. Windgassen, *J. Amer. Chem. Soc.*, **89**, 1999 (1967).

4) Y. Ohgo, S. Takeuchi, and J. Yoshimura, This Bulletin, **44**, 283 (1971).

5) Y. Ohgo, S. Takeuchi, and J. Yoshimura, *ibid.*, **44**, 583 (1971); *Chem. Lett.*, **1973**, 265.

6) J. Kwiatek, "Catalysis Review," Vol. 1, ed. by H. Heinemann, Marcel Dekker, Inc., New York, (1968), p. 62.

7) It is known that α-AC is formed by the reaction of 5 or 6 with hydridopentacyanocobaltate. (Ref. 6, p. 54).

The Thermal [2+2] Cycloaddition of 1-Halo-2-(9-fluorenylidene)ethylene to Afford Fluorene-9-spiro-1′-[2′-halo-3′-(9-fluorenylidene)-4′-halomethylene]cyclobutane

Fumio Toda, Hiroharu Motomura, and (in part) Hirofumi Oshima
Department of Industrial Chemistry, Faculty of Engineering, Ehime University, Matsuyama 790
(Received July 21, 1973)

The thermal [2+2]cycloaddition products of 1-chloro-(II) and 1-bromo-2-(9-fluorenylidene)ethylene (X) were found to be two head-to-tail dimers, fluorene-9-spiro-1′-[2′-chloro-3′-(9-fluorenylidene)-4′-chloromethylene]-cyclobutane (VI) and its bromo-analog (XI) respectively.

It has previously been reported[1] that the previously-assigned structure[2] 1-chloro-2-(9-fluorenylidene)ethylene (II) for the compound which was produced by the reaction of 9-ethynyl-9-hydroxyfluorene (I) with $SOCl_2$, is erroneous; rather, it is the head-to-head [2+2] cycloaddition dimer of II, 3,4-dichloro-1,2-bis(9-fluorenylidene)cyclobutane (III) (Scheme 1). We have now studied on the structures of the dimers of II and its Br-analog (X), and found that these dimers are two head-to-tail cycloaddition products, fluorene-9-spiro-1′-[2′-chloro-3′-(9-fluorenylidene)-4′-chloromethylene]cyclobutane (VI) and its Br-analog (XI) respectively.

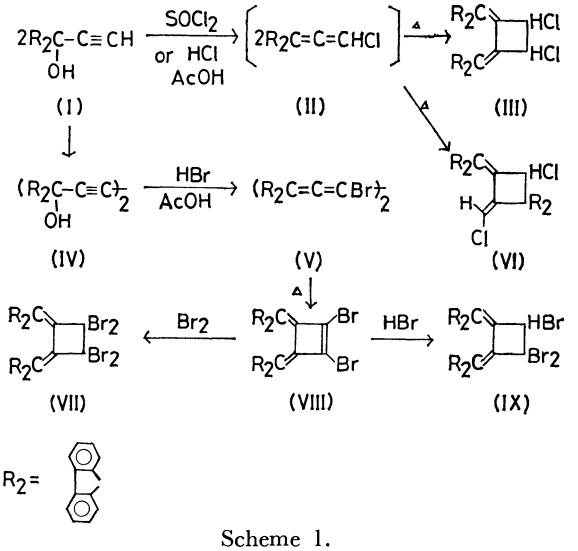

Scheme 1.

On the reaction of I with concd HCl in AcOH at 0 °C, II could not be isolated, but its head-to-tail cycloaddition dimer (VI) was obtained. The UV spectral data of VI were identical with those recorded for the dimer of II.[1] The heating of the Br-analog of II (X), which could be isolated by the reaction of I with concd HBr in AcOH, afforded the head-to-tail cycloaddition dimer (XI). The spectral data of XI were comparable to those of VI.

It is clear that the dimers of II and X were not the heat-to-head dimers, III and XII respectively, because the UV spectra of VI (276 (ε, 54000) and 375 nm (30000)) and XI (274 (ε, 51400) and 380 nm (32800)) differ widely from those of 3,3,4,4-tetrabromo- (VII) (278 (ε, 38600), 338 (9000) and 502 nm (23900)) and 3,3,4-tribromo-1,2-bis(9-fluorenylidene)cyclobutane (IX) (270 (ε, 30500), 328 (12700) and 472 nm (21400)), which were prepared by the addition of Br_2 and HBr

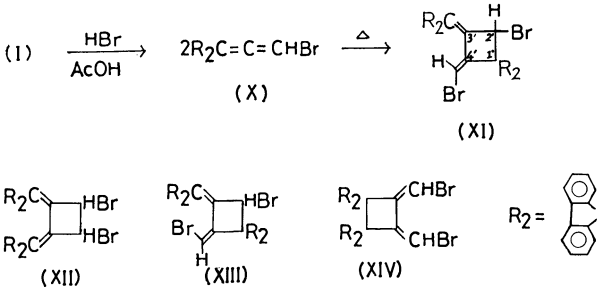

Scheme 2.

respectively to 1,2-dibromo-3,4-bis(9-fluorenylidene)-cyclobut-1-ene (VIII). The cyclobutene (VIII) was prepared by the intramolecular cycloaddition of 2,3-dibromo-1,4-bis(9-fluorenylidene)buta-1,3-diene (V), which had itself been obtained by the reaction of the diacetylenediol (IV) with concd HBr in AcOH.

Any possibility that the dimer of II and X are the tail-to-tail cyclodimerization products (for example, XIV for the dimer of X) can be rejected, because the absorption bands of the dimers of II and X in the visible region are not assignable to the tail-to-tail dimers containing only a buta-1,3-diene chromophore. In order to clarify the structures of VI and XI, some addition and elimination reactions were investigated on XI.

The reaction of XI with HBr afforded the 1,4-

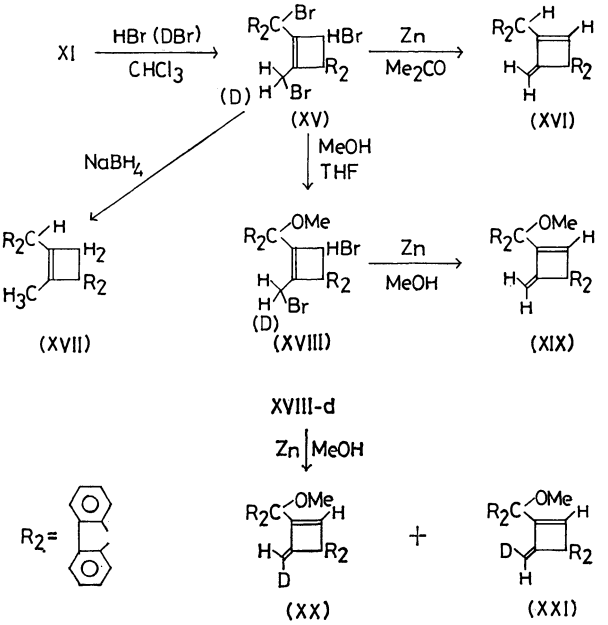

Scheme 3.

addition product (XV). The heating of XV in MeOH-THF afforded the methanolysis product (XVIII). On the NMR spectra, the CH_2 of both XV and XVIII appeared as two AB-type doublets, centered at 6.20 and 6.45 and at 5.88 and 6.11 τ respectively. Because these signals were little affected by raising temperature to 150 °C, the magnetic nonequivalence of the two hydrogens of CH_2 is probably due to an assymmetry effect. The CHD proton signals of XV-*d* and XVIII-*d* appeared as two singlets at 6.22 and 6.43 and at 5.92 and 6.13 τ respectively. This splitting of the CHD proton singal is also due to an assymmetry effect. These data support the structure of XI.

The reduction of XV with $NaBH_4$ afforded XVII, which showed CH, CH_2, and CH_3 signals at 4.95 (s), 7.54 (q), and 8.53 τ (t) respectively. This formation of the CH_3 group supports the presence of the *exo*-methylene moiety in XI. The multiplicity of the latter two signals suggests the presence of a long-range coupling between them.

The reaction of XV and XVIII with Zn afforded XVI and XIX respectively. The NMR signals of the $=CH_2$ protons of XVI and XIX appeared at 5.83 and 5.98 and at 5.93 and 6.06 τ respectively. The absence of spin-spin coupling between the two geminal protons of $=CH_2$ is likely, because it has been established that such a coupling of the *exo*-methylene bonded to cyclobutene ring is not detectable.[3] Of the two $=CH_2$ proton signals of XVI and XIX, that at higher magnetic field can be assigned to the hydrogen directed toward the spiro-fluorene ring, therefore it is shielded by this ring.

XVIII-*d*, which was derived from XV-*d*, was allowed to react with Zn to afford a 1 : 1 mixture of XX and XXI. In the NMR spectrum of this mixture, the intensities of the signals at both 5.96 and 6.09 τ were about one half of those of the corresponding signals of XIX. These results also support the structure of XI.

The addition of Br_2 to XI afforded the 1,4-addition product (XXII). The treatment of XXII with KOH–MeOH at room temperature and at an elevated temperature under reflux afforded XXIII and XXVI respectively. The latter may be formed by the 1,4-elimination of HBr, accompanied by the methanolysis of Br on the fluorene ring, because the heating with KOH–MeOH of XXV, which had been prepared by the methanolysis of XXII, afforded XXVI (Scheme 4).

The heating of XI with Zn in MeOH afforded XXIV, which showed three proton signals at 3.28 (=CH), 5.08 (=CH), and 5.15 τ (CH), in an equal integral ratio. The addition of Br_2 to XXIV afforded XXVII in a 60% yield. The dehydrobromination of XXVII with KOH–MeOH afforded the original dimer (XI). All these reactions again support the structure of XI (Scheme 4).

The geometry around the bromomethylene moiety of XI was determined on the basis of the following data. The signal of the olefinic proton of XI appeared at such a lower field that it overlapped the signals of aromatic protons (1.90—2.86 τ), probably because of a deshielding effect by the biphenylene moiety bonded to *exo*-methylene carbon. For by the same reason, the olefinic proton of VI appeared at 2.85 τ. If the reverse geometry of XI (XIII) is correct, this olefinic proton must be shielded by the spiro-fluorene ring and resonate at a much higher magnetic field. Studies of a molecular model also suggest that the geometry of XIII is unfavorable, because of a serious steric repulsion between the 9-fluorenylidene group and the Br of the bromomethylene moiety.

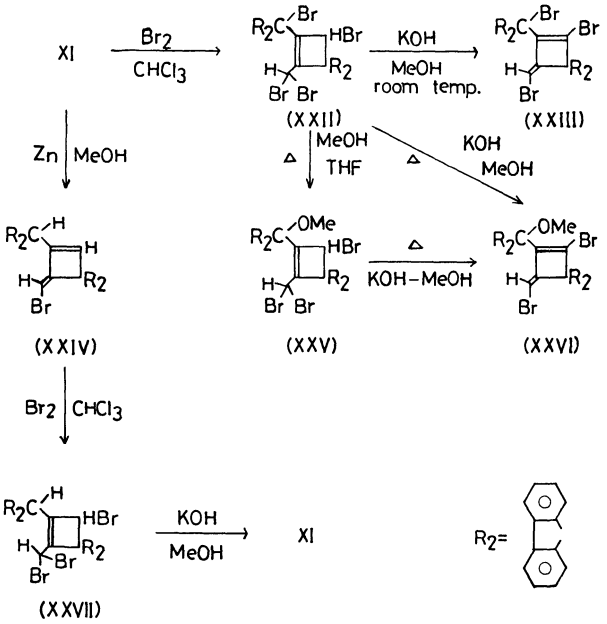

Scheme 4.

However, there is still a question why the difference between the chemical shifts of the two methylene protons of XVI or XIX is so small-less than 0.15 ppm. A plausible answer to the question is that the H_A of XVI or XIX is shielded by the fluorene-ring (A) which is arranged almost perpendicular to the four-membered ring and then faces H_A, and that the shielding is comparable to that of H_B by the fluorene-ring (B) (see the XXVIII shown in Scheme 5).

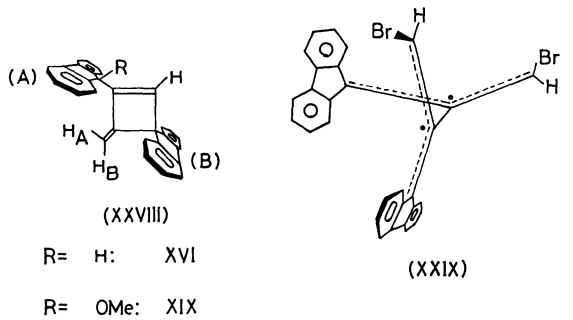

Scheme 5.

It has been reported[4,5] that the thermal [2+2] cycloaddition of allene often proceeds *via* the biallyl biradical intermediate, and that the most easily formed conformation for the biradical was that in which the two flat allylic ends were orthogonal and in which the larger one of the substituents on each terminal carbon was inward; ring closure was assumed to be faster than the rotation of the parts of the allylic system to form other conformers. However, some instances which do not follow this tendency because of steric bulkiness have also been reported.[6,7]

The dimerization of X can be formulated by assuming XXIX as an intermediate (Scheme 5). So as to avoid the steric interaction between the fluorene ring and Br, the cyclization of XXIX must proceed *via* its favorable conformation, in which Br is outward, thus finally affording the dimer of the most favorable geometry around the *exo*-methylene moiety (XI).

The contrast between the unusual[8,9] head-to-tail dimerization of X to afford XI and the head-to-head dimerization of 3-chloro-1,1-diphenylpropa-1,2-diene (II) to afford 3,4-dichloro-1,2-bis(diphenylmethylene)-cyclobutane (III)[1] is probably due to a much bigger steric interaction between non-flexible fluorene rings than that between flexible diphenylmethyl groups. It has been reported that the four phenyl rings of III are arranged as a propeller, and that they are free from steric interactions among them.[4]

Experimental

All the melting points are uncorrected. The IR, UV, and NMR spectra were measured in Nujol mull, $CHCl_3$, and $CDCl_3$ respectively. The mass spectra were measured with an ionization energy of 75 eV.

Reaction of II with HCl. To an ice-cooled solution of II (6.2 g) in AcOH (60 ml), we added concd HCl (10 ml) under stirring over a period of 30 min. The stirring was continued for 1.5 hr under cooling with an ice-bath. The solid thus precipitated was filtered and washed with water and then with MeOH. The recrystallization of the dried solid from AcOEt afforded VI as orange prisms; 5.5 g (80%); mp 225 °C (lit,[1] mp 223—224 °C). NMR: 1.9—2.8 (m, Ph, 16H), 2.85 (s, =CH, 1H), and 4.24 τ (s, CH, 1H).

Isolation of X. Into an ice-cooled solution of II (4.73 g) in AcOH (60 ml), concd HBr (10 ml) was stirred over a of 30 min; the stirring was then continued for 1.5 hr under cooling with an ice-bath. The solid thus precipitated was filtered and washed repeatedly with water and then with MeOH. The solid was dissolved in ice-cooled acetone. Water was added to this solution, after which the solution was allowed to remain in a refrigerator to afford X as yellow needles; 5.15 g (86%). During the measurement of the melting point, X dimerized to XI and melted at 207.5—208.5 °C. IR: 1940 cm^{-1} (C=C=C).

Found: C, 67.15; H, 3.35%. Calcd for $C_{15}H_9Br$: C, 66.94; H, 3.37%.

Thermal Dimerization of X. A solution of X (3.8 g) in benzene (50 ml) was heated under reflux for 30 min. The crude crystals which remained after the evaporation of the solvent were recrystallized from AcOEt to afford XI as orange prisms; 3.0 g (80%); mp 207.5—208.5 °C. IR: 1150 cm^{-1}; λ_{max}: 266 (ε, 46800), 274 (51400), and 380 nm (32800); NMR: 1.9—2.8 (m, Ph and =CH, 17H) and 4.15 τ (s, CH, 1H).

Found: C, 67.25; H, 3.34%. Calcd for $C_{30}H_{18}Br_2$: C, 66.94; H, 3.37%.

Synthesis of VIII. Into an ice-cooled solution of IV (0.6 g) in AcOH (30 ml), we added concd HBr (5 ml) over a period of 30 min. The stirring was continued for 1.5 hr. The reddish-purple crystals thus formed were filtered and washed repeatedly with water and then with MeOH to afford V; 0.46 g (54%); IR: 1945 cm^{-1} (C=C=C). A solution of V (0.4 g) in benzene (10 ml) was heated under reflux for 30 min. The recrystallization from AcOEt of the crude product obtained by the evaporation of benzene afforded VIII as orange yellow needles; 0.28 g (70%); mp 221.5—222 °C. λ_{max}: 226 (ε, 53700), 275 (54900), 343 (32300), and 375 nm (31600).

Found: C, 67.46; H, 2.90%. Calcd for $C_{30}H_{16}Br_2$: C, 67.19; H, 3.01%.

Addition of Br_2 to VIII. Into a solution of VIII (0.2 g) in $CHCl_3$ (50 ml), a solution of Br_2 (0.15 g) in $CHCl_3$ (5 ml) was stirred over a period of 20 min. After the stirring had continued for 30 min, the solvent was evaporated to leave crude crystals. The recrystallization of the crystals from AcOEt afforded VII as reddish-purple prisms; 0.22 g (80%); mp 235—237 °C. λ_{max}: 278 (ε, 38600), 338 (8950), and 502 nm (23900); NMR: 1.35—3.36 τ (m, Ph).

Found: C, 51.53; H, 2.40%. Calcd for $C_{30}H_{16}Br_4$: C, 51.77; H, 2.32%.

Addition of HBr to VIII. Through a solution of VIII (0.2 g) in $CHCl_3$ (50 ml), HBr was bubbled for 10 min. The subsequent evaporation of the solvent left crude crystals. Recrystallization from AcOEt afforded IX as reddish-purple needles; 0.22 g (85%); mp 219—221 °C. λ_{max}: 270 (ε, 30500), 328 (12700), and 472 nm (21400); NMR: 1.55—3.25 (m, Ph, 16H) and 3.90 τ (s, CH, 1H).

Found: C, 58.54; H, 2.82%. Calcd for $C_{30}H_{17}Br_3$: C, 58.38; H, 2.78%.

Addition of HBr to XI. Through a solution of XI (0.93 g) in $CHCl_3$ (20 ml), HBr was bubbled for 5 min. The subsequent evaporation of the solvent left crude crystals. Recrystallization from AcOEt afforded XV as pale yellow plates; 1.0 g (94%) mp 165—167 °C. λ_{max}: 253 (ε, 90000), 280 sh (53600), 295 sh (34500), and 306 sh nm (19200); NMR: 1.9—2.9 (m, Ph, 16H), 4.79 (s, CH, 1H), 6.20 (d, J=10 Hz, CH, 1H), and 6.45 τ (d, J=10 Hz, CH, 1H).

Found: C, 57.92; H, 2.94%. Calcd for $C_{30}H_{19}Br_3$: C, 58.19; H, 3.09%.

The addition of DBr to XI by means of the same procedure as that of HBr addition afforded XV-*d* in a 90% yield. NMR: 1.9—2.9 (m, Ph, 16H), 4.79 (s, CH, 1H), 6.22 (s, CHD, 1/2H), and 6.43 τ (s, CHD, 1/2H).

Methanolysis of XV. A solution of XV (0.46 g) in MeOH–THF (1 : 1) (30 ml) was heated under reflux for 1 hr. The recrystallization from AcOEt of the crude crystals obtained by the evaporation of the solvent afforded XVIII as pale yellow plates; 0.39 g (93%); mp 173—175 °C. IR: 1085 cm^{-1} (OMe); λ_{max}: 274 (ε, 64300), 285 sh (5000), and 305 sh nm (1100); NMR: 2.0—2.8 (m, Ph, 16H), 5.13 (s, CH, 1H), 5.88(d, J=10 Hz, 1H), 6.11 (d, J=10 Hz, 1H), and 7.06 τ (s, OCH_3, 3H).

Found: C, 65.48; H, 3.73%. Calcd for $C_{31}H_{22}OBr_2$: C, 65.28; H, 3.88%.

The methanolysis of XV-*d* by means of the same procedure as was used for XV afforded XVIII-*d* in a 90% yield. NMR: 2.1—2.8 (m, Ph, 16H), 5.13 (s, CH, 1H), 5.91 (s, CHD, 1/4H), 6.12 (s, CHD, 3/4H), and 7.07 τ (s, OCH_3, 3H).

Debromination of XVIII. A mixture of XVIII (0.2 g), Zn-powder (0.7 g), and MeOH (70 ml) was heated under reflux for 1 hr. The Zn-powder was then filtered off, after which the filtrate was evaporated to dryness to leave crude crystals. Recrystallization from AcOEt then afforded XIX as pale yellow prisms; 0.99 g (68%); mp 175.5—177 °C. IR: 1665 (C=C) and 1110 and 1080 cm^{-1} (OMe); λ_{max}: 249 (ε, 27400), 268 (25600), 273 sh (24700), 297 sh (10000), and 310 nm (9300); NMR: 2.2—2.8 (m, Ph, 16H), 3.28 (s, =CH, 1H), 5.93 (s, =CH, 1H), and 6.06 τ (s, =CH, 1H); *m/e* (relative intensity): 410 (M^+, 10), 379 (M^+–OMe, 10), 215 (M^+–(9-methoxyfluorenyl), 24), 195 (9-methoxyfluorenyl, 100), and 180 (fluorenone, 22).

Found: C, 90.59; H, 5.22%. Calcd for $C_{31}H_{22}O$: C, 90.69; H, 5.40%.

The debromination of XVIII-*d* with Zn by means of the same procedure as was used for XVIII afforded a 1 : 1 mixture of XX and XXI. NMR: 2.2—2.8 (m, Ph, 16H), 3.29 (s, =CH, 1H), 5.96 (s, =CHD, 1/2H), 6.09 (s, =CHD, 1/2H), and 7.01 τ (s, OCH_3, 3H).

Debromination of XV. A mixture of XV (0.7 g), Zn-powder (2 g), and acetone (50 ml) was heated under reflux for 1.5 hr. The Zn-powder was then filtered off, after which the filtrate was evaporated to dryness to leave crude crystals. Recrystallization from AcOEt afforded XVI pale yellow prisms; 0.38 g (90%); mp 177—179 °C. IR: 1660 (C=C) and 880 cm^{-1} (=CH); λ_{max}: 252 (ε, 87700), 264 (79500), 290 (32700), 303 (29200), and 309 nm (23400); NMR: 2.1—2.9 (m, Ph, 16H), 3.41 (s, =CH, 1H), 4.99 (s, CH, 1H), 5.83 (s, $=CH_2$, 1H), and 5.98 (s, $-CH_2$, 1H); *m/e* (relative intensity): 380 (M^+, 11), 215 (M^+-fluorenyl, 100), and 165 (fluorenyl, 30).

Found: C, 94.77; H, 5.06%. Calcd for $C_{30}H_{20}O$: C, 94.70; H, 5.30%.

Reduction of XV with $NaBH_4$. A solution of XV (0.68 g) and $NaBH_4$ (0.4 g) in MeOH-THF (1 : 1) (80 ml) was allowed to remain at room temperature for 1 hr. The subsequent evaporation of the solvent left crude crystals, which were then washed with water and dried. Recrystallization from MeOH-AcOEt afforded XVII as pale yellow needles; 0.4 g (90%); mp 162—163 °C. λ_{max}: 266 sh (ε, 25900), 269 (26200), 274 sh (22700), 280 sh (19400), 296 (10000), and 304 nm (10800); NMR; 2.1—2.9 (m, Ph, 16H), 4.95 (s, CH, 1H), 7.54 (q, J=2.5 Hz, CH_2, 2H), and 8.53 τ (t, J=2.5 Hz, CH_3, 3H).

Found: C, 94.05; H, 5.50%. Calcd for $C_{30}H_{22}$: C, 94.20; H, 5.80%.

Addition of Br_2 to XI. To a solution of XI (0.5 g) in $CHCl_3$ (20 ml), we added a solution of Br_2 (0.5 g) in $CHCl_3$ (5 ml) over a period of 30 min. The crude crystals which remained after the evaporation of the solvent were recrystallized from acetone to afford XXII as pale yellow prisms; 0.48 g (83%); mp 161—162 °C. λ_{max}: 253 (ε, 90000), 280 sh (53600) 295 sh (34500), and 306 sh nm (19200); NMR: 1.95—2.85 (m, Ph, 16H), 3.34 (s, $CHBr_2$, 1H), and 4.89 τ (s, CHBr, 1H).

Found: C, 51.55; H, 2.74%. Calcd for $C_{30}H_{18}Br_4$: C, 51.62; H, 2.60%.

Methanolysis of XXII. A solution of XXII (1.08 g) in MeOH-THF (1 : 1) (60 ml) was heated under reflux for 2 hr. The subsequent evaporation of the solvent left crude crystals. Recrystallization from acetone afforded XXV as pale yellow prisms; 0.84 g (90%); mp 170.5—171.5 °C. IR: 1645 (C=C) and 1100 and 1090 cm^{-1} (OMe); λ_{max}: 244 (ε, 26000), 275 (24300), and 285 nm (19900); NMR: 2.1—2.7 (m, Ph, 16H), 2.80 (s, $CHBr_2$, 1H), 5.28 (s, CHBr, 1H), and 7.07 τ (s, OCH_3, 3H).

Found: C, 57.10; H, 2.95%. Calcd for $C_{31}H_{21}OBr_3$: C, 57.35; H, 3.25%.

Dehydrobromination of XXII. A mixture of finely-powdered XXII (0.53 g), KOH (1 g), and MeOH (20 ml) was stirred at room temperature for 1 hr. The crude crystals thus formed were filtered and washed with water and MeOH. Recrystallization from AcOEt afforded XXIII as pale yellow prisms; 0.41 g (86%); mp 166.5—168 °C. λ_{max}: 253 (ε, 50300), 297 sh (13300), and 308 sh (7200); NMR: 2.15—2.85 τ (m, Ph and =CH).

Found: C, 58.50; H, 2.76%. Calcd for $C_{30}H_{17}Br_3$: C, 58.38; H, 2.78%.

Reaction of XXII with KOH-MeOH. A mixture of finely-powdered XXII (0.53 g), KOH (1.5 g) and MeOH (60 ml) was heated under reflux for 2 hr. The crude porduct formed by the addition of water to the reaction mixture was filtered, washed with water, and dried. Recrystallization from AcOEt afforded XXVI as pale yellow prisms; 0.37 g (63%); mp 179.5—181.5 °C. IR: 1070 cm^{-1} (OMe); λ_{max}: 243 (ε, 33600), 257 (33200), 271 (35800), and 309 nm (5900); NMR: 2.15—2.80 (m, Ph, 16H), 3.10 (s, =CH, 1H), and 7.15 τ (s, OCH_3, 3H).

Found: C, 65.55; H, 3.23%. Calcd for $C_{31}H_{20}OBr$: C, 65.52; H, 3.55%.

Dehydrobromination of XXV. A mixture of XXV (0.15 g), KOH (0.5 g), and MeOH (20 ml) was heated under reflux for 1 hr. The crude product formed by the addition of water to the reaction mixture was filtered, washed with water, and dried. Recrystallization from AcOEt afforded XXVI: 0.14 g (71%).

Reduction of XI with Zn. A mixture of XI (1 g), Zn-powder (2.5 g), and MeOH (100 ml), was heated under reflux for 2 hr. The Zn-powder was then filtered off, after which the evaporation of the solvent left crude crystals. Recrystallization from AcOEt afforded XXIV as colorless plates; 0.6 g (70%); mp 161—163 °C. IR: 1650 cm^{-1} (C=C); λ_{max}: 258 (ε, 75000) and 303 nm (28000); NMR: 2.2—2.9 (m, Ph, 16H), 3.28 (s, =CH, 1H), 5.08 (s, CHBr, 1H), and 5.15 τ (s, CH, 1H).

Found: C, 78.17; H, 3.91%. Calcd for $C_{30}H_{19}Br$: C, 78.44; H, 4.17%.

Addition of Br_2 to XXIV. A solution of XXIV (0.32 g) and Br_2(0.2 g) in $CHCl_3$ (10 ml) was allowed to remain at room temperature for 2 hr. The subsequent evaporation of the solvent left an oil, which was crystallized by the addition of a small amount of MeOH. Recrystallization from AcOEt afforded XXVII as colorless plates; 0.26 g (60%); mp 178—179 °C. λ_{max}: 270 (ε, 27800) and 304 nm (4600); NMR: 1.8—2.9 (m, Ph, 16H), 3.64 (s, $CHBr_2$, 1H), 4.93 (s, CHBr, 1H), and 5.23 τ (s, CH, 1H).

Found: C, 57.88; H, 2.98%. Calcd for $C_{30}H_{19}Br_3$: C, 58.16; H, 3.07%.

Dehydrobromination of XXVII. A mixture of XXVII (0.15 g), KOH (0.5 g), and MeOH (20 ml) was heated under reflux for 2 hr. The crude crystals obtained by the addition of water to the reaction mixture were recrystallized from AcOEt to afford XI; 0.12 g (92%).

References

1) T. Nagase, This Bulletin, **34**, 139 (1961).

2) G. F. Hennion and B. R. Fleck, *J. Amer. Chem. Soc.*, **77**, 3253 (1955).

3) C. F. Wilcox and D. L. Nealy, *J. Org. Chem.*, **28**, 3446 (1963).

4) S. R. Byrn, E. Maverick, O. J. Muscio, Jr., K. N. Trueblood, and T. L. Jacobs, *J. Amer. Chem. Soc.*, **93**, 6680 (1971), and the references cited therein.

5) T. L. Jacobs and R. C. Kammerer, *ibid.*, **94**, 7190 (1972).

6) W. R. Moore, R. D. Bach, and T. M. Ozretich, *ibid.*, **91**, 5918 (1969).

7) E. V. Dehmlow and G. C. Ezimora, *Tetrahedron Lett.*, **1972**, 1265.

8) It has been reported that the great majority of the [2+2]cyclodimerizations of allenes proceeds in a head-to-head or tail-to-tail manner; J. R. McClenon, Ph, D. Thesis, University of California, 1964; N. D. Epiotis, *J. Amer. Chem. Soc.*, **95**, 5624 (1973), and the references cited therein.

9) Recently, an unusual head-to-tail cyclodimerization of 1,1-dialkyl-3-cyanopropa-1,2-diene was reported; C. W. N. Cumper, Z. T. Fomum, P. M. Greaves, and S. R. Landor, *J. Chem. Soc. Perkin II*, **1973**, 885.

Peptides. V. Some Carbonates of Ethyl 2-Hydroximino-2-cyanoacetate and Related Compounds as Esterification Reagents for Peptide Synthesis

Masumi ITOH

Research Laboratories, Fujisawa Pharmaceutical Co., Ltd. Kashima-cho, Higashiyodogawa-ku, Osaka 532

(Received August 22, 1973)

Some carbonates (III) of ethyl 2-hydroximino-2-cyanoacetate (Ia) and 2-hydroximino-2-cyanoacetamide (Ib) were prepared and utilized as simple esterification reagents for acylamino acids.

The applications of some carbonates in the preparation of acylamino acid esters[1,2] have been reported, but the reactivity of these carbonates is rather low and these applications have been limited to the preparation of aryl esters. The present author wishes to report a generally-applicable esterification of acylamino acids by the use of carbonates (III) of strongly acidic oximes such as ethyl 2-hydroximino-2-cyanoacetate (Ia),[3] which has previously been proposed as an additive for racemization suppression.[4]

The oxime carbonates were prepared, as is shown in Scheme 1, by the reaction of oximes with alkyl or aryl chloroformates under the conditions of a Schotten-Baumann reaction (method A), or through a labile chloroformate, ethyl 2-chloroformyloximino-2-cyanoacetate (IV), prepared from Ia with phosgene in an anhydrous organic solvent (method B). The carbonates thus prepared are listed in Table 1. These carbonates are generally stable enough and remain unchanged over one year in closed bottles, but some of them are extremely unstable and are difficult to prepare. Ethyl 2-*t*-amyloxycarbonyloximino-2-cyanoacetate (IIIm; R_1=*t*-amyl), for example, was prepared by Method B, but it decomposed instantly after characterization by taking its infrared (IR) spectrum.

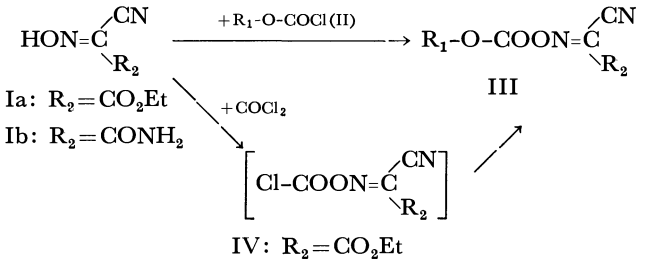

Scheme 1.

Preliminary experiments on the reaction of oxime carbonates with *N*-benzyloxycarbonylglycine in an attempt to prepare the corresponding esters were done in the presence of a tertiary base at room temperature; by the help of thin layer chromatography (tlc) on silica gel G, it was noticed that the reaction does not take place in the absence of base or in the presence of water. The reactivity of carbonates (III) is parallel to the acidity of the parent oximes, and the carbonates of 2-hydroximinopropane,[5] 1-hydroximinoethane,[6] 1-hydroximino-2-propanone[7] (pK_a 8.4), and diethyl 2-hydroximinomalonate[8] (pK_a 7.1) were less reactive. Thus, Ia (pK_a 4.6) and 2-hydroximino-2-cyanoacetamide[9] (Ib, pK_a 5.2) were selected as suitable parent oximes from among them. The rate of esterification depends largely on the basicity of the tertiary amines

TABLE 1. SOME CARBONATES OF VARIOUS OXIMES

R_1-O-COON=C(R_2)(R_3) (III)

	R_1	R_2	R_3	Method	Yield (%)	IR $\nu^{C=O}$ (cm^{-1})
IIIa	Me	$CONH_2$	CN	A	82	1810, 1720, 1685
b	Et	$CONH_2$	CN	A	84	1800, 1715, 1685
c	Bu (iso)	$CONH_2$	CN	A	58	1795, 1720, 1690
d	Me	COOEt	CN	A	82	1800, 1740
				B	87	
e	Et	COOEt	CN	A	74	1805, 1755, 1735
f	Bu (iso)	COOEt	CN	A	58	
g	Bzl	COOEt	CN	A	80	1795, 1735
h	Allyl	COOEt	CN	A	62	1810, 1735
i	C_6H_4-NO_2 (*p*)	COOEt	CN	B	37	1810, 1735
j	C_6H_2-Cl_3 (2, 4, 5)	COOEt	CN	B	83	1815, 1740
k	C_6Cl_5	COOEt	CN	B	42	1820, 1745
l	CH_2CCl_3	COOEt	CN	A	80	1810, 1755
m	Amyl (*t*)	COOEt	CN	A	40	1810, 1740
n	Et	Me	Me	A	80	1770
o	Et	H	Me	A	33	1765
p	Et	H	COMe	A	45	1780, 1700
q	Et	COOEt	COOEt	A	79	1795, 1745

Table 2. The yields of esters VI and VII under the various conditions

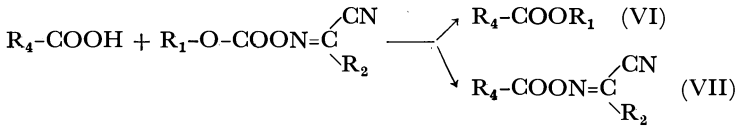

	R_1	R_2	R_4	Base/Solvent	Yield (%) VI	Yield (%) VII
1	Me	COOEt	C_6H_5-	TEA/MeOH	66.1	0
2	Me	COOEt	C_6H_5-	DMA/CH_2Cl_2	0	56.8
3	Et	$CONH_2$	C_6H_5-	TEA/THF	66.7	11.2
4	Et	COOEt	C_6H_5-	TEA/EtOAc	44.0	36.6
5	Bu (iso)	COOEt	C_6H_5-	TEA/EtOAc	95.5	trace
6	Et	$CONH_2$	-$(CH_2)_2$-[a]	TEA/THF	64.4	11.9
7	Et	COOEt	$HOCH_2$-[a]	TEA/THF	95.0[17]	
8	Me	COOEt	Z-Gly-	NEM/CH_2Cl_2	90.9	
9	Me	$CONH_2$	Z-Gly-	TEA/$CHCl_3$-MeOH (2 : 1)	98.0	
10	Et	$CONH_2$	Z-Gly-	TEA/EtOAc-THF (1 : 1)	92.4	
11	Bu (iso)	COOEt	Z-Gly-	TEA/THF	98.0	
12	Bzl	COOEt	Z-Gly-	TEA/Dioxane	95.0	
13	Et	COOEt	Z-Trp-	TEA/EtOAc	92.9	
14	Et	$CONH_2$	Z-Phe-	TEA/EtOAc	95.0	
15	Me	COOEt	H-Phe-[a]	TEA/$CHCl_3$	50.6	

a) Two equivalents of reagents were used. TEA = triethylamine, DMA = *N*,*N*-dimethylaniline, NEM = *N*-ethylmorpholine. Abbreviations used throughout this work are those recommended by IUPAC-IUB commission on biochemical nomenclature (*J. Biol. Chem.*, **247**, 977 (1972)).

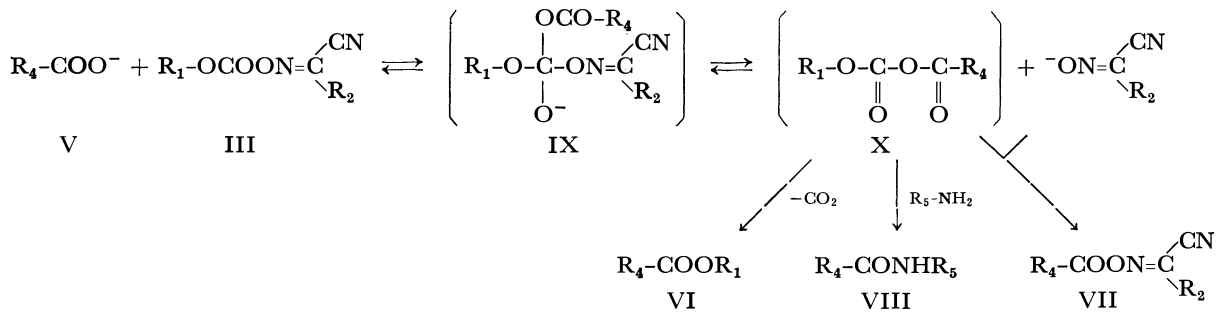

Scheme 2.

used and on the polarity of the solvents used. The reaction was completed fast by the use of a stronger base in a polar solvent.

When benzoic acid was used as a model, reverse esters, ethyl 2-benzoyloximino-2-cyanoacetate (VIIa) or 2-benzoyloximino-2-cyanoacetamide (VIIb), were obtained as by-products, accompanied by ordinary esters. The yield of the reverse esters varied depending upon the substituents of the carbonates, bases, and solvents used. The yield of VIIa increased up to 56.8% when the reaction of benzoic acid with ethyl 2-methyloxycarbonyloximino-2-cyanoacetate (IIId) was carried out using *N*,*N*-dimethylaniline in dichloromethane, while it was suppressed completely by the use of triethylamine in methanol.

In the case of *N*-benzyloxycarbonylglycine, on the contrary, the yields of such reverse esters are negligible. The esters prepared are summarized in Table 2. IIId and ethyl 2-ethyloxycarbonyloximino-2-cyanoacetate (IIIe) were also allowed to react with L-phenylalanine and hydroxyacetic acid to afford fully-protected acids, methyl *N*-methyloxycarbonyl-L-phenylalaninate and ethyl ethyloxycarbonyloxyacetate respectively. Some of the esters prepared were subjected to gas chromatography (Examples 6 and 7 in Table 2) and to mass spectrometry (Examples 8, 12, and 15 in Table 2) in order to characterize them. This procedure might be suitable for obtaining a simple characterization of multifunctional acids.

This esterification may proceed through a mixed anhydride-type intermediate (X), as is shown in Scheme 2. When the intermediate, X, is stable enough and when its decarboxylation is rather slow, it may react with the oxime anion to afford the reverse ester, VII. This mechanism is supported by the peptide formation from *N*-benzyloxycarbonylamino acids with amino acid esters, using ethyl 2-isobutyloxycarbonyloximino-2-cyanoacetate (IIIf) as a coupling reagent, at −15 °C. However, its use does not show remarkable advantages over the usual mixed anhydride method, because it requires conditions similar to the usual ones and it will act as an esterification reagent

Table 3. Some active esters of acylamino acids

$$R_4\text{-COOH} + R_1\text{-O-COON=C}\begin{matrix}\text{CN}\\ R_2\end{matrix} \longrightarrow R_4\text{-COOR}_1 + \text{HON=C}\begin{matrix}\text{CN}\\ R_2\end{matrix}$$

R_1	R_2	R_4	Base/Solvent	Yield (%)	Ref.
$-C_6H_4$-NO_2 (*p*)	$CONH_2$	Z-Phe	TEA/THF	60.0	10a
$-C_6H_4$-NO_2 (*p*)	COOEt	Z-Phe	NEM/CH_2Cl_2	47.0	
$-C_6H_4$-NO_2 (*p*)	COOEt	Z-Pro	TEA/EtOAc	54.0	10a
$-C_6H_4$-NO_2 (*p*)	COOEt	Z-Gly	TEA/EtOAc	63.0	11
$-C_6H_4$-NO_2 (*p*)	COOEt	Z-Cys (Bzl)	TEA/EtOAc	62.0	12
$-C_6H_4$-NO_2 (*p*)	COOEt	Z-Glu	TEA/DMF	44.3	12
$-C_6H_2Cl_3$ (2,4,5)	COOEt	Z-Phe	TEA/EtOAc	79.5	11
$-C_5H_2Cl_3$ (2,4,5)	COOEt	Z-Gly	TEA/EtOAc	80.2	14
$-C_6Cl_5$	COOEt	Z-Gly	TEA/EtOAc	78.6	10b, 11
$-C_6Cl_5$	COOEt	Z-Glu	TEA/DMF	62.5	13

for acylamino acid unless the reaction is performed at low temperature.

The aryl esters of *N*-benzyloxycarbonylamino acids were prepared by the use of ethyl 2-(*p*-nitrophenyl)-oxycarbonyloximino-2-cyanoacetate (IIIi), ethyl 2-(2,4,5-trichlorophenyl)-oxycarbonyloximino-2-cyanoacetate (IIIj) and ethyl 2-(pentachlorophenyl-)oxycarbonyloximino-2-cyanoacetate (IIIk), in moderate yields, as is shown in Table 3.

Experimental

The capillary melting points were observed on a Hoover "Uni-Melt" apparatus and are uncorrected. The optical rotations were determined with a JASCO optical rotatory dispersion recorder, Model ORD/UV-5. The gas-liquid chromatographic work was done with a Varian Aerograph, Model A-700, using a column (3/8 in×10 ft) packed with SF-96 on Neopak (60/80), and on a Shimadzu gas chromatograph, GC-2C, using a column (3 mm×1.5 m) packed with 5% SE-30 on Shimailte W (60/80). The spectrometers used throughout this work were as follows: IR spectra: Hitachi Model EPI-S2; nuclear magnetic resonance spectra: Varian A-60, and mass spectra: JEOLCO Model JMS 01 SG.

Materials. Commercially-available methyl, ethyl, isobutyl, trichloroethyl, and benzyl chloroformates were purchased and used for the preparation of the carbonates. The allyl chloroformate was prepared according to the literature.[15]

The Preparation of Oxime Carbonates (III). A-i) In an Aqueous Solution: Chloroformate (II, 0.1 mol) was added dropwise to a suspension of ethyl 2-hydroximino-2-cyanoacetate sodium salt[3] (16.4 g, 0.1 mol) or 2-hydroximino-2-cyanoacetamide sodium salt[3] (13.5 g, 0.1 mol) in a mixture of acetone (15 ml) and water (100 ml) at 0—+5 °C. The mixture was then stirred for 3 hr while the pH of the solution was maintained at 7—8. The product was then extracted from the solution by ether (IIId,e,n,o,p, and q) or ethyl acetate (EtOAc) (IIIf,g and h). The extract was washed with water and dried over magnesium sulfate. After evaporation, the residue was distilled or recrystallized from a suitable solvent, as will be shown below. In some cases (IIIb,c and g), a crude product was obtained by the filtration of the reaction mixture. The compounds (III, R_1-O-COON=CR_2R_3) prepared in this manner are as follows: (R_1, R_2, R_3, mp °C or bp °C/mmHg, recrystallization solvent, elemental analysis (calcd) shown) IIIb: Et, $CONH_2$, CN, 194—196, EtOAc, C, 39.12; H, 3.69; N, 22.78% (C, 38.92; H, 3.81; N, 22.70%); IIIc: *iso*-Bu, $CONH_2$, CN, 156—158, EtOAc, C, 44.86; H, 5.27; N, 19.57% (C, 45.07; H, 5.20; N, 19.71%); IIId: Me, COOEt, CN, 69—71, C_6H_6-hexane, C, 41.99; H, 3.90; N, 14.10% (C, 42.00; H, 4.03; N, 14.00%); IIIe: Et, COOEt, CN, 127.5/0.8, ···, C, 45.08; H, 4.63; N, 13.17% (C, 44.86; H, 4.71; N, 13.08%); IIIf: *iso*-Bu, COOEt, CN, 60—62, EtOAc-petroleum ether, C, 56.98; H, 4.30; N, 10.25% (C, 56.52; H, 4.38; N, 10.14%); IIIh: allyl, COOEt, CN, 122—124/0.9, --, C, 47.56; H, 4.40% (C, 47.79; H, 4.46%); IIIn: Et, Me, Me, 66—66.5/5, --, C, 49.81; H, 7.68% (C, 49.65; H, 7.64%); IIIo: Et, H, Me, 67—70/6, --, C, 46.38; H, 7.01; N, 10.49% (C, 45.80; H, 6.92; N, 10.68%); IIIp: Et, H, COMe, 81—85/8.5, --, C, 44.96; H, 5.62; N, 8.45% (C, 45.28; H, 5.70; N, 8.80%); IIIq: Et, COOEt, COOEt, 120/0.1, C, 46.27; H, 5.69; N, 5.53% (C, 45.98; H, 5.78; N, 5.36%).

A-ii) In Organic Solvents; A typical example is as follows. A solution of *β,β,β*-trichloroethyl chloroformate (10.5 g, 0.05 mol) in benzene (C_6H_6) (35 ml) was added dropwise to a solution of ethyl 2-hydroximino-2-cyanoacetate (Ia, 7.2 g, 0.05 mol) and triethylamine (TEA) (7.0 ml, 0.05 mol) in C_6H_6 (50 ml) under ice-cooling. The mixture was then stirred for 1 hr below 10 °C and allowed to stand overnight at room temperature. The solution was washed with water and dried over magnesium sulfate. After evaporation, the residue was triturated with petroleum ether and filtered to give IIIl; 12.3 g, mp 50—52 °C. A part of the sample was recrystallized from EtOAc-petroleum ether; mp 51—53 °C.

Found: C, 30.59; H, 2.14; N, 9.29; Cl, 32.70%, Calcd for $C_8H_7O_5N_2Cl_2$: C, 30.26; H, 2.22; N, 8.82; Cl, 33.50%.

For the preparation of IIIa, chloroform was used as the solvent. For IIIm, a solution of Ia and TEA in C_6H_6 was added to a solution of *t*-amyl chloroformate in an ether-toluene mixture.[16] The carbonates prepared in this manner are as follows: (R_1, R_2, R_3, mp °C, recrystallization solvent, elemental analysis (calcd) shown) IIIa: Me, $CONH_2$, CN, 174—175 (decomp), EtOAc, C, 35.33; H, 2.99; N, 24.31% (C, 35.09; H, 2.95; N, 24.56%); IIIm: *t*-Amyl, COOEt, CN, oil, ···, ···. This decomposed spontaneously after IR measurement.

B-i) Preparation of Ethyl 2-Chlorocarbonyloximino-2-cyanoacetate (IV): A solution of Ia (7.2 g) and TEA (7.0 ml) in dry C_6H_6 (50 ml) was added dropwise to a solution of phosgene in C_6H_6 (52.5 ml, 0.05 mol) at 5 °C. The mixture was stirred for 2 hr, allowed to stand overnight, and used for the next step without further treatment. In another run, the

reaction mixture was filtered and evaporated to dryness under reduced pressure. The pale yellow oil (8.6 g) thus obtained showed IR absorptions at 1870 and 1740 cm^{-1} and was very unstable toward moisture.

B-*ii) Preparation of Oxime Carbonates (III)*: A typical example is as follows. A solution of pentachlorophenol (13.3 g, 0.05 mol) and *N,N*-dimethylaniline (6.0 g, 0.05 mol) in CH_2Cl_2 (50 ml) and C_6H_6 (50 ml) was added dropwise into the stirred solution of IV described in B-i) at 5—10 °C. The mixture was then stirred for 2 hr and allowed to stand overnight. The mixture was subsequently washed with water, dried over magnesium sulfate, and evaporated to dryness under reduced pressure. The residue was filtered with a small amount of ether to give a crude powder; 5.5 g. Recrystallization from EtOAc-petroleum ether gave needles (IIIk); mp 122—124 °C.

Found: C, 33.02; H, 1.09; N, 6.25; Cl, 40.70%. Calcd for $C_{12}H_5O_5N_2Cl_5$: C, 33.17; H, 1.16; N, 6.45; Cl, 40.80%.

IIId, IIIi and IIIj were prepared by a similar procedure except for the following modifications: C_6H_6 (40 ml) for IIId, CH_2Cl_2 (50 ml) for IIIi and pyridine in C_6H_6 (50 ml) for IIIj. The following are the R_1, R_2, R_3, mp °C, recrystallization solvent, elemental analysis (calcd) shown; IIId: Me, COOEt, CN, 68—70, C_6H_6-hexane, ···; IIIi; C_6H_4-$NO_2(p)$, COOEt, CN, 90—93, C_6H_6-petroleum ether, C, 47.41; H, 2.90; N, 13.77% (C, 46.91; H, 2.95; N, 13.68%); IIIj: $C_6H_2Cl_3(2,4,5)$, COOEt, CN, 101—103, C_6H_6-petroleum ether, C, 39.29; H, 1.88; N, 6.95; Cl, 29.18% (C, 39.42; H, 1.93; N, 7.66; Cl, 29.10%.)

Preliminary Reactions of N-*Benzyloxycarbonylglycine with Some Oxime Carbonates. A) A Comparison of The Reactivity of Carbonates by The Help of Tlc*: The stoichiometric amount of oxime carbonate (2 mmol) cited below was added to a solution of *N*-benzyloxycarbonylglycine (0.42 g, 2 mmol) and TEA (0.28 ml, 2 mmol) in dioxane (5.0 ml) at room temperature. The reaction mixture was checked by tlc on silica gel G (solvent: $CHCl_3$–MeOH (9 : 1)). With 2-ethyloxycarbonyloximinopropane (IIIn), ethyloxycarbonyloximinoethane (IIIo), 1-ethyloxycarbonyloximinopropan-2-one (IIIp) and diethyl 2-ethoxycarbonyloximinomalonate (IIIq), the reaction did not take place at all. When dimethylformamide was used as the solvent, the reaction proceeded slightly with only IIIq. The reaction was completed with ethyl 2-ethoxycarbonyloximino-2-cyanoacetate (IIIe) and 2-ethoxycarbonyloximino-2-cyanoacetamide (IIIb) within 20 min and 2 hr respectively.

B) Comparison of The Solvent Effects: 2-Isobutyloxycarnyloximino-2-cyanoacetamide (IIIc, 0.43 g, 2 mmol) was allowed to react with *N*-benzyloxycarbonylglycine (0.42 g, 2 mmol) and TEA (0.28 ml, 2 mmol) in the following solvent (5.0 ml) for 3 hr at room temperature. The rate of ester formation was compared by tlc as has been described in A). The rate increased in the following order: THF≒dioxane<MeCN<dimethylformamide.

General Procedure for The Preparation of Esters. Oxime carbonate (III, 0.01 or 0.02 mol, according to the number of functional groups) was added portionwise to a solution of carboxylic acid (0.01 mol) and tertiary amine (0.01 or 0.02 mol) in a suitable solvent (20 ml), as is shown in Table 2, at room temperature. The mixture was then stirred for a further 2 hr and extracted with EtOAc, $CHCl_3$ (ex. 6) or ether (ex. 7). The organic layer was washed with water, 1M $NaHCO_3$ solution, water, 1M HCl and water successively, and dried over magnesium sulfate. The subsequent evaporation of the solvent gave a product, which was purified or analyzed by the method cited below for each section. Reverse esters (VII) were less soluble than normal esters (VI) and were easily separated by treatment with EtOAc containing petroleum ether. Remarks on each experiment shown in Table 2 follows: ex. 2) ethyl 2-benzoyloximino-2-cyanoacetate (VII), mp 99—101 °C (from EtOAc-petroleum ether), C, 58.60; H, 3.93; N, 11.60% (calcd for $C_{12}H_{10}O_4N_2$: C, 58.53; H, 4.09; N, 11.38%), IR (Nujol, cm^{-1}) 1770, 1745; ex. 3) 2-benzoyloximino-2-cyanoacetamide (VII), mp 223—226 °C (from THF), C, 55.69; H, 3.05; N, 19.30% (calcd for $C_{10}H_7O_3N_3$: C, 55.30; H, 3.25; N, (19.35%), IR (Nujol, cm^{-1}) 1770, 1695; ex. 6) diethyl adipate (VI) was checked by gas-liquid chromatography (glc) and identified with an authentic sample; 1,4-bis(α-cyano-α-carbamoylmethyleniminoxycarbonyl)butane (VII), mp 200—202 °C (from THF), C, 42.63; H, 3.54; N, 24.67% (calcd for $C_{12}H_{12}O_6N_6$: C, 42.86; H, 3.60; N, 24.99%), IR (Nujol, cm^{-1}) 3450, 3200, 1795, 1705; ex. 7) ethyl 2-ethoxycarbonyloxyacetate (VI), fractionated by preparative glc, IR (neat, cm^{-1}) 1745, nuclear magnetic resonance (in $CDCl_3$, ppm) 1.29 (methyl, 3H, triplet, J=7.5 Hz), 1.31 (methyl, 3H, triplet, J=7.5 Hz), 4.25 (two methylene, 4H, quartet, J=7.5 Hz), 4.61 (methylene, 2H, singlet); ex. 8) mass spectrometry *m/e* 223 (M^+), IR (neat, cm^{-1}) 3350, 1740, 1700; ex. 11) IR (neat, cm^{-1}) 3350, 1730, 1700; ex. 12) mass spectrometry *m/e* 299 (M^+); ex. 13) ethyl *N*-benzyloxycarbonyl-L-tryptophanate, mp 80—83 °C (from EtOAc-petroleum ether), C, 68.56; H, 6.05; N, 7.64% (calcd for $C_{21}H_{22}O_4N_2$: C, 68.83; H, 6.05; N, 7.65%), IR (Nujol, cm^{-1}) 3350, 1730, 1700; ex. 14) ethyl *N*-benzyloxycarbonyl-L-phenylalaninate, checked by tlc and identified with an authentic sample, IR (neat, cm^{-1}) 3350, 1730, 1700; ex. 15) methyl *N*-methoxycarbonyl-L-phenylalaninate, mass spectrometry *m/e* 237 (M^+), IR (neat, cm^{-1}) 3350, 1730, 1700.

Peptide Formation by the Use of Ethyl 2-isobutyloxycarbonyloximino-2-cyanoacetate (IIIf). A) Ethyl N-*Benzyloxycarbonylglycyl-*L-*leucinate*: To a solution of *N*-benzyloxycarbonylglycine (1.05 g, 5 mmol) and TEA (0.70 ml, 5 mmol) in EtOAC (15 ml), a solution of IIIf (1.21 g, 5 mmol) in EtOAc (10 ml) was added dropwise at —15 °C. The mixture was then stirred for 30 min at the same temperature. A solution of ethyl L-leucinate hydrochloride (1.0 g) and TEA (0.70 ml) in CH_2Cl_2 (15 ml) was subsequently added dropwise to the solution described above, and the mixture was stirred for 1 hr. The product was taken up into EtOAc. The extract was washed with water, 1M $NaHCO_3$ solution, water, 1M HCl, and water again, and dried over magnesium sulfate. Evaporation gave an oily product; 1.4 g (80%). To confirm the structure, the product was saponified to give *N*-benzyloxycarbonylglycyl-L-leucine; mp 100—102 °C (lit,[18] 101—102 °C). The sample was identified with an authentic specimen by means of its IR spectra.

B) Methyl N-*Benzyloxycarbonylglycyl-*L-*phenylalaninate*: This compound was prepared in a similar manner in an 86% yield. A part of the product was saponified to give *N*-benzyloxycarbonylglycyl-L-phenylalanine; mp 124—126 °C (lit,[19] mp 125—126 °C). An admixture of the sample and an authentic specimen melted at 124—126 °C.

The author wishes to express his thanks to Mr. Daizo Morino and Mr. Yoshiaki Yasuda for their skillful technical assistance.

References

1) R. Glatthard and M. Matter, *Helv. Chim. Acta*, **46**, 795 (1963).

2) T. Wieland, B. Heinke, K. Vogler, and H. Morimoto, *Ann. Chem.*, **655**, 189 (1962).

3) M. Conrad and A. Schulze, *Ber.*, **42**, 735 (1909).
4) M. Itoh, This Bulletin, **46**, 2219 (1973).
5) W. L. Semon, *J. Amer. Chem. Soc.*, **45**, 188 (1923).
6) V. Meyer and A. Janny, *Ber.*, **15**, 1525 (1882).
7) P. Freon, *Ann. Chim.*, **11**, 453 (1939); *Chem. Abstr.*, **33**, 7733 (1939).
8) V. Cerchez, *Bull. Soc. Chim. Fr.*, **47**, 1279 (1930); *Chem. Abstr.*, **25**, 919 (1931).
9) J. M. Ross and W. C. Smith, *J. Amer. Chem. Soc.*, **86**, 2861 (1964).
10) a) S. Sakakibara and N. Inukai, This Bulletin, **37**, 1231 (1964); b) *idem*, *ibid.*, **38**, 1979 (1965).
11) Y. Wolman, D. Ladkany, and M. Frankel, *J. Chem. Soc.*, **1967**, 689.
12) M. Bodanszky and V. du Vigneaud, *J. Amer. Chem. Soc.*, **81**, 5688 (1959).
13) J. Kovacs, M. Q. Ceprini, C. A. Dupraz, and G. N. Schmit, *J. Org. Chem.*, **32**, 3696 (1967).
14) J. Pless and R. A. Boissonnas, *Helv. Chim. Acta*, **46**, 1609 (1963).
15) P. Schving and S. Sabetay, *Bull. Soc. Chim. Fr.*, **43**, 857 (1928).
16) S. Sakakibara, M. Shin, M. Fujino, Y. Shimonishi, S. Inouye, and N. Inukai, This Bulletin, **38**, 1522 (1965).
17) Heintz, *Ann. Chem.*, **154**, 264; Beilsteins Handbuch der Organischen Chemie, III, 237 (1921).
18) D. Theodoropoulos and J. Tsangaris, *J. Org. Chem.*, **29**, 2272 (1964).
19) K. Hofmann and M. Bergmann, *J. Biol. Chem.*, **134**, 225 (1940).

The Reaction of Ethyl Ethoxymethylenecyanoacetate with Its Hydrazino Derivatives[1]

Koji SAITO,** Isaburo HORI,*,[2] Minoru IGARASHI,*,*** and Hiroshi MIDORIKAWA*

*The Institute of Physical and Chemical Research, Wako, Saitama 351

**Oyama Technical College, Oyama, Tochigi 323

***Department of Chemistry, Faculty of Science, Ibaraki University, Mito, Ibaraki 310

(Received October 5, 1973)

The reaction of ethyl ethoxymethylenecyanoacetate with its hydrazino derivative in the presence of pyridine in ethanol at room temperature gave ethyl (4-ethoxycarbonyl-5-aminopyrazol-1-yl)methylenecyanoacetate(**6**) and two geometric isomers of ethyl (4-ethoxycarbonylpyrazol-5-ylamino)methylenecyanoacetate(**7**). Compound **6** itself, under the same conditions, rearranged to compound **7**. Both compounds, **6** and **7**, upon heating cyclized exclusively to the same product, diethyl 7-aminopyrazolo[1,5-*a*]pyrimidine-3,6-dicarboxylate(**8**). From the results of other combination reactions on methylenecyanoacetic ester homologs, a plausible reaction mechanism involving a rearrangement is discussed.

A previous work[3] has been shown that the reaction of (1-alkoxyalkylidene)cyanoacetic esters (**1**: R=*n*-alkyl groups) with their hydrazino derivatives (**2**) in the presence of pyridine in ethanol at room temperature gave bis(substituted vinyl)hydrazines, whose cyclization led to the formation of only 5-hydroxypyrazolo[1,5-*a*]pyrimidines(**4**), while methyl (α-methoxybenzylidene)-cyanoacetate(**1**: R=Ph) or (1-ethoxyethylidene)malononitrile reacted with the hydrazino reactant(**2**: R=Me) to afford 7-hydroxy(or amino)pyrazolopyrimidine (**5**) as a major product directly, along with the 5-hydroxy (or amino) one. It has also been found that similar condensations on methylenecyanoacetic ester homologs(**1** and/or **2** being R=H) all lead to the 7-amino product as the only final product. The formation of the 7-amino (or hydroxy) product in these reactions suggests that a certain rearrangement must occur if **2** itself does not initially cyclize to 5-aminopyrazole(**3**) during the reaction.

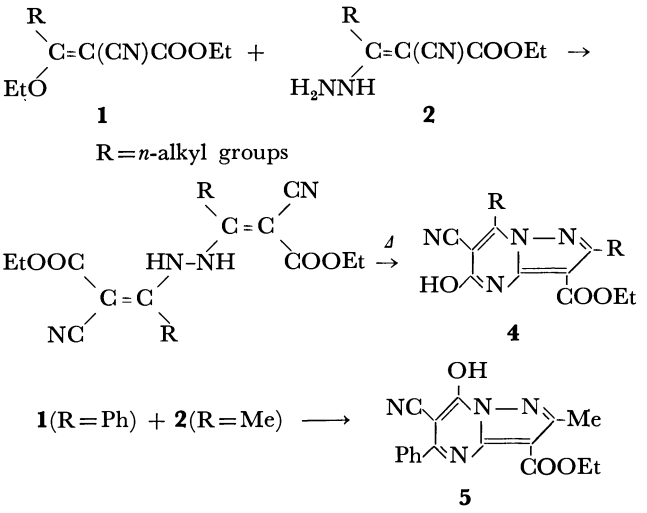

The reaction of ethyl ethoxymethylenecyanoacetate (**1**: R=H) with its hydrazino derivative (**2**: R=H)[4,5] under the same conditions as have been described in the earlier paper, Reaction **A**, afforded at first ethyl (4-ethoxycarbonyl-5-aminopyrazol-1-yl)methylenecyanoacetate(**6a**) instead of the expected intermediate(**Xa**), followed by two geometric isomers of ethyl (4-ethoxycarbonylpyrazol-5-ylamino)methylenecyanoacetate, (*E*)- and (*Z*)-**7a**. The elemental analyses of all these compounds indicated that they all had the same composition ($C_{12}H_{14}O_4N_4$). Their structures were chiefly verified by the following spectral studies. As can be seen from Table 1, the NMR spectrum of **6a** shows two sharp singlet signals(both 1H), corresponding to the vinyl proton and C–H proton on the pyrazole ring, and a broad singlet signal(2H) of the NH_2 protons. The IR spectrum of **6a** shows the pre-

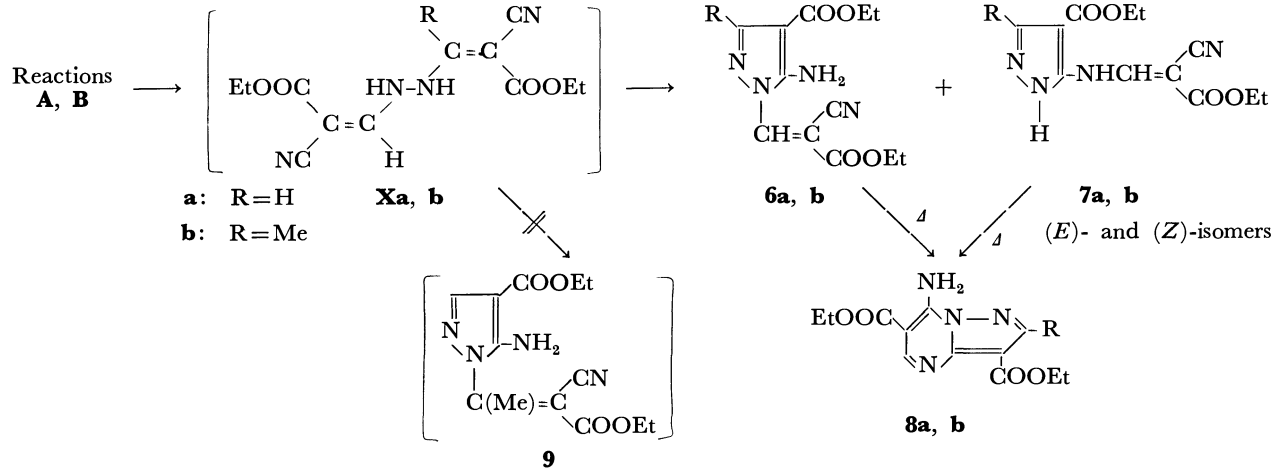

Scheme 1.

Table 1. Characteristic NMR and IR data of compounds **6** and **7**

Compd	Solv.	NMR (δ-Values from TMS)			NH (Ring)	IR (cm^{-1}, Nujol)		
		R (Ring)	=CH	NH (Exo)		ν NH_2		ν NH
6a	$CDCl_3$	8.29(H)	8.19	5.23(NH_2)		2478	3372	
	CD_3SOCD_3	8.57(H)	8.69	6.35(NH_2)				
6b	$CDCl_3$	2.64(Me)	8.16	5.31(NH_2)		3475	3350	
	CD_3SOCD_3	2.65(Me)	8.18	6.26(NH_2)				
(*E*)-**7a**	CD_3SOCD_3	8.27(H)	8.48 d (J=15 Hz)	9.40 d	13.39		3310(sh)	3250
(*Z*)-**7a**	CD_3SOCD_3	8.26(H)	8.28 d (J=14 Hz)	11.42 d	13.39		3312(sh)	3250
(*E*)-**7b**	$CDCl_3$	2.53(Me)	8.83 d (J=14 Hz)	9.30 d	10.80 br		3309(sh)	3251
	CD_3SOCD_3	2.37(Me)	8.48 d (J=14 Hz)	9.25 d	13.10			
(*Z*)-**7b**	$CDCl_3$	2.53(Me)	8.30 d (J=13 Hz)	11.58 d	10.60 br		3310(sh)	3252
	CD_3SOCD_3	2.38(Me)	8.28 d (J=13 Hz)	11.38 d	13.15			

sence of a typical primary amino group. On the other hand, the NMR spectra of the two isomers of **7a** show the doublet signal due to the vinyl proton coupled with the adjacent NH proton. The downfield NH signal attributed to an intramolecular hydrogen-bonding between the amino and the ester groups was assigned to that of the (*Z*)-form.[5]

Also, a similar reaction of the ethoxy reactant(**1**: R=H) with ethyl (1-hydrazinoethylidene)cyanoacetate(**2**: R=Me), Reaction **B**, gave the corresponding compounds, ethyl (3-methyl-4-ethoxycarbonyl-5-aminopyrazol-1-yl)methylenecyanoacetate (**6b**)[6] and two isomers of ethyl (3-methyl-4-ethoxycarbonylpyrazol-5-ylamino)methylenecyanoacetate, (*E*)- and (*Z*)-**7b**.

The two isomers of **7** were also prepared by the condensation of the ethoxy reactant(**1**: R=H) with ethyl 5-aminopyrazole-4-carboxylates(**3**), derived from the hydrazino reactants(**2**: R=H and Me), under the same conditions, and upon heating above 210 °C or by refluxing in acetic acid or in ethanolic hydrochloric acid they were cyclized to form the corresponding diethyl 7-aminopyrazolopyrimidine-3,6-dicarboxylates(**8**) exclusively.[7] Also, a similar treatment of **6** resultsed in the same product(**8**) instead of the 5-amino one. This fact implies that **6** must rearrange to **7** prior to its cyclization. In fact, when only **6** was placed under the same conditions as in the original reaction, a rearrangement occurred and a mixture of the geometric isomers of **7** resulted.

In view of the above facts, it seems reasonable to assume that both reactions, **A** and **B**, proceed through an initial intermediate(**X**) which cyclizes partially to **6** without the occurrence of an initial cyclization of the reactant(**2**) to **3**. In Reaction **B** the absence of ethyl [1-(4-ethoxycarbonyl-5-aminopyrazol-1-yl)ethylidene]cyanoacetate(**9**) suggests that the partial cyclization of an initial intermediate(**Xb**) takes place preferentially at the side of the methylvinyl group to give **6b**.

On the other hand, when ethyl (1-ethoxyethylidene)-cyanoacetate(**1**: R=Me) reacts with the hydrazino reactant(**2**: R=H), Reaction **C**, the same result as in Reaction **B** should be obtained because the same initial intermediate(**Xb**) is involved. In practice, however, this reaction afforded, besides **7b**, two unexpected compounds, **6a** and **7a**, which were identical with those obtained previously from Reaction **A**, and a minor compound, ethyl [1-(4-ethoxycarbonylpyrazol-5-ylamino)ethylidene]cyanoacetate(**10**). Compound **10** was also obtained by the condensation of **1**(R=Me) and **3**(R=H) under similar conditions, and when refluxed in ethanolic hydrochloric acid it cyclized to the 7-hydroxy and 7-aminopyrazolopyrimidines(**11** and **12**). These results may be elucidated by the following assumptions.

In connection with the present work, it was found that some 1-acyl-5-aminopyrazoles, on fusing or upon refluxing in acetic acid, rearrange to the corresponding 5-acylaminopyrazoles.[8] Considering that the acyl group of 1-acylpyrazoles is labile and is readily transacylated by aminolysis with strong amines,[9] the rearrangement of 1-(substituted vinyl)-5-aminopyrazoles(**6**) as well as 1-acyl-5-aminopyrazoles, would seem to be based on an intermolecular aminolysis rather than a Dimroth-type intramolecular rearrangement mechanism. In the reaction system, the aminolysis of **6** may occur not only with another molecule of the same type, but also with the hydrazino reactant molecule (**2**). The fact that the isolated **6a** and **6b**, when treated with aniline under the same conditions as in the original reaction, both underwent aminolysis to give the same product, ethyl anilinomethylenecyanoacetate,[5] lends some support to the above speculation.

The present competitive reactions are shown in Scheme 2 below. In Reactions **A** and **B**, the aminolysis of **6** with the hydrazino reactant(**2**) reproduces itself *via* the intermediate (**X**) and simultaneously gives 5-aminopyrazoles(**3**), which then condense with the ethoxy reactant(**1**) to form the same compound (**7**) as that obtained by the aminolysis of **6** with another molecule of the same type. On the other hand, Reaction **C** is complicated by the presence of the different hydrazino reactants(**2**) from Reaction **B**. Thus, **6b** undergoes aminolysis with **2**(R=H) to give **6a** *via*

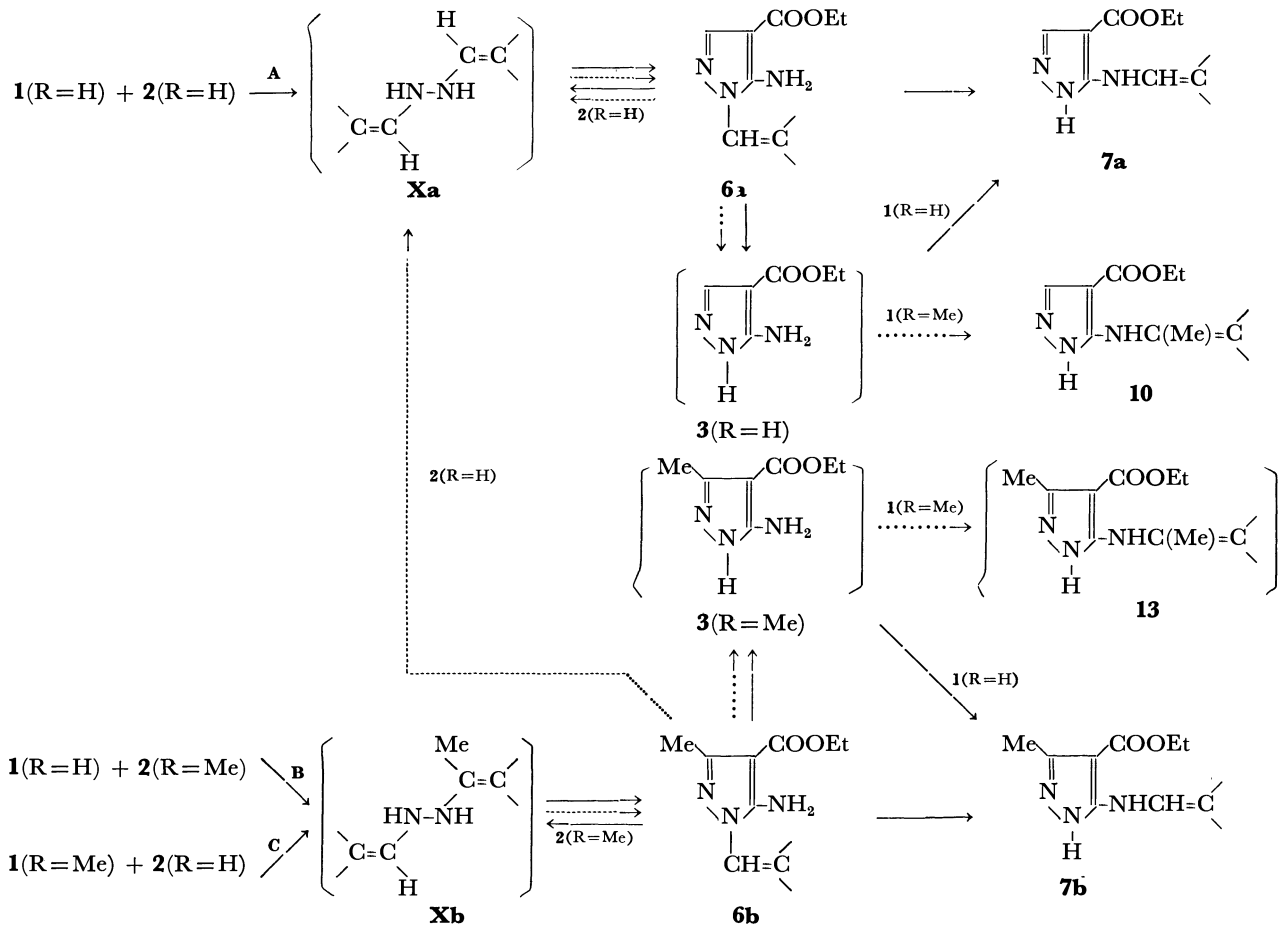

Scheme 2.

Xa with 5-aminopyrazole(**3**: R=Me), and the additional aminolysis of **6a** with **2**(R=H) leads to **3** (R=H), with the reproduction of **6a**. The condensation of the two resulting 5-aminopyrazoles(**3**: R=H and Me) with the ethoxy reactant(**1**: R=Me) ought to yield compounds **10** and **13** respectively, but an attempt to isolate **13** was unsuccessful. It can, therefore, be presumed that the formation of both **7a** and **7b** in Reaction **C** is based on the intermolecular aminolysis.

Experimental

All the melting points are uncorrected. The melting points of compounds **6** and **7** were determined with rapid heating because they varied with slow heating due to the ease of isomerization or cyclization. The NMR spectra were taken on a Varian HA-100 spectrometer, using TMS as the internal reference. The chemical shifts are expressed in terms of δ values(s: singlet, d: doublet, t: triplet, q: quartet). The IR spectra were recorded on a Hitachi 215 grating spectrophotometer.

*Reaction of Ethyl Ethoxymethylenecyanoacetate(**1**: R=H) with Its Hydrazino Derivative(**2**: R=H); Reaction **A**.* To a solution of 1.69 g (0.01 mol) of **1**(R=H) and 1.55 g(0.01 mol) of **2**(R=H) dissolved in ethanol at room temperature, a few drops of pyridine were added, and then the mixture was allowed to stand overnight at the same temperature. The crystals thus formed were collected and washed with ethanol to give 0.93 g(33.4%) of light yellow needles of ethyl (4-ethoxycarbonyl-5-aminopyrazol-1-yl)methylenecyanoacetate(**6a**), which were later recrystallized from acetone; mp 173—176 °C.

Found: C, 51.98; H, 5.10; N, 20.46%. Calcd for $C_{12}H_{14}O_4N_4$: C, 51.80; H, 5.04; N, 20.14%.

The mother liquor was allowed to stand until the following day at room temperature. The usual work-up of the resulting precipitate, followed by recrystallization from ethanol afforded 1.35 g(47.5%) of colorless needles of ethyl (*E*)-(4-ethoxycarbonylpyrazol-5-ylamino)methylenecyanoacetate (**7a**); mp 181.5—183 °C.

Found: C, 52.10; H, 4.98; N, 21.02%. Calcd: the same value as **6a** above.

Further, after the above filtrate had been allowed to stand for 3 days, the deposit was separated and washed with ethanol. The recrystallization of this from ethanol gave 0.24 g (8.6%) of colorless needles of ethyl (*Z*)-(4-ethoxycarbonylpyrazol-5-ylamino)methylenecyanoacetate(**7a**); mp 178—182 °C.

Found: C, 51.92; H, 4.85; N, 20.06%. Calcd: the same value as **6a** above.

The same esters, (*E*)- and (*Z*)-**7a**, were also prepared *via* a reaction between equimolecular amounts of **1**(R=H) and ethyl 5-aminopyrazole-4-carboxylate(**3**: R=Me) under the conditions described above; yields, 47.0 and 6.1% respectively.

*Reaction of the Ethoxy Reactant(**1**: R=H) with Ethyl (1-Hydrazinoethylidene)cyanoacetate(**2**: R=Me); Reaction **B**.* This reaction was carried out in the same manner as with Reaction **A**. Thus, from 1.69 g(0.01 mol) of **1**(R=H) and 1.69 g(0.01 mol) of **2**(R=Me), there was obtained the following three compounds.

Ethyl (3-methyl-4-ethoxycarbonyl-5-aminopyrazol-1-yl)-

methylenecyanoacetate(**6b**): light yellow needles; mp 184—185.5 °C from ethanol; yield, 0.35 g(12.0%).

Found: C, 53.50; H, 5.44; N, 18.92%. Calcd for $C_{13}H_{16}O_4N_4$: C, 53.40; H, 5.48; N, 19.17%.

When the reaction was conducted at a lower temperature (at about 5 °C), this ester(**6b**) was obtained as a mixture containing mostly another geometric isomer which melted at 164—165 °C. The characteristic NMR data of the other isomer are shown below; NMR($CDCl_3$): 2.41(s, Me-ring), 8.18(s, =CH), 6.05 (s, NH_2); (CD_3SOCD_3): 2.27(s, Me), 8.66(s, =CH), 7.68 (s, NH_2).

Ethyl (*E*)-(3-methyl-4-ethoxycarbonylpyrazol-5-ylamino)-methylenecyanoacetate(**7b**): colorless needles; mp 150—152 °C from ethanol; yield, 1.64 g(55.7%).

Found: C, 53.49; H, 5.37; N, 18.96%. Calcd: the same value as **6b** above.

Ethyl (*Z*)-(3-methyl-4-ethoxycarbonylpyrazol-5-ylamino)-methylenecyanoacetate(**7b**): colorless needles; mp 152—188.5 °C from ethanol; yield, 0.90 g (30.8%).

Found: C, 53.60; H, 5.48; N, 19.08%. Calcd: the same value as **6b** above.

The same esters, (*E*)- and (*Z*)-**7b**, were also obtained by the reaction of an equimolecular mixture of **1**(R=H) and ethyl 3-methyl-5-aminopyrazole-4-carboxylate(**3**: R=Me) under the conditions described above; yield, 24.0 and 31.0% respectively.

Cyclization of **6** *and* **7**. Each compound was treated under the following conditions to yield the corresponding cyclization products(**8**).

i) After the heating of each compound above 210 °C for 2 hr, the reaction mass was recrystallized from ethanol. The yields of **8** were over 80%.

ii) Each compound was refluxed in acetic acid for 3—5 hr, and then the reaction mixture was concentrated to an appropriate volume by means of a rotary evaporator. The resulting crystals were collected and washed with water. The recrystallization of the crystals from ethanol gave **8** in yields of 62—84%.

iii) A mixture of each compound(2 mmol) in ethanol (50 ml) containing a few drops of concentrated hydrochloric acid was refluxed for 4 hr. After the reaction mixture had been evaporated to dryness by means of a flash evaporator, the residue was diluted with water, and then the solution was made alkaline with sodium carbonate. The precipitate thus formed was purified by recrystallization from ethanol. The yields of **8** were 69—93%.

Diethyl 7-aminopyrazolo[1,5-*a*]pyrimidine-3,6-dicarboxylate (**8a**): colorless plates; mp 243—244 °C; IR(Nujol, cm^{-1}): 3344, 3236, 3125, 1727, 1692; NMR($CDCl_3$): 8.48(s, C_2–H), 8.99(s, C_5–H), 1.42(t), 4.43(q) and 4.44(q) (2COOEt).

Found: C, 51.66; H, 5.05; N, 20.02%. Calcd for $C_{12}H_{14}O_4N_4$: C, 51.80; H, 5.04; N, 20.14%.

Diethyl 2-methyl-7-aminopyrazolo[1,5-*a*]pyrimidine-3,6-dicarboxylate(**8b**): colorless needles; mp 192—194 °C; IR (Nujol, cm^{-1}): 3344, 3247, 3215, 1730, 1698; NMR($CDCl_3$): 2.64(s, C_2–H), 8.90(s, C_5–H), 1.40(t), 4.39(q) and 4.42(q) (2COOEt).

Found: C, 53.36; H, 5.47; N, 19.10%. Calcd for $C_{13}H_{16}O_4N_4$: C, 53.40; H, 5.48; N, 19.17%.

Rearrangement of **6** *to* **7**. To a solution of **6a**(1 mmol) dissolved in ethanol containing acetone at room temperature, a few drops of pyridine were added, and then the mixture was allowed to stand at the same temperature for 5 days. After the mixture had then been evaporated to dryness at 40 °C by means of a rotary evaporator, the recrystallization of the residue from ethanol gave **7a** as a mixture of the geometric isomers in a yield of 80.5%; it was identified by comparison with samples prepared as has been described in Reaction **A**.

When **6b** was treated in the same manner, (Z)-**7b**, identical with the sample described in Reaction **B**, was obtained in a yield of 67.2%.

*Reaction of Ethyl (1-Ethoxyethylidene)cyanoacetate(***1***: R=Me) with the Hydrazino Reactant(***2***: R=H); Reaction* **C**. A mixture of 1.83 g(0.01 mol) of **1**(R=Me) and 1.55 g(0.01 mol) of **2**(R=H) was dissolved in ethanol(70 ml) at room temperature, and to this a few drops of pyridine were added. After it had then been allowed to stand at room temperature for 2 days, the reaction mixture was concentrated to one-half of its volume at 40 °C by means of a rotary evaporator. The resulting precipitate was recrystallized from ethanol to give 0.32 g (11.5%) of colorless needles; mp 172—174 °C; the results of the elemental analysis and the IR spectrum of the product were identical with those of **6a**.

The mother liquor was further concentrated and allowed to stand overnight in a refrigerator. The recrystallization of the precipitate formed from ethanol gave colorless needles of 0.42 g(14.4%); mp 178—180 °C; the results of the elemental analysis and the IR spectrum of the product were identical with those of (*Z*)-**7a**.

Furthermore, the above filtrate was evaporated almost to dryness, and then allowed to stand until the following day. There was thus obtained 0.47 g (16.1%) of colorless needles which, on recrystallization from ethanol, melted at 169—180 °C and were identical with (*Z*)-**7b** previously prepared.

Finally, after it had stood in a refrigerator, the resulting viscous filtrate gave 0.05 g(1.6%) of colorless needles of ethyl [1-(4-ethoxycarbonylpyrazol-5-ylamino)ethylidene]cyanoacetate(**10**); mp 201—203 °C from ethanol; IR(Nujol, cm^{-1}): 3300(sh), 3216, 2117, 1672, 1595; NMR(CD_3SOCD_3): 2.68(s, Me), 8.41(s, H-ring), 12.40(s, NH-*exo*), 13.55(s, NH-ring), 1.27(t), 1.30(t), 4.25(q) and 4.31(q) (2COOEt).

Found: C, 53.60; H, 5.42; N, 19.01%. Calcd for $C_{13}H_{16}O_4N_4$: C, 53.40; H, 5.48; N, 19.17%.

Compound **10** was also prepared by the reaction of equimolecular amounts of **1**(R=Me) and the aminopyrazole(**3**: R=H) under the conditions described above; yield, 14.0%. Upon admixture with a sample obtained as has been described above, the melting point was not depressed.

Cyclization of **10**. A solution of **10**(3 mmol) in ethanol containing a few drops of concentrated hydrochloric acid was refluxed for 7 hr, and then the reaction mixture was concentrated to a small volume by means of a rotary evaporator. The precipitate thus formed was collected and recrystallized from ethanol to give 0.4 g(55.2%) of colorless needles of ethyl 5-methyl-6-cyano-7-hydroxypyrazolo[1,5-*a*]pyrimidine-3-carboxylate(**11**); mp 244—246 °C; IR(Nujol, cm^{-1}): 3190, 3078, 2233, 1705, 1700, 1675, 1625; NMR(CD_3SOCD_3): 2.63(s, C_5–Me), 8.21(s, C_2–H), 1.32(t) and 4.28(q)(COOEt).

Found: C, 53.82; H, 4.21; N, 22.74%. Calcd for $C_{11}H_{10}O_3N_4$: C, 53.66; H, 4.07; N, 22.76%.

The mother liquor was further allowed to stand overnight in a regrigerator, and the precipitate thus formed was restallized from ethanol to yield 0.05 g(5.7%) of colorless needles of diethyl 5-methyl-7-aminopyrazolo[1,5-*a*]pyrimidine-3,6-dicarboxylate(**12**); mp 134—136 °C; IR(Nujol, cm^{-1}): 3350, 3245, 1693, 1663, 1620, 1597; NMR(CD_3SOCD_3): 2.67(s, C_5–Me), 8.52(s, C_2–H), 8.64(s, NH), 1.31(t), 1.35(t), 4.28(q) and 4.30(q)(2COOEt).

Found: C, 53.42; H, 5.40; N, 19.12%. Calcd for $C_{13}H_{16}O_4N_4$: C, 53.40; H, 5.48; N, 19.17%.

Aminolysis of **6** *with Aniline*. A mixture of **6a**(1 mmol)

and aniline(1 mmol) was dissolved in ethanol (15 ml) containing one drop of pyridine at room temperature, and then the mixture was allowed to stand overnight at the same temperature. After the solution had been concentrated to a small volume by means of a flash evaporator and cooled in a refrigerator for 2 hr, the collection of the resulting crystals, followed by the recrystallization from ethanol, afforded 0.15 g(69.5%) of long colorless needles of ethyl anilinomethylenecyanoacetate consisting of a mixture of the geometric isomers; mp 108—113 °C.

Found: C, 66.99; H, 5.62; N, 13.08%. Calcd for $C_{12}H_{12}O_2N_2$: C, 66.65; H, 5.59; N, 12.96%.

Also, a similar treatment of **6b** with aniline gave the same product as that prepared above in a yield of 73.0%. This compound was identical with the product prepared from the ethoxy reactant (**1**: R=H) and aniline.[5]

The authors are indebted to Dr. Kiyoko Yamamoto for her fruitful discussions and to Mr. Shigenobu Murakami and Miss Keiko Tanaka for their helpful technical assistance. Thanks are also due to Dr. Haruo Homma and his staff for their elemental analyses and to Mr. Jun Uzawa for his help in taking the NMR spectra.

References

1) The Formation of Pyrazolo[1,5-*a*]pyrimidine Derivatives. II. Part I: Ref. 3.

2) To whom correspondence should be addressed.

3) I. Hori, K. Saito, and H. Midorikawa, This Bulletin, **43**, 849 (1970).

4) This ester was prepared from the ethoxy reactant(**1**: R=H) and hydrazine hydrate as the geometric isomers(mp 93—94 °C and 99—100 °C); *cf.* P. Schmidt and J. Druey, *Helv. Chim. Acta*, **39**, 986 (1956), mp 89—90 °C. The present reaction using both isomers led to the same result.

5) H. Baba, I. Hori, T. Hayashi, M. Igarashi, and H. Midorikawa, unpublished data; the structure of these *N*-substituted aminomethylenecyanoacetates will be discussed in more detail in a later communication.

6) When this reaction was carried out under a lower temperature, this ester was obtained as a mixture of the geometric isomers; see experimental section.

7) The formation of the 7-amino and 7-hydroxypyrazolo-[1,5-*a*]pyrimidines by the reaction between the ethoxy reactant(**1**) and 5-aminopyrazoles has been reported; Y. Makisumi *Chem. Parm. Bull.*(Tokyo), **10**, 620(1962); Ref. 3.

8) K. Saito, I. Hori and H. Midorikawa, unpublished result; the detailed result will be reported at a later data.

9) A. N. Kost and I. I. Grandberg, "Advances in Heterocyclic Chemistry," Vol. 6, ed. by A. R. Katritzky and A. J. Boulton, Academic Press, New York, N. Y. (1966), p. 420.

Autoxidation of Aromatic Hydrocarbons Catalyzed with Cobaltic Acetate in Acetic Acid Solution. III. Oxidation of *p*-Toluic Acid[1]

Mikito KASHIMA and Yoshio KAMIYA[2]

Polymer Research Laboratory, Ube Ind. Ltd., 8-2, *Goi, Ichihara-city, Chiba*, 290

(Received March 20, 1973)

The oxidation of *p*-toluic acid catalyzed with cobaltic acetate was studied kinetically in acetic acid. The maximum absorption rate of oxygen was obtained in the initial stage of reaction, being represented by the same equation as in the case of toluene, ethylbenzene and cumene. That is, the kinetic equation is of first order with respect to the initial concentration of *p*-toluic acid, of second order with respect to the initial concentration of Co(III), and of inverse first order with respect to the initial concentration of Co(II). The relative reactivity of *p*-toluic acid per active hydrogen was lower than that of toluene, but higher than that of ethylbenzene and cumene. The apparent chain-length in the oxidation of *p*-toluic acid was much shorter than that of *p*-xylene oxidation.

Many procedures have been developed for obtaining terephthalic acid by the autoxidation of *p*-xylene under applied oxygen pressure with cobaltous salts of aliphatic acids as catalyst, together with various promoters such as aldehydes[3,4] and ketones.[5,6] The roles of transition metal ion used as the catalyst are not yet fully clarified since the main purpose of these methods was to increase the yield of terephthalic acid.

Recently, aromatic oxidation catalyzed with cobaltic acetate has received considerable attention.[7-9] The reactions were mainly studied under nitrogen atmosphere for academic purposes, but they should be carried out under oxygen atmosphere for practical purposes. Thus we have reported the reaction mechanism and the role of catalyst in the liquid-phase oxidation of aromatic hydrocarbons catalyzed with cobaltic acetate under oxygen atmosphere.

It has been clarified that *p*-toluic acid was easily oxidized to terephthalic acid with cobaltic acetate under oxygen pressure in acetic acid. The oxidation of *p*-toluic acid to terephthalic acid was apparently initiated by the electron transfer equilibrium between *p*-toluic acid and cobaltic acetate. The oxidation proceeds with a short chain-length comparable to the one obtained in the oxidation of toluene catalyzed with Co(III).

Experimental

Materials. Glacial acetic acid of reagent grade was used. *p*-Toluic acid was vigorously stirred in boiling water and filtered after cooling. The procedure was repeated until no chloride ion was detected. It was then recrystallized from methanol-water solution. Cobaltous acetate was of special grade. The preparation and titration of cobaltic acetate, and the determination of water content in the solution were carried out by the same method as reported in part I.[10]

Procedure. The reaction mixture was charged into a 300 ml. stainless-steel autoclave, and temperature was increased gradually under applied oxygen pressure. The amount of absorbed oxygen was calculated on the basis of pressure drop. To keep oxygen pressure as constant as possible, fresh oxygen was charged into the autoclave as fresh oxygen was charged into the autoclave as soon as a pressure drop of 1 kg/cm^2 had been observed.

Analysis. The solid materials formed by the addition of 150 ml. of water into the reaction mixture were filtered from the aqueous solution, and washed twice with 50 ml of methanol. The crude terephthalic acid was dried at 100 °C.

The filtrate and methanol washings were mixed and concentrated to a syrup containing catalyst, *p*-toluic acid and other substances. It was dissolved in 10% sodium carbonate aqueous solution. The resulting solution was filtered and then acidified with hydrochloric acid. The resulting precipitate was filtered, washed twice with water, and dried at 60 °C to give unreacted *p*-toluic acid and terephthalaldehydic acid. A known weight of this precipitate was dissolved in a portion of M/10 sodium hydroxide. Hydrochloric acid of M/10 was added to this alkaline solution until pH of solution decreased to 3.8. An ethanol solution of hydroxylamine hydrochloride was then added to the solution and pH was again adjusted to 3.8 by adding M/10 sodium hydroxide. The amount of terephthalaldehydic acid contained in the precipitate was calculated by the following equation.

Yield of terephthalaldehydic acid (%)

$$= 1.50(x-y)/w$$

where x and y are the values of volume (ml) of NaOH and HCl aqueous solution, respectively, and w is weight (g) of precipitate.

Results and Discussion

Rate Law. When *p*-toluic acid (TA) was oxidized with cobaltic acetate under applied oxygen pressure in acetic acid at 80 °C, the reaction proceeded without an induction period. The maximum rate of oxygen absorption (v_m) was obtained in the initial stage of reaction.

The effect of oxygen partial pressure on v_m was studied in the case of the constant concentration of TA (0.333 M) and cobaltic acetate (0.084 M) in acetic acid at 100 °C with an agitation velocity of 1000 rpm. The maximum rate of oxygen absorption was independent of oxygen pressure above 4 kg/cm^2. All experiments were therefore carried out under oxygen pressure of 5 kg/cm^2 unless otherwise stated.

The relation between TA concentration and the maximum rate of oxygen absorption is shown in Fig. 1. The rate of oxidation is proportional to TA concentration below about 2 in the molar ratio of TA to cobaltic acetate, and is inversely proportional to that above the molar ratio 2. Two factors might be considered for explaining the above result: (a) acetate anions on cobaltic ion are replaced by *p*-toluate anions to form a less active cobaltic ion,[11] and (b) the solubility tof TA in acetic acid may be constant from the fac

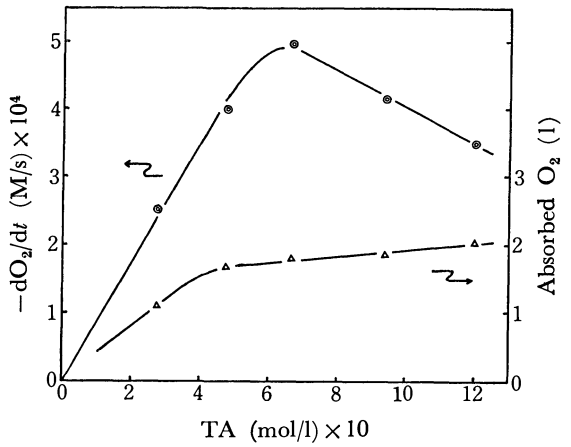

Fig. 1. The effect of TA concentration on the oxidation rate and the amount of O_2 absorbed at 80 °C under 5 kg/cm².
Co(III), 0.253 M; Co(II), 0.005 M.

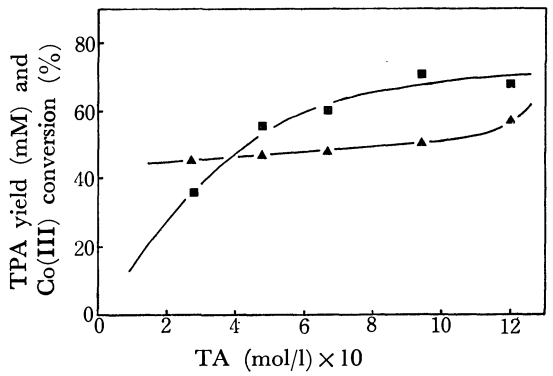

Fig. 2. The effect of TA concentration on TPA yield and Co(III) conversion under the same condition as Fig. 1.
■ TPA yield, ▲ Co(III) conversion

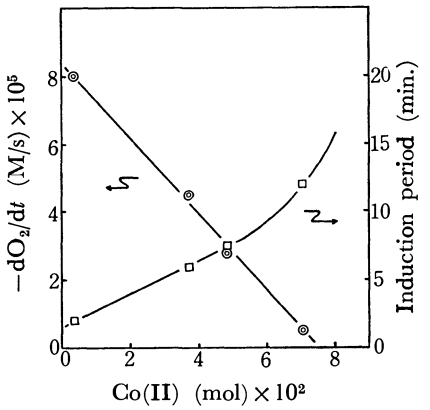

Fig. 3. The effect of Co(II) concentration on the oxidation rate and induction period at 80 °C under 5 kg/cm².
TA, 0.333 M; Co(III), 0.128 M.

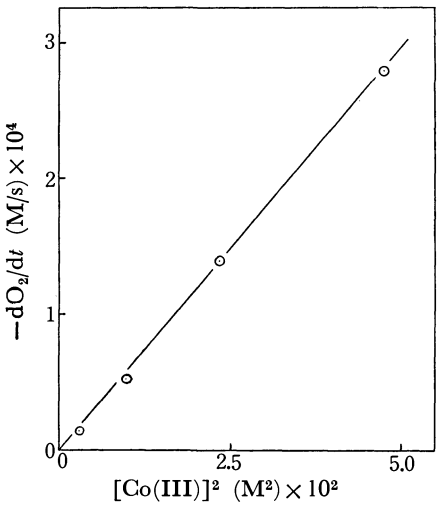

Fig. 4. The effect of Co(III) concentration on the oxidation rate at 80 °C under 5 kg/cm².
TA, 0.467 M; Co(II), 0.0116 M.

that the yield of terephthalic acid and the amount of oxygen absorbed are constant even when the ratio of TA to cobaltic acetate exceeds 2 (see Fig. 2). The cohesion of undissolved TA may cause a decrease in the apparent concentration of cobaltic acetate.

The effect of the initial concentration of cobaltous acetate on the maximum rate of oxygen absorption and the induction period are shown in Fig. 3. It is clear that cobaltous ion inhibits oxidation remarkably and the induction period increases with the concerntration of Co(II). The reaction proceeds very slowly when the ratio Co(III)/Co(II) is nearly equal to 1. Figure 4 shows a plot of v_m against the square of the initial concentration of cobaltic ion when the concentrations of *p*-toluic acid and cobaltous ion are maintained constant. It is evident that the reaction is of second order with respect to the concentration of Co(III).

Thus v_m obtained in oxidizing TA with cobaltic acetate under oxygen pressure can evidently be represented by the equation

$$v_m = k[TA][Co(III)]^2[Co(II)]^{-1} \quad (I)$$

which is similar to the equation obtained in the oxidation of toluene,[10] ethylbenzene and cumene.[1]

Thus the oxidation of TA catalyzed with cobaltic acetate is also initiated by the electron transfer equilibrium between TA and cobaltic acetate.

Effect of Temperature. The rate of oxygen absorption becomes maximum at 100 °C. Both the yield of terephthalic acid (TPA) and the amount of absorbed oxygen showed a similar change in the temperature range 60—120 °C, giving maximum value at 100 °C (see Fig. 5). However, the molar ratio of TPA formed to cobaltic ion consumed decreased gradually with temperature rise. The tendency was most remarkable above 100 °C. This indicates that the self-decomposition of cobaltic acetate occurs considerably above 100 °C as follows:

$$Co(OAc)_3 \rightarrow \cdot CH_3 + Co(OAc)_2 + CO_2$$
$$Co(OAc)_3 \rightarrow \cdot CH_2COOH + Co(OAc)_2$$

In view of the fact the yield of TPA shows only a slow decrease above 100 °C, methyl and carboxymethyl radicals do not seem to contribute to the formation of TPA. The apparent activation energy was cal-

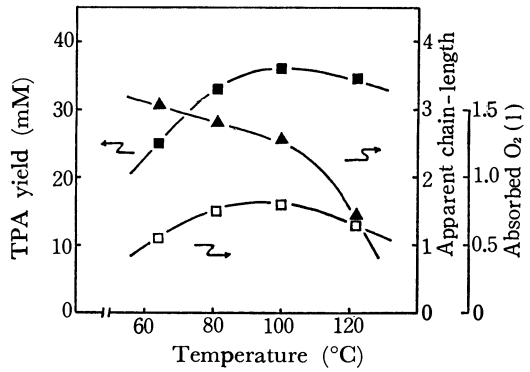

Fig. 5. The effect of temperature on TPA yield, the amount of absorbed O_2, and the apparent chain-length in the oxidation of TA (50 mM).
■ TPA yield, □ absorbed O_2,
▲ apparent chain-length

culated to be 10 kcal/mol, comparable to the one obtained by Kamiya *et al.*[12]

We have reported that the decreasing order of relative reactivities toward cobaltic acetate was as follows; primary>secondary>tertiary hydrogen, which was entirely inverse to the order for free radicals. The reactivity of TA per active hydrogen toward Co(III) was slightly smaller than that found in the oxidation of toluene with Co(III), but larger than that obtained for ethylbenzene and cumene (see Table 1). This result is not explicable in terms of the C–H bond rupture process, but supports the view that the electron transfer process is rate-determining step.

Table 1. Relative reactivities per active hydrogen of aromatic compounds toward Co(III) at 60 °C

Hydrocarbon	$k\times10^5$, ($M^{-1}s.^{-1}$)	Ratio
Toluene	3.08	1
p-Toluic acid	2.29	0.74
Ethylbenzene	1.67	0.54
Cumene	1.57	0.51

Reaction Products. Terephthalic acid was mainly obtained by the oxidation of TA with cobaltic acetate in acetic acid. A small amount of terephthalaldehydic acid (TAA) was also obtained as a by-product. The yield of TPA increased gradually with time, taking the constant value of 42% after 90 min, while the yield of TAA reached the steady value of 2% soon after the reaction started (see Fig. 6). It is thus apparent that the reaction proceeds successively TA→TAA→TPA, and that the oxidation of TAA is very fast.

The conversion of Co(III) and the ratio of Co(III)/(total Co) were found to take the constant value, 55% and 0.35, respectively after 90 min. Accordingly, the molar ratio of the yield of TPA to the consumed Co(III) was calculated to be 3.1 after 90 min, indicating that the apparent chain-length is much shorter than that obtained in the autoxidation of *p*-xylene. This suggests that the reaction is continued not by the abstraction of hydrogen from TA with peroxy radical, but by the regeneration of Co(III) from the oxidation of Co(II) with peracid or peroxy radical.

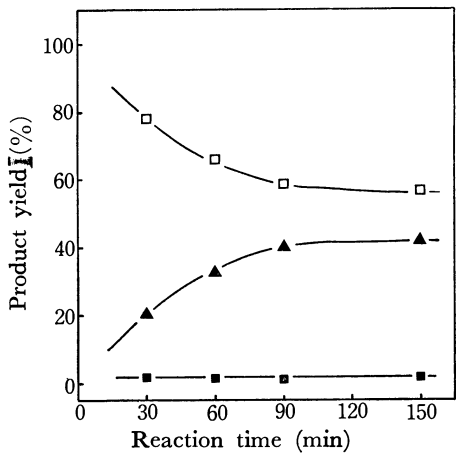

Fig. 6. Product yield and TA conversion in the oxidation of TA at 100 °C under 10 kg/cm².
TA, 0.333 M; Co(III), 0.081 M; Co(II), 0.02 M.
□ TA conversion, ▲ TPA, ■ TAA

Reaction Mechanism. It is clear that the oxidation of TA catalyzed with cobaltic acetate also proceeds through the electron transfer equilibrium as in the case of toluene, ethylbenzene and cumene, since the rate of oxygen absorption can be represented by the same equation independent of substrates, the apparent activation energies are almost equal to each other, and the relative reactivity of TA toward Co(III) is only a little smaller than that of toluene.

For the kinetics of second-order dependence on Co(III) and inverse first-order dependence on Co(II) of v_m, the following elementary reactions might play an important role in the early stage of reaction assuming that the active species of catalyst is the dimer of cobaltic acetate.

$$2\mathrm{Co(III)} \overset{K_1}{\rightleftarrows} \mathrm{Co(III)_2} \quad (1)$$

$$\mathrm{R\text{-}CH_3} + \mathrm{Co(III)_2} \overset{K_2}{\rightleftarrows} [\mathrm{R\text{-}CH_3{}^+AcO^-Co(III)}] + \mathrm{Co(II)} \quad (2)$$

$$[\mathrm{R\text{-}CH_3{}^+AcO^-Co(III)}] \overset{k_3}{\longrightarrow} \mathrm{R\text{-}CH_2\cdot} + \mathrm{Co(III)} + \mathrm{AcOH} \quad (3)$$

$$\mathrm{R\text{-}CH_2\cdot} + \mathrm{O_2} \overset{k_4}{\longrightarrow} \mathrm{R\text{-}CH_2OO\cdot} \quad (4)$$

$$\mathrm{R\text{-}CH_2OO\cdot} + \mathrm{Co(III)} \overset{k_5}{\longrightarrow} \mathrm{R\text{-}CHO} + \mathrm{Co(II)} + (1/2)\mathrm{O_2} + \mathrm{AcOH} \quad (5)$$

When the concentration of *p*-tolyl and *p*-tolylperoxy radicals reaches a stationary concentration in the early stage of reaction, the following equation can be introduced.

$$[\mathrm{R\text{-}CH_2\cdot}] = k_3[\mathrm{X}],\ [\mathrm{R\text{-}CH_2OO\cdot}] = k_3k_5^{-1}[\mathrm{X}][\mathrm{Co(III)}]^{-1}$$

where (X) is $K_1K_2k_3[\mathrm{R\text{-}CH_3}][\mathrm{Co(III)}][\mathrm{Co(II)}]^{-1}$ and R is C_6H_4COOH. The absorption rate of oxygen can then be represented by $(-dO_2/dt)=(1/2)k_3[\mathrm{X}]$. Then, v_m is abbreviated as

$$v_m = (1/2)K_1K_2k_3[\mathrm{R\text{-}CH_3}][\mathrm{Co(III)}]^2[\mathrm{Co(II)}]^{-1} \quad (\mathrm{II})$$

This equation is qualitatively in agreement with the experimental results. However, it will become more complicated or changed as the oxidation proceeds,

since the oxidation of aldehyde plays an important part.

We postulated that the active species of catalyst was the dimer of cobaltic acetate since no spectroscopic evidence could be found for the formation of Co(IV). However, it is possible that the active species of catalyst is Co(IV) produced by the disproportionation,

$$2\text{Co(III)} \overset{K_1'}{\rightleftarrows} \text{Co(IV)} + \text{Co(II)}$$

We can thus consider the following elementary reactions in the early stage of reaction.

$$\text{R-CH}_3 + \text{Co(IV)} \xrightarrow{k_2'} \text{R-CH}_2\cdot + \text{Co(III)} + \text{AcOH}$$

$$\text{R-CH}_2\cdot + \text{O}_2 \xrightarrow{k_3'} \text{R-CH}_2\text{OO}\cdot$$

$$\text{R-CH}_2\text{OO}\cdot + \text{Co(III)} \xrightarrow{k_4'} \text{R-CHO} + \text{Co(II)} + (1/2)\text{O}_2 + \text{AcOH}$$

Resolving these elementary reactions by the same method as mentioned above, we obtain

$$v_m = K_1'k_2'[\text{R-CH}_3][\text{Co(III)}]^2[\text{Co(II)}]^{-1}$$

This equation is also in agreement with Eqs. (1) and (II).

References

1) Part II, Y. Kamiya and M. Kashima, This Bulletin, **46**, 905 (1973).
2) Department of Reaction Chemistry, Faculty of Engineering, University of Tokyo, Hongo, Bunkyo-ku, Tokyo.
3) J. Yamashita, K. Kurashima, M. Hida, and H. Hashimoto, *Kogyo Kagaku Zasshi*, **67**, 1153 (1965).
4) D. C. Hull, U. S. P. 2,673,217/1954.
5) W. F. Brill, *Ind. Eng. Chem.*, **52**, 837 (1960).
6) T. Koga and T. Hara, This Bulletin, **39**, 664 (1966).
7) T. Morimoto and Y. Ogata, *J. Chem. Soc. B*, **1967**, 62.
8) T. A. Cooper and W. A. Waters, *ibid.*, **1967**, 687.
9) E. I. Heiba, R. M. Dessau, and W. J. Koehl, Jr. *J. Amer. Chem. Soc.*, **91**, 6830 (1969).
10) Y. Kamiya and M. Kashima, *J. Catal.*, **25**, 326 (1972).
11) R. Kawai and Y. Kamiya, *Nippon Kagaku Kaishi*, **1973**, 1538.
12) Y. Kamiya, M. Ohzu, and N. Ohta, *Kogyo Kagaku Zasshi*, **71**, 999 (1968).

Phenanthro[4,5-*bcd*]furan Derivatives. II. A Synthesis of 3-Hydroxyphenanthro[4,5-*bcd*]furan (Morphenol)

Takaaki HORAGUCHI and Takahachi SHIMIZU

Department of Chemistry, Faculty of Science, Niigata University, Igarashi, Niigata 950-21

(Received September 28, 1973)

3-Hydroxyphenanthro[4,5-*bcd*]furan (I) was synthesized by the dehydrogenation, with 20% palladium on charcoal, of 3-oxo-1,2,3,8,9,9a-hexahydronaphtho[4,5-*bcd*]furan (XII), which had itself been prepared *via* a naphtho[1,8-*bc*]furan derivative (IX) starting from 8-hydroxy-1-tetralone (IV).

3-Hydroxyphenanthro[4,5-*bcd*]furan (I), which is a degradation product of morphine, had not been synthesized in spite of many attempts. These failures have been attributed to the presence of a ring strain[1] in the phenanthro[4,5-*bcd*]furan derivative which is the fundamental ring skeleton of morphenol. Recently, though, 5-hydroxy-1-methoxyphenanthro[4,5-*bcd*]furan (II) was synthesized,[2] as the first synthetic phenanthro[4,5-*bcd*]furan derivative, starting from methyl 3-(8-hydroxy-5-methoxy-1-oxo-1,2,3,4-tetrahydro-2-naphthyl)propionate (III), however, the product (II), unlike morphenol, has a methoxyl group at the 1-position. This paper will show that this synthetic course is applicable also to morphenol (I) and, therefore, would be useful for the preparation of general phenanthro[4,5-*bcd*]furan derivatives.

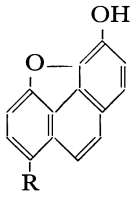

I: R=H
II: R=OMe

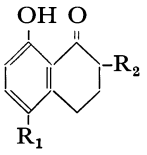

III: R_1=OMe, R_2=$(CH_2)_2CO_2Me$
IV: R_1=H, R_2=H
V: R_1=H, R_2=CHOH
VI: R_1=H, R_2=$(CH_2)_2CO_2Me$
VII: R_1=H, R_2=$(CH_2)_2COOH$

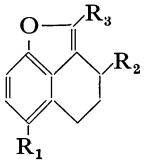

VIII: R_1=H, R_2=$(CH_2)_2COOH$, R_3=COOH
IX: R_1=H, R_2=$(CH_2)_2COOH$, R_3=H
X: R_1=OMe, R_2=$(CH_2)_2COOH$, R_3=COOH
XI: R_1=OMe, R_2=$(CH_2)_2COOH$, R_3=H

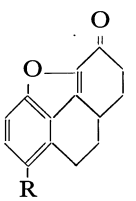

XII: R=H
XIII: R=OMe

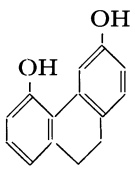

XIV

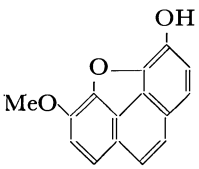

XV

Fig.

Results and Discussion

8-Hydroxy-1-tetralone (IV) was condensed[3] with ethyl formate in the presence of sodium methylate to give 8-hydroxy-2-hydroxymethylidene-1-tetralone (V). When a mixture of V and methyl acrylate was heated under reflux in aqueous methanol containing triethylamine, methyl 3-(8-hydroxy-1-oxo-1,2,3,4-tetrahydro-2-naphthyl)propionate (VI) was obtained along with IV; the ester (VI) gave an absorption corresponding to the phenolic hydroxyl group at τ −2.04 in the nuclear magnetic resonance spectrum and a conjugated-carbonyl band at 1634 cm^{-1} in the infrared spectrum. The ester was saponified to the corresponding carboxylic acid (VII) for practical separation from IV.

When VII was treated with ethyl bromoacetate at 170 °C, followed by hydrolysis, the expected di- and monocarboxylic acids, 3-(2-carboxy-4,5-dihydro-3*H*-naphtho[1,8-*bc*]furan-3-yl)propionic acid (VIII) and 3-(4,5-dihydro-3*H*-naphtho[1,8-*bc*]furan-3-yl)propionic acid (IX), were obtained in yields of 34 and 2% respectively; on the other hand, the use of VI in place of VII gave slightly increased yields (42% and 6%), which were comparable to those of the corresponding carboxylic acid (X and XI) in the synthesis of II (43% and 8%).[2] The monocarboxylic acid (IX), which was also obtained from the dicarboxylic acid by decarboxylation (59%), was subjected to polyphosphoric acid-catalyzed intramolecular cyclization to give 3-oxo-1,2,3,8,9,9a-hexahydrophenanthro[4,5-*bcd* furan (XII) in a 45% yield.

Finally, the aromatization[3,4] of XII with 20% palladium on charcoal afforded two phenolic compounds with different melting points, 142.5—143 °C and 175—179 °C (dec.), in 16 and 10% yields respectively. The lower-melting product was identified as 3-hydroxyphenanthro[4,5-*bcd*]furan (I) from its physical and spectral properties. It showed a purple fluorescence in a potassium hydroxide solution and a green fluorescence in concentrated sulfuric acid. The infrared spectrum gave absorptions at 3220 (OH) and at 814 and 822 cm^{-1} (2H), the ultraviolet spectrum was almost concordant with that of methyl morphenol,[5] and the nuclear magnetic resonance spectrum corresponded to the structure of I.

The other phenolic product, although it has not been subjected to elemental analysis, is perhaps 3,5-dihydroxyphenanthrene (XIV) in view of the following facts: (i) the nuclear magnetic resonance spectrum exhibited absorptions corresponding to two phenolic hydroxyl groups at τ 0.58 and 1.23, (ii) an isomeric 3,4-dihydroxyphenanthrene has been known to have a melting point of 143 °C,[6] (iii) the infrared spectrum is similar to that of morphenol in the 700—900 cm^{-1} region, showing the existence of two and three neighboring hydrogen atoms on the aromatic ring system.

Our synthetic course leading to 5-hydroxy-1-methoxyphenanthro[4,5-*bcd*]furan (II) is applicable also to morphenol. This suggests that the synthetic course would be generally useful for phenanthro[4,5-*bcd*]furan derivatives. It seemed that almost no effects of a methoxyl group appeared except in the intramolecular cyclization reaction (IX→XII). The yield (45%) of XII from IX was considerably lower than that (67%) of XIII. The cause of the difference in yields might be due to the steric effect of a methoxyl group; however, it is not yet clear. The effect of a methoxyl group will be further investigated by preparing 3-hydroxy-5-methoxyphenanthro[4,5-*bcd*]furan (XV).

Experimental

All the melting points are uncorrected. The column chromatography was performed over silica gel (WAKOGEL C-200, Wako Pure Chemical Industries, Ltd.). The polyphosphoric acid was prepared from 85% phosphoric acid (100 ml) and phosphorus pentoxide (123 g) by heating it at 160—165 °C for 5 hr. Unless otherwise stated, sodium sulfate was employed as the drying agent. The infrared spectra were determined with a JASCO Model DS 402G infrared spectrophotometer. The ultraviolet spectra were determined with a Shimadzu Model UV-200 spectrophotometer. The nuclear magnetic resonance spectra were determined at 100 MHz with a JEOL Model 4H-100 NMR spectrometer, using tetramethylsilane as the internal standard. Their chemical shifts are presented in terms of the τ value.

8-Hydroxy-2-hydroxymethylidene-1-tetralone (V). Ethyl formate (14.5 ml) was added to a mixture of sodium methylate (8.0 g) and benzene (50 ml) over a 5-min period, with stirring and cooling at 0 °C in nitrogen atmosphere; the stirring was then continued for one more hr. To the solution, IV (10 g) in benzene (50 ml) was added over a 30-min period at 0 °C, after which the mixture was stirred for an additional 4.5 hr at room temperature. The viscous mixture was then decomposed with 80 ml of 1 M sulfuric acid and extracted with benzene. The benzene layer was extracted with seven 55-ml portions of aqueous 1 M potassium carbonate. The alkaline solution thus obtained was acidified with 6 M hydrochloric acid, and the resulting precipitates were collected by filtration and recrystallized from *n*-hexane to give 5.35 g (76%) of V as yellow needles; mp 63—64 °C. IR(KBr): 1622 cm^{-1} (C=O). NMR($CDCl_3$): τ −3.45, −3.32 (d, C=CHOH), −1.90 (ϕ-OH).

Found: C, 69.65; H, 5.34%. Calcd for $C_{11}H_{10}O_3$: C, 69.83; H, 5.33%.

3-(8-Hydroxy-1-oxo-1,2,3,4-tetrahydro-2-naphthyl)propionic Acid (VII). A mixture of V (4.0 g), methyl acrylate (20.0 g), triethylamine (1.8 g), and 80% methanol (50 ml) was heated under reflux at 112 °C for 8 hr. The solution was then extracted with ether, and the ether layer was washed with four 30 ml-positions of aqueous 1 M potassium carbonate and with water, and dried. The ether was then evaporated, and the residue was hydrolyzed with a 3 M potassium hydroxide solution. The alkaline solution was acidified with 6 M hydrochloric acid, and the resulting precipitates were collected by filtration. They were then recrystallized from aqueous ethanol to give 3.7 g (75%) of VII as colorless needles; mp 164—165 °C. IR(KBr): 1717 (COOH), 1630 cm^{-1}(C=O).

Found: C, 66.78; H, 6.02%. Calcd for $C_{13}H_{14}O_4$: C, 66.68; H, 6.03%.

3-(2-Carboxy-4,5-dihydro-3H-naphtho[1,8-bc]furan-3-yl)propionic Acid (VIII) and 3-(4,5-Dihydro-3H-naphtho[1,8-bc]furan-3-yl)propionic Acid (VIII) and 3-(4,5-Dihydro-3H-naphtho[1,8-bc]furan-3-yl)propionic Acid (IX). A mixture of VII (2.0 g), ethyl bromoacetate (18.6 g) and potassium carbonate (12.8 g) was heated slowly up to 170 °C and then refluxed for 7 more hr at this temperature. The dark brown mixture was extracted with acetone, and then the acetone was evaporated. The residue was then separated after saponification with a 3 M potassium hydroxide solution into two moieties, one of which is insoluble in benzene. The benzene-insoluble moiety was recrystallized from tetrahydrofuran-benzene to give 0.8 g (34%) of VIII as colorless needles; mp 219—220 °C. IR (KBr): 1700 cm^{-1} (COOH).

Found: C, 68.37; H, 5.49%. Calcd for $C_{15}H_{14}O_5 \cdot 0.43\ C_6H_6$: C, 68.37; H, 5.40%.

The other moiety, in benzene, was chromatographed over silica gel and eluted with benzene-ether (97 : 3). A yellow fraction was collected, and the solvent was evaporated. The residue was crystallized from benzene-*n*-hxeane to give 40 mg (2%) of IX as colorless plates; mp 98—99 °C. IR(KBr): 1705 cm^{-1} (COOH). NMR ($CDCl_3$): τ −1.13 (COOH), 2.55 (H on the furan ring). UV: λ_{max}^{EtOH} 250 nm (ε 9500).

Found: C, 73.16; H, 6.10%. Calcd for $C_{14}H_{14}O_3$: C, 73.03; H, 6.13%.

When 1.3 g of the ester (VI) was used in place of the acid (VII), 0.6 g (41%) of VIII and 80 mg (6%) of IX were obtained.

Decarboxylation of VIII. A mixture of 10.0 g of quinoline, 1.0 g of VIII, and 1.0 g of copper powder was heated at 155 °C for 1.5 hr and then at 160 °C for 10 more min. The mixture was acidified with 1 M hydrochloric acid and extracted with ether. The ether extract was washed with four 30-ml portions of 2 M hydrochloric acid and with water, and dried, and then the ether was evaporated. The residue was crystallized from benzene-*n*-hexane to give 0.5 g (59%) of IX as colorless plates; mp 98—99 °C.

3-Oxo-1,2,3,8,9,9a-hexahydrophenanthro[4,5-bcd]furan (XII). A mixture of 0.5 g of IX and 69 g of polyphosphoric acid was stirred at 75 °C for 4 hr. The reaction mixture was poured onto ice and extracted with ether. The ether was washed with water, with four 45-ml portions of 1M aqueous potassium carbonate, and with water, and then dried. The ether was evaporated to give crystals. Recrystallization from ethanol–*n*-hexane gave 0.21 g (45%) of XII as colorless needles; mp 109—110 °C. IR(KBr): 1670 cm^{-1} (C=O). NMR($CDCl_3$): τ 2.45—2.90 (multiplet, ϕ-H), 6.57—7.03 (m, $-CH_2-$, -CH-), 7.40—7.72 (m, $-CH_2-$), 7.95—8.73 (m, $-CH_2-$).

Found: C, 79.13; H, 5.67%. Calcd for $C_{12}H_{12}O_2$: C, 79.23; H, 5.70%.

3-Hydroxyphenanthro[4,5-bcd]furan (I). A mixture of XII (0.2 g), 20% palladium on charcoal (0.4 g), and α-methylnaphthalene (3.5 g) was heated at 230 °C for 30 hr under nitrogen atmosphere. The reaction mixture was filtered, and the filtrate was extracted with ether. The ether layer was extracted with five 45 ml-portions of a 1 M potassium hydroxide solution, and the alkaline solution thus obtained was washed with three 30 ml-portions of carbon tetrachloride and then made acidic with 6 M hydrochloric acid. The resulting precipitates were extracted with ether, and the ether extract was washed with water, dried, and then concentrated. The residue was chromatogtaphed over silica gel and eluted with benzene-ether (9 : 1) to give colorless crystals from the first fraction. Recrystallization from benzene gave 32 mg (16%) of I as colorless needles; mp 142.5—143 °C. IR(KBr): 3220 (OH), 822, 813 (2H), 760 cm^{-1} (3H). NMR($CDCl_3$): τ 0.49(OH), 2.0—2.56 (ϕ-H). UV: λ_{max}^{EtOH} 234 (ε 47500), 240 (ε 49300), 257 (ε 23900), 269 (ε

17500), 317 (ε 13400), 335 (ε 4300), 353 nm (ε 6100).

Found: C, 80.75; H, 3.96%. Calcd for $C_{14}H_8O_2$: C, 80.76; H, 3.87%.

The latter fraction was also collected to give a phenolic compound. Recrystallization from benzene gave 20 mg (10 %) of colorless needles, which may be 3,5-dihydroxyphenanthrene (XIV) judging from the following spectral properties. IR(KBr): 3240 (OH), 840, 814 (2H), 762 cm^{-1} (3H). NMR(CD_3COCD_3): τ 0.58, 0.78 (d, ϕ-H), 1.23 (OH), 2.24—2.96 (m, ϕ-7H). UV: λ_{max}^{EtOH} 235 (ε 38700), 252 (ε 61400), 285 (ε 9800), 310 (ε 10900), 328 (ε 2600), 345 (ε 6000), 365 nm (ε 8300).

The authors wish to thank Mr. Y. Takahashi for the elemental analyses, Mr. H. Saisu for the infrared analyses, and Mr. T. Ono for the nuclear magnetic resonance analyses.

References

1) A. V. Dendy, J. H. P. Tyman, and W. B. Wahlley, *J. Chem. Soc.*, **1963**, 4040.
2) T. Shimizu, T. Horaguchi, and A. Watanabe, This Bulletin, **46**, 1772 (1973).
3) R. B. Turner, D. E. Nettleton, J. R. Ferebee, *J. Amer. Chem. Soc.*, **76**, 5923 (1956).
4) E. Mosetig and H. M. Duvoll, *ibid.*, **59**, 367 (1937).
5) H. Rapoport, A. D. Batchs, and J. E. Gordon, *ibid.*, **80**, 5767 (1958).
6) O. Fischer and Vongerichten, *Ber.*, **19**, 792 (1886).

NOTES

BULLETIN OF THE CHEMICAL SOCIETY OF JAPAN, VOL. 47(2), 488—489 (1974)

Charge Transfer Complexes and Self-association of Flavin Adenine Dinucleotide

Fujio TAKAHASHI and Hirotoshi MAEDA

Research Laboratory of Resources Utilization, Tokyo Institute of Technology, Ookayama, Meguro-ku, Tokyo 152

(Received July 20, 1973)

Synopsis. Spectrophotometric studies on the formation of FAD-L-tryptophane and FAD-D-tryptophane complexes, and the optical rotatory and polarographic studies of FAD have been carried out. The steric influence of ribosyl and ribityl groups on FAD for the complex formation is discussed. The dimerization of FAD in solution is suggested.

Many papers have appeared on the charge transfer complexes of flavins with tryptophane.[1] Flavin adenine dinucleotide (FAD) is known to form the charge transfer complex as an electron acceptor with caffeine,[2] while the intramolecular interaction between the flavin and adenine moieties in FAD has been established.[3] The ribosyl and ribityl groups in FAD are so bulky that they may sterically influence the complex formation with an electron donor. It was expected that FAD complex formation with L-tryptophane and D-tryptophane causes a difference in equilibrium constants and the thermodynamic parameters. If we suppose that ribosyl and ribityl groups interact with a side chain of indole, the molecular rotations of FAD-tryptophane complexes might differ from the sum of the individual molecular rotations of pure samples of FAD and tryptophanes. For optical rotatory dispersion studies, the molecular of FAD has been measured at very low concentration (10^{-4} mol/l) in the region of shorter wavelength than 450 nm.[4] In our studies, it was necessary to make the concentrations of FAD and tryptophanes higher (10^{-3}~10^{-2} mol/l) for the facilitation of complex formation. For comparison the molecular rotation of FAD was determined at the same concentration. It was found that the molecular rotation of FAD at 590 nm changes with concentration. This paper presents spectrophotometric studies on the formation of FAD-L-tryptophane and FAD-D-tryptophane complexes, and the optical rotatory and the polarographic studies of FAD.

TABLE 1. ANALYTICAL DATA OF FAD AND TRYPTOPHANES

Compound	UV, visible molar extinction coefficient	$[\alpha]_D^{28}$	Paper chromatograph, R_f
FAD	1.11×10^4	—	0.15[a]
	1.13×10^4		
	(450 nm)		
L-Tryptophane	5.9×10^3	−31.4	0.69[b]
D-Tryptophane	5.9×10^3	+32.4	0.70[b]
	5.6×10^3	±31.5	
	(280 nm)		

a) *n*-PrOH : *n*-BuOH : 5%Na_2HPO_4 aq. = 50 : 15 : 30,
b) *n*-BuOH : AcOH : H_2O = 4 : 1 : 1.

Experimental

The analytical data of FAD and tryptophane are given in Table 1. Requisite amounts of FAD and/or tryptophane were dissolved in 0.1 mol/l of phosphate buffer (pH 7.0) for the measurements. The adsorption spectra and the optical activities were determined with a Shimadzu spectrophotometer SV50AS and a JASCO automatic spectropolarimeter Model J-5, respectively. The polarograms were determined with a dropping mercury electrode.

Results and Discussion

From the differential absorption spectrum, the absorption maximum was found to appear at 505 nm and the absorbance of FAD-trypotphane systems was thus determined at 505 nm. The results are plotted according to Benesi-Hildebrand's equation[5] in Fig. 1. The equilibrium constant K for each temperature T was obtained from the values of slopes and intercepts. From the plots of log K vs. $1/T$, the enthalpy changes and entropy changes were calculated. The results are summarized in Table 2. It can be expected that FAD, in which flavin and adenine groups form an intramolecular complex, can form a complex weaker than flavin mononucleotide (FMN). Thus it is reasonable that the ΔH for FAD-tryptophane complexes is smaller than that for FMN-tryptophane complex (−7.4 kcal/mol).[1] The values of ΔH and ΔS for FAD-L-tryptophane and FAD-D-tryptophane systems,

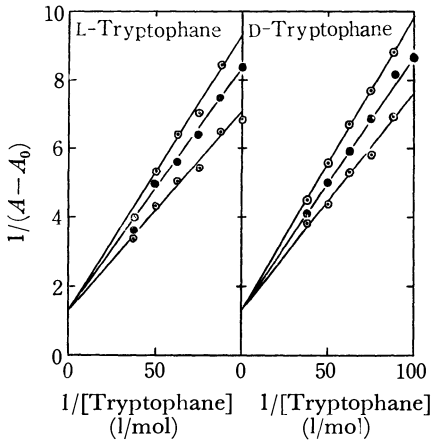

Fig. 1. Plots of $1/(A-A_0)$ at 505 nm *vs.* 1/(Tryptophane)
FAD: 4×10^{-4} mol/l, Tryptophane: 1—2.7×10^{-2} mol/l in 0.1 mol/l phosphate buffer (pH 7.0)
A: The absorbance of FAD-tryptophane solution
A_0: The absorbance of FAD solution
---- $1/(A-A_0)$ *vs.* 1/(Tryptophane) (l/mol)

Table 2. Thermodynamic data for the complex formation

System	K (l/mol) 25 °C	35 °C	45 °C	ΔH (kcal/mol)	ΔS (eu)
FAD-L-Tryptophane	$22._3$	$18._3$	$16._2$	−3.0	−3.9
FAD-D-Tryptophane	$20._5$	$17._6$	$15._2$	−2.8	−3.5

respectively, actually show no difference. It seems that ribosyl and ribityl groups can not sterically influence the complex formation. The side chain of indole might be located on the site opposite the ribosyl and ribityl groups in the FAD-tryptophane complex. Equimolar concentrations of FAD and tryptophane solutions were mixed for the determination of the molecular rotation of the complex. In the solution of 0.015 mol/l FAD and 0.015 mol/l L-tyrptophane or D-tryptophane, 20.3% or 19.2% FAD forms the complex at 28 °C as calculated from the values in Table 2. The molecular rotation of the mixture of FAD and tryptophane was compared with the sum of the individual molecular rotations of pure samples at 28 °C, and found to be almost the same. We see that the ribosyl and ribityl groups might not influence the molecular rotation for complex formation.

The plots of the molecular rotation *vs.* the concentration of FAD are given in Fig. 2. The molecular rotation of FAD was estimated to be $[M]^{28}_{590}$ -3.5×10^2 by the extrapolation to the zero concentration of FAD. In contrast to the extrapolation to higher concentration, the molecular rotation was found to be in the direction of positive value. Wave heights of polarograms are plotted against the concentration of FAD (Fig. 2). It seems that the reduction velocity of FAD decreases in higher concentration. The half-wave potential of FAD was found to be −0.55 V *vs.* SCE. The wave height is proportional to concentration in the region $10^{-3}\sim10^{-2}$ mol/l. Dimerization of FAD was suggested as a result of the nuclear magnetic resonance study.[6] The concentration dependence of the molecular rotation might confirm the dimerization of FAD. The dimer of FAD might hardly be reduced at the electrode, if the two flavin moieties associate with each other back to back and are enclosed by the two adenine moieties in FAD. If this is the case, the dimer can not form FAD-tryptophane complex. This can be justified because the plots in Fig. 1 fall on a line according to Benesi-Hildebrand's equation, which is derived by assuming the formation of 1 : 1 complex.

Dimerization constant K_2 could be calculated if we assume the observed molecular rotation R of FAD to be the weight average of monomer R_1 and dimer R_2:

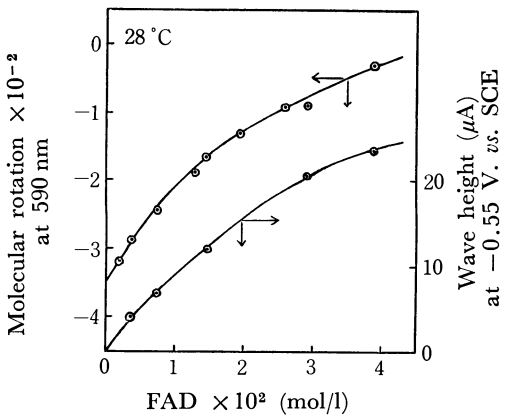

Fig. 2. The optical activities and the polarographic data of FAD 0.1 mol/l phosphate buffer (pH 7.0)

$$R = (M/C)R_1 + (2D/C)R_2, \quad C = M + 2D \tag{1}$$

where C, M, and D are FAD concentrations of total, monomer and dimer, respectively.

$$K_2 = D/M^2 \tag{2}$$

From Eqs. (1) and (2), we obtain,

$$R = -\left\{(R_2-R_1)2K_2\right\}^{1/2}\left\{(R-R_1)/C\right\}^{1/2} + R_2. \tag{3}$$

Plots of R *vs.* $\{(R-R_1)/C\}^{1/2}$ by means of this equation with data in Fig. 2 gives a straight line, from which the values of K_2 and R_2 are determined to be 22±5 l/mol and $+6.5\times10^2$ (28 °C), respectively. In the systems in Fig. 1, less than 3.3% FAD dimerizes and more than 17% FAD forms the charge transfer complex with tryptophane, which are calculated from the values of K_2 and the data in Table 2. The dimer concentration is not very high in the systems. The values of data in Table 2 might be reliable within 5% error.

The authors express their sincere thanks to Professor Shuichi Suzuki of Tokyo Institute of Technology for his encouragement.

References

1) M. A. Slifkin, "Charge Transfer Interactions of Biomolecules," Academic Press, London and New York (1971).
2) K. Yagi and Y. Matsuoka, *Biochem. Z.*, **328**, 138 (1956).
3) D. W. Miles and D. W. Urry, *Biochemistry*, **7**, 2791 (1968); P. S. Song, *J. Amer. Chem. Soc.*, **91**, 1850 (1969).
4) R. T. Simpson and B. L. Vallee, *Biochem. Biophys. Res. Commun.*, **22**, 712 (1966).
5) F. Takahashi, M. Okamoto, and H. Maeda, *Nippon Kagaku Kaishi*, **1972**, 2017.
6) R. H. Sarma, P. Dannies, N. O. Kaplan, *Biochemistry*, **7**, 4359 (1968).

BULLETIN OF THE CHEMICAL SOCIETY OF JAPAN, VOL. 47(2), 490 (1974)

Carbonylation of Phenylacetylene by Rhodium Carbonyl Chloride

Jitsuo KIJI, Susumu YOSHIKAWA, and Junji FURUKAWA

Department of Synthetic Chemistry, Faculty of Engineering, Kyoto University, Sakyo-ku, Kyoto 606

(Received July 16, 1973)

Synopsis. The reaction of phenylacetylene with carbon monoxide catalyzed by rhodium carbonyl chloride ($Rh_2(CO)_4Cl_2$) gives 3,6-diphenyl-1-oxa-[3,3,0]bicycloocta-3,6-diene-2,4-dione.

Although acetylenic compounds are known to react with carbon monoxide under the influence of transition-metal catalysts,[1] there have been few studies of the carbonylation of acetylene with rhodium carbonyl chloride ($Rh_2(CO)_4Cl_2$, I); the carbonylation of diphenylacetylene giving a cyclopentadienone and a quinone is catalyzed by I in benzene.[2] This paper will deal with a novel carbonylation of phenylacetylene with I.

Results and Discussion

The reaction was carried out in a benzene solution under the pressure of carbon monoxide. After the reaction, no phenylacetylene was recovered and deep-red needles were separated from the reaction mixture. The elemental analysis and the mass spectrum indicated that the product (II) is composed of two molecules of phenylacetylene and three molecules of carbon monoxide. The infrared spectrum taken with a KBr disk has three carbonyl bands, at 1788 (sh), 1753 and 1740 cm^{-1}, which can be assigned to an unsaturated γ-lactone and a five-membered cyclic ketone. The NMR spectrum in hexa-deuteriodimethyl sulfoxide at 90 °C shows a sharp singlet at 6.2 τ due to methylene protons and complicated peaks at 1.7—2.6 τ due to phenyl protons. The hydrogenation of II over platinum on carbon absorbed two moles of hydrogen to form a saturated compound, $C_{19}H_{16}O_3$ (by mass spectrometry). The reaction of II with 2,4-dinitrophenylhydrazine gave the corresponding hydrazone, in which the γ-lactone ring remained unchanged. From these observations, the product was proved to be 3,6-diphenyl-1-oxa-[3,3,0]bicycloocta-3,6-diene-2,4-dione (II).

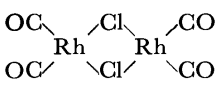

I

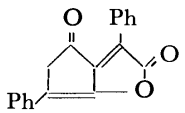

II

This reaction is characteristic of terminal acetylenes. The formation of II can be explained by the following mechanism; phenylacetylene adds oxidatively to rhodium to form a rhodium hydride,[3] and this is followed by the insertion of phenylacetylene and carbon monoxide. These processes involve two internal cyclizations, which give five-membered cycles. Many examples of a similar internal cyclization to form a lactone have been reported by Chiusoli and Cassar.[4]

The products other than II were oily polymeric materials containing a γ-lactone moiety, but their structure could not be determined. The formation of this polymeric product can presumably be explained on the assumptions that the mode of the insertion of phenylacetylene was not uniform and that the resulting intermediates were not suitable for the cyclization giving II, but gave a linear structure containing the γ-lactone group.

Similarly, from the reaction of *t*-butylacetylene a colorless carbonylated product was obtained.[5] Methylacetylene gave a 1,4-quinone derivative. In this carbonylation of α-acetylene, the substituent on the acetylenic carbon has a great influence on the course of the reaction.

Experimental

Carbonylation. A benzene solution containing 400 mg of $Rh_2Cl_2(CO)_4$ and an excess of phenylacetylene (8 g) was allowed to react with carbon monoxide under a pressure of 50 kg/cm^2 at 120 °C. After 12 hr, II was separated from the reaction mixture, gathered, and washed with benzene to give deep-red needles (yield, 1.07 g); mp 234—235 °C. Found: C, 79.08; H, 4.46; O, 16.42%. Calcd for $C_{19}H_{12}O_3$: C, 79.01; H, 4.19; O, 16.63%.

Hydrogenation of II. Compound II (370 mg) was hydrogenated in ethyl acetate (150 ml) at room temperature under an atmospheric pressure, using Pt on carbon (5%, 500 mg) as the catalyst. Subsequent chromatography on silica gel with ethyl acetate gave 146 mg of colorless product (III); mp 140—141.5 °C. IR (KBr): 1770, 1750 cm^{-1} (ν_{CO}). Found: C, 78.16; H, 5.70; O, 16.27. Calcd for $C_{19}H_{16}O_3$: C, 78.10; H, 5.48; O, 16.42.

References

1) C. W. Bird, "Transition Metal Intermediates in Organic Synthesis," Academic Press, New York (1967), p. 205.
2) S. McVey and P. M. Maitlis, *J. Organometal. Chem.*, **19**, 169 (1969).
3) J. P. Collman and J. W. Kang, *J. Amer. Chem. Soc.*, **89**, 844 (1967).
4) C. P. Chiusoli and L. Cassar, *Angew. Chem.*, **79**, 177 (1967).
5) Chromatography of the reaction mixture on Florisil (Floridin Co., U.S.A.), using benzene as the solvent, gave colorless prisms; mp 175 °C. Mass m/e 330 (M^+); IR (KBr) 1755, 1710 cm^{-1} (ν_{CO}); NMR ($CDCl_3$, TMS) τ 9.00, 8.76, 8.70 (27H of *t*-butyl) and 7.00, 2.40, 2.64 (3H).

BULLETIN OF THE CHEMICAL SOCIETY OF JAPAN, VOL. 47(2), 491—492 (1974)

The Relation between the Electronic Spectra and the Oxidation and Reduction Potentials of Benzenoid Hydrocarbons

Tanekazu KUBOTA, Hiroshi MIYAZAKI, Kiyoshi EZUMI, and Masumi YAMAKAWA

Shionogi Research Laboratory, Shionogi & Co., Ltd., Fukushima-ku, Osaka 553

(Received April 5, 1973)

Synopsis. It was shown that the ^1L_a band of benzenoid hydrocarbons is in a linear relation to $(E_{1/2}^{red}-E_{1/2}^{oxd})$ value led from the half-wave reduction and oxidation potentials. The theoretical background and the binding conditions of the application of this relation were clearly given.

In an earlier paper[1] we have theoretically shown the linear relation of the electronic spectra to the non-aqueous oxidation and reduction potentials of organic substances. That is, we wrote:[1]

$$E_{1/2}^{red} - E_{1/2}^{oxd} = k_1 \cdot {}^1E_{HO\to LV}^{UV} + k_2 \quad (1)$$

where $E_{1/2}^{red}$ and $E_{1/2}^{oxd}$ are the half-wave potentials (in volts) of the non-aqueous reduction and oxidation respectively. The ${}^1E_{HO\to LV}^{UV}$ is the singlet electronic transition energy, in which the contribution from the highest occupied molecular orbital (HOMO) to the lowest vacant MO (LVMO) is predominant. The absolute value of the k_1 constant equal 1 theoretically under suitable conditions[1] when an electron volt is taken as the energy unit for ${}^1E_{HO\to LV}^{UV}$. It should be noticed that Eq. (1) is an extension of Eq. (2) (given below), which also satisfies the experimental results quite well.[1] Here, ε_{LV} and ε_{HO} are the energy at the LVMO and the HOMO respectively:

$$E_{1/2}^{red} - E_{1/2}^{oxd} = k_1(\varepsilon_{LV}-\varepsilon_{HO}) + k_3 \quad (2)$$

In order to derive Eq. (1) from Eq. (2), however, there are necessary some binding conditions regarding the treatment of electronic transitions from the viewpoint of the electronic structures of molecules;[1] these conditions limit the applicability of Eq. (1) to the ${}^1E_{HO\to LV}^{UV}$ transition. Previously Pysh and Yang,[2] and Peover[3] reported the linear relation of the p-band of benzenoid alternant hydrocarbons (AH) to the value of $E_{1/2}^{red}-E_{1/2}^{oxd}$. However, there have been no detailed discussions of this physical meaning from the standpoint of electronic structures, *i.e.*, the nature of applied electronic transitions and the value of k_1 in Eq. (1) and (2). Note particularly that the k_2 value in Eq. (1) should depend not only on solvation energy of the cation or anion radical,[3] generated by electrolysis, but also on the electronic-state terms.[1]

Although Eqs. (1) and (2) can well explain the ^1L_a band of the electronic spectra of heterocyclic amine *N*-oxide,[1] it seems to be theoretically important to check whether or not these equations can be applied to other systems, especially to AH substances. This is because the AH's are the fundamental substances for testing theoretical treatments concerning molecular physics. The ^1L_a band (*p*-band)[4] reported in the literature is adopted as the value of ${}^1E_{HO\to LV}^{UV}$. Actually, the energies at the ^1L_a and ^1L_b (α-band) bands are cited from Clar's book,[5] in which the main vibrational peaks at the ^1L_a and ^1L_b bands are given. Either the vibrational peak appearing on the longest-wavelength side or that showing the strongest intensity was selected. However, the derived conclusion has the same, regardless of the choice. In addition, Peover *et al.*[6] reported the value of $E_{1/2}^{red}$ and $E_{1/2}^{oxd}$ of AH's measured in acetonitrile. As the molecular orbital energies we have used those calculated by Koutecký,[7] adopting the variable β method within the PPP π electron technique, since his purpose was to interpret the polarographic reduction and oxidation potentials. All the experimental and theoretical data mentioned above are collected in Table 1.

Figure 1 gives the linear relation of the $(E_{1/2}^{red}-E_{1/2}^{oxd})$ values against the ^1L_a band energies, the relation of Eq. (1) being well satisfied. The slope of $|k_1|=0.941$ is quite reasonable from the theoretical point of view.[1] Also, note that the good linear relation of Eq. (2), $(E_{1/2}^{red}-E_{1/2}^{oxd}=-0.815\ (\varepsilon_{LV}-\varepsilon_{HO})+1.701)$, also holds with the standard deviation of $\sigma=\pm0.071$ volt. We have also checked the constancy of the electron repulsion and CI terms,[1] given by $(J_{ho\cdot lv}-2K_{ho\cdot lv}-{}^1E_{CI})$, for the ^1L_a band of the compounds listed in Table 1. Our results[8] calculated using the PPP approximation with a constant β value (−2.37 eV) indicate that $(J_{ho\cdot lv}-2K_{ho\cdot lv})$ and $(J_{ho\cdot lv}-2K_{ho\cdot lv}-{}^1E_{CI})$ are within the maximum variations of 2.25±0.30 and 2.35±0.35 ev respectively in all the compounds except for benzene,[4] for which they are 2.92 and 3.33 eV respectively. It is possible to put these values as a constant, this condition being required for deriving Eq. (1).[1] In the case of ^1L_b band, however, each point is considerably scattered from the relation of Eq (1). Since the effect of the configuration interaction on the ^1L_b band seems to be much larger than that on the ^1L_a band,[9] the above result is reasonably expected. It is now clear, from the facts thus far presented, that Eqs. (1) and (2) can be safely applied also to the benzenoid AH's, and that, conversely speaking, the treatment of Eqs. (1) and (2) is reasonable.

Next, let us consider some other points. For the AH's this equation: I_p (ionization potential)$+E_A$ (electron affinity)=constant is well known.[4b] In other words, when Koopmans' theorem[4b,10] is applied, the ε_{HO} (or ε_{LV}) can be expressed in terms of the ε_{LV} (or ε_{HO}) on the basis of the above relation. Therefore, using Eq. (2), $(E_{1/2}^{red}-E_{1/2}^{oxd})$ can be linearly expressed by either the ε_{LV} or the ε_{HO}. Since $(E_{1/2}^{red}-E_{1/2}^{oxd})$ is proportional to ${}^1E_{HO\to LV}^{UV}$ (Eq. (1)),[1] we can conclude that the ε_{LV} or ε_{HO}, thus, $E_{1/2}^{red}$ or $E_{1/2}^{oxd}$, is also in a linear relation only to the ^1L_a band for the AH substances.[11] That is, this relation is easily given by this equation: $E_{1/2}^{red}$ (or $-E_{1/2}^{oxd}$)$=(k_1/2){}^1E_{ho\to lv}^{UV}+k_4$ (new constant). This kind of plot employing the data given in Table 1

Table 1. Various benzenoid hydrocarbons, with their half-wave oxidation and reduction potentials (V *vs.* SCE), SCF-MO energies at LVMO and HOMO, and observed positions (eV) at ^1L_a (p) and ^1L_b (α) bands

Compound	Oxidation and reduction potentials[a]		SCFMO energies[b]		Observed band positions[c]	
	$E_{1/2}^{oxd}$	$E_{1/2}^{red}$	ε_{HO}	ε_{LV}	^1L_a-band (p)	^1L_b-band (α)
Benzene	2.38[6)d)]	(−3.53)[e)]	−10.661	−1.339	6.205[f)]	4.761[f)]
Naphthalene	1.65	−2.63	−9.700	−2.300	4.350[f)]	4.174[f)]
Anthracene	1.19	−2.07	−9.086	−2.914	3.310[f)]	—
1,2-Benzanthracene	1.33	−2.11	−9.169	−2.831	3.491[g)]	3.219[g)]
1,2,5,6-Dibenzanthracene	1.40	−2.12	—	—	3.542[h)]	3.147[h)]
Pyrene	1.25	−2.19	−9.092	−2.908	3.718[f)]	3.337[f)]
1,2-Benzpyrene	1.34	−2.22	−9.200	−2.800	3.741[i)]	3.563[i)]
3,4-Benzpyrene	1.10	−1.95	−8.857	−3.143	3.225[i)]	3.076[i)]
3,4,9,10-Dibenzpyrene	1.17	−1.90	—	—	3.160[g)]	2.863[g)]
Perylene	1.04	−1.73	−8.808	−3.192	2.857[f)]	3.674[f)]

a) Taken from the Ref. 6 unless otherwise noted. These values were measured *vs.* SCE in CH_3CN containing 0.1 N. Et_4NClO_4. Generally speaking $E_{1/2}^{red}$ values correspond to those of a good reversible one-electron reduction wave at a dropping mercury electrode.[6)] The values of $E_{1/2}^{oxd}$ are also for the reversible one-electron oxidation at a rotating platinum electrode,[6)] except for anthracene, 1,2-benzanthracene, and 1,2-benzpyrene where the reversibility is not so good as an overall electrode reaction.[6)] In turn the reversibility on the $E_{1/2}^{oxd}$ values of benzene, naphthalene, and perylene is not clearly given in the cited literature.[6)] b) See Ref. 7. The relation of I_p+E_A = constant is well known for AH's[4b,c)] (see text). ε_{LV} was obtained from ε_{HO} by adopting the 12.0 eV for the constant.[7)] c) Taken from the Ref. 5 (see text). d) This is the value[6)] corrected *vs.* SCE on the data reported by H. Lund, *Acta Chem. Scand.*, **11**, 1323 (1957), where the potential was measured in CH_3CN *vs.* Ag electrode. e) This value was estimated from the extrapolation of the linear relation between $E_{1/2}^{red}$ and ε_{LV} in a series of benzenoid AH's.[6,7)] f) Obtained in CH_3OH-C_2H_5OH mixture. g) Obtained in benzene. For comparative purpose the 300 cm^{-1} was added to the value of the recorded ^1L_a band alone for correcting to that in ethanol. See E. Clar, *Spectrochim. Acta*, **4**, 116 (1950). h) Obtained in dioxane. i) Obtained in ethanol.

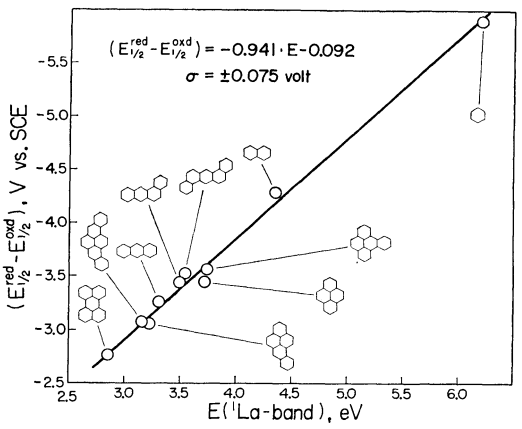

Fig. 1. The relationship between the observed values of ^1L_a band and $(E_{1/2}^{red}-E_{1/2}^{oxd})$ for benzenoid hydrocarbons.

also leads to a good linear relation with the slopes of −0.536 and −0.405 for the $E_{1/2}^{red}$ and $E_{1/2}^{oxd}$ plottings respectively. These absolute values of the slope are near the theoretical one, 0.5.

References

1) H. Miyazaki, T. Kubota, and M. Yamakawa, This Bulletin, **45**, 780 (1972).

2) E. S. Pysh and N. C. Yang, *J. Amer. Chem. Soc.*, **85**, 2124 (1963).

3) M. E. Peover, *Electrochim. Acta*, **13**, 1083 (1968).

4) a) In the case of benzene, the effect of the configuration interaction on the ^1L_a band as well as on the ^1L_b band is large because of its high symmetry.[b,c)] However, benzene is the most fundamental AH for the interpretation of the electronic spectra, so this ^1L_a band was also included in the present linear plotting. b) N. Mataga and T. Kubota, "Molecular Interactions and Electronic Spectra," Marcel Dekker, New York (1970), p. 80, etc. c) T. Kubota, Progress Reports on Electronic Processes in Chemistry, No. 2 (1960), published by the Japanese Research Group on Electronic States.

5) E. Clar, "Polycyclic Hydrocarbons," Vols. 1 and 2, Academic Press, London (1964).

6) T. A. Gough and M. E. Peover, "Polarography," Vol. 2, 1017, Macmillan, London (1964).

7) J. Koutecký, *Z. Phys. Chem., (N. F.)*, **52**, 8 (1967).

8) A. FACOM 270—30 computer was employed here. See also M. Yamakawa, T. Kubota, and H. Akazawa, *Theoret. Chim. Acta*, **15**, 244 (1969).

9) J. R. Platt, "Systematics of the Electronic Spectra of Conjugated Molecules," John Wiley & Sons (1964).

10) T. Koopmans, *Physica*, **1**, 104 (1935).

11) See also T. Tani and K. Honda, *J. Electrochem. Soc. Japan*, **36**, 700 (1968).

BULLETIN OF THE CHEMICAL SOCIETY OF JAPAN, VOL. 47(2), 493—494 (1974)

The Decomposition of Organic Substances by Laser Heating

Pil Hyon KIM,* Susumu NAMBA,* and Ko TAKI**

*The Institute of Physical and Chemical Research, Wako-shi, Saitama 351

**Faculty of Industrial Hygiene, Kitasato University, Sagamihara-shi, Kanagawa 228

(Received July 26, 1973)

Synopsis. Gaseous organic substances were decomposed by the laser heating of various solid targets (boiling points are different) which were placed in them. This method gives the products which have never been obtained by means of the conventional heat decomposition.

The laser irradiation of a solid target causes the vaporization of the target material. Laser irradiations of graphite carbon and copper cyanide have been reported previously by the present authors.[1-3] In these cases, the vaporized or fragmented species produced by the laser irradiation (carbon atoms or CN radicals) have reacted with gaseous substances to give various products containing the target material.

In the reaction of carbon vapor with hydrocarbons, an isotopic experiment[4] using carbon-14 labeled ethane as the substrate or carbon-14 enriched graphite as the target showed that the carbon vapor not only reacts with the substrate, but also decomposes the substrate by means of the collision. This decomposition may be considered to be heat decomposition.

The pulse-laser irradiation of the target produces a vapor of the target material, the temperature of which is about the boiling point of the target. It is expected that the collision of this vapor with a gaseous substance or the heated target surface induces the heat decomposition of the substance. In this case, it is considered that the decomposition temperatures of the substances have distributed from the boiling point of the target material to the lower temperature.

In pulse-laser irradiation, the vapor is produced so quickly (less than 10^{-3} s), and the temperature of vapor or the heated target surface decreases so rapidly, that decomposition at the boiling point of the target is possible. In the conventional heating method, however, the heating rate is not so fast as the pulse-laser heating, so the heat decomposition at a temperature above the decomposition temperature of the organic compound is not exactly possible because the organic compound is decomposed during the heating process before reaching the desired temperature.

In laser heating, as, in view of the above considerations, the decomposition temperature of the substance may be decided by the boiling point of the target material, the gaseous substances can be decomposed at various temperatures by using various targets. For instance, in case of the nickel target the maximum decomposition temperature is about 2850 °C (the boiling point of nickel).

In this investigation, the decomposition of gaseous organic substances has been studied by means of the pulse-laser irradiation of various targets of nickel, zinc and red phosphorus.

TABLE 1. RELATIVE PRODUCT YIELD IN THE DECOMPOSITION OF METHANE, ETHANE, TOLUENE AND ETHANOL FOR 7 PULSE LASER IRRADIATIONS ON NICKEL, ZINC OR PHOSPHORUS TARGET

Substance	Product	Relative yield		
		Ni target	Zn target	P target
Methane	C_2H_6	0.26	1.3	($\sim10^{-7}$ mol)
	C_2H_4	0.03	0.12	
	C_2H_2	1.00 ($\sim10^{-6}$ mol)	1.00 ($\sim10^{-7}$ mol)	(0)
Ethane	CH_4	0.86	0.57	2.2
	C_2H_4	2.08	2.4	42.4
	C_2H_2	1.00	1.00	1.00
	C_4H_{10}	0.23	0.58	10.4
Toluene	CH_4	0.40	0.12	
	C_2H_6	0.13	0.16	
	C_2H_4	0.04	0.07	
	C_2H_2	1.00	1.00	
Ethanol	CH_4	4.13		
	C_2H_6	0.23		
	C_2H_4	4.7		
	C_2H_2	1.00		

Experimental

The decomposition techniques were almost the same as those reported previously.[1-4] Nickel (bp 2850 °C) and zinc (bp 908 °C) plates, and a red phosphorus (bp 280 °C) tablet were used as the targets. Each target, placed in a 7-cm^3 cell filled with the substance gas, was irradiated by means of a focused laser beam. The laser used was a normal ruby laser, the output energy and pulse duration of which were 3J and 0.5 ms respectively. The gas pressure of the gaseous substance was 600—700 Torr, while that of the liquid substance was the saturated vapor pressure at 60—70 °C.

The volatile products were collected and analyzed by gas chromatography using silica gel and squalane columns. The most reliable value of the detection was about 10^{-8} mol.

Results and Discussion

The relative product yields in the decomposition of methane, ethane, toluene, and ethanol are shown in Table 1.

In methane decomposition, the acetylene yield goes down with the decrease in the boiling point of the target material; finally, at the decomposition temperature under the phosphorus boiling point no acetylene is obtained at all but the ethane yield increases. It is roughly estimated that the high-temperature decomposition gives C, CH, and CH_2, mainly resulting in acetylene, while low-temperature decomposition gives

CH_3 mainly resulting in ethane. The main processes of the decomposition may be estimated to be as follows:

(1) $CH_4 \xrightarrow{\text{Ni target}}$ fragmented C, CH and CH_2 $\longrightarrow C_2H_2$

(2) $CH_4 \xrightarrow{\text{Zn target}}$ fragmented C, CH, CH_2 and CH_3 $\longrightarrow C_2H_2$ and C_2H_6

(3) $CH_4 \xrightarrow{\text{P target}}$ fragmented $CH_3 \longrightarrow C_2H_6$

The fact that the acetylene yield is decreased by lowering the decomposition temperature was also observed by the following experiment. When the power density of the irradiated laser beam was decreased to about 1/10 by the use of a filter, no vapor was produced from the nickel target and the substance was decomposed at the heated target surface whose temperature was below the boiling point of nickel. In this case, the acetylene yield decreased to 1/40, but the ethylene yield was not so affected.

The conventional heat decomposition[5] of methane at 800—1120 °C gives two elements (C and H). The main reaction process is the elimination of hydrogen from methane. On the other hand, the arc discharge gives traces of acetylene and ethane. The products are the same as those in the case of laser heating.

In ethane decomposition, acetylene was produced mainly at high temperatures and butane was produced mainly at low temperatures, as is shown in Table 1. The shock-wave heating of ethane[6] at 1250—1660 K gives methane, ethylene, and acetylene as in laser heating. The acetylene yield increases with the temperature, as in laser heating. However, no butane is detected. This is probably because the butane produced is broken down rapidly by staying at the high temperature. The proposed mechanism may be similar to that in laser heating, but the butane produced in laser heating may be not broken down by the rapid quenching.

In toluene decomposition, the gaseous hydrocarbons were obtained as is shown in Table 1; traces of bibenzyl and biphenyl were also detected. In this case, the substituted methyl group may be cleaved easily, and these fragments undergo further product formation. However, the decomposition at the phosphorus boiling point did not give acetylene or other gaseous hydrocarbons.

The decomposition of methanol gave hydrogen, carbon monoxide, and a small amount of hydrocarbon, but no acetylene was obtained at various temperatures. Methyl iodide and dimethylamine gave acetylene, but methylamine did not give acetylene. In the conventional decomposition of methanol[5] above 500 °C, the processes are considered to be the elimination of hydrogen, giving formaldehyde, and the subsequent decomposition to carbon monoxide and hydrogen. In methanol and methylamine, it may be difficult to form the carbon species which are the precursors of acetylene because carbon monoxide and the CN radical are easily produced; consequently, acetylene is not obtained.

In the decomposition of ethanol, methane, acetylene, and, ethylene were obtained as is shown in Table 1. In the conventional heating,[5] the main products are ethylene and methane, but acetylene is not obtained. In arc discharge,[5] however, the acetylene yield is comparable with that of ethylene.

It may be noted that the laser heating induces the decomposition of organic substances at high temperatures and gives products which are not obtained in the conventional heating, such as acetylene in methane decomposition and butane in ethane decomposition. These results may be caused by the rapid heating and rapid quenching which are the characteristics of the pulse-laser heating.

References

1) K. Taki, P. H. Kim, and S. Namba, This Bulletin, **42**, 823 (1969).

2) K. Taki, P. H. Kim, and S. Namba, *Sci. Pap. Inst. Phys. Chem. Res.* (Tokyo), **63**, 41 (1969).

3) K. Taki, P. H. Kim, and S. Namba, This Bulletin, **45**, 2052 (1972).

4) K. Taki, P. H. Kim, and S. Namba, *ibid.*, **46**, 1556 (1973).

5) C. D. Hurd, "The Pyrolysis of Carbon Compounds," Chem. Catalog Co, New York (1929).

6) J. N. Bradley and M. A. Frend, *J. Phys. Chem.*, **75**, 1492 (1971).

BULLETIN OF THE CHEMICAL SOCIETY OF JAPAN, VOL. 47(2), 495—496 (1974)

The Pyrolysis of Hexyl Phosphates and Their Salts

Yoshiki OKAMOTO, Norio KIMURA, and Hiroshi SAKURAI

The Institute of Scientific and Industrial Research, Osaka University, Yamada-kami, Suita-shi Osaka 565

(Received September 5, 1973)

Synopsis. The isomer distribution of hexene from the tri-*n*-hexyl phosphate changes gradually as the decomposition proceeded. However the formation of the isomers other than 1-hexene was appreciably depressed by the addition of anhydrous disodium hydrogen phosphate.

There have been several reports on the thermal decomposition of alkyl phosphates,[1] alkyl phosphorochloridates,[2] and alkyl phosphites.[3] The olefins obtained by these procedures were mixtures of the isomers. The isomer distributions of the olefin and the mechanism of the formation of the isomer on the thermal decomposition of phosphate had not yet been studied.

In the present paper, the isomer distributions of the *n*-hexene obtained from the pyrolysis of *n*-hexyl phosphates under several different conditions were determined, and the pyrolysis method of obtaining 1-hexene as the sole product has been investigated.

Mono-(I), di-(II), and tri-*n*-hexyl phosphate (III) were prepared in the usual way.[4]

The sodium dihexyl phosphate and the disodium hexyl phosphate were prepared by the addition of an equivalent of alcoholic sodium hydroxide to II and to I respectively; after the solvent had then been distilled off, the residues were dried *in vacuo*. The lithium salts were prepared in the same manner. The magnesium or calcium hexyl phosphate was prepared by the double decomposition in the aqueous solution of sodium hexyl phosphate and the corresponding metal halide respectively. The precipitate was filtered and, after several washing with water, dried *in vacuo*.

In every run of pyrolysis, 0.1 mol of the phosphate was decomposed in a 10-ml distilling flask heated by means of a metal bath at reduced pressure (30 mmHg). The decomposition of phosphate began in the range from 280° to 310 °C, and was over in a few minutes. The pyrolysis products were trapped in a tube cooled with liquid nitrogen in 90—95% yields. They were analyzed with glc on two columns: a 3 m×3 mmϕ column (A), packed with PEG 1000 (10%) on Chromosorb W (60—80 mesh), at the column-temperature of 110 °C, and a 15 m×3 mmϕ column (B), packed with ODPN (40%) on C-22 fire brick (60—80 mesh), at the column-temperature of 25 °C, using nitrogen gas as the carrier. The glc peaks were identified by comparing their retention times with those of authentic samples. The A column was used for the determination of the yields of *n*-hexene and *n*-hexanol. The B column was used for the determination of the relative ratio of the *n*-hexene isomers.

The isomer distribution of hexene from the pyrolysis of III changed gradually as the decomposition proceeded. (Fig. 1) At the beginning of the decomposition, only 1-hexene was produced, but the ratio of 1-hexene to the other isomers gradually decreased with the progress of the decomposition; finally it approached the ratio which was attained by refluxing 1-hexene with phosphoric acid for 24 hr. When a small amount of

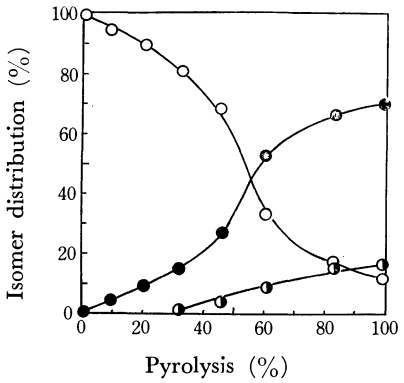

Fig. 1. Relationship between the isomer distribution of tri-*n*-hexyl phosphate. ○: 1-hexene, ●: 2-hexene, ◑: 3-hexene.

TABLE 1. THE RELATIVE YIELDS OF HEXENE AND HEXANOL OBTAINED FROM PYROLYSIS OF TRI-*n*-HEXYL PHOSPHATE AND METAL HEXYL PHOSPHATES

Phosphate[a]	Product from the pyrolysis of phosphates (mol%)					
	Hexene isomer					Hexanol
	1-	*cis*-2-	*trans*-10-	*cis*-3-	*trans*-3-	
$PO(OR)_3$	68	16	10	2	4	t
$ROPO(ONa)_2$	50	t[b]	t	0	0	50
$ROPO(OLi)_2$	50	t	t	0	0	50
$ROPO(O_2Ca)$	65	14	14	3	4	t
$ROPO(O_2Mg)$	29	34	23	5	9	t
$(RO)_2PO(ONa)$	30	t	t	0	0	70
$(RO)_2PO(OLi)$	51	2	3	0	0	64
$[(RO)_2PO]_2Ca$	59	21	20	t	t	t

a) R; *n*-C_6H_{13}, b) t; trace

TABLE 2. THE EFFECTS OF THE ADDITION OF Na_2HPO_4 OR $Na_4P_2O_7$ ON THE PYROLYSIS OF TRI-*n*-HEXYL PHOSPHATE

Additive	Amount of Additive [A] [a] / $(RO)_3PO$	Products from the pyrolysis of phosphate (mol%)					
		Hexene isomer					Hexanol
		1-	*cis*-2-	*trans*-2-	*cis*-3-	*trans*-3-	
Na_2HPO_4	14	72	t [b]	t	0	0	28
Na_2HPO_4	7	62	5	3	t	t	30
$Na_4P_2O_7$	14	73	t	t	0	0	27
$Na_4P_2O_7$	7	64	4	2	t	t	30

a) molar ratio, b) t; trace.

phosphoric acid was added to III, from the beginning of the decomposition the hexene isomers were produced.

The isomer distributions of the hexene obtained by the overall pyrolysis of III and the metal *n*-hexyl phosphates are shown in Table 1.

Although III gave a mixture of all the hexene isomers, disodium or dilithium hexyl phosphate gave 1-hexene and *n*-hexanol. The temperatures of the beginning of the decomposition of alkali metal hexyl phosphates were higher (300 °C) than that of III (280 °C), but that of calcium or magnesium hexyl phosphate was the same as that of III, according to the results of TGA analysis. Calcium or magnesium hexyl phosphate also gave a mixture of all the hexene isomers.

When a few tablets of sodium hydroxide were added to III, the formation of any isomer other than 1-hexene was inhibited, but a considerable amount of *n*-hexanol was produced (74%).

The formation of the isomers of hexene other than 1-hexene by means of the pyrolysis of III was appreciably depressed (at least the formation of *n*-hexanol was) by the addition of a large excess of anhydrous disodium phosphate or tetrasodium pyrophosphate. (Table 2)

The formation of the isomer of hexene by means of the pyrolysis of III may be autocatalyzed with the phosphoric acid resulting from its decomposition. The effect of the addition of sodium hydroxide or the salt may be explained on the basis of the neutralization of the acid. The differences in the behavior of the decompositions of sodium, lithium, calcium, and magnesium hexyl phosphates may be due to the differences in the valences and electronegativities of the metals.[5,6]

The hexanol may be produced by means of the hydrolysis of the hexyl phosphate by the alkali metal hydroxide resulting from the hydrolysis of the alkali metal hexyl phosphate.

References

1) H. E. Baumgarten and R. A. Setterquist, *J. Amer. Chem. Soc.*, **79**, 2605 (1957).
2) W. Gerrard, *J. Chem. Soc.*, **1944**, 84.
3) A. E. Arbuzov and F. G. Valitova, *Izvest. Akad. Nauk., U.S.S.R., Otdel. Khim. Nauk*, 801 (1952).
4) K. Sasse, "Methoden der Organischen Chemie, XII/2, Organische Phosphorverbindungen," ed. by E. Müller, Georg Thieme Verlag, Stuttgart (1964).
5) A. Toda, Y. Yamamoto, M. Itoh, and A. Suzuki, *Kogyo Kagaku Zasshi*, **73**, 1069 (1970).
6) A. Toda, Y. Yamamoto, M. Itoh, and A. Suzuki, *ibid.*, **73**, 1886 (1970).

BULLETIN OF THE CHEMICAL SOCIETY OF JAPAN, VOL. 47(2), 497—498 (1974)

The ESR Spectra of Bis(*t*-butyl and ethyl acetoacetato)copper(II) Complexes in Various Hydrocarbon Solvents

Hiroshi YOKOI

Chemical Research Institute of Non-aqueous Solutions, Tohoku University, Katahira, Sendai 980

(Received September 10, 1973)

Synopsis. The X-band ESR spectra of bis(*t*-butyl acetoacetato)copper(II) and bis(ethyl acetoacetato)copper-(II) in several non-coordinating solvents of hydrocarbon were measured at 77 K. Remarkable solvent effects on dimer formation were revealed for the complexes.

Recently, it has been revealed through ESR investigations that various copper(II) chelates of β-diketones, N-alkylsalicylaldimines, and related compounds are dimerized into triplet-state dimers to varying extents in toluene and chloroform.[1-5] However, there are many points to be clarified as to the factors on which the dimer formation depends. It is the purpose of this paper to investigate the solvent effects on such dimer formation using various hydrocarbon liquids as non-coordinating solvents.

Experimental

The copper(II) chelates employed here are bis(*t*-butyl acetoacetato)copper(II) and bis(ethyl acetoacetato)copper(II) (hereinafter abbreviated as Cu(*t*-Buoac)$_2$ and Cu(Etoac)$_2$ respectively). They were prepared and purified according to the usual method.[6] The chelate reagents were commercially available. The solvents used were ethylbenzene, toluene, methylcyclohexane, and 2-methylpentane, all of which were purchased as G. R. grade reagents. The first three solvents were further purified by succesive shaking with sulfuric acid and sodium hydroxide, followed by drying over sodium and, finally, fractional distillation. The methylcyclohexane was also passed through a column packed with silica gel. The ESR spectra were recorded at the temperature of liquid nitrogen over the field range of 0 to 6000 G by means of a Hitachi 771 X-band ESR spectrometer. All the sample solutions used for the ESR measurements were in the concentration of 1.0×10^{-2} M. The approximate solubilities of the Cu(*t*-Buoac)$_2$ in the solvents were determined at room temperature by the usual spectrophotometric method.

Results and Discussion

The ESR spectra of Cu(*t*-Buoac)$_2$ in the three solvents, toluene, methylcyclohexane, and 2-methylpentane, are shown in Fig. 1. The spectrum in ethylbenzene was analogous in line shape to that in toluene. The (A) spectrum in Fig. 1 is a typical one for mononuclear copper(II) complexes in a magnetically-diluted polycrystalline state.[7] On the other hand, it is clear that both the (B) and (C) spectra in the figure are made up of the superposition of a monomer spectrum quite similar to the (A) spectrum and a triplet-state spectrum resulting from dimers: this is quite analogous to the situation previously reported for Cu(Etoac)$_2$ in toluene.[1] Accordingly, it may be concluded that Cu(*t*-Buoac)$_2$ also is dissolved in methylcyclohexane and 2-methylpentane in the form of the monomeric and dimeric species which are at equilibrium ($2M \rightleftharpoons M_2$). Moreover, both of the triplet-state ESR spectra observed for Cu(*t*-Buoac)$_2$ in this work and for Cu(Etoac)$_2$ in toluene are quite similar in line shape.

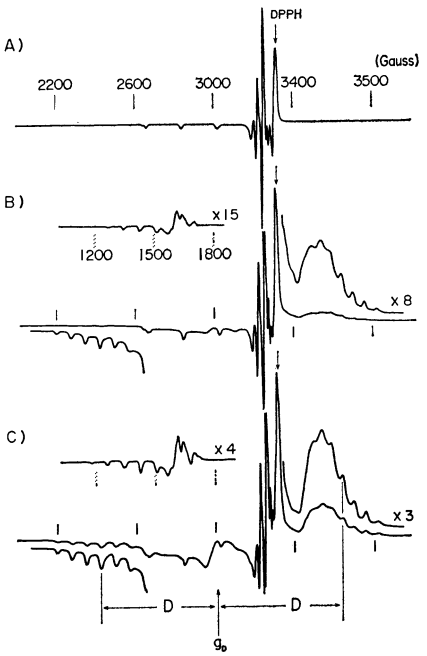

Fig. 1. The X-band ESR spectra of bis(*t*-butyl acetoacetato)copper(II) at 77 K in the following solvent at a concentration of 1.0×10^{-2} M.
(A): toluene, (B): methylcyclohexane, (C): 2-methylpentane.

The large absorption line observed at the highest field in Fig. 1 (A) is due to the extra-hyperfine structure of $M_I=3/2$.[8] As this figure shows, accordingly, this complex in toluene has nearly tetragonal g and A tensors. The magnetic parameters for the monomers of (A) in Fig. 1 were as follows; $g_{//}=2.270$, $g_{\perp}=2.052$, $|A_{//}|=192\times10^{-4}$ cm^{-1}, and $|A_{\perp}|=25\times10^{-4}$ cm^{-1}. On the other hand, the parameters for the triplet-state dimers of (B) and (C) in Fig. 1, g_D and D, which are defined in Fig. 1 (C), were as follows; $g_D=2.185$ and $D=623\times10^{-4}$ cm^{-1}. The copper-copper distance in the dimers, R, could then be estimated to be 3.65 Å from the equation of $R=(0.650\,g_D/D)^{1/3}$, using the above-determined g_D and D values.[1-3] These g_D, D, and R values are also close to those for the dimers of Cu(Etoac)$_2$ in toluene.[1] Therefore, the two dimeric structures seem to be almost the same; in these dimers, monomeric halves are situated with parallel planes, and the directly-coordinating oxygen atoms of adjacent molecules occupy the apical positions of the copper atom.[1]

Figure 1 indicates that there are remarkable solvent effects on the dimer formation for these kinds of copper(II) complexes; that is, the equilibrium constant, K, of $2M \rightleftharpoons M_2$ is largely dependent upon the property of the solvents. The K value for Cu(*t*-Buoac)$_2$ in toluene is close to zero, as has been described above. On the other hand, the K value for the complex in methylcyclohexane is quite small compared with that in 2-methylpentane, since it is clear that the ratio of the intensity of triplet-state ESR signals to that of doublet-state ones in (B) is smaller than that in (C).[1] Thus, the K values increase remarkably in this order: toluene<methylcyclohexane<2-methylpentane. On the other hand, the dielectric constants decrease in the same order: toluene(2.38)>methylcyclohexane(2.02)>2-methylpentane (1.88).[9] Moreover, it was found that the solubilities of the complex also decrease in the same order: toluene (1.30 M)>methylcyclohexane (0.37 M)>2-methylpentane (0.26 M), where the concentrations written in parentheses express the approximate concentrations of saturated solutions at room temperature. These facts suggest that the solubility of a complex in a solvent becomes smaller as the dielectric constant of the solvent decreases and, furthermore, that the complex tends to be dissolved in a solvent with a low dielectric constant in the form of dimers rather than in the form of monomers.

There seems to be no significant difference in property between toluene and ethylbenzene.[9] The ESR spectra of Cu(Etoac)$_2$ in both of the solvents are shown in Fig. 2. These two spectra are different in line shape, especially over the field range of 3100 to 3400 G. However, since their half-field ESR spectra for $\Delta M=2$ transitions are almost the same, there is no doubt that the same triplet-state dimers are formed in both solutions. Accordingly, it can be expected from the line shape of (B) that, in this solution, there exists another species, which may possibly be a polymer, besides the dimer and monomer species. In any event, it is obvious from Figs. 1 and 2 that the dimer formation for these kinds of copper(II) complexes is susceptible to a slight difference in the properties of the solvents.

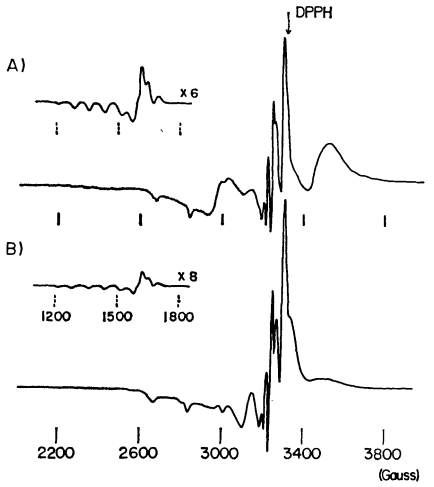

Fig. 2. The X-band ESR spectra of bis(ethyl acetoacetato)copper(II) at 77 K in the following solvents at a concentration of 1.0×10^{-2} M.
(A): toluene, (B): ethylbenzene.

The author is grateful to Professor Taro Isobe for his encouragement throughout this work.

References

1) H. Yokoi and T. Isobe, This Bulletin, **46**, 447 (1973).
2) H. Yokoi, *Chem. Lett.*, **1973**, 1023.
3) M. Chikira and T. Isobe, This Bulletin, **45**, 3006 (1972).
4) M. Chikira, H. Yokoi, and T. Isobe, to be published.
5) J. R. Pilbrow, A. D. Toy, and T. D. Smith, *J. Chem. Soc. A*, **1969**, 1029; A. D. Toy, S. H. H. Chaston, J. R. Pilbrow, and T. D. Smith, *Inorg. Chem.*, **10**, 2219 (1971).
6) D. P. Graddon and E. C. Watton, *J. Inorg. Nucl. Chem.*, **21**, 49 (1961).
7) T. Vanngard and R. Aasa, Proc. 1st Intern. Congr. "Paramagnetic Resonance," Jerusalem, 1962, Academic Press, New York (1963), p. 509, and the references therein.
8) H. Yokoi and T. Kishi, *Chem. Lett.*, **1973**, 749.
9) J. Riddick and W. B. Bunger, "Organic Solvents," Wiley-Interscience, New York (1970).

BULLETIN OF THE CHEMICAL SOCIETY OF JAPAN, VOL. 47(2), 499—500 (1974)

Computer-assisted In-phase AC Polarography: Determination of Cadmium(II) Ions

Shizuo FUJIWARA, Michio HIROTA, Katsuhiko SAWATARI,
Hiroyuki KOJIMA, and Yoshio UMEZAWA

Department of Chemistry, Faculty of Science, The University of Tokyo, Hongo, Tokyo 113

(Received August 17, 1973)

Synopsis. An on-line polarograph is used to detect the in-phase component of the ac response. The applied ac voltage and resulting current are sampled simultaneously and multiplied and then integrated. The detection limit of Cd(II)(0.1 M KCl) is 1.85×10^{-7} M by accumulation.

In ac polarography, two kinds of electrolytic currents flow at the mercury solution interface: one is the faradaic current which has in-phase and out-of phase components with applied alternating voltage, and the other is the charging current, which is an out-of-phase component. Both phase components provide meaningful information about the electrode kinetics. In quantitative analysis, the in-phase component of the ac electrolytic current must be selectively detected without the superposition of any out-of-phase charging current, because the elimination of the charging current plays the most decisive role in enhancing the signal-to-noise (S/N) ratio. In view of the above concideration, analog-type phase-sensitive ac polarography has successfully been used in trace analysis.[1-8]

In the present study, a computer-assisted on-line polarograph was used to perform phase-sensitive(in-phase) ac polarography. In recent years, many instruments have been interfaced for purposes of sampling, handling, and data collecting and processing. With the availability of such systems, the purchase of various pieces of hardware is sometimes no longer necessary; *i.e.*, a digital computer sometimes performs functions numerically similar to those of hardware.[9]

Method

Figure 1 shows the principle of the present method. By means of two channels of an analog to digital(A/D) converter, the polarographic current $I(t_i)$ and the applied alternating voltage $\Delta E(t_i)$ are sampled at the same time. The product of $I(t_i)$ and $\Delta E(t_i)$ is then integrated over the period of each cycle of the alternating voltage. The summed-up products give the in-phase (sine) component of the fundamental current.[1,3] It is a great convenience that the method does not require any troublesome adjustment of the timing circuit which triggers the start of sampling at the time when the applied alternating voltage is zero.[10] Furthermore, the limitation of the detection may be improved by the aid of the accumulation(ensemble average).

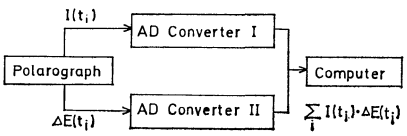

Fig. 1. The principle of the in-phase ac polarography.

Experimental

Apparatus. The block diagram of the present system is shown in Fig. 2. The polarograph used in the present work was built in our laboratory. The alternating voltage is applied by means of a Yokogawa Hewlett-Packard(YHP) function generator Model 3310B. Trigger pulses from a YHP frequency counter Model 5326B are fed into the computer to initiate the sampling.

Computer. Model JRA-5 of JEOLCO is used. The memory capacity of this computer is 4096 words, and the basic cycle time is 20 μs. The output voltage of the puncher-driving circuit is used to control the drop synchronizer. The waiting time before sampling can be set beforehand. The reference voltage signal and the current signal are input to a two-channel A/D converter, converted into 8-bit digital data, and stored in the memory. These two channels of the A/D converter are conveniently used in the present ex-

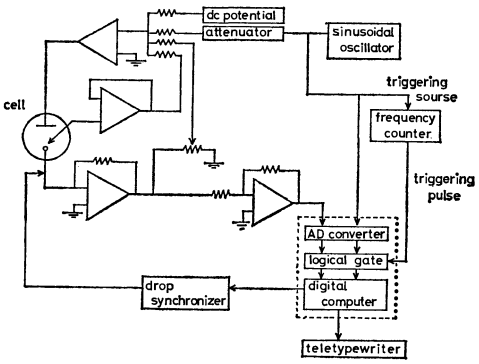

Fig. 2. The block diagram of the apparatus.

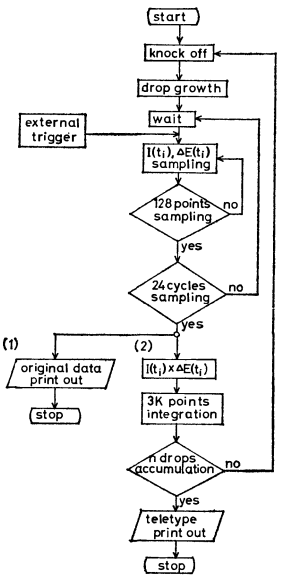

Fig. 3. The flow chart of the program.

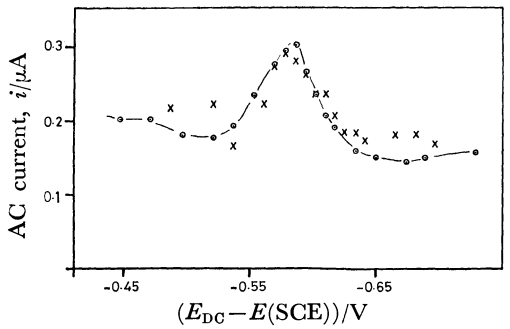

Fig. 4. In-phase ac polarogram of cadmium(II); the effect of accumulation.
$[Cd^{2+}]=7.5\times10^{-6}$ M, [KCl]=0.1 M,
frequency=27.9 Hz, peak-to-peak voltage=30 mV,
○: ensemble average for 4 drops.
×: 1 drop.

periment to perform a simultaneous sampling of both the polarographic current $I(t_i)$ and the applied alternating voltage $\Delta E(t_i)$. These two digitalized signals($I(t_i)$ and $\Delta E(t_i)$) are multiplied, and the product is integrated over n cycles, where $n=24$. The output of the computer is usually typed on a teletypewriter or is converted into analog voltages and written on the chart paper of a recorder. In addition, the experimental data can be perforated on paper tapes in the digital form of 6 holes if necessary.

Program. A machine language is used for programing in which the number of instructions are 17, including the orders for A/D and D/A conversions. The flow chart of the present experiment is shown in Fig. 3.

Conditions. An alternating voltage of 27.9 Hz and 30 mV (peak-to-peak) was superposed on the direct voltage. The mercury reservoir height was 35.0 cm. The measurements were done at (25.0±0.5)°C.

Procedure

(1) Fix the electrode potential at an appropriate value.
(2) Knock off a mercury drop with a pulse from the computer.
(3) Wait $200n$ μs and then begin to sample the analog data of both the polarographic current and applied voltage simultaneously every $(180+20m)$ μs, where $n=2^{14}$ and $m=5$. Thus, 3072 words of the data storage capacity of the computer are occupied.
(4) Calculate Eq. (1) by means of the computer:

$$X=\sum_i I(t_i)\cdot\Delta E(t_i) \qquad (1)$$

(5) In order to calculate the average of many drops, repeat the above procedures(2—4) and add the results.
(6) Write the results using a teletypewriter.

The above procedure is repeated above 20 times by changing the applied dc potential every 10 mV around the peak potential.

Results

The working curve of the present method was obtained by taking the Cd^{2+} ion in a 0.1 M KCl solution as an example. The peak current in this case is linearly proportional to the concentration of the Cd^{2+} ion in the range from 10^{-6} M to 5×10^{-4} M. As has been mentioned, in the present method, the calculation of the ensemble average of the output data for many drops easily be performed by means of the computer. A typical example showing the effect of ensemble average for 4 drops is demonstrated in Figure 4, where as appreciable enhancement of S/N ratio can be observed. The detection limit of this system was found to be 1.85×10^{-7} M for an accumulation of 8 drops, which is almost equivalent to that of conventional analog-type phase-sensitive ac polarography. For obtaining a larger S/N ratio, an accumulation of many more mercury drops would be necessary. Even with the advantages presented above, it should be mentioned that new developments which would avoid some time-consuming processes in the experiment are strongly desired: i) If much larger bit numbers of an A/D converter were available, the data for many mercury drops could be directly accumulated as they are, resulting in a decrease in the total experimental time. ii) A decrease in the cycle time of the computer would effectively reduce the time needed for the experiment.

References

1) D. E. Smith, *Anal. Chem.*, **35**, 1811 (1962).
2) J. W. Hayes and C. N. Reilley, *ibid.*, **37**, 1322 (1965).
3) D. E. Smith and W. H. Reinmuth, *ibid.*, **37**, 1892 (1965).
4) D. E. Smith, in A. J. Bard (ed.), "Electroanalytical Chemistry," Marcel Dekker, New York (1966), Vol. 1, p. 122.
5) R. F. Evilia and A. J. Diefenderfer, *Anal. Chem.*, **39** 1885 (1967).
6) R. de Levie and A. A. Muskovsky, *J. Electroanal. Chem.*, **20**, 181 (1969).
7) K. Matsuda, K. Takahashi, and R. Tamamushi, *Sci. Papers Inst. Phys. Chem. Research*, **64**, 62 (1970).
8) D. L. McAllister and G. Dryhust, *Anal. Chim. Acta*, **58**, 273 (1972).
9) G. M. Hieftje, R. I. Bystroff, and R. Lim, *Anal. Chem.*, **45**, 253 (1973).
10) H. Kojima and S. Fujiwara, This Bulletin, **44**, 2158 (1971).

BULLETIN OF THE CHEMICAL SOCIETY OF JAPAN, VOL. 47(2), 501—502 (1974)

Catalytic Activities of Salicylaldehyde Derivatives. IV. A Synthesis of 2-Formyl-3-hydroxyphenyltrimethylammonium Chloride

Makoto Ando and Sakae Emoto
The Institute of Physical and Chemical Research, Wako-shi, Saitama 351

(Received July 2, 1973)

Synopsis. 4-Ethoxy-1,3-benzodioxan-5-yltrimethylammonium salt, prepared from 4-ethoxy-5-nitro-1,3-benzodioxane *via* 5-dimethylamino-4-ethoxy-1,3-benzodioxane, was hydrolyzed to obtain 2-formyl-3-hydroxyphenyltrimethylammonium chloride in a good yield.

In a previous paper,[1] among the salicylaldehyde derivatives tested 4-formyl-3-hydroxyphenyltrimethylammonium bromide was found to be the most powerful catalyst in the racemization of L-glutamic acid in the presence of cupric ions at pH 10 and at 80 °C. Yoshikawa *et al.*[2] pointed out that the catalytic effects of nitrosalicylaldehydes on the racemization under the conditions described above were decreased in the order of 4-, 6-, 5-, and 3-nitrosalicylaldehydes at an early stage of the reaction. Accordingly, it was expected that 2-formyl-3-hydroxyphenyltrimethylammonium chloride (**1**) might also be an effective catalyst in the racemization.

The reductive methylation of 6-nitrosalicylaldehyde (**2**)[3] over palladium on carbon (Pd-C) in the presence of formaldehyde did not give 6-dimethylaminosalicylaldehyde (**3**), although a similar treatment of *m*-nitrobenzaldehyde afforded *m*-dimethylaminobenzaldehyde.[4] On the other hand, 4-ethoxy-5-nitro-1,3-benzodioxane (**4**)[3] gave 5-dimethylamino-4-ethoxy-1,3-benzodioxane (**5**), which was then hydrolyzed to **3** with acid. With the usual methylating reagents, the *N*-methylation of **3** and **5** was unsuccessful. However, when methyl fluorosulfate (MFS)[5] was used, the *N*-methylation of **5** took place easily to give syrupy 4-ethoxy-1,3-benzodioxan-5-yltrimethylammonium fluorosulfate, (**6**), together with crystalline 2-formyl-3-hydroxyphenyltrimethylammonium fluorosulfate (**7**), a hydrolysis product of **6**. On the other hand, no separable product was obtained from **3**. Both fluorosulfates, **6** and **7**, were converted, separately or not separately, into **1** via the corresponding picrates, (**8**) and (**9**), the former being then easily hydrolyzed to **1**.

Some other methods of preparing **1** from 5-amino-1,3-benzodioxane derivatives were also attempted. The catalytic reduction of 5-nitro-1,3-benzodioxane (**10**)[3] and **4** over Pd-C gave the corresponding 5-amino derivatives, (**11**) and (**12**). 5-Dimethylamino-1,3-benzodioxane (**13**) was prepared from **10** by reductive methylation. The *N*-methylation of **13** with MFS gave 1,3-benzodioxan-5-yltrimethylammonium fluorosulfate (**14**) alone. The corresponding picrate (**15**) and then chloride (**16**) were obtained in the usual way. The attempted bromination of benzodioxane rings of **11**, **13**, and **16** to **1** proceeded with unsatisfactory results. The catalytic activity of **1** will be discussed together with that of other salicyalaldehydes in the near future.

Experimental

All the mps and bps are uncorrected. The hydrogenation was carried out at room temperature under atmospheric pressure with 10% Pd-C.

*5-Dimethylamino-4-ethoxy-1,3-benzodioxane (**5**).* A solution of 4-ethoxy-5-nitro-1,3-benzodioxane (**4**) (15 g) and aqueous 37% formaldehyde (40 ml) in ethanol (300 ml) was hydrogenated with Pd-C (6 g). After 5 mol of hydrogen had been absorbed, the filtrate from the catalyst was concentrated under reduced pressure to a syrup, which was then extracted with ether. The extracts, washed with a dil sodium hydroxide solution and then with water, were fractionally distilled in a vacuum to afford 12.3 g (83%) of **5**; bp 123—124 °C/4 mmHg.

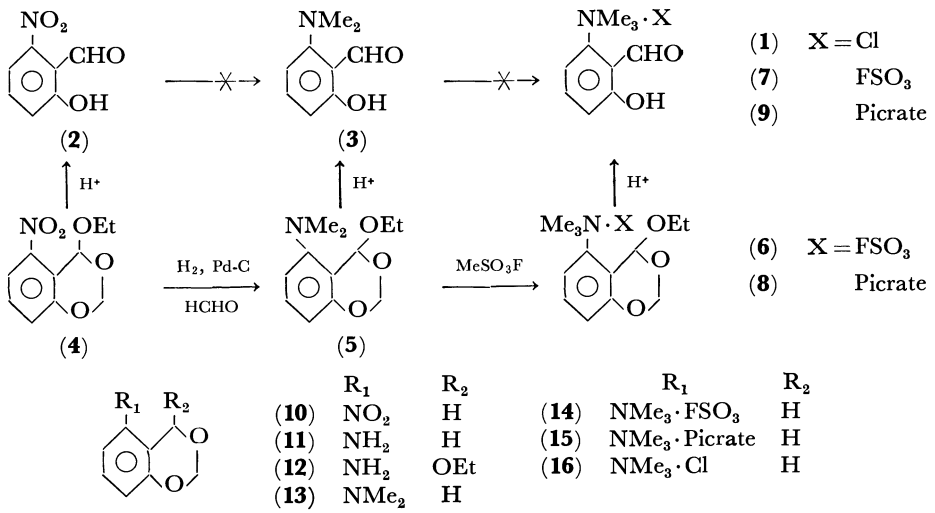

Scheme.

Found: C, 64.66; H, 7.69; N, 6.15%. Calcd for $C_{12}H_{17}O_3N$: C, 64.55; H, 7.68; N, 6.27%.

*6-Dimethylaminosalicylaldehyde (**3**).* A mixture of **5** (13.6 g), sulfuric acid (55 ml), ethanol(150 ml), and water (150 ml) was refluxed for 1 hr while being stirred. To the cold mixture, 4 M sodium hydroxide aqueous solution (550 ml) was added, and it was all shaken with ether. The aqueous solution, treated with charcoal, was neutralized with dil hydrochloric acid. Benzene extracts of an oily product were concentrated under diminished pressure; the residue was passed through a silica gel column (250 g). At first **3** was eluted with benzene; fractional distillation then gave 4.8 g (48%) of **3**; bp 114—117 °C/2 mmHg.

Found: C, 65.35; H, 6.78; N, 8.28%. Calcd for $C_9H_{11}O_2N$: C, 65.44; H, 6.71; N, 8.48%.

Hydrochloride: Mp>280 °C.

Found: C, 53.61; H, 6.01; N, 7.02; Cl, 17.78%. Calcd for $C_9H_{12}O_2NCl$: C, 53.60; H, 6.00; N, 6.95; Cl, 17.58%.

*2-Formyl-3-hydroxyphenyltrimethylammonium Fluorosulfate (**7**) and 4-Ethoxy-1,3-benzodioxan-5-yltrimethylammonium Picrate (**8**).* Into ice-cooled MFS (5 g), ice-cooled **5** (10 g) was stirred all at once. Within 30 min it became viscous and difficult to stir. After 2 hrs' stirring, the reaction mixture was allowed to stand overnight at room temperature. The resultant glassy mixture was dissolved in a mixture of water and ethyl acetate. The aqueous layer, treated with charcoal, was concentrated under diminished pressure to a syrup, which was then treated with acetone to precipitate 2.2 g (17%) of **7**; mp 192—193 °C (decomp). The filtrate, concentrated to a syrup, was treated with picric acid (5 g) in methanol. Recrystallization from methanol gave 8.3 g (40%) of **8**; mp 163—164 °C. Although the total yield of **7** and **8** was nearly constant, each yield was considerably variable.

Compound **7**: Found: C, 42.90; H, 5.24; N, 4.90; S, 11.38%. Calcd for $C_{10}H_{14}O_5NFS$: C, 43.01; H, 5.05; N, 5.02; S, 11.48%.

Compound **8**: Found: C, 49.00; H, 4.73; N, 12.20%. Calcd for $C_{19}H_{22}O_{10}N$: C, 48.93; H, 4.75; N, 12.01%.

*2-Formyl-3-hydroxyphenyltrimethylammonium Picrate (**9**).* By the usual treatment, **7** was converted into **9**, which was then recrystallized from methanol; mp 209—210 °C; yield 94%.

Found: C, 46.94; H, 3.95; N, 13.83%. Calcd for $C_{16}H_{16}O_9N_4$: C, 47.06; H, 3.95; H, 13.72%.

*2-Formyl-3-hydroxyphenyltrimethylammonium Chloride (**1**).*

a) From 9: By the usual process, **1** was obtained; it was then recrystallized from methanol; mp 217 °C (decomp); yield 92%.

Found: C, 55.88; H, 6.51; N, 6.50; Cl, 16.41%. Calcd for $C_{10}H_{14}O_2NCl$: C, 55.69; H, 6.54; N, 6.49; Cl, 16.44%.

b) From 8: In the usual way, upon treatment with dil hydrochloric acid, hydrolysis occurred to give **1** in a 58% yield.

c) From 5: MFS (5 g) and **5** (10 g) were treated as has been described in the preparation of **7** and **8**. A resultant syrupy mixture of **6** and **7** was treated with picric acid (10 g) in methanol. Diluting the solution with water gave, upon the removal of a clear supernatant, a non-crystalline residue, which was then treated with nitrobenzene and dil hydrochloric acid. The aqueous layer, washed with ether, was concentrated to give **1**. Recrystallization from methanol afforded 4.2 g (43%) of **1**.

*5-Amino-1,3-benzodioxane (**11**).* A solution of 5-nitro-1,3-benzodioxane (**10**) (10 g) in ethanol (250 ml) was hydrogenated with Pd-C (2.5 g). After 3 mol of hydrogen had been absorbed, the treatment of the reaction mixture as has been described in the preparation of **5** gave 7.8 g (94%) of **11**; mp 71—72 °C.

Found: C, 63.41; H, 5.96; N, 9.21%. Calcd for $C_8H_9O_2N$: C, 63.56; H, 6.00; N, 9.27%.

Hydrochloride: Mp>280 °C.

Found: C, 51.35; H, 5.36; N, 7.42; Cl, 18.76%. Calcd for $C_8H_{10}O_2NCl$: C, 51.21; H, 5.37; N, 7.47; Cl, 18.90%.

N-*Acetyl Derivative*: Mp 154—155 °C.

Found: C, 62.28; H, 5.75; N, 7.15%. Calcd for $C_{10}H_{11}O_3N$: C, 62.16; H, 5.74; N, 7.25%.

*5-Amino-4-ethoxy-1,3-benzodioxane (**12**).* A solution of **4** (5 g) in ethanol (150 ml) was hydrogenated with Pd-C (1 g) to give 3.7 g (85%) of **12**; bp 120—123 °C/3 mmHg.

Found: C, 61.61; H, 6.50; N, 7.17%. Calcd for $C_{10}H_{13}O_3N$: C, 61.52; H, 6.71; N, 7.18%.

N-*Acetyl Derivative*: Mp 146 °C.

Found: C, 60.66; H, 6.37; N, 5.78%. Calcd for $D_{12}H_{15}O_4N$: C, 60.75; H, 6.37; N, 5.90%.

*5-Dimethylamino-1,3-benzodioxane (**13**).* In a way similar to that used in the synthesis of **5**, **13** was given from **10** in a 77% yield; bp 104—105 °C/4 mmHg.

Found: C, 67.12; H, 7.05; N, 7.86%. Calcd for $C_{10}H_{13}O_2N$: C, 67.02; H, 7.31; N, 7.82%.

Hydrochloride: Mp 182 °C (decomp).

Found: C, 55.88; H, 6.49; N, 6.51; Cl, 16.48%. Calcd for $C_{10}H_{14}O_2NCl$: C, 55.69; H, 6.54; N, 6.49; Cl, 16.44%.

*1,3-Benzodioxan-5-yltrimethylammonium Fluorosulfate (**14**).* MFS (3.3 g) and **13** (5 g) were treated as has been described for the *N*-methylation of **5**. The addition of ethyl acetate to the final residue precipitated 6.5 g (84%) of **14**; mp 142 °C. It was soluble in acetone.

Found: C, 45.12; H, 5.45; N, 4.84; S, 10.97%. Calcd for $C_{11}H_{16}O_5NFS$: C, 45.03; H, 5.50; N, 4.78; S, 10.93%.

*1,3-Benzodioxan-5-yltrimethylammonium Picrate (**15**).* In the usual way, **15** was obtained from **14** in a 98% yield; mp 162 °C.

Found: C, 48.32; H, 4.21; N, 13.27%. Calcd for $C_{17}H_{18}O_9N_4$: C, 48.34; H, 4.30; N, 13.27%.

*1,3-Benzodioxan-5-yltrimethylammonium Chloride (**16**).* In the usual way, **16** was obtained from **15** in a 73% yield; mp 202—203 °C (decomp).

Found: C, 57.48; H, 6.97; N, 6.29; Cl, 15.51%. Calcd for $C_{11}H_{16}O_2NCl$: C, 57.52; H, 7.02; N, 6.10; Cl, 15.43%.

The authors wish to thank Dr. Haruo Homma and his co-workers of this Institute for their elemental analyses. This work was partially supported by a Research Grant of Life Sciences given by this Institute.

References

1) M. Ando and S. Emoto, This Bulletin, **42**, 2628 (1969).
2) S. Yoshikawa, K. Kuga, Y. Ueda, M. Goto, and H. Sugiyama, *Kogyo Kagaku Zasshi*, **70**, 331 (1967).
3) Part III of this series: M. Ando and S. Emoto, This Bulletin, **46**, 2903 (1973).
4) V. M. Ingram, *J. Chem. Soc.*, **1950**, 2247.
5) M. G. Ahmed, R. W. Alder, G. H. James, M. L. Sinott, and M. C. Whiting, *Chem. Commun.*, **1968**, 1533.

BULLETIN OF THE CHEMICAL SOCIETY OF JAPAN, VOL. 47(2), 503—504 (1974)

The Reaction of Styryl Sulfoxides or Sulfones with Boranes[1)]

Norioki MIYAMOTO, Daisuke FUKUOKA, Kiitiro UTIMOTO, and Hitosi NOZAKI

Department of Industrial Chemistry, Faculty of Engineering, Kyoto University, Yoshida, Sakyo-ku, Kyoto 606

(Received July 24, 1973)

Synopsis. The title reaction produces β-alkylated styrene **3** in preparative yields. The formation of *trans* **3** from the *cis* sulfoxide **2** or the sulfone **7** is explained by considering the vinylic radical **8** as the intermediate.

Studies of the reaction of the trialkylboranes with the α,β-unsaturated carbonyl compounds[2)] have opened a valuable route to the β-alkylated ketones. We now wish to describe the reaction of the boranes with the styryl sulfoxides or sulfones,[3)] which are formally the S-analogs of the α,β-enones.

The reaction of methyl styryl sulfoxide (**2**) with a trialkylborane (**1**) in THF was performed under reflux in a nitrogen atmosphere; it gave mainly the β-alkylated styrene (**3**),[4)] along with *trans*-β-(2-tetrahydrofuryl)styrene (**4**), styrene itself, methyl styryl sulfide (**5**),[5-7)] and methyl 2-tetrahydrofuryl sulfide (**6**).[8)] Practically the same results were obtained in toluene, except for the formation of *trans*-1,3-diphenylpropene[9)] instead of **4**. Each product was characterized by glc analyses prior to the oxidative work-up of the reaction mixture to decompose the remaining **1**. The results are summarized in Table 1.

Whereas no trace of *cis* **3**[4)] was produced from the *trans* sulfoxide **2**,[5)] a similar reaction of the *cis* isomer of **2** with **1** gave rise to a mixture of *trans* and *cis* **3**.[4)] In sharp contrast to the vinylic sulfoxides, both of the corresponding *trans*[5)] and *cis*[6)] sulfones (**7**) afforded the *trans* **3** exclusively; the *cis* isomer of **3** was not observed in the reaction mixture.[11)] The vinylic sulfoxides and sulfones were found to be stable in the absence of **1**.[12)] Apparently, the formation of styrene and the solvent-incorporation product (**4** or *trans*-1,3-diphenylpropene) should be ascribed to the formation of the vinylic radical (**8**)[13)] resulting from the homolytic cleavage of the C–S bond induced by the attack of **1**. The exclusive formation[14)] of the *trans* isomers of **3** and **4** from the *cis* sulfones (**7**)[6)] may be ascribed to the rapid equilibration[13)] between the sterically-hindered *cis* form and the more reactive *trans* form of the vinylic radical (**8**). Similarly, the formation of the *trans* isomers of **3** and **4** from the *cis* sulfoxide (**2**) can be explained by assuming the vinylic radical (**8**)[13)] as the intermediate. Meanwhile, the preferential formation of the *cis* **3** from the *cis* sulfoxide (**2**) is presumably due to the ionic pathway (**9** or **10**), which is reminiscent of the S_N1 mechanism. Thus, the two competing routes would account for the formation of the mixture of *trans* and *cis* **3** from the *cis* sulfoxide (**2**) (Scheme 1).

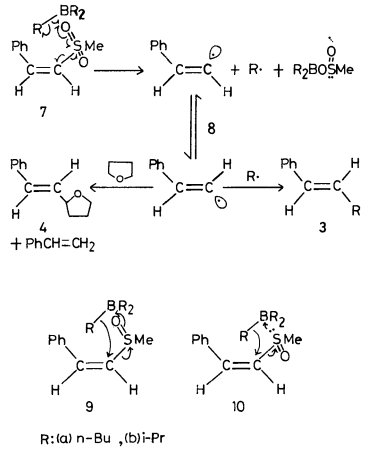

Scheme 1

The substitution reaction has been successfully extended to the methyl phenethynyl sulfone.[15)] The products isolated were found to be the 1-phenylalkyne-1 (*a*,[16)] 70%; *b*,[17)] 73%),[10)] phenyl(2-tetrahydrofuryl)-acetylene (8.4% and 10% respectively),[10)] and phenylacetylene (6.3% and 3.2% respectively).[10)] The corresponding sulfoxides[15)] gave practically the same results, though the reaction proceeded rather sluggishly.

TABLE 1. REACTION OF STYRYL SULFOXIDES OR SULFONES WITH BORANES

Sulfoxide or sulfone	Borane R:	Yield[a)] (%)						
		3[b)]		4	styrene	5		6[e)]
		trans	*cis*			*trans*[c)]	*cis*[d)]	
trans **2**[c)]	*n*-Bu	57	—	11	8.0	3.2	—	*trace*
	i-Pr	68	—	3.0	9.2	2.1	—	*trace*
cis **2**	*n*-Bu	11	58	6.3	5.2	—	1.5	*trace*
	i-Pr	26	46	9.2	5.0	—	1.5	*trace*
trans **7**[c)]	*n*-Bu	70	—	10	5.0	—	—	—
	i-Pr	75	—	5.0	8.1	—	—	—
cis **7**[d)]	*n*-Bu	76	—	3.2	4.5	—	—	—
	i-Pr	78	—	3.6	4.3	—	—	—

a) See Foot-note 10. b) See Ref. 4. c) See Ref. 5. d) See Ref. 6. e) See Ref. 8.

Experimental

The IR spectra were obtained on a Shimadzu IR-27-G spectrometer in neat liquid films unless otherwise stated. The NMR spectra were obtained on a JEOL-60-H spectrometer in $CDCl_3$. The chemical shifts are given in ppm from the TMS internal standard; the abbreviations of s, d, t, q, and m are used with their common meanings.

Preparation of cis *Methyl Styryl Sulfoxide (2).* The oxidation was carried out according to the method of Russell and Ochrymowycz.[13] An aqueous solution (50 ml) of $NaIO_4$ (4.5 g, 21 mmol) was added to an acetonitrile (50 ml) solution containing *cis* methyl styryl sulfide[6] (**5**, 3.0 g, 20 mmol) at −10 °C. The mixture was stirred at room temperature for 12 hr, filtered to remove $NaIO_3$, and extracted with chloroform. The removal of the solvent *in vacuo* and subsequent column chromatography afforded the *cis* sulfoxide (**2**) (3.1 g, 93%[10]) as a viscous oil; bp 130—134 °C/0.3 mmHg IR 1030 cm^{-1}, NMR δ 2.56 (s, 3H, Me), 6.50 (d, 1H, vinylic), and 7.00 ppm (d, 1H, vinylic). Found: C, 65.1; H, 6.1%. Calcd for $C_9H_{10}OS$: C, 65.4; H, 6.2%.

Reaction of Methyl Styryl Sulfoxide (2), the Corresponding Sulfone (7), or Methyl Phenethynyl Sulfone with the Boranes (1). The borane (**1**, 3.1 mmol) was added to a THF (20 ml) solution of the sulfoxide or the sulfone (3.0 mmol) under nitrogen. The mixture was stirred under reflux. The progress of the reaction was followed by the tlc analyses of the aliquots. After 48 hr, the reaction mixture was oxidized with alkaline H_2O_2 and extracted twice with ether. The extracts were dried (Na_2SO_4), and concentrated *in vacuo*, and the residue was distilled (or alternatively chromatographed on silica gel). The products were purified by means of preparative glc (HVSG 20%, 2 m, 200°). *trans-β-*(2-Tetrahydrofuryl)styrene (**4**): bp 120—123 °C/4 mmHg, IR 1050 and 963 cm^{-1}; NMR δ 4.33 (m, 1H, methine) and 6.11—6.62 ppm (m, 2H, vinylic). Found: C, 83.1; H, 8.0%. Calcd for $C_{12}H_{14}O$: C, 82.7; H, 8.1%. Phenyl(2-tetrahydrofuryl)acetylene: bp 118—120 °C/5 mmHg. IR 1050 cm^{-1}, NMR δ 4.92 ppm (m, 1H, methine). Found: C, 83.4; H, 6.9%. Calcd for $C_{12}H_{12}O$: C, 83.7; H, 7.0%.

References and Footnotes

1) Part of this work was presented in a preliminary form. See N. Miyamoto, K. Utimoto, and H. Nozaki, *Tetrahedron Lett.*, **1972**, 2895.

2) H. C. Brown and G. W. Kabalka, *J. Amer. Chem. Soc.*, **92**, 710 (1970); *ibid.*, **92**, 714 (1970).

3) (a) The vinylic sulfoxides or sulfones with an aliphatic carbon-chain instead of a phenyl group gave rise to a complicated mixture of products, whose structures have not yet been determined. (b) The styryl sulfide (**5**) failed to react with **1**.

4) K. Yasufuku, S. Hirose, S. Nozakura, and S. Murahashi, This Bulletin, **40**, 2149 (1967).

5) G. A. Russell, E. Sabourin, and G. J. Mikol, *J. Org. Chem.*, **31**, 2854 (1966).

6) W. E. Truce and J. A. Simms, *J. Amer. Chem. Soc.*, **78**, 2756 (1956).

7) The reduction of the sulfoxide with **1** has been recorded with respect to dimethyl sulfoxide. See A. Arase, Y. Masuda, M. Itoh, M. Itoh, and A. Suzuki, *Nippon Kagaku Kaishi*, **1972**, 395.

8) H. C. Brown and M. M. Midland, *J. Amer. Chem. Soc.*, **93**, 3291 (1971).

9) M. Tout and M. Guyard, *Bull. Soc. Chim. Fr.*, **1947**, 1086.

10) The yields were based on the compounds containing the sulfur atom.

11) The isomerization of the sulfoxide **2** or the sulfone **7** initially employed was not observed upon the NMR analyses during the reaction.

12) The heating of **2** or **7** dissolved in THF for 48 hr afforded only a trace of **4** (<0.1%) besides the recovered **2** or **7**.

13) O. Simamura, "Topics in Stereochemistry," Vol. 4, ed. by E. L. Eliel and N. L. Allinger, Wiley-Interscience, New York (1969), p. 1.

14) The addition-elimination mechanism for the formation of the β-alkylstyrene **3** seems to be improbable, if it involves the 1,2-addition of **1** to the double bond of **7** and the following vicinal elimination of R_2B–SO_2Me. This is because that the more electron-rich sulfide **5** than the sulfone **7** failed to react with **1**. See footnote **3b**.

15) G. A. Russell and L. A. Ochrymowycz, *J. Org. Chem.*, **35**, 2107 (1970).

16) H. K. Black, D. H. S. Horn, and B. C. L. Weedon, *J. Chem. Soc.*, **1954**, 1704.

17) H. H. Schlubach and K. Reppenning, *Ann. Chem.*, **614**, 37 (1958).

BULLETIN OF THE CHEMICAL SOCIETY OF JAPAN, VOL. 47(2), 505—506 (1974)

The Reactions of 2-Hydroxystilbenes with Lead Tetraacetate and Manganic Acetate

Keifumi NOGAMI and Kazu KUROSAWA

Department of Chemistry, Faculty of Sceince, Kumamoto University, Kurokami-2-39-1, Kumamoto 860

(Received August 23, 1973)

Synopsis. Four 2-hydroxystilbenes (Ia~Id) were oxidized with lead tetraacetate to give corresponding 3-arylbenzofurans (IIa~IId) in moderate yields. IId and IIe were also obtained by the reactions of Id and Ie respectively with manganic acetate in poor yields.

In the reactions of lead tetraacetate and manganic acetate with phenolic compounds, an oxidative cyclization has been observed when a compound possesses a hydroxy group and an aromatic or a vinylic hydrogen which are located in spatially suitable positions.[1-4] It is now demonstrated that 2-hydroxystilbenes gave 2-arylbenzofurans with lead tetraacetate in moderate yields.

When 4'-methoxy-2-hydroxystilbene(Ib), prepared from salicylaldehyde and 4-methoxybenzyl-triphenylphosphonium chloride by the Wittig reaction, was treated with lead tetraacetate, a compound (IIb) was isolated. This compound (IIb)(mp 146 °C), $C_{15}H_{12}O_2$, showed no absorption in the hydroxyl region (3500 cm^{-1}) in its IR spectrum. The NMR spectrum of this compound did indicate, however, the presence of a *p*-substituted phenyl group[δ 6.87 (d, 2H) and δ 7.73)(d, 2H)(AA'XX'-system)], a methoxy group [δ 3.80 (s, 3H)], four aromatic protons [δ 7.0—7.6 (m, 4H)], and a singlet [δ 6.80 (1H)]. These spectroscopic properties indicated that the structure of this compound is 2-(4'-methoxyphenyl)-benzofuran.

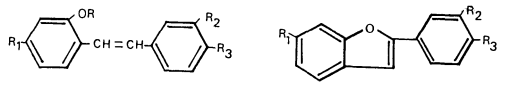

Ia–e (R=H)
IIIa–d (R=OAc)

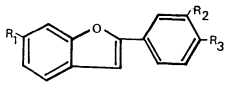

IIa–e

a $R_1=R_2=R_3=H$
b $R_1=R_2=H$, $R_3=OCH_3$
c $R_1=OCH_3$, $R_2=R_3=H$
d $R_1=R_3=OCH_3$, $R_2=H$
e $R_1=H$, $R_2=R_3=OCH_3$

Three other 2-hydroxystilbenes (Ia, Ic and Id) were prepared, their reactions with lead tetraacetate gave 2-arylbenzofurans (IIa, IIc and IId). The results are shown in Table 1. It seems that the reaction of 2-hydroxystilbenes with lead tetraacetate can be used as a convenient one-step synthesis of 2-arylbenzofurans, although the yields are not very good and depend on the reaction temperature and solvent used.

The reaction of 2-hydroxystilbenes with manganic acetate also yielded 2-arylbenzofurans (IId and IIe) in poor yields.

Experimental

The NMR spectra were recorded in a deuteriochloroform solution by means of a Hitachi R-24 NMR spectrometer, with tetramethylsilane as the internal reference; The IR spectra were recorded in a chloroform solution by means of a JASCO IRA-1 grating spectrometer; The UV spectra were measured for a methanol solution by means of a Hitachi EPS-3T spectrophotometer. The melting points were determined by means of a Yanagimoto hot-stage apparatus and are uncorrected.

Preparation of 2-Hydroxystilbenes. The general procedure for the preparation of 2-hydroxystilbene was as follows. Benzyl-triphenylphosphonium chloride[5] (22 mmol) was treated with sodium ethoxide, prepared from metallic sodium (20 mmol) and ethanol (50 ml). To this solution we then added 2-hydroxybenzaldehyde (15 mmol), and the solution was heated at 90 °C with stirring until all the aldehyde had disappeared. After the removal of the ethanol *in vacuo*, the residue was triturated with water and extracted with benzene. The benzene layer was washed with aqueous sodium bisulfite, and the benzene was removed *in vacuo*. The product was then purified through a silica column [a mixture of Wakogel C 100 (180 g) and B 10 (20 g)], eluted with benzene, and recrystallized from benzene; it could thus be characterized as an acetate. Thus, 2-hydroxystilbene (Ia) (mp 137—138 °C(lit,[6] mp 147 °C)) was obtained in a in 66% yield. ν_{max}: 3580 and 3300 cm^{-1} (OH); $\lambda_{max}(\varepsilon)$: 304 (35000) and 316 nm (25300). 2-Acetoxystilbene (IIIa) (mp 54 °C(lit.[7] mp 54 °C)). ν_{max}: 1760 cm^{-1}. 2-Hydroxy-4'-methoxystilbene (Ib); mp 145—146 °C; 23% yield. ν_{max}: 3580 and 3300 cm^{-1} (OH); $\lambda_{max}(\varepsilon)$: 310 (36,100) and 324 nm(23,600). Found: C, 79.61; H, 6.41%. Calcd for $C_{15}H_{14}O_2$: C, 79.62; H, 6.24%. 2-Acetoxy-4'-methoxy-

TABLE 1. OXIDATION OF 2-HYDROXYSTILBENE WITH LEAD TETRAACETATE

Compd.	Reaction conditions				Benzofuran (%)
	Molar ratio of I : oxidant	Solvent	Temperature (°C)	Time (min)	
Ia	1 : 1.5	C_6H_6	17	5	IIa(21)
Ib	1 : 1.5	C_6H_6	17	15	IIb(25)
Ic	1 : 1.5	AcOH	18	300	IIc(13)
Ic	1 : 1.5	C_6H_6	18	40	IIc(24)
Id	1 : 1.5	C_6H_6	17	15	IId(4)

stilbene (IIIb); mp 75.8 °C; ν_{max}: 1760 cm^{-1}(OAc). Found C, 75.99; H, 6.03%. Calcd for $C_{17}H_{16}O_3$: C, 76.10; H, 6.01%. 2-Hydroxy-4-methoxystilbene (Ic); mp 117—118 °C; 56% yield. ν_{max}: 3580 and 3300 cm^{-1}(OH); $\lambda_{max}(\varepsilon)$: 316 (32,400) and 329 nm(27,100). Found: C, 79.62; H, 6.38%. Calcd for $C_{15}H_{14}O_2$: C, 79.62; H, 6.24%. 2-Acetoxy-4-methoxystilbene (IIIc); mp 156 °C; ν_{max}: 1760 cm^{-1}(OAc). Found: C, 75.80; H, 6.02%. Calcd for $C_{17}H_{16}O_3$: C, 76.10; H, 6.01%. 4,4′-Dimethoxy-2-hydroxystilbene (Id); mp 168—169 °C; 44% yield. ν_{max}: 3500 cm^{-1}(OH); $\lambda_{max}(\varepsilon)$: 319 (36700) and 332 nm (29600). Found: C, 74.83; H, 6.33%. Calcd for $C_{16}H_{16}O_3$: C, 74.98; H, 6.29%. 2-Acetoxy-4,4′-dimethoxystilbene (IIId); mp 140 °C; ν_{max}: 1760 cm^{-1}(OAc). Found: C, 72.23; H, 6.22%. Calcd for $C_{18}H_{18}O_4$: C, 72.46; H, 6.08%. 3′,4′-Dimethoxy-2-hydroxystilbene (Ie): mp 109 °C; 21% yield. ν_{max}: 3580 and 3300 cm^{-1}(OH); $\lambda_{max}(\varepsilon)$: 316 (33,600) and 327 nm(25,500). Found: C, 75.09; H, 6.31%. Calcd for $C_{16}H_{16}O_3$: C, 74.98; H, 6.29%.

Oxidation of 2-Hydroxystilbene with Lead Tetraacetate. The general procedure for the oxidation of 2-hydroxystilbenes was as follows. 2-Hydroxystilbene (4.4 mmol) was heated with lead tetraacetate (6.6 mmol) in a solvent (70 ml) with stirring for a period of time as is shown in the table. After the removal of the solvent *in vacuo*, the residue was triturated with water and extracted with chloroform. The crude products were purified either on silica plates or through a silica column, with chloroform as the eluting solvent, and then recrystallized from ethanol. Ia gave 2-phenylbenzofuran (IIa) (mp 118 °C(lit,[8] mp 120 °C)) in a 21% yield. ν_{max}: 1560, 920 and 880 cm^{-1}; $\lambda_{max}(\varepsilon)$: 290 (19,000), 300 (16,800) and 327 nm(18,800); δ: 6.92(s, -CH) and 7.0—8.0(m, 9H). Ib gave 2-(4′-methoxyphenyl)benzofuran (IIb) (mp 146 °C) in a 25% yield. ν_{max}: 1570, 920 and 880 cm^{-1}; $\lambda_{max}(\varepsilon)$: 294 (21,400), 303 (20,000) and 331 nm(24,400). Found: C, 80.19; H, 5.57%. Calcd for $C_{15}H_{12}O_2$: C, 80.33; H, 5.29%. Ic gave 6-methoxy-2-phenylbenzofuran (IIc) (mp 81 °C) in a 24% yield. ν_{max}: 1560, 960 and 920 cm^{-1}; $\lambda_{max}(\varepsilon)$: 293 (18,200), 300 (17,600) and 331 nm(23,100); δ: 3.79 (s, OCH_3), 6.85(s, -CH) and 6.8—7.8 (m, 8H, aromatic). Found: C, 80.04; H, 5.45%. Calcd for $C_{15}H_{12}O_2$: C, 80.33; H, 5.29%. Id gave 6-methoxy-2-(4′-methoxyphenyl)benzofuran (IId) (mp 159 °C (lit,[9] mp 159 °C)) in a 4% yield. ν_{max}: 1560, 960 and 920 cm^{-1}; $\lambda_{max}(\varepsilon)$: 295 (22,500) and 334 nm(26,000); δ: 6.89(d, 2H) and 7.67 (d, 2H)(*p*-substituted phenyl), 3.79(s, OCH_3), 3.80(s, OCH_3), 7.33(d, 1H) and 6.8—7.0 (m, 2H)(aromatic), and 6.73(s, 1H, vinylic).

The oxidation of 2-hydroxystilbenes with manganic acetate was also carried out in a similar manner. Id gave IId (3%) and IIId (13%). Ie yielded 2-(3′,4′-dimethoxyphenyl)-benzofuran (IIe) (5%); mp 112—114 °C. ν_{max}: 1570, 920 and 880 cm^{-1}; $\lambda_{max}(\varepsilon)$: 294 (14500) and 333 nm(20800); δ: 3.89(s, OCH_3), 3.94(s, OCH_3), 6.89(s, -CH) and 6.8—7.7 (m, 7H, aromatic). Found: C, 75.28; H, 5.35%. Calcd for $C_{16}H_{14}O_3$: C, 75.57; H, 5.55%.

References

1) F. F. Stephens and J. D. Bower, *J. Chem. Soc.*, **1949**, 2971.
2) K. Kurosawa, This Bulletin, **42**, 1456 (1969).
3) K. Kurokawa and J. Higuchi, *ibid.*, **45**, 1132 (1972).
4) K. Kurosawa, Y. Sasaki, and M. Ikeda, *ibid.*, **46**, 1498 (1973).
5) K. Friedrich and H. G. Henning, *Chem. Ber.*, **92**, 2756 (1959).
6) "Beilsteins Handbuch der Organischen Chemie", VI, p. 692.
7) *ibid.*, VI, p. 693.
8) *ibid.*, XVII, p. 78.
9) J. C. Sheehan and R. Wilson, *J. Amer. Chem. Soc.*, **86**, 5277 (1964).

BULLETIN OF THE CHEMICAL SOCIETY OF JAPAN, VOL. 47(2), 507—508 (1974)

The Activating Effects of Amino Groups in Diazo-coupling Reactions

Yōji HASHIDA, Junichi TAKENAKA, and Kohji MATSUI

Department of Synthetic Chemistry, Faculty of Engineering, Gunma University, Tenjincho, Kiryu, Gunma 376

(Received August 27, 1973)

Synopsis. The rates of the reactions of various aromatic amines with diazotized sulfanilic acid have been studied. It was found that, among the *N,N*-disubstituted anilines, the activating effect of amino groups is roughly proportional to their pK_a values.

The kinetics of diazo-coupling reactions have been studied extensively in order to elucidate the reaction mechanism and the structural effects of the reactions on the reactivity.[1] As to the structural effect of the azo components on the reactivity, studies of phenols[2-4] and active methylene compounds[5] have been reported. However, much less work has been done on the reactions of aromatic amines; quantitative studies of the effects of amino groups in the electrophilic aromatic substitution have not been extensively undertaken, probably because of their basic properties and powerful substituent effects.[6]

This paper will report the quantitative results of the reactions of various aromatic amines with diazotized sulfanilic acid.

Experimental

Materials. *N,N*-Di-*iso*-propylaniline and *N*-ethyl-*N*-methylaniline were prepared by alkylating aniline and *N*-methylaniline with the corresponding alkyl iodides.[7] 9-Aminoanthracene was synthesized by the method of Kaufler.[8] The other aromatic amines were of commercal origin and were purified by distillation under reduced pressure. Their purities were confirmed by means of their physical constants and by vaporphase chromatography.

Kinetic Measurements. The diazo-coupling reaction of aromatic amines is known to be expressed by Eq. (1):[1]

$$\text{Rate} = k_2(\text{Ar-}\overset{+}{\text{N}}_2)(\text{Ar}'\text{-NH}_2) \quad (1)$$

In our experiment, the rate measurements were carried out spectrophotometrically in the presence of a large excess of amine in an aqueous buffer solution at a constant ionic strength of 0.04 at 20 °C. Then, the apparent rate constant (k') was calculated from Eq. (2):

$$k't = \ln\frac{E_\infty}{E_\infty - E_t} \quad (2)$$

where E_t and E_∞ represent the concentrations of the dyestuff formed at time t, and at an infinite time, respectively. The second-order rate constant (k_2) was obtained by dividing the k' value by the concentration of free amine, which can be calculated from the pK_a value, the concentration of amine, and the pH value of the medium. The buffering agents were of conventional CH_3COONa–CH_3COOH or CH_3COONa–HCl systems.

pK_a *Measurements.* The pK_a values of amines were determined spectrophotometrically under conditions identical with those of the kinetic experiments (20 °C, μ: 0.04, Table 1). As can be seen from Table 1, excepting the results for *N,N*-di-*n*-propylaniline, there is no serious disagreement between the present results and the published values; the slight disagreement may be ascribed to the differences in temperature and ionic strength.

Results and Discussion

The kinetic results are summarized in Table 1. As is shown in Table 1, the structural change of amine does not affect the reaction rate to any marked degree.

From the results (No. 1—3), it can be seen that the reactivity increases in the order of; primary<secondary <tertiary amine. This reactivity order is essentially the same as that obtained for alkylation;[9] it may be explained by an increased resonance donation of the lone pair of electrons of the amino nitrogen atom due to the alkyl group in the amino substituent.[6]

TABLE 1. RATE CONSTANTS OF THE REACTION OF DIAZOTIZED SULFANILIC ACID WITH AROMATIC AMINES AT 20 °C

No.	Amine	pK_a	k_2 (l/mol·min)
1	*m*-Toluidine	4.84(4.70)[a]	1.65×10^3
2	*N*-Methyl-*m*-toluidine	4.94	1.24×10^4
3	*N,N*-Dimethyl-*m*-toluidine	5.47(5.24)[b]	1.54×10^4
4	*N,N*-Dimethylaniline	5.17(5.06)[b]	7.34×10^2
5	*N*-Ethyl-*N*-methylaniline	5.98(5.98)[b]	1.72×10^3
6	*N,N*-Diethylaniline	6.72(6.56)[b]	3.92×10^3
7	*N,N*-Di-*n*-propylaniline	6.69(5.59)[b]	1.27×10^4
8	*N,N*-Di-iso-propylaniline	7.50(7.37)[c]	3.71×10^3
9	*N,N*-Di-*n*-butylaniline	6.37(6.21)[c]	7.71×10^3
10	*N*-Benzyl-*N*-ethylaniline	5.75	1.96×10^3
11	*N*-(2-Hydroxyethyl)-*N*-ethylaniline	5.86	1.84×10^3
12	*N,N*-Di-(2-hydroxyethyl)-aniline	4.31	2.67×10^2
13	*N*-(2-Cyanoethyl)-*N*-ethylaniline	3.47	3.49×10^1
14	*N*-(2-Cyanoethyl)-*N*-(2-hydroxyethyl)aniline	2.71	1.86×10^1
15	*N,N*-Dimethyl-*o*-toluidine	6.04(6.11)[d]	2.73×10^1
16	*N,N*-Diethyl-*o*-toluidine	7.64	2.90×10^2
17	1-Naphthylamine	4.09(3.92)[a]	7.09×10^4
17′	1-Naphthylamine	(3.70	1.53×10^5)[e]
18	*N,N*-Dimethyl-1-naphthylamine	4.76	1.12×10^3
19	2-Naphthylamine	4.11(4.16)[a]	4.16×10^4
20	9-Aminoanthracene	(3.25	3.29×10^5)[e]

a) A. Bryson, *J. Amer. Chem. Soc.*, **82**, 4858 (1960). b) N. F. Hall and M. R. Sprinkle, *ibid.*, **54**, 3469 (1932). c) G. Girault-Vexlearschi, *Bull. Soc. Chim. Fr.* **1956**, 589. d) B. M. Wepster, *Rec. Trav. Chim.*, **76**, 357 (1957). e) Data in 50% methanolic solution.

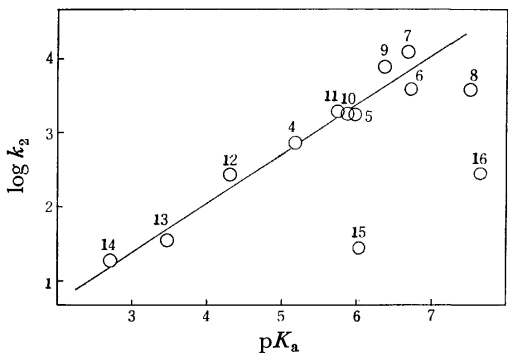

Fig. 1. Relationship between pK_a-value and rate constant. Figures refer to compounds in Table 1.

From the results of *N,N*-disubstitued anilines (No. 4—14), it was found that, among the di-*n*-alkyl-substituted amines (No. 4—7, 9), the activating effect of the amino group increases in the following order: NMe_2< $NMe(Et)\approx NEt_2$<N-*n*-$Pr_2\approx$N-*n*-Bu_2. This order is in accord with that of the inductive effect of the alkyl group, which may be explained on the basis of the effect of the alkyl group on the electron density at the amino nitrogen atom. On the other hand, the replacement of the hydrogen atom in the amino alkyl group by such an electron-attracting group as a hydroxy or cyano group (NO. 12—14) lowered the reactivity of dialkylaniline considerably.

Thus, it may be expected that a parallel correlation holds between the basicities of amines and the activating effects of their amino groups, since the electron-donating abilities of amino groups are considered generally proportional to their electron densities at the amino nitrogen atom. The relation between the basicity and the activating effect of a series of *N,N*-disubstituted anilines (No. 4—14) is shown in Fig. 1. From Fig. 1, it can be seen that a linear correlation holds between the basicities and the activating effects; an increase in the pK_a value by three units results in an increase in the reactivity by a factor of about 100.

The results (No. 15, 16) in Table 1 show that the introduction of methyl group into the ortho position leads to an increase in the basicity, but decreases the rate constant of *N,N*-dialkylaniline by a factor of about ten. The increase in the basicity may be ascribed mainly to the steric inhibition of the resonance; a departure from the coplanarity of the dialkylamino group with an aromatic ring as a result of the presence of an ortho methyl group should result a decrease in the electron donating ability of the amino group and is, therefore, base-strengthening. Consequently, although the methyl group s electrondonating, a methyl group in the ortho position of dialkylaniline lowers the reactivity of amine; thus, the plots of *o*-methyl-dialkylamines deviated markedly from the pK_a—log k line, as is shown in Fig. 1. In this sense, a linear relation between the basicities and the reactivities of the amines is considered to hold when the coplanarities of the amines are not hindered.

In the cases of 1-naphthylamine (No. 17) and 9-aminoanthracene (No. 20), the hydrogen atom at the peri position in the former, and the two hydrogen atoms the 1,8-positions in the latter, are considered to inhibit the interaction between the amino group and the aromatic ring to some extent. This inhibition is expected to become significant in the cases of secondary and tertiary amines. This estimation can easily be seen in the case of *N,N*-dimethyl-1-naphthylamine (No. 18), in which the reactivity is lower than that of 1-naphthylamine (No. 17), unlike the cases of the aniline series. Generally, it is well known that, in the electrophilic aromatic substitution, the reactivities of fused aromatic ring systems are much higher than those of monocyclic aromatic systems; there is a tendency for the reactivity to increase with an increase in the number of the condensed ring.[10] However, it can be seen from a comparison of the results of (No. 17′) and (No. 20) that the reactivities of 1-naphthylamine and 9-aminoanthracene are of the same order, suggesting that the steric inhibition by the hydrogen atom is larger in the latter than in the former.

References

1) H. Zollinger, "Azo and Diazo Chemistry," Interscience Publishers, New York, N. Y. (1961), p. 221.

2) I. Dobáš, V. Štěrba, and M. Večeřa, *Chem. Ind.* (London), **1968**, 1814.

3) I. Dobáš, V. Štěrba, and M. Večeřa, *Collect. Czech. Chem. Commun.*, **34**, 3746 (1969).

4) Y. Hashida, I. Shimoda, S. Sekiguchi, and K. Matsui, *Kogyo Kagaku Zasshi*, **74**, 73 (1971).

5) Y. Hashida, M. Kobayashi, and K. Matsui, This Bulletin, **44**, 2506 (1971).

6) G. Chuchani, "Directing and Activating Effects, The Chemistry of the Amino Group," ed. by S. Patai, Interscience Publishers (1968), p. 205.

7) G. Spielberger, "Amine durch Austaschreaktion" in "Methoden der Organischen Chemie. Stickstoffverbindungen II," ed. by E. Müller, Georg Thieme Verlag, Stuttgart (1957), p. 34.

8) K. Kaufler and W. Suchanneck, *Ber.*, **40**, 518 (1907).

9) V. Kese and G. Chuchani, *J. Org. Chem.*, **27**, 2032 (1962).

10) a) H. Noller, "Electrophilic Substitution in Benzenoid Compounds," Elsevier Publishing Co., New York (1965), p. 52. b) L. M. Stock and H. C. Brown, "Advances in Physical Organic Chemistry," Vol. 1, ed. by V. Gold, Academic Press Inc., New York (1963), p. 108.

BULLETIN OF THE CHEMICAL SOCIETY OF JAPAN, VOL. 47(2), 509—510 (1974)

Hydroxyl Stretching Frequencies and Conformations of 4-Chromanol, 4-Thiochromanol, and 4-Thiochromanol 1,1-Dioxide

Kaoru HANAYA, Shinji ONODERA,* Sachio AWANO,** and Hideaki KUDO

Department of Chemistry, Faculty of Science, Yamagata University, Koshirakawa-cho, Yamagata 990

**Chemical Research Institute of Non-Aqueous Solutions, Tohoku University, Katahira-2-chome, Sendai 980*

***Department of Industrical Chemistry, Tsuruoka Technical College, 104 Inooka, Tsuruoka, Yamagata 997*

(Received September 3, 1973)

Synopsis. Conformations of ten epimeric alcohols have been examined by the measurements of the OH stretching absorptions. The preference of the OH quasi-axial conformations was shown.

Iwamura and Hanaya[1] measured the O–H stretching absorption bands of epimeric 1-tetralols and 4-chromanols in carbon tetrachloride and pointed out that the epimer with the quasi-axial OH group shows a singlet absorption band and that with the quasi-equatorial OH group a doublet band. The doublet OH absorption of tetralol (**1**) was ascribed to the coexistence of the isomers with the quasi-axial and quasi-equational OH groups with the ratio 1 : 0.54.[2] The apparent conformational energy ($-\Delta G_{25°C}$) of the benzylic OH group was estimated to be 0.37 kcal/mol.

This paper reports on the measurements of the OH stretching absorptions and an estimation of the conformational energies for 4-chromanol (**2**), 4-thiochromanol (**3**), 4-thiochromanol 1,1-dioxide (**4**), and their derivatives which are considered to have a configuration similar to that of 1-tetralol. The OH absorption bands are analyzed in a similar way to that used for 1-tetralol.[1] The NMR spectra of these compounds were also examined to confirm the conformations.

Results and Discussion

The OH stretching absorption maxima of 4-chromanol (**2**), 4-thiochromanol (**3**), 4-thiochromanol 1,1-dioxide (**5**), and their derivatives (**5a**～**7b**) including 5,8-dimethyl-4-chromanol (**8**) are given in Table 1. The NMR measurements are summarized in Table 2 for the signals assigned to the protons at 4-positions of these compounds. Bolger and co-workers[3] have determined the conformations of **5a** and **5b** by NMR study. The NMR spectra of **6a**, **6b**, **7a**, and **7b** are interpreted in a similar manner to those of **5a** and **5b**. A double doublet signal due to the proton at 4-position of **6a** indicates that the hydroxyl group of this compound has quasi-equatorial conformation as regards the heterocyclic ring. The same situation is also suggested for the conformation of **7a**. The triplet signals observed for the protons at the 4-positions of **6a** and **7b** indicate quasi-axial conformations.

Epimers with a quasi-axial OH group each show a single absorption maximum, while those with the quasi-equatorial OH group have a doublet absorption band (Table 1). From the fact that the infrared spectra of these epimers are similar to those of 1-tetralols, it is assumed that these compounds have a similar conformation to that of 1-tetralol, in which the heterocyclic ring prefers a half-chair conformation.

The conformational free energies ($-\Delta G$) of the benzylic OH group for compounds **2**, **3**, and **4** were calculated by means of the graphical devision of the infrared OH absorptions in a similar manner to that for 1-tetralol[1] (Table 3). These values lead to the conclusion that the quasi-axial OH conformation is predominant in compounds **2**, **3**, and **4** and component of the epimer with this conformation increases in the order **1**<**4**≈**3**<**2**. This is consistent with the results by Katekar and Moritz,[4] who showed the preference of the quasi-axial OH conformation in **2** and **3** by examination of their infrared and NMR spectra.

From the half-chair conformations of the heterocyclic rings in **2**, **3**, and **4**, preference of the quasi-axial OH conformation should be attributed to the large steric repulsion between the equatorially oriented OH group and the aromatic hydrogen atom disposed parallel to the OH group, over the one 1,3-diaxial H···OH interaction in the heterocyclic ring.[5] The assumption is consistent with the result for 5,8-dimethyl-4-thiochro-

TABLE 1. ν_{OH} ABSORPTION MAXIMA OF 4-CHROMANOL, 4-THIOCHROMANOL, 4-THIOCHROMANOL 1,1-DIOXIDE AND THEIR ALLIED COMPOUNDS

Compound	ν_{max} (cm^{-1})	$\Delta\nu^{a}_{1/2}$ (cm^{-1})	ε
2	3616	16	84
	3597	14	20
3	3614	15	66
	3595	14	14
4	3611	21	108
	3586	13	23
5a	3623	23	34
	3596	14	75
5b	3616	16	89
6a	3625	18	32
	3594	12	52
6b	3613	18	91
7a	3617	27	30
	3588	15	74
7b	3612	22	145
8	3616	16	91

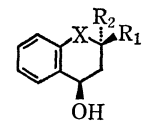

2 : X=O, R_1=R_2=H
3 : X=S, R_1=R_2=H
4 : X=SO_2, R_1=R_2=H
5a : X=O, R_1=Ph, R_2=H
5b : X=O, R_1=H, R_2=Ph
6a : X=S, R_1=CH_3, R_2=H
6b : X=S, R_1=H, R_2=CH_3
7a : X=SO_2, R_1=CH_3, R_2=H
7b : X=SO_2, R_1=H, R_2=CH_3

Table 2. NMR spectra of 4-chromanol, 4-thiochromanol and 4-thiochromanol 1,1-dioxide and their derivatives

Compound	Position of peaks in ppm	Assignment	Remarks (Hz)
5a[a]	6.55	4-H	Double doublet $J_{3a.4}+J_{3e.4}=16.2$
5b[a]	6.26	4-H	Triplet $J_{3a.4}+J_{3e.4}=6.0$
6a	4.65	4-H	Double doublet $J_{3a.4}+J_{3e.4}=15.3$
6b	4.47	4-H	Triplet $J_{3a.4}+J_{3e.4}=5.9$
7a	4.77	4-H	Double doublet $J_{3a.4}+J_{3e.4}=15.3$
7b	4.83	4-H	Triplet $J_{3a.4}+J_{3e.4}=6.8$

a) NMR spectrum of benzoyloxyflavan.

Table 3. Conformational free energies ($-\Delta G_{25°C}$) for the benzylic OH groups of **1**, **2**, **3**, and **4**

Compound	$-\Delta G_{25°C}$ (kcal/mol)[a]
1	0.37
2	0.65
3	0.56
4	0.51

a) With an error of about ±0.1 kal/mol.

manol (**8**). The infrared spectrum of **8** shows a singlet OH absorption maximum at 3616 cm^{-1} which can be assigned to the quasi-axial OH group. In this case, the steric repulsion between the equatorially oriented OH group and the bulky methyl group at 8-position would be more serious than that between the OH group and the hydrogen atom at 8-position, leading to an overwhelming selection of the quasi-axial conformation in **8**.

Experimental

Materials. *cis*-(**5a**) and *trans*-4-Flavanol (**5b**),[6] 4-chromanol (**2**),[7] 4-thiochromanol (**3**),[8] and 4-thiochromanol 1,1-dioxide (**4**)[9] were prepared by standard procedures. *cis*-(**6a**) and *trans*-2-Methyl-4-thiochromanol (**6b**), *cis*-(**7a**) and *trans*-2-m thyl-4-thiochromanol 1,1-dioxide (**7b**) were prepared by the sodium borohydride reduction or the Merewein-Ponndorf reduction of 2-methyl-4-thiochromanone 1,1-dioxide, respectively. *cis*-2-Methyl-4-thiochromanol (**6a**): mp 74—75 °C (lit, 74—75.5 °C).[10] *trans*-2-Methyl-4-thiochromanol (**6b**): bp 116—118 °C/1 mmHg; the *p*-nitrobenzoate crystallized from ethyl acetate, mp 156—157 °C. Found: C, 61.75; H, 4.69; N, 4.25%. Calcd for $C_{17}H_{15}O_4NS$: C, 62.00; H, 4.25%. *cis*-2-Methyl-4-thiochromanol 1,1-dioxide (**7a**): mp 130—131.5 °C. Found: C, 56.70; H, 5.95%. Calcd for $C_{10}H_{12}O_3S$: C, 56.60; H, 5.70%. *trans*-2-Methyl-4-thiochromanol 1,1-dioxide (**7b**): mp 105—106 °C. Found: C, 56.82; H, 5.74%. Calcd for $C_{10}H_{12}O_3S$: C, 56.60; H, 5.70%. 5,8-Dimethyl-4-chromanol (**8**): Reduction of 5,8-Dimethyl-4-chromanone with sodium borohydride yielded 5,8-dimethyl-4-chromanol (**8**) as colorless needles from ligroin, mp 108—110 °C. Found: C, 73.75; H, 7.80 %. Calcd for $C_{11}H_{14}O_2$: C, 74.13; H, 7.92%.

Measurements. The NMR spectra were measured in $CDCl_3$ using a Hitachi H-60 spectrometer with TMS as an internal standard. The infrared spectra were recorded with a Perkin-Elmer 125 or a JASCO DS-403G double beam grating spectrophotometer. A KCl cell of 30 mm in optical length was used. The concentration of the solution was *ca.* 0.005 mol/l in carbon tetrachloride purified by distillation over phosphorus pentoxide. The band due to intermolecular hydrogen bonding was not observed at this concentration.

The authors wish to express their gratitude to Associate Professor Hiizu Iwamura, the University of Tokyo, for his helpful discussions and suggestions during this work.

References

1) H. Iwamura and K. Hanaya, This Bulletin, **43**, 3901 (1970).
2) Preference of the quasi-axial OH conformation for tetralol has also been demonstrated by Mori *et al.*: N. Mori, M. Yoshifuji, Y. Asabe, and Y. Tsuzuki, *ibid.*, **44**, 1137 (1971).
3) B. J. Bolger, A. Hirwe, K. G. Marathe, E. M. Philbin, M. A. Vickars, and C. P. Lillya, *Tetrahedron*, **22**, 621 (1966).
4) G. F. Katekar and A. G. Moritz, *Aust. J. Chem.*, **22**, 2337 (1969).
5) A similar steric interaction has been recognized for several 1-substituted cyclohex-2-enes: K. Hanaya, *Nippon Kagaku Zasshi*, **91**, 82 (1970); E. W. Garblish, Jr., *J. Org. Chem.*, **27**, 4249 (1962).
6) S. Mitsui, and A. Kasahara, *Nippon Kagaku Zasshi*, **79**, 1382 (1958).
7) G. P. Thakar, N. Janaki, and B. C. Subba Rao, *Indian J. Chem.*, **3**, 74 (1965).
8) W. Bonthrone, and D. H. Reid, *Chem. Ind.* (London), **1960**, 1192.
9) I. W. J. Still, and M. T. Thomas, *J. Org. Chem.*, **33**, 2730 (1968).
10) T. E. Young, and C. J. Ohnmacht, *ibid.*, **32**, 1558 (1967).

BULLETIN OF THE CHEMICAL SOCIETY OF JAPAN, VOL. 47(2), 511—512 (1974)

MO Calculation for Interactions of Cu(II) and Co(III) with Hydroperoxides

Sei-ichiro IMAMURA and Shigeyoshi SAKAKI*

Department of Chemistry, Kyoto Institute of Technology, Matsugasaki, Sakyo-ku, Kyoto 606

**Department of Hydrocarbon Chemistry, Faculty of Engineering, Kyoto University, Sakyo-ku, Kyoto 606*

(Recieved September 20, 1973)

Synopsis. By means of MO calculation, cobalt(III) and copper(II) were considered to decompose primary and secondary hydroperoxides through the oxidative fission of their O–H bond. However, in basic solvents such as pyridine, copper(II) was found to promote the fission of their C–H bond of the α-position by the complex formation with them.

By the use of the extended Hückel and the simple Hückel MO method, Yonezawa *et al.* discussed the catalytic decomposition of *t*-butyl hydroperoxide (*t*-butyl HPO) by transition metals.[1] The interaction of methyl HPO with lower-valent transition metals was also studied by MO calculation.[2] However, no calculation has been carried out for the Cu(II)-HPO system, in which Cu(II) shows interesting catalytic activities.[3]

Previously, we have ourselves studied the catalytic action of copper(II) chloride in the decomposition of primary and secondary HPOs (—1,2,3,4-tetrahydro-1-naphthyl, benzyl and cyclohexenyl HPOs—) in pyridine and suggested that the reaction proceeds through an ionic dehydration by the pyridine-Cu(II) system.[4] The carbon-hydrogen bond of the α-position is considered to be weakened by the coordination of the HPOs to Cu(II) through the O lone-pair electron.

The present study has been undertaken in an attempt to obtain support for the mechanism of the ionic dehydration and also to elucidate the catalytic action of Cu(II) in the radical decomposition of HPO by the comparison with that of Co(III).

Method of Calculation

The semi-empirical SCF-MO method with the CNDO-type approximation was used. The reasonance integral, H_{rs}, was calculated by means of Wolfsberg-Helmholz approximation:[6] $H_{rs}=-kS_{rs}(I_r+I_s)$ where k was taken as 0.5 for the atomic orbital (AO) pair including the d-orbital and as 0.4 for the AO pair including only s- and p-AOs. For an atom pair which do not form a bond, H_{rs} is taken as zero. Slater-type AOs were used for the s- and p-AOs, and the double-ζ type orbital was used for the d-orbital.[7] The two-atomic part of the total energy, E_{AB}, proposed by Pople *et al.*,[8] was used as a measure of the strength of the bond between A and B, atoms.[5] The MO calculations were carried out for a closed-shell system, followed by the correction for an unpaired electron, because Cu(II)-HPO systems have odd numbers of electrons.

As model compounds for primary and secondary HPOs, methyl HPO (MHPO) and 1-methylallyl HPO(MAHPO) were employed. Square planar Cu(II)$(NH_3)Cl_2$ was used as a model catalyst in pyridine, and Co(III)$(OH)_5$ was employed as a cobalt catalyst in the non-basic solvent. The bond lenghts and bond angles of these compounds were estimated from the values in the literature;[9] the distance between Cu(II) or Co(III) and the oxygen atom of HPO was taken as 1.95 or 2.22 Å respectively.

Results and Discussion

Cu(II) Catalyst. Cu(II) is considered to form a complex with HPOs, as is shown in Fig. 1. Calculations were carried out for both the O_1- and O_2-coordinations; the results are given in Tables 1 and 2.

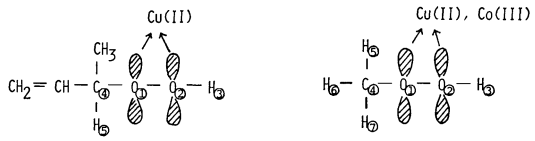

Fig. 1. Coordination position of MHPO and MAHPO.

The values of E_{total} and E_{Cu-O} show that, in both MHPO and MAHPO complexes, O_1 coordination is preferable to O_2 one. These results disagree with those of the previous study[1] in which it was proposed, from the consideration of the orbital electron density of free HPO, that the metal ion forms a complex with HPO through the O_2 lone pair. However, it is more probable that the O_1 complex is a major species in the reaction, because the Cu(II)-HPO complex seems more suitable than free HPO for the discussion of the coordination position. As can be seen from the tables, the C–H bonds of the α-position are weakened by the coordination of the HPOs to Cu(II), since the absolute value of E_{C-H} is decreased by 0.09—0.16 eV. Therefore, these results support the reaction mechanism for the ionic dehydration of primary and secondary HPOs by the Cu(II)-pyridine system previously proposed:

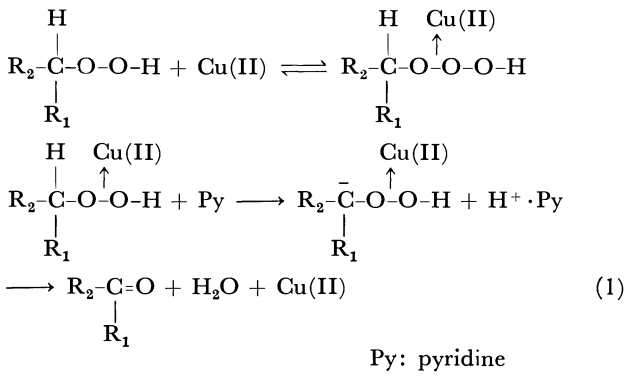

Co(III) Catalyst. Higher-valent transition metals are known to decompose HPO by the one-electron oxidation of a peroxidic bond to produce the peroxy radical and proton:

Table 1. MHPO and Cu(II)-MHPO complex

		MHPO	Cu-MHPO comp'ex	
			Cu-O_1	Cu-O_2
E_{total}/eV			−3073.68	−3073.48
Atom population	O_1	6.340	6.321	6.239
	O_2	6.373	6.281	6.365
	H_3	0.642	0.570	0.614
	$H_{5,6,7}$	1.023	0.970	0.970
	Cu		11.241	11.249
$E_{O_1-O_2}$		−14.81	−14.69	−14.23
$E_{O_2-H_3}$		−23.69	−22.94	−22.63
$E_{C_4-H_{5,6,7}}$	av./eV.	−20.37	−20.21	−20.23
$E_{Cu-O_1 \text{ or } O_2}$			−12.13	−12.06

Table 2. MAHPO and Cu(II)-MAHPO complex

		MAHPO	Cu-MAHPO complex	
			Cu-O_1	Cu-O_2
E_{total}/eV			−3612.50	−3610.26
Atom population	O_1	6.333	6.310	6.283
	O_2	6.396	6.317	6.417
	H_3	0.647	0.583	0.636
	H_5	0.953	1.035	0.981
	Cu		11.229	11.088
$E_{O_1-O_2}$		−14.69	−14.64	−13.61
$E_{O_2-H_3}$		−23.77	−23.19	−22.76
$E_{C_4-H_5}$	vs./eV.	−20.19	−20.10	−20.18
$E_{Cu-O_1 \text{ or } O_2}$			−12.40	−12.30

Table 3. MHPO and Co(III)-MHPO complex

		MHPO	Co-MHPO complex	
			Cu-O_1	Cu-O_2
E_{total}/eV.			−3750.28	−3749.78
Atom population	O_1	6.340	6.283	6.233
	O_2	6.373	6.290	6.297
	H_3	0.642	0.701	0.613
	$H_{5,6,7}$	1.023	0.997	1.050
	Co		8.043	8.049
$E_{O_1-O_2}$		−14.81	−14.87	−14.94
$E_{O_2-H_3}$		−23.67	−23.51	−22.60
$E_{C_4-H_{5,6,7}}$	av./eV.	−20.37	−20.19	−20.38
$E_{Co-O_1 \text{ or } O_2}$			−10.03	−9.73

$$ROOH + M^{+(n+1)} \longrightarrow ROO\cdot + H^+ + M^{n+} \quad (2)$$

When MHPO coordinates to Co(III) through the O_1 or O_2 lone-pair, it may be seen from Table 3 that the absolute value of $E_{O_1-O_2}$ is increased, but that of $E_{O_2-H_3}$ is decreased: this is in good agreement with the experimental result (Eq. (2)). The decrease in the absolute value of $E_{O_2-H_3}$ is larger in the O_2 coordination (about 1.1 eV) than that in the O_1 coordination (about 0.16 eV), suggesting that Reaction (2) proceeds more easily from the O_2 coordination than from the O_1 coordination. On the other hand, the O_1 coordination seems more favorable than O_2 coordination from the consideration of E_{total} and E_{Co-O}. Therefore, it is plausible that Co(III) forms two complexes with HPO in equilibrium with one another (see A and B below) and that the B complex, in high concentration, cannot contribute to Reaction (2) so much as the A complex. That is, the rate of the decomposition of the B complex in a higher concentration is small compared with that of the A complex in a low concentration. In this way, the decomposition of HPO seems to be catalyzed by Co(III).

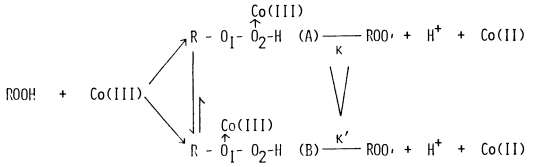

Cu(II), though effective in the decomposition of HPO, is considered not to promote the fission of the O_2–H_3 bond of HPO (Eq. (2)).[3] However, it can be seen from Tables 1 and 2 that the absolute value of $E_{O_2-H_3}$ is decreased by 0.7 eV (O_1 coordination)—1.1 eV (O_2 coordination), which suggests that Cu(II) can promote Reaction (2) as well as Co(III). Therefore, it can be expected that, in a non-basic solvent, Cu(II) promotes the direct decomposition of HPO (Eq. (2)) at the initial stage of the reaction (induction period), where the transformation of Cu(II) to Cu(I) occurs, and that, at the later stages of the reaction, the rapid oxidation of the alkyl radical by Cu(II) (Eq. 3) would predominate over Reaction (2):[3,10]

$$R\cdot + Cu(II) \longrightarrow R^+ + Cu(I) \quad (3)$$

The authors are very much indebeted to Professor Hiroshi Kato for his helpful advice and discussions.

References

1) T. Yonezawa, O. Yamamoto, H. Kato and K. Fukui, *Nippon Kagaku Zasshi*, **87**, 26 (1966).
2) K. Ohkubo and H. Kaneda, This Bulletin, **45**, 2646 (1971).
3) J. K. Kochi, *J. Amer. Chem. Soc.*, **85**, 1958 (1963).
4) S. I. Imamura, T. Banba, M. Teramoto, H. Teranishi, and Y. Takegami, *Nippon Kagaku Kaishi*, **1972**, 2113.
5) S. Sakaki, *Theoret. Chim. Acta*, **30**, 159 (1973).
6) M. Wolfsberg and L. Helmholz, *J. Chem. Phys.*, **20**, 837 (1952).
7) J. W. Richardson, W. C. Niewpoort, R. R. Powell, and W. F. Edgell, *J. Chem. Phys.*, **36**, 1057 (1962).
8) J. A. Pople, D. P. Santry, and G. A. Segal, *J. Chem. Phys.*, **43**, S129 (1965).
9) L. E. Sutton, Editor, "Tables of Interatomic Distances and Configurations in Molecules and Ions," Chem. Soc., London (1958).
10) S.-I. Imamura, K. Fukumoto, H. Teranishi, and Y. Takegami, *Nippon Kagaku Kaishi*, **1973**, 573.

BULLETIN OF THE CHEMICAL SOCIETY OF JAPAN, VOL. 47(2), 513—514 (1974)

Preferential Precipitation of Δ-$[Co(en)_3]_2(d\text{-}C_4H_4O_6)_3$ by Alcohol Addition to the $[Co(en)_3]^{3+}$–$d\text{-}C_4H_4O_6^{2-}$ Aqueous Systems

Hayami YONEDA, Gen TAKEMOTO, and Ushio SAKAGUCHI

Department of Chemistry, Faculty of Science, Hiroshima University, Higashi-Sendamachi, Hiroshima 730

(Received December 18, 1973)

Synopsis. Alcohol addition to the aqueous $[Co(en)_3]^{3+}$—*d*-tart systems causes the preferential precipitation of Δ-$[Co(en)_3]_2(d\text{-tart})_3$. The yield lies in between 54—55% under experimental conditions employed.

Tris(ethylenediamine)cobalt(III) ($[Co(en)_3]^{3+}$) ion is the prototype of many tris-chelated cobalt complexes. The optical activity and the interaction with $d\text{-}C_4H_4O_6^{2-}$ (*d*-tart) ions of $[Co(en)_3]^{3+}$ have attracted much interest of many workers.[1-6] The fact that the Λ-form of $[Co(en)_3]^{3+}$ can easily be precipitated by *d*-tart ions while the Δ-form can not has long been used as the method of resolution[7] of $[Co(en)_3]^{3+}$ by way of Λ-$[Co(en)_3]X\cdot(d\text{-tart})$ (X=Cl$^-$, Br$^-$). Thus, the specific interaction, as found[8,9] for the system Λ-$[Co(en)_3]^{3+}$—PO_4^{3-}, between Λ-$[Co(en)_3]^{3+}$ and *d*-tart ions may be supposed operative in such resolution processes.

It is reported here that the alcohol addition to the aqueous $[Co(en)_3]^{3+}$—*d*-tart systems causes the precipitation of $[Co(en)_3]_2$ $(d\text{-tart})_3$ and that the dominant diastereoisomer is Δ-$[Co(en)_3]_2(d\text{-tart})_3$. This result is somewhat contrary to the expectation from the above-mentioned method of resolution.

Experimental

Complexes used in this work are prepared after the literature methods.[10,11] Sixty-eight grams of $[Co(en)_3]Cl_3.3H_2O$ and 172 g of $KNa(d\text{-}C_4H_4O_6)$ are dissolved in water to a volume of 1500 ml. To every 100 ml of the solution is added the varying amount of alcohol. The identity of the precipitated complex has been confirmed by chemical analysis. Found: C, 25.69; H, 6.91; N, 15.01%. Calcd for $[Co(C_2H_8N_2)_3]_2(d\text{-}C_4H_4O_6)_3\cdot 11(12)H_2O$: C, 25.72(25.31) H, 7.37(7.43); N, 15.00(14.76)%. The precipitate redissolved in water is passed through an anion exchanger (Dowex-1 X8) to convert the tartrate to the chloride. The optical rotation has been measured on a Yanaco OR-50D automatic digital polarimeter and the concentration of the complex is determined spectrophotometrically. The CD spectra are recorded on a JASCO Model ORD/UV-5 spectrometer with a CD attachment. Similar procedure has been applied to tris(ethylenediamine)cobalt(III) bromide and acetate.

Results

The results are summarized in Fig. 1, which shows the variation of the amount of Δ-$(-)_{589}$-$[Co(en)_3]_2$ $(d\text{-tart})_3$ precipitated against the volume of added alcohol. It is clear that more precipitation of Δ-diastereoisomer than the Λ-isomer is induced by the alcohol addition to the aqueous $[Co(en)_3]^{3+}$—*d*-tart systems(see, Fig. 2). Tris(ethylenediamine)cobalt(III) acetate behaves in a similar manner to the corresponding chloride and bromide and the result for the acetate has been deleted. The best attainable yield of the Δ-form is low and lies in between 54—55%. The above results contrast, in two points, well with the case of the usual method for resolution of $[Co(en)_3]^{3+}$;[7] first, $[Co(en)_3]_2(d\text{-tart})_3$ is precipitated while in the latter case $[Co(en)_3]X\cdot d\text{-tart}$ precipitates; second, Δ-$[Co(en)_3]_2(d\text{-tart})_3$ predominates, though slightly, while in the latter Λ-$[Co(en_3]X\cdot d\text{-tart}$ is dominant.

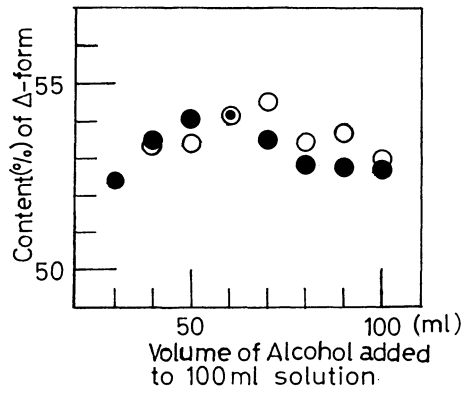

Fig. 1. The variation of the fraction of Δ-$(-)_{589}$-$[Co(en)_3]_2(d\text{-tart})_3$ precipitated against the volume of added alcohol. Open and closed circles refer to chloride and bromide starting materials, respectively.

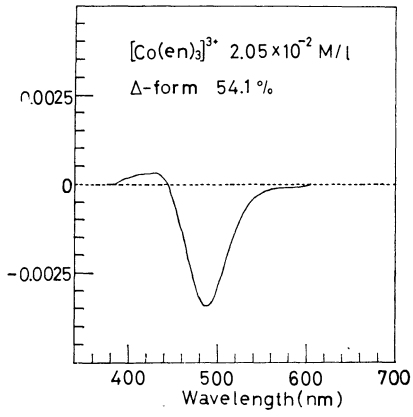

Fig. 2. The CD spectrum obtained when 60 ml alcohol is added to the 100 ml chloride solution.

Concentration by evaporation of the solution containing $[Co(en)_3]X_3$(X=Cl$^-$, Br$^-$) and *d*-tart ions yields Λ-$(+)_{589}$-$[Co(en)_3]X\cdot d\text{-tart}$, which is consistent with the conventional procedure for resolution. Of the two diastereoisomers Δ-$(-)_{589}$-$[Co(en)_3]_2(d\text{-tart})_3$ was observed to be the first to precipitate also in aqueous solution, because the reaction of $[Co(en)_3]X_3$(X=Cl$^-$, Br$^-$) with $Ag_2(d\text{-tart})$ precipitates first the Δ-diastereoisomer when evaporated. Alcohol is responsible, there-

fore, for the formation of $[Co(en)_3]_2(d\text{-tart})_3$ and the preferential precipitation of the Δ-diastereoisomer occurs both in pure and alcoholic water.

The problem remains to be settled why alcohol addition causes the precipitation of the form $[Co(en)_3]_2(d\text{-tart})_3$ rather than $[Co(en)_3]X\cdot d\text{-tart}$. More interesting is why *d*-tart ions prefer Δ-$[Co(en)_3]^{3+}$ in the case of $[Co(en)_3]_2(d\text{-tart})_3$ while Λ-$[Co(en)_3]^{3+}$ in $[Co(en)_3]X\cdot d\text{-tart}$. The association constant between Δ- and Λ-$[Co(en)_3]^{3+}$ and *d*-tart ions may shed some light on these problems. The work along this direction is in progress.

References

1) A. J. McCaffery and S. F. Mason, *Mol. Phys.*, **6**, 359 (1963).
2) H. Yoneda and T. Miura, This Bulletin, **45**, 2126 (1972).
3) K. Nakatsu, M. Shiro, Y. Saito, and H. Kuroya, *ibid.*, **30**, 158 (1957).
4) W. Moffit, *J. Chem. Phys.*, **25**, 1189 (1956).
5) T. S. Piper and A. Karipides, *Mol. Phys.*, **5**, 475 (1962).
6) M. Shinada, *J. Phys. Soc. Japan*, **19**, 1607 (1964).
7) J. A. Broomhead, F. P. Dwyer, and J. W. Hogarth, "Inorganic Syntheses," Vol. **6**, p. 183 (1960).
8) S. F. Mason and B. J. Norman, *Proc. Chem. Soc.*, **1964**, 339, *Chem. Commun.*, **1965**, 73, and *J. Chem. Soc., A*, **1966**, 73.
9) H. L. Smith and B. E. Douglas, *J. Amer. Chem. Soc.*, **86**, 3885 (1964).
10) J. B. Work, "Inorganic Syntheses," Vol. **2**, p. 221 (1946).
11) A. Werner and M. Sasyrin, *Ber.*, **46**, 3230 (1913).

Magnetic Susceptibilities of Octacoordinated Uranium (IV) Complexes

Tetsuhiko YOSHIMURA,* Chie MIYAKE, and Shosuke IMOTO

Department of Nuclear Engineering, Faculty of Engineering, Osaka University, Suita, Osaka 564

(Received March 6, 1973)

Magnetic susceptibility measurements were carried out on octacoordinated uranium(IV) complexes, such as tetrakis(acetylacetonato)uranium(IV), tetrakis(trifluoroacetylacetonato)uranium(IV), tetrakis(benzoylacetonato)-uranium(IV), tetrakis(dibenzoylmethanato)uranium(IV), tetrakis(thenoyltrifluoroacetonato)uranium(IV), tetrakis(cupferronato)uranium(IV), and uranium(IV)tetrachloride, in the temperature range from room temperature to the temperature of liquid nitrogen or liquid helium. The Curie-Weiss law holds above the temperature of liquid nitrogen, with a magnetic moment of 3.5—2.92 BM. For the latter two complexes, a temperature-independent paramagnetism was observed in the low temperature range; the other complexes also seemed to show the same trend. We tried to interpret the magnetic behavior on the basis of the crystal-field model of the square antiprism structure or the dodecahedron structure of the complexes.

The measurement of the magnetic behavior is one of the most useful and effective methods for the study of the electronic state of a complex. Particularly, the temperature-independent paramagnetism (TIP) at low temperatures often gives decisive information on the ground state of the central metal ion being studied. The configuration of the valence electrons of the uranium ion was early considered to be $(6d)^2$, because uranium dioxide magnetically diluted with thorium dioxide had a magnetic moment nearly equal to the spin-only value. Indeed, the quenching of the orbital angular momentum leading to the contribution only of the spin angular momentum to the observed magnetic momentum is, in many cases, characteristic of the d-electron, while in lanthanoid ions, which have unfilled 4f shell, the Russell-Saunders coupling has been found to be more feasible. Hutchison and Candela have, however, shown that the configuration $(5f)^2$ of the uranium ion (IV) with the $^3H_4$ term as the ground state is also capable of giving a magnetic moment near the spin-only value if the ion is influenced by the crystal field with cubic symmetry.[1] The TIP of the octahedral Cs_2UCl_6 at low temperatures could be reasonably explained by this scheme, taking into consideration the high-frequency interaction between the ground singlet state $^1\Gamma$ of the $^3H_4$ term and the lowest excited state (about 1 kcm^{-1} above the former). If the configuration be assumed to be $(6d)^2$, the ground state resulting from the splitting of $^3F_2$ in the octahedral crystal field would be the triplet $^3\Gamma_4$, which does not show the TIP at low temperatures. Recently, Mulak and Czopnik measured the magnetic susceptibility of $U(SO_4)_2 \cdot 4H_2O$ and $U(CH_3COCHCOCH_3)_4$ and explained the observed TIP on the basis of the splitting behavior of the $^3H_4$ term in a crystal field of a slightly distorted archimedian antiprism symmetry.[2] In the present study, the magnetic susceptibility of octacoordinated uranium (IV) complexes with the structure of dodecahedron as well as that of square antiprism is measured in the range from room temperature to the temperature of liquid nitrogen or liquid helium, and the results are interpreted on the basis of the crystal field theory.

* Present address: The Environmental Science Institute of Hyogo Prefecture, Hyogo-ku, Kobe.

Experimental

Magnetic susceptibility measurements in the range from room temperature to the temperature of liquid nitrogen were carried out with a torsion magnetometer of the Faraday type in the magnetic field of 5.0 kOe, and the measurements from the temperature of liquid nitrogen to that of liquid helium, with the Torsion Magnetic balance MB2 of the Shimadzu Seisakusho Ltd. in 10.66 and 8.685 kOe. The temperature was measured using an Au-Co/Cu thermocouple or a carbon-resistance thermometer. The value of the magnetic susceptibility was calibrated by using $NiCl_2$ powder as the standard. The measurements were made for seven complexes: tetrakis(acetylacetonato)uranium(IV) ($U(acac)_4$), tetrakis(trifluoroacetylacetonato)uranium(IV) ($U(tfac)_4$), tetrakis(benzoylacetonato)uranium(IV) ($U(bac)_4$), tetrakis-(dibenzoylmethanato)uranium(IV) ($U(dbm)_4$), tetrakis-(thenoyltrifluoroacetonato)uranium(IV) ($U(TTA)_4$), tetrakis (cupferronato) uranium(IV) ($U(cupf)_4$), and uranium(IV) tetrachloride (UCl_4); the methods of preparation have been described elsewhere.[3] UCl_4 is so deliquescent that it was sealed into a glass tube in a vacuum; the correction for the glass tube was made by measuring the magnetic susceptibility of the empty glass tube under the same conditions as were used for the specimen. Correction for diamagnetism was made for the U(IV) ion and the chloride ion by using the value reported by Dawson;[4] for H_2O and the acetylacetonato ion, by using the value reported by Earnshaw,[5] for benzoylacetone, by using the value reported by the Handbook,[6] and for all others, by using the value of Pascal's constant. The values of the diamagnetic increment used for the correction were as follows: $U(acac)_4$, -240; $U(tfac)_4$, -280; $U(bac)_4$, -404; $U(dbm)_4$, -592; $U(TTA)_4$, -368; $U(cupf)_4$, -315; UCl_4, -123 ($\times 10^{-6}$ cgs emu).

Results

Figure 1 shows the relationships between the reciprocal molar magnetic susceptibility and the temperature for $U(acac)_4$, $U(tfac)_4$, $U(bac)_4$, $U(dbm)_4$, $U(TTA)_4$, and $U(cupf)_4$. These complexes are found to follow the Curie-Weiss law over the temperature range measured except for the lowest part, where a slight positive deviation from the straight line is observed. The magnetic moment and the Weiss constant calculated from the straight line are shown in Table 1. Figure 2 represents the temperature dependence of the magnetic susceptibility for $U(cupf)_4$ and UCl_4 in the

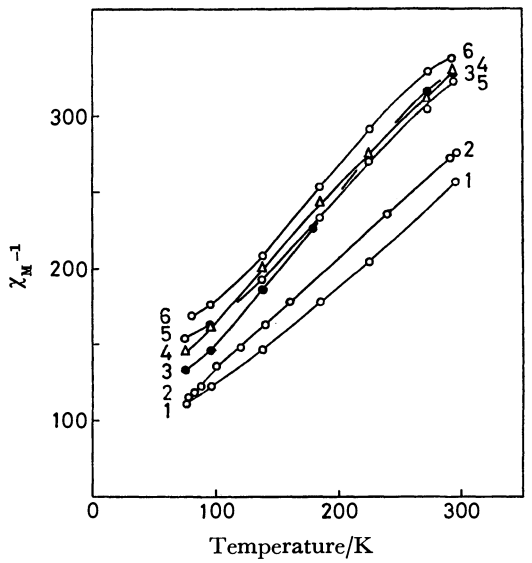

Fig. 1. Reciprocal susceptibility of complexes as a function of temperature.
1: $U(dbm)_4$, 2: $U(cupf)_4$, 3: $U(acac)_4$, 4: $U(tfac)_4$, 5: $U(bac)_4$, 6: $U(TTA)_4$.

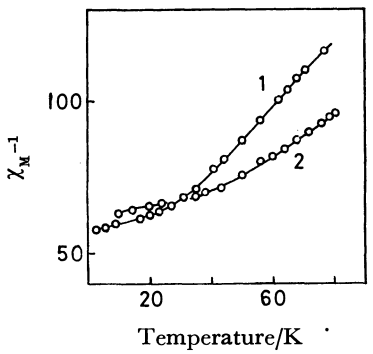

Fig. 2. Reciprocal susceptibility of complexes as a function of temperature.
1: $U(cupf)_4$. 2: UCl_4.

Table 1. Structure and magnetic constants of octacoordinated U(IV) complexes

Complexes	Structure	μ	Weiss const. (K)	Ref.
$U(dbm)_4$	DH	3.43	− 77	
$U(cupf)_4$		3.5	−120	
$U(acac)_4$	SA	2.92	− 68	
$U(tfac)_4$		3.16	−116	
$U(bac)_4$		3.08	− 91	
$U(TTA)_4$		3.01	−101	
UCl_4	DH	3.29	− 62	4
UF_4	SA	3.30	−102	4
UF_4 in ThF_4	SA	2.92	− 25	4
γ-Na_2UF_6	cube	3.18	− 86	8
$(NH_4)_4UF_8$	SA			
$U(SO_4)_2 \cdot 4H_2O$	SA	3.14[a)]	−125	2
UO_2	cube	3.11	−208	9
UO_2 in ThO_2	cube	2.86	− 42	9
$K_4U(NCS)_8$	cube	3.26	−119	10

a) Estimated from the figure in Ref. 2.

temperature range from the temperature of liquid nitrogen to the temperature of liquid helium.[7] TIP is suggested for both complexes from the curved χ^{-1} *vs.* T relationships at low temperatures. The magnetic moment and the Weiss constant of $U(cupf)_4$ and UCl_4, as estimated from the linear part of the curve in the higher temperature range, are also given in Table 1.

Discussion

Among the octacoordinated uranium(IV) complexes studied in the present experiment, only $U(acac)_4$, $U(dbm)_4$, and UCl_4 have been elucidated as to the structure around the central uranium ion. In Table 1 we have summarized the structures and the magnetic moments of the octacoordinated uranium(IV) compounds already determined, together with those obtained in the present study. From the table, it seems that the complexes with the square antiprism structure show relatively lower magnetic moments than do those with dodecahedron structure.

Dodecahedron. In UCl_4 and $U(dbm)_4$ the nearest surrounding anions around the central U(IV) ion are known to form a dodecahedron and to produce a tetragonal crystal field with D_{2d} symmetry. The ground state of the uranium ion with the ground term of $^3H_4$ in the configuration $(5f)^2$ is then split into five singlets and two doublets under the influence of the electric field. From his study of the visible absorption spectra of UCl_4 at the temperature of liquid helium, McLaughlin inferred that the ground state is the singlet, $^1\Gamma_{t4}$, with the lowest excited state of $^1\Gamma_{t1}$, spaced 551 cm^{-1} above.[11] However, the TIP observed in the present experiment does not agree with this scheme, because such a large splitting as 551 cm^{-1} would give rise to TIP in the temperature range below about 500 K.

Another example of the analysis of the absorption spectra for the complex of dodecahedron coordination has been given in the case of $ZrSiO_4$ doped with the U(IV) ion, where the ground state was also assigned to be $^1\Gamma_{t4}$, but where the lowest excited state was estimated to be the doublet, $^2\Gamma_{t5}$ 155 cm^{-1}, above the singlet.[12] Recently Troc *et al.* carried out a detailed analysis of the magnetic susceptibility measured for uranium compounds with a Th_3P_4-type structure, in which each cation is surrounded by eight nearest anions, thus forming an octaverticon with the point symmetry D_{2d}.[13] According to these results, the ground

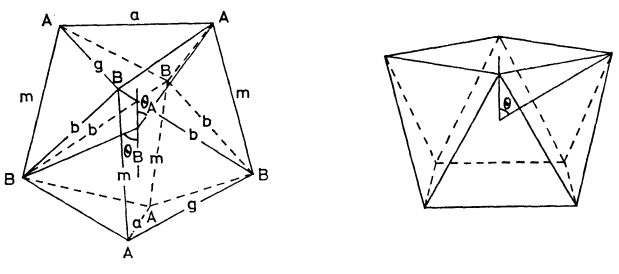

Fig. 3.

state for U_3P_4 was found to be composed of two close-spaced singlets, $^1\Gamma_{t3}$ and $^1\Gamma_{t2}$, with a separation of 8.9 cm^{-1}.

Here we shall apply the crystal field theory straightforwardly to the octacoordinated U(IV) complexes with a dodecahedron environment. The dodecahedron is characterized by two angles, θ_A and θ_B, as is shown in Fig. 3. As the values of θ_A and θ_B for several known complexes all fall into a relatively narrow range, that is, $\theta_A=34$—$37°$ and $\theta_B=72$—$74°$, it will be assumed in the following calculation that $\theta_A=35°$ and $\theta_B=73°$. The potential function of the crystal field is given by:

$$V = B_2^0O_2^0 + B_4^0O_4^0 + B_4^4O_4^4 + B_6^0O_6^0 + B_6^4O_6^4,$$

where O_2^0, O_4^0, O_4^4, O_6^0, and O_6^4 are equivalent operators, and where

$$B_2^0 = e^2Z(3\cos^2\theta_A+3\cos^2\theta_B-2)\alpha\langle r^2\rangle/a^3$$

$$B_4^0 = e^2Z(35\cos^4\theta_A+35\cos^4\theta_B-30\cos^2\theta_A - 30\cos^2\theta_B+6)\beta\langle r^4\rangle/16a^5$$

$$B_4^4 = -35e^2Z(\sin^4\theta_A+\sin^4\theta_B)\beta\langle r^4\rangle/16a^5$$

$$B_6^0 = e^2Z(231\cos^6\theta_A+231\cos^6\theta_B-315\cos^4\theta_A - 315\cos^4\theta_B+105\cos^2\theta_A+105\cos^2\theta_B-10)\cdot \gamma\langle r^6\rangle/64a^7$$

$$B_4^6 = -63e^2Z[(11\cos^2\theta_A-1)\sin^4\theta_A+(11\cos^2\theta_B-1)\cdot \sin^4\theta_B]\gamma\langle r^6\rangle/64a^7.$$

The α, β, and γ are the multiplying factors and are given for the $^3H_4$ term as $\alpha=-2.10\times10^{-2}$, $\beta=-7.346\times10^{-3}$, and $\gamma=6.099\times10^{-5}$. The U–O distance, a, was taken as 2.32 A, the value determined for tetrakis(acetylacetonato)uranium(IV), and the mean values of the n-th power of the radial distance of the 5f electron, $\langle r^2\rangle$, $\langle r^4\rangle$, and $\langle r^6\rangle$, were taken from the literature; $\langle r^2\rangle=1.68$, $\langle r^4\rangle=5.00$ and $\langle r^6\rangle=24.4$ a.u.[14] Z is the charge of the anion ligated to the central metal ion. The values of the coefficients, B_n^m, assuming that $Z=2$, are then given in cm^{-1} as follows: $B_6^0=-49.53$, $B_4^0=2.54$, $B_4^4=123.37$, $B_6^0=-1.97$, and $B_6^4=-16.67$. The splitting scheme of the $^3H_4$ term calculated on the basis of this potential function is shown in Fig. 4. This scheme shows that the ground state is the singlet, $^1\Gamma_{t3}$, with the lowest excited state, $^1\Gamma_{t2}$, located 23 cm^{-1} (33 K) above. A similar calculation showed the splitting to be 45 cm^{-1} if the two characteristic angles were taken to be $\theta_A=37°$ and $\theta_B=74°$.

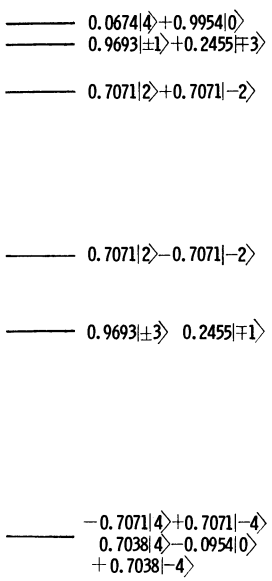

Fig. 4.

The magnetic susceptibility is written in the form:

$$\bar{\chi} = N\mu^2\mu_B^2/3kT(1-\exp(-\delta/kT))/(1+\exp(-\delta/kT))2kT/\delta \quad (1)$$

where δ is the splitting between $^1\Gamma_{t2}$ and $^1\Gamma_{t3}$ and where μ_B is the Bohr magneton. The magnetic moment is given by $\mu=\sqrt{32}\,pg$, where g is the spectroscopic splitting factor and where p is the coefficient of $|1\pm4\rangle$ in the eigenvector of the $^1\Gamma_{t3}$ state. The value of p is $1/\sqrt{2}$ for $\delta=0$; it is slightly decreased with an increase in δ, but it hardly reaches 0.69 in the present model. The spectroscopic splitting factor is 0.8 for the pure $^3H_4$ term, but is calculated to be 0.83 in the intermediate coupling scheme; this gives $\mu=3.27$—3.32 within the range of $p=0.696$—0.707. The temperature dependence of Eq. (1) with $\mu=3.30$ is presented in

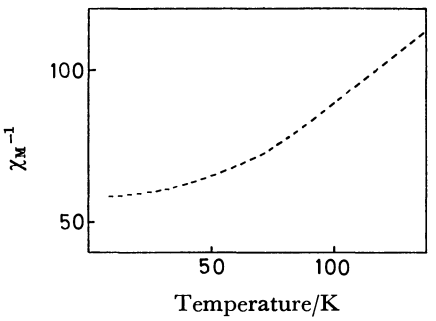

Fig. 5. Reciprocal susceptibility theoretically obtained as a function of temperature.
μ: 3.3, δ: 108 cm^{-1}, δ/k: 160

Fig. 5, where it may be seen that the reciprocal susceptibility shows a marked deviation from the straight line below about $T=\delta/2k$, suggesting the TIP at lower temperatures. The apparent magnetic moment gained from this figure is $\mu=3.43$, which is about 5% larger than that obtained in the higher temperature range, $\delta \ll kT$. Thus, the magnetic behavior of octacoordinated U(IV) complexes which would show TIP at low temperatures (below about 100 K (70 cm^{-1})) and which have the apparent magnetic moment of $\mu=3.4$—3.5 seems likely to be explained by the present scheme. From the values in Table 1, $U(cupf)_4$ is also considered to belong to this group along with $U(dbm)_4$ and UCl_4; it seems very possible that dodecahedron is the coordination polyhedron of $U(cupf)_4$.

Square Antiprism. For the complexes having the coordination polyhedron of archimedian antiprism with the octahedral symmetry of D_{4d}, the energy level scheme was calculated by Mulak and Czopnik using the c/a ratio as a parameter, and it was shown that either the singlet state, $|0\rangle$, or the doublet states, $|\pm4\rangle$ and $|\pm3\rangle$, can be the ground state, according to the value of c/a.[2] They assumed that the ground

state was $|\pm 3>$, which would be split into two closely-spaced singlets under the distortion of the rhombic or lower symmetry. However, the value of c/a determined by X-ray analysis for $Zr(acac)_4$, which is isomorphous with $U(acac)_4$, is 0.908; this value leads to the ground state being $|0>$, with the lowest excited level being $|\pm 1>$. According to Lippard and Russ, the polyhedron of $Zr(acac)_4$ is a distorted square antiprism; it is approximately formed by twisting the perfect square antiprism around the 8 axis by 10—20 degrees.[15] This twisting gives rise to the splitting of the $|\pm 2>$ state and markedly lowers the $1/\sqrt{2}$ $(|2>-|-2>)$ state. The calculation carried out along the lines of the analysis by Mulak and Czopnik, with the value of $c/a=0.908$, showed that the splitting between $|0>$ and $|\pm 1>$ is about 30 cm^{-1} and that the $1/\sqrt{2}$ $(|2>-|-2>)$ state is located near the $|\pm 1>$ doublet if the twisting angle is 10—15 degrees, as is shown in Fig. 3. We shall show that this energy level scheme can also be used in explaining the magnetic behavior of octacoordinated U(IV) complexes with a distorted square antiprism structure.

As the magnetic susceptibility is anisotropic in the tetragonal crystal field, components both parallel to and perpendicular to the symmetry axis should be considered. The parallel component of the magnetic susceptibility is given as follows;

$$\chi_{//} = Ng^2\mu_B^2/kT \cdot 2\exp(-\delta/kT)/(1+2\exp(-\delta/kT)) \quad (2)$$

where δ is the splitting between $|0>$ and $|\pm 1>$. The $\chi_\perp$ component is given by;

$$\chi_\perp = 2Ng^2\mu_B^2[10(1-\exp(-\delta/kT))/\delta + 4.5(1-\exp(-\delta/kT))\exp(-\Delta/kT)/\Delta]/ (1+2\exp(-\delta/kT)+\exp(-(\delta+\Delta)/kT)) \quad (3)$$

taking into account the high-frequency interaction between $|0>$ and $|\pm 1>$ and that between $|\pm 1>$ and $1/\sqrt{2}(|2>-|-2>)$, where Δ is the splitting between $|\pm 1>$ and $1/>\sqrt{2}(|2>-|-2>)$. When $\Delta \ll kT$,

$$\chi_\perp = 2Ng^2\mu_B^2[10(1-\exp(-\delta/kT))/\delta + 4.5\exp(-\delta/kT)/kT]/(1+3\exp(-\delta/kT)) \quad (4)$$

The average magnetic susceptibility, χ, is represented by Eq. (5); at lower temperatures ($Tk \ll \delta$) it becomes $40Ng^2\mu_B^2/3\delta$.

$$\bar{\chi} = 1/3\chi_{//} + 2/3\chi_\perp \quad (5)$$

Under these conditions, the only contribution to the paramagnetic susceptibility is the temperature-independent paramagnetism due to the high-frequency interaction between the excited levels, $|\pm 1>$, and the ground state of $|0>$. In Fig. 6 are plotted the average magnetic susceptibilities of Eq. (5), with the values of g and Δ/δ being assumed to be 0.827 and 0.1 respectively. TIP is seen at the lower temperatures, and the apparent magnetic moment of 3.24 is obtained from the straight part of the curve. This value is somewhat larger than the values experimentally obtained for $U(acac)_4$, $U(bac)_4$, $U(tfac)_4$, and $U(TTA)_4$, as in the case of the complexes with a dodecahedron structure. Thus, the behavior of magnetic susceptibility observed seems likely to be explained by the crystal field model with D_{2d} or D_{4d} symmetry, corresponding to dodecahedron or square antiprism respectively.

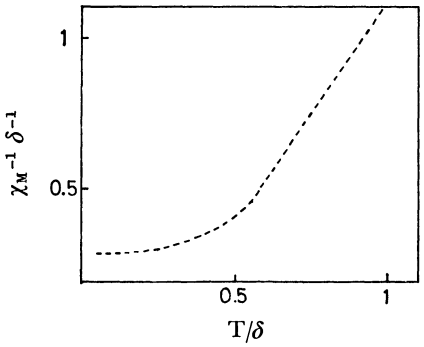

Fig. 6. Reciprocal susceptibility theoretically obtained as a function of temperature measured by energy difference between ground state and first excited state. $g=0.827$, Δ/δ: 0.1.

References

1) C. A. Hutchison and G. A. Candela, *J. Chem. Phys.*, **27**, 707 (1957).
2) J. Mulak and A. Czopnik, Preprint No. 13/45/71, Wroclaw. To be published in *Bull. Acad. Pol. Sci., Sér. Sci. Chim.*.
3) T. Yoshimura, C. Miyake, and S. Imoto, This Bulletin, **46**, 2096 (1973).
4) J. K. Dawson, *J. Chem. Soc.*, **1951**, 429, 2889; **1952**, 1185.
5) A. Earnshaw, "Introduction to Magnetochemistry," Academic Press, London (1968).
6) "Handbook of Chemistry and Physics," 47th edition (1966)-(1967), Chemical Rubber Co.
7) T. Yoshimura, C. Miyake, and S. Imoto, *J. Nucl. Sci. Tech.*, **8**, 498 (1971).
8) C. A. Hutchison and C. M. Herzfeld, *J. Chem. Phys.* **23**, 1650 (1955).
9) E. Slowinski and N. Elliott, *Acta Crystallogr.*, **5**, 768 (1952).
10) K. W. Bagnall, D. Brown, and R. Colton, *J. Chem. Soc.*, **1964**, 2527.
11) R. McLaughlin, *J. Chem. Phys.*, **36**, 2699 (1962).
12) I. Richman, P. Kislink, and E. Y. Wong, *Phys. Rev.*, **155**, 262 (1967).
13) R. Troć, J. Mulak, and W. Suski, *Physica Status Solidi*, **43**, 147 (1971).
14) C. J. Lenander, *Phys. Rev.*, **130**, 1033 (1963).
15) S. J. Lippard and B. J. Russ, *Inorg. Chem.*, **7**, 1686 (1968).

Theory of Ion Cyclotron Resonance Power Absorption for Nonreactive and Reactive Ions

Katsuyuki AOYAGI[1)]

Faculty of Engineering, Hokkaido University, Sapporo 060

(Received March 22, 1973)

An exact solution of the equation of motion and exact expressions of the ion current in ion cyclotron resonance power absorption were obtained. Instantaneous and total power absorptions together with power absorption line shapes were derived. Ion current expressions were also derived for both nonreactive and reactive ions over the whole range of pressure. The results agreed with those obtained previously for high and low pressures with appropriate approximation. The rate constants for the disappearance of primary ions and for the formation of nonreactive secondary ions were obtained from the ion cyclotron resonance experiments. The results showed good agreement with those obtained by other methods.

A charged particle moving in a strong uniform magnetic field describes a helical orbit which is a combination of a translation along a field line and a circular motion in a plane perpendicular to the direction of the magnetic field. The motion along the magnetic field is independent of the strength of the magnetic field. The circular motion in the plane is independent of the translational motion along the field lines. The angular frequency or cyclotron frequency ω of the circular motion is independent of the velocity of the ion and is given by

$$\omega = \frac{e\mathbf{H}}{mc}, \tag{1}$$

where e is the charge of the particle, $\mathbf{H}$ the magnetic field strength, m the particle mass, and c the velocity of light.[2)]

If a sinusoidal time-varying electric field $\mathbf{E}(t)$ with the frequency ω_1 is applied perpendicular to a static magnetic field $\mathbf{H}$, and the magnetic field is swept, the ion resonates at $\omega=\omega_1$ and absorbs energy from the sinusoidal time-varying electric field. The ion is accelerated and the radius of its orbit increases with time. An absorption of energy by the ions can be readily observed by a marginal oscillator detector[3,4)] or a bridge detector.[5,6)] With a fixed observing frequency, a spectrum obtained by sweeping the magnetic field is linear in the mass.

In the average chemically nonreactive ion undergoing ion cyclotron resonance, the phenomenological equation of motion for an ion is given by[5,9)]

$$\frac{d\mathbf{v}}{dt} = \frac{e}{m}\mathbf{E}(t) + \frac{e}{mc}\mathbf{v}\times\mathbf{H} - \xi\mathbf{v}, \tag{2}$$

where $\mathbf{v}$ is the nonrandom part of the average ion velocity, and ξ the reduced collision frequency that specifies the rate of momentum relaxation of the ion. If the ion undergoes only elastic collisions with the neutral species, the reduced collision frequency is given by[10)]

$$\xi = \frac{nm}{m+M}\langle v\sigma_d(v)\rangle, \tag{3}$$

where n and M are the number density and mass of the neutral species, respectively, and $\sigma_d(v)$ and v are the diffusion cross section and relative velocity of the ion to the neutral pair, respectively. The angle bracket indicates an average over the distribution of relative velocities.

Wobschall *et al.*[5)] and Beauchamp[9)] obtained a steady-state solution of Eq. (2) which leads to the Lorentzian line-shape expression for power absorption. The steady-state power absorption of an ion results in the broadening of ion cyclotron resonance (ICR) line shapes in the high-pressure limit where many collision occur during the ion transit time. The steady-state theory assumes equilibrium between power absorption and collision dissipation, ignoring the transient effect. However, it has been successfully applied to the determination of the collision frequency or the nonreactive cross section of ions from the line-shapes.[5,9)] Beauchamp[5)] and Buttrill[11)] obtained an approximated solution of Eq. (2) for the case $\xi=0$, which leads to an expression for low-pressure power absorption. Line-shapes calculated from the low-pressure theory show good agreement with experimental results at low pressure.[11)] In the presence of ion-molecule reactions, the theory has been extended successfully for determining of ion-molecule reaction rates using ICR signal intensity. The calculated rates show a substantial agreement with those measured by other techniques.[12)]

Recently, a more general solution for the phenomenological equation of motion of an ion in the ICR cell has been given by Comisarow[10)] and Dunbar[13)] which bridges the gap between the low- and high-pressure theories. This "total-pressure theory" has clarified the power absorption expressions for the chemically reactive ions.[10)] The theory has also been used for obtaining the collision relaxation rate and substantial probability for charge transfer by transient ICR experiment.[13)] However, in this theory, the ion current expression is not treated in detail.

In this paper, we propose exact expressions of ion current in the ICR cell, and an exact solution of the phenomenological equation of motion for the velocity of an ion used for deriving the power absorption of an ion and the ion kinetics. The ion-molecule reaction rate constants for the disappearance of primary ions and for the formation of nonreactive secondary ions are determined from ion cyclotron single resonance (ICSR) spectra. Rate constants are compared with values obtained by other methods. Close agreement between the present and previous values was obtained.

Theory

Ion Motion in the ICR Cell. The Cartesian coordinate system is chosen so that the static magnetic field is parallel to the z axis, the electrostatic drift field and the rf electric field are parallel to the x axis, and the ions drift to the y axis. Then ion motion in the x-y plane is independent of motion in the z direction.

The electrostatic trapping field is parallel to the z axis, as usually employed in the ICR cell.[3] The trapping field should not affect the power absorption of an ion.[3] The trapping voltage, however, shifts the ion cyclotron resonance frequency.[14,16] In the ICR cell, the electrostatic drift field only determines the residence time of the center of guide of the circular motion for an ion in the absence of collision.[3]

The actual motion of the ion in the analyzer region of the ICR cell consists of different types motion. A circular motion due to the Lorentz force in the x-y plane with increasing orbit radius with time, in which the ion absorbs energy from the applied rf electric field, and a motion of drift at constant velocity along the $-y$ axis lead to a trochoidal motion of increasing radius in the x-y plane. Furthermore, the ion describes an executed harmonic motion in a parabolic potential field in the x-z plane between the trapping electrodes. The exact solution of Eq. (2) leads to the above complicated motion of the ion in the analyzer region of the ICR cell.

Solution of Equation of Motion. In the absence of reactive collisions, the motion of an ion in the ICR cell can be described by Eq. (2). In the ICR cell, homogeneous electric and magnetic field distributions are assumed, the following electric and magnetic field configurations also being assumed:

$$\mathbf{H} = H_0\boldsymbol{k}, \tag{4}$$

$$\mathbf{E} = E_d\boldsymbol{i} + E_1 \sin(\omega_1 t + \phi_1)\boldsymbol{i} + E_t\boldsymbol{k}, \tag{5}$$

where H_0 is the static magnetic field strength, $\boldsymbol{i}$, $\boldsymbol{j}$, and $\boldsymbol{k}$ unit vectors of the coordinate system, E_d is the electrostatic drift field strength, E_t a function of z giving the electrostatic trapping field strength, and E_1 the observed rf electric field strength from the marginal oscillator or the oscillator for the bridge with frequency ω_1. The phase factor of ϕ_1 has been introduced because the rf phase at $t=0$ is not fixed.

Equation (2) is now separated into an equation of v_z only and two coupled equations of v_x and v_y. The relevant equations of motion are then;

$$\frac{dv_x}{dt} = \frac{e}{m}[E_d + E_1 \sin(\omega_1 t + \phi_1)] + \omega v_y - \xi v_x, \tag{6a}$$

$$\frac{dv_y}{dt} = -\omega v_x - \xi v_y. \tag{6b}$$

In the present investigation, the motion in the z direction does not affect the power absorption and will not be considered further.

An ion whose initial velosity v_0 is due to the thermal velocity leads to a circular motion with phase angle ϕ_0, $v_x(0) = -v_0\cos\phi_0$ and $v_y(0) = v_0\sin\phi_0$ at $t=0$. The exact solution of Eq. (6) is given by[7]

$$\begin{aligned} v_x = {} & v_0 \sin(\omega t - \phi_0) \exp(-\xi t) \\ & + \frac{eE_d}{m}\left[\frac{\xi - (\xi\cos\omega t - \omega\sin\omega t)\exp(-\xi t)}{\omega^2 + \xi^2}\right] \\ & + \frac{eE_1}{m}\{A\sin(\omega_1 t + \phi_1) - B\cos(\omega_1 t + \phi_1) \\ & - [(C\cos\phi_1 + D\sin\phi_1)\sin\omega t \\ & - (B\cos\phi_1 - A\sin\phi_1)\cos\omega t]\exp(-\xi t)\}, \end{aligned} \tag{7a}$$

$$\begin{aligned} v_y = {} & v_0 \cos(\omega t - \phi_0) \exp(-\xi t) \\ & + \frac{eE_d}{m}\left[\frac{\omega - (\xi\sin\omega t + \omega\cos\omega t)\exp(-\xi t)}{\omega^2 + \xi^2}\right] \\ & + \frac{eE_1}{m}\{D\sin(\omega_1 t + \phi_1) + C\cos(\omega_1 t + \phi_1) \\ & - [(B\cos\phi_1 - A\sin\phi_1)\sin\omega t \\ & + (C\cos\phi_1 + D\sin\phi_1)\cos\omega t]\exp(-\xi t)\}, \end{aligned} \tag{7b}$$

where

$$\begin{aligned} A &= [\xi(\xi^2 + \omega_1^2 - \omega^2) + 2\xi\omega^2]/F, \\ B &= \omega_1(\xi^2 + \omega_1^2 - \omega^2)/F, \\ C &= 2\xi\omega\omega_1/F, \\ D &= [\omega(\xi^2 + \omega_1^2 - \omega^2) - 2\xi^2\omega]/F, \\ F &= [(\omega_1 - \omega)^2 + \xi^2][(\omega_1 + \omega)^2 + \xi^2]. \end{aligned}$$

Line Shape Expression for Nonreactive Ion. a) Power Absorption of an Average Nonreactive Ion: Power absorption A of an ion from the rf electric field is given by

$$A = \langle e\mathbf{E}(t)\cdot\mathbf{v}(t)\rangle = eE_1 v_x \sin(\omega_1 t + \phi_1), \tag{8}$$

where v_x represents only the third term of Eq. (7a), because there is no observed effect of either the drift field or the initial velocity of an ion on the power absorption. The third term of Eq. (7b) has an effect on the power dispersion for an ion. The initial velocity of an ion with phase angle ϕ_0 will not contribute to the actual power absorption. Since an ensemble of ions enters the analyzer region in the ICR cell at time dt, the phase angles are expected to be distributed randomly so that the average over a period is 0.

Substituting the third term of Eq. (7a) into Eq. (8), the power absorption can be obtained by averaging over the phase angle ϕ_1 since all values of ϕ_1 are equally probable. With the approximation that

$$\omega_1 + \omega \approx 2\omega, \tag{9}$$

$$\xi \ll \omega_1, \tag{10}$$

the instantaneous power absorption by an ion is found to be

$$\begin{aligned} A(\omega_1 = \omega) = {} & \frac{e^2 E_1^2}{4m[(\omega_1 - \omega)^2 + \xi^2]}\{\xi + [(\omega_1 - \omega)\sin(\omega_1 - \omega)t \\ & - \xi\cos(\omega_1 - \omega)t]\exp(-\xi t)\}, \end{aligned} \tag{11}$$

which is a function of t, ω, ω_1, and ξ. The first term is a steady-state power absorption observed under slow passage conditions. The second term is a transient term of a damped oscillation with frequency $|\omega_1 - \omega|$, giving the ICR heterodyne spectrum.[13] The absorption giving by Eq. (11) agrees with that of Comisarow[10] and that of Dunber[13] who used slightly different methods.

At resonance $\omega_1 = \omega$, the instantaneous power absorption is shown to be

$$A(\omega_1=\omega) = \frac{e^2{E_1}^2}{4m\xi}[1-\exp(-\xi t)]. \quad (12)$$

If the pressure is sufficiently high for each ion to suffer many nonreactive collisions, Eq. (11) is reduced to

$$A(\xi t \gg 1) = \frac{e^2{E_1}^2}{4m}\frac{\xi}{(\omega_1-\omega)^2+\xi^2} \quad (13)$$

by application of the approximation

$$\xi t \gg 1. \quad (14)$$

This high-pressure power absorption represents the Lorentzian line shape and agrees with the results of Beauchamp[9] and Comisarow.[10] In the collisionless limit $\xi \to 0$, Eq. (11) is reduced to

$$A(\xi \to 0) = \frac{e^2{E_1}^2}{4m(\omega_1-\omega)}\sin(\omega_1-\omega)t. \quad (15)$$

This low-pressure power absorption agrees with that of Beauchamp,[9] of Buttrill[11] and also of Comisarow.[10]

b) Total Power Absorption for Nonreactive Ion: Under idealized experimental ICR conditions, the homogeneous electric and magnetic field distributions are assumed in the ICR cell. Ions are produced in a source region with electron impact at a rate n_0 ions per second, and then drift through an anlyzer region at constant drift velocity. It has been assumed that the distribution of ions is uniform inside the ICR cell. There is a constant number $n_0\tau$ of ions in time τ for an ion drift through the analyzer, each absorbing energy at the rate given in Eq. (11). Thus the total power absorption $A(T)$ is obtained by averaging the integration from 0 to τ, the time required for the ions to absorb energy from the applied rf electric field. The averaged total power absorption is given by

$$A(T) = \frac{1}{\tau}\int_0^\tau n_0\tau A(\omega_1=\omega)\mathrm{d}t$$

$$= \frac{n_0e^2{E_1}^2}{4m[(\omega_1-\omega)^2+\xi^2]}\left\{\xi\tau+\frac{(\omega_1-\omega)^2-\xi^2}{(\omega_1-\omega)^2+\xi^2}\right.$$

$$+\left[\frac{\{\xi^2-(\omega_1-\omega)^2\}\cos(\omega_1-\omega)\tau-2\xi(\omega_1-\omega)\sin(\omega_1-\omega)\tau}{(\omega_1-\omega)^2+\xi^2}\right]$$

$$\left.\times\exp(-\xi\tau)\right\}, \quad \text{for } \omega_1=\omega, \quad (16a)$$

and

$$A(T) = \frac{n_0e^2{E_1}^2}{4m\xi}\left\{1-\frac{1}{\xi\tau}[1-\exp(-\xi\tau)]\right\} \quad \text{for } \omega=\omega_1. \quad (16b)$$

Application of (14) in Eq. (16a) gives

$$A(T, \text{High-pressure}) = \frac{n_0e^2{E_1}^2\tau}{4m}\frac{\xi}{(\omega_1-\omega)^2+\xi^2}. \quad (17)$$

This represents the average total high-pressure power absorption expression.

In the collisionless limit $\xi \to 0$, Eq. (16a) is reduced to

$$A(T, \xi \to 0) = \frac{n_0e^2{E_1}^2}{4m(\omega_1-\omega)^2}[1-\cos(\omega_1-\omega)]. \quad (18)$$

The line shapes of ICR total power absorption for an ensemble of ions are represented by Eqs. (16)—(18). The results agree with those of Comisarow.[10]

Line Shape Expression for Reactive Ion. a) Ion Current in the Analyzer Region: When the pressure in the ICR cell is so high that the reactive collision cannot be ignored, ion-molecule reactions occur. In special cases where all ion-molecule collisions are reactive, the calculation of power absorption is particularly simple, since the reactive collision removes the ion as a power-absorption entity. Here, only one species of neutral reactant molecule is present assuming that no two ions formed in different steps have the same mass.

The cross section of ion-molecule reaction is the function of ion velocity. The thermal reaction cross section σ_θ can be estimated from the corresponding rate constant, and is given by[17]

$$\sigma_\theta = \frac{k}{v_\theta}, \quad (19)$$

where v_θ is the average thermal velocity of the reactant ion. The reaction cross section of ion-molecule reaction is also given by[18]

$$\sigma = \frac{S}{P_0Ml}, \quad (20)$$

where P_0 is the rate of primary ion formation in the electron beam, S the total secondary ion current after the primary ion has traveled a distance l from the origin (the electron beam), and M the neutral reactant molecule. In the source region, the angular velocity of the ion is almost equal to its thermal velocity, but is not the same at resonance in the analyzer region. Similarly, the path lengths of the ions in the source and analyzer regions are not the same. Thus, the cross sections of ion-molecule reaction in the source and in the anlyzer regions are not the same, the rate constants in the source and anlyzer regions also being different.

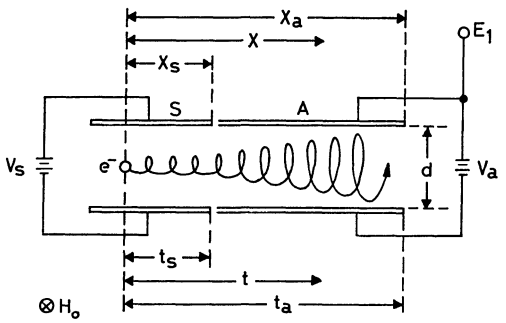

Fig. 1. Side view of the ICR cell showing parameters for kinetic analysis. e^- indicates the location of electron beam which forms the primary ions. The distances x_s, x and x_a are defined by the figure. t_s and t_a are the drift times through the source S and analyzer A regions, respectively.

Figure 1 shows a side cross-sectional view of the ICR cell required for kinetic analysis. Ions are produced in the source region by electron impact which are then made to drift through the analyzer region by the effect of the electrostatic drift field. Drift voltages are applied to the source and analyzer regions of the ICR cell separately. The time at each point x in the analyzer region, which is associated with the drift time t from the electron beam, is given by

$$t = \frac{x_s}{v_s} + \frac{x-x_s}{v_a}, \quad (21a)$$

where x_s and x are the distances indicated in Fig. 1, and v_s and v_a the drift velocities in the source and analyzer regions, respectively. The source exit time t_s and the analyzer exit time t_a for an ion are respectively given by

$$t_s = \frac{v_s}{v_{ds}} = \frac{x_s Hd}{cV_s} \tag{21b}$$

and

$$t_a = t_s + \frac{x_a - x_s}{v_{da}} = t_s + \frac{(x_a - x_s)Hd}{cV_a}, \tag{21c}$$

where V_s and V_a are the source drift and analyzer drift voltages, respectively. x_s, x_a, and d are the parameters defined in Fig. 1.

The equations for the change of ion current with time in the analyzer region are derived for the following primary, secondary, and tertiary chemical systems:[19,20]

Primary ion,

$$M + e^- \longrightarrow P^+, \tag{22}$$

Source-Formed Nonreactive Secondary (*SFNS*) ion,

$$P^+ + M \xrightarrow{k_{ps}} S_n^+ + N, \tag{23a}$$

Analyzer-Formed Nonreactive Secondary (*AFNS*) ion,

$$P^+ + M \xrightarrow{k_{pa}} S_n^+ + N, \tag{23b}$$

Source-Formed Reactive Secondary (*SFRS*) ion,

$$P^+ + M \xrightarrow{k_{ps},\, k_{ss}} S^+ + N, \tag{24a}$$

Analyzer-Formed Reactive Secondary (*AFRS*) ion,

$$P^+ + M \xrightarrow{k_{pa},\, k_{sa}} S^+ + N, \tag{24b}$$

Source-Formed Nonreactive Tertiary (*SFNT*) ion,

$$S^+ + M \xrightarrow{k_{ss}} T_n^+ + N, \tag{25a}$$

Analyzer-Formed Nonreactive Tertiary (*AFNT*) ion,

$$S^+ + M \xrightarrow{k_{sa}} T_n^+ + N. \tag{25b}$$

These obey the following equations in the analyzer region:

$$\frac{dP(t)_a}{d(t-t_{ps})} = -nk_{pa}P(t)_a, \tag{26}$$

$$\frac{dS(t)_{na}}{d(t-t_{ns})} = nk_{pa}P(t)_a, \tag{27}$$

$$\frac{dS(t)_a}{d(t-t_{ss})} = nk_{pa}P(t)_a - nk_{sa}S(t)_a, \tag{28}$$

$$\frac{dT(t)_a}{d(t-t_{ts})} = nk_{ss}S(t)_a. \tag{29}$$

The solutions are found to be

$$P(t)_a = P_0 \exp(-nk_{ps}t_{ps}) \exp[-nk_{pa}(t-t_{ps})], \tag{30}$$

$$S(SFNS, t)_a = P_0\{1-\exp(-nk_{ps}t_{ns}) \times \exp[-nk_{pa}(t-t_{ns})]\}, \tag{31a}$$

$$S(AFNS, t)_a = P_0\{1-\exp[-nk_{pa}(t-t_{ns})]\} \times \exp(-nk_{ps}t_{ns}), \tag{31b}$$

$$S(SFRS, t)_a = P_0\{(\alpha_s+\beta_s)\exp[-nk_{sa}(t-t_{ss})] - \alpha_s \exp[-nk_{pa}(t-t_{ss})]\}, \tag{32a}$$

$$S(AFRS, t)_a = P_0\alpha_s\{\exp[-nk_{sa}(t-t_{ss})] - \exp[-nk_{pa}(t-t_{ss})]\}, \tag{32b}$$

$$T(SFNT, t)_a = P_0\{1-(\alpha_t+\beta_t)\exp[-nk_{sa}(t-t_{ts})] + \gamma_t \exp[-nk_{pa}(t-t_{ts})]\}, \tag{33a}$$

$$T(AFNT, t)_a = P_0\{\alpha_t+\beta_t+\gamma_t-(\alpha_t+\beta_t) \times \exp[-nk_{sa}(t-t_{ts})] + \gamma_t \exp[-nk_{pa}(t-t_{ts})]\}, \tag{33b}$$

where

$$\alpha_s = \frac{k_{pa}}{k_{pa}-k_{sa}} \exp(-nk_{ps}t_{ss}),$$

$$\beta_s = \frac{k_{ps}}{k_{ps}-k_{ss}}[\exp(-nk_{ss}t_{ss}) - \exp(-nk_{ps}t_{ss})],$$

$$\alpha_t = \frac{k_{pa}}{k_{pa}-k_{sa}} \exp(-nk_{ps}t_{ts}),$$

$$\beta_t = \frac{k_{ps}}{k_{ps}-k_{ss}}[\exp(-nk_{ss}t_{ts}) - \exp(-nk_{ps}t_{ts})],$$

$$\gamma_t = \frac{k_{sa}}{k_{pa}-k_{sa}} \exp(-nk_{ps}t_{ts}).$$

Here P_0 is the rate of primary ion formation in ions per second at the electron beam in the source region, n the number density of neutral reactant molecule, k_{ps} and k_{pa} are the ion-molecule reaction rates for the primary ion and k_{ss} and k_{sa} those for the secondary ion in the source and analyzer regions, respectively, and t_{ps}, t_{ns}, t_{ss}, and t_{ts} the source exit times of primary, nonreactive-secondary, reactive-secondary, and nonreactive-tertiary ions, respectively.

In the limits $k_{sa}\to 0$ and $k_{ss}\to 0$, Eq. (32a) is reduced to Eq. (31a). In the limit $k_{sa}\to 0$, Eq. (32b) is reduced to Eq. (31b).

Equations (30) and (31a) can be now rewritten in the following forms:

$$P(t)_{a1} = P_0 \exp[-nk_{pa}(t-t_{ps})] \quad \text{for } k_{pa} \gg k_{ps} \sim 0, \tag{34a}$$

$$P(t)_{a2} = \text{Eq. (30)} \quad \text{for } k_{pa} \neq k_{ps}, \tag{34b}$$

$$P(t)_{a3} = P_0 \exp(-nk_{pa}t_{ps}) \exp[-nk_{pa}(t-t_{ps})] \quad \text{for } k_{pa} \approx k_{ps}, \tag{34c}$$

$$S(SFNS, t)_{a1} = P_0 - P_0 \exp[-nk_{pa}(t-t_{ns})] \quad \text{for } k_{pa} \gg k_{ps} \sim 0, \tag{35a}$$

$$S(SFNS, t)_{a2} = \text{Eq. (31a)} \quad \text{for } k_{pa} \neq k_{ps}, \tag{35b}$$

$$S(SFNS, t)_{a3} = P_0 - P_0 \exp(-nk_{pa}t_{ns}) \times \exp[-nk_{pa}(t-t_{ns})] \quad \text{for } k_{pa} \approx k_{ps}. \tag{35c}$$

Eqs. (34a) and (35a), corresponding to the primary and nonreactive-secondary ion current expressions, have been reported in a slightly different form.[11,17]

b) Total Power Absorption for Primary Ions: Equation (11) can be rewritten in terms of t', the time an ion commences to absorb the power, and t'', the time an ion ceases to absorb the power in the analyzer region, as follows:

$$A(t''-t') = \frac{e^2E_1^2}{4m[(\omega_1-\omega)^2+\xi^2]} \times\{\xi + [(\omega_1-\omega)\sin(\omega_1-\omega)(t''-t') - \xi\cos(\omega_1-\omega)(t''-t')]\exp[-\xi(t''-t')]\}. \tag{36}$$

In the time $t-t_{ps}$ required for a primary ion to drift into the analyzer region, there are $P(t)_a\cdot(t-t_{ps})$ number of ions, each of which absorbs the energy at the rate given by Eq. (36). The total power absorption $A(T,P)$ is thus obtained by averaging the integration from t_{ps} to t_{pa}. The average total power absorption is given by

$$A(T,P)=\frac{1}{(t-t_{ps})}\int_{t_{ps}}^{t_{pa}}P(t)_a\cdot(t-t_{ps})\cdot A(t''-t')dt$$
$$=\frac{P_0e^2E_1^2\exp(-nk_{ps}t_{ps})}{4m_p[(\omega_1-\omega)^2+\xi_p^2]}F(p), \tag{37}$$

where

$$F(p)=\xi_pK_{1p}+K_{2p}-K_{3p}[K_{4p}\cos(\omega_1-\omega)(t_{pa}-t_{ps})$$
$$+K_{5p}\sin(\omega_1-\omega)(t_{pa}-t_{ps})],$$

m_p is the mass of the primary ion, t_{ps} and t_{pa} are the source exit and analyzer exit times, respectively, for the primary ion. $K_{1p}\sim K_{5p}$ are given in Appendix II. Equation (37) is the line shape expression of the total power absorption for the primary ions.

c) Total Power Absorption for Nonreactive Secondary Ions: In time $t-t_{ns}$ required for a nonreactive and stable secondary ion to drift into the analyzer region, there are $S(t)_{na}\cdot(t-t_{ns})$ number of ions, each of which absorbs energy at the rate given by Eq. (36). Thus the total power absorption $A(T,SFNS)$ due to source-formed nonreactive and stable secondary ions is given by averaging the integration from t_{ns} to t_{na}:

$$A(T,SFNS)=\frac{1}{(t-t_{ns})}\int_{t_{ns}}^{t_{na}}S(SFNS,t)_a\cdot(t-t_{ns})\cdot A(t''-t')dt$$
$$=\frac{P_0e^2E_1^2}{4m_n[(\omega_1-\omega)^2+\xi_n^2]}$$
$$\times\{f(NS)-F(NS)\exp(-nk_{ps}t_{ns})\}, \tag{38}$$

where

$$f(NS)=\xi_n(t_{na}-t_{ns})+N_{1n}$$
$$-N_{2n}[N_{3n}\cos(\omega_1-\omega)(t_{na}-t_{ns})$$
$$+N_{4n}\sin(\omega_1-\omega)(t_{na}-t_{ns})],$$
$$F(NS)=\xi_nK_{1n}+K_{2n}-K_{3n}[K_{4n}\cos(\omega_1-\omega)(t_{na}-t_{ns})$$
$$+K_{5n}\sin(\omega_1-\omega)(t_{na}-t_{ns})],$$

m_n is the mass of the nonreactive and stable secondary ion, t_{ns} and t_{na} are the source exit and analyzer exit times for the nonreactive and stable secondary ion, respectively. $N_{1n}\sim N_{4n}$ and $K_{1n}\sim K_{5n}$ are given in Appendix II.

Similarly, the total power absorption $A(T,AFNS)$ due to analyzer-formed nonreactive and stable secondary ions is given by averaging the integration from t_{ns} to t_{na}:

$$A(T,AFNS)=\frac{1}{(t-t_{ns})}\int_{t_{ns}}^{t_{na}}S(AFNS,t)_a\cdot(t-t_{ns})\cdot A(t''-t')dt$$
$$=\frac{P_0e^2E_1^2\exp(-nk_{ps}t_{ns})}{4m_n[(\omega_1-\omega)^2+\xi^2]}[f(NS)-F(NS)]. \tag{39}$$

Equations (38) and (39) are the line shape expressions of total power absorption for the source-formed and analyzer-formed nonreactive and stable secondary ions, respectively. The total power absorption due to nonreactive and stable secondary ions is given by the sum of Eqs. (38) and (39):

$$A(T,S_n)=A(T,SFNS)+A(T,AFNS)$$

d) Total Power Absorption for Reactive Secondary Ions: In time $t-t_{ns}$ required for a reactive secondary ion to drift into the analyzer region, there are $S(t)_a\cdot(t-t_{ns})$ number of ions, each of which absorbs energy at the rate given by Eq. (36). Thus the total power absorption $A(T,SFRS)$ due to source-formed reactive secondary ions is given by averaging the integration from t_{ss} to t_{sa}:

$$A(T,SFRS)=\frac{1}{(t-t_{ss})}\int_{t_{ss}}^{t_{sa}}S(SFRS,t)_a\cdot(t-t_{ss})\cdot A(t''-t')dt$$
$$=\frac{P_0e^2E_1^2}{4m_s[(\omega_1-\omega)^2+\xi_s^2]}[(\alpha_s+\beta_s)R(s)-\gamma_sF(s)], \tag{40}$$

where

$$R(s)=\xi_sR_{1s}+R_{2s}-R_{3s}[R_{4s}\cos(\omega_1-\omega)(t_{sa}-t_{ss})$$
$$+R_{5s}\sin(\omega_1-\omega)(t_{sa}-t_{ss})],$$
$$F(s)=\xi_sK_{1s}+K_{2s}-K_{3s}[K_{4s}\cos(\omega_1-\omega)(t_{sa}-t_{ss})$$
$$+K_{5s}\sin(\omega_1-\omega)(t_{sa}-t_{ss})],$$

m_s is the mass of the reactive secondary ion, t_{ss} and t_{sa} are the source exit and analyzer exit times of the reactive secondary ion, respectively. $R_{1s}\sim R_{5s}$ and $K_{1s}\sim K_{5s}$ are given in Appendix II.

Similarly, the total power absorption $A(T,AFRS)$ due to analyzer-formed reactive secondary ions is given by averaging the integration from t_{ss} to t_{sa}:

$$A(T,AFRS)=\frac{1}{(t-t_{ss})}\int_{t_{ss}}^{t_{sa}}S(AFRS,t)_a\cdot(t-t_{ss})\cdot A(t''-t')dt$$
$$=\frac{P_0e^2E_1^2\alpha_s}{4m_s[(\omega_1-\omega)^2+\xi_s^2]}[R(s)-F(s)]. \tag{41}$$

Equation (40) and (41) are the line shape expressions of total power absorption for the source-formed and analyzer-formed reactive secondary ions, respectively. The total power absorption due to reactive secondary ions is given by the sum of Eqs. (40) and (41):

$$A(T,S)=A(T,SFNS)+A(T,AFRS).$$

In the limits $k_{sa}\to0$ and $k_{ss}\to0$, Eq. (40) is reduced to Eq. (38). In the limit $k_{sa}\to0$, Eq. (41) is reduced to Eq. (39).

e) Total Power Absorption for Nonreactive Tertiary Ions: In time $t-t_{ts}$ required for a nonreactive and stable tertiary ion to drift into the analyzer region, there are $T(t)_a\cdot(t-t_{ts})$ number of ions, each of which absorbs energy at the rate given by Eq. (36). Thus the total power absorption $A(T,SFNT)$ due to source-formed nonreactive and stable tertiary ions is obtained by averaging the integration from t_{ts} to t_{ta}:

$$A(T,SFNT)=\frac{1}{(t-t_{ts})}\int_{t_{ts}}^{t_{ta}}T(SFNT,t)_a\cdot(t-t_{ts})\cdot A(t''-t')dt$$
$$=\frac{P_0e^2E_1^2}{4m_t[(\omega_1-\omega)^2+\xi_t^2]}$$
$$\times\{f(T)-(\alpha_t+\beta_t)R(T)+\gamma_tF(T)\}, \tag{42}$$

where

$$f(T)=\xi_t(t_{ta}-t_{ts})+N_{1t}-N_{2t}[N_{3t}\cos(\omega_1-\omega)(t_{ta}-t_{ts})$$
$$+N_{4t}\sin(\omega_1-\omega)(t_{ta}-t_{ts})],$$

$$R(T) = \xi_t R_{1t} + R_{2t} - R_{3t}[R_{4t}\cos(\omega_1-\omega)(t_{ta}-t_{ts}) + R_{5t}\sin(\omega_1-\omega)(t_{ta}-t_{ts})],$$
$$F(T) = \xi_t K_{1t} + K_{2t} - K_{3t}[K_{4t}\cos(\omega_1-\omega)(t_{ta}-t_{ts}) + K_{5t}\sin(\omega_1-\omega)(t_{ta}-t_{ts})],$$

m_t is the mass of the nonreactive and stable tertiary ion, t_{ts} and t_{ta} are the source exit and analyzer exit times of the nonreactive and stable tertiary ion, respectively. $N_{1t}\sim N_{4t}$, $R_{1t}\sim R_{5t}$, and $K_{1t}\sim K_{5t}$ are given in Appendix II.

Similarly, the total power absorption $A(T,AFNT)$ due to analyzer-formed nonreactive and stable tertiary ions is given by averaging the integration from t_{ts} to t_{ta}:

$$A(T,AFNT) = \frac{1}{(t-t_{ts})}\int_{t_{ts}}^{t_{ta}} T(AFNT,t)_a\cdot(t-t_{ts})\cdot A(t''-t')dt$$
$$= \frac{P_0e^2E_1^2}{4m_t[(\omega_1-\omega)^2+\xi_t^2]}\{(\alpha_t+\beta_t+\gamma_t)f(T) - (\alpha_t+\beta_t)R(T)+\gamma_t F(T)\}. \quad (43)$$

Equations (42) and (43) are the line shape expressions of total power absorption for the source-formed and analyzer-formed nonreactive and stable tertiary ions, respectively. The total power absorption due to nonreactive and stable tertiary ions is given by the sum of Eqs. (42) and (43):

$$A(T,T) = A(T,SFNT) + A(T,AFNT).$$

Intensity Formula at Resonance. *a) Primary Ion*: In general, a full line shape expression is not required for the experimental determination of rate constant. The formula required for the ICSR signal intensity for an ion-molecule reaction described by Eqs. (22)—(25), is given as follows:

Applying the limit $\omega_1\to\omega$ to Eq. (37), we obtain the following intensity equation for primary ions;

$$I(P) = \frac{P_0e^2E_1^2\exp(-nk_{ps}t_{ps})}{4m_p\xi_p}\left\{\frac{1-\exp[-nk_{pa}(t_{pa}-t_{ps})]}{nk_{pa}} - \frac{1-\exp[-(nk_{pa}+\xi_p)(t_{pa}-t_{ps})]}{nk_{pa}+\xi_p}\right\}. \quad (44)$$

Under the approximation $k_{pa}\approx k_{ps}$, the first term of Eq. (44) corresponds to the intensity equation with the primary ion.[19] The second term points out the disadvantage of the old treatment, since k_{pa} should not be equal to k_{ps}. Under the collisionless limit $\xi\to 0$ and approximation $k_{pa}\approx k_{ps}$, Eq. (44) agrees with the intensity equation.[11] It is worthwhile noting that in our case the term of collision frequency ξ_p does not appear in the third order expansion of Eq. (44), and that no effect of collision frequency on signal intensity is considered.

b) Nonreactive Secondary Ion: The limit $\omega_1\to\omega$ in Eqs. (38) and (39) gives the following intensity equations for source-formed and analyzer-formed nonreactive and stable secondary ions, respectively;

$$I(SFNS) = \frac{P_0e^2E_1^2}{4m_n\xi_n}\Big\langle(t_{na}-t_{ns}) - \frac{1-\exp[-\xi_n(t_{na}-t_{ns})]}{\xi_n} - \left\{\frac{1-\exp[-nk_{pa}(t_{na}-t_{ns})]}{nk_{pa}} - \frac{1-\exp[-(nk_{pa}+\xi_n)(t_{na}-t_{ns})]}{nk_{pa}+\xi_n}\right\} \times\exp(-nk_{ps}t_{ns})\Big\rangle, \quad (45)$$

and

$$I(AFNS) = \frac{P_0e^2E_1^2\exp(-nk_{ps}t_{ns})}{4m_n\xi_n}\left\{(t_{na}-t_{ns}) - \frac{1-\exp[-\xi_n(t_{na}-t_{ns})]}{\xi_n} - \frac{1-\exp[-nk_{pa}(t_{na}-t_{ns})]}{nk_{pa}} + \frac{1-\exp[-(nk_{pa}+\xi_n)(t_{na}-t_{ns})]}{nk_{pa}+\xi_n}\right\}. \quad (46)$$

In the collisionless limit $\xi\to 0$, we can obtain the intensity equations of collisionless limiting case for source-formed and analyzer-formed nonreactive secondary ions. Under the approximation $k_{pa}\approx k_{ps}$, the intensity equation for source-formed nonreactive ion of collisionless limiting case corresponds to the secondary ion intensity expression.[11] The limit $k_{ps}\to 0$, applied to Eq. (46) and collisionless limiting case of Eq. (46), gives Eq. (45) and the collisionless limiting case of Eq. (45), respectively.

c) Reactive Secondary Ion: The intensity equations for the source-formed and analyzer-formed reactive secondary ions were similarly calculated:

$$I(SFRS) = \frac{P_0e^2E_1^2}{4m_s\xi_s}\Big\langle\frac{(\alpha_s+\beta_s)\{1-\exp[-nk_{sa}(t_{sa}-t_{ss})]\}}{nk_{sa}} - \frac{\alpha_s\{1-\exp[-nk_{pa}(t_{sa}-t_{ss})]\}}{nk_{pa}} - \frac{(\alpha_s+\beta_s)\{1-\exp[-(nk_{sa}+\xi_s)(t_{sa}-t_{ss})]\}}{nk_{sa}+\xi_s} - \frac{\alpha_s\{1-\exp[-(nk_{pa}+\xi_s)(t_{sa}-t_{ss})]\}}{nk_{pa}+\xi_s}\Big\rangle, \quad (47)$$

and

$$I(AFRS) = \frac{P_0e^2E_1^2\alpha_s}{4m_s\xi_s}\left\{\frac{1-\exp[-nk_{sa}(t_{sa}-t_{ss})]}{nk_{sa}} - \frac{1-\exp[-(nk_{sa}+\xi_s)(t_{sa}-t_{ss})]}{nk_{sa}+\xi_s} - \frac{1-\exp[-nk_{pa}(t_{sa}-t_{ss})]}{nk_{pa}} + \frac{1-\exp[-(nk_{pa}+\xi_s)(t_{sa}-t_{ss})]}{nk_{pa}+\xi_s}\right\}. \quad (48)$$

In the expansion of Eqs. (47) and (48) with respect to ξ, we obtain intensity equations of collisionless limiting case for the source-formed and analyzer-formed reactive secondary ions, respectively.

d) Nonreactive Tertiary Ion: By a similar calculation the following intensity equations for source-formed and analyzer-formed nonreactive and stable tertiary ions are obtained.

$$I(SFNT) = \frac{P_0e^2E_1^2}{4m_t\xi_t}\Big\langle(t_{ta}-t_{ts}) - \frac{1-\exp[-\xi_t(t_{ta}-t_{ts})]}{\xi_t} - \frac{(\alpha_t+\beta_t)}{nk_{sa}}\{1-\exp[-nk_{sa}(t_{ta}-t_{ts})]\} + \frac{\gamma_t}{nk_{pa}}\{1-\exp[-nk_{pa}(t_{ta}-t_{ts})]\} + \frac{(\alpha_t+\beta_t)}{nk_{sa}+\xi_t}\{1-\exp[-(nk_{sa}+\xi_t)(t_{ta}-t_{ts})]\} - \frac{\gamma_t}{nk_{pa}+\xi_t}\{1-\exp[-(nk_{pa}+\xi_t)(t_{ta}+t_{ts})]\}\Big\rangle, \quad (49)$$

and

$$I(AFNT) = \frac{P_0e^2E_1^2}{4m_i\xi_t}\Big\langle(\alpha_t+\beta_t+\gamma_t)\Big\{(t_{ta}-t_{ts}) - \frac{1-\exp[-\xi_t(t_{ta}-t_{ts})]}{\xi_t}\Big\} - \frac{(\alpha_t-\beta_t)}{nk_{sa}}\{1-\exp[-nk_{sa}(t_{ta}-t_{ts})]\} + \frac{\gamma_t}{nk_{pa}}\{1-\exp[-nk_{pa}(t_{ta}-t_{ts})]\} + \frac{(\alpha_t+\beta_t)}{nk_{sa}+\xi_t}\{1-\exp[-(nk_{sa}+\xi_t)(t_{ta}-t_{ts})]\} - \frac{\gamma_t}{nk_{pa}+\xi_t}\{1-\exp[-(nk_{pa}+\xi_t)(t_{ta}-t_{ts})]\}\Big\rangle. \quad (50)$$

In the collisionless limit $\xi\to 0$ of Eqs. (49) and (50) which are expanded to third order with respect to ξ, we obtain the intensity equations of collisionless limiting case for the source-formed and analyzer-formed nonreactive tertiary ions.

Calculation of Rate Constant for the Disappearance of Primary Ions. In ion-molecule reactions, the power absorption due to the primary ion is decreased by the reactive collisions with neutral reactant molecules. The ion-molecule collision rate or reaction rate constant for disappearance of the primary ion can be obtained from Eq. (44). However, there is no effect of collision frequency on ICSR signal intensity. Thus, the collisionless limit $\xi\to 0$ is a fairly good approximation except at the high pressure where the collision broadening occurs.

Equation (44) can be now expanded to give

$$I(P_1, \xi\to 0) = \frac{P_0e^2E_1^2(t_{pa}-t_{ps})^2}{8m_p^2}[1-nk_{pa}(t_{pa}-t_{ps})] \quad \text{for } k_{pa}\gg k_{ps}\sim 0, \quad (51a)$$

$$I(P_2, \xi\to 0) = \frac{P_0e^2E_1^2}{8m_p^2}(t_{pa}-t_{ps})\Big\{(t_{pa}-t_{ps}) - \frac{n}{k_{pa}}[k_{pa}t_p-(k_{pa}-k_{ps})t_{ps}]^2\Big\} \quad \text{for } k_{pa}\neq k_{ps}, \quad (51b)$$

$$I(P_3, \xi\to 0) = \frac{P_0e^2E_1^2}{8m_p^2}(t_{pa}-t_{ps})[(t_{pa}-t_{ps})-nk_{pa}t_{pa}^2] \quad \text{for } k_{pa}\approx k_{ps}. \quad (51c)$$

Solving Eqs. (51a), (51b), and (51c) for k_{pa}, we have

$$k_{pa} = \frac{1}{n(t_{pa}-t_{ps})}\left[1-\frac{I(P_1, \xi\to 0)}{\alpha}\right] \quad \text{for } k_{pa}\gg k_{ps}\sim 0, \quad (52a)$$

$$k_{pa} = \frac{1}{n(t_{pa}-t_{ps})}\left[1-2nk_{ps}t_{ps}-\frac{I(P_2, \xi\to 0)}{\alpha}\right] \quad \text{for } k_{pa}\neq k_{ps}, \quad (52b)$$

and

$$k_{pa} = \frac{(t_{pa}-t_{ps})}{nt_{pa}^2}\left[1-\frac{I(P_3, \xi\to 0)}{\alpha}\right] \quad \text{for } k_{pa}\approx k_{ps}, \quad (52c)$$

where k_{pa} is the collision rate or the rate constant for the disappearance of the primary ions, and

$$\alpha = \frac{P_0e^2E_1^2}{8m_p^2}(t_{pa}-t_{ps})^2.$$

Calculation of Rate Constant for the Formation of Nonreactive Secondary Ions. Single-resonance spectra are usually obtained at constant rf frequency ω_1 by sweeping the magnetic field. The magnetic field at which an ion is in resonance is proportional to m/e as indicated by Eq. (1).

The source exit and analyzer exit times for the primary ion are given by Eqs. (21b) and (21c), respectively. The values of t_{ps} and t_{pa} are related by

$$t_{ns} = (m_n/m_p)t_{ps}, \quad (53a)$$

$$t_{ss} = (m_s/m_p)t_{ps}, \quad (53b)$$

$$t_{ts} = (m_t/m_p)t_{ps}, \quad (53c)$$

$$t_{na} = (m_n/m_p)t_{pa}, \quad (54a)$$

$$t_{sa} = (m_s/m_p)t_{pa}, \quad (54b)$$

and

$$t_{ta} = (m_t/m_p)t_{pa}. \quad (54c)$$

If $nk_it_j<1$, $(i, j=ps, pa, ns, na)$, then the exponentials in the collisionless limit of Eq. (44) can be expanded to the third order. Using Eqs. (53a) and (54a), they can be solved for k_{pa} giving the approximations:

$$k_{pa} = \frac{m_p^2I(NS, \xi\to 0)\cdot(t_{pa}-t_{ps})}{n[m_n^2I(P, \xi\to 0)\cdot\alpha_k+m_p^2I(NS, \xi\to 0)\cdot\beta_k]} \quad \text{for } k_{ps}\neq k_{pa}, \quad (55a)$$

$$k_{pa} = \frac{m_p^2I(NS, \xi\to 0)}{n[2m_n^2I(P, \xi\to 0)+m_p^2I(NS, \xi\to 0)](t_{pa}-t_{ps})} \quad \text{for } k_{pa}\gg k_{ps}\sim 0, \quad (55b)$$

and

$$k_{pa} = \frac{m_p^2I(NS, \xi\to 0)\cdot(t_{pa}-t_{ps})}{n\{m_n^2I(P, \xi\to 0)[2t_{pa}^2-(t_{pa}-t_{ps})t_{ps}]+m_p^2I(NS, \xi\to 0)t_{pa}^2\}} \quad \text{for } k_{pa}\approx k_{ps}, \quad (55c)$$

where

$$\alpha_k = 2(t_{pa}-t_{ps})^2+\frac{3k_{ps}}{k_{pa}}(t_{pa}-t_{ps})t_{ps}+\frac{2k_{ps}^2}{k_{pa}^2}t_{ps}^2$$

and

$$\beta_k = (t_{pa}-t_{ps})^2+\frac{2k_{ps}}{k_{pa}}(t_{pa}-t_{ps})t_{ps}+\frac{2k_{ps}^2}{k_{pa}^2}t_{ps}^2.$$

Under high pressure, if $nk_it_j<1$, $(i,j=pa, ps, na, ns)$, then exponentials in Eqs. (44), (45), and (46) can be expanded to fourth order. Using Eqs. (53a) and (54a), they can be solved for k_{pa} giving the approximations:

$$k_{pa} = \frac{m_p^2I(NS)[3-3nk_{ps}t_{ps}-\xi_p(t_{pa}-t_{ps})]-3m_n^2I(P)nk_{ps}t_{ps}}{2n[2m_n^2I(P)+m_p^2I(NS)](t_{pa}-t_{ps})} \quad \text{for } k_{ps}\neq k_{pa}, \quad (56a)$$

$$k_{pa} = \frac{m_p^2I(NS)[3-\xi_p(t_{pa}-t_{ps})]}{2n[2m_n^2I(P)+m_p^2I(NS)](t_{pa}-t_{ps})} \quad \text{for } k_{pa}\gg k_{ps}\sim 0, \quad (56b)$$

and

$$k_{pa} = \frac{m_p^2I(NS)[3-\xi_p(t_{pa}-t_{ps})]}{n[m_n^2I(P)\cdot(4t_{pa}-t_{ps})+m_p^2I(NS)\cdot(2t_{pa}+t_{ps})]} \quad \text{for } k_{ps}\approx k_{pa}. \quad (56c)$$

Equations (55a)—(56c) were derived on the assumption that a secondary ion does not suffer any reactive collisions in the resonance region of the ICR cell. If

a large fraction of secondary ions react with neutrals in the analyzer region, Eqs. (55a)—(56c) could not be applied. In this case, the rate constant for the formation of reactive secondary ion can be derived from Eqs. (44), (47), and (48).

Results and Discussion

Single- and Double-resonance Spectra. The ion-molecule reactions of acetonitrile have been studied by high-pressure mass spectrometry[21] and ICR spectroscopy.[22] Twenty-three ion-molecule reactions have been observed in acetonitrile by ICDR technique,[22] and the rate constants for the disappearance of ion-molecule reactions in acetonitrile has been measured with a time-of-flight mass spectrometer.[21]

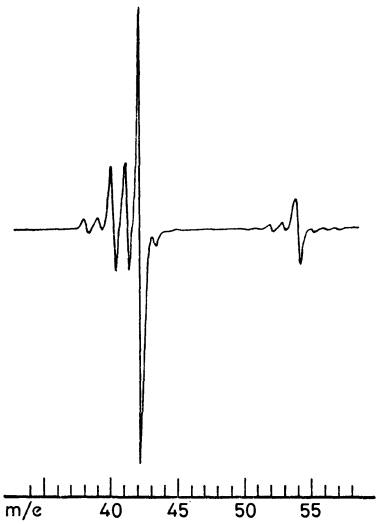

Fig. 2. Single-resonance spectrum of acetonitrile at 60 eV electron energy and 1.1×10^{-5} Torr.

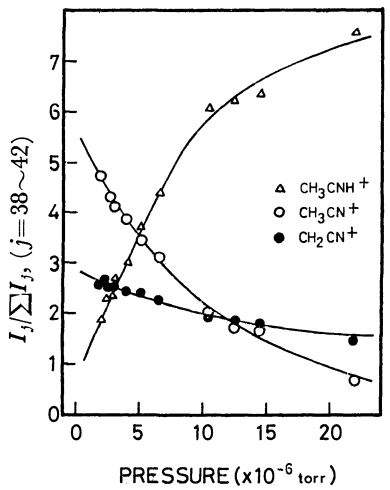

Fig. 3. Variation of single-resonance intensities of the various observed with pressure, at 60 eV electron energy.

However, the rate constant for the disappearance has not been reported by ICR spectroscopy. Equation (52) is applied to determine the rate constant for the disappearace of ions in acetonitrile.

Figure 2 shows a single-resonance spectrum of acetonitrile obtained at 1.1×10^{-5} Torr and electron energy of 60 eV. The spectrum is essentially the same as that reported.[22] The variations of single-resonance intensities with pressure are given in Fig. 3. The primary ion CH_2CN^+ and CH_3CN^+ decrease with increasing pressure. The secondary product CH_3CNH^+ increases with increasing pressure. The weak signal of $CHCN^+$ reaches a maximum, at around 6×10^{-6} Torr, and then decreases with increasing pressure. At a high electron energy, the sequence of reactions becomes complicated, probably because of possible generation of several reactant ions. By ICDR technique, however, one can readily identify the processes that produce each product ion. The ion-molecule reactions, identified by ICDR technique, are listed in Table 1. The results of ICDR experiments are in good agreement with those reported.[22]

Table 1. Ion-molecule reaction in acetonitrile

R1.	$C_2H_2^+$	+ CH_3CN	⟶	CH_3CNH^+	+ C_2H
R2.	HCN^+	+ CH_3CN	⟶	CH_3CNH^+	+ CN
R3.	H_2CN^+	+ CH_3CN	⟶	CH_3CNH^+	+ HCN
R4.	N_2H^+	+ CH_3CN	⟶	CH_3CNH^+	+ N_2
R5.	CH_2CN^+	+ CH_3CN	⟶	CH_3CNH^+	+ CHCN
R6.	CH_3CN^+	+ CH_3CN	⟶	CH_3CNH^+	+ CH_2CN
R7.	CH_2CN^+	+ CH_3CN	⟶	$C_3H_4CN^+$	+ HCN

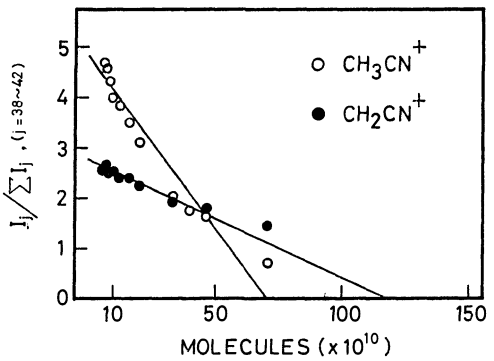

Fig. 4. $I_j/\sum I_j$, (j=38—42), *vs.* number density of neutral reactant molecules for the reaction disappearing CH_3CN^+ with CH_3CN and for the reaction disappearing CH_2CN^+ with CH_3CN.

Determination of Rate Constant for the Disappearance of Primary Ion. From Eqs. (52a, b, c), it is evident that a plot of I *versus* n should give a straight line passing through a point (0, n) with a slope proportional to $1/k_{pa}$. The factor α is generally very small, and has been omitted in plotting Fig. 4. On the assumption that $k_{ps}\ll k_{pa}$, k_{ps} has been ignored in the calculation. Therefore, when $I=0$, Eq. (52a) is reduced to

$$k_{pa}(t_{pa}-t_{ps}) = 1/n,$$

where the source exit time t_{ps} and the analyzer exit time t_{pa} are given by Eqs. (21b) and (21c), respectively. The behavior of single-resonance signal intensities of primary ions CH_2CN^+ and CH_3CN^+ are interpreted by means of Eq. (52a).

The values of $k_{pa}(\mathrm{R5})=1.34\times10^{-9}$ and $k_{pa}(\mathrm{R6})=1.99\times10^{-9}$ cc mol^{-1} s^{-1} for the reactions (R5) and

(R6) obtained from Fig. 4 are in excellent agreement with previous values of $k(\mathrm{R5})=1.78\times10^{-9}$ and $k(\mathrm{R6})=2.01\times10^{-9}$ ml mol^{-1} s^{-1} determined by the conventional technique.[21]

Determination of Rate Constant for the Formation of Nonreactive Secondary Ion. In ion-molecule reactions of acetonitrile, CH_3CNH^+ is not essentially a nonreactive secondary ion. But tertiary ions formed from CH_3CNH^+ are so few that CH_3CNH^+ can be considered to be the nonreactive secondary ion.

In the limits $\xi\to0$ and $k_{ps}\to0$, it is evident that a plot of n *versus* $m_p^2I(NS,\ \xi\to0)/[2m_n^2I(P,\ \xi\to0)+m_p^2I(NS,\ \xi\to0)](t_{pa}-t_{ps})$ of Eq. (55) should give a straight line with a slope proportional to k_{pa} as shown in Fig. 5. The analysis supports the above results for reactions (R5) and (R6).

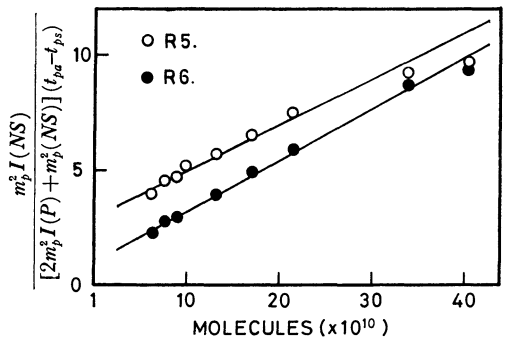

Fig. 5. $m^2{}_pI(NS)/[2m^2{}_nI(P)+m^2{}_pI(NS)](t_{pa}-t_{ps})$ *vs.* number density of neutral reactant molecules for the reaction of R(5) and for the reaction of R(6) listed in Table 1, respectively.

The values $k_{pa}(\mathrm{R5})=2.1\times10^{-9}$ and $k_{pa}(\mathrm{R6})=2.3\times10^{-9}$ cc mol^{-1} s^{-1} for reactions (R5) and (R6) are in very good agreement with previous results. Gupta *et al.*[23] reported $k(\mathrm{R6})=2.15\times10^{-9}$ cc mol^{-1} s^{-1} at 3.7 eV exit ion energy. Martin and Melton[24] reported $k(\mathrm{R6})=3.5\times10^{-9}$ cc mol^{-1} s^{-1} determined by conventional techniques. However, no value of $k(\mathrm{R5})$ has been reported.

Experimental

The ICR spectra recorded with a JEOL JIC-3B spectrometer have been described in detail.[15] The ICR cell was of a three-section square type similar to the conventional one,[3] the grid electrode being added to improve the distribution of the electric field. Ions were produced in the source region by the electron impact and then forced to drift into the analyzer region where they were observed by a Twin-T bridge detector.[6] Single-resonance spectra were obtained in the field modulation mode, and double-resonance experiments were performed in the pulsed modulation mode.[8]

The experimental conditions were as follows: Energy of ionizing electrons=60 eV, source and analyzer drift field strengths=0.2 V/cm, trapping voltage=0.26 V, the observed rf electric field strength and frequency=0.02 V/cm and 100 kHz. Acetonitrile of reagent grade (Wako Pure Chem. Ind., Ltd.) was purified by trap-to-trap distillation before use. The sample was degassed under vacuum utilizing freeze-pump-thaw cycles.

The author would like to thank Professor Koichiro Hayashi for his encouragement, and Professor Junkichi Sohma for advice and discussions. The author is also indebted to Dr. Tetsuo Maruyama of JEOL (U.S.A.), INC. for his support, helpful suggestions and encouragement. The support of JEOL Co., Ltd. is gratefully acknowledged.

Appendix

I) Ion Kinetic Energy in the Absence of Collisions. Kinetic energy of an ion is also derived from Eq. (7) as follows.

$$W(\omega_1=\omega)=\frac{mv_0^2}{2}+\frac{v_0eE_1}{2}\left[t\cos(\phi_0+\phi_1)-\frac{1}{\omega}\sin\omega t\cos(\omega t-\phi_0+\phi_1)\right]+\frac{e^2E_1^2}{8m}\left[t^2+\frac{\sin^2\omega t}{\omega^2}-\frac{2t\sin\omega t\cos(\omega t+2\phi_1)}{\omega}\right]$$

for $\omega_1=\omega$.

If $\phi_0=0$ and $\phi_1=0$, the equation from which the oscillating terms are ignored agrees with that reported previously.[11]

II) List of Notations Used in the Text.

$K_{1p}=\{1-\exp[-nk_{pa}(t_{pa}-t_{ps})]\}/nk_{pa}$,
$K_{2p}=[(\omega_1-\omega)^2-\xi_p(nk_{pa}-\xi_p)]/[(nk_{pa}+\xi_p)^2+(\omega_1+\omega)^2]$,
$K_{3p}=\exp[-(nk_{pa}+\xi_p)(t_{pa}-t_{ps})]/[(nk_{pa}+\xi_p)^2+(\omega_1-\omega)^2]$,
$K_{4p}=(\omega_1-\omega)^2-\xi_p(nk_{pa}+\xi_p)$,
$K_{5p}=(\omega_1-\omega)(nk_{pa}+2\xi_p)$,
$N_{1n}=[(\omega_1-\omega)^2-\xi_n^2]/[(\omega_1-\omega)^2+\xi_n^2]$,
$N_{2n}=\exp[-\xi_n(t_{na}-t_{ns})]/[(\omega_1-\omega)^2+\xi_n^2]$,
$N_{3n}=(\omega_1-\omega)^2-\xi_n^2$,
$N_{4n}=2\xi_n(\omega_1-\omega)$,
$K_{1n}=\{1-\exp[-nk_{pa}(t_{na}-t_{ns})]\}/nk_{pa}$,
$K_{2n}=[(\omega_1-\omega)^2-\xi_n(nk_{pa}-\xi_n)]/[(nk_{pa}+\xi_n)^2+(\omega_1-\omega)^2]$,
$K_{3n}=\exp[-(nk_{pa}+\xi_n)(t_{na}-t_{ns})]/[(nk_{pa}+\xi_n]^2+(\omega_1-\omega)^2]$,
$K_{4n}=(\omega_1-\omega)^2-\xi_n(nk_{pa}+\xi_n)$,
$K_{5n}=(\omega_1-\omega)(nk_{pa}+2\xi_n)$,
$R_{1s}=\{1-\exp[-nk_{sa}(t_{sa}-t_{ss})]\}/nk_{sa}$,
$R_{2s}=[(\omega_1-\omega)^2-\xi_s(nk_{sa}+\xi_s)]/[(nk_{sa}+\xi_s)^2+(\omega_1-\omega)^2]$,
$R_{3s}=\exp[-(nk_{sa}+\xi_s)(t_{sa}-t_{ss})]/[(nk_{sa}+\xi_s)^2+(\omega_1-\omega)^2]$,
$R_{4s}=(\omega_1-\omega)^2-\xi_s(nk_{sa}+\xi_s)$,
$R_{5s}=(\omega_1-\omega)(nk_{sa}+2\xi_s)$,
$K_{1s}=\{1-\exp[-nk_{pa}(t_{sa}-t_{ss})]\}/nk_{pa}$,
$K_{2s}=[(\omega_1-\omega)^2-\xi_s(nk_{pa}+\xi_s)]/[(nk_{pa}+\xi_s)^2+(\omega_1-\omega)^2]$,
$K_{3s}=\exp[-(nk_{pa}+\xi_s)(t_{sa}-t_{ss})]/[(nk_{pa}+\xi_s)^2+(\omega_1-\omega)^2]$,
$K_{4s}=(\omega_1-\omega)^2-\xi_s(nk_{pa}+\xi_s)$,
$K_{5s}=(\omega_1-\omega)(nk_{pa}+2\xi_s)$,
$N_{1t}=[(\omega_1-\omega)^2-\xi_t^2]/[(\omega_1-\omega)^2+\xi_t^2]$,
$N_{2t}=\exp[-\xi_t(t_{ta}-t_{ts})]/[(\omega_1-\omega)^2+\xi_t^2]$,
$N_{3t}=(\omega_1-\omega)^2-\xi_t^2$,
$N_{4t}=2\xi_t(\omega_1-\omega)$,
$R_{1t}=\{1-\exp[-nk_{sa}(t_{ta}-t_{ts})]\}/nk_{sa}$,
$R_{2t}=[(\omega_1-\omega)^2-\xi_t(nk_{sa}+\xi_t)]/[(nk_{sa}+\xi_t)^2+(\omega_1-\omega)^2]$,

$$R_{3t} = \exp[-(nk_{sa}+\xi_t)(t_{ta}-t_{ts})]/[(nk_{sa}+\xi_t)^2+(\omega_1-\omega)^2],$$
$$R_{4t} = (\omega_1-\omega)^2 - \xi_t(nk_{sa}+\xi_t),$$
$$R_{5t} = (\omega_1-\omega)(nk_{sa}+2\xi_t),$$
$$K_{1t} = \{1-\exp[-nk_{pa}(t_{ta}-t_{ts})]\}/nk_{pa},$$
$$K_{2t} = [(\omega_1-\omega)^2-\xi_t(nk_{pa}+\xi_t)]/[(nk_{pa}+\xi_t)^2+(\omega_1-\omega)^2],$$
$$K_{3t} = \exp[-(nk_{pa}+\xi_t)(t_{ta}-t_{ts})]/[(nk_{pa}+\xi_t)^2+(\omega_1-\omega)^2],$$
$$K_{4t} = (\omega_1-\omega)^2 - \xi_t(nk_{pa}+\xi_t),$$
$$K_{5t} = (\omega_1-\omega)(nk_{pa}+2\xi_t).$$

References

1) JEOL Fellow, 1970–1972. On leave of absence from Division of Industrial Physical Chemistry, Faculty of Engineering, Hokkaido University, Sapporo 060. Present address: JEOL Co., Ltd. 1418 Nakagami, Akishima-shi, Tokyo 196

2) Gaussian CGS units are employed unless otherwise stated.

3) J. L. Beauchamp, L. R. Anders, and J. D. Baldeschwieler, *J. Amer. Chem. Soc.*, **89**, 4569 (1967).

4) K. Aoyagi, (a) *Bunseki-kiki.*, **10**, 703 (1972). (b) Unpublished data.

5) D. Wobschall, J. R. Graham, and D. P. Malone, *Phys. Rev.*, **131**, 1565 (1963).

6) K. Aoyagi, T. Miyamae, M. Irie, K. Hayashi, and J. Sohma, 5th Annual Conference on Applied Spectrometry., Tokyo (1969).

7) See, for example, K. Yoshida and T. Kato, "Ohyo-sugaku-1", Syokabo. Tokyo (1967).

8) K. Aoyagi, T. Miyamae, T. Seki, and S. Fujiwara, 4th Annual Conference on Applied Spectrometry., Tokyo (1968).

9) J. L. Beauchamp, *J. Chem. Phys.*, **46**, 1231 (1967).

10) M. B. Comisarow, *ibid.*, **55**, 205 (1971).

11) S. E. Buttrill, *ibid.*, **50**, 4125 (1969).

12) References 10, 11, 13, 17 and 19.

13) R. C. Dunbar, *J. Chem. Phys.*, **54**, 711 (1971).

14) S. Fujiwara, K. Aoyagi, and T. Miyamae, This Bulletin **43**, 561 (1970)

15) K. Aoyagi, K. Hayashi, and J. Sohma, *Bull. Fac. Eng. Hokkaido Univ.*, No. **62**, 65 (1971).

16) J. L. Beauchamp and J. T. Armstrong, *Rev. Sci. Instr.*, **40**, 123 (1969).

17) M. T. Bowers, D. D. Elleman, and J. King, *J. Chem. Phys.*, **50**, 4787 (1969).

18) J. M. S. Henis, *ibid.*, **52**, 282 (1970).

19) M. T. Bowers, D. D. Elleman, and J. L. Beauchamp, *J. Phys. Chem.*, **72**, 3599 (1968).

20) W. J. Moore, "Physical Chemistry," 3rd Ed, Maruzen Asian Edition, Maruzen Co., Ltd. (1962), p. 226.

21) J. L. Franklin, Y. Wada, P. Natalis, and P. M. Hierl, *J. Phys. Chem.*, **70**, 2353 (1966).

22) G. A. Gray, *J. Amer. Chem. Soc.*, **90**, 2177 (1968); *ibid.*, **90**, 6002 (1968).

23) S. K. Gupta, E. G. Jones, A. G. Harrison, and J. J. Myher, *Can. J. Chem.*, **45**, 3107 (1967).

24) T. W. Martin and C. E. Melton, *J. Chem. Phys.*, **32**, 700 (1960).

Chemical Behavior of Intermediates Produced in Sulfuric Acid Glass by Gamma Irradiation. I. Reactivities of Mobile Electrons with Inorganic Ions

Teikichi SASAKI

Chemistry Division, Japan Atomic Energy Research Institute, Tokai-mura, Ibaraki 319-11

(Received March 31, 1973)

The yield of the trapped hydrogen atom, H_t, produced in the 6 M sulfuric acid matrix at 77 K was decreased by the presence of an electron scavenger. Based on the competition reaction kinetics, the reactivities of mobile electrons, e_m^-, with metallic and oxygen-containing ions were determined from the decrease in the H_t yield. It was found that e_m^- is scavenged most efficiently with the TeO_4^{2-} ion. The relative reaction rates of e_m^- with oxyanions were generally larger than those of the corresponding e_{aq}^- reactions. On the other hand, a good accordance in the reaction rates for both forms of electrons was observed in the cases of the reactions with metallic ions. An interpretation was given to the discrepancy in the observed reaction rates that e_m^- in the epithermal energy region goes over the Coulomb barrier, which is too high for e_{aq}^- to pass through, and thus reacts more efficiently with anionic species than does e_{aq}^-. Some unstable intermediates produced at 77 K polymerized with the solute during the thermal annealing. The ESR and optical spectra of the polymerized cadmium and molybdenum are shown, together with those of the primarily-produced species.

It is well recognized that e_m^- in an acidic matrix is converted into H_t:[1]

$$e_m^- + P \longrightarrow H_t \quad (1)$$

where P is a reaction partner of e_m^-, such as an H^+ or HSO_4^- ion. The addition of an electron scavenger, S, depresses the H_t formation:

$$e_m^- + S \longrightarrow S^- \quad (2)$$

From competition reaction kinetics applied to the e_m^- concentration, the following equation is obtained:[2]

$$G_0(H_t)/G(H_t) = 1 + k_s[S]/k_p[P] \quad (3)$$

where $G_0(H_t)$ and $G(H_t)$ are the G values of H_t in the absence and in the presence of the electron scavenger, and where k_s and k_p are the rate constants for the reaction of e_m^- with S and P respectively.

Kevan[2] has reported on the reactivities of e_m^- in the acidic matrix and concluded that the relative rates, except that of the reaction of e_m^- with the H^+ ion, were approximately proportional to those of e_{aq}^- at room temperature. However, similar studies using the other matrices[3,4] showed some deviations from the results which would be expected from the corresponding e_{aq}^- reactions. The disagreement might arise from a difference in the experimental method; Kevan employed acidic matrices with a low H_t yield ($G(H_t)=0.14$—0.27),[5] while the latter authors directly measured the disappearance of trapped electrons, e_t^-, in the matrices of high e_t^- yields ($G(e_t^-)=2.8$).[4]

Recently, Steen and Kongshaug[6] found, by employing an ethylene glycol-water matrix, that the relative scavenging efficiency of such anionic solutes as NO_3^- and $ClCH_2COO^-$ ions diminished with a decrease in the energy of the electron, *i.e.*, in the order of the dry electron, e^-, e_m^-, and the stabilized electron, e_s^-, produced in an ethylene glycol-water matrix at 77 K. We ourselves have also reported[4] that the relative rates of the e_m^- reactions in the same matrix are not always in accordance with those of the e_{aq}^- reactions, and that larger relative e_m^- rates were obtained, especially in the reaction with polynegative complex ions.

For the e_m^- reactions in sulfuric acid glass, Brown and Dainton[7] have studied the reactivities with Ag^+, Cd^{2+}, and In^{3+} ions by means of spectrophotometry. However, no correlation with the reactivity has been derived from their data.

The H_t yield in the frozen solution of 6M sulfuric acid is comparatively large ($G(H_t)=1.3$ at 77 K[8]) and the matrix becomes homogeneously glassy upon rapid freezing, which is convenient for the estimation of the reactivity of e_m^- from the decrease in the H_t yield. In the present paper, the relative rates of the e_m^- reactions in the acidic matrix were determined for 18 inorganic ions. Though it is qualitative, a distinct difference in the reactivity was observed between the e_m^- and e_{aq}^- reactions. This discrepancy seems to arise from an essential difference in the average kinetic energy possessed by the two entities at the time of the scavenging reaction rather than from the difference in the matrix or phase employed.

Experimental

Materials. The water was redistilled, and the ethylene glycol was fractionally distilled. As matrices, a 67 vol % ethylene glycol-water solution was used in the case of the e_m^- reaction with the H^+ ion, while in the other cases 6M sulfuric acid was employed.

Sulfates or alkali metal salts were generally used for the reactivity determinations of e_m^-. In the case of the reaction with the Ag^+ ion, silver nitrate was used as a solute. Since the NO_3^- ion itself is a strong e_m^- scavenger, the reaction rate was estimated from the summation of the efficiencies for Ag^+ and NO_3^- ions. All of the chemicals tabulated in Tables 1 and 2 were of an analytical reagent grade and were used without further purification.

Irradiation and Measurement. The samples which were made into a glassy state without any degassing treatment were exposed to gamma rays from a ^{60}Co source for 2 hr at 77 K. The dose rate was 4×10^{18} eV g^{-1} hr^{-1}. The ESR measurements were performed at 77 K in the absence of power saturation, and the optical measurements were carried out as has previously been described.[4] The H_t yield was determined from the ESR signal intensity in the higher magnetic field, while the estimation of the e_t^- yield was based

TABLE 1. RELATIVE RATES OF e_m^- AND e_{aq}^- REACTIONS WITH METALLIC IONS

Ion (S)	Compound	Relative rates $k(e_m^-+S)$ at 77K	Relative rates $k(e_{aq}^-+S)$ at 300K[a)]
Mg^{2+}	$MgSO_4 \cdot 7H_2O$	0.15	—
Al^{3+}	$KAl(SO_4)_2 \cdot 12H_2O$	0.09	0.07
Cr^{3+}	$Cr_2(SO_4)_3 \cdot 15H_2O$	1.0	1.5
Fe^{3+}	$Fe_2(SO_4)_3 \cdot 10H_2O$	3.0	—
Cu^{2+}	$CuSO_4 \cdot 6H_2O$	1.0	1.1
Ag^+	$AgNO_3$	2.2	1.0
Cd^{2+}	$CdSO_4 \cdot 2.7H_2O$	1.0	1.0
Ce^{4+}	$Ce(SO_4)_2 \cdot 6H_2O$	0.65	—
Hg^{2+}	$HgCl_2$	2.9	—
Tl^+	Tl_2SO_4	0.72	0.98

a) The data were cited from the table compiled by Anbar and Neta.[13)]

TABLE 2. RELATIVE RATES OF e_m^- AND e_{aq}^- REACTIONS WITH OXYGEN CONTAINING IONS

Ion (S)	Compound	Relative rates $k(e_m^-+S)$ at 77K	Relative rates $k(e_{aq}^-+S)$ at 300K[a)]
$B_4O_7^{2-}$	$Na_2B_4O_7 \cdot 10H_2O$	<0.03	—
NO_3^-	KNO_3	1.9	0.35
HSO_4^-[b)]	H_2SO_4	0.95[b)]	—
$Cr_2O_7^{2-}$	$K_2Cr_2O_7$	4.2	1.1
MnO_4^-	$KMnO_4$	0.58	0.71
MoO_4^{2-}	$Na_2MoO_4 \cdot 2H_2O$	1.1	—
TeO_4^{2-}	$H_2TeO_4 \cdot 2H_2O$	4.4	0.52
UO_2^{2+}	$UO_2SO_4 \cdot 3H_2O$	1.4	2.4 (pH ?)

a) The data were cited from the table compiled by Anbar and Neta.[13)] b) Activity coefficient of HSO_4^- ion was assumed to be 0.34.

on the method which will be described in the following section.

The thermal treatments above 77 K were done by using a variable-temperature accessory. The sample vessel was composed of double tubes of Pyrex glass which were covered with adiabatic material. An inner tube, 20 cm long and 1.5 cm in *i.d.*, was covered with paraffin wax, and a heating coil was wound on the outside of the wall. This tube was then inserted into a larger Pyrex tube covered with asbestos. The vessel was dipped in liquid N_2. The temperature of the sample was measured with a platinum resistance thermometer and held within ± 1 °C with a Chino E501 temperature controller.

Results and Discussion

Electron-scavenging Efficiency of Sulfuric Acid. The total scavenging efficiency of sulfuric acid for e_m^- was estimated from the decrease in the e_t^- concentration. On exposure to gamma rays, the ethylene glycol-water glass acidified with sulfuric acid develops a deep blue color which arise from the e_t^-. The color completely disappears above the acidic concentration of *ca.* 0.5 M or upon photobleaching with a light of wavelengths $\lambda \geq 390$ nm. The SO_4^- radical, which is

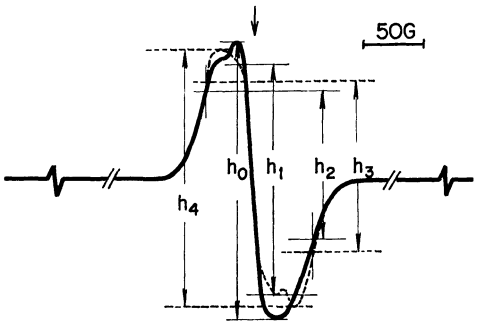

Fig. 1. ESR spectra of gamma-irradiated 67 vol % ethylene glycol-water glass containing 5×10^{-2}M sulfuric acid.
——— before photobleaching
---------- after bleaching by light of tungusten lamp

characterized by its bright yellow color, is not observed in the region of sulfuric-acid concentrations employed.

The ESR spectra (the 1st differential) of the gamma-irradiated sample are shown in Fig. 1. The shapes are essentially the same as those reported previously.[4)] After photobleaching, the central singlet which mainly arises from e_t^- disappears and the triplet which is probably due to the ethylene glycol radical increases, as may be seen in Fig. 1. The H_t yield is dependent upon neither the photobleaching procedure nor the concentration of sulfuric acid.

The absolute e_t^- concentration is proportional to the difference in the intensity of the integrated ESR spectra at the e_t^- position before and after photobleaching. In the preliminary examinations, however, the following simple method was confirmed to give a reliable estimate of the relative e_t^- concentration. By photobleaching, the singlet spectrum of e_t^- is probably converted to the triplet spectrum of the ethylene glycol radical.[9)] Consequently, the contribution of the triplet at the e_t^- position increases by h_1h_3/h_2, where h_1 is the signal intensity of the triplet at the e_t^- position and where h_2 and h_3 are the intensities of the triplet before and after photobleaching respectively. Therefore, the relative e_t^- concentration, $C(e_t^-)$, is approximately given as follows:

$$C(e_t^-) \simeq (h_0 - h_1h_3/h_2)/h_4 \quad (4)$$

where h_0 is the signal intensity at the e_t^- position before photobleaching. A normalization factor, h_4, is the total intensity of the ethylene glycol radical, regardless of the concentration of sulfuric acid employed. These notations are also presented in Fig. 1.

Based on the competition reaction kinetics described previously,[4)] the value of $[C_0(e_t^-)/C(e_t^-) - 1]$, where $C_0(e_t^-)$ is the relative e_t^- concentration in the absence of sulfuric acid, is plotted against the acidic concentration in Fig. 2. The total scavenging efficiency of 8.0 M^{-1} obtained for sulfuric acid is 0.21 of that for the NO_3^- ion in the same matrix. The chemical species which can scavenge e_m^- in the sulfuric acid matrix are H^+ and HSO_4^- ions.[1,10)] Because the reaction rate of e_m^- with the H^+ ion was given as 0.12 $k(e_m^- + NO_3^-)$ in the experiment using chloric acid,[3)] the rate with the HSO_4^- ion is estimated as follows:

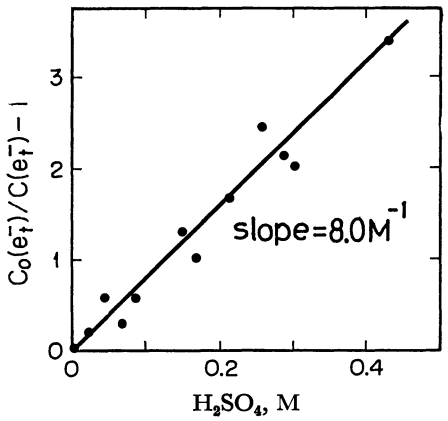

Fig. 2. Relationship between $[C_0(e_t^-)/C(e_t^-)-1]$ and sulfuric acid concentration.

$$k(e_m^- + HSO_4^-) = k(\text{total}) - k(e_m^- + H^+)$$
$$= (0.21/a - 0.12) \times k(e_m^- + NO_3^-) \quad (5)$$

where a is an activity coefficient of the HSO_4^- ion in the medium. Assuming that the coefficient is the same as that in the 0.1 M solution at 0 °C, *i.e.*, 0.34, the reaction rate of e_m^- with the HSO_4^- ion is found to be equal to 0.50 $k(e_m^- + NO_3^-)$.

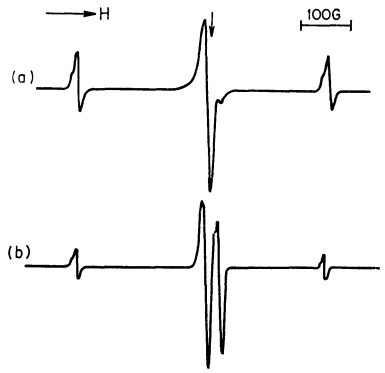

Fig. 3. ESR spectra of gamma-irradiated specimens.
(a) 6M sulfuric acid glass immediately after the irradiation.
(b) 6M sulfuric acid glass containing 1×10^{-2}M Cd^{2+}.

Electron-scavenging Efficiencies of Inorganic Ions. The ESR spectra of the gamma-irradiated samples which contained the Cd^{2+} ion are displayed in Fig. 3. The spectrum of the 6 M sulfuric acid glass is also shown for purposes of comparison. The doublet pattern of H_t is diminished efficiently by the presence of the Cd^{2+} ion. Because the reduction of the Cd^{2+} ion with e_{eq}^- is very fast ($k < 5.2 \times 10^{10}$ M^{-1} s^{-1}),[11] whereas that of the Cd^{2+} ion with the hydrogen atom is negligibly slow at room temperature ($k = 10^5$ M^{-1} s^{-1}),[12] the above observation implies that the reaction partner of the Cd^{2+} ion is not the hydrogen atom, but e_m^-. This finding allows us to estimate the reactivity of e_m^- from the decrease in the H_t yield.

Frohlinde *et al.* have reported that the H_t in the 6 M sulfuric acid glass is subject to thermal decay, even at 77 K.[14] This was confirmed in the present study; the rate was increased by the addition of the electron scavenger. The fraction decaying in the first

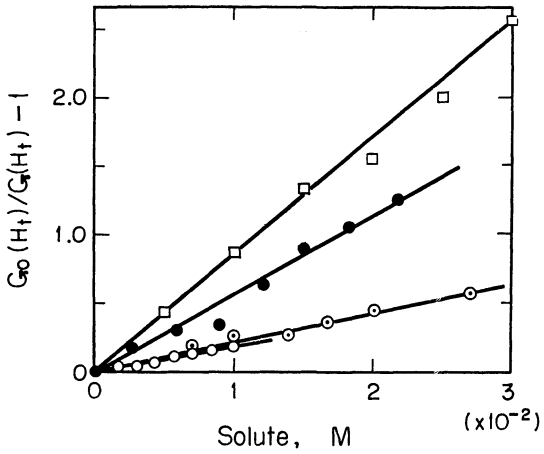

Fig. 4. Relationships between $[G_0(H_t)/G(H_t)-1]$ and solute concentration.
○: Cd^{2+}, ●: Fe^{3+}, ⊙: MoO_4^{2-}, □: TeO_4^{2-}.

2 hr amounted to 18% for the pure matrix and 27% for the matrix containing 5×10^{-2} M Cu^{2+} ions respectively. Therefore, the precise H_t yields were obtained by correcting the thermal decay at 77 K.

Based on Eq. (3), the relative rates of the e_m^- reaction can be determined from the slope of the straight line obtained by plotting $[G_0(H_t)/G(H_t)-1]$ against $[S]$. Some of the plottings are shown in Fig. 4. The relative reaction rates are summarized in Tables 1 and 2. The corresponding data known about the reactivities of e_{aq}^- in neutral solution are also presented. All the values normalized to unity for the reaction of $(e_m^- + Cd^{2+})$ or $(e_{aq}^- + Cd^{2+})$. As may be seen in the tables, the most effective e_m^- scavengers are the Fe^{2+} ion in the cationic solutes and the TeO_4^{2-} ion in the anionic solutes.

In the reaction of the Cr^{3+} ion with e_m^-, the relative rate is less than that which would be expected from the corresponding e_{aq}^- reaction, while in the case of the Ag^+ ion the reactivity amounts to 2.2 times the expected value. At present, it is impossible to give a reasonable interpretation of this irregularity. In the cases of the other metallic ions, the relative rates of the e_m^- reaction are roughly proportional to those of the e_{aq}^- reaction. These results are consistent with the previous observations for e_m^- in the ethylene glycol-water matrix.[4] On the other hand, in the cases of the oxyanions listed in Table 2 the reactivities of e_m^- seem to be independent of those of e_{aq}^-, and they are mostly larger than those of the e_{aq}^- reaction. This discrepancy seems to be closely related to the difference in the kinetic energy at the time of the scavenging reaction. The maximum concentration of e_t^- in alkaline glass has been determined to be 5.4×10^{17} g^{-1}, *viz.*, 2.4×10^{-2} M.[15] Assuming a homogeneous spatial distribution, the e_t^-'s are estimated to be 41 Å distant from each other. Furthermore, the e_t^- yield is reduced to 50% by the addition of 2.5×10^{-2} M acrylamide, an effective electron scavenger.[16] After all, the e_m^- in the acidic glass is also expected to travel a distance of over 20.5 Å before it is captured by the solute. Therefore, the electron in the system containing a

sufficient amount of the scavenger may encounter the solute a few times during the slowing-down processes. It is probable that the e_m^- in the epithermal energy region goes over the Coulomb barrier, which is too high for e_{aq}^- to pass through, and thus reacts more efficiently with the anionic species. In other words, the present results suggest that the electron can be scavenged even in the somewhat higher-energy region before slowing down to the thermal energy. This postulation is supported by the results of a previous experiment,[4] where the relative rates of the e_m^- reaction with polynegative cyano and oxalato complex ions are also larger than those which would be expected from the e_{aq}^- reaction.

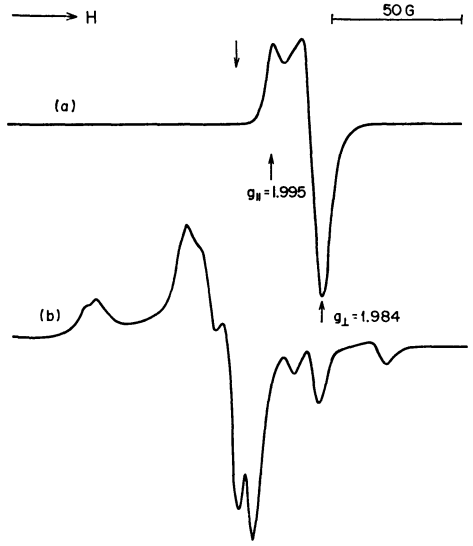

Fig. 5. ESR spectra of gamma-irradiated 6M sulfuric acid glasses containing 1×10^{-2}M Cd^{2+}.
(a) difference spectrum; Figs. 3(b)—(a)
(b) after thermal annealing at 152 K

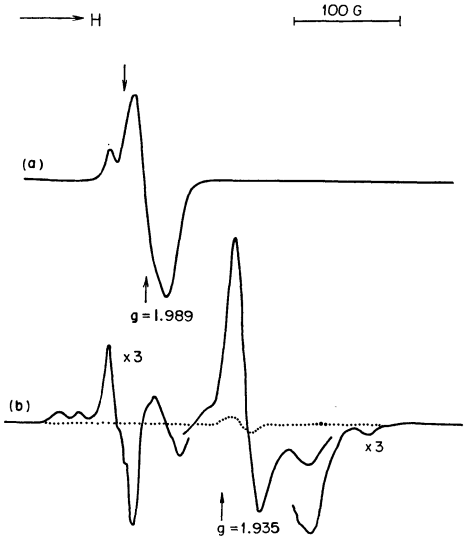

Fig. 6. ESR spectra of gamma-irradiated 6M sulfuric acid glasses containing
(a) 3×10^{-2}M TeO_4^{2-}. The sample has been annealed at 152 K.
(b) 4×10^{-2}M MoO_4^{2-}. The sample has been annealed at 154 K.

Spectra of the Reaction Products. Several fine spectra of the reaction intermediates could be obtained by thermal annealing at *ca.* 150 K, where the SO_4^- radical completely disappears. A difference spectrum (Figs. 3(b)—(a)) and a spectrum after thermal annealing for the samples containing the Cd^{2+} ion, both of which have axially symmetric *g*-factors, are shown in Fig. 5. The spectrum in Fig. 5(a) has a line shape attributable to the Cd^{1+} ion primarily formed.[17,18] The most intense signal in Fig. 5(b), which is complicated by the superposition of the Cd^{1+} ion, is assigned to a diatomic cation, *i.e.*, the Cd_2^{3+} ion found previously at 233 K.[18] These observations indicate that even in the solid phase, the migration of the Cd^{1+} ion takes precedence over the electron transfer from the Cd^{1+} ion to the SO_4^- radical.

Figure 6(a) shows the irradiated specimen containing the TeO_4^{2-} ion. The tellurium of the 5-valency state has an unpaired electron in its 4d shell, and it is expected to give rise to an intense singlet with a weak doublet due to ^{125}Te (6.99%, $I=1/2$). Therefore, the spectral pattern in Fig. 6(a) may be attributed to Te(V), *i.e.*, the TeO_4^{3-} ion. However, this assignment remains somewhat tentative, because no information is known about the spectral characteristics of the Te(V) species.

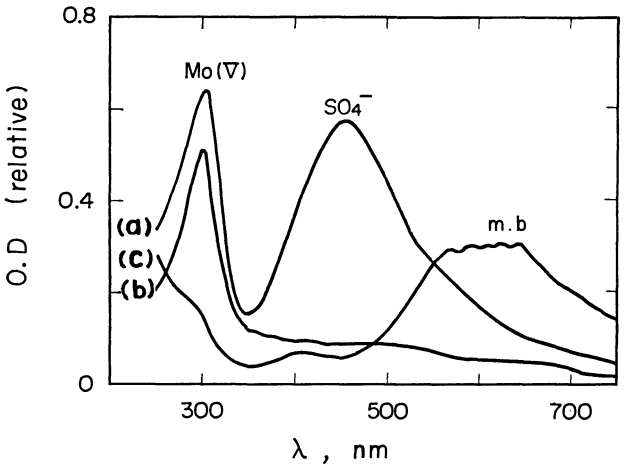

Fig. 7. Optical spectra of gamma-irradiated 6 M sulfuric acid glasses containing 4×10^{-2}M MoO_4^{2-}.
(a) after irradiated at 77 K
(b) after thermal annealing at 154 K
(c) after thermal annealing at 250 K

After the thermal annealing at 154 K, the irradiated glass containing the MoO_4^{2-} ion remained bright yellow, but it turned dark blue above *ca.* 190 K. The optical absorption spectra are displayed in Fig. 7. The spectrum of the blue species is assigned to molybedenum blue,[19] which is a nonstoichiometric polymolybdate composed of the Mo(V) and the Mo(VI) oxides.[20] The ESR pattern of the bright yellow species is shown in Fig. 6(b). There are two magnetic isotopes of molybdenum in natural abundance, ^{95}Mo (15.7%, $I=5/2$) and ^{97}Mo (9.45%, $I=5/2$). The molybdenum of the 5-valency state has unpaired electron in the 4d shell. Hence, we may assign the sixtet splitting to

the hyperfine coupling of ^{95}Mo and ^{97}Mo, which is overlapped with a stronger central singlet due to the nonmagnetic molybednum nuclei.

From these observations it may be concluded that the Mo(V) species primarily produced polymerize with some MoO_4^{2-} ions during the thermal annealing as in the case of the Cd^{1+} ion. By performing thermal-annealing experiments on the frozen specimen, much information would be obtained on the inorganic polymerized species, which are hard to be detected at room temperature.

References

1) L. Kevan, P. N. Moorthy, and J. J. Weiss, *J. Amer. Chem. Soc.*, **86**, 771 (1964); L. Kevan, *Progr. Solid State Chem.*, **2**, 304 (1965); S. Ohno, T. Sasaki, and M. Koike, This Bulletin, **45**, 2383 (1972).

2) L. Kevan, *J. Amer. Chem. Soc.*, **89**, 4238 (1967); "Radiation Chemistry of Aqueous Systems", ed. by G. Stein, Weizmann Science Press, Israel (1968), p. 62.

3) H. B. Steen, O. Kaalhus, and M. Kongshaug, *J. Phys. Chem.*, **75**, 1941 (1971).

4) T. Sasaki and S. Ohno, This Bulletin, **44**, 2626 (1971).

5) L. Kevan and C. Fine, *J. Amer. Chem. Soc.*, **88**, 869 (1966).

6) H. B. Steen and M. Kongshaug, *J. Phys. Chem.*, **76**, 2217 (1972).

7) D. M. Brown and F. S. Dainton, *Trans. Faraday Soc.*, **62**, 1139 (1966).

8) R. Livingston and A. J. Weinberger, *J. Chem. Phys.*, **33**, 499 (1960).

9) J. Moan, *Int. J. Radiat. Phys. Chem.*, **5**, 293 (1973).

10) B. G. Ershov and A. K. Pikaev, *Radiat. Res. Rev.*, **2**, 66 (1969).

11) J. H. Baxendale, E. M. Fielden, and J. P. Keene, *Proc. Royal Soc., Ser. A*, **286**, 320 (1965).

12) E. Hayon and M. Moreau, *J. Chim. Phys.*, 391 (1965).

13) M. Anbar and P. Neta, *Int. J. Appl. Radiat. Isotopes*, **18**, 493 (1967).

14) W. Kohnlein and D.S. Frohlinde. *Radiat. Res.*, **38**, 173 (1969).

15) H. Hase and L. Kevan, *J. Phys. Chem.*, **73**, 3290 (1969).

16) W. A. Seddon and D. R. Smith, *Can. J. Chem.*, **45**, 3083 (1967).

17) P. N. Moorthy and J. J. Weiss, *Nature*, **201**, 1318 (1964).

18) R. S. Eachus and M. C. R. Symons, *J. Chem. Soc. A*, **1970**, 3080.

19) F. L. Conde and L. Prat, *Anal. Chim. Acta*, **16**, 473 (1957).

20) "Advanced Inorganic Chemistry", ed. by P. J. Durrant and B. Durrant, Longmans, London (1962), p. 1001.

The Dianion of 9,9′-Bixanthenylidene and Its Reaction with Oxygen. A Contribution to Photochromism

Mikio HOSHINO, Masao MATSUI, and Masashi IMAMURA
The Institute of Physical and Chemical Research, Wako, Saitama 351
(Received April 16, 1973)

The anion produced by the reduction of 9,9′-bixanthenylidene with sodium or potassium metal was identified with the dianion by pulse radiolysis. It appears that the dianion is twisted around the central ethylenic bond. The dianion reacts with oxygen at 100 K to produce a colored form, the spectrum of which is in accord with that of the transient species observed in the flash photolysis of 9,9′-bixanthenylidene. The colored form is expected to be produced *via* a twisted 9,9′-bixanthenylidene, because the oxygen is considered to remove electrons from the twisted dianion. This twisted intermediate may also participate in the photochromic or thermochromic reaction in which the same-colored form is produced.

9,9′-Bixanthenylidene is known to be one of the thermochromic ethylenes, and the structure of the colored form has been assumed to be a dihydro-form of a species, A, which is obtained as the stable photoproduct.[1,2]

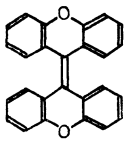
Species A

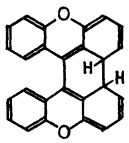
Dihydro- form of A

The same color is observed on UV irradiation at low temperatures, and it fades reversibly in the dark in a few minutes.[3] The above structure of the colored form was assumed by analogy from the facts that *cis*-stilbene, which has the same ethylenic bond, shows photochromism in a deaerated solution and, that its colored form is considered to be the dihydro-form of phenanthrene.[4,5]

A similar dihydro-form has been assumed for the colored form of thermochromic 10,10′-bianthrone. It has been found that, in the presence of oxygen, helianthrone and *meso*-naphthobianthrone are produced; the dihydro-forms of these stable photoproducts are produced in the absence of oxygen.[6–8]

It seems, therefore, that in many cases the colored form of the thermochromic ethylenes is a dihydro-form of the stable photoproducts.

In 1959, Woodward and Wasserman[9] showed that the reaction of the anion of 10,10′-bianthrone with methanol gave rise to the formation of the colored form. We ourselves have found that the colored form of 9,9′-bixanthenylidene is produced by the reaction of its anion with oxygen at low temperatures. The mechanism of this reaction has now been studied by using flash photolysis and pulse radiolysis with the aim of elucidating the mechanism of the photochromic reactions.

Experimental

9,9′-Bixanthenylidene was prepared by the reduction of xanthone with zinc powder and acetic acid in the presence of hydrochloric acid. The purification was done by recrystallization from a methanolic solution. The tetrahydrofuran (THF) and 2-methyltetrahydrofuran (MTHF) were stored on the metallic alloy of potassium and sodium *in vacuo*. The benzene and ethanol were extra-pure reagents from Wako Pure Chemical Industries.

The details of the flash photolysis apparatus have been described previously.[10] The photolysis flash consisted of two xenon lamps, 80 J in power and 50 μs in duration.

The pulse radiolysis was carried out by using 2.7 MeV pulsed electrons, 0.5 or 1.0 μs in duration, generated from a Van de Graaff accelerator; the details have been described elsewhere.[11]

The absorption spectra of stable products were recorded on a Cary 14 R spectrophotometer.

Results and Discussion

Flash Photolysis. Figure 1 shows the transient absorption spectrum observed immediately after the flash photolysis of 9,9′-bixanthenylidene in a deaerated benzene solution. The spectrum had an absorption peak at 620 nm and decayed with a first-order rate constant of $1.8\times10^4\ s^{-1}$ at room temperature. In an aerated solution, the same spectrum was observed; the amount of intermediate species produced (at 620 nm) per flash and the decay rate were identical with those in a deaerated solution within the limits of experimental errors. These results indicate that the transient species may be produced *via* the excited singlet state.

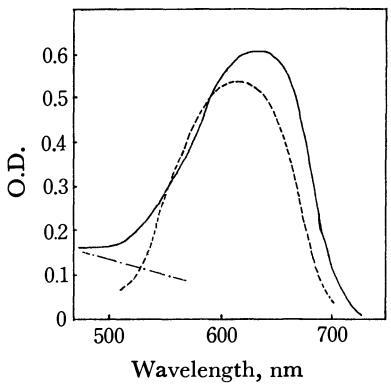

Fig. 1. Absorption spectra of the colored substance.
------: The transient species formed upon flash photolysis in benzene at room temperature;
——: The colored substance produced by the reaction of the dianion of 9,9′-bixanthenylidene with oxygen at low temperature (100 K) in MTHF.

On the other hand, Hirshberg and Fischer[3] found that the colored form is produced on the UV irradiation of 9,9′-bixanthenylidene at low temperatures. The spectrum is in accord with the transient spectrum obtained by the present flash photolysis. They also studied the dependence of the decay rate of the colored form on the temperature, and evaluated the kinetic parameters of a "critical increment" [12] and a frequency factor over the temperature range from −150 to −170 °C. Using these parameters, one can estimate the rate constant of the decay at room temperature to be $2.5 \times 10^4\ s^{-1}$; this value is in agreement with that obtained for the transient species by the flash photolysis.

From these results, it may be concluded that the transient absorption in the flash photolysis is due to the colored form of 9,9′-bixanthenylidene produced by UV irradiation at low temperatures.

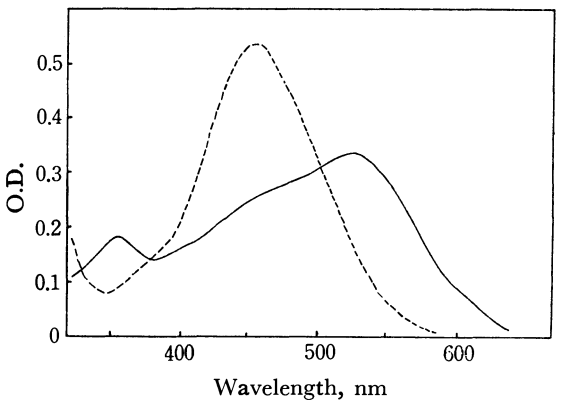

Fig. 2. Absorption spectra of the dianion of 9,9′-bixanthenylidene (——) and potassium xanthenylide (------) in MTHF at room temperature.

Reaction of Dianion with Oxygen. When 9,9′-bixanthenylidene was reduced in a MTHF solution by metallic sodium or potassium, the solution turned reddish-brown and had an absorption peak at 520 nm, as is shown in Fig. 2. The colored species may be regarded as a monoanion or a dianion because the color of the solution fades rapidly upon the introduction of air. It was identified with the dianion by pulse radiolysis, as will be described in the next section.

The solution turned brilliant blue and had an absorption peak at 630 nm when the dianion was in contact with the air at a low temperature (100 K). The resulting spectrum is similar to that of the transient species produced by the flash photolysis, as is shown in Fig. 1, indicating that the two species are identical.

The colored form was stable so long as the solution was kept at 77 K, but it disappeared rapidly with an increase in the temperature. This suggests that the viscosity of the solution plays an important role in the reversion reaction (colored→colorless).

Hirshberg and Fischer[3] found that photochromism occurs above −120 °C in the mixed glassy media of methanol and ethanol. They also mentioned that the phenomenon takes place only in a fluid solution.

Pulse Radiolysis of 9,9′-Bixanthenylidene. Figure 3 shows the transient spectrum of the monoanion of

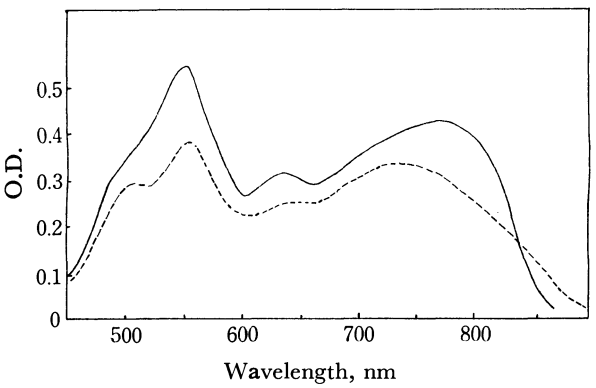

Fig. 3. Absorption spectra of the monoanion of 9,9′-bixanthenylidene.
——: Produced by γ-ray irradiation at 77 K;
------: Produced by pulse radiolysis at room temperature.

9,9′-bixanthenylidene produced by pulsed electron irradiation in a MTHF solution at room temperature. The ion is produced according to:

$$\text{MTHF} \rightsquigarrow e^- + \text{MTHF}^+$$

$$e^- + \text{M} \longrightarrow \text{M}^- \quad (\text{M: solute}).$$

A similar spectrum of the monoanion was observed by the steady Co^{60}-γ rays irradiation of 9,9′-bixanthenylidene in MTHF at 77 K.

In view of the difference between the spectrum of this monoanion and that of the ion produced by the reduction of 9,9′-bixanthenylidene with alkali metals, the latter one may possibly be regarded as being due to the dianion.

It is also noted that the monoanion does not appear to change in structure in going from 77 K to room temperature, because the electronic spectra are similar at both temperatures.

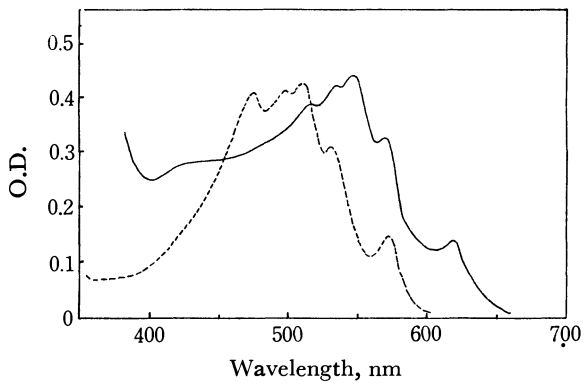

Fig. 4. Absorption spectra of the dianion of 9,9′-bixanthenylidene (——) and potassium xanthenylide (------) at 77 K in MTHF.

Structure of the Dianion. In Fig. 4, the absorption spectrum of the dianion is compared with that of potassium xanthenylide, both of which were obtained in MTHF solutions at 77 K.

If the dianion is assumed to be twisted around the ethylenic bond, the spectrum is expected to be similar to that of the xanthenyl carbanion. Although the

absorption band of the dianion is located in a longer wavelength region compared with that of the carbanion, the same vibrational progression is found in both spectra. It is, therefore, reasonable to assume that the dianion has a twisted structure at 77 K. The slight shift of the absorption band of the dianion to longer wavelengths may be interpreted in terms of the bathochromic effect due to the substituted xanthenyl moiety.

The structure of the stilbene dianion was discussed by Garst *et al.*,[13] who proposed a geometry in which the two benzylidene moieties are rotated around the central ethylenic bond to an angle of 90°. Suzuki *et al.*[14] studied the twisted forms of the dianion of stilbene derivatives and interpreted the absorption spectra on the basis of the MO calculation.

The dianion with a central ethylenic bond is likely to be twisted around the bond.

Intermediate as a Precursor of the Colored Form. The reaction of oxygen with anions of aromatic molecules is considered to give rise to the formation of the original molecules:

$$M^- \text{ (or } M^{2-}) + O_2 \longrightarrow M \text{ (M: aromatic molecule)}$$

where oxygen is assumed to act simply as an electron acceptor.

In the case of the 9,9′-bixanthenylidene dianion, the reaction with oxygen at low temperatures has been shown to produce a colored compound, not original 9,9′-bixanthenylidene. This result may be explained by assuming that the elimination of two electrons from the twisted dianion gives rise to the formation of a metastable intermediate which is also twisted and which immediately forms the colored compound:

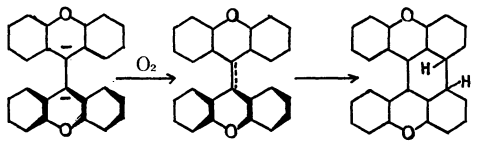

(Twisted intermediate)

In view of the fact that the same colored substance is formed in either the photochromic or thermochromic reaction, this intermediate is formed in both cases, although it could not be detected by the flash photolysis.

We wish to thank Miss. Yuriko Moribe for her assistance with the flash photolysis study, and Dr. Tadamasa Shida and Dr. Shigeyoshi Arai for thier enlightening discussions.

Literatures

1) A. Schönberg and O. Schutz, *Chem. Ber.*, **61**, 478(1928).
2) W. Theilacker, G. Kortüm, and G. Friedheim, *ibid.*, **83**, 508 (1950).
3) Y. Hirshberg and E. Fischer, *J. Chem. Soc.*, **1953**, 629.
4) A. Schönberg and K. Junghaus, *Chem. Ber.*, **98**, 2539 (1965).
5) W. M. Moore, D. D. Morgan, and F. R. Stermitz, *J. Amer. Chem. Soc.*, **85**, 829 (1963).
6) H. Meyer, R. Bondy, and A. Eckert, *Monatsh. Chem.*, **33**, 1451 (1912).
7) H. R. Huber, U. Wild, and Hs. H. Gunthard, *Helv. Chim. Acta*, **50**, 598 (1967).
8) G. Kortüm, *Angew. Chem.*, **70**, 14 (1958).
9) R. B. Woodward and E. Wasserman, *J. Amer. Chem. Soc.*, **81**, 5007 (1959).
10) A. Kira and K. Nishi, *Rep. Inst. Phys. Chem. Rev.*, **44**, 56 (1968).
11) A. Kira, S. Arai, and M. Imamura, *ibid.*, **47**, 139 (1971).
12) The critical increment was calculated from the temperature dependence of the reversion time(colored→colorless). The actual activation energy may be somewhat higher than this value.
13) J. F. Garst, J. G. Pacific, and E. R. Zabolontny, *J. Amer. Chem. Soc.*, **88**, 3872 (1966).
14) H. Suzuki, K. Koyano, and T. L. Kunii, This Bulletin, **45**, 1979 (1972).

The Crystal Structure of *dl*-1,1,4a*α*-Trimethyl-2*α*-hydroxy-8*β*-methoxy-1,2,3,4,4a,5,6,7,8,9-decahydrophenanthrene

Akio FURUSAKI, Nobuyuki HAMANAKA, and Takeshi MATSUMOTO
Department of Chemistry, Faculty of Science, Hokkaido University, Sapporo 060
(Received April 24, 1973)

The crystal structure of the title compound has been determined from three-dimensional data collected on an automatic, four-circle diffractometer. The racemic crystals are triclinic, with two molecules in a unit cell of these dimensions; $a=10.502$, $b=11.706$, $c=7.488$ Å, $\alpha=71°33'$, $\beta=91°46'$, and $\gamma=116°22'$. The space group is $P\bar{1}$. The structure was solved by the symbolic addition method and was then refined by the block-diagonal-matrix least-squares method, with isotropic temperature factors for the hydrogen atoms and with anisotropic ones for the others. The final R value was 6.7%. The length of the C–C single bond opposite to the double bond in the cyclohexene ring is only 1.34 ± 0.01 Å. This apparent remarkable shortening can be well explained on the assumption that the two atoms concerned vibrate vigorously with parallel and antiparallel harmonic components perpendicular to the plane of the ring. It is shown that, if the root-mean-square amplitudes of the former components are taken to be equal to that of the thermal vibration of the carbon atom adjacent to one of the two atoms, the above C–C distance, corrected for these antiparallel motions, becomes quite reasonable: 1.60 Å.

It has recently been reported that the Birch reduction of 1,1,4a*α*-trimethyl-2*α*-hydroxy-8-methoxy-1,2,3,4,4a,9-hexahydrophenanthrene, I, produced an unexpected product, II.[1] The X-ray study of the *p*-bromobenzoate of II has revealed that the C ring of cyclohexene-type shows an unusual thermal behavior in the crystalline state.[2] In order to obtain more accurate information about the behavior of the C ring, an X-ray crystallographic analysis of II itself has now been carried out.

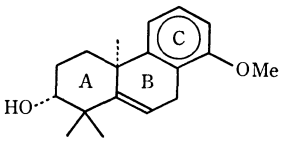

I

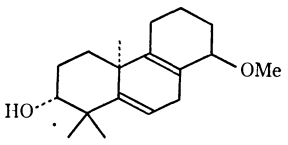

II

Experimental

Colorless, single crystals of II (racemate), $C_{18}H_{28}O_2$ (mp 162—164 °C), were obtained from a chloroform solution. A crystal with dimensions of about $0.2\times0.3\times0.4$ mm was used for the X-ray measurement. The crystal data are summarized in Table 1. The cell dimensions were measured by using a single-crystal diffractometer with Cu$K\alpha$ radiation ($\lambda=1.54178$ Å). The space group was assumed to be $P\bar{1}$ at the beginning of the study; this choice was later confirmed by a successful refinement. The intensity data were collected on an automatic, four-circle diffractometer at this University, using Cu$K\alpha$ radiation monochromatized with a LiF crystal. The intensity measurement was made by using an ω-2θ continuous scan at a rate of about 0.5°(ω)/min; the background was measured for 30—60 s at each end of the scan range. The intensities thus obtained were corrected for the Lorentz and polarization factors, but not for either the absorption or the extinction effect. In all, out of the structure factors of reflections with 2θ values up to 140°, 2276 above $3\,\sigma(F)$ were selected for the structural study.

Table 1. The crystal data

Crystal system Space group	Triclinic $P\bar{1}$
a	10.502 ± 0.002 Å
b	11.706 ± 0.003
c	7.488 ± 0.002
α	$71°33'\pm2'$
β	$91°46'\pm3'$
γ	$116°22'\pm2'$
Z	2
D_x	1.183 g/cm^3

Structure Determination

The structure was solved by the direct method on the basis of 511 $|E|$ values above 1.30.[3] The origin was specified by assigning positive signs to three linearly-independent reflections, as is shown in Table 2. At the early stage of the structure determination, the symbolic addition procedure was carried out by the use of three symbols, A, B, and C. However, this procedure turned out to be unsuccessful, for no E-maps calculated from the eight possible combinations of the numerical values of the symbols afforded an acceptable structure. This difficulty was overcome by adding a fourth symbol, D. The correct combination of the values of the symbols, $A=B=C=\pi$ and $D=0$, was chosen by the method that had been used in the structure determination of the acetolysis product of II.[4] An E-map calculated with 461 phases clearly revealed the positions of all twenty non-hydrogen atoms. The structure thus obtained was refined at first by the block-diagonal-matrix least-squares method with isotropic temperature factors. After it had been ascertained that there was no other remarkable peak in a Fourier diagram, the structure was further refined by the

Table 2. The starting set

h	k	l	$\|E\|$	φ
2	7	3	4.73	0
$\bar{8}$	1	2	4.54	0
$\bar{3}$	4	6	4.10	0
4	10	4	5.00	A
$\bar{8}$	1	1	4.30	B
$\bar{2}$	2	0	3.26	C
9	0	4	3.96	D

TABLE 3. THE FINAL ATOMIC PARAMETERS WITH THEIR STANDARD DEVIATIONS

(a) The non-hydrogen atoms

The parameters are multiplied by 10^4.

(1) The fractional coordinates

Atom	x/a	y/b	z/c	Atom	x/a	y/b	z/c
O(1)	7614(2)	3884(2)	2840(4)	C(9)	2049(3)	−455(2)	3124(3)
O(2)	54(2)	−3306(2)	6912(4)	C(10)	3300(2)	987(2)	2556(3)
C(1)	4636(3)	1006(3)	1695(4)	C(11)	1763(4)	−1146(4)	1637(5)
C(2)	5988(3)	2344(3)	1338(4)	C(12)	560(6)	−2519(6)	2233(9)
C(3)	6330(3)	2656(3)	3166(4)	C(13)	−480(8)	−2948(6)	3641(8)
C(4)	5115(3)	2772(2)	4069(3)	C(14)	−139(3)	−2411(3)	5248(4)
C(5)	3686(2)	1494(2)	4256(3)	C(15)	5499(3)	2903(3)	6021(5)
C(6)	2812(3)	833(2)	5878(3)	C(16)	5044(3)	4088(3)	2903(5)
C(7)	1435(3)	−423(3)	6264(4)	C(17)	2804(3)	1898(3)	1032(4)
C(8)	1192(3)	−1056(2)	4762(3)	C(18)	−1218(3)	−4389(3)	8017(5)

(2) The anisotropic temperature factors

These are expressed as

$$\exp\left[-(\beta_{11}h^2+\beta_{22}k^2+\beta_{33}l^2+\beta_{12}hk+\beta_{23}kl+\beta_{31}lh)\right].$$

Atom	β_{11}	β_{22}	β_{33}	β_{12}	β_{23}	β_{31}
O(1)	86(2)	104(2)	338(6)	41(3)	−102(6)	−15(5)
O(2)	88(2)	94(2)	357(6)	42(3)	4(6)	−19(6)
C(1)	117(3)	101(3)	188(5)	82(5)	−115(6)	32(6)
C(2)	107(3)	110(3)	210(6)	70(5)	−81(6)	70(7)
C(3)	89(3)	80(2)	224(5)	67(4)	−55(6)	−24(6)
C(4)	92(3)	74(2)	171(5)	53(4)	−79(5)	−28(5)
C(5)	90(2)	70(2)	145(4)	71(4)	−77(5)	−33(5)
C(6)	101(3)	93(2)	145(4)	64(4)	−111(5)	−28(5)
C(7)	102(3)	103(3)	153(5)	39(4)	−89(6)	27(6)
C(8)	91(2)	80(2)	166(4)	54(4)	−83(5)	−38(5)
C(9)	105(3)	91(2)	146(4)	75(4)	−108(5)	−52(5)
C(10)	98(3)	78(2)	123(4)	71(4)	−59(5)	−16(5)
C(11)	165(4)	128(3)	223(6)	32(6)	−209(8)	−1(8)
C(12)	241(8)	224(7)	450(14)	−116(13)	−506(19)	153(18)
C(13)	336(12)	208(7)	379(13)	−266(16)	−374(17)	192(20)
C(14)	103(3)	94(3)	211(5)	38(5)	−86(6)	−41(6)
C(15)	124(3)	108(3)	227(6)	42(5)	−160(7)	−73(7)
C(16)	129(3)	87(3)	288(7)	92(5)	−99(7)	−54(8)
C(17)	134(3)	107(3)	169(5)	112(5)	−67(6)	−65(6)
C(18)	117(3)	103(3)	302(8)	45(5)	−34(8)	10(8)

(b) The hydrogen atoms

The positional and thermal parameters are multiplied by 10^3 and 10 respectively.

Atom	x/a	y/b	z/c	B(Å^2)	Atom	x/a	y/b	z/c	B(Å^2)
H(1-1)	476(4)	28(3)	255(5)	19(6)	H(15-1)	547(5)	203(4)	688(6)	34(8)
H(1-2)	446(4)	83(4)	57(5)	23(6)	H(15-2)	640(4)	361(4)	586(6)	30(7)
H(2-1)	680(4)	226(4)	83(5)	24(6)	H(15-3)	487(5)	308(5)	663(7)	43(9)
H(2-2)	587(5)	301(4)	50(6)	31(7)	H(16-1)	421(5)	410(5)	345(7)	37(8)
H(3)	643(3)	192(3)	404(4)	9(5)	H(16-2)	597(5)	486(5)	303(7)	42(9)
H(6)	309(3)	123(3)	693(5)	16(5)	H(16-3)	510(6)	418(6)	164(9)	56(12)
H(7-1)	70(5)	−19(4)	642(6)	33(8)	H(17-1)	349(5)	277(5)	42(7)	42(9)
H(7-2)	139(4)	−104(4)	741(5)	27(7)	H(17-2)	206(5)	202(5)	151(7)	46(10)
H(11-1)	159(8)	−54(8)	46(11)	79(17)	H(17-3)	249(5)	155(5)	11(7)	41(9)
H(11-2)	255(6)	−97(6)	104(8)	49(11)	H(18-1)	−94(6)	−491(6)	911(8)	48(11)
H(12-1)	42(5)	−293(5)	134(7)	44(10)	H(18-2)	−183(7)	−479(6)	727(9)	58(12)
H(13-1)	−118(7)	−354(6)	389(9)	56(12)	H(18-3)	−183(9)	−415(8)	883(12)	80(17)
H(14)	−98(4)	−231(4)	568(5)	26(7)	H(O)	832(6)	366(5)	292(8)	47(10)

least-squares method, anisotropic thermal motions being assumed for all the non-hydrogen atoms. In this way, the discrepancy factor, R, was reduced to 11.9%. Out of the twenty-eight hydrogen atoms in the molecule, twenty-six were located in a difference Fourier map. The least-squares refinement was further repeated including these hydrogen atoms. In this refinement, the following weighting scheme was used:

$$W = 1/\{\sigma(F_o)^2 \exp(AX^2+BY^2+CXY+DX+EY)\},$$

where $X=|F_o|$ and $Y=\sin\theta/\lambda$.[4] The intensity data were grouped with constant intervals along two coordinates, $|F_o|$ and $\sin\theta/\lambda$. The coefficients, A, B, C, D, and E, were determined by the least-squares fit so as to give as equal values of $\langle W|\Delta F|^2\rangle$ for all the groups as possible. The final R value was 6.7%. The atomic parameters thus obtained are listed in Table 3.

The calculations for the present study were performed on a FACOM 230-60 computer at the Computer Center of Hokkaido University, using our own programs. The atomic scattering factors were taken from International Tables for X-ray Crystallography (1962), Vol. III. The tables of the observed and calculated structure factors are preserved by the Chemical Society of Japan (Document No. 7408).

Results and Discussion

The molecular framework of II and the torsion angles for the tricyclic system are given in Figs. 1 and 2 respectively. The molecular conformation of II is found to resemble closely that of its *p*-bromobenzoate derivative, hereafter called III;[2] the A and B rings take a distorted chair- and a somewhat flattened boat-form respectively, while the C ring has a considerably flattened half-chair conformation, with the methoxyl group oriented axially. A closer examination of the torsion angles shows that the conformational differences between the corresponding A, B, and C rings of II and III become greater in that order. This seems strange at first sight, since II differs from III simply in having a free hydroxyl group instead of a *p*-bromobenzoyloxy group in the A ring. However, this might be explained in terms of the theory that the unstable and flexible conformation of the C ring is more or less influenced by the hydrogen-bond formation of the methoxyl oxygen atom, with the hydroxyl group in another molecule.

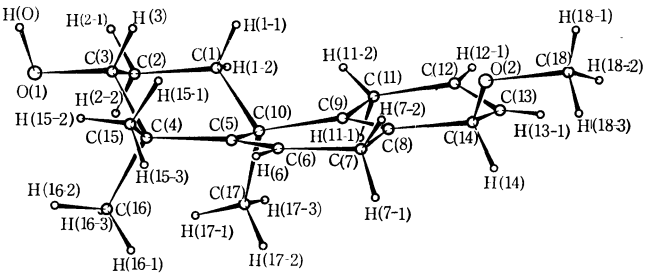

Fig. 1. The molecular configuration of II and the numbering system of the atoms.

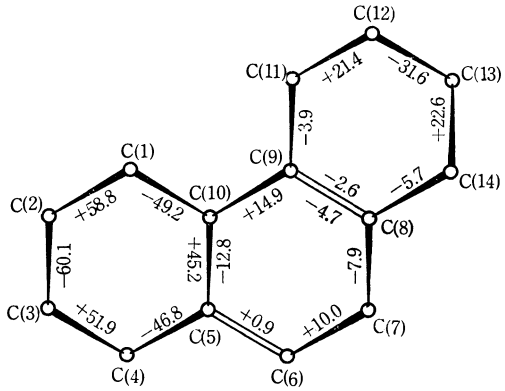

Fig. 2. The torsion angles (°) for the tricyclic system.

Table 4. The bond distances with their standard deviations (Å)
The standard deviations given in parentheses refer to the last decimal position.

(a) The bond distances between the non-hydrogen atoms

C(1)–C(2)	1.525(3)	C(5)–C(6)	1.326(3)	C(10)–C(17)	1.548(4)
C(1)–C(10)	1.551(4)	C(5)–C(10)	1.539(4)	C(11)–C(12)	1.468(6)
C(2)–C(3)	1.518(5)	C(6)–C(7)	1.485(3)	C(12)–C(13)	1.343(10)
C(3)–C(4)	1.539(5)	C(7)–C(8)	1.491(4)	C(13)–C(14)	1.491(8)
C(3)–O(1)	1.422(3)	C(8)–C(9)	1.330(3)	C(14)–O(2)	1.427(4)
C(4)–C(5)	1.548(3)	C(8)–C(14)	1.516(3)	C(18)–O(2)	1.405(3)
C(4)–C(15)	1.541(4)	C(9)–C(10)	1.538(3)		
C(4)–C(16)	1.545(4)	C(9)–C(11)	1.522(5)		

(b) The bond distances involving the hydrogen atoms

C(1)–H(1-1)	0.95(4)	C(11)–H(11-2)	0.86(7)	C(16)–H(16-3)	0.92(7)
C(1)–H(1-2)	0.92(4)	C(12)–H(12-1)	0.92(7)	C(17)–H(17-1)	0.92(4)
C(2)–H(2-1)	1.00(5)	C(13)–H(13-1)	0.73(5)	C(17)–H(17-2)	0.95(7)
C(2)–H(2-2)	0.88(5)	C(14)–H(14)	1.02(5)	C(17)–H(17-3)	0.89(6)
C(3)–H(3)	0.95(3)	C(15)–H(15-1)	1.01(5)	C(18)–H(18-1)	0.98(6)
C(6)–H(6)	1.01(4)	C(15)–H(15-2)	0.92(4)	C(18)–H(18-2)	0.91(7)
C(7)–H(7-1)	0.95(6)	C(15)–H(15-3)	0.94(7)	C(18)–H(18-3)	1.08(11)
C(7)–H(7-2)	0.91(4)	C(16)–H(16-1)	0.98(6)	O(1)–H(O)	0.88(7)
C(11)–H(11-1)	1.01(8)	C(16)–H(16-2)	1.02(5)		

Table 5. The bond angles with their standard deviations (°)
The standard deviations given in parentheses refer to the last decimal position.

C(2)–C(1)–C(10)	113.1(2)	C(4)–C(3)–H(3)	107(2)
C(1)–C(2)–C(3)	110.9(2)	O(1)–C(3)–H(3)	110(2)
C(2)–C(3)–C(4)	112.3(3)	C(5)–C(6)–H(6)	117(2)
C(2)–C(3)–O(1)	110.8(2)	C(7)–C(6)–H(6)	117(2)
C(4)–C(3)–O(1)	108.6(2)	C(6)–C(7)–H(7-1)	107(3)
C(3)–C(4)–C(5)	108.9(2)	C(6)–C(7)–H(7-2)	110(2)
C(3)–C(4)–C(15)	107.2(2)	C(8)–C(7)–H(7-1)	111(4)
C(3)–C(4)–C(16)	111.0(2)	C(8)–C(7)–H(7-2)	110(2)
C(5)–C(4)–C(15)	111.6(2)	H(7-1)–C(7)–H(7-2)	105(4)
C(5)–C(4)–C(16)	112.0(2)	C(9)–C(11)–H(11-1)	107(5)
C(15)–C(4)–C(16)	106.0(3)	C(9)–C(11)–H(11-2)	111(4)
C(4)–C(5)–C(6)	120.1(2)	C(12)–C(11)–H(11-1)	111(5)
C(4)–C(5)–C(10)	119.5(2)	C(12)–C(11)–H(11-2)	121(4)
C(6)–C(5)–C(10)	120.4(2)	H(11-1)–C(11)–H(11-2)	90(6)
C(5)–C(6)–C(7)	125.6(3)	C(11)–C(12)–H(12-1)	113(4)
C(6)–C(7)–C(8)	114.0(2)	C(13)–C(12)–H(12-1)	122(4)
C(7)–C(8)–C(9)	122.4(2)	C(12)–C(13)–H(13-1)	129(4)
C(7)–C(8)–C(14)	113.9(2)	C(14)–C(13)–H(13-1)	109(4)
C(9)–C(8)–C(14)	123.6(3)	C(8)–C(14)–H(14)	108(3)
C(8)–C(9)–C(10)	123.1(3)	C(13)–C(14)–H(14)	110(3)
C(8)–C(9)–C(11)	120.5(2)	O(2)–C(14)–H(14)	104(3)
C(10)–C(9)–C(11)	116.2(2)	C(4)–C(15)–H(15-1)	109(3)
C(1)–C(10)–C(5)	108.9(2)	C(4)–C(15)–H(15-2)	109(2)
C(1)–C(10)–C(9)	109.3(2)	C(4)–C(15)–H(15-3)	114(4)
C(1)–C(10)–C(17)	109.9(2)	H(15-1)–C(15)–H(15-2)	110(4)
C(5)–C(10)–C(9)	112.2(2)	H(15-1)–C(15)–H(15-3)	108(5)
C(5)–C(10)–C(17)	110.6(2)	H(15-2)–C(15)–H(15-3)	107(5)
C(9)–C(10)–C(17)	106.0(2)	C(4)–C(16)–H(16-1)	109(3)
C(9)–C(11)–C(12)	114.5(3)	C(4)–C(16)–H(16-2)	105(3)
C(11)–C(12)–C(13)	122.0(7)	C(4)–C(16)–H(16-3)	109(4)
C(12)–C(13)–C(14)	119.8(5)	H(16-1)–C(16)–H(16-2)	111(4)
C(8)–C(14)–C(13)	113.5(3)	H(16-1)–C(16)–H(16-3)	117(5)
C(8)–C(14)–O(2)	107.0(2)	H(16-2)–C(16)–H(16-3)	105(5)
C(13)–C(14)–O(2)	113.6(4)	C(10)–C(17)–H(17-1)	116(3)
C(14)–O(2)–C(18)	115.2(3)	C(10)–C(17)–H(17-2)	114(4)
C(2)–C(1)–H(1-1)	111(2)	C(10)–C(17)–H(17-3)	110(4)
C(2)–C(1)–H(1-2)	109(3)	H(17-1)–C(17)–H(17-2)	103(5)
C(10)–C(1)–H(1-1)	107(2)	H(17-1)–C(17)–H(17-3)	105(4)
C(10)–C(1)–H(1-2)	109(3)	H(17-2)–C(17)–H(17-3)	108(6)
H(1-1)–C(1)–H(1-2)	107(4)	O(2)–C(18)–H(18-1)	107(4)
C(1)–C(2)–H(2-1)	108(3)	O(2)–C(18)–H(18-2)	110(4)
C(1)–C(2)–H(2-2)	110(3)	O(2)–C(18)–H(18-3)	117(6)
C(3)–C(2)–H(2-1)	109(3)	H(18-1)–C(18)–H(18-2)	121(6)
C(3)–C(2)–H(2-2)	109(3)	H(18-1)–C(18)–H(18-3)	96(7)
H(2-1)–C(2)–H(2-2)	110(4)	H(18-2)–C(18)–H(18-3)	105(7)
C(2)–C(3)–H(3)	107(2)	C(3)–O(1)–H(O)	106(5)

The bond lengths and angles calculated with the final coordinates are listed in Tables 4 and 5 respectively. In the present molecule also, the C(12)–C(13) distance is found to be unusually shorter than the normal C–C single bond length. A detailed account of this remarkable shortening will be given later. The intramolecular hydrogen-hydrogen distances less than 2.40 Å are listed in Table 6.

The conformation of the A ring in II is closely parallel to that in III; for example, the greatest of the differences between the corresponding torsion angles is only 2.6°, and the average torsion angles for the two

Table 6. The intramolecular H···H contacts (Å)
The standard deviations are given in parentheses.

H(1-1)···H(2-1)	2.35(4)	H(3)	···H(O)	2.06(5)	H(11-2)···H(12-1)	2.34(7)
H(1-2)···H(2-1)	2.33(5)	H(6)	···H(7-2)	2.36(5)	H(12-1)···H(13-1)	2.30(9)
···H(2-2)	2.29(6)		···H(15-1)	2.25(6)	H(13-1)···H(14)	2.21(9)
···H(11-2)	2.10(6)		···H(15-3)	2.09(5)	H(15-2)···H(16-2)	2.33(7)
H(2-1)···H(3)	2.32(5)	H(11-1)	···H(12-1)	2.37(10)	H(16-3)···H(17-1)	2.19(8)
H(2-2)···H(16-3)	2.24(11)		···H(17-3)	2.12(10)		

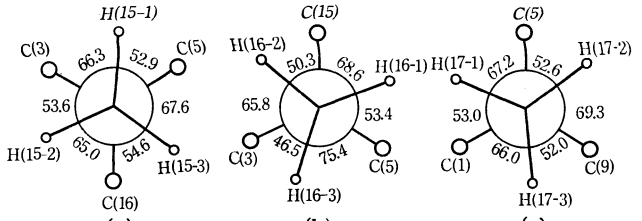

Fig. 3. The Newman projections along the bonds, (a) C(4)–C(15), (b) C(4)–C(16), and (c) C(10)–C(17).

rings are also in good agreement with each other. The distribution of the valence angles in the A ring is similar to those in III and in the acetolysis product of II, hereafter called IV;[4] *i.e.*, the valence angles at the C(1) and C(3) atoms are significantly greater than the normal tetrahedral angle. This may be due to the existence of the exocyclic double bond, C(5)=C(6). The conformations of the three methyl groups attached to the A ring are shown in Fig. 3. The deviations of the two axial methyl groups, $C(16)H_3$ and $C(17)H_3$, from the staggered conformation, 10° and 7°, are both slightly smaller than the corresponding values for III. On the other hand, the conformation of the equatorial methyl group, $C(15)H_3$, deviates by about 6° from the staggered arrangement; this value is about 3° larger than that for III. These small variances of the rotation angles found in II and III probably result from the delicate difference in the conformations of the tricyclic systems. The hydroxyl group, O(1)H, is equatorially bonded to the A ring. The azimuthal angle of the O(1)–H(O) and C(3)–H(3) bonds around the C(3)–O(1) bond is about 33°. This approach to the eclipsed arrangement may be attributable to the formation of the O(1)–H(O)···O(2′) hydrogen bond. In fact, the O(1)–H(O)–O(2′) angle is about 180°.

Table 7. The deviations (Å) of the atoms from the least-squares plane

C(7)	0.030	C(11)	0.027
C(8)	0.019	C(12)[a]	0.105
C(9)	0.029	C(13)[a]	−0.246
C(10)	−0.053	C(14)	−0.052

a) These atoms were omitted from the calculation of the least-squares plane.

With respect to the plane which bisects the C(5)–C(10)–C(9) or C(6)–C(7)–C(8) angle, the conformation of the B ring in II is less symmetrical than that in IV. Although one of the two ethylenic parts, >C(5)=C(6)<, holds a good planarity, the other, >C(8)=C(9)<, deviates to some extent from a planar configuration. The deviations of the atoms from the least-squares plane through the C(7), C(8), C(9), C(10), C(11), and C(14) atoms are given in Table 7. The angle between this plane and the least-squares plane through the C(4), C(5), C(6), C(7), and C(10) atoms is about 11.8°; this is about 3.3° and 8.2° smaller than the corresponding angles for III and IV respectively.

As will be seen in Fig. 1, the C ring in II is unusually flattened, although it keeps approximately the C_2 symmetry characteristic of the half-chair conformation. The C(12) and C(13) atoms are, respectively, only about 0.14 and 0.18 Å displaced above and below the mean plane through the other four atoms in the ring; the sum of these deviations, 0.32 Å, is remarkably smaller than that in IV, 0.73 Å, and that in cyclohexene, 0.7346 Å.[5] It is of great interest to examine why the C ring in II is forced to take such an unusually-flattened conformation. The closest approach of the methylene groups, $C(1)H_2$ and $C(11)H_2$, is found between the two equatorial hydrogen atoms, H(1–2) and H(11–2), their distance being about 2.10 Å; this is only slightly greater than the distance between the overcrowded hydrogen atoms in phenanthrene, 2.04 Å.[6] Since the less the equatorial nature of the H(11–2) atom is, the more distant the H(1–2) and H(11–2) atoms become, it is clear that the flattened conformation of the C ring prevents the two hydrogen atoms from approaching each other at an extremely small distance. The unusual conformation of the C ring is, therefore, perhaps caused mainly by the strong steric repulsion between the H(1–2) and H(11–2) atoms. On the other hand, an X-ray study of IV has revealed that the C ring in IV takes the normal half-chair form in which the axial positions in II become equatorial and *vice versa*.[4] This is probably because the equatorial hydrogen atoms, H(1–2) and H(11–1), maintain a distance of about 2.23 Å without any large deformation of the C ring. If this is the reason, then the question arises of why the C ring in II does not take the same conformation as that in IV. The most conceivable reason is that the allylic axial methoxyl group might have the effect of stabilizing the cyclohexene system, probably by allowing the transfer of some π-electrons on the C(8)=C(9) double bond into the overlapping antibonding orbital of the C(14)–O(2) bond.[7] The stabilization due to the delocalization of π-electrons would overcome the energy loss resulting from the great deformation of the C ring.

The length of the C(12)–C(13) bond is found to be about 1.343 Å; this is almost equal to the value for III, 1.340 Å. However, both the results of elemental analysis and the NMR spectrum clearly show that the C(12)–C(13) bond should be a single one.[1] This conflict may be resolved by taking account of the unusual thermal vibrations of the C(12) and C(13) atoms. The thermal ellipsoids of atoms in the C ring are shown in Fig. 4, while the root-mean-square deviations and direction cosines in the principal axes of the ellipsoids are given in Table 8. It is found that all

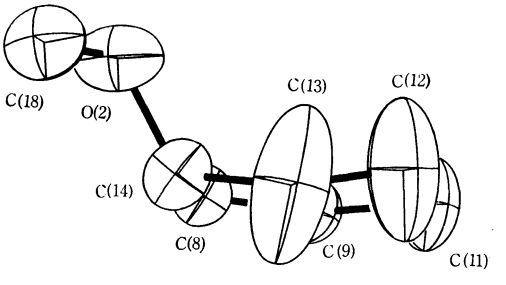

Fig. 4. The thermal behavior of the C ring. The thermal ellipsoids are scaled to enclose 50% probability.

Table 8. The root-mean-square deviations and direction cosines in the principal axes of the thermal ellipsoids

$B_i=8\pi^2u_i^2$ where u_i is the root-mean-square deviation corresponding to the ith axis of the ellipsoid. C_{ia}, C_{ib}, and C_{ic} are the direction cosines of the i axis with respect to the orthogonal coordinate axes by **b** $\times$ **c***, **b**, and **c***.

Atom	Axis i	B_i (Å^2)	u_i (Å)	C_{ia}	C_{ib}	C_{ic}
C (8)	1	2.75	0.187	−0.827	−0.549	−0.120
	2	3.31	0.205	−0.069	−0.113	0.991
	3	4.03	0.226	−0.558	0.828	0.056
C (9)	1	2.45	0.176	−0.412	−0.471	−0.780
	2	3.55	0.212	0.661	0.435	−0.611
	3	4.13	0.229	−0.627	0.768	−0.132
C (11)	1	2.67	0.184	−0.398	−0.674	−0.623
	2	4.52	0.239	−0.686	−0.233	0.690
	3	9.07	0.339	−0.610	0.702	−0.369
C (12)	1	2.55	0.180	−0.534	−0.718	−0.446
	2	5.89	0.273	−0.662	0.027	0.749
	3	21.36	0.520	−0.526	0.695	−0.489
C (13)	1	2.57	0.180	−0.718	−0.677	−0.160
	2	5.82	0.271	−0.310	0.105	0.945
	3	27.76	0.593	−0.624	0.728	−0.285
C (14)	1	2.92	0.192	−0.860	−0.499	0.102
	2	4.16	0.229	0.171	−0.092	0.981
	3	5.59	0.266	0.480	−0.862	−0.165
O (2)	1	2.72	0.186	−0.848	−0.389	0.359
	2	4.32	0.234	0.527	−0.681	0.508
	3	9.16	0.341	−0.047	−0.620	−0.783
C (18)	1	3.18	0.201	−0.747	−0.467	0.473
	2	5.68	0.268	0.664	−0.548	0.508
	3	7.35	0.305	−0.022	−0.694	−0.720

the six atoms in the C ring vibrate most vigorously in a direction almost perpendicular to the mean plane of the ring. Above all, the anisotropy of the thermal motions of the C(12) and C(13) atoms is very conspicuous; their greatest root-mean-square deviations are about 0.52 and 0.59 Å respectively. In a previous paper,[2] we pointed out that, even though the C(12)–C(13) bond distance is corrected for these large thermal motions, the correction is very small so long as the riding motion is assumed, but that if a highly-correlated antiparallel motion is assumed for the two atoms, the corrected distance becomes too large (1.73 Å). This suggests that the thermal motions of the C(12) and C(13) atoms may contain both parallel and antiparallel components.

Let us consider a one-dimensional harmonic oscillator which moves along the x axis, with the point 0′ as the equilibrium position. If the 0′ point further vibrates harmonically round the origin of the coordinates, 0, much more slowly than the oscillator moves round the 0′ point, then the probability of finding simultaneously the 0′ point between X and $X+dX$ and the oscillator between x and $x+dx$, $P(x, X)dxdX$, may be represented approximately by the following equation:

$$P(x,X)dxdX \propto \exp\left\{-\frac{X^2}{2\bar{u}_1^2}\right\}\times\exp\left\{-\frac{(x-X)^2}{2\bar{u}_2^2}\right\}dxdX$$

$$=\exp\left\{-\frac{1}{2}\left(\frac{1}{\bar{u}_1^2}+\frac{1}{\bar{u}_2^2}\right)\left(X-\frac{x}{1+\bar{u}_2^2/\bar{u}_1^2}\right)^2\right\}$$

$$\times\exp\left\{-\frac{x^2}{2(\bar{u}_1^2+\bar{u}_2^2)}\right\}dxdX,$$

where $\bar{u}_1$ and $\bar{u}_2$ are, respectively, the root-mean-square amplitude of the 0′ point and that of the oscillator with respect to the vibrating point, 0′. Accordingly, the probability of finding the oscillator between x and $x+dx$, $P(x)dx$, is given by the equation:

$$P(x)dx=\int_{-\infty}^{\infty}P(x,X)dxdX\propto\exp\left\{-\frac{x^2}{2(\bar{u}_1^2+\bar{u}_2^2)}\right\}dx$$

$$=\exp\left\{-\frac{x^2}{2\bar{u}^2}\right\}dx.$$

The apparent mean-square amplitude of the oscillator, $\bar{u}^2$, is thus given by the sum of $\bar{u}_1^2$ and $\bar{u}_2^2$. The thermal motions of the C(12) and C(13) atoms in the direction perpendicular to the mean plane of the C ring might be approximated by such a special harmonic oscillator model. In this case, the oscillation of the 0′ point corresponds to the parallel vibrational components of the two atoms arising from the thermal motion of the whole molecule as a rigid body, while the harmonic motion of the oscillator with respect to the 0′ point corresponds to the antiparallel components resulting from the internal vibration of the C ring. Since the thermal vibration of the C(11) atom does not seem to be very closely related to the antiparallel motions of the C(12) and C(13) atoms, it would be reasonable to use its greatest root-mean-square deviation as the approximate $\bar{u}_1$ value of the two atoms. From this value of $\bar{u}_1$, 0.34 Å, and the observed values of $\bar{u}$ for the C(12) and C(13) atoms, 0.52 and 0.59 Å, we obtain $\bar{u}_2$=0.39 and 0.48 Å for these two atoms respectively. In case of the antiparallel motions, the mean-square distance, $\bar{r}^2$, is given by the equation: $\bar{r}^2=s^2+\bar{r}_0^2$, where s is the sum of the $\bar{u}_2$ values of the two atoms and where r_0 is the observed distance between their equilibrium positions. Since both the effect on the $\bar{r}^2$ of the parallel motions of the C(12) and C(13) atoms and that of their thermal vibrations in the directions parallel with the mean plane of the C ring seem to be very small, it is expected that the C(12)–C(13) distance can be corrected to a considerable extent by using this equation. In fact, the value thus obtained, 1.60 Å, is much closer to the standard C–C distance, 1.54 Å, than the uncorrected value, 1.34 Å. That the correction is too great is probably in part due to the underestimation of the $\bar{u}_1$ value used in the calculation, and in part to the presence of the anharmonic components in the thermal motions of the C(12) and C(13) atoms.

The complicated thermal motions found in II are probably caused by the highly-strained conformation of the C ring. Compared with the ordinary half-chair form, such an unusually-flattened conformation is considerably unstable. This would bring about the vigorous, antiparallel vibrations of the C(12) and C(13) atoms. That, in the cyclohexene ring, the bond corresponding to the C(12)–C(13) is too short has previously

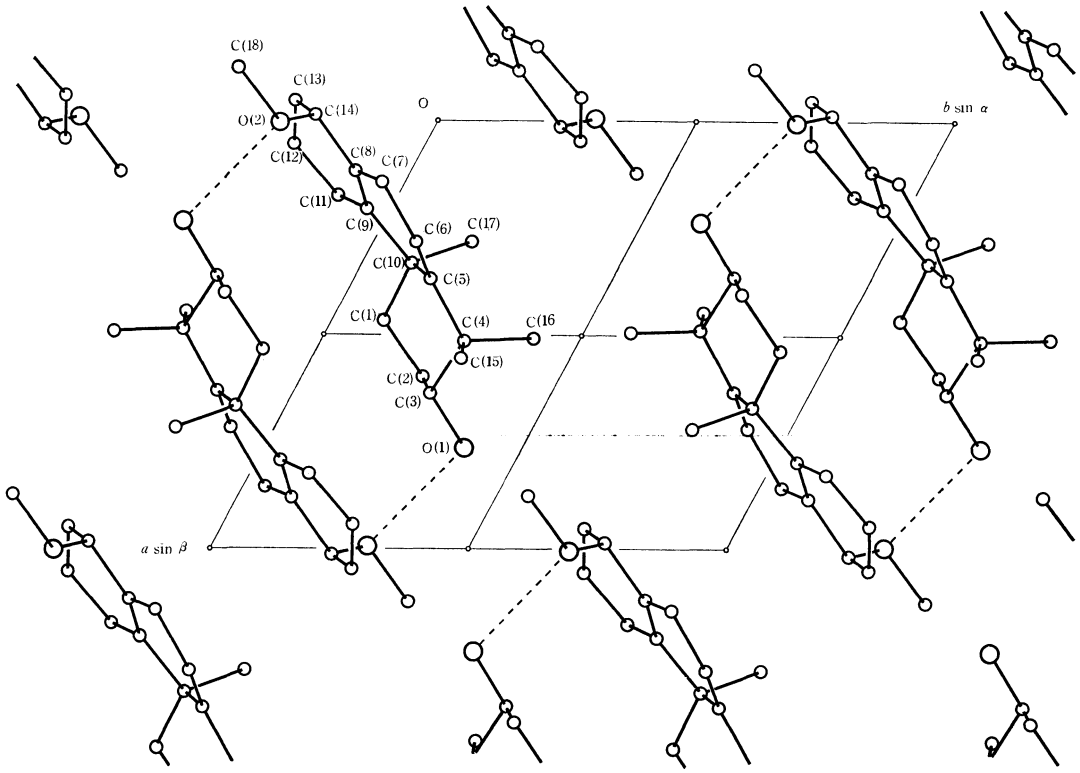

Fig. 5. The molecular arrangement viewed along the c axis.

been noticed in canthaxanthin[8] and in the *trans* isomer of β-ionylidenecrotonic acid.[9] In the former case, the shortening was interpreted as being due to the existence of two separate ring conformations in one single crystal, while, in the latter case, it was not clear whether the shortening was attributable to the conformational disorder or to the large asymmetric vibrations of the ring. When the C ring in II flips from one normal half-chair form to the other, the O(2) atom is shifted by about 0.7 Å. This shows that, if the present crystal had a disordered structure with respect to the two possible half-chair conformations of the C ring, it would contain two kinds of O(2)···O(1′) hydrogen bonding; for the normal half-chair form (A-form) where the O(2) atom is axial, the O(2)···O(1′) distance is estimated to be about 2.7 Å, while, for the other (B-form) where the O(2) atom is equatorial, it is about 3.2 Å.* In the case of such a disordered structure, the number of molecules with the A-form would be considerably larger in the crystal of II than in the crystal of III; in other words, the apparent conformation of the C ring in II would be much closer to the A-form than that in III, because, although the O(2) atom does not take part in the hydrogen-bond formation in the latter crystal, it can form a stable hydrogen bond in the former crystal if the C ring takes the A-form. However, in fact, almost the same conformations are observed for II and III. Accordingly, in the present case, it seems more reasonable to consider the remarkable shortening of the C(12)–C(13) bond as due to the special thermal vibrations of the C(12) and C(13) atoms rather than to the conformational disorder.

As has already been mentioned, out of the twenty-eight hydrogen atoms in a molecule, two were not located in the difference Fourier map. These two are the same axial hydrogen atoms at the C(12) and C(13) atoms that could not be found in the crystal structure of III. The fact that the axial hydrogen atoms are difficult to locate is obviously related to the complicated thermal vibrations of the C(12) and C(13) atoms.

The O(2)–C(18) bond makes an azimuthal angle of about 41° with the C(14)–H(14) bond and one of about 78.8° with the C(13)–C(14) bond around the C(14)–O(2) bond.

The molecular arrangement viewed along the c axis

Table 9. The principal intermolecular distances (Å)
The standard deviations are given in parentheses.

(1) I···II(III···I)		(4) I···VIII(VIII···I)	
C(7)···C(11)	3.878(4)	C(7)···C(7)	3.841(6)
C(15)···C(2)	3.882(5)	···C(8)	3.803(5)
(2) I···IV(V···I)		···C(14)	3.960(5)
O(1)···C(12)	3.849(6)	(5) I···IX(IX···I)	
···C(13)	3.586(7)	O(1)···O(2)	2.803(4)
(3) I···VI(VII···I)		···C(14)	3.784(4)
O(1)···C(18)	3.476(4)	···C(18)	3.607(5)
C(2)···C(18)	3.726(3)	O(2)···C(3)	3.525(4)
		C(3)···C(8)	3.865(4)

I: $x/a, y/b, z/c$ (given in Table 3). II: $x/a, y/b, 1+z/c$. III: $x/a, y/b, -1+z/c$. IV: $1+x/a, 1+y/b, z/c$. V: $-1+x/a, -1+y/b, z/c$. VI: $1+x/a, 1+y/b, -1+z/c$. VII: $-1+x/a, -1+y/b, 1+z/c$. VIII: $-x/a, -y/b, 1-z/c$. IX: $1-x/a, -y/b, 1-z/c$.

* In this estimation, it was assumed that the C(13) atom deviates by 0.367 Å from the plane of the C(8)=C(9) double bond, and that the bond distances and angles for the C(8) and C(14) atoms are equal to those in Tables 4 and 5.

is shown in Fig. 5, while the short intermolecular distances are listed in Table 9. The molecules make a hydrogen bond, O(1)–H···O(2′), with each other at a distance of about 2.80 Å to form a dimer around a center of symmetry. The hydrogen-bonded dimers thus formed are further held together mainly by the ordinary van der Waals interactions.

References

1) N. Hamanaka, T. Okuno, T. Nakajima, A. Furusaki, and T. Matsumoto, *Chem. Lett.*, **1972**, 1037.

2) A. Furusaki, N. Hamanaka, and T. Matsumoto, This Bulletin, **46**, 434 (1973).

3) J. Karle and I. L. Karle, *Acta Crystallogr.*, **21**, 849 (1966).

4) A. Furusaki, N. Hamanaka, and T. Matsumoto, This Bulletin, **46**, 1021 (1973).

5) J. F. Chiang and S. H. Bauer, *J. Amer. Chem. Soc.*, **91**, 1898 (1969).

6) M. I. Kay, Y. Okaya, and D. E. Cox, *Acta Crystallogr.*, **B27**, 26 (1971).

7) R. Hoffmann, L. Radom, J. A. Pople, P. v. R. Schleyer, W. J. Hehre, and L. Salem, *J. Amer. Chem. Soc.*, **94**, 6221 (1972).

8) J. C. J. Bart and C. H. MacGillavry, *Acta Crystallogr.*, **B24**, 1587 (1968).

9) B. Koch, *ibid.*, **B28**, 1151 (1972).

The Crystal and Molecular Structure of *meso*-(2*S*, 4*s*, 6*R*)-2,4,6-Heptanetriol

Shunsuke KURIBAYASHI

Government Industrial Research Institute, Osaka, Midorigaoka, Ikeda 563

(Received June 20, 1973)

The crystal structure of *meso*-(2*S*,4*s*,6*R*)-2,4,6-heptanetriol has been determined by means of X-ray methods. The crystal belongs to monoclinic system (space group Ic), with four molecules in a unit cell with dimensions of a=8.133, b=9.374, c=11.248 Å, and β=93.24°. The structure was solved by three-dimensional Patterson and trial-and-error methods. The final R factor was 0.076. The molecule has the GTTḠ conformation, and all of the OH groups are linked together by intermolecular hydrogen bonds.

The crystal and molecular structures of stereoregular vinyl polymers are of great interest. The structure of stereoregular polyvinyl alcohol has been proposed on the basis of the IR and NMR spectra and X-ray diffractions.[1-9] The configurations and conformations of 2,4,6-heptanetriol as a model compound have been studied by NMR and IR spectroscopy.[10-14] The present paper will report on the crystal and molecular structure of *meso*-(2*S*,4*s*,6*R*)-heptanetriol as a model compound of isotactic polyvinyl alcohol.

Experimental

The sample was prepared by the method reported by Fujii.[15] This compound was a highly viscous liquid, but it crystallized gradually upon standing in cold storage overnight. The specimens suitable for X-ray analysis were crystallized from a dioxane solution. They were colorless and needle-like elongated along the c axes or of a lozenge shape. Since the sample was very hygroscopic, it was enclosed in a glass capillary during exposure to X-rays.

The dimensions of the unit cell were determined by using a Syntex, on-line-controlled, four-circle diffractometer.

The density of the crystal, measured by the flotation method, was about 1.15 g cm^{-3}; this is in good agreement with the calculated value.

The probable space group is Ic or I2/c; the former was chosen, as the molecule can be placed neither on the center of symmetry nor on the two-fold axis. The crystallographic data are listed in Table 1.

Table 1. Crystallographic data

$C_7H_{16}O_3$	Systematic absences
a=8.133(2) Å	of the reflections
b=9.374(2)	hkl for $h+k+l=2n+1$
c=11.248(3)	$0k0$ for $k=2n+1$
β=93.24(2)°	D_x=1.149 g/cm^3
Mol. wt. 148.2	D_m=1.15
V=856.3(4) Å^3	mp 67°C
Z=4	
Space group Ic	

Multiple-film equi-inclination Weissenberg methods were applied to the layer lines from 0 to 8 and from 0 to 6 about the c and a axes respectively, using Ni filtered Cu$K\alpha$ radiation. The diffracted intensities were estimated visually by comparison with the standard scale. A total of 874 non-zero independent reflections were observed by these procedures. The corrections for Lorentz polarization and the spot-shape factors were made in the usual way, but no correction was made for absorption or extinction.

Structure Determination

From the three-dimensional Patterson function, it was deduced that the molecular axis made an angle of about 55° with the c axis and that the zigzag plane was nearly perpendicular to the b axis. From the consideration of the interatomic distances and internal rotation angles about the C–C–C–C–C bonds, it was deduced that five molecular models having different sequences of T, G, and/or Ḡ must be taken into account; they were (i) TTTT, (ii) GTTT, (iii) GTTḠ, (iv) TTGT, and (v) GTGT. We rotated each molecular model at an interval of 6° in Eulerian angles, fixing the middle carbon atom at x=0, and z=0, so that the lower-order calculated structure factors, $|F(h0l)|$'s, agreed relatively well with the observed $|F(h0l)|$'s. As a good agreement was obtained for the third model, we terminated these procedures without examining TTGT or GTGT.

The y parameters for all the atoms were introduced on the assumption that the y coordinate of the molecule is very close to 0, as the 020 is much stronger than the other $0k0$ reflections. With these parameters, the block-diagonal least-squares methods with isotropic temperature factors were applied on the TOSBAC 3400-41 using a program, HBLS IV, written by T. Ashida. After ten cycles of iterations, the discrepancy factor, R, for all the observed reflections decreased to 0.14. Further refinements were carried out with anisotropic temperature factors. After six cycles of iterations, the R factor decreased to 0.098. All of the hydrogen atoms were found in the difference Fourier map calculated at this stage, but their coordinates were thought not to be reliable. All of thier positions except for those bonded to oxygen were, therefore, determined assuming C–H bond lengths of 1.09 Å and bond angles of 109.5°. Fixing the calculated coordinates of the hydrogen atoms, six cycles of least-squares refinements were carried out. The R reduced to 0.076. The function to be minimized was $\sum w\Delta^2$, where:

$$w = (20.0/|F_0|) \quad \text{for } |F_0| > 20.0$$
$$w = 1 \quad \text{for } 20.0 \geq |F_0| \geq 5.0, \text{ and}$$
$$w = 0.3 \quad \text{for } |F_0| < 5.0$$

The final atomic coordinates and temperature factors, with their standard deviations, are listed in Tables 2 and 3. A list of observed and calculated

TABLE 2. THE FINAL ATOMIC COORDINATES WITH THEIR STANDARD DEVIATIONS

Atom	x/a	y/b	z/c
C(1)	0.3071(8)	0.1395(7)	0.1079(6)
C(2)	0.2517(5)	−0.0038(5)	0.1529(4)
C(3)	0.0671(5)	−0.0320(6)	0.1278(4)
C(4)	0.0000(5)	−0.0210(4)	0.0000(3)
C(5)	−0.1847(6)	−0.0565(5)	−0.0067(4)
C(6)	−0.2710(5)	−0.0392(5)	−0.1302(4)
C(7)	−0.2891(7)	0.1145(5)	−0.1695(5)
O(1)	0.2773(4)	−0.0153(4)	0.2777(3)
O(2)	0.0825(4)	−0.1211(3)	−0.0734(3)
O(3)	−0.4354(4)	−0.0951(4)	−0.1286(3)
H(14)	0.372(9)	0.015(7)	0.294(6)
H(15)	0.155(10)	−0.076(7)	−0.125(6)
H(16)	−0.438(9)	−0.170(7)	−0.076(6)

TABLE 3. THE ANISOTROPIC TEMPERATURE FACTORS OF NONHYDROGEN ATOMS IN THE FORM $\exp\{-10^{-4}\times(h^2\beta_{11}+k^2\beta_{22}+l^2\beta_{33}+2hk\beta_{12}+2hl\beta_{13}+2kl\beta_{23})\}$. Their estimated standard deviations are given in parentheses

Atom	β_{11}	β_{22}	β_{33}	β_{12}	β_{13}	β_{23}
C (1)	190(11)	150(8)	89(5)	−71(7)	−32(6)	27(5)
C (2)	68(5)	112(5)	46(3)	−7(4)	−13(3)	3(3)
C (3)	83(6)	130(7)	62(4)	−13(5)	−18(4)	3(4)
C (4)	91(5)	81(4)	48(3)	−1(4)	−8(3)	−9(3)
C (5)	94(6)	112(6)	55(3)	−7(4)	−24(3)	11(3)
C (6)	93(6)	93(5)	50(3)	−2(4)	−21(3)	2(3)
C (7)	176(9)	100(6)	71(4)	4(6)	−30(5)	18(4)
O (1)	85(4)	145(5)	56(2)	−20(4)	−15(2)	7(3)
O (2)	119(4)	101(4)	65(2)	6(3)	1(2)	−18(2)
O (3)	95(4)	110(4)	108(4)	−18(3)	−56(3)	23(3)

structure factors is given in Table 4.*

Results and Discussion

The crystal structure projected along the b and c axes are shown in Figs. 1 and 2 respectively. The molecular structure is schematically shown in Fig. 3. As may clearly be seen from this figure, the molecule has a GTTḠ conformation, all of the hydroxyl groups are linked together by intermolecular hydrogen bonds, and their mean distances is 2.71 Å. The shortest van der Waals contact is 3.86 Å for C···C and 3.47 Å for C···O. The torsional angles about the C–C bonds are listed in Table 5. The best plane, composed of C(2) C(3), C(4), C(5), C(6), O(1), and O(3), is expressed by the equation:

$$-0.2495x + 0.9529y + 01856z + 0.1630 = 0$$

where x, y, and z are in Å units with respect to the crystallographic axes. The deviations from this plane are listed in Table 6.

The C–C and C–O bond lengths and the C–C–C

TABLE 5. TORSIONAL ANGLES

	Torsional angles (°)
C(1)-C(2)-C(3)-C(4)	55.2
C(2)-C(3)-C(4)-C(5)	178.5
C(3)-C(4)-C(5)-C(6)	175.9
C(4)-C(5)-C(6)-C(7)	−70.3
O(1)-C(2)-C(3)-C(4)	177.5
O(3)-C(6)-C(5)-C(4)	171.6
C(2)-C(3)-C(4)-O(2)	59.4
C(6)-C(5)-C(4)-O(2)	−63.8

* Table 4 has been deposited with the Chemical Society of Japan (Document No. 7403)

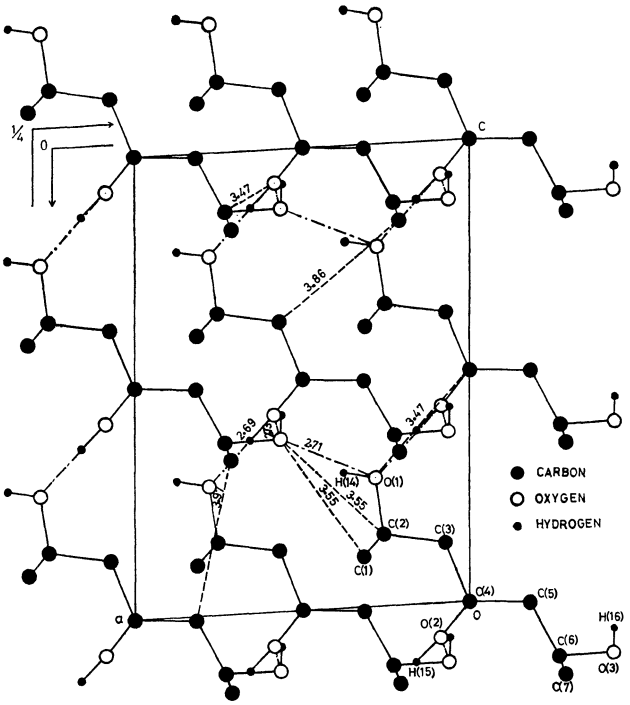

Fig. 1. The crystal structure viewed along the b axis. Only the hydrogen atoms attached to oxygen are indicated. The van der Waals distances shorter than 4.0 Å for C-----C and 3.6 Å for C-----O are shown by broken lines. The hydrogen bonds are also shown by chain lines.

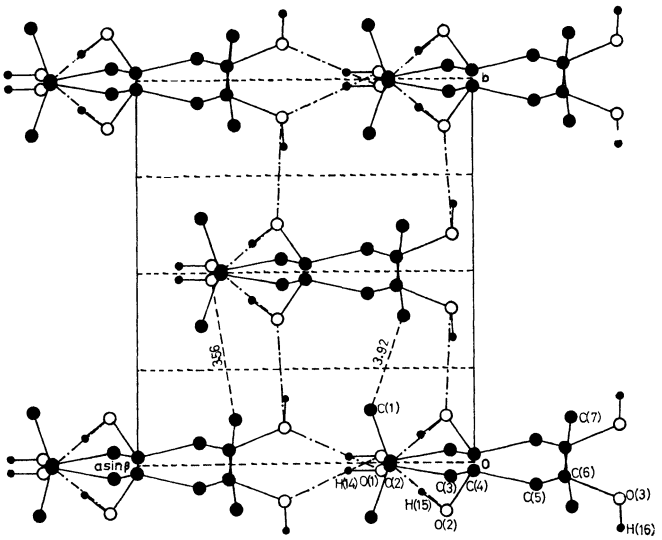

Fig. 2. The crystal structure viewed along the c axis. The hydrogen bonds are shown by chain lines.

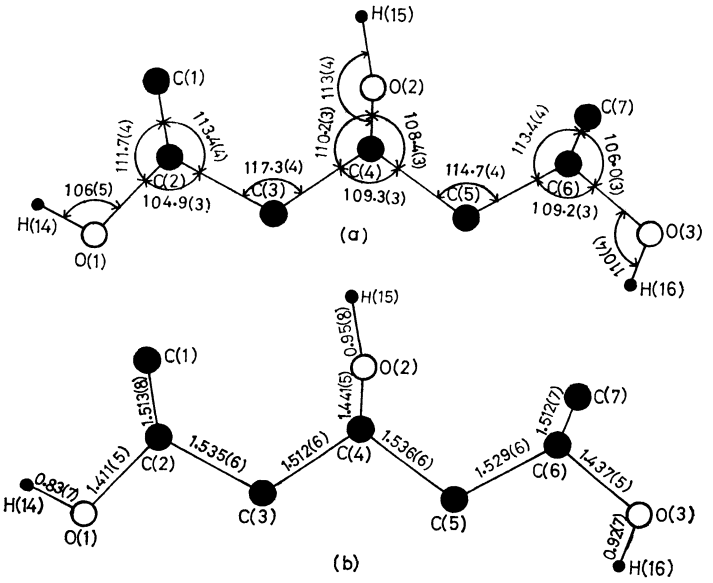

Fig. 3. Bond angles (degree) (a) and lengths (Å) (b).
Hydrogen atoms attached to carbon are omitted.

Table 6. Deviation of each atom from the best plane

Atom	Deviation (Å)
C(2)	−0.063
C(3)	0.007
C(4)	−0.024
C(5)	0.018
C(6)	0.090
O(1)	0.042
O(3)	−0.071

and C–C–O bond angles agree well with those observed in ordinary aliphatic compounds, except for C(2)–C(3)–C(4), which is remarkably large.

It is thought to be unwize to discuss these results in comparison with those obtained by NMR or IR spectroscopy in solution,[10–14] as the solvents and thermal effects may affect the conformations and hydrogen bondings of the molecule. The structure of isotactic polyvinyl alcohol has a TTT sequence, and all of the hydroxyl groups are linked together by intermolecular hydrogen bonds,[1–3] which is quite different from the present trimer structure. There might be some metastable states or polymorphism. We expect to elucidate these points by future studies.

The author is indebted to Mr. Takahiko Kawaguchi of Ritsumeikan University for his assistance in experiments and helpful discussions. The author also wishes to express his thanks to Dr. Tamaichi Ashida and Dr. Toshio Sakurai for providing him computing facilities.

References

1) S. Murahashi, H. Yuki, T. Sano, U. Yonemura, H. Tadokoro, and Y. Chatani, *J. Polym. Sci.*, **62**, S77 (1962).
2) T. Shimanouchi, *ibid.*, **C7**, 85 (1963).
3) K. Fujii, T. Mochizuki, S. Imoto, J. Ukida, and M. Matsumoto, *ibid.*, **A2**, 2327 (1964).
4) W. C. Tincher, *Makromol. Chem.*, **85**, 46 (1965).
5) J. Bargon, K.-H. Hellwege, and U. Johnsen, *ibid.*, **85**, 291 (1965).
6) K. C. Ramey and N. D. Field, *Polym. Lett.*, **3**, 63 (1965).
7) S. Murahashi, S. Nozakura, and M. Sumi, *ibid.*, **3**, 245 (1965).
8) S. Murahashi, S. Nozakura, M. Sumi, and K. Matsumura, *ibid.*, **4**, 59 (1966).
9) K. C. Ramey and D. C. Lini, *ibid.*, **5**, 39 (1967).
10) T. Moritani, I. Kuruma, K. Shibatani, and Y. Fujiwara, *Macromolecules*, **5**, 577 (1972).
11) J. Štokr and B. Schneider, *Collection Czech. Chem. Commun.*, **28**, 1946 (1963).
12) Y. Fujiwara, S. Fujiwara, and K. Fujii, *J. Polym. Sci.*, **A4**, 257 (1966).
13) D. Lím, E. Votavová, J. Stokr, and J. Petránek, *Polym. Lett.* **4**, 581 (1966).
14) D. Doskočilova, J. Stokr, E. Votavová, B. Schneider, and D. Lím, *J. Polym. Sci., Part C*, **16**, 2225 (1967).
15) K. Fujii, *ibid.*, **B3**, 375 (1965).

The Thermal Decomposition of Formaldehyde in the Presence of Nitric Oxide

Kohji TADASA,* Naomi IMAI, and Tetsuo INABA

Faculty of Liberal Arts and Sciences, University of Osaka Prefecture, Sakai, Osaka 591

(Received June 21, 1973)

The pyrolysis of formaldehyde was investigated in the presence of nitric oxide at 500 °C. The kinetics of the reaction suggests that the pyrolysis proceeds by means of a mechanism which is initiated by this reaction:

$$NO + CH_2O \longrightarrow HNO + CHO$$

and which involves this reaction:

$$HNO + HNO \longrightarrow N_2 + 2OH$$

as one of the chain-carrying steps.

Nitric oxide has generally been used as an inhibitor in the free-radical reactions in the gaseous phase. This compound, however, has been found to have an accelerative effect on the free-radical reaction in addition to an inhibitive one. Thus, the mechanisms of reactions containing nitric oxide are so complex that the reaction schemes proposed by various workers do not necessarily coincide with each other.

Both effects of nitric oxide are typically exhibited in the pyrolysis of dimethyl ether;[1-3] that is, the pyrolysis is suppressed almost completely by the addition of a small amount of nitric oxide, and, after maximal inhibition, it is linearly accelerated by an increased amount of nitric oxide. Thus, the inhibitive and accelerative parts in the kinetics are very clearly separated in the case of dimethyl ether, suggesting that this compound is suitable for a study of the effects of nitric oxide.

It is known that the free-radical decomposition of dimethyl ether follows this stoichiometric relation:

$$CH_3OCH_3 \longrightarrow CH_4 + CH_2O$$

and that the formaldehyde thus formed decomposes easily by a chain reaction following this stoichiometric relation:

$$CH_2O \longrightarrow CO + H_2.$$

In the presence of nitric oxide, however, the amount of hydrogen in the product of dimethyl-ether pyrolysis is very small compared with that of carbon monoxide, in contrast to the case of the absence of nitric oxide, suggesting that the reaction mechanism is complex, though the kinetics is very simple.

This work was attempted in order to investigate the effect of nitric oxide on the thermal decomposition of formaldehyde; we expected to obtain valuable information about its effect on that of dimethyl ether.

Experimental

Materials. The formaldehyde was prepared by the distillation of paraformaldehyde at about 120 °C, condensing the methanol and water involved by means of at −78 °C. The nitric oxide was obtained from the Takachiho Kagaku Co. Ltd. in a research-grade purity of 99.6%. It was subjected to several trap-to-trap distillations.

Apparatus. The reaction was studied in a conventional static system, and was carried out in a cylindrical Pyrex glass vessel of 210 cm^3 placed in an electric furnace, which was itself wrapped in asbestos and placed inside a cylindrical aluminium collar (20 cm in length, 9 cm in diameter, and with walls 1.6 cm thick) to hold the temperature constant.

Procedure. Required quantities of formaldehyde and nitric oxide were introduced into the vessel, which had until then been kept at the experimental temperature. In order to avoid the decomposition of the formaldehyde alone, the two substances were introduced in the order of (i) nitric oxide and (ii) formaldehyde. The products of decomposition were analyzed quantitatively by means of a gas chromatograph.

Analysis. After the pyrolysis, using a Toepler gauge, the unreacted reactants and products were passed through a trap at −78 °C, where a part of the unreacted formaldehyde and the high-boiling-point products, methanol and water, were condensed. The uncondensable fraction at −78 °C was passed through a trap at −196 °C, where the remaining parts of the unreacted formaldehyde, the unreacted nitric oxide, the carbon dioxide, and the nitrous oxide were condensed, while the uncondensable fraction at −196 °C was collected and measured by means of the Toepler gauge. That fraction was composed of carbon monoxide, hydrogen, and nitrogen. The quantity of each fraction of the products was measured by means of a gas chromatograph. Carbon monoxide, hydrogen, and nitrogen were analysed on a 2 m Molecular Sieve 5A column at room temperature, the carbon dioxide and nitrous oxide, on a 4 m Porapak Q column at room temperature, and the methanol, on a 2 m PEG-400 column at 80 °C. No quantitative analysis of formaldehyde was carried out; some of it polymerized on a glass tube of the collecting system, so accurate measurement was very difficult. Identification was achieved by using IR, a mass spectrometer, NMR measurements, and an elemental analyzer as well as a gas chromatograph.

Results

The yields of carbon monoxide, hydrogen, methanol, nitrogen, nitrous oxide, and carbon dioxide were measured at various times during the uninhibited and inhibited pyrolyses of formaldehyde. Some results are shown in Fig. 1. The figure shows that the amount of each product increases linearly with the time after 5 min even though the rate is higher at the beginning of the reaction. In this work the initial rate of the formation of each product was determined from the

* Present address: Department of Agricultural Chemistry, College of Agriculture, Shinshu University, Ina, Nagano 396

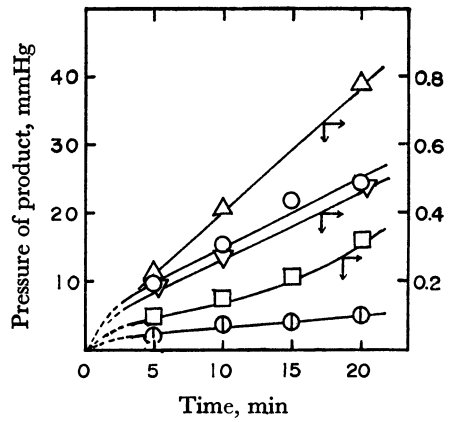

Fig. 1. Yields of products in the pyrolysis of 100 mmHg formaldehyde for 50 mmHg nitric oxide at 500°C.
○: CO, ⊕: N_2, □: N_2O, △: H_2, ▽: CO_2

slope of the line in the yield-time curve, except for the true initial part of the curve.

A series of runs was carried out at 500 °C using a fixed pressure of formaldehyde (100 mmHg) and various pressures of nitric oxide between 10 and 100 mmHg. The results for each product are shown in Figs. 2 and 3. The amount of water, which was measured by means of a gas chromatograph, is not very accurate. The rate of carbon monoxide formation follows a typical inhibition curve. It has a lower limit and then tends to increase with the nitric oxide pressure.

The formation of hydrogen is also inhibited, but after maximal inhibition the rate of its formation is very low compared with that of carbon monoxide, just as in the case of dimethyl ether. The rate of nitrogen formation increases linearly with the pressure of nitric oxide. This means that nitrogen formation is dependent on the first-order kinetics of nitric oxide.

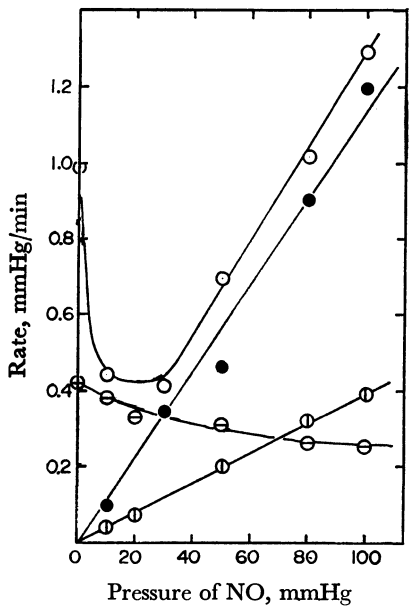

Fig. 2. The rates of product formation as a function of nitric oxide pressure in the pyrolysis of 100 mmHg formaldehyde at 500°C.
○: CO, ●: H_2O, ⊕: N_2, ⊖: CH_3OH.

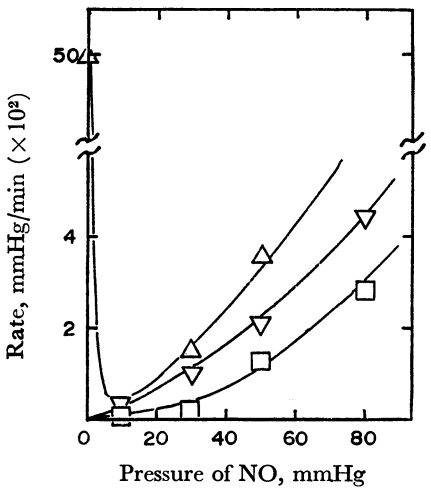

Fig. 3. The rates of product formation as a function of nitric oxide pressure in the pyrolysis of 100 mmHg formaldehyde at 500 °C.
△: H_2, ▽: CO_2, □: N_2O.

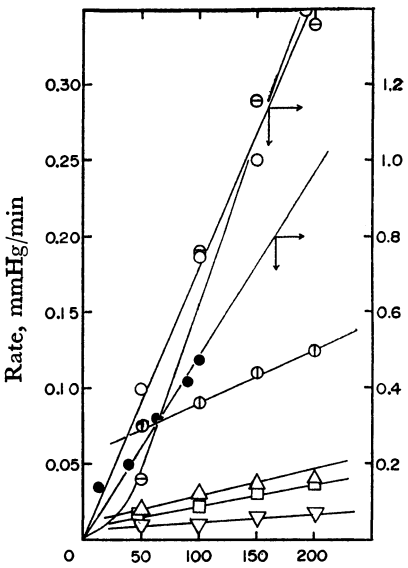

Fig. 4. The rates of product formation as a function of formaldehyde pressure in the pyrolysis of 50 mmHg nitric oxide at 500 °C.
○: CO, ●: H_2O, ⊕: N_2, ⊖: CH_3OH, △: H_2, ▽: N_2O, □: CO_2

The rates of both carbon dioxide and nitrous oxide formation also increase with the nitric oxide pressure, but their dependencies on nitric oxide are not clear because of a poor reproducibility.

Figure 4 shows the change in the rates of product formation at 500 °C using a fixed pressure of nitric oxide (50 mmHg) and various pressures of formaldehyde between 20 and 200 mmHg. These results show that each rate of product formation depends linearly on the formaldehyde pressure between 50 and 200 mmHg. However, the amount of water is not so accurate as in the case of Fig. 2.

Discussion

It has been well known that formaldehyde decomposes thermally *via* the reaction resulting from these two simulatneous stoichiometric equations:

$$2CH_2O \longrightarrow CO + CH_3OH \quad (I)$$

$$CH_2O \longrightarrow CO + H_2 \quad (II)$$

The former is a surface reaction,[4] while the latter is the following free-radical chain reaction.[5,6]

$$2CH_2O \longrightarrow CHO + H + CH_2O \quad (1)$$

$$CHO \longrightarrow CO + H \quad (2)$$

$$H + CH_2O \longrightarrow H_2 + CHO \quad (3)$$

$$CHO + CHO \longrightarrow CO + CH_2O \quad (4)$$

Methanol formation decreases slightly upon the addition of nitric oxide; therefore, Reaction (I) may be affected to only a small extent by the addition of nitric oxide. (A slight reduction of the rate of methanol formation by the addition of nitric oxide presumes a mild inactivation of the surface of a reaction cell by nitric oxide.)

On the contrary, the rate of carbon monoxide formation decreases greatly upon the addition of a small amount of nitric oxide; after the rate reaches its minimum, it increases linearly with the amount of nitric oxide added. The minimum rate of carbon monoxide formation, furthermore approximately equals that of methanol, indicating that the free-radical decomposition (II) is inhibited almost completely and that the increased rate after the minimum value is the result of free-radical decomposition accelerated by the addition of nitric oxide. In this paper, hereafter, the effect of nitric oxide on the free-radical decomposition will be described (mainly the accelerated part). The quantity of carbon monoxide produced by the free-radical process may be regarded as the difference between the total amount of carbon monoxide and that of methanol.

In the free-radical chain decomposition of formaldehyde alone (II), equal amounts of carbon monoxide and hydrogen are formed. On the other hand, in the presence of nitric oxide, as is shown in Figs. 2—4, very little hydrogen is produced after maximal inhibition; water, nitrogen, nitrous oxide, *etc.* are formed instead. A very rough ratio of the main products is:

$$CO:H_2O:N_2 = 1:1:1/2$$

The rates of their formation are first-order both for formaldehyde and nitric oxide after maximal inhibition.

The addition of nitric oxide to the pyrolysis should cause inhibition by means of the scavenging reaction of the hydrogen atom (3i) and, at the same time, acceleration by means of the inhibition reaction (1i):

$$H + NO \rightleftharpoons HNO \quad (3i)\ (-3i)$$

$$NO + CH_2O \longrightarrow HNO + CHO \quad (1i)$$

The formyl radicals formed by (1i) follow produce a hydrogen atom by means of Reaction (2). The very little formation of hydrogen in the inhibited decomposition shows that hydrogen atoms do not abstract the hydrogen atom as in (3); consequently, the chain decomposition of the formaldehyde propagated by (2) and (3) does not occur. Almost all of the H atom should undergo scavenging (3i), and the nitroxyl thus formed should react further. This reaction of nitroxyl should yield a nearly stoichiometric amount of water, since two atoms of hydrogen are formed for one molecule of carbon monoxide and nearly equal amounts of water and carbon monoxide are produced.

Nitroxyl is known to react as:[7]

$$HNO + HNO \longrightarrow N_2O + H_2O \quad (5)$$

The very low yield of nitrous oxide, however, indicates that (5) is not the main reaction for nitroxyl under the present conditions. Two reactions have been proposed between nitroxyl and nitric oxide:

$$HNO + 2NO \longrightarrow N_2 + H + NO_3 \quad (6)^{7}$$

$$HNO + 2NO \longrightarrow HNO_3 + N_2 \quad (7)^{8}$$

Since neither reaction yields water, neither is the main nitroxyl reaction. As another nitrogen formation step, Reaction (8) has been proposed:[9]

$$N_2O + H \longrightarrow N_2 + HO \quad (8)$$

This reaction, combined with Reaction (5) as a nitrous oxide source, should yield nitrogen with a half amount of water. If nitrogen is produced mainly by Reaction (8), however, the nitrogen yield-time curve should have a sigmoidal form and the rate of nitrous oxide formation should fall off. As shown in Fig. 1, this is not the case, indicating that Reaction (8) does not play an important role. (Reaction (8) is known to have a comparatively high activation energy *ca.* 11 kcal/mol.[10])

In the present work, an alternative reaction of nitroxyl (9) is proposed:

$$HNO + HNO \longrightarrow N_2 + 2OH \quad (9)*$$

As far as the energetics of this reaction are concerned, this is likely to occur: ΔH=3.6 kcal/mol.** The OH radical may produce water *via* Reactions (10)[11] and (11):

$$HO + HNO \longrightarrow H_2O + NO \quad (10)$$

$$HO + CH_2O \longrightarrow H_2O + CHO \quad (11)$$

If most of the hydroxyl radicals react as in Reaction (11), formaldehyde decomposes by means of a chain mechanism propagated by Reactions (3i), (9), (11), and (2). In the chain decomposition, the terminating step should be (5), (7), or (10), since nitroxyl radicals are the most abundant radicals. If formaldehyde does not decompose by means of a chain reaction, nitroxyl radicals are formed by Reactions (1i), (2), and (3), and the radical-consuming step should be Reactions (5), (7), or (10). Table 1 lists the simplified reaction mechanisms using the reactions described above and the rate equations derived from them. In this table, a sufficient long chain is assumed for the chain reactions.

Only Cases (i) and (vi) in the table are consistent

* This may proceed in a manner such as;

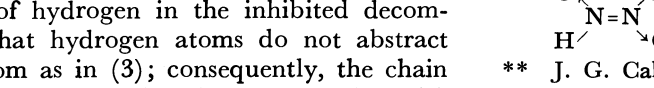

** J. G. Calvert and J. N. Pitts, Jr., "Photochemistry," John Wiley and Sons, New York, N. Y. (1966), p. 819.

TABLE 1. RATE EQUATIONS FROM VARIOUS REACTION SCHEMES

Chain reaction[a)]

	Terminating step		
	(5)	(7)	(10)
Reaction scheme	(1i) (2) (3i) (9) (11) (5)	(1i) (2) (3i) (9) (11) (7)	(1i) (2) (3i) (9) (11) (10)
rate equation	$R_{CO}=R_{H_2O}=(2k_{1i}k_9/k_5)$-$[CH_2O][NO]$ $R_{N_2}=(1/2)R_{H_2O}$ $R_{N_2O}=k_{1i}[CH_2O][NO]$	$R_{CO}=R_{H_2O}$ $=(2k_{1i}k_9/k_7^2)[CH_2O]^2$	$R_{CO}=R_{H_2O}=(k_{1i}k_9k_5^2/$ $2k_{10}^2)^{1/3}[CH_2O]^{4/3}[NO]^{2/3}$ $R_{N_2}=(1/2)R_{H_2O}$ $R_{N_2O}=(k_5/2k_9)R_{H_2O}$
case	(i)	(ii)	(iii)

Non chain reaction

	Radical consuming step		
	(5)	(7)	(10)
Reaction scheme	(1i) (2) (3i) (5)	(1i) (2) (3i) (7)	(1i) (2) (3i) (9) (10)
rate equation	$R_{H_2O}=R_{N_2O}$	$R_{H_2O}=0$	$R_{CO}=R_{H_2O}=k_{1i}$- $[CH_2O][NO]$ $R_{N_2}=(1/2)R_{H_2O}$ $R_{N_2O}=(k_5/2k_9)R_{H_2O}$
case	(iv)	(v)	(vi)

a) sufficient long chain is assumed

with the experimental results (excepting the molecular reaction); that is, both stoichiometric relation:

$$CH_2O + NO \longrightarrow CO + H_2O + (1/2)N_2$$

and the rate equation:

$$R_{CO} = k[CH_2O][NO]$$

hold approximately. We suggest that Reaction (11) progresses fast enough at the present temperature; hence, Case (i) is prefarable to (vi). As there is only a little change in the reaction order in the case of (iii), Reaction (10), besides (5), may be adopted as the termination step.

Nitrous oxide, since its formation is dependent on more than the first-order kinetics of nitric oxide, may be formed by (12) besides (5), which, as described in (i), leads to a linear relation to nitric oxide upon the nitrousoxide formation:

$$HNO + NO \longrightarrow N_2O + OH \qquad (12)$$

Thus we obtain: $R_{N_2O(12)}=k_{12}[HNO][NO]=(k_{12}k_{11}^{1/2}/k_5^{1/2})[CH_2O]^{1/2}[NO]^{3/2}$. The occurrence of this reaction (12) has little effect on the values of R_{H_2O} and R_{N_2}.

It has been established that nitric oxide is disproportionated by the chain reaction propagated by (3i) and (6) in the presence of the H atom at low temperatures. (This reaction, however, does not affect the rate of CH_2O decomposition reaction.) Judging from the results, the N_2 formation by (6) is negligible in comparison with that by (9):

$$R_{N_2(6)} = k_6[HNO][NO]^2 = (k_6k_{11}^{1/2}/k_5^{1/2})[CH_2O]^{1/2}[NO]^{5/2}$$

Even if, instead of (2), Reaction (13) occurs, it may produce no variation in the kinetics:

$$CHO + NO \longrightarrow CO + HNO \qquad (13)$$

Several workers have proposed different reaction schemes for the accelerating effect of nitric oxide on the gas-phase decomposition of simple organic compounds. Laidler *et al.* studied the pyrolysis of various organic compounds and proposed a chain mechanism.[12)] Applying their scheme to formaldehyde pyrolysis, the chain is initiated by (1i) and propagated by (2) and (3); consequently, hydrogen should be produced in the same amount of carbon monoxide.

Sabo *et al.* studied the pyrolysis of nitric oxide and acetaldehyde or higher aldehydes and proposed a different chain mechanism, where the propagating steps are:[13)]

$$R + NO \rightleftarrows RNO$$
$$RNO + RNO \longrightarrow RCO + RH + NO$$
$$RCO \longrightarrow R + CO$$

Applying this scheme, formaldehyde should yield equal amounts of CO and RH, that is H_2. Clearly, neither of these two schemes can be accepted for formaldehyde pyrolysis because of the low yield of hydrogen.

Pratt's scheme,[14)] which involves the isomerization of a nitroso compound to an oxime, also can not be applied to our system, because the nitroso compound in this system is nitroxyl.

Bibliography

1) N. Imai and O. Toyama, This Bulletin, **35**, 860 (1962).

2) D. J. McKenney, B. W. Wojciechowski, and K. J. Laidler, *Can. J. Chem.*, **41**, 1993 (1963).

3) K. Tadasa, N. Imai, and T. Inaba, unpublished work.

4) J. G. Calvert and E. W. R. Steacie, *J. Chem. Phys.*, **19**, 176 (1951).

5) E. W. R. Steacie, "Atomic and Free Radical Reactions," Vol. 1, Reinhold Publishing Corporation, New York, N. Y. (1954), p. 205.

6) R. Klein, M. D. Sheer, and L. J. Schoen, *J. Amer. Chem. Soc.*, **78**, 50 (1956).

7) E. A. Arden and L. Phillips, *J. Chem. Soc. A*, **1964**, 5118.

8) O. P. Strausz and H. E. Gunning, *Trans. Faraday Soc.*, **60**, 347 (1964).
9) K. Schofield, *Planet. Space Sci.*, **15**, 643 (1967).
10) F. Kaufman, *Can. J. Chem.*, **47**, 1917 (1969).
11) E. M. Bulewicz and T. M. Sudgen, *Proc. Roy. Soc. Ser. A*, **277**, 143 (1964).
12) M. Eusuf and K. J. Laidler, *Can. J. Chem.*, **42**, 1861 (1964); K. J. Laidler and M. Eusuf, *ibid.*, **43**, 268, 278 (1965); B. W. Wojciechowski and K. J. Laidler, *Trans. Faraday Soc.*, **59**, 369 (1963); K. J. Laidler and D. J. McKenney, *Proc. Roy. Soc. Ser. A*, **278**, 517 (1964).
13) Z. G. Sabo, *Nature*, **170**, 246 (1952); Z. G. Sabo, P. Huhn, and A. Bergh, *Adv. Catal.*, **9**, 343 (1957); Z. G. Sabo and F. Marta, *J. Amer. Chem. Soc.*, **83**, 768 (1961); F. Marta, *Acta Chim. Acad. Sci. Hung.*, **31**, 415 (1962).
14) G. L. Pratt and J. H. Purnell, *Proc. Roy. Soc. Ser. A*, **260**, 317 (1961); R. G. W. Norrish and G. L. Pratt, *Nature*, **199**, 143 (1963); G. L. Pratt, *Proc. Roy. Soc. Ser. A*, **293**, 235 (1966).

The Thermal Behavior of Silanol Groups of Silica Gel as Studied by Infrared Spectroscopy. I*

Seiichi KONDO,*1 Masa-aki MUROYA,*2 and Kenzo FUJII*1

*1*Osaka University of Education, Tennoji, Osaka 543*

*2*Osaka Electrocommunication University, Neyagawa, Osaka 572*

(Received July 4, 1973)

The thermal behavior of the silanol of silica gel has been studied by quantitative infrared spectroscopy. Transparent and glass-like plates of silica gel of high purity, after they had been heat-treated at various temperatures below 680 °C, were used for the measurement of OH stretching vibrations ranging from 3100 to 3800 cm^{-1}. These absorption bands were analysed into the several component bands by the simulation method using a Dupont Co. Curve Resolver. The intensity of these bands in area were proportional to the OH concentrations as measured by the thermal method. Each component band disappeared at a temperature which was roughly equal to that obtained from the dielectric and conductivity measurements. From these results, assignment was attempted on the basis of these bands.

The nature of the silanol group of high-specific-surface-area silicas, such as silica gel, aerosil, and porous glass, has been studied in many laboratories in relation to its electric, thermodynamic, optical, and many other physical properties.[1,2] Among them, infrared spectroscopy has been proved to be one of the most useful tools for the investigation of the bond nature of the surfaces of these substances. In the case of aerosil, the broad absorption band of the silanol group has been extensively studied, and a few absorption bands have been reported to exist in this broad band. However, the analysis of these bands is not clear enough except for those very near to 3750 cm^{-1}. Also, few infrared absorption experiments have been carried out on silica gel because of the difficulty of preparing a specimen suitable for the infrared measurement. The purpose of this paper is to try to make a quantitative analysis of the absorption band of silica gel and to study some properties of the resolved component bands.

Experimental

Materials. Ethyl orthosilicate was hydrolyzed to silica sol in the presence of hydrochloric acid at about 70 °C and gelled on a plastic plate such as Teflon. The hydrogel thus formed was dried in air at room temperature. A thin glass-like plate, about 0.15 mm thick and 1 cm^2 wide, was obtained; the infrared transmittance of this sample at 4000 cm^{-1} was about 80%. The specific-surface-area, as determined by the BET N_2 method, and the weight loss of this sample when heat-treated at various temperatures are shown in Fig. 1. The pore volume was 0.33 cc/g. No alkali and alkali earth impurities were detected with the flame spectroscopic analysis within limits of experimental error of about ±1 ppm in the case of the sodium ion in silica gel.

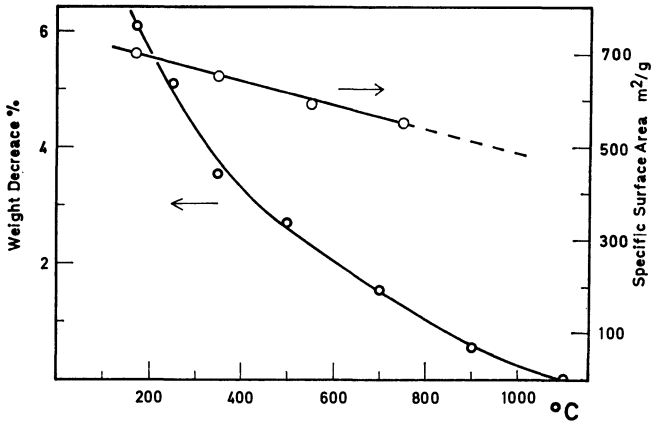

Fig. 1. The effect of heat-treatment on the weight decrease and the specific-surface-area of silica gel

Infrared Spectroscopy. The spectrophotometers used in this work were Japan Spectroscopy Co. types IRA-2 and 402G, and Hitachi Works Co. type IR 225. The absorp-

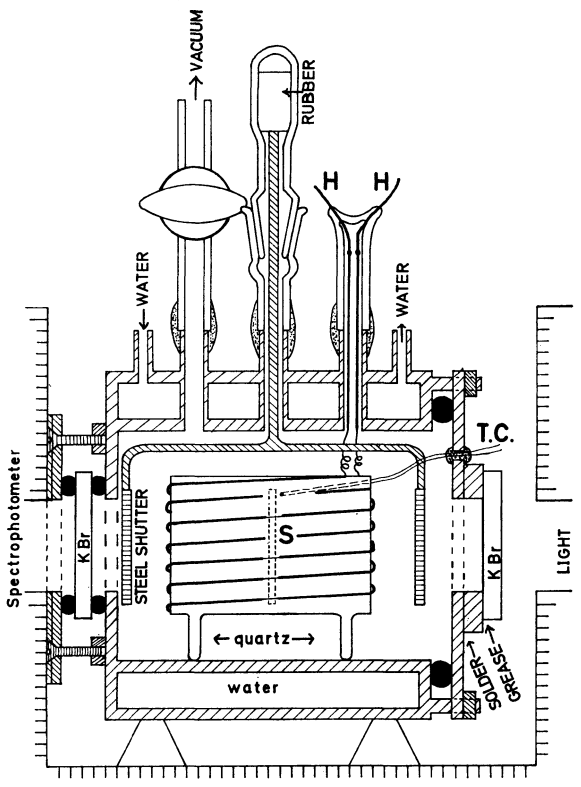

Fig. 2. High temperature vacuum cell for the infrared spectroscopy. The shaded, blank, black, and dotted areas show brass, glass, O ring and "Torr Seal" adhesive respectively unless otherwise specified.

* presented at the 23th (1969) and 27th (1973) annual meetings of the chemical Society of Japan and the 23th (1970) Colloid and Surface Chem. Symposium.

tion cell used in this experiment is shown in Fig. 2. The specimen was kept fixed in a furnace capable of heating the sample up to about 680 °C under a vacuum of 1×10^{-3} Torr. The absorption band was taken at room temperature *in vacuo*. No contamination of silica gel by the oil used in producing the vacuum was seen as far as the infrared spectra were concerned. The absorption intensity was estimated with the accuracy of about ±4% by measuring the area of the absorption curve within the range of the transmittance from about 80 to 20%; in this range the transmittance is practically linear to the extinction coefficient.

The absorption bands thus obtained were resolved into their component bands with Lorentz, Gauss, and mixed types by means of a Dupont Co. Curve Resolver, type 310. It was fairly easy to find the most reasonable combination of component bands with this simulation method. More details of the infrared measurement will be shown elsewhere.[3] The experimental error of the temperature measurement of the specimen was about ±4%.

Results and Discussion

As is well known, the broad absorption band between 3800 and 3000 cm^{-1}, as is shown in Fig. 3(a), can be assigned generally to the OH bond of silanol groups and adsorbed water of silica gel at 70 °C. Upon repeated heavy water adsorption, this band shifts quickly and uniformly to the OD stretching region, keeping its original OH band shape quite well. By elevating the heat-treatment temperature, this broad band at 70 °C becomes narrower—for example, at 180 and 360 °C, as is shown in Figs. 3(b) and (c) respectively; at 680 °C in Fig. 3(d) the band shape is sharp as a result of the condensation and dehydration reaction of silanol. Heating was done sufficiently long to attain the equilibrium condition (constant absorption intensity), as is shown in the upper part of Fig. 5.

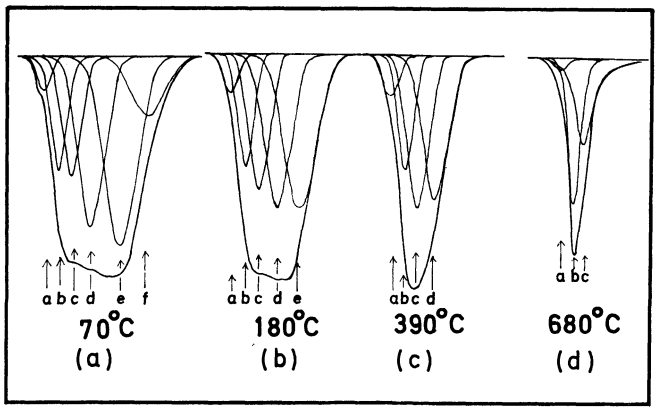

Fig. 3. OH stretching absorption bands and their component bands of silanol in various heat-treatment temperatures. *a*, *b*, *c*, *d*, *e*, and *f* show the maximum wave numbers of the component bands at 3870, 3750, 3630, 3470, 3260, and 3030 cm^{-1}, respctively.

In Fig. 4 a good linear relationship can be seen between the intensity of these bands, being equal to the area of the absorption curve and the hydroxyl concentration of the sample at the corresponding temperature; this relationship can be obtained from Fig. 1

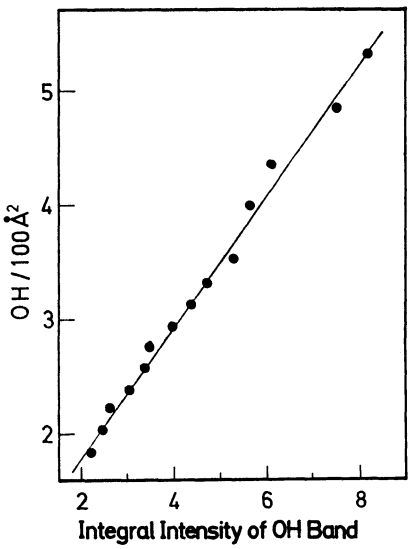

Fig. 4. The relation of the integral intensity of OH band in arbitrary scale to the concentration of silanol per 100 Å².

by dividing the weight decrease by the specific-surface-area. Therefore, the concentration of the silanol under given conditions can be estimated by using this curve derived from the infrared spectra.

The shape of the band at 680 °C is not symmetrical; it can be satisfactorily simulated as the sum of the three component bands at 3870, 3750, and 3630 cm^{-1} ± 10 cm^{-1}, as is shown in Fig. 3(d). The 3750 and 3630 cm^{-1} bands agree with the literature,[1,2] while the 3870 cm^{-1} band seems to be newly found in silica gel in this work. The shapes of the 3750 and 3630 cm^{-1} bands were nearly Lorentzian, while that of the 3870 cm^{-1} band was almost Gaussian in type. The broader

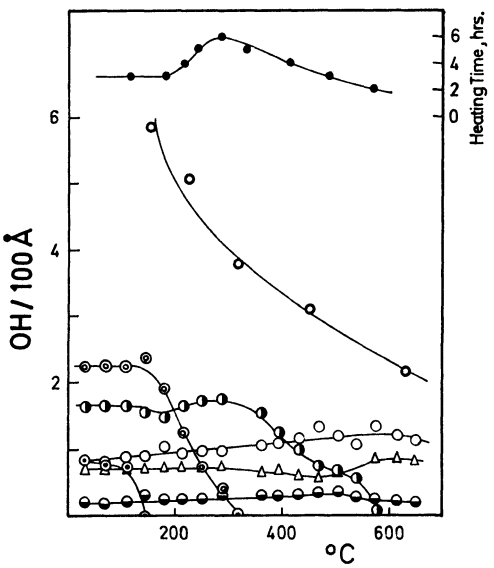

Fig. 5. The relation of the silanol concentration of the absorption bands and their component bands and the heating time to the heat-treatment temperature of silica gel.
○: Total OH, ⊙: 3030 cm^{-1}, ◎: 3260 cm^{-1},
◑: 3470 cm^{-1}, ○: 3630 cm^{-1}, △: 3750 cm^{-1},
◒: 3870 cm^{-1}.

bands at lower temperatures could easily be analyzed to their component bands in a similar manner; in order they were shown from the higher to the lower temperatures, in Figs. 3(c), (b), and (a). At 70 °C, the broad band was found to consist of six component bands, with their maxima at 3870, 3750, 3630, 3470, 3260, and 3030 $cm^{-1} \pm 10$ cm^{-1}. The existence of the 3470, 3260, and 3030 cm^{-1} bands seems to have been made clear in this work. The concentration of silanol corresponding to each of these component bands can be obtained from the total concentration of silanol at a given temperature multiplied by the fraction of the area of each of these component bands in relation to the total area of the absorption band at this temperature. The results are plotted in Fig. 5. In this figure, the OH concentration of each component band decreases successively by elevating the heat-treatment temperature. The 3030 cm^{-1} band disappears at about 150 °C and can be assigned to adsorbed water, since this temperature agrees well with the temperature of the desorption of adsorbed water obtained from our TGA, dielectric, and conductivity measurements.[4-6] The intensity of the 3260 cm^{-1} band began to decrease at about 150 °C, the temperature of disappearance of the 3030 cm^{-1} band. The same is true for the 3470 cm^{-1} band as may be seen in this figure. These two bands disappear at about 330° and 580 °C respectively. These bands can be assigned to the hydrogen-bonded silanols with various bond energies. During the decrease in these bands, the maximum wave numbers of these bands shift slightly to higher wave numbers, as is shown in Fig. 6. This blue shift may be interpreted in the following two ways: 1) it may be the result of the weakening of the hydrogen-bond interaction of the neighboring atoms following the dehydration reaction; 2) more likely, each component band may be composed of a few secondary components and the dehydration reaction may proceed from the lower-wave-number part of these secondary components.

Since the decrease in the intensity of one band and the increase in that of the other type does not seem to have occurred simultaneously in Fig. 6, the possibility of such a generation of one type of silanol as

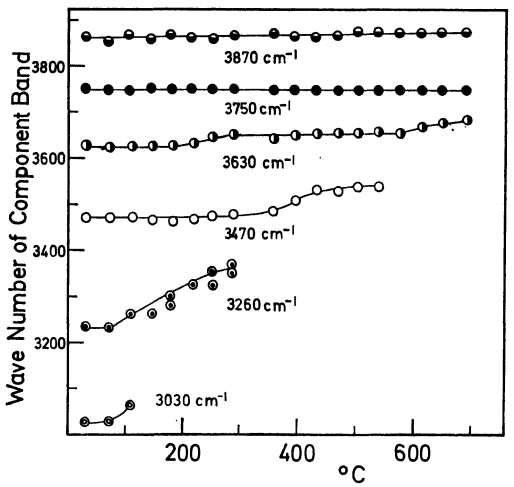

Fig. 6. The shift of the component bands by the elevation of the heat-treatment temperature.

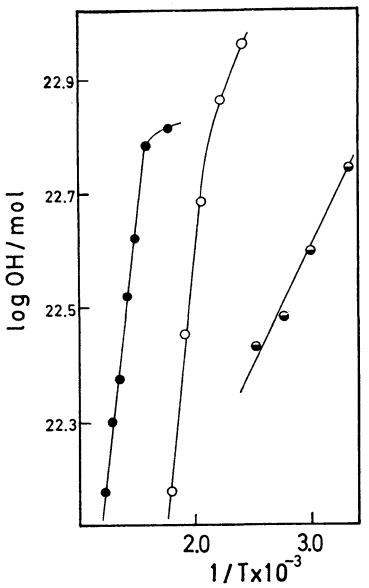

Fig. 7. The logarithm of the silanol concentration of component bands as a function of the reciprocal temperature of heat-treatment.
◒: 3030 cm^{-1}, ○: 3260 cm^{-1}, ●: 3470 cm^{-1}

Table 1.

OH band in cm^{-1} ± 10 cm^{-1}	Temperature of dissociation in °C $\pm$ 4%	ΔH kcal/mol ± 0.2 kcal/mol	O-H···O Distances in Å	Assignment
3030	150	1.9	—	Adsorbed water
3260	330	8.9	2.7	H-bond OH
3470	580	8.1	2.8	H-bond OH
3630	—	—	3.0	? H-bond OH
3750	—	—	—	Free OH
3870	—	—	—	?

a result of the condensation of another type or types of silanols is very small.

The OH equilibrium concentrations of 3030, 3260, 3470, and 3630 cm^{-1} bands are proportional to the reciprocal temperatures in the temperature range of dehydration reaction, as may be seen in Fig. 7. From these relations, we can obtain the enthalpy values, ΔH, of the dehydration reaction of these silanols, as is shown in Table 1. These values are very small compared with that of the usual chemical reaction. Table 1 also shows the O—H···O bond distances estimated from the relation between the absorption frequencies and the O—H···O distances of various compounds,[7] and their possible assignments.

The intensities of the 3630, 3750, and 3870 cm^{-1} bands did not change in the temperature range measured in this study. The 3750 cm^{-1} band, which is assigned to the free silanol, can also be found in other types of silica. However, this band of silica gel overlapped with the 3870 and 3630 cm^{-1} bands pretty heavily even at 680 °C, in contrast with that of aerosil, which can be clearly seen without overlapping at 700 °C.[1] Therefore, it was not possible to resolve

the 3750 cm^{-1} band into its components as in the case of aerosil.[8,9] The OH band at about 3630 cm^{-1} was also found in aerosil.[10-12] However, there are some differences in the deuterium exchange behavior and, hence, in the interpretations between these two materials.

References

1) L. H. Little, "Infrared Spectra of Adsorbed Species," Academic press Inc., London, 1966.
2) S. Kondo, *Hyomen*, **10**, 321 (1972).
3) M. Muroya and S. Kondo, *The Memoirs of Osaka Electrocommunication University*, **10**, 1974, under publication.
4) S. Kondo and M. Muroya, This Bulletin, **43**, 2657 (1970).
5) S. Kondo and M. Muroya, *ibid.*, **42**, 1165 (1969).
6) M. Muroya and S. Kondo, presented at the 26th spring meeting of the Chem. Soc. Japan, 1972.
7) E. Schwartzman, *Z. Anorg. Allgem. Chem.*, **317**, 176 (1962).
8) F. H. Van Cauwelaert, P. A. Jacobs, and J. B. Uytterhoeven, *J. Phys. Chem.*, **76**, 1434 (1972).; M. L. Hair and W. Hertle, *ibid.*, **73**, 2372 (1969).
9) I. Tsuchiya, presented at the 28th annual meeting of the Chemical Society, Japan, April, 1973.
10) R. S. McDonald, *J. Amer. Chem. Soc.*, **79**, 850 (1957).
11) A. N. Sidorov, *Optika Spectrosk.*, **8**, 806 (1957).
12) V. Ya. Davidov, A. V. Kiselev, and L. T. Zhuravlev, *Trans. Faraday Soc.*, **60**, 2254 (1964).

Partially-occupied d-Orbitals Participating in the Activation of Molecular Oxygen

Katsutoshi OHKUBO

Department of Synthetic Chemistry, Faculty of Engineering, Kumamoto University, Kumamoto 860

(Received July 4, 1973)

UV spectroscopic and semiempirical SCFMO investigations have been performed on the partially-occupied (formally unoccupied) *d*-orbitals participating in the activation of the ground state, $^3\Sigma_g^-O_2$, with special attention being given to the catalytic activities of onium compounds. The order of the red shifts of the $(p_z)^2 \rightarrow (p_z)(d)$ transition of the onium compounds in an oxygen atmosphere is in satisfactory accordance with those of the magnitude, of the partial occupancy of the *d*-orbitals and of the catalytic activities of the onium compounds in hydrocarbon oxidations. The d_{xz} (or d_{yz}) and $d_{x^2-y^2}$ orbitals are most favorably disposed for the interactions between the Group VI and V onium compounds and the $(1\pi_g)_x$-orbital of the $^3\Sigma_g^-O_2$ respectively. The partial occupation of the formally unoccupied *d*-orbitals results from the *d*-π delocalization between the onium central atom and the neighboring atoms of substituents and the counter-anion.

The liquid-phase oxidation of hydrocarbons such as cumene, tetraline, xylenes, *etc.*, with onium compounds proceeds without any appreciable incubation period and accumulates only hydroperoxide as an oxidation product, at least for 1 hr after the start of reaction under the usual conditions.[1] Among onium compounds involving C, N, O, P, S, As, Se, and Te as their central atoms, the third-row onium (phosphonium and sulfonium) ones have been proved to be the most effective catalysts.[2,3] The distinguished activity of phosphonium compounds as well as of sulfonium compounds may be ascribed to their catalytic activation of the ground state, $^3\Sigma_g^-O_2$, during the initial stage of the reaction:[4,5]

$$\text{onium cat.} + O_2 \underset{2.898\times10^9\sqrt{Te}\,e^{-21370/RT}}{\overset{9.389\times10^9\sqrt{Te}\,e^{-19930/RT}}{\rightleftharpoons}} \text{onium cat.}^{\delta+}\cdots O_2^{\delta-}$$

$$\text{onium cat.}^{\delta+}\cdots O_2^{\delta-} + RH \xrightarrow[\text{(rate determining)}]{1.447\times10^{10}\sqrt{Te}\,e^{-22460/RT}} R\cdot + HO_2\cdot + \text{onium cat.}$$

$$R\cdot + O_2 \xrightarrow{8.538\times10^9\sqrt{Te}\,e^{-6280/RT}} RO_2\cdot$$

$$RO_2\cdot + RH \xrightarrow{1.592\times10^{10}\sqrt{Te}\,e^{-19300/RT}} ROOH + R\cdot$$

$$RO_2\cdot + RO_2\cdot \xrightarrow{1.582\times10^{10}\sqrt{Te}\,e^{-10745/RT}} \text{inactive product}$$

$$\text{onium cat.} \xrightarrow{2.243\times10^{10}\sqrt{Te}\,e^{-18104/RT}} \text{inactive form}$$

where the rate constants ($M^{-1}\,s^{-1}$ or s^{-1} unit) are those in the case of cumene oxidation catalyzed by triphenylsulfonium chloride.

With respect to the catalytic activation of the $^3\Sigma_g^-O_2$, other types of catalysts, such as copper phthalocyanine,[6,7] Cu-pc, and hemoglobin,[8-12] Globin-Fe, participate in the activation of the $^3\Sigma_g^-O_2$:

$$\text{Cu-pc} + O_2 \longrightarrow \text{Cu-pc}^{\delta+}\cdots O_2^{\delta-}$$

$$\text{Globin-Fe} + O_2 \rightleftharpoons \text{Globin-Fe}^+\cdots O_2^-$$

No successful SCFMO calculation has hitherto been reported on the reaction systems mentioned above,[13] perhaps because there is difficulty in the accurate assessment of the relative locations of the states of O^+, O, and O^- on the energy scale and in the divergency of the SCF calculations.

The goal of the present study is to elucidate the role of partially-occupied (formally unoccupied) *d*-orbitals of onium compounds in the catalytic activation of the ground state, $^3\Sigma_g^-O_2$, on the basis of UV spectroscopic measurements[14] and semi-empirical SCFMO calculations.[15]

Method of Calculation

The following three systems were investigated in this work: (a) trimethylsulfonium compounds, $(CH_3)_3SX$ (X=Cl, Br, I, BF_4, and ClO_4), (b) tetramethylphosphonium compounds, $(CH_3)_4PX$ (X=Cl, Br, I, BF_4, and ClO_4), and (c) trimethyl-selenonium and telluronium chlorides, $(CH_3)_3SeCl$ and $(CH_3)_3TeCl$. The method of calculation is a semiempirical SCFMO, similar to the one described by Yonezawa *et al.*,[15] using the parametrization given in Ref. 16. The geometries used for calculations are illustrated in Fig. 1.

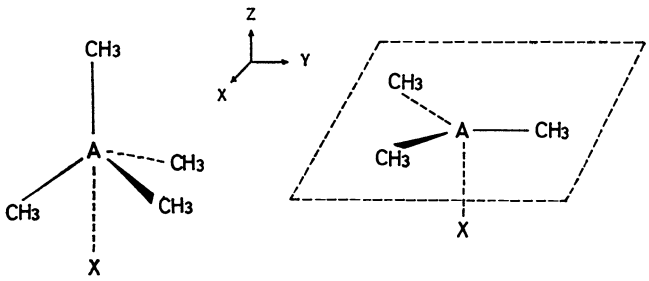

A=P C-P=1.87 Å C-H=1.10 Å CAX=CAC=109°28′
A=S, Se, or Te C-S=1.82 Å: C-Se=1.95 Å; C-Te=2.09 Å C-H=1.10 Å CAC=120°; CAX=90°

Fig. 1. Geometries of the onium compounds.

Results and Discussion

UV Spectroscopic Phenomena. Let us first discuss the UV spectroscopic phenomena concerned with the interaction between onium compounds and the $^3\Sigma_g^-O_2$. Figure 2 presents the UV absorption spectra of $(C_6H_5)_4PCl$, $(C_6H_5)_3SCl$, $(C_6H_5)_3SeCl$, and $(C_6H_5)_3TeCl$ in absolute ethyl alcohol at 25±1 °C in a nitrogen or oxygen atmosphere; the absorption curves of the said compounds indicate strong and reproducible peak, with absorption maxima, $\lambda_{max}(\log\varepsilon)$, of 204 (4.81)

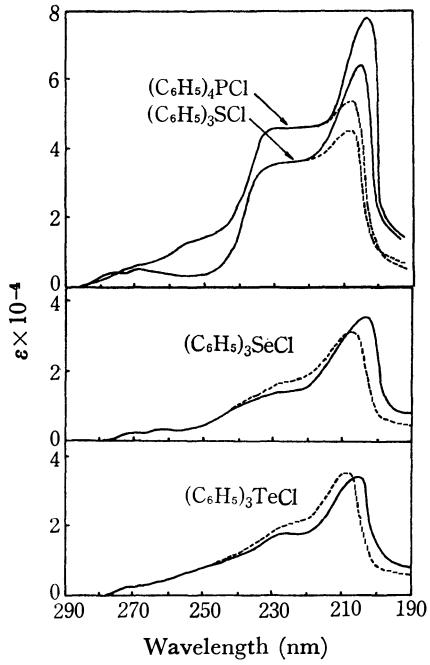

Fig. 2. UV absorption spectra of onium chlorides in C_2H_5OH at 25+1 °C. (Solid and dotted curves indicate the spectra in N_2 and O_2 atmospheres respectively.)

204 (4.88), 204 (4.56), and 205 nm (4.54) respectively in a N_2 atmosphere. These absorption peaks can be assigned to the electron excitation from the *p*-orbitals of the onium central atom to its *d*-orbitals, especially that from the p_z-orbital to the d_{z^2}-one, in view of the singlet excitation energies as evaluated by the SCFMO calculations. (Those for phosphonium chloride are shown in Fig. 3, while those for the others have already been discussed in Ref. 14.)

In an oxygen atmosphere, the above-mentioned peaks

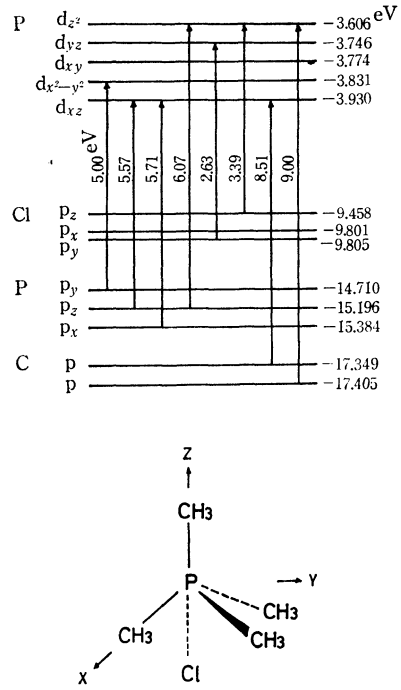

Fig. 3. Calculated excitation energies of $(CH_3)_4PCl$.

are shifted to longer wavelength regions ($\lambda_{max}(\log \varepsilon)$= 208 (4.65), 209 (4.73), 207.5 (4.50), and 208 nm (4.55) respectively). This is a result of the lowering of the low-lying, partially-occupied *d*-orbitals of the onium central atom, which results from the electron migration from the *d*-orbitals to the $1\pi_g$-orbitals of molecular oxygen through the plausible *dp*-σ type orbital overlappings to be shown later in this paper. That is, the more the electron densities of the *d*-orbitals decrease, the more their MO energy levels become lowered.

Interaction between the Partially-occupied d-Orbitals of Onium Compounds and the $1\pi_g$*-Orbitals of the* $^3\Sigma_g^- O_2$. Let us interpret briefly the molecular structures of onium compounds before discussing their interaction with the $^3\Sigma_g^- O_2$ in hydrocarbon oxidation. The energetically-stable phosphonium halides involve tetrahedral T_d onium cations, while the other oniums possess planar C_{3v} cations; the bond distance between the onium central atom and the counteranion has been proved to be a purely ionic one, particularly in polar solvents.[17] With regard to the structures of onium tetrafluoroborates and perchlorates (BF_4 and ClO_4), the planar C_{4v} counter-anions (B–F=1.40 Å; Cl–O=1.50 Å; ∠FBF=∠OClO=90°) have been, shown to give energetically-stable species.[18]

We should now consider the interaction between the partially-occupied *d*-orbitals and the $1\pi_g$-orbitals of the $^3\Sigma_g^- O_2$. In the Group VI onium (sulfonium, selenonium, and telluronium) compounds, a *dp*-σ type overlap between the d_{xy} (or d_{yz}) and the $(1\pi_g)_z$ is most predominant,[19] while in phosphonium compounds a *dp*-σ type orbital overlapping between the $d_{x^2-y^2}$ and the $1\pi_g$ is most probable, as is indicated in Fig. 4. It may be deduced, therefore, that the magnitude of the electron density on the *d*-orbitals (*viz.*, d_{xz} or d_{xy} and/or $d_{x^2-y^2}$) most favorably disposed for the interaction with the $1\pi_g$-orbitals of the $^3\Sigma_g^- O_2$ can be taken as a measure of the activation of the molecular oxygen.

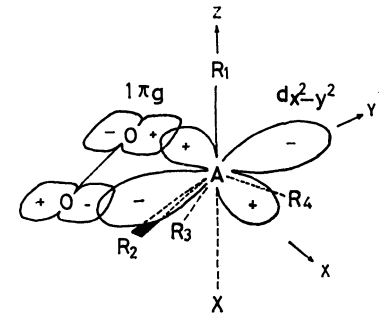

Fig. 4. Orbital overlap between phosphorus d-orbitals and $1\pi_g$-orbitals of O_2.

Correlation between the Partial Occupancy of the d-Orbitals and the Amount of the Red Shift. In this section, the discussion will be focused on the correlation between the electron densities of the *d*-orbitals of onium compounds and the amount of the red shift, $\Delta\lambda$, observed by the UV spectroscopic measurements. From earlier discussions, it is believed that the more the electron density of the *d*-orbitals of the onium central atom

increases, the larger becomes the red shift of $\Delta\lambda$(eV), because the electron is expected to transfer from the onium compound to the $^3\Sigma_g^-$ O_2. Moreover, a parallelism may be expected between the $\Delta\lambda$ values and the catalytic activities of onium compounds, as defined by the maximum rate of oxygen absorption, R_{max}, in M/s units, during the initial stage of hydrocarbon (10 ml) oxidation with the onium compound (3.0 mM) at 85 °C. As can be seen from Table 1, the order of the electron densities of the d_{xz} (or d_{xy}) and/or $d_{x^2-y^2}$ orbitals accords with that of the $\Delta\lambda$ values and also with that of the R_{max} values.

Table 1. Correlation of electron density of partially-occupied *d*-orbitals, amount of red shift, $\Delta\lambda$, and maximum oxidation rate, R_{max}

Onium compound	Electron density			$\Delta\lambda$ (eV)	$R_{max}\times10^4$ (Ms^{-1})	
	d_{xz}	d_{yz}	$d_{x^2-y^2}$		tetralin	cumene
$(CH_3)_4PCl$	0.216	0.191	0.189	0.12	7.44	
$(CH_3)_3SCl$	0.249		0.264	0.14	11.20	1.12
$(CH_3)_3SeCl$	01.05		0.162	0.104		1.04
$(CH^3)^3TeCl$	0.073		0.153	0.09		0.45
None					0.062	0.17

The correlation mentioned above is also realized in a series of sulfonium compounds, as is indicated in Table 2. Table 3 shows that the electron densities of the phosphorus $d_{x^2-y^2}$ orbital correlate well with the R_{max} values obtained from the tetralin oxidation under the conditions listes previously. The results shown in Tables 1, 2, and 3 are in harmony with the idea that the partially-occupied *d*-orbitals participate directly in the catalytic activation of the $^3\Sigma_g^-$ O_2. However, the *d*-orbital energy and the diffuseness of the *d*-orbital expansion should also be taken into consideration in discussing the interaction between the *d*-orbitals and O_2. In this respect, the relatively low activities of the fourth- or fifth-row onium compounds, such as selenonium and telluronium halides, may be ascribed to the diffuse 4*d* or 5*d* orbitals,[16,20] which may be unable to interact strongly with the $1\pi_g$-orbital of O_2.

Table 2. Correlation of electron density of sulfur *d*-orbitals, amount of red shift, $\Delta\lambda$, and maximum oxidation rate, R_{amx}

Sulfonium compound	Electron density $d_{xz}=d_{yz}$	$\Delta\lambda$(eV)	$R_{amx}\times10^4$ (Ms^{-1}) tetralin
$(CH_3)_3SCl$	0.249	0.14	11.20
$(CH_3)_3SBr$	0.230	0.10	10.88
$(CH_3)_3SI$	0.212	0.05	3.80
$(CH_3)_3SBF_4$	0.171	0.03	0.56
$(CH_3)_3SClO_4$	0.148	0.02	0.30

Here, it is necessary to discuss the chemical nature of the activated molecular oxygen. In an interacting system between the partially-occupied *d*-orbitals and the $1\pi_g$-orbitals, electron migrations from the former to the latter and from the $1\pi_u$-orbitals of the $^3\Sigma_g^-$ O_2

Table 3. Correlation between electron density of phosphorus *d*-orbitals and maximum oxidation rate, R_{amx}

Phosphonium compound	Electron density					$R_{max}\times10^4$ (Ms^{-1})
	d_{xy}	d_{yz}	d_{xy}	$d_{x^2-y^2}$	d_{z^2}	tetralin
$(CH_3)_4PCl$	0.216	0.191	0.180	0.189	0.450	7.44
$(CH_3)_4PBr$	0.216	0.194	0.179	0.185	0.342	7.00
$(CH_3)_4PI$	0.209	0.183	0.179	0.183	0.333	3.72
$(CH_3)_4PBF_4$	0.193	0.200	0.184	0.185	0.239	0.45
$(CH_3)_4PClO_4$	0.191	0.166	0.184	0.182	0.218	0.12

to the former may be expected. Such electron migrations increase the O–O bond distance of the oxygen molecule by means of the electron repulsion, and an odd-electron may be localized on each oxygen atom, thus increasing the radical nature of O_2. In this situation, the half-occupied, doubly-degenerate $1\pi_g$-orbitals come to be free from the degenerate state: for instance, a long-range interaction between $(CH_3)_3SCl$ and O_2 (S-Center of the O–O=3.0 Å) brings about the separation of the MO-energies of the $1\pi_g$-orbitals in an energy scale over 0.01 eV.[21] It may be worthy of emphasis here that the order of the catalytic activities: sulfonium≳phosphonium>selenonium>telluronium, is almost contrary to the lowering order of the energy levels of the d_{xz} (or d_{xy}) or the $d_{x^2-y^2}$: −4.8 eV for $(CH_3)_3TeCl$>−4.69 eV for $(CH_3)_3SeCl$>−4.38 eV for $(CH_3)_3SCl$>−3.83 eV for $(CH_3)_4PCl$. This may imply that the *d*-orbitals follow the initial charge to a higher π_g orbital (−0.15 eV[22,23]) rather than the $1\pi_g$ orbital (−12.075 eV) of the $^3\Sigma_g^-$ O_2.

Partial Occupation of the Formally Unoccupied d-Orbitals. Finally, mention should be made of the partial occupation of the formally unoccupied *d*-orbitals of onium compounds. The neighboring atoms of substituents and counter-anion participate directly in the partial occupation of the *d*-orbitals by the aid of the *d*-π (mainly, *dp*-π) delocalization between the central atom of the onium compound and the neighboring atoms. Table 4 shows the circumstances mentioned above in the case of phosphonium chloride; the *dd*-π delocalization between the phosphorus and the counter chlorine *d*-orbitals should also be taken into consideration.

Table 4. Partial occupation of phosphorus *d*-orbitals of $(CH_4)_4PCl$

Species	Basis set		Atom population		Electron density	
	P	Cl	P	Cl	$d_{x^2-y^2}$	d_{z^2}
$(CH_3)P_4^+$	*s,p*		5.089			
$(CH_3)_4P^+$	*s,p,d*		5.430		0.1706	0.1716
$(CH_3)_4PCl$	*s,p*	*s,p*	5.061	7.982		
$(CH_3)_4PCl$	*s,p,d*	*s,p*	5.629	7.538	0.1889	0.1803
$(CH_3)_4PCl$	*s,p,d*	*s,p,d*	5.647	7.520	0.1895	0.1805

Therefore, the more electron-releasing groups of substituents or counteranions are attached to the central atoms, the higher becomes the catalytic activity of the onium compounds. This is in harmony with the experimental phenomena observed in the liquid-

phase oxidation of hydrocarbons with various onium compounds.[2,3]

References

1) K. Ohkubo, T. Yamabe, and K. Fukui, This Bulletin, **42**, 2220 (1969).
2) K. Fukui, K. Ohkubo, and T. Yamabe, *ibid.*, **42**, 312 (1969).
3) K. Ohkubo and T. Yamabe, *Bull. Japan Petrol. Inst.*, **12**, 130 (1970).
4) K. Ohkubo, T. Yamabe, and K. Fukui, This Bulletin, **42**, 1800 (1969).
5) K. Ohkubo and T. Hashimoto, *ibid.*, **45**, 3350 (1972).
6) H. Kropf, *Ann.*, **637**, 73 (1960).
7) H. Kropf and Hd. Hoffmann, *Tetrahedron Lett.*, **1967**, 659.
8) L. Pauling and C. D. Coryell, *Proc. Natl. Acad. Sci. U. S.*, **22**, 210 (1936).
9) L. Pauling, *Nature*, **203**, 182 (1964).
10) J. S. Griffith, *Proc. Roy. Soc., Ser. A*, **235**, 23 (1956).
11) J. J. Weiss, *Nature*, **202**, 83 (1964); *ibid.*, **203**, 183 (1964).
12) R. D. Harcurt, *Int. J. Quantum Chem.*, **5**, 479 (1971).
13) The extended Hückel MO treatment of the interacting system between sulfonium compounds and the $^3\sum_g^- O_2$ can be seen in the following paper: K. Ohkubo and H. Kanaeda, This Bulletin, **45**, 11 (1972).
14) With respect to the technique of the UV spectroscopic measurements, see K. Ohkubo and T. Yamabe, *J. Org. Chem.*, **36**, 3149 (1971).
15) For instance, see H. Kato, H. Konishi, and T. Yonezawa, This Bulletin, **40**, 1017 (1967).
16) K. Ohkubo and H. Kanaeda, *J. Chem. Soc., Faraday Trans. II*, **68**, 1164 (1972).
17) K. Ohkubo and H. Kanaeda, This Bulletin, **45**, 1571 (1972).
18) K. Ohkubo and H. Sakamoto, *Chem. Lett.*, **1973**, 209.
19) K. Ohkubo and T. Yamabe, This Bulletin, **44**, 1183 (1971).
20) K. Ohkubo, *Tetrahedron Lett.*, **1971**, 2571.
21) K. Ohkubo, *ibid.*, **1971**, 2897.
22) D. S. Burch, S. J. Smith, and L. M. Branscomb, *Phys. Rev.*, **112**, 171 (1958).
23) R. S. Mulliken, *ibid.*, **115**, 1225 (1959).

The Magnetic Properties of Manganese(II) Phthalocyanine. II

Hirokazu MIYOSHI

Department of Chemistry, Faculty of Science, Kyoto University, Kyoto 606

(Received July 11, 1973)

The magnetic susceptibilities of manganese(II) phthalocyanine (PcMn) have been measured in the paramagnetic region between 13.8 and 280 K. The deviation from the Curie-Weiss law was found at a moderately high temperature (about 70 K), and the Weiss constant was obtained as 23 K. Comparing the ratio of T_c to θ (0.37) with that of the 2- or 3-dimensional lattice, the data were analysed on the basis of the ferro-magnetic linear-chain model. The magnitude of the intra-chain interaction (J) was deduced as $5.64k$ by comparison with Fisher's classical form of the theory of the ferromagnetic Heisenberg chain. We have also measured the magnetic susceptibilities of cobalt(II) phthalocyanine (PcCo) and of copper(II) phthalocyanine (PcCu), which are isomorphous with manganese(II) phthalocyanine, from 1.8 to 77 K. In PcCo, a broad maximum has been observed, and the data were analysed in terms of the theory of the antiferromagnetic Ising-chain model. On the other hand, PcCu obeyed the Curie law down to 1.8 K. A qualitative explanation of the exchange interactions in PcMn, PcCo, and PcCu was presented on the basis of their electronic states.

Most of the transition-metal phthalocyanines are known to be paramagnetic.[1] So far as the present author knows, most reports of their magnetic properties have been concentrated upon the investigation of their electronic structures within one molecule, though there have been a few of the intermolecular exchange interaction. However, the magnetic interaction revealed by the measurements of the magnetic susceptibility in the low-temperature region is of some interest, since the crystal is composed of discrete molecules at the van der Waals' radii; thus, the magnetic interaction is primarily intermolecular in origin.

Our earlier report[2] has shown that a ferromagnetic transition occurs in manganese(II) phthalocyanine $C_{32}H_{16}N_8Mn$ (hereafter simply denoted as PcMn) at $T_c=8.6$ K. However, no detailed measurements or discussion of the exchange interaction have been made.

TABLE 1. CONSTANTS OF CRYSTAL STRUCTURES[3]

	PcMn	PcCo	PcCu	PcNi
a Å	20.2	20.2	19.6	19.9
b	4.75	4.77	4.79	4.71
c	15.1	15.0	14.6	14.9
β°	121.7	121.3	120.6	121.9
Space group	$P2_1/a$	$P2_1/a$	$P2_1/a$	$P2_1/a$
No of 3d-electron	5	7	9	8
Spin number	3/2	1/2	1/2	0

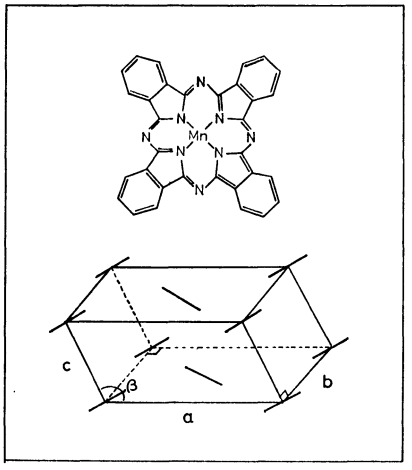

Fig. 1. Molecular and schematic crystal structures of PcMn. The molecular plane is approximately normal to the ab-plane.

To study the magnetic exchange interaction in the phthalocyanines, the magnetic susceptibilities of PcMn, PcCo, and PcCu were measured. They have been shown to be isomorphous with PcNi, whose structure is known[3] (see Table 1). The molecule is almost perfectly square-planar. The base-centered arrangement of two molecules per unit cell is shown in Fig. 1. The planar molecules are stacked along the short b axis at intervals of 4.7 Å, and the molecular planes are inclined to the ac plane at an angle of about 45°. The vertical distance between the nearest neighbors is 3.4 Å; this seems to be the minimum intermolecular separation when only van der Waals' forces are operative. As was pointed out by Mitra *et al.*,[4] this distance may provide a possible pathway for the magnetic exchange interaction. Therefore, the phthalocyanine may form magnetic linear chains along the b axis.

PcMn gives a large positive deviation from the Curie-Weiss law, and PcCo shows a broad maximum. These results are analysed in terms of the theory of linear-chain models. On the other hand, PcCu obeys the Curie law and may not form a magnetic linear chain. These results are also discussed on the basis of their electronic states.

Experimental

PcMn, PcCo and PcCu were prepared by the methods of Linstead *et al.*[5] and of McQueen *et al.*[6] The products were washed with benzene, ethanol, and acetone, and then sublimed at around 500 °C in an atmosphere of pure nitrogen. The single crystal grown by sublimation was in the shape of an elongated flat plate. The results of the elemental analysis of the carbon, hydrogen, and nitrogen of each sample corresponded closely to the calculated values. PcMn: Found: C, 67.70; H, 2.94; N, 19.67%, (Calcd: C, 67.73; H, 2.84; N, 19.75%), PcCo: Found: C, 67.86; H, 2.74; N, 19.57%, (Calcd: C, 67.76; H, 2.82; N, 19.61%), PcCu: Found: C, 66.87; H, 2.57; N, 19.42%, (Calcd: C, 66.72; H, 2.80; N, 19.45%).

All the measurements were carried out in the polycrystalline state. The static (dc) susceptibility measurements

were done by means of a magnetic torsion balance described elsewhere[7] on the samples of 50—150 mg in a field of 10.2 kG. The measurements on PcMn were performed between 1.8 K and 280 K in the temperature region attainable by pumping out the liquid helium and liquid nitrogen. The measurements on PcCo and PcCu were carried out between 1.8 K and 77 K. The temperatures of the samples were measured with a carbon resistor and AuCo-Cu thermocouple calibrated by measuring not only the known magnetic susceptibility of Mn-Tutton salt, but also the vapor pressures of liquid helium, liquid hydrogen, and liquid nitrogen. The ac-susceptibility measurements of PcMn were done by means of a Hartshorn bridge zero-field method (90 Hz) between 13.8 K and 20.2 K by pumping out the liquid hydrogen. The temperature was determined from the susceptibility of the standard sample, $Cr(NH_3)_6Cl_3$,[8] and from the vapor pressures of liquid hydrogen. With this method, the initial susceptibility in the limit of zero field is fairly well approximated because the amplitude of the measuring field may be kept very small.

A diamagnetic correction of -290×10^{-6} emu/mol was used to correct the susceptibility data, following the recent results on diamagnetic PcNi reported by Mitra *et al.*[9]

Results and Discussion

a) PcMn. The dc susceptibility in 10.2 kG appears to deviate from the Curie-Weiss law below 70 K, as is shown in Fig. 2. Below 7 K, it reaches a constant maximum value dependent on the magnetic field strength, as has already been reported.[2] To study the magnetic behavior in the low-temperature region, it is more advantageous to plot $(\chi_m T)^{-1}$ against T^{-1}, which enlarges the deviation from the Curie-Weiss law.[10] The data are plotted as $1/\chi_m T$ to $1/T$ in Fig. 3. The molecular-field result (the Curie-Weiss law) appears as a straight line; $1/\chi_m T=1/C-\theta/CT$. The deviation from the molecular-field result is very large. The Curie constant, C, and the Weiss constant, θ, are estimated as 2.13 and 23 K respectively in the high-temperature region. The susceptibility seems to

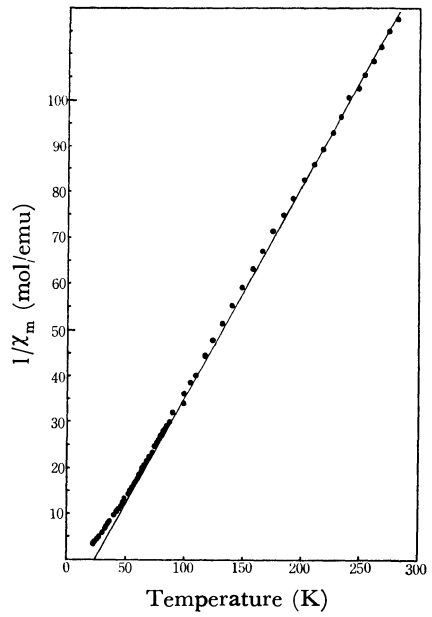

Fig. 2. Reciprocal susceptibilities of PcMn as a function of temperature (H= 10.2 kG).

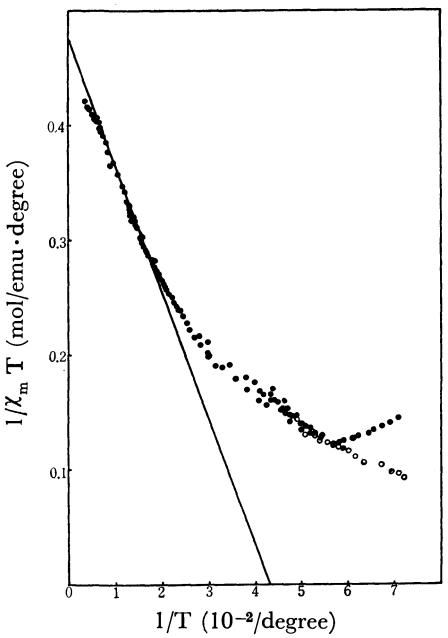

Fig. 3. Reciprocal susceptibilities ($1/\chi_m T$) of PcMn as a function of $1/T$. (●: H=10.2 kG, ○: $H\approx0$ G.)

become dependent on the field at $1/T$=0.057, (T= 17 K). The results of ac-susceptibility measurements have been included in Fig. 3; they coincide with those measured in 10.2 kG above 17 K. This field dependence of the susceptibility is consistent with the results of the magnetization measurements[2] at 4.2, 11.1, and 20.2 K.

It has been reported[1,4] that the ground electronic state of PcMn is a quartet (S=3/2). However, the ground state is not completely understood for the reason that no single crystal ESR data have been reported, though ESR measurements have been made of the powder sample (g=2.0).[11] Because of the lack of detailed information about the magnetic anisotropy, the exchange interaction in PcMn is assumed to be isotropic.

Now, let us compare the ratio of T_c to the θ of PcMn with that of the 2- or 3-dimensional lattice. On the Curie points of Heisenberg model magnetics, many theoretical studies have been made all along the line. Rushbrooke and Wood[12] have obtained an approximate formula for the Curie temperatures of 3-dimensional lattices for $S>1/2$; $T_c=(5/96)(z-1)[11S(S+1)-1](J/k)$, where z is the coordination number of the lattice. Moreover, Stanley and Kaplan[13] have

Table 2. The values of T_c/θ and kT_c/J[12-14] (Heisenberg model of S=3/2)

Lattice	Dimension	z[a]	T_c/θ	kT_c/J
Simple cubic	3	6	0.68	10.48
b. c. c.	3	8	0.73	14.67
f. c. c.	3	4	0.77	6.28
triangle	2	6	0.43	6.5
quadratic	2	4	0.39	3.9
PcMn	—	2	0.37	1.53

a) the coordination number.

given the transition temperature in 2-dimensional lattices for $S>1/2$ as follows; $T_c=(1/5)(z-1)[2S(S+1)-1](J/k)$. The Weiss constant, θ, has also been obtained by the molecular-field model; $\theta=(2/3)zS(S+1)(J/k)$. Using these formulas, the (T_c/θ) ratio can be calculated theoretically in individual lattice. The results are tabulated for $S=3/2$ in Table 2. The experimentally-obtained ratio of PcMn is 0.37, much smaller than that of the 2- or 3-dimensional lattice. This suggests that the dominant exchange interactions in PcMn may form a magnetic linear-chain system.

In the second place, taking into account the crystal structure, PcMn is treated approximately as a ferromagnetic-chain system and the results are compared with the definite theory. At first sight, it seems plausible to apply Fisher's classical Heisenberg result.[15] Fisher replaced the quantum mechanical spin operators with classical vectors. The resulting Hamiltonian for a chain of $N+1$ may be written in a magnetic field. H, as;

$$\mathcal{H} = -2JS(S+1)\sum_{i=1}^{N} \boldsymbol{s}_i \boldsymbol{s}_{i-1} - g\mu_B[S(S+1)]^{1/2}\sum_{i=0}^{N} \boldsymbol{H}\cdot\boldsymbol{s}_i, \quad (1)$$

where the unit vector, $\boldsymbol{s}_i$, is associated with the ith spin, whose magnetic moment is $g\mu_B[S(S+1)]^{1/2}$. Fisher's expression for the magnetic susceptibility of the chain then becomes;[16]

$$\chi_m = Ng^2S(S+1)\mu_B^2/3kT\cdot(1+u)/(1-u), \quad (2)$$

where $u=\coth[2JS(S+1)/kT]-kT/2JS(S+1)$. If the interaction is ferromagnetic ($J>0$), χ_m diverges as $T\to 0$. We may conveniently rewrite the above formula;

$$C/X_mT = (1-u)/(1+u). \quad (3)$$

Using $S=3/2$ and the obtained C value of 2.13, Eq. (3) is fitted to the data in the high-temperature range by adjusting J. The best fit is obtained with $J=5.64k$. The resulting curve of C/χ_mT *versus* J/kT is shown together with the data in Fig. 4. Although the theory

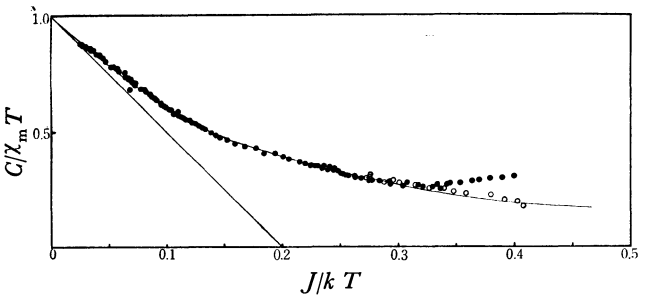

Fig. 4. Reciprocal susceptibilities (C/χ_mT) of PcMn *versus* J/kT (dimensionless units). (●: $H=10.2$ kG, ○: $H\approx 0$ G) C; 2.13, $J/k=5.64$.

is restricted within the classical limits and the real system of PcMn may be more complex, the data agree rather well with Fisher's theory over quite a wide temperature region. Using the value of $J=5.64k$, it is found that kT_c/J is 1.53 (8.6/5.64), smaller than the value of the theory of the 2- or 3-dimensional lattice (see Table 2).

Thus, the preceding discussion confirms the 1-dimensionality of the dominant exchange interactions in PcMn. It is well known theoretically[13,17] that isolated

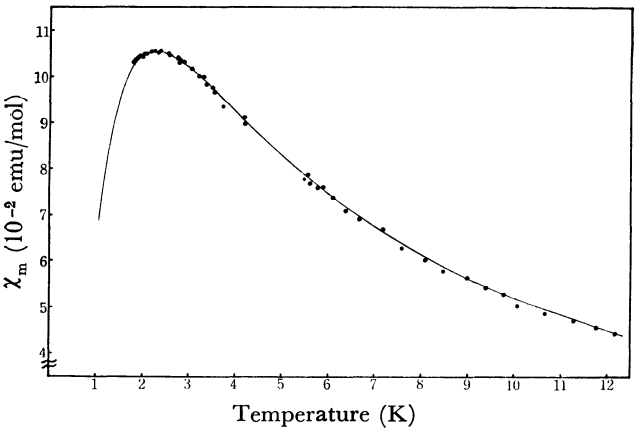

Fig. 5. Molar susceptibilities of PcCo as a function of temperature. The solid line; the parallel susceptibilities of the 1-dimensional Ising theory ($J/k=2.3$, $g=2.66$).

magnetic chains do not give rise to a magnetic transition, and that there occurs a magnetic transition in the presence of a small interaction between chains. Therefore, the magnetic transition in PcMn presumably results from an interchain interaction much smaller than the intrachain interaction.

b) PcCo. The magnetic susceptibilities of PcCo are shown in Fig. 5. The results obey the Curie-Weiss law above 5 K. One feature of the results is the presence of antiferromagnetic interaction among molecules, suggested by the negative Weiss constant, $\theta(-3$ K). Another feature is the existence of a broad maximum at 2.3 K ($\chi_{max}=10.55\times10^{-2}$ emu). Such a maximum can be expected for an antiferromagnetic linear-chain system. Of course, the broad susceptibility maxima could occur also in systems of isolated clusters or 2-dimensional sheets of spins. The structural consideration of phthalocyanines presented earlier does, however, favor the linear-chain model rather than any other one.

The electronic structure of PcCo has been studied by means of ESR measurements.[18] The experimental results confirm that PcCo exists as a doublet ($S=1/2$) and has anisotropic g values. The experimentally-obtained g-value (2.66), determined from the slope of $1/\chi_m-T$ plots, is consistent with the reported data ($g_{//}=1.89$, $g_\perp=2.94$).

Let us analyse the results using the theory of the 1-dimensional antiferromagnetic Ising model, because of the anisotropy shown in g values. The exchange interaction is represented as $-2JS_{iz}S_{jz}$. The expression for the magnetic susceptibility of the Ising chain thus becomes;[19]

$$\left.\begin{aligned}\chi_{//} &= (Ng^2\mu_B^2/4kT)\exp(J/kT)\\ \chi_\perp &= (Ng^2\mu_B^2/4|J|)[\tanh(|J|/2kT)\\ &\quad +(|J|/2kT)\,\mathrm{sech}^2(|J|/2kT)]\\ \chi_p &= (\chi_{//}/3)+(2\chi_\perp/3),\end{aligned}\right\} \quad (4)$$

where $\chi_{//}$, $\chi_\perp$, and χ_p indicate the parallel, perpendicular, and powder susceptibilities respectively. χ_p is the spatial average of $\chi_{//}$ and $\chi_\perp$. χ_p has a broad maximum (χ_{max}) at $kT_{max}/|J|\simeq 0.47$. By comparing

the experimental and theoretical values of the temperature (T_{max}) which corresponds to the broad maximum (χ_{max}), the exchange interaction is estimated to be $J/k=-4.89$. However, using this value, the calculated maximum susceptibility (11.91×10^{-2} emu) does not agree with the experimental one (10.55×10^{-2} emu); this discrepancy is beyond the limits of experimental error. Strangely, the data are quantitatively in good accord with $\chi_{//}$ rather than with χ_p. $\chi_{//}$ exhibits a broad maximum at $kT_{max}=J$; thus, it is found that $J/k=-2.3$ K for $T_{max}=2.3$ K. Using the values of $g=2.66$ and $J=-2.3k$, the theoretical curve of $\chi_{//}$ is shown against T as a solid curve, together with the data shown in Fig. 5. The agreement is very good. The Weiss constant is expressed as $\theta=(2/3)zS(S+1)(J/k)$. By substituting the values of $\theta=-3$ K, $z=2$ and $S=1/2$, it is found that $J=-3k$, which is consistent with the value of $J=-2.3k$ rather than with that of $J=-4.89k$.

These facts can not be understood well, but they may come from the fact that PcCo is not the ideal Ising spin system, since the anisotropy of g values is small compared with those of the usual Co(II) compounds of the Ising type.[20]

c) PcCu. The results are subjected to the Curie law in the temperature region where the measurements were carried out (1.8—77 K). This implies that the exchange interaction in the PcCu crystal is very small; thus, PcCu may not form a magnetic linear chain. The g value was determined as 2.07 from the slope of the $1/\chi_m-T$ plots; this value is consistent with those obtained from the ESR measurements ($g_{//}=2.18$, $g_\perp=2.05$).[21]

d) Exchange Interactions in PcMn, PcCo, and PcCu. Through their crystal structures are isomorphous, the exchange interactions in PcMn, PcCo, and PcCu are multifarious. Because the nature of the magnetic interaction is dependent on the electronic configuration of each molecule, it will be useful to comment on the characteristics of the electronic state of the present system. The phthalocyanine ring has a well-developed π-system and generally has been treated by the molecular orbital method. The central metal orbitals interact weakly with the π-system. Let us consider the orbitals occupied by the unpaired electrons. Based upon the discussion of the results calculated by Gouterman *et al.*[22] and the results observed experimentally by ESR measurements, *etc.*[1,4,18,21] for PcCu, PcCo, and PcMn, the features can be described as follows.

The ordering of energy levels may be identical for the three compounds, as is shown in Fig. 6. The rise in the d_{zx} and d_{yz} levels above the d_{xy} level originates in the π-bonding with the phthalocyanine molecular orbitals.[21] In PcCu, the $d_{x^2-y^2}$ orbital is occupied by the unpaired electron which spreads into the molecular plane and has a σ-characteristic. In PcCo, the unpaired electron is localized in a d_{z^2} orbital which is almost pure. This orbital has a characteristic of an out-of-plane spreading. In PcMn, three unpaired electrons occupy the d_{z^2}, d_{zx}, and d_{yz} orbitals. The unpaired electrons in the d_{zx} and d_{yz} orbitals can spread

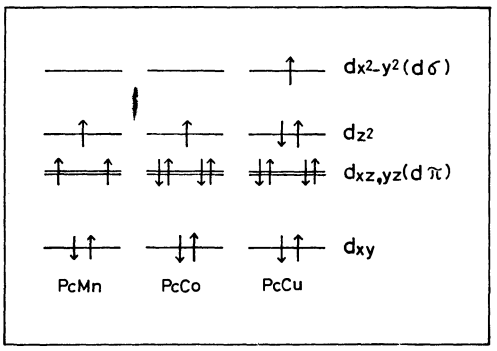

Fig. 6. Schematic representation of electronic structures of PcCu, PcCo, and PcMn.

on the liganding phthalocyanine ring *via* the π-bonding.

In our previous report[2] on PcMn, the paramagnetic shifts of hydrogens were observed by means of proton magnetic resonance measurements (12 MHz) in the liquid-hydrogen-temperature region. These maesurements showed that the unpaired electrons in PcMn are spreading on the ligand. On the other hand, in PcCo and PcCu, only one nonshifted absorption is observed down to 1.8 K in the helium temperature range (PcCo: the linewidth is 9—10 G at 30 MHz; PcCu: the linewidth is 15—18 G at 17 MHz). These results support the above description of the electronic states.

The exchange interaction originates from an overlap of the wave function of the unpaired electrons. The nearest vertical distance between adjacent parallel molecules is 3.38 Å and may ensure a weak overlap of the out-of-plane orbitals. In PcCu, the $d_{x^2-y^2}$ unpaired orbital has a σ-characteristic; hence, the overlap of the wave function between adjacent molecules may be very small. Both PcCo and PcCu have out-of-plane unpaired orbitals; therefore, the overlap may be present. In PcCo, since the unpaired orbital d_{z^2} is almost pure, the overlap may be attributed to the direct one between the d_{z^2} orbitals of adjacent molecules. On the other hand, in PcMn there exists a delocalization of the unpaired spins onto the molecular plane *via* the π-bonding. This may enhance the overlap and afford the possibility of an exchange interaction between the nonparallel molecules (interchain interaction). However, for the nonparallel molecules, the metal-metal distance is 10.3 Å and the orbitals are at right angles to each other. Accordingly, the overlap of the wave functions between nonparallel molecules may be smaller than that between the parallel molecules.

The author is much obliged to Professor Yasuo Deguchi and Dr. Hiroaki Ohya-Nishiguchi for their continuous encouragement throughout this work, and also to Professor Mamoru Mekata, Dr. Yoshitami Ajiro, and the other members of his laboratory for their illuminating discussions. Thanks are also due to Professor Ikuji Tsujikawa and Dr. Hanako Kobayashi for offering him a chance to use the Hartshorn bridge apparatus.

References

1) A. B. P. Lever, *J. Chem. Soc.*, **1965**, 1821.
2) H. Miyoshi, H. Ohya-Nishiguchi, and Y. Deguchi, This Bulletin, **46**, 2724 (1973).
3) J. M. Robertson, *J. Chem. Soc.*, **1935**, 615; **1937**, 219. R. P. Linstead and J. M. Robertson, *J. Chem. Soc.*, **1936**, 1736. C. J. Brown, *ibid.*, **1968A**, 2488.
4) C. G. Barraclough, R. L. Martin, and S. Mitra, *J. Chem. Phys.*, **53**, 1638 (1970).
5) P. A. Barrett, C. E. Dent, and R. P. Linstead, *J. Chem. Soc.*, **1936**, 1719.
6) H. A. Rutter Jr. and J. D. McQueen, *J. Inorg. Nucl. Chem.*, **12**, 362 (1960).
7) M. Mekata, *J. Phys. Soc. Jap.*, **17**, 796 (1962).
8) H. Kobayashi, T. Haseda, and M. Mori, This Bulletin, **38**, 1455 (1965).
9) C. G. Barraclough, R. L. Martin, and S. Mitra, *J. Chem. Phys.*, **55**, 1426 (1971).
10) A. Danielian, *Proc. Phys. Soc.*, **80**, 981 (1962).
11) D. J. E. Ingram and J. E. Bennett, *J. Chem. Phys.*, **22**, 1136 (1954).
12) G. S. Rushbrooke and P. J. Wood, *Mol. Phys.*, **1**, 257 (1958).
13) H. E. Stanley and T. A. Kaplan, *Phys. Rev. Lett.*, **17**, 913 (1966).
14) J. Kanamori, "Jisei", Baifukan, Tokyo (1969), p. 97.
15) M. E. Fisher, *Am. J. Phys.*, **32**, 343 (1964).
16) T. Smith and S. A. Friedberg, *Phys. Rev.*, **176A**, 660 (1968).
17) L. Onsager, *Phys. Rev.*, **65**, 117 (1944).
18) J. F. Gibson, D. J. E. Ingram, and D. Schonland, *Discuss. Faraday Soc.*, **26**, 72 (1958). J. S. Griffith, *ibid.*, **26**, 81 (1958). J. M. Assour and W. K. Kahn, *J. Amer. Chem. Soc.*, **87**, 207 (1965).
19) M. E. Fisher, *J. Math. Phys.*, **4**, 124 (1963).
20) N. Achiwa, *J. Phys. Soc. Jap.*, **27**, 561 (1969). K. Takeda, S. Matsukawa, and T. Haseda, *ibid.*, **30**, 1330 (1971)
21) S. E. Harrison and J. M. Assour, *J. Chem. Phys.*, **40**, 365 (1964).
22) M. Zerner and M. Gouterman, *Theoret. Chim. Acta.* (Berl.), **4**, 44 (1966).

Ultrasonic Study on Solute-Solvent Interaction in Aqueous Systems of Ethers

Nobuo TAKENAKA and Kiyoshi ARAKAWA

Research Institute of Applied Electricity, Hokkaido University, Sapporo 060

(Received July 12, 1973)

Ultrasonic velocity and absorption were measured for binary mixtures of water and ethers (1,2-dimethoxyethane, bis(2-ethoxyethyl)ether, bis(2-methoxyethyl)ether, ethylether, diethoxymethane, 1,1-diethoxyethane and 1,2-diethoxyethane) in the frequency range 15—45 MHz at 10—30 °C. Vibrational relaxation was observed in the pure liquid of 1,2-dimethoxyethane. For each solution of 1,2-dimethoxyethane and bis(2-methoxyethyl)-ether, the maximum absorption at the intermediate composition was ascribed to the formation of dihydrate and trihydrate, respectively. The difference between the behavior of ethyl group in water and that of methyl group was discussed from the absorption data.

It has been accepted that hydrocarbon-water interaction (hydrophobic interaction) plays an important role in the conformation of biopolymers in aqueous solutions. For the elucidation of the nature of the interaction, we have studied the aqueous solutions of polyethyleneoxide,[1] dioxane,[2,3] alkyl-substituted urea,[4] amino acid,[5] diamine,[6] tetraalkylammonium salt[7] *etc.* in relation to the structure theory of water.[8-10]

Ultrasonic studies of the aqueous solution of polyethyleneoxide have been carried out by several workers.[1,11-15] It was concluded that "the local water structure formation around the polymer consists of water molecules hydrogen-bonded to oxygen atoms of the chain and hydrophobic water structure around the $-CH_2CH_2-$ groups",[12] and also that it is the origin of the ultrasonic relaxation in the MHz region in the solution. From a study on the aqueous solution of dioxane,[2,3] the presence of dioxane dihydrate was proposed. It was concluded that, concerning the water structure, the structure-breaking ability due to two etheral oxygens is diminished in part by the structure-forming ability due to two $-CH_2CH_2-$ groups.

Many problems concerning the interaction between water and alkyl groups with polar groups remain nusolved.

An ultrasonic measurement is one of the most useful methods for studying the structure of liquids and solutions.[16-18] We have undertaken a comprehensive study of aqueous solutions of ethers by means of an ultrasonic pulse technique with the intention to investigate ethyleneoxide-water and alkyl group-water interactions.

Experimental

Apparatus and Procedures. The ultrasonic pulse method was used for the measurement of absorption coefficient and velocity. The apparatus and procedures were described previously.[1,19] The sound velocity and absorption coefficient were measured at 5 MHz and in the frequency range 15—45 MHz, respectively at temperatures 10—30 °C. The data of the absorption coefficient were reproducible within ±2% and sound velocity data ±1 m/s.

Samples. The samples of ethers were obtained from Wako Pure Chemical Ind. Co. Ltd. (Table 1). Before purification, ethylether was treated with a saturated potassium permanganate solution containing 5% sodium hydroxide, with 50% sulfuric acid and then with water.[20] To bis(2-ethoxyethyl)ether and bis(2-methoxyethyl)ether, a small amount of water was added and the mixture was distilled. Impurities such as xylene were azeotropically removed.

All the samples were refluxed over potassium–sodium alloy after desiccation with potassium hydroxide, and then fractionally distilled through a Widmer column. Distillation was carried out under reduced pressure for 1,2-diethoxyethane and bis(2-ethoxyethyl)ether and for bis(2-methoxyethyl)ether under nitrogen atomsphere. The boiling points observed are given in Table 1.

Results

Sound Velocity. 1,2-Dimethoxyethane, bis(2-ethoxyethyl)ether and bis(2-methoxyethyl)ether are miscible with water in all compositions, while other ethers are partially miscible at room temperature. The aqueous solution of bis(2-ethoxyethyl)ether has a lower critical solution temperature (L.C.S.T., 28 °C, 63.5% ether).[25] The sound velocity *vs.* concentration curves for aqueous solutions of 1,2-dimethoxyethane, bis(2-ethoxyethyl)ether and bis(2-methoxyethyl)ether are shown in Figs. 1(a)—(c), where the concentration is given in vol %.[26] The sound velocity data for dilute aqueous solutions of ethylether, diethoxymethane,

Table 1. Boiling points of ethers

Sample		Bp (°C) Present work	Ref.
Ethylether	$C_2H_5OC_2H_5$	34.4	34.55[20]
Diethoxymethane	$C_2H_5OCH_2OC_2H_5$	87.9	87.9[21]
1,1-Diethoxyethane	$(C_2H_5O)_2CHCH_3$	103.5	103.6[20]
1,2-Diethoxyethane	$C_2H_5OC_2H_4OC_2H_5$	43.5 (47.5 mmHg)	
Bis(2-ethoxyethyl)ether	$(C_2H_5OC_2H_4)_2O$	70.9 (10 mmHg)	
1,2-Dimethoxyethane	$CH_3OC_2H_4OCH_3$	85.1	85.2[22] 84.6[23]
Bis(2-methoxyethyl) ether	$(CH_3OC_2H_4)_2O$	163.0	162[24]

1,1-diethoxyethane and 1,2-diethoxyethane at 20 °C are shown in Fig. 2, including those for 1,2-dimethoxyethane, bis(2-ethoxyethyl)ether and bis(2-methoxyethyl)ether solutions. We see that the velocity *vs.* concentration relation is similar to each other in dilute aqueous solutions of all these materials, and that the relation is represented by a single curve for all the solutions.

Ultrasonic Absorption. Ultrasonic absorption, α/f^2, where α is absorption coefficient and f frequency, is plotted against temperature for pure 1,2-dimethoxyethane, bis(2-ethoxyethyl)ether and bis(2-methoxyethyl)ether (Fig. 3). In the frequency range studied, no relaxation was observed. The absorption of bis(2-ethoxyethyl)ether and bis(2-methoxyethyl)ether decreases and that of 1,2-dimethoxyethane increases with temperature rise. This indicates the presence of a vibrational relaxation mechanism in the pure liquid of 1,2-dimethoxyethane like dioxane.[2)]

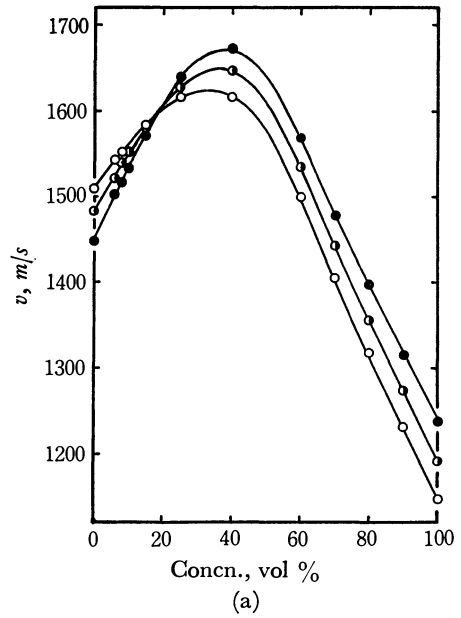

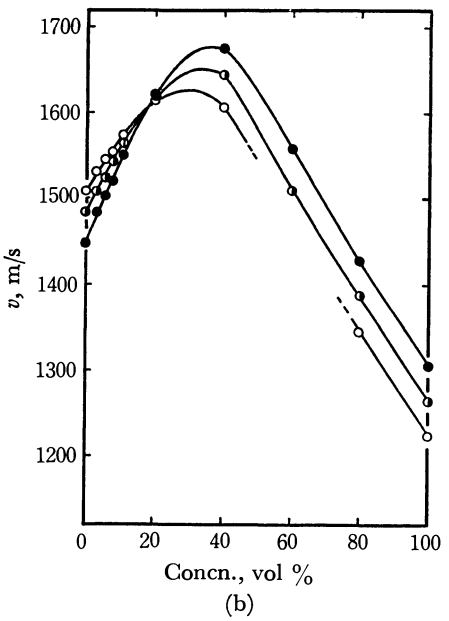

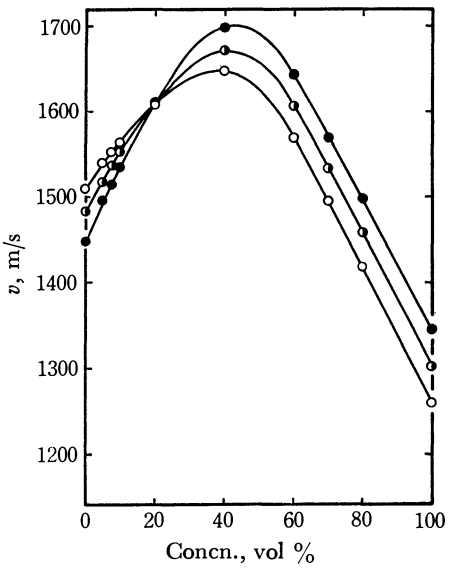

Fig. 1. The plot of ultrasonic velocity *vs.* concentration of ethers (vol %) in aqueous systems of ethers, (a): 1,2-dimethoxyethane, (b): bis(2-ethoxyethyl)ether, (c): bis(2-methoxyethyl)ether, ●: 10 °C, ◑: 20 °C, ○: 30 °C.

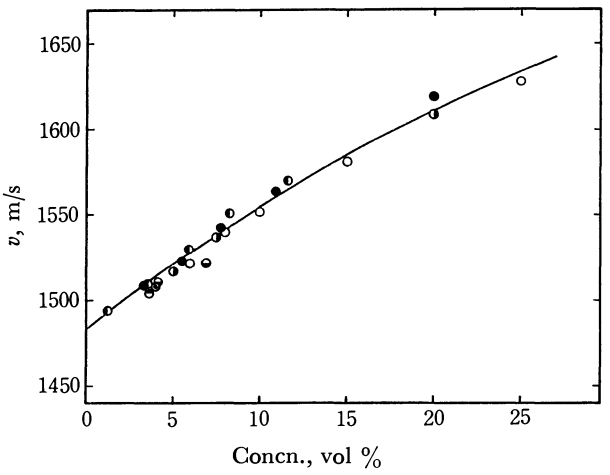

Fig. 2. Ultrasonic velocity in aqueous solutions of ethers at 20 °C, ○: 1,2-dimethoxyethane, ●: bis(2-ethoxyethyl)ether, ◑: bis(2-methoxyethyl)ether, ◒: ethylether, ⊙: diethoxymethane, ◓: 1,1-diethoxyethane, ◐: 1,2-diethoxyethane.

The absorptions of aqueous solutions of these ethers at 15 MHz are plotted against concentration (Figs. 4(a)—(c)). They are also plotted at various frequencies at 20 °C for the 1,2-dimethoxyethane–water system (Fig. 5). The absorption *vs.* concentration curves have a peak at about 60—80 vol %. The maximum value decreases with increasing frequency. In the aqueous solutions of 1,2-dimethoxyethane and bis(2-methoxyethyl)ether, the maximum value decreases with increasing temperature, while in the solutions of bis(2-ethoxyethyl)ether it increases. In Fig. 6, the absorption of the aqueous solutions of 1,2-dimethoxyethane and that of bis(2-methoxyethyl)ether at 10 °C and at 35 MHz are plotted against concentration

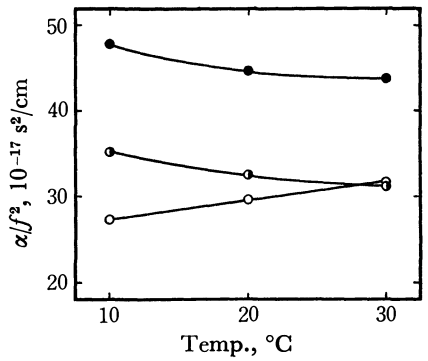

Fig. 3. Ultrasonic absorption in pure ethers,
○: 1,2-dimethoxyethane, ●: bis(2-ethoxyethyl)ether,
◑: bis(2-methoxyethyl)ether.

(mol %), including that of 1,2-ethanediol-water mixtures reported by Blandamer *et al.* (at 0 °C, 70 MHz).[27]

The ultrasonic absorption for all solutions at low concentrations is plotted against concentration by vol% in Fig. 7. No relaxation has been observed in the frequency range measured. The absorption *vs.* vol %

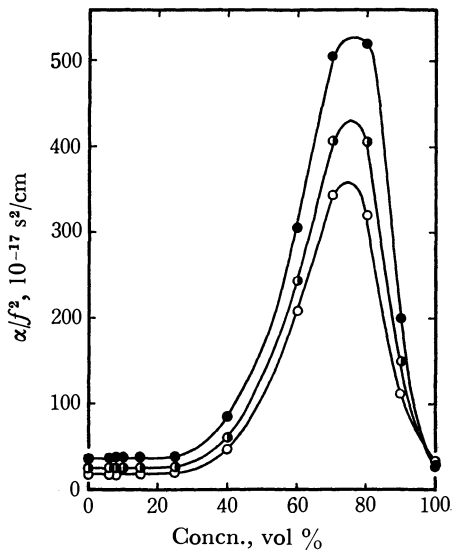

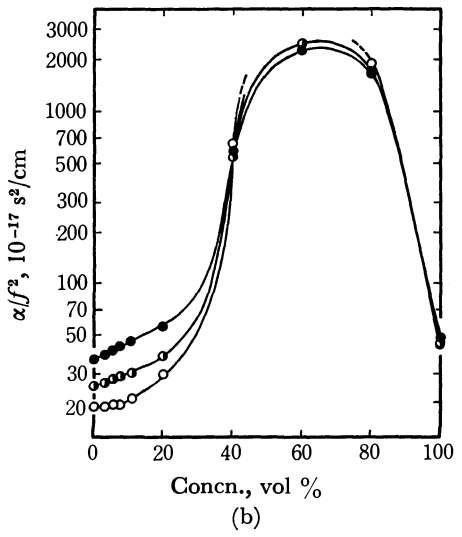

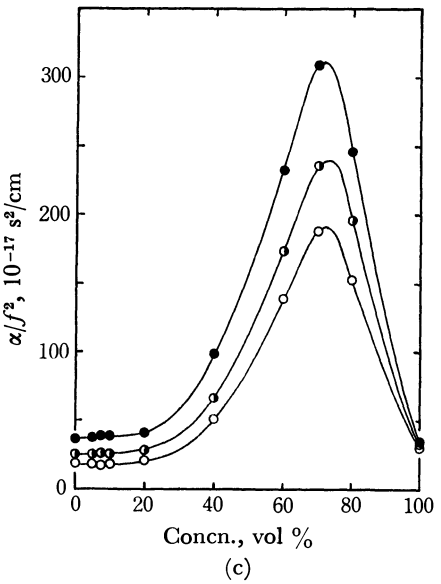

Fig. 4. The plot of ultrasonic absorption *vs.* concentration of ethers (vol %) in aqueous systems of ethers, (a): 1,2-dimethoxyethane, (b): bis(2-ethoxyethyl)ether, (c): bis(2-methoxyethyl)ether, ●: 10 °C, ◑: 20 °C, ○: 30 °C.

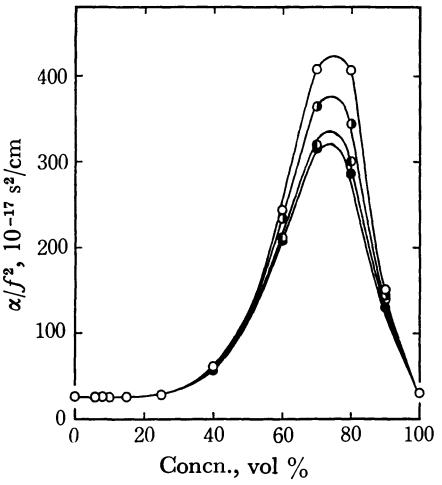

Fig. 5. The plot of ultrasonic absorption *vs.* concentration of ether (vol %) in the 1,2-dimethoxyethane-water system, ○: 15 MHz, ◑: 25 MHz, ◐: 35 MHz, ●: 45 MHz.

relations in these solutions are classified into two groups, each of which is represented by a single curve. The upper curve is for the ethers with ethyl groups at each end of a molecule, the lower curve for those with methyl groups at each end.

Partial molar volume has been calculated graphically[28] from the density data obtained for the bis(2-ethoxyethyl)ether-water system and is plotted in Fig. 8.

Discussion

The Origin of the Maximum in Ultrasonic Absorption. A marked peak appears at an intermediate composition in each absorption *vs.* composition curve. The behavior of the curve for bis(2-ethoxyethyl)ether (Fig. 4(b))

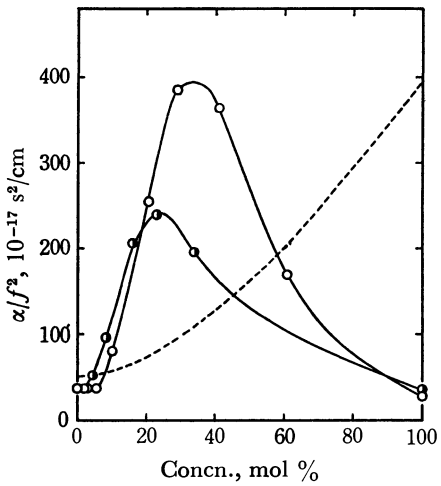

Fig. 6. The plot of ultrasonic absorption *vs.* concentration of ethers (mol %) in aqueous systems of ethers at 10 °C and 35 MHz, ○: 1,2-dimethoxyethane, ◑: bis(2-methoxyethyl)ether, dashed line: 1,2-ethanediol (at 0 °C 70 MHz, ref. 27).

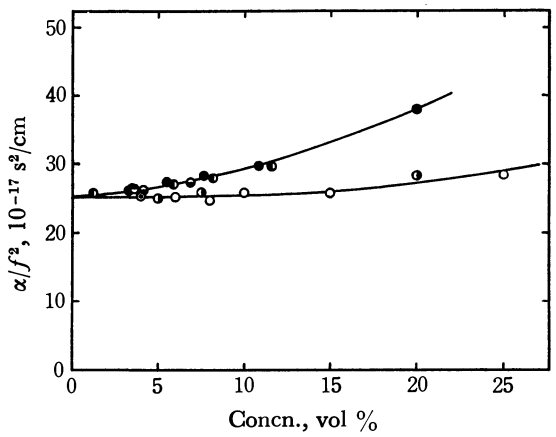

Fig. 7. Ultrasonic absorption in aqueous solutions of ethers at 20 °C. ○: 1,2-dimethoxyethane, ●: bis(2-ethoxyethyl)ether, ◑: bis(2-methoxyethyl)ether, ◒: ethylether, ⊙: diethoxymethane, ◓: 1,1-diethoxyethane, ◐: 1,2-diethoxyethane.

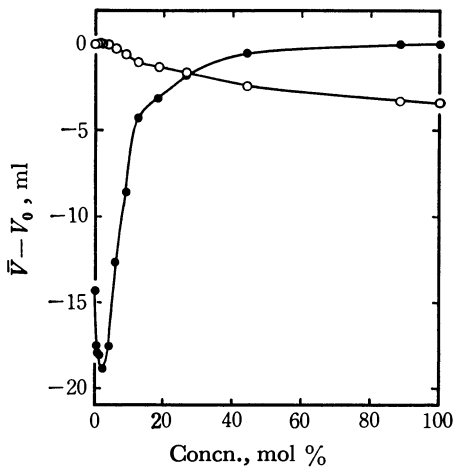

Fig. 8. Partial molar volumes for the bis(2-ethoxyethyl)-ether-water system. ●: the ether, ○: water.

differs from that for other ethers (Figs. 4(a) and (c)), the temperature dependence of absorption near the maximum being the reverse of that at each side. This is ascribed to the presence of L.C.S.T. It is well-known that ultrasonic absorption increases rapidly near L.C.S.T.[29]

In the aqueous solution of 1,2-dimethoxyethane and bis(2-methoxyethyl)ether the maximum of the ultrasonic absorption could be attributed to other sources. At the composition of each maximum (Figs. 4(a), (c), and 6) the molar ratio between ether and water is 1 : 2 and 1 : 3 for 1,2-dimethoxyethane and bis(2-methoxyethyl)ether, respectively. Thus, the molar ratio between etheral oxygen and water becomes 1 : 1 exactly at the composition for both ethers, because each ether has two and three etheral oxygen atoms per molecule, respectively. In the case of the dioxane-water mixture a similar feature was found and the formation of dioxane dihydrate was proposed.[2] Thus it is tentatively assumed that the origin of the maximum absorption is mainly attributed to the presence of hydrates (1,2-dimethoxyethane dihydrate and bis(2-methoxyethyl)ether trihydrate).

Absorption vs. Composition Curves for Low Concentrations. A deep minimum is found in the partial molar volume of the solute *vs.* composition curve for the bis(2-ethoxyethyl)ether-water system (Fig. 8), similar to other aqueous solutions of organic substance.[22,24,30] The composition of the minimum is about 2.5 mol % (about 20% by volume).

The sound velocity *vs.* concentration curves at various temperatures shown in Figs. 1(a)—(c) have a crossing point, where sound velocity is independent of temperature. The solute concentration at the point is about 15—20 vol % for every ether (Fig. 1). As to the ultrasonic absorption, each curve for the absorption *vs.* concentration relation has a flat region at low concentrations (below about 15—20 vol %) (Figs. 4, 5, and 7). The concentration at which the rapid increase of absorption begins is the same as that at the crossing point of velocity *vs.* concentration curves and nearly the same as that at the minimum of partial molar volume. This suggests that all these features are related to some common molecular process in dilute aqueous solutions. As regards the aqueous solutions of dioxane and other substances,[3] we proposed an explanation of a similar feature in absorption *vs.* concentration curves, based on a model of water structure. The underlying molecular process has been assumed to be the "cooperative formation" of the short-lived "ice-like structure" in liquid water.[10]

Difference between the Behavior of Ethyl and Methyl Groups in Water. As seen in Fig. 7, the absorption *vs.* concentration relation for ethers with ethyl groups at each end of a molecule is represented by a single curve (upper curve), and that for ethers with methyl group by another single curve (lower curve).

The difference between the upper and lower curves could be ascribed to the different behavior of ethyl and methyl groups in water. A methyl group at the end of a molecule is considered to rotate almost freely in water at room temperature.[31] Thus, from the

large absorption of ethers with ethyl in comparison with that of ethers with methyl, the ethyl group at the molecular end is supposed to be hindered in its motion by the formation of the water structure about itself. The formation of "water structure" about ethyl group and its disruption by the direct contact of the hydrocarbon is considered to be the origin of "hydrophobic interaction" between hydrocarbons in general with exception of the methyl group.[10,32]

Literatures

1) K. Arakawa and N. Takenaka, This Bulletin, **40**, 2063 (1967).
2) K. Arakawa and N. Takenaka, *ibid.*, **42**, 5 (1969).
3) K. Arakawa, N. Takenaka, and K. Sasaki, *ibid.*, **43**, 636 (1970).
4) K. Sasaki and K. Arakawa, *ibid.*, **42**, 2485 (1969).
5) K. Sasaki and K. Arakawa, *ibid.*, **44**, 3223 (1971).
6) K. Sasaki and K. Arakawa, *ibid.*, **45**, 3287 (1972).
7) F. Hirata and K. Arakawa, *ibid.*, **45**, 2715 (1972).
8) K. Arakawa and K. Sasaki, *ibid.*, **42**, 303 (1969).
9) K. Arakawa and K. Sasaki, *ibid.*, **43**, 3048 (1970).
10) K. Arakawa and K. Sasaki, *Kagaku to Kogyo*, **24**, 444 (1971), K. Arakawa, *Kagaku*, **26**, 1172 (1971).
11) G. G. Hammes and T. B. Lewis, *J. Phys. Chem.*, **70**, 1610 (1966).
12) G. G. Hammes and P. R. Schimmel, *J. Amer. Chem. Soc.*, **89**, 422 (1967).
13) G. G. Hammes and P. B. Roberts, *ibid.*, **90**, 7119 (1968).
14) S. A. Hawley and F. Dunn, *J. Chem. Phys.*, **50**, 3523 (1969).
15) L. W. Kessler, W. D. O'Brien, Jr. and F. Dunn, *J. Phys. Chem.*, **74**, 4096 (1970).
16) K. F. Herzfeld and T. A. Litovitz, "Absorption and Dispersion of Ultrasonic Wave," Academic Press, New York, N. Y., (1959), p. 353.
17) V. F. Nozdrev, "Application of Ultrasonics in Molecular Physics," translated into English, Gordon and Breach Sci. Pub. Ltd., New York, N. Y. (1963), p. 354.
18) T. A. Litovitz and C. M. Davis, "Physical Acoustics," vol. IIA, ed. by W. P. Mason, Academic Press, New York, N. Y. (1965), p. 282.
19) K. Arakawa and N. Takenaka, This Bulletin, **39**, 447 (1966).
20) J. A. Riddick and W. B. Bunger, "Organic Solvents," 3rd ed., ed. by A. Weissberger, Wiley Interscience, New York, N. Y. (1970).
21) J. Timmermans, "Physyco-Chemical Constants of Pure Organic Compounds", vol. 2, Elsevier Pub. Co., New York, N. Y. (1965).
22) W. J. Wallace and A. L. Mathews, *J. Chem. Eng. Data*, **8**, 496 (1963).
23) E. Tommila and V. Turkki, *Suomen Kem.*, **B40**, 207 (1967).
24) W. J. Wallace and A. L. Mathews, *J. Chem. Eng. Data*, **9**, 267 (1964).
25) N. Murata and Y. Masuda, *Oyobutsuri*, **40**, 180 (1971).
26) The volume fraction (or vol %) used in this study was determined from the mixing ratio, the excess volume on mixing was safely ignored for the present purpose.
27) J. M. Blandamer, N. J. Hidden, M. C. R. Symons and N. C. Treloar, *Trans. Faraday Soc.*, **65**, 1805 (1969).
28) G. N. Lewis and M. Randall, "Thermodynamics", 2nd ed. revised by K. S. Pitzer and L. Brewer, McGraw-Hill Book Co., New York, N. Y., (1961) p. 205.
29) M. Fixman, *J. Chem. Phys.*, **36**, 1957, 1961, 1965 (1962).
30) D. N. Glew, H. D. Mak, and N. S. Rath, "Hydrogen-Bonded Solvent Systems," ed. by A. K. Covington and P. Jones, Taylor and Francis Ltd., London, (1968) p. 195.
31) K. Sasaki and K. Arakawa, This Bulletin, **46**, 2738 (1973).
32) K. Shinoda, *Kagaku to Kogyo*, **21**, 1400 (1968).

Isomerization of 2-Pinene Catalyzed by Solid Acids

Ryuichiro OHNISHI, Kozo TANABE,* Shinsuke MORIKAWA,* and Tadao NISHIZAKI

Research Institute for Catalysis, Hokkaido University, Sapporo 060
**Department of Chemistry, Faculty of Science, Hokkaido University, Sapporo 060*

(Received July 13, 1973)

The isomerization of 2-pinene (I) and 2(10)-pinene (II) in the liquid phase has been studied at 50 °C over solid acid catalysts such as silica–alumina, aluminum phosphate, nickel sulfate and zinc sulfide which have different acid strengths. The primary reaction products were camphene (III), 1,7,7-trimethyl-tricyclo[2.2.1.$0^{2,6}$]-heptane (IV) and *p*-mentha-1,8-diene (VI). The catalytic activities increased with increasing acid strength and acid amount of the catalysts. The selectivities for the formation of III+IV and VI from I were about 90 and 10% respectively over $NiSO_4$, but about 10 and 70% respectively over SiO_2–Al_2O_3 and $AlPO_4$. Those for the formation of I, III+IV and VI from II also depended on the acid strength. In the isomerization of VI, *p*-mentha-1,4(8)-diene (VII) was formed predominantly over $NiSO_4$ and *p*-cymene (IX) over SiO_2–Al_2O_3. From these results together with those of the isomerizations of III and IV, a reaction mechanism is proposed which consists of two parallel reactions proceeding *via* a common intermediate between I and II: one which gives monocyclic terpenes and the other bi- and tricyclic terpenes.

The isomerization of 2-pinene (I) over solid catalysts in the liquid phase was first reported by Gurvich in 1915.[1] Since then, a number of studies have been made on the isomerization and the following reaction products have been reported: bi- or tricyclic terpenes such as 2(10)-pinene (II), camphene (III), 1,7,7-trimethyl-tricyclo[2.2.1.$0^{2,6}$]heptane (IV), bornene (V) *etc.*, monocyclic terpenes such as *p*-menthadienes (VI, VII, VIII *etc.*), *p*-cymene (IX) and polymers[2,3] (See Fig. 4 for structures of the compounds).

Catalysts used for the isomerization were mineral clay, active carbon, silica–alumina, titanium oxide, magnesium sulfate *etc.* which can be classified as solid acids. It was reported recently that alumina, a strong acid, showed a tendency to give monocyclic terpenes, while alkali poisoned aluminas, weak acids, form bi- or tricyclic terpenes in vapor phase reactions.[4] However, no systematic work has been done on the correlation between acidic property of solid acids and their catalytic activity or selectivity. In the present work, the correlation was examined by employing as catalysts nickel sulfate which has moderate acid strength and whose acidity can be easily changed by calcination,[5–7] silica–alumina and aluminum phosphate which have high acid strength and zinc sulfide which has weak acid strength[8] in liquid phase.

On the basis of the observed results, the reaction paths and intermediates of the isomerization are discussed.

Experimental

Reagents and Catalysts. 2-Pinene was purified from turpentine oil (Wako Pure Chemical Co.) by distillation over sodium, passage through a preparative gas chromatography (Perkin–Elmer F-21) with a 3 m×8 mm column containing 20% polyethylene glycol 1500 on Chromosorb W and distillation again over sodium under a stream of nitrogen. The purified material was stored in sealed ampoules. 2(10)-Pinene and camphene (Takasago Perfumery Co.) and 1,7,7-trimethyl-tricyclo[2.2.1.$0^{2,6}$]heptane, synthesized from camphor according to the method of Meerwein and Emster,[9] were purified similarly to 2-pinene.

Nickel sulfate catalysts were prepared by calcining the heptahydrate (guaranteed reagent, Kanto Chemical Co.) in the temperature range 150—550 °C in air, grinding after cooling and calcining again at the original temperature for 3 hr. Aluminum phosphate, prepared from H_3PO_4 and $AlCl_3 \cdot 6H_2O$,[10] was calcined in air at 450 °C for 3 hr. Silica–alumina (15 wt. % Al_2O_3, Nikki Chemical Co.) and zinc sulfide (guaranteed reagent, Nakarai Chemical Co.) were calcined in air at 600 and 450 °C respectively. All catalysts were stored in sealed ampoules.

Acidity and Kinetic Measurements The acid amounts at various acid strengths of the catalysts were measured by *n*-butylamine titration using various indicators,[5] or by the ultraviolet spectrophotometric method.[11] The indicators used for the titration method were phenylazonaphthylamine ($pK_a = +4.0$), *p*-dimethylaminoazobenzene (+3.3), dicinnamalacetone (−3.0) and anthraquinone (−8.2). 2,6-Dichloro-4-nitroaniline ($pK_a = -3.27$) was used for the spectrophotometric method.

The reaction was carried out under helium gas since it is sensitive to air. The reaction temperature was 50 °C unless otherwise stated. Reaction products were analyzed by a gas chromatograph with FID (Hitachi-Perkin-Elmer F-6D), using a 45 m capillary column of Ucon LB-500-X. The amount (mole %) of each product was obtained by measuring each peak area with an integrator (DISC Co.) and by multiplying by the respective correction coefficient.

Results

Acidity of Catalysts. The acid amounts at various strengths of the catalysts are shown in Table 1. Silica–alumina and aluminum phosphate have high acid strength ($pK_a = -8.2$), while zinc sulfide has a weak one ($pK_a = +4.0$). The acid strength of the nickel sulfates was moderate. The acid amount increased with the rise in calcination temperature, attaining a maximum value at 350 °C, and then decreased at higher temperatures.[5]

Isomerization of Camphene (III), 1,7,7-Trimethyl-tricyclo-[2.2.1.$0^{2,6}$]heptane (IV) and p*-Mentha-1,8-diene (VI).* Before the reaction of I, the isomerization of III, IV, and VI, main reaction products of I, was studied. The products of the isomerization of III (or IV) were IV (or III) and a small amount of V over nickel sulfates. Over silica–alumina and aluminum phosphate which

Table 1. Acid amounts at various acid strengths of catalysts

Catalysts Calcination temp., °C	(pK_a)	$NiSO_4$ 150	200	250	350	450	550	SiO_2–Al_2O_3 600	$AlPO_4$ 450	ZnS 400
Acid amounts	+4.0	—	—	—	—	—	—	—	—	1.08
(mmol/g) at	+3.3	0.029	0.064	0.11	0.13	0.088	0.046	—	—	0
various acid	−3.0	0	—	0.016	0.046	0	0	—	—	—
strengths (pK's)	−3.27	—	0	0	0	—	—	—	—	—
	−8.2	—	—	—	—	—	—	0.25	0.42	—

Table 2. Equilibrium constants between camphene(III) and 1,7,7-trimethyltricyclo[2.2.1.$0^{2,6}$]heptane (IV)

Catalysts Reaction temp., °C	$NiSO_4$ 50	70	80	90	100	110	140	150	$KHSO_4$ 200	Co/Al_2O_3 250	Al_2O_3 275
K=IV/III	0.20—0.23	0.23	0.20	0.20	0.19	0.21	0.20	0.20	0.25—0.28[a]	0.33[b]	0.33[c]

a) Cited from Ref. 18, b) Ref. 19, c) Ref. 20

Table 3. Selectivities of varopis catalysts for isomerization of p-mentha-1,8-diene (VI) at 50 °C

Catalysts		$NiSO_4$ calcined at 400 °C	SiO_2–Al_2O_3	$AlPO_4$
Selectivity	VI→VII	0.84	—	0.21
	VI→IX	0.03	0.86	0.52

have high acid strength, considerable amounts of polymers were obtained in addition to the above products. The isomerization to I did not occur on any of the catalysts.

The equilibrium constants between III and IV, obtained from the mole % ratio of III to IV in equilibrium, are listed in Table 2. The values above 200 °C were cited from literature.

The main reaction products of VI were p-mentha-1,4(8)-diene (VII), p-mentha-1,3-diene (VIII) and p-cymene (IX). From initial slopes of the plots of VI, VII, and IX against reaction time the selectivity for the formation of VII and IX was obtained (Table 3). VII was formed predominantly over metal sulfates which have moderate acid strength, while IX was formed predominantly over strong solid acids, where polymers were also found.

Isomerization of 2-Pinene. The % conversion of 2-pinene (I) plotted against reaction time is shown in Fig. 1a. Since the isomerization did not obey the rate equation of a first- or second- order reaction, the initial rate per unit weight of catalyst was taken as the catalytic activity. The activities of various catalysts are given in Table 4. Because of high activity of silica–alumina, the reaction over the catalyst was carried out at ambient temperature. High activities were found for silica–alumina and aluminum phosphate and a low activity for zinc sulfide as expected from their acid strengths (Table 1). Calcined nickel sulfates showed intermediate activity, varying with changes in the calcination temperature. A correlation exists between the activity and the acid amount or strength.

It should be noted that the rate of isomerization is considerably affected by the presence of air. The reaction rate in the presence of air was too slow to measure at 50 °C but became measurable at 150 °C, at which temperature the reaction in the absence of air was too fast to follow. Thus, the unusual curve

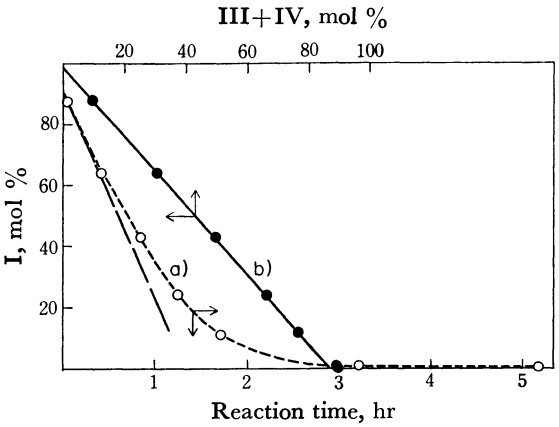

Fig. 1. a) Time dependence in mol % of 2-pinene (I). b) Mol % of 2-pinene (I) *vs.* mol % of camphene (III)+1,7,7-trimethyl-tricyclo[2.2.1.$0^{2,6}$]heptane (IV). Reaction temp.: 50 °C, Catalyst: 0.877 g of nickel sulfate calcined at 350 °C.

Table 4. Activities and selectviities of various catalysts for isomerization of 2-pinene (I) at 50 °C

Catalysts Calcination temp., °C	$NiSO_4$ 150	200	250	300	350	400	450	600	SiO_2–Al_2O_3 600	$AlPO_4$ 450	ZnS 400
Selectivity I→III+IV	0.93	0.77	0.83	0.84	0.89	0.78	0.79	0.87	0.14[a]	0.12	0.61
I→VI	—	0.14	0.11	0.10	0.09	0.10	0.15	0.08	0.67[a]	0.68	0.33
Initital velocity $hr^{-1}g^{-1}\times 10^{-2}$	0.01	0.02	0.5	0.8	0.8	2.3	1.4	0.9	51[a]	41	0.3

a) Values at room temperature.

of % conversion *vs.* reaction time in Fig. 1a is considered to be due to the poisoning effect of a very small amount of oxygen or moisture in the reaction system.

In order to see the selectivity of this reaction, % of I remaining at reaction time t was plotted against % of III+IV formed at time t in Fig. 1b.[12] The plots fell on a straight line. This indicates that there is no backward reaction to I and that III and IV are not converted into any other compounds under the reaction conditions, in accordance with the results of the reactions of III and IV. This indicates that III and/or IV are primary products of I. A linear relation was also found between I and VI, indicating that there is no backward reaction from VI to I.

The selectivities for the formation of III+IV and VI from I, calculated from the slopes of the straight lines over various catalysts, are shown in Table 4. The selectivity did not change much over nickel sulfates calcined at various temperatures, 80—90% of bicyclic terpenes (III+IV) and about 10% of monocyclic terpene (VI) being formed. On the other hand, a high selectivity (about 70%) for VI was found for silica–alumina and aluminum phosphate which have high acid strength. This is in agreement with the result which showed that monocyclic terpenes are formed more readily over alumina than over alkali poisoned alumina;[4] it also explains the result observed by Okada and Fushizaki where the yield of camphene was increased by the addition of magnesium oxide to mineral clay used as a solid acid,[13] since magnesium oxide, recently recognized to be a strong solid base,[14,15] is considered to weaken the acid strength of a mineral clay catalysts.

The relation between III and IV which were formed from I is shown in Fig. 2, where the catalyst used was nickel sulfate calcined at 300 °C. The slope of IV/III increased with the progress of reaction and finally reached the equilibrium value, the plots of I *vs.* III+IV falling on a straight line until the end of the reaction (Fig. 3a). The results suggest that the isomerization between III and IV takes place during a later stage of the reaction. It is shown in Fig. 3b that limonene (VI) is also converted into other compounds during a later stage of the reaction. Similar results observed

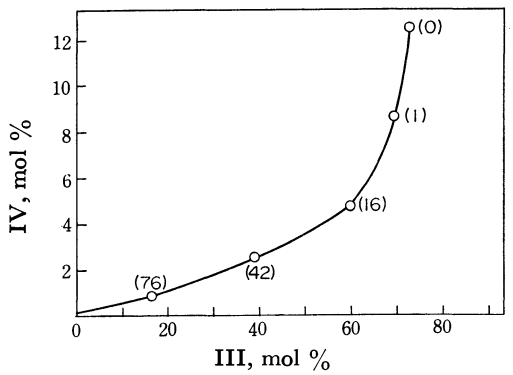

Fig. 2. Mol % of 1,7,7-trimethyl-tricyclo[2.2.1.$0^{2,6}$]heptane (IV) *vs.* mol % of camphene (III). Catalyst: nickel sulfate calcined at 300 °C, Figures in parentheses show the mol % of 2-pinene (I).

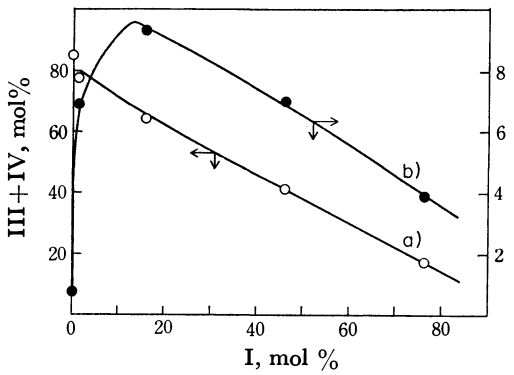

Fig. 3. Mol % of III+IV and *p*-mentha-1,8-diene (VI) *vs.* mole % of I. Catalyst: the same as in Fig. 2.

by Rudakov *et al.* for titanium oxide[16] indicate that both III and IV are primary products.

Isomerization of 2(10)-Pinene (II). The isomerization products of II were the same as those of I. The plots of III+IV *vs.* II, VI *vs.* II and I *vs.* II gave straight lines in the range 100—20 mol % of II as in Fig. 3. This indicates that III and/or IV, VI, and I are the primary products of II and that there is no backward reaction to II. This is in line with the result by Ivanova *et al.* which showed that I, III, and VI are not readsorbed on silica–alumina to react further until the concentration of II becomes less than 20—30%.[17] The selectivities for the formation of III+IV, VI and I from II, calculated from the slopes of the straight lines, are shown in Table 5, where the activity of various catalysts for the isomerization is also given. The values in parentheses, which show the selectivity recalculated by using the formula, selectivity of III+IV from II/(1−selectivity of I from II), can be compared with the selectivity values for the reactions from I given in Table 4, since II is not formed from I. The values are in fairly good accord with those in Table 5 except for silica–alumina, suggesting that III, IV, and VI are formed through a common intermediate from both.

Table 5. Activities and selectivities of various catalysts for isomerization of 2(10)-pinene(II) at 50 °C

Catalysts calcination temp., °C		$NiSO_4$ 250	$NiSO_4$ 450	SiO_2–Al_2O_3 600	ZnS 450
Selectivity	II→III+IV	0.52	0.66	0.31[a]	0.55
		(0.76)	(0.84)	(0.41)[a]	(0.62)
	II→VI	0.08	0.12	0.30[a]	0.20
		(0.12)	(0.15)	(0.40)[a]	(0.22)
	II→I	0.32	0.21	0.27[a]	0.11
Initial velocity $hr^{-1}g^{-1}\times 10^{-2}$		0.6	2.4	4.4[a]	0.1

a) Values at 15—20 °C.

Discussion

The maximum acidity of nickel sulfate was observed when the sulfate is calcined at 350 °C (Table 1). It is known that the acidity as measured by titrating with *n*-butylamine is the sum of Brönsted and Lewis acidity.

According to the infrared study on pyridine adsorbed on nickel sulfates, maximum Brönsted acidity appears at 250 °C and maximum Lewis acidity at 400 °C.[21] The fact that, in the isomerization of 2-pinene (I), maximum activity was observed when the sulfate was calcined at 400 °C seems to indicate that Lewis acid sites are active for the reaction. However, the isomerization of I is not catalyzed by Lewis acids such as BF_3, $AlCl_3$, $TiCl_4$ *etc.*, in the presence of an aprotic solvent such as benzene although polymers including dimer *etc.* were formed during the course of reaction.[22] The isomerization took place, however, in the presence of protic solvents such as alcohols which have proton donating ability.[23] Ozaki and Kimura reported that Lewis acid sites were converted into Brönsted acid sites by the adsorption of olefin and that the converted sites were active for olefin isomerization.[24] Thus, it can be said that the number of Lewis acid sites are correlated with the catalytic activity for the isomerization, but the actual active sites under the reaction conditions are all Brönsted acids.

Important results obtained are summarized as follows. 1) III, IV, and VI are formed through a common protonated intermediate from I and II. 2) There is no reverse reaction to I or II from III, IV, and VI. 3) VI is formed through a reaction path differing from that which III and IV are formed. 4) III, IV, and VI are not readsorbed on catalysts to react further in the presence of I or II, but turn to other compounds when the amount of I or II becomes small. 5) Over strong acid catalysts, VI is formed predominantly as compared with III and/or IV, polymers being formed from III and IV. 6) The reaction between III and IV is reversible, if I is absent. 7) The main products in the isomerization of VI are VII and IX, the latter being formed predominantly over strong solid acids.

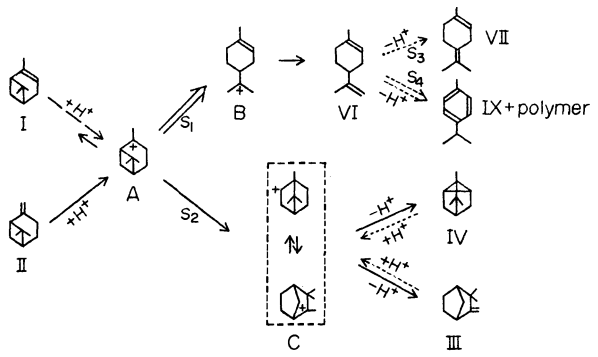

Fig. 4. Reaction scheme.

A, B, C: reaction intermediates.

⟶ steps taking place independently of the amount of I.

⟶ a step taking place when the amount of II becomes small.

⇢ steps taking place when the amounts of both I and II become small.

Steps S_1 and S_4 take place more predominantly than steps S_2 and S_3, respectively, as the acid strength of catalyst becomes higher.

These results lead us to the reaction scheme shown in Fig. 4, where the inferred structures of the reaction intermediates are also given. It is considered that the structures of intermediate A and an intermediate between VI and VII or IX change depending on the acid strength of catalyst.

The authors wish to thank Professor K. Miyahara and Professor T. Masamune for their helpful discussions.

References

1) L. G. Gurvich and J. Russ, *Phys. Chem. Soc.*, **47**, 827 (1915); *Chem. Abstr.*, **9**, 3005 (1915).
2) D. V. Banthorpe and D. Whittaker, *Quart. Rev.*, **20**, 373 (1966).
3) J. L. Simonsen and L. N. Owen, "The Terpenes," 2nd ed., Cambridge Univ. Press, London (1949).
4) A. Stanislaus and L. M. Yeddenapalli, *Can. J. Chem.*, **50**, 61 (1972).
5) K. Tanabe and R. Ohnishi, *J. Res. Inst. Catal. Hokkaido Univ.*, **10**, 229 (1962).
6) T. Takeshita, R. Ohnishi, T. Matsui, and K. Tanabe, *J. Phys. Chem.*, **69**, 4077 (1965).
7) K. Tanabe and T. Takeshita, *Adv. Catal. Relat. Subj.*, **17**, 315 (1967).
8) K. Tanabe and T. Yamaguchi, *J. Res. Inst. Catal. Hokkaido Univ.*, **14**, 93 (1966).
9) H. Meerwein and K. van Emster, *Ber.*, **53**, 1815 (1920).
10) K. Kearby, "Actes du Deuxieme Congres Intern. de Catalyse," Paris, 1960, Sect. III-134.
11) R. Ohnishi, S. Ishikura, and K. Tanabe, *Nippon Kagaku Kaishi*, **1973**, 183.
12) If I is absent, III is converted into IV and *vice versa*, as mentioned.
13) Y. Okada and Y. Fushizaki, *Kogyo Kagaku Zasshi*, **59**, 719 (1956).
14) T. Iizuka, H. Hattori, Y. Ohno, J. Sohma, and K. Tanabe, *J. Catal.*, **22**, 130 (1971).
15) J. Take, N. Kikuchi, and Y. Yoneda, *ibid.*, **21**, 164 (1971).
16) G. A. Rudakov, Z. S. Khomenko, and M. M. Shestaeva, *Zhur. Obshei Khim.*, **24**, 549 (1954); *Chem. Abstr.*, **49**, 6186d (1955).
17) L. S. Ivanova, A. G. Borovskaya, and G. A. Rudakov, *Zh. Org. Khim.*, **3**, 2162 (1967); *Chem. Abstr.*, **68**, 69138x (1968).
18) P. Hirsjarvi, K. Heinonen, and L. Pirila, *Suomen Kemistil.*, **b37**, 77 (1964).
19) R. Maurel, M. Guisnet, and M. Garin-Place, *Bull. Soc. Chim. Fr.*, **1969**, 4112.
20) K. Watanabe, C. N. Pillai and H. Pines, *J. Amer. Chem. Soc.*, **84**, 3934 (1962).
21) H. Hattori, S. Miyashita, and K. Tanabe, This Bulletin, **44**, 893 (1971).
22) M. O. Carmody and W. H. Carmody, *J. Amer. Chem. Soc.*, **59**, 1312 (1937); W. J. Roberts and A. R. Day, *ibid.*, **72**, 1226 (1950).
23) R. Lombard and A. Kress, *Bull. Soc. Chim. Fr.*, **1959**, 1415; K. Nagai, This Bulletin, **34**, 1825 (1961).
24) A. Ozaki and K. Kimura, *J. Catal.*, **3**, 395 (1964).

Studies on the Mechanism of Methanol Oxidation on Zinc Oxide by Dynamic Treatments of Chemisorbed Species under the Reaction Conditions

A. C. HERD, Takaharu ONISHI, and Kenzi TAMARU

Department of Chemistry, Faculty of Science, The University of Tokyo, Hongo, Tokyo 113

(Received June 4, 1973)

The mechanism of methanol oxidation on zinc oxide was studied by quantitatively observing the dynamic behaviour of the surface species during the course of the reaction. It was concluded that the mechanism was similar to that of the decomposition reaction, with an additional step, the oxidation of the carbon monoxide formed. As a key step in the oxidation of methanol, the decomposition of adsorbed methoxide groups in the presence of oxygen at temperatures between 140 and 180 °C has been studied by infrared spectroscopy. The methoxide groups decompose to formate ions until a maximum surface concentration is reached. The rate of decomposition at first increases with methoxide concentration, then decreases as the surface coverage approaches saturation. The observed kinetics can be explained by a mechanism which postulates that negatively charged surface species repel electrons from the surface of the zinc oxide, thus inhibiting decomposition of the methoxide groups.

In order to elucidate the mechanisms of heterogeneous catalytic reactions, it is advantageous to be able to quantitatively observe the dynamic behaviour of the surface species during the course of the reaction.[1] Infrared spectroscopy provides a means of achieving this, but progress has been limited, mainly because of experimental difficulties.[2]

Recently, a paper from this laboratory[3] elucidated the mechanism of methanol decomposition on zinc oxide, by the use of simultaneous infrared and kinetic measurements. It was shown that methanol is adsorbed as methoxide and hydroxide groups. At temperatures above approximately 150 °C, the methoxide groups decompose to give formate ions, which at temperatures above 200 °C and in the absence of methanol vapour, decompose to give carbon monoxide.

Because of this successful application of quantitative infrared spectroscopy, it was felt that it would be profitable to extend this work to a detailed study of the individual reaction steps of a similar system. The oxidation of methanol was chosen because the presence of oxygen decreases the infrared absorption by zinc oxide. Experiments showed that the mechanism was similar to that of the decomposition reaction, with an additional step, the oxidation of the carbon monoxide formed. This paper reports on the decomposition of surface methoxide groups on zinc oxide in the presence of oxygen.

Experimental

The zinc oxide, Kadox 25, a product of the New Jersey Zinc Co., was the same as that used in the previous work,[3] and had a B.E.T. surface area of 10 $m^2 g^{-1}$. It was pressed into self-supporting disks (ca. 0.1 g cm^{-2}) and a single disk placed in a previously described infrared cell,[4] part of a conventional closed circulating system. The infrared spectrometer employed was a JASCO 402G Grating Spectrometer (Japan Spectroscopic Co.), and the spectra of the adsorbed species were studied within the 4000 to 900 cm^{-1} range.

Before each experiment, the catalyst disk was given the following outgassing treatment at 400 °C. Evacuation (*ca.* 10^{-5} Torr) for three hours, followed by 5 minutes in 1 cmHg of oxygen, a further 1 hour evacuation, 30 minutes in 1 cmHg of oxygen, and finally cooled to the reaction temperature (usually 150 °C) under oxygen. During the oxygen treatments, the gas phase was circulated through the infrared cell and a liquid nitrogen trap in order to remove any CO_2 that had desorbed from the catalyst surface. This treatment gave a highly oxidised catalyst, and the residual hydroxyl and carbon dioxide peaks were reduced to a satisfactory level.

The reactions were carried out in the absence of gas phase methanol, under 1 cmHg of oxygen. Methoxide groups are strongly bound to the zinc oxide surface, and at the temperatures studied, the rate of desorption was small, especially at lower coverages.

Results

Oxidation of Methanol and Decomposition of Methoxide Groups. The spectra observed for the methoxide, hydroxide and formate surface species on zinc oxide in the presence of oxygen, were the same as those reported by Ueno *et al.*[3] on reduced zinc oxide, with the addition of a methoxide band overlapping the ZnO band at 1070 cm^{-1}, which is assigned to C–O stretching.

At temperatures above 150 °C in vacuum, ZnO slowly loses oxygen,[5] giving an increase in the number of conduction electrons. This causes a marked decrease in the background transmission, and affects the optical density of the absorption bands due to adsorbed

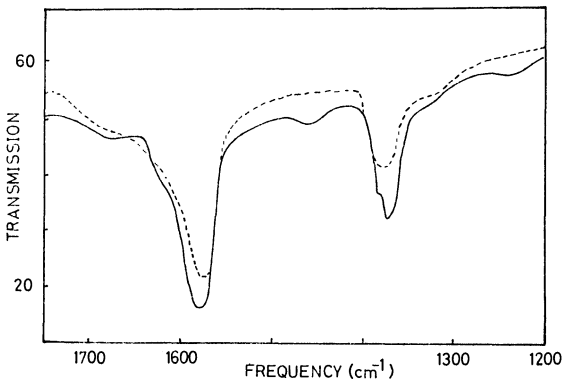

Fig. 1. The effect of adsorbed methanol on the spectrum of formate ions on ZnO.
------ the spectrum of adsorbed formic acid, —— the same spectrum after the addition of methanol.

species, especially those at lower frequencies. This loss of lattice oxygen appears to be enhanced by the adsorption of methanol. In the presence of oxygen, however, the background transmission is greatly improved, and the intense formate O–C–O asymmetric stretching band at 1570 cm^{-1} can be used for quantitative measurements.

It was found that the band shape and optical density of the formate 1570 cm^{-1} band were affected by the presence of other surface species as illustrated in Fig. 1. Therefore, for this band, the integrated optical density was used, as this was shown to be independent of the presence or absence of the other surface species occurring in this work.

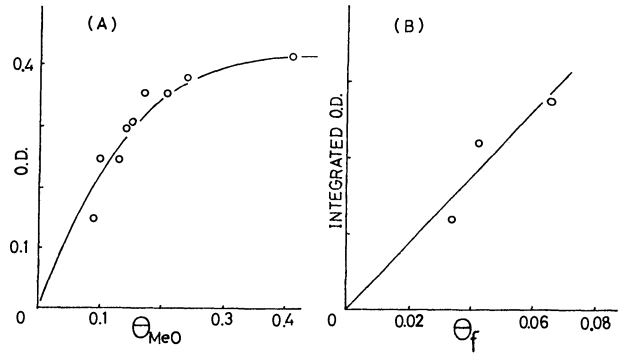

Fig. 2. Calibration curves. (A) Optical density of the 2830 cm^{-1} methoxide band *versus* methoxide group coverage. (B) Integrated optical density of the 1570 cm^{-1} formate ion band *versus* formate ion coverage.

The calibration curves for the methoxide group and formate ion shown in Fig. 2 were determined by measuring the 2830 and 1570 cm^{-1} bands when measured amounts of methanol and formic acid respectively were adsorbed at 100 °C. The concentration of surface sites on the zinc oxide was assumed to be 10^{15} cm^{-2}.

It is of significant interest to note that methanol oxidation proceeds in the presence of oxygen in a manner similar to that of methanol decomposition in the absence of oxygen, with an additional step, the oxidation of the carbon monoxide formed.

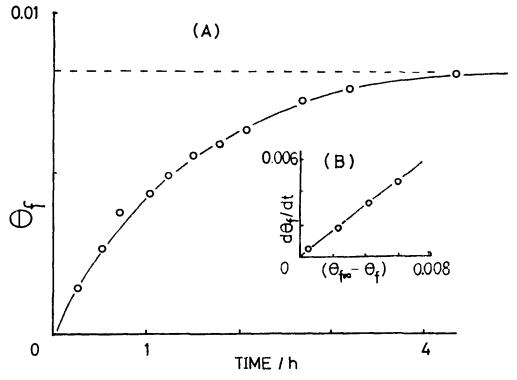

Fig. 3. Formate ion formation at 150 °C and $\theta_{MeO}=0.095$

When methanol was adsorbed on zinc oxide at 150 °C, the methoxide groups decomposed to give formate ions, until the surface formate ion coverage, θ_f, reached a saturation value, $\theta_{f\infty}$, which increased with increasing temperature. A typical result is shown in Fig. 3(A). It was found that the results, when plotted as $d\theta_f/dt$ against $(\theta_{f\infty}-\theta_f)$, as in Fig. 3(B), gave a straight line, and hence could be expressed as

$$d\theta_f/dt = k(\theta_{f\infty}-\theta_f).$$

Although the limited accuracy of the experimental results does not exclude other expressions, this form was found to be useful in defining a first order rate constant k, and in cases where the reaction was very slow, in estimating $\theta_{f\infty}$.

When formic acid was preadsorbed on the catalyst disk at 150 °C, to give a coverage of $\theta_f=0.01$, the integrated optical density of the 1570 cm^{-1} band remained constant with time, and did not change even when methoxide groups were introduced onto the surface. This showed that the methoxide groups did not decompose in the presence of this surface coverage of formate ions, and that the rate of formate ion decomposition at 150 °C is negligible.

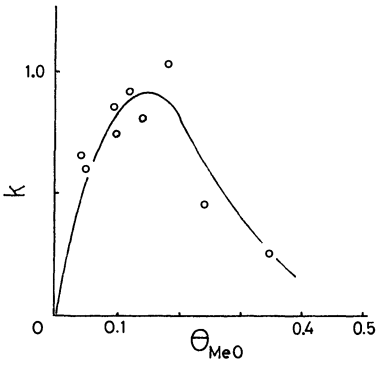

Fig. 4. The dependence of k on the methoxide group coverage.

Figure 4 shows the dependence of k on the methoxide surface coverage, θ_{MeO}. As $\theta_{f\infty}$ was always small compared to θ_{MeO}, the methoxide coverage was approximated as being constant during each run, although the gradual desorption of methanol may lead to errors of up to 10% in the value of θ_{MeO} at higher coverages. The results from Fig. 4 suggest that the rate equation for the reaction could be written as

$$d\theta_f/dt = k'(\theta_{f\infty}-\theta_f)\theta_{MeO}^{x}(1-\theta)^{y}$$

where θ is the total surface coverage. Although the scatter of the experimental points cannot justify putting exact values to x and y, it seems probable that $y \geq x \approx 1$.

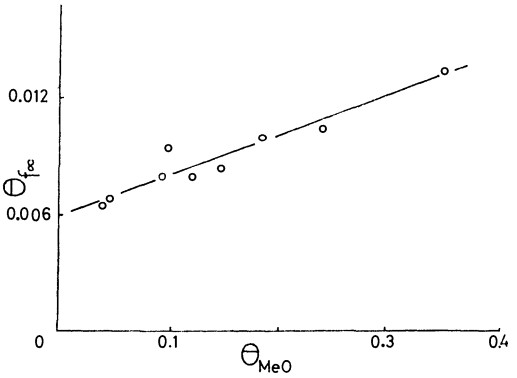

Fig. 5. The saturation formate ion coverage at 150 °C *versus* methoxide group coverage.

Support for the $(1-\theta)^y$ term was given by the results of an experiment in which the methoxide coverage was increased in the middle of a normal run. θ increased from 0.27 to 0.75 and the rate of formate ion formation was drastically reduced. As shown in Fig. 5, $\theta_{f\infty}$ depends linearly on θ_{MeO}.

It was found that there was no measureable dependence of either $\theta_{f\infty}$ or k on oxygen pressure in the range 1 to 12 cmHg. At oxygen pressures of less than about 0.5 cmHg, the zinc oxide appeared to lose oxygen, and the formate ion coverage was impossible to measure quantitatively.

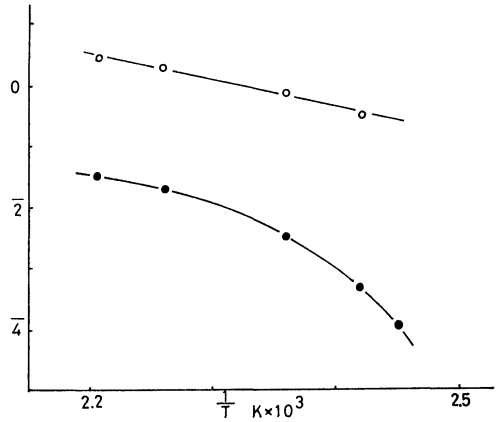

Fig. 6. Arrhenius plots of k —●—, and the initial rate of formate ion formation —○—.

Arrhenius plots of k and the initial rate of formate formation, for constant $\theta_{MeO}=0.16$, are shown in Fig. 6. The slope of the straight line given by $\log_{10} k$ against $1/T$ is equivalent to an activation energy of 85 kJ·mol^{-1}.

Preadsorbed Carbon Dioxide. The effect of CO_2 on the rate of the formate ion decomposition and on $\theta_{f\infty}$ was also investigated. CO_2 was admitted onto the zinc oxide in the presence of oxygen at 150 °C, then the circulated gas phase was trapped with liquid nitrogen. Figure 7 shows the spectrum immediately after the CO_2 was removed from the gas phase, and after a further 40 min trapping. The addition of methanol caused a large proportion of the remaining carbon dioxide to desorb.

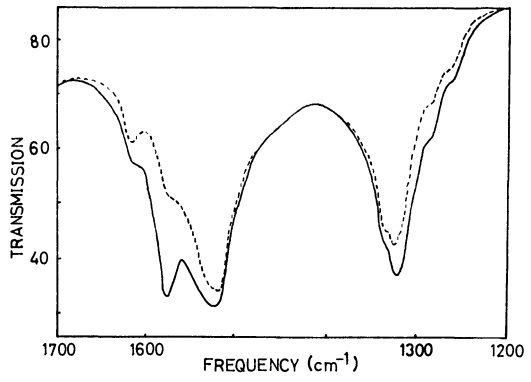

Fig. 7. The spectrum of CO_2 adsorbed on ZnO at 150 °C.
—— immediately after trapping the gas phase CO_2.
---- after 40 minutes trapping.

Despite a considerable amount of literature, the assignment of the infrared bands of CO and CO_2 adsorbed on metals and metal oxides remains very uncertain.[2] However, it seems probable that the two strong bands at 1530 and 1325 cm^{-1} should be assigned to the asymmetric and symmetric O–C–O stretching vibrations of

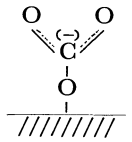

because of the close correlation with the spectrum of $Na_2[Cu(OCO_2)_2]\cdot 3H_2O$, which has bands at 1529 and 1326 cm^{-1}.[6] The unstable species absorbing at 1575 and probably 1325 cm^{-1} is possibly.[7]

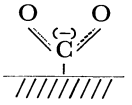

Although it is difficult to determine exactly the amount of chemisorbed carbon dioxide species, it was found that the chemisorption of an estimated θ_{CO_2} of 0.02 halved the formate ion coverage at saturation. This effect is obviously too great to be attributed solely to the $(1-\theta)^y$ term.

Discussion

It appears unlikely that the apparent saturation of the formate ion is caused by its simultaneous decomposition, because the rate of decomposition of formate ions was shown to be negligible at 150 °C, and because this explanation would predict a linear Arrhenius plot for the initial rate.

A possible explanation for the results arises from the observation that negatively charged surface ions such as adsorbed CO_2 and formate ions appear to inhibit the decomposition of the methoxide groups. If the methoxide group must capture an electron from the zinc oxide before it can decompose,

$$CH_3O(a) + e \rightleftharpoons CH_3O^-(a) \quad (1)$$

$$CH_3O^-(a) + \text{free surface sites} \longrightarrow HCOO^-(a) + 2OH(a) \quad (2)$$

and it is assumed that the concentration of $CH_3O^-(a)$ is small, and that the latter reaction is rate controlling, we can write

$$d\theta_f/dt = k''(1-\theta)^a[CH_3O(a)][e_s]K \quad (3)$$

where e_s is the concentration of free electrons at the surface of the zinc oxide and K is the equilibrium constant for Eq. (1). The concentration of electrons at the surface can be written as[8]

$$[e_s] = N_c \exp\{-(\mu + eQ^2/2N_d\varepsilon\varepsilon_0)/kT\} \quad (4)$$

where N_c is the number of free electrons, μ is the energy difference between the Fermi level and the bottom of the conduction band in the bulk, N_d the donor density, ε the dielectric constant of the ZnO, ε_0 the permittivity of the ambient gas, and eQ^2 the surface charge arising from charged surface species ($HCOO^-(a)$, $CO_2^-(a)$, and $O^-(a)$). Substitution of this term into Eq. (3) gives a rate equation similar to the experimentally derived rate equation, except that the $(\theta_{f\infty}-\theta_f)$ term

has been replaced by an expression for the surface electron concentration which is exponential in $-eQ^2$. It is very unlikely that the experimental results could distinguish between these two forms, especially in view of the approximations of constant θ_{MeO} and θ, and the lack of information about chemisorbed oxygen. The proposed mechanism therefore suggests that the slowing down of the reaction is caused by the negatively charged layer of surface formate ions (or adsorbed CO_2^-) repelling electrons from the surface.

The increase of $\theta_{f\infty}$ with increasing temperature and increasing θ_{MeO} can be explained by their effects on the amount of chemisorbed O^-. Both would tend to decrease [O^-(a)] thus decreasing the number of negatively charged species at the surface. Although no oxygen pressure dependence was found at oxygen pressures above 1 cmHg, it is possible that the surface is virtually saturated with O^-(a) below this pressure. In support of this, increasing the oxygen pressure from 1 to 12 cmHg had little effect on the background ZnO infrared absorption. Further, values of $\theta_{f\infty}$ (ignoring formate ion decomposition) in the absence of gas phase oxygen, calculated from the results of Ueno *et al.*[3] are approximately 10 times larger than those found in this work.

Doping of the zinc oxide should also affect $\theta_{f\infty}$, though not to the same extent as changes in the surface charge, and this may help to explain the direct relationship between the electrical conductivity of zinc oxides and their activities for the decomposition of methanol.[9]

A. C. H. gratefully acknowledges the financial support of a research fellowship from The Japan Society for the Promotion of Science.

References

1) K. Tamaru, *Adv. Catal.*, **15**, 65 (1964).
2) L. H. Little, "Infrared Spectra of Adsorbed Species," Academic Press, N. Y. (1966).
3) A. Ueno, T. Onishi, and K. Tamaru, *Trans. Faraday Soc.*, **67**, 3585 (1971).
4) Y. Noto, K. Fukuda, T. Onishi, and K. Tamaru, *ibid.*, **63**, 3081 (1967).
5) M. L. Hair, "Infrared Spectroscopy in Surface Chemistry," Marcel Dekker, N. Y. (1967).
6) B. M. Gatehouse, S. E. Livingston, and R. S. Nyholm, *J. Chem. Soc.*, **1958**, 3137.
7) J. H. Taylor and C. H. Amberg, *Can. J. Chem.*, **39**, 535 (1961).
8) S. R. Morrison, *J. Catal.*, **20**, 110 (1971).
9) G. K. Boreskov and K. I. Matveyev, *Problemy Kinet. Katal.*, **8**, 165 (1955), cited by F. F. Volkenshtein, "The Electronic Theory of Catalysis on Semiconductors," Pergamon Press, Oxford (1963).

A New Technique Using the Polynomials Approximation and Trapezoidal Average Method for Estimating Kinetic Rate Constants in Systems of Linear or Nonlinear Differential Equations

Katsutoshi OHKUBO, Kohji TSUCHIHASHI, and Hiroyuki SAKAMOTO

Department of Synthetic Chemistry, Faculty of Engineering, Kumamoto University, Kurokami, Kumamoto 860

(Received August 9, 1973)

A new technique using the polynomials approximation and the trapezoidal average method, has been proposed for estimating kinetic rate constants. It is implemented by minimizing the error of the concentration (of a product) obtained from the polynomial-approximated least square-error analysis of the observed concentrations during the initial reaction stage relative to that obtained theoretically from the trapezoidal average of the calculated concentration (of a product) on the basis of the law of mass action. The technique is useful for easily and exactly estimating the rate constants in systems of linear or nonlinear differential equations. A kinetic model, $A \longrightarrow B \rightleftarrows C$, was used to illustrate and develop the present technique.

In usual kinetic studies of chemical-reaction mechanisms, we often find it difficult to estimate exactly the kinetic rate constants of the elementary steps of the reaction. Some numerical integration methods, such as the Runge-Kutta integration,[1] Taylor's series expansion,[2] and Picard's method,[3] are usually used to estimate the rate constants. These methods, however, require a precision fit to dense data or much computation time.

The new technique presented in this paper requires only a few kinetic data (usually concentrations) about the species participating in the reaction. It is based on the polynomial approximation of the given kinetic data and the trapezoidal average of the minute change in the concentration of the species (typically, that of a product). The following kinetic model was used to illustrate and develop the present technique:

$$A \xrightarrow{k_1} B \underset{k_3}{\overset{k_2}{\rightleftarrows}} C \qquad (1)$$

where A=reactant; B=intermediate; C=product; k_i= rate constant i, and i=1, 2, and 3. The type of reaction depicted by Eq. (1) is found in such an organic reaction progress as chlorosulfonation:

$$RH \xrightarrow{ClSO_2OH} RSO_2OH + HCl \overset{ClSO_2OH}{\rightleftarrows} RSO_2Cl + H_2SO_4 \quad (R=\text{alkyl or aryl}).$$

Computation Method

The kinetic model illustrated by Eq. (1) can be described by the following differential equations drawn from the law of mass action:

$$d(A)/dt = -k_1(A) \qquad (A)_0 \neq 0 \qquad (2a)$$

$$d(B)/dt = k_1(A) - k_2(B) + k_3(C) \qquad (B)_0 = 0 \qquad (2b)$$

$$d(C)/dt = k_2(B) - k_3(C) \qquad (C)_0 = 0 \qquad (2c)$$

where the parentheses denote concentrations and where the subscript zeros stand for the initial concentrations of the species.

We will now explain the computation method of the present technique for estimating the rate constants, basing on the above differential equations. According to Eqs. (2a—c), the increments for the three components, A, B, and C, at the reaction time of t, $D(A)_t$, $D(B)_t$, and $D(C)_t$, are defined as:

$$D(A)_t = -k_1(A)_t dt, \quad (A)_{t+dt} = (A)_t + D(A)_t \qquad (3a)$$

$$D(B)_t = k_1(A)_t dt - k_2(B)_t dt + k_3(C)_t dt, \quad (B)_{t+dt} = (B)_t + D(B)_t \qquad (3b)$$

$$D(C)_t = k_2(B)_t dt - k_3(C)_t dt, \quad (C)_{t+dt} = (C)_t + D(C)_t \qquad (3c)$$

where the notations of $(\text{Component})_t$ and $(\text{Component})_{t+dt}$ indicate the concentrations of the components at t and $t+dt$ respectively.

The concentrations of the components at $t+mdt$ (m=1,2,3,$\cdots$), $(\text{Component})_{t+mdt}$ are, then, defined by:

$$(\text{Component})_{t+mdt} = (\text{Component})_t + \sum_{p=1}^{m} D(\text{Component})_{t+(p-1)dt} \qquad (4)$$

The $D(\text{Component})_{t+(p-1)dt}$ values in Eq. (4) are evaluated by the following trapezoidal average:

$$\begin{aligned} D(\text{Component})_{t+(p-1)dt} &= (D(\text{Component})_{t+(p-1)dt} + D(\text{Component})_{t+pdt})/2 \\ &= 1.5D(\text{Component})_{t+(p-1)dt} - 0.5D(\text{Component})_{t+(p-2)dt} \end{aligned} \qquad (5)$$

where $D(\text{Component})_{t+(p-1)dt}$ is defined by

$$D(\text{Component})_{t+(p-1)dt} = (D(\text{Component})_{t+pdt} + D(\text{Component})_{t+(p-2)dt})/2.$$

We will use the product of C as the Component and assume that p=2. Then, the above relationships can be rewritten as:

$$\begin{aligned} D(C)_{t+dt} &= (D(C)_{t+dt} + D(C)_{t+2dt})/2 \\ &= 1.5D(C)_{t+dt} - 0.5D(C)_t \end{aligned} \qquad (5')$$

where $D(C)_{t+dt}=(D(C)_{t+2dt}+D(C)_t)/2$.

In the evaluation of the $D(C)_{t+dt}$ values, the rate constants, k_i, are supplied by:

$$k_t = \min k_t + \sum^{n} 10^{(\gamma-\beta)} \min k_t, \quad \gamma = \text{gauss}\left[\frac{n-1}{9\alpha}\right] \qquad (6)$$

(n=1, 2, 3, $\cdots$, β=0, 1, 2, $\cdots$, $\alpha=10^{\beta}$)

where min k_i=lower limit of k_i ($1.0\times10^{\delta}$; δ=constant); γ=integral number; β=constant; α=parameter determining the number of significant figure for k_i (*viz.*, k_i=(β+1) significant figures at $\alpha=10^{\beta}$).

On the other hand, the time conversion of the observed concentration of C, $(C)_{t,obsd}$, is represented by the following series of polynomials, resulting from the least square-error analysis of the $(C)_{t,obsd}$ values:

$$(C)_{t,obsd} = a_0 + a_1 t + a_2 t^2 + a_3 t^3 + \cdots + a_n t^n \quad (n=0, 1, 2, \cdots) \tag{7}$$

where a_n (n=0,1,2,$\cdots$) denote coefficients. The average increment observed at $t+dt$, $D(C)_{t+dt,obsd}$, is, then, defined as:

$$D(C)_{t+dt,\,obsd} = (C)_{t+2dt,\,obsd} - (C)_{t+dt,\,obsd} \tag{8}$$

where the $(C)_{t+2dt,obsd}$ and $(C)_{t+dt,obsd}$ values are calculated by Eq. (7).

The best rate constants are estimated by minimizing the following relative error, ε:

$$\varepsilon = |D(C)_{t+dt} - D(C)_{t+dt,\,obsd}| / D(C)_{t+dt,\,obsd} < \delta\varepsilon \tag{9}$$

where $\delta\varepsilon$ is the error norm for converging the computation. In the evaluation of the ε value, the iteration procedure is necessary: that is, the rate constants, k_j (j=1, 2, or 3), are changed in turn until one gets the smallest ε value while the other constants, $k_{i(i\neq j)}$, are fited.

The $D(C)_{t+dt}$ values in Eq. (9) are computed by the following equation, derived from Eqs. (3c), (4), and (5′):

$$\begin{aligned} D(C)_{t+dt} = {} & [k_2((A)_0 - (A)_{t+dt}) - (k_2+k_3)(C)_{t+dt})]dt \\ & + 1.5[k_2(k_1+k_2+k_3)(A)_{t+dt} \\ & + (k_2+k_3)^2(C)_{t+dt} - k_2(k_2+k_3)(A)_0]dt^2 \end{aligned} \tag{10}$$

In Eq. (10), the following approximation is taken for simplicity of computation:

$$(A)_{t+dt} \approx (A)_t \tag{11}$$

In order to avoid any technical error caused by the above approximation, a very small dt value should be used for the computation. However, it is better to discard the above approximation when the $(A)_{t+dt}$ value can be evaluated from the time conversion of (A).

The conditions used throughout in this paper are dt=0.01—0.1, min k_i=1.0×10^{-5}, n=1—991, β=1, and α=10.

Computed Results and Discussion

Table 1 shows the kinetic data, $(Component)_{t,obsd}$, obtained by the simulation[4] of the kinetic model with specifications of $(A)_0$=10.0, $(B)_0=(C)_0$=0, k_1=0.1, k_2=0.6, k_3=0.2, and dt=0.001. We used the simulation data as the given kinetic data, because the preliminarily known k_i values facilitate the checking of the accuracy of the estimated rate constants, $k_{i,estimated}$. The coefficients (a_n) of the polynomials of Eq. (7) were, then, determined by the least square-error analysis of the $(C)_{t,obsd}$ values at t=0, 1, 2, $\cdots$, n in Table 1 (n corresponds to the subscript n of a_n in the highest-order term of Eq. (7)). Table 2 lists the a_n values,

Table 1. Given kinetic data

t[a]	(A)	(B)	(C)
0	10.00000	0.00000	0.00000
1	9.04838	0.72595	0.22567
2	8.18731	1.11407	0.69863
3	7.40818	1.34449	1.24733
4	6.70320	1.49872	1.79807
5	6.06531	1.61390	2.32079
6	5.48812	1.70717	2.80472
7	4.96585	1.78663	3.24752
8	4.49329	1.85632	3.65039
9	4.06570	1.91839	4.01592
10	3.67880	1.97410	4.34711
11	3.32871	2.02431	4.64698
12	3.01195	2.06965	4.91841
13	2.72532	2.11063	5.16405
14	2.46597	2.14770	5.38632
15	2.23131	2.18123	5.58746
16	2.01897	2.21157	5.76946
17	1.82684	2.23902	5.93414
18	1.65299	2.26386	6.08315
19	1.49569	2.28633	6.21798
20	1.35335	2.30666	6.33998
21	1.22457	2.32506	6.45037
22	1.10803	2.34171	6.55026
23	1.00259	2.35677	6.64064
24	0.90718	2.37040	6.72242
25	0.82085	2.38273	6.79642
26	0.74274	2.39389	6.86337
27	0.67206	2.40399	6.92395
28	0.60810	2.41313	6.97877
29	0.55023	2.42139	7.02837
30	0.49787	2.42887	7.07326

a) Arbitrary time unit.

Table 2. Coefficinets (a_n) for the polynomial approximation

a_n	Order of polynomials					
	n=2	n=3	n=4	n=5	n=6	n=10
a_0	1.934×10^{-16}	2.680×10^{-16}	6.413×10^{-15}	2.709×10^{-13}	-1.946×10^{-14}	8.648×10^{-10}
$10^2\,a_1$	10.202	4.4842	2.0379	0.95372	0.45605	0.039630
$10\,a_2$	1.2365	2.0942	2.5427	2.7686	2.8822	2.9879
$10^2\,a_3$		−2.8592	−5.3054	−6.8865	−7.8197	−8.8519
$10^3\,a_4$			4.0771	8.5946	12.120	17.256
$10^4\,a_5$				−4.5175	−10.738	−25.089
$10^5\,a_6$					4.1472	27.338
$10^5\,a_7$						−2.1602
$10^6\,a_8$						1.1613
$10^8\,a_9$						−3.7742
$10^{10}a_{10}$						5.5664

Table 3. $(C)_{t+dt}$ (and/or $(C)_{t+2dt}$) used for the present computations

t	Order of polynomials						Simulation[a]
	$n=2$	$n=3$	$n=4$	$n=5$	$n=6$	$n=10$	
1	0.22567	0.22567	0.22567	0.22567	0.22567	0.22567	0.22567
1.01	0.22917	0.22946	0.22954	0.22957	0.22958	0.22958	0.22959
1.02	0.23270	0.23327	0.23344	0.23349	0.23351	0.23352	0.23353
1.04	0.23983	0.24097	0.24129	0.24140	0.24144	0.24146	0.24147
1.06	0.24706	0.24977	0.24925	0.24940	0.24945	0.24948	0.24950
1.08	0.25439	0.25666	0.25729	0.25749	0.25756	0.25760	0.25760
1.10	0.26219	0.26465	0.26542	0.26567	0.26534	0.26580	0.26581
1.12	0.26934	0.27272	0.27363	0.27392	0.27402	0.27408	0.27409
1.16	0.28469	0.28915	0.29032	0.29069	0.29081	0.29089	0.29090
1.20	0.30044	0.30592	0.30733	0.30777	0.30792	0.30801	0.30802

a) See Ref. 5 ($(A)_0=10.0$; $(B)_0=(C)_0=0$; $k_1=0.1$; $k_2=0.6$; $k_3=0.2$; $dt=0.001$).

and Table 3 shows the $(C)_{t+dt,obsd}$ and $(C)_{t+2dt,obsd}$ values evaluated by the polynomial approximation.

Now, let us examine the effect of the dt values on the estimation of the rate constants. The rate constants for the kinetic model were estimated using the polynomials ($n=10$) with the following specifications: $(A)_0=10.0$; $(B)_0=(C)_0=0$; $dt=0.01$—0.1; $(C)_t=(C)_{1.0}$; $(C)_{t+dt}=(C)_{1.0+dt}$; $(C)_{t+2dt}=(C)_{1.0+2dt}$. Table 4 shows the change in the $k_{i,estimated}$ values due to the dt values, together with the relative errors of ε and ε_i ($i=1$, 2, and 3), defined by Eq. (9) and (12) respectively:

$$\varepsilon_i = |k_{i,estimated}-k_{i,given}|/k_{i,given} \quad (12)$$

where $k_{i,given}$ stands for the exact k_i values (*viz.*, $k_1=0.1$, $k_2=0.6$, and $k_3=0.2$). It may be seen from Table 4 that the smaller the dt value becomes, the more the ε_i values are lowered. Since the best k_i values should be given by the $k_{i,estimated}$ values, which are not appreciably influenced by the dt value, it is desirable to establish the following relationship:

$$|(A)_{t+dt}-(A)_t|/(A)_t \approx 0 \quad (13)$$

where the $(A)_{t+dt}$ and $(A)_t$ values are, respectively, obtained from Eq. (3a) and Table 1.

It is of interest here to compare the $k_{i,estimated}$ values presented in Table 4 with those calculated by means of the following equation:

$$\begin{aligned} D(C)_{t+dt} &= (C)_{t+2dt}-(C)_{t+dt} \\ &= [k_2((A)_0-(A)_{t+dt})-(k_2+k_3)(C)_{t+dt}]dt \\ &\quad + [k_2(k_1+k_2+k_3)(A)_{t+dt}+(k_2+k_3)^2(C)_{t+dt} \\ &\quad -k_2(k_2+k_3)(A)_0]dt^2 \end{aligned} \quad (14)$$

where $(A)_{t+dt}$ is approximated by $(A)_t$. The $k_{i,estimated}$ values evaluated by Eq. (14) were found to be inaccurate in some measure as compared with those listed in Table 4; for example, $k_1=0.14$, $k_2=0.60$, $k_3=0.20$, and $\varepsilon=0.221\%$ at $dt=0.1$, and $k_1=0.13$, $k_2=0.60$, $k_3=0.20$, and $\varepsilon=0.028\%$ at $dt=0.01$ under the specifications mentioned before. It may be deduced, therefore, that the trapezoidal average method depicted by Eq. (5′) is superior to the usual technique illustrated by Eq. (14) for estimating the rate constants.

Next, let us notice the effect of the order (n) of the polynomial approximation on the evaluation of the $k_{i,estimated}$ values. Table 5 lists the $k_{i,estimated}$ values

Table 4. Effect of the dt value on the estimation of rate constants

dt	k_i			$\varepsilon_i(\%)$			$\varepsilon(\%)$
	k_1	k_2	k_3	ε_1	ε_2	ε_3	
0.1	0.097	0.60	0.20	3.0	0.0	0.0	0.063
0.08	0.097	0.60	0.20	3.0	0.0	0.0	0.003
0.06	0.098	0.60	0.20	2.0	0.0	0.0	0.048
0.04	0.098	0.60	0.20	2.0	0.0	0.0	0.026
0.02	0.098	0.60	0.20	2.0	0.0	0.0	0.004
0.01	0.10	0.60	0.20	0.0	0.0	0.0	0.029

Computations were carried out with the polynomials of $n=10$. (Iteration=2; Computation time with FACOM 230-25=1.7 min in every case.)

obtained by the trapezoidal method using the polynomials of $n=2$, 3, 4, 5, 6, and 10. As we expected, the increase in the n value of the polynomials decreases the ε_i ($i=1$—3) values as defined by Eq. (12), and the polynomials of $n=10$ offer the exact rate constants. The present technique requires a polynomial approximation involving a relatively high order of terms, because it takes the rough approximation depicted by Eq. (11).

Table 5. Estimated rate constants and relative errors

n	k_i[a]			$\varepsilon_i(\%)$			$\varepsilon(\%)$
	k_1	k_2	k_3	ε_1	ε_2	ε_3	
2	0.01	0.55	0.19	90.0	8.33	5.0	0.0494
3	0.010	0.59	0.19	90.0	1.67	5.0	0.187
4	0.052	0.60	0.20	48.0	0.0	0.0	0.0068
5	0.077	0.60	0.20	23.0	0.0	0.0	0.0023
6	0.089	0.60	0.20	11.0	0.0	0.0	0.0034
10	0.10	0.60	0.20	0.0	0.0	0.0	0.0298

a) k_i=2 significant figures. Computations were carried out with $dt=0.01$. In every case, iteration=2 and computation time=1.7 min by FACOM 230-25.

Finally, it may be worth emphasis that the present technique will be useful for estimating the kinetic rate constants in the systems of linear or nonlinear differential equations.

The calculations were carried out on a FACOM

320–25 computer at the Engineering Research Center of Kumamoto University.

References

1) For instance, see H. Margenau and G. H. Murphy, "The Mathematics of Physics and Chemistry," D. van Nostrand, New York (1943), p. 450.
2) I. G. Darvey, S. J. Prokhovnik, and J. F. Williams, *J. Theor. Biol.*, **11**, 459 (1966).
3) R. Tanner, *Ind. Eng. Chem. Fundam.*, **11**, 1 (1972).
4) K. Ohkubo and T. Hashimoto, This Bulletin, **45**, 3350 (1972).

The Molecular and Crystal Structure of the Cyclic Tetramer of Formaldehyde, 1,3,5,7-Tetroxocane

Yozo CHATANI,* Tadafumi YAMAUCHI,** and Yasuhiko MIYAKE**

*Department of Polymer Science, Faculty of Science, Osaka University, Toyonaka, Osaka 560

**Central Research Loboratory, Mitsui-Toatsu Chemicals, Inc., Tozuka, Yokohama 274

(Received August 10, 1973)

The crystal structure of the cyclic tetramer of formaldehyde, 1,3,5,7-tetroxocane, has been determined by the X-ray diffraction method. The unit cell is monoclinic, with $a=11.455$, $b=4.160$, $c=12.232$ Å, and $\beta=108.4°$. The space group is C2/c, and there are four molecules per unit cell. The structure was solved by using a molecular transform method and was refined by the block-diagonal least-squares method to a final R factor of 0.051, using 728 reflections measured with an automated four-circle diffractometer. The molecules in the crystal are of the so-called crown form, with an approximate C_{4v} symmetry but an exact C_2 symmetry. The torsion angles about the four independent C–O bonds appear in two distinguishable values: two bonds with 83.7 and −83.6°, and the other two bonds with 93.6 and −94.1°. The average C–O bond length is 1.403 Å, while the average C–O–C and O–C–O bond angles are 116.6 and 113.8° respectively. The deformation from a regular crown form by taking the two distinguishable torsion angles and the increase in bond angles is favorable to compensating for the intramolecular H···H repulsions; the close H···H distances in the deformed crown form are 2.16 and 2.20 Å.

The cyclic tetramer of formaldehyde, 1,3,5,7-tetroxocane $(-CH_2-O-)_4$, presents two interesting problems which can be investigated by X-ray study. One is the molecular conformation of this eight-membered cyclic compound, and the other is the radiation-induced solid-state polymerization of tetroxocane, by which tetroxocane molecules in the crystal are converted into highly crystalline linear polyoxymethylene $(-CH_2-O-)_n$.[1] Studies along similar lines have been performed on some cyclic oligomers of formaldehyde: 1,3,5-trioxane $(-CH_2-O-)_3$,[2] 1,3,5,7,9-pentoxecane $(-CH_2-O-)_5$,[3,4] and 1,3,5,7,9,11-hexoxecane $(-CH_2-O-)_6$.[5] As for tetroxocane, a structural study of the solid-state polymerization has already been reported,[6] in which the crystal structure of this substance has been shown; also, it has been stated that the molecular conformation in the crystal is of a crown form. On the other hand, the presence of two conformations is suggested by the study of the temperature dependence of the NMR spectra of the tetroxocane in solutions:[7,8] one has a boat-chair or a distorted boat-chair conformation, and the other, preponderant at low temperatures, presumably has a crown form which was expected to be found in the crystal. The present paper will describe the crystal structure of tetroxocane in detail.

Experimental

The tetroxocane was synthesized by the method of Staudinger and Luthy.[9] The melting point of tetroxocane is 114 °C. Recrystallization from a benzene solution or sublimation yielded prismlike crystals elongated along the b axis. Because of its high vapor pressure, single crystals were sealed in thin-walled Lindemann glass capillaries. The cell dimensions were determined from Weissenberg photographs and from θ values as measured with a single-crystal diffractometer. Crystal data:

1,3,5,7-Tetroxocane, $(-CH_2-O-)_4$
Molecular weight 120.1
Monoclinic $a=11.455\pm0.007$ Å
$b=4.160\pm0.006$
$c=12.232\pm0.009$
$\beta=108.4\pm0.1°$
$Z=4$
Volume of the unit cell: $V=553.0$ Å^3
Density, calculated: $D_x=1.442$ g/cm^3; measured: $D_m=1.435$ g/cm^3
Number of electrons per unit cell: $F(000)=256$
Absorption coefficient for $\lambda_{MoK\alpha}$(=0.7107 Å): $\mu=1.40$ cm^{-1}

The systematic extinctions occur for hkl with $h+k$ odd, for $h0l$ with either h or l odd, and for $0k0$ with k odd. The space group is, therefore, either Cc or C2/c, of which the latter was adopted on the basis of the plot of the intensity distribution.[10,11]

The intensity measurements were performed using a Rigaku-Denki automated four-circle diffractometer. The crystal used for the intensity measurements was $0.4\times0.4\times0.5$ mm^3 in size. The integrated intensities were measured using the $\theta-2\theta$ (moving-crystal, moving-counter) technique for all the reflections in the sphere of the $\sin\theta/\lambda<0.70$ Å^{-1} radius, with MoKα radiation. The scanning speed was 2°/min, and the scan range was calculated by this formula:

$$\text{scan range}=(0.8+1.0\tan\theta)\text{ degrees.}$$

The background counts were measured at the beginning and at the end of the scan range for a period of 20 seconds and corrected for the time factor. No correction was made for absorption. The F values of 52 out of the 780 non-equivalent reflections within the sphere were set as equal to zero, since the F values were smaller than the estimated standard deviation of the values, and were not included in the refinement. In a previous paper[6] solid-state polymerization by X- or γ-irradiation was reported. The yield of the polymer depends upon the irradiation temperature. The present measurements were performed at 19 °C; judging from the approximate constancy of the intensities of the three reference reflections measured every 25 reflections, such a polymerization was almost suppressed, the gradual decrease in the observed F values being 2% at the end of the measurements (the total exposure was 42 hours). Therefore, the correction for the time dependence was made for the observed F values. It was also noticed that the diffraction spots of tetroxocane crystal were not altered in location and remained fairly sharp in spite of the polymerization.

* To whom correspondence should be addressed.

Structure Determination

b-Projection. There are eight equivalent general positions in the C2/c space group, while the number of molecules in the unit cell is four. Therefore, the molecules in the unit cell must be situated at one of the twofold positions. There are, in this space group, four sets of centers of symmetry and a set of twofold rotation axes along the b axis. In the b-projection, however, these two kinds of symmetry elements are not distinguishable, and a smaller cell with one molecule can be chosen. The shortness of the b dimension (4.160 Å) indicates that there can be no superposition of atoms in the b-projection, and the eight-membered rings are oriented almost perpendicularly to the b axis. On the b-projection, we could assume a regular octagonal ring as a gross structure of the projected molecule, although the molecular conformation was still uncertain. Accordingly, as a first step, the molecular transform of a regular octagonal ring of the tetroxocane molecule was calculated, taking the polar coordinates (r, ϕ) and (R, ψ) in the real space and the reciprocal space respectively. On the regular octagonal model, there is a fourfold rotation symmetry. The molecular transform, F_m, thus can be written by analogy with the molecular transform of a helix proposed by Cochran, Crick, and Vand:[12]

$$F_m(R, \psi) = 4\sum_n\sum_j f_j J_n(2\pi R r_j) \exp\{in(\psi-\phi_j+\pi/2)\},$$

where J_n is the Bessel function of the n-th order. In the present case, only $n=0$, ±4 and ±8 need be considered in the range of $\sin\theta/\lambda<0.70$ Å^{-1}, and the ϕ_j's for the reference oxygen and carbon atoms are 0 and $\pi/4$ respectively. By using this expression, the molecular transform was evaluated very fast by handwork. A satisfactory fitting of the squares of the molecular transform, F_m^2, to the weighted reciprocal lattice points, as is shown in Fig. 1a, was obtained when the oxygen atom was oriented at an angle of 27° from the c axis (Fig. 1b). The signs of all the observed $F(h0l)$'s except for a few weak ones were determined from the molecular transform. By two cycles of two-dimensional Fourier syntheses, the atomic coordinates were refined up to the discrepancy factor, $R(=\sum||F_o|-|F_c||/\sum|F_o|)$, of 0.12 without hydrogen atoms.

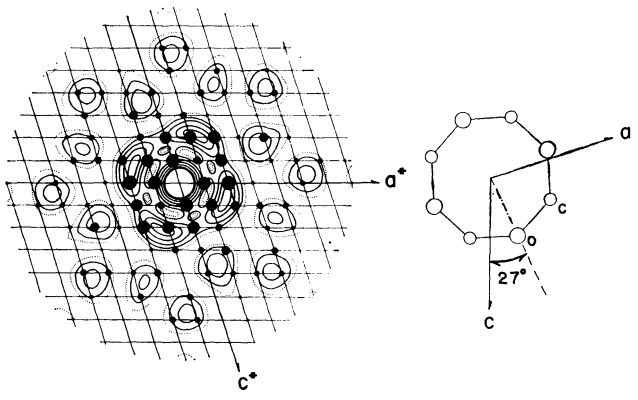

Fig. 1. (a) Contour map of $F_m^2(R, \psi)$ of the regular octagonal shape model of tetroxocane molecule and the weighted $(h0l)$ reciprocal lattice points. (b) Orientation of the model in the crystal lattice.

Three-dimensional Structure. A good agreement of F_o and F_c was obtained when the molecular conformation was a crown form with a twofold rotation axis and when the center of gravity of the molecule was at approximate $y=0.25$. Further refinement was made using the block-diagonal least-squares method.[13] The R value was reduced to 0.14 by using isotropic thermal factors. The anisotropic thermal factors were then introduced, and the R value dropped to 0.09 after six cycles. Hydrogen atoms were located at this stage from a difference Fourier synthesis (Fig. 2) and were included in the least-squares refinement with isotropic thermal factors. In the last stage, the 002 and $\bar{1}11$ reflections were excluded from the least-squares calculation because they appeared to be seriously affected by extinction. The $\sum w(F_o-kF_c)^2$ quantity was minimized, where w is the weight function and k is the scale factor. At the final stage of the refinement, the following weighting scheme was employed: $w=(4F_{min}/F_o)^2$ if $F_o\geq4F_{min}$, $w=1$ if $4F_{min}>F_o\geq F_{min}$, and $w=0.2$ if $F_o<F_{min}$, where $F_{min}=2.0$. The R value dropped to 0.048 for all the observed reflections except 002 and $\bar{1}11$, and to 0.051 including these two reflections. The atomic scattering factors used for the carbon and oxygen atoms were those in the International Tables for X-ray Crystallography, Vol. III,[14] while for hydrogen the values of Stewart *et al.*[15] were used. The final atomic coordinates and thermal parameters are listed in Table 1. A comparison of the observed and calculated structure factors is given in Table 2.

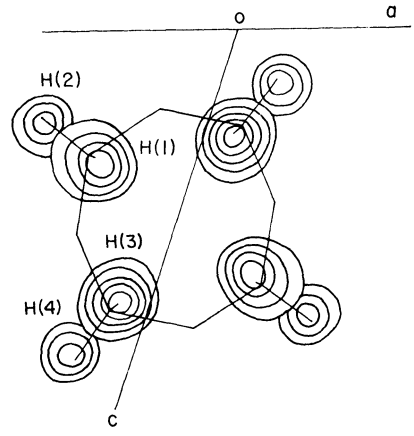

Fig. 2. Sections of three-dimensional difference Fourier synthesis through the atomic centers parallel to the (010). The contours are at intervals of 0.1 e/Å^3, starting with 0.2 e/Å^3.

Results and Discussion

The molecular dimensions derived from the final atomic coordinates are shown in Table 3 and Fig. 3. The molecular conformation of tetroxocane in the crystal was established to have a crown form, like that of methaldehyde[16] and sulphur,[17] though 1,3,5,7-tetrathiocane $(-CH_2-S-)_4$[18] was found to exist not in

TABLE 1. THE FINAL ATOMIC PARAMETERS AND THEIR ESTIMATED STANDARD DEVIATIONS

	x	y	z	$B_{ij}\times 10^5$					
				$B_{11}(B)$	B_{22}	B_{33}	B_{12}	B_{13}	B_{23}
C(1)	−0.1477(2)	0.2911(5)	0.1633(2)	809(15)	7216(127)	729(13)	642(72)	328(22)	−93(67)
C(2)	−0.0476(2)	0.2907(4)	0.3672(2)	1042(17)	5981(109)	663(12)	10(70)	748(23)	−99(61)
O(1)	−0.0714(1)	0.1648(3)	0.1030(1)	1001(12)	7094(90)	683(9)	−281(53)	464(17)	−1153(46)
O(2)	−0.1309(1)	0.1446(3)	0.2702(1)	911(11)	5942(77)	827(10)	−618(49)	640(17)	72(45)
H(1)	−0.142(2)	0.538(6)	0.169(2)	5.4(5)					
H(2)	−0.235(2)	0.233(5)	0.112(2)	6.0(5)					
H(3)	−0.038(2)	0.528(5)	0.354(2)	4.2(4)					
H(4)	−0.074(2)	0.247(5)	0.434(2)	5.7(5)					

The anisotropic temperature factors are of the form: $\exp[-(B_{11}h^2+B_{22}k^2+B_{33}l^2+B_{12}hk+B_{13}hl+B_{23}kl)]$.
The isotropic temperature factors for hydrogen atoms are of the form: $\exp(-B\sin^2\theta/\lambda^2)$ and are given in Å^2.

TABLE 2. THE OBSERVED AND THE FINAL CALCULATED STRUCTURE FACTORS ($\times 10$)

H	L	F_o	F_c
	(K = 0)		
0	2	519	-626
0	4	501	-554
0	6	180	-180
0	8	242	247
0	10	7	-7
0	12	9	12
0	14	17	-17
0	16	20	-20
2	0	533	548
2	2	480	484
2	4	238	-236
2	6	320	-323
2	8	191	191
2	10	87	-95
2	12	55	56
2	14	21	17
-2	2	234	-223
-2	4	624	-596
-2	6	187	176
-2	8	39	51
-2	10	244	246
-2	12	188	-190
-2	14	27	-27
-2	16	30	31
4	0	619	-619
4	2	354	354
4	4	40	50
4	6	57	55
4	8	157	-179
4	10	25	28
4	12	14	17
4	14	24	22
-4	2	562	573
-4	4	577	-563
-4	6	93	83
-4	8	296	289
-4	10	39	38
-4	12	189	-180
-4	14	19	-19
-4	16	69	73
6	0	84	-97
6	2	230	-240
6	4	185	172
6	6	209	216
6	8	178	-175
6	10	29	-26
6	12	24	26
-6	2	96	-93
-6	4	162	151
-6	6	9	-11
-6	8	224	217
-6	10	205	-203
-6	12	27	31
-6	14	30	-31
-6	16	40	40
8	2	204	-197
8	4	111	110
8	6	47	45
8	8	31	29
8	10	70	-68
-8	2	155	-155
-8	4	392	385
-8	6	67	-67
-8	8	158	-158
-8	10	33	28
-8	12	37	41
-8	14	11	-11
10	0	168	-171
10	2	17	-22
10	4	39	45
10	6	15	-21
10	8	21	28
-10	2	161	172
-10	4	92	92
-10	6	45	-46
-10	8	184	-186
-10	10	122	124
-10	12	3	0
-10	14	18	18
12	0	32	-37
12	4	14	-15
-12	2	110	113
-12	4	45	-42
-12	6	18	-23
-12	8	33	-31
-12	10	4	0
-12	12	68	62
-12	14	15	-11
14	0	49	48
14	2	12	9
-14	4	18	16
-14	6	6	-10
-14	10	24	-23
-14	12	52	53
	(K = 1)		
1	0	250	221
1	1	652	-691
1	2	78	-79
1	3	389	-404
1	4	255	246
1	5	38	-33
1	6	327	-317
1	7	299	296
1	8	65	61
1	9	130	-126
1	10	41	39
1	11	62	63
1	12	32	32
1	13	17	-20
1	14	35	-36
1	15	23	-22
-1	1	1072	-1116
-1	2	89	-82
-1	3	182	-172
-1	4	74	-70
-1	5	289	281
-1	6	96	-89
-1	7	118	123
-1	8	55	54
-1	9	21	25
-1	10	73	74
-1	11	113	-120
-1	12	41	-41
-1	15	24	21
-1	16	15	-13
3	0	128	-123
3	1	388	378
3	2	310	302
3	3	255	-263
3	4	6	-9
3	5	97	-98
3	6	71	-69
3	7	48	48
3	8	53	-51
3	10	17	18
3	11	34	35
3	12	44	43
3	13	10	8
3	14	21	-19
-3	1	215	214
-3	2	27	-22
-3	3	413	-408
-3	4	347	-325
-3	5	319	313
-3	6	330	311
-3	7	97	100
-3	8	62	-54
-3	9	17	17
-3	10	22	23
-3	11	235	-233
-3	12	35	-38
-3	13	69	71
-3	14	6	5
-3	15	67	63
5	0	186	-189
5	1	184	175
5	2	285	284
5	3	132	132
5	4	65	-56
5	5	9	7
5	6	36	33
5	7	217	-217
5	8	62	-62
5	9	92	93
5	10	17	16
5	11	27	24
5	12	2	-1
5	13	4	5
-5	1	243	247
-5	2	213	-205
-5	3	119	-126
-5	4	73	74
-5	5	151	142
-5	6	160	149
-5	7	154	156
-5	8	7	4
-5	9	230	-222
-5	10	87	-87
-5	11	22	-20
-5	12	22	22
-5	13	38	31
-5	14	12	-10
-5	15	56	55
-7	0	15	-20
-7	1	108	-113
-7	2	31	-34
-7	3	222	217
-7	4	76	79
-7	5	36	35
-7	6	9	-12
-7	7	115	-110
-7	8	2	-4
-7	9	27	-26
-7	10	2	-2
-7	11	51	48
-7	12	34	-40
-7	13	163	-160
-7	3	290	291
-7	4	213	216
-7	5	160	-165
-7	6	44	-46
-7	7	31	-29
-7	8	47	43
-7	9	46	-46
-7	10	92	-92
-7	11	67	72
-7	12	12	17
-7	13	31	-32
-7	14	23	23
-7	15	22	23
-7	16	5	7
9	0	26	23
9	1	20	23
9	2	85	-83
9	3	78	81
9	4	36	37
9	5	20	-22
9	7	27	25
9	8	18	17
9	9	46	-44
9	10	16	-16
9	1	110	115
-9	2	18	14
-9	3	111	111
-9	4	12	12
-9	5	172	-170
-9	6	26	31
-9	7	95	-100
-9	8	40	-43
-9	9	162	167
-9	10	10	-7
-9	11	30	-28
-9	12	9	-8
-9	13	8	-9
-9	14	42	43
-9	15	13	-11
-9	16	22	-19
11	0	3	-5
11	1	39	35
11	2	1	0
11	3	17	19
11	4	39	-36
11	5	7	-6
11	6	20	20
11	7	8	0
-11	1	146	149
-11	2	59	56
-11	3	85	-87
-11	4	51	-49
-11	5	43	-46
-11	6	32	33
-11	7	27	-27
-11	8	46	-47
-11	9	81	84
-11	10	23	24
-11	11	11	3
-11	12	1	3
-11	13	20	-18
-11	15	25	-25
13	0	4	3
13	1	19	-20
13	2	9	10
13	3	20	-15
13	4	24	-21
13	5	13	8
-13	1	18	-16
-13	2	14	14
-13	3	12	-15
-13	4	8	-4
-13	6	31	-31
-13	8	18	18
-13	10	11	4
-13	11	53	52
-13	12	13	8
-13	13	48	-47
15	0	56	55
15	1	58	64
15	2	63	52
15	3	42	40
15	4	53	54
15	5	40	-41
15	6	62	60
15	7	7	4
15	8	30	-31
15	9	6	-2
15	10	64	-65
15	11	11	-6
15	12	26	25
15	13	12	13
15	1	59	61
15	3	47	45
15	4	184	-187
15	5	35	-32
-15	1	4	-3
-15	2	2	-5
-15	3	48	46
-15	4	44	42
-15	5	31	34
-15	6	23	-24
-15	7	16	-16
-15	8	35	34
-15	9	10	8
-15	10	9	-13
-15	11	17	-16
17	0	8	-6
17	1	106	101
17	2	195	-198
17	3	123	-118
17	5	9	-6
17	6	37	38
17	7	19	20
17	8	23	-21
	(K = 4)		
0	0	41	-45
0	2	43	47
0	3	9	-9
0	4	60	-58
0	5	82	85
0	6	66	65
0	7	48	-52
0	8	22	-25
0	9	39	-38
0	10	19	-17
0	11	17	18
2	1	31	-33
2	2	11	-10
2	4	37	-37
2	5	78	80
2	6	56	55
2	8	4	-5
2	9	48	-47
2	10	10	-11
-2	1	19	18
-2	3	26	29
-2	4	54	54
-2	5	52	-56
-2	6	59	-56
-2	8	20	16
-2	10	13	-11
-2	12	17	18
-2	13	53	55
4	1	78	-84
4	2	101	-101
4	3	55	58
4	4	41	37
4	5	7	8
4	6	6	-2
4	7	18	18
4	8	21	21
4	9	14	-17
4	1	50	48
4	2	22	17
-4	1	33	-31
-4	2	72	-76
-4	3	53	-51
-4	4	133	-137
-4	5	30	-31
-4	6	12	13
-4	7	32	31
-4	8	38	-37
-4	9	41	-39
-4	10	26	25
-4	11	14	17
-4	12	8	-5
-4	13	16	-12
-4	14	32	-32
-4	11	14	-17
-4	12	8	-5
6	0	24	21
6	1	56	-58
6	2	38	-40
6	3	10	14
6	4	7	-1
6	5	20	18
6	6	11	7
6	7	2	-6
6	8	14	12
6	9	27	26
6	1	27	26
6	2	52	50
6	3	92	-96
6	4	57	-54
6	5	10	9
6	6	8	8
6	7	21	21
6	8	15	-17
6	9	30	34
6	10	45	42
6	11	13	-19
6	12	12	-15
8	0	26	-24
8	1	10	13
8	2	38	34
8	3	27	-30
8	4	31	-30
8	5	11	9
8	6	26	26
8	7	11	-12
8	8	19	-23
8	9	12	12
8	10	16	-11
8	11	8	-13
8	12	26	24
8	13	11	10
10	0	3	0
10	1	7	-10
10	2	31	27
10	3	26	22
10	4	24	-29
10	5	19	-25
10	6	22	23
-10	1	18	23
-10	2	9	2
	(K = 5)		
1	0	36	-31
1	1	24	25
1	2	19	17
1	3	14	-13
1	4	29	30
1	5	37	38
1	6	19	-24
1	7	29	-33
1	1	35	34
-1	2	21	17
-1	3	9	0
-1	4	8	6
-1	6	16	-18
-1	7	1	-11
-1	8	10	-3
3	0	1	5
3	1	37	-37
3	2	12	14
3	3	28	27
3	4	13	12
3	5	14	10
3	6	6	-4
3	1	9	-2
3	2	34	-31
3	3	16	19
3	4	8	0
3	5	50	-52
3	6	18	19
3	7	29	26
5	0	5	0
5	1	41	-41
5	2	25	27
5	3	21	22
5	4	4	0
5	5	48	-3
5	6	48	-50
5	3	21	-19
-5	4	15	20
-5	5	6	-8
-5	6	26	25
-5	7	6	7
-5	8	14	-9
-7	1	13	12
-7	2	5	-7
-7	3	30	-32
-7	4	8	1
-7	5	19	20
-7	6	16	15

TABLE 3. MOLECULAR DIMENSIONS OF TETROXOCANE

Bond lengths (Å)			
O(1)–C(1)	1.411(3)	C(1)–H(1)	1.03(2)
C(1)–O(2)	1.399(2)	C(1)–H(2)	1.03(3)
O(2)–C(2)	1.405(3)	C(2)–H(3)	1.01(2)
C(2)–O(1′)	1.396(3)	C(2)–H(4)	0.97(3)
Bond angles (°)			
O(1)–C(1)–O(2)	113.6(2)	O(1)–C(1)–H(2)	104(1)
C(1)–O(2)–C(2)	117.2(2)	O(2)–C(1)–H(1)	113(1)
O(2)–C(2)–O(1′)	113.9(2)	O(2)–C(1)–H(2)	107(1)
C(1)–O(1)–C(2′)	116.0(2)	O(2)–C(2)–H(3)	112(1)
H(1)–C(1)–H(2)	108(2)	O(2)–C(2)–H(4)	109(2)
H(3)–C(2)–H(4)	113(2)	O(1′)–C(2)–H(3)	105(1)
O(1)–C(1)–H(1)	111(1)	O(1′)–C(2)–H(4)	105(1)
Torsion angles (°)			
C(2′)–O(1)	83.7	C(1)–O(2)	93.6
O(1)–C(1)	−83.6	O(2)–C(2)	−94.1
Intramolecular H···H distances (Å)			
H(1)···H(3)	2.20(3)	H(1)···H(3′)	2.16(3)

Estimated standard deviations shown in parentheses refer to the last decimal positions.

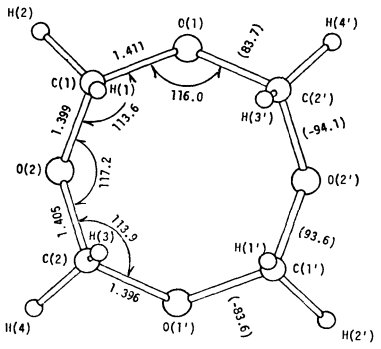

Fig. 3. Bond lengths, bond angles and torsion angles (shown in parentheses) of tetroxocane molecule.

a crown form but in a boat-chair form in the crystalline state. On a closer examination, the molecular conformation of tetroxocane in the crystal is found to depart from the regular crown form: the molecular shape has an approximate C_{4v} symmetry but an exact C_2 symmetry. That is, the crown is elongated in the direction of O(1)···O(1′) (3.448 Å) and is shrunk along the direction of O(2)···O(2′) (3.190 Å). The difference, 0.258 Å, is significant. The torsion angles about the four independent C–O bonds thus appear in two distinguishable values: two bonds with 83.7 and −83.6°, and the other two bonds with 93.6 and −94.1°. The average C–O bond length is 1.403 Å, and the average C–O–C and O–C–O bond angles are 116.6 and 113.8° respectively. This deformation from the regular crown form with the tetrahedral angle may be due to the steric effects of the hydrogen atoms. If a regular crown form is constructed from the normal bond lengths and the tetrahedral angle, the torsion angle is calculated to be 96°58′ and the H···H distances become 1.90 Å, while the actual short H···H distances in the distorted crown form were found to be 2.16 and 2.20 Å. Table 4 shows the molecular dimensions of the cyclic oligomers of formaldehyde from trimer to hexamer. The average C–O bond length in the tetroxocane is the shortest. This may be partly due to the thermal motions. Except for trioxane, the C–O–C bond angles are larger than the O–C–O bond angles, but all the C–O–C and O–C–O bond angles are evidently larger than the tetrahedral angle, 109°28′. The increase in the bond angles, especially those of the C–O–C bond angles, may compensate for the intramolecular steric hindrances. The bending force constant of C–O–C is smaller than that of O–C–O. Therefore, the larger increase in the C–O–C bond angles might be favorable in terms of the conformation energy.

Table 5 lists the root-mean-square vibration am-

TABLE 4. MOLECULAR DIMENSIONS[a] OF CYCLIC OLIGOMERS OF FORMALDEHYDE

Molecular symmetry	$(-CH_2-O-)_3$ C_{3v}–3m			$(-CH_2-O-)_4$ C_2–2	$(-CH_2-O-)_5$ C_2–2	$(-CH_2-O-)_6$ C_{3i}–$\bar{3}$
Method	X[b]	M[c]	ED[d]	X	X	X
C–O (Å)	1.421	1.411	1.411	1.403	1.410	1.411
C–H (Å)	1.07	1.09[e]	1.116	1.01	1.00	1.06
O–C–O (°)	109.6	111.2	111.0	113.8	111.8	114.0
C–O–C (°)	110.4	108.2	109.2	116.6	115.6	115.4
H–C–H (°)	114	109.5[e]	111.8	111	112	116
Intramolecular H···H distance (Å)	2.46			2.16 2.20	2.17 2.20	2.13
C–O torsion angle (°)	58.8 −58.8			83.7 −83.6 93.6 −94.1	−72.9 118.7 −84.2 123.4 −69.8	−84.3 85.5
Ref.	19) (at −170 °C) 20)		21)	This work	22)	5)

a) Average values of independent bond lengths and bond angles when there are independent values. b) X-ray diffraction c) Microwave d) Electron diffraction e) Assumed value.

Table 5. Temperature parameters (B_i) and r.m.s. displacements (U_i) along the principal axes of the thermal ellipsoids and the angles between the principal axes and the crystallographic a, b, and c* axes (ω_{ia}, ω_{ib}, and ω_{ic}*)

	i	B_i(Å^2)	U_i(Å)	ω_{ia}(°)	ω_{ib}(°)	ω_{ic}*(°)
C(1)	1	3.48	0.210	39	107	56
	2	4.40	0.236	125	90	36
	3	5.13	0.255	103	163	99
C(2)	1	3.13	0.199	119	84	30
	2	4.14	0.229	87	6	95
	3	4.97	0.251	30	91	61
O(1)	1	3.03	0.196	93	60	30
	2	4.86	0.248	177	91	92
	3	5.59	0.266	90	30	120
O(2)	1	3.48	0.210	42	50	101
	2	4.51	0.239	99	97	169
	3	4.74	0.245	49	139	90

plitudes along the principal axes of the thermal ellipsoids and the angles between the principal axes and the crystallographic a, b, and c* axes. The thermal motion of each skeletal atom is predominant in the direction perpendicular to the plane formed by the atom and both neighboring atoms. Such a feature has previously been found in the cases of pentoxecane[22] and hexoxecane.[5] In the case of hexoxecane, a rigid body approximation[23,24] was undertaken for the molecule of the $\bar{3}$ symmetry, but no reasonable result could be obtained. These facts might imply that, besides the translational and vibrational motions, intramolecular motions, *e.g.*, torsional and bending motions, are also appreciable in these cyclic oligomers. Since we do not yet know the mode of the intramolecular motions, corrections of bond lengths and bond angles for the thermal motions were not made.

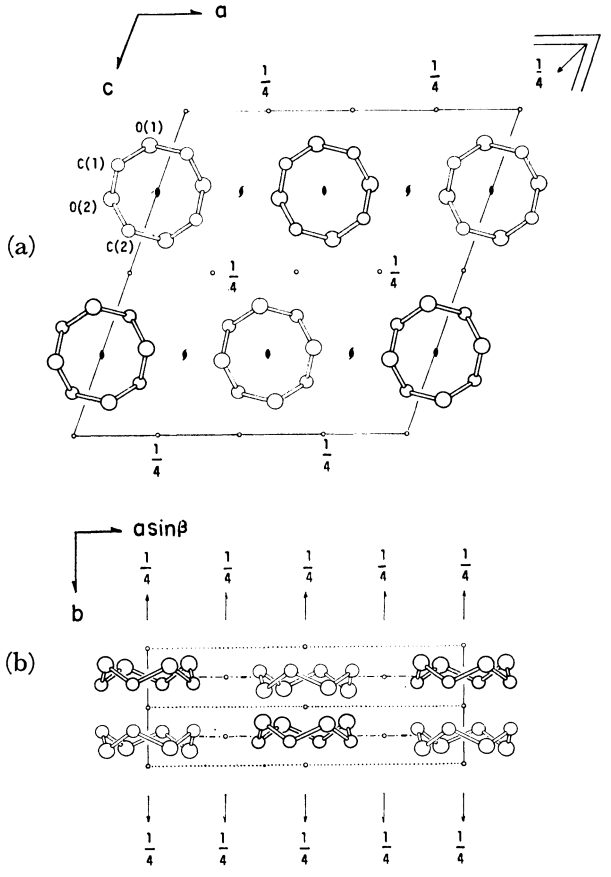

Fig. 4. (a) Crystal structure viewed along the b axis. (b) Crystal structure viewed along the c axis.

Table 6. Intermolecular atomic distances

C···O (Å)		C···C (Å)	
C(1,a)···O(1,b)	3.86	C(2,a)···C(2,f)	3.54
C(1,a)···O(2,b)	3.77	C(2,a)···C(2,g)	3.92
C(2,a)···O(2,b)	3.77	C(1,a)···C(1,h)	4.18
C(2,a)···O(1,c)	3.86	C(1,a)···C(2,h)	3.98
C(2,a)···O(1,d)	3.75	C(2,a)···C(1,h)	3.98
C(2,a)···O(1,e)	3.53	C(1,a)···C(1,i)	3.96
C(1,a)···O(2,h)	3.25		
C(1,a)···O(1,i)	3.79		

a: x, y, z; b: $x, 1+y, z$; c: $-x, 1+y, 1/2-z$; d: $x, 1-y, 1/2+z$; e: $x, -y, 1/2+z$; f: $-x, 1-y, 1-z$; g: $-x, -y, 1-z$; h: $-1/2-x, 1/2+y, 1/2-z$; i: $-1/2-x, 1/2-y, -z$.

The molecular packing is shown in Fig. 4. The ring molecules are piled up along the b axis. The shortest intermolecular (between centers of gravity) distance of 4.16 Å is in the b direction, along which the dipole moment vectors of all the molecules in a row are parallel. Some short intermolecular atomic distances are shown in Table 6. The closest C···O distance is 3.25 Å. The C···C distances are longer than 3.92 Å except for the 3.54 Å of C(2,a)···C(2,f).

The authors wish to thank Professor H. Tadokoro of Osaka University for his interest in the work and his constant encouragement.

References

1) K. Hayashi, M. Nishii, and S. Okamura, *J. Polym. Sci.*, **C4**, 839 (1963).
2) G. Carazzolo, S. Leghissa, and M. Mammi, *Makromol. Chem.*, **60**, 171 (1965).
3) Y. Chatani, K. Kitahama, H. Tadokoro, T. Yamauchi, and Y. Miyake, *J. Macromol. Sci.-Phys.*, **B4**, 61 (1970).
4) M. Nishii, K. Hayashi, and S. Okamura, *J. Polym. Sci.*, **B7**, 891 (1969).
5) Y. Chatani, T. Ohno, T. Yamauchi, and Y. Miyake, *J. Polym. Sci.-Polym. Phys.*, **11**, 369 (1973).
6) Y. Chatani, T. Uchida, H. Tadokoro, K. Hayashi, M. Nishii, and S. Okamura, *J. Makromol. Sci.-Phys.*, **B2**, 567 (1968).
7) J. Dale, T. Ekeland, and J. Krane, *J. Amer. Chem. Soc.*, **94**, 1389 (1972).
8) F. A. L. Anet and P. J. Degen, *ibid.*, **94**, 1390 (1972).
9) H. Staudinger and M. Luthy, *Helv. Chim. Acta*, **8**, 65 (1925).
10) A. J. C. Wilson, *Acta Crystallogr.*, **2**, 318 (1949).
11) E. R. Howells, D. C. Phillips, and D. Rogers, *ibid.*, **3**, 210 (1950).
12) W. Cochran, F. H. C. Crick, and V. Vand, *ibid.*, **5**,

581 (1952).
13) Y. Okaya and T. Ashida, "HBLS IV, The Universal Crystallographic Computing System (I)," The Crystallographic Society of Japan, Tokyo (1967), p. 65.
14) "International Tables for X-Ray Crystallography," Vol. III, Kynoch Press, Birmingham (1962), p. 202.
15) R. F. Stewart, E. R. Davidson, and W. T. Simpson, *J. Chem. Phys.*, **42**, 3175 (1965).
16) L. Pauling and D. C. Carpenter, *J. Amer. Chem. Soc.*, **58**, 1274 (1936).
17) S. L. Abrahams, *Acta Crystallogr.*, **8**, 661 (1955).
18) G. W. Frank, P. J. Degen, and F. A. L. Anet, *J. Amer. Chem. Soc.*, **94**, 4792 (1972).
19) V. Busetti, A. Del Pra, and M. Mammi, *Acta Crystallogr.*, **B25**, 1191 (1969).
20) T. Oka, K. Tsuchiya, S. Iwata, and Y. Morino, This Bulletin, **37**, 4 (1964).
21) A. H. Clark and T. G. Hewitt, *J. Mol. Structure*, **9**, 33 (1971).
22) Y. Chatani and K. Kitahama, This Bulletin, **46**, 2300 (1973).
23) D. W. Cruickshank, *Acta Crystallogr.*, **9**, 754 (1956).
24) V. Schomaker and K. N. Trueblood, *ibid.*, **23**, 1049 (1968).

Proton Nuclear Magnetic Resonance Spectroscopy of Partially-deuterated *n*-Pentanes

Masahiro KONDO, Isao ANDO, Riichirô CHÛJÔ, and Atsuo NISHIOKA

Department of Polymer Chemistry, Tokyo Institute of Technology, Ookayama, Meguro-ku, Tokyo 152

(Received August 24, 1973)

The proton NMR spectra of some partially deuterated *n*-pentanes were observed under both proton-deuteron (H–D) spin-coupled and -decoupled conditions. With using the spectrum-simulation method, it was confirmed experimentally that the chemical shift of the $CH_2(3)$ protons appears at a higher field than that of the $CH_2(2)$ protons.

It is well known[1] that, in the case of molecules with rotational isomers, in which rotation about the C–C bond is very quick, the observed NMR chemical shift is averaged with the statistical weight for each isomer. *n*-Pentane can take seven preferred isomeric forms[2] (TT, TG, GT, TG', G'T, GG, G'G'), while GG' and G'G conformations are ignored because of the steric hindrance or the so-called "pentane effect." In a previous paper,[3] the proton NMR chemical shift of *n*-pentane has been calculated theoretically, taking into account the above conformations, and then the energy difference between *trans* and *gauche* conformations and the magnetic anisotropy of the C–C bond was estimated. According to the results obtained there, the $CH_2(3)$ proton peak would appear at a field higher than that of the $CH_2(2)$ proton by 0.03—0.04 ppm.

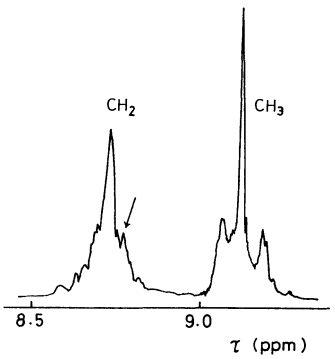

Fig. 1. The proton NMR spectrum of non-deuterated *n*-pentane in CCl_4 solution at 22.5 °C. The chemical shift of methyl protons appears at 9.125τ. The shoulder of the $CH_2(3)$ proton is indicated by an arrow.

As is shown in Fig. 1, the observed spectrum of the methylene groups in *n*-pentane has a weak shoulder at a higher field in the main peak. This shoulder was previously tentatively assigned to the $CH_2(3)$ protons, and the main peak, to the $CH_2(2)$ protons.[3] Such an assignment, however, was made without taking into account the effect of the nuclear spin-spin coupling. Since the difference in the chemical shift between the $CH_2(2)$ and $CH_2(3)$ protons is very small, it may be considered that the spin-spin coupling plays an important role in determining the pattern of the spectrum. Hence, we attempted to confirm whether the previous assignment is true or not. In doing this, we may encounter inconvenience due to the large number of protons. Therefore, we prepared some partially-deuterated *n*-pentanes and made spectrum-simulation in order to determine whether or not the chemical shift of the $CH_2(3)$ protons appears at a field higher than that of the $CH_2(2)$ protons.

Experimental

Materials. The partially-deuterated *n*-pentanes, (II)—(V), used here are as follows:

$CH_3CH_2CH_2CH_2CH_3$ (I)

$CH_2DCH_2CH_2CH_2CH_2D$ (II)

$CHD_2CH_2CH_2CH_2CHD_2$ (III)

$CD_3CH_2CH_2CH_2CD_3$ (IV)

$CH_3CH_2CD_2CH_2CH_3$ (V)

They were prepared by the method to be described below.

Preparation. $CD_3CH_2CH_2CH_2CD_3$: Dimethyl glutarate (25 g) was added, drop by drop, to a well-stirred solution of lithium aluminum deuteride (7 g) in dry ether (150 ml). After this addition and stirring for 2 hr, the excess lithium aluminum deuteride was carefully decomposed with water to give a product like white clay. 1,5-Pentanediol-1,1,5,5-d_4 (12 g) was extracted from the product with ether by using a Soxhlet extractor for 2 days. The ether was then evaporated, and the resulting alcohol was treated with potassium iodide (50 g) in a mixture of phosphoric anhydride (12 g) and 85% phosphoric acid (40 ml) to give 1,5-diiodopentane-1,1,5,5-d_4. After drying, it was converted to *n*-pentane-1,1,1,5,5,5-d_6 with heavy water by the usual Grignard reaction. This product (*ca.* 1 ml) was separated from ether by washing with cold, concentrated sulfuric acid, and then distilled. The NMR spectrum of the deuterated *n*-pentane showed the absence of methyl protons.

$CH_3CH_2CD_2CH_2CH_3$: Diethyl ketone (25 g) was reduced with lithium aluminum deuteride (3 g) in dry ether (100 ml) in the usual way to give 3-pentanol-3-d_1 (14 ml). A mixture of this alcohol and freshly-distilled methanesulfonyl chloride in methylene chloride (70 ml) was treated with pyridine (15 ml) below −5 °C. After having been stirred for 1 hr in an ice-salt bath, the mixture was stored in a refrigerator for 24 hr and then poured into dilute sulfuric acid. The washed and dried organic layer was evaporated at room temperature, and the residue was pumped for several hours to yield 3-penthyl-3-*d* methanesulfonate (13 ml). This product was added, drop by drop, to a solution of lithium aluminum deuteride (4 g) in dry ether (100 ml). A mixture of *n*-pentane-3,3-d_2 and ether was distilled, and the deuterated *n*-pentane (2 ml) was separated from ether by washing with cold concentrated sulfuric acid. According to the NMR spectrum of this product, the deuterium content was more than 95%.

Method: The proton NMR spectra of partially-

deuturated *n*-pentanes were measured by means of a JEOL PS-100-type spectrometer at 100 MHz, in a solution of carbon tetrachloride at room temperature. Tetramethylsilane (TMS) was used as the internal standard. The deuteron spin decoupling (D-decoupling) was done using JNM SD-HC (hetero spin decoupler) equipment.

Calculations of the NMR spectra were carried out by means of the HITAC 5020E of the Computer Centre of the University of Tokyo, using a LAOCOON III program.

Results and Discussion

The observed spectra of some deuterated *n*-pentanes are shown in Figs. 2, 3, 4, and 5, where (a) and (b) were obtained under proton-deuteron (H–D) spin-coupled and -decoupled conditions respectively. The following features may be noted: In *n*-pentane-1,5-d_2, $CH_2DCH_2CH_2CH_2CH_2D$ (II), each line of the methyl proton triplet, moreover, splits into a triplet (Fig. 2(a)) as a result of the geminal H–D spin-spin coupling, the constant of which is $J_{H\text{-}D}^{gem}=1.9$ Hz. In *n*-pentane-1,1,5,5-d_4, $CHD_2CH_2CH_2CH_2CHD_2$ (III), it splits into a quintet (Fig. 3(a)). While Fig. 4(a) shows only a single methylene proton peak, which is somewhat broad because of the vicinal H–D spin-spin coupling,

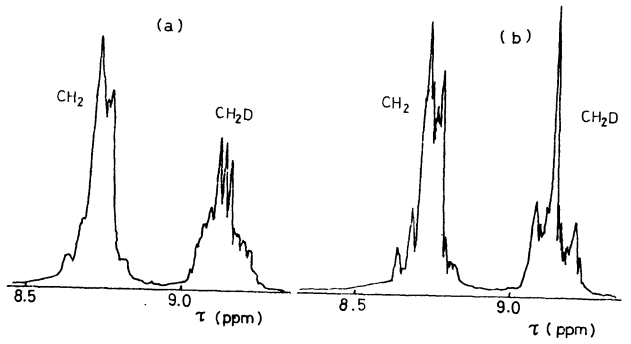

Fig. 2. The proton NMR spectrum of *n*-pentane-1,5-d_2 in CCl_4 solution at 22.5 °C. The chemical shift of methyl protons appears at 9.141τ.
(a) Taken under H–D spin-undecoupled condition.
(b) Taken under H–D spin-decoupled condition.

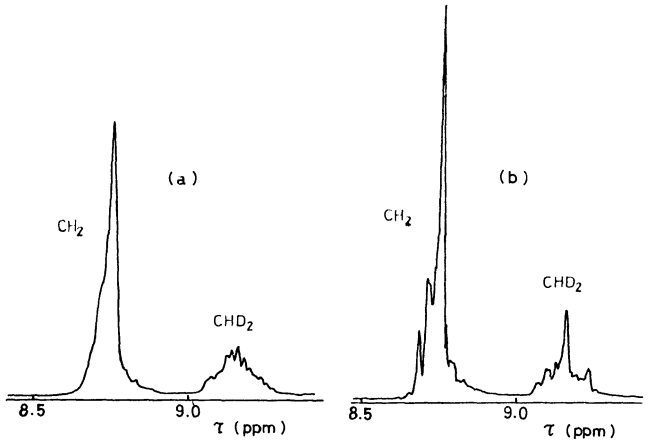

Fig. 3. The proton NMR spectrum of *n*-pentane-1,1,5,5-d_4 in CCl_4 solution at 22.5 °C. The chemical shift of methyl protons appears at 9.158τ.
(a) Taken under H–D spin-undecoupled condition.
(b) Taken under H–D spin-decoupled condition.

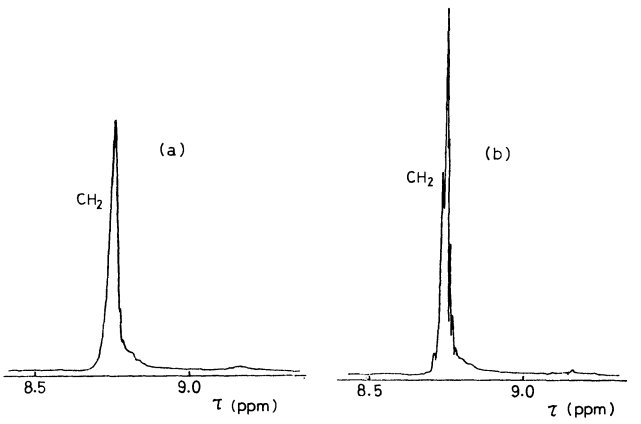

Fig. 4. The proton NMR spectrum of *n*-pentane-1,1,1,5,5,-5-d_6 in CCl_4 solution at 22.5 °C.
(a) Taken under H–D spin-undecoupled condition.
(b) Taken under H–D spin-decoupled condition.

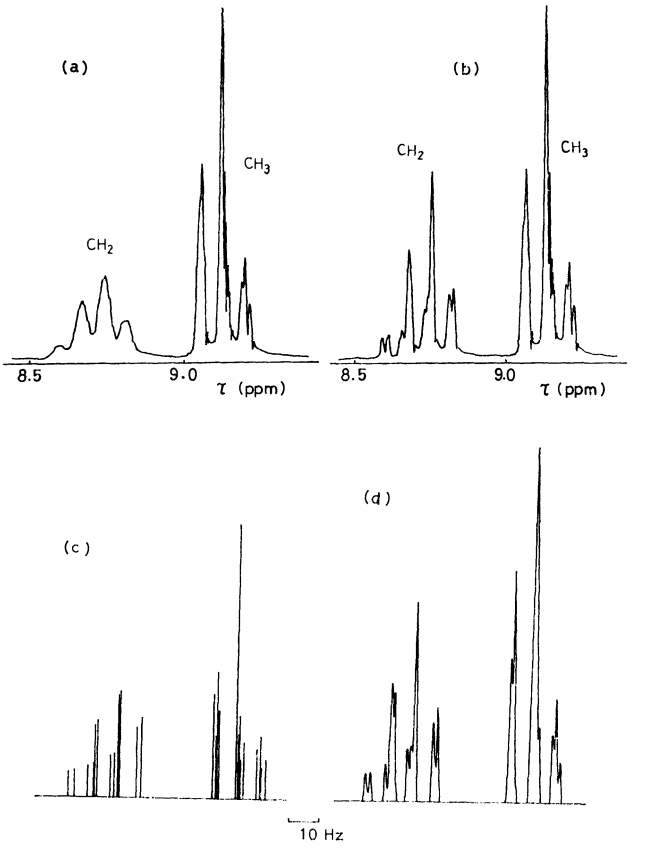

Fig. 5. The proton NMR spectrum of *n*-pentane-3,3-d_2 in CCl_4 solution at 22.5 °C. The chemical shift of methyl protons appears at 9.127τ.
(a) Taken under H–D spin-undecoupled condition.
(b) Taken under H–D spin-decoupled condition.
(c) Calculated "Stick" spectrum.
(d) Calculated spectrum in Lorentzian line shapes. with half-height-width of 0.4 Hz.

the D-decoupled spectrum (Fig. 4(b)) shows a fine structure, which may be expected to come from the chemical-shift difference between the methylene protons in *n*-pentane-1,1,1,5,5,5-d_6, $CD_3CH_2CH_2CH_2CD_3$ (IV). *n*-Pentane-3,3-d_2, $CH_3CH_2CD_2CH_2CH_3$ (V), gives a A_3B_2-type spectrum of the five-spin system (Fig. 5(b))

if the deuteron is irradiated. As is shown in Fig. 5(a), line broadening occurs in the methylene proton quartet because of the vicinal H–D spin-spin coupling, the constant of which is probably about 1 Hz, but the methyl proton triplet remains sharp. This means that the long-range H–D spin-spin coupling separated by more than four bonds is negligibly small.

As we have stated above, we are mainly concerned with the problem of the chemical-shift difference between the $CH_2(2)$ and $CH_2(3)$ protons, which was previously predicted by means of theoretical calculations.[3] Thus, let us first compare the spectra of the partially-deuterated *n*-pentane measured under two different conditions, in which one was under undecoupled conditions and the other, under D-decoupled conditions. As for Sample (II), a comparison between Figs. 2(a) and 2(b) shows the following features: the shoulders which appear on the down-field side of the methylene peak in Fig. 2(a), which may be expected to come from the line broadening due to the vicinal H–D spin-spin coupling, change into rather sharp peaks upon D-decoupling, as is shown in Fig. 2(b) but there is almost no significant difference on the up-field side. Also, in the case of Sample (III), similar features are noted in comparing the spectra shown in Figs. 3(a) and 3(b). The $CH_2(2)$ protons are placed on the vicinal position against the deuterium atom in the methyl group, while the $CH_2(3)$ protons are on the position of four-bond separation from the deuterium atom. We may, therefore, conclude qualitatively that the chemical shift of the $CH_2(2)$ protons should appear at a lower field than that of the $CH_2(3)$ protons: this is in agreement with the previous results.

Table 1. The parameters used in doing the spectrum simulation of deuterated *n*-pentanes

$CH_3CH_2CD_2CH_2CH_3$	
	$\delta_{CH_3(1)-CH_3(2)}=0.415$ ppm
	$J^{gem}_{CH_3(1)-CH_3(1)}=J^{gem}_{CH_3(2)-CH_3(2)}=12.4$ Hz
	$J^{vic}_{CH_3(1)-CH_3(2)}=7.4$ Hz
$CD_3CH_2CH_2CH_2CD_3$	
	$\delta_{CH_3(3)-CH_3(2)}=0.05$, 0.03, and -0.03 ppm
	$J^{gem}_{CH_3(2)-CH_3(2)}=J^{gem}_{CH_3(3)-CH_3(3)}=12.4$ Hz
	$J^{vic}_{CH_3(3)-CH_3(2)}=7.4$ Hz
	$J^{long}_{CH_3(2)-CH_3(4)}=1$ Hz

Next, let us examine the spectrum of Sample (IV) by the aid of the spectrum-simulation method. Before doing this, though, we shall preliminarily simulate the spectrum of Sample (V) in order to estimate the vicinal coupling constant. The simulated spectra shown in Figs. 5(c) and 5(d) were obtained by using the "stick" type and the Lorentzian line shape respectively. When the parameters listed in Table 1 are used, the spectrum fairly well fits the observed one except that the calculated methylene part is somewhat sharper than the observed one: this may come from the neglect of the long-range coupling between the $CH_2(2)$ and $CH_2(4)$ protons. Although these parameters are not necessarily the best-fitting ones, they seem to be reasonable. In doing the spectrum simulation of Sample (IV) we

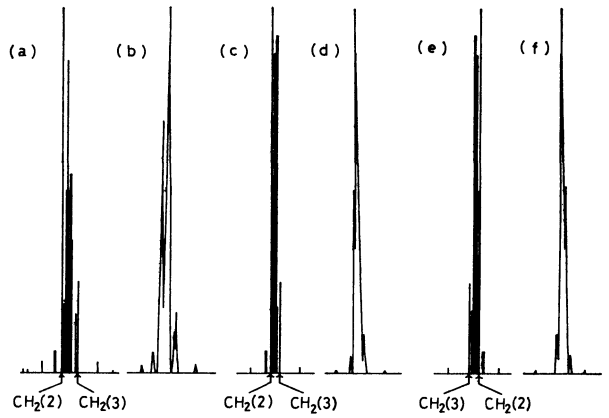

Fig. 6. The calculated spectra of *n*-pentane-1,1,1,5,5,5-d_6 for various values as the chemical shift difference between the $CH_2(3)$ and $CH_2(2)$ protons ($\delta_{CH_3(3)-CH_3(2)}$).
(a), (c), (e):
Calculated "stick" spectra using the values of 0.05, 0.03, and -0.03 ppm as $\delta_{CH_3(3)-CH_3(2)}$, respectively. The input chemical shifts of the $CH_2(3)$ and $CH_2(2)$ protons are indicated by the arrow.
(b), (d), (f):
Calculated spectra in Lorentzian line shapes with half-height-width of 0.4 Hz corresponding to (a), (c) and (e), respectively.

will tentatively use the parameters obtained above, that is, the vicinal coupling constant of 7.4 Hz and the long-range coupling of 1 Hz, since we cannot decide the detailed parameters because of the lack of characteristic peaks in Fig. 4(b). These values are, then, approximated such that the coupling constant between the $CH_2(2)$ and $CH_2(3)$ protons is nearly equal to that between the $CH_3(1)$ and $CH_2(2)$ protons: the long-range coupling constant may be somewhat overestimated. Figure 6 shows the calculated spectra of Sample (IV) with the various values for the chemical-shift difference between the $CH_2(2)$ and $CH_2(3)$ protons. As the observed spectrum (Fig. 4(b)) shows a rather sharp shoulder on the lower-field side of the main peak, we shall compare the calculated spectra with the observed one with regard to this shoulder. As is shown in Figs. 6(e) and 6(f), when the chemical shift of the $CH_2(2)$ protons is at a higher field than that of the $CH_2(3)$ protons, the calculated spectrum shows a shoulder on the higher-field side of the main peak: this is in disagreement with the observed spectrum. On the contrary, when the chemical shift of the $CH_2(3)$ protons is at a higher field, the shoulder in the calculated spectrum (Figs. 6(a), (b), (c), and (d)) appears on the lower-field side: this agrees with the observed spectrum. As the difference in chemical shift between the $CH_2(2)$ and $CH_2(3)$ protons becomes large, this shoulder moves away from the center of the main peak and becomes a resolved peak. When the value of 0.03 ppm is used as the chemical shift difference, a better-fitting spectrum seems to be obtained. From the "stick" spectrum (Fig. 6) it is found that the shoulder can be assigned to the $CH_2(2)$ protons, while a weak peak at the foot of the higher-field side, which is hardly shown in the observed spectrum because

of wiggle, can be assigned to the $CH_2(3)$ proton, and that the position of the main peak corresponds to something like the mean value of the chemical shifts between the $CH_2(2)$ and $CH_2(3)$ protons. Thus, we obtained results in accordance with the previous ones[3] by means of the simulation method for Sample (IV) as well as for Samples (II) and (III).

It is well known[4] that the replacement of a hydrogen atom by a deuterium atom causes a small up-field shift in the proton NMR: this is called the isotope shift. We shall examine this effect upon the deuterated *n*-pentanes, since we are concerned with a slight difference in the chemical shift between the methylene protons. The observed isotope shifts of the methyl protons in the deuterated *n*-pentanes are tabulated in Table 2. As has been reported in methane and other molecules by Bernheim *et al.*[5] and Barfield *et al.*[6] it was noted that the magnitude of the isotope shift is proportional to the number of the geminally isotopic substitution. We could not measure the isotope shift of the methylene protons, for we could not decide the exact chemical shifts of the $CH_2(2)$ and $CH_2(3)$ protons in deuterated *n*-pentanes. However, we can expect a very small isotope effect between the $CH_3(1)$ and $CH_2(3)$ groups, because the observed isotope shift of the methyl proton in Sample (V) is very small. Further, if we assume that the isotope effect of the vicinally isotopic substitution is smaller than that of the geminally one, it may not be because of the isotope shift, but because of the difference in the original chemical shift, that the $CH_2(3)$ protons appear at a field higher than the $CH_2(2)$ ones by *ca.* 0.03 ppm in the deuterated *n*-pentanes. Though we could not obtain any information on whether or not the shoulder on the higher-field side of the main peak in the non-deuterated *n*-pentane (Sample (I)) was the signal of the $CH_2(3)$ protons, we obtained experimental results which were in accordance with the theoretically-predicted ones.[3]

TABLE 2. ISOTOPE SHIFTS OF METHYL PROTONS OF *n*-PENTANE IN CCl_4 SOLUTION FOR VARIOUS AMOUNTS OF DEUTERIUM SUBSTITUTION (22.5 °C)

Sample	Isotope shift (ppm)
$CH_3CH_2CH_2CH_2CH_3$	0
$CH_2DCH_2CH_2CH_2CH_2D$	0.016
$CHD_2CH_2CH_2CH_2CHD_2$	0.033
$CH_3CH_2CD_2CH_2CH_3$	0.002

The authors wish to thank Dr. Tsuneo Hirano of the University of Tokyo for the use of the LAOCOON III program. Their thanks are also due to Mr. Masao Kambe of our laboratory for his kind assistance in the D-decoupling technique.

References

1) J. A. Pople, W. G. Schneider, and H. J. Bernstein, "High Resolution Nuclear Magnetic Resonance," McGraw Hill Book Co., New York (1959), Chapter 13.
2) S. Mizushima, "Structure of Molecules and Internal Rotation", Academic Press, Inc., New York (1954).
3) I. Ando and A. Nishioka, This Bulletin, **46**, 1040 (1973)
4) J. W. Emsley, J. Feeney, and L. H. Sutcliffe, "Progress in NMR Spectroscopy," Pergamon Press, Oxford (1967) Vol. 3, Chapter 2.
5) R. A. Bernheim and B. J. Lavery, *J. Chem. Phys.*, **42**, 1461 (1965).
6) M. Barfield and D. M. Grant, *J. Amer. Chem. Soc.*, **83**, 4726 (1961).

Phase Equilibria of the Systems Containing Silver Iodide and Alkali Iodide. II.† AgI-NaI-H_2O System

Norio NISHIMURA and Tatsuo HIGASHIYAMA*

Department of Chemistry, Faculty of Science, Okayama University, Tsushima, Okayama 700
**College of Liberal Arts, Okayama University, Tsushima, Okayama 700*

(Received September 10, 1973)

Phase diagrams were constructed for the equilibria of the AgI–NaI–H_2O system at temperatures 0—70 °C. A compound $AgI \cdot NaI \cdot 3H_2O$ was isolated, and the compound was found by means of X-ray analysis to belong to the orthorhombic system with cell constants $a=8.78$, $b=33.5$, and $c=6.48$ Å.

The formation of a series of compounds, probably of the type $K_n[AgI_{1+n}]$, was recognized for the binary system of AgI and KI.[1-4] They can be formed by a solid state reaction at high temperatures or by mixing the components with a small amount of water or from a concentrated aqueous solution. This type of compound often crystallizes with a solvent of crystallization. Marsh and Rhymes[5] described a series of crystalline compounds such as $2AgI \cdot KI \cdot 2C_3H_6O$, where C_3H_6O denotes acetone. The present authors[6] have studied the phase equilibria of the AgI–KI–H_2O system and reported the formation of a new compound $2AgI \cdot KI \cdot 2H_2O$.

The phase equilibria of the AgI–NaI–H_2O system at 25 °C were studied by Krym.[7] His phase diagram, however, is obviously incomplete, since he did not notice the existence of the solid phase of $NaI \cdot 2H_2O$. The present paper deals with an investigation of this system over a wide temperature range together with an X-ray study of a compound formed in this system.

Experimental

Materials. Silver iodide of extra pure grade was used. It was found by means of X-ray powder method to be γ-AgI (cubic), containing a small amount of β-AgI(hexagonal). Sodium iodide of extra pure grade was dried at 110—120 °C to a constant weight.

Determination of Composition. Desired amounts of AgI, NaI and water were introduced into a stoppered flask and thermostated for various periods of time depending on the experimental temperature (*ca.* 3 hr(70 °C)—24 hr(0 °C)). After the equilibrium had been attained, the solution was pipetted out and weighed, and then dried to a constant weight. The loss in weight was regarded to correspond to the quantity of the water involved. A large amount of water was added to the residue. After complete precipitation of AgI, the supernatant solution was carefully removed. The NaI in the residue was removed completely by repeating the procedure several times. It was confirmed that recovery of AgI was over 99%.

At temperatures below 40 °C, the formation of a crystalline compound, other than the components, was observed in a range of appropriate proportions of the components. As this compound crystallized from very concentrated solutions, supersaturation of the solutions often occurred. In the determination of the number of the water of crystallization, high temperature and humidity were avoided as far as possible, since the crystal is unstable in air and easily decomposes to the components even at room temperature. The crystals were washed with a small amount of acetone and dried quickly on a sheet of filter paper and weighed. The weight percentage of each component of the crystal was determined by the same method as that for solutions.

X-Ray Analysis. For the determination of the cell constants of the crystal, a single crystal was inserted into a thin-walled Pyrex glass capillary with a small amount of the mother liquid and sealed off. X-ray oscillation and Weissenberg photographs were taken using Ni-filtered Cu$K\alpha$ radiation. The density measurement was carried out with a picnometer of *ca.* 5 cm^3 and liquid paraffin.

Results and Discussion

The overall compositions of the AgI–NaI–H_2O system and the compositions of the liquid phases in equilibrium with solid phases are given in Table 1.

Table 1. Compositon of the AgI–NaI–H_2O system

Temp. (°C)	Overall composition (wt%) AgI	Overall composition (wt%) NaI	Composition of liquid phase in equilibrium with solid phase (wt%) AgI	Composition of liquid phase in equilibrium with solid phase (wt%) NaI	Solid phase
0	11.4	26.6	6.8	28.0	AgI
	16.1	29.8	11.4	31.4	
	25.9	31.5	18.1	34.7	
	28.8	35.5	24.3	37.6	
	24.2	45.3	18.7	47.7	Complex[b]
	29.8	40.7	21.7	43.7	
	24.8	46.8	18.9	49.5	
	6.8	60.6	7.5	58.4	$NaI \cdot 2H_2O$
	13.6	56.4	13.8	56.1	
			0	61.7[a]	
			24.9	40.6	AgI+Complex
			23.9	41.6	
			17.2	54.0	$NaI \cdot 2H_2O$+Complex
30	0.4	10.2	0.2	10.1	AgI
	0.6	19.9	0.8	19.7	
	5.3	28.6	5.1	29.0	
	15.4	33.8	14.3	34.2	
	26.1	36.9	23.4	38.1	
	37.4	38.1	32.5	40.8	
			35.9	42.3	AgI+Complex
	37.0	43.0	30.2	47.4	Complex
	34.0	45.4	29.1	48.5	

† Part 1 of this series: see Ref. 6.

Table 1. (Continued)

Temp. (°C)	Overall composition (wt%) AgI	Overall composition (wt%) NaI	Composition of liquid phase in equilibrium with solid phase (wt%) AgI	Composition of liquid phase in equilibrium with solid phase (wt%) NaI	Solid phase
	30.1	50.0	26.6	51.1	NaI·2H$_2$O+Complex
	28.1	52.0	27.5	51.0	
	23.1	53.7	23.7	52.7	NaI·2H$_2$O
	16.6	58.3	17.5	56.2	
	12.2	59.5	12.6	58.6	
	7.4	63.3	7.9	61.2	
	3.5	64.4	3.6	63.8	
			0	65.7[a)]	
40	4.4	19.2	0.8	19.9	AgI
	11.3	26.1	4.4	28.0	
	17.1	31.8	12.1	33.7	
	24.5	36.3	21.8	37.2	
	33.9	33.5	24.3	37.9	
	37.4	37.4	32.3	40.4	
	39.3	39.4	35.5	41.7	
	40.8	42.9	38.0	44.5	AgI+Complex
			38.1	44.7	
	42.5	41.6	38.2	44.4	
	41.6	42.8	37.7	44.9	
			36.7	46.4	Complex
			35.5	47.3	
			36.3	46.1	
			33.4	48.8	Complex+NaI·2H$_2$O
	3.5	67.8	4.2	65.1	NaI·2H$_2$O
	11.4	61.3	11.3	61.1	
	15.3	61.3	18.3	57.2	
			26.4	53.3	
			0	67.3[a)]	
50	4.6	18.8	0.9	19.6	AgI
	11.1	25.9	4.7	28.1	
	17.7	26.2	6.5	30.1	
	29.1	31.9	19.9	36.3	
	35.8	37.2	30.5	40.1	
	41.5	41.0	39.5	42.2	
			0	69.4[a)]	NaI·2H$_2$O
			3.2	67.9	
	5.0	67.3	4.7	66.9	
	10.3	64.9	11.0	63.4	
	14.9	62.3	15.7	60.5	
			21.2	58.0	
			34.9	50.5	NaI
	29.4	54.8	30.6	52.8	
			25.7	55.2	NaI+NaI·2H$_2$O
			37.7	49.7	AgI+NaI
70	11.4	26.4	4.8	28.6	AgI
	27.5	33.5	22.5	37.1	
	41.1	41.1	38.9	41.7	
			36.8	53.2	AgI+NaI
	4.5	76.3	5.5	71.0	NaI
	11.3	70.8	13.2	65.5	
	17.9	69.5	22.4	61.2	
			0	74.2[a)]	

a) Solubility of NaI.[8)] b) AgI·NaI·3H$_2$O.

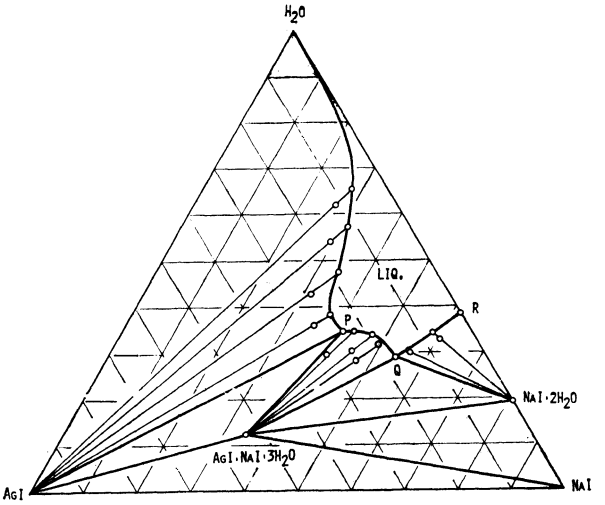

Fig. 1. Phase diagram of the AgI–NaI–H$_2$O system at 0 °C (wt%).

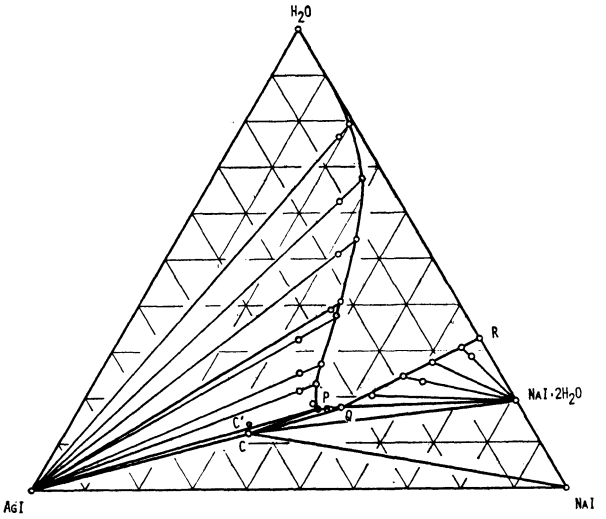

Fig. 2. Phase diagram of the AgI–NaI–H$_2$O system at 40 °C (wt%).

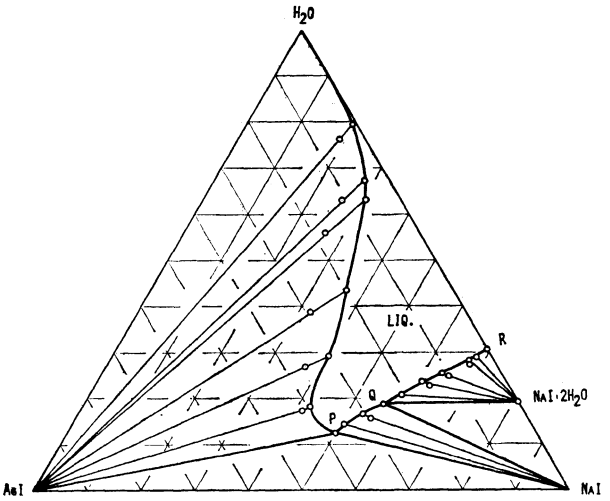

Fig. 3. Phase diagram of the AgI–NaI–H$_2$O system at 50 °C (wt%).

The weight percentages of the components were plotted on an equilateral triangle. Examples are shown in Figs. 1—3. Each corner of the triangle represents pure components. Points P and Q in these figures are invariant points, and R denotes the solubility of NaI in pure water.

A compound containing all the three components crystallizes under appropriate conditions. It should be identical with the one Krym[7] found in his study of the AgI–NaI–H_2O system at 25 °C, and to which he gave the formula $AgI \cdot NaI \cdot 3.5H_2O$. The compound was analyzed and the results are given in Table 2.

Table 2. Chemical composition (wt%)

	AgI	NaI	H_2O
	50.7	36.2	13.1
	52.3	34.9	12.8
	51.4	35.7	12.9
	52.5	34.7	12.8
Mean	51.7	35.4	12.9
Calcd as $AgI \cdot NaI \cdot 3H_2O$			
	53.5	34.2	12.3
Calcd as $AgI \cdot NaI \cdot 3.5H_2O$			
	52.4	33.5	14.1

It is evident that the mole ratio of AgI to NaI is 1:1, but the number of water of crystallization is not clear. It seems to be a $3H_2O$ rather than a $3.5H_2O$ compound.

An alternative way to presume the chemical formula is the Schreinemaker plot. In the region in which the compound coexists with solution, total composition–solution composition tie lines should converge on the point which represents the true composition of the compound. However, from the data at 0 °C as well as at other temperatures, no decisive conclusion has been drawn, since the experimental points have uncertainties due to errors in the chemical analysis. Nevertheless, a $3H_2O$ compound is considered more plausible on the following grounds. The invariant point P (filled circle) in Fig. 2 represents the average composition of the solution in equilibrium with both the solid AgI and the compound (see Table 1). The position of C′ ($3.5H_2O$ compound) is incompatible with the positions of P and AgI, making it impossible to construct the phase diagram at 40 °C. On the other hand, if the $3H_2O$ compound is assumed, no inconsistency is found in constructing the phase diagrams at 40 °C and other temperatures.

King *et al.*[9] studied the dependence of the solubility of AgI in water on the common ion concentration and indicated the existence of anionic and cationic complex ions in solution. Greenslade and Symons[10] measured the UV spectra of the solutions containing AgI and KI in various solvents. They assigned the band at 43800 cm^{-1} to AgI_2^-. The existence of this band was also confirmed by us. Thus the compound is considered to be a complex with the formula $Na[AgI_2] \cdot 3H_2O$.

The complex is a colorless, needle-like crystal. It loses the water of crystallization on exposure to dry air, deliquescing and at the same time decomposing in contact with water vapor. The crystal data of this compound are given in Table 3.

Table 3. Crystal data

Formula	$AgI \cdot NaI \cdot 3H_2O$
Molecular weight	438.7
Melting point	42—43 °C; decompose
Crystal system	Orthorhombic
a	8.78 Å
b	33.5 Å
c	6.48 Å
V	1908 Å^3
d_m	3.11 g cm^{-3}
d_c	3.05 g cm^{-3}
Z	8
Absent spectra	$0kl$ when k is odd and $h0l$ when l is odd
Possible space group	Pbcm or $Pbc2_1$

It is interesting to note that the solubility curves of AgI are s-shaped and almost independent of temperature. On the other hand, the solubility of NaI is temperature dependent and the extrapolated point to zero concentration of AgI agrees with the solubility of NaI in pure water at each temperature.[8]

According to the phase rule, no more than three phases can coexist in this system. In a region where all three phases are solid, AgI and $NaI \cdot 2H_2O$ can never coexist. Other sets of solids were observed to coexist depending on conditions. Identification of these solids was made by visual observation and the X-ray diffraction method: silver iodide was of yellow powder or thin yellow flakes; NaI white powder or brilliant flakes; $NaI \cdot 2H_2O$ large transparent plates, and the complex transparent needle-like crystals or white spherulites.

Figure 4 was constructed on the basis of the phase diagrams at each temperature. We see that the liquid phase is surrounded with four kinds of surfaces (S_1—S_4), the edges of which are shown with heavy solid lines. Surfaces S_1, S_2, S_3, and S_4 consist of the points repre-

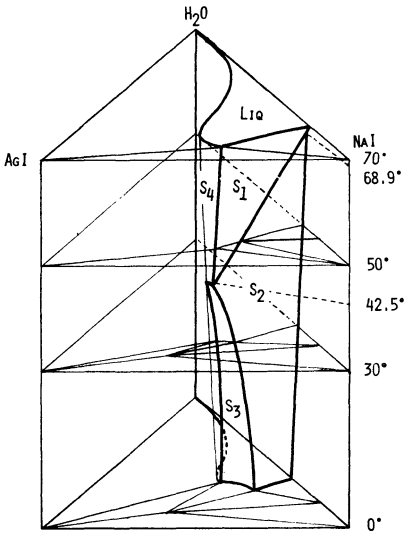

Fig. 4. Three-dimensional representation of the AgI–NaI–H_2O system (wt%).

senting the compositions of the liquid phase in equilibrium with the solids NaI, $NaI \cdot 2H_2O$, $Na[AgI_2] \cdot 3H_2O$, and AgI, respectively. The edges of the surfaces consist of the invariant points. Surfaces S_1 and S_2 are almost flat; S_3 is curved and S_4 is waved. Surface S_3 disappears above the melting point of the complex, and surface S_2 above 68.9 °C[8] (or 68.1 °C[11]), the decomposition point of $NaI \cdot 2H_2O$. It is not certain whether S_1 is in contact with S_3 or not, since it is difficult to make a study of the phase equilibria in the vicinity of the melting point of the complex. No ambiguity other than this seems to remain in Fig. 4 from the viewpoint of the phase rule.

References

1) G. Burley and H. E. Kissinger, *J. Res. Natl. Bur. Stand.*, **64A**, 403 (1960).
2) J. N. Bradley and P. D. Greene, *Trans. Faraday Soc.*, **62**, 2069 (1966).
3) C. Brink and H. A. S. Kroese, *Acta Crystallogr.*, **5**, 433 (1952).
4) W. van Dam and A. D. Donk, *Chem. Weekblad.*, **8**, 846 (1911).
5) J. E. Marsh and W. C. Rhymes, *J. Chem. Soc.*, **1913**, 781.
6) N. Nishimura, T. Higashiyama, S. Yamamoto, and S. Hasegawa, *Nippon Kagaku Kaishi*, **1973**, 1059.
7) V. Krym, *J. Russ. Phys. Chem. Soc.*, **41**, 382 (1909); *Chem. Abstr.*, **5**, 1565 (1911).
8) "International Critical Table," Vol. 4 (1928), p. 238.
9) E. King, H. J. Krall, and M. L. Pandow, *J. Amer. Chem. Soc.*, **74**, 3492 (1952).
10) D. J. Greenslade and M. C. R. Symons, *Trans. Faraday Soc.*, **62**, 307 (1966).
11) A. F. Scott and E. J. Durham, *J. Phys. Chem.*, **34**, 1424 (1930).

An ESR Study of Nitric Oxide Adsorbed on Silica Gel

Masamoto IWAIZUMI, Shozo KUBOTA, and Taro ISOBE

Chemical Research Institute of Non-Aqueous Solutions, Tohoku University, Katahira 2-1-1, Sendai 980

(Received October 1, 1973)

Nitric oxide adsorbed on silica gel was investigated by ESR. It was found that there are at least two adsorption sites for nitric oxide; one of them is on the silica gel which has been pretreated at low temperatures (below *ca.* 500 °C) (Site L), while the other is predominantly on the silica gel which has been pretreated at high temperatures (above *ca.* 500 °C) (Site H). The crystal-field splitting of the π_X^* and π_Y^* states, which are originally degenerate, was determined to be 0.26 eV for the nitric oxide adsorbed on Site L and 0.52 eV for the nitric oxide on Site H. The temperature dependence of the ESR spectrum was also examined, and the average crystal field acting on nitric oxide was found to decrease with an increase in the temperature.

Previously, the magnetic properties of nitric oxide adsorbed on silica gel surfaces have been studied by Solbakken *et al.*[1] by the measurement of the magnetic susceptibility. They reported that, at 181 and 193 K, nitric oxide is adsorbed entirely in a state with a magnetic moment the same as in the excited $^2\Pi_{3/2}$ state, while at 273 and 293 K it is adsorbed in the same average magnetic state of $^2\Pi_{1/2}$ and $^2\Pi_{3/2}$as in the gas phase. On the other hand, the ESR of nitric oxide adsorbed on solid surfaces has been observed in several adsorbent systems at the temperature of liquid nitrogen and at −180 °C.[2-10] In the ESR studies, it has been shown that, when nitric oxide is adsorbed on the solid surfaces, the orbital degeneracy of the $2p\pi^*$ level, which an odd number of electron occupy, is lifted by the surface field and the orbital angular momentum is quenched; that is, the ESR of nitric oxide in the adsorbed state can be explained by a spin-only paramagnetism and well reflects the nature of the interaction with the surfaces. A few attempts have been made to observe the ESR of nitric oxide adsorbed on the silica-gel surface.[5,7] However, no successful observation has yet been reported, although the ESR investigation of nitric oxide in the silica-gel system seemed to be interesting in connection with Solbakken's work and also for purposes of comparison with other adsorbent systems. In the course of studies of radicals trapped on solid surfaces, we could observe the ESR of nitric oxide adsorbed on silica gel. In this paper we will present the ESR observed for nitric oxide on silica gel and will discuss the interaction of nitric oxide with the surface.

Experimental

The nitric oxide was obtained commercially from the Takachiho Chem. Ind. Co., Ltd., and was dried with P_2O_5. The silica gel used was a Tokyo Chem. Ind. Co. product for chromatography, with a surface area of 422 m^2/g. The gel was heated *in vacuo* at 10^{-6} Torr overnight prior to the adsorption of nitric oxide. The heating *in vacuo* was attempted at several temperatures between 300 °C and 600 °C. After the pretreatment of the silica gel, the nitric oxide was adsorbed onto the silica gel at −60 °C and at pressures ranging from 2 to 60 Torr. When the silica gel was evacuated at low temperatures (below 450 °C), an appreciable decrease of radical concentration was observed when the sample was left standing at room temperature. All the samples for ESR measurements, therefore, were immediately immersed in the liquid nitrogen after the nitric oxide had been adsorbed and the sample tube had been sealed off from the vacuum line.

The measurements of the ESR were carried out with a Hitachi model 771 ESR spectrometer with 100 kHz field modulation. The number of nitric-oxide molecules responsible for the ESR was determined by using a freshly-crystallized $CuSO_4 \cdot 5H_2O$ crystal as the standard.

Results and Discussion

The ESR of nitric oxide observed at −196 °C are shown in Fig. 1. The hyperfine pattern observed is similar to those observed for the other adsorbent systems,[2-10] except that the linewidth is rather broader and the nitrogen hyperfine splitting is observed only as a shoulder. In Fig. 1, the sharp line with a *g*-value of 2.004 (indicated by A) is a background spectrum of silica gel which is produced by heating *in vacuo*. When the silica gel is preheated at temperatures higher than 550 °C, as Fig. 1b shows, a new additional absorption is observed on the low-field side of the nitric oxide spectrum (marked with B). This new absorption may be considered to be due to a paramagnetic center produced on the surface by the reaction with nitric oxide.

The ESR absorption due to nitric oxide changes appreciably with the preheating temperature of the silica gel. As Fig. 1 shows, when the silica gel is

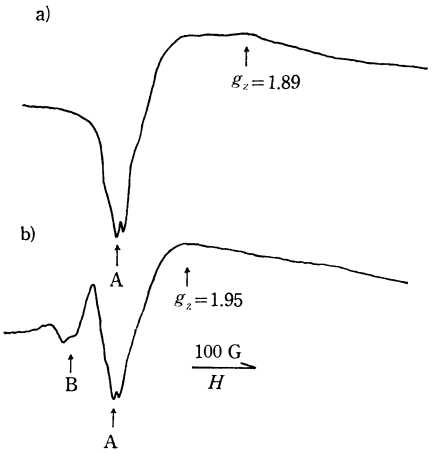

Fig. 1. ESR spectra, recorded at −196 °C, of nitric oxide on silica gel preheated at 500 °C (a), and at 600 °C (b).

pretreated at low temperatures (below *ca.* 500 °C), nitric oxide shows a spectrum with g_z value of 1.89,[11] whereas when the silica gel is pretreated at temperatures above *ca.* 500 °C, the signal intensity at the absorption maximum corresponding to the g_z value weakens appreciably and the maximum appears on the low-field side corresponding to $g_z=1.95$. These facts indicate that there are at least two different adsorption sites for nitric oxide on the silica-gel surface; one of the sites is on the silica gel which has been preheated at low temperatures (Site L), while the other is predominantly on the silica gel preheated at high temperatures (Site H). However, it is imagined that there may still be some small variety in these two adsorption sites, since the spectra show broad absorption bands.

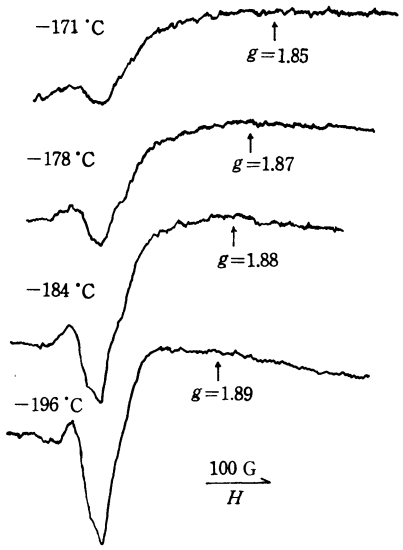

Fig. 2. Variation of ESR spectra of nitric oxide on silica gel with temperature. The silica gel was preheated at 550 °C.

When the ESR are measured at temperatures higher than −196 °C, the ESR absorption extensively broadens, losing its intensity, and above *ca.* −160 °C no ESR absorption attributable to the adsorbed nitric oxide can be detected. However, it was observed that, as the temperature increases, the absorption maximum in the g_z region gradually shifts toward the high-field side (Fig. 2). In a way similar to that reported by Kanzig *et al.* for the O_2^- molecule,[12] the following expression is derived for the g_z-value of nitric oxide:

$$g_z = g_e - 2\left(\frac{\lambda^2}{\lambda^2+\Delta^2}\right)^{1/2}. \quad (1)$$

Here, λ is the spin-orbit coupling constant and is estimated to be ~0.01 eV from the interval between the $^2\Pi_{3/2}$ and and $^2\Pi_{1/2}$ states, while Δ is the crystal-field splitting of the Π_x^* and Π_y^* states. According to the equation, the increase in the g_z value with the elevation of the temperature indicates that the effective surface field acting on the nitric oxide molecule weakens as the temperature is elevated and as the molecular motion becomes more active, implying that the orbital angular momentum, quenched by the interaction with the surface, recovers as the temperature is elevated. The marked linewidth broadening observed with the elevation of the temperature may be attributed to the large spin-orbit coupling, the magnitude of which is modulated with the fluctuation in the interaction of nitric oxide with the surface by the thermal agitation of nitric oxide.

Recetnly, Huang and Van Vleck tried to explain Solbakken's magnetic-susceptibility measurements by theoretical calculations.[13] They showed that Solbakken's observation may be explained by assuming that the average crystal field per molecule increases as the temperature is elevated. Our observation indicates, however, that the average crystal field acting on nitric oxide, rather, decreases as the temperature is elevated. It seems likely that the average magnetic moment of nitric oxide at low temperatures in the adsorbed state is much higher than that of nitric oxide in the gas phase at the same temperature, because the orbital angular momentum is quenched by the interaction with the surface and the molecule in the ground state, $^2\Pi_{1/2}$, which originally has no magnetic moment because of the cancellation of the orbital magnetic moment and the spin magnetic moment, comes to show paramagnetism due to electron spin.

Table 1. Values of Δ for nitric oxide

Solid	(eV)	Ref.
Silica gel { site L	0.26	This work
Silica gel { site H	0.52	This work
MgO	0.30	2
ZnS	0.33	3
ZnO	0.50	3
Silica–alumina	0.60	5
Silica–magnesia	0.33, 0.60	5
γ-Alumina	0.75	5

The crystal-field splitting of the Π_x^* and Π_y^* states, Δ, was evaluated as 0.26 eV for nitric oxide on Site L and 0.52 eV for nitric oxide on Site H by means of Eq. (1). These Δ values are compared with those obtained in the other systems in Table 1. It should be noticed here that the value relates to the field gradient in the X or Y direction of the nitric oxide molecule;[9] therefore, it relates also to the adsorbed structure of nitric oxide. It is not necessarily proportional to the field strength primarily existing on the surface if there is any difference in the adsorbed structure in the solid systems.

The maximum concentration of nitric oxide responsible for the ESR absorption was obtained for the sample pretreated at temperatures higher than 500 °C as 0.9×10^{18} spin/g, which corresponds to 2×10^{11} spin/cm^2, with an error of ±30%, while for the sample pretreated at *ca.* 300 °C the spin concentration was much less (1/3~1/4), suggesting that the sites for adsorption were produced by the loss of a hydroxyl group, such as a siloxane group. The presence of the two adsorption sites, Site L and Site H, may be due to a difference in the surroundings of the two sites; Site L may be the siloxane group, with silanol groups

surrounding it, while Site H may be the siloxane group, with no silanol groups surrounding it. The increase in the pressure of nitric oxide over 30 Torr at the adsorption process in the sample preparation did not seem to result in any appreciable increase in the radical concentration. This may be mainly due to the formation of the diamagnetic dimer of nitric oxide, N_2O_2, on the surface.

The authors wish to express their thanks to Dr. Hiroshi Utsuki for his help in the measurement of the surface area of silica gel and also for his valuable discussions.

This work was supported by a grant from the Japanese Ministry of Education. This financial support is gratefully acknowledged.

References

1) A. Solbakken and L. H. Reyerson, *J. Phys. Chem.*, **63**, 1622 (1959).
2) J. H. Lunsford, *J. Chem. Phys.*, **46**, 4347 (1967).
3) J. H. Lunsford, *J. Phys. Chem.*, **72**, 2141 (1968).
4) J. H. Lunsford, *ibid.*, **72**, 4163 (1968).
5) J. H. Lunsford, *J. Catal.*, **14**, 379 (1969).
6) B. M. Hoffman and N. J. Nelson, *J. Chem. Phys.*, **50**, 2598 (1969).
7) M. Shelef, *J. Catal.*, **15**, 289 (1969).
8) J. H. Lunsford, *J. Phys. Chem.*, **74**, 1518 (1970).
9) C. L. Gardner and M. A. Weinberger, *Can. J. Chem.*, **48**, 1317 (1970).
10) P. H. Kasai and R. J. Bishop, Jr., *J. Amer. Chem. Soc.*, **94**, 5560 (1972).
11) z Axis coincides with N–O bond axis.
12) W. Kanzig and M. H. Cohen, *Phys. Rev. Lett.*, **3**, 509 (1959).
13) N. L. Huang and J. H. Van Vleck, *J. Chem. Phys.*, **50**, 2932 (1969).

A New Method for Determination of Self-diffusion Coefficients in Solid Solutions

Seiichi KURIHARA, Kazuo FUEKI, and Takashi MUKAIBO

Department of Industrial Chemistry, Faculty of Engineering, The University of Tokyo, Hongo, Bunkyo-ku, Tokyo 113

(Received October 8, 1973)

A new method for obtaining the self-diffusion coefficients of A in the AY–BY solid solution has been proposed. In this method, the tracer diffusion of A* and the interdiffusion between AY and BY are carried out simultaneously, and the self-diffusion coefficients are determined as a function of composition over the whole range of composition in a similar way as the Boltzmann-Matano analysis. Since this method employs a diffusion couple consisting of single crystals of AY and BY, one can avoid troubles and errors due to segregation and/or phase separation which are often encountered in experiments using solid solutions as specimens. In order to confirm the validity of the proposed method, D_{Cl}* in the TlCl–TlBr system and D_{Ag}* and D_{Na}* in the AgBr–NaBr system have been determined at 400 °C by this method and compared with the results obtained by the conventional method. A good agreement has been found between them.

Self-diffusion coefficients in solid solutions are usually determined as a function of composition by using single crystals of various compositions. However, segregation occurs during solidification of melts and segregated crystals cannot be easily homogenized by annealing. Sometimes, phase separation occurs with lowering temperature and the single crystal changes into a polycrystal. In such a case, it is difficult to obtain self-diffusion coefficients by the conventional method.

The purpose of this paper is to propose a new method for obtaining self-diffusion coefficients in solid solutions as a function of composition. In this method, the tracer diffusion of an element and the interdiffusion between the component salts are carried out simultaneously, and the concentration profiles are analysed in a similar way as the Boltzmann[1]-Matano[2] method which is usually used to obtain interdiffusion coefficients. Employment of this new method can avoid experimental difficulties due to the segregation and/or the phase separation.

Theoretical

1. Flux and Mass Balance Equations. Let us assume that ionic crystals AY and BY form a solid solution. If pure AY and BY containing a small amount of A*, a radioactive isotope of A, are in contact with each other and allowed to diffuse mutually, the concentration curve for A including both radioactive and stable isotopes and that for A* would be as shown in Fig. 1. Denoting the fluxes of A and A*, relative to one end of the specimen, by J'° and J'^{*} and those relative to the local lattice by J° and J^{*}, respectively, we obtain

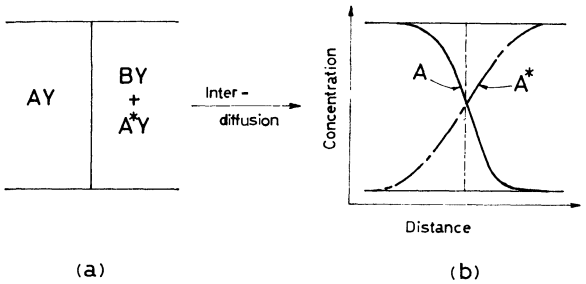

Fig. 1. Schematic diagram for interdiffusion in AY–(B,A*)Y system.

$$J'^{\circ} = J^{\circ} + c^{\circ}v \tag{1}$$

$$J'^{*} = J^{*} + c^{*}v, \tag{2}$$

where v is the velocity of the local lattice relative to one end of the specimen and c is the molar concentration. Symbols ° and * express the quantities with respect to A and A*, respectively. Neglecting cross terms, we have the following phenomenological equations,

$$J^{\circ} = -\frac{D^{*}c^{\circ}}{RT}\frac{\partial\tilde{\mu}^{\circ}}{\partial x} \tag{3}$$

$$J^{*} = -\frac{D^{*}c^{*}}{RT}\frac{\partial\tilde{\mu}^{*}}{\partial x}, \tag{4}$$

where x is the distance, D^* is the self-diffusion coefficient of A and $\tilde{\mu}$ is the electrochemical potential. $\tilde{\mu}^{\circ}$ and $\tilde{\mu}^{*}$ are written as follows:

$$\tilde{\mu}^{\circ} = \mu^{\circ} + ZF\phi \tag{5}$$

$$\tilde{\mu}^{*} = \mu^{*} + ZF\phi, \tag{6}$$

where μ, ZF and ϕ are the chemical potential, electric charge per mole and electric potential, respectively. μ° is the chemical potential of A in the system of (A, B)Y and μ^{*} is that of A* in the system of (radioactive A, stable A, B)Y which has the same concentration of B as the former system.

Because A* atoms have the same chemical properties as stable A atoms, A* atoms are expected to be distributed in stable A atoms with complete randomness and to interact with others in a quite same manner as stable A atoms. Therefore, μ^{*} is expressed as

$$\mu^{*} = \mu^{\circ} - T\bar{S}_c, \tag{7}$$

where $\bar{S}_c$ is the partial molal configurational entropy of A* in both radioactive and stable A atoms. $\bar{S}_c$ is written as

$$\bar{S}_c = R\ln(c^{\circ}/c^{*}). \tag{8}$$

Combination of Eqs. (7) and (8) gives

$$\mu^{*} = \mu^{\circ} + RT\ln(c^{*}/c^{\circ}). \tag{9}$$

Combination of Eqs. (5), (6), and (9) yields

$$\tilde{\mu}^* = \tilde{\mu}^\circ + RT\ln(c^*/c^\circ). \quad (10)$$

Substituting Eq. (10) into Eq. (4) and comparing Eq. (4) with Eq. (3), we obtain

$$J^* = \frac{c^*}{c^\circ}J^\circ + D^*\left(\frac{c^*}{c^\circ}\frac{\partial c^\circ}{\partial x} - \frac{\partial c^*}{\partial x}\right). \quad (11)$$

Substitution of Eq. (11) into Eq. (2) and comparison of Eq. (2) with Eq. (1) results in

$$J'^* = \frac{c^*}{c^\circ}J'^\circ + D^*\left(\frac{c^*}{c^\circ}\frac{\partial c^\circ}{\partial x} - \frac{\partial c^*}{\partial x}\right). \quad (12)$$

Assuming that the molal volume of the AY–BY solid solution is independent of the composition, we obtain

$$J'^\circ = -\tilde{D}\frac{\partial c^\circ}{\partial x} \quad (13)$$

where $\tilde{D}$ is the interdiffusion coefficient of the AY–BY system. Equation (13) gives the mass balance equation,

$$\frac{\partial c^\circ}{\partial t} = \frac{\partial}{\partial x}\left(\tilde{D}\frac{\partial c^\circ}{\partial x}\right). \quad (14)$$

Substituting Eq. (13) into Eq. (12) we obtain the flux equation of A* as follows:

$$J'^* = -\frac{c^*}{c^\circ}\tilde{D}\frac{\partial c^\circ}{\partial x} + D^*\left(\frac{c^*}{c^\circ}\frac{\partial c^\circ}{\partial x} - \frac{\partial c^*}{\partial x}\right). \quad (15)$$

The mass balance equation of A* is

$$\frac{\partial c^*}{\partial t} = \frac{\partial}{\partial x}\left\{\frac{c^*}{c^\circ}\tilde{D}\frac{\partial c^\circ}{\partial x} - D^*\left(\frac{c^*}{c^\circ}\frac{\partial c^\circ}{\partial x} - \frac{\partial c^*}{\partial x}\right)\right\}. \quad (16)$$

Equations (14) and (16) give the concentration curves in such a system where the interdiffusion and the tracer diffusion proceed simultaneously.

2. Equation for Determination of D.* The concentration of A obtained experimentally is not c° but the mole fraction N. Also, the normalized A* concentration n^* which is defined as the ratio of $c^*(x,t)$ to the initial value of c^* in BY, is obtained experimentally as the concentration of A*. Therefore, equations for N and n^* are required for the purpose of application, instead of Eqs. (14) and (16). Since Eqs. (14) and (16) are linear with respect to c° and c^* and the molar volume of the solid solution is assumed to be independent of composition, they are rewritten in the following forms:

$$\frac{\partial N}{\partial t} = \frac{\partial}{\partial x}\left(\tilde{D}\frac{\partial N}{\partial x}\right) \quad (17)$$

$$\frac{\partial n^*}{\partial t} = \frac{\partial}{\partial x}\left\{\frac{n^*}{N}\tilde{D}\frac{\partial N}{\partial x} - D^*\left(\frac{n^*}{N}\frac{\partial N}{\partial x} - \frac{\partial n^*}{\partial x}\right)\right\}. \quad (18)$$

If the initial conditions for Eq. (17) are described in terms of the Boltzmann variable $\eta \equiv x/(2\sqrt{t})$, N is a function of η only and Eq. (17) can be transformed into an ordinary differential equation,

$$-2\eta\frac{dN}{d\eta} = \frac{d}{d\eta}\left(\tilde{D}\frac{dN}{d\eta}\right). \quad (19)$$

Similarly, if the initial conditions for n^* in addition to those of N are described as a function of η, Eq. (18) is rewritten as

$$-2\eta\frac{dn^*}{d\eta} = \frac{d}{d\eta}\left\{\frac{n^*}{N}\tilde{D}\frac{dN}{d\eta} - D^*\left(\frac{n^*}{N}\frac{dN}{d\eta} - \frac{dn^*}{d\eta}\right)\right\}. \quad (20)$$

Assuming that the mole fraction of A*Y is very small, we can describe the initial conditions in Fig. 1 as follows:

$$N = 0, \quad n^* = 1 \quad \text{for } \eta = +\infty$$
$$N = 1, \quad n^* = 0 \quad \text{for } \eta = -\infty.$$

Integrating Eqs. (19) and (20) with respect to η and rearranging them, we obtain the following expressions for D^*,

$$-D^*(N_m) = \frac{2N_m\int_0^{n_m^*}\eta dn^* - 2n_m^*\int_0^{N_m}\eta dN}{N_m\left(\frac{dn^*}{d\eta}\right)_{\eta=\eta_m} - n_m^*\left(\frac{dN}{d\eta}\right)_{\eta=\eta_m}}$$
$$= \frac{N_m\int_0^{n_m^*}x dn^* - n_m^*\int_0^{N_m}x dN}{2t\left\{N_m\left(\frac{\partial n^*}{\partial x}\right)_{x=x_m} - n_m^*\left(\frac{\partial N}{\partial x}\right)_{x=x_m}\right\}}, \quad (21)$$

where N_m and n_m^* are N and n^* at $\eta_m\{=x_m/(2\sqrt{t})\}$, respectively and $D^*(N_m)$ is the self-diffusion coefficient of A in a homogeneous solid solution of composition N_m. The so-called Matano interface is taken as the origin of η or x. If the concentration profiles of both interdiffusion and tracer diffusion are obtained experimentally, we can determine the self-diffusion coefficients of A and B in the AY–BY solid solution by means of Eq. (21).

Experimental

In order to confirm the results of the aforementioned theory experimentally, the self-diffusion coefficients of Cl in the TlCl–TlBr system and those of Ag and Na in the AgBr–NaBr system were determined by the new method and compared with the results obtained by the conventional method.

1. TlCl–TlBr System. Single crystals of TlCl and TlBr were prepared in a similar way as reported previously.[3] Disks, 2 mm in thickness and 10 mm in diameter, were cut from these crystals. A few drops of aqueous TlCl*(^{36}Cl) solution were applied to both ends of the disk. After the drying, the disk was sealed in an evacuated Pyrex-glass ampoule and annealed at about 400 °C for several days to distribute Cl* uniformly in the disk. Then, the disk was finished to obtain flat end surfaces. The doped disk was coupled with an undoped one as follows:

Couple A: TlCl(Cl*)/TlBr

Couple B: TlCl/TlBr(Cl*)

where TlCl(Cl*) and TlBr(Cl*) are ^{36}Cl-doped disks, and TlCl and TlBr are undoped disks. Couple A was used for obtaining the interdiffusion profile, because the concentration of Cl* is proportional to the concentration of Cl. Couple B was employed for determining the profile of tracer diffusion accompanied by interdiffusion. The couple was sealed in a Pyrex-glass ampoule evacuated to 10^{-3} Torr and annealed at 400 °C. Then, the couple was taken out and sectioned serially from one end. The procedures of diffusion annealing and sectioning are described elsewhere.[3,4] The weight and radioactivity of each sectioned layer were measured. Mole fraction of TlCl of each layer was determined from the radioactivity. Density of the layer was calculated from the mole fraction and lattice constant of this system.[5] The thickness of each layer was determined from the weight, the cross sectional area and the density. As the interface between

the disks acts as a natural marker during the interdiffusion, it was taken as the standard plane for determining the distance. In this way, the mole fraction of TlCl was determined as a function of distance from the interface.

The relation between radioactivity and weight per cross sectional area was also obtained for couple B. As the annealing time required for couple A was different from that for couple B, the weight per cross sectional area for couple A was multiplied by the square root of the ratio of the annealing time for couple B to that for couple A, to obtain the corresponding profiles of self-diffusion and interdiffusion. The mole fraction of TlCl in couple B was determined from the corresponding profiles with the same origin of distance, and the normalized concentration of Cl* was calculated as a function of distance from the interface.

2. AgBr–NaBr System. According to the results by previous investigators, the self-diffusion coefficients of this system depend on the purity of crystals in a composition range rich in NaBr.[6] Therefore, in the present study the experiment was carried out in a composition range from $N_{AgBr}=0.4$ to 1.0. Commercially obtained AgBr of G. R. grade was further purified in an evacuated and sealed Pyrex-glass tube by the zone refining technique. The refining operation was repeated 30 times so that the concentration of impurity might decrease to the order of 10 ppm. NaBr of Merck's Suprapur grade (99.9995% pure) was used.

Single crystals were prepared by the Bridgeman method, and cut into disks, 2 mm in thickness. Radioisotope ^{110m}Ag or ^{22}Na was applied to the disks of $Ag_{0.4}Na_{0.6}Br$, which were then annealed at about 410 °C for 20 days in an evacuated ampoule in order to homogenize the composition and distribute the radioisotopes uniformly in them. Concentration profiles were obtained by using the following couples,

Couple C: $AgBr/Ag_{0.4}Na_{0.6}Br(Na^*)$

Couple D: $AgBr/Ag_{0.4}Na_{0.6}Br(Ag^*)$

Couple E: $AgBr(Na^*)/Ag_{0.4}Na_{0.6}Br$.

Couples C, D and E were used for obtaining the concentration profiles of interdiffusion, tracer diffusion of Ag* and tracer diffusion of Na*, respectively. Annealing was carried out at 400 °C, and the determination of concentration profile was performed in a similar way as the TlCl–TlBr system.

Results and Discussion

1. TlCl–TlBr System. The profile of the interdiffusion obtained by using couple A, is given in Fig. 2 as a plot of N_{TlCl} *vs.* distance. The diffusion profile of tracer Cl* is shown in Fig. 3, as a plot of n_{Cl}^* *vs.* distance. In both figures, the interface between the crystals was taken as the origin of the distance and are shown by symbol B. Figure 4 shows the profiles of self-diffusion and interdiffusion, expressed as a plot of concentration *vs.* η. Plane A in the figure indicates the Matano interface and it was taken as the origin of the distance.

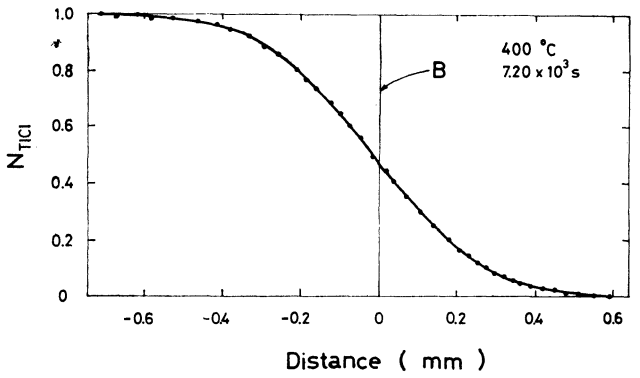

Fig. 2. Interdiffusion profile for TlCl–TlBr system.

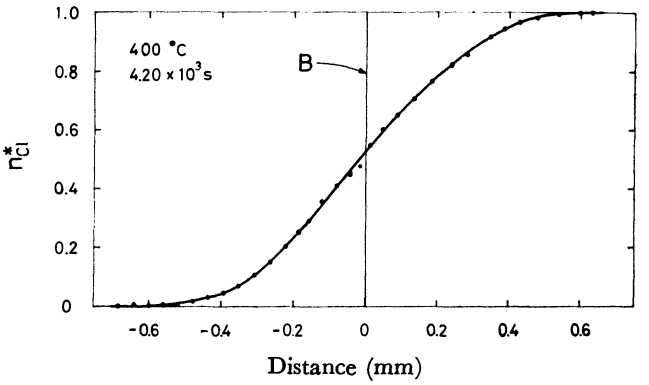

Fig. 3. Tracer diffusion profile of Cl* in TlCl/TlBr interdiffusion couple.

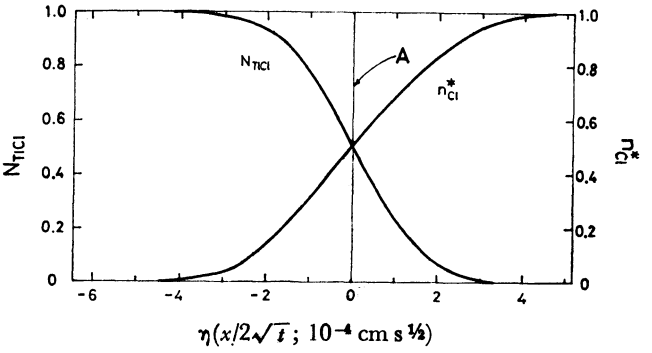

Fig. 4. Concentration profiles of TlCl and Cl* at 400 °C.

The self-diffusion coefficients of Cl, D_{Cl}^*, at 400 °C were calculated from the curves given in Fig. 4 by using Eq. (21). The results are shown by solid circles in Fig. 5. For comparison, the values of D_{Cl}^* obtained by the conventional method[4] are shown by open circles in the same figure. Agreement between them is fairly good. The maximum difference is only 15% of D_{Cl}^*.

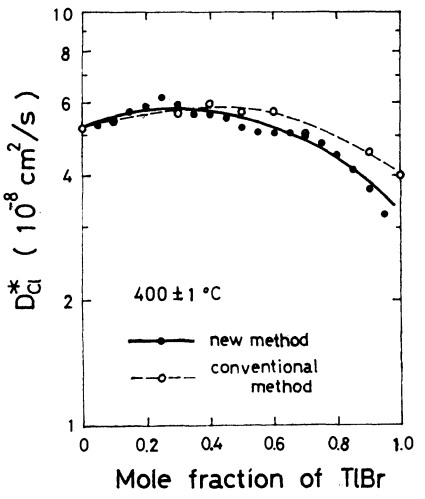

Fig. 5. D_{Cl}^* in TlCl-TlBr system.

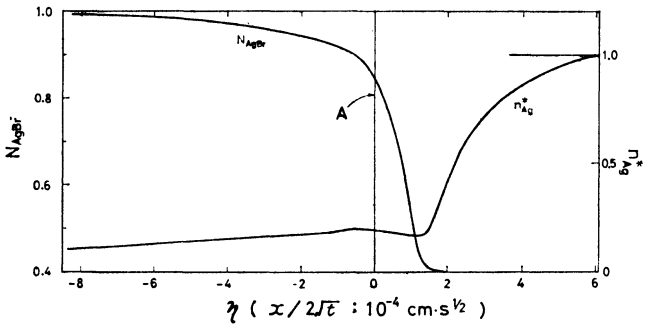

Fig. 6. Concentration profiles of AgBr and Ag* at 400 °C.

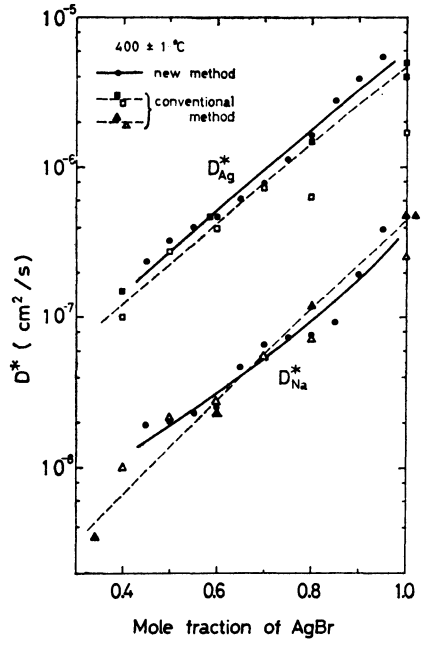

Fig. 7. D_{Ag}* and D_{Na}* in AgBr–NaBr system.
□, △: Tsuji *et al.*[6] ■, ▲: the authors
⊠: Friauf[7] ⊠, ◬: Wynnyckyj *et al.*[8]

2. AgBr–NaBr System. Figure 6 shows N_{AgBr} and n_{Ag}* as functions of η. These profiles were obtained from couples C and D, by assuming that Vegard's law holds for molar volume of the solid solution. D_{Ag}* at 400 °C were calculated from the curves shown in Fig. 6 by using Eq. (21). The results are shown by solid circles in the upper part of Fig. 7. D_{Na}* at 400 °C was calculated from the results for couples C and E. They are given by solid circles in the lower part of Fig. 7. The values of D_{Ag}* and D_{Na}* obtained by the conventional method are also shown in Fig. 7. Self-diffusion coefficients obtained by the new method well agree with those by the conventional method.

It is concluded that self-diffusion coefficients in solid solutions can be obtained by the method proposed in this paper.

Summary

(1) A new method has been proposed to obtain self-diffusion coefficients of A in AY–BY solid solution as a function of composition.

(2) D_{Cl}* in TlCl–TlBr system and D_{Ag}* and D_{Na}* in AgBr–NaBr system at 400 °C have been obtained by the new method and compared with the values obtained by the conventional method. A good agreement was found between them.

References

1) L. Boltzmann, *Ann. Phys.*, **53**, 960 (1893).
2) C. Matano, *Jap. J. Phys.*, **8**, 109 (1933).
3) S. Kurihara, K. Fueki, and T. Mukaibo, *Chem. Lett.*, **1972**, 831.
4) S. Kurihara, K. Fueki, and T. Mukaibo, *J. Solid State Chem.*, **8**, 229 (1973).
5) M. A. Popova, T. I. Darvoid, and M. A. Gurevicz, *Z. Neorg. Chim.*, **11**, 1236 (1966).
6) T. Tsuji, K. Fueki, T. Mukaibo, T. Ohta, and T. Watanabe, *J. Solid State Chem.*, **2**, 563 (1970).
7) R. J. Friauf, *Phys. Rev.*, **105**, 843 (1957).
8) J. R. Wynnyckyj, H. Schmalzried, and H.-G. Sockel, *Z. Phys. Chem. N. F.*, **68**, 30 (1969).

The Triplet States of 1,3,5-Tricyanobenzene Complexes with Methyl Substituted Benzenes

Satoru MATSUMOTO,* Saburo NAGAKURA,*,** Yasuyuki SHIMOZATO,**
Hisaharu HAYASHI, and Junko NAKAMURA**

*The Institute for Solid State Physics, The University of Tokyo, Roppongi, Minato, Tokyo 106
**The Institute of Physical and Chemical Research, Wako, Saitama 351

(Received October 15, 1973)

Triplet-triplet absorption, phosphorescence, and ESR spectra have been measured on the 1,3,5-tricyanobenzene complexes with toluene, mesitylene, durene, and hexamethylbenzene. Four triplet-triplet absorption bands were commonly observed in the wave number region of 10000—30000 cm^{-1} for all the complexes. The observed phosphorescence and T-T absorption spectra could be understood systematically by considering the interaction among zero-order charge-transfer triplet states and zero-order locally (within the acceptor) excited triplet states. From an analysis of the zero-field splitting values obtained from the observed ESR spectra, the contribution of the zero-order charge-transfer triplet state to the lowest triplet state was determined to be 76, 65, 25, and 9% for the 1,3,5-tricyanobenzene complexes with hexamethylbenzene, durene, mesitylene, and toluene, respectively. From the consideration on the results obtained for various polycyanobenzene complexes, the phosphorescence lifetime was found to decrease remarkably for the complexes with the charge-transfer character higher than 50% in their lowest triplet states.

The triplet states of electron donor-acceptor (EDA) complexes have been studied in detail through measurements of the phosphorescence and ESR spectra.[1-7] In particular, concerning the TCNB complexes with benzene and methyl substituted benzenes, the nature of their lowest triplet states was investigated quantitatively and the appearance of the charge-transfer (CT) phosphorescence characteristic of the electron donor-acceptor interaction was confirmed.[4,5]

Triplet-triplet (T-T) absorption spectra have been measured with some EDA complexes.[8-12] The analysis of the results on the TCNB complexes with methyl substituted benzenes supports the conclusions obtained from the phosphorescence and ESR spectra.[10,12]

In the present paper, for the purpose of studying the effects of the electron accepting ability and molecular symmetry of the acceptor upon the triplet states of EDA complexes, we have undertaken a study of the phosphorescence, ESR, and T-T absorption spectra of the 1,3,5-tricyanobenzene complexes with toluene, mesitylene, durene, and hexamethylbenzene.

Experimental

1,3,5-Tricyanobenzene (TRCNB) used as electron acceptor was prepared and purified by the method described in literature.[13,14]

Hexamethylbenzene (HMB), durene, mesitylene, and toluene were used as electron donors. HMB and durene were recrystallized from ethanol. Mesitylene was shaken with concentrated sulfuric acid, washed with water, dried over calcium chloride, and finally distilled. Toluene (Dotite spectrosol grade) was used without further purification.

T-T absorption spectra were measured at 77 K for the TRCNB–toluene complex in a toluene–ethyl ether (1:1) mixed solvent and for the other TRCNB complexes in an ethyl ether–isopentane (1:1) mixed solvent (EP). The samples were excited by a 500 W super-high pressure mercury lamp combined with a Toshiba UV-D 25 filter. The details of the measurement were described in a previous paper.[12]

The electronic absorption spectra as shown in Fig. 2 were measured with a Cary recording spectrophotometer model 14M. Phosphorescence spectra were measured with a phosphoroscope and a grating monochromator (Spex 1700-111) attached with an EMI 9558 QB photomultiplier, and excitation of the samples was effected with a 100 W high pressure mercury lamp.

ESR spectra of the phosphorescent states were measured in rigid solutions at 77 K with a JEOL ME 3X spectrometer (9225.9 MHz, 100 kHz magnetic field modulation), the samples being excited with a 500 W super-high pressure mercury lamp. The microwave magnetic field was perpendicular to the external field.

Theoretical

In order to assign the observed T-T absorption spectra and clarify the nature of the triplet states of the complexes, theoretical studies were made by considering the interaction among the zero-order CT triplet states and the zero-order locally (within TRCNB) excited (LE) triplet states. The details of the method were described in the previous paper.[12] In actuality, we took six zero-order CT triplet states and three zero-order LE triplet states shown in Table 1.

The molecular orbitals of TRCNB were calculated by the Pariser-Parr-Pople SCF MO method,[15,16] the same parameters as those used for TCNB[17] being adopted. The results are shown in Table 2. The zero-order CT triplet states in Table 1, ${}^3\Phi_{CT_1}({}^3\Phi_{CT_2})$, ${}^3\Phi_{CT_3}({}^3\Phi_{CT_4})$, and ${}^3\Phi_{CT_5}({}^3\Phi_{CT_6})$, correspond to the electron transfer from the highest occupied orbital of the donor, $\theta_2(\theta_3)$, to the lowest three vacant orbitals of TRCNB, ϕ_7, ϕ_8, and ϕ_9, respectively. The zero-order LE triplet states, ${}^3\Phi_{LE_1}$, ${}^3\Phi_{LE_2}$, and ${}^3\Phi_{LE_3}$ are represented as follows:

$$
\begin{aligned}
{}^3\Phi_{LE_1} = {} & -0.64638\,{}^3\Psi_{6\to7} + 0.64719\,{}^3\Psi_{5\to8} + 0.00040\,{}^3\Psi_{5\to9} \\
& - 0.00081\,{}^3\Psi_{4\to8} + \cdots \\
{}^3\Phi_{LE_2} = {} & 0.52383\,{}^3\Psi_{6\to7} + 0.52037\,{}^3\Psi_{5\to8} + 0.33223\,{}^3\Psi_{5\to9} \\
& - 0.31785\,{}^3\Psi_{4\to8} + \cdots \\
{}^3\Phi_{LE_3} = {} & -0.02656\,{}^3\Psi_{6\to7} - 0.02695\,{}^3\Psi_{5\to8} - 0.44357\,{}^3\Psi_{5\to9} \\
& + 0.31901\,{}^3\Psi_{4\to8} + \cdots
\end{aligned}
$$

Table 1. Configurations and their estimated energies used in the calculation for the TRCNB–HMB complex

Configuration	$^3\Phi_{CT_1}$	$^3\Phi_{CT_2}$	$^3\Phi_{CT_3}$	$^3\Phi_{CT_4}$	$^3\Phi_{CT_5}$	$^3\Phi_{CT_6}$	$^3\Phi_{LE_1}$	$^3\Phi_{LE_2}$	$^3\Phi_{LE_3}$
Energy (eV)	3.0	3.0	3.0	3.0	5.25	5.25	3.20	3.92	5.11

Table 2. Orbital energies and their wave functions of TRCNB

	Orbital energy (eV)	Wave function[a]
ϕ_1	−14.430	$0.3704\chi_1+0.3262\chi_2+0.3715\chi_3+0.3267\chi_4+0.3715\chi_5+0.3262\chi_6+0.2377\chi_7$ $+0.2340\chi_8+0.2340\chi_9+0.1774\chi_{N_1}+0.1793\chi_{N_2}+0.1793\chi_{N_3}$
ϕ_2	−13.148	$-0.0009\chi_1+0.1600\chi_2+0.2811\chi_3+0.0005\chi_4-0.2802\chi_5-0.1605\chi_6-0.0014\chi_7$ $+0.4522\chi_8-0.4508\chi_9-0.0014\chi_{N_1}+0.4358\chi_{N2}-0.4372\chi_{N3}$
ϕ_3	−13.142	$0.3255\chi_1+0.0945\chi_2-0.1600\chi_3-0.1839\chi_4-0.1616\chi_5+0.0937\chi_6+0.5210\chi_7$ $-0.2593\chi_8-0.2620\chi_9+0.5050\chi_{N_1}-0.2521\chi_{N_2}-0.2544\chi_{N_3}$
ϕ_4	−11.857	$0.1708\chi_1+0.2399\chi_2+0.1721\chi_3+0.2409\chi_4+0.1721\chi_5+0.2399\chi_6-0.2991\chi_7$ $-0.2973\chi_8-0.2973\chi_9-0.3979\chi_{N1}-0.3963\chi_{N_2}-0.3963\chi_{N_3}$
ϕ_5	−10.208	$-0.4827\chi_1-0.2622\chi_2+0.2464\chi_3+0.5356\chi_4+0.2362\chi_5-0.2735\chi_6+0.1483\chi_7$ $-0.0754\chi_8-0.0723\chi_9+0.3534\chi_{N_1}-0.1803\chi_{N_2}-0.1729\chi_{N_3}$
ϕ_6	−10.208	$-0.0059\chi_1-0.4672\chi_2-0.4151\chi_3+0.0065\chi_4+0.4210\chi_5+0.4607\chi_6+0.0018\chi_7$ $+0.1271\chi_8-0.1289\chi_9+0.0043\chi_{N_1}+0.3037\chi_{N_2}-0.3080\chi_{N_3}$
ϕ_7	−1.669	$0.1570\chi_1-0.5328\chi_2+0.2605\chi_3+0.2003\chi_4-0.4174\chi_5+0.3324\chi_6+0.1016\chi_7$ $+0.1680\chi_8-0.2693\chi_9-0.1319\chi_{N_1}-0.2185\chi_{N_2}+0.3502\chi_{N_3}$
ϕ_8	−1.669	$-0.3912\chi_1+0.0761\chi_2+0.3315\chi_3-0.4992\chi_4+0.0596\chi_5+0.4233\chi_6-0.2532\chi_7$ $+0.2139\chi_8+0.0384\chi_9+0.3288\chi_{N_1}-0.2782\chi_{N_2}-0.0500\chi_{N_3}$
ϕ_9	−0.339	$-0.1354\chi_1+0.2922\chi_2-0.1370\chi_3+0.2306\chi_4-0.1370\chi_5+0.2292\chi_6-0.3683\chi_7$ $-0.3672\chi_8-0.3672\chi_9+0.3566\chi_{N_1}+0.3558\chi_{N_2}+0.3558\chi_{N_3}$
ϕ_{10}	1.209	$-0.3895\chi_1+0.1198\chi_2+0.1926\chi_3-0.2354\chi_4+0.1939\chi_5+0.1191\chi_6+0.5463\chi_7$ $-0.2728\chi_8-0.2746\chi_9-0.4007\chi_{N_1}+0.2004\chi_{N_2}+0.2018\chi_{N_3}$
ϕ_{11}	1.216	$-0.0007\chi_1-0.2043\chi_2+0.3366\chi_3-0.0004\chi_4-0.3359\chi_5+0.2047\chi_6+0.0010\chi_7$ $-0.4740\chi_8+0.4731\chi_9-0.0008\chi_{N_1}+0.3480\chi_{N_2}-0.3473\chi_{N_3}$
ϕ_{12}	2.807	$-0.3834\chi_1+0.3410\chi_2-0.3844\chi_3+0.3415\chi_4-0.3844\chi_5+0.3410\chi_6+0.2274\chi_7$ $+0.2291\chi_8+0.2911\chi_9-0.1304\chi_{N_1}-0.1316\chi_{N_2}-0.1316\chi_{N_3}$

a) χ_n is the AO of the n-th carbon atom. The numbering of the atoms is shown in the figure next to Table 2.

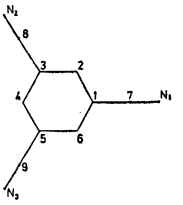

where $^3\Psi_{j\to k}=|\theta_1\theta_1\cdots\phi_1\phi_1\cdots\phi_j\phi_k|$, ϕ_j and ϕ_k being the j-th (occupied) and k-th (vacant) SCF MO's of TRCNB, respectively.

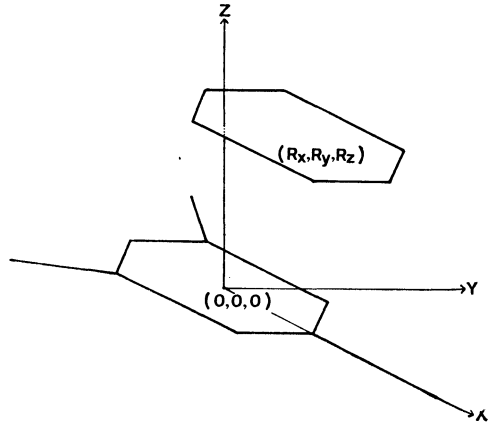

Fig. 1. Models assumed for the TRCNB–benzene complex.

Model	R_x (Å)	R_y (Å)	R_z (Å)
1	0.0	0.0	3.4
2	0.695	0.0	3.4
3	1.274	0.602	3.4
4	1.39	0.0	3.4
5*	0.0	0.0	3.4

* One of the benzene rings is rotated about the z axis by 30° from the other.

The geometrical structure of this complex is not yet known. Therefore, the actual calculation was made with five tentative geometrical models shown in Fig. 1. The separation between the two benzene rings was fixed to 3.4 Å. The off-diagonal elements of the total electronic Hamiltonian representing the interactions between the zero-order CT triplet states and the zero-order LE triplet states were taken to be $\beta=-kS_{ij}$, where the parameter k was assumed to be 10[17] and the overlap integral $S_{ij}=\int\theta_i(1)\phi_j(1)d\tau$ was calculated by the use of the SCF MO's. The energies of the zero-order triplet states were determined by the procedures described in the previous paper.[12] The result on the TRCNB–HMB complex is shown in Table 1.

Results and Discussion

Electronic Absorption Spectra. The donors used in the present study show absorption bands in the wavelength region shorter than 280 nm.[18] The acceptor, TRCNB, exhibits the longest wavelength band at 300 nm. Methanol solutions containing TRCNB as an electron acceptor and HMB or durene as an electron donor exhibit a weak CT band in the 300—360 nm region. TRCNB in mesitylene also shows a CT band at 290 nm. The CT band of the TRCNB–HMB complex, as an example, is shown in Fig. 2. No CT band could be observed with TRCNB in toluene.

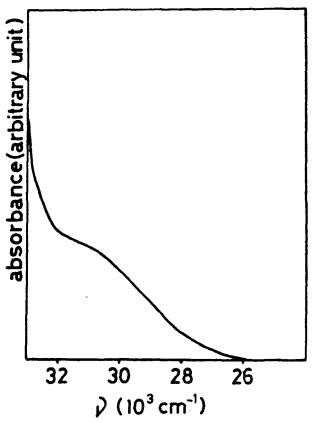

Fig. 2. The electronic absorption spectrum of the methanol solution of the TRCNB–HMB complex.

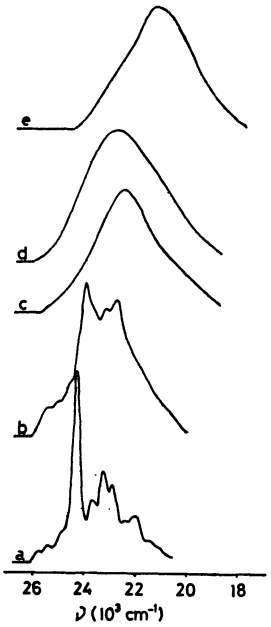

Fig. 3. Phosphorescence spectra of TRCNB and its Complexes in EP at 77 K. (a) TRCNB (b) TRCNB–toluene (c) TRCNB–mesitylene (d) TRCNB–durene (e) TRCNB–HMB.

It is expected to appear around 270 nm and may be covered with the strong absorptions of the component molecules.

The Phosphorescence Spectra. The phosphorescence spectra of the TRCNB complexes were measured by use of a Toshiba UV-D2 filter so that the excitation was effected only in the CT bands. The observed phosphorescence spectra are shown in Fig. 3, together with that of TRCNB. Their peak positions are shown in Table 3, together with the phosphorescence lifetimes. The characteristics of the phosphorescences of the TRCNB complexes are as follows: (1) the vibrational structures appearing in the phosphorescence spectrum of TRCNB disappear or become obscure in the spectra of the CT complexes; (2) the phosphorescence spectra shift to the longer wavelengths for the complexes than for the acceptor; (3) the phosphorescence lifetimes are slightly shorter for the complexes than for the acceptor. These characteristics are similar to those observed for the TCNB complexes[4] and suggest that the lowest excited states of the complexes under consideration have the CT character to some extent.

TABLE 3. PHOSPHORESCENCE MAXIMA (ν_{max}) AND LIFETIMES (τ) OBSERVED FOR TRCNB AND ITS COMPLEXES WITH METHYL SUBSTITUTED BENZENES

	ν_{max} (10^3 cm^{-1})	τ (s)
TRCNB	25.8	7.0
TRCNB–Toluene	24.0	7.0
TRCNB–Mesitylene	22.8	6.7
TRCNB–Durene	23.0	5.5
TRNCB–HMB	21.5	5.0

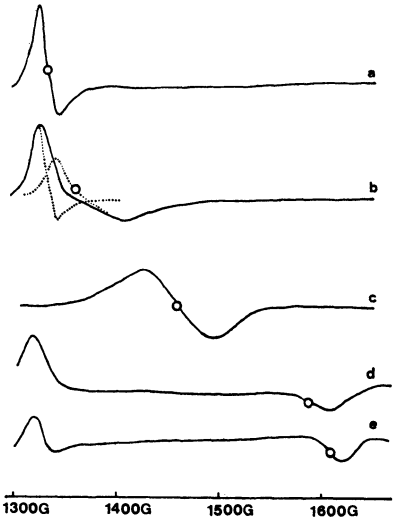

Fig. 4. ESR spectra ($\Delta m=\pm 2$) observed with the ternary solutions containing TRCNB and various donors in EP at 77 K. (a) TRCNB (b) TRCNB–toluene (c) TRCNB–mesitylene (d) TRCNB–durene (e) TRCNB–HMB. Open circles denote the position of H_{min} The signal due to the TRCNB was not observed for curve (c) because of the high concentration of mesitylene. The signals due to the complex and the TRCNB are close to each other in curve (b). The H_{min} value in this case was obtained with the curve corrected for the contribution from the TRCNB.

The ESR Spectra. In order to discuss the character of the lowest triplet state quantitatively, we measured ESR spectra for TRCNB and its complexes. ESR spectra due to the $\Delta m=\pm 2$ transitions of the lowest triplet states were observed for the EP solutions of the CT complexes and of the acceptor itself by steady irradiation with the 500 W mercury lamp through a UV-D25 filter. The observed spectra are shown in Fig. 4. The lowest possible resonance fields (H_{min}) were determined as the midpoint between the maximum and minimun of each of the observed derivative curves. From the H_{min} value, the zero-field splitting constant, D^*, was evaluated by the following equation:[19]

$$D^* = \left\{\frac{3}{4}(h\nu)^2 - 3(g\beta H_{min})^2\right\}^{1/2}$$

where $D^*=(D^2+3E^2)^{1/2}$. D, E, ν, g, and β have their conventional meanings. The g value was assumed

Table 4. The observed D^* values and the CT characters

Donor	TRCNB		TCNB[a]	
	D^* (cm^{-1})	CT(%)	D^* (cm^{-1})	CT(%)
Toluene	0.1478	9	0.1189	11
Mesitylene	0.1237	25	0.0844	42
Durene	0.0698	65	0.0502	72
HMB	0.0557	76	0.0231	95
	0.1567[b]		0.1317[b]	

a) Ref. 4). b) Values for the acceptors.

to be 2.003 and 2.000 for the acceptor and the complexes, respectively.[5] From the D^* values obtained for the complexes we evaluated the degree of CT, x(%), in the lowest triplet state for the molecular complexes by the following equation.[5]

$$D^* = xD_{CT}^* + (1-x)D_A^*$$

Here D_A^* is the observed valueof TRCNB itself (0.1567 cm^{-1}) and D_{CT}^* is the theoretical value of the zero-order CT triplet state. By considering the electron spin dipolar interaction, D_{CT}^* was calculated to be 0.0243, 0.0228, 0.0229, and 0.0250 cm^{-1} for the zero-order CT triplet states represented by Φ_{CT_1}, Φ_{CT_2}, Φ_{CT_3}, and Φ_{CT_4}, respectively. Since they are close to one another, the average value, 0.0238 cm^{-1} was used as D_{CT}^*. The D^* and x values are given in Table 4, together with those for the TCNB complexes.

The results show that the CT character of the lowest triplet state increases for the TRCNB complexes with the decreasing I_p of the donor. This tendency was also found for the TCNB and dicyanobenzene complexes. Table 4 shows that the lowest triplet state is mainly contributed by the CT structure in the TRCNB complexes with HMB and durene, whereas by the LE structure in those with mesitylene and toluene.

T-T Absorptions of the TRCNB Complexes with Methyl Substituted Benzenes. The T-T absorption spectra observed for the TRCNB complexes with HMB, durene, mesitylene, and toluene are shown in Fig. 5. The spectrum of each complex apparently consists of four bands, bands A and B in 10000—15000 cm^{-1}, and bands C and D in >20000 cm^{-1}.[20] Neither TRCNB

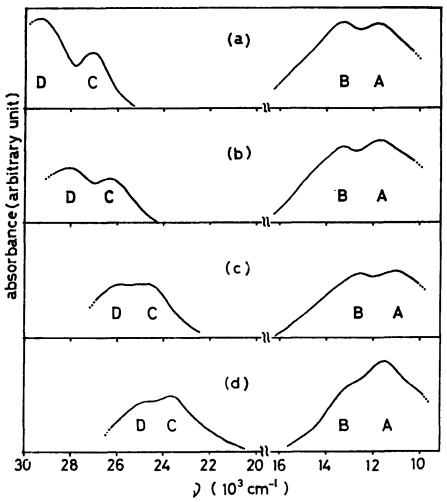

Fig. 5. T-T absorption spectra observed with the TRCNB complexes with (a) toluene (b) mesitylene (c) durene (d) HMB.

Table 5. T-T absorption maxima (in 10^3 cm^{-1}) observed for the TRCNB complexes with methyl substituted benzenes

Donor	Band A	Band B	Band C	Band D
Toluene	11.8	13.3	27.0	29.4
Mesitylene	11.6	13.2	26.3	28.0
Durene	10.9	12.5	24.7	26.0
HMB	11.6	13.2	23.8	25.0

Table 6. Observed and calculated transition energies (10^3 cm^{-1}) and oscillator strengths (in parentheses) for the TRCNB–HMB complex

	Calcd					Obsd[a]
	1	2	3	4	5	
$T_2 \leftarrow T_1$	2.6(0.004)	3.0(0.003)	2.2	2.6(0.003)	2.6	
$T_3 \leftarrow T_1$	4.5(0.004)	3.9(0.004)	2.3	2.7(0.001)	4.5	
$T_4 \leftarrow T_1$	4.5(0.001)	3.9(0.001)	2.3	2.7(0.000)	4.5	
$T_5 \leftarrow T_1$	10.6(0.330)	8.9(0.220)	5.6	6.4(0.150)	10.6	11.6(S)
$T_6 \leftarrow T_1$	13.5(0.000)	12.5(0.090)	10.5	11.0(0.110)	13.5	13.2(M)
$T_7 \leftarrow T_1$	19.7(0.075)	19.8(0.030)	19.4	19.4(0.020)	19.7	
$T_8 \leftarrow T_1$	22.7(0.170)	22.0(0.280)	20.5	20.9(0.240)	22.7	23.8(M)
$T_9 \leftarrow T_1$	24.9(0.100)	23.4(0.050)	20.5	21.4(0.090)	24.9	25.0(M)

a) S and M in parentheses mean strong and medium intensities, respectively.

TABLE 7. WAVE FUNCTIONS CALCULATED FOR THE TRCNB–HMB COMPLEX (MODEL 2)

$^3\psi_1 = 0.5963\,{}^3\Phi_{CT_1} + 0.3399\,{}^3\Phi_{CT_2} - 0.1784\,{}^3\Phi_{CT_3} + 0.3089\,{}^3\Phi_{CT_4} + 0.6179\,{}^3\Phi_{LE_1} - 0.1395\,{}^3\Phi_{LE_2}$

$^3\psi_2 = -0.4179\,{}^3\Phi_{CT_1} - 0.2363\,{}^3\Phi_{CT_2} - 0.4085\,{}^3\Phi_{CT_3} + 0.7066\,{}^3\Phi_{CT_4} + 0.1261\,{}^3\Phi_{LE_1} + 0.2988\,{}^3\Phi_{LE_2}$

$^3\psi_3 = 0.8618\,{}^3\Phi_{CT_3} + 0.4981\,{}^3\Phi_{CT_4}$

$^3\psi_4 = -0.4929\,{}^3\Phi_{CT_1} + 0.8648\,{}^3\Phi_{CT_2}$

$^3\psi_5 = -0.3446\,{}^3\Phi_{CT_1} - 0.1965\,{}^3\Phi_{CT_2} + 0.2224\,{}^3\Phi_{CT_3} - 0.3850\,{}^3\Phi_{CT_4} + 0.7579\,{}^3\Phi_{LE_1} + 0.2618\,{}^3\Phi_{LE_2}$

$^3\psi_6 = 0.3288\,{}^3\Phi_{CT_1} + 0.1874\,{}^3\Phi_{CT_2} + 0.1090\,{}^3\Phi_{CT_6} - 0.1670\,{}^3\Phi_{LE_1} + 0.8975\,{}^3\Phi_{LE_2}$

$^3\psi_7 = 0.2820\,{}^3\Phi_{CT_5} - 0.4882\,{}^3\Phi_{CT_6} + 0.8193\,{}^3\Phi_{LE_3}$

$^3\psi_8 = 0.8659\,{}^3\Phi_{CT_5} + 0.5002\,{}^3\Phi_{CT_6}$

$^3\psi_9 = -0.4078\,{}^3\Phi_{CT_5} + 0.7061\,{}^3\Phi_{CT_6} + 0.5712\,{}^3\Phi_{LE_3}$

nor the donors show any T-T absorption in these wave number regions. The observed absorption bands for the respective complexes decay at the same rate as the corresponding phosphorescences. Therefore, we can safely assign them to the T-T absorption bands of the complexes. The observed band positions are given in Table 5.

Assignment of the T-T Absorptions. We interpreted the observed absorption spectra considering the calculated transition energies and oscillator strengths, the TRCNB–HMB complex being taken as an example. The observed and the calculated transition energies for this complex are shown in Table 6. The calculations were made with five geometrical models shown in Fig. 1. In Table 6 are also shown the calculated oscillator strengths for three of the models.

The calculated band positions and intensities vary considerably with the choice of models. Model 1 (face-to-face model) is rather favorable from the comparison between the observed and calculated transition energies, but the calculated intensities for this model can not explain even qualitatively the observed ones; particularly the intensity predicted for band B is too weak. The transition energies calculated for models 3 and 4 become too low compared with the observed data (particularly for band A). As a whole, the overall feature of the observed spectrum (the appearance of the two pairs of bands with comparable intensities) seems to be reproduced by model 2.[21]

The wave functions calculated for model 2 are given in Table 7.[22] Since the lowest four zero-order CT triplet states (3.0 eV) and the lowest zero-order LE triplet state (3.2 eV) are close to each other in the TRCNB–HMB complex, they mix with each other efficiently and give rise to the five states, T_1—T_5. The bands corresponding to the transitions from T_1 to T_2—T_4 are expected to be too weak to be observed. A fairly strong band due to the transition between T_1 and T_5 is expected to appear in the lowest energy region. Therefore, we assign band A in the near-infrared region to the $T_5 \leftarrow T_1$ transition. As is clearly seen in Table 6, bands B, C, and D can reasonably be assigned to the transitions from T_1 to T_6, T_8, and T_9, respectively.[23]

From the wave functions given in Table 7, it is found that T_1 is mainly contributed by the zero-order CT triplet states, while the main components of T_5 and T_6 are $^3\Phi_{LE_1}$ and $^3\Phi_{LE_2}$, respectively. Therefore, bands A and B are assigned to the LE←CT transitions.

The $T_8 \leftarrow T_1$ and $T_9 \leftarrow T_1$ transitions may be interpreted as due to the local excitations within the TRCNB anion. The T_8 and T_9 states arise mainly from the interaction between the $^3\Phi_{CT_5}$ and $^3\Phi_{CT_6}$ structures. This means that the $T_8 \leftarrow T_1$ and $T_9 \leftarrow T_1$ transitions correspond to the strong absorption of the TRCNB anion appearing at 18500 cm^{-1}.[24] The shifts to the higher frequencies (5300 and 6500 cm^{-1}) caused by the complex formation may partly be due to the stabilization of the lowest zero-order triplet state.

Effect of Electron Donors. The calculated (model 2) and observed triplet levels are shown in Fig. 6, in which the triplet-state energies of the complexes are plotted against the ionization potentials of the donors,

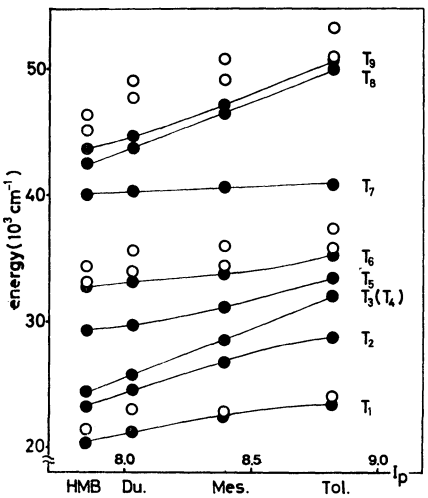

Fig. 6. The triplet state energy diagrams calculated (model 2) and observed for the TRCNB complexes. ○: observed, ●: calculated.

TABLE 8. CT CHARACTERS (%) ESTIMATED FOR THE TRIPLET STATES OF THE TRCNB COMPLEXES (MODEL 2)

Donor	T_1[a]	T_2	T_3	T_4	T_5	T_6	T_7	T_8	T_9
Toluene	25 (9)	42	100	100	76	76	4	100	96
Mesitylene	37 (25)	72	100	100	57	34	8	100	92
Durene	53 (65)	86	100	100	42	21	19	100	80
HMB	60 (76)	89	100	100	36	16	32	100	67

a) The values in parentheses are estimated from the ESR spectra.

I_p. The calculated energy levels, though they are commonly about 0.25 eV smaller for the T_5, T_6, T_8, and T_9 states of all the complexes than the observed values, can well explain the observed energy dependences upon I_p.

The calculated contributions of the zero-order CT triplet states to the $T_1 \sim T_9$ states of the complexes are given in Table 8. The character of T_1 is mainly of the CT triplet for the complexes with HMB and durene and mainly of the LE triplet for those with mesitylene and toluene. A similar tendency was found for the TCNB complexes with these methyl substituted benzenes. The contributions of the zero-order CT triplet states to T_1 are 60, 53, 37, and 25% for the TRCNB complexes with HMB, durene, mesitylene, and toluene, respectively. This estimation is semi-quantitatively consistent with the results of the ESR study. The CT characters of the T_5 state are 36, 42, 57, and 76% for the TRCNB complexes with HMB, durene, mesitylene, and toluene. Consequently, it is confirmed that the character of band A is of the LE←CT transition for the TRCNB–HMB and TRCNB–durene complexes, and of the CT←LE transition for the TRCNB–mesitylene and TRCNB–toluene complexes.

Band B is comparatively insensitive to the electron donors. The calculation shows that the energies of the upper and lower states of this band, T_1 and T_6, change almost in parallel with each other by changing the electron donor from toluene to HMB. This is a reason why band B does not shift remarkably from donor to donor.

Bands C and D shift toward the higher frequencies with the increasing I_P of the donor. The upper states of these bands, T_8 and T_9, are mainly of the CT character and their energies increase more steeply than that of the T_1 state.

Comparison among Polycyanobenzene Complexes. Table 9 shows the observed values of $\Delta\nu_p = \nu_{00}^A - \nu_{max}^C$, x, and τ_C/τ_A for the phthalonitrile (PN), TRCNB, TCNB complexes with various donors. Here ν_{00}^A and ν_{max}^C are the phosphorescence 0-0 band frequency of

Table 9. $\Delta\nu_p$, x, and τ_C/τ_A for various polycyanobenzene complexes

$\Delta\nu_p(10^3\ cm^{-1})$	PN[a]	TRCNB	TCNB[b]
HMB	3.6	4.5	4.4
Durene	2.8	2.8	3.2
Mesitylene	2.8	3.0	2.9
Toluene		1.8	2.1
x(%)	PN[a]	TRCNB	TCNB[b]
HMB	48	76	95
Durene		65	72
Mesitylene	10	25	42
Toluene		9	11
τ_C/τ_A	PN[a]	TRCNB	TCNB[b]
HMB	0.89	0.71	0.44
Durene	0.84	0.79	0.60
Mesitylene	0.95	0.96	1.0
Toluene		1.0	1.0

a) Taken from Ref. 6. b) Taken from Ref 4.

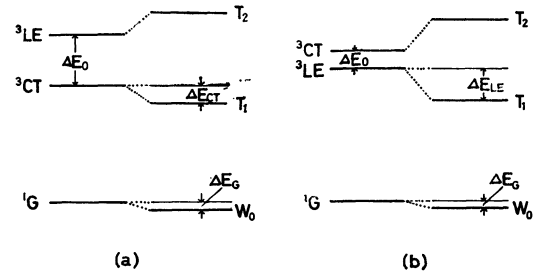

Fig. 7. Schematic energy diagrams of the lower triplet states of the HMB complexes with (a) TCNB or TRCNB; (b) PN.

the acceptor and the phosphorescence maximum frequency of the complex, respectively, x is the CT character of the phosphorescent state of the complex obtained from the ESR spectrum, and τ_A and τ_C are the phosphorescence lifetimes obtained for the acceptor and the complex, respectively.

As clearly seen in Table 9, $\Delta\nu_p$ and x increase, while τ_C/τ_A decreases, for a fixed acceptor with the decreasing I_p of the donor. This holds for all the complexes under consideration. On the other hand, for a fixed donor, $\Delta\nu_p$ is the largest for the TRCNB complex. For example, taking HMB as donor, $\Delta\nu_p$ is 4500, 4400, and 3600 cm^{-1} for the TRCNB, TCNB, and PN complexes, respectively. The phosphorescent states are mainly of the CT character for the TCNB and TRCNB complexes and of the LE character for the PN complex. As is seen in Fig. 7, $\Delta\nu_p$ is expressed as follows;

$$\Delta\nu_p = \Delta E_0 + \Delta E_{CT} - \Delta E_G \quad \text{for the TCNB and TRCNB complexes}$$

$$\Delta\nu_p = \Delta E_{LE} - \Delta E_G \quad \text{for the PN complex.}$$

The energy difference between the zero-order CT and LE triplet states, ΔE_0, is estimated to be 2480 and 1600 cm^{-1} for the TCNB and TRCNB complexes, respectively. The stabilization energy of the ground configuration, ΔE_G, is estimated to be 240—480 cm^{-1} for the TCNB complex,[17] and is expected to be smaller for the TRCNB and PN complexes. Thus, the stabilization energy of the lowest zero-order CT or LE triplet state (ΔE_{CT} or ΔE_{LE}, respectively), is expected to be the greatest for the PN complex and the smallest for the TCNB complex. This is reasonable in view of the fact that the ΔE_0 value is the greatest for the TCNB complex and the smallest for the PN complex (160 cm^{-1}).

According to Table 9, the x values for a fixed donor decrease in the following order of acceptors; TCNB> TRCNB>PN. This is consistent with the expectation that the electron affinities of the acceptors decrease in the same order.

Finally let us consider the relation between the phosphorescence lifetime of a complex and the CT character in its lowest triplet state.[4] The τ_C/τ_A values are plotted *versus* x in Fig. 8. The figure shows that τ_C/τ_A decreases with the increasing x, and the decrease becomes appreciable, in particular, in the region of x>50%. This may suggest that such phosphorescence quenching processes as ion-pair formation and ioniza-

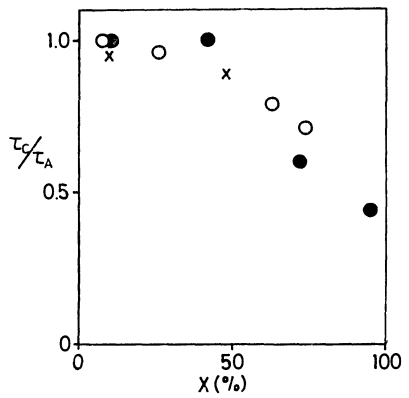

Fig. 8. Plots of τ_C/τ_A *versus* x for the complexes.
●: TCNB complexes, ○: TRCNB complexes, ×: PN complexes.

tion become important in that region of x.

The authors express their sincere thanks to Professor Jiro Higuchi, Yokohama National University, for his kindness in putting the ESR spectrometer at their disposal.

References

1) C. Reid, *J. Chem. Phys.*, **20**, 1212 (1952).
2) J. Czekalla and K. J. Mager, *Z. Elektrochem.*, **66**, 65 (1962).
3) N. Christdouleas and S. P. McGlynn, *J. Chem. Phys.*, **40**, 166 (1964).
4) S. Iwata, J. Tanaka, and S. Nagakura, *ibid.*, **47**, 2203 (1967).
5) H. Hayashi, S. Iwata, and S. Nagakura, *ibid.*, **50**, 993 (1969).
6) H. Hayashi and S. Nagakura, *Mol. Phys.*, **19**, 45 (1970).
7) P. Krebs, E. Sackmann, and J. Schwarz, *Chem. Phys. Lett.*, **8**, 417 (1971).
8) G. Briegleb, H. Schuster, and W. Herre, *ibid.*, **4**, 53 (1963).
9) K. B. Eisenthal, *J. Chem. Phys.*, **46**, 3268 (1967).
10) S. Matsumoto, S. Nagakura, S. Iwata, and J. Nakamura, *Chem. Phys. Lett.*, **13**, 463 (1972).
11) H. Masuhara, N. Tsujino, and N. Mataga, *ibid.*, **15** 360 (1972).
12) S. Matsumoto, S. Iwata, J. Nakamura, and S. Nagakura, *Mol. Phys.*, to be published.
13) G. M. Bennett and R. L. Wain, *J. Chem. Soc.*, **1936** 1108.
14) A. S. Bailey, B. R. Henn, and Janet M. Langdon, *Tetrahedron*, **19**, 161 (1963).
15) R. Pariser and R.G. Parr, *J. Chem. Phys.*, **21**, 466 (1953).
16) J. A. Pople, *Proc. Phys. Soc., Ser. A.* **68**, 81 (1955).
17) S. Iwata, J. Tanaka, and S. Nagakura, *J. Amer. Chem. Soc.*, **88**, 894 (1966).
18) "UV Atlas of Organic Compounds," Verlag Chemie, Weinheim, (1966).
19) M. S. de Groot and J. H. van der Waals, *Mol. Phys.*, **3**, 190 (1960).
20) We could observe no T-T absorption band for the complexes in the region below 10000 cm^{-1}.
21) The overlap integral between the highest occupied orbital of the donor and the lowest vacant one of the acceptor, and consequently the stabilization energy of the ground state, is larger for models 2, 3, and 4 than for model 1. Thus, the former models favor the formation of a stable complex.
22) The calculated energy levels have a general tendency to be about 2000 cm^{-1} lower than the observed ones. This tendency was also seen to some extent in the TCNB complexes.[12] These discrepancies may originate from the underestimation of the interaction term. As the interaction is expected to increase in the excited state, the constant k should be taken to be greater than 10.
23) We did not assign band C to the $T_7 \leftarrow T_1$ transition. The $T_7 \leftarrow T_1$ transition is predicted to show a red shift with the increasing I_p of the donor, while as shown in Fig. 6, band C shifts to the higher frequencies with the increasing I_p.
24) Private communication from Dr. T. Shida, The Institute of Physical and Chemical Research.

Metachromasy. II.* Interaction between Sodium Polyphosphates and Crystal Violet with Special Emphasis on the Effect of Chain Lengths of the Polymer on the Metachromasy Band

Kiwamu YAMAOKA, Mineo TAKATSUKI, Kunio YAGUCHI,** and Masaji MIURA
Faculty of Science, Hiroshima University, Hiroshima 730
(Received October 22, 1973)

The interaction of crystal violet with sodium polyphosphate in aqueous solutions at neutral pH has been investigated by means of visible absorption spectroscopy and electric conductivity. The mixing ratio of polymer residue to dye was varied from 0.1 to 10000. The metachromasy band at 506 nm was found to fully develop between 3 and 10, whereas conductometric titration showed that crystal violet saturates the polymer site. Emphasis was placed on the effect of the polymer chain length on the metachromasy band. To study this effect, 17 fractionated and 13 refractionated polymer samples with degrees of polymerization extending from 4 to 300 were utilized. A critical range of the degree of polymerization from the metachromasy band exists between 7 and 20. The effect of small ions on metachromasy was also studied using sodium phosphates. An increase in Na^+ ions tends to suppress the metachromasy band. This effect is more pronounced with shorter polymer lengths. In order to explain the observed metachromasy phenomena, two mechanisms were postulated; one attributes metachromasy to the flexibility of the polymer backbone when dye is present, and the other deals with specific interaction of dye and polymer site.

A characteristic change of color is exhibited by certain cationic dyes in aqueous solutions, as their concentration is increased or the temperature is lowered. A similar change occurs when such dyes are bound to certain polyelectrolytes with anionic groups in low concentrations where the dyes alone obey Beer's law. This is the phenomenon of *metachromasy*, as originally termed by Ehrlich, in contrast with *orthochromasy* which signifies the relative lack in such a color change of basic dyes at higher concentrations or when bound to polyelectrolytes.[2] The metachromatic change, which is most pronounced in the visible spectrum, is frequently characterized by the appearance of a new absorption band (or bands)—metachromasy band—or prominent shoulders in the wavelength region shorter than the original band of a pure dye. The change has been interpreted as due to the formation of various aggregates of the bound dye molecules on the polymer sites.[3]

Such metachromatic changes are frequently specific rather than general and constitute an experimental basis of histo- and cytochemical applications. For a particular dye the metachromatic behavior is characteristic of the polyelectrolyte species and its conformation under given experimental conditions.[3-5] For a particular polymer species it often depends on the specific substituents attached to the dyes even if they belong to a class of the same chemical structure.[6,7] The differentiation of nucleic acids between themselves or from proteins *in vitro* as well as *in vivo* is based on the delicate color shades of a bound metachromatic dye.

A simple polymeric model of nucleic acids is indisputably polyphosphoric acid which is one of the simplest polyelectrolytes with ionizable phosphate groups in the polymer chain. The interactions between polyphosphates and metachromatic cationic dyes have been studied and the results compared with the interaction with nucleic acids. Dyes studied so far are toluidine blue,[8] 4,5,4′,5′-dibenzo-3,3′-diethyl-9-methylthiacarbocyanine,[9] acridine orange,[3,10-14] and proflavine.[10] Polyphosphates utilized in these studies were randomly chosen from small oligomeric samples to very high polymeric Kurrol's salts. Few attempts, however, have been made to find the relation between the critical polymer dimension and metachromasy.

In this paper we present, for the first time, detailed results of the effect of the length of polymer chain on induction of metachromasy and, in particular, evidence for the existence of a critical range of the chain lengths. We prepared a large number of fractionated polyphosphate samples with degrees of polymerization in the range 4—300. As a metachromatic dye we chose crystal violet, purer and more representative of triphenylmethane dyes, instead of acridines. The optical properties of crystal violet have been studied to the same extent as acridine orange or proflavine both in the absence [15-17] and presence of various polyelectrolytes.[6,7,18-20,25,26] Crystal violet is particularly suitable, since, under certain conditions, it exhibits a new, well-defined metachromasy band at 506 nm separated from its principal band, when bound to polyphosphate.[1]

Experimental

Materials. Sodium polyphosphate (NaPP) was synthesized from sodium dihydrogen phosphate used as a monomer by the method of pyropolymerization.[1] The degree of polymerization of each preparation was controlled by adding an appropriate amount of disodium hydrogen phosphate, as a chain terminator, to the monomer. The reactants were mixed and preheated in a platinum crucible below 200 °C to dryness and then heated at 800 °C in an electric furnance for about 8 hr. The melt was then quickly solidified in a liquid nitrogen bath.

Eight NaPP preparations were each fractionated into five to eight fractions of approximately equal volume by the method of fractional precipitation from aqueous solution (ca. 7%) with acetone. Each fraction was separated from the mother liquor by decantation, redissolved in water, lyophilyzed, and dried *in vacuo* at room temperature and then at 57 °C. Samples were stored in a desiccator over

* Part I of this series is Ref. 1.
** Present Address: Toda Kōgyō & Co., Hiroshima.

phosphorus pentoxide. The number-average degree of polymerization, $\bar{n}$, of the total fifty fractions was determined by the method of end-group titration with sodium hydroxide and found to be in the range 4—300. In order to prepare better-defined samples with respect to molecular weight distribution, a mixture of four fractions, whose $\bar{n}$'s were in the neighborhood of 11, was refractionated into eight fractions. Another mixture of two fractions with $\bar{n}$'s of approximately 120 was also refractionated into eight fractions.

Crystal violet (CV) in the chloride form (Chroma Gesellschaft, Schmid & Co.) was purified by recrystallization from hot water and dried to be anhydrous at 80 °C *in vacuo*.[1] The purity of CV was tested by thin-layer chromatography (1: 4 methanol–chloroform mixed solvent as an eluent). The vacuum-dried dye sample was weighed as anhydrous chloride to prepare a stock solution, which was stored in the dark at room temperature. All glassware was equilibrated with a concentrated dye solution and rinsed thoroughly with water before use to avoid the undesirable adsorption of dye. The maximum molar extinction coefficient at 592 nm was 94000 at 1.12×10^{-5}M.

Procedures. An anhydrous polymer sample was dissolved in distilled water to prepare a stock solution which was stored in the cold. Just prior to measurements, one part of the dye stock solution was added dropwise to one part of the polymer solution, while the mixture was being stirred. The dye–polymer solution was then equilibrated for about 15 min. This order of mixing was observed throughout. The final concentration of dye in the dye–polymer solution was maintained at a fixed value of 1.12×10^{-5}M, unless otherwise stated. The ratio of monomer residue (or anionic site) to dye, P/D, was defined as before.[4]

The buffered dye–polymer solution was prepared by using the Na_2HPO_4–NaH_2PO_4 buffer system, the components of which are both monomeric units of NaPP. One part of the buffer solution was first added to one part of the polymer solution, followed by two parts of the dye solution. The pH of buffered dye–polymer solutions was adjusted to about 6.5. Part of this solution was saved for pH determination. The final buffer concentration was kept at five times higher than that of NaPP, except for the study of the effect of concentration of added salt (Na_2HPO_4–NaH_2PO_4) on the dye–polymer complex formation.

Measurements. A Hitachi Model EPS-3T recording spectrophotometer was used together with a matched pair of 1 cm long quartz cells. The temperature was controlled at 25 °C by circulating regulated water through a cell holder. The solution was always equilibrated for 5—10 min before the measurement of an absorption spectrum which was scanned at least twice to ascertain reproducibility. Conductometric titration was carried out on a Jones type 1000-Hz bridge.[21,22] The electrodes of a conductivity cell with a cell constant of 0.0333 were made of bright platinum to avoid the adsorption of NaPP. No time dependence of the cell resistance was observed in the presence of the solution of NaPP or CV. 1 ml of a 1.3×10^{-3}M NaPP solution was added (0.04 ml at a time) through a burette to 25 ml of a 2.26×10^{-5}M CV solution in the cell. The mixture was stirred and allowed for about 2 min each time for equilibration before reading the resistance.

Results

Spectra of Crystal Violet in the Presence of NaPP in Aqueous Solutions. The visible absorption spectra of CV in the presence of a high molecular weight NaPP are shown in Fig. 1. The values of P/D were varied by adjusting the polymer concentration at a fixed CV concentration. The absorption maximum of CV at 592 nm decreases with an increase in P/D values up to 3 by the addition of NaPP, while its absorption at 506 nm increases steadily to a distinct band—a metachromasy band. There is an isosbestic point at 639 nm in the longer wavelength side in a family of the NaPP–CV spectra at P/D values less than unity. The spectral trend reverses very slowly at first and then gradually, as the polymer concentration is increased to about 100 in terms of P/D. At exceedingly high P/D values, the 592 nm band regains its intensity, whereas the metachromasy band at 506 nm diminishes. Thus, the overall spectrum becomes almost the same as that of pure CV. An isosbestic point also appears at 636 nm in the spectra of NaPP–CV systems at P/D values higher than 100. It should be noted that in the spec-

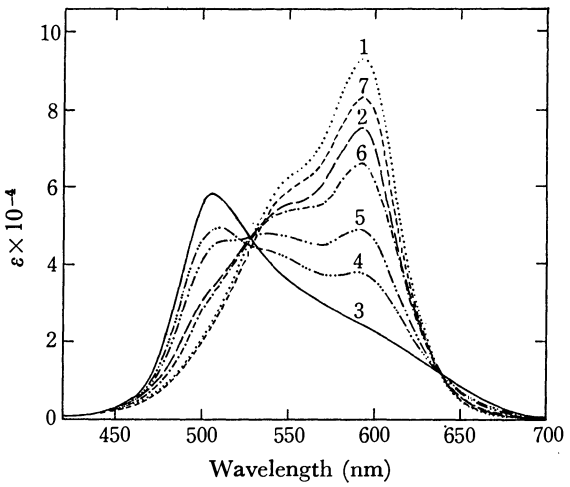

Fig. 1. Spectra of CV in the presence of NaPP ($\bar{n}$=154) at various P/D values in aqueous solutions.
(1) Pure CV (P/D=0) for comparison, (2) P/D=0.3, (3) P/D=3, (4) P/D=80, (5) P/D=150, (6) P/D=300, (7) P/D=1000.

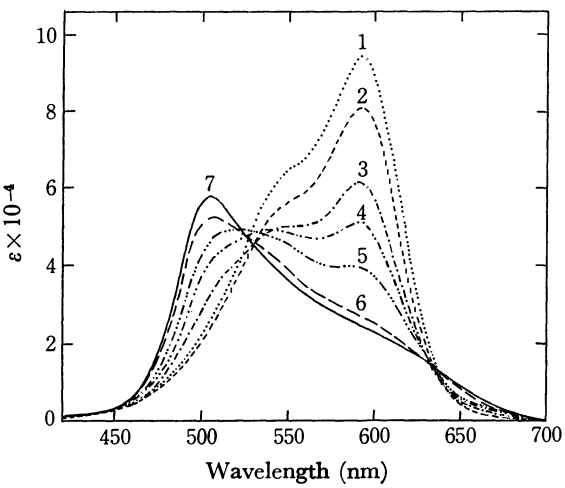

Fig. 2. Spectra of CV in the presence of NaPP with various chain lengths at a P/D value of 3 in aqueous solutions.
(1) Pure CV (P/D=0) for comparison, (2) $\bar{n}$=7.77, (3) $\bar{n}$=12.9, (4) $\bar{n}$=15.6, (5) $\bar{n}$=24.4, (6) $\bar{n}$=63.0, (7) $\bar{n}$=154.

trum of CV there is a weak, probably forbidden band between 340 and 380 nm which is also affected by the presence of NaPP.[1] No quantitative analysis of this band is given because of the small changes in intensity and band position.

The effect of the chain length of NaPP on the visible absorption spectra of CV is shown in Fig. 2. The P/D value is held at 3 which is one of the most favorable values for the appearance of the metachromasy band. The spectra for $\bar{n}$ values less than about 5 are essentially the same as the pure CV spectrum. As the values of $\bar{n}$ increase, the principal band intensity at 592 nm decreases, while the metachromasy band intensity increases for the NaPP samples. A sharp transient region of $\bar{n}$ lies approximately between 7 and 20. The intensities of both bands become unchanged as $\bar{n}$ exceeds 20. It is interesting to note that the spectral behavior shown in Fig. 2 is closely related to that shown in Fig. 1. This indicates that, with respect to the 506 nm metachromasy band, some correlation exists between changes in P/D values at a given $\bar{n}$ and changes in $\bar{n}$ at a given P/D value. All results are hereafter described in terms of absorptions at the 592 and 506 nm bands with which the metachromasy of CV can be characterized most conveniently.

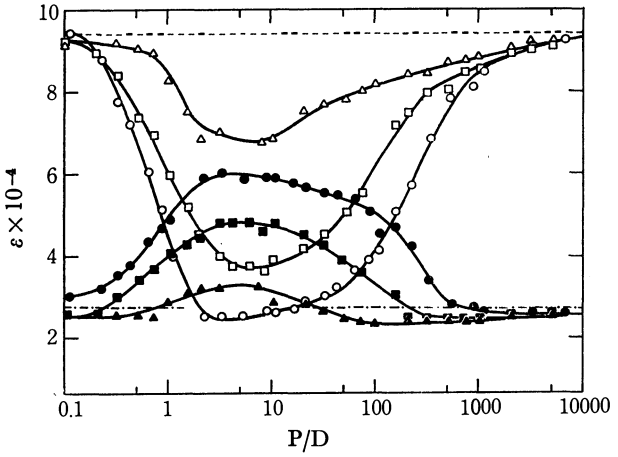

Fig. 3. The dependence of metachromasy on the P/D values for NaPP–CV systems with different chain lengths in aqueous solutions.
Open symbols are the molar extinction coefficients of CV at 592 nm and filled ones are those at 506 nm. -○- and -●- for $\bar{n}$=154, -□- and -■- for $\bar{n}$=24, -△- and -▲- for $\bar{n}$=11.

Effect of the P/D Values on the Absorption of NaPP–CV Complexes with Various Degrees of Polymerization. In Fig. 3, the molar extinction coefficients of CV at 592 and 506 nm in the presence of three different NaPP samples ($\bar{n}$=154, 24, and 11) are plotted against P/D on a logarithmic scale. The effect of P/D is such that, at both low and extremely high P/D values, the molar extinction coefficients at 592 and 506 nm are about the same as those of pure CV. The 506 nm band becomes most outstanding and the 592 nm band is diminished to a minimum for each NaPP sample at P/D values between about 3 and 10. The extreme values of the extinction coefficients differ with the chain length of NaPP. This indicates that, while the metachromasy is developed to be maximum for each NaPP sample in this P/D range, the magnitude of the 506 nm metachromasy band is affected by the polymer chain length. The three NaPP samples were so chosen that the metachromasy band is induced to a small ($\bar{n}$=11), medium ($\bar{n}$=24), or large ($\bar{n}$=154) extent.

Effects of the Chain Length and Fractionation of NaPP on the Absorption of NaPP–CV Complexes at Various Values of P/D. The effects of chain length and frac-

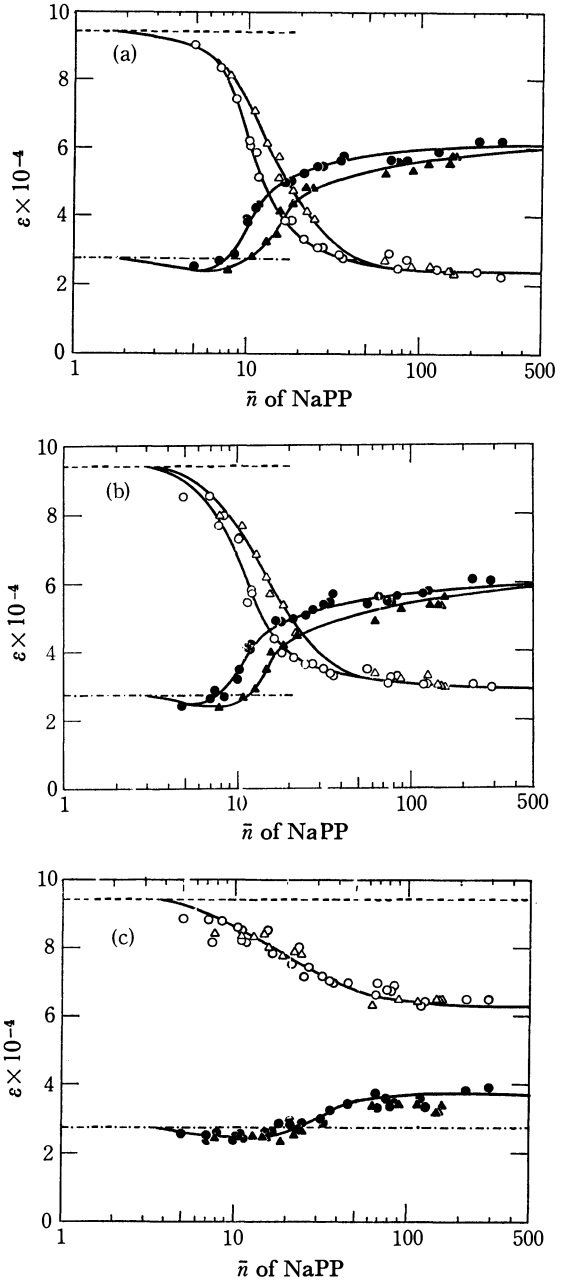

Fig. 4. The dependence of metachromasy on the chain lengths of fractionated and refractionated NaPP samples at (a) P/D=3, (b) P/D=30, and (c) P/D=300 in aqueous solutions.
In each figure, open symbols are the molar extinction coefficients of CV at 592 nm and filled ones are those at 506 nm. -○- and -●- for fractionated NaPP, and -△- and -▲- for refractionated NaPP.

tionation on the induction of metachromasy band are shown in Figs. 4a—4c, where the molar extinction coefficients of the NaPP–CV system are plotted against the chain length of both fractionated and refractionated NaPP samples on a logarithmic scale. The concentration of each NaPP sample is so chosen that the metachromasy is most distinctive (P/D=3), medium (P/D=30), or very weak (P/D=300). At P/D values of 3 and 30 the principal band at 592 nm decreases, while the metachromasy band at 506 nm increases, very sharply in a narrow range of the chain length 7—20. Both band intensities then level off, as $\bar{n}$ reaches about 100. The midpoints of these sigmoidal changes in ε_{506nm} and ε_{592nm} correspond to $\bar{n}=17$ and 14 (P/D=3), and $\bar{n}=18$ and 16 (P/D=30), respectively, for refractionated samples. The midpoint is slightly displaced to $\bar{n}=30$ and 20 at a P/D value of 300, which indicates that a longer chain length is required for metachromasy. In any case, it is evident that metachromasy is dependent on the polymer chain length and is critically associated with the oligomeric dimensions.

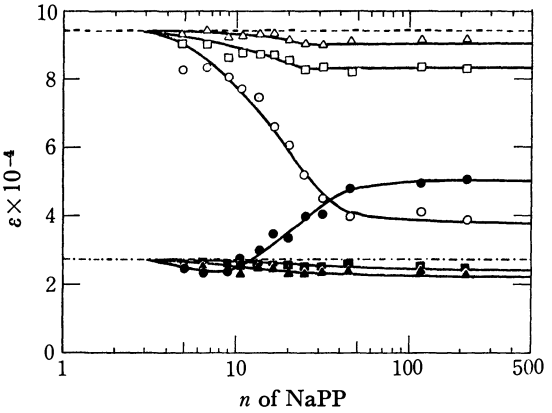

Fig. 5. The dependence of metachromasy on the chain lengths of NaPP at various P/D values and at fixed pH's.
Open symbols are the molar extinction coefficients of CV at 592 nm and filled ones are those at 506 nm. -○- and -●- for P/D=5 at pH=7.0, -□- and -■- for P/D=50 at pH=6.8, -△- and -▲- for P/D=500 at pH=6.5.

The pH value of NaPP in aqueous solutions varies slightly with the chain length at a given value of P/D and the polymer concentration at a given value of $\bar{n}$. An attempt was made to examine the effect of $\bar{n}$ on metachromasy at a constant pH using a sodium phosphate buffer five times more concentrated than NaPP (Fig. 5). As the data in Figs. 4a—4c and 5 indicate, the optical behavior is all the same except that the development of the metachromasy is somewhat suppressed in the buffered solution. This is, not a direct consequence of maintaining pH at a fixed value*,

* The slight variation of pH in the neutral region is due to the fact that the degree of ionization of end-groups of a polymer chain (other phosphate residues are all ionized in this pH region) depends on the chain length. For a given NaPP sample, the metachromasy is confirmed to be independent of pH between 5.5 and 9 for CV.

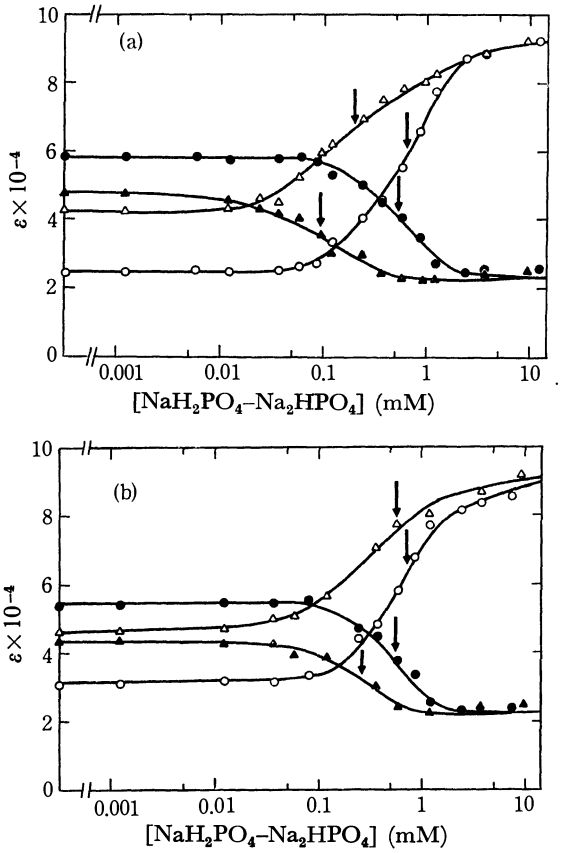

Fig. 6. The effect of small electrolytes on metachromasy at (a) P/D=3, and (b) P/D=30.
Open symbols in each figure are the molar extinction coefficients of CV at 592 nm and filled ones are those at 506 nm. -○- and -●- for NaPP with n=154, and -△- and -▲- for NaPP with n=24. Arrows indicate the mid-points of the changes in ε.

but due to the effect of the ionic strength of the buffering small ions on metachromasy (*vide infra*).

Effect of Addition of Small Electrolytes on Metachromasy. The effect of small ions on the absorption bands at 592 and 506 nm is shown for two NaPP samples ($\bar{n}$=154 and 24) at P/D values 3 and 30, respectively (Figs. 6a and 6b). At each P/D the effect of the concentration of the added small ion on metachromasy is insignificant up to about 1×10^{-5} M, a concentration comparable with that of CV. However, a further increase in the salt concentration gives rise to a gradual decrease in metachromasy. The absorptions at 592 and 506 nm become indistinguishable with those of pure CV at salt concentration higher than 10^{-2} M, up to which the pure CV spectrum is independent of the amount of added salts. The chain length effect on this process, which has been attributed to the competitive binding between CV^+ cations and Na^+ ions toward polymer sites,[1,19] reflects the prevailing relationship between molecular weight of polymer and metachromasy. The 506 and 592 nm sigmoidal curves for the higher $\bar{n}$ sample are clearly displaced to the right. More small ions are required to dissociate the bound dye. The arrows in Figs. 6a and 6b indicate the midpoints of either increasing or decreasing curves of molar extinction coefficients.

Conductometric Titration of CV with NaPP of Three Different Chain Lengths. In order to establish the relation between the binding of CV to polymer site and the chain length of NaPP, conductometric titrations of CV with representative NaPP samples were carried out. The results are shown in Figs. 7a—7c, where each corresponding blank titration is also plotted. In the absence of CV the conductivity of each NaPP sample increases with the increase of the concentration, although the slope depends on the chain length. In the presence of CV, however, the conductivity of the titrated solution increases in two steps on the dropwise addition of the NaPP titrant. A sharp break always appears at a P/D value of about unity (1.01, 1.01, and 1.02) for each NaPP sample ($\bar{n}$=11, 24, and 154) as shown by an intersection of two interpolated lines (Figs. 7a—7c). This indicates that, regardless of the chain length of NaPP, *i.e.*, either oligomeric or polymeric sample, CV binds to the NaPP site at most up to a one-to-one ratio at a total CV concentration of 2.26×10^{-5} M. After the P/D=1 break, a further addition of NaPP increases the conductivity of the NaPP–CV solution practically in parallel with the increase in conductivity of a pure NaPP solution.

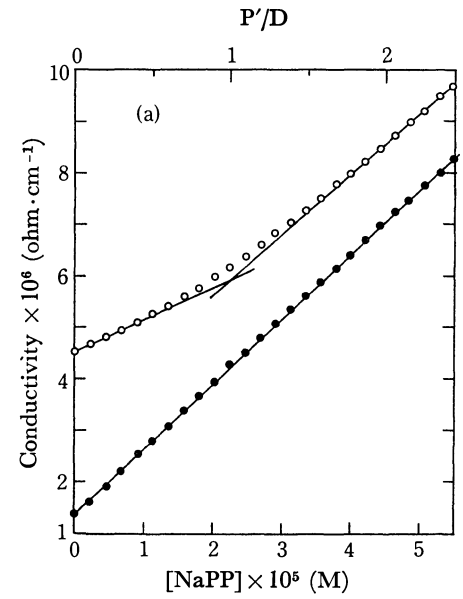

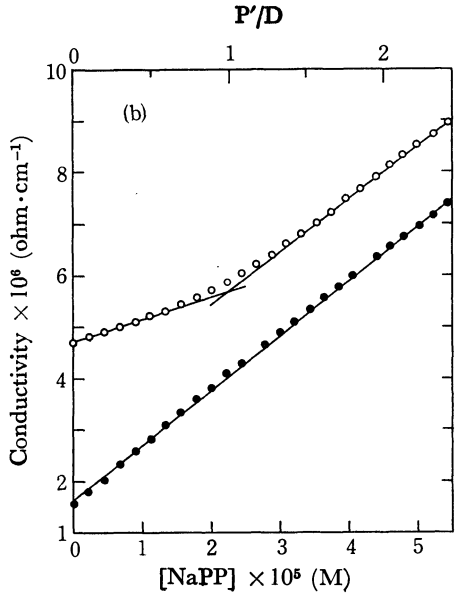

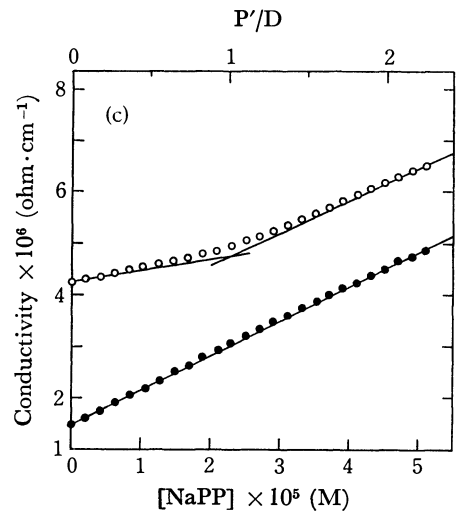

Fig. 7. Conductometric titration of CV with NaPP with various chain lengths (a) n=11, (b) n=24, and (c) n=154.
—●— for blank solution titrated with NaPP for comparison. The concentration of NaPP is corrected for volume increase. P′ is the concentration of the ionized group of the polymer and corrected as equal to $P(1+1/n)$ where P is the residue concentration. Other conditions are given in Experimental.

Discussion

Effects of Mixing Ratio and Polymer Chain Length on Metachromasy. The fact that an abrupt change in metachromasy of CV occurs in the presence of NaPP with chain lengths in the range 7—20 at P/D values of 3 and 30 (Figs. 4a—4b) should be taken as evidence that a certain degree of polymerization is required for a polyphosphate to show metachromasy in a dilute concentration range of 10^{-5} M. This finding newly confirms the previous incomplete reports[8,11,12] and definitely establishes the existence of a critical range of polymer chain lengths for metachromasy. It is not known at present why the polyelectrolyte should have a certain degree of polymerization to induce metachromasy, or why such a critical range should lie in the relatively short oligomeric dimensions. However, there can be no doubt that some action of water on the NaPP–CV complex is involved. The conformation of the complex in aqueous media can be strongly affected by factors such as dielectric constant, hydration and dissociation. Such effects may vary with the chain length of polymer—less pronounced in the case of higher molecular weight. Gekko reported a sudden change in the second virial coefficients of dextran oligomers in aqueous solutions.[23] He attributes the sharp break, which occurs at a degree of polymerization close to 12, to the conformational transition from uncoiling stretched-form for lower molecular weight to random-coil form for higher molecular weight

oligodextrans. Goodman *et al.* have also demonstrated that a critical range exists between $\bar{n}=7$ and 9 for γ-methyl-L-glutamate oligomers forming a helix in dimethylformamide.[24]

The effect of the refractionation of NaPP samples is apparent from Figs. 4a—4c. From the data which show that the sigmoidal curves of the samples are shifted toward the higher $\bar{n}$ relative to the fractionated ones, each refractionated sample should have a narrower molecular weight distribution. This is because the ability of inducing the metachromasy band is unproportionally high with the longer chain length components, which conceivably are included in larger proportions in once-fractionated oligomeric samples than in the twice-fractionated ones. We have studied competitive interactions between a higher ($\bar{n}=154$) and a lower ($\bar{n}=11$) molecular weight NaPP toward the binding of CV. The presence of the small amount (10%) of the higher NaPP in the mixture is sufficient to produce spectra identical with those of the higher NaPP–CV complex at several P/D values. The molecular weight distributions have thus been estimated to be reasonably narrow enough for establishing the critical range of the chain lengths.

Comparison of Optical Titrations with Conductometric Titrations. The optical titration curves in Fig. 3 can be divided into two parts; the region of P/D smaller than unity, where CV in solution is in excess of NaPP residues, and the rest of P/D, where the situation reverses. This option can be justified particularly for polyphosphates, since the only functional group is ionizable phosphates. The first region represents, at a fixed dye concentration (1.12×10^{-5} M), the state of equilibrium between free and bound dyes in solution. This is manifest when the pure CV spectrum is compared with any one of NaPP–CV spectra at very low P/D. They are essentially superimposable. The 592 and 506 nm band intensities are restored almost linearly with P/D between approximately unity and zero. An isosbestic point exists at 639 nm. Hence, it is unlikely that any strong interaction is involved between unbound and bound CV molecules.

With regard to the transition from the first to the second region, the present results (Fig. 3) corroborate the fact that not only the magnitude of metachromasy but also the break at a P/D value near unity depends on the chain lengths of oligomeric polyphosphates ($P/D=1.3$, 1.6, and 2.0 with the uncertainty of about $\pm20\%$ for $\bar{n}=154$, 24, and 11 in this order). The conductometric data (Figs. 6a—6c) show a sharp break at a P/D value of about unity for each NaPP sample. The break is almost independent of the chain length (P/D=1.01, 1.01, and 1.02 with the uncertainty of about $\pm5\%$ for $\bar{n}=11$, 24, and 154 in this order). The unexpected conductometric finding may be taken to be an indication that CV can bind to the phosphate residue of the polymer up to the 1 : 1 ratio at maximum, *i.e.*, the saturation of sites irrespective of the polymer chain length; thus a simple electrostatic binding between cationic CV moiety and anionic phosphate residue should not be the direct cause for the generation of metachromasy. If such an electric charge neutralization by the Coulombic force were sufficient to give rise to metachromasy, then the fact that the metachromasy is less developed for smaller NaPP samples could not be correctly explained without modifying the interpretation of the conductometric data.

Critical Views of the Origin of Metachromasy. As regards the restoration of the 592 nm band intensity observed at higher P/D portion of the second region where polymer sites are in large excess of dye, Bradley *et al.* proposed a mechanism in which metachromasy is generated as a result of the interaction between adjacent bound dyes on the sites of a polymer of infinite length.[3] As the number of the polymer sites becomes in great excess of dye molecules, the bound dyes are unstacked from the adjacent sites and tend to redistribute themselves on the sites and, consequently, they are separated from one another by some vacant sites on a single polymer. Or they are transferred to the isolated sites of other polymer molecules. Pal and Chaudhuri have considered the interaction between adjacent bound dyes to be of hydrophobic nature.[25] According to the original stacking theory, however, the magnitude of metachromasy induced by CV bound to NaPP should remain practically constant over a wide P/D range (particularly between 1 and 10) irrespective of the polymer chain length. This conclusion apparently contradicts the present experimental results.

We alternatively offer two possible but tentative views on the origin of metachromasy, recognizing in both the important role of solvent water molecules. The first view is a modified version of the stacking theory which associates metachromasy with the conformation, more specifically flexibility, of the polymer backbone to which dyes are bound. Since the high molecular weight NaPP is more flexible, the sparsely bound dyes may approach one another while being shielded from hydrophilic environments even in a relatively high P/D range. The forces are thus exerted between the approaching dyes sufficiently to induce metachromasy. Low molecular weight oligomers are too short to be flexible. Because of the stiffness of the short chain, the bound dyes can hardly be enclosed so that they are adjacent. When all the polymer sites are filled with dye molecules (P/D=1), the chain of either short or long polymer would have to be elongated stiffly rather than compactly coiled because of the geometric constraint of the dye-bound moiety. Therefore, the development of metachromasy is optimum in the P/D range 3—10 rather than near unity. One drawback is the difficulty of explaining the fact that the metachromasy band position at 506 nm remains independent of P/D values over almost the entire range while only its intensity varies, and that CV shows a metachromasy band with NaPP, but malachite green does not.[1]

The second view is the dye-site interaction theory which emphasizes the local and specific binding resulting from the dye-site interaction more than the general effect of gross polymer conformations and bound dye-bound dye interactions. The theory attaches primary importance to the following factors: the specific chemical

structure and symmetry of a dye, alteration of the electronic states of dye and site upon formation of a bond which is more than a pure Coulombic one, and the distortion of the bond by some steric perturbation which should increase as more dye molecules are bound in a given crowded area (the lower P/D region). When the bonding between dye and site is purely electrostatic with little orbital overlapping and unsheathing of hydrated water, no metachromasy band should be expected (higher P/D region). In this case, the overall electronic structures of the excited and ground states of the bonding site probably closely resemble those of the pure CV in organic solvents. The second theory does not exclude contributions, to metachromasy, of the flexibility of the polymer chain, which should increase the steric constraints on the bound dye as the chain length increases (high $\bar{n}$ samples), and of the bound dye-bound dye interaction which is probably affected by the conjugated π-electron system of triphenylmethane skeleton. These factors are not to be sufficient for elucidating metachromasy; thus, the first view may be considered to be supplementary to the second.

Closing Remarks. The primary importance should be the class and functional substituent of triphenylmethane dyes for metachromatic behavior. While malachite green with a C_{2v} symmetry, which is short of a substituted amino group as compared with CV, behaves very similarly in the presence of NaPP but shows no metachromasy band under the closely related conditions, ethyl violet and parafuchsin, both of which are homologs of CV with a point symmetry of D_{3h}, show the metachromasy band. In this connection, systematic work relating the development of metachromasy to the chemical structures of triphenylmethane and acridine dyes is highly desirable.[6]

References

1) K. Yamaoka, T. Suenaga, A. Fujita, and M. Miura, *J. Sci. Hiroshima Univ., Ser. A*, **34**, 1 (1970).
2) J. A. Bergeron and M. Singer, *J. Biophys. Biochem. Cytol.*, **4**, 433 (1958).
3) D. F. Bradley and M. K. Wolf, *Proc. Natl. Acad. Sci. US.*, **45**, 945 (1959).
4) K. Yamaoka and R. A. Resnik, *J. Phys. Chem.*, **70**, 4051 (1966).
5) R. A. Resnik and K. Yamaoka, *Biochem. Biophys. Res. Comm.*, **41**, 958 (1970).
6) K. Yamaoka, *Biopolymers*, **11**, 2537 (1972).
7) K. Yamaoka, *Chem. Lett.*, **1973**, 305.
8) J. M. Wiame, *J. Amer. Chem. Soc.*, **69**, 3146 (1947).
9) R. C. Bean, W. C. Shepherd, R. E. Kay, and E. R. Walwick, *J. Phys. Chem.*, **69**, 4368 (1965).
10) G. Weill and M. Calvin, *Biopolymers*, **1**, 401 (1963).
11) B. L. Van Duuren, in "Fluorescence and Phosphorescence Analysis," ed. by D. M. Hercules, John Wiley & Sons, New York, N. Y. (1966), p. 201.
12) M. Miura and Y. Kubota, This Bulletin, **40**, 466 (1967).
13) V. Kleinwächter and J. Koudelka, *Biophysik*, **5**, 119 (1968).
14) G. Löber and V. Kleinwächter, *Stud. Biophys.*, **33**, 73 (1972).
15) R. Itoh, *J. Phys. Soc. Jap.*, **12**, 644 (1957).
16) W. T. Simpson, *J. Amer. Chem. Soc.*, **75**, 597 (1953).
17) W. H. J. Stork, G. J. M. Lippits, and M. Mandel, *J. Phys. Chem.*, **76**, 1772 (1972).
18) M. Schubert and A. Levine, *J. Amer. Chem. Soc.*, **77**, 4197 (1955).
19) T. Soda and K. Yoshioka, *Nippon Kagaku Zasshi*, **86**, 1019 (1965); **87**, 324 (1966).
20) C. L. Greenblatt, N. E. Sharpless, and K. Yamaoka, *Mol. Pharm.*, **6**, 649 (1970).
21) G. Jones and R. C. Josephs, *J. Amer. Chem. Soc.* **50**, 1049 (1928).
22) M. Miura and S. Otani, *Nippon Kagaku Zasshi*, **77**, 517 (1956).
23) K. Gekko, *J. Sci. Hiroshima Univ., Ser. A*, **34**, 1 (1970).
24) M. Goodman, E. E. Schmitt, and D. Yphantis, *J. Amer. Chem. Soc.*, **82**, 3483 (1960).
25) M. K. Pal and M. Chaudhuri, *Makromol. Chem.*, **133**, 151 (1970).
26) M. K. Pal and M. Biswas, *ibid.*, **151**, 121 (1972).

Dielectric Relaxation and Molecular Structure. IX. Dielectric Behavior of 1-Propanol and 1-Butanol in a Variety of Solvents

Taro KOSHII, Eiji ARIE,* Masahiko NAKAMURA, Hiroaki TAKAHASHI, and Keniti HIGASI

Department of Chemistry, Waseda University, Shinjuku, Tokyo 160

(Received November 22, 1973)

The dielectric constants and losses of 1-propanol and its mixtures with benzene, chlorobenzene, 1,4-dioxane or pyridine, and 1-butanol and its mixtures with benzene or pyridine have been measured in the frequency range of 0.35—2.1 GHz at 25.0 °C. Concentrations of alcohols are 1—0.6 mol fraction of the mixtures. Densities and refractive indices have also been determined. The dielectric data were used to calculate the relaxation times of the alcohols. The Cole-Cole plots for these systems showed Debye-type semicircles in lower frequencies where the principal relaxation of alcohols dominates. Deviations from the semicircle, however, have been observed in the region of upper frequencies, where the second dispersion of alcohol, the dispersion of solvent itself and of hydrogen-bonded species between alcohol and solvent may occur. The principal relaxation times of alcohols calculated from the data of lower frequencies change with concentration in two different manners by solvents, and this difference is due to whether the solvent has hydrogen-bonding capacity or not, and does not depend upon the dielectric constant and/or the polarity of the solvent.

Since Mizushima published his measurements on a number of liquid alcohols in 1926,[1] the monoalcohols have been considered to provide an example with which the Debye dispersion of polar molecules occurs in the liquid state. Later, Smyth *et al.*[2] studied ten normal alcohols from propyl through dodecyl in a wide frequency range up to 150 GHz, and established that the dielectric dispersion of primary aliphatic alcohols in the liquid state is characterized by three relaxation regions the most important (the principal relaxation) being at the lower frequency region, and that the principal relaxation cannot be accounted for as arising from rotation of single alcohol molecules. Although a number of dielectric investigations have been made on alcohols since, the precise mechanism of the principal relaxation is still unknown.

In this report the dielectric behavior of normal alcohols has been investigated in the frequency range in which the principal relaxation occurs. Several solvents having different properties in the dielectric constant, the dipole moment and the hydrogen-bonding capacity were added to alcohols and the effect of this addition on the principal relaxation was examined.

Experimental

Materials. All the samples were of the best grade available from commercial sources. They were dehydrated by the usual methods and fractionally distilled prior to their use. The observed refractive indices at 25.0 °C: 1-propanol $n_D=1.3830$, 1-butanol $n_D=1.3968$ are in agreement with the literature values[3].

Apparatus. The apparatus (UHF Material Characteristics Test Assembly) is a coaxial-slotted line type, manufactured by Rohde and Schwarz Co. Ltd., (München, Germany). The principle of the measurement is the standing-wave method, that is, if there is any attenuation in the dielectrics there will be a reduction in the voltage standing-wave ratio (E_{max}/E_{min}), since all the incident wave intensity would not be reflected. A water-jacket surrounding the cell allows for the temperature control of samples within 0.05 °C during a run.

Densities were determined with a Lipkin type pycnometer calibrated with pure water. Refractive indices for sodium D line were measured with a Pulfrich type refractometer.

Evaluation of data. Dielectric constants and losses were calculated as follows. The measured value of the standing-wave ratio E_{max}/E_{min} is mathematically related to the propagation constant γ of the wave along the coaxial line within the sample in the following equation.

$$\frac{\tanh \gamma d}{\gamma d} = -j\left(\frac{\lambda}{2\pi d}\right)\frac{\frac{E_{min}}{E_{max}} - j\tan\left(\frac{2\pi x}{\lambda}\right)}{1 - j\frac{E_{min}}{E_{max}}\tan\left(\frac{2\pi x}{\lambda}\right)} \quad (1)$$

where x is the distance from the first electric field strength minimum of the standing-wave to the surface of the sample, d the specimen length and λ the wavelength along the coaxial line outside the sample. A graphical solution of Eq. (1) has been given by von Hippel[4] in the charts of the following equation.

$$Ce^{j\zeta} = \frac{\tanh Te^{j\delta}}{Te^{j\delta}} \quad (2)$$

where $T\exp(j\delta)$ is the polar form of γd and $C\exp(j\zeta)$ is the polar form of the right hand side of Eq. (1). The charts given in Ref. 4 are limited in range. A computer solution of Eq. (2) was used in order to extend the range. Then the dielectric constant and loss factor are calculated by the following equation.

$$\varepsilon' - j\varepsilon'' = -\left(\frac{\lambda}{2\pi d}\right)^2(\gamma d)^2 \quad (3)$$

When the value of E_{min}/E_{max} is large enough (more than 0.7), it can be measured directly. If the value is small, the distance between the points of twice minimum power Δl is measurable and it connects with E_{max}/E_{min} as follows.

$$\frac{E_{max}}{E_{min}} = \frac{\sqrt{2-\cos^2\left(\frac{\pi\Delta l}{\lambda}\right)}}{\sin\left(\frac{\pi\Delta l}{\lambda}\right)} \quad (4)$$

If the dielectric constant of the sample is approximately

* Present address: Mitsubishi Monsanto Chemical Company, Iwatsuka, Nakamura, Nagoya 453.

known, the optimum length d is given by the condition that d should be at least a quarter wavelength in the material[5], that is,

$$d = \frac{\lambda}{4\sqrt{\varepsilon'}} \tag{5}$$

To determine the relaxation time τ, the distribution parameter α and the high-frequency dielectric constant ε_∞, the Cole-Cole equation[6]

$$\varepsilon' - j\varepsilon'' = \varepsilon_\infty + \frac{\varepsilon_0 - \varepsilon_\infty}{1 + (j\omega\tau)^{1-\alpha}} \tag{6}$$

was fitted to the data by an iterative method using an electronic computer.

Results and Discussion

The dielectric constants and losses of alcohols and their mixtures obtained in this experiments are recorded in Table 1. Dielectric spectra for 1-propanol–benzene and 1-butanol–pyridine mixtures are shown in Fig. 1. (See also Fig. 1 of the preceding letter[7] regarding those for 1-propanol–pyridine mixtures.) It is found for all the mixtures that with increasing amount of solvent the intensity of the maximum absorption decreases and the critical frequency shifts to the higher frequency side. The shift of the frequency is more pronounced in the 1,4-dioxane and in the pyridine mixtures than those in the benzene and in the chlorobenzene mixtures.

The high frequency intercepts of the Cole-Cole plots (ε_∞) for pure alcohols are always much larger than the square of refractive indices for sodium D line (Table 2). It suggests that the second and the third dispersions of alcohols exist in higher frequency range. Values of ε_∞ for the pyridine and chlorobenzene mixtures increase with increasing concentration of solvent, (see *e.g.* Fig. 2-a), while those of ε_∞ for the 1,4-dioxane and benzene mixtures do not change with an increase in the concentration, (see *e.g.* Fig. 2-b). The above difference is due to whether the dispersion of polar solvent contributes to this effect or not. Deviation from the Debye-type semicircle was observed in the frequency range higher than 1 GHz for pure alcohols. For pyridine mixtures the deviation in higher frequency range increases with increasing amount of solvent, while such is not observed for benzene mixtures as in Fig. 2-a and 2-b. The above trend is an indication for the existence of the dispersions of polar solvent, of interaction species between solute and solvent, of second dispersion of the alcohol, *etc.*

Using Eq. (6) the distribution parameter α of the Cole-Cole plot and the relaxation time τ were evaluated

Table 1 (a). Dielectric constant and loss of pure alcohols at 25.0 °C

Substance	1-Propanol		1-Butanol	
f(GHz)	ε'	ε''	ε'	ε''
0.356	14.41	7.97	9.44	6.84
0.515	11.64	8.43	7.35	6.17
0.697	8.92	7.71	5.85	5.24
1.00	7.06	6.39	4.79	3.99
1.50	5.55	4.93	4.01	2.95
2.11	4.67	3.92	3.70	2.11

Table 1(b). Dielectric constant and loss for alcohol mixtures (mole fraction of alcohol, mf) at 25.0 °C

f(GHz)	ε'	ε''	ε'	ε''	ε'	ε''	ε'	ε''
	1-Propanol in benzene							
	mf=0.899		mf=0.857		mf=0.741		mf=0.633	
0.356	13.33	6.79	12.75	6.10	11.30	4.83	9.61	3.35
0.515	11.11	7.22	10.76	6.72	9.56	5.33	8.43	3.82
0.697	8.48	6.54	8.98	6.59	8.08	5.25	7.47	4.09
1.00	6.79	5.70	6.75	5.42	6.45	4.63	6.07	3.67
1.50	5.36	4.48	5.55	4.37	5.16	3.77	4.87	3.07
2.11	4.41	3.55	4.52	3.42	4.45	3.07	4.24	2.47
	1-Propanol in chlorobenzene							
	mf=0.929		mf=0.887		mf=0.822		mf=0.690	
0.356	13.92	6.95	14.17	6.31	13.63	5.42	11.76	3.91
0.515	11.23	7.36	11.67	6.96	10.87	5.92	10.43	4.47
0.697	8.53	6.48	9.64	6.66	9.45	5.90	8.96	4.45
1.00	7.30	5.81	7.36	5.67	7.82	5.27	7.59	4.07
1.50	5.90	4.75	5.41	4.38	6.12	4.13	6.32	3.33
2.11	5.00	3.53	5.27	3.55	5.25	3.26	5.71	2.82
	1-Propanol in 1,4-dioxane							
	mf=0.940		mf=0.856		mf=0.790		mf=0.581	
0.356	14.90	6.12	13.83	4.02	12.63	2.79	8.19	0.85
0.515	12.63	6.94	12.63	4.98	11.89	3.67	8.20	1.13
0.697	9.79	6.85	10.54	5.64	10.96	4.28	7.94	1.51
1.00	8.23	6.36	9.15	5.53	9.20	4.63	7.51	1.93
1.50	6.21	5.21	7.19	5.03	7.47	4.43	6.81	2.21
2.11	5.52	4.43	6.05	4.38	6.57	4.17	6.22	2.32

f(GHz)	ε'	ε''	ε'	ε''	ε'	ε''	ε'	ε''
	1-Propanol in pyridine							
	mf=0.980		mf=0.960		mf=0.947		mf=0.917	
0.356	15.37	7.63	15.81	7.14	16.07	6.82	16.86	6.06
0.515	12.37	8.14	13.12	7.82	13.38	7.56	14.51	7.12
0.697	9.71	7.72	10.62	7.85	10.93	7.76	12.66	7.60
1.00	7.57	6.55	9.35	7.16	8.55	6.78	9.58	6.82
1.50	5.97	5.15	6.19	5.30	6.64	5.57	7.94	5.96
2.11	4.97	4.12	5.34	4.41	5.48	4.55	6.05	4.86
	mf=0.905		mf=0.855		mf=0.719		mf=0.577	
0.356	16.52	6.06	17.48	4.78	17.44	2.83	16.75	1.76
0.515	14.75	6.84	15.51	6.08	16.95	3.77	16.27	2.29
0.697	12.69	7.25	13.58	6.77	15.99	4.72	15.93	3.10
1.00	9.94	6.85	11.30	6.76	14.24	5.69	14.84	4.14
1.50	7.93	5.93	8.73	6.16	12.32	6.10	13.18	4.69
2.11	6.38	4.99	7.23	5.49	10.27	5.87	12.01	5.22
	1-Butanol in benzene							
	mf=0.899		mf=0.806		mf=0.670		mf=0.620	
0.356	9.40	6.09	9.02	5.27			7.77	3.15
0.515	6.78	5.61	7.20	5.04	6.79	3.89	6.57	3.34
0.697	5.86	4.88	5.78	4.47	5.62	3.39	5.67	3.20
1.00	4.82	3.81	4.80	3.46	4.73	3.00	4.68	2.71
1.50	3.99	2.78	4.01	2.64	3.99	2.28	3.98	2.14
2.11	3.67	2.22	3.64	2.10	3.64	1.85	3.65	1.70
	1-Butanol in pyridine							
	mf=0.894		mf=0.807		mf=0.699		mf=0.568	
0.356	12.62	5.69	13.96	4.18	14.52	2.90	14.59	1.77
0.515	10.35	5.91	12.56	5.00	13.67	3.74	14.10	2.44
0.697	8.88	5.93	11.14	5.43	12.70	4.40	13.51	3.10
1.00	7.17	5.11	9.15	5.51	10.87	4.84	12.53	3.79
1.50	5.67	4.20	7.18	4.69	9.00	4.89	10.91	4.33
2.11	5.00	3.48	6.20	4.26	8.08	4.67	9.90	4.64

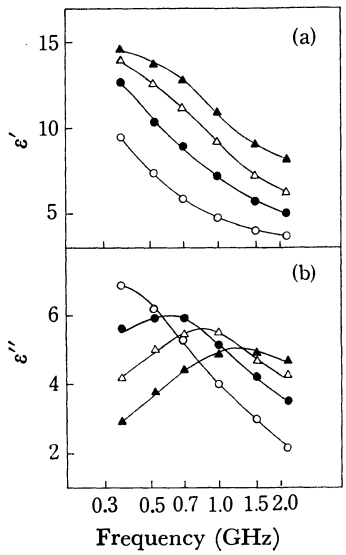

Fig. 1-1. (a) Dielectric dispersion and (b) absorption curves for 1-butanol mixtures with pyridine.
Mole fraction of alcohol
○: 1.00, ●: 0.894, △: 0.807, ▲: 0.699

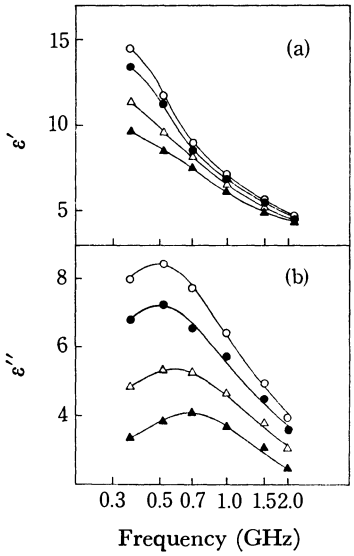

Fig. 1-2. (a) Dielectric dispersion and (b) absorption curves for 1-propanol mixtures with benzene.
Mole fraction of alcohol
○: 1.00, ●: 0.899, △: 0.741, ▲: 0.633

in two ways, that is, (1) the higher frequency data over 1 GHz are neglected and (2) all the data are taken into equal consideration. The values of α calculated from (1) are nearly equal to zero in all the mixtures, *viz.* α=0.00—0.03, while those of calculated from (2) are larger, *viz.* α=0.04—0.07. Presumably

Table 2. Values of ε_∞, n_D^2 and τ

Substance	ε_∞	n_D^2	τ ps (25.0 °C) This work	Lit.[2)a)]	Lit.[8)]
1-Propanol	3.93	1.91	340	350	330
1-Butanol	3.50	1.95	505	540	480

a) Recalculated from low-frequency data and corrected to 25.0 °C.

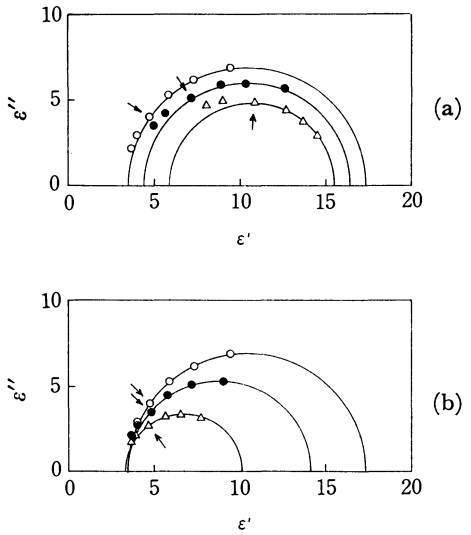

Fig. 2. Cole-Cole plots for 1-butanol mixtures with (a) pyridine and (b) benzene.
Mole fraction of alcohol
(a) ○: 1.00, ●: 0.894, △: 0.699
(b) ○: 1.00, ●: 0.806, △: 0.620
Arrows indicate the points measured at the frequency of 1.00 GHz.

the Debye dispersions observed in the frequency range lower than 1 GHz are of the principal relaxation.** The values of principal relaxation times of normal alcohols are thus determined from (1) and compared with those of the literature in Table 2.

The principal relaxation times of 1-propanol and 1-butanol against the molarity of the alcohols are plotted in Fig. 3. With increasing alcohol molarity, τ increases; in other words, decrease in τ is accompanied with decrease in the molarity, *i.e.*, with increasing amount of solvent added. It will be seen that this decrease in τ is more pronounced when hydrogen-bonding solvent, pyridine or 1,4-dioxane, is added to 1-propanol. And the plots of τ *vs.* molarity fall into the same curve A for these two solvents inspite of the fact that pyridine has a large dipole moment 2.25 D and high dielectric constant (ε=12.3)*** and 1,4-dioxane

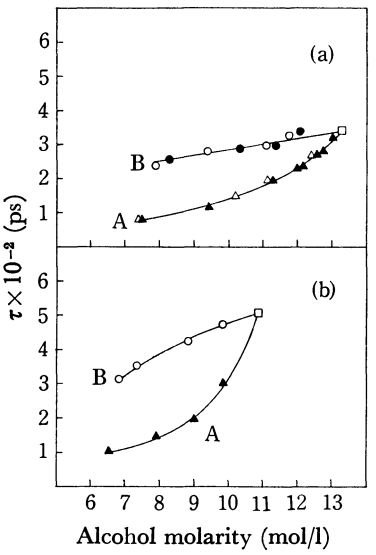

Fig. 3. Relaxation time τ *vs.* concentration for (a) 1-propanol and (b) 1-butanol mixtures with solvent.
Solvent:
○: Benzene, ●: Chlorobenzene, △: 1,4-Dioxane,
▲: Pyridine, □: Pure alcohol

is non-polar and has a low dielectric constant (ε=2.21). In sharp contrast to this, the same plots for the addition of two non-hydrogen-bonding solvents, benzene or chlorobenzene, give the identical curve B in which the degree of decrease in τ is much smaller with decreasing molarity. Again the dipole moments μ and the dielectric constants ε differ greatly in benzene (μ=0.0 D, ε=2.27) and in chlorobenzene (μ=1.70 D, ε=5.62).

The principal relaxation time of 1-butanol is studied with addition of hydrogen-bonding pyridine and non-hydrogen-bonding benzene. Again the decrease in τ is more pronounced in pyridine mixtures (curve A) than benzene mixtures (curve B).

The dependence of relaxation time upon the concentration in highly concentrated mixture of alcohols has been reported by Sarojini[9)] and Hanna *et al.*[10)] Both of these authors observed that the relaxation time did not change monotonously with the concentration. A minimum in τ was observed in 1-propanol mixture with pyridine,[9)] while a maximum was detected in 1-butanol mixture with carbon tetrachloride and with other viscous non-polar solvents.[10)] These results are inconsistent with ours. Perhaps their choice of the frequency range was inadequate for determining the pure principal relaxation, that is, they failed in eliminating the effects from other dispersions.

We wish to present our sincere thanks to Professor Mansel Davies of University College of Wales for his helpful suggestions and also correcting English in the manuscript. We also thank Toray Science Foundation for the financial aids.

** Errors due to the losses of polar solvents, *viz.* pyridine and chlorobenzne, were estimated and the relaxation times with this correction were found to be almost identical with those calculated without the correction. The relaxation times reported in the preceding letter[7)] were those of calculated from the method (2). New relaxation times calculated by use of the Debye equation (α=0) are employed in the present paper.

*** The dielectric constants cited here are those at 25.0 °C.

References

1) S. Mizushima, This Bulletin, **1**, 163 (1926).
2) S. K. Garg and C. P. Smyth, *J. Phys. Chem.*, **69**, 1294

(1965).
3) Landolt-Börnstein, "Zahlenwerte und Funktionen aus Physik, Chemie, Astronomie, Geophysik und Technik," 2 Band, 8 Teil, Optische Konstanten.
4) A. R. von Hippel, "Dielectric Materials and Applications," John Wiley and Sons (1954).
5) R. Payne and I. E. Theodorou, *Rev. Sci. Instr.*, **42**, 218 (1971).
6) K. S. Cole and R. H. Cole, *J. Chem. Phys.*, **9**, 341 (1941).
7) E. Arie, M. Nakamura, H. Takahashi, and K. Higasi, *Chem. Lett.*, **1973**, 533.
8) A. Sugget, P. A. Mackness, M. J. Tait, H. W. Loeb, and G. M. Young, *Nature*, **228**, 456 (1970).
9) V. Sarojini, *Trans. Faraday Soc.*, **58**, 1729 (1962).
10) F. F. Hanna and I. K. Hakim, *Z. Naturforsch.*, **26a**, 1194 (1971).

Dielectric Relaxation and Molecular Structure. X. Dielectric Behavior of 2-Propanol, 2-Methylpropanol, and 2-Butanol in a Variety of Solvents

Taro KOSHII, Eiji ARIE,* Masahiko NAKAMURA, Hiroaki TAKAHASHI, and Keniti HIGASI

Department of Chemistry, Waseda University, Shinjuku, Tokyo 160

(Received November 22, 1973)

The dielectric constants and losses of 2-propanol and its mixtures with benzene, chlorobenzene, 1,4-dioxane or pyridine and 2-methylpropanol or 2-butanol and their mixtures with benzene or pyridine have been measured in the frequency range of 0.35—2.1 GHz at 25.0 °C. Concentrations of alcohols are 1—0.6 mol fractions of the mixtures. The principal relaxation times and the Kirkwood correlation factor g were evaluated. Variation of the principal relaxation times against the concentrations of these branched alcohol mixtures is not much different from that of normal alcohol mixtures. The g factor decreases almost monotonously with increasing amount of solvent exception being found in case for propanol–benzene mixtures.

Smyth *et al.*[1] have made dielectric measurements on several isomeric octanols in non-polar solvent (*n*-heptane). For those isomers in which a methyl group is attached to the same carbon atom as the hydroxyl group or to the adjacent carbon, the dielectric absorption is characterized by two relaxation times and the principal relaxation does not appear at the concentrations employed. However, the isomers containing a relatively less shielded hydroxyl group exhibit an additional low-frequency relaxation at the higher alcohol concentrations. Crossley *et al.*[2] have made dielectric investigation on several isomeric butanols with various solvents in a wide concentration range. He found that the basicity of the solvent plays an important role in determining the extent of self association of alcohol, that is, cyclohexane was regarded as an inert solvent and the other three solvents had a disassociating effect which increases in the order of *p*-xylene$\leq$mesitylene$<$1,4-dioxane.

We have made dielectric measurements on branched-alcohol mixtures with solvents having various properties such as different dipole moments, dielectric constants or hydrogen-bonding capacities. The side chain of those alcohols is expected to have an effect on the relaxation mechanism. The relaxation time observed in our frequency range was the principal (long) relaxation time and its variation with the concentration of solvents was examined.

Experimental

The purification of the samples has been given in the previous paper[3]. The observed refractive indices: 2-propanol n_D=1.3750, 2-methylpropanol n_D=1.3932, 2-butanol n_D=1.3945 at 25.0 °C are in agreement with the literature values[4]. The dielectric constants and losses were measured by use of the method previously described[3]. Viscosities were measured with an Ostwald type viscometer.

The Kirkwood correlation factor g is represented in the following equation[5].

$$g = \frac{9kT(\varepsilon_0-\varepsilon_\infty)(2\varepsilon_0+\varepsilon_\infty)}{4\pi N\varepsilon_0(\varepsilon_\infty+2)^2\mu_0^2} \quad (1)$$

where μ_0 is the dipole moment of the molecule, N the number of molecules per unit of volume, k the Boltzmann constant and T the absolute temperature. ε_0 and ε_∞ are the static and the high frequency dielectric constants, respectively. We used the values of ε_0 and ε_∞ obtained from the low and the high frequency intercepts of the Debye-type semicircle, respectively and μ_0 from the values in the gaseous state.[6] The values of ε_0 obtained above are compared with those measured at the frequency of 10 kHz; both are generally in good agreement.

Results and Discussion

The measurements in dielectric constants and losses are recorded in Table 1. The dispersion and absorption curves of branched-alcohol mixtures are similar to those observed in normal-alcohol mixtures. (See Fig. 1 of Ref. 3).

The principal relaxation times were calculated by the method previously employed[3] and are plotted against the concentration in Fig. 1. The trend similar to normal-alcohol mixtures is observed, that is, the plots can be grouped into two groups (curves A and B). The relaxation times of 2-propanol depend very little upon the polarity of the solvent; the dipole moments of pyridine, chlorobenzene, 1,4-dioxane, and benzene are 2.25, 1.70, 0.4, and 0.0 D in gaseous state, respectively. They are also independent of the dielectric constant (ε for pyridine, chlorobenzene, 1,4-dioxane, and benzene are 12.3, 5.62, 2.21, and 2.27 at 25 °C, respectively) and depend only upon the hydrogen-bonding capacity. These facts strongly suggest that the principal relaxation times of the alcohol may be mainly dominated by hydrogen bonding of alcohol molecules.

A similar study on the relaxation times for 2-butanol dioxane mixture was reported by Sakellaridis and Hinopoulos.[7] Their relaxation times are, however, much lower than those of our experiment: possibly it may come from their measurement at the single frequency of 9.3 GHz.

The separation between curves A and B is not the same for all the alcohols. This separation is more pronounced in 1-propanol** than in 2-propanol, while

* Present address: Mitsubishi Monsanto Chemical Company, Iwatsuka, Nakamura, Nagoya, 453.

** Data for 1-propanol and 1-butanol are given in Ref. 3.

Table 1(a). Dielectric constant and loss of pure alcohols at 25.0 °C

Substance f(GHz)	2-Propanol		2-Methylpropanol		2-Butanol	
	ε'	ε''	ε'	ε''	ε'	ε''
0.356	13.77	7.58	8.10	6.74	9.23	6.44
0.515	10.28	7.81	6.31	5.80	7.20	5.90
0.697	8.44	7.31	5.06	4.71	5.77	4.98
1.00	6.18	5.76	4.24	3.47	4.67	3.83
1.50	4.57	4.23	3.60	2.52	3.97	2.88
2.11	4.07	3.36	3.43	1.92	3.62	2.21

Table 1(b). Dielectric constant and loss for alcohol mixtures (mole fraction of alcohol, mf) at 25.0°C

f(GHz)	ε'	ε''	ε'	ε''	ε'	ε''	ε'	ε''
	2-Propanol in benzene							
	mf=0.900		mf=0.827		mf=0.742		mf=0.618	
0.356	12.56	6.01	11.96	5.01	10.58	3.76	8.75	2.34
0.515	10.36	6.44	10.05	5.51	9.19	4.40	7.80	2.83
0.697	8.46	6.36	8.25	5.60	7.76	4.66	6.99	3.24
1.00	6.85	5.49	6.39	4.87	6.25	4.22	5.72	3.21
1.50	4.75	4.16	5.01	3.90	4.85	3.47	4.74	2.70
2.11	4.25	3.39	4.10	2.95	4.23	2.93	4.19	2.35
	2-Propanol in chlorobenzene							
	mf=0.937		mf=0.894		mf=0.814		mf=0.625	
0.356	12.86	6.46	13.11	5.79	12.21	4.48	9.97	2.16
0.515	10.91	6.90	10.85	6.27	10.43	5.10	9.18	2.76
0.697	8.30	6.53	8.94	6.24	8.73	5.18	8.44	2.97
1.00	6.72	5.57	6.58	5.26	7.27	4.73	7.45	2.97
1.50	5.18	4.26	5.43	4.27	5.88	3.85	6.40	2.75
2.11	4.51	3.36	4.69	3.35	5.16	3.29	5.90	2.48
	2-Propanol in 1,4-dioxane							
	mf=0.919		mf=0.856		mf=0.769		mf=0.601	
0.356	13.38	5.44	12.73	3.80	11.15	2.39	7.85	0.91
0.515	11.50	6.05	11.47	4.67	10.43	3.08	7.59	1.15
0.697	9.66	6.32	9.85	5.24	9.62	3.72	7.33	1.43
1.00	7.18	5.56	8.13	5.08	8.18	3.83	6.90	1.76
1.50	5.54	4.64	6.24	4.52	6.60	3.77	6.04	2.03
2.11	4.70	3.76	5.23	3.83	5.66	3.54	5.50	2.21
	2-Propanol in pyridine							
	mf=0.912		mf=0.822		mf=0.752		mf=0.550	
0.356	15.08	5.86	16.00	4.09	16.07	3.09	15.49	1.44
0.515	13.11	6.59	14.64	5.13	15.14	4.04	15.19	2.26
0.697	10.44	6.71	13.13	5.87	14.27	4.58	14.85	2.62
1.00	8.62	6.28	10.94	6.01	12.24	5.46	14.03	3.40
1.50	6.60	5.23	8.59	5.75	10.18	5.46	12.65	4.19
2.11	5.44	4.55	7.39	5.24	8.55	5.39	11.50	4.98
	2-Methylpropanol in benzene							
	mf=0.888		mf=0.799		mf=0.664		mf=0.609	
0.356	8.36	6.06	8.43	5.14	7.86	3.65	7.42	2.96
0.515	6.69	5.35	6.67	4.83	6.51	3.71	6.33	3.10
0.697	5.47	4.55	5.39	4.21	5.44	3.31	5.30	2.97
1.00	4.42	3.47	4.46	3.26	4.49	2.78	4.52	2.46
1.50	3.71	2.56	3.81	2.51	3.89	2.19	3.85	2.01
2.11	3.44	1.96	3.45	1.96	3.53	1.74	3.52	1.62
	2-Methylpropanol in pyridine							
	mf=0.904		mf=0.801		mf=0.701		mf=0.619	
0.356	11.49	6.03	13.54	3.98	14.12	2.98	14.21	2.12
0.515	9.38	6.09	12.08	5.03	13.11	3.76	13.64	2.98
0.697	7.74	5.56	10.62	5.46	12.31	4.44	12.90	3.68
1.00	6.36	4.72	8.73	5.14	10.54	4.78	11.76	4.13
1.50	5.07	3.72	6.99	4.50	8.11	4.84	10.10	4.52
2.11	4.53	3.11	5.90	4.11	7.68	4.59	8.88	4.56

f(GHz)	ε'	ε''	ε'	ε''	ε'	ε''	ε'	ε''
	2-Butanol in benzene							
	mf=0.897		mf=0.809		mf=0.675		mf=0.533	
0.356	9.23	5.34	8.95	4.25	7.86	2.52	6.04	1.31
0.515	7.38	5.36	7.42	4.41	6.87	2.74	5.78	1.51
0.697	5.85	4.47	5.96	4.02	5.93	2.96	5.21	1.62
1.00	4.64	3.64	5.01	3.42	4.99	2.57	4.80	1.60
1.50	3.92	2.80	4.10	2.71	3.98	2.06	4.09	1.53
2.11	3.52	2.20	3.68	2.10	3.73	1.83	3.77	1.35
	2-Butano lin pyridine							
	mf=0.900		mf=0.809		mf=0.699		mf=0.616	
0.356	11.56	5.31	12.99	3.76	13.52	2.51	13.49	1.72
0.515	9.60	5.55	11.71	4.51	12.80	3.10	13.03	2.42
0.697	8.06	5.37	10.28	4.92	11.86	3.80	12.59	3.14
1.00	6.56	4.54	8.57	4.70	10.10	4.25	11.54	3.63
1.50	5.25	3.71	6.89	4.33	8.79	4.38	9.44	4.43
2.11	4.59	3.15	5.89	3.93	7.72	4.32	8.85	4.48

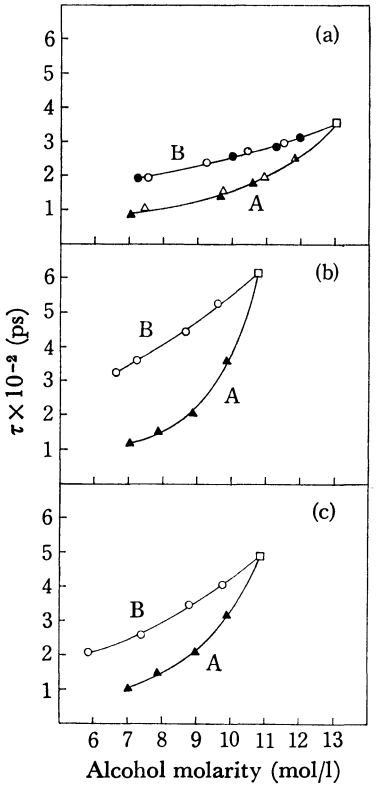

Fig. 1. Relaxation time τ *vs.* concentration for (a) 2-propanol, (b) 2-methylpropanol and (c) 2-butanol mixtures with solvent.
Solvent:
○: Benzene, ●: Chlorobenzene, △: *p*-Dioxane,
▲: Pyridine, □: Pure alcohol

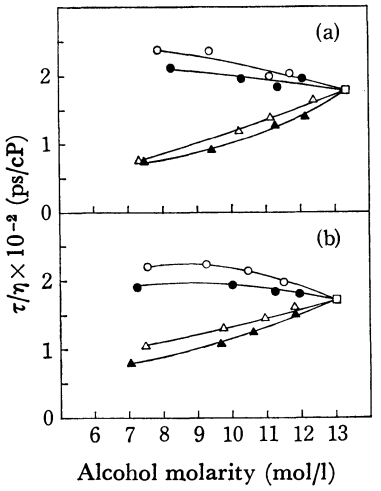

Fig. 2. Reduced relaxation time τ/η *vs.* concentration for (a) 1-propanol and (b) 2-propanol mixtures with solvent. Same notations as in Fig. 1.

for 1-butanol** and 2-methyl propanol it is similar to each other, being much diminished in 2-Butanol Thus, the relaxation process of normal alcohols is more strongly effected by hydrogen-bonding capacity of solvents than that of *iso* and *secondary* alcohols in which hydrogen bonding of the hydroxyl group is hindered by the screening effect of side chains.

The reduced relaxation time τ/η in which τ is the relaxation time and η is the viscosity of the mixture is considered. Plots of τ/η against the molarity are shown in Fig. 2. We find four curves in Fig. 2 instead of two curves A and B in Fig. 1. Again in the pyridine and 1,4-dioxane mixtures the decrease in τ/η, which represents the volume of rotating units in the Stokes assumption, is sharper with increasing amount of solvent than that in the benzene and chlorobenzene mixtures.

Figure 3 shows the Kirkwood correlation factor g against the concentration of mixture. The values of g were calculated by means of Eq. (1). A large value of g, a parameter for the self association, is found in the pure liquid alcohols, and the value of g decreases with increasing amount of solvent (see Fig. 3). At infinite dilution, or, for free molecules g is equal to unity.[2] Small g values less than the unity found *e.g.*, in pyridine mixtures, might reveal the formation of multimers having smaller dipole moments than the free monomer. Further, if the g factor represents the short-range interaction of molecules, the observed decrease in g would suggest that the degree of this interaction decreases in dilution. It will be seen that the decrease is sharpest in case of the mixture with hydrogen-bonding pyridine (ε=12.3, μ=2.25 D) and followed by

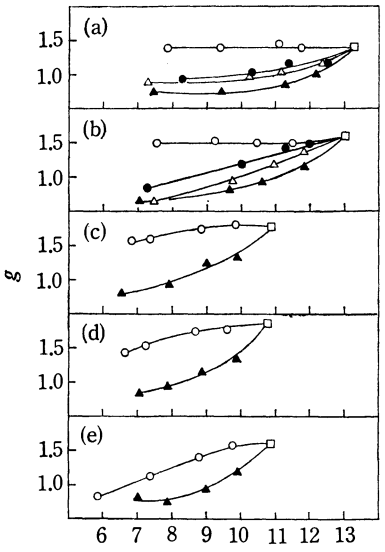

Fig. 3. Kirkwood correlation factor g *vs.* concentration for (a) 1-propanol, (b) 2-propanol, (c) 1-butanol, (d) 2-methylpropanol and (e) 2-butanol mixtures with solvent. Same notations as in Fig. 1.

another hydrogen-bonding 1,4-dioxane (ε=2.21, μ=0.4 D), non-hydrogen-bonding chlorobenzene (ε=5.62, μ=1.7 D) and benzene (ε=2.27, μ=0.0 D). This order of decrease in g agrees with that in reduced relaxation time in Fig. 2. This would suggest that the multimer is associated with the volume of rotating unit. The fact that g is almost independent of the concentration in propanol–mixtures with benzene would indicate that the interaction between alcohol and solvent molecule does not change with dilution.

We wish to present our sincere thanks to Professor Mansel Davies of University College of Wales for his helpful suggestions and also for correcting English in the manuscript. We also thank Toray Science Foundation for the financial aids.

References

1) J. Crossley, L. Glasser, and C. P. Smyth, *J. Chem. Phys.*, **55**, 2197 (1971).
2) G. E. Rajala and J. Crossley, *Can. J. Chem.*, **49**, 3617 (1971).
3) T. Koshii, E. Arie, M. Nakamura, H. Takahashi and K. Higasi, This Bulletin **47**, 618 (1974).
4) Landolt-Börnstein, "Zahlenwerte und Funktionen aus Physik, Chemie, Astronomie, Geophysik und Technik," 2 Band, 8 Teil, Optische Konstanten.
5) J. G. Kirkwood, *J. Chem. Phys.*, **7**, 911 (1939).
6) A. L. McClellan, "Tables of Experimental Dipole Moments," W. H. Freeman and Company (1963).
7) P. Sakellaridis and B. Hinopoulos, *J. Appl. Chem. Biotechnol.*, **22**, 1077 (1972).

Vibrational Structures in the He(I) Photoelectron Spectra of Carboxylic Acids

Iwao WATANABE, Yu YOKOYAMA, and Shigero IKEDA

Department of Chemistry, Faculty of Science, Osaka University, Toyonaka, Osaka 560

(Received August 17, 1973)

The first and the second bands of the photoelectron spectra of acetic, propionic, and isobutyric acids were recorded, and the vibrational structures in the spectra were studied by comparing with the results of formic acid. The first band exhibits a $\nu_{C=O}$, a δ_{OH}, and a ρ_{COOH} vibrational progression, and this implies that an oxygen lone pair orbital, from which the first band of the spectra originates, contributes not only to a C=O bonding and the bonding between carbonyl oxygen and hydroxyl hydrogen, but to the settling of carboxyl group in the molecular plane. The second band exhibits a $\nu_{C=O}$, a ν_{C-O}, and a δ_{OCO} vibrational progression with very high frequency for the $\nu_{C=O}$ as observed in the case of formic acid. Thus the vibrational features of the second band are consistent with the ionization of an antisymmetric π orbital localized mainly on carbonyl and hydroxyl oxygen atoms. Since the 0-0 vibrational transitions for the second ionization are out of the Franck-Condon region, the second adiabatic ionization potential was estimated by comparing the vibrational fine structures of the spectra with that of formic acid. The second adiabatic ionization potential of acetic acid so determined is 11.63 eV.

It is predicted from theoretical calculations that the most easily ionized orbitals, from which the first and the second bands of photoelectron spectra of aliphatic carboxylic acids originate, are an oxygen lone pair (n_o) and an antisymmetric π (π_2) orbital.[1-3] It is reasonable to expect that these bands have quite similar appearances among these molecules, since the calculations predict that the n_o orbital is localized mainly on a carbonyl oxygen and the π_2 on carbonyl and hydroxyl oxygens. In other words, if some features in the photoelectron bands are found which are common in all carboxylic acids, they must be the features intrinsic to the carboxyl group.

In the previous report,[3] the vibrational structures in the spectra of formic acid and its deuterium derivatives have been studied in detail, and the most interesting phenomenon found in the spectra of formic acid is the extraordinarily strengthened C=O bond by the ionization of the π_2 orbital. If the n_o and the π_2 orbitals are really the intrinsic orbitals localized on the carboxyl group, similar vibrational structures to those of formic acid should be revealed in the spectra of acetic acid and/or higher carboxylic acids, too.

The only vibrational structures reported in the spectrum of acetic acid are a $\nu_{C=O}$ (C=O stretching vibration) mode in the first band, and a 1050 cm^{-1} mode unassigned in the second.[4,5] Any other vibrational structures in the second or deeper bands for acetic or higher carboxylic acids have not been reported.

This paper deals with the first and the second bands of improved resolution spectra of acetic, propionic, and isobutyric acids together with the comparison of their fine structures with those of formic acid to find intrinsic features in the photoelectron spectra of carboxylic acids.

Experimental

The photoelectron spectra were measured with an apparatus already reported[6] and a modified helium resonance lamp. The new lamp has a shorter collimating capillary of wider inner diameter and two hollow electrodes aligned in the optical axis of the lamp. The modification increased the intensity of the exciting light (He(I) 584 Å), and better performance was attained.

All samples were of G. R. grade and used without any further purification. Variations of appearance potentials of photoelectron peaks for carboxylic acids during measurements were so large that preliminary mixing of reference gas, xenon, into the sample gas was essentially needed to measure the ionization potentials accurately. Usually the spectra were measured after running of sample gas more than 30 minutes, since shift of the kinetic energy of photoelectron to lower energy side with the elapse of time was always noticed. The measurements were repeated many times for more than five hours until it was confirmed that the differences between consecutive runs were not detected.

The point which an attention should be paid to is the dependence of the resolving power of this apparatus on the sample pressure. The spectra of acetic acid at high and low pressures have very different appearances. The spectrum at low sample pressure has adequate signal intensity and very similar appearance to the expanded spectrum reported by Sweigart *et al.*[4] On the other hand, the high pressure spectrum has sharper bands with finer vibrational structures. To study whether the association of sample molecules or the change of sample density in an ionization chamber gives rise to the phenomenon, the sample gas was mixed with xenon gas and the spectra of the sample were measured with varying the xenon gas pressure while the partial pressure of the sample gas remained constant. It was found that by introducing the xenon in relatively high pressure the spectrum features resemble those of the high pressure spectrum, and that the resolving power strongly depends on the gas density in the ionization chamber. The similar phenomena have been noticed in the cases of other molecules. The factors influencing the variation of the electron kinetic energy[6] can cause the broadening of the photoelectron peaks. It was found that the degree of the photoelectron spectrum degradation by the broadening depends on the character of the sample gas, the gas density in the ionization chamber, and the history of the apparatus, that is, the sample flowed just before the measurement, the period of the apparatus left at rest in vacuum or in air, and so on.

Results and Discussion

The First Bands. The expanded spectra of the first band of acetic, propionic, and isobutyric acids are

shown in Figs. 1, 2, and 3, respectively, and their vibrational frequencies are summarized in Table 1. The spectra of other aliphatic carboxylic acids do not exhibit clear vibrational structures and are not shown.

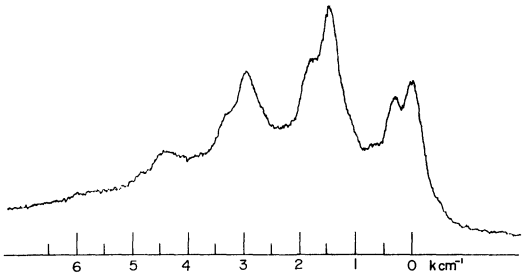

Fig. 1. The first band of the photoelectron spectrum of acetic acid.

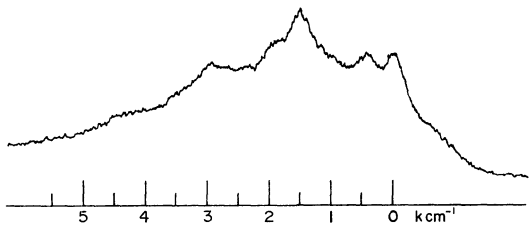

Fig. 2. The first band of the photoelectron spectrum of propionic acid.

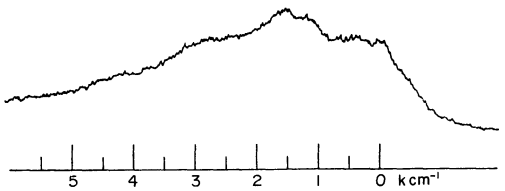

Fig. 3. The first band of the photoelectron spectrum of isobutyric acid.

For comparison the fundamental vibrational frequencies of the ground molecular state of acetic acid are taken from the work by Berney *et al.*,[7] which utilized an inert-gas matrix method and are included in Table 1. The usual gas phase IR spectra of the monomers of carboxylic acids have been measured at a high temperature, 150 °C, to decrease dimer equilibrium ratio and thus the appearance of their IR spectra becomes broad and complex. The matrix-isolation technique at temperatures near 4 K sharpens the absorption peaks, removes hot bands, and allows an accurate determination of the band origins.

Obviously the first ionization is accompanied by the excitation of not only a $\nu_{C=O}$ mode but some other vibrational modes in all carboxylic acids. The main spacings (*ca.* 1500 cm^{-1}) of the $\nu_{C=O}$ present in all molecules almost agree with that of formic acid (1486 cm^{-1}).[3]

The frequencies for the next strongest vibrational progression are 310, 420, and 360 cm^{-1} in acetic, propionic, and isobutyric acid, respectively. This structure has not been reported yet. It is difficult to find a fundamental mode of acetic acid corresponding to such a low vibrational frequency and thus the two possibilities are considered to interpret this low frequency component by attributing to one of the vibrational frequencies of dimer molecule. (1) The photoelectron spectra of dimers of carboxylic acids have the same profiles as those of monomers with the ionization potential blue shifted by *ca.* 38 meV (~300 cm^{-1}). The orbital energies, obtained from the *ab initio* MO calculations performed by Ady *et al.*,[8] of the highest occupied σ orbital of monomer and dimer molecule of formic acid are −0.4510 and −0.4526 (in atomic units) and the difference is about the same as the observed ionization potential shift. (2) The adiabatic ionization potentials of monomers and dimers are almost or just the same and thus the peaks separated

TABLE 1. VIBRATIONAL FREQUENCIES IN THE FIRST BAND SPECTRA OF SOME CARBOXYLIC ACIDS, AND FUNDAMENTAL FREQUENCIES OF GROUND STATE ACETIC ACID[a] (cm^{-1})

Acetic	Propionic	Isobutyric	Assignments
1500±20	1500±30	1510±40	$\nu_{C=O}$
1470±20	1430±40		
1450±30			
310±20	420±30	360±40	ρ_{gear}
320±40	430±50		
380±50			
1170±50	1090±100	1150±50	δ_{OH}
1190±50	1170±50		
710±50	850±50		ν_{CC}, ν_{C-O}, or ρ_{CH_3}
730±50			
910±50			

a′ block						a″ block		
ν_1	ν_{OH}	3583	ν_7	ν_{C-O}	1259	ν_{13}	ν_{HCH_2}	2996
ν_2	ν_{HCH_2}	3051	ν_8	δ_{OH}	1181	ν_{14}	δ_{HCH_2}	1439
ν_3	ν_{CH_3}	2944	ν_9	ρ_{CH_3}	987	ν_{15}	ω_{CH_3}	1044
ν_4	$\nu_{C=O}$	1788	ν_{10}	ν_{CC}	847	ν_{16}	τ_{OH}	535
ν_5	δ_{HCH_2}	1434	ν_{11}	δ_{OCO}	581	ν_{17}	γ	639
ν_6	δ_{CH_3}	1380	ν_{12}	ρ_{gear}	428	ν_{18}	τ_{CH_3}	93

a) From C. V. Berney, R. L. Redington, and K. C. Lin, Ref. 7.

from the main progression by 300—400 cm^{-1} correspond to the vibrational components of dimer ions.

Although low frequency modes are easily found in the IR or Raman spectra of dimers,[9-11] both explanations mentioned above are based on the assumption of very near or almost equal ionization potentials for monomer and dimer molecules and this is unlikely if the photoelectron experiment of carboxylic acid dimers performed by Thomas[5] is considered. His spectra for dimers are very broad and structureless and he has concluded that the ionization potentials of dimers are 0.2—0.3 eV lower than those of the corresponding monomers. The peaks observed in the present spectra should have been broadened if the peaks were attributed to the dimers, because of many low frequency hydrogen bond vibrations of dimer ions and the thermal population of the low frequency vibrational states of the dimer molecules.

Therefore above-mentioned two models are discarded and the low frequency mode is more likely to be attributed to the monomer ions. The present experiments in which the pressure of ionization chamber was changed by introducing inert gas strongly support that the spectra obtained are from monomers.

This low frequency structure is not observed in the spectrum of formic acid, and then should originate from the vibration accompanying the geometrical alteration of methyl group. With regard to a ν_{17} (γCOOH wagging) or a ν_{18} (τ_{CH_3}, CH_3 torsion) among the modes in an a'' block their doubled frequencies are too high or too low[12] compared with 310 cm^{-1} and it is unlikely that the vibrational mode of a'' symmetry is so strongly excited by the ionization of the n_o orbital.

It is concluded, therefore, that the most reasonable assignment is a ν_{12} (ρ gear, COOH rocking or CCO angle deformation). Other modes in an a' block are thought to arise from vibrations involving more rigid bonds and are too high frequencies. This ν_{12} mode excitation in acetic acid could be considered to be an evidence supporting the assignments that the first band of formic acid exhibits not only a δ_{OH} but a δ_{CH} vibrational component.[3]

Another structure observed in all spectra of the three carboxylic acids is *ca.* 1100 cm^{-1} vibration and this mode could be assigned as a δ_{OH} by analogy with the case of formic acid.[3] The peaks appear weakly as shoulders on the slopes of the $\nu_{C=O}$ progression in formic and acetic acid, and are separated from the peaks of the $\nu_{C=O}$ progression by the deuterium substitution of hydroxyl hydrogen in the formic acid molecule.

The remaining vibration unassigned, 700—900 cm^{-1}, could be attributed either to a ν_{CC}, a ρ_{CH_3} (CH_3 rocking), or a ν_{C-O}.

A broad band in Figs. 2 or 3 at the lower ionization potential region than a 0-0 peak might be attributed to the ionization of corresponding dimer, since the appearance is quite similar to that of the mixture of monomer and dimer molecules reported by Thomas.[5]

The Second Bands. The appearances of the second band spectra of acetic, propionic, and isobutyric acids are quite different from that of formic acid, but the three spectra resemble each other. At least six vibrational peaks are clearly distinguishable in the spectrum of acetic acid. The vibrational analysis assuming the first or the second peak as arising from an adiabatic ionization process have not led to any reasonable vibrational assignments.

Then, for the identification of the position of the 0-0 peak, namely, the adiabatic ionization potential, the second band spectrum of acetic acid has been superimposed on that of formic acid and the best fit obtained is shown in Fig. 4, together with the bands of propionic and isobutyric acids. It is shown in Fig. 4 that the vibrational fine structures in the spectra of the three acids are quite the same as that of formic acid, and that the 0-0 transition for acetic and higher carboxylic acids is out of the Franck-Condon region.

The adiabatic ionization potential of the second band of acetic acid so determined is 11.63 eV and is included in Table 2 with other ionization potentials determined by the same procedures.

The vibrational assignments are summarized in Table 3. The frequencies measured in practice are the peak separations from the postulated 0-0 peak and therefore the small differences of the frequencies of formic acid

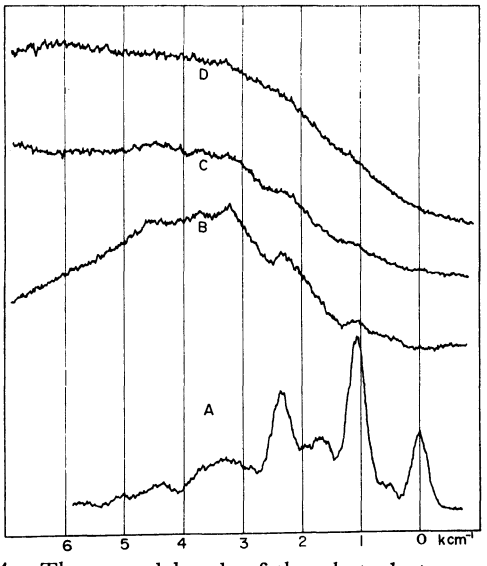

Fig. 4. The second bands of the photoelectron spectra of A; formic acid, B; acetic acid, C; propionic acid, and D; isobutyric acid.

Table 2. Ionization potentials for n_o and π_2 orbitals of some carboxylic acids (eV)

		Acetic	Propionic	Isobutyric
n_o	Adiabatic	10.664±0.003	10.525±0.003	10.329±0.005
	Vertical	10.848±0.003	10.711±0.003	10.519±0.005
π_2	Adiabatic	11.63 ±0.01	11.52	11.39
	Vertical	12.02 ±0.01	11.91	12.80

TABLE 3. VIBRATIONAL FREQUENCIES IN THE SECOND BAND OF ACETIC ACID SPECTRUM (cm^{-1})

Frequencies from 0—0 peak (postulated)	Assignments
510	δ_{OCO}
1050	ν_{C-O}
2320	$\nu_{C=O}$
3260	$\nu_{C-O}+\nu_{C=O}$ (3370)
3760	$\nu_{C-O}+\nu_{C=O}+\delta_{OCO}$ (3770)
4500	$2\nu_{C=O}$ (4640)

from those of acetic or other carboxylic acids do not have any significance.

The spectra in Fig. 4 become broad and structureless as the substituted alkyl group becomes larger, but still the band structures seem to correspond well to those of formic acid.

Thus the vibrational modes appearing in the second band for the molecules from formic to isobutyric acid are a $\nu_{C=O}$, a ν_{C-O}, and a δ_{OCO}, and are all fundamental modes intrinsic to the main framework of carboxyl group.

Conclusion

The technique of photoelectron spectroscopy provides the information about the structures of various ions produced by the ionization of one of the electrons in the corresponding molecule. This capability of the technique could be described in other way that the technique is able to give the information how each electron plays a role in the molecule.

From the study of the photoelectron spectra it is concluded that the n_0 and the π_2 orbitals have a number of inherent properties common to all the carboxylic acids studied.

1. The photoelectron spectra of carboxylic acids have a characteristic band, n_0, of carboxyl group corresponding to the first ionization and the n_0 orbital is so separated in energy from other deeper orbitals that the corresponding photoelectron band always appears as a strong isolated band overlapped by no other bands and easily identified from the spectrum. Such bands exhibiting vibrational structures as those originating either from the n_0 or π_2 orbital for carboxylic acids can be directly assigned without the aid of theoretical calculations.

2. The photoelectron peak corresponding to an adiabatic ionization from the n_0 orbital is always detected and this fact implies that the n_0 orbital is almost of "non-bonding" character; the ionization from the n_0 orbital does not alter the geometry of the molecule greatly.

3. The n_0 orbital is strongly localized on the carbonyl oxygen atom. The loss of an electron from this orbital excites a $\nu_{C=O}$ vibration and weakens the C=O bond slightly. The orbital also contributes to bonding of hydroxyl hydrogen to carbonyl oxygen. It is further conceived that the orbital plays an important role in settling the carboxyl group in a molecular plane as it is, since the ionization of the n_0 orbital is accompanied by the excitation of a δ_{CH} mode in formic acid and a ρ_{COOH} mode in acetic and higher carboxylic acids.

4. The second band of carboxylic acids is verified to originate from the π_2 ionization by inspecting vibrational structures. It is found from a study of formic acid and its deuterium derivatives, that the second band has an unexpected feature, *i.e.*, the extraordinarily high frequency for the $\nu_{C=O}$ mode of the ion, and it is the case for other higher carboxylic acids, also.

Thus it is concluded that the characteristic properties of the π_2 orbital are the anti-bonding character with regard to the C=O bond, and that the π_2 orbital contributes to settling the geometrical structure of carboxyl group, since the ionization of the π_2 orbital excites only the $\nu_{C=O}$, a ν_{C-O}, and a δ_{OCO} modes which are all intrinsic vibrational modes within the carboxyl group.

5. The lack of a 0-0 peak for the second band of acetic and higher carboxylic acids corresponding to the π_2 ionization implies that the equilibrium geometry of the corresponding ions is out of the Franck-Condon region and that the ions considerably change in geometry from the neutral molecules.

References

1) C. R. Brundle, D. W. Turner, M. B. Robin, and H. Basch, *Chem. Phys. Lett.*, **3**, 292 (1969).
2) I. Watanabe, Y. Yokoyama, and S. Ikeda, This Bulletin, **46**, 1959 (1973).
3) I. Watanabe, Y. Yokoyama, and S. Ikeda, *Chem. Phys. Lett.*, **19**, 406 (1973).
4) D. A. Sweigart and D. W. Turner, *J. Amer. Chem. Soc.*, **94**, 5592 (1972).
5) R. K. Thomas, *Proc. Roy. Soc., Ser. A*, **331**, 249 (1972).
6) Y. Yokoyama, I. Watanabe, and S. Ikeda, *Bunseki Kagaku*, **20**, 1502 (1971).
7) C. V. Berney, R. L. Redington, and K. C. Lin, *J. Chem. Phys.*, **53**, 1713 (1970).
8) E. Ady and J. Brickmann, *Chem. Phys. Lett.*, **11**, 302, (1971).
9) A. Witkowski, *J. Chem. Phys.*, **52**, 4403 (1970).
10) G. L. Carlson, R. E. Witkowski, and W. G. Fateley, *Spectrochim. Acta*, **22**, 1117 (1966).
11) R. L. Redington and K. C. Lin, *J. Chem. Phys.*, **54**, 4111 (1971).
12) However, there is a possibility that the ν_{18} mode has a frequency of about a half of 310 cm^{-1}, since the frequency of 93 cm^{-1} for the ν_{18} of acetic acid has not been experimentally determined but is a theoretically predicted value. See Ref. 7.

Molecular Structure of *N*-Methylformamide as Studied by Gas Electron Diffraction

Mitsuo KITANO and Kozo KUCHITSU

Department of Chemistry, Faculty of Science, The University of Tokyo, Hongo, Bunkyo-ku, Tokyo 113

(Received December 6, 1973)

The bond distances (r_g) and angles (r_α) in *N*-methylformamide $HCONHCH_3$ have been determined by gas electron diffraction as follows: N–C(methyl) = 1.459±0.006 Å, C(carbonyl)–N = 1.366±0.008 Å, C=O = 1.219±0.005 Å, C–H(methyl) = 1.114±0.025 Å, ∠N–C=O = 124.6±0.5° and ∠C–N–C = 121.4±0.9°, where uncertainties represent estimated limits of experimental error. Systematic trends are observed among the skeletal structures of formamide, acetamide, *N*-methylformamide and *N*-methylacetamide. A conformer with the C(carbonyl)–H and N–C(methyl) bonds *trans* to each other is found to be dominant in the gas phase. The presence of a small fraction of the *cis* conformer is suggested, but the experimental evidence is not conclusive.

The present work is a part of our systematic study of simple amide structures by gas electron diffraction. In the preceding studies of formamide,[1] acetamide,[2] and *N*-methylacetamide,[3] significant differences in the C′–N[4] and C′=O distances and in the N–C′=O angles were observed. The question was then raised whether the skeletal structure of *N*-methylformamide (Fig. 1), which has never been reported,[5] conforms to these trends.

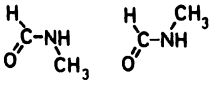

trans *cis*

Fig. 1. *N*-methylformamide.

As for the possibility of rotational isomerism about the C′–N bonds, Phillips[6] observed a single methyl-proton NMR spectrum and reported that only one of the two possible conformers (*trans* and *cis* relative to the C′–H and N–C bonds) was present. Jones[7] remarked that the general character of the infrared spectrum in the vapor phase was more consistent with the *cis* model and that the rotation about the C′–N bond was severely hindered. However, his assignment was questioned by Miyazawa[8] and Suzuki,[9] who interpreted the spectrum as that of the *trans* conformer, though a small fraction of the *cis* conformer could exist. The abundance ratio of the *cis* form in a dilute solution of carbon tetrachloride was estimated from the N–H stretching bands to be about 5% by Russell and Thompson.[10]

Experimental

A commercial sample was heated to about 130 °C by a high-temperature nozzle,[11] and diffraction photographs were taken with 40 kV electrons[12] at camera distances of 112.30 mm (short) and 246.86 mm (long). The scale factors of the diffraction patterns were calibrated to within 0.10% with reference to the r_a (C=O) distance of carbon dioxide (1.1646 Å).[12] The densities of four plates taken at each camera distance (D=0.82—0.25) were measured by a digital microphotometer.[13] Other experimental conditions are described elsewhere.[11-14]

Molecular intensities in the ranges s=2.2—15.7 and 9.4—37.7 Å^{-1} were obtained[15] from the long and short distance data, respectively, by use of hand-drawn backgrounds.

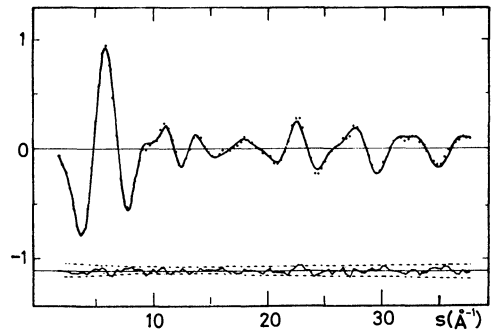

Fig. 2. Experimental and theoretical molecular intensities for *N*-methylformamide. Typical observed $sM(s)$ values are shown in dots, and the best-fit theoretical intensity based on a mixture model of 83% *trans* and 17% *cis* conformers is shown in the solid curve. The lower solid and broken curves represent the residual and the error limits in the $sM(s)$ to a fractional error of 1×10^{-3} of the original photocurrent, respectively. A 100% *trans* model gives residuals of nearly equal magnitude.

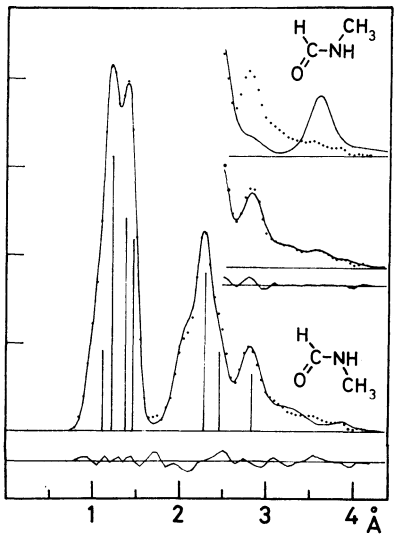

Fig. 3. Experimental (dots) and theoretical radial distribution curves for 100% *cis* (top), 83% *trans* and 17% *cis* (middle), and 100% *trans* (bottom) models. Vertical bars represent principal atom pairs. A damping factor, $\exp(-0.0016\,s^2)$ is used. Residuals are shown below.

Since they agreed with each other in the overlapping region within experimental error (about 0.03 in the absolute $sM(s)$ scale), they were joined at $s=12.7$ Å^{-1} (Fig. 2). The corresponding radial distribution curve, shown in Fig. 3, confirmed that the dominant conformer has the C'–H and N–C bonds *trans* to each other. Most of the calculations were carried out on a HITAC-5020E and a HITAC-8800 in the Computer Centre of the University of Tokyo.

Analysis

Skeletal Structure. The skeletal parameters were determined by a least-squares analysis of molecular intensities with conventional diagonal weights[16] under the following assumptions:

1) All the atoms except for two hydrogen atoms in the methyl group are coplanar.

2) The C'–H and N–C bonds are *trans* to each other.

3) The *N*-methyl group is in the staggered conformation with the C'–N bond.[17]

4) The methyl group has local C_{3v} symmetry and has no tilt.

5) The H–C–H angle (r_α defined in Ref. 18) is equal to that in dimethylamine,[19] 108.6°.

6) The r_g(C'–H) and r_g(N–H) distances are equal to the corresponding distances in formamide,[1] 1.125 and 1.027 Å, respectively.

7) The C'–N–H and N–C'–H angles (r_α) are equal to the corresponding angles in formamide,[1,20] 118.7 and 112.7°, respectively.

8) The barriers hindering the skeletal and methyl torsions, V_2 and V_3, are 20 kcal/mol[21] and 1 kcal/mol, respectively.

9) The asymmetry parameters κ for the bonded C–H and N–H distances are 1.8×10^{-5} Å^3, and the rest of the κ parameters are zero.[22]

Mean vibrational amplitudes and vibrational corrections for shrinkage effects (r_a-r_α)[18,23] were calculated by use of the modified Urey-Bradley force constants reported by Suzuki[9] with a number of additional force constants for out-of-plane displacements for *N*-methylacetamide reported by Itoh,[24,25] both determined from frequencies observed in the liquid phase. The results are given in Table 1. Contributions to the vibrational corrections from the skeletal and methyl torsions were estimated in the way described in a previous paper[3] by use of assumption 8. All the mean amplitudes except for those of the C'=O and C'–N bonds were fixed to the values listed in Table 1.

TABLE 1. MEAN AMPLITUDES AND VIBRATIONAL CORRECTIONS FOR *N*-METHYLFORMAMIDE (in 10^{-4} Å)

	l	r_a-r_α		l	r_a-r_α
C'=O	394	31	O···H_t	901	35
C'–N	426	27	O···H_1	1268	−609
N–C	498	22	O···H_2	4293	−335
N–H_t	718	44	N···H_a	960	−12
C'–H_a	799	0	N···H_1	1032	33
C–H_1	800	70	C···H_a	1011	27
N···O	531	5	C···H_t	1017	46
C'···C	719	−11	H_a···H_t	1549	35
C···O	1128	12	H_a···H_1	1349	88
C'···H_t	949	−9	H_a···H_2	2120	44
C'···H_1	1027	−591	H_t···H_1	1670	103
C'···H_2	2493	−14	H_t···H_2	2035	120
O···H_a	906	4	H_1···H_2	1298	35

a) Calculated at 130 °C. The carbonyl carbon atom is denoted as C'. The amide hydrogen and carbonyl hydrogen atoms are denoted as H_t and H_a, respectively; H_1 and H_2 are the in-plane and out-of-plane hydrogen atoms of the *N*-methyl group, respectively. The shrinkage effects due to the skeletal and methyl torsions are included as described in Ref. 3.

TABLE 2. STRUCTURAL PARAMETERS FOR *N*-METHYLFORMAMIDE AND RELATED MOLECULES[a]

	HCONH(CH_3)[b]	$HCONH_2$[c]	CH_3CONH_2[d]	$CH_3CONH(CH_3)$[e]
C–H (methyl)[f]	1.114(25)	—	1.124(10)	1.107 (5)
C'=O	1.219 (5)	1.212 (3)	1.220 (3)	1.225 (3)
C'–N	1.366 (8)	1.368 (3)	1.380 (4)	1.386 (4)
N–C	1.459 (6)	—	—	1.469 (6)
∠N–C'=O	124.6 (5)	125.0 (4)	122.0 (6)	121.8 (4)
∠C–N–C'	121.4 (9)	—	—	119.7 (8)
l(C'=O)	0.043 (4)	0.043 (3)	0.043 (5)	—
l(C'–N)	0.044 (5)	0.050 (4)	0.049 (5)	—

a) Distances r_g and mean vibrational amplitudes l in Å, and angles r_α in degrees.[18] Estimated limits of experimental error attached to the last significant decimal places are enclosed in parentheses. The carbonyl carbon atom is denoted as C'. b) Structure of *N*-methylformamide determined in the present least-squares analysis. c) Formamide, Ref. 1. d) Acetamide, Ref. 2. e) *N*-Methylacetamide, Ref. 3. f) Average r_g(C–H) distances for the *N*-methyl group in *N*-methylformamide, for the *C*-methyl group in acetamide, and the mean value for the *N*-methyl and *C*-methyl groups in *N*-methylacetamide.

Table 3. Error matrix for *N*-methylformamide[a)]

	X_1	X_2	X_3	X_4	X_5	X_6	l_1	l_2	k_1	k_2
X_1	17	8	8	12	−10	−20	−6	−7	18	−66
X_2		20	9	8	−16	−9	−4	−16	22	52
X_3			11	15	−6	−14	5	−9	−13	40
X_4				45	−5	−17	13	−9	−48	54
X_5					45	12	6	13	−11	−20
X_6						35	5	10	−11	65
l_1							12	9	−12	52
l_2								18	−10	−42
k_1									110	−77
k_2										458

a) X_1=C′–N, X_2=N–C, X_3=C′=O, X_4=C–H, X_5=∠C–N–C′, X_6=∠N–C′=O, l_1=l(C′=O), l_2=l(C′–N), k_1, k_2= indices of resolution for long and short distance data (0.98 and 0.97), respectively. Units ($\times 10^{-4}$) for the distances and mean amplitudes are Å, those for the angles are rad, and those for the indices are dimensionless.

The r_g distances and the r_α angles derived from the least-squares analysis are listed in Table 2 with limits of error estimated from random and systematic errors.[16,26,27)] The skeletal parameters are not sensitive to any of the above assumptions 1—9, and systematic errors caused by uncertainties in the assumptions are included in the quoted error limits. The error matrix[28)] is given in Table 3.

Skeletal Torsion. The observed radial distribution curve shown in Fig. 3 seems to have a small hump around 3.6 Å, which can be assigned to the O···C (methyl) distance in a *cis* conformer. Though the hump is almost comparable with the noise level of the observed radial distribution curve, the peak is reproducible, and a fraction of about 17% is suggested. Accordingly, the molecular intensity was further examined by a least-squares analysis. The system was assumed to be a mixture of *trans* and *cis* conformers with identical frame structures, and their fractions were taken as an additional variable. The analysis gave identical structural parameters and 17±10% for the *cis* fraction, corresponding to a free energy difference ΔG of about 1.3 kcal/mol. This estimate is compatible with the spectroscopic prediction by Miyazawa.[8)] This model was also acceptable according to a further analysis of background functions[29,30)] based on a criterion of their smoothness. However, a 100% *trans* model was equally acceptable in this criterion within experimental error. Furthermore, the *cis* fraction derived from the least-squares analysis mentioned above was found to have strong correlation with the assumptions about the methyl conformation and the methyl torsional barrier. The *cis* fraction decreased to 11± 10% when the methyl torsion was assumed to be essentially free. In further consideration of the uncertainties in the experimental molecular intensity and in the above-mentioned assumptions made in the analysis, it was im possible to unambiguously demonstrate the presence of the *cis* conformer. Further precise spectroscopic or diffraction experiments are necessary for a definite confirmation of the rotational isomerism.

Methyl Torsion. Theoretical radial distribution curves were calculated with different conformations of the methyl hydrogens and with different barrier heights for the methyl torsion. When the V_3 value was assumed to be less than 1 kcal/mol, theoretical curves based on any equilibrium position agreed with the observed curve within the range of experimental error. The agreement became worse when the barrier height was increased, and for $V_3 \simeq 3.8$ kcal/mol, which corresponds to a methyl torsional frequency of about 242 cm^{-1} assigned by DeGraaf and Sutherland,[31)] only a model with a dihedral angle of about 30° between the C′–N and one of the C–H bonds remained acceptable. Consequently, it seems to be the case that either the barrier is lower than those in methylamine,[32)] 2.0 kcal/mol, and in dimethylamine,[33)] 3.2 kcal/mol, or the equilibrium dihedral angle is about 30°.

The theoretical molecular intensity and radial distribution curves based on the most probable structure are compared with the corresponding observed curves in Figs. 2 and 3, respectively.

Discussion

In comparison with the skeletal structures of formamide, acetamide, and *N*-methylacetamide listed in Table 2, the following trends are observed:

1) The C(carbonyl)–N bond lengths in formamide and *N*-methylformamide are essentially equal to each other and are about 0.01 Å shorter than those in acetamide and *N*-methylacetamide.

2) The N–C=O angles in formamide and *N*-methylformamide are nearly equal to each other and are about 3° larger than those in acetamide and *N*-methylacetamide. As remarked in Ref. 1, this trend conforms to the similar trends observed in other systems, where X–CH=Y angles are consistently larger than the corresponding X–C(CH_3)=Y angles by about 3°.

3) On the other hand, the C=O bond lengths in *N*-methylformamide and acetamide are nearly equal to each other and are slightly longer than that in formamide and slightly shorter than that in *N*-methylacetamide.

4) The N–C(methyl) bond length in *N*-methylformamide appears to be shorter than that in *N*-methylacetamide.

5) The C–N–C angle in *N*-methylformamide is larger than that in *N*-methylacetamide.

The authors are indebted to Professor R. K. Bohn for his critical reading of the manuscript and to Professor R. H. Schwendeman for his communication of his microwave data prior to publication.

References

1) M. Kitano and K. Kuchitsu, This Bulletin, **47**, 67 (1974).
2) M. Kitano and K. Kuchitsu, *ibid.*, **46**, 3048 (1973).
3) M. Kitano, T. Fukuyama, and K. Kuchitsu, *ibid.*, **46**, 384 (1973).
4) The carbonyl carbon atom is denoted as C'.
5) The structure of *N*-methylformamide is now being studied by microwave spectroscopy. R. A. Elzaro and R. H. Schwendeman, Symposium on Molecular Structure and Spectroscopy, CC6, Columbus, Ohio, June, 1973.
6) W. D. Phillips, *J. Chem. Phys.*, **23**, 1363 (1955).
7) R. L. Jones, *J. Mol. Spectrosc.*, **2**, 581 (1958).
8) T. Miyazawa, *ibid.*, **4**, 155 (1960).
9) I. Suzuki, This Bulletin, **35**, 540 (1962).
10) R. A. Russell and H. W. Thompson, *Spectrochim. Acta*, **8**, 138 (1956).
11) A. Yokozeki and K. Kuchitsu, This Bulletin, **44**, 72 (1971).
12) Y. Murata, K. Kuchitsu, and M. Kimura, *Jap. J. Appl. Phys.*, **7**, 591 (1970).
13) Y. Morino, K. Kuchitsu, and T. Fukuyama, This Bulletin, **40**, 423 (1967).
14) M. Tanimoto, K. Kuchitsu, and Y. Morino, *ibid.*, **43**, 2776 (1970).
15) Numerical experimental data of the leveled total intensity and the background have been deposited with the Chemical Society of Japan (Document No. 7404).
16) Y. Morino, K. Kuchitsu, and Y. Murata, *Acta Crystallogr.*, **18**, 549 (1965).
17) Note, however, that Yan *et al.* favored the eclipsed conformation of the C'–N bond and one of the C(methyl)–H bonds from their CNDO/2 and extended Hückel calculations. J. F. Yan, F. A. Momany, R. Hoffman, and H. A. Scheraga, *J. Phys. Chem.*, **74**, 420 (1970).
18) K. Kuchitsu and S. J. Cyvin, "Molecular Structures and Vibrations," ed. by S. J. Cyvin, Chapter 12, Elsevier, Amsterdam (1972).
19) J. E. Wollrab and V. W. Laurie, *J. Chem. Phys.*, **48**, 5058 (1968).
20) E. Hirota, R. Sugisaki, C. J. Nielsen, and G. O. Sørensen, *J. Mol. Spectrosc.*, in press.
21) A. Warshel, M. Levitt, and S. Lifson, *ibid.*, **33**, 84 (1970).
22) K. Kuchitsu, This Bulletin, **40**, 505 (1967).
23) K. Kuchitsu and S. Konaka, *J. Chem. Phys.*, **45**, 4342 (1966).
24) K. Itoh, Ph. D. Thesis, The University of Tokyo (1969).
25) K. Itoh and T. Shimanouchi, *Biopolymers*, **9**, 383 (1970).
26) K. Kuchitsu, T. Fukuyama, and Y. Morino, *J. Mol. Structure*, **1**, 463 (1958).
27) K. Kuchitsu, "Molecular Structures and Vibrations," ed. by S. J. Cyvin, Chapter 10, Elsevier, Amsterdam (1972).
28) O. Bastiansen, L. Hedberg, and K. Hedberg, *J. Chem. Phys.*, **27**, 1311 (1957).
29) Y. Morino and K. Kuchitsu, *ibid.*, **28**, 175 (1958).
30) M. M. Abe, K. Kuchitsu, and T. Shimanouchi, *J. Mol. Structure*, **4**, 245 (1969).
31) D. E. DeGraaf and G. B. B. M. Sutherland, *J. Chem. Phys.*, **26**, 716 (1957).
32) K. Takagi and T. Kojima, *J. Phys. Soc. Jap.*, **30**, 1145 (1971).
33) J. E. Wollrab and V. W. Laurie, *J. Chem. Phys.*, **54**, 532 (1971).

The Chemistry of Americium. II. The Behavior of Am(III), Am(V), and Am(VI) in Column Chromatography, with Bis(2-ethylhexyl)phosphoric Acid Used as the Extractant

Mitsuo HARA and Shin SUZUKI

The Research Institute for Iron, Steel and Other Metals, Tohoku University, Katahira 2-chome, Sendai 980

(Received January 5, 1973)

The behavior of Am(III), Am(V), and Am(VI) in column chromatography with bis(2-ethylhexyl)phosphoric acid(HDEHP) used as the extractant were investigated in comparison with that of Np(IV), Np(V), and Np(VI). When the solution of Am(VI) was submitted to the column chromatography, it was found that Am(VI) was rapidly reduced to Am(V) and partially to Am(III) by HDEHP, irrespective of the conditions, such as the flow rate, the acidity, and the composition and temperature of the influent. The optimum conditions for the separation of Am(V) and Am(III) and for the preparation of the Am(V) solution were established by utilizing the difference in the adsorbability on the column bed between Am(III) and Am(V). When a freshly-prepared Am(V) solution was submitted to column chromatography, it was found that Am(V) was also reduced to Am(III) as well as Am(VI) by HDEHP. The percentage of the Am(V) fraction eluted strongly depended on the conditions in the column chromatography, but it was found to be constant within the limits of experimental error under definite conditions as long as the same column was used. This fact was applied to the determination of the Am(V) content in the mixed solution of Am(III) and Am(V). The content of Am(V) decreased slowly in the nitrate, acetate, sulfate, and perchlorate solutions at lower temperatures, but it rapidly decreased in the chloride, iodide, sulfite, and hydrogen peroxide solutions even at 0 °C. The content of Am(V) decreased more rapidly at higher temperatures, and the kinetic analysis showed that the reduction of Am(V) apparently followed the first-order kinetics in the acetate solutions.

Americium is the heaviest of the actinoid element which are known to have penta- and hexa-valent states. In the solution involving higher concentrations of americium, the disproportionation reaction of Am(V) is remarkable, but it is negligible at lower concentrations of americium. The α-decay of ^{241}Am leads to the radiolytic reduction of both Am(V) and Am(VI) at rates of 1.2 and 3.1%/h respectively, irrespective of the concentration of ^{241}Am.[1] Therefore, the stabilities of Am(V) and Am(VI) must be discussed in connection with the participation of these reactions.

It is well known that Am(VI) is relatively stable in strongly acidic solutions,[2] but Stokely and Moore have reported that the addition of an acetate buffer to a cooled solution of Am(VI) causes the reduction of Am(VI) to Am(V).[3] It has also been reported that Am(VI) in a dilute nitric acid solution not containing silver ion was rapidly reduced to Am(V) in the absence of such stabilizing anions as fluoride.[4] Zangen investigated the solvent extraction of Am(VI) with several extractants such as HDEHP in CCl_4 from nitric acid solutions containing $(NH_4)_2S_2O_8$ and $AgNO_3$ as holding oxidants, but he gave no information about the stability of Am(VI) during the extraction.[5]

The standard potentials for the Am(III)–Am(V) and Am(V)–Am(VI) couples are 1.74 and 1.60 volts respectively.[6] It can be expected from these potentials that Am(V) and Am(VI) are powerful oxidants and that they are easily reduced by normal reductants and organic materials. Our information concerning the instabilities of Am(V) and Am(VI) in both the aqueous and organic phases is rather poor, especially at lower concentrations of americium. Only a little information was obtained by the previous work in which the rates of reduction of Am(V) in several media were investigated by means of solvent extraction with 2-thenoyltrifluoroacetone(TTA).[7]

In this work the behavior of Am(III), Am(V), and Am(VI) in column chromatography, using HDEHP as an extractant, has been studied in comparison with that of neptunium in various valency states. Furthermore, the instabilities of Am(V) and Am(VI) with respect to reduction by HDEHP and by some coexisting materials have been investigated.

Experimental

Reagents. The nuclides used in this study were ^{241}Am (433 y), ^{243}Am(7400 y), ^{237}Np(2.14×10^6 y), and ^{239}Np (2.355 d); their radiochemical purities were certified by γ-ray and α-particle spectrometry. The solutions of Am(III) and Am(VI) were prepared in a manner which has been described before using ^{241}Am,[7] and the concentration of americium was adjusted to about 10^{-6}M. $^{243}AmO_2$, obtained from the Oak Ridge National Laboratory, was dissolved in concentrated nitric acid, and a 10M nitric acid solution of ^{243}Am was used for the tri-*n*-octylamine (T-*n*-OA) extraction to isolate ^{239}Np,[8] which was a daughter of ^{243}Am and which was used as a tracer of neptunium. ^{237}Np in a 1M nitric acid solution, obtained from the Radiochemical Centre, Amersham, England, was purified by the TTA extraction method[9] and was used as a carrier of neptunium within two hours after the purification in order to minimize the interference from its daughter. The solutions of Np(IV), Np(V), and Np(VI) were prepared by the literature methods.[10-12]

HDEHP, obtained from Tokyo Kasei, was purified by the solvent extraction method[13] and diluted with distilled acetone. The TTA, T-*n*-OA, and other chemicals were of a G. R. grade. Celite 545, obtained from Jones–Mannville, was used as a supporting medium for the extractant. It had been washed with acid, treated with dimethyldichlorosilane, and sized in 80—100 meshes.

Apparatus. A Kobe Kogyo Model PS-500 flat-type NaI(Tl) scintillation probe connected with a Toshiba 800-channel pulse-height analyzer was used for the measurement of the γ-ray spectra, while an Osaka Dempa Gridded Ioniza-

tion Chamber connected with the same pulse-height analyzer was used for the measurement of the α-particle spectra. The γ-ray assay was performed by the use of the scintillation probe connected with a Kobe Kogyo Model SA-400 scaler.

A Toa-Dempa-Kogyo pH meter Model PE-2 was used for the pH measurements. A Shimadzu Ozone Generator was used to bubble ozone gas through the testing solutions in order to eliminate the reducing materials as much as possible. Most of the column chromatographic experiments were performed at a temperature determined with an accuracy of ±0.5 °C in an Ohishi Netsu-Kagaku thermostatted box.

Procedure. Column Preparation: 5 grams of Celite 545 and 20 ml of 1M HDEHP–acetone were mixed in a beaker. The mixture was allowed to settle overnight, and then the excess solution was decanted. After air drying at room temperature, the powder was suspended in distilled water; the mixture was then added to a glass tube plugged with glass wool to the desired height. The column was subsequently washed with a 2M nitric acid solution and with water.

Column Chromatography: 50—100 μl portions of sample solutions were fed onto the top of the column bed, which had preliminarily been washed with the influent. The column was operated by the usual chromatographic procedures. Suitable aliquots of the effluent were put in polyethylene test tubes or on aluminium dishes for γ-ray measurements.

If the separation of Am(III) and Am(V) was desired, it was done as follows: Am(V) was eluted from the column with a few milliliters of an influent whose acidity was lower than 0.1M; then the Am(III) was eluted with a few milliliters of a 2M nitric acid solution. After the measurement of the total γ-ray activity in both the Am(V) and Am(III) fractions, the percentage of Am(V) was calculated.

Results and Discussion

Elution of Am(III), Am(VI), Np(IV), Np(V), and Np(VI). The Am(III), Am(VI), and Np(V) in the nitric acid solutions were fed onto the top of a column bed and then eluted with nitric acid solutions of various acidities. Some typical elution curves are shown in Fig. 1. The peak of Np(V) in the elution curve did not shift in the 10^{-4}—0.5 M acidity range; Np(V) passed through the column without adsorption. On the other hand, the peak of Am(III) shifted remarkably with the change in the acidity of the influent. In the case of the Am(VI) sample solution, the major part of the americium was eluted within two column volumes of the influent, while the minor part was eluted with the same volume of the influent as Am(III); the major peak did not shift in the 10^{-4}—0.5 M acidity range like the peak of Np(V), and the minor peak showed the same behavior as that of Am(III).

The Np(IV) and Np(VI) fed onto the column bed could not be eluted with the nitric acid solution in the 0.01—2 M acidity range. However, Np(VI) was gradually eluted with influents of acidities higher than 5 M, though Np(IV) was not eluted at all with the nitric acid solution of the acidity up to 10 M adsorbed tightly on the column bed.

It is known that the actinoid(III, IV, VI) ions are adsorbed tightly on the column bed containing HDEHP.[4] Therefore, it may be concluded that the species which passed through the column without adsorption in the elution of the Am(VI) sample solution was Am(V), since it showed a behavior in the column chromatography similar to that of Np(V) among the various valency states of neptunium.

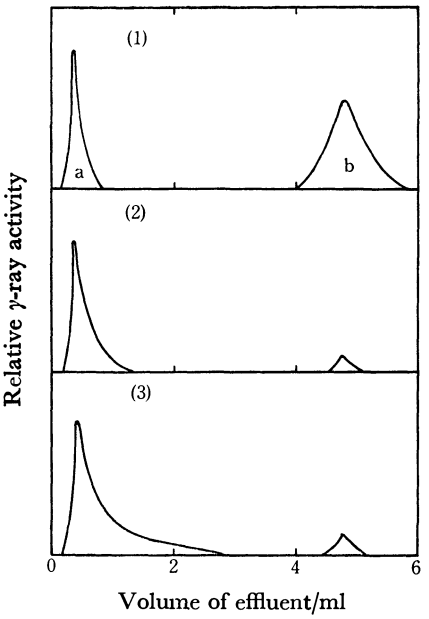

Fig. 1. Behaviors of Am(III), Am(VI) and Np(V) in column chromatography.
Column: 5 mmφ × 30 mm, Influent: 0.2 M HNO_3, Flow rate: 80 μl/min
1. a) Np(V), b) Am(III). 2. Am(VI) sample solution. 3. Am(VI) sample solution (Influent: 0.2 M HNO_3, 0.1 M peroxydisulfate, trace $AgNO_3$).

Reduction of Am(VI) during the Column Chromatography. Before the Am(VI) sample solution was submitted to the column chromatography, the valency state of americium had been confirmed as hexavalent by means of the LaF_3 coprecipitation method.[14] Therefore, it is clear that Am(VI) was rapidly reduced to Am(V) during the column chromatography. It is well known that Am(VI) is relatively stable in the presence of such holding oxidants as $(NH_4)_2S_2O_8$ with an $AgNO_3$ catalyst and without any contact with organic materials.[14] In the elution curve with an influent containing the holding oxidant (Fig. 1(3)), the peak corresponding to Am(V) had a tail. The rate of reduction decreased somewhat in the presence of the holding oxidant, but it was found that most of the americium was eluted in the pentavalent state.

As causes of the reduction of Am(VI), two factors are possible: the supporting medium and the extractant (HDEHP) in the column bed. In the preliminary experiments, it was confirmed that the powder used as the supporting medium was inert to the redox reaction of americium. Thus, the Am(VI) was probably reduced by the extractant even though the holding oxidant was added. The rapid reduction of Am(VI) by the extractant was also observed in the column chromatography with the Am(VI) solutions of acetate, sulfate, perchlorate, bromate, chloride and hypochlorite in the acidity range of 10^{-4}—0.1 M.

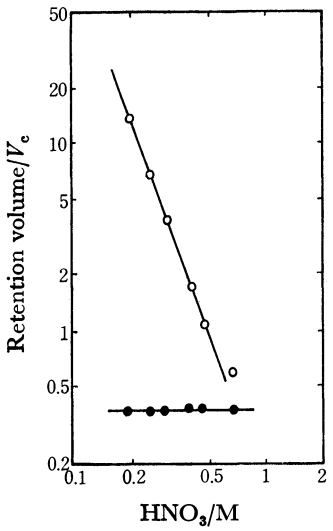

Fig. 2. Dependence of the retention volume on the acidity of the influent.
○: Am(III) ●: Am(V)

Reduction of Am(V) during the Column Chromatography. The log-log plot of the retention volume (the volume of the effluent at the peak position in the elution curve) *vs.* the acidity of the influent is shown in Fig. 2, where the retention volume, subtracted by one column volume (V_c), is expressed in V_c units. The difference between Am(III) and Am(V) in their adsorbability on the column bed suggests that the recommended procedure for the separation of Am(V) from Am(III) should be as follows: using a column more than 1 ml in bed volume, the Am(V) should be eluted with an influent with an acidity of less than 0.1 M and a volume of less than two column volumes, and the Am(III) should be rapidly stripped with a 2 M nitric acid solution.

Table 1. Elution of Am(VI) sample solution with 0.1 M nitrate solution

pH	Temperature °C	Am(V) fraction %	
2.0	0	86.5±0.8[a)]	
2.5	0	85.1±0.8	
3.0	0	84.1±1.0	
3.5	0	84.7±0.8	
2.0	0	89.8±0.8[b)]	77.7[c)]
2.0	10	87.8±1.0	70.5
2.0	20	88.9±1.0	69.5
2.0	30	87.4±1.0	68.6
2.0	40	80.8±1.0	61.0

Oxidant a) and b): $(NH_4)_2S_2O_8+AgNO_3$ c): $(NH_4)_2S_2O_8$
Column a): 6 mmϕ×30 mm b) and c): 6 mmϕ×25 mm

Following the procedure described above, Am(VI) sample solutions were eluted with nitrate solutions under various conditions and the percentage of the Am(V) fraction was determined radiometrically. As is postulated in Table 1, the percentage of the Am(V) fraction was almost constant in the 2.0—3.5 pH range at 0 °C, but it decreased with a rise in the temperature at a constant acidity. The percentage of the Am(V) fraction did not reach 100% even at 0 °C. These findings are probably the result of the instability of Am(V) during the column chromatography.

Table 2. Elution of Am(V) sample solution with 0.01 M nitrate solution (pH 2.5) at 0 °C

Bed volume mmϕ, mm	Flow rate ml/min	Am(V) fraction %
8×50	0.1	3.0
8×40	0.4	15.1
8×35	1.0	42.4
8×30	1.1	60.3
8×30	1.6	64.8
10×20	2.0	91.5
10×15	2.5	95.0

The Am(V) solution freshly prepared by the elution of the Am(VI) solution was submitted to column chromatography, and the percentage of the Am(V) fraction was measured with respect to the different volume of the column bed. It is clear from the results presented in Table 2 that the bigger the column bed, the smaller the percentage of the Am(V) fraction. These results can be explained easily in connection with the duration of passing over the column bed: Am(V) was obviously reduced by the extractant to Am(III) just like Am(VI). The percentage of the Am(V) fraction depended on the conditions of the column chromatography, such as the temperature, the flow rate, the composition of the influent, and the volume of the column bed. However, it was found that the percentage of the Am(V) fraction was constant within limits of experimental error, as is shown in Fig. 3, when the same column was used in the elution

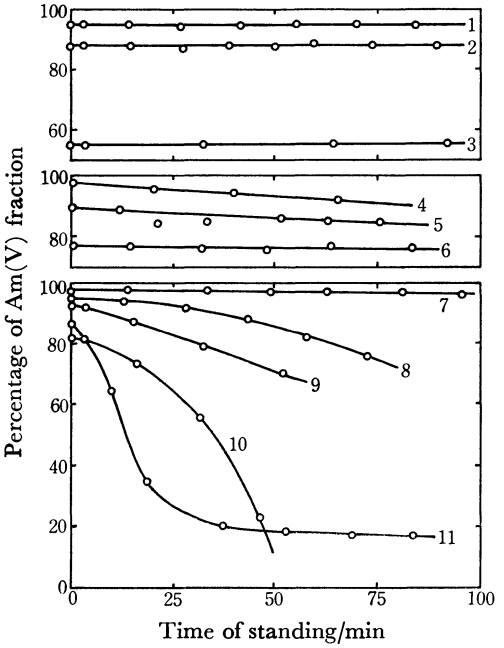

Fig. 3. Time-dependence of percentage of Am(V) fraction in 0.1 M solutions of pH 2.5 at 0 °C
1–3: Nitrate, 4: Acetate, 5: Sulfate, 6: Perchlorate, 7: Peroxydisulfate, 8: Chloride, 9: Hydrogen peroxide, 10: Potassium bromate, 11: Peroxydisulfate freshly prepared (The different column was used except for two couples, 1–8 and 2–11)

of Am(V) in a 0.1 M nitric acid solution. This finding suggests that Am(V) is stable in the nitrate solutions and that the rate of Am(V) decreased by the column chromatography is constant so long as the same column is used. Thus, the content of Am(V) in the mixed solution of Am(III) and Am(V) can be determined by a simple correction for the percentage of the Am(V) fraction obtained by the column chromatography under definite conditions using the same column.

Stability of Am(V) in Several Kinds of Solutions.

Aliquots of an Am(V) solution kept at various temperatures were submitted to column chromatography at 0 °C in order to investigate the dependence of the percentage of the Am(V) fraction on the standing time. Some of the results are shown in Fig. 3. The percentage of the Am(V) fraction in the perchlorate, sulfate, acetate, and aged peroxydisulfate solutions decreased slowly, but it readily decreased in the chloride, iodide, sulfite, hydroxylamine, hydrogen peroxide, bromate, and freshly-prepared peroxydisulfate solutions, even at 0 °C. The unexpected results with the common oxidant, the bromate, and the freshly-prepared peroxydisulfate solutions can be explained in terms of the following phenomena: the bromate obviously eluted a portion of the extractant and the peroxydisulfate formed bubbles in the column bed. The decreases in the percentage of the Am(V) fraction in the solution kept at lowered temperatures did not result from the oxidation of Am(III) and Am(V), but from the reduction of Am(V) to Am(III) because of the higher redox potentials for two couples, Am(III)–Am(V) and Am(V)–Am(VI).

Then, the dependence of the content of Am(V) in the acetate solutions on the standing time was investigated at various temperatures. As is shown in Fig. 4, the semilog arithmic plot of $[Am(V)]_t/[Am(V)]_0$ *vs.* the standing time showed a linearity, where $[Am(V)]_0$ and $[Am(V)]_t$ were the concentrations of Am(V) at the standing times of 0 and t respectively. The slope of the straight line somewhat increased with an increase in the pH in the 2—3 range examined at the same temperature. Consequently, the reduction of Am(V) in an acetate solution apparently follows the first-order kinetics. The reduction rate of Am(V) to Am(III) decreased to as low as a few percentages per hour at 0 °C, though the radiolytic reduction rate of 1.2%/h should remain even at sufficiently lowered temperatures. Therefore, the experiments using Am(V) solutions have to be performed at lower temperatures and have to be finished within a few hours after the preparation of Am(V) solutions in order to minimize the interference from Am(III).

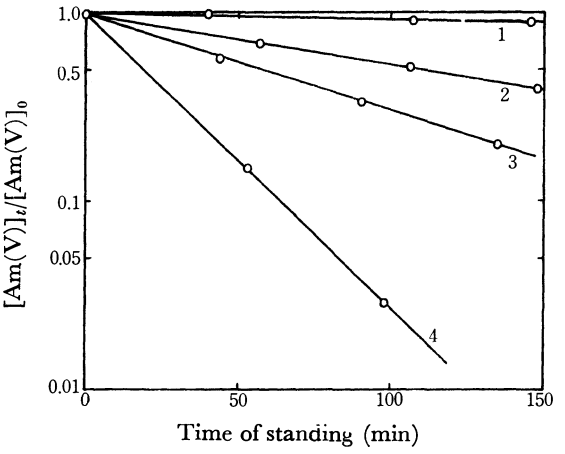

Fig. 4. Time-dependence of $[Am(V)]_t/[Am(V)]_0$ in 0.1 M acetate solution of pH 2.0
1: 0 °C, 2: 40 °C, 3: 60 °C, 4: 80 °C.

References

1) G. R. Hall and T. L. Markin, *J. Inorg. Nucl. Chem.*, **4**, 296 (1957).
2) J. S. Coleman, T. K. Keenan, L. H. Jones, W. T. Carnall and R. A. Penneman, *Inorg. Chem.*, **2**, 58 (1963).
3) J. R. Stokely, Jr. and F. L. Moore, *Anal. Chem.*, **39**, 994 (1967).
4) F. L. Moore, *ibid*, **40**, 2130 (1968).
5) M. Zangen, *J. Inorg. Nucl. Chem.*, **28**, 1693 (1966).
6) R. A. Penneman and L. B. Asprey, Proc. Intern. Conf. Peaceful Uses At. Energy, Geneva, 1955, Paper 838, **7**, 355 (1956).
7) M. Hara, This Bulletin, **43**, 89 (1970).
8) C. W. Sill, *Anal. Chem.*, **38**, 802 (1966).
9) F. L. Moore, *ibid*, **29**, 941 (1957).
10) E. Nakamura, *Nippon Genshiryoku Gakkaishi*, **3**, 684 (1961).
11) A. G. Rykov and G. N. Yakovlev, *Radiokhimiya*, **8**, 20 (1966).
12) B. Weaver and D. E. Honer, *J. Chem. Eng. Data*, **5**, 260 (1960).
13) D. F. Peppard, J. R. Ferraro, and G. W. Mason, *J. Inorg. Nucl. Chem.*, **7**, 231 (1958).
14) F. L. Moore, *Anal. Chem.*, **35**, 715 (1963).

ESR of Copper(II) Complexes in Magnetically Non-dilute Crystals. II. Polycrystals of Various Bis(amino acidato)copper(II) Complexes

Hiroshi Yokoi

Chemical Research Institute of Non-aqueous Solutions, Tohoku University, Katahira, Sendai 980

(Received February 24, 1973)

The molecular g values of several bis(amino acidato)copper(II) complexes in crystals, whose crystal structures with two molecules per unit cell are known, have been estimated from the crystal g values by considering the effect of the spin-exchange interaction between the dissimilar copper(II) ions. All the crystal g values have been determined here from the powder K-band ESR spectra. Many other complexes with unknown crystal structures have also been dealt with in a similar way. The results have indicated that most of the complexes probably have a tetragonal or nearly tetragonal copper(II) ion environment in crystals, and a tendency for the estimated $g_{//}$ value to decrease with an increase in the energy of the visible absorption peak in crystals have been noted. A discussion about the correlation between an axial molecular g tensor and the two copper-ligand bond lengths of Cu–O and Cu–N has been given.

In previous papers,[1,2] it has been suggested that the copper(II) ion environment in most bis(amino acidato)-copper(II) complexes in crystals may be rhombically distorted because of two different kinds of atoms (O and N) directly coordinating to the metal ion. This has been supported by the fact that almost all the powder ESR spectra of the complexes show three different principal g values.[1] On the other hand, however, it has been reported that some bis(amino acidato)copper(II) complexes in magnetically diluted crystals and almost all the complexes in frozen aqueous methanolic solutions are of an axial symmetry in their g values.[1-3] Recently, an ESR study of bis(L-alaninato)copper(II) in undiluted single crystals has also revealed that a tetragonal molecular g tensor can be estimated from the observed rhombic g tensor of the crystal bulk by considering the crystal structure and the effect of the spin-exchange interaction between the dissimilar copper(II) ions.[4] Therefore, it seems necessary at present to reinterpret the powder ESR results previously reported after giving thought to the spin-exchange interaction in magnetically non-dilute crystals.

The purpose of this paper is to estimate the molecular g values from the crystal values for various bis(amino acidato)copper(II) complexes in crystals in view of the above-mentioned spin-exchange effect, and to discuss the correlation among the estimated molecular g values, the crystal structures, and the ligand-field properties.

Experimental

The K-band ESR spectra were measured in a polycrystalline state at room temperature with a Hitachi ESR spectrometer, Model-4001. The principal crystal g values (the principal g values of the crystal bulk) were determined from the powder ESR spectra by the use of the approximation of Kneubühl.[5]

The copper(II) complexes of amino acids employed in the present ESR measurements were as follows: bis(α-amino-isobutyrato)copper(II), bis(L-threoninato)copper(II) monohydrate, bis(*N*,*N*-dimethylglycinato)copper(II) trihydrate, and bis(L-hydroxyprolinato)copper(II) monohydrate (abbreviated as $[Cu(Aib)_2]$, $[Cu(L\text{-}Thr)_2]\cdot H_2O$, $[Cu(Dmg)_2]\cdot 3H_2O$, and $[Cu(L\text{-}Hypro)_2]\cdot H_2O$ respectively). They were all prepared according to the usual method,[6] using commercial G.R.-grade α-amino acids, were recrystallized from water, and were identified by elemental analysis. The visible absorption spectra for these complexes in a polycrystalline state were measured using the opal-glass method previously described.[1] Only the absorption peak positions (λ_{max}) will

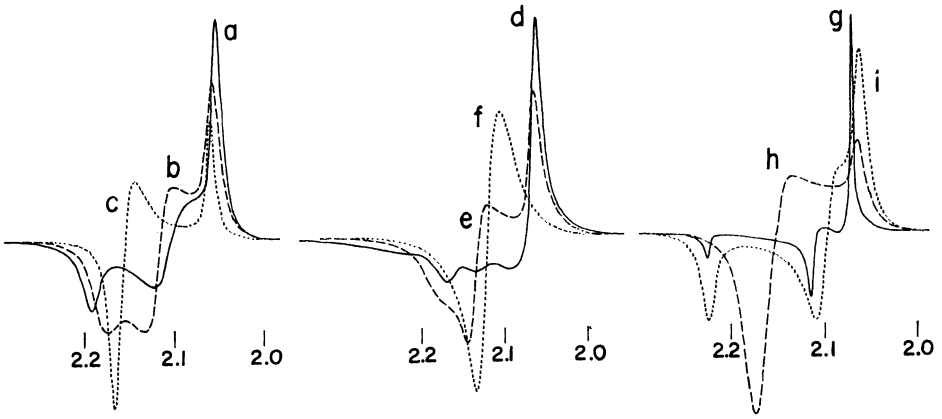

Fig. 1. Powder K-band ESR spectra at room temperature (numbers represent g values). (a): $[Cu(Aib)_2]$, (b): $[Cu(L\text{-}Thr)_2]\cdot H_2O$, (c): $[Cu(Dmg)_2]\cdot 3H_2O$, (d): $[Cu(DL\text{-}Pro)_2]\cdot 2H_2O$, (e): $[Cu(L\text{-}Hypro)_2]\cdot H_2O$, (f): $[Cu(L\text{-}Pro)_2]\cdot 0\text{-}1H_2O$, (g): $[Cu(\beta\text{-}Ala)_2]\cdot 6H_2O$, (h): $[Cu(\beta\text{-}Ala)_2]\cdot 2H_2O$, (i): $[Cu(\beta\text{-}Ala)_2]\cdot 0\text{-}1H_2O$.

be reported here, with an error of ±4 nm.

Bis(β-alaninato)copper(II) hexahydrate is known to effloresce in air at room temperature. After the powdered hexahydrate complex had been allowed to stand in air at room temperature for several hours (resulting in Compound (I)), its powder K-band spectrum was measured; then, the K-band spectrum also was measured for the complex obtained by heating Compound (I) *in vacuo* at 120 °C for two hours (resulting in Compound (II)).[7] Recently, Misumi *et al.* determined the hydration degree for each of the complexes obtained in the course of the dehydration of the hexahydrate complex; they also measured the powder X-band ESR spectra of the complexes.[8] By a comparison between the ESR spectra reported by them and those shown in this paper, Compounds (I) and (II) can be regarded as $[Cu(\beta\text{-Ala})_2]\cdot 2H_2O$ and $[Cu(\beta\text{-Ala})_2]\cdot 0\text{—}1H_2O$ respectively. $[Cu(L\text{-Pro})_2]\cdot 2H_2O$ was also dehydrated *in vacuo* at 120 °C for two hours (the degree of hydration for this complex, which is abbreviated as $[Cu(L\text{-Pro})_2]\cdot 0\text{—}1H_2O$, was not checked here). The powder ESR spectrum of $[Cu(DL\text{-Pro})_2]\cdot 2H_2O$ was again measured after repeated recrystallizations from water. All the powder ESR spectra measured in this work are shown in Fig. 1. $[Cu(\beta\text{-Ala})_2]\cdot 6H_2O$, $[Cu(L\text{-Pro})_2]\cdot 2H_2O$, and $[Cu(DL\text{-Pro})_2]\cdot 2H_2O$ are the complexes which had been prepared in previous works.[1,2] The abbreviations for the other bis(amino acidato)copper(II) complexes cited in this paper are the same as have been reported previously.[1,2]

Results and Discussion

Estimation of Molecular g Values. We will now consider the case of a unit cell containing only two sets of crystallographically non-equivalent axial molecules, whose principal g values are represented by $g_{//}$ and $g_\perp$ ($g_{//}>g_\perp$). Let the two principal axes of the molecules be inclined at an angle of 2γ. In the condition of $2J>(g_{//}-g_\perp)\beta H$, the three principal crystal g values ($g_1\leq g_2\leq g_3$ for $0°\leq\gamma\leq 45°$) are expressed as follows:[9]

$$g_1 = g_\perp \tag{1}$$

$$g_2 = \sqrt{g_\perp^2+(g_{//}^2-g_\perp^2)\sin^2\gamma} \tag{2}$$

$$g_3 = \sqrt{g_\perp^2+(g_{//}^2-g_\perp^2)\cos^2\gamma} \tag{3}$$

where the g_3 and g_2 axes are directed to the internal and external bisectors respectively of the axes normal to the two non-equivalent molecular planes, and where the g_1 axis is perpendicular to both the g_2 axis and the g_3 axis. The powder ESR line shape of a reverse-type ($g_1<g_2=g_3$) is observed for any one of the complexes, with $\gamma=45°$ in crystals. Strictly speaking, Eqs. (1)—(3) are incorrect for the above-described system, since g_2 and g_3 must be expressed as $g_\perp+(g_{//}-g_\perp)\sin^2\gamma$ and $g_\perp+(g_{//}-g_\perp)\cos^2\gamma$ respectively, because of the following form of the Zeeman term in the effective spin Hamiltonian under such a spin-exchange field: $(\beta/2)(\boldsymbol{S}^1+\boldsymbol{S}^2)(\boldsymbol{g}_a+\boldsymbol{g}_b)\boldsymbol{H}$, where the two paramagnetic species are denoted by a and b and where the electrons are denoted by 1 and 2.[10] However, as the anisotropy in the molecular g tensor for copper(II) complexes is not so large, Eqs. (1)—(3) can be used in numerical calculations without any serious errors in this work; so can Eq. (4), which will be discussed later.

Equations (1)—(3) were successfully applicable to the case of $[Cu(L\text{-Ala})_2]$ in crystals. The results alone are presented in Table 1. The $g_{//}$ and $g_\perp$ values of $[Cu(Pen)_2]$ in crystals were determined from Eqs. (1)—(3), using the γ value determined by X-ray analysis so as to minimize the equation of $(g_2^{ob}-g_2^{calc})^2+(g_3^{ob}-g_3^{calc})^2$.[11] The results are listed in Table 1. The values of g_2^{calc} and g_3^{calc} for this complex are in agreement with the experimentally-determined values of g_2^{ob} and g_3^{ob} respectively within the limits of experimental error. $[Cu(DL\text{-}\alpha\text{-}NH_2but)_2]$ and $[Cu(DL\text{-Met})_2]$, whose γ values are not known,[12,13] show powder ESR line shapes similar to those of $[Cu(L\text{-Ala})_2]$ and $[Cu(Pen)_2]$; the values of $g_{//}$, $g_\perp$, and γ for the former two complexes were tentatively calculated from Eqs. (1)—(3) using the observed crystal g values. The γ values thus calculated were close to those of the latter two complexes, as is shown in Table 1. This result can be well understood from the point of view of crystal structure; all these four complexes are monoclinic, with a space group of the $P2_1$ type, and all may be expected to have almost the same inter-molecular interaction in crystals. The molecular g values thus estimated, therefore, may be substantially correct.

The powder ESR spectrum of $[Cu(L\text{-Ser})_2]$ has a typical reverse-type line shape ($g_1^{ob}<g_2^{ob}\fallingdotseq g_3^{ob}$), as has been shown previously.[2] The γ value of this complex was determined by X-ray analysis to be close to 45°.[14] Its observed crystal g values, therefore, can be qualitatively explained from Eqs. (1)—(3) using such a large γ value as is listed in Table 1. The powder ESR line shape of $[Cu(DL\text{-Pro})_2]\cdot 2H_2O$ is also of a reverse-type, as is shown in Fig. 1. Its reverse-type line shape alone can be qualitatively explained in terms of the fact that its γ value is close to 45°. Some other complicated factors, however, must be considered in order to explain the complexity of its line shape.

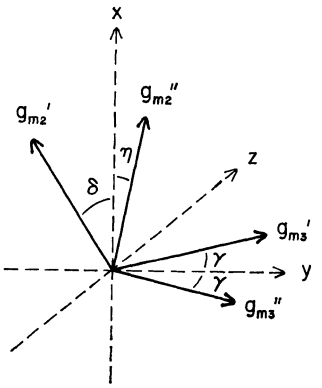

Fig. 2. A coordinate system for two non-axial molecules per unit cell.

The possibility, however, can not be denied that certain complexes might have non-axial molecular tensors. The equations corresponding to Eqs. (1)—(3) are complicated for this non-axial case;[15,16] besides γ, they require two new angles (δ and η), which will be defined below. The three principal molecular g values are denoted by g_{m1}, g_{m2}, and g_{m3} in order of increasing magnitude. The y and z axes are defined so as to bisect the angle between the two non-equivalent molecular axes (the two g_{m3} axes) internally and ex-

TABLE 1. CRYSTAL g VALUES, MOLECULAR g VALUES, AND CRYSTAL STRUCTURES

No.	Copper(II) complex	Crystal g values		Molecular g values	λ_{max} (nm)	Crystal structures			Ref.
		Obsd[c]	Calcd	$g_\perp$ $g_{//}$		(degree) γ	Bond lengths (Å) (the mean) Cu–N	Cu–O	
1	[Cu(L-Ala)$_2$][b]	2.049	2.049	2.049	590	28.5	2.015	1.965	17
		2.096	2.096	2.247					
		2.203	2.204						
2	[Cu(Pen)$_2$]	2.053	2.053	2.053	535	29.8	1.98	1.91	11
		1.089	2.089	2.195					
		2.160	2.161						
3	[Cu(β-Ala)$_2$]·6H$_2$O	2.068	2.068	2.068	635	29.8	2.04	2.01	18
		2.109	2.119	2.266					
		2.223	2.219						
4	[Cu(L-Ser)$_2$][d]	2.056	2.056	2.056	603	41.8	1.982	1.961	14
		2.157	2.146	2.254					
		2.157	2.168						
5	[Cu(DL-Pro)$_2$]·2H$_2$O[e]	(reverse-type g values)		(rhombic g values)	605	40.2	1.99	2.03	19
6	[Cu(DL-α-NH$_2$but)$_2$][f]	2.052	2.052	(2.052)	585	(28.5)			12
		2.098	2.098	(2.247)					
		2.204	2.204						
7	[Cu(DL-Met)$_2$][f]	2.053	2.053	(2.053)	580	(30.1)	1.983	1.951	13
		2.100	2.100	(2.234)					
		2.190	2.190						
8	[Cu(β-NH$_2$but)$_2$]·2H$_2$O	2.044			655	0	1.992	2.004	20
		2.090							
		2.280							

a) All the complexes have two molecules per unit cell except [Cu(β-NHbut)$_2$]·2H$_2$O, which has one molecule per unit cell. b) See Ref. 4. c) Experimental errors in g factors were $\pm$ 0.003. d) Larger errors may be expected in the two large crystal g values, because the powder ESR line shape of this complex deviates slightly from a complete reverse-type. e) See the text. f) The assumed values are expressed in parentheses (see the text).

ternally respectively, while the x axis is defined as perpendicular to the plane containing the two molecular axes (Fig. 2). In this coordinate system, δ and η specify the inclination of the two sets of g_{m2} axes to the x-axis. In general, the relation of $\delta=180°-\eta$ holds, since molecules are often related by screw-diad axes, as in the case of the complexes in Table 1. Accordingly, the elements of the g^2 matrix in this coordinate system may be expressed as follows:

$$g_{xx}^2 = g_{m1}^2 + (g_{m2}^2-g_{m1}^2)\cos^2\delta$$
$$g_{yy}^2 = g_{m2}^2\cos^2\gamma + g_{m3}^2\sin^2\gamma - (g_{m2}^2-g_{m1}^2)\sin^2\gamma\cos^2\delta$$
$$g_{zz}^2 = g_{m3}^2\sin^2\gamma + g_{m2}^2\cos^2\gamma - (g_{m2}^2-g_{m1}^2)\cos^2\gamma\cos^2\delta$$
$$g_{xz}^2 = (1/2)(g_{m2}^2-g_{m1}^2)\cos\gamma\sin 2\delta \qquad (4)$$

Here, g^2_{yz} and g^2_{xy} are reduced to zero by the relation of $\delta=180°-\eta$. The observed principal crystal g values (g_a, g_b, and g_c) are obtained by diagonalizing the above matrix; in this case, the following convenient equations can be derived:

$$g_a^2 = g_{yy}^2$$
$$g_a^2 + g_c^2 = g_{xx}^2 + g_{zz}^2$$
$$g_a^2\cdot g_c^2 = g_{xx}^2\cdot g_{zz}^2 - (g_{xz}^2)^2 \qquad (5)$$

There have been almost no data concerning the δ except for a few copper(II) complexes. The crystal g values (g_a, g_b, and g_c) for each of the properly-assumed

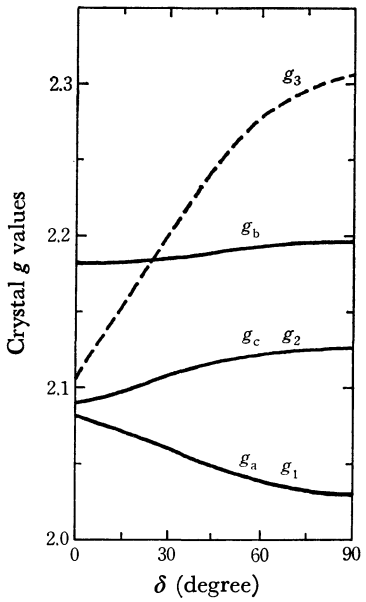

Fig. 3. The three principal crystal g values (g_a, g_b, and g_c; they are expressed as solid lines) derived from Eqs. (4) and (5) using $g_{m1}=2.030$, $g_{m2}=2.090$, $g_{m3}=2.230$, and $\gamma=30°$. The dashed line represents the g_3 value derived from Eq. (3) on the assumption of $g_1=g_a$ and $g_2=g_c$ in Eqs. (1) and (2).

sets of the g_{m1}, g_{m2}, g_{m3}, γ, and δ values were calculated from Eqs. (4) and (5). Then, it was examined whether or not the g_1, g_2, and g_3 values derived from Eqs. (1)—(3) using a proper set of the $g_{//}$ and $g_{\perp}$ values and the same γ value could be fitted to the g_a, g_b, and g_c values calculated above. Some of the results are shown in Fig. 3. This figure indicates that the g_a, g_b, and g_c values calculated for $\gamma=30°$, $g_{m1}=2.030$, $g_{m2}=2.090$, and $g_{m3}=2.230$ are not equal to the g_1, g_3, and g_2 values respectively except for the case of $\delta=25°$ (an intersection of solid and dashed lines in this figure). Furthermore, it became apparent that such an intersection varies over a wide range of δ according to the g_{m1}, g_{m2}, g_{m3}, and γ values. Since it is very rare for an actual case to correspond to the case of such an intersection, it is highly probable that the g tensors of copper(II) complexes in crystals are of an axial or nearly axial symmetry, if their crystal g values, as calculated from Eqs. (1)—(3) using proper sets of the $g_{//}$ and $g_{\perp}$ values, can be fitted to the observed values within the limits of experimental error. Accordingly, there is very little doubt that [Cu(Pen)$_2$] in crystals has an axial g tensor as well as [Cu(L-Ala)$_2$], as has been mentioned above. On the other hand, it was found that, when γ is close to 45°, g_b becomes close to g_c for any value of δ; accordingly, it is difficult to judge whether the observed crystal g values of a reverse-type ($g_1^{ob}<g_2^{ob}=g_3^{ob}$) correspond to the g_a, g_b, and g_c values or to the g_1, g_2, and g_3 ones. In this case, another method for judging whether or not the $g_{//}$ and $g_{\perp}$ values tentatively estimated from the observed g values are correct is required.

Support for the view that all the $g_{//}$ and $g_{\perp}$ values listed in Table 1 are close to the true molecular g values comes also from the fact that the tendency for the $g_{//}$ value to decrease regularly with an increase in the energy of λ_{max}, as is shown by full circles in Fig. 4, is consistent with the same tendency previously recognized for a great numer of copper(II) complexes in frozen solutions.[21]

The values of $g_{//}$, $g_{\perp}$, and γ for a number of bis-

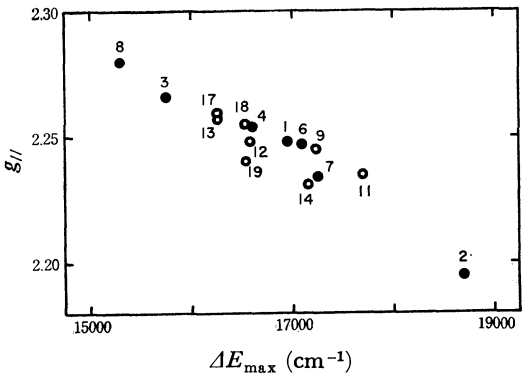

Fig. 4. A plot of $g_{//}$ against ΔE_{max} (numbers correspond to the complexes in Tables 1 and 2; open circles correspond to the complexes with unknown crystal structures listed in Table 2).

(amino acidato)copper(II) complexes whose crystal structures are not known were determined from the observed crystal g values using Eqs. (1)—(3), on the assumption that all these complexes have axial g tensors in crystals; the results are listed in Table 2. All the reverse-type crystal g values observed for several complexes led to the result of $\gamma=45°$. The fact that all the determined γ values of the anhydrous complexes in Table 2 are close to 30° is consistent with the fact noted for the anhydrous complexes in Table 1. There is also a slight tendency for the $g_{//}$ value thus estimated to decrease with an increase in the energy of λ_{max} in crystals, as is shown by open circles in Fig. 4. The molecular g values listed in Table 2 may, therefore, be substantially correct.

The ESR spectra of the hydrated copper(II) complexes generally show drastic changes in line shape when the complexes are dehydrated to a varying extent, as is shown by some examples in Fig. 1. It seems unnatural, however, that the molecular g values of the hydrates are markedly altered only by such a dehydration. For instance, [Cu(β-Ala)$_2$]·6H$_2$O and [Cu(DL-Ala)$_2$]·H$_2$O showed almost no marked changes in the

Table 2. Crystal and molecular g values for the complexes with unknown crystal structures

No.	Copper(II) complex	Observed values: Crystal g values[a] g_1^{ob}	g_2^{ob}	g_3^{ob}	λ_{max} (nm)	Assumed values[b]: Molecular g values $g_{\perp}$	$g_{//}$	γ (degree)
9	[Cu(DL-Ala)$_2$]·H$_2$O	2.053	2.122	2.180	580	2.053	2.245	36.2
10	[Cu(DL-Ala)$_2$]	2.054	2.100	2.202		2.054	2.245	28.8
11	[Cu(Aib)$_2$]	2.051	2.102	2.187	565[c]	2.051	2.235	31.2
12	[Cu(DL-Val)$_2$]	2.056	2.105	2.202	603	2.056	2.248	29.8
13	[Cu(DL-Ser)$_2$]	2.058	2.111	2.208	615	2.058	2.257	30.4
14	[Cu(L-Thr)$_2$]·H$_2$O	2.058	2.116	2.176	583	2.058	2.231	34.8
15	[Cu(β-Ala)$_2$]·2H$_2$O	2.062	2.171	2.171		2.062	2.275	45.0
16	[Cu(β-Ala)$_2$]·0—1H$_2$O	2.060	2.095	2.224		2.060	2.256	24.5
17	[Cu(Dmg)$_2$]·3H$_2$O	2.058	2.161	2.161	615	2.058	2.259	45.0
18	[Cu(L-Pro)$_2$]·2H$_2$O	2.056	2.158	2.158	605	2.056	2.255	45.0
19	[Cu(L-Hypro)$_2$]·H$_2$O	2.061	2.129	2.175	605	2.061	2.240	37.5

a) Experimental errors in g factors are ±0.003. b) The observed crystal g values can be calculated from Eqs. (1)—(3) using the assumed γ and molecular g values. c) Since the absorption spectrum is composed of two broad bands (about 525 and 610 nm), the mean was adopted for convenience.

estimated molecular g values upon dehydration, as is shown in Table 2, nor were there any remarkable accompanying color changes. It is of interest that the reverse-type powder ESR line shape of [Cu(L-Pro)$_2$]·2H$_2$O changed into a nearly symmetric one when this complex was dehydrated to a certain degree, as is shown in Fig. 1(f). It is more likely that the molecular g values for this complex also are not markedly altered upon dehydration, and that the symmetric powder ESR line shape is due to a special type of molecular packing in crystals; for instance, such a symmetrical line is observed if the four axial molecules are arranged with their molecular axes pointing towards the corners of a tetrahedron.[16]

Symmetry of the Ligand Field. Recently, many ESR studies have indicated that the molecular g tensors of the copper(II) complexes with different coordinating atoms in the molecular plane are of an axial or nearly axial symmetry. Almost all of the mixed-ligand complexes of copper(II) in solution so far examined have shown ESR line shapes of an axial type.[22] It is a well-known fact that the ability of some familiar ligand atoms to coordinate to the copper atom is in the order of S>N>O. The copper(II) chelates of monothio-β-diketones also have nearly axial g and A tensors in various magnetically-diluted states.[23] These facts suggest that, especially in solution, most copper(II) complexes generally tend to be of an axial or nearly axial symmetry in the g and A tensors, even if their coordinating atoms are different in kind.

Most of the complexes listed in Table 1 also have axial or nearly axial molecular g tensors in crystals; it is worthy of special attention that all the Cu–O bonds of these complexes are shorter by 0.03—0.07 Å than the Cu–N ones. On the other hand, the Cu–O bonds of [Cu(β-NH$_2$but)$_2$]·2H$_2$O are slightly longer than the Cu–N ones, and its molecular g tensor is clearly rhombic. [Cu(L-Ser)$_2$] is known to adopt a *cis*-configuration. The Cu–O bonds of this complex also are shorter by 0.020 Å (the mean) than the Cu–N ones. In general, the *cis*-complexes of copper(II), whose four coordinating atoms take a planar conformation of C_{2v} symmetry, as is approximately the case with [Cu(L-Ser)$_2$], tend to have axial or nearly axial g tensors, since even the possible lateral distortions (a distortion type of $Y_{1,3}^1$ in the crystal-field theory) in such *cis*-complexes do not destroy the axial symmetry in the molecular g tensor.[24]

Let us now consider the above-mentioned relation between the coordinate bond lengths and the axial g tensor. An axial molecular g tensor roughly means that $2-2\lambda_0(\alpha^2\mu^2/\Delta E_{xz})=2-2\lambda_0(\alpha^2\nu^2/\Delta E_{yz})$, where λ_0 represents the spin-orbit coupling constant for the free copper(II) ions, where $\Delta E_{xz}=E_{x^2-y^2}-E_{xz}$ and $\Delta E_{yz}=E_{x^2-y^2}-E_{yz}$, and where α, μ, and ν are the coefficients of the metal $3d$ atomic orbitals in the following antibonding molecular orbitals: $\phi_\alpha=\alpha d_{x^2-y^2}-\alpha'\phi_\alpha^{\mathrm{L}}$, $\phi_\mu=\mu d_{xz}-\mu'\phi_\mu^{\mathrm{L}}$, and $\phi_\nu=\nu d_{yz}-\nu'\phi_\nu^{\mathrm{L}}$ (ϕ^{L}s express the proper ligand orbitals).[25] One of the conditions which satisfy the equation of $(\alpha^2\mu^2/\Delta E_{xz})=(\alpha^2\nu^2/\Delta E_{yz})$ for the *trans*-complexes is as follows: the energy levels of ϕ_μ^{L} and ϕ_ν^{L} are close to each other, and, in addition, the square values of the overlap integral in the ϕ_μ and ϕ_ν molecular orbitals are almost equal.[26] Although the oxygen $2s$ and $2p$ atomic orbitals generally lie at lower energy levels than the respective nitrogen ones, it can reasonably be considered that the oxygen energy levels in the complexes of amino acids are raised to a great extent because of the oxygen atoms coordinated to the metal atom as a part of negatively-charged carboxyl anions.[27]

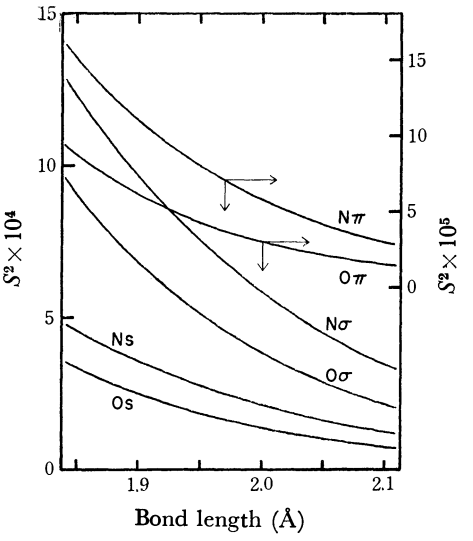

Fig. 5. Variations of the squares of overlap integrals with bond length (Ns, Nσ, and Nπ represent [S(3dσ–2s)]^2, [S(3dσ—2pσ)]^2, and [S(3πd—2pπ)]^2 respectively for the Cu–N bond, and Os, Oσ, and Oπ do so for the Cu–O bond).

The square values of the overlap integral, S, for the Cu–O and Cu–N bonds were calculated from the Slater atomic orbitals by the use of the single-ζ exponent values given by Clementi and Raimondi,[28] assuming that the copper and nitrogen atoms are electrically neutral and that the oxygen atom is negatively charged by a half unit; for the oxygen $2s$ and $2p$ orbitals, $\zeta=\zeta_n-0.35\ (q/n)$, where ζ_n represents the ζ value of electrically-neutral oxygen atoms, where 0.35 means the shielding constant, and where q is the charge, and n, the principal quantum number ($q=1/2$, $n=2$).[29] The numerical calculations were carried out on the NEAC-2200 Model-700 (TSS) computer at Tohoku University. The results are shown in Fig. 5. This figure indicates that the square values of S(3dσ-2s), S(3dσ-2pσ), and S(3dπ-2pπ) for the Cu–O bonds become equal to those for the respective Cu–N bonds when the Cu–O bonds are shorter than the Cu–N ones by about 0.07 Å for the former two S's and by about 0.09 Å for the latter. This result can qualitatively explain the above-mentioned fact that it is required for an axial g tensor that the Cu–O bonds are shorter by about 0.05 Å than the Cu–N ones. This result is also almost consistent with the concept of covalent bond radii; the covalent radius of N is larger by 0.04 Å than that of O.[30]

It may be concluded from all the experimental results listed in Tables 1 and 2 that almost all bis(amino acidato)copper(II) complexes in crystals, except for

a small number, are of an axial or nearly axial symmetry in the copper(II) ion environment.

The author is grateful to Professor Taro Isobe for his encouragement throughout this work.

References

1) H. Yokoi, M. Sai, T. Isobe, and S. Ohsawa, This Bulletin, **45**, 2189 (1972).
2) H. Yokoi, M. Sai, and T. Isobe, *ibid.*, **45**, 3488 (1972).
3) H. A. Kuska and M. T. Rogers, *J. Chem. Phys.*, **43**, 1744 (1965); H. C. Allen, Jr., M. I. Mandrioli, and J. W. Becker, *ibid.*, **56**, 997 (1972); M. Fujimoto and Y. Tomkiewicz, *ibid.*, **56**, 746 (1972).
4) H. Yokoi and S. Ohsawa, This Bulletin, **46**, 2766 (1973).
5) F. K. Kneubühl, *J. Chem. Phys.*, **33**, 1074 (1960).
6) E. Abderhalden and E. Schnitzler, *Z. Physiol. Chem.*, **163**, 94 (1927).
7) H. Yokoi and T. Isobe, Abstract of the 6th ESR Symposium (The Chemical Society of Japan), p. 24 (1967).
8) S. Misumi, T. Isobe, and S. Kimoto, *Chem. Lett.*, **1972**, 1101.
9) H. Abe and K. Ono, *J. Phys. Soc. Japan*, **11**, 947 (1956).
10) K. Itoh, H. Hayashi, and S. Nagakura, *Mol. Phys.*, **17**, 561 (1969).
11) C. A. Barklay and F. S. Stephens, *J. Chem. Soc.*, **1963**, 2027.
12) A. J. Stosick, *J. Amer. Chem. Soc.*, **67**, 362 (1945).
13) M. V. Veidis and G. J. Palenik, *Chem. Commun.*, **1969**, 1277.
14) D. van der Helm and W. A. Franks, *Acta Crystallogr.*, **B25**, 451 (1969).
15) D. E. Billing and B. J. Hathaway, *J. Chem. Phys.*, **50**, 1476 (1969).
16) B. J. Hathaway and D. E. Billing, *Coordin. Chem. Rev.*, **5**, 143 (1970).
17) A. Dijkstra, *Acta Crystallogr.*, **20**, 588 (1966).
18) K. Tomita, This Bulletin, **34**, 297 (1961).
19) A. McL. Mathieson and H. K. Welsh, *Acta Crystallogr.*, **5**, 599 (1952).
20) R. F. Bryan, R. J. Poljak, and K. Tomita, *ibid.*, **14**, 1125 (1961).
21) H. Yokoi, M. Otagiri, M. Sai, and T. Isobe, Abstract of the 10th ESR Symposium (the Chemical Society of Japan), p. 62 (1971); H. Yokoi and T. Kishi, *Chem. Lett.*, **1973**, 749.
22) H. Yokoi, M. Otagiri, and T. Isobe, This Bulletin, **44**, 2395 (1971); *ibid.*, **46**, 442 (1973); H. Yokoi, M. Sai, and T. Isobe, *ibid.*, **43**, 1078 (1970).
23) A. D. Toy, S. H. H. Chaston, J. R. Pilbrow, and T. D. Smith, *Inorg. Chem.*, **10**, 2219 (1971).
24) W. E. Blumberg, "The Biochemistry of Copper," ed. by J. Peisach, P. Aisen, and W. E. Blumberg, Academic Press, New York (1966), p. 49.
25) B. R. McGarvey, "Transition Metal Chemistry," Vol. 3, ed. by R. L. Carlin, Marcel Dekker, New York (1967), p. 89.
26) C. J. Ballhausen and H. B. Gray, "Molecular Orbital Theory," W. A. Benjamin, Inc., New York (1964), p. 92.
27) T. Anno, *Theoret. Chim. Acta*, **18**, 223 (1970).
28) E. Clementi and D. L. Raimondi, *J. Chem. Phys.*, **38**, 2686 (1963).
29) A. Loftus, *Mol. Phys.*, **5**, 105 (1962).
30) L. Rauling, "The Nature of the Chemical Bond," 3rd Edition, Cornell Univ. Press., Ithaca (1960). p. 221.

The Reaction of Bis(2-pyridinecarbonitrile)copper(II) Chloride with Methanol and Various Amines

Shinnichiro SUZUKI,[1] Masayoshi NAKAHARA,* and Ken-ichi WATANABE

Department of Chemistry, Faculty of Science, Tokyo Metropolitan University, Setagaya, Tokyo 158
**Department of Chemistry, Faculty of Science, Rikkyo University, Nishi-ikebukuro, Toshima, Tokyo 171*

(Received April 12, 1973)

On treatment of bis(2-pyridinecarbonitrile)copper(II) chloride with various amines in methanol, the alkoxylation of the nitrile group in the complex took place; in some cases, the alkoxylation and the ligand substitution of the complex occurred at the same time. The reaction products were classified into three types depending on the amines used; two of the types consisted of new complexes. The complexes of $CuCl_2$(MeOpy)(Amine) (MeOpy: *O*-methylpyridine-2-carboximidate), were obtained on the addition of ammonia, methylamine, dimethylamine, ethylamine, benzylamine, or piperidine to a methanol solution of bis(2-pyridinecarbonitrile)copper(II) chloride. On the other hand, the addition of trimethylamine, diethylamine, or triethylamine afforded the complex of $CuCl_2$-$(MeOpy)_2$. These types of complexes were not obtained by the use of aniline or pyridine; but the previously known complex, $CuCl_2$(MeOpy), was obatined in this case. It has been assumed that the formation of the three types of complexes is essentially the result of both the basicities and the steric factors of the amines.

It has been reported that 2-pyridinecarbonitrile readily gives the chelates of 2-pyridinecarboxamide or *O*-methylpyridine-2-carboximidate(MeOpy) upon heating with transition-metal ions, *e.g.*, Cu(II) or Ni(II), in water[2,3] or methanol[3] respectively. Although 2-pyridinecarbonitrile coordinates *via* the nitrogen atom of the pyridine ring to the metal ions, the nitrile group in the 2-position is presumed to have an interaction with the metal ions and to be easily attacked by the nucleophilic reagents, water or alcohols.

The amination of the nitrile group in $PtCl_2(CH_3CN)_2$ has been reported by Stephenson.[4] We tried the addition of amines to bis(2-pyridinecarbonitrile)copper(II) chloride in methanol. However, no amination products but the following three types of copper(II) complexes were obtained (Fig. 1); the complexes of Type

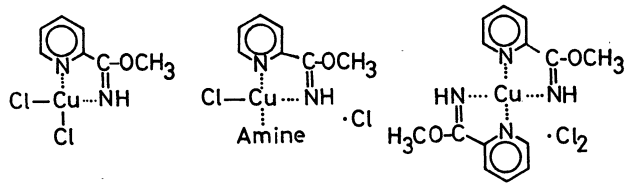

$CuCl_2$(MeOpy), Type I — $CuCl_2$(MeOpy)(Amine), Type II — $CuCl_2(MeOpy)_2$ Type III

Fig. 1. Three types of copper(II) complexes.

II and III were new ones. A brief note has been already reported.[5] In this paper, the relationship between the cause of the formation of the different types of complexes and their structures will be discussed.

Experimental

Preparation of Bis(2-pyridinecarbonitrile)copper(II) Chloride. Commercial 2-pyridinecarbonitrile was purified by recrystallization from ether; mp 26.5—27.5 °C. A dry methanol solution of 2-pyridinecarbonitrile(2 mol) was added to a dry methanol solution of copper(II) chloride dihydrate (1 mol) at 0 °C. The mixture was stirred vigorously to yield deep blue crystals. The crystals were immediately collected by filtration, and washed with ether. They were then dried over phosphorus pentoxide *in vacuo*. Found: C, 42.04; H, 2.48; N, 15.99; Cu, 18.45% Calcd for $CuCl_2(C_5H_4NCN)_2$: C, 42.06; H, 2.36; N, 16.35; Cu, 18.54%.

Reaction of Bis(2-pyridinecarbonitrile)copper(II) Chloride with Methanol and Various Amines. Bis(2-pyridinecarbonirile)-copper(II) chloride was suspended by stirring it in dry methanol at 0 °C, and then a methanol solution of an amine (1 or 2 mol) was immediately added to it. After the mixture had been stirred for 45—60 min at 0 °C, ether was added until bluish green crystals were precipitated; these crystals were then separated by filtration. They were instantly washed with ether several times and dried over silica gel *in vacuo*. All the products were obtained quantitatively. For recrystallization, the precipitates were dissolved in methanol, and ether was added until fine crystals were deposited. Since the recrystallization of ethylamine complex was not easy, its methanol solution was kept overnight at room temperature. The various complexes thus obtained are shown in Table 1, while the analytical data of the new complexes are given in Table 2.

$CuCl_2(NH_3)$(MeOpy)–No. 2– was also synthesized by means of the following method. At room temperature, ammonia gas was bubbled into 50 ml of a methanol solution containing 1.0 g of $CuCl_2$(MeOpy), No. 1. The reaction occurred immediately, and the color of the reaction mixture changed from bluish green to violet. Then the reaction mixture was concentrated to about 15 ml. The violet precipitates of the tetraamminecopper (II) chloride which had been initially deposited were filtered off, and pale blue $CuCl_2(NH_3)$-(MeOpy), crystals were obtained by adding ether to the filtrate. It was recrystallized from methanol ether mixture three times.

Instraments. The electronic and infrared spectra were obtained with Hitachi Recording Spectrophotometers, ESP-3T and EPI-G-2 respectively.

Results and Discussion

Absorption Spectra. The absorption spectra of the complexes synthesized are listed in Table 3. All the copper(II) complexes have d-d bands in the 12900—15000 cm^{-1}, $\log \varepsilon = 1.8$—2.0, while the bands of $\log \varepsilon = 3.85$ in the ultraviolet region (36600 cm^{-1}) are mainly due to the pyridine ring in the ligand. As for the infrared spectra of all the complexes, the bands of the

TABLE 1. REACTION PRODUCTS OF BIS(2-PYRIDINECARBONITRILE)COPPER(II) CHLORIDE AND VARIOUS AMINES IN METHANOL

Type	Compound No.	Amine	pK_a	Products	Color
I	1	Aniline Pyridine	4.60 5.18	$CuCl_2$(MeOpy)	Bluish green
	2	Ammonia	9.25	$CuCl_2(NH_3)$(MeOpy)	Pale blue
	3	Methylamine	10.62	$CuCl_2(CH_3NH_2)$(MeOpy)	Bluish green
	4	Dimethylamine	10.77	$CuCl_2(CH_3)_2NH$(MeOpy)	Light green
II	5	Ethylamine	10.63	$CuCl_2(CH_3CH_2NH_2)$(MeOpy)	Bluish green
	6	Benzylamine	9.35	$CuCl_2$(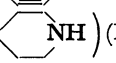)(MeOpy)	Deep blue
	7	Piperidine	11.12	$CuCl_2$(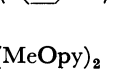)(MeOpy)	Light green
		Trimethylamine	9.80		
III	8	Diethylamine	10.93	$CuCl_2(MeOpy)_2$	Pale blue
		Triethylamine	10.87		

TABLE 2. ANALYTICAL DATA OF COMPLEXES

Compound No.	Formula	Cu(%)		C(%)		H(%)		N(%)	
		Found	Calcd	Found	Calcd	Found	Calcd	Found	Calcd
2	$CuCl_2C_7H_{11}ON_3$	22.56	22.09	29.07	29.23	3.75	3.86	14.59	14.61
3	$CuCl_2C_8H_{13}ON_3$	21.06	21.06	32.07	31.85	4.32	4.35	13.40	13.93
4	$CuCl_2C_9H_{15}ON_3$	19.95	20.13	34.24	34.24	4.58	4.80	13.07	13.31
5	$CuCl_2C_9H_{15}ON_3$	19.9	20.13	34.33	34.24	4.85	4.80	13.20	13.31
6	$CuCl_2C_{14}H_{17}ON_3$	16.70	16.82	44.35	44.51	4.32	4.54	11.18	11.13
7	$CuCl_2C_{12}H_{19}ON_3$	17.81	17.86	40.34	40.51	5.10	5.39	11.44	11.81
8	$CuCl_2C_{14}H_{16}O_2N_4$	15.72	15.62	40.67	41.33	4.06	3.97	13.33	13.78

TABLE 3. ABSORPTION MAXIMA IN VISIBLE, ULTRAVIOLET AND INFRARED REGION

No.	ν_{max} in cm^{-1} and log ε (in parentheses, ε=molar extinction coefficient) in methanol		C=N (cm^{-1})	C–O–C (cm^{-1})
1	13300 (1.81)	36600 (3.85)	1658[a]	1380[a]
2	14900 (1.89)	36600 (3.85)	1655	1388
3	14700 (1.93)	36600 (3.85)	1646	1382
4	14600 (1.92)	36600 (3.85)	1644	1386
5	15000 (1.85)	36600 (3.85)	1646	1385
6	14600 (1.95)	36600 (3.85)	1655	1381
7	14600 (1.87)	36600 (3.83)	1647	1388
8	12900 (2.02)	36600 (4.06)	1646	1398

a) Ref. 2.

N–H stretching vibrations of amines or of the imidate group appeared at 3000—3300 cm^{-1}. The C–N stretching and antisymmetric C–O–C stretching vibrations of the imidate group appeared at about 1650 and 1380 cm^{-1} respectively.

The Formation of the Type I Complex. The complex of Type I, which is prepared by heating equimolar amounts of 2-pyridinecarbonitrile and copper(II) chloride in methanol, has already been reported by Barnard.[3] In our studies, it was also prepared easily when aniline or pyridine was added to a methanol solution containing an equimolar amount of bis(2-pyridinecarbonitrile)copper(II) chloride. However, by adding an excess of amine —but less than two moles—, a mixture of the Type I complex and the copper(II) complex of aniline or pyridine was obtained.

The Formation of the Type II Complexes. The complexes of Type II (Nos. 2—7, Table 1) were obtained by adding amines to a methanol solution of bis(2-pyridinecarbonitrile)copper(II) chloride. The amines used are shown in Table 1. The amount of amines employed was 1—2 mol for bis(2-pyridinecarbonitrile)copper(II) chloride. On the contrary, each aminecopper(II) complex was formed by employing more than two moles of amines. The difference in the composition of the Type II complexes from that of the other types is observed in the absorption spectra data (d-d bands, λ_{max}=14600—15000 cm^{-1}) in Table 3. In particular, the d-d band of No. 2 (Type II) was shifted to the range of shorter wavelengths and increased in its absorption intensity as compared with that of No. 1. This indicates the coordination of ammonia in the No. 2. From the infrared spectral data in Table 3, the bands of C–N stretching vibrations of the imino group (Nos. 2—7) are known to be shifted to the range of lower wave numbers than that of the Type I complex (1658 cm^{-1}). Accordingly, it is presumed that these shifts may be attributed to the coordination of various amines in the complexes.

The Formation of the Type III Complexes. The addition of trimethylamine, diethylamine, or triethylamine to bis(2-pyridinecarbonitrile)copper(II) chloride in methanol always afforded a complex of Type III, $CuCl_2(MeOpy)_2$. With regard to the ultraviolet absorp-

tion bands due to the ligand, MeOpy (in Table 3), the absorption intensity of No. 8 is about twice that of No. 1, hence, No. 8 obviously contains two molecules of MeOpy.

The Effect of Amines. It was concluded that 2-pyridinecarbonitrile coordinated to the copper(II) ion underwent alkoxylation and/or ligand-exchange reaction in the presence of various amines. However, the complex formations of the different types, from I to III, are mainly dependent on the basicities and steric factors of the amines used.

In the case of Type I complex formation, in the presence of a weaker base, such as aniline or pyridine, the interaction of the amine with the metal ion is not strong enough to form a mixed-ligand complex such as Type II. However, when a large excess of the amine was employed, only an amine complex was obtained by the ligand exchange (*e.g.* an aniline or pyridine copper-(II) complex).

It is conceivable that the distinction between the formation of Types II and III complexes is due mainly to steric effects between amines and the MeOpy group. The basicities of the amines belonging to Types II and III are similar (Table 1, pK_a). The amines which afford the complexes of Type II have little steric hindrance and easily coordinate to the metal ion by means of the ligand exchange. On the other hand, the amines which have bulky alkyl groups, *e.g.*, trimethylamine, diethylamine, and triethylamine, do not afford amine complexes by the steric hindrance; they only act as catalysts for the alkoxylation (Type III). In order to prepare a Type III complex without amines, it is necessary for the reaction mixture to be refluxed more than 5 hr.

Reference and Footnote

1) Present address: Institute of Chemistry, College of General Education, Osaka University, Toyonaka, Osaka.
2) K. Sakai, T. Ito, and K. Watanabe, This Bulletin, **40**, 1660 (1967).
3) P. F. B. Barnard, *J. Chem. Soc., A*, **1969**, 2140.
4) N. C. Stephenson, *J. Inorg. Nucl. Chem.*, **24**, 801 (1962).
5) S. Suzuki, M. Nakahara, and K. Watanabe, This Bulletin, **44**, 1441 (1971).

Syntheses of *N,N'*-Bis(1-acetonylethylidene)ethylenediamine Complexes of Rare Earth Perchlorates

Norifumi YOSHIDA, Akira MATSUMOTO, and Jiro SHIOKAWA

Department of Applied Chemistry, Faculty of Engineering, Osaka University, Yamadakami, Suita, Osaka 565

(Received May 28, 1973)

N,N'-Bis(1-acetonylethylidene)ethylenediamine(AEH_2) complexes were prepared by the reaction of hydrous rare earth perchlorates with AEH_2 in methanol. Elemental analysis, X-ray powder diffraction analysis, pH titration, IR and luminescence spectrometries indicated that the complexes of the lighter rare earths were $Ln(AEH_2)_4(ClO_4)_3$, where Ln are La, Pr, Nd, and Sm, while the complexes of the heavier rare earths were hydroxocomplexes, $Ln(AEH_2)_2(ClO_4)_2(OH)\cdot H_2O$, where Ln are Gd, Dy, and Er. Anhydrous gadolinium perchlorate was reacted with AEH_2 in methanol under anhydrous conditions to give $Gd(AEH_2)_4(ClO_4)_3$. It was possible that a water molecule played an important role in the complexation of rare earth perchlorates with AEH_2 in methanol. The formation of the hydroxocomplexes with AEH_2 was related to the low coordinating ability of the perchlorate ion and to the charge densities of the rare earth ions as well as to the basicity of AEH_2.

A number of the rare earth complexes with neutral ligands have been prepared in organic solvents to avoid the coordination of the water molecule.[1,2] In the case of highly basic ligands such as amines,[3,4] the complexes have been prepared under anhydrous conditions to prevent hydrolysis. The number of the given ligands attached to rare earth ions depends on the ionic radii of the rare earth ions and on the coordinating abilities of the anions.

N,N'-Bis(1-acetonylethylidene)ethylenediamine-(AEH_2) complexes have previously been prepared from the hydrous rare earth salts, such as chlorides, nitrates, and thiocyanates, in ethanol[5] or in a methanol–acetone mixture,[6] while the AEH_2 complexes of rare earth perchlorates have not been reported. The present paper will deal with the preparation of the complexes obtained by the reaction of AEH_2 with hydrous rare earth perchlorates and anhydrous gadolinium perchlorate in methanol. The AEH_2 complexes of the lighter rare earth perchlorates include more ligand molecules attached to the metal ion than those[5,6] of the lighter rare earth salts. The complexes obtained from hydrous, heavier rare earth perchlorates were hydroxocomplexes. Scarcely no hydroxocomplexes with neutral ligands are found in the literature.

Experimental

Materials. Rare earth oxides of a 99.9% purity were obtained from the Shin-etsu Chem. Ind. Co., Ltd. The hydrous rare earth perchlorates were prepared by dissolving a known amount of oxide in dilute perchloric acid and by then evaporating the mixture carefully on a hot plate. Anhydrous gadolinium perchlorate was obtained by heating the hydrate slowly up to 250 °C *in vacuo*.[3] The AEH_2 was prepared by the method shown in the literature.[7]

Preparation of Complexes Using Hydrous Rare Earth Perchlorates. The complexes were prepared by adding 10 ml of methanol containing an appropriate amount of AEH_2 (7 mM or 14 mM) to 15 ml of a methanol solution of rare earth perchlorate (3 mM). Lanthanum and praseodymium complexes were precipitated immediately. In the case of the other rare earths, the mixed solution was stirred for a few minutes and then allowed to stand overnight at room temperature to precipitate crystalline complexes.

Preparation of a Complex Using Anhydrous Gadolinium Perchlorate. The procedure was carried out in a dry nitrogen atmosphere. Anhydrous gadolinium perchlorate (*ca.* 3 mM) was dissolved in 15 ml of methanol, and then a small amount of the insoluble residue was filtered off. The filtrate was added to 10 ml of methanol including 14 mM of AEH_2, and the mixture was allowed to stand overnight at room temperature to give a crystalline product.

All the products were filtered, washed with methanol, and then dried *in vacuo*.

Elemental Analysis. A known amount of the complex was dissolved in dilute hydrochloric acid. The rare earth elements were determined gravimetrically.[8] The perchlorate ion was determined spectrophotometrically.[9]

Measurements. The IR spectra were recorded with a Perkin-Elmer 225 and a Hitachi EPI-L spectrophotometer. X-ray powder diffraction patterns were obtained with a Rigaku Denki diffractometer "Geiger-flex", using Ni-filtered Cu$K\alpha$ radiation. The luminescence spectra of the complexes and AEH_2 in the solid state excited at 260 nm were measured with a Hitachi MPF model 3 spectrophotometer. The pH was measured by a Hitachi-Horiba F-7 pH meter.

Results and Discussion

The analytical data listed in Table 1 indicate that the complexes obtained may be classified into two types—the 'D' type[6] including the complexes obtained from the hydrous, lighter rare earth (La, Pr, Nd, and Sm) and anhydrous gadolinium perchlorates, and the 'E' type including the complexes obtained from the hydrous, heavier rare earth (Gd, Dy, and Er) perchlorates. The formulas are estimated to be $Ln(AEH_2)_4(ClO_4)_3$ for the 'D' type and $Ln(AEH_2)_2(ClO_4)_2(OH)\cdot H_2O$ for the 'E' type on the basis of the analytical data and the data to be described hereinafter. The X-ray diffraction spectra shown in Fig. 1 also support the above classification into two types.

The pH titration curves for the two types of complexes are compared in Fig. 2. The pH value of the aqueous solution of the praseodymium complex (the 'D' type) varied little from the initial pH value upon the addition of a standard acid solution. On the other hand, the titration curve of the erbium complex (the 'E' type) shows a pH break which corresponds to *ca.* one equivalence of the acid. When the titration was continued, the pH titration curves of both 'D'- and

Table 1. Analytical data of complexes (%)

Ln	Type[a]		Ln	C	H	N	ClO_4
La	D	Found	10.5	42.93	6.04	8.21	22.0
		Calcd	10.4	43.22	6.00	8.40	22.4
Pr	D	Found	10.7	43.80	6.24	8.51	
		Calcd	10.5	43.16	5.99	8.39	22.3
Nd	D	Found	10.9	42.77	6.12	8.20	22.8
		Calcd	10.8	43.05	5.97	8.37	22.3
Sm	D	Found	11.4	42.08	5.90	8.10	
		Calcd	11.2	42.85	5.95	8.33	22.2
Gd[b]	D	Found	11.7	41.60	5.89	8.15	
		Calcd	11.6	42.61	5.97	8.28	22.1
Gd	E	Found	18.9	33.82	5.33	6.70	23.2
		Calcd	18.7	34.30	5.24	6.67	23.7
Dy	E	Found	19.4	33.71	5.01	6.24	
		Calcd	19.2	34.08	5.20	6.63	23.5
Er	E	Found	19.8	33.70	5.20	6.44	23.1
		Calcd	19.7	33.80	5.17	6.59	23.4

a) 'D' type: $Ln(AEH_2)_4(ClO_4)_3$, 'E' type: $Ln(AEH_2)_2(ClO_4)_2(OH)\cdot H_2O$. b) Complex was prepared from anhydrous gadolinium perchlorate. Other complexes were prepared from hydrous rare earth perchlorates.

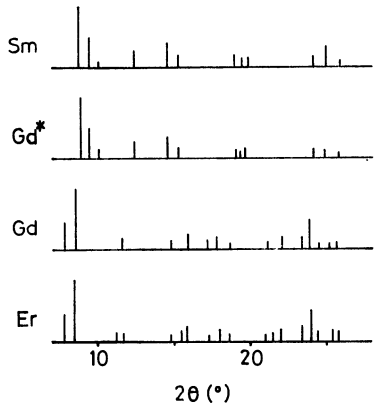

Fig. 1. X-ray powder diffraction diagrams of complexes. * Complex was prepared from anhydrous gadolinium perchlorate. The other complexes were prepared from hydrous rare-earth perchlorates.

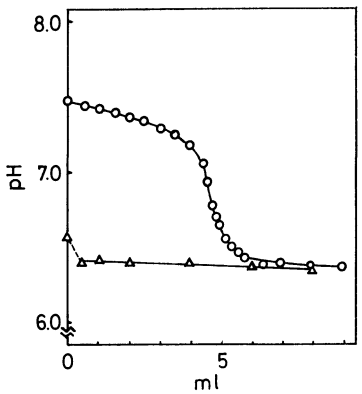

Fig. 2. Titration curves of complexes with 0.012 M HCl. —△—: Pr complex ('D' type), —○—: Er complex ('E' type).

'E' types leveled off at a pH value of *ca.* 6.4. An odor of acetylacetone was also detected; it seems to be caused by a decomposition of AEH_2 into acetyl-

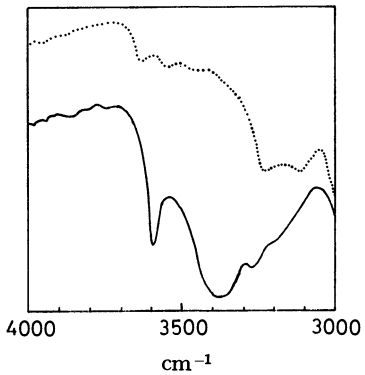

Fig. 3. Infrared spectra of gadolinium complexes in the OH and NH stretching region. ---------: 'D' type, ———: 'E' type

acetone and diazepine.[10,11] The results of the pH titration are considered to indicate that 'E'-type complexes contain a hydroxyl group.

The presence of the hydroxyl group in the 'E'-type complexes is also suggested by the IR absorption spectra. The IR absorption spectra of gadolinium complexes in the 3000—4000 cm^{-1} region are shown in Fig. 3. For the 'E'-type complex of gadolinium, a sharp band is observed at 3594 cm^{-1}. The corresponding bands are also observed at 3596 cm^{-1} for the dysprosium complex and at 3600 cm^{-1} for the erbium complex. These sharp bands are assignable to the OH stretching of the hydroxyl group. In other reports, a similar assignment has been made for the sharp absorption bands of the rare earth hydroxo-compounds, *e.g.*, at 3600—3610 cm^{-1} (hydroxides),[12] 3585—3620 cm^{-1} (hydroxo-oxides),[12] 3425—3550 cm^{-1} (hydroxocarbonates)[13] and 3588 cm^{-1} (neodymium azide).[14] The broad band at 3380 cm^{-1} of the 'E' type might arise from the OH stretching vibration of the inherent water of the complex.[15,16] On the other hand, the 'D'-type complex of gadolinium shows no absorption bands due to hydroxyl and water molecule.

In Fig. 3, the broad band at 3100—3300 cm^{-1} observed in both 'D'- and 'E'-type complexes indicates that hydrogen-bonded O–H···N or O···H–N groups are present in the complexes.[5,17] The IR absorption bands of the complexes in the region of the C=O, C=N, and C=C stretching vibrations[17] are summarized in Table 2. In the case of the thorium(IV) complex[18]

Table 2. Characteristic infrared absorption bands (cm^{-1}) of complexes and ligand

Ln	Type	(C=O)	(C=C) or (C=N)
La	D	1605s 1593sh	1542s 1496m
Pr	D	1605s 1592sh	1542s 1495m
Nd	D	1605s 1595s	1540s 1495m
Sm	D	1606s 1592s	1542s 1493m
Gd	D	1606s 1590s	1547s 1498m
Gd	E	1594s	1550s 1495m
Dy	E	1597s	1550s 1499m
Er	E	1596s	1550s 1495m
Ligand		1610s	1582s 1565m
			1550m 1520s

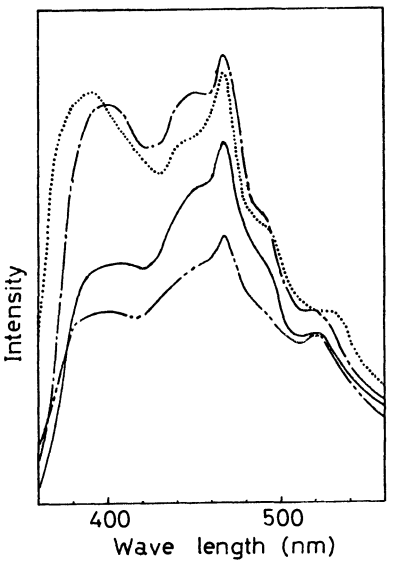

Fig. 4. Luminescence spectra of gadolinium complexes and AEH_2.
----: 'C' type complex, — — —: 'D' type complex, ———: 'E' type complex, ·····: AEH_2.

containing both neutral and ionic ligands, $Th(AEH_2)(AE)(NO_3)_2$, the absorption intensity of $\nu_{(C=O)}$ at 1600 cm^{-1} is rather weaker than those of $\nu_{(C=N)}$ and $\nu_{(C=C)}$. Since the absorption bands $\nu_{(C=O)}$ of both 'D'- and 'E'-type complexes are very strong, these complexes seem not to contain an ionic ligand such as AEH^- or AE^{2-}.

Furthermore, the luminescence spectra in the solid state of AEH_2 and three gadolinium complexes with AEH_2 were recorded in the 360—560 nm range. The results are shown in Fig. 4. The fluorescence of the terpositive gadolinium ion could not be observed in the visible region because of the ^6P level of Gd^{3+} being in the ultraviolet region (—32 kK).[19] The luminescence spectra of the three gadolinium complexes are quite similar to that of AEH_2. The close similarity in the luminescence spectra suggests that the ligand molecules in the 'D'- and 'E'-type complexes of gadolinium are neutral, as are those in the 'C'-type complex of gadolinium.

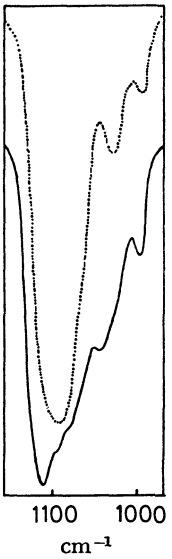

Fig. 5. Infrared spectra of complexes in the region of perchlorate absorption.
------: Pr complex ('D' type), ——: Dy complex ('E' type).

In Table 2, the $\nu_{(C=O)}$ bands of the 'D'-type complexes are found to split weakly into two peaks; this is not observed for the 'A'-, 'B'-, 'C'-, and 'E'-type complexes. The splitting suggests that the ligands in the 'D'-type complexes are coordinated and/or not coordinated with oxygen atoms.[20]

Figure 5 presents the IR absorption spectra assigned to perchlorate ions in the praseodymium and dysprosium complexes. The praseodymium complex shows two peaks in the 1100 cm^{-1} region. The perchlorate ion in the 'E'-type complexes appears to be coordinated weakly with the rare earth ions.[21]

Table 3. Metal-ligand stretching vibrations (cm^{-1})

Type	La	Pr	Nd	Sm	Gd	Dy	Er
D	418	418	418	422	422		
E					429	430	432

The bands assignable to the metal-ligand stretching vibrations[6] are listed in Table 3. The absorption frequencies of these bands increase in the order of the atomic numbers of the rare earths.

The number of the ligand molecules attached to a metal ion in the 'D'-type complexes is more than those of the AEH_2 complexes of the other lighter rare earth salts, such as chlorides, nitrates, and thiocyanates.[5] The increasing of the ligand molecules is probably due to the low coordinating ability of the perchlorate ion.[2]

Gadolinium perchlorate forms a 'D'-type complex under anhydrous conditions, while it forms an 'E'-type complex under hydrous conditions. Therefore, it is obvious that a water molecule plays an important role in the formation of hydroxo complexes ('E' type). Since the hydroxo complexes with AEH_2 are obtained only from the hydrous, heavier rare earth perchlorates, the increase in the charge densities of rare earth ions and the low coordinating ability of the perchlorate ion are considered to result from the formation of the hydroxide ion. The hydroxide ion, which has a strong tendency to coordinate toward rare earth ions,[2] seems to be produced from a water molecule in the complex cation of heavier rare earths, $[Ln(H_2O)_x(Solvent)_y]^{3+}$. Actually, the perchlorate ion is present in the outer coordination sphere, and the other anionic species are present in inner coordination sphere of rare earth ions in alcohol,[22,23] though the coordination of the perchlorate ion in the 'E'-type complexes can not be explained.

Consequently, it may be presumed that the formation of the hydroxo complexes ('E' type) is related to the low coordinating ability of the perchlorate ion and the charge densities of the rare earth ions as well as to the basicity of AEH_2.

References

1) S. P. Sinha, "Complexes of the Rare Earths," Pergamon Press, New York (1966), Chapters 3 and 5.
2) T. Moeller, "MTP International Review of Science, Lanthanides and Actinides," K. W. Bagnall, Ed., Butterworths, London, Chapter 7 (1972).
3) J. H. Forsberg and T. Moeller, *Inorg. Chem.*, **8**, 883 (1969).
4) L. J. Carpenter and T. Moeller, *J. Inorg. Nucl. Chem.*, **32**, 3575 (1970).
5) N. K. Dutt and K. Nag, *ibid.*, **30**, 3273 (1968).
6) N. Yoshida, A. Matsumoto and J. Shiokawa, *Nippon Kagaku Kaishi*, **1973**, 860.
7) P. J. McCarthy, R. J. Horey, K. Ueno, and A. E. Martell, *J. Amer. Chem. Soc.*, **77**, 5820 (1955).
8) S. Misumi, *Bunseki Kagaku*, **7**, 260 (1958).
9) "Colorimetric Determination of Nonmetals", D. F. Bolty, Ed., Interscience Pub. Inc., New York (1958), p. 176.
10) G. Schwarzenbach and K. Lütz, *Helv. Chim. Acta*, **23**, 1139 (1940).
11) C. N. O'Callaghan and D. Twony, *J. Chem. Soc. C*, **1967**, 2400.
12) P. V. Klevstov, R. F. Klevstova, and L. P. Sheina, *Zh. Strukt. Khim.*, **8**, 268 (1967); *Chem. Abstr.*, **67**, 94769 (1967).
13) P. E. Caro, J. O. Sawyer, and L. Eyring, *Spectrochim. Acta*, **28A**, 1167 (1972).
14) H. Rosenwasser and J. I. Bryant, "Rare Earth Research," Vol. 2, K. Vorres, Ed., Gordon and Breach, New York (1963), p. 75.
15) L. J. Bsile, D. Gronert, and J. R. Ferraro, "Solvent Extraction Research," A. S. Kertes and Y. Marcus, Ed., John Wiley & Sons Inc., New York (1969), p. 299.
16) M. F. Lichardson, W. F. Wagner, and D. E. Sands, *J. Inorg. Nucl. Chem.*, **32**, 1417 (1969).
17) K. Ueno and A. E. Martell, *J. Phys. Chem.*, **59**, 988 (1955).
18) C. G. Macarovici, E. Perte, and E. Motiu, *Rev. Roumain Chim.*, **11**, 59 (1966).
19) Chapter 8 of Ref. 1.
20) Y. Baskin and J. R. Ferraro, *J. Inorg. Nucl. Chem.*, **30**, 241 (1968).
21) R. C. Grandey and T. Moeller, *ibid.*, **32**, 333 (1970).
22) C. K. Yørgensen, *Mat. Fys. Medd. Dan. Vid. Selsk.* **30 No. 22**, 19 (1956).
23) J. C. Barnes, *J. Chem. Soc.*, **1964**, 3880.

Thermal Reaction in a Series of Ammineisothiocyanatochromium(III) Complexes in Solid State.[1]

Hisaya Oki,* Meiji Yasuoka,* and Ryokichi Tsuchiya**

*Department of Chemistry, Faculty of Education, Fukui University, Fukui 910

**Department of Chemistry, Faculty of Science, Kanazawa University, Kanazawa 920

(Received June 27, 1973)

The thermal decomposition of $[Cr(NH_3)_6](SCN)_3$, $[Cr(NCS)(NH_3)_5](SCN)_2$ and *cis*-$[Cr(NCS)_2(NH_3)_4]SCN$ in solid state was studied by isothermal as well as continuous temperature-rise methods. Under isothermal heating at 140 °C, $[Cr(NH_3)_6](SCN)_3$ changed stepwise to *cis,trans*-$[Cr(NCS)_3(NH_3)_3]$ through *trans*-$[Cr(NCS)_2(NH_3)_4]$-SCN, $[Cr(NCS)(NH_3)_5](SCN)_2$ turning to the *cis-trans* complex over the *trans* complex in the same manner as $[Cr(NH_3)_6](SCN)_3$. Under the continuous temperature-rise, $[Cr(NH_3)_6](SCN)_3$, $[Cr(NCS)(NH_3)_5](SCN)_2$ as well as *trans*-$[Cr(NCS)_2(NH_3)_4]SCN$ were found to be directly converted into *cis,trans*-$[Cr(NCS)_3(NH_3)_3]$.

The thermal decomposition of various chromium(III) compiexes has been extensively investigated.[2] As regard the thermal decomposition of several hexaamminechromium(III) halides, Wendlandt and Chou[3] reported that decomposition is initiated by the substitution reaction of a coordinated ammonia by halide ion in outer sphere, but gave no discussion on the structure of the decomposition products. Tanaka and Nagase carried out kinetic studies of the thermal decomposition reaction of $[Cr(NH_3)_6]Cl_3$, $[CrCl(NH_3)_5]Cl_2$, and *cis*-$[CrCl_2(NH_3)_4]Cl$ in solid state,[4] and proposed the following possible pathway for the deamminationanation reaction of these chromium(III) ammine complexes:

$[Cr(NH_3)_6]Cl_3$

↓

$[CrCl(NH_3)_5]Cl_2$

↓

trans-$[CrCl_2(NH_3)_4]Cl \overset{\text{isomerization}}{\rightleftharpoons}$ *cis*-$[CrCl_2(NH_3)_4]Cl$

↓

cis, trans-$[CrCl_3(NH_3)_3] \overset{\text{isomerization}}{\longleftarrow}$ *cis, cis*-$[CrCl_3(NH_3)_3]$

Recently, they made it clear that *trans*-$[CrCl_2(NH_3)_4]Cl$ is reversibly isomerized to the corresponding *cis*-form.[5]

So far systematic pathways for the thermal decomposition of the chromium(III) ammine isothiocyanato complexes are not known. Werner and Halben[6] obtained a pale rose insoluble product $[Cr(NCS)_3(NH_3)_3]$ by isothermal heating of $[Cr(NCS)(NH_3)_5](SCN)_2$ at 130—140 °C, but its geometrical structure has not been identified.

In order to examine the structural changes along with the thermal reaction pathways of the ammine chromium(III) thiocyanate, we have studied the decomposition reactions of $[Cr(NH_3)_6](SCN)_3$, $[Cr(NCS).(NH_3)_5](SCN)_2$, and *cis*-$[Cr(NCS)_2(NH_3)_4]SCN$ in solid state by the isothermal and the continuous temperature-rise methods. The structures of the decomposition products obtained upon heating were clarified by the measurement of their infrared and electronic spectra. Possible reaction pathways in the thermal reaction of these chromium(III) ammine complexes were proposed.

Experimental

Preparation of Complexes. Hexaamminechromium(III) thiocyanate, $[Cr(NH_3)_6](SCN)_3$, was prepared by adding potassium thiocyanate to the corresponding chloride obtained by the method in literature.[7]

Isothiocyanatopentaamminechromium(III) thiocyanate, $[Cr(NCS)(NH_3)_5](SCN)_2$, and *cis*-diisothiocyanatotetraamminechromium(III) thiocyanate, *cis*-$[Cr(NCS)_2(NH_3)_4]$-SCN, were prepared by the method given by Werner and Halben[6] and by Kyuno *et al.*[8] All the complexes were identified by elemental analysis and absorption spectral measurement.

trans-Diisothiocyanatotetraamminechromium(III) thiocyanate, *trans*-$[Cr(NCS)_2(NH_3)_4]SCN$, was prepared by the isothermal heating of $[Cr(NH_3)_6](SCN)_3$ at 140 °C for 10 min.

cis, trans-Triisothiocyanatotriamminechromium(III), *cis, trans*-$[Cr(NCS)_3(NH_3)_3]$, was prepared by the isothermal heating of $[Cr(NH_3)_6](SCN)_3$ at 140 °C for seven hours and was prepared by the known method.[6]

Isothermal Measurement. Isothermal measurement for these complexes was carried out in a Toyo Roshi Air Oven, the temperature of the sample being controlled within ±1 °C at 140 °C. In each run a 500 mg sample smaller than 200 mesh in size was weighed.

Continuous Temperature-rise Measurement. The continuous temperature-rise measurement was carried out with a Metrimpex Derivatograph Type-OD-102 and a Tokyo Koki thermobalance. Derivatographic measurement was made in a nitrogen stream under heating rate of 1 °C/min, 500 mg of the sample being used in each run. TG curve was obtained with the thermobalance in an open system under the heating rate of 1 °C/min for 500 mg of the sample. The results obtained by the above two instruments were in good agreement with each other.

Apparatus for Measurement. Molar conductivity, electronic and IR absorption spectra and X-ray diffraction were measured with a Yanagimoto conductivity-measuring equipment, a Hitachi EPU-2A spectrophotometer, a JASCO IR spectrophotometer DS-301 and with a Toshiba EO-60B X-ray Analyser, respectively.

Results and Discussion

Thermal Reaction of $[Cr(NH_3)_6](SCN)_3$ under Isothermal Heating at 140±1 °C. The starting yellow complex liberated two moles of ammonia in the initial stage of 10 min heating, turning to reddish orange. The molar conductivity of the product in a 5×10^{-3} M aqueous

Table 1. IR spectral bands of ammine-isothiocyanato chromium(III) complexes

	ν_{CH}	δ_{aNH_3}	δ_{SNH_3}	ρ_{NH_3}
$[Cr(NH_3)_6(SCN)_3]$	2050	1600	1310	766
$[Cr(NCS)(NH_3)_5](SCN)_2$	2050	1605	1290	730
cis-$[Cr(NCS)_2(NH_3)_4]SCN$	2080	1607	1292	720
$[Cr(NCS)_2(NH_3)_4]SCN$[a]	2050	1588	1263	722
$[Cr(NCS)_3(NH_3)_3]$	2050[b]	1599[b]	1270[b]	722[b]

δ_a: degenerate deformation, δ_S: symmetric deformation, ρ: rocking

a) Obtained from $[Cr(NH_3)_6](SCN)_3$ by isothermal heating. b) These values were in agreement with those obtained from $[Cr(NH_3)_6](SCN_3)$ by the continuous temperature-rise method.

solution was 125 ohm^{-1} cm^2/mol. This value corresponds to that of 1:1 valency type complex. Found: N, 33.13; C, 12.07; H, 4.06%. Calcd for $[Cr(NCS)_2(NH_3)_4]SCN$: N, 33.01; C, 12.24; H, 4.11%. The product is soluble in acetone, differing from *cis*-$[Cr(NCS)_2(NH_3)_4]SCN$ insoluble.

The wave numbers of some IR spectral bands are listed in Table 1 for the ammine-isothiocyanato chromium(III) complexes. We see that the thermal reaction product $[Cr(NCS)_2(NH_3)_4]SCN$ gives the absorption band assigned to the NH_3 symmetric deformation vibration at 1263 cm^{-1}, while the corresponding *cis*-form complex gives the corresponding band at 1292 cm^{-1}. The X-ray diffraction pattern of this compound was found to differ from that of *cis*-$[Cr(NCS)_2(NH_3)_4]SCN$.

The electronic spectral data of a series of ammine-isothiocyanato chromium(III) complexes are shown in

Table 2. Absorption maxima of chromium(III) complexes

	ν_1 (logε)	ν_2 (logε)	ν_3 (logε)
$[Cr(NH_3)_6](SCN)_3$	21.6 (1.65)	28.5 (1.58)	
$[Cr(NCS)(NH_3)_5](SCN)_2$	20.4 (1.87)	27.1 (1.69)	33.8 (3.43)
cis-$[Cr(NCS)_2(NH_3)_4]SCN$	20.2 (1.93)	26.9 (1.72)	33.1 (3.71)
$[Cr(NCS)_2(NH_3)_4]SCN$[a]	19.9 (1.93)	26.5 (1.85)	33.2 (3.72)
$[Cr(NCS)_2(NH_3)_4]SCN$[b]	19.9 (1.95)	26.5 (1.85)	33.2 (3.75)
$[Cr(NCS)_3(NH_3)_3]$[a]	19.3 (2.04)	25.5 (1.95)	30.9 (3.84)
$[Cr(NCS)_3(NH_3)_3]$[c]	19.3 (2.04)	25.5 (1.95)	30.9 (3.84)
$[Cr(NCS)_3(NH_3)_3]$[b]	19.3 (2.02)	25.5 (1.96)	30.9 (3.82)
$[Cr(NCS)_3(NH_3)_3]$[d]	19.3 (2.02)	25.5 (1.96)	30.8 (3.82)
$[Cr(NCS)_3(NH_3)_3]$[e]	19.3 (2.02)	25.5 (1.97)	30.8 (3.84)

a) obtained from $[Cr(NH_3)_6](SCN)_3$ by isothermal heating. b) obtained from $[Cr(NCS)(NH_3)_5](SCN)_2$ by isothermal heating. c) obtained from $[Cr(NH_3)_6](SCN)_3$ by continuous temperature-rise method. d) obtained from $[Cr(NCS)(NH_3)_5](SCN)_2$ by the continuous temperature-rise method. e) obtained from a) by the continuous temperature-rise method.

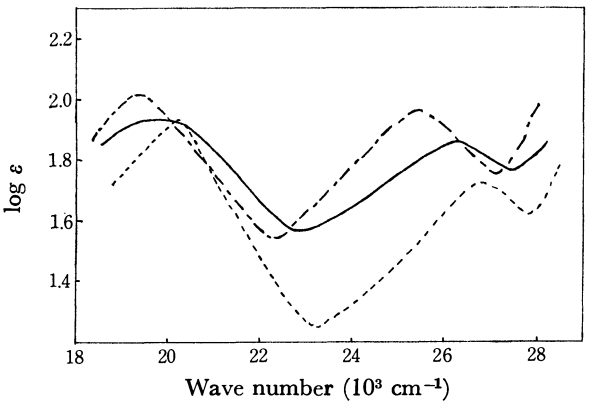

Fig. 1. The electronic spectra of $[Cr(NCS)_2(NH_3)_4]SCN$ (——) and $[Cr(NCS)_3(NH_3)_3]$ (– – –) obtained from $[Cr(NH_3)_6](SCN)_3$ by the isothermal heating along with that of cis-$[Cr(NCS)_2(NH_3)_4]$ SCN (------).

Table 2. The spectra of $[Cr(NCS)_2(NH_3)_4]SCN$ and $[Cr(NCS)_3(NH_3)_3]$, obtained by the isothermal heating of $[Cr(NH_3)_6](SCN)_3$ are given in Fig. 1 together with that of *cis*-$[Cr(NCS)_2(NH_3)_4]SCN$. It is seen that the spectra of $[Cr(NCS)_2(NH_3)_4]SCN$ specimens obtained from $[Cr(NH_3)_6](SCN)_3$ and $[Cr(NCS)(NH_3)_5](SCN)_2$ are in complete agreement with each other, and that they differ from the spectrum of *cis*-$[Cr(NCS)_2(NH_3)_4]SCN$.

It is concluded that the geometrical configuration of the thermal product formed by liberating two moles of ammonia from $[Cr(NH_3)_6](SCN)_3$ is *trans*-$[Cr(NCS)_2(NH_3)_4]SCN$.

The starting hexaammine complex liberated three moles of ammonia after seven hours heating with a color change to reddish purple. The product is soluble in acetone but not in water. Found: N, 30.67; C, 12.63; H, 3.34%. Calcd for $[Cr(NCS)_3(NH_3)_3]$: N, 30.30; C, 12.99; H, 3.25%. No composition change

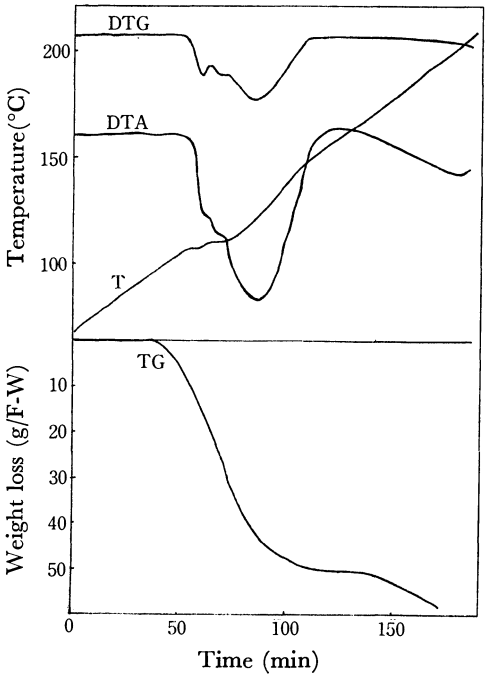

Fig. 2. The derivatogram for $[Cr(NH_3)_6](SCN)_3$.

took place even after heating for 11 hr. As the geometrical isomers of this product, either *cis-trans* or *cis-cis* configuration is possible. However, since the product at the first thermal decomposition step has a *trans*-configuration, it is likely that the product at the second step is *cis,trans*-$[Cr(NCS)_3(NH_3)_3]$. It is reasonable to consider that the *cis,cis*-configuration is less stable than the *cis,trans* one from the viewpoint of the steric hindrance, as has been reported by Tanaka and Nagase.[4]

Thermal Reaction of $[Cr(NH_3)_6](SCN)_3$ *under Continuous Temperature-rise.* The derivatogram of $[Cr(NH_3)_6](SCN)_3$ is shown in Fig. 2. The TG curve shows that the weight loss starts at 110 °C, and the weight remains almost constant untill 170 °C. The DTA curve gives an endothermic peak with two shoulders. The DTG curve also shows a similar feature to that of the DTA curve. The weight loss in the TG curve corresponds to the loss of three moles of ammonia. The analytical data of the product are as follows: Found: N, 29.68; C, 12.61; H, 3.33%. Calcd for $[Cr(NCS)_3(NH_3)_3]$: N, 30.30; C, 12.99; H, 3.25%.

The data listed in Tables 1 and 2 support the view that the product has *cis,trans*-configuration. It is obvious from the spectral data that *cis,trans*-$[Cr(NCS)_3(NH_3)_3]$ produced in the derivatograph is identical with the final product obtained by isothermal heating at 140 °C. The X-ray diffraction pattern also supports this conclusion. The shoulders and the peak in DTA can be attributed to the liberation of one and two moles of ammonia from the starting material, respectively. However, it can not be confirmed whether $[Cr(NCS)(NH_3)_5](SCN)_2$ is formed in the intermediate step or not.

Thermal Reaction of $[Cr(NCS)(NH_3)_5](SCN)_2$ *under Isothermal Heating at 140±1 °C.* The starting complex seems to change to *trans*-$[Cr(NCS)_2(NH_3)_4]SCN$ after eight minutes heating and finally to *cis,trans*-$[Cr(NCS)_3(NH_3)_3]$ as judged by the weight loss. But the stoichiometry was not complete. Even after 18 hr heating, the weight loss amounted to only 98% of two moles of ammonia. Werner and Halben[6] reported that $[Cr(NCS)_3(NH_3)_3]$ was obtained from $[Cr(NCS)(NH_3)_5](SCN)_2$ by isothermal heating (at 130—140 °C) for 30—40 hr. The results we obtained are not contradictory to theirs.

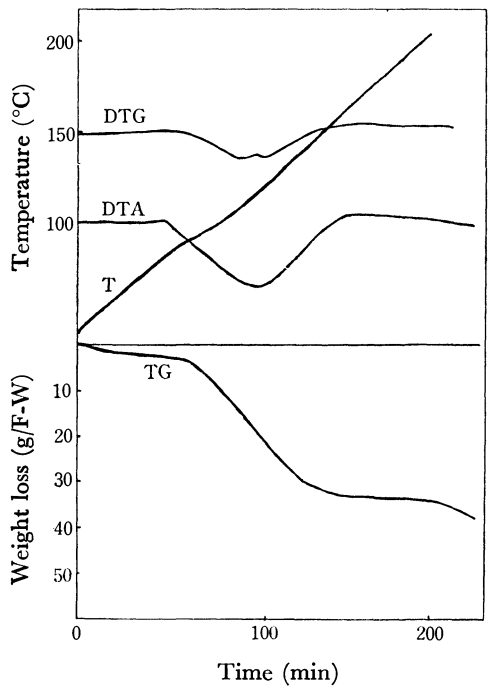

Fig. 3. The derivatogram for $[Cr(NCS)(NH_3)_5](SCN)_2$.

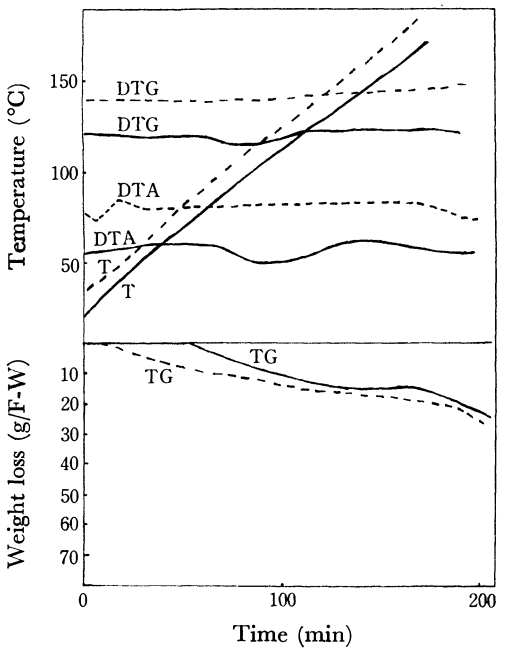

Fig. 4. The derivatograms for *trans*-$[Cr(NCS)_2(NH_3)_4]SCN$ obtained from $[Cr(NH_3)_6](SCN)_3$ by the isothermal heating (——) and *cis*-$[Cr(NCS)_2(NH_3)_4]SCN$ (------).

Thermal Reaction of $[Cr(NCS)(NH_3)_5](SCN)_2$ *under Continuous Temperature-rise.* The derivatogram of this complex is shown in Fig. 3. The TG, DTA, and DTG curves support an endothermal reaction one step. The weight loss corresponds to only 90% of two moles of ammonia. The result suggests that the reaction in the derivatograph is not completely stoichiometric and is similar to the isothermal reaction. The main product was confirmed to have a *cis,trans*-configuration from the spectral measurements.

Thermal Reaction of trans- *and* cis-$[Cr(NCS)_2(NH_3)_4]SCN$ *under Continuous Temperature-rise.* The derivatograms of these complexes are shown in Fig. 4. The thermal product obtained from the *trans* complex was identified by electronic spectra to be *cis,trans*-$[Cr(NCS)_3(NH_3)_3]$, whereas the configuration of the product obtained from the *cis* complex was difficult to be determined. For the *cis* complex, the derivatogram showed no distinct plateau corresponding to the weight loss of one mole of ammonia. The product obtained at the heating step by the thermobalance was not pure due to its hygroscopic character. The decomposition process of the *cis* complex must be a complicated one and the isomerization could not be clearly observed in both the isothermal measurement as well as the con-

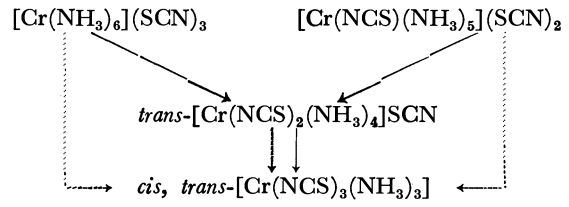

(——) The isothermal reaction (at 140°±1°C)
(------) The continuous temperature-rising reaction (1 °C/min)

Fig. 5. The possible reaction processes of isothiocyanato-ammine chromium(III) complexes.

tinuous temperature-rise method. The results differ remarkably from those in the decomposition processes of *cis*-$[CrCl_2(NH_3)_4]Cl$ reported by Tanaka and Nagase.[4]

Possible decomposition reaction processes of a series of isothiocyanato-ammine chromium(III) complexes can be represented as shown in Fig. 5.

References

1) Presented at the 20th Symposium on Coordination Chemistry, Tokyo, 18 November, 1970.
2) W. W. Wendlandt and J. P. Smith, "The Thermal Properties of Transition-Metal Ammine Complexes," Elseiver, Amsterdam (1967), p. 109.
3) W. W. Wendlandt and C. Y. Chou, *J. Inorg. Nucl. Chem.*, **26**, 943 (1964).
4) N. Tanaka and K. Nagase, This Bulletin, **42**, 2854 (1969).
5) *Idem.*, *ibid.*, **45**, 1907 (1972).
6) A. Werner and J. Halben, *Ber.*, **39**, 2668 (1906).
7) M. Mori. *Nippon Kagaku Zasshi*, **74**, 253 (1953).
8) E. Kyuno, M. Kamada, and N. Tanaka, This Bulletin, **40**, 1848 (1967).

Infrared Spectra of Nitrosylplatinum (^{14}NO and ^{15}NO) Complexes

Eiichi Miki, Kunihiko Mizumachi, Tatsujiro Ishimori, and Hisateru Okuno
Department of Chemistry, College of Science, Rikkyo University, Nishi-Ikebukuro, Toshima, Tokyo 171
(Received September 3, 1973)

The ^{15}NO-complexes for *trans*-$[PtCl(NH_3)_4(NO)]Cl_2$, *trans*-$K_2[PtCl(NO_2)_4(NO)]$ and $M_2[PtX_5(NO)]$ (M=K and Cs, X=Cl and Br) were prepared. The effect of ^{15}N-substitution on infrared spectra indicated that the weak absorption band at *ca.* 290 cm^{-1} is assigned to the Pt-(NO) stretching vibration and the absorptoin band in the region 530—570 cm^{-1} to the Pt-(NO) bending vibration.

For transition-metal nitrosyl compounds, the isotopic effects of ^{15}N in the NO group on infrared spectra were measured. The isotopic shifts observed were compared with those calculated by a three-body model of the metal and the NO group. This method is found to be useful for assigning the skeletal vibrations between the metal and the NO group; the isotopic shift of the metal–(NO) stretching vibration is smaller than that of the metal–(NO) bending vibration.[1]

We have measured the isotopic shifts for ^{15}NO-substitution in *trans*-$[PtCl(NH_3)_4(NO)]Cl_2$, *trans*-$[PtCl(ND_3)_4(NO)]Cl_2$, *trans*-$K_2[PtCl(NO_2)_4(NO)]$ and $M_2[PtX_5(NO)]$ (M=K and Cs, X=Cl and Br). The Pt-(NO) binding states are discussed on the basis of the following: comparison of the infrared spectra with those for ammine- and chloro-complexes of Pt(II) and Pt(IV), the approximate force constant for the Pt-(NO) stretching vibration and the isotopic shift of the N–O stretching vibration upon ^{15}NO-substitution.

Experimental

Preparation of Nitrosylplatinum Compounds. The complexes were prepared by the method of Griffith *et al.*[2] Their ^{15}NO-complexes were prepared in a vacuum line with the use of ^{15}NO, ^{15}NO–$^{15}NO_2$, or $^{15}NOCl$ derived from 3—10 mmol of $K^{15}NO_3$ (^{15}N atom %=95—99.7). Nitrosyl chloride was prepared from nitric oxide and potassium chloride by the method of Ratcliffe.[3] The elementary analyses and IR spectra showed that the desired products were obtained.

trans-$[PtCl(NH_3)_4(NO)]Cl_2$: (A) By cooling with liquid nitrogen, 3 mmol of NO gas was trapped into a reaction vessel containing 0.3 mmol of $[Pt(NH_3)_4]Cl_2 \cdot H_2O$ in 10 ml of 6M hydrochloric acid. The reaction vessel was shaken in running water until the frozen solution was molten. Air was then introduced into the reaction vessel to instantly give green precipitates with shaking. The products were filtered out and dried under vacuum. $\chi_g = -0.27 \times 10^{-6}$ (c.g.s.). Found: Pt, 48.9; N, 17.5; H, 4.3; Cl, 25.2%. Calcd for $[PtCl(NH_3)_4(NO)]Cl_2$: Pt, 48.82; N, 17.53; H, 3.03; Cl, 26.62%. (B) Finely powdered $[Pt(NH_3)_4]Cl_2 \cdot H_2O$ (0.3 mmol) was stirred with 5 mmol of NOCl in 5 ml of freshly distilled chloroform for 70 hr at about 0 °C. Found: Pt, 49.5; N, 16.3; H, 2.9; Cl, 26.9%.

trans-$[PtCl(ND_3)_4(NO)]Cl_2$: 3 mmol of NO gas was trapped into a reaction vessel containing a solution prepared by adding 5 ml of concentrated hydrochloric acid to 0.3 mmol of $[Pt(NH_3)_4]Cl_2 \cdot H_2O$ in 5 ml of D_2O. Green products were obtained by the same produre as for *trans*-$[PtCl(NH_3)_4(NO)]Cl_2$. The IR spectra showed that deuteration was accomplished by hydrogen exchange with D_2O.

trans-$K_2[PtCl(NO_2)_4(NO)]$: This compound was synthesized with NOCl in a similar procedure to that for $[PtCl(NH_3)_4(NO)]Cl_2$. Found: K, 14.3; Pt, 36.7; N, 11.0%. Calcd for $K_2[PtCl(NO_2)_4(NO)]$: K, 14.96; Pt, 37.32; N, 13.40%.

$K_2[PtCl_5(NO)]$: $K_2[PtCl_4]$ (0.3 mmol) was stirred with 5 mmol of NOCl in 5 ml of freshly distilled chloroform for 50 hr at about 0 °C to convert it into olive green products. The products were washed with chloroform and dried under vacuum. Found: K, 16.3; Pt, 41.1; Cl, 38.5; N, 2.7%. Calcd for $K_2[PtCl_5(NO)]$: K, 16.57; Pt, 40.45; Cl, 36.75; N, 2.91%.

$Cs_2[PtCl_5(NO)]$: An aqueous solution of $K_2[PtCl_4]$ (1 mmol in 5 ml) was passed through a 5 cm column (1 cm diameter) of cation exchange resin, Diaion SK#1, in hydrogen form. CsCl (2 mmol) in 5 ml of H_2O was added to the effluent. NO–NO_2 gas was bubbled into the solution to give dark brown products. $\chi_g = -0.08 \times 10^{-6}$ (c.g.s.). To prepare the ^{15}NO-complex, 0.5 mmol of $K_2[PtCl_4]$ and 3 mmol of ^{15}NO–$^{15}NO_2$ gas were used. Found: Cs, 39.9; Pt, 29.3; N, 2.1; Cl, 26.4%. Calcd for $Cs_2[PtCl_5(NO)]$: Cs, 39.78; Pt, 29.20; N, 2.10; Cl, 26.53%.

$K_2[PtBr_5(NO)]$ (*contaminated with a large amount of* $K_2[PtBr_6]$): 5 mmol of NO gas was trapped with liquid nitrogen into a reaction vessel containing 1 mmol of $K_2[PtBr_4] \cdot 2H_2O$ in 3 ml of 1M hydrobromic acid. After the frozen solution was melted in running water, the solution was stirred for *ca.* 6 hr. $K_2[PtBr_6]$ formed was removed by filtration and the filtrate was added to 25 ml of ice-cooled ethyl alcohol to give dark brown powder. The product was washed with ether and dried in air. Stirring of NO with $K_2[PtBr_4] \cdot 2H_2O$ in hydrobromic acid over a long period gave only $K_2[PtBr_6]$. Found: N, 1.3; Br, 57.8%. Calcd for $K_2[PtBr_5(NO)]$: N, 1.99; Br, 56.85%.

The synthetic procedure for the complexes shows the possibility that nitro-complex contaminates the nitrosyl complex. However, infrared spectra showed no characteristic absorption bands of nitro-complex.

Apparatus. Infrared spectra were measured in the region 200—4000 cm^{-1} as Nujol mull and hexachlorobutadiene mull in sodium chloride and in polyethylene plates. The spectra at room temperature were recorded on JASCO DS-402G and JASCO model IR-F infrared spectrophotometers. The spectra of *trans*-$[PtCl(NH_3)_4(NO)]Cl_2$ and $K_2[PtCl_5(NO)]$ at liquid nitrogen temperature were measured *in vacuo* as Nujol mull on KRS-5 plates in the range *ca.* 300—600 cm^{-1} on a Hitachi EPI-L infrared spectrophotometer. The wave numbers of the observed bands were calibrated with polystyrene film, 1,2,4-trichlorobenzene and water vapour. The magnetic susceptibility was measured by the Gouy method.

Results

Assignments of Infrared Spectra. The IR spectra and isotopic shifts upon ^{15}NO-substitution for *trans*-

Table 1. Wave numbers, observed isotopic shifts and assignments of infrared absorption bands due to the PtNO group

Compound	NO str. ($\Delta\nu_{obsd}$)	Pt–(NO) bend. ($\Delta\nu_{obsd}$)	Pt–(NO) str. ($\Delta\nu_{obsd}$)
trans-$[PtCl(NH_3)_4(NO)]Cl_2$	1684 vs. (23)	569 s. (11)	not observed
trans-$[PtCl(ND_3)_4(NO)]Cl_2$	1685 vs. (23)	564 s. (13)	not observed
trans-$K_2[PtCl(NO_2)_4(NO)]$	1729 vs. (20)	552 m. (3)	
		540 sh. (11)	not observed
$K_2[PtCl_5(NO)]$	1728 vs. (30)	558 s. (12)	291 w. (2)
	1712 vs. (30)		
$Cs_2[PtCl_5(NO)]$	1723 vs. (29)	559 s. (13)	283 w. (4)
	1709 vs. (30)		
$K_2[PtBr_5(NO)]$	1681 vs. (43)	544 s. (10)	287 w. (3)

$\Delta\nu_{obsd} = \nu$ ^{14}NO-complex (obsd) $-$ ν ^{15}NO-complex (obsd)
Abbreviations: str.=stretching; bend.=bending; vs.=very strong; s.=strong; *m.*=medium; w.=weak; sh.=shoulder.

$[PtCl(NH_3)_4(NO)]Cl_2$ prepared with the use of $NO-NO_2$ gas were almost the same as those prepared with NOCl.

Pt–NH_3 stretching vibration was expected in the region where the skeletal vibrations between the metal atom and the NO group are usually observed. This absorption band for *trans*-$[PtCl(NH_3)_4(NO)]Cl_2$ was ascertained on the basis of considerable isotopic shifts upon deuterium substitution and no isotopic shifts upon ^{15}NO-substitution. It was found that the band did not overlap with the bands due to the PtNO skeleton.

The wave numbers, isotopic shifts and assignments of infrared absorption bands due to the PtNO group of the examined complexes are shown in Table 1. The N–O stretching vibrations were observed in the region 1680—1730 cm^{-1}, the isotopic shifts upon ^{15}NO-substitution being 20—40 cm^{-1}.

Of the absorption bands in the region 200—700 cm^{-1}, only strong ones in the region 530—570 cm^{-1} shifted downwards by 10—15 cm^{-1} upon ^{15}NO-substitution for all the compounds. For $K_2[PtCl(NO_2)_4(NO)]$, the absorption bands in this region were broad and the isotopic shifts could not be measured exactly.

The infrared spectra at liquid nitrogen temperature showed that the bands in the region 530—570 cm^{-1} shifted downwards but did not split; the band at 575 cm^{-1} shifted to 565 cm^{-1} for $[PtCl(NH_3)_4(NO)]Cl_2$, that at 570 to 555 cm^{-1} for $[PtCl(ND_3)_4(NO)]Cl_2$, and that at 565 to 552 cm^{-1} for $K_2[PtCl_5(NO)]$. In the region other than 530—570 cm^{-1}, no isotopic shifts could be observed for $[PtCl(NH_3)_4(NO)]Cl_2$, $[PtCl(ND_3)_4(NO)]Cl_2$, and $K_2[PtCl(NO_2)_4(NO)]$. On the other hand, for $M_2[PtX_5(NO)]$ (M=K and Cs, X=Cl and Br) the weak absorption bands at about 290 cm^{-1} shifted downwards by 2—4 cm^{-1} (Table 1 and Fig. 1). Such absorption bands for the examined complexes except for $M_2[PtX_5(NO)]$ could not be observed because of the overlapping with the strong absorption bands due to the H_3N–Pt–NH_3 bending and the NO_2 rocking vibrations.

The IR study on $[MCl_5(NO)]^{n-}$ anion (M=Ru, Os, and Ir) by Cleare *et al.*[4] has shown that two or three M–Cl stretching, two or three Cl–M–Cl bending and (ON)–M–Cl bending vibrations are observed in the regions 280—340 cm^{-1}, 120—185 cm^{-1}, and 70—90 cm^{-1}, respectively. For $[MBr_5(NO)]^{n-}$ anion (M=Ru, Os, and Ir), M–Br stretching, Br–M–Br bending and (ON)–M–Br bending vibrations are observed in the regions 180—260 cm^{-1}, 120—140 cm^{-1}, and 60—90 cm^{-1}, respectively. No isotopic shifts upon ^{15}NO-substitution are shown for all of the absorption bands. The possibility of assigning the *ca.* 290 cm^{-1} bands to the (ON)–Pt–halogen bending vibrations can be excluded. Thus the weak bands at *ca.* 290 cm^{-1} and the strong bands at 530—570 cm^{-1} are considered to be assigned to the skeletal vibrations between the platinum and the NO group. The strong absorption band at 339 cm^{-1} with a shoulder at *ca.* 330 cm^{-1} and the broad 212 cm^{-1} band for $K_2[PtCl_5(NO)]$ can be assigned to the Pt–Cl stretching and the Cl–Pt–Cl bending vibrations, respectively. The 240 cm^{-1} band for $K_2[PtBr_5(NO)]$ can be assigned to the Pt–Br stretching vibration.

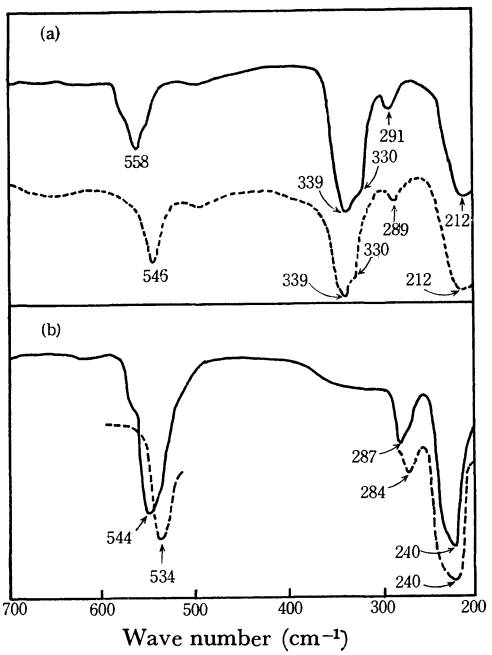

Fig. 1. Infrared spectra of $K_2[PtCl_5(NO)]$ (a) and $K_2[PtBr_5(NO)]$ (b) in the region 200—700 cm^{-1}. ^{14}NO-complex, ——; ^{15}NO-complex, ------.

Table 2. Observed and calculated isotopic shifts ($\Delta\nu_{obsd}$ and $\Delta\nu_{calcd}$ in cm^{-1}), and force constants of $K_2[PtCl_5(NO)]$

Assignment	Observed		Calculated		$\Delta\nu_{obsd}$	$\Delta\nu_{calcd}$	Force constants (mdyn/Å)
	^{14}NO-complex	^{15}NO-complex	^{14}NO-complex	^{15}NO-complex			
Pt–N–O arrangement							
NO str.	1712	1682	1712	1682	30	30	$f_{11}=12.9$, $f_{12}=0.2$
PtNO bend.	558	546	559	546	12	13	$f_{13}=0.2$, $f_{22}=1.3$
PtN str.	291	289	291	288	2	3	$f_{23}=0.3$, $f_{33}=0.6$
Pt–O–N arrangement							
NO str.	1712	1682	1712	1682	30	30	$f_{11}=12.8$, $f_{12}=0.2$
PtON bend.	558	546	558	546	12	12	$f_{13}=0.2$, $f_{22}=1.6$
PtO str.	291	289	291	289	2	2	$f_{23}=0.8$, $f_{33}=0.8$

$\Delta\nu_{obsd}=\nu^{14}$NO-complex (obsd) $-\nu^{15}$NO-complex (obsd). $\Delta\nu_{calcd}=\nu^{14}$NO-complex (calcd) $-\nu^{15}$NO-complex (calcd). Abbreviations: str.=stretching; bend.=bending; f_{11}=force constant of N–O stretching vibration; f_{22}=force constant of Pt–(NO) stretching vibration; f_{33}=force constant of Pt–(NO) bending vibration; f_{12}=force constant associated with N–O stretching and Pt–(NO) stretching vibrations (assumed to be 0.2 mdyn/Å); f_{13}=force constant associated with N–O stretching and Pt–(NO) bending vibrations (assumed to be 0.2 mdyn/Å); f_{23}=force constant associated with Pt–(NO) stretching and Pt–(NO) bending vibrations.

Calculation of Isotopic Shifts. No structural study on monomeric nitrosylplatinum complex has been reported. IR studies for the examined complexes show that the oxidation state of the platinum atom is considered to be IV and that of the NO group −I. X-ray diffraction studies on several nitrosyl complexes formulated as NO^- complexes have shown that the metal–(NO) bond angle is almost equal to 120° and the N–O bond distance is 1.1—1.2 Å.[5] The Pt–(NO) bond distance is considered to be 1.9—2.0 Å.[6]

Calculation of the ^{15}N-isotopic shifts by means of the three-body model of the metal atom and the NO group is useful for determining the coordination atom of the NO group and for assigning distinctly the skeletal vibrations between the metal and the NO group, when the metal atom and the ligands other than the NO group are much heavier than nitrogen and oxygen.[1] Thus the calculation is considered to be useful in the case of $K_2[PtCl_5(NO)]$ as well as $K_2[RuCl_5(NO)]$. The isotopic shifts were calculated with two angular three-body models, Pt–N–O and Pt–O–N (the metal–(NO) bond angle is 120°) and by assuming that the N–O distance is 1.1 Å and the Pt–(NO) distance 2.0 Å. The force constants f_{12} and f_{13} were assumed to be 0.2 mdyn/Å[1] (Table 2). The calculation was carried out with a Hitachi 5020E at the Computer Centre of the University of Tokyo.

The observed isotopic shifts, calculated ones and the force constants for $K_2[PtCl_5(NO)]$ are shown in Table 2. The wave numbers and isotopic shifts calculated from the bent Pt–N–O model were almost the same as those from the bent Pt–O–N one. Application of ^{15}NO-substitution to determine the coordinating atom of the NO group in the case of the NO^- complexes seems to be useless even though metal and ligands are much heavier than nitrogen and oxygen. From a comparison of the observed isotopic shifts with the calculated ones, the absorption bands observed in the region 530—570 cm^{-1} can be assigned to the Pt–(NO) bending vibration, and the *ca.* 290 cm^{-1} bands which could be observed on $M_2[PtX_5(NO)]$ (M=K and Cs, X=Cl and Br) to the Pt–(NO) stretching vibration. The *ca.* 290 cm^{-1} band is in the same region as that of the 259 cm^{-1} band which was assigned to the Co–(NO) stretching vibration for $Co(NO)(S_2CN(CH_3)_2)_2$.[1] The calculation shows that the isotopic shift for the Pt–(NO) stretching vibration is smaller than that of the Pt–(NO) bending vibration for the nitrosylplatinum complexes as observed on other nitrosyl complexes.[1]

Discussion

IR studies on ammine- and chloro-complexes have shown that the NH_3 rocking and the Pt–Cl stretching vibrations are sensitive to the oxidation state of the metal atom.[7,8] The NH_3 rocking vibrations of Pt(II)- and Pt(IV)-ammine complexes are observed in the region 810—840 cm^{-1} and *ca.* 940 cm^{-1}, respectively. The Pt–Cl stretching vibrations of Pt(II)- and Pt(IV)–chloro complexes are observed at *ca.* 320 and 340 cm^{-1}, respectively. For *trans*-$[PtCl(NH_3)_4(NO)]Cl_2$, the NH_3 rocking vibration and the Pt–Cl stretching vibration were observed at 918 and 350 cm^{-1}, respectively. The Pt–Cl stretching vibration of $K_2[PtCl_5(NO)]$ was observed at 339 cm^{-1}. This seems to support the view that the oxidation state of the platinum atom is IV and that of the NO group −I.

For $Ir(NO)Cl_2(P(C_6H_5)_3)_2$ and $[Co(NO)(NH_3)_5]Cl_2$ formulated as NO^- complexes, two skeletal vibrations between the metal and the NO group were observed in the region 560—620 cm^{-1}.[1] The Pt–(NO) bending vibration was observed in this region but the Pt–(NO) stretching vibration was observed at extraordinarily low wave numbers. An X-ray diffraction study on nitrosyl complexes by Mingos and Ibers[5] has shown that the N–O bond distance for nitrosyl complex formulated as NO^- complex is almost equal to that formulated as NO^+ complex, a multiple bond character existing in the NO group of the NO^- complex. This might reflect the suggestion that the Pt–(NO) bending vibration is left behind in the region 530—570 cm^{-1} where the skeletal vibrations between the metal and the NO

group would have been observed even though the Pt–(NO) stretching vibration shifts to *ca.* 290 cm^{-1}. The same phenomenon has been observed on octahedral cyanides. IR studies on $[M(CN)_6]^{n-}$ and $[M(CN)_5L]^{m-}$ have shown that bands at *ca.* 460—590 cm^{-1} and at *ca.* 340—420 cm^{-1} are assigned to metal–(CN) bending and metal–(CN) stretching vibrations, respectively, and that the stretching vibrations are in a lower region than the bending vibrations by *ca.* 50—150 cm^{-1}.[8]

If another possibility of overlapping of the Pt–(NO) stretching vibration with the strong absorption band assigned to the Pt–(NO) bending vibration exists, the *ca.* 290 cm^{-1} band might be assigned to one of the Pt–Cl stretching vibrations for $[PtCl_5(NO)]^{2-}$ anion, but a reasonable explanation cannot be given to the *ca.* 290 cm^{-1} band for $[PtBr_5(NO)]^{2-}$ anion.

Our recent study has shown that the isotopic shifts observed on the N–O stretching vibration for the NO^- complexes are smaller than those for the NO^+ complexes which are almost equal to those calculated by assuming the linear metal–N–O model.[1] Thus the extent of isotopic shift for N–O stretching vibration might be used as a measure for determining the oxidation state of the NO group. The isotopic shifts of the N–O stretching vibrations observed on the examined complexes are in the region 20—30 cm^{-1}, and the shift calculated by assuming a linear Pt–N–O model is 38 cm^{-1}. This seems to suggest a bent Pt–N–O linkage. The isotopic shift observed on $K_2[PtBr_5(NO)]$ was 43 cm^{-1}. The abnormally large value may be attributed to the change of Pt–(NO) bond angle due to the great size of the bromide ion in $[PtBr_5(NO)]^{2-}$ anion. However, no details can be given.

The force constants of the metal–(NO) stretching vibrations calculated by means of the three-body model are in the region 4—7 mdyn/Å. The approximate force constant of the Pt–(NO) stretching vibration for $K_2[PtCl_5(NO)]$ was calculated to be 1.3 mdyn/Å. This is considered to reflect the suggestion that the metal–(NO) bond distances for the NO^- complexes are generally longer than those for the NO^+ complexes.[5] The force constant for the Pt–(NO) stretching vibration is considered to be comparable to the force constants for the Pt–NH_3 stretching vibrations; for the Pt(II) and the Pt(IV)-ammine complexes, the force constants of the Pt–NH_3 stretching vibrations have been reported to be 1.92 and 2.13 mdyn/Å, respectively.[9]

For $M_2[PtX_5(NO)]$ (M=K and Cs, X=Cl and Br), the effects of outer sphere cations and halide ions on IR spectra were observed on the absorption bands due to the Pt–(NO) skeleton. The wave numbers of the N–O stretching, Pt–(NO) bending and Pt–(NO) stretching vibrations increase in the order Br and Cl for the potassium salts, and the wave numbers of the N–O stretching and Pt–(NO) stretching vibrations increase in the order Cs and K for the chloro-complexes. These tendencies were similar to those observed on the absorption bands due to the Ru–(NO) skeleton for $M_2[RuX_5(NO)]$ (M=K, Rb, and Cs; X=Cl, Br, and I).[10]

The authors wish to express their appreciation to Prof. Ichiro Nakagawa of Tohoku University and Mr. Yoshiyuki Morioka of the University of Tokyo for measurement of the IR spectra at liquid nitrogen temperature, and to Dr. Shigeru Nagashima and Mr. Akira Tamura for their technical assistance. The present work was supported in part by a Grant for Scientific Research from the Ministry of Education.

References

1) E. Miki, K. Mizumachi, T. Ishimori, and H. Okuno, This Bulletin, **46**, 3779 (1973).
2) W. P. Griffith, J. Lewis, and G. Wilkinson, *J. Chem. Soc.*, **1961**, 775.
3) C. T. Ratcliffe and J. M. Shreeve, "Inorganic Syntheses," Vol. 11, (1968), p. 194.
4) M. J. Cleare, H. P. Fritz, and W. P. Griffith, *Spectrochim. Acta*, **28A**, 2013 (1972).
5) D. M. P. Mingos and J. A. Ibers, *Inorg. Chem.*, **10**, 1479 (1971).
6) R. C. Evans, "An Introduction to Crystal Chemistry," 2nd. Ed., Cambridge University Press, (1964), p. 74.
7) T. Shimanouchi and I. Nakagawa, *Inorg. Chem.*, **3**, 1805 (1964).
8) D. M. Adams, "Metal-Ligand and Related Vibrations," Edward Arnold Publishers Ltd., London (1967).
9) T. Shimanouchi and I. Nakagawa, *J. Amer. Chem. Soc.*, **79**, 3313 (1957).
10) E. Miki, T. Ishimori, H. Yamatera, and H. Okuno, This Bulletin, **42**, 3007 (1969).

Derivatographic Studies on Transition Metal Complexes. XIII.[1] Thermal Decomposition of $[Ni(N_2H_4)_6]X_2$ Complexes[2]

Ryokichi TSUCHIYA, Masaaki YONEMURA,* Akira UEHARA, and Eishin KYUNO

Department of Chemistry, Faculty of Science, Kanazawa University, Kanazawa 920

(Received November 10, 1973)

The thermal decomposition of $[Ni(N_2H_4)_6]X_2$ (X=Cl, Br, I) in solid phase was investigated by means of derivatography and IR spectral measurement. It was found from the derivatography that the decomposition of the chloride and bromide proceeded *via* tris-, bis-, and mono-hydrazine complexes as metastable reaction intermediates, while tetra-hydrazine complex was produced in the decomposition of the iodide instead of the tris-one which appeared in the chloride and bromide. IR spectra showed that, although the hexa-hydrazine complex as a starting material contains only unidentate hydrazine coordinated by either one of terminal nitrogen atoms, all the reaction intermediates have bidentate one bridging between two nickel ions. In particular, it was of much interest that the decomposition of these hydrazine complexes was remarkably exothermic, a part of the reasons being discussed.

Systematic studies on thermal decomposition in solid phase for [Ni(II)N_6]-type complexes seem to be still rare except for $[Ni(NH_3)_6]X_2$.[3] Tanaka *et al.*[4] proposed from the thermogravimetry for hexaammine-nickel(II) complexes that it decomposed in two or three steps through lower ammine intermediates $NiX_2 \cdot n NH_3$: n=2, 1 for X=Cl; n=2 for X=Br, I and n=4 for X=NO_3.

Because of d^8 electronic configuration in nickel(II) ion, the tendency of the complex formation of either octahedral (O_h symmetry) six-coordinated, square planar (D_{4h}) or tetrahedral (T_d) four-coordinated structure apparently could exist depending upon the changes in trivial steric hindrance or the nature of surroundings for the central metal ion.[5,6] In the thermal decomposition of hexaamminenickel(II) complexes described above, however, the latter two forms, square planar and tetrahedral, could not be found, but the intermediates were presumed to be polymers from the diffuse reflectance spectral measurement in which nickel ions were octahedrally coordinated with ammonia molecules and bridging halogen atoms.

Hydrazine (NH_2NH_2), in general, behaves either as unidentate ligand coordinated by either one of terminal nitrogen atoms or as bidentate one bridging between two metals[7-9] because of the difficulty of the formation of bidentate coordination with a same metal ion owing to its short N–N distance despite of keeping two nitrogen atoms capable of coordinating to metal in one hydrazine molecule itself.

From these standpoints, hydrazine may be expected to form the complex like [NiN_6]-type. On the other hand, the thermal decomposition of the complexes of nickel(II),[10] iron(II),[11] and cobalt(II)[12] oxalates with hydrazine had been investigated.

Thus, as the object of the present work, it was undertaken to find whether or not the nickel(II) complexes with hydrazine undergo the analogous structural transformation to that of hexaamminenickel(II) complexes in the course of thermal decomposition, and whether or not any unique changes can be found in terms of the peculiar behavior of hydrazine to coordination form as described above.

* Present address: Matsushita Denki Sangyo Co. Ltd., Yamato-koriyama, Nara.

Experimental

Preparation of Complexes. Complexes $Ni(N_2H_4)_6X_2$ (X=Cl, Br, I) were prepared in the similar manner to that described in the literature.[13] Compounds of $Ni(N_2H_4)_3X_2$ type as well as $Ni(N_2H_4)_2X_2$ type were also obtained by the known method[8] to identify the corresponding intermediates in the thermal reaction of hexehydrazinenickel(II) complexes. Their chemical formulae were determined by elemental analysis and spectral measurement.

Derivatographic Measurements. The derivatograms were obtained with a MOM Derivatograph Typ-OD-102. All the measurements were carried out in a constant flow of nitrogen stream under the heating rate of 1 °C/min. In each run 0.4 or 0.5 g sample was used. The thermal functions, activation energies (E_a) and enthalpy changes (ΔH), were calculated in each step of thermal reaction by analyzing the DTA curves in the derivatograms obtained.[14]

Spectral Measurements. In order to examine the structural change or bonding feature of the reaction intermediates during the course of the thermal decomposition, the reaction intermediates were taken out of a furnace at various desired temperatures during the continuous heating by a Shimadzu TM-1A thermobalance and their electronic and infrared absorption spectra were measured with a Hitachi EPS and EPU-2A spectrophotometers in both solution and powder state and with a JASCO Model IR-E spectrophotometer in mull state, respectively.

Magnetic Measurements. The effective magnetic moments of the samples as well as the reaction intermediates were evaluated from the magnetic susceptibilities of the sample corrected by applying the Pascal's constant of the elements involved.

X-Ray Powder Diffraction. X-ray powder diffraction patterns of the sample and its thermal reaction intermediates were obtained with a Rigaku-denki Geiger-flex X-ray Analyzer.

Results and Discussion

Derivatography. When $Ni(N_2H_4)_6X_2$ (X=Cl, Br) was heated in solid phase, the decomposition accompanying the liberation of hydrazine took place stepwise with some color changes. Figure 1 shows the derivatograms for the chloride and bromide.

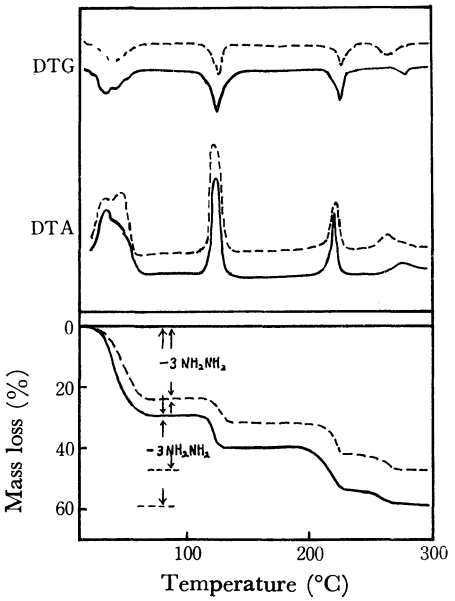

Fig. 1. Derivatograms for $Ni(N_2H_4)_6Cl_2$ (——) and $Ni(N_2H_4)_6Br_2$ (------).

As seen in this figure, two reaction intermediates formed as the result of the evolution of three and four moles of hydrazine are obviously detected successively in the TG curves up to 60 °C and in the temperature range of 100—140 °C, respectively, being confirmed to have the compositions, $Ni(N_2H_4)_3X_2$ (X=Cl, Br) and $Ni(N_2H_4)_2X_2$, by the electronic and IR spectra which will be described in the later sections. The further heating of these compounds leads to the decomposition to nickel(II) halides as the final products at 240—320 °C *via*, as a whole, the formation of monohydrazine complexes, $Ni(N_2H_4)X_2$ (Cl, Br), at 190—230 °C as the third reaction intermediates.

The DTA curves show one broad and two sharply exothermic peaks in the three decomposition steps, $Ni(N_2H_4)_6X_2$ to $Ni(N_2H_4)_3X_2$, $Ni(N_2H_4)_3X_2$ to $Ni(N_2H_4)_2X_2$ and $Ni(N_2H_4)_2X_2$ to $Ni(N_2H_4)X_2$, and a small exothermic peak in the last step of the decomposition to nickel(II) halides.

Although the evolution of ammonia or water molecules in the thermal decomposition of aquo or ammine cobalt(III) or chromium(III) complexes gives, in general, endothermic peak,[14,15] an appearance of exothermic peaks as mentioned above is of much interest. Such a phenomenon will be attributed to the characteristic properties of hydrazine, and the discussion concerned will be briefly made in the later section.

In the case of the iodide, on the other hand, the tetrahydrazine complex was found in place of tris(hydrazine) complex in the case of chloride and bromide, and bis(hydrazine) complex undersent the complete decomposition without the formation of monohydrazine complex as shown in Fig. 2: the two decomposition steps, hexa-to-tetra and tetra-to-bis complex, appear at about 30—85 °C and at 100—135 °C, respectively, and the final decomposition occurs at 240—290 °C. The most striking difference between the chloride, bromide and iodide is that, in the former two, the final decomposition product is nickel(II) halides, whereas the iodide finally decomposes without the formation of nickel(II) iodide. It may be in part due to the essential decomposition with iodine liberation.

Magnetic Susceptibilities. The effective magnetic moments evaluated from the magnetic susceptibilities of the hexahydrazine complexes and their thermal reaction intermediates are listed in Table 1 together with their colors.

The complexes $Ni(N_2H_4)_6X_2$ (Cl, Br) did not give a constant value on account of the sensitivity of the composition in air exposure, and hence are expressed as paramagnetic. That the complexes, $Ni(N_2H_4)_3X_2$ and $Ni(N_2H_4)_2X_2$, give the magnetic moments corresponding to the electronic structure with two free spins suggests that their structures are not, at least, the square planar. The values for the iodide could not be obtained because of the comparative instability against the chloride and bromide.

Electronic Spectra. In order to clarify the coordination structures of the hexahydrazinenickel(II) complexes, $Ni(N_2H_4)_6X_2$, and their thermal reaction intermediates, their electronic spectra were measured in the powdered state by the diffuse reflectance method, which are shown in Fig. 2 for the chloride, in Fig. 3 for the bromide and in Fig. 4 for the iodides.

As seen in these figures and in Table 1, tris(hydrazine)nickel(II) chloride, $Ni(N_2H_4)_3Cl_2$, and the bromide, $Ni(N_2H_4)_3Br_2$, and tetra-hydrazine iodide, $Ni(N_2H_4)_4I_2$, as well as the hexahydrazinenickel(II)

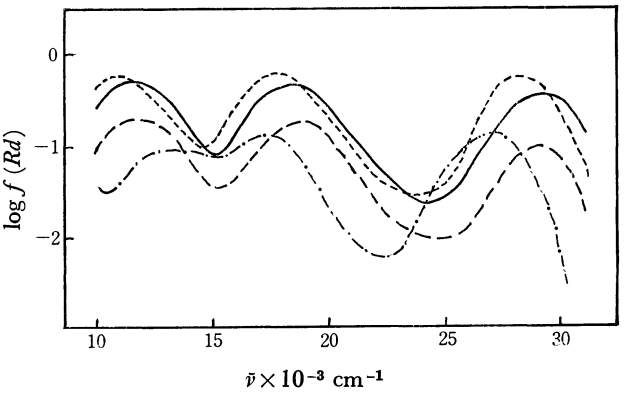

Fig. 2. Electronic spectra of $[Ni(N_2H_4)_6]Cl_2$ (——), $Ni(N_2H_4)_3Cl_2$ (– – – –), $Ni(N_2H_4)_2Cl_2$ (— – —), and $[Ni(NH_3)_6]Cl_2$ (-------).

Table 1. Magnetic moments (25 °C) and colors of $[Ni(N_2H_4)_n]X_2$

n	X	μ_{eff}(B.M.)	Color	n	X	μ_{eff}(B.M.)	Color	n	X	Color
6	Cl	paramag.	pale violet	6	Br	paramag.	pale violet	6	I	pale violet
3	Cl	2.96	pale violet	3	Br	3.43	pale violet	4	I	pale violet
2	Cl	3.17	pale blue	2	Br	3.20	grayish blue	2	I	yellowish green
1	Cl		yellow	1	Br		yellowish brown			

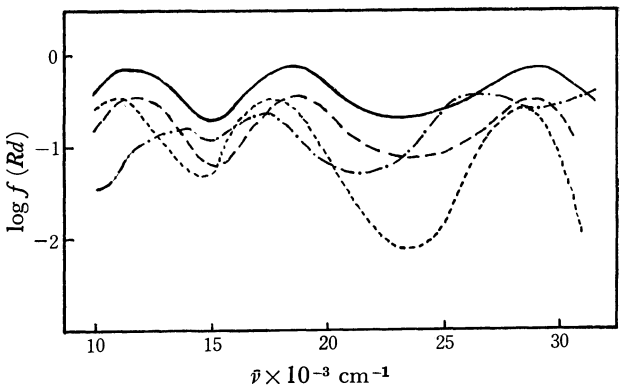

Fig. 3. Electronic spectra of $[Ni(N_2H_4)_6]Br_2$ (——), $Ni(N_2H_4)_3Br_2$ (----), $Ni(N_2H_4)_2Br_2$ (— — —) and $[Ni(NH_3)_6]Br_2$ (-------).

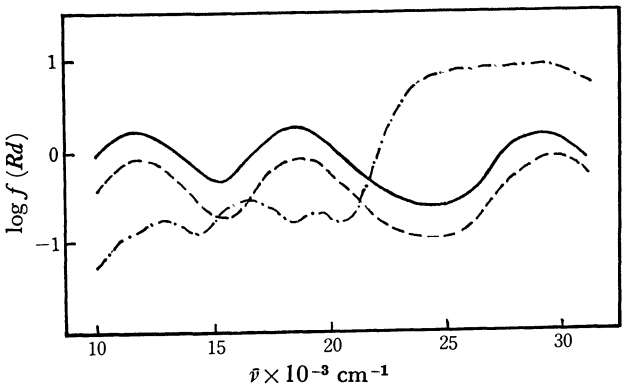

Fig. 4. Electronic spectra of $[Ni(N_2H_4)_6]I_2$ (——), $Ni(N_2H_4)_4I_2$ (----) and $Ni(N_2H_4)_2I_2$ (— — —).

complexes as the starting materials are all pale violet in color, and their spectra are in approximate agreement with each other in the chlorides, bromides and iodides, respectively. These facts exhibit that these complexes have commonly the same $[NiN_6]$-type coordination structure.

In the bis-type complexes, $Ni(N_2H_4)_2X_2$, on the other hand, the spectra assigned to $^3T_{2g}\leftarrow{}^3A_{2g}$, $^3T_{1g}\leftarrow{}^3A_{2g}$, and $^3T_{1g}(P)\leftarrow{}^3A_{2g}$ are found to slightly shift to the longer wavelength region than that of hexahydrazine complexes without the remarkable change of the spectral form. These shifts are understood to be attributed to the substitution of the ligand hydrazine by halide ions in the lower position of the spectrochemical series, and they support the color change to pale blue for the chloride, grayish blue for the bromide and yellowish green for the iodide from yellow in the starting complexes upon heating, in a similar manner in the case of heating $Ni(NN\text{-}deen)_2Cl_2\cdot 2H_2O$(NN-deen=*N*,*N*-diethylethylenediamine), where two chloride ions existing as a counter ion anate by entering the coordination sphere after the liberation of water.[5]

IR Spectra. Closely related to the structural determination from electronic spectra, it may be very important to know whether the hydrazine coordinates as unidentate or as bidentate ligand bridging between two nickel ions from IR spectral measurement in the course of thermal reaction. Above all, the strikingly decisive factor for the above informations is the N–N stretching vibration, ν_{N-N}.

It is well known that the vibration ν_{N-N} in the hydrazine coordinated as unidentate ligand by either one of terminal nitrogen atoms appears in the 920—940 cm^{-1} region with considerably high intensity, whereas in the hydrazine coordinated as bidentate ligand bridging between two metal ions, the ν_{N-N} frequency is expected to shift to higher wave number side, lying in the 960—985 cm^{-1} region.[8,9] Therefore, the ν_{N-N} frequency mentioned above is thought to be the most immediately useful identification method which type of coordinated hydrazine are contained in the complexes.

The IR spectra of the hexahydrazinenickel(II) complexes and their thermal reaction intermediates were given in Fig. 5.

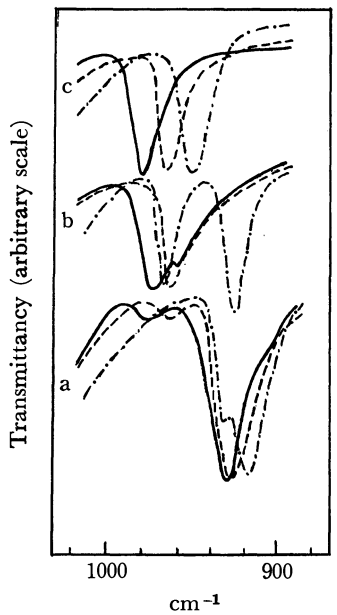

Fig. 5. IR spectra of (a) $[Ni(N_2H_4)_6]X_2$, (b) $Ni(N_2H_4)_4X_2$ (X=I) and $Ni(N_2H_4)_3X_2$ (X=Cl, Br) and (c) $Ni(N_2H_4)_2X_2$.
—— chloride, ---- bromide, — — — iodide

As seen in this figure, the N–N stretching vibration are found at around 932, 928, and 936(sh)—915 cm^{-1} for the chloride, bromide and iodide of $[Ni(N_2H_4)_6]X_2$ complexes as starting materials, respectively. These facts indicate that all the hydrazine molecules coordinate to central nickel(II) ion as unidentate ligand with either one of terminal nitrogen atoms in these type complexes. In $Ni(N_2H_4)_3X_2$ type complexes of the first reaction intermediates, on the other hand, the ν_{N-N} band is shifted to 968 cm^{-1} for the chloride and 966 cm^{-1} for the bromide, respectively.

Upon heating $[Ni(N_2H_4)_6]I_2$, the original peak, 936—915 cm^{-1}, is diminished gradually and a new peak at 966 cm^{-1} grows strong until $Ni(N_2H_4)_4I_2$ is formed, with the liberation of two moles of hydrazine. These facts suggest that tris(hydrazine)nickel(II) chloride and bromide contain bidentate bridging hydrazine alone, while the tetrahydrazinenickel(II) iodide does both unidentate terminal and bidentate bridging hydrazine as ligands.

In the bis(hydrazine)nickel(II) chloride and bromide as the second reaction intermediates, the ν_{N-N} band is observed at around 980 and 966 cm^{-1}, respectively, as the same as the corresponding tris complexes, and in the bis(hydrazine)nickel(II) iodide, only the band at 966 cm^{-1} remains, the band at a around 930 cm^{-1} being quenched. These results indicate that all the hydrazines are the bidentate bridging ligand.

It was concluded, therefore, from the information shown by IR spectra as above along with no color change in the first reaction step for $[Ni(N_2H_4)_6]X_2$ to tris(hydrazine)nickel(II) chloride and bromide or to tetrahydrazinenickel(II) iodide that these processes are "Dehydrazination-Bridging" reaction, and from the electronic spectra that the second step reactions are "Dehydrazination-Anation."

X-Ray Powder Diffraction Pattern. The structural determination of $[Zn(N_2H_4)_2]Cl_2$ has been done by X-ray diffraction method.[16] The powder patterns of $Ni(N_2H_4)_2Cl_2$ and $Ni(N_2H_4)_2Br_2$ obtained in the present work were similar to that of the corresponding Zn(II) complex, as shown in Fig. 6. Therefore, they seem to have isostructure, which is also supported by the spectral measurements.

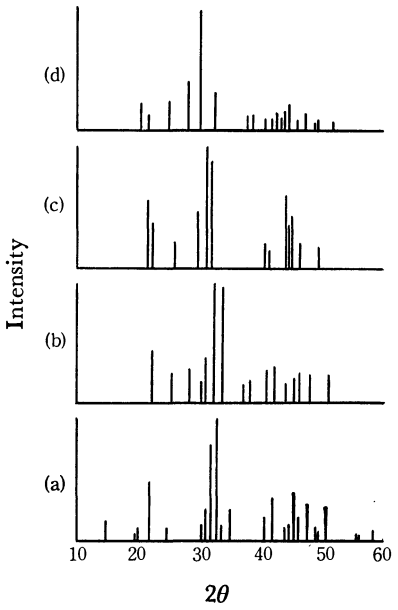

Fig. 6. X-ray diffraction patterns of (a) $ZnCl_2(NH_2-NH_2)_2$, (b) $NiCl_2(NH_2NH_2)_2$, (c) $NiBr_2(NH_2NH_2)_2$ and (d) $NiI_2(NH_2NH_2)_2$.

In the case of $Ni(N_2H_4)_2I_2$, however, the powder pattern may be somewhat different from those of the chloride and bromide. Although details on the structure except by the informations in the electronic and IR spectra are still unknown the tetra-, tris-, and bis-(hydrazine) type complexes probably have polymer structures.

Summarily, on the basis of the experimental results obtained above, the thermal reactions of hydrazine complexes are presumed to be portrayed by the following schemes:

for chloride and bromide:

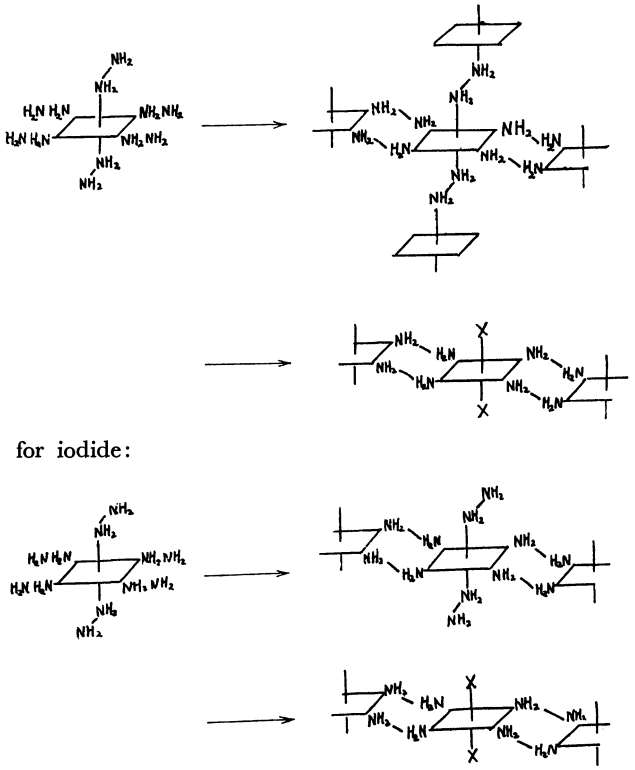

for iodide:

Thermochemical Functions. The values of the enthalpy changes (ΔH) and the activation energies (E_a) were calculated from the derivatograms, which are summarized in Table 2, along with the temperatures of each decomposition step.

As shown in derivatograms and in Table 2, the striking feature appearing in the hydrazine complexes treated in the present work is great exothermicity in the dehydrazination in contrast to the endothermicity in the general dehydration. This abnormal character may be considered to be in part attributed to the following reaction predicted to occur in the dehydrazination process.

Table 2. Thermochemical functions for decomposition of $[Ni(N_2H_4)_6]X_2$ (X=Cl, Br)

Decomposition step		Complex	
		$[Ni(N_2H_4)_6]Cl_2$	$[Ni(N_2H_4)_6]Br_2$
$Ni(N_2H_4)_6X_2$ to $Ni(N_2H_4)_3X_2$	T(°C)[a]	−60	−50
	ΔH[b]	−20.5	−18.6
	E_a[c]	—	—
$Ni(N_2H_4)_3X_2$ to $Ni(N_2H_4)_2X_2$	T(°C)	100—140	110—140
	ΔH	−19.6	−13.7
	E_a	46.5	43.8
$Ni(N_2H_4)_2X_2$ to $Ni(N_2H_4)X$	T(°C)	190—230	190—230
	ΔH	−16.8	−8.5
	E_a	26.3	33.7
$Ni(N_2H_4)X_2$ to NiX_2	T(°C)	240—320	250—310
	ΔH	−16.7	−8.6
	E_a	—	—

a) Decomposition temperature. b) kcal per one mole of hydrazine liberated. c) kcal per one mole of complexes.

If hydrazine is decomposed by the following mode,

$$NH_2NH_2\,(g) = 4/3NH_3\,(g) + 1/3N_2\,(g),$$

the enthalpy change is expected as $\Delta H_1 = -36.77$ kcal/mol.[17] On the other hand, the enthalpy change of deammonation in the reaction,

$$Ni(NH_3)_6Br_2\,(s) = Ni(NH_3)_2Br_2\,(s) + 4NH_3\,(g),$$

is known as $\Delta H_2 = 15.79$ kcal/mol,[18] which is assumed to be equal to the energy required to break the bond between nickel(II) ion and four nitrogen atoms.

$$Ni(NH_2NH_2)_3Br_2\,(s) = Ni(NH_2NH_2)_2Br_2\,(s) + 4/3NH_3\,(g) + 1/3N_2\,(g),$$

Therefore, for example, the enthalpy change of the thermal decomposition of tris(hydrazine)nickel(II) bromide is calculated as $\Delta H = \Delta H_1 + 2\Delta H_2 = -5.19$ kcal/mol. Although this value is relatively lower than the observed value, $\Delta H = -13.7$ kcal/mol in Table 2, the exothermicity can be, to some extent, explained by the results calculated as above.

References

1) Part XII in this series: See R. Tsuchiya, A. Uehara and E. Kyuno, This Bulletin, **46**, 3737 (1973).
2) Presented at the 22nd Symposium on Coordination Chemistry, Osaka, November, 1972.
3) T. D. George and W. W. Wendlandt, *J. Inorg. Nucl. Chem.*, **25**, 395 (1963).
4) N. Tanaka, M. Kagawa, and M. Kamada, This Bulletin, **41**, 2908 (1968).
5) R. Tsuchiya, S. Joba, A. Uehara and E. Kyuno, This Bulletin, **46**, 1454 (1973).
6) E. Uhlig, *Coord. Chem. Rev.*, **10**, 227 (1973).
7) W. G. Paterson and M. Onyszghuk, *Can. J. Chem.*, **39**, 986 (1961).
8) D. Nicholls, M. Rowley and R. Swindells, *J. Chem. Soc.*, (**A**) **1966**, 950.
9) L. Sacconi and A. Sabantini, *J. Inorg. Nucl. Chem.*, **25**, 1389 (1963).
10) E. A. Nikonenko, E. I. Krilov, and V. A. Sharov, *Zh. Neorg. Khim.*, **14**, 669 (1969), **18**, 1569 (1973); E. I. Krilov, E. A. Nikonenko, V. A. Sharov, and Y. M. Ovchinnikov, *ibid.*, **15**, 38 (1970).
11) T. B. Shkodina, E. I. Krilov, and V. A. Sharov, *ibid.*, **17**, 353 (1972).
12) Idem, *ibid.*, **17**, 1823 (1972).
13) K. H. Linke, F. Durholtz, and D. Handicke, *Z. Anorg. Allg. Chem.*, **356**, 113 (1968).
14) R. Tsuchiya, Y. Kaji, A. Uehara, and E. Kyuno, This Bulletin, **42**, 1881 (1969).
15) R. Tsuchiya, S. Nakagawa, A. Uehara, and E. Kyuno, This Bulletin, **46**, 169 (1973).
16) A. Ferrari, A. Braibanti, and G. Brigdiardi, *Acta Cryst.*, **16**, 498 (1963).
17) W. A. Roth, *Z. Elektrochem.*, **50**, 111 (1944).
18) F. Ephraim, *Ber.*, **58**, 2262 (1925).

Reactions of Bis(acetylacetonato)palladium(II) with Triphenylphosphine and Nitrogen Bases

Shigeru BABA, Tetsuya OGURA, and Shinichi KAWAGUCHI*

Department of Chemistry, Faculty of Science, Osaka City University, Sumiyoshi, Osaka 558

(Received November 12, 1973)

Bis(acetylacetonato)palladium(II) reacts with triphenylphosphine and nitrogen bases such as pyridine, diethylamine, and *N*-methylbenzylamine to transform one of the chelating ligands into the carbon-bonded state. The product complexes of the type $Pd(acac)_2L$ have been isolated in high yields and characterized by IR and NMR spectra. Several reactions of $Pd(acac)_2PPh_3$ and $Pd(acac)_2py$ were also examined.

Acetylacetone is a very versatile ligand showing various modes of bonding to metal atoms.[1] Most usually the acetylacetonate anion coordinates to a metal atom *via* the two oxygen atoms, forming a six-membered chelate ring.[2] The unidentate linkage *via* the central carbon atom is also well known for platinum(II) and other rather soft metal ions,[3] but no example of carbon-bonded palladium(II) complexes of acetylacetone has yet been reported.

The complex $K[PtCl(acac)_2]$ was prepared by Werner[4] in 1901 by the reaction of $K_2[PtCl_4]$ with potassium acetylacetonate in aqueous solution, and was shown by X-ray crystal analysis[5] to have one carbon-bonded and one oxygen-bonded ligands. On the other hand, similar reactions of $K_2[PdCl_4]$ with acetylacetonate anions under various conditions produce only the simple chelate $Pd(acac)_2$.[3] However, in our study of the reaction between $Pd(acac)_2$ and triphenylphosphine in benzene to prepare $Pd(PPh_3)_4$, the carbon-bonded acetylacetonate complex $Pd(acac)_2(PPh_3)$ was obtained as a stable intermediary product.[6] This paper reports the preparation and characterization of several palladium(II) complexes containing the carbon-bonded acetylacetonate ligand.

Results and Discussion

Preparation. Bis(acetylacetonato)palladium(II), $Pd(acac)_2$, reacts with excess triphenylphosphine in benzene at room temperature to produce $Pd(PPh_3)_4$ or $PdO_2(PPh_3)_2$ in the absence or presence of oxygen, respectively. However, an equimolar amount of triphenylphosphine gave a carbon-bonded acetylacetonate complex, $Pd(acac)_2(PPh_3)$ [**1a**], in a high yield. Nitrogen bases such as pyridine, diethylamine, and *N*-methylbenzylamine also reacted with $Pd(acac)_2$ to transform one of the chelating ligands into the carbon-bonded state (Eq. (1)). The analytical data of the products are summarized in Table 1.

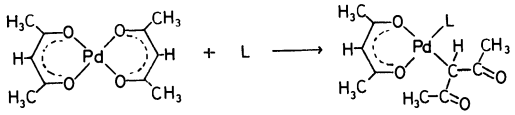

(1)

L=PPh_3[**1a**], Py[**1b**], $NHEt_2$[**1c**], or $NH(Me)CH_2Ph$[**1d**]

Triphenylarsine and benzonitrile did not react with $Pd(acac)_2$. Either twice as many moles of triphenylphosphine or excess nitrogen bases did not afford the palladium(II) complex containing two carbon-bonded acetylacetonate ligands, but resulted in the compounds **1** alone. The bidentate bases such as 1,2-bisdiphenylphosphinoethane, 2,2′-bipyridine, 1,10-phenanthroline, ethylenediamine, and *N*,*N*′-dimethylethylenediamine did not produce the aimed compounds, either. It is not yet clear why the palladium(II) complex containing two carbon-bonded acetylacetonate ligand can not be obtained, but the existence of one acetylacetonate chelate ring might be necessary to stabilize the carbon-bonding of the other acetylacetonate ligand.

Infrared and NMR Spectra. The characteristic stretching vibrations in the carbon-bonded acetylacetonate complexes are summarized in Table 2. The ν(C=O) and ν(C=C) bands of the chelating acetylacetonate ligand appear in the 1500—1600 cm^{-1} region, and the absorption bands in the 1600—1700 cm^{-1} region which are not observed for $Pd(acac)_2$ can be unequivocally assigned to the ν(C=O) vibrations of the carbon-bonded acetylacetonate ligand.[7] The strong band which is observed in the 500—550 cm^{-1} region

Table 1. Analytical data of palladium(II) complexes

Complex	Found %			Calcd %			Mol. wt. Found (Calcd)	Color	Dec. pt. °C
	C	H	N	C	H	N			
$Pd(acac)_2PPh_3$	59.38	5.77		59.32	5.16		560 (567)	yellow-orange	142
$Pd(acac)_2py$	46.92	5.06	3.92	46.95	4.99	3.65	381 (383)	yellow-green	150
$Pd(acac)_2NHEt_2$	44.20	6.84	4.27	44.51	6.67	3.71	380 (377)	yellow	106
$Pd(acac)NH(Me)CH_2Ph$	51.93	6.04	3.74	52.12	5.75	3.20	410 (437)	yellow	156
$PdCl(acac)PPh_3$	55.60	4.79		54.90	4.40		500 (503)	orange	162
$PdCl(acac)py$	37.53	3.76	4.79	37.52	3.78	4.40	302 (320)	reddish orange	160
$PdOCOCH_3(acac)PPh_3$	56.75	5.19		56.99	4.78		510 (527)	yellow	135
$PdOCOCH_3(acac)py$	42.01	4.78	4.04	42.31	4.44	4.11	340 (310)	orange	117

* Correspondences should be addressed to this author.

Table 2. Infrared spectra in nujol mull (cm^{-1})[a]

Complex	C-bonded acac ν(C=O)	ν(Pd–C)	O-bonded acac ν(C=O)+ν(C=C)	ν(Pd–Cl)	CH_3COO ν(C=O)
$Pd(acac)_2PPh_3$	1665 vs	540 vs	1572 vs, 1550 s		
	1632 s		1523 vs		
$Pd(acac)_2py$	1680 vs	524 vs	1568 vs, 1548 m, sh		
	1640 m		1521 vs		
$Pd(acac)_2NHEt_2$	1675 vs	519 vs	1575 vs, 1562 s, sh		
	1630 m		1521 vs		
$Pd(acac)_2NH(Me)CH_2Ph$	1678 vs	518 s	1570 vs, 1558 s		
	1630 m		1521 s		
$PdCl(acac)PPh_3$			1568 s, 1545 m, sh	360 s	
			1521 vs		
PdCl(acac)py			1567 s, 1558 m, sh	348 vs	
			1520 vs		
$PdOCOCH_3(acac)PPh_3$			1578 vs, 1558 m, sh		1640 vs
			1515 s		
$PdOCOCH_3(acac)py$			1561 s, 1550 m, sh		1632 vs
			1520 vs		

a) vs: very strong, s: strong, m: medium, sh: shoulder

can be attributed to the ν(Pd–C) vibration.

The coexistence of one oxygen-chelating and one carbon-bonded acetylacetonate ligands in the complexes **1a**—**1d** is clearly revealed by the proton NMR spectra listed in Table 3. The NMR spectra of platinum(II) complexes containing the carbon-bonded acetylacetonate ligand have been studied extensively by Lewis and his co-workers,[8] and are referred to here in assigning the present spectra.

In a spectrum of $Pd(acac)_2PPh_3$ [**1a**] three methyl-proton signals are observed each as a singlet at 8.46, 7.96, and 7.86 τ with the intensity ratio of 1 : 1 : 2. The lowest-field peak is assigned to the two methyl groups of the carbon-bonded acetylacetonate ligand, indicating

Table 3. NMR data recorded at 60 MHz in $CDCl_3$ (τ Values relative to internal TMS)[a]

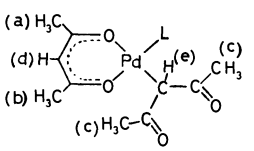

L	O-Bonded acac ligand CH_3(a)	CH_3(b)	CH(d)	C-Bonded acac ligand CH_3(c)	CH(e)
PPh_3	8.46	7.96	4.70	7.86	6.46[b]
py	8.10	8.00	4.66	7.86	5.76
$NH(Me)CH_2Ph$	8.03	7.99	4.63	7.80	5.50

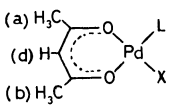

L	X	CH_3(a)	CH_3(b)	CH(d)	CH_3COO
PPh_3	Cl	8.46	7.93	4.70	
py	Cl	7.96	7.90	4.53	
PPh_3	$OCOCH_3$	8.36	7.96	4.66	8.50
py	$OCOCH_3$	8.06	8.00	4.63	8.00

a) All signals except the following one are singlets.
b) Doublet, J_{P-H}=6.3 Hz.

that the two methyl groups are equivalent on account of free rotation of the ligand around the Pd–C bond. The two peaks of equal intensity at 8.46 and 7.96 τ are attributed to the two methyl groups of the chelating acetylacetonate ligand. As is noticed in Table 3, the highest-field signal is shifted appreciably when triphenylphosphine is replaced by other ligands, while the lower-field one is not sensitive to the nature of L. Such an anisotropic shielding effect of the triphenylphosphine ligand is expected to be experienced by the methyl group nearer to this ligand, and thus the highest-field signal is assigned to the acetylacetonate-methyl group in the *cis* position of L. Similar situations have also been found for PtCl(acac)L complexes containing various tertiary phosphines and other bases as L.[8,9]

It has been well established for the platinum(II) complexes[10] that the methine proton of the carbon-bonded acetylacetone absorbs at higher field in comparison with that of the chelating acetylacetone. This assignment holds also for the palladium(II) complexes, and the methine proton signal of the carbon-bonded acetylacetone in the phosphine complex **1a** appears as a doublet because of coupling with the phosphorus nucleus (J_{P-H}=6.3 Hz).

Reactions of Pd(acac)$_2$L. The compound **1a** reacts with more than three mole equivalents of triphenylphosphine to produce tetrakis(triphenylphosphine)palladium(0). Benzoyl chloride reacts with **1a** in benzene at room temperature to replace the carbon-bonded acetylacetonate ligand with a chloride anion, affording $PdCl(acac)PPh_3$ [**2a**]. The loss of the carbon-bonded acetylacetone is clearly evidenced by the IR and NMR spectra (Tables 2 and 3). The compound **2a** can be transformed again to **1a** by the reaction with thallium(I) acetylacetonate. **2a** also reacts with thallium(I) acetate to form $Pd(OCOCH_3)(acac)PPh_3$ [**3a**], which can alternatively derived from **1a** by the direct reaction with acetic acid. It should be noted that $Pd(acac)_2$ does not react with acetic acid, but the carbon-bonded acetylacetonate group in **1a** can be easily displaced by the reaction with acetic acid.

The mechanism of the reaction of **1a** with acetic acid or benzoyl chloride is not clear at the present stage of investigation, but the oxidative addition of the reactant to **1a** might have occurred, being followed by the reductive elimination of acetylacetone or its benzoyl derivative.

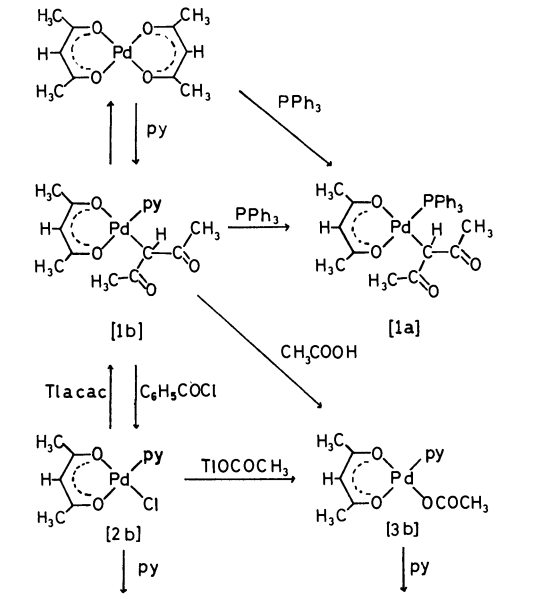

Scheme

As is summarized in the Scheme, similar reactions are also observed for the compound **1b** to produce PdCl(acac)py [**2b**] and $PdOCOCH_3$(acac)py [**3b**]. The compound **1b** was prepared by the reaction of $Pd(acac)_2$ with pyridine, but the reaction can be reversed. When **1b** was dissolved in benzene, refluxed for about one hour, and the solvent was distilled off under reduced pressure, $Pd(acac)_2$ was recovered. The ligand pyridine can also be replaced by triphenylphosphine to give **1a**.

It is very interesting that the compound **2b** reacts with pyridine to produce *trans*-$PdCl_2py_2$ and $Pd(acac)_2$-py [**1b**]. These products correspond to the disproportionation of **2b** to form $PdCl_2py_2$ and $Pd(acac)_2$ followed by the reaction of $Pd(acac)_2$ with pyridine to give **1b**. However such a disproportionation reaction of **2b** does not occur spontaneously, but needs pyridine as a trigger reagent. The acetate complex **3b** also reacts with pyridine to afford *trans*-$Pd(OCOCH_3)_2py_2$ and **1b**.

The mechanism of this kind of interesting reaction is not yet clear, but the reaction proceeds quite readily and offers a useful and convenient route for the synthesis of *trans*-$Pd(OCOCH_3)_2py_2$. Bis(acetylacetonato)-palladium(II) readily reacts with pyridine and acetic acid in benzene at room temperature to form *trans*-$Pd(OCOCH_3)_2py_2$ in a high yield.

Experimental

Reactions of $Pd(acac)_2$ with Bases. A mixture of $Pd(acac)_2$ (0.272 g, 0.89 mmol) and PPh_3 (0.240 g, 0.91 mmol) was stirred in benzene (6 ml) at room temperature until the solution became transparent. Then petroleum ether (bp 30 —60 °C) was added to separate the product. Yield 0.473 g, 87%. Yellow-orange crystals of $Pd(acac)_2PPh_3 \cdot \frac{1}{2}C_6H_6$ were obtained by recrystallization from benzene–petroleum ether, but those recrystallized from chloroform did not involve the lattice solvent.

A mixture of $Pd(acac)_2$ (0.290 g, 0.95 mmol) and pyridine (5 ml) was warmed at about 80 °C until a clear solution resulted. Petroleum ether was added to precipitate $Pd(acac)_2py$. Yield 0.332 g, 91%. Yellow-green crystals were obtained by recrystallization from benzene–petroleum ether. $Pd(acac)_2NH(Me)CH_2Ph$ was also prepared by a similar reaction in a yield of 90%.

A mixture of $Pd(acac)_2$ (0.353 g, 1.15 mmol) and $NHEt_2$ (5 ml) was stirred at room temperature until a clear solution was obtained. Then the amine was evaporated spontaneously to leave the product $Pd(acac)_2NHEt_2$, which was recrystallized from cyclohexane. Yield 0.39 g, 87%.

The Reaction of $Pd(acac)_2PPh_3$ with Excess Triphenylphosphine. The complex $Pd(acac)_2PPh_3$ (0.202 g, 0.35 mmol) was allowed to react with triphenylphosphine (0.380 g, 1.45 mmol) in benzene at room temperature in an atmosphere of nitrogen. Petroleum ether was added to the dark red solution to separate out the product $Pd(PPh_3)_4$. Yield 0.335 g, 81%.

The Reactions of $Pd(acac)_2PPh_3$ and $Pd(acac)_2py$ with Benzoyl Chloride. A mixture of $Pd(acac)_2PPh_3$ (0.205 g, 0.35 mmol) and benzoyl chloride (2 ml) was stirred in benzene (5 ml) at room temperature until a reddish orange solution resulted. Petroleum ether was then added to precipitate the product $PdCl(acac)PPh_3$. Yield 0.172 g, 95%. Reddish orange crystals were obtained by recrystallization from benzene–petroleum ether. Orange crystals of PdCl(acac)py were similarly prepared in a yield of 85%.

The Reactions of $PdCl(acac)PPh_3$ and PdCl(acac)py with Thallium(I) Acetylacetonate. Thallium(I) acetylacetonate (0.015 g, 0.05 mmol) was added to a solution of $PdCl(acac)$-PPh_3 (0.024 g, 0.05 mmol) in chloroform (10 ml) and the mixture was stirred at room temperature for 30 min. Thallium(I) chloride was filtered off and the filtrate was concentrated by evaporation under reduced pressure to separate out $Pd(acac)_2PPh_3$. Yield 0.024 g, 88%. $Pd(acac)_2py$ was also derived from PdCl(acac)py by a similar procedure in a yield of 90%.

Reactions of $Pd(acac)_2py$ to $Pd(acac)_2$ and $Pd(acac)_2PPh_3$. A solution of $Pd(acac)_2py$ in benzene was refluxed for 1 hr and the solvent was distilled off. $Pd(acac)_2$ was recovered. In another experiment, triphenylphosphine (0.300 g, 0.12 mmol) was added to a solution of $Pd(acac)_2py$ (0.348 g, 0.11 mmol) in benzene. After stirring for 10 min, the solution was concentrated to separate out $Pd(acac)_2PPh_3$. Yield 0.500 g, 90%.

Preparations of $PdOCOCH_3(acac)PPh_3$ and $PdOCOCH_3(acac)py$. To a solution of $PdCl(acac)PPh_3$ (0.162 g, 0.32 mmol) in methylene chloride (10 ml) was added thallium(I) acetate (0.102 g, 0.39 mmol), and the mixture was stirred for 30 min at room temperature. Thallium(I) chloride was filtered off, and the filtrate was concentrated by evaporation under reduced pressure to separate out $PdOCOCH_3(acac)PPh_3$. Yield 0.167 g, 97%.

The corresponding pyridine complex $PdOCOCH_3(acac)py$ was similarly prepared from PdCl(acac)py in a yield of 86%. The acetate complex was also prepared by the direct reaction of $Pd(acac)_2py$ (0.167 g, 0.04 mmol) with acetic acid (2 ml) in benzene. The solution was stirred for 3 hr at room temperature. After the evaporation of benzene and acetic acid under reduced pressure, the residue was recrystallized from

benzene–petroleum ether. Yield 0.125 g, 84%.

The Reactions of PdCl(acac)py and PdOCOCH$_3$(acac)py with pyridine. Pyridine (2 ml) was added to a solution of PdCl(acac)py (0.114 g, 0.36 mmol) in benzene (10 ml). The reaction occurred rapidly to precipitate *trans*-PdCl$_2$py$_2$ (yield 0.054 g, 44% on the basis of palladium). Petroleum ether was added to the concentrate of the filtrate to separate out Pd(acac)$_2$py (yield 0.067 g, 48%).

Pyridine (2 ml) was added to a solution of PdOCOCH$_3$-(acac)py (0.139 g, 0.41 mmol) in benzene (10 ml). After stirring for 3 hr at room temperature the solution was concentrated to yield precipitates. Concentration to separate out precipitate was repeated further twice. Resultant yield of *trans*-Pd(OCOCH$_3$)$_2$py$_2$·H$_2$O was 0.075 g, 46%. From the final filtrate Pd(acac)$_2$py was obtained in a yield of 0.059 g, 38%.

Preparation of trans-*Pd(OCOCH$_3$)$_2$py$_2$ from Pd(acac)$_2$.* When pyridine (2 ml) and acetic acid (2 ml) were added to a suspension of Pd(acac)$_2$ (0.241 g, 0.79 mmol) in benzene (12 ml), the mixture became transparent immediately and changed its color from red to pale yellow. After stirring for 20 min petroleum ether was added to the solution to yield *trans*-Pd(OCOCH$_3$)$_2$py$_2$. Yield 0.300 g, 94%. White needles were obtained by the recrystallization from methylene chloride–petroleum ether. Found: C, 42.00; H, 4.63; N, 7.08%. Calcd for Pd(OCOCH$_3$)$_2$py$_2$·H$_2$O: C, 41.96; H, 4.52; N, 6.99%. The ν(C=O) absorption is observed at 1600 cm^{-1}, and the CH$_3$–proton signal at 8.16 τ.

Measurements. Infrared absorption spectra in the 4000—600 cm^{-1} region were measured with a JASCO IR-E spectrophotometer and those in the 700—200 cm^{-1} region with a Hitachi grating infrared spectrophotometer EPI-L. The NMR spectra were recorded at 60 MHz with tetramethylsilane as the internal reference on a C-60 HL spectrometer of Japan Electron Optics. The molecular weight was determined in dichloromethane at 25 °C by the method of vapor pressure osmometry with an apparatus manufactured by Knauer, Germany.

We are indebted to Mr. J. Gohda and Miss M. Iwao for the elemental analyses and NMR measurements. Financial aid by the Ministry of Education and the kind supply of acetylacetone by the Daicel Co., Ltd. are also acknowledged.

References

1) D. W. Thompson, *Structure and Bonding*, **9**, 27 (1971); B. Bock, K. Flatau, H. Junge, M. Kuhr, and H. Musso, *Angew. Chem.*, **83**, 239 (1971).
2) J. P. Fackler, Jr., *Progress Inorg. Chem.*, **7**, 361 (1966).
3) D. Gibson, *Coord. Chem. Rev.*, **4**, 225 (1969).
4) A. Werner, *Ber.*, **34**, 2584 (1901).
5) R. Mason, G. B. Robertson, and P. J. Pauling, *J. Chem. Soc. (A)*, **1969**, 485.
6) A short communication appeared in S. Baba, T. Ogura, and S. Kawaguchi, *Inorg. Nucl. Chem. Lett.*, **7**, 1195 (1971).
7) K. Nakamoto, "Infrared Spectra of Inorganic and Coordination Compounds," 2nd. ed., Wiley–Interscience, New York (1970), pp. 247—256.
8) G. Hulley, B. F. G. Johnson, and J. Lewis, *J. Chem. Soc., (A)*, **1970**, 1732 and references cited therein.
9) C. E. Holloway, G. Hulley, B. F. G. Johnson, and J. Lewis, *ibid.*, **1970**, 1653.
10) J. Lewis, R. F. Long, and C. Oldham, *J. Chem. Soc.*, **1965**, 6740.

Proton Magnetic Resonance Spectra of Metal Ammine Complexes. I. Cobalt(III) Pentammine Series

Hayami YONEDA and Yoshiaki NAKASHIMA*

Department of Chemistry, Faculty of Science, Hiroshima University, Hiroshima 730

(Received December 21, 1973)

The proton magnetic resonance spectra have been measured in dimethylsulfoxide on some cobalt(III) complexes of the type $[CoX(NH_3)_5]$. Ammine protons show two peaks, except in a complex with $X=NO_2^-$. The major peak, due to *cis* NH_3, appears downfields and the minor one, due to *trans* NH_3, upfields as compared with the shift in $[Co(NH_3)_6]^{3+}$. In the case of $X=CN^-$, the shift pattern is reversed. For $[Co(NO_2)(NH_3)_5]^{2+}$, the spectrum is a single peak. This chemical shift behavior is explained by a simple model based on Ramsay's theory for chemical shift. It is concluded that the behavior arises primarily from paramagnetic anisotropy of the central cobalt(III) ion. The model used in this work is shown to be applicable also to the assignment of the PMR spectra for complexes of the types *cis*-$[CoX_2(NH_3)_4]$ and *cis*-$[CoX_2(en)_2]$.

Only a few works have been made on the proton magnetic resonance (PMR) spectra of metal–ammine complexes. This is partly due to the paucity of suitable solvents. Cliffton and Pratt[1] may be the first, to our knowledge, to show that the PMR spectra of cobalt(III) ammine complexes can be obtained when dissolved in acidified heavy water. Recently, Jolly and co-workers[2,3] have measured the PMR spectra of pentammine complexes of cobalt(III), rhodium(III), and iridium(III) in sulfuric acid. It is reported that two peaks with an intensity ratio of 4 to 1 can be obtained for cobalt(III) complexes while single peaks are observed in rhodium(III) and iridium(III) complexes. They have suggested that two-peak patterns in cobalt complexes may be explained by taking into consideration the contribution to the proton shift from the paramagnetic anisotropy of the central cobaltic ion. They have not made, however, even qualitative order-of-magnitude estimations and further no clear-cut explanation has been given to the fact that $[Co(CN)(NH_3)_5]^{2+}$ has *trans* ammine protons shifted to lower field than *cis* protons. Other complexes have reversed shift patterns with *trans* protons shifted to higher field.

We have measured the PMR spectra of some pentammine complexes of cobalt(III) in dimethyl sulfoxide. Herein reported are the shift patterns for these complexes and a simple explanation is given to the shift behavior. The model is based on Ramsay's theory of chemical shift. The major contribution to the proton shift is attributed to the anisotropy of temperature-independent paramagnetism of cobalt(III) ion. This model can account for the change in proton chemical shifts of $[CoX(NH_3)_5]$ when X is varied along the spectrochemical series. Further, some applications are given to the assignment of the PMR spectra of *cis*-$[CoX_2(NH_3)_4]$ and *cis*-$[CoX_2(en)_2]$ (en=ethylenediamine).

Experimental

The complexes used in this work are $[Co(NH_3)_6](NO_3)_3$, $[Co(H_2O)(NH_3)_5](NO_3)_3$, $[Co(CN)(NH_3)_5](NO_3)_2$, and $[CoX(NH_3)_5](NO_3)_2$ ($X=NO_2^-$, OH^-, Cl^-, Br^-, HCO^-, $CH_3CO_2^-$, $CH_2ClCO_2^-$, and $CCl_3CO_2^-$). These complexes are prepared after the well-established methods.[4]

All the spectra are recorded on a Varian A-60 spectrometer. Dimethyl sulfoxide of spectrograde or deuterated dimethyl sulfoxide (Merck) as the case may be is used as solvent. Chemical shifts are measured relative to an internal standard of sodium 2,2-dimethyl-2-silapentane-5-sulfonate (DSS).

Results

As illustrated in Fig. 1, the observed PMR spectra of cobalt(III)–pentammine complexes may be grouped into three categories. Category A; most of the complexes investigated belong to this category. The major peak, due to *cis* NH_3, appears downfields and the minor one, due to *trans* NH_3, upfields as compared with the shift of $[Co(NH_3)_6]^{3+}$. Category B; the spectrum of $[Co(NO_2)(NH_3)_5]^{2+}$ is an example. The shift difference between *cis* and *trans* ammine protons is not observed. The single peak lies slightly upfields relative to the hexammine complex. In trifluoroacetic acid, it also shows a single peak. Category C; the spectrum of cyanopentammine complex belongs to this group. The spectrum pattern is reversed in that the major peak is situated at higher field than the minor one.

The PMR data are summarized in Table 1. Note

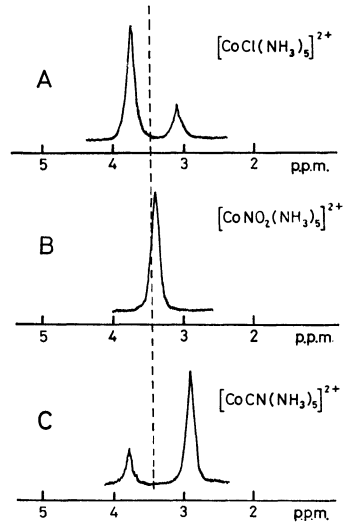

Fig. 1. Three types of PMR spectra for pentammine cobalt(III) complexes. Shift values are relative to DSS internal standard.

* On leave from Wakayama University.

TABLE 1. CHEMICAL SHIFTS (in Hz) OBSERVED FOR PENTAMMINE COBALT(III) COMPLEXES IN DIMETHYLSULFOXIDE SOLUTION

Measurements have been made at 60 MHz with DSS internal standard.

X	*trans* NH_3	*cis* NH_3
CN^-	227	174
NO_2^-	205 (singlet)	
H_2O	173	240
OH^-	175	220
Cl^-	186	222
Br^-	185	~224
HCO_2^-	a)	230
$CH_3CO_2^-$	a)	227
$CH_2ClCO_2^-$	169	232
$CHCl_2CO_2^-$	173	235
$CCl_3CO_2^-$	174	238
NO_3^-	a)	240
$[Co(NH_3)_6]^{3+}$	207	

a) Overlapped with the methyl signal of dimethylsulfoxide.

that all X's in $[CoX(NH_3)_5]$ of Category A are observed to lie lower in the spectrochemical series than NH_3. Further, the lower in the spectrochemical series the ligand X lies, the greater the shift difference between *cis* and *trans* ammine protons. In $[Co(CN)(NH_3)_5]^{2+}$ of Category C, CN^- is a representative of strong-field ligands and lies highest in the spectrochemical series.

The Model

We assume that three protons of each ammine group are situated at an average position, *i.e.*, at one of the points indicated by open circles in Fig. 2. Figure 2 defines the coordinate axes x, y, and z for complexes $[CoX(NH_3)_5]$. Chemical shift of specific ammine protons of a complex in solution is characterized by

$$\sigma = \frac{1}{3}(\sigma_{xx}+\sigma_{yy}+\sigma_{zz}). \quad (1)$$

Here, σ_{xx}, σ_{yy}, and σ_{zz} are the shielding constants for protons of interest when the magnetic field is applied along the x, y, and z axes, respectively, defined in Fig. 2. These constants consist of two contributions, namely the so-called paramagnetic and diamagnetic terms. It can be shown,[5] however, that diamagnetic terms are at least two orders of magnitude smaller than paramagnetic ones. Thus, we attribute the chemical shift behavior in pentammine cobalt complexes to the paramagnetic shielding constant, σ^P.

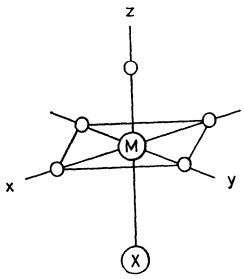

Fig. 2. The definition of the frame of reference for $[CoX(NH_3)_5]$-type complexes. Open circles are assumed to represent the position of ammine protons.

Calculation of the paramagnetic shielding constant for complexes of C_{4v} symmetry has been made by Buckingham and Stephens.[6] They have discussed the PMR spectra of hydride complexes of cobalt and iron. We will follow their procedure. They have modified Ramsay's formula for chemical shift of protons in C_{4v} cobalt complex to the form

$$\sigma^P_{xx} = -\frac{e^2}{2m^2c^2}\frac{1}{E_E-E_{A1}}[\langle {}^1A_1|\sum_j L_{xj}|{}^1E_x\rangle\langle {}^1E_x|\sum_k L_{xk}/r_k^3|{}^1A_1\rangle + \langle {}^1A_1|\sum_k L_{xk}/r_k^3|{}^1E_x\rangle\langle {}^1E_x|\sum_j L_{xj}|{}^1A_1\rangle], \quad (2)$$

and

$$\sigma^P_{zz} = -\frac{e^2}{2m^2c^2}\frac{1}{E_{A2}-E_{A1}}[\langle {}^1A_1|\sum_j L_{zj}|{}^1A_2\rangle\langle {}^1A_2|\sum_k L_{zk}/r_k^3|{}^1A_1\rangle + \langle {}^1A_1|\sum_k L_{zk}/r_k^3|{}^1A_2\rangle\langle {}^1A_2|\sum_j L_{zj}|{}^1A_1\rangle]. \quad (3)$$

We have retained paramagnetic terms only. In the above, $|{}^1A_1\rangle$, and $|{}^1A_2\rangle$ and $|{}^1E_x\rangle$ are the ground and the excited states of the central cobalt(III) ion and E_{A1}, E_{A2}, and E_E are the corresponding energies, respectively (see Fig. 3). L_{xj} and L_{zj} are the x and z components of orbital angular momentum operator for j-th electron of cobalt ion. The distance from protons in question to k-th electron is denoted by r_k. The summation is over all 3d electrons of cobalt. Operators subscripted with M and H are on the metal and proton centers, respectively.

Figure 3 shows the ground and the low-lying excited states of Co(III) ion under C_{4v} symmetry. Wave functions associated with these levels are given in Table 2. $|{}^1E_x\rangle$ and $|{}^1E_y\rangle$ are degenerate. To a first approximation, we neglect hybridization of 3d with 4s and 4p orbitals and covalency with ligand orbitals.

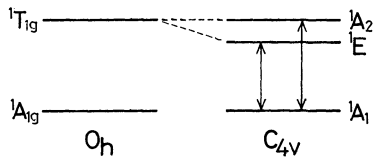

Fig. 3. The ground and the low-lying excited states of Co(III) ion under crystal fields of O_h and C_{4v} symmetries.

TABLE 2. WAVEFUNCTIONS ASSOCIATED WITH THE GROUND AND THE LOW-LYING EXCITED STATES OF Co(III) ION UNDER C_{4v} CRYSTAL FIELD

Superscripts 2, and + and − refer to the fully occupied orbital and orbitals with up and down spins, respectively.

$\|{}^1A_1\rangle$	$\|d_{yz}^2 d_{zx}^2 d_{xy}^2\|$
$\|{}^1A_2\rangle$	$\frac{1}{\sqrt{2}}[\|d_{yz}^2 d_{zx}^2 d_{xy}^+ d_{x^2-y^2}^-\| - \|d_{yz}^2 d_{zx}^2 d_{xy}^- d_{x^2-y^2}^+\|]$
$\|{}^1E_x\rangle$	$\frac{1}{\sqrt{2}}[\|d_{yz}^+ d_{y^2-z^2}^- d_{zx}^2 d_{xy}^2\| - \|d_{yz}^- d_{y^2-z^2}^+ d_{zx}^2 d_{xy}^2\|]$
$\|{}^1E_y\rangle$	$\frac{1}{\sqrt{2}}[\|d_{yz}^2 d_{zx}^+ d_{z^2-x^2}^- d_{xy}^2\| - \|d_{yz}^2 d_{zx}^- d_{z^2-x^2}^+ d_{xy}^2\|]$

Further, contributions can be shown small to be neglected from levels into which T_{2g} state in O_h symmetry is split under the influence of the crystal field of C_{4v} symmetry. Under these simplifying assumptions, calculation of Eqs. (2) and (3) renders Eqs. (4) and (5) for *cis* and *trans* ammine protons, respectively.

$$\sigma_C^P = \frac{1}{3}(\sigma_{xx}^P+\sigma_{yy}^P+\sigma_{zz}^P) = \frac{4e^2\hbar^2}{3m^2c^2}\frac{1}{R^3}\left(\frac{1}{E_{A2}-E_{A1}}-\frac{1}{E_E-E_{A1}}\right). \quad (4)$$

$$\sigma_T^P = \frac{1}{3}(2\sigma_{xx}^P+\sigma_{zz}^P) = \frac{8e^2\hbar^2}{3m^2c^2}\frac{1}{R^3}\left(\frac{1}{E_E-E_{A1}}-\frac{1}{E_{A2}-E_{A1}}\right). \quad (5)$$

Quantities subscripted with C and T refer to *cis* and *trans*, respectively. R is the distance between the protons of interest and the cobalt nucleus. If R and excitation energies are measured in units of a.u. and cm^{-1}, $\sigma_C{}^P$ and $\sigma_T{}^P$ are expressed as dimensionless quantities.

$$\sigma_C^P = \frac{4}{3}\times 11.7\frac{1}{R^3}\left(\frac{1}{E_{A2}-E_{A1}}-\frac{1}{E_E-E_{A1}}\right). \quad (6)$$

$$\sigma_T^P = \frac{8}{3}\times 11.7\frac{1}{R^3}\left(\frac{1}{E_E-E_{A1}}-\frac{1}{E_{A2}-E_{A1}}\right). \quad (7)$$

The above result may be visualized in the following way (see Fig. 4).

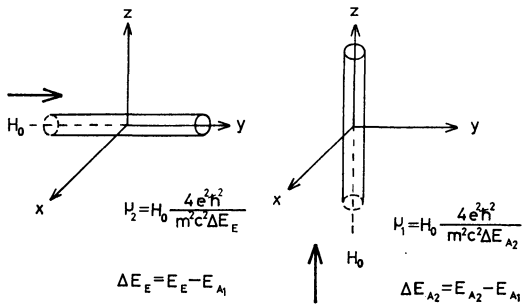

Fig. 4. The schematic presentation of induced paramagnetic moments. All notations have their usual singnificance.

On applying the magnetic field along the, say, x direction, magnetic moment will be induced. This induced moment, μ_2, is known as second-order paramagnetism and in magnetism as temperature-independent paramagnetism or the highfrequency term. This is given by

$$\mu_2 = H_0\frac{4e^2\hbar^2}{m^2c^2}\frac{1}{E_E-E_{A1}}. \quad (8)$$

Induced moments when the magnetic field is applied along the y and z directions are depicted in Fig. 4. These induced moments will be sensed by protons of interest as dipolar fields. Summing up over these dipolar fields, the same result as in Eqs. (6) and (7) is obtained. These reasoning is equivalent to regarding the shift as caused by the anisotropy in paramagnetic moment of Co(III) ion.

Comparison with Experiment

We first note that the energy E_E changes upon substitution of X, while the energy E_{A_2} is unaffected by substitution because the latter energy corresponds to the transition from d_{xy} to $d_{x^2-y^2}$. The ordering of the ligand field levels is determined, from spectroscopic and spectrophotometric studies,[7] as $E_E<E_{A_2}$ except for strong-field ligands such as CN^- and NO_2^-, for which the ordering is reversed. Therefore, σ_C^P is generally positive and σ_T^P is negative, which means that *trans* ammine protons are shifted to high fields and *cis* protons to low fields (from the shift of hexammine cobalt(III) ion). This corresponds to the case of Category A. Further, the weaker spectrochemically the ligand X is, we can expect the smaller E_E, and hence, the bigger shift difference between *cis* and *trans* protons. This trend is consistent with experimental results already mentioned. In contrast, when X is a strong-field ligand, *e.g.*, $X=CN^-$, we can expect the shift pattern reversed to that in Category A, as has the case really been observed. So far so good.

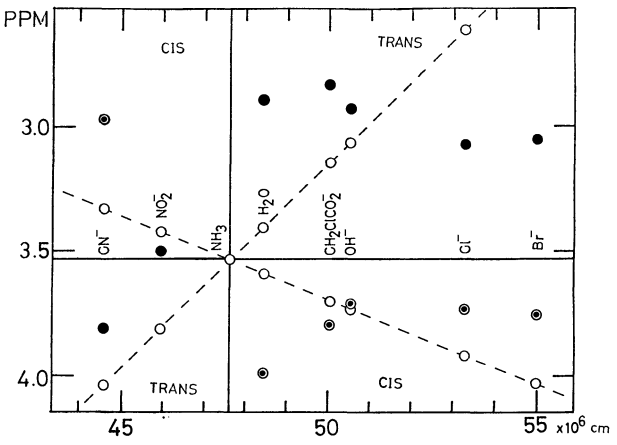

Fig. 5. Comparison of the calculated shift values (○) with observed values (⊙ and ●). Shift values are from DSS internal standard and the abscissa is the reciprocal of the excitation energy E_E-E_{A1}.

If we examine more closely the correlation between the experimental results and Eqs. (6) and (7), agreement is not so satisfactory. Setting $R=5.7$ a.u.[8] and using reported values for excitation energies,[9] we can plot the calculated shift values against the reciprocal of the energy difference E_E-E_{A1}. Figure 5 shows the comparison of the calculated and the observed shift values. As seen in Fig. 5, shift patterns of Categories A, B, and C appear to be roughly explained. It seems difficult to explain by using only metal 3d orbitals that the complex with $X=NO_2^-$ goes into Category B.

The model used in this work is applicable also to the interpretation of the PMR spectra of *cis*-$[CoX_2(NH_3)_4]$ and *cis*-$[CoX_2(en)_2]$. For these complexes, *trans* (to ligand X) ammine or NH_2 protons and *cis* protons have the same intensity. The assignment is therefore not straightforward. We assume, after Yamatera,[10] that three electronic transitions comprising the first absorption band are approximated, irrespective of the symmetry of the complex in question, by the following transitions under O_h symmetry.

$$d_{xy}\rightarrow d_{x^2-y^2},\ \frac{1}{2}\delta+\Delta \quad (9)$$

$$d_{yz} \rightarrow d_{y'z'},\ \frac{1}{4}\delta+\Delta \quad (10)$$

$$d_{zx} \rightarrow d_{z'x'},\ \frac{1}{4}\delta+\Delta \quad (11)$$

To the right are given the corresponding transition energies.

δ is the splitting factor defined by Yamatera and Δ the transition energy of the first absorption band in $[Co(NH_3)_6]^{3+}$ or $[Co(en)_3]^{3+}$ [11] as the case may be. Substitution of these energies into Eqs. (4) and (5) yields

$$\sigma^P(5,6) = -2\left(\frac{4e^2\hbar^2}{3m^2c^2}\frac{1}{R^3}\right)\left(\frac{1}{\Delta+\delta/2}-\frac{1}{\Delta+\delta/4}\right), \quad (12)$$

$$\sigma^P(2,3) = +\left(\frac{4e^2\hbar^2}{3m^2c^2}\frac{1}{R^3}\right)\left(\frac{1}{\Delta+\delta/2}-\frac{1}{\Delta+\delta/4}\right). \quad (13)$$

Shielding constants $\sigma^P(5,6)$ and $\sigma^P(2,3)$ are for *cis* and *trans* NH_3 or NH_2 protons, respectively. For complexes with weak-field ligand X, δ is negative by definition, rendering $\sigma^P(5,6)$ negative and $\sigma^P(2,3)$ positive. Therefore, we can expect, except for strong-field ligands, that 5- and 6-protons are shifted to low fields and 2- and 3-protons to high fields. For strong-field ligands, such as X=CN⁻, the situation may be the reverse of the above.

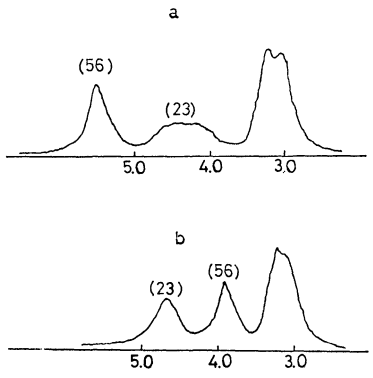

Fig. 6. The PMR spectra of (a) $[CoCl_2(en)_2]^+$ and (b) $[Co(CN)_2(en)_2]^+$ in trifluoroacetic acid. Shift values are from an internal standard of tetramethylsilane. Numbers in parentheses represent the proposed assignments (see text).

Let us illustrate how this result works in actual cases. Figure 6 depicts the PMR spectra of *cis*-$[CoCl_2(en)_2]^+$ and *cis*-$[Co(CN)_2(en)_2]^+$ in trifluoroacetic acid. Chloride ion is a representative of weak-field ligands. Thus, the broader peak situated around 4.4 ppm is assigned as *trans* NH_2 protons and the lowest-field peak as *cis* NH_2. Since CN^- is strong-field ligand, the assignment given in Fig. 6-b will hold.

Conclusion

The PMR spectra of pentammine cobalt(III) complexes can be explained primarily by the paramagnetic anisotropy of the central cobalt(III) ion. The results derived in this work may be summarized as the following rules (see Fig. 7).

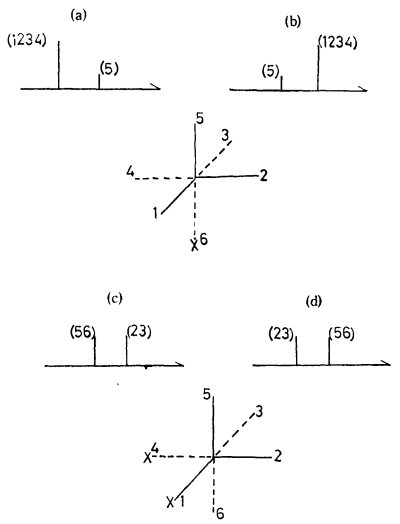

Fig. 7. The predicted behavior of the PMR spectra for $[CoX(NH_3)_5]$ and *cis*-$[CoX_2(NH_3)_4]$ or *cis*-$[CoX_2(en)_2]$. (a) and (b) are for pentammine complexes with weak- and strong-field ligands, respectively. (c) and (d) are for the *cis*-type complexes with weak- and strong-field ligands, respectively.

For $[CoX(NH_3)_5]$;

(1) If X is spectrochemically lower than NH_3, ammine protons *trans* to X appear at high fields (Fig. 7-a).

(2) If X is a strong-field ligand, the reverse is expected (Fig. 7-b).

For *cis*-$[CoX_2(NH_3)_4]$ or *cis*-$[CoX_2(en)_2]$;

(1) If X is a weak-field ligand, the high-field peak is due to 2- and 3-protons (Fig. 7-c).

(2) If X is strong, protons situated at 5- and 6-positions will appear at higher field (Fig. 7-d).

This work was supported in part by a Grant for Scientific Research by the Ministry of Education.

References

1) P. Cliffton and L. Pratt, *Proc. Chem. Soc.*, **1963**, 339.
2) W. L. Jolly, A. D. Harris, and T. S. Briggs, *Inorg. Chem.*, **4**, 1064 (1965).
3) D. N. Hendrickson and W. L. Jolly, *ibid.*, **9**, 1197 (1970).
4) See, for example, F. Basolo, and R. K. Murmann, "Inorganic Syntheses," Vol. 4, p. 171 (1953).
5) H. Yoneda and Y. Nakashima, to be published.
6) A. D. Buckingham and P. J. Stephens, *J. Chem. Soc.*, **1964**, 2747.
7) See, for example, "Mukikagaku-zensho," Vol. XV-2, ed. by K. Yamasaki and S. Inoue, Maruzen, Tokyo (1959), p. 264.
8) This value has been selected by assuming the Co–N and H–H distances of 2.0 and 1.43 Å,[7] respectively.
9) M. Shibata, M. Mori, and E. Kyuno, *Inorg. Chem.*, **3**, 1573 (1964). See, also, Ref. 7 and references cited therein.
10) H. Yamatera, This Bulletin, **31**, 95 (1958).
11) See, *e.g.*, Ref. 7.

The Cyclopolymerization of Triallyl Citrate

Akira MATSUMOTO, Tetsuji OHATA, and Masayoshi OIWA

Department of Applied Chemistry, Faculty of Engineering, Kansai University, Senriyama, Suita, Osaka 564

(Received June 12, 1973)

The radical polymerization of triallyl citrate was carried out at 60 °C, benzoyl peroxide being used as the initiator and benzene as the solvent; here it has been considered kinetically in terms of cyclopolymerization. Thus, the kinetic equations for the polymerization of the triallyl ester were first derived by an extension of the kinetic treatment for the cyclopolymerization of the diallyl ester. Next, they were applied to the polymerization of triallyl citrate. In consequence, the following results were obtained: (i) the rate of polymerization, R_p, was not proportional to either the square root or first power of the initiator concentration, [I]; rather, $R_p/[I]^{1/2}$ and $[I]^{1/2}$ had a linear relationship, (ii) the relation between the rate of polymerization over the degree of polymerization, $R_p/\bar{P}_{n,o}$, and the monomer concentration, [M], was also linear, and (iii) the ratio of the unimolecular cyclization reaction to the bimolecular propagation reaction of the uncyclized radical, K_c, was estimated to be 4.5 mol/l from the dependence of the residual unsaturation on the monomer concentration.

In our previous papers,[1-4] the polymerizations of various diallyl esters of dicarboxylic acids have been kinetically discussed in detail in terms of cyclopolymerization and allyl polymerization, including the degradative chain transfer[5] characteristic of allyl compounds.

The present paper will be concerned with the polymerization kinetics of triallyl citrate; the kinetic treatment for the polymerization of the diallyl ester involving the intramolecular cyclization reaction is developed for application and the radical polymerization results are discussed in detail.

Experimental

Materials. The triallyl citrate was prepared by the esterification of citric acid with allyl alcohol according to the literature[6]; bp 130 °C/0.005 mmHg, d_4^{20} 1.135 (lit. bp 207—208 °C/12 mmHg, d_4^{17} 1.1358). The purity of triallyl citrate was confirmed further by spectral and chemical analyses.

The benzoyl peroxide (BPO) was purified by repeated precipitations from a chloroform solution with methanol.

The benzene was distilled over metallic sodium after purification by the usual method.

Polymerization Procedure. Measured amounts of triallyl citrate, BPO, and benzene were placed in a glass ampoule (10—50 ml capacity), which was then evacuated under reduced pressure and flushed with nitrogen. The ampoule was then sealed under a vacuum and put into a thermostat regulated at 60±0.1 °C.

After a definite reaction time, the polymer thus produced was precipitated by pouring the reaction mixture into more than a tenfold volume of cooled petroleum ether. The polymer thus obtained was then washed repeatedly with petroleum ether and dried *in vacuo* until a constant weight was obtained. The percentage conversion was calculated from the weight of the polymer isolated. The polymer was then purified by dissolving it in acetone and by subsequent reprecipiation with petroleum ether.

Analyses of the Polymer. The unreacted pendant allyl groups of the purified polymer were determined by the method of Simpson *et al.*[7] The polymer was dissolved in methanol and saponified in excess potassium hydroxide, and then the free allyl alcohol was determined by the bromide–bromate technique. The residual unsaturation of the polymer was then expressed as percentages of the corresponding pure triallyl citrate.

The number-average molecular weight of the polymer was measured with a Hewlett-Packard 302 vapor pressure osmometer in acetone at 37 °C.

Results and Discussion

Kinetics. The polymerization mechanism of triallyl citrate must be virtually equivalent to that of the diallyl ester.[1] Thus, the following reaction scheme can be presented for the polymerization of triallyl citrate; in the scheme it is assumed that the three allyl groups of triallyl citrate behave equivalently and that the possibility of a bicyclo-intramolecular propagation[8] accompanying the formation of a bicyclic ring is negligible, as will be discussed later.

Decomposition: $I \longrightarrow 2R\cdot$	$2k_d[I]$
Initiation: $R\cdot + M \longrightarrow M\cdot$	$3k_i[R\cdot][M]$
Cyclization: $M\cdot \longrightarrow M_c\cdot$	$2k_c[M\cdot]$
Propagation: $M\cdot + M \longrightarrow M\cdot$	$3k_p[M\cdot][M]$
$M_c\cdot + M \longrightarrow M\cdot$	$3k_{cp}[M_c\cdot][M]$
Chain transfer: $M\cdot + M \longrightarrow P + M\cdot *$	$3k_{t1}[M\cdot][M]$
$M_c\cdot + M \longrightarrow P + M\cdot *$	$3k_{t2}[M_c\cdot][M]$
Re-initiation: $M\cdot * + M \longrightarrow M\cdot$	$3k_i'[M\cdot *][M]$
Stabilization: $M\cdot * + M\cdot * \longrightarrow M*\text{–}M*$	$k_{t3}[M\cdot *]^2$

where I denotes an initiator; M, a triallyl citrate monomer; P, the polymer; R·, the initiator radical; M·, the initial radical derived from the attack of a radical on M (the uncyclized radical); $M_c\cdot$, the radical formed by the intramolecular cyclization of M· (the cyclized radical), and M·*, the radical derived from the abstraction of an allylic hydrogen of M by the growing polymer chain (the degraded radical).

If a steady state is assumed for the different types of radicals, Eqs. (1)—(4) can be obtained:

$$[R\cdot] = 2fk_d[I]/3k_i[M] \tag{1}$$

$$[M\cdot] = \frac{2fk_d[I] + 3k_i'(2fk_d[I]/k_{t3})^{1/2}[M]}{3k_{t1}[M] + 2k_ck_{t2}/(k_{cp}+k_{t2})} \tag{2}$$

$$[M_c\cdot] = \frac{\{2k_c/3(k_{cp}+k_{t2})[M]\}\{2fk_d[I] + 3k_i'(2fk_d[I]/k_{t3})^{1/2}(M)\}}{3k_{t1}[M] + 2k_ck_{t2}/(k_{cp}+k_{t2})} \tag{3}$$

$$[M\cdot *] = (2fk_d[I]/k_{t3})^{1/2} \tag{4}$$

where f denotes the efficiency of the initiation of chain radicals by R·.

In previous papers on the polymerization of diallyl esters,[1-3] the kinetic equations were derived for two cases. In one case, where the loss of a monomer by initiation, chain termination, and re-initiation reaction is not negligible compared with that by the propagation, the kinetic chain length is small. In the other case, where the propagation reaction is predominant, the kinetic chain length is quite large and the simplified kinetic equations can, therefore, be used instead of the elaborate ones. In the polymerization of triallyl citrate investigated in this paper, the degree of polymerization was quite large, as can be seen in Table 2: therefore, the polymerization of triallyl citrate is of the latter type, as for the diallyl esters of aliphatic dicarboxylic acids.[2,3]

Thus, the rate of polymerization is given by:

$$\begin{aligned} R_p &= 3k_p[M\cdot][M] + 3k_{cp}[M_c\cdot][M] \\ &= \{2fk_d[I] + 3k_i'(2fk_d[I]/k_{t3})^{1/2}[M]\} \\ &\quad \times \left\{ \frac{3k_p[M] + 2k_ck_{cp}/(k_{cp}+k_{t2})}{3k_{t1}[M] + 2k_ck_{t2}/(k_{cp}+k_{t2})} \right\} \end{aligned} \quad (5)$$

The initial degree of polymerization is also given by:

$$\begin{aligned} \bar{P}_{n,o} &= R_p/(3k_{t1}[M\cdot][M] + 3k_{t2}[M_c\cdot][M]) \\ &= \frac{3k_p[M] + 2k_ck_{cp}/(k_{cp}+k_{t2})}{3k_{t1}[M] + 2k_ck_{t2}/(k_{cp}+k_{t2})} \end{aligned} \quad (6)$$

The combination of Eqs. (5) and (6) gives:

$$R_p/\bar{P}_{n,o} = 2fk_d[I] + 3k_i'(2fk_d[I]/k_{t3})^{1/2}[M] \quad (7)$$

On the other hand, the rate of the formation of the pendant unreacted allyl groups in the polymer is given by:

$$d[allyl]/dt = 6k_p[M\cdot][M] + 3(1-\alpha)k_{cp}[M_c\cdot][M] \quad (8)$$

where α denotes the ratio of the non-consecutive cyclization as seen in the polymerization of diallyl terephthalate[4] to the consecutive intramolecular cyclization in the same monomer unit.

Equation (8) is true in the absence of crosslinking reactions, since these reactions will consume the pendant unreacted allyl groups in the polymer. However, in the early stage of polymerization, the loss of allyl groups by the crosslinking reaction should be small compared with that during propagation.

By using Eqs. (2) and (3), we obtain:

$$\begin{aligned} d(allyl)/dt &= \{2fk_d[I] + 3k_i'(2fk_d[I]/k_{t3})^{1/2}[M]\} \\ &\quad \times \left\{ \frac{6k_p[M] + 2(1-\alpha)k_ck_{cp}/(k_{cp}+k_{t2})}{3k_{t1}[M] + 2k_ck_{t2}/(k_{cp}+k_{t2})} \right\} \end{aligned} \quad (9)$$

Equatins (5) and (9) give:

$$\begin{aligned} -\frac{d[allyl]}{d[M]} &= 3R_{us} \\ &= \frac{6k_p[M] + 2(1-\alpha)k_ck_{cp}/(k_{cp}+k_{t2})}{3k_p[M] + 2k_ck_{cp}/(k_{cp}+k_{t2})} \end{aligned} \quad (10)$$

where R_{us} denotes the degree of unsaturation of the polymer.

From Eq. (10) we obtain:

$$(3R_{us})_{M\to 0} = 1 - \alpha \quad (11)$$

On the other hand, the rearrangement of Eq. (10) gives:

$$(2-3R_{us})^{-1} = \frac{1}{1+\alpha} + \frac{3(1+x)}{2(1+\alpha)} \cdot \frac{1}{K_c}[M] \quad (12)$$

where $x = k_{t2}/k_{cp} = (\bar{P}_{n,o})^{-1}_{M\to 0}$, $K_c = k_c/k_p$.

Polymerization Results. The bulk polymerization of triallyl citrate was investigated under different initiator concentrations at 60 °C; the initial rates of polymerization as calculated from the slope of the straight lines of the time-conversion curves, are summarized in Table 1; they are proportional neither to the square root nor to the first power of the initiator concentration, as was observed in the polymerization of diallyl esters.[1-4]

Table 1. Relation between the rate of polymerization and initiator concentration in the bulk polymerization of triallyl citrate at 60 °C

[I] (mol/l)	$R_p \times 10^5$ (mol/l·s^{-1})	$(R_p/[I]^{1/2}) \times 10^4$ (mol/l·s^{-2})$^{1/2}$	$(R_p/[I]) \times 10^3$ (s^{-1})
0.01	1.39	1.39	1.39
0.02	2.31	1.63	1.16
0.04	3.42	1.71	0.86
0.10	8.24	2.61	0.82

Table 2. Polymerization of triallyl citrate (60 °C, [BPO] = 0.02 mol/l, Solvent; benzene)

[M] (mol/l)	$R_p \times 10^5$ (mol/l·s^{-1})	$\bar{P}_{n,o}$	R_{us}
3.63	2.33	—	0.500
2.42	1.20	58.9	0.465
1.82	0.74	52.3	0.435
1.21	0.45	44.2	0.405
0.73	0.25	36.5	0.362
0.40	0.13	29.5	0.327

On the other hand, the influence of the monomer concentration on the rate of polymerization, the residual unsaturation, and the degree of polymerization was also examined at a constant initiator concentration at 60 °C. The results obtained are given in Table 2.

Figure 1 shows the relation between the residual unsaturation, R_{us}, and the monomer concentration; R_{us} tends to decrease with a decrease in the monomer con-

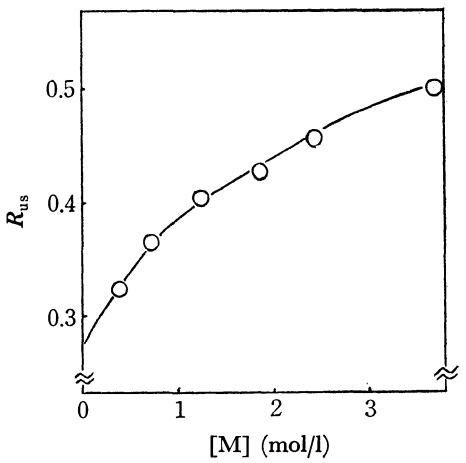

Fig. 1. Dependence of R_{us} on monomer concentration.

centration, and it reaches 0.284 by the extrapolation of the monomer concentration to zero. Thus, α is estimated from Eq. (11) to be 0.148.

Now, it should be noted that R_{us} must be 0.667 if neither cyclization nor crosslinking reaction occurs; conversely, it reaches zero in an infinitely diluted solution if the bicyclo-intramolecular cyclization reaction occurs completely. On the other hand, in the absence of the bicyclo-intramolecular cyclization, R_{us} approaches 0.333, assuming that the intramolecular cyclization reaction occurs only in the same monomer unit. Consequently, the result obtained above, *i.e.*, $(R_{us})_{M\to 0}=$ 0.284, may be understood by considering the absence of the bicyclo-intramolecular cyclization and the occurrence of the non-consecutive intramolecular addition reaction, as was observed in the polymerization of diallyl terephthalate.[4,9,10]

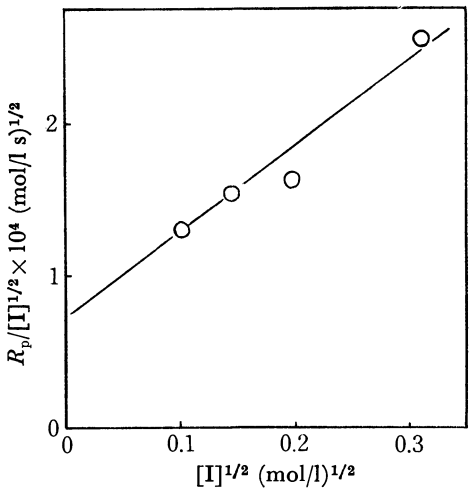

Fig. 2. Relationship between $R_p/[I]^{1/2}$ and $[I]^{1/2}$ based on Eq. (6).

Kinetic Evaluation. Figure 2 shows the relation between $R_p/[I]^{1/2}$ and $[I]^{1/2}$ based on the data of Table 1; there is a fairly good linear relationship, as can be expected from Eq. (5). Similarly, if the initiator concentration is kept constant and the monomer concentration is varied, a linear relationship between $R_p/\bar{P}_{n,o}$ and [M] can be expected from Eq. (7) (See Fig. 3). These results seem to demonstrate the validity

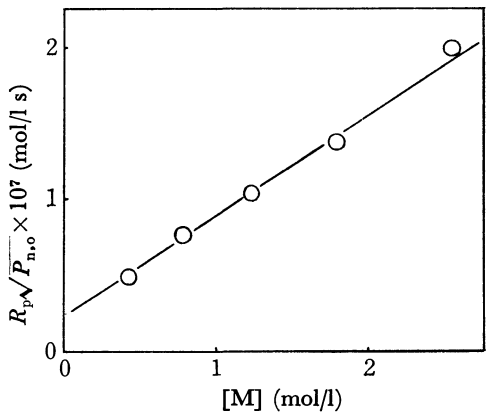

Fig. 3. Relationship between $R_p\sqrt{\bar{P}_{n,o}}$ and [M] based on Eq. (9).

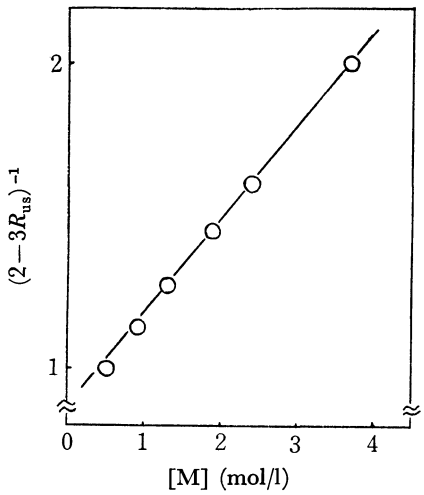

Fig. 4. Evaluation of K_c based on Eq. (14).

of the kinetics discussed in the previous section.

On the other hand, the ratio of the unimolecular cyclization reaction to that of the bimolecular propagation reaction of the uncyclized radical, K_c, can be obtained from the dependence of the residual unsaturation on the monomer concentration by employing Eq. (12), since, in the early stage of polymerization, the crosslinking reaction is negligible and the deviation of R_{us} from 0.667 can predominantly be attributed to the intramolecular cyclization reaction. Figure 4 shows the plot of $(2-3R_{us})^{-1}$ *vs.* [M]; there is a good linear relationship, and K_c was estimated to be 4.5 mol/l from the slope of the straight line. K_c is a critical factor determining the microstructure of the polymer; the monomer concentration required for obtaining the polymer carrying 50% of the cyclic recurring unit is 3.0 mol/l, which corresponds to around a 82.5% dilution of the pure monomer.

Now, it should be noted that the values of K_c for diallyl phthalate and diallyl succinate, which are considered to be diallyl esters structurally corresponding to triallyl citrate, are 7.5 mol/l[1] and 2.8 mol/l[3] respectively, in which the free rotation between the two ester groups is possible in diallyl succinate, whereas in diallyl phthalate it is impossible. Thus, the fact that the value of the K_c of triallyl citrate is intermediary between those of diallyl phthalate and diallyl succinate suggests a limited rotation among the three ester groups; we may imagine the structural feature of triallyl citrate to be that the three allyl groups are symmetrical about the hydroxide group. From such a standpoint, the equivalency of the three allyl groups of triallyl citrate mentioned above can also be understood.

References

1) A. Matsumoto, K. Asano, and M. Oiwa, *Nippon Kagaku Zasshi*, **90**, 290 (1969).

2) A. Matsumoto, K. Takashima, and M. Oiwa, This Bulletin, **42**, 1959 (1969).

3) A. Matsumoto and M. Oiwa, *J. Polym. Sci., Part A-1*, **8**, 751 (1970).

4) A. Matsumoto and M. Oiwa, *Nippon Kagaku Zasshi*, **90**, 1278 (1969).

5) P. D. Bartlett and R. Altschul, *J. Amer. Chem. Soc.*, **67**, 812 (1945).
6) V. Avwes and Moosbrugger, *Ann. Chem.*, **387**, 199 (1912).
7) W. Simpson, T. Holt, and R. J. Zetie, *J. Polym. Sci.*, **10**, 489 (1953).
8) D. S. Trifan and J. J. Hoglen, *J. Amer. Chem. Soc.*, **83**, 2021 (1961).
9) A. Matsumoto, H. Sasaki, and M. Oiwa, *Nippon Kagaku Kaishi*, **1972**, 166.
10) A. Matsumoto, H. Sasaki, and M. Oiwa, *Makromol. Chem.*, **166**, 179 (1973).

Bromine Addition to Chloronorbornene Derivatives[1]

Yūji YANAGIDA, Hideo SHIGESATO, Masakatsu NOMURA, and Shōichi KIKKAWA

Department of Applied Chemistry, Faculty of Engineering, Osaka University, Yamadakami, Suita, Osaka 565

(Received July 6, 1973)

The reaction of bromine with both *trans*-5,6-dichloro-2-norbornene (I) and *exo-cis*-5,6-dichloro-2-norbornene (III) in an acetic acid solution gave *trans*-adducts in a 100% yield, while the bromination of *endo-cis*-5,6-dichloronorbornene (II) afforded the *exo-cis* adduct in a *ca.* 100% yield. The latter observation was explained in terms of a sterical inhibition of the bromide ion's attack in the *endo*-direction by the two *endo*-chloro substituents. In the CCl_4 solution, however the reaction of I with bromine afforded the *exo-cis* adduct in a 64% yield, together with the *trans*-adduct (36% yield). Then, the reaction of I with bromine was carried out in several other solvents (CH_3OH, $Cl(CH_2)_2Cl$, $CH_3CO_2C_2H_5$, and CCl_4). As the polarity of the solvents (the E_T values are used here as a measure of the solvents' polarity) decreased, the formation of the *exo-cis* adduct became progressively more predominant, while the addition of bromide salt retarded the formation of the *exo-cis* adduct. Such results and the kinetic studies suggested that the *exo-cis* adduct was formed through the carbonium bromide ion-pair mechanism. The stereoisomers obtained in this study were assigned on the basis of the NMR spectra.

The authors have found, in a previous investigation,[2] that, under mild conditions, (in an acetic acid solution) favoring the polar mechanism rather than the free radical mechanism, the addition of bromine to *trans*-5,6-dicyano-2-norbornene gave the *exo-cis* adduct in a 24% yield, along with the *trans* adduct in a 76% yield. Such a formation of the *exo-cis* adduct could not be interpreted only in terms of the steric effects of cyano-substituents. In order to obtain further information on the nature of substituent effect on the *exo-cis* formation, we undertook a study of the addition of bromine to *trans*-5,6-dichloro-2-norbornene(I), *endo-cis*-5,6-dichloronorbornene(II), and *exo-cis*-5,6-dichloronorbornene(III). The chlorine atom was chosen as a substituent because of its similarity in steric environment[3] to the cyano group, but it has less inductive effect than that of the cyano group.

Experimental[4]

Starting Materials. The starting chlorides I and II. were prepared according to the procedure of Roberts[5] and were comfirmed to be the desired *trans-endo, exo*-5,6-dichloronorbornene (I) and *cis-endo*-5,6-dichloronorbornene (II) on the basis of the NMR spectral data. Their purities were above 99%, as determined by means of glc analysis. (I), mp 79—80 °C (from *n*-Hexane); yield, 11% (Found; C, 51.05; H, 5.03%). (II), bp 72.5—73 °C/15 mmHg; yield, 74% (Found; C, 51.33; H, 5.03%).

cis-exo-5,6-Dichloronorbornene was also isolated from the reaction mixture of cyclopentadiene with *cis*-dichloroethylene, along with I, in a yield of about 0.3% (bp 88 °C/20 mmHg); its identity was confirmed on the basis of NMR datum and elementary analysis (Found C, 51.56; H, 4.93%. Calcd C, 51.56; H, 4.95%), while glc analysis showed some (ca. 3%) contamination with the *endo*-isomer.

Bromination and Kinetic Study. The bromine addition reactions were carried out in the usual way in solutions of CCl_4, $CH_3CO_2C_2H_5$, CH_3CO_2H, $Cl(CH_2)_2Cl$, and CH_3OH. The addition products were isolated, according to their situation, by means of recrystallization (A), vacuum distillation (B) and preparative gas chromatography (C).[6]

The rate of addition was determined by the titration method described in the previous paper[2].

Results and Discussion

The brominations of the substrates, I, II, and III, in acetic acid were stereospecific, giving the *trans* adduct, the *exo-cis* adduct, and the *trans* adduct respectively. The stereochemistry of the addition products was confirmed on the basis of the NMR spectra. The results of microanalysis and the assignments of the NMR spectra of the adducts obtained in this investigation are listed in Tables 1 and 2 respectively.

Table 1. Results of micro analysis of adducts

Adducts	Bp or Mp	C%		H%	
		Calcd	Found	Calcd	Found
(I_t)	59—60 °C (C, A)[c] (*n*-hexane)	26.04	25.90	2.50	2.44
(I_c)[a]	57.5—58.5 °C (B)	26.04	26.14	2.50	2.43
(II_c)	164.5—165.5 °C (A) (cyclohexane)	26.04	26.14	2.50	2.49
(III_t)	83—85 °C/ 10^{-3} mmHg (C)	26.04	26.11	2.50	2.30
(I_m)[b]	(B)	35.07	35.01	4.05	4.16

a) The preparative gas chromatography of the reaction mixture of I with bromine in CCl_4 afforded the *exo-cis* adduct as a crystalline compound. b) The methoxy derivative was isolated as an oily product together with I_t by the preparative gas chromatography from the reaction mixture of I with bromine in methanol. Bp of the mixture of I_t and I_m was 60—75 °C/10^{-3} mmHg. c) Alphabet in brackets shows the preparative method described in Experimental part.

As to the orientation of bromine addition, the results for the substrates, I, II, and III, show an inclination to dicyanonorbornene derivatives similar to that described in the previous paper[2] except that the bromination of *endo*-2,*exo*-3-dicyanonorbornene gave *exo-cis* adduct in a 24% yield even in acetic acid, while the bromination of I gave stereospecifically the *trans* adduct (*ca.* 100% yield). Steric terms could not interpret the difference described above because the chlorine atom may be considered to have a bulkiness similar to that of the cyano group. Such results may presumably be explained in terms of the different inductive effects.

TABLE 2. NMR SPECTRAL DATA OF ADDUCTS[a)]

Adduct[g)]	H_2	H_3	H_1 and H_4	H_5	H_6	H_{7a}	H_{7b}
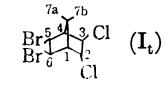 (I_t)	5.72 (6.31)	5.60 (6.14)	7.28[b)] (8.00)	5.50 (5.61)	5.50 (5.61)	7.78 (8.57)[c)]	
	$J_{2exo-1}=J_{5exo-4}=3.0$ Hz, $J_{2exo-3endo}=3.0$ Hz, $J_{7a-3endo}=2.0$ Hz						
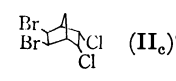 (II_c)[d)]	5.40 (6.66)	5.40 (6.66)	7.13 (7.77)	5.13 (5.43)	5.13 (5.43)	7.56 (9.50)	8.24 (—)
	$J_{2exo-1 \text{ and } 3exo-4}=2.8$ Hz, $J_{7b-5endo \text{ and } 6endo}=2.0$ Hz, $J_{7a-7b}=13.0$ Hz, $J_{5endo-6}=0$ Hz						
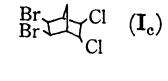 (I_c)	5.77 (6.50)	6.28 (7.06)	7.23 (7.81)	5.77 (6.74)	5.19 (5.68)	7.59 (7.99)	7.94 (8.67)
	$J_{5endo-6endo}=7.0$ Hz, $J_{7b-5endo \text{ and } 6endo}=1.8$ Hz, $J_{7a-7b}=11.7$ Hz, $J_{2exo-1}=4.5$ Hz						
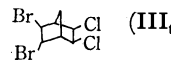 (III_t)	5.26 (5.70)	5.86 (6.79)	7.30 (7.90)	6.15 (6.92)	5.59 (6.29)	7.91 (8.64)	7.67 (8.06)
	$J_{2endo-3endo}=6.5$ Hz, $J_{6exo-1}=5.1$ Hz, $J_{7a-7b}=11.0$ Hz, $J_{5endo-6exo}=3.5$ Hz, $J_{7a-2endo \text{ and } 3endo}=1.8$ Hz, $J_{7b-5endo}=2.0$ Hz						
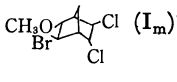 (I_m)[e),f)]	5.81 (6.12)	5.94 (6.33)	7.29 7.39 (7.79)	5.74	5.80	7.89	7.89
	$J_{2exo-3endo}=4.5$ Hz, $J_{6endo-7b}=1.8$ Hz, $J_{1-4}=0.8$ Hz, $J_{7a-3endo}=1.6$ Hz, $J_{5exo-4}=3.0$ Hz, $J_{5exo-6endo}=3.1$ Hz						

a) Chemical shifts are in ppm downfield from TMS (τ-units, in $CDCl_3$). b) Band width at half-height= 14 Hz. c) Chemical shifts in parentheses were measured in C_6H_6. This solvent was useful for separation of the overlapped signals. d) Measured in solution of $CDCl_3$ and $(CD_3)_2CO$ in the ratio of 1:1. e) Measured in solution in CCl_4. f) τ-Value for CH_3O was 6.57 ppm in CCl_4 solution. g) At first such numbering as shown in (I_t) were employed for convenience of stereochemical studies of bromine adducts. Stereochemistry of bromine atoms of adducts was elucidated by means of the magnitude of coupling constants between C_5 proton and C_6 proton and the presence of 4σ long range coupling between 7b proton and C_5 or C_6 *endo* proton (refer to assignments of lines in the previous paper[2)]). An example of the assignment of peaks in I_t is afforded here. The 100 MHz NMR spectrum of I_t shows two resonances equivalent to two protons at upfield positions. Based upon the discussion presented in the previous paper, the absorptions around τ 7.28 and 7.78 are assigned to the 1,4 protons and 7a, 7b protons, respectively. The absorptions around τ 5.72 and 5.60 exhibits a complicated AB pattern in which the upfield part is assigned to C_2 *exo* proton with great certainty compared with the chemical shift of C_2 *exo* proton in I_c. Spin decoupling experiments also revealed that the proton in I_t at τ 5.72 was coupled with the C_1 proton to the extent of 3 Hz, leading to the assignment of 3 Hz of the resulting doublet as the coupling between C_2 *exo* and C_3 *endo* protons. Irradiation of C_{7a} proton removes the 2.0 Hz coupling from the absorption at τ 5.60, confirming 2.0 Hz as a coupling of C_3 *endo* proton with C_{7a} proton. The complicated resonance at τ 5.50 is equivalent to two protons. The value of 5.0 Hz as band width at half-height may eliminate the presence of *cis* coupling between C_5 and C_6 protons. However, the presence of two stereoisomers would be possible with I_t adduct. This is the same with the *trans*-adduct I_t' of bromine to 5,6-dicyanonorbornene (I') obtained in the previous paper whose conformational assignment remained obscure. NMR spectra of these adducts (I_t and I_t') showed the formation of only one isomer of each two stereoisomers. With I_t', one of them, 5-*exo*,6-*endo*-dibromo, 2-*endo*, 3-*exo*-dicyanonorbornane which seemed to be least probable according to their intramolecular repulsion between C_6-*endo* bromine and C_2-*endo* cyano group, does not take place intramolecular lactonization on hydrolysis. Treatment of I_t' with 15% HBr solution under reflux conditions over a 30 min period, afforded a solid material which was recrystallized from hot 15% HBr solution. mp 228—230 °C. The IR spectrum (KBr disk) exhibited a strong absorption band at 1770 cm^{-1} (γ-lactone). The NMR spectrum (DMSO-d_6) gave signals at 5.34 (1H, C_{6exo}, $J_{6-exo-1}=4.8$ Hz), 5.33 (1H, C_{5exo}, $J_{5exo-4}=3.5$ Hz, $J_{6exo-5exo}=7.1$ Hz), suggesting this compound 3-*exo*-carboxy-5-*endo*-bromo-6-*endo*-hydroxybicyclo[2,2,1]heptane-2-*endo*-carboxylic acid lactone (Found: C, 40.85; H, 3.40; Br, 30.36%; Calcd: C, 41.40; H, 3.47; Br, 30.61%). As a chlorine atom is considered to have a bulkiness similar to that of cyano group from their van der Waals radii,[7)] I_t may be also assigned to a less strained structure shown in Table 2. (The structure of I_m was also considered to be that one listed in Table 2 in connection with those of I_t' and I_t).

Kinetic studies showed that the reactions of bromine with I and II in acetic acid follow the second-order rate equation (first-order in bromine concentration and first-order in substrate concentration); the rate constants observed in these studies are summarized in Table 3. The reaction of bromine with the III substrate was too fast to be determined by such a titration method ($k(25\ °C)>273\times10^{-3}$ mol/l·s).

Table 3 shows that the reactivity increased in the substrate order of III>I>II, indicating that the *endo*-chlorine atoms retarded the bromine addition reaction. Such results appear to be analogous to the reactivities reported in the previous paper[2)] with 2,3-dicyano-5-norbornene derivatives, although the rate constants are about six times larger than those of the corresponding 2,3-dicyano-5-norbornenes.

Unlike the results of the reaction of I with bromine in acetic acid, in a relatively nonpolar solvent such as CCl_4, the *trans*-adduct (I_t) and the *exo-cis* adduct (I_c) were obtained in 37 and 63% yields respectively; their

Table 3. Rate constants of bromine addition in acetic acid

Sutbsrate	Concentration of substrate (mol/l)	Temp. (°C)	Completion (%)	$k\times10^3$ (l/mol·s)
(I)	0.0299 (0.0483)[a]	20.0	91.3	43.9
	0.0313 (0.0481)	24.9	93.2	50.0
	0.0301 (0.0484)	24.9	94.2	51.7
	0.0299 (0.0481)	29.8	91.0	62.1
	0.0309 (0.0487)	29.8	90.5	62.9
(II)	0.0301 (0.0483)	20.0	61.6	6.33
	0.0300 (0.0476)	24.7	60.1	7.58
	0.0400 (0.0475)	35.0	66.7	9.88

a) Values in brackets indicate the initial bromine concentration (mol/l).

compositions were estimated by glc.[9] As the compositions of these dibromides were estimated to depend upon the polarity of solvents, the addition of bromine to the substrate I was carried out in various solvents whose polarities had been evaluated in terms of the E_T value.[10]

Table 4 summarizes the approximate compositions of I_t and I_c obtained from the addition reaction, along with the E_T value of each solvent. Table 4 indicates that the addition became progressively less stereospecific and gave more and more *exo-cis* adduct as solvents of lower E_T values (relatively non-polar solvents) were used. Since free-radical addition has often been reported to lead to the *exo-cis* adduct[11,12] as the major product, the addition of bromine was carried out in the presence of nitrobenzene, which has been reported to be a radical inhibitor[13] (Runs No. 9 and 10), but as is shown in Table 4, no inhibiting effect by nitrobenzene was observed. The increase in the *trans*-adduct with Run No. 10 compared with that of Run No. 9 was observed. This may be considered to be the result of the increase in solvent polarity caused by the addition of nitrobenzene (polar media, E_T value=42.0). Such a finding may exclude the possibility of a radical mechanism in bromine addition in relatively non-polar solvents.

Kinetic studies showed that the addition reaction in CCl_4 followed the third-order rate equation ($dc/dt = k[Br_2]^2\times[\text{substrate}]$, $[Br_2]=0.0511$ mol/l, [substrate]=0.0309 mol/l, percentage of completion=64%, k(29.7 °C)$=5.86\times10^{-1}$ l²/mol²·s) rather than the second-order rate equation ($dc/dt=k\times[Br_2]\times[\text{substrate}]$). Such results suggest that the *exo-cis* adduct may be produced through the ion-pair mechanism shown in Scheme 1. Such an intermediate would be most stable in relatively nonpolar solvents. As the polarities of solvents increase, the ion-pair intermediate may become progressively less stable and be replaced by the bromonium-ion intermediate.

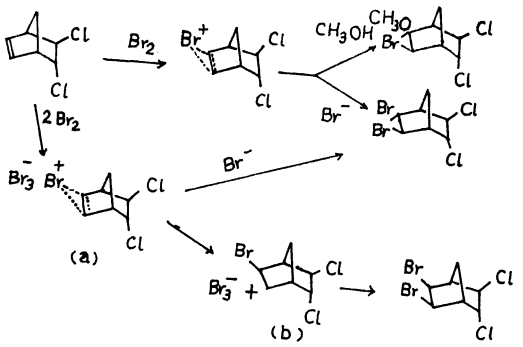

Scheme 1. Probable reaction mechanism.

The interpretation of the *cis* addition of bromine in terms of ion-pair mechanism was employed in Tamelen's report[14] with regard to the bromination of Dewar benzene in an octane solution. The formation of the *trans*-adduct from the ion-pair intermediate (b) or its precursor [(a) in Scheme 1, most probably] is possible, as is shown in Scheme 1. In order to confirm this possibility, additions were carried out with a bromide salt(tetra-*n*-butylammonium bromide) present (listed in Table 4).[15] The presence of bromide salt[16] as a source of bromide ions increases the ratio of the *trans* adduct in three different solvents ($Cl(CH_2)_2Cl$, $CH_3CO_2C_2H_5$, CCl_4), suggesting that the increase in the *trans* adduct compared with that in the absence of bromide salt may result from the bromide ion attack on this intermediate from the *endo* direction. Accordingly, the finding that the bromination of *trans*-

Table 4. Results of bromine addition to substrate I in different solvents

Run No.	Concentration of substrate (mol/l)	Solvent (ml)	Temp. (°C)	E_T-value[a]	I_t (%)	I_c[b] (%)
1	0.0188	MeOH (170)	30	55.5	100[d]	0
2	0.0124	AcOH (100)	room temp.	51.9	*ca.* 100	trace[e]
3	0.0061	$Cl(CH_2)_2Cl$ (70)	30—32	41.9	94.3	5.7
4	0.00319	$Cl(CH_2)_2Cl$ (100)	30[c]		99.0	1.0
5	0.00312	AcOEt (100)	30	38.1	80.6	19.4
6	0.00312	AcOEt (100)	30[c]		99.0	1.0
7	0.0184	CCl_4 (100)	30	32.5	37.0	63.0
8	0.00316	CCl_4 (100)	30[c]		64.5	35.5
9	0.00619	CCl_4 (70)+$C_6H_5NO_2$ (6)	66—70		32.5	67.5
10	0.00619	CCl_4 (70)+$C_6H_5NO_2$ (18)			46.9	53.1

a) These values were taken from Ref. 10. b) Analyzed by means of glc. c) Addition of 1.6 g of tetra-*n*-butyl ammonium bromide. d) 6-Bromo-5-methoxy-1-*endo*, 2-*exo*-dichloronorbornane (refer to Tables 1 and 2) was also obtained along with *trans* dibromide, (I_t). e) Small amounts of (I_c) was detected by means of glc analysis.

5,6-dicyano-2-norbornene in acetic acid afforded the *exo-cis* adduct in a 24% yield, whereas the bromination of I gave the *trans* adduct stereospecifically, may be explained in terms of the coexistence of a carbonium bromide ion pair[17] along with the bromonium ion in the former reaction. With the bromonium ion as an intermediate, a full positive charge develops through olefin carbons, which may be destabilized to some extent by a stronger electron-attracting group such as the cyano group, while, in the ion-pair intermediate, where the bromide ion may remain associated with the carbonium ion, the above substituent will not exert such an influence on the destabilization of the ion pair as is imagined in the case of the bromonium ion. Therefore, in the bromination of *trans*-5,6-dicyano-2-norbornene in acetic acid, the bromonium-ion intermediate may be destabilized to the extent of permitting the coexistence of an ion pair by the more electronegative group (C≡N).

References

1) Presented at the 25th Annual Meeting of the Chemical Society of Japan, Tokyo, April, 1972; Proceedings, Vol. III, p. 1551.

2) S. Kikkawa, M. Nomura, Y. Uno, M. Matsubara, and Y. Yanagida., This Bulletin, **45**, 2523 (1972).

3) L. Pauling, "The Nature of the Chemical Bond," 3rd ed., Cornell University Press, Ithaca, New York (1960), p. 261.

4) All the melting points were determined on a Yanagimoto micro-melting-point apparatus and are uncorrected. The NMR spectra were obtained with a JNM-Ps-100 spectrometer, using TMS as the internal standard. Glc analysis was carried out on a Shimadzu-GC 3AH gas chromatograph equipped with a TCD apparatus using a 3 m×3 mm stainless steel column packed with Silicone DC-550 on Celite 545 (carrier gas, H_2).

5) J. D. Roberts, F. O. Johnson, and R. A. Carboni, *J. Amer. Chem. Soc.*, **76**, 5692 (1954).

6) Preparative glc was carried out with a Shimadzu gas chromatograph GC-2C, equipped with a 4.38 m×10 mm stainless steel column packed with Silicone DC-550 on Celite 545.

7) Referring to the A-value,[8] the bulkiness of chlorine (A-value=0.4) may be expected to be rather larger than that of cyano group (A-value=0.2).

8) E. L. Eliel, N. L. Allinger, S. J. Angyal, and G. A. Morrison., "Conformational Analysis," John Wiley & Sons, Inc, New York (1965), p. 44.

9) In addition, the studies of the product composition as a function of the reaction time showed that the product composition did not vary with the degree of conversion.

10) K. Dimroth, C. Reichardt, T. Siepmann, and F. Bohlmann, *Ann. Chem.*, **661**, 1 (1963); **669**, 95 (1963).

11) J. A. Berson and R. Swiuler, *J. Amer. Chem. Soc.*, **75**, 4366 (1953).

12) J. A. Berson, *ibid.*, **76**, 5748 (1954).

13) B. Miller and C. Walling, *ibid.*, **79**, 4187 (1957).

14) E. E. van Tamelen and D. Carty, *ibid.*, **93**, 6102 (1971).

15) R. E. Buckles, J. M. Bader, and R. J. Thurmaier, *J. Org. Chem.*, **27**, 4523 (1962).

16) When tetra-*n*-butylammonium bromide is dissolved in a bromine solution, the equilibrium may be considered to involve bromine, monobromide salt, and tribromide salt. However, in the bromination by these salts, it is said that active species is bromine, so that the addition of monobromide in this experiment will exert little effect upon the stereochemical distribution of adducts.

Some Electrophilic Substitution Reactions of 2-Hydroxyazulene Derivatives[1]

Tetsuo Nozoe,* Toyonobu Asao,** and Masaji Oda
Department of Chemistry, Faculty of Science, Tohoku University, Aramaki, Aoba, Sendai 980
(Received July 18, 1973)

The bromination, chlorination, and nitration of 1,3-disubstituted 2-hydroxyazulenes were investigated. Bromination by bromine or NBS afforded 1-bromoazulan-2-one derivatives as kinetically-controlled products and 6-bromo-2-hydroxyazulene derivatives as thermodynamically-controlled products. Chlorination by NCS gave 1-chloroazulan-2-one derivatives, while that by chlorine afforded further chlorine addition products. Nitration afforded a mixture of 1-nitroazulan-2-one and 6-nitro-2-hydroxyazulene derivatives. The ultraviolet, infrared, and NMR spectra of the products were discussed.

It has been established[2,3] that the electrophilic substitutions of azulenes occur at the 1 and 3 positions; positions which coincide with the calculated positions[4] thought to have the highest electron density by theoretical considerations, and that the 5, 7, and 2 positions, with the next higher electron density, undergo the reaction in the case of 1,3-disubstituted azulenes.[5]

However, 1,3-disubstituted azulenes with strongly electron-releasing groups, such as an amino or a methylamino group, at the 2-position have been known to undergo facile bromination at the 6-position,[6] and 1,3-dicyano-2-hydroxy-5-isopropylazulene have also been known to afford 6,8-dibromo derivative by bromination.[7] These facts indicate that the strongly electron-releasing group at the 2-position governs the substitution at the 4, 6, and 8 positions.

In the present research, some electrophilic substitutions of 1,3-disubstituted 2-hydroxyazulenes were investigated; the results will be reported herein.

The bromination of diethyl 2-hydroxyazulene-1,3-dicarboxylate (I)[8] with 1.5 molar equivalents of bromine in acetic acid in the presence of sodium acetate afforded a reddish pink solid (II). When the solid was dissolved in ethanol, it gradually turned yellow; from it 90% of the starting azulene (I) and 5.5% of yellow needles (III) (mp 163 °C) were then obtained. Compound III, corresponding to the monobromide of I, shows an ultraviolet spectrum (Fig. 1) similar to that of I; its infrared spectrum displays an out-of-plane deformation band due to adjacent two hydrogens at 830 cm^{-1}. Furthermore, the NMR spectrum of III shows two doublets with the same coupling constant (J=11.8 Hz) at δ 7.86 and 8.93, each corresponding to two protons. These data clearly show that Compound III is diethyl 6-bromo-2-hydroxyazulene-1,3-dicarboxylate.

When the reddish pink solid (II) was washed with ether and then recrystallized from benzene–petroleum ether, a pure specimen of II was obtained as reddish prisms (mp 129 °C) in a yield of 68%. Compound II was also obtained by the reaction of I and NBS in CCl_4 in a 75% yield. Elemental analyses show that Compound II is also a monobromide of I; its UV spectrum (Fig. 1) is completely different from that of I or III, but rather similar to those of 1-oxaazulan-2-one (1*H*-1-oxaazulene-2-one) derivatives[9] or 8,8-dicyanoheptafulvene[10] in methanol.

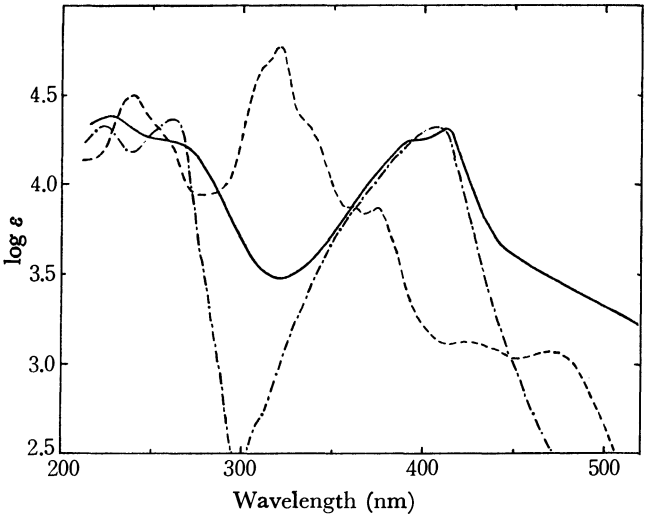

Fig. 1. UV spectra of II (——), III (----), and ethyl 1-oxa-2-oxo-azulane-3-carboxylate (— - —) in methanol.

The IR spectrum of II shows carbonyl bands at 1749 and 1689 cm^{-1}; the former one is comparable to that of 1-oxaazulan-2-one.[9] The NMR spectrum of II exhibits signals at δ 8.40 (bd, J=12 Hz, Ha), 6.7—7.2 (m, Hb–He), 4.31 (q), 4.20 (q), 1.36 (t), and 1.1 (t). From the above data, it is clear that II is diethyl 1-bromo-2-oxo-azulane-1,3-dicarboxylate (diethyl 1*H*-1,2-dihydro-1-bromo-2-oxoazulene-1,3-dicarboxylate), with a heptafulvenoid chromophore. The formation of II can be explained by considering that Compound I reacts as a β-keto ester form (Ia) under the present reaction conditions. The reactivity is similar to that of β-naphthol.[11]

It has been found that 2-hydroxyazulene (IV) exists in the enol form (IV) in methanol and in the keto form, 1,2-dihydroazulene-2-one (IVa), in $CHCl_3$ or water, and that the IR of 2-hydroxyazulene in KBr disk does not show any carbonyl band.[12] Meanwhile, Nozoe *et al.* have reported, in their azulene synthesis from the reactive troponoids with active methylene compounds, that there are three principal interme-

* Present address: No. 811, 2-5-1, Kamiyoga, Setagaya-ku, Tokyo 158.
** Present address: Department of Chemistry, College of General Education, Tohoku University, Kawauchi, Sendai 980.

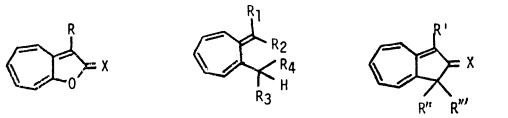

(A) X = O, NH (B) (C) X = O, NH

diates: "oxaazulanone" (A), "heptafulvene" (B), and "azulanone" (C).[13] However, the B and C intermediates are so unstable in the basic reaction conditions that they could not be isolated. Compound II is the first example of stable azulanone type compound obtained from azulene derivatives, and from the above view points, it is of interest to investigate the properties of II and the similar compounds obtained below.

Compound II is unstable to protic solvents, especially to bases, and in these solvents II liberates the bromine cation, which can easily be detected by the iodine-starch test, to give mainly I and a small amount of III at room temperature. Even on standing in air, II is gradually decomposed, presumably by moisture, to give I and III. Compound II immediately gave the sodium salt of hydroxyazulene (I) by the action of a sodium hydroxide solution, while the reaction with potassium iodide in acetone afforded potassium salt of I. The reaction of II with 2,4-dinitrophenylhydrazine or hydrazine yielded I and the hydrazine salt of I respectively.

On the other hand, the heating of II in DMF at 90 °C afforded 55% of I and 45% of III. When II was heated in DMF at 90 °C in the presence of an equimolar amount of dimethyl 2-hydroxyazulene-1,3-dicarboxylate (V),[10] dimethyl 6-bromo-2-hydroxyazulene-1,3-dicarboxylate (VI) (mp 210 °C) was obtained besides I, III, and V by intermolecular reaction. Therefore, it is clear that the bromination of I afforded at first the 1-bromo derivative (II) as a kinetically controlled product; then it afforded the 6-bromo derivative (III) as a thermodynamically controlled product under more severe reaction conditions. For the purpose of the direct synthesis of III, the bromination of I at an elevated temperature was attempted. Thus, the action of bromine on I in acetic acid–sodium acetate or in DMF–sodium acetate at 100 °C afforded III in yields of 45 and 70% respectively, besides I.

The bromination of the dimethyl ester (V) by bromine in $CHCl_3$ in the presence of sodium acetate at room temperature afforded 1-bromo compound (VII) as reddish prisms (mp 136 °C), whose UV and IR spectra are very similar to those of Compound II. When the reaction was carried out in DMF in the presence of sodium acetate and then the mixture was left standing at room temperature for 10 hr, the 6-bromo derivative (VI) was obtained in a 76% yield. Compound VI was also obtained by heating VII in DMF.

Similarly, the bromination of ethyl 1-cyano-2-hydroxyazulene-3-carboxylate (VIII)[13] with bromine in acetic acid–sodium acetate or with NBS in benzene afforded ethyl 1-bromo-3-cyano-2-oxo-azulane-1-carboxylate (IX) (mp 109 °C); the bromination of VIII in acetic acid–sodium acetate at 100 °C afforded ethyl 6-bromo-3-cyano-2-hydroxyazulene-1-carboxylate (X) (mp 207 °C).

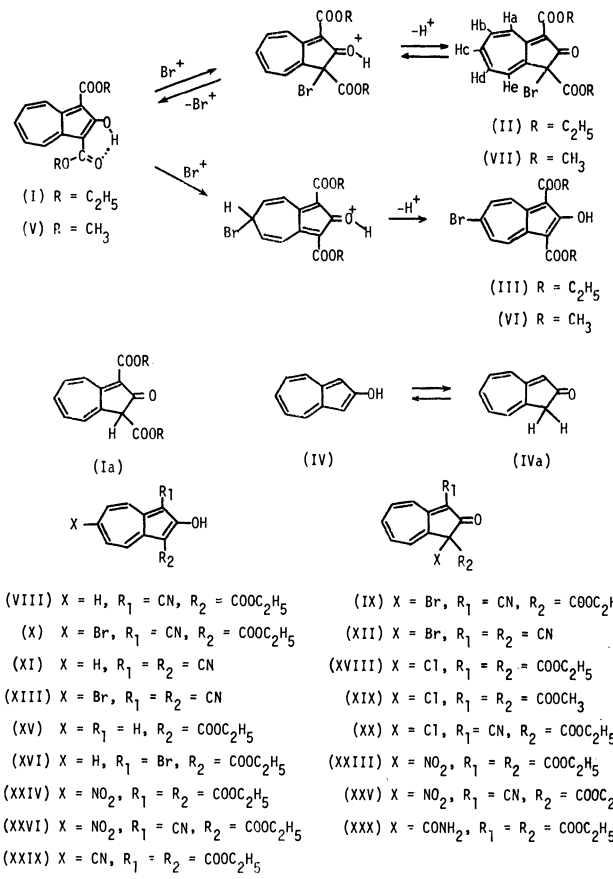

(I) R = C_2H_5
(V) R = CH_3
(II) R = C_2H_5
(VII) R = CH_3
(III) R = C_2H_5
(VI) R = CH_3
(Ia) (IV) (IVa)

(VIII) X = H, R_1 = CN, R_2 = $COOC_2H_5$
(X) X = Br, R_1 = CN, R_2 = $COOC_2H_5$
(XI) X = H, R_1 = R_2 = CN
(XIII) X = Br, R_1 = R_2 = CN
(XV) X = R_1 = H, R_2 = $COOC_2H_5$
(XVI) X = H, R_1 = Br, R_2 = $COOC_2H_5$
(XXIV) X = NO_2, R_1 = R_2 = $COOC_2H_5$
(XXVI) X = NO_2, R_1 = CN, R_2 = $COOC_2H_5$
(XXIX) X = CN, R_1 = R_2 = $COOC_2H_5$

(IX) X = Br, R_1 = CN, R_2 = $COOC_2H_5$
(XII) X = Br, R_1 = R_2 = CN
(XVIII) X = Cl, R_1 = R_2 = $COOC_2H_5$
(XIX) X = Cl, R_1 = R_2 = $COOCH_3$
(XX) X = Cl, R_1 = CN, R_2 = $COOC_2H_5$
(XXIII) X = NO_2, R_1 = R_2 = $COOC_2H_5$
(XXV) X = NO_2, R_1 = CN, R_2 = $COOC_2H_5$
(XXX) X = $CONH_2$, R_1 = R_2 = $COOC_2H_5$

The bromination of 1,3-dicyano-2-hydroxyazulene (XI)[13] by bromine in $CHCl_3$ in the presence of sodium acetate at room temperature afforded a reddish oily product (XII), which did not crystallize and which could not be purified because of its instability. The IR of XII exhibits a strong carbonyl band at 1724 cm^{-1} and a weak cyano band at 2215 cm^{-1}. The UV of XII shows a curve similar to that of II, with maxima at 290, 406, and 425 nm. From these data, the oil is assumed to be 1-bromo-1,3-dicyanoazulan-2-one (XII). When the solution of the oil (XII) in $CHCl_3$ was allowed to stand at room temperature for 30 min, it turned yellow and 50% of the 6-bromo-1,3-dicyano-2-hydroxyazulene (XIII) was obtained, besides XI. The structure of XIII was determined by means of the spectroscopic data.

When a solution of XI, 1.5 molar equivalents of bromine, and sodium acetate in acetic acid was allowed to stand at room temperature for 1 hr, the 6-bromo derivative (XIII) was obtained in a yield of 67% besides an unidentified yellowish-brown mixture. The reaction of XI with 3 molar equivalents of bromine in acetic acid in the presence of sodium acetate afforded 4,6,8-tribromo-1,3-dicyano-2-hydroxyazulene (XIV) besides XIII and an unidentified brown solid.

On the bromination of ethyl 2-hydroxyazulene-1-carboxylate (XV),[8] the unsubstituted 3-position was exclusively attacked, and ethyl 3-bromo-2-hydroxyazulene-1-carboxylate (XVI) was obtained in a good yield.

When the 6-bromo compound (III) was further

treated with NBS in benzene, the solution turned red, and the UV of the solution showed a curve similar to that of 1-bromide (II); therefore, the 1,6-dibromo compound (XVII) seems to be formed. However, the working-up of the solution afforded only the starting compound (III), and no XVII or 4,6-dibromo derivative could be isolated; such unreactivity may due to a steric interaction of ethoxycarbonyl groups at the 1 and 3 positions to the peri-position of the nucleus.

The reactions of I, V, and VIII with *N*-chlorosuccinimide (NCS) in benzene afforded three 1-chloro derivatives, XVIII (mp 98 °C), XIX (mp 161 °C), and XX (mp 132 °C), in good yields. The structures of these products were determined by their spectroscopic properties. These compounds are more stable than the corresponding bromides (II and VII), and do not change easily on standing in the air.

The reaction of I and VIII with chlorine in CCl_4 afforded two pale yellow oils (XXI and XXII respectively). The results of the analyses of these products almost accord with those of trichloride of the starting compounds, and their UV maxima appear only at 261 nm in both compounds. The IR of XXI displays bands at 1790 and 1767 cm^{-1}, while that of XXII shows them at 2205 (vw), 1975, and 1767 cm^{-1}. From these data, the structures of the compounds can tentatively be assigned as is shown in the figure. Compound XXI is quite stable; however, XXII gradually changes when allowed to stand at room temperature and gives a reddish solid, from which the 1-chloro compound (XX) is subsequently isolated in a 50% yield.

The nitration of I with concentrated nitric acid in acetic acid was carried out, and two kinds of mononitro derivatives, were isolated. One consisted of brown needles (XXIV) (41% yield), while the other consisted of reddish crystals (XXIII) with a low melting point (36% yield). Compound XXIV was determined to be diethyl 2-hydroxy-6-nitroazulene-1,3-dicarboxylate from its spectroscopic data; the UV is similar to those of azulenes, and the NMR in $CDCl_3$ shows A_2B_2-type doublets at δ 9.48 and 8.43, with the same coupling constant (J=12 Hz). From the similarity of UV and IR spectra of XXIII to those of II, Compound XXIII is assumed to be diethyl 1-nitro-2-oxo-azulane-1,3-dicarboxylate.

A similar nitration of VIII afforded 6-nitro derivative (XXVI) as brown crystals in a 39% yield and 1-nitro derivative (XXV) as reddish crystals in a 42% yield. In these nitrations of I and VIII, reddish powders were obtained in 10—15% yields; however, attempts to purify them were not successful.

As has been mentioned at the beginning, diethyl 2-aminoazulene-1,3-dicarboxylate (XXVII) undergoes a facile bromination by bromine at the 6-position in a $CHCl_3$ solution to give orange crystals with UV maxima at 473, 410, 332, 320, and 245 nm.[6] The UV spectrum of a solution of XXVII and NBS in benzene displays maxima at 395 and 375 nm characteristic of heptafulvene chromophore, therefore, the 1-bromoazulan-2-imine derivative (XXVIII) must be formed in the solution. However, the compound could not be isolated.

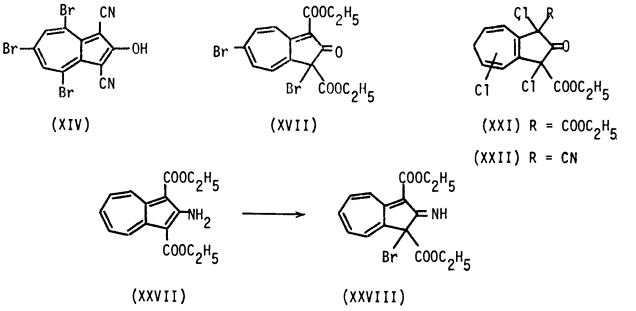

In order to synthesize the model compound (C; R′=R″=$COOC_2H_5$, R‴=CN or $CONH_2$) of the "azulanone" intermediate in the azulene synthesis,[13] the reaction of II with cyanogen bromide or urea was attempted. The reaction of silver salt of I with cyanogen bromide afforded II, III, and a small amount of a compound assumed to be diethyl 6-cyano-2-hydroxyazulene-1,3-dicarboxylate (XXIX). On the heating of I with urea in acetic acid in the presence of a few drops of sulfuric acid, reddish orange needles, which were assumed to be diethyl 1-carbamoyl-2-oxo-azulan-2-one-1,3-dicarboxylate (XXX), were obtained once in a 5% yield; also the starting azulene was recovered. However, the structure and the reactivity of XXX were not clarified because of the lack of a sample.

Experimental***

Bromination of Diethyl 2-Hydroxyazulene-1,3-dicarboxylate (I). (a) To a stirred solution of I (1 g) and sodium acetate (427 mg) in acetic acid (10 ml), a solution of bromine (834 mg) in acetic acid was added at room temperature. The solution turned deep red. After 2 hr, a 40 ml portion of water was added, thus giving a reddish oil, which was subsequently solidified by allowing to stand. The reddish pink solid that resulted was washed with ether, and 870 mg (68%) of reddish crystals were obtained. Recrystallization from benzene–petroleum ether gave II as reddish needles; mp 128—129 °C.

Found: C, 52.66; H, 4.29; Br, 22.00%. Calcd for $C_{16}H_{15}O_5Br$: C, 52.32; H, 4.12; Br, 21.76%.

λ_{max}^{MeOH} nm (log ε); 228 (4.39), 260 (4.24), 395 (4.24) and 414 (4.31).

By treating the filtrate with sodium hydroxide, sodium salt of I was recovered in a 25% yield.

(b) NBS (354 mg) was added to a stirred solution of I (500 mg) and sodium acetate in benzene (20 ml). After 15 min, the solvent was removed until the volume was about 10 ml, and then succinimide was removed by filtration. The filtrate was further condensed to about 5 ml, and petroleum ether was added to give reddish crystals (495 mg, 79%), which were subsequently washed with petroleum ether and recrystallized from benzene–petroleum ether to give red needles (mp 128—129 °C), whose infrared spectrum was superimposable upon that of II obtained by Procedure (a).

(c) A solution of I (1 g), sodium acetate (427 mg), and bromine (894 mg) in acetic acid was warmed on a water bath for 2 hr; then it was allowed to stand overnight at room temperature. The precipitate was filtered to give 490 mg

*** All melting points are uncorrected.

of yellow crystals; when water was then added to the filtrate to yield a reddish oil which was subsequently crystallized by the addition of ethanol, 80 mg of the same yellow crystals and 500 mg of the starting materials were obtained. The combined product was then recrystallized from ethanol to give III as yellow needles (470 mg, 73%); mp 162—163 °C

Found: C, 52.44; H, 4.32%. Calcd for $C_{16}H_{15}O_5Br$: C, 52.32; H, 4.12%.

λ_{max}^{MeOH} nm (log ε); 240 (4.50), 263^{sh} (4.23), 313^{sh} (4.67), 322 (4.78), 360 (3.87), 375 (3.87), 420 (3.13) and 470 (3.07).

$\lambda_{max}^{MeOH-0.1N\ NaOH}$nm (log ε); 247 (4.42), 275 (3.99), 320^{sh} (4.60), 334 (4.73), 420 (3.77) and 490 (3.72).

Methyl Ether: Methyl ether was obtained by the reaction of III with diazomethane; reddish orange needles; mp 124—125 °C.

Found: C, 53.39; H, 4.80%. Calcd for $C_{17}H_{17}O_5Br$: C, 53.55; H, 4.50%.

Ethyl Ether: Ethyl ether was obtained by the reaction of III with diazoethane; reddish orange needles; mp 109—110 °C.

Found: C, 54.53; H, 4.70%. Calcd for $C_{18}H_{19}O_5Br$: C, 54.71; H, 4.85%.

(d) A solution of I (200 mg), sodium acetate (85 mg), and bromine (166 mg) in dimethyl formamide (4 ml) was allowed to stand at room temperature for 2 days. When water (15 ml) was then added, 245 mg solid was obtained. The fractional recrystallization of the solid afforded 175 mg (68%) of III and 50 mg of I.

Thermal Reaction of Diethyl 1-Bromo-2-oxo-azulan-2-one-1,3-dicarboxylate (II). A solution of II (100 mg) in DMF (2 ml) was heated at 100 °C for 3 hr. When water was then added and the precipitate was fractionally recrystallized from ethanol, 45 mg (45%) of III and 40 mg (50%) of I were obtained.

Reaction of II and Dimethyl 2-Hydroxyazulene-1,3-dicarboxylate (V). A solution of II (200 mg) and V (142 mg) in DMF (6 ml) was heated at 100 °C for 3 hr. The crystals (80 mg) which were precipitated out were recrystallized from ethyl acetate to give 75 mg (40%) of pale yellow needles (mp 210 °C). The crystals were identified as dimethyl 6-bromo-2-hydroxyazulene-1,3-dicarboxylate (VI) by a mixed-melting-point comparison and by a comparison of the infrared spectra. The filtrate of the reaction was diluted with water and extracted with chloroform. When the extract was then evaporated, 215 mg of crystals were obtained. The crystals were proved to be a mixture of I, V, and a small amount of III by separation using thin-layer chromatography on silica gel.

Bromination of Dimethyl 2-Hydroxyazulene-1,3-dicarboxylate (V). (a) To a stirred solution of V (100 mg) and sodium acetate (42 mg) in chloroform (5 ml), a solution of bromine (80 mg) in chloroform was added at room temperature. After 15 min, the inorganic substance thus precipitated was filtered off, and to the filtrate petroleum ether was added to obtain reddish crystals. The crystals were then recrystallized from $CHCl_3$–petroleum ether to give VII as reddish prisms (25 mg); mp 136 °C.

Found: C, 49.49; H, 3.24%. Calcd for $C_{14}H_{11}O_5Br$: C, 49.60; H, 3.27%.

λ_{max}^{MeOH} nm (log ε); 227 (4.38), 270^{sh} (4.21), 395^{sh} (4.20) and 415 (4.26).

The treatment of the filtrate with sodium hydroxide afforded 70 mg of a sodium salt of V.

(b) A solution of V (200 mg), sodium acetate (77 mg), and bromine (148 mg) in DMF (5 ml) was allowed to stand at room temperature for 12 hr. Water (20 ml) was then added, and the crystals thus precipitated were washed with methanol and recrystallized from ethyl acetate to give VI (200 mg, 76%) as pale yellow needles; mp 210 °C.

Found: C, 49.39; H, 3.34%. Calcd for $C_{14}H_{11}O_5Br$: C, 49.60; H, 3.27%.

λ_{max}^{MeOH} nm (log ε); 240 (4.52), 264^{sh} (4.27), 310^{sh} (4.65), 321 (4.77), 335^{sh} (4.47), 374 (4.28), 420 (3.48) and 470 (3.30).

$\lambda_{max}^{MeOH-0.1N\ NaOH}$ nm (log ε); 247 (4.50), 280^{sh} (4.14), 325^{sh} (4.70), 333 (4.76), 415 (4.28) and 488 (4.18).

Bromination of Ethyl 3-Cyano-2-hydroxyazulene-1-carboxylate (VIII). (a) To a suspended solution of VIII (200 mg) and sodium acetate (88 mg) in acetic acid (20 ml) was added a solution of bromine (162 mg) in acetic acid at room temperature. After the solution had been stirred for 30 min, water (30 ml) was added and the solution was extracted with benzene. The extract was dried, the solvent was removed to a small volume, and petroleum ether was added to give reddish crystals (175 mg, 66%). Subsequent recrystallization from benzene–petroleum ether afforded ethyl 1-bromo-3-cyano-2-oxo-azulane-1-carboxylate (IX) as reddish prisms; mp 109 °C.

Found: C, 52.41; H, 3.15; N, 4.69; Br, 25.02%. Calcd for $C_{14}H_{10}O_3NBr$: C, 52.54; H, 3.40; N, 4.38; Br, 24.97%.

λ_{max}^{MeOH} nm (log ε); 225 (4.27), 258 (4.15), 395 (4.19) and 417 (4.25).

When the combined filtrates were treated with a sodium hydroxide solution, 55 mg of the sodium salt of VIII were recovered.

(b) To a stirred solution of VIII (500 mg) in benzene (25 ml), NBS (445 mg) was added at room temperature. After 20 min, the solvent was removed to about 10 ml and the precipitated succinimide was filtered off. A large amount of petroleum ether was then added to the filtrate, and 630 mg (95%) of reddish crystals were obtained. Recrystallization from benzene–petroleum ether afforded IX as reddish prisms; their infrared spectrum was superimposable on that of IX obtained by Procedure (a).

(c) A solution of VIII (300 mg), sodium acetate (154 mg), and bromine (298 mg) in acetic acid (15 ml) was heated at 100 °C for 3 hr. After the solution had stood overnight, 300 mg of crystals were obtained; they were recrystallized from ethyl acetate to give ethyl 6-bromo-3-cyano-2-hydroxy-azulene-1-carboxylate (X) (230 mg, 60%) as yellow needles; mp 206—207 °C. From the combined filtrate, VIII (60 mg) and X (20 mg) were obtained.

Found: C, 52.21; H, 3.30; N, 4.07%. Calcd for $C_{14}H_{10}O_3$-NBr: C, 52.54; H, 3.40; N, 4.38%.

λ_{max}^{MeOH} nm (log ε); 235 (4.54), 315^{sh} (4.74), 319 (4.82), 375 (3.93) and 450 (2.95).

$\lambda_{max}^{MeOH-0.1N\ NaOH}$nm (log ε); 247 (4.50), 270^{sh} (3.86), 320^{sh} (4.69), 332 (4.79), 422 (3.95) and 485 (3.77).

Bromination of 1,3-Dicyano-2-hydroxyazulene (XI). (a) To a suspended solution of XI (200 mg) and sodium acetate (127 mg) in $CHCl_3$ (10 ml), a solution of bromine (248 mg) in $CHCl_3$ was added. After 15 min, the precipitate was filtered off, a 50 ml portion of petroleum ether was added to the filtrate, and a reddish oil (200 mg, 70%) was obtained by decantation. The oil could not be crystallized or purified. A solution of the oil in $CHCl_3$ showed UV maxima at 290, 406, and 425 nm. The precipitate obtained from the reaction mixture was identified as a mixture of XI and the 6-bromo derivative (XIII) by a comparison of the infrared spectra.

(b) Bromine (620 mg) was added to a suspension of XI (500 mg) and sodium acetate (317 mg) in acetic acid (10 ml) at room temperature. After 1 hr, the crystals which were precipitated out were filtered and 470 mg of yellow crystals were obtained; these crystals were recrystallized from ethanol

to give 6-bromo-1,3-dicyano-2-hydroxyazulene (XIII) as yellow crystals; mp over 300 °C.

Found: C, 52.74; H, 2.02; N, 9.97%. Calcd for $C_{12}H_5ON_2Br$: C, 52.79; H, 1.85; N, 10.26%.

λ_{max}^{MeOH} nm (log ε); 228 (4.54), 250^{sh} (4.18), 315 (4.78), 328 (4.88), 426 (3.91) and 473 (3.63).

The filtrate obtained from the reaction mixture was diluted with water; a reddish brown solid, which could not be purified, was thus obtained.

(c) To a stirred suspension of XI (500 mg) and sodium acetate (640 mg) in acetic acid (15 ml), bromine (1.24 g) was added at room temperature. The suspension turned deep red, and yellow crystals began to precipitate after 20 min. After 3 hr, the crystals (480 mg) were filtered out and recrystallized from DMF to give 1,3-dicyano-2-hydroxy-4,6,8-tribromoazulene (XIV) (290 mg, 25%) as orange yellow crystals; mp over 300 °C.

Found: C, 32.47; H, 0.67; N, 5.87%. Calcd for $C_{12}H_3ON_2Br_3$: C, 33.43; H, 0.70; N, 6.50%.

λ_{max}^{MeOH} nm; 227, 283, 325, 338 and 440.

From the filtrate of the recrystallization, the 6-bromo derivative (XIII) (150 mg) was obtained. When water was then added to the filtrate of the reaction mixture, 410 mg of a reddish brown solid was obtained.

Ethyl 3-Bromo-2-hydroxyazulene-1-carboxylate (XVI). A solution of ethyl 2-hydroxyazulene-1-carboxylate (XV) (100 mg) and NBS (100 mg) in CCl_4 (4 ml) was gently heated for 20 min. Working up as usual sebsequently afforded XVI (110 mg) as deep orange needles; mp 106—107 °C after recrystallization from ethanol.

Found: C, 53.34; H, 3.82%, Calcd for $C_{13}H_{11}O_3Br$: C, 52.93; H, 3.76%.

λ_{max}^{MeOH} nm (log ε); 247 (4.36), 320 (4.53), 375 (3.75), 390^{sh} (3.77) and 408 (3.81).

$\lambda_{max}^{MeOH-0.1N\ NaOH}$nm (log ε); 245 (4.36), 320 (4.58), 369 (4.76) and 407 (3.70).

Chlorination of Diethyl 2-Hydroxyazulene-1,3-dicarboxylate (I), (a) A solution of I (250 mg), NCS (150 mg), and sodium acetate (100 mg) in $CHCl_3$ (10 ml) was gently heated for 30 min. The resulting reddish solution was washed with water, dried over anhydrous sodium sulfate, and chromatographed on silica gel column, using $CHCl_3$ as the solvent, to give 230 mg of reddish crystals. Subsequent recrystallization from benzene–cyclohexane afforded diethyl 1-chloroazulan-2-one-1,3-dicarboxylate (XVIII) as reddish prisms; mp 97—98 °C.

Found: C, 59.33; H, 4.60%. Calcd for $C_{16}H_{15}O_5Cl$: C, 59.54; H, 4.69%.

λ_{max}^{MeOH} nm (log ε); 225 (4.40), 258 (4.25), 395 (4.26) and 414 (4.30).

(b) To a stirred solution of I (250 mg) in $CHCl_3$, two molar equivalents of a solution of chlorine in CCl_4 were slowly added under gentle heating. The solution first turned red and then pale yellow. The solvent was then removed to give a pale yellow oil (XXI) which could not be purified further.

Found: C, 47.52; H, 3.81%. Calcd for $C_{16}H_{15}O_5Cl_3$: C, 48.85; H, 3.86%.

Dimethyl 1-Chloro-2-oxo-azulane-1,3-dicarboxylate (XIX). By the reaction of dimethyl 2-hydroxyazulene-1,3-dicarboxylate (V) with NCS, XIX was obtained in an 80% yield as reddish prisms (from benzene–cyclohexane); mp 160—161 °C.

Found: C, 57.49; H, 3.83%. Calcd for $C_{14}H_{11}O_5Cl$: C, 57.06; H, 3.76%.

λ_{max}^{MeOH} nm (log ε); 225 (4.38), 265 (4.20), 395 (4.25) and 415 (4.30).

Chlorination of Ethyl 3-Cyano-2-hydroxyazulene-1-carboxylate (VIII). (a) The reaction of VIII with NCS afforded ethyl 1-chloro-3-cyano-2-oxo-azulane-1-carboxylate (XX) as reddish prisms (from benzene–cyclohexane); mp 131—132 °C.

Found: C, 60.97; H, 3.95; N, 5.28%. Calcd for $C_{14}H_{10}O_3NCl$: C, 61.00; H, 3.95; N, 5.08%.

λ_{max}^{MeOH} nm (log ε); 222 (4.38), 255 (4.30), 395 (4.28) and 416 (4.31).

(b) To a solution of VIII (300 mg) in $CHCl_3$ (5 ml), a solution of chlorine in CCl_4 was added. The solution became pale yellow. The solvent was then removed to give a pale yellow oily product, which was assumed to be trichloride (XXII); however, it could not be purified. The oil was gradually decomposed to give a reddish solid. When a part (180 mg) of the solid was dissolved in $CHCl_3$ and chromatographed on silica gel, a compound (91 mg) (mp 132 °C) was obtained whose IR was superimposable upon that of XX obtained by Method (a).

Nitration of Diethyl 2-Hydroxyazulene-1,3-dicarboxylate (I). To a stirred solution of I (1 g) in acetic acid (10 ml), concentrated nitric acid (5 ml) was added at room temperature. A small amount of the solution was then placed in a test tube and heated until the solution turned deep red. The solution was then added to the original reaction mixture, and the mixture was stirred at room temperature. The mixture thereupon turned deep red; then it was cooled with ice. After 10 min, water (3 ml) was added and the precipitate was filtered and washed with ethanol to give 410 mg of brown crystals. The filtrate was diluted with water (50 ml) and extracted with $CHCl_3$. The extract was dried and chromatographed on silica gel, using $CHCl_3$ as the solvent. From the first effluent, 100 mg of the starting azulene (I) was obtained; the second effluent gave 420 mg of a reddish oil, which could not be crystallized or purified completely. The compound was considered to be diethyl 1-nitro-2-oxoazulane-1,3-dicarboxylate (XXIII) from the analytical results and the UV spectrum.

Found: C, 58.01; H, 4.90; N, 3.98%. Calcd for $C_{16}H_{15}O_7N$: C, 57.66; H, 4.54; N, 4.20%.

λ_{max}^{MeOH} nm; 225, 256, 395, and 416.

From the third effluent, 70 mg of brown crystals were obtained. The combined brown crystals (480 mg) were recrystallized from ethyl acetate to give diethyl 2-hydroxy-6-nitroazulene-1,3-dicarboxylate (XXIV) as brown needles; mp 219—220 °C.

Found: C, 57.44; H, 4.64; N, 4.13%. Calcd for $C_{16}H_{15}O_7N$: C, 57.66; H, 4.54; N, 4.20%.

λ_{max}^{MeOH} nm (log ε); 247 (4.54), 328 (4.64), 342 (4.59), 370 (3.98), 385 (3.95), 408 (3.92) and 465 (4.22).

$\lambda_{max}^{MeOH-0.1N\ NaOH}$nm (log ε); 243 (4.50), 342 (4.55), 382 (3.96), 405 (3.92) and 487 (4.41).

From the last effluent of the chromatography using ethanol as the solvent, 105 mg of a deep red powder were obtained.

Methyl Ether of XXIV: The methylation of XXIV with diazomethane afforded methyl ether as brownish green needles; mp 143.5—144.5 °C (from ethyl acetate).

Found: C, 58.47; H, 4.54; N, 4.25%. Calcd for $C_{17}H_{17}O_7N$: C, 58.79; H, 4.93; N, 4.03%.

λ_{max}^{MeOH} nm (log ε); 247 (4.49), 318 (4.78), 374 (3.84), 390 (3.86), 406 (3.89) and 470 (3.24).

Ethyl Ether of XXIV: Ethyl ether was obtained by the reaction of XXIV with diazoethane; green needles; mp 106—107 °C (from ethyl acetate).

Found: C, 60.23; H, 5.31%. Calcd for $C_{18}H_{19}O_7N$: C, 59.83; H, 5.30%.

Nitration of Ethyl 3-Cyano-2-hydroxyazulene-1-carboxylate (VIII). A solution of VIII (600 mg) and concentrated nitric acid (10 ml) in acetic acid (20 ml) was gently heated until a

reddish color appeared. When the solution was cooled and water was added 175 mg of brown crystals was obtained. The filtrate was then worked up as in the case of the nitration of I; 220 mg of reddish crystals (XXV), 100 mg of brown crystals, and 84 mg of a reddish powder were thus obtained. The reddish crystals (XXV) showed a mp of 105—108 °C and UV maxima at 225, 257, 397 and 417 nm, but they could not be purified further.

Found: C, 59.20; H, 3.60; N, 9.56%. Calcd for $C_{14}H_{10}O_5N_2$: C, 58.74; H, 3.52; N, 9.79%.

The combined brown crystals (275 mg) were recrystallized from ethyl acetate to give ethyl 3-cyano-2-hydroxy-6-nitroazulene-1-carboxylate (XXVI) as brown needles; mp 231—232 °C.

Found: C, 59.12; H, 3.38; N, 9.57%. Calcd for $C_{14}H_{10}O_5N_2$: C, 58.74; H, 3.52; N, 9.79%.

λ_{max}^{MeOH} nm (log ε); 236 (4.56), 325 (4.65), 340^{sh} (4.63), 370 (4.10), 385 (4.10) and 468 (4.16).

$\lambda_{max}^{MeOH-0.1N\ NaOH}$nm (log ε); 233 (4.55); 327 (4.51), 338 (4.54), 380 (4.02) and 476 (4.34).

Reaction of Silver Salt of I with Cyanogen Bromide. Silver salt of I was obtained by the reaction of I with silver oxide in ethanol and was used after drying under reduced pressure. To a stirred solution of silver salt of I (396 mg) in DMF (4 ml) at 100 °C, cyanogen bromide (400 mg) was added, whereupon the solution immediately turned red. After 30 min, the precipitated silver bromide was filtered off and washed with $CHCl_3$; the solvent was then removed under reduced pressure to leave a reddish oily product. A solution of the oil in $CHCl_3$ was chromatographed on silica gel. The crystals obtained from the reddish effluent was fractionally recrystallized from $CHCl_3$–petroleum ether; 120 mg of II, 20 mg of III, and 55 mg of reddish needles (XXIX) (mp 128—130 °C) were thus obtained.

Found: C, 64.95; H, 4.78; N, 4.19%. Calcd for $C_{17}H_{15}O_5N$: C, 65.23; H, 4.83; N, 4.48%.

λ_{max}^{MeOH} nm; 237, 262, 301, 312, and 410.

IR (KBr disk); 2242 and 1690 cm^{-1}.

NMR ($CDCl_3$); δ 1.52 (t), 4.53 (q), 7.92 (2H, d, J=8.6 Hz) and 10.03 (2H, d, J=8.6 Hz).

Reaction of I with Urea. A solution of I (400 mg) and urea (250 mg) in acetic acid (5 ml) was heated at *ca.* 90 °C for 4 hr in the presence of 5 drops of concentrated sulfuric acid. The solution was then diluted with water and extracted with $CHCl_3$, after which the extract was dried and chromatographed on a silica gel column. From the first effluent, 130 mg of the starting azulene (I) was recovered; the next effluent afforded 50 mg of a reddish oil, which was crystallized from benzene–petroleum ether, and also 10 mg of XXX as reddish-orange needles (mp 154—155 °C) was obtained (from benzene–petroleum ether).

Found: C, 63.55; H, 5.51%. Calcd for $C_{17}H_{17}O_6N$: C, 61.63; H, 5.17%.

This work was financially supported by grants from the Ministry of Education of Japan and the Sankyo Co., Ltd., to which the authors' thanks are due.

References

1) Presented at 18th Annual Meeting of the Chemical Society of Japan, Osaka, April, 1965.

2) A. G. Anderson, Jr., and J. A. Nelson, *J. Amer. Chem. Soc.*, **72**, 3824 (1950); A. G. Anderson, Jr., J. A. Nelson, and J. J. Tazuma, *ibid.*, **75**, 4980 (1953); A. G. Anderson, Jr., R. Scotoni, Jr., E. J. Cowles, and C. J. Fritz, *J. Org. Chem.*, **22**, 1193 (1957).

3) For reviews, see; W. Treibs, W. Kirchhof, and W. Ziegenbein, *Fortschr. Chem. Forsch.*, **3**, 334 (1955); K. Hafner, *Angew. Chem.* **70**, 419 (1958); W. Keller-Schierlein, and E. Heilbronner, "Non-Benzenoid Aromatic Compounds," ed. by D. Ginsburg, Interscience Publ., New York, N. Y., (1959), p. 310; T. Nozoe and T. Asao, "Dai-Yuki Kagaku," Vol. 13, Asakura Shoten, Tokyo (1960), p. 439; T. Nozoe and S. Ito, *Fortschr. Chem. Org. Naturstoffe*, **19**, 32 (1961).

4) R. D. Brown, *Trans. Farady Soc.*, **44**, 984 (1948); A. Julg, *J. Chim. Phys.*, **52**, 377 (1955); R. Pariser, *J. Chem. Phys.*, **25**, 1112 (1956); H. Spiesecke and W. G. Schneider, *Tetrahedron Lett.*, **1961**, 468; E. Heilbronner, "Non-Benzenoid Aromatic Compounds," ed. by D. Ginsburg, Interscience Publ., New York, N. Y. (1959), p. 196.

5) (a) A. G. Anderson, Jr., and L. L. Replogle, *J. Org. Chem.*, **25**, 1275 (1960); **28**, 2578 (1963); K. Hafner and K.-K. Moritz, *Ann. Chem.*, **656**, 40 (1962); (b) For the formylation of guaiazulene, see; T. Ukita, M. Miyazaki, and M. Hayashi, *Chem. Pharm. Bull.* (Tokyo), **6**, 223 (1958); (c) See also W. Treibs, *Angew. Chem.*, **67**, 76 (1955); S. J. Assony and N. Kharasch, *J. Amer. Chem. Soc.*, **80**, 5978 (1958).

6) T. Nozoe, S. Seto, and S. Matsumura, This Bulletin, **35**, 1990 (1962); S. Matsumura, *Chem. Pharm. Bull.* (Tokyo), **10**, 1024 (1962); T. Arai, Dr. Thesis, Tohoku University, 1965.

7) T. Asano, Dr. Thesis, Tohoku University, 1959.

8) T. Nozoe, K. Takase, and N. Shimazaki, This Bulletin, **37**, 1644 (1964).

9) *Cf.* T. Sato, *Bull. Chem. Research Inst. Non-Aqueous Soln., Tohoku University*, **8**, 47 (1959).

10) T. Nozoe, T. Mukai, K. Osaka, and N. Shishido, This Bulletin, **34**, 1384 (1961).

11) H. Burton, *J. Chem. Soc.*, **1945**, 280.

12) K. Takase, T. Asao, Y. Takagi, and T. Nozoe, *Chem. Commun.*, **1968**, 368; R. Hagen, E. Heilbronner, and P. A. Straub, *Helv. Chim. Acta*, **50**, 2504 (1967).

13) T. Nozoe, S. Seto, S. Matsumura, and T. Asano, *Proc. Japan Acad.*, **33**, 339 (1956); T. Nozoe, S. Seto, K. Takase, S. Matsumura, and T. Nakazawa, *Nippon Kagaku Zasshi*, **86**, 346 (1965).

Photo-Beckmann Rearrangements of Oximes of Androsterone and 13α-Androsterone[1]

Hiroshi SUGINOME and Tsutomu UCHIDA

Department of Chemistry, Faculty of Science, Hokkaido University, Sapporo 060

(Received July 26, 1973)

The photolysis of androsterone oxime and 13α-androsterone oxime affords isomeric lactams with and without the original configuration of the C-13 substituent of the starting oxime, although there were poor yields and no products due to photo-Beckmann fission. The formation of an epimeric pair of lactams from an oxime is at variance with our previous results on the photolysis of 5α- and 5β-cholestan-6-one oximes, in which the stereochemical integrity of the terminus of the migrating carbon in the photo-Beckmann rearrangement was observed. The implication of the present results for the migration step of the photo-Beckmann rearrangement is discussed.

In our previous papers it has been shown that in the photo-Beckmann rearrangement of steroidal oximes the bond migration of the oximes to amides proceeds in a stereospecific manner, the migration of carbon α to the oximino group occurring with the retention of the original configuration, and in these unsymmetrically α-substituted oximes the relative amounts of the two isomeric lactams due to the migration of the tri-substituted carbon (C_5) and the disubstituted carbon (C_7) are not significantly different.[2,3] This finding was subsequently confirmed by Just *et al.*[4] They showed that the photo-Beckmann rearrangements of menthone oxime and isomenthone oxime afforded the corresponding lactams with retention of the original configuration at carbon α to the oximino group of the starting oximes.

In this paper we wish to report on further results with respect to the stereospecificity of the migration stage in the photo-Beckmann rearrangement. In the present studies we used the title steroidal substrates in which one of the migrating carbons of the oximes is tetra-substituted and therefore, if any radical pair or ion pair is involved in the rearrangement, these species would be more stable and the original configuration of the migrating carbon would be lost more readily in the product lactams.

Results

The oximation of *O*-acetylandrosterone[5] was found to give a single oxime **1** as described previously.[6] The ground state Beckmann rearrangement of **1** has already been described by Regan and Hayes,[6] and later by Barton and his colleagues.[7] Our repetition of this Beckmann rearrangement with thionyl chloride led to a lactam, $C_{21}H_{33}O_3N$, mp 291—292 °C (50% yield), described by the previous investigators, and a mixture of olefins. The structure of the former was confirmed to be 17a-aza-*D*-homo-5α-androsterone **2** both by the NMR spectrum (no signal corresponding to methylene protons adjacent to the nitrogen) and by the mass spectrum in which distinct fragments were observed at *m/e* 347 (M^+), at *m/e* 332, at *m/e* 272, and at *m/e* 150. The respective fragments of the mass spectrum are attributable to the following fragments A, B, and C.[8] The olefins also obtained in a substantial

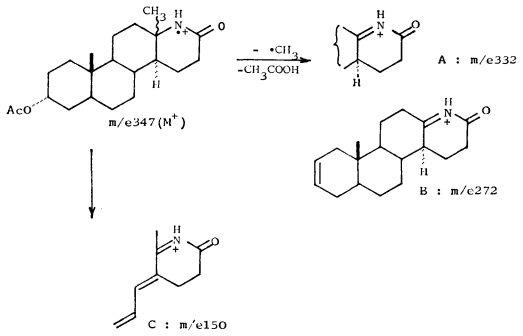

amount (31%) were amorphous. The elemental analysis and the mass spectrum of this was in accord with the molecular formula $C_{21}H_{31}O_2N$. The infrared spectrum of this revealed the characteristic bands at 2280, 1735, 1643, and 900 cm^{-1} attributable to C≡N stretching, acetoxy C=O stretching, C=C stretching and terminal methylene out-of-plane deformation vibrations. The NMR spectrum of this, however, showed it to be a mixture of 3α-acetoxy-13,17-seco-enoic nitriles, **3a**, **3c**, and **3e** with the double bond at 13, 18, at 12, 13 and at 13, 14. Thus, the NMR spectrum showed a broad singlet at τ 5.00, a couple of singlets of equal intensity at τ 5.23 and 5.54, two singlets at τ 7.96 and 9.29. These signals are safely assignable to the 3β-proton, the exocyclic methylene protons on a cyclohexane ring, the 3-*O*-acetyl group, and the C-10 methyl protons of **3a**. Besides these signals the spectrum showed a doublet at τ 4.38 (J=6.0 Hz) ascribable to the C-12-H of **3c** and a singlet at τ 9.26 ascribable to the 10β-methyl protons of **3c** and **3e**. Based on the peak areas the ratio of **3a**, **3c**, and **3e** were estimated to be 2:2:3. The hydrolysis of this mixture with methanolic KOH at room temperature resulted in the formation of a mixture of the corresponding 3β-ols. In the NMR spectrum two singlets at τ 5.25 and 5.56 and a broad singlet at τ 6.00 were observable and these are attributable to the exocyclic methylene protons and the 3β-proton of **3b**. No signal due to an olefinic proton at C-12 was observed but in the methyl part of the spectrum, in addition to the singlet at τ 9.33 ascribable to 10β-methyl protons of **3b**, another singlet at τ 9.29 and a doublet at τ 7.98 (J=2.4 Hz) were observable. We attribute this to the signal due to 10β-methyl protons and 13-methyl protons of **3f**. Based on the intensities of each signals the ratio of **3b** and

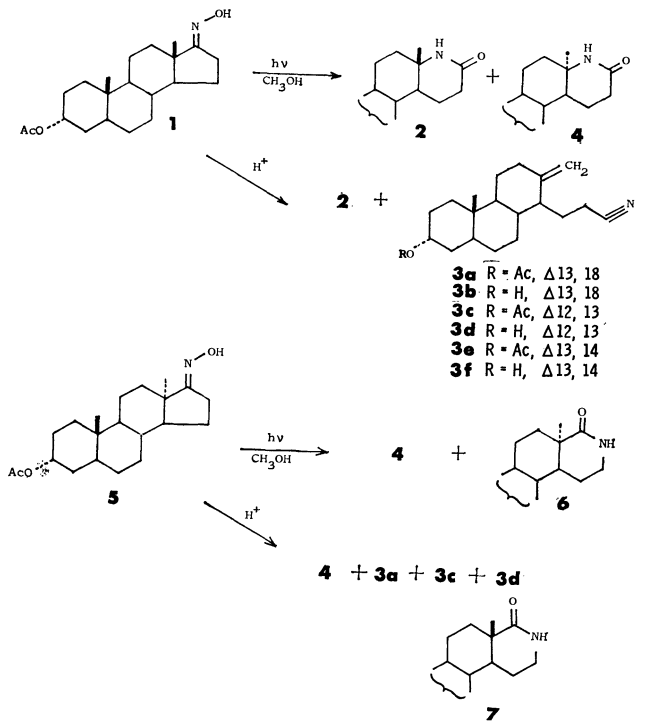

Scheme 1

3f was estimated to be approximately 3:2. The nitriles may be derived either by a second-order Beckmann rearrangement[9] of **1** or by the conversion of the lactam **2** under the reaction condition.[10] But the treatment of **2** in dioxane with $SOCl_2$ did not afford nitriles. Thus, it is certain that these are derived through a second-order Beckmann rearrangement of **1** and is not a secondary reaction product. It is noted that a product due to Beckmann fission of *cis*- and *trans*-8-methyl-1-hydrindanone oximes was a compound with an endocyclic double bond.[11] The obtaining of lactam **2** confirmed that the hydroxyl group is in *anti* position with respect to the C-13 methyl group.

The parallel experiments were then performed with 13α-androsterone oxime. 13α-Androsterone (lumiandrosterone) was first prepared by Butenandt and Poschmann by the photochemical isomerization of androsterone in 1944.[12] In the present study, the irradiation of 3-*O*-acetylandrosterone in dioxane afforded 3-*O*-acetyl-13α-androsterone, mp 122—124 °C, in *ca.* 21% yield. The oximation of this by the usual method afforded a single oxime **5**, mp 186—187 °C, and no isomeric oxime was formed as revealed by tlc. The Beckmann rearrangement of this oxime under the same condition as with androsterone oxime yielded a lactam **4**, mp 193—194 °C* and a mixture of olefins (57 mg) **3a**, **3c**, and **3e** in the ratio of approximately 2:5:3 as was judged by the NMR spectrum. The lactam **4** was isomeric with the lactam **2** and revealed IR bands at 1663 and 3200 cm^{-1} attributable to lactam C=O stretching and lactam NH stretching vibrations. The structure of the lactam **4** should be either 17a-aza-*D*-homo-5α,13α-androsterone or 17-aza-*D*-homo-5α, 13α-androsterone and the former was found to be correct by the NMR and mass spectra. The NMR spectrum of **4** revealed three three-proton singlets at τ 8.74, and at τ 7.96 ascribable to the C-10 methyl, the C-13 methyl and the 3-*O*-acetyl groups, and a three-proton singlet at τ 5.03 and a broad one-proton singlet at τ 3.52 (which vanished on the addition of D_2O), ascribable to the 3βH and the NH. Since no signals due to methylene protons attached to the lactam nitrogen are found, the structure of the lactam **4** should be 17a-aza-*D*-homo-5α,13α-androsterone. This structure was confirmed by the mass spectrum which showed qualitatively the same major fragmentation patterns with that of the lactam **2**. Therefore, the configuration of the hydroxyl group of **5** should be *anti* with respect to the C-13 methyl group.

The oxime **1** in methanol was photolyzed by a 15 W low pressure Hg arc lamp[13] for 30 hr under argon atmosphere to afford a product in which the presence of major four compounds was evidenced by the tlc analysis. Careful separation of the less polar lactam part by the preparative tlc afforded only two lactams, **2** (3%) and **4** (1%), which were identical with the lactams obtained by the ground state Beckmann rearrangements of **1** and **5**. Apart from these lactams a mixture of 3-*O*-acetylandrosterone and 3-*O*-acetyl-13α-androsterone[14] was obtained in 5% yield, together with the oxime **1** in 6% yield.

The photolysis of 3-*O*-acetyl-13α-androsterone oxime **5** was then studied under the same conditions as **1** and afforded a complex mixture of the products. Tlc analysis of this mixture indicated a similar pattern to that in the photolysis of **1** and disclosed the formation of the four major products. Careful preparative tlc gave the crystalline **4** (1%), a mixture of 3-*O*-acetyl-13α-androsterone and 3-*O*-acetylandrosterone (11%) and a gum **6** (3%), apart from the recovered starting oxime (6%). The product **4** was identical with the lactam obtained by the ground state Beckmann rearrangement of **5**. The NMR and IR spectra of the gum **6**, unobtainable in the pure crystalline form (although the near homogeneity of the material was revealed by the tlc examination), were taken and they revealed that gum **6** might be a 3-*O*-acetyl-17-aza-*D*-homo-5α,13α-androsterone. Thus, the mass spectrum of **6** revealed the M^+ peak at *m/e* 347, corresponding to $C_{21}H_{33}O_3N$, and a significant peak at *m/e* 288 due to the elimination of acetic acid from the parent ion. The IR spectrum of **6** revealed the NH band at around 3400 cm^{-1}, the OAc at 1733 cm^{-1} and the lactam C=O group at 1643 cm^{-1}. The NMR spectrum showed three three-proton singlets at τ 9.32, at τ 8.76, and at τ 7.97, a singlet at τ 5.05 and a multiplet from τ 6.2—7.0. These may be attributable to the C-10 methyl, the C-13 methyl, the 3-*O*-acetyl, the 3βH and the C-16-methylene protons.

Through the studies of these two photolyses, the lactam parts of the crude products were very carefully examined. However, none of **6** or **7** from the photolysis of **1**, and none of **2** or **7** from the photolysis of **5**, could be detected in the reaction mixture. Moreover, no nitriles stemming from the photo-Beckmann fission

* Described previously[1] as mp 180—182 °C.

were detected in the photolysates of **1** and **5**.

Discussion

It is notable that while camphor oxime, in which the carbon α to the oximino group is in the bridgehead position and tetra-substituted and is comparable to the present system, gives solely nitriles due to the photo-Beckmann fission,[15] the photolysis of the oximes **1** or **5** does not give any nitriles on photolysis. It is interesting to speculate on the reason for this difference in the modes of photolysis between camphor oxime and steroidal 17-oximes.

One of the rationale for this difference would be the following. In camphor oxime the C_1–C_6 bond may cleave without the intervention of an oxaziridine intermediate since the oxaziridine, if it is formed, should be in the high energy state and would be unstable due to the interaction between the oxaziridine ring and both the C_1-methyl and the extra C_7-methyl. Therefore, the excited camphor oxime would prefer the lower energy reaction pathway, forming an imino radical instead of forming the corresponding oxaziridine ring.

In agreement with this, norcamphor oxime, in which the α-carbon is in bridgehead position but is tri-substituted and there are no C_1- and C_7-methyl groups, affords no cleaved products but the products due solely to normal photo-Beckmann rearrangements.[16]

On the basis of these considerations, we suggest that among several factors which result in the photo-Beckmann fission, the relative stabilities of the intermediate oxaziridine and the N–O bond cleaved species should be the crucial factor together with the strength of the C–C bond to be cleaved.

The formation of an epimeric pair of lactams from an oxime **1** is at variance with the mechanistic pattern on the breakdown of oxaziridine we previously suggested, although we were unable to isolate the lactam **2** from the photolysate of the oxime **5**.[2] The observed non-stereospecificity in the migration from the oxaziridine intermediate to the lactams cannot be due to secondary photolysis of the lactam **2**, which reveals UV absorption maximum at 207 nm (ε: 7300, CH_3OH), as **2** was found to be stable under the condition of the photolysis. The present results would, therefore, require the intervention of a radical or a charged intermediate species, such as **8**, in the rearrangement in liquid phases; in this intermediate[17] the C_{13}–C_{17} bond of the androsterone framework is broken and the C-17 end is released prior to bonding to the nitrogen. The failure in isolating **2** in the photolysis of oxime **5** can either be due to inadequacy of the analysis or due to some complicated origin.

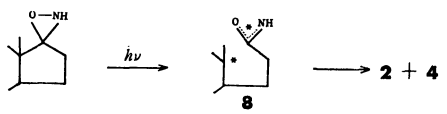

8

With regard to the implication of the present results for the migration step of the photo-Beckmann rearrangement, on the basis of our results together with those of others, the following possibilities on the mode of the formation of lactam from oxaziridine may be considered.

The first would be a unifying mechanism for the whole saturated oximes involving the intervention of an intermediate in which the C–C bond between oxaziridine and the migrating α-carbon is released. If this is the case, our previous results on the oximes of cholestane series should be reinterpreted in terms of the involvement of an intermediate with the configurationally stable ion pairs or radical pairs.

Another possibility is dual mechanism for the saturated oximes. Oximes of cholestan-6-ones, menthone, isomenthone and norcamphor bear the tri-substituted migrating carbon whereas in the oximes of androsterone and 13α-androsterone, one of the migrating carbons is tetra-substituted. Thus we might suspect that the dual mechanisms are operative in the saturated oximes, depending on their structural features, particularly the immediate surrounding of the relevant oximino group, and the oxime which can afford stable ionic or radical species by the cleavage would be able to rearrange through an intermediate in which the migrating group becomes free of the migration terminus. In this instance, we cannot exclude the possibility of amide formation without an involvement of the intermediary oxaziridine although this seems less likely.

Between these, a unifying mechanism would have some difficulty in accommodating the fact that the two isomeric lactams are formed in nearly equal amounts in the case of cholestan-6-one oximes,[2] 3α,5-cyclo-5α-cholestan-6-one oxime,[3] unsymmetrically α-substituted cyclohexanone oximes[4] and norcamphor oxime.[16] Results in these oximes, would be better understandable if we assume both the migrating carbons of oxaziridines migrate to lactams without intermediate. Therefore, with reservation, the preference appears to be for the operation of the dual mechanism.

In the present experiments although we obtained only 17a-aza-*D*-homo-androsterones as the product lactam, the photolysis of the oxime **5** afforded 17-aza-*D*-homo-isomer in addition to 17a-aza-*D*-homo-androsterone.

In terms of the dual mechanism these results may be explicable as follows; in the oxime **5**, the C-13 end may rearrange through the open-chain intermediate such as **8** from oxaziridine but the C-16 end may still be able to migrate to lactam **6**, in this case, without intermediate.

This would mean that in the oxime **1** or **5** two mechanistic modes of the breakdown of oxaziridine appear to operate at the same time although we failed to isolate the lactam **7** in the photolysis of the oxime **1**. Further examination of the stereochemistry of the reaction on the various steroidal substrates will obviously be required to clear up the problem.

Experimental

All mp's were determined by a Yanagimoto type hot-stage and were uncorrected. Unless stated otherwise, IR was determined in Nujol using a Jasco model IR-E spectrophotometer. All NMR spectra were determined on a

Japan Electron Optics PS-100 high resolution NMR spectrometer in $CDCl_3$ solution using TMS as an internal reference. Wako gel B 5 for the preparative tlc was used. The progress of the reactions was followed by the tlc.

Beckmann Rearrangement of 3-O-Acetylandrosterone Oxime. Oxime **1** (300 mg) and thionyl chloride (0.1 ml) in dioxane were stirred for 10 minutes at room temperature. The reaction mixture was neutralized with aqueous 10% KOH and was extracted with chloroform. The solution was worked up in the usual manner. The residue (305 mg) revealed two spots on tlc and column chromatography (Mallinkrodt, silica gel 100 mesh, 3 g) afforded 88 mg of colorless gum and 154 mg of crystals **2**. The latter was recrystallized from acetone, yielding **2**, mp 291—292 °C. (lit., mp 280—284 °C).[7] IR; 3180 cm^{-1} (NH) 1747 cm^{-1} (OAc). 1678 cm^{-1} (lactam C=O). NMR; τ 5.01 (1H, 3β-H), τ 7.96 (3H, OAc), τ 8.86 (3H, C-13 methyl), τ 9.23 (3H, C-10 methyl). The colorless gum was proved to be a mixture of olefins **3a**, **3c**, and **3e** be the NMR spectrum. (See text.)

The Hydrolysis of 3a, 3c, and 3e. The gum above (88 mg) in 5% methanolic KOH (8 ml) was stirred for 5 hr at room temperature. The usual work-up of this reaction mixture afforded an unsaturated nitrile **3b** and **3f** (84 mg) in the ratio of 3: 2.

Photolysis of 3-O-Acetylandrosterone Oxime. Oxime **1** (960 mg) in dry methanol (400 ml) was irradiated by a 15-W low pressure Hg arc lamp under argon atmosphere at room temperature for 104 hours. The solvent was removed under reduced pressure and the residue showed four major spots on tlc. The reaction mixture was submitted to the preparative tlc. (chloroform–acetone 4: 1). Four fractions A, B, C and D were obtained in the order of their increasing polarity. The fraction A (157 mg) was recrystallized from ether, yielding the lactam **2** (57 mg) identical with the lactam **2** obtained by the ground state Beckmann rearrangement of **1**. The fraction B (84 mg) was recrystallized from ether, yielding the lactam **4**, mp 180—182 °C. The fraction C (157 mg) was recrystallized from acetone to yield the pure starting oxime (57 mg). The fraction D (215 mg) was a gum and the NMR spectrum of this showed it to be a mixture of 3-*O*-acetylandrosterone and 3-*O*-acetyl-13α-androsterone.

3-O-Acetyl-13α-androsterone. 3-*O*-Acetylandrosterone (1.27 g) in dioxane (400 ml) was irradiated for 5 hr by a 100 W high pressure Hg arc lamp. After the evaporation of the solvent, the residue was submitted to the preparative tlc. The separation of 3-*O*-acetylandrosterone and the 13α isomer with the similar R_f values could be achieved by twelve times developments of the thin-layer with a mixed solvent of petroleum ether and benzene with an increasing amount of the latter. The number of developments and the proportions of the volumes of petroleum ether and benzene are as follows; twice with 5 (petroleum ether): 1 (benzene), three times with 3: 1, once with 2: 1, twice with 1: 1, twice with 1: 1, twice with 1: 2 containing a few drops of ethyl acetate. Thus, 3-*O*-acetyl-13α-androsterone (263 mg, 21%) was obtained and showed mp 122—124 °C. Butenandt and Poschmann reported mp 121—122 °C for this compound. NMR τ 9.37 and τ 9.04 (C-10 methyl and C-13 methyl) τ 8.03 (OAc) τ 5.09 (3β-H). IR; 1740 cm^{-1} (OAc, five-membered ring ketone).

Oxime of 3-O-Acetyl-13α-androsterone. 3-*O*-acetyl-13α-androsterone (165 mg), hydroxylamine hydrochloride (180 mg) and sodium acetate (120 mg) in ethanol (7 ml) were stirred for 6 hours at room temperature and then were warmed for 17 hours at 50—60 °C. The usual work-up of the reaction mixture afforded the crude oxime **5** (129 mg). This was recrystallized from hexane, yielding 111 mg of the oxime **5**, mp 186—187 °C. Found: C, 72.71; H, 9.37; N, 3.88%; Calcd for $C_{21}H_{33}O_3N$: C, 72.58; H, 9.57; N, 4.03%. IR 3440 cm^{-1} (OH), 1710 cm^{-1} (OAc), 1665 cm^{-1} (C=N), Mass *m/e* 347 (M^+). NMR τ 9.34 and τ 8.96 (C-10 methyl and C-13 methyl) τ 7.97 (OAc), τ 4.97 (3β-H).

Beckmann Rearrangement of 3-O-Acetyl-13α-androsterone Oxime. To the solution of **5** (100 mg) in dioxane (1 ml) there was added thionyl chloride (0.5 ml). The solution was stirred for 20 min at room temperature. Work-up as was described in the case of the oxime **1** afforded a crude product (157 mg). This showed to be a mixture of nonpolar and polar substances by the tlc. Purification by the preparative tlc afforded a crude lactam **4** (40 mg) and a mixture of olefins. The former was recrystallized from a mixture of ether and hexane to yield the lactam **4**, mp 193—194 °C (25 mg). Found: C, 72.57; H, 9.62; N, 3.77%. Calcd for $C_{21}H_{33}O_3N$: C, 72.58; H, 9.57; N, 4.03%. IR 3200 cm^{-1} (NH), 1741 cm^{-1} (OAc), 1633 cm^{-1} (lactam C=O). Mass *m/e* 347 (M^+), *m/e* 332, 272, 150. The latter was a colorless gum and it was proved to be a mixture of the three olefinic nitriles **3a**, **3c**, and **3e** in the ratio of 2: 5: 3 as was judged by the NMR spectrum in the same manner as in the case of Beckmann rearrangement of **1**. The hydrolysis of this mixture (43 mg) afforded a mixture of **3b**, **3d**, and **3f** (33 mg) in a ratio of 2: 5: 3 as was judged by the NMR spectrum. The presence of **3d** was apparent by the presence of a broad doublet signal at τ 4.39 (J=4.5 Hz). The 10β-methyl protons of **3d** and **3f** appeared as a coincident singlet at τ 9.29. Moreover, there were two doublets at τ 7.98 (J=2.4 Hz) and at τ 8.05 (J=2.7 Hz), which are attributable to the 13-methyl protons of **3f** and **3d**. The observed small splittings are due to allyl couplings.

Phytolysis of 3-O-Acetyl-13α-androsterone Oxime. Oxime (500 mg) in dry methanol (200 ml) was irradiated by a 15-W low pressure Hg arc lamp under argon atmosphere at room temperature for 30 hr. The solvent was removed under reduced pressure and the residue showed four major spots on tlc. This reaction product was submitted to the preparative tlc. (chloroform–acetone 5: 1). The four fractions A. B, C and D in the order of increasing polarity were obtained. The fraction A (46 mg) was recrystallized from ether to yield 5 mg of the lactam **4** identical with lactam obtained by the ground state Beckmann rearrangement of **5**. The fraction B (30 mg) was purified again by the preparative tlc, yielding 13 mg of gum. It was not in a crystalline state, but the NMR and IR spectra of the gum showed it to be probably a crude lactam **6**. The fraction C (105 mg) was recrystallized from acetone to yield 31 mg of the starting oxime **5**. The fraction D (55 mg) was found to be a mixture of 3-*O*-acetyl-13α-androsterone and 3-*O*-acetylandrosterone from its NMR and IR spectra.

The authors are grateful to the Ministry of Education of Japan for financial assistance. We thank Mrs. Satoko Araki in this department for the measurements of 100 MHz NMR spectra. Microanalyses and the measurements of the mass spectra were carried out by the staffs of the laboratories of the Faculty of Pharmaceutical Sciences of this university, and we thank them for these measurements.

References

1) Photoinduced Transformations XXIII. The previous paper: H. Suginome and T. Uchida, *Tetrahedron Lett.*, **1973,**

2289.

2) H. Suginome and H. Takahashi, *ibid.*, **1970**, 5119.

3) H. Suginome, H. Takahashi, and T. Masamune, This Bulletin, **45**, 1836 (1972).

4) M. Cunningham, L. S. N. Lim, and G. Just, *Can. J. Chem.*, **49**, 2891 (1971).

5) A. Butenandt, *Angew. Chem.*, **45**, 655 (1932).

6) B. M. Regan and F. N. Hayes, *J. Amer. Chem. Soc.*, **78**, 639 (1956).

7) C. H. Robinson, O. Gnoj, A. Mitchell, E. P. Oliveto, and D. H. R. Barton, *Tetrahedron*, **21**, 743 (1965).

8) H. Budzikiewicz, F. Compernolle, K. V. Cauwenberghe, K. Schulze, H. Wolf, and G. Quinkert, *ibid.*, **24**, 6797 (1968).

9) L. G. Donaruma and W. Z. Heldt, "Organic Reaction," Vol. 11, p. 1 (1960).

10) G. DiMaio and V. Permutti, *Tetrahedron*, **22**, 2059 (1966).

11) E. J. Moriconi and M. A. Stemniski, *J. Org. Chem.*, **37**, 2035 (1972). DiMaio and Permutti[10] described that the treatment of *cis*-8-methyl-1-hydrindanone oxime with PCl_5 in ether afforded a fission product with an exocyclic double bond. This product is not a true Beckmann fragmentation product since these investigators converted a lactam obtained by the Beckmann rearrangement into the fission product in question.

12) A. Butenandt and L. Poschmann, *Ber.*, **77**, 394 (1944).

13) In our previous papers[2,3] 15-W Hg arc lamp was erroneously described as 150 W.

14) These two isomeric ketones were readily discernible by the difference of the chemical shift of either the C-10 methyl groups or the C-13 methyl groups. (*O*-acetylandrosterone, C-10 methyl at τ 9.18, C-13 methyl at τ 9.14, *O*-acetyl-13α-androsterone, C-10 methyl at τ 9.37, C-13 methyl at τ 9.04) The isomeric *syn* oxime was neither observed on tlc nor isolated. This is understandable by assuming that in steroid 17-oximes the thermal relaxation of photochemically formed *syn* oxime to *anti* is very rapid even at room temperature. (*cf.* G. Wettermark, "The Chemistry of the Carbon-Nitrogen double bond," ed. by S. Patai, Interscience, London (1970), p. 565).

15) T. Sato and H. Obase, *Tetrahedron Lett.*, **1967**, 1633. T. Sato, *Asahi-garasukogyo Gijutushorekai Report*, **14**, 425 (1968).

16) B. L. Fox and H. M. Rosenberg, *Chem. Commun.*, **1969**, 1115.

17) This naturally implies a solvated species.

The Chlorination of Olefins with Antimony(V) Chloride[1]

Sakae UEMURA,* Akira ONOE, and Masaya OKANO
Institute for Chemical Research, Kyoto University, Uji, Kyoto 611

(Received August 8, 1973)

Antimony(V) chloride was revealed to be a good reagent for the *cis*-chlorination of simple olefins in chlorinated hydrocarbon solvents, such as 1,2-dichloroethane, dichloromethane, chloroform, and carbon tetrachloride. The higher the reaction temperature or the solvent polarity was, the higher the selectivity for *cis*-chlorination became. From 1,3-butadiene, *cis*-1,4-dichloro-2-butene was formed together with the *trans*-1,4- and 1,2-dichloro isomers. In the cases of cyclopentene and norbornene, the *trans*-1,2-dichloride and other various dichlorides were obtained without any formation of the *cis*-1,2-isomer. Probable mechanisms for this chlorination are briefly discussed.

Although antimony(V) chloride has been used as a reagent for the chlorination of aromatic hydrocarbons[2] and alkanes[3] and as an active catalyst for chlorine molecule addition to olefins,[4-6] the direct chlorination of olefins with this reagent has not yet been studied except for only one case with α,β-dibromoethylene.[7] After we published our preliminary data[1] concerning a predominant *cis*-chlorination of certain olefins with antimony(V) chloride in carbon tetrachloride, an additional study of the same reaction in a more polar solvent, liquid SO_2, was described by Akiyama *et al.*[8] In this report, all the results of the chlorination of several kinds of mono-olefins and 1,3-butadiene in less polar solvents, mainly chlorinated hydrocarbons, will be described in detail. In contrast to other metal or metalloidal chlorides,[9] this chloride showed a striking product selectivity.

Results and Discussion

Reaction with Simple Olefins. When an olefinic hydrocarbon was added to a light-yellow homogeneous solution of antimony(V) chloride in carbon tetrachloride at room temperature, the reaction occurred exothermally to give the corresponding *vic*-dichloroalkane (**1**) in a good yield, occasionally together with small amounts

$$RCH{=}CHR' \xrightarrow[CCl_4]{SbCl_5} \underset{\mathbf{1}}{RCH(Cl)-CHR'(Cl)} + \underset{\mathbf{2}}{RCH_2-CHR'(Cl)} \quad (1)$$

of monochloride (**2**). Some typical data for several olefins are shown in Table 1. In contrast to the usual complete or predominant *trans*-addition in the chlorination using chlorine gas or other metal and metalloidal chlorides[9] (*e.g.*, PCl_5, $CuCl_2$, $AuCl_3$, and $TlCl_3$), a favorable *cis*-addition is the most remarkable feature of this chlorination.[10] Separate experiments revealed that no interconversion of *cis*- and *trans*-1,2-dichlorocyclohexanes occurred under the present reaction conditions. Moreover, as can be seen in Table 1, an elongation of the reaction time does not affect the ratio of *cis*- to *trans*-addition in the chlorination of *trans*-2-butene. Therefore, the observed ratio of *cis*- and *trans*-addition appears to be kinetically controlled. It should be noted that a rise in the reaction temperature resulted in a considerable increase in the *cis*-selectivity of this chlorination. The temperature dependence on the isomer ratio would indicate that both isomers may not arise from a common intermediate, as will be discussed later.

The reaction is clearly of an electrophilic nature,

Table 1. Chlorination of simple olefins by antimony(V) chloride in carbon tetrachloride [$SbCl_5$ 25 mmol, CCl_4 100 ml]

Run	Olefin	mmol	Temp. °C	Time min	Products, mmol				Ratio of *cis*- to *trans*-add.
					1			**2**	
					cis-add.	*trans*-add.	total yield, %[a]		
1	*trans*-2-Buetne[b]	71	73	10	19.7[f]	4.3[g]	96	0	4.6[l]
2	*trans*-2-Butene[b]	54	73	60	19.5[f]	4.2[g]	94	0	4.7[l]
3	*trans*-2-Butene[b]	30	2—6	10	17.5[f]	7.5[g]	100	0	2.3[l]
4	*cis*-2-Butene[c]	45	76	10	20.6[g]	3.8[f]	98	0	5.4[l]
5	*cis*-2-Butene[c]	61	0	10	18.0[g]	5.9[f]	96	0	3.1[l]
6	*cis*-2-Octene[d]	50	76	10	13.4[h]	2.1[i]	62	4.5	6.4[l]
7	2-Octene[e]	50	30—35	10	12.4[h]	7.5[i]	80	5.3	1.7
8	Cyclohexene	20	76	10	15.0[j]	3.0[k]	90	1.7	5.0
9[m]	Cyclohexene	100	0—10	10	11.9[j]	13.0[k]	92	4.0	0.9
10	1-Octene	50	30—35	10	25.0		100	0	—
11	Allyl chloride	50	30	30	23.1		92	0	—

a) Based on $SbCl_5$. b) Contains 1% of *cis*-isomer. c) Contains 2.4% of *trans*-isomer. d) Contains 0.2% of *trans*-isomer. e) A mixture of *cis*- and *trans*-isomer (1: 1). f) *dl*-Isomer. g) *meso*-Isomer. h) *erythro*-Isomer. i) *threo*-Isomer. j) *cis*-Isomer. k) *trans*-Isomer. l) Correction based on contamination is not made. m) $SbCl_5$, 27 mmol.

because no reaction occurred with olefins having strong electron-withdrawing groups, such as acrylonitrile, ethyl maleate, ethyl fumarate, and tetrachloroethylene, even at the refluxing temperature in carbon tetrachloride, and all the olefins were recovered qualitatively. In a reaction with styrene or ethyl vinyl ether, a vigorous reduction of antimony(V) to antimony(III) occurred even at 0 °C, but only a resinous product was obtained; all attempts to isolate the dichlorinated compound were unsuccessful.

A radical pathway for the formation of **1** can be excluded by considering the following facts. First, no trace of 4-chloro-1-cyclohexene was found in the chlorination products from cyclohexene. Second, when the reaction was carried out in the presence of *m*-dinitrobenzene or oxygen, no change in the yield or in the *cis*/*trans* ratio of **1** was observed.

In order to ascertain the effect of solvents upon the stereoselectivity of the reaction, the chlorination of cyclohexene was carried out in several solvents. Some results are given in Table 2a. All the reaction mixtures were homogeneous. In chlorinated hydrocarbon solvents, the *cis*-dichloride generally predominated, and an increase in the ratio of *cis*- to *trans*-addition was observed when the dielectric constant of the solvent was increased. On the contrary, in a donor solvent such as carbon disulfide, a favorable *trans*-addition was observed. Certain polar solvents were not adequate for this chlorination; *i.e.*, when nitromethane was used as a solvent, only a slight amount of dichloride was formed from cyclohexene, and the reaction in acetonitrile afforded a tarry product. Alcohols, ethers (diethyl ether, 1,4-dioxane and tetrahydrofuran), dimethylformamide, and dimethyl sulfoxide could not be used as solvents because of a vigorous reaction or adduct formation between the solvent and antimony(V) chloride itself.

We should also consider briefly the source of hydrogen chloride, which gives **2** by addition to olefins. As the hydride-ion abstraction from triphenylmethane, 9,10-dihydroanthracene and cycloheptatriene with antimony(V) chloride has been established[11] to give hexachloroantimonate salts of stable carbonium ions, $SbCl_3$, and hydrogen chloride, it might be possible to assume that a similar abstraction may occur with olefins to produce hydrogen chloride. In fact, though we failed to isolate the corresponding antimonate salts or the hydrogen chloride addition product, α-chloroethylbenzene (**2**), because of the polymerization of styrene, the evolution of much hydrogen chloride was observed during the reaction of styrene. As the addition of hydrogen chloride is much easier to internal olefins than to terminal ones, **2** was not obtained from 1-octene and allyl chloride. Furthermore, the rate of the formation of **2** seems much slower than that of **1**; when the reaction was carried out using a smaller amount of cyclohexene than of antimony(V) chloride, the yield of chlorocyclohexane (**2**) became very low without affecting that of **1**. This may be a reason why **2** was not obtained from either *trans*- or *cis*-2-butenes, where the contact time of olefin and antimony(V) chloride is considered not to be very long. Another possible source of hydrogen chloride is the decomposition of antimony(III) chloride (formed through a reaction) or antimony(V) chloride by moisture.[12] However, even in the careful reaction under N_2 in a dried condition, the formation of **2** was observed, and so this possibility may be excluded.

Table 2. Chlorination of cyclohexene by antimony(V) chloride

(a) Effect of solvents on the isomer ratio [$SbCl_5$ 25 mmol, solvent 100 ml]

Cyclohexene mmol	Solvent (ε)	Temp. °C	Time min	1,2-Dichlorides Yield,[a] %	1,2-Dichlorides *cis*/*trans* Ratio
20	$ClCH_2CH_2Cl$ (10.37)	83	10	88	8.3
20	$ClCH_2CH_2Cl$ (10.37)	20—30	10	89	4.6
100	CH_2Cl_2 (8.9)	40	10	89	4.0
100	$CHCl_3$ (4.70)	30—40	10	67	3.2
20	CCl_4 (2.23)	76	10	90	5.0
20	CCl_4 (2.23)	20—30	10	94	1.5
100	CCl_4 (2.23)	20—40	10	98	1.5
100	CS_2 (2.64)	30	10	77	0.81

(b) Effect of additives on the isomer ratio [Cyclohexene 100 mmol, $SbCl_5$ 25 mmol, CCl_4 100 ml, 76 °C, 10 min]

Additive mmol	1,2-Dichlorides Yield,[a] %	1,2-Dichlorides *cis*/*trans* Ratio
None	67	5.0
$SbCl_3$, 25	67	4.3
$TiCl_4$, 25	85	3.7
SbF_3, 25	52	1.2
$AlCl_3$, 25	25	0.8

a) Based on $SbCl_5$.

Table 3. Chlorination of 1,3-butadiene by antimony(V) chloride in carbon tetrachloride [$SbCl_5$ 25 mmol, CCl_4 100 ml]

Diene mmol	Temp. °C	Time min	Products (mmol) and yield[a] (%) Dichlorides 3[b]	4[c]	5[d]	Total yield	Tetrachlorides 6[e]	7[f]	Total yield
78	0	10	3.7	2.5	5.6	47	0.3	0.3	5
86	30	10	4.5	2.5	4.6	46	0.9	1.2	17
62	76	10	6.9	3.6	6.1	66	1.4	2.7	33

a) Based on $SbCl_5$. b) 3,4-Dichloro-1-butene. c) *cis*-1,4-Dichloro-2-butene. d) *trans*-1,4-Dichloro-2-butene. e) *dl*-1,2,3,4-Tetrachlorobutane. f) *meso*-1,2,3,4-Tetrachlorobutane.

Reaction with 1,3-Butadiene. By passing 1,3-butadiene through a CCl_4 solution of antimony(V) chloride, the following compounds were obtained as products: 3,4-dichloro-1-butene (**3**), *cis*- and *trans*-1,4-dichloro-2-butenes (**4** and **5** respectively), and two stereoisomers of tetrachlorobutanes [**6** (*dl*) and **7** (*meso*)]. Some typical data are shown in Table 3. Separate experiments eliminated the possibility of the interconversion of **3**, **4**, and **5** under the present reaction conditions. At higher temperatures the formation of **6** and **7** became prominent; they were apparently formed by a further reaction of **3**, **4**, and **5** with antimony(V) chloride. A rather high proportion of **4** (21—22%) to all the products should be noted here, together with the results of chlorination using $TlCl_3 \cdot 4H_2O$[13] (11%) and $CuCl_2$[14] (5%), because **4** has never[15] or only slightly (1%)[16] been formed in chlorination with a chlorine molecule. This fact suggests the existence of a certain interaction between metal chloride and both terminal carbons of 1,3-butadiene.

$$CH_2{=}CH{-}CH{=}CH_2 \xrightarrow[CCl_4]{SbCl_5} \underset{\mathbf{3}}{CH_2{=}CHCHClCH_2Cl} + \underset{\mathbf{4}\ (cis)\ \&\ \mathbf{5}\ (trans)}{ClCH_2CH{=}CHCH_2Cl} + \underset{\mathbf{6}\ (dl)\ \&\ \mathbf{7}\ (meso)}{ClCH_2CHClCHClCH_2Cl} \quad (2)$$

Reaction with Cyclopentene and Norbornene. For cases of cyclopentene and norbornene, which might resist the *cis*-addition or *cis*-attack of the bulky species, the *trans*-1,2-dichloride and various unexpected dichlorides were obtained without the formation of the *cis*-1,2-isomer (Eqs. (3) and (4), where the figures in parentheses indicate a product distribution). All the dichlorides for each reaction seem to be formed by way of the corresponding carbonium ions, *i.e.*, the classical chlorocyclopentyl cation and the nonclassical chloronorbornyl cation, as will be discussed later. The reaction of cyclopentene with chlorine gas (neat or in CCl_4) has been reported[17] to yield only **10**; we found

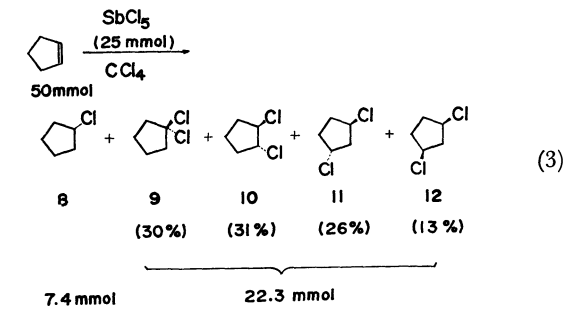

(3)

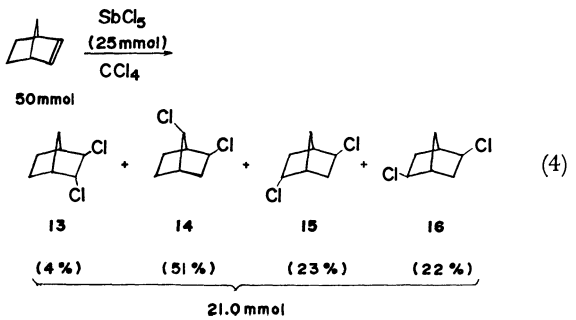

(4)

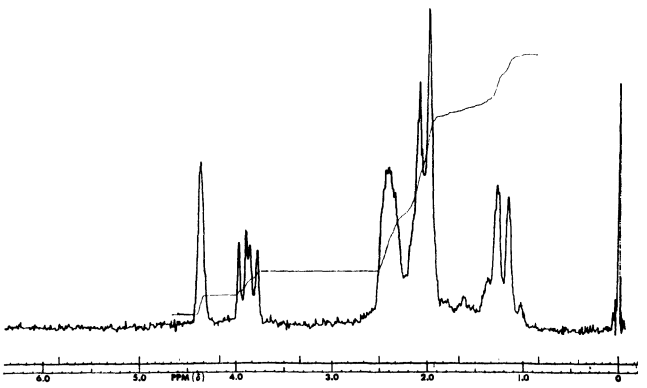

Fig. 1. NMR spectrum of **14** in CCl_4.

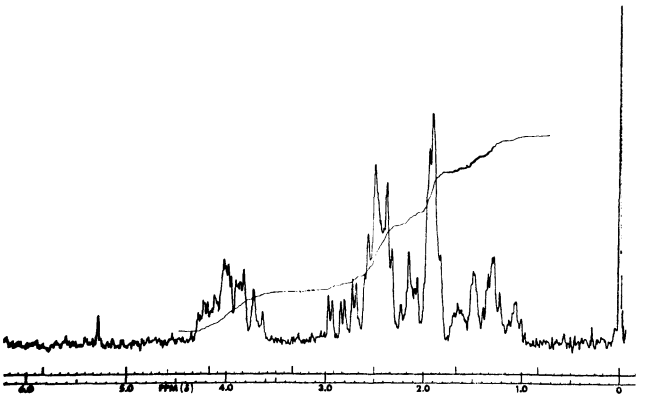

Fig. 2. NMR spectrum of **15** in CCl_4.

such a case also with copper(II) chloride (in acetonitrile). As to the chlorination of norbornene, the diversity of reaction products has previously been established. Thus, the chlorination with chlorine gas (in CCl_4) affords nortricyclyl chloride and *exo*-2-*syn*-7-dichloronorbornane, together with smaller amounts of *trans*-2,3- (**13**) and *exo*-*cis*-2,3-dichloronorbornane, by the ionic pathway,[18] and the reaction with gold(III) chloride (in cyclohexane) gives a mixture of *exo*-*cis*-2,5-dichloronorbornane (**16**), *exo*-2-*syn*-7-dichloronorbornane, and two unidentified isomeric dichlorides.[19] We have also confirmed that the chlorination with copper(II) chloride (in acetonitrile) yields mainly the *trans*-2,3- (**13**) and *exo*-*cis*-2,3-dichlorides, just as does the reaction with iodobenzene dichloride.[20]

Probable Reaction Mechanisms. The nature of antimony(V) chloride in solutions appears to depend on the polarity of the solvents. Thus, in acetonitrile (ε 37.5) the conductivity data have shown that $SbCl_5$ is in equilibrium with $SbCl_4^+$ and $SbCl_6^-$,[21] while in carbon tetrachloride (ε 2.23) it has been established that the vibrational spectra are consistent with the D_{3h} symmetry expected for covalent antimony(V) chloride; *i.e.*, the predominant species is the monomeric molecules.[22] In contrast to such thermodynamic data, Kovacic and Sparka have assumed the attack of the $SbCl_4^+$ moiety formed from two molecules of antimony(V) chloride (see Eq. (5)) in the reaction of benzene, toluene, and chlorobenzene with antimony(V) chloride (below 40 °C), where an excess aromatic component (ε 2.27—5.61) is used as the solvent.[2] Since the re-

action conditions of our chlorination and the electrophilic nature of the reaction are apparently similar to those of this aromatic chlorination, a similar participation of the ionic species—an initial attack of $SbCl_4^+$ on olefins, followed by a Cl^- transfer from $SbCl_6^-$ to give *trans*-dichlorides—might be expected, though the concentration of these species is believed to be very low. In this connection, a considerable decrease in the ratio of *cis*- to *trans*-addition was observed upon the addition of a strong Lewis acid (*e.g.*, $AlCl_3$ and SbF_3) to our chlorinating system (see Table 2b), where a complex formation of antimony(V) chloride with Lewis acid is to be expected (Eq. (6)).

$$2SbCl_5 \rightleftharpoons (SbCl_5)_2 \rightleftharpoons SbCl_4^+\|SbCl_6^- \quad (5)$$

17 **18** **19**

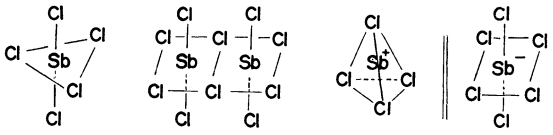

17 **18** **19**

$$SbCl_5 + MXn \rightleftharpoons SbCl_4^+\|MXnCl^- \quad (6)$$

20

On the other hand, the formation of *cis*-dichlorides can presumably be explained by a concerted or near-concerted molecular addition of **17** or **18** to olefins, as has been proposed in connection with the chlorination of olefins by iodobenzene dichloride.[23] The distance

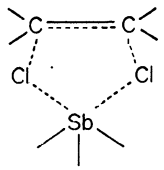

of any two chlorines is about 3.2—4.0 Å, assuming that the antimony-chlorine bond length of antimony(V) chloride is 2.29—2.34 Å[24] even in the liquid state; this is large enough for the interaction of two chlorines with two p-orbitals of simple olefins and even of 1,3-butadiene at the 1,4-position. The rather high proportion of *cis*-1,4-dichloro-2-butene (**4**) in the reaction products of 1,3-butadiene may be explained by assuming this interaction at the *s-cis*-conformation of 1,3-butadiene.

Since the ionization step in Eq. (5) is considered to be exothermic, like that of PCl_5,[25] the amount of **19** can be expected to increase when the temperature is lowered. The observed temperature effect on the isomer ratio in each solvent agreed with this expectation (see Table 2a). It is also anticipated that an increase in the solvent polarity would increase the proportion of ionized species. However, apparently a different trend was observed within a range of selected chlorinated hydrocarbon solvents (ε 2.23—10.37): namely, the higher the solvent polarity was, the higher the *cis*-selectivity became (see Table 2a). This may be explained by considering the large difference in the solvent effect on the rate between two chlorination reaction; *i.e.*, a change to a more polar solvent will increase the rate of the *cis*-addition (the reaction between two uncharged species) and will decrease that of the *trans*-addition (the reaction between uncharged and charged species).[26] The low *cis*-selectivity in carbon disulfide (ε 2.64) compared with that in carbon tetrachloride (ε 2.23) might be ascribed to the stabilization of **19** by solvation.

Another possible scheme for the chlorination is the addition of both chlorine and tetrachloroantimony species to olefin, followed by the displacement of antimony with chlorine (Eq. (7)), as has been established in the case of PCl_5.[27] However, the *trans* compound should be obtained preferably or exclusively by this scheme, as in the case of a reaction using PCl_5;[27] also, even careful experiments have failed to isolate the intermediate antimony compound. From these facts, this scheme can be excluded from consideration.

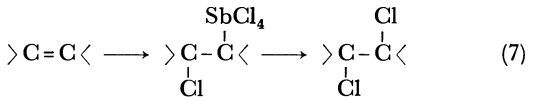

(7)

Finally, reasonable pathways to various unexpected chlorides derived from cyclopentene and norbornene were considered. If the *cis*-addition proceeds through a concerted or near-concerted transfer of chlorine between **17** or **18** and olefin, as has been described previously, quite a large steric hindrance would be unavoidable for both olefins and the attack of the $SbCl_4^+$ moiety of **19** may become important. In addition, an eclipsing effect at the Cl^--transfer step may affect the reaction products. In fact, the obtained 1,2-dichlorides consisted entirely of the *trans*-isomer. Further, the formation of 1,1- and 1,3-dichlorocyclopentanes from cyclopentene can be explained by assuming the deprotonation of the cation, **22** (Eqs. (8) and (9)). In the case of norbornene, the attack of $SbCl_6^-$ from a less crowding site upon each of the nonclassical

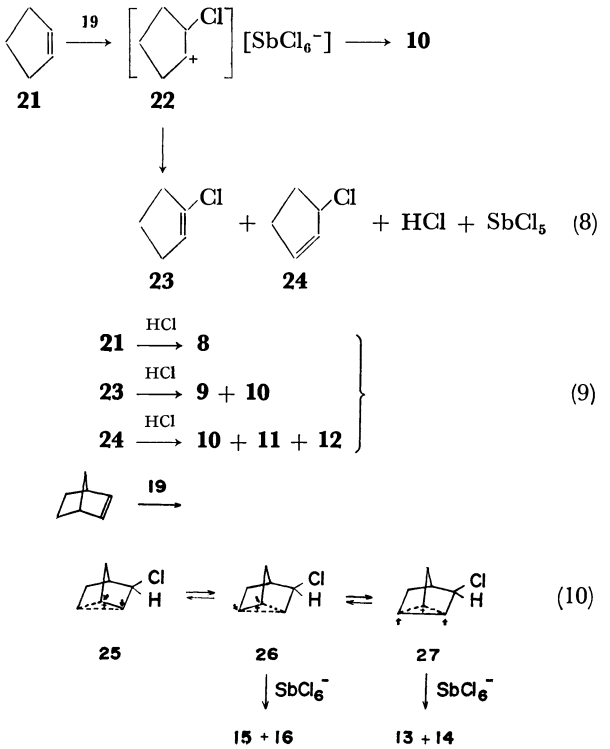

21 **22** **23** **24** (8)

(9)

(10)

25 **26** **27**

15 + 16 **13 + 14**

ions in equilibrium[28] may be expected, and all expected dichlorides were obtained except for those from **25** (Eq. (10)). The results seem to provide chemical evidence for the existence of such an equilibrium.

Experimental

Materials. Commercially-available *trans*-2-butene (contains 1% of the *cis*-isomer), *cis*-2-butene (contains 2.4% of the *trans*-isomer), and 1,3-butadiene were used without further purification, while $SbCl_5$ and all the other organic substrates and solvents were purified by distillation before use.

General Procedure. An appropriate amount of an olefinic hydrocarbon was added or bubbled into a homogeneous yellow solution of $SbCl_5$ (sometimes containing another Lewis acid salt as an additive) in a suitable solvent under stirring. The resulting black-red reaction mixture was cooled, aqueous NaOH was added, and the antimony(III) oxychloride or pentoxydichloride formed was filtered out.* The products in the filtrate sepatated from water were analyzed by glc with an appropriate internal standard material. The product composition was almost unchanged in the reverse reaction, *i.e.*, the drop-by-drop addition of $SbCl_5$ to a solution containing olefin.

a) 1,3-Butadiene: 1,3-Butadiene gas (4.6 g, 86 mmol) was bubbled into a CCl_4 (100 ml) solution of $SbCl_5$ (7.5 g, 25 mmol) at 30 °C for 10 min. The mixture was then treated as described above; the subsequent glc analysis of the CCl_4 layer showed the presence of these five components as products; 3,4-dichloro-1-butene (**3**; 0.56 g, 4.5 mmol), *cis*-1,4-(**4**; 0.31 g, 2.5 mmol) and *trans*-1,4-dichloro-2-butene (**5**; 0.58 g, 4.6 mmol), and *dl*-1,2,3,4- (**6**; 0.22 g, 1.2 mmol) and *meso*-1,2,3,4-tetrachlorobutane (**7**; 0.17 g, 0.9 mmol). A mixture of **4** and **5** (**4**: **5**=*ca.* 1: 2) was isolated by distillation (bp 51—53 °C/22 mmHg) from the reaction products of several runs. NMR (in $CDCl_3$) of the mixture; δ 6.05—5.7 (m, 2H), 4.2—4.0 (m, 4H). Found: C, 37.64; H, 4.72; Cl, 56.38%. Calcd. for $C_4H_6Cl_2$: C, 38.43; H, 4.84; Cl, 56.73%.

When 1,3-butadiene (3.5 g, 65 mmol) was passed into a CCl_4 (25 ml) solution of $SbCl_5$ (15 g, 50 mmol) at 76 °C for 10 min, a mixture of isomeric tetrachlorobutanes (**6** and **7**) was obtained as the main product (12.7 mmol, **6**: **7**=1: 2.7). Found: C, 24.53; H, 3.14; Cl, 72.33%. Calcd. for $C_4H_6Cl_4$: C, 24.52; H, 3.08; Cl, 72.39%. **7** was isolated as a solid and was revealed to be a *meso*-isomer; mp 72 °C from ethanol (lit.,[15] 72 °C).

b) Cyclopentene: The reaction of cyclopentane (3.4 g, 50 mmol) with $SbCl_5$ (7.5 g, 25 mmol) in CCl_4 (100 ml) at 25 °C for 5 min afforded a mixture of five products: **8** (7.4 mmol) and **9**—**12** (22.3 mmol, **9**: **10**: **11**: **12**=30: 31: 26: 13 by g.l.c.). A simple distillation gave 2.6 g, (18.7 mmol) of a mixture of **9**—**12**, which was revealed by analysis to be composed of isomeric dichlorocyclopentanes; bp 61—64 °C/42 mmHg. Found: C, 43.19; H, 5.97%. Calcd for $C_5H_8Cl_2$: C, 43.19; H, 5.80%. Further products, **9**, **10**, **11**, and **12**, were purely isolated by preparative glc, and comparisons of the NMR spectra and retention time on glc with those of the reported ones[29] revealed the compounds to be 1,1-, *trans*-1,2-, *trans*-1,3-, and *cis*-1,3-dichlorocyclopentane respectively. The chlorination of cyclopentene with a chlorine molecule in CCl_4[17] at room temperature afforded only **10** (by glc). **10** (1.2 g) could also be prepared by the reaction of cyclopentene (3.4 g) with $CuCl_2$ (3.4 g) in acetonitrile (25 ml) containing LiCl (1.1 g) at 80 °C for 3 hr; bp 50—51 °C/22 mmHg (lit.,[17] 53—53.5 °C/25 mmHg).

The reaction using 1,2-dichloroethane as a solvent at 84 °C for 10 min gave **9**, **10**, **11**, and **12** in the ratio of 18: 32: 30:: 20 (19 mmol).

c) Norbornene: The reaction of norbornene (4.7 g, 50 mmol) with $SbCl_5$ (7.5 g, 25 mmol) in CCl_4 (100 ml) at 26 °C for 10 min gave a mixture of four products (21 mmol, **13** : **14** : **15** : **16**=4 : 51 : 23: 22 by glc), all of which were revealed to be isomeric dichloronorbornanes by analysis; bp 92—98 °C/18 mmHg. Found: C, 50.72; H, 6.16%. Calcd for $C_7H_{10}Cl_2$: C, 50.93; H, 6.11%. After the fractional distillation of the mixture (a, bp 83—86 °C/13 mmHg; b, 86—87 °C/13 mmHg; c, 54—55 °C/2 mmHg), three products, **14**, **15**, and **16**, were purely isolated from Fraction a, b, and c respectively, by preparative glc. The NMR spectrum (in CCl_4) and the retention time on glc of **13** were identical with those of *trans*-2,3-dichloronorbornane, which was obtained from the reaction of norbornene (4.7 g) and $CuCl_2$ (13.4 g) in acetonitrile (200 ml) containing LiCl (4.2 g) at 84 °C for 3 hr; δ 4.3—4.1 (m, 1H), 3.7—3.6 (t, J=2 Hz, 1H) 2.6—2.3 (m, 2H), 2.1—1.1 (m, 6H). In the chlorination with $CuCl_2$, a slight formation of the *cis-exo*-2,3-dichloroisomer was also detected, together with **13** (yield, 6.7 g; *cis*: *trans*=*ca.* 1: 8). The NMR spectrum (in CCl_4) of **16** was identical with that of *exo-cis*-2,5-dichloronorbornane reported by Hüttel *et al.*;[19] δ 3.8—3.6 (t, J=5.5 Hz, 2H), 2.6—2.4 (m, 2H), 2.0—1.8 (m, 6H). The NMR spectra (in CCl_4) of **14** and **15** are shown in Figs. 1 and 2; **14**, δ 4.35 (s, 1H), 4.0—3.75 (m, 1H), 2.5—2.25 (m, 2H), 2.2—1.9 (m, 4H), 1.4—1.1 (m, 2H); **15**, δ 4.3—3.6 (m, 2H), 3.0—2.0 (m, 4H), 2.0—1.8 (m, 2H), 1.8—1.0 (m, 2H). The possibility of **14** and **15** being *cis-exo*-2,3- and *exo*-2-*syn*-7-dichloronorbornanes was eliminated, as well as the possibility of their being *cis-endo*-2,3-dichloroisomer (lit.,[18b] mp 70—72 °C), by a comparison of the retention time on glc and of the boiling point with the samples prepared by the reported method.[18a] Thus, **14** and **15** should be either *exo*-2-*anti*-7-, *trans*-2,5-, or *cis*- or *trans*-2,6-dichloronorbornane. In deuterated pyridine, a broad resonance near δ 2.4 of **14** in CCl_4 was split into two kinds of peaks, δ 2.15 (m) and 2.35 (m). Further, the sharp singlet peak at δ 4.35 of **14** can most reasonably be explained by identifying it as the *syn*-proton on C_7 bearing Cl. Thus, **14** is assigned to *exo*-2-*anti*-7-dichloronorbornane (lit.,[30] bp 77—81 °C/10 mmHg). A multiplet absorption at δ 4.3—3.6 in **15** shows the presence of both *exo*- (δ 4.3—4.0) and *endo*-(δ 4.0—3.6) protons; this appears to favor a *trans*-dichloride structure. If **15** is the *trans*-2,6-isomer, the peak of 2-*endo*-H can be expected to appear at a much lower field than usual because of the anisotropy of 6-*endo*-Cl. Thus, **15** can be assigned to *trans*-2,5-dichloronorbornane.

The reaction using 1,2-dichloroethane as a solvent at 84 °C for 10 min gave **13**, **14**, **15**, and **16** in the ratio of 5: 22: 40: 33 (20 mmol).

Attempted Isomerization of cis- *and* trans-*1,2-Dichlorocyclohexanes.* A mixture of the *cis*- and *trans*-dichlorides (2 g, *cis*/*trans*=1.6) was heated in 40 ml of CCl_4 containing 0.2 g of $SbCl_3$ and 0.3 g of $SbCl_5$ at a refluxing temperature (76 °C). Glc analysis after 2 hr gave an almost unchanged isomer ratio, *i.e.*, *cis*/*trans*=1.68.

Authentic Samples for glc. Both *meso*-2,3- (containing

* In separate experiments we have confirmed that the decomposition of $SbCl_3$ with water gave hydrogen chloride, which reacted easily with cyclohexene and 2-octene to afford monochloroalkanes (**2**) at room temperature. In order to avoid the formation of **2** by this route, the reaction mixture was treated with aqueous NaOH instead of water.

9.5% *dl*-isomer) and *dl*-2,3-dichlorobutane (containing 9.4% *meso*-isomer) were prepared by the reported method[31] by the reaction of *trans*- and *cis*-2-butenes with chlorine respectively at −40 °C. The *cis*-1,2-dichlorocyclohexane was obtained from the reaction of *trans*-2-chlorocyclohexanol with thionyl chloride in pyridine.[32] *trans*-1,2-Dichlorocyclohexane, 1,2-dichlorooctane, and *threo*-2,3-dichlorooctane were prepared by the reaction of the corresponding olefins with Cl_2 or $CuCl_2$.[33] The *erythro*-2,3-dichlorooctane was isolated by the reaction of *cis*-2-octene with $SbCl_5$; bp 77—79 °C/10 mm, Found: C, 52.33; H. 8.91; Cl 38.24%. Calcd. for $C_8H_{16}Cl_2$: C, 52.47; H, 8.81; Cl, 38.73%. The monochloroparaffins, 1,2,3-trichloropropane, 3,4-dichloro-1-butene, and *trans*-1,4-dichloro-2-butene were commercially available.

Analytical Instruments. The IR and NMR spectra were determined by the use of a Hitachi EPT-S2 apparatus and a Varian A-60 (CCl_4 or $CDCl_3$ solvent, with TMS as the internal standard) apparatus respectively. Gas chromatographies were carried out by the use of two Shimadzu apparatuses 5APTF and 4BMPF [PEG 20M (25%)-Shimalite (3 m), PEG 6000 (25%)-Chromosorb-W (3 m), Apiezon L (30%)-Celite (1 m) and DEGS (25%)-Shimalite (3 m) columns; carrier gas, He].

References

1) Preliminary communication, S. Uemura, O. Sasaki, and M. Okano *Chem. Commun.*, **1971**, 1064.

2) P. Kovacic and A. K. Sparka, *J. Amer. Chem. Soc.*, **82**, 5740 (1960).

3) P. Kovacic and J-H. C. Chang, *J. Org. Chem.*, **36**, 3138 (1971) and references therein.

4) M. R. Radcliffe and C. E. Best, U. S. 2445729; *Chem. Abstr.*, **42**, 8207 (1948).

5) M. C. Hoff, K. W. Greenlee, and C. E. Boord, *J. Amer. Chem. Soc.*, **73**, 3329 (1951).

6) R. E. Buckles and D. F. Knaack, *J. Org. Chem.*, **25**, 20 (1960).

7) H. van de Walle, *Bull. Soc. Chim. Belg.*, **28**, 304 (1919).

8) F. Akiyama, T. Horie, and M. Matsuda, This Bulletin, **46**, 1888 (1973).

9) For a recent review, see S. Uemura and M. Okano, *Bull. Inst. Chem. Res. Kyoto Univ.*, **50**, 423 (1972).

10) A favorable *cis*-chlorination has been known for some olefins such as stilbene and acenaphtylene.[10a] Recent report of *cis*-chlorination of olefins by iodobenzene dichloride is also worth to be referred.[10b]

a) P. B. D. de la Mare and R. Bolton, "Electrophilic Additions to Unsaturated Systems", Elsevier, Amsterdam 1966, p. 92. b) M. Devillier and H. Bodot, *Bull. Soc. Chim. France*, **1972**, 227.

11) J. Holmes and R. Pettit, *J. Org. Chem.*, **28**, 1695 (1963).

12) In connection to this, see a footnote of experimental section.

13) S. Uemura, O. Sasaki, and M. Okano, This Bulletin, **45**, 1482 (1972).

14) W. C. Baird, Jr., J. H. Surridge, and M. Buza, *J. Org. Chem.*, **36**, 2088, 3324 (1971).

15) a) I. E. Muskat and H. E. Northrup, *J. Amer. Chem. Soc.*, **52**, 4043 (1930). b) K. Mislow and H. M. Hellman, *ibid.*, **73**, 244 (1951).

16) M. L. Poutsma, *J. Org. Chem.*, **31**, 4167 (1966).

17) H. L. Goering and F. H. McCarron, *J. Amer. Chem. Soc.*, **78**, 2270 (1956). We have confirmed the stereospecificity of the reaction by glc.

18) a) M. L. Poutsma, *ibid.*, **87**, 4293 (1965). b) J. D. Roberts, F. O. Johnson, and R. A. Carboni, *ibid.*, **76**, 5692 (1954).

19) R. Hüttel, H. Reinheimer, and K. Nowak, *Chem. Ber.*, **101**, 3761 (1968).

20) D. D. Tanner and G. C. Gidley, *J. Org. Chem.*, **33**, 38 (1968).

21) L. Kolditz and H. Preiss, *Z. Anorg. Allg. Chem.*, **310**, 242 (1961).

22) a) G. L. Carlson, *Spectrochim. Acta*, **19**, 1291 (1963). b) I. R. Beattie, T. Gilson, K. Livingston, V. Fawcett, and G. A. Ozin, *J. Chem. Soc., A*, **1967**, 712. Further, we have confirmed that no appreciable absorption assigned to $SbCl_6^-$ is found in the Laser Raman spectrum (excited by Ar^+ 4880 Å) of $SbCl_5$ (in CCl_4). Measurement was kindly furnished by Professor T. Takenaka of our Institute.

23) D. H. R. Barton and E. Miller *J. Amer. Chem. Soc.*, **72**, 370 (1950).

24) S. M. Ohlberg, *ibid.*, **81**, 811 (1959).

25) R. W. Suter, H. C. Knachel, V. P. Petro, J. H. Howatson, and S. G. Shore, *ibid.*, **95**, 1474 (1973).

26) For leading references, *e.g.*, a) C. K. Ingold, "Structure and Mechanism in Organic Chemistry," 2nd Ed. Cornell University Press, Ithaca (1969), p. 457. b) K. B. Wiberg, "Physical Organic Chemistry", John Wiley, New York (1964), p. 374.

27) D. P. Wyman, J. Y. C. Wang and W. R. Freeman, *J. Org. Chem.*, **28**, 3173 (1963).

28) A spectral evidence for equilibrium of non-classical norbornyl (unsubstituted) cations was given by G. A. Olah *et al.* [*J. Amer. Chem. Soc.*, **92**, 4627 (1970)].

29) G. A. Russel and A. Ito, *ibid.*, **85**, 2983 (1963).

30) H. Kwart and R. K. Miller, *ibid.*, **78**, 5678 (1956).

31) H. J. Lucas and C. W. Gould, Jr., *ibid.*, **63**, 2541 (1941).

32) B. Carroll, D. G. Kubler, H. W. Davis, and A. M. Whaley, *ibid.*, **73**, 5382 (1951).

33) K. Ichikawa, S. Uemura, T. Hiramoto, and Y. Takagaki, *Kogyo Kagaku Zasshi.*, **71**, 1657 (1968).

Studies of Peptide Antibiotics. XXX.[1] Syntheses of Gramicidin S Analogs Containing *N*-Methylleucine in Place of Leucine

Hiroshi SUGANO,* Hayao ABE,** Muneji MIYOSHI,* Tetsuo KATO,** and Nobuo IZUMIYA**

**Department of Synthetic Chemistry, Research Laboratory of Applied Biochemistry, Tanabe Seiyaku Co., Ltd., Kashima, Higashiyodogawa, Osaka 532*

***Laboratory of Biochemistry, Faculty of Science, Kyushu University, Hakozaki, Fukuoka 812*

(Received August 20, 1973)

Two analogs of gramicidin S, *cyclo*(–Val–Orn–Leu–D-Phe–Pro–Val–Orn–MeLeu–D-Phe–Pro–), *i.e.*, [3-*N*-Methylleucine]–gramicidin S, and *cyclo*(–Val–Orn–MeLeu–D-Phe–Pro–Val–Orn–MeLeu–D-Phe–Pro–), *i.e.*, [3,3′-di-*N*-Methylleucine]–gramicidin S, were prepared in an attempt to investigate the contribution of the NH group of the leucine residue with regard to antibacterial activity. These analogs were almost as active as gramicidin S in the antibacterial test in reaction to microorganisms. The optical rotatory dispersions of these two analogs and of gramicidin S were measured in solvents of ethanol and 8 M aqueous urea. These studies suggested that both of the analogs containing *N*-methylleucine have a molecular conformation very similar to that of gramicidin S, and that the NH group of the leucine residues is not necessary for stabilizing the conformation in order to exhibit the biological properties.

In studies of the structure-activity relationship of gramicidin S, various analogs have been synthesized.[2] From these works and the optical rotatory dispersion (ORD) studies, it has been suggested that the biological activity of gramicidin S and its analogs has a close correlation to their conformation, and that a specific conformation may be necessary for a molecule to exhibit antibacterial activity.[3]

For the conformation of gramicidin S in the solid- and the solution-state, several models have been proposed. A possible model which was first suggested on the basis of X-ray studies by Hodgkin and Oughton is the intramolecular antiparallel β-form, with four hydrogen bondings between the valyl and the leucyl residues.[4] A similar structure was proposed by Schwyzer,[5] by Craig's group,[6] and by Urry's group.[7] These proposals prompted us to synthesize analogs which lack some of the four intramolecular hydrogen bondings in order to investigate to what extent these hydrogen bondings will stabilize the conformation.

The present paper will deal with the syntheses, antibacterial properties, and ORD measurements of two analogs of gramicidin S, [3-*N*-Methylleucine]- and [3,3′-di-*N*-Methylleucine]-gramicidin S, in which the leucyl residues in positions 3 and 3′ are replaced, singly or together, by *N*-methylleucine residues. These analogs are lacking in one or two of the four hydrogen bondings of the proposed model.

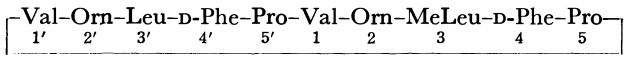

[3-*N*-Methylleucine]-gramicidin S

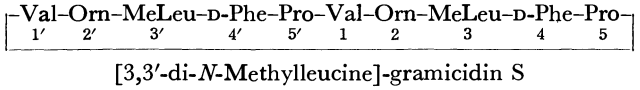

[3,3′-di-*N*-Methylleucine]-gramicidin S

The synthesis of [3-*N*-Methylleucine]-gramicidin S is outlined in Scheme 1.[8] The strategy of the synthesis was chosen specifically to preclude the *N*-methylamino acid from the *N*- and *C*-terminus of the decapeptide, since acylation of the secondary amino group in *N*-methylamino acid residue and acylation by the activated carboxyl group in *N*-methylamino acid residue seems not to be favored.[9,10] Proline was chosen as the *C*-terminal residue in order to avoid racemization in the final cyclization step.

α-*t*-Butoxycarbonyl (Boc)-δ-benzyloxycarbonyl (Z)-ornithine was coupled with *N*-methylleucine methyl ester in the presence of dicyclohexylcarbodiimide (DCC) to yield the protected dipeptide, **1**, as an oil, together with the *N*-acylurea derived from the carboxyl component. All attempts at purification, such as crystallization and column chromatography, were unsuccessful. The corresponding reaction using the water-soluble carbodiimide gave the protected dipeptide, **1**, in a pure state in a 50% yield. The NMR evidence of the three *N*-methyl protons supported the proposed structure. Saponification of **1** easily gave the corresponding acid, **2**, as fine crystals. It was reported previously that, when the *C*-terminal amino acid residue of a carboxyl component was an *N*-methylamino acid residue, a system of DCC plus 1-hydroxybenzotriazole (HObt)[11] was a useful coupling agent;[10] therefore α-Boc-δ-Z-ornithyl-*N*-methylleucine was coupled with D-phenylalanylproline ethyl ester by the aid of DCC and HObt. The consequent yield of α-Boc-δ-Z-ornithyl-*N*-methylleucyl-D-phenylalanylproline ethyl ester (**3**) was nearly quantitative. After removal of the Boc group of **3**, the resulting tetrapeptide ester was coupled with Boc-valine *N*-hydroxysuccinimide ester to yield Boc-valyl-δ-Z-ornithyl-*N*-methylleucyl-D-phenylalanylproline ethyl ester (**4**) in an 80% yield; this ester was then converted to the corresponding acid **5** by saponification and subsequently to hydrochloride of valyl-δ-Z-ornithyl-*N*-methylleucyl-D-phenylalanylproline (**6**) by the action of hydrogen chloride in ethyl acetate. Condensation of the azide derived from Boc-valyl-δ-Z-ornithylleucyl-D-phenylalanylproline hydrazide with the pentapeptide, **6**, gave the acyldecapeptide acid, **7**, which was then isolated by column chromatography on silica gel. The acid, **7**, was then transformed into the Boc-decapeptide *N*-hydroxysuccinimide ester, **8**, by the reaction of *N*-hydroxysuccinimide (HONSu) and the water-soluble carbodiimide. After removal of the Boc group of **8** with trifluoroacetic acid, the decapeptide ester trifluoroacetate thus obtained was cyclized in pyridine at room temperature by the high-

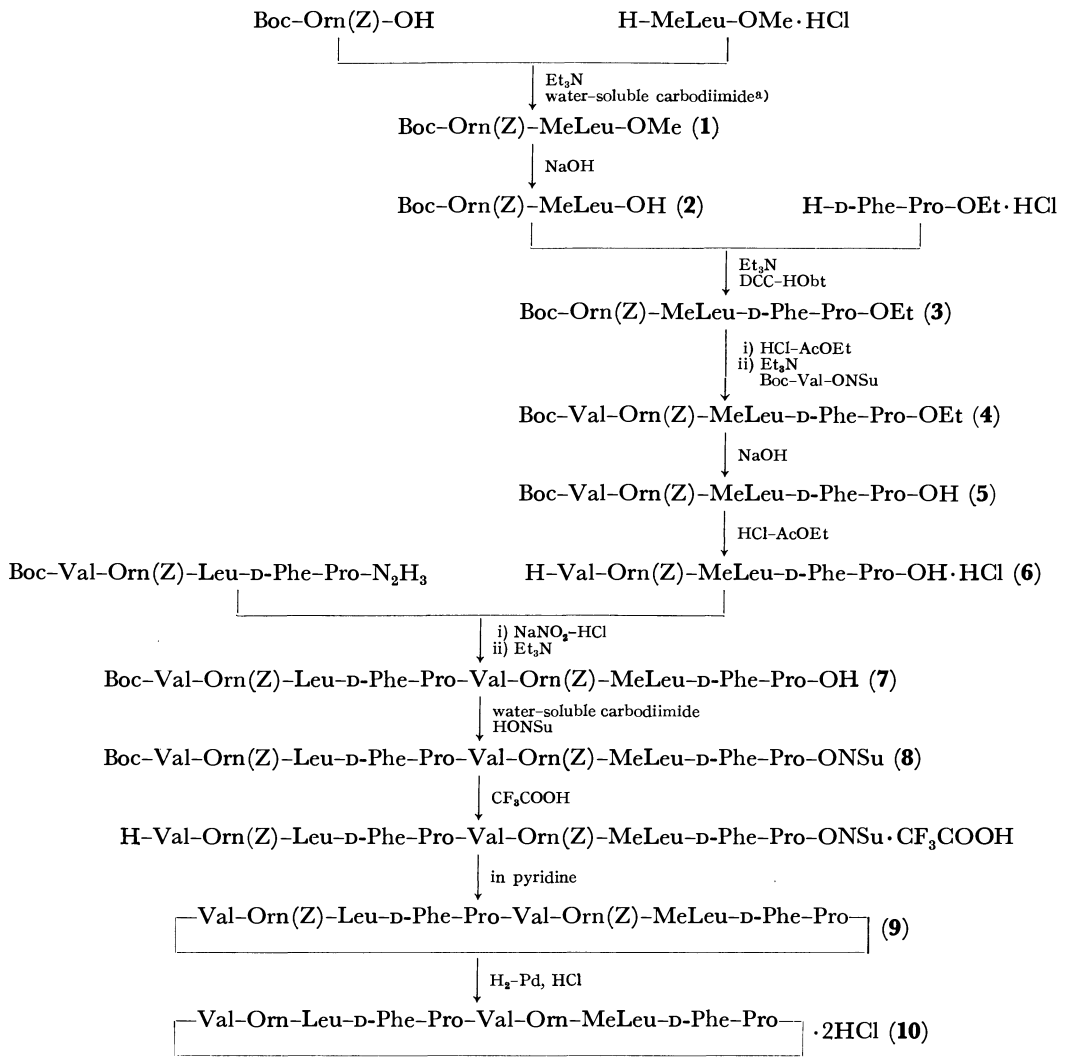

a) 1-Ethyl-3-(3-dimethylaminopropyl)-carbodiimide

Scheme 1.

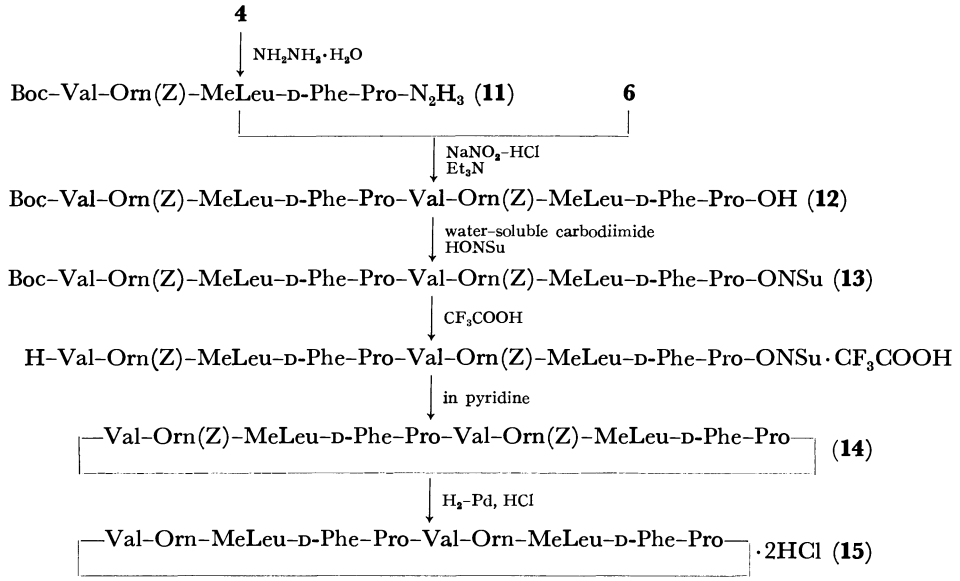

Scheme 2.

dilution method.[12] Purification through ion-exchange columns, followed by fractionation on silica gel, gave the Z-substituted cyclic decapeptide, **9**, as colorless needles in a 56% yield. Hydrogenolysis of **9** afforded the desired [3-*N*-Methylleucine]-gramicidin S as a crystalline dihydrochloride, **10**.

[3,3'-Di-*N*-Methylleucine]-gramicidin S was prepared in a similar manner (Scheme 2). The Z-substituted cyclic derivative, **14**, was obtained in a 67.5% yield. These results indicate that the cyclization reaction is not affected by the *N*-methyl group. These two synthetic analogs gave satisfactory results in elemental and amino acid analyses, and were homogeneous by the criteria of paper electrophoresis and paper chromatography with various solvent systems.

Table 1. Antibacterial activity of the compounds
(Minimum inhibitory concentration, μg/ml)

Strain	Gramicidin S	[MeLeu³]-Gramicidin S (**10**)	[MeLeu³,³']-Gramicidin S (**15**)
Staphylococcus aureus	6.25 (1.56)[a]	6.25 (3.12)[a]	6.25 (6.25)[a]
Bacillus subtilis	3.12	3.12	3.12
Escherichia coli	100	50	50
Shigella flexneri	100	100	100
Candida albicans	50	50	25

a) ( ): Knight modified semisynthetic medium.

The results of the biological comparison of the two analogs to gramicidin S are shown in Table 1. In the antibacterial activities toward microorganisms, both of the analogs were almost identical with gramicidin S in potency. This indicates that the NH's of the leucine residues are not necessary for exhibiting the biological activity. Izumiya *et al.* have reported that the biologically-active gramicidin S analogs possess conformations similar to one another, irrespective of their primary structures.[3] Accordingly, we assume that these two

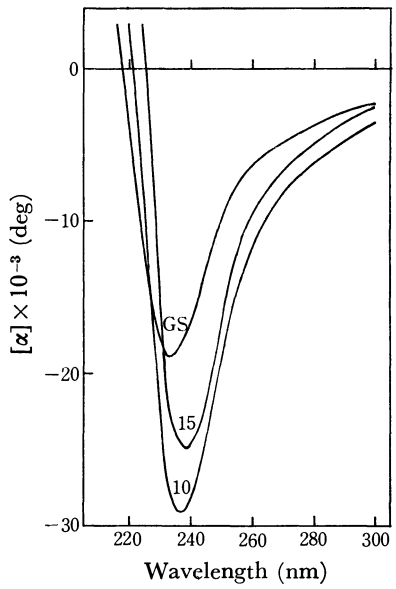

Fig. 1. ORD curves of [MeLeu³]-gramicidin S (**10**), [MeLeu³,³']-gramicidin S (**15**), and gramicidin S (GS) in ethanol, concentration 0.24 mg/ml.

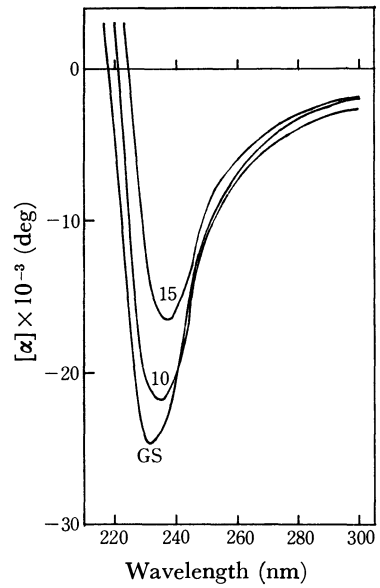

Fig. 2. ORD curves of [MeLeu³]-gramicidin S (**10**), [MeLeu³,³']-gramicidin S (**15**), and gramicidin S (GS) in 8 M urea, concentration 0.24 mg/ml.

analogs containing *N*-methylleucine also have conformations similar to that of gramicidin S. To confirm our assumption, ORD measurements were undertaken.

The ORD's of [3-*N*-methylleucine]- and of [3,3'-di-*N*-methylleucine]-gramicidin S in ethanol are shown in Fig. 1, along with that of gramicidin S. The shapes of the three ORD curves are very similar to each other. The troughs of the former two compounds are at 236—238 nm, whereas that of gramicidin S is at 232 nm. In a solvent of 8 M aqueous urea, which causes the denaturation of some polypeptides (*e.g.*, the biologically-inactive analogs of gramicidin S[12]), the positions of the troughs of the analogs (**10** and **5**) remained unchanged, as does that of gramicidin S (Fig. 2). In both solvents, their dispersions are different in their minimum rotations, and the positions of the troughs are slightly different, but the shapes of the curves are very similar even in 8 M urea, suggesting that all these three molecules have very similar and stable conformations. Judging from these results, two of the four hydrogen bondings in the β-type structure of gramicidin S proposed by several authors are not necessary for stabilizing the conformation. Furthermore, another model in which the NH's of the leucine residues do not participate in the intramolecular hydrogen bondings can be put forward. In this respect, as has been mentioned by Balasubramanian,[13] the Hodgkin-Oughton mixed α,β-structure and the Scheraga model can not be disregarded.[4,14] Further studies of this question are in progress.

Experimental

Thin-layer chromatography (tlc) was carried out on silica gel G (Merck) with the solvent systems: R_f^1, chloroform–methanol–acetic acid (95: 5: 3), R_f^2, acetone —28% aqueous ammonia (100: 5). The NMR spectra were recorded at 60 MHz, with tetramethylsilane as the internal standard and using a Hitachi R-20A apparatus. The optical rotations

were measured with a Perkin-Elmer polarimeter 141.

Boc-Orn(Z)-MeLeu-OMe (1). Into a solution of Boc-Orn(Z)-OH[15] (7.3 g, 20 mmol), H-MeLeu-OMe·HCl[10] (4 g, 20 mmol), and triethylamine (2.8 ml) in tetrahydrofuran (100 ml), was added 1-ethyl-3-(3-dimethylaminopropyl)-carbodiimide[16] (3.1 g, 20 mmol) at −5—0 °C over a period of 10 min. After the mixture had been stirred overnight at room temperature, the solvent was distilled off under reduced pressure and the residue was taken up in ethyl acetate. The ethyl acetate solution was then washed successively with M hydrochloric acid, 4% sodium bicarbonate, and water, and then dried over magnesium sulfate. The solvent was evaporated under reduced pressure to leave a colorless oil; yield, 5 g (50%); $[\alpha]_D^{25}$ −38.0° (*c* 1.5, methanol). NMR δ ($CDCl_3$): 1.45 (s, 9H, $(CH_3)_3C$–), 2.93 (s, 3H, CH_3N–), 3.65 (s, 3H, CH_3OCO–), 5.07 (s, 2H, $-C\underline{H}_2C_6H_5$), 7.30 (s, 5H, phenyl protons).

Boc-Orn(Z)-MeLeu-OH (2). A solution of compound **1** (4.7 g, 9.4 mmol) and 4M sodium hydroxide (2.5 ml) in methanol (18 ml) was stirred for 6 hr at 20—25 °C. The solution was then evaporated under reduced pressure below 40 °C to remove methanol, diluted with water (300 ml), and washed with ether. The aqueous solution was acidified with 2M hydrochloric acid, and the oil separated was repeatedly extracted with ether. The extract was washed with M hydrochloric acid and water. After drying over magnesium sulfate, the solution was evaporated to leave an oil which was subsequently crystallized in a refrigerator. The product was recrystallized from ether–*n*-hexane; yield, 3.4 g (73%); mp 95—97 °C; $[\alpha]_D^{25}$ −32.0° (*c* 1, methanol). Found: C, 60.62; H, 7.61; N, 8.50%. Calcd for $C_{25}H_{39}N_3O_7$: C, 60.83; H, 7.96; N, 8.51%.

Boc-Orn(Z)-MeLeu-D-Phe-Pro-OEt (3). To a stirred solution of **2** (9 g, 18 mmol), HObt (2.4 g, 18 mmol), HCl·H-D-Phe-Pro-OEt[17] (6 g, 18 mmol), and triethylamine (2.5 ml) in tetrahydrofuran (90 ml), DCC was added at −10—−5 °C. After the stirring had been continued for 2 hr at −5—0 °C, and for a further 2 hr at room temperature, the mixture was left to stand overnight. The mixture was then evaporated under reduced pressure, and the residue was diluted with ethyl acetate (500 ml). The solution which was separated from the dicyclohexylurea by filtration was washed successively with water, 4% sodium bicarbonate, and water, and then dried over magnesium sulfate. The solvent was distilled off under reduced pressure to leave an oil; yield, 13.4 g (98%); R_f^1, 0.44; $[\alpha]_D^{25}$ −82.1° (*c* 0.55, methanol). NMR δ ($CDCl_3$): 1.45 (s, 9H, $(CH_3)_3C$–), 2.87 (s, 3H, CH_3-N–), 5.10 (s, 2H, $-OC\underline{H}_2C_6H_5$), 7.17—7.35 (m, 10H, phenyl protons).

Boc-Val-Orn(Z)-MeLeu-D-Phe-Pro-OEt (4). Compound **3** (7.65 g, 10 mmol) was dissolved in 3M hydrogen chloride in ethyl acetate (100 ml) and allowed to react for 30 min at room temperature. The solvent was distilled off under reduced pressure to dryness. The tetrapeptide ethyl ester hydrochloride thus obtained was dissolved in chloroform (30 ml), neutralized with triethylamine (1.4 ml), and subjected to a reaction with Boc-Val-ONSu[18] (3.45 g, 11 mmol) overnight at room temperature. To this solution, a few drops of *N*-2-aminoethylpiperazine were added, and the mixture was allowed to stand for 30 min. The solution was then diluted with chloroform (200 ml), washed successively with M hydrochloric acid and 4% sodium bicarbonate, and dried over magnesium sulfate. The solvent was distilled off under reduced pressure, and the residue was crystallized by adding dry ether; yield, 7.7 g (80%); mp 88—99 °C; $[\alpha]_D^{25}$ −91.2° (*c* 0.25, methanol). Found: C, 63.74; H, 7.85; N, 9.73%. Calcd for $C_{46}H_{68}N_6O_{10}$: C, 63.86; H, 7.92; N, 9.71%.

Boc-Val-Orn(Z)-MeLeu-D-Phe-Pro-OH (5). To a solution of **4** (6.5 g, 7.5 mmol) in methanol (70 ml), M sodium hydroxide (15 ml) was added; the solution was then allowed to stand for 6 hr at room temperature. The solution was evaporated under reduced pressure to remove methanol, diluted with water (100 ml), and acidified with 2M hydrochloric acid. The oil thus separated was extracted with ethyl acetate, and the extract was washed with water and dried over magnesium sulfate. The solvent was distilled off under reduced pressure to yield an oily product; 6.4 g (100%); $[\alpha]_D^{25}$ −80.5° (*c* 1, methanol). Found: C, 61.71; H, 7.72; N, 9.37%. Calcd for $C_{44}H_{64}N_6O_{10}\cdot H_2O$: C, 61.80; H, 7.78; N, 9.82%.

H-Val-Orn(Z)-MeLeu-D-Phe-Pro-OH·HCl (6). Compound **5** (6.4 g, 7.5 mmol) was treated with 3M hydrogen chloride in ethyl acetate (80 ml) for 30 min at room temperature. The solution was then evaporated under reduced pressure, and the residue was triturated with dry ether. The product was collected by filtration, washed well with ether, and dried *in vacuo* over sodium hydroxide; yield, 5.8 g (100%).

Boc-Val-Orn(Z)-Leu-D-Phe-Pro-Val-Orn(Z)-MeLeu-D-Phe-Pro-OH (7). To a solution of Boc-Val-Orn(Z)-Leu-D-Phe-Pro-$NHNH_2$[12] (3.3 g, 4 mmol) and 3M hydrochloric acid (4 ml) in dimethylformamide (100 ml), was added a chilled solution of sodium nitrite (300 mg, 4.4 mmol) in water (1 ml) at −15 °C. After 15 min, the reaction mixture was neutralized with triethylamine (0.56 ml), and a solution of **6** (3 g, 4 mmol) and triethylamine (1.2 ml, 8 mmol) in dimethylformamide (40 ml) was added to the mixture. After 2 days at 3 °C, the solvent was evaporated under reduced pressure below 40 °C. The residue was added to 10% citric acid (50 ml), and the resulting oil was extracted with ethyl acetate. The ethyl acetate solution was washed successively with 10% citric acid and water and dried over magnesium sulfate. After removal of the solvent, the residue was subjected for purification to chromatography on a column of silica gel 60 (Merck), first with a mixture of acetone and 28% aqueous ammonia (100: 5). In this solvent system, the by-products (R_f^2, 0.9 and 0.8) were eluted; the main product (R_f^2, 0.1) was not eluted. The desired product was then removed with methanol. The fractions containing the product, as detected by tlc (R_f^1, 0.53), were pooled and evaporated to dryness. The residue was dissolved in ethyl acetate (200 ml), and the ethyl acetate solution was washed with 10% citric acid until the washings became acidic, and then with water. After drying over magnesium sulfate, the solvent was distilled off; yield of oil, 3.3 g (53%); $[\alpha]_D^{25}$ −96.9° (*c* 1, methanol). Found: C, 62.67; H, 7.77; N, 9.97%. Calcd for $C_{82}H_{116}N_{12}O_{17}\cdot 2H_2O$: C, 62.41; H, 7.66; N, 10.65%.

Boc-Val-Orn(Z)-Leu-D-Phe-Pro-Val-Orn(Z)-MeLeu-D-Phe-Pro-ONSu (8). To a solution of **7** (2.1 g, 1.3 mmol) in dimethylformamide (6 ml), HONSu (300 mg, 2.6 mmol) and 1-ethyl-3-(3-dimethylaminopropyl)-carbodiimide (400 mg, 2.6 mmol) were added at 0 °C. After 12 hr at room temperature, the mixture was diluted with ethyl acetate (200 ml). The solution was washed with M hydrochloric acid, 4% sodium bicarbonate, and water. After drying over magnesium sulfate, the solvent was distilled off under reduced pressure. The crude product was reprecipitated from ethyl acetate–petroleum ether; yield, 2.0 g (95%); mp 105—111 °C; $[\alpha]_D^{25}$ −125.0° (*c* 0.6, ethyl acetate). Found: C, 62.21; H, 7.20; N, 10.92%. Calcd for $C_{86}H_{119}N_{13}O_{19}\cdot H_2O$: C, 62.33; H, 7.36; N, 10.98%.

cyclo(*-Val-Orn(Z)-Leu-D-Phe-Pro-Val-Orn(Z)-MeLeu-D-*

Phe–Pro–) (9). The decapeptide *N*-hydroxysuccinimide ester, **8** (400 mg), was dissolved in trifluoroacetic acid (15 ml). After 30 min, the solution was evaporated, and the residual powder was collected by filtration with the aid of dry ether and dried over sodium hydroxide *in vacuo*; yield, 340 mg. The *N*-hydroxysuccinimide ester trifluoroacetate thus obtained (340 mg) was dissolved in dimethylformamide (10 ml), and the solution was added, drop by drop, to pyridine (100 ml) at 30—40 °C over a period of 2 hr; stirring was then continued for an additional 2 hr at room temperature. The solvent was removed, and the residue was dissolved in a mixture of methanol (50 ml) and water (10 ml). The solution was passed through columns (1.9×40 cm, each) of Dowex 1 (OH^- form) and Dowex 50 (H^+ form). The columns were washed with the same solvent (500 ml), the combined effluent was evaporated, and the oil was extracted with ethyl acetate. The extract was dried over magnesium sulfate and evaporated to dryness. The oily product was further purified by a column (1.5×15 cm) with silica gel 60 (Merck). After the column had been washed with a mixture of ethyl acetate and benzene (1: 1) (200 ml), the desired product, as determined by tlc, was eluted with ethyl acetate (100 ml). The solvent was evaporated to leave an oil, which was subsequently crystallized by the addition of a mixture of ethyl acetate and petroleum ether; yield, 163 mg (56%); mp 212—214 °C; $[\alpha]_D^{25}$ −248° (*c* 0.31, methanol). Found: C, 63.45; H, 7.46; N, 11.71%; molecular weight 1450.[19] Calcd for $C_{77}H_{106}N_{12}O_{14}\cdot 2H_2O$: C, 63.35; H, 7.59; N, 11.51%; molecular weight 1460.

cyclo*(–Val–Orn–Leu–*D*-Phe–Pro–Val–Orn–MeLeu–*D*-Phe–Pro–)·2HCl ([3-*N*-Methylleucine]-gramicidin S Dihydrochloride) (10).* The protected cyclic decapeptide **9** (100 mg) was dissolved in 0.01M hydrogen chloride in methanol (20 ml), after which hydrogenation was carried out for 4 hr, using palladium black as a catalyst. After removal of the catalyst by filtration, the filtrate was evaporated under reduced pressure. The syrup which remained was treated with M hydrochloric acid (2 ml), and the crystals formed were filtered, washed in portions with M hydrochloric acid (2 ml), and dried *in vacuo* over sodium hydroxide; yield, 60 mg. Recrystallization from ethanol–M hydrochloric acid gave colorless crystals; yield, 50 mg; mp 237—239 °C; $[\alpha]_D^{25}$ −272° (*c* 0.05, ethanol). Amino acid ratios in acid hydrolyzate: Val 2.11, Orn 1.82, Leu 0.98, Pro 2.08, MeLeu 1.00, Phe 2.12.[10] Found: C, 57.89; H, 7.82; N, 13.23%. Calcd for $C_{61}H_{94}N_{12}O_{10}\cdot 2HCl\cdot 2H_2O$: C, 57.94; H, 7.97; N, 13.29%.

*Boc–Val–Orn(Z)–MeLeu–*D*-Phe–Pro–N_2H_3 (11).* A solution of **4** (8.56 g, 10 mmol) and hydrazine hydrate (15 ml, 300 mmol) in dimethylformamide (20 ml) was allowed to stand at 30 °C for 7 days. The solution was evaporated below 40 °C, and then ethyl acetate (200 ml) was added to the residue. The solution was washed with M hydrochloric acid, 4% sodium bicarbonate, and water. After drying over magnesium sulfate, the solution was evaporated to dryness; yield of oil, 8.6 g (100%); $[\alpha]_D^{25}$ −88.6° (*c* 1.5, ethyl acetate). Found: C, 60.74; H, 7.72; N, 12.44%. Calcd for $C_{44}H_{66}N_8O_9\cdot H_2O$: C, 60.80; H, 7.88; N, 12.89%.

*Boc–Val–Orn(Z)–MeLeu–*D*-Phe–Pro–Val–Orn(Z)–MeLeu–*D*-Phe–Pro–OH (12).* Compound **11** (2.9 g, 3.3 mmol), in a mixture of 3M hydrochloric acid (3.5 ml) and dimethylformamide (100 ml), was treated with sodium nitrite (280 mg, 4 mmol) as in the case of **7**. To the azide solution was added a solution of **6** (2.6 g, 3.3 mmol) in dimethylformamide (40 ml) containing triethylamine (1.8 ml). After the mixture had been stirred for 24 hr at 3 °C, the solvent was evaporated under reduced pressure. The residue was dissolved in ethyl acetate (500 ml), and the ethyl acetate solution was washed with 10% citric acid and water and dried over magnesium sulfate. After removal of the solvent, the residue was triturated with petroleum ether. The product was reprecipitated from ethyl acetate–petroleum ether; yield, 2.0 g (39%), mp 94—106 °C; $[\alpha]_D^{25}$ −115.0° (*c* 1, methanol). Found: C, 62.58; H, 7.30; N, 10.76%. Calcd for $C_{83}H_{118}N_{12}O_{17}\cdot 2H_2O$; C, 62.62; H, 7.72; N, 10.55%.

*Boc–Val–Orn(Z)–MeLeu–*D*-Phe–Pro–Val–Orn(Z)–MeLeu–*D*-Phe–Pro–ONSu (13).* The decapeptide acid **12** (1.55 g, 1 mmol) was converted to the active ester, **13**, by the method described for the preparation of **8**; yield, 1.27 g (77%); mp 95—110 °C; $[\alpha]_D^{25}$ −111.7° (*c* 0.5, ethyl acetate). Found: C, 63.01; H, 7.18; N, 10.88%. Calcd for $C_{87}H_{121}N_{13}O_{19}$: C, 63.21; H, 7.37; N, 11.01%.

cyclo*(–Val–Orn(Z)–MeLeu–*D*-Phe–Pro–Val–Orn(Z)–MeLeu–*D*-Phe–Pro–) (14).* Compound **13** (1.27 g, 0.77 mmol) was treated with trifluoroacetic acid (10 ml) as in the case of **9**. The decapeptide *N*-hydroxysuccinimide ester trifluoroacetate thus obtained (1.2 g) was dissolved in dimethylformamide (10 ml), and the solution was added to pyridine (700 ml). The solvent was removed, and the residue was dissolved in a mixture of methanol (50 ml) and water (10 ml). The solution was passed through columns (1.9×40 cm, each) of Dowex 1 (OH^- form) and Dowex 50 (H^+ form). The columns were washed with the same solvent (700 ml), the combined effluent was evaporated, and the oil was extracted with ethyl acetate. The extract was dried and evaporated. The oily product was further purified by column chromatography with silica gel 60 (Merck). After the column had been washed with a mixture of ethyl acetate and benzene (1: 1) (50 ml), the desired product, as determined by tlc (R_f^1, 0.5), was eluted with a mixture of chloroform, methanol, and acetic acid (95: 5: 3). The fractions (105—240 ml) containing the product were pooled and evaporated to an amorphous powder; yield, 770 mg (67.5%); mp 105—115 °C; $[\alpha]_D^{25}$ −173° (*c* 0.4, methanol). Found: C, 63.49; H, 7.18; N, 11.17%; molecular weight 1465.[19] Calcd for $C_{78}H_{108}N_{12}O_{14}\cdot 2H_2O$: C, 63.56; H, 7.65; N, 11.40%; molecular weight 1474.

cyclo*(–Val–Orn–MeLeu–*D*-Phe–Pro–Val–Orn–MeLeu–*D*-Phe–Pro–)·2HCl ([3,3′-di-*N*-Methylleucine]-gramicidin S Dihydrochloride) (15).* The protected cyclic derivative, **14** (340 mg, 0.23 mmol), was converted to **15** by the method described for the preparation of **10**; yield, 255 mg (85%); mp 233—235 °C; $[\alpha]_D^{25}$ −235.7° (*c* 0.05, ethanol). Amino acid ratios in acid hydrolyzate: Val 1.10, Orn 0.89, MeLeu 1.00, Phe 0.98, Pro 1.05.[10] Found: C, 57.47; H, 7.68; N, 12.78%. Calcd for $C_{62}H_{96}N_{12}O_{10}\cdot 2HCl\cdot 3H_2O$: C, 57.43; H, 8.08; N, 12.96%.

Paper Electrophoresis. To ascertain further the purities of the analogs of gramicidin S synthesized here, paper electrophoresis was carried out as has been described before.[20] Each peptide revealed a single spot, and the mobilities were comparable with that of gramicidin S.

Microbiological Assays. The minimum amounts of the compounds necessary for the complete inhibition of growth were determined by a dilution method, using a bouillon agar and a semisynthetic medium; the results are shown in Table 1.

ORD Measurements. The measurements were performed with a JASCO spectropolarimeter model ORD/UV-5, over the wavelength range from 210 to 300 nm. A cell with a path length of 0.2 cm was used, and the runs were made at an ambient temperature. Patterns in the solvents of ethanol and 8M aqueous urea are shown in Figs. 1 and 2 respectively.

The authors wish to express their thanks to Dr. I. Chibata of Tanabe Seiyaku Co., Ltd., for his encouragement in the course of this study. Thanks are also due to Associate Professor Y. Mukohata of Osaka University for his help in the ORD measurements, and to Dr. K. Enomoto of Tanabe Seiyaku Co., Ltd., for the biological assay.

References

1) Part XXIX: N. Takahashi, T. Kato, and N. Izumiya, *Memoirs Fac. Sci., Kyushu Univ., Series C*, in press.
2) T. Kato and N. Izumiya, "Chemistry and Biochemistry of Amino acids, Peptides, and Proteins," Vol. 2, ed. by B. Weinstein, Marcel Dekker, New York (1972), in press.
3) T. Kato, M. Waki, S. Matsuura, and N. Izumiya, *J. Biochem.* (Tokyo), **68**, 751 (1970).
4) D. C. Hodgkin and B. M. Oughton, *Biochem. J.*, **65**, 752 (1957).
5) R. Schwyzer, *Chimia*, **12**, 53 (1958); R. Schwyzer and U. Ludesher, *Biochemistry*, **7**, 2519 (1968).
6) A. Stern, W. A. Gibbons, and L. C. Craig, *Proc. Nat. Acad. Sci. U.S.*, **61**, 734 (1968).
7) M. Ohnishi and D. W. Urry, *Biochem. Biophys. Res. Commun.*, **36**, 194 (1969).
8) The abbreviations recommended by the IUPAC-IUB Commission on Biochemical Nomenclature (*J. Biol. Chem.*, **247**, 977 (1972)) have been used throughout. In addition, DCC: dicyclohexylcarbodiimide, HONSu: *N*-hydroxysuccinimide, and HObt: 1-hydroxybenzotriazole. Amino acid symbols except D-Phe denote the L-configuration.
9) E. Schröder and K. Lübke, "The Peptides," Academic Press, New York and London (1966), p. 143.
10) H. Sugano, K. Higaki, and M. Miyoshi, This Bulletin, **46**, 231 (1973).
11) W. König and R. Geiger, *Chem. Ber.*, **163**, 788 (1970).
12) S. Matsuura, M. Waki, T. Kato, and N. Izumiya, This Bulletin, **46**, 977 (1973).
13) D. Balasubramanian, *J. Amer. Chem. Soc.*, **89**, 5445 (1967).
14) G. Vanderkooi, S. J. Leach, G. Nemethy, R. Scott, and H. A. Scheraga, *Biochemistry*, **5**, 2991 (1966).
15) E. Schnabel, *Ann. Chem.*, **702**, 188 (1967).
16) J. C. Sheehan, P. A. Cruickshank, and G. L. Boshart, *J. Org. Chem.*, **26**, 2525 (1961).
17) M. Ohno, T. Kato, S. Makisumi, and N. Izumiya, This Bulletin, **39**, 1738 (1966).
18) M. Fujino, C. Hatanaka, and O. Nishimura, *Chem. Pharm. Bull.* (Tokyo), **18**, 1288 (1970).
19) Molecular weight was determined on a Hitachi Osmometer, type 115, using methanol as a solvent.
20) H. Aoyagi, T. Kato, M. Waki, O. Abe, R. Okawa, S. Makisumi, and N. Izumiya, This Bulletin, **42**, 782 (1969).

Effect of Pressure on the Rate of Solvolysis. Formolysis of 1-(*p*-Substituted benzyl)ethyl Tosylates[1,2]

Akira SERA, Chisako YAMAGAMI, and Kazuhiro MARUYAMA

Department of Chemistry, Faculty of Science, Kyoto University, Sakyo-ku, Kyoto 606

(Received September 10, 1973)

The effect of pressure on the formolysis of 1-(*p*-substituted benzyl)ethyl tosylates was investigated, and the activation volumes, ΔV_o^* were estimated. The apparent values of activation volume were found to correlate nicely with σ^*. Because the present substrates were believed to be formolyzed through two separate processes, anchimerically assisted (k_Δ) and unassisted (k_s), the apparent values of activation volume were partitioned into the corresponding activation volumes, ΔV_Δ^* and ΔV_s^*. The dependence of ΔV_Δ^* and ΔV_s^* on the substituents was examined, and the correlation between the mechanisms of solvolysis and ΔV_Δ^* and ΔV_s^* was discussed.

In a previous paper we have shown the utility of the activation volumes as a diagnostic tool for studying solvolytic reaction mechanisms.[3]

The activation volume, ΔV^*, defined as difference in the partial molal volumes between the transition and the initial states, can be determined experimentally from the rate data under pressure by means of the following equation;

$$\Delta V^* = -RT(\partial \ln k/\partial P)_T \qquad (1)$$

In general, solvolytic reactions of neutral substrates are characterized by activation volumes with a negative sign; that is, the rate constant increases by the application of pressure. This volume contraction is known to be caused mainly by the electrostrictive reorientation of the solvent molecules around the newly-charged transition state species.[4] The magnitude of activation volume is considered to reflect the charge density of the transition state species; a more delocalized charge yields a less negative value of ΔV^*. It may, then, be anticipated that the application of this concept to neighboring group participation reactions could provide a more comprehensive understanding of the carbonium-ion problem. le Noble and his co-workers studied the solvolysis of *exo*-2- and *endo*-2-norbornyl systems and showed that the less negative value of ΔV^* observed for the *exo*-epimer could be well reconciled with the σ-participation.[5] The aryl participations were also studied for primary substrates, and it was shown that the participation processes resulted in less negative activation volumes than the non-participation processes.[6]

However, little is known about the substituent effects on the activation volume for reactions proceeding through the participation mechanism. It seems that a series of β-arylalkyl compounds would be a suitable model for the investigation of this problem because the solvolytic behavior of β-arylalkyl arenesulfonates has been extensively studied[7] since the first proposal of phenonium-ion intermediate[7a] and because the presence of the aryl participation has been actually proved in some cases.[7c~e] Accordingly, we chose the formolysis of 1-(*p*-substituted benzyl)ethyl tosylates (System I) as our model reaction. It is now accepted that tosylates (I) are solvolyzed through two distinct pathways, the anchimerically assisted (k_Δ) and anchimerically unassisted (k_s) routes, as shown in Scheme 1.[7c,8]

In this paper, we shall describe an attempt to partition the activation volume (ΔV^*) of the reaction into the activation volume for the anchimerically assisted process (ΔV_Δ^*) and that for the anchimerically unassited process (ΔV_s^*) in order to obtain a further insight into the reaction mechanism in terms of the activation volume.

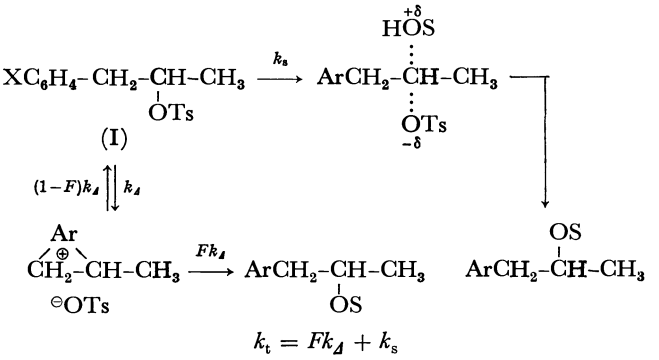

Scheme 1.

Results

The apparent activation volumes at atmospheric pressure, ΔV_o^*, for the formolysis of I and some typical secondary alkyl tosylates (System II) at 25.0 °C are summarized in Table 1, together with their rate constants at atmospheric pressure. These data were taken from our previous papers.[2,3] In order to examine the effect of an aryl moiety on the activation volume, the formolysis of γ-phenylalkyl tosylates (System III), a model possessing a non-participating aryl ring, was also studied (see Table 4). Their activation volumes, ΔV_o^*, were determined according to Eq. (1) by using the following first-order expression;

$$\ln k = a + bP \qquad (2)$$

The slope b was calculated by the method of least-squares in the range from 1 to 700 kg/cm^2, as has previously been described.[3] The results are given in Table 1.

As is shown in Table 1, the activation volume is dependent on the substituents in all systems. Figure 1 shows the correlations between ΔV_o^* and σ_{add}^*.[9] Two systems, I and II, were found to give approximately parallel correlation lines. The plot of ΔV_o^* against σ_{add}^* for System III gave another correlation line with a slope similar to the two others, whereas

Table 1. Formolysis rate constants and activation volumes for secondary tosylates at 25.0 °C

$XC_6H_4CH_2CH(OTs)CH_3$ (I)[a]			$R_1CH(OTs)R_2$ (II)[b]				$C_6H_5CH_2CH_2CH(OTs)R$ (III)[c]		
X	10^5k[d]	ΔV_o^*[e]	R_1	R_2	10^5k[d]	ΔV_o^*[e]	R	10^5k[d]	ΔV_o^*[e]
p-OCH_3 (**1**)	47.8	−7.3	Me	Me (**6**)	2.47	−14.7	Me (**9**)	1.42	−9.8
p-CH_3 (**2**)	9.84	−7.1	Me	Et (**7**)	6.04	−12.9	Et (**10**)	4.15	−8.5
H (**3**)	1.60	−7.8	Et	Et (**8**)	13.1	−11.2			
p-Cl (**4**)	0.229	−9.1							
p-NO_2 (**5**)	0.0394	−13.1							

a) Ref. 2. b) Ref. 3. c) For rate constants at other pressures, see Experimental. d) Rate constant at atmospheric pressure, s^{-1}. e) Activation volume at atmospheric pressure, cm^3/mol. Accurate to within 1 cm^3/mol.

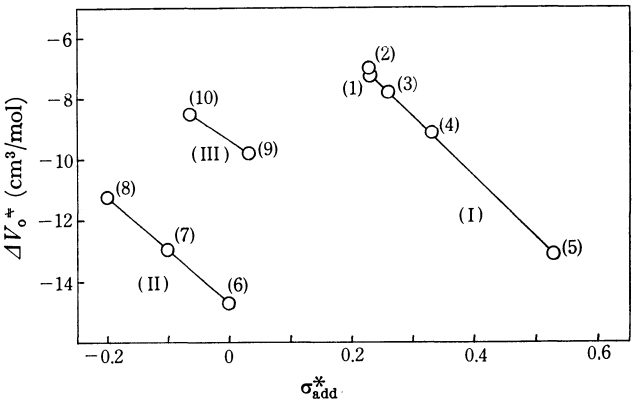

Fig. 1. Correlation of activation volume (ΔV_o^*) with σ^*_{add}. Roman numerals indicate system numbers and arabic numerals correspond to substrate numbers in Table 1.

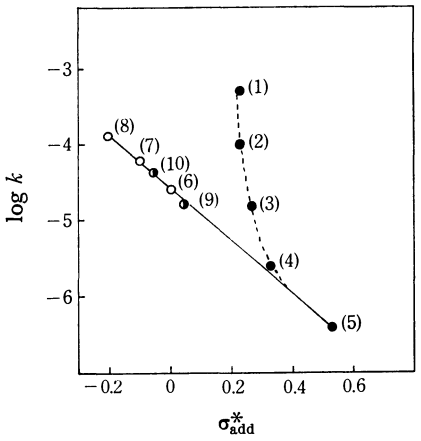

Fig. 2. Hammett-Taft plot of formolysis of secondary alkyl tosylates at atmospheric pressure.
●: $XC_6H_4CH_2CH(OTs)CH_3$, (system I); ○: $R_1CH(OTs)R_2$, (system II); ◑: $C_6H_5CH_2CH_2CH(OTs)R$, (system III). Numerals correspond to substrate numbers in Table 1.

the Hammett-Taft plot of log k against σ^*_{add} revealed a single correlation line including the points for System II (Fig. 2).

Partitioning of the Activation Volume. In order to partition solvolysis rates (k_t) for the β-arylalkyl system into anchimerically assisted (k_Δ) and unassisted (k_s) rate constants (Scheme 1), Schleyer and his coworkers[7c] have successfully utilized the deviation from the Hammett-Taft relation of the reaction rates for the substrates with activating substituents. The present method of partition of ΔV_o^* into ΔV_s^* and ΔV_Δ^* was essentially the same in principle. The plot of log k against σ^*_{add} (Fig. 2) shows that four substrates, **5**, **6**, **7**, and **8**, define a nicely correlated k_s line with the ρ*-value of −3.475.[8b] From this correlation line we estimated the k_s values for the other substrates with activating substituents. The values of Fk_Δ were then readily calculated from the relationship; $k_t = Fk_\Delta + k_s$. The same treatments of the rate-data at other pressures allow us to estimate the values of k_s and Fk_Δ at the given pressure. By knowing the values of k_s and Fk_Δ at each pressure, we can evaluate the magnitudes of ΔV_Δ^* and ΔV_s^* by means of the same method employed to determine the apparent ΔV_o^*. The representative results obtained for the unsubstituted compound (**3**) are presented in Table 2; the ρ*-value at each pressure is also given. Table 3 summarizes the activation volumes thus evaluated and the partitioned rate constants at atmospheric pressure for all the substrates. A set of parameters, ΔV_o^*, ΔV_Δ^*, and ΔV_s^*, allows us to calculate the fraction undergoing the k_Δ process, X_Δ, from the equation; $\Delta V_o^* = X_\Delta \cdot \Delta V_\Delta^* + (1 - X_\Delta) \cdot \Delta V_s^*$. The results are presented in the last column in Table 3. The rate ratio, Fk_Δ/k_t, is considered to be an alternative parameter providing the fraction of the contribution of the k_Δ-process. The excellent agreement of these two values (see Table 3) may confirm the reliability of the present analysis.

Table 2. Partitioning of formolysis rates for $PhCH_2CH(OTs)CH_3$ and ρ*-values under pressure at 25.0 °C

Pressure (kg/cm^2)	$10^5 k_t$ (s^{-1})	$10^5 k_s$ (s^{-1})	$10^5 Fk_\Delta$ (s^{-1})	ρ*[a]
1	1.60	0.336	1.26	−3.475
300	1.76	0.396	1.36	−3.467
500	1.87	0.433	1.44	−3.450
700	2.01[b]	0.488	1.52	−3.446
	$\Delta V_0^* = -7.8$[c]	$\Delta V_s^* = -13.2$[c]	$\Delta V_\Delta^* = -6.5$[c]	

a) Established from **5**, **6**, **7**, and **8**, see text and Fig. 2. b) Extrapolated from data at other pressures. c) Activation volume at atmospheric pressure, cm^3/mol.

Discussion

All the activation volumes shown in Table 1 are negative as had been predicted. Figure 1 shows that

TABLE 3. ESTIMATE OF $\Delta V_s^{\ddagger}$- AND $\Delta V_\Delta^{\ddagger}$- VALUES FOR $XC_6H_4CH_2CH(OTs)CH_3$ AT 25.0 °C

X	$10^5 k_t$ [a]	$\Delta V_o^{\ddagger}$ [b]	$10^5 k_s$ [a]	$\Delta V_s^{\ddagger}$ [b]	$10^5 Fk_\Delta$ [a]	$\Delta V_\Delta^{\ddagger}$ [b]	Fk_Δ/k_t	X_Δ [c]
p-OCH_3 (**1**)	47.8	−7.3	0.420	−13.3	47.4	−7.3	0.99	1.0
p-CH_3 (**2**)	9.84	−7.1	0.441	−13.4	9.40	−6.8	0.96	0.96
H (**3**)	1.60	−7.8	0.336	−13.2	1.26	−6.5	0.79	0.80
p-Cl (**4**)	0.229	−9.1	0.192	−13.6	0.04	—	0.17	—
p-NO_2 (**5**)	0.0394	−13.1	0.0394	−13.1	—	—	—	—

a) Rate constant at atmospheric pressure, s^{-1}. (b) Activation volume at atmospheric pressure, cm^3/mol.
c) Calculated from $\Delta V_o^{\ddagger} = X_\Delta \cdot \Delta V_\Delta^{\ddagger} + (1-X_\Delta) \cdot \Delta V_s^{\ddagger}$.

all the systems presently studied exhibit a considerable dependence of the $\Delta V_o^{\ddagger}$ on σ_{add}^*. The conformity of $\Delta V_o^{\ddagger}$ to the Hammett-type correlation for II was previously discussed in terms of the k_c-k_s hybrid nature of the substrates.[3] The reaction of I is known to be accelerated more effectively by an electron-donating substituent. Accordingly, the shown trend that a less negative activation volume is associated with a more electron-donating substituent is in good accordance with the general concept that the transition state accompanying the neighboring group participation is sufficiently stabilized by the charge delocalization into the aryl moiety. The results of the partition of $\Delta V_o^{\ddagger}$ clearly indicate that the anchimerically assisted process (k_Δ) is characterized by a less negative activation volume (about −7 cm^3/mol) than the value (about −13 cm^3/mol) evaluated for the non-assisted process (k_s). This trend seems to correspond to the prediction that a k_Δ-process has a less negative activation entropy, $\Delta S^{\ddagger}$, than a k_s-process.[10] The difference of about 6 cm^3/mol observed between the two processes is noteworthy. This magnitude is thought to be large enough for us to distinguish these two reaction mechanisms.

It should be noted that the values of $\Delta V_\Delta^{\ddagger}$ and $\Delta V_s^{\ddagger}$ were found to be independent of the substituents in spite of the presence of a significant substituent effect on the apparent activation volumes, $\Delta V_o^{\ddagger}$. Since the $\Delta V_o^{\ddagger}$-σ^* correlation was observed for secondary alkyl tosylates,[3] the dissimilar features between Systems I and II will require some consideration. In the present treatments, the accumulation of errors causes the values of $\Delta V_o^{\ddagger}$ to be less precise. Hence, it is obscure whether $\Delta V_\Delta^{\ddagger}$ reveals a substituent effect or not.[11] Therefore, we will here discuss only the case of the non-assisted pathway. The independence of $\Delta V_s^{\ddagger}$ on the substituents for System I must result from the presence of the aryl ring in these substrates. As has been presented in Table 1 and Fig. 1, the substituent effect on $\Delta V_o^{\ddagger}$ for System III was actually observed. Accordingly, the possibility that the aryl moiety functions in some way effectively to exhibit a leveling effect on $\Delta V_s^{\ddagger}$ for System I could be excluded. Another effect induced by the presence of the aryl moiety is an inductive rate deceleration. Therefore, the most likely explanation of the insensitivity of $\Delta V_s^{\ddagger}$ to σ_{add}^* may be that the anchimerically unassisted reaction in the system under consideration actually undergoes a solvent assisted process, that is, a nearly pure k_s-process,[12] whereas simple alkyl tosylates are solvolyzed with some k_c-character.[3] The leveling effect on the activation volumes associated with the k_s-mechanism (solvent assisted) has already been discussed in the case of methanolyses.[3] The k_s-character (solvent assisted) of the non-participating process of β-arylalkyl system has been accepted by several workers;[7c,7e] another evidence can be supplied on the basis of activation volume parameters. We have suggested that, as a reaction mechanism shifts from a k_c- to k_s-process, its activation volume becomes more negative.[3,13] The study of the formolyses of *n*-propyl and isopropyl tosylates at 45.0 °C yielded the activation volumes of −16.5 cm^3/mol for the former and −15.6 cm^3/mol for the latter.[14] These two values agree well with each other within the limits of experimental error. These results lead us to conclude that the reaction of isopropyl tosylate, even in formolysis, has a sufficient k_s-character rather than a k_c-character.[15] It may, then, be reasonably predicted that the non-participating process of I, for all substituents, is actually nearly the pure k_s-process (solvent assisted) because the rate-retarding inductive effect of the aryl ring makes it more difficult for the reaction to proceed *via* a carbonium-ion intermediate (k_c-character).

As has been shown above, the apparent slope associated with System I (Fig. 1) does not reflect the substituent dependence of $\Delta V_\Delta^{\ddagger}$ and/or $\Delta V_s^{\ddagger}$. From Table 3, the value of X_Δ is seen to vary with the substituents. Therefore, it is the change in X_Δ which is responsible for the apparent substituent dependence of $\Delta V_o^{\ddagger}$. In other words, the slope of the correlation line for System I is determined by the change in the degree of the contribution of each process, k_Δ and k_s, to the over-all reaction. The fact that the correlation lines between $\Delta V_o^{\ddagger}$ and σ_{add}^* for Systems I and II show similar slopes is also of interest. In the discussion of the $\Delta V_o^{\ddagger}$-σ_{add}^* correlation for the formolysis of secondary alkyl tosylates, we have suggested the importance of the k_c-character of the reaction.[3] Therefore, it may be considered that the difference in the degree of the solvent assistance in contributing to the over-all reactions decides the correlation slope. The similarity of the slopes for Systems I and II implies that the change in the degree of the solvent assistance is controlled by the substituents in a similar manner in these two cases. This interpretation supports the k_c-k_s hybrid mechanism proposed for secondary alkyl tosylates.

The comparison of the activation volumes for System II with those for System III indicates that the introduction of a non-participating aryl substituent into the alkyl system results in an increase in $\Delta V_o^{\ddagger}$ by several cubic centimeters/mol (see Fig. 1). Since all the points for the substrates of System II and III fall on a single

Hammett-Taft correlation line (Fig. 2), it is hard to consider that the observed increase in ΔV_0^* is a result of a change in the mechanism. Accordingly, the presence of an aryl group is considered to result in the difference in solvation. The activation volume is represented as follows;

$$\Delta V^* = \bar{V}_t - \bar{V}_g \quad (3)$$

where $\bar{V}_g$ and $\bar{V}_t$ are the partial molal volumes of the initial and the transition sates respectively. The measurements of the partial molal volumes of the substrates can provide information on this problem.[16] A rough estimate of $\bar{V}_g$ in formic acid gave the values of 194.6 cm³/mol for (**6**) and 295 cm³/mol for (**10**).[14] These data indicate that, taking into account the molar volumes (V_m) of 188.2 cm³/mol for neat (**6**) and 287 cm³/mol for neat (**10**), the volume changes in the solvent system accompanied by the addition of the solute ($\bar{V}_g - V_m$) are nearly the same. Hence, the difference in ΔV_0^* between the two systems (II and III) can be thought to reflect the difference in $\bar{V}_t$ rather than that in $\bar{V}_g$. This means that, in the transtion state, System III reveals a less significant volume contraction than System II. An explanation is possible in terms of the steric effect; that is, the bulky aryl group exerts some effect in hindering the electrostrictive solvation. Unfortunately, unambiguous evidence supporting this interpretation is now lacking.

Experimental

Materials. Formic acid was purified as has been described previously.[3] All the tosylates were prepared from the corresponding alcohols in the usual way. The purity of all the tosylates was confirmed by NMR analysis. Tosylate (**10**) was found to contain a small amount of impurity, but it did not interfere with the kinetic measurements.

Rate Measurements. A high-pressure apparatus described previously[17] was used without further modification. The bath temperature was kept at 25.0±0.01 °C. The reactions were followed by a conductometric method described previously.[3] The rate constants of γ-phenyl tosylates at various pressures are given in Table 4.

Table 4. Formolysis rate constants of $PhCH_2CH_2CH(OTs)R$ under pressure at 25.0 °C

Pressure (kg/cm²)	R=Me $10^5k(s^{-1})$	R=Et $10^5k(s^{-1})$
1	1.42	4.15
300	1.60	4.53
500	1.73	4.86
700	—	5.25
1000	2.07	—

References

1) Organic Reaction under High Pressure. XIII. Part XII, see K. Seguchi, A. Sera, and K. Maruyama, This Bulletin, Submitted.

2) A part of this work was briefly reported. C. Yamagami and A. Sera, *Chem. Lett.*, **1972**, 741.

3) A. Sera, C. Yamagami, and K. Maruyama, This Bulletin, **46**, 3864 (1973).

4) a) S. D. Hamann, "Physico-Chemical Effects of Pressure", Butterworths Scientific Publications, London (1957). b) W. J. le Noble, "Progress in Physical Organic Chemistry," Vol. 5, ed. by A. Streitwieser, Jr. and R. W. Taft, Jr., Interscience Publisher, New York (1967). p. 207.

5) a) W. J. le Noble and B. L. Yates, *J. Amer. Chem. Soc.*, **87**, 3515 (1965); b) W. J. le Noble, B. L. Yates, and A. W. Scaplehorn, *ibid.*, **89**, 3751 (1967).

6) W. J. le Noble and B. Gabrielsen, *Tetrahedron Lett.*, **1970**, 45.

7) a) D. J. Cram, *J. Amer. Chem. Soc.*, **71**, 3863 (1949); b) C. J. Kim and H. C. Brown, *ibid.*, **91**, 4286, 4287 (1969); c) C. J. Lancelot, J. J. Harper, P. von R. Schleyer, *ibid.*, **91**, 4294 (1969), and references cited therein.; d) A. F. Diaz and S. Winstein, *ibid.*, **91**, 4300 (1969); e) H. C. Brown and C. J. Kim, *ibid.*, **93**, 5765 (1971).

8) a) For definition of the terms, we follow Ref. 7c. Therefore, k_s designates the anchimerically unassisted pathway. F was reported to be nearly unity for the unsubstituted compound in formic acid.[7] b) Schleyer and coworkers reported the ρ* value of −3.38 for the same system in formic acid.[7c]

9) $\sigma^*_{add} = \sigma^*_{R_1} + \sigma^*_{R_2}$ for R_1–CH(OTs)–R_2. R. W. Taft, Jr., "Steric Effects in Organic Chemistry", ed. by M. S. Newman, John Wiley and Sons, Inc., New York (1956), p. 556.

10) a) S. Winstein and R. Hech, *J. Amer. Chem. Soc.*, **78**, 4801 (1956). b) D. J. Cram and L. A. Singer, *ibid.*, **85**, 1075 (1963).

11) It should be noted that in the present system the partitioned Fk_Δ-values do not correlate well with σ⁺-constants, see also D. S. Noyce and R. L. Castenson, *J. Amer. Chem. Soc.*, **95**, 1247 (1973). In order to examine the substituent effect on ΔV_Δ^*, therefore, a model system in which a linear Fk_Δ-σ⁺ relationship is fulfilled must be chosen.

12) In the present discussion, the definition of the term k_s is somewhat troublesome To refer to the solvent assisted pathway, a word "solvent assisted" was parenthesized.

13) For such a generalization, the partial molal volume of the initial state must be, of course, taken into account. Details will be presented elsewhere.

14) Unpublished data.

15) For the difference in k_s-characters between primary and secondary systems, see ref. 7e and the references cited therein.

16) For the studies of initial state volumes in solvolytic reactions, see for example, H. S. Golinkin, I. Lee, and J. B. Hyne, *J. Amer. Chem. Soc.*, **89**, 1307 (1967).

17) A. Sera, T. Miyazawa, T. Matsuda, Y. Togawa, and K. Maruyama, This Bulletin, **46**, 3490 (1973).

Carbon-13 Nuclear Magnetic Resonance Studies of Biphenyl Derivatives II. FT-NMR of Halobiphenyls[1)]

Mamoru IMANARI,* Masahiro KOHNO,* Muneki OHUCHI,* and Kazuhiko ISHIZU**

*Analytical Instrument Division JEOL, Akishima, Tokyo 196

**Department of Chemistry, Faculty of Science, Ehime University, Bunkyocho, Matsuyama, Ehime 790

(Received September 13, 1973)

The natural-abundance ^{13}C NMR spectra of the *ortho*- or the *para*-halobiphenyls were obtained by the pulse Fourier transform NMR (FT-NMR). For the *para*-derivatives, the observed chemical shifts of the C_1, C_2, and C_3-positions gave an excellent linear dependence on the electronegativity of the substituents. The dependence for the C_4-position, which showed a deviation from the linear plot, may be due to the heavy atom effects. The additivity of the chemical shifts holds also for the *ortho*-derivatives except for the cases of the bridgehead carbons, the C_1 and C_1'-positions. In particular, the observed chemical shifts of the C_2, C_3, and C_4 positions for 2,2',6,6'-tetrachlorobiphenyl showed a good agreement with the predicted values, whereas a large discrepancy can be seen between the observed and the assumed values for the C_1 and C_1' positions. The effects on the chemical shifts due to the steric hindrance are discussed by comparison with the results of the hindered alkylbiphenyls. The temperature dependence of the spin-lattice relaxation time was investigated for 4,4'- and 2,2'-dichlorobiphenyls. The activation energies of the molecular reorientation are negligibly small at the C_1, and C_4-positions for the *para*-derivative, but the *ortho*-derivatives have higher values at these positions, indicating anisotropy for the molecular motion.

The recent greater facility of ^{13}C FT-NMR spectroscopy has promised to better results from structural and dynamic studies of organic molecules. In particular, the measurements of the spin-lattice relaxation time (T_1) can yield useful information about molecular motion.[2,3)] In the present work, ^{13}C FT NMR measurements were carried out on 4,4'-dihalobiphenyls, 4-halobiphenyls and several *ortho*-substituted chlorobiphenyls. The substituent effects of halogen atoms were studied in terms of the electronegativity of the substituents. The effects on the chemical shifts due to the steric hindrance were investigated on the basis of the additivity calculation and compared with the results of the previous works on the hindered alkylbiphenyls.[4)] The spin-lattice relaxation times of the ring carbons were measured for 4,4'-dichlorobiphenyl and 2,2'-dichlorobiphenyl, and the activation energies of the molecular reorientation were estimated from the temperature dependence of the spin-lattice relaxation time. The activation energies for the C_1 and C_4 positions were negligibly small, and those for C_2 and C_3 showed nearly the same value in the case of the *para*-derivative. This means that the molecule is likely to rotate around the long axis of biphenyl. In the case of the *ortho*-derivative, however the activation energy values increased at both C_1 and C_4 positions, suggesting that a molecular motion may be greatly hindered in the direction of the long molecular axis. The D_2O used for the NMR lock was also filled outside the spherical tube. The concentration of the samples used for the T_1 measurements was adjusted so as to make a 30% solution in THF. The reproducibility of the T_1 values was better than 10%.

Experimental

All the ^{13}C NMR spectra were recorded with a JEOL PS/PFT-100 spectrometer equipped with a Fourier transform operation at 25.15 MHz under a complete proton decoupling. Benzene was used as the external reference, and the chemical shifts were measured within limits of experimental error of about 0.1 ppm. The following materials were synthesized and recrystallized from ethanol (the physico-chemical indices are given): 4-fluorobiphenyl (mp 74.2—75 °C), 4-chlorobiphenyl (mp 72—72.5 °C), 4-bromobiphenyl (mp 79.5—80 °C), 4-iodobiphenyl (mp 112—113 °C), 4,4'-difluorobiphenyl (mp 88—89 °C), 4,4'-dichlorobiphenyl (mp 149—150 °C), 4,4'-dibromobiphenyl (mp 162—163 °C), 4,4'-diiodobiphenyl (mp 199—202 °C), and 2,2'-dichlorobiphenyl (mp 58—59 °C). The 2,2',6,6'-tetrachlorobiphenyl and 2,6-dichlorobiphenyl were purchased from the Japan chromatograph Co., Ltd. The purity of the material was checked by means of the proton NMR spectra. The samples were prepared as approximately a 10—30% solution in tetrahydrofuran (THF).

The measurements of the spin-lattice relaxation time (T_1) were carried out using the Inversion Recovery Method[5)] and the Progressive Saturation Method.[6)] The pulse width was 20 μs for 90° pulse in all the experiments. In these experiments, spherical tubes, which were placed in standard tubes, were employed to reduce the inhomogenity of the external field (H_0) and the rf field (H_1).

Results and Discussion

The ^{13}C NMR spectra of 4,4'-difluorobiphenyl and 4,4'-dichlorobiphenyl observed at room temperature are given in Fig. 1. The spectra can be easily analyzed on the basis of the predictions of additivity calculations.[7)] An extra splitting of the ^{19}F ($I=1/2$) nucleus can be seen in Fig. 1, where the magnitude of the spin-spin coupling constant alters as a function of the distance between the ^{13}C and ^{19}F nuclei. The calculated chemical shifts of 4,4'- and 4-halobiphenyls, summarized in Table 1, are in satisfactory agreement with the observed values. In order to study the substituent effects in the *para*-derivatives, plots were made between the observed chemical shifts and the electronegativity. As is shown in Fig. 2, the plots for C_1 and C_3 give straight lines, indicating that they are positive-dependent on the absolute value of the electronegativity, conversely, those for the C_2 and C_4 positions show a

Table 1. The ^{13}C chemical shifts of 4,4′-dihalobiphenyl and 4-halobiphenyl (ppm)

4,4′-Dihalobiphenyl		C-1	C-2	C-3	C-4				
H	Observed	−13.1	1.3	−0.5	1.1				
F[a)]	Observed	−8.4	−0.4	12.7	−37.0				
	Predicted	−8.8	−0.5	12.7	−33.8				
Cl	Observed	−10.3	−0.1	−0.8	−5.4				
	Predicted	−11.3	−0.2	−0.7	−4.9				
Br	Observed	−10.7	−0.4	−3.8	6.4				
	Predicted	−11.7	−0.5	−3.7	6.9				
I	Observed	−16.6	−0.4	−9.9	34.9				
	Predicted	−12.2	−0.7	−9.7	34.9				
4-Halobiphenyl		C-1	C-2	C-3	C-4	C-1′	C-2′	C-3′	C-4′
F[b)]	Observed	−9.4	−0.3	12.7	−34.5	−12.1	1.3	−0.8	0.9
	Predicted	−8.8	−0.4	12.4	−38.7	−13.1	1.3	−0.5	1.1
Cl	Observed	−11.3	−0.2	−0.7	−5.4	−11.5	1.4	−0.7	1.1
	Predicted	−11.3	−0.2	−0.7	−4.9	−12.1	1.3	−0.5	1.1
Br	Observed	−11.8	−0.9	−3.9	6.7	−12.2	0.3	−0.8	1.2
	Predicted	−7.7	−1.3	−4.8	7.6	−13.3	1.2	−0.8	1.0
I	Observed	−12.4	−0.5	−9.6	35.5	−11.7	1.6	−0.5	0.7
	Predicted	−16.6	−0.4	−9.9	34.9	−13.1	1.3	−0.5	1.1

The chemical shifts are indicated that positive is to high field (to the right side) from benzene.
a) J_{C-F}=245 Hz J_{C-C-F}=22 Hz $J_{C-C-C-F}$=8 Hz
b) J_{C-F}=255 Hz J_{C-C-F}=21 Hz $J_{C-C-C-F}$=8 Hz

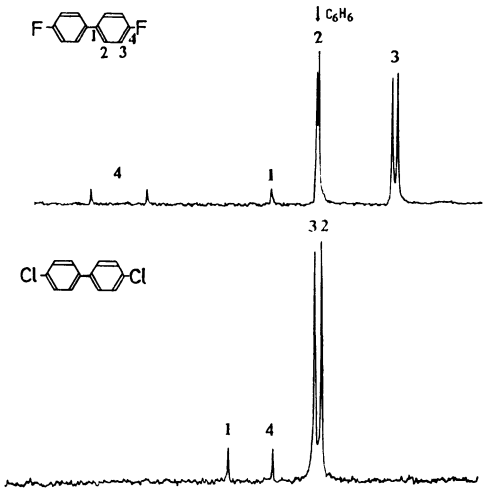

Fig. 1. ^{13}C FT-NMR spectra of 4,4′-difluorobiphenyl and 4,4′-dichlorobiphenyl.

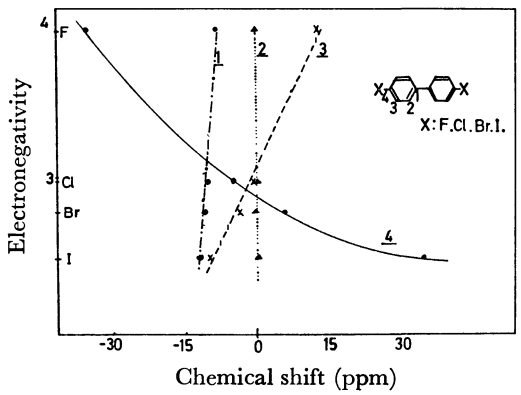

Fig. 2. Relation between the observed chemical shifts and the electronegativity of the substituents in 4,4′-dihalobiphenyls.
The electronegativity were taken from L. Pauling, "The Nature of the Chemical Bond," Cornell University Press, New York (1940).

negative-dependence. Similar alternative effects of the substituents, which were previously confirmed by the proton NMR of the 4,4′-dihalobiphenyl, have also been reported in ^{13}C NMR studies of the alkylbiphenyls. The plots of the C_4-position only revealed a remarkable deviation from the straight line. This can probably be attributed to the heavy-atom effects of the halogen atoms.[8)] It is of interest to compare the observed chemical shifts and predicted values in the *ortho*-derivatives, since the discrepancy between them may be attributed to the effect of a steric hindrance. In Table 2 we give the observed and the predicted ^{13}C

Table 2. The ^{13}C chemical shifts of 2,6-dichlorobiphenyl, 2,2′-dichlorobiphenyl and 2,2′,6,6′-tetrachlorobiphenyl

		C-1	C-2	C-3	C-4	C-1′	C-2′	C-3′	C-4′
2,6-Cl	Observed	−12.6	−6.9	−0.4	−1.8	−9.2	0.4	−1.6	0.2
	Predicted	−14.9	−7.0	−0.4	−1.7	−13.1	1.3	−0.5	1.1
		C-1	C-2	C-3	C-4	C-5	C-6		
2,2′-Cl	Observed	−10.5	−5.5	−3.4	−1.5	1.8	−1.5		
	Predicted	−13.3	−4.6	−0.7	−0.5	1.3	−0.2		
2,2′,6,6′-Cl	Observed	−7.2	−7.0	−0.3	−3.0				
	Predicted	−14.9	−7.6	−0.4	−3.0				

2,6-Cl: 2,6-dichlorobiphenyl 2,2′-Cl: 2,2′-dichlorobiphenyl 2,2′,6,6′-Cl: 2,2′,6,6′-tetrachlorobiphenyl

chemical shifts of 2,2'-dichlorobiphenyl, 2,6-dichlorobiphenyl, and 2,2',6,6'-tetrachlorobiphenyl. It is rather surprising that the additivity calculation gave more or less suitable results for the ring carbons, except for the values of the bridgehead C_1 and C_1' positions. Similar results for the proton NMR chemical shifts have previously been reported for 2,2'-dichlorobiphenyl.[9] This suggests that the anisotropic effect of the ring current is reduced by the large electronegativity of the halogen atoms. As can be seen in Table 2, however, the observed shifts of the C_1 and C_1' atoms show a remarkable deviation, shifting higher by about from 2.3 to 2.5 ppm in dichlorobiphenyl and by 7.7 ppm in 2,2',6,6'-tetrachlorobiphenyl, exceeding the calculated values by the additivity rule. A similar large discrepancy between the observed and the predicted C_1 chemical shifts has already been demonstrated for hindered alkylbiphenyl. One may consider several cooperative mechanisms[10] which modify the chemical shift for the *ortho*-derivatives. The first is the perturbation of the π-bond order between the central C_1–C_1' bond or that of the charge density on the bridgehead carbon atoms due to the steric hindrance. In the present case, however, the first effect is not important, because the observed chemical shifts of the other position (C_2, C_3, C_4) are nearly the value calculated for the planar biphenyl. Recently, the importance of the short-range interaction has been demonstrated between non-bonded atoms which are accessibly located in hindered molecules.[4,11,12] In such a case, a large higher shift (a so-called compression shift) has been observed for the carbon atoms bonded to the carbon interacting together this shift is due to the electronic repulsion. No such effect can be seen for the *ortho*-carbon atoms of the present derivatives. This suggests that the two phenyls are almost perpendicularly twisted in the hindered halobiphenyls.[13] In such a case, these anomalous discrepancies in the C_1-chemical shift may be considered to result from some interaction between the chlorine and $2p_z$ carbon atomic orbitals, but a more rigorous explanation will need further investigations.

Carbon-13 Spin-lattice Relaxation Time. When analyzing ^{13}C spin-lattice relaxation time, three possible relaxation mechanisms may be considered. One is the chemical-shift anisotropy (CSA), and another is spin-rotation (SR) and ^{13}C–^1H dipole-dipole interactions.[2,14,15] The third mechanism is expected to be predominant for the protonated carbons. It has been relatively easy to observe the ^{13}C relaxation under complete proton decoupling.[16] In this case, if the rotational reorientation of the molecule is isotropic, the ^{13}C–^1H dipole relaxation contributes to the $1/T_1$ of all the protonated carbons to the same extent. The ^{13}C–^1H dipole-dipole relaxation becomes:

$$1/T_1 = K\{f(\omega_H-\omega_C)+3f(\omega_C)+6f(\omega_H+\omega_C)\} \quad (3)$$

where:

$$f(\omega_i) = \tau_R(1+\omega_i^2\tau_R^2)^{-1} \quad (4)$$

$$K = \hbar^2\gamma_H^2\gamma_C^2 r^{-6} \quad (5)$$

The τ_R is the rotational correlation time, r is the C–H distance, and γ_H and γ_C are the gyromagnetic ratios of the proton and carbon nuclei respectively. For all cases, we have $(\omega_C+\omega_H)\tau_R \ll 1$, and Eq. (3) can be reduced to the familiar results;

$$1/T_1 = \hbar^2\gamma_H^2\gamma_C^2\tau_R r^{-6} \quad (6)$$

Equations (3)—(6) can be suitably modified, however, either when the rotational reorientation of the molecule is anisotropic or when an internal motion of the functional group must be considered.[15] If the anisotropic motion (τ_G) is much slower than the overall reorientation ($\tau_R(\tau_G \gg \tau_R)$), the relaxation time becomes identical to the suitably-modified Eq. (6). In this case, an internal motion has little effect on $1/T_1$, and τ_G can be estimated only with difficulty. On the other hand, however, if an anisotropic motion is much faster than the overall reorientation ($\tau_G \ll \tau_R$), the relaxation can be easily understood on the basis of Eqs. (3) and (6). One may thus expect that T_1 values do not depend on the correlation time for the overall reorientation, but will be affected by an internal motion. In the *para*-position, T_1 is shorter than those for the carbon atoms at the *ortho*- and the *meta*-positions as a result of the preferred rotation about the symmetry axis. The bulky substituents of benzene that are axially symmetric causes the T_1 *ortho*/T_1 *para* and T_1 *meta*/T_1 *para* ratios to become larger, while substituents without axial symmetry lead to these ratios approaching 1.0.[17] In rod-shaped molecules such as diphenyl diacetylene, the T_1 value for the *para*-carbons is five times shorter than the T_1 for the *ortho*- and *meta*-carbons.[2]

In order to see the motional anisotropy in the present biphenyl derivatives, the temperature dependence of the T_1 values was investigated for 4,4'-dichlorobiphenyl and 2,2'-dichlorobiphenyl.

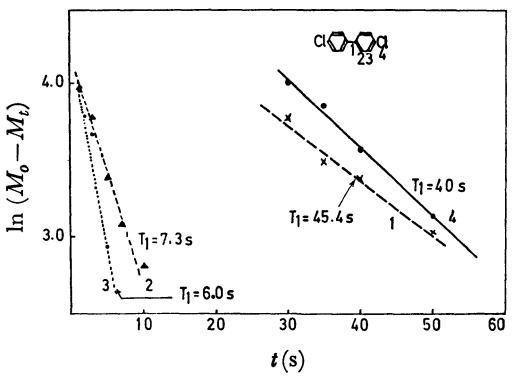

Fig. 3. Spin-lattice relaxation times of ^{13}C nuclei in proton decoupled 4,4'-dichlorobiphenyl.

The relaxation behavior of the ring carbons in 4,4'-dichlorobiphenyl is shown in Fig. 3.[18] The *ortho*-carbon relaxation of 4,4'-dichlorobiphenyl is nearly identical with that of the *meta*-carbons, since the anisotropic motion of this molecule dominates around the long biphenyl axis.

In general, the observed spin-lattice relaxation time T_1 can be divided into two contributions:

$$1/T_1 = (1/T_1)_D + (1/T_1)_0 \quad (7)$$

where the first term is the contribution of the dipole-dipole interaction and where the second term includes those of all the other mechanisms, in which the spin-rotation mechanism and the chemical-shift anisotropy

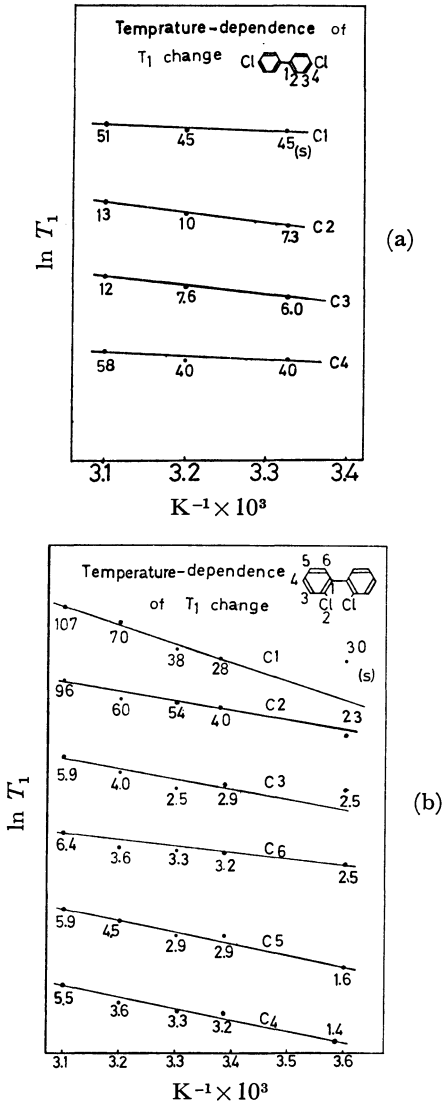

Fig. 4. Temperature dependence of the spin-lattice relaxation times for chloroderivatives.
a) 4,4′-dichlorobiphenyl, b) 2,2′-dichlorobiphenyl.

have been considered to be most important.[2] If the contribution of the spin-rotation relaxation is really important, the temperature dependence on the relaxation time will show a tendency opposite to those due to the other relaxation mechanisms.[14] At present, we have no strong experimental basis on which to characterize the relaxation mechanism of each carbon atom, but we have assumed that the dipole relaxation will be dominant for all carbon atoms; that is, $(T_1)_D \simeq T_1$, since the ^{13}C-resonance lines show nearly the same intensity ratio as that calculated from the numbers of the equivalent carbon atoms in the biphenyl ring. As is illustrated in Fig. 4, the T_1 curves show a temperature dependence of the Arrhenius type on the high-temperature side of their minima and the temperature dependence of τ_R is given by:

$$\tau_R = \tau_R^0 \exp(E_a/RT) \quad (8)$$

where E_a is the activation energy for the molecule reorientation. The apparent activation energy can be calculated from the slope of the plot, as is summarized in Table 3. The E_a values of the C_2 and C_3 positions are almost equal, but those for C_1 and C_4 positions are all negligibly small in the case of the *para*-derivative. This indicates that the rotation of the moecule is overwhelmingly dominant around the long axis of biphenyl. On the other hand, the E_a values of both C_1 and C_4 positions become much higher than those of the other positions in the *ortho*-derivative. This indicates that the partial motion of the phenyl would be greatly modified by the steric hindrance, in particular around the long axis of biphenyl.

Table 3. Activation energy (kcal/mol)

	C1	C2	C3	C4	C5	C6
4,4′-Cl	—	5.1	5.6	—		
2,2′-Cl	9.8	5.7	6.3	8.1	6.0	5.8

4,4′-Cl: 4,4′-dichlorobiphenyl.
2,2′-Cl: 2,2′-dichlorobiphenyl.

The temperature dependence of the C_1 and C_3 positions, which changes the slope at around 10 °C, suggests some contribution from the other relaxation mechanisms. The spin-rotational relaxation is most probable, but detailed investigations are now under way.

References

1) Presented at the 11th NMR symposium of the Chemical Society of Japan, Osaka, October 1972.
2) G. C. Levy and G. L. Nelson, *J. Amer. Chem. Soc.*, **94**, 4897 (1972).
3) G. C. Levy, J. D. Cargioli, and F. A. L. Anet, *ibid.*, **95**, 1527 (1973).
4) H. Hasegawa, M. Imanari, and K. Ishizu, This Bulletin **45**, 1153 (1972)
5) R. L. Vold, J. S. Waugh, M. P. Klein, and D. E. Phelps, *J. Chem. Phys.* **48**, 3831 (1968).
6) R. Freeman and H. D. W. Hill, *ibid.*, **54**, 3367 (1971).
7) G. B. Savatisky, *ibid.*, **67**, 2723 (1963).
8) W. M. Lichman and D. M. Grant, *J. Amer. Chem. Soc.*, **90**, 1400 (1968).
9) A. R. Tarpley, Jr. and J. H. Goldenstein, *J. Phys. Chem.*, **75**, 421 (1971)
10) M. Karphus and J. A. Pople, *J. Chem. Phys.*, **38**, 2803 (1963).
11) Warner R. Woolfenden and D. M. Grant, *J. Amer. Chem. Soc.*, **88**, 1496 (1966).
12) D. M. Grant and B. Vernon Cheney, *ibid.*, **89**, 5315 (1967).
13) A. C. Littlejohn and L. W. Smith, *J. Chem. Soc.*, 4637 (1956).
14) T. C. Farrar and E. D. Becker, "Pulse and Fourier Transform NMR," Academic Press, N. Y. (1971), p. 46.
15) G. C. Levy, *Accounts Chem. Res.*, **6**, 161 (1973)
16) K. F. Kuhluman and D. M. Grant, *J. Chem. Phys.*, **55**, 2998 (1971).
17) D. Doddrell, V. Gluskko, and A. Allrehand, *ibid.*, **56**, 3683 (1972).
18) M_0 is the line intensity of longest pulse sequence ($t \simeq 4T_1$) and M_t is that of a given pulse interval (t) in the steady state. For any line, the quantity (M_0–M_t) was found to be an exponential function of t, and the time constant was given to the spin-lattice relaxation time.

Radical Addition Reactions to the Carbonyl Group. I. The Reaction of Aliphatic Aldehydes with Di-*t*-butyl Peroxide

Kazuhiro MARUYAMA,* Mamoru TANIUCHI, and Shinzaburo OKA

**Department of Chemistry, Faculty of Science, Kyoto University, Kyoto 606*
Institute for Chemical Research, Kyoto University, Gokashō, Uji, Kyoto 611

(Received September 22, 1973)

The thermal decomposition of di-*t*-butyl peroxide in aliphatic aldehydes has been carefully examined. *n*-Aldehydes and β-substituted aldehyde gave appreciable amounts of *sec*-alcohols in the reactions. *sec*-Alcohol arose from the addition of the alkyl radical to the carbonyl group of aldehyde. α-Substituted aldehydes, however, did not give *sec*-alcohol, but instead gave considerable amounts of enol ether-aldehydes and dialdehydes. The addition of the alkyl radical to the carbonyl group and the decarbonylation of aldehydes were influenced remarkably by the structures of the aldehydes.

The cleavage reaction of the *t*-alkoxy radical to form ketone and the alkyl radical has been extensively studied. The relative ease of the bond scission of the *t*-alkoxy radical has been determined quantitatively by various methods.[1] On the other hand, only a few studies have been reported on the addition of the alkyl radical to the carbonyl groups of aldehyde and ketone, which is considered to be the reverse of the well-known cleavage reaction of the *t*-alkoxy radical.[2] However, no quantitative investigation has been published.

In this work, the formation of *sec*-alcohols by the reaction of aliphatic aldehydes with di-*t*-butyl peroxide has been examined in order to ascertain the possibility of the radical addition reaction to carbonyl groups.

Results and Discussion

The thermal decomposition of di-*t*-butyl peroxide in *n*-aldehydes yielded considerable amounts of *sec*-alcohols, accompanied by paraffin hydrocarbons and carbon monoxide. The yields of the reaction products were determined by gas chromatography. The reproducibility of the experimental results was fairly good: same typical experimental results are summarized in Table 1. The *sec*-alcohols, obtained in *ca.* 8% yields based on the aldehydes consumed (Table 1), were isolated by distillation and were identified by a comparison of the retention times in gas chromatography, and by a comparison of the IR, NMR, and mass spectra, with those of authentic samples. The main products obtained from the reaction of *n*-aldehydes with di-*t*-butyl peroxide can be explained by the mechanism shown in Eqs. (1)—(6):[2a]

$$(CH_3)_3COOC(CH_3)_3 \longrightarrow 2(CH_3)_3CO\cdot \quad (1)$$

$$(CH_3)_3CO\cdot + RCHO \longrightarrow (CH_3)_3COH + R\dot{C}O \quad (2)$$

TABLE 1. TYPICAL EXPERIMENTAL RESULTS OBTAINED IN THE REACTION OF ALDEHYDES WITH DI-*t*-BUTYL PEROXIDE (REACTION TIME 6 hr)

	Aldehyde used						
	Heptanal	Octanal	Nonanal	Decanal	2-Ethyl-heptanal	2-Methyl-octanal	3-Ethyl-heptanal[a]
Reactants, m mol							
Aldehyde	87.5	87.5	87.3	87.3	87.3	87.3	87.3
Di-*t*-butyl peroxide	26.6	26.6	26.6	26.6	26.6	26.6	26.6
Products, m mol							
t-Butyl alcohol	2.8	7.5	6.8	6.4	8.1	10.6	4.0
Paraffin hydrocarbon	29.1	46.6	62.0	60.2	33.7	18.0	70.2
Di-*t*-butyl peroxide	25.3	23.2	22.4	22.2	22.0	21.4	24.0
Aldehyde	39.9	22.3	11.5	10.4	43.2	56.7	7.4
sec-Alcohol	1.8	2.6	2.9	3.4			1.5
Enol ether-aldehyde					1.0	1.7	
Dialdehyde					0.3	0.7	
Carbon monoxide	48.8	65.0	72.4	74.0	41.5	26.4	80.6
Conversion, %							
Aldehyde	54.4	74.5	86.8	88.1	50.5	35.0	91.5
Di-*t*-butyl peroxide	4.9	12.8	15.8	16.5	17.3	19.5	9.8
Product Yields, mol/100 mol of aldehyde consumed							
Paraffin hydrocarbon	61.2	71.5	81.8	78.3	76.5	58.9	88.0
sec-Alcohol	7.6	8.0	7.7	8.9			3.8
Enol ether-aldehyde					4.5	11.1	
Dialdehyde					1.4	4.6	
Carbon monoxide	102.0	99.7	95.5	96.3	94.0	86.3	101.0

a) Reaction was carried out in 4 hr.

$$R\dot{C}O \longrightarrow R\cdot + CO \quad (3)$$

$$R\cdot + RCHO \longrightarrow R_2CHO\cdot \quad (4)$$

$$R\cdot + RCHO \longrightarrow RH + R\dot{C}O \quad (5)$$

$$R_2CHO\cdot + RCHO \longrightarrow R_2CHOH + R\dot{C}O \quad (6)$$

The main products—*t*-butyl alcohol, carbon monoxide, paraffin hydrocarbons, and *sec*-alcohols—are formed by Reactions 2, 3, 5, and 4—6 respectively. Reaction 4 implies the addition of the alkyl radical to the carbonyl group and is the reverse reaction of the decomposition of the *t*-alkoxy radical. Thus, the yield of *sec*-alcohol is a measure of the facility of the addition of the alkyl radical to the carbonyl group. β-Substituted aldehyde also yielded *sec*-alcohol, but its yield was considerably lower than those of *n*-aldehydes (Table 1). On the other hand, the reaction of α-substituted aldehydes with di-*t*-butyl peroxide led to the formation of enol ether-aldehydes and dialdehydes, much as in the oxidative coupling of α-substituted aldehydes by activated manganese dioxide.[3] In spite of our efforts, no *sec*-alcohol was detected in the products of these reactions. The formation of enol ether-aldehydes and dialdehydes may be explained by the following scheme:

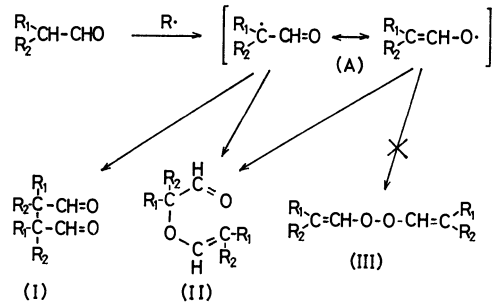

α-Substituted aldehydes may suffer hydrogen abstraction on the α-carbon by a radical to a significant degree, thus giving the resonance-stabilized hybrid radicals (A). The hybrid radicals are considered to be fairly well stabilized by the hyperconjugation of two alkyl groups. However, with *n*-aldehydes and β-substituted aldehyde, an analogous conjugation would not be so important, because the radicals derived from α-hydrogen abstraction have only one alkyl group which contributes to such a stabilization. This would be the reason why the hybrid radical (A) plays an important role in the reaction of α-substituted aldehydes. Dialdehyde (I) and enol ether-aldehyde (II) can be produced through the dimerization of the radical (A). None of the other symmetrical coupling product, the divinyl peroxide (III), was found in the products. Moreover, 2-methyloctanal yielded quite large amounts of enol ether-aldehydes and dialdehyde compared with 2-ethylheptanal (Table 1). This can be explained by the greater capacity for the hyperconjugation effect of the methyl group, because it is well-known that this effect is much greater in the methyl group than in the ethyl group.[4] The lack of *sec*-alcohol may be interpreted in terms of steric factors. That is to say, the alkyl radicals derived from α-substituted aldehydes are *sec*-radicals, while the radicals from *n*-aldehydes and β-substituted aldehyde are prim-radicals. Thus, in adding to the carbonyl group, the radicals derived from α-substituted aldehydes are more sterically inhibited than those from *n*-aldehydes and β-substituted aldehyde. Similarly, the alkyl radical derived from β-substituted aldehyde is more sterically crowded than those from *n*-aldehydes. This would cause the lower yield of *sec*-alcohol in the reaction of β-substituted aldehyde (Table 1). As the other products, carbon monoxide was formed almost quantitatively except in the cases of α-substituted aldehydes, in which considerable amounts of enol ether-aldehydes and dialdehydes were formed: paraffin hydrocarbons were obtained in yields ranging from *ca.* 60 to 90%, depending on the structures of the aldehydes used. *t*-Butyl alcohol was obtained almost quantitatively with respect to the peroxide decomposed. Finally, in comparison with the rate of the decarbonylation of the three isomers of nonanal (Table 1), it was found that their rates were remarkably influenced by the structures of the aldehydes, decreasing in the following order: β-substituted aldehyde>*n*-aldehydes>α-substituted aldehydes. Therefore, the radical-induced decarbonylation of aliphatic aldehydes does not depend only on the structure of the attacking radical, but also on the structure of aldehydes.

Experimental

Materials. The heptanal, octanal, 2-ethylhexanal, nonanal, decanal, and di-*t*-butyl peroxide were all purchased from commercial sources. The 2-methyloctanal and 3-ethylheptanal were prepared by the Grignard procedure from the corresponding halides and ethyl orthoformate: 2-methyloctanal: bp 65—67 °C/18 mmHg; $n_D^{25.8}$ 1.4180: 3-ethylheptanal: bp 74—76 °C/18 mmHg; $n_D^{29.0}$ 1.4213. Their purities were confirmed by gas chromatography. The aldehydes were purified by vacuum distillation under nitrogen immediately before use.

Apparatus. The product analyses were performed by means of Yanagimoto Model GCG-220 and G-8 chromatographs equipped with thermal conductivity detectors. A Varian Model 920 aerograph was used in the preparations. The product identifications were carried out by a comparison of retention times in gas chromatography, and, if necessary, by a comparison of the IR spectra (Perkin-Elmer 521 spectrometer), the NMR spectra (Varian A-60 spectrometer), and the mass spectra (JMS-01SG spectrometer) of the products with those of authentic specimens.

Procedure. A three-necked reaction flask was equipped with a thermometer, a reflux condenser, and a gas inlet tube. The inlet tube was connected to a cylinder of nitrogen of 99.99 mol% purity. The reflux condenser was connected to a dry ice-acetone trap and then in turn to a water gas holder. A mixture of aldehyde and di-*t*-butyl peroxide was added to the reaction flask. The air in the reaction apparatus was then replaced by nitrogen prior to heating. The flask was heated to 120 °C in an oil bath. The reaction time was determined after the temperature of the oil bath had reached 120 °C. The gas liberated in the reaction was passed through the cold trap (−78 °C) and collected over water in the gas holder. The quantity of carbon monoxide was determined by means of the gaseous volume collected in the gas holder. At given time intervals, the oil bath was removed and the reaction flask was cooled by standing in air in order to quench the reaction. The reaction mixture in the flask and the volatile

products found in the cold trap were then combined. The resultant mixture was analyzed quantitatively by gas chromatography, using a suitable substance as an internal standard. The analyses of the products were mainly carried out, for lower-boiling materials by the use of a Model GCG-220 gas chromatograph equipped with a column (2.5 m) packed with 25% of Squalane on Firebrick C-22, 60—80 mesh, at 80 and 140 °C: for higher-boiling materials, we used a Model G-8 gas chromatograph equipped with a column (0.75 m) packed with 5.0% of Silicone Gum SE-30 on Chromosorb W, 60—80 mesh, at temperatures from 100 to 160 °C.

Preparation of Enol Ether-aldehydes and Dialdehydes by the Oxidative Coupling of α-Substituted Aldehydes. As a typical example, the procedure for the oxidative coupling of 2-ethylhexanal will be described. Activated manganese dioxide was prepared by a modified Attenburrow procedure[5] and activated by the azeotropic distillation of the excess water with benzene.[6] 2-Ethylhexanal (18.0 g) was added under nitrogen to a stirred mixture of activated manganese dioxide (69.5 g) in dioxane (150 ml). Then, the resultant mixture was heated for 24 hours at the reflux temperature of dioxane. The reaction mixture was subsequently filtered, and the filtrate evaporated. The residue was vacuum distilled under nitrogen. 2-Ethyl-2-(2'-ethyl-1'-hexenyloxy)hexanal (enol ether-aldehyde) and 2,3-diethyl-2,3-dibutyl-succinaldehyde (dialdehyde) were obtained in yields of 31 and 21% respectively. Essentially the same results were obtained from 2-methyloctanal.

References

1) K. Maruyama and K. Murakami, This Bulletin, **41**, 1401 (1968); J. D. Bacha and J. K. Kochi, *J. Org. Chem.*, **30**, 3272 (1965); J. K. Kochi, *J. Amer. Chem. Soc.*, **84**, 1193 (1962); D. G. Hoare and W. A. Waters, *J. Chem. Soc.*, **1964**, 2552.

2) a) F. F. Rust, F. H. Seubold, and W. E. Vaughan, *J. Amer. Chem. Soc.*, **70**, 4253 (1948); G. Fuller and F. F. Rust, *ibid.*, **80**, 6148 (1958); b) W. H. Urry, A. Nishihara, and J. H. Y. Niu, *J. Org. Chem.*, **32**, 347 (1967); W. G. Bentrude and K. R. Darnall, *J. Amer. Chem. Soc.*, **90**, 3558 (1968).

3) J. C. Leffingwell, *Chem. Commun.*, **1970**, 357.

4) C. L. Deasy, *Chem. Rev.*, **36**, 145 (1945).

5) E. F. Pratt and S. P. Suskind, *J. Org. Chem.*, **28**, 638 (1963).

6) I. M. Goldman, *ibid.*, **34**, 1979 (1969).

The Unsensitized Photooxidation of (+)-Limonene, 1,2-Dimethylcyclohexene, and *endo*-Dicyclopentadiene

Tadashi SATO and Eigoro MURAYAMA

Department of Applied Chemistry, Waseda University, Shinjuku-ku, Tokyo 160

(Received November 9, 1973)

The unsensitized photooxidation of (+)-limonene (**1**), 1,2-dimethylcyclohexene (**2**) and *endo*-dicyclopentadiene (**3**) were carried out with Pyrex-filtered light. The singlet-oxygen oxidation was found to occur concurrently with the radical oxidation to the extent of 41% with **1** and 66% with **2**, but not at all with **3**. A reaction path *via* a complex was proposed.

Although sensitized photooxidation has been the subject of a number of recent investigations in connection with the reactivity of singlet oxygen, unsensitized photooxidation has attracted less attention. It has generally been accepted that, in unsensitized photooxidation, the light energy can be assumed to be used for the formation of a radical initiator, and that the reaction proceeds in the same reaction pattern as that of the radical-initiated oxidation.[1] In the present study, we observed that (+)-limonene (**1**), 1,2-dimethylcyclohexene (**2**), and *endo*-dicyclopentadiene (**3**), each possessing only isolated double bonds, suffered oxidation under the influence of the light of a longer wavelength (Pyrex-filtered light) to give results different from those obtained by the radical oxidation; an investigation was then undertaken in order to clarify the relation between the unsensitized photooxidation and the radical oxidation.

Results

(+)-Limonene (**1**), 1,2-dimethylcyclohexene (**2**), and *endo*-dicyclopentadiene (**3**) were oxidized with oxygen in three ways; Ox I—by heating a neat sample at 40—60 °C; Ox II—by irradiation with visible light in the presence of rose bengal (0.5 M in 1 : 1 *t*-butyl alcohol–methanol), and Ox III—by irradiation with Pyrex-filtered light in the absence of any sensitizer (0.5 M in 1 : 1 *t*-butyl alcohol–methanol). The products and product distribution after the reduction ($Na_2S_2O_3$+KI) of the primarily-formed hydroperoxide mixture are summarized in Tables 1—3. The product identification was carried out spectroscopically (see Experimental). The relative retention times on gas chromatography were also compared with those reported[2] in the case of the oxidation products of **1**.

It has been reported[3] that Compounds **10** and **11**, when obtained by the radical oxidation of **1**, are racemic, while both are optically-active when obtained by singlet-oxygen oxidation. In the latter case, Compounds **9** and **12** have also been known to be optically-active. The optical activities obtained in the present study are included in Table 1. It should be noted that the optical activities of **10** and **11**, obtained by Ox III, were reduced compared to those obtained by Ox II, whereas those of **9** and **12** were unchanged irrespective of the oxidation methods (Ox II or Ox III). We inferred from these facts that, in Ox III, some radical oxidation occurs concurrently with the singlet-oxygen oxidation. From the $[\alpha]_D$ values of **10** and **11**, it was estimated that the ratio of both reaction types is 41 : 59 (singlet-oxygen oxidation: radical oxidation). The product distribution also coincided

Table 2. Yields of oxidation products from **2**

	Products				
	13	**14**	**15**	**16**	**17**
Ox I	12	7	39	34	8
Ox II	0	92	8	0	0
Ox III	1	64	22	7	6

Table 3. Yields of oxidation products from **3**

	Products				
	18	**19**	**20**	**21**	**22**
Ox I	8	42	0	18	32
Ox II	0	0	0	0	100
Ox III	15	38	17	0	30

Table 1. Yields and optical activities of oxidation products from **1**[a,b]

	Products								
	4	**5**	**6**	**7**	**8**	**9**	**10**	**11**	**12**
Ox I	14	3	16	14	7	0	26 (0)[d]	20 (0)[c]	0
Ox II	0	0	30	7	3	23 (+92.4)[c]	8 (−178)[d]	3 (−71.8)[c]	26 (+5.71)[c]
Ox III	16	3	22	11	13	10 (+92.1)	11 (−32)	5 (−5.6)	10 (+7.2)

a) The unparenthesized figures refer to the yield (%), and figures in the parentheses refer to optical activities ($[\alpha]_D$). b) The product distribution in Ox I and Ox II are almost identical with those reported.[2,13] c) Data from Ref. 2. d) As the value in Ref. 2 was that of a mixture, the value from Ref. 14 was indicated.

fairly well with the calculated values based on this ratio.*

It is evident from the results in Table 2 that, in the case of **2** also, the singlet-oxygen oxidation and the radical oxidation occur concurrently in Ox III, the ratio in the present case being 66: 34.** This ratio became larger as the reaction was carried out with a more dilute solution in the case of **2**, while it was almost independent of the concentration in the case of **1** (Tables 4 and 5).

Table 4. The ratio of singlet-oxygen participation as a function of concentration in case of **1** (after 20 hr)

Concentration (M)	0.25	0.5	0.1	1.5	Neat
Percent of singlet-oxygen participation	39	41	40	35	26

Table 5. The ratio of singlet-oxygen participation as a function of concentration in case of **2** (after 5 hr)

Concentration (M)	0.19[a]	0.22	0.5	Neat[b]
Percent of singlet-oxygen participation	90	77	66	35

a) After 20 hr. b) Unfiltered or Pyrex-filtered light.

Contrary to the results obtained with the Ox-III oxidations of **1** and **2**, where singlet-oxygen oxidation constituted a considerable part of the reaction, only radical oxidation was observed in the Ox-III oxidation of **3** (Table 3). This conclusion was derived from the observation that the same product distribution as obtained by Ox III was obtained when Ox I and irradiation in the absence of oxygen were applied consecutively to **2**. Obviously, Ox III is essentially the same as the radical oxidation (Ox I) and the apparent differences in product distributions (with **18**, **20**, and **21**) in Ox I and Ox III may be assumed to arise from a secondary phototransformation of the primary products. This reasoning was supported by the facts that **21** afforded **20** on irradiation with Pyrex-filtered light[6] and that the hydroperoxide **23**, which is a presumable intermediate in the Ox-I oxidation of **3**, and which is actually obtained in an almost pure state by the singlet-oxygen oxidation of **3**, afforded **18**, in addition to **20**, under the irradiation.

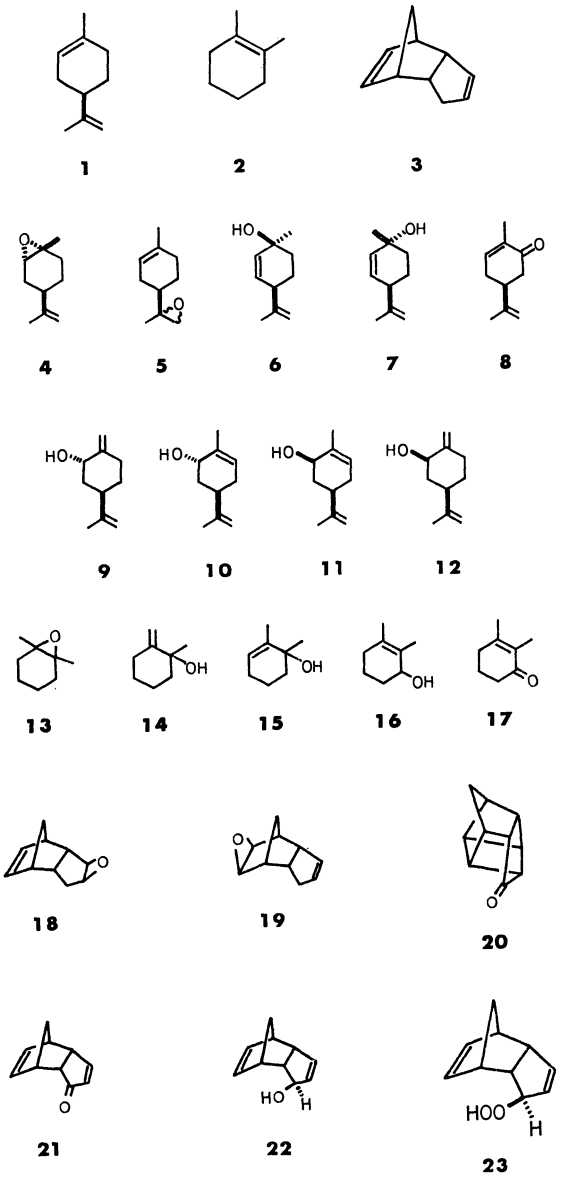

Discussion

It was amusing that olefins which should not absorb the working light underwent photoreaction, and that the participation of singlet-oxygen oxidation was observed only in cases of **1** and **2**. Chien[7] has studied the mechanism of the initiation of the photooxidation of hydrocarbons in the wavelength region where there are no allowed transitions. He postulated, mainly on the basis of the kinetic data, two processes, the charge-transfer excitation and the oxygen-perturbed S–T ex-

* The unsensitized photooxidation of **1** has been reported by Schenck and his co-workers,[2] where a product distribution almost identical with that in the radical oxidation is obtained. This result contradictory to ours is conceivable since, under their reaction conditions (irradiation for 43 hr at 50 °C in a quartz vessel), the radical reaction would necessarily become more important than the inherent photochemical reaction of the olefin.

** The Ox-I and Ox-II oxidations of **2** have been reported by Foote.[4] Although results identical with ours have been obtained in case of Ox II, no description of **13** and **17** has appeared in the case of Ox I, in contrast to our results. This might be due to their over-reducing of the primary products by using $NaBH_4$ as a reducing reagent. Farmer and Sutton[5] have obtained a 1: 1 mixture of two hydroperoxides which are presumable precursors of **15** and **16** by the unsensitized photooxidation of **2**, and claimed an identity in mechanism between unsensitized photooxidation and radical oxidation. We traced the reaction under their reaction conditions (at 35 °C with a neat sample in a quartz vessel) and obtained **14** (38.6%) and **15** (32.8%) as the main products after the reduction of the hydroperoxide intermediates. The ratio of **16** was quite low (6%); it might be suspected that they were led to an erroneous conclusion as to the structure of the product deluded by the isomerization during the chemical-identification process of the products.

citation, as the most probable primary processes for this type of photooxidation. The possible formation of singlet oxygen has been suggested, but as a process of minor importance in the cases he studied.

We considered that singlet oxygen might be produced through a) sensitization by some impurities present in the reactants, b) sensitization by the primarily-formed radical oxidation products, and c) charge-transfer excitation.

The UV spectrum of **1** (1 cm path length, neat) showed a fine structure in the 250—270 nm region which was ascribable to some aromatics. The fine structure could not be removed by ordinary purification methods (distillation, column chromatography on alumina). *p*-Cymene, whose UV spectrum was very similar to the fine structure observed with the limonene sample, is the most probable candidate for the aromatic impurity. We, therefore, carried out the Ox-III oxidation of **1** in the presence of varying amounts of *p*-cymene, but the reaction pattern was unchanged in the *p*-cymene concentration region of 0—3.5 mg/8 ml. Thus, the Path a could be ruled out. As for the Path b, we considered that the most probable radical oxidation product which could sensitize the singlet-oxygen formation was carvone (**8**, λ_{max} 315 nm (ε 47)); therefore, Ox III with varying amounts of **8** was carried out. The results are shown in Fig. 1. Evidently **8** acted

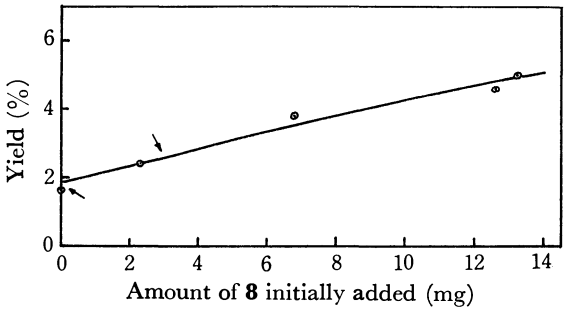

Fig. 1. Total yield of products from singlet-oxygen oxidation after 20 hr *vs.* amount of initially added **8** (mg in 8 ml of 0.5 M solution of **1** in 1 : 1 *t*-butyl alcohol–methanol).

as a sensitizer for the singlet-oxygen formation, but the following consideration revealed that this sensitization is not responsible for the total of the singlet-oxygen participation observed in Ox III. The amounts of **8** present in the reaction mixture obtained by the Ox-III oxidation of **1** with (3 mg) and without the initial addition of **8** are indicated by Lines I and II respectively in Fig. 2. The amount of **8** corresponding to the A area must be responsible for the extra singlet-oxygen participation of 0.7% (=2.6—1.9%; see arrows in Fig. 1), effected by the initial addition of **8**. The singlet-oxygen participation induced solely by the primarily-formed **8**, whose amount corresponds to the B area, should thus amount to 0.6% (=0.7%×(area B/areaA)), which corresponds to only one-third of the total singlet-oxygen oxidation observed in the Ox-III oxidation of **1**. A similar treatment was undertaken for the Ox-III oxidation of **2** by assuming **17** (λ_{max} 305 nm(ε 60)) as the possible sensitizer. From the

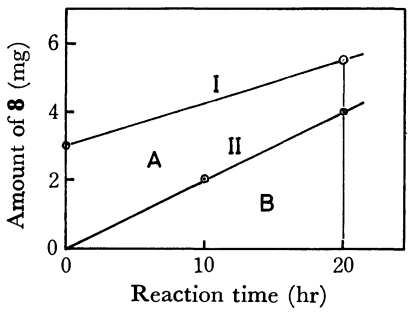

Fig. 2. Amount of **8** present in the reaction mixture as a function of time. (8 ml of 0.5 M solution of **1** in 1 : 1 *t*-butyl alcohol–methanol).
I: With initial addition of 3 mg of **8**. II: Without initial addition.

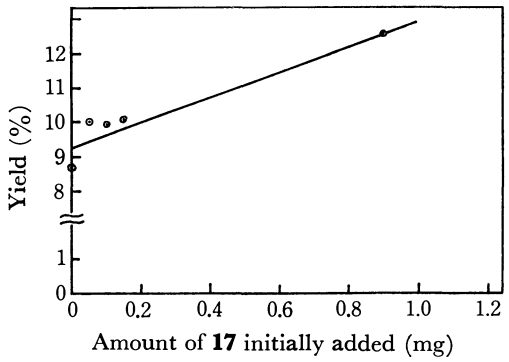

Fig. 3. Total yield of products from singlet-oxygen oxidation after 5 hr *vs.* amount of initially added **17** (mg in 2 ml of 0.5 M solution of **2** in 1 : 1 *t*-butyl alcohol–methanol).

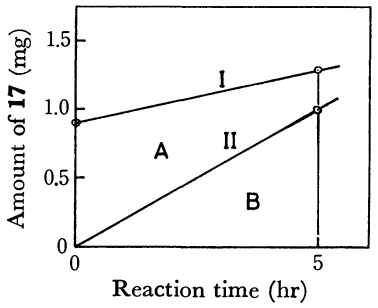

Fig. 4. Amount of **17** present in the reaction mixture as a function of time. (2 ml of 0.5 M solution of **2** in 1 : 1 *t*-butyl alcohol–methanol). I: With initial addition of 9 mg of **17**. II: Without initial addition.

results shown in Figs. 3 and 4, it was calculated that only one-third of the singlet-oxygen participation was ascribable to the sensitization by **17**. Further support that a mechanism other than unsaturated ketone sensitization for the singlet-oxygen formation was probably operating was obtained from the following observation. If the carvone sensitization were the sole path for the singlet-oxygen formation in the Ox III oxidation of **1**, then:

$$\{d[\text{singlet-oxygen products}]/dt\}_{t=0} = 0$$

and $\{d[\text{radical products}]/dt\}_{t=0} > 0$.

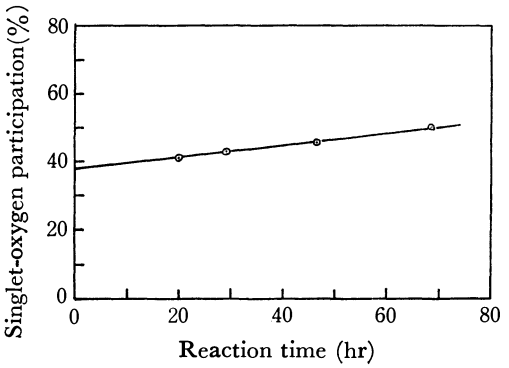

Fig. 5. Percent of singlet-oxygen participation as a function of time.

Therefore, the plots of

$$\frac{d[\text{singlet-oxygen products}]/dt}{d[\text{radical products}]/dt} \approx \frac{[\text{singlet-oxygen products}]}{[\text{radical products}]}$$

should extrapolate to zero at zero time. Such a plot is shown in Fig. 5, which does not intercept zero, in contrast to the above assumption. As another scheme for the singlet-oxygen formation, we considered a route *via* a C–T complex (Path c). When the UV spectra were measured with neat samples of **1**, **2**, and **3** which had been bubbled with 1 atom of oxygen for 5 min prior to the measurement, the end absorption moved to a wavelength longer by about 10 nm as compared with those of the oxygen-free samples. The original spectra were restored when the samples were bubbled with nitrogen. It might be reasonable, therefore, to assume that a C–T excitation is the primary step in Ox III, and that singlet oxygen would be formed by Reaction (1). With these arguments, we should consider why no singlet-oxygen participation was observed with **3**, in contrast to the observations with **1** and **2**. One is inclined to believe that only Path b is operative here, since this path would clearly explain the absence of singlet-oxygen participation in the case of **3** because of the photo-instability of the unsaturated ketone **21**, a potential sensitizer. However, we still persist in Path c for the following reason. Previous work[4] has shown that the reaction of singlet oxygen is quite sensitive to the electron density in the double bond of the olefin, and that the reactivity towards singlet oxygen increases with the number of alkyl groups attached to the double-bond carbon. Therefore, **1** and **2**, which have tri- and tetra-alkyl-substituted olefins respectively, would react with singlet oxygen more rapidly than **3**, disubstituted olefin. The situation is also clearly demonstrated by the fact that, with **1**, only trisubstituted olefin is attacked by singlet oxygen. If the rate of the reaction between singlet oxygen and **3** is fairly slow, the competing reactions of triplet species or Σ^1O_2, which are other products of Reaction (1) and possible initiators for the radical reaction, would become important and only radical-oxidation products would result. The dependence of the ratio of the singlet-oxygen participation on the concentration in the case of **2** (Table 5) would be another support for the involvement of the complex, since it is conceivable that the chain reaction would be easily terminated in a dilute solution, while the reaction through a complex would proceed as effectively in a dilute solution as in the more concentrated solution. However, the absence of a definite concentration dependence in the case of **1** can not be clearly interpreted.

$$\text{Olefin} + {}^3O_2 \xrightarrow{h\nu} (\text{Olefin-}O_2)^* \longrightarrow \text{Olefin} + {}^1O_2\ (\Delta \text{ or } \textstyle\sum) \quad (1)$$

In conclusion, we are inclined to favor the idea that the participation of charge-transfer excitation in the unsensitized photooxidation of olefin induces a competing singlet-oxygen oxidation and radical oxidation, but it remains uncertain, at this stage of the investigation, to what degree Path b is involved, particularly there is uncertainty as to the analyses of **8** or **17**; the possibility that compounds other than **8** or **17** could also serve as sensitizers for singlet-oxygen formation was also taken into account.

Experimental

The IR spectra were obtained in neat form with liquid samples and in KBr pellet form with solid samples. The NMR spectra were measured on a JEOL MH 60 (60 MHz) spectrometer with a CCl_4 solution; the chemical shifts are represented in δ values relative to the internal TMS standard. The mass spectra were measured on a Hitachi RMS-4 mass spectrometer.

Starting Materials. **1**: A commercial sample was passed through an alumina column. $[\alpha]_D^{26.5}=+112.6°$. Lit:[3] $[\alpha]_D^{20}=+122.4°$. **2**: A material prepared by the dehydration of 1,2-dimethylcyclohexanol[8] was purified by preparative gas chromatography. The sample could not be freed from 2,3-dimethylcyclohexene (5—7%), as revealed by the NMR spectrum. **3**: A commercial sample was fractionated through a packed column 80 cm in length.

General Methods of Oxidation. *Ox. I*: The sample was kept at 40—60 °C for 5—10 hr while oxygen was bubbled through. *Ox. II*: A 0.5M solution of the sample in *t*-butyl alcohol–methanol (1: 1) containing a small amount of rose bengal was irradiated at 18—20 °C with a tungsten lamp (200 W) for 10—20 hr, while oxygen was bubbled through. *Ox. III*: A 0.5M solution of the sample in *t*-butanol-methanol (1: 1) was irradiated at 18—20 °C with Pyrex-filtered light for 5—20 hr while oxygen was bubbled through.

The oxidized mixture obtained by each oxidation method was stirred vigorously with a solution containing KI (3 g) and $Na_2S_2O_3\cdot 5H_2O$ (4.5 g) in 10 ml of water for 40 hr. The organic material was extracted with ether, and the solvent was evaporated *in vacuo*. The residue was analyzed on a gas chromatograph, *p*-cymene being used as the internal reference. Although calibration curves were not obtained with all the oxidation products, we assumed that the relative sensitivities for the gas chromatographic detection did not deviate very much from each other; a calibration curve was obtained only with **10** in the case of **1** and with **14** in the case of **2**. Each product was obtained in a pure state by preparative gas chromatography.

*Product Identification.**** **4**: IR; Identical with the reported datum.[9] NMR; δ 1.27 (3H, s), 1.72 (3H, s), 2.93 (1H, dist. t), 4.75 (2H, s). **5**: IR; 1680, 842, and 795 cm^{-1}. NMR; δ 1.20 (3H, s), 1.63 (3H, s), 2.45 (2H, ABq) and 5.35 (1H, b. s). **6**: IR; Identical with the reported value.[2] NMR; δ 1.21 (3H, s), 1.71 (3H, s), 3.69 (1H, b.s, OH), 4.78

*** Abreviations: dist.: distorted, b: broad.

(2H, s), and 5.62 (2H, s). **7**: IR; Identical with the reported value.[2] NMR; δ 1.23 (3H, s), 1.72 (3H, s), 3.60 (1H, b.s, OH), 4.6—4.8 (2H, m), and 5.5—5.65 (2H, m). **8**: IR; 3075, 1675, 895, and 800 cm^{-1}. NMR; δ 1.80 (6H, s), 2.45 (5H, b.s), 4.83 (2H, s), and 6.75 (1H, dist. t). **9**: IR; Identical with the reported value.[2] NMR; δ 1.70 (3H, s), 4.25 (1H, dist. t), 3.50 (1H, b.s), and 4.69 (4H, b.s). **10**: IR; 3330, 1644, 1055, 889, and 810 cm^{-1}. NMR; δ 1.75 (6H, s), 3.65 (1H, s, OH), 3.89 (1H, dist. t), 4.68 (2H, s), and 5.45 (1H, b.s). **11**: IR; 3330, 1645, 1038, 889, and 810 cm^{-1}. NMR; δ 1.73 (3H, s), 1.74 (3H, s), 4.10 (1H, b.s, OH), 4.71 (2H, s), and 5.45 (1H, b.s). **12**: IR; Identical with the reported value.[2] NMR; δ 1.72 (3H, s), 3.80 (1H, b.s, OH), 4.70 (3H, s), and 4.96 (1H, s). **13**: IR; No characteristic band. NMR; δ 1.21 (6H, s), and 1.2—1.8 (m). **14**: IR; 3380, 1640, and 890 cm^{-1}. NMR; δ 1.23 (3H, s), 1.50 (6H, b.s), 1.9—2.4 (2H, b.d), 3.27 (1H, s, OH), 4.40 (1H, b.s), and 4.64 (1H, d). **15**: IR; 3380 cm^{-1}. NMR; δ 1.16 (3H, s), 1.62 (b.s), 2.64 (1H, s, OH), and 5.13 (1H, b.s). **16**: IR; 3380, and 1640 cm^{-1}. NMR; δ 1.66 (s), 1.73 (s), 1.6—2.0 (m), 2.30 (1H, s, OH), and 3.85 (1H, b.s). **17**: IR; 1660 cm^{-1}. NMR; 1.74 (3H, s), 1.95 (3H, s), and 2.2—2.4 (m). **18**[10]: MS; *m/e* 148, 117, 91, and 66. IR; 1573, and 832 cm^{-1}, NMR; δ 1.42 (2H, dist. q, for endomethylene) and 5.98 (2H, d). **19**[10]: MS; *m/e* 148, 117, 91, 82, and 66. IR; 1616, and 844 cm^{-1}. NMR; δ 1.10 (2H, ABq, endomethylene with an anisotropic effect by the epoxy ring) and 5.75 (2H, m). **20**[6], **21**[11], and **22**[12]: Identical with those of the authentic samples.

References

1) O. L. Magelli and C. S. Sheppard, "Organic Peroxides," Vol. 1, ed. by D. Swern, Wiley-Interscience, New York, N. Y. (1969), p. 15.

2) G. O. Schenck, O. -A. Neumuller, G. Ohloff and S. Schroeter, *Ann.*, **687**, 26 (1965).

3) G. O. Schenck, K. Gollnick, G. Buchwald, S, Schroeter, and G. Ohloff, *ibid.*, **674**, 93 (1964).

4) C. S. Foote, *Accounts. Chem. Res.*, **1**, 104 (1968).

5) E. H. Farmer and D. A. Sutton, *J. Chem. Soc.*, **1946**, 10.

6) R. C. Cookson, J. Hudec, and R. O. Williams, *J. Chem. Soc., C*, **1967**, 1382.

7) J. C. W. Chien, *J. Phys. Chem.*, **69**, 4317 (1965). *Cf.* N. Kulevsky, P. V. Sneeringer, L. D. Grina, and V. I. Stenberg, *Photochem. Photobiol.*, **12**, 395 (1970).

8) F. K. Signaigo and P. L. Cramer, *J. Amer. Chem. Soc.*, **55**, 3326 (1933).

9) W. F. Newhall, *J. Org. Chem.*, **29**, 185 (1964).

10) *Cf.* N. Muto, T. Nagase, Y. Goto, and S. Fujiki, Abstracts of Papers presented at the 22nd meeting of the Chemical Society of Japan, Tokyo, April, 1969, Vol. III, p. 1234.

11) K. Alder and F. H. Flock, *Chem. Ber.*, **87**, 1916 (1954).

12) R. B. Woodward and T. J. Katz, *Tetrahedron*, **5**, 70 (1959).

13) C. S. Foote, S. Wexler, and W. Ando, *Tetrahedron Lett.*, **1965**, 4111.

14) K. Gollnick, T. Franken, G. Schade, and G. Dörhöfer, *Ann. N. Y. Acad. Sci.*, **171**, 89 (1970).

A New Reagent for the Syntheses of *N*-Monoalkylated Hydroxylamines; *N*-Tosyl-*O*-2,4,6-trimethylbenzylhydroxylamine

Yoshikazu Isowa and Hideaki Kurita

Sagami Chemical Research Center, Nishionuma, Sagamihara, Kanagawa 229

(Received November 2, 1973)

The reactions of *N*-tosyl-*O*-2,4,6-trimethylbenzylhydroxylamine with primary alkyl halides yielded the protected hydroxylamines. The simultaneous cleavage of *N*-tosyl- and *O*-2,4,6-trimethylbenzyl groups with hydrogen bromide in acetic acid gave the corresponding *N*-monoalkylated hydroxylamines such as *N*-benzylhydroxylamine, 1-amino-3-hydroxyaminopropane and DL-3-hydroxyamino-2-aminopropionic acid.

Syntheses of naturally-occurring hydroxylamines,[1] which exist as hydroxamates or *N*-nitroso derivatives, have been accomplished using various methods including method A to E;

Method A: Zinc dust reduction of nitro group[2] in aqueous solution containing ammonium chloride.

Method B: Acid hydrolysis or hydrazinolysis of nitrone,[3] which is obtainable by the reaction of alkyl halides or acrylic acid derivatives with the appropriate aldoxime in the presence of base.

Method C: Direct conversion of alkyl halides[4] by hydroxylamine itself in the absence or presence of solvents.

Method D: Reduction of oxime.[5]

Method E: Hydrolysis of oxazirane,[6] which is obtained by the oxidation of Schiff's base.

In our previous papers, *N*-tosyl-*O*-benzylhydroxylamine (I) has been used for the syntheses of alanosine,[7] 5-*N*-hydroxy-L-ornithine,[8] rhodotorulic acid,[9] and ferrichrome.[10] The *N*-protecting tosyl group of I is always deprotected by the action of 36% hydrogen bromide in acetic acid, while the *O*-protecting benzyl group, after the *N*-acylation, is deblocked by the hydrogenation. In some cases,[8] *N*-tosyl and *O*-benzyl groups may be removed simultaneously by the treatment with 36% hydrogen bromide–acetic acid after long days, but in almost all cases, benzyl group remained intact with the action of this reagent.

In this paper, we describe a new reagent for the syntheses of *N*-monosubstituted hydroxylamines; *N*-tosyl-*O*-2,4,6-trimethylbenzylhydroxylamine (II). 2,4,6-Trimethylbenzyl group has been used for the first time by Stewart[11] for the masking of carboxyl groups in the peptide chemistry and is known to be acid-sensitive.

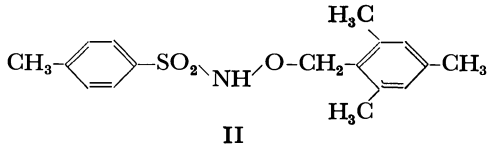

II

The reagent (II) was prepared according to the procedure[8] for the analogue (I); the tosylation of *O*-2,4,6-trimethylbenzylhydroxylamine, which was prepared by the 2,4,6-trimethylbenzylation of *N*-carboethoxyhydroxylamine and the subsequent alkaline hydrolysis, afforded II. Using this reagent, *N*-benzylhydroxylamine (III), 1-amino-3-hydroxyaminopropane (IV), and DL-3-hydroxyamino-2-aminopropionic acid (DL-V) were synthesized.

Synthesis of N-*Benzylhydroxylamine (III) and the Conditions of the Removal of the Protecting Groups.* Reaction of benzyl chloride and II in the presence of sodium methoxide gave *N*-benzyl-*N*-tosyl-*O*-2,4,6-trimethylbenzylhydroxylamine (VI).

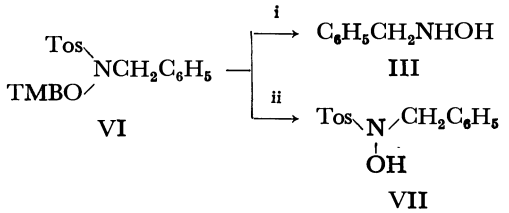

Fig. 1. Tos: tosyl, TMB: 2,4,6-trimethylbenzyl.
i: hydrogen bromide–acetic acid
ii: trifluoroacetic acid

The treatment of VI with 36% hydrogen bromide-acetic acid in the presence of phenol gave III. 18% Hydrogen bromide–acetic acid was also effective for the simultaneous removal of the two protecting groups. The use of trifluoroacetic acid as a deprotecting agent gave another result; only the 2,4,6-trimethylbenzyl group was removed and the *N*-tosyl group remained intact. The product was *N*-benzyl-*N*-tosylhydroxylamine, whose structure was determined by the elemental analysis, IR, and NMR spectra. Absorption of *N*-hydroxy group of VII appeared at 3360 cm^{-1} in IR and δ 10.19 in NMR.

Synthesis of 1-Amino-3-hydroxyaminopropane (IV). 1-Amino-3-hydroxyaminopropane (IV) is a component of schizokinen, an iron-transport compound from *Bacillus megaterium* and was synthesized by Neilands *et al.*[2a] by method A. The higher analogues of IV, 1-amino-4-hydroxyaminobutane[2c] and 1-amino-5-hydroxyaminopentane,[2d,e] were also synthesized previously by the same method. Condensation of 3-bromopropylphthalimide and II in the presence of sodium methoxide gave 1-phthalimido-3-(*N*-tosyl-*N*-2,4,6-trimethylbenzyloxy)aminopropane (VIII). VIII was converted by the action of hydrazine hydrate to 1-amino-3-(*N*-tosyl-*N*-2,4,6-trimethylbenzyloxy)aminopropane (IX), which was identified as the hydrochloride. The action of 36% hydrogen bromide-acetic acid on IX gave IV as the di-hydrobromide.

Synthesis of DL-*3-Hydroxyamino-2-aminopropionic Acid (DL-V).* First synthesis[4c,d] of DL-V was achieved by method C; condensation of methyl L- or DL-3-chloro-2-acetaminopropionate (X) with hydroxylamine in the absence of solvents and the subsequent acid

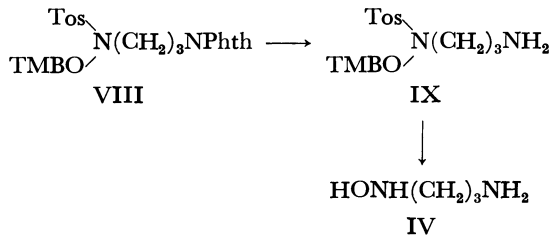

Fig. 2. Phth: phthalyl

hydrolysis gave DL-V. In recent years, improved synthesis[3g] of DL-V using method B was reported; the reaction of X with *anti*-benzaldoxime and the subsequent acid hydrolysis gave DL-V in excellent yield.

The higher homologues of DL-V, 5-*N*-hydroxy-DL-ornithine[2b,3e,f,4d] and 6-*N*-hydroxy-DL-lysine,[2b,3e,4d] were obtained by method A, B, or C.

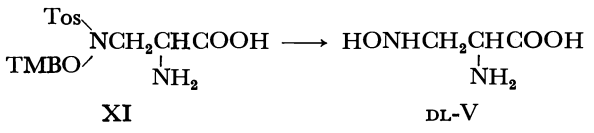

Fig. 3.

DL-2-Amino-3-(*N*-tosyl-*N*-2,4,6-trimethylbenzyloxy)-aminopropionic acid (XI) was synthesized, according to the procedure[7] for DL-2-amino-3-(*N*-tosyl-*N*-benzyloxy)aminopropionic acid, from ethyl 2,3-dibromopropionate and II as the starting materials. The protected amino-hydroxyamino acid (XI) was converted to DL-V by the treatment with 36% hydrogen bromide-acetic acid in the presence of phenol at room temperature.

Experimental

Melting points were determined with a Yanagimoto electric micromelting point apparatus, unless otherwise indicated and are uncorrected. Infrared spectra were recorded on a Hitachi EPI G-3 spectrophotometer as KBr disk. Nuclear magnetic resonance spectra were run on a Hitachi Perkin-Elmer R-20 High Resolution spectrometer, using tetramethylsilane as an internal standard.

N-*Carboethoxy*-O-*2,4,6-trimethylbenzylhydroxylamine.* To an ice-cooled solution of *N*-carboethoxyhydroxylamine (23.1 g, 0.22 mol) in methanol (50 ml) was added a solution of potassium hydroxide (12.3 g, 0.22 mol) in methanol (50 ml). After stirring for 30 min, 2,4,6-trimethylbenzyl chloride (33.7 g, 0.2 mol) in methanol (50 ml) was added at room temperature and the mixture was refluxed for 1 hr. The precipitated potassium chloride was removed and the filtrate was evaporated *in vacuo*. Ether (150 ml) and water (50 ml) were added. The organic layer was separated and dried. After evaporation of the solvent, the residue was distilled to give a pure product. Yield, 25.5 g (53.8%); bp 148—153 °C/0.9 mmHg.

Found: C, 65.40; H, 7.78%. Calcd for $C_{13}H_{19}NO_3$: C, 65.80; H, 8.07%.

O-*2,4,6-Trimethylbenzylhydroxylamine.* A mixture of *N*-carboethoxy-*O*-2,4,6-trimethylbenzylhydroxylamine (47.5 g, 0.2 mol) and potassium hydroxide (45 g, 0.8 mol) in water (200 ml) was refluxed for 5 hr. After 12 hr, the crystallized substance was collected and washed with water. Yield, 23.6 g (70.6%). Recrystallization from ether–petroleum ether gave an analytical sample, mp 54—55 °C.

Found: C, 72.51; H, 8.95; N, 8.23%. Calcd for $C_{10}H_{15}NO$: C, 72.69; H, 9.15; N, 8.48%.

N-*Tosyl*-O-*2,4,6-trimethylbenzylhydroxylamine (II).* To an ice-cooled solution of *O*-2,4,6-trimethylbenzylhydroxylamine (16.5 g, 0.1 mol) in pyridine (80 ml) was added a solution of tosyl chloride (19.2 g, 0.101 mol) in pyridine (60 ml). Stirring was continued for another 5 hr at room temperature and then the solvent was evaporated *in vacuo*. Ethyl acetate (150 ml) was added to the residue and washed successively with 1M hydrochloric acid and water. The organic layer was dried over magnesium sulfate and evaporated *in vacuo* to give crystals. Yield, 26.8 g (84%); mp 132—134 °C. Recrystallization from ether–petroleum ether gave an analytical sample, mp 135—136 °C.

Found: C, 63.85; H, 6.67; N, 4.32%. Calcd for $C_{17}H_{21}NO_3S$: C, 63.92; H, 6.63; N, 4.39%.

N-*Benzyl*-N-*tosyl*-O-*2,4,6-trimethylbenzylhydroxylamine (VI).* To a stirred solution of sodium (1.2 g) in methanol (150 ml) were added II (14.8 g, 40 mmol) and benzyl chloride (6.3 g, 50 mmol) and then the mixture was refluxed for 3 hr. The deposited crystals were collected and washed successively with water and ether. Yield, 12.8 g (78.1%); mp 128—131 °C. Recrystallization from ethanol gave an analytical sample, mp 129—131 °C.

Found: C, 70.22; H, 6.64; N, 3.38%. Calcd for $C_{24}H_{27}NO_3S$: C, 70.38; H, 6.65; N, 3.42%.

N-*Benzylhydroxylamine (III).* *a*): A solution of VI (1.64 g, 4 mmol) in 36% hydrogen bromide–acetic acid (10 ml) containing phenol (1.5 g) was stirred for 20 hr and then concentrated *in vacuo*. To the residual oil was added ether (30 ml) and water (10 ml). The aqueous layer was separated, concentrated to a small volume, and adjusted to pH 8 with solid sodium carbonate. The crystals were collected, after the solution was stored in an ice box for 12 hr. Yield, 0.24 g (49%); mp 56—56.5 °C (lit,[18] mp 57 or 58 °C). Recrystallization from petroleum ether unchanged the mp. Triphenyltetrazolium test was positive. IR: 3255 and 3150 cm^{-1}.

b): III was also obtained from VI by the treatment with 18% hydrogen bromide- acetic acid. Yield, 32.7%.

N-*Benzyl*-N-*tosylhydroxylamine (VII).* A solution of VI (0.82 g, 2 mmol) in trifluoroacetic acid (5 ml) containing phenol (0.4 g) was stirred at room temperature for 20 hr. The deposits were collected. Yield, 0.43 g (79.5%); mp 171—173 °C. Recrystallization from ethanol gave an analytical sample, mp 175—177 °C. This compound gave negative ferric chloride and triphenyltetrazolium tests. IR: 3375, 1595, 1380 and 1170 cm^{-1}. NMR (d_6-DMSO): δ 2.45 (s, 3H), 4.02 (s, 2H), 7.33, 7.50 and 7.84 (9H), and 10.18 (s, 1H).

Found: C, 60.58; H, 5.45; N, 5.00%. Calcd for $C_{14}H_{15}NO_3S$: C, 60.63; H, 5.45; N, 5.05%.

*1-Phthalimido-3-(*N-*tosyl*-N-*2,4,6-trimethylbenzyloxy)aminopropane (VIII).* To a stirred solution of sodium (1.38 g, 60 mmol) in methanol (150 ml) were added 3-bromopropylphthalimide (13.4 g, 50 mmol) and II (15.95 g, 50 mmol). The mixture was refluxed for 3 hr and concentrated *in vacuo*. To the residue, water (50 ml) and ether (50 ml) were added and the mixture was stirred for 5 hr. Then crystals were collected, dried and recrystallized from *n*-propyl alcohol. Yield, 17.2 g (68.0%); mp 139—140 °C.

Found: C, 66.32; H, 6.17; N, 5.27%. Calcd for $C_{28}H_{30}N_2O_5S$: C, 66.38; H, 5.97; N, 5.53%.

*1-Amino-3-(*N-*tosyl*-N-*2,4,6-trimethylbenzyloxy)aminopropane (IX).* A suspension of VIII (2.53 g, 5 mmol) in ethanol (130 ml) was warmed at 60—65 °C. To the resultant solution, hydrazine hydrate (2.5 g, 50 mmol) was added.

After stirring for 6 hr at 60—65 °C, the mixture was adjusted to pH 5 with acetic acid and the precipitates were filtered off. The filtrate was concentrated *in vacuo* and water (50 ml) was added. Insoluble substance was removed and the filtrate was extracted with ethyl acetate (50 ml). The aqueous layer was evaporated. To the residual oil, ethanol (20 ml) was added and evaporated. This operation was repeated three times and finally water (30 ml) was added. The solution was adjusted to pH 8 with 7% aq. ammonia and extracted with ethyl acetate (50 ml×2). The organic layer was dried over sodium sulfate and concentrated *in vacuo* to give IX quantitatively as a colorless oil. IX was characterized as the monohydrochloride monohydrate. Recrystallization from methanol–ether gave an analytical sample. mp 99—102 °C.

Found: C, 55.87; H, 7.27; N, 6.50%. Calcd for $C_{20}H_{28}N_2O_3S \cdot HCl \cdot H_2O$: C, 55.73; H, 7.25; N, 6.50%.

1-Amino-3-hydroxyaminopropane Dihydrobromide (IV·2HBr). To the crude oil (IX), which was obtained from VIII (5 mmol) as described above, phenol (2 g) and 36% hydrogen bromide-acetic acid (10 ml) were added. After stirring for 24 hr at room temperature, dry ether (150 ml) was added. The deposited crystals were collected and washed with dry ether. Yield, 1.13 g (90%). Recrystallization from methanol–ether gave an analytical sample, mp 157—159 °C. Triphenyltetrazolium test was positive.

Found: C, 14.77; H, 5.02; N, 10.97%. Calcd for $C_3H_{12}N_2OBr_2$: C, 14.30; H, 4.80; N, 11.12%.

Ethyl 2-Bromo-3-(N-tosyl-N-2,4,6-trimethylbenzyloxy)aminopropionate. To a solution of sodium (2.8 g) in ethanol (500 ml) was added II (31.9 g, 0.1 mol). Then ethyl 2,3-dibromopropionate (29 g, 0.11 mol) was added dropwise at room temperature. After stirring for 12 hr, the deposited crystals were collected and washed with water. Yield, 18 g. The filtrate was concentrated *in vacuo* to a small volume to give 12 g of a second crop. Total yield, 30 g (60%). Recrystallization from ethanol gave an analytical sample, mp 98—99 °C. IR: 1740 cm^{-1}.

Found: Br, 15.65%. Calcd for $C_{22}H_{28}NO_5SBr$: Br, 16.03%.

2-Bromo-3-(N-tosyl-N-2,4,6-trimethylbenzyloxy)aminopropionic Acid. To a solution of the ester (12.5 g, 25 mmol), obtained as described above, in acetone (300 ml) was added M sodium hydroxide (40 ml) and the mixture was stirred at room temperature. After 72 hr, the solution was adjusted to pH 4 with M citric acid and then concentrated *in vacuo*. Ethyl acetate (300 ml) and water (100 ml) were added to the residue and the organic layer was dried over sodium sulfate. The solvent was removed to give a crystalline product. Yield, 8.1 g (69%). Recrystallization from carbon tetrachloride gave an analytical sample, mp 168—170 °C. IR: 1700 cm^{-1}.

Found: Br, 16.93%. Calcd for $C_{20}H_{24}NO_5SBr$: Br, 16.99%.

DL-*2-Amino-3-(N-tosyl-N-2,4,6-trimethylbenzyloxy)aminopropionic Acid (XI).* A solution of the bromide (9.4 g, 20 mmol), obtained as described above, in concd. aq. ammonia (500 ml) was stored at room temperature for 10 days and then concentrated *in vacuo* to a small volume. After acidified with acetic acid to pH 4, the crystals were collected and washed successively with water, hot methanol and water. Yield, 5.3 g (65%); mp 189—191 °C (decomp.).

Found: C, 58.97; H, 6.47; N, 6.84%. Calcd for $C_{20}H_{26}N_2O_5S$: C, 59.09; H, 6.45; N, 6.89%.

DL-*2-Amino-3-hydroxyaminopropionic Acid* (DL-*V*). A solution of XI (1.02 g, 2.5 mmol) in 36% hydrogen bromide–acetic acid (5 ml) containing phenol (1 g) was stirred at room temperature. After 45 hr, dry ether (70 ml) was added. The deposits were collected and dissolved in water. The aqueous solution was extracted with ether and concentrated *in vacuo*. The residue redissolved in a small quantity of water was adjusted to pH 8 with 7% aq. ammonia and ethanol was added until the solution was cloudy. The precipitated crystals were collected, after the solution was stirred in an ice box for 12 hr. Yield, 0.17 g (56.7%). Recrystallization from water–ethanol gave an analytical sample, mp 167—168 °C (decomp.) in an open capillary in a liquid bath (lit. mp 163—165 °C (decomp.)[4c,d] 180—181 °C (decomp.)[3g]). Triphenyltetrazolium test was positive. IR: 3275, 3250, 1635, 1585, and 1525 cm^{-1}.

Found: C, 29.97; H, 6.57; N, 22.91%. Calcd for $C_3H_8N_2O_3$: C, 30.00; H, 6.71; N, 23.33%.

Bibliography and Footnotes

1) Recent reviews of hydroxylamine derivatives: a) B. Zeeh and H. Metzger, "Houben-Weyl: Methoden der organischen Chemie," Band, X/I, Georg Thieme Verlag, Stuttgart (1971), pp. 1091—1279. b) P. A. S. Smith, "The Chemistry of Open-chain Nitrogen Compounds," Vol. II, Benjamin, New York (1966).

Recent reviews of naturally-occurring hydroxylamines: c) H. Maehr, *Pure Appl. Chem.*, **28**, 603 (1971). d) J. B. Neilands, *Struct. Bond.*, **1**, 59 (1966).

2) a) K. B. Mullis, J. R. Pollack, and J. B. Neilands, *Biochemistry*, **10**, 4894 (1971). b) S. J. Rogers and J. B. Neilands, *ibid.*, **3**, 1850 (1964). c) W. Keller-Schierlein, P. Mertens, V. Prelog, and A. Walser, *Helv. Chim. Acta*, **48**, 710 (1965). d) R. F. C. Brown, G. Buchi, W. Keller-Schierlein, V. Prelog, and J. Renz, *ibid.*, **43**, 1868 (1960). e) H. Bickel, B. Fechtig, G. E. Hall, W. Keller-Schierlein, V. Prelog, and E. Vischer, *ibid.*, **43**, 901 (1960). f) W. Keller-Schierlein and B. Maurer, *ibid.*, **52**, 603 (1969).

3) a) E. Bellasio, F. Parravicini, A. Vigevani, and E. Testa, *Gazz. Chim. Ital.*, **98**, 1014 (1968). b) E. Bellasio, F. Parravicini, T. La Noce, and E. Testa, *Ann. Chim*, **58**, 407 (1968). c) E. Buehler and G. B. Brown, *J. Org. Chem.*, **32**, 265 (1967): some of the earlier synthetic methods of α-*N*-hydroxy-DL-amino acids have been reviewed. d) E. Falco and G. B. Brown, *J. Med. Chem.*, **11**, 142 (1968). e) Y. Isowa and M. Sato, Japan 680165 (1973). f) Ref. 1c) pp. 608—609. g) C. N. Eaton, G. H. Denny, Jr., M. A. Ryder, M. G. Ly, and R. D. Babson, *J. Med. Chem.*, **16**, 289 (1973); some of the precedent for this method of introducing hydroxylamino group are summarized.

4) a) T. La Noce, E. Bellasio, and E. Testa, *Ann. Chim.*, **58**, 393 (1968). b) Y. Chigira, M. Masaki, and M. Ohta, This Bulletin, **42**, 224 (1969). c) G. C. Lancini, A. Diena, and E. Lazzari, *Tetrahedron Lett.* **1966**, 1769. d) G. C. Lancini, E. Lazzari, and A. Diena, *Farmaco, Ed. Sci.*, **24**, 169 (1969). e) K. Kaminski and T. Sokolowska, *Rocz. Chem.*, **47**, 653 (1973). f) T. Takemoto, N. Takagi, T. Nakajima, S. Arihara, and K. Koike, 16th Symposium papers on the chemistry of natural products, Osaka, 1972, p. 256.

5) a) A. Murayama and S. Tamura, *Agr. Biol. Chem.* (Tokyo), **34**, 130 (1970). b) H. Feuer, B. F. Vincent, Jr., and R. S. Bartlett, *J. Org. Chem.*, **30**, 2877 (1965).

6) M. Ohno, H. Iinuma, N. Yagisawa, S. Shibahara, Y. Suhara, S. Kondo, K. Maeda, and H. Umezawa, *Chem. Commun.*, **1973**, 147.

7) Y. Isowa, H. Kurita, M. Ohmori, M. Sato, and K. Mori, This Bulletin **46**, 1847 (1973).

8) Y. Isowa, T. Takashima, M. Ohmori, H. Kurita, M. Sato, and K. Mori, *ibid.*, **45**, 1461 (1972).

9) *Idem, ibid.*, **45**, 1467 (1972).

10) Y. Isowa, M. Ohmori, and H. Kurita, *ibid.*, **47**, 215 (1973).

11) F. H. C. Stewart, *Aust. J. Chem.*, **19**, 1067, 1511 (1966).

Stable Crystalline Complexes of Diphenylcyclopropenone with Substituted Acetic Acids[1]

Israel AGRANAT* and Shmuel COHEN
Department of Organic Chemistry, The Hebrew University of Jerusalem, Jerusalem, Israel
(Received August 16, 1973)

Diphenylcyclopropenone (DCP) forms 1 : 1 stable crystalline complexes with dichloroacetic acid, phenylacetic acid, diphenylacetic acid, trichloroacetic acid and cyanoacetic acid. The physical properties of these complexes are consistent with a hydrogen-bonded complexation between the carbonyl oxygen of DCP and the acidic hydrogen of the substituted acetic acid.

Diphenylcyclopropenone (DCP) (I) has been shown to form stable solid complexes with Lewis acids (BF_3, $SbCl_5$),[2] water,[3] and acetylenic dialcohols;[3] with methanol, a complex was formed in solution.[4] We wish to report that DCP forms 1 : 1 stable crystalline complexes with substituted acetic acids. The physical properties of these complexes are consistent with a hydrogen-bonded complexation between the carbonyl oxygen of DCP and the acidic hydrogen of the substituted acetic acid.

Treatment of DCP with an equimolar quantity of dichloroacetic acid (II) in boiling cyclohexane solution afforded a crystalline adduct of DCP and (II), mp 88—89 °C, in 78% yield, which analyzed for $C_{17}H_{12}Cl_2O_3$. The properties of this adduct (III) indicated that it was a 1 : 1 complex of DCP and II. In the solid state, the infrared molecular bands of DCP (II)[5] were shifted to lower frequencies: (KBr) 1850 cm^{-1} (I)→ 1820 cm^{-1} (III); 1630 cm^{-1} (I)→1595 cm^{-1} (III). (Similar shifts were observed in nujol.) The NMR spectrum of the complex III in $CDCl_3$ solution (100 MHz, δ=7.59 (m, 6H, *meta*+*para*) and 7.98 ppm (m, 4H, *ortho*)) showed a downfield shift of the aromatic protons relative to the respective absorptions of DCP.[6] It is noteworthy that the extent of the shift of the *ortho* protons (8 Hz) was identical to that of the *meta*+*para* protons. Thus, these shifts cannot be rationalized as due to a greater contribution of the "aromatic" dipolar structure of the cyclopropenium type in the complex (III). The longest wavelength maximum in the UV spectrum of I in cyclohexane solution, at 362 nm (ε=960), was absent in the corresponding spectrum of the complex (III). Instead, only a tailing towards the visible was observed. It has previously been suggested, on the basis of the wavelength, the relatively low extinction and the response to solvent, that the 362 nm band was due to intramolecular charge transfer of the "aromatic" 1,2-diphenylcyclopropenium oxide type.[4] The behaviour of this band in the UV spectrum of the complex is consistent with this interpretation.

Most revealing is the mass spectrum of the complex (III). It is not simply a superposition of the mass spectra of DCP and dichloroacetic acid (II). Certain of its features originate from the complex. Whilst the molecular ion ($[C_{17}H_{12}{}^{35}Cl_2O_3]^{+\cdot}$, *m/e* 334) was absent, the mass spectrum contained a most intense signal at *m/e* 207 (36% relative to that of *m/e* 206 $[DCP]^{+\cdot}$). It is most probably due to the 3-hydroxy-1, 2-diphenylcyclopropenium ion (IV). Thus, the mass spectrum strongly supports the proposed structure of the complex (III).

It appears that the chlorine substituents in the acetic acid moiety are not a prerequistite for the complexation. The formation of such a 1 : 1 complex between DCP and a substituted acetic acid proved to be a general reaction (at least for acetic acids with $pK_a<$ 4.3). DCP reacts with phenylacetic acid, diphenylacetic acid, trichloroacetic acid, and cyanoacetic acid, in boiling cyclohexane solution to form, in each case, a 1 : 1 complex (see experimental section). The physical properties of these complexes closely resemble those of (III). The mass spectrum of each complex contained the prominent signal at *m/e* 207 representing the 3-hydroxy-1,2-diphenylcyclopropenium ion (IV). It should be noted that in solution, the complexation

TABLE 1. THE IR SPECTRA OF DCP–SUBSTITUTED ACETIC ACID COMPLEXES (2000—1500 cm^{-1} region)

Compound	Medium	ν (cm^{-1})		
DCP–$PhCH_2CO_2H$	Nujol	1870(m),	1845(s),	1825(s),
		1810(s),	1710(vs),	1595(vs),
		1580(vs),	1570(s)	
	KBr	1880_{sh}(m),	1860_{sh}(s),	1850(s),
		1835(s),	1820(s),	1775(w),
		1720(vs),	1605(vs),	1590(vs),
		1575(s)		
DCP–Ph_2CHCO_2H	Nujol	1875(m),	1845(s),	1830(s),
		1815(s),	1750(m),	1710(vs),
		1600(vs),	1585(vs),	1570(s)
	KBr	1890(w),	1860(s),	1845(s),
		1825(s),	1785(w),	1720(vs),
		1610(vs),	1595(vs),	1580(s)
DCP–Cl_2CHCO_2H	Nujol	1880(w),	1865_{sh}(s),	1850(s),
		1820(s),	1730(s),	1600(vs),
		1580(s),	1570(s)	
	KBr	1880(w),	1850(s),	1820(vs),
		1745(vs),	1620(m),	1595(vs),
		1575(vs),	1560(vs)	
DCP–Cl_3CCO_2H	Nujol	1845_{sh}(m),	1820_{sh}(s),	1795(vs),
		1700_{sh}(s),	1675(s),	1600(vs),
		1570(s)		
	KBr	1850(s),	1810(s),	1745(m),
		1600(vs),	1580(s),	1565(s)
DCP–$NCCH_2CO_2H$	Nujol	1875(w),	1850(m),	1815(vs),
		1750(m),	1720(vs),	1600(vs),
		1580(vs),	1570(vs)	
	KBr	1850(s),	1820(s),	1755(m),
		1720(vs),	1600(vs),	1585(vs),
		1575(vs)		

TABLE 2. THE NMR SPECTRA OF DCP-SUBSTITUTED ACETIC ACID COMPLEXES (in ppm)

Compound	δ (COOH)	δ (*ortho*[a])	δ (*meta*+*para*[a])	δ (Phenyl)	δ (CH)	δ (CH_2)	Δ
DCP		7.90	7.51				0.39
DCP-$PhCH_2COOH$	10.84	7.89	7.50	7.26		3.62	0.39
DCP-$Ph_2CHCOOH$	11.16	7.92	7.50	7.28	5.06		0.42
DCP-$Cl_2CHCOOH$	13.38	7.98	7.59		6.04		0.39
DCP-Cl_3CCOOH	14.56	7.98	7.59				0.39
DCP-$NCCH_2COOH$	12.72	7.94	7.57			3.55	0.37

a) (*ortho*) and (*meta*+*para*) refers to the chemical shifts of the center of the corresponding multiplets of the AB_2C_2 systems of the DCP residue.

could be effected directly by dissolving equimolar quantities of DCP and the substituted acetic acid in the appropriate solvent. Under such conditions, both the NMR spectra and the UV spectra were identical with those obtained from the respective solutions of crystalline complexes.

It is plausible to assume that the complexation involves a hydrogen bond between the oxygen of the polar carbonyl group of DCP and the acidic hydrogen of the substituted acetic acid. The shift to lower frequencies of the cyclopropenone bands in the infrared spectra in the solid state supports this hypothesis. Likewise, the strong signal in the mass spectra of the complexes at *m/e* 207 is consistent with the proposed structure. In solution (CH_2Cl_2), however, the infrared spectrum was, in each case, a superposition of the respective spectra of the two components. The exact structure of the complexes of DCP with the substituted acetic acids must await an X-ray-crystallographic determination.

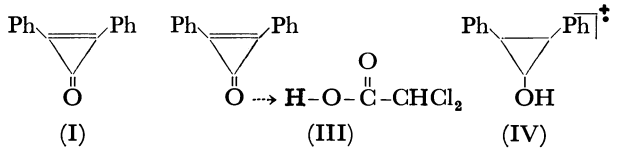

(I) (III) (IV)

Cl_2CHCO_2H

(II)

Experimental

Melting points were taken on a Unimelt Thomas and Hoover capillary mp apparatus and are uncorrected. IR spectra were recorded on a Perkin-Elmer 457 Spectrophotometer. UV spectra were recorded on a Unicam SP 800 spectrophotometer. NMR spectra were recorded at 100 MHz on a Varian HA-100 spectrometer in $CDCl_3$ solutions. ^1H chemical shifts are reported in parts per million, downfield from Me_4Si. Mass spectra were recorded on a Varian MAT-311 spectrometer operating at 70 eV.

The Reaction of DCP (I) with Dichloroacetic Acid (II). DCP (0.515 g, 2.5 mmol)[7] and dichloroacetic acid (0.32 g, 2.5 mmol) were dissolved in 50 ml of boiling cyclohexane; the solution was refluxed for 15 min and gradually cooled to room temperature. The complex (III) crystallized from the solution. It was obtained as colourless crystals, mp 88—89 °C (cyclohexane) (78% yield). Found: C, 61.13; H, 3.38; Cl, 21.20%. Calcd for $C_{17}H_{12}Cl_2O_3$: C, 60.92; H, 3.61; Cl, 21.15%. ν_{max} (KBr) 3050 (w), 3000 (w), 2895 (w), 2845 (w), 2450 (w), 1880(w), 1850 (s), 1820 (vs), 1745 (vs), 1620 (m), 1595 (vs), 1575 (s), 1560 (s), 1480 (w), 1450 (s), 1370 (vs), 1290 (s), 1210 (m), 1175 (s), 1000 (w), 925 (w), 810 (s), 790 (w), 767 (vs), 687 (s), 590 (m), 520 (m), 473 (m), and 440 (m) cm^{-1}. λ_{max} (C_6H_{12}) 218, 222, 237_{sh}, 249_{sh}, 253_{sh}, 266, 274, 280, 289, 298, and 314_{sh} nm (ε 18900, 17900, 7200, 8200, 9300, 17100, 19600, 25600, 20400, 24000, and 4600); λ_{max} (CH_3CN) 219, 226, 230_{sh}, 265_{sh}, 280, 288, 296, 310_{sh}, and 330 nm (ε 18800, 16900, 14400, 13000, 24000, 24400, 28000, 13500, and 1820).

The following complexes were prepared in a similar manner:

DCP-Phenylacetic Acid Complex. Mp 76—77 °C, 75% yield. Found: C, 80.73; H, 5.18%. Calcd for $C_{23}H_{18}O_3$: C, 80.68; H, 5.30%. λ_{max} (C_6H_{12}) 217_{sh}, 222_{sh}, 227_{sh}, 249_{sh}, 267, 274_{sh}, 281, 289, 298, 314_{sh} and 356 nm (ε 23500, 20500, 15200, 6700, 15000, 18000, 22200, 19800, 22400, 7400, and 880).

DCP-Diphenylacetic Acid Complex. Mp 89—90 °C, 50% yield. Found: C, 83.56; H, 5.37%. Calcd for $C_{29}H_{20}O_3$: C, 83.23; H, 5.30%. λ_{max} (C_6H_{12}) 216_{sh}, 222_{sh}, 237, 249_{sh}, 266, 274, 281, 289, 298, 314_{sh}, and 344 nm (ε 36000, 28000, 9200, 10200, 19700, 21500, 27800, 19600, 24000, 1040, and 460).

DCP-Trichloroacetic Acid Complex. Mp 83—83.5 °C, 72% yield. Found: C, 55.33; H, 3.14; Cl, 28.43%. Calcd for $C_{17}H_{11}Cl_3O_3$: C, 55.24; H, 3.00; Cl, 28.77%. λ_{max} (C_6H_{12}) 219, 222, 227_{sh}, 266, 274, 281, 289, 298, and 314_{sh} nm (ε 18600, 18200, 14600, 14500, 17800, 21200, 18800, 22000, and 770).

DCP-Cyanoacetic Acid Complex. Mp 86—86.5 °C, 48% yield. Found: C, 73.94; H, 4.58; N, 5.03%. Calcd for $C_{18}H_{13}NO_3$: C, 74.22; H, 4.50; N, 4.89%. λ_{max} (C_6H_{12}) 221, 228, 290, 301, 314_{sh}, and 352_{sh} nm (ε 11500, 10900, 14100, 8200, and 440). For the preparation of this complex, a cyclohexane–benzene (50: 1) solution was employed.

The IR and the NMR spectra of the complexes are given in Tables 1 and 2.

We are deeply grateful to Professor Ernst David Bergmann of the Hebrew Universtiy of Jerusalem for his encouragement and his interest.

References

1) Fulvenes and Thermochromic Ethylenes. Part 78.
2) Z. Yoshida and H. Miyahara, This Bulletin, **40**, 3219 (1971).
3) F. Toda and K. Akagi, *Tetrahedron Lett.*, **1968**, 3735.
4) E. Osawa, K. Kitamura, and Z. Yoshida, *J. Amer. Chem. Soc.*, **89**, 3814 (1967).
5) A. Krebs, B. Schroder, and F. Hofler, *Tetrahedron Lett.*, **1968**, 5935.
6) E. D. Bergmann and I. Agranat, *J. Amer. Chem. Soc.*, **86**, 3897 (1964).
7) R. Breslow, T. Eicher, A. Krebs, R. A. Peterson, and J. Posner, *ibid.*, **87**, 1320 (1965).

Implication of Diazonium Cations as Intermediates in the Photorearrangement of Azoxybenzenes

Nigel James BUNCE
Department of Chemistry, University of Guelph, Guelph, Ontario, Canada
(Received March 28, 1973)

Photolysis of azoxybenzene and 2,2′-azoxytoluene in the presence of 2-naphthol gives, in addition to *o*-hydroxyazocompounds, 1-arylazo-2-naphthols, sometimes as the major products. This implies that cleavage into diazonium ions may sometimes be a major pathway in the irradiation of aromatic azoxycompounds. A mechanism is proposed to account for the formation of azonaphthols as well as the various side products that have previously been obtained from these reactions.

The photorearrangement of azoxybenzene (**1a**) to *o*-hydroxyazobenzene (**2a**) is an intramolecular process in which the azoxy oxygen migrates to a free *ortho* position in the more distant aromatic ring.[1] Tanikaga showed[2] that the reaction involves the singlet π,π^* state of **1a** because, when the triplet excited state is populated by photosensitisation, oxygen migration is suppressed and photoreduction occurs instead. Iwata and Emoto[3] observed minor products additional to **2a** on photolysis of **1a** in chloroform solution; photoreduction concurrent with rearrangement occurred even in the absence of a photosensitiser, and *p*-hydroxyazobenzene (**3a**) was also formed. The authors speculated that photodissociation of **1a** into azobenzene and an oxygen atom might account for these minor products.

Side products have also been observed in irradiations of 2,2′-azoxytoluene (**1b**). Lewis and Reiss[4] observed the azocompounds (**3b**) and **4** in addition to expected product (**2b**), when ethanol was used as the solvent. Recently we have obtained **2b**, **4**, and the bis-azocompound **5** in our laboratory on photolysis of **1b** in benzene.[5] Similar behaviour was also observed with 2,2′-dibenzylazoxybenzene.

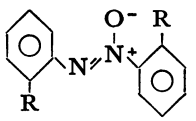

1a R=H
1b R=CH_3

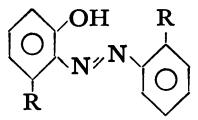

2a R=H
2b R=CH_3

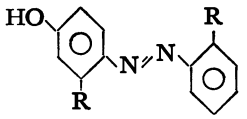

3a R=H
3b R=CH_3

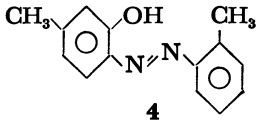

4

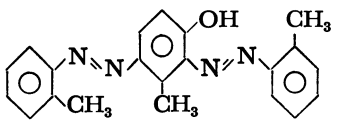

5

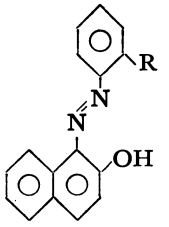

6a R=H
6b R=CH_3

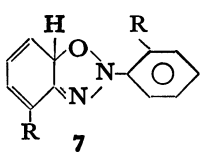

7

The abnormal products **3b** and **5** especially are reminiscent of the coupling products of a diazonium ion cation with an appropriate phenol; however, both we and Lewis and Reiss noted that **2b** is stable to the photolysis conditions and hence that the abnormal products do not arise as secondary products through the photochemical cleavage of **2b** into diazonium cations. By contrast, in this paper are reported observations which strongly implicate the participation of diazonium ion intermediates at some stage in the reaction. A modification of the widely accepted Badger and Buttery[6] rearrangement mechanism is proposed to account for the various side products that have been observed in the photolyses alluded to above.

Irradiation in ethanol of **1b** in the presence of 2-naphthol gave the usual rearrangement product **2b**, but the anomalous products **3**—**5** were suppressed. Instead there were obtained *m*-cresol and 1-*o*-tolylazo-2-naphthol (**6b**), the coupling product of an *o*-toluenediazonium cation with 2-naphthol. Photolysis of **2b** in the presence of 2-naphthol gave none of this compound. Observation of *m*-cresol and **6b** thus suggests that fragmentation of some intermediate is occurring, with one of the fragments being the *o*-toluenediazonium cation. The photostability of **2b** implies that such diazonium ions are formed not from **2b** but from one of its precursors. Tentatively, the accompanying reaction scheme is proposed to account for those observations. The Badger and Buttery cyclic intermediate **7** may either cleave the N–O bond to yield eventually **2b** as Badger and Buttery proposed; alternatively, the *o*-toluenediazonium ion may be expelled with the formation of a phenoxide anion. The diazonium ion reacts with the *m*-cresol or its anion, giving **3b** and **4**, or couples with preformed **2b**, when the bis-azocompound **5** results. In the presence of 2-naphthol the side products are suppressed because the diazonium ion is trapped by 2-naphthol.

An attractive feature of this proposal is that the ejection of the diazonium ion from **7** will be facilitated by the bulky alkyl group already in the 6-position of the intermediate. This is consistent with the fact that abnormal rearrangement products have only been observed during photolyses of 2,2′-disubstituted azoxybenzenes. It was thus anticipated that azoxybenzene **1a** itself, being sterically unencumbered, would afford

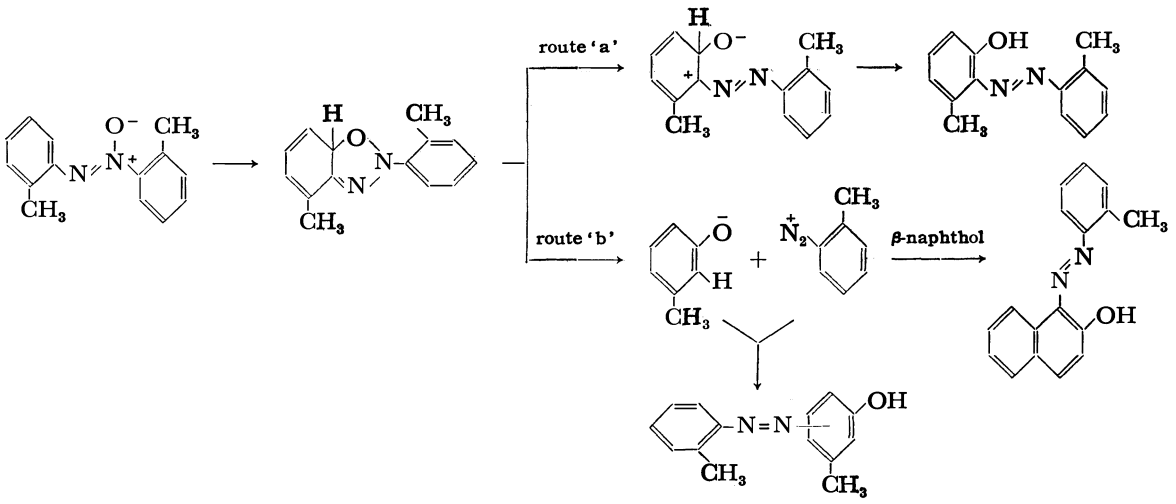

only small quantities of products arising from diazonium ion precursors. From an irradiation in ethanol, this was indeed the case, but unexpectedly, irradiation of **1a** and 2-naphthol in benzene gave 1-phenylazo-2-naphthol (**6a**) as the major product (60% based on reacted **1a**) together with 22% of **2a**. If formation of (**6a**) may be considered diagnostic of a diazonium ion precursor, it follows that, in this system at least, most azoxybenzene molecules photolyse by cleavage to a trappable diazonium cation. This implies that in the absence of 2-naphthol, even the normal product **2a** may arise, at least in part, by recombination of a geminate pair of diazonium cation and phenoxide ion (or phenol). Clearly the diazonium cation and the phenoxide anion never become free of each other, else *p*-hydroxyazobenzene would be a major product, since diazonium couplings invariably take place at an available *para* position.[7] The above implication opens up the question of whether aromatic azoxycompounnds in general photorearrange by the Badger and Buttery pathway (route 'a') or whether cleavage into diazonium ions (route 'b') can be a major, or even the exclusive, route to *o*-hydroxyazocompounds. Further work is in progress to test this possibility and to try to determine the cause of the marked change in product distribution observed when the solvent is changed from ethanol to benzene. Thus, photolysis of **1b** with 2-naphthol in benzene led to an increase in the proportion of the azonaphthol **6b** in the product mixture, analogous with the observations with **1a**.

An additional, minor product of the reaction of **1a** with 2-naphthol in benzene was an isomer of **6a** according to mass spectrometry, although insufficient material was obtained for complete identification. The isomer appears to be much too stable thermally to be the *cis* isomer of **6a**, aside from which, previous attempts to prepare *cis*-*o*-hydroxyazocompounds have been without success.[8] The new compound was not produced by photolysis of **6a** either alone or in the presence of either **1a** or 2-naphthol. It was felt that this could be a constitutional isomer of **6a** formed by a photochemical coupling reaction between a benzenediazonium cation and 2-naphthol. However, photolysis of sodium phenylazosulphonate (which gives diazonium ions on irradiation[9]) in the presence of 2-naphthol gave **6a**, but none of the other isomer, whose origin is therefore still a mystery.

The *p*-hydroxyazobenzene obtained by Iwata and Emoto may now be accounted for as the product of reaction of a separated diazonium ion with phenol. Their isolation of azobenzene however most likely involves a quite different mechanism, since Tanikaga[2] showed that, while **2a** derives from singlet excited **1a**, azobenzene is a triplet state product. Heavy atom solvents are well known to promote intersystem crossing, so it is likely that in chloroform solution intersystem crossing would occur more readily than in ethanol, and the resultant population of the triplet state of **1a** would allow a small amount of photoreduction to occur. On the scale of his experiments, Tanikaga did not observe any photoreduction in heavy atom solvents; perhaps the quantum yield for photoreduction is low.

TABLE 1. PHOTOREARRANGEMENT OF **1a** TO **2a** IN ETHANOLIC MIXTURES

Added solvent	**2a**, mg.	Recovered **1a**, mg	**2a**/**1a**
None	186	223	0.83
$CH_3CH_2CH_2Cl$	117	248	0.47
$CHCl_3$	112	252	0.44
$CH_3CH_2CH_2Br$	88	287	0.31
CCl_3Br	58[a]	252	0.23
CH_3CH_2I	78	296	0.26

a) Brominated *o*-hydroxyazobenzenes (61 mg) were formed in addition.

In support of a heavy atom effect, the photorearrangement of **1a** in ethanol has been found to be retarded considerably when halogenated compounds are added to the solvent (see Table 1) and the heavier the halogen concerned, the slower the reaction. On the scale of these experiments, azobenzene was again not formed in isolable quantities; nevertheless, the results are consistent with the idea of a heavy atom effect promoting intersystem crossing, with the consequent removal of some of the singlet excited **1a** molecules, making them unavailable for photorearrangement. In one solvent, ethanol/bromotrichloromethane, brominated *o*-hydroxy-

Table 2. Physical properties of brominated *o*-hydroxyazobenzenes

Compound	Mp	UV data: Conc. mg/100 ml	UV data: λ_{max} nm(A) in ethanol	UV data: λ_{max} nm(A) in ethanol/0.1 M KOH
Monobromide (photoreaction)	117—120°	0.9	376(0.43), 320(0.97)	462(0.44)
Dibromide (photoreaction)	132—134°	1.9	380(0.40), 325(1.10)	470(0.38)
Monobromide (**2a**+equimolar Br_2)	110—115°	2.0	377(0.94), 317(2.08)	467(1.04)
Dibromide (**2a**+equimolar Br_2)	125—129°	2.1	382(0.43), 327(1.13)	474(0.35)
Dibromide (**2a**+excess Br_2)	173—175°	2.7	380(0.55), 334(1.33)	480(0.45)
5-Bromo-**2a**($C_6H_5N^+_2$+*p*-BrC_6H_4OH)	120—122°	1.9	378(0.57), 317(1.24)	465(0.42)

azobenzenes were formed additionally; these probably arise through photolysis of bromotrichloromethane to molecular bromine,[10] which brominates the **2a** already produced. Indeed, independent bromination of **2a** gave the same mixture of mono- and di-bromohydroxyazobenzenes, but isolation of pure compounds from these mixtures was difficult because of problems of separation (see Experimental section).

Experimental

Separation and analytical procedures have been described in detail previously.[5]

Irradiation of ***1b*** *with 2-Naphthol.* i) A solution of **1b** (0.650 g) and 2-naphthol (2.0 g) in ethanol (30 ml) was irradiated with an external source for 17 hr. After evaporation of the solvent, the residue was taken up in chloroform and extracted with 3 M sodium hydroxide solution. The organic phase was dried, evaporated, and separated by preparative tlc on silica gel (E. Merck No. 7747) (benzene: ligroin, 1:4) to give three bands, each of which was shown after extraction to be pure (tlc). Band 1 (129 mg) was **2b**, red needles from ethanol, mp 92—94 °C (lit,[5] 96 °C). Band 2 (81 mg) was an oil, which crystallised from ethanol, mp 50—52 °C, and was starting material. Band 3 (226 mg), red leaflets from ethanol, had mp 126—128 °C. Its mass spectrum, m^+/e 262 (M+ 74%), 245 (11), 234 (17), 171 (17), 144 (14), 143 (100), 128 (10), 115 (61), 107 (12), 106 (22), 91 (68), and mp were identical with those of an authentic sample of 1-(*o*-tolylazo-)-2-naphthol, **6b**, (lit, mp[11] 131 °C), obtained by coupling *o*-toluenediazonium chloride with 2-naphthol.

The sodium hydroxide extract of the crude photolysis mixture was acidified and extracted into chloroform, dried and evaporated. Vapour phase chromatography of the extract (10% SE30 on 30/80 Celite, 100°) showed a peak of retention time identical to that of *m*-cresol. The residue was distilled from a bulb using an oilbath at 260 °C to give *m*-cresol (99 mg) having IR spectrum identical to that of an authentic sample.

ii) A solution of **1b** (0.650 g) and 2-naphthol (2.0 g) in benzene (20 ml) was irradiated with an external source for 21 hr. After removal of most of the 2-naphthol by base extraction, the organic material was separated by preparative tlc as described above. The bands obtained were, in increasing order of polarity, **2b** (16 mg), recovered **1b** (0.26 g) and **6b** (133 mg), mp 128—129 °C. UV spectra of each of these compounds were identical with those of authentic samples.

Photolysis of **2b**. A solution of **2b** (26 mg) in benzene (2.0 ml) was irradiated for 6 hr in a 5 ml Pyrex flask equipped with reflux condenser, using an external source. Analytical tlc showed only one spot in the reaction mixture, and passage of the reaction mixture through a short column of silica gel, eluting with benzene, allowed recovery of **2b** (22 mg), mp 94—96 °C. Similar results were obtained in a 6 hr irradiation of **2b** (45 mg) in the presence of 2-naphthol (199 mg).

Irradiation of ***1a*** *with 2-Naphthol.* (i) A solution of **1a** (0.45 g) and 2-naphthol (2.0 g) in 95% ethanol (40 ml) was irradiated in a corked Pyrex test tube for 90 hr using an external source. After extraction with 0.5 M NaOH solution to remove most of the 2-naphthol, the residue was resolved by preparative tlc (benzene: ligroin, 1:9) affording **2a** (110 mg), mp 80—81 °C, recovered **1a** (322 mg), and **6a** (0.6 mg), estimated from its UV spectrum which was identical with that of an authentic sample (see below).

(ii) A solution of **1a** (0.40 g) and 2-naphthol (1.00 g) in dry benzene (20 ml) was irradiated for 12 hr in a stoppered Pyrex ampoule using a Hanovia 450 W medium pressure mercury arc. Analytical tlc on silica gel (benzene: ligroin, 1:4) showed three compounds besides starting materials. After removal of most of the 2-naphthol by extraction with 0.5 M NaOH, the organic residue was resolved by preparative tlc on silica gel.

The most mobile band was **2a** (43 mg), red needles from ethanol, mp 78—80 °C. Band 2 (213 mg) was recovered **1a**. Band 3 (19 mg) separated incompletely from band 2; fractional crystallisation from ethanol gave dark red needles (3 mg), mp 130—132 °C, softened at 117 °C. Mass spectrum (70 eV): m^+/e 248 (M+, 100%), 171 (18), 143 (90), 115 (52), 77 (42); UV (EtOH): λ_{max} 487 nm (log ε 4.6), 352 (4.5), 288 (4.6). The least mobile material on the tlc plate was **6a** (153 mg), mp 130—131 °C (lit,[6] 133 °C). Mass spectrum: m^+/e 248 (M+, 100%), 171 (25), 143 (98), 115 (72), 77 (49); UV (EtOH): λ_{max} 475 nm. (log ε 4.17), 413 sh (4.00), 309 (3.85), 258 sh (3.99), 251 (4.02) very similar to that reported.[6]

Despite the similarity of physical properties of bands 3 and 4, they were shown to be different as follows. Band 3 was a red spot (R_f 0.25) on analytical tlc whereas band 4 gave an orange spot (R_f 0.15). Band 3 was not converted to band 4 either by fusion at 150 °C or by heating in chlorobenzene to 160 °C for 21 hr. Likewise band 4 could not be converted to band 3 by photolysis either alone in benzene solutions of varying concentration, or by photolyses in benzene solution in the presence of either **1a** or 2-naphthol. In each case **6a** was recovered unchanged.

Irradiation of Sodium Phenylazosulphonate with 2-Naphthol. A solution of sodium phenylazosulphonate[9] (2.0 g) and 2-naphthol (1.0 g) in 100 ml ethanol and 225 ml water was irradiated in an immersion well apparatus with an unfiltered mercury arc for 1 hr by which time a suspension of a red substance was present. Extraction into chloroform gave a solution containing **6a**, unreacted 2-naphthol, and a tarry

residue, but no other products, according to tlc on silica gel (benzene: ligroin, 1: 9). Passage through a short column of alumina eluting with benzene: chloroform, 4: 1 gave **6a** (0.43 g), which crystallised as red needles from ethanol, mp 131—132 °C.

Irradiation of ***1a*** *in Mixtures of Ethanol and Halogenated Solvents.* Solutions of **1a** (0.40 g) in equal volumes of ethanol and the halogenated solvent (total volume 40 ml) were irradiated simultaneously for 100 hr using a Rayonet "Merry-go-round". The solvent was evaporated and each residue was separated by preparative tlc (benzene: ligroin, 1: 9), giving the quantities of **1a** and **2a** recorded in Table 1. When ethanol/bromotrichloromethane was the solvent the *o*-hydroxyazobenzene was obtained contaminated with other products. These could not be resolved on silica gel or by fractional crystallisation; partial separation was achieved by preparative tlc on alumina (J. T. Baker, Type 9F; developing solvent benzene, or benzene: ether, 9: 1), followed by repeated crystallisation from ethanol.

Physical characteristics of the purest samples obtained from both the photoreaction and from the bromination of **2a** in CCl_4 are given in Table 2. The identities of the products were established by mass spectrometry, but since the mass spectra of the monobromide always showed small amounts of the dibromide and *vice versa*, the raw UV absorbance data are recorded rather than the molar extinction coefficients. It seems most likely that the monobromide is 5-bromo-2-hydroxyazobenzene since its mp, mass spectrum, and UV correspond closely to those of authentic material, prepared in low yield by coupling benzenediazonium chloride with *p*-bromophenol. Also given for comparison are the physical properties of a second dibromohydroxyazobenzene, which crystallises from solution when **2a** is treated with a large excess of bromine.

The author thanks the National Research Council of Canada for generous financial support.

References

1) G. G. Spence, E. C. Taylor, and O. Buchardt, *Chem. Rev.*, **70**, 231 (1970); E. Buncel, in "Mechanisms of Molecular Migrations," Vol. 1, Ed. B. S. Thyagarajan, Interscience, (1969), pp. 104—110.
2) R. Tanikaga, This Bulletin, **41**, 1664, 2151 (1968).
3) M. Iwata and S. Emoto, *ibid.*, **43**, 946 (1970).
4) G. E. Lewis and J. A. Reiss, *Aust. J. Chem.*, **19**, 1887 (1966).
5) D. J. W. Goon, N. G. Murray, J-P. Schoch, and N. J. Bunce, *Can. J. Chem.*, **51**, 3827 (1973).
6) G. M. Badger and R. G. Buttery, *J. Chem. Soc.*, **1954**, 2243.
7) H. Zollinger, "Azo and Diazo Chemistry," Interscience (1961), p. 253.
8) Ref. 7, pp. 59—61.
9) R. Dijkstra and J. de Jonge, *Rec. Trav. Chim.*, **77**, 538 (1958).
10) E. S. Huyser, *J. Amer. Chem. Soc.*, **82**, 391 (1960).
11) T. Zincke and F. Rathgen, *Ber.*, **19**, 2482 (1886).

A Reinvestigation of the Normal Vibrations of Thioacetamide

Arabinda RAY and D. N. SATHYANARAYANA

Department of Inorganic and Physical Chemistry, Indian Institute of Science, Bangalore, 560012 India

(Received January 30, 1973)

The normal coordinate treatments of thioacetamide and its seven isotopic molecules have been carried out using Urey-Bradley force constants refined by a least-squares procedure. The laser Raman spectrum of thioacetamide has also been recorded.

A satisfactory assignment of the infrared frequencies of thioacetamide (TAM) and its *N*-deuterated molecule was made by Suzuki[1] with the aid of a normal coordinate analysis using Urey-Bradley force field. Walter and Kubersky[2] reinvestigated the infrared spectra of TAM and its several isotopic molecules. They appear to doubt the applicability of the results of the normal coordinate treatment (of Suzuki) to the isotopic molecules of TAM and have proposed considerable revision of the assignments of the infrared spectrum of TAM. It is of particular interest that the C=S stretching frequency was assigned around 975 cm^{-1}, as was done by some earlier workers[3,4] instead of a band near 720 cm^{-1} as favoured by the normal coordinate treatment.[1] It was therefore considered worthwhile to reinvestigate the infrared spectral assignments of this simplest thioamide, the results of which could be of considerable interest for other molecules. We report here the results of the normal coordinate treatments of TAM and its seven isotopic molecules—CH_3CSND_2, CD_3CSNH_2, CD_3CSND_2, $CH_3CS^{15}NH_2$, $^{13}CH_3CSNH_2$, $^{13}CH_3CSND_2$, and $CH_3{}^{13}CSNH_2$. The laser Raman spectrum of TAM has also been recorded.

Experimental

Infrared Spectra: We recorded the infrared spectra of thioacetamide (E. Merck) and its *N*-deuterated molecule in the range 4000—250 cm^{-1}. The frequency data agree with those of Walter and Kubersky[2] within 2—3 cm^{-1}. In order to utilize the infrared data of other isotopes and for uniformity, the data from the latter were only employed in the calculations.

Raman Spectrum: The Raman spectrum of powdered TAM sealed in a capillary tube was taken on a Cary 81 Raman spectrophotometer using argon laser. The spectrum was kindly recorded for us by Dr. J. R. Scherer of the U. S. Department of Agriculture, Albany, California, to whom we are grateful for this help. The Raman bands are included in Table 2.

Normal Coordinate Treatment

The structural parameters and the internal symmetry coordinates were the same as those employed by Suzuki.[1] The NH and CH stretching modes, however, were retained in the calculations. The initial force constants were taken from Suzuki. Twelve of these force constants were refined by a least-squares technique[5] from 14 frequencies by keeping all stretching constants and three bending constants around the thioamide carbon fixed. The final force constants are given in Table 1. They are comparable to the initial set except for $F_{HNH}(=-0.33$ mdyn/Å). We have preferred keeping the force constants within the framework of Urey-Bradley field to the alternate method of keeping F_{HNH} as zero, and introducing a non Urey-Bradley term between two NH bonds, as was done in the case of acetamide and other molecules.[6-8] If the force constant F_{HNH} is kept zero, the NH_2 stretching frequencies deviate largely and the force filed does not converge satisfactorily. The frequencies of the isotopic molecules were calculated employing the refined force constants. All the numerical calculations were made on an IBM 360/44 computer.

Table 1. Force constants (mdyn/Å) for thioacetamide

Stretching		Bending		Repulsion	
K_{CH}	4.50	H_{SCN}	0.240	F_{NCS}	0.991
K_{NH}	5.52	H_{NCC}	0.270	F_{NCC}	0.894
K_{CN}	5.70	H_{CCS}	0.270	F_{CCS}	0.286
K_{CS}	3.40	H_{CNH}	0.308	F_{CCH}	0.479
K_{CC}	2.70	H_{HNH}	0.567	F_{CNH}	0.481
		H_{CCH}	0.279	F_{HCH}	0.122
$k^{a)}{}_{CH_3}$	−0.071	H_{HCH}	0.391	F_{HNH}	−0.332
				F'	$-0.1F$

a) Intramolecular tension in mdyn·Å

Results and Discussion

The observed and calculated frequencies for TAM are given in Table 2, and for *N*- and *C*-deuterated TAM in Table 3, where the assignments obtained from the potential energy distribution (PED) are also shown. The agreement between the observed and calculated frequencies for TAM is excellent and that for isotopes of TAM listed in Tables 3 and 4 is fairly good. The calculated ND stretching frequencies deviate somewhat in the deuterated molecules. This may be attributed to the effects of hydrogen bonding.

The assignments given in Table 2 are practically the same as Suzuki's, and will therefore not be discussed. The satisfactory reproduction of the frequency shifts for several isotopic molecules of TAM (Tables 3 and 4) reflects the validity of the Urey-Bradley force constants and also the assignmtens derived therefrom. The revision of Suzuki's infrared assignments for TAM by Walter and Kubersky[2] therefore finds no support from isotopic molecules. When extensive coupling of the vibrations are involved, correlation by inspection of the frequency variations in the isotopic molecules with the assignments may be difficult as in the case of *N,N*-dimethylformamide.[9]

The C=S stretching mode has been attributed by Suzuki to a band at 720 cm^{-1} which has a mjaor contribution (approx. 60%) from the mode. This

Table 2. Vibrational frequencies (cm^{-1}) and assignments for thioacetamide

Raman	Infrared[a]	Calcd	Assignments (PED, %)	Raman	Infrared[a]	Calcd	Assignments (PED, %)
	3295	3295	ν_aNH(100)	975 vw	972	973	νCC(37)+rCH$_3$(21)+rNH$_2$(17)+νCS(11)
	3080	3080	ν_sNH(98)	—	760wsh[b]	—	τNH$_2$(A″)
	2977	2978	ν_aCH(100); νCH(A″)	720 vs	719	717	νCS(60)+νCC(16)
	2945	2945	ν_sCH(100)	712 s	709	—	wNH$_2$(A″)
1650 vw	1650 1648	1650	δNH$_2$(84)+νCN(10)	515 mw	512	—	πCC(A″)
1474 mb	1479	1479	δ_aCH$_3$(55)+rCH$_3$(21)+νCN(15)	471 s 463	471 460	465	δNCS(74)+νCS(14)
1432 vw	—	—	δCH$_3$(A″)	379 w	377w[b]	377	δCS(63)+δNCS(21)
1406 wb	1390	1390	νCN(54)+δ_aCH$_3$(23)	372 vw			
1370 m	1362	1361	δ_sCH$_3$(88)	220 w	n.i.	—	—
1312 wsh 1297 mw	1303	1303	rNH$_2$(42)+νCC(24)+νCS(13)+δNCS(12)	162 ms 120 s	n.i.	—	τCH$_3$(A″)
—	1130w[b]	—	rCH$_3$(A″)	101 m 80 s	n.i.		Lattice modes
1038 s	1025	1025	rCH$_3$(46)+rNH$_2$(24)+δ_aCH$_3$(11)				

A″ vibrations are tentatively assigned (*cf.* Table 3) a) From Ref. 2. b) From present investigation. n.i. denotes not investigated.

assignment is supported by the large red shift of the band, by 30—60 cm^{-1}, in metal complexes, where the thiocarbonyl sulfur is the donor[10,11] and the shift of the band to 675 cm^{-1} on *S*-methylation.[12] A comparison of the infrared spectrum of TAM with that of selenoacetamide ("Selenation") has also confirmed this assignment.[12] Thus the attribution of C=S stretching vibration to ~975 cm^{-1} frequency by Walter and Kubersky and others is not supported.[2-4,13] This band has, however, about ~10% C=S stretching mode and shows minor changes on complex formation, *S*-methylation and selenation.[10-12]

The C=S stretching vibration generally occurs as a split band in isotopic molecules. It appears at considerably lower wave numbers in deuterated molecules (Tables 3 and 4) depending on the nature of vibrational coupling.

Out-of-plane Vibrations. A tentative assignment for the seven A″ vibrations of TAM is given in Table 2.

The CH_3 out-of-plane rocking mode generally occurs at a higher frequency than CH_3 in-plane rocking and is of weaker intensity in amides. Accordingly, a weak broad band near 1130 cm^{-1} is attributed to CH_3 out-of-plane rocking in TAM, the band being slightly intensified in metal complexes.[10,11] Identification of CH_3 torsional mode is difficult since lattice modes

Table 3. Infrared frequencies and their assignments for *N*- and *C*- deuterated thioacetamide

Frequencies, cm^{-1}		CH_3CSND_2 Assignments (PED, %)	Frequencies, cm^{-1}		CD_3CSNH_2 Assignments (PED, %)
Obsd[a]	Calcd		Obsd[a]	Calcd	
2981	2978	ν_aCH(100); νCH(A″)	3296	3295	ν_aNH(100)
2924	2945	ν_sCH(100)	3077	3080	ν_sNH(98)
2485	2443	ν_aND(99)	—	2211	ν_aCD(98); νCD(A″)
2285	2238	ν_sND(95)	—	2112	ν_sCD(99)
1506 1486	1487	νCN(30)+δ_aCH$_3$(40)+rCH$_3$(18)	1653 1648	1650	δNH$_2$(84)+νCN(10)
1424	1416	νCN(44)+δ_aCH$_3$(34); δCH(A″)	1438	—	
1360	1361	δ_sCH$_3$(91)	1393	1403	νCN(69)
1240	1231	νCC(35)+νCS(21)+rND$_2$(16)+NCS(14)	1303	1301	rNH$_2$(43)+νCC(25)+νCS(14)
1164	1179	δND$_2$(73)	1234	—	
979	983	rCH$_3$(62)+δ_aCH$_3$(12)+νCN(11)	1094	1086	δ_sCD$_3$(61)+νCC(26)+rNH$_2$(11)
836	838	rND$_2$(60)+νCC(33)	1034	1038	δ_aCD$_3$(87); δCD$_3$(A″)
700 694	691	νCS(64)+νCC(10)	975	—	rCD$_3$(A″)
580 556	—	τND$_2$(A″)	957	954	rNH$_2$(31)+νCS(22)+δ_sCD$_3$(17)+νCC(15)
523	—	πCC(A″)	812	817	rCD$_3$(58)+νCN(11); τNH$_2$(A″)
480	—	wND$_2$(A″)	709	—	wNH$_2$(A″)
428	420	δNCS(64)+δCS(17)+rND$_2$(13)	670 664	663	νCS(55)+rCD$_3$(22)+νCC(13)
—	374	δCS(61)+δNCS(24)	461 448	453	δNCS(78)
			—	343	δCS(65)+δNCS(15)

a) From Ref. 2.

TABLE 4. OBSERVED AND CALCULATED FREQUENCIES (cm^{-1}) FOR SOME ISOTOPIC MOLECULES OF THIOACETAMIDE

CD_3CSND_2		$CH_3CS^{15}NH_2$		$^{13}CH_3CSNH_2$		$^{13}CH_3CSND_2$		$CH_3{}^{13}CSNH_2$	
Obsd[a]	Calcd	Obsd[a]	Calcd	Obsd[a]	Calcd	Obsd[a]	Calcd	Obsd[a]	Calcd
2477	2443	3288	3285	3292	3295		2967	3297	3295
2285	2238	3081	3075	3082	3080		2942	3082	3080
—	2210	2980	2978	2978 2967	2967		2443	2979	2978
—	2112	2934	2945	2942	2941		2238	2944	2945
1488	—	1654 1640	1642	1652 1648	1650	1506 1502	—	1653 1647	1649
1462	1439	1475	1477	1478	1478	1485	1487	1475	1471
1236	1229	1387 1382	1383	1389	1389	1421	1415	1464	—
1197	—	1361	1361	1364	—	1367	—	1370	1367
1172	1174	1300	1298	1351	1352	1351	1352	1360	1355
—	1056	1024	1022	1303	1299	1236	1225	1304	—
1028	1036	970	969	1022	1018	—	1177	1286	1280
814	809	714	712	973	—	973	976	1026	1022
—	802	704	—	965	964	831	831	963	966
694	—	512	—	718 710	712	700	—	714	713
663									
658	652	466 453	460	703	—	693 689	687	705	—
573	—	—	376	512	—	580	—	512 501	—
546	—	—		470 459	463	— 557	—	471 460	468
523	—	—	—	—	372	523	—	—	379
438	—	—	—	—	—	478	—	—	—
416	410	—	—	—	—	426	418	—	—
—	341	—	—	—	—	—	369	—	—

a) From Ref. 2.

interfere in this region. A band at 162 cm^{-1} in Raman may be favoured to methyl torsion in comparison with that at 155 cm^{-1} in acetamide.[14]

Both the wagging and torsional vibrations of the NH_2 group in TAM were assigned[1] earlier to a fairly sharp band at 709 cm^{-1}. In the Raman spectrum also the corresponding band is sharp. Careful observation of the infrared spectrum of TAM shows a weak shoulder at 760 cm^{-1} to the main absorption at 720 cm^{-1}. In metal complexes of TAM, the 760 cm^{-1} band acquires intensity and is sometimes observed as a farily strong band as in the case of copper(I) and palladium(II) chloride complexes.[10,11] We favour therefore the weak band at 760 cm^{-1} in TAM to NH_2 torsion in comparison with that at 810 cm^{-1} (weak) in acetamide.[14] The intense band at 709 cm^{-1} is attributed to NH_2 wagging mode in agreement with the earlier assignment.[1] This is compatible with the NH_2 wagging in acetamide assigned[14] to a strong band at 700 cm^{-1}.

The remaining three A″ vibrations of TAM are easily assigned as indicated in Table 2. In the deuterated molecules CD_3 out-of-plane rocking is expected near *ca.* 1000 cm^{-1}, and the torsional and wagging modes of ND_2, respectively, around δ 550 and 500 cm^{-1}. It is satisfying to note that bands are observed in this region in deuterated molecules (Tables 3 and 4). For a more definite assignment of the A″ vibrations, a normal coordinate analysis would be helpful.

The authors wish to thank Prof. W. Walter for a copy of his paper, and Prof. C. C. Patel for helfpul discussions.

References

1) I. Suzuki, This Bulletin, **35**, 1449 (1962).
2) W. Walter and H. P. Kubersky, *Ann. Chem.*, **694**, 56 (1966).
3) E. Spinner, *Spectrochim. Acta*, **15**, 95 (1959).
4) W. Kutzelnigg and R. Mecke, *ibid.*, **17**, 530 (1961).
5) T. Shimanouchi and I. Suzuki, *J. Mol. Spectrosc.*, **6**, 277 (1961).
6) T. Uno, K. Machida, and Y. Saito, This Bulletin, **42**, 897 (1969).
7) I. Nakagawa and T. Shimanouchi, *Spectrochim. Acta*, **18**, 513 (1962).
8) K. Kuchizu and L. S. Bartell, *J. Chem. Phys.*, **36**, 2460 (1962).
9) G. Durgaprasad, D. N. Sathyanarayana, and C. C. Patel, This Bulletin, **44**, 316 (1971).
10) C. D. Flint and M. Goodgame, *J. Chem. Soc., A*, **1968**, 750.
11) R. R. Iyengar, D. N. Sathyanarayana, and C. C. Patel, *J. Inorg. Nucl. Chem.*, **34**, 1088 (1972).
12) K. A. Jensen and P. H. Nielsen, *Acta Chem. Scand.*, **20**, 597 (1966).
13) C. Collard-Charon and M. Rensen, *Bull. Soc. Chem. Belges*, **72**, 304 (1963).
14) T. Uno, K. Machida, and Y. Saito, *Spectrochim. Acta*, **27A**, 833 (1971).

The Magnetic Circular Dichroism of Some Copper(II) β-Diketone Chelate Complexes in Various Media

Hajime KATÔ and Takahide KIMURA

Department of Chemistry, Faculty of Science, Kobe University, Nada-ku, Kobe 657

(Received May 15, 1973)

The magnetic circular dichroism (MCD) and absorption spectra of $Cu(acac)_2$, $Cu(bzac)_2$, $Cu(acest)_2$, $Cu(TFacac)_2$, and $Cu(HFacac)_2$ in benzene, chloroform, methylene chloride, 1,4-dioxane, pyridine, and piperidine are observed. The behavior of these spectra can be well explained by proposing this order of energy levels: d_{xz}, $d_{yz} < d_{x^2-y^2} < d_{z^2} < d_{xy}$. The MCD spectra in pyridine do not show any dispersion in the neighbourhood of the absorption peak which seems to correspond to the d_{xz}, $d_{yz} \rightarrow d_{xy}$ transition; this fact suggests that the B-term of the MCD parameters is dominant at room temperature. There is no serious difference between the MCD of $Cu(acac)_2$ and $Cu(bzac)_2$, or between $Cu(HFacac)_2$ and $Cu(TFacac)_2$. It appears that this lowering of symmetry is not important in interpreting the MCD spectra.

The magnetic circular dichroism (MCD) spectra of several Cu(II) complexes have been studied, and the B-term of the MCD parameters has been found to be dominant in the MCD of the Cu(II) complexes at room temperature.[1] The MCD spectrum of bis(acetylacetonato)copper(II), $Cu(acac)_2$, dissolved in chloroform was also studied.[2] The absorption spectra of $Cu(acac)_2$ in various media have been reported, and the positions and intensities have been shown to depend primarily upon the solvent basicity.[3] Therefore, MCD studies of the solvent effects are expected to yield a great deal of information about the assignments of the transitions and the properties of the MCD spectra. Furthermore, we have thought it worth while to investigate the MCD spectra for several substituted β-diketone complexes of copper(II). From this investigation, we expect to ascertain the effect of the lowering of symmetry around copper(II) upon the MCD and to ascertain the effect of various electron-withdrawing abilities of substituted acetylacetonates upon the MCD.

Experimental

Five copper(II) β-diketone chelate complexes, *i.e.*, bis(acetylacetonato)copper(II), bis(benzoylacetonato)copper(II), bis(ethylacetoacetato)copper(II), bis(trifluoroacetylacetonato)copper(II), and bis(hexafluoroacetylacetonato)copper(II) (abbreviated as $Cu(acac)_2$, $Cu(bzac)_2$, $Cu(acest)_2$, $Cu(TFacac)_2$, and $Cu(HFacac)_2$) were prepared and purified according to the methods described in the literature.[4-7] The absorption and MCD spectra of these compounds in the benzene, chloroform, methylene chloride, 1,4-dioxane, pyridine, and piperidine series of solvents were measured by the techniques described in an earlier paper.[1]

Results and Discussion

Figure 1 gives the MCD and absorption spectra of $Cu(acac)_2$ in the chloroform, methylene chloride, 1,4-dioxane, pyridine, and piperidine series of solvents. The MCD datum of $Cu(acac)_2$ in benzene was not available because of its poor solubility. Belford and his co-workers[3] have studied the absorption spectra, in the visible and near infrared region, of $Cu(acac)_2$ and bis(3-ethylacetylacetonato)copper(II) in various

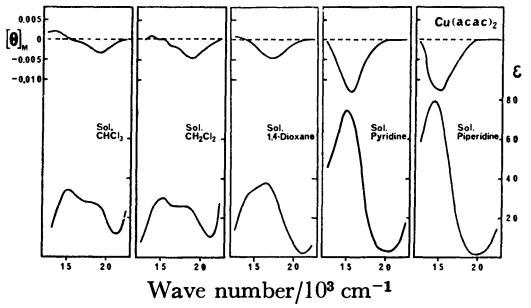

Fig. 1. The MCD (upper) and absorption (lower) spectra of $Cu(acac)_2$ dissolved in various solvents at room temperature.

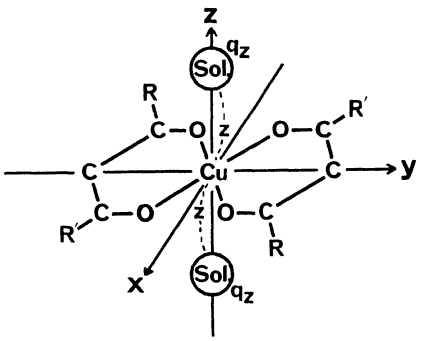

Fig. 2. The coordinate system and geometrical model for the calculation of solvent effects.

media. The behavior of these absorption bands upon the alternation of the solvent have been quite successfully explained in terms of the crystal field theory. Let us adopt the same model. The effect of the solvent is considered as two axial ligands (two charges, q_z, at (0, 0, z) and (0, 0, −z), as is shown in Fig. 2) are added to a square planar complex. $Cu(acac)_2$ molecule in a noninteracting solvent, chloroform, may be considered as an isolated square-planar complex. If we assign the bands at 18810 and 15190 cm^{-1} observed for $Cu(acac)_2$ in chloroform to the d_{yz}, $d_{yz} \rightarrow d_{yz}$ and $d_{x^2-y^2} \rightarrow d_{xy}$ transitions respectively,[3] the transition energies in the presence of an interacting solvent are given by:

$$\delta E_1(|xz\rangle, |yz\rangle \rightarrow |xy\rangle) = 18810 + (-9\langle r^2\rangle/z^2 + 5\langle r^4\rangle/z^4)2q_z e^2/21z,$$
$$\delta E_2(|x^2-y^2\rangle \rightarrow |xy\rangle) = 15190,$$
$$\delta E_3(|z^2\rangle \rightarrow |xy\rangle) = 14950 + (-12\langle r^2\rangle/z^2 - 5\langle r^4\rangle/z^4)2q_z e^2/21z \quad (1)$$

in units of cm^{-1}. The values of $\langle r^2\rangle$ and $\langle r^4\rangle$ are evaluated by using the analytical SCF function for Cu obtained by Clementi:[8] $\langle r^2\rangle_{Cu}=1.106\ a_0^2$, $\langle r^4\rangle_{Cu}=3.301\ a_0^4$. If we assume the distance, z, between the metal and the solvent charge, q_z, to be 2 A, then the excitation energies given by Eq. (1) are reduced to functions of q_z only. The results are shwon schematically in Fig. 3. $\delta E_2(|^2x-y^2\rangle \rightarrow |xy\rangle)$ displays little variation from solvent to solvent. $\delta E_1(|xz\rangle, |yz\rangle \rightarrow |xy\rangle)$ approaches $\delta E_2(|x^2-y^2\rangle \rightarrow |xy\rangle)$ as the solvent basicity is increased. The variation in the absorption bands upon the alternation of the solvent can be well explained by assuming the q_z values to be about 0.0, 0.1, 0.3, 0.7, and 0.9 for the spectra of $Cu(acac)_2$ in chloroform, methylene chloride, 1,4-dioxane, pyridine, and piperidine respectively. These values seem to be of a plausible order of magnitude.

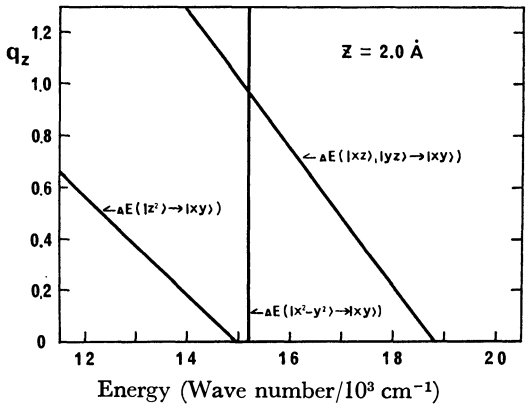

Fig. 3. Excitation energy diagram as a function of solvent charges q_z, which are assumed to be located axially to a square-planar complex at (0, 0, 2A) and (0, 0, −2A).

The interpretation of the polarized visible absorption spectrum of $Cu(acac)_2$ has been the subject of speculation and controversy as attempts have been made to remove the ambiguity of the assignment.[9-12] Unfortunately, however, the type of packing of molecules in the crystal was inadequate for the attempt.[13] Hitchman and Belford[13] studied the temperature-dependent polarized spectra of $Cu(bzac)_2$; they assigned the band at 18.1 kK to d_{xz}, $d_{yz} \rightarrow d_{xy}$, the band at 15.6 kK to $d_{x^2-y^2} \rightarrow d_{xy}$ and the band at 14.2 kK to $d_{z^2} \rightarrow d_{xy}$ on the basis of the temperature dependence and the relative polarization. This ordering of the d levels is the same as that suggested for bis(3-phenyl acethylacetonato)copper.[14] The positions of the d-d bands in $Cu(bzac)_2$ at 14.2, 15.6, and 18.1 kK, are very similar to those of the bands in $Cu(acac)_2$, at 14.5, 16.3, and 18.0 kK;[13] this suggests the same ordering of the d levels. Katô and Gohda[2] proposed the same order of energy levels (d_{xz}, $d_{yz} < d_{x^2-y^2} < d_{z^2} < d_{xy}$) for $Cu(acac)_2$ in chloroform on the basis of the MCD analysis.

The variation in the absorption bands upon the alternation of the solvent can be well explained by proposing this order of energy levels, as we have seen above. On the other hand, if we assign the bands at 18810 and 15190 cm^{-1} observed for $Cu(acac)_2$ in chloroform to the $d_{x^2-y^2} \rightarrow d_{xy}$ and d_{xz}, $d_{yz} \rightarrow d_{xy}$ transitions respectively, we can not explain the observed red shift of the bands as the basicity of the solvent increases. The energy for the $d_{x^2-y^2} \rightarrow d_{xy}$ transition should undergo little change from the variation in the basicity of solvent which coordinates axially to a square-planar complex. This property is due to the geometrical structure of the d_{xy} and $d_{x^2-y^2}$ orbitals and does not depend greatly on the model of the calculation.

The MCD spectra of $Cu(acac)_2$ display a remarkable change on going to a more basic solvent. This change can be explained on the basis of the above discussion about the transition energies and the previous analysis about the MCD of the Cu(II) complexes.[1] The d_{xz}, $d_{yz} \rightarrow d_{xy}$ transition, which shows an MCD with a positive B-term, approaches the $d_{x^2-y^2} \rightarrow d_{xy}$ transition band, which shows an MCD with a small positive B-term, as the solvent basicity is increased. The $d_{z^2} \rightarrow d_{xy}$ transition, which shows an MCD with a negative B-term, shifts to the lower frequency region, in which we can not measure the MCD spectra because of our instrumental restriction. Therefore, $Cu(acac)_2$ values in pyridine and piperidine display only a negative MCD in the region of 12.5—20.0 kK.

The MCD spectra of $Cu(acac)_2$ in 1,4-dioxane and pyridine do not show any dispersion in the neighbourhood of the absorption peak which seems to correspond to the d_{xz}, $d_{yz} \rightarrow d_{xy}$ transition. This fact strongly suggests that the B-term of the MCD parameters is dominant in the MCD of $Cu(acac)_2$ at room temperature. This conclusion is consistent with the theoretical prediction previously proposed by one of the present authors.[1]

The MCD and absorption spectra of $Cu(bzac)_2$, $Cu(acest)_2$, $Cu(TFacac)_2$, and $Cu(HFacac)_2$ in the benzene, chloroform, methylene chloride, 1,4-dioxane, pyridine, and piperidine series of solvents are shown in Figs. 4—7. In these spectra, the effect of changing the substituents is smaller than the effect of changing the solvent. However, the MCD and absorption spectra in the solvent with a weak basicity suggest a correla-

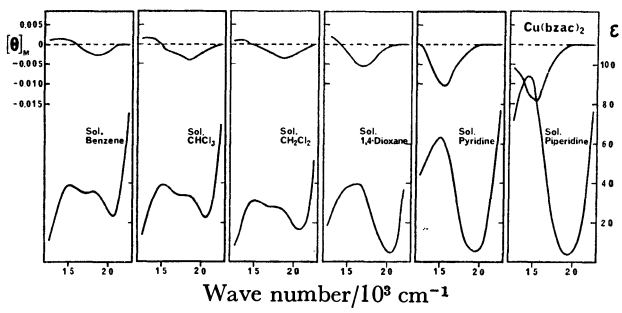

Fig. 4. The MCD and absorption spectra of $Cu(bzac)_2$ dissolved in various solvents at room temperature.

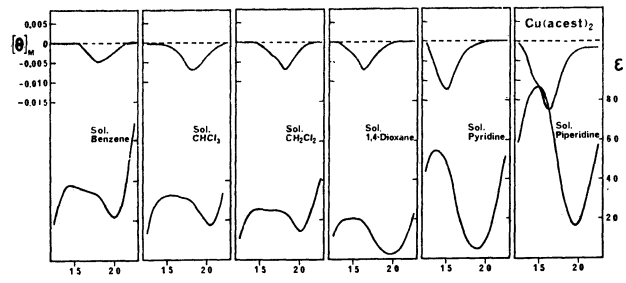

Fig. 5. The MCD and absorption spectra of Cu(acest)$_2$ dissolved in various solvents at room temperature.

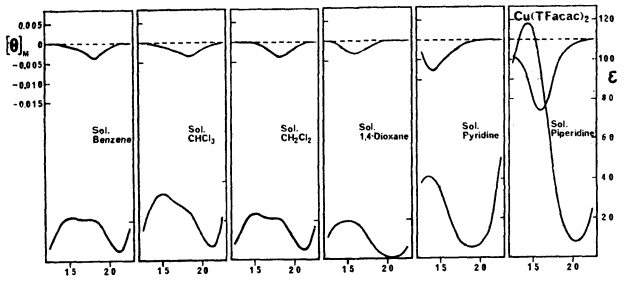

Fig. 6. The MCD and absorption spectra of Cu(TFacac)$_2$ dissolved in various solvents at room temperature.

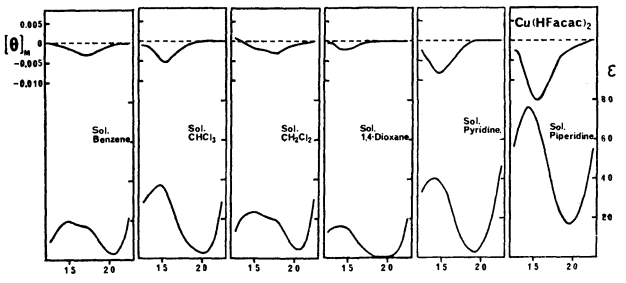

Fig. 7. The MCD and absorption spectra of Cu(HFacac)$_2$ dissolved in various solvents at room temperature.

tion between the relative electron-withdrawing ability of substituents and the energy levels of copper d electrons; the more electronegative the substituent, the smaller the energy separation. The order of electronegativity must be CF_3>OC_2H_5>Ph>H>CH_3. The MCD of the positive B-term of the d_{xz}, d_{yz}→d_{xy} transition would overcome the MCD of the negative B-term of the d_{z^2}→d_{xy} transition in Cu(acest)$_2$, Cu(TFacac)$_2$, and Cu(HFacac)$_2$.

Of course, the coordinating form and the steric effect of the solvent in each case is important. Kuska and Rogers[15] have reported that increasing the basicity of the solvent has the same effect on the d electron energy levels and on the unpaired electron density of copper as increasing the electronegativity of the substituents. To be sure, there are also similarities in the ESR parameters for Cu(HFacac)$_2$ in a chloroform solution and for Cu(acac)$_2$ in a pyridine solution, and the same similarity in the absorption and MCD spectra. However, the spectrum of Cu(HFacac)$_2$ in chloroform is rather a special case; the spectrum of Cu(HFacac)$_2$ in solvents of a weak basicity, benzene or methylene chloride, is similar to that of Cu(acac)$_2$ in chloroform. Chloroform would be an interacting solvent for Cu(HFacac)$_2$.

The symmetry of Cu(bzac)$_2$ or Cu(TFacac)$_2$ is lower than that of Cu(acac)$_2$ or Cu(HFacac)$_2$, but there is no serious difference between the MCD spectra of Cu(acac)$_2$ and Cu(bzac)$_2$ or between those of Cu(HFacac)$_2$ and Cu(TFacac)$_2$. It appears that this lowering of the symmetry is not important in interpreting the MCD spectra.

This work was partially supported by a Scientific Research Grant from the Ministry of Education of Japan.

References

1) H. Katô, *Mol. Phys.*, **24**, 81 (1972).
2) H. Katô and J. Gohda, This Bulletin, **46**, 636 (1973).
3) R. L. Belford, M. Calvin, and G. Belford, *J. Chem. Phys.*, **26**, 1165 (1957).
4) W. C. Fernelius and B. E. Bryant, *Inorg. Synthesis*, **5**, 105 (1957).
5) Ping-Kay Hon, C. E. Peluger, and R. L. Belford, *Inorg. Chem.*, **5**, 516 (1966).
6) D. P. Graddon, *J. Inorg. Nucl. Chem.*, **14**, 161 (1960).
7) R. L. Belford, A. E. Martell, and M. Calvin, *ibid.*, **2**, 11 (1956).
8) E. Clementi, *J. Chem. Phys.*, **41**, 295 (1964).
9) J. Ferguson, *ibid.*, **34**, 1609 (1961).
10) T. S. Piper and R. L. Belford, *Mol. Phys.*, **5**, 169 (1962).
11) J. Ferguson, R. L. Belford, and T. S. Piper, *J. Chem. Phys.*, **37**, 1569 (1962).
12) H. C. Allen, Jr., *ibid.*, **45**, 553 (1966).
13) M. A. Hitchman and R. L. Belford, *Inorg. Chem.*, **10**, 984 (1971).
14) R. L. Belford and J. W. Carmichael, Jr., *J. Chem. Phys.*, **5**, 516 (1966).
15) H. A. Kuska and M. T. Rogers, *ibid.*, **43**, 1744 (1965).

Hole-particle Formalism for the Electronic Spectra of Long Chain Polyenes

Sadhan BASU

Department of Chemistry, University College of Science, Calcutta-9, India

(Received June 15, 1973)

From the hole-particle description of the many-Fermion system of long chain polyenes it has been shown that the convergence limit in the electronic spectra may be accounted for by the electron-hole pairing interaction.

It is well-known that the wavelength of the lowest N–V transition of polyenes does not grow proportionately with the number n of the conjugated double bonds as is true for symmetrical cyanines, but tends to a limit as n becomes large.[1] Kuhn[2] related this behavior to the unequal length of single and double bonds, which generates a perturbing potential with a period of the bond length and thus introduces a Brillouin gap between the highest occupied and the lowest unoccupied level. Dewar[3] accounts for this phenomenon by assuming different exchange integrals for single and double bonds. On the other hand, simple free electron theory as well as molecular orbital theory predict a rapid equalization of bond lengths with increasing n and therefore invalidates the above reasoning. Further it has been found that mono- and dinegative ions of diphenyl polyenes show bond alternation,[5] although dinegative ions show convergence and mono-negative ions do not. Unequal bonds do not appear to lead to convergence. Araki[4] tried to correlate the convergence limit with the plasma oscillation in many-electron system, but it fails to explain different behavior of cyanines and polyenes.

In the usual treatment of many-Fermion problem each particle is supposed to move independently, the effect of the interaction between particles being simply replaced by an average field of force. This treatment does not take interparticle correlation into account. A step towards the improvement of the method so as to include correlation was taken by Euler,[6] who calculated the effect of interparticle interaction, which causes the correlation, by perturbation theory assuming the interaction to be small. The calculation of such a type is carried out in the following manner. In the zeroth approximation each particle is in some one-particle quantum state, which we consider a "level". Let us consider the lowest state for the sake of definiteness. In this state all levels up to some highest, which we call the Fermi maximum (λ), are each filled by the particles. The perturbation energy due to the interparticle force, has non-vanishing matrix elements which cause virtual transitions to states in which particles are excited to levels higher than the Fermi maximum. The state which results from the interparticle force is thus a superposition of zero order state and various excited states. Such a mixture of excited states gives rise to correlation between particles.

Accepting the above model we may approach the problem of π-electronic spectra of long chain polyenes in a different way. In the single-particle level scheme of "electron in a box" the levels up to λ (Fermi level) are occupied and the levels above it are unoccupied. The state obtained by exciting a particle from an occupied level to an unoccupied level is called a state of one hole-one particle type, because in this process of excitation a vacancy (hole) is left in the occupied level and a "particle" is produced, instead, in one of the unoccupied level. If we use single-particle creation operator and destruction operator in the treatment of many-body-Hamiltonian, then we will be able to get the elementary excitation energy of a hole-particle pair or a quasiparticle.

The physics and mathematics of quasiparticles have been rigorously developed and applied with great success in nuclear physics[8,8e] and in the theory of superconductivity.[7] In what follows we use this formulation in a simplified and somewhat approximate form.

Quasiparticle Hamiltonian

The second quantized version of the many-body Hamiltonian is given as[9]

$$H = \sum_{\alpha,\beta}\langle\alpha|T|\beta\rangle C_\alpha^+ C_\beta + \frac{1}{2}\sum_{\alpha,\beta,\gamma,\delta}\langle\alpha\beta|v|\gamma\delta\rangle C_\alpha^+ C_\beta^+ C_\gamma C_\delta \cdots, \quad (1)$$

$$\left(v = \frac{1}{r_{ij}}\right)$$

where C_α^+ is the creation operator for the state α and C_β, the destruction operator for the state β. The ground state $|\psi_0\rangle$contains a set of occupied single particle states h, h^1, $\cdots$ and hence it is impossible to create another particle in an occupied state h. Therefore

$$C_h^+|\psi_0\rangle = 0$$

The state $|\psi_0\rangle$ does not contain any of the unoccupied single particle states p, p^1 $\cdots$ and hence it is impossible to destroy any such state in

$$C_p|\psi_0\rangle = 0$$

If we now define a new destruction operator for the single particle state by the following relation;

$$b_i = C_i^+ \text{ when } i = h,$$
$$= C_i \text{ when } i = p.$$

Then we have

$$b_i|\psi_0\rangle = 0 \text{ for all } i.$$

We interpret the state $|\psi_0\rangle$ as the vacuum state for the new object which we created by b_i^+, such that

$$b_i^+ = C_i \text{ where } i = h,$$
$$= C_i^+ \text{ where } i = p.$$

We call these new-objects quasiparticles and the $|\psi_0\rangle$ state plays the role of vacuum state for these objects.

We now replace the Hamiltonian (1) by its expectation value with respect to ground state $|\psi_0\rangle$ and get

$$\langle H\rangle = \sum_{\alpha,\beta}\langle\alpha|T|\beta\rangle\langle C_\alpha^+ C_\beta\rangle + \frac{1}{2}\sum_{\alpha,\beta,\gamma,\delta}\langle\alpha\beta|v|\gamma\delta\rangle \times\{\langle C_\alpha^+ C_\beta^+\rangle\langle C_\gamma C_\delta\rangle + \langle C_\alpha^+ C_\gamma\rangle\langle C_\beta^+ C_\delta\rangle - \langle C_\alpha^+ C_\delta\rangle\langle C_\beta^+ C_\gamma\rangle\} \quad (2)$$

where the exceptation values $\langle C_\alpha^+ C_\beta\rangle$ *etc.* are pure numbers and is defined as density functions

$$\langle\beta|\rho|\alpha\rangle = \langle\psi_0|C_\alpha^+ C_\beta|\psi_0\rangle \quad (3)$$

With this definition the last two terms combine to give us the self-consistent potential V, made up of both Coulomb and exchange terms. We then get

$$\langle H\rangle = \sum_{\alpha,\beta}\langle\alpha|T+\frac{1}{2}V|\beta\rangle\langle\beta|\rho|\alpha\rangle + \frac{1}{2}\sum_{\alpha,\beta,\gamma,\delta}\langle\alpha\beta|v|\gamma\delta\rangle\langle C_\alpha^+ C_\beta^+\rangle\langle C_\gamma C_\delta\rangle \quad (4)$$

We notice that the energy expression contains an extra-potential term than what is present in Hartree-Fock state, so these states are called Hartree-Fock-Bogolyubov (HFB) states.[8] Now following (3) we define $\langle C_\delta C_\gamma\rangle = K_{\delta\gamma}$ a density function and following anticommutation of destruction operators we have $\langle C_\gamma C_\delta\rangle = -K_{\delta\gamma}$. We therefore write the second term in (4) as

$$\frac{1}{4}\sum_{\alpha,\beta,\gamma,\delta}\langle\alpha\beta|v|\gamma\delta\rangle K^*_{\beta\alpha}(K_{\delta\gamma}-K_{\gamma\delta}) = \frac{1}{2}\sum_{\alpha,\beta}\Delta_{\alpha\beta}K^*_{\beta\alpha}, \quad (5)$$

where $\Delta_{\alpha\beta}$ may be defined as a pairing potential. So we get

$$\langle H\rangle = \sum_{\alpha,\beta}\{\langle\alpha|T+\frac{1}{2}V|\beta\rangle\langle\beta|\rho|\alpha\rangle+\frac{1}{2}\Delta_{\alpha\beta}K^*_{\beta\alpha}\} \quad (6)$$

Variation of Calculation of Quasiparticle Energy

We now try to determine the ground state energy by a variational calculation,[8] *i.e.*, we try to minimise $\langle\psi_0|H-\lambda N|\psi_0\rangle$ where λ is the Lagrangian multiplier and N is the operator for total number of particles

$$N = \sum_\alpha C_\alpha^+ C_\alpha. \quad (7)$$

We now follow a two-step minimising procedure on $H(\lambda)=H-\lambda N$. We first omit the second term in (6) and define a single-particle state as

$$|i\rangle = \sum X_\alpha^i|\alpha\rangle \text{ and } H|i\rangle = \varepsilon_i|i\rangle$$

then the variation parameters X_α^i which makes $\langle H(\lambda)\rangle$ a minimum satisfy

$$\sum_\beta\langle\alpha|T-\lambda\mathbf{1}+\frac{1}{2}V|\beta\rangle X_\beta^i = (\varepsilon_i-\lambda)X_\alpha^i. \quad (8)$$

That is at this stage we now have single particles with energies $(\varepsilon_i-\lambda)$. In the next step we write $H(\lambda)$ using $|i\rangle$ as the basis

$$\langle H(\lambda)\rangle = \sum_{i,j}\langle i|T-\lambda\mathbf{1}+\frac{1}{2}V|j\rangle\langle j|\rho|i\rangle + \frac{1}{2}\sum_{ij}\Delta_{ij}K^*_{ij}, \quad (9)$$

Now we make a transformation[8]

$$b_i^+ = u_i C_i^+ + v_i C_{-i}, \quad (10)$$

where the coefficients u_i and v_i are the variation parameters. One can create a particle in a state if it is empty and destroy a particle if it is occupied. Therefore u_i^2 and v_i^2 are the probabilities of getting the state i empty and occupied respectively. We therefore have

$$u_i^2 + v_i^2 = 1,\ u_i = u_{-i},\ v_i = -v_{-i}. \quad (11)$$

Similarly we get

$$b_i = u_i C_i + v_i C_{-i}^+. \quad (12)$$

Inverting these relations we get

$$C_{-i}^+ = u_i b_{-i}^+ + v_i b_i,$$
$$C_i = u_i b_i - v_i b_{-i}^+. \quad (13)$$

With this transformations we have

$$\langle j|\rho|i\rangle = \langle C_i^+ C_j\rangle = \langle\psi_0|(u_i b_i^+ - v_i b_{-i})(u_j b_j - v_j b_{-j}^+)|\psi_0\rangle = \langle\psi_0|b_i b_j^+|\psi_0\rangle v_i v_j = v_i^2\delta_{ij}, \quad (14)$$

$$K_{ij} = \langle\psi_0|(u_i b_i - v_i b_{-j}^+)(u_j b_j - v_j b_{-j}^+)|\psi_0\rangle = -\langle\psi_0|b_i b_j^+|\psi_0\rangle u_i v_j = u_i v_{-i}\delta_{i,-j}. \quad (15)$$

Now b_i's in (10) and (12) are the creation and destruction operators for quasiparticles in the HFB[8] formulation and they differ from relations given for HF state because in HFB formulation the particle number is not conserved. In simplifying these relations we have used the Fermion anticommutation relations of quasiparticle operators

$$\{b_i, b_j\} = \{b_i^+, b_j^+\} = 0,$$

and

$$\{b_i, b_j^+\} = \delta_{ij}.$$

With these transformation we get

$$\langle H(\lambda)\rangle = \sum_i\langle i|T-\lambda\mathbf{1}+\frac{1}{2}V|i\rangle v_i^2 + \frac{1}{2}\sum_i\Delta_{i,-i}u_i v_{-i}. \quad (16)$$

We now minimise (16) by requiring $\delta H(\lambda)/\delta v_i=0$, using $u_i^2=1-v_i^2$, $v_{-i}=-v_i$ and we get

$$(\varepsilon_i-\lambda)2v_{-i}u_i+\frac{1}{2}\Delta_{i,-i}(u_i^2-v_i^2) = 0. \quad (17)$$

Putting $\cos\theta_i=u_i$ and $\sin\theta_i=v_{-i}$ we have

$$(\varepsilon_i-\lambda)\sin 2\theta_i = \Delta\cos 2\theta_i,\ \Delta = -\Delta_{i,-i}/2,$$

$$\text{or } \tan 2\theta_i = \frac{\Delta}{\varepsilon_i-\lambda},$$

$$2u_i v_{-i} = \sin 2\theta_i = \frac{\Delta}{\sqrt{(\varepsilon_i-\lambda)^2+\Delta^2}}, \quad (18)$$

$$u_i^2 - v_i^2 = \cos 2\theta_i = \frac{\Delta}{\sqrt{(\varepsilon_i-\lambda)^2+\Delta^2}}. \quad (19)$$

We set E_i equal to

$$E_i = \sqrt{(\varepsilon_i-\lambda)^2+\Delta^2}. \quad (20)$$

Significance of E_i

While simplifying the Eq. (1) we have used the product of the creation and destruction operator in the contracted form which gives us information about

the ground state only. Terms containing the normal products of the operator will give us informations about the states in which there are one, two, three, four, *etc.* pairs of creation and destruction operators. If we pick up only terms in which there is only one pair of creation and destruction operator, then we have

$$H_1(\lambda) = \sum_j(\varepsilon_j-\lambda)C_j^+C_j + \frac{1}{2}\sum_j \Delta_{j,-j}C_j^+C_{-j}^+. \quad (21)$$

Expressing the creation operators in terms of quasiparticle operators and following the algebraic procedure outlined in the proceeding section we get

$$\begin{aligned} H_t(\lambda) &= \sum_j[(\varepsilon_j-\lambda)(u_j^2-v_j^2)+\Delta_{j,-j}u_jv_{-j}]b_j^+b_j \\ &= \sum_j[(\varepsilon_j-\lambda)\cos 2\theta_j+\Delta_{j,-j}\sin 2\theta_j]b_j^+b_j \\ &= \sum_j E_jb_j^+b_j. \end{aligned} \quad (22)$$

The new Hamiltonian is thus

$$H = \langle H_0(\lambda)\rangle + \sum_j E_jb_j^+b_j. \quad (23)$$

Let us now consider a state i with one quasiparticle, *i.e.*, the state $b_i^+|\psi_0\rangle$. The energy of the state is given as

$$\begin{aligned} &\langle\psi_0|b_i\{\langle H_0(\lambda)\rangle+\sum_j E_jb_j^+b_j\}b_i^+|\psi_0\rangle \\ &= \langle H_0(\lambda)\rangle\langle\psi_0|b_ib_i^+|\psi_0\rangle + \sum_j E_j\langle\psi_0|b_ib_j^+b_jb_i^+|\psi_0\rangle \\ &= \langle H_0(\lambda)\rangle + E_i. \end{aligned} \quad (24)$$

The energy of the state ψ_0 is $\langle H_0(\lambda)\rangle$ and the energy of the state with one quasiparticle is $\langle H_0(\lambda)\rangle+E_i$. Hence we conclude that E_i is the energy carried by one hole-particle pair, *i.e.* a quasiparticle and it is given as

$$E_i = \sqrt{(\varepsilon_i-\lambda)^2+\Delta^2}, \quad \Delta^2 = \left(\frac{\Delta_{i,-i}}{2}\right)^2. \quad (25)$$

Exactly same expression has been obtained by solving HFB equation by Green function technique.[11] This partially justifies our assumption that Δ's are constant in variation calculation.

Significance of λ

From the relation

$$v_i^2 = \frac{1}{2}\left[1-\frac{\varepsilon_i-\lambda}{E_i}\right] \quad (26)$$

it is evident that when ε_i is much greater than λ, $v_i^2=0$ while when it is much less than λ, $v_i^2=1$ assuming Δ to be small. In the usual description of π-electron system the levels upto Fermi-maximum are occupied while those above it are all empty. So the occupation probability above Fermi-maximum is zero and below it is one. This suggests that λ is to be associated with ε_F, the energy of the Fermi-maximum. Hence the quasiparticle energy is given.

$$E_i = \sqrt{(\varepsilon_i-\varepsilon_F)^2+\Delta^2} \quad (27)$$

Convergence Limit and Δ

Equation (27) shows that when ε_i becomes equal to ε_F, the hole-particle energy is Δ and not zero and the minimum value of all quasiparticles is Δ. If the long-wavelength transition in linear polyene is associated with the electron jump from the top-most filled orbital to the first empty orbital, then in the quasiparticle scheme the energy should go over to Δ as the energy difference $\varepsilon_i-\varepsilon_F$ goes to zero, *i.e.*, as the length of the chain goes to infinity.

A Chemist's View of Δ

From the relation (18) we have

$$2u_iv_{-i} = \frac{\Delta}{\sqrt{(\varepsilon_i-\varepsilon_F)^2+\Delta^2}}.$$

Now for HF state we have

$u_i=1$ for a particle state
$=0$ for a hole state,
$v_{-i}=1$ for a hole state
$=0$ for a particle state.

In HFB case u_i and v_i will deviate from these unique values and will be somewhere between zero and one. This means that even for HFB case should be positive. So Δ must be a positive quantity. Now Δ has been set equal to $-(\Delta_{i,-i})/2$, which means that $\Delta_{i,-i}$ must be negative. $\Delta_{i,-i}$ is related to pairing potential which in the present formulation must be Coulombic in origin as $v=1/r_{ij}$. The Coulombic potential is negative if the interaction is between two particles of opposite charges. This suggests that we may associate this interaction with the attraction between a particle and a hole. This interaction is not taken into account at any stage in HF calculation.

If the Hamiltonian (1) is written out in full, then there will appear terms which can be correlated with interaction arising from hole-particle, particle-particle hole-hole, *etc.* These points have been thoroughly discussed in Random-Phase-Approximation Scheme.[10] Instead of going into details of that calculation we only state that whenever we go over to calculate energy values for states other than ground state we must take into account interactions arising from hole-hole, hole-particle terms in the Hamiltonian (1).

With this formulation we now proceed to analyse the case of cyanine. In the π-electron calculation on cyanines, the systems are considered to be open-chain systems like polyenes, but carry a positive charge *i.e.* a hole in Fermi sea. The interaction of this charge with the π-electrons is taken into account in the usual HF calculation. In the expression for quasiparticle energy

$$E_i = \sqrt{(\varepsilon_i-\varepsilon_F)^2+\Delta^2},$$

the Δ should be made up of two terms, the hole-particle attraction and the hole-hole repulsion, the terms which are not taken care of in HF calculation. It may not be too unfair to assume that these two terms will be nearly equal and cancel each other. The quasiparticle energy will then reduce to

$$E_i = (\varepsilon_i-\varepsilon_F),$$

and the system will not show any convergence limit as is actually the case.

While considering biphenyl-polyene dinegative and mononegative ions, we may consider the mononegative ion to be the same as dinegative ion with a formal hole in the Fermi sea. Consequently mononegative ion will show no convergence limit like cyanines, while dinegative ion will.

It appears that the hole-particle formulation with some chemical intuition can give a reasonable account for the convergence limit in π-electronic spectra of open-chain compounds.

References

1) L. G. S. Brooker, *Rev. Mod. Phys.*, **14**, 275 (1942); K. Hiramaya, *J. Amer. Chem. Soc.*, **77**, 372 (1955).
2) H. Kuhn, *J. Chem. Phys.*, **17**, 1198 (1949).
3) M. J. S. Dewar, *J. Chem. Soc.*, **1952**, 3544.
4) G. Araki, *J. Chem. Phys.*, **24**, 1269 (1956).
5) P. H. Van der Meij, Thesis, Amsterdam, 1958.
6) Euler, *cf.* S. Tomonaga, *Prog. Theor. Phys.*, **5**, 544 (1950).
7) J. Bardeen, L. N. Cooper, and J. R. Schrieffer, *Phys. Rev.*, **108**, 1175 (1957).
8) N. N. Bogolyubov, *Dokl. Akad. Nauk SSSR*, **110**, 936 (1958).
8e) M. Pal, *IAEA*-SMR-6125, (1970).
9) J. Hubbard, *Proc. Roy. Soc.* (London), **276A**, 242 (1963).
10) P. L. Altick and A. E. Glass Gold, *Phys. Rev.*, **133**, 632 (1964).
11) V. J. Kresin, *Zh. Strukt. Khim.*, **12**, 745 (1971).

NOTES

BULLETIN OF THE CHEMICAL SOCIETY OF JAPAN, VOL. 47 (3), 739—740 (1974)

Estimation of the Structures and Electronic States of Radicals Using the INDO-SCF MO Method. I. Alkoxyl Radicals

Katsutoshi OHKUBO and Futoshi KITAGAWA

Department of Synthetic Chemistry, Faculty of Engineering, Kumamoto University, Kurokami, Kumamoto 860

(Received July 2, 1973)

Synopsis. The most energetically stable alkoxyl radicals take the following configuration: r(C–O)=1.36 Å, r(C–H)=1.12 Å, and ∠OCH=109°28′ for $CH_3O\cdot$, and r(C–O)=1.36 Å, r(C–C)=1.47 Å, and ∠OCC=108° for $C_2H_5O\cdot$. The pseudo π orbital is observed in the C–O bond.

Alkoxyl radicals (referred to as RO·) have been postulated as momentarily-living intermediates participating in the oxidation and polymerization reactions. Recently, they have been considered to play an important role in the air-pollution cycle:

$$-\underset{\text{H}}{\text{C}}=\text{C}-\text{C}- + {}^1\text{O}_2 \longrightarrow -\text{C}(\text{OOH})-\text{C}=\text{C}-$$

$$\xrightarrow{\text{dec.}} \text{Radicals such as RO}\cdot$$

$$\text{RO}\cdot + {}^3\text{O}_2 \longrightarrow \text{RO}_3\cdot$$

$$\xrightarrow{\text{NO}} \text{RO}_2\cdot + \text{NO}_2 \text{ (or } \text{RO}_3\text{NO)}$$

$$\text{RO}_2\cdot + \text{NO} \longrightarrow \text{RO}\cdot + \text{NO}_2$$

The molecular structures and electronic states of RO radicals, however, seem to be open to question, although some rough estimates of the said aspects of the radicals have been established by the iterative extended Hückel[1] and CNDO/2[2] treatments of some lower molecules.

In the present study, we will estimate the molecular structures and electronic states of RO radicals by means of the INDO-SCF MO method,[3] taking methoxyl and ethoxyl radicals as examples.

Method of Calculation

The following two systems were investigated in this work: (a) the methoxyl radical, $CH_3O\cdot$ and (b) the ethoxyl radical, $CH_3CH_2O\cdot$. The geometric parameters of the above species are shown in Fig. 1. In

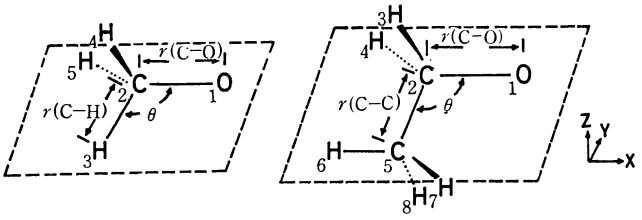

Fig. 1. Geometries used for calculations. (r(C–O), θ, r(C–H), and r(C–C) stand for geometric parameters.)

$CH_3CH_2O\cdot$, the interatomic distance of C–H and the valence angle of H–C–H of the CH_3 group were uniformly taken to be 1.09 Å and 109°28′ for the sake of simplicity.

The method of calculation was a semiempirical INDO, using the integrals and parametrization described in Ref. 3.

Results and Discussion

Methoxyl Radical. The INDO calculations were first performed on $CH_3O\cdot$ with two variables of the bond distances, r(C–O) and r(C–H), and one variable of the valence-bond angle, θ, by changing r(C–O), θ, and r(C–H) in turn.[4] As Table 1 indicates, the set of r(C–O)=1.36 Å, r(C–H)=1.12 Å, and θ=109°28′ give the lowest SCF total energy (E_{SCF}) of $CH_3O\cdot$. The bond angle of θ is in accordance with the usual sp^3 hybrid valence angle, while the bond lengths of r(C–O) and r(C–H) differ appreciably from those (r(C–O)≈1.44 Å[5] and r(C–O)≈1.09 Å[5]) of usual alcohols and carboxylic acids. In particular, the large estimated r(C–H) value of 1.12 Å is distinctive. It may also be seen in Table 1 that the formal charges (Q_A) of +0.240 for C and −0.178 for O give the dipole

Table 1. Changes in total energy and electronic state of $CH_3O\cdot$ as a function of three variables, r(C–O), θ, and r(C–H)

r(C–O)/Å	θ	r(C–H)/Å	E_{SCF}/a.u.	Q_A C	Q_A O	Odd-electron density	μ/D
1.35	109°28′	1.09	−26.6063	+0.242	−0.180	1.037	1.80
1.36	109°28′	1.09	−26.6064	+0.240	−0.180	1.035	1.81
1.37	109°28′	1.09	−26.6060	+0.236	−0.180	1.034	1.82
1.36	109°	1.09	−26.6063	+0.239	−0.181	1.075	1.81
1.36	109°28′	1.09	−26.6064	+0.240	−0.180	1.035	1.81
1.36	110°	1.09	−26.6063	+0.240	−0.179	1.238	1.81
1.36	109°28′	1.11	−26.6101	+0.240	−0.179	1.058	1.79
1.36	109°28′	1.12	−26.6106	+0.240	−0.178	1.056	1.78
1.36	109°28′	1.13	−26.6103	+0.240	−0.177	1.101	1.77

moment (μ) of 1.78 D, working mainly in the direction of the C–O bond axis.

The odd-electron (its density=1.056) is predominantly localized in the following occupied MO, ϕ_{occ}^{odd}:

$$\phi_{occ}^{odd} = 0.734Y_O + 0.112Z_O - 0.358Y_C + 0.456S_{3H} - 0.287S_{4H} - 0.167S_{5H}$$ [6]

while the lowest unoccupied MO, ϕ_{unocc}^{odd}, is also occupied strongly by the oxygen $2p_y$-orbital as:

$$\phi_{unocc}^{odd} = 0.849Y_O + 0.129Z_O + 0.174Y_O + 0.386S_{3H} - 0.248S_{4H} - 0.146S_{5H}$$ [6]

Here, let us illustrate the orbital contour maps of both MOs in Fig. 2 in order to aid understanding of the MOs.

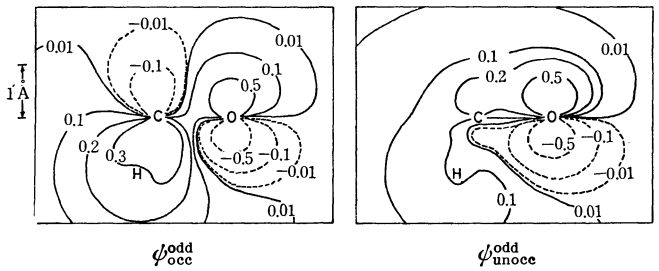

Fig. 2. Orbital Contour Maps of ϕ_{occ}^{odd} and ϕ_{unocc}^{odd} of $CH_3O\cdot$.
(x-y cross-section; solid and dotted curves are positive and negative MO signs respectively.)

Ethoxyl Radical. The INDO calculations were performed further on $CH_3CH_2O\cdot$ with three variables (r(C–O), θ, and r(C–C) in Fig. 1). The computation results with respect to the most energetically stable $CH_3CH_2O\cdot$ are shown in Table 2, together with the results from the CNDO/2 calculations. The bond angle of θ differs by 1°28′ from the sp^3 hybrid valence angle, and the r(C–C) of 1.47 Å is shorter than the usual single C–C bond (~1.54 Å). Moreover, the Q_A values of 2C and O atoms are more positively or negatively charged than those of $CH_3O\cdot$, although the magnitude of the odd-electron density (1.045) is weak in comparison with $CH_3O\cdot$.

With regard to the ionization energies (I_p), the INDO evaluations are relatively large, as we expected, for such open-shell molecules as the $CH_3O\cdot$ and CH_3-$CH_2O\cdot$ radicals as well as for the closed-shell molecules. The I_p values[7] of 0.526 a.u. for $CH_3O\cdot$ and 0.509 a.u. for $CH_3CH_2O\cdot$ differ considerably from those derived from experiments (0.339 a.u.[8] for the former and 0.337 a.u.[9] for the latter).

Finally, it is worthy of emphasis that, in the INDO calculations, the pseudo π orbital consisting of the $2p_z$-orbitals of the C and O atoms is observed in the C–O bond (for instance, see AO populations of the C and O and the bond-orders of the C–O bond in Table 2), as well as that in the iterative extended Hückel calculations.[1]

Table 2. Molecular structure and electronic state of $CH_3CH_2O\cdot$

Minimum E_{SCF}/a.u.		−35.056	(−36.385)
r(C–O)/Å		1.36	(1.36)
r(C–C)/Å		1.47	(1.54[a])
θ/deg.		108	(109°28′[a])
Dipole moment μ/D		1.94	(1.95)
Q_A	O	−0.200	(−0.162)
	2C	+0.262	(+0.158)
	5C	+0.039	(−0.019)
N_O[b]	p_x	1.369	(1.355)
	p_y	1.045	(1.044)
	p_z	1.961	(1.968)
N_C[b]	p_x	−0.8246	(−0.8769)
	p_y	1.001	(1.022)
	p_z	0.9139	(0.9524)
P_{C-O}[c]	p_x–p_x	−0.7504	(−0.7463)
	p_y–p_y	0.2335	(0.2426)
	p_z–p_z	0.2052	(0.1834)

a) Fixed values in the CNDO/2 calculations.
b) AO populations of O and C. c) Bond-orders of C–O. Values in parentheses denote those resulted from the CNDO/2 calculations.

The calculations were carried out on a FACOM 230-60 computer at the Data Processing Center of Kyushu University.

References

1) O. Yamamoto, H. Kato, and T. Yonezawa, *Nippon Kagaku Zasshi*, **91**, 907 (1970).
2) K. Ohkubo and F. Kitagawa, *Nippon Kagaku Kaishi*, **1973**, 2147.
3) J. A. Pople and D. L. Beveridge, "Approximate Molecular Orbital Theory," McGraw-Hill, New York (1970).
4) Strictly speaking, a molecule involving three variables requires 3^2 SCF evaluations for estimating its minimum SCF energy, but the present study did not follow this procedure for the simplicity of computations.
5) L. E. Sutton, editor, "Interatomic Distances," The Chemical Society, London (1958).
6) The notations of Y_O, Y_C, S_{3H}, *etc.* stand for the $2p_y$ of O the $2p_y$ of C, the s of 3H, *etc.* respectively. The eigenvectors below 0.09 were neglected for simplicity.
7) Estimated from the orbital energy of the highest occupied MO.
8) M. S. B. Munson and J. L. Franlkin, *J. Phys. Chem.*, **68**, 3191 (1964).
9) R. R. Bernecker and F. A. Long, *ibid.*, **65**, 1565 (1961).

BULLETIN OF THE CHEMICAL SOCIETY OF JAPAN, VOL. 47 (3), 741—742 (1974)

Very-high-dose-rate Radiolysis of *n*-Butane in the Gas Phase. The Effect of the Addition of Electron Scavengers

Yoshihiko HATANO, Satoshi TAKAO, Hideki NAMBA, Takumi UENO, and Shoji SHIDA

Laboratory of Physical Chemistry, Tokyo Institute of Technology, Meguro, Tokyo 152

(Received June 21, 1973)

Synopsis. The dose rate and its pulse-to-pulse reproducibility of very-high-intensity electron pulses have been measured. The effect of the addition of electron scavengers on the neutralization processes in the gas-phase radiolysis of *n*-butane has been examined by using this very high dose-rate electron pulse.

Several tests on the current waveforms of electron pulses from a high-intensity electron-pulse generator and on the pulse-to-pulse reproducibility of its intensity have been carefully undertaken. The results have shown that this pulsed-electron source gives very high dose rates of about 10^{27} eV g^{-1} s^{-1} with a good reproducibility. These high dose rates must cause some differences in the neutralization processes compared to those in the ordinary γ-radiolysis[1-3] of the lower dose rates. In this note, therefore, the effect of the addition of electron scavengers, SF_6 and N_2O, on the gas-phase radiolysis of *n*-C_4H_{10} under these very high dose rates has been examined. The results were compared with those of the γ-radiolysis.

Experimental

The electron pulses were obtained from a Febetron 706 with a model 5515 electron tube at a charging voltage of 27 kV and a nitrogen pressure of 14.4 atm in it. The current waveform of an electron pulse was measured directly using a Faraday cup bolted to the face of the Febetron electron window. The gap between the fringes of the electron window and of the Faraday cup was covered with aluminum foil to exclude the electromagnetic noise on the oscilloscope. A very small part of the electron beam was admitted through a collection aperture to strike the Faraday cup, which was coupled through a impedance matched attenuator and a cable to the 50Ω-input resistance of a 150 MHz oscilloscope (Tektronix 454 A MOD 163 D), equipped with a self-shield and self-filter for the electromagnetic noise. The signal cable was 4 m long and was equipped with a 50Ω feed-through terminator on each end to avoid any reflection. The display on the oscilloscope was photographed by means of an oscilloscope camera (Tektronix C-30A) equipped with an enhancer ($f=1.9$; image ratio, 0.7; shutter speed, 5 s) with Polaroid Land roll film, 10000 speed/type 410. The shape showed rather a sharp triangle with little noise. From this current shape, the value of 7.6 ns was obtained for the half-duration of the electron pulse, which is about twice as large as the nominal value. The rise time of this overall detection system is definitely less than 7.6 ns.

All the irradiations for dosimetry and pulse radiolysis were done in cylindrical vessels 20 cm long, 3 cm in o.d., 1 mm walls with a 80 μ thick aluminum window on one end, and equipped with an arm for the sample preparations. They were positioned to face the Febetron electron window. The aluminum windows were attached to the vessels by means of epoxy cement. The irradiation of these vessels caused the production of some gases in an amount less than 0.1 μmol. These were identified as H_2, N_2, and CO_2 by gas chromatography and mass spectrometry. These amounts, however, result in little error in this study; therefore, most of the irradiations were done with these vessels. This problem was overcome by soldering a thin film (20 μ) of stainless steel as a window material to a Kovar-to-glass seal. The dosimetry was based on a nitrogen yield of $G(N_2)=12.3$[4] in the radiolysis of N_2O at 800 mmHg. The absorbed dose in *n*-C_4H_{10} was calculated by an appropriate correction for the electron density. The gases were of a very high purity and were used without further purifications except for the usual degassing, the stated purities being *n*-C_4H_{10} (>99.7%), SF_6 (>98%), and N_2O (>99.9%). The products, H_2 and N_2, were measured by gas chromatography using a 5 m column of Molecular Sieve-5A at 60 °C.

Results and Discussion

The pulse-to-pulse reproducibility of an electron-pulse intensity has been examined by using the nitrous oxide dosimetry described above. The results are shown in Fig. 1. From the straight line in Fig. 1, the total dose in N_2O has been found to be $(1.45\pm0.07)\times 10^{19}$ eV g^{-1} $pulse^{-1}$. This corresponds to a mean dose rate of the order of 10^{27} eV g^{-1} s^{-1}. The pulse-to-pulse reproducibility is very excellent, with a maximum deviation of less than 5%; the additivity of the pulses is also excellent.

The fact that the dose rate of the above electron pulses is much higher than those in usual ^{60}Co-γ ray-irradiation facilities invites the following interest. Some new results might be obtained under these very high dose rates, especially in neutralization reactions. About 800 mmHg of *n*-C_4H_{10} has been pulse-radiolyzed at room temperature, and the effect of the addition of SF_6 on the hydrogen yield at the total dose of 8.5×10^{19} eV g^{-1} has been examined. The results are shown

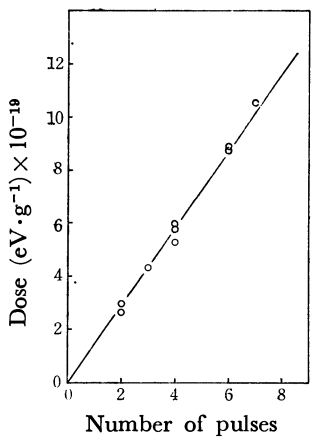

Fig. 1. The total dose as a function of the number of electron pulses.

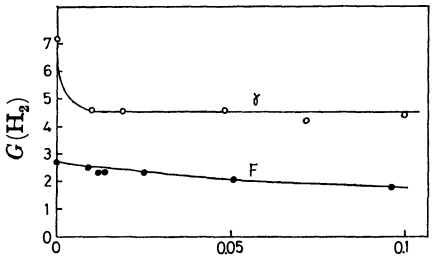

Fig. 2. The effect of the addition of SF_6 on $G(H_2)$ in the gas-phase radiolysis of n-C_4H_{10}.
γ; γ-radiolysis at a dose rate of 1.79×10^{15} eV $g^{-1}s^{-1}$.
F; pulsed electron radiolysis at a dose rate of 2.2×10^{27} eV $g^{-1}s^{-1}$.

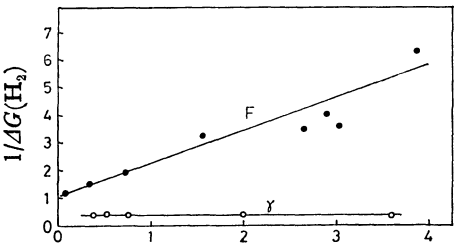

Fig. 3. Reciprocal plot of the decrement in the hydrogen yield *vs.* concentration of SF_6 added.

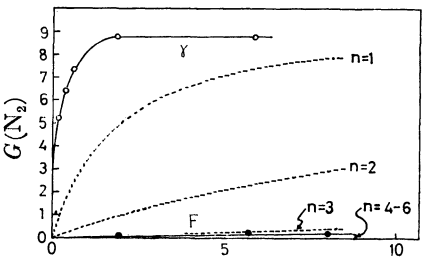

Fig. 4. The effect of the addition of N_2O in the gas-phase radiolysis of n-C_4H_{10}. The dotted lines correspond to the calculated results described in the text.

in Fig. 2, where the results for the same system obtained by γ-ray radiolysis[5] are also presented. The G-value of hydrogen from pulse-radiolyzed n-C_4H_{10} is 2.6, less than one-half of that in the γ-radiolysis of the same system. Figure 2 clearly shows the poor effect of SF_6 on $G(H_2)$, contrary to its very great effectiveness in the γ-radiolysis, where only 0.01 mol% of SF_6 is enough to suppress the neutralization completely. Following the reaction scheme accepted in γ-radiolysis,[1-3] the simple reaction scheme for the ionic processes for the hydrogen formation in the pulsed-electron radiolysis of n-C_4H_{10}–SF_6 mixtures may be depicted as:

$$n\text{-}C_4H_{10} \overset{D}{\rightsquigarrow} M^+ + e^-$$

$$M^+ + e^- \xrightarrow{k_1} H_2 \qquad (1)$$

$$SF_6 + e^- \xrightarrow{k_2} SF_6^- \qquad (2)$$

$$M^+ + SF_6^- \xrightarrow{k_3} \text{no } H_2 \text{ formation} \qquad (3)$$

where M^+ denotes the positive species in the system. Assuming that the steady-state treatment to be applied to this scheme, one may derive the following relation between the decrease in $G(H_2)$ in the presence of SF_6, $\Delta G(H_2)$, and the concentration of SF_6:

$$\frac{1}{\Delta G(H_2)} = \frac{1}{\Delta G_\infty(H_2)} \times \left(1+\frac{k_1[M^+]}{k_2[SF_6]}\right) \qquad (4)$$

with $[M^+]=(100^{-1}G(e^-)D/k_a)^{1/2}$, where $\Delta G_\infty(H_2)$ is the decrease in $G(H_2)$ at an infinite concentration of SF_6, where D is the dose rate in eV $cm^{-3}s^{-1}$, and where k_a is the averaged value of the neutralization rate constants, k_1 and k_3. Since no large significant difference has been observed[6] between them, it may be reasonable to use the k_a value. It can be expected from Eq. (4) to obtain the linear relation between $1/\Delta G(H_2)$ and $1/[SF_6]$ shown in Fig. 3. Good linearities were obtained in both cases, with a very large difference in the slopes. An almost zero slope was obtained in the case of γ-radiolysis. This large difference can be explained in terms of the large difference in the dose rates. If it is assumed in Eq. (4) that the rate constants and the other values are not very different from each other, then the ratio of the slopes is proportional to $D^{1/2}$. The ratio is calculated as high as 10^6, which may explain why the slope in γ-radiolysis is nearly equal to zero.

The effect of the addition of N_2O has also been examined (Fig. 4). Contrary to the large yields of N_2, which are well known in γ-radiolysis, very small yields of N_2 were observed in pulsed-electron radiolysis. This large difference can be explained as in the same way as in the addition of SF_6. The experimental results in Fig. 4 give good linear relationships between $1/G(N_2)$ and $1/[N_2O]$, as expected.[7] The slope in γ-radiolysis being multiplied by 10^n(n=1—6), one can obtain the dotted lines in Fig. 4. The observed yields in pulsed-electron radiolysis are at least below the curve at n=3, and might be near that at n=6. After the correction for the direct radiolysis of N_2O by using $G(N_2)=12.3$ from pure N_2O,[4] the slope becomes slightly less than zero. It is not easy to determine the curve which best fits them. More accurate and reasonable corrections for the direct radiolysis of N_2O are required, as has been suggested for the radiolysis of hydrocarbon solutions of N_2O,[8] in view of the small amount of N_2 formed. There remains, moreover, an important part unexplained—why $\Delta G_\infty(H_2)$ is not equal. More detailed experiments and discussions will be required to the clear and final understanding of the effect of very-high-dose-rate radiolysis.

References

1) S. Shida, N. Fujisaki, and Y. Hatano, *J. Chem. Phys.*, **49**, 4571 (1968).
2) N. Fujisaki, S. Shida, and Y. Hatano, *ibid.*, **52**, 556 (1970).
3) N. Fujisaki, I. Fujimoto, and Y. Hatano, *J. Phys. Chem.*, **76**, 1260 (1972).
4) C. Willis, A. W. Boyd, and O. A. Miller, *Rad. Res.*, **46**, 428 (1971).
5) The addition of SF_6 at higher concentration than 0.1 mol% has already been reported.[3]
6) S. G. Lias, R. E. Rebbert, and P. Ausloos, *J. Chem. Phys.*, **57**, 2080 (1972).
7) K. Okazaki, R. Yugeta, and S. Sato, This Bulletin, **46**, 2066 (1973).
8) Y. Hatano, K. Takeuchi, and S. Takao, *J. Phys. Chem.*, **77**, 586 (1973).

BULLETIN OF THE CHEMICAL SOCIETY OF JAPAN, VOL. 47 (3), 743—744 (1974)

The Effect of Copper(II) on the Formation and Thermal Change of Synthetic β-FeOOH

Katsuya INOUYE, Hiroyuki IMAMURA, Katsumi KANEKO, and Tatsuo ISHIKAWA

Department of Chemistry, Faculty of Science, Chiba University, Chiba 280

(Received July 10, 1973)

Synopsis. The effect of Cu(II) added to β-FeOOH in various ratios up to 6% Cu/Fe was examined by X-ray diffraction, electron microscope, BET surface area, DTA, TGA and chemical analyses. Differing from other cases reported previously, Cu(II) showed no effect, but thermal changes of the Cu-doped samples indicated a reinforcement of bonding by Cu.

In order to obtain a more definitive fundamental elucidation of the role of copper added to anti-weathering steels, which have been widely recognized to be appreciably anti-corrosive in atmospheric and, perhaps in a lesser extent, marine environments, the present authors have examined the effect of Cu(II) doped in every component of the corrosion product. These studies have covered the following cases: oxide-oxyhydroxide mixtures produced by the air oxidation of $Fe(OH)_2$,[1,2] magnetite from mutual interaction between $Fe(OH)_2$ and $Fe(OH)_3$ colloids,[3] magnetite from the self-decomposition of $Fe(OH)_2$[4] and α-FeOOH produced by the hydrolysis of a Fe(III)-sulfate solution.[5] The explanation of the phenomena observed as the copper effects is by no means simple, but it appears plausible to conclude that Cu(II) invariably impedes the formation and growth of those oxides and/or oxyhydroxides.

The present study is concerned with an examination of the similarly-expected copper effect on the crystallization of β-FeOOH, together with some thermal changes in Cu-doped β-FeOOH. It is interesting to note that β-FeOOH, as one of the corrosion products of iron-base alloys, is produced only when the Cl^- ion (or possibly other halide ions) is present and further, that the β-FeOOH crystal embraces chlorine as a genuine component.[6-8] It thus appears that the behavior of chlorine is an essential problem in any case involving the characteristics of β-FeOOH.

β-FeOOH was prepared from solutions of 0.2 M $FeCl_3$ added by 0.2 M $CuCl_2$ in 0, 1, 2, 3, 4, 5, and 6 Cu/Fe atomic % through hydrolysis with and without the addition of urea (30 g per 500 ml of a mixed solution) at 95—99 °C for 5 hr; up to this temperature range the solution was warmed at the rate of 1 °C/min. When aged, the suspension was kept at 30± 0.5 °C for various times up to 10, 20, 30, and 50 days. During the aging procedure, the pH values of the suspensions were kept at 7.5—8.0 with daily stirring. The suspensions were then filtered, and the crystals thus obtained were washed thoroughly with distilled water and dried at 80 °C for 2 hr.

The Fe, Cu, and Cl contents were conventionally determined after dissolving β-FeOOH in HCl by $K_2Cr_2O_7$ titration, by colorimetry in the presence of Cupferazone, and by Volhard method respectively, based on the crystal dried at 105—110 °C for 1 hr. Correction for the co-existing Cu(II) on Fe determination was done by means of a calibration curve. X-Ray diffraction, BET surface area determination, electron microscopy, differential thermal analysis (DTA), and thermal gravimetric analysis (TGA) were carried out by procedures similar to those described in preceding reports.[3-5,7,8]

It is noteworthy, first, that any Cu(II) over 6% Cu/Fe added to the original solution is excluded from the precipitates into medium during the course of hydrolysis, though the reason why 6% is the limit has not yet been understood.

The electron micrographs of each sample, with or without addition of Cu(II) and after aging at 30 °C for various durations, showed almost identical rod-like crystals approximately $1.8—1.9\times10^{-5}$ cm in length. The specific BET surface area measurements also gave almost identical values, ranging from 41 to 51 m^2/g. X-Ray diffraction patterns were exactly the same, irrespective of the variation in Cu content and aging time. There is no recognizable shift in any diffraction peak of the samples with different amounts of Cu present. The crystallite size calculated showed no appreciable variation with regard to the Cu content and aging time, giving values mostly in the range of 250—290 Å.

These results were inconceivable on the basis of our knowledge of previous experimental results, which indicated comprehensively that Cu is more or less destructive in the formation of oxyhydroxides or oxides. The disappearance of the Cu effect in the present case was thought at first to be possibly due to the presence of urea in the hydrolysis because of the homogeneous precipitation. The preparation of β-FeOOH without

Table 1. Chemical composition of β-FeOOH

Aging time (day)	Cu/Fe, intended (%)	Cu/Fe, analyzed (%)	Cl/Fe, analyzed (%)	Cl/(Fe+Cu), calculated (%)
0	0	0.0	8.2	8.2
	1	0.9	8.2	8.1
	3	2.9	8.7	8.4
	6	5.8	9.2	8.7
20	0	0.0	8.7	8.7
	1	0.9	8.9	8.8
	3	3.1	9.3	9.0
	6	5.2	9.3	8.8
50	0	0.0	8.3	8.3
	1	0.8	8.8	8.7
	3	2.8	9.1	8.8
	6	5.5	9.0	8.5

the addition of urea under conditions otherwise the same was attempted in order to confirm the effect of urea. The X-ray diffraction patterns and other examinations of the resultant crystals showed them to be entirely identical with those which came out of suspensions upon the addition of urea.

The chemical analyses of each sample give us the Cu/Fe and Cl/Fe atomic ratios which are tabulated in Table 1. It seems that in crystals Fe is replaced by Cu at each intended ratio, except in the cases of 6% Cu/Fe, when only somewhat lower ratios were obtained. As for the Cl/Fe atomic ratio, values were observed in only the limited range of 8—9%, although a slight increase with the rise in the Cu/Fe ratio was observed. However, a constant Cl content was obtained by calculating Cl/(Fe+Cu). It is thus implied that Cl interacts not only with the Fe but also with the Cu included in the crystal.

According to Mackay,[6] β-FeOOH has the α-MnO_2 or hollandite ($BaMn_8O_{16}$) structure in a tetragonal system with a=10.48 Å and c=3.023 Å. Channels parallel to the *c*-axis are contained in crystals, where Cl^- and H_2O can be accomodated and sometimes mutually exchanged. In other words, the β-FeOOH structure is like a bundle of fine tubes, the walls of which are composed of O^- and OH^- ions surrounding the Fe^{3+}. Each Fe^{3+} is surrounded octahedrally by six (O^-, OH^-) ions. The octahedra are linked to form tubes parallel to the *c*-axis, sharing edges and some corners of the octahedra. In this context, therefore, it may be concluded that β-FeOOH crystals are so strongly stabilized by the presence of Cl^- that the destructive action of replacing Cu does not show up.

TGA curves in Fig. 1 on pure β-FeOOH and the 6% Cu/Fe sample illustrate the difference in the temperature region where the weight loss increases steeply, corresponding to the evolution of $FeCl_3$ sublimed, accompanied by a transformation of β-FeOOH to α-Fe_2O_3.[7,8] The shift in the "decomposition temperature" with the Cu indicates an increase in the bonding in the Cu-doped crystals. From the DTA curves in Fig. 2, we can conceive a bonding between the Cu added and the Cl constitutionally present. After the evolution of H_2O and the degradation of the β-FeOOH crystals to an amorphous state below 300 °C, a rather sudden recrystallization to α-Fe_2O_3 occurs at the temperatures characteristic of the Cu content; the recrystallization temperature corresponds to the sharp exothermic DTA peak, which shifts to higher temperatures proportionally with the increase in the Cu/Fe ratio. It is noted further that shallow endothermic DTA peaks appear in Fig. 2 just below 500 °C, presumably as a result of the melting of the resulting $CuCl_2$ (mp 498 °C).

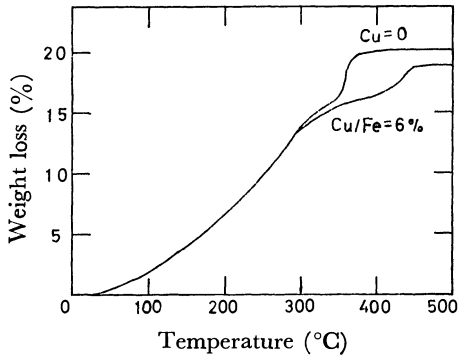

Fig. 1. TGA curves of β-FeOOH with 6% Cu/Fe and without addition of Cu.

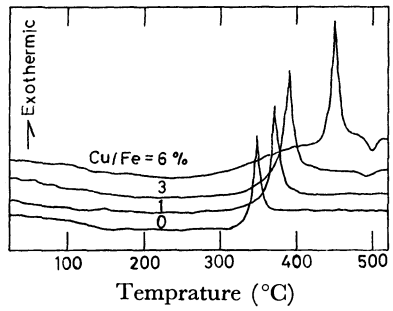

Fig. 2. DTA curves showing the shift of exothermic peaks.

All the facts observed seem to coincide with the unexpectedly high consistency of β-FeOOH crystals doped with Cu(II), if one accepts that it is likely to produce an interaction between Cu and Cl.

This work has been partly supported by the Government Science Research Fund of the Ministry of Education.

References

1) K. Inouye, *J. Colloid Interface Sci.*, **27**, 171 (1968).
2) K. Inouye and T. Ishikawa, *Corrosion Engineering, Japan*, **20**, 460 (1971).
3) K. Inouye, T. Hozumi, and T. Ishikawa, *Kolloid-Z. Z. Polym.*, **250**, 262 (1972).
4) K. Inouye, K. Murata, and T. Ishikawa, *Z. Anorg. Allg. Chem.*, **386**, 340 (1971).
5) K. Inouye, S. Ishii, K. Kaneko, and T. Ishikawa, *ibid.*, **391**, 86 (1972).
6) A. L. Mackay, *Miner. Mag.*, **32**, 545 (1960).
7) T. Ishikawa and K. Inouye, This Bulletin, **45**, 2350 (1972).
8) T. Ishikawa and K. Inouye, Paper presented at the 25th Symposium of Colloid and Interface Chem., Chem. Soc. Jap., Nov., 1972.

BULLETIN OF THE CHEMICAL SOCIETY OF JAPAN, VOL. 47 (3), 745—746 (1974)

Flash-Spectroscopic Study of Phthalazine[1)]

Nobuaki KANAMARU,* Saburo NAGAKURA,** and Katsumi KIMURA

Physical Chemistry Laboratory, Institute of Applied Electricity, Hokkaido University, Sapporo 060

***The Institute for Solid State Physics, The University of Tokyo, Minato, Tokyo 106*

(Received July 19, 1973)

Synopsis. The phthalazine triplet and the hydrogen-abstracted radical were obtained in ethanol *etc.* at room temperature, suggesting that the T_1 is of $n\pi^*$ type, whereas only the T–T absorption spectrum was obtained in acidic ethanol as reported in EPA glass at 77 K.

The lowest triplet states of hetero-cyclic aromatic compounds containing nitrogen are known to be mostly of the $\pi\pi^*$ type.[2)] Azobenzenes containing more than two nitrogen atoms, however, have been concluded to have the lowest excited triplet states of the $n\pi^*$ type from several spectroscopic studies on T←S transitions in gas phase as well as on phosphorescence in rigid glasses.[3)]

Hetero-polycyclic aromatic compounds containing nitrogen have also received much attention in connection with the assignment of the lowest excited singlet and triplet states.[2)] Phosphorescence and triplet-triplet (T–T) absorption studies[2,4–8)] of some hetero-polycyclic compounds in EPA glasses at 77 K have indicated that their lowest triplet states are of the $\pi\pi^*$ type at least in the 77 K EPA glasses. Phthalazine is one of typical examples in which a large interaction between two adjacent nitrogen atoms might cause the $^3n\pi^*$ state to be the lowest triplet. Recently, Baba *et al.*[7)] have concluded from phosphorescence and phosphorescence-polarization studies that the phosphorescent state of phthalazine should be of $^3B_2(\pi\pi^*)$ in EPA glass at 77 K. The $^3n\pi^*$ and $^3\pi\pi^*$ states of phthalazine are thought to be so close that the order of these two energy levels might be dependent on solvent and temperature. It is still unknown which state $^3n\pi^*$ or $^3\pi\pi^*$ is the lowest in solution at room temperature.

Since no flash photolysis studies have been reported for phthalazine in solution at room temperature, we have attempted to carry out flash photolysis experiments with a variety of solutions of phthalazine, with particular emphasis on studying the solvent effects of transient species.

Experimental

Flash experiments at room temperature were carried out with degassed solutions containing 10^{-4}—10^{-5} M phthalazine in ethanol, ether, *n*-hexane, benzene and acidic ethanol, 20 cm quartz cells being used. Low-temperature flash experiments were performed at 77 K in rigid glasses of a mixture of ether, isopentane and alcohol (EPA, 5 : 5 : 2) and a mixture of methylcyclohexane and isopentane (MP, 1 : 1) with a 1 cm quartz cell immersed in liquid nitrogen. The flash spectroscopic apparatus used here was the same as that described previously.[9)] Phthalazine was purchased from Aldrich Chemical Co. and purified by vacuum sublimation. Ethanol, ether, isopentane, *n*-hexane and benzene were purified by usual methods.[10)]

* Present address: Department of Chemistry, Wayne State University, Detroit, Michigan, U.S.A.

Results and Discussion

The transient absorption spectra obtained by the flash photolysis of phthalazine (10^{-4}—10^{-5} M) in ethanol, ether, *n*-hexane and benzene at room temperature are shown by curves a—d in Fig. 1 and that obtained for an acidic ethanol solution of 1×10^{-2} M phthalazine by curve e. The transient absorptions were observed only under degassed condition immediately after flash, a considerable amount of photoproducts being finally obtained. Each transient spectrum shown in Fig. 1 was obtained by subtracting the spectrum measured a few minutes after flash from that immediately after flash. The shorter wavelength parts of the spectra shown by broken lines are suffered from the absorption of the phthalazine molecule in the ground state. Thus, the absorption intensity in this region is somewhat smaller than the true value.

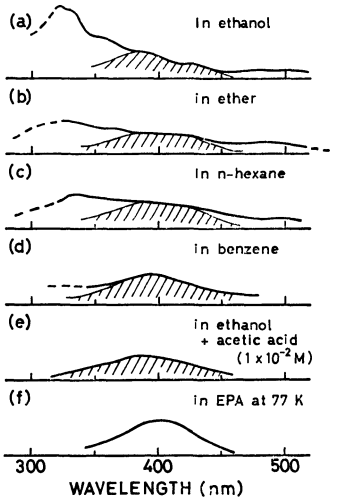

Fig. 1. Transient absorption spectra obtained for photoirradiated phthalazine. Curves a–e were obtained at room temperature under degassed condition with 20 cm quartz cells. Shaded portions indicate the absorption bands due to T-T transition. Concentrations of phthalazine: (a) 3×10^{-5}M; (b, c) 5×10^{-5}M; (d, e) 1×10^{-4}M. Curve f was obtained in EPA glass at 77 K, with a 1 cm quartz cell.

The flash photolysis of phthalazine in the EPA glass at 77 K gave rise to a transient spectrum shown by curve f in Fig. 1. In an MP glass at 77 K, the transient absorption was too weak to obtain a well-defined spectrum. The lifetime of the transient 390 nm band in the EPA glass was found to be roughly consistent with

the available phosphorescence lifetime of phthalazine (0.4 s).[7] Furthermore, the transient spectrum (curve f in Fig. 1) is in good agreement with the T–T absorption spectrum recently obtained by Alvarez and Hadley[11] in a rigid matrix of *n*-butanol and isopentane at 77 K and by Yamazaki and Baba[12] with a laser flash technique in EPA at 77 K. Therefore, there may be no doubt that the 77 K spectrum obtained here is due to the T–T transition of phthalazine.

As seen from Fig. 1, the transient spectra obtained in benzene and acidic ethanol solutions (spectra d and e) seem to differ considerably from those in ethanol, ether and *n*-hexane (spectra a—c), and are similar to the T–T spectrum of phthalazine (curve f). Thus, spectra d and e may be mainly due to the phthalazine triplet. As revealed from its shape, spectrum d may have a minor contribution of another transient species.

The transient spectra obtained with the ethanol, ether and *n*-hexane solutions at room temperature (curves a—c in Fig. 1) indicate the existence at least two sorts of transient species. The absorption intensities in the range 380 to 450 nm are independent of the solvents used, whereas those in the two ranges 300—380 and 450—520 nm considerably depend on the solvents. According to the time-resolved spectrophotographs obtained in the present study, the 380—450 nm bands decay much faster than the 300—380 nm and 450—520 nm bands: The 380—450 nm bands were detected only within several μs, whereas the 300—380 and 450—520 nm bands were observed until about 100 μs. Therefore, we may conclude that there exists another transient species in ethanol, ether and *n*-hexane, in addition to the triplet phthalazine.

The order of the yield of the transient species with the bands at 300—380 nm and 450—520 nm is:

$$n\text{-hexane} < \text{ether} < \text{ethanol}$$

This order seems to be correlated with the hydrogen-donating ability of the solvents. By adding acetic acid (1×10^{-2} M) to the ethanol solution, the ability of hydrogen abstraction of phthalazine is expected to be reduced significantly, since the nature of its lowest triplet excited state is changed by protonation from the $n\pi^*$ type to the $\pi\pi^*$ one. (It should be mentioned that the absorption spectrum of the ground state phthalazine in an acidic ethanol solution containing more than 10^{-3} M acetic acid shows no absorption corresponding to the $n\pi^*$ band of the ethanol solution of phthalazine appearing at about 330 nm, although this fact gives no direct information as to the triplet-state energy levels.) The $n\pi^*$ state of phthalazine is considered to have a greater ability of hydrogen abstraction than the $\pi\pi^*$ state, as is well known with carbonyl compounds.[13,14]

The experimental facts presented here concerning the second transient species may be explained by considering that this species is ascribed to the 2-hydrophthalazyl radical. It is interesting to note that the transient bands appearing at 330 and 480 nm resemble those of the naphthalene anion radical showing absorption maxima at 370 and 450 nm.[15] This fact strongly supports the assignment of the second species to the 2-hydrophthalazyl radical, which is isoelectronic to the naphthalene anion in π-electron structure. Judging from the short lifetimes (a few μs) of the T–T bands observed in ethanol, ether, *n*-hexane and benzene at room temperature, we may conclude that the lowest triplet states of phthalazine are of the $n\pi^*$ type but the lowest $\pi\pi^*$ and $n\pi^*$ triplet states are close to each other and mix to a considerable extent.

The present authors wish to express their sincere thanks to Professor H. Baba and Dr. I. Yamazaki for their helpful discussions.

References

1) This study was partly submitted as a doctor thesis to the University of Tokyo by one of the authors (N.K.), 1968.
2) S. P. McGlynn, T. Azumi, and M. Kinoshita, "Molecular Spectroscopy of the Triplet States," Prentice-Hall, Englewood Cliffs, New Jersey (1969).
3) For reviews, see, K. K. Innes, J. P. Byrne, and I. G. Ross, *J. Mol. Spectrosc.*, **22**, 125 (1967); M. Sundbom, *Acta Chem. Scand.*, **25**, 487 (1971).
4) D. P. Craig and I. G. Ross, *J. Chem. Soc.*, **1954**, 1589.
5) B. R. Henry and M. Kasha, *J. Chem. Phys.*, **44**, 411 (1966).
6) P. Loustauneau and G. Nouchi, *C. A. Rcad. Sci., Paris*, **261**, 4693 (1966).
7) H. Baba, I. Yamazaki, and T. Takemura, *Spectrochim. Acta*, **27A**, 1271 (1971).
8) R. Li and E. C. Lim, *J. Chem. Phys.*, **57**, 605 (1972).
9) N. Kanamaru and K. Kimura, *Mol. Photochem.*, in press (1973).
10) A. Weissberger and E. S. Proskauer, "Technique of Organic Chemistry Vol. VII, Organic Solvents," Interscience Publishers, Inc. (1935).
11) V. L. Alvarez and S. G. Hadley, *J. Phys. Chem.*, **76**, 3937 (1972).
12) I. Yamazaki, Ph. D. Dissertation, Hokkaido University, 1973; I. Yamazaki and H. Baba, to be published.
13) N. J. Turro, "Molecular Photochemistry," Benjamin, Inc. (1965).
14) T. S. Godfrey, G. Porter, and P. Suppan, *Discuss. Faraday Soc.*, **39**, 194 (1965).
15) P. Balk, G. T. Hoijtink, and J. W. H. Schreurs, *Rec. Trav. Chem. Pays-Bas*, **76**, 813 (1957); T. Shida and S. Iwata, *J. Amer. Chem. Soc.*, **95**, 3473 (1973).

BULLETIN OF THE CHEMICAL SOCIETY OF JAPAN, VOL. 47 (3), 747—748 (1974)

A Solvent-Extraction Study of Zinc(II) Complexes with Several Divalent Anions of Carboxylic and Inorganic Acids

Hiromitsu MORIYA and Tatsuya SEKINE

Department of Chemistry, Science University of Tokyo, Kagurazaka, Shinjuku-ku, Tokyo 165

(Received August 3, 1973)

Synopsis. Stability constants of zinc(II) mono- and biscomplexes with C_2 to C_6 dicarboxylic acids and with sulfate, thiosulfate and selenate ions determined at 25 °C by solvent extraction are described. The stability order of the dicarboxylate complexes decreases in an order of $C_2>C_3>C_4\simeq C_5\simeq C_6$ whereas that of the inorganic acids are nearly similar.

In previous papers of the present authors, the stability constants of zinc(II) with thiocyanate,[1] halide,[2] and monocarboxylate[3] ions in sodium perchlorate media at 25 °C have been determined. In the present paper, a further determination of the stability constants of zinc(II) complexes with several divalent anions has been made in 1 M sodium perchlorate media at 25 °C, using a chelate extraction method with β-isopropyltropolone (IPT).

Experimental

All the experiments were done in a thermostated room at 25±0.3 °C in a way similar to that described in the previous papers.[1-4] Ghe initial concentration of the zinc(II) in the aqueous phase was 1×10^{-6} M. Ghe aqueous phase in some experiments was buffered with acetate (the initial aqueous concentration was 0.01 M). It was confirmed that at this concentration the buffer has no effect on the extraction of zinc(II). Ghe dissociation constants of certain dicarboxylic acids were determined by the method described by Speakman.[5]

Results and Discussion

The statistical treatment of the experimental data was the same as in the previous papers.[1-3]

$$\beta_n = [ZnL_n^{2-2n}][Zn^{2+}]^{-1}[L^{2-}]^{-n} \quad (1)$$

The extraction of zinc(II) with IPT (HA) is generally written as:[6]

$$Zn^{2+} + 2HA(org) \rightleftarrows ZnA_2(org) + 2H^+ \quad (2)$$

$$ZnA_2(org) + HA(org) \rightleftarrows ZnA_2HA(org) \quad (3)$$

$$D_0 = ([ZnA_2]_{org}+[ZnA_2HA]_{org})/[Zn^{2+}] = K_{ex0}[HA]_{org}^2[H^+]^{-2}(1+K_{org}[HA]_{org}) \quad (4)$$

where K_{ex0} and K_{org} are the equilibrium constants for the reactions in Eqs. (2) and (3) respectively. When the concentration, $[HA]_{org}$, is kept constant in a series of experiments, Eq. (4) can be rewritten as:

$$D_0[H^+]^2 = K_0 \quad (5)$$

where $K_0=K_{ex0}[HA]_{org}^2(1+K_{org}[HA]_{org})$. It was confirmed that the value of K_0 is constant, at least when $D_0<10$ (K_0 is $10^{-11.76}$, $10^{-10.44}$, or $10^{-8.39}$ when $[HA]_{org}$ is 5.0×10^{-3} M, 2.0×10^{-2} M, or 1.0×10^{-1} M respectively). The distribution ratio when zinc(II) forms complexes with the L^{2-} is written as follows if the $[HA]_{org}$ value is also kept the same:

$$D = ([ZnA_2]_{org}+[ZnA_2HA]_{org})/([Zn^{2+}]+[ZnL]+[ZnL_2^{2-}]+\cdots) \quad (6)$$

and from Eqs. (1), (5), and (6):

$$D[H^+]^2K_0^{-1} = (1+\beta_1[L^{2-}]+\beta_2[L^{2-}]^2+\cdots)^{-1} \quad (7)$$

It was confirmed that the distribution ratio at a certain ligand concentration is proportional to $[H^+]^{-2}$ with all the ligands studied; thus, it was concluded that Eq. (7) can be used for the analysis of the experimental data.

Figures 1 and 2 show the decrease in the zinc(II) extraction as a function of the ligand-anion concentration in the aqueous phase. The ranges of the hydrogen-ion concentration in the aqueous phase were $10^{-6.1}$—$10^{-6.8}$ M (divalent carboxylate), $10^{-3.6}$—$10^{-3.7}$ M (sulfate), and $10^{-4.5}$—$10^{-5.2}$ M (selenate and thiosulfate), and the association of the ligand anion with protons in these hydrogen-ion concentration ranges was corrected by using the acid dissociation constants in Table 1 and in Ref. 8. Since the relative concentration of the HL^--type anion is rather low (the protonated species of oxalate and the inorganic ligand anions were negligible whereas the contributions of the HL^- and H_2L species were 7 and 0.2% respectively at the maximum for the other divalent carboxylate ligands), and since the stability constants of the complexes containing the HL^--form ligand may be much smaller than those for the ZnL and ZnL_2^{2-} complexes, as has been reported by, for example, Ostacoli and his co-workers,[9] the formation of such species as $ZnHL^+$ could be excluded from consideration. On these assumptions, the data in the figures were analyzed graphically and the stability constants listed in Tables 1(a) and 1(b) were obtained. The solid curves in the

Table 1. Stability constants

(a) Carboxylate complexes[a]

Ligands	pK_{a1}	pK_{a2}	$\log\beta_1$	$\log\beta_2$
Oxalate	—	3.54[b]	3.42	6.16
Malonate	2.68	5.15	2.47	3.80
Succinate	3.97	5.13	1.48	2.00
Glutarate	4.18	4.94	1.25	1.74
Adipate	4.29	4.97	1.23	1.78

(b) Sulfate, thiosulfate and selenate complexes[c]

Ligands	$\log\beta_1$	$\log\beta_2$
Sulfate	0.69	1.48
Thiosulfate	0.62	2.28
Selenate	0.73	1.38

a) The organic phase was chloroform containing 2×10^{-2}M IPT (oxalate) or containing 5×10^{-3}M IPT (the others). b) Ref. 7. c) The organic phase was chloroform containing 1×10^{-1}M IPT.

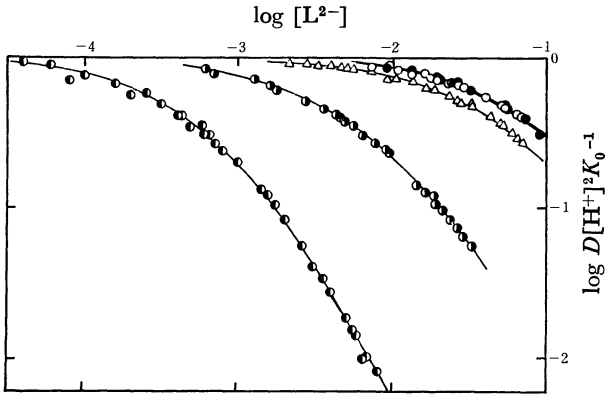

Fig. 1. Decrease in the IPT extraction of Zn(II) as a function of the ligand concentration. Org. phase: $CHCl_3$ containing 2×10^{-2}M IPT for oxalate and 5×10^{-3}M IPT for others. Aq. phase: 1M $Na(\frac{1}{2}L^{2-}, ClO_4^-)$ where L^{2-} is oxalate (◐), malonate (◑), succinate (△), glutarate (○), and adipate (●). The solid curves were drawn by using the following equation in which K_0 is defined by Eq. (5) and the values are given in the text; $\log D[H^+]^2K_0^{-1} = -\log(1+\beta_1[L^{2-}]+\beta_2[L^{2-}]^2)$.

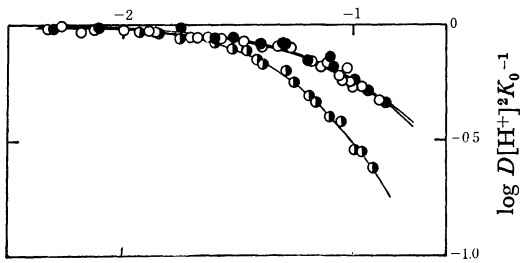

Fig. 2. Decrease in the IPT extraction of Zn(II) as a function of the ligand concentration. Org. phase: $CHCl_3$ containing 1×10^{-1}M IPT. Aq. phase: 1M $Na(\frac{1}{2}L^{2-}, ClO_4^-)$ where L^{2-} is sulfate (●), thiosulfate (◑), and selenate (○). The solid curves were drawn by using the following equation in which K_0 is defined by Eq. (5) and the values are given in the text; $\log D[H^+]^2K_0^{-1} = -\log(1+\beta_1[L^{2-}]+\beta_2[L^{2-}]^2)$.

figures were drawn by introducing these constants into Eq. (7).

There have been several literature values of the stability constants of zinc(II) complexes with these dicarboxylate ions,[9-15] but these stability constants were determined at lower ionic concentrations; furthermore, only a few data are available on the ZnL_2^{2-}-type.

Schwarzenbach and his co-workers[16-19] pointed out that the stability is the greatest with complexes having a five-membered chelate ring, it is less with those having a six-membered ring, and it reaches almost a constant value even when the member of the CH_2 group increases more. Such a tendency was also found with zinc(II) complexes with these divalent carboxylate ligands.[11-13]

This tendency may also be observed in the present results (Table 1(a)). It is remarkable that the same tendency can also be found among the second complexes, as may also be seen in Table 1(a). The β_2 values for the zinc(II) complexes with oxalate and malonate previously reported also show such a decrease with the increase in the member of the ring.[13] The tendency for the stabilities of the complexes with succinate, glutarate, and adipate to be similar to each other has been explained by previous workers[11,16-19] on the assumption that more members than seven is too large a number to form a stable chelate ring with the metal ion. The present results also seem to support this concept.

There have been some literature values of the stability constants of zinc(II) complexes with sulfate,[20] thiosulfate,[21,22] and selenate[23] ions. However, since the ionic concentrations in the literature (0 to 0.05 M) are different from that in the present study, a comparison of the values under different conditions is difficult.

References

1) H. Moriya and T. Sekine, This Bulletin, **44**, 3347 (1971).
2) H. Moriya and T. Sekine, *ibid.*, **45**, 1626 (1972).
3) H. Moriya and T. Sekine, *ibid.*, **46**, 1178 (1973).
4) T. Sekine, M. Isayama, S. Yamaguchi, and H. Moriya, *ibid.*, **40**, 27 (1967).
5) J. C. Speakman, *J. Chem. Soc.*, **1940**, 855.
6) T. Sekine and D. Dyrssen, *J. Inorg. Nucl. Chem.*, **26**, 1726 (1964).
7) T. Sekine, *Acta Chem. Scand.*, **19**, 1476 (1965).
8) L. G. Sillén and A. E. Martell, "Stability Constants," spec. pub. no. 17, The Chemical Society, London (1964).
9) G. Ostacoli, A. Vanni, and E. Roletto, *Scienze Chimiche*, **38**, 318 (1968).
10) R. K. Cannan and A. Kibrick, *J. Amer. Chem. Soc.*, **60**, 2314 (1938).
11) M. Yasuda, K. Yamasaki, and H. Ohtaki, This Bulletin, **33**, 1067 (1960).
12) D. L. G. Rowlands and C. B. Monk, *Trans. Faraday Soc.*, **62**, 945 (1966).
13) C. E. Evans and C. B. Monk, *ibid.*, **66**, 1491 (1970).
14) J. Schubert, E. L. Lind, W. M. Westfall, R. Pelger, and N. C. Li, *J. Amer. Chem. Soc.*, **80**, 4799 (1958).
15) A. McAuley, G. H. Nancollas, and K. Torrance, *Inorg. Chem.*, **6**, 136 (1967).
16) G. Schwarzenbach and H. Ackermann, *Helv. Chim. Acta*, **31**, 1029 (1948).
17) G. Schwarzenbach, B. Maissen, and H. Ackermann, *ibid.*, **35**, 2334 (1952).
18) G. Schwarzenbach and G. Anderegg, *Z. Anorg. Alleg. Chem.*, **282**, 286 (1955).
19) G. Schwarzenbach, H. Senn, and G. Anderegg, *Helv. Chim. Acta*, **40**, 1886 (1957).
20) B. B. Owen and R. W. Gurry, *J. Amer. Chem. Soc.*, **69**, 3074 (1938).
21) F. G. R. Gimblett and C. B. Monk, *Trans. Faraday Soc.*, **51**, 793 (1958).
22) L. V. Nazarova, T. M. Efamova, and S. I. Orenshtein, *Zh. Neorg. Khim.*, **17**, 357 (1972).
23) W. H. Banks, *J. Chem. Soc.*, **1934**, 1010.

BULLETIN OF THE CHEMICAL SOCIETY OF JAPAN, VOL. 47 (3), 749—750 (1974)

The Migration of Electronic Excitation Energy in Copolymers of *N*-Vinylcarbazole with a Small Content of Styrene or Vinyl Acetate[1]

Kenichi OKAMOTO,* Akikazu YANO,** Shigekazu KUSABAYASHI,* and Hiroshi MIKAWA

Department of Applied Chemistry, Faculty of Engineering, Osaka University, Yamadakami, Suita, Osaka 565

(Received August 9, 1973)

Synopsis. The migration of electronic excitation energy in films of copolymers rich in *N*-vinylcarbazole has been studied by fluorescence quenching experiments using dimethyl terephthalate and perylene as guest molecules. The efficiency of the singlet exciton migration is almost the same for the copolymers and for poly-*N*-vinylcarbazole.

The present authors have reported on the significant decrease in the photocurrent in the copolymers of *N*-vinylcarbazole(VCz) with a small content of styrene (St) or vinylacetate(VAc).[1] For understanding this phenomenon, the efficiency of the migration of the electronic excitation energy in the copolymer films should be compared with the efficiency in a PVCz film.

The migration of the electronic excitation energy in a PVCz film has been studied by Schneider[2] and by Klöpffer.[3] Klöpffer has concluded that the energy transfer in a PVCz film occurs by means of the exciton migration mechanism.

Dimethyl terephthalate (DMTP) is a weak electron acceptor and interacts with a carbazole (Cz) chromophor to produce an exciplex which emits a broad fluorescence at 21000 cm^{-1}.[6] The single-step (dipole-dipole resonance) energy transfer from a Cz chromophor to a DMTP molecule is impossible, because DMTP has no absorption in the wavelength region longer than 300 mμ. DMTP is, therefore, expected to be useful in studying the efficiency of the singlet exciton migration.

Experimental

The polymers were prepared by a method similar to that described perviously.[1] The molecular weights of the polymers ranged from 7000 to 100000. DMTP and perylene were purified by repeated recrystallizations and then by vacuum sublimation. A spectrophotofluorometer was constructed using a high-intensity grating monochrometor equipped with a 1P 28 photomultiplier. The light from a 500W super-high-pressure mercury lamp was monochromatized by means of interference filters and then used for excitation. The emission spectra were measured with 90° excitation at 20 °C in the air and corrected using quinine sulfate and β-naphthol. A film (1 μ thick) was cast onto a quartz plate from a benzene solution and dried at 50 °C *in vacuo*.

Results and Discussion

Figure 1 shows the fluorescence spectra of the VCz–St copolymers in solution. The copolymers rich in VCz show almost the same fluorescence spectra as that of PVCz. With a decreasing VCz content, the excimer fluorescence (I_E) is reduced and the monomer fluorescence (I_M) is enhanced. The I_E/I_M ratio in the VCz–St copolymer is much smaller than that in the VCz–VAc copolymer with the same VCz content, as is shown in Fig. 2. From the monomer reactivity ratio,[5] the VCz sequence in the former is considered to be much shorter than that in the latter. Furthermore, the I_E/I_M value in the alternate VCz–fumaronitrile copolymer[6] is less than 0.1, as is shown by a cross mark in Fig. 2; this is much smaller than the corresponding value (0.4) in the VCz–St copolymer. These results suggest that excimer formation in a dilute solution of PVCz and of the VCz copolymers is mainly between nearest neighboring chromophores in a polymer chain rather than between far-distant neighboring ones.

The host-sensitized energy transfer in films of PVCz and of copolymers rich in VCz doped with DMTP or perylene was investigated. The fluorescence spectra of the films doped with DMTP are shown in Fig. 3.

According to the hopping model of exciton migration, the quenching factor of the host (monomer and excimer) fluorescence (Q_H) can be expressed by Eq. (1), in a way similar to that of the excimer fluorescence (Q_E) in Ref. 3, when that of the monomer fluorescence (Q_M) due to excimer-forming sites is much larger than unity:

$$Q_H = C/C_E \quad (1)$$

where C and C_E are the concentrations of the guest and the excimer-forming site (mol/mol VCz unit).

The values of Q_H were calculated from Eq. (2):[3]

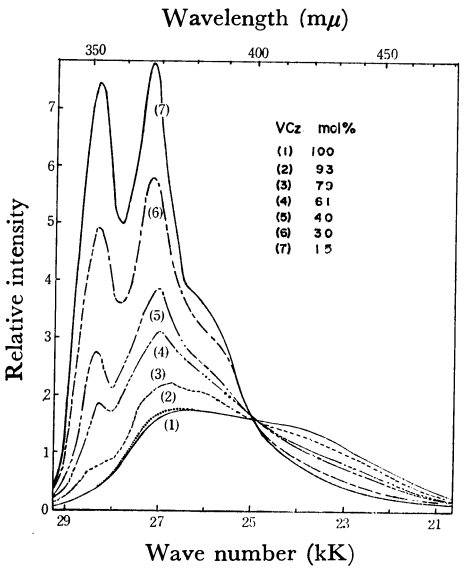

Fig. 1. Fluorescence spectra of VCz–St copolymers in benzene solution (1.5×10^{-4} mol VCz unit/l), 310 mμ excitation.

* Present address: Department of Chemical Engineering, Faculty of Engineering, Yamaguchi University, Ube 755.

Table 1. Energy transfer by exciton diffusion process in polymer films

No	Host	Guest	η_H	η_G	$C_E \times 1000$ (mol/mol VCz unit)	$1/C_E$
1	PVCz	DMPT	0.03	0.036	2.9	350
2	VCz–St copolymer (VCz 93 mol%)	DMPT	0.03	0.036	3.3	300
3	PVCz	Perylene	0.03	0.3	1.5	670
4	VCz–St copolymer (VCz 79 mol%)	Perylene	0.047	0.4	1.6	630
5	VCz–VAc copolymer (VCz 91 mol%)	Perylene	0.03	0.3	1.1	900
6	VCz–VAc copolymer (VCz 83 mol%)	Perylene	0.035	0.35	1.9	530

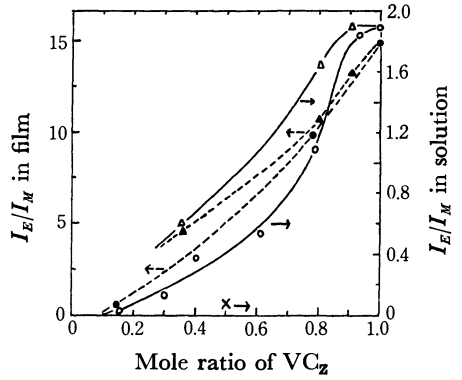

Fig. 2. Dependence of I_E/I_M ratios for benzene solution (1.5×10^{-4} mol VCz unit/l) and for films on VCz content in copolymers. (○) and (●), VCz–St copolymers; (△) and (▲), VCz–VAc copolymers; (X), VCz–fumaronitrile, 310 mμ excitation.

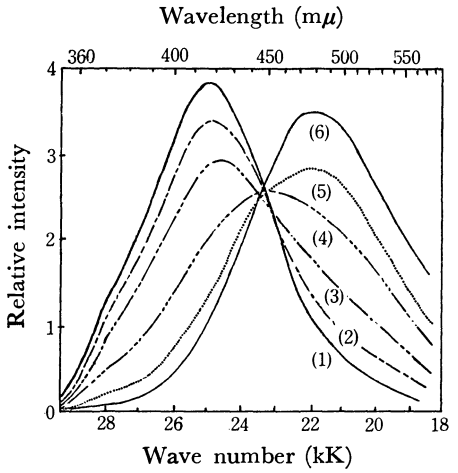

Fig. 3. Fluorescence spectra of PVCz films doped with DMTP, 334 mμ excitation. DMTP concentration; (1) 0, (2) 8×10^{-4}, (3) 2×10^{-3}, (4) 5×10^{-3}, (5) 1×10^{-2} and (6) 3×10^{-2} mol/mol VCz unit.

$$Q_H = (I_G/I_H)(\eta_H/\eta_G) \quad (2)$$

where I_H and I_G are the fluorescence intensities of the host and the guest and where η_H and η_G are quantum yields. The quantum yields of the exciplex fluorescence (η_G) between a Cz chromophore and DMTP in the films were determined from the exciplex fluorescence intensity in the heavy doping films (C=0.1) where no host fluorescence was observed.

Figure 4 shows the bilogarithumic plots of Q_H thus obtained and C. Straight lines with a slope of 1.0

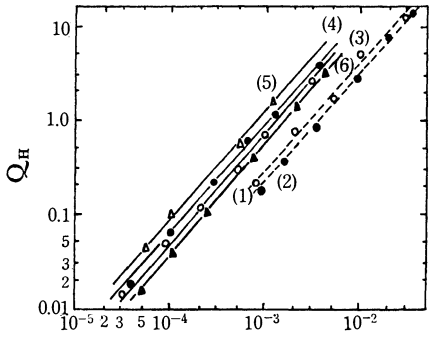

Fig. 4. Q_H *versus* C. See Table 1 as to the number in parentheses.

were obtained for every film as was to be expected from Eq. (1). In the films doped with DMTP, where the single-step energy transfer by the dipole-dipole resonance is impossible, the host fluorescence is quenched significantly by a small amount of DMTP, according to Eq. (1), as in the case of perylene doping. This indicates that the energy transfer both in a PVCz film and in films of copolymers rich in VCz occurs by means of the exciton migration mechanism. The values of C_E were obtained from Fig. 4: they are tabulated in Table 1. The values of C_E obtained from films doped with DMTP are somewhat larger than the values obtained from films doped with perylene. This may imply that in films doped with perylene the single-step energy transfer plays an important role when a singlet exciton comes close to a perylene molecule. In both doping systems, the values of C_E are, however, almost the same for PVCz and for copolymers.

Both in a PVCz film and in films of copolymers rich in VCz, the exciton migration is limited by excimer-forming sites, and the number of Cz rings covered by an exciton during the life-time is represented by $1/C_E$. This number is almost the same for a PVCz film and for copolymers films, it ranges from 400 to 900.

References

1) K. Okamoto, K. Kato, K. Murao, S. Kusabayashi, and H. Mikawa, This Bulletin, **46**, 2883 (1973).
2) F. Schneider, *Z. Naturforsch.*, *A*, **24**, 863 (1969).
3) W. Klöpffer, *J. Chem. Phys.*, **50**, 2337 (1969).
4) K. Okamoto, S. Kusabayashi, and H. Kikawa, This Bulletin, **46**, 2613 (1973).
5) R. Hart, *Makromol. Chem.*, **47**, 143 (1961).
6) Y. Shirota and H. Mikawa, *Polym. J.*, **3**, 643 (1972).

BULLETIN OF THE CHEMICAL SOCIETY OF JAPAN, VOL. 47 (3), 751—752 (1974)

INDO Calculation of ^{13}C Chemical Shifts by the Finite Perturbation Method

Hiroyuki FUKUI

Kitami Institute of Technology, 165 Koencho, Kitami 090

(Received October 11, 1973)

Synopsis. The approximate SCF-MO calculation of ^{13}C nuclear magnetic shielding constants was performed using the finite perturbation method. The results indicated that the INDO finite perturbation method calculates ^{13}C chemical shifts in poor agreement with experiment.

The previous theories of the ^{13}C chemical shifts[1,2] have referred the shifts to the changes in the effective nuclear charge, the mobile bond order, and the average excitation energy and have given good results in many cases. However, in these semiempirical calculations, there is a certain degree of arbitrariness in the choice of an appropriate average excitation energy value. Especially the comparison of the shieldings between different types of molecules depends greatly on the choice of excitation energies. In the finite perturbation theory[3] this arbitrariness is eliminated. Ditchfield, Miller, and Pople[4] have presented *ab initio* results for the shieldings of small molecules using the finite perturbation method. The aim of this note is to examine the effectiveness of the finite perturbation calculation of ^{13}C chemical shifts in the simple molecular orbital method.[5]

In the finite perturbation theory, the shielding constant of the nucleus, A, in a liquid sample is expressed as:

$$\sigma^A = \sigma_d{}^A + \sigma_p{}^A,$$

$$\sigma_d{}^A = \frac{e^2}{3mc^2}\sum_{\mu\nu}P_{\mu\nu}(0)\langle\phi_\mu|r_A{}^{-1}|\phi_\nu\rangle,$$

$$\sigma_p{}^A = -\frac{1}{3}\sum_{\mu\nu}\sum_{\alpha}(H^{(0,1)}_{A\mu\nu})_\alpha(\partial/\partial H_\alpha[P^{Im}_{\mu\nu}(H_\alpha)])_{H=0},$$

$$(H^{(0,1)}_{A\mu\nu})_\alpha = (e\hbar/mc)\langle\phi_\mu|(r_A\wedge\nabla)_\alpha r_A{}^{-3}|\phi_\nu\rangle, \quad (\alpha=x, y, z), \tag{1}$$

where the gauge origin of the vector potential is set at the position of the nucleus, A. $P_{\mu\nu}(0)$ and $P_{\mu\nu}(H_\alpha)$ are the density-matrix elements without and with the magnetic perturbation, H_α, respectively. $P_{\mu\nu}(H_\alpha)$ is allowed to be complex to accommodate the purely imaginary nature of the perturbation, and $P_{\mu\nu}{}^{Im}(H_\alpha)$ represents its imaginary part. Then,

$$P_{\mu\nu}(H_\alpha) = 2\sum_i^{occ}C^*_{\mu i}C_{\nu i} = P^{Re}_{\mu\nu} + iP^{Im}_{\mu\nu}. \tag{2}$$

The LCAO coefficients, $C_{\mu i}$, are found by solving the Roothaan equation with the finite perturbation. The Fock matrix with the perturbation is given by:

$$F_{\mu\nu}(H_\alpha) = H^{core}_{\mu\nu} + iH_\alpha(H^{(1,0)}_{\mu\nu})_\alpha + \sum_{\lambda\sigma}P_{\lambda\sigma}(H_\alpha)[(\mu\nu|\lambda\sigma) - 1/2(\mu\sigma|\lambda\nu)],$$

$$(H^{(1,0)}_{\mu\nu})_\alpha = (e\hbar/2mc)\langle\phi_\mu|(r_A\wedge\nabla)_\alpha|\phi_\nu\rangle. \tag{3}$$

The equation used in the present calculation was simplified by means of the Alger, Grant, and Paul assumption[2] for the angular momentum operators. Then,

$$\langle\phi_\mu{}^A|\phi_\nu{}^B\rangle = \langle\phi_\mu{}^A|l_\alpha{}^A|\phi_\nu{}^B\rangle = 0,$$

$$\langle\phi_\mu{}^A|r_A{}^{-3}l_\alpha{}^A|\phi_\nu{}^B\rangle = \langle\phi_\mu{}^B|r_A{}^{-3}l_\alpha{}^A|\phi_\nu{}^B\rangle = 0,$$

$$l_\alpha{}^A = (r_A\wedge\nabla)_\alpha. \tag{4}$$

There is only one integral which survives the assumptions of Eq. (4) and that does not place all the orbitals on the A atom. It is the integral of the $\langle\phi_\mu{}^B|l_\alpha{}^A|\phi_\nu{}^B\rangle$ form, whose evaluation requires a translation of the coordinates, $l_\alpha{}^A = L_\alpha{}^{AB} + l_\alpha{}^B$. The term arising from the $L_\alpha{}^{AB}$ portion of $l_\alpha{}^A$ could be shown to be negligible; then:

$$\langle\phi_\mu{}^B|l_\alpha{}^A|\phi_\nu{}^B\rangle = \langle\phi_\mu{}^B|l_\alpha{}^B|\phi_\nu{}^B\rangle. \tag{5}$$

It was assumed here that the diamagnetic contribution, $\sigma_d{}^A$, is determined by the carbon 1s electrons. This assumption led to the value of 202.4 ppm for the diamagnetic contribution. The paramagnetic contribution, $\sigma_P{}^A$, was calculated from the INDO approximate molecular orbitals with Eqs. (1)—(5). The integral of $\langle\phi_\mu{}^A|r_A{}^{-3}l_\alpha{}^A|\phi_\nu{}^A\rangle$ in Eq. (1) reduces to the evaluation of $\langle r_A{}^{-3}\rangle_{2p}$. This was estimated by using the Slater 2p orbitals and by choosing the appropriate nuclear charge, Z_A. The effective nuclear charge was given by Eq. (6):

$$Z_A = 3.25 - 0.35(P_A - 4), \quad P_A = \sum_\lambda^A P_{\lambda\lambda}(0). \tag{6}$$

Since $P_{\mu\nu}{}^{Im}(H_\alpha)$ is an odd function of H_α, the derivatives in Eq. (1) are given approximately by:

$$(\partial/\partial H_\alpha[P^{Im}_{\mu\nu}(H_\alpha)])_{H=0} = P^{Im}_{\mu\nu}(H_\alpha)/H_\alpha. \tag{7}$$

The magnitude of H_α used was 5×10^6 Gauss; this gave about 10^{-3} a.u. as the perturbation energy. The diagonalization of the Hermitian matrix, F, was performed by means of a FACOM 230-60 computer in the Hok-

Table 1. Calculated and experimental values of ^{13}C chemical shift (ppm)

		σ_p	σ	Exptl σ
C_2H_2		−103.6	98.8	−76[a]
C_2H_4		−158.7	43.7	−126[a]
C_2H_6		−120.5	81.9	−8.0[a]
C_6H_6		−161.3	41.1	0[b]
C_6H_5F	C–F	−164.1	38.3	−34.8[b]
	o	−160.2	42.2	12.9[b]
	m	−162.8	39.6	−1.4[b]
	p	−160.9	41.5	4.5[b]

a) Shielding constant relative to CH_4. Ref. 4.
b) Shielding constant relative to C_6H_6. G. L. Nelson, G. C. Levy, and J. D. Cargioli, *J. Amer. Chem. Soc.*, **94**, 3089 (1972).

kaido University Computer Center, using a CDIAG program written by the author. The results are given in Table 1.

Although the approximation of the above calculation is of the same degree as that of Karplus and Pople[1b] or of Alger, Grant, and Paul's[2] semiempirical calculations, the estimated values of σ_p in Table 1 are about a half the values obtained by the latter average excitation approximation. Ditchfield, Miller, and Pople's *ab initio* calculation by the finite perturbation indicated an excellent agreement with the experimental values. However, the finite perturbation calculation in the simple molecular orbital method indicates rather poorer agreement with the experiment than does the average excitation method. This seems to be because the average excitation approximation cancels the neglect of the overlap integrals of the angular momentum operators. Recently Maciel *et al.*[5] have reported that he INDO finite perturbation calculation of ^{13}C chemical shifts with an altered set of parameters reproduced successfully the experimental results. However, they have not shown clearly why the standard INDO parameters should be altered.

References

1) (a) M. Karplus and T. D. Das, *J. Chem. Phys.*, **34**, 1683 (1961). (b) M. Karplus and J. A. Pople, *ibid.*, **38**, 2803 (1963). (c) J. A. Pople, *Mol. Phys.*, **7**, 301 (1964).

2) T. D. Alger, D. M. Grant, and E. G. Paul, *J. Amer. Chem. Soc.*, **88**, 5397 (1966).

3) J. A. Pople, J. W. McIver, Jr., and N. S. Ostlund, *J. Chem. Phys.*, **49**, 2960 (1968).

4) (a) R. Ditchfield, D. P. Miller, and J. A. Pople, *ibid.*, **54**, 4186 (1971). (b) R. Ditchfield, *ibid.*, **56**, 5688 (1972).

5) (a) P. D. Ellis, G. E. Maciel, and J. W. McIver, Jr., *J. Amer. Chem. Soc.*, **94**, 4069 (1972). (b) G. E. Maciel, J. L. Dallas, R. L. Elliott, and H. C. Dorn, *ibid.*, **95**, 5857 (1973).

BULLETIN OF THE CHEMICAL SOCIETY OF JAPAN, VOL. 47(3), 753—754 (1974)

Reactions of Tris(acetylacetonato)manganese(III) and -cobalt(III) with 1,10-Phenanthroline and α-Methylstyrene

Kyoji KAERIYAMA

Research Institute for Polymers and Textiles, Sawatari-4, Kanagawa-ku, Yokohama 221

(Received November 28, 1972)

Synopsis. Lower-valence-state compounds, bis(acetylacetonato)manganese(II) and bis(acetylacetonato)(1,10-phenanthroline)manganese(II), were prepared from tris(acetylacetonato)manganese(III). ESR spectra of manganese(II) compounds were shown. Bis(acetylacetonato)(1,10-phenanthroline)Co(II) was also prepared. The results were compared with activity for the initiation of radical polymerization.

In the course of studying the initiation reaction of radical polymerization by tris(acetylacetonato)manganese(III), $Mn(acac)_3$, and tris(acetylacetonato)cobalt(III), $Co(acac)_3$, the present author has found that these chelates react with α-methylstyrene and 1,10-phenanthroline to give anhydrous crystalline bis(acetylacetonato)manganese(II), $Mn(acac)_2$, bis(acetylacetonato) (1,10-phenanthroline)manganese(II), $Mn(acac)_2$-phen, and bis(acetylacetonato)(1,10-phenanthroline)-cobalt(II), $Co(acac)_2$phen.

The kinetic data of the polymerization can be explained by assuming that $Mn(acac)_3$ dissociats into $Mn(acac)_2$ and an acetylacetonyl radical on heating, and that $Mn(acac)_2$ and the acetylacetonyl radical recombine in the absence of a radical scavenger such as a vinyl monomer.[1] Bamford and Ferrar found that $Mn(acac)_3$/amine systes were much more active than $Mn(acac)_3$ and proposed a ligand-exchange mechanism.[2] In fact, Nishikawa, Nakanuma, and Kawaguchi obtained heterochelates of $Mn(acac)_2$ with primary amines from $Mn(acac)_3$ and $Mn(acac)_2(H_2O)_2$.[3] It was reported in previous papers that 1,10-phenanthroline accelerated the elimination of the acetylacetonyl radical from $Mn(acac)_3$.[4,5] In the present investigation, the effects of α-methylstyrene and 1,10-phenanthroline have been examined and discussed in connection with the activity of the initiation of radical polymerization.

A concentrated $Mn(acac)_3$ solution was heated in the presence of a radical scavenger, α-methylstyrene, which was not polymerized to a high polymer above room temperature. Crystalline $Mn(acac)_2$ was thus obtained in a high yield. This crystal remained anhydrous over a month under atmospheric conditions. Figure 1 shows its unique ESR spectrum. Its solution in pyridine gives a spectrum of six lines, as is shown in Fig. 2, although their separations are insufficient. They agree with the nuclear spin of Mn 5/2. These spectra may rise from the paramagnetic Mn(II) ion, which has a long relaxation time. Crystalline $Mn(acac)_2$ was also obtained in the presence of cyclohexanone. The $Mn(acac)_2$ gives the same ESR spectra as those shown in Figs. 1 and 2.

The reaction of $Mn(acac)_3$ with 1,10-phenanthroline resulted in the formation of heterochelate, $Mn(acac)_2$-phen, in a high yield. The chelate gives a symmetrical

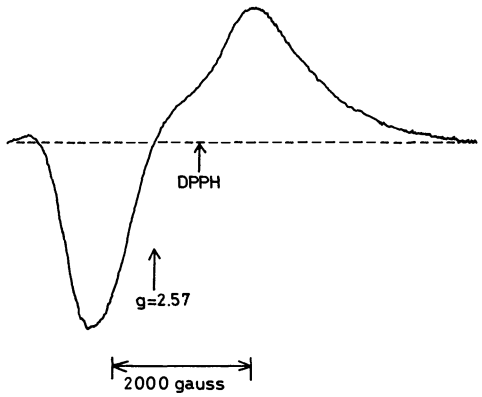

Fig. 1. ESR spectrum of $Mn(acac)_2$.

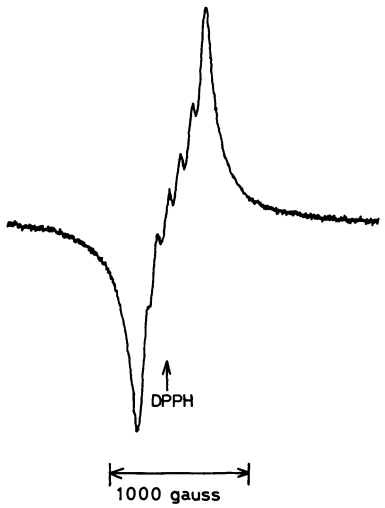

Fig. 2. ESR spectrum of $Mn(acac)_2$ solution in pyridine. $g = 2.0$

ESR spectrum, as is shown in Fig. 3. Its solution in pyridine gives the same spectrum as that shown in Fig. 2.

When a benzene solution of $Mn(acac)_3$ was heated without any such additives as α-methylstyrene, cyclohexanone, and 1,10-phenanthroline, no evidence of $Mn(acac)_2$ was obtained.

$Co(acac)_2$ could not be prepared from $Co(acac)_3$ in the presence of α-methylstyrene, but $Co(acac)_2$phen was obtained after the long heating of $Co(acac)_3$ in the presence of both α-methylstyrene and 1,10-phenanthroline. Although chromium and iron have the same two oxidation states as manganese and cobalt, it was impossible to get lower-valence-state chelates from their higher homologs.

$Mn(acac)_3$ is the most active for the initiation of radical polymerization, $Co(acac)_3$ is the second most

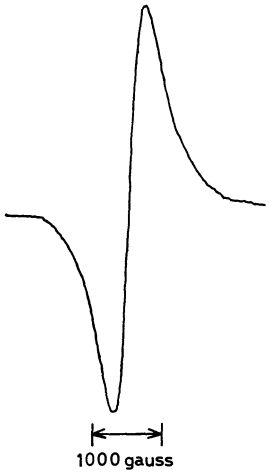

Fig. 3. ESR spectrum of 1,10-phenanthroline $Mn(acac)_2$.
$g = 2.0$

active, and $Fe(acac)_3$ and $Cr(acac)_3$ are inactive.[5] The same order of activity is observed in the present preparation of lower-valence-state compounds.

Experimental

A solution of 750 mg of $Mn(acac)_3$ in 5 ml of benzene and 5 ml of α-methylstyrene was heated for 40 hr at 70 °C under a high vacuum in a sealed tube. A yellow precipitate was thus separated. The solution was cooled to room temperature, and then the precipitate was collected on a sintered glass filter, washed with a small portion of benzene, and dried. Yield, 452 mg (84%). Found: C, 47.35; H, 5.35%. Calcd for $MnC_{10}H_{14}O_4$: C, 47.44; H, 5.57%.

Instead of α-methylstyrene, a 5 ml portion of cyclohexanone was used. The same procedure as that described above gave a yield of 231 mg (43%). Found: C, 48.34; H, 5.34%.

In 10 ml of benzene were heated 750 mg of $Mn(acac)_3$ (2.13×10^{-3} mol) and 422 mg of 1,10-phenanthroline (2.13×10^{-3} mol) for 22 hr at 70 °C. A yellow precipitate was thus obtained. Yield, 848 mg (92%). Found: C, 61.89; H, 4.68; N, 6.18%. Calcd for $MnC_{10}H_{14}O_4 \cdot C_{12}H_8N_2$: C, 60.97; H, 5.11; N, 6.47%.

A solution of 1.0 g of $Co(acac)_3$ and 587 mg of 1,10-phenanthroline in 5 ml of benzene and 5 ml of α-methylstyrene was heated for 5 days at 70 °C. $Co(acac)_2$ phen was thus precipitated from the solution. Yield, 717 mg (58.4%). Found: C, 60.53; H, 4.75; N, 6.85%. Calcd for $CoC_{10}H_{14}O_4 \cdot C_{12}H_8N_2$: C, 60.42; H, 5.07; N, 6.41%.

ESR measurements were made on samples in a capillary by using the JES-3BS-X apparatus of the Japan Electron Optics Laboratory. The frequency of the microwave was around 9450 Mc.

The author is grateful to Dr. M. Suzuki, Dr. S. Ueda, and Mr. Y. Shimura for their interest and encouragement during this work, and also to Dr. K. Someno for his useful suggestion with regard to the ESR spectroscopy.

References

1) K. Kaeriyama, This Bulletin, **43**, 1511 (1970).
2) C. H. Bamford and A. N. Ferrar, *Proc. Roy. Soc.*, **A321**, 425 (1971).
3) Y. Nishikawa, Y. Nakamura, and S. Kawaguchi, This Bulletin, **45**, 155 (1972).
4) K. Kaeriyama, *Makromol. Chem.*, **150**, 189 (1971).
5) K. Kaeriyama and Y. Yamazaki, *Kogyo Kagaku Zasshi*, **74**, 1718 (1971).

BULLETIN OF THE CHEMICAL SOCIETY OF JAPAN, VOL. 47 (3), 755—756 (1974)

The Synthesis of Crystalline Hydrated Double Carbonates of Rare Earth Elements and Sodium

Akihiko MOCHIZUKI, KOZO NAGASHIMA, and Hisanobu WAKITA*

Department of Chemistry, Faculty of Science, Tokyo Kyoiku University, Otsuka, Bunkyo-ku, Tokyo 112

**Department of Chemistry, Faculty of Science, Fukuoka University, Fukuoka 814*

(Received June 25, 1973)

Synopsis. Crystalline hydrated double carbonates of rare-earth elements and sodium were obtained by adding sodium carbonate solutions to rare-earth chloride solutions. The formula of the precipitates was determined to be $LnNa(CO_3)_2 \cdot 6H_2O$ (Ln=La, Ce, Nd, Sm, Gd, Dy, and Y). The products have similar X-ray powder diffraction patterns, which were indexed assuming a tetragonal symmetry. The cell parameters of the products were calculated, they decrease linearly with the decrease in the ionic radii of the rare-earth elements.

In preceding papers,[1] the preparation, formation temperature, optical properties, infrared spectra, and TG data of crystalline hydrated oxocarbonates and crystalline hydrated normal carbonates of rare-earth elements were reported. One of the articles[1] also included the formation of the crystalline hydrated double carbonates of rare-earth elements and sodium (rare-earth element: sodium=1: 1). As for the double carbonates with a 1: 1 composition, though, very little has been known so far. Tselik *et al.*[2] reported the formation of Y: Na=1: 1 double carbonate by mixing solutions of sodium carbonate and yttrium chloride. It is not clear, however, whether their product is of a crystalline or an amorphous phase.

In this study, the synthesis of crystalline double carbonates of rare-earth elements and sodium was attempted at various temperature in order to make clear the formation temperatures of double carbonates. Some other properties of the products were also studied.

Experimental

To solutions of 0.05 M rare-earth chlorides we added acetic acid-sodium acetate buffer solutions of pH 5; then we vigorously stirred in excessive amounts of solutions of sodium carbonates. The solutions containing the precipitates were stored in an air bath kept at the temperatures of 20, 30, 40, 50, 60, 70, and 80 °C, for four days. The changes in the crystallinity of the product during the aging were checked by X-ray powder diffractometry. In the dry air, the precipitates are not stable and slowly change into another phase; therefore, studies such as chemical analysis, X-ray powder diffractometry, thermal analysis, infrared spectrometry, and the measurement of the refractive index were carried out immediately after filtration.

Results

Chemical Analysis. The rare-earth elements used for the preparation of the double carbonates were La, Ce, Nd, Sm, Gd, Dy, Y, Er, Yb, and Sc. The products of La, Ce, Nd, Sm, Gd, Dy, and Y were obtained in crystalline form, while those of Er, Yb, and Sc were obtained in amorphous form. The results of the chemical analysis of Gd and Y compounds are shown in Table 1. On the basis of these results, the chemical formulas for the synthesized double carbonates were determined to be $LnNa(CO_3)_2 \cdot 6H_2O$ (Ln=rare-earth elements).

Table 1. Chemical analysis of double carbonates

Rare earth element	M_2O_3 :	CO_2 :	H_2O :	Na_2O
Gadolinium	1.00	1.97	6.05	0.98
Yttrium	1.00	1.97	5.95	1.00

The formation temperatures of the double carbonates by means of the present procedure are shown in Fig. 1. The La and Ce precipitates were found to be mixtures of double carbonates and lanthanite-type carbonates, $Ln_2(CO_3)_3 \cdot 8H_2O$, while the Nd, Sm, Gd, Dy, and Y compounds were double carbonates showing the same X-ray powder diffraction pattern.

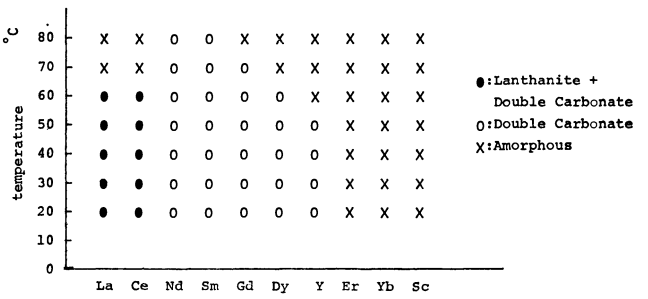

Fig. 1. Diagram showing the formation temperature of double carbonates.

X-Ray Data. The X-ray powder patterns were recorded on a Rigaku Denki Co., Ltd. The data of the synthesized crystalline, hydrated double carbonates of rare-earth elements and sodium are given in Table 2. The sample grains are too fine to be submitted to single crystal X-ray analysis. The indexing of the X-ray powder lines was done by the use of the indexing charts given by Bell *et al.*[3] The probable indices for the powder data, assuming a tetragonal symmetry, are listed in Table 2. The assumed tetragonal symmetry is consistent with the optical properties. Based on these indexings, the unit-cell dimensions and unit-cell volumes were calculated. The results are also shown in Table 2. The relations between the unit-cell parameters and the ionic radii of rare-earth elements are shown in Fig. 2. Using the cell parameters and measured density (2.31 g/cm^3 at 20 °C) for the Y compound, the number of formula units per unit cell was calculated as eight. Since all the reflexions of $h00$ are observed in the X-ray powder patterns, the space group of the materials may be one

TABLE 2. X-RAY POWDER DATA OF DOUBLE CARBONATES

Nd			Sm		Gd		Dy		Y	
d(Å)	I	Probable hkl	d(Å)	I	d(Å)	I	d(Å)	I	d(Å)	I
13.31	100	100	13.17	100	13.08	100	13.02	100	12.98	100
6.61	80	200	6.56	80	6.53	80	6.47	70	6.44	70
4.37	80	300	4.35	100	4.33	90	4.31	50	4.30	50
3.28	20	302	3.26	20	3.24	5	3.22	5	3.21	5
2.62	60	500, 332	2.61	60	2.60	60	2.58	30	2.57	30
2.18	40	600, 252	2.17	20	2.16	30	2.15	10	2.15	20
1.87	10	353, 550	1.86	10	1.85	10	1.84	5	1.84	10
a=13.11Å			a=13.05Å		a=12.99Å		a=12.93Å		a=12.90Å	
c=9.93Å			c=9.85Å		c=9.77Å		c=9.69Å		c=9.65Å	
V=1706.7Å^3			V=1677.5Å^3		V=1648.6Å^3		V=1620.0Å^3		V=1605.8Å^3	

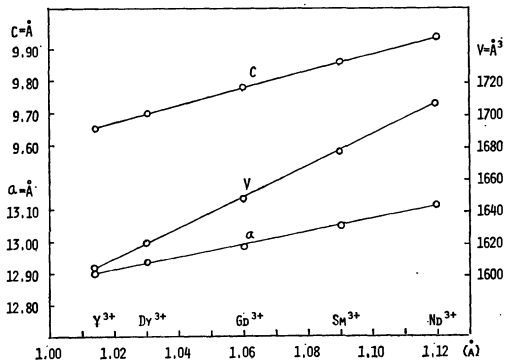

Fig. 2. Relationships between ionic radii of rare earth elements and unit cell parameters.

of P4 symmetries. These space groups have a four-fold axis in the unit cell, which is consistent with the fact that the materials have eight formula in a unit cell.

Refractive Indices. Under the microscope, the synthesized materials were very small rectangles and exhibited a straight extension. The refractive indices of the materials were determined by the immersion method. The immersion media were checked with an Abbe refractometer. The refractive indices of the Nd, Sm, Gd, and Dy compounds were found to have the same values of $\gamma=1.554$ and $\alpha=1.546$ within the limits of experimental error (± 0.001). The refractive indices of the Y compound are $\gamma=1.541$ and $\alpha=1.534$. The size of the crystals was so small that β and 2V could not be determined.

Infrared Absorption Spectra. The infrared absorption spectra were obtained by the KBr disk method. The absorption curve of the Nd compound is shown in Fig. 3 as an example. All the double carbonates of the rare-earth elements show spectra very similar as that in Fig. 3. The ν_1 band of CO_3^{2-} appears at 1070 cm^{-1} as a singlet absorption. On the other hand, the ν_2 and ν_3 band appears as doublet bands. The ν_2 band has peaks at 875 and 850 cm^{-1}, while ν_3 has its at 1530 and 1385 cm^{-1}. These splittings of ν_2 and ν_3 are rather common in rare-earth carbonates.[1] They may be due to the coupling between neighboring carbonate ions and/or to occupying two structurally different sites in the unit cell.

Thermal Analysis. The TG and DSC curves of Nd and Gd compounds are shown in Fig. 4. Based

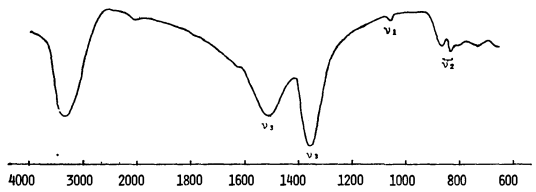

Fig. 3. Infrared absorption spectrum of double carbonate of neodymium and sodium.

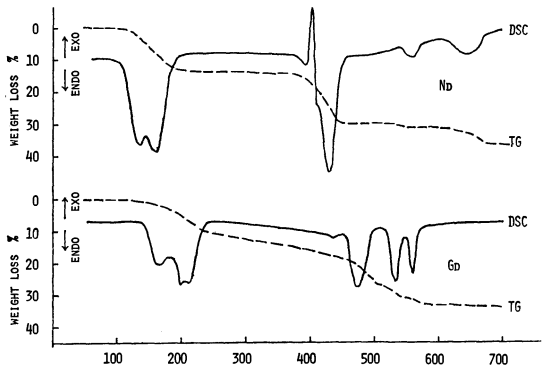

Fig. 4. TG and DSC curves of double carbonates.

on the TG data, the process of the thermal decomposition of each sample may be considered to take place in one of the following ways.

(1) $NdNa(CO_3)_2\cdot 6H_2O \xrightarrow[120\sim200°C]{} NdNa(CO_3)_2\cdot 3H_2O \xrightarrow[370\sim450°C]{} NdNa(CO_3)_2 \xrightarrow[650°C]{} NdNaO(CO_3)$

(2) $GdNa(CO_3)_2\cdot 6H_2O \xrightarrow[70\sim200°C]{} GdNa(CO_3)_2\cdot 2H_2O \xrightarrow[370\sim450°C]{} GdNa(CO_3)_2\cdot H_2O \xrightarrow[400\sim600°C]{} GdNaO(CO_3)$

The decomposition process of Sm carbonate is very similar to that of Nd carbonate, while the processes of Dy and Y carbonates are similar to that of Gd carbonate.

References

1) For instance, K. Nagashima, H. Wakita, and A. Mochizuki, This Bulletin, **46**, 152 (1972).

2) I. N. Tselik, G. F. Denieka, V. Ya. Shvartsman, and V. D. Fedorenko, *Russ. J. Inorg. Chem.*, **13**, 53 (1968).

3) J. C. Bell and A. E. Austin, "Battelle Indexing Charts for Diffraction Patterns of Tetragonal, Hexagonal and Orthorhombic Crystals," Battelle Memorial Institute, Columbus 1, Ohio, U.S.A.

BULLETIN OF THE CHEMICAL SOCIETY OF JAPAN, VOL. 47 (3), 757—758 (1974)

Studies on Preparation of High Purity Sulfur. II. Removal of Trace Amounts of Selenium and Tellurium in Sulfur by Means of Distillation with Silver

Hiroshi SUZUKI, Yasuaki OSUMI, Masanori NAKANE, and Yoshizo MIYAKE

Government Industrial Research Institute, Osaka, Midorigaoka, Ikeda, Osaka 563

(Received June 30, 1973)

Synopsis. In the distillation without silver, most of the selenium and tellurium in crude sulfur appeared in the distillate. However, these impurities were removed by distillation using a column which was filled with silver and heated at 600—700 °C. The removal of them in the process was confirmed in a tracer experiment.

Selenium and tellurium are the main impurities in sulfur; however, few works have been published on the removal of trace amounts of these impurities.

Slepanov *et al.*[1] reported that 84.6% of the selenium in sulfur could be removed by treating molten sulfur in an aqueous magnesium chloride with nitric acid. Devyatykh *et al.*[2] reported that the removal of selenium was difficult during the purification of sulfur, by passing sulfur vapor through a high-temperature zone, because it formed a compound with sulfur. Nothing can be found in literature concerning the removal of tellurium in sulfur.

A method offers an investigation of distillation with silver as for the removal of selenium and tellurium in sulfur. A tracer experiment using ^{75}Se and ^{127m}Te has been undertaken in order to ascertain the effect of silver on the removal of trace amounts of the impurities.

Experimental

Determination of Selenium in Sulfur.[3] The sample solution was prepared by heating 5 g of sulfur with 15 ml of bromine and 60 ml of 30% nitric acid. To an aliquot of a sample solution (0.5 g sulfur), after neutralization, 12 g of ammonium chloride and 2 ml of 2 M formic acid were added and its pH was adjusted to 2—3. Ten ml of a 10% ethylenediaminetetraacetic acid solution and 2 ml of a 0.5% of diaminobenzidine solution were then added, the mixture was heated on a water both for 5 minutes and cooled, and its pH was adjusted to 6—7. The selenium complex in the solution was subsequently extracted in 10 ml of toluene, and its absorbance was measured at 420 nm.

Determination of Tellurium in Sulfur.[4] To an aliquot of a sample solution (1—4 g sulfur), about a 30 mg portion of ferric ions was added, precipitated with ammonia water, filtered, and washed with water. The solution obtained by dissolving the precipitate in 2 ml of 2 M hydrochloric acid and by then diluting the mixture to 10 ml with water was passed through an ion-exchange resin column (1 cm × 10 cm, Amberlite IR-120, H-form, 60 mesh). To the residue, obtained by evaporating the effluent and washing solution, 2.8 ml of water, 1 ml of a 40% ammonium citrate solution, and 2 ml of a 0.1% diethyldithiocarbamate solution were added, and the mixture was diluted to 10 ml with water. The tellurium complex in the solution was extracted in 5 ml of tributyl phosphate and measured at 400 nm.

Filling Material Containing Silver. The material, such as activated alumina, alumina ball, silica gel or a pumiceous substance, was digested in a silver nitrate solution. That containing silver was dried at 100 °C and then heated at 800 °C for 1 hr.

Preparation of Sulfur Containing ^{75}Se and ^{127m}Te. Into a flask of distillatory ^{75}Se (20 μCi, as Na_2SeO_3, 2.14 mCi/mg Se) and ^{127m}Te (450 μCi, as H_2TeO_3, 0.228 mCi/mg Te), 1 ml of hypophosphorous acid was added, and the mixture was dried at 100 °C. Into the flask a 30 g portion of sulfur was then taken, heated at 200 °C for 1 hr, and then distilled under a nitrogen atmosphere. The ^{75}Se and ^{127m}Te in the distilled sulfur were 41.5% and 92.6% respectively of these added to the flask.

Measurement of ^{75}Se and ^{127m}Te in Sulfur. In a 19-mmϕ aluminium dish, 0.5 g of sulfur was placed; then it was heated at 140 °C to melt and cooled slowly. The γ-rays from ^{75}Se and ^{127m}Te were simultaneously measured by the method described by Lee,[5] using a 100-channel scintillation spectrometer.

Distillation of Sulfur. The distilling apparatus used was the same as has been described in a previous paper.[6] The sulfur sample was distilled with a heated column, filled with filling material.

Results and Discussion

Table 1 shows the effect of silver on the removal of

TABLE 1. THE EFFECT OF SILVER FILLED IN COLUMN ON THE REMOVAL OF Se AND Te IN DISTILLATION OF SULFUR[a]

Filling material[b]			Distilled sulfur			Removal rate	
Silver (g)	Support (g)		Yield (%)	Se (ppm)	Te (ppm)	Se (%)	Te (%)
.....	.....	.....	c) 98	117	46	10	18
Null	Pumiceous substance	(4—8 mesh)	20 98	117	26	10	54
Null	Activated alumina	(4—8 mesh)	42 98	117	30	10	46
12.6	Alumina ball[d]	(2 mm ϕ)	81 96	75	17	42	70
4.2	Silica gel	(4—8 mesh)	40 96	87	12	33	79
8.6	Activated alumina	(4—8 mesh)	42 94	2.5	0.9	98	98
9.0	Pumiceous substance	(5—8 mm grain)	20 94	4.8	3.3	96	94

a) Sulfur sample: Amount; 10 g, Se content; 130 ppm, Te content; 56 ppm. Column temperature: 600 °C. b) The bed of filling material was about 20 cm long. c) Distillation without filling material. d) Commercial support for catalyst.

TABLE 2. THE RESULT OF TRACER EXPERIMENT ON DISTILLATION OF SULFUR CONTAINING ^{75}Se AND ^{127m}Te[a)]

Filling material[b)]			Distilled sulfur					Removal rate	
Silver (g)	Support (g)		Yield (%)	Se total activity (cpm)	Te total activity (cpm)	Se (ppm)	Te (ppm)	Se (%)	Te (%)
	c)		99	265685	42276	2.71	5.57	9.7	11.6
	c)		99	286198	45886	2.92	6.04	2.7	4.1
Null	Pumiceous substance	3	97	272309	37121	2.78	4.89	7.4	22.4
Null	Activated alumina	5	97	271639	29777	2.77	3.92	7.6	37.8
0.85	Pumiceous substance	3	96	2472	790	0.025	0.104	99.2	98.4
0.85	Activated alumina	5	96	2261	408	0.023	0.063	99.2	99.0

a) Sulfur sample: Amount; 2 g, Se content; 3.00 ppm, Te content; 6.30 ppm, Se total activity; 293959 cpm, Te total activity; 47839 cpm. Column temperature: 600 °C. The bed of filling material was about 7 cm long. b) 8—12 mesh. c) Distillation without filling material.

selenium and tellurium. In the distillation without silver, most of the selenium and tellurium in crude sulfur appeared in the distillate. However, both the impurities were removed by distillation using a column filled with silver supported on a pumiceous substance or activated alumina. The effect of silver is related to the affinity of silver for selenium and tellurium. It has been established that silver has more affinity for selenium than for sulfur.[7] It seemes that silver reacts slowly with sulfur, but reacts rapidly with selenium and tellurium in the process. Consequently, sulfur passed through the column, while selenium and tellurium remained in the column.

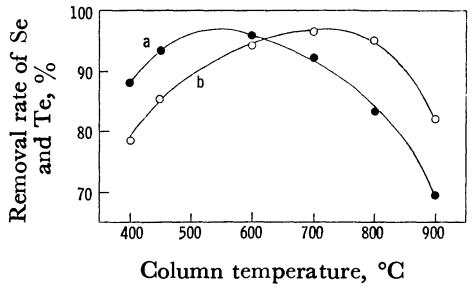

Fig. 1. The effect of temperature of column filled with silver on the removal of Se (a) and Te (b).
Sulfur sample: Amount; 10 g, Se content; 117 ppm, Te content; 56 ppm. The column was filled with 2 g of silver supported on 20 g of pumiceous substance (4—8 mesh) about 20 cm long.

Figure 1 shows the effect of the column temperature on the removal of the impurities. Both impurities were effectively removed with the column heated at 600—700 °C.

Figure 2 shows the effect of the amount of silver in the column on the removal of the impurities during the distillation of 10 g of sulfur. Effective removals of selenium and tellurium were shown when more than 1.7 and 1.0 g of silver respectively were present in the column. The reduction of the amount of silver in the column caused a decrease in the removal rates of the impurities; this was because the sulfuration of silver in the column progressed rapidly, while produced

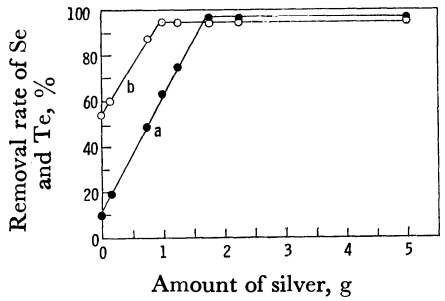

Fig. 2. The effect of amount of silver in column on the removal of Se (a) and Te (b).
Sulfur sample: Amount; 10 g, Se content; 117 ppm, Te content; 56 ppm. The columns were filled with various amounts of silver supported on 20 g of pumiceous substance (4—8 mesh) about 20 cm long. Column temperature: 600 °C.

sulfide did not react with selenium and tellurium.

The reproduction of the column in which silver had been converted into sulfide was easily carried out by passing air or oxygen through the column heated at more than 600 °C.

The removal of them was confirmed in a tracer experiment as shown in Table 2.

References

1) M. N. Slepanov, S. N. Remner, and I. I. Berger, *J. Chem. Ind.*, (U.S.S.R.) **18**, No. 20, 4 (1941); *Chem. Abstr.*, **38**, 6057, (1944).

2) G. G. Devyatykh, V. A. Umilin, and A. I. Odnosevtsev, *Tr. po. Khim. i Khim. Teknol*, **2**, 306 (1962); *Chem. Abstr.*, **59**, 7135f (1963); G. G. Devyatykh, A. I. Odnosevtsev and V. A. Umilin, *Zhur. Priklad. Khim.*, **34**, 1969 (1961); *Chem. Abstr.*, **56**, 165 (1962).

3) K. L. Cheng, *Anal. Chem.*, **28**, 1738 (1956): I. Iwasaki, A. Kishioka, and Y. Yoshida, *Bunseki Kagaku*, **10**, 479 (1961).

4) M. Inarida, *Bunseki Kagaku*, **7**, 449 (1958).

5) W. Lee, *Anal. Chem.*, **31**, 800 (1959).

6) H. Suzuki, E. Ishii, and Y. Miyake, *Nippon Kagaku Kaishi*, **1973**, 1416.

7) J. M. Mellor, "A Comprehensive Treatise on Inorganic and Theoretical Chemistry," Vol. 3, Longman, Green and Co., London (1923), p. 444.

BULLETIN OF THE CHEMICAL SOCIETY OF JAPAN, VOL. 47 (3), 759—760 (1974)

Studies on Preparation of High Purity Sulfur. IV. Effect of the Distillation with Adsorbent and Silver on the Removal of the Impurities in Sulfur[1)]

Hiroshi SUZUKI, Kunishige HIGASHI, and Yoshizo MIYAKE

Government Industrial Research Institute, Osaka, Midorigaoka, Ikeda, Osaka 563

(Received July 16, 1973)

Synopsis. The distillation was shown to be effective in removing arsenic, selenium, tellurium, carbon, and common elements in sulfur. However, there was the disadvantage that trace amounts of common elements were not reduced further by the repetition of the distillation. This could be carried out by the zone refining.

In the course of studies of the preparation of high-purity sulfur, the removals of trace amounts of the main impurities, such as arsenic, selenium, tellurium, and carbon, have been separately presented in previous papers.[2-4)]

In order to remove the impurities simultaneously, a distillation of sulfur, using an adsorbent and silver, was proposed. In the distillation, the removal of the impurities was ascertained. Simultaneously, the ignition residue of the distilled sulfur and the common elements in the ignition residue were investigated.

The distillation was shown to be effective in removing various impurities in sulfur. At the same time it was found that trace amounts of the common elements remained in the distilled sulfur.

The zone refining of sulfur[5-8)] was carried out parallel with the distillation. The experimental results suggest that trace amounts of the common elements in the distilled sulfur can be further reduced by the technique.

Experimental

Distillation of Sulfur. The distilling apparatus and the silver supported on a pumiceous substance were the same as have been described in a previous paper.[3)] The column of the distilling flask, 50 cm long, was filled with the silver. In the flask, 50 g of a sulfur sample and 5 g of activated carbon (24—40 mesh) were then taken. The column was heated at 600 °C, the flask was heated below 500 °C, and the sulfur was distilled in a flow of inert gas.

Zone Refining. Sixty grams of sulfur were placed in a glass tube (15 mmϕ) and heated at 140 °C for several hours. After the atmosphere of the tube had then been replaced with nitrogen, the tube (30 cm long) was sealed. It was kept horizontal, heated to melt the sulfur, and then cooled slowly. A horizontal zone-refining apparatus was used. The conditions of the zone refining were as follows: zone width, 3 cm; speed of zoning, 1 cm per hour; pass of zone, 10 times.

Determination of the Impurities in Sulfur. The arsenic, selenium, and tellurium were separately determined by the spectrophotometric methods described in previous papers.[2,3)]

The common elements in the ignition residue of sulfur were determined by the spectrographic method. A sulfur sample was mixed with graphite powder in a proportion of 10: 1 in a platinum crucible and then heated to the melting point. Then, the graphite powder remaining in the crucible was heated at 650 °C for 3 hr; it was afterward transferred into a capsule and shaken sufficiently with the mixer mill. A weighed portion of this was used as the sample for measurements. The intensities of the spectral lines of the elements, such as Co, Si, Fe, Pb, Cu, Mg, Ca, Al, Cd, B, Bi, Ag, and Sn, were simultaneously measured by using a direct-reading emission spectrometer (Shimadzu, Ebert Grating Spectrometer GEM-340).

Results and Discussion

The distillation with an adsorbent and silver was compared with the distillations without them with respect to the removal of various impurities. The former distillation was more effective than the latter, as is shown in Table 1.

Arsenic was adsorbed to the activated carbon, and it remained in the flask. While sulfur vapor passed through the column, selenium and tellurium were caught in it, because they reacted rapidly with the heated silver in it. The removal rates of arsenic, selenium, and tellurium by the distillation were about 99, 95, and 95% respectively. The repetition of the

Table 1. Contents of the impurities in raw and distilled sulfurs

	Impurities, ppm																
	Co	Si	Fe	Pb	Cu	Mg	Ca	Al	Cd	B	Bi	Ag	Sn	As	Se	Te	Ignition residue
Raw sulfur	0.36	>10	>10	1.1	0.96	1.2	3.4	>10	0.40	0.80	0.52	*	0.28	43	130	56	290
Sulfur distilled with adsorbent and silver	*	0.56	0.16	*	0.04	*	0.04	0.12	*	*	0.04	*	*	0.4	6.5	2.8	2.4
Sulfur distilled without ones	0.04	0.72	1.0	*	0.12	*	0.24	0.24	*	*	0.08	*	0.04	26	117	45	43
Sulfur redistilled without ones	*	0.72	0.56	*	0.12	0.04	0.04	0.04	*	*	0.04	*	0.04	16	105	36	3.7

* No detection.

Table 2. Contents of the impurities in fractions of sulfur traversed by molten zones

Distance in zone lengths (cm)	Impurities, ppm													Distance in zone lengths (cm)	Impurities, ppm		
	Co	Si	Fe	Pb	Cu	Mg	Ca	Al	Cd	B	Bi	Ag	Sn		As	Se	Te
0—10	0.59	1.50	2.66	0.43	0.26	0.13	0.68	0.98	0.01	1.94	0.21	0.18	0.40	0— 6	0.9	79	20
10—20	0.02	0.42	0.81	0.05	0.26	0.10	0.20	0.14	0.01	*	*	*	*	6—12	1.3	79	20
20—30	0.02	0.33	0.50	0.04	0.10	0.09	0.20	0.13	0.01	*	*	*	*	12—18	1.9	79	20
														18—24	1.9	79	20
														24—30	3.2	79	20

* No detection.

distillation was effective in removing trace amounts of the impurities.

Although it is not shown in Table 1, most of the carbonaceous impurity was removed, and the halogen was removed somewhat. The carbonaceous impurity was decomposed rapidly and separated from the sulfur in the process, by which it was brought in contact with the heated silver in the column.

The common elements were effectively removed, too. Their contents in the sulfur were all reduced to the range of $n \times 10^{-1}$—10^{-2} ppm. However, there was the disadvantage that trace amounts of the common elements remaining in the distilled sulfur were not reduced further by the repetition of the distillation.

Table 2 shows the contents of various impurities in the fraction of sulfur traversed by molten zones. The results of the experiment showed that the contents of most of the common elements were reduced, and suggested that trace amounts of the impurities in sulfur could be reduced by zone refining. At the same time, it was found that the contents of arsenic, selenium, and tellurium could not be expected to be reduced, for the impurities in sulfur had unfavorable coefficients.

By the distillation, such impurities as arsenic, selenium, tellurium, and carbon were effectively removed, and the common elements were reduced to trace amounts. The further reduction of the common elements could be carried out by the zone refining.

References

1) A part of this work was presented at 21th Annual Meeting of Chemical Society of Japan, Osaka, April, 1968.

2) H. Suzuki, E. Ishii, and Y. Miyake, *Nippon Kagaku Kaishi*, **1973**, 1416.

3) H. Suzuki, Y. Osumi, M. Nakane, and Y. Miyake, This Bulletin, **47**, 757 (1974).

4) H. Suzuki, M. Nakane, and Y. Miyake, Japan Pat. 617354 (1971).

5) M. V. Pashkovskii, R. V. Lutsiv, and I. V. Savitskii, *Ukrain. Fiz. Zhur.*, **5**, 418 (1960); *Chem. Abstr.*, **55**, 25177h (1961).

6) F. Feher and H. D. Lutz, *Z. Anorg. Allg. Chem.*, **334**, 235 (1964).

7) F. Feher, H. D. Lutz, and K. Obst, *Z. Anal. Chem.*, **224**, 407 (1967).

8) W. E. Medcalf and R. H. Fahing, *J. Electrochem. Soc.*, **105**, 719 (1958).

BULLETIN OF THE CHEMICAL SOCIETY OF JAPAN, VOL. 47 (3), 761—762 (1974)

The Extraction and Spectrophotometric Determination of Vanadium(IV) with Tiron[1]

Yoshinobu WAKAMATSU and Makoto OTOMO*

Department of Industrial Chemistry, Hachinohe Technical College, Hachinohe 031

**Department of Synthetic Chemistry, Nagoya Institute of Technology, Showa-ku, Nagoya 466*

(Received August 6, 1973)

Synopsis. The vanadium(IV)-Tiron chelate can be extracted into a mixed solvent of 1:4 isopentyl alcohol-chloroform in the presence of 1,3-diphenylguanidinium salt. Beer's law was obeyed up to 36 μg vanadium per 10 ml of the solvent.

Tiron reacts with vanadium(IV, V) to form water-soluble chelates. Tserkovnitskaya *et al.*[2] studied the complex formation between vanadium(IV) and Tiron in an aqueous solution. On the other hand, Sarma[3] and Nishikawa *et al.*[4] applied the vanadium(V)-Tiron chelate to the visible and ultraviolet spectrophotometric determination of vanadium(V) in an aqueous solution.

The present paper will describe the spectrophotometric determination of vanadium(IV), which is based on the extraction of the vanadium(IV)-Tiron chelate into a mixed solvent of 1:4 isopentyl alcohol–chloroform in the presence of excessive 1,3-diphenylguanidinium-(DPG) salt. The combining ratio of vanadium, Tiron, and DPG in the extracted species has also been determined by a spectrophotometric method.

Experimental

Reagents and Apparatus. A stock solution of vanadium (IV) (about 0.01 M) was prepared by dissolving a reagent grade vanadium(IV) sulfate in distilled water and then standardized against a standard EDTA solution, using Cu–PAN as the indicator.[5] All the other reagents and apparatus used were the same as those reported previously.[6]

Standard Procedure. To a sample solution containing up to 36 μg of vanadium in a 50 ml separatory funnel we added 1.0 ml of a 0.56 M ascorbic acid solution, 4.0 ml of a 0.2 M Tiron solution, and 10.0 ml of a 0.34 M DPG solution which had been adjusted to pH 3.5 with a 0.2 M monochloroacetic acid solution and a 0.2 M sodium acetate solution. The solution was diluted with water to 20.0 ml, allowed to stand for 20 min, and shaken for 10 min with 10.0 ml of a mixed solvent of 1:4 isopentyl alcohol–chloroform. The absorbance of the organic phase was then measured at 585 nm using a reagent blank as the reference.

Results and Discussion

Absorption Spectra. The absorption spectra of the vanadium(IV)-Tiron chelate in an aqueous solution and the ion association complex extracted into the solvent are shown in Fig. 1. The absorption maxima of the vanadium(IV) Tiron chelate and the ion-association complex are found at 565 and 585 nm respectively. Tiron is not extracted into the solvent, not even in the presence of DPG salt at pH 3.5.

The Effect of the pH. The effect of the pH of the aqueous phase on the extraction is shown in Fig. 2.

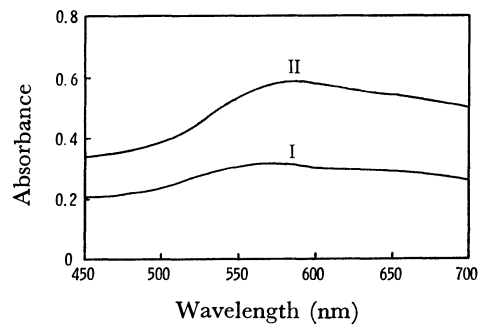

Fig. 1. Absorption spectra of the V(IV)-Tiron chelate in aqueous phase and the association complex in organic phase.
Tiron: 4.0×10^{-2}M, Ascorbic acid: 2.8×10^{-2}M, pH: 3.5, I: V(IV)-Tiron chelate, V(IV); 38.$_8$ μg, II: association complex, V(IV); 28.$_5$ μg, DPG; 0.17M.

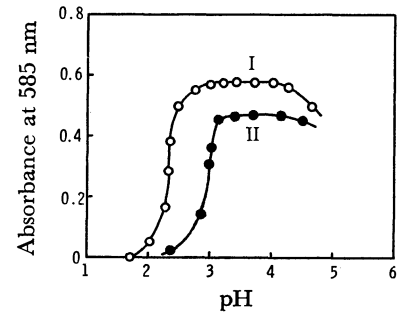

Fig. 2. Effect of pH on the extraction of V(IV)-Tiron-DPG.
V(IV): 28.$_5$ μg, DPG: 0.17M, Ascorbic acid: 2.8×10^{-2}M, Tiron: I; 4.0×10^{-2}M, II; 5.0×10^{-3}M.

The maximum extraction is reached at pH 2.9—4.1 when the association complex is extracted into the solvent from an aqueous solution containing 4.0×10^{-2} M Tiron. The wavelength of maximum absorption was independent of the pH of the aqueous phase.

The Effect of the Additives. The effect of the Tiron and the DPG concentrations on the extraction was investigated separately by varying the Tiron and the DPG concentrations respectively. It was found that the absorbances of the organic phase were essentially constant provided that the Tiron and the DPG concentrations in the initial aqueous phase were more than 3.0×10^{-2} M and 0.13 M respectively.

Choice of Solvent. The vanadium(IV)-Tiron-DPG association complex can be readily extracted into aliphatic alcohols; its extractability is analogous to those of the corresponding titanium complex.[6] A 1:4 mixed solvent of isopentyl alcohol and chloroform, which proved to give the highest absorbance, was chosen as the solvent.

The Effect of the Standing Time. The formation of the vanadium(IV)-Tiron chelate does not occur instantaneously in an aqueous solution, about 20 min being required to obtain the maximum absorbance. The absorbance of the organic phase remains almost constant for at least 5 hr if the vanadium(IV)-Tiron-DPG association complex is extracted into the solvent after the reaction mixture has been allowed to stand for 20 min.

The Effect of the Shaking Time. It was found that shaking for 5 min sufficed; for safety, though, a shaking time of 10 min was selected. The aqueous phase was colorless after one extraction, indicating that only one extraction is needed for the complete extraction of the association complex.

Calibration Curve. A calibration curve for the determination of vanadium(IV) was prepared under the optimum conditions. A good linear relationship was obtained over the concentration range from 0 to 36 μg of vanadium per 10 ml of the solvent. The molar absorptivity of the extracted species was approximately 1.03×10^4 at 585 nm, 1.4 times as high as that of the vanadium(V)-Tiron chelate at 310 nm.[4] The proposed method is comparable in sensitivity to the Methylthymol Blue method.[7]

Table 1. Effect of metal ions

V(IV): 2.8×10^{-5}M (28.5 μg), Tiron: 4.0×10^{-2}M, DPG: 0.17M, Ascorbic acid: 2.8×10^{-2}M, pH: 3.5

Metal ion	Amount added (μg)	V(IV) found (μg)
Fe(III)	30	28.5
	200	28.4
Al(III)	30	28.3
	200	28.8
Ti(IV)	60	28.3
	960	34.3
	960	28.2[a]
Th(IV)	200	29.0
U(VI)	200	28.9
W(VI)	30	28.4
	200	29.7
Mo(VI)	200	29.7

a) 2 ml of NaF (0.1M) was added.

The Effect of Diverse Ions. The effect of diverse ions on the determination of vanadium(IV) was examined. The effect of metal ions is summarized in Table 1. Divalent metal ions such as nickel, lead, cadmium, copper, calcium, and magnesium up to at least 200 μg do not interfere with the determination. Molybdenum(VI) and tungsten(VI), when present in large quantities, give positive errors. The interferences from iron(III) and titanium(IV) can be eliminated by the addition of ascorbic acid and sodium fluoride (0.01 M) respectively. Of the anions tested, chloride, sulfate, nitrate, phosphate, fluoride, and tartrate have no effect on the determination even when present in a molar concentration 500 times that of vanadium(IV). Chelating agents such as EDTA and CyDTA, however, interfere seriously.

The Composition of the Extracted Species. The combining ratios of Tiron and DPG to vanadium(IV) in the extracted species were deduced by a spectrophotometric method.[6] The number of moles of Tiron in the association complex was determined by plotting log(the distribution ratio of vanadium, D_v) against log(the total concentration of Tiron, $[H_2R]_t$). The pH and the total concentration of DPG were kept constant at 3.5 and 0.17 M respectively. The slope of the straight-line portion indicates that the vanadium: Tiron ratio is 1: 2. In the same manner, the number of moles of DPG in the association complex was determined by plotting $\log D_v$ against log(the total concentration of DPG, $[DPG]_t$), the pH and the total concentration of Tiron being kept constant. The slope of 6.1 suggests that one vanadium(IV)-Tiron chelate anion associates with six DPG cations to form an extractable neutral species. The pH dependence of the extraction was then examined by plotting $\log D_v$ against the pH value of the aqueous phase. The results are shown in Fig. 3. The slope of 4.1, which is calculated by the method of least-squares, indicates that four protons are concerned with the extraction process.

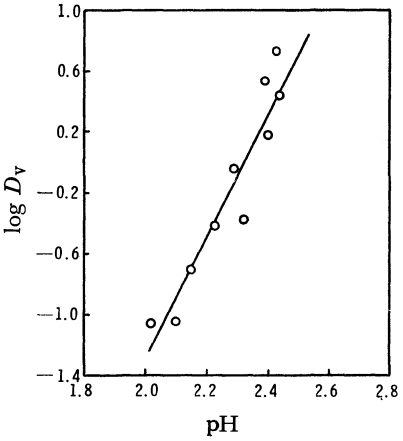

Fig. 3. Relationship between log D_v and pH for the V(IV)-Tiron-DPG system.
V(IV): 2.8×10^{-5}M, Tiron: 4.0×10^{-2}M, DPG: 0.17M, Ascorbic acid: 2.8×10^{-2}M.

From the foregoing observations, it seems natural to express the extraction equilibrium expression in the simplest form:

$$VO^{2+} + 2H_2R^{2-} + 6(DPG)^+ \rightleftarrows VO(R)_2(DPG)_6 + 4H^+$$

$$[VO(R)_2(DPG)_6] \rightleftarrows [VO(R)_2(DPG)_6]_0$$

References

1) Presented at the Tohoku Branch Meeting of the Chemical Society of Japan, Yonezawa, October, 1972.
2) I. A. Tserkovnitskaya and M. F. Grigor'eva, *Ser. Fiz. Khim.*, **3**, 130 (1966); *Chem. Abstr.*, **66**, 16346 (1967).
3) B. Sarma, *J. Sci. Ind. Research India*, **16B**, 569 (1957).
4) S. Nishikawa, Y. Nakagawa, M. Satake, and T. Matsumoto, *Bunseki Kagaku*, **15**, 944 (1966).
5) K. Ueno, "Kireto Tekitei (Chelatometric Titration)" (in Japanese), Nankodo, Tokyo (1960), p. 220.
6) Y. Wakamatsu and M. Otomo, This Bulletin, **45**, 2764 (1972).
7) Y. Wakamatsu and M. Otomo, *Nippon Kagaku Zasshi*, **90**, 595 (1969).

BULLETIN OF THE CHEMICAL SOCIETY OF JAPAN, VOL. 47(3), 763—764 (1974)

A Novel Type of Penta-Coordinated Iron(III) Complex $FeCl[SSeCNR_2]_2$ ($R=CH_3$, C_2H_5)

Shunji NAKAJIMA and Toshio TANAKA

Department of Applied Chemistry, Faculty of Engineering, Osaka University, Yamada-kami, Suita, Osaka 565

(Received October 6, 1973)

Synopsis. The titled compounds were prepared, and the magnetic susceptibility and electronic spectrum were measured; the two weak bands observed in the near-infrared region are assigned as spin-forbidden d-d bands.

We have previously reported on some *N,N*-dialkylthioselenocarbamate complexes of tin(IV),[1] nickel(II), palladium(II), platinum(II),[2] and gold(III),[3] in which the thioselenocarbamate, $\left[\begin{matrix}S\\Se\end{matrix}\!\!\diagdown\!\!\!\!\diagup C{=}N\!\!\diagup\!\!\!\!\diagdown\begin{matrix}R\\R\end{matrix}\right]^-$ ($R=CH_3$, C_2H_5), coordinates through both the sulfur and selenium atoms. Recently, Heber *et al.*[4] prepared a variety of metal *N,N*-diethylthioselenocarbamates by the reaction of metal ions with $(C_2H_5)_2NH_2\cdot SSeCN(C_2H_5)_2$.

Our recent study has shown that the reaction of $FeCl_3$ with dimethylchlorotin(IV) *N,N*-dialkylthioselenocarbamate, $(CH_3)_2ClSn[SSeCNR_2]$ ($R=CH_3$ and C_2H_5), gave a novel type of penta-coordinate complex, $FeCl[SSeCNR_2]_2$. This paper will report the preparation and properties of this complex.

Experimental

Materials. Dimethylchlorotin(IV) *N,N*-dimethyl-[1] and *N,N*-diethylthioselenocarbamates,[2] $(CH_3)_2ClSn$(dmtsc) and $(CH_3)_2ClSn$(detsc) (dmtsc=$SSeCN(CH_3)_2$, detsc=$SSeCN(C_2H_5)_2$), were prepared as has been described elsewhere.

Preparation. An ethanol–ligroin (1 : 3 vol/vol) solution (20 ml) of $FeCl_3$ (1.2 mmol) was added, drop by drop, into $(CH_3)_2ClSn$(dmtsc) (3.7 mmol) in an ethanol–ligroin (1 : 5 vol/vol) mixture (100 ml) on an ice-bath, after which the solution was stirred for a further 30 min at 0 °C. The precipitate thus obtained was washed with chloroform several times and then dried *in vacuo* to give a black powder of $FeCl$(dmtsc)$_2$ (1.1 mmol) (mp >250 °C).

Found: C, 17.28; H, 3.15; N, 6.80%. Calcd for $C_6H_{12}N_2S_2Se_2ClFe$: C, 16.93; H, 2.81; N, 6.58%. ν(C=N) 1551 cm^{-1} and μ^{eff} 4.00 BM.

$FeCl(detsc)_2$ was similarly prepared by the reaction of $FeCl_3$ (6.2 mmol) with $(CH_3)_2ClSn$(detsc) (12—18 mmol). Recrystallization was done from a chloroform–ethanol mixture to give black crystals (3.0 mmol) (mp ~240 °C (decomp.)).

Found: C, 24.66; H, 4.36; N, 5.73%, mol wt, 487 in $CHCl_3$ by a vapor-pressure osmometer. Calcd for $C_{10}H_{20}N_2S_2Se_2ClFe$: C, 24.93; H, 4.19; N, 5.82%; mol wt, 482. ν(C—N) 1509 cm^{-1} and μ^{eff} 3.90 BM.

Physical Measurements. Magnetic susceptibility was measured for micro-crystalline materials by the Gouy method at room temperature. The infrared spectra were recorded in Nujol mulls on a Hitachi-Perkin Elmer 225 spectrophotometer, while the electronic spectra covering the near-infrared region were measured on a Hitachi EPS-03 or 124 spectrophotometer with a 1 cm quartz cell at 25 °C.

Results and Discussion

The reaction of $FeCl_3$ with $(CH_3)_2ClSn$(dmtsc) or its *N,N*-diethyl derivative at the mole ratio of 1 : 3 was carried out with a view to obtaining $Fe(dmtsc)_3$ or $Fe(detsc)_3$. We have not, however, been successful in isolating the tris-carbamate complex, even in several reaction conditions differing from that described in the Experimental section, such as at an elevated temperature and with prolonged stirring. Instead, the reaction yielded two complexes of a novel type, $FeCl(dmtsc)_2$ and $FeCl(detsc)_2$. This is in contrast with the results reported by Heber *et al.*,[4] who obtained $Fe(detsc)_3$ by the reaction of the Fe(III) ion with $(C_2H_5)_2NH_2$(detsc) in a methanol–water mixture.

Both the complexes obtained are somewhat sensitive to humidity in air. Molecular-weight determination indicates that the detsc complex is essentially monomeric in chloroform; the dmtsc complex is not sufficiently soluble in common organic solvents to determine the molecular weight.

The magnetic moments of the dmtsc and detsc complexes indicate the presence of three unpaired electrons. This may be compared with the results reported for halogenoiron(III) bis(*N,N*-dialkyldithiocarbamate), $FeX[S_2CNR_2]_2$ (X=Cl, R=CH_3, C_2H_5, and *sec*-C_4H_9; X=Br and I, R=C_2H_5),[5] the chloroiron(III) *N,N*-diethyl derivative of which has been reported to have an approximate square pyramidal structure, with the iron atom lying above the basal plane formed by the four sulfur atoms.[6] The electronic configuration suggested for these dithiocarbamates, $[(3d_{xy})^2(3d_{xz}3d_{yz})^2(3d_{z^2})^1(3d_{x^2-y^2})^0]$,[5] will be found in $FeCl(dmtsc)_2$ and $FeCl(detsc)_2$.

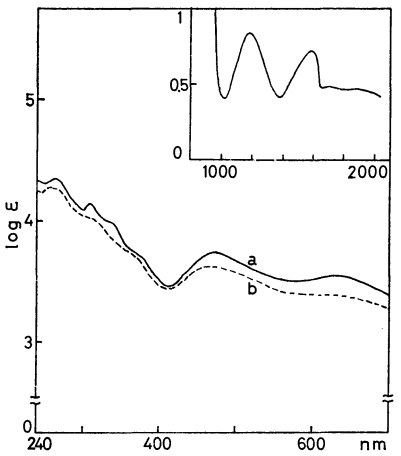

Fig. 1. Electronic spectra of $FeCl(detsc)_2$ (a) and $FeCl(dmtsc)_2$ (b) in dichloromethane.

Table 1. Electronic spectra in dichloromethane; band maxima (kK) and log ε (in parenthesis)

Complex	d-d band	CT band	Ligand band
$FeCl(dmtsc)_2$	16.0 (3.39)	26.5 (3.76)	32.3 (4.04)
	21.4 (3.62)	28.5 (3.82)	38.5 (4.27)
$FeCl(detsc)_2$	6.25 (0.72)	26.6 (3.72)	32.3 (4.14)
	8.40 (0.83)	29.9 (4.01)	37.6 (4.36)
	15.6 (3.54)		
	21.1 (3.75)		

Figure 1 depicts the electronic spectra of the Fe(III) complexes, while the data are listed in Table 1. The spectrum of $FeCl(detsc)_2$ is rich in absorption band and in appearance resembles the spectrum of $FeCl[S_2CN(C_2H_5)_2]$.[5] The bands observed above 25 kK have their origin in charge-transfer and intra-ligand transitions, while the two succeeding bands at around 21 and 16 kK arise from spin-allowed d-d transitions. These assignments seem reasonable in view of the fact that the bands around 20 and 16 kK of $M(detsc)_n$ ($n=3$ when M=Cr(III) and Co(III); $n=2$ when M=Ni(II)) have been identified as d-d transitions,[4] while the 15.9 kK band[7] of $Cu(detsc)_2$ is missing.[4] Moreover, the corresponding dmtsc complexes exhibit similar spectra.[7] There is, however, little information about the d-d bands of square pyramidal complexes,[8] and we have to await further studies of this type of complexes before we can make detailed assignments. It is noticed that there are two weak bands of $FeCl(detsc)_2$ in the near-infrared region. In view of the ε values, they are most likely to be spin-forbidden d-d bands, while the analogous weak bands of $FeCl[S_2CN(C_2H_5)_2]_2$ have been assigned as spin-allowed transitions.[5] No corresponding absorption has been observed in $FeCl(dmtsc)_2$, because of its limited solubility.

References

1) T. Kamitani and T. Tanaka, *Inorg. Nucl. Chem. Lett.*, **6**, 91 (1970).
2) T. Tanaka and N. Sonoda, *Inorg. Chem.*, **10**, 2337 (1971).
3) N. Sonoda and T. Tanaka, *J. Inorg. Nucl. Chem.*, **35**, 1145 (1973).
4) R. Heber, R. Kirmse, and E. Hoyer, *Z. Anorg. Allgem. Chem.*, **393**, 159 (1972).
5) R. L. Martin and A. H. White, *Inorg. Chem.*, **6**, 712 (1967).
6) B. F. Hoskins, R. L. Martin, and A. H. White, *Nature*, **211**, 627 (1966).
7) S. Nakajima and T. Tanaka, unpublished work.
8) B. N. Figgis, "Introduction to Ligand Fields," Chapter 12 (1966), Interscience.

BULLETIN OF THE CHEMICAL SOCIETY OF JAPAN, VOL. 47 (3), 765—766 (1974)

Notiz über neue $\overset{+}{S}$–$\overset{-}{N}$-Ylid-Komplexe von Platin(II)

Gen-etsu MATSUBAYASHI, Masaharu TORIUCHI, und Toshio TANAKA

Abteilung für Angewandte Chemie, Technische Fakultät der Universität Osaka, Yamadakami, Suita, Osaka 565

(Eingegangen den Oktober 12, 1973)

Synopsis. The reaction of $(CH_3)_2SNC(O)R$ (R= C_6H_5, $C_6H_4CH_3$-*p*)(Y) with K_2PtCl_4 in water gives a stable ylide complex, $PtCl_2(Y)(DMSO)$, in which Y coordinates to the Pt(II) *via* nitrogen and DMSO *via* the sulfur to form a *cis*-configuration.

In Rahmen einer Untersuchung der Komplexbildung von Yliden haben wir in früheren Mitteilungen über die stabilen $\overset{+}{S}$–$\overset{-}{C}$H Ylid-Komplexe[1] der Palladium(II)- und Platin(II)-dihalogenide und die isoelektronischen $\overset{+}{S}$–$\overset{-}{N}$ Ylid-Komplexe des Typs $PdCl_2 \cdot 2Y$, $PdCl_2 \cdot (Y)(P(C_6H_5)_3)$ und $PtCl_2 \cdot 2Y$ (Y=*S,S*-Dimethyl-*N*-benzoyl- oder *S,S*-Dimethyl-*N*-*p*-methylbenzoylsulfilimin) berichtet.[2] Für die letzten Komplexe wurde IR-spektrometrisch bestätigt, dass der negative Stickstoff gegenüber dem Metallatom als Donator wirkt.

Bei der Umsetzung des $\overset{+}{S}$–$\overset{-}{N}$ Ylids mit K_2PtCl_4 in Wasser beobachteten wir die Bildung eines neuen Komplexes, der Ylid und Dimethylsulfoxid als Liganden enthält.

Wäßrige Lösungen von K_2PtCl_4 wurden mit einem Überschluß an *S,S*-Dimethyl-*N*-benzoylsulfilimin mehr als 10 Stdn bei Raumtemperatur gerührt. Die Niederschläge wurden nach dem Abfiltrieren wiederholt mit Methylenchlorid gewaschen. Nach der Entfernung des Lösungsmittels kristallisiert *S,S*-Dimethyl-*N*-benzoylsulfilimin–dimethylsulfoxid–dichloroplatin (II) (i) als gelbe Nadeln aus Methylenchlorid/Petroläther. Schmpt. 129—131.5 °C. $C_{11}H_{17}Cl_2NO_2S_2Pt$. (Mol.-Gew. 525.4) Ber. C; 25.15, H; 3.26, N; 2.67. Gef. C; 25.46, H; 3.24, N; 2.85, (Mol.-Gew. osmometr. in Chloroform 508). *S,S*-Dimethyl-*N*-*p*-methylbenzoylsulfilimin–dimethylsulfoxid–dichloroplatin(II) (ii) wurde genauso wie (i) dargestellt. Schmpt. 135.5—137.5 °C. $C_{12}H_{19}Cl_2NO_2S_2Pt$. (Mol.-Gew. 539.4) Ber. C; 26.72, H; 3.55, N; 2.60. Gef. C; 26.90, H; 3.63, N; 2.84. (Mol.-Gew. osmometr. in Chloroform 534).

Das ungebundene Ylid hydrolysiert langsam in Wasser, wobei Benzamid und Dimethylsulfoxid entstehen.[3] Die zugleich im System befindlichen Platin(II)-Ionen beschleunigen die Spaltung der S-N-Bindung des Ylids. Dabei entsteht Dimethylsulfoxid, welches mit dem Metallion koordiniert. In der wäßrigen Lösung kann Benzamid oder *p*-Methylbenzamid nachgewiesen werden. In den hier in Frage kommenden Versuchen werden Bis(ylid)dichloroplatin(II) und Bis(dimethylsulfoxid)dichloroplatin(II) auch als in Methylenchlorid unlöslichen Niederschläge erhalten.

Die Daten der IR- und ^{1}H-NMR-Spektren der Ylid-Komplexe werden in Tabelle 1 wiedergegeben. Die Frequenz der C=O Streckschwingung liegt beim komplexierten Ylid um 81 bzw. 105 cm^{-1} höher als beim freien. Daraus ist zu schliessen, dass das Ylid mit dem Stickstoffatom an Platin gebunden wird, wie wir bereits für die Bis(ylid)-Komplexe gefunden haben.[2] Im freien Dimethylsulfoxid tritt ν(S–O) bei 1045 cm^{-1} auf, während bei den Komplexen eine langwellige Verschiebung dieser Bande nach 1118 bzw. 1120 cm^{-1} beobachtet wird. Das spricht für das Vorliegen einer Metal-Schwefel-Bindung. Dementsprechend erscheint ν(Pt–S) bei 437 bzw. 442 cm^{-1}, wie es ähnlich für $PtCl_2 \cdot 2DMSO$ beobachtet wurde.[4] Aus den ν(Pt–Cl)-Daten in der Tabelle wird auf eine *cis*-Konfiguration am Platinatom geschlossen, was in Übereinstimmung mit änderen Dihalogenidplatin(II)-Komplexen[4,5] steht.

Die ^{1}H-NMR-Spektren weisen auf eine erhöhte Abschirmung der Ylid- und Dimethylsulfoxidprotonen in den Addukten gegenüber den freien Liganden hin. Aus den Molgewichtsbestimmungen geht hervor, dass es sich um monomere Moleküle handelt, die ihrerseits in Chloroform keine Liganden abspalten. Im ^{1}H-NMR-Spektrum findet man dementsprechend nach Zusatz von überschüssigem Dimethylsulfoxid und Ylid für komplexierte und freie Liganden getrennte Signale. Das bedeutet, dass die Ylid-Metall-Bindung wesentlich

TABELLE 1. CHARAKTERISTISCHE IR-ABSORPTIONEN[a] UND ^{1}H-NMR-DATEN[b] DER PLATIN(II)-YLID-KOMPLEXE

Verbindung	ν(C=O)	ν(S–O)	ν(Pt–S)	ν(Pt–Cl)
Y_H[c]	1539	—	—	—
$PtCl_2 \cdot 2Y_H$[e]	1611	—	—	326, ?[f]
$PtCl_2 \cdot (Y_H)(DMSO)$	1620	1118	437	344, 323
Y_{CH_3}[d]	1532	—	—	—
$PtCl_2 \cdot 2Y_{CH_3}$[e]	1603	—	—	339, 326
$PtCl_2 \cdot (Y_{CH_3})(DMSO)$	1632	1120	442	358, 344
$PtCl_2 \cdot 2DMSO$[g]	—	1157	450, 430	344, 309

Verbindung	Ylid δ (S–CH_3)	Ylid δ (*o*-H)	Ylid δ(*m*-H oder *m,p*-H)	DMSO δ (S–CH_3)	DMSO J(^{195}Pt–S–CH_3)
Y_H	2.76	8.05	7.38	——	——
$PtCl_2 \cdot (Y_H)$ (DMSO)	3.28	8.18	7.50	3.23	21.7
Y_{CH_3}	2.73	7.93	7.16	——	——
$PtCl_2 \cdot (Y_{CH_3})$ (DMSO)	3.24	8.06	7.27	3.20	21.3
$PtCl_2 \cdot 2DMSO$[h]	——	——	——	3.51	22.0
DMSO	——	——	——	2.51	——

a) In Nujol (cm^{-1}), b) Bei 25 °C in Methylenchlorid gegen TMS als internen Standard (δ, ppm; J, Hz), c) $Y_H = (CH_3)_2\overset{+}{S}\overset{-}{N}C(O)C_6H_5$, d) $Y_{CH_3} = (CH_3)_2\overset{+}{S}$-$\overset{-}{N}C(O)C_6H_4CH_3$-*p*, e) Lit. 2, f) Verdeckt durch Ligandbande g) Lit. 4, h) Lit. 4 in Nitromethan.

stärker ist als in Triphenylphosphin-Ylid-Palladium-Komplexen,[2] die zum Teil in Lösung dissoziieren. Auf Zusatz von Dimethylsulfid oder Triphenylphosphin zur Komplexlösung liefert aber bald Bis(dimethylsulfid)- oder Bis(triphenylphosphin)dichloroplatin(II). Die Spin-Spin-Kopplungskonstante zwischen ^{195}Pt und Methylprotonen des koordinierten Dimethylsulfoxids, die dem Wert des Bis(dimethylsulfoxid)dichloroplatins(II) sehr ähnlich ist, zeigt ebenfalls die *cis*-Konfiguration am Platinatom auf.

Wir danken Herrn Dr. F. H. Köhler, Technische Universität München, für die Durchsicht des Manuskript.

Literatur

1) H. Koezuka, G. Matsubayashi, und T. Tanaka, *Inorg. Chem.*, **13**, 443 (1974).

2) G. Matsubayashi, M. Toriuchi, und T. Tanaka, *Chem. Lett.*, **1973**, 985.

3) In der Literatur (A. Papa, *J. Org. Chem.*, **35**, 2837 (1970)) wird berichtet, dass *S,S*-Dimethyl-*N*-benzoylsulfilimin nicht hydrolysiert. Wir haben jedoch durch die ^1H-NMR-Messung beobachtet, dass nach langer Zeit sogar aus dem Ylid allein in Wasser Dimethylsulfoxid und Benzamid entstehen.

4) J. H. Price, A. N. Williamson, R. F. Schramm, und B. B. Wayland, *Inorg. Chem.*, **11**, 1280 (1972).

5) J. R. Farraro, "Low-Frequency Vibrations of Inorganic and Coordination Compounds," Plenum Press, N. Y. (1971), p. 165.

BULLETIN OF THE CHEMICAL SOCIETY OF JAPAN, VOL. 47 (3), 767—768 (1974)

Benzo[*h*]quinolin-10-yl-*N* Iridium(III) Complexes

Matsuo NONOYAMA

Department of Chemistry, Faculty of Science, Nagoya University, Chikusa, Nagoya 464

(Received November 5, 1973)

Synopsis. Benzo[*h*]quinoline(bhqH) is metallated with iridium(III) to give $[Ir(bhq)_2Cl]_2$ in which bhq is coordinated at 1-N and 10-C atoms. This complex reacts with a ligand(L) such as tri-*n*-butylphosphine and diethylsulfide to yield $[Ir(bhq)_2ClL]$.

The metallation reactions of organic nitrogen compounds with palladium(II) and platinum(II) to form a metal-carbon σ-bond have been studied widely, but the same reactions with other platinum metals have scarcely been investigated at all. A nitrogen heterocyclic base, benzo[*h*]quinoline(abbreviated as bhqH), has been reported[1] to form a π-complex with chromium hexacarbonyl, $Cr(CO)_3(bhqH)$. A different type of a benzo[*h*]quinoline complex has been prepared with palladium(II),[2,3] platinum(II),[3] and rhodium(III)[4] halides. In these complexes, the ligand loses one proton and coordinates to a metal ion through the carbon (10-C) and nitrogen (1-N) atoms, thus forming a five-membered chelate ring containing a metal-carbon σ-bond (Formula I). As a part of our studies of the metallation reactions of this ligand, the reaction of bhqH with $Na_3[IrCl_6]$ will be reported here.

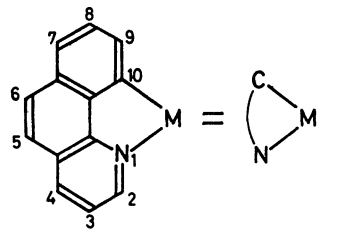

I

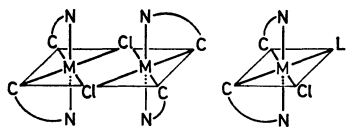

II III

Experimental

The Reaction of bhqH with $Na_3[IrCl_6]$. To a solution of 0.5 g of $Na_3[IrCl_6]$ in 2-methoxyethanol (30 ml), we added 0.6 g of bhqH. The mixture was stirred for 8 hr at room temperature and then refluxed for 24 hr. A brownish-yellow precipitate was obtained. The crude product was washed with ethanol and extracted three times with 100 ml of chloroform. The extract was then concentrated to a small volume to give a yellowish-orange powder (0.3 g), $[Ir(bhq)_2Cl]_2 \cdot 2/3CHCl_3$, which decomposed above 305 °C.

Found: C, 50.80; H, 2.70; N, 4.54; Cl, 11.12%. Calcd for $Ir_2C_{52}H_{32}N_4Cl_2 \cdot 2/3CHCl_3$: C, 50.70; H, 2.64; N, 4.49; Cl, 11.37%.

When this chloroform adduct was recrystallized from benzene, an unsolvated complex, $[Ir(bhq)_2Cl]_2$, was obtained.

Found: C, 53.55; H, 2.92; N, 4.52%. Calcd for $Ir_2C_{52}H_{32}N_4Cl_2$: C, 53.47; H, 2.76; N, 4.80%.

In a similar manner, $Na_3[IrBr_6]$ gave yellowish-orange $[Ir(bhq)_2Br]_2 \cdot 1/2CHCl_3$.

Found: C, 47.80; H, 2.37; N, 4.31%. Calcd for $Ir_2C_{52}H_{32}N_4Br_2 \cdot 1/2CHCl_3$: C, 47.89; H, 2.49; N, 4.25%.

The Reactions of $[Ir(bhq)_2Cl]_2$ with Tri-n-butylphosphine and Diethylsulfide. To a chloroform suspension (20 ml) of 0.3 g of $[Ir(bhq)_2Cl]_2$, we added 0.1 g of tri-*n*-butylphosphine (PBu_3). The suspension became transparent, and upon the addition of *n*-hexane, a yellow powder, $[Ir(bhq)_2Cl(PBu_3)]$, was precipitated. It melted at 214—217 °C.

Found: C, 57.51; H, 5.29; N, 3.49; P, 3.44%. Calcd for $IrC_{38}H_{43}N_2PCl$: C, 58.04; H, 5.51; N, 3.56; P, 3.94%.

A similar reaction of $[Ir(bhq)_2Cl]_2$ with diethylsulfide (SEt_2) in benzene gave a yellow powder, $[Ir(bhq)_2Cl(SEt_2)]$, which decomposed above 300 °C.

Found: C, 53.18; H, 3.83; N, 4.11; S, 4.82%. Calcd for $IrC_{30}H_{26}N_2SCl$: C, 53.44; H, 3.89; N, 4.15; S, 4.76%.

Measurements. All the spectral measurements were carried out by the methods reported previously.[2,4]

Results and Discussion

The reaction of bhqH with iridium(III) halides requires more drastic conditions than that with rhodium(III) halides, which has been reported to proceed in boiling ethanol and to give a similar complex, $[Rh(bhq)_2Cl]_2 \cdot 1/4CHCl_3$.[4] This fact is consistent with the general inertness of iridium(III) compared with rhodium(III).

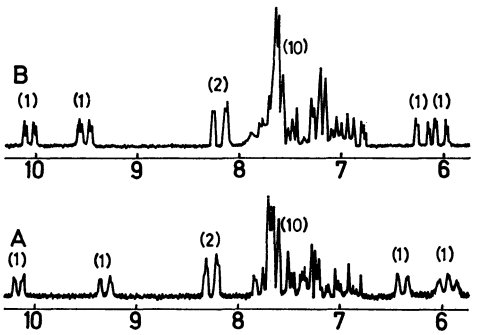

Fig. 1. 60 MHz PMR spectra of (A) $[Ir(bhq)_2Cl(PBu_3)]$ and (B) $[Ir(bhq)_2Cl(SEt_2)]$. Relative intensities of the signals are given in parentheses.

The iridium complex, $[Ir(bhq)_2Cl]_2$, is not sufficiently soluble in common solvents for precise PMR measurements. However, the gross features of the spectrum of its dilute deuterochloroform solution are similar to those of $[Rh(bhq)_2Cl]_2 \cdot 1/4CHCl_3$. Three isolated doublet-like signals were observed at $\delta = ca.$ 9.4, 8.3, and 6.0 ppm, and several overlapped peaks in the 6.7—8.0 ppm region. The former three signals are

assigned, respectively, to 2-H, 4-H, and 9-H of the metallated ligand on the basis of the assignments reported for the rhodium analogue.[4] The entire infrared spectrum of $[Ir(bhq)_2Cl]_2$ is very similar to that of the rhodium complex and shows ν_{Ir-Cl} at 219 and 240 cm^{-1}. The structure of the iridium complex seems, therefore, to be similar to that of the rhodium analogue (Formula II).

The PMR spectra of deuterochloroform solutions of $[Ir(bhq)_2Cl(PBu_3)]$ and $[Ir(bhq)_2Cl(SEt_2)]$ are shown in Fig. 1. The spectrum of the phosphine complex is very similar to that of the corresponding $[Rh(bhq)_2Cl(PBu_3)]$. In the spectra of the phosphine and sulfide complexes, the signals due to 2-H and 9-H of $[Ir(bhq)_2Cl]_2$ split into two components, implying that the two bhq moieties are not equivalent, while that of 4-H remains unsplit, probably because 4-H exists in a distant position from the donor atoms. One of the two components of the 9-H of the phosphine complex is a broad doublet at 6.39 ppm (J=6 Hz), and the other is a triplet at 5.95 ppm (J=6 Hz), while both of the sulfide complex are double doublets (at 6.22 and 6.04 ppm (J=6 and 1.5 Hz)). The triplet of the former complex may be due to the coupling of 9-H with the phosphorus atom (I=1/2), which is at the *trans*-position to the metallated carbon atom (10-C) (Formula III, L=PBu_3).

The signals due to 2-H are observed at 10.15 and 9.29 ppm for $[Ir(bhq)_2Cl(PBu_3)]$ and at 10.05 and 9.54 ppm for $[Ir(bhq)_2Cl(SEt_2)]$. The large splitting can be explained in terms of the proposed structure III, in which one proton is directed towards the coordinated chlorine atom and the other towards the phosphorus or sulfur atom. The two 2-H protons are, therefore, not equivalent.

The infrared spectrum of the phosphine complex is similar to that of the corresponding $[Rh(bhq)_2Cl(PBu_3)]$, and the band assignable to ν_{Ir-Cl} is observed at 247 cm^{-1}. The corresponding band, ν_{Ir-Cl}, for the sulfide complex is at 245 cm^{-1}. The low frequencies of these bands may be attributed to the fact that the chlorine atom is situated at *trans* position to a carbon atom with a high *trans*-influence (Formula III).[5] A new band observed for the phosphine complex at 397 cm^{-1} is tentatively assigned to δ_{CPC}.

Recently, the octahedral structure of acetatobis(2-(phenylazo)phenyl-*N*)rhodium(III) has been determined by X-rays;[6] the metallated carbon atoms have been found to be located mutually *cis*, and the nitrogen atoms *trans*, to each other. This is consistent with the structures proposed for the rhodium and iridium complexes of benzo[*h*]quinoline, and it is evident that the reaction of bhqH with $Na_3[IrCl_6]$ forms a carbon-iridium bond to give a five-membered metallocycle (Formula I).

References

1) E. O. Fischer, H. A. Goodwin, C. G. Kreiter, H. D. Simmons, Jr., K. Sonogashira, and S. B. Wild, *J. Organometal. Chem.*, **14**, 359 (1968).

2) M. Nonoyama, K. Suzuki, and K. Yamasaki, *Proc. Japan Acad.*, **45**, 909 (1968); M. Nonoyama and K. Yamasaki, *Nippon Kagaku Zasshi*, **91**, 1058 (1970).

3) B. N. Cockhurn, D. V. Howe, T. Keating, B. F. G. Johnson, and J. Lewis, *J. Chem. Soc., Dalton*, **1973**, 404.

4) M. Nonoyama and K. Yamasaki, *Inorg. Nucl. Chem. Lett.*, **7**, 943 (1971).

5) D. F. Gill, B. E. Mann, and B. L. Shaw, *J. Chem. Soc., Dalton*, **1973**, 270 and references therein.

6) R. J. Hoare and O. S. Mills, *ibid.*, **1972**, 2138, 2141.

BULLETIN OF THE CHEMICAL SOCIETY OF JAPAN, VOL. 47 (3), 769—770 (1974)

Kinetic Studies of the Nickel Glycolate Complex Formation in Solution by the Pressure-Jump Method

Shoji HARADA, Yozo OKUUE, Haruki KAN, and Tatsuya YASUNAGA

Department of Chemistry, Faculty of Science, Hiroshima University, Higashisenda-machi, Hiroshima 730

(Received December 17, 1973)

Synopsis. The nickel glycolate complex formation reaction was studied by the pressure-jump method and the kinetic parameters were obtained. The rate-determining step of the reaction was revealed to be the chelate-ring formation process.

Glycolate ion makes a chelate complex with a metal ion where COO^- group and OH group are coordinated. The step-by-step model will be, then, proposed for the complex formation mechanism.[1,2] In the previous studies on the kinetics of the nickel lactate complex formation,[3] the authors showed that the rate-determining step is the chelate-ring closure and compared the results with those of the nickel glycolate. On the nickel glycolate complex formation reaction, a few kinetic data have been provided[4-6] but the detailed interpretations have not been reported. By obtaining the kinetic data on the nickel glycolate in the same procedures as that applied to the nickel lactate,[3] the authors aimed to study the ligand effects on the complex formation reaction.

Experimental

All of the chemicals used were of a reagent grade. Sample solutions were prepared in the same way as that described in the previous papers.[3,7] Kinetic studies were carried out by the pressure-jump method which has been described elsewhere.[3,7] The measurements were carried out at 10, 15, 20, 25, and 30 °C in the concentration range from 1.01×10^{-3} to 5.04×10^{-2} M of the nickel glycolate. Experiments were carried out at least five times for each solution and the quoted relaxation times were the mean values.

Results and Discussion

The concentration dependency of the relaxation times showed that the relaxation phenomena can be interpreted in terms of the following mechanism:

$$M^{2+} + L^- \underset{k_d}{\overset{k_f}{\rightleftharpoons}} ML^+ \qquad (1)$$

where M^{2+} is the metal ion, L^- is the ligand ion, ML^+ is the complex, k_f and k_d are the formation and the dissociation rate constants respectively. In Eq. (1), the relaxation time, τ, is related to the rate constants as follows:

$$1/\tau = k_f\gamma_M\gamma_L(C_M+C_L) + k_d\gamma_{ML} \qquad (2)$$

where γ is the activity coefficient, C is the equilibrium concentration of the species, and the subscripts indicate the corresponding species. Assuming that $\gamma_{ML}=\gamma_L$, Eq. (2) is converted to:

$$1/(\tau\cdot\gamma_{ML}) = k_f\gamma_M(C_M+C_L) + k_d \qquad (3)$$

If the stability constant, $K(=k_f/k_d)$, is given appropriately, the plot of $1/(\tau\cdot\gamma_{ML})$ *vs.* $\gamma_M(C_M+C_L)$ will be linear; then k_f and k_d can be obtained from the slope and the intercept of the straight line respectively. Here, the activity coefficients were calculated by the Davies equation.[8] Most probable plots at each temperatures are shown in Fig. 1. The rates and the stability constants obtained are summarized in Table 1. Activation parameters were calculated in the same way as that described in the previous papers.[3] They are listed in Table 2. Taking into account the differences of the experimental conditions and the method, the

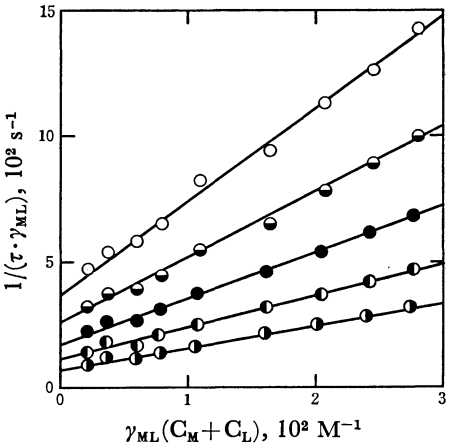

Fig. 1. $1/(\tau\cdot\gamma_{ML})$ *vs.* $\gamma_M(C_M+C_L)$ plot at 10 °C (◑), 15 °C (◐), 20 °C (●), 25 °C (◒), and 30 °C (○).

Table 1. The formation and the dissociation rate constants and the stability constants of the nickel glycolate ($\mu\rightarrow0$)

t, °C	k_f (10^3 M^{-1} s^{-1})	k_d (s^{-1})	K (10^2M^{-1})
10	8.7±0.6	72±5	1.2±0.1
15	12.5±0.6	114±5	1.1±0.1
20	18.7±0.6	170±10	1.1±0.1
25	26.0±1.0	260±15	1.0±0.1
30	37.0±1.5	370±20	1.0±0.1

Table 2. Kinetic data of the nickel glycolate complex formation at 25 °C ($\mu\rightarrow0$)

K, M^{-1}	$1.0(\pm0.1)\times10^2$
k_f, M^{-1}s^{-1}	$2.60(\pm0.10)\times10^4$
k_d, s^{-1}	$2.60(\pm0.15)\times10^2$
ΔE_f^*, kcal·mol^{-1}	12.5±1.1
ΔE_d^*, kcal·mol^{-1}	13.8±1.0
ΔG_f^*, kcal·mol^{-1}	11.4±1.1
ΔH_f^*, kcal·mol^{-1}	11.9±1.1
ΔS_f^*, cal·deg^{-1}·mol^{-1}	2±4

TABLE 3. THE RATE AND THE STABILITY CONSTANTS FOR THE NICKEL CARBOXYLATE COMPLEXES AT 25 °C

Ligand	K (M^{-1})	k_f ($M^{-1}s^{-1}$)	k_d (s^{-1})	K_0k_1 ($M^{-1}s^{-1}$)	k_{-1} (s^{-1})	k_2 (s^{-1})	k_{-2} (s^{-1})	ΔE_f^* (kcal·mol^{-1})	μ	Ref.
Oxalate	2.1×10^4	7.4×10^4	3.6	8.5×10^5	7×10^3	6.7×10^2	4	15	0.1	2a)
Malonate	1.0×10^4	4.5×10^5	45	8.5×10^5	3.5×10^3	4.5×10^3	1×10^2	—	—	5
	1.2×10^4	4.2×10^5	35	8.5×10^5	3.5×10^3	3.4×10^3	70	14.2	→0	12a)
Lactate	1.5×10^2	2.6×10^4	1.7×10^2	1.5×10^5	9×10^3	1.9×10^3	2.1×10^2	13.5	→0	3
Glycolate	1.0×10^2	2.6×10^4	2.6×10^2	1.5×10^5	9×10^3	1.9×10^3	3.2×10^2	12.5	→0	This work
	1.7×10^2	3.3×10^4	2.0×10^2	1.5×10^5	9×10^3	2.5×10^3	2.6×10^2	—	—	6

a) The rate constants of the individual steps were calculated from the original data in the same way as that carried out in the nickel glycollate system.

stability constants in Table 2 are in good agreement with the literature values.[9-11] The rate constants at 25 °C are in fair agreement with the data of the nickel glycolate reported by Hoffmann.[6] The activation parameters are close, not only, to those of the lactate but also to the oxalate and the malonate.[12] These resembrances imply that the same step of the reaction, *e.g.*, chelate-ring closure, is responsible for the present relaxation phenomena.

The detailed model of the nickel glycolate complex formation can be expressed as follows:

$$\underset{\text{(I)}}{Ni^{2+} + L^-} \overset{K_0}{\rightleftharpoons} \underset{\text{(II)}}{Ni^{2+}O\begin{matrix}H\\ \diagdown\\ H\end{matrix}L^-} \overset{k_1}{\underset{k_{-1}}{\rightleftharpoons}} \underset{\text{(III)}}{Ni^+ - L} \overset{k_2}{\underset{k_{-2}}{\rightleftharpoons}} \underset{\text{(IV)}}{Ni^+ = L} \qquad (4)$$

where (I) is the free ions, (II) is the outer-sphere complex, (III) is the unidentated complex, (IV) is the chelate complex, and K_0 is the outer-sphere complex formation constant.

Assuming that the complex is stable as a chelate complex and the intermediate state (II) and (III) are in the steady state, the rate constants in Eq. (4) are related to k_f and k_d in Eq. (1) as follows:

$$k_f = K_0k_1\left(\frac{k_2}{k_2+k_{-1}}\right) \qquad (5)$$

$$k_d = k_{-1}\left(\frac{k_{-2}}{k_2+k_{-1}}\right) \qquad (6)$$

As that described in the previous paper,[3] K_0k_1 and k_{-1} can be estimated to be $1.5\times10^5\ M^{-1}\ s^{-1}$ and $9\times10^3\ s^{-1}$, respectively. Then, k_2 and k_{-2} can be obtained by Eqs. (5) and (6). They are listed in Table 3 along with the rate constants of the other nickel bidentate complexes.

In the nickel glycolate complex formation, the rate-determining-step is the chelate-ring closure step. The kinetic data are very close to those of the nickel lactate. This fact shows that the methyl group of the lactate ion does not give effective contributions to the kinetic values of the complex formation. In Table 3, the rate constants of the chelate-ring closure, k_2, are of the order of $\sim10^3\ s^{-1}$, which is about an order of magnitude smaller than the water exchange rate constant of the nickel ion. This fact means that the values of the rate constants of the chelate-ring rupture, k_{-2}, reflect the stabilities of the chelate complexes.

References

1) M. Eigen and L. DeMaeyer, "Technique of Organic Chemistry," Vol. VIII, 2nd Ed., S. L. Friess, Interscience Publishers Inc., New York, N. Y. (1963), Part 2, p. 895.

2) G. H. Nancollas and N. Sutin, *Inorg. Chem.*, **3**, 360 (1964).

3) S. Harada, H. Tanabe, and T. Yasunaga, This Bulletin, **46**, 3125 (1973).

4) H. Hoffmann, J. Stuehr, and E. Yeager, "Chemical Physics of Ionic Solutions," B. Conway and R. Barradas Eds., John Wiley & Sons, Inc., New York, (1966), Chapter 14, p. 255.

5) H. Hoffmann and E. Yeager, *Rev. Sci. Instrum.*, **39**, 1151 (1968).

6) H. Hoffmann, *Ber. Bunsenges. Physik. Chem.*, **73**, 432 (1969).

7) S. Harada and T. Yasunaga, This Bulletin, **46**, 502 (1973).

8) C. W. Davies, "Ion Association," Butterworths, London (1962).

9) W. P. Evans and C. B. Monk, *J. Chem. Soc.*, 550 (1954).

10) B. Grabaric and I. Filipovic, *Croat. Chem. Acta*, **42**, 479 (1970).

11) I. Filipovic, T. Matusinovic, B. Mayer, I. Piljac, B. Bach-Dragutinovic, and A. Bujak, *ibid.*, **42**, 541 (1970).

12) J. L. Bear and C. T. Lin, *J. Phys. Chem.*, **72**, 2026 (1968).

BULLETIN OF THE CHEMICAL SOCIETY OF JAPAN, VOL. 47 (3), 771—772 (1974)

Micellar Effect of Lauryldimethylsulfonium Halides on the Hydrolysis of *p*-Nitrophenyl Decanoate

Tsuneo OKONOGI, Yumihiko YANO, and Waichiro TAGAKI

Department of Chemistry, Faculty of Technology, Gunma University, Kiryu, Gunma 376

(Received July 23, 1973)

Synopsis. Micellar effects of lauryldimethylsulfonium chloride, bromide, and iodide on the hydrolysis of *p*-nitrophenyldecanoate were found to be very similar to those of the corresponding lauryltrimethylammonium halides.

Ester hydrolysis catalyzed by cationic micelles of quaternary ammonium salts has been extensively investigated in recent years.[1] In most cases, the rate of hydrolysis is first order with respect to hydroxide ion. Meanwhile, we have observed,[2] previously, that the rate of base catalyzed H–D exchange reaction of the methyl group of lauryldimethylsulfonium halides is non-linear with respect to the concentration of hydroxide ion under micellar conditions, but follows to a Michaelis-Menten type saturation kinetics, and we have suggested that the binding of hydroxide ion occurs on a cationic micellar surface prior to the hydrogen abstraction. Although such a difference in the behavior of hydroxide ion between ester hydrolysis and H–D exchange reaction is probably due to different ranges of hydroxide ion concentration which is much higher for the latter than for the former reaction, another possibility is due to some difference in micellar properties between ammonium and sulfonium salts. Incidentally, the micellar effects of sulfonium salts on the ester hydrolysis has little been investigated. Therefore we have compared the micellar effects of lauryltrimethylammonium and lauryldimethylsulfonium halides on the hydrolysis of *p*-nitrophenyl decanoate.

Results and Discussion

The rates of hydrolysis were followed by a conventional spectrophotometric determination of *p*-nitrophenol liberated. The dependency of the rates on detergent concentration is shown in Fig. 1. The Figure indicates typical micellar effects: 1) The rates increase rapidly by increasing detergent concentration near the CMC[1,3] and reach to a maximum, then decrease gradually by further increase of detergent. 2) The rates are affected markedly by the counter anion (X) and increase in the order of X=I<Br<Cl. These two trends are almost the same for each series of sulfonium and ammonium salts. The effects of added salts on the rates are shown in Table 1. The rate of sulfonium chloride observed in the absence of KI was reduced to one fifth by the addition of a half molar amounts of KI over the detergent concentration. The rate of the sulfonium iodide is also reduced by the addition of KCl, but the extent of rate reduction is very small. These salt effects appears to be essentially the same as observed in the micellar effects of quaternary ammonium salts.[4]

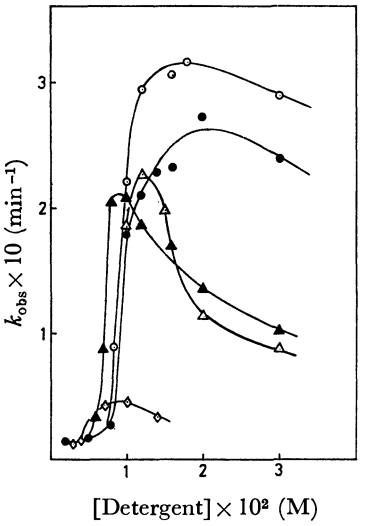

Fig. 1. Plots of k_{obs} *vs.* detergent concentration: Ester, 1×10^{-5}M; pH 10.1 (Na_2CO_3–$NaHCO_3$ buffer, 5×10^{-3}M), 25 °C.
○: *n*-$C_{12}H_{25}N^+(CH_3)_3Cl^-$, ●: *n*-$C_{12}H_{25}S^+(CH_3)_2Cl^-$,
△: *n*-$C_{12}H_{25}N^+(CH_3)_3Br^-$, ▲: *n*-$C_{12}H_{25}S^+(CH_3)_2Br^-$,
◇: *n*-$C_{12}H_{25}S^+(CH_3)_2I^-$.

Table 1. Salt effect on the hydrolysis of *p*-nitrophenyl decanoate (1×10^{-5}M) catalyzed by *n*-$C_{12}H_{25}S^+(CH_3)_2X^-$ (X=I; 1×10^{-2}M, X=Cl; 2×10^{-2}M): pH 10.1 (Na_2CO_3–$NaHCO_3$ buffer; 5×10^{-3}M), 25°

X=I		X=Cl	
KCl ($\times 10^2$M)	k_{obs} (min^{-1})	KI ($\times 10^3$M)	k_{obs} (min^{-1})
0	4.57×10^{-2}	0	2.73×10^{-1}
3	3.82×10^{-2}	2	1.90×10^{-1}
5	3.33×10^{-2}	4	1.58×10^{-1}
10	3.01×10^{-2}	10	5.06×10^{-2}

The dependency of the rates on hydroxide ion concentration was also examined. For all the salts shown in Fig. 1, the plots of log ($k_{obs}-k_o$) *vs.* log [OH^-] gave straight lines (slope=1.0) up to [OH^-]=10^{-2} M, and no saturation phenomenon as observed in the H–D exchange reaction was detected. It was difficult to use more higher base concentration as in the H–D exchange reactions ([OH^-]=0.1—0.2 M)[2] because the rates become too fast to measure by the present method.

The above results indicate that long chain alkyl sulfonium and ammonium salts behave quite similarly in the hydrolysis of *p*-nitrophenyl decanoate.

Experimental

Materials. *p*-Nitrophenyldecanoate was prepared by the method of Bodansky,[5] mp 35 °C (lit,[6] 35—35.7 °C).

Lauryldimethylsulfonium halides, $n\text{-}C_{12}H_{25}S^{+}(CH_3)_2X^{-}$, were reported previously:[2] iodide, mp 87 °C; bromide, mp 68—70 °C; chloride, mp 64—66 °C.

Lauryltrimethylammonium halides: bromide, mp 243 °C (lit,[7] 243—244 °C); chloride, mp 247 °C (lit,[8] 247 °C).

Kinetics were performed spectrophotometrically with Hitachi 124 spectrophotometer according to our previous method.[9] The pH of the reaction mixture was determined with Hitachi-Horiba pH meter (F-7DE).

References

1) a) E. H. Cordes and R. B. Dunlap, *Accounts Chem. Res.*, **2**, 329 (1969). b) E. J. Fendler and J. H. Fendler, "Advances in Physical Organic Chemistry," Vol. 8, ed. by V. Gold, Academic Press, London and New York, (1970), p. 271.

2) Y. Yano, T. Okonogi, and W. Tagaki, *J. Org. Chem.*, **38**, 3912 (1973).

3) The CMC values of $C_{12}H_{25}S^{+}(CH_3)_2X^{-}$ in pure water are; 1.65×10^{-2} M (X=Cl), 1.14×10^{-2} M (X=Br), and 0.689×10^{-2} M (X=I).

4) L. R. Romsted and E. H. Cordes, *J. Amer. Chem. Soc.*, **90**, 4404 (1968).

5) M. Bondansky and V. Duvigneaud, *ibid.*, **81**, 5688 (1959).

6) C. A. Blyth and J. R. Knowles, *ibid.*, **93**, 3017 (1971).

7) J. A. Cella, D. N. Eggenberg, D. R. Noel, L. A. Harriman, and H. J. Harwood, *ibid.*, **74**, 2061 (1952).

8) M. J. McDowell and C. A. Kraus, *ibid.*, **73**, 2170 (1951).

9) a) W. Tagaki, M. Chigira, T. Amada, and Y. Yano, *Chem. Commun.*, **1972**, 219. b) W. Tagaki, T. Amada, Y. Yamashita, and Y. Yano, *ibid.*, **1972**, 1131.

BULLETIN OF THE CHEMICAL SOCIETY OF JAPAN, VOL. 47 (3), 773—774 (1974)

The Reaction of Substituted Tropones with Diphenylketene

Toyonobu Asao, Noboru Morita, and Nobuo Iwagame

Department of Chemistry, College of General Education, Tohoku University, Kawauchi, Sendai 980

(Received July 25, 1973)

Synopsis. The reaction of 2-methoxytropone and diphenylketene afforded (2+8)cycloadduct and 1-methoxy-8,8-diphenylheptafulvene which must be formed by the decarboxylation of the initially-formed (2+2)cycloadduct. 2-Dimethylaminotropone also gave the heptafulvene derivative. However, 2-chloro-, 2-cyano-, and 2,5-dimethoxytropone yielded only (2+8)cycloadducts.

The reaction of 4,5-benzotropone with diphenylketene has long been known to give diphenylbenzoheptafulvene[1] by the decarboxylation of the initially-formed (2+2)cycloadduct. The reactions of tropone with diphenylketene[2] and dichloroketene[3] have also been studied; two (8+2)cycloadducts (I and II respectively) were obtained. However, the reaction of tropone with activated isocyanates has been shown to give troponeimine derivatives; presumably they are formed by the elimination of CO_2 from the (2+2)cycloadducts.[4] Furthermore, we have recently found that 8-oxoheptafulvene, which has a cyclic conjugated ketene moiety, reacts with tropones to give (8+2)cycloadducts and heptafulvalenes and its derivatives, which are formed by the decarboxylation of the (2+2)cycloadducts; we have also found that the (8+2)cycloadducts might be the isomerization products of the (2+2)-cycloadducts.[5]

These results prompted us to investigate the reaction of substituted tropones and diphenylketene; this paper will describe the results of this study.

The refluxing of a mixture of 2-methoxytropone and diphenylketene (1: 1.2 molar ratio) in anhydrous benzene and subsequent chromatographic separation afforded two products, yellow plates (III) and colorless plates (IV), in 6.5 and 50% yields respectively.

Compound (III) was proved to be 1-methoxy-8,8-diphenylheptafulvene[6] from elemental analyses and its spectroscopic data, as well as by hydrolysis with hydrochloric acid which gave 2-benzhydryltropone (V). It is clear that Compound (III) is formed by the decarboxylation of the (2+2)cycloadduct intermediate (VI).

Compound (IV) was proved to be the (8+2)cycloadduct by the elemental analyses and by the spectroscopic data. The alternative structure (VII) for Compound (IV) could be excluded on the basis of the existence of a signal ascribable to Ha hydrogen in its NMR spectrum. This result is similar to that in the case of the (8+2)cycloadducts of 8-oxoheptafulvene with substituted tropones.[5]

The reaction of 2-dimethylaminotropone with diphenylketene afforded 1-dimethylamino-8,8-diphenylheptafulvene (VIII) and an unidentified product. However, the reaction of diphenylketene with 2-chloro-, 2-cyano-, and 2,5-dimethoxytropone afforded only (8+2)cycloadducts (IX—XI); no heptafulvene derivatives could be obtained.

It is clear that electron-releasing groups, such as a methoxy or dimethylamino group, stabilize 8,8-diphenylheptafulvene; however, the influence of the substituents of tropone on the mode of the reaction with diphenylketene is not clear.

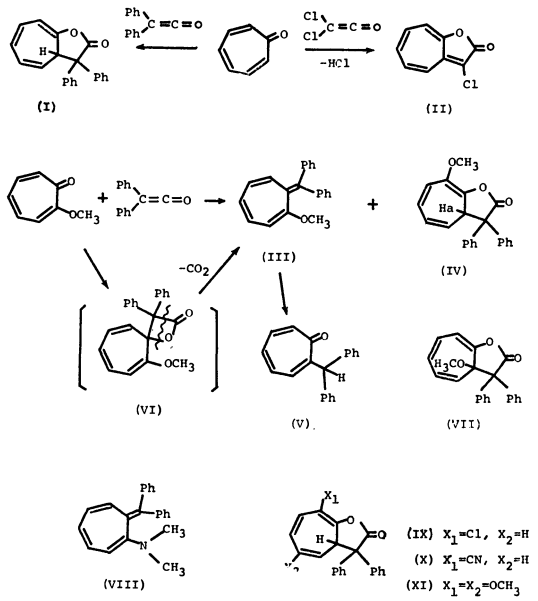

Experimental

Reaction of 2-Methoxytropone with Diphenylketene. A solution of 2-methoxytropone (500 mg) and diphenylketene (800 mg) in anhydrous benzene (5 ml) was refluxed for 2 hr under a nitrogen atmosphere. The solvent was then removed and chromatographed on a silica-gel column, using $CHCl_3$ as the solvent. From the first effluent, 70 mg of yellow plates (III) (mp 115—116 °C (from ethanol)) were obatined. Compound (III) is stable when standing in the air at room temperature. λ_{max}^{MeOH} nm(log ε); 255^{sh} (3.48) and 333 (3.95). NMR ($CDCl_3$); δ 3.30 (OCH_3), 5.48 (1H, d, J=7.0 Hz), 5.8—6.4 (4H, m) and 6.8—7.4 (10H, m).

Found: C, 88.21; H, 6.40%. Calcd for $C_{21}H_{18}O$: C, 88.08; H, 6.34%.

From the second effluent, 646 mg of colorless plates (IV) (mp 122—123 °C (from ethanol)) were obtained. NMR ($CDCl_3$); δ 3.48 (Ha, d.d, J=4.5, 1.5 Hz), 3.75 (OCH_3), 4.62 (1H, d.d, J=10.0, 4.5 Hz), 5.8—6.5 (3H, m) and 6.9—7.6 (10H).

Found: C, 79.96; H, 5.59%. Calcd for $C_{22}H_{18}O_3$: C, 79.98; H, 5.49%.

Reaction of 2-Dimethylaminotropone with Diphenylketene. A solution of 2-dimethylaminotropone (750 mg) and diphenylketene (970 mg) in dry benzene (5 ml) was refluxed for 6 hr. The solution was then chromatographed on a silica-gel column and eluted with benzene; 117 mg (7.8%) of pale yellow needles (VIII) (mp 118—120 °C (from ethanol)), 246 mg of colorless needles (mp 131.5—132 °C,

(Found: C, 87.33; H, 5.97%, λ_{max}^{EtOH} nm; 249)), and 368 mg (49%) of the starting tropone were thus obtained. Compound (VIII) is also stable for standing in the air at room temperature. λ_{max}^{MeOH} nm(log ε); 246 (4.17), 310 (3.91), and 356 (4.03), NMR ($CDCl_3$); δ 2.42 ($N(CH_3)_2$), 6.6—7.5 (15H, m).

Found: C, 88.52; H, 7.22; N, 4.41%. Calcd for $C_{22}H_{21}N$: C, 88.25; H, 7.07; N, 4.68%.

Reaction of 2-Chlorotropone with Diphenylketene. A solution of 2-chlorotropone (560 mg) and diphenylketene (800 mg) in dry benzene (5 ml) was refluxed for 2 hr. The solvent was then removed, leaving colorless crystals; these crystals were subsequently recrystallized from ethanol to give 1.087 g (82%) of colorless prisms (IX) (mp 149—150 °C). NMR ($CDCl_3$); δ 3.72 (1H, d.d, J=4.5, 2.0 Hz), 4.66 (1H, d.d, J=10.0, 4.5 Hz), 5.90—6.65 (3H, m) and 7.18—7.50 (10H).

Found: C, 75.08; H, 4.50%. Calcd for $C_{21}H_{15}O_2Cl$: C, 75.34; H, 4.52%.

Reaction of 2-Cyanotropone with Diphenylketene. A solution of 2-cyanotropone (262 mg) and diphenylketene (450 mg) in dry benzene (15 ml) was refluxed for 1.5 hr. The solvent was then removed, and the residue was washed with $CHCl_3$ to give 530 mg of colorless crystals. Recrystallization from $CHCl_3$–ethanol gave X as colorless prisms; mp 175—176 °C. NMR ($CDCl_3$); δ 3.70 (1H, d.d, J=4.0, 2.0 Hz), 4.65 (1H, d.d, J=10.0, 4.0 Hz), 6.1 (1H, m), 6.60 (2H) and 7.15—7.5 (10H).

Found: C, 81.02; H, 4.58; N, 4.13%. Calcd for $C_{22}H_{15}O_2N$: C, 81.21; H, 4.65; N, 4.31%.

Reaction of 2,5-Dimethoxytropone with Diphenylketene. A solution of 2,5-dimethoxytropone (336 mg) and diphenylketene (400 mg) in dry benzene (8 ml) was refluxed for 1.5 hr. When the solution was then chromatographed on a silica-gel column, 697 mg of a colorless powder were obtained. Recrystallization from $CHCl_3$–ethanol afforded XI as colorless prisms; mp 125—126 °C. NMR ($CDCl_3$); δ 3.20 (OCH_3), 3.65—3.75 (OCH_3 and 2H), 6.07 (1H, d, J=11.5 Hz), 6.28 (1H, d, J=11.5 Hz) and 7.3 (10H).

Found: C, 76.43; H, 5.54%. Calcd for $C_{23}H_{20}O_4$: C, 76.65; H, 5.59%.

2-Benzhydryltropone (V). A solution of heptafulvene (III, 109 mg) in methanol (16 ml) and 3M HCl (3 ml) was refluxed for 25 min. The solvent was then removed, water was added, and the solution was extracted with $CHCl_3$. The subsequent removal of the solvent gave 90 mg of a pale yellow powder; recrystallization from $CHCl_3$–cyclohexane afforded V as pale yellow plates; mp 123—124 °C. λ_{max}^{MeOH} nm(log ε); 219^{sh} (4.46), 230^{sh} (4.36), and 313 (3.88). NMR ($CDCl_3$); δ 6.04 (1H, s) and 6.5—7.5 (16H, m).

Found: C, 88.27; H, 5.95%. Calcd for $C_{20}H_{16}O$: C, 88.20; H, 5.92%.

References

1) H. Staudinger and H. Kon, *Ann.*, **384**, 38 (1911).

2) C. Jutz, I. Rommel, I. Lengyel, and J. Feeney, *Tetrahedron*, **22**, 1809 (1966); G. Gommper, A. Studenere, and W. Elser, *Tetrahedron Lett.*, **1968**, 1019; A. S. Kende, *ibid.*, **1967**, 2661.

3) J. Ciabattoni and H. W. Anderson, *ibid.*, **1967**, 3377.

4) L. A. Paquette and N. Horton, *ibid.*, **1968**, 2289.

5) N. Morita, Y. Kitahara, and T. Asao, *ibid.*, **1972**, 869; T. Asao, N. Morita, and Y. Kitahara, *Synthetic Commun.*, **2** (6), 353 (1972); T. Asao, N. Morita, C. Kabuto, and Y. Kitahara, *Tetrahedron Lett.*, **1972**, 4379; N. Morita, T. Asao, N. Iwagame, and Y. Kitahara, *Chem. Lett.*, **1973**, 67.

6) 8,8-Diphenylheptafulvene itself has been synthesized as red-brown needles; mp 59—60 °C. It is stable under nitrogen, but reacts readily with atmospheric oxygen; H. J. Dauben, Jr., and R. B. Medz, 145th Meeting of American Chemical Society (September 1963), *Abstracts of Papers*, p. 7s. For 1,8,8-triphenylheptafulvene, see J. A. Myers, R. C. Joines, and W. M. Jones, *J. Amer. Chem. Soc.*, **92**, 4740 (1970).

BULLETIN OF THE CHEMICAL SOCIETY OF JAPAN, VOL. 47 (3), 775—776 (1974)

The Reaction of Isocyanates with Carboxylic Acids and Thiocarboxylic Acids

Shinichi MOTOKI, Takao SAITO, and Hiroaki KAGAMI

Department of Chemistry, Faculty of Science, Science University of Tokyo, Kagurazaka, Shinjuku-ku, Tokyo 162

(Received July 27, 1973)

Synopsis. Thiocarboxylic acids reacted with isocyanates or acyl isocyanates to give the stable addition products. However, similar products obtained from benzoic acid and acyl isocyanates dissociated into their components in solution.

Isocyanates are known to react with carboxylic acids to give mixed carbamic carboxylic anhydrides (I).[1-3] These anhydrides are relatively unstable and decompose to give a mixture of amide, *sym*-substituted urea and carboxylic anhydride with evolution of carbon dioxide on heating.[2,3] Some of them dissociate into isocyanates and carboxylic acids in solution.[2,4] It appeared of interest to study the reactions of isocyanates and acyl isocyanates with carboxylic acids and thiocarboxylic acids.

Thiobenzoic acid was allowed to react with phenyl isocyanate in *n*-hexane at room temperature. The reaction proceeded immediately and benzoyl phenylcarbamoyl sulfide (IIa) was obtained as white precipitates. Though I* was readily decomposed on heating and difficult to be recrystallized, IIa was relatively stable and could be purified by recrystallization. Thus analogous sulfides (IIa)—(IIf) were prepared by a similar procedure. The results are summarized in Table 1. The IR spectra of II showed a N–H band at 3220—3250 cm^{-1}, two C=O bands at 1700—1730 cm^{-1} and 1675—1680 cm^{-1} and no absorption due to S–H in the region 2500—2600 cm^{-1}.** The reaction of phenyl isocyanate with thioacetic acid gave acetyl phenylcarbamoyl sulfide (IIg), mp 37—39 °C. IIg decomposed on standing for a few days. Elementary analyses were not in good agreement with the calculated values, but the structure was confirmed by IR spectra (3250 cm^{-1} (N–H), 1720, and 1680 cm^{-1} (C=O)) and NMR spectra (2.67 τ (5H, C_6H_5) and 7.66 τ (3H, CH_3)). The reaction of methyl isocyanate with thioacetic acid or thiobenzoic acid resulted in the corresponding decomposition products, *N*-methylacetamide and *N*-methylbenzamide.

Table 1. RNH–COSCO–R′ (II)

Compd	R	R′	Yield (%)	Mp (°C)
IIa	C_6H_5	C_6H_5	86	95—97
IIb	*m*-$O_2NC_6H_4$	C_6H_5	95	124
IIc	*m*-$O_2NC_6H_4$	CH_3	83	98
IId	C_6H_5	*p*-$O_2NC_6H_4$	76	125—126
IIe	C_6H_5	*p*-ClC_6H_4	81	118—120
IIf	C_6H_5	*p*-$CH_3C_6H_4$	93	109

* For the preparation of I, it is necessary to carry out the reaction in a very concentrated solution.[2]

** Wheeler, who examined the reaction of phenyl isocyanate and thiobenzoic acid, erroneously gave the structure *N*-benzoyl phenyl thiocarbamic acid to the product. (H. L. Wheeler, *J. Amer. Chem. Soc.*, **23**, 444 (1901)).

Table 2. RCONH–COSCO–R′ (III)

Compd	R	R′	Yield (%)	Mp (°C)
IIIa	C_6H_5	C_6H_5	93	75—76
IIIb	C_6H_5	*p*-ClC_6H_4	69	85—86
IIIc	C_6H_5	*p*-$O_2NC_6H_4$	74	82—83
IIId	C_6H_5	CH_3	85	59—61
IIIe	*p*-ClC_6H_4	C_6H_5	91	83—84
IIIf	*p*-$O_2NC_6H_4$	C_6H_5	89	105—106
IIIg	CH_2Cl	C_6H_5	81	107—109
IIIh	$CHCl_2$	C_6H_5	84	105—108
IIIi	CCl_3	C_6H_5	89	112—114

Acyl isocyanates reacted with thiocarboxylic acids also to give acyl acylcarbamoyl sulfides (IIIa)—(IIIi). The results are shown in Table 2. The IR spectra of III showed a broad N–H band at 3100—3400 cm^{-1} and three C=O bands at 1750—1790 cm^{-1}, 1660—1720 cm^{-1} and 1640—1660 cm^{-1}.

Table 3. RCONH–COOCO–R′ (IV)

Compd	R	R′	Yield (%)	Mp (°C)	Dissociation percent (25 °C) (0.5 mol/l)	
					$CHCl_3$	C_6H_6
IVa	C_6H_5	C_6H_5	82	62—65	100	100
IVb	CH_2Cl	C_6H_5	54	101—103	55	100
IVc	$CHCl_2$	C_6H_5	48	102—105	70	100
IVd	CCl_3	C_6H_5	80	70—73	80	100

Satisfactory analytical data (±0.3% for C, H, N, S) were obtained for all new compounds listed in Tables 1, 2, and 3.

The reaction of mono- or dichloroacetyl isocyanate with benzoic acid proceeded similarly to give carbamic benzoic anhydride (IVb) or (IVc). Treatment of benzoyl isocyanate or trichloroacetyl isocyanate with benzoic acid in ether at room temperature gave no precipitate of the product. However, the corresponding anhydride (IVa) or (IVd) was obtained in good yield by evaporation of the solvent. The results are shown in Table 3. The IR spectra of solid IVa—IVd were those of true anhydride (3200—3300 cm^{-1} (N–H), 1800—1820, 1740—1760, 1690—1720 cm^{-1} (C=O)). In $CHCl_3$, however, the spectra apparently consist of both of the absorption of the anhydride and its dissociated components, acyl isocyanate (2250 cm^{-1}

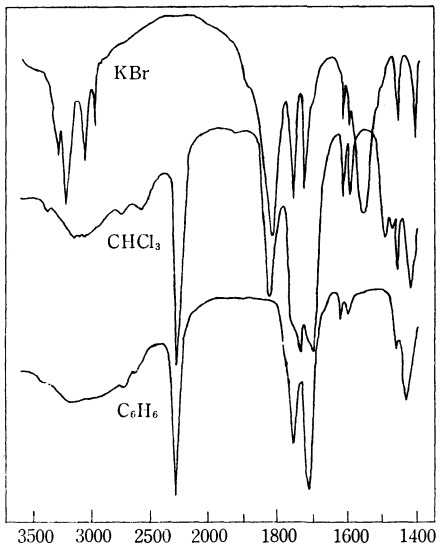

Fig. 1 IR spectra of IVb

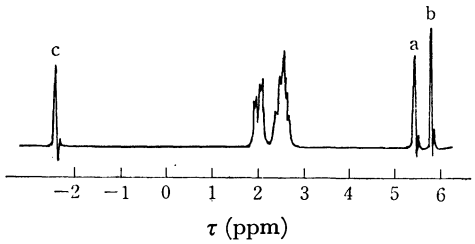

Fig. 2 NMR spectra of IVb ($CDCl_3$)

$ClCH_2CONHCOOCOC_6H_5 \rightleftharpoons ClCH_2CONCO + C_6H_5COOH$

a 5.42 τ b 5.79 τ c −2.24 τ

(NCO), and 1705—1760 cm^{-1} (C=O)) and benzoic acid (1700 cm^{-1} (C=O)). In C_6H_6, the spectra showed only those of dissociation components. The dissociation percentage of IVa—IVd were estimated by means of their NMR absorption. For illustration the spectra of IVb are given in Figs. 1 and 2. From the results shown in Table 3, it is concluded that the compounds IVa—IVd are partly dissociated into their components in solution, the degree of dissociation depending on the structure of the anhydrides and nature of the solvents. In the IR spectra of II and III, a very weak absorption of NCO appeared in $CHCl_3$ or C_6H_6 solution. The amount of dissociated species seemes to be negligible.

$$R\text{-}N{=}C{=}O + R'COOH \longrightarrow R\text{-}\underset{H}{N}\text{-}\underset{O}{C}\text{-}O\text{-}\underset{O}{C}\text{-}R' \quad (I)$$

$$I \longrightarrow RNHCONHR + (R'CO)_2O + CO_2$$

$$I \longrightarrow RNHCOR' + CO_2$$

$$R\text{-}N{=}C{=}O + R'COSH \longrightarrow R\text{-}\underset{H}{N}\text{-}\underset{O}{C}\text{-}S\text{-}\underset{O}{C}\text{-}R' \quad (II)$$

$$R\text{-}CO\text{-}N{=}C{=}O + R'COX \longrightarrow R\text{-}\underset{O}{C}\text{-}\underset{H}{N}\text{-}\underset{O}{C}\text{-}X\text{-}\underset{O}{C}\text{-}R'$$

X=S III
X=O IV

Experimental

Materials. Commercial phenyl isocyanate, methyl isocyanate, thioacetic acid and thiobenzoic acid employed were used. *p*-Nitrothiobenzoic, *p*-chlorothiobenzoic and *p*-thiotoluic acids were prepared according to the method given in literature.[5] *m*-Nitrophenyl isocyanate was prepared from *m*-nitroaniline and phosgene.[6] Acyl isocyanates were prepared from the corresponding amides and oxalyl chloride.[7,8]

Acylcarbamoyl Sulfides (IIa)—(IIf). To a solution of 4.76 g (0.04 mol) of phenyl isocyanate in 50 ml of *n*-hexane was added a solution of 5.52 g (0.04 mol) of thiobenzoic acid in 10 ml *n*-hexane at room temperature with vigorous stirring. The yellow color of thiobenzoic acid disappeared and white precipitates formed. Recrystallization of the product from *n*-hexane yielded 8.2 g (86%) of IIa melting at 95—97 °C with decomposition. The other compounds (IIb)—(IIf) were prepared in a similar way. The results are shown in Table 1.

Acyl Acylcarbamoyl Sulfides (IIIa)—(IIIi), Chloroacetylcarbamoyl Benzoic Anhydride (IVb) and Dichloroacetylcarbamoyl Benzoic Anhydride (IVc). To a solution of 7.36 g (0.05 mol) of benzoyl isocyanate in 80 ml of ether was added a solution of 6.91 g (0.05 mol) of thiobenzoic acid in 50 ml of ether at 0 to −5 °C with stirring. The yellow color of thiobenzoic acid soon disappeared. Colorless needles were formed immediately. Recrystallization of the product from ligroin yielded 13.3 g (93%) of IIIa melting at 75—76 °C with decomposition. The other compounds (IIIb)—(IIIi), (IVb) and (IVc) were prepared in a similar way. The results are shown in Tables 2 and 3.

Benzoylcarbamoyl Benzoic Anhydride (IVa) and Trichloroacetylcarbamoyl Benzoic Anhydride (IVd). To a solution of 7.36 g (0.05 mol) of benzoyl isocyanate in 50 ml of ether was added a solution of 6.10 g (0.05 mol) of benzoic acid in 50 ml of ether at room temperature with stirring. After the addition of benzoic acid, the solvent was immediately evaporated under reduced pressure. White solid thus obtained was washed with ether and dried to yield 11.2 g (82%) of VIa melting at 62—65 °C with decomposition. As the compound was difficult to be recrystallized, it was analyzed without further purification. IVd was prepared in a similar way. The results are shown in Table 3.

References

1) C. Naegeli and A. Tyabji, *Helv. Chim. Acta*, **17**, 931 (1934).
2) C. Naegeli and A. Tyabji, *ibid.*, **18**, 142 (1935).
3) W. Dieckmann and F. Breest, *Ber.*, **39**, 3052 (1906).
4) Krzysztof Colankiewicz and M. Dezor-Mazur, *Bull. Acad. Pol. Soc., Ser. Sci. Chim.*, **17** (10), 575—578 (1969).
5) P. Noble, Jr., and D. S. Tarbell, "Organic Syntheses," Coll. Vol. IV, p. 924 (1963).
6) R. L. Shriner and R. F. B. Cox, *J. Amer. Chem. Soc.*, **53**, 1603 (1931).
7) A. J. Speziale and L. R. Smith, *J. Org. Chem.*, **28**, 1805 (1963).
8) O. Tsuge and R. Mizuguchi, *Kogyo Kagaku Zasshi*, **69** (5), 939 (1966).

BULLETIN OF THE CHEMICAL SOCIETY OF JAPAN, VOL. 47 (3), 777—778 (1974)

The Induced Optical Rotatory Dispersion of Mercury Orange-Phosphoenolpyruvate Carboxylase*

Masataka MIYAMURA and Shuichi SUZUKI

Research Laboratory of Resources Utilization, Tokyo Institute of Technology, Meguro-ku, Tokyo 152

(Received August 16, 1973)

Synopsis. On reacting with a SH group, the mercury orange enzyme formed, showed a positive Cotton effect near 500 nm, and the optical activity of which was remarkably induced by adding ADP or PEP. It seemed that ADP or PEP might move to the vicinity of the active amino acid residues.

It has been reported that phosphoenolpyruvate carboxylase (EC4.1.1.a), which is activated by the manganous ion, has a sulfhydryl group in the active center, judging from the fact that the activity of this enzyme is inhibited by the addition of *p*-chloromercury benzoate.[1-3] A kinetic study of this enzyme has been carried out by us.[4] It is, however, necessary to accumulate more data for a better understanding of the active center of this enzyme.

It is known that 1-(4-chloromercuriphenylazo)naphthol-2 (mercury organge) reacts with enzyme to form mercury–sulfur bondings.[5,6] It has been found that phosphoenolpyruvate carboxylase reacts with mercury orange and that the product shows an absorption maximum near 492 nm because of the azochromophore of mercury orange. This chromophoric group at the active center of the enzyme has been found to be environmentally sensitive to the optical activity.

This paper will show how the environment of the active center of phosphoenolpyruvate carboxylase can be studied using mercury orange by means of the optical rotatory dispersion spectrophotometric method.

Experimental

The phosphoenolpyruvate carboxylase was prepared from Baker's yeast in the way described in a previous paper.[4] The optical rotatory dispersion (ORD) and the visible spectra were measured by means of the JASCO ORD/UV/CD-5 spectrometer. The enzyme and the substrates were dissolved into a 0.25 mol/l phosphate buffer solution (pH 6.0), and the ORD spectra were measured at 18 °C.

Results and Discussion

Mercury orange exhibits an absorption maximum at 500 nm and shoulders near 450 nm and near 550 nm on a visible spectrum, as is shown in Fig. 1. The shoulder near 450 nm and λ_{max} at 500 nm might be assigned to the *cis* and *trans* isomers respectively, for it is known that a diazo-containing compound gives *cis* and *trans* configurations upon transformation, and because the absorption maximum of the *cis* isomer generally appears at a shorter wavelength than that of the *trans* isomer.[7] The mercury orange-binding enzyme (MO–enzyme) shows an absorption spectrum similar to that of mercury orange. The absorbance near 500 nm decreases and the absorbance near 450 nm increases upon the addition of adenosine-5'-diphosphate (ADP) or phosphoenolpyruvate (PEP) into the MO-enzyme (Fig. 1). It could be said that ADP or PEP are located near the mercury orange group in the MO-enzyme and affect the transformation of a

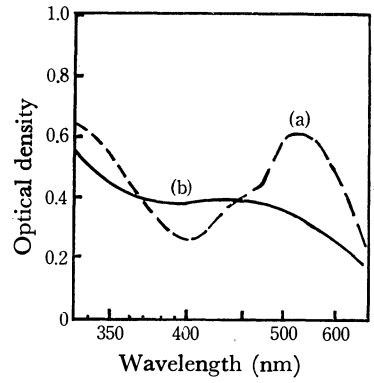

Fig. 1. Absorption spectra of mercury orange–phosphoenolpyruvate carboxylase complex.
a): MO–enzyme (1.0 mmol/l) and MO (1.0 mmol/l, pH 6.0)
b): MO–enzyme (1.0 mmol/l)+ADP (1.0 mmol/l) and MO–enzyme (1.0 mmol/l)+PEP (1.0 mmol/l)

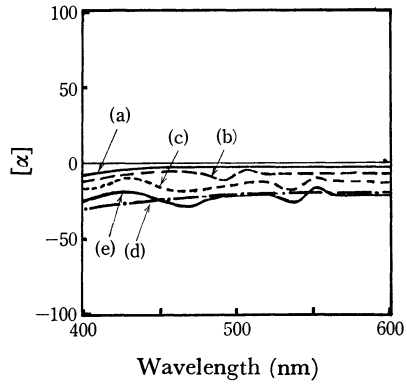

Fig. 2. ORD spectra of mercury orange–phosphoenolpyruvate carboxylase complex.
a): base line, manganous ion, bicarbonate ion, phosphoenolpyruvate and mercury orange
b): MO–enzyme (1.0 mmol/l), MO–enzyme (1.0 mmol/l)+Mn^{2+} (1.0 mmol) and MO–enzyme (1.0 mmol/l)+bicarbonate ion (1.0 mmol/l)
c): MO–enzyme ((1.0 mmol/l)+PEP (1.0 mmol/l)
d): ADP (1.0 mmol/l)
e): MO–enzyme (1.0 mmol/l)+ADP (1.0 mmol/l)

* The Chemical Modification of Biopolymers. VII.

diazo group of mercury orange.

The MO–enzyme showed a positive Cotton effect near 500 nm (Fig. 2). Neither mercury orange nor the enzyme exhibits an optical activity in the same region. The ORD spectrum of the MO–enzyme is not influenced by the addition of manganous ion (Fig. 2), which means that there is no interaction between the manganous ion and the active center of the enzyme. This is to be expected if mercury orange might be located in the active center, thus forming mercury-sulfur binding, and if the manganous ion should bind with the sulfhydryl group in the active center, thus activating the enzyme. In this connection, the bicarbonate ion was found not to interact with the MO–enzyme. The optical activity of the MO–enzyme is remarkably induced by adding ADP or PEP. It can be deduced from the visible absorption and the ORD spectra that the diazo group in the MO–enzyme has the *trans* configuration mainly, and that this configuration can be influenced by the interaction between the mercury orange goup and ADP or PEP. It seemed that ADP or PEP might move to the vicinity of the active site of the enzyme.

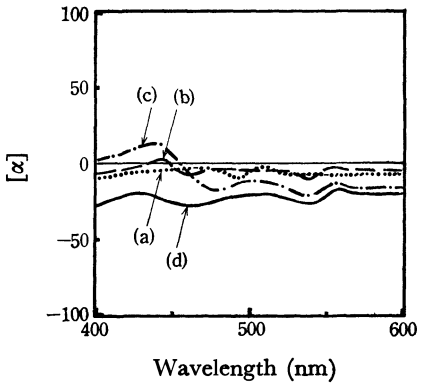

Fig. 3. ORD spectra of mercury orange–phosphoenolpyruvate carboxylase–adenine derivatives complex.
a): MO–enzyme (1.0 mmol/l)
b): a)+adenine (1.0 mmol/l)
c): a)+adenosine (1.0 mmol/l)
d): a)+ADP (1.0 mmol/l)

The optical activity of the MO–enzyme was induced by the addition of adenine, adenosine, or adenosine-5′-triphosphate (ATP) instead of ADP, as is shown in Fig. 3. The ORD spectrum of ATP seems almost the same as ADP, and those of adenine and adenosine exhibit a tendency similar to that of ADP. In every case, another Cotton effect appears around 400 nm. It seems that the adenine or adenine group of adenosine, ADP or ATP, may be located at the binding site of the active center, thus transform in the diazo group from the *trans* to the *cis* configuration as follows:

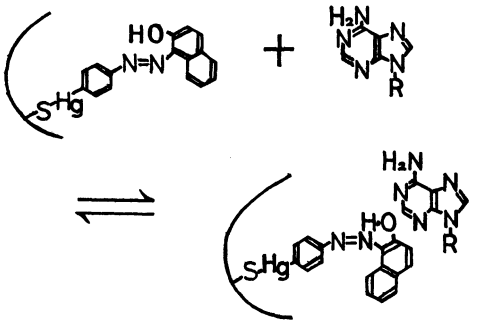

References

1) J. J. B. Cannata and A. O. M. Stoppani, *J. Biol. Chem.*, **238**, 1196 (1963).
2) J. J. B. Cannata and A. O. M. Stoppani, *ibid.*, **238**, 1208 (1963).
3) J. J. B. Cannata and A. O. M. Stoppani, *ibid.*, **238**, 1919 (1963).
4) M. Miyamura, F. Takahashi, and S. Suzuki, unpublished results.
5) H. S. Bennet and D. A. Yphantis, *J. Amer. Chem. Soc.*, **70**, 3552 (1948).
6) P. D. Boyer, *ibid.*, **76**, 4331 (1954).
7) H. H. Jaffe, S. J. Yeh, and R. W. Gardner, *J. Mol. Spectrosc.*, **2**, 120 (1958).

BULLETIN OF THE CHEMICAL SOCIETY OF JAPAN, VOL. 47 (3), 779—780 (1974)

A Study on Phosphorylation by Means of 8-Quinolyl Phosphates

Hiroshi TAKAKU, Yoshifusa SHIMADA, and Kenichi ARAI

Department of Chemistry, Chiba Institute of Technology, Narashino, Chiba 275

(Received August 31, 1973)

Synopsis. Phosphorylation of phosphates and nucleosides forming unsymmetrical pyrophosphates and nucleotides by the use of 8-quinolyl phosphates has been investigated. According to this method, various pyrophosphates and nucleotides were obtained in high yields.

Recently, we reported[1] that mixed diesters of phosphoric acid (**2**) were prepared in a high yield by treating an active ester, phenyl 8-quinolyl phosphate (**1**), with alcohols as shown in the following scheme.

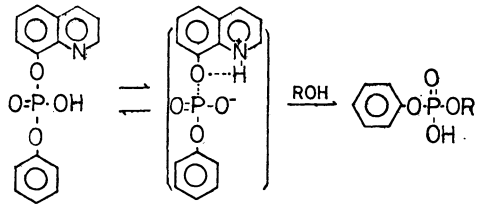

1 **1′** **2**

This paper deals with the reaction of 8-quinolyl phosphates[2] such as **1** or tris-(8-quinolyl) phosphate (**5**), with phosphates and nucleosides which give unsymmetrical pyrophosphates and nucleotides that are expected from the above reaction.

First, an attempt was made to synthesize unsymmetrical pyrophosphate (**3**) by the reaction of **1** with phosphates. When a mixture of one equiv. of **1** and 1.5 equiv. of *p*-chlorophenyl phosphate in dry pyridine was allowed to stand at 50 °C for 5 hr, the corresponding P^1-*p*-chlorophenyl P^2-phenyl pyrophosphate (**3a**) was obtained in 78% yield. However, when a small quantity of triethylamine was added to the pyridine solvent, the yield of **3a** decreased markedly.[3]

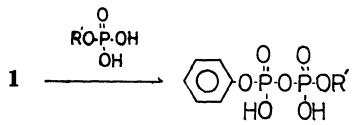

3

In a similar manner, various unsymmetrical pyrophosphates (**3**) were obtained in a high yield as shown in Table 1. When adenosine 5′-phosphate was used in the above experiments, P^1-adenosine-5′ P^2-phenyl pyrophosphate (**3d**) was obtained in 54% yield. Thus it can be said that phenyl 8-quinolyl phosphate (**1**) is effective for the synthesis of pyrophosphates.

Next, the synthesis of nucleoside 5′-phosphate was tried by the use of a phosphorylating reagent, tris-(8-quinolyl) phosphate (**5**). The reagent (**5**) was prepared in 75% yield by treating six equiv. of 8-quinolinol (**4**) with one equiv. of phosphoryl chloride.

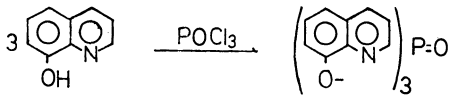

4 **5**

When a mixture of one equiv. of 2′,3′-*O*-isopropylideneadenosine and two equiv. of **5** in dry pyridine was heated at 80 °C for 8 hr, 2′,3′-*O*-isopropylideneadenosine 5′-bis-(8-quinolyl) phosphate (**6a**) was formed. The phosphate (**6a**) without isolation, was further treated with aqueous solution of cupric chloride and 2′,3′-*O*-isopropylideneadenosine 5′-phosphate was obtained. After removal of the protecting group, adenosine 5′-phosphate (**7a**) was obtained in 70% yield, which was determined by UV absorption after separation by paper chromatography. Nucleoside 5′-phosphates were characterized by comparison of ultraviolet absorption properties with those of authentic samples,[4] R_f values in paper chromatography, and paper electrophoresis.

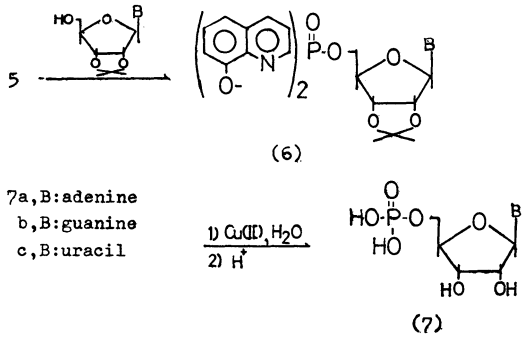

(6)

7a,B:adenine
b,B:guanine
c,B:uracil

(7)

Similarly, other nucleoside 5′-phosphates were ob-

Table 1. Preparation of unsymmetrical pyrophosphates (**3**)

Compd No.	R′	Yield (%)	Mp[a] (°C)	R_f[b]	Formula	Calcd (%) C	Calcd (%) H	Calcd (%) N	Found (%) C	Found (%) H	Found (%) N
3a	*p*-Chlorophenyl	78	262—264	0.60	$C_{24}H_{37}ClN_2O_7P_2$	51.25	6.58	4.98	50.97	6.74	5.01
3b	Benzyl	73	218—220	0.58	$C_{25}H_{40}N_2O_7P_2$	55.15	7.33	5.15	55.53	8.01	5.24
3c	β-Naphthyl	82	226—227	0.59	$C_{28}H_{40}N_2O_7P_2$	58.13	6.92	4.84	58.45	7.03	4.97

a) Bis-cyclohexylammonium salt. b) Paper chromatography was carried out by the descending technique using Toyo Roshi No. 51 paper. Solvent system used was: isopropyl alcohol–concentrated ammonia–water (8:1:1 v/v).

Table 2. Preparation of nucleotides (7)

Compd No.	Nucleotide	Yield (%)	R_f Value[a] Solv. C	Solv. D	UV spectra (pH 2) $\lambda_{max}^{H_2O}$(mμ)	$\lambda_{min}^{H_2O}$(mμ)
7a	Adenosine 5′-phosphate	70	0.30	0.29	257	230
7b	Guanosine 5′-phosphate	68	0.49	0.23	256	228
7c	Uridine 5′-phosphate	65	0.68	0.31	262	230

a) Paper chromatography was carried out by the descending technique using Toyo Roshi No. 51 paper. Solvent systems used were: 2-propyl alcohol–saturated ammonium sulfate–water (2:79:19 v/v) (Solvent C) and *n*-propyl alcohol–concentrated ammonia–water (20:20:3 v/v) (Solvent D).

tained in a high yield as shown in Table 2.

Experimental

Paper chromatography was carried out the descending technique using Toyo Roshi No. 51 paper. The solvents used were isopropyl alcohol–concentrated ammonia–water (8:1:1 v/v) (Solvent A), or (7:1:2 v/v) (Solvent B), 2-propyl alcohol–saturated ammonium sulfate–water (2:79:19 v/v) (Solvent C), and *n*-propyl alcohol–concentrated ammonia–water (20:20:3 v/v) (Solvent D). Paper electrophoresis was carried out on Toyo Roshi No. 51A paper at 80 V/cm in system E (0.05 M potassium phosphate (pH 7.5)). Nucleotides were confirmed by Hanes and Isherwood spray,[5] followed by ultraviolet irradiation.

Phenyl 8-quinolyl phosphate (**1**) was prepared from the phosphorylation of 8-quinolinol (**4**) with phenyl phosphorodichloridate according to the previous paper.[1]

P^1-p-*Chlorophenyl* P^2-*Phenyl Pyrophosphate (3a).* A mixture of 602 mg (2 mmol) of phenyl 8-quinolyl phosphate (**1**) and 624 mg (3 mmol) of *p*-chlorophenyl phosphate in dry pyridine (10 ml) was allowed to stand at 50 °C for 5 hr. To the reaction mixture, 991 mg (10 ml) of cyclohexylamine and water (10 ml) was added, and the mixture was kept overnight in a refrigerator. The precipitate was collected by filtration and washed with water and acetone. The precipitate was recrystallized from a mixture of ethanol and water (1:1 v/v). Bis-cyclohexylammonium salt of *P*^{1}-*p*-chlorophenyl *P*^{2}-phenyl pyrophosphate (**3a**) (876 mg, 78%) was obtained as white prisms; mp 262—264 °C; R_f 0.60 (Solvent A).

Found: C, 50.97; H, 6.74; N, 5.01%. Calcd for $C_{24}H_{37}ClN_2O_7P_2$: C, 51.25; H, 6.58; N, 4.98%.

P^1-*Adenosine-5′* P^2-*Phenyl Pyrophosphate (3d).*[6] A solution of 452 mg (1.5 mmol) of phenyl 8-quinolyl phosphate (**1**) and 347 mg (1 mmol) of adenosine 5′-phosphate in dry pyridine (10 ml) was allowed to stand at 50 °C for 8 hr. The pyridine solution was evaporated *in vacuo* and the residue mixed with water (10 ml). The solution was adjusted to pH 8 and passed through a column of Amberlite IR-120 (H^+) (50—100 mesh) ion-exchange resin. The eluate was neutralized with 6 M ammonium hydroxide and evaporated to dryness. The residue was dissolved in methanol (10 ml). Bis-ammonium salt of *P*^{1}-adenosine-5′ *P*^{2}-phenyl pyrophosphate (**3d**) (339 mg, 54%) was separated by the addition of ether; R_f 0.40 (Solvent B).

Found: C, 30.17; H, 5.41; N, 15.49%. Calcd for $C_{16}H_{25}N_7O_{10}P_2 \cdot 5H_2O$: C, 30.60; H, 5.62; N, 15.56%.

Tris-(8-Quinolyl) Phosphate (5). To a solution of 8.70 g (60 mmol) of 8-quinolinol (**4**) in dry pyridine (20 ml) was added dropwise a solution of 1.53 g (10 mmol) of phosphoryl chloride in dry pyridine (10 ml) with stirring at 0 °C. The mixture was stirred for 2 hr and further at room temperature for 3 days. After removal of pyridinium chloride, the filtrate was concentrated *in vacuo*. Tris-(8-quinolyl) phosphate (**5**) was separated and collected 3.59 g (75%). It was recrystallized from dimethylformamide; mp 202—203 °C; R_f 0.90 (Solvent B). IR ν_{max}^{KBr} cm^{-1}: 1620—1570. (C=C and C=N) and 1253 (P=O).

Found: C, 67.39; H, 3.75; N, 8.97%. Calcd for $C_{27}H_{18}N_3O_4P$: C, 67.64; H, 3.75; N, 8.76%.

Adenosine 5′-Phosphate (7a). A mixture of 286 mg (0.60 mmol) of tris-(8-quinolyl) phosphate (**5**) and 92 mg (0.30 mmol) of 2′,3′-*O*-isopropylideneadenosine in dry pyridine (3 ml) was heated at 80 °C for 8 hr. The mixture was treated 0.48 ml of 43% aqueous cupric chloride at 100 °C for 1.5 hr and concentrated. The residue was treated with 80% acetic acid at 70 °C for 1.5 hr. Adenosine 5′-phosphate (**7a**) was obtained in an over-all yield of 70%, as determined by means of the ultraviolet absorption after separation with paper chromatography. This sample is identical with an authentic specimen of adenosine 5′-phosphate[4] by paper chromatography and paper electophoresis. The R_f values are summarized in Table 2; ultraviolet absorption was $\lambda_{max}^{H_2O}$ 257 mμ.

Similarly, guanosine and uridine 5′-phosphate were obtained in high yields as shown in Table 2.

References

1) H. Takaku and Y. Shimada, *Chem. Pharm. Bull.* (Tokyo), **21**, 445 (1973).

2) Hydrolysis of 8-quinolyl phosphate was studied recently by Murakami and his co-workers (Y. Murakami and J. Sunamoto, This Bulletin, **44**, 1827, 1939 (1971)).

3) W. Kampe, *Chem. Ber.*, **98**, 1038 (1965).

4) Purchased from Sigma Chemical Corp.

5) C. S. Hanes and F. A. Isherwood, *Nature*, **164**, 1107 (1949).

6) J. G. Moffatt and H. G. Khorana, *J. Amer. Chem. Soc.*, **80**, 3756 (1958).

BULLETIN OF THE CHEMICAL SOCIETY OF JAPAN, VOL. 47 (3), 781—782 (1974)

Direct Syntheses of Methyl 2-Deoxy-2-alkoxycarbonylamino-D-glucopyranoside from 2-Amino-2-deoxy-D-glucose

Sinichi OTANI

Department of Chemistry, College of Liberal Arts and Science, Kyoto University, Yoshida, Sakyo-ku, Kyoto 606

(Received November 20, 1973)

Synopsis. Methyl 2-deoxy-2-methoxycarbonylamino- and methyl 2-deoxy-2-ethoxycarbonylamino-D-glucopyranosides were synthesized by the reaction of 2-amino-2-deoxy-D-glucose with alkyl chlorocarbonate and sodium carbonate in methanol by a one-step process.

This note deals with the direct syntheses of methyl 2-deoxy-2-methoxycarbonylamino-α- (MI-α), methyl 2-deoxy-2-methoxycarbonylamino-β- (MI-β), methyl 2-deoxy-2-ethoxycarbonylamino-α- (MII-α) and methyl 2-deoxy-2-ethoxycarbonylamino-β-D-glucopyranoside (MII-β) starting from 2-amino-2-deoxy-D-glucose hydrochloride.

MI-β and MII-β were synthesized in two steps with 15—28% yield,[1,2] the first step being the formation of 2-deoxy-2-methoxycarbonylamino- (I) and 2-deoxy-2-ethoxycarbonylamino-D-glucose (II) by the reaction of 2-amino-2-deoxy-D-glucose with a half equivalent of methyl and ethyl chlorocarbonate respectively in methanol, and the second step the glycosidation with methanolic hydrogen chloride. Recently, MI-α has been synthesized in 78% yield[3] by the reaction of 2-amino-2-deoxy-D-glucose with an equivalent of methyl chlorocarbonate and sodium carbonate in aqueous acetone, followed by evaporation to dryness and the glycosidation with methanolic hydrogen chloride without isolation of I. The author has found that 2-amino-2-deoxy-D-glucose reacts with excess methyl or ethyl chlorocarbonate in methanol to give the main product MI-α, MI-β, MII-α, or MII-β in a good yield. The reaction might be utilized as a convenient procedure for the syntheses.

2-Amino-2-deoxy-D-glucose hydrochloride was dissolved in methanol containing an equivalent of sodium. After the addition of finely powdered anhydrous sodium carbonate, excess methyl or ethyl chlorocarbonate was added under stirring. The components of the reaction products were detected by thin-layer chromatography with silica gel and *n*-propanol–concd ammonia water–water (6: 2: 1). It was confirmed that, after the formation of I or II, β-glycoside appeared, gradually changing into α-glycoside. Separation of the components was carried out by column chromatography using silicic acid and ethyl acetate–methanol (9: 1). Evaporation of the elution and crystallization gave the pure products. At refluxing temperature overnight, the thermodynamically stable α-glycoside was the major product in 83% yield accompanied by a small amount of the kinetically favorable β-glycoside in 9—10% yield. After being stirred at room temperature for three days, the β-glycoside was found to be the main product in 65—66% yield, in addition to a considerable amount of the α-glycoside as a by-product in 29% yield.

The α- and β-glycoside were identified by elementary analysis and the physical constant measurements.[1,2] The melting point of MI-α differed from that of the reference,[3] MII-α being an unknown compound. In the NMR spectrum of MI-α in deuterium oxide the protons OCH_3 (singlet, τ 6.60), $NHCOOCH_3$ (singlet, τ 6.32) and H-2,3,4,5,6,6′ (multiplet, τ 6.1—6.6) were identical with those of the reference.[3] However, the proton of H-1, reported[3] to appear at τ 5.18 (doublet, J=2 Hz), could not be detected because of the overlapping with HOD signal (τ 5.15—5.4). The data are in good agreement with the NMR spectrum of MI-β except the protons OCH_3 and H-1. In the NMR spectrum of MII-α in deuterium oxide, protons $NHCOOCH_2CH_3$ (triplet, τ 8.78), $NHCOOCH_2CH_3$ (quartet, τ 5.91) and H-2,3,4,5,6,6′ (multiplet, τ 6.1—6.6) were essentially identical with those of MII-β, and protons OCH_3 (singlet, τ 6.62) were in good agreement with those of MI-α, differing from those of MI-β (τ 6.50) and MII-β (τ 6.52). As in the case of MI-α the proton of H-1 of MII-α could not be detected at τ 5.2. Therefore, by measuring the NMR spectra in acetic acid-d_4, protons of H-1 of MI-α and MII-α were detected at τ 5.26 (doublet, J=1.8 Hz) and at τ 5.27 (doublet, J=1.7 Hz), respectively. These NMR data were compatible with those of the α-glycoside.

The reaction mechanism is considered to consist of the formation of I or II and the subsequent methyl glycosidation catalyzed with hydrogen chloride liberated by the decomposition of alkoxy chlorocarbonate.

Experimental

All melting points were taken in capillaries with a Yamato melting point apparatus model MP-21. NMR spectra were measured with a JEOL PS-100 spectrometer. Sodium 4,4-dimethyl-4-silapentane-1-sulfonate (for the solution of deuterium oxide) and tetramethyl silane (for the solution of acetic acid-d_4) were used as an internal standard. Thin-layer chromatography (tlc) was carried out on precoated plates of silica gel G (E. Merck) with the solvent (*n*-propanol–concd ammonia water–water (6: 2: 1)), and the spots were visualized with iodine vapor. Column chromatography was carried out with silicic acid (AR 100 mesh, Mallincrodt).

Reaction at Refluxing Temperature in Methanolic Solution. 2-Amino-2-deoxy-D-glucose hydrochloride (2 g) was dissolved in methanol (50 ml) containing sodium (0.23 g). After the addition of finely powdered anhydrous sodium carbonate (1 g), methyl chlorocarbonate (6 ml) was added dropwise to the mixture under stirring. When the mixture was refluxed overnight, tlc showed two spots corresponding to MI-α (R_f

0.65, major spot) and MI-β (R_f 0.57, minor spot). The mixture was neutralized with lead carbonate and filtered. The clear solution was evaporated to a crystalline residue, which was chromatographed on a column of silicic acid (65×4.5 cm) with ethyl acetate–methanol (9: 1). The two components were obtained as needles after evaporation of the elution. MI-α was recrystallized from methanol–ether; 1.85 g (83%), mp 150—151 °C, $[\alpha]_D^{22}$ +137° (*c* 2, methanol); (lit,[3] mp 126—128 °C, $[\alpha]_D^{22}$ +135° (*c* 2, methanol)).

Found: C, 42.75; H, 7.00; N, 5.49%. Calcd for $C_9H_{17}NO_7$: C, 43.02; H, 6.82; N, 5.58%.

NMR (in D_2O): τ 6.61 (3H, s, OCH_3), 6.32 (3H, s, $NHCOOCH_3$), 6.1—6.6 (6H, m, H-2,3,4,5,6,6′). (in CD_3COOD): 6.63 (3H, s, OCH_3), 6.33 (3H, s, $NHCOOCH_3$), 6.0—6.5 (6H, m, H-2,3,4,5,6,6′), 5.26 (1H, d, J=1.8 Hz, H-1).

MI-β was recrystallized from methanol: 0.21 g (9%), mp 197—198 °C, $[\alpha]_D^{22}$ −35° (*c* 1, water); (lit,[1] mp 196—197 °C, $[\alpha]_D^{18}$ −33.8° (water)). (Found: C, 42.86; H, 6.82; N, 5.53%).

NMR (in D_2O): τ 6.50 (3H, s, OCH_3), 6.32 (3H, s, $NHCOOCH_3$), 6.1—6.7 (6H, m, H-2,3,4,5,6,6′), 5.58 (1H, d, J=8 Hz, H-1).

When ethyl chlorocarbonate (6 ml) was used, the reaction gave MII-α (R_f 0.70, major product) and MII-β (R_f 0.61, minor product) on tlc. MII-α was recrystallized from methanol–ether; 2.05 g (83%); mp 113—115 °C, $[\alpha]_D^{21}$ +114° (*c* 1, water), +127° (*c* 1, methanol).

Found: C, 45.46; H, 7.26; N, 5.37%. Calcd for $C_{10}H_{19}NO_7$: C, 45.27; H, 7.22; N, 5.28%.

NMR (in D_2O): τ 8.78 (3H, t, $NHCOOCH_2\underline{CH_3}$), 6.62 (3H, s, OCH_3), 6.1—6.6 (6H, m, H-2,3,4,5,6,6′), 5.89 (2H, q, $NHCOOC\underline{H_2}CH_3$). (in CD_3COOD): 8.78 (3H, t, $NHCOOCH_2\underline{CH_3}$), 6.64 (3H, s, OCH_3), 6.05—6.5 (6H m, H-2,3,4,5,6,6′), 5.91 (2H, q, $NHCOOC\underline{H_2}CH_3$), 5.27 (1H, d, J=1.7 Hz, H-1).

MII-β was recrystallized from methanol; 0.24 g (10%), mp 188—189 °C, $[\alpha]_D^{22}$ −30° (*c* 1, water); (lit,[2] mp 188—189 °C, $[\alpha]_D^{15}$ −31° (*c* 3.2, water). (Found: C, 45.05; H, 7.24; N, 5.30%).

NMR (in D_2O): τ 8.78 (3H, t, $NHCOOCH_2\underline{CH_3}$), 6.52 (3H, s, OCH_3), 6.1—6.8 (6H, m, H-2,3,4,5,6,6′), 5.91 (2H, q, $NHCOOC\underline{H_2}CH_3$), 5.62 (1H, d, J=8 Hz, H-1).

Reaction at Room Temperature. 2-Amino-2-deoxy-D-glucose hydrochloride (2 g) was dissolved in methanol (50 ml) containing sodium (0.23 g). After addition of finely powdered anhydrous sodium carbonate (1 g) methyl chlorocarbonate (4 ml) was added dropwise to the mixture under stirring. When the mixture was stirred for 3 days at room temperature, tlc showed MI-β (major product) and MI-α (minor product). The same treatment gave the two components which yielded on crystallization; 1.53 g (66%) of MI-β and 0.68 g (29%) of MI-α.

When ethyl chlorocarbonate (4 ml) was used, the reaction gave MII-β yielding 1.60 g (65%) and MII-α yielding 0.72 g (29%).

The author is grateful to Dr. Jyun'ichi Hayami for his helpful discussions and for the NMR spectra measurements.

References

1) M. Viscontini and J. Meier, *Helv. Chim. Acta*, **35**, 807 (1952).

2) S. Akiya and T. Osawa, *Yakugaku Zasshi*, **77**, 726 (1957).

3) D. Ikeda, T. Tsuchiya, and S. Umezawa, This Bulletin, **44**, 2529 (1971).

BULLETIN OF THE CHEMICAL SOCIETY OF JAPAN, VOL. 47 (3), 783—784 (1974)

The Use of Hydroxybenzoic Acids to Polymers. II. Polyether-amides Obtained from the Interfacial Polycondensation of *p*-Carboxyphenoxyacetic Acid Dichloride with Aliphatic Diamines

Ichiro HIRAO, Taketoshi KITO, Tsutomu FUJIMOTO, and Hideo YOSHIHARA

Laboratory of Industrial Chemistry, Department of Chemical Engineering, Kyushu Institute of Technology, Tobata-ku, Kitakyushu-shi, 804

(Received September 10, 1973)

Synopsis. Five polyether-amides were prepared from the title reaction. The physical properties ([η], T_m, T_g, and decomp. temp.) and the effects of the reaction conditions were examined. These polymers were superior in some physical properties to the polymers obtained from the melt polycondensation.

We have previously reported[1] on polyether-amides obtained from the condensation of ω-(*p*-carboxyphenoxy)alkanoic acids (CPAA) with aliphatic diamines, in which three types of polymers were included in the variety of diamines; ethylenediamine, hexamethylenediamine, and piperazine. The polymers prepared from CPAA and hexamethylenediamine, Hm, showed higher intrinsic viscosities and moderate melting points (200—240 °C), but the polymer prepared from *p*-carboxyphenoxyacetic acid (CPAC) and hexamethylenediamine, Hl, showed a low intrinsic viscosity (0.38). Similarly, other polymers prepared from CPAC and ethylenediamine, El, or piperazine, Pl, also showed low intrinsic viscosities. In the second polymer, El, it was concluded that the small difference between the decomposition temperature (293 °C) and the melting point (294 °C) may cause a low intrinsic viscosity because the polymerization was carried out in a molten state. However, in the first polymer, Hl, we found that the polymer set to gel or was partially insoluble in *m*-cresol when it was heated at an elevated temperature (higher than 250 °C). This may be caused by the active methylene group placed between the oxygen atom and the carboxyl group of CPAC. A similar reason may be deduced as one of the causes of the intrinsic viscosity of El being low.

Therefore, we investigated the interfacial polymerization of CPAC dichloride and aliphatic diamines.

Results and Discussion

White polyether-amides were prepared by the interfacial polymerization of CPAC dichloride and such diamines as ethylenediamine, propylenediamine, 1,3-diaminopropane, hexamethylenediamine, or piperazine, whose polymers will be abbrebiated here as Ed, P-2, P-3, Hm, and Pz (the Ed, Hm, and Pz are essentially equal to El, Hl, and Pl respectively, but the latter were obtained by the melt polycondensation). The melting point (T_m), the glass transition temperature (T_g) and the intrinsic viscosity ([η]) of five polyether-amides are summarized in Table 1. These polymers were superior in some physical properties to the polyether-amides obtained by the melt polycondensation. For example, the intrinsic viscosity of Ed was 0.68; this value is 0.56 higher than that of the intrinsic viscosity of El. Ed did not melt on a hot plate below 325 °C. The thermal analysis of Ed showed that the weight loss of Ed began at about 300 °C; no endothermic peak was detected below that temperature. The *T*m of Pz was determined only by observing the temperature at which melting was complete, because Pz showed no endothermic peak in the DTA analysis.

The reaction conditions (the effects of the volume of tetrachloroethylene and of the molar ratio of diamine to CPAC dichloride) were also examined; the results are summarized in Table 2. The relationship between the diamine partition coefficient and the intrinsic

TABLE 1. POLYETHER-AMIDES

Repeating unit	Diamine/Dichloride[a] (mol/mol)	[η]	T_m (°C)	T_{m2}[b] (°C)	T_{m3}[c] (°C)	T_d[d] (°C)	T_g (°C)	Yield (%)
-CO-⟨⟩-$OCH_2CONH(CH_2)_2NH$- (Ed)	1.1	0.68	>325	—	294 (El)	324	—	92.3
-CO-⟨⟩-$OCH_2CONHCHCH_2NH$- (P-2)	1.1	0.56	263.5—264.5	256	—	318	58	52.3
-CO-⟨⟩-$OCH_2CONH(CH_2)_3NH$- (P-3)	1.1	0.96	242—246	217	—	—	—	86.9
-CO-⟨⟩-$OCH_2CONH(CH_2)_6NH$- (Hm)	1.1	0.90	239—240	242	236 (Hl)	370	50—52	82.7
-CO-⟨⟩-OCH_2CON N- (Pz)	1.03	0.39	188—192	—	151 (Pl)	316	—	89.1

a) *p*-Carboxyphenoxyacetic acid dichloride. b) Melting points estimated by DTA. c) Melting points of polyether-amides obtained by the melt polycondensation (see Ref. 1). d) Temperature at which 10% weight loss occurs. T_d of nylon 66: 404 °C.

Table 2. Effects of the concentration of CPAC dichloride and the molar ratio[a]

Aqueous layer		Organic layer		HMDA	
HMDA[c] (mol)	NaOH (mol)	Dichloride[d] (mol)	TCE[e] (ml)	Dichloride (mol/mol)	[η]
0.02	0.04	0.018	20	1.11	0.58
0.02	0.04	0.018	50	1.11	0.68
0.02	0.04	0.018	100	1.11	0.78
0.02	0.04	0.018	150	1.11	0.80
0.02	0.04	0.018	200	1.11	0.82
0.02	0.004	0.002	150	10	0.80
0.02	0.008	0.004	150	5	0.92
0.02	0.020	0.010	150	2	0.87
0.02	0.040	0.020	150	1	0.84
0.02	0.080	0.040	150	0.5	0.25
0.02	0.200	0.100	150	0.2	0.06

a) A series of polymerization (the first five and the last six) was carried out using the same reagents. b) Total volume is 300 ml, containing ice. c) Hexamethylenediamine. d) See Table 1. e) Tetrachloroethylene.

Table 3. Effect of the diamine partition coefficient on the intrinsic viscosity of H_m[a]

Organic solvent	Diamine partition coefficient K[b]	[η]
Carbon tetrachloride	66.0	1.07
Tetrachloroethylene	43.7	0.91
1,2-Dichloroethane	13.1	0.85
Chloroform	1.03	0.54

a) H_m: See Table 1. b) K is the equilibrium partition coefficient at 25 °C for hexamethylenediamine ($C_{H_2O}/C_{solvent}$).

viscosity is shown in Table 3.

Morgan and Kwolek[2] said that the polyamidation takes place near the interface in the organic phase. The results listed in Tables 2 and 3 can best be explained on the basis of their idea. When the polymer terminates at the chlorocarbonyl group, it reacts with the diamine or it is hydrolyzed by water; the latter case leads to the termination of the polymerization. Therefore, the amino group is desirable as the polymer-end; that is, a higher diamine/CPAC dichloride ratio may be favorable so long as the transfer rate of the diamine from the aqueous layer to the organic layer is not as fast as the reaction rate of diamine and CPAC dichloride. The low concentration of CPAC dichloride is also favorable.

The following results were obtained by Morgan and Kwolek;[2,3] In the unstirred polymerization, a solvent which extracts diamine strongly, such as chloroform, gives a polymer with a higher intrinsic viscosity, and the optimum reactant diamine/dichloride ratio at which the highest polymer is obtained shifts to a lower value. On the contrary, in the stirred polymerization, the intrinsic viscosities in the optimum reactant ratio are nearly equal when the solvent is changed. In this paper, the polymerization was carried out in four solvents, with the ratio of diamine/dichloride kept at a constant value (1.11). As a result, the intrinsic viscosity increased with an increase in the diamine partition coefficient.

CPAA, unlike CPAC, was not chlorinated by a similar method, so other polyether-amides with a repeating unit of 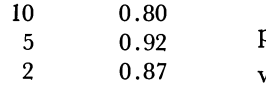
were not obtained.

Experimental

p-Carboxyphenoxyacetic Acid Dichloride. A mixture of 58.9 g (0.3 mol) of *p*-carboxyphenoxyacetic acid (CPAC) and 107 g of (0.9 mol) thionyl chloride was refluxed for 5 hr. After an excess amount of thionyl chloride had been distilled off, the CPAC dichloride was distilled under a vacuum. Distillation was then repeated two times. bp 164—165 °C /0.9 mmHg (lit,[4] bp 107—108 °C/0.08 mmHg) Yield, 95.0%.

Interfacial Polycondensation. A typical example will be shown as follows. A mixture of 0.02 mol of diamine, 0.04 mol of sodium hydroxide, and 60 g of ice was diluted with water to 300 ml. The aqueous solution was placed in a home-mixer (Matsushita Electric, type MX-83). While the solution was being stirred vigorously, a solution of 0.02 mol of CPAC dichloride in 150 ml of tetrachloroethylene was prepared and then poured rapidly into the aqueous solution. After 10 min, the resulting polymer was collected on a glass filter, washed with a sufficient amount of hot water, and dried in a vacuum.

Intrinsic Viscosity. The specific viscosity was measured in *m*-cresol at 25 °C with an Ubbelohde viscometer, plotted *versus* the concentration, and extrapolated to zero.

Melting Point. The melting point was determined by observing the temperature at which the sample on a hot plate reached a completely molten state (T_m) or by DTA (T_{m2}).

Glass Transition Temperature (T_g). The T_g was measured by means of a dilatometer.

Decomposition Temperature (T_d). The T_d was measured by TGA (Cho Keiryoki, TRDA$_1$-L; heating rate, 2.8 °C/min in N_2).

Diamine Partition Coefficient. Conditions: hexamethylenediamine, 0.002 mol; sodium hydroxide, 0.004 mol; water, 60 ml; organic solvent, 30 ml; temperature, 25 °C.

References

1) Part I of this series: T. Kito, T. Fujimoto, R. Mikami, and I. Hirao, This Bulletin, **46**, 209 (1973).
2) P. W. Morgan and S. L. Kwolek, *J. Polym. Sci.*, **62**, 33 (1962).
3) P. W. Morgan and S. L. Kwolek, *ibid.*, **40**, 299 (1959).
4) V. Rosnati, *Chem. Abstr.*, **52**, 7216g (1958).

BULLETIN OF THE CHEMICAL SOCIETY OF JAPAN, VOL. 47 (3), 785—786 (1974)

The Preparation of 2,2-Bis(trifluoromethyl)-1,3-heterocycles from 2,2,4,4-Tetrakis(trifluoromethyl)-1,3-dithietane

Tomoya KITAZUME and Nobuo ISHIKAWA

Tokyo Institute of Technology, Department of Chemical Engineering, Ookayama, Meguro-ku, Tokyo 152

(Received October 16, 1973)

Synopsis. 2,2-Bis(trifluoromethyl)-1,3-heterocyclic compounds, **3**, **4**, **6**, **7**, and **8**, were prepared by the reaction of 2,2,4,4-tetrakis(trifluoromethyl)-1,3-dithietane (**1**) with bifunctional compounds such as amino alcohols, *o*-aminophenol, *o*-aminothiophenol and *o*-phenylenediamine.

In earlier communications we reported on several nucleophilic reactions of 2,2,4,4-tetrakis(trifluoromethyl)-1,3-dithietane (**1**), which can be obtained from hexafluoropropene and sulfur. Alkyl- and arylamines reacted with **1** to give *N*-substituted hexafluoroisopropylideneimines,[1] while neither alcohol nor thiol reacted without the catalytic fluoride ion.[2] In this paper, we wish to report on the reactions of aminoalcohols, *o*-aminophenol, *o*-aminothiophenol, or *o*-phenylenediamine with **1**. In these cases, we found that both functional groups in a molecule, an amino and a hydroxyl for example, reacted with the positive carbon atom of **1** to afford 2,2-bis(trifluoromethyl)-1,3-heterocyclic compounds.

2-Aminoethanol and **1** reacted at room temperature in methylene chloride with a liberation of sulfur, which is usual in the reactions between amines and **1**.[1] The structure of the reaction product, 2,2-bis(trifluoromethyl)oxazolidine (**3**), was elucidated by means of its IR and NMR spectra.

In the IR spectrum, the presence of N–H and C–O–C was shown by the bands at 3370 and 1265 cm^{-1} respectively, but no O–H band was observed. In the ^{19}F NMR spectrum, only one singlet signal, at −2.1 ppm from external CF_3CO_2H in CCl_4, appeared. This is in contrast to the spectra of the hexafluoroisopropylidene imines, which have two ^{19}F signals corresponding to *syn* and *anti* CF_3. 3-Amino-1-propanol gave a similar compound, **4**.

Anilines with a functional group in the *ortho*-position reacted with **1** in dimethylformamide. *o*-Aminophenol, *o*-aminothiophenol, and *o*-phenylenediamine gave 2,2-bis(trifluoromethyl)benzoxazolidine (**6**), -benzothiazolidine (**7**), and -benzimidazolidine (**8**) respectively. The structures of these compounds were also elucidated by the IR, NMR, and mass spectra. The presence of the N–H group was proved by the band at 3200—3300 cm^{-1} in their IR spectra. In the ^{19}F NMR spectra, there was only one singlet signal each at about −3 ppm from external CF_3CO_2H in CCl_4. In the mass spectrum of **8**, for example, the strong molecular ion (M^+ 256) was observed, together with the appropriate fragment peaks,[3] such as *m/e* 187 ($C_8H_6F_3N_2$), 167 ($C_8H_5F_2N_2$), 117 ($C_7H_5N_2$), 90 (C_6H_4N), and 69 (CF_3). When **6** was treated with methyl iodide, the *N*-methyl compound was obtained as expected.

Since alkyl- or arylamines are known to give hexafluoroisopropylideneimines by reacting with **1**,[1] the ring formations mentioned above were estimated to proceed by the addition reaction of ZH across the neighboring >C=N double bond of **2** or **5**.

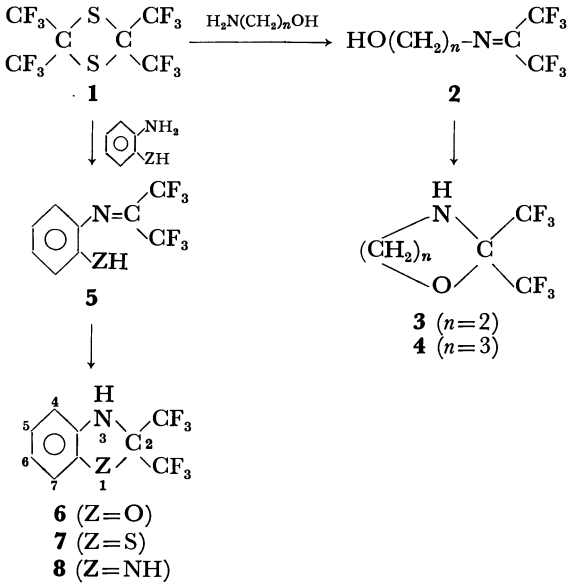

Table 1. Preparation and physical properties of compounds

Compound	Yield (%)	Bp (°C/mmHg)	IR (cm^{-1}) N–H	IR (cm^{-1}) C–O–C	NMR $^{19}F^{a)}$ CF_3	NMR ^1H (τ) NH	F (%) Found	F (%) Calcd
3	23	48—51/760	3370	1265	−2.10	4.80	54.8	54.5
4	31	52—54/760	3440	1272	−2.30	4.75	50.4	51.1
6	61	91—93/21	3220	1265	−3.20	4.70	43.7	44.3
5-Me-**6**	54	97—98/25	3240	1260	−3.20	5.30	42.5	42.1
7	48	103—105/25	3370	——	−3.15	5.20	41.9	41.6
8	42	113—114/28	3360	——	−3.80	5.00	44.8	44.5
5-F-**8**	20	60—63/3	3385	——	−3.10	5.10	48.0	48.5

a) Given δ in ppm from ext. CF_3CO_2H in CCl_4.

Experimental

2,2-Bis(trifluoromethyl)oxazolidine (3). To a stirred mixture of 2-aminoethanol (5.0 g, 0.08 mol) and methylene chloride (30 ml), **1** (18.2 g, 0.05 mol) was added, drop by drop, at room temperature. The stirring was continued for 1 hr at that temperature, and then the liberated sulfur was removed by filtration. The filtrate was distilled to give **3** (n=2) (3.8 g); bp 48—51 °C.

2,2-Bis(trifluoromethyl)tetrahydro-1,3-oxazine (4). This compound was prepared by using 3-amino-1-propanol (6.0 g) instead of the 2-aminoethanol used in the preceding reaction.

2,2-Bis(trifluoromethyl)benzoxazolidine (6). A mixture of **1** (7.30 g, 0.02 mol), 2-aminophenol (2.18 g, 0.02 mol). and dimethylformamide (30 ml) was stirred for 4 hr at room temperature, and then filtered. The filtrate was poured into water, and the oily material thus separated was extracted with ethyl ether. The extract was dried over magnesium sulfate, and the solvent was removed. A fraction with a bp of 91—93 °C/21 mmHg was collected to give **6** (3.15 g, 61%).

5-Methyl-substituted **6** was prepared in a similar manner, using 4-methyl-2-aminophenol.

N-*Methyl Derivative of* **6**. Into a mixture of **6** (2.57 g, 0.01 mol), potassium hydroxide (0.56 g, 0.01 mol) and ethyl alcohol (15 ml), methyl iodide (1.44 g, 0.01 mol) was added, drop by drop, after which the whole was stirred for 10 hr at room temperature. The reaction mixture was poured into water, and the oily material was extracted with ethyl ether. The extract was then dried over magnesium sulfate, and the solvent was removed. The vaccum distillation of the residue gave an *N*-methyl derivative (bp 109—110 °C/29 mmHg), in a yield of 63%. Found: F, 42.5%. Calcd for $C_{10}H_7F_6NO$: F, 42.1%.

2,2-Bis(trifluoromethyl)benzothiazolidine (7). A mixture of **1** (14.6 g, 0.04 mol), 2-aminothiophenol (6.00 g, 0.04 mol), and dimethylformamide (30 ml) was stirred for 4 hr at room temperature. The usual work-up process gave a product (**7**) (6.5 g).

2,2-Bis(trifluoromethyl)benzimidazolidine (8). *o*-Phenylenediamine (4.32 g, 0.04 mol), **1** (14.6 g, 0.04 mol), and dimethylformamide (30 ml) were used as in the preceding reaction, and then worked up similarly. Subsequent distillation gave **8** (4.3 g). 5-Fluoro-**8** was prepared similarly by using 4-fluoro-*o*-phenylenediamine.

References

1) N. Ishikawa and T. Kitazume, This Bulletin, **46**, 3260 (1973).
2) T. Kitazume and N. Ishikawa, *ibid.*, **46**, 3285 (1973).
3) Q. N. Porter and J. Baldas, "Mass Spectrometry of Heterocyclic Compounds," Wiley-Interscience (1971), Chap. 11—14.

BULLETIN OF THE CHEMICAL SOCIETY OF JAPAN, VOL. 47 (3), 787—788 (1974)

Die Kinetische Racemat-Spaltung des 1-Phenyläthanols und 1-Phenyläthylamins durch die aktivierten *N*-Tosyl-L-prolin-ester

Takeo SAKAN, Yutaka MORI, Tomio YAMAZAKI, Tetsushi YAMASHITA, und Nobuo NAKAMURA

Chemische Abteilung, Naturwissenschaftliche Fakultät, Städliche Universität Osaka, Sugimoto-cho, Sumiyoshi-ku, Osaka 558

(Eingegangen den Dezember 18, 1973)

Synopsis. Die optische Ausbeute von 10—50% wird erzielt. Einander entgegengesetztes Reaktionsverhalten zeigen die Magnesiumbromide des 1-Phenyläthanols und des 1-Phenyläthylamins bei der Umsetzung mit den Reagenzien.

Bisher wurden zur kinetischen Racemat-Spaltung der Alkohole optisch aktive Carbonsäureanhydride[1] oder Aminosäuren[2] verwendet, und die Horeausche Regel war in zahlreichen Fällen zur Konfigurationsbestimmung dieser Alkohole anwendbar. Wir haben die Reaktionsverhalten der aktivierten *N*-Tosyl-L-prolin-ester, d. h. Chinolyl-(8)-, (I),[3] *p*-Nitrophenyl-, (II),[4] und Naphthyl-(1)-ester, (III),[5] bei der Umsetzung mit Alkoxymagnesiumbromid des racem. 1-Phenyläthanols untersucht. Die Racemat-Spaltung durch die *S*-konfigurierten Reagenzien (I), (II), und (III), die aus *N*-Tosyl-L-prolylchlorid und dem betreffenden Phenol hergestellt wurden, läßt sich wie folgt durchführen:

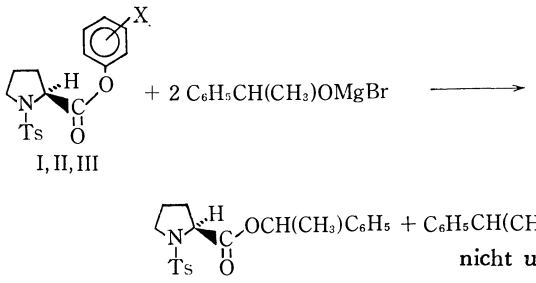

Die Versuche wurden gleichartig durchgeführt. Als Beispiel sei ein Versuch durch das Reagenz (I) beschrieben: Bei Raumtemperatur fügte man unter Rühren zu 16.4 mMol Alkoxymagnesiumbromid des 1-Phenyläthanols in 15 ccm Äther und 18 ccm Benzol 8.2 mMol von I in 30 ccm Benzol zu und rührte 4 Stdn. bei dieser Temperatur. Anschliessend versetzte man das Gemisch mit 10 ccm Wasser und filtrierte den abgetrennten Niederschlag. Die organische Phase wurde mit 2M HCl und Wasser gewaschen. Nach Trocknen und Verdampfen des Lösungsmittels erhielt man ölige Rohprodukte und destillierte den nicht umgesetzten Alkohol vorsichtig im Vakuum ab. Zur Hydrolyse des dabei zurückbleibenden Esters kochte man 2 Stdn. mit 5% iger wäßriger Natronlauge unter Rückfluß und ätherte mehrfach aus. Der umgesetzte Alkohol wurde durch Destillation gereinigt.

Unter den selben Bedingungen versuchten wir auch die Racemat-Spaltung des 1-Phenyläthylamins, um seine Konfigurationspriorität mit der des 1-Phenyläthanols zu vergleichen. Dabei wurde das Amin als Aminomagnesiumbromid oder als freies Amin eingesetzt.

In Tabelle 1 sind die Ergebnisse der kinetischen Racemat-Spaltung des 1-Phenyläthanols und 1-Phenyläthylamins zusammengestellt.

Die Magnesiumbromide des 1-Phenyläthanols und des 1-Phenyläthylamins zeigen einander entgegengesetztes Reaktionsverhalten bei der Umsetzung mit den Reagenzien (I) (II), und (III) (Versuch Nr.

TABELLE 1. ERGEBNISSE DER KINETISCHEN RACEMAT-SPALTUNGEN DURCH I, II, UND III

Versuch Nr.	Reagenz	Umgesetzt				Nicht-umgesetzt			
		Destilliert (%)	$[\alpha]_D$	o.A. (%)	(*R*), (*S*)	Destilliert (%)	$[\alpha]_D$	o.A. (%)	(*R*), (*S*)
	Substrat, $C_6H_5CH(CH_3)OMgBr$								
1	I	45	−6.8°	13	*S*	39	+8.6°	17	*R*
2	II	39	−12.6°	25	*S*	53	+9.4°	19	*R*
3	III	22	−18.4°	37	*S*	34	+18.3°	37	*R*
	Substrat, $C_6H_5CH(CH_3)OH$								
4	I	6	+6.4°	13	*R*	80	−0.83°	1.6	*S*[a]
	Substrat, $C_6H_5CH(CH_3)NHMgBr$								
5	I	17	+4.5°	11	*R*	36	−2.6°	6.2	*S*
6	II	20	+7.3°	17	*R*	35	−5.7°	14	*S*
7	III	9.7	+6.5°	16	*R*	31	−3.2°	7.6	*S*
	Substrat, $C_6H_5CH(CH_3)NH_2$								
8	I	21	−20.3°	48	*S*	44	+20.3°	48	*R*
9	I	27	−23.6°	56	*S*	44	+22.2°	53	*R*[b]
10	II	23	−9.1°	23	*S*	40	+10.5°	25	*R*
11	III	1.5	−12.2°	29	*S*	79	+0.97°	2.3	*R*

o.A.=optische Ausbeute, (*R*),(*S*)=Konfiguration

a) Das Ganze wurde 2 Tage in Benzol gekocht. Die Reagenzien (II) und (III) reagierten mit 1-Phenyläthanol so schwer, daß die optischen Drehungen nicht genau bestimmt werden konnten. b) bei −78 °C in Toluol versetzt. Zur Berechnung der optischen Ausbeuten dienten folgende Vergleichswerte: (*S*)-1-Phenyläthanol, $[\alpha]_D^{27}=-50.6°$ (Toluol)[6] (*R*)-1-Phenyläthylamin, $[\alpha]_D^{15}=+41.8°$ (Benzol)[7]

1—3 und 5—7). Man findet auch eine interessante Konfigurationskorrelation, daß bei der Umsetzung mit dem Reagenz (I) das Alkoxymagnesiumbromid und das freie Amin die gegenteilige Priorität als der freie Alkohol und das Aminomagnesiumbromid zeigen (Versuch Nr. 1, 4, 5, und 8). Die optischen Ausbeuten bei den Versuchen (Nr. 8 und 9) sind genug hoch. Außer den Ergebnissen von Tabelle 1 fanden wir, daß das Magnesiumbromid des *S*-konfigurierten 1-Phenyl-1-propanols bevorzugt mit I zum Ester reagiert (optische Ausbeute=14%).

Referenzen

1) A. Horeau, *Tetrahedron Lett.*, **1961**, 506. A. Horeau, *ibid.*, **1962**, 965. R. Weidmann und A. Horeau, *Bull. Soc. Chim. Fr.*, **1967**, 117. vgl. H. Brockmann, Jr. und J. Bode, *Ann. Chem.*, **748**, 20 (1971).

2) B. Halpern und J. W. Westley, *Aust. J. Chem.*, **19**, 1533 (1966).

3) Schmp. 141—141.5 °C, $[\alpha]_D^{18}=-115°$ (Chloroform, $c=4.1$).

4) Schmp. 106—107 °C, $[\alpha]_D^{18}=-130°$ (Chloroform, $c=3.8$).

5) Schmp. 133.5—134.5 °C, $[\alpha]_D^{23}=-86°$ (Chloroform, $c=4.4$).

6) W. von E. Doering und T. C. Aschner, *J. Amer. Chem. Soc.*, **71**, 838 (1949).

7) W. Leithe, *Monatsh. Chem.*, **51**, 385 (1929).

Role of Germanate Catalyst in the Transformation of Germanium Dioxide

Michiko YONEMURA and Yoshihide KOTERA

National Chemical Laboratory for Industry, Mita, Meguro-ku, Tokyo 153

(Received July 4, 1973)

The role of alkali germanates as catalysts in the polymorphic transformation of germanium dioxide was investigated by high-temperature X-ray diffraction method. Lithium germanate and sodium germanate catalyze the transformation in a solid state, the activation energies being larger than 80 kcal/mol. Potassium germanate catalyst plays its role in a liquid state, the activation energy being smaller than that of other catalysts.

It was found[1] that pure germanium dioxide does not undergo transformation on being heated up to 1000 °C, but it is transformed into tetragonal modification from hexagonal modification in the presence of lithium carbonate or potassium chloride. It was confirmed by means of DTA and high-temperature X-ray diffraction that a solid state reaction first occurs between the alkali salt and germanium dioxide to form germanate compounds which, in a crystalline or glassy state, catalyze the transformation.[2] Since it is expected that the occurence of such a reaction may disturb the determination of the transformation rate, it is necessary to investigate the transformation with an alkali germanate salt which is prepared by separate procedure. The phase diagrams of alkali oxide and germanium dioxide having been studied by Murthy *et al.*,[3-5] it was possible to elucidate the role of alkali germanate salts during the course of transformation.

We have studied the role of the alkali germanate salt during the course of phase transformation in detail under standardized conditions. It was found that lithium germanate and sodium germanate catalyze the transformation in solid state, while potassium germanate does so in liquid state, the activation energy being smaller than that of other salts.

Experimental

The starting materials were much the same as previously reported. Alkali germanate was prepared by a solid state reaction between Li_2CO_3, K_2CO_3 or Na_2CO_3 and GeO_2, as follows.

1) Lithium germanate: Li_2CO_3 and GeO_2 were mixed in a 1 : 7 mole ratio and ignited at 750 °C for 5 hr or at 1020 °C for 40 min. The end point of formation of $Li_2O \cdot 7GeO_2$ was confirmed by comparing the X-ray diffraction patterns of the product with the data given by Murthy and Ip.[3] The catalyst ignited at high temperature is of a larger crystal size than that at low temperature.

2) Potassium germanates: In order to prepare $3K_2O \cdot 11GeO_2$, K_2CO_3 and GeO_2 were mixed in a 3 : 11 mole ratio and ignited at 800 °C for 4 hr or at 1020 °C for 30 min, while K_2CO_3 and GeO_2 were mixed in a 1 : 7 mole ratio and ignited at 940 °C for 30 min, the product being $K_2O \cdot 7GeO_2$.[4] The end point of formation of these salts was confirmed by the same procedure as described above. In the case of $K_2O \cdot 7GeO_2$, the sintering was observed to occur, and the salt was used as catalyst after being finely ground.

3) Sodium germanate: $2Na_2O \cdot 9GeO_2$ was prepared by igniting a mixture of Na_2CO_3 and GeO_2 in a 2 : 9 mole ratio at 1050 °C for 40 min and the X-ray diffraction patterns of the product were compared with that reported by Murthy and Aguayo.[5]

High-temperature X-ray diffraction and measurements of transformation rate were carried out as reported.[2] All the experiments were carried out in dry nitrogen atmosphere.

Results

Some typical plots of logarithm of a hexagonal fraction, α, against time are shown in Figs. 1 and 2, where α was calculated by $H/H+T$, H or T being the peak height of hexagonal or tetragonal modification. The catalyst and its amount in weight percentage are given in the figures.

Activation energies were calculated from the Arrhenius plots (Figs. 3 and 4), where k was determined from the slope of straight lines. The results are given in Tables 1 and 2.

Discussion

From the study on the role of catalyst during the phase transformation of germanium dioxide[2] it was found that lithium and potassium salts added react with germanium dioxide to form germanate compounds. It was clarified for lithium salt that the formation of lithium germanate, $LiO_2 \cdot 7GeO_2$, occurs at a lower temperature than that of the transformation. Lithium germanate thus formed seems to catalyze the transformation in solid state. Potassium germanate, in contrast, seems to act as a catalyst in liquid state. It is expected that the kinetics of the transformation differ for the two cases. Murthy *et al.*[4] reported that there are many stable or metastable states in the K_2O-GeO_2 system, but since the added amount of potassium salt is rather small, it is desirable to select stable compounds rich in GeO_2. $3K_2O \cdot 11GeO_2$ and $K_2O \cdot 7GeO_2$ were prepared and used as catalysts, and it was found that the difference exists between them.

The phase transformation proceeds with alkali germanate salts. The plots of $\log \alpha$ against time (Figs. 1 and 2) consist of two straight lines, which can be explained by the assumption that the transformation proceeds in two stages, probably nucleation and propagation. However, activation energies calculated for two stages (Figs. 3 and 4) do not differ as much for lithium and sodium germanate as in the case of potassium germanate. This might be accounted for by the difference of solid and liquid catalyst. It could be concluded that lithium and sodium germanate remain in solid state even during the course of transformation, while potassium germanate turns to liquid.

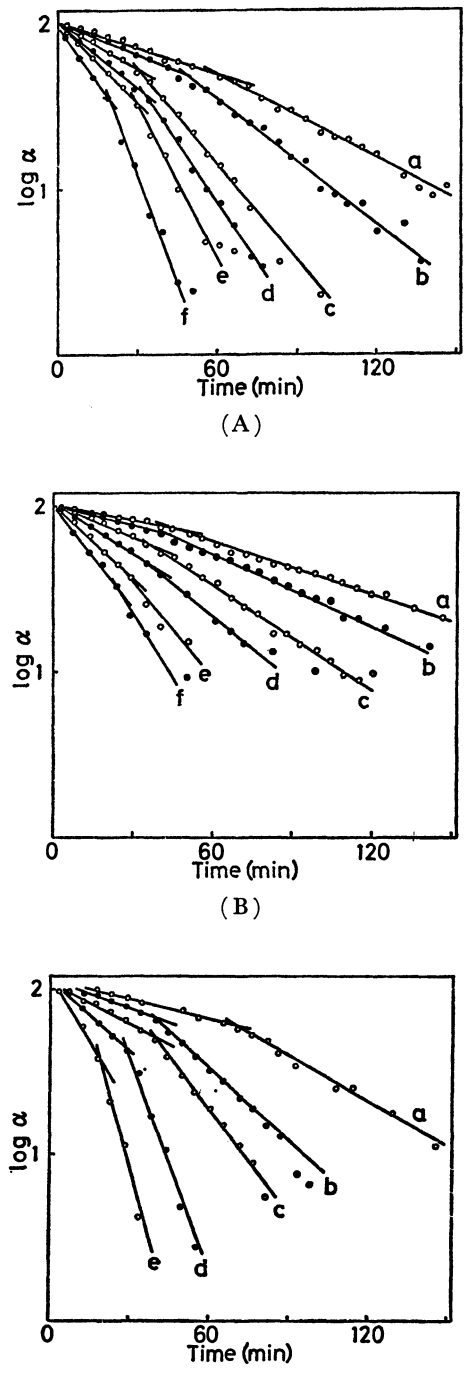

Fig. 1. First-order plot of conversion of hexagonal to tetragonal germanium dioxide (with catalyst of lithium germanate; $Li_2O \cdot 7GeO_2$); α is the percentage of hexagonal form present.

(A) Catalyst amount: 5 wt%
temperature a : 880 °C b : 890 °C c : 900 °C
d : 910 °C e : 920 °C f : 930 °C

(B) Catalyst amount: 10 wt%
temperature a : 870 °C b : 880 °C c : 890 °C
d : 900 °C e : 910 °C f : 920 °C

(C) Catalyst was prepared at low temperature and added amount was 5 wt%
temperature a : 840 °C b : 850 °C c : 860 °C
d : 870 °C e : 880 °C

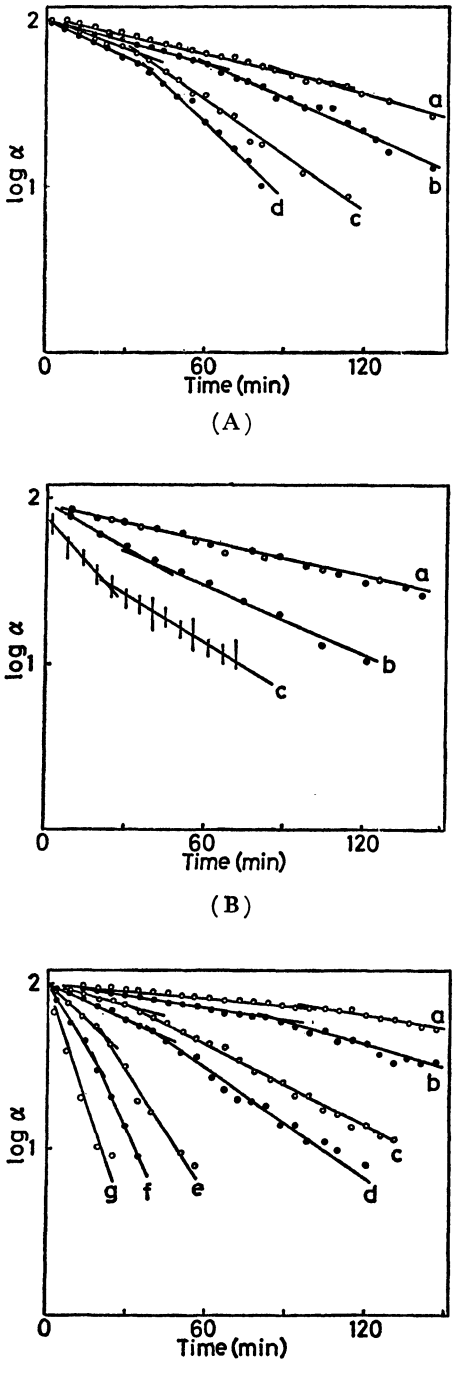

Fig. 2. First-order plot of conversion of hexagonal to tetragonal germanium dioxide (with catalyst of potassium or sodium germanate).

(A) $3K_2O \cdot 11GeO_2$ catalyst was prepared at low temperature and added amount was 1 wt%
temperature a : 840 °C b : 850 °C c : 860 °C
d : 870—890 °C

(B) Catalyst amount: 2 wt% of $K_2O \cdot 7GeO_2$
temperature a : 850—860 °C b : 870 °C
c : 880—940 °C

(C) Catalyst amount: 5 wt% of $2Na_2O \cdot 9GeO_2$
temperature a : 870 °C b : 880 °C c : 890 °C
d : 900 °C e : 910 °C f : 920 °C
g : 930 °C

Table 1. Activation energy of transformation (in N_2)

Catalyst	$Li_2O \cdot 7GeO_2$	$3K_2O \cdot 11GeO_2$	$K_2O \cdot 7GeO_2$	$2Na_2O \cdot 9GeO_2$
wt%	5	1	2	5
Activation energy	83— 91(A) 122—123(B)	72—102(A) 70— 98(B)	50±5	157—149

Note: 1) The first number denotes the value for the initial stage of the transformation, and the second number that for the final stage. 2) Catalyst A was prepared at 1020 °C for 30—40 min. Catalyst B was prepared at 750—800 °C for 4—5 hr.

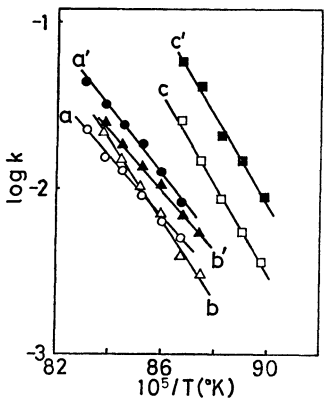

Fig. 3. Arrhenius plot of $\log k$ (k is obtained from Fig. 1) against reciprocal absolute temperature.
a : initial stage of transformation (Fig. 1-A)
a' : final stage of transformation (Fig. 1-A)
b : initial stage of transformation (Fig. 1-B)
b' : final stage of transformation (Fig. 1-B)
c : initial stage of tuansformation (Fig. 1-C)
c' : final stage of transformation (Fig. 1-C)

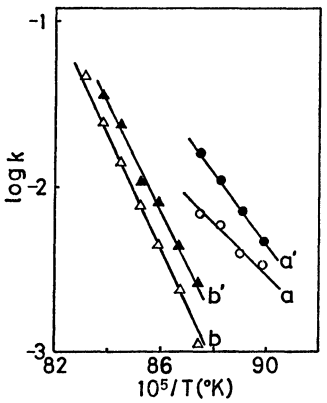

Fig. 4. Arrhenius plot of $\log k$ (k is obtained from Fig. 2) against reciprocal absolute temperature.
a : initial stage of transformation (Fig. 2-A)
a' : final stage of transformation (Fig. 2-A)
b : initial stage of transformation (Fig. 2-C)
b' : final stage of transformation (Fig. 2-C)

This is also supported by the fact that the temperature where the phase transformation occurs is lower in the case of liquid than in solid catalyst.

In the case of $K_2O \cdot 7GeO_2$ the results seem to be caused by the change of its state, as shown in Fig. 2 (B). The mean value of activation energy obtained from the Arrehnius plot is 50±5 kcal/mol between 850 °C and 900 °C (Table 1). Such a phenomenon was not observed with germanates other than $K_2O \cdot 7GeO_2$.

Table 2. Effect of amount of catalyst upon activation energy (in N_2)

Catalyst	$Li_2O \cdot 7GeO_2$	$3K_2O \cdot 11GeO_2$
1 wt%	110—100	70—98
5 wt%	83— 91	92—
10 wt%	109— 83	—

In the case of $3K_2O \cdot 11GeO_2$ it is probable that the interaction between the salt and germanium dioxide would occur during the course of the transformation and $K_2O \cdot 7GeO_2$ is formed.[4] However, this change was not detected by high-temperature X-ray diffraction, probably because of an insufficient amount of the catalyst for detection. The small values of the activation energy obtained for $3K_2O \cdot 11GeO_2$ may be the result of such an interaction. The catalyst, whose melting point is known to be 1055 °C, would be solid during the transformation so far as no interaction took place.

In the case of sodium germanate the results shown in Figs. 2(C) and 4 are much the same as in the case of lithium germanate. The activation energy obtained is 157 and 149 kcal/mol for first and final stages, respectively. The large values of activation energy would be explained by the fact that sodium germanate is stable and would catalyze the transformation in solid state.

The effect of the preparative method of catalysts on the transformation was observed for lithium germanate as an example for the solid catalyst (Table 1). The rate constant, k, was larger for the catalyst prepared at low temperature than prepared at high temperature, the activation energies differing a great deal from each other. No such effects were observed when potassium germanate was used. It would be concluded that the transformation carried out with solid catalysts is affected by characteristics such as particle size and morphology of the catalyst.

The amount of catalysts used in the transformation has in general no influence upon the activation energy of the transformation (Table 2). In the case of $LiO_2 \cdot 7GeO_2$, the transformation rate increased with 1—5 wt% increase in amount and it becomes saturated at 5—10 wt%. In the case of $3K_2O \cdot 11GeO_2$, the increase in amount causes the sintering of germanium dioxide. This would be accelerated by the presence of the catalyst in liquid state. As a result the calculation of activation energy could not

be carried out in the case of large amounts of $3K_2O \cdot 11GeO_2$.

The role of lithium salt in this transformation was recently reported.[6] The intermediate phase found by the same method as that applied in the transforma- of silicon dioxide[7] increased during the course of the transformation of germanium dioxide.

References

1) Y. Kotera and M. Yonemura, *Trans. Faraday Soc.*, **59**, 147 (1963).
2) Y. Kotera and M. Yonemura, *J. Amer. Ceram. Soc.*, **52**, 210 (1969).
3) M. K. Murthy and J. Ip, *ibid.*, **47**, 328 (1964).
4) M. K. Murthy, L. Long, and J. Ip, *ibid.*, **51**, 661 (1968).
5) M. K. Murthy and J. Aguayo, *ibid.*, **47**, 444 (1964).
6) M. Kunugi, A. Konishi, and S. Fukutani, *Zairyo*, **22**, 319 (1973).
7) A. C. D. Chaklader and A. L. Roberts, *J. Amer. Ceram. Soc.*, **44**, 35 (1961).

Effect of Surrounding Atmosphere in the Transformation of Germanium Dioxide

Michiko YONEMURA and Yoshihide KOTERA

National Chemical Laboratory for Industry, Mita, Meguro-ku, Tokyo 153

(Received July 4, 1973)

The effect of surrounding atmosphere on the phase transformation of germanium dioxide with alkali germanate catalysts was investigated by high temperature X-ray diffraction method. The catalysts were $Li_2O \cdot 7GeO_2$, $3K_2O \cdot 11GeO_2$, $K_2O \cdot 7GeO_2$ and $2Na_2O \cdot 9GeO_2$. The ambient atmospheres were dry or wet nitrogen and oxygen. The effect of atmosphere was found to be not so large as that of the catalyst. Water vapor has prominent effects upon the transformation as in other solid state reactions.

The role of the catalyst during the phase transformation of germanium dioxide was elucidated in a previous paper.[1] It is known that the surrounding atmosphere affects the rate and activation energy of the transformation singnificantly. It is thought that the atmosphere has a different effect on the transformation depending upon the catalyst used. In the present study the role of the surrounding atmosphere during the transformation was studied in detail under standardized conditions.

Experimental

The starting materials and the procedure of high-temperature X-ray diffraction were similar to those reported.[1] A high-temperature X-ray cell was filled with gas, dry or wet nitrogen and oxygen being used for the ambient atmospheres. Nitrogen and oxygen were dried by passing through concd. sulfuric acid and anhydrous calcium chloride; or wetted by allowing the gas to flow through water at 0 or 51±1 °C (water vapor pressure 5 or 100 mmHg, respec-

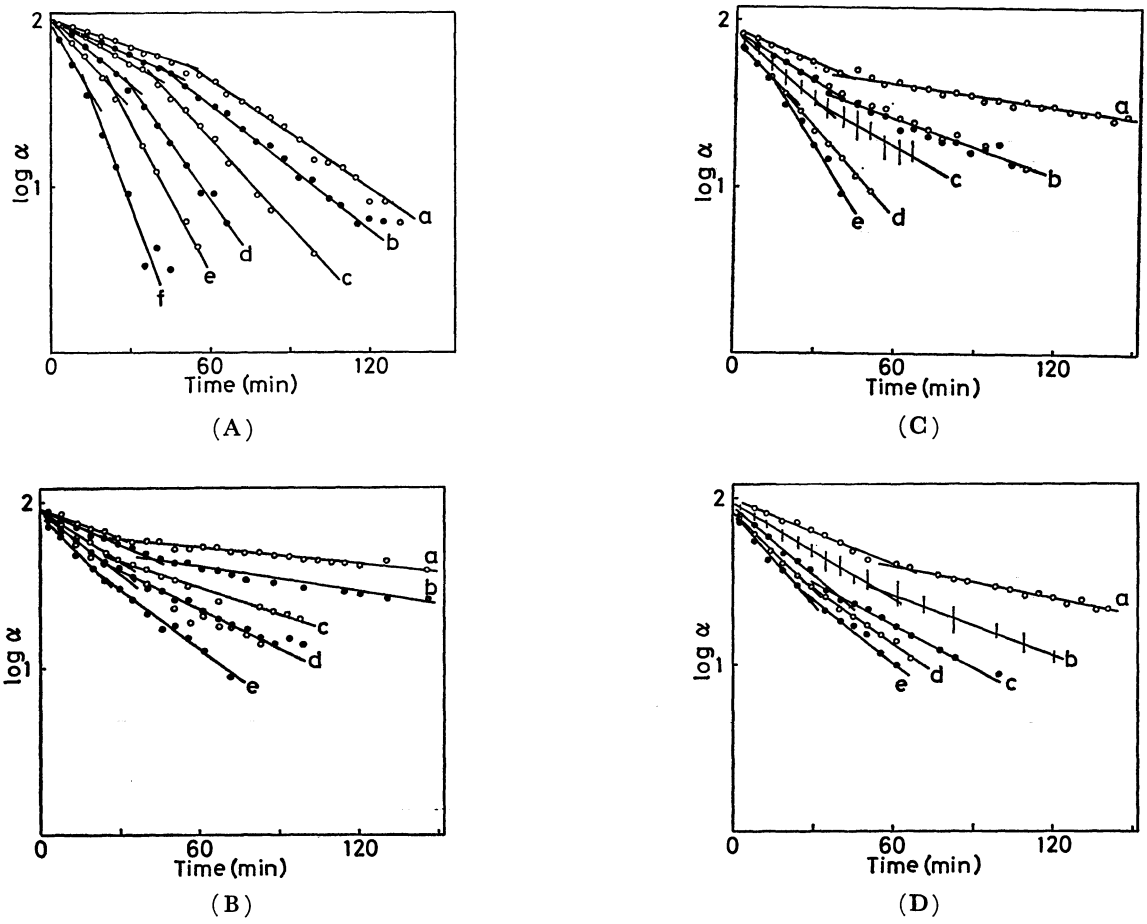

Fig. 1. First-order plot of conversion of hexagonal to tetragonal germanium dioxide.

(A) Catalyst: $Li_2O \cdot 7GeO_2$ 5wt%
Atmosphere: dry O_2
temperature a : 880 °C b : 890 °C c : 900 °C
d : 910 °C e : 920 °C f : 930 °C

(B) Catalyst: $3K_2O \cdot 11GeO_2$ 1 wt%
Atmosphere: wet N_2 (water vapor 5 mmHg)
temperature a : 840 °C b : 850 °C c : 860 °C
d : 870 and 880 °C e : 890 °C

(C) Catalyst: $3K_2O \cdot 11GeO_2$ 1 wt%
Atmosphere: wet O_2 (water vapor 5 mmHg)
temperature a : 840 °C b : 850 and 860 °C
c : 870 °C d : 880 °C e : 890 °C

(D) Catalyst: $K_2O \cdot 7GeO_2$ 2 wt%
Atmosphere: wet O_2 (water vapor 100 mmHg)
temperature a : 860 °C b : 870 °C c : 880 °C
d : 890 °C e : 900 °C

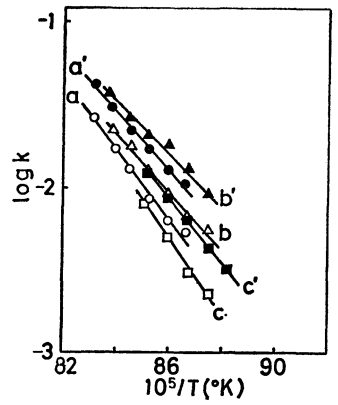

(A) a : initial stage of transformation (Fig. 1-A)
a' : final stage of transformation (Fig. 1-A)
b : initial stage of transformation[1)]
b' : final stage of transformation[1)]
c : initial stage of transformation[2)]
c' : final stage of transformation[2)]
1) Catalyst: $Li_2O \cdot 7GeO_2$ 5 wt%
Atmosphere: Wet O_2 (water vapor 100 mmHg)
2) Catalyst: $2Na_2O \cdot 9GeO_2$ 5 wt%
Atmosphere: Wet N_2 (water vapor 5 mmHg)

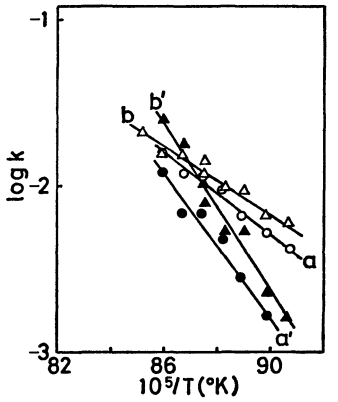

(B) a : initial stage of transformation (Fig. 1-B)
a' : final stage of transformation (Fig. 1-B)
b : initial stage of transformation (Fig. 1-C)
b' : final stage of transformation (Fig. 1-C)

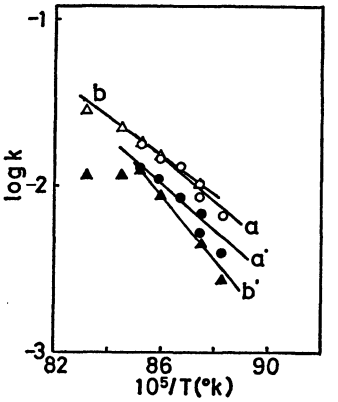

(C) a : initial stage of transformation (Fig. 1-D)
a' : final stage of transformation (Fig. 1-D)
b : initial stage of tranformation[3)]
b' : final stage of transformation
3) Catalyst: $K_2O \cdot 7GeO_2$ 2 wt%
Atmosphere: Wet N_2 (water vapor 5 mmHg)

Fig. 2. Arrhenius plot of $\log k$ (k is obtained from the figures of $\log \alpha - t$ plot) against reciprocal temperature.

TABLE 1. ACTIVATION ENERGY OF TRANSFORMATION

Atmosphere			Activation energy (kcal/mol)			
			$Li_2O \cdot 7GeO_2$ 5 wt%	$3K_2O \cdot 11GeO_2$ 1 wt%	$K_2O \cdot 7GeO_2$ 2 wt%	$2Na_2O \cdot 9GeO_2$ 5 wt%
N_2	Dry		83—91 (122—123)	70—98 (72—102)	50±5	157—149
	Wet	5 mmHg	96—91	55—98	52—90	101— 90
		100 mmHg	92—78			
O_2	Dry		93—80 (92—82)	47—130 (52—128)	40±5	142—106
	Wet	5 mmHg	83—90	46—114	115—119	107—83
		100 mmHg	81—74		60—65	

$\ln k = \ln A - E/RT$ k: rate const. E: activation energy (kcal/mol). A: pre-exponential factor
Note: 1) The first number denotes the value for the initial stage of the transformation, and the second number that for the final stage. 2) Data given in parentheses were calculated for $Li_2O \cdot 7GeO_2$ catalyst prepared at low temperature and $3K_2O \cdot 11GeO_2$ catalyst prepared at high temperature.

tively). The flow rate of gas was held constant by a tube flowmeter.

Results

Typical plots of logarithm of hexagonal fraction against time are shown in Fig. 1. Rate constant, k, was calculated in the same way as that described in the previous paper for the initial and final stages. The catalyst and atmosphere used are given in the Figures.

Activation energies were calculated from Arrhenius plots (Fig. 2). The experimental data with the atmosphere of dry nitrogen were reported.[1] The values of activation energy and pre-exponential factor are given in Tables 1 and 2.

Discussion

It was found that lithium or potassium salt added reacts with germanium oxide to form a germanate compound,[1,2] and that the surrounding atmosphere affects the rate and activation energy of the transformation significantly.[3] In these cases a different effect depending on the kind of germanate was expected, especially between one acting in solid state and one in liquid state.

From the values of activation energy it was confirmed that the effect of the surrounding atmosphere upon the phase transformation is smaller than that of the catalyst. While the values of activation energy do not change so much, the pre-exponential factor of transformation was dependent upon the surrounding atmosphere (Table 1).

A comparison of the relative positions of initial and final stages in the Arrhenius plot (Fig. 2), shows that they do not intersect in the temperature range studied in the cases of $Li_2O \cdot 7GeO_2$, ((A) a and a', b and b'), $2Na_2O \cdot 9GeO_2$ ((A) c and c') and $K_2O \cdot 7GeO_2$ ((C) a and a', b and b') catalysts. Their positions are in contrast to those of the two former catalysts acting in a solid state and the latter in a liquid one. This indicates that the rate k is higher in the final stage than in the initial stage for solid catalysts and lower for liquid ones. In the case of $3K_2O \cdot 11GeO_2$ ((B) a and a', b and b') the lines cross, the points of intersection lying between 870 and 890 °C. These temperatures lie near the eutectic point between $K_2O \cdot 7GeO_2$ and GeO_2 in the phase diagram reported by Murthy *et al.*[4] This salt would be formed by the reaction of $3K_2O \cdot 11GeO_2$ and GeO_2.

The effect of oxygen atmosphere is shown in Table 1, where oxygen makes the activation energy in the final stage small for $Li_2O \cdot 7GeO_2$ and $2Na_2O \cdot 9GeO_2$ which act in a solid state. However the difference between nitrogen and oxygen is not so large for liquid $K_2O \cdot 7GeO_2$ as in the two former catalysts. The effect of oxygen could be explained by the formation of germanium monoxide, which is assumed to be stable at high temperature. The effect of germanium monoxide seems to be more prominent on the transformation with a solid catalyst than with a liquid one.

The effects of the preparing conditions of solid catalysts upon the activation energy of the phase transformation, recognized in the nitrogen atmosphere,[1] were not observed in the present experiment in which oxygen atmosphere was used. They were not observed for liquid catalysts independent of the atmosphere during the transformation. The effect upon the rate of transformation is independent of the atmosphere and a high rate was found for catalysts prepared at lower temperature. It seems that the effect of the surrounding atmosphere upon the transformation is larger than that of the preparing conditions of the catalyst.

The effect of water vapor was observed only for the initial stage for low pressure. It was found also for the final stage when its pressure is as high as 100 mmHg. We see that water vapor influences the pre-exponential factor (Table 2), such phenomena being often found in the solid state reaction. When the vapor pressure was as high as 500 mmHg, the transformation rate was found to be high especially in the final stage, but the lowering of X-ray intensity made accurate determination of the rate impossible.

The effect of oxygen or water vapor upon the transformation rate is observed to be similar by independent

Table 2. Values of pre-exponential factor

Atmosphere			log A (A : pre-exponential factor) Catalyst			
			$Li_2O \cdot 7GeO_2$ 5 wt%	$3K_2O \cdot 11GeO_2$ 1 wt%	$K_2O \cdot 7GeO_2$ 2 wt%	$2Na_2O \cdot 9GeO_2$ 5 wt%
N_2	Dry		13.4 15.3	11.3 16.9		27.2 26.0
			(21.6 22.1)	(11.7 19.9)		
	Wet	5 mmHg	15.9 15.0	8.7 16.7	8.0 14.8	18.0 14.8
		100 mmHg	15.1 12.6			
O_2	Dry		15.9 13.2	6.9 23.1	5.5	24.5 17.8
			(15.9 14.3)	(7.8 22.3)		
	Wet	5 mmHg	13.4 15.1	6.8 19.9	19.9 20.3	17.8 13.5
		100 mmHg	13.1 12.1	15.6 23.7	9.5 10.2	

Note: See Table 1.

of the catalyst; k is larger for oxygen than for nitrogen and for wet atmosphere than for dry one. However, the log α–t plot (Fig. 1) scatters more in the wet atmosphere than in the oxygen atmosphere.

The co-operative effect of oxygen and water vapor is so complicated that it is difficult to give an explanation. They might compensate each other when the catalyst is $Li_2O \cdot 7GeO_2$ and the vapor pressure of water as low as 5 mmHg. For the catalyst $3K_2O \cdot 11GeO_2$, the co-operative effect is very clear.

The so-called "compensation effect" was observed (Tables 1 and 2) and the linearity between activation energy and common logarithm of pre-exponential factor was established. This might be the first time for it to be found in the solid state reaction.

References

1) M. Yonemura and Y. Kotera, This Bulletin, **47**, 789 (1974).
2) Y. Kotera and M. Yonemura, *J. Amer. Ceram. Soc.*, **52**, 210 (1969).
3) Y. Kotera and M. Yonemura, *Trans. Faraday Soc.*, **59**, 147 (1963).
4) M. K. Murthy, L. Long, and J. Ip., *J. Amer. Ceram. Soc.*, **51**, 661 (1968).

Vibrational Spectrum of Trisdimethylaminocyclopropenium Perchlorate

Zen-ichi YOSHIDA, Yoshiyuki TAWARA, Shizue HIROTA, and Hisanobu OGOSHI
Department of Synthetic Chemistry, Kyoto University, Yoshida, Kyoto 606

(Received July 6, 1973)

Infrared spectrum in the region 4000—100 cm^{-1} and Raman spectrum of trisdimethylaminocyclopropenium perchlorate (1) have been measured. Band assignments have been made on the basis of normal coordinate analysis and deuteration of the methyl groups. Remarkable stabilization of cyclopropenium ion due to the peripheral amino groups is attributed to a marked delocalization of the positive charge of the ring on the amino groups through conjugation. Peculiar electronic structure of trisaminocyclopropenium ion is explained in terms of its vibrational spectrum.

Cyclopropenium cations have received much attention in both the field of organic chemistry and molecular spectroscopies, mainly because of the fact that the smallest non-benzenoid aromatic cation (2π electron system) possesses high strain energy. The infrared spectrum of this system is usually discussed on the characteristic bands assigned to the skeletal vibrations of the three membered ring (C_3^+ core). The normal coordinate analysis of parent,[11] trimethyl-[11] and trichloro-cyclopropenium cations[1,11] was carried out using the Urey-Bradley force field. The calculation by the GVFF method was also reported for trichloro- and triphenyl-cyclopropenium cations in the simplified model.[2] However, no vibrational spectra of the cyclopropenium ion substituted with the strongly electron donating group (X) have been found so far. Such a tri-X-substituted cyclopropenium ion is considered to offer a good model for the investigation of physical and chemical properties of the strongly perturbed cyclopropenium ion.

Recently we have succeeded in the synthesis of triaminocyclopropenium ion[3] which is very stable (even in hot water) in contrast to the cyclopropenium ions reported so far. Thus the unusual physico-chemical properties of triaminocyclopropenium ion are expected to reflect on its vibrational spectrum. The present paper deals with the vibrational spectra of tris(dimethylamino)cyclopropenium ion(1) and its deutero analog in order to elucidate its structural feature at the ground state.

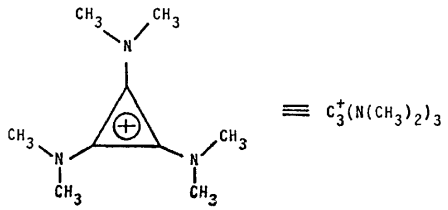

(1)

Experimental

1,2,3-Trisdimethylaminocyclopropenium perchlorate (1) was obtained by the treatment of tetrachlorocyclopropene with dimethylamine in methylene chloride.[3] Deuteration was performed with dimethylamine hydrochloride-d_6 (99%, E. Merck Co.) as a starting material.

The infrared spectra between 4000 and 300 cm^{-1} were recorded on a Perkin-Elmer Model 521 spectrophotometer and the far-infrared spectra on a Perkin-Elmer-Hitachi FIS-3 far-infrared photometer. The KBr-pellet technique was used for the former and the Nujol mull technique with a polyethylene window for the latter. Raman spectrum in the solid state was recorded on a JASCO R-1100 spectrophotometer with He-Ne laser (6328 Å).

Normal Coordinate Analysis

Figure 1 illustrates the molecular model and the internal coordinates used for normal coordinate analysis. According to a recent crystallographic study[4] of (1), the molecular symmetry can be approximated to D_{3h}. Out-of-plane deviations of six methyl groups are found to be very small. In order to simplify the calculation, each of the six methyl groups is treated as a single atom having a mass of 15.035. The G-matrix elements were evaluated by using the structure parameters listed in Table 1. These values were slightly changed from those of the original X-ray study in order to adjust the molecular dimension to D_{3h} symmetry.[6] Thus in this model, thirty normal vibrations, 30 ($12\times3-6$), are grouped into $4A_1'+3A_2'+$

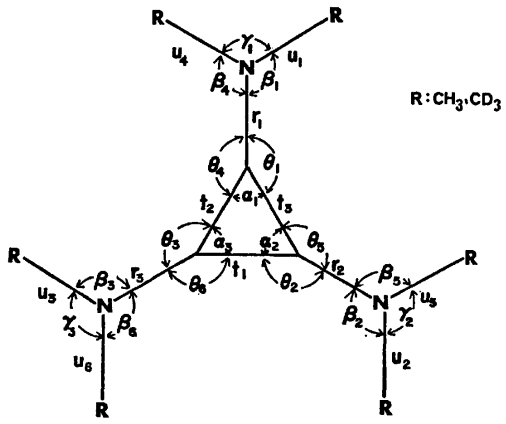

Fig. 1. Internal coordinates for the in-plane vibrations of trisdimethylaminocyclopropenium ion.

TABLE 1. MOLECULAR DIMENSIONS

Bond length (Å)	Bond angle
d(N-R)=1.457 (1.457)	∠C-N-R=120° (119.5°)
d(C-N)=1.332 (1.333)	∠R-N-R=120° (119.0°)
d(C-C)=1.362 (1.363)	∠N-C-C=150° (150.0°)
	∠C-C-C=60° (60.0°)

Values in brackets indicate the average value from X-ray analysis.[4]

Table 2. Symmetry coordinates for in-plane vibrations

	Symmetry coordinate	Vibration mode[a]
A_1'	$S_1=(\Delta t_1+\Delta t_2+\Delta t_3)/\sqrt{3}$	ν(C-C)
	$S_2=(\Delta r_1+\Delta r_2+\Delta r_3)/\sqrt{3}$	ν(C_3^+-R)
	$S_3=(\Delta s_1+\Delta s_2+\Delta s_3+\Delta s_4+\Delta s_5+\Delta s_6)/\sqrt{6}$	ν(N-R)
	$S_4=(2\Delta\gamma_1-\Delta\theta_1-\Delta\theta_4+2\Delta\gamma_2-\theta_2-\Delta_5+2\Delta\gamma_3-\Delta\theta_3-\Delta\theta_6)/3\sqrt{2}$	δ(R-N-R)
E′	$S_5=(2\Delta t_1-\Delta t_2-\Delta t_3)/\sqrt{6}$	ν(C-C)
	$S_6=(2\Delta r_1-\Delta r_2-\Delta r_3)/\sqrt{6}$	ν(C-N)
	$S_7=(2\Delta s_1+2\Delta s_4-\Delta s_3-\Delta s_6-\Delta s_2-\Delta s_5)/\sqrt{12}$	ν(N-R)
	$S_8=(\Delta s_2+\Delta s_6-\Delta s_3-\Delta s_5)/2$	ν(N-R)
	$S_9=(4\Delta r_1-2\Delta\theta_1-2\Delta\theta_4-2\Delta\gamma_2+\Delta\theta_2+\Delta\theta_5-2\Delta\gamma_3+\Delta\theta_3+\Delta\theta_6)/(6)$	δ(R-N-R)
	$S_{10}=(\Delta\theta_2+\Delta\theta_6-\Delta\theta_3-\Delta\theta_5)/(2)$	δ(C_3^+-N-R)
	$S_{11}=(4\Delta\alpha_1-2\Delta\beta_1-2\Delta\beta_4-2\Delta\alpha_2+\Delta\beta_2+\Delta\beta_5-2\Delta\alpha_3+\Delta\beta_3+\Delta\beta_6)/(6)$	ring def.
	$S_{12}=(\Delta\beta_2-\Delta\beta_5-\Delta\beta_3+\Delta\beta_6)/2$	δ(C-C-N)

a) Symbols ν and δ denote stretching and in-plane bending vibrations, respectively.

$7E'+1A_2''+3E'')$. There are sixteen infrared active modes; 7E′ (in-plane) and $2A_2''$ (out-of-plane), and twenty four Raman active modes; 7E′ (in-plane), $4A_1'$ (in-plane) and 3E″ (out-of-plane). We have calculated eleven in-plane vibrations (7E′ and $4A_1'$) by means of Wilson's GF matrix method. The twelve symmetry coordinates used in the calculation are given in Table 2.

The F-matrix elements are expressed by the simple Urey-Bradley force field. In the first calculation, the stretching force constants K(C–C), K(C–N), and K-(N–CH_3) were estimated from those of trichlorocyclopropenium ion,[1] guanidium salt,[7] and alkyl urea,[8] respectively. The bending and repulsive forec constants were transferred from those of the amide compounds.[9]

The computational procedures were carried out by using the FACOM in Kyoto University. The final set of force constants were obtained by referring to the Jacobian matrix elements followed by further refinement using the least squares method (Table 3). Calculated frequencies are compared with those observed for (1) and (1)-d_{18} (Table 4). We see that agreement is quite satisfactory in spite of a single mass approximation for the methyl group. For the band assignments, the potential energy distribution was calculated for each normal vibration in terms of the symmetry coordinates are shown in the last column of Table 4.

Table 3. Urey-Bradley force constants of trisdimethylaminocyclopropenium ion (in mdyn/Å)

K(C-C)	6.622
K(C-N)	5.741
K(N-R)	4.270
H(C-C-C)	−1.014
H(C-C-N)	0.615
H(C_3^+-N-R)	0.203
H(R-N-R)	0.353
F(C----N)	0.659
F(C----R)	0.430
F(R----R)	0.039

Table 4. Comparison of observed and calculated frequencies

		Obsd	Calcd	PED
		(I)		
(A_1')	ν_1	1985	1985	S_1(80), S_2(38)
	ν_2	1135	1140	S_1(11), S_2(30), S_3(45), S_4(14)
	ν_3	614	607	S_2(21), S_3(55), S_4(14)
	ν_4	324	310	S_2(15), S_4(74)
(E′)	ν_5	1553	1545	S_5(42), S_6(70), S_{11}(11)
	ν_6	1280	1278	S_6(12), S_8(52), S_{10}(13), S_{12}(20)
	ν_7	1120	1097	S_5(42), S_7(18), S_8(37), S_{11}(11)
	ν_8	790	780	S_6(12), S_7(60)
	ν_9	460	463	S_5(10), S_7(13), S_9(55), S_{10}(13)
	ν_{10}	316	319	S_5(22), S_9(35), S_{10}(30)
	ν_{11}	130	131	S_{10}(40), S_{12}(50)
		(II)-d_{18}		
(A_1')	ν_1	—	1985	S_1(80), S_2(38)
	ν_2	—	1124	S_1(12), S_2(32), S_3(41), S_4(14)
	ν_3	—	561	S_2(19), S_3(60), S_4(12)
	ν_4	—	283	S_2(14), S_4(74)
(E′)	ν_5	1534	1544	S_5(42), S_6(70), S_{11}(11)
	ν_6	1252	1262	S_6(13), S_8(45), S_{10}(14), S_{12}(22)
	ν_7	1060	1074	S_5(41), S_7(14), S_8(42), S_{11}(11)
	ν_8	732	738	S_6(11), S_7(60)
	ν_9	410	435	S_5(10), S_7(16), S_9(52), S_{10}(13)
	ν_{10}	306	295	S_5(21), S_9(37), S_{10}(29)
	ν_{11}	125	120	S_{10}(41), S_{12}(49)

Results

Band Assignments. The infrared spectra of (1) and (1)-d_{18} from 4000 to 400 cm^{-1} and from 400 to 100 cm^{-1} are shown respectively in Figs. 2 and 3. The Raman spectrum of (1) in the solid state is shown in Fig. 4. In normal coordinate analyses, we have approximated the methyl group as a single atom having masses of 15.035 and 18.035 for (1) and (1)-d_{18}, respectively. Thus the absorptions due to the methyl group were confirmed by comparing the spectrum of (1) with that of (1)-d_{18}. The four bands at 2970, 2935, 2892, and 2842 cm^{-1} are assigned to the C–H stretching vibrations, which disappear upon deuteration of the methyl groups. The deutero analog (1)-d_{18} shows three bands at 2370, 2235 and 2079 cm^{-1} assigned to the C–D stretching vibrations. The broad and strong absorption at 1553 cm^{-1} is mainly due to the C_3^+–N< stretching vibration and the C–C ring stretching vibration according to the potential energy distribution. However, the calculation indicates a slight shift of ν_5 upon deuteration. The observed value shows a

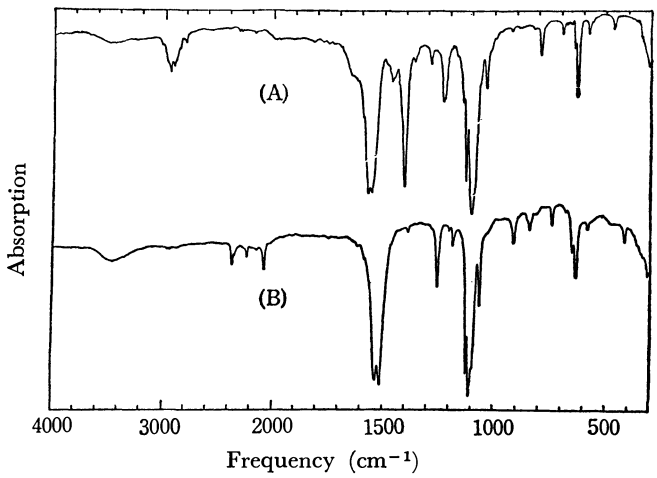

Fig. 2. Infrared spectra of trisdimethylaminocyclopropenium perchlorate (A) and its deutero analog (B).

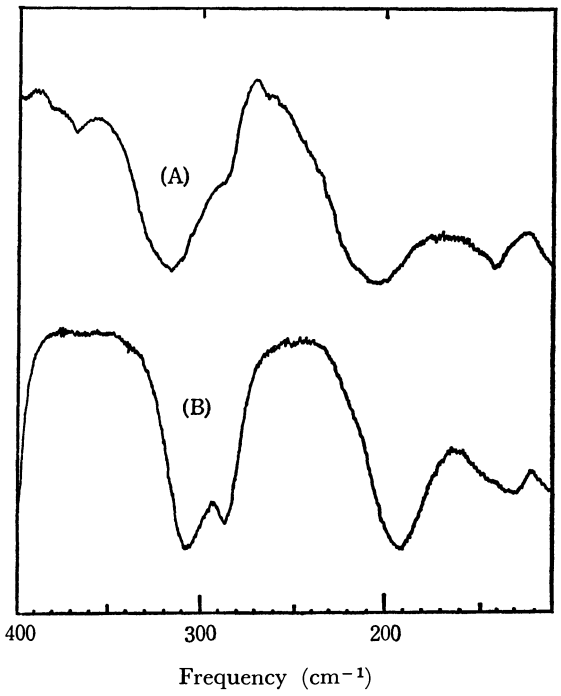

Fig. 3. Far-infrared spectrum of trisdimethylaminocyclopropenium perchlorate (A) and its deutero analog (B).

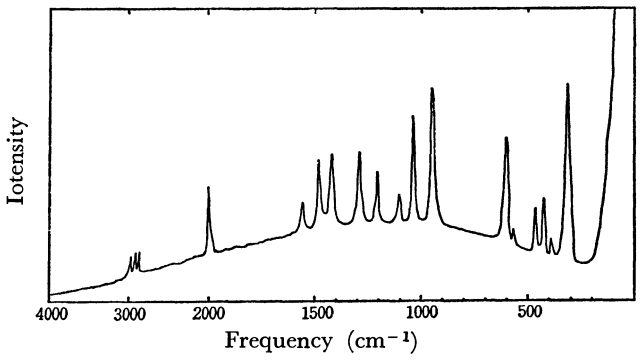

Fig. 4. Raman spectrum of trisdimethylaminocyclopropenium perchlorate.

lower frequency-shift of about 20 cm^{-1} upon deuteration. The discrepancy is attributed to the one mass approximation of the CH_3 and CD_3 groups. Breslow *et al.* reported that the degenerate ring deformation of the $C_3H_3^+$ mode appears at 1276 cm^{-1}.[10] We have assigned the corresponding absorption of the $C_3(CH_3)_3^+ \cdot SbCl_6^-$ to 1490 cm^{-1} referring to the spectra of the $C_3(CD_3)_3^+ \cdot SbCl_6^-$.[11]

The Raman line at 1135 cm^{-1} is assigned to the symmetric C_3^+–N< stretching (ν_2) coupled with the N–CH_3 symmetric stretching (ν_3). The band at 1238 cm^{-1} is assigned to the C_3^+–N< stretching vibration. The Raman line at 1985 cm^{-1} of medium intensity is assigned to the totally symmetric C–C stretching vibration S_1(C_3^+ core breathing) coupled with the C_3^+–N stretching mode (S_2). The C_3^+ core stretching (S_1) shows the largest contribution to ν_1. The calculation indicates that the coupling of the C_3^+ ring stretching vibration with the C–N< stretching mode in E′ species is stronger than that in A_1' species.

The bands at 1455 and 1405 cm^{-1} of (1) are interpreted to be the CH_3 asymmetric and symmetric deformation modes. No CH_3 deformation band appears for (1)-d_{18} in this region. The two bands of (1)-d_{18} appear at 1180 and 1120 cm^{-1} as shoulder bands of the strong absorption (1100 cm^{-1}) of the ClO_4^-. A lower frequency band of the CH_3 rocking of (1) appears at 1225 cm^{-1} and 1134 cm^{-1}. The deutero compound (1)-d_{18} shows two absorptions due to the CD_3 rocking modes at 904 and 835 cm^{-1}.

The sharp band at 1060 cm^{-1} of (1)-d_{18} is explained to be the C–C stretching of the C_3^+ ring and the N–CD_3 stretching vibration. The corresponding absorption of (1) seems to shift to a slightly higher frequency region resulting in the overlapping with the strong absorption of the ClO_4^- ion. The band at 790 cm^{-1} of (1) can be assigned to the N–CH_3 stretching mode, which is confirmed by deuteration of the methyl group. The N–CD_3 stretching appears at 732 cm^{-1} in accordance with the calculation. The Raman line at 614 cm^{-1} is assigned to the symmetric N–CH_3 stretching vibration. The bands at 455, 316, and 130 cm^{-1} of (1) are assigned to the CH_3–N–CH_3 bending, the C_3^+–N–CH_3 bending and the $C_3^+N(CH_3)_2$ bending modes, respectively. The bands shift to a slightly lower frequency region upon deuteration. A weak band at 290 cm^{-1} and a band at 206 cm^{-1} are presumably due to the out-of-plane deformations of the N–$(CH_3)_2$ groups. The presence of perchlorate ion is confirmed by the bands at 1100 and 680 cm^{-1} assigned to the Cl–O stretching and bending modes of ClO_4^- ion.

Discussion

It is noted that extremely stable triaminocyclopropenium ion (1) shows the highest frequency of the totally symmetric C–C stretching vibration of the C_3^+ core among the various cyclopropenium ions reported so far (Table 5). For example, the ions $C_3(CH_3)_3^+$, $C_3(C_6H_5)_3^+$ and $C_3Cl_3^+$ exhibit the C–C stretching mode (A_1') at 1880, 1845 and 1791 cm^{-1} in their Raman spectra respectively. It is noteworthy that there is

Table 5. Frequencies of ring deformation vibration and pK_{R^+} values of various cyclopropenium ions $C_3X_3^+$

X=	H	Cl	C_6H_5	CH_3	$N(CH_3)_2$
A_1' (Raman)	—	1791[b]	1845[c]	1875[h]	1985[g]
E′ (IR)	1276[a]	1321[b]	1411[c]	1446[h]	1553[g]
pK_{R^+}	−7.4[a]	−3[f]	3.1[d]	7.4[e]	13[f]

a) R. Breslow and J. T. Groves, *J. Amer. Chem. Soc.*, **92**, 984 (1970). b) R. West, A. Sadô and S. W. Jobey, *ibid.*, **88**, 2488 (1966). c) F. Höfler, B. Schrader, and A. Krebs, *Z. Naturforsch.*, **24a**, 1617 (1969). d) R. Breslow, J. Rockhart, and H. W. Chang, *J. Amer. Chem. Soc.*, **83**, 2375 (1961). e) J. Ciabattoni and E. C. Nathan, III, *Tetrahedron Lett.*, **57**, 4997 (1969). f) Ref. 12. g) This work. h) Ref. 11.

an empirical linear relationship between the stability (pK_{R^+}) of C_3^+ core and the frequencies of the C_3^+ core vibrations (A_1' and E′).[12] The two frequencies shift towards a higher frequency region with the increase of the relative stability of the cyclopropenium ion. Although pK_{R^+} of (1) could not be determined by the usual potentiometric titration because of its alkaline hydrolysis,[5] we could estimate this value to be 13 from the relationship between pK_{R^+} values of cyclopropenium ions and their degenerate ring deformation (Table 5). Such a remarkable stabilization of cyclopropenium ion by amino-substitution has also been observed in the case of aminodiphenylcyclopropenium ion[14] ($pK_{R^+}=10$). The INDO calculation of triaminocyclopropenium ion suggests that its high stability is due to the large electron-donating π conjugative effect of amino group on the C_3^+ ring.[15] Since the frequency of ring deformation vibration is sensitive to the peripheral substituent, the vibrational spectrum of highly strained cyclopropenium ion may provide an accessible and convenient method to estimate its relative stability.

Of the force constants obtained for trisdimethylaminocyclopropenium ion (Table 3), the force constant (6.62) of the C–C stretching vibration of (1) is larger than the force constants (6.22 and 6.31) of trichloro- and trimethyl-cyclopropenium ions.[11] The values ($Cl< CH_3<N(CH_3)_2$) seem to be strange, since electron-donating π conjugative effect of the amino group (+0.190) is larger than that of Cl- and CH_3- (+0.005) groups.[15] Since the C–C π bond order ($CH_3> N(CH_3)_2$) of the C_3^+ ring decreases with increase in electron-donating nature of substituent, the observed increase of the ring stretching force constant ($CH_3< N(CH_3)_2$) might be responsible for the marked increase of the C–C σ-bond order in (1). This is a peculiar property of the cyclopropenium ring. The X-ray crystallographic study[6] of (1) indicates that the C–C bond length of (1) is about 0.01 Å shorter than that of triphenylcyclopropenium ion.[13] The result seems to support the larger C–C stretching force constant of (1). It is possible to explain the increase in the K(C–C) on the basis of the decrease in the replusion between the carbon nuclei of the three membered ring due to the strong electron donating amino groups. It is of particular interest to compare the C–N stretching vibration of (1) with that of the guanidine hydrochloride, for which Yamaguchi[7] assigned the infrared

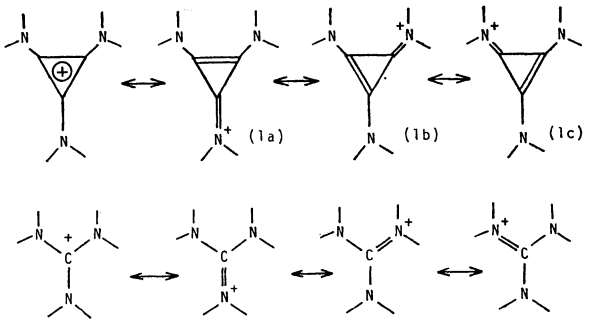

absorption at 1640 cm^{-1} and Raman line at 1015 cm^{-1} to the degenerate C–N stretching vibration and symmetric C–N stretching vibration, respectively. The large contribution of the C_3^+–N< stretching mode to this band indicates a strong π-conjugative interaction between the amino group and the C_3^+ core. The canonical structures of (1) can be shown as above in analogy with guanidium salt. The INDO type calculation shows a considerable migration of the positive charge from the C_3^+ ring to the peripheral amino groups,[15] suggesting a large contribution of the charge-delocalized structures (Ia, Ib, and Ic).

It is interesting to note that the C_3^+–N stretching force constant is very large and comparable to that of guanidium salt.[7] This can be interpreted in terms of the large delocalition of the positive charge to the peripheral amino groups. The C–N bond lengths of (1) and guadinium salt obtained by X-ray analysis are 1.333 Å and 1.34 Å, respectively, which are markedly smaller than the length of the ordinary C–N single bond (*ca.* 1.47 Å). The small negative bending force constant of the C_3^+ core is derived from the transformation of the internal coordinates to the symmetry involving the redundant condition of the ring C_3^+ system.[11]

References

1) R. West, A. Sadô, and S. W. Tobey, *J. Amer. Chem. Soc.*, **88**, 2488 (1966).
2) F. Höfler, B. Schrader, and A. Krebs, *Z. Naturforsch.*, **24a**, 1617 (1969).
3) Z. Yoshida and Y. Tawara, *J. Amer. Chem. Soc.*, **93**, 2573 (1971).
4) Z. Yoshida, H. Konishi, Y. Tawara, and H. Ogoshi, *ibid.*, **95**, 3043 (1973).
5) Z. Yoshida, H. Konishi, Y. Tawara, K. Nishikawa, and H. Ogoshi, *Tetrahedron Lett.*, **1973**, 2619.
6) A. T. Ku and M. Sundaralingam, *J. Amer. Chem. Soc.*, **94**, 1688 (1972).
7) A. Yamaguchi, *Nippon Kagaku Zasshi*, **78**, 672, 694 (1957).
8) R. K. Dosavi, U. Agarwala, and C. N. Rao, *J. Amer. Chem. Soc.*, **89**, 235 (1967).
9) S. Mizushima and T. Schimanouchi, "Infrared absorption and the Raman Effect," Kyoritsu, Tokyo (1958).
10) R. Breslow, H. Hofler, and H. W. Chang, *J. Amer. Chem. Soc.*, **84**, 3168 (1962).
11) Z. Yoshida, S. Hirota, and H. Ogoshi, *Spectrochim. Acta*, in press.
12) Z. Yoshida, H. Ogoshi, and S. Hirota, *Tetrahedron Lett.*, **1973**, 869.
13) M. Sundaralingam and L. H. Densen, *J. Amer. Chem. Soc.*, **88**, 198 (1966).
14) R. C. Kerber and C. Hsu, *ibid.*, **95**, 3239 (1973).
15) Z. Yoshida, "Topics in Current Chemistry," Vol. 40, Springer-Verlag, Berlin (1973), p. 50, "Three Membered Ring."

Characteristic Studies on Dealumination of Faujasite-type Zeolite

Kazuo TSUTSUMI, Hisao KAJIWARA, and Hiroshi TAKAHASHI

Institute of Industrial Science, The University of Tokyo, Roppongi, Minato-ku, Tokyo 106

(Received July 11, 1973)

Aluminium ion was extracted stoichiometrically from the framework of the faujasite-type zeolite by EDTA treatment. Dealuminated zeolites with various silica/alumina ratios (from 4.80 to 10.29) were obtained. A dealuminated zeolite does not necessarily show the molecular-sieve-type adsorption isotherm of nitrogen. The lattice constant of zeolite decreases with the silica/alumina ratio. The zeolite with an increased silica/alumina ratio has a higher catalytic activity for a cumene-cracking reaction than the parent H-$Y_{4.80}$ zeolite. It is suggested, on the basis of infrared spectroscopic and calorimetric measurements, that the total number of acid sites decreases with dealumination, while the number of strong acid sites increases. These strong aicd sites seem to contribute to the catalytic activity of dealuminated zeolite.

The catalytic properties of zeolite depend mostly on the type of zeolite, the kind and degree of the exchanged cation, and the silica/alumina ratio. The first three factors have been reported on by many authors, but the effect of the silica/alumina ratio has scarcely been investigated at all. Ward showed that the Brönsted acidity of Ca- or Mg- exchanged faujasite-type zeolite and the catalytic activity for the isomerization of *o*-xylene increased[1] with the silica/alumina ratio.

We have investigated the acidity,[2] and catalytic activity for cumene cracking[3] and the electrostatic-field strength[4] of faujasite-type zeolite as functions of the silica/alumina ratio. In the case of Ca-exchanged zeolite, the electrostatic-field becomes stronger with the increase in the silica/alumina ratio. The cumene-cracking activity of Ca-form zeolite follows in magnitude the change in the electrostatic-field strength. The number of acid sites and the catalytic activity of decationated zeolite increase with the increase in the silica/alumina ratio.

It has been established that the aluminium ion can be readily extracted from the framework of clinoptilolite[5] or erionite[6] by a mineral-acid treatment. The removal of aluminium from mordenite frameworks can also be performed by hydrochloric-acid treatment without distroying the crystal structure as far as the X-ray diffraction patterns are concerned. The catalytic activity and other physicochemical properties of Al-deficient mordenite have been examined by several authors in order to make clear the effect of the dealumination on the diffusion behavior of reactants.[7,8]

It was recently reported that aluminium could also be removed from faujasite-type zeolite frameworks by ethylenediamine-tetraacetic acid (H_4EDTA) treatment.[9] Topchieva and T'huoang reported that the highest activity was exhibited by a specimen in which half of the aluminium atoms had been removed from the faujasite frameworks.[10] Beaumont and Barthomeuf[11–13] and Beaumont *et al.*[14] measured the acidity of the dealuminated zeolite by means of *n*-butylamine titration and infrared spectroscopy.

This paper reports on studies of the effect of the silica/alumina ratio in correlation with the structure, adsorption, acidity, acid strength and catalytic activity, by using the EDTA-treated faujasite-type zeolites.

Experimental

Synthetic sodium faujasite (Linde SK-40) was used as the starting material. The ion exchange for the ammonium ion was performed in an aqueous solution of ammonium chloride by the conventional method. Twenty grams of NH_4^+-exchanged zeolite was treated with an EDTA aqueous solution of an appropriate concentration by means of a Soxhlet extractor. The samples obtained were washed, dried and then equilibrated with saturated vapor of water and the compositions were determined by chemical analysis.

The X-ray powder diagrams were recorded with an X-ray diffractometer (Rigaku Denki Co., Ltd., D-9C Type) using Cu$K\alpha$ radiation, the scanning speed being 1° or 1/8° 2θ/min, the time constant 4 s, receiving slit 0.15 mm, and angular aperture 1°. Silicon was used as an internal standard for the measurement of the lattice constant. The (642) diffraction line of zeolite was used for the measurement.

Mid-infrared spectroscopy has been applied to changes in the zeolite structure with dealumination. The spectra were obtained using the KBr wafer technique. The wafer concentrations were adjusted to obtain the desired absorbance. The spectra were recorded with a Hitachi Model EPI-G3 spectrophotometer.

The nitrogen adsorption isotherms were obtained with a conventional volumetric adsorption apparatus. The pore distribution was calculated by the Inkley method.

The catalytic activity for the cumene-cracking reaction was measured by means of a pulse reactor. The apparatus has been described in detail.[3]

The second infrared spectroscopic technique was used to measure the spectra in the OH stretching region and those of the adsorbed pyridine. The zeolite samples were pressed into a wafer with a thickness of about 10 mg/cm^2. The sample was set in a quartz cell fitted with NaCl windows and heated to 450 °C under 10^{-5} mmHg. The cell was then cooled to room temperature under vacuum; the spectrum was thus obtained. The spectrum of the pyridine adsorbed was also observed. Excess pyridine was adsorbed on the sample and allowed to equilibrate for 3 hr. The spectrum of the adsorbate was obtained after the sample-adsorbate had been evacuated at 250 °C in order to remove the physically adsorbed pyridine.

The differential heats of the adsorption of ammonia were measured in order to estimate the acid strength of zeolite. About one gram of zeolite was placed in the stainless-steel cell, and evacuated at 400 °C under 10^{-5} mmHg over a period of several hours. The cell was set in a twin con-

duction-type calorimeter until thermal equilibrium was reached at 25 °C. Gaseous ammonia was then introduced into the cell. The heat liberated was recorded and calibrated by a known amount of heat.

Results and Discussion

Chemical Compositions. The compositions of the samples obtained are shown in Table 1. Zeolite becomes cation-deficient with dealumination. The silica/alumina ratios are plotted against the moles of EDTA used in Fig. 1. The broken line indicates the relation calculated by Eq. (1).

$$x\mathrm{H_4EDTA} + \mathrm{NH_4AlO_2(SiO_2)_{2.40}} \longrightarrow x\mathrm{NH_4AlEDTA} + (\mathrm{NH_4AlO_2})_{1-x}(\mathrm{H_2O})_{2x}(\mathrm{SiO_2})_{2.40} \quad (1)$$

The close fit of the points shows that the dealumination reaction proceeds stoichiometrically as Kerr suggested.[9]

Table 1. Zeolite compositions

Sample	Composition
H-$Y_{4.80}$	$0.78(NH_4)_2O\cdot 0.15Na_2O\cdot Al_2O_3\cdot 4.80SiO_2$
H-$Y_{5.97}$	$0.71(NH_4)_2O\cdot 0.17Na_2O\cdot Al_2O_3\cdot 5.97SiO_2$
H-$Y_{6.54}$	$0.70(NH_4)_2O\cdot 0.18Na_2O\cdot Al_2O_3\cdot 6.54SiO_2$
H-$Y_{7.38}$	$0.68(NH_4)_2O\cdot 0.19Na_2O\cdot Al_2O_3\cdot 7.38SiO_2$
H-$Y_{10.29}$	$0.67(NH_4)_2O\cdot 0.16Na_2O\cdot Al_2O_3\cdot 10.29SiO_2$

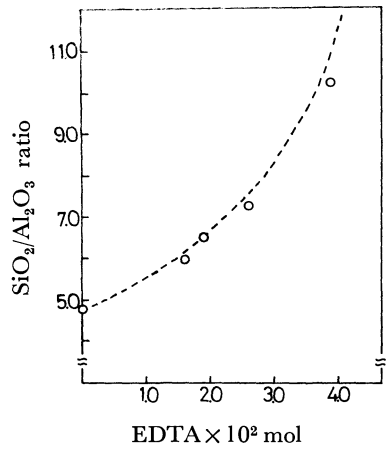

Fig. 1. Correlation between silica/alumina ratio of zeolites and the moles of EDTA added.
----: Calcd

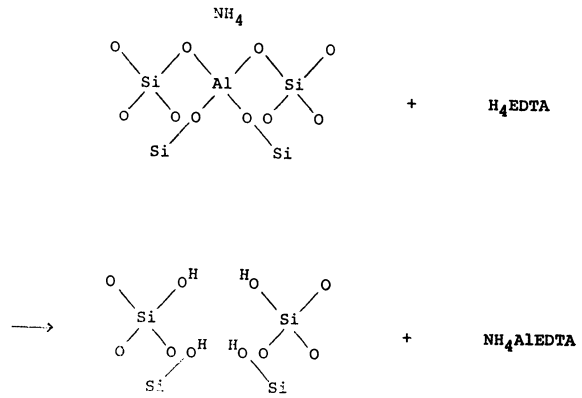

Fig. 2. Two-dimentional representation of the dealuminated zeolite.

The resulting model of zeolite when aluminium ion was removed from the framework according to Eq. (1) is illustrated two-dimensionally in Fig. 2.

Structural Characters. The X-ray diffraction diagrams are illustrated in Fig. 3. It can be seen that the structure of zeolite is not essentially destroyed by the treatment with EDTA. However, on the basis of the changes in the half-value of the breadth and integral intensity, amorphous species were partially produced as EDTA treatment became severe.

The correlation between the lattice constant and the silica/alumina ratio is plotted in Fig. 4. The lattice is contracted as the silica/alumina ratio becomes higher, which seems to be due to the removal of the constitutional aluminium of the zeolite lattice. It is well-known that the lattice constant decreases with the increase in the silica/alumina ratio in X- and Y-type zeolites.[15–17] The results obtained are of interest in the light of this fact.

The mid-infrared spectra of H-$Y_{4.80}$, H-$Y_{7.38}$ and H-$Y_{10.29}$ are shown in Fig. 5. The absorption bands were assigned in detail by Flanigen and Khatami.[18]

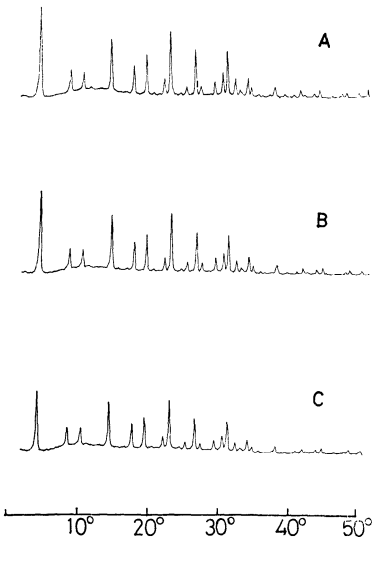

Fig. 3. X-Ray diffraction patterns of zeolites.
A: H-$Y_{4.80}$, B: H-$Y_{7.38}$, C: H-$Y_{10.29}$

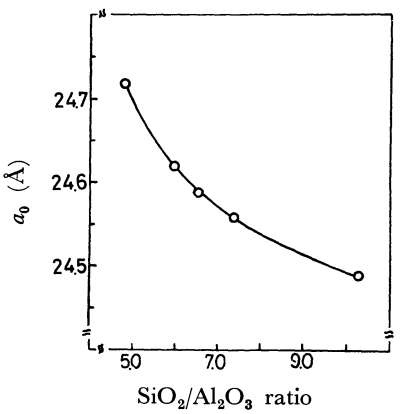

Fig. 4. Correlation between silica/alumina ratio of zeolites and lattice constant.

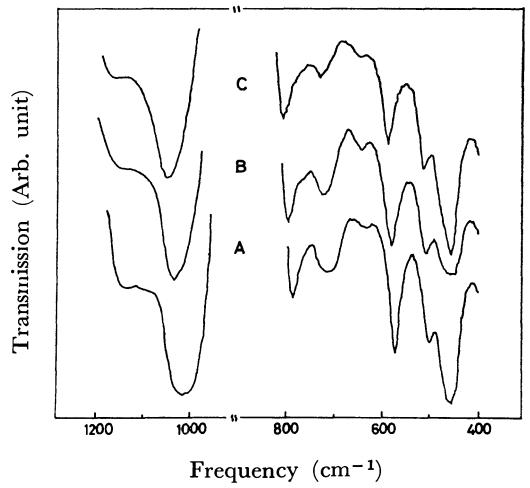

Fig. 5. Mid-infrared spectra of zeolite.
A: H-$Y_{4.80}$, B: H-$Y_{7.38}$, C: H-$Y_{10.29}$

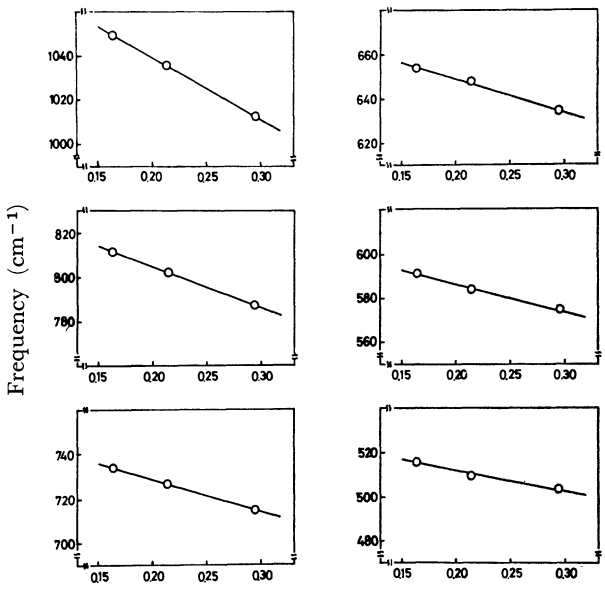

Fig. 6. Correlations between silica/alumina ratio and frequency of various adsorption bands.

Except for the band at about 460 cm^{-1}, the bands are shifted to higher frequency with an increase in the silica/alumina ratio.[19,20] The most intense absorption band, caused by the T–O (T represents Si or Al) asymmetric stretching vibration in the 1010—1050 cm^{-1} region, is very sensitive to the silica/alumina ratio. The absorption wave numbers change linearly with the Al fraction in the zeolite frameworks as is shown in Fig. 6. Since the masses of Al and Si are similar, the increase in frequency with the decrease in Al content is due to the difference in bond length and bond order. The fact that the bond length of Al–O is longer and Al is more electronegative seems to cause a decrease in the force constant of the T–O bond.

Nitrogen Adsorption Behaviors. N_2 adsorption isotherms at the temperature of liquid nitrogen are shown in Fig. 7. H-$Y_{4.80}$ shows a typical molecular-sieve adsorption isotherm; H-$Y_{7.38}$ and H-$Y_{10.29}$ samples with

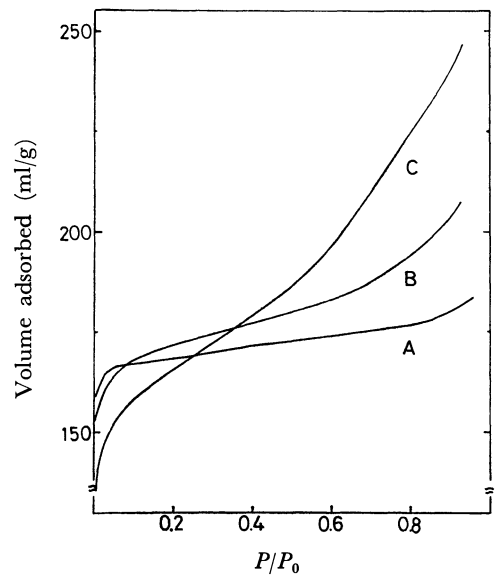

Fig. 7. Nitrogen adsorption isotherms.
A: H-$Y_{4.80}$, B: H-$Y_{7.38}$, C: H-$Y_{10.29}$

higher silica/alumina ratios adsorb increased amounts of nitrogen at higher relative pressures. This is probably due to the presence of amorphous parts. The cumulative pore volume distributions calculated from the adsorption isotherm show that, as the silica/alumina ratio increases, the pore size becomes widely distributed and the typical regular pore structure of zeolite must be partially destroyed.

Catalytic and Acid Properties. Figure 8 shows the cracking activity *vs.* silica/alumina ratio. With the rise in silica/alumina ratio the activity increases reaching a maximum and then decreases. Since Brönsted acid sites are effective for a cumene-cracking reaction, the increased activity seems to be due to the change in the surface-acid properties.

The infrared spectra and the heat of adsorption were studied in order to estimate the acidity and the acid strength.

Hydroxyl bands were detected on H-$Y_{4.80}$ zeolite near 3640 and 3550 cm^{-1} after evacuation at 450 °C.[21] Both hydroxyl groups are known to be acidic. An additional band was observed at 3750 cm^{-1} in the case of Al-deficient zeolite. The band agrees with that of the isolated silanol on the silica surface.[22]

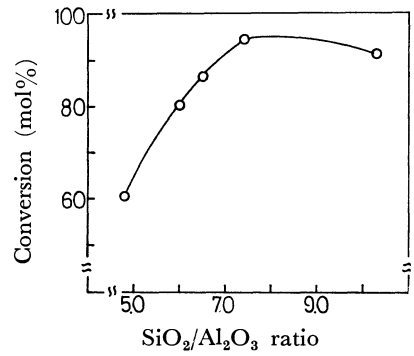

Fig. 8. Correlation between silica/alumina ratio and cumene-cracking activity.
Pretreatment, 550 °C; Reaction, 300 °C

Since four Si–OH bonds are expected to be newly formed by treatment with EDTA, it is probable that the additional band appears at 3750 cm^{-1} (Fig. 2).

Under pyridine adsorption, all the hydroxyl bands were eliminated and new bands were detected at 1400—1700 cm^{-1}. The integrated adsorptivities were measured for the 1540 cm^{-1} band, which was assigned to the pyridinium ion bonded to the Brönsted acid site.[21] From the adsorptivities, the Brönsted acid site was calculated using the apparent integrated molar adsorption intensity of 2.5 cm/μmol.[23] The results are shown in Table 2 for H-$Y_{4.80}$, H-$Y_{7.38}$, and H.$Y_{10.29}$ zeolite. The order of the number of acid sites is H-$Y_{7.38}$>H-$Y_{4.80}$>H-$Y_{10.29}$. Since the protonic acid site is combined with a zeolite negative site, that is $(AlO_2)^-$ ion, Brönsted acid sites are considered to decrease in proportion to dealumination. However, H-$Y_{7.38}$ zeolite showed an increased acidity. This can be explained as follows. The proton becomes mobile as the negative shield of the structural aluminium ion is decreased. As a result, an increased number of sites become effective for the acid. The ratio of Brönsted sites to Lewis sites was also calculated from the integrated absorptivities of the 1490 cm^{-1} band. The ratio of $\varepsilon^{B}_{1490}/\varepsilon^{L}_{1490}$ is assumed to be 5.2.[24] The ratio increases with the silica/alumina ratio. This results from the fact that the distance between Brönsted acid sites becomes longer as Al is removed, and the conversion of the Brönsted sites into Lewis sites on dehydroxylation becomes unfavorable. The H-$Y_{10.29}$ zeolite shows a higher cracking activity than would be expected from its acidity, suggesting the contribution of acid strength to be significant.

Table 2. Brönsted and Lewis acid site concentrations measured by the infrared spectra of adsorbed pyridine

Sample	$\log [T_0/T]d\nu$[a] (cm^{-1})	B acid[b] (mmol/g)	B/L
H-$Y_{4.80}$	8.9	0.44	0.9
H-$Y_{7.38}$	10.8	0.66	5.8
H-$Y_{10.29}$	3.3	0.18	10.2

a) 1540 cm^{-1} band of adsorbed pyridine. b) Apparent integrated molar adsorption intensity taken as 2.5 cm/μmol.

The effects of dealumination on the strength and distribution of acid sites were investigated by measuring the differential heats of adsorption of ammonia. The differential heats of adsorption are plotted against the ammonia molecules adsorbed in Fig. 9. The region of initial adsorption seems to be important in interpreting the relation between the energy distribution and the activity. The initial heats on the samples used are all over 25 kcal/mol at the adsorbed amount of 3×10^{-2} mmol/g. If we assume that one ammonia molecule is adsorbed on each acid site, the number of acid sites with a heat of adsorption of ammonia of over 23 kcal/mol is larger in H-$Y_{10.29}$ than in others. As the amount adsorbed increases to about 1.75 mmol/g, heats of adsorption on H-$Y_{10.29}$ and H-$Y_{7.38}$ fall off steeply to about 14 kcal/mol; on the other hand, the

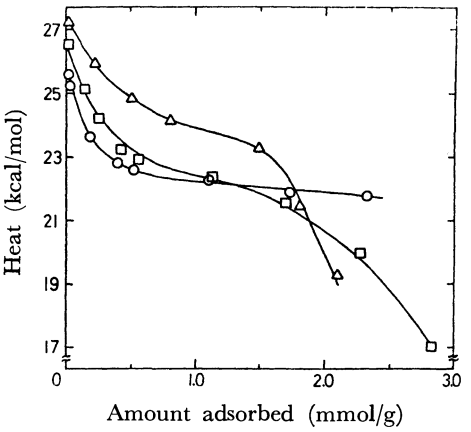

Fig. 9. Differential heats of adsorption of ammonia at 25 °C.
—○—: H-$Y_{4.80}$, —□—: H-$Y_{7.38}$, —△—: H-$Y_{10.29}$

heats of adsorption on H-$Y_{4.80}$ decrease gradually. As a result, the total number of acid sites with heats of adsorption of over 20 kcal/mol of H-$Y_{4.80}$ is larger than that of H-$Y_{10.29}$ and H-$Y_{7.38}$. This would not contradict the infrared spectroscopic data, since the heat of adsorption of ammonia would depend on both Brönsted and Lewis acids and the conversion of the former into the latter could easily occur on H-$Y_{4.80}$.

It is thus evident that the ratio of strong acid sites to all sites increases with dealumination. Beaumont *et al.* showed by means of infrared spectroscopy that the concentration of weak acid sites was lower in aluminium-deficient zeolite than in Y zeolite, while the concentration of strong acid sites was higher.[14] The results agree with ours. The strong acid sites thus formed seem to produce the higher cracking activity of H-$Y_{10.29}$, though the pyridinium-ion concentration of H-$Y_{10.29}$ is lower than that of H-$Y_{4.80}$.

It can be concluded that the change in acid properties with dealumination predominantly influences catalytic activity for the cumene-cracking reaction. However, the appearance of amorphous parts might play a role in the catalytic activity, especially in the case of H-$Y_{10.29}$. The effect of the pore volume on catalytic activity seems to be significant in the structure-sensitive reaction.

References

1) J. W. Ward, *J. Catal.*, **17**, 355 (1970).
2) M. Ikemoto, K. Tsutsumi, and H. Takahashi, This Bulletin, **45**, 1330 (1972).
3) K. Tsutsumi and H. Takahashi, *J. Catal.*, **24**, 1 (1972).
4) K. Tsutsumi and H. Takahashi, *J. Phys. Chem.*, **76**, 110 (1972).
5) R. M. Barrer and M. B. Makki, *Can. J. Chem.*, **42**, 1481 (1964).
6) S. P. Zhdanov and B. G. Novikov, *Dokl. Akad. Nauk. S. S. S. R.*, **166**, 1107 (1966).
7) P. E. Eberly, Jr., C. N. Kimberlin, Jr., and A. Voorhies, Jr., *J. Catal.*, **22**, 419 (1971).
8) W. L. Kranich, Y. H. Ma, L. B. Sand, A. H. Weiss, and I. Zwiebel, "Molecular Sieve Zeolite-I," (R. F. Gould, ed.), p. 502, Adv. Chem. Ser.-101, (1971).

9) G. T. Kerr, *J. Phys. Chem.*, **72**, 2594 (1968).
10) K. V. Topchieva and H. S. T'houang, *Kinet. Katal.*, **11**, 490 (1970).
11) R. Beaumont and D. Barthomeuf, *C. R. Acad. Sc. Paris, Ser. C.*, **1971**, 363.
12) R. Beaumont and D. Barthomeuf, *J. Catal.*, **26**, 218 (1972).
13) R. Beaumont and D. Barthomeuf, *ibid.*, **27**, 45 (1972).
14) R. Beaumont, P. Pichat, D. Barthomeuf, and Y. Trambouze, Prep. 5th Int. Cong. Catal., Miami (1972).
15) A. C. Wright, J. P. Rupert, and W. T. Granquist, *Amer. Mineral.*, **53**, 1293 (1968); **54**, 1484 (1969).
16) E. Dempsey, G. H. Kuhl, and D. H. Olson, *J. Phys. Chem.*, **73**, 387 (1969).
17) J. V. Smith, "Molecular Sieve Zeolite-I," (R. F. Gould, ed.), p. 171, Adv. Chem. Ser.-101, (1971).
18) E. M. Flanigen and H. Khatami, *ibid.*, p. 201.
19) P. Pichat, R. Beaumont, and D. Barthomeuf, *C. R. Acad. Sci., Paris, Ser. C*, 612 (1971).
20) O. L. Šarc, *J. Phys. Chem.*, **75**, 2408 (1971).
21) For example, J. M. Ward, *J. Catal.*, **9**, 225 (1967).
22) For example, R. S. McDonald, *J. Phys. Chem.*, **62**, 1168 (1958).
23) Y. Watanabe and H. W. Habgood, *ibid.*, **72**, 3066 (1968).
24) M. Lefrancois and G. Malbois, *J. Catal.*, **20**, 350 (1971).

Normalization of Potentials in Propylene Carbonate, Ethylene Carbonate, *N,N'*-Dimethylformamide, and Dimethyl Sulfoxide to the Water Scale Studied by Polarographic Method

Niro MATSUURA, Kisaburo UMEMOTO, Masako WAKI, Zen'ichi TAKEUCHI, and Mariko OMOTO

Department of Pure and Applied Sciences, College of General Education, The University of Tokyo, Komaba, Meguro-ku, Tokyo 153

(Received July 28, 1973)

The polarographic behavior of alkali metal ions were studied in propylene carbonate(PC), ethylene carbonate(EC), water, *N,N'*-dimethylformamide(DMF), and dimethyl sulfoxide(DMSO). The polarographic half-wave potentials measured in these solvents against an aqueous saturated calomel electrode(SCE) were normalized to the potential of SCE in aqueous system by making corrections of potential required for transfer of rubidium ion from water to these solvents. The free energies of transfer of rubidium ion from water to other solvents were calculated by the application of the modified Born equation. The potential series on the normalized potential scale were given in the order DMSO<DMF<water<PC<EC, indicating that the metal ion-solvent interaction increases with increasing the electron donor property of the solvent. The solvent shifts in potential calculated by the application of the modified Born equation disagreed with the experimental results. In order to fit well the calculated solvent shifts in potential with the experimental results, following values of liquid junction potential must be assumed for these solvents; +0.090 V for DMSO, +0.085 V for DMF, +0.004 V for PC, and −0.064 V for EC against the aqueous phase.

One of the most urgent problems in non-aqueous electrochemistry is to find a way of intercorrelating the potential series measured in different solvents. A direct comparison of electrode potentials measured in various solvents is impossible in the thermodynamic sense. The main difficulty is that the unknown liquid junction potential is inevitably introduced when one attempts to calibrate the potential of a reference electrode in a given solvent against a universal common reference point *viz.* hydrogen electrode or SCE in the aqueous medium. Some efforts have been devoted to estimate the magnitude of the shift in potential for the transfer of a reference redox system from one solvent to another by the application of extrathermodynamic methods.[1,2] In one of these approaches, the standard potentials of redox systems of rubidium,[3,4] ferrocene,[5] cobaltocene,[5] or iron(II–III) complexes of phenanthroline and of its derivatives[6] have been assumed to be respectively constant in various solvents. The ion, constructing each redox system, has been considered to exert a similar type of a weak electrostatic interaction with various solvents, since the ion is symmetrical in shape and slightly polarizable and has large radius but small charge. Accordingly, there should be practically no difference in solvation energies by transfer of these preferred redox systems from one solvent to another. In an alternative way of approach the change in the solvation energy in the process of transferring the ion from one solvent to another was estimated on the assumption of "modified Born equation." The application of the Born equation[7] is in principle seriously limited owing to the ignorance of specific solvation or dielectric saturation effect of solvent towards solute ions. Nevertheless, a consistent value of free energy of solvation has been plausibly obtained, provided a correction term for crystal radius of an ion is introduced in Born equation as effective ionic radius which fits with the radius of a cavity present in the dielectric medium.[8] A similar approximation has been also proposed for Born equation by taking into account the dielectric properties of solvent in the nearest neighborhood of ions.[9] The classical method of Latimer's effective radii of hydrated ions has been recently revalued since there is no other reliable data on the variation of dielectric constant of solvent in the vicinity of solute ions.[10] In this connection, Koepp *et al.*[11] have estimated the solvation energies for rubidium ion in non-aqueous solvents by measuring the solubility products of alkali metal halides in various solvents. Still more, Coetzee *et al.*[12,13] calculated the free energy of transfer for rubidium ion in various nitriles by measuring the polarographic half-wave potentials.

Takaoka[14] proposed an experimental method to refer the polarographic half-wave potentials in DMF to an aqueous SCE. As a reference electrode, he used an aqueous SCE equipped with a non-aqueous salt bridge. He estimated the liquid junction potential at the interphase between the aqueous and the non-aqueous media negligibly small. However, his argument for estimating the liquid junction potential was based on only the transference phenomena of solute ions and the solvent shift in the activity coefficients of ions was not taken into account. Accordingly, his conclusion should be open to further examination.

In this work, polarographic behaviors of alkali metal ions in several selected organic solvents were studied for examining the reversibility of the electrode process. The free energy changes in transfer of rubidium ion from water to other solvents were evaluated from the reversible polarographic half-wave potentials by using the modified Born equation. The liquid junction potentials of the interphase between water and non-aqueous solvent were estimated by comparing the calculated solvent shift in potentials with the experimental results.

Experimental

Solvent. DMF was dehydrated over oven-dried potassium carbonate and DMSO was freed from impurities with activated alumina prior to distillation. PC and EC were

treated with *p*-toluenesulfonic acid for the removal of basic contaminants.[15] All these solvents were distilled twice in a current of dry nitrogen gas at a reduced pressure of about 20 Torr. The water content of the middle fraction of the distillates was always less than 0.01%, as determined by the Karl-Fischer titration. Triply distilled water was used throughout the runs for the measurement in aqueous medium.

Electrolyte. Tetraethylammonium perchlorate(TEAP) was prepared by the double decomposition of tetraethylammonium iodide with sodium perchlorate.[16] The starting material, tetraethylammonium iodide, was synthesized by heating an equimolar mixture of triethylamine and ethyliodide at 80 °C for two hours in nitrobenzene.[17] Tetrabutylammonium perchlorate(TBAP) was prepared in a similar way as TEAP from tetrabutylammonium bromide which was synthesized by refluxing an equimolar mixture of tributylamine and butyl bromide in acetonitrile for 36 hours.[18] TEAP was recrystallized from hot water for five times. TBAP was purified by dissolving it in hot ethyl alcohol followed by precipitation with the addition of water, and this treatment was repeated for five times. Conversions into perchlorate of potassium, rubidium, caesium and thallium were made by the double decomposition of their chlorides or nitrates with perchloric acid. Zinc perchlorate was prepared by heating zinc metal to dryness with an excess of perchloric acid. Lithium and sodium perchlorates were obtained commercially. All these perchlorates were recrystallized from water for several times. The G. R. grade barium and silver perchlorates, and cadmium nitrate were used without further purification. All these electrolytes were kept over phosphorus pentoxide, and before use TEAP and TBAP were dried at 70 °C and other perchlorates at 100 °C in vacuum-oven.

Polarography. The polarographic measurement was made by using an H-type cell with compartments A and B separated by a sintered glass diaphragm. The dropping mercury electrode(DME) was inserted into compartment A and an agar salt bridge into compartment B. The salt bridge was prepared as follows: the lower half portion of a glass tubing sealed with a fine porosity sintered glass at one end was filled with agar solution composed of 70% DMF-30% water mixture containing 0.5 M TEAP, and then the upper half portion with aqueous agar solution containing 1.0 M sodium chloride. The potential drift caused by the salt bridge amounts to several tens of milli-volts immediately after the preparation of the salt bridge, while it fell to minimum after several tens of days of aging by immersing it in DMF. The potential of the SCE with the salt bridge was calibrated against an auxiliary aqueous SCE of common type. As the SCE of the former special type being kept in compartment B of the H-type cell, the DME in compartment A was replaced with another SCE of common type. Potential measurement between these two SCE was performed by allowing the KCl solution to flow out slightly from the latter aqueous SCE through a sintered glass.[14] Polarogram was recorded after the passage of nitrogen gas for 20 min. The potential was supplied manually with an accuracy of ± 0.1 mV and iR drop was corrected. During the runs the temperature was kept at 40 °C for EC and at 25 °C for all other solvents. The DME has following characteristics; $m=0.620$ mg/s and $t=4.0$ s for water, $m=0.764$ mg/s and $t=3.9$ s in DMSO and $m=0.727$ mg/s and $t=4.0$ s in PC.

Results and Discussion

Reversibility. The DC and AC polarograms of alkali metal perchlorated indicated that the electrode process is one electron reduction process not only in aqueous medium but also in the non-aqueous solvents. The DC polarographic waves were diffusion-controlled as evidenced by the limiting currents proportional to the square root of the height of mercury head. The peak current of the AC polarogram was independent of the height of mercury head. A trace of water left unremoved in the non-aqueous media, if it is less than 0.1%, did not affect the half wave potential $E_{1/2}$ and the peak potential E_p. The reversibility of the electrode reaction was examined from the slope of $\log(i_d-i)/i$ *vs.* E plots, the half-width of E_p peak ($\delta E_{p/2}$) and the reversibility factor defined by the current ratio $i_p/i_d\tau^{1/2}$.[19] All these data are represented together with the potential values in Table 1. The observed waves were all reversible or quasi-reversible except for a few example, particularly for lithium ion.

Potentials in Aqueous Medium. In Table 1(a) the half wave potentials and the peak potentials of alkali metal ions at a fixed concentration of 1×10^{-3} M in 0.1 M TEAP aqueous solution are represented. The values of half-wave potential for alkali metal ions are in good agreement with those given in literatures.[4,20] The reversibilities were shown excellent as examined from the slope of log-plots, $\delta E_{p/2}$, $i_p/i_d\tau^{1/2}$ ratio and $(E_p-E_{1/2})$ by comparing them with the referred values of thallium(I) ion whose reversibility in perchlorate solution is well accepted.[21] By varing the concentration of supporting electrolyte in the range between 0.025 and 0.25 M, the $E_{1/2}$ values differed less than several milli-volts. Consequently, it is possible to assume that there is no association between the alkali metal cations and the perchlorate anion, at least in a TEAP concentration range cited above.[22-24]

Potentials in PC and EC. The results in Tables 1(b) and (c) for the potentials of alkali metal ions in PC and EC can be regarded as potential values of reversible process except for caesium in EC and lithium in both PC and EC. Despite of reversibility, an unusual form of polarogram was obtained in PC, showing an appreciable deviation of slope of log-plots, depending on whether a maximum or an average current is taken for DC ploarogram. The values in parentheses in Table 1(b) for the slope of log-plot made with the average current showed deviation from values of reversible wave. A correct analysis of DC polarogram in solvent of high viscosity,[13] PC, must be made with the maximum current polarogram.

Potentials in DMF and DMSO. The results in Tables 1(d) and (e) show that all the alkali metal ions except for lithium ion gave reversible wave in DMF and DMSO containing 0.1 M TEAP. The irreversibility of the polarographic wave of lithium ion was improved by using TBAP in place of TEAP as supporting electrolyte. However, in this time, there appeared a polarographic maximum, which made the accurate determination of the half-wave potential difficult. Since there was found no effective suppressor for the maximum in these solvents, the obtained potentials were less accurate for lithium. For this reason, with the exception for lithium, all the potential measurements were made by the use of TEAP. The half-

TABLE 1. POLAROGRAPHIC RESULTS OF ALKALI METAL IONS IN (a) WATER, (b) PC, (c) EC, (d) DMF AND (e) DMSO[a)]

	DC polarography			AC polarography			
	$-E_{1/2}$ (V)	I_d	slope (mV)	$-E_p$ (V)	$\delta E_{p/2}$ (mV)	$i_p/i_d\tau^{1/2}$	$E_p-E_{1/2}$ (V)
			(a) water				
Li^+	2.332	2.38	56	2.339	105	38	−0.007
Na^+	2.113	3.02	62	2.114	105	40	−0.001
K^+	2.136	3.44	61	2.140	135	35	−0.004
Rb^+	2.131	3.66	62	2.140	138	35	−0.009
Cs^+	2.108	3.77	65	2.128	140	39	−0.020
			(b) PC				
Li^+	2.001	0.94	77[1)] (82)[2)]	2.039	155	11	−0.038
Na^+	1.848	1.08	65 (65)	1.854	120	44	−0.006
K^+	1.965	1.11	63 (62)	1.970	110	45	−0.005
Rb^+	1.989	1.16	63 (67)	1.991	120	42	−0.002
Cs^+	1.981	1.22	60 (72)	1.982	125	43	−0.001
			(c) EC				
Li^+	2.009	1.27	73	2.046	140	10	−0.037
Na^+	1.861	1.28	70	1.862	150	29	−0.001
K^+	1.986	1.45	70	1.986	130	33	0.000
Rb^+	2.009	1.60	75	2.009	135	29	0.000
Cs^+	2.011	1.59	77	2.046	170	27	−0.035
			(d) DMF				
Li^+	2.385[b)]	1.65	91	2.425	170	2	−0.040
Na^+	2.035	1.83	62	2.035	105	34	0.000
K^+	2.055	1.84	63	2.060	108	35	−0.005
Rb^+	2.045	1.91	62	2.050	105	42	−0.005
Cs^+	2.011	2.04	58	2.013	98	39	−0.002
			(e) DMSO				
Li^+	2.578[b)]	0.93	90	2.688	260	2	−0.110
Na^+	2.075	1.24	60	2.075	120	38	0.000
K^+	2.093	1.34	63	2.095	115	45	−0.002
Rb^+	2.075	1.33	60	2.075	120	46	0.000
Cs^+	2.047	1.46	61	2.050	120	49	−0.003

1) Values obtained from maximum current polarogram.
2) Values obtained from mean current polarogram.

a) $E_{1/2}$ and E_p are half-wave and peak potentials directly measured against aq. SCE. I_d is polargraphic diffusion current constant; $i_d/Cm^{2/3}t^{1/6}$. $\delta E_{p/2}$ is the half width of AC current peak. $i_p/i_d\tau^{1/2}$ is the reversibility factor, τ is the drop time at AC peak, in s. b) The half-wave potentials of lithium ion in DMF and DMSO are 2.308 and 2.461, respectively when TBAP was used as supporting electrolyte.

wave potentials of alkali metal ions showed a good internal consistency with those given in literatures.[25,26)]

The shifts in half-wave potentials with increasing the concentration of TEAP are shown in Fig. 1. The shift in the half wave potential of lithium ion was found to be abnormally large to an extent of exceeding the usual effect of increasing ionic strength. The unusual behavior of lithium ion has not been clearly explained. As the reversibility was found to be recovered for lithium ion by the use of TBAP, the ion-pair formation of lithium ion with perchlorate anion in TEAP solution is not the primary reason for the unusually large negative shift of the half-wave potential. It is worthy to note the similar observation made by Izutsu *et al.*, *i. e.* an unexpectedly large negative values of the half-wave potential of alkali metal ions of small radius with TEAP or TMAP(tetramethylammonium perchlorate) in hexamethylphosphoramide, but a small shift with TPAP(tetrapropylammonium perchlorate) or TBAP.[27)]

Significance of Half-Wave Potential. A systematic survey on the reversible polarograhpic half-wave potentials for a group of cations provides data for evaluating the free energy of solvation of the cations. An approach for obtaining a common potential scale in various solvents is undertaken by evaluating the free energy of transfer of cation from one solvent to another. The evaluation of transfer free energy is based on the assumption that the standard potential of metal-ion system can be obtained by Born-Haber cycle, involving the free energies of sublimation $\Delta G°$(sub), ionization $\Delta G°$(ion), photoelectric work function $\Delta G°$(w). The thermodynamic expression for standard potential $E°$ in absolute scale is given by Eq. (1).

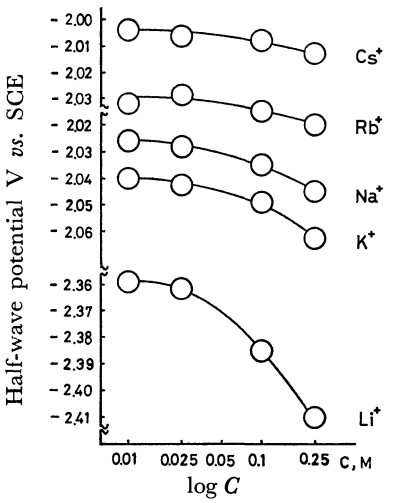

Fig. 1. Half-wave potentials of alkali metal ions in DMF at various concentration of TEAP (A similar result was obtained for DMSO).

$$nE^{\circ}F = \Delta G^{\circ}(\text{sub}) - \Delta G^{\circ}(\text{ion}) - \Delta G^{\circ}(\text{w}) + \Delta G^{\circ}(\text{solv}) \quad (1)$$

The reversible polarographic half-wave potentials are related to the standard potential of amalgam electrode by Eq. (2),

$$E_{1/2} = E^{\circ}_{\text{amalgam}} - \frac{RT}{nF}\ln\frac{f'}{f} - \frac{RT}{nF}\ln\frac{\sqrt{D}}{\sqrt{D'}} \quad (2)$$

where f and f' are activity coefficients, and D and D' are diffusion coefficients respectively, the values being concerned with metallic ion in solution and metal in amalgam. The second and third terms of Eq. (2) make a very small contribution to $E_{1/2}$, since the ratio f'/f and D/D' deviate not largely from unity. The reversible polarographic half-wave potential is regarded as a good approximation of standard amalgam potential.[29] The difference between the standard electrode potential and the standard amalgam electrode potential is given by the free energy of amalgamation. In as much as the calculation of the transfer free energy of ions between solvents is concerned, the free energy of amalgamation can be out of consideration, because of the cancellation of this free energy term by computing the potential difference of identical amalgam electrode in two different solvents.

The ambiguity involved in the evaluation of transfer free energy of ions from the observed polarographic half wave potential data is due to the undetermined activity coefficients and diffusion coefficients in Eq. (2). However, these ambiguous terms can be excluded from consideration by taking the potential difference between a pair of cations i_+ and j_+, $\underset{i_+-j_+}{\Delta} E_{1/2}$, for each solvent and then by taking the difference of this difference in two solvents k and l, $\underset{k-l}{\Delta}\underset{i_+-j_+}{\Delta} E_{1/2}$. The ratio of the activity coefficients as well as the ratio of the diffusion coefficients for a pair of ions, appearing in the double comparison cited above, are nearly constant irrespective of the kind of solvent, as being evidenced from Eq. (2) by calculating the activity coefficient with the Debye-Hückel equation and by replacing the diffusion coefficient with the polarographic diffusion current constant given in Table 1. Accordingly, by taking the solvation energy difference between a pair of ions $\Delta\Delta G^{\circ}$(solv) from Eq. (1), the expression for the transfer free energy is written as

$$nF\underset{k-l}{\Delta}\underset{i_+-j_+}{\Delta} E_{1/2} = (\Delta\Delta G^{\circ}_{i_+,j_+}(\text{solv}))_k - (\Delta\Delta G^{\circ}_{i_+,j_+}(\text{solv}))_l \quad (3)$$

Effective Radii of Solvated Ions by the Application of Born Equation. The free energy change in electrostatic work for transfering a pair of gaseous ions, with diameters r_+ and r_- and charges z^+ and z^-, to a medium of dielectric constant ε is given by the modified Born equation.

$$\Delta G_{\pm}^{\circ}(\text{solv}) = -(Ne^2/2)\left(1-\frac{1}{\varepsilon}\right) \times \{z_+^2/(r_+ + R_+') + z_-^2/(r_- + R_-')\} \quad (4)$$

In Eq. (4) R_+' and R_-' are empirical correction terms for solvated cations and anions, respectively, and N denotes Avogadro's number. There are two most basic assumptions in Eq. (4); first, the interaction of alkali metal ions with solvent is predominantly electrostatic in nature, and second, the contribution of the neutral part of solvation energy is to the same extent for all the solvents according to the zero energy assumption.[9]

In this work the perchlorate salts were employed as common anion and the specific interaction between alkali metal cations and perchlorate anion is unimportant even at 0.1 M of TEAP concentration as evidenced by the concentration dependence of half-wave potentials on TEAP (Fig. 1). Consequently, the contribution of anionic species to the solvation energy can be discounted because of its invariant values for any couple of the ion pairs. On this ground the double comparison procedure in Eq. (3) is a reasonable way of calculation for relative values of cationic solvation energy by eliminating the contribution from the anionic part.

The expression for $\Delta\Delta G^{\circ}_{i_+,j_+}$ (solv) is, then, given by Eq. (5), showing the solvation energy difference between a couple of cations i_+ and j_+ in each solvent. For simplification, $\Delta\Delta G^{\circ}_{i_+,j_+}$ (solv) is denoted by $\Delta\Delta G^{\circ}_{i_+,j_+}$ in the following discussion.

$$\Delta\Delta G^{\circ}_{i_+,j_+} = -(Ne/2)(1-1/\varepsilon)\{1/(r_{i_+}+R_+') - 1/(r_{j_+}+R_+')\} \quad (5)$$

The expression for calculating the transference free energy between non-aqueous solvent S and aqueous solution is given by Eq. (6).

$$(\Delta\Delta G^{\circ}_{i_+,j_+})_{\text{aq}} - (\Delta\Delta G^{\circ}_{i_+,j_+})_{\text{S}} = -(Ne^2/2)[(1-1/78.5) \times \{1/(r_{i_+}+R'_{+\text{aq}}) - 1/(r_{j_+}+R'_{+\text{aq}})\} - (1-1/\varepsilon_{\text{S}})\{1/(r_{i_+}+R'_{+\text{S}}) - 1/(r_{j_+}+R'_{+\text{S}})\}] \quad (6)$$

The value for dielectric constant for aqueous solution ε_{aq} is taken as 78.5 esu at 25 °C and for radius correction term the value of 0.72 Å was tentatively assigned to $R'_{+\text{aq}}$ in Eq. (6). All values except for $R'_{+\text{S}}$ have been found; r_+ from crystal data, ε_{S} from dielectric data and $\Delta\Delta G^{\circ}$ from our potential data. The values of radius correction term $R'_{+\text{S}}$ were obtained from Eq. (6) and the results are shown in Table 2. A comparison was made in Table 2 with the published data for the solvents other than our's. In the solvent system so far investigated, there exists a

Table 2. Estimation of the radius correction term R_+'

	Donor number[a]	R_+' (Å)	ε[b]
Benzonitrile	11.9	0.83[c]	25.2
Acetonitrile	14.1	0.82[c]	38.0
Sulpholane	14.8	0.80[c]	43.0
Propylene carbonate	15.1	0.82	65.1
Iso-butyronitrile	15.4	0.79[c]	20.2
Propionitrile	16.1	0.80[c]	26.1
Ethylene carbonate	16.4	0.86	89.6(40 °C)
Acetone	17.0	0.74[c]	20.7
Water	18.0	0.72[d]	78.5
N,N'-Dimethylformamide	26.6	0.69	36.7
Dimethyl sulfoxide	29.8	0.68	46.4

a) Taken from V. Gutmann and E. Wychera, *Inorg. Nucl. Lett.*, **2**, 257 (1966). b) Dielectric constant at 25 °C. c) Taken from Ref. 13. d) Taken from Ref. 9.

close relation with the donor number rather than the dielectric constant of the solvent for the radius correction term. The value R_+' decreases with increasing value of the donor number. This means that a solvent of large donor number shows a strong interaction with the solute cation. The theoretical values of $\Delta\Delta E_{1/2}$ were calculated by the use of R_+' given in Table 2. A comparison was made for $\Delta\Delta E_{1/2}$ between experimental and the theoretical values in Table 3. The agreement is reasonablly good except for lithium ion, indicating that the radius correction term is a convenient and very useful parameter for computing the solvation energy of free ions in these solvents.

Transfer Energy of Rubidium Ion. The estimation of the potential shift caused by changing the solvent for rubidium ion was made by use of the R_+' values in Table 2. The results are given in Table 4, along with the experimental potential shifts. If the liquid junction potentials were properly calibrated the calculated values of solvent shift in potential should coincide with the experimental values. The data represented in Table 4 show poor agreements between the theoretically expected values and the experimentally obtained ones. The deviations shown in fourth row of Table 4 are far greater than a limit of 10 mV expected inevitably for the difference in salt activity coefficient and diffusion coefficient in Eq. (2). This discrepancy can mainly be attributed to the liquid junction potential appeared in the interface between the aqueous SCE and applied organic solvent containing 0.1 M of TEAP. The liquid junction potentials shown in the fifth row of Table 4 are the average values for the difference of half-wave potentials of alkali metal ions between the theoretically computed and experimentally obtained data. These liquid junction potentials must be reduced from the experimentally obtained half-wave potentials for the purpose to intercorrelate the potentials in different solvents on the common potential scale (Corrected Rubidium Scale). The half-wave potential series of cations on the common potential scale are alined in the order DMSO<DMF<water<PC<EC, the more negative value indicating the stronger solvation, showing a good agreement with the cationic solvation property of these solvents.[30,31]

Comment to the Ferrocene Scale and the Rubidium Scale. Half-wave potentials of cations referred to those of ferrocene and rubidium are given in Table 5. A con-

Table 3. Comparison of the calculated and the observed $\Delta\Delta E_{1/2}$ by taking rubidium as reference[a]

	DMSO		DMF		PC		EC	
	Obsd	Calcd	Obsd	Calcd	Obsd	Calcd	Obsd	Calcd
Li^+	−0.185[b]	−0.075	−0.062[b]	−0.038	+0.189	+0.203	+0.201	+0.266
Na^+	−0.018	−0.034	−0.008	−0.015	+0.123	+0.094	+0.129	+0.124
K^+	−0.013	−0.008	−0.005	−0.004	+0.029	+0.022	+0.028	+0.028
Rb^+	0.000	0.000	0.000	0.000	0.000	0.000	0.000	0.000
Cs^+	+0.005	+0.007	+0.011	+0.003	−0.015	−0.023	−0.025	−0.031

a) $\Delta\Delta E_{1/2}=(\Delta E_{1/2})_S-(\Delta E_{1/2})_W$: $(\Delta E_{1/2})_S$ is the difference of the half-wave potential of metal ions with respect to that of rubidium ion in solvent S, and $(\Delta E_{1/2})_W$ is that in water. b) Half-wave potential obtained by using TBAP as supporting electrolyte.

Table 4. Estimation of the solvent shift of rubidium standard potential and of liquid junction potential *vs.* the aqueous saturated calomel electrode

	DMSO	DMF	PC	EC
$E_{tr}(Rb)$[a]	−0.069	−0.029	+0.109	+0.155
$E_{tr}(Rb)_{obsd}$[b]	+0.056	+0.086	+0.142	+0.122
$E_{s,m}$[c]	−0.035	−0.034	−0.040	−0.034
$E_{LJ}(Rb)$[d]	+0.090	+0.081	−0.007	−0.067
E_{LJ}[e]	+0.090	+0.085	+0.004	−0.064

a) Calculated solvent shift of rubidium standard potential. Correction for the solvent molality is included. b) Observed solvent shift of the half-wave potential of rubidium. c) Correction for the solvent molality on the solvent shift of the standard potential. d) Estimated liquid junction potential. The value of b)-a)-c). e) Average value of the estimated liquid junction potentials for all alkali metals.

Table 5. Comparison of half wave potentials in various solvents on the rubidium scale, using 0.1 M TEAP as the supporting electrolyte[a)]

	DMSO	DMF	Water	PC	EC	ACN[b)]
Li^+	−0.386[c)] (−0.297)	−0.263[c)] (−2.83)	−0.201 (−2.47)	−0.012 (−2.36)	0.000	+0.03 (−2.36)
Na^+	0.000 (−2.55)	+0.010 (−2.52)	+0.018 (−2.27)	+0.141 (−2.22)	+0.147	+0.13 (−2.25)
K^+	−0.018 (−2.53)	−0.010 (−2.52)	−0.005 (−2.28)	+0.024 (−2.32)	+0.023	+0.02 (−2.34)
Rb^+	0.000	0.000	0.000	0.000	0.000	0.000
Cs^+	+0.028	+0.034	+0.023	+0.008	−0.002	+0.01
Tl^+	+1.557	+1.566	+1.676	+1.722	d)	+1.71
Zn^{2+}	+1.003 (−1.50)	+1.060 (−1.43)	+1.147 (−1.14)	+1.722 (−1.02)	d)	+1.71 (−1.03)
Cd^{2+}	+1.388	+1.471	+1.569	+1.697	d)	+1.72
Ba^{2+}	+0.024	+0.004	+0.094	+0.203	d)	+0.35
Ag^+	+2.387	e)	e)	e)	d)	+2.40

a) The values given in parentheses are the half-wave potentials on the ferrocene scale cited in T. Fujinaga and K. Izutsu, *Kagaku to Kogyo*, **23**, 117 (1970). b) Data from Ref. 4. The other data were determined in this work. c) Half-wave potential obtained by using TBAP as supporting electrolyte. d) Not measured. e) Immeasurable.

tradictory behavior is noticed between the rubidium and the ferrocene scale for the transfer of potassium ion from water to acetonitrile(ACN). On the ferrocene scale, the shift in the half-wave potential of potassium for the transfer of potassium ion from water to ACN, $\Delta_{\text{A-W}}\Delta_{\text{K}^+\text{-Fe}}E_{1/2}$, is given as −0.06 V, whereas on the rubidium scale, $\Delta_{\text{A-W}}\Delta_{\text{K}^+\text{-Rb}^+}E_{1/2}$ is given as +0.03 V; opposite signs of $\Delta\Delta E_{1/2}$ were obtained whether the half-wave potential of potassium was referred to the ferrocene scale or to the rubidium scale. Suzuki *et al.*[32)] have reported a similar observation; the half-wave potentials of thallium and cadmium referred to the ferrocene scale shifted to more negative with increasing content of ACN in ACN–water mixture, while half-wave potentials referred to the rubidium scale shifted to less negative.

ACN is a poor solvent for inorganic electrolyte and yields a smaller solvation energy for inorganic ions. Accordingly, the free energy in transfer of ions from water to ACN is positive, resulting in a positive value of $\Delta\Delta E_{1/2}$. The observed contradiction in $\Delta\Delta E_{1/2}$ is probably due to the inaccuracy of the ferrocene scale. The solubility of ferrocene in ACN is greater than in water by a factor of 10^4.[6,12)] A large increase of the ferrocene solubility in ACN results in a large shift of the redox potential of ferrocene-ferricinium couple to less negative side by the change of solvent from water to ACN. Accordingly, it is quite probable that such a potential shift to the negative direction is expected by the transfer of ions from water to a solvent of high ferrocene solubility, when ferrocene is chosen as reference. In fact, it can be seen from the potential data in Table 5 that the ferrocene scale gives about 0.1 V more negative shift of potential in transfer of cations from water to ACN than the rubidium scale does.

Furthermore, it would be worthy to give a comment to the method employed by Strehlow and his coworkers to correct the ferrocene scale. They calculated the electrostatic free energy change in transfer of ferricinium ion from water to ACN by the modified Born equation with a radius correction term R_+' which was obtained for alkali metal cations. It should be noticed that the radius correction term is very sensitive to the specific interaction between solute ion and solvent molecules, and accordingly, a value of R_+' obtained for a series of alkali metal ions, whose interaction with solvent is similar among them, should not be applied for ferricinium ion whose interaction with solvent is quite different from that of alkali metal ions.

References

1) H. Strehlow, "The Chemistry of Non-Aqueous Solvents," Vol. 1, ed. by J. J. Lagowski, Academic Press, New York and London (1966), Chap. 4.

2) S. Misumi, "Hisui Yoeki Hanno (The Chemistry of Non-Aqueous Solvents)," ed. by N. Ise, N. Tokura, and T. Fujinaga, Kagakudojin, Kyoto (1971), p. 131.

3) V. S. Pleskov, *Usp. Khim.*, **16**, 254 (1947).

4) J. F. Coetzee, D. K. McGuire, and J. L. Hedrick, *J. Phys. Chem.*, **67**, 1814 (1963).

5) H. Strehlow, *Z. Elektrochem.*, **56**, 827 (1952).

6) I. M. Kolthoff and F. G. Thomas, *J. Phys. Chem.*, **69**, 3049 (1965).

7) M. Born, *Phys. Z.*, **1**, 45 (1920).

8) W. M. Latimer, K. S. Pitzer, and C. M. Slansky, *J. Chem. Phys.*, **7**, 108 (1939).

9) R. M. Noyes, *J. Amer. Chem. Soc.*, **84**, 513 (1962).

10) R. H. Robinson and R. H. Stokes, "Electrolyte Solution," 2nd ed., Butterworth Co., London (1959).

11) H. M. Koepp, H. Wendt, and H. Strehlow, *Z. Elektrochem.*, **64**, 483 (1960).

12) J. F. Coetzee and J. J. Campion, *J. Amer. Chem. Soc.*, **89**, 2513 (1967).

13) J. F. Coetzee, J. M. Simon, and R. J. Bertozzi, *Anal. Chem.*, **41**, 766 (1969).

14) K. Takaoka, *Rev. Polarog.* (Kyoto), **14**, 63 (1966).

15) T. Fujinaga and K. Izutsu, *Pure Appl. Chem.*, **27**, 273 (1971); p. 122 in Ref. 2.

16) K. Umemoto, This Bulletin, **40**, 1058 (1967).

17) P. H. Given, M. E. Peover, and J. Schoen, *J. Chem. Soc.*, **1958**, 2674.
18) T. Fujinaga, K. Izutsu, K. Umemoto, T. Arai, and K. Takaoka, *Nippon Kagaku Zasshi*, **89**, 105 (1968).
19) M. Senda, M. Senda, and I. Tachi, *Denkikagaku*, **27**, 83 (1959).
20) W. E. Clark, *J. Amer. Chem. Soc.*, **75**, 6042 (1953).
21) A. Saito, *Nippon Kagaku Zasshi*, **82**, 715 (1961).
22) J. J. Lingane, *J. Amer. Chem. Soc.*, **61**, 2099 (1939).
23) D. D. Deford and D. L. Anderson, *ibid.*, **72**, 3918 (1950).
24) W. B. Shaap, *ibid.*, **82**, 1837 (1960).
25) G. H. Brown and R. Al-Urfali, *ibid.*, **80**, 2113 (1958).
26) D. L. McMasters, R. B. Dunlap, J. R. Kuempel, L. W. Kreider, and T. R. Shearer, *Anal. Chem.*, **39**, 103 (1967).
27) K. Izutsu, S. Sakura, and T. Fujinaga, This Bulletin, **45**, 445 (1972).
28) See text. *Cf.* N. Matsuura, "Denki Kagaku (Electrochemistry)," Shokabo, Tokyo (1965).
29) J. Heyrovsky and J. Kuta, "Principle of Polarography," Academic Press, New York and London (1966), Chap 7. For a more accurate thermodyanmic calculation, a half-wave potential extrapolated to zero ionic strength $\mu=0$ in such a way as shown in Fig. 1 is recommended. Such extrapolated half-wave potentials have been found to agree with half-wave potentials calculated from standard potentials. (*cf.* A. A. Vlcek, *Chem. Listy*, **48**, 1474 (1954); *Collection Czechoslov. Chem. Communc.*, **20**. 400 (1955)).
30) J. F. Coetzee, "Progress in Physical Organic Chemistry," ed. by A. Cohen, A. Streitwieser, and R. W. Taft, Jr., Interscience, New York (1967), Vol. 4.
31) J. B. Headridge, "Electrochemical Techniques for Inorganic Chemists," Academic Press, London and New York (1969).
32) M. Suzuki, S. Sawada, and K. Yasuda, *Rev. Polarog.* (Kyoto), **18**, 1 (1972).

Standard Potentials of Alkali Metals, Silver, and Thallium Metal/Ion Couples in *N,N'*-Dimethylformamide, Dimethyl Sulfoxide, and Propylene Carbonate

Niro MATSUURA, Kisaburo UMEMOTO, and Zen'ichi TAKEUCHI

Department of Pure and Applied Sciences, College of General Education, The University of Tokyo, Komaba, Meguro-ku, Tokyo 153

(Received August 7, 1973)

The relative standard potentials of alkali metals, silver, and thallium metal/ion couples in *N,N'*-dimethylformamide(DMF), dimethyl sulfoxide(DMSO), and propylene carbonate(PC) were measured against an aqueous saturated calomel electrode(SCE). These standard potentials of lithium, sodium, potassium, rubidium, caesium, thallium, and silver are −3.237, −2.898, −3.116, −3.079, −3.079, −0.643, and +0.372 V *vs.* SCE respectively in DMSO, and −3.163, −2.830, −3.067, −3.040, −3.048, −0.559, and +0.538 V *vs.* SCE respectively in DMF, and −2.906, −2.691, −3.002, −2.980, −2.986, −0.402, and +0.813 V *vs.* SCE respectively in PC. The thallium electrode was found to be stable enough to be used as a reference electrode in these solvents. For the purpose of examining the Debye-Hückel equation for estimating the activity coefficient, the formal potentials of the thallium electrode were measured at various ionic strengths. The Debye-Hückel equation was confirmed to be applicable in these solvents, provided a proper value was chosen for the ionic radius parameter, *a*, for each solvent—3.6 for DMSO, 5.0 for DMF and 0.0 for PC.

The measurements of the standard potentials of metal/ion couples in non-aqueous media have been made for only a few media, such as alcohols, acetonitrile, and liquid ammonia.[1] In this connection, we have attempted to determine the standard potentials of alkali metals, silver, and thallium metal/ion couples in DMF, DMSO, and PC. The method employed by Lewis and his co-workers[2–4] for the determination of the potentials of alkali metal electrodes in aqueous solutions is applicable for a variety of non-aqueous solvents. According to a modification of Lewis *et al.*'s method, we determined the potential of a dilute metal amalgam electrode against aqueous SCE equipped with a specially-constructed non-aqueous salt bridge. After correcting the difference in potential between the metal amalgam and the pure metal electrode, a relative potential series was determined for each solvent. The purpose of determining the potential of an electrode in a non-aqueous solvent is to find a stable electrode which can be used as a reference electrode in the solvent. For this purpose we studied the stability of alkali metal, silver, and thallium electrodes and found the potential of the thallium electrode to be very stable in these solvents. It is also important to confirm the applicability of the Debye-Hückel equation for calculating the activity coefficient in these solvents. In order to examine the applicability of the Debye-Hückel equation, the shifts of the formal potentials of the thallium amalgam electrodes were determined at various ionic strengths.

Experimental

Solvents and Electrolytes. The purification of DMF, DMSO, and PC, as well as the preparation and purification of tetraethylammonium perchlorate (TEAP) and perchlorates of alkali metals and thallium, have been described elsewhere.[5] The silver perchlorate was obtained commercially. The electrolytes were dried in a vacuum oven for several tens of hours at 70—100 °C.

Preparation of Metal Amalgams. The alkali metal amalgams were prepared by electrolysis; the aqueous solution of alkali metal chloride or nitrate was electrolyzed with a mercury cathode and a plutinum anode. The thallium amalgam was prepared by adding pure thallium metal to distilled mercury, heating them with an infrared lamp under a nitrogen atmosphere. The metal contents in the amalgams were determined by acidimetric titration;[6] the amalgams were decomposed in a 0.01 M H_2SO_4 solution, and then the excess acid was titrated with a standard NaOH solution. A pure silver rod was used as the silver electrode. The silver rod was polished well with fine emery paper and then with filter paper until a stable potential was obtained. The silver electrode was kept immersed in the solvent for several hours before use.

Measurement of the Potential with an Amalgam Electrode. The apparatus for storing the amalgam and measuring the potential was a modification of Lewis *et al.*'s cell. The cell equipment is given in Fig. 1. The reservoir (B) was evacuated first. The amalgam was introduced into the com-

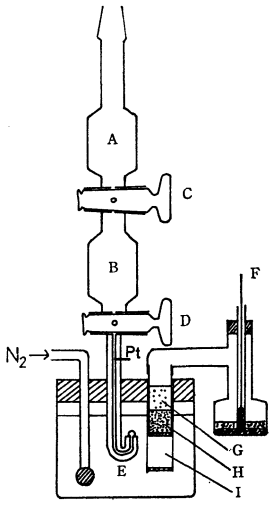

Fig. 1. Cell equipment for measurement of the potential of amalgam electrode.
A, B: amalgam reservoir. C, D: stopcock. E: capillary electrode. F: aqueous SCE. G: agar salt bridge composed of DMF-water mixture containing 0.05 M TEAP. H: agar salt bridge composed of aqueous solution containing 0.1 M NaCl. I: non-aqueous salt bridge containing 0.01 M TEAP.

partment (A) and then evacuated in order to remove the trace of water and oxygen, after which the amalgam was filtered into the reservoir (B) through the stopcock (C) by opening the stopcock (C) slightly with great caution. The prospect of the amalgam in the reservoir was the same as with pure mercury. Before measurement, the reservoir (B) was filled with pure nitrogen gas at a pressure of about 1.5 atm. Nitrogen gas was bubbled through the solution for 30 min, and an atmosphere of nitrogen was maintained during the measurement. The amalgam was admitted to the capillary electrode (E) from the reservoir (B) through the stopcock (D). The potential of the amalgam electrode was measured against an aqueous SCE equipped with a non-aqueous salt bridge.[7] The potential of the electrode was measured at various concentrations of electroactive species, ranging from 1×10^{-4} to 2×10^{-3} M, under a constant ionic strength kept by TEAP. During the measurements, the cell was thermostated at 25.0±0.05 °C. The potential measurement was made with Yokogawa Hewlett-Paccard Model 2727 potentiometer.

Results and Discussion

The cell arrangement is as follows:

$$\text{SCE} \;\Big|\; \underset{\text{(I)}}{\text{TEAP 0.01 M}} \;\Big|\; \underset{\text{(II)}}{\begin{matrix}\text{TEAP 0.01 M}\\ \text{MClO}_4\ C\ \text{M}\end{matrix}} \;\Big|\; \text{M(Hg)} \qquad (1)$$

Phase (I) is a salt bridge consisting of the same solvent as Phase (II). The electromotive force (e.m.f.) of this combination changed slowly on standing. A little more amalgam was admitted into the capillary electrode (E), thus effecting a removal of the electrode surface. When the surface was removed, the e.m.f. almost always returned to a given constant value, although occasionally it deviated from this value by several milli-volts. This was the case for alkali metal amalgams, especially when the concentration of the electroactive species was lower than 5×10^{-4} M. The potential was continuously monitered for a few hours. The total potential drift during this time was typically of the order of a few milli-volts for alkali metal amalgams and of several milli-volts for the silver electrode. The potential drift of the thallium amalgam was of the order of one to two milli-volts. The thallium amalgam electrode was very stable, especially when the concentration of Tl^+ in the solution was greater than 1×10^{-3} M, the potential drift did not exceed one milli-volt.

The overall potential of Cell (1) is given by;

$$E_{\text{cell}} = E_{\text{M}^+/\text{M(Hg)}} - E_{\text{SCE}} - E_{\text{LJ1}} - E_{\text{LJ2}} \qquad (2)$$

where E_{LJ1} and E_{LJ2} represent the liquid junction potentials of the left- and the right-hand junctions of the salt bridge respectively. By defining E'_{SCE} as $E'_{\text{SCE}}=E_{\text{SCE}}+E_{\text{LJ1}}$, and by assuming initially that the liquid junction potential, E_{LJ2}, is negligible and that the Debye-Hückel equation applies, the following relations can be written:

$$E'_{\text{cell}} = E_{\text{cell}} - 0.0591\ \log C \qquad (3)$$

$$E'_{\text{cell}} = E^{\circ\prime}_{\text{M}^+/\text{M(Hg)}} - E'_{\text{SCE}} - (0.0591)\frac{A\sqrt{\mu}}{1+Ba\sqrt{\mu}} \qquad (4)$$

$$E^{\circ\prime}_{\text{M}^+/\text{M(Hg)}} = E^{\circ}_{\text{M}^+/\text{M}} + E_{\text{A}} \qquad (5)$$

where E'_{cell} is the formal potential of Cell (1) and where $E^{\circ\prime}_{\text{M}^+/\text{M(Hg)}}$ is the potential of the amalgam electrode when the activity of the metal ion in the solution is unity; $E^{\circ}_{\text{M}^+/\text{M}}$ is the standard potential of the metal/ion couple, and E_{A}, the e.m.f. of the following cell:

$$\text{M}\,|\,\text{M}^+\,|\,\text{M(Hg)} \qquad (6)$$

viz. the difference between the potentials of the metal and the amalgam electrode. The other terms have their usual meanings.

The E_{A} values of our amalgam electrodes were calculated from the literature values of the potential of Cell (6), in which the concentration of metal in the amalgam is different from ours. The concentrations of metal in our amalgams are given in Table 1, along with those in the amalgams used for the direct measurement of the potential of Cell (6) in the literature. The concentration of metal in the amalgams used in this work does not greatly differ from that used in the literature. Accordingly, the activity coefficients of metal in the two amalgams can reasonably be assumed to be equal. The potential of our amalgam electrode against the metal electrode can, therefore, be calculated from the following equation:

$$E_{\text{A2}} = E_{\text{A1}} - 0.0591\ \log\frac{x_2}{x_1} \qquad (7)$$

where E_{A1} and E_{A2} indicate the e.m.f. of Cell (6), consisting of amalgam electrode used in the literature and in this work respectively, and where x_1 and x_2 are, respectively, the mole fraction of metal in each amalgam. The values of E_{A2} thus calculated are given in Table 1, along with the values of E_{A1}. The potential of the

Table 1. The potential of amalgam electrode against metal elfctrode

	Concentration of metal in amalgam (mole fraction)		Potential of amalgam *vs.* metal electrode (V)	
	Amalgam given in literature	Amalgam used in this work	Amalgam given in literature	Amalgam used in this work
Lithium	0.01002[a]	0.00212	0.9502[a]	0.990
Sodium	0.01834[b]	0.0168	0.8456[b]	0.848
Potassium	0.01127[c]	0.0176	1.0481[c]	1.037
Rubidium	0.00540[d]	0.00384	1.0745[d]	1.083
Caesium	0.002827[e]	0.00438	1.119[e]	1.108
Thallium		0.00750		0.154

a) Ref. 3b. b) Ref. 2. c) Ref. 3a. d) Ref. 4. e) H. E. Bent, G. S. Forbes, and A. F. Forziati, *J. Amer. Chem. Soc.*, **61**, 709 (1939).

thallium amalgam electrode against the metallic thallium electrode was calculated by using Lewis and Randlall's results, which give the relation among the concentration of thallium in the amalgam, the activity coefficient of thallium, and the potential of the amalgam electrode against the matallic thallium electrode.[8] The potential of the thallium electrode thus estimated is also given in Table 1.

The equilibrium potential of Cell (1) was measured at various concentrations of electroactive species by maintaining the concentration of TEAP at 0.01 M. The values of the cell potential, E_{cell}, and the formal potential, E'_{cell}, are given in Tables 2—4. As the concentrations of electroactive species approach zero, the contents of bothphases, (I) and (II), in Cell (1) approach an identical solution of TEAP. Upon extrapolation to zero concentration of electroactive species, a potential, E'_{cell}, is obtained at a fixed ionic strength from which the liquid junction potential, E_{LJ2}, has been eliminated. For this purpose, the data were analyzed by the method of least squares; the results are also given in Tables 2, 3, and 4.

From the values of E'_{cell} at a fixed ionic strength, $E^{\circ\prime}_{M^+/M(Hg)}-E'_{SCE}$ can be calculated from Eq. (4) if we know the radius parameter, a, in the Debye-Hückel equation. The radius parameter, a, was determined as follows.

From Eq. (4) a plot of the formal potential of the cell against the $\sqrt{\mu}/(1+Ba\sqrt{\mu})$ term should be a straight line with the slope of $-0.0591\,A$. In DMSO, DMF, and PC at 25 °C, A and B are calculated to be 1.18 and 0.435 for DMSO, 1.73 and 0.493 for DMF, 0.717 and 0.363 for PC, respectively. The a term can be varied to give the best fit.

For the purpose of examining this relation, the formal potentials of the thallium amalgam electrode were measured at various concentrations of TEAP in the right-hand-half cell of Cell (1) by maintaining the concentration of TEAP in the Phase (I) at 0.01 M. This time, the measured formal potentials include the liquid junction potential, E_{LJ2}. In this case, the liquid interphase between Phases (I) and (II) is composed of the same solvent; only the concentrations of the same electrolyte TEAP differ from each other. For such a simple liquid interphase, Henderson equation for estimating the liquid junction potential can be used with sufficient accuracy. E_{LJ2} was calculated by the following Henderson equation:

$$E_{LJ2} = 0.0591\frac{u_+-u_-}{u_++u_-}\log\frac{a_{II}}{a_I} \qquad (8)$$

Table 2. Data from cell 1 in DMSO
(Potential: V *vs.* aq. SCE, C: mol l^{-1})

Lithium			Caesium		
$C\times10^3$	$-E_{cell}$	$-E'_{cell}$	$C\times10^3$	$-E_{cell}$	$-E'_{cell}$
0.298	2.454	2.248	0.302	2.184	1.976
0.680	2.447	2.260	0.690	2.170	1.983
1.047	2.437	2.261	1.063	2.164	1.988
2.312	2.424	2.258	2.346	2.148	1.992
$E'_{cell}=-2.253\pm0.004$ at $\mu=0.01$			$E'_{cell}=-1.977\pm0.002$ at $\mu=0.01$		
Sodium			Thallium		
$C\times10^3$	$-E_{cell}$	$-E'_{cell}$	$C\times10^3$	$-E_{cell}$	$-E'_{cell}$
0.295	2.262	2.054	0.145	0.723	0.496
0.673	2.247	2.060	0.332	0.705	0.486
1.037	2.237	2.061	0.512	0.694	0.499
2.289	2.219	2.063	1.130	0.675	0.502
$E'_{cell}=-2.056\pm0.002$ at $\mu=0.01$			$E'_{cell}=-0.495\pm0.001$ at $\mu=0.01$		
Potassium			Silver		
$C\times10^3$	$-E_{cell}$	$-E'_{cell}$	$C\times10^3$	$+E_{cell}$	$+E'_{cell}$
0.303	2.294	2.086	0.215	0.136	0.364
0.693	2.272	2.085	0.308	0.163	0.370
1.068	2.263	2.087	0.472	0.175	0.372
2.358	2.244	2.088	1.050	0.196	0.372
$E'_{cell}=-2.085\pm0.001$ at $\mu=0.01$			$E'_{cell}=+0.366\pm0.002$ at $\mu=0.01$		
Rubidium					
$C\times10^3$	$-E_{cell}$	$-E'_{cell}$			
0.298	2.210	2.002			
0.679	2.191	2.004			
1.047	2.182	2.006			
2.312	2.164	2.008			
$E'_{cell}=-2.002\pm0.001$ at $\mu=0.01$					

Table 3. Data from cell (1) in DMF
(Potential: V *vs.* aq. SCE, C: mole l^{-1})

Lithium			Caesium		
$C\times10^3$	$-E_{cell}$	$-E'_{cell}$	$C\times10^3$	$-E_{cell}$	$-E'_{cell}$
0.298	2.388	2.179	0.299	2.155	1.947
0.679	2.371	2.183	0.683	2.139	1.952
1.047	2.360	2.183	1.052	2.119	1.950
2.312	2.339	2.182	2.323	2.108	1.952
$E'_{cell}=-2.181\pm0.001$ at $\mu=0.01$			$E'_{cell}=-1.948\pm0.001$ at $\mu=0.01$		
Sodium			Thallium		
$C\times10^3$	$-E_{cell}$	$-E'_{cell}$	$C\times10^3$	$-E_{cell}$	$-E'_{cell}$
0.303	2.199	1.989	0.146	0.638	0.412
0.693	2.182	1.994	0.333	0.620	0.413
1.068	2.173	1.995	0.514	0.610	0.416
2.358	2.155	1.997	1.133	0.590	0.410
$E'_{cell}=-1.990\pm0.001$ at $\mu=0.01$			1.676	0.577	0.413
Potassium			$E'_{cell}=-0.413\pm0.001$ at $\mu=0.01$		
$C\times10^3$	$-E_{cell}$	$-E'_{cell}$	Silver		
0.306	2.246	2.038	$C\times10^3$	$+E_{cell}$	$+E'_{cell}$
0.699	2.229	2.042	0.151	0.301	0.527
1.078	2.221	2.045	0.345	0.326	0.531
2.381	2.204	2.048	0.532	0.336	0.529
$E_{cell}=-2.038\pm0.001$ at $\mu=0.01$			1.173	0.355	0.528
Rubidium			1.735	0.363	0.526
$C\times10^3$	$-E_{cell}$	$-E'_{cell}$	$E'_{cell}=+0.530\pm0.001$ at $\mu=0.01$		
0.303	2.171	1.963			
0.693	2.156	1.969			
1.068	2.144	1.968			
2.358	2.126	1.970			
$E'_{cell}=-1.965\pm0.002$ at $\mu=0.01$					

Table 4. Data from cell (1) in PC
(Potential: V *vs.* aq. SCE, C: mol l^{-1})

Lithium			Caesium		
$C\times10^3$	$-E_{cell}$	$-E'_{cell}$	$C\times10^3$	$-E_{cell}$	$-E'_{cell}$
0.307	2.128	1.920	0.296	2.090	1.882
0.703	2.112	1.925	0.676	2.076	1.889
1.084	2.102	1.926	1.042	2.070	1.894
2.393	2.087	1.932	2.300	2.057	1.901
$E'_{cell}=-1.920\pm0.001$			$E'_{cell}=-1.882\pm0.002$		
at $\mu=0.01$			at $\mu=0.01$		
Sodium			Thallium		
$C\times10^3$	$-E_{cell}$	$-E'_{cell}$	$C\times10^3$	$-E_{cell}$	$-E'_{cell}$
0.306	2.054	1.846	0.148	0.477	0.251
0.700	2.040	1.853	0.340	0.458	0.253
1.078	2.029	1.854	0.523	0.448	0.254
2.381	2.014	1.858	1.155	0.429	0.254
$E'_{cell}=-1.847\pm0.002$			1.708	0.420	0.256
at $\mu=0.01$			$E'_{cell}=-0.252\pm0.001$		
Potassium			at $\mu=0.01$		
$C\times10^3$	$-E_{cell}$	$-E'_{cell}$	Silver		
0.299	2.177	1.969	$C\times10^3$	$+E_{cell}$	$+E'_{cell}$
0.683	2.162	1.975	0.144	0.581	0.808
1.052	2.154	1.978	0.330	0.606	0.810
2.323	2.140	1.984	0.509	0.618	0.813
$E'_{cell}=-1.969\pm0.001$			1.124	0.639	0.813
at $\mu=0.01$			1.664	0.652	0.816
Rubidium			$E'_{cell}=+0.809\pm0.001$		
$C\times10^3$	$-E_{cell}$	$-E'_{cell}$	at $\mu=0.01$		
0.305	2.107	1.899			
0.696	2.095	1.908			
1.073	2.084	1.908			
2.369	2.069	1.913			
$E'_{cell}=-1.901\pm0.002$					
at $\mu=0.01$					

where a_I and a_{II} are the mean activities of ions in the Phases (I) and (II) respectively, and where u_+ and u_- are the ionic mobilities of the tetraethylammonium cation and the perchlorate anion respectively, which were obtained from conductance measeurments as 16.8 and 24.6 ohm^{-1} cm^2 in DMSO, as 36.9 and 50.6 ohm^{-1} cm^2 in DMF, and as 13.8 and 18.3 ohm^{-1} cm^2 in PC, respectively.[9] The contribution of the small amount of thallium perchlorate in the right-hand-half cell was neglected in this calculation. Plot of E'_{cell} against $\sqrt{\mu}/(1+Ba\sqrt{\mu})$ should, then, give a straight line with a slope of $-0.0591A\{1-(u_+-u_-)/(u_++u_-)\}$, again, a was used as a fitting parameter to obtain the best fit to the straight line. By means of this method we have determined the values of a for the solvents to be 3.6, 5.0, and 0.0 for DMSO, DMF, and PC respectively. The results, the plots of E'_{cell} corrected for the liquid junction potentials E_{LJ2} from Eq. (8) by the use of estimated a values, are shown in Fig. 2.

A satisfactory best fit was obtained for each solvent; these best fits indicate that the slopes of the straight lines are −0.073, −0.10, and −0.060 for DMSO, DMF, and PC respectively. For DMSO and DMF the experimentally-determined slopes are nearly equal to the theoretical values, −0.070 for DMSO and −0.102 for DMF, but for PC the experimental value

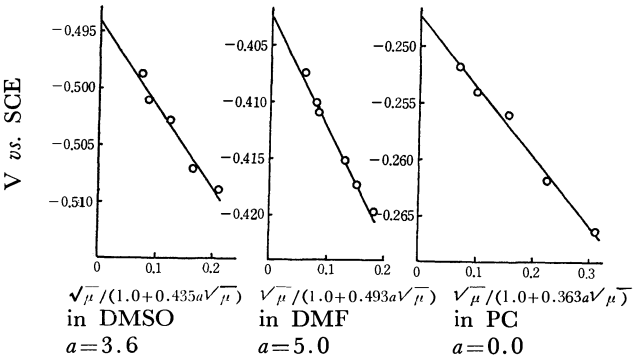

Fig. 2. Formal potential of thallium amalgam electrode as a function of ionic strength.

is slightly different from the theoretical value, −0.042. In order to obtain the theoretical slope for PC, a value of −2.0 must be estimated for a. However, in this case the best fit to the straight line is not obtained; moreover, the negative value of a is not understandable. Accordingly, we tentatively estimate the value of a for PC to be 0.0. With the use of these values of a, small corrections in the potential due to the activity coefficient were calculated, and the values of $E^{\circ\prime}_{M^+/M(Hg)}-E'_{SCE}$ were obtained from Eq. (4). Then, the standard potentials, relative to the aqueous SCE, were calculated from Eq. (5); they are given in Table 5.

These standard potentials include the liquid junction potential between the aqueous and non-aqueous interphase, E_{LJ1}. The estimation of the liquid junction potential is made by comparing the experimentally-determined potential scale with the common potential scale established in a previous work.[5] The solvent shifts in the potential of rubidium by the transfer of the rubidium ion from water to these solvents have been estimated as −0.034 V for DMSO, +0.005 V for DMF, and +0.149 V for PC. Accordingly, the standard potentials of rubidium should be −3.200, −3.161, and −3.017 V *vs.* SCE in DMSO, DMF, and PC respectively, since the standard potential of rubidium in an aqueous solution has been given as −3.166 V *vs.* SCE.[10] By comparing these potentials of rubidium with the experimental values, the liquid junction potentials of aqueous and non-aqueous interphases were estimated as +0.121 V for DMSO, +0.121 V for DMF, and +0.037 V for PC against the aqueous phase. By correcting these liquid junction potentials, the standard potentials on the common potential scale—Corrected Rubidium Scale—were obtained; these values are shown in Table 5.

The liquid junction potentials estimated in this work are different from the values previously estimated from the polarographic half-wave potentials by +0.031 V for DMSO, by +0.036 V for DMF, and by +0.033 V for PC. These differences may be attributed partly to the different concentration of electrolyte in the non-aqueous phase in the two experiments: in present work the non-aqueous phase includes 0.01 M TEAP, while in the previous polarographic study it included 0.1 M TEAP. Moreover, these differences

Table 5. Standard potentials of metal/ion couples on the corrected rubidium scale and estimation of the liquid junction potential *vs.* the aqueous saturated calomel electrode

	DMSO		DMF		PC		Water[d]
	E°[a]	E°[b]	E°[a]	E°[b]	E°[a]	E°[b]	E°
Lithium	−3.237	−3.358	−3.163	−3.284	−2.906	−2.943	−3.27
Sodium	−2.898	−3.019	−2.830	−2.951	−2.691	−2.728	−2.954
Potassium	−3.116	−3.237	−3.067	−3.188	−3.002	−3.039	−3.166
Rubidium	−3.079	−3.200	−3.040	−3.161	−2.980	−3.017	−3.166
Caesium	−3.079	−3.200	−3.048	−3.169	−2.986	−3.023	−3.164
Thallium	−0.643	−0.764	−0.559	−0.680	−0.402	−0·439	−0.577
Silver	+0.372	+0.251	+0.538	+0.417	+0.813	+0.776	+0.553
E_{LJ1}[c]		+0.121		+0.121		+0.037	

a) Standard potential measured directly against aqueous SCE. b) Standard potential on the corrected rubidium scale. Solvent shift in rubidium standard potential is −0.034 V for DMSO, +0.005 V for DMF and +0.149 V for PC by transfer of rubidium ion from water to these solvents as determined in Ref. 5. c) Estimated liquid junction potential against aqueous phase. d) Ref. 10.

may also be due to the solvent shift in the polarographic half-wave potentials caused by the variation in the diffusion constants and the salt activity coefficients of ions for changing the solvent.

At first, the present authors intended to estimate the solvent shift in the potential of rubidium by the application of the modified Born equation by the use of the standard potential series determined in this work. However, this attempt was unsuccessful, because the accuracy of the determined standard potentials was not good enough to be used for this purpose. The authors found that the potentials of an amalgam measured with different capillary electrodes showed a deviation of several milli-volts among them, although the potential of each electrode was stable by itself. The potential of the amalgam electrode must be affected by the structure of the capillary electrode. In this connection, for the purpose of obtaining more accurate and reproducible potentials, it would be worth-while to examine the utility of the dropping amalgam electrode used by Ulich and Spiegel.[11]

The authors wish to express their thanks to Miss Mariko Omoto, Mr. Toshio Shingyouchi, and Mr. Mikio Ochi for their cooperation in the experimental work.

References

1) H. Strehlow, "The Chemistry of Non-Aqueous Solvents," Vol. 1, ed. by J. J. Lagowski, Academic Press, New York and London (1966), Chap. 4.
2) G. N. Lewis and C. A. Kraus, *J. Amer. Chem. Soc.*, **32**, 1459 (1910).
3) a) G. N. Lewis and F. G. Keyes, *ibid.*, **34**, 119 (1912). b) *ibid.*, **35**, 340 (1913).
4) G. N. Lewis and W. L. Argo, *ibid.*, **37**, 1990 (1915).
5) N. Matsuura, K. Umemoto, M. Waki, Z. Takeuchi, and M. Omoto, This Bulletin, **47**, 806 (1974).
6) T. W. Richards and F. Daniels, *J. Amer. Chem. Soc.*, **41**, 1732 (1919).
7) The construction and the calibration of the agar non-aqueous salt bridge has been described in detail in Ref. 5.
8) G. N. Lewis and M. Randall, 'Thermodynamics," revised by K. S. Pitzer and L. Brewer, McGraw-Hill Book Co., New York (1961), Chap. 20, p. 259.
9) N. Matsuura, K. Umemoto, and Y. Takeda, to be published.
10) G. Charlot, "Selected Constants. Oxido-Reduction Potentials," Pergamon Press, New York (1958).
11) H. Ulich and G. Spiegel, *Z. Phys. Chem.*, **177**, 103 (1936).

Infrared Absorption Spectra and Normal Coordinate Analysis of Metal-DL-Tyrosine Chelates

Yoshie INOMATA, Tadaaki INOMATA, and Takao MORIWAKI

Department of Chemistry, Faculty of Science and Technology, Sophia University, Chiyoda-ku, Tokyo 102

(Received August 8, 1973)

The infrared absorption spectra of DL-tyrosine and six metal DL-tyrosine chelates have been investigated from 4000 to 300 cm^{-1}. A detailed normal coordinate analysis was performed for the metal chelates as a 39-body problem and an approximate description of the vibrational modes has been assigned to the observed frequencies. DL-Tyrosine chelates are found to be coordinated with the metal through nitrogen and oxygen and to have a *trans* configuration; the same is true for other aliphatic amino acid chelates. The bond-stretching force constants for the metal-nitrogen bonds have been found to decrease in the order Pd(II)>Cu(II)>Zn(II)>Cd(II)>Ni(II)>Co(II). The calculated frequencies, which were obtained using the same force constants as in other aliphatic amino acid chelates, were in good agreement with the observed frequencies.

The infrared absorption spectra and the normal coordinate analysis for aliphatic α-amino acid chelates have already been studied.[1-4] However, amino acids having a substituent in the β-position and their metal-chelates have not yet been studied in detail. Recently, the authors have investigated the infrared spectra and the normal coordinate analysis for DL-α-serine[5] having a hydroxy group and DL-phenylalanine[6] having a benzene ring in the β-position.

Laurie[7] has synthesized three isomers of bis(DL-tyrosino)-copper(II) and reported that two isomers have a *trans* configuration, and the third is 4-coordinated with either a *trans* or *cis* configuration. He used both diffuse reflectance spectra and infrared absorption spectra for this configuration assignment.

In the present investigation, detailed assignments for the infrared absorption bands of DL-tyrosine and its six metal chelates have been made by a comparison with the results of the normal coordinate analysis. In addition, we discuss how the phenolic group in the β-position influences the order of the metal-ligand bond strength which has already been found in aliphatic α-amino acid chelates.[8]

Experimental

Preparation of Compounds. *Bis(DL-tyrosino)-palladium(II)* was prepared by adding 0.81 g (0.0025 mol) of K_2PdCl_4 to hot water in which 0.91 g (0.005 mol) of DL-tyrosine was thoroughly dissolved, and stirring for half an hour. The yellow crystals which precipitated were washed with hot water and dried at room temperature *in vacuo* for several hours.

Found: C, 45.75; H, 4.22; N, 5.98% Calcd for Pd-$[C_6H_4OHCH_2CHNH_2CO_2]_2$: C, 46.31; H, 4.33; N, 6.00%

Bis(DL-tyrosino)-copper(II) was prepared by the method of Laurie,[7] which yielded the blue, prismatic form of bis(DL-tyrosino)-copper(II).

Found: C, 45.95; H, 5.47; N, 5.90% Calcd for $Cu[C_6H_4OHCH_2CHNH_2CO_2]_2\cdot 2\frac{1}{2}H_2O$: C, 46.09; H, 5.38; N, 5.97%.

Bis(DL-tyrosino)-nickel(II) was prepared by adding 1.2 g (0.005 mol) of $NiCl_2\cdot 6H_2O$ to a hot solution of 1.81 g (0.01 mol) of DL-tyrosine and 0.56 g (0.01 mol) of KOH and stirring. After filtering while hot, the filtrate was allowed to stand overnight. The sky blue precipitate separated was recrystallized from hot water and dried at room temperature *in vacuo* for several hours.

Found: C, 45.91; H, 5.41; N, 5.93% Calcd for $Ni[C_6H_4OHCH_2CHNH_2CO_2]_2\cdot 2\frac{1}{2}H_2O$: C, 46.57; H, 5.44; N, 6.04%.

Bis(DL-tyrosino)-cobalt(II)

Found: C, 48.99; H, 5.10; N, 6.35% Calcd for $Co(C_6H_4OHCH_2CHNH_2CO_2]_2\cdot 1\frac{1}{3}H_2O$: C, 48.43; H, 5.20; N, 6.28%.

Bis(DL-tyrosino)-cadmium(II)

Found: C, 44.90; H, 4.20; N, 5.74% Calcd for $Cd[C_6H_4OHCH_2CHNH_2CO_2]_2$: C, 45.72; H, 4.27; N, 5.93%.

Bis(DL-tyrosino)-zinc(II)

Found: C, 45.61; H, 5.08; N, 5.86% Calcd for $Zn[C_6H_4OHCH_2CHNH_2CO_2]_2\cdot 2\frac{1}{2}H_2O$: C, 45.92; H, 5.36; N, 5.95%.

These three chelates were prepared by employing essentially the same procedure as for the nickel(II) chelate. For cobalt(II) chelate, after filtering the solution while it was hot, the pink filtrate was allowed to stand for several days at room temperature. The precipitates of cobalt(II), cadmium(II), and zinc(II) chelates were washed twice in hot water and dried at room temperature *in vacuo*.

Deuteration of Compounds. The deuterated DL-tyrosine and copper(II) chelate were prepared by dissolving DL-tyrosine and copper(II) chelate, which had been dried thoroughly, in 99.75% deuterium oxide at 80 °C and drying them *in vacuo*. The NH and OH groups were deuterated by this method. The perfect deuteration of the other chelates was difficult, since they were insoluble in water.

Thermal Analysis of Chelates. Thermal analysis was carried out with a Rigaku Denki TG–DTA from room temperature 250 °C in air; the decrease in weight was measured when an endothermic reaction occurred. It was found that the nickel(II), the copper(II), and the zinc(II) chelates had $2\frac{1}{3}$ molecules of water and cobalt(II) had $1\frac{1}{2}$ molecules. The cadmium(II) and the palladium(II) chelates had no water.

Absorption Measurement. Infrared absorption spectra from 4000 cm^{-1} to 300 cm^{-1} were obtained with Hitachi EPI-G2 and EPI-L spectrophotometers, which were calibrated with polystyrene and atmospheric water vapor. Samples were prepared as potassium bromide discs and nujol mulls. The observed absorption frequencies and assignments for DL-tyrosine and the metal chelates are listed in Table 1.

Discussion

The assignments for DL-tyrosine and its metal chelates have been based on a comparison of the observed spectra with those of aliphatic α-amino acids,[1-5] DL-phenylalanine,[6] and those metal chelates which had

TABLE 1. OBSERVED FREQUENCIES AND ASSIGNMENTS FOR DL-TYROSINE AND METAL-DL-TYROSINE CHELATES (cm^{-1})

RH	Pd(II)	Cu(II)	Ni(II)	Zn(II)	Co(II)	Cd(II)	Assignments
			3599 m	3519 m	3399 sb		OH str. (water of crystallization)
			3359 vs	3348 s		3345 s	
	3294 sb	3307 sb	3302 vs	3328 s	3277 sb	3331 s	NH str. for chelates
3212 s	3239 s	3255 sb		3267 s	3244 sb	3283 s	OH str.
	3159 sh					3272 sh	
	3125 sh	3144 sb		3187 sb	3159 sb	3109 wb	
3117 s							
3046 s						3069 w	
						3037 m	NH_3^+ str. for the ligand
3029 s	3029 w	3016 m	3029 m	3015 w	3026 w	3019 m	CH str. of benzene ring
2971 s	2976 vw	2959 w		2959 m	2969 sh	2952 m	
	2951 w			2936 m	2959 sh		
2943 s	2919 w	2931 sh	2937 m	2917 w	2935 w	2915 m	CH str. of CH_2 and CH
2882 sh							
	2849 w	2853 sh	2860 w	2858 w	2855 sh	2846 m	
2827 s	2784 sh	2806 m		2813 wb	2819 w	2819 m	
2747 s			2760 sh	2736 w		2758 w	
	2694 sh	2689 w		2679 w	2694 sh	2694 mb	NH_3^+ str. for the ligand
2652 s							
2601 s		2608 w	2628 sh	2604 w	2612 w	2624 m	
2501 m		2512 w		2514 vw		2517 w	
2094 m							
		1652 sh					
		1647 sh	1648 sh		1654 sh		
		1633 sh	1632 sh		1648 sh		COO^- asym. str. + C=C str.
1627 s	1636 sb	1630 s	1625 s		1636 s		NH_3^+ deg. def. + C=C str. for ligand
1608 s		1607 s		1597 vs	1629 s	1608 m	
	1584 s	1591 s	1592 s	1570 sh	1610 sh	1584 s	NH_2 scissors + C=C str.
1588 s							COO^- asym. str. + C=C str. for ligand
1528 s						1548 s	
1510 s	1503 m	1507 m	1512 m	1511 s	1510 m	1512 s	C=C str.
1448 m			1458 m	1468 vw	1457 sh	1458 sh	
				1458 sh		1450 w	
1434 m	1433 m	1437 m	1447 sh	1445 m	1445 m	1435 m	C=C str. + CH_2 scissors
				1411 s	1439 m	1412 m	
						1382 sh	
1410 m	1357 s	1373 s	1391 s	1357 m	1378 s	1357 m	COO^- sym. str. + CH bending (metal chelates)
1367 s		1341 m		1349 sh			
1330 s	1321 vw	1330 m	1336 m	1331 w	1330 m	1341 m	CH bending + C=C str.
	1306 vw	1304 sh	1308 sh	1307 vw	1307 sh	1315 w	CH_2 wagging
1289 w	1290 m						CH in plane deformation of benzene ring
1269 w							CH_2 twisting
1249 s	1261 m	1265 m		1255 s	1264 sh	1255 m	C-O str.
1216 m	1205 s	1235 m	1247 s	1242 m	1237 s	1231 w	OH in plane def.
1199 m							NH_3^+ rocking
				1212 w		1215 m	
1180 m	1171 vw	1167 w	1171 w	1172 vw	1184 vw	1178 m	CH in plane deformation of benzene ring
					1172 vw		
1150 m	1151 sh		1139 w	1146 w			CCN asym. str.
	1137 s					1141 w	
1113 m		1105 m	1099 m	1115 m	1102 w	1113 m	CH in plane deformation of benzene ring
	1097 w			1100 s			
	1084 w	1085 m		1081 s	1093 sh	1077 m	NH_2 wagging
1098 m							NH_3^+ rocking

Table 1. (continued)

RH	Pd(II)	Cu(II)	Ni(II)	Zn(II)	Co(II)	Cd(II)	Assignments
1047 m	1062 sh		1057 s			1047 w	CH_2-C str.
1018 w	1021 vw	1010 sh	1013 vw	1020 vw	1010 w	1013 w	CH in plane deformation of benzene ring
	1011 vw						
989 w							
985 w	976 vw	989 w	985 w	978 m		986 m	
	963 vw					952 vw	C=C def.
	947 vw			945 vw			
938 w	932 w	932 wb	924 w	936 w	945 wb	926 vw	CH out of plane deformation of benzene ring
897 w	919 sh					903 w	
						897 m	
876 m	860 w	864 w	868 w	871 vw	864 sh	871 m	CCN sym. str.
842 s			850 sh	851 vw	851 sh		
	837 sh			831 sh		831 m	C-C str.
834 m	822 s	824 m	821 s	820 m	816 m	817 m	CH out of plane deformation of benzene ring
808 m	805 m	810 m	811 s	806 m		810 m	COO^- scissors
797 m	782 w			775 vw		773 vw	CH_2 rocking
738 m	724 w	730 w	741 w	727 m	744 sh	735 m	
711 w	707 vw	714 sh	719 w	707 w	713 wb	715 m	C=C out of plane deformation
			683 w				
644 m	668 sh	650 m	650 vw	665 m	658 w	672 w	OH out of plane deformation
	660 w					658 vw	
639 m	641 vw		639 vw	640 vw	638 w	638 vw	in plane benzene ring deformation
	622 vw					621 sh	
	613 w		587 m	603 w	582 m	599 m	NH_2 rocking
575 s	583 w		577 sh	590 vw		572 sh	COO^- wagging
559 vw							
534 s	542 m	553 sh	532 m	534 m	543 m	539 m	CCC def.
	524 w	539 m	512 sh	523 w	533 m	520 vw	C=C def.
498 m	486 w	486 w	494 w	498 w	487 m	496 w	COO^- rocking
478 vw				484 vw		484 w	
452 vw	443 vw			458 vw	447 m	463 w	
434 m	432 w	408 w	411 wb	410 w	423 w	439 w	C=C out of plane deformation
	429 w						
					400 w		
	407 m						M-N str.
385 s	392 m	393 w	381 wb	376 vw	385 sh	390 vw	CCO def.
	377 sh	372 vw	377 sh	370 vw	375 sh	370 vw	CCCN sym. def.
337 m	342 m				341 vw	352 w	CO out of plane def.
325 m		320 mb	317 m	359 w	315 w	316 w	M-N str. for the chelates
		317 mb					
308 m	305 w	305 w	305 vw		302 vw		

Abbreviations: RH=DL-tyrosine, s=strong, m=medium, w=weak, sh=shoulder, b=broad

been thoroughly studied.

The spectra of DL-tyrosine chelates are similar to the spectra of those which have a *trans* configuration. Laurie[7] reported that the blue prismatic DL-tyrosine copper(II) chelate had a *trans* configuration. Therefore, in spite of the lack of X-ray data for the metal chelates, it seems reasonable that they have a *trans* configuration.

Assignment of Observed Frequencies. *DL-Tyrosine*: The sharp band at 3212 cm^{-1} is assigned to the OH stretching vibration, because of its disappearance on deuteration and the absence of bands in this region for DL-phenylalanine.[6] The broad bands from 3100 to 2800 cm^{-1} are due to NH_3^+ and CH stretching vibrations of the benzene ring. The CH stretching vibration bands are assigned easily, since they do not shift on deuteration. The CH stretching vibrations of an aliphatic group are observed in a lower frequency region than those of a benzene ring.

The bands at 1627, 1528, 1199, and 1098 cm^{-1} which shift on deuteration are due to NH_3^+ deformation vibrations, since no corresponding bands appear in the metal chelates.

It is very difficult to assign C–O stretching and OH

deformation vibrations in the phenolic group. Jakobsen[9] has reported about the group frequencies of *para*-substituted phenols in detail. He shows that *p*-cresol has bands at 1253, 1215, 1170, and 555 cm^{-1}, which have been assigned to C–O and C–CH_3 stretching and OH deformation vibrations. The frequencies of DL-tyrosine, however, may be different from those of *p*-cresol on account of the intermolecular hydrogen bonding. Therefore it is reasonable to assign the bands at 1249 and 1216 cm^{-1} to the C–O stretching and the OH in plane deformation vibrations, and the band at 644 cm^{-1} to the OH out of plane deformation vibration by a comparison with the *N*-deuterated compound and with phenylalanine.[6]

CN and CC stretching and skeletal deformation vibrations are assigned by a comparison with the spectra of the metal chelates.

If the phenolic group (C_6H_4OH) is treated as possessing C_{2v} symmetry, it has thirty normal vibrations which are divided into symmetry classes as follows: $(11A_1+10B_1)$planar and $(3A_2+6B_2)$ non planar. The A_2 symmetry class is infrared inactive. The eight vibrations $(4A_1+3B_1+B_2)$ of these normal vibrations have already been mentioned above. The remaining 19 vibrations are assigned by referring to the assignments in *p*-cresol and phenylalanine.[6]

Metal-Chelates: As the bands above 3500 cm^{-1} of the nickel(II) and the zinc(II) chelates disappear in the spectra are obtained after DTA analyses, these bands are assigned to the OH stretching vibrations in the water of crystallization.

Although the bands from 3400 to 3100 cm^{-1} are due to NH_2 symmetric and antisymmetric and OH stretching vibrations, it is difficult to assign them separately, since all bands shift on deuteration. The CH stretching vibrations are observed at the same region as in the ligand.

In the region 1700 to 500 cm^{-1} the assignment of the observed bands is accomplished by a comparison of the spectrum of each chelate with that of the ligand.

For the metal chelates, the NH_2 deformation vibrations appear instead of NH_3^+ deformation vibrations of the ligand. The COO^- antisymmetric stretching vibrations for all chelates are intense and overlap with the C=C stretching vibrations of the benzene ring and the NH_2 scissors vibrations to some extent. The COO^- antisymmetric stretching vibrations are observed at higher frequencies and symmetric stretching vibrations are at lower frequencies than those of the ligand. The OH in plane and out of plane deformation vibrations shift to higher frequencies. The vibrations of the phenolic group and the skeletal deformation vibrations occur at the same regions as in the ligand.

From 500 to 300 cm^{-1}, absorption bands which cannot be observed in the ligand appear at 407 cm^{-1} for palladium(II) chelate, 393 cm^{-1} for copper(II) chelate, 359 cm^{-1} for zinc(II) chelate, 317 cm^{-1} for nickel(II) chelate, 316 cm^{-1} for cadmium(II) chelate and 315 cm^{-1} for cobalt(II) chelate. They are assigned to the metal-nitrogen stretching vibration by comparison of chelate spectra with the ligand spectrum and by referring to the metal chelates of DL-phenylalanine,[6] DL-serine[5] and other amino acids.[1-4]

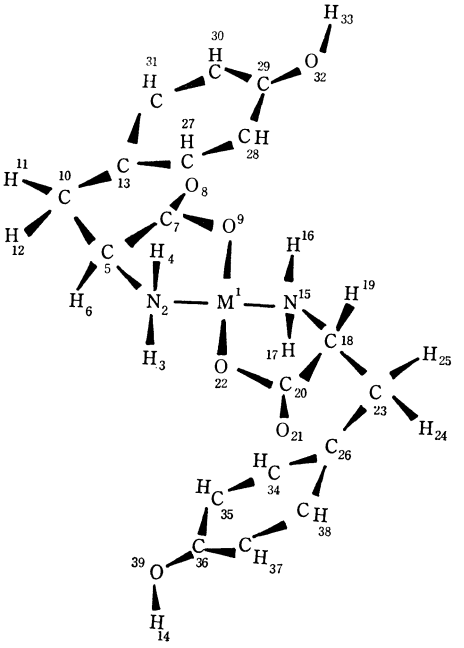

Fig. 1. Structure of DL-tyrosine chelates.

Normal Coordinate Analysis. The normal coordinate analysis for a metal chelate was performed as a 39-body problem using the model illustrated in Fig. 1. Major calculations were carried out on HITAC 5020E and 8700/8800 computers.[10]

The model adopted has M_1 as a center of symmetry. The atoms M, N(2,15), C(5,18), C(7,20), O(9,22) form planar five-membered chelate rings and O(8,21) is in the same plane. The atoms C(5,18), C(10,25), C(13, 26), C(29,36), and O(32,39) are in the same plane, which is perpendicular to these chelate rings. The atoms C(10,23) and phenolic groups are in the same plane, which makes half of a tetrahedral angle with

Table 2. Bond lengths and bond angles used in the calculation for DL-tyrosine chelate

Bond lengths (Å)			
M-N	1.86[5]	C-H	1.09
N-H	1.01	C_5-C_{10}	1.55
N-C	1.48 [11]	C_{10}-C_{13}	1.57 [11]
C_5-C_7	1.50	C=C	1.37
C_7-O_8	1.25	C_{29}-O_{32}	1.43[12]
C_7-O_9	1.271583[a]	O-H	0.960[13]
O-M	1.881279[a]		

Bond angles (°)			
O_9-M_1-N_2	90	O_8-C_7-O_9	120
C_5-C_7-O_8	120	C_7-O_9-M_1	$330-2\theta$
C_5-C_7-O_9	120	C_{29}-O_{32}-H_{33}	109[14]
C-C=C	120		
	θ : 109°28′		

All other angles are assumed to be 109° 28′. The same bond lengths and bond angles are used for second chelate ring.

a) Calculated to insure ring closure.

these chelate rings.

The CH groups in the phenolic groups are considered as one unit. (Mass=13.007825)

In the absence of X-ray data, the bond lengths and bond angles listed in Table 2 were used for all DL-tyrosine metal chelates in the calculation.

The frequencies for the infrared active vibrations were calculated using the same symmetry coordinates as those of Ref. 4 except for the phenolic group vibrations.

Wilson's GF matrix method was used and all results were obtained using FORTRAN program designed by Shimanouchi.[15] The potential field employed was the modified Uray-Bradley type, similar to that used for the chelates of DL-α-serine.[5]

Most of the force constants in Table 3 were transferred from the corresponding values determined for the DL-α-serine[5] and other amino acids chelates. The remaining force constants were evaluated so as to obtain the best fit between the calculated and observed frequencies. Adjustment of the force constant values was accomplished by a trial and error method guided by the values of a Jacobian matrix.

Calculated frequencies for the palladium(II)chelate are shown in Table 4. An approximate description of the vibrational mode is given for each observed frequency, which is based on the potential energy distribution to the symmetry coordinates and force constants. In this model, the CH groups in the phenolic groups were considered as a single unit. Therefore, the frequencies corresponding to the stretching and deformation vibrations of those groups will not appear in the calculations.

A similar calculation was accomplished for the cadmium(II), copper(II), zinc(II), nickel(II) and cobalt(II) chelates and good agreement was obtained between the observed and calculated frequencies for these chelates.

Metal-ligand Bonds. The important frequencies and the force constants related to the metal-ligand bonds are summarized for each chelates in Table 5 and 6.

As shown in Table 5, the frequency separation of the COO^- antisymmetric and symmetric stretching vibrations of chelates which have the same number of molecules of water increases in the order Ni(II)< Zn(II)<Cu(II). This trend is the same as that in many aliphatic α-amino acid chelates.[1-4,8]

In Table 6, the F_{dia} terms represent the diagonal elements of the symmetrized F matrix: *i. e.*, the

TABLE 3. FORCE CONSTANTS USED IN THE CALCULATION FOR THE PALLADIUM(II) CHELATE (mdyn/Å)

Stretching		Bending		Repulsion	
K(M-N)	0.75	H(MNH)	0.15	F(MHN)	0.07
K(N-H)	5.68	H(MNC)	0.05	F(MNC)	0.10
K(N-C)	2.50	H(HNH)	0.57	F(HNH)	0.06
K(C_5-C_7)	1.50	H(HNC)	0.17	F(HNC)	0.40
K(C_7-O_8)	8.30	H(NCH)	0.26	F(NCH)	0.54
K(C_7-O_9)	5.60	H(NCC_R)	0.20	F(NCC_R)	0.20
K(C_5-H_6)	4.13	H(NCC)	0.20	F(NCC)	0.20
K(C_5-C_{10})	1.50	H(HCC_R)	0.23	F(HCC_R)	0.43
K(C-H)	4.13	H(CCC)	0.40	F(CCC)	0.30
K(C-C_{13})	1.50	H(HCC)	0.23	F(HCC)	0.43
K(O-H_{33})	5.27	H(CCO)	0.40	F(CCO)	0.70
K(C_{13}-C_{27})	6.25	H(CCO_R)	0.50	F(CCO_R)	0.70
K(C_{27}-C_{28})	6.25	H(OCO)	0.35	F(OCO)	3.50
K(C_{28}-C_{29})	6.25	H(COM)	0.05	F(COM)	0.10
K(C_{29}-O_{32})	2.50	H(CCH)	0.23	F(CCH)	0.43
		H(CCC_B)	0.40	F(CCC_B)	0.37
		H(HCH)	0.42	F(HCH)	0.05
		H(HCC_B)	0.23	F(HCC_B)	0.43
		H(CC_BC$_B$)	0.23	F(CC_BC$_B$)	0.37
		H(C$_B$C$_B$C$_B$)	0.33	F(C$_B$C$_B$C$_B$)	0.27
		H(C$_B$C$_O$C$_B$)	0.23	F(C$_B$C$_O$C$_B$)	0.37
		H(C$_B$C$_{13}$C$_B$)	0.23	F(C$_B$C$_{13}$C$_B$)	0.37
		H(CC$_B$O)	0.23	F(CC$_B$O)	0.37
		H(C$_B$OH)	0.30	F(C$_B$OH)	0.67

Out-of-plane wagging		mdyn·Å			
P(C_{13}-C)	0.18	P(C_{29}-O)	0.08	P(OCO)	0.50

Torsion		mdyn·Å			
T(C_{13}-C_{27})	0.15	T(C_{10}-C_{13})	0.15	T(C_{27}-C_{28})	0.15
T(C_5-C_7)	0.15	T(C_{28}-C_{29})	0.15	T(C_5-C_{10})	0.065
T(C_{29}-O)	0.19				

TABLE 4. OBSERVED AND CALCULATED FREQUENCIES FOR THE INFRARED ACTIVE VIBRATIONS OF THE PALLADIUM(II) CHELATE

Obsd cm^{-1}	Calcd cm^{-1}	Description	Obsd cm^{-1}	Calcd cm^{-1}	Description
3294	3294	NH_2 asym. str.	976		
3239	3247	NH_2 sym. str.		941	C=C def. + C_{10}-C str.
3159	3159	OH str.	932		CH[a] out of plane bending of benzene ring
3125					
3029		CH[a] str. of benzene ring	860	901	CH_2 rocking + CH_2-C str.
2976			837	837	CH_2-C str. + CH_2 rocking
2951	2950	CH str.	805		
2919	2905	CH_2 asym. str.	782	797	CH_2 rocking + CCC def.
2849	2860	CH_2 sym. str.		740	C-O str. + C=C str.
2784			724		
2694			707		
1636	1630	CO_2 asym. str.	668	663	C-O torsion
	1620	C=C str.	660		
1584	1583	NH_2 scissors	641		
	1581	C=C str.	622		
1503	1523	C=C str.	613	647	NH_2 rocking
1433	1440	CH_2 scissors		627	C-CO_2 str. + CCC def.
1357	1369	CO_2 sym. str. + CH bending	583	586	CO_2 wagging
1321	1339	CH_2 wagging + CH bending		559	C=C torsion
	1315	CH bending + CH_2 wagging	542	541	CO_2 rocking + C_{10}-C str.
1306	1301	CH bending + C=C str.	524		
1290		CH[a] in plane bending of benzene ring	486	519	CO_2 rocking + C=C def.
1261	1277	C=C str.	432	517	C=C def.
	1231	CH bending + CH_2 wagging	429	412	C=C torsion
1205	1204	CH_2 twisting + COH def.	407	410	M-N str. + CCCN asym. def.
	1174	COH def. + C=C str.	392	397	CCO def. + C-C in plane def.
1171		CH[a] in plane bending of benzene ring	377	367	C=C def. + C-O in plane def.
1151			342	351	CO out of plane def. + CCCN sym. def.
1137					
1097	1085	NH_2 wagging	317	311	CCCN asym. def. + CCO def.
1084				257	C_{10}-C torsion + C_5-C torsion
	1085	C=C str.		248	CCCN asym. def. + M-N str.
1062	1054	C-N str. + NH_2 twisting		228	C_{10}-C_{13} out of plane def. + C=C torsion
	1048	NH_2 twisting			
1021		CH[a] in plane bending of benzene ring		216	O-M str. + CCCN asym. def.
	999	CO_2 scissors + C-CO_2 str.			

a) As the CH groups on the phenolic groups are considered as a single unit, the frequencies corresponding to the stretching and deformation vibrations of those groups will not appear in the calculations.

TABLE 5. OBSERVED AND CALCULATED FREQUENCIES RELATED TO THE METAL-LIGAND BOND (cm^{-1})

	Pd(II)		Cu(II)		Zn(II)		Cd(II)		Ni(II)		Co(II)	
	Obsd	Calcd	Obsd	Calcd	Obsd	Calcd	Obsd	Calcd	Obsd	Calcd	Obsd	Calcd
NH_2 asym. str.	3294	3294		3355	3348	3363	3345	3363	3359	3358	3277	3285
NH_2 sym. str.	3239	3247	3307	3306	3328	3314	3331	3314	3302	3308	3244	3238
OH str.	3159	3159	3255	3256	3267	3267	3283	3283		3209	3159	3159
COO^- asym. str.	1636	1630	1630	1622	1597	1588	1608	1602	1625	1623	1629	1623
NH_2 scissors	1584	1583	1591	1587	1570	1575	1584	1584	1592	1598	1610	1616
COO^- sym. str.	1357	1369	1373	1388	1357	1368	1357	1371	1391	1387	1378	1388
OH in plane def.	1205	1204	1235	1234	1242		1231	1230	1247	1240	1237	1233
NH_2 wagging	1097											
	1084	1085	1085	1088	1081	1074	1077	1078		1033		1047
OH out of plane def.	668	663	650	647	665	664	672	664	650	647	658	664
NH_2 rocking	613	647		642	603	587	599	601	587	582	582	584
COO^- wagging	583	586		574	590	591	572	574	577	574		574
COO^- rocking	486	519	486	522	498	503	496	503	494	521	487	519
MN str.	407	410	393	385	359	357	316	330	317	327	315	325

TABLE 6. VALUES OF FORCE CONSTANTS AND F_{dia} RELATED TO THE METAL-LIGAND BONDS

Force constant (mdyn/Å)	Pd(II)	Cu(II)	Zn(II)	Cd(II)	Ni(II)	Co(II)
K(MN)	0.75	0.52	0.33	0.20	0.14	0.12
K(NH)	5.68	5.90	5.93	5.93	5.91	5.65
$K(C_7\text{-}O_8)$	8.30	8.00	7.90	8.10	8.00	8.00
$K(C_7\text{-}O_9)$	5.60	6.10	5.80	5.80	6.00	6.10
$K(C_{29}\text{-}O_{32})$	2.50	2.50	2.50	2.50	2.50	2.50
K(OH)	5.27	5.62	5.66	5.72	5.45	5.27
H(MNH)	0.15	0.14	0.10	0.11	0.10	0.10
H(HNH)	0.57	0.57	0.55	0.56	0.59	0.60
H(CCO)	0.40	0.45	0.35	0.35	0.50	0.45
$H(CCO_R)$	0.50	0.50	0.35	0.35	0.50	0.50
H(OCO)	0.35	0.35	0.35	0.35	0.35	0.35
$H(C_{13}OH)$	0.30	0.40	0.40	0.40	0.43	0.40
T(COH) mdyn·Å	0.19	0.18	0.19	0.19	0.18	0.19
P(OCO) mdyn·Å	0.50	0.48	0.51	0.48	0.48	0.48
$F_{dia}(NH_2$ asym. str.) mdyn/Å	5.90	6.12	6.15	6.15	6.13	5.87
$F_{dia}(COO^-$ asym. str.) mdyn/Å	7.27	7.37	7.17	7.27	7.32	7.37
F_{dia}(MN str.) mdyn/Å	0.98	0.75	0.56	0.43	0.37	0.35
$F_{dia}(NH_2$ rocking) mdyn·Å	0.41	0.41	0.41	0.41	0.36	0.38
F_{dia}(CO torsion) mdyn·Å	0.19	0.18	0.19	0.19	0.18	0.19

strengths of the forces opposing the corresponding vibrational modes.

The values for the M–N bond-stretching force constants and the values of F_{dia} (M–N str.) vary in the order Pd(II)>Cu(II)>Zn(II)>Cd(II)>Ni(II)>Co(II), which demonstrates a corresponding order in the strengths of the metal-nitrogen bonds.

Similar trends are found for the M–N stretching, the NH_2 wagging, and the NH_2 rocking frequencies.

The frequencies of NH_2 scissors vibrations show a different trend. This may be due to an overlap with the COO^- stretching and C=C stretching vibrations to some extent.

These facts show that the phenolic group in the β-position of DL-tyrosine has no influence on the order of metal ligand bond strengths which has already been found in aliphatic α-amino acid chelates.

References

1) T. J. Lane, J. A. Durkin, and R. J. Hooper, *Spectrochim. Acta*, **20**, 1017 (1964).
2) I. Nakagawa, R. J. Hooper, J. L. Walter, and T. J. Lane, *ibid.*, **21**, 1 (1965).
3) J. F. Jackovitz and J. L. Walter, *ibid.*, **22**, 1393 (1966).
4) J. F. Jackovitz, J. A. Durkin, and J. L. Walter, *ibid.*, **23A**, 67(1967).
5) Y. Inomata, T. Inomata, and T. Moriwaki, This Bulletin, **44**, 365 (1971).
6) Y. Inomata, T. Inomata, T. Moriwaki, and J. L. Walter, *Spectrochim. Acta*, **29A**, 1933 (1973).
7) S. H. Laurie, *Aust. J. Chem.*, **20**, 2609 (1967).
8) K. Nakamoto, "Infrared Spectra of Inorganic and Coordination Compounds," John Wiley & Sons, Inc., New York(1963), p. 201.
9) R. J. Jakobsen, *Write Air Development Division Technical Report*, pp. 60—402.
10) These calculations are performed at Computer Centre, The University of Tokyo.
11) B. K. Vainshtein and G. V. Gurskaya, *Soviet Physics-Doklady*, **9**, 335 (1964) translated from *Doklady Akad. Nauk SSSR*, **156**, No. 2, 312 (1964).
12) C. Scheringer, O. J. Wehrhahn, and M. v. Stackelberg, *Z. Electrochem.*, **64**, 381 (1960).
13) Y. Morino and M. Tsuboi, "Gendai Butsurikagaku Koza" Vol. 3, "Bunshi no Kozo" p. 151, Tokyo Kagaku Dojin, Tokyo (1966).
14) P. Venkateswarlu and W. Gordy, *J. Chem. Phys.*, **23**, 1200 (1955).
15) T. Shimanouchi, "Computer Programs for Normal Coordinate Treatment of Polyatomic Molecules," The University of Tokyo, Tokyo (1968).

Crystal and Molecular Structure of (−)-*erythro*-1′-(2,5-Dimethoxyphenyl)-3′-diethylaminobutyl Acetate Hydrobromide[1]

Yoshihiro MASUDA, Yoichi IITAKA and Hiroaki HAMANO*

Faculty of Pharmaceutical Sciences, University of Tokyo, Hongo, Tokyo 113

**Research Laboratory, Pharmaceutical Division, Nippon Kayaku Co., Ltd., Kita-ku, Tokyo 115*

(Received September 21, 1973)

In order to determine the stereospecificity and absolute configuration of 1′-(2,5-dimethoxyphenyl)-3′-diethylamino-*n*-butanol, X-ray structure analysis of its acetate hydrobromide has been carried out. The crystal of the derivative belongs to the monoclinic space group C2, with lattice constants $a=14.21_8$, $b=8.29_0$, $c=18.18_7$Å, $\beta=108.1°$, containing four formula units of $C_{18}H_{29}O_4N\cdot HBr$ in a unit cell. The structure was solved by the heavy atom method and refined by the block-matrix least squares method to an R value of 0.06. The absolute configuration was determined by the use of the anomalous dispersion method, the configuration at the two asymmetric carbon atoms being found to be *S*.

In the course of a study on antitussives, it was found that 1′-(2,5-dimethoxyphenyl)-3′-diethylamino-*n*-butanol (I) strongly potentiates the antitussive activity of codein.[2] However, this compound has four stereoisomers and it seemed to be of importance to compare their pharmacological activities. One of us (H. H.) attempted to synthesize each isomer stereoselectively and obtained two diastereomers I_a and I_b.[3] The diastereomer, I_a, was then acetylated, being resolved by using *d*-camphorsulfonic acid. Their infrared spectra showed that the hydroxyl group forms an intramolecular hydrogen bonding to the diethylamino nitrogen. The nuclear magnetic resonance spectrum of I_a, on the other hand, showed a nuclear Overhauser effect between the protons H_a and H_d. Thus the relative configuration of I_b was presumed to be *erythro* type and that of I_b *threo* type.

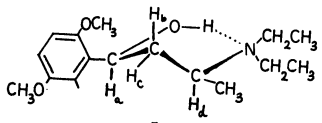

Ia

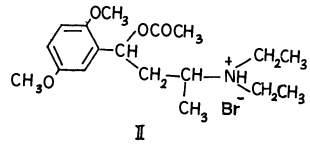

II

An X-ray analysis was undertaken to establish the absolute configuration of I_a. The crystal of its levorotatory acetate hydrobromide(II) was used for the analysis.

Experimental

(−)-*erythro*-1′-(2,5-Dimethoxyphenyl)-3′-diethylamino-*n*-butyl acetate hydrobromide (II) was prepared as follows. To a solution of I_a-acetate (100 mg) in absolute ether (10 ml) was added dropwise a 2% solution of HBr in absolute ether (10 ml) at −60°. Ether was evaporated *in vacuo* to obtain a crystal (110 mg). The cyrstal was recrystallized from absolute ether–methanol mixture under exclusion of moisture. Colorless thin plates parallel to (001); mp 147—148 °C, IR (KBr) 1745, 1505, 1230, 1210, 1045 cm^{-1}. $[\alpha]_D^{20}$ −82.5° (*c* 0.627, EtOH). ORD (*c* 4.8×10^{-4}, MeOH) $[\phi]_{400}$ −116°, $[\phi]_{350}$ −168°, $[\phi]_{300}$ −402°, $[\phi]_{250}$ −2940°, $[\phi]_{233}$ −8800° (trough). Found: C, 53.16; H, 7.38; N, 3.34%. Calcd for $C_{18}H_{30}O_4NBr$: C, 53.46; H, 7.48; N, 3.46%.

The Laue symmetry and systematic extinction on the precession photographs taken with Zr-filtered Mo radiation indicated that the space group is C2 or Cm or C2/m. The density of the crystal (1.32 g cm^{-3}) measured by the flotation method is in good agreement with the calculated value of 1.317 g cm^{-3} assuming four formula units in a unit cell. The space group was taken to be C2 considering the asymmetry of the molecule.

Crystal Data. (−)-*erythro*-1′-(2,5-Dimethoxyphenyl)-3′-diethylaminobutyl acetate hydrobromide, $C_{18}H_{29}O_4N\cdot HBr$, mol wt 404.35. Monoclinic, $a=14.218\pm0.008$, $b=8.290\pm0.005$, $c=18.187\pm0.010$ Å, $\beta=108.1\pm0.1°$, $Z=4$, $D_m=1.32$ g cm^{-3}, $D_x=1.317$ g cm^3, Space group: C2.

The lattice constants and intensity data were obtained by using a four-circle X-ray differentometer with Zr-filtered Mo$K\alpha$ radiation. Intensities were measured by the θ–2θ scanning method with a scan speed of $2\theta=4°$/min. The backgrounds were counted on both sides of each diffraction peak for 10 sec. Out of about 3310 possible hkl and $\bar{h}kl$ reflections having a 2θ value less than 60°, 1647 structure factors were evaluated as being observed since they have net intensities greater than three times their estimated standard deviations.

Determination and Refinement of the Structure

The crystal structure was determined by the heavy atom method. The two methoxy groups attached to the benzene ring have large temperature factors and it was hard to find their exact positions on the Fourier map. One of the terminal methyl groups, C(14) of the methoxy group at C(9), could not be found and the atom was excluded from the present analysis. Refinement of the atomic parameters was carried out by the block-matrix least-squares method using the HBLS program.[4] Several cycles of calculations with anisotropic temperature factors for non-hydrogen atoms reduced the R value to 0.063 for 1647 observed structure factors. The weighting scheme used was:

$$w = 1 \text{ when } F_o > 2.5$$

$$w = 0 \text{ when } F_o \leq 2.5 \ .$$

The final atomic parameters are listed in Table 1 with their estimated standard deviations. A comparison of the observed and calculated structure factors is given in Table 2†. The final difference Fourier map showed only a trace of the peak which might be as-

† Table 2 has been deposited at the office of the Chemical Society of Japan (Document No. 7406).

Table 1. Atomic parameters and their estimated standard deviations

Temperature factors are of the form: $T=\exp\{-(\beta_{11}h^2+\beta_{22}k^2+\beta_{33}l^2+2\beta_{12}hk+2\beta_{13}hl+2\beta_{23}kl)\}$. To represent the absolute configuration, x, y and z should be referred to the left-handed coordinate system.

	x	y	z	β_{11}	β_{22}	β_{33}	β_{12}	β_{13}	β_{23}
Br	0.6862(1)	0.5000(0)	1.0738(1)	0.0052(0)	0.0164(1)	0.0034(0)	-0.0000(2)	0.0012(0)	-0.0004(1)
O(1)	0.3423(5)	0.4281(10)	0.7279(5)	0.0051(4)	0.0191(14)	0.0049(3)	0.0017(6)	0.0013(3)	-0.0001(5)
O(2)	0.2213(7)	0.2465(14)	0.7196(6)	0.0072(6)	0.0337(25)	0.0079(5)	-0.0047(10)	0.0032(5)	-0.0049(10)
O(3)	0.4191(8)	-0.0148(26)	0.6926(6)	0.0110(7)	0.0304(24)	0.0070(4)	0.0024(21)	0.0002(4)	-0.0024(17)
O(4)	0.3560(9)	0.4032(26)	0.4544(6)	0.0108(8)	0.1014(73)	0.0046(4)	0.0025(19)	0.0016(5)	0.0096(14)
N	0.6264(4)	0.4968(19)	0.8853(4)	0.0034(3)	0.0108(10)	0.0040(3)	-0.0000(13)	0.0013(22)	-0.0014(11)
C(1)	0.4084(7)	0.2935(14)	0.7287(6)	0.0049(6)	0.0150(18)	0.0034(4)	-0.0006(8)	0.0008(4)	-0.0025(7)
C(2)	0.5138(6)	0.3580(13)	0.7679(6)	0.0036(5)	0.0128(16)	0.0039(8)	-0.0005(8)	0.0009(3)	-0.0011(7)
C(3)	0.5329(6)	0.3874(12)	0.8524(5)	0.0036(4)	0.0122(15)	0.0032(3)	-0.0009(7)	0.0007(3)	0.0002(6)
C(4)	0.5474(9)	0.2312(15)	0.8979(8)	0.0057(7)	0.0163(21)	0.0062(6)	-0.0014(10)	0.0018(5)	0.0010(9)
C(5)	0.2461(8)	0.3800(17)	0.7219(7)	0.0056(6)	0.0242(25)	0.0041(4)	0.0012(11)	0.0019(4)	-0.0010(9)
C(6)	0.1848(9)	0.5316(25)	0.7237(8)	0.0070(7)	0.0294(50)	0.0053(5)	0.0048(16)	0.0016(5)	-0.0007(12)
C(7)	0.3953(8)	0.2454(17)	0.6446(7)	0.0052(6)	0.0215(24)	0.0045(5)	0.0005(11)	0.0018(4)	-0.0016(9)
C(8)	0.3787(9)	0.3501(21)	0.5857(6)	0.0066(7)	0.0344(34)	0.0031(4)	0.0015(14)	0.0012(4)	0.0010(10)
C(9)	0.3717(12)	0.3006(30)	0.5122(8)	0.0090(10)	0.0525(55)	0.0043(6)	0.0056(21)	0.0007(6)	0.0016(15)
C(10)	0.3774(11)	0.1292(34)	0.5008(10)	0.0072(9)	0.0700(75)	0.0060(7)	0.0049(24)	0.0008(7)	-0.0053(21)
C(11)	0.3945(11)	0.0291(32)	0.5570(8)	0.0096(10)	0.0387(59)	0.0057(6)	0.0053(22)	0.0000(6)	-0.0064(18)
C(12)	0.4025(9)	0.0732(21)	0.6297(9)	0.0055(7)	0.0327(37)	0.0067(6)	0.0002(13)	0.0007(5)	-0.0085(12)
C(13)	0.4066(15)	-0.1911(26)	0.6718(14)	0.0126(15)	0.0231(39)	0.0142(14)	0.0017(21)	-0.0025(12)	-0.0058(21)
C(15)	0.7140(7)	0.4230(14)	0.8646(7)	0.0034(5)	0.0177(18)	0.0048(4)	0.0007(8)	0.0014(4)	-0.0025(8)
C(16)	0.8110(7)	0.5060(40)	0.9154(7)	0.0038(4)	0.0217(23)	0.0067(5)	-0.0014(17)	0.0015(4)	-0.0024(18)
C(17)	0.6113(8)	0.6707(14)	0.8624(7)	0.0056(6)	0.0126(18)	0.0050(5)	0.0002(9)	0.0018(4)	0.0001(8)
C(18)	0.5349(8)	0.7479(13)	0.8959(7)	0.0069(7)	0.0093(15)	0.0064(6)	0.0016(9)	0.0033(5)	0.0000(8)

sociated with C(14), but it was almost impossible to locate the atom.

Determination of the Absolute Configuration

The absolute configuration was determined by use of the anomalous dispersion method. The dispersion corrections for the atomic scattering factors of bromine for Mo$K\alpha$ radiation were taken to be $\Delta f'=-0.3$, $\Delta f''=2.5$.[5] The calculated values of intensity ratio between the Friedel pair of reflections agreed with those observed on the $hk0$, $hk1$ and $0kl$ precession photographs if one takes the left-handed coordinate system. A comparison of observed and calculated intensity ratios is given in Table 3. The Figures in this paper are drawn with the correct absolute configuration.

Table 3. Comparison of calculated and observed intensity ratios of Friedel pair reflections

$h\ k\ l$	$I(hkl)/I(h\bar{k}l)$ Calcd	$I(hkl)/I(h\bar{k}\bar{l})$ Obsd
0 2 0	0.88	<1
1 1 0	0.91	<1
3 1 0	0.94	<1
7 1 0	1.23	>1
8 2 0	1.07	>1
1 3 0	0.77	<1
3 3 0	0.87	<1
5 3 0	0.84	<1
3 1 1	1.80	>1
$\bar{5}$ 1 1	0.61	<1
6 2 1	0.58	<1
$\bar{2}$ 2 1	1.06	>1
5 3 1	0.79	<1
$\bar{5}$ 3 1	1.20	>1
0 2 2	1.12	>1
0 2 4	1.21	>1
0 2 6	0.92	<1
0 4 1	0.89	<1

Discussion of the Structure

Figure 1 shows a stereoscopic view of the molecule drawn by the plotter program ORTEP.[6] We see

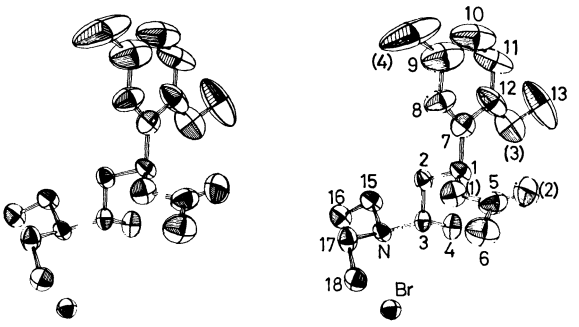

Fig. 1. Stereoscopic view of the molecule.
The ellipsoid covers the area in which the center of the atom is found with a probability 50%. The numbers in parentheses indicate those of oxygen atoms.

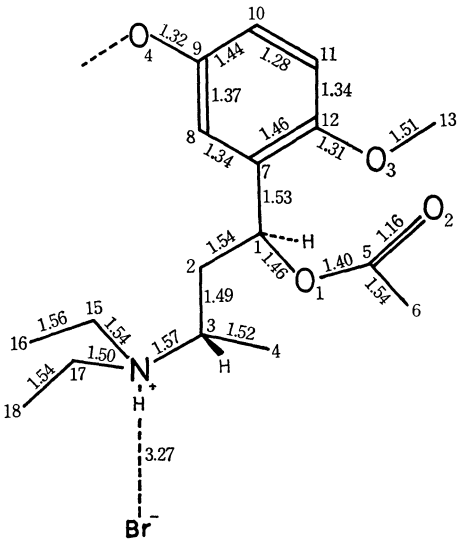

Fig. 2. Bond lengths (Å).

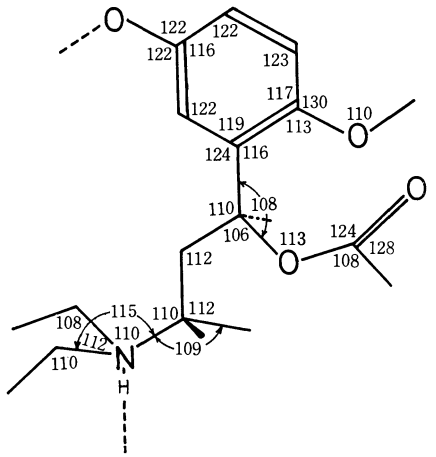

Fig. 3. Bond angles (°).

Table 4. Deviations of atoms from the least-squares plane

Benzene ring			
C(7)	0.00 Å	C(1)[a]	0.04 Å
C(8)	−0.01	O(3)[a]	0.01
C(9)	0.02	C(13)[a]	−0.26
C(10)	−0.02	O(4)[a]	0.01
C(11)	0.01		
C(12)	0.00		
Acetyl group			
O(1)	0.00 Å	C(1)[a]	0.02 Å
C(5)	−0.02		
O(2)	0.01		
C(6)	0.01		

a) Not included in the least-squares calculation.

Table 5. Internal rotation angles

A-B-C-D	τ
O(1)-C(1)-C(2)-C(3)	−70°
C(1)-C(2)-C(3)-C(4)	−74
C(1)-C(2)-C(3)-N	−164
C(2)-C(3)-N-C(15)	53
C(2)-C(3)-N-C(17)	−74
O(1)-C(1)-C(7)-C(8)	−36
C(11)-C(12)-O(3)-C(13)	13

The torsion angle τ of the bonded group A-B-C-D is defined as the angle between planes A-B-C and B-C-D. It is positive if clockwise and negative if anticlockwise from the near atom A to the further D.

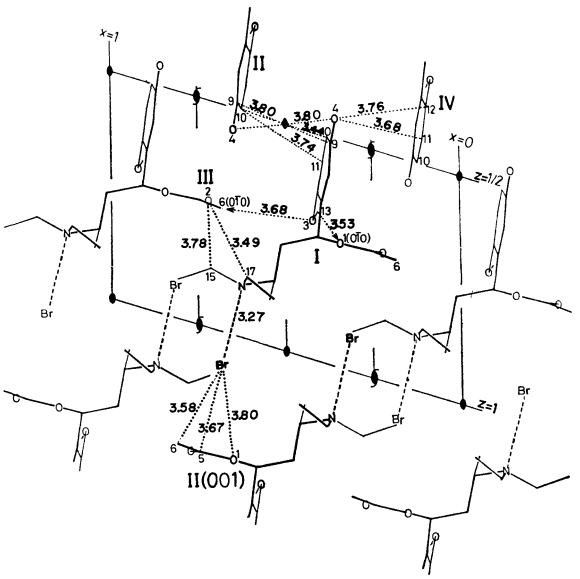

Fig. 4. Projection of crystal structure along the b axis. Intermolecular short contacts of atoms less than 3.8 Å are shown by dotted lines. The positions of the molecules are: I at x, y, z; II at $1-x$, y, $1-z$; III at $1/2+x$, $1/2+y$, z; IV at $1/2-x$, $1/2+y$, $1-z$, where x, y and z are given in Table 1. Translations are shown in parentheses, thus, II (001) be at $1-x$, y, $2-z$.

that the absolute configurations at C(1) and C(3) are both *S* configuration. The bond lengths and angles are shown in Figs. 2 and 3, respectively. The standard deviations of the values for light atoms are about 0.01—0.02 Å and 1°, respectively, except for those involving C(9), C(13), O(3) and O(4) atoms for which they are about 0.04 Å and 2°. The large values for these atoms are due to the extremely large anisotropic thermal vibrations. No abnormal lengths and angles are found in the structure. The diethylamino nitrogen is protonated and takes a tetrahedral configuration. The bromide anion is 3.27 Å apart from the nitrogen atom and a hydrogen bond is formed between them. The planarities of the benzene ring and acetyl group are shown in Table 4.

The skeleton of the butyl acetate group, C(6), C(5), O(1), C(1), C(2), C(3), and C(4), is strongly folded at C(2) and C(3). The C(6), C(5), O(1) and C(1) atoms are extended in a *trans* planar form while the C(4) atom is folded back and closer to C(1) at 3.12 Å, the internal rotation angles about the C(1)–C(2), C(2)–C(3) bonds being −70° and −74°, respectively. The reason for the *gauche* conformation about the C(2)–C(3) bond is to make the nitrogen atom *trans* with respect to C(1) and to locate the charged diethylamino group far from the acetyl group. As for the rotation about the C(1)–C(2) bond, it is easy to see that if it were a *trans* conformation, either the methyl group $C(4)H_3$ or the diethylamino group would be too close to the phenyl group. Some internal rotation angles to be noted are listed in Table 5.

The projection of the crystal structure along the b axis is shown in Fig. 4, together with short intermolecular distances less then 3.8 Å. The diethylamino nitrogen atom is protonated and forms a hydrogen bond to the bromide ion. There are many van der Waals contacts among molecules I, III and their translation equivalents along the a and b axes. The bromide ion also interacts with the acetyl group of the neighboring molecule mainly through van der Waals forces. The methoxyphenyl groups are stacked in **a** direction and several close contacts are found between them.

The authors would like to express their sincere thanks to Mr. W. Tanaka, Manager of the Research Laboratory, Nippon Kayaku Co., Ltd., for permission to publish the present work, and also to Professors Y. Kasuya and S. Okuda of the University of Tokyo for their valuable discussions.

References

1) Presented at the 92nd Annual Meeting of the Pharmaceutical Society of Japan, Osaka, April 4, 1972.
2) Presented at the 87th Annual Meeting of the Pharmaceutical Society of Japan, Kyoto, April 6, 1967.
3) H. Hamano and S. Okuda, *Chem. Pharm. Bull.* (Tokyo), in press.
4) T. Ashida, HBLS IV, The Universal Crystallographic Computing System (I), The Crystallographic Society of Japan (1967), p. 65.
5) C. H. Dauben and D. H. Templeton, *Acta Crystallogr.*, **8**, 841 (1955).
6) C. K. Johnson, ORTEP, A Fortran Thermal Ellipsoids Plot Program for Crystal Structure Illustration, Report ORNL-3794, Oak Ridge National Laboratory, Oak Ridge, Tennessee (1965).

Novel Radical Salt Polymers as Hydrogenation Catalyst of α-Olefins

Hiroshi KAWAZURA,* Yoshiro YAMAMOTO, Toshio OHMORI, Kentaro MURANO,** and Hiroo INOKUCHI**

Research Laboratory, Japan Synthetic Rubber Co., Ltd., 7569 Ikuta, Tama, Kawasaki 214

***The Institute for Solid State Physics, The University of Tokyo, Roppongi, Tokyo 106*

(Received October 4, 1973)

Novel polymeric radical salts prepared by inserting alkali-metals into semi-conductive polymers derived from poly(tetrahalophenylene sulfides) were found to be effective hydrogenation catalyst for α-olefins; their activity trends as to the sort of alkali-metal and halogen of the matrix polymer were Cs>K>Na and F>Cl>Br respectively. The catalyst also showed an activity for the *cis-trans* isomerization of hex-2-ene which was proportional to that for the hydrogenation. The activities of the catalyst were discussed in terms of its steric confinement.

The enhanced *para-ortho* hydrogen conversion catalysis[1] found for polymeric radical salts prepared by alkali-metal insertion into poly(tetrahalophenylene sulfides) and the semi-conductive polymers derived therefrom[2] prompted us to examine their catalytic activity for the hydrogenation of unsaturated compounds. Along these lines, we investigated the hydrogenation activity of these novel polymeric radical salts for some olefins referring to their *para-ortho* hydrogen conversion activity. We will report here that the present radical salts, despite a lack of metal with a d-electron shell, are effective hydrogenation catalysts for α-olefins.

Experimental

Hydrogenation was carried out at 140 °C for 3 hr in an autoclave (volume, 100 ml) containing 4 ml of olefin, 0.5 g of the radical salt, and hydrogen pressurized up to 35 kg/cm² unless otherwise noted. The reaction products were identified with authentic samples and were quantitatively determined by using gas-liquid partition chromatography (DMS 30 wt%, 6 m).

Commercial reagents, hex-1-ene, hex-2-ene, 4-methylpent-1-ene, 4-methylpent-2-ene, and cyclohexene were purified by distillation over metallic sodium. Propylene, but-1-ene, and *cis*-but-2-ene in commercial cylinders were simply dried over calcium hydride. All the olefins were confirmed before use to contain no appreciable amount of any impurity detected by the glc.

The radical-salt complexes were prepared by bringing poly(tetrahalophenyl sulfides) or semi-conductive polymers (*vide infra*) into contact with alkali-metal vapor in a vacuum at the evaporation temperature of alkali-metals up to their saturated insertion into the polymers. The amounts of the inserted alkalimetals were determined by means of atomic-absorption spectroscopy.

We utilized poly(tetrahalophenylene sulfides) prepared by careful polycondensation of sodium pentahalothiophenoxide, and semi-conductive polymers prepared by a dehalogenation condensation of poly(tetrahalophenylene sulfides), as described previously.[2] In this investigation we also used new semi-conductive polymers which were obtained by treating the radical salt complexes with water in a Soxhlet extractor for an extended period until no trace of alkali-metal was detected in the extract. Some characteristics of those modified semi-conductive polymers are given in Table 1, together with those of the poly(tetrahalophenylene sulfides) and semi-conductive polymers previously prepared.

TABLE 1. CHARACTERISTICS OF ACCEPTOR POLYMERS

Acceptor polymers[a)]	Elemental Analysis, %					Free spins per g
	C	H	N	X	S	
PTF	40.2	0	0	—	19.0	nil
PTCl	29.3	0	0	57.4	12.8	nil
PTBr	18.9	0	0	73.0	8.0	nil
SMF	44.8	0.7	2.9	—	18.0	1.2×10^{16}
SMCl	40.8	1.2	3.1	38.9	12.5	4.2×10^{18}
SMBr	26.6	0.5	1.8	61.0	8.5	1.2×10^{18}
mSMF	60.3	1.8	5.4	—	11.2	1.8×10^{19}
mSMCl	76.0	2.9	9.0	1.9	2.7	8.1×10^{18}
mSMBr	62.5	2.8	7.7	2.9	10.5	4.0×10^{18}

a) PTX (X : F, Cl, Br), SMX (X : F, Cl, Br) and mSMX (X : F, Cl, Br) are abbreviations for the poly(tetrahalophenylene sulfides), the semi-conductive polymers, and the modified semi-conductive polymers, respectively, mentioned in the text. mSMX(X : F, Cl, Br) were prepared from SMX-Cs(X : F, Cl, Br) radical salts (see Table 3)

The free spin concentrations of the acceptor polymers and the radical-salt complexes were determined by means of their ESR spectra measured at 9000 MHz in 100 kHz modulation, in comparison with the DPPH spectra obtained under the same operating conditions as with the polymers and the complexes.

Results and Discussion

Table 2 shows the results of the hydrogenation of some olefins in the presence of the semi-conductive polymer alkali-metal complexes as catalyst. It can be seen that the present catalyst hydrogenates α-olefins fairly well, but not inner olefins and cyclic olefins. This may be interpreted as a consequence of the severe steric requirements of the present catalyst, which controls an effective interaction with olefins on the surface of the catalyst.

Thus, the study was focused on the hydrogenation activity of the polymeric radical salt for α-olefin, *i.e.*, hex-1-ene. The results of the hydrogenation of hex-1-ene in the presence of the poly(tetrahalophenylene sulfide)–Cs complex and the semi-conductive polymer–Cs complex are given in Table 3. The hydrogenation

* Present Address: Faculty of Pharmaceutical Sciences, Josai University, 1076 Tawame, Sakado, Saitama 350-02.

TABLE 2. HYDROGENATION OF OLEFINS WITH THE RADICAL SALT POLYMERS

Olefins	Radical salts	Conversion, %	Selectivity, %
Propylene[a)]	SMBr-K	90	100
But-1-ene[a)]	SMBr-K	99	60
cis-But-2-ene[a)]	SMF-K	—	0
Hex-1-ene	SMCl-Cs	50	24
Hex-2-ene	SMCl-Cs	—	0
4-Methylpent-1-ene	SMCl-Cs	31	40
4-Methylpent-2-ene	SMCl-Cs	—	0
Cyclohexene	SMCl-Cs	0	0

a) Olefin 200 mmHg and H_2 300 mmHg were introduced into a 300 ml volume reactor containing SMX (X : F, Br) 0.2 g and distilled potassium 0.3 g, the hydrogenation being carried out at 100°C for 2.5 hr.

selectivity was low because of the concurrent isomerization of hex-1-ene to hex-2-ene; however, the activity of the present catalyst can be fully appreciated when one considers that no hydrogenation of hex-1-ene occurred in the presence of alkali-metal alone under the same reaction conditions. Further, the present catalysts incorporating the halogen were more effective on the hex-1-ene conversion, and hence on the hexane yield, than the poly(phenylene sulfide)–Cs complex (abbreviated as PPS–Cs), which contained no halogen, although the *para-ortho* hydrogen conversion activity of the PPS–Cs, as is shown in Table 3, was not inferior to that of the present catalysts. Here, it should be noted that the *cis/trans* isomer ratios of the hex-2-ene isomerized from hex-1-ene were larger than the thermodynamic equilibrium ratio about 0.43.† This suggests a correlation between the hydrogenation and the *cis-trans* isomerization activity of the catalyst, as will be discussed below in conjunction with a later experiment.

In spite of the characteristics detailed above, the rather poor activity of the hydrogenation, together with the obscure activity trend as to the sort of halogen, forced us to prepare the catalyst more elaborately. The poor activity was considered to be due to a partial destruction of the radical-salt structure of the catalyst, followed by the formation of alkali-metal halide. The catalysts were, therefore, treated with water (see Experimental) to remove the alkali-metal halide, thus giving newly modified semi-conductive polymers from which we could again prepare radical salts of alkali-metals.

The results of the hydrogenation of hex-1-ene in the presence of these modified radical salt polymers are given in Table 4. It can be seen that there is a clear trend for the activities of the catalysts as to sort of halogen and also as to sort of alkali-metal, together with enhanced hydrogenation activity as was collated by their extraordinarily high *para-ortho* hydrogen conversion rate constant.

This activity trend, increasing towards the catalyst with less electronegative alkali-metals, has frequently been observed in radical salts previously studied.[4,5] It should be interpreted on the basis of the nature of alkali-metals, *viz.*, the ionization potential, the electron affinity, the ion radius, and finally the structure of the catalysts in which alkali-metals are located.

The activity trend for this sort of halogen—*viz.*, the larger the electronegativity of halogen, the stronger the hydrogenation activity—is the first experimental evidence, as far as we are aware, as to radical salts containing halogen; however, the extremely low halogen content of the catalyst (see Table 1) compels us to postpone a discussion of the role of the halogen until a structural elucidation of the catalyst has been made.

TABLE 3. HYDROGENATION OF HEX-1-ENE WITH THE RADICAL SALT POLYMER

Radical salts	Cs inserted wt%	Conversion, %	Selectivity, %	Hex-2-ene isomer ratio, *cis/trans*	*Para-ortho* conversion rate const. at 20 °C min^{-1}
PTF-Cs	57.2	73.2	14.4	0.56	1.9×10^{-1}
PTCl-Cs	68.8	79.6	27.3	0.82	3.7×10^{-1}
PTBr-Cs	70.2	40.5	23.3	0.47	1.2×10^{-1}
SMF-Cs	70.0	32.6	16.6	0.62	1.2×10^{0}
SMCl-Cs	77.6	49.7	23.9	0.52	2.3×10^{-1}
SMBr-Cs	79.5	53.0	61.3	1.4	2.0×10^{-1}
PPS-Cs	—	17.2	20.3	—	3.0×10^{-1}

TABLE 4. HYDROGENATION OF HEX-1-ENE WITH THE MODIFIED RADICAL SALT POLYMER

Radical salts	Alkali-metal wt%	Conversion, %	Selectivity, %	Hex-2-ene isomer ratio, *cis/trans*	*Para-ortho* conversion rate const. at 20 °C, min^{-1}
mSMF-Cs	62.2	100	90.5	3.8	2.5×10^{0}
mSMF-K	60.7	90.0	80.3	3.1	—
mSMF-Na	62.3	78.6	67.0	1.8	—
mSMCl-Cs	76.9	99.6	83.7	2.8	1.8×10^{0}
mSMBr-Cs	71.4	85.4	24.0	1.7	2.5×10^{-1}

† This value was obtained in the glc analysis of commercial hex-2-ene.

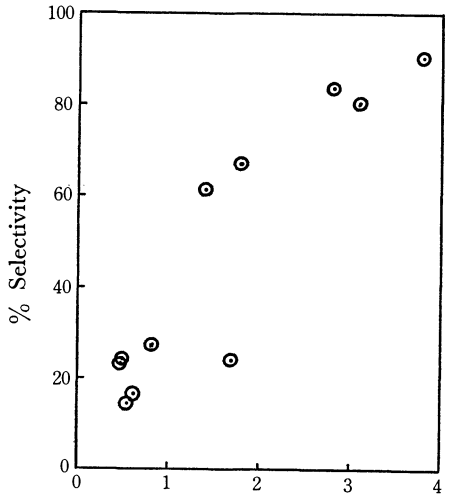

Fig. 1. A correlation between the selectivity in the hydrogenation of hex-1-ene and the *cis/trans* isomer ratio of hex-2-ene.

Also notable was a prominent elevation of the *cis/trans* isomer ratio of the hex-2-ene isomerized from hex-1-ene, as may also be seen from Table 4. The relation between the hydrogenation selectivity of hex-1-ene and the *cis/trans* isomer ratio of hex-2-ene, by using the values in Tables 3 and 4 is shown in Fig. 1. In the present catalyst the hydrogenation activity for hex-1-ene is nearly proportional to the *cis-trans* isomerization activity for hex-2-ene. This result confirms the correlation between the hydrogenation and the *cis-trans* isomerization activity of the catalyst. The linear relation and the high *cis-trans* isomer ratio at high selectivity imply that the active site for the hydrogenation is also active for the *cis-trans* isomerization. The steric requirement of olefins for the hydrogenation and the activity for the *cis-trans* isomerization process lead us to suspect that the active site of the catalyst consists of a sterically-confined structure.

Thus, attention should again be directed to the structural characteristics of the catalysts, especially those of the acceptor polymers prepared through the extraction; however, because of the scarcity of appropriate analytical methods, only their element compositions and free spin concentrations have been collected (Table 1). As was noted in a previous paper,[2] the semi-conductive polymers tightly bind the pyridine used in the preparation. Although the bound pyridine remained, giving rise to its enriched presence in the extracted polymers (Table 1), it could not execute a dramatic enhancement in the hydrogenation activity since no activity difference was observed between the radical salts from poly(tetrahalophenylene sulfides) and those from the semiconductive polymers. One rather troublesome thing for the enhancement might be the role of oxygen, which mainly filled†† the residual composition, amounting to about 10%, of the extracted polymers, besides the role of the halogens, as has already been noted. In addition, it may be useful to note that the extracted polymers have no hydrogen bound by any such reaction as an ion exchange of alkali-metals in the radical salt polymer with the water, since the binding of alkali-metals in the radical salt was considered to be a loose one which lead to such reaction as hydrogen evolution.

In any case, however, the increase in the free-spin concentrations of the extracted polymers from that of the original polymer might lead to some inferences, such as that the extracted polymers came to have largely developed conjugated networks favorable for the accommodation of large amounts of free spins, thus increasing the sterically-confined active sites for the hydrogenation.

Eventually, the low content of halogen and the large amount of free spins in the extracted polymer may be a consequence of the acceptor polymer acquiring a structure functionable for the present catalysis at high densities.

References

1) K. Murano, H. Kawazura, H. Inokuchi, and T. Ohmori, This Bulletin, **45**, 3230 (1972).
2) H. Kawazura and T. Taketomi, *Polymer Lett., Ser. B*, **10**, 265 (1972).
3) H. Inokuchi, N. Wakayama, T. Kondow, and Y. Mori, *J. Chem. Phys.*, **46**, 837 (1967).
4) N. Wakayama and H. Inokuchi, *J. Catal.*, **15**, 417 (1969).
5) Y. Mori, N. Wakayama, and H. Inokuchi, *ibid.*, **14**, 1 (1969).

†† Among the extracted polymers, mSMCl and mSMBr gave 6.3% and 9.6% oxygen respectively (see Table 1).

The Crystal Structure of 2,4,6-Triphenylpyrylium-1,1,3,3-tetracyanopropenide, $[(C_{23}H_{17}O)^+ \cdot (C_7HN_4)^-]$[1]

Toshiaki TAMAMURA, Takashi YAMANE*,[2], Noritake YASUOKA and Nobutami KASAI[3]

Department of Applied Chemistry, Faculty of Engineering, Osaka University, Yamadakami, Suita, Osaka 565

**Institute for Protein Research, Osaka University, Yamadakami, Suita, Osaka 565*

(Received October 4, 1973)

The crystal structure of an organic charge transfer salt 2,4,6-triphenylpyrylium-1,1,3,3-tetracyanopropenide has been determined by means of X-ray diffraction. The crystals are monoclinic in the space group $P2_1/a$. The unit cell dimensions are: $a=13.024$, $b=21.357$, $c=8.324$ Å, $\beta=94.56°$. The cation and the anion are nearly planar and form an "ion-pair." The crystal is built up from infinite columns stacked by these ion-pairs along the c axis. Between two adjacent anions in the neighboring columns, a weak hydrogen bond (C–H···N 3.265 (5), H···N 2.185(4) Å) is present. The charge transfer interaction between the anion and the cation seems to have less influence on the crystal structure than the electrostatic force or the hydrogen bonding.

The charge transfer interaction has been observed spectroscopically in a number of ionic compounds composed of an electron-donating anion and an electron-accepting cation.[4] However, few systematic studies have been made on the physical properties and the crystal structure of these organic charge transfer salts. The effect of interionic charge transfer force on the crystal structure is almost unknown, because of the presence of the strong electrostatic force in addition to the charge transfer and van der Waals interaction between the anion and the cation.

In this paper we describe the crystal structure of an organic charge transfer salt 2,4,6-triphenylpyrylium (TPP)-1,1,3,3-tetracyanopropenide (TCP). A series of structural studies have been made on organic charge transfer salts,[5] as well as on the interionic charge transfer interaction in organic charge transfer salts consisting of a polycyanoacid anion and a heteroaromatic cation.[1,6] The charge transfer absorption of TPP-TCP is observed in non-polar solvents and also in solid state.[7] The study was also promoted by the interesting relationship between the crystal structure and the charge transfer dichroism.

Experimental

Crystal Data. $[(C_{23}H_{17}O)^+ \cdot (C_7NH_4)^-]$, F.W.=450.5, monoclinic, $a=13.024$, $b=21.357$, $c=8.324$ Å, $\beta=94.56°$, $Z=4$, $D_m=1.38$ g·cm^{-3}(CCl_4–C_6H_6), $D_x=1.32$ g·cm^{-3}, space group; $P2_1/a$, absent spectra; $h0l$: $h\neq 2n$, $0k0$: $k\neq 2n$.

Dark red needles of TPP-TCP were recrystallized from a methanol solution.

Oscillation and Weissenberg photographs showed that the crystals belong to the monoclinic system, the space group being $P2_1/a$. Both the determination of cell constants and the collection of intensity data were carried out on a Rigaku four-cycle diffractometer.

The crystal used for the intensity measurement had the dimension $0.32\times0.45\times0.15$ mm. The crystal was mounted on a goniometer-head along the c axis. Nickel-filtered Cu$K\alpha$ radiation was used. The ω-2θ scan technique was applied. The scan range, $\Delta(2\theta)$, of each reflection, was computed by the equation: $\Delta(2\theta)=(2.0°+0.3°\tan\theta_c)$. The starting angle of the scan is $(2\theta_c-1.0)°$, where θ_c is the calculated value of the Bragg angle for λ(Cu$K\alpha_1$) (=1.5405 Å), the scanning speed being 4° min^{-1}. The background was measured at both ends of each scan range. A total of 3394 independent reflections was obtained. No absorption correction was made ($\mu=8.2$ cm^{-1} for Cu$K\alpha_1$).

Structure Determination and Refinement

The phases of the reflections were determined by means of the symbolic addition procedure.[8] SIGMA program was used to compute the normalized structure factor magnitude $|E|$, and to list the Σ_2 relationships for each reflection. Three reflections, 0 3 2, 1 10 6, 11 5 5, were chosen in order to specify the origin, and two other reflections were assigned as phases A and B in order to facilitate the symbolic addition procedure (Table 1). The signs of 108 reflections out of 143 reflections ($|E|\geq2.0$) were determined by hand calculations. TANGENT FORMULA program was then used to calculate the phases of 628

Table 1(a). Distribution of normalized structure factors and statistical averages

	Distribution of $\|E\|$	
	Experimental (%)	Theoretical (centrosymmetric) (%)
$\|E\|\geqq3.0$	0.8	0.5
$\|E\|\geqq2.0$	4.2	5.0
$\|E\|\geqq1.8$	29.0	32.0
$\langle\|E\|\rangle$	0.752	0.798
$\langle\|E\|^2\rangle$	0.996	1.000
$\langle\|E\|^2-1\rangle$	1.027	0.968

Table 1(b). Starting set of application of Σ_2 formula

h	k	l	$\|E\|$	Phase
0	3	2	4.44	+
1	10	6	4.91	+
11	5	5	3.59	+
0	4	2	5.55	A
9	13	$\bar{2}$	4.83	B

Table 1(c). Process of the symbolic addition procedure

Run number	Number of reflections	$\|E\|$	Number of phases determined
0	5		Starting set
1	143	$\geqq2.0$	108 (hand calculations)
2	628	$\geqq1.3$	579

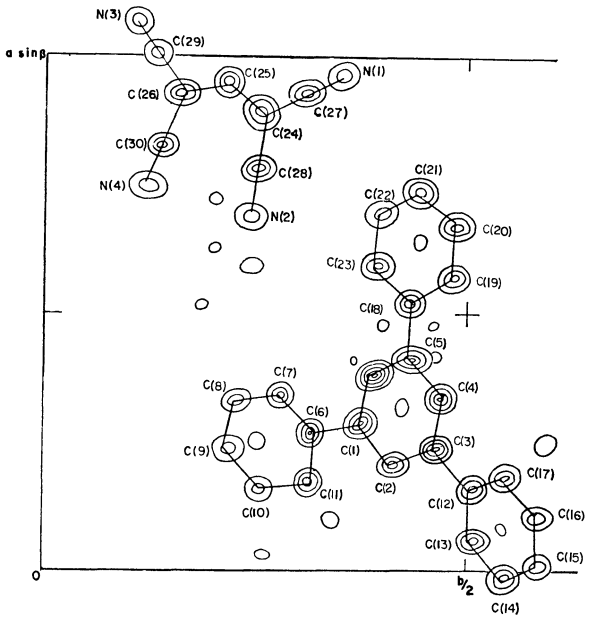

Fig. 1. *E* map viewed along the c axis.

reflections with $|E| \geq 1.3$. From the interaction list the signs of phases A and B were both assigned to be negative.

The positions of all non-hydrogen atoms were found from *E* map (Fig. 1). The oxygen atom in the pyrylium ring was identified by the Fourier synthesis based on these atomic coordinates assuming that all the atoms in the ring are carbon ($B=3.5$ Å^2). This was confirmed by the block-diagonal least-squares refinement using the FBLS program. Four cycles of isotropic refinement reduced the *R* value to 0.150. Three cycles of anisotropic refinement using 2867 reflections ($\sin\theta/\lambda \leq 0.53$) reduced the *R* value to 0.084. The positions of hydrogen atoms were found from the difference Fourier synthesis computed at this stage. Further refinement including hydrogen atoms gave the final *R* value as 0.053 for non-zero reflections (0.058 for all reflections). In the refinement the function minimized was $\sum w(F_o - k|F_c|)^2$, where $w=1.00$ for all reflections. The atomic scattering factors were taken from the values determined by Hanson and his co-workers.[9]

The final positional and anisotropic thermal parameters of non-hydrogen atoms are listed in Tables 2 and 3, respectively, the coordinates and isotropic temperature factors of hydrogen atoms in Table 4, and the observed and calculated structure factors in Table 5.[10]

Results and Discussion

Structure of TPP Cation. The bond lengths and bond angles in the TPP cation are given in Fig. 2(a). The dimensions of the pyrylium ring, which contains 6π electrons as well as benzene and pyridinium rings, have so far not been reported. The pyrylium ring is almost planar with a maximum deviation of 0.015 Å from the best plane (Table 6). The bond angle of oxygen is 122.5(3)° and the two C–O bond lengths

Table 2. Positional parameters of non-hydrogen atoms and their estimated standard deviations (in parentheses)

Atom	*x*	*y*	*z*
O	0.3831(2)	0.3841(1)	0.9618(3)
C(1)	0.2826(3)	0.3723(2)	0.9807(4)
C(2)	0.2089(3)	0.4100(2)	0.9053(4)
C(3)	0.2366(3)	0.4616(2)	0.8153(4)
C(4)	0.3418(2)	0.4718(2)	0.8022(4)
C(5)	0.4139(3)	0.4325(2)	0.8728(4)
C(6)	0.2671(3)	0.3181(2)	1.0825(4)
C(7)	0.3486(3)	0.2785(2)	1.1292(4)
C(8)	0.3331(3)	0.2272(2)	1.2262(5)
C(9)	0.2375(3)	0.2152(2)	1.2788(5)
C(10)	0.1554(3)	0.2548(2)	1.2328(5)
C(11)	0.1694(3)	0.3062(2)	1.1351(5)
C(12)	0.1590(3)	0.5041(2)	0.7371(4)
C(13)	0.0582(3)	0.5052(2)	0.7858(5)
C(14)	−0.0143(3)	0.5453(2)	0.7115(5)
C(15)	0.0105(3)	0.5838(2)	0.5881(5)
C(16)	0.1091(3)	0.5828(2)	0.5387(5)
C(17)	0.1833(3)	0.5437(2)	0.6125(5)
C(18)	0.5257(2)	0.4360(2)	0.8651(4)
C(19)	0.5689(3)	0.4831(2)	0.7782(5)
C(20)	0.6755(3)	0.4859(2)	0.7703(5)
C(21)	0.7376(3)	0.4415(2)	0.8477(5)
C(22)	0.6959(3)	0.3953(2)	0.9359(5)
C(23)	0.5904(3)	0.3921(2)	0.9462(5)
C(24)	0.3866(3)	0.2438(2)	0.7116(4)
C(25)	0.4501(3)	0.2833(2)	0.6323(4)
C(26)	0.4260(3)	0.3355(2)	0.5401(4)
C(27)	0.4289(3)	0.1928(2)	0.8027(5)
C(28)	0.2785(3)	0.2507(2)	0.7078(5)
C(29)	0.5052(3)	0.3679(2)	0.4661(5)
C(30)	0.3261(3)	0.3616(2)	0.5066(5)
N(1)	0.4621(3)	0.1507(2)	0.8756(5)
N(2)	0.1913(3)	0.2563(2)	0.7064(5)
N(3)	0.5670(3)	0.3947(2)	0.4040(5)
N(4)	0.2487(3)	0.3855(2)	0.4769(5)

are both 1.355(4)Å, which are slightly shorter than that for conjugated *O*-heterocyclic, furan (1.371(5) Å).[11] The bond lengths of C(1)–C(2) and C(4)–C(5) are significantly shorter, however, those of C(2)–C(3) and C(3)–C(4) are slightly longer than the value accepted for the benzene ring (1.397 Å).[12]

The three C–C bond lengths connecting the benzene rings with the pyrylium ring (1.456(5), 1.471(5) and 1.461(5)Å) gave value for a single bond between two sp^2 hybridized carbon atoms. The considerably small angles of O–C(1)–C(6) and O–C(5)–C(18), 113.6 (3) and 113.3(3)° might be due to the absence of a hydrogen atom bonded with the oxygen atom. The three benzene rings are planar within experimental error, but tilt from the plane of the pyrylium ring at angles of 10.4, 18.0 and 2.3° for A, B and C rings, respectively. No unusual bond lengths and bond angles were found.

Structure of TCP Anion. The bond lengths and bond angles in the anion are given in Fig. 2(b). The

Table 3. Anisotropic thermal parameters of non-hydrogen atoms ($\times 10^5$) expressed in the form: $\exp\{-(\beta_{11}h^2+\beta_{22}k^2+\beta_{33}l^2+\beta_{12}hk+\beta_{13}hl+\beta_{23}kl)\}$

Atom	β_{11}	β_{22}	β_{33}	β_{12}	β_{13}	β_{23}
O	476	202	1655	12	77	60
C(1)	471	210	1409	−76	160	−179
C(2)	443	200	1461	−20	11	−45
C(3)	472	196	1321	−16	33	−197
C(4)	425	186	1346	29	−18	−76
C(5)	515	182	1308	−63	137	−43
C(6)	510	196	1342	−64	6	−86
C(7)	647	234	1639	14	35	150
C(8)	755	269	2094	28	−51	133
C(9)	866	252	1863	−136	−106	167
C(10)	693	286	2084	−232	139	58
C(11)	564	247	1839	−64	35	129
C(12)	441	189	1477	−1	−70	−170
C(13)	492	260	2118	44	222	22
C(14)	485	275	2689	77	143	−57
C(15)	584	230	2458	80	−363	−133
C(16)	726	265	2058	67	−225	211
C(17)	547	234	1752	2	51	97
C(18)	431	185	1354	5	141	−54
C(19)	555	249	1717	30	219	180
C(20)	585	282	1903	−91	472	100
C(21)	540	287	2080	88	235	161
C(22)	584	274	2403	194	72	162
C(23)	501	242	2076	89	107	183
C(24)	428	213	1610	−1	−9	−147
C(25)	406	221	1573	15	−22	−202
C(26)	394	231	1683	34	122	−117
C(27)	461	239	1796	−69	75	−76
C(28)	397	292	1844	−88	52	−75
C(29)	541	244	2052	104	249	83
C(30)	515	231	1562	16	−37	−89
N(1)	649	283	2548	−30	68	230
N(2)	505	471	2924	−112	120	75
N(3)	723	341	3265	93	837	626
N(4)	602	342	2498	223	−219	−73

Table 4. Atomic coordinates and isotropic temperature factors for hydrogen atoms

Each hydrogen atom bears the same number as that of the carbon atom to which it is attached.

Atom	x	y	z	B (Å^2)
H(3)	0.130	0.400	0.913	1.8
H(5)	0.366	0.510	0.735	1.6
H(7)	0.424	0.287	1.089	1.9
H(8)	0.396	0.196	1.260	2.2
H(9)	0.226	0.176	1.353	1.9
H(10)	0.081	0.145	1.275	2.2
H(13)	0.038	0.475	0.883	1.9
H(14)	−0.090	0.546	0.750	2.0
H(15)	−0.047	0.614	0.531	2.3
H(16)	0.129	0.613	0.440	2.3
H(17)	0.259	0.543	0.573	2.1
H(19)	0.520	0.517	0.715	2.3
H(20)	0.708	0.523	0.703	2.3
H(21)	0.819	0.443	0.840	2.1
H(22)	0.745	0.361	0.997	2.3
H(23)	0.558	0.355	1.016	2.1
H(25)	0.529	0.272	0.644	1.6

The average estimated standard deviations are $\sigma(x)=0.002$, $\sigma(y)=0.001$, and $\sigma(z)=0.003$ and $\sigma(B)=0.6$Å^2.

Table 6. Least-squares planes and deviations of the atoms

Equation of the plane: $AX+BY+CZ=D$, where $X=ax+cz\cdot\cos\beta$, $Y=by$, $Z=cz\cdot\cos\beta$.

(I) Best plane through the TPP cation					
$0.0168X+0.5961Y+0.8027Z=4.7142$					
O	−0.005 Å	C(8)	0.245 Å	C(16)	0.338 Å
C(1)	0.041	C(9)	0.069	C(17)	0.329
C(2)	0.078	C(10)	−0.112	C(18)	−0.060
C(3)	0.013	C(11)	−0.119	C(19)	−0.086
C(4)	−0.052	C(12)	0.010	C(20)	−0.092
C(5)	−0.037	C(13)	−0.306	C(21)	−0.055
C(6)	0.058	C(14)	−0.306	C(22)	−0.040
C(7)	0.234	C(15)	0.018	C(23)	−0.049
(II) Best plane through the pyrylium ring					
$-0.0205X+0.5773Y+0.8163Z=4.3721$					
O	−0.002 Å	C(2)	0.015 Å	C(4)	−0.011 Å
C(1)	−0.012	C(3)	−0.003	C(5)	0.014
(III) Best plane through benzene ring-A					
$0.1608X+0.5625Y+0.8110Z=4.9282$					
C(6)	0.001 Å	C(8)	0.003 Å	C(10)	−0.001 Å
C(7)	−0.003	C(9)	−0.001	C(11)	0.001
(IV) Best plane through benzene ring-B					
$0.2160X+0.7150Y+0.6649Z=6.7314$					
C(12)	−0.000 Å	C(14)	−0.004 Å	C(16)	0.004 Å
C(13)	0.005	C(15)	−0.000	C(17)	−0.004
(V) Best plane through benzene ring-C					
$0.0196X+0.5815Y+0.8138Z=4.6481$					
C(18)	0.006 Å	C(20)	−0.008 Å	C(22)	0.001 Å
C(19)	0.001	C(21)	0.007	C(23)	−0.007
(VI) Best plane through the TCP anion					
$0.0680X+0.5773Y+0.8138Z=8.1201$					
C(24)	−0.001 Å	C(28)	0.036 Å	N(2)	0.053 Å
C(25)	−0.012	C(29)	0.012	N(3)	0.042
C(26)	−0.015	C(30)	−0.024	N(4)	−0.051
C(27)	−0.020	N(1)	−0.020		

TCP anion is also approximately planar, the maximum deviations from the least-squares plane being 0.053 Å (above) for N(2) and −0.051 Å (below) for N(4). However, two C–C(CN)$_2$ groups are planar within 0.0017 Å, and both tilt at an angle of 1.3° from the best plane of the anion. The large bond angle of C(24)–C(25)–C(26), 129.6°, presumably indicates a steric repulsion between the C(CN)$_2$ groups. The conjugated C–C bonds between two sp^2 carbon atoms, C(24)–C(25)=1.388(5) and C(25)–C(26)=1.379(5)Å, are significantly shorter than the C–C bond associated with the CN group, the average value being 1.41 Å. Molecular orbital calculation shows that the bond order is 0.61 for the former and 0.49 for the latter. The result is consistent with the observed bond lengths. The average C≡N bond length, 1.145 Å, is in agreement with that observed in other polycyanoacid anions.[5c,13]

Crystal Structure. The packings of cations and anions in the unit cell viewed along the c and a axes are respectively shown in Figs. 3 and 4. Interionic atomic contacts less than 3.6 Å are given in Table 7.

The crystal structure consists of parallel columns

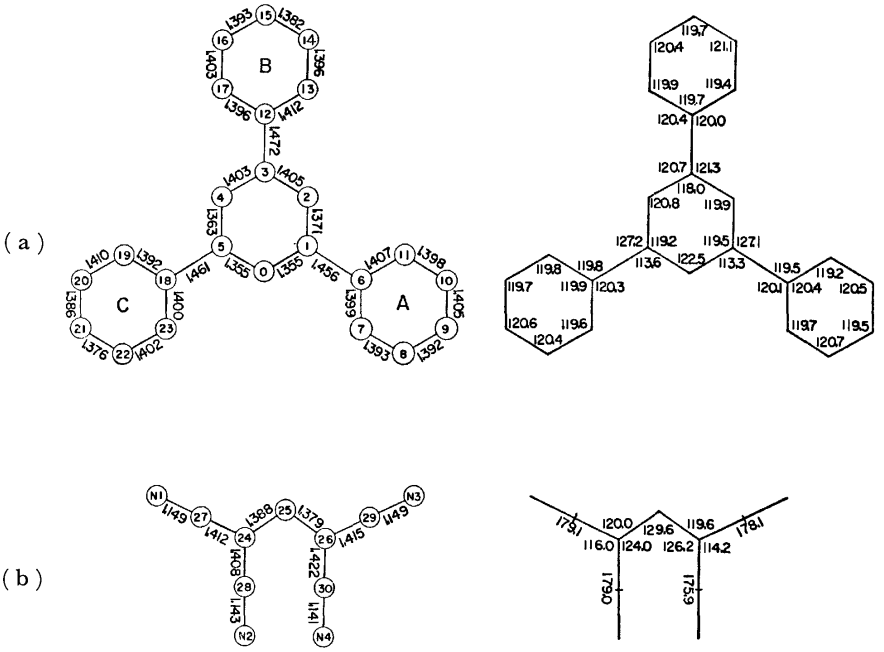

Fig. 2. Bond lengths (Å) and bond angles (°).
The estimated standard deviations are in 0.004—0.006Å for bond lengths and in 0.3—0.4° for bond angles.
(a) TPP cation, (b) TCP anion.

Table 7. Interionic atomic contacts (less than 3.6 Å)

Within an ion-pair.			
C(26)···C(5)	3.472(5) Å	N(2)···C(1)	3.512(5) Å
C(27)···C(7)	3.504(5)	N(2)···C(6)	3.468(5)
C(28)···C(1)	3.449(5)	N(4)···C(3)	3.267(5)
C(28)···C(6)	3.450(5)	N)4)···C(4)	3.417(5)
C(30)···C(4)	3.400(5)	N(4)···C(12)	3.588(5)
C(30)···C(5)	3.511(5)		
Between ion-pairs.			
$N(4)^{i}\cdots C(11)^{ii}$	3.401(5) Å		
Between anions.			
$C(25)^{i}\cdots N(2)^{iv}$	3.265(5) Å		
Between cations.			
$C(5)^{i}\cdots C(19)^{iii}$	3.411(5) Å	$O^{i}\cdots(19)^{iii}$	3.480(5) Å
$C(3)^{i}\cdots C(21)^{iii}$	3.480(5)		
Between nonoverlapping anion and cation.			
$N(3)^{i}\cdots C(4)^{iii}$	3.579(5) Å	$N(1)\cdots C(11)^{iv}$	3.446(5) Å
$N(3)^{i}\cdots C(17)^{iii}$	3.520(6)	$N(1)\cdots C(21)^{vi}$	3.517(6)
$N(3)^{i}\cdots C(19)^{iii}$	3.438(6)	$N(3)\cdots C(9)^{v}$	3.446(6)
$N(1)^{i}\cdots C(2)^{iv}$	3.457(5)	$N(4)\cdots C(15)^{vii}$	3.439(6)

Codes for superscripts

i	x, y, z	v	$\frac{1}{2}+x, \frac{1}{2}-y, -1+z$
ii	$x, y, -1+z$	vi	$-\frac{1}{2}+x, \frac{1}{2}-y, z$
iii	$1-x, \frac{1}{2}-y, 1-z$	vii	$-x, 1-y, 1-z$
iv	$\frac{1}{2}+x, \frac{1}{2}-y, z$		

of infinite length along the c axis in which the cations and anions stack alternately (Fig. 4). The least-squares planes of the cation and the anion are almost parallel to the a axis, the former inclining to the c axis at 53.0° and the latter at 53.7°, and the dihedral angle

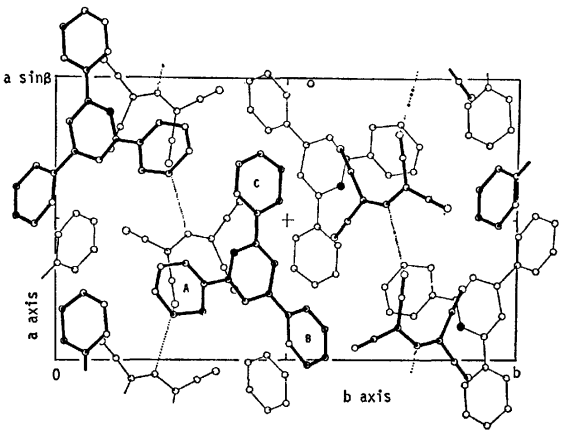

Fig. 3. The crystal structure viewed along the c axis. The dotted lines show the presence of the hydrogen bonding.

between them being 3.2°. In the column, although the TCP anion is sandwiched by TPP cations and *vice versa*, the TCP anion has a larger overlap and closer contact with one of the cations than the other. Thus, the TCP anion and TPP cation can be considered to form an "ion-pair" in the crystal as a stacking unit.

The relative arrangement between the cation and the anion in the column is shown in Fig. 5. In the ion-pair the anion overlaps mainly with the pyrylium ring of the cation. The average interplanar spacing between the best planes of the anion and the pyrylium ring is 3.31 Å, and the closest atomic contact is N(4)–C(3), 3.267(5)Å. They are slightly shorter than the corresponding van der Waals distances. In addition to the alternate arrangement and close contact of the

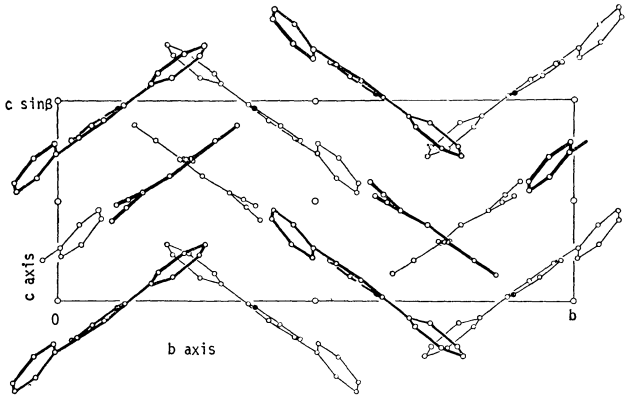

Fig. 4. The crystal structure viewed along the a axis. The benzene ring-B in each TPP cation (shown in Fig. 3) is omitted.

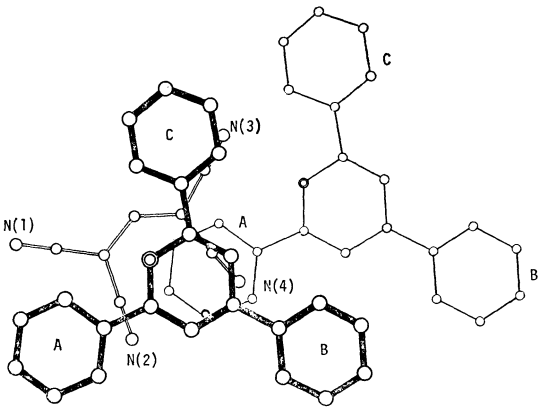

Fig. 5. The relative arrangement of the cation and the anion in the column projected on the best plane of the anion.

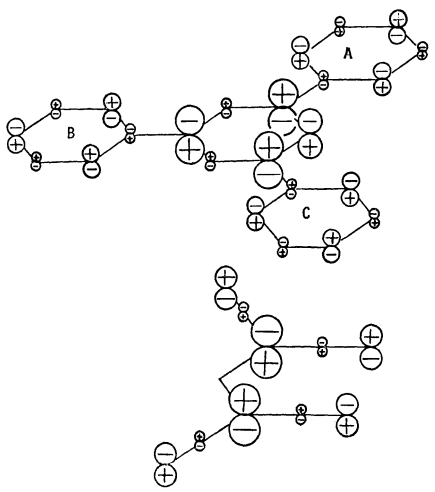

Fig. 6(a). The shapes of the lowest vacant molecular orbital of the cation and the highest occupied molecular orbital of the anion calculated by Hückel MO method using ω-technique.
The parameters were assumed as follows; the resonance integrals are $1.0\beta_0$ for all C-C bonds, $0.9\beta_0$ for two C-O bonds, and $1.2\beta_0$ for C-N bonds, and the Coulombic integrals are α_0 for all C atoms, $\alpha_0+2.5\beta_0$ for O atom, and $\alpha_0+1.0\beta_0$ for four N atoms, and the parameters $\omega=1.4$.

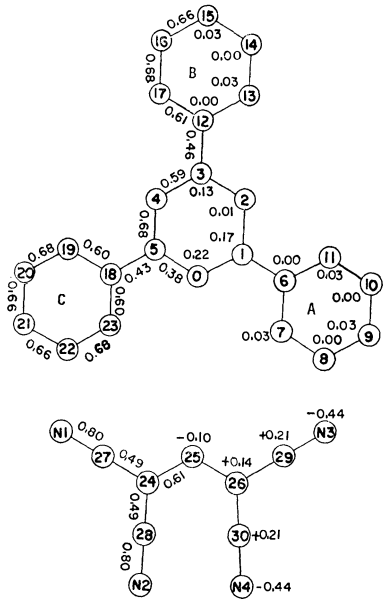

Fig. 6(b). The charge distributions (shown in the right half of the molecule) and the bond orders (shown in the left half of the molecule) calculated by Hückel MO method using ω-technique. The negative values of the charge density indicate the excess of negative charge.

two components characteristic of organic charge transfer complexes, the overlap between the highest occupied molecular orbital of the anion and the lowest vacant molecular orbital of the cation can be considered as a measure of the charge transfer interaction. The shapes of these orbitals, charge distributions and bond orders, shown in Figs. 6(a) and 6(b), were calculated by the Hückel MO method using the ω-technique.[14] However, they cannot explain the observed overlapping between the cation and the anion in terms of the interionic charge transfer interaction. Only slight coincident overlaps between the atoms are observed in Fig. 5. This does not indicate an appreciable contribution of charge transfer force on the relative arrangement of the cation and the anion.

Figure 6(b) shows that the negative charge in the anion is significantly distributed on four nitrogen atoms, whereas the positive charge in the cation is localized at the oxygen and neighboring carbon atoms in the pyrylium ring. The observed overlap of the cation with the anion in which the oxygen atom of the cation is located approximately above the center of the anion, can thus be explained mainly by the electrostatic interaction.

A short atomic contact between the C(25) atom of the TCP anion and the N(2) atom of the adjacent TCP anion along the a axis (dotted line in Fig. 3) indicates the existence of a strong interaction like hydrogen bond between anions in the neighboring columns. The C(25)···N(2)^{iv} and H(25)···N(2)^{iv} distances are 3.265(5) and 2.185(5) Å, respectively, and the C(25)–H(25)···N(2)^{iv} angle is 170°. Although the C–H···N hydrogen bond was scarcely observed, in the present case this type of hydrogen bond is present, which is probably caused by the activation of H(25) atom by four electron-withdrawing cyano groups. The relative

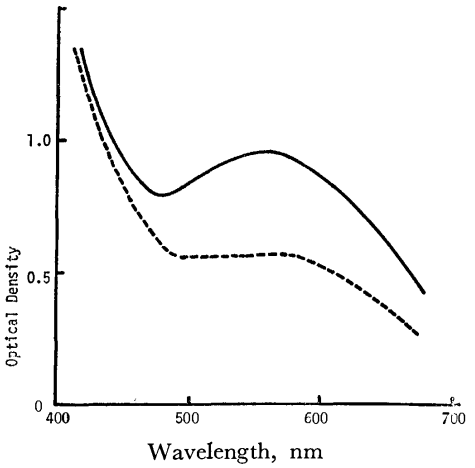

Fig. 7. Polarized absorption spectrum of TPP-TCP single crystal.
—— // c axis, ---- ⊥ c axis.

arrangement of the anion also seems to be affected by this interaction.

The tilt angles of the three benzene rings from the pyrylium ring may be affected by the degree of the overlap with the TCP anion. The C-ring, with the least tilt angle, overlaps the anion in the ion-pair where the interplanar spacing is fairly short. However, the contact between the A-ring and the anion is in the van der Waals distance, which may slightly restrict free rotation of the benzene ring (Fig. 5). On the other hand, the slight overlap observed between the B-ring and the anion allows rotation of the B-ring.

The polarized absorption spectrum of a single crystal of this salt is given in Fig. 7. The optical density of the absorption band at 535 nm, usually assigned to interionic charge transfer band, is about 1.65 times higher in the c-polarization spectrum than the other. Assuming that the direction of the transition moment is perpendicular to the planes of the anion and the cation, which is inclined to the c axis by *ca.* 37°, the ratio of two components of the dipole moment parallel and perpendicular to the c axis is given by cos 37°/cos 53° (=1.32). The dichroism ratio, therefore, is $(\cos 37°/\cos 53°)^2$, 1.74. This agrees approximately with the observed dichroism ratio. Thus the polarized absorption spectrum can be explained in terms of the crystal structure.

All the programs used for the structure analysis were written by Professor T. Ashida. The program of ω-technique used for the molecular orbital calculations was written by one of us (T. T.). Most of the calculations were carried out at Kyoto university on a FACOM 230-60 computer.

The authors wish to express their deep thanks to Prof. Masao Kakudo, and Prof. Tamaichi Ashida for their valuable suggestions and encouragement in the X-ray structure analysis, and also to Prof. Hiroshi Mikawa and Prof. Shigekazu Kusabayashi for their helpful discussions.

References

1) Organic Charge Transfer Salts. IV. Part II of this series; T. Tamamura, M. Yokoyama, S. Kusabayashi and H. Mikawa, This Bulletin, **47**, 442 (1974).

2) Present address; Welding Research Institute, Osaka University, Suita, Osaka 565.

3) To whom any correspondence should be addressed.

4) *a*) E. M. Kosower and P. A. Klinedinst, Jr., *J. Amer. Chem. Soc.*, **78**, 3493 (1956). *b*) S. F. Mason, *J. Chem. Soc.*, **1960**, 2437. *c*) E. L. Goff and R. B. LaCount, *J. Amer. Chem. Soc.*, **85**, 1354 (1963). *d*) G. Briegleb, W. Jung, und W. Herr, *Z. Phys. Chem.* (Frankfurt), **38**, 253 (1963). *e*) A. T. Balaban, M. Mocanu, and Z. Simon, *Tetrahedron*, **20**, 119 (1964).

5) *a*) S. Sakanoue, Y. Kai, N. Yasuoka, N. Kasai, and M. Kakudo, This Bulletin, **43**, 1306 (1970). *b*) K. Nakamura, N. Yasuoka, N. Kasai, H. Mikawa, and M. Kakudo, *Chem. Commun.*, **1970**, 1135. *c*) S. Sakanoue, N. Yasuoka, N. Kasai, and M. Kakudo, This Bulletin, **44**, 1 (1971).

6) T. Tamamura, H. Yasuba, K. Okamoto, T. Imai, S. Kusabayashi, and H. Mikawa, This Bulletin, **47**, 448 (1974).

7) H. Yasuba, T. Imai, K. Okamoto, S. Kusabayashi, and H. Mikawa, *ibid.*, **43**, 3101 (1970).

8) J. Karle and I. L. Karle, *Acta Crystallogr.*, **21**, 849 (1966).

9) H. F. Hanson, F. Hermann, J. D. Lea, and S. Skillman, *ibid.*, **17**, 1040 (1964).

10) Table 5 is filed at the Chemical Society of Japan, (Document No. 7407), 1–5, Kanda-Surugadai, Chiyoda-ku, Tokyo.

11) A. Almennings, O. Bastiansen, and L. Hansen, *Acta Chem. Scand.*, **9**, 1306 (1955).

12) L. Pauling, "The Nature of the Chemical Bond," Cornell Univ. Press, Ithaca N. Y. (1960).

13) *a*) R. Desiderato and R. L. Sass, *Acta Crystallogr.*, **18**, 1 (1965). *b*) J. Konnert and D. Britton, *Inorg. Chem.*, **6**, 1193 (1967). *c*) P. Andersen, B. Klewe, and E. Thom, *Acta Chem. Scand.*, **21**, 1530 (1967). *d*) D. A. Beoke, P. K. Gantzel, and K. N. Trueblood, *Acta Crystallogr.*, **22**, 657 (1967).

14) A Streitwieser, Jr., *J. Amer. Chem. Soc.*, **82**, 4123 (1960).

The Relative Determination of the Soret Coefficients of Electrolytes. IV

Toshio IKEDA and Yasuki YAMAMOTO

Department of Chemistry, Shizouka University, Shizouka 420

(Received October 29, 1973)

The relative values of the Soret coefficients of 0.01 M aqueous solutions of symmetric tetraalkylammonium chlorides (R_4NCl, R=Me, Et, *n*-Pr, *n*-Bu, and *n*-Am) were determined by measuring the initial thermoelectric power of "combined thermocells" made up of AgCl electrode systems, taking LiCl as a reference. The results obtained were found to be rather high, higher by about 20% than those previously found on the combined thermocells made up of calomel-electrode systems.

In a previous paper,[1] the Soret coefficients of a series of symmetric tetraalkylammonium chlorides were determined by using a "combined thermocell" made up of calomel-electrode systems. The merit of using a combined thermocell for the determination of the Soret coefficients is that thereby the nature of the electrode system used in the cell is completely canceled out. On the other hand, the electrode potentials of calomel-electrodes have rather high temperature coefficients as much as 950 μV/deg at 0.01 M; accordingly, a considerable error may be caused in the thermoelectric power by an occasional slight shift in the temperature of an electrode system, thereby losing the merit of using combined thermocells. For this reason, in the present work, silver chloride electrodes with a relatively low temperature coefficient of about 600 μV/deg were used in place of the calomel-electrodes.

A combined thermocell of the following system was constructed:

$$\underset{T}{\text{Ag-AgCl}},\ \text{LiCl}(m),\ \underset{T+\Delta T}{\text{AgCl-Ag-AgCl}},\ \text{R}_4\text{NCl}(m),\ \underset{T}{\text{AgCl-Ag}} \qquad (1)$$

where R_4NCl represents a symmetric tetraalkylammonium chloride of the same concentration, m, as that of lithium chloride. Lithium chloride was chosen here as a reference substance because it shows a very slight Soret effect. From the measured initial thermoelectric power, $(dE/dT)_0$, of the cell (1), the Soret coefficient, σ, of R_4NCl can be calculated by means of the following equation:[2]

$$\sigma^{\text{QCl}} = \frac{t_{\text{Li}^+}^{\text{LiCl}} B^{\text{LiCl}}}{t_{\text{Q}^+}^{\text{QCl}} B^{\text{QCl}}}\sigma^{\text{LiCl}} - \frac{F(dE/dT)_0}{2RTt_{\text{Q}^+}^{\text{QCl}} B^{\text{QCl}}} - \frac{\bar{\bar{S}}_{\text{Cl}^-}^{\text{QCl}} - \bar{\bar{S}}_{\text{Cl}^-}^{\text{LiCl}}}{2RTt_{\text{Q}^+}^{\text{QCl}} B^{\text{QCl}}} \qquad (2)$$

where Q stands for R_4N, where σ's are the Soret coefficients, where t's are the ionic transport numbers for the ions indicated by the subscripts corresponding to the solution phases indicated by the superscripts, where F is the Faraday constant, where T is the absolute temperature, and where the B's are defined by:

$$B^{\text{LiCl}} = (1 + d\ \ln\gamma_{\pm}^{\text{LiCl}}/d\ \ln m)_{T,P}$$

$$B^{\text{QCl}} = (1 + d\ \ln\gamma_{\pm}^{\text{QCl}}/d\ \ln m)_{T,P}$$

where the $\gamma_{\pm}$'s are the mean activity coefficients on the molality scale in an m molal solution and where the $\bar{\bar{S}}_{\text{Cl}^-}$'s represent the transported entropies of the chloride ions in the solution phases indicated by the superscripts. In the present work, the third term on the right-hand side of Eq. (2) was omitted in the practical calculation because this contribution is negligible in the present experimental accuracy.

Experimental

Materials. The symmetrical tetraalkylammonium chlorides, R_4NCl (R: Me=CH_3, Et=C_2H_5, *n*-Pr=*n*-C_3H_7, *n*-Bu=*n*-C_4H_9, and *n*-Am=*n*-C_5H_{11}), were of the C. P. grade, while the lithium chloride was of a Guaranteed Reagent grade obtained from Wako Pure Chemical Industry, Ltd. All the solutions were prepared to a concentration of 0.01 M± 0.3% using conductivity water.

Silver Chloride Electrodes. Two ways of preparation were tried: (a) the chlorination of the silver electrode by electrolysis and (b) a modification of Haase's process of thermal decomposition.[3] These two processes were found to give practically the same electrochemical stability, and so both were used conveniently. The practice of these processes was as follows: (a) the silver-plated surface of a silver electrode (10×10 mm² in area) was converted into silver chloride by anodic electrolysis in 1 N hydrochloric acid under a current of 15—20 mA for about 5 min, washed with water, and dried in the open air. After it had been heated in an electric furnace at about 500 °C for 15 min, it was left overnight in the furnace to allow for natural cooling for annealing. (b) A silver electrode, 10×10 mm² in area, the surface of which was coated with a muddy paste of a 4 : 1 mixture of silver oxide and silver chloride in weight, was heated in an electric furnace at about 500 °C for about 15 min and then cooled for a few minutes in the open air. This process of coating the surface with paste and heating was repeated several times, and then finally the electrode was subjected overnight to natural cooling from 600 °C to room temperature for annealing.

Cells and Measurements. An H-type cell was used to make single thermocells of LiCl and R_4NCl. The outside of the H-cell was painted black to keep the silver chloride electrode from the light. The temperature of the cell was controlled by thermostated water in a Dewar vessel as has been described previously;[2] however, it was changed in a descending way from room temperature (about 25°) down to about 15° in order to minimize the vertical thermal convection of electrolytes in the legs of the H-cell. The temperature near the silver chloride electrode was measured directly by the aid of a mercury thermometer of 0.1 degree divisions which was inserted near the electrode in a leg of the H-cell. The electromotive force of the combined thermocell was measured with a Yokogawa D. C. potentiometer, Type P-7B, using a sensitive Yokogawa electronic galvanometer, Type 2700, as a zero indicator accurately to 0.1 μV.

Results and Discussion

Some typical results are represented in Fig. 1. The initial thermoelectric powers, $(dE/dT)_0$, of the combined thermocells were determined by the method of the least squares; they are listed in Table 1. Despite the lower temperature coefficient of the electrode potential of the silver chloride electrode used here, fairly large fluctuations were unexpectedly found in the observed values of $(dE/dT)_0$. This may possibiy be caused by a thermal convection occasionally occurring in the electrolyte solutions in the cell. The Soret coefficient of lithium chloride, which was used as a reference in the present work, was assigned to be -0.01×10^{-3} deg^{-1}, a value obtained by adjusting Snowdon and Turner's value[4] of -0.02×10^{-3} deg^{-1} at 0.01 M and at 25.3 °C to the value at 25 °C. Using this value and our data on $(dE/dT)_0$, the relative values of the Soret coefficients, σ^{QCl}, at 25 °C and at 0.01 M were determined by the aid of Eq. (2) taking $\bar{\bar{S}}^{QCl}_{Cl^-}=\bar{\bar{S}}^{LiCl}_{Cl^-}$; the results are listed in Table 1. Here, the σ-values determined in the present work are found to be rather higher (by about 20%) than our previous results[1] and the value of tetraalkylammonium chloride found by the use of the direct method by Snowdon and Turner.[4] Though the mean temperature is not 25° but 20° in the present work, such a large difference in the σ-values cannot be explained by the difference in mean temperature, because, in many cases, the influence of the mean temperature upon the σ-values of univalent electrolytes at 0.01 M is known to be of an order of magnitude of 0.1×10^{-3} deg^{-2}.[5] For the present, it is difficult to judge which of them is proper; however, the results of the present work may be nicely compared with the σ-values of symmetrical tetraalkylammonium bromides, R_4NBr: σ in 10^{-3} deg^{-1} are -5.78 for R=Me, -9.65 for R=Et, -13.4 for R=*n*-Pr, -16.3 for R=*n*-Bu, and -18.5 for R=*n*-Am, all of which were previously estimated by one of the present authors[6] from the initial thermoelectric powers[7] of single thermocells of the $HgBr/R_4NBr$(0.01 M) system at 25 °C. Further, Agar and Turner[5] reported a value of -9.20×10^{-3} deg^{-1} for Et_4NCl at 0.01 M and at 25 °C. Upon taking into consideration the fact that the σ-values of the bromides should, accodring to Snowdon and Turner,[4] be higher by only about 0.06×10^{-3} deg^{-1} in absolute value than those of the chlorides at 25° in 0.01 M aqueous solutions of univalent salts, the σ-values found for the symmetrical tetraalkylammonium chlorides in the present work seem likely to be more reasonable.

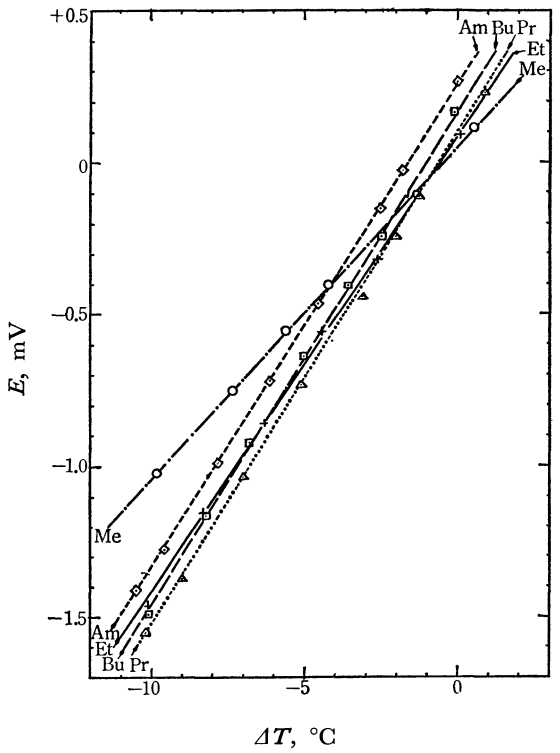

Fig. 1. Plots of emfs of the combined thermocells (1) *vs.* temperature difference, ΔT.

Table 1. Soret coefficients of symmetric tetraalkylammonium chlorides in water at 25 °C and at 0.01 M

Chlorides	t_+	B	$(dE/dT)_0$ μV/deg	$10^3\sigma$, deg^{-1}		
				This work	Ref. 4	Ref. 1
LiCl	0.3289[a]	0.969	—	(+0.01)†	+0.01	(0.01)†
Me_4NCl	0.3699[b]	0.941[d]	94.0±4.1	−5.25	—	−5.17
Et_4NCl	0.2996[b]	0.943[d]	146.8±3.8	-10.0_9	−8.38	−8.61
n-Pr_4NCl	0.2350[b]	0.945[d]	160.9±2.7	-14.0_8	—	−10.91
n-Bu_4NCl	0.2004[b]	0.947[d]	161.5±3.7	-16.5_3	—	−13.27
n-Am_4NCl	0.180_0[c]	0.949[c]	160.7±3.2	-18.3_0	—	—

a) B. E. Conway, "Electrochemical Data," Elsevier Publishing Co., Amsterdam, (1952). b) Calculated from the data on the ionic mobilities at 25 °C, Landolt-Börnstein, "Zahlenwerte und Funktionen aus Physik, Chemie, Astronomie, Geophysik und Technik," 6. Auflage, II. Band, 7. Teil., Elektrische Eigenschaften II, Springer-Verlag, Berlin (1960). c) An extrapolated value. d) Graphical determination from S. Lindenbaum and G. E. Boyd, *J. Phys. Chem.*, **68**, 911 (1964). Values for the concentrations below 0.1 M were estimated by extrapolation.

† A value adopted as a standard for the relative determination of σ.

References

1) T. Ikeda and H. Miyoshi, *J. Phys. Chem.*, **70**, 3361 (1966).
2) T. Ikeda and H. Kimura, *ibid.*, **69**, 41 (1965).
3) R. Haase and H. Schönert, *Z. Phys. Chem.* (Frankfurt), **25**, 193 (1960).
4) P. N. Snowdon and J. C. R. Turner, *Trans. Faraday Soc.*, **56**, 1409 (1960).
5) J. N. Agar and J. C. R. Turner, *Proc. Roy. Soc., Ser. A*, **255**, 307 (1960).
6) T. Ikeda, *Rep. Liberal Arts Sci. Fac. Shizuoka Univ.* (*Nat. Sci.*), **2**, 153 (1959).
7) J. C. Goodrich, F. M. Goyan, E. E. Morse, R. G. Preston, and M. B. Young, *J. Amer. Chem. Soc.*, **72**, 4411 (1950).

Thermal Decomposition Reaction of Halogenoammineruthenium(III) Halide Complexes[1)]

Akira OHYOSHI, Shunichi HIRAKI, and Hideo KAWASAKI

Department of Industrial Chemistry, Faculty of Engineering, Kumamoto University, Kumamoto 860

(Received April 17, 1973)

The thermal decomposition of halogenopentaammine- and *cis*-dihalogenotetraammineruthenium(III) complexes was studied by the techniques of thermogravimetry(TG), differential thermal analysis(DTA), and evolved gas analysis(EGA). The stoichiometry of the decomposition reaction was determined by the analysis of the reaction intermediates and products. The order of decreasing thermal stability, as well as order of temperature of mass-loss initiation, seems to be: $[RuCl(NH_3)_5]Cl_2 > [RuBr(NH_3)_5]Br_2 > [RuI(NH_3)_5]I_2$ for monohalogeno complexes, and *cis*-$[RuCl_2(NH_3)_4]Cl$ > *cis*-$[RuBr_2(NH_3)_4]Br$ > *cis*-$[RuI_2(NH_3)_4]I$ for dihalogeno complexes. Trihalogeno-triammine complexes were observed as intermediates for the cases of dichloro and bromo complexes. a simple decomposition reaction was found for the iodo complexes, and then the activation energy for the following reaction was determined: $[RuI(NH_3)_5]I_2 \rightarrow RuI_3 + 5NH_3$, $E_a = 41.9$ kcal/mol and *cis*-$[RuI_2(NH_3)_4]I \rightarrow RuI_3 + 4NH_3$, $E_a = 27.8$ kcal/mol. The reaction mechanisms may be summarized as follows: (a) an electron-transfer mechanism, in which the ruthenium(III) was reduced by the ammonia molecule or the halide ion, (b) the thermal splitting of the ruthenium-ammine bond, and (c) the bond formation between the ruthenium(III) and the halide ion after the ion migration from the outersphere to the innersphere of the complex. The predominant factors which control these mechanisms may be the coordinate bond strength of the ruthenium(III) and various ligand species, the relative potential of electron transfer from the ligand to the ruthenium(III), and the ease of halide-ion migration from the outersphere to the innersphere of the complex.

The thermal decomposition of a number of cobalt(III)[2-9)] and chromium(III)[10-15)] ammine complexes has been previously reported. Recently, the thermal decomposition of hexaammineruthenium(III) chloride only has been studied by Trehoux *et al.*[16)] It is thus the object of this investigation to study the thermal decomposition of complexes of the $[RuX(NH_3)_5]X_2$ and $[RuX_2(NH_3)_4]X$ type, where X is Cl^-, Br^-, and I^-, by the techniques of thermogravimetry(TG), differential thermal analysis(DTA), and evolved gas analysis(EGA). The reaction intermediates and products were analyzed by spectrophotometry.

Experimental

Preparation of Ruthenium Complexes. $[RuCl(NH_3)_5]Cl_2$, $[RuBr(NH_3)_5]Br_2$, and $[RuI(NH_3)_5]I_2$ were prepared from ruthenium trichloride, hydrazine hydrate, and the respective hydrohalogenic acid by the method of Allen and Senoff.[17)] The $[RuX_2(NH_3)_4]X$, (X=Cl^-, Br^- and I^-) were prepared by the method of Gleu and Breuel.[18)] The compounds thus prepared were analyzed by the usual elemental analysis and confirmed by studying their electronic spectra.

Apparatus and Procedure. A Shimadzu D. T. 20B micro-differential thermal analyzer connected with an EGD 20 evolved gas detector was used for a series of thermal-decomposition reactions. Another series of experiments formed the thermogravimetry of a complex by using a Shimadzu T.G.C. 20-type microthermobalance. A Shimadzu UV 200 recording spectrophotometer was used for the measurement of the absorption spectra of the initial complexes, reaction intermediates, and products.

Samples of about 5—8 mg were pyrolyzed in a dynamic helium atmosphere in a furnace at a heating rate of 5 °C per min. The electric responses corresponding to the variation in the temperature, the gas evolution, and the sample massloss were recorded as functions of the furnace temperature on a potentiometric recorder with a sensitivity of ±50 μV.

The reaction products were analyzed as follows. The sample of about 30—40 mg was pyrolyzed in dynamic helium by using a differential thermal analyzer connected with a gas evolution detector. The liberated ammonia gas was absorbed in a series of traps containing 0.02 M sulfuric acid. For all the aliquots of the trap solution, the concentration of ammonia was determined by potentiometric titration with a 0.02 M sodium hydroxide standard solution. An aliquot of the solution was also used for the colorimetric determination of ammonia with the Nessler reagent.

The liberated halogen gas was dissolved in a dilute potassium iodide solution and titrated with a standard sodium thiosulfate solution.

The reaction products, which were condensed on the wall of apparatus, were collected and identified by the tests for ammonium ion and halide ions. The final reaction product was analyzed by direct weighing and found to be ruthenium oxide after heating in the air. To analyze the halide content, titration with the potassium thiocyanate standard solution was carried out after dissolving the product in water and adding an excess of a standard silver nitrate solution.

The UV and visible spectra were measured in order to identify some decomposition intermediates and products.

Results and Discussion

Differential Thermal Analysis-Gas Evolution Studies. The DTA and GE curves of the monohalogenopentaammineruthenium(III) and *cis*-dihalogenotetraammineruthenium(III) halogenides are given in Figs. 1 and 2. All of the DTA curves of the monohalogenopentaammineruthenium(III) halogenides are characterized by an endothermic peak: at 313 °C (chloro complex), 319 °C (bromo complex), and 258 °C (iodo complex) respectively. A small peak was also observed at 388 °C for the last complex. Each endothermic peak corresponds well to the respective peak on the GE curves. This fact shows that the main decomposition reaction, probably taking place during the first endothermic reaction, is accompanied by the evolution of such gases as ammonia, free halogen and/or ammonium halide. The DTA curves of the *cis*-dihalogenotetra-

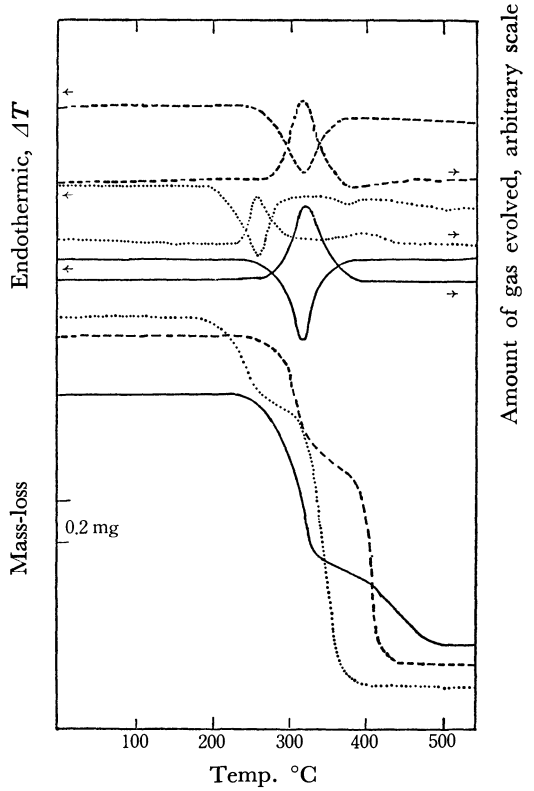

Fig. 1. DTA, GE and TG curves of $[RuX(NH_3)_5]X_2$, in a helium atmosphere. —— X=Cl, ---- X=Br, ····· X=I.

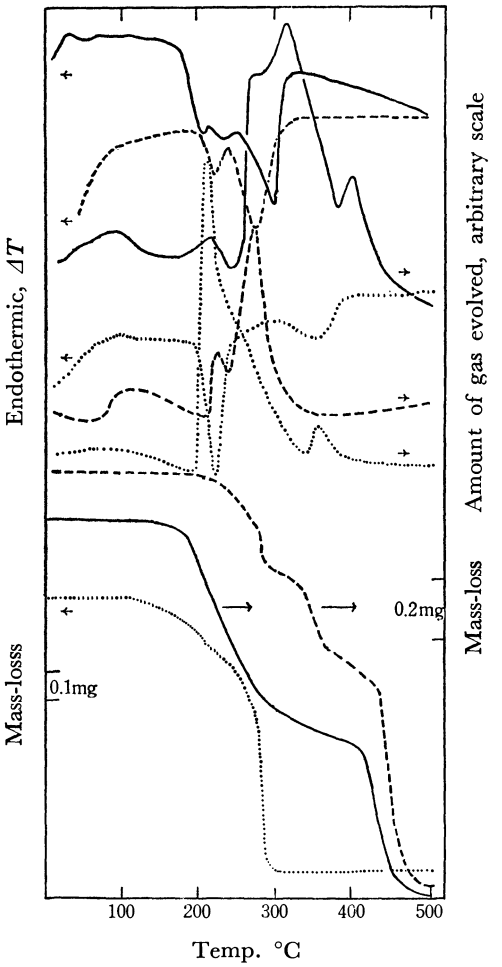

Fig. 2. DTA, GE and TG curves of $[RuX_2(NH_3)_4]X$, in a helium atmosphere. —— X=Cl, ---- X=Br, ····· X=I.

ammineruthenium(III) halogenides (Fig. 2) are different from each other and also from those of the monohalogeno complexes. In particular, that of the dichloro complex shows an endothermic peak at 246 °C between the first (220 °C) and the third (310 °C) peaks. For both the dibromo and the diiodo complex, the DTA curves show two endothermic peaks; however, the relative intensities of the first to the second peak is different. For the dichloro and dibromo complexes, the last peak is the largest, while for the diiodo complex, first peak at 220 °C is sharper and larger than the last one (353 °C). The temperature at each peak on the GE curves in Fig. 2 corresponds to that at the respective endothermic peak on the DTA curves. From this fact, it may be concluded that all the decomposition reactions are endothermic and gas-evolving.

Thermogravimetric Analysis. The curves obtained by the thermogravimetry(TG) are given in Figs. 1 and 2. The thermal decomposition is initiated at 246 °C (chloro complex), 244 °C (bromo complex), 174 °C (iodo complex), 200 °C (dichloro complex), 210 °C (dibromo complex), and 114 °C (diiodo complex). The initial decomposition temperature of each dihalogeno complex is generally lower than that of the corresponding monohalogeno complex, while the final temperature for the mass-loss is higher than that of the monohalogeno complex, except in the case of the iodo complex.

The orders of the decrease in thermal stability, along with the temperature of mass-loss initiation, seem to be: $[RuCl(NH_3)_5]Cl_2 > [RuBr(NH_3)_5]Br_2 > [RuI(NH_3)_5]I_2$ for the monohalogeno complexes and *cis*-$[RuCl_2(NH_3)_4]Cl > cis$-$[RuBr_2(NH_3)_4]Br > cis$-$[RuI_2(NH_3)_4]I$ for the dihalogeno complexes. The complexes containing iodide were certainly least stable. Similar relations have been reported in the thermal decomposition studies of halogenoammine complexes of cobalt(III)[3,5,7] and chromium(III).[13]

Table 1 shows the numerical data of mass-loss studies along with those of evolved gas analysis. The calculated mass-loss values for chloro complexes could not be determined because of their continuous thermal decompositions. From these results, the intermediate products were estimated to be as follows: $RuBr_2$ at 398 °C for the monobromo complex and at 431 °C for the dibromo complex; RuI_3 at 268 °C for the monoiodo complex and at 222 °C for the diiodo complex.

Product-analysis Studies. Table 2 shows the results of the evolved-ammonia-gas analyses, the mass of the final reaction products, and the molar ratios of ammonia to ruthenium metal. The mass of the final product is nearly in agreement with that of the ruthenium metal in each complex. The molar ratios (NH_3/Ru) are different from each other, however all the ammine ligands in the iodo complexes are liberated as ammonia molecules, while only three molecules for bromo complexes and only one or two for chloro complexes are liberated. These facts suggest that the

Table 1. Mass-loss data for halogenoammineruthenium(III) complexes

Complex		Mass-loss (%)		
$[RuCl(NH_3)_5]\cdot Cl_2$	Temp. (°C)	246—396	396—466	
	Experimental	47.0	16.0	
	Theoretical	—	—	
	Evolved gas	NH_3, NH_4Cl, HCl	HCl, Cl_2	
$[RuBr(NH_3)_5]\cdot Br_2$	Temp. (°C)	244—398	398—440	
	Experimental	35.8	39.3	
	Theoretical	38.7	37.5	
	Evolved gas	NH_3, NH_4Br	Br_2	
$[RuI(NH_3)_5]I_2$	Temp. (°C)	136—268	268—476	
	Experimental	16.5	65.2	
	Theoretical	15.0	67.2	
	Evolved gas	NH_3	I_2	
$[RuCl_2(NH_3)_4]\cdot Cl\cdot 2/5H_2O$	Temp. (°C)	63—200	200—419	419—521
	Experimental	2.6	37.2	25.1
	Theoretical	—	—	—
	Evolved gas	H_2O	HH_3, NH_4Cl, HCl	HCl, Cl_2
$[RuBr_2(NH_3)_4]\cdot Br$	Temp. (°C)		210—431	431—473
	Experimental		37.7	37.4
	Theoretical		36.9	39.1
	Evolved gas		NH_3, NH_4Br	Br_2
$[RuI_2(NH_3)_4]\cdot I$	Temp. (°C)		114—222	222—320
	Experimental		13.3	68.3
	Theoretical		12.4	69.2
	Evolved gas		NH_3	I_2

Table 2. Determination of evolved ammonia gas and residue

Complex	Sample weight (mol)	NH_3 Calcd	Residue (%) Obsd	Ru (%) Calcd	Molar ratio, NH_3/Ru
$[RuCl(NH_3)_5]Cl_2$	8.60×10^{-5}	1.93×10^{-4}	35.0	34.6	2.2
$[RuBr(NH_3)_5]Br_2$	9.65×10^{-5}	3.25×10^{-4}	24.8	23.7	3.4
$[RuI(NH_3)_5]I_2$	5.43×10^{-5}	2.65×10^{-4}	17.4	17.8	4.9
cis-$[RuCl_2(NH_3)_4]Cl2/5H_2O$	1.14×10^{-4}	1.52×10^{-4}	35.9	36.7	1.3
cis-$[RuBr_2(NH_3)_4]Br$	9.56×10^{-5}	2.59×10^{-4}	25.6	24.7	2.7
cis-$[RuI_2(NH_3)_4]I$	6.35×10^{-5}	2.70×10^{-4}	20.0	18.4	4.1

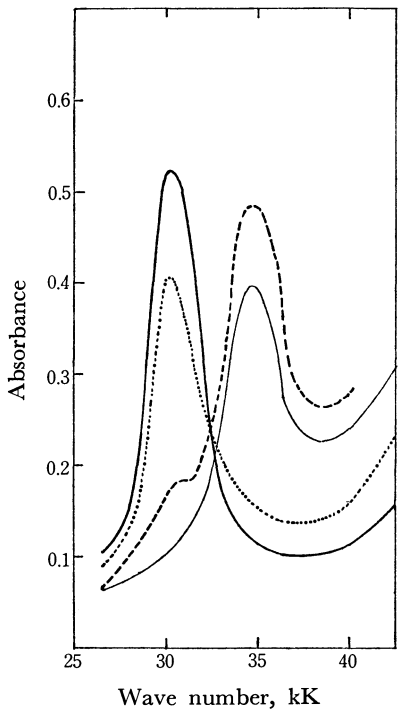

Fig. 3. Absorption spectra of thermal decomposition products for $[RuCl(NH_3)_5]Cl_2$. —— room temp., ····· 260 °C, ---- 297 °C, —— 396 °C.

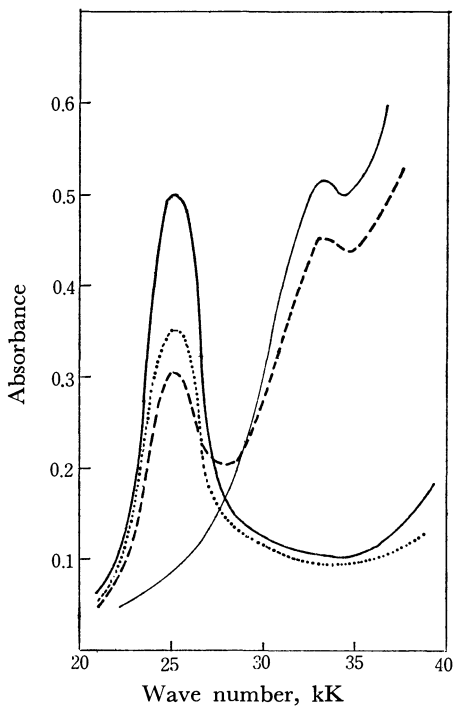

Fig. 4. Absorption spectra of thermal decomposition products for $[RuBr(NH_3)_5]Br_2$. —— room temp., ····· 265 °C, ---- 300 °C, —— 320 °C.

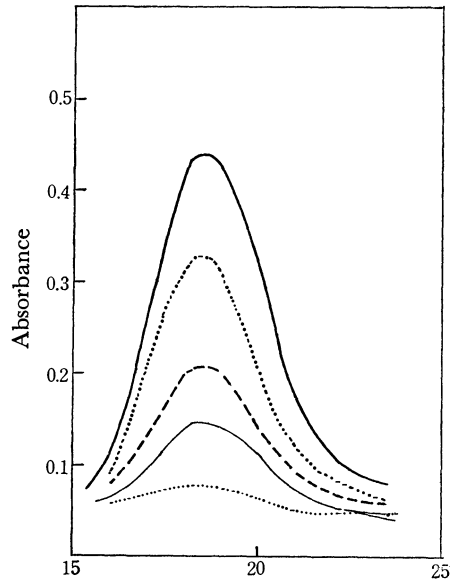

Fig. 5. Absorption spectra of thermal decomposition products for $[RuI(NH_3)_5]I_2$ —— room temp., ···· 203 °C, ---- 210 °C, —— 230 °C, ····· 240 °C.

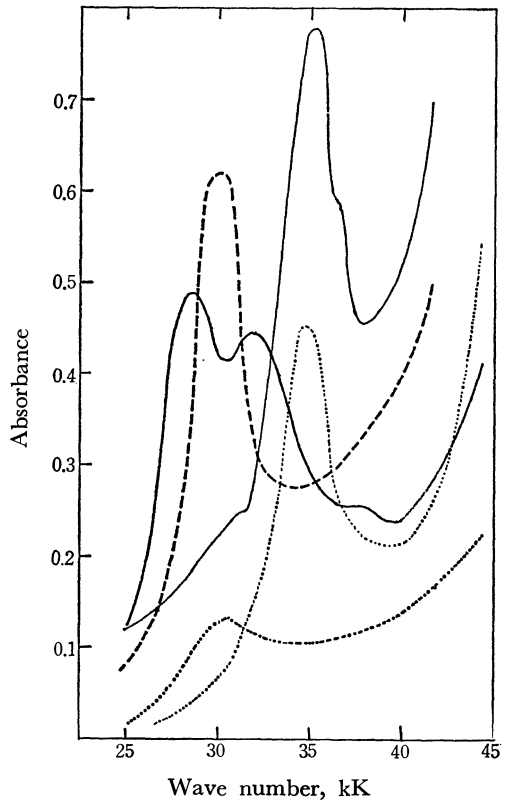

Fig. 6. Absorption spectra of thermal decomposition products for *cis*-$[RuCl_2(NH_3)_4]Cl$. —— room temp., ···· 215 °C, ---- 235 °C, —— 300 °C, ····· 419 °C.

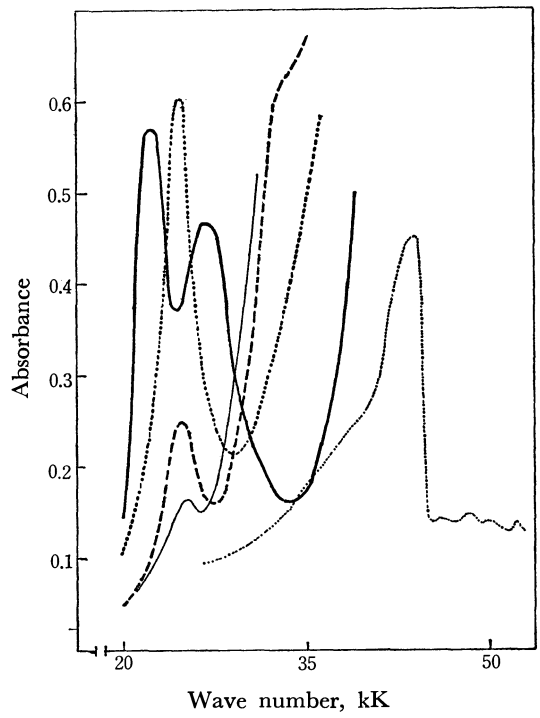

Fig. 7. Absorption spectra of thermal decomposition products for *cis*-$[RuBr_2(NH_3)_4]Br$. —— room temp., ···· 215 °C, ---- 240, 260 °C, —— 280 °C, ····· 416 °C.

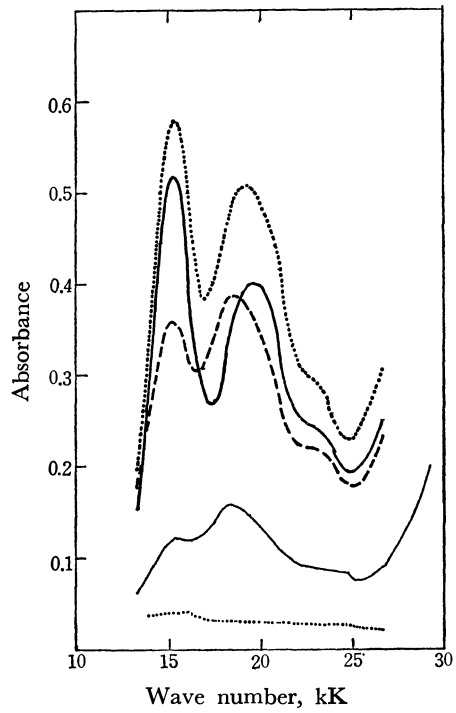

Fig. 8. Absorption spectra of thermal decomposition products for *cis*-$[RuI_2(NH_3)_4]I$. —— room temp., ···· 150 °C, ---- 180 °C, —— 200 °C, ····· 230 °C.

contribution of the halide ion to the weakening of the strength of the ruthenium–ammine coordinate bond is variable.

The absorption spectra of the initial complexes and the decomposition intermediates are shown in Figs. 3—8. The temperature for the sampling of the intermediates was selected by reference to the variation points on the DTA and TG curves. The initial spectrum of the monochloro complex shows an absorption peak at 30.5 kK which decreases with the progress of

the thermal decomposition, and a new peak appears at 34.7 kK. The formation of trichlorotriammine complex was apparently confirmed by the appearance of a peak at 30.2 kK in the spectra of the intermediates obtained at 215 and 235 °C only in the case of the dichloro complex, as is shown in Fig. 6, while it was difficult to identify this complex in the case of the monochloro complex. A similar complex has been assumed to be the same as an intermediate in the thermal decomposition of the hexaammineruthenium(III) trichloride by Trehoux *et al.*[16] The absorption peak at 34.7 kK in the spectra of the final products in Figs. 3 and 6 has not yet been assigned definitely. The chemical formula of this product was estimated to be Ru_2Cl_2-NH_3 from the results of elemental analysis. These facts suggest that the ruthenium(III) has already been reduced to the low valence state when the temperature is elevated to 297 °C.

As is shown in Fig. 4, the absorption peak at 25.1 kK ascribed to the monobromo complex decreases with a slight shift toward the side of higher wave numbers. A new peak at 33.1 kK begins to appear in the spectrum of the intermediate obtained at 300 °C (Fig. 4). In the spectrum of the intermediate obtained at 320 °C, the 25.1 kK peak has entirely disappeared, and the spectrum is found to consist of 33.1 kK peak and a continuous absorption in the region of ultraviolet wavelengths (Fig. 4). This 33.1 kK peak has not yet been assigned. The variations in the absorption spectra in the course of thermal decomposition for *cis*-dibromotetraammine appear to be somewhat complex. The character of the spectrum of the initial complex has entirely vanished in that of the intermediate obtained at 215 °C (Fig. 7). At this temperature, the deammonation has already started, as is shown by the endothermic peak at 226 °C and the mass-loss curve starting at 210 °C in Fig. 2. The absorption peak at 24.9 kK in the spectrum of the intermediate obtained at 215 °C may be attributable to the tribromotriammine complex because the spectral change is similar to that corresponding to the transformation from *cis*-dichlorotetraammine to the trichlorotriammineruthenium(III) complex.

The absorption spectra of intermediates produced in both the thermal decompositions of iodopentaammine and *cis*-diiodotetraammineruthenium(III) iodides show the continuous variation, as is shown in Figs. 5 and 8. Such a variation in the spectrum suggests that only deammonation is continuously proceeding because of the difficulty of the substitution reaction by the iodide ions in the outerspheres of complexes.

Stoichiometry of the Thermal-decomposition Reaction. In view of the results obtained from the DTA, EGA, and TG and the product analysis, the following thermal decomposition reactions are presumably established. For the chloroammineruthenium(IIII) complexes:

$$[RuCl(NH_3)_5]Cl_2 \rightarrow [RuCl_3(NH_3)_3] + 2NH_3 \quad (1)$$

$$\rightarrow Ru + 2NH_3 + 2NH_4Cl + HCl + 1/2\,N_2 \quad (2)$$

$$[RuCl_2(NH_3)_4]Cl \rightarrow [RuCl_3(NH_3)_3] + NH_3 \quad (3)$$

$$\rightarrow Ru + NH_3 + 2NH_4Cl + HCl + 1/2\,N_2 \quad (4)$$

For the bromoammineruthenium(III) complexes:

$$2[RuBr(NH_3)_5]Br_2 \rightarrow 2[RuBr_3(NH_3)_3] + 4NH_3 \quad (5)$$

$$\rightarrow 2RuBr_2 + 7NH_3 + 2NH_4Br + 1/2\,N_2 + 1/2\,H_2 \quad (6)$$

$$\rightarrow 2Ru + 2Br_2 + 7NH_3 + 2NH_4Br + 1/2\,N_2 + 1/2\,H_2 \quad (7)$$

$$2[RuBr_2(NH_3)_4]Br \rightarrow 2[RuBr_3(NH_3)_3] + 2NH_3 \quad (8)$$

$$\rightarrow 2RuBr_2 + 5NH_3 + 2NH_4Br + 1/2\,N_2 + 1/2\,H_2 \quad (9)$$

$$\rightarrow 2Ru + 2Br_2 + 5NH_3 + 2NH_4Br + 1/2\,N_2 + 1/2\,H_2 \quad (10)$$

For the iodoammineruthenium(III) complexes:

$$[RuI(NH_3)_5]I_2 \rightarrow RuI_3 + 5\,NH_3 \quad (11)$$

$$\rightarrow Ru + 3/2\,I_2 + 5\,NH_3 \quad (12)$$

$$[RuI_2(NH_3)_4]I \rightarrow RuI_3 + 4\,NH_3 \quad (13)$$

$$\rightarrow Ru + 3/2\,I_2 + 4\,NH_3 \quad (14)$$

The intermediates of the above reactions, the trichlorotriammineruthenium(III), $[RuCl_3(NH_3)_3]$, and the ruthenium dibromide, $RuBr_2$, were confirmed by the elemental analysis.

Found: H, 3.60; N, 16.52%. Calcd for $[RuCl_3(NH_3)_3]$: H, 3.48, N, 16.24%.

Found: Br, 61.6%. Calcd for $RuBr_2$: Br, 62.2%.

From the above reaction scheme, we have noted that the complexes are dissociated by two different mechanisms, that is, that in which the ruthenium(III) is reduced by the halide ion and that in which the ruthenium(III) is reduced by the ammonia molecule. Of course, the displacement of ligand species by the halide ions in the outersphere of the complex was also observed.

One of the probable factors controlling the two different mechanisms may be the relative reducing power of the ligands, which is presumed, from the order of their reduction potentials, to be $I^- > Br^- > NH_3 > Cl^-$. By this assumption, it can be interpreted that the ruthenium(III) is reduced by the ammonia molecule in the thermal-decomposition reactions of chloro- and bromopentaammine complexes, while the ruthenium(III) is reduced by iodide in the iodopentaammine complex.

The monohalogenopentaammine complexes are thermochemically more stable than the corresponding dihalogeno complexes, while the iodo complexes are the least stable of the series of complexes. This means that the bond nature of the ruthenium(III)-ammine ligand may be reflected by the bond strength of the ruthenium(III)-halogen ligand.

The order of the thermal stability, chloro complexes > bromo complex > iodo complex, is also in agreement with that of the strength of the ruthenium(III)-ammine bond as estimated from the vibrational frequencies of the complexe, *i. e.*, the ν(Ru–N) values are 485, 463 and 451 cm^{-1} for chloropentaammines > 479, 459 and 448 cm^{-1} for bromopentaammine > 468, 450, 442 and 424 cm^{-1} for iodopentaammine, as has been re-

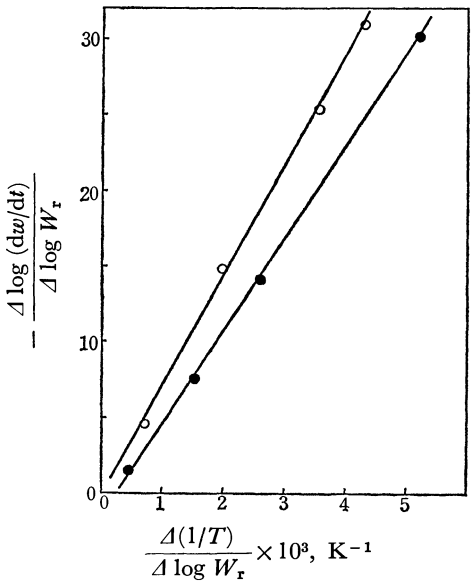

Fig. 9. The plots of Freeman-Carroll equation for the reaction, $[RuI_n(NH_3)_{6-n}]I_{3-n} \rightarrow (6-n)NH_3 + 3/2\ I_2$, $n=1$ and 2. $W_r = w_0 - w$, w_0 = weight loss at completion of reaction, w = total weight loss up to time t. ○ diiodo complex, ● monoiodo complex

ported by Allen and Senoff.[17]

The Thermal-reaction Kinetics. Since the decompositions of iodo complexes were definitely observed to consist of ammonia-gas and free-iodine liberations, the kinetic treatment of the ammonia-gas evolution reaction for two iodo complexes was made using the method of Freeman and Carroll.[19] These kinetic plots are shown in Fig. 9; the activation energies were calculated as follows:

$[RuI(NH_3)_5]I_2 \rightarrow 5NH_3 + RuI_3$, 41.7 ± 0.7 kcal/mol

$[RuI_2(NH_3)_4]I \rightarrow 4NH_3 + RuI_3$, 27.8 ± 0.2 kcal/mol

Wendlandt and Smith[4] reported the activation energy for the deammonia reaction of halogenopentaamminecobalt(III) to be 28 kcal/mol for chloropentaammine and 21 kcal/mol for bromopentaammine. Though the species of the halide ligands are different, these values are smaller than that of iodopentaammineruthenium(III). This fact may suggest that the metal-ammine bond is stronger in the ruthenium(III) complex than in the cabalt(III) complex, because the metal-halide bond strength is rather the reverse.

The authors wish to thank the Ministry of Education for the financial support granted to this research.

References

1) Part V of this series: A. Ohyoshi, S. Shida, F. Kitagawa, and K. Ohkubo, This Bulletin, **46**, 2431 (1973).
2) W. Bilts, *Z. Anorg. Chem.*, **83**, 177 (1913).
3) M. Mori and T. Tsuchiya, This Bulletin, **33**, 841 (1960).
4) W. W. Wendlandt and J. P. Smith, *J. Inorg. Nucl. Chem.*, **25**, 843 (1963).
5) W. W. Wendlandt and J. P. Smith, *ibid.*, **25**, 1267 (1963).
6) G. W. Watt, *Inorg. Chem.*, **3**, 325 (1964).
7) N. Tanaka and M. Nanjo, This Bulletin, **37**, 1330 (1964),
8) N. Tanaka and K. Nagase, *ibid.*, **40**, 546 (1967).
9) N. Tanaka, K. Nagase, and S. Nagakura, *ibid.*, **41**, 1143 (1968).
10) H. I. Schlesinger and R. K. Worner, *J. Amer. Chem. Soc.*, **51**, 3520 (1929).
11) H. I. Schlesinger and D. N. Rickles, *ibid.*, **51**, 3523 (1929).
12) W. W. Wendlandt and C. Y. Chou, *J. Inorg. Nucl. Chem.*, **26**, 943 (1964).
13) N. Tanaka and K. Nagase, This Bulletin, **42**, 2854 (1969).
14) K. Nagase and N. Tanaka, *ibid.*, **45**, 1097 (1972).
15) K. Nagase and N. Tanaka, *ibid.*, **46**, 2435 (1973).
16) J. Trehoux, G. Nowogrocki, D. Thomas, and G. Tridot, *J. Thermal Anal.*, **1**, 171 (1969).
17) A. D. Allen and C. V. Senoff, *Can. J. Chem.*, **45**, 1337 (1967).
18) K. Gleu and W. Breuel, *Z. Anorg. Allg. Chem.*, **237**, 335 (1938).
19) E. S. Freeman and B. Carroll, *J. Phys. Chem.*, **62**, 394 (1958).

The Synthesis and Spectroscopic Study of Some Bis(tertiary-phosphine)bis(*N,N*-dialkylselenocarbamate) Complexes of Palladium(II) and Platinum(II)

Koji TANAKA and Toshio TANAKA

Department of Applied Chemistry, Faculty of Engineering, Osaka University, Yamada-kami, Suita, Osaka 565

(Received July 20, 1973)

Ten *N,N*-dialkylselenocarbamate complexes of palladium(II) and platinum(II), $[(C_6H_5)_3P]_2Pd[SeC(O)NR_2]_2$ (**1**), $[(C_6H_5)_3P]_2Pt[SeC(O)NR_2]_2$ (**2**) (R=CH_3, C_2H_5, *n*-C_3H_7, and *n*-C_4H_9), $[CH_3(C_6H_5)_2P]_2Pd[SeC(O)N(CH_3)_2]_2$ (**3**), and $[CH_3(C_6H_5)_2P]_2Pt[SeC(O)N(CH_3)_2]_2$ (**4**), have been prepared. The infrared spectra and molecular-weight determinations indicate that the selenocarbamate ligand is bonded to the palladium(II) or platinum(II) through the selenium atom, with a free carbonyl group in the solid state, while in **1** and **2** two and one triphenylphosphine dissociate in a dilute solution to exist as compounds with bidentate selenocarbamate, $Pd[SeC(O)NR_2]_2$ and $[(C_6H_5)_3P]Pt[SeC(O)NR_2]_2$, respectively. The ^1H- and ^{31}P-NMR spectra of **3** and **4** reveal that they have a *trans*-configuration. The same configuration is suggested for the *N,N*-dibutyl derivative of **2** on the basis of the spin-spin coupling constant between the ^{31}P and ^{195}Pt nuclei.

Although *N,N*-dialkyldithiocarbamate- and -diselenocarbamate-metal complexes have widely been investigated, there have not been many studies of metal complexes of carbamate with hetero ligand atoms.[1-5] They have been limited only to the *N,N*-dialkylthiocarbamate and *N,N*-dialkylthioselenocarbamate complexes, and a little attention has been paid to the difference in coordination ability to metal between oxygen and sulfur[6] or between sulfur and selenium.[7]

The present work was undertaken in an attempt to prepare a series of *N,N*-dialkylselenocarbamate complexes of palladium and platinum, $[(C_6H_5)_3P]_2M[SeC(O)NR_2]_2$ and $[CH_3(C_6H_5)_2P]_2M[SeC(O)N(CH_3)_2]_2$ (M=Pd(II) and Pt(II); R=CH_3, C_2H_5, and *n*-C_3H_7), in order to elucidate their configurations by the infrared, ^1H-, and ^{31}P-NMR techniques.

Experimental

Physical Measurements. The molecular-weight determinations were carried out by means of a Hitachi-Perkin-Elmer 115 vapor pressure osmometer in chloroform at 30.5 °C. The infrared spectra were recorded on a Hitachi-Perkin-Elmer 225 spectrophotometer in Nujol mulls, and the electronic spectra were measured on a Hitachi 124 spectrophotometer in a dichloromethane solution, using a 1-cm quartz cell. The proton and P-31 NMR spectra were recorded on a Japan Electron Optics PS-100 spectrometer at 100 and 40.5 MHz respectively. The chemical shifts were measured against tetramethylsilane as the internal standard and 85% H_3PO_4 as the external standard, and were calibrated by the audio-frequency side-band technique.

Preparation. *N,N*-Dialkylammonium *N,N*-dialkylselenocarbamates were prepared by the reaction of the appropriate dialkylamine with selenium powder and carbon monoxide in tetrahydrofuran, as has been described elsewhere;[8] they were used as the solutions to prepare metal complexes without isolating them.

The method of preparing the complexes, $[(C_6H_5)_3P]_2M[SeC(O)NR_2]_2$ (M=Pd(II) and Pt(II); R=CH_3, C_2H_5, and *n*-C_3H_7), was basically the same as that for the *N,N*-dibutyl derivatives described in a previous paper;[5] the yields were almost quantitative. A suspension of $[(C_6H_5)_3P]_2MCl_2$ (M=Pd(II) and Pt(II)) (0.5 mmol) in dry benzene (20 ml) was stirred, drop by drop, into a tetrahydrofuran solution (10 ml) of dialkylammonium *N,N*-dialkylselenocarbamate (1.0 mmol) at room temperature, and then the mixture was further stirred for 4 hr. With the *N,N*-dimethyl and *N,N*-diethyl derivatives, the precipitates which appeared were filtered and washed with methanol several times to remove the dialkylammonium chloride. The products were then reprecipitated from a large amount of a chloroform–ether mixture.

$[(C_6H_5)_3P]_2Pd[SeC(O)N(CH_3)_2]_2$ (**1a**), mp 207 °C(decomp).

Found: C, 53.30; H, 4.51; N, 3.01%. Calcd for $C_{42}H_{42}N_2O_2P_2Se_2Pd$: C, 54.06; H, 4.53; N, 3.02%.

$[(C_6H_5)_3P]_2Pd[SeC(O)N(C_2H_5)_2]_2$ (**1b**), mp 202—203 °C (decomp).

Found: C, 56.05; H, 5.23; N, 2.72%. Calcd for $C_{46}H_{50}N_2O_2P_2Se_2Pd$: C, 55.86; H, 5.01; N, 2.83%.

$[(C_6H_5)_3P]_2Pt[SeC(O)N(CH_3)_2]_2$ (**2a**), mp 203—204 °C.

Found: C, 48.68; H, 4.24; N, 2.52%. Calcd for $C_{42}H_{42}N_2O_2P_2Se_2Pt$: C, 49.37; H, 4.14; N, 2.74%.

$[(C_6H_5)_3P]_2Pt[SeC(O)N(C_2H_5)_2]_2$ (**2b**), mp 217—220 °C.

Found: C, 50.79; H, 4.52%. Calcd for $C_{46}H_{50}N_2O_2P_2Se_2Pt$: C, 51.26; H, 4.68%.

In the case of the *N,N*-di-*n*-propyl derivatives, the ammonium chloride appearing in the reaction was filtered off, and the filtrate was evaporated to dryness under reduced pressure at room temperature. The resulting product was washed with a small amount of methanol and was recrystallized from benzene.

$[(C_6H_5)_3P]_2Pd[SeC(O)N(n\text{-}C_3H_7)_2]_2$ (**1c**), mp 185 °C.

Found: C, 57.45; H, 5.59; N, 2.68%; mol wt, 624 (6.83×10^{-3} M), 465 (4.12×10^{-3} M). Calcd for $C_{50}H_{58}N_2O_2P_2Se_2Pd$: C, 57.46; H, 5.59; N, 2.86%; mol wt, 1045.

$[(C_6H_5)_3P]_2Pt[SeC(O)N(n\text{-}C_3H_7)_2]_2$ (**2c**), mp 225 °C.

Found: C, 52.78; H, 5.27; N, 2.52%; mol wt, 832 (5.76×10^{-3} M), 764 (4.61×10^{-3} M). Calcd for $C_{50}H_{58}N_2O_2P_2Se_2Pt$: C, 52.96; H, 5.16; N, 2.47%; mol wt, 1134.

The characterization of the di-*n*-butyl derivatives, $[(C_6H_5)_3P]_2M[SeC(O)N(n\text{-}C_4H_9)_2]_2$ (M=Pd(**1d**) and Pt(**2d**)), was previously reported.[5]

Into $[(CH_3)_2NH_2][SeC(O)N(CH_3)_2]$ (1.0 mmol) in tetrahydrofuran (10 ml), we stirred a suspension of $[CH_3(C_6H_5)_2P]_2PdCl_2$ (0.5 mmol) in benzene (20 ml) over a 3 hr period at room temperature. The resulting dark red solution was filtered to remove the dimethylammonium chloride precipitated, and the solution was evaporated under reduced pressure to yield a red solid. Recrystallization from toluene gave orange crystals of $[CH_3(C_6H_5)_2P]_2Pd[SeC(O)N(CH_3)_2]_2$ (**3**) (0.47 mmol), mp 186—188 °C.

Found: C, 47.61; H, 4.92; N, 3.68%; mol wt, 701 (4.98×10^{-3} M), 745 (1.42×10^{-2} M). Calcd for $C_{32}H_{38}N_2O_2P_2$-

Se_2Pd: C, 47.51; H, 4.74; N, 3.46%; mol wt, 809.

The $[CH_3(C_6H_5)_2P]_2Pt[SeC(O)N(CH_3)_2]_2$ (**4**) was similarly prepared by the reaction of $[CH_3(C_6H_5)_2P]_2PtCl_2$ (0.5 mmol) with the *N*,*N*-dimethylselenocarbamate salt (1.0 mmol); it was recrystallized from toluene to give light yellow crystals (0.45 mmol), mp 182—184 °C.

Found: C, 43.26; H, 4.45; N, 3.18%; mol wt, 800 (3.99×10^{-3} M), 841 (1.33×10^{-2} M). Calcd for $C_{32}H_{38}N_2O_2P_2Se_2Pt$: C, 42.82; H, 4.27; N, 3.12%; mol wt, 898.

Results and Discussion

Properties. The palladium(II) and platinum(II) complexes obtained are stable in air; their solubilities are dependent on the nature of the *N*-alkyl group as well as on the phosphine coordinated. Among the triphenylphosphine complexes, **1d** and **2d** are fairly soluble in non-polar solvents, but less soluble in polar ones, such as acetone, alcohol, and water. **1c** and **2c** are somewhat soluble only in non-polar solvents, but **1a**, **1b**, **2a**, and **2b** are not sufficiently soluble to undergo spectroscopic study. On the other hand, both **3** and **4** are fairly soluble in common organic solvents.

In a previous communication,[5] the molecular-weight determination and the infrared spectra of **1d** and **2d** at various concentrations in solution have been reported to establish that: (i) the selenocarbamate ligand acts as a monodentate through the selenium atom in the solid state, (ii) in solution, partial dissociations of triphenylphosphine result in the ligand acting in a bidentate manner, and (iii) in a dilute solution, the palladium(II) and platinum(II) complexes dissociate into three and two species, and mainly exist as the following species, A and B respectively. Al-

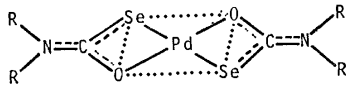

A

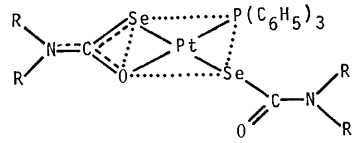

B

though the molecular-weights of **1c** and **2c** could not be determined at high concentrations due to their limited solubility, they exhibit a concentration dependence of the molecular weight similar to the cases of **1d** and **2d**, as is shown in Fig. 1.

The infrared spectra of **1c** and **2c** in the solid state show a strong band due to the ν(C=O) at about 1600 cm^{-1}, while in dichloromethane solution an additional weak band appears around 1540 cm^{-1}, as is listed in Table 1. The band in the 1540 cm^{-1} region is intensified by a decrease in the concentration of the solution, and at the same time the 1600 cm^{-1} band is weakened; these bands may be assigned to the carbonyl groups coordinated and uncoordinated to the metal atom. This infrared behavior is coincident with that of **1d** and **2d**.[5] Thus, conclusions (i)—(iii) for **1d** and **2d**

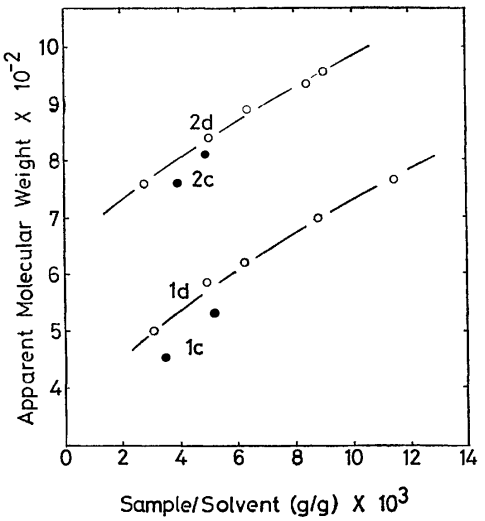

Fig. 1. Apparent molecular weights of $[(C_6H_5)_3P]_2Pd[SeC(O)N(n\text{-}C_3H_7)_2]_2$ (**1c**), $[(C_6H_5)_3P]_2Pt[SeC(O)N(n\text{-}C_3H_7)_2]_2$ (**2c**), $[(C_6H_5)_3P]_2Pd[SeC(O)N(n\text{-}C_4H_9)_2]_2$ (**1d**), and $[(C_6H_5)_3P]_2Pt[SeC(O)N(n\text{-}C_4H_9)_2]_2$ (**2d**) at various concentrations in chloroform.

TABLE 1. ν(C=O) FREQUENCY (cm^{-1}) OF THE COMPLEXES

Complex[a]		ν(C=O)[b]
$[(C_6H_5)_3P]_2Pd(dmsc)_2$	(**1a**)	1599 s
$[(C_6H_5)_3P]_2Pd(desc)_2$	(**1b**)	1589 s
$[(C_6H_5)_3P]_2Pd(dpsc)_2$	(**1c**)	1590 s (1589 s, 1537 m)
$[(C_6H_5)_3P]_2Pd(dbsc)_2$	(**1d**)	1600 s (1592 s, 1532 m)
$[CH_3(C_6H_5)_2P]_2Pd(dmsc)_2$	(**3**)	1599 s (1592 s, 1540 vw)
$[(C_6H_5)_3P]_2Pt(dmsc)_2$	(**2a**)	1603 s
$[(C_6H_5)_3P]_2Pt(desc)_2$	(**2b**)	1595 s
$[(C_6H_5)_3P]_2Pt(dpsc)_2$	(**2c**)	1598 s (1599 s, 1540 sh)
$[(C_6H_5)_3P]_2Pt(dbsc)_2$	(**2d**)	1603 s (1595 s, 1540 sh)
$[CH_3(C_6H_5)_2P]_2Pt(dmsc)_2$	(**4**)	1603 s (1603 s)

a) dmsc: $SeC(O)N(CH_3)_2$, desc: $SeC(O)N(C_2H_5)_2$, dpsc: $SeC(O)N(n\text{-}C_3H_7)_2$, and dbsc: $SeC(O)N(n\text{-}C_4H_9)_2$. b) s, strong; m, medium; sh, shoulder; vw; very weak. The wave number in parentheses are those in dichloromethane solution (1.0 mm cell, 0.8 wt%).

presented above are reasonable for **1c** and **2c** also.

On the other hand, the molecular-weight determination indicates that both **3** and **4** are less dissociated than the triphenylphosphine complexes in solution. In accordance with this, the infrared spectra of these complexes show little change between the solid state and in solution, even in a very dilute solution.

NMR Spectra. As is shown in Table 2, the complexes of **3** and **4** in dichloromethane exhibit two N–CH_3 proton signals resulting from the restricted rotation around the carbamate C—N bond at low temperatures, although at room temperature broad singlets due to the N–CH_3 are observed. The approximate coalescence temperature was about −5 °C for both complexes. This temperature is considerably lower than that of $(CH_3)_2Sn[SeC(O)N(CH_3)_2]_2$ (50 °C) in nitrobenzene, which has a bidentate selenocarbamate, though the coordination of the carbonyl oxygen to the tin atom is weak.[4] This result suggests that the

Table 2. ^{1}H- and ^{31}P-NMR parameters of the complexes in chloroform solution; concd. 5.0 and 12 wt%, respectively

Complex		δ(N-CH_3) ppm	δ(P-CH_3) ppm	$\Delta(^{31}P)$[a] ppm
$[(C_6H_5)_3P]_2Pd(dbsc)_2$	(**1d**)			−29.0
$[CH_3(C_6H_5)_2P]_2Pd(dmsc)_2$	(**3**)	2.56 2.57[b] 2.46	2.35	−35.2
$[(C_6H_5)_3P]_2Pt(dbsc)_2$	(**2d**)			−25.6
$[CH_3(C_6H_5)_2P]_2Pt(dmsc)_2$	(**4**)	2.57 2.56[b] 2.49	2.43	−31.2

a) $\Delta=\delta(^{31}P)_{complexed}-\delta(^{31}P)_{free}$; $\delta(^{31}P)_{(C_6H_5)_3P}=5.6$ and $\delta(^{31}P)_{CH_3(C_6H_5)_2P}=28.1$ ppm from 85% H_3PO_4. b) Measured at −15°C.

double-bond character of the carbamate C–N bond of **3** and **4** is small, resulting from the fact that only the selenium atom attaches to the palladium(II) or platinum(II).

The P–CH_3 signal of **3** and **4** appears as a triplet, and the latter compound exhibits an additional triplet of the satellite in the higher magnetic field (this triplet results from spin interaction between the ^{195}Pt and (P-)CH_3 protons), whereas the lower satellite is obscured by the N-CH_3 signal, as is depicted in Fig. 2. This kind of "virtual coupling" phenomenon[9] establishes a *trans* disposition of the phosphine in the square-planar complexes of **3** and **4**.

Fig. 3 shows the ^{31}P-NMR spectra of the complexes, together with those of the free phosphines. **1d** shows a broad signal of the ^{31}P nucleus, which may be due to a dissociative exchange of $(C_6H_5)_3P$ in solution. On the other hand, a sharp signal of the ^{31}P is observed in the remaining complexes. In addition, the Pt(II) complexes exhibit the satellite due to a spin-spin interaction with the ^{195}Pt nucleus, while no coupling between the ^{31}P and ^{77}Se nuclei has been observed. Moreover, no appreciable change in the ^{31}P chemical shift occurred, even when a large excess of the phosphines was added to the solution, in contrast to the the case of **1d**. That the $J(^{195}Pt-^{31}P)$ value of **2d** is comparable to those of **4** and some *trans*-bis(tertphosphine)platinum(II) dichlorides (J=2385—2531Hz)[10,11] leads us to the conclusion that **2d** is also of a *trans* configuration.

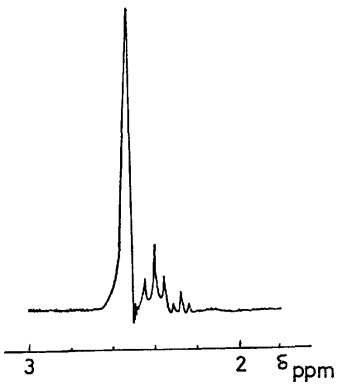

Fig. 2. PMR spectrum of $[CH_3(C_6H_5)_2P]_2Pt(dmsc)_2$ (**4**); 5wt% in $CHCl_3$.

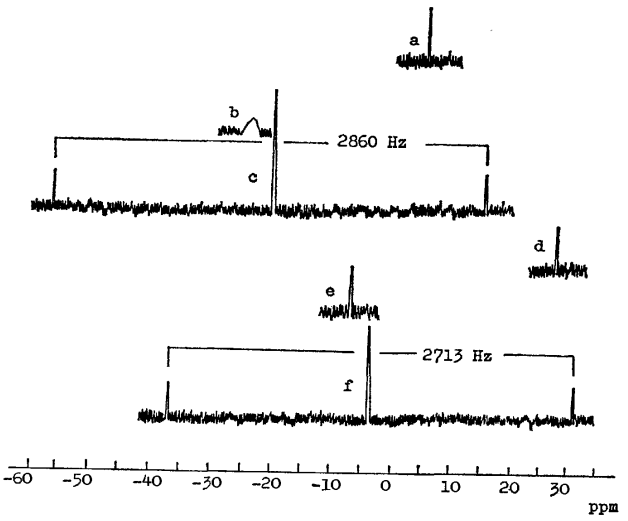

Fig. 3. ^{31}P-NMR spectra of $(C_6H_5)_3P$ (a), $[(C_6H_5)_3P]_2M(dbsc)_2$ (M=Pd (b), Pt (c)), $CH_3(C_6H_5)_2P$ (d), and $[CH_3(C_6H_5)_2P]_2M(dmsc)_2$ (M=Pd (e), Pt (f)) in $CHCl_3$; conc. 12 wt%.

Table 2 also lists the coordination chemical shifts, which are defined as the ^{31}P chemical shifts (relative to 85% H_3PO_4) of the complexes minus that of the free phosphine.[12] It may be noted that the coordination chemical shifts of the methyldiphenylphosphine complexes are larger than those of the triphenylphosphine complexes, while the reverse is true for the $J(^{195}Pt—^{31}P)$ value. A similar finding with regard to the ^{31}P-NMR spectra has been reported on *cis*-bis-(triphenylphosphine)-[13] and bis(methyldiphenylphosphine)-platinum-(II) dichloride,[10] in which the phosphines acting as good σ donors produce a large down-field shift upon coordination, whereas the π bonding with the platinum-(II) causes an up-field shift. Thus, the difference in coupling constants between **2d** and **4** may be ascribed to an increase in the π bonding character of the Pt–P bond in the former complex.

Electronic Spectra. The electronic spectra of some complexes are summarized in Table 3. The apparent spectrum of **1d** changes gradually with an increase in the amounts of triphenylphosphine added to the solution, possibly because of a considerable dissociation of triphenylphosphine of **1d** in the measured concentration. Thus, the data for **1d** are those measured in the presence of a large excess of triphenylphosphine.

TABLE 3. ELECTRONIC SPECTRA OF SOME COMPLEXES IN DICHLOROMETHANE; BAND MAXIMA IN nm AND log ε IN PARENTHESES

		CT band	d-d band	
$[(C_6H_5)_3P]_2Pd(dbsc)_2$	(**1d**)	340 (4.12)	494 (2.52)	410 (3.47)
$[CH_3(C_6H_5)_2P]_2Pd(dmsc)_2$	(**3**)	325 (4.20)	474 (2.52)	390 (3.40)
$[(C_6H_5)_3P]_2Pt(dbsc)_2$	(**2d**)	280 (4.23)	398 (2.50)	336 (3.46)
$[CH_3(C_6H_5)_2P]_2Pt(dmsc)_2$	(**4**)	273 (4.35)	383 (2.68)	322 (3.45)

On the contrary, there was no appreciable change in the spectra of the remaining complexes when an excess amount of the phosphines was added to the solution. As may be seen in Table 3, the d-d bands of **3** and **4** appear at wavelength shorter by about 20 nm than those of **1d** and **2d**, indicating a stronger ligand field for methyldiphenylphosphine than for triphenylphosphine.

References

1) E. M. Krankovits, R. J. Magee, and M. J. O'Connor, *Inorg. Nucl. Chem. Lett.*, **7**, 541 (1971).
2) B. J. McCormick and B. P. Stomer, *Inorg. Chem.*, **11**, 729 (1972).
3) E. W. Abel and M. O. Dunster, *J. Chem. Soc., Dalton*, **1973**, 98.
4) K. Tanaka, S. Araki, and T. Tanaka, This Bulletin, **46**, 2136 (1973).
5) K. Tanaka and T. Tanaka, *Inorg. Nucl. Chem. Lett.*, **9**, 429 (1973).
6) R. F. Dalton and K. Jones, *J. Chem. Soc., A*, **1970**, 590.
7) T. Kamitani and T. Tanaka, *Inorg. Nucl. Chem. Lett.*, **6**, 91 (1970); N. Sonoda and T. Tanaka, *J. Inorg. Nucl. Chem.*, **35**. 1145 (1973).
8) N. Sonoda, T. Yasuhara, K. Kondo, T. Ikeda, and S. Tsutsumi, *J. Amer. Chem. Soc.*, **93**, 6344 (1971); K. Kondo, Sonoda, Y. Yoshida, M. Koishi, and S. Tsutsumi, *Chem. Lett.*, **1972**, 401.
9) J. M. Jenkins and B. L. Shaw, *J. Chem. Soc., A*, **1966**, 770.
10) S. O. Grim, R. L. Keiter, and W. McFarlane, *Inorg. Chem.*, **6**, 1123 (1967).
11) The J values of *cis*-bis(*tert*-phosphine)platinum(II) dichlorides are in the range of 3500—3641 Hz; Ref. 10.
12) S. O. Grim, D. A. Wheatland, and W. McFarlane, *J. Amer. Chem. Soc.*, **89**, 5573 (1967).
13) J. F. Nixon and A. Pidcock, *Ann. Rev. NMR Spectroscopy*, **2**, 345 (1969).

Kinetic Studies of the Electron Transfer Reaction in Iron(II) and Iron(III) Systems. VI. Reaction in *N,N*-Dimethylformamide[1]

Goro WADA, Yoshiko SAHIRA, Kyoko OHSAKI, and Fusako SHINODA

Department of Chemistry, Nara Women's University, Nara 630

(Received August 2, 1973)

The electron transfer reaction between Fe(II) and Fe(III) in *N,N*-dimethylformamide (DMF) was found to be influenced by the presence of perchloric acid, chloride ion, and water in the reaction system. This suggests that the reaction involves chemical species such as partially hydrated iron, its deprotonated iron, and $FeCl^{2+}$ and $FeCl_2^+$. The individual rate constants in DMF, containing a small amount of water, are $k_0=33.6\ M^{-1}s^{-1}$ for Fe^{2+}–Fe^{3+}, $k_1=1.2\times10^2\ M^{-1}s^{-1}$ for Fe^{2+}–$FeCl^{2+}$, and $k_2=\sim10^3\ M^{-1}s^{-1}$ for Fe^{2+}–$FeCl_2^+$ at $\mu=0.20$ M and 25 °C. The formation constant for $FeCl^{2+}$ was determined to be $K_1=(2.0\pm0.3)\times10^4\ M^{-1}$ at $\mu=0.20$ M and 25 °C. In the mixed solvents of DMF and water, the apparent rate constant exhibited a minimum at a certain water concentration. The activation parameters for the reactions Fe^{2+}–Fe^{3+} and Fe^{2+}–$FeCl^{2+}$ are $\Delta H_0^{\neq}=8.3$ kcal/mol, $\Delta S_0^{\neq}=-24$ cal/deg·mol, $\Delta H_1^{\neq}=4.5$ kcal/mol, and $\Delta S_1^{\neq}=-34$ cal/deg·mol, respectively. The results are compared with those in H_2O, D_2O, and DMSO.

The electron transfer reaction between iron(II) and iron(III) has been investigated in various solvents. In protic solvents such as water[2,3] and mixed solvents of water with some alcohols,[1,4,5] the predominant reaction path in the absence of catalytical bridging ligand was deduced to be one *via* a hydrogen-atom-transfer mechanism, first proposed by Reynolds and Lumry.[6] On the other hand, in dimethyl sulfoxide (DMSO)[7] as an aprotic solvent, the reaction was found to proceed faster than in water, although the hydrogen-atom-transfer mechanism does not seem to occur in aprotic solvents. In such a medium, therefore, an inner-sphere mechanism should be more favorable.

In this study, *N,N*-dimethylformamide(DMF), another aprotic solvent, of a little larger basicity than DMSO,[8,9] was adopted in order to see how its properties reflect on the reaction mechanism. Dependence upon the concentrations of acid, chloride ion, and water was investigated.

Experimental

Materials. Commercial DMF of E. P. grade (Nakarai Chemicals, Ltd.) was dried over potassium carbonate and sodium sulfate, and distilled twice under reduced pressure of nitrogen at about 40 °C. DMF solution of perchloric acid, prepared by mixing 70% perchloric acid of reagent grade and pure DMF, was used soon after preparation. The water content introduced by this method was about twice in molarity of the acid concentration in DMF. The concentration of water was kept constant at 0.3 M, unless otherwise stated.

An extremely anhydrous acid solution could be made up either by dissolving an anhydrous solid acid such as crystal of toluenesulfonic acid in DMF, or by passing a DMF solution of ammonium perchlorate through a column of cation-exchange resin of H-form. However, the former method was not free from the anion effect upon the reaction and the latter was accompanied by a small degree of decomposition of DMF during the treatment, deteriorating the reproducibility of the rate measurements considerably. Thus neither method was employed in the present preparation.

Other materials used were prepared by the procedure described elsewhere.[7,10] The ionic strength of the solution was controlled with sodium perchlorate at $\mu=0.20$ M. Radioactive iron-59 was used as a tracer.

Apparatus and Procedure. The methods for determining the formation constants and the rate constants were similar to those described previously.[7,10,11]

Results and Discussion

Reaction Order with Respect to Iron Concentrations. The reaction rate R of the electron transfer reaction, Fe(II)+*Fe(III)→Fe(III)+*Fe(II), is expressed by the following McKay's relation,[12]

$$R=\frac{0.693[\mathrm{Fe(II)}][\mathrm{Fe(III)}]}{\{[\mathrm{Fe(II)}]+[\mathrm{Fe(III)}]\}t_{1/2}} \quad (1)$$

where [Fe(II)] and [Fe(III)] represent the total concentrations of iron(II) and iron(III) species, respectively, and $t_{1/2}$ the half-life period of the reaction. If the reaction is of the first order with respect to each of [Fe(II)] and [Fe(III)], the apparent second-order rate constant k_{app} of the reaction can be obtained by the following equation, which should give a constant value at different iron concentrations under a fixed condition, this being proved in Table 1.

$$k_{app}=\frac{0.693}{\{[\mathrm{Fe(II)}]+[\mathrm{Fe(III)}]\}t_{1/2}} \quad (2)$$

Acid Dependence. The reaction rate was influenced by the concentration of perchloric acid in the concentration range 0.03—0.15 M; the higher the acid concentration the slower the reaction. When k_{app} was plotted against the reciprocal acid concentra-

Table 1. Constancy of second-order rate constants at fixed acid and water concentrations at $\mu=0.20$ M and 25 °C

$[HClO_4]$ M	$[H_2O]$ M	[Fe(II)] 10^{-4} M	[Fe(III)] 10^{-4} M	$t_{1/2}$ s	k_{app} $M^{-1}s^{-1}$
0.15	0.3	1.55	0.10	112	37.5
		1.26	0.34	120	36.9
		0.972	0.12	172	36.9
0.05	1.80	1.61	0.12	155	25.9
		1.22	0.20	161	30.6
		0.73	0.23	272	26.5
		0.59	0.21	305	28.7

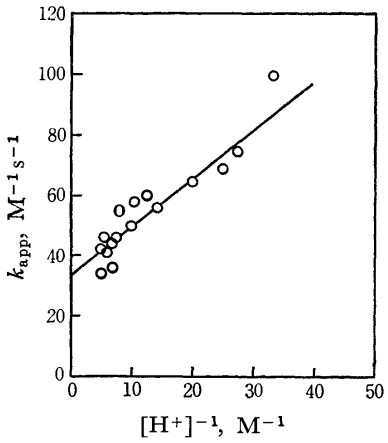

Fig. 1. Dependence of k_{app} upon $[H^+]^{-1}$ at $[H_2O]=0.3$ M, $\mu=0.20$ M, and 25 °C in DMF.

tion, a straight line was obtained with an intercept 33.6 $M^{-1}s^{-1}$ and a slope 1.71 s^{-1} at 25 °C, as is shown in Fig. 1. This implies that the reaction involves a path with a deprotonated species of the reactant. Thus, the acid-dependent reaction scheme in the presence of water in DMF is deduced as follows:

$$Fe^{2+} + {}^*Fe^{3+} \rightarrow Fe^{3+} + {}^*Fe^{2+} \quad (k_o) \qquad (3)$$

$$Fe^{2+} + {}^*Fe(-H)^{2+} \rightarrow Fe(-H)^{2+} + {}^*Fe^{2+} \quad (k_H) \qquad (4)$$

where $Fe(-H)^{2+}$ stands for an iron(III) species, of which one coordinated solvent molecule is deprotonated, keeping an equilibrium with acid concentration in the medium, and Fe^{2+} and Fe^{3+} stand for normally solvated ones.

Since DMF is more basic than DMSO,[8,9] it is not likely that the solvating DMF dissociates to lose a proton as an acid. The deprotonated species $Fe(-H)^{2+}$ might be one attributed to a coordinating water molecule which is present in the solvent. Thus, k_{app} can be expressed by the following equation, in which K_H is defined as the dissociation constant of the equilibrium $Fe^{3+} \rightleftarrows Fe(-H)^{2+} + H^+$.

$$k_{app} = \frac{k_o + k_H K_H/[H^+]}{1 + K_H/[H^+]} \qquad (5)$$

Accordingly, $k_{app}(1+K_H/[H^+])$ should have a linear relationship with $[H^+]^{-1}$. The value of K_H is not known here but since $K_H/[H^+]$ seems to be negligibly small as compared with unity, k_{app} would also exhibit an approximate linearity with $[H^+]^{-1}$, as is evident from Fig. 1. Thus, k_0 and $k_H K_H$ are found to be $k_0=33.6$ $M^{-1}s^{-1}$ and $k_H K_H=1.71$ s^{-1}, respectively.

The value of k_0 is very close to that of the corresponding reaction in DMSO, 34.4 $M^{-1}s^{-1}$.[10] On the other hand, the value of $k_H K_H$ is difficult to be quantitatively analyzed. However, when *N*-methylacetamide or *N*,*N*-dimethylacetamide partially coordinates with iron(III) in aqueous solution, the electron transfer reaction is known still to occur *via* path 4.[13] It is not absurd to consider that the reaction can occur in a similar way in water-containing DMF.

Formation Constants of Fe(III)-Cl⁻ Complex. When sodium chloride is added to iron(III) perchlorate solution at $[Cl]=3.53\times10^{-4}$ M, $[Fe(III)]=4.92\times10^{-5}$ M, $[H^+]=0.15$ M in DMF, the optical absorbance in

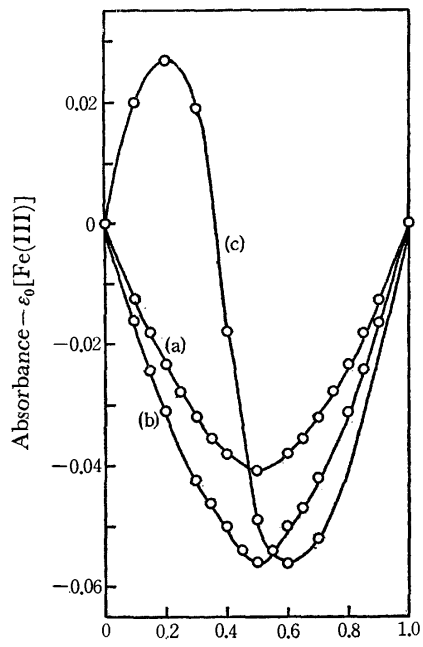

Fig. 2. Job's continuous variation curves for Fe(III) and Cl^- at $[H^+]=0.15$ M, $[H_2O]=0.3$ M, $\mu=0.20$ M, and 25 °C in DMF.
(a) $[Fe(III)]+[Cl]=1.4\times10^{-4}$ M at 290 nm
(b) $[Fe(III)]+[Cl]=1.8\times10^{-4}$ M at 290 nm
(c) $[Fe(III)]+[Cl]=2.0\times10^{-3}$ M at 440 nm

the wavelength range 280—400 nm diminishes as a whole with a peak at *ca.* 340 nm and a minimum at *ca.* 290 nm. In Fig. 2, Job's curves are given at different total concentrations of iron(III) and chloride ion at $[H_2O]=0.3$ M, $\mu=0.2$ M, and $[H^+]=0.15$ M, where the acid concentration is so high that the influence of the deprotonation of iron(III) species is removed. Curves (a) and (b) indicate that a 1 : 1 complex is formed between iron(III) and chloride ion at lower total concentrations and curve (c) that, at a higher concentration, a higher complex, probably of a composition of $FeCl_2^+$, is formed. The formaiton constant, $K_1=[FeCl^{2+}]/[Fe^{3+}][Cl^-]$, and the molar absorptivity ε_1^{290} for $FeCl^{2+}$ are calculated[11] from the curves (a) and (b) at 25 °C and 16 °C as follows.

$$\left.\begin{aligned} K_1 &= (2.0\pm0.3)\times10^4\ M^{-1} \\ \varepsilon_1^{290} &= (5.35\pm0.06)\times10^3\ M^{-1}cm^{-1} \end{aligned}\right\} \ 25\ °C$$

$$\left.\begin{aligned} K_1 &= (1.9\pm0.4)\times10^4\ M^{-1} \\ \varepsilon_1^{290} &= (5.20\pm0.05)\times10^3\ M^{-1}cm^{-1} \end{aligned}\right\} \ 16\ °C$$

Both K_1 and ε_1^{290} seem to be independent of temperature. The K_1 value at 25 °C is about five times greater than that in DMSO, $K_1=3.7\times10^3$ M^{-1}.[11]

Catalysis by Chloride Ion. The electron transfer reaction is accelerated by the presence of chloride ion; its apparent rate constant grows higher as the concentration of chloride ion increases at a constant acid concentration, $[H^+]=0.15$ M. If chloroiron(III) complexes such as $FeCl^{2+}$ and $FeCl_2^+$ are involved in the reaction, the following two paths may occur in addition to 3 and 4:

$$Fe^{2+} + {}^*FeCl^{2+} \rightarrow FeCl^{2+} + {}^*Fe^{2+} \quad (k_1) \qquad (6)$$

$$Fe^{2+} + {}^*FeCl_2^+ \rightarrow FeCl_2^+ + {}^*Fe^{2+} \quad (k_2) \qquad (7)$$

The apparent rate constant k_{app} is expressed by

$$k_{app} = \frac{k_0 + k_H K_H/[H^+] + k_1 K_1 [Cl^-] + k_2 K_1 K_2 [Cl^-]^2}{1 + K_H/[H^+] + K_1[Cl^-] + K_1 K_2 [Cl^-]^2} \qquad (8)$$

where K_2 represents the second stepwise formation constant of $FeCl_2^+$, which is roughly estimated to be about $10^3\ M^{-1}$ from a simple comparison with that of DMSO. According to Eq. 8, the following linearity between Y and $[Cl^-]$ should be established, where D is the denominator in Eq. 8.

$$Y = \frac{k_{app} \cdot D - (k_0 + k_H K_H/[H^+])}{[Cl^-]}$$

$$= k_1 K_1 + k_2 K_1 K_2 [Cl^-] \qquad (9)$$

The linearity is proved in Fig. 3. The intercept and slope of the straight line give the values $k_1K_1 = 2.37 \times 10^6 M^{-2} s^{-1}$ and $k_2K_1K_2 = 4.64 \times 10^{10} M^{-3} s^{-1}$, respectively. By using the values of K_1 and K_2, the individual rate constants are obtained as follows.

$$k_1 = 1.2 \times 10^2\ M^{-1} s^{-1}$$

$$k_2 = \sim 10^3\ M^{-1} s^{-1}$$

Dependence upon Water Concentrations. Since the DMF we used inevitably contained a small amount of water, it was necessary to examine the influence of water upon the rate constants. When the water concentration was changed in DMF as mixed solvents, the value of k_{app} decreases with the increase in water concentration and reaches a broad minimum, beyond which it increases at a constant acid concentration. The minimum points of k_{app} appear at about 2 and 4 M of water concentration when the fixed acid concentrations are 0.01 M and 0.05 M, respectively. Such behaviors of water are reproduced in Fig. 4. The value of k_{app} is always smaller at higher acid concentrations within the water concentration range studied.

In aqueous DMF, the partially-hydrated iron species such as $Fe(III)(H_2O)_x(DMF)_{6-x}$ should be considered

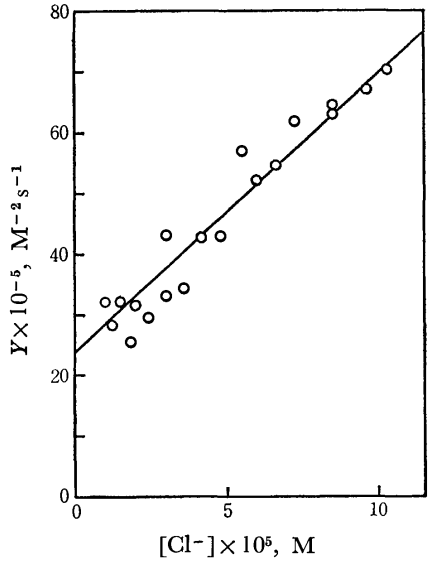

Fig. 3. Linear relationship between Y and $[Cl^-]$ at $[H^+] = 0.15$ M, $[H_2O] = 0.3$ M, $\mu = 0.20$ M, and 25 °C in DMF.

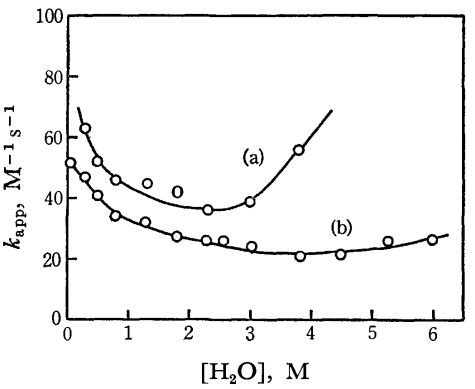

Fig. 4. Dependence of k_{app} upon $[H_2O]$ at $\mu = 0.20$ M and 25 °C in DMF.
(a) $[H^+] = 0.01$ M, (b) $[H^+] = 0.05$ M

to be involved in the electron transfer reaction. Judging from the fact that k_{app} is dependent upon the acid concentration, the deprotonated species of the hydrated iron, $Fe(III)(OH^-)(H_2O)_{x-1}(DMF)_{6-x}$, seems also to take part in the reaction with a larger rate constant than that due to the unhydrolyzed one. Since the formation constants and hydrolysis constants for the iron species hydrated to various extents are not known, the individual rate constants cannot be estimated.

The phenomenon that k_{app} exhibits a minimum at a certain water concentration when the acid concentration is constant, has been also observed in the cases of mixed solvents of DMSO and water.[7] As the water content varies from zero to 100%, the predominant mechanism of the reaction may also turn from an inner-sphere type to a hydrogen-atom-transfer one in DMF as in DMSO.

The DMSO used for the first investigation on the electron transfer reaction between iron(II) and iron(III) contained water at as high as $[H_2O] = 0.015$ M.[7] The water concentration was much higher than those of reactants 10^{-5}—10^{-4} M. However, since DMSO is very hydrophilic[14] and water is likely to be preferentially excluded from the coordination sphere of metal ions in DMSO-rich mixed solvents of DMSO and water,[15] the occurrence of partially hydrated iron species was not so great as expected. This might be the case with DMF, although the water concentration is larger.

An important difference between DMSO and DMF is as follows. In the former, the acid dependence of k_{app} tends to disappear[7] or become smaller at least[10] as the water concentration is lowered. In the latter, it tends to remain according to the extrapolation of water concentration to zero. The reason for this is not clear at present.

Activation Parameters and General Discussion. Kinetic measurements were carried out at 10 °C—35 °C at intervals of five degrees. The activation parameters, $\Delta H_0^{\neq}$, $\Delta S_0^{\neq}$, $\Delta H_1^{\neq}$, and $\Delta S_1^{\neq}$ were calculated from the linearity between $\log(k_0/T)$ and $\log(k_1/T)$ *vs.* T^{-1}, respectively. The results are listed in Table 2, along with various related data in other solvents in literature. The data related to DMF may be approximately regarded as those in pure DMF.

TABLE 2. SUMMARY OF RATE CONSTANTS AND ACTIVATION PARAMETERS IN VARIOUS SOLVENTS

Solvent	Dielectric constants	Condition μ, temp. °C	k_0 $M^{-1}s^{-1}$	k_1 $M^{-1}s^{-1}$	k_2 $M^{-1}s^{-1}$	$\Delta H_0^{\neq}$ kcal/mol	$\Delta S_0^{\neq}$ cal/deg·mol	$\Delta H_1^{\neq}$ kcal/mol	$\Delta S_1^{\neq}$ cal/deg·mol	$\log K_1$ (M^{-1})
H_2O[3,16]	80	0.5, 25°	4.0	22.8(20°)	53(20°)	10.5	−20.6	11.0	−15	1.48
D_2O[3,16]	79	0.5, 25°	1.0	9.1(20°)	—	—	—	13.2	−10	—
DMSO[7,10,17]	46.7	0.2, 20°	34.4(25°)	1.3×10^2 (μ=0.1)	1.02×10^3 (μ=0.1)	9.7	−19	5.2	−27	3.62
DMF	36.1	0.2, 25°	33.6	1.2×10^2	$\sim10^3$	8.3	−24	4.5	−34	4.30

The rate constants and activation parameters for DMSO and DMF are very close. This suggests that the solvent effects on the reaction are similar to each other, and accordingly the reaction scheme is the same. DMF, as well as DMSO, is a unique aportic solvent in which the value of k_0 is larger than that in water.

A DMF molecule coordinates with an iron ion on the oxygen atom,[18] and has a tendency to be hydrolyzed to give formate ion and dimethylamine in the presence of hydroxide ion in DMF–water mixture.[19] Thus, it is probable that hydroxide ion reacts with DMF intramolecularly in the coordination sphere of an $Fe(OH^-)(DMF)$-type complex in the case of DMF–water mixed solvents, making the electron transfer reaction somewhat more complicated.

The value of the formation constant of $FeCl^{2+}$, $\log K_1$ in Table 2, varies in the sequence H_2O <DMSO <DMF, being in line with what is expected from the dielectric constants of the solvents.

References

1) Part V of this series: G. Wada and A. Endo, This Bulletin, **45**, 1073 (1972).
2) J. Silverman and R. W. Dodson, *J. Phys. Chem.*, **56**, 846 (1952).
3) S. Fukushima and W. L. Reynolds, *Talanta*, **11**, 283 (1964).
4) N. Sutin, *J. Phys. Chem.*, **64**, 1766 (1960).
5) R. A. Horne, "Exchange Reactions," I.A.E.A., Vienna, (1965), p. 67.
6) W. L. Reynolds and R. W. Lumry, *J. Chem. Phys.*, **23**, 2460 (1955).
7) J. Menashi, W. L. Reynolds, and G. van Auken, *Inorg. Chem.*, **4**, 299 (1965).
8) G. Wada, This Bulletin, **42**, 890 (1969).
9) G. Wada and T. Takenaka, *ibid.*, **44**, 2877 (1971).
10) G. Wada, N. Yoshizawa, and Y. Sakamoto, *ibid.*, **44**, 1018 (1971).
11) G. Wada, *ibid.*, **41**, 882 (1968).
12) H. A. C. McKay, *Nature*, **42**, 997 (1938).
13) G. Wada and R. Yoshihara, *Kogyo Kagaku Zasshi*, **73**, 2309 (1970).
14) G. Wada and M. Aoki, This Bulletin, **44**, 3056 (1971).
15) S. Thomas and W. L. Reynolds, *Inorg. Chem.*, **9**, 78 (1970).
16) N. Sutin, J. K. Rowley, and R. W. Dodson, *J. Phys. Chem.*, **65**, 1248 (1961).
17) G. Wada and W. L. Reynolds, *Inorg. Chem.*, **5**, 1354 (1966).
18) C. I. Lin and N. C. Li, *J. Inorg. Nucl. Chem.*, **32**, 2796 (1970).
19) E. Buncel, S. Kesmarky, and E. A. Symons, *Chem. Commun.*, **1971**, 120.

Association Involving Optically Active Ions. III. Pfeiffer Effect in Tris(phenanthroline)-zinc(II) or -nickel(II) -Alkaloid Systems

Kazuko OGINO* and Tokue KUMAGAI**

Department of Chemistry, Faculty of Science, Tohoku University, Aoba, Aramaki, Sendai 980

(Received October 11, 1973)

Pfeiffer effect was studied in aqueous solutions containing tris(phenanthroline)metal(II) (metal=zinc or nickel) complexes and various alkaloids. The results were interpreted quantitatively from the viewpoint of stereoselective association and the resulting equilibrium shift. The contribution of π-π interaction between the complex and the alkaloid conjugate systems to the stereoselective association is suggested. NMR data were found to be consistent with the π-π interaction. Relation between the sign of the Pfeiffer rotation and the absolute configuration of the complex is presumed.

The induction of new optical activity by the addition of some resolvable complexes to a solution containing optically active substances is known as Pfeiffer effect.[1] It has been interpreted from the viewpoint of equilibrium shift,[1-6] configurational activity,[3] differential association,[2] hydrophobic bonding,[6] *etc.* However, few quantitative analyses based on the mechanisms listed above have been reported. In this paper, Pfeiffer rotation was measured in solutions containing various alkaloids, and a quantitative analysis of Pfeiffer rotation from the viewpoint of differential association and the resulting equilibrium shift was attempted.

Experimental

Optical rotatory dispersion curves were obtained with a Jasco UV/ORD 5 spectrophotometer equipped with a constant temperature cell compartment. Nuclear magnetic resonance spectra were recorded on a Varian A-60 spectrometer. The complexes $[Zn(phen)_3]Cl_2 \cdot 6H_2O$ and $[Ni(phen)_3]Cl_2 \cdot 6H_2O$ were obtained by mixing the corresponding metal chloride with stoichiometric amount of phenanthroline and recrystallized from water. Alkaloid hydrochlorides were obtained by neutralizing the free base with an equivalent amount of hydrochloric acid. All other chemicals were of guaranteed reagent grade.

Results and Discussion

Optical rotatory dispersion curves were recorded from 350 to 650 nm in aqueous solutions containing phenanthroline complexes, alkaloid monohydrochloride and some electrolyte in a 1 cm cell. Fig. 1 shows the curves in a solution containing 0.02 M $[Ni(phen)_3]^{2+}$, 0.02 M cinchonine hydrochloride and 0.5 M NaCl. An instantaneous change in rotation takes place after mixing the solution. Rotation at this stage is denoted by α_i. A further change in rotation proceeds gradually and after *ca.* 70 hours a final value, α_∞ is reached. This slow change is considered to be due to the inversion of configuration of the complex. The rotatory dispersion curve of cinchonine hydrochloride (denoted by α_X) is also given in Fig. 1. In the case of zinc complex, the inversion of configuration is so rapid

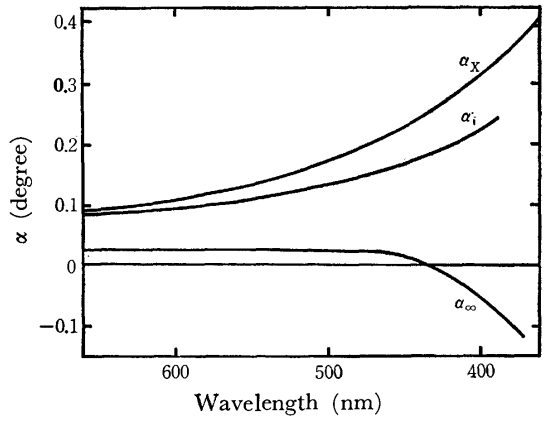

Fig. 1. Optical rotatory dispersion curves of 0.02 M cinchonine hydrochloride (α_X) and a solution containing 0.02 M cinchonine hydrochloride, 0.02 M $[Ni(phen)_3]Cl_2$ and 0.5 M NaCl(α_i and α_∞). The α_i curve was measured immediately after mixing and the α_∞ curve at equilibrium. Cell lengh, 1 cm; temperature, 30 °C.

that only the α_∞ value is measured. The overall rotational change is defined as the Pfeiffer rotation in this paper:

$$\alpha_P = \alpha_\infty - \alpha_X$$

Nature of Alkaloids. The Pfeiffer rotations with various alkaloids are tabulated in Table 1. The α_P values were obtained most accurately at 400 nm, and data at this wavelength are given. The magnitude of Pfeiffer rotation decreases in the order, cinchonine and cinchonidine>strychinine and brucine≳quinine and quinidine for both zinc(II) and nickel(II) complexes. The same order was obsreved at other wave-

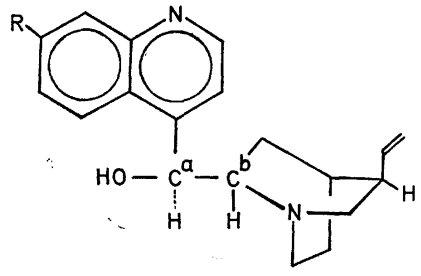

I. R=H: cinchonine
II. R=OCH_3: quinidine

* Present address: College of Medical Sciences, Tohoku University, Seiryo-machi, Sendai.

** Present address: Research Institute for Catalysis, Hokkaido University, Sapporo.

Table 1. Pfeiffer rotation at 400 nm in solutions containing 0.02 M alkaloid hydrochloride and 0.02 M $[Zn(phen)_3]Cl_2 \cdot 6H_2O$ or $[Ni(phen)_3]Cl_2 \cdot 6H_2O$, 30°C

Alkaloid	$[Zn(phen)_3]^{2+}$			$[Ni(phen)_3]^{2+}$				
	α_X	α_∞	α_P	α_i	α_∞	$\alpha_i-\alpha_X$	$\alpha_\infty-\alpha_i$	α_P
Cinchonine	0.308°	0.028°	−0.280°	0.263°	0.130°	−0.045°	−0.133°	−0.178°
Cinchonidine	−0.248°	−0.043°	0.205°	−0.178°	−0.069°	0.070°	0.109°	0.179°
Quinine	−0.405°	−0.324°	0.081°	−0.334°	−0.305°	0.071°	0.029°	0.100°
Quinidine	0.505°	0.420°	−0.085°	0.425°	0.418°	−0.080°	−0.007°	−0.087°
Strychinine	−0.075°	−0.175°	−0.100°	−0.083°	−0.180°	−0.008°	−0.097°	−0.105°
Brucine	−0.110°	−0.195°	−0.085°	−0.105°	−0.214°	−0.005°	−0.109°	−0.104°

Table 2. 60 MHz NMR data. The chemical shifts are against external TMS* standard (Hz)

Solution	Cinchonine		Phenanthroline[b]			
	Quinolyl[a]	$-CH=CH_2$	2, 9	3, 8	4, 7	5, 6
0.05 M Cinchonine hydrochloride	542	372, 326				
0.05 M Cinchonine hydrochloride + 0.01 M $[Zn(phen)_3]^{2+}$	534	366, 321	501	469	527	493
0.01 M $[Zn(phen)_3]^{2+}$			504	472	531	497

a) The chemical shift is for the proton on the carbon atom adjacent to the quinolyl nitrogen atom. b) The assignment is after J. D. Miller and R. M. Prince, *J. Chem. Soc*, **1965**, 3185.

lengths in 350~700 nm region. Cinchonidine is a stereoisomer of cinchonine(I)[7] with reversed configurations of the two carbon atoms C^a and C^b. The magnitude of Pfeiffer rotation caused by these alkaloids are similar to each other except the sign. Quinine and quinidine(II) are methoxyl derivatives of cinchonidine and cinchonine respectively. The magnitudes of Pfeiffer rotations by these alkaloids are much smaller than those by cinchonine and cinchonidine. These differences should be related to the presence of a methoxyl group on the quinolyl part in quinine or quinidine. This fact suggests that there is π-π interaction between the conjugate system of phenanthroline rings of the complex and the quinolyl group of cinchonine or cinchonidine, and that stereoselectivity in such an interaction is responsible for Pfeiffer rotation. The presence of methoxyl group at the quinolyl part of quinine or quinidine would make π-π interaction less favorable sterically than in cinchonine or cinchonidine. As will be mentioned later, such stereoselectivity is related more directly to $(\alpha_\infty-\alpha_i)$ values than to α_P values (see Eq. 11). It is seen in Table 1 that $\alpha_\infty-\alpha_i$ values for cinchonine or cinchonidine are much larger than those for quinine or quinidine for nickel(II) complexes. The π-π interaction mentioned above has hydrophobic nature. Brasted *et al.*[6] reported that the effects of solvent and urea on the Pfeiffer effect in $[Zn(phen)_3]^{2+}$–alkaloid(cinchonine hydrochloride or strychinine hydrosulfate) systems and in other systems indicate hydrophobic bonding between the complex and the optically active substance.

The magnitudes of the Pfeiffer rotations of strychinine(III)[8] hydrochloride and brucine(IV) hydrochloride are of the same order to each other and much smaller than those of cinchonine or cinchonidine hydrochloride. This fact shows that the methoxyl groups in brucine do not exert significant influence on Pfeiffer effect. The π-π interaction between the phenanthroline rings of the complex and the phenyl group of strychinine may be smaller than that between the complex and the quinolyl group of cinchonine or contribution of other interactions may be larger.

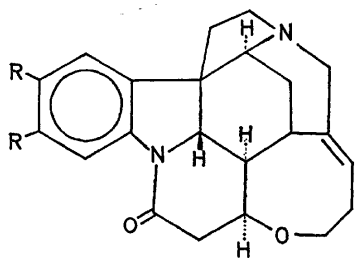

III. R=H; strychinine
IV. R=OCH_3: brucine

NMR Data. Table 2 gives NMR data of cinchonine hydrochloride and $[Zn(phen)_3]^{2+}$. Chemical shifts were given in cps from sodium trimethylsilyl sulfonate(TMS*) used as external standard.[9] The data in the table indicate that the quinolyl protons of cinchonine are shifted toward higher field by 8 or 9 cps by the addition of 0.01 M $[Zn(phen_3)]^{2+}$. Other protons in cinchonine are shifted by only 5 to 6 cps. The phenanthroline protons of the complex are also affected by the addition of cinchonine hydrochloride: 2, 9 and 3, 8 protons are shifted by 2 or 3 cps and 4, 7 and 5, 6 protons by *ca.* 4 cps toward higher field. These shifts can be due to the effect of the ring current of the phenanthroline or the quinolyl group. These results are not inconsistent with the π-π interaction mentioned above.

Influence of Indifferent Electrolyte. Both the complex ion and the monoprotonated alkaloid ion are positively charged. Association between these cations by hydrophobic bonding or π-π interaction should overwhelm the electrostatic repulsion between them.

Table 3. Effect of electrolyte on Pfeiffer rotation at 400 nm in $[Zn(phen)_3]^{2+}$- cinchonidine hydrochloride system

Cell lengh, 1 cm; temperature, 30 °C

$[Zn(phen)_3]Cl_2$, M	Cinchonidine, M	Electrolyte	α_P
0.02	0.02	None	0.205°
0.02	0.02	0.02 M NaCl	0.314°
0.02	0.02	0.02 M $CaCl_2$	0.403°
0.02	0.02	0.5 M NaCl	0.52°
0.01	0.02	0.03 M $CaCl_2$	0.248°
0.01	0.02	0.5 M NaCl	0.294°

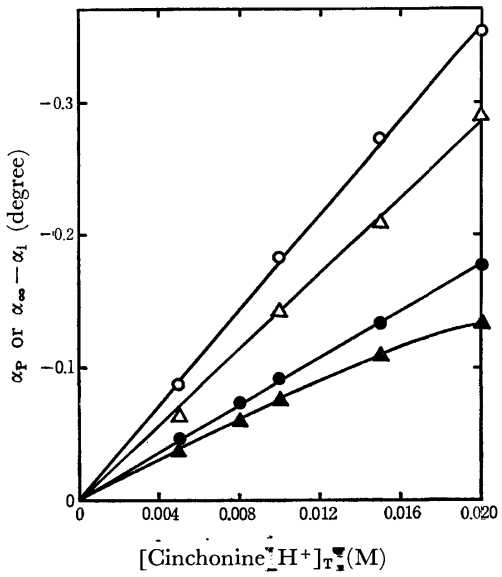

Fig. 2. Dependence of α_P (○, ●) and $\alpha_\infty - \alpha_i$ (△, ▲) values on cinchonine hydrochloride concentration in solutions with (○, △) and without (●, ▲) 0.5 M NaCl. Cell length, 1 cm; temperature, 30 °C; $[Ni(phen)_3]Cl_2$, 0.02 M.

Addition of electrolyte would diminish such a repulsion. Table 3 and Fig. 2 give Pfeiffer rotations in the presence and in the absence of electrolytes. It is seen that both sodium chloride and calcium chloride have considerable enhancing effect on Pfeiffer rotation. The enhancing effect seems to be more than that to be understood from simple electrostatic consideration.

Concentrations of Alkaloids and the Complex. The dependencies of Pfeiffer rotation on concentrations of the complexes and alkaloids were studied (Figs. 2 to 4). In these solutions 0.5 M NaCl was added in order to maintain ionic strength of the solution constant. The concentration ranges of the complexes and alkaloids were restricted because of the limited solubility. In the following, concentration dependence is analyzed quantitatively in terms of stereoselective association between the complex and the alkaloid cations. As is mentioned later, 1 : 1 association seems to be predominant under the experimental condition and only 1 : 1 association was taken into consideration in the following treatment. The association of the optically active alkaloid with one enantiomer of the complex

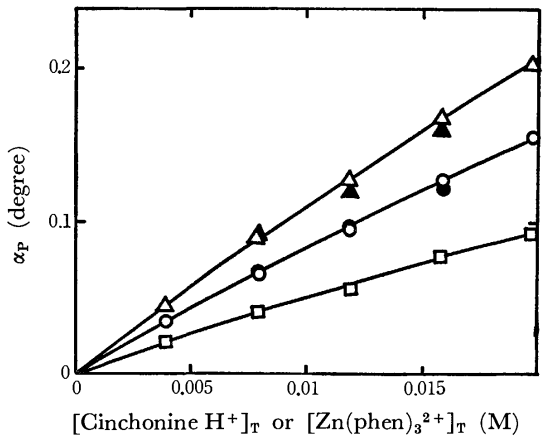

Fig. 3. Dependence of Pfeiffer rotation on cinchonine hydrochloride concentration in solutions containing 0.0049 M $[Zn(phen)_3]Cl_2$ and 0.5 M NaCl at 380 (△), 400 (○) and 450 (□) nm. Dependence on $[Zn(phen)_3]^{2+}$ concentration in solutions containing 0.0049 M cinchonine hydrochloride and 0.5 M NaCl at 380 (▲) and 400 (●) nm is also shown. Cell length, 1 cm; temperature, 30 °C.

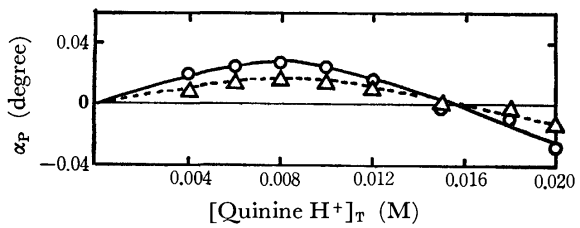

Fig. 4. Pfeiffer rotation at 400 (○) and 450 (△) nm in solutions containing 0.01 M $[Zn(phen)_3]Cl_2$, 0.5 M NaCl and various amount of quinine hydrochloride. Cell length, 1 cm; temperature, 30 °C.

can be different from that with the other enantiomer:

$$d\text{-M} + d\text{-X} \rightleftharpoons d\text{-M}\cdot d\text{-X},$$

$$K_{dd} = [d\text{-M}\cdot d\text{-X}]/([d\text{-M}][d\text{-M}][d\text{-X}]) \quad (1)$$

$$l\text{-M} + d\text{-X} \rightleftharpoons l\text{-M}\cdot d\text{-X},$$

$$K_{ld} = [l\text{-M}\cdot d\text{-X}]/([l\text{-M}][d\text{-X}]) \quad (2)$$

where *d*-M and *d*-X denote one enantiomer of the complex and the optically active substance(*e. g.* alkaloid cation), respectively and *l*-M and *l*-X their antipodes. A stereoselective association has been reported between some tervalent complex ions and tartrate ions.[10,11]

The optical rotation of the solution containing a racemic salt of the complex and alkaloid in a cell of unit cell length is given by

$$\alpha = \theta_X[d\text{-X}] + \theta_d([d\text{-M}] - [l\text{-M}]) + \theta_{dd}[d\text{-M}\cdot d\text{-X}] + \theta_{ld}[l\text{-X}\cdot d\text{-X}] \quad (3)$$

where θ_X, θ_d, θ_{dd} and θ_{ld} denote molecular rotations of *d*-X, *d*-M, *d*-M·*d*-X and *l*-M·*d*-X, respectively. Until inversion of the complex takes place, the concentrations of the two enantiomers of the complex should be equal:

$$[d\text{-M}]_i + [d\text{-M}\cdot d\text{-X}]_i = [l\text{-M}]_i + [l\text{-M}\cdot d\text{-X}]_i = [M]_T/2 \quad (4)$$

where the suffix i denotes the time immediately after

mixing before any inversion takes place. It follows from Eqs. (1) to (4) that a new optical activity is induced even when no inversion occurs unless $K_{dd}=K_{ld}$ and $\theta_{dd}=-\theta_{ld}$. It was shown previously that θ_{dd} is considerably different from θ_{ld} in some Co(III) complex-tartrate systems.[11] In the case of the nickel complex, the rate of inversion is slow and the α_i values in Table 1 are considered to correspond to the optical rotations given by Eqs. (3) and (4).

When K_{dd} is not equal to K_{ld}, assoications represented by Eqs. (1) and (2) cause differences in concentrations of free *d*-M and *l*-M, and inversion of the complex will take place to make them equal:

$$[d\text{-M}]_\infty=[l\text{-M}]_\infty \tag{5}$$

where the parenthesis with suffix ∞ denotes the concentration at equilibrium. The optical rotation of the equilibrated solution, α_∞, is given by

$$\alpha=\theta_X[d\text{-X}]_\infty+(\theta_{dd}K_{dd}+\theta_{ld}K_{ld})[d\text{-M}]_\infty[d\text{-X}]_\infty \tag{6}$$

If the extent of association is small, the equation

$$[d\text{-X}]_T\simeq[d\text{-X}]_\infty \tag{7}$$

holds, where $[d\text{-X}]_T$ is the total concentration of the alkaloid salt, and the Pfeiffer rotation is expressed as

$$\alpha_P=a[d\text{-M}]_\infty[d\text{-X}]_\infty \tag{8}$$

where

$$\alpha=\theta_{dd}K_{dd}+\theta_{ld}K_{ld} \tag{9}$$

Eq. (8) is transformed to

$$[\text{d-X}]_\infty/\alpha_P=2(1+K_{app}[d\text{-X}]_\infty)/(a[M]_T) \tag{9}$$

where

$$K_{app}=(K_{dd}+K_{ld})/2 \tag{10}$$

The plot of the left-hand side of Eq. (9) *vs.* $[d\text{-X}]_\infty$ should be a straight line, and the ratio of slope to intercept is equal to K_{app}.

This procedure was applied to the data in Fig. 3. A correction was made for Eq. (7) by stepwise approximation. The values of K_{app} thus obtained are listed in Table 4. Values obtained from data at different wavelengths are in agreement with one another. It is in accord with the assumption of the absence of the higher order association.[11] Theoretical curves calculated by use of Eq. (8) and K_{app} values in Table 4 are given in Fig. 3 by solid lines. They are in agreement with experimental plots. From the temperature dependence of Pfeiffer rotation and that of K_{app} value, the ΔH° for the association between $[Zn(phen)_3]^{2+}$ and cinchonine hydrochloride was calculated to be -3 kcal/mol. This value is comparable with those reported for some systems where hydrophobic bonding is concerned.[12]

Table 4. Association constants between $[Zn(phen)_3]^{2+}$ and monoprotonated alkaloid cations in solutions containing 0.5 M NaCl obtained by use of Eq. (9)

Alkaloid	Temp.	K_{app}[a]
Cinchonine	30°	8.3 (380 nm) 8.3 (400 nm) 8.4 (450 nm)
	35°	7.7 (400 nm)
	25°	8.9 (400 nm)
Cinchonidine	30°	7.3 (400 nm) 7.0 (420 nm) 9.5 (450 nm)

a) Because of the uncertainty in the measurement in optical rotation the precision of K_{app} values is ±1.5. The values in parentheses are wavelengths at which measurement was made.

Figure 4 shows concentration dependence of Pfeiffer rotation in $[Zn(phen)_3]^{2+}$–quinine hydrochloride system. The magnitude is much smaller than those observed in cinchonine or cinchonidine hydrochloride systems, and the sign of α_P changes with change in quinine concentration, positive for $[X]<0.015$ M and negative for $[X]>0.015$ M at 400 nm. It may be because of the presence of higher order association to a considerable extent.

As is seen in Fig. 2, α_P is proportional to the alkaloid concentration within experimental error in $[Ni(phen)_3]^{2+}$–cinchonine hydrochloride system. Though K_{app} value could not be obtained in this system, an upper limit is given: $K_{app}\lesssim8$. From a comparison of Eqs. (3) and (6), it follows that the value $\alpha_\infty-\alpha_i$ can be approximated as

$$\alpha_\infty-\alpha_i\simeq\theta_d([d\text{-M}]_i-[l\text{-M}]_i)\simeq\theta_d([l\text{-M}]_{T,\infty}-[d\text{-M}]_{T,\infty}) \tag{11}$$

within $\pm10\%$ if $K_{app}\lesssim8$, $0.5<K_{dd}/K_{ld}<2$ and $0.5<|\theta_{dd}/\theta_{ld}|<2$. From data in Fig. 2 and optical rotation of pure $(-)_D$-$[Ni(phen)_3](ClO_4)_2$, it is calculated that when a solution containing 0.02 M $[Ni(phen)_3]Cl_2$, 0.02 M cinchonine hydrochloride and 0.5 M NaCl is equilibrated, the total amount of *l*-rotatory complex is more than that of the *d*-rotatory complex by about 3 %. Taking $K_{app}<8$ for this system into account, it follows that K_{ld} is considerably larger than K_{dd} for the association between $[Ni(phen)_3]^{2+}$ and cinchonine hydrochloride.

Sign of Pfeiffer Rotation and Absolute Configuration. The more favorable conformation of cinchonine is presumed to be one in which the two hydrogen atoms on the two carbon atoms adjacent to quinolyl group, H^a and H^b, are *trans* to each other as depicted in V. If π-π interaction between the phenanthroline rings of the complex and the quinolyl group of cinchonine is contributing to the association (see V), cinchonine seems to associate more favorably with tris(phenanthroline)complex of Λ configuration than with that of Λ configuration. The absolute configuration of $(+)_D$-$[Ni(phen)_3]^{2+}$ was determined to be Λ by X ray

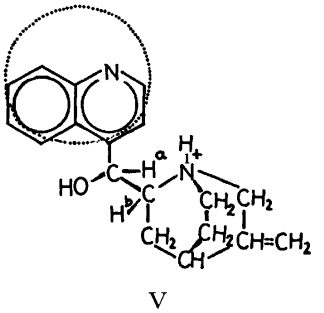

V

The dotted circle denotes interaction between the quinolyl group and the phenanthroline rings of the complex.

analysis.[13] Hence the sign of the Pfeiffer rotation in $[Ni(phen)_3]^{2+}$–cinchonine system should be minus. This is in accord with the experimental results. It is concluded that the absolute configuration of phenanthroline complexes can be deduced from the sign of Pfeiffer rotation with certain types of alkaloid. The sign of Pfeiffer rotation in $[Zn(phen)_3]^{2+}$–cinchonine system is minus. It follows from above argument that the absolute configuration of $(+)_D$-$[Zn(phen)_3]^{2+}$ is *Λ*.

The prediction of the absolute configuration of Pfeiffer active complexes has also been proposed by Kirschner and Pollock[14] using optically active dibasic acids.

The authors wish to thank Professors Kazuo Saito and Junnosuke Fujita for their helpful discussions.

References

1) P. Pfeiffer and K. Quehl, *Ber.*, **64**, 2267 (1931); **65**, 560 (1932); P. Pfeiffer and Y. Nakatsuka, *ibid.*, **66**, 410, 415 (1933).
2) E. E. Turner and M. M. Harris, *Quart. Rev.* (London), **1**, 299 (1947).
3) F. P. Dwyer and E. C. Gyarfas, *Nature*, **168**, 28 (1951).
4) E. C. Gyarfas and F. P. Dwyer, *Rev. Pure Appl. Chem.*, **4**, 73 (1954).
5) S. Kirschner and N. Ahmad, in S. Kirschner ed., "Coordination Chemistry", Plenum Press, New York, 1969, p. 42 and references therein.
6) R. C. Brasted, V. J. Landis, E. J. Kuhajek, P. E. R. Nordquist, and L. Mayer, *ibid.*, p. 64 and references therein.
7) V. P. Prelog and O. Hafliger, *Helv. Chim. Acta* **33**, 2021 (1950).
8) K. Nagarajan, Ch. Weissman, H. Schmid, and P. Karrer, *ibid.*, **46**, 1212 (1963).
9) Proton signals of TMS* is affected by the phenanthroline complex. Presence of 0.025 M $[Zn(phen)_3]Cl_2$ makes TMS* signal move by *ca.* 30 cps toward higher field. The phenanthroline signals of the complex were also found to be dependent on its concentration.
10) K. Ogino and U. Saito, This Bulletin, **40**, 826 (1967).
11) K. Ogino, *ibid.*, **42**, 447 (1969).
12) P. Molyneur and H. P. Frank, *J. Amer. Chem. Soc.*, **83**, 3169 (1961).
13) K. R. Butler and M. R. Snow, *J. Chem. Soc. A*, **1971**, 565.
14) S. Kirschner and R. J. Pollock, Proc. XIV ICCC, Toronto, 1972, p. 545.

Bromine Addition Reaction to Olefins with Magnesium Bromide and Aroyl Peroxides

Masao Ōkubo, Hisahiro Kusakabe, Tsunenori Hiwatashi, and Kazuo Kishida
Department of Chemistry, Faculty of Science and Engineering, Saga University, Honshō-chō, Saga 840
(Received June 11, 1973)

When $MgBr_2$ prepared in anhydrous tetrahydrofuran was added to a mixture of olefin and benzoyl peroxide, the peroxide decomposed at a moderate rate at room temperature. Olefin dibromide and magnesium benzoate were obtained in nearly quantitative yields. The effects of *p*- and *m*-substituents of peroxide and of the structure of olefin were studied. A complex consisting of $MgBr_2$ and peroxide was formed. Abstraction of brominium cation from the complex by the olefinic double bond was proposed.

The addition of bromine to cyclohexene in an orange-colored solution of a complex prepared from PhCOOMgBr and benzoyl peroxide(BPO) in tetrahydrofuran(THF) has been reported.[1] The results and the fact that $MgBr_2$ is considered to be a component of Grignard reagents[2] prompted us to examine the reaction of BPO and $MgBr_2$ in anhydrous THF. When equimolar BPO was added to a solution of $MgBr_2$, an orange color appeared. The colored solution has the ability to add bromine to cyclohexene giving *trans*-1,2-dibromocyclohexane in a good yield. Results of studies of this reaction are given in this paper.

Results and Discussion

The same reaction was reported by Yang and Lawesson,[3] who obtained *trans*-1,2-dibromocyclohexane almost quantitatively. They suggested the reaction to be a simple addition of molecular bromine produced in the reaction of BPO and $MgBr_2$ (Reaction 1), but gave no precise mechanism. Whereas they used ethyl ether

$$(PhCOO)_2 + MgBr_2 \rightarrow (PhCOO)_2Mg + Br_2 \qquad (1)$$

as solvent, we used THF. It should be noted that ethyl ether cannot maintain the reaction components in solution and forms a heavy precipitate easily. In contrast, the reaction mixture is homogeneous in THF when the concentration is about 40 mmol/l.

When equimolar BPO was added to a clear solution of $MgBr_2$ in anhydrous THF[4] at 15 °C, the mixture turned yellow, deepening to orange in the course of 45 to 60 min. No more deepening took place after the solution has been left to stand for several hours under nitrogen atmosphere. The color is similar to that of "Complex II"[5] prepared from PhCOOMgBr and a half equimolar BPO. The coloration is not due to molecular bromine, since Br_2 attacks the THF molecule easily even at 0 °C giving hydrogen bromide. Neither molecular bromine nor hydrogen bromide was detected in the distillate of the orange colored solution. The color did not fade and the peroxide-content(determined by iodometry) did not decrease when the solution was left to stand overnight. Turbidity appeared when ethyl ether was added to the concentrated solution at 0 °C. Orange-red crystals were obtained after the mixture was left to stand in a refrigerator for about two weeks. Thus, it was confirmed that $MgBr_2$ and BPO from a complex(Reaction 2), hereafter called Complex III.[5] Reaction

$$(PhCOO)_2 + MgBr_2 \rightleftharpoons [\text{Complex III}] \qquad (2)$$

2 will be expressed as an equilibrium process.

When equimolar cyclohexene was added to the solution of Complex III, the peroxide-content decreased and became nearly 10% after about two hours(Fig. 1, case A) accompanied by fading of the color.[6] From the reaction mixture, magnesium benzoate and *trans*-1,2-dibromocyclohexane were obtained almost quantitatively. When anhydrous THF solution of $MgBr_2$ was added to the mixture of BPO and cyclohexene dissolved in THF(Fig. 1, case B),

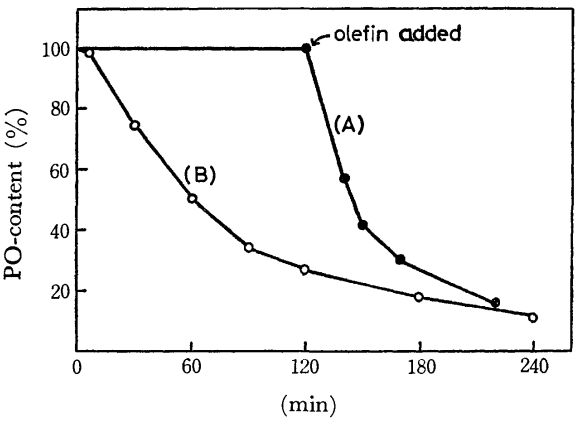

Fig. 1. Consumption of BPO-content at 20 °C.
Concn: 0.0042 mol in 100 ml THF.
Curve A: After 2 hr, olefin is added to Complex III.
Curve B: $MgBr_2$ is added to the mixt. of BPO and olefin.

the peroxide-content decreased immediately. The reaction was slow and a longer time was needed for it to be completed, the products being the same as those in case A. The two curves in Fig. 1 show that Complex III liberates the first bromine atom on access of olefin molecule (Reaction 3).

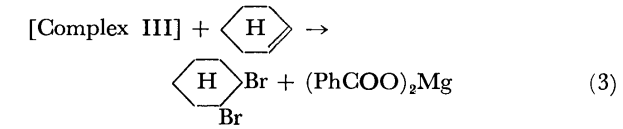

(3)

Kochi and his co-workers reported the formation of *p*-bromoanisole in the reaction of lithium bromide with BPO in a mixture of acetic acid and anisole[7] (Reaction 4).

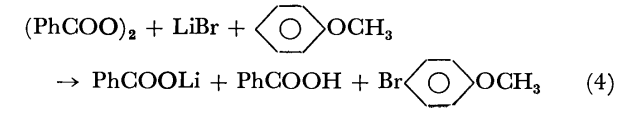

(4)

Table 1. Reaction of case B at 20 °C
Concentration: 0.0042 mol in 100 ml THF.

Time (s)	P. O.-content consumed (%)	Rate consts. calcd. on 1st-order eq.[a] (s^{-1}) $\times 10^4$	2nd-order eq. ($l \cdot mol^{-1} \cdot s^{-1}$) $\times 10^3$	3rd-order eq. ($l^2 \cdot mol^{-2} \cdot s^{-1}$) $\times 10^1$
480	3.2	0.68	1.63	0.39
1740	22.5	1.46	3.95	1.07
3420	46.4	1.82	6.00	2.04
4320	58.0	2.01	7.58	3.03
5520	66.6	1.99	8.56	4.05
7020	72.5	1.84	8.90	4.89

a) The latter four numbers were used to calculate the mean value of the apparent-first-order rate constant.

An equimolar mixture of Complex III and anisole in THF at 25 °C slowly gave *p*-bromoanisole(Reaction 5).

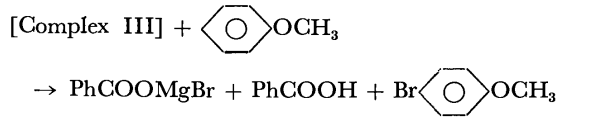

$$[\text{Complex III}] + \text{C}_6\text{H}_5\text{OCH}_3 \rightarrow \text{PhCOOMgBr} + \text{PhCOOH} + \text{Br-C}_6\text{H}_4\text{-OCH}_3 \quad (5)$$

This suggests that anisole as well as cyclohexene abstract brominium cation from Complex III in reactions 5 and 3, respectively.

The possibility that Complex III consists of benzoyl hypobromite and benzoyloxymagnesium bromide(Reaction 6), could be excluded since no Hunsdiecker-Prévost-type product such as 2-bromocyclohexyl benzoate[8] was detected in cases A and B.

$$(PhCOO)_2 + MgBr_2 \rightarrow [PhCOOBr][PhCOOMgBr] \quad (6)$$

Since Complex III no longer has characteristic infrared absorption bands of BPO itself,[9] it cannot be pictured as a simple mixture of $MgBr_2$ and BPO. If the structure of Complex III were to be depicted, the Mg-Br bond and O–O bond might be said to have excited characters. Bromine atom may have a positive charge as the result of coordination of electron-seeking peroxide molecules to the Mg-atom. This is justified by the formation of *p*-bromoanisole. Complex III liberates bromine when it is treated with water.[5]

Since a straight line was obtained when the olefin had not yet been added(Fig. 1, case A) and no appreciable fluctuation which we came across in the lithium bromide–BPO system[7] was not observed(Fig. 1, case B), the features of decomposition of Complex III could be followed by iodometry. Typical results of measurements in case B are listed in Table 1. The first-order rate constants show a smaller fluctuation as compared with the other two series of values. The apparent-first-order rate constants remained virtually unchanged when two molar equivalents of cyclohexene were used. $MgBr_2$ in slight excess, however, greatly accelerates the reaction as shown in Fig. 2. In case A, no satisfactory rate constant was obtained by using any of the first-, second- and third-order rate equations. This might be due to the change of degree of association(or dissociation) of Complex III(Reaction 2) caused by the change in

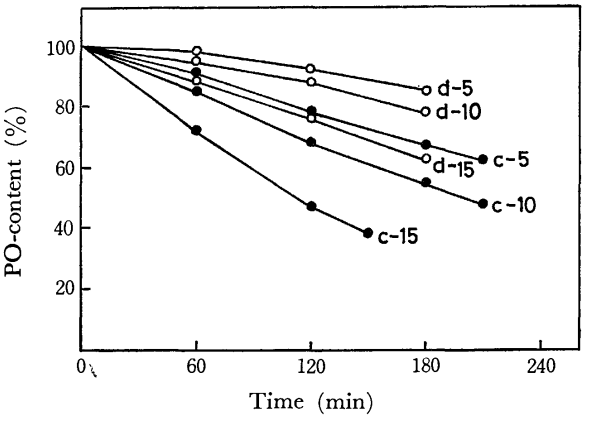

Fig. 2. Consumption of BPO-content (case B). Effect of temperature and $MgBr_2$-concentration.
i) Concn. of BPO and cyclohexene are fixed to 0.00238 mol in 45 ml THF. ii) Numbers (5, 10 and 15) denote the temperature (°C). iii) "c" and "d" denote the concn. of $MgBr_2$-soln (15 ml). c: 0.173 M, d: 0.159 M.

concentration. Addition of olefin-THF solution at the initial stage of case A alters the concentration at that time, affecting the rate of decomposition of Complex III. The overall path of reaction should thus consist mainly of i) equilibrium(2), and ii) abstraction of brominium cation from Complex III to form 2-bromocyclohexyl carbonium ion, which may combine rapidly with the bromide ion in the subsequent step.

Effects of the substituent of BPO and the structure of olefin were examined mainly for case B. *p,p'*-Dinitrobenzoyl peroxide greatly accelerates the reaction which completed within 20 min. at 20 °C (Table 2, and Fig. 3-a, b). Since the species abstracted by the π-electron system of cyclohexene should be brominium cation, the facilitation of this step by the electron-attracting substituent is reasonable.[10] We see from Fig. 3-b and 3-c that the difference between the rate of BPO and that of *m,m'*-dimethoxy derivative decreases with the lowering in temperature. Weakly electron-attracting *m*-methoxy group should be less favorable to complex-formation(Reaction 2). The tendency might become greater at a higher temperature; thus, the overall rate of *m,m'*-dimethoxy derivative becomes relatively lower(Fig. 3-b). Both equilibrium(2) and the rate of abstraction of bromi-

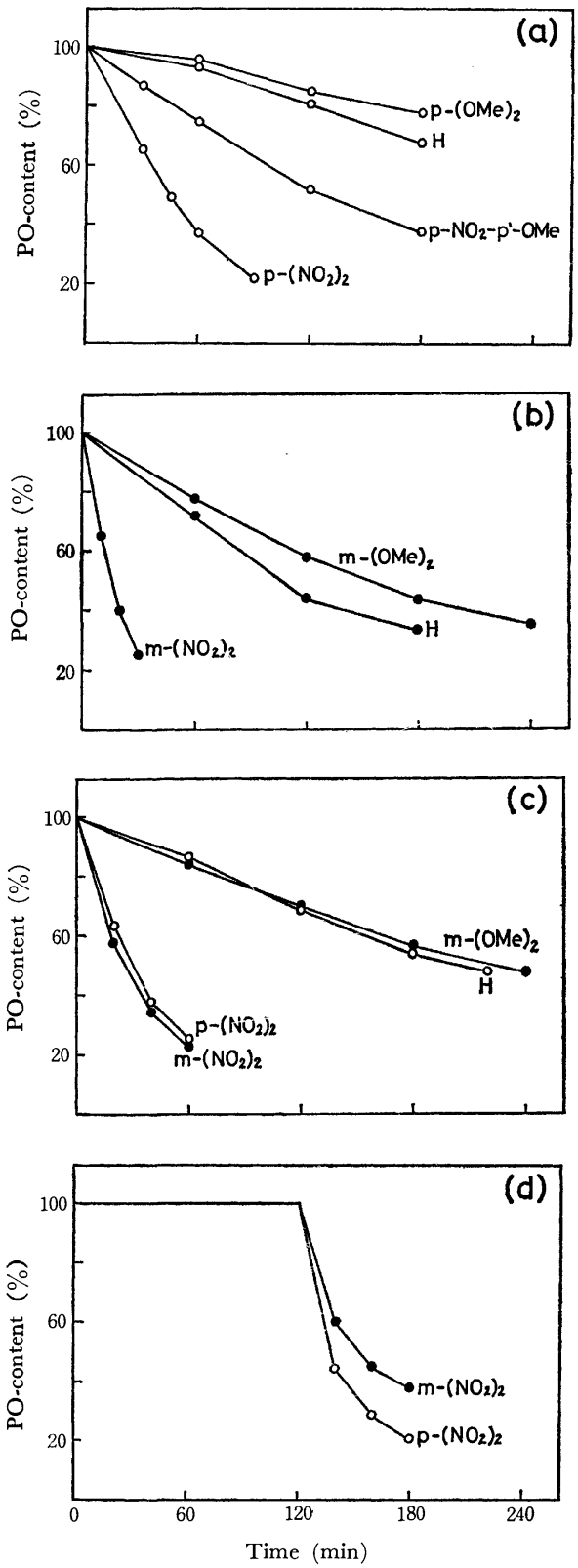

Fig. 3. Comsumption of PO-content for cases A and B.
a) case B, 15 °C, *p*-substituted BPO, $MgBr_2$: 0.159 M. b) case B, 15 °C, *m*-substituted BPO, $MgBr_2$: 0.173 M. c) case B, 10 °C, *p*- and *m*-substituted BPO, $MgBr_2$: 0.173 M. d) case A, 5 °C, *p*- and *m*-nitro derivatives, $MgBr_2$: 0.173 M.
Concn of peroxides and cyclohexene are to 0.00238 mol in 45 ml THF.

Table 2. Apparent-first-order rate constants for substituted BPO in reaction with cyclohexene at 20 °C (case B)
Concentration: 0.0042 mol in 100 ml.

Peroxides	Rate constant (s^{-1}) $\times 10^4$
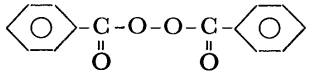	1.9
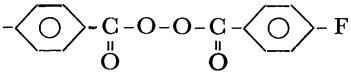	2.4
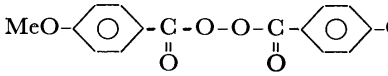	0.8

Table 3. Apparent-first-order rate constants for olefins in reaction with BPO at 20 °C (case B)
Concentration: 0.0042 mol in 100 ml.

Olefins	Rate constant (s^{-1}) $\times 10^5$
t-Bu-CH=CH_2	1.4
CH_3-(-CH_2-)$_5$-CH=CH_2	3.2
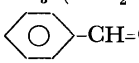	2.8
	19.0
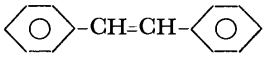	Very slow

nium cation by the olefinic system should change with temperature and substituent. Lower temperature and an electron-donating substituent favor the association of Complex III; higher temperature and an electron-attracting substituent favor the abstraction of brominium cation. At 10 °C, *m,m'*-dinitro-derivative decomposed at a rate somewhat higher than that for *p,p'*-derivative(Fig. 3-c). In case A at 5 °C, however, the *p,p'*-derivative decomposed much faster than the *m,m'*-derivative(Fig. 3-d). Thus the *m*-nitro group should be more favorable to the association of Complex III than the *p*-nitro group; the *p*-nitro group accelerates the abstraction of brominium cation to a greater extent than the *m*-nitro group.

Apparent-first-order rate constants(case B) for several olefins were obtained when unsubstituted BPO was used (Table 3). The rate decreases in the following order:

cyclohexene > 1-octene > styrene > *t*-butylethylene > *cis*-stilbene > *trans*-stilbene.

The rate of *trans*-stilbene at room temperature is so low that the peroxide-content was consumed after about 30 days. The rate of *cis*-isomer was as high as twice that of *trans*-isomer. π-Electron density of the ethylene groups of stilbenes and styrene is lower than that of alkyl-substituted ethylenes owing to delocalization of electrons on the whole of molecule, and might be unfavorable to the abstraction of brominium cation. Bulkiness of the phenyl and *t*-butyl groups may also be

another retarding factor. The fact that cyclohexene reacts very fast and that *cis*-stilbene reacts faster than *trans*-isomer shows that the olefins having *cis*-type configuration favor the reaction.

The course of the reaction in the case of cyclohexene could be formulated as follows:

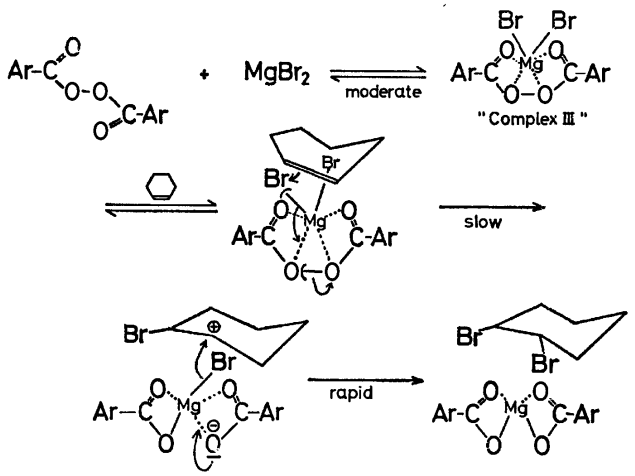

Experimental

Materials. A clear solution of $MgBr_2$(about 0.2 M) in anhydrous THF was prepared from Mg-turnings and ethylene dibromide.[4] Its concentration was determined by the magnesium-oxinate method.[11] When necessary benzoyl peroxide was purified by reprecipitation with methanol from its chloroform solution. *p,p'*-Difluoro-, *p,p'*-dimethoxy-, *m,m'*-dimethoxy-, *p,p'*-dinitro- and *m,m'*-dinitro-benzoyl peroxides were prepared from the corresponding acyl chlorides and peroxide.[12] *p*-Nitro-*p'*-methoxybenzoyl peroxide was prepared by the condensation of *p*-nitroperoxybenzoic acid and *p*-anisic acid with dicyclohexylcarbodiimide.[13] Cyclohexene and styrene were purified by distillation before use. *trans*- and *cis*-Stilbene were prepared from *trans*- and *cis*-α-phenylcinnamic acids, respectively.[14] *t*-Butylethylene was prepared from pinacolone by reduction and dehydration by means of the methylxanthate method.[15]

Rate Measurements. A typical procedure for case B is described in the following. Anhydrous THF(60 ml) was introduced into the N_2-purged reaction flask at 20 °C and 1.0113 g (0.0042 mol) of BPO was added. Cyclohexene (0.346 g, 0.0042 mol) dissolved in 10 ml THF was added to the solution. Twenty milliliters of $MgBr_2$ solution (0.211 M) and 10 ml THF were successively introduced into the reservoir,[16] and the apparatus was set up under a slow stream of nitrogen. The mixture in the reaction flask was vigorously stirred and the $MgBr_2$ solution was added at once by turning the reservoir upside-down. After mixing, the total volume of the reaction mixture was 100 ml. One milliliter portions of the reaction mixture were pipetted out at definite intervals, introduced into a CO_2-purged flask containing acetic acid and potassium iodide, and titrated.[17]

For case A, BPO and $MgBr_2$ were mixed in THF under N_2-atmosphere. The reaction flask was kept in a water bath controlled at a definite temperature for over 8 hr, when the solution turned orange. Cyclohexene dissolved in 10 ml THF was added at once, and the peroxide-content was followed by iodometry.

Analysis of Products. After the peroxide-content became zero, the reaction mixture was concentrated under reduced pressure to a small volume, decomposed by saturated ammonium chloride solution, extracted with ether and worked up as usual. Benzoic acid was obtained quantitatively. From the neutral part, *trans*-1,2-dibromocyclohexane was obtained in 82—90% yields. 2-Bromocyclohexyl benzoate was prepared[8] and used for comparison with the products of this reaction on tlc. The yield of dibromide was determined on vpc using hexachloroethane as an internal reference. The conformation of the dibromide was identified by comparing its retention time on vpc with that of the dibromide prepared by adding bromine to cyclohexene in CCl_4.[18]

p-Nitro-*p'*-methoxybenzoyl peroxide is known to decompose with ionic mechanism *via* carboxy-inversion.[19] However, in our reaction no *p*-methoxyphenol was detected.

Electrophilic Bromination. A solution of Complex III was prepared from 0.726 g (0.003 mol) of BPO and equimolar $MgBr_2$ solution (total volume: 60 ml). Anisole(0.324 g) dissolved in 10 ml THF was added. After the mixture was stirred at 25 °C for 6 hr, the peroxide-content fell to 69%. The yield of *p*-bromoanisole was determined to be 13% on vpc.

The authors are grateful to Professor Kazuhiro Maruyama, Kyoto University, for his stimulating discussions.

References

1) M. Ōkubo, K. Maruyama, and J. Ōsugi, This Bulletin, **44**, 1365 (1971).
2) W. Schlenk and W. Schlenk, *Ber.*, **64**, 739(1931); E. C. Ashby, *Quart. Rev.* (London), **1967**, 259.
3) N. C. Yang and S. O. Lawesson, *J. Amer. Chem. Soc.*, **81**, 4230 (1959).
4) H. Edelstein and E. I. Becker, *J. Org. Chem.*, **31**, 3375 (1966).
5) M. Ōkubo, K. Maruyama, and J. Ōsugi, This Bulletin, **42**, 1162 (1969).
6) The curve, obtained in the case when cyclohexene was added to the solution of Complex II, was nearly the same as curve A.
7) J. K. Kochi, B. M. Graybill, and M. Kurz, *J. Amer. Chem. Soc.*, **86**, 5257 (1964).
8) A. C. Cope, H. L. Holmes, and H. O. House, "Organic Reactions", Vol. 9, Chap. 4, John Wiley & Sons, Inc., New York (1957).
9) Infrared absorption bands(in THF) of C=O stretching vibration shifted from 1770 cm^{-1} in the case of free BPO to 1640 cm^{-1} in that of Complex III.
10) Considering this and the results described later, we can exclude the other possibility that Complex III is a molecular compound in which molecular bromine is adsorbed on magnesium benzoate.
11) I. M. Kolthoff and E. B. Sandell, "Textbook of Quantitative Inorganic Analysis", Macmillan Co., New York, (1955), p. 362.
12) C. G. Swain, W. H. Stockmayer, and J. T. Clarke, *J. Amer. Chem. Soc.*, **72**, 5426 (1950).
13) F. D. Greene and F. Kazan, *J. Org. Chem.*, **28**, 2168 (1963).
14) L. F. Fieser, *J. Chem. Educ.*, **31**, 296 (1954).
15) H. R. Nace, "Organic Reactions", Vol. 12, p. 88 (1962)
16) M. Ōkubo, K. Maruyama, and J. Ōsugi, This Bulletin, **44**, 125 (1971).
17) J. P. Wibaut, H. B. van Leewen and B. van der Wal, *Rec. Trav. Chim. Pays-Bas*, **73**, 1033 (1954).
18) Bender, D. L. Flowers, and H. L. Goering, *J. Amer. Chem. Soc.*, **77**, 3464 (1955).
19) J. E. Leffler, *J. Amer. Chem. Soc.*, **72**, 67 (1950).

Photoreactions of *N*-Vinylcarbazole Induced by Metal Salts. VI. Cyclodimerization Catalyzed by Copper(II) Perchlorate in Aprotic Solvents

Michihiko ASAI,* Hiroshi MATSUI, and Shigeo TAZUKE**

Department of Polymer Chemistry, Faculty of Engineering, Kyoto University, Kyoto 606

(Received June 15, 1973)

Photocyclodimerization of *N*-vinylcarbazole(VCZ) catalyzed by $Cu(ClO_4)_2 \cdot 6H_2O$(Cu(II)) in tetrahydrofuran was investigated under irradiation at 365 nm. At $[Cu(II)]_0 = 10^{-2}$ M in air, when $[VCZ]_0$ was less than 0.4 M, only 1,2-*trans*-dicarbazylcyclobutane(D) was formed, but when $[VCZ]_0$ was higher than 0.5 M, rapid cationic polymerization commenced after about 0.3 M of VCZ had been converted to D. Any consumption of Cu(II) could not be detected in the course of reaction. The change of reaction course from dimerization into polymerization in the midway of reaction was presumably brought about by the consumption of oxygen. Kinetic expression for dimerization rate(R_d) was obtained as follows:

$$R_d \propto I_0^{1.0}[VCZ]_0^{1.0}[Cu(II)]_0^0$$

The quantum yield for D production was much larger than 1, indicating production of D *via* chain mechanism.

A number of metal salts have been found to be effective catalyst for the photosensitized polymerization and cyclodimerization of *N*-vinylcarbazole (VCZ) in organic solution. Sensitizing effect of the group Ib metal salts such as gold(III), silver(I) and copper(II) salts in various aprotic solvents upon these reactions have been preliminarily reported.[1] Due to the subtle changes in the reaction modes, polymerization or cyclodimerization, from system to system and remarkable effects of atmosphere and ligand in some cases, the mechanisms of sensitization by these metal salts seem to be very intricate and to vary with cases. Breitenbach[2] has reported also the photoinduced cyclodimerization in the presence of mercury(II) cyanide, lead(II) thiocyanate or cadmium(II) nitrate in acetonitrile. Ledwith[3] and Wang[4] have investigated the thermal cyclodimerization of VCZ with iron(III) and cerium(IV) in methanolic media to propose two different chain mechanisms involving initiation with the cation radical of VCZ.

The photoreaction of organic substrate in the presence of metal salt can be classified roughly into three categories in terms of the effective light absorption species:

$$\left.\begin{array}{ll} \text{Type I;} & M \xrightarrow{h\nu} M^* \xrightarrow{L} \\ \text{Type II;} & L \xrightarrow{h\nu} L^* \xrightarrow{M} \\ \text{Type III;} & M + L \rightleftharpoons ML \xrightarrow{h\nu} \end{array}\right\} \text{reaction products}$$

where M and L denote metal salts and organic substrate, respectively. As described previously,[1] the photodimerization of VCZ catalyzed by copper(II) perchlorate belongs to the Type II analogous to the photopolymerization of VCZ with silver(I) salts.[5] Type II, the reaction of an excited organic molecule with a metal salt, is very unique and has been unequivocally confirmed in a few limited systems.[6] On the other hand, quenching of fluorescence and phosphorescence from excited molecules by metal ions has been studied with emphasis of physical viewpoint.[7] As to photoreactions catalyzed by copper(II) salts, such as cyclodehydrogenation and oxidative fission of stilbene derivatives by copper chloride,[8] methanolysis of styrene by copper(II) perchlorate[9] and chlorination of simple organic substrate by copper(II) chloride[10] examined qualitatively.

In the present article, kinetic and mechanistic studies on the photosensitized cyclodimerization catalyzed by copper(II) perchlorate were undertaken under irradiation of 365 nm light in tetrahydrofuran at 20 °C in air. While effect of solvent, ligand or anion, and atmosphere were examined, cationic polymerization was observed under specific conditions. Furthermore, interaction of the excited VCZ with copper(II) perchlorate as well as with oxygen were investigated quantitatively.

Experimental

N-Vinylcarbazole (Koch-Light Lab. Ltd.) was recrystallized twice from hot *n*-hexane and dried *in vacuo*. $Cu(ClO_4)_2 \cdot 6H_2O$ and $Cu(NO_3)_2 \cdot 3H_2O$ were used after drying *in vacuo* at room temperature. Anhydrous $CuCl_2$ was prepared by drying commercial $CuCl_2 \cdot 2H_2O$ at 110 °C *in vacuo*. $Cu(ClO_4)_2 \cdot 2H_2O$, acetylacetonatocopper(II) and $Cu(ClO_4)_2(pyridine)_4 \cdot 2H_2O$ were prepared.[11] Tetrahydrofuran(THF), ethyl methyl ketone(EMK), ethyl acetate(EA), benzonitrile (BN), acetophenone(AP), and dimethyl sulfoxide (DMSO) were purified by the conventional methods. Purification of all other materials and apparatus for photoreaction were described previously.

Monochromatic light of 365 nm was selected by filtering the emission from a 300 W high pressure Hg lamp with combination of UV-DlA and UV-35 (Toshiba Electric Co. Ltd.) The incident intensity of light was 4×10^{-8} Einstein/min. cm^2 as determined by the Hatchard-Parker actinometry[12] and controlled with wire meshes. The reaction rate was determined by dilatometry, using a cylindrical quartz cell with parallel flat windows (optical length 10 mm, diameter 44 mm) connected to a capillary with glass joint. No special care was taken to remove dissolved air and trace amount of moisture from the reaction mixture, unless otherwise stated. Pure oxygen or nitrogen was bubbled into the reaction mixtures at least ten minutes prior to reaction if required. To identify 1,2-*trans*-dicarbazylcyclobutane after the comple-

* Present address: Research Institute for Polymers and Textiles, Sawawatari, Kanagawa-ku, Yokohama, Kanagawa 221.

** Present address: Research Laboratory of Resources Utilization, Tokyo Institute of Technology, Meguro, Tokyo 152

tion of reaction as confirmed by volume contraction, the reaction mixture was poured into an excess of methanol to precipitate polymer which might be produced simultaneously. After filtration, the filtrate was evaporated to dryness. The residue was confirmed as the cyclodimer from its melting point(195 °C) and its NMR spectra.[13]

The molecular weight of polymer was determined by viscosity measurement according to the equation, $[\eta]=3.35\times 10^{-4}M^{0.58}$, at 20 °C in benzene.[14]

Absorption and emission spectra were measured by Shimadzu spectrophotometer MPS-50 and Hitachi fluorescence photometer MPF-3, respectively.

Results

Exploratory experiments were carried out using various kinds of copper(II) species in THF, EMK and DMSO. As shown in Table 1, photo and thermal reactions were dramatically affected by combinations of anion, ligand and solvent. Both hexa- and dihydrate of copper perchlorate gave the same initial rate of photodimerization in THF. Anhydrous copper(II) chloride induced photosensitized cationic polymerization in THF, which was confirmed by additive effects of cationic inhibitors, to produce polyVCZ with molecular weight of about 30000. Meanwhile, acetylacetonato complex and nitrate salt were completely inert in THF. The perchlorate salt seems to be the best catalyst because of its unique reactivity for cyclodimerization indifferent of the kinds of solvent. The reaction modes and the time-conversion curves of the copper perchlorate catalyzed as well as the non-catalyzed photoreactions in a number of solvents under

Table 1. Effect of anion and ligand

System	THF	EMK	DMSO
$Cu(ClO_4)_2\cdot 6H_2O$	D^p	D^p	D^{no}
$Cu(ClO_4)_2\cdot 2H_2O$	D^{no}		
$CuCl_2$	P^{no}	$NO^{d>p}$	
$Cu(NO_3)_2\cdot 3H_2O$	NO	$NO^{d<p}$	
$Cu(acac)_2$	NO		
$Cu(ClO_4)_2(Py)_4\cdot 2H_2O$	—		D^{no}

$[VCZ]_0=0.25$ M, $[Cu^{II}]_0=10^{-6}-10^{-2}$ M, in air, at 20—25 °C, for 2—3 hr. D,P; photo-dimerization, -polymerization. d,p; thermal dimerization, polymerization. no; no reaction in photosensitized or thermal system. ——; catalyst is insoluble.

Table 2. Reaction products in the absence and presence of $Cu(ClO_4)_2\cdot 6H_2O$ in air

System	No catalyst	$Cu(ClO_4)_2\cdot 6H_2O$
THF	P	D
DMSO	$P\gg D$	D
EMK	D	D
AP	D	D
EA	D	D
BN	D	D

$[VCZ]_0=0.25$ M, $[Cu^{II}]_0=10^{-6}-10^{-2}$ M, $\lambda=365$ nm, P; polymer, D; cyclodimer.

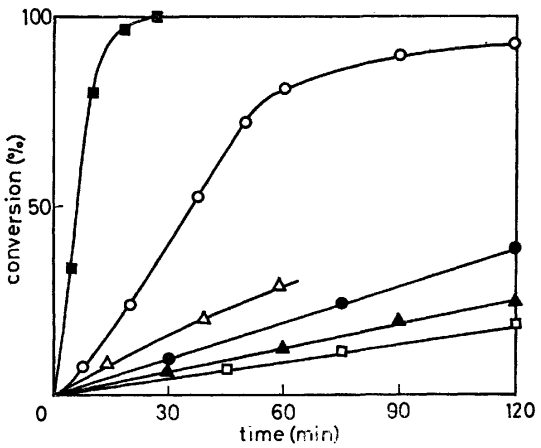

Fig. 1. Effect of solvent on photodimerization of VCZ catalyzed by $Cu(ClO_4)_2\cdot 6H_2O$ in air.
-■-: in BN*1, $[Cu^{II}]_0=10^{-5}$ M, $\lambda=365$ nm, 30 °C.
-○-: in THF, $[Cu^{II}]_0=10^{-2}$ M, $\lambda>365$ nm, 25 °C.
-△-: in AP*2, $[Cu^{II}]_0=10^{-5}$ M, $\lambda=365$ nm, 30 °C.
-●-: in EMK, $[Cu^{II}]_0=10^{-6}$ M, $\lambda=365$ nm, 25 °C.
-▲-: in DMSO, $[Cu^{II}]_0=10^{-2}$ M, $\lambda>365$ nm, 20 °C.
-□-: in EA, $[Cu^{II}]_0=5\times 10^{-6}$ M, $\lambda=365$ nm, 30 °C.
*1 including thermal polymerization.
*2 including photopolymerization without Cu(II).

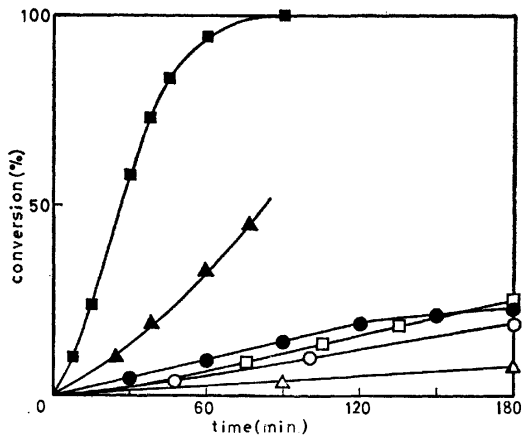

Fig. 2. Effect of solvent on non-catalyzed photoreaction of VCZ in air.
$[VCZ]_0=0.25$ M, 30 °C.
-■-: in BN, $\lambda=365$ nm. -●-: in AP, $\lambda>365$ nm. -□-: in THF, $\lambda>365$ nm. -○-: in EMK, $\lambda=365$ nm. -▲- in DMSO, $\lambda>365$ nm. -△-: in EA, $\lambda=365$ nm.

various reaction conditions are depicted in Figs. 1 and 2, respectively, and summarized in Table 2. The behaviors of non-catalyzed photoreaction agreed with the results reported by Mikawa.[15] Remarkable change in the reaction mode from the non-catalyzed photosensitized radical polymerization to the catalyzed photodimerization in THF and DMSO is particularly interesting. The VCZ–$Cu(ClO_4)_2\cdot 6H_2O$–THF system was chosen for detailed investigation.

Photoreactions Induced by Copper(II) Perchlorate in THF. Under the standard conditions ($[VCZ]_0=0.25$ M, $[Cu^{II}]_0=10^{-2}$ M, 20 °C, $\lambda=365$ nm, in air), the thermal

and non-catalyzed* photoreactions along with photodimerization were negligibly slow.

Light Absorbing Species. Absorption spectra of relevant compounds under the present reaction conditions are shown in Fig. 3. Absorption bands of copper perchlorate appeared in the near ultraviolet region and near infrared region which are assigned to the charge transfer band and the d-d band, respectively. On the other hand, the absorption band of VCZ in the ultraviolet region was scarcely affected by the addition of Cu(II), except negligibly weak 1 : 1 interaction between VCZ and Cu(II). Consequently, the photoenergy at 365 nm was absorbed almost exclusively by VCZ molecule. Meanwhile, it was confirmed that the prolonged irradiation at the d-d band of Cu(II) in longer wavelength region by means of a 500 W incandescent lamp with a cut-off glass filter (λ_{max}= 550 nm) induced no photoreaction of VCZ. These facts indicate that the effective absorbing species leading to photoreactions is VCZ itself.

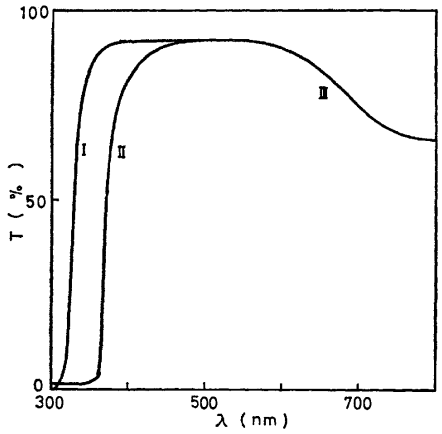

Fig. 3. Absorption spectra of VCZ and $Cu(ClO_4)_2 \cdot 6H_2O$ in THF.
I; $[Cu^{II}]_0=10^{-2}$ M (CT band), III; $[Cu^{III}]_0=10^{-2}$ M (d-d band), II; $[VCZ]_0=0.25$ M, room temperature.

Effect of Additives. The photodimerization in the presence of dissolved air was not affected at all by the addition of methanol(10^{-2} M). Addition of a trace amount(10^{-2} M) of water did not affect the initial rate, whereas large amounts of water exceeding 5×10^{-2} M reduced the stationary rate(R_d) as expressed by the following relation.

$$R_d \propto 1/[H_2O]_0$$

Under standard conditions the dimerization proceeded up to the complete conversion after a short acceleration period, while the bubbling of oxygen into reaction mixture prior to irradiation retarded the rate at the early stage of reaction as shown in Fig. 4. When the atmosphere was replaced with nitrogen, remarkably different features of reaction were observed that the rate was accelerated in the midway and polymerization proceeded simultaneously with dimerization. In this case, the fraction of polymer was about 70 percent. This polymerization was of cationic nature as judged by the inhibitory effect of methanol.

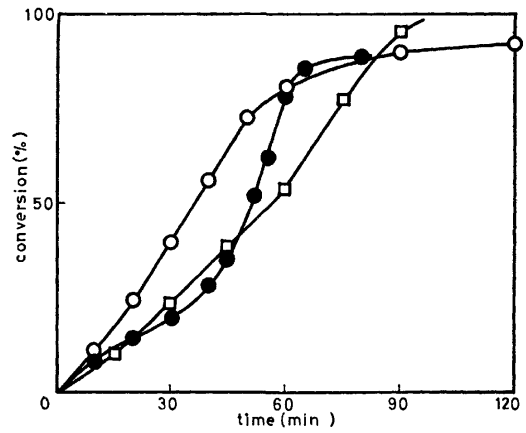

Fig. 4. Effect of atmosphere.
$[VCZ]_0=0.25$ M, $[Cu^{II}]_0=10^{-2}$ M, 25 °C.
-○-: in air. -□-: in oxygen. -●-: in nitrogen.

Effect of Monomer Concentration. At $[Cu^{II}]_0=10^{-2}$ M in air, when $[VCZ]_0$ was less than approximately 0.4 M, cyclodimer was formed. When $[VCZ]_0$ was higher approximately 0.5 M, the authors have found an unusual phenomenon that rapid polymerization commenced after the conversion of 0.25—0.3 M of VCZ to the cyclodimer, as demonstrated in Fig. 5. This polymerization was inhibited by methanol(5×10^{-2} M) but not by DPPH (2×10^{-4} M), indicating cationic polymerization. On the other hand, when the reaction system was saturated with oxygen

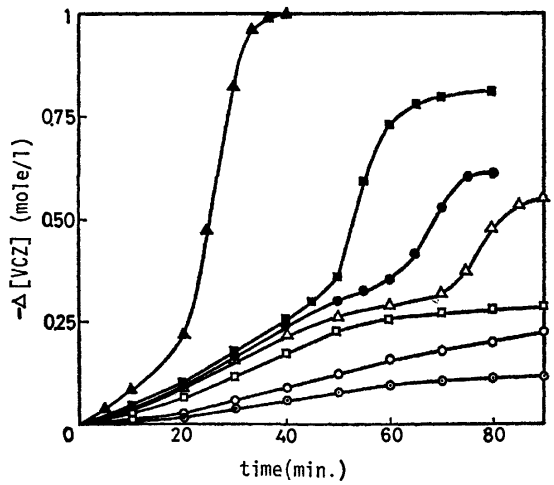

Fig. 5. Effect of the initial concentration of VCZ on the photoreaction.
$[Cu^{II}]_0=10^{-2}$ M, 20 °C, in air.
$[VCZ]_0$(M): -⊙-: 0.125. -○-: 0.25. -□-: 0.40. -△-: 0.50. -●-: 0.60. -■-: 0.75. -▲-: 1.0.

* This photopolymerization was completely inhibited by 1,1-diphenyl-2-picrylhydrazyl(10^{-4} M) but not affected by methanol (10^{-2} M), indicating radical propagation. Since the rate of polymerization(R_p) *in vacuo* was less than a half of that in the presence of dissolved air, oxygen seems to participate more or less in the initiation processes. The R_p was expressed as follows:

$$R_p \propto I_0^{0.45}[VCZ]_0^{1.4}$$

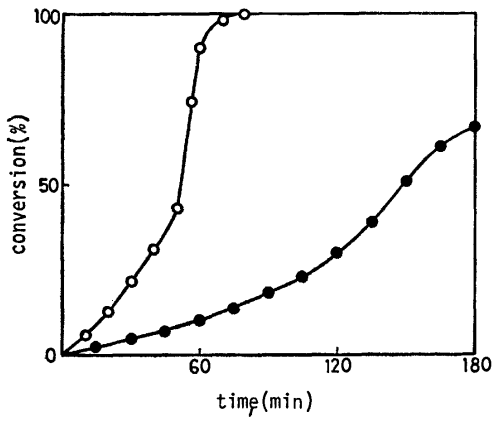

Fig. 6. Effect of an excess of oxygen.
$[VCZ]_0=0.75$ M, $[Cu^{II}]_0=10^{-2}$ M, 20 °C.
-○-: in air. -●-: in saturated oxygen.

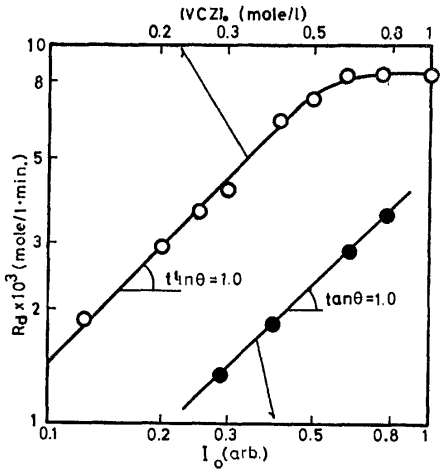

Fig. 7. Dependence of R_d on $[VCZ]_0$ and I_0.
$[Cu^{II}]_0=10^{-2}$ M, 20 °C, in air.
-○-: $[VCZ]_0$=variable, I_0=constant.
-●-: $[VCZ]_0=0.25$ M, I_0=variable.

before photoirradiation, the cationic polymerization in the later stage was suppressed, and the cyclodimer alone was obtained all through the reaction with a slower rate, as shown in Fig. 6. This fact suggests that oxygen plays some major roles in either the production of the cyclodimer or the inhibition of the polymer formation, and that the subsequent polymerization starts after the consumption of oxygen.

Dependence of the stationary rate (R_d) after the short acceleration period on the initial concentration of VCZ is shown in Fig. 7. Although R_d saturated at higher concentration, R_d was proportional to $[VCZ]_0$ up to 0.5 M VCZ.

Effects of Copper(II) Perchlorate Concentration. In the concentration range of 10^{-3}—10^{-1} M of copper perchlorate the initial R_d is nearly constant. The saturation of time conversion curve was observed at lower conversion with increasing $[Cu^{II}]_0$. This saturation effect seems to be attributed to the different concentration of water involved in these Cu(II) salts, since the same effect was observed when water was added into the reaction mixture. Another finding in support of this assumption is the fact that the dimerization by dihydrate copper(II) perchlorate proceeded up to nearly the complete conversion without saturation.

Changes of $[Cu^{II}]$ during the reaction were measured spectroscopically by following the d-d absorption band of Cu(II). Any consumption of Cu(II) could not be detected in the course of both dimerization ($[VCZ]_0=0.25$ M) and polymerization($[VCZ]_0=0.75$ M) subsequent to dimerization, indicating the role of Cu(II) to be purely catalytic.

Quantum Yield for Dimer Production. Linear dependence of R_d on the incident intensity of light(I_0) was depicted in Fig. 7. Upon interrupting irradiation, the dimerization stopped completely after a short after-effect, as shown in Fig. 8, indicating the production of relatively short lived species. The apparent quantum yield for dimer production including the after-effect was calculated from Fig. 8 to be about 15. This value of more than unity suggests that the cyclodimer is formed *via* some type of chain mechanism.

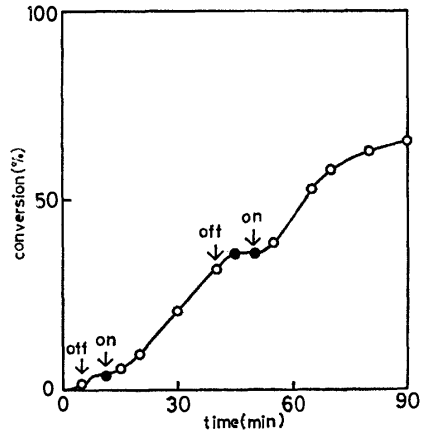

Fig. 8. On-off test.
$[VCZ]_0=0.25$ M, $[Cu^{II}]_0=10^{-2}$ M, 20 °C, in air.

Interaction of the Excited Singlet State of VCZ with Copper(II) Perchlorate or Oxygen. As shown in Table 3, under excitation at 345 nm VCZ emitted monomer and excimer fluorescence at 365—370 nm and at 460 nm, respectively. The mirror image relation of absorption and monomer emission spectra was held very well. Excimer fluorescence was observed only at high concentration of VCZ. Both fluorescences were quenched by Cu(II), where the Stern-Volmer plots fall on a straight line as typically depicted in Fig. 9. The quenching constants $K_{q,Cu}(=k_{q,Cu}\cdot\tau_0)$ for monomer and excimer emission were exactly identical as shown in the first row in Table 3. On the other hand, oxygen also quenched both emissions to nearly an equal extent(the second row). Therefore, $K_{q,Cu}$ must depend on the concentration of oxygen. Assuming the concentration of dissolved oxygen as 10^{-3} M and conformity to the Stern-Volmer equation as well, K_{q,O_2} was calculated from measurements of emission in air, nitrogen and oxygen in the presence of an appropriate concentration of Cu(II). Dependence of atmosphere on $K_{q,Cu}$ was also tabulated in Table 3 (the third row). The value of K_{q,O_2} (the forth row) thus

Table 3. Quenching constants

[VCZ] (M)	Atmosphere or $[Cu^{II}]_0$	λ_{ex} (nm)	λ_{em} (nm)	$K_{q,Cu}$	K_{q,O_2}
10^{-1}	in air	345	370	206	—
	in air	345	460	206[a]	—
	$[Cu^{II}]_0=0$ M	345	370	—	500
	$[Cu^{II}]_0=0$ M	345	460	—	680[a]
	$[Cu^{II}]_0=10^{-2}$ M	345	370	—	190
10^{-4}	in N_2	345	365	119	—
	in air	345	365	84	—
	in O_2	345	365	55	—
	$[Cu^{II}]_0=0$ M	345	365	—	590
	$[Cu^{II}]_0=10^{-2}$ M	345	365	—	430
	$[Cu^{II}]_0=5\times10^{-2}$ M	345	365	—	180
	$[Cu^{II}]_0=10^{-1}$ M	345	365	—	80

a) For excimer emission

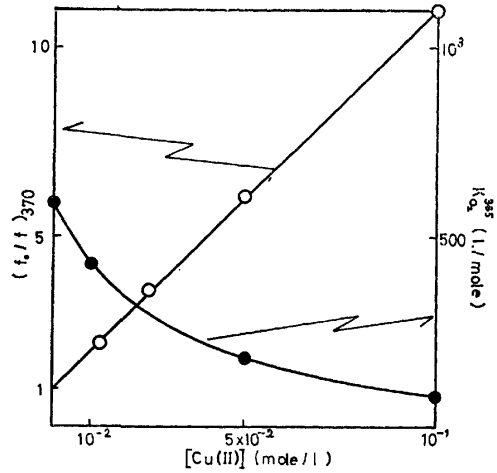

Fig. 9. The Stern-Volmer plot and K_{q,O_2} as a function of $[Cu^{II}]_0$.
-○-: $[VCZ]_0=0.1$ M, $\lambda_{ex}=365$ nm, in air.
-●-: $[VCZ]_0=10^{-4}$ M, $\lambda_{ex}=345$ nm.

calculated was depicted as a function of $[Cu^{II}]$ in Fig. 9.

Discussion

Photoreactions of VCZ in the presence of copper(II) salts exhibited very intricate features depending on various factors such as anion or ligand of the salt, solvent, atmosphere, water or concentration of VCZ. The fact that copper perchlorate induces the photocyclodimerization alone indifferent of solvent under the condition of $[VCZ]_0=0.25$ M and in the presence of air is the characteristic nature of this metal salt in contrast to gold(III) complexes or silver(I) salts.[1] The authors classified[1] the photoreactions of VCZ with these metal salts into three categories in terms of the effective light absorbing species: Type I; metal salt, Type II; VCZ and Type III; VCZ/metal salt complex. The copper perchlorate-THF-365 nm system belongs to the Type II similar to the photoreaction with silver(I) salts. In the latter system, however, cyclodimerization and/or cationic polymerization took place depending upon solvents.

The sequences of the rate of photocyclodimerization in both Cu(II) catalyzed and non-catalyzed systems seem to depend upon the donor-number of solvent (DN) proposed by Gutmann,[16] which is an indication of donating power of solvent to cation, as follows:

$Cu(ClO_4)_2\cdot6H_2O$ system:

R_d; BN>EMK~AP>EA>THF>DMSO

DN; 12< <17< 20 < 30

Non-catalyzed system: R_d; BN≫EMK≧AP>EA

The parallelism between the Cu(II) catalyzed and non-catalyzed photoreactions with respect to the solvent effect on R_d suggests that the major solvent effect is not to influence the activity of Cu(II). The cyclodimerization in DMSO in the presence of Cu(II) should be noted since such reaction has not been reported in the cases of photo- or γ-ray induced reactions both in the presence and absence of organic acceptors.

Effect of atmosphere on the reaction mode is of interest. When $[VCZ]_0$ is higher than 0.5 M, the rapid cationic polymerization commences after about 0.3 M of VCZ has been converted to the cyclodimer and in the presence of an excess of oxygen this polymerization is completely suppressed and cyclodimerizaiton alone proceeds. These findings suggest that oxygen is indispensable to the formation of cylcodimer or for the inhibition of cationic polymerization, and that oxygen is consumed in the course of the cyclodimerization. This oxygen effect is also supported by the fact that cationic polymerization predominates in nitrogen atmosphere.

Kinetic relation, $R_d\propto I_0[VCZ]_0\,[Cu^{II}]_0^0$, is identical with that of the photodimerization by $Hg(CN)_2$ in acetonitrile briefly described by Breitenbach.[2] Apparent quantum yield for the production of cyclodimer is observed to be about 15, suggesting the chain mechanism as proposed by Ledwith in the photocyclodimerization sensitized by organic dyes.[3]

Fluorescence of VCZ was quenched by both Cu(II) and oxygen. Provided that the actions of Cu(II) and oxygen on fluorescence are mutually independent, the following equations are derived, respectively.

$$K_{q,O_2}=\frac{K^\circ_{q,O_2}}{1+K^\circ_{q,Cu}[Cu^{II}]},\quad K_{q,Cu}=\frac{K^\circ_{q,Cu}}{1+K^\circ_{p,O_2}[O_2]}$$

where, K°_{q,O_2} and $K^\circ_{q,Cu}$ denote the intrinsic quenching constants of oxygen and Cu(II) in the absence of the other, respectively. These hyperbolic relations agree with the experimental results qualitatively. Fluorescence of VCZ is supposed to be quenched dynamically by Cu(II), since interaction between VCZ and Cu(II) in the ground state is negligible. Meanwhile, dynamic quenching by oxygen may not be characterized unequivocally because of possible formation of the ground state charge-transfer complex. The equal quenching constants for monomer and excimer emissions indicate that apparent quenching of excimer emission was attributed to a result of quenching of monomer fluoresence. Quantitative studies on the quenching of or-

ganic fluorescence by metal ion have been scarcely reported.[7] On the other hand, the quenching effect of inorganic ion on phosphorescence has been investigated systematically by several authors to some extent.[7] Although in the present study no phosphorescence was observed under reaction conditions, at room temperature and in air, interactions of the excited triplet state of VCZ with Cu(II) ion seem to be also very likely, as inferred from quenching action of Cu(II) to the triplet state of aromatic molecules.[7] Quenching mechanisms may be roughly classified into three categories: i) energy-transfer ii) electron-transfer iii) enhancement of intersystem crossing S*→T*. Similar quenching action of oxygen to the excited aromatic molecule has been reported in details.[17]

As to the mechanism of cyclodimerization of VCZ, the following different two types of mechanisms have been proposed by Ledwith[3] and by Wang,[4] respectively.

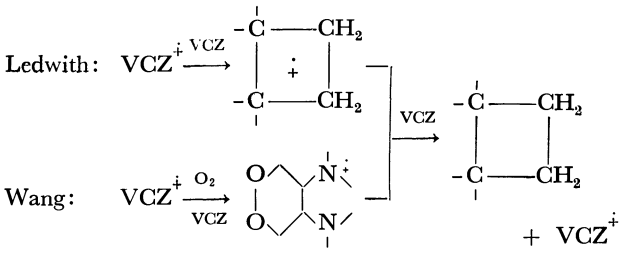

Both mechanisms are common in the sense of assuming chain reaction *via* radical-cation intermediate ($M^{\dot{+}}$). The former assumed the cyclodimer radical cation intermediate ($D^{\dot{+}}$) whereas the latter considered the six-membered ring peroxide intermediate. However, the problem of oxygen consumption has never been investigated by them. Recently, the direct evidence for the following equilibrium

$$M^{\dot{+}} + VCZ \rightleftharpoons D^{\dot{+}}$$

was obtained by means of the pulse radiolysis technique by Imamura.[18] They have proposed that $D^{\dot{+}}$ is a common precursor for both cyclodimerization and cationic polymerization of VCZ.

The following reaction scheme is proposed. Either excited singlet or triplet state ($VCZ^{*1,3}$) would collide with Cu(II), while one electron transfer from $VCZ^{*1,3}$ to Cu(II) produces $VCZ^{\dot{+}}$ and Cu^{I}. Simultaneously, Cu^{I} would interact with radical part of the $VCZ^{\dot{+}}$ in either the formation of organometallic bond or radical complex[19] to stabilize the free spin and consequently, cationic polymerization is initiated from the carbonium ion. The role of oxygen is to oxidize Cu^{I} to Cu^{II} accompanied by the production of radical-anion of oxygen ($O_2^{\dot{-}}$) and the free $VCZ^{\dot{+}}$ which reacts with VCZ to produce the cyclodimer cation-radical (D^{+}). Subsequent processes would be almost similar to the Ledwith's chain mechanism with the exception of the role of $O_2^{\dot{-}}$ and termination reaction. In this mechanism, propagation proceeds *via* $D^{\dot{+}}$ with a counter-ion $O_2^{\dot{-}}$ and termination takes place by electron-transfer between them resulting none of consumption of molecular oxygen. In the present study, however, it is suggested that oxygen is consumed through the main route of the reaction but not as side reactions, since about 0.3 M VCZ was always converted into the cyclodimer indifferent of the initial concentration of VCZ if it is over 0.4 M, as shown in Fig. 5, under the standard conditions. Therefore, $O_2^{\dot{-}}$ might be consumed by some types of bimolecular reaction as reported in the pulse radiolysis studies[20] or the cerium(IV) salt catalyzed reaction of hydroperoxide.[21]

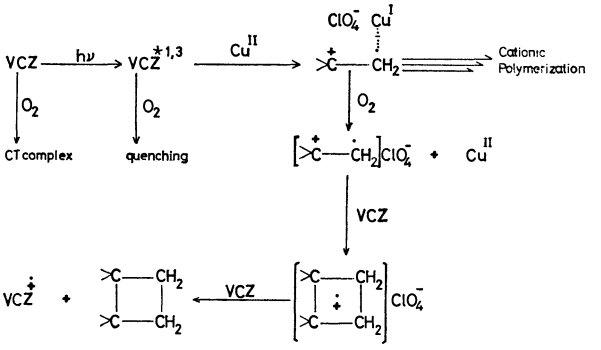

Scheme

Termination is assumed as monomer termination, for example, the Friedel-Crafts type reaction of carbonium ion with the carbazyl ring as proposed previously.[22] By applying the assumption of stationary concentration $M^{\dot{+}}$, $D^{\dot{+}}$ and $\overset{+}{C}—\dot{C}\cdots\cdots Cu^{I}$, the following rate expression is derived.

$$R_d \propto I_{abs}^{M}[Cu^{II}]_0^0 = I_0\{1-\exp(-\varepsilon_M[VCZ]_0)\}\ [Cu^{II}]_0^0$$

This kinetic relation explains the experimental results very well. Another role of oxygen in this mechanism is the interaction with either ground state or excited state of VCZ to quench the emission of VCZ, which may result the retardation of the rate in the presence of an excess of oxygen in the reaction system. Further detailed investigations on the vacuum system and the direct measurement of oxygen consumption as well as the effects of water would be future problems.

The authors are indebted to professors Seizo Okamura and Toshinobu Higashimura for their encouragement and helpful discussion and express their thanks to Mr. I. Umehara for his help in measuring molecular weight of polymer.

References

1) M. Asai, H. Matsui, Y. Takeda, and S. Tazuke, IUPAC Symposium on Macromolecular Chemistry held at Helsinki, July 1972.

2) J. W. Breitenbach, F. Sommer, and G. Unger, *Monatsh. Chem.*, **101**, 32 (1970).

3) A. Ledwith, *Accounts Chem. Res.*, **5**, 133 (1972) and references cited therein.

4) C. H. Wang, *J. Org. Chem.*, **35**, 2045 (1970).

5) M. Asai, Y. Takeda, and S. Tazuke, Part IV and V in this series, *Polymer J.*, in press.

6) For example, J. Feitelson, and N. Shaklay, *J. Phys.*

Chem., **71**, 2582 (1967); J. Fujihara, S. Hirayama, S. Kusuhara, and J. Osugi, This Bulletin, **44**, 3495 (1971); D. H. Paskovich, A. H. Reddoch, and D. F. Williams, *Chem. Commun.*, **1972**. 1195.

7) For example, G. Porter and M. R. Wright, *Discuss. Faraday Soc.*, **27**, 18 (1959); C. Steel and H. Linschitz, *J. Amer. Chem. Soc.*, **66**, 2577 (1962); A. W. Varnes, R. B. Dodson, and E. L. Wehry, *ibid.*, **94**, 946 (1972); M. Koizumi, "Ko-Kagaku Gairon", Asakura-Shoten, Tokyo (1963).

8) D. J. Collins and J. J. Hobbs, *Aust. J. Chem.*, **20**, 1905 (1967).

9) S. Murai and S. Tsutsumi, This Bulletin, **39**, 198 (1966).

10) J. K. Kochi, *J. Amer. Chem. Soc.*, **84**, 2121 (1962). M. L. Poutma, *ibid.*, **87**, 2161 (1965).

11) B. J. Hathaway and A. E. Underhill, *J. Chem. Soc.*, **1961**, 3091; R. D. Peacock, *J. Chem. Educ.*, **48**, 133 (1971); P. C. Sinha and R. C. Ray, *J. Indian Chem.*, **20**, 32 (1943).

12) C. G. Hatchard and C. A. Parker, *Proc. Roy. Soc., Ser. A.*, **235**, 518 (1956).

13) L. P. Ellinger, J. Feeney, and A. Ledwith, *Monatsh. Chem.*, **96**, 131 (1965).

14) K. Ueberreiter and J. Springer, *Z. Phys. Chem.*, **36**, 299 (1963).

15) Y. Shirota, K. Tada, M. Shimizu, S. Kusabayashi, and H. Mikawa, *Chem. Commun.*, **1970**, 1110.

16) V. Gutmann, "Coordination Chemistry in Non-aqueous Solution," Springer, New York (1968).

17) D. R. Kearns, *Chem. Rev.*, **71**, 395 (1971); T. Brewer, *J. Amer. Chem. Soc.*, **93**, 775 (1971).

18) S. Tagawa, S. Arai, M. Imamura, Y. Tabata, and K. Oshima, *J. Polym. Sci., B*, **10**, 295 (1972) and JSPS 21st Symposium on Macromolecules, Osaka(1972).

19) P. Clopath and A. v. Zelewsky, *Chem. Commun.*, **1971**, 47; F. Leh and J. K. S. Wan, *Can. J. Chem.*, **50**, 999 (1972).

20) G. E. Adams, J. W. Boag, and B. D. Micheal, *Proc. Roy. Soc. Ser. A*, **289**, 321 (1966); G. Czapski and L. M. Dorfman, *J. Phys. Chem.*, **68**, 1169 (1964).

21) E. Saito and B. H. J. Bielski, *J. Amer. Chem. Soc.*, **83**, 4467 (1961); *J. Phys. Chem.*, **66**, 2266 (1962).

22) M. Asai, S. Tazuke, and S. Okamura, *J. Polym. Sci., A-1.*, **12**, 45 (1974).

A Study of the Interaction of Diethylcadmium with Lewis Bases as Solvents

Osami NAKASUGI, Michihiro ISHIMORI, and Teiji TSURUTA

Department of Synthetic Chemistry, Faculty of Engineering, The University of Tokyo, Bunkyo-ku, Tokyo 113

(Received June 21, 1973)

The infrared spectra of diethylcadmium($CdEt_2$) in a variety of different solvents were measured. The affinity of $CdEt_2$ toward oxygen and sulfur bases was studied by infrared frequency shifts of $CdEt_2$. Linear relationships were observed for the plots of the two frequency shifts $\Delta\nu_a$(C–Cd–C) of $CdEt_2$ *vs.* $\Delta\nu_a$(C–Zn–C) of $ZnEt_2$ and $\Delta\nu_a$(C–Cd–C) *vs.* $\Delta\nu$(O–D) of CH_3OD. The deviation of the plots for the systems of $CdEt_2$ with cyclic sulfides from the linear behavior was interpreted in terms of dative back-bonding from $CdEt_2$ to sulfides. The enhanced reactivity of the Cd–S compound toward propylene oxide compared to that of the Cd–O compound was considered to result from a harder acid character of the Cd atom in the Cd–S compound caused by its back-bonding nature.

Several studies of organozinc compounds as catalysts for propylene oxide polymerization have been reported.[1-3] The polymerization proceeds by a coordinate anionic mechanism, in which the coordination of the monomer molecule to the zinc atom is considered to be important in the activation of the monomer and of the catalyst, and also for the high stereoregulation observed in this polymerization.

The binary system of diethylzinc with water[2,4] or alcohol[1,5] has an excellent activity for propylene oxide polymerization. In contrast, the corresponding binary system of diethylcadmium with water or alcohol has little or no activity for the ring-opening reaction of propylene oxide.[6] It was recently found, however, that systems of $CdEt_2$ with thiocarboxylic acid[6] and of $CdEt_2$ with mercaptan[7] have favorable catalyst activities for the ring-opening reactions of propylene oxide; especially, $CdEt_2$–RCOSH systems gave high-molecular-weight polymers in satisfactory yield. A marked difference in catalyst activity between Cd-S and Cd-O compounds has been noted.

In order to elucidate the factors influencing the catalytic activities of Group IIb organometallic compounds, the mode of the interaction of $CdEt_2$ with an oxygen base and a sulfur base was studied in terms of the magnitude of the infrared frequency shifts of $CdEt_2$ and was compared with those of $ZnEt_2$ and methanol-*d*. It was previously reported that cadmium metal ions are classified into "soft"[8] or "class b"[9] acids, whereas zinc ions are "borderline" acids. The bonding natures of Group IIb organometallic compounds with oxygen (hard) and sulfur (soft) bases are of considerable interest.

Results and Discussion

Infrared Spectrum of Diethylcadmium. The infrared spectrum of $CdEt_2$ in the region of 4000 to 200 cm^{-1} was measured. The spectrum in the range of 4000 to 650 cm^{-1} is approximately identical to the data reported by Kaesz and Stone.[10] However, the bands[10] at 1186 (assigned to the CH_2 rocking vibration), 670, and 663 cm^{-1} ($C–CH_3$ rocking) were not observed in our spectrum. These bands may be due to the contamination of diethylmercury (*cf.* the spectrum in Ref. 10), which could itself be formed by the reaction of $CdEt_2$ with mercury metal.[11]

Three bands for $CdEt_2$ at 614, 494, and 441 cm^{-1} were observed in the region of 700 to 200 cm^{-1}. To obtain a reasonable assignment for the infrared frequencies, it is necessary to consider its plausible symmetry form. It was previously reported that methyl derivatives of Group IIb metals, $Cd(CH_3)_2$, $Zn(CH_3)_2$, and $Hg(CH_3)_2$, have linear C–M–C chains (M=Cd, Zn and Hg).[12] We interpreted the bands of $CdEt_2$ on the basis of the reasonable assumption that the C–Cd–C skeleton is linear in a similar way to $ZnEt_2$.[1] From the general similarity of the spectra between $CdEt_2$ and $ZnEt_2$ shown in Table 1, the bands at 614, 494, and 441 cm^{-1} were assigned to the CH_2 rocking $\gamma_r(CH_2–(Cd))$, C–Cd–C antisymmetric ν_a(C–Cd–C), and C–Cd–C symmetric ν_s(C–Cd–C) vibrations, respectively. Although the C–Cd–C skeleton is considered to be linear, a very weak band of ν_s(C–Cd–C) was observed similarly to the ν_s(C–Zn–C) of $ZnEt_2$;[3] this indicates some deviation of the above C–Cd–C symmetric vibration from the ideal one, probably due to the interaction of $CdEt_2$ with another $CdEt_2$ or solvent molecule and/or the free internal rotation of the ethyl groups of the $CdEt_2$ molecule itself. The deformation frequency of the C–Cd–C chain is expected to lie beyond the range of our measurement.

Table 1. INFRARED FREQUENCIES OF DIETHYLCADMIUM IN KBr REGION[a]

$CdEt_2$	Ref. $ZnEt_2$[3]	Assignment
614(s)	617(s)	$\gamma_r(CH_2–(M))$
494(s)	561(s)	ν_a(C–M–C)
441(w)	479(w)	ν_s(C–M–C)

a) Measured without solvent. cm^{-1}. (s): strong; (w): weak

The reliability of the above assignment for $CdEt_2$ was roughly checked for the spectra of reaction products between $CdEt_2$ and CH_3OH. The frequencies of $EtCdOCH_3$ and $Cd(OCH_3)_2$ in the region of 700 to 200 cm^{-1} are shown in Table 2. Tentative assignments for the frequencies of $EtCdOCH_3$ and $Cd(OCH_3)_2$ were made on the assumption of bending structures of the C–Cd–O and O–Cd–O chains, with reference to the corresponding zinc systems.[1,3] The bands of $CdEt_2$ at 494 and 441 cm^{-1} ascribed respectively to the ν_a(C–Cd–C) and ν_s(C–Cd–C) vibration disappeared completely in the spectra of $EtCdOCH_3$ and $Cd(OCH_3)_2$. The CH_2 rocking vibration of $EtCdOCH_3$ was observed at 608 cm^{-1}, a frequency somewhat lower than that of $CdEt_2$; no sign of the corresponding band was observed in the spectrum of

TABLE 2. INFRARED FREQUENCIES (cm^{-1}) OF $Cd(C_2H_5)_2$-CH_3OH SYSTEM[a]

	$\gamma_r(CH_2)$	ν(OCdO)	ν_a(CCdC)	ν_a(CCdO)	ν_s(CCdC)	ν_s(CCdO)	ν(OCdO)
$CdEt_2$	614(s)	—	494(s)	—	441(w)	—	—
EtCdOMe	608(s)	—	—	461(s)	—	345(s)	—
$Cd(OMe)_2$	—	550(m)	—	—	—	—	245(s)

a) cm^{-1}. (s): strong; (w): weak; (m): medium

TABLE 3. INFRARED FREQUENCY SHIFTS OF DIETHYLCADMIUM IN SOLVENTS[a]

No.	Solvent	Et_2Cd $\gamma_r(CH_2)$ (s)	Et_2Cd ν_a(C-Cd-C) (s)	Et_2Cd ν_s(C-Cd-C) (w)	Et_2Cd $\Delta\nu_a$(C-Cd-C)	Et_2Zn[b] $\Delta\nu_a$(C-Zn-C)	CH_3OD[b] $\Delta\nu$(O-D)
1	*n*-Heptane	617.5	497	441	0	0	—
2	Benzene	620	495.5	440	1.5	2.0	29
3	Toluene	620	495.5	—	1.5	2.0	26
4	Diethyl ether	613.5	491	—	6.0	10.5	96
5	Propylene oxide	612.5	489.5	—	7.5	14.0	99
6	Styrene oxide	617	491	—	6.0	11.0	85
7	Epichlorohydrin	614.5	491.5	—	5.5	9.5	80
8	Dioxane	—	488	435	9.0	17.0	111
9	Tetrahydrofuran	611.5	487.5	433	9.5	{19.0 {30.0	117
10	Diethyl sulfide	613	489	434	8.0	14.5	106
11	Propylene sulfide	—	487	433	10.0	15.5	99
12	Tetrahydrothiophene	610	485	429	12.0	20.0	117

a) An instrument of EPI-G3 was used. See "Experimental" section. (—): not observed due to the bands of solvents. b) ν_a(C-Zn-C) of $ZnEt_2$[3] and ν(O-D) of CH_3OD[15] for the solvents (No. 1—9) were previously reported. Differences between the values in this paper and those in the previous ones were ± 1 cm^{-1}.

$Cd(OCH_3)_2$. The two strong bands at 461 and 345 cm^{-1} in the spectrum of $EtCdOCH_3$ were assigned to the pseudoantisymmetric and pseudosymmetric ν(C-Cd-O) vibrations, respectively. The bands at 550(m) and 245(s) cm^{-1} in $Cd(OCH_3)_2$ could be assigned to the skeletal vibrations of the O-Cd-O chain, ν(O-Cd-O), from the spectral similarity between $Cd(OCH_3)_2$ and $Zn(OCH_3)_2$.[1]

In the light of these spectral changes, the above-mentioned assignments for the frequencies of $CdEt_2$ are considered to be reasonable.

Interaction between $CdEt_2$ and Lewis Bases. The infrared spectra of $CdEt_2$ in a variety of different solvents were measured in the KBr region. The frequencies of $CdEt_2$, $\gamma_r(CH_2)$, ν_a(C-Cd-C), and ν_s(C-Cd-C) in a series of Lewis base solvents are summarized in Table 3, together with three frequency shifts, $\Delta\nu_a$(C-Cd-C) of $CdEt_2$, $\Delta\nu_a$(C-Zn-C) of $ZnEt_2$, and ν(O-D) of CH_3OD. The frequency shifts of $CdEt_2$ and $ZnEt_2$ were calculated by reference to each frequency in *n*-heptane solvents. The shifts of methanol-d were calculated on the basis of the value in carbon tetrachloride.

Since the frequency shifts in donor solvents are due to the formation of donor-acceptor complexes between Lewis acids and bases, the magnitudes of the frequency shifts are considered to reflect the strength of the bondings of these complexes. For instance, some enthalpy data for hydrogen bondings have been reported to generate linear relationships with the infrared OH frequency shifts.[13]

The $\Delta\nu_a$(C-Cd-C) shifts of $CdEt_2$ are plotted against the corresponding shifts, $\Delta\nu_a$(C-Zn-C), of $ZnEt_2$, in Fig. 1. The $\Delta\nu_a$(C-Zn-C) *vs.* $\Delta\nu_a$(C-Cd-C) plots lie on a straight line for most of the Lewis base solvents examined.

In tetrahydrofuran solution, the ν_a(C-Zn-C) of $ZnEt_2$ showed a doublet band at 543 and 532 cm^{-1}; it was assigned to the vibrations of the $ZnEt_2$·THF and $ZnEt_2$·2THF complexes, respectively.[3] On the other hand, the spectrum of $CdEt_2$ in the same solvent showed a singlet band of ν_a(C-Cd-C). The plot for $CdEt_2$ in tetrahydrofuran (No. 9) against the one-to-one complex of $ZnEt_2$·THF lies on the straight line of $\Delta\nu_a$-(C-Zn-C) *vs.* $\Delta\nu_a$(C-Cd-C) in Fig. 1, indicating the presence of $CdEt_2$·THF as the sole complex in the tetrahydrofuran solution of $CdEt_2$. The difference in affinity with tetrahydrofuran between $CdEt_2$ and $ZnEt_2$ indicates the difference between their Lewis acidities toward ether-oxygen. The weaker Lewis acidity of $CdEt_2$ than that of $ZnEt_2$ is also suggested by the slope of the plots in Fig. 1, which is much smaller than unity. It was previously reported by Bellamy, Hallam and Williams (BHW)[14] that a linear relationship held between the relative frequency shifts of the common characteristic bands of two different solutes in a variety of different solvents; the $\Delta\nu/\nu$ (O-D) of CH_3OD, for example, has a linear relationship with the $\Delta\nu/\nu$ (N-H) of $C_6H_5NH_2$ or the $\Delta\nu/\nu$ (S-H) of H_2S. It has been suggested that the slopes of the plots for solutes against a standard acid are a measure of their Lewis acidities. The BHW plots between $\Delta\nu/\nu$(C-Cd-C) and $\Delta\nu/\nu$(C-Zn-C) gave a linear relationship, the slope of

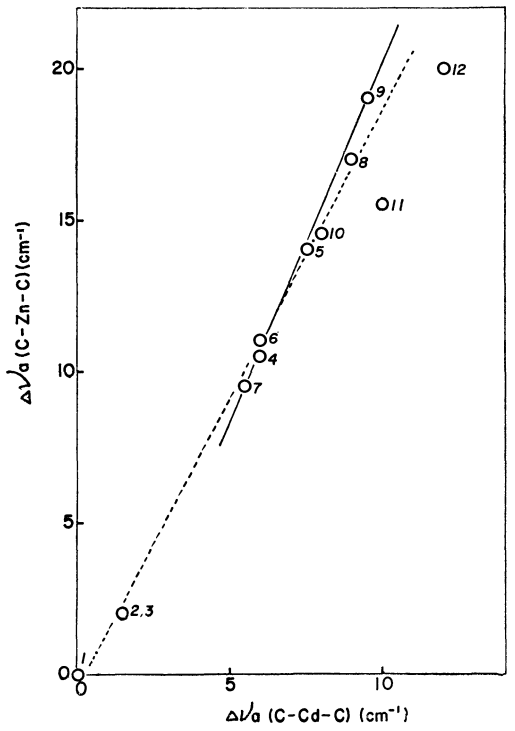

Fig. 1. Frequency shifts of $\Delta\nu_a$(C-Zn-C) of $ZnEt_2$ *vs.* frequency shifts of $\Delta\nu_a$(C-Cd-C) for a series of Lewis base solvents.
1: *n*-heptane, 2: benzene, 3: toluene, 4: diethyl ether, 5: propylene oxide, 6: styrene oxide, 7: epichlorohydrin, 8: dioxane, 9: tetrahydrofuran, 10: diethyl sulfide, 11: propylene sulfide, 12: tetrahydrothiophene.

Table 4. Frequency shifts of ν(C-O) of dioxane

Organometal. compd.	ν(C-O)(cm^{-1})	$\Delta\nu$(cm^{-1})
None	873	0
$CdEt_2$	832	41
$ZnEt_2$	830	43
$InEt_3$	831	42
$AlEt_3$	823	50

which again suggested a weaker acidity for $CdEt_2$. Then the relative Lewis acidity of $CdEt_2$ toward ether-oxygen was precisely examined by measuring the magnitude of the infrared band shift of ν(C-O) of dioxane[2] at 873 cm^{-1} due to the coordination of oxygen to metal. The results are shown in Table 4, toegther with those for $AlEt_3$ and $InEt_3$ as references. The Lewis acidity toward ether-oxygen increases in the order: $CdEt_2 < InEt_3 < ZnEt_2 < AlEt_3$.

The most remarkable point about the $\Delta\nu_a$(C-Zn-C) *vs.* $\Delta\nu_a$(C-Cd-C) relationship in Fig. 1 is the anomaly of the plots for propylene sulfide and tetrahydrothiophene (No. 11 and 12) from the linear behavior. Namely, the relative affinity of $CdEt_2$ with the sulfur base compared with that with oxygen bases is different from that of $ZnEt_2$. The greater affinity of $CdEt_2$ toward soft bases of sulfide than that of $ZnEt_2$ is coincident with the "softer"[8] nature of the cadmium ion.

The rocking vibration of the CH_2 group of $CdEt_2$ in π-bases of benzene and toluene (No. 2 and 3) was observed at higher frequencies than that for *n*-heptane, similarly to the case of $ZnEt_2$.[3] Another type of interaction, *i. e.*, that of the π-complex of $CdEt_2$ with benzene rings, is suggested by the deviation of the plots for benzene, toluene, and styrene oxide (No. 6) from the linear relationship of $\Delta\gamma_r CH_2$ (calculated from the value in *n*-heptane) *vs.* $\Delta\nu_a$(C-Cd-C), as is shown in Fig. 2.

In order to examine in detail the above difference

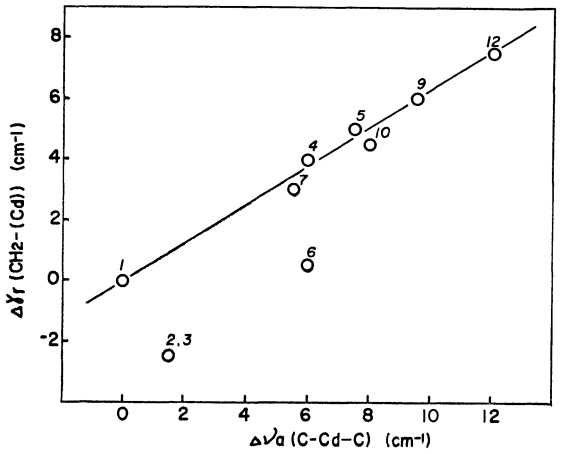

Fig. 2. Frequency shifts of $\Delta\gamma_r$(CH_2-(Cd)) *vs.* frequency shifts $\Delta\nu_a$(C-Cd-C) of $CdEt_2$ for a series of Lewis base solvents. Numbers for solvents as in Fig. 1.

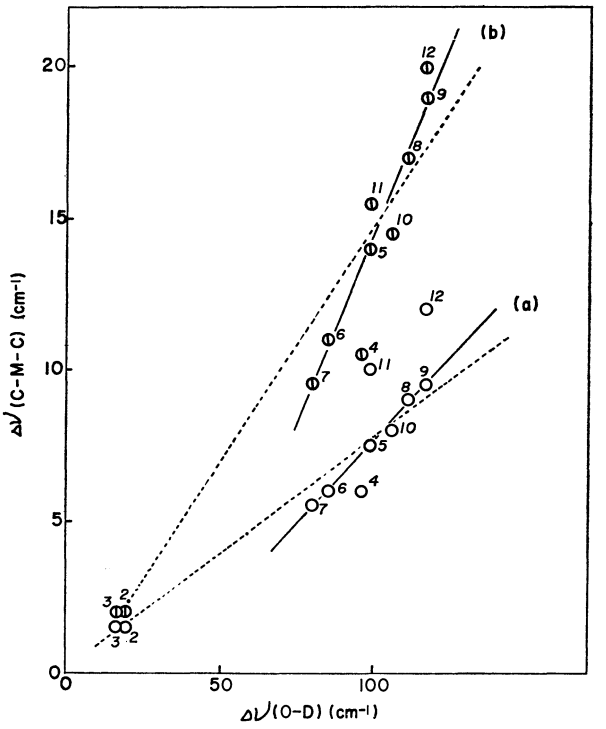

Fig. 3. Frequency shifts of $\Delta\nu_a$(C-M-C) of $CdEt_2$ and $ZnEt_2$ *vs.* frequency shifts of $\Delta\nu$(OD) of CH_3OD for a series of Lewis base solvents. Numbers for solvents as in Fig. 1.
(a): $CdEt_2$, (b): $ZnEt_2$

Table 5. Interactions of $Cd(C_2H_5)_2$ and $Zn(C_2H_5)_2$ with cyclic sulfides and ethers[a]

Lewis base	$CdEt_2$		$ZnEt_2$		CH_3OD
	$\Delta\nu_a$(C-Cd-C) (cm^{-1})	$\Delta\nu/\nu$ ($\times 10^3$)	$\Delta\nu_a$(C-Zn-C) (cm^{-1})	$\Delta\nu/\nu$ ($\times 10^3$)	$\Delta\nu$(OD) (cm^{-1})
Propylene sulfide	10.0	20	15.5	27	100
Propylene oxide	7.5	15	14.0	25	99
Tetrahydrothiophene	12.0	24	20.0	35	116
Tetrahydrofuran	9.5	19	19.0 30.0	34 53	117
Diethyl sulfide	8.0	16	14.5	26	106
Diethyl ether	6.0	12	10.5	19	96

a) The frequencies ν of $\Delta\nu/\nu$ for $CdEt_2$ and $ZnEt_2$ are each value in *n*-heptane solvents.

between $CdEt_2$ and $ZnEt_2$, the frequency shifts of $CdEt_2$ and $ZnEt_2$ for a series of Lewis base solvents are plotted against the $\Delta\nu$(O–D) of methanol-*d* in Fig. 3. The steric requirement of a hard acid of CH_3CD is small, and its frequency shift, $\Delta\nu$(O–D), is known as a scale of the basicity in the usual sense.[15]

The plots of $\Delta\nu_a$(C–Cd–C) *vs.* $\Delta\nu$(O–D) in Fig. 3(a) indicate again a special interaction of $CdEt_2$ with such cyclic sulfides as propylene sulfide and tetrahydrothiophene. In contrast, such a special interaction is considerably weak in the systems of $ZnEt_2$ with cyclic sulfur bases, as is shown by the $\Delta\nu_a$(C–Zn–C) *vs.* $\Delta\nu$(O–D) plots in Fig. 3(b). This phenomenon is more clearly shown by the relative frequency shifts of $CdEt_2$, $ZnEt_2$, and CH_3OD with cyclic sulfides and ethers, as are listed in Table 5. The shifts of $CdEt_2$ with cyclic sulfides are much greater than those with the corresponding ethers. Namely, the "soft" characters of the above Lewis acids are in this order: $CdEt_2 > ZnEt_2 \gtrsim CH_3OD$.

However, the plot for $CdEt_2$ with diethyl sulfide (No. 10) falls onto a straight line in Fig. 3. The apparent lack of any special interaction for this system is considered to be caused by the steric hindrance between ethyl groups of $CdEt_2$ and those of diethylsulfide. The marked deviation of the plots for diethyl ether with $CdEt_2$ and $ZnEt_2$ from the linear behavior in the direction of the methanol-*d* side (No. 4 in Fig. 3) can also be explained in terms of the above steric hindrance.

The special interaction of $CdEt_2$ with sulfide can be interpreted in terms of dative back bonding[9,16] from the occupied 4d orbital of the cadmium atom of $CdEt_2$ to the 3d vacant orbital of the sulfur atom of sulfide.

It was described in the "Introduction" section that Cd–S compounds are much more reactive toward propylene oxide than the Cd–O compounds. This fact can be interpreted as follows; Cd atoms in Cd–S compounds are "harder" than those of Cd–O compounds because of their back-bonding nature which increases the positive charge of Cd atoms by a process of electron transfer from Cd to S; accordingly, they are much more reactive toward a hard oxygen base of propylene oxide.

Experimental

All the experiments concerned with organometallic compounds were carried out under purified nitrogen atmosphere.

Reagents. Diethylcadmium[17] and triethylindium[18] were prepared by the methods which involve the reactions of metal halides with Grignard reagents. Organometallic compounds ($CdEt_2$, $ZnEt_2$, $AlEt_3$ and $InEt_3$) were purified by fractional distillation under reduced pressure. Methanol-*d* was used after distillation.

Propylene sulfide was prepared by the reaction between propylene oxide and potassium thiocyanate.[19] Solvents (hydrocarbons, ethers, and sulfides) were purified by the standard methods[20] and were fractionally distilled.

Infrared Measurements. A Hitachi EPI-G3 and a JASCO DS-402G grating infrared spectrometers were used to collect the infrared data. The spectrum of diethylcadmium was measured as a liquid film. The spectra of diethylcadmium, diethylzinc, and methanol-*d* in solvents were measured using liquid cells with KBr windows at the concentration of 1.0 mol/l. Ethylcadmium methoxide and cadmium dimethoxide were measured as mulls in dry liquid paraffin. Expanded frequency scales were used to obtain accurate values of the shifts, $\Delta\nu$. The frequencies in the KBr region were corrected by reference to the band of CO_2 at 667 cm^{-1}. The data in Tables 1 and 2 were recorded with a DS-402G instrument, while the data in Tables 3, 4 and 5 were recorded with an EPI-G3 instrument. A slight difference in frequency for any sample, but especially for γ_r (CH_2), was observed when it was measured with the above two instruments, however, the magnitude of the frequency shifts ($\Delta\gamma_r$) was approximately the same (± 1 cm^{-1}).

References

1) M. Ishimori and T. Tsuruta, *Makromol. Chem.*, **64**, 190 (1963).
2) M. Ishimori, O. Nakasugi, N. Takeda, and T. Tsuruta, *ibid.*, **115**, 103 (1968).
3) M. Ishimori and T. Tsuruta, *Kogyo Kagaku Zasshi* **70**, 378 (1967).
4) R. Sakata, T. Tsuruta, T. Saegusa, and J. Furukawa, *Makromol. Chem.*, **40**, 64 (1960).
5) M. Ishimori, G. Hsiue, and T. Tsuruta, *ibid.*, **128**, 52 (1969).
6) M. Ishimori, O. Nakasugi, K. Yokobori, and T. Tsuruta, *ibid.*, **171**, 41 (1973).
7) O. Nakasugi, M. Ishimori, and T. Tsuruta, unpublished data.
8) R. G. Pearson, *J. Amer. Chem. Soc.*, **85**, 3533 (1963).
9) S. Ahrland, J. Chatt, and N. R. Davies, *Quart. Rev.* (London), **12**, 265 (1958).
10) H. D. Kaesz and F. G. A. Stone, *Spectrochim. Acta*, **15**, 360 (1959).
11) K. Henold, J. Soulati, and J. P. Oliver, *J. Amer. Chem. Soc.*, **91**, 3171 (1969).

12) H. S. Gutowsky, *J. Amer. Chem. Soc.*, **71**, 3194 (1949); *J. Chem. Phys.*, **17**, 128 (1949).
13) T. D. Epley and R. S. Drago, *J. Amer. Chem. Soc.*, **89**, 5770 (1967); A. D. Sherry and K. F. Purcell, *J. Phys. Chem.*, **74**, 3535 (1970).
14) L. J. Bellamy, H. E. Hallam, and R. L. Williams, *Trans. Faraday Soc.*, **54**, 1120 (1958).
15) W. Gordy and S. C. Stanford, *J. Chem. Phys.*, **9**, 204 (1941); E. M. Arnett, "Progress in Physical Organic Chemistry", Vol. 1, Ed. by S. G. Cohen, A. Streitwieser and R. W. Taft, Wiley New York, 1963, p. 223.
16) D. P. Craig, A. Maccoll, R. S. Nyholm, L. E., Orgel, and L. E. Sutton, *J. Chem. Soc.*, **1954**, 332.
17) E. Krause, *Ber.*, **50**. 1813 (1917).
18) F. Runge, W. Zimmermann, H. Pfeiffer, and I. Pfeiffer, *Z. Anorg. Allgem. Chem.*, **267**, 39 (1951).
19) H. R. Snyder, J. M. Stewart, and J. B. Ziegler, *J. Amer. Chem. Soc.*, **69**, 2672 (1947).
20) J. A. Riddick and W. B. Bunger, "Techniques of Organic Chemistry," Vol. 2, 3rd Ed., Organic Solvents, John Wiley and Sons Inc., New York (1970).

Products Obtained by the Reaction of Trichlorotrimethylbenzenes with Fuming Nitric Acid. Side-chain Nitrooxylation *versus* Oxidation to Unsaturated Cyclic Ketones[1)]

Hitomi SUZUKI, Shigeru MARUYAMA, and Terukiyo HANAFUSA

Department of Chemistry, Faculty of Science, Hiroshima University, Higashi-sendamachi, Hiroshima 730

(Received August 23, 1973)

The reaction of trichlorotrimethylbenzenes with fuming nitric acid has been investigated. Trichloropseudocumene underwent both side-chain nitrooxylation and nuclear oxidation to give 2,5,6-trichloro-3,4-dimethylbenzyl nitrate, 3,5,6-trichloro-2,4-dimethylbenzyl nitrate, and 3,6-dichloro-4-nitro-2,4,5-trimethylcyclohexa-2,5-dienone. Trichloromesitylene yielded a mixture of several carbonyl compounds, from which 3,5-dichloro-4-hydroxy-2,4,6-trimethylcyclohexa-2,5-dienone and two nitro-ketones, tentatively formulated as 2,4,6-trichloro-5-hydroxy-6-nitro-2,3,5-trimethylcyclohex-3-enone and 3,5-dichloro-2-hydroxy-6,6-dinitro-2,4,5-trimethylcyclohex-3-enone, were obtained as crystalline products by chromatography and fractional extraction. Trichlorohemimellitene behaved similarly towards the nitrating agent to give 2,6-dichloro-4-hydroxy-3,4,5-trimethylcyclohexa-2,5-dienone as the major product. The competitive modes of side-chain nitrooxylation and formation of cyclic ketones have been described.

In recent years attention has been paid to several new aspects of aromatic nitration, including various substitutions on alkyl side-chain of polyalkylbenzenes,[2)] acyloxylation,[3)] nitrative coupling,[4)] and oxidation to cyclic ketones.[5)] Although these reactions have so far been regarded as discrete and anomalous, they could be classified as branched-off processes of ordinary nitration. Nitronium ion attacks a polyalkylbenzene to form a nitrobenzenium ion, which could undergo four different types of reactions; loss of proton or some cationic species from the ring to give a nitrobenzene derivative (path *a*), proton release from the alkyl side-chain to yield a nitromethylenecyclohexadiene which could be transformed into benzylic compound (path *b*), capture of nucleophile to give an addition product which will collapse to form unsaturated cyclic ketone or acyloxylated product (path *c*), and attack on another aromatic ring to give a coupling product such as nitrobiaryl (path *d*). When the normal course *a* is suppressed, an unusual path *b*, *c*, or *d* will emerge. With highly alkylated benzene derivatives, the major nitrative processes are the side-chain nitrooxylation (path *b*) and the formation of unsaturated cyclic ketones (path *c*), the competitive modes of which are best illustrated by the behaviors of three isomeric trichlorotrimethylbenzenes towards fuming nitric acid.

Trichloropseudocumene (1): A solution of **1** and excess of fuming nitric acid (d=1.5) in dichloromethane was left standing at room temperature overnight. Quenching with water, followed by removal of the solvent *in vacuo* gave a syrupy substance, which was passed over alumina to give two trichlorodimethylbenzyl alcohols, mp 197—198 °C and 204—206 °C, and a carbonyl compound, mp 146—147 °C. Benzyl alcohols were identified as 2,5,6-trichloro-3,4-dimethylbenzyl alcohol (**12**) and 3,5,6-trichloro-2,4-dimethylbenzyl alcohol (**13**), respectively, by a comparison of their melting points, infrared spectra and ^{1}H NMR spectra with those of the authentic specimens prepared from xylidines according to the sequences shown in Scheme 4. There was no indication of isomeric 3,4,6-trichloro-2,5-dimethylbenzyl alcohol (**14**) in the product.

A carbonyl compound with the molecular formula

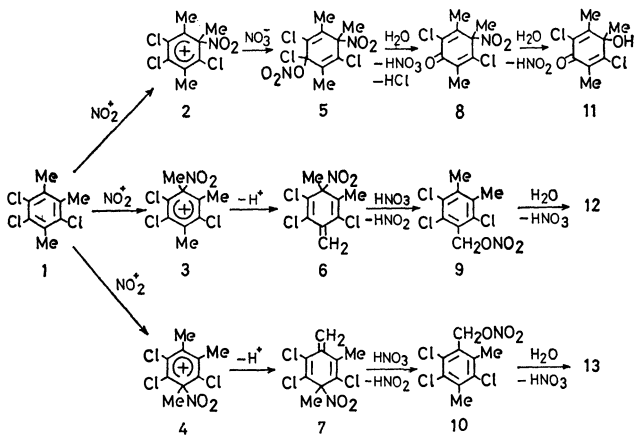

Scheme 1

$C_9H_{10}O_2Cl_2$ showed mass peaks at *m/e* 220 (M^+), 205 (M^+-CH_3), and 185 (M^+-Cl). Its infrared spectrum showed carbonyl absorption at 1666 cm^{-1}, carbon-carbon double bond absorption at 1621 cm^{-1}, and hydroxyl absorption at 3240—3400 cm^{-1}, suggesting a cross-conjugated hydroxy-ketone. Its ultraviolet spectrum exhibited absorption maxima at 246—247 (log ε=4.08) and 286—287 nm (log ε=3.34) characteristic of a 2,5-cyclohexadienone structure.[6)] Proton NMR spectrum showed three peaks due to methyls at 8.40, 7.96, and 7.73 τ, and a broad peak due to hydroxyl at *ca.* 7.3 τ. The dienone was thus presumed to be either 3,6-dichloro-4-hydroxy-2,4,5-trimethylcyclohexa-2,5-dienone (**11**) or 5,6-dichloro-4-hydroxy-2,3,4-trimethylcyclohexa-2,5-dienone, the former being favored upon an examination of the chemical shifts given in Table 1. Since the crude product mixture prior to chromatographic treatment showed intense infrared bands due to nitro and nitrooxy groups, products **11**, **12** and **13** no doubt were formed by the hydrolysis of the nitro-ketone **8** and benzyl nitrates **9** and **10**, respectively, during the elution.

Nitronium ion attacks **1** to form a mixture of benzenium ions, in which **2**—**4** would be important, since the electron-donating methyl group is bonded direct to the reaction site (Scheme 1). Proton release form

Table 1. Physical properties of some 4-hydroxycyclohexa-2,5-dienones

Compound	Mp (°C)	^{1}H NMR spectra (τ) CH_3	^{1}H NMR spectra (τ) OH	IR spectra cm^{-1}	UV spectra (nm)	UV spectra log ε
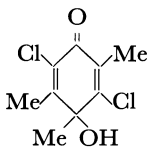	146—147	8.40(Me; C-4) 7.96(Me; C-2) 7.73(Me; C-5)	*ca.* 7.3	764, 984, 1068, 1200, 1260, 1621, 1656, 3240—3400	246—247 286—287	4.08 3.34
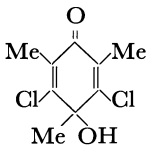	96—98	8.31(Me; C-4) 7.99(2Me; C-2, C-6)	*ca.* 7.3	724, 987, 1073 1222, 1341, 1632, 1652, 3430—3400	245 284—286	4.03 3.29
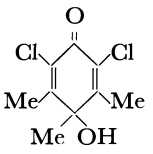	204—205	8.51(Me; C-4) 7.74(2Me; C-3, C-5)	*ca.* 7.1	760, 1012, 1044, 1209, 1262, 1602, 1658, 3420	249 289	4.06 3.27
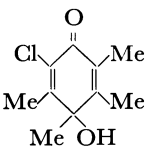	178—179[12]	8.61(Me; C-4) 8.19(Me; C-3) 7.94(Me; C-2) 7.80(Me; C-5)	*ca.* 7.0	766, 902, 1073, 1221, 1270, 1612, 1636, 3400[b]	246—247 286—287	4.08 3.34
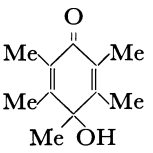	138—140[13]	8.63(Me; C-4) 8.16(2Me; C-3, C-5) 7.96(2Me; C-2, C-6)[a]	*ca.* 7.0	768, 919, 1001, 1028, 1084, 1276, 1613, 1662, 3390[b]	242	4.20

a) In carbon tetrachloride solution. b) With a KBr disc.

the most activated methyl groups of **3** and **4** would lead to the formation of nitromethylenecyclohexadienes **6** and **7**, which will pass over a benzylic intermediate—nitrite ion pair to give the corresponding benzyl nitrates **9** and **10**. Capture of the nitrate ion by **2** will give an unstable chloro-nitrate **5**, from which nitryl chloride is eliminated to yield ketone **8**. No change in the pseudocumene skeleton was observed in the products.

*Trichloromesitylene (**15**)*: A similar treatment of **15** with fuming nitric acid gave a mixture of several carbonyl compounds as a yellow pasty solid, which on chromatography over alumina gave a new carbonyl compound, mp 96—98 °C, from ether eluates. It had the molecular formula $C_9H_{10}O_2Cl_2$ and showed mass peaks at *m/e* 220 (M^+), 205 (M^+–CH_3), and 185 (M^+–Cl). Proton NMR spectrum showed peaks at 8.31, 7.99, and *ca.* 7.3 τ with an intensity ratio of 6 : 3 : 1. The infrared and ultraviolet data given in Table 1 are consistent with a cyclohexa-2,5-dienone structure. A lower shift of C=O frequency indicated the absence of chlorine atoms on both sides of the carbonyl group. These spectral evidences readily led to the formulation of 3,5-dichloro-4-hydroxy-2,4,6-trimethylcyclohexa-2,5-dienone (**19**) for the carbonyl compound.

When the product was subjected to fractional extractions with a mixture of light petroleum and dichloromethane, another ketone was obtained with the composition $C_9H_{10}NO_4Cl_3$, mp 153—154 °C with decomposition. Its mass spectrum showed fragment ion peaks derived from non-detectable molecular ion at *m/e* 220 (M^+–NO_2–Cl), 185 (M^+–NO_2–2Cl), 177 (M^+–NO_2–Cl–CO–CH_3), and 142 (M^+–NO_2–2Cl–CO–CH_3). The lower mass spectrum consisted of the prominent peak clusters centered at *m/e* 107 ($C_7H_6OH^+$), 91 ($C_7H_7^+$), and 77 ($C_6H_5^+$) in accord with a structure related to the benzenoid compound. Its ultraviolet spectrum showed no maximum above 220 nm, suggesting a cyclohex-3-enone structure. Proton NMR spectrum contained three methyl singlets at 8.21, 7.76, and 7.73 τ and one hydroxyl peak at *ca.* 5.5 τ (broad, exchangeable with D_2O). Its infrared spectrum showed absorption due to an aliphatic nitro group at 1572, 1560, 1359, and 1342 cm^{-1}; a carbonyl group at 1715 cm^{-1}; a carbon-carbon double bond at 1650 cm^{-1}; and a hydroxy group at 3440 cm^{-1}. The asymmetric vibration bands of nitro group are shifted towards a high-frequency region, while the symmetric frequency is lowered. This may reflect the presence of a geminal chloro-nitro grouping,[7] which can be attached to C-2, C-5, or C-6 of the cyclohex-3-enone skeleton. Chlorine atoms do not undergo intramolecular migration under the nitrating conditions. The nitro group on the activated allylic carbon atom usually undergoes a facile solvolytic replacement during aqueous work-up. This makes it possible for three chlorine atoms to be placed on C-2, C-4, and C-6, respectively, and favors the chloro-nitro grouping to be placed on the less

activated C–6. Thus the hydroxy group must be located on C–5, and three methyl groups on the remaining C–2, C–3, and C–5. The product may be represented by the formula 2,4,6-trichloro-5-hydroxy-6-nitro-2,3,5-trimethylcyclohex-3-enone (**24**).

When the reaction mixture was flash-evaporated *in vacuo* and the resulting pasty substance was immediately chromatographed over silica gel, a third carbonyl compound melting at 131—135 °C under the liberation of a brown fume was eluted from benzene. It had the formula $C_9H_{10}N_2O_6Cl_2$ and showed mass peaks at *m/e* 249 (M^+–NO_2–OH), 220 (M^+–$2NO_2$), 185 (M^+–$2NO_2$–Cl), 177 (M^+–$2NO_2$–CO–CH_3), and 142 (M^+–$2NO_2$–Cl–CO–CH_3). Prominent peak clusters centered at *m/e* 107, 91, and 77 are typical of a structure closely related to the benzenoid compound. The absence of ultraviolet maximum above 220 nm suggests a cyclohex-3-enone structure. Its proton NMR spectrum displayed three methyl peaks at 8.39, 7.88, and 7.76 τ and one hydroxyl absorption at *ca.* 7.7 τ (broad, exchangeable with D_2O). Its infrared spectrum indicates the presence of geminal nitro groups (1582, 1572, 1333, and 850 cm^{-1}), a carbonyl group (1750 cm^{-1}), a carbon-carbon double bond (1628 cm^{-1}), and a hydroxy group (3495 cm^{-1}). It is unlikely that chlorine atoms underwent the intramolecular migration or replacement by nitro group during the course of reaction.[8] Two chlorine atoms could reasonably be assigned to C–3 and C–5 of the cyclohex-3-enone. The unusually higher shift of the C=O stretching vibration at 1750 cm^{-1} is attributed to the presence of a *gem*-dinitro grouping adjacent to the carbonyl group. We lean toward the location of this grouping at the non-allylic C–6 position because of its stability toward solvolytic replacement. Placing the hydroxy group on C-2 and three methyl groups on C-2, C-4, and C-5, respectively, we can formulate the product as 3,5-dichloro-2-hydroxy-6,6-dinitro-2,4,5-trimethylcyclohex-3-enone (**25**).

The infrared and proton NMR spectra of the crude product from **15** indicated the presence of some additional carbonyl compounds which, however, could not be isolated as crystalline solid. Formation of the side-chain substitution products could not be observed.

Scheme 2 outlines one possible pathway from **15** to these carbonyl compounds. Nitrobenzenium ion **16**[9] derived from **15** has neither a good leaving group nor a methyl group favorably situated for proton release. Thus it will take up the nitrate ion to give **18** *via* **17**, or undergo isomerization to **20** followed by the anion capture to give **21**, from which **24** and **25** could be derived through an addition-elimination sequence and subsequent hydrolysis.

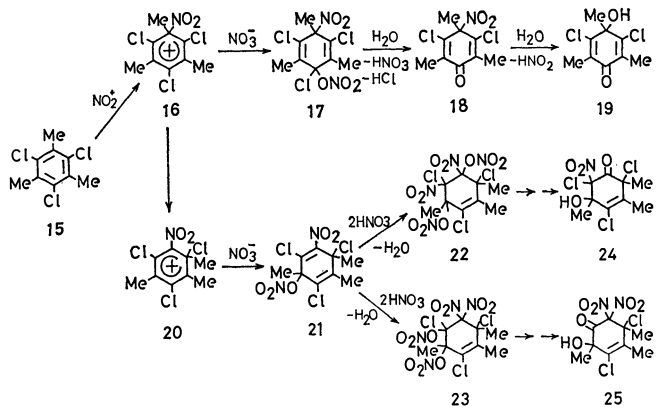

Scheme 2

*Trichlorohemimellitene (**26**)*: A similar treatment of **26** with fuming nitric acid followed by ordinary work-up gave a carbonyl compound, mp 204—205 °C, as the major product. Its formula, as established by mass spectrometric molecular weight determination and elemental analysis, was $C_9H_{10}O_2Cl_2$. On the basis of the spectroscopic data (Table 1), it was readily identified as 2,6-dichloro-4-hydroxy-3,4,5-trimethylcyclohexa-2,5-dienone (**30**). Formation of **30** from **26** can be rationalized by Scheme 3; preferential attack of nitronium ion will occur at C-2 of **26** to give ion **27**. Capture of the nitrate ion by **27** followed by elimination of nitryl chloride from unstable chloro-nitrate **28** would give a nitro-ketone **29**, which undergoes a facile hydrolysis during aqueous work-up to yield **30** as the final product.

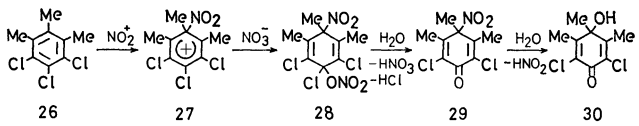

Scheme 3

The presence of a pair of methyl groups in position *para* to each other seems critical for the facile formation of benzyl nitrates. A pair of *para* methyl groups at C-1 and C-4 in **1** undergo side-chain nitrooxylation to form two benzyl nitrates **9** and **10**, whereas the unpaired methyl group at C-2 remains intact during the course of reaction. In contrast to **1**, **15** and **26** both bearing no paired methyl groups in *para* positions undergo only addition-elimination sequences to give unsaturated cyclic carbonyl compounds **19**, **24**, **25**. and **30**. No side-chain substitution was observed with these compounds.

The process of the side-chain nitrooxylation could be explained by the intermediacy of 1-methyl-1-nitro-4-methylenecyclohexa-2,5-dienes **6** and **7**, which would undergo the heterolytic scission of the carbon-nitrogen bond to give a benzyl cationic species—nitrite ion pair; recombination at benzyl carbon atom followed by oxidation affords side-chain nitrooxylation products **9** and **10**. The required disposition of methyl groups in position *para* one another might be taken to indicate that the transition state of the conversion of nitromethylenecyclohexadiene to benzyl nitrite is closer to the benzylic structure and stabilized more effectively by the electron-donating methyl group at *para* position. **1** bearing a pair of methyl groups reacts with the nitrating agent more readily than **15** and **26** which lack such structural advantage, indicating the high propensity of the nitrobenzenium ions **3** and **4** to form nitromethylenecyclohexadienes **6** and **7** rather than to take up anion or undergo isomerization. Oxidation to unsaturated cyclic ketone (path *c*) could effectively compete with side-chain nitrooxylation (path *b*) only under the conditions in which the formation of 1-nitro-4-methyl-

enecyclohexa-2,5-diene intermediate is structurally disfavored. Thus, on dissolution in excess fuming nitric acid (d=1.5) at room temperature, tetrachloro-*p*-xylene gave 2,3,5,6-tetrachloro-4-methylbenzyl nitrate (mp 80—82 °C) in 88% yield,[10] while a similar treatment of tetrachloro-*o*-xylene and tetrachloro-*m*-xylene led to the formation of a mixture of carbonyl compounds. Addition of sulfuric acid to the reaction system was found to facilitate the proton removal from the side-chain in favor of path *b* over path *c*. This is best exemplified by the nitration of 5,6-dinitroprehnitene; treatment with fuming nitric acid afforded 4,5-dinitro-2,3,6,6-tetramethylcyclohexa-2,4-dienone and 2,3,4,5-tetranitro-2,3,6,6-tetramethylcyclohex-3-enone, whereas the action of the mixed acid gave 5,6-dinitro-2,3,4-trimethylbenzyl nitrate as the major product.[11]

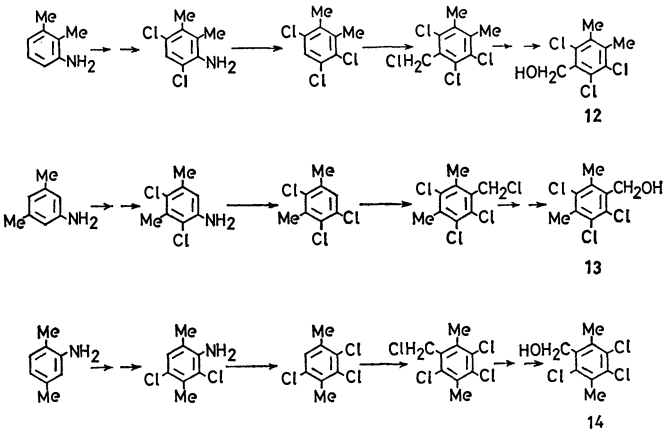

Scheme 4

Experimental

Melting points are uncorrected. IR spectra were determined in mulls on a Jasco 402G spectrophotometer. Proton NMR spectra were obtained in deuteriochloroform on a Hitachi Perkin-Elmer spectrometer using TMS as internal standard. Ultraviolet spectra were measured in methanol with a Shimadzu QV-50 spectrophotometer. Mass spectra were recorded on a Hitachi RMU-6E instrument.

Trichloropseudocumene, trichloromesitylene, and trichlorohemimellitene were prepared by the chlorination of the corresponding hydrocarbons and purified through chromatography on alumina. 2,5,6-Trichloro-3,4-dimethylbenzyl alcohol, 3,5,6-trichloro-2,4-dimethylbenzyl alcohol, and 3,4,6-trichloro-2,5-dimethylbenzyl alcohol were obtained from the corresponding chlorides *via* hydrolysis of acetates, which in turn were prepared from 3-*o*-xylidine, 5-*m*-xylidine, and *p*-xylidine, respectively, following the sequences shown in Scheme 4. Physical properties of trichlorodimethylbenzyl compounds obtained in context with the present work are summarized in Table 2. All new compounds gave satisfactory analytical results.

Nitration of Trichlorotrimethylbenzenes: The general procedure is illustrated below, taking an example from the reaction of trichloropseudocumene **1**.

To a stirred solution of **1** (7.5 g; 0.034 mol) in dichloromethane (38 ml) maintained at 0—5 °C, fuming nitric acid (d=1.5; 17.4 g; 0.375 mole) was added dropwise over a period of 30 min. After standing at room temperature overnight, the reaction mixture was poured into a large excess of

Table 2. Physical properties of some trichlorodimethylbenzyl compounds

Compound	Mp (°C)	^{1}H NMR spectra (τ)			IR spectra cm^{-1}
		CH_3	CH_2	OH	
2,5,6-Trichloro-3,4-dimethylbenzyl series					
Chloride	73—74	7.60 7.57	5.07		687, 756, 893, 1009, 1149, 1170, 1274
Nitrate	54—56	7.59 7.52	4.19		847, 981, 1170, 1276 1643
Alcohol	197—198	7.60 7.56	5.01	7.92	692, 1037, 1166, 1255 3260—3300
3,5,6-Trichloro-2,4-dimethylbenzyl series					
Chloride	96—97	7.50 7.46	5.20		685, 747, 878, 932, 997, 1145, 1170, 1261
Nitrate	102—103	7.52 7.43	4.28		887, 976, 1170, 1276, 1298, 1614, 1646
Alcohol	204—206	7.48 7.45	5.11	8.22	690, 973, 1003, 1030, 1161, 3240
3,4,6-Trichloro-2,5-dimethylbenzyl series					
Chloride	96—98	7.45 7.45	5.20		709, 756, 892, 934 993, 1144, 1184, 1273
Nitrate	98—99	7.48 7.46	4.28		887, 976, 1170, 1276, 1298, 1614, 1646
Alcohol	204—205	7.47 7.47	5.11	8.30	631, 980, 1007, 1034, 1164, 3240

water, and the organic layer was separated, thoroughly washed with water and aqueous sodium hydrogen carbonate, and dried over anhydrous sodium sulfate. Removal of the solvent under reduced pressure gave a reddish brown syrupy substance, a part (4.0 g) of which was chromatographed on silica gel with light petroleum as eluant to give a mixture of benzyl nitrates **9** and **10** (0.24 g), and with light petroleum–benzene a bisbenzyl ether (0.05 g); mp 213—215 °C; ^{1}H NMR, 7.57 (2 Me), 7.48 (2 Me), and 5.20 τ (2 CH_2); IR, 1170, 1070, and 966 cm^{-1}; MS, *m/e* 458 (M^+); Found: C, 46.97; H, 3.21%. Calcd for $C_{18}H_{16}OCl_6$: C, 46.85; H, 3.47%. Elution with benzene furnished some noncrystallizable gummy substance (0.02 g). Further elution with benzene–ether afforded two benzyl alcohols **13** (0.51 g) and **12** (0.22 g) in this order, and finally ketone **11** (0.59 g) was obtained from ether eluates.

*3,5,6-Trichloro-2,4-dimethylbenzyl Alcohol (**13**)*: Found: C, 45.13; H, 3.67%. Calcd for $C_9H_9OCl_3$: C, 45.09; H, 3.76%.

*2,5,6-Trichloro-3,4-dimethylbenzyl Alcohol (**12**)*: Found: 45.19; H, 3.73%. Calcd for $C_9H_9OCl_3$: C, 45.09; H, 3.76%.

*3,6-Dichloro-4-hydroxy-2,4,5-trimethylcyclohexa-2,5-dienone (**11**)*: Found: C, 48.85; H, 4.50%. Calcd for $C_9H_{10}O_2Cl_2$: C, 48.87; H, 4.50%.

*3,5-Dichloro-4-hydroxy-2,4,6-trimethylcyclohexa-2,5-dienone (**19**)*: Found: C, 49.00; H, 4.62%. Calcd for $C_9H_{10}O_2Cl_2$: C, 48.87; H, 4.50%.

*2,4,6-Trichloro-5-hydroxy-6-nitro-2,3,5-trimethylcyclohex-3-enone (**24**)*: Found: C, 35.09; H, 3.73%. Calcd for $C_9H_{10}NO_4Cl_3$: C, 35.72; H, 3.34%.

*3,5-Dichloro-2-hydroxy-6,6-dinitro-2,4,5-trimethylcyclohex-3-enone (**25**)*: Found: C, 34.86; H, 3.33; N, 8.89; O, 30.87; Cl, 22.56%. Calcd for $C_9H_{10}N_2O_6Cl_2$: C, 34.53; H, 3.23; N, 8.94; O, 30.66; Cl, 22.64%.

*2,6-Dichloro-4-hydroxy-3,4,5-trimethylcyclohexa-2,5-dienone (**30**)*: Found: C, 48.97; H, 4.53%. Calcd for $C_9H_{10}O_2Cl_2$: C, 48.87; H, 4.50%.

References

1) The Reaction of Polysubstituted Aromatics. Part XXXIV; Part XXXIII: H. Suzuki and T. Hanafusa This Bulletin, **46**, 3607 (1973).

2) H. Suzuki and K. Nakamura, *ibid.*, **43**, 473 (1970); K. Nakamura, *ibid.*, **44**, 133 (1971); H. Suzuki and K. Nakamura, *ibid.*, **44**, 227 (1971); H. Suzuki and K. Nakamura, *ibid.*, **44**, 303 (1971); S. Isaev, L. A. Ostaschevskaya, A. A. Morozov, L. M. Bestchetonova, and V. A. Koptyug, *Zh. Org. Khim.*, **7**, 2321 (1971); E. Hunziker, J. R. Penton, and H. Zollinger, *Helv. Chim. Acta*, **54**, 2043 (1971); R. Astolfi, E. Baciocchi, and G. Illuminati, *Chemica e Industria*, (Milano) **53**, 1153 (1971).

3) A. Fischer, J. Vaughan, and G. J. Wright, *J. Chem. Soc., B*, **1967**, 368; D. J. Blackstock, A. Fischer, K. E. Richards, J. Vaughan, and G. J. Wright, *Chem. Commun.*, **1970**, 641.

4) I. Puskas and E. K. Fields, *J. Org. Chem.*, **31**, 4205 (1966).

5) H. Suzuki, M. Sawaki, and R. Sakimoto, This Bulletin **45**, 1834 (1972); H. Suzuki and K. Nakamura, *ibid.*, **45**, 2534 (1972); D. J. Blackstock, M. P. Hartshorn, A. J. Lewis, K. E. Richards, J. Vaughan, and G. J. Wright, *J. Chem. Soc., B*, **1971**, 1212; A. J. M. Reuvers, F. F. van Leewen, and A. Sinnema, *Chem. Commun.*, **1972**, 828.

6) H. H. Jaffe and M. Orchin, "Theory and Application of Ultraviolet Spectroscopy," Wiley, New York (1962), p. 204; A. I. Scott, "Interpretation of the Ultraviolet Spectra of Natural Products," Pergamon, London (1964), p. 55.

7) J. F. Brown, *J. Amer. Chem. Soc.*, **77**, 6341 (1955).

8) Dichloronitromesitylene was found to be stable towards fuming nitric acid under the same condition.

9) G. A. Olah, H. C. Lin, and Y. K. Mo, *J. Amer. Chem. Soc.* **94**, 3667 (1972).

10) Unpublished results.

11) H. Suzuki and K. Nakamura, *Synthesis*, **1972**, 606.

12) H. Suzuki and K. Nakamura, This Bulletin, **45**, 1270 (1972).

13) H. Suzuki and K. Nakamura, *ibid.*, **44**, 227 (1971).

Effect of Pressure on the Rate of Solvolysis. Volume Parameters and Solvolysis Mechanism[1)]

Chisako YAMAGAMI, Akira SERA, and Kazuhiro MARUYAMA

Department of Chemistry, Faculty of Science, Kyoto University, Sakyo-ku, Kyoto 606

(Received September 10, 1973)

The effect of pressure on the solvolysis rates of representative primary, secondary, and tertiary tosylates was investigated in three representative solvents—formic acid, aqueous acetone, and methanol. The calculated activation volumes for these reactions were found to depend on the substrate structure and on the nature of solvent in a systematic manner. The activation volumes for k_c-like reactions were less negative than those for k_s-like reactions. In the case of the nearly k_s-like reactions, the activation volume was found to be governed by the partial molal volume of the initial state.

In previous papers concerning the pressure dependence of the solvolytic rates of secondary tosylates,[2)] we have discussed some correlations between the activation volumes, $\Delta V^{\neq}$, and the reaction mechanisms. It was suggested that the activation volume for the reactions of a series of substrates in a given solvent became less negative with an increase in the k_c-character of the substrate. It was also found that a reaction in formic acid resulted in a less negative value of activation volume than the corresponding reaction in methanol. If these observations are common to various types of substrates and solvents, this activation parameter could be expected to provide an additional criterion for examining the detailed reaction mechanisms. However, much of the published data on the activation volume is of limited usefulness for this purpose; there has been no systematic investigation of the activation volume upon changes in the type of substrate and the nature of solvent.

From this point of view, in this report we wish to extend our solvolytic studies under pressure to primary, secondary, and tertiary substrates in three different types of solvent—formic acid, 85% aqueous acetone (v/v), and methanol. It is generally accepted that primary substrates are solvolyzed by a solvent assisted pathway (k_s), and tertiary substrates by a solvent unassisted pathway (k_c). It may, then, be anticipated from our previous assumption[2)] that the activation volume for a tertiary system is less negative than for a primary system. Methyl, isopropyl, and adamantyl tosylates were chosen as model compounds for primary, secondary, and tertiary systems respectively. Methyl tosylate, possessing the lowest m-value[3)] of 0.30, has often been used as a reference standard for k_s-type behavior.[4)] On the other hand, adamantyl system has been well established to exhibit limiting behavior (k_c).[5)] Formic acid was chosen as a polar solvent which facilitates the k_c-process, whereas methanol was employed as a solvent of high nucleophilicity promoting the k_s-process. An aqueous organic solvent was expected to be intermediate in character between the above two solvents. The composition of the aqueous binary solvent (85%, v/v) was adopted so as to give appropriate rate constants at the temperatures employed in this investigation.

Results and Discussion

The solvolysis rate constants of typical primary, secondary, and tertiary alkyl tosylates were measured at various pressures (Table 1), and the activation volumes, $\Delta V^{\neq}$, were estimated by means of the following equations;

$$\Delta V^{\neq} = -RT(\partial \ln k/\partial P)_T \quad (1)$$

$$\ln k = a + bP \quad (2)$$

The parameter b in Eq. (2) was determined by the least-squares method in the range from 1 to 700 kg/cm^2.

The activation volumes obtained at atmospheric pressure, $\Delta V_0^{\neq}$, are summarized in Table 2 and are also illustrated in Fig. 1. As the wide range of reactivities of the substrates prevented rate measurements at a common temperature, two temperatures were employed for each solvent (25 °C and 45 °C for formolysis, and 25 °C and 40 °C for methanolysis and hydrolysis). The check of the temperature dependence of $\Delta V_0^{\neq}$ was performed in the case of isopropyl tosylate. The results indicate that an increase in the temperature results in a slight decrease in $\Delta V_0^{\neq}$ (Table 2).[6)] However, these differences are considered to be small enough to advance our argument without any corrections. In the case of formolysis, 2-adamantyl tosylate was used in the place of 1-adamantyl tosylate because all tertiary tosylates are too reactive to be measured at 25 °C. This replacement is reasonable since secondary 2-adamantyl tosylate is well known to behave like tertiary substrates.[5)]

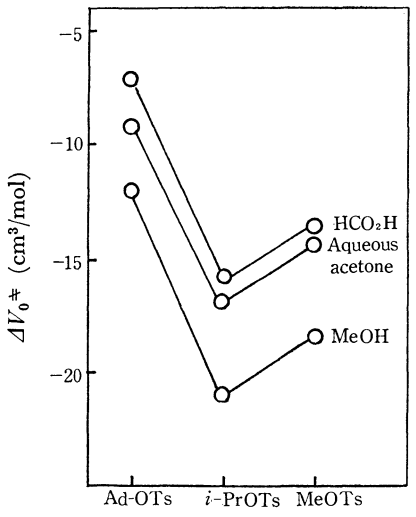

Fig. 1. Dependence of activation volume on substrate structure and solvent.

TABLE 1. SOLVOLYSIS RATE CONSTANTS OF PRIMARY, SECONDARY AND TERTIARY ALKYL TOSYLATES UNDER PRESSURE

Solvent	Temperature (°C)	Pressure (kg/cm²) 1	100	200	300	500	700	1000
		Methyl tosylate 10^6k (s^{-1})[a]						
HCOOH	45.0	—[c]	0.684	—	0.757	0.834	0.924	—
aq-Acetone[b]	40.0	1.12	1.14	—	1.27	1.41	1.57	—
MeOH	40.0	3.72	4.05	—	4.76	5.36	6.03	—
		Isopropyl tosylate 10^6k (s^{-1})[a]						
HCOOH	45.0	265	286	—	321	363	397	—
aq-Acetone[b]	40.0	1.62	1.70	—	1.97	2.21	2.50	—
MeOH	40.0	7.08	7.72	—	9.22	10.6	12.3	—
		Adamantyl tosylate 10^4k (s^{-1})[a]						
HCOOH[d]	25.0	0.275	—	—	0.300	0.318	0.332	0.354
aq-Acetone[b,e]	25.0	1.88	2.00	—	2.19	2.35	2.48	—
MeOH[e]	25.0	5.63	6.13	6.57	6.87	7.42	—	—

a) The average of duplicate runs. b) 15% Water-85% acetone (v/v). c) An accurate value was not obtained due to the decomposition of formic acid. d) 2-Adamantyl. e) 1-Adamantyl.

TABLE 2. ACTIVATION VOLUMES FOR SOLVOLYSIS OF PRIMARY SECONDARY AND TERTIARY TOSYLATES IN VARIOUS SOLVENTS

ROTs R=	$\Delta V_0^{\neq}$ (cm³/mol)[a] HCOOH	aq-Acetone[b]	MeOH
Methyl	−13.4(45°)	−14.2(40°)	−18.2(40°)
Isopropyl	−14.7(25°)[c]	—	−18.9(25°)[c]
	−15.6(45°)	−16.7(40°)	−20.9(40°)
2-Adamantyl	−6.9(25°)	—	—
1-Adamantyl	—	−9.0(25°)	−11.8(25°)[d]

a) Accurate to within 1 cm³/mol. b) 15% Water-85% acetone (v/v). c) Taken from Ref. 2a. d) See Ref. 2a, footnote 8.

TABLE 3. PARTIAL MOLAL VOLUMES AND MOLAR VOLUMES OF METHYL AND ISOPROPYL TOSYLATES AT 25.0±0.001 °C

ROTs R=	Solvent	$\bar{V}_g$[a]	V_m[b]	$\bar{V}_g - V_m$[c]
Methyl	HCOOH	154.4	151.8	2.6
	MeOH	142.9		−8.9
Isopropyl	HCOOH	194.5	188.2	6.3
	MeOH	181.6		−6.6

a) Partial molal volume of the initial state, cm³/mol. The average deviation from the mean of several trials is ±0.5 cm³/mol. b) Molar volume of substrate, cm³/mol. c) cm³/mol.

The partial molal volumes ($\bar{V}_g$) of methyl and isopropyl tosylates were measured at 25.0±0.001 °C by the dilatometric method.[7] The results are presented in Table 3, together with the molar volumes of the substrates (V_m).

Dependence of Activation Volume on the Nature of Solvent. All the activation volumes listed in Table 2 are negative. The invariable observation of negative activation volumes in solvolyses of neutral substrates is consistent with the view that the volume contraction by the electrostriction of the solvent predominates over the volume expansion due to bond extension during the activation process.[8] Accordingly, the activation volume which reflects the degree of solvation should, of course, be sensitive to the solvent change. In fact, Fig. 1 clearly shows the solvent dependence of $\Delta V_0^{\neq}$. The magnitude of $\Delta V_0^{\neq}$ for a given substrate is seen to decrease in the order; formic acid, aqueous acetone, and methanol. Such behavior is compatible with the previous observation in the Menschutkin reactions that the change in solvent from a non-polar to a polar one causes a remarkable increase in $\Delta V_0^{\neq}$.[9] The explanation was given that a polar solvent should be less constricted by the partly ionic transition state because of its low compressibility. Our results may also be considered to conform to this generalization.

In the case of limiting adamantyl systems, in which the volume contraction due to the partial bond formation is negligible, it may be said that the change in $\Delta V_0^{\neq}$ with solvent directly reflects the difference in the degree of the electrostrictive volume contraction of the solvent. Accordingly, the magnitude of the difference in $\Delta V_0^{\neq}$ between any two solvents could be regarded as a measure of the relative solvating ability of the solvent.

It is also interesting to note that a more favorable solvent for the k_c-process gives a less negative activation volume. Two solvent parameters, Y-[3] and N_{BS}-[4] values, are useful for describing the solvent character under discussion. The comparison of the Y-values (Y=2.05, −1.27,[10] and −1.09 for formic acid, aqueous acetone, and methanol respectively) indicates that formic acid is the most favorable for the k_c-process, whereas the N_{BS}- values, recently established solvent nucleophilicity parameters (N_{BS}=−2.05, −0.4,[10] and 0.01 for formic acid, aqueous acetone, and methanol respectively), indicate that methanol is the most favorable for the k_s-process.

The above-mentioned behavior will become more obvious if we examine the volumes of the initial state ($\bar{V}_g$) presented in Table 3.[11] The most important point to be noted is that $\bar{V}_g$ in formic acid is greater than V_m for a given substrate, while the reverse trend

is observed in methanol. The observed increase in the volume of the solution in the case of formic acid, when one mole of a solute was dissolved in the solvent, is most likely attributable to the inherent structuredness of the solvent. On dissolving the solute, the polar formic acid, already highly oriented itself, should be compelled to expand in order to make a "hole" to accept the solute. On the other hand, in methanol, a less structured medium, the process of the reorientation of solvent molecules around the dissolved solute becomes more important than the hole-making process; hence, the total contraction of the solvent system may result. As the activation volume is represented by the following equation;

$$\Delta V^{\neq} = \overline{V}_t - \overline{V}_g \quad (3)$$

the partial molal volume of the transition state species, $\overline{V}_t$, can be calculated from the values of $\overline{V}_g$ and $\Delta V_0^{\neq}$. Calculations were made for $\overline{V}_t$ of isopropyl tosylate to give rise to values of 162.7 cm^3/mol in methanol and 179.8 cm^3/mol in formic acid. The difference in $\overline{V}_t$ for isopropyl tosylate in these two solvents amounts to 17 cm^3/mol. This large difference in $\overline{V}_t$ is understandable in terms of the general concept in organic chemistry that methanol has a powerful solvating ability, while formic acid is a solvent of low nucleophilicity.

Dependence of Activation Volume on the Structure of Substrate. An inspection of Fig. 1 indicates that the variation in $\Delta V_0^{\neq}$ with the substrate structure reveals a similar behavior in all solvents. In each case, the $\Delta V_0^{\neq}$ for adamantyl tosylate is less negative by about 8 cm^3/mol than that for isopropyl tosylate. This finding is compatible with our assumption that the more k_c-like process results in a less negative activation volume.[2] However, a conflicting tendency was observed in the case of the primary system; a change in structure from isopropyl to methyl is accompanied by an increase in $\Delta V_0^{\neq}$ by 2—3 cm^3/mol, in spite of the fact that the latter is inevitably a more k_s-like substrate than the former. This observed discrepancy can be explained by assuming a larger contribution of the initial state volume to $\Delta V_0^{\neq}$ in the case of methyl tosylate than in that of isopropyl tosylate. In our previous discussion we have considered the activation volume to reflect chiefly the degree of solvation in the transition state. Such a view is quite reasonable as long as the systematic change of the substrate structure can govern the systematic alteration of solvation, in situation and degree, in the transition state. However, once the intensely solvated transition state is attained, that is, when the reaction is thought to be classifiable as a nearly pure k_s-process, the transition state volume ($\overline{V}_t$) can no longer be expected to be modified by a further change in the substrate structure. In this case, the contribution of the initial state volume becomes important, and the activation volume, $\Delta V_0^{\neq}$, must be controlled by $\overline{V}_g$ rather than by $\overline{V}_t$. This may be the case for methyl tosylate. In order to get information about the initial state contribution,[7] it would be useful to examine the quantity of $\overline{V}_g - V_m$. It may be seen from Table 3 that the value of $\overline{V}_g - V_m$ for methyl tosylate is smaller than that for isopropyl tosylate in each solvent. Although $\Delta V_0^{\neq}$ and $\overline{V}_g$ were not measured at the same temperature, the observed decreases in $\overline{V}_g - V_m$ with the substrate change from isopropyl to methyl tosylate (about 4 cm^3/mol for formic acid and about 2 cm^3/mol for methanol at 25 °C) seem to correspond approximately to the increases in $\Delta V_0^{\neq}$ in the same structural change (2—3 cm^3/mol for both of the solvents at either 40 or 45 °C). This suggests that $\overline{V}_g$ is more sensitive to the change in the substrate structure from the secondary to primary system than is $\overline{V}_t$. That is, the transition state of isopropyl tosylate constricts the surrounding solvent to nearly the same extent as that of methyl tosylate. The importance of the k_s-character of isopropyl tosylate has already been described in the case of methanolysis.[2] It is worthwhile to note again that the behavior of isopropyl tosylate is far from limiting solvolysis, even in formic acid. The same conclusion has been reported by Schleyer and his-coworkers[5] on the basis of a scrutiny of the relative rates of the corresponding substrates.

It can be seen from our results that the change in mechanism from a k_s- to a k_c-process causes a considerable variation in $\Delta V_0^{\neq}$ (about 8 cm^3/mol). As has been reported,[2a] this mechanistic change in the case of formolysis was achieved by means of the successive introduction of alkyl groups into the parent substrate, isopropyl tosylate. A good linear regression of the activation volume with the characteristics of the substrate was actually observed; the more k_c-like substrate was characterized by the less negative activation volume. The most k_c-like substrate, 2-adamantyl tosylate, gave the least negative-value (−6.9 cm^3/mol), while the most k_s-like substrate, isopropyl tosylate, gave the most negative value (−14.7 cm^3/mol). The others exhibited values between these two. However, the leveling effect on the activation volume[2a] in the case of the pure k_s-substrate, methyl tosylate, embosses the importance of the initial state partial molal volume. These observations lead us to conclude that the activation volume is a quite useful parameter or criterion for the study of solvolytic reaction mechanisms, especially for a series of reactions in which the degree of the k_s-contribution to the whole kinetic process varies.

Experimental

Materials. Methyl tosylate was a commercial material. Isopropyl and 2-adamantyl tosylates were prepared from the corresponding alcohols by the usual method. 1-Adamantyl tosylate was prepared from 1-adamantyl iodide and silver *p*-toluenesulfonate according to the procedure in the literature.[12] All the tosylates were found by NMR analysis to be satisfactorily pure.

Formic acid and methanol were purified as has previously been described.[2a] Acetone was dried over Drierite and distilled. The distilled water used was stored out of contact with air.

Rate Measurements. The high-pressure apparatus has previously been described.[6c] Temperature was controlled within 0.03 °C for all the kinetic runs. The reaction rate was measured using the conductance technique.[2a] The concen-

trations of the kinetic solutions were 0.019, 0.005, and 0.003 M for formolysis, hydrolysis, and methanolysis respectively. The rate constants for all the reactions of adamantyl tosylates and for the formolysis of isopropyl tosylate were determined by the Guggenheim method.[13] Pre-cooling of the medium in the high-pressure vessel was required to establish the thermal equilibrium rapidly.[2a] For the other slow reactions, we employed the procedure previously described for the methanolysis of secondary alkyl tosylates.[2a]

Partial Molal Volume Measurements. The technique used here was the dilatometric method recommended by Hyne and his co-workers.[7] 30 μl of tosylate was injected into a dilatometer consisting of a 190 cm^3 bulb containing a magnetic spin bar and fitted with precision bore capillary, 25 cm in length. The bath temperature during the measurement was kept within 0.002 °C. The density of the substrate used in calculating the molar volume was determined by the usual picnometer technique.

The present work has been supported by a Grant-in-aid for Scientific Research from the Ministry of Education.

References

1) Organic Reaction under High Pressure XIV. Part XIII, A. Sera, C. Yamagami, and K. Maruyama, This Bulletin, **47**, 704 (1974).

2) a) A. Sera, C. Yamagami, and K. Maruyama, *ibid.*, **46**, 3864 (1973); b) *Idem*, *ibid.*, **47**, 704 (1974).

3) a) S. Winstein and H. Marshall, *J. Amer. Chem. Soc.*, **74**, 1120, (1952); b) A. H. Fainberg and S. Winstein, *ibid.*, **78**, 2770, (1956).

4) T. W. Bentley, F. L. Schadt, and P. v. R. Schleyer, *ibid.*, **94**, 992 (1972).

5) J. L. Fry, C. J. Lancelot, L. K. M. Lam, J. M. Harris, R. C. Bingham, D. J. Raber, R. E. Hall, and P. v. R. Schleyer, *ibid.*, **92**, 2538 (1970), and references cited therein.

6) This is the expected result because the volume of the transition state in solvolysis is less sensitive to the temperature change than the initial state, see a) A. B. Lateef and J. B. Hyne, *Can. J. Chem.*, **47**, 1369 (1969); b) M. J. MacKinnon, and J. B. Hyne, *ibid.*, **49**, 3840 (1971); c) A. Sera, T. Miyazawa, T. Matsuda, Y. Togawa, and K. Maruyama, This Bulletin, **46**, 3490 (1973).

7) H. S. Golinkin, I. Lee, and J. B. Hyne, *J. Amer. Chem. Soc.*, **89**, 1307 (1967).

8) a) S. D. Hamman, "Physico-Chemical Effects of Pressure," Butterworths Scientific Publications, London (1957); b) W. J. le Noble, "Progress in Physical Organic Chemistry," Vol. 5, ed. A. Streitwieser, Jr. and R. W. Taft, Jr. by Interscience Publisher, New York (1967), p. 207.

9) K. R. Brower, *J. Amer. Chem. Soc.*, **85**, 1401 (1963), and references cited therein.

10) Estimated value.

11) For the study of the initial state contribution to the activation volume, see Ref. 7.

12) D. N. Kevill, K. C. Kolwyck, and F. L. Weitl, *J. Amer. Chem. Soc.*, **92**, 7300 (1970).

13) E. A. Guggenheim, *Phil. Mag.*, **2**, 538 (1926).

The Structure of Ternstroemiaxanthin, a New Aldehydic C_{40}-Carotenoid*

Kiyoshi KIKUCHI** and Masaru YAMAGUCHI

Department of Chemistry, Faculty of Science, Kyushu University, Higashi-ku, Fukuoka 812

(Received September 10, 1973)

A new carotenoid, ternstroemiaxanthin, was isolated as a main constituent from the red seeds of "*Ternstroemia japonica*," and the structure of the pigment was determined to be 3-hydroxy-β,ψ-caroten-18′-al (I) by spectral and chemical methods.

The deep red coloration of the seeds of "*Ternstroemia japonica*" (Mokkoku) is mainly due to the presence of a new phytocarotenoid, which is named ternstroemiaxanthin. In this paper we will describe its isolation and the structural studies which led to the conclusion that the pigment has the formula (3-hydroxy-β,ψ-caroten-18′-al)[1] represented by I. This is the first example of the presence of aldehydic C_{40}-carotenoid in higher plants.

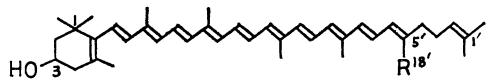

I R=CHO
II R=CH_2OH

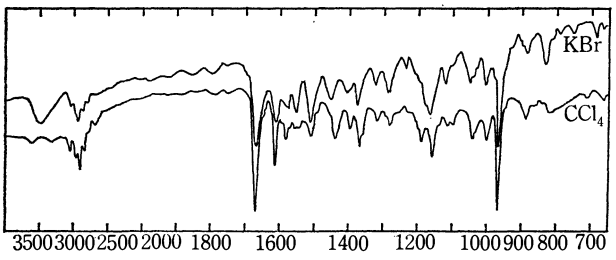

Fig. 1. Infrared spectra of ternstroemiaxanthin (I).

Results and Discussion

Ternstroemiaxanthin has the molecular formula of $C_{40}H_{54}O_2$ (elementary analysis and mass spectra). The presence of a hydroxyl group is indicated by the solubilities, the partition ratio,[2] the IR spectrum (3500, 1050—1040 cm^{-1}),[3] the mass spectrum (ions associated with m/e 18), and the formation of acetate or trimethylsilyl ether. The possibility of a tertiary nature of the group is eliminated by the absence of the characteristic 1150—1130 and 905 cm^{-1} IR absorptions.[4] The possibility of the allylic hydroxyl group can also be excluded by the negative result in the oxidation with chloranil[5] or by the difficulty in an attempted dehydration of the pigment with an acid–chloroform reagent.[6a,b] From the 1042 cm^{-1} position of ν_{C-O} (in carbon tetrachloride), the hydroxyl group seems likely to be secondary and to be on an alicyclic system.[7]

The presence of a formyl group is indicated by the IR [2720 cm^{-1} (in carbon tetrachloride); 1667 (conjugated) and 1160 cm^{-1}] and NMR spectra [δ 9.30]. The conjugated nature of the group can also be seen in the large red shift (10 nm) and the disappearance of fine structures in the UV spectrum taken in a polar solvent.[8]

In *cis,trans*-isomerization with iodine under light,[9] no particular evidence has been obtained to contradict the assumption that the compound has a normal all-*trans* configuration, at least in the central part of the polyene chain. This means that complications due to the presence of thermostable poly-*cis*-,[9] hindered *cis*-,[10] or *cis*-structures with a cross-conjugated aldehyde group[11] can be eliminated in the estimation of the length or the type of chromophore of the pigment from the UV data. A central *cis* or retro-type structure of the chromophore may also be excluded on the basis of the appearance of the δ_{CH} absorption at 965 cm^{-1} (sharp singlet).[12] The pigment absorbs thirteen moles of hydrogen, presumably twelve for double bonds and one for a carbonyl group; it appears, therefore, to be monocyclic. From the λ_{max} of ternstroemiaxanthin (486 nm, petroleum benzin) and its moderately-developed fine structures, it can be inferred that one of the double bonds is out of conjugation and that a part of the chromophore is in a substituted cyclic structure, such as a β-ionone ring, where the effective conjugation of that part with the main chromophore is hindered.[6b] If a partial chromophore involving the terminal carbonyl group is in the cyclic system, however, the fine structures should almost disappear and the λ_{max} should further shift toward blue to a considerable extent, as can be seen in compounds with a 4-keto-β,ψ-carotene chromophore (λ_{max} 462 nm).[13] Therefore, the chromophore given by I, for example, seems appropriate for the pigment. The similarity in the UV spectra of the pigment and of 4′-apo-β,ψ-caroten-4′-al[14] supports this conclusion. The above arguments are also supported by the fact that dihydroternstroemiaxanthin (II) or its diacetate exhibits absorption maxima almost identical with those of β,ψ-carotene,[15] β,ψ-caroten-3-ol[16] or 4′-apo-β,ψ-caroten-4′-ol.[14]

The ions [m/e 413(M–153) and 373(M–193)] in the mass spectrum are considered to give strong evidence for the presence of a hydroxylated β-ionone ring;[17] this is further confirmed by the mass spectra of the trimethylsilyl ether[18] of the pigment and the bistrimethylsilyl ether of the dihydro derivative (II).

The 4-position of the hydroxyl group can be eliminated because of its non-allylic nature. The NMR signal (δ 3.95) of the methine proton adjacent to the hydroxyl group is quite similar to that (δ 4.00) of β,β-carotene-3,3′-diol[19] and different from that (δ 3.55) of β,β-caroten-2-ol.[20] The hydroxyl group can, therefore,

* Presented in part at the 10th Symposium on the Chemistry of Natural Products, Osaka, October, 1972.

** Present address: Kowa Chemical Industries Co., Ltd., Kitakojiya, Ota-ku, Tokyo 144.

be assigned to the 3-position on the β-ionone ring.

The ions associated with *m/e* 69 clearly indicate the presence of a isopentenyl group which is common in ψ-type carotenoids.[17] The NMR spectrum, however, shows only nine methyl groups and shows the absence of the δ 1.81 signal which is characteristic of the 5'-methyl group in β,ψ-type carotenoids.[19] This indicates that the formyl group is at the 5'-position in the pigment.

Further confirmations of the structure have been made by chemical means. The lithium aluminium hydride or sodium borohydride reduction of the pigment gave a dihydro compound (II), which gave diacetate or bistrimethylsilyl ether. An attempt to oxidize the aldehyde group into carboxylic acid with silver oxide failed completely. A similar observation regarding the resistance of polyene aldehyde toward oxidation has been previously reported.[21]

Experimental

Anhydrous sodium sulfate was used for drying the solutions. The calcium carbonate or calcium hydroxide used for chromatography was activated by heating it at 150 °C for 3 hr just before use. The instruments used for the measurements of the spectra were as follows: UV spectra, Hitachi, Model EPS-3T. IR spectra, Hitachi, Model 215. NMR spectra, JEOL, Model TS 100. Mass spectra, Hitachi, Model TMS-4, and JEOL, Model JMS-01SG.

Isolation and Properties of Ternstroemiaxanthin (I). The seeds were repeatedly extracted with acetone, the pigment was transferred into petroleum benzin (bp 60—70 °C) by the addition of water, and the solution was concentrated to a deep red oil. The oil was diluted with petroleum benzin and chromatographed on alumina (Merck, neutral; grade II). The ternstroemiaxanthin ester formed a wide violet zone in the middle of the column, besides several minor zones above and below it. A colorless vegetable oil was removed as thoroughly as possible by prolonged washing. The main zone was eluted (petroleum benzin containing a little methanol), and the evaporation residue of the elute was saponified with 10% methanolic potassium hydroxide in petroleum benzin at room temperature for 20 hr. The solution was washed with water, dried, and concentrated to give a reddish-black resinous residue, which was then chromatographed on calcium carbonate from a petroleum benzin solution. A wide, purplish-red main zone (the fourth from the top) was eluted (10% methanolic benzene) and concentrated under reduced pressure. The residue, redissolved in a small amount of methylene chloride, crystallized on the drop-by-drop addition of methanol. Several recrystallizations from the same mixture gave pure ternstroemiaxanthin as blackish-violet needles (8 mg from 1 Kg seeds); mp 160.5 °C (uncorr.). Found: C, 84.32; H, 10.00%. Calcd for $C_{40}H_{54}O_2$: C, 84.75; H, 9.60%. UV spectra: 518(ε 98000), 486(ε 127000), 460_{sh} nm(hexane); 496 nm(ε 115000) (ethanol); 536, 504, 472_{sh} nm(benzene). IR spectra: Fig. 1. NMR spectrum: δ ($CDCl_3$) 1.08(6H, s; 1,1-dimethyl); 1.58 and 1.64(each 3H, s; 1',1'-dimethyl); 1.73(3H, s, 5-methyl); 1.97(12H, s; 9,13,9',13'-tetramethyl); 4.00(1H, m, 3-proton); 5.15(1H, m, 2'-proton); 5.98—6.95 (15H, m, polyene chain protons); 9.30(1H, s, aldehyde). Mass spectrum: 566.4132(M, calcd for $C_{40}H_{54}O_2$, 566.4124), 548 (M−18, 2.6%), 497(M−69, 1.1), 487(M−79, 0.8), 479 (M−69−18, 0.6), 474(M−92, 2.5), 460(M−106, 4.5), 456 (M−92−18, 0.7), 442(M−106−18, 1.1), 413(M−153, 1.3), 408(M−158, 1.8), 405 (M−92−69, 1.0), 391 (M−106 −69, 1.7), 373(M−193, 1.0), 368(M−106−92, 1.6), 106(32), 91(63), 69(17), 28(100), 18(53).

cis,trans-*Isomerization.* After equilibration in benzene in the presence of iodine and light, the 504-nm maximum of the pigment shifted to 500 nm, accompanied with a decrease in the extinction coefficient, and a *cis*-peak was newly formed at 381 nm, with a shoulder at 361 nm.

Catalytic Hydrogenation:[22] 13.28 mol of hydrogen were absorbed (PtO_2, acetic acid; reference substance, β,β-carotene-3,3'-diol).

The partitioning ratio[2] between petroleum ether (bp 50—60 °C) and 90% methanol was 42 : 58.

The pigment (0.1 mg) dissolved in chloroform (0.2 ml) was treated with three drops of an acid-chloroform reagent[6a] for fifteen minutes. Most of the pigment was recovered unchanged, and no dehydrated product was observed on working up, including a chromatographic examination. The pigment (0.1 mg) was also treated with chloranil (0.09 mg) in a mixture of benzene (0.6 ml) and ethanol (0.07 ml) at room temperature for 20 hr. No product exhibiting wavelength maxima longer than those of the starting pigment was observed in the chromatographic analysis of the mixture.

Acetate. Acetate was prepared by the usual procedure from the pigment and acetic anhydride in pyridine and was purified by chromatography on calcium carbonate. A reddish-black precipitate. Partition ratio: 95.5:4.5 (petroleum benzin and 90% methanol). λ_{max} 518, 486, 457_{sh} nm(petroleum benzin). IR; 2960, 2880, 1738 (CH_3COO), 1670, 1242, 962 cm^{-1}.

Trimethylsilyl Ether. This was prepared from the pigment, hexamethyldisilazane, and trimethylchlorosilane in pyridine,[18] and was purified by chromatography (calcium carbonate, petroleum benzin). Some characteristic peaks in the mass spectrum were as follows: *m/e* 638 [M, for $C_{40}H_{53}O_2Si(CH_3)_3$], 569(M−69), 566(M−72), 548(M−90), 546(M−92), 532(M−106), 480(M−158), 477(M−69−92), 463(M−69−106), 413(M−72−153), 373(M−72−193), 41 (base peak).

Dihydroternstroemiaxanthin (II). Ternstroemiaxanthin (2 mg) dissolved in ethanol (15 ml) was treated with sodium borohydride (50 mg) for thirty minutes. The mixture was then treated as usual, and after chromatographic purification (calcium carbonate, petroleum benzin), a dihydro derivative was obtained as red needles (1.1 mg); mp 174 °C (from benzene-petroleum benzin). Lithium aluminium hydride gave a poorer yield. λ_{max}: 490(ε 107000), 459(ε 122000), 434_{sh} nm(petroleum benzin); 508, 476, 447_{sh} nm(benzene).

Diacetate; λ_{max} 492, 461, 434 nm(petroleum benzin).

Bistrimethylsilyl ether, prepared by the usual procedure,[18] gave the following characteristic peaks: *m/e* 712(M for $C_{46}H_{72}O_2Si_2$), 643(M−69), 622(M−90), 620(M−92), 606 (M−106), 532(M−90−90), 487(M−72−153), 447(M−72−193), 73(base peak).

The authors wish to thank Dr. Michio Nakanishi of the Yoshitomi Pharmaceutical Co. Ltd., for the help he gave them in the measurement of the NMR and mass spectra, and the members of the authors' laboratory for their help in the collection of materials.

References

1) The new carotenoid nomenclature, recommended by IUPAC (O. Isler, "Carotenoids," Birkhäuser, Basel (1971), p. 851), is used in this report.

2) F. J. Petracek and L. Zechmeister, *Anal. Chem.*, **28**, 1484 (1956).
3) If not specified, the IR data are those taken in potassium bromide pellets.
4) S. Liaaen-Jensen and A. Jensen, *Progr. Chem. Fats Lipids*, **8**, Part 2, 150 (1965).
5) C. K. Warren and B. C. L. Weedon, *J. Chem. Soc.*, **1958**, 3972; S. Liaaen-Jensen, *Acta Chem. Scand.*, **19**, 1166 (1965).
6) a) P. Karrer and E. Leumann, *Helv. Chim. Acta*, **34**, 445 (1951); R. Entschel and P. Karrer, *ibid.*, **41**, 402 (1958). b) S. Liaaen-Jensen, *Pure Appl. Chem.*, **14**, 227 (1967).
7) C. Bodea, E. Nicoară, V. Tămaș, and H. Mantsch, *Ann. Chem.* **666**, 189 (1963).
8) F. Feichtmayr, E. Heilbronner, A. Nürrenbach, H. Pommer, and J. Schlag, *Tetrahedron*, **25**, 5383 (1969).
9) L. Zechmeister, *Fortschr. Chem. Org. Naturstoffe*, **18**, 223 (1960).
10) O. Isler, L. H. Chopard-Dit-Jean, M. Montavon, R. Rüegg, and P. Zeller, *Helv. Chim. Acta*, **40**, 1256 (1957); Ref. 9, p. 275.
11) A. J. Aasen and S. Liaaen-Jensen, *Acta Chem. Scand.*, **21**, 2185 (1967).
12) K. Lunde and L. Zechmeister, *J. Amer. Chem. Soc.*, **77**, 1647 (1955); E. Nicoară, V. Tămaș, G. Neamțu, and C. Bodea, *Ann. Chem.*, **697**, 201 (1966).
13) A. P. Leftwick and B. C. L. Weedon, *Acta Chem. Scand.*, **20**, 1195 (1966).
14) R. Rüegg, M. Montavon, G. Ryser, G. Saucy, U. Schwieter, and O. Isler, *Helv. Chim. Acta*, **42**, 845 (1959).
15) P. Karrer and E. Jucker, "Carotinoide," Birkhäuser, Basal (1948), p. 167.
16) *Ibid.*, p. 173.
17) a) C. R. Enzell, G. W. Francis, and S. Liaaen-Jensen, *Acta Chem. Scand.*, **23**, 727 (1969). b) U. Schwieter, G. Englert, N. Rigassi, and W. Vetter, "Carotenoids Other than Vitamin A," Vol. 2, Butterworths, London (1969), p. 402.
18) A. McCormick and S. Liaaen-Jensen, *Acta Chem. Scand.*, **20**, 1989 (1966).
19) Ref. 17b, p. 382.
20) H. Kjøsen, N. Arpin, and S. Liaaen-Jensen, *Acta Chem. Scand.*, **26**, 3053 (1972).
21) Ref. 11; R. Kuhn and C. Grundmann, *Ber.*, **65**, 1880 (1932).
22) R. Kuhn and E. E. Möller, *Angew. Chem.*, **47**, 145 (1934).

Kinetic Studies on the Hydrolysis of Ethyl Benzenesulfinates[1]

Michio KOBAYASHI, Ritsuko NISHI, and Hiroshi MINATO

Department of Chemistry, Faculty of Science, Tokyo Metropolitan University, Fukazawa, Setagaya, Tokyo 158

(Received September 22, 1973)

The rates of hydrolysis of ethyl *p*-substituted benzenesulfinates were determined in acidic and alkaline media; the rates were greater in the former with the sulfinates containing electron-releasing substituents, $\rho = -0.54$ (20 °C); and in the latter with the sulfinates containing electron-withdrawing substituents, $\rho = 1.60$. The mechanisms of the hydrolysis are discussed.

By use of oxygen-18, Bunton and Hendy established that hydrolysis of methyl *p*-toluenesulfinate proceeds with S(O)–O bond fission under both alkaline and acidic conditions.[2] The alcoholysis of alkyl *p*-toluenesulfinates catalyzed by potassium acetate was found to proceed also with S(O)–O bond fission and inversion on the sulfur atom.[3] The hydrolysis of benzhydryl arenesulfinates, however, was found to proceed with S(O)–O bond fission and inversion on the sulfur atom.[3] The hydrolysis of benzhydryl arenesulfinates, however, was found to proceed with O–C bond fission; part of the sulfinate anion-benzhydryl cation ion pair formed recombined, forming a sulfone.[4,5]

The only kinetic study on the hydrolysis of sulfinates carried out by Bunton and Hendy[2] described the hydrolysis of methyl *p*-toluenesulfinate under acidic conditions, and no substituent effects were investigated. Concerning the alkaline hydrolysis, they stated that the reaction proceeds too rapidly to determine the rates, and gave only one approximate value.

We have determined the rates of hydrolysis of ethyl *p*-substituted benzenesulfinates in aqueous ethanol under acidic and alkaline conditions, and calculated the activation parameters. The results are given in this paper together with their implication.

Results and Discussion

Ethyl arenesulfinates (I) show a strong absorption near 250 nm due to n→pdπ transition, whereas arenesulfinate anions show a weak one.[6] Thus, the rates of hydrolysis of I in alkaline media can be determined by observing the decrease of the absorption near 250 nm.

Arenesulfinic acids are fairly strong acids (p*K*a< 2),[7] and dissociate almost completely in dilute aqueous solutions, their UV spectra showing the absorption of the sulfinate anions alone.[4] Thus, the rates of hydrolysis of I in acidic media also can be determined by observing the decrease of the absorption near 250 nm.

Rates of Hydrolysis in Alkaline Media. An ester was dissolved in a 2/3 (v/v) mixture of ethanol and a dilute NaOH solution (the concentration of the ester, $\sim 10^{-3}$ M). Aliquots were withdrawn at suitable intervals, cooled with ice, diluted with a 0.1 N H_2SO_4 aqueous solution (20 times), and the UV absorption of the mixture was determined. An example of such a spectrum, exhibiting an isosbestic point, is shown in Fig. 1. The rates of hydrolysis were calculated from the decrease of the absorbance near 240—250 nm, and were of first order both in [ester] and in [OH^-]. Since the rate of hydrolysis of ethyl *p*-nitrobenzenesulfinate in alkaline media near room temperature was very large, the reaction was carried out in a UV cell, and its absorption was repeatedly determined at suitable intervals without acidifying the reaction mixture.

Rates of Hydrolysis in Acetic Media. An ester was dissolved in a 2/3 (v/v) mixture of ethanol and a dilute

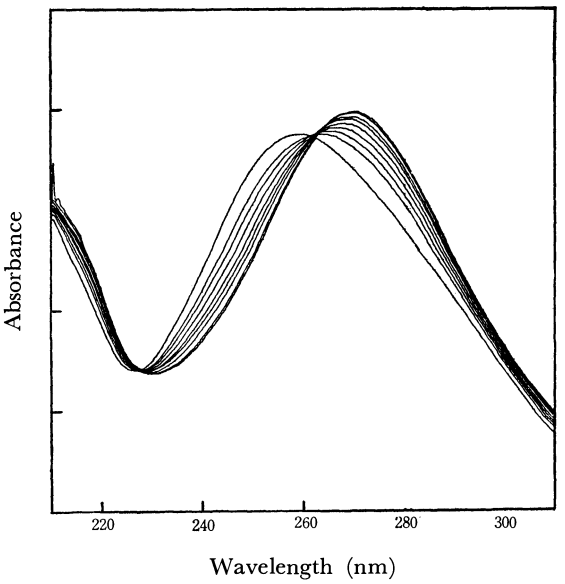

Fig. 1. Changes of the UV absorption of ethyl *p*-nitrobenzenesulfinate in alkaline hydrolysis.

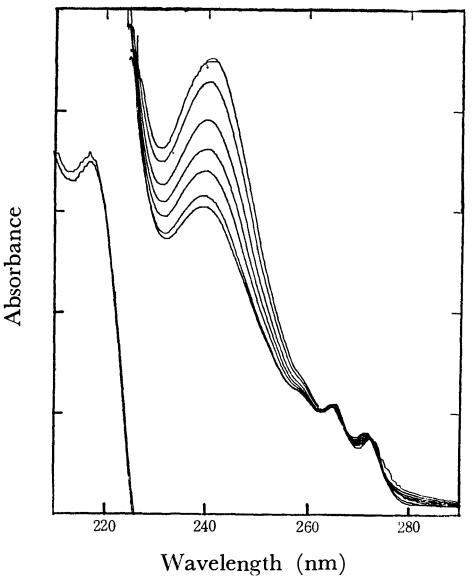

Fig. 2. Changes of the UV absorption of ethyl benzenesulfinate in acidic hydrolysis.

H_2SO_4 solution (the concentration of the ester was about 10^{-3} M and that of H_2SO_4 was 2~5 N). Aliquots were withdrawn at suitable intervals, cooled with ice, diluted with distilled water (20 times), and the UV absorption of the mixture was determined. A group of spectra obtained possessed an isosbestic point (Fig. 2).

Table 1. Rate constants and activation parameters for the hydrolysis of ethyl *p*-substituted benzensulfinates, *p*-X-$C_6H_4SO_2Et$, in acidic media

X	Temp. (°C)	$[H_2SO_4]$ (N)	$10^5 \times k$ ($M^{-1}s^{-1}$)	$\Delta H^{\neq}$ (kcal/mol)	$\Delta S^{\neq}$ (e.u.)
CH_3O	20.8	4.38	2.31	18.1	−18.4
	30.3	4.38	3.25		
	39.5	4.12	15.6		
CH_3	20.8	4.28	1.49	17.1	−22.6
	24.0	4.56	2.03		
	34.2	3.98	5.21		
	38.5	4.58	8.26		
H	21.2	4.14	1.38	20.8	−10.2
	31.3	3.92	4.33		
	40.1	4.34	12.2		
Br	21.3	4.90	1.35	15.4	−27.7
	31.1	4.80	3.16		
	39.5	2.14	5.75		
	39.5	4.00	7.20		
	39.5	4.32	7.70		
	39.5	5.48	7.93		
NO_2	21.4	4.14	0.592	7.62	−56.7
	30.2	4.38	0.648		
	39.7	4.14	1.34		

Table 2. Rate constants and activation parameters for the hydrolysis of ethyl *p*-substituted benzenesulfinates, *p*-X-$C_6H_4SO_2Et$, in alkaline media

X	Temp. (°C)	[NaOH] (M)	$10^2 \times k$ ($M^{-1}s^{-1}$)	$\Delta H^{\neq}$ (kcal/mol)	$\Delta S^{\neq}$ (e.u.)
CH_3O	0.0	0.0193	1.39	10.1	−30.0
	10.6	0.0201	3.44		
	21.4	0.0197	5.84		
CH_3	0.0	0.0182	6.12	6.67	−39.9
	0.6	0.0184	5.07		
	10.4	0.0180	7.90		
	11.3	0.0195	8.87		
	15.7	0.0195	9.73		
	21.6	0.0208	14.4		
	22.6	0.0196	13.1		
	23.0	0.0193	16.9		
	25.7	0.0195	17.5		
H	0.2	0.0130	7.62	6.37	−40.5
	11.9	0.0132	10.4		
	20.2	0.0129	16.7		
Br	0.0	0.0817	18.7	7.86	−33.0
	10.6	0.0825	34.8		
	17.4	0.0935	44.5		
	21.2	0.0710	59.5		
NO_2	2.0	0.0062	104	8.79	−25.8
	8.4	0.0025	184		
	16.2	0.0017	313		

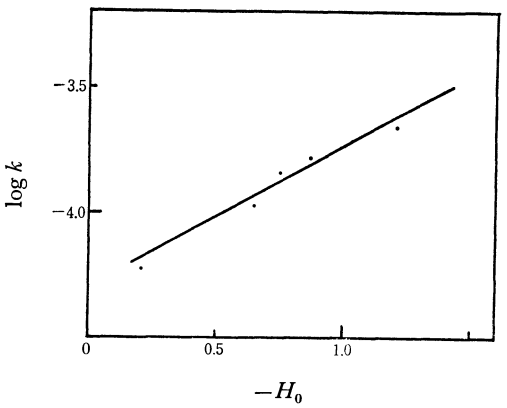

Fig. 3. The relationship between $\log k$ and acidity function H_0 in the hydrolyses of ethyl *p*-bromobenzenesulfinate.

In strongly acidic media, benzenesulfinic acids undergo disproportionation, forming a 1 : 1 mixture of thiolsulfonate and sulfonic acid, the disproportionation being much slower than the hydrolysis of sulfinates. The UV absorption of a disproportionated mixture near 240—260 nm was weak, its molar absorbance differing from that of a hydrolyzed mixture (sulfinate anion). Thus, the rates of hydrolysis of I were calibrated by determining the rates of disproportionation of sulfuric acids under the same conditions.

The rates of hydrolysis of I in acidic media were of first order in I, and were nearly proportional to acid concentration. The rate constants were calculated by assuming a second-order rate equation, (Tables 1 and 2). The values of $\log k$ were found to show a linear relationship with acidity function H_0 (Fig. 3).[8] In the case of the hydrolysis of methyl *p*-toluenesulfinate catalyzed by perchloric acid in aqueous dioxane, Bunton and Hendy reported a similar linear relationship between $\log k$ and H_0.

Hammett Relationship. For the hydrolysis in alkaline media, good linear relationship was found between the rate constants and Hammett σ-values (the ρ value was 1.60 at 0, 10, and 20 °C; the correlation coefficient, γ was 0.99 in every case). For the hydrolysis in acidic media, fair linear relationship was found ($\rho=-0.54$ at 21 °C ($\gamma=0.96$); $\rho=-0.85$ at 30 °C ($\gamma=0.93$); $\rho=-0.95$ at 40 °C ($\gamma=0.95$)).

Reaction Mechanism. For the hydrolysis in alkaline media, the following mechanism is proposed on the basis of the findings that the Hammett ρ value was positive (+1.60), the value of the activation entropy is a large negative value (~−30 e.u.), and the reaction involves S(O)–O fission.[3]

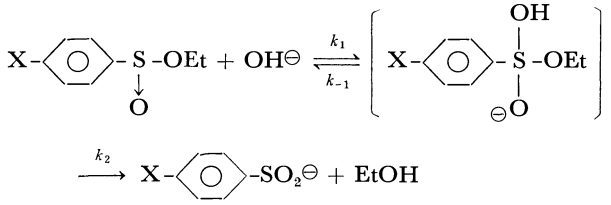

The positive ρ value suggests that the first step (*i.e.*, the addition of OH^- to I) is rate-determining. When the hydrolysis of ethyl *p*-toluenesulfinate in ^{18}O-enriched

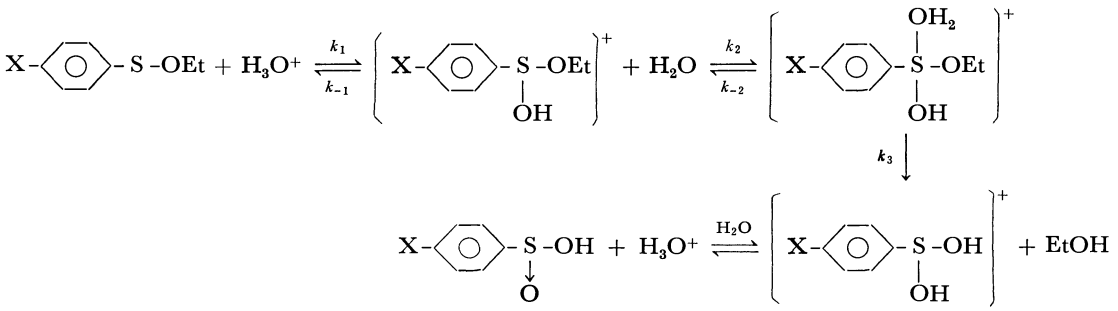

water was stopped before completion and the unchanged ester was recovered, no incorporation of ^{18}O in the ester was found.[10] Therefore, k_2 should be far greater than k_{-1}. Thus, the life time of the tetracoordinated intermediate should be very short, and the addition-elimination mechanism described above is kinetically indistinguishable from that which involves a one-step S_N2-type displacement of OEt of I with OH^-. However, nucleophilic attack on an atom containing a double bond (for example, C=O, C=N) is usually not a one-step S_N2-type displacement (for example, the hydrolysis of carboxylate esters proceed by an addition-elimination mechanism similar to that presented for I), and the S–O bonds in sulfinate esters and sulfoxides are considered to have semipolar double bond character. Hence, we prefer the addition-elimination mechanism, but we admit that there is no concrete evidence for the choice between the two mechanisms.

For the hydrolysis in acidic media, the mechanism shown above is proposed on the basis of the following findings; the ρ value is negative and relatively small, $\log k$ is proportional to H_0, the entropy of activation is fairly large negative value characteristic of an A2 type reaction, and the reaction involves S(O)–O fission.

The ρ value of the first step is expected to be negative, that of the second step positive, and that of the third step negative. If the rate-determining step is the second or third step, the ρ value of the overall reaction will be small. The ρ value experimentally obtained was a small and negative value. The linear relationship between $\log k$ and H_0 is consistent with the hypothesis that the first step is the protonation of I and the rate-determining step is the second step (*i. e.*, the addition of water to the conjugate acid of I) or a later step.

The hydrolysis in acidic media proceeds *via* several steps, and the effect of substituents varies in each step. Therefore, it is reasonable that the linearity of the Hammett relationship between $\log k$ of the overall reaction and the σ values was not too good and that of the Arrhenius plots ($\log k$ vs $1/T$) was poorer than that observed in alkaline hydrolysis.

When ethyl *p*-toluenesulfinate was partially hydrolyzed in ^{18}O-enriched water and the unchanged ester was recovered, no increase in its ^{18}O content was found.[10] Hence, k_3 must be far greater than k_{-2}.

Experimental

Materials. Ethyl arenesulfinates were prepared by adding dicyclohexylcarbodiimide (0.90—0.95 mol per mol of sulfinic acids) to an anhydrous ethanol solution of a sulfinic acid at 0 °C, and by allowing the mixture to stand overnight;[11] the ester was purified by vacuum distillation or recrystallization (in the case of ethyl *p*-nitrobenzenesulfinate).

Kinetics. Acid Hydrolyses. Stock solutions were prepared by dissolving a weighed amount of I in ethanol. The stock solution (2~5 ml) was diluted with an EtOH–dil.H_2SO_4 mixture (v/v, 2/3) to 100 ml, and the reaction mixture was placed in a constant temperature bath. At suitable intervals, a 5 ml sample was withdrawn, diluted to 100 ml with distilled water, and its UV spectrum was determined.

Alkaline Hydrolysis. Two to five ml of a stock solution of I was diluted with an EtOH–NaOH aq mixture (v/v, 2/3) to 100 ml, and the reaction mixture was placed in a constant temperature bath. At suitable intervals, a 5-ml sample was withdrawn, diluted to 100 ml with a 0.1 N H_2SO_4, and its spectrum was determined. In a 0.1 N H_2SO_4, arenesulfinic acids ($\sim 10^{-4}$ M) are almost completely dissociated.[4]

When the rates were very large, the hydrolysis was carried out in a UV cell. A stock solution was diluted with an EtOH–NaOH aqueous mixture, and the UV spectrum of the ester solution ([I]=about 10^{-5} M) was repeatedly determined.

The rate was determined several times for each case. The average values are given in Tables 1 and 2.

References

1) Organic Sulfur Compounds XLVIII.
2) C. A. Bunton and B. N. Hendy, *J. Chem. Soc.*, **1962**, 2562.
3) H. Phillips, *ibid.*, **127**, 2552 (1925).
4) D. Darwish and R. A. McLaren, *Tetrahedron Lett.*, **1962**, 1231.
5) A. H. Wragg, J. S. McFadyen, and T. S. Stevens, *J. Chem. Soc.*, **1958**, 3603.
6) M. Kobayashi and N. Koga, This Bulletin, **39**, 1788 (1966).
7) C. D. Ritchie, J. D. Saltiel, and E. S. Lewis, *J. Amer. Chem. Soc.*, **83**, 4601 (1961).
8) H_0 values in 20 vol% Ethanol-H_2SO_4 aq[9] were used for this plot since those in 40 vol% ethanol were not available.
9) D. Dolman and R. Stewart, *Can. J. Chem.*, **45**, 903 (1967).
10) "One-step and two-step processes in nucleophilic substitution at organic sulfur," a plenary lecture given by A. Fava at IVth Symposium on Organic Sulphur at Venice, Italy, on June 15, 1970.

Hydrogen Exchange Reactions of Sulfilimines and Sulfoximines[1)]

Michio KOBAYASHI, Akira MORI, and Hiroshi MINATO

Department of Chemistry, Faculty of Science, Tokyo Metropolitan University, Fukazawa, Setagaya, Tokyo 158

(Received September 22, 1973)

Alkyl phenyl sulfilimines, benzyl phenyl sulfilimine and the corresponding sulfoximines were found to exchange their α-hydrogens with deuteriums in heavy water when the medium was alkaline. No exchange was observed when the medium was acidic or neutral. The rates of exchange in a sulfilimine were greater than those of the corresponding sulfoximine. The kinetics of these H-D exchange reactions were investigated by use of pyridine as a catalyst, and the reaction mechanism was discussed.

The α-hydrogens of sulfoxides and sulfones are known to undergo H-D exchange, and the stereochemistry has been studied.[2)] However, H-D exchange in sulfilimines(I) and sulfoximines(II) has not been studied. In order to determine whether or not they also undergo H-D exchange and, if so, whether or not the exchange is stereospecific, an investigation was carried out.

Results and Discussion

When benzyl phenyl sulfilimine(Ia) or benzyl phenyl sulfoximine(IIa) was heated in a dioxane–D_2O mixture at 95 °C, no decrease in their NMR benzyl signals was observed. Addition of acetic acid or dilute HCl did not cause exchange either.

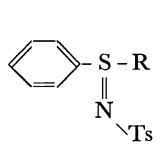

Ia: R=$PhCH_2$
Ib: R=CH_3
Ic: R=C_2H_5

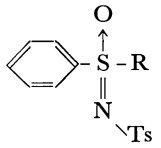

IIa: R=$PhCH_2$
IIb: R=CH_3
IIc: R=C_2H_5

However, when a small amount (2～5 mol%) of sodium hydroxide was added as a catalyst, the benzyl hydrogens of Ia undergo complete exchange on being heated at 95 °C for 10 min. The two benzyl hydrogens of Ia show an AB quartet in the NMR spectrum owing to chirality on the sulfur atom. However, the rates of exchange of these two hydrogens did not appear to differ, and no stereospecificity was observed. This finding differs from what was observed with benzyl sulfoxides.[3)]

The α-hydrogens of Ib, Ic, IIa and IIb also undergo exchange readily in D_2O in the presence of sodium hydroxide. The rates of H-D exchange in a 95% dioxane–5% D_2O mixture were determined by means of NMR with the tosyl methyl signal as a built-in standard, since the tosyl methyl hydrogens do not undergo exchange at all. In alkaline media, I is slowly hydrolyzed, but its rate is far smaller than that of H-D exchange and can be neglected.

The rates of H-D exchange of Ia～Ic were determined with [NaOH]=0.013 M at 10 °C. The exchange was of first order in I, and the pseudo first-order rate constants per one exchangeable hydrogen atom are as follows.

Ia: $k_{obs}=6.35\times10^{-5}\ s^{-1}$
Ib: $k_{obs}=2.10\times10^{-6}$
Ic: $k_{obs}=1.39\times10^{-6}$

The ratio of reactivities per one α-hydrogen is Ia : Ib : Ic=30 : 1 : 0.66. The presence of an adjacent phenyl group promotes the H-D exchange, whereas the presence of an adjacent methyl group retards the exchange.

These results show that the S=N bond of I is strongly polarized and α-carbanions are readily formed. However, in order to compare the effect of the S=N group with those of >C=O, $>SO_2$ and >S=O groups, accurate determination of the H-D exchange rate constants is necessary. For this, sodium hydroxide is unsuitable since the reaction proceeds too rapidly. When a very small amount of sodium hydroxide was used in the later stages of the reaction, part of the catalyst was neutralized with the *p*-toluenesulfonamide formed by hydrolysis of I. Pyridine was, therefore, chosen as catalyst, and the H-D exchange in pyridine–D_2O was studied.

Sulfilimines (Ia or Ib) or sulfoximines (IIa or IIb) (1～2 mmol) were dissolved in pyridine (5 ml), and D_2O (0.5～2.0 g, 24～102 mmol) was added. The mixture was allowed to react in ampoules at a constant temperature. At suitable intervals, ampoules were cooled in ice, and their NMR absorptions were determined. The rates of exchange were calculated from the decrease of integrated intensity of α-methyl or α-methylene absorptions. Since D_2O is present in far excess of I or II, the backward reaction (D-H exchange) can be neglected. The apparent rate constants were calculated by using the following equation, as in the case of the NaOH-catalyzed reaction. The tosyl

$$k_{obs}=\frac{2.303}{t}\log\frac{(M/R)_\infty-(M/R)_0}{(M/R)_\infty-(M/R)_t}$$

R: Integrated intensity of the tosyl methyl signal.
M: Integrated intensity of the α-methyl or α-methylene signal.
$(M/R)_\infty$: Value calculated for $t=\infty$.
$(M/R)_0$: Value calculated for $t=0$; it is 1 for Ib or IIb, and 2/3 for Ia or IIa.

methyl group was used as a built-in standard. This method is similar to that of Hine *et al.*, who determined base-catalyzed H-D exchange rates of $CH_3OCH_2CO_2$-CH_3 by using the methoxy methyl NMR signal as a built-in standard.[4)]

For the calculation of rate constants, the first-order rate equation described above was used with assumption that the H-D exchange is not stereospecific and rates of exchange of three α-methyl or two α-methylene hydrogens are equal. This might be reasonable since the rates of exchange of two benzyl hydrogens of Ia were equal.

TABLE 1. RELATIONSHIP BETWEEN k_{obs} AND D_2O CONCENTRATION

Substrate	$[D_2O]$ (mol/l)	Temperature (°C)	k_{obs}[a] (s^{-1})
Ia	4.31	60.0	1.57×10^{-5}
	8.60	60.0	3.26×10^{-5}
	4.48	70.0	3.91×10^{-5}
	8.60	70.0	8.15×10^{-5}
Ib	4.69	70.0	1.94×10^{-5}
	8.14	70.0	2.78×10^{-5}

a) k_{obs} was calculated for one α-hydrogen atom.

Since pyridine was the catalyst and the solvent, the catalyst concentration was constant. When the relationship between k_{obs} and $[D_2O]$ was examined at 60 °C and 70 °C, k_{obs} was approximately proportional to $[D_2O]$ as shown in Table 1. Thus, the rate constant k was calculated by dividing k_{obs} with $[D_2O]$.

$$v = k_{obs}[Ia]$$
$$= k[D_2O][Ia]$$
$$= k'[Py][D_2O][Ia]$$

The values of k_{obs}, k ($=k_{obs}/[D_2O]$) and the activation parameters are shown in Table 2. No exchange was observed with Ic and IIc under these conditions.

The data in Table 2 show that the H-D exchange in benzyl sulfilimine and benzyl sulfoximine is faster than that in the corresponding methyl analog. This is probably due to the stabilization of the carbanion by resonance with the adjacent phenyl group.

The H-D exchange in sulfoximines (IIa and IIb) is much slower than that in sulfilimines(Ia and Ib). If the effect of the >S=N′ or >S(=O)=N′ group is only inductive effect alone, the >S(=O)=N′ group containing an additional oxygen atom should facilitate the abstraction of α-hydrogens to a greater extent. However, the experimental findings are to the contrary; the H-D exchange in I is 10 times that in II and its activation energy is about 1 kcal/mol smaller than that of II. These results are surprising, and the only possible explanation seems to be the more extensive stabilization of the carbanion by the resonance with the >S=N′ group than with the >S(=O)=N′ group, but at present no other data supporting such difference are available.

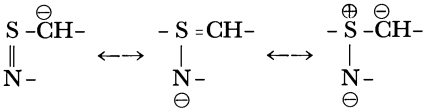

In order to compare the ability of >S=N′ and >S(=O)=N′ for stabilizing carbanions with that of >C=O, the H-D exchange of benzyl *p*-methoxyphenyl ketone(III) was measured in pyridine–D_2O by using its methoxy hydrogens as a built-in standard. The reaction was of first-order in III, and at 70 °C k_{obs} was 2.68×10^{-4} s^{-1} and k ($=k_{obs}/[D_2O]$) was 5.85×10^{-5} $M^{-1}s^{-1}$ (both k_{obs} and k were calculated for one methylene hydrogen). These values are about 7 times that of Ia and 60 times that of IIa. Thus the ability of >S=N′ or >S(=O)=N′ for stabilizing carbanions is much less than that of >C=O.

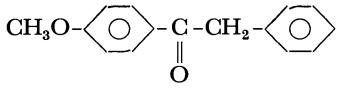

(III)

The base-catalyzed H-D exchange of sulfilimines is considered to proceed *via* the following steps (similar steps can be formulated for the H-D exchange of sulfoximines).

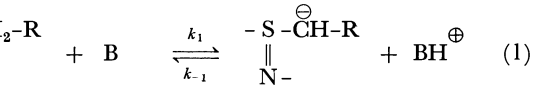

(1)

TABLE 2. H-D EXCHANGE RATES AND ACTIVATION PARAMETER[a]

Substrate	Temperature (°C)	$[D_2O]$ (mol/l)	$10^6\times k_{obs}$ (s^{-1})	$10^6\times k$ ($s^{-1}M^{-1}$)	$\Delta H^{\neq}$ (kcal/mol)	$\Delta S^{\neq}$ (e. u.)
Ia	49.5	4.48	5.00	1.12		
	54.0	4.48	7.75	1.73		
	60.0	4.31	15.7	3.63		
	65.0	4.48	22.9	5.10		
	70.0	4.48	39.1	8.70	21.4	−19.6
Ib	60.0	4.69	3.70	0.79		
	65.0	4.69	10.7	2.28		
	70.0	4.69	19.4	4.13		
	75.0	4.44	26.4	5.93		
	80.0	4.44	68.0	14.8	31.4	+8.6
IIa	60.0	4.75	1.67	0.352		
	75.0	4.32	7.85	1.82		
	80.0	4.32	11.6	2.68		
	85.0	4.32	16.2	3.73	22.2	−21.5
IIb	60.0	5.08	0.0453	0.00893		

a) Both k_{obs} and k were calculated for one α-hydrogen atom, error ranges being ±20%.

$$-S(=N-)-\overset{\ominus}{C}H-R + D_2O \underset{k_{-2}}{\overset{k_2}{\rightleftharpoons}} -S(=N-)-CHD-R + OD^{\ominus} \quad (2)$$

$$-S(=N-)-CHD-R + B \underset{k'_{-1}}{\overset{k'_1}{\rightleftharpoons}} -S(=N-)-\overset{\ominus}{C}D-R + BH^{\oplus} \quad (3)$$

$$-S(=N-)-\overset{\ominus}{C}D-R + D_2O \underset{k'_{-2}}{\overset{k_2'}{\rightleftharpoons}} -S(=N-)-CD_2-R + OD^{\ominus} \quad (4)$$

For the sake of simplicity, only steps (1) and (2) are considered, since (3) and (4) are repetitions of (1) and (2), and $k_1'=k_1$, $k'_{-1}=k_{-1}$, $k_2'=k_2$ and $k'_{-2}=k_{-2}$. Since I and II are very weak acids, the concentration of carbanions must be very small. On the basis of the usual steady-state assumption, the following equation is derived.

$$v = \frac{k_1k_2}{k_{-1}[BH^+]+k_2[D_2O]}[I][B][D_2O]$$

If $k_{-1}[BH^+] \gg k_2[D_2O]$,

$$v = \frac{k_1}{k_{-1}[BH^+]}k_2[I][B][D_2O]$$

and

$$k_{obs} = \frac{k_1}{k_{-1}[BH^+]}k_2[B][D_2O]$$

If $k_{-1}[BH^+] \ll k_2[D_2O]$,

$$v=k_1[I][B] \quad \text{and} \quad k_{obs}=k_1[B]$$

In this case, a large kinetic isotope effect is expected, and changes in $[D_2O]$ should not alter the rate.

In fact, two types of H-D exchange in labile hydrogens have been reported. In the case of the exchange of α-hydrogens of toluene in cyclohexylamine in the presence of lithium cyclohexylimide, the isotopc effect (k_H/k_D) was greater than 10, indicating that the first step (the abstraction of proton) is rate-determining.[5] In the case of the exchange of α-hydrogens of toluene in DMSO in the presence of potassium *t*-butoxide, k_H/k_D was 0.6, indicating that the second step is rate-determining.[6]

When the D-H exchange of α,α-dideuteriobenzyl phenyl sulfilimine (Ia-d_2) was measured in pyridine–H_2O at 70 °C, the following values were obtained.

$$k_{obs} = 2.07\times10^{-5}\,s^{-1}$$
$$k_D^{70°} = k_{obs}/[H_2O] = 4.84\times10^{-6}\,s^{-1}\,M^{-1}$$
$$(k_H/k_D)_{70°C} = 1.80$$

For α,α,α-trideuteriomethyl phenyl sulfilimine (Ib-d_3), the following values were obtained.

$$k_{obs} = 8.40\times10^{-6}\,s^{-1}$$
$$k_D = k_{obs}/[H_2O] = 1.89\times10^{-6}\,M^{-1}\,s^{-1}$$
$$(k_H/k_D) = 2.19$$

Ph-S(=N-Ts)-CD_2Ph (Ia-d_2) Ph-S(=N-Ts)-CD_3 (Ib-d_3)

Thus, kinetic isotope effect was observable, and the abstraction of the α-hydrogens must be involved in the rate-determining steps. However, the k_H/k_D values were not so great, and k_{obs} was proportional to the concentration of water. Thus, $k_{-1}[BH^+]$ might be slightly greater than $k_2[D_2O]$.

Experimental

Materials. *N-p*-Toluenesulfonylsulfilimines (Ia, Ib and Ic) were prepared from the reaction between the corresponding sulfides and chloramine-T in methanol.[7]

N-p-Toluenesulfonylsulfoximines (IIa, IIb and IIc) were prepared by the oxidation of the corresponding sulfilimines with perbenzoic acid in chloroform,[8] and recrystallized from methanol.

α,α,α-Trideuteriomethyl phenyl *N-p*-toluenesulfonylsulfilimine(Ib-d_3). An anhydrous dioxane solution (60 g) of Ib (2.88 g) was mixed with an NaOH (20 mg) solution in D_2O (99.75%, 4.0 g). After the mixture was heated at 80 °C for several hours, it was concentrated under reduced pressure and cooled. Colorless crystals obtained were washed with D_2O and recrystallized from methanol.

α,α-Dideuteriobenzyl phenyl *N-p*-toluenesulfonylsulfilimine(Ia-d_2). A mixture of Ia (4.0 g), dioxane (40 g), D_2O (4.0 g) and NaOH (16 mg) was heated at 70 °C for 1 hr. After the solvents were removed under reduced pressure, the residue was washed with D_2O and recrystallized from methanol.

Kinetics. Exchange in Ia in the presence of NaOH. A mixture of Ia (1.200 g), D_2O (99.75 atom%, 5.0 ml, containing 2.23×10^{-2} mol/l NaOH) and spectroscopic-grade dioxane (100 ml) was allowed to stand at 10 °C. At suitable intervals, 10-ml samples were withdrawn, acidified with acetic acid and evaporated under reduced pressure. The residue was washed with D_2O, dried in vacuum and its NMR spectrum was determined in $CDCl_3$. The rate of exchange was calculated from the decrease in the methylene signal in comparison with the tosyl methyl signal.

Exchange in Ib in pyridine. A mixture of Ib (1.708 g) and pyridine (15.56 ml, containing 5.175 mol/l D_2O) was divided into ampoules (0.5 ml each), which were placed in a constant-temperature bath. Ampoules were withdrawn at suitable interval and cooled with ice. The rate of exchange was calculated from the decrease in the *S*-methyl signal in comparison with the tosyl methyl signal.

References

1) Organic Sulfur Compounds. Part XLIX.
2) J. N. Roitman and D. J. Cram, *J. Amer. Chem. Soc.*, **93**, 2225 (1971); D. J. Cram, "Fundamentals of Carbanion Chemistry," Academic Press, New York (1965), p. 105; E. J. Corey, H. König, and T. H. Lowry, *Tetrahedron Lett.*, **1962**, 515; G. Maccagnari, F. Montanari, and F. Taddei, *J. Chem. Soc., (B)*, **1968**, 453.
3) K. Nishihata and M. Nishio, *J. Chem. Soc., Perkin II*, **1973**, 912.
4) J. Hine, K. G. Hamptom, and B. C. Menon, *J. Amer. Chem. Soc.*, **89**, 2664 (1967).
5) A. Streitwieser, W. C. Langworthy, and D. E. Van Sickle, *ibid.*, **84**, 251 (1962).
6) D. J. Cram, "Fundamentals of Carbanion Chemistry," Academic Press, New York (1965), p. 28, footnote.
7) F. G. Mann and W. J. Pope, *J. Chem. Soc.*, **121**, 1052 (1922); A. Kucsman, I. Kapovits, and M. Balla, *Tetrahedron*, **18**, 75 (1962); K. Tsujihara, N. Furukawa, K. Oae, and S. Oae, This Bulletin, **42**, 2631 (1969).
8) D. R. Rayner, D. M. Von Schriltz, J. Day, and D. J. Cram, *J. Amer. Chem. Soc.*, **90**, 2721 (1968).

Cationic Arylation. VII. Cationic Phenylation and Benzoyloxylation of Aromatic Compounds with Benzoyl Peroxide in Trifluoroacetic Acid

Nobumasa KAMIGATA, Hiroshi MINATO, and Michio KOBAYASHI

Department of Chemistry, Faculty of Science, Tokyo Metropolitan University, Fukazawa, Setagaya, Tokyo 158

(Received October 9, 1973)

Benzoyl peroxide (BPO) was decomposed in benzene in the presence of trifluoroacetic acid. The thermal reaction is first order in BPO, and the activation energy and activation entropy are 18.7 kcal/mol and −26.3 e. u., respectively. The isomer distributions in the phenylation and benzoyloxylation of substituted benzenes determined indicate that the phenylation and benzoyloxylation are electrophilic substitution reactions. The reaction mechanisms are discussed.

Studies on the decomposition of the arylazo and aryldiazonium compounds revealed that both phenyl radical and phenyl cation can be generated by selecting the suitable reaction conditions from an arylazo or aryldiazo compound.

Benzenediazonium salts spontaneously decompose in aprotic polar solvents, yielding phenyl cation;[1,2] but they form phenyl radical when nitrite ion,[3] hydroxide ion[4] or pyridine[5] is added to the reaction medium. Phenylazo *p*-tolyl sulfone decomposes homolytically basic agents such as pyridine, quinoline, and magnesium oxide are present,[6] while ionic decomposition yielding phenyl cation takes place in the presence of a large excess of trifluoroacetic acid.[7] Phenylazotriphenylmethane (PAT), regarded as a dependable source for the phenyl radical,[8] decomposes heterolytically, yielding phenyl cation when trifluoroacetic acid is added.[9]

Decomposition of benzoyl peroxide (BPO) has been extensively investigated,[10] but the generation of phenyl cation from BPO has not been reported.

In order to determine whether or not phenyl cation could be generated, BPO was decomposed in aromatic solvents in the presence of excess trifluoroacetic acid, and the isomer distributions in the phenylation and benzoyloxylation of substituted benzenes were determined.

In this paper, the results of this investigation are described and the mechanism of the reaction discussed.

Results and Discussion

BPO was thermally decomposed in a mixture of benzene and trifluoroacetic acid, and the reaction was followed by iodometry. The results are summarized in Table 1. The decomposition was found to be of first order in BPO. The rate constant at 70 °C in benzene–trifluoroacetic acid mixture is larger than that in pure benzene at the same temperature (by about 24%), but the extent of acceleration is much less than those in the cases of azosulfone[7] or PAT.[9] The data in Table 1 satisfied the Arrhenius equation, and the activation parameters calculated (E_a=18.7 kcal/mol, $\Delta S^{\neq}$=−26.3 e.u.) are quite different from those reported for the decomposition of BPO in pure benzene (E_a=33.6 kcal/mol, $\Delta S^{\neq}$=13.8 e.u.);[11] the activation energy is much smaller and the activation entropy has a large negative value. The results suggest that the mechanism of the decomposition of BPO in trifluoroacetic acid differs from that in neutral solvents. The products of decomposition of BPO in benzene–trifluoroacetic acid were benzoic acid (95.9%), biphenyl (6.1%), phenyl benzoate (20.2%), a trace of phenol, and some resinous materials. When BPO was decomposed in a mixture of an arene and trifluoroacetic acid, both phenyl benzoate and aryl benzoate were formed. The results indicate that the part of phenyl benzoate observed in the reaction in benzene–trifluoroacetic acid is formed by intermolecular benzoyloxylation, while other parts could be attributed to the intramolecular rearrangement.[12,13]

Table 1. Rate constants for the decomposition of BPO in benzene–trifluoroacetic acid[a]

Temp. (°C)	$10^5 \times k_1$ (s^{-1})		E_a (kcal/mol)	$\Delta S^{\neq}$ (e.u.)
	C_6H_6–CF_3CO_2H	C_6H_6		
49.7	0.69			
55.0	1.03			
60.0	1.82		18.7	−26.3
65.2	2.51			
78	4.5[b]	3.62[c]		

a) The initial concentration of BPO is 0.200 M. b) Calculated by extrapolation of the rate constants at lower temperatures. c) G. B. Gill and G. H. Williams, *J. Chem. Soc.*, **1965**, 995: the initial concentration of BPO is 0.218 M.

Tables 2 and 3 show the isomer distributions for the phenylation and benzoyloxylation of anisole, toluene,

Table 2. Isomer distributions for the phenylation of C_6H_5X with BPO in the presence of trifluoroacetic acid at 40 °C

X of C_6H_5X	Position	Phenylating agent		
		BPO in CF_3CO_2H	PhN_2^+ $CF_3CO_2^-$ [2]	PhN(NO)-Ac[14]
OCH_3	*o*-	45	61.6	69
	m-	19	9.7	18
	p-	36	28.7	13
C_2H_2	*o*-	55	45.5	71[a]
	m-	25	28.1	18[a]
	p-	20	26.4	11[a]
Cl	*o*-	63	55.2	64
	m-	14	19.9	21
	p-	23	24.9	15
NO_2	*o*-	23	27.8	62
	m-	64	69.4	8
	p-	13	2.8	30

a) The isomer distribution of $PhC_6H_4CH_3$.

Table 3. Isomer distributions for the benzoyloxylation of C_6H_5X with BPO

X of C_6H_5X	Temp. (°C)	Oxidizing agent	Isomer distribution (%)			Reference
			o-	*m*-	*p*-	
OCH_3	40		29	0	71	This work
	60	$CuCl_2$	67	1	33	17)
	79	O_2	28	1	71	18)
	80	I_2	35	(65)		19)
CH_3	40		51	9	40	This work
	60	$CuCl_2$	58	18	26	17)
	81	O_2	38	17	45	18)
	80	I_2	53	16	31	19)
Cl	40		45	5	50	This work
	45	O_2	16	43	41	20)
NO_2	40		1>	88	12	This work

Table 4. Partial rate factors for the phenylation of C_6H_5Cl

Phenylating agent	Temp. (°C)	Partial rate factors		
		k_o/k	k_m/k	k_p/k
BPO in CF_3CO_2H	40	1.27	0.29	0.91
$PhN_2^+BF_4^-$	40	0.67	0.17	0.56
$PhN_2^+CF_3CO_2^-$	40	0.83	0.30	0.75
PhN_2CPh_3 in CF_3CO_2H	40	0.89	0.16	0.48
PhN(NO)Ac	20	3.09	1.01	1.48
BPO	80	2.2	1.4	1.6

chlorobenzene, or nitrobenzene by BPO in the presence of trifluoroacetic acid.

The isomer distributions in the phenylation (Table 2) are similar to those observed for the phenylation with phenyl cation (benzenediazonium trifluoroacetate[2]), but differ from those with phenyl radical (*N*-nitrosoacetanilide[14]). The difference is conspicuous in the phenylation of nitrobenzene, in which the nitro group behaves as a *meta* director towards phenyl cation but behaves as an *ortho-para* director fowards phenyl radical.

The partial rate factors in the phenylation of chlorobenzene shown in Table 4 are also similar to those for the phenylation with phenyl cation generated from benzenediazonium tetrafluoroborate,[1] benzenediazonium trifluoroacetate,[2] or phenylazotriphenylmethane in the presence of trifluoroacetic acid,[9] but differ from those for the phenylation with phenyl radical generated from *N*-nitrosoacetanilide[14] or BPO.[15] Isomer distributions and partial rate factors for the phenylation of substituted benzenes suggest that the decomposition of BPO in trifluoroacetic acid is heterolytic and phenyl cation is formed as a reactive intermediate.

Edward, Chang, and Samad reported that phenyl cation was not formed in the decomposition of BPO in the presence of aluminum chloride, since they could not detect chlorobenzene by gas-chromatographic analysis of the reaction mixture.[16] The discrepancy might be ascribed to the difference in the reaction conditions; their reaction medium is heterogeneous while ours is homogeneous.

It was reported that benzoyloxylation of aromatic compounds with BPO does not occur unless oxidizing agent such as cupric chloride,[17] oxygen,[18] or iodine[19] is present in the reaction system. However, in our reaction system (when trifluoroacetic acid is present) benzoyloxylation occurred. It is of interest that benzoyloxylation takes place in the absence of oxidizing agents.

The figures of isomer distribution for anisole (Table 3) are similar to those reported for the benzoyloxylation with BPO in the presence of oxygen which has been considered to involve benzoyloxy radical. However, the isomer distributions for anisole with benzoyloxy radical reported vary with the kind of oxidizing agent. The isomer distribution for toluene is similar to that for the benzoyloxylation with BPO–iodine but differs from that with BPO–oxygen. As for the benzoyloxylation of chlorobenzene with benzoyloxy radical, there has been only one report,[20] the isomer distribution differing a great deal from the present. Hitherto, the benzoyloxylation of nitrobenzene was considered to be improbable. The present result (Table 3) is the first case of the benzoyloxylation of nitrobenzene. The fact that it took place mainly at the *meta* position suggests that the benzoyloxylation with BPO in the presence of trifluoroacetic acid is electrophilic.

Table 5 shows the ratio of the total yield of aryl benzoates to that of arylbenzenes, and the yield of phenyl benzoate formed from BPO itself (probably by carboxy-inversion followed by decarboxylation). The ratio of the yield of aryl benzoates to that of arylbenzenes decreases in the order X=MeO, Me, Cl, NO_2. The results indicate that the arenes containing electron-releasing substituents react rapidly with the protonated BPO before decarboxylation or carboxy-inversion takes place. The absence of phenyl benzoate in the reaction product in the benzoyloxylation of anisole suggests that anisole is readily benzoyloxylated before carboxy inversion takes place.

Table 5. Ratio of the yield of $PhCO_2C_6H_4X$ to that of PhC_6H_4X in the decomposition of BPO in C_6H_5X in the presence of CF_3CO_2H

X	OCH_3	CH_3	Cl	NO_2
$\frac{PhCO_2C_6H_4X}{PhC_6H_4X}$	14.3	4.5	1.0	0.2
Yield of $PhCO_2Ph$	0	20	35	14

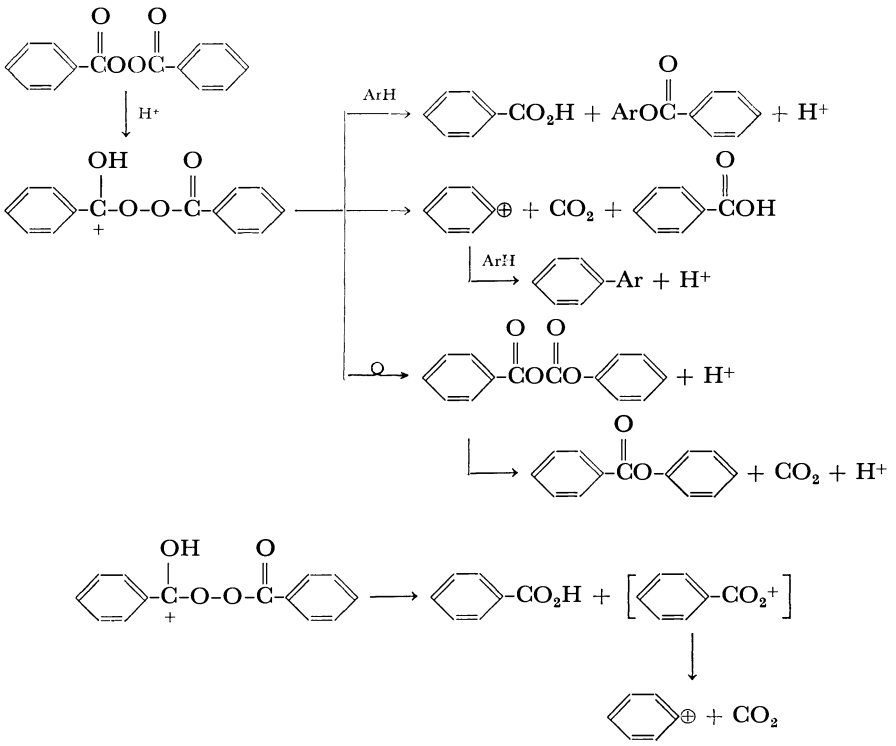

The following mechanism seems plausible for the decomposition of BPO in the presence of trifluoroacetic acid. The first step is the protonation of BPO, and then the protonated BPO reacts with arenes or undergoes carboxy-inversion.

It is possible that the protonated BPO spontaneously decomposes to benzoic acid and benzoyloxy cation. The benzoyloxy cation reacts with arenes or decomposes to carbon dioxide and phenyl cation, which reacts with arenes yielding arylbenzenes.

The mechanism of the formation of phenyl benzoate from BPO in the presence of trifluoroacetic acid is probably similar to that proposed by Leffler,[12] and Denney, Valega and Denney[13] for the decomposition of BPO in the presence of a Lewis acid.

Experimental

Materials. BPO of Wako Pure Chemical Industries LTD. was purified by recrystallization from chloroform-methanol. Trifluoroacetic acid of Wako Pure Chemical Industries LTD. was used without further purification. Purification of benzene and arenes, and preparation of authentic samples of arylbenzenes were described previously.[1b]

Kinetic Measurement of the Decomposition of BPO in the Presence of Trifluoroacetic Acid. BPO (2.422 g, 10 mmol) was dissolved in 25.0 ml of trifluoroacetic acid, and the solution was diluted to 50.0 ml with benzene ([BPO]=0.2 M). The solution was placed in a constant-temperature bath (regulated within ±0.1 °C). At suitable intervals aliquots (5.0 ml) were withdrawn and subjected to the iodometric analysis of Wagner, Smith, and Peters,[21] using a 0.1 N sodium thiosulfate solution.

Products of Decomposition of BPO in the Presence of Trifluoroacetic Acid. BPO (2.319 g, 9.57 mmol) was dissolved in 25.0 ml of trifluoroacetic acid, and the mixture was diluted to 50.0 ml with benzene. The decomposition was carried out at 60±0.1 °C for 70 hr. The dark gray solution obtained was washed with water and then with a 10% sodium hydrogen carbonate solution. The sodium hydrogen carbonate extracts were acidified by hydrochloric acid, and the benzoic acid liberated was extracted with ether, and determined gravimetrically. The benzene layer was dried over anhydrous magnesium sulfate, and the products were separated by elution chromatography after removal of benzene (Wakogel Q-22 200 mesh; eluant, n-hexane-benzene).

Determination of Isomer Ratios and Partial Rate Factors for the Phenylation and Benzoyloxylation of Arenes with BPO in the Presence of Trifluoroacetic Acid. BPO (2.00 g, 8.26 mmol) dissolved in an arene (200 mmol) and trifluoroacetic acid (40.0 g) was decomposed at 40±0.1 °C for 18 days. The reaction mixture was diluted with ether, washed with water and a 10% of aqueous sodium carbonate solution, and then dried over anhydrous magnesium sulfate. After removal of the ether and about 70% of the unchanged arene, the biphenyl isomers and aryl benzoates in the residue were determined by glc. Details of the glc analysis were described previously.[1b,20]

References

1) a) R. A. Abramovitch and F. F. Gadallah, *J. Chem. Soc., B.* **1968**, 497; b) M. Kobayashi, H. Minato, E. Yamada, and N. Kobori, This Bulletin, **43**, 215 (1970).

2) N. Kamigata, R. Hisada, H. Minato, and M. Kobayashi, *ibid.*, **46**, 1016 (1973).

3) M. Kobayashi, H. Minato, N. Kobori, and E. Yamada, *ibid.*, **43**, 1131 (1970).

4) N. Kamigata, T. Kurihara, H. Minato, and M. Kobayashi, *ibid.*, **44**, 3152 (1971).

5) R. A. Abramovitch and J. G. Saha, *Tetrahedron*, **21**, 3297 (1965).

6) M. Kobayashi, H. Minato, M. Kojima, and N. Kamigata, This Bulletin, **44**, 2501 (1970); C. G. Overberger and A. J. Rosenthal, *J. Amer. Chem. Soc.*, **82**, 108, 117 (1960).

7) M. Kobayashi, H. Minato, and N. Kobori, This Bulletin, **43**, 219 (1970).

8) D. H. Hey, C. J. N. Stirling, and G. H. Williams, *J. Chem. Soc.*, **1955**, 3963; D. H. Hey, M. J. Perkins, and G. H. Williams, *ibid.*, **1965**, 110; W. A. Pryor, J. F. Echols, Jr., and K. Smith, *J. Amer. Chem. Soc.*, **89**, 1189 (1967); C. M. Camaggi, R. Leardini, M. Tiecco, and A. Tundo, *J. Chem. Soc., B*, **1969**, 1251; M. Harada, R. Ito, T. Migita, and O. Simamura, *Kogyo Kagaku Zasshi*, **69**, 962 (1966).

9) N. Kamigata, M. Kobayashi, and H. Minato, This Bulletin, **45**, 1231 (1972).

10) D. Swern, "Organic Peroxides," Vol. II, Wiley Interscience, New York (1971).

11) P. D. Bartlett and R. R. Hiatt, *J. Amer. Chem. Soc.*, **80**, 1398 (1958).

12) J. F. Leffler, *ibid.*, **72**, 67 (1950).

13) D. Z. Denney, T. M. Valega, and D. B. Denney, *ibid.*, **86**, 46 (1964).

14) R. Ito, T. Migita, N. Morikawa, and O. Simamura, *Tetrahedron*, **21**, 955 (1965).

15) G. H. Williams, "Homolytic Aromatic Substitution," Pergamon Press, Oxford (1960).

16) J. T. Edward, H. S. Chang, and S. A. Samad, *Can. J. Chem.*, **40**, 804 (1962).

17) M. E. Kurz and P. Kovacic, *J. Org. Chem.*, **33**, 1950 (1968).

18) K. Tokumaru, *Nippon Kagaku Zasshi*, **92**, 887 (1971).

19) S. Hashimoto, W. Koike, and M. Yamamoto, This Bulletin, **42**, 2733 (1969); P. Kovacic, C. G. Reid, and M. J. Brittain, *J. Org. Chem.*, **35**, 2152 (1970).

20) R. Hisada, M. Kobayashi, and H. Minato, This Bulletin, **45**, 2902 (1972).

21) C. D. Wagner, R. H. Smith, and E. D. Peters, *Ind. Eng. Chem., Anal. Ed.*, **19**, 976 (1947).

The Action of Alkali on Inosine. The Formation of 5-Amino-1-β-D-ribofuranosyl-4-imidazolecarboxamide and 9-β-D-Ribopyranosyl Hypoxanthine

Yoshihisa SUZUKI

Central Research Laboratories, Ajinomoto Co., Inc., Suzuki-cho, Kawasaki 210

(Received October 8, 1973)

On treating inosine with aqueous dilute alkali hydroxide (pH 10) over 100 °C, three types of reactions have been found to occur in competition with one another: (1) the hydrolysis of the glycosidic bond to give hypoxanthine and D-ribose, (2) the opening of the pyrimidine ring at C-2 to give 5-amino-1-β-D-ribofuranosyl-4-imidazolecarboxamide, and (3) the isomerization of the ribose moiety to give mainly 9-β-D-ribopyranosyl hypoxanthine. The last two are newly-found reactions, and the products were isolated through column chromatography using Dowex 50W. The products are obtainable in yields of 30 and 10% respectively under optimum conditions. Hypoxanthine was cleaved in an alkaline solution to give 5-amino-4-imidazolecarboxamide, and 5′-inosinic acid was supposed to give 5-amino-1-β-D-ribofuranosyl-4-imidazolecarboxamide-5′-monophosphate. The ring-opening reaction at C-2 was not observed for adenosine or guanosine.

In the course of an investigation of the stability of inosine to acid and alkali, 5-amino-1-β-D-ribofuranosyl-4-imidazolecarboxamide (AICA-riboside) and 9-β-D-ribopyranosyl hypoxanthine were obtained when inosine was heated over 100 °C for several hours with aqueous dilute alkali hydroxide (pH 10). The reactions are considered to be useful for preparing those compounds conveniently from inosine.

It is well known that the acid treatment of inosine causes a hydrolysis at the *N*-glycosyl bond to give hypoxanthine and D-ribose. Such a hydrolysis is regarded as an acid-base catalyzed reaction; therefore, the same reaction was expected to take place when inosine was treated with alkali. This expectation was right. However, under alkaline conditions, especially in a dilute alkaline solution (pH 10), two other interesting reactions have been found to take place besides hydrolysis.

One of these reactions is a ring-opening reaction at C-2 in the pyrimidine of the purine ring to give AICA-riboside. The cleavage has been found to occur predominantly at C-2 rather than at the glycosyl bond at pH 10. Shaw[1] and Montgomery *et al.*[2] have reported that the N-1 substitution of inosine makes it susceptible to a nucleophilic attack of a hydroxide ion at C-2 in alkali, while they considered that inosine itself is extremely stable to alkali.[3] Therefore, what the present author found is somewhat contradictory to their considerations. A brief account of the present work has already appeared elsewhere.[4]

It was once considered, without actual isolation and identification, that purine ribonucleosides undergo an attack by the hydroxide ion at C-8, resulting in the opening of the imidazole ring without the hydrolysis of the *N*-glycosyl bond. For instance, 5-amino-4-ribosylaminopyrimidine is considered to be formed from 9-β-D-ribofuranosylpurine,[5] and also a reaction product, from 7-[β-(*N*-methyl-*N*-4-formylphenylamino) ethyl] guanosine.[6] It is considered that whether the ring-opening reaction takes place at C-2 or at C-8 depends upon the nature of the purine ribosides.

Another remarkable reaction in an alkaline solution would be an isomerization in the ribose moiety to give mainly 9-β-D-ribopyranosyl hypoxanthine. Although an isomerization of the riboside has been shown for aniline riboside[7] in alcohol, no such isomerization has yet been reported in the literature for usual ribonucleosides. This is probably because the *N*-glycosyl bond is labile in the usual nucleosides, so that this bond is cleaved before the isomerization takes place. On the other hand, for an abnormal ribonucleoside, such as pseudouridine, which involves the C-C glycosyl bond in the molecule, the isomerization has been found in acid and alkali.[8] This is probably because the C-glycosyl bond is stable. 9-β-D-Ribopyranosyl hypoxanthine has been obtained by Baddiley *et al.*[9] by the deamination of the 9-β-D-ribopyranosyl adenine which had been synthesized from 4,6-diaminopyrimidine and D-ribose.

Results and Discussion

The three reactions found in the action of alkali on inosine are summarized in Fig. 1. The results of the paper chromatography of the reaction mixture are shown in Table 1. The spots were revealed by the color development of diazotizable amine and by UV absorption. The two spots on the paper chromatogram, named X_1 and Y in Table 1, were coincident with

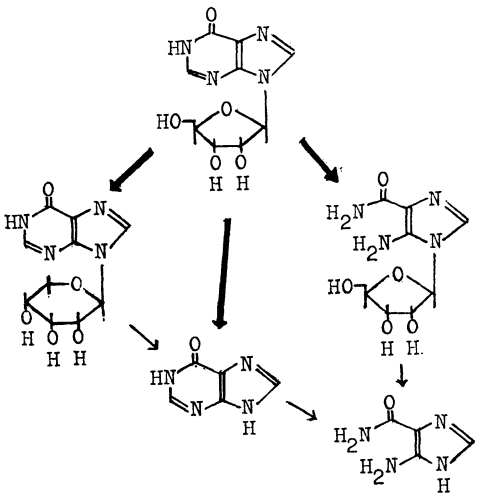

Fig. 1

Table 1. Reaction products of alkaline treated inosine[a]

Component	R_f[b]	UV-absorption	Color development
K	0.96	−[c]	−
X_2	0.83	+	+ (orange)
Hypoxanthine	0.74	++	−
X_1	0.64	++	+ (purple-red)
R	0.55	−	± (purple-red)
Inosine	0.52	++	−
Y	0.43	++	−

a) Initial pH 9.6 at 120 °C for 16 hr. b) On the paper chromatogram in solvent A (thrice development). c) Fluorescence was observed.

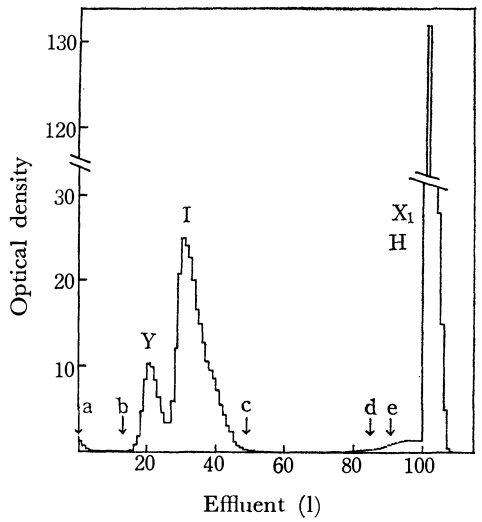

Fig. 2. Fractionation of alkaline treated reaction mixture of inosine by Dowex 50 W.
Y: 9-β-D-Ribopyranosyl hypoxanthine, I: Inosine, X_1: AICA-riboside, H: Hypoxanthine, (a) water, (b) 0.004 M NH_4Cl, (c) 0.01 M NH_4OH, (d) 0.05 M NH_4OH, (e) 0.1 M NH_4OH.

those of AICA-riboside and 9-β-D-ribopyranosyl hypoxanthine respectively. They were later identified by isolation through column chromatography using Dowex 50 W (Fig. 2).

The analytical data, the UV spectrum and the melting point of X_1 agreed with those reported for AICA-riboside by Greenberg and Spilman.[10] The X-ray diffraction data agreed with those of authentic AICA-riboside (Table 2).

On the other hand, the melting point (253 °C, decomp., uncorrected) of Y agreed with that (259—260 °C decomp., only available datum) reported for 9-β-D-ribopyranosyl hypoxanthine by Baddiley.[9] Elementary analysis data supported the assumption that Y was 9-β-D-ribopyranosyl hypoxanthine. The acid hydrolysis of Y gave two components, hypoxanthine and D-ribose. The fact that the UV spectrum of Y is similar to that of inosine indicated that the glycosyl bond of Y was attached at N-9. Therefore, Y may be considered to be 9-ribosyl hypoxanthine. By examining the periodate oxidation, the ring structure of Y

Table 2. X-ray diffraction data

9-β-D-Ribopyranosyl hypoxanthine				AICA-riboside	
α-Form		β-Form			
d(Å)	I/I_1[a]	d(Å)	I/I_1[a]	d(Å)	I/I_1[a]
10.78	60	17.00	100	10.74	5
6.86	80	5.52	60	7.44	40
5.34	100	5.25	20	5.40	40
4.58	60	5.16	30	5.13	20
3.60	20	4.73	80	4.77	30
3.56	40	4.62	15	4.70	70
3.48	10	4.51	15	4.62	20
3.40	5	4.20	5	4.53	20
3.34	10	3.73	5	4.44	20
3.30	5	3.52	5	4.08	95
3.15	20	3.18	20	3.71	30
		3.06	25	3.56	30
				3.55	35
				3.35	100

a) Peak heights scaled that the most intense line is given a value of 100.

Table 3. Optical rotations of some ribonucleosides

Nucleosides	$[\alpha]_D$(°) in water
Adenosine	−65.5[b], −60.4[c], −60.7[d]
9-β-D-Ribopyranosyl adenine	−38[e,f], −37[g,h], −30[d]
9-α-D-Ribofuranosyl adenine	+24[c]
Inosine	−49.2[a]
Y	−26.5

a) The Merck Index. b) J. Davoll and B. A. Lowry, *J. Amer. Chem. Soc.*, **73**, 1650 (1951). c) R. S. Wright, G. M. Tener, and H. G. Khorana, *ibid.*, **80**, 2004 (1958). d) Y. Furukawa and M. Honjo, *Chem. Pharm. Bull.*, **16**, 1076 (1968). e) Ref. 7. f) M. Viscontini and S. Huwyler, *Helv. Chim. Acta*, **43**, 782 (1960). g) J. Davoll and B. A. Lowry, *J. Amer. Chem. Soc.*, **74**, 1563 (1952). h) K. Onodera, S. Hirano, N. Kashimura, F. Masuda, T. Yajima, and N. Miyazaki, *J. Org. Chem.*, **31**, 1291 (1966).

was assumed to have a pyranosyl form; the slow velocity on acid hydrolysis as compared with inosine supported this assumption. (Ribopyranosyl adenine has been known to be hydrolyzed by acid slower than ribofuranosyl adenine.[11]) The optical rotation data are shown in Table 3, along with some available data on adenosine derivatives. As β-pyranosyl adenine has about one-half the value of β-furanosyl adenine, Y also showed about one-half the value of inosine (β-furanoside). Thus, it is very likely that Y is 9-β-D-ribopyranosyl hypoxanthine. The X-ray diffraction patterns of Y were obtained in two forms (Table 2). One of the forms seems to be unstable (named the α-form) and to be changed into another stable form (named the β-form) during storage. The crystals of the α-form were obtained on the first experimental run; afterward they were never obtainable in several succeeding experimental runs. These facts suggest that there is a large energy difference between the two crystal forms.

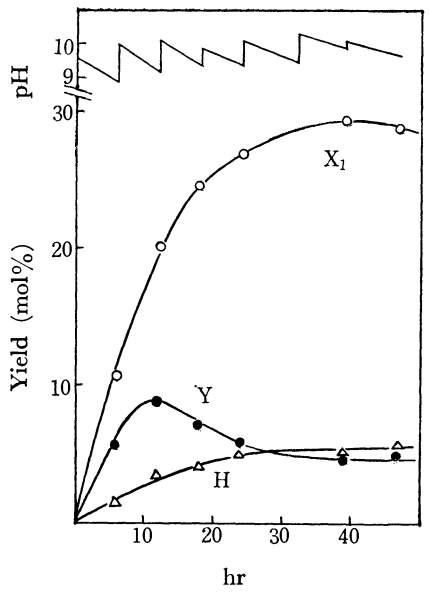

Fig. 3. Dependence of the yield of three major products on the reaction period in alkaline treatment of inosine at 130 °C (pH between 10 and 9).
X_1(○): AICA-riboside, Y(●): 9-β-D-Ribopyranosyl hypoxanthine H(△): Hypoxanthine

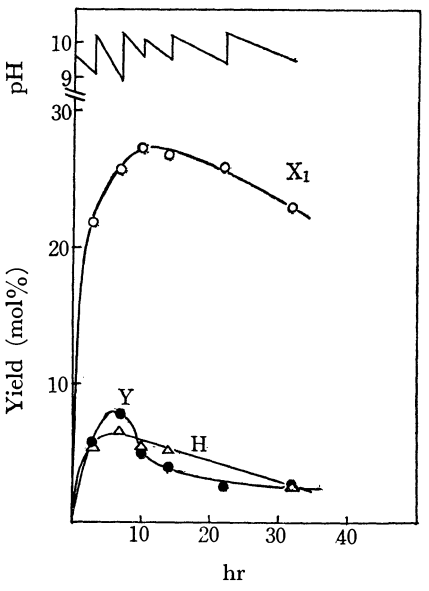

Fig. 4. Dependence of the yield of three major products on the reaction period in alkaline treatment of inosine at 150 °C (pH between 10 and 9).
X_1(○): AICA-riboside, Y(●): 9-β-D-Ribopyranosyl hypoxanthine, H(△): Hypoxanthine

In the alkaline treatment of inosine, the dependence of the yield of the three major UV-absorbing products on the reaction time is shown in Figs. 3 and 4. When the pH's of the solutions were kept between 9 and 10, the maximum yield of AICA-riboside reached 28—30% and that of 9-β-D-ribopyranosyl hypoxanthine, 8—9% (that of hypoxanthine was 6—7%). The relative amount of the yield was found to be independent of the temperature in the 130 °C—150 °C range. The reaction time for the maximum yield, however, depends on the temperature. The higher the temperature, the shorter was the reaction period needed to give the maximum yield of both compounds. The amounts of the three major products (including hypoxanthine) all decreased when too long a reaction period was employed. This fact suggested that a further degradation occurs into simple compounds which have no more UV-absorption.

Among the minor reaction products of the alkaline treatment of inosine, X_2 in Table 1 is considered to be 5-amino-4-imidazolecarboxamide (AICA) on the basis of its UV spectrum, the characteristic orange color caused by the NBDF reagent,* and the R_f value on the paper chromatogram (compared with the authentic standard of AICA). Undoubtedly AICA is obtained by a base-catalyzed hydrolysis at the glycosyl bond of AICA-riboside. AICA may be also obtainable by a base-catalyzed ring-opening reaction at C-2 in the pyrimidine ring of hypoxanthine (Fig. 1). In an acid solution AICA has been obtained from hypoxanthine both in the presence of zinc[12] and in its absence.[13] In this report the AICA formation from hypoxanthine in 0.4 M NaOH at 150 °C is shown (Table 4) in a yield of 30%, corresponding with the reaction period of 4 hr. Under these conditions, the original hypoxanthine remained 52%, though 99% of the hypoxanthine has been reported by Albert and Brown[14] to remain unreacted in 10 M NaOH at 100 °C for 1 hr.

A ring-opening reaction at C-2 in the pyrimidine section of the purine ring was also postulated for 5'-inosinic acid to give 5-amino-1-β-D-ribofuranosyl-4-imidazolecarboxamide-5'-monophosphate (AICA-ribotide) on the basis of a characteristic color reaction found by the NBDF reagent and a comparison of its R_f value with that of authentic AICA-ribotide (Table 5). It should be pointed out here that, for the purpose

Table 4. Reaction products of alkaline treated hypoxanthine[a]

Component	R_f[b]	UV-absorption	Color development
AICA[c]	0.71	+	+ (orange)
Hypoxanthine	0.50	++	−

a) Initial pH 11.8 at 150 °C for 4 hr. b) On the paper chromatogram in Solvent B. c) 5-Amino-4-imidazolecarboxamide.

Table 5. Reaction products from disodium 5'-inosinic acid[a]

Component	R_f[b]	UV-absorption	Color development
Hypoxanthine	0.44	+	−
X_1 (AICA-riboside)	0.33	+	+
Inosine	0.23	++	−
5'-Inosinic acid+X_0[c]	0.07	++	±
AICA-ribotide standard	0.07	++	+

a) Initial pH 7.8 at 120 °C for 8 hr. b) On the paper chromatogram in Solvent A. c) Suspected to be AICA-ribotide.

* See Experimental Section.

of obtaining AICA-ribotide through the ring-opening at C-2, Shaw[1c] made the N-1 substitution of isopropylidene-inosine-5′-di(*p*-nitrophenyl)phosphate and left out the direct cleavage of inosinic acid. Also, Magrath and Brown[15] reported a ring-opening reaction at C-8 in the imidazole section of the purine ring on 9-β-D-ribofuranosylpurine-5′-phosphate in dilute aqueous alkali.

Guanosine and adenosine were subjected to alkaline treatment under the same conditions as those used for inosine. By the NBDF reagent, however, no compounds with the ring opened at C-2 were detected on the chromatogram. The amino group at the 2 position of guanosine probably interferes with the approach of the hydroxide ion and prevents its attack at C-2. In adenosine, on the other hand, the amino group at the 6 position may increase the electron density at C-2, and this would prevent a nucleophilic attack at C-2; the attack may take place, however, at C-8.[3] However, it is known that the alkaline treatment of adenosine causes some deamination, thus giving inosine,[3] so that it may be expected that a little AICA-riboside can be obtained, through inosine. It may need longer reaction period than that in the present study. The characteristic spots corresponding with β-pyranoside in the case of inosine were detected in both nucleosides with UV light on the chromatogram. The mechanism of the alkaline isomerization of these usual ribonucleosides including inosine is expected to occur through an intermediate of the oxide anion, whose negative charge is located on one of the oxygen atoms in the ribose moiety. Such an intermediate, *i. e.*, a mono oxide anion in which an electron is shared by the ring oxygen and the 5′-oxygen in the ribose moiety, is suspected to induce the formation of β-pyranoside. However, if the case of pseudouridine, examined by Chambers *et al.*[8a] is taken into consideration, the concomitant formation of the α-anomer can be expected in the present experiments. The α-anomer was not isolated here, probably because too little of it was formed to be perceived in this brief period of detection. In this respect, detailed experimental results and a discussion will be given in a later paper.

Experimental

Material and Equipment. Inosine, hypoxanthine, disodium 5′-inosinic acid, adenosine, and guanosine crystals, all indicated free from any impurities by paper chromatography, and the authentic standard samples of AICA, AICA-riboside, and AICA-ribotide were all prepared by the Ajinomoto Co., Inc. The ultraviolet absorbance was measured with a Hitachi 139 spectrophotometer, and the pH's of the solutions were measured at room temperature with a Toa Dempa pH meter HM-5A. Automatic Polarimeter Bendix-NPL 143-A was used for the measurement of the optical rotation. The X-ray powder diffraction patterns were obtained by means of a Rigaku Denki X-ray diffractometer.

Paper Chromatography. One-dimensional ascending paper chromatography was carried out on Toyo-Roshi No. 51A, the following two solvent systems being used: Solvent A, *n*-butanol-acetic acid-water (4 : 1 : 1); Solvent B, distilled-*i*-butylic acid-*n*-butanol-28% ammonia aq.-water (36 : 30 : 3 : 31). The papers were developed thrice if necessary for the complete separation of the components on the chromatogram. The components of the reaction mixture were detected on the paper by two different methods: (a) absorption in ultraviolet light was used to detect the ultraviolet absorbing compounds, (b) color development with NBDF reagent was used to detect the diazotizable amines. The NBDF reagent was prepared by an addition of 100 mg of *p*-nitrobenzenediazonium fluoroborate to 100 ml of 2 M acetic acid.

Alkaline Treatment on Inosine. Inosine (0.6 g) was dissolved in 20 ml of 0.1 M NaOH and heated in a sealed stainless steel tube at 120 °C on an oil bath for 16 hr. The pH of the solution was varied from 9.6 to 9.1 during the reaction period. The reaction mixture was paperchromatographed in Solvent A three times (Table 1).

Isolation of Y (9-β-D-ribopyranosyl hypoxanthine) and X_1 (AICA-riboside) in the Crystalline Form. Potassium hydroxide (4.1g) and inosine (20 g) were dissolved in 45 ml of water, and the mixture was heated in a sealed tube at 130 °C for 6 hr. The pH of the solution was varied from 10.1 to 9.5 during the reaction period. A granule of potassium hydroxide was added to correct the pH of the solution to 10.0. Then, the reaction was continued for 6 hr more. The reaction mixture was acidified (pH 2) by 10 ml of conc. HCl and applied to a column (95 cm × 3.7 cm) of Dowex 50W X-8 (H^+-form, 50—100 mesh, 1 l). The column was developed with 13 l of water and 36 l of 0.004 M NH_4Cl, 36 l of 0.01 M NH_4OH, 6 l of 0.05 M NH_4OH, and 23 l of 0.1 M NH_4OH in turn. The fraction was collected every 1 l. The optical densities of the fractions at 250 nm were measured. The first and the second UV-absorbing peaks appeared in the fractions with NH_4Cl. The first peak contained Y, and the second, inosine. The third peak appeared in the fractions with 0.1 M NH_4OH; it was found to be a mixture of a large amount of X_1 and a little hypoxanthine. The fractions between No. 17 and No. 25 (9 l) in the first peak were neutralized with ammonia and concentrated *in vacuo* until 20 ml. When the concentrated solution was cooled, crystallization occurred. The crystals were washed with cold 50% aqueous methanol and weighed (1.5 g). Recrystallization from water gave 0.7 g (dry) of plate-like crystals (Y). The fractions between No. 101 and No. 107 (7 l) in the third peak were concentrated *in vacuo* until 90 ml. The concentrated solution was neutralized (pH 7) with a drop of dil. HCl and cooled for precipitation. After the removal of the precipitated fine powder of hypoxanthine, the filtrate was concentrated *in vacuo* until 5 ml and then cooled again. The precipitated powder crystals were triturated with water and the insoluble parts (hypoxanthine) removed by filtration. The filtrate was evaporated in a desiccator; thus some large cubic crystals and fine powder crystals different in appearance from each other were obtained. On filtration with a fiber net of 50 mesh, the fine powder crystals were passed out through the net with the mother liquor. The large cubic crystals remaining on the net were collected and recrystallized from water. The filtration with a fiber net was repeated again; subsequent recrystallization gave 1.4 g of large cubic crystals (X_1) which were free from any contaminant on the paper chromatogram.

Characterization of AICA-riboside. The large cubic crystals (X_1) were analyzed as follows. (a) Paper chromatography. The R_f agreed with the authentic standard in Solvent A; 0.64 (thrice developed). (b) UV spectrum. Agreed with the data of Greenberg and Spilman in 0.1 M HCl and in 0.1 M NaOH. (c) Melting point. Found; 213 °C (decomp.) uncorrected. (d) X-ray diffraction data (Cu K_α). Identical with the authentic standard under a diffraction angle of 30 degrees (2θ).

Characterization of 9-β-D-Ribopyranosyl Hypoxanthine. The

plate-like crystals (Y) were analyzed as follows. (a) Paper chromatography. The R_f was a little lower than that of inosine in Solvent A [0.43 (thrice-developed)] and the same as that of inosine in Solvent B [0.55 (twice-developed)]. (b) UV spectrum. The same behavior as inosine in 0.1 M HCl, H_2O, and 0.1 M NaOH. (c) Elementary analysis. Agreed with inosine or 9-β-D-ribopyranosyl hypoxanthine. Found: C, 44.49; H, 4.57; N, 21.15%. Calcd for $C_{10}H_{22}O_5N_4$: C, 44.78; H, 4.51; N, 20.89%. (d) Components of acid hydrolysate. In 1 ml of water 10 mg of crystals were dissolved, and then 1 ml of conc. HCl was added. The mixture was heated at 80 °C for 1 hr and chromatographed in Solvent A. Hypoxanthine (R_f 0.29) was revealed by UV light and D-ribose (R_f 0.25), by periodate oxidation, by Ohkuma.[16] (e) Periodate oxidation. The Fleury-Lange[17] method was employed for a 1% solution of crystals. The consumptive mole number of periodate was 1.92, which could be regarded as nearly 2. (f) Velocity of acid hydrolysis. In 1 ml of 0.1 M HCl, 10 mg of crystals were dissolved, and then the mixture was heated at 85 °C for 1 hr. Inosine was also used for control. Paper chromatogram in Solvent A showed two UV-absorbing spots, hypoxanthine (R_f 0.40) and the original compounds (R_f 0.22). The spots were cut off and eluted with 0.1 M HCl, and the absorbance of the eluate was measured at 250 nm. The absorption ratio of hypoxanthine to the original compounds was 12 : 88 for these plate crystals and 90 : 10 for ionsine. (g) Optical rotation. Found: $[\alpha]_D^{25}$ −26.5° (*c*, 1 water). (h) Melting point. 252—254 °C (decomp.) uncorrected. (i) X-ray diffraction data (Cu K_α). The measurements were carried out under a diffraction angle of 30 degrees (2θ).

Dependence of the Yields of the Three Major Reaction Products on the Reaction Period on the Alkaline Treatment of Inosine. Potassium hydroxide (7.5 g) and inosine (40 g) were dissolved in 90 ml of water to obtain a clear alkaline solution (pH 9.6). After the solution had been heated in a sealed tube at 130 °C or 150 °C for an appropriate period of several hours, it was cooled quickly and sampled (1 ml). The pH's of the solutions were usually decreased to some extent. A granule of potassium hydroxide was added to correct the pH to about 10, and the solution was again heated for several hours; these treatments were repeated many times over. Aliquots of 1 ml samples were diluted to 25 ml, and 10 μl of the diluted solution was spotted on the paper for chromatography in Solvent A (thrice-developed). Ten microliters of a 1% solution of three compounds, hypoxanthine, AICA-riboside, and inosine (used in place of 9-β-D-ribopyranosyl hypoxanthine), were also spotted on the same paper as the standard. The UV-absorbing spots on the chromatogram corresponding to the three compounds were cut off, together with their appropriate blanks, and eluted with 0.1 M HCl, and the absorbances of the eluates were measured at 267 nm for AICA-riboside and at 250 nm for the hypoxanthine derivatives. The concentration of each component in the reaction mixture was calculated from the absorbance compared with that of the standard references. The yields of the three compounds in mol% were computed from the known concentration of the initial solution.

Identification of X_2 as AICA. The R_f of the X_2 spot on the chromatogram shown in Table 1 was identical with that of the authentic reference sample of AICA. The spot was cut off and eluted with water, and the spectra of the eluate were measured in 0.1 M HCl (λ_{max} 267 nm and 240 nm; λ_{min} 250 nm and 220 nm) and in 0.1 M NaOH (λ_{max} 278 nm and λ_{min} 240 nm). An orange color development which was characteristic of AICA was found on the paper with the NBDF reagent.

Formation of AICA from Alkaline-treated Hypoxanthine. Hypoxanthine (0.8 g) was dissolved in 20 ml of 0.4 M NaOH and heated in a sealed tube at 150 °C for 4 hr. The pH of the solution varied from 11.8 to 10.6 during the reaction period. The reaction mixture showed two major UV-absorbing spots on the paper; one was estimated to be AICA, and the other, unreacted hypoxanthine. A clear separation of the two spots was achieved in Solvent B (AICA, R_f 0.71; hypoxanthine, R_f 0.50); three developments were required in Solvent A (AICA, R_f 0.83; hypoxanthine, R_f 0.74). The R_f value, a characteristic orange color development with the NBDF reagent, and the behavior of the UV spectra in acid and alkali were all in accordance with the authentic reference sample of AICA and also with the X_2 described before. The spots on the paper were cut off, together with their appropriate blanks, and eluted with 0.1 M HCl, and the absorbances of the eluates were measured at 267 nm for AICA and at 250 nm for hypoxanthine. The yield of AICA was determined to be 30%, and that of the unreacted hypoxanthine, 52%.

Formation of AICA-ribotide from 5′-Inosinic Acid. Disodium 5′-inosinic acid crystals (0.28 g) were dissolved in 20 ml of water and heated in a sealed tube at 120 °C for 8 hr. The pH value of the solution was varied from 7.8 to 7.2 during the reaction period. The chromatography with UV light of the resultant solution in Solvent A revealed the formation of as much inosine (R_f 0.23) as of unreacted 5′-inosinic acid (R_f 0.07), along with other minor reaction products. On the spot corresponding with 5′-inosinic acid, a pale purple-red color development was found with the NBDF reagent. The R_f value of the authentic AICA-ribotide was superimposed on 5′-inosinic acid in Solvent A.

Alkaline Treatment on Adenosine and Guanosine. Adenosine (0.1 g) was added to 20 ml of 0.008 M NaOH and heated in a sealed tube at 130 °C for 3 hr. The reaction mixture showed three UV-absorbing spots on the chromatogram in Solvent A: R_f 0.6 Adenine; R_f 0.47 Unreacted adenosine; R_f 0.34 presumably pyranoside. Nothing of the colored spot with the NBDF reagent was detected. Guanosine (0.5 g) was added to 20 ml of 0.038 M NaOH, and the mixture was heated in a sealed tube at 130 °C for 8 hr. The pH of the solution was varied from 11.0 to 9.8. The reaction mixture showed five UV-absorbing spots on the chromatogram in Solvent A (thrice developed): R_f 0.7 Guanine; R_f 0.54 Unreacted Guanosine; R_f 0.43 Presumably pyranoside; R_f 0.34 Unknown; R_f 0.27 Unknown. Nothing of the spot with the NBDF reagent was detected.

The author wishes to thank Mr. Kentaro Hara and Mr. Takashi Sato for their technical assistance, and also Dr. Akihiro Yamazaki for his interest in this work. He is also indebted to Prof. Dr. Masamichi Tsuboi for reading the manuscript.

References

1) a) E. Shaw, *J. Amer. Chem. Soc.*, **80**, 3899 (1958); b) E. Shaw, *ibid.*, **81**, 6021 (1959); c) E. Shaw, *ibid.*, **83**, 4770 (1961).

2) J. A. Montgomery and H. J. Thomas, *J. Med. Chem.*, **15**, 1334 (1972).

3) A. S. Jones, A. M. Mian, and R. T. Walker, *J. Chem. Soc.*, **1966** 692.

4) Y. Suzuki, *Chem. Lett.*, **1973**, 547.

5) M. P. Gordon, V. S. Weliky, and G. B. Brown, *J. Amer. Chem. Soc.*, **79**, 3245 (1957).

6) A. M. Belikova, N. I. Grineva, and G. G. Karpova,

Khim. Geterotsikl. Soedin., **1**, 109 (1972).
7) a) J. Lee, E. Fells, and L. Berger, U. S. 2384104 (1945); b) G. A. Howard, G. W. Kenner, B. Lythgoe, and A. R. Todd, *J. Chem. Soc.*, **1946**, 855.
8) a) R. W. Chambers, V. Kurkov, and R. Shapiro, *Biochemistry*, **2**, 1192 (1963); b) W. E. Cohn, *J. Biol. Chem.*, **235**, 1488 (1960).
9) J. Baddiley, G. W. Kenner, B. Lythoge, and A. R. Todd, *J. Chem. Soc.*, **1944**, 657.
10) R. Greenberg and E. L. Spilman, *J. Biol. Chem.*, **219**, 411 (1956).
11) J. Davoll, B. Lythgoe, and A. R. Todd, *J. Chem. Soc.*, **1946**, 833.
12) S. Friedeman and J. S. Gots, *Biochem. Biophys.*, **39**, 254 (1952).
13) Y. Hirata, K. Iwashita, and T. Teshima, *Nagoya Sangyo Kogaku Kenkyujo Kenkyu Hokoku*, **9**, 83 (1957).
14) A. Albert and D. J. Brown, *J. Chem. Soc.*, **1954**, 2060.
15) D. I. Magrath and G. B. Brown, *J. Amer. Chem. Soc.*, **79**, 3245 (1957).
16) S. Ohkuma and C. Miyauchi, *Seikagaku*, **34**, 166 (1962).
17) P. F. Fleury and J. Lange, *J. Pharm. Chim.*, **17**, 107, 196 (1933).

Reactions of 2-Cyano-2-dimethylamino-1,3-dithiolane[1]

Kazuhisa HIRATANI, Takeshi NAKAI, and Makoto OKAWARA

Research Laboratory of Resources Utilization, Tokyo Institute of Technology, Ookayama, Meguro-ku, Tokyo 152

(Received October 23, 1973)

The reactions of 2-cyano-2-dimethylamino-1,3-dithiolane (**2**) with electrophiles (organic halides and perchloric acid) and nucleophiles were investigated. It was found that **2** dissociated partially to 2-dimethylamino-1,3-dithiolan-2-ylium (**1**) and cyanide ions in polar solvents. In the reactions of **2** with electrophiles, nitriles were obtained along with the formation of salts of **1**. The reactions of **2** with nucleophiles were studied since **2** was expected to be a precursor of the cation **1**. In some cases, its reactivity differs from that of perchlorate of **1**. A mechanism was discussed in which the cyanide ion might behave as a base to abstract a proton from the nucleophiles.

In a previous paper[2] it was reported that 2-dialkylamino-1,3-dithiolan-2-ylium ions (**1**) were ambident electrophiles capable of undergoing reactions with nucleophiles at three sites, a, b, and c. In the case of the reaction of perchlorate of **1** (R=Me) with cyanide ion as a nucleophile, 2-cyano-2-dimethylamino-1,3-dithiolane (**2**) was obtained in a good yield.[3] In this work the reactions of **2** with various electrophiles and nucleophiles have been studied.

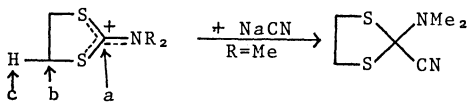

1 **2**

Little information has been given on the reactions of α-cyanoacetal and α-cyanoorthoester derivatives. It has only been reported that treatment of 2-cyano-2-methyl 1,3-dioxolane[4] and 2-cyano-2-morpholino-1,3-dithiolane[5] with acids gives 2-methyl-1,3-dioxolan-2-ylium ion and 2-morpholino-1,3-dithiolan-2-ylium ion, respectively.

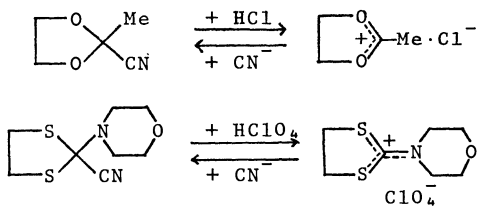

Thus, compound **2** is expected to be capable of cyanogenating electrophiles along with the formation of the cation **1**. On the other hand, **2** is expected to behave as a precursor of **1** in the reaction with nucleophiles. The limitation of the use of **2** in this reaction was also studied by comparing the reactivity of **2** with that of perchlorate of **1**.

Results and Discussion

Reactions of 2 with Electrophiles. The reactions of **2** with the following electrophiles were studied: methyl iodide, *n*-butyl iodide, benzyl bromide, benzoyl chloride, phenacyl bromide, and perchloric acid. Firstly, in order to find the influence of solvent on the reactions of **2** with electrophiles, the reaction of **2** with methyl iodide was carried out in ethyl ether, acetonitrile, and nitromethane[6] to obtain iodide of **1** in all cases. It was found that the yield of iodide of **1** was higher in polar solvents (acetonitrile and nitromethane) than in nonpolar one (ethyl ether). Thus, the reactions of **2** with other electrophiles were carried out in polar solvents. The yields of salts of **1** and nitrile **3** obtained simultaneously are summarized in Table 1. These products were found to be identical with authentic samples.[7]

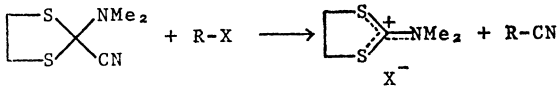

2 **1** **3**

Thus, electrophile can react with **2** giving nitrile along with the formation of salt of **1**. It should be noted that **2** is useful as a precursor of cyanide ion which is soluble in organic solvents and product **3** can readily be isolated from another product, salt of **1**.

The fact that the yield of salts of **1** increases with the increase in polarity of solvent as observed in the case of the reaction of **2** with methyl iodide suggests that **2** dissociates first to cation **1** and cyanide ion, and then cyanide ion attacks methyl iodide giving acetonitrile and iodide of **1**. In order to investigate the influence of solvents on the dissociation of **2** to cation **1** and cyanide ion, the UV spectrum of **2** was measured in the following solvents: cyclohexane, tetrahydrofuran, chloroform (containing 1% ethanol), 99% etha-

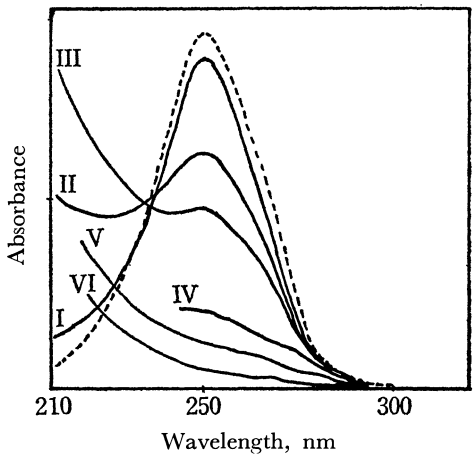

Fig. 1. Ultraviolet spectra of **2** and salt **1**.
……: **1** [ClO_4^-] in MeOH, ——: **2**
I: MeOH, II: EtOH[99%], III: MeCN, IV: $CHCl_3$-[Containing 1% EtOH], V: THF, XI: C_6H_{12}.

Table 1. Reactions of 2 with electrophiles

Electrophile	Conditions: Solvent	Temp. °C	Time hr (day)	Products: 1 X	1 Yield, %[b]	3[c]	3 Yield, %[b]
Methyl iodide	Et_2O	reflux	4	I	5	(MeCN)	—
	MeCN	40	3	I	35	(MeCN)	—
	$MeNO_2$	rt	(2)	I	53	(MeCN)	—
n-Butyl iodide	$MeNO_2$	rt	(2)	I	22	*n*-BuCN	15
Benzyl bromide	$MeNO_2$	rt	(2)	Br[a]	41	$PhCH_2CN$	36
Benzoyl chloride	MeCN	reflux	3	Cl[a]	97	PhC(=O)-CN	63
Phenacyl bromide	MeCN	50	2	Br[a]	73	PhC(=O)-CH_2CN	57
Perchloric acid	EtOH	rt	1	ClO_4	80	(HCN)	—

a) Cation **1** was isolated as perchlorate which was more stable than the bromide and chloride. b) Based upon **2**. c) In the cases of methyl iodide and perchloric acid, acetonitrile and hydrogen cyanide, respectively, were formed but not identified.

Table 2. Ultraviolet spectra of 2 and salt, 1

	Solvent	λ_{max}, nm	ε[b]
2	MeOH	250.5	1.09×10^4
	EtOH (99%)	250	2.70×10^3
	MeCN	250 (sh)[c]	$<1.54\times10^3$
	$CHCl_3$[a]	250 (sh)[c]	$\ll10^2$
	THF	—	—
	C_6H_{12}	—	—
1 (ClO_4^-)	MeOH	250.5	1.30×10^4
	MeCN	250	0.94×10^4

a) Containing 1% ethanol. b) The apparent molecular extinction coefficient at absorption maxima. c) Shoulder band.

nol, acetonitrile, and methanol (Fig. 1). The absorption maxima (λ_{max}) and the molecular extinction coefficients (ε) of **2** and perchlorate of **1** in various solvents are given in Table 2. The absorption band (λ_{max}~250 nm) in Fig. 1 is evidently assigned to the cation **1** since salts (iodide, perchlorate, and tetrafluoroborate) of **1** show the same absorption band as that of **2** in the same solvents. It was observed that the values of the apparent molecular extinction coefficient (ε) at λ_{max} (~250 nm) of **2** were larger in polar solvents than in nonpolar solvents. The values of apparent ε at λmax of **2** in acetonitrile and methanol are smaller than those of perchlorate of **1** in the same solvents (Table 2). Thus it can be concluded that **2** dissociates partially to the cation **1** and cyanide ion in polar solvents. The reactions of **2** with electrophiles can be interpreted by the following scheme.

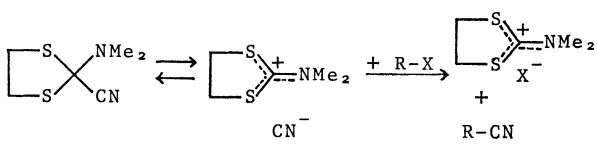

Reactions of 2 with Nucleophiles. Compound **2**, soluble in organic solvents, is expected to be useful as a precursor of cation **1** since **2** can dissociate partially to cation **1** and cyanide ion in polar solvents. The reactions of **2** with the following nucleophiles were studied: aniline, *p*-nitroaniline, 2,4-dinitroaniline, benzamide, *p*-toluenesulfonylamide (tosylamide), phenylhydrazine, *p*-toluenesulfonylhydrazide (tosylhydrazide), sodium thiophenoxide, and sodium *N*,*N*-dimethyldithiocarbamate. The difference in the reactivity of **2** from that of perchlorate of **1** was also investigated.

The equimolar reaction of **1** with nucleophiles was carried out in benzene or acetonitrile at refluxing temperature for 5 hr giving the products shown in Table 3. In the cases of aniline, *p*-nitroaniline, 2,4-dinitroaniline, and benzamide, the reactants were recovered unchanged. Treatment of **2** with tosylamide, phenylhydrazine, and tosylhydrazide gave 2-tosylimino-1,3-dithiolane, 2-phenylhydrazo-1,3-dithiolane, and 2-tosylhydrazo-1,3-

Table 3. Reactions of 2 with nucleophiles

Nucleophile	Product	Yield[a] %	Mp °C
Aniline, *p*-Nitroaniline, 2,4-Dinitroaniline, Benzamide	No reaction		
Tosylamide	Tos-N=	70[b] 47[c]	121—123
Tosylhydrazide	Tos-N(H)-N=	47[b] 28[c]	193—195
Phenylhydrazine	PhNH-N=	88	90— 92
Sodium thiophenoxide		84	liq.
Sodium *N*,*N*-Dimethyldithiocarbamate		17	187—190

a) For reaction conditions, see Experimental. b) In acetonitrile. c) In benzene.

dithiolane, respectively, in moderate yields (path a). On the other hand, treatment of **2** with sodium thiophenoxide and sodium *N,N*-dimethyldithiocarbamate gave β-(phenylthio)ethyl-*N,N*-dimethyldithiocarbamate and ethylenebis(*N,N*-dimethyldithiocarbamate), respectively (path b). The structures of the products were elucidated by elemental analysis and spectroscopic methods. The yield and melting point of the products are summarized in Table 3.

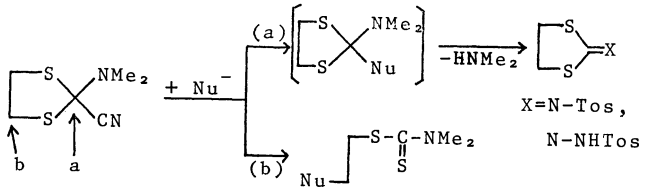

2

The salt of **1** reacts with aniline, sodium thiophenoxide, and sodium *N,N*-dimethyldithiocarbamate giving 2-phenylimino-1,3-dithiolane, β-(phenylthio)ethyl-*N,N*-dimethyldithiocarbamate, and ethylenebis(*N,N*-dimethyldithiocarbamate), respectively.[2] On the other hand, perchlorate of **1** does not react with tosylamide and tosylhydrazide at all.

From these results it was found that i) compound **2** reacted with some nucleophiles along with the elimination of cyanide ion; ii) it reacted with nucleophiles at two sites, a and b, in formula (**2**); iii) in the case of sodium thiophenoxide and sodium *N,N*-dimethyldithiocarbamate as nucleophile, both **2** and perchlorate of **1** reacted with them giving the same products; and iv) **2** reacted with nucleophiles such as tosylamide and tosylhydrazide, with which perchlorate of **1** did not react, but it did not react at all with nucleophiles such as aniline with which perchlorate of **1** reacted to give 2-phenylimino-1,3-dithiolane.[2]

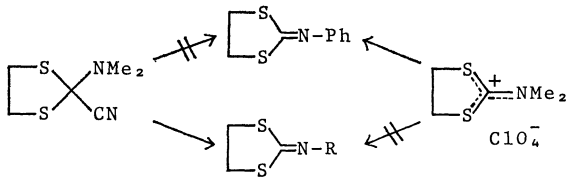

R = Tos, NHTos

It is to be noted that the reactivity of **2** differs from that of salt of **1**. It is considered that cyanide ion participates in the reaction of **2** with nucleophiles. In order to clarify the difference in reactivity between **2** and salt of **1**, the following reactions were attempted with tosylamide and tosylhydrazide as nucleophiles.

The equimolar reaction of **2** with tosylhydrazide at refluxing temperature for 5 hr in a polar solvent (acetonitrile) and a nonpolar solvent (benzene) gave 2-tosylhydrazo-1,3-dithiolane in 47 and 28% yields, respectively. Under the same conditions, the reaction of **2** with tosylamide in acetonitrile and benzene gave 2-tosylimino-1,3-dithiolane in 70 and 47% yields, respectively (Table 3). The reaction seems to be more favorable in a polar solvent than in a nonpolar one.

The reactants were quantitatively recovered unchanged in the reaction of perchlorate of **1** with tosylhydrazide at refluxing temperature for 5 hr in acetonitrile and dimethylformamide and also in the case of tosylamide in acetonitrile. The reaction of salt of **1** with tosylamide including sodium cyanide was attempted. The reactions in the presence of equimolar, 0.6 molar, and 0.4 molar of sodium cyanide at refluxing temperature for 5 hr in acetonitrile gave 2-tosylimino-1,3-dithiolane in 34, 25, and 14% yields, respectively. The reaction of salt of **1** with sodium tosylamide prepared by the treatment of tosylamide with sodium hydride in tetrahydrofuran, at refluxing temperature for 5 hr in the mixture of acetonitrile and tetrahydrofuran also gave 2-tosylimino-1,3-dithiolane in 17% yield.

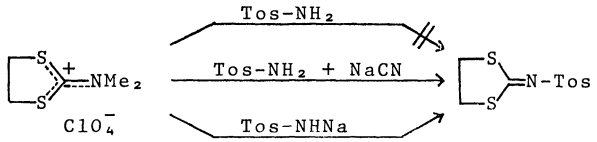

1

It can thus be concluded that cyanide ion evidently participates in the reaction of **2** with tosylamide. The result of the reaction of salt of **1** with sodium tosylamide suggests that cyanide ion behaves as a base in the reaction of **2** with tosylamide to abstract a proton from the amide. This assumption may be supported by the fact that compound **2** tends to react with tosylamide ($pK_a=10.2$)[8] which has a smaller basicity than aniline ($pK_a=27$).[9]

The reaction of **2** with tosylamide and tosylhydrazide can be interpreted by the following processes: i) compound **2** dissociates partially to 2-dimethylamino-1,3-dithiolan-2-ylium ion (**1**) and cyanide ion in solution (Eq. 1); ii) cyanide ion abstracts a proton from the nucleophiles to give anion **5** and hydrogen cyanide (Eq. 2); and iii) the cation **1** reacts with the anion **5** to afford the corresponding product (Eq. 3). An important point in this reaction seems to be that the hydrogen cyanide formed is removed from the reaction mixture to displace the equilibrium (Eq. 2).

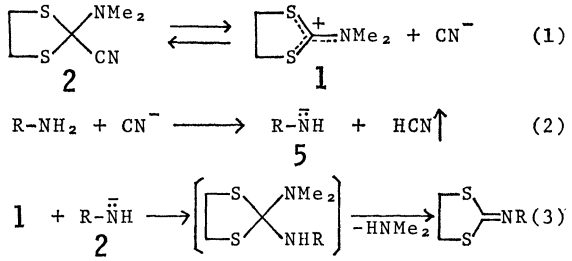

An alternative formation of the product arising from the direct reaction of **2** with nucleophiles ($R-NH_2$) *via* S_N2 type mechanism might be disregarded since the reaction was slow in nonpolar solvent and nucleophiles having small nucleophilicity reacted preferentially with **2**.

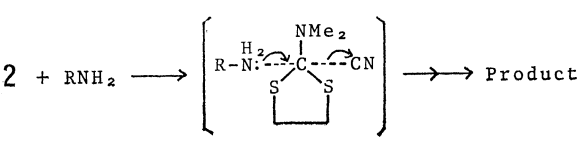

Thus, it was proved that cyanide ion behaved as a base, and **2** could react with nucleophiles having small nucleophilicity with which salt of **1** did not react.

Experimental

General. All melting and boiling points are uncorrected. IR and UV spectra were recorded with Hitachi EPI-S2 and EPS-3T spectrophotometers, respectively. NMR spectra were obtained with Japan Electron Optics JNN PS-100 and MH-60 spectrometers. Chemical shifts are given in ppm from tetramethylsilane as an internal standard.

2-Cyano-2-dimethylamino-1,3-dithiolane (2). Dithiolane **2** was prepared by the procedure previously reported:[2] bp 119—121 °C/2.0 mmHg, yield 74%.

Reaction of 2 with Methyl Iodide. a) In Acetonitrile. In a 50-ml round-bottomed flask equipped with reflux condenser was placed 0.58 g (3.3 mmol) of **2** and 2.0 g (14 mmol) of methyl iodide in 20 ml of acetonitrile (MeCN). The solution was stirred for 4 hr at 40 °C. After MeCN was removed by distillation, the residue (white precipitates) was washed with ether and dried *in vacuo*. Recrystallization of the precipitates from ethanol gave 0.32 g (35%) of 2-dimethylamino-1,3-dithiolan-2-ylium iodide; mp 191—192 °C. NMR (DMSO-d_6); δ 3.47(s, 6H, NCH_3) and 3.98 (s, 4H, SCH_2).

b) In Ether. In a similar manner, the reaction of **2** (0.58 g) with methyl iodide (2.0 g) in 20 ml of ether at refluxing temperature for 4 hr gave 0.05 g (5%) of iodide of **1**.

c) In Nitromethane. In a similar manner, the reaction of **2** (1.9 g) with methyl iodide (4.0 g) in 50 ml of $MeNO_2$ at room temperature for 2 days gave 1.6 g (53%) of iodide of **1**.

Reactions of 2 with Other Electrophiles. In a similar manner, the reaction of **2** with equimolar electorphile under the conditions shown in Table 1 gave salt of **1** in a moderate yield along with nitrile **3**. The products were identified by spectroscopic methods and comparison of their physical properties with those of authentic samples.

Reaction of 2 with Perchloric Acid. To a solution of **2** (1.74 g, 10 mmol) in 20 ml of ethanol with stirring at room temperature was added dropwise 70% aqueous perchloric acid (1.5 g, 15 mmol), and the solution was stirred for 1 hr at room temperature. The precipitates formed were filtered off and washed with cooled ethanol. 2.0 g (80%) of perchlorate of **1** was obtained and recrystallized with ethanol. The IR spectrum of the product was in complete agreement with that of an authentic sample.

Reaction of 2 with p-Toluenesulfonylhydrazide. In a 100-ml flask was placed a solution of 1.74 g (10 mmol) of **2** and 1.86 g (10 mmol) of *p*-toluenesulfonylhydrazide (tosylhydrazide) in 40 ml of MeCN. The reaction mixture was refluxed for 8 hr. After removal of MeCN, a small amount of chloroform was added to the liquid residue. The white precipitates were filtered off and recrystallized from benzene giving 0.45 g of 2-tosylhydrazo-1,3-dithiolane. The filtrate was subjected to chromatography on silica gel with chloroform. The first eluent gave 0.24 g of a pale yellow liquid (unidentified). The second eluent gave 0.23 g of 2-tosylhydrazo-1,3-dithiolane:[10] total yield 0.68 g (47%); mp 193—195 °C. UV (EtOH): λ_{max} 225 and 254 (sh.)nm; NMR ($CDCl_3$): δ 2.30 (s, 3H, CH_3), 3.43 (s, 4H, $S-CH_2$), 7.22 (d, 2H, aromatic-H), 7.51 (d, 2H, aromatic-H), and 10.05 (s, 1H, N–H).

Found: C, 41.72; H, 3.99; N, 10.09%. Calcd for $C_{10}H_{12}NS_3O_2$: C, 41.67; H, 4.06; N, 9.92%.

In the case of benzene as solvent, 2-tosylhydrazo-1,3-dithiolane was obtained in 28% yield.

Reaction of 2 with Phenylhydrazine. In a similar manner, the reaction of **2** (0.35 g, 2.0 mmol) with phenylhydrazine (0.22 g, 2.0 mmol) in 20 ml of benzene at refluxing temperature for 5 hr gave 0.37 g (88%) of 2-phenylhydrazo-1,3-dithiolane which was isolated by means of column chromatography (alumina, chloroform) and recrystallized from ethanol: 90—92 °C (lit,[11] 91 °C). UV (EtOH): λ_{max}=242, 288, and 315 (sh.)nm; NMR ($CDCl_3$): δ 3.16—3.56 (m, 4H, $S-CH_2$), 6.53(s, 1H, N–H), and 6.70—7.30 (m, 5H, aromatic-H).

Found: C, 50.56; H, 4.95; N, 13.12%. Calcd for $C_9H_{10}N_2S_2$: C, 51.42; H, 4.76; N, 13.33%.

Reaction of 2 with p-Toluenesulfonylamide. a) In MeCN: In a similar manner, the reaction of **2** (0.58 g, 3.3 mmol) with *p*-toluenesulfonylamide (tosylamide) (0.57 g, 3.3 mmol) in 20 ml of MeCN at refluxing temperature for 5 hr gave 0.64 g (70%) of 2-tosylimino-1,3-dithiolane which was recrystallized from the mixture of benzene and cyclohexane; mp 121—123 °C (lit,[12] 126—127 °C). UV (EtOH): λ_{max}=228 and 268 nm; NMR ($CDCl_3$): δ 2.42 (s, 3H, CH_3), 3.58 (s, 4H, $S-CH_2$), 7.47 (d, 2H, aromatic-H), and 7.87 (d, 2H, aromatic-H).

Found: C, 44.56; H, 4.21; N, 5.43%. Calcd for $C_{10}H_{11}NO_2S_3$: C, 43.96; H, 4.03; N, 5.13%.

b) In Benzene: In a similar manner, the reaction of **2** (0.30 g, 1.7 mmol) with tosylamide (0.30 g, 1.7 mmol) in 20 ml of benzene at refluxing temperature for 5 hr gave 0.22 g (47%) of 2-tosylimino-1,3-dithiolane. The IR spectrum of the product was in complete agreement with that of an authentic sample.

Reaction of 2 with Sodium N,N-*Dimethyldithiocarbamate.* In a similar manner, the reaction of **2** (0.35 g, 2.0 mmol) with sodium *N,N*-dimethyldithiocarbamate (0.50 g, 2.8 mmol) in 20 ml of MeCN at refluxing temperature for 5 hr gave 0.09 g (17%) of ethylenebis(*N,N*-dimethyldithiocarbamate) which was recrystallized from ethanol giving colorless crystals, mp 187—190 °C (lit,[2] 188—189 °C). The IR spectrum was in complete agreement with that of an authentic sample.

Reaction of 2 with Sodium Thiophenoxide. In a similar manner, the reaction of **2** (0.35 g, 2.0 mmol) with sodium thiophenoxide (0.40 g, 3.0 mmol) in 20 ml of MeCN at refluxing temperature for 5 hr gave 0.43 g (84%) of β-phenylthioethyl-*N,N*-dimethyldithiocarbamate which was purified by means of column chromatography (alumina, $CHCl_3$) giving a pale yellow liquid. NMR (CCl_4): δ 3.15 and 3.35 (s, 6H, $N-CH_3$), 2.96—3.56 (m, 4H, SCH_2), and 6.94—7.44 (m, 5H, aromatic-H).

Reaction of Perchlorate of 1 with Tosylhydrazide. A mixture of **1** (2.48 g, 0.01 mol) and tosylhydrazide (1.86 g, 0.01 mol) in 40 ml of MeCN was refluxed for 8 hr. After removal of MeCN, the residual solid was dried (weight: 4.30 g). It was then poured into water and the white precipitates were filtered and dried *in vacuo*. The product (1.80 g) was identified to be tosylhydrazide by comparison of the IR spectrum with that of an authentic sample.

In a similar manner, the reaction of **1** with tosylhydrazide in dimethylformamide (DMF) was attempted. The reactants were recovered unchanged.

Reaction of Perchlorate of 1 with Tosylamide. The reaction of perchlorate of **1** (1.24 g, 5.0 mmol) with tosylamide (0.86 g, 5.0 mmol) in 20 ml of MeCN at refluxing temperature for 5 hr resulted in the recovery of perchlorate of **1** (1.16 g) and tosylamide (0.83 g).

Reaction of Perchlorate of 1 with Tosylamide and Sodium Cyanide. In a 50-ml round-bottomed flask equipped with reflux con-

denser was placed a solution of perchlorate of **1** (1.24 g, 5.0 ml), tosylamide (0.86 g, 5.0 mmol), and sodium cyanide (0.25 g, 5.0 mmol) in 20 ml of MeCN. After the solution was refluxed for 5 hr, the solvent was removed by distillation. The residue was subjected to chromatography on alumina with chloroform. The first eluent gave 0.46 g (34%) of 2-tosylimino-1,3-dithiolane. The second eluent contained 0.46 g of the starting material, tosylamide. The IR spectrum of the product was in complete agreement with that of an authentic sample.

In a similar manner, the reaction of perchlorate of **1** (1.24 g) with tosylamide (0.86 g) and sodium cyanide (0.15 g, 3.0 mmol) gave 0.34 g (25%) of 2-tosylimino-1,3-dithiolane. On addition of 0.10 g (2.0 mmol) of sodium cyanide, the product was obtained in 14% yield.

*Reaction of Perchlorate of **1** with Sodium Tosylamide.* To a suspension of sodium tosylamide prepared *in situ* by the treatment of 0.83 g (4.8 mmol) of tosylamide with 0.15 g of 50% sodium hydride in 50 ml of tetrahydrofuran, was added 1.24 g (5.0 mmol) of perchlorate of **1** in 20 ml of MeCN. The mixture was stirred at 60—70 °C for 5 hr. After removal of the solvents by distillation, water was added to the residue. White precipitates separated were filtered off and washed with a small amount of ether. 2-Tosylimino-1,3-dithiolane (0.23 g, 17%) was obtained and recrystallized from the mixture of benzene and cyclohexane. The IR spectrum of the product was in complete agreement with that of an authentic sample.

References

1) Presented in part at the 26th Annual Meeting of the Chemical Society of Japan, Hiratsuka, 1 April, 1972; Reprint, Vol. III, p. 1115 (1972).

2) T. Nakai and M. Okawara, This Bulletin, **43**, 1864 (1970).

3) The reaction of perchlorate of **1** (R=Et) with cyanide ion unexpectedly gave *S*-vinyl-*N*,*N*-diethyldithiocarbamate, identical with an authentic sample.[2] The same reaction gave a yellow oil unconfirmed which was proved not to be 2-cyano-2-diethylamino-1,3-dithiolane.[2]

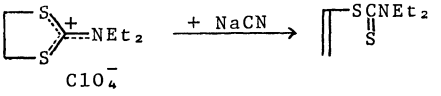

4) H. Meerwein, K. Bodenbenner, P. Borner, F. Kunert, and K. Wunderlich, *Ann. Chem.*, **632**, 38 (1960).

5) R. Mayer and K. Schäfer, *J. Prakt. Chem.*, **26**, 279 (1964).

6) Protic solvents, ethanol and methanol, were not used in this reaction since **2** might be subjected to solvolysis in protic solvents.[2]

7) For the preparation and physical properties of salt of **1**, see T. Nakai, Y. Ueno, and M. Okawara, This Bulletin, **43**, 156 (1970).

8) A. W. Willi, *Helv. Chim. Acta*, **39**, 46 (1956).

9) J. B. Hendrickson, D. J. Cram, and G. S. Hammond, "Organic Chemistry," 3rd Ed., McGraw-Hill Book Co., New York (1970), Chap. 8.

10) D. M. Lemal and E. H. Banitt, *Tetrahedron Lett.*, **1964**, 245.

11) F. Runge, Z. El-Hewehi, H. J. Renner, and E. Taeger, *J. Prakt. Chem.*, **11**, 284 (1960).

12) R. Gompper and W. Hägele, *Chem. Ber.*, **99**, 2885 (1966).

Synthesis and Reactions of 4-Dimethylsulfuranylidene-2,3-dioxotetrahydrofuran Derivatives

Katsuaki HAGIO, Naoto YONEDA, and Hisashi TAKEI*

Research Laboratory of Applied Biochemistry, Tanabe Seiyaku Co., Ltd., Kashima-cho, Higashiyodogawa-ku, Osaka 532

**Laboratory of Organic Chemistry, Tokyo Institute of Technology, Ookayama, Meguro-ku, Tokyo 152*

(Received, November 5, 1973)

The cyclic sulfonium ylides, 4-dimethylsulfuranylidene-2,3-dioxotetrahydrofuran derivatives (**8**), were synthesized in good yields by reactions of methyl and ethyl dimethylsulfuranylidenepyruvates (**3** and **4**) with carbonyl compounds. The reactions of **8** with *p*-toluenesulfonyl chloride and benzoyl chloride gave 4-methylthio-3-(*p*-toluenesulfonyloxy)- and 4-methylthio-3-benzoyloxy-2-oxo-2,5-dihydrofuran derivatives respectively in high yields. The ylides (**8**) reacted with mercaptans to afford 4-substituted products (**14**—**16**), whereas, on the reactions with thiourea, the demethylation of the dimethylsulfonium group proceeded exclusively.

Recently, a number of carbonyl-stabilized sulfonium ylides have been synthesized and their properties studied.[1-3] These ylides are of interest because reactions using them provide useful methods for the syntheses of many organic compounds.[1,2,4,5] Among the synthetic methods of cyclic sulfonium ylides, the conversion of simple carbonyl-stabilized sulfonium ylides into cyclic sulfonium ylides, such as 3-dimethylsulfuranylidene-2,4,5-pyrrolidinetrione and 5-dimethylsulfuranylidene-2,6-diacetyl-2,6-dimethyl-4-oxo-1,3-dioxane, have been reported only by Howard[6] and Payne.[7]

In the course of the synthetic study of sulfonium ylides in our laboratory,[5] the cyclic sulfonium ylides, 4-dimethylsulfuranylidene-2,3-dioxotetrahydrofuran derivatives (**8**), were successfully synthesized by the reactions of methyl and ethyl dimethylsulfuranylidenepyruvates (**3** and **4**), and their reactivity was investigated.

Synthesis of 8. The sulfonium ylides, **3** and **4**, were prepared from the corresponding sulfonium bromides or picrates (**1** and **2**) by a procedure similar to that used for ordinary carbonyl-stabilized sulfonium ylides.[2] The use of stable sulfonium picrates (**1** and **2**, X=$(NO_2)_3C_6H_2O$) was advantageous for this conversion, since the corresponding bromides (**1** and **2**, X=Br)[8] were very hygroscopic and were less stable compounds which decomposed slowly upon exposure to air.

The treatment of **2** (X=$(NO_2)_3C_6H_2O$) with 1 equivalent of 50% aqueous sodium hydroxide and saturated potassium carbonate solution in methylene chloride gave ethyl dimethylsulfuranylidenepyruvate (**4**) as pale yellow hygroscopic crystals. The IR spectrum showed bands at 1720 and 1550 cm^{-1} attributable to the ester and the ylide carbonyl group[9] respectively. The NMR spectrum was consistent with the structure of **4**; a singlet at δ 4.68 (1H) for the methine proton and a singlet at δ 3.00 (6H) for the two methyl groups attached to the sulfonium group. In a similar way, **3** was prepared from the corresponding sulfonium salt (**1**) in a 64% yield. The treatment of **3** and **4** with picric acid in ethanol yielded the corresponding sulfonium picrates quantitatively.

The reactions of **3** and **4** with carbonyl compounds were carried out in expectation of the formation of 4-dimethylsulfuranylidene-2,3-dioxotetrahydrofuran derivatives (**8**) *via* the intermediate betaine (**6**), which would be cyclized by an intramolecular nucleophilic

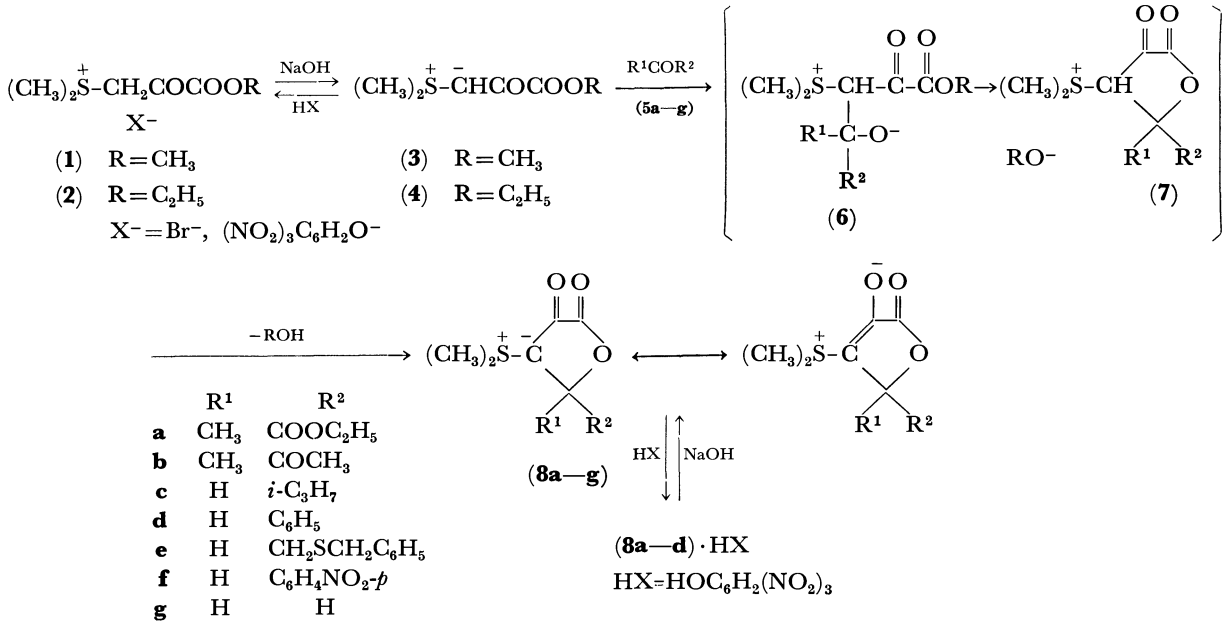

(1) R=CH_3 (3) R=CH_3
(2) R=C_2H_5 (4) R=C_2H_5
X⁻=Br⁻, $(NO_2)_3C_6H_2O^-$

(6) (7)

	R^1	R^2
a	CH_3	$COOC_2H_5$
b	CH_3	$COCH_3$
c	H	i-C_3H_7
d	H	C_6H_5
e	H	$CH_2SCH_2C_6H_5$
f	H	$C_6H_4NO_2$-*p*
g	H	H

Scheme 1.

attack of the alkoxide anion on the alkoxycarbonyl group.

The reaction of **4** with ethyl pyruvate proceeded at room temperature. However, an attempt to isolate the new sulfonium ylide directly from the reaction mixture failed. The addition of picric acid to the mixture gave yellow crystals (mp 142—143 °C (dec)), whose elemental analysis agreed with the expected picrate of **8a**. The IR spectrum showed the characteristic bands of a five-membered lactone and an ester at 1790 and 1775 cm^{-1}. The picrate in methylene chloride was treated with 50% aqueous sodium hydroxide to give 5-ethoxycarbonyl-4-dimethylsulfuranylidene-5-methyl-2,3-dioxotetrahydrofuran (**8a**) (mp 132—134 °C (dec)), which was then recrystallized from ethanol–ether. The ylide (**8a**) reverted to the picrate quantitatively by means of picric acid in ethanol. The IR spectrum showed an absorption at 1620 cm^{-1} attributable to the ylide carbonyl,[9] and the NMR spectrum (δ, in $CDCl_3$) showed two singlets, at 3.30 (3H) and 3.14 (3H), ascribable to the two methyl groups of the sulfonium group. The nonequivalence of the two methyl groups at the sulfonium group was observed also in DMSO-d_6 or at temperature between 30 and 100 °C. It may be due to the assymentric carbon (C_5).

In a similar manner, the reactions of **4** with carbonyl compounds (**5b—d**) gave the corresponding new sulfonium ylides (**8b—d**), which were isolated as their picrates.

The reaction of **4** with benzylthioacetaldehyde in methanol precipitated the new sulfonium ylide (**8e**) as crystals (mp 147—148 °C (dec)) directly from the reaction mixture. The structural assignment of **8e**

Table 1. Reactions of methyl and ethyl dimethylsulfuranylidenepyruvates(**3** and **4**) with carbonyl compounds(**5a—g**)

Sulfonium ylide	Carbonyl Compound	R^1	R^2	Solvent	Time (day)	Product (**8**)[a]	Yield(%)	Mp(dec)(°C)
4	**5a**	CH_3	$COOC_2H_5$	EtOH	2	**8a**-pic	71	142—143
4	**5a**	CH_3	$COOC_2H_5$	THF	2	**8a**-pic	41	
3	**5b**	CH_3	$COCH_3$	MeOH	0.5	**8b**-pic	66	148—149
4	**5b**	CH_3	$COCH_3$	MeOH	1	**8b**-pic	61	
4	**5b**	CH_3	$COCH_3$	EtOH	2	**8b**-pic	44	
4	**5b**	CH_3	$COCH_3$	THF	2	**8b**-pic	41	
4	**5c**	H	*i*-C_3H_7	MeOH	1	**8c**-pic	49	128—130
4	**5d**	H	C_6H_5	MeOH	1	**8d**-pic	52	145—146
4	**5e**	H	$CH_2SCH_2C_6H_5$	MeOH	1	**8e**	78	147—148
3	**5f**	H	$C_6H_4NO_2$-*p*	MeOH	0.5	**8f**	70	170
4	**5f**	H	$C_6H_4NO_2$-*p*	MeOH	1	**8f**	71	
4	**5f**	H	$C_6H_4NO_2$-*p*	EtOH	2	**8f**	41	
4	**5f**	H	$C_6H_4NO_2$-*p*	THF	2	**8f**	0	
4	**5g**[b]	H	H	MeOH	1	**8g**	80	139—140

a) pic: picrate. b) Paraformaldehyde was used.

Table 2. Physical constants of new sulfonium ylides(**8**)

Sulfonium ylide	R^1	R^2	Mp(dec)(°C) (solvent)	$IR^{KBr}_{\nu C=O}$ (cm^{-1})	NMR (δ) $(CH_3)_2S^+$-	NMR (δ) Others	Solvent[b]
8a	CH_3	$COOC_2H_5$	132—134 (EtOH-Et_2O)	1765, 1750, 1625	3.30(3H, s) 3.14(3H, s)	1.30(3H, t), 1.71(3H, s), 4.23(2H, q)	A
8b	CH_3	$COCH_3$	120—122 (MeOH-Et_2O)	1765, 1760, 1715, 1625	3.30(3H, s) 3.11(3H, s)	1.61(3H, s), 2.26(3H, s)	A
8c	H	*i*-C_3H_7	124—125 (THF)	1775, 1740, 1620	3.25(6H, s)	0.84(3H, d), 1.06(3H, d), 1.7—2.2(1H, m), 4.87(1H, d)	A
8d	H	C_6H_5	162—163 (MeOH-Et_2O)	1750(sh)[a], 1745, 1620	3.07(3H, s) 2.89(3H, s)	5.83(1H, s), 7.35(5H, m)	A
8e	H	$CH_2SCH_2C_6H_5$	147—148 (MeOH-H_2O)	1740, 1620	3.02(6H, s)	2.76(2H, d), 3.79(2H, s), 5.16(1H, t), 7.28(5H, m)	A
8f	H	$C_6H_4NO_2$-*p*	170 (EtOH-H_2O)	1750, 1620	2.92(6H, s)	6.16(1H, s), 7.67(2H, d), 8.28(2H, d)	B
8g	H	H	139—140 (MeOH)	1750, 1635	2.98(6H, s)	4.83(2H, s)	B

a) sh: shoulder absorption. b) Solvent: A, $CDCl_3$; B, DMSO-d_6.

was made on the basis of its spectral data and elemental analysis. However, the two methyl groups at the sulfonium group of **8e** appeared as a single peak at δ 3.02, which was in striking contrast to that of **8a**. In the case of the reaction with *p*-nitrobenzaldehyde or paraformaldehyde, the ylides (**8f** and **8g**) were also obtained as stable crystals. The results and physical data of **8** are shown in Tables 1 and 2 respectively. Further attempts were made to improve the yields of **8** in the reactions with diacetyl and *p*-nitrobenzaldehyde. As is shown in Table 1, methanol was proved to be the best solvent among the solvents examined, and **3** was more favorable than **4** to these reactions. Although the reaction of **3** or **4** in methanol with 1 equivalent of the carbonyl compound at room temperature produced good results in each case, at an elevated temperature or in the presence of excess carbonyl compound the desired products were not obtained.

The results are different from those for carbonyl-stabilized sulfonium ylides, such as dimethylsulfuranylideneacetophenone and ethyl dimethylsulfuranylideneacetate, which have been reported to be relatively unreactive toward ordinary carbonyl compounds.[2,3] It is reasonable to consider that the reaction of **3** or **4** with carbonyl compounds proceed through the intermediate betaine (**6**), which in turn cyclizes to form **8**, as is shown in Scheme 1. The cyclization, effected by the formation of a stable five-membered ring from **6**, must be the driving force of this reaction.

Reactivities of 8. In the presence of a catalytic amount of pyridine, the treatment of **8a** with *p*-toluenesulfonyl chloride in methylene chloride at room temperature afforded 5-ethoxycarbonyl-5-methyl-4-methylthio-2-oxo-3-(*p*-toluenesulfonyloxy)-2,5-dihydrofuran (**10a**) as colorless needles (mp 69—70 °C). The IR spectrum showed absorptions at 1785 (five-membered lactone), 1745 (ester), and 1615 cm^{-1} (double bond). The NMR spectrum exhibited two singlets, at δ 2.45 (3H) and 2.75 (3H), attributable to the methylthio group and the methyl protons of the tolyl group. Similar reactions of **8b** and **8g** afforded 3-*O*-tosylate (**10b** and **10g**) in good yields (see Table 3). The reaction of **8a** with benzoyl chloride in methylene chloride was completed in 30 min under ice-cooling to give 3-benzoyloxy-5-ethoxycarbonyl-5-methyl-4-methylthio-2-oxo-2,5-dihydrofuran (**11a**) as colorless needles (mp 95—96 °C). Similarly, **11b** and **11e—g** were readily obtained from the corresponding sulfonium ylides **8** (see Table 3). Although the evolution of methyl chloride was not detected, it seems likely that the formations of **10** and **11** result from the loss of methyl chloride from the intermediate sulfonium salt (**9**) derived from the betaine structure in **8**.

O-Benzoate (**11a**) was relatively stable under acidic conditions, whereas hydrolysis occurred in ethanolic sodium hydroxide to yield 5-ethoxycarbonyl-3-

Table 3. Reactions of **8** with *p*-toluenesulfonyl chloride and benzoyl chloride

Compound **8**	R^1	R^2	Chloride[a]	Product	Yield (%)	Mp (°C)
8a	CH_3	$COOC_2H_5$	TsCl	**10a**	87	69—70
8b	CH_3	$COCH_3$	TsCl	**10b**	83	79—80
8g	H	H	TsCl	**10g**	88	84—85
8a	CH_3	$COOC_2H_5$	BzCl	**11a**	84	95—96
8b	CH_3	$COCH_3$	BzCl	**11b**	88	Syrup
8e	H	$CH_2SCH_2C_6H_5$	BzCl	**11e**	89	54—55
8f	H	p-$NO_2C_6H_4$	BzCl	**11f**	72	153—154
8g	H	H	BzCl	**11g**	76	83—84

a) TsCl: *p*-toluenesulfonyl chloride; BzCl: benzoyl chloride.

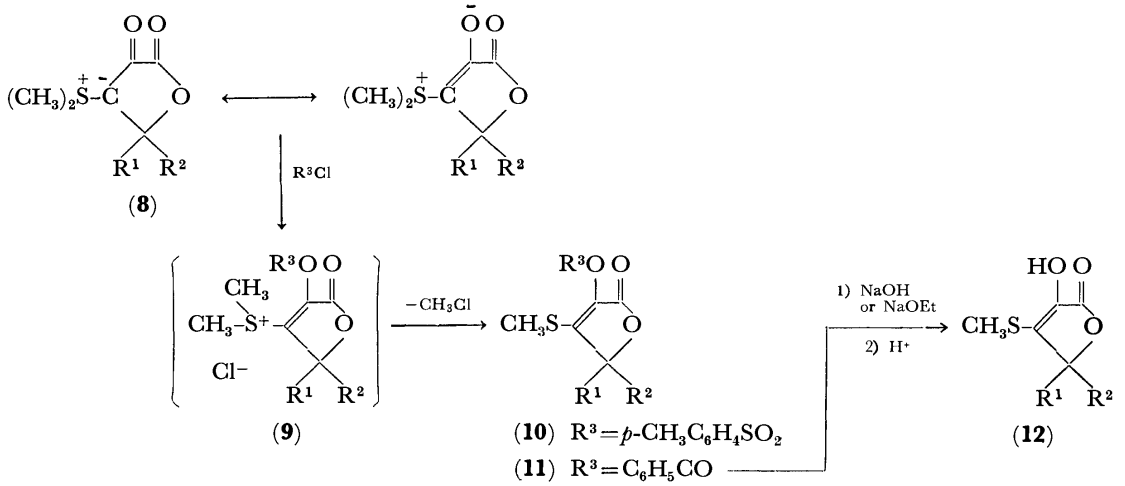

Scheme 2.

hydroxy-5-methyl-4-methylthio-2-oxo-2,5-dihydrofuran (**12a**) (mp 67—68 °C), which gave a blue color with ferric chloride. Under similar conditions, **11e** was also converted into the 3-hydroxy derivative (**12e**) in a good yield.

Methyl iodide and benzyl bromide, unexpectedly, were unreactive toward **8** under similar conditions. A prolonged reaction at an elevated temperature resulted in the formation of intractable products.

The reactions with nucleophilic reagents, such as mercaptans or thiourea, were also examined. When a mixture of **8e** and benzylmercaptan in 90% aqueous ethanol was refluxed, 4-benzylthio-5-benzylthiomethyl-3-hydroxy-2-oxo-2,5-dihydrofuran (**15e**) was obtained in a 67% yield (mp 89—91 °C). The product combined with ferric chloride to give a blue color. The structural assignment for **15e** was made on the basis of the elemental analysis and its spectral properties. In this manner, various 4-substituted products (**14**—**16**) were obtained from **8** and mercaptans (see Table 4). As is shown in Table 4, the yields increase with a decrease in the bulkiness of the mercaptans and substituents at the C_5-position of **8**. The reactions probably proceed through the nucleophilic displacement of the dimethylsulfonium group by the mercaptide anion of the intermediate sulfonium salt (**13**) formed by protonation. The reaction of **8a** which has two substituents at C_5, however, afforded the 4-substituted product in a low yield. In this case, the nucleophilic attack of the mercaptide anion on the C_4-position of **13** is unfavorable because of the steric hindrance.

On the other hand, the reaction of **8e** with thiourea in the presence of *p*-toluenesulfonic acid in refluxing ethanol yielded **12e** (95%) and *S*-methylisothiouronium *p*-toluenesulfonate. The analogous reactions of picrate of **8a** and **8c** gave demethylated products exclusively in a good yield. However, complicated reactions occurred in the absence of an acid.

In this reaction, it seems not unreasonable to explain that the preferential attack of thiourea on the less reactive methyl group rather than on the C_4-position

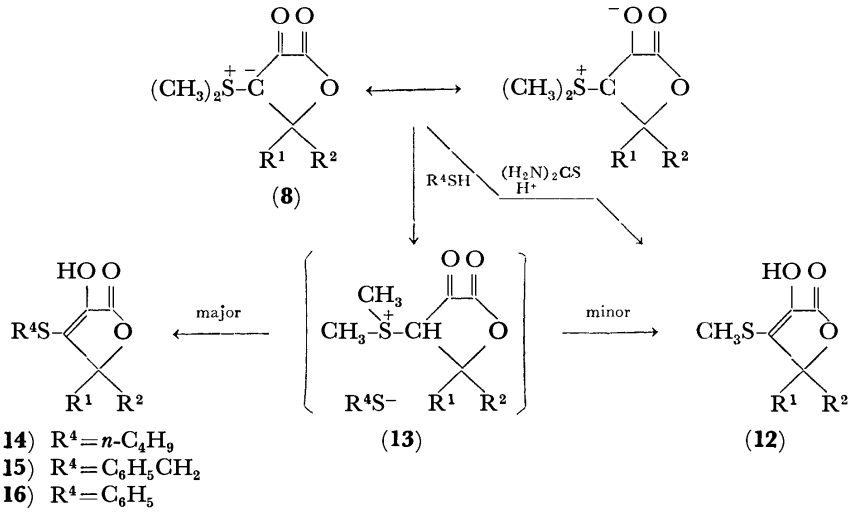

Scheme 3.

TABLE 4. REACTIONS OF **8** WITH MERCAPTANS AND THIOUREA

Compound **8**	R^1	R^2	Nucleophilic reagent	Product	Yield (%)	Mp (°C)
8a	CH_3	$COOC_2H_5$	*n*-C_4H_9SH	**14a**	22	Syrup
8a	CH_3	$COOC_2H_5$	$C_6H_5CH_2SH$	**15a**	26	74—75
8a	CH_3	$COOC_2H_5$	C_6H_5SH	**16a, 12a**[b]	(30)	(Syrup)
8a	CH_3	$COOC_2H_5$	$(H_2N)_2CS$[a]	**12a**	84	67—68
8c	H	*i*-C_3H_7	*n*-C_4H_9SH	**14c**	76	59—61
8c	H	*i*-C_3H_7	$C_6H_5CH_2SH$	**15c**	70	97—98
8c	H	*i*-C_3H_7	C_6H_5SH	**16c**	56	103—104
8c	H	*i*-C_3H_7	$(H_2N)_2CS$[a]	**12c**	75	125—126
8e	H	$CH_2SCH_2C_6H_5$	*n*-C_4H_9SH	**14e**	75	52—54
8e	H	$CH_2SCH_2C_6H_5$	$C_6H_5CH_2SH$	**15e**	67	89—90
8e	H	$CH_2SCH_2C_6H_5$	C_6H_5SH	**16e**	32	Syrup
8e	H	$CH_2SCH_2C_6H_5$	$(H_2N)_2CS$[a]	**12e**	95	85—86
8g	H	H	*n*-C_4H_9SH	**14g**	81	40—42
8g	H	H	$C_6H_5CH_2SH$	**15g**	83	107—108
8g	H	H	C_6H_5SH	**16g**	85	140—142

a) The reactions were carried out in the presence of acid. b) The mixture of **12a** and **16a** in the ratio of 1 : 2.

is due to a steric hindrance.

Furthermore, although the reactions with active methylene compounds, such as malononitrile and ethyl cyanoacetate, were examined under similar conditions, the desired reaction did not proceed. However, the cyclic sulfonium ylides (**8**) can be used as intermediates for the synthesis of 3-hydroxy-4-mercapto-2-oxo-2,5-dihydrofuran derivatives.[10]

Experimental

All the melting points are uncorrected. The IR spectra were determined with a Shimadzu IR-27G spectrophotometer. The NMR spectra were recorded on a Hitachi R-20A instrument, using TMS as the internal standard. The elemental analyses of all the new compounds except for **1** and **2** are listed in Table 7.

*Dimethyl(methoxalylmethyl)sulfonium Picrate (**1**) and Dimethyl(ethoxalylmethyl)sulfonium Pictrate (**2**).* Dimethyl(ethoxalylmethyl)sulfonium bromide[8] (194 g, 0.753 mol) and picric acid (174 g, 0.76 mol) in water were stirred for 1 hr at room temperature. The precipitate thus formed was collected by filtration and washed with ethyl acetate to give 261 g (81%) of the picrate (**2**, X=$(NO_2)_3C_6H_2O$). Recrystallization from ethyl acetate gave a pure sample as yellow needles; mp 95—97 °C (dec), $\nu_{C=O}$ (KBr) 1740 cm^{-1}.

Found: C, 36.93; H, 3.67; N, 9.88; S, 7.78%. Calcd for $C_{13}H_{15}N_3O_{10}S\cdot H_2O$: C, 36.89; H, 3.62; N, 9.93; S, 7.75%.

In a similar manner, 70.3 g of dimethyl(methoxalylmethyl)sulfonium picrate (**1**, X=$(NO_2)_3C_6H_2O$) was prepared from 86.5 g of the bromide (**1**, X=Br)[8] and 82 g of picric acid. Recrystallization from acetone-ether gave yellow needles; mp 106—108 °C (dec), $\nu_{C=O}$ (KBr) 1745 cm^{-1}.

Found: C, 35.24; H, 3.69; N, 10.18; S, 7.59%. Calcd for $C_{12}H_{13}N_3O_{10}S\cdot H_2O$: C, 35.21; H, 3.69; N, 10.26; S, 7.83%.

*Methyl and Ethyl Dimethylsulfuranylidenepyruvate (**3** and **4**).* *a) Preparation of **4** from the Picrate (**2**):* A mixture of the picrate (**2**, X=$(NO_2)_3C_6H_2O$, 11.15 g, 0.0265 mol), 50% aqueous sodium hydroxide (2.15 g, 0.0265 mol), and a saturated potassium carbonate solution (6.5 ml) in methylene chloride (50 ml) was stirred vigorously under ice-cooling for 30 min. After the removal of the inorganic precipitate by filtration, the methylene chloride layer was separated and dried over potassium carbonate. The removal of the solvent under reduced pressure at room temperature gave 3.69 g (80%) of **4** as pale yellow hygroscopic crystals: $\nu_{C=O}$ (KBr) 1720 and 1550 cm^{-1}; NMR (δ in $CDCl_3$) 4.68 (1H, s), 4.25 (2H, q), 3.00 (6H, s) and 1.34 (3H, t). This ylide was treated with picric acid in ethanol to give the picrate (**2**) quantitatively.

*b) Preparation of **4** from the Bromide (**2**):* By the same procedure, the bromide (**2**, X=Br, 2.57 g, 0.01 mol) afforded 1.27 g (72%) of **4**.

*c) Preparation of **3** from the Picrate (**1**):* According to the procedure described above, 3.95 g (64%) of **3** was obtained from 15.7 g of the picrate (**1**, X=$(NO_2)_3C_6H_2O$): pale yellow crystals; $\nu_{C=O}$ (KBr) 1725 and 1565 cm^{-1}; NMR (δ in $CDCl_3$) 4.68 (1H, s), 3.78 (3H, s) and 2.99 (6H, s). This ylide was converted to the picrate (**1**) quantitatively by treatment with picric acid in methanol.

*4-Dimethylsulfuranylidene-2,3-dioxotetrahydrofuran Derivatives(**8**).* *a) Preparation of **8a—d**:* A solution of **4** (1.76 g, 0.01 mol) and ethyl pyruvate (**5a**, 1.16 g, 0.01 mol) in ethanol was allowed to stand at ambient temperature for 2 days. The addition of picric acid (2.3 g) to the reaction mixture and the removal of the solvent under reduced pressure left a syrup, which was crystallized by the addition of ethyl acetate. Filtration and washing with ethyl acetate gave 3.37 g (71%) of the picrate of 4-dimethylsulfuranylidene-5-ethoxycarbonyl-5-methyl-2,3-dioxotetrahydrofuran (**8a**), which was subsequently recrystallized from ethanol to afford a pure sample as yellow needles; mp 142—143 °C (dec), $\nu_{C=O}$ (KBr) 1790 and 1775 cm^{-1}. The analytical data are shown in Table 7.

To a vigorously stirred suspension of the picrate of **8a** (1.80 g, 3.8 mmol) in methylene chloride (10 ml) was added, in one portion, 50% aqueous sodium hydroxide (0.31 g, 3.8 mmol) and a saturated potassium carbonate solution (3 ml). After 30 min the methylene chloride layer was separated and dried over potassium carbonate. The subsequent removal of the solvent gave 0.71 g (76%) of the sulfonium ylide (**8a**) as pale yellow needles which was crystallized from ethanol-ether (mp 132—134 °C (dec)). The ylide was treated with picric acid in ethanol to give the picrate of **8a** quantitatively.

Similarly, the reactions of **3** and **4** with **5b—d** afforded picrates of **8b—d**, which were converted into **8b—d** in 82, 78, and 72% yields respectively. The results and the spectral data are listed in Tables 1 and 2.

*b) Preparation of **8e—g**:* A solution of **4** (21.0 g, 0.119 mol) and benzylthioacetaldehyde (**5e**, 19.6 g, 0.119 mol) in methanol (100 ml) was allowed to stand at room temperature for 24 hr. The precipitates thus formed were collected by filtration and washed with methanol to give 27.3 g (78%) of 4-dimethylsulfuranylidene-5-benzylthiomethyl-2,3-dioxotetrahydrofuran (**8e**) as light yellow needles; it was subsequently recrystallized from aqueous methanol; mp 147—148 °C (dec).

In this way, **8f** and **8g** were obtained by the reactions of **3** and **4** with *p*-nitrobenzaldehyde (**5f**) and paraformaldehyde (**5g**) respectively. The results and the spectral properties are shown in Tables 1 and 2.

*Reactions of **8** with p-Toluenesulfonyl Chloride.* A solution of **8a** (2.31 g, 9.4 mmol), *p*-toluenesulfonyl chloride (1.82 g, 9.5 mmol), and 3 drops of pyridine in methylene chloride (10 ml) was refluxed for 1 hr, and then washed with water and dried over sodium sulfate. The removal of the solvent gave 2.56 g (87%) of 5-ethoxycarbonyl-5-methyl-4-methylthio-2-oxo-3-(*p*-toluenesulfonyloxy)-2,5-dihydrofuran (**10a**) (mp 69—70 °C), which was subsequently recrystallized from benzene-cyclohexane.

By a similar procedure, **10b** and **10g** were obtained from the corresponding **8**. The results and the spectral data are given in Tables 3 and 5.

*Reactions of **8** with Benzoyl Chloride.* To a solution of **8a** (1.37 g, 5.85 mmol) in methylene chloride (7 ml) stirred under ice-cooling was added drop by drop benzoyl chloride (0.84 g, 5.9 mmol). After stirring for 30 min, the reaction mixture was washed with water, dried, and then evaporated to give a solid. Recrystallization from benzene-cyclohexane afforded 1.64 g (84%) of 3-benzoyloxy-5-ethoxycarbonyl-5-methyl-4-methylthio-2-oxo-2,5-dihydrofuran (**11a**) as colorless needles; mp 95—96 °C. Similarly, **8b** and **8e—g** furnished the corresponding benzoates (**11**). The results and the spectral properties are shown in Tables 3 and 5.

The structural assignment of the syrupy product (**11b**) was made on the basis of the IR and NMR spectra with a sample purified by the chromatography of silica gel G (methylene chloride).

*Hydrolysis of **11**.* To a solution of **11a** (1.67 g, 5 mmol) in ethanol (9 ml) stirred under ice-cooling was added drop by drop a solution of sodium hydroxide (0.20 g, 5 mmol)

Table 5. Spectral data of tosylates(**10**) and benzoates(**11**)

Compd	ν_{max}^{Nujol} cm^{-1}	NMR (δ, in $CDCl_3$)
10a	1785, 1746, 1615, 1380, 1175	1.28(3H, t), 1.74(3H, s), 2.45(3H, s), 2.74(3H, s), 4.25(2H, q), 7.37(2H, d), 7.95(2H, d)
10b	1770, 1730, 1600, 1375, 1170	1.14(3H, s), 2.20(3H, s), 2.47(3H, s), 2.67(3H, s) 7.40(2H, d), 7.79(2H, d)
10g	1765, 1600, 1377, 1175	2.46(3H, s), 2.45(3H, s), 4.87(2H, s), 7.39(2H, d), 7.94(2H, d)
11a	1785, 1745, 1630	1.52(3H, t), 1.83(3H, s), 2.56(3H, s), 4.30(2H, q), 7.3—8.2(5H, m)
11b	1780, 1775, 1733,[a] 1627	1.70(3H, s), 2.29(3H, s), 2.56(3H, s), 7.3—8.3(5H, m)
11e	1775, 1750, 1630	2.48(3H, s), 2.69(1H, q), 3.04(1H, q), 3.85(2H, s), 5.06(1H, q), 7.2—8.2(10H, m)
11f	1780, 1750, 1637, 1525, 1355	2.44(3H, s), 6.00(1H, s), 7.2—8.5(9H, m)
11g	1768, 1740, 1630	2.46(3H, s), 4.92(2H, s), 7.2—8.3(5H, m)

a) Measured as a film.

Table 6. Spectral data of 3-hydroxy-2-oxo-2,5-dihydrofuran derivatives

Compd	ν_{max}^{Nujol} cm^{-1}	NMR (δ, in $CDCl_3$)
12a	3240, 1770, 1725, 1665	1.30(3H, t), 1.74(3H, s), 2.67(3H, s), 4.26(2H, q), 6.8—7.3(1H)[b]
12c	3300, 1725, 1665	0.67(3H, d), 1.15(3H, d), 2.10(1H, m), 2.67(3H, s), 4.73(1H, d), 6.5—7.2(1H)[b]
12e	3320, 1735, 1665	2.53(1H, q), 2.63(3H, s), 2.90(1H, q), 3.76(2H, s), 4.85(1H, q), 6.8—7.5(1H)[b], 7.24(5H, s)
14a	3310, 1760, 1663[a]	0.90(3H, m), 1.1—1.9(4H, m), 1.29(3H, t), 1.73(3H, s), 3.20(2H, t), 4.25(2H, q), 6.0—7.0(1H)[b]
14c	3310, 1735, 1663	0.74(3H, d), 0.9(3H, m), 1.15(3H, d), 1.1—1.9(4H, m), 2.1(1H, m), 3.21(2H, t), 4.69(1H, d), 6.4—7.2(1H)[b]
14e	3300, 1738, 1660	0.93(3H, m), 1.2—1.9(4H, m), 2.60(1H, q), 2.98(1H, q), 3.16(2H, t), 3.79(2H, s), 4.90(1H, q), 6.9(1H, broad s)[b], 7.28(5H, s)
14g	3200, 1740, 1057	0.93(3H, m), 1.1—2.0(4H, m), 3.09(2H, t), 4.72(2H, s), 6.8—7.3(1H)[b]
15a	3300, 1760, 1743, 1665	1.21(3H, t), 1.54(3H, s), 4.12(2H, q), 4.36(2H, s), 7.28(5H, s), 7.35(1H, broad s)[b]
15c	3310, 1728, 1660	9.63(3H, d), 1.08(3H, d), 2.06(1H, m), 4.40(2H, s), 4.60(1H, d), 7.0—7.5(1H)[b], 7.24(5H, s)
15e	3300, 1730, 1665	2.39(1H, q), 2.84(1H, q), 3.72(2H, s), 4.30(2H, s), 4.76(1H, q), 6.6—7.5(1H)[b], 7.25(10H, s)
15g	3250, 1720, 1650	4.37(2H, s), 4.55(2H, s), 6.6—7.2(1H)[b], 7.30(5H, s)
16c	3300, 1730, 1668	0.84(3H, d), 1.03(3H, d), 2.10(1H, m), 4.73(1H, d), 6.0—6.6(1H)[b], 7.2—7.6(5H, m)
16e	3270, 1740, 1670[a]	2.52(1H, q), 2.92(1H, q), 3.70(2H, s), 4.94(1H, q), 5.4—6.1(1H)[b], 7.1—7.6(10H, m)
16g	3280, 1750, 1665	4.50(2H, s), 6.0—6.8(1H)[b], 7.2—7.7(5H, m)

a) Measured as a film. b) D_2O-exchangeable peak.

in ethanol (4 ml). After stirring for 30 min at room temperature, the reaction mixture was concentrated to dryness under reduced pressure. The residue was dissolved in water and washed with ether. The aqueous solution was acidified with hydrochloric acid and then extracted with ether. The removal of the solvent left a syrup, which was subsequently crystallized by the addition of cyclohexane. Recrystallization from benzene–cyclohexane afforded 0.95 g (81%) of 5-ethoxycarbonyl-3-hydroxy-5-methyl-4-methylthio-2-oxo-2,5-dihydrofuran (**12a**); colorless needles; mp 67—68 °C.

When sodium ethoxide was employed, **11a** (1.67 g) gave **12a** (0.88 g) in a 76% yield.

Similarly, the treatment of **11e** (1.93 g) with ethanolic sodium hydroxide gave **12e** (1.14 g, 81%); mp 85—86 °C.

Both products were treated with ferric chloride in ethanol to give a blue color.

The IR and NMR spectra are shown in Table 6.

Reactions of 8 with Mercaptans. A solution of **8c** (1.01 g, 5 mmol) and *n*-butylmercaptan (0.63 g, 7 mmol) in ethanol (10 ml) was refluxed for 1 hr and evaporated under reduced pressure to give a colorless syrup. The resulting residue was dissolved in warm cyclohexane and allowed to stand overnight at room temperature. Filtration and washing with cyclohexane afforded 0.87 g (76%) of 4-butylthio-3-hydroxy-5-isopropyl-2-oxo-2,5-dihydrofuran (**14c**) as colorless needles; it gave a blue color with ferric chloride.

According to the procedure described above, the reactions of **8** with mercaptans furnished 4-substituted products (**14**—**16**) except for the treatment of **8a** with phenylmercaptan. The results and the spectral data are summarized in Tables 4 and 6 respectively. The structures of the syrupy products (**14e** and **16e**) were confirmed by the IR and NMR spectra of the sample purified by column chromatography on silica gel G (methylene chloride).

The reaction of **8a** (1.00 g, 4.07 mmol) with phenylmercaptan (0.66 g, 6 mmol) in refluxing ethanol (10 ml) for 9 hr gave 0.34 g of a mixture of **12a** and **16a** in the ratio of 1 : 2 (total yield of 30%) as a viscous syrup. Since the separation of the mixture was unsuccessful, the product composition was determined from the peak areas of the protons of the methylthio group (δ 2.66) and the phenylthio group (δ 7.2—7.6) in the NMR spectrum.

Reactions of 8 with Thiourea. A mixture of **8e** (2.96 g, 10 mmol), thiourea (1.14 g, 15 mmol), and *p*-toluenesulfonic acid in 90% ethanol (30 ml) was refluxed for 4 hr and then evaporated to dryness. The residue was combined with water and extracted with benzene, and the organic layer was washed with water, dried, and evaporated to give 2.68 g (95%) of 4-benzylthio-5-benzylthiomethyl-3-hydroxy-2-oxo-2,5-dihydrofuran (**12e**) as colorless needles after recrystallization from benzene–cyclohexane. The ethanolic solution of **12e** was combined with ferric chloride to give a blue color. The aqueous phase which was separated from the organic layer was treated with picric acid (2.3 g) to afford *S*-methylisothiuronium picrate (2.52 g, 79%) as yellow needles (mp 223 °C) after recrystallization from ethanol.

By the procedure described above, **12a** and **12c** were obtained from the picrates of **8a** and **8c** in 84 and 65% yields respectively.

The IR and NMR spectra are shown in Table 6.

Table 7. Elemental analyses of new compounds

Compd No	Formula	Calcd (%)				Found (%)			
		C	H	N	S	C	H	N	S
8a-picrate	$C_{16}H_{17}N_3O_{12}S$	40.43	3.60	9.04	6.74	40.70	3.46	8.95	6.76
8b-picrate	$C_{15}H_{15}N_3O_{11}S$	40.46	3.39	9.43	7.20	40.66	3.42	9.50	7.47
8c-picrate	$C_{15}H_{17}N_3O_{10}S$	41.76	3.97	9.74	7.43	41.85	3.99	9.76	7.21
8d-picrate	$C_{18}H_{15}N_3O_{10}S$	46.46	3.25	9.03	6.89	46.41	3.35	9.08	6.91
8e	$C_{14}H_{16}O_3S_2$	56.73	5.44		21.36	56.60	5.52		21.59
8f	$C_{12}H_{11}NO_5S$	51.25	3.94	4.98	11.41	51.31	4.00	4.94	11.63
8g	$C_6H_8O_3S$	44.99	5.03		20.01	45.19	5.17		19.82
10a	$C_{16}H_{18}O_7S_2$	49.74	4.69		16.56	50.01	4.75		16.38
10b	$C_{15}H_{16}O_6S_2$	50.54	4.53		17.98	50.67	4.64		17.79
10g	$C_{12}H_{12}O_5S_2$	47.98	4.02		21.34	48.10	4.09		21.02
11a	$C_{16}H_{16}O_6S$	57.13	4.80		9.53	56.94	4.96		9.27
11e	$C_{20}H_{18}O_4S_2$	62.15	4.69		16.59	61.98	4.80		16.48
11f	$C_{18}H_{13}NO_6S$	58.21	3.52	3.77	8.63	58.16	3.62	3.69	8.72
11g	$C_{12}H_{10}O_4S$	57.58	4.02		12.81	57.60	4.03		12.64
12a	$C_9H_{12}O_5S$	46.54	5.21		13.81	46.26	5.37		13.67
12c	$C_8H_{21}O_3S$	51.06	6.42		17.04	51.01	6.54		17.02
12e	$C_{13}H_{14}O_3S_2$	55.29	4.99		22.70	55.23	5.15		22.76
14c	$C_{11}H_{18}O_3S$	57.36	7.87		13.92	57.63	7.79		13.70
14e	$C_{16}H_{20}O_3S_2$	59.22	6.21		19.76	59.33	6.16		19.61
14g	$C_8H_{12}O_3S$	51.04	6.42		17.03	51.20	6.36		17.20
15a	$C_{15}H_{16}O_5S$	58.43	5.23		10.05	58.52	5.55		10.24
15c	$C_{14}H_{16}O_3S$	63.60	6.10		12.15	63.49	6.27		12.05
15e	$C_{19}H_{18}O_3S_2$	63.66	5.06		17.88	63.93	5.09		17.82
15g	$C_{11}H_{10}O_3S$	59.44	4.53		14.42	59.51	4.67		14.28
16c	$C_{13}H_{14}O_3S$	62.37	5.64		12.81	62.28	5.82		12.90
16g	$C_{10}H_8O_3S$	57.76	3.83		15.39	57.77	4.07		15.27

The authors wish to thank Professer Teruaki Mukaiyama for his helpful suggestions in this work. They also wish to thank Director Dr. Ichiro Chibata and Dr. Muneji Miyoshi for their encouragement in this study.

References

1) a) H. Nozaki, M. Takaku, D. Tsunemoto, Y. Yamamoto, and K. Kondo, *Nippon Kagaku Zasshi*, **81**, 1 (1967). b) A. F. Cook and J. G. Moffatt, *J. Amer. Chem. Soc.*, **90**, 740 (1968).

2) a) G. B. Payne, *J. Org. Chem.*, **32**, 3351 (1967). b) A. W. Johnson and R. T. Amel, *ibid.*, **34**, 1240 (1969).

3) K. W. Ratts and A. N. Yao, *ibid.*, **31**, 1185, 1689 (1966).

4) a) B. M. Trost, *J. Amer. Chem. Soc.*, **88**, 1587 (1966); *ibid.*, **89**, 138 (1967). b) M. Higo and T. Mukaiyama, *Tetrahedron Lett.*, **1950**, 2565. c) Y. Hayashi and H. Nozaki, *Tetrahedron*, **27**, 3085 (1971). d) P. Bravo, G. Gaudiano, P. P. Ponti, and C. Ticozzi, *ibid.*, **28**, 3845 (1972). e) O. Tsuge and K. Sakai, *ibid.*, **29**, 1983 (1973).

5) T. Mukaiyama, K. Hagio, H. Takei, and K. Saigo, This Bulletin, **44**, 161 (1971).

6) E. G. Howard, A. Kotch, R. V. Lindsay, Jr., and R. E. Putnam, *J. Amer. Chem. Soc.*, **80**, 3924 (1958).

7) G. B. Payne, *J. Org. Chem.*, **33**, 3417 (1968).

8) N. F. Blau and C. G. Stuckwisch, *ibid.*, **22**, 82 (1957).

9) It has been reported in the following papers that the sulfonium ylides show characteristic absorption of carbonyl group shifted 100—150 cm^{-1} to longer wavelength in comparison to ordinary carbonyl groups. a) H. Nozaki, Z. Morita, and K. Kondo, *Tetrahedron Lett.*, **1966**, 2913. b) Refs. 1 and 2.

10) Synthetic methods of 2,3-dioxotetrahydrofuran derivatives, α-tetronic acid, have been reported in the following papers. a) H. Shinz and M. Hinder, *Helv. Chim. Acta*, **30**, 1349 (1947). b) A. Rossi and H. Schinz, *ibid.*, **31**, 473, 1953 (1948); *ibid.*, **32**, 1967 (1949). c) E. D. Stecher and E. Gelblum, *J. Org. Chem.*, **26**, 2693 (1961). d) E. Galantay, C. Hoffman, and N. Paolella, *ibid.*, **35**, 4277 (1970).

Synthesis of 6-(2-Amino-2-deoxy-β-D-glucopyranosylamino)- and 6-(β-D-Glucopyranosylamino)purine

Shunzo FUKATSU,* Aiko SAWA,** and Sumio UMEZAWA

Department of Applied Chemistry, Faculty of Engineering, Keio University, Hiyoshi, Yokohama 223

(Received November 17, 1973)

6-(β-Glycosylamino)purines have been synthesized in good yields by condensation of 4-amino-5-nitro-6-chloropyrimidine with masked glycosylamines followed by hydrogenation of nitro group, cyclization with triethyl orthoformate and removal of protecting groups.

Since kinetin[1] and zeatin,[2] factors inducing cell division, were discovered, many related compounds such as 6-acylaminopurines,[3] reversed nucleosides,[4] and modified nucleosides,[5] have been synthesized. Furthermore, 6-(aminoheptosylamino)purine was found in septacidin,[6] an antifungal and cytotoxic antibiotic. In order to investigate further the structure-activity relationships, we have synthesized the title compounds.

The synthesis of 6-(glycosylamino)purines has rarely been reported. The elegant synthesis of reversed nucleosides by Leonard and Carraway[4] involved condensation of a 9-masked derivative of 6-chloropurine with a masked derivative of 5-amino-5-deoxyribose. Ikehara and Tada[7] found that carbon disulfide ring-closure of 6-(2,3,4,6-tetra-*O*-acetyl-β-D-glucopyranosylamino)-4,5-diaminopyrimidine gave a mixture of masked derivatives of 9-(β-D-glucopyranosyl)purine and 6-(β-D-glucopyranosyl)purine.

For the preparation of 6-substituted purines, the condensation of 6-chloropurine[8] or 6-mercaptopurine[1,9] with an amine, and the direct alkylation of adenine derivatives[1] have been developed. Our attempts to prepare 6-(glycosylamino)purines by these procedures were unsuccessful. However, we have found that the 6-(β-glycosylamino)purines could be synthesized in good yields by condensation of 4-amino-6-chloro-5-nitropyrimidine with masked glycosylamines followed by cyclization with triethyl orthoformate.

We have prepared 6-(2-amino-2-deoxy-β-D-glucopyranosylamino)purine (**8**) as an aminonucleoside (Scheme 1). In this synthesis, the base-labile *N*-trifluoroacetyl group was used for the protection of the amino group of the sugar. Ikehara and Tada[7] discussed the formation of N^6-glucosyladenine together with N^9-isomer and ascribed it to the presence of hydrogen bond between the 2′-*O*-acetyl and 6-NH group of pyrimidine base. Since the *N*-trifluoroacetyl group is known to be less participating, we were interested in the influence of this function on the ring-closure.

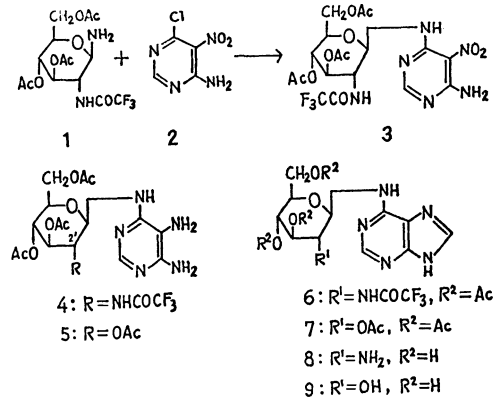

Scheme 1

3,4,6-Tri-*O*-acetyl-2-deoxy-2-trifluoroacetamido-β-D-glucopyranosyl azide[10,11] was hydrogenated with Raney nickel to give the glycosylamine (**1**) in high yield. Condensation of **1** with 4-amino-6-chloro-5-nitropyrimidine[12] (**2**) in dioxane afforded 6-(3,4,6-tri-*O*-acetyl-2-deoxy-2-trifluoroacetamido-β-D-glucopyranosylamino)-4-amino-5-nitropyrimidine (**3**) in a 58% yield. Catalytic reduction with Raney nickel then gave 6-(3,4,6-tri-*O*-acetyl-2-deoxy-2-trifluoroacetamido-β-D-glucopyranosylamino)-4,5-diaminopyrimidine (**4**). Cyclization of **4** with triethyl orthoformate and acetic anhydride afforded, in a 66% yield, 6-(3,4,6-tri-*O*-acetyl-2-deoxy-2-trifluoroacetamido-β-D-glucopyranosylamino)purine (**6**), which, after removal of the protecting groups by treatment with methanolic ammonia at room temperatures, led to 6-(2-amino-2-deoxy-β-D-glucopyranosylamino)purine (**8**) in a 39% overall yield from **1**.

Next, we prepared 6-(β-D-glucopyranosylamino)-purine (**9**) by the analogous procedure. 6-(2,3,4,6-Tetra-*O*-acetyl-β-D-glucopyranosylamino)-4,5-diaminopyrimidine (**5**) was prepared by the method described by Ikehara and Tada,[7] and, in the present paper, we have described purification of this compound and its physical properties. Cyclization of **5** with triethyl

Table 1. Ultraviolet spectral data

Compounds	λ_{max} mμ	($\varepsilon \times 10^{-3}$)
3	325.5	(16.3)[a]
4	286.5	(6.56)[a]
5	286	(8.4)[a]
6	263.5	(19.5)[a]
7	263	(16.4)[a]
8	271.5	(21.0)[b]
	262	(18.45)[c]
	271	(18.4)[d]
9	273	(17.5)[b]
	263	(16.4)[c]
	272	(14.3)[d]

a) MeOH, b) 0.01 M HCl, c) Water, d) 0.01 M NaOH.

* Present address: Development Laboratories, Meiji Seika Kaisha, Ltd., 580 Horikawa-cho, Saiwai-ku, Kawasaki 210.

** Present address: Department of Pharmacology, School of Medicine, Keio University, Shinanomachi, Shinjuku-ku Tokyo 162.

Table 2. Physical properties and elemental analyses

Compound	Mp, °C	Formula	Calcd, %			Found, %			Yield %	$[\alpha]_D$[a]
			C	H	N	C	H	N		
3	245	$C_{18}H_{21}N_6O_{10}F_3$	40.16	3.93	15.62	40.26	4.27	16.00	58	−27.4 (*c* 0.55) m
4	122—135	$C_{18}H_{23}N_6O_8F_3$	42.52	4.53	16.54	42.28	4.80	16.29	96	−4.3 (*c* 0.9) m
5	113—115	$C_{18}H_{25}N_5O_9$	47.47	5.49	15.38	47.30	5.63	15.62	95.5	−12.0 (*c* 2.0) c
6	169—170	$C_{19}H_{21}N_6O_8F_3$	44.02	4.05	16.22	44.13	3.98	16.37	66	−4.9 (*c* 1.0) m
7	193—194	$C_{19}H_{27}N_5O_9$	48.61	5.80	14.92	48.88	5.75	14.54	60	−22.0 (*c* 0.5) m
8	225(dec)	$C_{11}H_{16}N_6O_4$	44.59	5.44	28.60	44.73	5.66	28.20	84	−70.0 (*c* 1.1) w
9	223(dec)	$C_{11}H_{15}N_5O_5$	44.44	5.09	23.56	44.50	5.33	23.53	70	−48.5 (*c* 1.0) w

a) Determined at room temperatures, m: methanol, c: chloroform, w: water

or thoformate and acetic anhydride gave, in a 60% yield, 6-(2,3,4,6-tetra-*O*-acetyl-*β*-D-glucopyranosylamino)purine (**7**), which, after deblocking, gave **9** in a 33% overall yield from **2**.

The above-mentioned yields of **6** and **7** suggested that the hydrogen bonding of 2′-*O*-acyl or 2′-*N*-acyl group with 6-NH group in the pyrimidine compounds (**4**, **5**) did not exert substantial influence on the ring-closure with triethyl orthoformate.

The structure and stereochemistry of the above-described products have been confirmed by UV (Table 1), IR and NMR spectral studies.

Experimental

*3,4,6-Tri-O-acetyl-2-deoxy-2-trifluoroacetamido-β-D-glucosylamine (**1**).* A solution of 3,4,6-tri-*O*-acetyl-2-deoxy-2-trifluoroacetamido-*β*-D-glucopyranosyl azide[11] (2.66 g, 6.24 mmol) in ethyl acetate (50 ml) was shaken with Raney nickel (W-2, 2 ml) and hydrogen (55 kg/cm²) at room temperatures for 18 hr. The catalyst was filtered off, and the filtrate was evaporated to dryness *in vacuo*. The residue was crystallized from 2-propanol-ethyl acetate (1 : 1) to yield 2.39 g (5.97 mmol, 96.5%) of **1** as needles; mp 174—176 °C, $[\alpha]_D^{15}$ −20.2° (*c* 1.12, MeOH) [lit,[11] mp 158 °C, $[\alpha]_D^{22}$ −14.4° (*c* 0.6, MeOH)]; ν_{max}^{KBr} (cm⁻¹), 1750, 1710 (-$COCH_3$, -$COCF_3$), 1230 (C-O-C); tlc, R_f 0.75 (benzene-ethyl acetate 1 : 6).

*6-(3,4,6-Tri-O-acetyl-2-deoxy-2-trifluoroacetamido-β-D-glucopyranosylamino)-4-amino-5-nitropyrimidine (**3**).* To a solution of **1** (2.22 g, 5.55 mmol) in anhydrous dioxane (5 ml) and triethylamine (0.77 ml, 5.55 mmol), a suspension of 4-amino-6-chloro-5-nitropyrimidine[12] (**2**) in anhydrous dioxane (30 ml) was added with stirring. The mixture was heated at 60—65 °C for 15 hr and filtered. The filtrate was evaporated to dryness *in vacuo*. The residue (3.78 g) was chromatographed on a column (3×38 cm) of silica gel (100 g, Wakogel C-200) and eluted with ether. The fractions containing **3** were combined and evaporated to dryness *in vacuo*. The residue was crystallized from ethanol to give **3** (1.73 g, 58%) as needles; ν_{max}^{KBr} (cm⁻¹), 1760, 1715 (-$COCH_3$, -$COCF_3$), 1625, 1595 (-C=N-), 1525, 1370 (-NO_2), 1235 (C-O-C); tlc R_f 0.6 (ethyl acetate-benzene 3 : 1).

*6-(3,4,6-Tri-O-acetyl-2-deoxy-2-trifluoroacetamido-β-D-glucosylamino)-4,5-diaminopyrimidine (**4**).* A sample of **3** (1.24 g, 2.31 mmol) was hydrogenated in the presence of Raney nickel as described in the preparation of **5**. The catalyst was filtered off and the filtrate was evaporated to dryness *in vacuo* to give a colorless glass of **4** (1.11 g, 96%); ν_{max}^{KBr} (cm⁻¹), 1760, 1740 (-$COCH_3$, -$COCF_3$), 1650, 1600 (-C=N-); tlc R_f 0.2 (ethyl acetate).

*6-(2,3,4,6-Tetra-O-acetyl-β-D-glucopyranosylamino)-4,5-diaminopyrimidine (**5**).* A sample of 6-(2,3,4,6-tetra-*O*-acetyl-*β*-D-glucopyranosylamino)-4-amino-5-nitropyrimidine[7] (1.52 g, 3.15 mmol) was dissolved in anhydrous methanol (55 ml) at 60 °C and cooled. To the solution Raney nickel (3.8 ml, W-2) was added and the mixture was shaken with hydrogen (hydrogen pressure 60 kg/cm²) at room temperature for 6 hr. The catalyst was filtered off and washed with methanol. The filtrate and washings were combined and evaporated to dryness *in vacuo*. The resulting solid (1.37 g) was crystallized from ethyl acetate to give colorless needles of **5** (1.01 g, 95.5%); ν_{max}^{KBr} (cm⁻¹), 3380 (-NH), 1750 (-$COCH_3$), 1660, 1630, 1595 (-C=N-); tlc R_f 0.5 (ethyl acetate-ethanol 6 : 1).

*6-(3,4,6-Tri-O-acetyl-2-deoxy-2-trifluoroacetamido-β-D-glucopyranosylamino)purine (**6**).* A solution of **4** (1.26 g, 2.31 mmol) in triethyl orthoformate and acetic anhydride (11.2 ml, 1 : 1) was refluxed for 85 min and the reaction mixture was evaporated to sirup *in vacuo*. The residue was chromatographed on a column (2.8×24 cm) of silica gel (70 g, Wakogel C-200) and eluted with ethyl acetate-ethanol (20 : 1). Fractions containing the product of R_f 0.5 (tlc, ethyl acetate-ethanol 20 : 1) were combined and evaporated to dryness. The residue was crystallized from ethyl acetate-isopropyl ether (1 : 1) to yield **6** (0.792 g, 66%) as colorless needles; ν_{max}^{KBr} (cm⁻¹), 1760 1725 (-$COCH_3$, -$COCF_3$), 1625, 1600 (-C=N-), 1245 (C-O-C); tlc R_f 0.5 (ethyl acetate-ethanol 6 : 1), 0.3 (ethyl acetate).

*6-(2,3,4,6-Tetra-O-acetyl-β-D-glucopyranosylamino)purine (**7**).* A solution of **4** (1.733 g, 3.82 mmol) in triethyl orthoformate and acetic anhydride (19 ml, 1 : 1) was heated at 125 °C (bath temperature) for 1.5 hr and the solution was evaporated to dryness *in vacuo*. The residue was chromatographed on a column of silica gel (50 g, Wakogel C-200) and eluted with benzene-ethanol (9 : 1). Fractions containing of the product of R_f 0.35 (tlc, benzene-ethanol 9 : 1) were combined and evaporated to dryness *in vacuo* to give **7** (1.074 g, 60%) as colorless needles, which were recrystallized from ethyl acetate; ν_{max}^{KBr} (cm⁻¹), 3430 (-NH), 1760 (-$COCH_3$), 1625, 1600 (-C=N-), 1060, 1035 (C-O-C); NMR (DMSO-d_6), δ 8.70 (1H s, purine H_2), 8.64 (1H d, J=8—9 Hz, purine C_6-NH), 8.50 (1H s, purine H_8), 5.85 (1H d, J=8—9 Hz, $C_{1'}$-H), 2.02 (3H s, -$OCOCH_3$), 1.97 (6H s, -$OCOCH_3$), 1.88 (3H s, -$OCOCH_3$); tlc R_f 0.35 (benzene-ethanol 9 : 1), 0.30 (ethyl acetate).

*6-(2-Amino-2-deoxy-β-D-glucopyranosylamino)purine (**8**).* A portion of **6** (0.60 g, 1.16 mmol) was treated with saturated methanolic ammonia (35 ml) at room temperature for 5 days. The solution was evaporated to dryness *in vacuo*. The resulting solid was recrystallized from water-ethanol to give 6-(2-amino-2-deoxy-*β*-D-glucopyranosyl)purine (**8**) (290 mg, 84%) as colorless needles; ν_{max}^{KBr} (cm⁻¹), 3380, 3320,

3180 (-NH, -OH), 1635, 1595 (-C=N-), 1105, 1080, 1057, 1048, 1026 (C-O-C); NMR (DMSO-d_6), δ 8.27 (1H s, purine H_2), 8.17 (1H s, purine H_8), 8.01 (1H d, J=9 Hz, purine C_6-NH), 5.43 (1H d, J=9 Hz, $C_{1'}$-H); tlc R_f 0.2 (*n*-butanol-water 86 : 14).

*6-(β-D-Glucopyranosylamino)purine (**9**).* A solution of **7** (335 mg, 0.715 mmol) in anhydrous methanol (35 ml) was saturated at 0 °C with dry ammonia. After storage in a refrigerator for 18 hr, the solution was evaporated to dryness *in vacuo*. The residue was recrystallized from water-ethanol to give 6-(β-D-glucopyranosylamino)purine (**9**) (148 mg, 70%) as colorless needles; ν_{max}^{KBr} (cm^{-1}), 3400, 3350, 3140 (-NH, -OH), 1625, 1600 (-N=C-), 1105, 1080, 1070 (C-O-C) NMR (DMSO-d_6), δ 8.26 (1H s, purine H_2), 8.17 (1H s, purine H_8), 7.84 (1H d, J=8.5 Hz, purine C_6-NH), 5.52 (1H broad, $C_{1'}$-H); tlc R_f 0.17 (*n*-butanol saturated with 2 M ammonia).

References

1) C. O. Miller, F. Skoog, M. H. Von Saltza, and F. M. Strong, *J. Amer. Chem. Soc.*, **77**, 1392 (1955). C. O. Miller, F. Skoog, F. S. Okumura, M. H. Von Saltza, and F. M. Strong, *ibid.*, **78**, 1375 (1956).

2) D. S. Letham, J. S. Shannon, and I. R. McDonald, *Proc. Chem. Soc.*, **1964**, 230.

3) M. M. Baizer, J. R. Clark, M. Dub, and A. Loter, *J. Org. Chem.*, **21**, 1276 (1956). H. Lettré and H. Ballweg, *Ann. Chem.*, **633**, 171 (1960).

4) N. J. Leonard and K. L. Carraway, *J. Heterocyclic Chem.*, **3**, 485 (1966).

5) J. Hildesheim, J. Gléophax, and S. D. Géro, *Tetrahedron Lett.*, **1967**, 5013.

6) J. D. Dutcher, M. H. Von Saltza, and F. E. Pansy, "Antimicrobial Agents and Chemotherapy," (1963) p. 83. H. Agahigian, G. D. Vickers, M. H. Von Saltza, J. Reid, A. I. Cohen, and H. Gauthier, *J. Org. Chem.*, **30**, 1085 (1965).

7) M. Ikehara and H. Tada, *Chem. Pharm. Bull.* (Tokyo), **11**, 1102 (1963).

8) M. W. Bullock, J. J. Hard, and E. L. R. Stokstad, *J. Amer. Chem. Soc.*, **78**, 3693 (1956).

9) G. B. Elion, E. Burgi, and G. H. Hitchings, *ibid.*, **74**, 411 (1952).

10) W. L. Wolfrom and H. B. Bhat, *J. Org. Chem.*, **32**, 1821 (1967).

11) D. E. Cowley, L. Hough, and C. M. Peach, *Carbohyd. Res.*, **19**, 231 (1971).

12) W. R. Boon, W. G. M. Jones, and G. R. Ramage, *J. Chem. Soc.*, **1951**, 96.

Synthesis of Alkoxythallium(III) Compounds of Olefins and Their Reaction with Copper Halides and Pseudohalides

Sakae UEMURA,* Kazuo ZUSHI, Akira TABATA, Akio TOSHIMITSU, and Masaya OKANO

Institute for Chemical Research, Kyoto University, Uji, Kyoto 611

(Received January 23, 1974)

Some new alkoxythallium(III) compounds of olefins, $C_6H_5C(R^1)(OR^3)CH_2Tl(OCOR^2)_2$ [I], are prepared from styrene and α-methylstyrene with thallium(III) acetate and isobutyrate in various alcohols. I(R^1=H) reacts with copper(I) iodide, bromide, chloride, cyanide and thiocyanate to afford the corresponding alkyl halides and pseudohalides, $C_6H_5CH(OR^3)CH_2X$ [II], in various organic solvents, acetonitrile being the solvent of choice for the purpose of preparing II. The addition of potassium salt has a remarkable effect in improving the yield of II. The halo- and pseudohalodethallation occur at the position where thallium is attached previously to alkyl carbon. An ionic concerted intermolecular scheme is proposed as a reaction mechanism for the preparation of II. The data of NMR and IR spectra of I are briefly discussed.

Compared to the corresponding mercury(II) compounds, oxythallium(III) compounds of olefins are known to be unstable, and so far only a few compounds have been isolated since the first report by Criegee.[1] The compounds from styrene,[2] *o*-allylphenol,[2] norbornene,[3] norbornadiene[3] and isobutylene[4] are the known examples. Recently oxythallation products from acetylene[5,6b] and allene[6a] have also been isolated from the reaction mixture in methanol or acetic acid. Earlier work on the decomposition of oxythallium(III) compounds of olefins has revealed that the carbon-thallium bond is cleaved to leave a carbonium cation which gives the oxidation products of olefins.[2] A recent report by Mitani *et al.*[7] that carbon-thallium bond fission of the compound occurs easily with potassium thiocyanate to give 1-methoxy-2-thiocyanoalkanes in good yield may add another use of oxythallation in organic synthesis. We have reported some reactions of arylthallium(III) compounds with copper halides and pseudohalides where the aryl carbon-thallium bond was cleaved, resulting in the introduction of halogens[8a] or pseudohalogens[8b,c] to the aromatic ring. In connection with this observation, it might be interesting to examine how alkyl carbon-thallium bonds of oxythallium(III) compounds of olefins behave to these copper salts. We have investigated the synthesis of some new oxythallium(III) compounds of olefins and also some reactions of the resulting compounds with copper(I) iodide, chloride, bromide, cyanide, and thiocyanate. As a result a number of new oxythallium(III) compounds have been isolated from styrene and α-methylstyrene and the replacement of thallium group in these compounds by halogens or pseudohalogens has been achieved in good yield.

Results and Discussion

Synthesis of Alkoxythallium(III) Compounds of Olefins. Kabbe has reported the synthesis of α-methoxy-β-diacetatothallium ethylbenzene from styrene and thallium(III) acetate in methanol.[2] Similarly we obtained various α-alkoxy-β-diacetatothallium ethylbenzenes in 60—86% yield by stirring a mixture of styrene and thallium(III) acetate in various alcohols at room temperature for 0.5—24 hr. The reaction proceeded with decreasing order through the following series of alcohols as solvent; methyl>ethyl>*n*-propyl, *n*-butyl>*i*-propyl, *i*-butyl≫*t*-butyl, reflecting both steric and polar factors of the solvents. Thus in methanol the reaction was almost completed at 0 °C after 15 min, while the corresponding compound was scarcely obtained in *t*-butanol even by stirring at 20 °C for 2 days. Thallium(III) isobutyrate could also be used instead of the acetate for the preparation of methoxy- and ethoxy-thallium(III) compounds of styrene, but a longer reaction time was required. Similar oxythallium(III) compounds were obtained from α-methylstyrene using thallium(III) acetate in methanol or ethanol, but not in higher alcohols under similar reaction conditions. All the compounds isolated were white amorphous solids, soluble in polar solvents and recrystallized from benzene. The reaction conditions for the preparation of I and the yields, melting points, and analytical data of I are summarized in Table 1 (Eq. (1)).

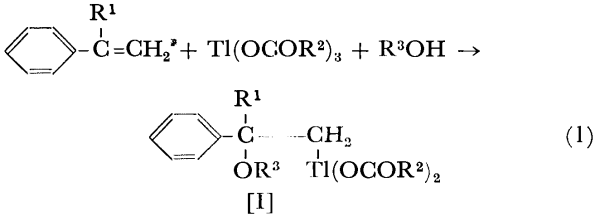

(1)

[I]

IR spectra (paraffin and hexachlorobutadiene mulls) of I (R^1=H, R^2=R^3=CH_3) showed four strong absorption bands in the acetate region which are assignable to two ν_{asym} (CO_2) (1600 and 1525 cm^{-1}) and two ν_{sym} (CO_2) (1422 and 1390 cm^{-1}) (Table 2). This suggests the presence of two types of acetate group, namely a bridging acetate group (1525 and 1422 cm^{-1}; strong and slightly broad) and a non-bridging one (1600 and 1390 cm^{-1}; strong and sharp), as in the case of methyl, ethyl and phenylthallium(III) dicarboxylates which were reported by Kurosawa and Okawara,[9] and Lee.[10] The expected large Tl–H spin-spin couplings were observed in NMR spectra (in $CDCl_3$ or CD_3OD) of I, but the clear separation of $J_{^{205}Tl-H}$ and $J_{^{203}Tl-H}$ was not obtained. Contrary to the known result that in ethyl-or *n*-propylthallium(III) compounds $J_{Tl-\beta-H}$ is generally larger than $J_{Tl-\alpha-H}$,[9a,11] the coupling constants of Tl-methylene protons ($J_{Tl-H_B \text{ or } H_C}$) in I were larger than that of Tl-methine proton (J_{Tl-H_A}) (Table 2). Similar result has been reported in the acetoxythallated compound of norbornene where

Table 1. Reaction conditions of alkoxythallation of styrene and α-methylstyrene and characterization of I

Olefin R^1 (mmol)	Tl-salt R^2 (mmol)	Alcohol R^3 (50 ml)	React. temp. (°C)	React. time (hr)	I Yield[a] (%)	I Mp(dec) (°C)	I Analysis Found (Calcd) C	I Analysis Found (Calcd) H
H	CH_3	CH_3	20	0.5	86	127—128[b]	33.9(34.1)	3.6(3.7)
H	CH_3	C_2H_5	20	1.3	60	115	35.5(35.6)	4.1(4.0)
H	CH_3	n-C_3H_7	20	4	72	103	37.0(37.2)	4.3(4.3)
H	CH_3	i-C_3H_7	20	22	64	115—117	37.1(37.2)	4.4(4.3)
H	CH_3	n-C_4H_9	20	2	60	118—119	38.2(38.6)	4.5(4.6)
H	CH_3	i-C_4H_9	25	15	58	102—103	39.0(38.6)	4.9(4.6)
H	i-C_3H_7	CH_3	20	24	60	124—125	39.8(39.7)	4.8(4.9)
H	i-C_3H_7	C_2H_5	25	24	74	91.5—93	38.7(41.0)[c]	4.8(5.2)
CH_3	CH_3	CH_3	20	0.5	70	134	35.6(35.6)	3.9(4.0)
CH_3	CH_3	C_2H_5	20	20	58	121—122	36.3(37.2)	4.1(4.3)

a) Based on Tl(III) salt charged. b) Reported,[2] 127.5—128 °C. c) After recrystallization four times from chloroform.

Table 2. Carboxylate absorption bands (in cm^{-1})[a] and J_{Tl-H} (in Hz) and δ (in ppm)[b,c] of I

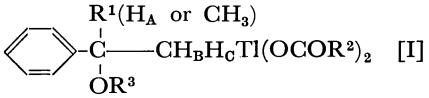

[I]

I R^1	I R^2	I R^3	J_{Tl-H_B} (δ_B)	J_{Tl-H_C} (δ_C)	J_{Tl-H_A} (δ_A)	$J_{Tl-CH_3(R^1)}$ (δ)	$\nu_{asym}(CO_2)$		$\nu_{sym}(CO_2)$	
H	CH_3	CH_3	760 (3.07)	920 (3.17)	748 (4.58)	—	1600(s)	1525(s)	1422(s)	1390(s)
H	CH_3	C_2H_5	768 (3.08)	921 (3.11)	737 (4.82)	—				
H	CH_3	n-C_3H_7	768 (3.07)	929 (3.18)	751 (4.66)	—				
H	CH_3	i-C_3H_7	786 (3.07)	921 (3.19)	818 (4.85)	—				
H	CH_3	n-C_4H_9	774 (3.03)	934 (3.18)	757 (4.66)	—	1600(s)	1530(s)	1425(s)	1380(s)
H	CH_3	i-C_4H_9	772 (3.07)	917 (3.18)	828 (4.65)	—	1598(s)	1527(s)	1415(s)	1380(sh)
H	i-C_3H_7	CH_3	758 (3.05)	906 (3.13)	752 (4.60)	—	1586(s)	1505(s)	1415(m)	1392(m)
H	i-C_3H_7	C_2H_5	759 (3.03)	904 (3.13)	716 (4.70)	—				
CH_3	CH_3	CH_3	810 (3.23)	892 (3.20)	—	29 (1.76)	1608(s)	1530(s)	1424(s)	1375(s)
CH_3	CH_3	C_2H_5	822 (3.25)	890 (3.17)	—	29 (1.76)				

a) Paraffin and hexachlorobutadiene mulls. In methylthallium(III) diacetate, 1613(s), 1530(s), 1428(s), and 1375(s) cm^{-1} were the observed bands.[9b] b) $CDCl_3$ and CD_3OD solvent; TMS as the internal standard. c) In ethylthallium (III) diisobutyrate, $J_{Tl-CH_2\underline{CH_3}}$ of 1626 Hz and $J_{Tl-\underline{CH_2}}$ of 822 Hz were reported.[9a]

$J_{Tl-\alpha-H}$ is larger than $J_{Tl-\beta-H}$ and this was attributed to a possible geometric effect in rigid molecule.[12] Since the interaction between mercury and oxygen is proposed in the oxymercuration of cycloalkenols,[13] it may be possible to assume that in I thallium interacts with oxygen of alkoxy group to restrict free rotation of C_α–C_β bond in some extent. This may be one reason for the unexpected small value of J_{Tl-H_A} in I. Electronic absorption spectra (in EtOH) of I showed a maximum at 226 mμ, and ε of I (R^1=H, R^2=R^3=CH_3), I (R^1=H, R^2=CH_3, R^3=C_2H_5) and I (R^1=H, R^2=i-C_3H_7, R^3=CH_3) were 1.8×10^4, 1.4×10^4 and 2.1×10^4, respectively.

From β-methylstyrene no alkoxythallium(III) compounds were isolated using methanol and ethanol as solvents after stirring at 20 °C for 5 hr. Similarly, attempts to isolate oxythallium(III) compounds from cyclohexene were unsuccessful either with thallium(III) acetate in chloroform or chloroform–acetic acid (10 : 1) as solvents, or with thallium(III) trifluoro-

acetate in trifluoroacetic acid–*n*-pentane (1 : 5) as solvent at 15 °C.

Reaction of Alkoxythallium(III) Compounds of Styrene with Copper Salts. A mixture of I (R^1=H, R^2=CH_3) and the copper(I) salt and/or potassium salt was stirred for 5 hr under reflux in various organic solvents such as acetonitrile, 1,4-dioxane, THF, methanol, chloroform, and DMF. As a result thallium was replaced by halogen or pseudohalogen to afford II along with small amounts of styrene [III] and α-alkoxyethylbenzene [IV], acetonitrile being the solvent of choice for the preparation of II (Eq. (2)). Although in the cases of iodide and thiocyanate the reaction

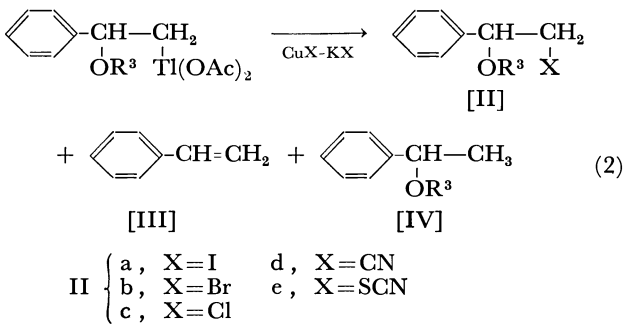

(2)

proceeded with the potassium salt alone as reported by Mitani *et al.*[7] in thiocyanate case, the addition of the corresponding copper(I) salts was found to increase the yield of II in both cases. For chloride, bromide, and cyanide, however, a replacement of thallium by halogen or pseudohalogen scarcely occurred with the potassium salt alone, while II was obtained in good yield using the corresponding copper(I) salts. Interestingly, the addition of the potassium salt to the reaction system containing copper(I) salt caused a remarkable improvement in the yield of II. In contrast to the aryl carbon–Tl bond,[8] the alkyl carbon–Tl bond of I was cleaved usually by copper(I) salts, and not so readily by copper(II) salts.

From the reaction using I (R^1=H, R^2=R^3=CH_3), the by-products such as phenylacetaldehyde [V], α-methoxy-β-acetoxy- [VI], β-acetoxy-β-methoxy- [VII], and β,β-dimethoxyethylbenzenes[VIII] were sometimes obtained, the distribution and the amount of these depending on the reaction conditions. These compounds are obviously the decomposition products of I, because, for example, Kabbe[2] reported the formation of VIII by stirring I (R^1=H, R^2=R^3=CH_3) in methanol at 65 °C for 4 days (64% yield). We have also examined the decomposition of I (R^1=H, R^2=R^3 CH_3) in various solvents by refluxing for 5 hr (without any copper and/or potassium salts) and the results in acetonitrile, 1,4-dioxane and methanol were shown in Eq. (3) where the yields of III and V were less than 3%. Only a slight amount of the decomposition products was formed in DMF, THF, CH_2Cl_2, and CCl_4.

a. Iodination (Table 3). Although the reaction mixture was heterogeneous in acetonitrile because of the insolubility of copper(I) iodide, the good yield of IIa was obtained in this solvent. Small or trace amounts of III and IV were always detected as by-products. Though IIa was obtained using either po-

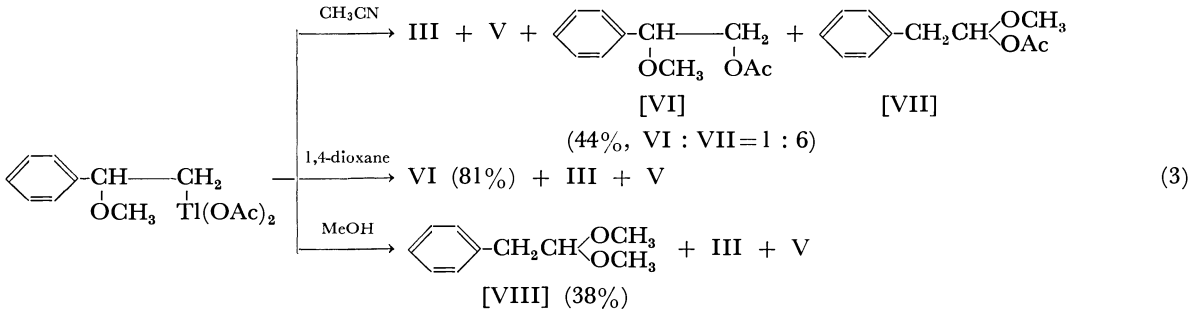

(3)

Table 3. Results of iodination

Reaction time, 5 hr

I(R^1=H, R^2=CH_3) R^3 (5 mmol)	CuI (mmol)	KI (mmol)	Solvent (25 ml)	React. Temp. (°C)	Products (yield, %)[a] IIa	III	IV	Remarks
CH_3	0	10	CH_3CN	81	64	trace	trace	V s. a.[b]
CH_3	10	0	CH_3CN	81	68	17	trace	V s. a.
CH_3	5	5	CH_3CN	81	71	5	trace	V s. a.
CH_3	5	10	CH_3CN	81	89	2	trace	V s. a.
C_2H_5	5	10	CH_3CN	81	82	trace	trace	V s. a.
n-C_3H_7	5	10	CH_3CN	81	73	2	trace	V s. a.
n-C_4H_9	5	10	CH_3CN	81	72	5	trace	V s. a.
CH_3	0	10	1,4-dioxane	101	21	trace	trace	VI 74
CH_3	10	0	1,4-dioxane	101	35	19	3	VI s. a.
CH_3	5	5	1,4-dioxane	101	44	15	4	VI s. a.
CH_3	5	10	1,4-dioxane	101	35	trace	26	VI 12
CH_3	5	5	THF	66	46	2	30	

a) Based on I. b) s. a.=a small amount (1—2%).

tassium iodide or copper(I) iodide alone, it was found that the reaction in the presence of both salts gave the best yield of IIa. The reaction of I with iodine or lithium iodide in acetonitrile gave only a trace amount of IIa.

b. Bromination and Chlorination (Table 4). In contrast to the iodination the reaction of I with potassium bromide alone gave only a small amount of IIb, while copper(I) bromide reacted with I to afford IIb in fairly good yield together with small amounts of III, IV, and bis(2-alkoxy-2-phenylethyl)thallium bromide, the disproportionation product of I (see Experimental). The yield of IIb was increased by the addition of potassium bromide as in the case of iodination. The addition of potassium chloride instead of the bromide also improved the yield of IIb and an additional formation of a small amount of IIc was observed in this case. Acetonitrile and methanol were revealed to be the solvent of choice, and 1,4-dioxane, DMF, and $CHCl_3$ could also be used as solvents, although the selectivity for IIb was low in the last three solvents. While it has been reported that methyl thallium diacetate reacted readily with aqueous solution of sodium chloride, bromide, or iodide to give the corresponding methyl halide,[9a] the reaction of I with potassium bromide in water at 20 °C or 100 °C for 1 hr afforded III, V, a trace amount of IIb, and thallium(I) bromide. The yields of III and V were 3% and 56% at 20 °C, and 2% and 31% at 100 °C respectively. This fact means that in water as solvent the decomposition of I to V and III is much faster than the formation of alkyl halide and that the nature of C–Tl bonds of I and methylthallium diacetate is different in some way. None of IIb was obtained from the reaction of I with copper(II) bromide in acetonitrile as solvent. The reaction of I with bromine in acetonitrile did not give any of IIb at 81 °C for 5 hr.

While only a slight amount of IIc was obtained from the reaction of I with potassium chloride in acetonitrile, the reaction proceeded smoothly in the presence of both copper(I) and potassium chlorides in the same solvent to afford IIc, III and IV. Here, the selectivity and also the yield of IIc were slightly lower than those of iodination and bromination. When the reaction of I with copper(I) chloride was carried out in the presence of potassium bromide, IIb and IIc were obtained, being the former predoninant. Bis(2-alkoxy-2-phenylethyl) thallium chloride was also obtained in a small amount as in the case of bromination and it became apparent that such disproportionated compounds could be formed in the presence of copper(I) halide and irrespective of the presence of potassium halide. Thus, bis-(2-methoxy-2-phenylethyl) thallium bromide and chloride were obtained in 15—20% yield by refluxing I (R^1=H, R^2=R^3=CH_3) and copper(I) bromide or chloride in acetonitrile respectively (see experimental part), and the disproportionation product[14] of I (R^1=H, R^2=CH_3, R^3=*n*-C_3H_7) was obtained in 10% yield

Table 4. Results of bromination and chlorination

I(R^1=H, R^2=CH_3) R^3 (5 mmol)	Cu salt (mmol)	K salt (mmol)	Solvent (25 ml)	React. temp. (°C)	React. time (hr)	Products (yield, %)[a] IIb	IIc	III	IV	Remarks
CH_3	0	KBr 10	CH_3CN	81	5	6	0	trace	0	V 24 VI 4
CH_3	CuBr 10	0	CH_3CN	81	1	29	0	5	trace	R_2TlBr[b] 20
CH_3	CuBr 10	KCl 10	CH_3CN	81	1	40	1	3	1	
CH_3	CuBr 10	0	CH_3CN	81	5	53	0	12	trace	R_2TlBr s. a.[c]
CH_3	CuBr 5	KBr 5	CH_3CN	81	5	69	0	4	4	R_2TlBr s. a.
CH_3	CuBr 10	KBr 10	CH_3CN	81	5	87	0	3	4	R_2TlBr s. a.
CH_3	CuBr 10	KBr 20	CH_3CN	81	5	83	0	4	4	R_2TlBr s. a.
C_2H_5	CuBr 10	KBr 10	CH_3CN	81	5	86	0	2	2	R_2TlBr s. a.
n-C_3H_7	CuBr 10	KBr 10	CH_3CN	81	5	79	0	3	4	R_2TlBr s. a.
n-C_4H_9	CuBr 10	KBr 10	CH_3CN	81	5	68	0	7	2	R_2TlBr s. a.
CH_3	CuBr 10	KBr 10	MeOH	56	5	84	0	2	0	VII 2 VIII trace
CH_3	CuBr 10	KBr 10	1,4-dioxane	101	5	38	0	36	trace	VI 20
CH_3	CuBr 10	KBr 10	DMF	80	5	54	0	10	trace	V 4
CH_3	CuBr 10	KBr 10	$CHCl_3$	61	5	72	0	9	6	VII 5
CH_3	CuBr 10	KBr 10	pyridine	117	5	0	0	2	0	
CH_3	0	KCl 10	CH_3CN	81	5	0	3	2	1	VI 4, VII 14 $RTlCl_2$ 15
CH_3	CuCl 10	0	CH_3CN	81	1	0	27	trace	1	R_2TlCl 15
CH_3	CuCl 10	KCl 10	CH_3CN	81	1	0	36	2	2	R_2TlCl 10
CH_3	CuCl 10	KBr 10	CH_3CN	81	1	27	12	3	2	
CH_3	CuCl 10	KCl 10	CH_3CN	81	5	0	59	18	7	R_2TlCl s. a.
C_2H_5	CuCl 10	KCl 20	CH_3CN	81	5	0	50	8	6	R_2TlCl s. a.
n-C_3H_7	CuCl 10	KCl 20	CH_3CN	81	5	0	60	9	6	R_2TlCl s. a.
n-C_4H_9	CuCl 10	KCl 20	CH_3CN	81	5	0	45	9	2	R_2TlCl s. a.

a) Based on I. b) R=$C_6H_5CH(OCH_3)CH_2$ c) s. a.=a small amount (2—8%).

TABLE 5. RESULTS OF CYANATION AND THIOCYANATION

Acetonitrile as solvent 25 ml; React. temp 81 °C; React. time 5 hr

I(R^1=H, R^2=CH_3) R^3 (5 mmol)	Cu salt (mmol)		K salt (mmol)		Products (yield, %)[a]				Remarks
					IId	IIe	III	IV	
CH_3	0		KCN	10	0	0	trace	0	
CH_3	CuCN	10	0		74	0	6	trace	VII 14
CH_3	CuCN	10	KCN	10	3	0	trace	trace	V 6, VI 5, VII 14
CH_3	CuCN	10	KBr	10	86	0	5	4	IIb trace
CH_3	CuCN·C_5H_5N[b]	10	0		65	0	2	trace	VII 7
CH_3	CuBr	10	KCN	10	60	0	6	4	IIb 5
CH_3	K[Cu(CN)$_2$][c]	10	0		1	0	1	1	V 2, VII 3
C_2H_5	CuCN	10	KBr	10	74	0	7	10	IIb trace
n-C_3H_7	CuCN	10	KBr	10	68	0	3	11	IIb trace
n-C_4H_9	CuCN	10	KBr	10	62	0	3	6	IIb trace
CH_3	Cu(CN)$_2$	5	0		48	0	6	0	VII 16
CH_3	0		KSCN	10	0	72	trace	trace	
CH_3	CuSCN	10	0		0	44	3	9	VII 8
CH_3	CuSCN	5	KSCN	10	0	96	0	0	
CH_3	Cu(NCS)$_2$	10	0		0	23	0	trace	V 7, VII 26

a) Based on I. b) CuCN-pyridine (1 : 1) complex. c) CuCN-KCN (1 : 1) complex.

(after recrystallization from methanol) together with IIc (35%) and small amounts of III, IV, and VI by refluxing I (10 mmol) and copper(I) chloride (20 mmol) in acetonitrile for 5 hr. None of IIc was obtained from the reaction of I with copper(II) chloride in acetonitrile as solvent.

c. Cyanation and Thiocyanation (Table 5). I did not react with potassium cyanide to give IId, while a good yield of IId was obtained from the reaction of I with copper(I) cyanide in acetonitrile. In contrast to the halogenation described above, the addition of potassium cyanide to the reaction mixture of I and copper(I) cyanide lowered strongly the yield of IId. Instead of potassium cyanide, potassium bromide showed some effect for improving the yield of IId with a formation of only a trace amount of IIb. Small amounts of disproportionated organothallium(III) compounds were sometimes detected as in the case of halogenation. The reaction seemed to be strongly affected by the kind of solvent and almost no reaction was observed in other solvents such as pyridine, 1,4-dioxane, and methanol which were the good solvents for the reaction of arylthallium(III) compounds with copper cyanide.[8b] Copper(II) cyanide could also be used for this reaction, but the activity was inferior to copper(I) salt. No isonitrile compounds were detected in all cases.

For thiocyanation, I(R^1=H, R^2=R^3=CH_3) is known to react easily with potassium thiocyanate to give IIe.[7] We found that copper(I) thiocyanate also reacted with I to give IIe, the best yield of which was obtained in the presence of both of copper(I) and potassium thiocyanates. The reaction with copper(II) thiocyanate afforded IIe in a low yield together with considerable amounts of the decomposition products. None of isothiocyanate compounds were obtained in all cases.

d. Attempts of the Reactions of I with Copper(II) Fluoride and Some Other Metal Salts. The reaction of I (R^1=H, R^2=R^3=CH_3) with copper(II) fluoride dihydrate in dioxane at refluxing temperature gave only the decomposition products such as V and VI together with α-methoxyethylbenzene. Similarly none of fluorinated compounds were obtained from the reaction even in the presence of potassium fluoride in DMF or acetonitrile as solvents. No appreciable reaction of I was observed with copper(II) acetate or acetylacetonate. In acetonitrile as solvent mercury(II) and silver cyanides or iron(II) chloride hydrate did not react with I to give IId or IIc respectively.

e. Some Consideration on the Reaction Scheme of Halogenation and Pseudohalogenation. Although it has been known that no substitution of mercury by halogen or pseudohalogen occurs in the reaction of oxymercurated compounds of olefins with potassium iodide, cyanide, or thiocyanate,[15] thallium in I was readily substituted by iodide or thiocyanate to afford IIa or IIe as described above. As proposed by Mitani *et al.*,[7] this reaction may proceed through the exchange of the acetate ligand of I by group X giving very unstable alkylthallium(III) diiodide or dithiocyanate [IX] followed by an intramolecular migration of X to alkyl carbon (Eq. (4)). For chloride and bromide, IX seemed to be rather stable and did not give II readily. We will describe in a separate paper about the isolation of IX (X=Cl or Br).

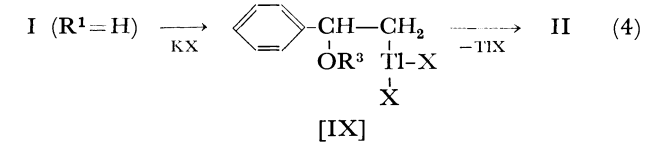

(4)

[IX]

In connection to this observation, it should be noted here that mercury in the oxymercurated compound of olefins has been known to be substituted electrophilically by iodine or bromine molecule,[15] while no such reaction was observed with I as described above. These facts may be explained by the difference of the oxidation potential between Hg and Tl; namely a reductive

cleavage of carbon-metal bonds would be much easier in thallium compound than in mercury one and so a favorable nucleophilic attack on carbon can be expected for the former and a favorable electrophilic attack for the latter.

Next the reaction scheme of I with copper salts should be considered. In contrast to the reaction of arylthallium(III) salt with copper salts,[8] it is not necessary to use copper(II) salt in this case. This fact may be explained as follows. Since it has been stated[16] that Pd(II) aryls are more stable than Pd(II) alkyls and require stronger oxidants to decompose them, it seems reasonable to assume that Tl(III) alkyls do not require stronger oxidant compared to Tl(III) aryls if the latter is more stable than the former. In fact arylthallium(III) compounds were quite stable and did not give any appreciable amount of decomposition products under the conditions shown in Eq. (3) where I gave many products. The reason why I did not react with copper(II) salts in acetonitrile so readily is not certain at present but the choice of a suitable solvent may improve the yield of II. Thus, the reaction of I with copper(II) bromide in the presence of potassium bromide in pyridine at refluxing temperature for 1 hr gave a 20% yield of IIb, while IIc was obtained in 30—50% yield by the reaction using copper (II) chloride in pyridine or dioxane as solvent.

As to the halogenation and pseudohalogenation of I with copper(I) salts, first, the reaction does not appear to involve radicals because the reaction of I (5 mmol) with copper(I) and potassium bromides (both of 10 mmol) in the presence of acrylonitile (10 mmol) at 81 °C for 5 hr in acetonitrile as solvent under N_2 gave neither polyacrylonitrile nor alkylated acrylonitrile[17] even though an appreciable amount of IIb (53% yield) was still obtained. Second there is no evidence of the substitution of thallium with copper salt, because none of α-alkoxystyrene or acetophenone and copper metal was obtained which may be derived from alkylcopper compound if formed.[18] Third a free carbonium cation is not formed in the reaction because halogenation or pseudohalogenation occurred at the position where thallium was attached previously, and none of phenyl migrated compounds was detected in the products. Fourth there is a clear difference in product distributions between the reaction with potassium salt alone and that with copper(I) salt alone in polar acetonitrile solvent. This may suggest that direct attack of unionized copper(I) species is operative. Considering all these facts an ionic concerted intermolecular scheme shown in Eq. (5) seems to be most reasonable.

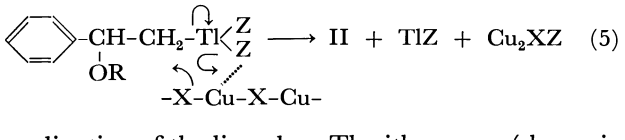

$$\longrightarrow \text{II} + \text{TlZ} + \text{Cu}_2\text{XZ} \quad (5)$$

Coordination of the ligand on Tl with copper (shown in dotted line) may be one of the driving forces of the reaction. In fact the reaction of I with copper(I) bromide in strong complexing solvent such as pyridine or *N,N*-tetramethylethylenediamine gave none of II at refluxing temperature for 5 hr, while IId was obtained in good yield (65%) in acetonitrile from the reaction of I with copper(I) cyanide–pyridine (1 : 1) complex where a coordination site of copper is still vacant.

As has been described above, the addition of potassium salt to the reaction mixture showed a remarkable effect for improving the yield of II. The reasons for this effect may be as follows. The solubility of copper(I) salt in solvents is increased by the coordination between potassium and copper salts, and the coordination makes Cu–X bond loosen and the attack of X on carbon easy. For example, 1.15 g out of 1.43 g (10 mmol) of copper(I) bromide or only 0.05 g out of 1.19 g (10 mmol) of potassium bromide was soluble in 25 ml of acetonitrile at 81 °C, while 1.51 g out of 2.62 g of a mixture of both bromides (each of 10 mmol) was soluble in the same amount of acetonitrile at 81 °C. It should be also noted that the deoxythallation of I to give styrene was prevented in the presence of potassium iodide, bromide, or thiocyanate. For cyanation with copper(I) cyanide, however, the addition of potassium cyanide prevented the formation of IId. This may be due to the formation of the unreactive coordination compound, $K[Cu(CN)_2]$, which is known to have a spiral polymeric structure in which each Cu atom is covalently bound to two carbon atoms and one nitrogen atom.[19] In fact the reaction of I with this compound prepared separately gave only 1% yield of IId in acetonitrile as solvent. When the reaction of I with copper(I) cyanide and potassium bromide was carried out in acetonitrile, IId was the main product and IIb was obtained only in a trace amount. In contrast to this, it may be interesting to note that the reaction of I with a mixture of copper(I) bromide and potassium cyanide in the same solvent, which was refluxed for 1 hr before the addition of I, gave a small amount of IIb and the main product was IId in this case. In connection to this the following observations are worth to refer. As shown in Table 4, the reaction of I with copper(I) bromide in the presence of potassium chloride gave almost IIb, while with copper(I) chloride and potassium bromide a mixture of IIc and IIb was obtained under similar conditions, the former being a minor product. These results can be explained by the consideration of the equilibrium shown in Eqs. (6) and (7) which are based on the HSAB principle;[20] *i.e.*, Cu^+ is soft acid and $CN^- > Br^- > Cl^-$ are soft bases with decreasing order of softness.

$$\text{CuCl} + \text{KBr} \rightleftarrows \text{CuBr} + \text{KCl} \quad (6)$$

$$\text{CuBr} + \text{KCN} \rightleftarrows \text{CuCN} + \text{KBr} \quad (7)$$

Although the precise nature of the formation of III and IV is uncertain at present, it is noteworthy to refer to the following facts. As to the formation of III, it is clear that the deoxythallation of I giving III was catalyzed by copper salt, because the amount of III formed is larger at the reactions in the presence of copper salt than at those without it. Halogen acid such as hydrogen chloride has been known to accelerate the deoxymercuration of alkoxymercurated compounds of olefins[21] and the elimination of the alkoxy group giving mercurinium ion followed by demercuration has been proposed as the reaction mechanism.[21] We

observed similar phenomena in I (R^1=H, R^2=R^3=CH_3) which gave 73% yield of III and 93% of Tl^{3+} salt by the reaction with hydrogen chloride (0.2 M) in an aqueous ethanol solvent under stirring at 20 °C for 2 hr. This fact suggests that similar reaction mechanism may be operative for the formation of III in Tl case as well. Copper salt may help the elimination of alkoxy group in the present reactions. In connection to the formation of IV, it is interesting to note that the action of water[22] or hydrogen iodide[23] on trialkylthallium split off the corresponding hydrocarbon RH and that the reaction of diorganothallium(III) carboxylate with tetramethyltin in methanol[24] gave also a hydrocarbon. This protodethallation can be explained by an electrophilic substitution on carbon by hydrogen. The action of water, which may exist in solvent or metal salts, on I might give IV by similar reaction scheme, but more work should be necessary to discuss it.

Experimental

The IR spectra were taken with Hitachi EPI-S2 and Perkin-Elmer 521 spectrometers in paraffin and hexachlorobutadiene mulls. The UV and visible spectra were taken with Hitachi EPS-2U spectrometer using ethanol as solvent. The NMR spectra were recorded by a Varian A-60 spectrometer in $CDCl_3$ or CD_3OD as solvents, using TMS as the internal standard. The glc analyses were carried out on Shimadzu 5APTF and 4BMPF apparatus, using PEG 6000 (25%)-Chromosorb W (3m) and Apiezon L (30%)-Celite (1 and 3m) columns (N_2 as the carrier gas).

Materials. All the organic materials except the alkoxythallium(III) compounds of olefins were purified before use by distillation, while commercially available copper and and potassium salts and other inorganic materials were used without further purification. $Cu(NCS)_2$ was prepared by the reported method from $CuSO_4 \cdot 5H_2O$ and KSCN.[25] Copper(I) cyanide-pyridine (1 : 1) complex was prepared by the same method reported previously.[8a] $K[Cu(CN)_2]$[26] was prepared by stirring 77 mmol of KCN and 39 mmol of CuCN in 20 ml of water at 20 °C for 2 hr, collecting white crystals (3.3 g) precipitated after evaporating the reaction mixture to 5 ml, washing with a small amount of water and drying over silica gel; yield 54% (Found: C, 15.66; N, 18.68%. Calcd for C_2N_2KCu: C, 15.53; N, 18.11%). Thallium(III) acetate and isobutyrate were prepared by stirring thallium(III) oxide in acetic acid and isobutyric acid at 65 °C for 20 hr and at 90 °C for 2 hr respectively, collecting white amorphous crystals formed after cooling, and drying over CaO.

Preparation of Alkoxythallium(III) Compounds of Olefins, I. The following example of I (R^1=R^2=R^3=CH_3) shows a typical experimental procedure. To a yellow-orange homogeneous solution of thallium(III) acetate (19.4 g, 0.05 mol) in methanol (50 ml), α-methylstyrene (11.8 g, 0.1 mol) was added drop by drop at 15—20 °C. The mixture was stirred at 20 °C for 30 min during which period the color of the homogeneous solution turned to colorless. The mixture was added by 200 ml of petroleum ether (30—70 °C), stored in an ice-box at −10 °C for 2 hr. The white precipitates of I (R^1=R^2=R^3=CH_3) (16.0 g, 70% yield) thus formed were collected by filtration and were recrystallized from benzene. I is very soluble in pyridine, DMF, DMSO, carbon disulfide, methanol, acetic acid, and dichloromethane, soluble in acetone, acetonitrile, dioxane, nitromethane, chloroform, dichloroethane, ethanol, ethyl acetate, diglyme, THF, and sparingly soluble in ether, benzene, petroleum ether (30—70 °C), carbon tetrachloride, and water. NMR spectral data of I except those of methine and methylene protons shown in Table 2 are as follows: δ 2.0 (s, 6H, $OCOCH_3$) when R^2 is methyl; 1.23 (d, 12H, J_{H-H}=7 Hz, $-COCH(CH_3)_2$) and 2.57 (septet, 2H, J_{H-H}=7 Hz, $OCOCH(CH_3)_2$) when R^2 is isopropyl; some peaks due to respective alkoxy group; 6.9—7.7 (m, 5H, phenyl).

Decomposition of I (R^1=H, R^2=R^3=CH_3) in Dioxane. A mixture of I (4.58 g, 10 mmol) and dioxane (50 ml) was stirred for 5 hr at 100 °C. The precipitates thus formed (TlOAc: 1.53 g, 5.8 mmol) were filtered off after cooling and the filtrate was added by 200 ml of water and extracted with *n*-hexane. Glc analysis of a part of the extract using ethyl cinnamate as the internal standard showed that the products were VI (81%) and slight amounts of III and V. After drying over Na_2SO_4, the extract was distilled to give 1.0 g (52% yield) of VI; bp 103—110 °C/8 mmHg. NMR δ 2.07 (s, 3H, $OCOCH_3$), 3.30 (s. 3H, OCH_3), 4.12—4.48 (m, 3H, $>CHCH_2-$), 7.35 (s, 5H, phenyl). Found: C, 67.99; H, 7.43%. Calcd for $C_{11}H_{14}O_3$: C, 68.02; H, 7.27%.

Decomposition of I (R^1=H, R^2=R^3=CH_3) in Acetonitrile. After I (4.58 g, 10 mmol) was stirred in acetonitrile (50 ml) for 5 hr at 80 °C, the reaction mixture was worked up as described above. Glc analysis of the extract showed that the products were III (1.5%), VI (6%) and VII (38%). Distillation of the extract gave a mixture of VI and VII (VI : VII=1 : 3.5; 0.3 g); bp 65—76 °C/5 mmHg. NMR of VII, δ 2.00 (s, 3H, $OCOCH_3$), 2.93 (d, 2H, J_{H-H}=5.5 Hz, $-CH_2-$), 3.33 (s, 3H, OCH_3), 5.81 (t, 1H, J_{H-H}=5.5 Hz, $-CH<$), 7.17 (s, 5H, phenyl). Analysis of the mixture of VI and VII; Found: C, 67.78; H, 7.40. Calcd for $C_{11}H_{14}O_3$: C, 68.02; H, 7.27%.

Formation of Bis(2-methoxy-2-phenylethyl)thallium Bromide and Chloride. A pale green heterogeneous mixture of I (R^1=H, R^2=R^3=CH_3) (2.29 g, 5 mmol) and copper(I) bromide (1.43 g, 10 mmol) in acetonitrile (25 ml) was stirred at 81 °C for 1 hr during which period the colour of the solution turned to deep green. After the reaction mixture was cooled down, the pale yellow precipitates (1.59 g, IR inactive) thus formed were filtered off and water (200 ml) was added to the filtrate to afford 0.40 g of white solids which were revealed to be bis(2-methoxy-2-phenylethyl)thallium bromide. Recrystallization from acetonitrile gave 0.27 g of pure white needle crystals (19.5% yield based on I). IR; 1088 (s)cm^{-1} (ν_{C-O}); mp>300 °C. Found: C, 38.82; H, 4.02%. Calcd for $C_{18}H_{22}O_2BrTl$: C, 38.98; H, 4.00%.

The same procedure using copper(I) chloride gave white amorphous solid of bis(2-methoxy-2-phenylethyl)thallium chloride (0.19 g after recrystallization from acetonitrile; 14.9 % yield based on I). IR; 1090 (s)cm^{-1} (ν_{C-O}); mp, slowly decomposed over 205 °C. Found: C, 42.02; H, 4.42%. Calcd for $C_{18}H_{22}O_2ClTl$ C, 42.38; H, 4.35%.

Reaction of I with Copper Salts. The following example shows a typical experimental procedure.

Reaction of I(R^1=H, R^2=R^3=CH_3) with Copper(I) Cyanide in the Presence of Potassium Bromide. A white heterogeneous solution of I (2.29 g, 5 mmol), copper(I) cyanide (0.89 g, 10 mmol), and potassium bromide (1.19 g, 10 mmol) in acetonitrile (25 ml) was stirred at 81 °C for 5 hr during which period the blue precipitates came out gradually. The reaction mixture was worked up as in the case of the decomposition of I in dioxane and glc analysis of the benzene extract showed that the products were IId (R^3=CH_3) (86%), III (4%), IV (R^3=CH_3) (4%) and a trace amount of IIb. Distillation of the extract gave 0.76 g of pure IId; bp 109—

110 °C/5 mmHg. IR; 2250 (ν_{CN}) 1106 (ν_{C-O}), 760 and 703 (phenyl) cm^{-1}. NMR: δ 2.70 (d, 2H, J=6 Hz), 3.29 (s, 3H), 4.44 (t, 1H, J=6 Hz), 7.36 (s, 5H). All the other cyano compounds were isolated by distillation respectively, and explained reasonably by IR and NMR spectra. IId (R^3=C_2H_5), bp 140—142 °C/18 mmHg. IId (R^3=n-C_3H_7), bp 120—122 °C/6 mmHg. IId (R^3=n-C_4H_9), bp 139—140 °C/9 mmHg. Some spectroscopic data and boiling point of other II are as follows. IIa (R^3=CH_3), bp 105—108 °C/6 mmHg (lit,[27] bp 107—108 °C/5 mmHg). IIa (R^3=C_2H_5), bp 110—112 °C/6 mmHg [lit,[28] bp 142—144 °C/14 mmHg]. IIa (R^3=n-C_3H_7), bp 121—122 °C/6 mmHg, IR: 1110 (ν_{C-O}), 760 (phenyl), 700 (phenyl) and 580 (ν_{C-I}) cm^{-1}. NMR: δ 0.73 (t, 3H, J=7 Hz), 1.60 (m, 2H, J=7 Hz), 3.31 (d, 2H, J=6 Hz), 3.32 (t, 2H, J=7 Hz), 4.38 (t, 1H, J=6 Hz) and 7.32 (s, 5H). Found: C, 41.09; H, 4.24%. Calcd for $C_9H_{11}OI$: C, 41.24; H, 4.23%. IIa (R^3=n-C_4H_9), bp 124—125 °C/5 mmHg. IIb (R^3=CH_3), bp 98—99 °C/7.5 mmHg (lit,[29] bp 117—118 °C/15 mmHg), IR 1115 (ν_{C-O}), 760 (phenyl), 700 (phenyl) an 600 (ν_{C-Br}) cm^{-1}, NMR: δ 3.29 (s, 3H), 3.47 (d, 1H J=5.5 Hz), 3.48 (d, 1H, J=7 Hz), 4.37 (q, 1H, J=7 Hz and 5.5 Hz) and 7.33 (s, 5H). IIb (R^3=C_2H_5), bp 90—91 °C/4 mmHg (lit,[30] bp 78 °C/2 mmHg). IIb (R^3=n-C_3H_7), bp 96—98 °C/3.5 mmHg (lit,[29] bp 146—148 °C/27 mmHg). IIb (R^3=n-C_4H_9), bp 112—113 °C/4 mmHg (lit,[29] bp 165—166 °C/32 mmHg). IIc (R^3=CH_3), bp 79—82 °C/4 mmHg, (lit,[31] bp 92—93 °C/8 mmHg), IR, 1115 (ν_{C-O}), 756 (phenyl), 725 (ν_{C-Cl}) and 700 (phenyl) cm^{-1}. NMR: δ 3.32 (s, 3H), 3.62 (d, 1H, J=6 Hz), 3.64 (d, 1H, J=7 Hz), 4.37 (q, 1H, J=7 Hz and 6 Hz) and 7.37 (s, 5H). Found: C, 63.79; H, 6.72%. Calcd for $C_9H_{11}OCl$: C, 63.35; H, 6.50%. IIc (R^3=C_2H_5), bp 86—88 °C/5 mmHg (lit,[31] bp 101—103 °C/8 mmHg). IIc (R^3=n-C_3H_7), bp 88—91 °C/4 mmHg (lit,[31] bp 111—112 °C/8 mmHg). IIc (R^3=n-C_4H_9), bp 98—101 °C/4 mmHg (lit,[31] bp 122—125 °C/8 mmHg). IIe (R^3=CH_3), bp 146—147 °C/9 mmHg, IR, 2150 (ν_{SCN}), 1105 (ν_{C-O}), 770 and 700 (phenyl) cm^{-1}. NMR: δ 3.17 (d, 1H, J=6 Hz), 3.18 (d, 1H, J=7 Hz), 3.27 (s, 3H), 4.41 (q. 1H, J=7 Hz and 6 Hz) and 7.33 (s. 5H).

Authentic Samples for Glc Analysis. IV and IIc were prepared by the reported method[32] from styrene, copper(II) chloride and alcohols. α-Methoxyethylbenzene (IV, R^3=CH_3) was also prepared by alkaline $NaBH_4$ reduction of α-methoxy-β-acetoxymercuriethylbenzene: bp 71—72 °C/23 mmHg; NMR δ 1.42 (d, 3H, J=6.5 Hz), 3.20 (s. 3H), 4.28 (q, 1H, J=6.5 Hz) and 7.30 (s, 5H). VIII was prepared by refluxing 5 mmol of I (R^1=H, R^2=R^3=CH_3) for 5 hr in methanol (25 ml) containing 5 mmol of BF_3 etherate; yield 92%, bp 103—108 °C/28 mmHg, NMR δ 2.90 (d. 2H), 3.33 (s, 6H), 4.55 (t, 1H) and 7.28 (s, 5H). All of IIa were also obtained in pure state from the reaction of styrene with copper(II) chloride and potassium iodide in alcohols (at refluxing temperature for 2—3 hr).[33]

The authors are very grateful to Professor Katsuhiko Ichikawa, Kyoto University, for his helpful discussions.

References

1) R. Criegee, *Angew. Chem.*, **70**, 173 (1958).
2) H. J. Kabbe, *Ann. Chem.*, **656**, 204 (1962).
3) K. C. Pande and S. Winstein, *Tetrahedron Lett.*, **1964**, 3393.
4) K. Kruse and T. M. Bendarski, *J. Org. Chem.*, **36**, 1154 (1971).
5) S. Uemura, K. Sohma, H. Tara, and M. Okano, *Chem. Lett.*, **1973**, 545.
6) a) R. K. Sharma and E. D. Martinez, *Chem. Commun.*, **1972**, 1129. b) R. K. Sharma and N. H. Fellers, *J. Organometal. Chem.*, **49**, C69 (1973).
7) H. Mitani, T. Ando, and Y. Yukawa, *Chem. Lett.*, **1972**, 455.
8) a) S. Uemura, Y. Ikeda, and K. Ichikawa, *Tetrahedron*, **28**, 5499 (1972). b) S. Uemura, Y. Ikeda, and K. Ichikawa, *ibid.*, **28**, 3205 (1972). c) S. Uemura, S. Uchida, M. Okano, and K. Ichikawa, This Bulletin, **46**, 3254 (1973).
9) a) H. Kurosawa and R. Okawara, *J. Organometal. Chem.*, **10**, 211 (1967). b) H. Kurosawa and R. Okawara, *ibid.*, **19**, 253 (1969).
10) A. G. Lee, *ibid.*, **22**, 537 (1970).
11) J. P. Maher and D. F. Evans, *J. Chem. Soc.*, **1965**, 637.
12) F. A. L. Anet, *Tetrahedron Lett.*, **1964**, 3399.
13) For example; H. B. Henbest and B. Nicholls, *J. Chem. Soc.*, **1959**, 227; H, B. Henbest and R. S. McElhinney, *ibid.*, **1959**, 1834; S. Moon and B. H. Waxman, *Chem. Commun.*, **1967**, 1283.
14) White amorphous solid; mp, slowly decomposed over 210 °C. IR 1090 (s)cm^{-1} (ν_{C-O}). Found: C, 46.31; H, 5.60%. Calcd for $C_{22}H_{30}O_2ClTl$: C, 46.66; H, 5.34%.
15) J. Chatt, *Chem. Revs.*, **48**, 7 (1951).
16) P. M. Henry, *J. Org. Chem.*, **36**, 1886 (1971).
17) D. C. Nonhebel and W. A. Waters, *Proc. Roy. Soc., A.*, **242**, 16 (1957).
18) For example; G. M. Whitesides, E. R. Stedronsky, C. P. Casey, and J. San Filippo, Jr., *J. Amer. Chem. Soc.*, **92**, 1426 (1970); K. Wada, M. Tamura, and J. Kochi, *ibid.*, **92**, 6656 (1970).
19) F. A. Cotton and G. Wilkinson, "Advanced Inorganic Chemistry," 3rd Ed., Interscience Publishers, New York, N. Y. (1972), p. 907.
20) F. Basolo and R. G. Pearson, "Mechanism of Inorganic Reactions," 2nd Ed., John Wiley & Sons, New York, N. Y. (1967), p. 23; R. G. Pearson, *Chem. Brit.*, **3**, 103 (1967).
21) O. A. Reutov and I. P. Beletskaya, "Reaction Mechanisms of Organometallic Compounds," North-Holland, Amsterdam (1968), p. 352.
22) H. P. A. Groll, *J. Amer. Chem. Soc.*, **52**, 2998 (1930).
23) H. Gilman and R. G. Jones, *ibid.*, **68**, 517 (1946); H. Gilman and R. G. Jones, *ibid.*, **72**, 1760 (1950).
24) M. Tanaka, H. Kurosawa, and R. Okawara, *J. Organometal. Chem.*, **18**, 49 (1969).
25) C. L. Jenkins and J. K. Kochi, *J. Org. Chem.*, **36**, 3095 (1971).
26) E. Staritzky and D. Walker, *Anal. Chem.*, **28**, 419 (1956).
27) S. Winstein and L. L. Ingraham, *J. Amer. Chem. Soc.*, **77**, 1741 (1955).
28) M. Tiffeneau, *C. R. Acad. Sci., Paris*, **145**, 813 (1907).
29) W. M. Lauer and M. A. Spielman, *J. Amer. Chem. Soc.*, **55**, 4927 (1933).
30) K. Mislow, *ibid.*, **73**, 3954 (1951).
31) P. S. Belov and V. I. Isagnlyants, *Izv. Vyssh. Ucheb. Zaved., Nef i Gaz*, **1958**, 93; *Chem. Abstr.*, **53**, 18901 g (1959).
32) K. Ichikawa, S. Uemura, T. Hiramoto, and Y. Takagaki, *Kogyo Kagaku Zasshi*, **71**, 1657 (1968).
33) A. Onoe, S. Uemura, and M. Okano, to be published.

The Cyclocopolymerization of Triallyl Citrate with Several Vinyl Monomers

Tetsuji OHATA, Akira MATSUMOTO, and Masayoshi OIWA

Department of Applied Chemistry, Faculty of Engineering, Kansai University, Senriyama, Suita, Osaka 565

(Received June 12, 1973)

Triallyl citrate (TAC) was copolymerized with allyl benzoate (ABz), vinyl acetate (VAc), vinyl chloride (VC), acrylonitrile (AN), and styrene (St) at 60 °C with benzoyl peroxide or 2,2′-azobisisobutyronitrile as the initiator; it was considered kinetically in terms of cyclocopolymerization. The following monomer reactivity ratios were obtained: VAc: $r_1=1.29$, $r_2=0.76$, $r_c=0.61$; ABz: $r_1=1.63$, $r_2=1.10$, $r_c=0.47$; VC: $r_1=0.40$; $r_2=1.90$, $r_c=0.31$; AN: $r_1=0.01$, $r_2=8.7$; St: $r_1=0.03$, $r_2=53.0$, where r_1, r_c and r_2 denote the monomer reactivity ratio of the uncyclized, cyclized, and monovinyl radicals respectively. In the copolymerization of TAC with AN, the penultimate effect was also observed: $r_1=r_1'=0.01$, $r_2=k_{122}/k_{121}=11$, $r_2'=k_{222}/k_{221}=5$.

In a previous paper[1] we have suggested that the polymerization of triallyl citrate (TAC) proceeds by means of a cyclopolymerization mechanism analogous to that[2-4] proposed for the polymerization of the diallyl ester. It may, therefore, be expected that the behavior of the copolymerization of TAC with monovinyl monomers can also be accounted in terms of the extension of the cyclocopolymerization mechanism for the copolymerization of the diallyl ester with monovinyl monomer.[2-4]

Thus, this paper is concerned with the copolymerizations of TAC with several monovinyl monomers, including allyl benzoate (ABz), vinyl acetate (VAc), vinyl chloride (VC), acrylonitrile (AN), and styrene (St); radical copolymerizations were conducted, and the results thus obtained will be kinetically discussed in detail. It will deal also with the penultimate effect observed in the copolymerization of TAC with AN.

Experimental

Materials. TAC was prepared by the reaction of citric acid with allyl alcohol according to the method described in the literature.[1]

ABz was obtained as has been described in a previous paper.[2]

VAc,[4] AN,[6] St,[7] and VC[8] as comonomers, 2,2′-azobisisobutyronitrile (AIBN)[8] as an initiator, and *N*,*N*-dimethylformamide[6] as a solvent—these reagents were purified as has been described respectively.

Copolymerization Procedure. The copolymerizations of TAC with VAc,[4] ABz,[2] AN,[6] St,[7] and VC[8] were allowed to proceed in a sealed glass ampoule. After a definite reaction time, the copolymer thus produced was precipitated by pouring the reaction mixture into a large amount of a ethyl ether-petroleum ether mixture (1 : 4 by volume); it was then washed repeatedly with the mixed ether and dried *in vacuo* until a constant weight was obtained. The copolymer was then purified by dissolving in acetone and by subsequently reprecipitating with the mixed ether.

Analyses of Copolymers. The compositions of the purified copolymers were determined by elemental analyses. In the case of the copolymerization of TAC with VAc, the composition of the copolymer was indirectly calculated from the amounts of the unreacted monomer because of the difficulty of direct determination from the analyses of the copolymer; after a definite reaction time, the unreacted VAc monomer was determined by removing it at room temperature from the reaction mixture with a vacuum pump, after which the unreacted TAC monomer was determined by pouring the reaction mixture into a large amount of the ether. The unreacted pendant allyl groups of the TAC-VC copolymer were calculated from the iodine value using the Wijs method,[8] while in the other copolymers, it was calculated from the bromine value determined by the bromide-bromate technique.[1]

The residual unsaturation, R_{us}, was then exhibited as the molar ratio of the unreacted pendant allyl group to the total allyl groups of the TAC incorporated into the copolymer.

Results and Discussion

Figure 1 shows the relations between the relative rate of copolymerization, which is presented as a ratio of the rate of copolymerization to that of the homopolymerization of TAC under the same conditions, and the feed-monomer composition.

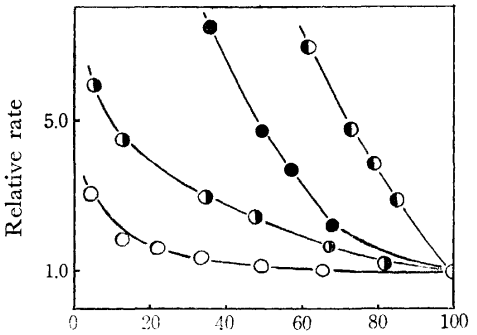

Fig. 1. Relation between the relative rate of copolymerization and the feed-monomer composition.
◐: St, ●: AN, ◑: VC, ○: VAc

The relative rate tended to decrease, as a whole, with an increase in the mole fraction of TAC in the feed; this may be ascribable to the degradative chain transfer of the growing chain end to TAC. On the other hand, its decreasing tendencies changed with the kind of comonomer from the linear lowering for the conjugated monomer (St) to the abrupt one in the low feed-mole fraction of TAC for the unconjugated monomer (VAc); this may be interpreted by considering that the ability of the growing radicals to abstract the allylic hydrogen of TAC decreases with an increase in the conjugation of comonomer, while the possibility of the allyl radical's re-initiating the comonomer is the reverse.

Figure 2 shows the copolymer composition curves based on the data shown in Tables 1—5. In the

Table 1. Copolymerization of TAC (M_1) with VAc (M_2)[a]

Monomer			Time (min)	Conversion (%)	Copolymer	
$[M_1]$ (mol/l)	$[M_2]$ (mol/l)	$[M_1]$ (mol %)			d$[M_1]$[b] (mol %)	R_{us}
3.09	1.63	65.49	210	9.18	84.99	0.494
2.73	2.71	50.12	200	9.19	70.94	0.488
2.18	4.34	33.44	180	9.57	63.25	0.485
1.64	5.97	21.40	160	9.90	48.16	0.481
1.09	7.60	12.55	90	6.15	34.74	0.479
0.73	8.68	7.73	60	4.44	—	0.476

a) In bulk, total volume 20 ml, [BPO] = 0.04 mol/l, polymerization temperature 60 °C. b) The composition of the copolymer was determined by tracing the unreacted monomer.

Table 2. Copolymerization of TAC (M_1) with ABz (M_2)[a]

Monomer			Time (min)	Conversion (%)	Copolymer		
$[M_1]$ (mol/l)	$[M_2]$ (mol/l)	$[M_1]$ (mol %)			Carbon contents (%)	d$[M_1]$ (mol %)	R_{us}
2.91	1.29	69.19	140	7.32	58.87	86.99	0.463
2.54	1.94	56.71	160	6.68	60.08	75.23	0.441
2.18	2.59	45.71	190	5.17	61.54	62.81	0.436
1.64	3.56	31.47	230	6.48	62.89	52.73	0.414
1.09	4.53	19.39	235	4.85	65.13	38.40	0.418
0.55	5.50	9.01	330	2.85	68.61	20.58	0.397

a) In bulk, total volume 10 ml, [BPO] = 0.1 mol/l, polymerization temperature 60 °C.

Table 3. Copolymerization of TAC (M_1) with VC (M_2)[a]

Monomer			Time (min)	Conversion (%)	Copolymer		
$[M_1]$ (mol/l)	$[M_2]$ (mol/l)	$[M_1]$ (mol %)			Chlorine contents (%)	d$[M_1]$ (mol %)	R_{us}
1.17	0	100	350	7.37	0	100	0.396
1.06	0.50	67.73	250	8.45	4.11	71.93	0.409
0.94	1.01	48.26	200	10.13	8.57	52.93	0.431
0.82	1.51	35.24	160	10.67	12.29	41.98	0.452
0.70	2.01	25.91	130	7.77	16.62	32.57	0.459
0.47	3.02	13.45	100	9.44	25.93	19.20	0.473
0.23	4.02	5.51	80	9.84	36.41	10.04	0.497
0	5.02	0	40	7.20	56.72	0	—

a) Benzene 10 ml, total monomer *ca.* 5 ml, [AIBN] = *ca.* 0.05 mol/l (123 mg), polymerization temperature 60 °C.

Table 4. Copolymerization of TAC(M_1) with AN(M_2)[a]

Monomer			Time (min)	Conversion (%)	Copolymer		
$[M_1]$ (mol/l)	$[M_2]$ (mol/l)	$[M_1]$ (mol %)			Nitrogen contents (%)	d$[M_1]$ (mol %)	R_{us}
1.82	0	100	300	3.51	0	100	0.435
1.73	0.38	81.97	260	3.57	4.93	42.52	0.448
1.64	0.76	68.29	220	5.60	6.71	33.27	0.501
1.54	1.14	57.55	180	7.44	8.11	27.70	0.522
1.45	1.52	48.90	150	8.02	9.47	23.29	0.540
1.27	2.28	35.82	120	10.15	11.85	17.26	—
1.09	3.04	26.41	90	9.61	13.23	14.46	—
0.73	4.56	13.75	70	10.38	17.51	7.94	—
0.36	6.08	5.64	50	7.30	22.03	3.37	—

a) Dimethylformamide 10 ml, total monomer 10 ml, [BPO] = 0.01 mol/l, polymerization temperature 60 °C.

TABLE 5. COPOLYMERIZATION OF TAC (M_1) WITH St (M_2)[a]

Monomer			Time (min)	Conversion (%)	Copolymer		
$[M_1]$ (mol/l)	$[M_2]$ (mol/l)	$[M_1]$ (mol %)			Carbon contents (%)	d$[M_1]$ (mol %)	R_{us}
3.39	0.58	85.36	250	2.95	73.80	27.65	0.560
3.27	0.87	78.94	250	4.03	77.47	19.96	—
3.15	1.16	73.02	230	4.70	80.46	14.73	—
2.91	1.75	62.48	210	6.38	84.56	8.72	0.565
2.67	2.33	53.38	200	7.02	86.71	6.00	0.575
2.42	2.91	45.44	190	8.35	87.59	4.95	0.595

a) In bulk, total volume 15 ml, [BPO] = 0.01 mol/l, polymerization temperature 60 °C.

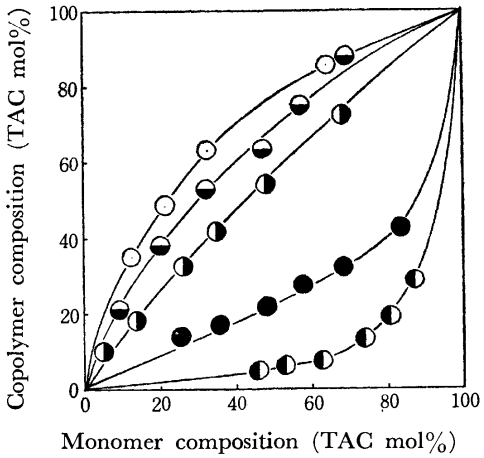

Fig. 2. Copolymer composition curves for the copolymerizations of TAC with several monovinyl monomer at 60 °C; (——) calculated curves based on the monomer reactivity ratios (see Table 6), (○) experimental results.
○: VAc, ◒: ABz, ◑: VC, ●: AN, ◐: St

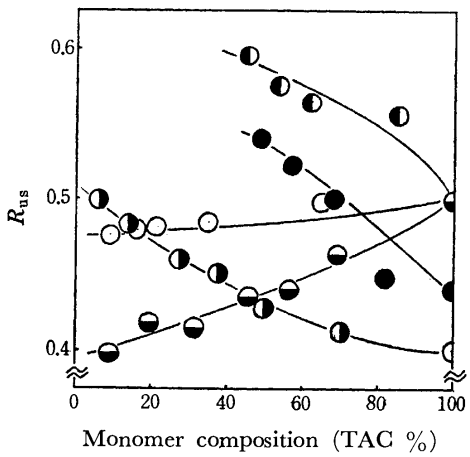

Fig. 3. Relationships between R_{us} and the feed-monomer composition.
◐: St, ●: AN, ○: VAc, ◒: ABz, ◑: VC

copolymerization with ABz, VAc, and VC, the mole fraction of TAC in the copolymer is always larger than that in the feed, but in the other copolymerization systems (M_2: AN and St) it is always smaller. These tendencies were also observed in the copolymerizations of diallyl phthalate.[2,4,6-8]

The relations between R_{us} and the mole fraction of TAC in the feed are shown in Fig. 3, where the different values of R_{us} denoted for the homopolymerization of TAC are due to the difference in the possibility of cyclization reaction between the bulk copolymerization for the TAC–St, VAc, and ABz copolymerization systems and the solution copolymerization for the TAC–AN and VC systems. In the copolymer of TAC with St, AN, and VC(M_2), R_{us} increases with an increase in mole fraction of M_2 in the feed, while with ABz and VAc (M_2) it decreases with an increase in the mole fraction of M_2. Now, it should be noted that R_{us} must be 0.667 if no cyclization and crosslinking reactions occur. On the other hand, in the early stage of polymerization the crosslinking reaction is probably negligible. The deviation of R_{us} from 0.667 may, therefore, be attributed predominantly to the intramolecular cyclization reaction. Thus, the above results suggest that, in the copolymerizations with St, AN, and VC, the cyclization reaction has a tendency to be hindered with an increase in the mole fraction of the comonomer in the feed, while in the copolymerizations with ABz and VAc the cyclization reaction comes to be promoted with an increase in the mole fraction of the comonomer. Similar results were also obtained in the copolymerizations of the diallyl ester;[2-4,6,8] these results can be understood by considering the competition among the unimolecular cyclizations with the allyl group of the same monomer unit, the bimolecular propagation with another diallyl-ester monomer or with the comonomer of the uncyclized radical produced by the radical attack on one allyl group of the diallyl ester.

Determination of the Monomer Reactivity Ratio. In the copolymerizations of TAC with several monovinyl monomers, the cyclization reaction of TAC is not negligible, as may be seen in Fig. 3. On considering the copolymerization mechanism of the triallyl ester (M_1) with the monovinyl monomer(M_2), it is necessary to discuss the possibility of a bicyclo-intramolecular propagation of M_1. However, in the copolymerization of TAC the occurrence of the bicyclo-intramolecular propagation reaction is negligible, as can be seen from the results of the homopolymerization of TAC in our previous paper.[1]

Thus, these copolymerizations may be treated as extensions of the mechanism of the cyclocopolymerization of the divinyl monomer with the monovinyl monomer.[4] The reactions, (1)—(7), can, then, be given as the propagation reactions for copolymerization.

$$M_1\cdot + M_1 \longrightarrow M_1\cdot \qquad 3k_{11}[M_1\cdot][M_1] \qquad (1)$$

$$M_1\cdot + M_2 \longrightarrow M_2\cdot \qquad k_{12}[M_1\cdot][M_2] \qquad (2)$$

$$M_1\cdot \longrightarrow m\cdot \qquad 2k_c[M_1\cdot] \qquad (3)$$

$$m\cdot + M_1 \longrightarrow M_1\cdot \qquad 3k_{c1}[m\cdot][M_1] \qquad (4)$$

$$m\cdot + M_2 \longrightarrow M_2\cdot \qquad k_{c2}[m\cdot][M_2] \qquad (5)$$

$$M_2\cdot + M_1 \longrightarrow M_1\cdot \qquad 3k_{21}[M_2\cdot][M_1] \qquad (6)$$

$$M_2\cdot + M_2 \longrightarrow M_2\cdot \qquad k_{22}[M_2\cdot][M_2] \qquad (7)$$

where M_1 is the TAC monomer; M_2, the monovinyl monomer, and m·, the cyclized radical formed by the intramolecular cyclization of M·. On the basis of the seven propagation reactions presented above, Eqs. (8)—(10) were derived:

$$\frac{3(2-3R_{us})}{3R_{us}+\alpha-1}[M_1]=2K_c-\frac{1}{r_1}\cdot\frac{2-3R_{us}}{3R_{us}+\alpha-1}\cdot[M_2] \qquad (8)$$

$$r_2=\frac{F}{f}\cdot\frac{(1+r_cF)(1+r_1F+2K_c'/[M_2])}{1+r_cF+2K_c'/[M_2]}-F \qquad (9)$$

$$r_2=\frac{F^2}{f(2-3R_{us})}\cdot\frac{2K_c'(r_c+1/F)}{2K_c'+3[M_1](r_c+1/F)}-F \qquad (10)$$

where $r_1=k_{11}/k_{12}$, $r_2=k_{22}/k_{21}$, $r_c=k_{c1}/k_{c2}$, $K_c=k_c/k_{11}$ $K_c'=k_c/k_{12}$ $(r_1\times K_c)$, $f=d[M_1]/d[M_2]$, and $F=3[M_1]/[M_2]$. Here, α is the ratio of the non-consecutive cyclization to the intramolecular cyclization in the same monomer unit, as in the homopolymerization of TAC.[1]

The experimental results may be discussed on the basis of Eqs. (8)—(10). First, in the copolymerizations of TAC with VC, VAc, and ABz, the values of r_1 and K were evaluated by using Eq. (8), and consequently K_c' was determined from $r_1\times K_c$. By using the results thus obtained, we can further evaluate the values of r_2 and r_c from Eq. (9) or (10). The results thus obtained are summarized in Table 6.

Table 6. Monomer reactivity ratios

M_2	r_1	r_2	r_c
VAc[a]	1.29	0.76	0.61
VBz[a]	1.63	1.10	0.47
VC[a]	0.40	1.90	0.31
AN[b]	0.01	8.7	—
St[b]	0.03	53.0	—

a) Estimated on the basis of cyclocopolymerization mechanism. b) Estimated from the general copolymer composition equation.

On the other hand, to the copolymerization of TAC with St the treatment of cyclocopolymerization could not be applied since the copolymerizability was very low; therefore, the accuracy of the analyses was significantly influenced by scatter of the experimental data. As a result, the value shown in Table 6 was obtained by using the usual copolymer composition equation.

Now, it should be noted that the penultimate effect was observed in the copolymerization of TAC with AN. Therefore, the relation between d[AN]/d[TAC] and [AN]/[TAC] was plotted in order to estimate the values of r_2 and r_2' using the method of Joshi[9] (Fig. 4); thus, $r_1=r_1'=0.01$, $r_2=11$, and $r_2'=5$. This suggests that the rate of the addition of the AN monomer to the AN radical with the penultimate TAC unit is twice as large as that with the penultimate AN unit.

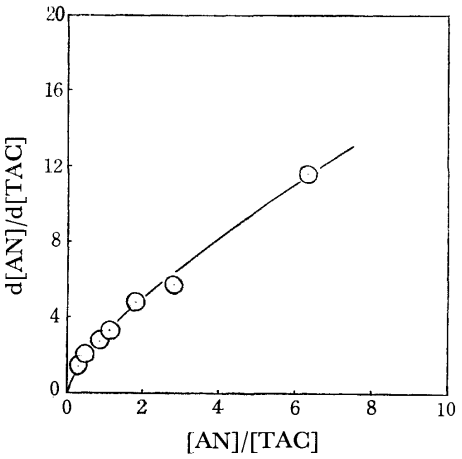

Fig. 4. Evalution of r_2 and r_2' in the copolymerization of TAC with AN.

The difference between r_1 and r_c is also a matter of interest, since r_1 and r_c correspond to the reactivities of the uncyclized and the cyclized radicals respectively. The experimental results show that r_1 is considerably larger than r_c; this may be due to the fact that the existence of steric hindrance in the addition reaction of the cyclized radical with TAC can be expected in light of the molecular model. Such a tendency has also been observed in the copolymerizations of diallyl phthalate with several monovinyl monomers, as has been reported previously.[2,4,8]

References

1) A. Matsumoto, T. Ohata, and M. Oiwa, This Bulletin, **47**, 673 (1974).
2) A. Matsumoto and M. Oiwa, *Kogyo Kagaku Zasshi*, **72**, 2127 (1969).
3) A. Matsumoto and M. Oiwa, *J. Polym. Sci., Part A-1* **7**, 3607 (1971).
4) A. Matsumoto, H. Muraoka, M. Taniguchi, and M. Oiwa, *Kogyo Kagaku Zasshi*, **74**, 1913 (1971).
5) V. Avwers and Moosbrugger, *Ann. Chem.*, **387**, 199 (1912).
6) A. Matsumoto, S. Shoda, T. Harada, and M. Oiwa, *Kogyo Kagaku Zasshi*, **70**, 1007 (1967).
7) A. Matsumoto and M. Oiwa, *ibid.*, **70**, 360 (1967).
8) A. Matsumoto, T. Ise, and M. Oiwa, *Nippon Kagaku Kaishi*, **1972**, 209.
9) R. M. Joshi, *J. Polym. Sci.*, **17**, 125 (1955).

The Reduction of Methyl Acetate with Several Hydrosilanes under γ Irradiation

Ren NAKAO, Tsugio FUKUMOTO, and Jitsuo TSURUGI

Radiation Center of Osaka Prefecture, Shinke-cho, Sakai, Osaka 593

(Received July 13, 1973)

The reduction of methyl acetate with chlorinated hydrosilanes, $HSiCl_{3-n}R_n$ ($R=CH_3$ or OCH_3, $n=0$—2), and triethylsilane under γ irradiation has been studied. The hydrosilanes other than triethylsilane reduce the ester to ethyl methyl ether. The reaction rate is proportional to the hydrosilane concentration and is independent of the methyl acetate concentration. The results indicate that the rate-determining step in the reduction reaction is the hydrogen abstraction from the hydrosilanes. The reactivities of the chlorinated hydrosilanes in the reaction increase with the progressive chlorine substitution on the silicon atom and may be due to the susceptibility of each H–Si bond toward free radicals, $CH_3\text{–}\dot{C}(\text{–}O\text{–}SiX_3)\text{–}OCH_3$.

Previously, we reported that the aliphatic carboxylates can be reduced to dialkyl ethers with trichlorosilane under γ irradiation.[1] Kinetic work[2] on this reduction and the reduction of acetals[3] with trichlorosilane have indicated that the mechanism for the reduction of the ester with trichlorosilane consists of three sequences. The first is the radical-chain addition of trichlorosilane to a carbonyl group of a carboxylate (Eqs. (1) and (2)). The second is the ionic chlorination of the adduct (I) by chlorosilanes, giving an α-chloro ether (II) (Eq. (3)). The third is the reduction of α-chloro ether to an ether with trichlorosilane (Eqs. (4) and (5)).

$$\cdot SiX_3 + R\text{-}\underset{\underset{O}{\|}}{C}\text{-}OR' \rightarrow R\text{-}\underset{\underset{O\text{-}SiX_3}{|}}{\dot{C}}\text{-}OR' \quad (1)$$

$$R\text{-}\underset{\underset{OSiX_3}{|}}{\dot{C}}\text{-}OR' + HSiX_3 \rightarrow R\text{-}\underset{\underset{O\text{-}SiX_3}{|}}{CH}\text{-}OR' \ (I) + \cdot SiX_3 \quad (2)$$

$$(I) + Cl\text{-}Si\lessgtr \rightarrow R\text{-}CHCl\text{-}OR' \ (II) + X_3SiOSi\lessgtr \quad (3)$$

$$(II) + \cdot SiX_3 \rightarrow R\text{-}\dot{C}H\text{-}OR' + ClSiX_3 \quad (4)$$

$$R\text{-}\dot{C}H\text{-}OR' + HSiX_3 \rightarrow R\text{-}CH_2\text{-}OR' + \cdot SiX_3 \quad (5)$$

It seems interesting to examine whether chlorinated hydrosilanes containing the general formula $HSiCl_{3-n}R_n$ ($R=CH_3$ or OCH_3, $n=0$—2) can be used in the reduction of the ester, and, if so, which is the most efficient reagent. With these points in view, trichlorosilane, methyldichlorosilane, dimethylchlorosilane, methoxydichlorosilane, dimethoxychlorosilane, and triethylsilane were allowed to react with methyl acetate and acetaldehyde dimethyl acetal under γ irradiation.[4]

Results and Discussion

All the reactions were carried out in tetrachlorosilane as a solvent. Our previous paper[3] reported that all chlorinated silanes including tetrachlorosilane can chlorinate an acetal-type intermediate (I) to an α-chloro ether (II) in Eq. (3), and that the chlorination is instantaneous. In the present experiments, tetrachlorosilane as a solvent behaves as the chlorinating agent[5] in Eq. (3), and the chlorinated hydrosilanes ($HSiCl_{3-n}R_n$) used may be regarded as participating only in the first sequence (Eqs. (1) and (2)) and the third sequence (Eqs. (4) and (5)).

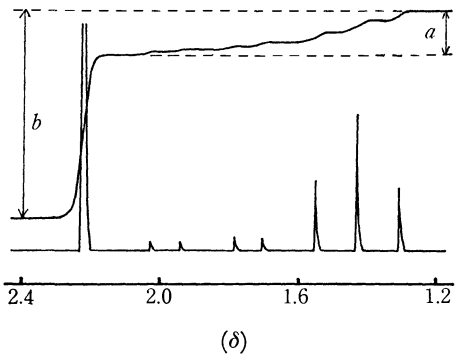

Fig. 1. NMR spectrum and integration curve of an irradiated mixture of methyl acetate and trichlorosilane (see the footnote (a) in Table 1), where singlet at δ 2.22 was attributable to $CH_3C(O)$- of methyl acetate, and two doublets at δ 1.74 and 1.98, and triplet at δ 1.43 were assigned to the corresponding methyl protons of the adduct, α-chloroethyl methyl ether, and ethyl methyl ether, respectively. Dose rate; 1.7 M rad/h and dose; 0.9 M rad.

A typical example of the NMR spectrum of a γ-irradiated mixture of methyl acetate and trichlorosilane in tetrachlorosilane is shown in Fig. 1. Small amounts of the adduct ((I), in which $R=R'=CH_3$ and $X=Cl$) and α-chloroethyl methyl ether were detected, together with the unchanged ester and the ethyl methyl ether produced.

In order to shed light on the mechanism, it seems necessary to determine the rates of the first sequence (adduct formation) and the third sequence (the reduction of α-chloro ether) separately. Because of the (ester→I→II→ether) sequence and the equimolar relationship[2] between species, the rate of the adduct formation at any given reactant concentration can be obtained by determining the total sum of the adduct, the α-chloro ether, and the ether in the reaction system. When a mixture of a hydrosilane and methyl acetate (3 : 1 molar ratio) in tetrachlorosilane was irradiated for various time periods, a plot of the total sum against the irradiation time was found to be a straight line up to *ca.* a 30% conversion of methyl acetate. The rates of the adduct formation, which were calculated from

Table 1. Rates of the reactions with several hydrosilanes

Hydrosilane	Rate of reduction[a] (mol/l·h), (A)	Rate of reduction[b] (mol/l·h), (B)	R_{add}/R_{red}[c] (2A/3B)
$HSiCl_3$	0.76	0.77	0.66
$HSiCl_2Me$	0.15	0.13	0.79
$HSiCl_2OMe$	0.09	0.14	0.44
$HSiClMe_2$	0.05	0.08	0.41
$HSiCl(OMe)_2$	0.03	0.05	0.39

Dose rate; 1.7 M rad/h. a) CH_3COOCH_3; 0.7 mmol; hydrosilane; 2.1 mmol, $SiCl_4$; 1 ml. b) $CH_3CH(OCH_3)_2$; 0.7 mmol, hydrosilane; 1.4 mmol, $SiCl_4$; 1 ml. c) This value was corrected by a factor of 2/3, since the addition and reduction reactions were carried out with 3 : 1 aad 2 : 1 molar excess of each hydrosilane, respectively, and the rates of both reactions were proportional to hydrosilane concentration as described in the text. Detailed calculations on the concentrations of each hydrosilane in both the addition and reduction reactions show that the factor 2/3 is approximately correct to obtain the ratio R_{add}/R_{red} at the same concentration.

the respective slopes of the straight lines for five hydrosilanes, are shown in Table 1.

As to the third sequence, we can utilize the following reaction. Our previous paper[3] reported that the simple mixing of acetaldehyde dimethyl acetal and tetrachlorosilane gave α-chloroethyl methyl ether.

$$CH_3CH(OCH_3)_2 + Cl_4Si \rightarrow CH_3CHClOCH_3 + Cl_3SiOCH_3$$

Therefore, acetaldehyde dimethyl acetal in tetrachlorosilane was allowed to react with hydrosilanes (1 : 2 molar ratio) under γ irradiation. The rates of the reduction of the α-chloro ether at given reactant concentrations can be obtained by determining the amount of ethyl methyl ether produced, these rates are shown in Table 1 (the time plot is a straight line in this case also). In both reactions (the addition to the carboxylate and the reduction of the α-chloro ether), the reactivities of the hydrosilanes increase with progressive chlorine substitution on the silicon atom, as Table 1 shows.

R_{add}/R_{red}, the ratio of the rate of the addition to that of the reduction at the same hydrosilane concentration for the individual hydrosilane, is given in the last column of Table 1. All of the ratios are smaller than unity. This result clearly indicates that the adduct formation is rate-determining. This is consistent with the fact that little α-chloroethyl methyl ether was detected in the reaction mixture when hydrosilanes other than methyldichlorosilane were used. When methyldichlorosilane was used, however, the α-chloro ether was detected by NMR. This result coincides with the R_{add}/R_{red} ratio for methyldichlorosilane, which is 0.79—the largest in the series.

The dependence of both rates on the reactant concentrations was investigated by using methoxydichlorosilane as a representative. The results for the addition to methyl acetate and for the reduction of α-chloroethyl

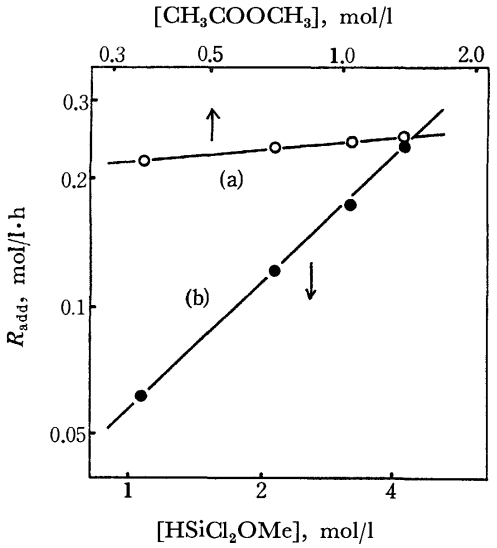

Fig. 2. Variation in the rate of the adduct formation with reactant concentrations under a given dose rate of 1.7 M rad/h. (a); $[HSiCl_2OMe]=4$ mol/l, (b); $[CH_3COOCH_3]=0.7$ mol/l.

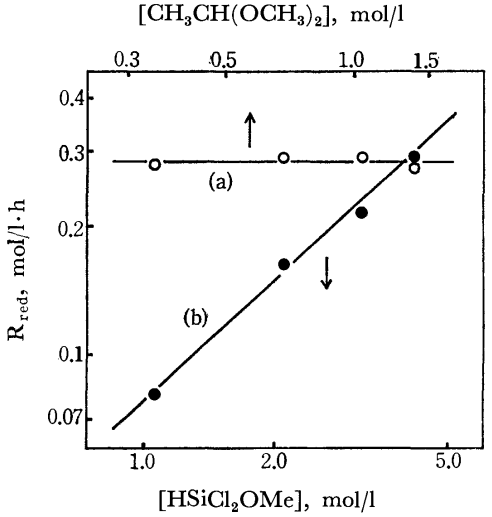

Fig. 3. Variation in the rate of the reduction of α-chloroethyl methyl ether with reactant concentrations under a given dose rate of 1.7 M rad/h. (a); $[HSiCl_2OMe]=4$ mol/l, (b); $[CH_3CH(OCH_3)_2]=0.7$ mol/l.

methyl ether are shown in Figs. 2 and 3 respectively, where the (a) lines give a run with a constant methoxydichlorosilane concentration and with various concentrations of methyl acetate or acetaldehyde dimethyl acetal, while the (b) lines show one with a constant concentration of the ester or the acetal and with various concentrations of the hydrosilane. The two slopes calculated from the (a) and (b) lines in Fig. 2 were 0.05 and 0.97, while those obtained from Fig. 3 were zero and 0.93, respectively. Thus, both the addition and reduction reaction rates were proportional to the methoxydichlorosilane concentration and were independent of the carboxylate or acetal concentration. The same dependence had been observed in the addition reaction of trichlorosilane[2] to the ester (the first sequence in the reduction of the ester). The results

presented above suggest that the rate-determining step of the addition sequence is Eq. (2), while that of the reduction sequence of the α-chloro ether is Eq. (5). The results mean that the hydrogen abstraction steps are rate-determining in both sequences.

When γ irradiation is carried out under the same conditions, the rate of the radical formation may be regarded as identical in all the reactions using any hydrosilane. Therefore, we concluded that the rates in Table 1 correspond to the reactivities of each Si–H bond toward either $CH_3-\dot{C}(O-SiX_3)-OCH_3$ or $CH_3-\dot{C}H-OCH_3$. The reactivity increases with the progressive introduction of chlorine, which is an electron-withdrawing atom, on the silicon atom. The reactivities of Me_3SiH, $MeCl_2SiH$, and Cl_3SiH for hydrogen abstraction by methyl radicals have been reported[6] to increase consistently with an increase in the amount of chlorine on the silicon atom. Nagai and Sakurai[7] described that an electron-withdrawing group on a silicon atom decreases the contribution of $\rangle Si^+H^-$ in the resonance formula: $\rangle Si-H \leftrightarrow \rangle Si^+H^-$, thus causing the bond strength of Si–H to become weak. In this connection, the reactivities of hydrosilanes on the hydrogen abstraction by the attack of halogenated methyl radicals, $Cl_3C\cdot$ or $Cl_2HC\cdot$, have been reported[8] to decrease with the progressive introduction of an electron-withdrawing group on the silicon atom. Kerr *et al.*[9] reported that the reaction rates of $F_2HC\cdot$ and $FH_2C\cdot$ radicals toward hydrogen abstraction from $HSiCl_3$ were lower than the corresponding rate for $H_3C\cdot$ radicals and explained the result in terms of a polar repulsion between $HSiCl_3$ and the fluorinated methyl radicals. It is clear from the above literature[6-9] that the $CH_3-\dot{C}(O-SiEt_3)-OCH_3$ and $CH_3-\dot{C}H-OCH_3$ radicals in this paper behave like methyl radicals rather than like halogenated methyl radicals.

We attempted the γ-induced reduction of methyl acetate with triethylsilane in tetrachlorosilane, but ethyl methyl ether was not detected by gas chromatography. On the other hand, acetaldehyde dimethyl acetal could be reduced to ethyl methyl ether in a high yield under the same conditions.[3] If the adduct, $CH_3-CH(O-Si_3)-OCH_3$, were produced, the adduct had to be reduced *via* α-chloroethyl methyl ether[10] to ethyl methyl ether under the same conditions. Consequently, these facts indicate that triethylsilane, containing no chlorine atom, cannot be added to the carbonyl group of methyl acetate.

Experimental

The NMR spectra were recorded on JNM 3H-60, with tetramethylsilane as the external standard. Gas chromatographies were determined by means of a Yanagimoto GCG-5DH, with a 3-m column containing 30% dioctyl phthalate on Celite 545 and using helium as the carrier gas.

Materials. The methoxydichlorosilane (bp 51 °C) was prepared by the methanolysis of trichlorosilane.[3] The dimethoxychlorosilane was synthesized in a similar manner: bp 70 °C (lit,[11] 70.5 °C).

The other reagents, commercial materials, were previously distilled and stored in an ampoule.

Procedure for γ Irradiation. To an NMR tube which was attached to a vacuum line, given amounts of tetrachlorosilane, methyl acetate, and hydrosilane were transferred successively by means of the vacuum line. Although the procedure on using acetaldehyde dimethyl acetal as a starting material was almost identical with those described above, a hydrosilane was added after the mixture of tetrachlorosilane and the acetal had stood for 30 min. The tube, after being sealed, was irradiated by γ-rays from a ^{60}Co source.

Estimation of Products. The adduct was estimated by the use of the NMR intensity of the methyl proton which resulted from the $CH_3C(O)$ in methyl acetate. The results were obtained from the average values of ten scannings. For example, the yield of the addition reaction was calculated by the use of the a/b ratio in Fig. 1, where (a) showed the total methyl intensity of the adduct, α-chloroethyl methyl ether, and ethyl methyl ether, and where (b) gave the sum of (a) and the intensity of the unchanged methyl acetate. The yield of the reduction reaction was estimated in the same manner as above by a comparison of the corresponding methyl intensity of the ether with that of α-chloroethyl methyl ether.

References

1) J. Tsurugi, R. Nakao, and T. Fukumoto, *J. Amer. Chem. Soc.*, **91**, 4587 (1969).

2) Y. Nagata, T. Dohmaru, and J. Tsurugi, *J. Org. Chem.*, **38**, 795 (1973).

3) R. Nakao, T. Fukumoto, and J. Tsurugi, *ibid.*, **37**, 4349 (1972).

4) The photoinduced decomposition of di-*tert*-butyl peroxide and UV irratiation can initiate the reduction as well as γ irradiation can. However, the use of the peroxide is inconveniently followed by the side reaction of hydrosilane with the acetone produced by the decomposition of the peroxide, and UV irradiation has to be carried out in a quartz NMR tube.

5) An earlier article (B. G. Gowenlock and K. E. Thomas, *J. Chem. Soc.*, **1965**, 5068) has reported an unusually weak Cl_3Si-Cl bond in tetrachlorosilane, leading to the view that tetrachlorosilane behaves exclusively as a chlorinating agent.

6) J. A. Kerr, D. H. Slater, and J. C. Young, *J. Chem. Soc., A*, **1966**, 104; **1967**, 134.

7) Y. Nagai and H. Sakurai, "Yuriki no Kagaku," Nankodo, Tokyo (1967), p. 246.

8) Y. Nagai, H. Matsumoto, M. Hayashi, E. Tajima, and H. Watanabe, This Bulletin, **44**, 3113 (1971).

9) J. A. Kerr and D. M. Timlin, *Int. J. Chem. Kinet.*, **3**, 1 (1971).

10) It was reported that $CH_3-CH(O-SiEt_3)-OC_2H_5$ reacted with chlorosilane to give α-chloroethyl ethyl ether in a high yield.[3] It is very natural that $CH_3-CH(O-SiEt_3)-OCH_3$ is also thought to give α-chloroethyl methyl ether.

11) O. J. Klejnot, *Inorg. Chem.*, **2**, 825 (1963).

Chemistry of Nitrosoimines. VI.[1] Attempted Syntheses of Some[1] Resonance Stabilized Nitrosoimines and Their UV Spectra

Kin-ya AKIBA, Satoru MATSUNAMI, Chikahiko EGUCHI, and Naoki INAMOTO

Department of Chemistry, Faculty of Science, The University of Tokyo, Hongo, Tokyo 113

(Received October 27, 1973)

1,1,3,3-Tetrasubstituted 2-nitrosoguanidines, the attempted syntheses and UV spectra of which are reported, are unstable, and decomposed into the corresponding ureas and nitrogen, only 2-nitroso-1,1,3,3-tetraphenylguanidine (**1f**) being obtained as a pure compound. The reaction of **1f** with phenyl isocyanate gave pentaphenylguanidine, probably through 1,4-cycloaddition.

N-Nitrosoaldimines were suggested as being intermediates to explain the formation of aldehydes during the course of reaction of alkylidenetriphenylphosphoranes with nitric oxide.[2] Thoman and Hunsberger reported the syntheses of sterically hindered *N*-nitrosoketimines and showed basic characters of *N*-nitrosoimines for the first time.[3]

We report herewith on the attempted syntheses of resonance stabilized *N*-nitrosoimines such as 1,1,3,3-tetrasubstituted 2-nitrosoguanidines, their UV spectra, decomposition rates of one of them in a few solvents and some reactions of 2-nitroso-1,1,3,3-tetraphenylguanidine (**1f**).

1,1,3,3-Tetrasubstituted guanidines (**2a—f**) and *S*-benzyl-*N*-ethyl-*N*-phenylisothiourea (**2g**) were nitrosated with nitrosyl chloride in carbon tetrachloride in the presence of anhydrous sodium acetate at *ca.* −20 °C according to the reported procedure.[3] Upon the mixing of two reagents, a yellow to orange red color appeared in the solution according to the structure of the product.

All the nitrosoimines (**1a—e,g**) except 2-nitroso-1,1,3,3-tetraphenylguanidine (**1f**) decomposed to the corresponding carbonyl compounds, *i.e.*, ureas (**3a—e**) and thiolcarbamate (**3g**), during the course of reaction and isolation.

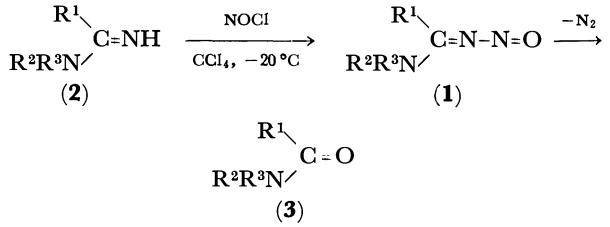

Scheme 1.

	R^1	R^2	R^3	Yield (%)
a :	Me_2N	Me	Me	53
b :	Et_2N	Et	Et	11*
e :		$(CH_2)_5$		65
d :		$(CH_2)_2O(CH_2)_2$		57
e :	PhMeN	Me	Ph	61
f :	Ph_2N	Ph	Ph	91
g :	$PhCH_2S$	Et	Ph	86

* The low yield is due to isolation procedure, during which the reaction mixture was kept at low pressure for a long time to evaporate the solvent before distillation.

Ths isolated yields of carbonyl compounds (**3**) are shown in Scheme 1.

Nitrosation of **2a—d** and **2g** was attempted at lower temperatures (−60 to −70 °C) in dichloromethane.

Table 1. Absorption spectra of nitrosoimines (**1**)

	Nitrosoimine	Solvent	λ_{max} (nm)[a] $\pi\rightarrow\pi^*$	$n\rightarrow\pi^*$
1a	$(Me_2N)_2C=N-N=O$	CH_2Cl_2	277 (sh)	[b]
1b	$(Et_2N)_2C=N-N=O$	CH_2Cl_2	277	458
1c		CH_2Cl_2	276	462
1d		CH_2Cl_2	276	473
1e	$(PhMeN)_2C=N-N=O$	$CHCl_3$	289 (sh)	488
1f	$(Ph_2N)_2C=N-N=O$	$CHCl_3$	330 (9550)	519 (183)
1g		CH_2Cl_2	330 (sh)	504
1h	$(4\text{-}ClC_6H_4)_2C=N-N=O$[c]	CCl_4	306 (8770)	522, 596 (107) (107)
1i		EtOH	310	523, 585
1j		$CHCl_3$	354 (11800)	506 (62)

a) Numerical values in parentheses show molar extinction coefficients. b) Decomposition too rapid for measurement. c) Ref. 3. d) Ref. 4a.

Table 2. UV spectra of guanidines (**2**)

	Guanidine	Solvent	λ_{max} (nm)	ε
2b	$(Et_2N)_2C=NH$	EtOH	225	9.5×10^3
2c		EtOH	224	7.0×10^3
2d		EtOH	224	1.1×10^4
2e	$(PhMeN)_2C=NH$	EtOH	231 250	1.5×10^4 1.2×10^4
2f	$(Ph_2N)_2C=NH$	EtOH	265 (broad)	2.3×10^4
2j		$CHCl_3$	281 288	5.3×10^3 5.9×10^3

The color of the resulting *N*-nitrosoimines (**1**) was deeper and more intense, yellow orange to red brown.

UV spectra of nitrosoimines are shown in Table 1 together with those of three reference compounds (**1h**—**j**).

Nitrosoimines have two characteristic bands (π-π^* and n-π^*). The π-π^* bands are shifted to longer wavelengths than those of the corresponding imines by 50—70 nm (Table 2).

These π-π^* bands can be attributed to neither the separate imino nor nitroso groups,[4] and are probably due to the nitrosoimino group with a large contribution of canonical structures **1'** and **1''**.

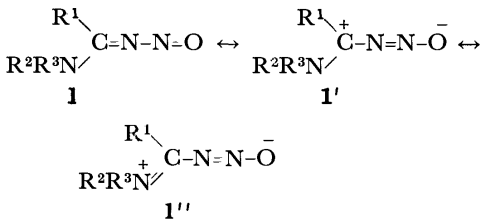

The π-π^* band shifts further toward a longer wavelength with substitution by a phenyl on the nitrogen (**1e**, **f**, **g**). The effect is common to the parent imines (**2**), but larger in the case of nitrosoimines (**1**).

It might be of interest to note that n-π^* bands of **1a**—**d** are shifted toward longer wavelengths while their π-π^* bands remain constant.

The n-π^* bands of **1** are expected to consist of two components at least, *viz.*, $_{N(C=N)}$n-π^* and $_{N(N=O)}$n-π^*. This was found in the case of nitrosoketimines (**1h**, **i**),[3] but not in our case (Table 1).

UV spectra and rates of decomposition of bis(morpholino)-*N*-nitrosomethyleneimine (**1d**) were measured in four solvents. The results are shown in Table 3. The blue shift of the n-π^* band is very large (473 nm in CH_2Cl_2 and 418 nm in H_2O). Three peaks appear as n-π^* bands in alcohols but the reason is not clear.

TABLE 3. SOLVENT EFFECT ON ABSORPTION SPECTRA AND DECOMPOSITION RATES OF BIS(MORPHOLINO)-*N*-NITROSOMETHYLENEIMINE (**1d**)

Solvent	λ_{max} (nm)		k (s^{-1}) (13.5 °C)
	$\pi\rightarrow\pi^*$	n$\rightarrow\pi^*$	
CH_2Cl_2	276	473	3.5×10^{-3}
EtOH	276 (sh)	404, 423.5, 443 (sh)	2.8×10^{-4}
MeOH	274.5	404, 425.5, 441 (sh)	4.0×10^{-4}
H_2O	268.5	418	1.5×10^{-5}

1d is fairly stable in water at room temperature, though the yellowish green color of **1d** fades rapidly with evolution of gas (N_2) at 90 °C. The rates of decomposition were followed by the decrease in π-π^* absorption. Plots of absorption intensity *vs.* time indicates that the rate of decomposition follows first-order kinetics and decreases with the increase in polarity of the solvents (Table 3).

This is consistent with the unimolecular decomposition mechanism in which a non-polar four-membered ring is assumed to be a transition state starting from a polar ground state.

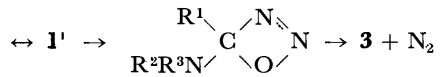

Thoman and Hunsberger also observed that the rate of decomposition of *N*-nitroso-2,4'-dimethyldiphenylmethyleneimine (**1i**) in cyclohexane indicates a first-order mechanism, followed by the rate of evolution of nitrogen.[3]

Guanidines are stable against hydrolysis, so there is no need to consider hydrolysis in contrast to the case of *N*-nitrosoketimines.

If nitrosoimines have a considerable polar character in ground state, they are expected to undergo 1,4-cycloaddition with appropriate dienophiles.

Attempts to react 2-nitroso-1,1,3,3-tetraphenylguanidine (**1f**) with ethyl vinyl ether and maleic anhydride in chloroform at 0 °C for a month were unsuccessful, tetraphenylurea being recovered quantitatively (thermal decomposition product).

Reaction of **1f** with phenyl isocyanate under the same conditions gave pentaphenylguanidine in 38% yield together with 43% of tetraphenylurea as shown below.

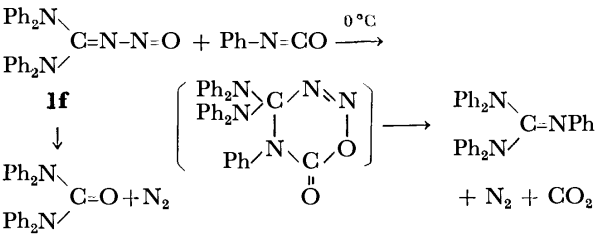

1,1,3,3-Tetramethyl-2-phenylguanidine reacted with *p*-toluenesulfonyl isocyanate to give 1,2-cycloaddition product.[5] 1,4-Cycloaddition mechanism might be preferred in the reaction.

Experimental

Materials. *(a) Guanidines*: Commercial 1,1,3,3-tetramethylguanidine (**2a**) was distilled before use (bp 160—161 °C). 1,1,3,3-Tetraethylguanidine (**2b**) was prepared from diethylcyanamide and diethylamine (bp 92 °C/13 mmHg).[6,7] Bis(piperidino)methyleneimine (**2c**) was prepared from piperidine and cyanogen bromide (bp 110—116 °C/0.15—0.2 mmHg).[7] Bis(morpholino)methyleneimine (**2d**) was prepared by the same method (mp 87—93 °C).[7] 1,3-Dimethyl-1,3-diphenylguanidine (**2e**) was prepared as follows: *N*-methylaniline hydrochloride (21.6 g) and *N*-methyl-*N*-phenylcyanamide (20 g) were heated in a sealed tube at 180—190 °C for 2 hr. The resulting mass was dissolved in ethanol. Sodium hydroxide was added to the solution until the pH of the solution became 11. The resulting NaCl was filtered off and ethanol was evaporated. The residue was extracted with benzene, and the residual liquid was distilled under reduced pressure after evaporation of benzene. Bp 124.5—127 °C/0.15 mmHg,[8] yield 51%. The yield decreased when the sealed tube was heated longer (4 or 6 hr) and it was necessary to adjust the pH of the solution to around 11. 1,1,3,3-Tetraphenylguanidine (**2f**) was prepared from diphenylcyanamide[9] (34 g) and diphenylamine hydrochloride (36 g) which were heated in a sealed tube at 175 °C for 6 hr. The resulting mass was extracted with aq. hydrochloric acid and the aq. solution was made alkaline with NaOH.

The resulting precipitates were filtered and recrystallized from ligroin, mp 132.0—132.5 °C, yield 32%.[10] Larger scale preparations gave lower yields (5—20%).

(b) Ureas and Thiolcarbamate: Ureas and thiolcarbamate were prepared from the corresponding secondary amines and phosgene according to methods given in literature; tetramethylurea (**3a**: bp 170.5—173.0 °C),[11] tetraethylurea (**3b**: 61—62 °C/6 mmHg),[12] bispiperidinoketone (**3c**: mp 39—42 °C),[13] bismorpholinoketone (**3d**: mp 139—141 °C)[13] *sym*-dimethyldiphenylurea (**3e**: mp 120—122 °C),[14] tetraphenylurea (**3f**: mp 179.5—180.0 °C),[14] and benzyl *N*-ethyl-*N*-phenylthiolcarbamate (**3g**: mp 46.2—47.0 °C).[15]

General Procedure of Nitrosation. (a) A solution of nitrosyl chloride (4.9 g, 75 mmol) in carbon tetrachloride (50 ml) was cooled under stirring to *ca.* −20 °C in a dry ice-acetone bath with anhydrous sodium acetate (14.8 g, 145 mmol). A cold solution of guanidine (50 mmol) in carbon tetrachloride (20 mmol) was then added dropwise for 20 min, the internal temperature being kept below −10 °C. The mixture was stirred for 20 min at −10 °C, and washed with cold 10% potassium hydrogen carbonate (150 ml) and then with ice-water (150 ml). The dried solution (with anhydrous magnesium sulfate) was evaporated under reduced pressure and the residue was distilled or recrystallized. Ureas thus produced were identified by a comparison with authentic samples.

(b) For UV measurement, dichloromethane was used as a solvent, and nitrosation was performed at *ca.* −70 °C, the dried solution being then used for the measurement. For the kinetic study of decomposition of **1d**, dichloromethane was evaporated below 0 °C, and the resulting yellow slurry was dissolved in an appropriate solvent.

(c) 1,1,3,3-Tetraphenylguanidine (**2f**) was nitrosated according to procedure (a). A red solid appeared during nitrosation which was quickly filtered off after addition of cold 10% potassium hydrogen carbonate. The filtered solid was dried in a vacuum desiccator over P_2O_5. The red solid (**1f**) was then recrystallized from chloroform–ether–petroleum ether at *ca.* −60 °C. Mp 80 °C (dec.); $\lambda_{max}^{CHCl_3}$ 330 (ε 9550) and 519 nm (183); yield, 81—92%.

The compound **1f** is stable in solid state at −20 °C but decomposes fairly rapidly in chloroform at room temperature. Decomposition was not detected when it was left to stand for a day in chloroform at −60 to −70 °C.

Found: C, 76.30; H, 5.43; N, 14.65%. Calcd for $C_{25}H_{20}N_4O$: C, 76.51; H, 5.14; N, 14.28%.

*Thermal Decomposition of 2-Nitroso-1,1,3,3-tetraphenylguanidine (**1f**).* A solution of **1f** (0.9 g, 2.3 mmol) in chloroform (20 ml) was left to stand at 0 °C for a month. The residue, after evaporation of chloroform, was chromatographed on silica gel, and tetraphenylurea (0.762 g, 2.1 mmol, 91%) was eluted with dichloromethane.

*Reaction of **1f** with Phenyl Isocyanate.* Phenyl isocyanate (1.83 g, 15.3 mmol) and **1f** (3.0 g, 7.7 mmol) were dissolved in chloroform (25 ml) and the solution was left to stand at 0 °C for a month. Ethanol (5 ml) was added to convert the residual phenyl isocyanate into the urethane, and the solvent was evaporated. The residue was chromatographed on silica gel to elute urethane and tetraphenylurea (1.19 g, 3.3 mmol, 43%) with dichloromethane. The residual component was eluted with ethanol and again chromatographed on alumina to elute pentaphenylguanidine (1.26 g, 2.9 mmol, 38%), mp 180.0—180.5 °C, $\nu_{C=N}$ 1625 cm^{-1}; M^+(437).

Found: C, 84.77; H, 5.90; N, 9.85%. Calcd for $C_{31}H_{25}N_3$: C, 84.71; H, 5.73; N, 9.56%.

References

1) Part V; K. Akiba, T. Kawamura, M. Ochiumi, and N. Inamoto, *Heterocycles*, **1**, 35 (1973).
2) K. Akiba, M. Imanari, and N. Inamoto, *Chem. Commun.*, **1969**, 166.
3) C. J. Thoman, S. J. and I. M. Hunsberger, *J. Org. Chem.*, **33**, 2852 (1968). References for earlier publications are cited with authors' interpretation.
4) a) K. Akiba, I. Fukawa, N. Nomura, and N. Inamoto, This Bulletin, **45**, 1867 (1972). b) S. F. Mason, *Quart. Rev.*, **15**, 314 (1961).
5) H. Ulrich, B. Tucker, and A. A. R. Sayigh, *Angew. Chem.*, **80**, 218 (1968).
6) R. H. McKee, *Amer. Chem. J.*, **36**, 208 (1906).
7) J. v. Braun, *Ber.*, **42**, 2040 (1909).
8) J. Stieglitz and R. H. McKee, *ibid.*, **33**, 808 (1900). H. King and I. M. Tonkin, *J. Chem. Soc.*, **1946**, 1063.
9) J. v. Braun, *Ber.*, **33**, 1450 (1900).
10) J. v. Braun, *ibid.*, **33**, 2724 (1900).
11) W. Michler and C. Escherich, *ibid.*, **12**, 1164 (1879).
12) W. Michler, *ibid.*, **8**, 1664 (1875).
13) O. Wallach and F. Lehman, *Ann. Chem.*, **237**, 250 (1887).
14) W. Michler and R. Zimmerman, *Ber.*, **12**, 1166 (1879). H. Erdmann and H. Smissen, *Ann. Chem.*, **361**, 56 (1908).
15) K. Akiba and N. Inamoto, unpublished results.

Preparation of Stable 2,3-Dihydroindolizines by the Reactions of Pyridinium Methylides with Various Acrylates

Akikazu KAKEHI and Suketaka ITO

Department of Industrial Chemistry, Faculty of Engineering, Shinshu University, Wakasato, Nagano 380

(Received November 17, 1973)

Pyridinium methoxycarbonylmethylides(**5**—**8**), readily obtainable from their corresponding salts(**1**—**4**), reacted with various acrylates to afford dimethyl 2,3-*trans*-dihydroindolizine-1,3-dicarboxylate derivatives(**9**—**20**) in moderate yields. These dihydroindolizines were very stable and were not aromatized by heating. However, treatment with lead tetraacetate gave the corresponding indolizine derivatives(**21**—**32**) in good yields. The configuration at C-2 and C-3 positions in these dihydroindolizines was assigned to *trans* from their NMR and by comparison with an authentic specimen(**12**).

Cycloaddition and cyclization of various pyridinium ylides are useful methods for synthesizing nitrogen-bridged heteroaromatics such as indolizines and pyrazolopyridines. However, because of their sensitiveness to air, hardly any reports have appeared on the isolation of primary dihydroadducts formed.

Sasaki *et al.*,[1] and Tamura *et al.*[2] have reported that 1,5-dipolar cyclization of pyridinium allylides gave only their aromatized indolizine derivatives. Pohjala[3] reported on the isolation of the primary dihydroadducts, 1,8a-dihydroindolizines by similar cyclization reactions.

Kabayashi *et al.*[4] obtained 2,3- and 3,8a-dihydro isomers from the 1,3-dipolar cycloaddition of isoquinolinium disubstituted methylides with dimethyl acetylenedicarboxylate.

This paper deals with 1,3-dipolar cycloaddition of pyridinium methoxycarbonylmethylides with various acrylates, and the isolation of the resulting stable 2,3-dihydroindolizines.

Results and Discussion

Reactions of Pyridinium Salts(1)-(4) with Various Acrylates in the Presence of Alkali. An equimolar mixture each of pyridinium salt(**1**)—(**4**) and dimethyl maleate (DMM) were stirred with excess potassium carbonate in chloroform at room temperature for 2—3 days to afford 2,3-dihydroindolizine derivatives(**9**)—(**12**) in 20—50% yields respectively. The same products(**9**) and (**10**) were obtained in 29 and 35% yields, respectively, when dimethyl fumarate(DMF) was used in place of DMM for the reactions with salts(**1**) and (**2**). Similar treatments of the salts(**1**)—(**4**) with methyl α-chlorocinnamate (MCC) and methyl α-bromocrotonate(MBC) also afforded the corresponding 2,3-dihydroindolizines(**13**)—(**20**). Compound (**13**) was also prepared from salt(**1**) and methyl cinnamate(MC), but the yield was low (6%). In these reactions, no product generated through the Micheal-type reaction of the pyridinium methylides(**5**)—(**8**) with the acrylates, such as observed in the reaction of *N*-ethoxycarbonyliminopyridinium ylide,[5] was detected. The results are shown in Scheme 1.

In contrast with the instability of the known 1,8a- and 3,8a-dihydroindolizine derivatives, 2,3-dihydroindolizines (**9**)—(**20**) were very stable. Compounds (**9**)—(**20**) remained unchanged on being put to stand for a few months on contact with air or when their

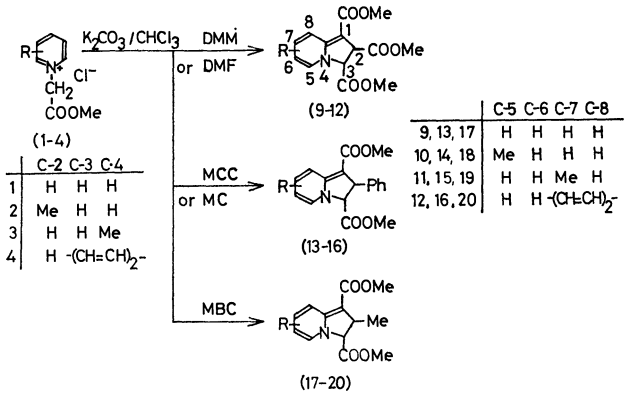

Scheme 1.

benzene solutions were refluxed. However, treatment with dehydrogenating agents gave the corresponding indolizine derivatives (**21**)—(**32**).

Aromatization of Dihydroindolizines(9)—(20). Dihydroindolizines(**9**)—(**20**) were treated with palladium on carbon in benzene at reflux temperature to afford the corresponding indolizine derivatives(**21**)—(**32**) in only 10—20% yields. However, increased yields were observed when lead tetraacetate was used as a dehydrogenating agent(Scheme 2).

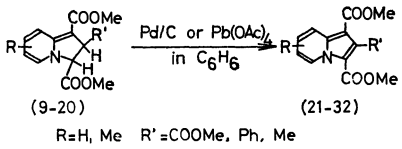

Scheme 2.

Structural Elucidation of 2,3-Dihydroindolizines(9)—(20). Structures of products(**9**)—(**20**) were established mainly by their physical and spectral data and by comparison with the authentic specimen(**12**) reported by Kobayashi.[4] The elemental analyses of the products (**9**), (**10**), (**12**)—(**14**), (**16**)—(**18**) and (**20**) were in good accordance with their proposed structures. The analyses of products(**11**), (**15**) and (**19**) were not performed, since the compounds were amorphous and preparation of the samples for analyses was unsuccessful. The spectral patterns of products (**9**)—(**20**), were extremely similar to each other. The NMR spectra, in particular, strongly supported the presence of the 2,3-dihydroindolizine skeleton; for example, compound(**9**) exhibited signals at δ 5.95, 6.99, 7.03 and

Table 1. NMR spectral data of 2,3-dihydroindolizines

Compd.[a]	Substituent													
	C-2		C-3		C-5		C-6		C-7		C-8		COOMe		R'(C-2)
9	4.18 d		5.01 d		7.03 dd		5.95 bt		6.99 bt		7.35 dd		3.67 s	3.75 s	3.80 s
	$J_{2,3}$=3.5,				$J_{5,6}$=7.0,				$J_{6,7}$=7.0,				$J_{7,8}$=9.0,		$J_{5,7}$=$J_{6,8}$=2.0
10	4.07 d		5.14 d		2.13 s		5.80 bd		6.93 q		7.31 dd		3.68 s	3.75 s	3.86 s
	$J_{2,3}$=3.0,				$J_{6,7}$=7.0,				$J_{7,8}$=9.0,				$J_{6,8}$=2.5		
11	4.13 d		4.99 d		7.03 d		5.84 dd		2.13 s		7.17 bs		3.66 s	3.72 s	3.78 s
	$J_{2,3}$=3.0,				$J_{5,6}$=7.0,				$J_{6,8}$=2.0						
12	4.29 d		4.83 d		6.74 d		6.22 d		7.1—7.6 m[b]				3.67 s	3.71 s	3.76 s
	$J_{2,3}$=3.5,				$J_{5,6}$=7.0										
13	4.52 s				6.87 bd		5.90 t		6.95 q		7.44 bd		3.53 s	3.83 s	7.0—7.4 m
	$J_{2,3}$=0,				$J_{5,6}$=6.0,				$J_{6,7}$=6.0,				$J_{7,8}$=9.0		
14	4.41 d		4.65 d		2.01 s		5.76 d		6.91 q[c]				3.55 s	3.84 s	7.0—7.3 m
	$J_{2,3}$=2.5,				$J_{6,7}$=6.0,				$J_{7,8}$=9.0						
15	4.44 s				6.76 d		5.75 d		2.10 s[c]				3.48 s	3.77 s	7.0—7.3 m
	$J_{2,3}$=0,				$J_{5,6}$=6.0										
16	4.42 d		4.55 d		6.62 d		6.17 d		7.0—7.5 m[d]				3.47 s	3.77 s	7.0—7.5 m
	$J_{2,3}$=2.5,				$J_{5,6}$=7.5										
17	3.35 m		4.19 d		6.84 bd		5.68 bt		6.80 bt		7.26 bd		3.62 s	3.72 s	1.29 d
	$J_{2,3}$=3.5,				$J_{2,Me}$=7.0,				$J_{5,6}$=6.0,				$J_{6,7}$=6.0,		$J_{7,8}$=8.0
18	3.28 m		4.33 d		2.03 s		5.67 d		6.80 q		7.20 dd		3.62 s	3.71 s	1.26 d
	$J_{2,3}$=2.5,				$J_{2,Me}$=7.0,				$J_{6,7}$=6.5,				$J_{7,8}$=8.0,		$J_{6,8}$=1.5
19	3.34 m		4.23 d		6.86 d		5.71 dd		2.05 s		7.10 d		3.60 s	3.69 s	1.27 d
	$J_{2,3}$=3.5,				$J_{2,Me}$=7.0,				$J_{5,6}$=7.0,				$J_{6,8}$=1.5		
20	3.45 m		4.14 d		6.65 d		6.13 d		7.1—7.5 m[e]				3.67 s	3.68 s	1.31 d
	$J_{2,3}$=2.5,				$J_{2,Me}$=7.0,				$J_{5,6}$=7.0						

a) All compounds were measured in deuteriochloroform. b) Plus 9.74(1H, d, J=8.0). c) Overlapped with phenyl protons. d) Plus 9.78(1H, d, J=7.5). e) Plus 9.81(1H, d, J=7.5).

7.35 due to the four protons on the six-membered ring, and at δ 4.18 and 5.01 attributable to the two protons on the five-membered ring, together with three methoxycarbonyl proton signals at δ 3.67, 3.75 and 3.80. The latter signals at δ 4.18 and 5.01 coupled with 3.5 Hz, which is indicative of its *trans* configuration. In the cases of compounds(**17**)—(**20**) the proposed structure, 2,3-dihydroindolizine, was verified by the presence of the coupling(J=7.0 Hz) between a proton and a methyl group at C-2 position. The NMR data of compounds (**9**)—(**20**) are listed in Table 1. Compound (**12**) was entirely in accord with an authentic specimen prepared by the alkali-methanolysis of the corresponding adduct of isoquinolinium bis(methoxycarbonyl)methylide and dimethyl acetylenedicarboxylate.[4]

From the results, products(**9**)—(**20**) were concluded to be dimethyl 2,3-*trans*-dihydroindolizine-1,3-dicarboxylate derivatives.

*Structural Elucidation of Indolizines(**21**)—(**32**).* The structures of the indolizine derivatives(**21**)—(**32**) were determined by their unequivocal syntheses(**21**)—(**28**) and by comparison with authentic specimens(**21**) and (**24**). Compounds(**21**)—(**28**) were in accord with the indolizines obtained from the 1,3-dipolar cycloaddition of pyridinium methoxycarbonylmethylides(**5**)—(**8**) with dimethyl acetylenedicarboxylate and methyl phenylpropiolate respectively.[6]

Reaction Mechanism. The formation of 2,3-dihydroindolizines (**9**)—(**20**) seems to proceed *via* the well-known 1,3-dipolar cycloaddition of pyridinium methoxycarbonylmethylides(**5**)—(**8**) with acrylates, followed by elimination of two hydrogen atoms or a hydrogen halide from C-1 and C-8a positions of the resulting tetrahydroindolizine derivatives(Scheme 3).

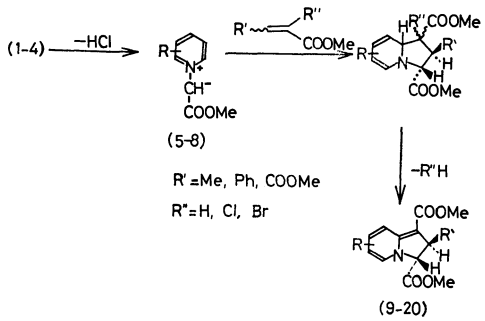

Scheme 3.

In these reactions, the appearance of the only *trans*-adducts at C-2 and C-3 positions may be considered as the result of the approach from each less hindered site of the reactants in the transition state, and rapid conversion from 1,2,3,8a-tetrahydro- into 2,3-dihydroindolizine can be ascribed to be parallel with the

instability of 1,8a-dihydroindolizine, which gave smoothly indolizine.[3] Although the primary tetrahydroadducts could not be detected and isolated, the pyridinium methylides reacted with various acrylates to afford the corresponding cycloadducts. 1,3-Dipolar cycloaddition of pyridinium ylides with such olefinic dipolarophiles has not been reported.

Experimental

Mps were measured with a Yanagimoto micromelting point apparatus and are uncorrected. Microanalyses were performed on a Perkin-Elmer 240 Elemental Analyser. The NMR spectra were determined with a JEOL JNM-4H-100 spectrometer in deuteriochloroform with tetramethylsilane as an internal standard. The chemical shifts are expressed in δ values. The IR spectra were taken with a JASCO DS-301 spectrophotometer.

*Preparation of Pyridinium Salts(**1**)—(**4**).* A mixture of a pyridine base and methyl chloroacetate was kept at room temperature without any solvent and the resulting mass of pyridinium salt was filtered and washed 3—4 times with ether. The corresponding pyridinium salts (pyridinium, α-, γ-picolinium and isoquinolinium salt, **1**—**4**) were obtained as very hygroscopic colorless crystals almost quantitatively. The salts were used for subsequent reactions without further purification.

*Reactions of Salts(**1**)—(**4**) with Various Acrylates in the Presence of Alkali.* A solution of the salt(4 mmol) and an acrylic derivative(4 mmol) in chloroform(50 ml) was stirred with potassium carbonate(10 g) at room temperature for 2—4 days. The reaction mixture was filtered to remove inorganic substances and the filtrate was concentrated under reduced pressure. The resulting yellowish or reddish oil was then separated by column chromatography (alumina) using ether as an eluent. Recrystallization from chloroform–ether–*n*-hexane gave the corresponding 2,3-dihydroindolizine derivatives(**9**)—(**20**) as yellow or red crystals, but not compounds (**11**), (**15**) and (**19**). The results and properties of 2,3-dihydroindolizines are listed in Table 2.

*Aromatization of 2,3-Dihydroindolizines(**9**)—(**20**).* A benzene solution of 2,3-dihydroindolizine was stirred with an equimolar amount of lead tetraacetate at room temperature for 6—12 hrs, the reaction mixture then being filtered.

Table 2. Data of 2,3-dihydroinodolizines

Compd.	Reactant		React. time (day)	Yield (%)	$\nu_{C=O}^{KBr}$ (cm^{-1})		Mp (°C)	Formula	Calcd%			Found%		
	Salt	Acrylate							C	H	N	C	H	N
9	**1**	DMM	2	35	1748	1762	103—106	$C_{14}H_{15}NO_6$	57.33	5.16	4.78	57.16	5.17	4.71
	1	DMF	2	29										
10	**2**	DMM	3	48	1734	1746	182—185	$C_{15}H_{17}NO_6$	58.63	5.58	4.56	58.36	5.67	4.32
	2	DMF	3	35										
11	**3**	DMM	3	33[a]	amorphous substance									
12	**4**	DMM	2	28	1725	1747	156—157[b]	$C_{18}H_{17}NO_6$	62.97	4.99	4.08	62.95	4.97	3.99
13	**1**	MCC	3	10	1740		137—140	$C_{18}H_{17}NO_4$	69.44	5.50	4.50	69.68	5.62	4.37
	1	MC	4	6										
14	**2**	MCC	3	27	1745		156—159	$C_{19}H_{19}NO_4$	70.14	5.89	4.31	70.25	6.01	4.32
15	**3**	MCC	4	15[a]	amorphous substance									
16	**4**	MCC	2	31	1737		205—208	$C_{22}H_{19}NO_4$	73.11	5.30	3.88	73.10	5.22	3.77
17	**1**	MBC	3	56	1751		124—126	$C_{13}H_{15}NO_4$	62.64	6.07	5.62	62.90	6.03	5.60
18	**2**	MBC	3	78	1750		79— 81	$C_{14}H_{17}NO_4$	63.86	6.51	5.32	63.89	6.47	5.19
19	**3**	MBC	3	57[a]	amorphous substance									
20	**4**	MBC	4	59	1745		106—108	$C_{17}H_{17}NO_4$	68.21	5.73	4.68	68.29	5.70	4.61

a) Crude yield. b) Lit[4] 155—156.

Table 3. Data of indolizines

Compd.	Reactant	Yield (%)	Mp (°C)	$\nu_{C=O}^{KBr}$ (cm^{-1})		Formula	Calcd%			Found%		
							C	H	N	C	H	N
21	**9**	85	145—147[a]	1696	1738							
22	**10**	70	113—115	1687	1741							
23	**11**	65	141—142	1692	1743							
24	**12**	75	149—150[b]	1706	1730							
25	**13**	75	139—142	1675								
26	**14**	60	115—118	1690	1710							
27	**15**	60	172—175	1680								
28	**16**	85	143—145	1695								
29	**17**	80	122—123	1680		$C_{13}H_{13}NO_4$	63.15	5.30	5.67	62.98	5.36	5.51
30	**18**	80	80— 82	1690		$C_{14}H_{15}NO_4$	64.36	5.79	5.36	64.26	5.80	5.14
31	**19**	85	117—119	1685	1708	$C_{14}H_{15}NO_4$	64.36	5.79	5.36	64.11	5.77	5.10
32	**20**	80	115—117	1685		$C_{17}H_{15}NO_4$	68.67	5.08	4.71	68.59	5.22	4.86

a) Lit.[4] 148—149 °C. b) Lit.[4] 150—151 °C.

The filtrate was concentrated under reduced pressure and the residue was separated by column chromatography (silica gel) using benzene as an eluent. Recrystallization from ether–*n*-hexane or methanol gave the corresponding indolizine derivative as colorless crystals. The results and properties of indolizines(**21**)—(**32**) are listed in Table 3. Compounds (**21**)—(**28**) were in accord with the products prepared from the 1,3-dipolar cycloaddition of the pyridinium salts(**1**)—(**4**) with dimethyl acetylenedicarboxylate and methyl phenylpropiolate in the presence of potassium carbonate. Compounds (**21**) and (**24**) were also in accord with the products reported by Kobayashi.[4]

The authors are grateful to Professor Tadashi Sasaki and Assistant Professor Ken Kanematsu of Nagoya University for their helpful advice and discussions.

References

1) T. Sasaki, K. Kanematsu, A. Kakehi, and G. Ito, *Tetrahedron*, **28**, 4942 (1972).

2) a) Y. Tamura, N. Tsujimoto, Y. Sumida, and M. Ikeda, *ibid.*, **28**, 21 (1972). b) Y. Tamura, Y. Sumida, S. Tamada, and M. Ikeda, *Chem. Pharm. Bull.* (Tokyo), **20**, 1139 (1972).

3) E. Pohjala, *Tetrahedron Lett.*, **1972**, 2585.

4) a) Y. Kobayashi, T. Kutsuma, and Y. Sekine, *ibid.*, **1972**, 3325. b) T. Kutsuma, K. Fujiyama, Y. Sekine, and Y. Kobayashi, *Chem. Pharm. Bull.* (Tokyo), **20**, 1558 (1972). c) T. Kutsuma, K. Fujiyama, and Y. Kobayashi. *ibid.*, **20**, 1809 (1972).

5) T. Sasaki, K. Kanematsu, and A. Kakehi, *Tetrahedron*, **28**, 1469 (1972).

6) V. Boekelheide and K. Fahrenholtz, *J. Amer. Chem. Soc.*, **83**, 458 (1961).

The Photochemistry of 2-Quinolinecarbonitriles. II. A Mechanism of the Photoinduced Substitution Reaction

Norisuke HATA and Tsugio SAITO

Department of Chemistry, College of Science and Engineering, Aoyama Gakuin University, Chitosedai, Setagaya-ku, Tokyo 157

(Received March 17, 1973)

In order to elucidate the mechanism of the photoinduced substitution reaction of 2-quinolinecarbonitrile in alcohols or ethers, measurements of the absorption and fluorescence spectra and the photochemical reactions were carried out in ethanol, *t*-butyl alcohol, or diethyl ether; consequently, an interesting relationship has been found to exist between the fluorescence intensity and the photoreactivity. The photosubstitution reaction can reasonably be assumed to be initiated by a hydrogen-atom abstraction from an alcohol or ether by the nitrogen atom of the quinoline nucleus. The experimental results indicated that such a hydrogen-atom abstraction was markedly facilitated by a hydrogen-bond formation of the nitrogen lone pair of the quinoline nucleus with ethanol or water: further, the reactive excited singlet state (S_1) was presumed to be of a π,π^* nature.

As has been reported in previous papers,[1,2] the irradiation of 2-quinolinecarbonitrile with ultraviolet light longer than 300 nm in alcohol (ethanol, 1-propanol, 2-propanol, or *t*-butyl alcohol) under an oxygen or nitrogen atmosphere resulted in the replacement of the cyano group at the 2-position of a quinoline nucleus by the hydroxyalkyl group. Under a nitrogen atmosphere, however, a certain triazapentaphene was also produced in addition to the photosubstitution product, except for the case of the *t*-butyl alcohol solution. Further, the photosubstitution reaction has been revealed, by triplet-quenching studies, to proceed directly from the lowest excited singlet state (S_1) of 2-quinolinecarbonitrile, whereas the lowest triplet state (T_1) was responsible for the formation of a triazapentaphene. The purpose of the present investigation is to elucidate the mechanism of such a photochemical substitution reaction.

Results and Discussion

It has recently been shown that the ultraviolet irradiation of quinoline itself in ethanol or *t*-butyl alcohol resulted in the corresponding hydroxyalkyl substituted products,[3] and also that 3,5-dicarbomethoxypyridines in alcohol were susceptible to the photochemical addition of alcohol.[4] These photoinduced reactions have been anticipated to be initiated by a hydrogen-atom abstraction from the solvent by the nitrogen atom of heterocycles. Such an assumption has been primarily supported by a flash-spectroscopic detection of the acridanyl radical formed during the photoreduction of acridine in hydrocarbon solvents,[5] and also by the observation of a corresponding radical from pyridine, quinoline, and isoquinoline during their photoreduction in alcohol or ether.[6] In view of these facts, it seems reasonable to assume that the photosubstitution reaction of 2-quinolinecarbonitrile is likewise initiated by a hydrogen abstraction from an alcohol or ether by the nitrogen atom of the quinoline nucleus; for example, as is shown in Scheme 1, an excited 2-quinolinecarbonitrile **1*** in ethanol abstracts a hydrogen atom from ethanol to give a quinolinium radical **2** which is then coupled with the 1-hydroxyethyl radical **3**, after which it loses a hydrogen cyanide to afford a 2-(1-hydroxyethyl)quinoline **5**.[7] In addition, an alternate pathway (Scheme 2), in which the 1-hydroxyethyl radical **3** thus formed attacks an unexcited 2-quinolinecarbonitrile **1**, can also be supposed to account for the substitution reaction.

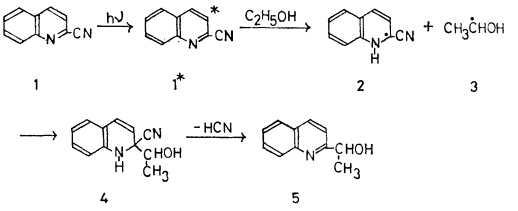

Scheme 1

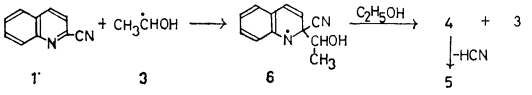

Scheme 2

In order to clarify whether or not the mechanism of Scheme 2 is operative in the photosubstitution reaction, the following experiments were undertaken. To a solution of 2-quinolinecarbonitrile (70 mg) in anhydrous ethanol (20 ml), we added 20 mg of di-*t*-butyl peroxyoxalate (DTBP); the mixture was kept at 35 °C for 4 hr under bubbling in oxygen or nitrogen, because DTBP is well known to decompose thermally to produce a *t*-butoxyl radical, which then abstracts a hydrogen atom from an ethanol to give a 1-hydroxyethyl radical.[8] Consequently, not even trace amounts of the substituted product, 2-(1-hydroxyethyl)-quinoline, were detected by means of gas chromatography (column: Silicone SE-30 on Chromosorb P). This appears to indicate that the mechanism of Scheme 2 is not responsible for the photosubstitution reaction.

Next, in order to obtain information about the nature of the reactive excited singlet state (S_1) of 2-quinolinecarbonitrile, measurements of the absorption and and fluorescence spectra and the photochemical reactions were carried out under various conditions at room temperature. The ultraviolet absorption spectrum of 2-quinolinecarbonitrile in anhydrous ethanol is shown in Fig. 1. Both the spectral shape and the maximum wavelength were essentially unchanged in either anhydrous diethyl ether or anhydrous *t*-butyl

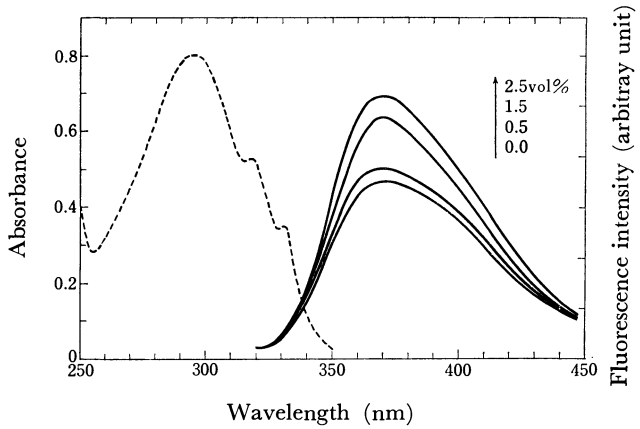

Fig. 1. The absorption and the fluorescence spectra of 2-quinolinecarbonitrile in ethanol at room temperature (concentration of 2-quinolinecarbonitrile: 1.9×10^{-4} M).
----: The absorption spectrum.
——: The fluorescence spectrum. Numbers refer to the concentration of water (vol%).

alcohol, although a slight change in the molar extinction coefficient was observed. On the other hand, the fluorescence spectrum of 2-quinolinecarbonitrile showed a markable dependence on the solvent used. A fairly strong fluorescence specturm was observed around 370 nm in anhydrous ethanol (Fig. 1), but the intensity was greatly diminished in anhydrous *t*-butyl alcohol and much more so in anhydrous diethyl ether. Moreover, the introduction of small amounts of water into these solutions caused the fluorescence intensity to increase, just as in the case of quinoline itself.[9] As an example, Fig. 1 shows the fluorescence enhancement with an increase in the concentration of water in ethanol, but the absorption spectrum of 2-quinolinecarbonitrile remained entirely unchanged under these circumstances. Curve (a) in Fig. 2 shows the results when the degree of increase in the fluorescence intensity is plotted against

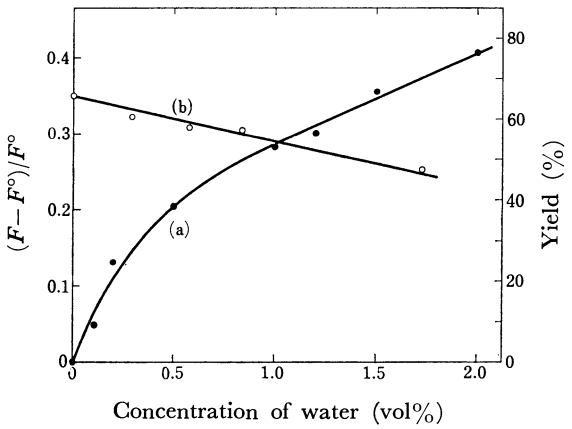

Fig. 2. The effect of small amounts of water on both the yield of photoproduct and the fluorescence intensity in ethanol at room temperature. F and F° represent the relative fluorescence intensity in the presence and the absence of water.
(a) —●—: The degree of increase in the fluorescence intensity.
(b) —○—: The yield of photoproduct.

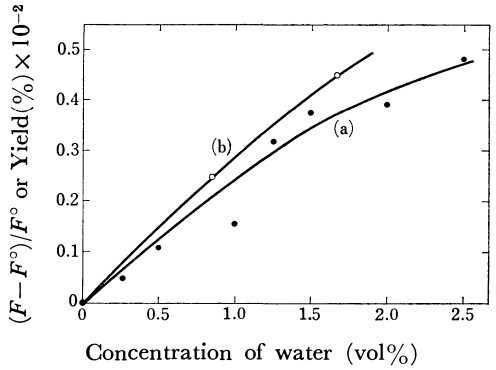

Fig. 3. The effect of small amounts of water on both the yield of photoproduct and the fluorescence intensity in *t*-butyl alcohol at room temperature. F and F° represent the relative fluorescence intensity in the presence and the absence of water.
(a) —●—: The degree of increase in the fluorescence intensity.
(b) —○—: The yield of photoproduct.

the concentration of water. Quite similar results were also obtained in the case of the *t*-butyl alcohol solution (Curve (a) in Fig. 3). The results described above indicate clearly that the 2-quinolinecarbonitrile becomes fluorescent in hydroxylic solvents, except in *t*-butyl alcohol, which can form a hydrogen bond with the nitrogen lone pair of the quinoline nucleus. The very weak fluorescence in anhydrous *t*-butyl alcohol, however, is probably to be ascribed to the shielding of the hydroxyl group responsible for the hydrogen-bond formation by the bulky *t*-butyl group.

The fluorescence activation of quinoline by hydroxylic solvents has been accounted for by assuming that the lowest excited singlet state $S_1(n, \pi^*)$ is raised considerably by the hydrogen-bonding interaction, so that the relative positions of the singlet n,π^* and π,π^* states are reversed and decrease the spin-orbit coupling and, hence, the rate of the intersystem crossing to the triplet manifold.[9] Recent studies by means of photoelectron spectroscopy,[10] however, appear to suggest that the lowest excited singlet state (S_1) of quinoline is of a π,π^* rather than n,π^* nature. Therefore, the fluorescence activation of quinoline by hydroxylic solvents may be interpreted as follows. The $S_1(\pi,\pi^*)$ state is probably close to the upper singlet n,π^* state, so that some mixing between them may occur through the vibronic coupling. Lim and Yu have described that such a vibronic coupling between the singlet π,π^* and n,π^* states can possibly occur in nitrogen heterocycles.[11] This mixing could become smaller in hydroxylic solvents, because the energy difference between the π,π^* and n,π^* states beomes larger because of a hydrogen bonding interaction, and could decrease the n,π^* character in the $S_1(\pi,\pi^*)$ state, resulting in a decrease in the rate of the intersystem crossing to the triplet manifold. Quite similar considerations can possibly account for the fluorescence activation of 2-quinolinecarbonitrile by hydroxylic solvents; that is, the S_1 state of 2-quinolinecarbonitrile is also assumed to be of a π,π^* configuration mixed with the n,π^* singlet state through the vibronic coupling; such an n,π^* nature in the $S_1(\pi,\pi^*)$ state may decrease in hydroxy-

lic solvents, which can form a hydrogen bond with the nitrogen atom of the quinoline nucleus, resulting in the fluorescence enhancement.

As has been reported in a previous paper,[2] the 2-quinolinecarbonitrile in commercial diethyl ether (containing *ca.* 0.2 vol% of water) undergoes photochemical substitution to afford the 2-(2-ethoxyethyl)quinoline in a 32% yield. When anhydrous diethyl ether was used as the reaction medium, however, the yield was greatly reduced to *ca.* 3.6%. In the case of the anhydrous *t*-butyl alcohol solution, also, the yield of the photoproduct, 2-(2-hydroxy-2-methylpropyl)quinoline, was found to be vanishingly low (*ca.* 0.8%), but it increased markedly as small amounts of water were introduced into the solution (Curve (b) in Fig. 3). These results imply that the presence of minute amounts of water in the solution (therefore leading to the hydrogen-bond formation with the nitrogen atom of quinoline nucleus) serves to facilitate remarkably the photosubstitution reaction of 2-quinolinecarbonitrile. In addition, it should be noticed that such an effect of water on the photoreactivity is closely parallel to that on the fluorescence intensity, indicating that the hydrogen-atom abstraction leading to the substitution reaction takes place in the fluorescent state $S_1(\pi,\pi^*)$.

On the other hand, the photosubstitution reaction in anhydrous ethanol occurred in a good yield (*ca.* 66%);[2] however, interestingly, the yield was found to decrease with the addition of small amounts of water to the solution (Curve (b) in Fig. 2). The results could be well explained as follows. In anhydrous ethanol, an excited 2-quinolinecarbonitrile can form a hydrogen bond with an ethanol; such a hydrogen-bonded ethanol molecule may be inferred to be subject to α-hydrogen abstraction by the nitrogen atom, thus resulting in the photosubstitution product in a good yield. When small amounts of water are present in the solution, the hydrogen bonding interaction also exists between excited 2-quinolinecarbonitrile and water. Such an excited 2-quinolinecarbonitrile hydrogen-bonded with water instead of ethanol is also assumed to be responsible for the hydrogen-atom abstraction from a solvent, just as in the case of diethyl ether or *t*-butyl alcohol solution. Therefore, it may be expected that, with an increase in the concentration of water, the yield approaches the value in a *t*-butyl alcohol or diethyl ether solution. In fact, the yield in an ethanol solution containing *ca.* 1.7 vol% of water was about 47%, a value approximately comparable in *t*-butyl alcohol containing *ca.* 1.7 vol% of water (*ca.* 45%) or in commercial diethyl ether (*ca.* 32%). This seems to support the above assumption. Quite similar considerations can be also made in the case of an 1-propanol solution, where the photosubstitution product arising from the β-hydrogen abstraction, different from that in an ethanol solution, may be expected in addition to that from the α-hydrogen abstraction. However, it has been shown in a previous paper[2] that only the 2-(1-hydroxy-2-methylethyl)quinoline arising from the α-hydrogen abstraction was obtained in a yield of 45%. This is probably because the β-hydrogen abstraction is quite difficult because of the steric hindrance of a cyano group at the 2-position of the quinoline nucleus. As will be described in a later paper,[13] the photochemical reaction of 4-quinolinecarbonitrile in 1-propanol provides a 2-(1-hydroxy-2-methylethyl)quinoline-4-carbonitrile and a 2-(1-hydroxymethylethyl)quinoline-4-carbonitrile in yields of 24% and 16%, indicating that the β-hydrogen abstraction takes place as well as the α-hydrogen abstraction. This also supports the idea that the photosubstitution reaction of quinolinecarbonitriles in such anhydrous alcohols as ethanol and 1-propanol is initiated by a hydrogen-atom were abstraction from the alcohol hydrogen-bonded with the nitrogen atom of the quinoline nucleus.

Experimental

The 2-quinolinecarbonitrile used in this experiment was prepared and purified according to the method given in the literature.[14] The ethanol, *t*-butyl alcohol, and diethyl ether used as solvents were reagent-grade products of Wako Pure Chemical Industries; the first two were refluxed over magnesium for dehydration, while the last was dehydrated by sodium and then calcium hydride. The di-*t*-butyl peroxyoxalate used in the thermal reaction of 2-quinolinecarbonitrile in anhydrous ethanol was kindly supplied by Dr. Katsumi Tokumaru of the University of Tokyo.

The ultraviolet absorption and fluorescence spectra were, respectively, measured with a Hitachi recording spectrophotometer EPS-3T and a Hitachi fluorescence spectrophotometer MPF-2A.

The photolytic procedure was similar to that described in a previous paper;[2] 2-quinolinecarbonitrile (0.5 g) dissolved in 350 ml of ethanol, *t*-butyl alcohol, or diethyl ether containing various amounts of water in a Pyrex vessel was irradiated with a 100W high-pressure immersion mercury lamp (Riko Kagaku Sangyo Co.) for 2 hr while oxygen was being bubbled in; the photoproduct and the starting material were then separated by means of silica gel chromatography.

In conclusion, the authors wish to thank Dr. Katsumi Tokumaru and Mr. Hiroyuki Ohta of the University of Tokyo and Professor Akira Sugimori of Sophia University for their kind discussions.

References

1) N. Hata, I. Ono, and S. Ogawa, This Bulletin, **44**, 2286 (1971).

2) N. Hata, I. Ono, S. Matono, and H. Hirose, *ibid.*, **46**, 942 (1973).

3) F. R. Stermitz, C. C. Wei, and C. M. O'Donnell, *J. Amer. Chem. Soc.*, **92**, 2745 (1970).

4) T. J. van Bergen and R. M. Kellogg, *ibid.*, **92**, 8451 (1972).

5) A. Kira, S. Kato, and M. Koizumi, This Bulletin, **39**, 1221 (1966); A. Kira and M. Koizumi, *ibid.*, **40**, 2486 (1967); M. Koizumi, Y. Ikeda, and H. Yamashita, *ibid.*, **41**, 1056 (1968).

6) G. Allan, A. Castellano, J. P. Catteau, and A. Lablache-Combier, *Tetrahedron*, **27**, 4687 (1971); S. Caplain, A. Castellano, J. P. Catteau, and A. Lablache-Combier, *ibid.*, **27**, 3541 (1971).

7) Natsume and Wada have reported that the 3-quinolinecarbonitrile in methanol underwent the photochemical addition of methanol to afford a 1,2-dihydro-2-hydroxymethylquinoline-3-carbonitrile, but a 2-hydroxymethylquinoline-3-

carbonitrile was not produced. M. Natsume and M. Wada, *Tetrahedron Lett.*, **1971**, 4503.

8) W. A. Pryor, "Free Radicals," McGraw-Hills (1966), p. 165.

9) N. Mataga and S. Tsuno, This Bulletin, **30**, 368 (1957).

10) F. Brogli, E. Heilbronner, and T. Kobayashi, *Helv. Chim. Acta*, **55**, 274 (1972).

11) E. C. Lim and J. M. H. Yu, *J. Chem. Phys.*, **45**, 4742 (1966); **47**, 3270 (1967).

12) The yield decreased with an increase of the irradiation time: for example, 66% at 2 hr, 51.6% at 4 hr and 45.4% at 8 hr. This is probably because that the photoproduct undergoes a secondary reaction with oxygen to form the diol, just as in the case of 2-hydroxymethylquinoline reported by Hamana and Noda. M. Hamana and H. Noda, *Chem. Pharm. Bull.* Tokyo, **17**, 2633 (1969).

13) N. Hata, I. Ono, and H. Suzuki, This Bulletin, in press.

14) H. Menze, *Ber.*, **69**, 1566 (1936).

2,3,5,6-Tetra-aryl-1,2,4,5-tetra-azapentalenes.[1] A New Heteroaromatic System

Akira MATSUMOTO, Joung Hee LEE, Masayuki YOSHIDA, and Osamu SIMAMURA

Department of Chemistry, Faculty of Science, The University of Tokyo, Hongo, Tokyo 113

(Received November 27, 1973)

2,3,5,6-Tetra-aryl-1,2,4,5-tetra-azapentalenes (II) have been prepared by the dimerization of arylazoethynylarenes (I). The properties of the new ring system are discussed on the basis of their reactivities.

1-Methylpentalene[2] was found so unstable as to dimerize even at −100 °C, but pentalene dianion,[3] a 10π-electron system, is known to show aromatic character. Thus, replacement of the ring carbon atoms of pentalenes by nitrogen atoms may yield stable azapentalenes containing 10π-electrons. We have recently synthesized 2,3,5,6-tetra-aryl-1,2,4,5-tetra-azapentalenes[4] (II) and 2-aryl-5-phenyl-*v*-triazolo[4,5-*d*]-*v*-triazoles,[5] both new *meso*-ionic heteroaromatics. These azapentalenes contain nitrogens at non-fused positions and examples of *meso*-ionic azapentalenes with nitrogens at fused positions have recently been described.[6] This paper presents the synthesis, structure, and properties of 2,3,5,6-tetra-aryl-1,2,4,5-tetra-azapentalenes.

p-Chlorophenylazoethynylbenzene[7] (Ia: Ar^1=Ph, Ar^2=*p*-ClC_6H_4), prepared from *p*-chlorobenzenediazonium chloride and silver phenylacetylide, on heating in cyclohexane deposited 2,5-bis-(*p*-chlorophenyl)-3,6-diphenyl-1,2,4,5-tetra-azapentalene (IIa: Ar^1=Ph, Ar^2=*p*-ClC_6H_4) in 60% yield. This compound shows ultraviolet absorption maxima at 292 and 398 nm (log ε=4.37 and 4.33, respectively) in chloroform. Tetra-azapentalene IIa is pale yellow crystalline solid, mp 328 °C, which is sparingly soluble in ordinary organic solvents giving strongly fluorescent solutions. It is weakly basic, being insoluble in dilute mineral acids, but dissolves readily in concentrated sulphuric acid and is reprecipitated when the solution is diluted with water. It is unaffected by heating in 65% sulphuric acid and can be sublimed unchanged *in vacuo* at about 300 °C. On prolonged heating with methyl iodide, it gives a crystalline methiodide, which is decomposed into its components at about 200 °C or when dissolved in solvents other than methyl iodide. Treatment of tetra-azapentalene IIa with silver nitrate in a mixture of acetonitrile and tetrahydrofuran gives a 1 : 1 adduct, mp 314 °C (decomp.).

Evidence for the structure of compound IIa was provided by its mode of formation, its spectral and analytical data, and the following degradations.

Its pyrolysis *in vacuo* at about 500 °C afforded pale yellow needles (26%), mp 93.5—94.5 °C, identified with α-(*p*-chlorophenylimino)phenylacetonitrile[8] (IIIa: Ar^1=Ph, Ar^2=*p*-ClC_6H_4).

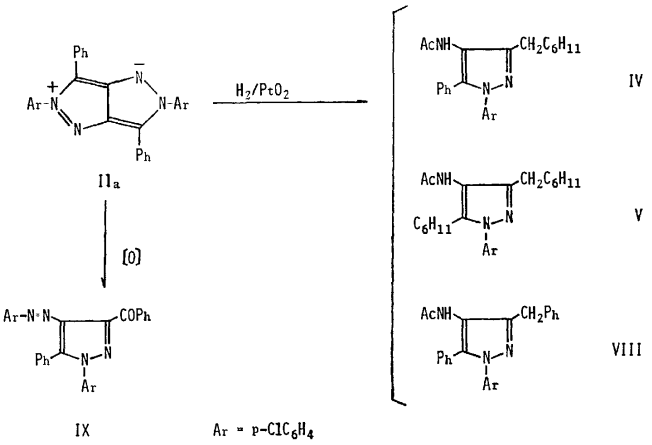

When compound IIa was hydrogenated in acetic acid at 60 °C with platinum oxide, two pyrazole derivatives, $C_{24}H_{26}ClN_3O$ (IV, 25%), mp 233—235 °C (decomp.), and $C_{24}H_{32}ClN_3O$ (V, 10%), mp 214—215 °C, were isolated, and they were assigned the structures of 4-acetamino-1-*p*-chlorophenyl-3-cyclohexylmethyl-5-phenylpyrazole (IV) and 4-acetamino-1-*p*-chlorophenyl-5-cyclohexyl-3-cyclohexylmethylpyrazole (V), respectively, on the basis of their spectral and analytical data and of the degradation of compound IV. Hydrolysis of compound IV and deamination of the resulting amine by reduction of the corresponding diazonium fluoroborate with sodium borohydride yielded 1-*p*-chlorophenyl-3-cyclohexylmethyl-5-phenylpyrazole (VI), mp 113—114 °C. The structure of this compound was established by an independent synthesis, in which condensation of *p*-chlorophenylhydrazine with 1,4-diphenylbutane-1,3-dione in ethanol yielded 3-benzyl-1-*p*-chlorophenyl-5-phenylpyrazole (VII), mp 111—112 °C. Catalytic hydrogenation of this pyrazole (VII) with platinum oxide in acetic acid at room temperature gave a product, which was identical with compound VI. Evidence for the presence of a cyclohexylmethyl instead of a benzyl group in compound VI is furnished by its NMR spectrum with a doublet at τ 7.41 (2H, J=6 Hz), whereas the NMR spectrum of compound VII shows a singlet at τ 5.94 due to a benzylic methylene. The observed spectral data are not incompatible with the isomeric structure of 1-*p*-chlorophenyl-5-cyclohexylmethyl-3-phenylpyrazole, which could be expected from

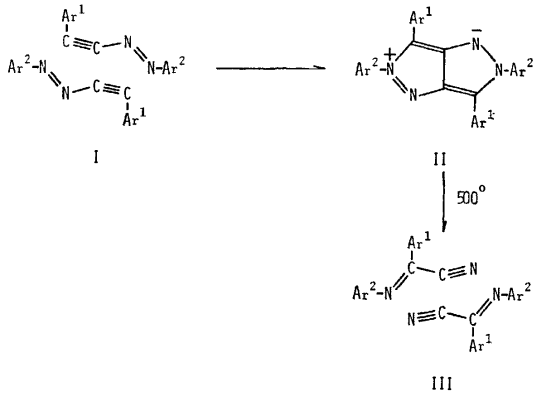

the above synthetic route. However, the fact that compound VI was obtained from the degradation of IIa excludes such an assignment to VI, and thus, supports the structure of 3-benzyl-1-*p*-chlorophenyl-5-phenylpyrazole for compound VII. Separate hydrogenation of IIa under similar conditions resulted in the cleavage of the parent ring to give another pyrazole derivative, 4-acetamino-3-benzyl-1-*p*-chlorophenyl-5-phenylpyrazole (VIII, 12%), mp 217—218 °C. Comparison of the NMR spectra of VII and VIII (a singlet signal at τ 5.90 due to a benzylic methylene) reveals their close similarity, and supports the above structure for compound VIII.

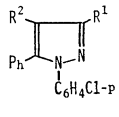

VI: R^1 = $C_6H_{11}CH_2$, R^2 = H
VII: R^1 = $PhCH_2$, R^2 = H
XI: R^1 = PhCO, R^2 = NH_2

Compound IIa was oxidized with potassium permanganate in a mixture of pyridine and water at 95 °C to yield 3-benzoyl-1-*p*-chlorophenyl-4-*p*-chlorophenylazo-5-phenylpyrazole (IX, 64%), mp 208—209.5 °C, the structure being determined on the basis of its spectral and analytical data and of its degradation. The IR spectrum of IX shows a band at 1665 cm^{-1} due to a carbonyl stretching vibration. The NMR spectrum shows a multiplet at τ 2.4—2.7. The mass spectrum shows the molecular ion *m/e* 496, and major fragments *m/e* 385($M^+-C_6H_4Cl$), 105(C_6H_5CO), and 77(C_6H_5). Compound IX was hydrogenated in acetic acid with 10% palladium on carbon to yield two products, 4-acetamino-3-benzyl-1-*p*-chlorophenyl-5-phenylpyrazole (VIII, 12%) and 4-amino-3-benzoyl-1-*p*-chlorophenyl-5-phenylpyrazole (XI, 16%), mp 182 °C. With peroxyacetic acid in chloroform, compound IIa also gave this arylazobenzoylpyrazole (IX, 9%).

Nitration of compound IIa with nitric acid (d= 1.38) in concentrated sulphuric acid at room temperature gave a dinitro derivative (IId: Ar^1=*p*-NO_2-C_6H_4, Ar^2=*p*-ClC_6H_4), mp 365 °C.

Treatment of compound IIa with bromine in chloroform gave a monobromo derivative (XII, 38%), mp 294.5—295.5 °C, together with a small quantity (6%) of a dibromo derivative (IIe: Ar^1=*p*-BrC_6H_4, Ar^2=*p*-ClC_6H_4), mp 349 °C. The structures of IId and IIe were substantiated by separate syntheses through dimerization of 4-(*p*-chlorophenylazoethynyl)-substituted nitro- and bromobenzene, respectively. The monobromide (XII) was assigned the structure of 2,5-bis-(*p*-chlorophenyl)-3-*p*-bromophenyl-6-phenyl-1,2,4,5-tetra-azapentalene. The position of the bromo substituent in the benzene ring was established by examination of the IR spectrum (ν_{max} 760 and 675 cm^{-1}, and 840 cm^{-1} due to mono- and 1,4-disubstituted benzene, respectively).

The tetra-azapentalenes listed in the Table have been prepared by dimerization of arylazoethynylarenes.

The parent structure, 2*H*,5*H*-pyrazolo[4,3-*c*]pyrazole, is *meso*-ionic, being satisfactorily represented only by several charge-separated structures such as XIII and XIV. The preferential electrophilic substitution observed at the *para* positions in the phenyl substituents of compound IIa indicates an electron-donating character of the parent structure due to the contribution of resonance structures such as XIV.

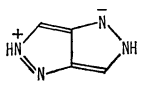

XIII

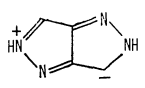

XIV

Experimental

*2,5-Bis-(*p*-chlorophenyl)-3,6-diphenyl-1,2,4,5-tetra-azapentalene (IIa).* A solution of *p*-chlorophenylazoethynylbenzene (Ia, 6.0 g) in 200 ml of cyclohexane was heated under reflux for 5 hr, and the solvent was removed by distillation. The crystalline residue was washed with acetone and recrystallized from benzene to yield 3.6 g (60%) of compound IIa (Found: C, 69.88; H, 3.77; N, 11.92%. Calcd for $C_{28}H_{18}Cl_2N_4$: C, 69.86; H, 3.77; N, 11.64%), mp 328 °C; λ_{max} (chloroform) 292 and 398 (log ε 4.37 and 4.33, respectively), and mass-spectral M, 480.

Other tetra-aryl-tetra-azapentalenes prepared in similar ways are listed in Table 1.

*2,5-Bis-(*p*-chlorophenyl)-3,6-diphenyl-1-methyl-1,2,4,5-tetra-azapentalenium Iodide.* A mixture of IIa (0.90 g) and methyl iodide (50 ml) was heated under reflux for one week. The mixture was filtered and the filtrate, on evaporation of solvent, gave 0.90 g (77%) of the methiodide as orange crystals. The crude material was dissolved in methyl iodide and the solvent was removed under reduced pressure. The residual crystals were similarly treated repeatedly with methyl iodide, and subjected to analysis (Found: C, 56.05; H, 3.51; N, 8.71%. Calcd for $C_{28}H_{18}Cl_2N_4 \cdot CH_3I$: C, 55.88; H, 3.40; N, 8.99%) The methiodide, heated at about 200 °C or dissolved in solvents other than methyl iodide, decomposed into methyl iodide and compound IIa.

Complex Formation of Compound IIa with Silver Nitrate. To a solution of compound IIa (0.22 g) in 100 ml of tetrahydrofuran was added a solution of silver nitrate (1.0 g) in 20 ml of acetonitrile. The mixture was stirred for 3 hr at room temperature, and the pale yellow precipitate was collected and washed with fresh acetonitrile and tetrahydrofuran to yield 0.3 g of the silver nitrate complex. Recrystallization from dimethylformamide gave a pure sample (Found: C, 52.00; H, 2.62; N, 11.02%. Calcd for $C_{28}H_{18}Cl_2N_4 \cdot AgNO_3$: C, 51.64; H, 2.79; N, 10.75%), mp 314 °C (decomp.).

Pyrolysis of Compounds IIa and IIb. α-(p-Chlorophenylimino)- and α-(p-Bromophenylimino)phenylacetonitrile (IIIa and IIIb): Compound IIa (1.2 g), when heated at about 500 °C under reduced pressure of 1 mmHg in a quartz tube, deposited yellow silky crystals on a cold part of the tube. The organic materials were dissolved in ether, and subjected to chromatography on silica gel in benzene. Evaporation of the eluate followed by recrystallization from ethanol gave 0.31 g (26%) of compound IIIa as yellow needles (Found: C, 70.37; H, 4.24; N, 11.66%. Calcd for $C_{14}H_9ClN_2$: C, 69.86; H, 3.77; N, 11.64%), mp 93.5—94.5 °C (lit,[8] mp 94 °C), ν_{max} (KBr) 1595, 1570, 1480, 1445, 1280, 1090, 1015, 1000, 835, 770, 740, 680, and 520 cm^{-1}. The product was identical (mixed melting point, and IR spectrum) with an authentic specimen.

Pyrolysis of compound IIb (1.0 g) in a similar way gave 0.159 g of α-(*p*-bromophenylimino)phenylacetonitrile[9] (Found: C, 59.16; H, 2.88; N, 10.00%. Calcd for $C_{14}H_9BrN_2$: C, 58.97; H, 3.18; N, 9.83%), mp 115.0—115.5 °C (lit,[9] mp 118 °C); ν_{max} (KBr) 1595, 1570, 1475, 1445, 1280, 1200, 1065, 1010, 840, 775, 740, 685, and 520 cm^{-1}.

TABLE 1. TETRA-AZAPENTALENES (II)

II	X in Ar^1 (p-XC_6H_4)	X in Ar^2 (p-XC_6H_4)	Mp (°C)	Yield (%)	Formula		Elementary analysis (%) C	H	N	λ_{max} ($CHCl_3$) nm (log ε)
IIa	H	Cl	328	60	$C_{28}H_{18}Cl_2N_4$	Found	69.86	3.77	11.64	292(4.37), 398(4.33)
						Calcd	69.88	3.77	11.92	
IIb	H	Br	342—343	50	$C_{28}H_{18}Br_2N_4$	Found	58.90	3.48	10.09	295(4.45), 398(4.33)
						Calcd	58.97	3.18	9.83	
IIc	H	NO_2	358—359	55	$C_{28}H_{18}N_6O_4$	Found	67.04	3.87	16.61	332(4.52), 439(3.96)
						Calcd	66.92	3.61	16.73	
IId	NO_2	Cl	>365	1	$C_{28}H_{16}Cl_2N_6O_4$	Found	59.34	2.92	13.95	270(3.43), 310(4.24),
						Calcd	58.86	2.82	14.71	448(4.53)
IIe	Br	Cl	349	40	$C_{28}H_{16}Br_2Cl_2N_4$	Found	52.64	2.47	8.63	292(4.31), 404(4.40)
						Calcd	52.61	2.52	8.77	
IIf	Br	NO_2	>370	40	$C_{28}H_{16}Br_2N_6O_4$	Found	50.78	2.61	12.68	330(4.54), 440(4.11)
						Calcd	50.93	2.44	12.73	
IIg	CH_3	Cl	321	50	$C_{30}H_{22}Cl_2N_4$	Found	71.02	4.60	10.70	292(4.40), 401(4.35)
						Calcd	71.26	4.35	11.00	
IIh	CH_3	NO_2	354—355	20	$C_{30}H_{22}N_6O_4$	Found	67.90	4.05	15.97	336(4.58), 448(3.98)
						Calcd	67.91	4.18	15.84	

Catalytic Hydrogenation of Compound IIa. (a) 4-Acetamino-1-p-chlorophenyl-3-cyclohexylmethyl-5-phenylpyrazole (IV) and 4-Acetamino-1-p-chlorophenyl-5-cyclohexyl-3-cyclohexylmethylpyrazole (V): A suspension of IIa (4.4 g) in 285 ml of acetic acid was hydrogenated over platinum oxide (0.44 g) with hydrogen (60 kg/cm²) at 60 °C for 2 days. The insoluble material was removed by filtration and the filtrate was concentrated under reduced pressure. The residue was poured into 100 ml of water and the mixture was neutralized with sodium bicarbonate. The brownish white solid was collected on a filter, washed with water, and dried. The crude product was chromatographed on silica gel in chloroform as eluant. Evaporation of the eluate followed by fractional recrystallization from ethanol gave two pyrazole derivatives: Compound VI (25 %) (Found: C, 70.89; H, 5.87; N, 10.38%. Calcd for $C_{24}H_{26}ClN_3O$: C, 70.66; H, 6.42; N, 10.30%), mp 233—235 °C (white needles), mass *m/e* 407 (M^+, 23%), 401(29), 359(17), 325(100), 283(17), 214(69), 141(15), 123(16), 111 (50), and 77(20); and compound V (10%) (Found: C, 69.81; H, 7.86; N, 10.02%. Calcd for $C_{24}H_{32}ClN_3O$: C, 69.63; H, 7.79; N, 10.15%), mp 214—215 °C (white leaflets), mass *m/e* 413 (M^+, 15%), 407(10), 331(100), 138(23), and 111(12).

(b) 4-Acetamino-3-benzyl-1-p-chlorophenyl-5-phenylpyrazole (VIII): Separate hydrogenation of IIa (1.0 g) over 0.1 g of platinum oxide with hydrogen (90 kg/cm²) at 60 °C for 47 hr followed by similar treatment to that described above yielded 0.1 g (12%) of compound VIII (Found: C, 71.71; H, 4.96; N, 10.31%. Calcd for $C_{24}H_{20}ClN_3O$: C, 71.73; H, 5.02; N, 10.46%), mp 217—218 °C (from chloroform and pentane).

Deamination of Compound IV. 1-p-Chlorophenyl-3-cyclohexylmethyl-5-phenylpyrazole (VI): Crude compound IV (1.0 g) was hydrolyzed by heating under reflux in 200 ml of 30% sulphuric acid for 45 min. After cooling, the solution was neutralized with aqueous sodium hydroxide, and the organic material was extracted with ether. After evaporation of the solvent, the residue was dissolved in a mixture of 8 ml of concentrated hydrochloric acid and 50 ml of water and treated with sodium nitrite (0.18 g) at 0—3 °C. The solution was stirred for 3 hr and filtered to remove insoluble matter. Fluoroboric acid (48%, 5 ml) was added to the filtrate, and the white precipitate of the resulting diazonium tetrafluoroborate was collected on a filter and washed with a small portion of tetrafluoroboric acid. Sodium borohydride (1 g) was added in small portions with stirring to a solution of the diazonium tetrafluoroborate in about 10 ml of dimethylformamide at 0—3 °C. Stirring was continued for 2 hr at 0 °C and for another 2 hr at room temperature. The reaction mixture was poured into a solution of 10 ml of concentrated hydrochloric acid and 20 ml of ice water. Gummy materials, which were separated by filtration were digested with ether, and the ethereal extract was evaporated to yield yellowish orange oil. The oil was chromatographed on silica gel in benzene. The eluate was concentrated and subjected to purification by preparative thin layer chromatography on silica gel. After development with benzene, the faster moving substance was collected and recrystallized from aqueous ethanol giving 4 mg of compound VI as white needles, mp 113.1—114.1 °C, which is identical (mixed mp and IR spectrum) with material described later.

3-Benzyl-1-p-chlorophenyl-5-phenylpyrazole (VII). A mixture of 1,4-diphenylbutane-1,3-dione (6.7 g) and *p*-chlorophenylhydrazine (5.4 g) in 75 ml of ethanol was heated under reflux for 3 hr. The reaction mixture was concentrated, and the product was separated by filtration and washed with dilute acetic acid and then with water. Recrystallization of the crude product from aqueous ethanol with active charcoal gave 7.4 g (77%) of compound VII (Found: C, 76.48; H, 4.90; N, 8.12%. Calcd for $C_{22}H_{17}ClN_2$: C, 76.62; H, 4.97; N, 8.13%), mp 109.2—110.2 °C (white needles).

Catalytic Hydrogenation of Compound VII. 1-p-Chlorophenyl-3-cyclohexylmethyl-5-phenylpyrazole (VI): A solution of compound VII (3.44 g) in 200 ml of acetic acid was hydrogenated with 0.4 g of platinum oxide with hydrogen (60 kg/cm²) for 48 hr. Removal of the catalyst and solvent left an oily residue. Chromatography on activated alumina in benzene gave a colourless oily product. Distillation at about 205 °C/1.5 mmHg gave 0.57 g (16.3%) of compound VI (Found: C, 75.53; H, 6.65; N, 7.68%. Calcd for

$C_{22}H_{23}ClN_2$: C, 75.31; H, 6.61; N, 7.99%, mp 113.1—114.5 °C; ν_{max} (KBr) 3050, 2920, 2840, 1595, 1550, 1490, 1440, 1370, 1170, 1095, 1000, 970, 830, 760, 700, 600, 560, 535, and 500 cm^{-1}.

*Oxidation of Compound IIa. 3-Benzoyl-1-*p*-chlorophenyl-4-*p*-chlorophenylazo-5-phenylpyrazole (IX). (a) With Potassium Permanganate*: To a mixture of compound IIa (2.50 g), 300 ml of pyridine, and 150 ml of water was added potassium permanganate (*ca.* 3 g) in small portions over a period of 4 days, the temperature being kept at about 95 °C. The resulting mixture was filtered while hot, and the filtrate was cooled to yield 1.60 g (64%) of 3-benzoyl-1-*p*-chlorophenyl-4-chlorophenylazo-5-phenylpyrazole (IX) (Found: C, 67.49; H, 3.80; N, 10.98%. Calcd for $C_{28}H_{18}Cl_2N_4O$: C, 67.62; H, 3.65; N, 11.26%), mp 208—209.5 °C (yellow needles from ethanol and acetone); λ_{max} (ethanol) 244 and 344 nm (log ε=4.65 and 4.33, respectively); mass *m/e* 496(M^+, 38%), 385(64), 214(53), 141(44), 105(82), and 77(100).

(b) With Peroxyacetic Acid: Compound IIa (1.50 g) in a mixture of 200 ml of chloroform and 280 ml of a solution (total activity, 2.2%) prepared from 30 ml of 30% hydrogen peroxide and 300 ml of acetic acid was heated under reflux for 11 hr. The mixture was cooled and poured into a large amount of cold aqueous sodium hydroxide solution. The organic layer was separated and evaporated to dryness. The residue was treated as described above to yield 0.13 g (9%) of compound IX and some starting material.

*Catalytic Hydrogenation of Compound IX. 4-Amino-3-benzoyl-1-*p*-chlorophenyl-5-phenylpyrazole (XI)*: Compound IX (0.82 g) in 100 ml of acetic acid was hydrogenated over 0.10 g of 10% palladium on carbon at a hydrogen pressure of 70 kg/cm^2 at 45 °C for 17 hr. The insoluble material was removed by filtration, and the filtrate was concentrated to dryness under reduced pressure. The residue was digested with ether and the ethereal extract was washed with dilute aqueous sodium bicarbonate. The ether was evaporated, and the residue was chromatographed on silica gel in dichloromethane and eluted with ether. The faster moving fraction gave 100 mg (16%) of compound XI on recrystallization from methanol (with active charcoal). It was subjected to purification by preparative thin layer chromatography on silica gel to give an analytical sample (Found: C, 70.64; H, 4.26; N, 11.38%. Calcd for $C_{22}H_{16}ClN_3O$: C, 70.69; H, 4.31; N, 11.24%), mp 182 °C (pale yellow); λ_{max} (ethanol) 259, 276(shoulder), and 369 nm (log ε=4.41, 4.35, and 3.64, respectively); ν_{max} (KBr) 3460, 3370, 1625, and 835 cm^{-1}; mass *m/e* 373(M^+, 19%) and 105(100); NMR ($CDCl_3$) τ 5.62(broad singlet, 2H, NH), 2.38—2.90(multiplet, 12H, aryl H), and 1.60(multiplet, 2H, aryl H). The later fraction gave 80 mg (12%) of compound VIII as white crystals on recrystallization from benzene, mp 217—218 °C, whose IR spectrum was identical with that of the product obtained by hydrogenation of compound IIa.

*Nitration of Compound IIa. 2,5-Bis-(*p*-chlorophenyl)-3,6-bis-(*p*-nitrophenyl)-1,2,4,5-tetra-azapentalene (IId)*: Nitric acid (0.33 ml, d=1.38) was added to a solution of compound IIa (1.0 g) in 11 ml of concentrated sulphuric acid. The mixture was stirred for 10 hr at room temperature and poured onto 200 ml of ice water. The yellow solid was collected, washed thoroughly with water, and dried to yield 1.27 g of a dinitro compound. Recrystallization from acetone gave a pure specimen (Found: C, 59.34; H, 2.92; N, 13.95%. Calcd for $C_{28}H_{16}Cl_2N_6O_4$: C, 58.86; H, 2.82; N, 14.71%), mp> 365 °C, whose IR spectrum was identical with that of compound IId, prepared by dimerization of 4-(*p*-chlorophenylazoethynyl)nitrobenzene.

*Bromination of Compound IIa. 3,6-Bis-(*p*-bromophenyl)-2,5-bis-(*p*-chlorophenyl)-1,2,4,5-tetra-azapentalene (IIe) and 3-(*p*-Bromophenyl-2,5-bis(*p*-chlorophenyl)-6-phenyl-1,2,4,5-tetra-azapentalene (XII)*: Bromine (0.19 g) in 31 ml of chloroform was added with stirring to a solution of compound IIa (0.29 g) in 20 ml of chloroform, and the mixture was allowed to stand overnight. It was then heated under reflux for 15 min to complete the reaction. After cooling, it was washed with aqueous sodium thiosulphate solution to remove excess of bromine. The organic layer was dried over anhydrous sodium sulphate, and the solvent was removed by distillation to yield 0.3 g of yellow solid. A part of the solid (10 mg) was subjected to preparative thin layer chromatography on silica gel in benzene. The first, the second, and the third bands were scraped off the plate and extracted with dichloromethane and evaporation of the extracts gave 0.8 mg (6%) of the dibromine, 4.3 mg (38%) of the monobromide, and 4.7 mg of the starting material, respectively. The dibromide, mp 349 °C, was identified with IIe by mixed melting point and comparison of its IR spectrum with that of an authentic sample. The monobromide (XII) (Found: C, 56.58; H, 3.05; N, 10.74%. Calcd for $C_{24}H_{17}BrCl_2N_4$: C, 56.28; H, 3.25; N, 10.94%) showed mp 294.5—295.5 °C (yellow needles); ν_{max} (KBr) 1515, 1485, 1465, 1400, 1340, 1190, 1160, 1010, 965, 840, 760, and 675 cm^{-1}.

References

1) The parent structure may be named 2*H*,5*H*-pyrazolo-[4,3-*c*] pyrazole.
2) R. Bloch, R. A. Marty, and P. de Mayo, *J. Amer. Chem. Soc.*, **93**, 3071 (1971).
3) T. J. Katz, M. Rosenberger, and R. K. O'Hara, *ibid.*, **86**, 249 (1964).
4) J. H. Lee, A. Matsumoto, O. Simamura, and M. Yoshida, *Chem. Commun.*, **1969**, 1393.
5) M. Yoshida, A. Matsumoto, and O. Simamura, This Bulletin, **43**, 3587 (1970).
6) a) S. Trofimenko, *J. Amer. Chem. Soc.*, **88**, 5588 (1966); b) T. W. G. Solomons and C. F. Voight, *ibid.*, **88**, 1992 (1966); c) R. A. Carboni, J. C. Kauer, J. E. Castle, and H. E. Simmons, *ibid.*, **89**, 2618 (1967).
7) A. M. Sladkov, L. Yu. Ukhin, and G. N. Gorshkova, *Zh. Org. Khim.*, **2**, 1456 (1966); *Chem. Abstr.*, **66**, 55143s (1967).
8) O. Mumm, *Ber.*, **43**, 886 (1910).
9) F. Sachs and M. Goldmann, *ibid.*, **35**, 3319 (1902).

Mechanisms for the Reaction of Phenol with Methanol over the $ZnO-Fe_2O_3$ Catalyst

Takeshi KOTANIGAWA

The Government Industrial Development Laboratory, Hokkaido, Higashi-Tsukisamu, Toyohiraku, Sapporo 061-01

(Received May 7, 1973)

It was confirmed from the infrared spectra of phenol chemisorbed on $ZnO-Fe_2O_3$ that the surface species were characterized by a loss of O-H stretching (3250 cm^{-1}) and by in-plane bending vibration (1370 cm^{-1}) as well as by a phenol ring vibration (1472 cm^{-1}) and a shift of the C-O stretching mode from 1230 cm^{-1} to 1248 cm^{-1}. From these data, phenoxide surface species were proposed. Furthermore, the dissociative adsorption of phenol was discussed by taking account of the acidity and basicity of the catalyst. That is, in the case of the adsorption, phenol was thought to sit on the acid and the base site. Based on the above discussion, a mechanism for the selective methylation at the *ortho* position of phenol was proposed. On the other hand, it was found from the infrared spectrum that a surface species similar to zinc formate appears on the chemisorption of methanol. Therefore, it may be possible to consider that methanol adsorbed on the base site decomposes *via* formate-like surface species to form carbon dioxide, carbon monoxide, and hydrogen.

Phenol reacts with alcohol over solid acidic catalysts such as alumina by means of vapor phase reaction to yield ring-alkylated products.[1] However, because of its low selectivity for a desired alkylphenol, the application of the reaction has not attracted special attention in industry. Since selective alkylation is of special interest[2] (mainly *ortho*-methylation), various catalysts have been reported.[3] These catalysts consist mainly of a solid basic component, such as magnesium oxide or zinc oxide. The products by the alkylation over solid acidic catalysts and solid basic catalysts differ significantly. This interest led to an attempt to study the mechanism of the alkylation of phenol. The mechanism of alkylation was studied by Cullinane and Chard.[4] As the intermediate of alkylation, Klemm and Taylor reported on cyclohexadienone[5] and Nishizaki *et al.* reported on alcoxybenzene.[6] Recently, Nishizaki and Tanabe studied the mechanism of the methylation of phenol over alumina, silica-alumina,[7] and $MgO-Al_2O_3$.[8] Taylor and Ludlum studied the structure of phenols chemisorbed on alumina by infrared techniques.[9]

Previously, the present author found that the $ZnO-Fe_2O_3$ catalyst promoted the selective methylation at the *ortho* position of phenol with methanol and also the simultaneous decomposition of methanol.[10] It is the purpose of this paper to report the mechanisms of the *ortho*-methylation of phenol and the decomposition of methanol over the $ZnO-Fe_2O_3$ catalyst.

Experimental

Materials. Phenol and benzene of an analytical reagent grade were distilled once. Because of the high solidifying point of phenol, an equimolar solution of phenol with benzene was used for measuring the basicity. Pyridine of an analytical reagent grade was dehydrated in potassium hydroxide, distilled, and used for measuring the acidity.

Equipment. The equipment employed for measuring the basicity and the acidity of the present catalyst was a conventional gas chromatograph constructed in our laboratories (Column; Silicone Oil DC 550, 2 m, 150 °C, 7 ml/min, TCD: 80 mA). The only modification was the incorporation of a special furnace designed to hold a 40 cm U-tube, made of 3mm-i.d. stainless steel pipe. Electric heating was supplied by means of a nickelchrome wire wound on the ceramic tube; the temperature of U-tube had a deviation range of 0.2 °C. The weight of the catalyst in the bed was about 500 mg (approximately 5 cm). Before adsorption, catalyst was heated in a stream of helium gas at 400 °C for 3 hr. Then, the catalyst bed was controlled at the prescribed temperature of 200 °C and 375 °C. The chromatogram was counted by using a digital integrator of the Takeda Riken Co., Ltd.

Measurement of the Basicity and the Acidity. As the present catalyst was colored, the acidity and the basicity could not be measured by the Benesi method (indicator method). Therefore, the basicity was measured by means of the adsorption of phenol vapor,[11] while the acidity was measured by means of the adsorption of pyridine vapor.[12]

A given phenol-benzene solution was injected into the catalyst bed in the U-tube by means of a microliter injector of the Hamilton type. The peak of phenol in the chromatogram is not observed upon the initial injection, but the peak is gradually observed on successive injections and finally reaches a constant height. Thus, the irreversible adsorption of phenol, *i. e.*, the basicity, can be evaluated. Similarly, the irreversible adsorption of pyridine, *i. e.*, the acidity, can also be evaluated.

Catalysts. The catalysts ($ZnO-ZnFe_2O_4$) used for the reaction of phenol with methanol were prepared by the procedures described in a previous report.[13] The methods of preparation and the properties of the catalysts are briefly summarized in Table 1. Zinc oxide and zinc ferrite were used for observations of the adsorption of phenol and methanol. The zinc oxide (4 m^2/g) was of an analytical reagent grade, and the zinc ferrite (24.2 m^2/g) was coprecipitated by adding

Table 1. Preparations and properties of $ZnO-Fe_2O_3$ catalysts

Starting materials Zn-Fe	Calcination temperature (°C)	Surface area (m^2/g)
O-O	600	7.5
CO_3-O	600	18.8
O-OH	600	14.5
	700	8.2
CO_3-OH	500	21.2
	600	19.6
	700	5.3
OH-OH	500	36.6
	600	12.6
	700	3.3

a 14% aqueous ammonium solution to a solution containing one mole of zinc nitrate and two moles of ferric nitrate.[10]

Infrared Spectrometry of Catalysts. A double-beam infrared spectrometer (Model 402G; Japan Spectroscopic Co., Ltd.) was used for measuring the spectra in the wave-number region between 4000 cm^{-1} and 430 cm^{-1}. The *in situ* cell used for the measurement of the adsorption spectra of phenol and methanol was the same as that described previously.[16] The cell was made from quartz, and its heating was electrically supplied by means of a nickelchrome wire wound outside the quartz tube. The catalyst disk placed in the cell was heated under a vacuum (10^{-4} Torr) up to 400 °C. The disk was made in the following manner: the catalyst was ground to a fine powder (325 mesh, 44 μ), and then about 150 mg of the catalyst powder was pressed into a disk. The adsorption spectra on the catalyst disk were measured under a vacuum at room temperature.

Results

Phenol Chemisorption. Before measuring the adsorption spectra of phenol, the background spectra were measured. The zinc ferrite and the zinc oxide were heated for 3 hr under a vacuum (10^{-4} Torr) at 200 °C and then cooled to room temperature. The zinc ferrite showed a broad band at about 3100 cm^{-1}, this band may be attributed to the surface O–H stretching frequencies. However, the zinc oxide did not show the background spectrum in the wave-number region 1150 and 4000 cm^{-1}. Then, after the exposure of the disk of zinc ferrite in the cell to phenol vapor for 30 minutes at room temperature, evacuation was carried out for 3 hr at room temperature and at 100, 350, and 400 °C. Similarly, after the exposure of the disk of zinc oxide in the cell to phenol vapor for 30 minutes at room temperature, evacuation was carried out for 3 hr at 200 °C. The infrared spectra are shown in Figs. 1 and 2. A comparison of the spectra in Fig. 1 with the spectrum of phenol in KBr indicates that the phenol O–H stretching vibration (3250 cm^{-1}) and the in-plane bending vibration (1370 cm^{-1}) as well as the phenol ring vibration (1472 cm^{-1}) disappeared upon chemisorption. Furthermore, the phenol C–O stretching vibration (1230 cm^{-1}) shifts at 1248 cm^{-1}. These results are quite similar to the results of the chemisorption of phenol on alumina reported by Taylor and Ludlum.[9] Variations in the chemisorption spectra with a rise in the evacuation

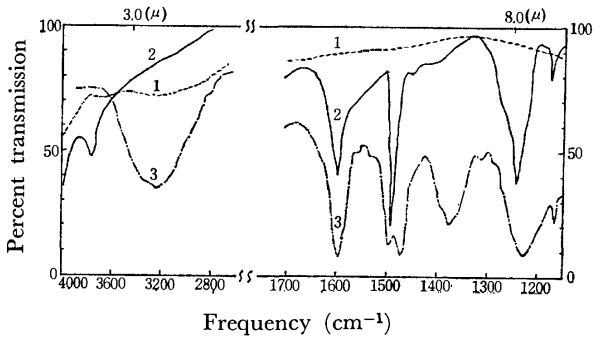

Fig. 1. Infrared spectra of phenol chemisorbed on ZnO.
(1) background, (2) phenol chemisorbed on ZnO, (3) phenol in KBr.

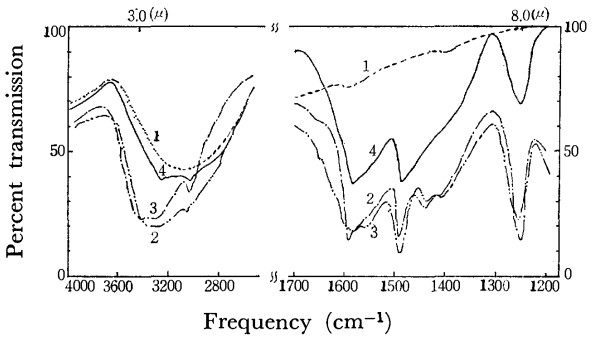

Fig. 2. Infrared spectra of phenol chemisorbed on $ZnFe_2O_4$.
(1) background, (2) phenol evacuated at 100 °C, (3) phenol evacuated at 350 °C, (4) phenol evacuated at 400 °C.

temperature are observed in Fig. 2. The phenol O–H stretching vibration gradually shifts from 3400 to 3150 cm^{-1} and disappears at the same time when the phenol O–H in-plane bending vibration (1390 cm^{-1}) disappears. The chemisorption spectra of phenol on zinc ferrite at 350 and 400 °C are similar to the spectrum on zinc oxide in Fig. 1. It is clear from these observations and the results of Taylor and Ludlum that the phenol molecule loses a proton on the surface and that the phenoxide anion is chemisorbed on the metal ion.

Methanol Chemisorption. Before measuring the adsorption spectrum of methanol, the background spectra were measured. The zinc ferrite and the zinc oxide were heated for 3 hr under a vacuum (10^{-4} Torr) at 200 °C and then cooled to room temperature. The background spectra of the zinc ferrite and zinc oxide were not observed in the wave-number region between 1300 and 1800 cm^{-1}. Then, the disk of zinc oxide in the cell was exposed to 30 Torr of methanol vapor for 5 minutes at 150 °C and then evacuated for 1 hr at 165, 200, and 315 °C. Similarly, the disk of zinc ferrite was also exposed to 30 Torr of methanol vapor for 5 minutes at 150 °C and then evacuated for 1 hr at 200 °C. The spectra are compared

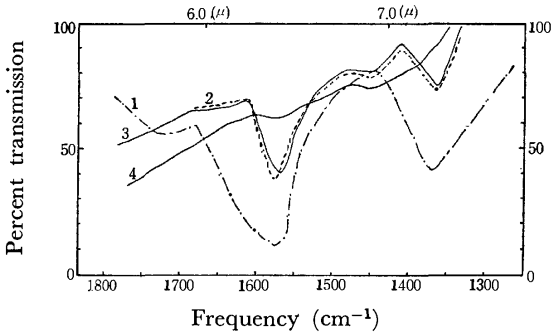

Fig. 3. Infrared spectra of methanol chemisorbed on ZnO and $ZnFe_2O_4$.
(1) zinc formate, (2) methanol evacuated at 200 °C on $ZnFe_2O_4$ (3) methanol evacuated at 165 and 200 °C on ZnO, (4) methanol evacuated at 315 °C on ZnO
* Background spectra of ZnO and $ZnFe_2O_4$ are shown in Figs. 1 and 2.

with the spectrum of zinc formate in Fig. 3. All of the spectra in Fig. 3 are quite similar to the spectrum of zinc formate. Tamaru *et al.* have reported that the methanol adsorbed on zinc oxide decomposes *via* the formate intermediate to form carbon monoxide, carbon dioxide, and hydrogen.[14] It can, therefore, be expected that the observed spectra (Fig. 3) are attributable to the intermediate of the decomposition of methanol over the present catalyst. However, no information about methylation was obtained from the present infrared spectra of methanol.

Acidic and Basic Properties. A typical relation between the acidic and basic properties of the catalyst is shown in Fig. 4. In obtaining the results in Fig. 4, we measured: (1) the saturated adsorption of pyridine on the fresh catalyst without the pre-adsorption of phenol (the acidity was 24.5 μmol/g-cat.); (2) the saturated adsorption of phenol on the fresh catalyst (the basicity was 98.5 μmol/g-cat.), and the adsorption of pyridine after the saturated adsorption of phenol (9.2 μmol/g-cat.); and (3) the adsorption of pyridine after the pre-adsorption of phenol. In those procedures, the amount of the adsorption of pyridine gradually decreased from 24.5 μmol/g-cat. to 9.2 μmol/g-cat. It is clear from these results that phenol is adsorbed on both the acid site and the base site of the catalyst.

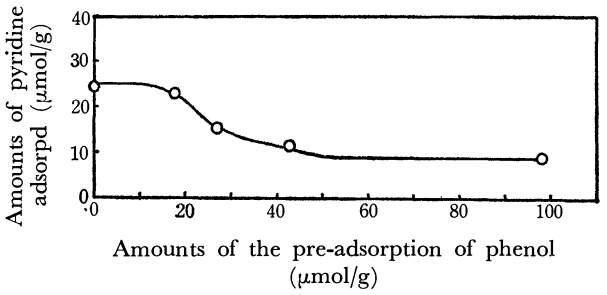

Fig. 4. Acidic and basic properties of $ZnCO_3$–$Fe(OH)_3$ calcined at 600 °C.

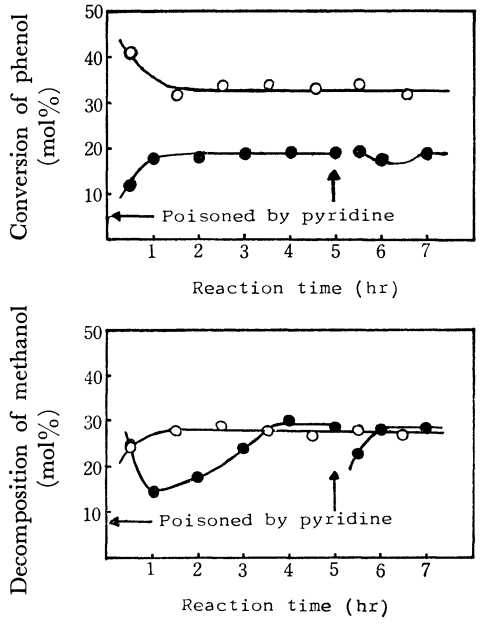

Fig. 5. Effects of poisoning by pyridine.
Reaction conditions;
W/F; 24 g-cat·hr/mol.
Reaction temp.; 375 °C
Reactants; methanol(5 mol)/phenol(1 mol)
Catalyst; From $ZnCO_3$-$Fe(OH)_3$ calcined at 500 °C
(○) Results of the reaction without poisoning by pyridine
(●) Results of the reaction after poisoning by pyridine

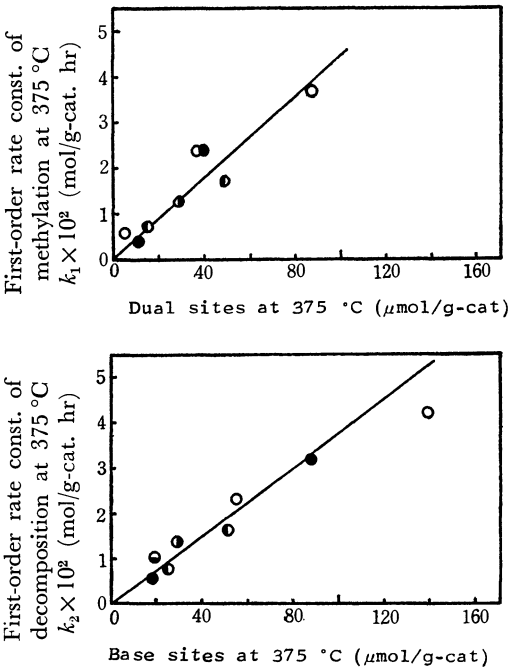

Fig. 6. Relations between rate constants and active sites of ZnO-Fe_2O_3 catalyst in several preparations. (-○-) prepared from $Zn(OH)_2$-$Fe(OH)_3$, (-●-) from $ZnCO_3$-$Fe(OH)_3$, (-◑-) from $ZnCO_3$-Fe_2O_3, (-◐-) from ZnO-$Fe(OH)_3$, (-◒-) from ZnO-Fe_2O_3.

In order to confirm the above results, the poisoning effects by pyridine were examined; the results are given in Fig. 5. The fresh catalyst was first placed in contact with small amounts of pyridine under the present reaction conditions. Then, the reaction of phenol with methanol was carried out under the same conditions. According to the experimental results, the methylation was considerably hindered by the first poisoning operation, but no further decrease in the activity occurred upon the second poisoning operation. Further, the experimental results show that the active site for the methylation is permanently poisoned by the first addition of pyridine. On the other hand, the decomposition of methanol was found to be temporarily poisoned by each operation and the activity was easily recovered. The relations between the number of active sites for the individual reaction and the first-order rate constant are given in Fig. 6. These facts seem to suggest that the methylation occurs on a dual site composed of an acid site and a base site, while the decomposition of methanol occurs only on a base site.

Discussion

With respect to the identification of the active sites for the methylation of phenol and the decomposition

of methanol, the above experimental results give obvious evidence. Now, let us discuss the mechanism for the selective methylation at the *ortho* position of phenol and the decomposition of methanol. It has been reported that the methylation of phenol over alumina proceeds *via* anisole as a key intermediate.[6] However, no reaction was found to take place when only anisole vapor or a mixed vapor of anisole and methanol was placed in contact with the present catalyst. Therefore, the methylation of phenol over the present catalyst cannot be considered to proceed *via* anisole.

The selective methylation of phenol at the *ortho* position may proceed by means of the following mechanism: phenol may dissociate into the phenoxide anion and proton on the catalyst surface, and methanol may be adsorbed onto the proton to form the methyl cation.[15] As the distance between the phenoxide species and the proton is inevitably governed by the O–H bond length of phenol, the methyl cation may be located at a site neighboring the *ortho* position of the phenoxide species. On the other hand, Fig. 3 strongly supports the idea that the decomposition of methanol proceeds *via* formate on both zinc oxide and zinc ferrite.[14] Therefore, the proposed mechanism is applicable to the reactions which occur on both zinc oxide and zinc ferrite.

The author is very grateful to Mr. Katsuyoshi Shimokawa for his assistance with the experiments.

References

1) E. Briner, W. Plüss, and H. Paillard, *Helv. Chim. Acta*, **7**, 1046 (1924).
2) A. S. Hay, G. F. Endres, and J. W. Eustance, *J. Amer. Chem. Soc.*, **81**, 6335 (1959).
3) U. S. 3446856 (1954). Japan 653986 (1972).
4) N. M. Cullinane and S. J. Chard, *J. Chem. Soc.*, **1954**, 821.
5) L. H. Klemm and D. R. Taylor, *J. Org. Chem.*, **35**, 3216 (1970).
6) T. Nishizaki, H. Hattori, and K. Tanabe, An abstract presented at the 23rd Annual Meeting of the Chemical Society of Japan, Tokyo, Part **I**, 53, No. 03419 (1970).
7) T. Nishizaki and K. Tanabe, *Shokubai*, **14**, 138p (1972).
8) Y. Fukuda, T. Nishizaki, and K. Tanabe, *Nippon Kagaku Kaishi*, **1972**, 1754.
9) D. R. Taylor and K. H. Ludlum, *J. Phys. Chem.*, **76**, 2882 (1972).
10) T. Kotanigawa, M. Yamamoto, K. Shimokawa, and Y. Yoshida, This Bulletin, **44**, 1961 (1971).
11) O. Krilov and E. A. Fokina, *The Problems of Kinetics and Catalysis*, **8**, 245 (1955).
12) R. L. Richardson and S. W. Benson, *J. Phys. Chem.*, **61**, 405 (1957).
13) T. Kotanigawa and M. Yamamoto, This Bulletin, **47**, 954 (1974).
14) A. Ueno, T. Onishi, and K. Tamaru, *Trans. Faraday Soc.*, **67**, 3585 (1971).
15) V. R. Padmanabhan and F. J. Eastburn, *J. Catal.*, **24**, 88 (1972).
16) G. Blyholder and L. D. Neff, *J. Phys. Chem.*, **66**, 1464 (1962).

The Pore Structure of the $ZnO-Fe_2O_3$ Catalyst

Takeshi KOTANIGAWA and Mitsuyoshi YAMAMOTO

The Government Industrial Development Laboratory, Hokkaido, Higashi-Tsukisamu, Toyohiraku, Sapporo 061-01

(Received May 7, 1973)

With regard to the $ZnO-Fe_2O_3$ catalyst used for the selective methylation at the *ortho* position of phenol, the pore structures of the catalysts prepared by five processes were studied. The pore structures of these catalysts were determined by converting the detailed nitrogen desorption isotherm data to the pore-volume distribution. These catalysts had two types of pores, a micropore at about 20 Å and a macropore at 80 Å or more. These pores were sensitive to the sintering conditions. The micropore sizes were independent of the calcination temperature, but the macropore sizes were made proportionally larger with a rise in the calcination temperature. The macropore sizes were related to the particle sizes of the zinc ferrite formed by the solid reaction of ZnO with Fe_2O_3.

As part of a series of studies of catalysts for the synthesis of 2,6-xylenol, we previously reported that the $ZnO-Fe_2O_3$ catalyst promoted selective methylation at the *ortho* position of phenol and that simultaneously the decomposition of methanol took place as a side reaction.[1] The present catalyst was used in the above reaction without a supporter. It is, therefore, of considerable importance for the preparation of the most-favored catalyst to clarify the relations between the preparative methods of the catalyst and their pore structures. As information of this type is useful in the estimation of effective diffusion coefficients,[2] the details of pore structure have been studied on industrially-important catalysts such as alumina.[3,4] However, papers on the pore structure of the $ZnO-Fe_2O_3$ system as a catalyst for the selective methylation of phenol are not available in the literature.

We have attempt here to clarify the pore structures of $ZnO-Fe_2O_3$ catalysts prepared by various processes.

Experimental

Measurement of the Pore Structure. The adsorption-desorption isotherms were measured by using conventional volumetric equipment, as has previously been described.[5] The desorption isotherms have been used to calculate the pore-size distribution by Barrett, Joyner, and Halenda.[6] Mercury porosimeter was used for measuring the large pore-size distribution.[7] The total pore volume was measured by helium-mercury techniques.[8]

X-Ray Analysis of the Catalyst. Rigaku Denki X-ray diffractometer, with Fe$K\alpha$ radiation, was used for this purpose. Using the Scherrer equation, the crystalline sizes were calculated from the half-width of the peak of the angles (2θ) of 42°, 44.8°, and 46.1° for ferric oxide, zinc ferrite, and zinc oxide respectively. The percentage of a given crystal can be measured by calculating the area under a suitable diffraction peak and by comparing this with the corresponding area for a known sample.

Catalyst Preparation. Catalysts were prepared by the following five processes: (A) After mixing 1 mol of ferric oxide with 2 mol of zinc oxide, the mixed powder was pressed into a tablet 3 mm in diameter under pressures up to 150 kg/cm^2. (B) After the addition of 71 g of water to a mixture of 1 mol of ferric oxide and 2 mol of zinc carbonate, the mixture was kneaded for six hours at 50 °C. The paste thus prepared was forced out in a wire form 3 mm in diameter by extrusion. (C) After the addition of 67 g of water to a mixture of 1 mol of ferric hydroxide and 1 mol of zinc oxide, the mixture and the paste were treated by the method used for the (B) catalyst. (D) After the addition of 85 g of water to a mixture of 1 mol of ferric hydroxide and 1 mol of zinc carbonate, the mixture and the paste were treated by the method used for the (B) catalyst. (E) After the dissolution of 1 mol of ferric nitrate and 1 mol of zinc nitrate in water, a 14% aqueous ammonium solution was added to the solution until it gave a pH value of 6.85 at room temperature. The coprecipitate was filtered, washed several times with water, and kneaded for six hours at 50 °C. The paste was then treated by the method used for the (B) catalyst.

These wires and tablets prepared by the five processes were first heated at 150 °C for several hours to remove any moisture and then individually calcined in an electric furnace at 500, 600, 700, and 800 °C respectively for three hours with dry air being pumped into the container. They were then crushed and sieved to 12—14 mesh-size particles.

Results

Catalyst (A). The catalyst calcined at 500 °C consists of 61% ZnO, 23% Fe_2O_3, and 16% $ZnFe_2O_4$, judging from X-ray analysis. In the previous study,[1] it was confirmed through thermal analysis that the solid reaction of ZnO and Fe_2O_3 occurred at 645 °C.

TABLE 1. CRYSTALLINE SIZES OF $ZnO-Fe_2O_3$ CATALYST IN SEVERAL PREPARATIONS

Catalyst symbol	Calcination (°C)	Crystalline sizes (Å)		
		$ZnFe_2O_4$	ZnO	Fe_2O_3
A	500	367	547	249
	600	405	684	467
	700	544	628	—
	800	609	684	—
B	500	—	234	346
	600	398	261	539
	700	462	305	619
	800	820	627	—
C	500	155	596	—
	600	424	627	—
	700	557	644	—
	800	661	684	—
D	500	340	254	—
	600	358	313	—
	700	634	393	—
	800	735	547	—
E	500	169	208	—
	600	347	255	—
	700	702	460	—
	800	772	562	—

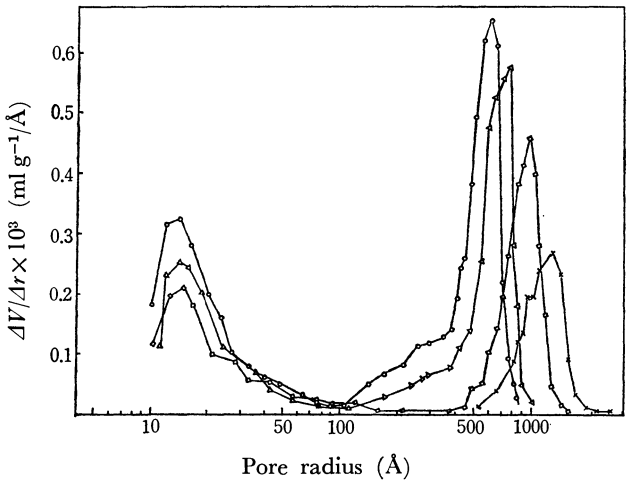

Fig. 1. Pore distribution of catalyst (A)
(-○-) at 500 °C, (-△-) at 600 °C,
(-□-) at 700 °C, (-×-) at 800 °C.

In the catalyst at 600 °C, 5% Fe_2O_3 is still present, but Fe_2O_3 is no longer present in it at 700 °C or more. The components in it are ZnO and $ZnFe_2O_4$. These crystalline sizes are shown in Table 1. The distribution of pore sizes is shown in Fig. 1. The fraction of the micropore volume per total pore volume is about 4% and is not drastically changed by the calcination temperature.

Catalyst (B). The X-ray diffraction pattern of the catalyst calcined at 500 °C does not show the line of $ZnFe_2O_4$; that is, the components in it are still ZnO and Fe_2O_3. The catalyst at 600 °C consists of 26% Fe_2O_3, 11% $ZnFe_2O_4$, and 63% ZnO. The catalyst at 700 °C consists of 24% Fe_2O_3, 14% $ZnFe_2O_4$, and 62% ZnO. However, Fe_2O_3 is no longer present in it at 800 °C. The distribution of pore sizes is shown in Fig. 2. The fraction of the micropore volume per total pore volume is 20.6% in the catalyst at 500 °C, 7.6% at 600 °C, and 6.3% at 700 °C. The micropore disappears rapidly with a rise in the calcination temperature.

Catalyst (C). In the X-ray analysis, the only components in the catalyst are found to be ZnO and $ZnFe_2O_4$, even in the catalyst calcined at 500 °C; that is, Fe_2O_3 is not detected in any catalyst. These crystalline sizes are shown in Table 1. The distribution of pore sizes is shown in Fig. 3. The fraction of the micropore volume per total pore volume is 22.7% in the calcined at 500 °C, 14.2% at 600 °C, 8.6% at

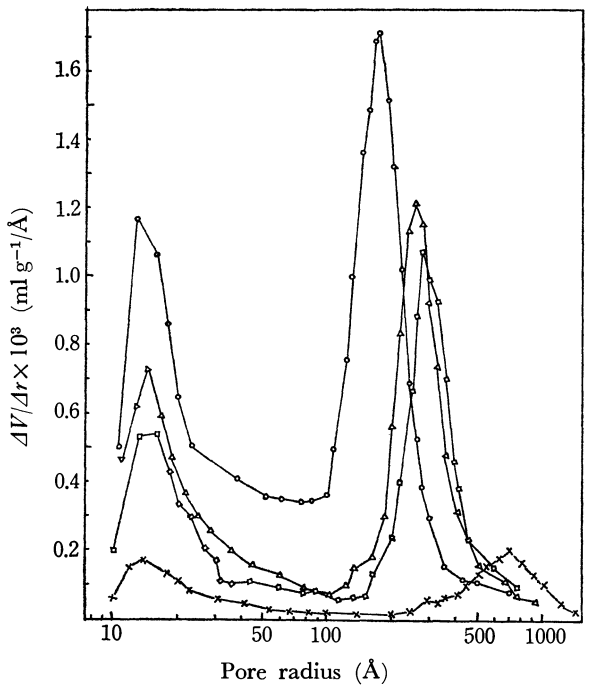

Fig. 2. Pore distribution of catalyst (B)
(-○-) at 500 °C, (-△-) at 600 °C,
(-□-) at 700 °C, (-×-) at 800 °C.

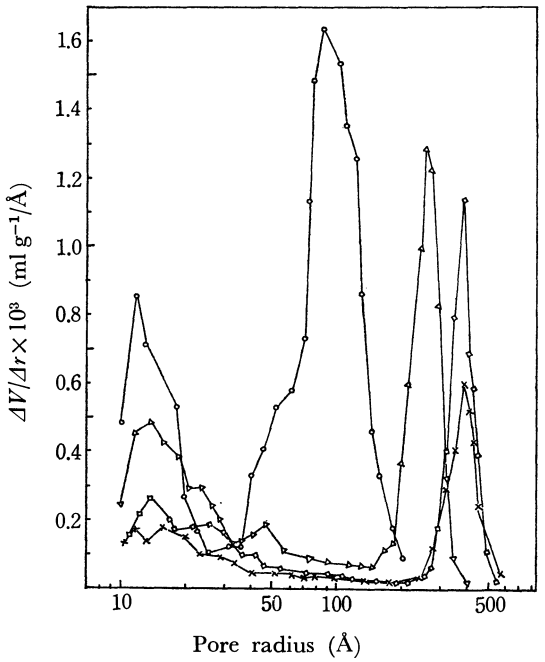

Fig. 3. Pore distribution of catalyst (C)
(-○-) at 500 °C, (-△-) at 600 °C,
(-□-) at 700 °C, (-×-) at 800 °C.

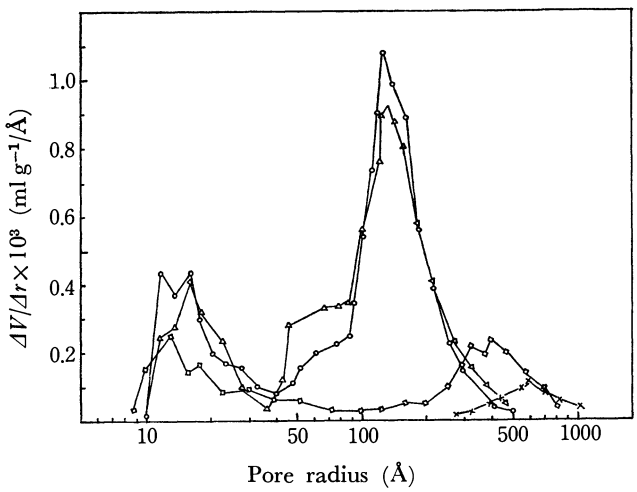

Fig. 4. Pore distribution of catalyst (D)
(-○-) at 500 °C, (-△-) at 600 °C,
(-□-) at 700 °C, (-×-) at 800 °C.

700 °C, and 8.4% at 800 °C. The disappearance of the micropore occurs rapidly with a rise in the calcination temperature.

Catalyst (D). In the X-ray analysis, the same components as in the (C) catalyst are obtained; that is, Fe_2O_3 is not detected in any catalyst. These crystalline sizes are shown in Table 1. The distribution of pore sizes is shown in Fig. 4. The fraction of the micropore volume per total pore volume is 35.1% in the catalyst calcined at 500 °C, 34.8% at 600 °C, 8.0% at 700 °C. The disappearance of the micropore occurs rapidly at 700 °C or more.

Catalyst (E). It has been reported that the formation of ferrite by the wet method depends upon pH value of the solution, but at a pH value below 10.0 the coprecipitate consists of hydroxides.[9] As the coprecipitate in the (E) catalyst is formed at a pH value of 6.85, it consists of zinc hydroxide and ferric hydroxide. In the X-ray analysis, Fe_2O_3 is not detected in any catalyst. The only components in the catalyst are ZnO and $ZnFe_2O_4$. The distribution of pore sizes is shown in Fig. 5. The fraction of the micropore volume per total pore volume is 16.6% in the catalyst calcined at 500 °C, 13.8% at 600 °C, and 6.5% at 700 °C. These crystalline sizes are shown in Table 1.

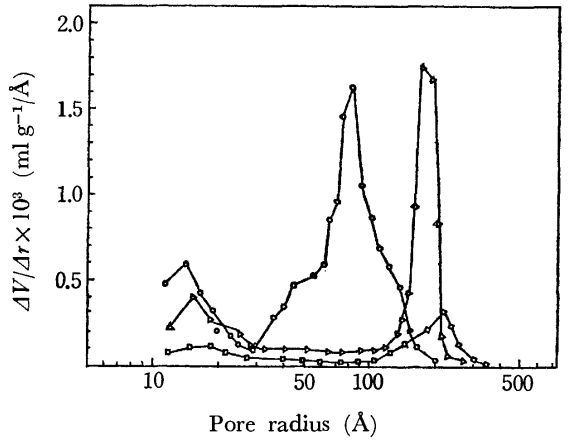

Fig. 5. Pore distribution of catalyst (E)
(-○-) at 500 °C, (-△-) at 600 °C,
(-□-) at 700 °C.

TABLE 2. PORE STRUCTURE OF ZnO-Fe_2O_3 CATALYST IN SEVERAL PREPARATIONS

Catalyst symbol	Calcination (°C)	Total pore volume (cm³/g)	Surface area (m²/g)	Pore radius (Å)
A	500	0.265	9.4	610
	600	0.294	7.5	710
	700	0.276	5.8	960
	800	0.192	5.3	1300
B	500	0.442	35.0	150
	600	0.418	18.8	250
	700	0.373	15.0	290
	800	0.308	5.5	700
C	500	0.190	40.4	80
	600	0.190	14.4	270
	700	0.170	8.2	380
	800	0.110	5.6	390
D	500	0.189	21.2	135
	600	0.203	19.6	140
	700	0.152	5.3	380
	800	0.100	2.3	700
E	500	0.134	36.6	85
	600	0.126	12.6	175
	700	0.058	3.3	215
	800	0.013	—	—

The pore volumes and surface areas of the present catalysts are summarized in Table 2. It may be concluded from Table 2 that the present catalysts are very sensitive to sintering.

Discussion

Three types of pores (the dehydration pore, the small interparticle pore, and the macropore (which consists of the voids between particles)) have previously been confirmed from a study of the origin of pores in the alumina.[3] However, the catalysts prepared by the five processes outlined above clearly form two types of pores, the micropore at about 20 Å and the macropore at 80 Å or more. With regard to the micropore, water and/or carbon dioxide are loosed from starting materials during the calcination. The amounts of the loss increase in the order of (D)→(B)→(E)→(C)→(A). The fraction of the micropore volume per total pore volume also corresponds to the order of the amounts of the loss of the small molecules from the starting materials. The micropore is considered to be formed by the loss of water and/or carbon dioxide from the starting materials and is considered to be a dehydration pore or a decarbonation pore.

On the other hand, the macropore becomes proportionally larger with a rise in the calcination temperature and with the growth of these crystalline sizes, as shown in Tables 1 and 2. Hence, the macropore is considered to consist of the voids between particles. In the present catalyst, zinc ferrite is formed by the

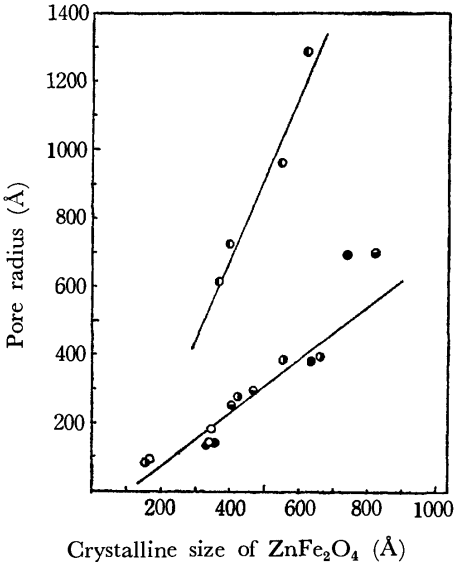

Fig. 6. Relations between pore radius and crystalline size of zinc ferrite
(-◐-) Catalyst A, (-◒-) Catalyst B, (-◑-) Catalyst C, (-●-) Catalyst D, (-○-) Catalyst E.

solid reaction of zinc oxide with ferric oxide.[1] In Table 1, the solid reaction may be seen to proceed easily in the (C), (D), and (E) catalysts, which include ferric hydroxide as a starting material. The crystalline sizes of the zinc ferrite grow considerably with a rise in the calcination temperature. Therefore, the crystalline sizes of zinc ferrite must be estimated for the formation of the macropore. The relationship between the macropore radius of these catalysts and the crystalline sizes of zinc ferrite is shown in Fig. 6. The plots of the catalysts prepared by the extrusion technique are on the same linear line, but the plot of the catalyst prepared by the tableting technique is on the other linear line. This may be expected to be due to the conditions of the preparation.

The micropore and the macropore volumes can be calculated by means of the total pore volumes and the distribution of pore sizes. From these results, the micropore may be determined to disappear mainly at temperatures below 700 °C and the macropore, to disappear suddenly at 800 °C. It may be found from the results in Table 2 that considerable decreases in the pore volume and the surface area occur with a rise in the calcination temperature. As a result, it may be concluded that the present catalyst is well crystallized and sensitive to sintering conditions.

References

1) T. Kotanigawa, M. Yamamoto, K. Shimokawa, and Y. Yoshida, This Bulletin, **44**, 1961 (1971).
2) J. M. Thomas and W. J. Thomas, "Introduction to the Principles of Heterogeneous Catalysis," Academic Press (1968).
3) M. F. L. Johnson and J. Mooi, *J. Catal.*, **10**, 342 (1968).
4) J. H. De Boer and B. C. Lippens, *ibid.*, **3**, 38 (1964).
5) H. E. Ries, M. F. L. Johnson, and J. S. Melik, *J. Phys. Colloid. Chem.*, **53**, 657 (1949).
6) E. P. Barrett, L. G. Joyner, and P. P. Halenda, *J. Amer. Chem. Soc.*, **73**, 373 (1951).
7) H. L. Ritter and L. C. Drake, *Ind. Eng. Chem. Anal. Ed.*, **17**, 782 (1945).
8) Y. Yoneda, "Shokubai Kogaku Koza," Vol. 4, Chijin Shokan, Tokyo, Vol. 4, p. 68.
9) T. Sato, M. Sugihara, and M. Saito, *Kogyo Kagaku Zasshi*, **65**, 1749 (1962).

Vacuum Ultraviolet Absorption and Photoelectron Spectra of Aliphatic Ketones

Hitoshi OGATA, Jun KITAYAMA, Masanori KOTO, Shinji KOJIMA, Yoshimasa NIHEI, and Hitoshi KAMADA

Department of Industrial Chemistry, Faculty of Engineering, The University of Tokyo, Bunkyo-ku, Tokyo 113

(Received December 1, 1972)

The vacuum ultraviolet absorption spectra down to 65000 cm^{-1} and HeI photoelectron spectra were measured for CH_3CHO and $RCOCH_3$ ($R=CH_3$ to t-C_4H_9). Assignments of the absorption bands are proposed with the aid of photoelectron spectra and CNDO/2 type molecular orbital calculations. Special notice has been paid to the similarity of the vibrational structure between the lowest ionization potential bands of photoelectron spectra and the second bands of vacuum ultraviolet absorption spectra.

Many experimental and theoretical studies have been made on the interpretation of the vacuum ultraviolet absorption spectra of aliphatic ketones and aldehydes.[1-8] Although some interpretation has been given, there is no agreement on the assignment of bands to electronic transitions. Recently, Lucazeau and Sandorfy measured the spectra of acetaldehyde and its deuterated homologues in the ultraviolet down to 85000 cm^{-1}, and gave detailed assignments to the individual absorption bands.[9] As for ketones, Ito *et al.* measured the spectra of aliphatic ketones, mainly methyl alkyl ketones, in the region from 50000 cm^{-1} to 60500 cm^{-1}, but they gave no definite assignment.[10] The present paper deals with the interpretation of these spectra with the aid of the photoelectron spectra (pes) of these molecules and CNDO/2 type SCF MO calculations.

Experimental

The vacuum ultraviolet absorption spectra were measured on a Jasco model VUV-2 vacuum ultraviolet self-recording spectrophotometer mounted with 1 m radius concave grating having 1200 grooves per mm, equipped with a ratio recording double beam system using the rotating-cell method. 3 cm gas cell blocks containing a sample cell and a reference cell with CaF_2 windows rotate at 8 Hz and function as a rotating sector.[11] The light sources were a hydrogen discharge tube and a zenon discharge tube. The spectra were measured in the vapor state at room temperature and recorded photoelectrically down to 65000 cm^{-1}.

A Jasco model PE-1 photoelectron spectrometer was used for measurements of the photoelectron spectra. The resonance line of He (584Å) was emitted by means of DC glow discharge. A hemispherical electrostatic condenser with 100mm diameter was used for electron energy analysis, a channel electron multiplier for detection and a pulse counting method for signal processing system. The terrestrial magnetic field and fluctuating magnetic field around the apparatus were removed by μ-metal shielding. In order to obtain ionization potentials from spectra, Xe gas was fed into the sample gas as an internal standard of ionization potential. The spectra were measured in gas phase at room temperature.

We have measured the absorption and photoelectron spectra of CH_3CHO, CH_3COCH_3, $C_2H_5COCH_3$, n-$C_3H_7COCH_3$, i-$C_3H_7COCH_3$, n-$C_4H_9COCH_3$, i-$C_4H_9COCH_3$, s-$C_4H_9COCH_3$ and t-$C_4H_9COCH_3$. These compounds were commercial products and used without further purification. Theoretical calculations were based on the CNDO/2 method.

Results and Discussion

Photoelectron Spectra. The photoelectron (pe) spectra of acetaldehyde and eight aliphatic ketones are shown in Fig. 1. Each pe spectrum of these molecules contains relatively a sharp peak located at the lowest ionization potential side (called the first band) and a series of broader peaks at the higher ionization potential region. We assume the validity of the Koopmans' theorem throughout.[12] Since the calculations have been performed in the ground state geometries, the calculated ionization potentials are compared with the experimental vertical ionization potentials throughout. Observed vertical ionization potentials and calculated ionization potentials of acetone and acetaldehyde are summarized in Table 1. For the sake of convenience,

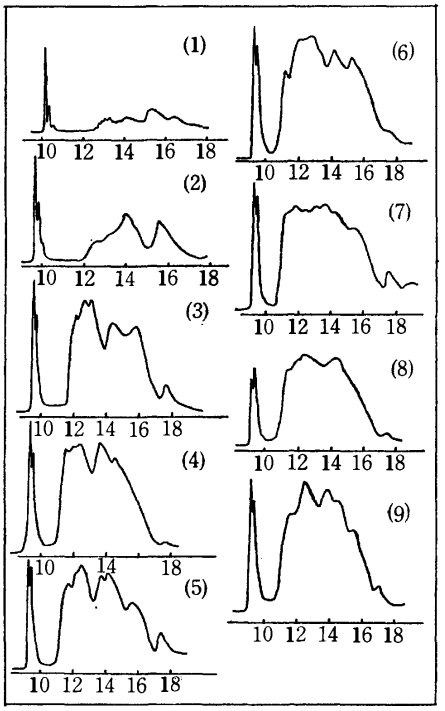

Fig. 1. The photoelectron spectra of ketones and acetaldehyde, Abscissa; ionization potential (eV). Ordinate; arbitrary unit. (1): CH_3CHO, (2): CH_3COCH_3, (3): $CH_3COC_2H_5$, (4): CH_3CO-n-C_3H_7, (5): CH_3CO-i-C_3H_7, (6): CH_3CO-n-C_4H_9, (7): CH_3CO-i-C_4H_9, (8): CH_3CO-s-C_4H_9, (9): CH_3CO-t-C_4H_9.

Table 1. Calculated and observed ionization potentials of acetone and acetaldehyde

CNDO/2		Obsd
I. P. (eV)	Symmetry	I. P. (eV)
Acetone		
13.12	$4b_2$ (n)	9.71
15.16	$2b_1$ (π)	12.62
17.06	$5a_1$ (σ)	13.70
17.62	$3b_2$ (σ)	14.18
Acetaldehyde		
13.71	7a' (n)	10.19
16.23	2a'' (π)	13.09
17.50	6a' (σ)	13.93
20.86	5a' (σ)	15.09

Table 2. The first pe bands and the second absorption bands of acetone and acetaldehyde

Acetone				
pes	peak position (eV)	9.71	9.86	10.02
	intensity (cps)	360	200	70
VUV	peak position (eV)	6.35	6.50	6.65
	intensity ($\varepsilon\times10^{-3}$)	10.30	6.10	2.05
Acetaldehyde				
pes	peak position (eV)	10.19	10.33	10.50
	intensity (cps)	690	250	60
VUV	peak position (eV)	6.83	6.96	7.13
	intensity ($\varepsilon\times10^{-3}$)	9.8	3.0	2.3

the types of molecular orbitals are roughly classified into n, π, and σ. The first bands of the pe spectra of acetone and acetaldehyde can be assigned to the ionization from the non-bonding orbital localized on the respective oxygen atom on the basis of their spectral features and calculated eigenvectors. The first bands of other aliphatic ketones can also be assigned to non-bonding orbitals from the same reason.

All the first bands of aliphatic ketones and aldehyde show vibrational fine structures. Peak positions and intensities of the fine structures for acetone and acetaldehyde are shown in Table 2. Three peaks can be found for acetone with spacings 0.15 and 0.16 eV and two peaks for other ketones with spacings ranging from 0.15 to 0.08 eV. In the spectrum of acetaldehyde, three peaks with spacings of 0.14 and 0.17 eV can be identified.

Results of calculations show that the second ionization bands of acetone and acetaldehyde can be assigned to the C=O π orbitals and the third bands to the C=O σ orbitals, other types of σ orbitals largely contributing to the third bands.

General Description of the VUV Spectra. The absorption spectra of acetone, first studied by Scheibe *et al.*,[13] have been investigated in detail by Lawson and Duncan,[14] Lake and Harrison,[5] and Ito *et al.*[10] Absorption spectra of acetone and acetaldehyde we obtained are shown in Fig. 2. For acetone, the absorption bands near 50000, 60000, and 65000 cm^{-1} are denoted by the second, third, and fourth absorption bands respectively, since aliphatic ketones have an

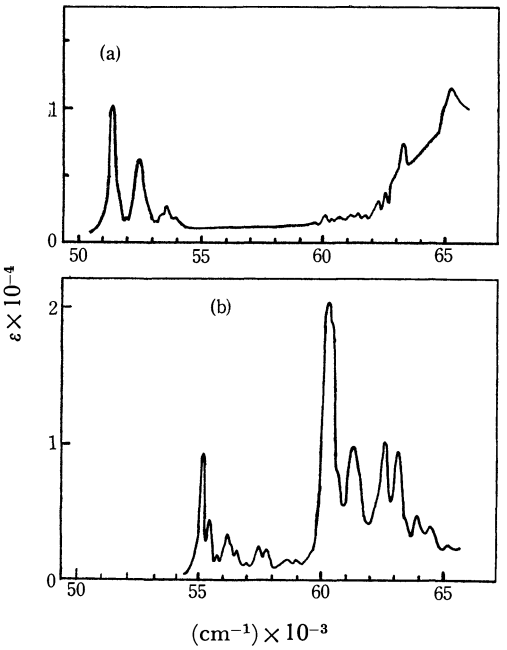

Fig. 2. The VUV absorption spectra of (a) acetone and (b) acetaldehyde.

absorption band near 36000 cm^{-1} assigned to the n-π^* transition. In the case of acetone, the third and fourth absorption bands are rather difficult to separate, but are separated at 62200 cm^{-1} by taking spectra of other ketones into consideration. The reproducibility of *f*-values is almost within 10 per cent and *f*-values are in fairly good agreement with those reported by Ito *et al.*,[10] except for methyl isobutyl ketone, methyl s-butyl ketone and methyl t-butyl ketone.[15] Because of overlapping with Ref. 10, the absorption spectra of aliphatic ketones are not shown except for acetone.

The Second and Third Absorption Bands of Ketones. The first problem in the spectral region beyond 50000 cm^{-1} is to distinguish the Rydberg bands from the valence shell bands. Duncan[16] assigned 65000 cm^{-1} band of acetone to the Rydberg band whose quantum defect is 0.495, but its limit was not confirmed by the photoionization experiments of Watanabe,[17] who made a different assignment and obtained a series leading to an ionization potential of 9.705 eV. In contrast, Barnes and Simpson[7] assigned the weak band near 60000 cm^{-1} to the 2p-3s Rydberg transition and the strong band near 65000 cm^{-1} to the π-π^* transition. Barnes and Simpson[7] and Ito *et al.*[10] assigned the sharp peaks locating from 50000 cm^{-1} to 55000 cm^{-1} to the n-σ^* valence shell transition.

The equilibrium geometries of the excited Rydberg species and the ionic species lacking one non-bonding electron are expected to be considerably close. A similarity of the Franck-Condon factors is therefore expected between the pe spectra and optical spectra assigned to Rydberg transitions. The vibrational structure of the pe band assigned to non-bonding orbital is thought to be very much alike that of a Rydberg transition which converges into the corresponding ionization.

The fine structures of the second absorption band and

of the first pe band of acetone are summarized in Table 2. As might be expected, the vibrational structure of first pe band bears a striking resemblance to that of the second absorption band. Fine structures of the second absorption bands of other ketones are considerably complicated, but the corresponding peaks can be found in the first pe bands with a few exceptions. This evidence strongly supports the assignment that the second absorption bands of aliphatic ketones are the Rydberg transitions. If we take the 51300 cm^{-1} peak of acetone for the first member of the Rydberg series and use the values obtained by Watanabe,[17] transition energies of each absorption peak satisfy the Rydberg equation, giving the quantum defect $\delta=1.02$. In other words, the peaks observed by Watanabe belong to the s-type Rydberg series in the range $n\geq 4$, and the 51300 cm^{-1} band is the $n=3$ Rydberg transition of the same series.

As regards the variation of the second absorption bands of aliphatic ketones by alkyl groupes, Ito *et al.* pointed out that methyl alkyl ketones could be classified into Group I, methyl *n*-alkyl ketones (including methyl isobutyl ketone) and Group II, the methyl alkyl ketones in which the α-carbons of the alkyl groups are the secondary or tertiary carbons, the shapes of these second bands being sensitive to alkyl groups.[10] In the second bands of Group I molecules, there are main vibrational progressions with frequencies *ca.* 1200 cm^{-1}. Hardly any vibrational fine structures can be seen in Group II molecules with the exception of methyl isopropyl ketone. In particular, the difference in band shape between methyl isobutyl ketone and methyl *s*-butyl ketone is remarkable. Although the former has a fairly distinct fine structure the latter has practically no structure. This is thought to be due to the existence of conformational isomers and the characteristics of the Rydberg orbitals.

The first member of the Rydberg transition series is related to the smallest Rydberg orbitals. The first Rydberg state undergoes a larger perturbation from the molecular skelton than higher members. Because of the localization character of the lone pair orbitals, the Rydberg spectra of methyl alkyl ketones caused by the transitions from the lone pair to Rydberg orbitals are mainly affected by the structure near the carbonyl group. In the case of Group I molecules, the methyl alkyl ketones with large normal alkyl groups have essentially the same vibrational structures as methyl ethyl ketone. On the other hand, Rydberg states of Group II molecules which have branched alkyl groups at α-position are strongly perturbed by their internal rotations. In the case of methyl isobutyl ketone which has a branched alkyl group at β-position, the absorption band is considered to show several vibrational fine structures, since the Rydberg state is not much perturbed.

The vacuum ultraviolet absorption spectra of aliphatic alcohols, ROH, and amines, RNH_2 were also measured R = (CH_3 to t-C_4H_9). Important results alone are presented here. The first electronic transition bands of ROH located at about 55500 cm^{-1} and of RNH_2 at about 47600 cm^{-1} can be assigned to the n-σ^* transitions. The variation of oscillator strengths f of the first

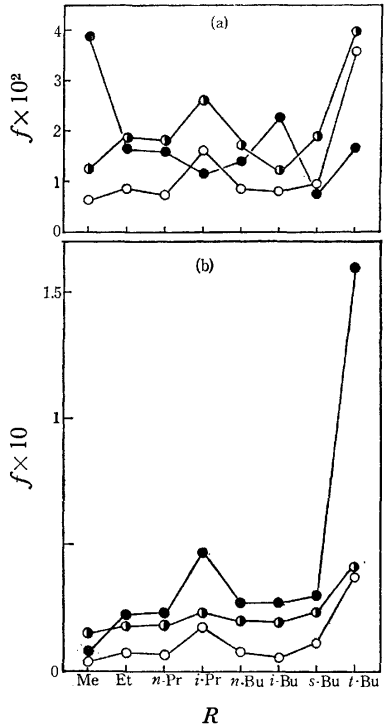

Fig. 3. The oscillator strengths of (a) the second and (b) the third absorption bands of $RCOCH_3$ and those of n-σ^* transitions of RNH_2 and ROH.
○: ROH, ◑: RNH_2, ●: $RCOCH_3$.

bands of ROH and RNH_2, and the oscillator strengths of the second absorption bands of $RCOCH_3$ are shown in Fig. 3(a). The f-values of the n-σ^* bands of alcohols and those of amines undergo the same variation by alkyl substituents, the second bands of ketones showing a different tendency. Similar plots for the n-σ^* bands of alcohols and amines and for the third absorption bands of ketones are shown in Fig. 3(b). The oscillator strengths vary considerably with the alkyl group, the methyl group giving the smallest f-value and the *t*-butyl group the largest f-value. However, the three series of molecules show the same variation by alkyl groups.

Taking into account the vibrational structure of the second absorption bands of ketones and the varation of the oscillator strentghs of the second and third bands, it seems reasonable to assign the second bands of ketones to the Rydberg transition and the third bands to the n-σ^* transition. The assignment is based only on experimental results, and therefore, attention should be paid to whether the lowest Rydberg orbital is distinguishable from the lowest σ^* orbital. For example, the $3sa_1$ Rydberg orbital of H_2O is identical with the antibonding orbital $4a_1$. However, in larger molecules with lower symmetry the lowest Rydberg orbital might not be identical with the lowest σ^* orbital, though mixing may occur. In this regard, the theoretical investigation by Salahub[18] is prerequisite.

In order to obtain further proof that the second bands can be assigned to the Rydberg transition, further measurements are necessary.[19-21] As for the second band of acetone, it was pointed out[19] that the upper state of the transition has the characteristic of a big

orbit, but the pressure effect by the use of nitrogen gas is not so extreme as methyl iodide, a well-known example. According to the assignment by Lucazeau and Sandorfy[9] acetaldehyde has the n-3s Rydberg state at 55045 cm^{-1}, the n-3p Rydberg state at 60154 cm^{-1} and the n-3d Rydberg state at 67985 cm^{-1}. Their spectra show that these peaks are very sharp and intense. In the case of acetone, on the contrary, no sharp and intense peak corresponding to n-3p or n-3d Rydberg peak of acetaldehyde can be found in this spectral region.

The Fourth Absorption Bands of Ketones. The fourth band starting at 62200 cm^{-1} could not be experimentally examined. The spectra obtained by Barnes and Simpson[7] show that this band extends to about 69000 cm^{-1} and has a large f-value. In the assignment of this band, CNDO/2 calculations were performed, orbitals with a higher principal quantum number being not included in the basis functions.

On the basis of experimental results, the third bands have been assigned to n-σ^* transitions. But CNDO/2 calculations show that the third band is π-π^* and the fourth band n-σ^*. If absorption intensities are taken into consideration and, further, from the fact that the calculated transition energies for π-π^* and n-σ^* are very close, it may not be appropriate to make direct use of calculations to assignments. The spectrum reported by Barnes and Simpson[7] shows that the f-value of the fourth band is more than ten times larger than that of the third band. Our calculations show that the f-value of π-π^* is about ten times larger than that of n-σ^*. This may support the assignment that the fourth band is the π-π^* transition.

Acetaldehyde. The first band of the pe spectrum of acetaldehyde can be assigned to the ionization from the non-bonding orbital localized on an oxygen atom. Fine structures of the first pe band and the 60000 cm^{-1} absorption band of acetaldehyde assigned to n-3s Rydberg state are summarized in Table 2. As in the case of acetone, similarity of the vibrational structure between pe and absorption spectra is recognized.

Though we could not identify it, Lucazeau and Sandorfy[9] found a very weak band in the region 53677—58254 cm^{-1} and assigned it to the n-σ^* transition on the basis of the following (1) In Rydberg series, the 0–0 component usually has maximum intensity. (2) The σ^* orbital has a conspicuous 3s Rydberg character. The f-value of this n-σ^* transition is calculated to be 0.12. This value is too large for an explanation of the weakness of this band. Our results show that the σ-π^* transition is the second transition having an f-value one tenth of the n-σ^* transition. It may thus be reasonable to assign this band to the σ-π^* rather than the n-σ^* transition, where the σ orbital has mainly CO bonding character. Calculations show that in the case of acetone the second lowest transition is also σ-π^*. In contrast with the presence of the weak band in the absorption spectrum of acetaldehyde in the region 53677—58254 cm^{-1}, no corresponding band has been found. Concerning transition energies, calculated results for acetaldehyde are consistent with the experimental results, the n-σ^* transition having lower energy than the π-π^* transition. Observed transition energies and assignments for acetone and acetaldehyde are shown in Table 3.

Table 3. The observed transition energies, ΔE, and oscillator strengths, f

Obsd		Assign.
ΔE (eV)	f	
Acetone		
4.50	4.14×10^{-4} [22]	n-π^*
6.35	3.9×10^{-2}	Rydberg
7.46	$<8.6\times10^{-3}$	n-σ^*
8.10	—	π-π^*
Acetaldehyde		
4.28	3.63×10^{-4} [22]	n-π^*
6.82	3.2×10^{-2}	Rydberg
7.46	1.8×10^{-1}	Rydberg[9]
7.75		n-σ^*[9]

References and footnotes

1) H. L. Mcmurry, *J. Chem. Phys.*, **9**, 231, 241 (1941).
2) A. D. Walsh, *Trans. Faraday Soc.*, **42**, 66 (1946).
3) W. C. Price, *J. Chem. Phys.*, **3**, 256 (1935).
4) W. C. Price, *Proc. Roy. Soc., Ser. A*, **162**, 110 (1937).
5) T. S. Lake and A. J. Harrison, *J. Chem. Phys.*, **30**, 361 (1959).
6) R. S. Holdsworth and A. B. F. Duncan, *Chem. Rev.*, **41**, 311 (1947).
7) E. E. Barnes and W. T. Simpson, *J. Chem. Phys.*, **39**, 670 (1963).
8) W. C. Johnson, Jr. and W. T. Simpson, *ibid.*, **48**, 2168 (1968).
9) G. Lucazeau and C. Sandorfy, *J. Mol. Spectrosc.*, **35**, 214 (1970).
10) H. Ito, Y. Nogata, S. Matsuzaki, and A. Kuboyama, This Bulletin, **42**, 2453 (1969).
11) Y. Nihei, S. Oda, E. Niki, and H. Kamada, *Spectrochim. Acta*, **24A**, 457 (1968).
12) T. Koopmans, *Physica*, **1**, 104 (1934).
13) G. Scheibe, F. Povenz, and C. Linstrom, *Z. Phys. Chem.*, **B20**, 283 (1933).
14) M. Lawson and A. B. F. Duncan, *J. Chem. Phys.*, **12**, 329 (1944).
15) Our experiments showed that the absorption spectra and related results of methyl isobutyl ketone and methyl *s*-butyl ketone should be named in reverse to those given in Ref. 10.
16) A. B. F. Duncan, *J. Chem. Phys.*, **3**, 131 (1935).
17) K. Watanabe, *ibid.*, **22**, 1564 (1954).
18) D. R. Salahub, *Theoret. Chim. Acta* (Berl.), **22**, 330 (1971).
19) M. B. Robin and N. A. Kuebler, *J. Mol. Spectrosc.*, **33**, 274 (1970).
20) H. Basch, M. B. Robin, N. A. Kuebler, C. Baker, and D. W. Turner, *J. Chem. Phys.*, **51**, 52 (1969).
21) J. W. Raymonda, *ibid.*, **56**, 3912 (1972).
22) E. F. Worden, *Spectrochim. Acta*, **22**, 21 (1966).

The Effects of the Composition of Raw Cadmium Sulfide on the Characteristics of Cadmium Pigments

Makoto TSUNASHIMA and Hiroshi TAKAHASHI*

Omiya Plant, Mitsubishi Metal Corporation, Kitabukuro, Omiya 330

** Institute of Industrial Science, The University of Tokyo, Roppongi, Minato, Tokyo 106*

(Received April 6, 1973)

The effects of the S/Cd mol ratios of cadmium sulfide precipitates on the particle size, the hexagonality, and the brightness of cadmium pigments were studied. The precipitates were prepared by mixing an aqueous solution of cadmium nitrate with either sodium sulfide or hydrogen sulfide. Then, cadmium pigments were made of these precipitates by heat-treatment under an atmosphere of oxygen or nitrogen. The characteristics of the pigments were affected by the following three factors; particle size, hexagonality, and brightness. These factors were closely related to the S/Cd mol ratio of the precipitates of the cadmium pigments. We found the minimum points on the curves of the particle size, the hexagonality, and the brightness in relation to the S/Cd mol ratio. From these results, it was concluded that the optimum range of the S/Cd mol ratios of the precipitates for the characteristics of the cadmium pigments was 0.98 ± 0.01.

Cadmium pigments are ordinarily composed of CdS or solid solutions of CdS and either ZnS, CdSe, or HgS. These pigments are mainly formed by two processes, precipitation and calcination. The former process is the precipitation reaction of a metal salt solution with alkali sulfide (selenium is sometimes dissolved in this solution); the latter, the calcination of the precipitates at 500—700 °C in a non-oxidizing atmosphere.

The characteristics of cadmium pigments have been reported in many papers[1-5] and patents.[6] Most of these reports have been concerned with the two processes mentioned above. The effects of the temperature, pH, additions, *etc.* on the pigments have been studied for the precipitation process, and those of the temperature, the atmosphere, the time, additions, *etc.*, for the calcination. However, the characteristics of the precipitated powders and their effects on the final pigments have been little investigated.

We have previously reported that on heat-treatment oxygen and sulfur affected the particle size, the hexagonality, and the color.[7,8] The results showed that the changes in the particle size and hexagonality were very similar to the conditions of heat-treatment. Especially in the heat-treatment, oxygen in an atmosphere distinctly brought about a brighter color than did nitrogen or helium. Therefore, the effects on the pigment characteristics in relation to the amount of cadmium hydroxide and sulfur in precipitates and that of oxygen in an atmosphere were studied.

In this paper, the effects of the S/Cd mol ratio of the CdS precipitates before heat-treatment of the pigment characteristics will be discussed. Some interesting correlations between the S/Cd mol ratios and the pigment characteristics were obtained.

Experimental

Raw Materials. The raw materials were precipitated by the reaction of cadmium sulfate and a sodium sulfide solution of each 1 molar concentration. Precipitates with various S/Cd mol ratios were prepared by the use of the sodium sulfides, dissolved sulfur powder for precipitates including excess sulfur, and mixed sodium hydroxide for those with excess cadmium. After the solution had been stirred for 3 hr at 80 °C, the precipitate was dried at 100 °C, then, it was pulverized to a fine powder. It was considered that all these, including cadmium polysulfides or cadmium hydroxide, were coprecipitated with CdS.

In addition to these materials, other raw materials were prepared by the bubbling of hydrogen sulfide gas. Sulfur or cadmium hydroxide powder was mixed with the suspension after it had been washed to obtain Cd or S excess raw materials. The precipitates prepared by sodium sulfide were classified as Group A, and those prepared by hydrogen sulfide, as Group B.

These raw materials were analyzed by the gravimetric method for sulfur and by the EDTA titration method for cadmium.

Heat-treatment. Each raw material was degassed at 200 °C for an hour under a pressure of 10^{-3} mmHg and then heat-treated for an hour at a constant temperature in pure nitrogen or oxygen gas of an atmospheric pressure. The temperature of the heat-treatment was fixed at 500 °C for Group B, for the precipitates of Group B were stable and no changes in hexagonality occurred at 500 °C, as has previously been reported.[9]

Properties of Products. The particle size was measured by the BET method, from the nitrogen gas adsorption at the temperature of liquid nitrogen, after the raw materials had been pretreated at 200 °C under a pressure of 10^{-3} mmHg.

CdS crystals have two polymorphic forms, *i. e.*, a hexagonal closely-packed structure (wurtzite) and a face-centered cubic (zincblende).

CdS polycrystals usually include both of the forms, and the term 'hexagonality' has been previously used[10,11] to describe the fraction of the hexagonal form in the crystal. We have also used this term 'hexagonality'.

Short and Steward[10] have shown that the 'hexagonality' (H) of CdS polycrystal is related to the ratio (R) between the integrated intensities (I) of the first and second Debye-Sherrer rings:

$$H = 4R/(3R+1.33)$$

where:

$$R = I(100)/I(002+111)$$

As is shown in the previous paper, in this equation the constant value, 1.33, was the lower estimation. From the many experimental results, the most reliable value was 1.70. Therefore, the above equation was modified as follows:

$$H = 4R/(3R+1.70)$$

The X-ray diffraction patterns were recorded by means of a Philips X-ray diffractometer, model PW. As an X-ray radiation source, nickel-filtered copper radiation at 30 kV and 20 mA was used.

The brightness of the specimen was investigated as one pig-

ment characteristic.

Specimens were mixed and kneaded with varnish on Hoover muller* by hand or by four times 25 revolutions under a 150 lb. weight. The spectral reflectance curve of each of these sheets was then measured by means of a spectrophotometer.

The brightness was represented by the slope of the spectral reflectance curve at the 50 percent reflectance point (in arbitrary units), but it agreed well with both the 'excitation purity' from the chromaticity diagram** and with observations. As the slope is proportional to the crystallinity, the brightness represents the purity of the color.[12]

Results and Discussion

Particle Size. The raw materials had particle sizes (surface area diameter) of 10—20 nm for Group A and of 150 nm for Group B. The particle sizes of the heat-treated specimens are shown in Fig. 1.

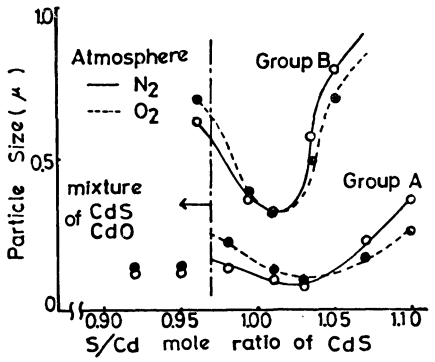

Fig. 1. The correlation between the S/Cd mol ratio of CdS precipitate and particle size of heat-treated specimen.

In Fig. 1, the changes in particle size according to the S/Cd mol ratio of the raw materials describe a curve with a minimum in the range from 1.02 to 1.03. The particle sizes also differed with the atmospheric gas.

It seems to be general that particles grow remarkably on heat-treatment in an excess of either S or Cd. Therefore, it is natural that a miniumm point exists on the curve. Parravano[13] showed that ZnO particles grew by the recombinations of zinc diffused in the crystal with oxygen on the surface. Further, Woodbury[14] and Whelan[15] reported that the diffusion of Cd in the CdS crystal was in proportion to the Cd vapor pressure.

These facts prove that an increase in particle size is promoted by the excess of either S or Cd, and that, because sulfur was more volatile than Cd and was reactive with atmospheric oxygen,*** the position of the minimum point in the curve shifts to a somewhat lower value of the S/Cd mol ratio.

Hexagonality. Changes in the hexagonality of heat-treated specimens of Group A are shown in Fig.

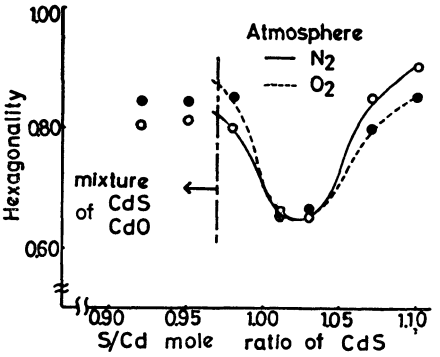

Fig. 2. The correlation between the S/Cd mol ratio of CdS precipitate and hexagonality of heat-treated specimen.

2 in relation to the S/Cd mol ratios of the original specimens. The curve of Group B has been abbreviated to be almost the same as for Group A. The changes in hexagonality showed the same tendency toward particle size.

According to Holt and Wilcox,[16] phase transformation to the hexagonal form was accelerated by the quantities of defects. It was supposed that specimens of Group A had more defects than those of Group B, since the particles of the former were fine.

The effect of the oxygen in the atmosphere on the hexagonality was almost the same as that on the particle growth.

Brightness. CdS pigments, prepared under similar conditions, took various hues, brightness, tinting strength, and hiding powers according to the differences in crystal structure, particle size, *etc.*

The correlation with the brightness and the S/Cd mol ratio is shown in Fig. 3 in the case of Group A; the curve is almost the same as Group B.

The changes in brightness showed results similar to those for both particle size and hexagonality, but the minimum point of the curve was less clear compared with the previous two characteristics.

The brightness of heat-treated specimens in an atmosphere of oxygen was higher than that in one of nitrogen. In general, cadmium pigments were pulverized and mixed with vehicles for practical use. As

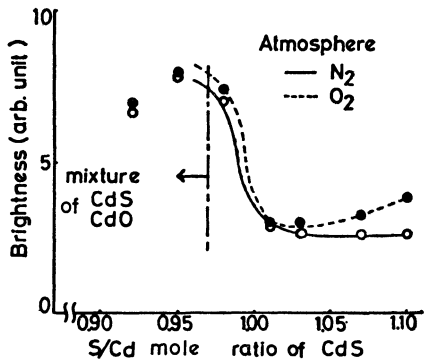

Fig. 3. The correlation between the S/Cd mol ratio of CdS precipipate and the brightness of heat-treated specimen.

* Japanese Industrial Standard, JIS K5101: Testing methods for pigments.

** Japanese Industrial Standard, JIS Z8701.

*** Observed by the generation of SO_2 gas.

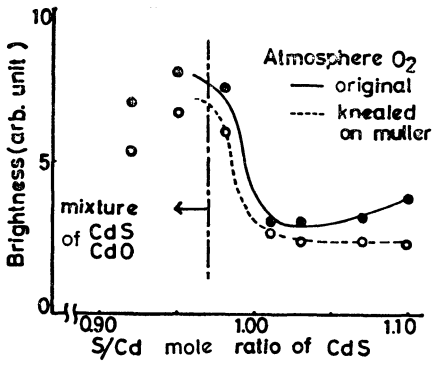

Fig. 4. Effects on brightness by the grinding of heat-treated specimens.

has previously been reported,[12] the brightness decreased upon such treatments, distortion also occurring in a crystal.

As is shown by the dotted lines in Fig. 4, the brightness of the specimens in this study was also reduced by kneading on muller; the reduction was especially remarkable in the specimens with a S/Cd mol ratio of over 1.00 and which has been heat-treated in an atmosphere of nitrogen.

Conclusion. Cadmium pigments with excellent characteristics must have the range in the particle size of 0.1—0.5 μ and as much high hexagonality and brightness as possible.

It has been established in this report that the value of the S/Cd mol ratio of the raw materials has a great effect on the quality of pigments obtained; the optimum value was 0.98±0.01. Under a ratio of 0.97, black cadmium oxide was formed by the decomposition of cadmium hydroxide; over one oxide of 0.99, the products were unsuitable as pigments because of their low brightness.

Further,if oxygen was present in the calcining atmosphere, it caused not only a decrease in the S/Cd mol ratio by the consumption of sulfur, but also an increase in the brightness. However, we could not confirm by any quantitative methods whether or not the oxygen was substituted for sulfur in a crystal.

References

1) W. O. Milligan, *J. Phys. Chem.*, **38**, 797 (1934).
2) E. S. Rittner, *ibid.*, **47**, 537 (1943).
3) R. Sato, *Acta Crystallogr.*, **15**, 1109 (1962).
4) A. J. Eroles and A. L. Friedberg, *J. Amer. Ceram. Soc.*, **48**, 223 (1965).
5) P. Cherin, E. L. Lind, and E. A. Davis, *J. Electrochem. Soc.*, **117**, 233 (1970).
6) For example, US Patent, W. J. Meister, 2134055 (1938); J. J. O'Brien, 2226573 (1940); G. C. Marcot, 2496587 (1950); G. C. Marcot, 2578363 (1951); A. Giordans, 3012899 (1961).
7) M. Tsunashima and H. Takahashi, *Nippon Kagaku Kaishi*, **1972**, 1788.
8) M. Tsunashima and H. Takahashi, *ibid.*, **1972**, 1794.
9) M. Tsunashima, *Shikizai Kyokai Shi*, **43**, 598 (1970).
10) M. A. Short and E. G. Steward, *Amer. Mineral.*, **44**, 189 (1959).
11) R. Sato, H. Itoh, and S. Yamashita, *Japan J. Appl. Phys.*, **3**, 626 (1964).
12) M. Tsunashima, K. Mohri, K. Tsutsumi, and H. Takahashi, *Kogyo Kagaku Zasshi*, **74**, 1733 (1971).
13) V. J. Lea and G. Parravano, *J. Appl. Phys.*, **30**, 1735 (1959).
14) H. H. Woodbury, *Phys. Rev.*, **134**, A492 (1964).
15) D. Shaw and R. C. Whelan, *Phys. Stat. Sol.*, **36**, 705 (1969).
16) D. B. Holt and D. M. Wilcox, *J. Cryst. Growth*, **9**, 193 (1971).

Molecular Vibrations and Force Fields of Alkyl Sulfides. VII. Polythiomethylene (PTM) and Polythiomethylene-d_2 (PTM-D2), and Their Model Compounds: $CH_3S(CH_2S)_nCH_3$ ($n=1-3$)

Masaru OHSAKU

Department of Chemistry, Faculty of Science, Hiroshima University, Higashisenda-machi, Hiroshima 730

(Received June 20, 1973)

Infrared spectra of polythiomethylene (PTM) and polythiomethylene-d_2 (PTM-D2) observed by a Nujol mull method are reported, and their spectra are assigned. Normal coordinates of bis(methylthio)methane, $CH_3SCH_2SCH_3$, bis(methylthiomethyl) sulfide, $CH_3SCH_2SCH_2SCH_3$, bis[methylthio(methylthio)]methane, $CH_3SCH_2SCH_2SCH_2SCH_3$, PTM, and PTM-D2 have been treated. The force field used in the computation is a modified Urey-Bradley type. The skeletal conformation of these model compounds in the solid state is confirmed to be the [G] form. The relations between the degree of n and their CH_2 deformation fundamentals are explained by the concept of the frequency-phase difference. The calculated frequencies are compared with those of experiment. A comparison of the force fields of PTM and polyoxymethylene (POM) is also briefly made.

Vibrational analyses[1-5] of the hexagonal polyoxymethylene (POM) and polyoxymethylene-d_2 (POM-D2), and those of their model compounds,[6,7] $CH_3O(CH_2O)_nCH_3$ ($n=1$—5), have been extensively treated. The X-ray analyses of the hexagonal POM have also been made.[8-11] For the sulfur analogs, in the first paper of this series[12] it has been described that the interaction terms on the methyl groups are indispensable in the force fields of dimethyl sulfide. In the second paper,[13] the analyses were made on the infrared spectra of this series: $CH_3S(CH_2S)_nCH_3$ ($n=0$—3). These are model compounds of polythiomethylene (PTM). The preparation methods of PTM have been investigated.[14,15] An identification by means of the infrared spectra of PTM, which was obtained by the polymerization of *s*-trithiane, was very briefly made.[16] Recently, Hendra *et al.*[17] reported the Raman and infrared spectra of PTM and polyselenomethylene (PSeM). They also tentatively assigned the observed bands. However, no reports on normal coordinates of PTM have been published. The vibrational treatments of deuterated PTM (PTM-D2) have not been reported either. The molecular structure of the hexagonal PTM has already examined by Carazzolo and Valle by means of X-ray analysis,[10] as is shown in Fig. 1. The PTM is only known in the hexagonal form. They suggest that polymer chains are helicoidal, with the axis of the helix parallel to *c*, and that the unit cell is comprised of seventeen $-CH_2S-$ units and nine turns of the helix: $a=5.07$ Å, and $c=36.52$ Å. They have also estimated the internal rotation angle to be 65°59′, *i. e.*, the [G] form. The infrared spectra of PTM and its deuterated species, which were prepared according to the method of Ref. 14, have been recorded. Then, we tried to discuss the transferability of the set of the force constants obtained on dimethyl sulfide. Another purpose of this paper is to clarify the skeletal conformation of $CH_3S(CH_2S)_nCH_3$ ($n=1$—3) in relation to the conformation of PTM. Still another purpose of this paper is to find the relations in the vibrational frequencies between PTM and POM. In the present paper, the molecular vibrations of the $CH_3S(CH_2S)_nCH_3$ ($n=1-3$), PTM, and PTM-D2 series are treated with a potential function of the modified Urey-Bradley type, assuming that all of the potential constants are common in this series.

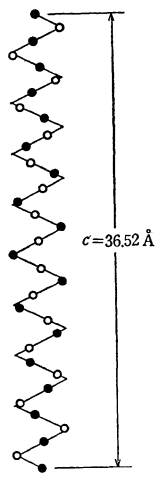

Fig. 1. Molecular structure of polythiomethylene (PTM) determined by the X-ray analysis.[10]
Open circle: methylene group. Closed circle: sulfur atom.

Experimental

The preparation of PTM and PTM-D2 was done by the method of Schmidt *et al.*[14] The melting point of the purified PTM was 195—200 °C, while that of PTM-D2 was 175—180 °C. The infrared spectra were recorded by a Nujol mull method in the 4000—200 cm^{-1} region at room temperature.

Vibrational Assignment

The obtained infrared data are summarized in Table 1. The spectroscopically active vibrations of the hexagonal PTM or PTM-D2 are subdivided into A_1, A_2, and E species. Seven vibrations (the C–H or C–D stretching, methylene bending, twisting, C–S stretching, CSC bending, and the torsional vibrations) belong to the A_1 species. Five vibrations (the C–H or C–D stretching, methylene wagging, rocking, C–S stretching, and the torsional vibrations) belong to the A_2 species. Twelve degenerate vibrations belong to the E species. The vibrations belonging to the A_1 species are infrared-inactive. The vibrations of the A_2 and E species are

Table 1. Infrared frequencies[a] (cm^{-1}), frequency ratios, and assignments of polythiomethylene (PTM) and polythiomethylene-d_2 (PTM-D2)

PTM[b]	PTM-D2[c]	$\nu_{PTM}/\nu_{PTM\text{-}D2}$	Assignment
1368 m	1012 m	1.352	CH_2, CD_2 bend
1225 vw	962 w	1.273	CH_2, CD_2 wag
1173 s	908 vs	1.292	CH_2, CD_2 wag
1155 sh, w	885 sh, w	1.305	CH_2, CD_2 twist
972 vvw	738 sh, vvw	1.32	—
946 vvw	675 sh, vvw	1.40	—
882 w	752 w	1.17	CH_2, CD_2 rock
742 w	635 sh, w	1.17	CH_2, CD_2 rock
735 m	697 m	1.05	C–S str
708 m	648 m	1.09	C–S str
671 w	603 w	1.11	C–S str
633 vw	585 sh, vw	1.08	—
511 vvvw	505 vvvw	1.01	—
467 vvvw	465 vvvw	1.00	—

s=strong, m=medium, w=weak, v=very, sh=shoulder. a) Obtained in a Nujol mull. b) The region above 1400 cm^{-1} is omitted. c) The region above 1100 cm^{-1} is omitted.

Table 2. Symmetry properties of PTM

Mode	A_1	A_2	E
νC-H	1	1	2
$B$$CH_2$	1	—	1
$W$$CH_2$	—	1	1
$T$$CH_2$	1	—	1
$R$$CH_2$	—	1	1
νC-S	1	1	2
BSCS	1	—	1
BCSC	1	—	1
τC-S	1	1	2
Infrared	inactive	//	⊥

ν, stretching; B, bending; W, wagging; T, twisting; R, rocking; τ, torsion.

infrared-active. Table 2 shows the numbers of the bands and the band types. The following bands may, then, be expected in our spectral region: one methylene bending, two wagging, one twisting, two rocking, three C–S stretching, and one skeletal bending vibrations. The numbers of the obtained bands correspond well with those expected.

Polythiomethylene. The spectra of PTM obtained are closely similar to those of polymethylene disulfide.[18] The spectra are virtually identical with those of Hendra *et al.*[17] As for the CH_2 deformation modes, the bands of the CH_2 bending, wagging, twisting, and rocking are expected in the 1400—740 cm^{-1} region. Hendra *et al.* did not completely assign the infrared bands obtained in this region. In the 1400—1100 cm^{-1} region, one CH_2 bending, two wagging, and one twisting bands may appear. The band at 1225 cm^{-1} is assignable to the CH_2 wagging vibration. This band, however, might be due to the other vibration. The result of the normal-coordinates fairly well reproduced this frequency. Although the CH_2 twisting band is expected around 1150 cm^{-1}, no effectively sharp bands appear around this region. There, the weak shoulder band around 1150 cm^{-1} may be identified to the CH_2 twisting vibration. To the CH_2 rocking vibrations, two bands, at 882 and 742 cm^{-1}, were assigned. To the C–S stretching vibrations, three bands at 735, 708, and 671 cm^{-1} are assignable. The bands at 742 and 735 cm^{-1} are very close to each other. These vibrations of the bands may be strongly coupled. Therefore, the assignments of these bands are ambiguous. Hendra *et al.*[17] did not assign the band at 742 cm^{-1} (their value—738 cm^{-1}) to any vibrational mode. They assigned the bands at 748 and 739 cm^{-1}, observed from the Raman spectra, to the C–S stretching vibrations belonging to the E_2 species, though. In the skeletal deformation region, below 400 cm^{-1}, none of the sharp bands appear. The extremely weak band at 511 cm^{-1} may be due to the vibration of the S–S bond. In that case, the PTM obtained is not completely constructed by the head-to-tail combination.

Polythiomethylene-d_2. Most of the bands of the fully-deuterated PTM shift to a frequency region lower than those of the normal species. To assign the bands, it is useful to ascertain the frequency ratios of $\nu_{PTM}/\nu_{PTM\text{-}D2}$. The CD_2 deformation band is conspicuous in the frequency shift. The band at 1012 cm^{-1} was assigned to the CD_2 bending vibration. The bands at 962 and 908 cm^{-1}, and the shoulder band at 885 cm^{-1} were assigned to the CD_2 wagging and twisting vibrations. In the 700—550 cm^{-1} region, the obtained spectra are more complicated than those of the normal species. Although, in this region, we can expect the CD_2 rocking and C–S stretching bands, each assignment is difficult since the vibrations may be strongly coupled with each other. In conclusion, we have assigned the fairly strong bands to the C–S stretching vibrations.

Normal Coordinate Treatment

In order to confirm the previous assignments, the normal coordinates, including all of the vibrational degrees of freedom, were treated for the n=1—3 species using a force function of the modified Urey-Bradley type. The force constants in relation to the methyl group were transferred from those of dimethyl sulfide,[12] while the other constants were referred to those of 1,2-ethanedithiol,[19] polymethylene disulfide,[18] and (methylthio)methanethiol.[20] The molecular parameters used in the computations were: r(C–H)=1.09 Å, r(C–S)=1.81 Å, and ϕ(CSC)=99°; the other bond angles were assumed to be tetrahedral. The correction terms used were p, p', n, t, g, t', g', and l. The corrections of p, p', n, t, g, and l have been explained in a previous paper.[20] Additional terms, t' and g', which were the *trans* and *gauche* coupling constants between the HCS and CSC angles in the methylene group, were introduced in order to explain the separation width of the CH_2 deformation bands. The force constants used in the computations are summarized in Table 3. The diagonal elements of the potential energy matrix, $\boldsymbol{F}$, are also listed in Table 4. The calculated frequencies are listed in Tables 5—7, toge-

Table 3. Modified Urey-Bradley force constants[a]

K(C-H)	4.250[b]	CH_3 and CH_2 groups
K(C-S)	1.691[b]	CH_3-S and S-CH_2 bond
H(HCS)	0.030	CH_3 group
H(HCH)	0.366	CH_3 group
H(CSC)	0.244[b]	CH_3-S-CH_2 and CH_2-S-CH_2 angles
H(SCS)	0.150[b]	S-CH_2-S angle
H(SCH)	0.160[b]	CH_2 group
H(HCH)	0.335[b]	CH_2 group
F(HCS)	0.763	
F(HCH)	0.200	
F(CSC)	0.210[b]	
F(SCS)	0.500[b]	
F(SCH)	0.390[b]	
F(HCH)	0.200[b]	
κ	0.060	CH_3 group
	−0.010[b]	CH_2 group
Y	0.054[b]	CH_3-S and S-CH_2 bonds
p	−0.115[b]	CH_3 and CH_2 groups
p'	−0.100[b]	CH_3-S and S-CH_2 bonds
n	0.033	CH_3 group ($\angle$HCS and $\angle$HCH)
t	0.070	CH_3 group ($\angle$HCS and $\angle$CSC, *trans*)
g	−0.050	CH_3 group ($\angle$HCS and $\angle$CSC, *gauche*)
t'	0.100[b]	CH_2 group ($\angle$HCS and $\angle$CSC, *trans*)
g'	−0.040[b]	CH_2 group ($\angle$HCS and $\angle$CSC, *gauche*)
l	−0.005[b]	S-CH_2-S

a) Unit of K, H, F, p, and p' is in mdyn/Å; κ, Y, n, t, g, t', g', and l is in mdyn·Å; $F'=-0.1F$. b) These constants are also used in polymers.

Table 4. Diagonal elements[a] of the potential energy matrix (F)

4.843	CH_3 stretching
4.724	CH_2 stretching
3.632	CH_3-S stretching
2.743	S-CH_2 stretching
0.675	CH_3 group, HCS bending
0.594	CH_3 group, HCH bending
1.129	CH_3-S-CH_2 and CH_2-S-CH_2 bending
1.136	S-CH_2-S bending
0.582	CH_2 group, SCH bending
0.482	CH_2 group, HCH bending
0.054	CH_3-S and S-CH_2 bonds, internal rotation

a) Element of the stretching is in mdyn/Å; element of the bending or internal rotation is in mdyn·Å.

ther with the experimental frequencies.

In order to confirm the transferability of the force constants, the normal coordinates of PTM and PTM-D2 were also treated with the common force field of the model compounds. Calculations were made according to the analogous method of Tadokoro *et al.*[1] The molecular parameters used were: r(C-H)=1.09 Å, r(C-S)=1.815 Å, ϕ(CSC) and ϕ(SCS)=106°52′, and ϕ(HCH)=109°28′, and the internal rotation angle was assumed to be 65°59′.

Molecular Forms. At first we will try to determine the stable conformation which exists in the solid state of the series of $n=1-3$. For the molecule of $n=1$, four forms are possible: TT, TG, GG, and GG′. For the $n=2$ and 3 species, a large number of forms are possible. In this treatment, however, we took into consideration the six most probable forms of TTTT, GGGG, TGTG, TTGT, TGGT, and TTGG for the $n=2$ species and of TTTTTT, GGGGGG, TGTGTG, TTGTTG, TGGTGG, and TTGGTT for the $n=3$ species. The calculated frequencies of the CH_2 rocking, C–S stretching, and skeletal deformation are fairly much affected by their internal angles. The observed frequencies are taken from the previous paper.[13] In the previous paper, however, more bands than those expected for one form are described in the 400—200 cm^{-1} region, even in the solid state. The bands of this region are essentially weak. Moreover, the reliability of the spectrophotometer is not very good in this region. Still another difficulty is due to the bands of water vapor in the atmosphere. A few of the bands which decrease in intensity in the solid state may be due to the imperfect annealing. Figure 2 shows the observed and calculated frequencies in relation to the skeletal vibrations through the $n=1-3$ species. On the molecule of $n=1$ the bands at 341 and 314 cm^{-1} are obviously due to the stable form in the solid state. The frequencies calculated for the GG form explain these bands well. On the species of $n=2$, the three bands at 339, 318, and 247 cm^{-1} can be assigned to the stable form in the solid state. These bands fit well to the frequencies calculated for the [G] form. In the same way, the calculated frequencies of the [G]

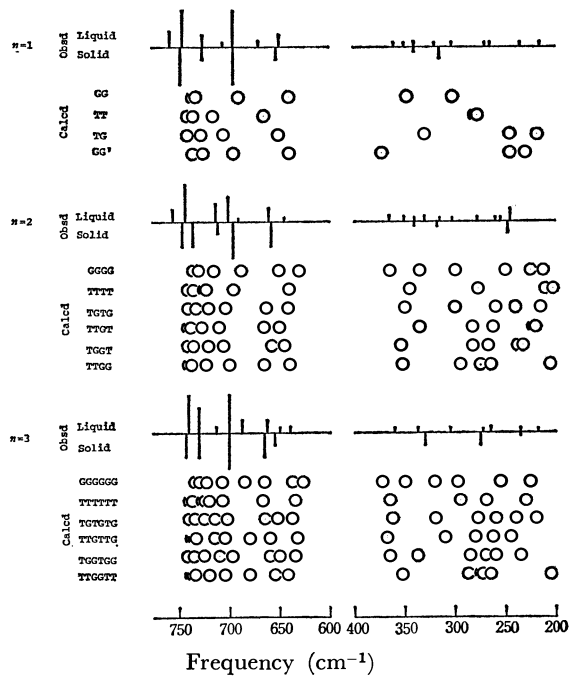

Fig. 2. Observed frequencies and relative intensities, and calculated frequencies of $CH_3S(CH_2S)_nCH_3$ ($n=1-3$) in relation to the skeletal vibrations.

Table 5. Observed and calculated frequencies (cm^{-1}), and potential energy distribution, PED,[a] of bis(methylthio)methane

Obsd[b]	Calcd							
	GG	PED	TT[c]	PED	TG	PED	GG′	PED
1441_a	1441	ΔCH_3	1441	ΔCH_3	1441	ΔCH_3	1441	ΔCH_3
1436_a	1441	ΔCH_3	1441	ΔCH_3	1441	ΔCH_3	1441	ΔCH_3
1421_a	1441	ΔCH_3	1441	ΔCH_3	1441	ΔCH_3	1441	ΔCH_3
1417_a	1441	ΔCH_3	(1441)	ΔCH_3	1441	ΔCH_3	1441	ΔCH_3
1387_l	1388	BCH_2	1391	BCH_2	1390	BCH_2	1388	BCH_2
1327_l	1317	$\sum CH_3$	1317	$\sum CH_3$	1317	$\sum CH_3$	1317	$\sum CH_3$
1318_l	1317	$\sum CH_3$	1317	$\sum CH_3$	1317	$\sum CH_3$	1317	$\sum CH_3$
1203_l	1206	WCH_2	1204	WCH_2	1205	WCH_2	1206	WCH_2
(1163_l)			(1143)	TCH_2	1144	TCH_2	1145	TCH_2
1155_l	1146	TCH_2						
(1124_l)								
986_l	994	RCH_3	991	RCH_3	990	RCH_3	990	RCH_3
986_l	986	RCH_3	986	RCH_3	988	RCH_3	989	RCH_3
959_l	967	RCH_3	968	RCH_3	967	RCH_3	968	RCH_3
959_l	967	RCH_3	(967)	RCH_3	967	RCH_3	967	RCH_3
874_l								
(824_l)					802	RCH_2		
806_l	817	RCH_2					800	RCH_2
—			780	RCH_2				
(758_l)			739	νC–S	739	νC–S	736	νC–S
746_l	733	νC–S	735	νC–S				
724_l	733	νC–S			728	νC–S	723	νC–S
(705_l)			715	νC–S	704	νC–S		
694_l	690	νC–S					695	νC–S
(669_l)			665	νC–S, BSCS				
649_l	639	νC–S, BSCS			651	νC–S, BSCS	640	νC–S, BSCS
(360_l)							372	BCSC
(350_l)					331	BCSC, BSCS		
340_l	347	BSCS, BCSC						
321_l	302	BCSC						
303_l								
(270_l)			279	BCSC				
(265_l)			277	BSCS, τC–S				
235_l*					245	BCSC	245	BSCS, BCSC, τC–S
216_l*					218	BSCS, BCSC, τC–S	228	BCSC
—	189	BCSC, τC–S, BSCS						
—			(182)	τC–S				
—	174	τC–S	173	τC–S	175	τC–S	173	τC–S
—	162	τC–S, BSCS	170	BCSC, BSCS	165	τC–S	164	τC–S
—	79	τC–S	(75)	τC–S	71	τC–S		
—			65	τC–S			65	τC–S
—					55	τC–S		
—	44	τC–S					48	τC–S

ν, stretching; Δ, degenerate deformation; $\sum$, symmetrical deformation; B, bending; W, wagging; T, twisting; R, rocking; τ, torsion. The region above 1500 cm^{-1} is omitted. a) Only the predominant modes are shown. b) From Ref. 13. Figures in parentheses show the bands which disappear in the solid state. a, annealed- and l, liquid-state bands. *See text. c) A_2 species in parentheses.

TABLE 6. OBSERVED AND CALCULATED FREQUENCIES (cm^{-1}), AND POTENTIAL ENERGY DISTRIBUTION, PED OF BIS(METHYLTHIOMETHYL) SULFIDE

Obsd	Calcd											
	GGGG	PED	TTTT	PED	TGTG	PED	TTGT	PED	TGGT	PED	TTGG	PED
1439_a	1441	ΔCH_3	1441	ΔCH_3	1442	ΔCH_3	1441	ΔCH_3	1442	ΔCH_3	1441	ΔCH_3
1434_a	1441	ΔCH_3	1441	ΔCH_3	1441	ΔCH_3	1441	ΔCH_3	1441	ΔCH_3	1441	ΔCH_3
1416_a	1441	ΔCH_3	1441	ΔCH_3	1441	ΔCH_3	1441	ΔCH_3	1441	ΔCH_3	1441	ΔCH_3
1410_a	1441	ΔCH_3	(1441)	ΔCH_3	1441	ΔCH_3	1441	ΔCH_3	1441	ΔCH_3	1441	ΔCH_3
1395_1	1389	BCH_2	1392	BCH_2	1390	BCH_2	1391	BCH_2	1390	BCH_2	1391	BCH_2
1379_1	1388	BCH_2	1389	BCH_2	1389	BCH_2	1390	BCH_2	1389	BCH_2	1389	BCH_2
1327_1	1317	ΣCH_3	1317	ΣCH_3	1317	ΣCH_3	1317	ΣCH_3	1317	ΣCH_3	1317	ΣCH_3
1317_1	1317	ΣCH_3	1317	ΣCH_3	1317	ΣCH_3	1317	ΣCH_3	1317	ΣCH_3	1317	ΣCH_3
1218_1	1206	WCH_2	1206	WCH_2	1207	WCH_2	1206	WCH_2	1206	WCH_2	1206	WCH_2
1193_1	1206	WCH_2	1203	WCH_2	1204	WCH_2	1204	WCH_2	1205	WCH_2	1204	WCH_2
1165_1	1148	TCH_2	1145	TCH_2	1149	TCH_2	1148	TCH_2	1149	TCH_2	1150	TCH_2
1132_1	1147	TCH_2	(1141)	TCH_2	1145	TCH_2	1141	TCH_2	1143	TCH_2	1144	TCH_2
(1119_1)												
974_1	991	RCH_3	989	RCH_3	990	RCH_3	989	RCH_3	989	RCH_3	990	RCH_3
974_1	990	RCH_3	989	RCH_3	989	RCH_3	989	RCH_3	989	RCH_3	989	RCH_3
961_1	968	RCH_3	967	RCH_3	968	RCH_3	968	RCH_3	968	RCH_3	968	RCH_3
961_1	967	RCH_3	(967)	RCH_3	967	RCH_3	967	RCH_3	968	RCH_3	968	RCH_3
(855_1)									830	RCH_2		
841_1	839	RCH_2										
(834_1)											826	RCH_2
(820_1)					815	RCH_2	808	RCH_2				
778_1	796	RCH_2	788	RCH_2	795	RCH_2	790	RCH_2	791	RCH_2	797	RCH_2
—			(775)	RCH_2								
(754_1)			741	νC–S	740	νC–S	739	νC–S	739	νC–S	738	νC–S
742_1	736	νC–S	734	νC–S	733	νC–S	737	νC–S	734	νC–S	736	νC–S
742_1	730	νC–S	723	νC–S			727	νC–S	721	νC–S	723	νC–S
712_1	716	νC–S	722	νC–S	719	νC–S	711	νC–S	706	νC–S		
700_1	688	νC–S	694	νC–S, BSCS, BCSC	703	νC–S					699	νC–S
(690_1)							667	νC–S, BSCS			667	νC–S, BSCS
661_1	649	νC–S, BSCS			662	νC–S, BSCS	649	νC–S, BSCS	657	νC–S, BSCS		
(645_1)	630	νC–S, BSCS	642	νC–S	642	νC–S, BSCS			647	νC–S, BSCS	640	νC–S, BSCS
(365_1)	364	BCSC, BSCS										
(350_1)			345	BSCS, BCSC	351	BSCS, BCSC, νC–S			353	BCSC, BSCS	352	BSCS, BCSC
(340_1)							336	BSCS, BCSC, νC–S				
331_1	331	BCSC, BSCS										
315_1	299	BCSC										
(305_1)					299	BSCS					294	BCSC
277_1*			278	BCSC			283	BCSC, BSCS	282	BSCS, νC–S	274	BCSC, BSCS, νC–S
(259_1)							263	τC–S	268	τC–S	266	τC–S
(254_1)					259	τC–S						
244_1	250	τC–S, BCSC			239	BCSC, BSCS			237	BCSC, BSCS		
—	225	τC–S					222	BCSC	233	BCSC		
—	213	BSCS, τC–S, BCSC	209	BCSC, BSCS	215	BCSC, τC–S	218	BSCS, BCSC				
—			202	BSCS, νC–S, BCSC	190	BCSC, τC–S, BSCS			195	τC–S	206	BSCS, BCSC
—			179	τC–S	179	τC–S, BCSC, BSCS						
—			(177)	τC–S			173	BCSC, τC–S, BSCS	172	BSCS, BCSC, τC–S		
—											145	BCSC, τC–S, BSCS
—					143	τC–S					143	τC–S

Table 6. Continued

Obsd	Calcd											
	GGGG	PED	TTTT	PED	TGTG	PED	TTGT	PED	TGGT	PED	TTGG	PED
—	131	*B*SCS, *B*CSC										
—							107	τC-S	107	τC-S	114	τC-S
—	99	τC-S	98	τC-S								
—			92	*B*CSC, *B*SCS								
—			(82)	τC-S	77	τC-S						
—	63	τC-S			67	τC-S	68	τC-S	71	τC-S	72	τC-S
—									62	τC-S	59	τC-S
—	46	τC-S	48	τC-S	52	τC-S	47	τC-S				
—			(38)	τC-S			42	τC-S				
—	28	τC-S			34	τC-S			32	τC-S		
—											22	τC-S

Notations are the same as in Table 5.

Table 7. Observed and calculated frequencies (cm^{-1}), and potential energy distribution, PED, of bis[(methylthio)methylthio]methane

Obsd	Calcd											
	GGGGGG	PED	TTTTTT	PED	TGTGTG	PED	TTGTTG	PED	TGGTGG	PED	TTGGTT	PED
1446_a	1442	ΔCH_3	1441	ΔCH_3	1441	ΔCH_3	1441	ΔCH_3	1441	ΔCH_3	1441	ΔCH_3
1441_a	1441	ΔCH_3	1441	ΔCH_3	1441	ΔCH_3	1441	ΔCH_3	1441	ΔCH_3	1441	ΔCH_3
1431_a	1441	ΔCH_3	1441	ΔCH_3	1441	ΔCH_3	1441	ΔCH_3	1441	ΔCH_3	1441	ΔCH_3
1418_a	1441	ΔCH_3	(1441)	ΔCH_3	1441	ΔCH_3	1441	ΔCH_3	1441	ΔCH_3	1441	ΔCH_3
(1401_l)							—					
1394_l	1389	BCH_2	1393	BCH_2	1390	BCH_2	1391	BCH_2	1390	BCH_2	1391	BCH_2
1378_l	1388	BCH_2	1391	BCH_2	1390	BCH_2	1391	BCH_2	1389	BCH_2	1391	BCH_2
1378_l	1388	BCH_2	1389	BCH_2	1389	BCH_2	1389	BCH_2	1388	BCH_2	1389	BCH_2
1316_l	1317	$\sum CH_3$	1317	$\sum CH_3$	1317	$\sum CH_3$	1317	$\sum CH_3$	1317	$\sum CH_3$	1317	$\sum CH_3$
1316_l	1317	$\sum CH_3$	1317	$\sum CH_3$	1317	$\sum CH_3$	1317	$\sum CH_3$	1317	$\sum CH_3$	1317	$\sum CH_3$
1223_l	1206	WCH_2	1206	WCH_2	1207	WCH_2	1207	WCH_2	1207	WCH_2	1207	WCH_2
(1205_l)			1204	WCH_2	1206	WCH_2	1205	WCH_2	1205	WCH_2	1205	WCH_2
1199_l	1206	WCH_2										
1188_l	1206	WCH_2	1202	WCH_2	1204	WCH_2	1203	WCH_2	1205	WCH_2	1204	WCH_2
1171_l	1148	TCH_2	(1146)	TCH_2	1149	TCH_2	1149	TCH_2	1149	TCH_2	1150	TCH_2
1145_l	1148	TCH_2	1143	TCH_2	1146	TCH_2	1145	TCH_2	1145	TCH_2	1146	TCH_2
1125_l	1147	TCH_2	(1140)	TCH_2	1142	TCH_2	1139	TCH_2	1141	TCH_2	1141	TCH_2
971_l	991	RCH_3	989	RCH_3	990	RCH_3	990	RCH_3	990	RCH_3	989	RCH_3
971_l	990	RCH_3	989	RCH_3	989	RCH_3	989	RCH_3	989	RCH_3	989	RCH_3
960_l	968	RCH_3	(967)	RCH_3	968	RCH_3	968	RCH_3	968	RCH_3	968	RCH_3
960_l	967	RCH_3	967	RCH_3	967	RCH_3	967	RCH_3	967	RCH_3	967	RCH_3
858_l	849	RCH_2							833	RCH_2	831	RCH_2
820_l	816	RCH_2			818	RCH_2	810	RCH_2	822	RCH_2		
(785_l)			791	RCH_2	804	RCH_2	800	RCH_2			798	RCH_2
763_l	788	RCH_2	(782)	RCH_2	788	RCH_2	790	RCH_2	788	RCH_2	783	RCH_2
763_l			773	RCH_2								
740_l	735	νC-S	740	νC-S	740	νC-S	738	νC-S	739	νC-S	737	νC-S
740_l	731	νC-S	737	νC-S	735	νC-S	737	νC-S	735	νC-S	737	νC-S
731_l	722	νC-S	727	νC-S	726	νC-S	731	νC-S	724	νC-S	732	νC-S
731_l			726	νC-S							721	νC-S
(712_l)			719	νC-S	714	νC-S	714	νC-S	710	νC-S		
700_l	708	νC-S	707	νC-S, *B*CSC, *B*SCS	702	νC-S	705	νC-S	698	νC-S	704	νC-S
(687_l)	687	νC-S					680	νC-S, *B*SCS			680	νC-S, *B*SCS
663_l	665	νC-S, *B*SCS	667	νC-S, *B*SCS	666	νC-S, *B*SCS	661	νC-S, *B*SCS	661	νC-S, *B*SCS	656	νC-S, *B*SCS
651_l	637	νC-S, *B*SCS			653	νC-S, *B*SCS			651	νC-S, *B*SCS		
(640_l)	627	νC-S, *B*SCS	636	νC-S	638	νC-S, *B*SCS	633	νC-S	636	νC-S, *B*SCS	643	νC-S, *B*SCS

Table 7. Continued

Obsd	Calcd											
	GGGGGG	PED	TTTTTT	PED	TGTGTG	PED	TTGTTG	PED	TGGTGG	PED	TTGGTT	PED
(360_1)	372	*B*SCS, *B*CSC	366	*B*SCS, *B*CSC	362	*B*SCS, *B*CSC, νC–S	368	*B*SCS, *B*CSC	364	*B*SCS, *B*CSC	353	*B*SCS, *B*CSC
338_1	349	*B*CSC, *B*SCS							337	*B*CSC, *B*SCS		
338_1	320	*B*CSC, *B*SCS			319	*B*CSC, *B*SCS						
(305_1)	297	*B*CSC	295	*B*SCS, *B*CSC, νC–S			310	*B*CSC, *B*SCS, νC–S				
272_1					277	*B*SCS, *B*CSC	281	*B*CSC, *B*SCS	286	*B*CSC	288	*B*CSC
272_1	256	*B*SCS, *B*CSC	271	*B*CSC					271	τC–S	275	*B*SCS, νC–S, *B*CSC
272_1											273	*B*CSC, *B*SCS
265_1					259	τC–S	263	τC–S	260	*B*SCS, τC–S	266	τC–S
235_1	227	τC–S	231	*B*CSC, *B*SCS	239	*B*CSC	244	*B*CSC, *B*SCS	234	*B*CSC		
217_1*					221	*B*CSC, *B*SCS, τC–S					205	*B*SCS, *B*CSC
—	191	*B*SCS, *B*CSC			188	*B*SCS, *B*CSC, τC–S	194	*B*SCS, *B*CSC			194	*B*CSC, *B*SCS
—			(178)	τC–S	185	*B*CSC, τC–S, *B*SCS			181	*B*SCS, *B*CSC	189	τC–S
—			178	τC–S			176	τC–S *B*CSC				
—	162	τC–S	160	*B*SCS, νC–S, *B*CSC	164	τC–S	166	*B*CSC, τC–S, *B*SCS	157	*B*CSC, *B*SCS, τC–S		
—									148	τC–S		
—			139	*B*CSC, *B*SCS			136	*B*SCS, *B*CSC, τC–S				
—	110	τC–S									119	τC–S
—	104	*B*CSC, *B*SCS	(109)	τC–S			107	τC–S	113	τC–S	104	*B*CSC, τC–S, *B*SCS
—			91	τC–S							86	τC–S
—	76	τC–S	(70)	τC–S	78	τC–S	78	τC–S	72	τC–S	71	τC–S
—					73	τC–S	67	τC–S	65	τC–S		
—			58	τC–S	60	τC–S						
—	50	τC–S	56	*B*CSC, *B*SCS			54	τC–S			51	τC–S
—			36	τC–S	42	τC–S			38	τC–S	41	τC–S
—	30	τC–S	(25)	τC–S	27	τC–S	30	τC–S				
—	25	τC–S			22	τC–S	22	τC–S	22	τC–S		
—	23	τC–S							21	τC–S		
—											12	τC–S

Notations are the same as in Table 5.

form explain well the bands which are observed in the solid state of the $n=3$ species. Therefore, it is likely that these three molecules stay in the [G] form in the solid state. In the C–S stretching region, the calculated frequencies of the [G] form fit the observed frequencies well.

The molecular conformations existing in the liquid state will now be briefly described. We will first consider the molecular species of $n=1$. In the region below 400 cm^{-1}, which was observed in the liquid state, there are bands which correspond to at least three forms. In a previous paper,[13] the GG′ form was excluded from the stable forms. In Table 5, however, the frequencies calculated for the GG′ form are listed for reference. The GG form, which is the stable form in the solid state, was also excluded from consideration in this section. Two forms then remain: TT and TG. In the C–S stretching region, the band at 758 cm^{-1} observed in the liquid state fits fairly well to the frequencies calculated for the TT and/or TG form. The band at 705 cm^{-1} fits well to the frequencies calculated for the TT and/or TG form. The weak band at 669 cm^{-1} fits well to the frequency calculated for the TT form. In the skeletal deformation region, nine bands appear in the liquid state. Two bands which disappear in the unannealed film were excluded from the fundamentals, since, around this region, there are not the corresponding calculated frequencies, although these bands may be due to the GG′ form. Four bands then remain at 270, 260, 235, and 220 cm^{-1}. Among these bands, the two bands at 270 and 260 cm^{-1} fit well to the frequencies calculated for the TT form, while the bands at 235 and 220 cm^{-1} fit well to the frequencies calculated for the TG form. Therefore, it may be concluded that three conformations, TT, TG, and GG, coexist in the liquid or gaseous state for the $n=1$ species. Moreover, the following descriptions can be postulated. The bands at 235 and

220 cm^{-1} may be identified as imperfect annealing: that is, a small amount of the TG form is present. Here, the order of the stability of the conformation may be supposed to be: GG>TG>TT.

The treatment was also extended to discuss the species of $n=2$ and 3. On the molecular species of $n=2$ and 3, the results are nearly the same as in the case of $n=1$. That is, if these three forms coexist in the species of $n=1$, the six forms now considered for the $n=2$ and 3 species are fully acceptable. However, we cannot give any more detailed descriptions on the basis of only the data thus for obtained.

Model Compounds. The C–H stretching, CH_3 deformation, C–S stretching, and skeletal deformation vibrations are reproduced well by this set. For the CH_2 deformation vibrations, on the species of $n=1$, one each of the CH_2 bending, CH_2 wagging, CH_2 twisting, and CH_2 rocking vibrations are expected for each form. These four bands are fairly well reproduced by the calculations. In the cases of the $n=2$ and 3 species, the separation widths between or among the same methylene deformation bands are not so well reproduced. However, in general the transferability of the force constants is very good.

PTM and PTM-D2. The calculated data of PTM and PTM-D2 are listed in Tables 8 and 9, along with the observed data. A part of the Raman and infrared data of PTM which were obtained by Hendra *et al.*[17] are also listed. It is shown that the calculated frequencies agree satisfactorily well with the observed frequencies. It is also shown that the transferability of the force constants used on the model compounds is very good. The vibrations in relation to the methylene group shifted directly upon deuteration. The observed shifts correspond well with those expected.

Table 8. Observed and calculated frequencies (cm^{-1}), and potential energy distribution, PED, of PTM

Species	Obsd[a]	Calcd	PED[b]
A_1	1373[c]	1406	BCH$_2$
	1180[c]	1129	TCH$_2$
	648[c]	614	νC-S, BSCS
	335[c]	331	BCSC, BSCS
	—	78	τC-S
	—	2	BSCS, BCSC
A_2	1225	1188	WCH$_2$
	742	805	RCH$_2$
	735	724	νC-S
	—	99	τC-S
E	1368	1406	BCH$_2$
	1173	1187	WCH$_2$
	1155	1129	TCH$_2$
	882	821	RCH$_2$
	708	723	νC-S
	671	624	νC-S, BSCS
	355[c]	343	BCSC, BSCS
	—	177	BSCS, BCSC
	—	90	τC-S
	—	27	τC-S

The region above 1500 cm^{-1} is omitted.
a) From Table 1. b) Notations are the same as in Table 5. c) From Ref. 17.

Table 9. Observed and calculated frequencies (cm^{-1}), and potential energy distribution, PED, of PTM-D2

Species	Obsd[a]	Calcd	PED[b]
A_1	—	1032	BCD$_2$
	—	808	TCD$_2$
	—	583	νC-S
	—	325	BCSC, BSCS
	—	42	τC-S
	—	2	BSCS, BCSC
A_2	962	924	WCD$_2$, νC-S
	697	696	νC-S
	635	618	RCD$_2$
	—	105	τC-S
E	1012	1031	BCD$_2$
	908	926	WCD$_2$, νC-S
	885	808	TCD$_2$
	648	686	νC-S, RCD$_2$
	752	654	RCD$_2$, νC-S
	603	587	νC-S
	—	318	BSCS, BCSC
	—	160	BCSC, BSCS
	—	66	τC-S
	—	42	τC-S

The region above 1100 cm^{-1} is omitted.
a) From Table 1. b) Notations are the same as in Table 5.

Frequency-phase Difference Curves

It has been seen[13] that the observed CH_2 deformation frequencies of the $CH_3S(CH_2S)_nCH_3$ ($n=1-3$) series have some regularities between the degree of n and their fundamentals. Table 10 shows the observed frequencies of the model compounds and PTM in the methylene deformation region. The CH_2 bending or twisting band of PTM is at nearly the same frequency as that of the central bands of the $n=3$ species. On the other hand, the wagging and rocking bands of PTM lie outside of the bands of the $n=3$ species. These will be explained more quantitatively in the following section.

From the concept of the frequency-phase difference,[21] when the degree of n and the molecular conformation are confirmed, the infrared-active bands of the species become easily recognizable. On the species of $-(CH_2S)_n-$, the number of atoms per polymer unit is four; the vibrational degrees of freedom, therefore, are $3\times4=12$. The phase-difference, δ_a, is defined thus: $\delta_a=(a-1)\pi/n$ ($a=1, 2, 3, \ldots, n$), where n denotes the degree of polymerization. The species of $n=1$ correspond to $CH_3SCH_2SCH_3$; $n=2$, to $CH_3SCH_2SCH_2SCH_3$, and $n=3$, to $CH_3SCH_2SCH_2SCH_2SCH_3$. Figure 3 shows the frequency-phase difference curves in relation to the CH_2 deformation modes. The curves show the [G]-type frequency-phase dif-

Table 10. Infrared frequencies (cm^{-1}) of methylene deformation vibrations of $CH_3S(CH_2S)_nCH_3$ ($n=1-3$) and PTM observed in the solid state

	$n=1$	$n=2$	$n=3$	PTM
BCH_2			1379	
		1381		
	1388[a]		1369	1368
		1372		
			1355	
WCH_2			1220	1225
		1219		
	1214[a]		1204	
		1193		
			1182	1173
TCH_2			1173	
		1167		
	1166		1153	1155
		1133		
			1126	
RCH_2			866	882
		844		
	808		811	
		780		
			760	742

a) Average of the doublet-band.

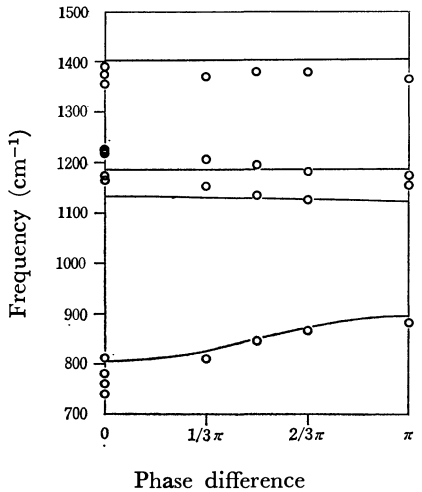

Fig. 3. Frequency-phase difference curves for the CH_2 bending, wagging, twisting, and rocking modes.

ference of PTM, and the plots are the observed ones. From this figure, the observed plots can be seen to correspond well with the calculated ones. The separation width of the observed CH_2 deformation bands can also be explained well by these curves. The tendency of the frequency-phase difference curve is conspicuous in the CH_2 rocking vibrations. For the [T]-type frequency-phase difference, detailed investigations have previously been made on polyethylene,[22] for example. The [T]-type frequency-phase difference curve is different from that of the [G] type. This is also conspicuous in the CH_2 rocking vibrations. In the [T] type, the frequency change due to phase difference is less than that of the [G] type. It is natural that the curves of the PTM resemble those of the hexagonal POM; the frequencies themselves are very different, though. Since the CH_2 deformation frequencies of the molecular species of $n=1$—3 are explained well by the [G]-type curves, it is also confirmed that these model molecules exist in the [G] form in the solid state. This shows also that the force fields in PTM and its model compounds are nearly the same, and that, in the determination of the force fields of polymers, it is important to determine the force fields of their model compounds.

Discussion

The regularities lying between the degree of n and the CH_2 deformation frequencies are reasonably explained by the frequency-phase difference curves. The relations lying between n and the terminal methyl deformation frequencies do not appear very clearly in the calculated frequencies. That is, the calculated frequencies of the CH_3 degenerate deformation, the CH_3 symmetrical deformation, and the CH_3 rocking vibrations are around 1440, 1317, and 990—970 cm^{-1}. In the observed frequencies, very interesting results were obtained. For the CH_3 symmetrical deformation in the annealed spectra, the separation widths of the two bands are 28, 14, 6, and 21 cm^{-1} for the $n=0$, $n=1$, 2, and 3 species respectively. For the CH_3 rocking vibrations, the separations of the side bands are 129, 43, 14, and 17 cm^{-1} respectively in the above-mentioned species. That is, the separation width between side bands rapidly decreases from the $n=0$ to $n=2$ species, and then increases a little. As has previously been described, the stable conformation of these molecules is the [G] form. The skeletal form of these compounds is shown in Fig. 4. Two methyl groups of the $n=1$ species stand at the same edge, and the methylene group stands at the opposite position. Therefore, the interactions between the methyl and methylene groups are small. In the case of the $n=2$ species, things are the same in the $n=1$ species. In the species of $n=3$, the distance between the methyl groups at both ends becomes large. However, the central methylene and two methyl groups are on the same side, and the interactions among these groups become large. In the potential energy distribution, PED, or in the L-matrix, however, this tend-

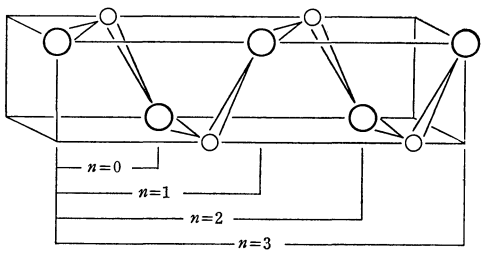

Fig. 4. Skeletal structures of $CH_3S(CH_2S)_nCH_3$ ($n=0$—3).
Large circle: methyl or methylene group. Small circle: sulfur atom.

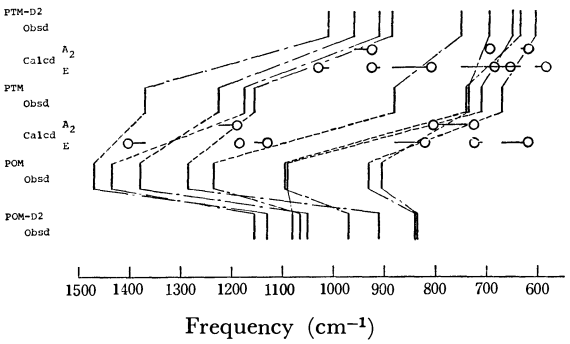

Fig. 5. Observed and calculated frequencies of PTM and PTM-D2, and obserbed frequencies of POM and POM-D2.

ency does not appear so clearly.

The vibrational spectra between PTM and POM will be briefly compared here. Figure 5 shows the observed frequencies of PTM, PTM-D2, POM, and POM-D2, along with the calculated frequencies of PTM and PTM-D2. The assignments of the observed bands of POM and POM-D2 have been made by several authors.[1,4,5] In this figure, the data obtained by Tadokoro *et al.*[1] are cited. The CH_2 bending, CH_2 wagging, and CH_2 twisting vibrations of PTM appear at frequencies lower by *ca.* 150—300 cm^{-1} than those of POM. In the case of the CH_2 rocking vibrations, the bands of PTM are much lower than the corresponding POM bands. However, the separation widths of the bands correspond well with PTM and POM. The stretching bands of PTM appear in a different spectral region from those of POM. The frequency shifts upon deuteration show nearly the same tendency.

The force constants of PTM may now be compared with the constants of POM, which are listed in Table 3 of Ref. 1. The set of No. 17 is used for comparison. The constants of PTM are much smaller than the corresponding constants of POM. The smaller values of the stretching constants show the weaker binding forces. The bending and repulsion constants, except for the constant of F(HCH), are also much smaller than the corresponding constants of POM. From these results it is seen that the binding forces in PTM are much weaker than those in POM, and that the interatomic interacitons in PTM are smaller than those in POM.

For the $CH_3O(CH_2O)_nCH_3$ (n=1—5) species, the stable conformation in the solid state is confirmed to be the [G] form; in the liquid state the [G] form may also persist.[6,7] In the same way, it may be concluded that the conformation of the sulfur analogs is the [G] form in the solid state. In the liquid state, the [G] form may persist. On the other hand, n-alkane and polyethylene[23] exist in the [T] form. Moreover, in the cases of normal alkyl ethers[24] and normal alkyl sulfides,[25-27] the skeletal conformation is confirmed to be the [T] form. In the cases of n-alkane and polyethylene, the lone-pair electrons are not involved. For n-ethers and n-sulfides, the directions of the lone pairs on the oxygen or sulfur atoms coincide with those of the C–H bonds of n-alkane and polyethylene. The present author has previously described[27] that the sulfur atom with lone-pair electrons can be regarded as a CH_2 group in the conformational analyses of alkyl sulfides. In the case of PTM, the molecular conformations of the [T] and [G] forms are shown below. In the case

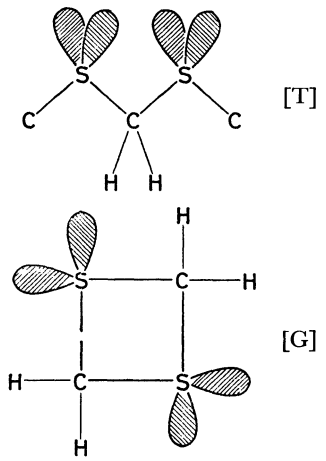

of the [G] form, the lone-pair electrons are coordinated in the center of the C–H bond directions. On the other hand, in the case of the [T] form, the lone-pair electrons on the sulfur atoms are in the same directions and the repulsion forces between lone pairs become large (rabbit-ear effect);[28] in consequence the [G] form may be stable. In the species of alkyl disulfides, sulfur atoms combine with each other. Therefore, the lone pairs on the sulfur atoms produce a powerful effect on the structure of these molecules. In conclusion, these molecules easily have a form which has almost a rectangle (*e.g.*, the internal angle of *ca.* 85° has been proposed for dimethyl disulfide[29]). Therefore, the analysis of the conformation has been done with reference to the concept of the lone pairs.

Conclusion

The results for the infrared spectra of PTM and PTM-D2, and the normal coordinates of $CH_3S(CH_2S)_n$-CH_3 (n=1—3), PTM, and PTM-D2 reveal that the molecular form and the force fields of the model compounds fit well with those of PTM. On the molecular form in the solid state, the model compounds and PTM are confirmed to be the [G] form. On the molecular species of n=1, three forms are confirmed to exist in the liquid or gaseous state: GG, TG, and TT. On the species of n=2 and 3, many of the forms may coexist in the liquid or gaseous state. A comparison of the force fields between PTM and POM reveals that, in PTM, the intramolecular binding forces and non-bonded interatomic interactions are much weaker than those in POM.

The author wishes to thank Professor Hiromu Murata and Associate Professor Yuji Shiro for their helpful advice and encouragement. The author is also indebted to Miss Kuniko Fujiwara for her help in the preparation of the samples.

References

1) H. Tadokoro, M. Kobayashi, Y. Kawaguchi, A. Kobayashi, and S. Murahashi, *J. Chem. Phys.*, **38**, 703 (1963).
2) V. Zamboni and G. Zerbi, *J. Polym. Sci.*, **C7**, 153 (1964).
3) H. Sugeta and T. Miyazawa, *Rept. Prog. Polym. Phys. Japan*, **9**, 177 (1966).
4) G. Zerbi and P. J. Hendra, *J. Mol. Spectrosc.*, **27**, 17 (1968).
5) H. Sugeta, T. Miyazawa, and T. Kajiura, *J. Polym. Sci.*, **B7**, 251 (1969).
6) H. Sugeta, H. Murata, and T. Miyazawa, The Annual Meeting of the Chemical Society of Japan, 16th, p. 373 (1963); 17th, p. 514 (1964); 18th, p. 467 (1965).
7) H. Sugeta, M. Ito, and T. Miyazawa, The 21st Annual Meeting of the Chemical Society of Japan, Vol. 1, p. 325 (1968).
8) G. Carazzolo, *J. Polym. Sci.*, *A*-1, **1**, 1573 (1963).
9) G. Carazzolo and G. Valle, *ibid.*, *A*-1, **3**, 4013 (1965).
10) G. Carazzolo and G. Valle, *Makromol. Chem.*, **90**, 66 (1966).
11) T. Uchida and T. Tadokoro, *J. Polym. Sci.*, *A*-2, **5**, 63 (1967).
12) Y. Shiro, M. Ohsaku, M. Hayashi, and H. Murata, This Bulletin, **43**, 609 (1970).
13) M. Ohsaku, Y. Shiro, and H. Murata, *ibid.*, **45**, 113 (1972).
14) M. Schmidt, K. Blaettner, P. Kochendörfer, and H. Ruf, *Z. Naturforsch.*, **21b**, 622 (1966).
15) J. B. Lando and V. Stannet, *J. Polym. Sci.*. **B2**, 375 (1964).
16) E. Gipstein, E. Wellisch, and O. J. Sweeting, *ibid.*, **B1**, 237 (1963).
17) P. J. Hendra, D. S. Watson, and M. Mammi, *Spectrochim. Acta*, **28A**, 351 (1972).
18) M. Hayashi, Y. Shiro, and H. Murata, This Bulletin, **39**, 1857 (1966).
19) M. Hayashi, Y. Shiro, T. Osima, and H. Murata, *ibid.*, **38**, 1734 (1965).
20) M. Ohsaku, Y. Shiro, and H. Murata, *ibid.*, **45**, 3035 (1972).
21) T. Miyazawa, *Nippon Kagaku Zasshi*, **88**, 111 (1967).
22) M. Tasumi, T. Shimanouchi, and T. Miyazawa, *J. Mol. Spectrosc.*, **9**, 261 (1962); **11**, 422 (1963).
23) R. G. Snyder, *J. Chem. Phys.*, **47**, 1316 (1967).
24) R. G. Snyder and G. Zerbi, *Spectrochim. Acta*, **23A**, 391 (1967).
25) D. W. Scott and M. Z. El-Sabban, *J. Mol. Spectrosc.*, **30**, 317 (1969).
26) M. Ohsaku, Y. Shiro, and H. Murata, This Bulletin, **46**, 1399 (1973).
27) M. Ohsaku, to be published.
28) R. O. Hutchins, L. O. Kopp, and E. L. Eliel, *J. Amer. Chem. Soc.*, **90**, 7174 (1968); M. Ōki and H. Nakanishi, This Bulletin, **45**, 3419 (1971).
29) D. Sutter, H. Dreizler, and H. D. Rudolph, *Z. Naturforsch.*, **20a**, 1676 (1965).

The Derivation of the r_s Structure by the Use of a Nondiagonal Weight Matrix for Rotational Constants

Chiaki HIROSE

Laboratory of Molecular Spectroscopy, Tokyo Institute of Technology, O-okayama, Meguro-ku, Tokyo 152

(Received July 7, 1973)

The use of a nondiagonal weight matrix in a least-squares analysis of the quantities which themselves are derived from another least-squares analysis is discussed in relation to the analysis of rotational constants in determining molecular geometry. The method is applied to the calculation of the r_s structure of ethylene oxide, and the result is compared with those obtained by Kraitchman's formula and by a least-squares fit by the use of a diagonal weight matrix.

Least-squares procedure are commonly used in microwave spectroscopy in two ways: (1) for deriving rotational constants and centrifugal distortion constants from observed transition frequencies, and (2) for deriving structural parameters and/or force constants from rotational or centrifugal distortion constants. In these procedures, however, not all the parameters to be determined are always linearly independent. Lees[1] described a procedure to diagonalize a matrix of the normal equation in order to decouple the equations which correlate the parameters. When the limits of uncertainties in the parameters can be estimated, a *diagonostic least-squares* described by Curl[2] can replace the estimated limits for those calculated by means of a least-squares fit.

As Kirchhoff[3] has pointed out, there is another difficulty in the correlated data. The values derived from a least-squares fit or from a linear combination of directly-observed values (*i.e.*, indirect or secondary observations) are, in general, correlated with one another. Since rotational constants are derived from transition frequencies, correlations among them should be accounted for in a calculation of structural parameters. Similar circumstances are encountered in a structure analysis of gas-electron diffraction,[4–6] where correlations are dealt with by the use of a nondiagonal weight matrix. The present paper will describe the use of a nondiagonal weight matrix in the least-squares fit of rotational constants for determining molecular geometry. The derivation of an r_s structure from the rotational constants for various isotopic species is considered. Following the definition of the r_s structure,[7] no explicit account of the systematic errors due to the neglect of zero-point vibrations is made. Though such systematic errors are usually much larger than the uncertainties originating from errors in the measurement, the correction requires knowledge of the force field; such an undertaking is beyond the range of the present statistical treatment. In the absence of a complete force field, as in the case of ethylene oxide, effective structures, such as r_0 and r_s, are the best one can derive from spectroscopic measurements.

Below, the r_s structure obtained by using a nondiagonal weight matrix will be compared with those derived by neglecting the correlations among rotational constants. The r_s structure calculated by Kraitchman's method is also examined: the formulation for the error analysis in this case is described in the Appendix.

Weight Matrix for Indirect Observations

As Morino *et al.* have pointed out,[4] when a set of observations, μ, which are linear combinations of direct observations, $\mathbf{y}$, is used as the data in the least-squares fit, the weight matrix is expressed by:

$$\mathbf{W} = (\mathbf{G}\mathbf{P}^{-1}\tilde{\mathbf{G}})^{-1} \tag{1}$$

where $\mathbf{G}$ is the matrix which relates $\mathbf{y}$ to μ as:

$$\mu = \mathbf{G}\mathbf{y}, \tag{2}$$

and where $\tilde{\mathbf{G}}$ is the transpose of $\mathbf{G}$. $\mathbf{P}$ is a weight matrix for the direct observations, $\mathbf{y}$, and is diagonal provided each direct observation is measured independently.

This idea can readily be applied to the case where a set of indirect observations, μ (rotational constants, for example), are derived from a set of direct observations, $\mathbf{y}$ (transition frequencies), by way of a least-squares fit. In that case, the matrix, $\mathbf{G}$, to be used is expressed as:

$$\mathbf{G} = \mathbf{B}^{-1}\tilde{\mathbf{J}}\mathbf{P}, \tag{3}$$

where:

$$\mathbf{B} = \tilde{\mathbf{J}}\mathbf{P}\mathbf{J}. \tag{4}$$

$\mathbf{J}$ is the Jacobian matrix used in deriving μ from $\mathbf{y}$, and matrix element, J_{ik}, is the first derivatives of the i-th observation, y_i, with respect to the k-th parameter, μ_k, at the point of convergence, that is, $J_{ik}=(\partial y_i/\partial \mu_k)_0$. Since the $\mathbf{P}$ and $\mathbf{B}$ matrices are symmetric, the substitution of Eq. 3 into Eq. 1 gives:

$$\mathbf{W} = (\mathbf{B}^{-1}\mathbf{J}\mathbf{P}\mathbf{P}^{-1}\mathbf{P}\mathbf{J}\mathbf{B}^{-1})^{-1} = \mathbf{B}. \tag{5}$$

Furthermore, when a set of indirect observations, γ, is a linear combination of the μ set like isotopic changes of rotational constants:

$$\gamma = \mathbf{F}\mu, \tag{6}$$

the weight matrix to be used for the γ set is given by:

$$\mathbf{W} = (\mathbf{F}\mathbf{G}\mathbf{P}^{-1}\tilde{\mathbf{G}}\tilde{\mathbf{F}})^{-1} = (\mathbf{F}\mathbf{B}^{-1}\tilde{\mathbf{F}})^{-1}. \tag{7}$$

In this scheme, the diagonal elements of the matrix $\mathbf{W}$ expressed in Eqs. 1, 5 and 7 account for the propagation of errors, and the off-diagonal terms represent correlations among the indirect observations.[4–6] When a set of indirect observations are composed of subsets, each obtained independently, such as the rotational constants for each isotopic species, the $\mathbf{W}$

matrix splits into submatrices.

Calculation of Structural Parameters

The r_0 structure of a molecule is the one which makes a best fit to the rotational constants in its ground state. In this case, the J_{ik} element of $\mathbf{J}$ is $(\partial\nu_i/\partial A_k)_0$, where ν_i and A_k are the i-th transition frequency and the k-th rotational constant (*i.e.*, A, B, or C) respectively. The i-th element, P_{ii}, of a diagonal matrix, $\mathbf{P}$, is inversely proportional to the square of the measurement error for the i-th frequency. Since an independent analysis is made for each isotopic species, the weight matrix is calculated by the use of Eqs. 4 and 5:

$$\mathbf{W}(r_0)=\begin{bmatrix}\mathbf{B}^{(1)} & & & \mathbf{0}\\ & \mathbf{B}^{(2)} & & \\ & & \cdots\cdots & \\ \mathbf{0} & & & \mathbf{B}^{(n)}\end{bmatrix}^{-1}, \tag{8}$$

where $\mathbf{B}^{(s)}=\mathbf{J}_s\mathbf{P}_s\mathbf{J}_s$ (s=1,2,..., n) is a 3×3 submatrix for the s-th isotopic species and where n is the number of isotopic species for which the rotational constants are obtained.

The r_s structure is defined as a set of parameters derived from isotopic changes in the rotational constants:

$$\Delta A_\alpha^{(s)} = A_\alpha^{(ref)} - A_\alpha^{(s)}, \tag{9}$$

where $A_\alpha^{(s)}$ is the rotational constants along the principal axis, α, for the s-th isotopic species. The value for the reference species (normal ethylene oxide in the present study) is denoted as $A_\alpha^{(ref)}$. The matrix, $\mathbf{F}$ (Eq. 6), consists of $3(n-1)$ rows and $3n$ columns:

$$\mathbf{F}=\begin{bmatrix}\mathbf{E} & -\mathbf{E} & \mathbf{0} & \mathbf{0} & \cdots\cdots & \mathbf{0}\\ \mathbf{E} & \mathbf{0} & -\mathbf{E} & \mathbf{0} & \cdots\cdots & \mathbf{0}\\ & & \cdots\cdots & & & \\ \mathbf{E} & \mathbf{0} & \mathbf{0} & \mathbf{0} & \cdots\cdots & -\mathbf{E}\end{bmatrix}, \tag{10}$$

where $\mathbf{E}$ is a three-dimensional unit matrix. From Eq. 7, the following weight matrix of rank $3(n-1)$ is obtained:

$$\mathbf{W}(r_s)=\begin{bmatrix}\mathbf{B}^{(ref)}+\mathbf{B}^{(1)} & \mathbf{B}^{(ref)} & \cdots\cdots & \mathbf{B}^{(ref)}\\ \mathbf{B}^{(ref)} & \mathbf{B}^{(ref)}+\mathbf{B}^{(2)} & \cdots\cdots & \mathbf{B}^{(ref)}\\ \cdots\cdots & \cdots\cdots & \cdots\cdots & \cdots\cdots\\ \mathbf{B}^{(ref)} & \mathbf{B}^{(ref)} & \cdots\cdots & \mathbf{B}^{(ref)}+\mathbf{B}^{(n-1)}\end{bmatrix}^{-1}. \tag{11}$$

This matrix represents the correlation among the ΔA_α values used for the r_s structure.

The r_s Structure of Ethylene Oxide. As an ap-

Table 1. Rotational constants and their variances of ethylene oxides (in MHz)[a]

	A	σ(A)	B	σ(B)	C	σ(C)
Normal	25483.96	0.070	22120.77	0.072	14097.81	0.069
^{13}C	25291.89	0.055	21597.77	0.058	13825.75	0.056
^{18}O	23992.83	0.112	22121.58	0.117	13628.56	0.126
D_1	24252.47	0.058	19905.34	0.057	13327.40	0.056
t-D_2	22943.19	0.030	18198.47	0.032	12585.27	0.030
t-D_2-^{13}C	22786.84	0.061	17852.32	0.072	12377.50	0.060
t-D_2-^{18}O	21646.74	0.092	18202.46	0.099	12186.66	0.093
c-D_2	22700.41	0.050	18318.39	0.054	12650.08	0.051
c-D_2-^{13}C	22555.61	0.037	17963.42	0.040	12438.85	0.038
c-D_2-^{18}O	21424.03	0.042	18317.20	0.050	12243.45	0.048

a) Identifications of the substances indicated in the first column are; *Normal*=$^{12}C_2H_4{}^{16}O$, ^{13}C=$^{12}C^{13}CH_4{}^{16}O$, ^{18}O=$^{12}C_2H_4{}^{18}O$, *t*-D_2=*trans*-$^{12}C_2H_2D_2{}^{16}O$, *t*-D_2-^{13}C=*trans*-$^{12}C^{13}CH_2D_2{}^{16}O$, *t*-$D_2$-$^{18}O$=*trans*-$^{12}C_2H_2D_2{}^{18}O$, *c*-$D_2$=*cis*-$^{12}C_2H_2D_2{}^{16}O$, *c*-$D_2$-$^{13}C$=*cis*-$^{12}C^{13}CH_2D_2{}^{16}O$, *c*-$D_2$-$^{18}O$=*cis*-$^{12}C_2H_2D_2{}^{18}O$, and D_1=$^{12}C_2H_3D^{16}O$.
Variances derived from a least-squares fit of the observed frequencies are listed. As for the details of the analysis see Ref. 7.

Table 2. Elements of weight matrix used in the calculation of r_s structure of ethylene oxide[a]

	A, A	A, B	A, C	B, B	B, C	C, C
$\mathbf{B}^{ref}$ [b]	0.1394	0.1354	0.1102	0.1460	0.1108	0.1382
$\mathbf{B}^{ref}+\mathbf{B}^1$	0.2850	0.2469	0.2473	0.3117	0.2159	0.2898
$\mathbf{B}^{ref}+\mathbf{B}^2$	0.2771	0.2653	0.2383	0.2955	0.2067	0.3113
$\mathbf{B}^{ref}+\mathbf{B}^3$	0.2749	0.2641	0.2322	0.2998	0.2253	0.2764
$\mathbf{B}^{ref}+\mathbf{B}^4$	0.2833	0.2462	0.2326	0.3418	0.2233	0.2772
$\mathbf{B}^{ref}+\mathbf{B}^5$	0.4024	0.3930	0.3511	0.4480	0.3454	0.4069
$\mathbf{B}^{ref}+\mathbf{B}^6$	0.2747	0.2641	0.2327	0.3046	0.2219	0.2772
$\mathbf{B}^{ref}+\mathbf{B}^7$	0.2755	0.2652	0.2308	0.3028	0.2262	0.2797
$\mathbf{B}^{ref}+\mathbf{B}^8$	0.2776	0.2671	0.2283	0.3034	0.2189	0.2822
$\mathbf{B}^{ref}+\mathbf{B}^9$	0.2883	0.2568	0.2365	0.2897	0.2244	0.2745

a) See Eqs. (4), (5) and (11). b) ref: normal ethylene oxide, which is the reference species, 1: ^{13}C-ethylene oxide, 2: ^{18}O-ethylene oxide, 3: *trans*-D_2-ethylene oxide, 4: *trans*-D_2-^{13}C-ethylene oxide, 5: *trans*-D_2-^{18}O-ethylene oxide, 6: *cis*-D_2-ethylene oxide, 7: *cis*-D_2-^{13}C-ethylene oxide, 8: *cis*-D_2-^{18}O-ethylene oxide, and 9: monodeutero-ethylene oxide.

TABLE 3. r_s STRUCTURES OF ETHYLENE OXIDE[a)]

	L. S. 1[b)]	L. S. 2[c)]	K. M. 1[d)]	K. M. 2[e)]
r(CO)	1.4309(10)	1.4303(13)	1.4313(31)	1.4294(24)
r(CC)	1.4663(18)	1.4657(28)	1.4648(16)	1.4630(23)
r(CH)	1.0854(10)	1.0858(10)	1.0859(18)	1.0824(34)
∠HCH	116.61(10)	116.57(13)	116.50(40)	——
θ[f]	21.99(15)	22.01(10)	21.95(28)	——

a) Bond lengths are in Å and the angles are in degrees. C_{2v} symmetry is assumed for the normal ethylene oxide. Uncertainties given in parentheses are 2.5 times the standard errors attached to the last digit. b) Derived from the least-squares analysis using the nondiagonal weight matrix given in Eq. (11). c) Derived from the least-squares analysis using a diagonal weight matrix following the law of propagation of errors. d) Derived from Kraitchman's method by combination of *normal*, ^{13}C-, ^{18}O-, and monodeutero ethylene oxide. e) Derived from Kraitchman's method by combination of *trans*-D_2-, *trans*-D_2-^{13}C-, *trans*-D_2-^{18}O-, and monodeutero ethylene oxide. f) θ is the dihedral angle of the C-C bond to the H_2C plane.

plication of the present method, the r_s structure of ethylene oxide was calculated by the use of the rotational constants of ten isotopic species.[8)] The observed rotational constants and the elements of $\mathbf{B}^{(s)}$ are shown in Tables 1 and 2 respectively.*

Calculation of the r_s structure were made with a nondiagonal weight matrix and with a diagonal matrix set up by leaving out the diagonal elements of the former. The molecule is assumed to have C_{2v} symmetry. Table 3 lists the derived values of the r_s parameters.

The converged values based on the two weight matrices are not significantly different, but the correlation factors based on the nondiagonal matrix are somewhat smaller than those based on the diagonal matrix. On the other hand, similar calculations based on nondiagonal weight matrices gave larger correlation factors in the r_0 and r_m structures.[9)]

For the sake of comparison, the parameter values obtained by Kraitchman's formula[10)] are also shown in Table 3. The reliability intervals of these values were estimated by way of the propagation of errors; the procedure is shown in the Appendix.

The author is grateful to Professor Kozo Kuchitsu for his helpful comments on the manuscript.

Appendix

Error Estimation of the r_s Structure Obtained by Kraitchman's Method. Kraitchman's formula is given in a matrix form as:

$$\mathbf{a} = \mathbf{Ax}\,, \tag{A1}$$

where

$$a_\alpha = (P_\alpha'-P_\alpha)(P_\alpha'-P_\beta)(P_\alpha'-P_\gamma) = p_{\alpha\alpha}p_{\alpha\beta}p_{\alpha\gamma}\,, \tag{A2}$$

$$A_{\alpha\alpha} = \mu(P_\alpha'-P_\beta)(P_\alpha'-P_\gamma) \equiv \mu p_{\alpha\beta}p_{\alpha\gamma}\,, \tag{A3a}$$

$$A_{\alpha\beta} = \mu(P_\alpha'-P_\alpha)(P_\alpha'-P_\gamma) \equiv \mu p_{\alpha\alpha}p_{\alpha\gamma}\,, \tag{A3b}$$

and

$$x_\alpha = \alpha_s^2 \tag{A4}$$

$(\alpha, \beta, \gamma = a, b \text{ or } c \text{ with } \alpha, \beta \neq \gamma \text{ and } \beta \neq \alpha$, and $p_{\alpha\beta} \equiv P_\alpha'-P_\beta)$.

In the above equations, P_α and P_α', are derived from the moments of inertia, I_α and I_α' for the reference and substituted species, respectively, as:

$$P_\alpha = (-I_\alpha+I_\beta+I_\gamma)/2\,, \tag{A5}$$

$$P_\alpha' = (-I_\alpha'+I_\beta'+I_\gamma')/2\,, \tag{A6}$$

μ is the reduced mass difined as $M\Delta m/(M+\Delta m)$, where M is the molecular weight of the reference molecule and Δm is the difference in molecular weight caused by the isotopic substitution, and α_s is the coordinate of the substituted atom referred to the principal axis α of the reference species. One gets from (Al) that

$$\mathbf{x} = \mathbf{A}^{-1}\mathbf{a}\,. \tag{A7}$$

If the moments of inertial, I_α and I_α' (α=a,b or c), contain error limits of ΔI_α and $\Delta I_\alpha'$ which are positive and independent of one another, error limits of P_α and P_α' can be estimated as:

$$\Delta P_\alpha = (\Delta I_\alpha+\Delta I_\beta+\Delta I_\gamma)/2 = \Delta\,, \tag{A8}$$

$$\Delta P_\alpha' = (\Delta I_\alpha'+\Delta I_\beta'+\Delta I_\gamma')/2 = \Delta'\,. \tag{A9}$$

Thus the error in $p_{\alpha\beta}$ is given by

$$\Delta p_{\alpha\beta} = \Delta + \Delta'\,. \tag{A10}$$

The error limits of a_α and $A_{\alpha\beta}$ are obtained by substituting (A10) into A(2) and A(3) to be:

$$\Delta a_\alpha = \Delta p_{\alpha\alpha}|p_{\alpha\beta}^0 p_{\alpha\gamma}^0| + \Delta p_{\alpha\beta}|p_{\alpha\alpha}^0 p_{\alpha\gamma}^0| + \Delta p_{\alpha\gamma}|p_{\alpha\alpha}^0 p_{\alpha\beta}^0|$$
$$= (\Delta+\Delta')(|A_{\alpha\alpha}^0| + |A_{\alpha\beta}^0| + |A_{\alpha\gamma}^0|)/|\mu| \tag{A11}$$

$$\Delta A_{\alpha\alpha} = |\mu|(\Delta+\Delta')(|p_{\alpha\beta}^0| + |p_{\alpha\gamma}^0|) \tag{A12a}$$

$$\Delta A_{\alpha\beta} = |\mu|(\Delta+\Delta')(|p_{\alpha\alpha}^0| + |p_{\alpha\gamma}^0|)\,. \tag{A12b}$$

When some of the $P_{\alpha\alpha}$'s are set to zero from a consideration of symmetry, $\Delta_\alpha'' = |P_{\alpha\alpha}^0|$ should be added to Δ and Δ', where $p_{\alpha\alpha}^0$ is the observed value which is set equal to zero. The errors are modified as:

$$\Delta a_\alpha' = \Delta a_\alpha + \Delta_\alpha''|A_{\alpha\alpha}^0|/|\mu| \tag{A11a}$$

and the corresponding modification on $\Delta A_{\alpha\beta}$. When $\mathbf{A}^0$ and $\mathbf{x}^0$ are given prior to the error analysis, the error limit $\Delta\mathbf{x}$ can be derived by use of the above equations.*

* The correlation factor between A and B, for instance, is given by $c_{AB}=B_{AB}^{-1}/(B_{AA}^{-1}\cdot B_{BB}^{-1})^{1/2}$. The value of c_{AB} for normal ethylene oxide, 0.9299, indicates that A and B in Table 1 are considerably correlated. The $0 \leqq |c_{AB}| \leqq 1$ relation holds, and the upper limit is realized when A and B are in exact linear dependence.

* Since the propagation of errors is dealt with in a matrix representation, the formula $\Delta\mathbf{x} = (\mathbf{A}^0)^{-1}(\Delta\mathbf{a} + \Delta\mathbf{A}\cdot\mathbf{x}^0)$ does not apply here when it is solved algebraically, but correct solutions are given as follows:

Referring to (A4), the error limits of the coordinates are derived following the law of propagation of errors as:

$$\Delta\alpha_s = \Delta x_\alpha / 2(x_\alpha{}^0)^{1/2} \quad (\text{when } x_\alpha{}^0 \neq 0) \ , \tag{A13a}$$

or

$$\Delta\alpha_s = 0 \quad (\text{when } x_\alpha{}^0 = 0 \text{ by symmetry}) \ . \tag{A13b}$$

(footnote continued)

$$\begin{aligned}
\Delta x_a = (&b_1(|A_{22}{}^0A_{33}{}^0| + |A_{23}{}^0A_{32}{}^0|) \\
&+ b_2(|A_{32}{}^0A_{13}{}^0| + |A_{12}{}^0A_{33}{}^0|) \\
&+ b_3(|A_{13}{}^0A_{22}{}^0| + |A_{12}{}^0A_{23}{}^0|))/|A^0|^* \ , \\
\Delta x_b = (&b_1(|A_{23}{}^0A_{31}{}^0| + |A_{21}{}^0A_{33}{}^0|) \\
&+ b_2(|A_{11}{}^0A_{33}{}^0| + |A_{31}{}^0A_{13}{}^0|) \\
&+ b_3(|A_{23}{}^0A_{11}{}^0| + |A_{21}{}^0A_{13}{}^0|))/|A^0|^* \ , \\
\Delta x_c = (&b_1(|A_{31}{}^0A_{22}{}^0| + |A_{21}{}^0A_{32}{}^0|) \\
&+ b_2(|A_{31}{}^0A_{12}{}^0| + |A_{11}{}^0A_{32_0}|) \\
&+ b_3(|A_{11}{}^0A_{22}{}^0| + |A_{12}{}^0A_{21}{}^0|))/|A^0|^* \ ,
\end{aligned}$$

where,

$$\mathbf{b} = \Delta\mathbf{A}\cdot\mathbf{x}^0 + \Delta\mathbf{a} \ ,$$

and $|A^0|^*$ denotes the absolute value of the determinant of the matrix $\mathbf{A}^0$.

The error limits Δr_{ij} of the distance between the i-th and the j-th atoms is given by,

$$\begin{aligned}
\Delta r_{ij} = [&|a_i{}^0 - a_j{}^0|(\Delta a_i + \Delta a_j) + |b_i{}^0 - b_j{}^0|(\Delta b_i + \Delta b_j) \\
&+ |c_i{}^0 - c_j{}^0|(\Delta c_i + \Delta c_j)]/r_{ij}{}^0 \ ,
\end{aligned} \tag{A14}$$

where

$$r_{ij}{}^0 = [(a_i{}^0 - a_j{}^0)^2 + (b_i{}^0 - b_j{}^0)^2 + (c_i{}^0 - c_j{}^0)^2]^{1/2} \ . \tag{A15}$$

References

1) R. M. Lees, *J. Mol. Spectrosc.*, **33**, 124 (1970).
2) R. F. Curl, Jr., *J. Compt. Phys.*, **6**, 367 (1970).
3) W. H. Kirchhoff, *J. Mol. Spectrosc.*, **41**, 333 (1972).
4) Y. Morino, K. Kuchitsu, and Y. Murata, *Acta Crystallogr.*, **18**, 549 (1965).
5) Y. Murata and Y. Morino, ibid., **20**, 605 (1966).
6) H. M. Seip and R. Stolevik, "Molecular Structures and Vibrations," Chap. 11, ed. by S. J. Cyvin, Elsevier Publishing Co., Amsterdam, Netherlands, (1972), p. 171.
7) C. C. Costain, *J. Chem. Phys.*, **29**, 864 (1958).
8) C. Hirose, This Bulletin, accepted.
9) J. K. G. Watson, Abstracts for the 24th Symposium on Molecular Structure and Spectroscopy, Ohio State University, p. 81, (1969).
10) J. Kraitchman, *Amer. J. Phys.*, **21**, 17 (1953).

Mechanistic Studies on the Photooxidation of Chlorpromazine in Water and Ethanol

Teiki IWAOKA and Michio KONDO

Central Research Laboratories, Sankyo Co., Ltd., Shinagawa-ku, Tokyo 140

(Received August 30, 1973)

It has been established that chlorpromazine undergoes photooxidation *via* its cation radical, yielding chlorpromazine 5-sulfoxide as an ultimate photoproduct. Molecular oxygen has been found indispensable not only for the formation of chlorpromazine cation radical but also for the formation of the sulfoxide from the radical. Oxygen atom in the sulfoxide originates from the atmospheric oxygen and not from water, which was ascertained by both tracer experiment and kinetic analysis. It was concluded that phenazathionium ion is not involved in the reaction. The possibility of singlet oxygen participation in the photooxidation was also ruled out. An intermediate, which is formed from the cation radical, was found as a precursor of the sulfoxide and was tentatively assigned as a peroxyl type radical.

Many photochemical and photobiological studies have been carried out on the photooxidation of chlorpromazine, but there are some discrepancies and ambiguities especially in the behavior of paramagnetic species and their assignment.

Lagercrants[1] showed that ultraviolet irradiation of an aqueous solution of chlorpromazine yielded a radical, the ESR signal of which decayed within about one minute in the dark, the resulting solution turning yellow. The ESR absorption could then be reproduced by blue light(435 nm) illumination inactive to initial chlorpromazine. Degassing of the solution had very little influence on the dynamical behavior of the ESR signal caused by the irradiation. The effect of ultraviolet irradiation of an aqueous solution of chlorpromazine was examined also by Boag and Cotzias.[2] They reported a pale pink(λ_{max}; 530 nm) paramagnetic species which was assigned to the semiquinone cation radical identical with the one produced by the action of trace metal ion(Ce^{4+}) or by potentiometric electrolysis. In spite of the fact that the same photochemical technique was employed, Piette and Forrest[3] reported another radical species, differing in color and in the pattern of ESR signal from those observed by Boag and Cotzias.[2] They assigned this paramagnetic species to the same radical as that detected in urinary metabolites from patients dosed with chlorpromazine drug.

Billon[4] carried out the first systematic investigation on the electrochemical oxidation of phenothiazine and its *N*-substituted derivatives, and showed that the two-electron oxidation yielded a very reactive dication (phenazathionium ion) which underwent hydrolysis to form sulfoxide even with a trace of water. Dismutative formation of the phenazathionium ion of chlorpromazine, suggested from the second-order decay of the cation radical of chlorpromazine formed in the enzymic oxidation systems of peroxidase–H_2O_2 was reported by Cavanaugh[5] and by Piette *et al.*[6] Dismutative formation and subsequent hydrolysis of this phenazathionium ion of chlorpromazine was also proposed by Merkle *et al.*,[7] based on the fact that a mixture of chlorpromazine and its sulfoxide was obtained by dissolving solid free radical in water, prepared with perchloric acid as oxidizing reagent. The formation of the sulfoxide through the phenazathionium ion derivatives was proposed for many oxidation systems, the oxidants being bromine,[8] manganic ion under aerobic conditions,[9] lead tetraacetate,[10] and sulfuric acid.[11] Thus, the phenazathionium ions have been assigned to the precursor of the sulfoxide. The indispensable hydrolysis causes the incorporation of oxygen atom into the sulfoxide from water. Though there have been many reports on sulfoxide formation through the phenazathionium ion, no direct evidence for its participation has been obtained except for the case of electrochemical oxidation.[4]

Photosensitized oxidation of chlorpromazine in the biological system is very interesting as regards photoallergic effects.[12] Blois[13] reported that the visible light irradiation of the melanine polymer into which chlorpromazine was incorporated gave a red pigmentation in the spot exposed to light. It may be worthwhile to mention the oxidation of dimethyl sulfide into the sulfoxide by photosensitization with the use of several dyes.[14]

We have investigated the photooxidation of chlorpromazine in water and in ethanol, especially on the dynamic characteristics of the radical cation and other transients formed as the intermediates by means of steady light and flash photolytic techniques. The possibility of the participation of singlet oxygen as an oxidizing agent was also examined. Strong evidence was obtained from tracer experiments for the view that molecular oxygen in air is incorporated as the oxygen atom in the sulfoxide, and the mechanism involving the hydrolysis of the phenazathionium ion was eliminated at least in the photochemical reaction. A peroxyl type radical was tentatively proposed as a favorable intermediate.

Experimental

Materials. Commercial chlorpromazine hydrochloride was used. Triethylamine(Iwaikagaku G. R. grade), ascorbic acid (G. R. grade, Tokyo Daiichikagaku) and ethanol of G. R. grade (Osaka Yukikagaku Kogyo) were used without further purification. Acetic acid-sodium acetate(pH 3.2—6.3) and hydrochloric acid-sodium acetate(pH 0.6—1.7) were used for the buffer systems. H_2O^{18} (40% isotopic content, Miles Laboratory Inc.) was used for the tracer experiment.

Method. The change in absorbance of chlorpromazine was measured by a monitoring light, perpendicular to the exciting light at 253.7 nm. Combinations of a hydrogen arc lamp, grating monochromator(Shimazu GF-16) and photomultiplier (HTV-109) were used. Contamination of the

scattered light from the source in the monitoring light was about 0.5% at the exciting wavelength. The light intensity was measured with a ferric oxalate actinometer. Flash photolytic experiments were carried out with a Ushio UFP-105(500 J) and a hand-made instrument[15] specially designed in our laboratory. Specially designed flash cell and apparatus were used for the bubbling of several gases (Ar, O_2, air) into the solution. The technique of freeze and thaw was applied for complete deaeration. The electrical power of 100 J for one flashing was used unless otherwise stated.

Results

General Features of the Steady Light Photooxidation.

Figure 1 shows the spectral change of chlorpromazine when its aerated solution in water(pH 4.7[16]) is irradiated by 253.7 nm light from a low pressure mercury lamp. Isosbestic points were clearly seen at 247, 263 nm, similar spectral changes with irradiation being observed in ethanol, methanol, 2-propanol, dioxane–water (20 : 1), and mixed solvent systems of water and ethanol. It was found for the sample bubbled with oxygen that these isosbestic points are observable till the later stage of the reaction and that the yield of the photoproduct exceeds the value in the aerated conditions. Lowering the pH of the aqueous solution of chlorpromazine from 4.7 to 0.7 did not alter the characteristics of the spectral change so much but the bleaching rates became smaller.

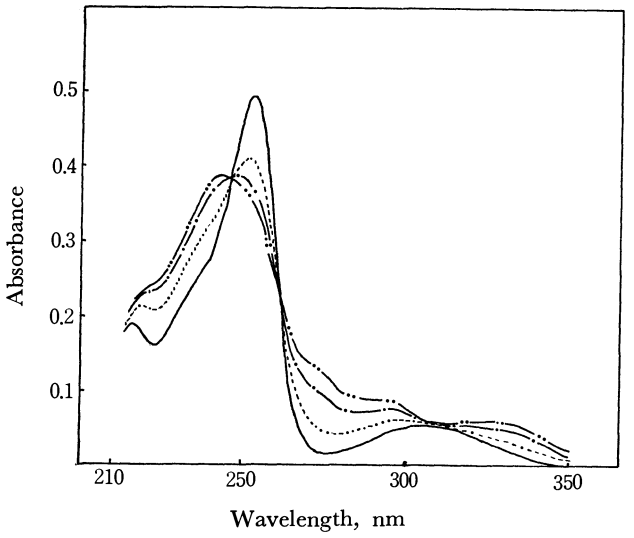

Fig. 1. Spectral change of chlorpromazine in the aerated aqueous solution of pH 4.7.
[CPZ] = 1.4×10^{-5} M. —— 0 s, ---- 8 s, —·— 23 s, —··— 40 s.

The ultraviolet spectrum obtained after the irradiation of 40 seconds in water could be ascribed to chlorpromazine sulfoxide(λ_{max}[17]: 240, 275, 298, and 342 nm) from a comparison with the spectra reported by several workers,[7,17,18] though a considerable amount of the starting chlorpromazine still remained. The mass spectra of the photoproducts in all the systems stated above gave a molecular peak assignable to chlorpromazine sulfoxide. It was established from a comparison of the thin layer chromatogram of the photoproduct with that of chlorpromazine that only one product was formed. Long irradiation which brought about a considerable deviation from the isosbestic point gave the sulfoxide in extremely low yield, the mass spectrum being composed of peaks of low mass number presumably as a consequence of the photochemical decomposition of the photoproduct.

In spite of the similarity in feature of the spectral change and the identity of photoproduct, the quantum yields for the disappearance of chlorpromazine at 253.7 nm are quite different for aqueous solution (Φ_{H_2O}; 5.6×10^{-2}) and ethanol solution($\Phi_{C_2H_5OH}$; 2.7×10^{-3}), suggesting that the solvent effect causes a drastic change in the efficiency in some elementary processes of the photooxidation, or that the formation of the photoproduct by hydrolysis of the reactive transients is involved.

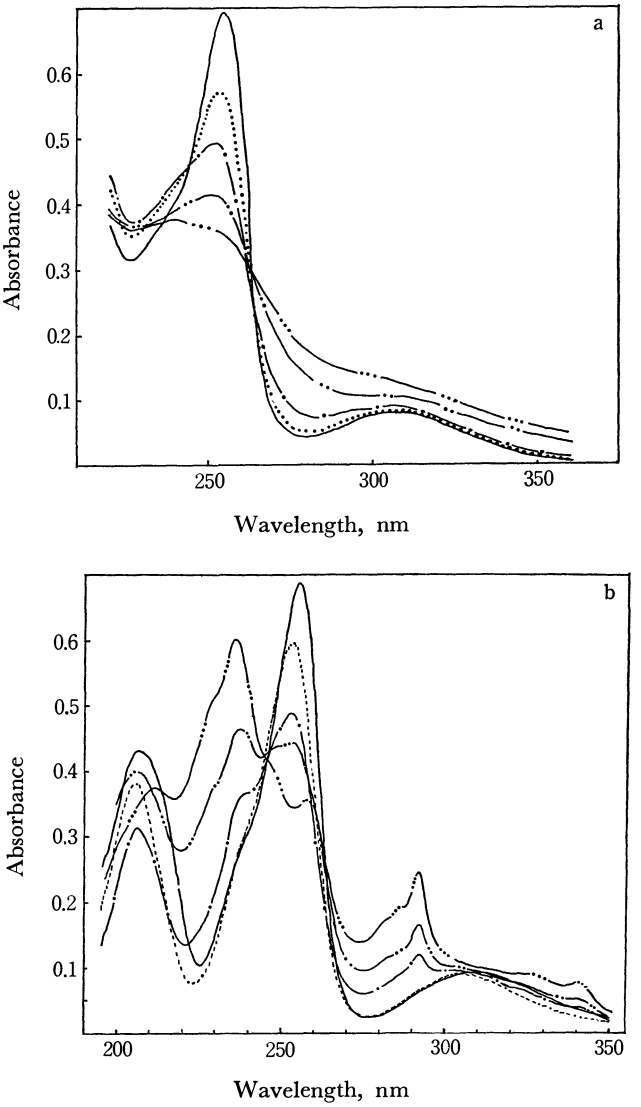

Fig. 2. Spectral change of chlorpromazine in the deaerated solutions.
a : Water (pH 4.7) [CPZ] = 2.0×10^{-5} M. —— 0 s, ---- 6 s, —·— 30 s, —··— 295 s, —···— 22 min.
b : Ethanol [CPZ] = 2.0×10^{-4} M. —— 0 s, ---- 15 s, —·— 19 min, —··— 31 min, —···— 71 min.

Effect of Degassing and H_2O^{18} Tracer Experiment. Spectral changes upon UV illumination of the completely degassed solutions of chlorpromazine in water (pH 4.7) and ethanol are shown in Fig. 2. The bleaching rate of chlorpromazine at 253.7 nm in the completely degassed aqueous solution was approximately the same as the one in the aerated solution, but in the absorption spectrum no peaks ascribable to the sulfoxide were observed. After prolonged irradiation the absorption spectrum showed absorption increase independent of wavelength but no characteristic peaks.

In the case of the degassed ethanol solution, a different photochemical reaction(Fig. 2(b)) occurs with a negligibly small rate ($\Phi_{\text{degassed } C_2H_5OH}$; *ca.* 8×10^{-5}) as compared with the aerated case. We may say that the photochemical reaction leading to the sulfoxide formation practically does not occur.

The effects of addition of oxygen on the quantum yield for the disappearance of chlorpromazine in water and ethanol are shown in Fig. 3. Even at such a small oxygen concentration as 10^{-5} M, the spectral changes of chlorpromazine in water are essentially the same as those in the air saturated solution as well as in the oxygen saturated one. This supports the view that a small amount of oxygen inhibits the reaction predominating under completely degassed conditions. This was further established by the following observation; the quantum yield for formation of the sulfoxide estimated from the absorption rise at 275 nm of the sulfoxide increases as oxygen concentration is increased, while the quantum yield for the disappearance of chlorpromazine is almost independent of oxygen concentration. The quantum yields for the two reactions, one *in vacuo* and the other in aerated condition, are equal. Dependence of the quantum yields upon oxygen concentration in ethanol differs from the case in the aqueous solution, suggesting a different reaction scheme, especially on the behavior of the dissolved oxygen.

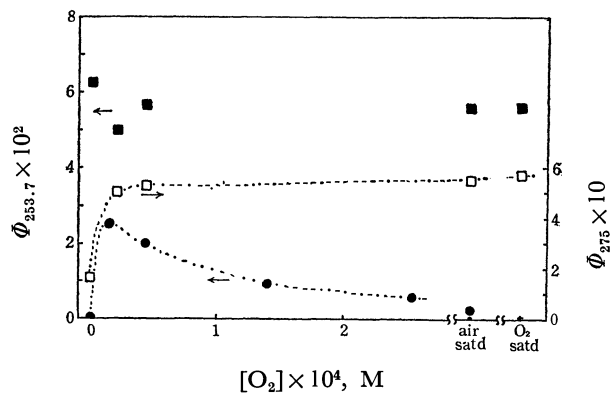

Fig. 3. Dependence of the quantum yields on the oxygen concentration in water and in ethanol. $[CPZ(H_2O)]=2.0\times10^{-5}$ M. $[CPZ(C_2H_5OH)]=1.7\times10^{-5}$ M.
■: Quantum yield for the disappearance of CPZ at 253.7 nm in water (pH 4.7). Inner filter effect is not corrected.
□: Quantum yield for the formation of the sulfoxide in water (pH 4.7) estimated from the absorption at 275 nm.
●: Quantum yield for the disappearance of CPZ at 253.7 nm in ethanol. Inner filter effect is not corrected.

TABLE 1. RELATIVE INTENSITY OF THE MASS PEAKS OF CHLORPROMAZINE SULFOXIDE OBTAINED BY PHOTOOXIDATION IN VARIOUS SOLVENTS

Medium		334	335	336	337
normal	H_2O	100	26	48	9
calcn[a]	H_2O^{18}	100	26	91	
exptl[b]	C_2H_5OH-H_2O^{18}	100	26	48	
exptl	H_2O^{18}	100	24	53	

a) The relative intensities are calculated from the results in normal H_2O on the assumption of 30% in O^{18} concentration. b) C_2H_5OH: $H_2O^{18}=100:1$ in volume ratio.

Tracer experiments using H_2O^{18} instead of normal H_2O were carried out in order to confirm the mechanism proposed by several workers,[4,5,7] according to which the sulfoxide is formed by the hydrolysis of the phenazathionium ion. Photochemical reactions in H_2O^{18} and in ethanol containing a small amount of H_2O^{18} occur with the same rates and with the same spectral changes as in the experiments with normal H_2O. Mass spectrometric measurement, details of which are given in Table 1, definitely excludes the possibility of oxygen incorporation into sulfoxide from H_2O^{18}. It may be concluded that the formation of sulfoxide by way of hydrolysis of the phenazathionium ion[7-11] is not involved in the photochemical oxidation of chlorpromazine and that the oxygen atom in the sulfoxide should originate from molecular oxygen in air, in line with the occurrence of quite different reactions under the degassed conditions.

$$CPZ + O_2(\text{air}) \xrightarrow{h\nu} CPZ{\rightarrow}O \qquad (1)$$

Effects of Light Intensity and Ionic Strength. Further experiments concerning the possible formation of the phenazathionium ion were carried out. In the photochemical reaction where no strong oxidant is involved, formation of the phenazathionium ion, if it occurs at all, should be due to the disproportionation of the cation radical[5,6] or with less probability to the direct photoionization of the cation radical by the absorption of the exciting light. The mechanisms require that the intensity of exciting light considerably affect the quantum yield. However, it was found that the quantum yield does not depend upon the light intensity for the aqueous, ethanol, and acetic acid–water (1 : 1) solutions (Fig. 4). A mechanism involving the quantitative disproportionation of the cation radical, by which no light intensity effect is expected on the quantum yield, was rejected by the dominant first-order decay of the cation radical in our flash photolytic experiments.

The increase of ionic strength which accelerates the reaction between the charged molecules with the same sign[19] should bring about an increase of the quantum yield, provided that the dismutative formation of the reactive phenazathionium ion from the cation radical occurs. However, a decreasing tendency in quantum yield was found with increasing ionic strength.

All these results strongly rejected the possibility of

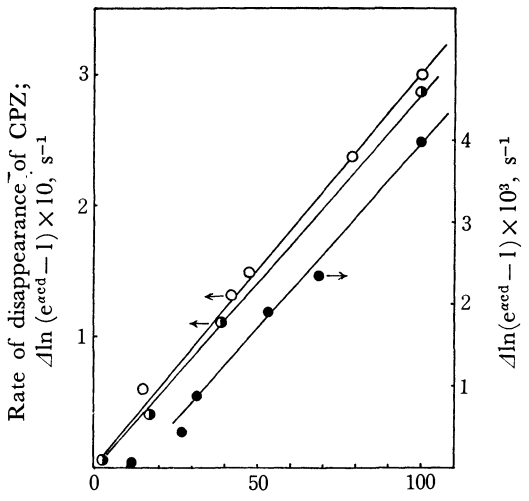

Fig. 4. Dependence of the rate of disappearance of chlorpromazine on the light intensity.
●: Ethanol, ○: Water (pH 4.7), ◑: Water-acetic acid (1:1)

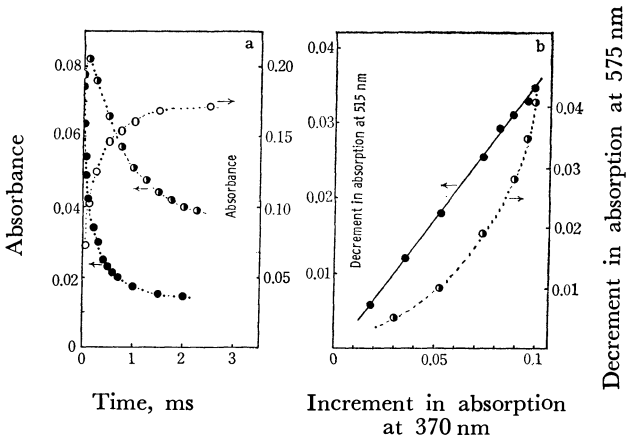

Fig. 6. Changes of the transient absorption with time at 515, 575 and 370 nm.
a: Plots of the absorbance *vs.* time. ●: 515 nm, ◑: 575 nm, ○: 370 nm.
b: Plots of the decrease in absorptions at 515(●) and 575(◑) nm against the increment in absorption at 370 nm.

the dismutative formation of phenazathionium ion from the cation radical. An alternative route for the sulfoxide formation through the cation radical should be considered.

Transient Intermediates by Flash Photolysis. The transient absorption spectra of chlorpromazine flashed in the aerated aqueous solution of pH 4.7 are shown in Fig. 5. A very short-lived intermediate easily discriminated as the absorption at about 515 nm is assigned to the chlorpromazine cation radical. A satisfactory agreement of this spectrum with that in concentrated H_2SO_4 solution of chlorpromazine and also with other spectra reported[2,5,7,9,17] as the chlorpromazine cation radical, supports the assignment. The transient absorption around 575 nm decayed with a little slower rate than that of the cation radical and a realtively slow rise of absorption around 370 nm was observed, acompanied with the decline of the cation radical. Thus three transient intermediates were clearly differentiated. The time characteristics of absorptions at 515, 575 and 370 nm after flashing are shown in Fig. 6(a). From the proportionality between the absorption increment at 370 nm and the decrease at 515 nm (Fig. 6(b)), it is very likely that the absorption at 515 nm due to the cation radical is replaced by the one at 370 nm with one to one correspondence. It should be noted that a small increase in absorption at 575 nm is equivocally observed at an early stage, till about 100 μs after flashing. Deaeration caused the extreme decrease in the yield of the cation radical. This suggests the involvement of oxygen in the reaction yielding the cation radical. No such considerable effect of deaeration on the yield of the 575 nm absorbing intermediate was observed.

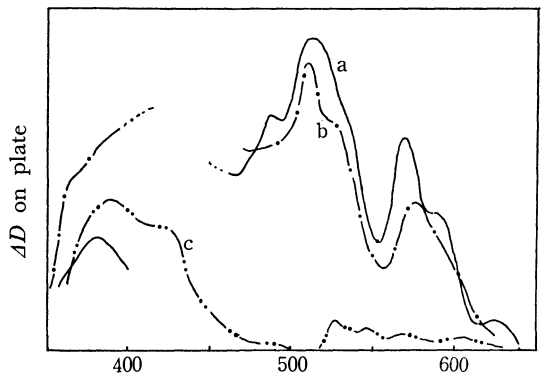

Fig. 5. Transient absorption spectra obtained by the flash photolysis of the aerated aqueous solution of chlorpromazine (pH 4.7).
a: 30 μs, b: 300 μs, c: 1 ms,

Flashing of the degassed ethanol solution of chlorpromazine gave the 575 nm light absorbing species as well as the chlorpromazine triplet state with an absorption around 480 nm, the assignment of which was made from a comparison of its shape and peak position with those of the phenothiazine triplet state[20] and also from the behavior of this species toward oxygen. The absorption around 370 nm was hardly detected in this case. Aerated ethanol solution gave only the cation radical in an extremely small amount upon flashing.

Influence of pH *and Oxygen Concentration on the Kinetics of the Transients.* The spectral change by ultraviolet irradiation is indifferent to the change of pH from 4.7 to 0.7 except for the bleaching rates. This makes it possible to determine the reactive intermediates by kinetical analysis of the reaction mechanism. The effect of pH on the yields and lifetimes of the transient intermediates are summarized in Table 2. The pH effect on the quantum yields for the steady light irradiation is shown in Fig. 7. The 370 nm light absorbing species(370-Int.) has smaller yields at low pH values, while the yield of 575 nm light absorbing species(575-Int.) remains almost constant over the whole pH range examined. The lifetimes of the above two

Table 2. pH effect on the yields of 575-Int. and 370-Int. in the aerated aqueous solution
[CPZ] = 1.1×10^{-4} M

pH	370-Int.		575-Int.		CPZ^+	
	Yield	Rate const.	Yield	Rate const.	Yield	Rate const.
0.65	0.03_2	—	0.05_3	7.8×10^2	0.07_8	5.1×10^3
1.7	0.01_8	—	0.04_4	8.5×10^2	0.03_4	—
3.2	0.06_6	1.2×10^2	0.05_0	1.1×10^3	0.04_6	6.1×10^3
4.7	0.10_1	1.4×10^2	0.03_9	1.2×10^3	0.03_6	6.1×10^3
6.3	0.12_0	1.2×10^2	0.03_5	1.1×10^3	0.03_2	5.8×10^3
8.0	0.11_6	—	0.03_1	1.3×10^3	0.03_1	5.1×10^3

Table 3. Yields of intermediates by flash photolysis of the aqueous solutions of CPZ, deaerated, and bubbled with argon, air, and oxygen
[CPZ] = 1.4×10^{-4} M

	370-Int.	575-Int.	CPZ^+	*d* O. D. (275)
Deaerated	0.06_1	0.04_7	0.03_1	
Argon	0.06_6	0.04_0	0.03_6	0.02_6
Air	$0.12_4(2.2)$	$0.08_8(1.6)$	0.05_6	0.03_3
Oxygen	$0.19_4(2.9)$	$0.11_0(1.5)$	0.06_6	0.05_2

Note) Values in parentheses are absorptions of the transient divided by the absorption of CPZ^+.

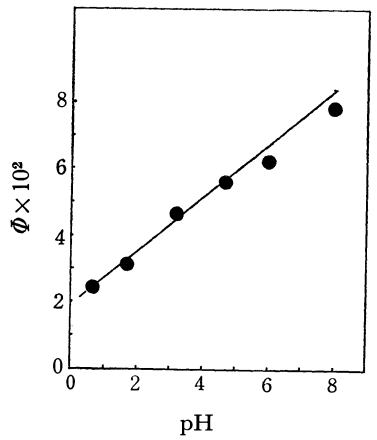

Fig. 7. Dependence of the quantum yield of chlorpromazine upon the value of pH in the aerated aqueous solution. [CPZ] = 1.5×10^{-5} M.

transients remain almost unchanged over the pH range tested. It is obvious that 370-Int. is a reactive intermediate judging from a similar tendency of decrease of the yield to that of the final product with lowering pH of the medium.

The initial yields of the intermediates upon flashing in our four different samples are shown in Table 3. One sample was degassed completely by the freeze-thaw technique, the others being saturated with argon, air, and oxygen. The absorption at 370 nm is moderately increased by the saturation of oxygen, while that at 575 nm is not much affected. The 370-Int. owes its origin to the cation radical which has been identified as the precursor of the sulfoxide as evidenced by several workers.[7,9] The significant increase of the 370-Int. with oxygen concentration supports the formation of 370-Int. through the reaction of the cation radical with oxygen.

Thus it may be concluded from the effect of pH and oxygen concentration on the reaction that the photoproduct, chlorpromazine sulfoxide, is formed from 370-Int. which comes from the cation radical.

$$CPZ^+ + O_2 \longrightarrow \text{370-Int.} \longrightarrow CPZ{\rightarrow}O \qquad (2)$$

Effect of the Intensity of Flashing Light. The decay curve of the cation radical could be reproduced by the first-order decay formulation, even if a high flashing power was supplied for the large concentration of the intermediates. Figure 8 shows the dependence on the flashing light intensity of the amounts of the transient intermediates in terms of their maxima in absorbance. It is evident that no biphotonic process contributes to the cation radical production nor to the formation of the other two intermediates. This is in line with the results of the light intensity effect in steady

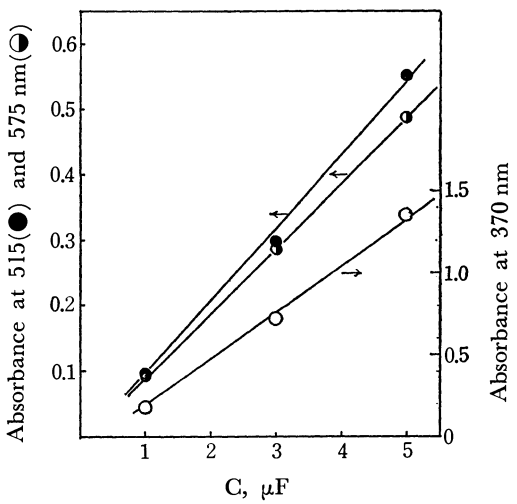

Fig. 8. Dependence of the yields of the transients on the intensity of flashing light in the aerated aqueous solution of pH 4.7. : $CPZ^{\cdot+}$, : 575-Int., ○: 370-Int.

light experiments. The phenazathionium ion, a two electron oxidized form of chlorpromazine, was not detected even in the photolysis of a high flashing light intensity.

Effect of the Addition of Radical Quenchers and of Singlet Oxygen Quencher. The effect of the addition of triethylamine(TEA) on the quantum yield in ethanol is shown in Fig. 9(a). TEA has a considerable affinity to the cation radical on account of its low ionization potential or high reducing power. The result suggests that the two reaction intermediates are involved in the reaction. The plot of $1/\Phi$ against [TEA] gives a curve consisting of two straight lines, which shows unequivocally the existence of two intermediates (Fig. 9(b)). One has a lifetime far longer than that of a typical triplet state in air saturated ethanol and might be assigned to some radical species. Assignment of the other species is unimportant, since the spectral change occuring in such a high concentration of TEA is very small, reflecting the occurrence of different reactions.

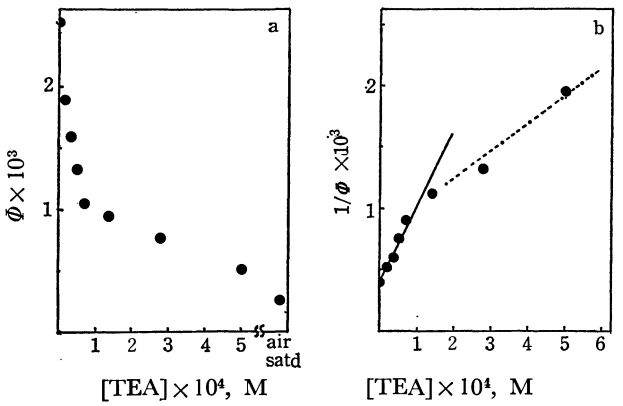

Fig. 9. Dependence of the quantum yield on the triethylamine (TEA) concentration in the aerated ethanol solution.
a: Plots of Φ *vs.*[TEA]. b: Plots of $1/\Phi$ *vs.*[TEA]

Similar quenching experiments using ascorbic acid as a radical quencher in the case of aqueous solution were performed in steady light and flash photolytic experiments. The results are summarized in Table 4. The quantum yields of the disappearance of chlorpromazine and the decay rates of the cation radical are affected considerably by the addition of ascorbic acid, which substantiates the mechanism of the sulfoxide formation through the chlorpromazine cation radical.

Tetramethylethylene, a prominent singlet oxygen quencher, showed no inhibitory effect in ethanol against chlorpromazine photooxidation even at a high concentration of 3.4×10^{-1} M. Thus the photooxidation of chlorpromazine *via* singlet oxygen mechanism can be excluded. This is consistent with the independence of quantum yield on the chlorpromazine concentration.

General Discussion

It is impossible to identify the 370-Int. conclusively, but the establishment of oxygen uptake from the atmospheric oxygen into the sulfoxide may reject the possibility of sulfonium ion(I) as the precursor of the sulfoxide. In support of this conclusion, the halosulfonium ion(R_2SX^+), known as a familiar intermediate for sulfoxide formation in the oxidation of the corresponding sulfide by halogen, undergoes hydrolysis and incorporation of the oxygen atom of water is attained.[21] The phenazathionium ion is also excluded definitely for the same reason.

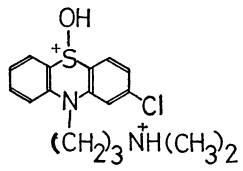

(I)

The electrochemical oxidation of phenothiazine leading to the formation of the cation radical requires 270 mV as half-wave potential for one electron oxidation, and 750 mV for the formation of the two electron oxidized form.[4] The reaction of this phenazathionium ion with the initial phenothiazine occurs rapidly and two molecules of the cation radical are obtained.[4] Thus the occurrence of the dismutative reaction of the cation radical of chlorpromazine is not thermodynamically possible. It is to be added that the absorption spectra of the phenazathionium ions have not been reported and the formation of the sulfoxide through the phenazathionium ion of chlorpromazine has been concluded only from the observation of the second-order decay of the cation radical.

Table 4. Effects of addition of ascorbic acid(AA) on the quantum yield and also on the yields of transients in water, and of tetramethyl ethylene(TME) on the quantum yield in ethanol

Solvent	Quencher concn(M)	370-Int.	575-Int.	CPZ^+	$Kd(CPZ^+)$	$\Phi_{253.7}$
H_2O(pH 4.7)	AA 0	0.18_1	0.07_6	0.09_0	6.1×10^3	5.3×10^{-2}
	1.0×10^{-4}	0.15_0	0.05_6	0.07_2	6.1×10^3	4.9×10^{-2}
	3.0×10^{-4}	0.13_8	0.05_0	0.08_0	8.2×10^3	2.9×10^{-2}
	5.0×10^{-4}	0.08_8	0.04_3	0.05_6	1.6×10^4	$8—9\times10^{-3}$ a)
C_2H_5OH	TME 0					2.5×10^{-3}
	5.3×10^{-5}					2.5×10^{-3}
	6.7×10^{-2}					3.0×10^{-3}
	3.0×10^{-1}					— b)

a) Error due to the inner filter effect; $\pm1\times10^{-3}$. b) Absorption overlap is very large but reaction occurs.

The assignment of 370-Int. is difficult in the present stage but we tentatively assume it to be a peroxyl radical(II) from its predominant formation with oxygen bubbling. A similar type of radical species was reported in the formation of dimethyl sulfoxide from dimethyl sulfide.[22]

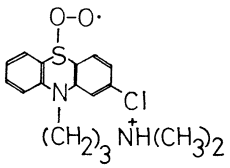

(II)

As to the formation of the cation radical, ionization by the consecutive absorption of two photons and singlet oxygen mechanism are both excluded, so that the remaining possibility is the electron transfer process with molecular oxygen as an acceptor.

The authors are indebted to Dr. M. Koizumi and Dr. H. Kokubun for their suggestions and encouragement. Thanks are due to Dr. Y. Kishida and T. Kinoshita for their valuable discussions.

References

1) C. Lagercrants, *Psychopharmacol. Serv. Centr. Bull.*, **2**, 53 (1962).
2) D. C. Boag and G. C. Cotzias, *Proc. Natl. Acad. Sci.*, **48**, 623 (1962).
3) L. H. Piette and I. S. Forrest, *Biochem. Biophys. Acta.*, **57**, 419 (1962).
4) J. P. Billon, *Bull. Soc. Chim. Fr.*, **1961**, 1784.
5) D. J. Cavanaugh, *Science*, **125**, 1040 (1957).
6) L. H. Piette, G. Bulow, and I. Yamazaki, *Biochem. Biophys. Acta.* **88**, 120 (1964).
7) F. H. Merkle, C. A. Disher, and A. Felmeister, *J. Pharm. Sci.*, **53**, 965 (1957).
8) C. McMartin and H. V. Street, *Acta. Pharmcol. Toxicol.*, **21**, 172 (1964).
9) D. C. Boag and G. C. Cotzias, *Proc. Natl. Acad. Sci.*, **48**, 643 (1962).
10) A. Berka, FlProchazkva, and J. Zyka, *Cesk. Farm.*, **13**, 121 (1964).
11) A. H. Beckett and S. H. Hurry, *J. Pharm. Pharmacol.*, **15**, Supple 246 (1963).
12) H. Ippen, *Proc. 3rd. Intrn. Congr. Dermatol.*, **1961**, 509. H. Ippen, *Proc. 12th. Intrn. Congr. Dermatol.*, **1962**, 1073.
13) M. S. Blois, *J. Invest. Dermatol.*, **44**, 475 (1965).
14) C. S. Foote and J. W. Peters, *J. Amer. Chem. Soc.*, **93**, 3795 (1971).
15) T. Iwaoka, M. Kondo, E. Enomoto, and T. Takahashi, *Ann. Sankyo. Res. Lab.*, *24*, **83** (1972).
16) T. Nakagawa, T. Kubota, and H. Miyazaki, *Ann. Rep. Shionogi. Res. Lab.*, **1957**, 319.
17) R. J. Warren, I. B. Eisdorfen, W. E. Thomson, and J. E. Zarenbo, *J. Pharm. Sci.*, **55**, 144 (1966).
18) D. C. Boag and G. C. Cotzias, *Proc. Natl. Acad. Sci.*, **48**, 617 (1962).
19) K. J. Laidler, "Reaction Kinetics," Mc Graw-Hill Book Company Inc. (1965).
20) T. Iwaoka, H. Kokubun, and M. Koizumi, This Bulletin, **44**, 341 (1971).
21) S. Oae and S. Kawamura, This Bulletin, **36**, 146 (1963). R. J. Gritter and D. J. Crarey, *J. Org. Chem.*, **29**, 1160 (1964). A. H. Fenselan and J. G. Moffat, *J. Amer. Chem. Soc.*, **88**, 1762 (1966).
22) D. Barnard, L. Bateman and J. I. Cunneen, "Organic Sulfur Compounds," Vol. 1, ed. by N. Kharasch, Pergamon Press, (1961).

Photocyclization of [2.2]Metacyclophane at 2537 Å[1]

Kenji SORIMACHI,[2] Toshifumi MORITA, and Haruo SHIZUKA*

Department of Chemistry, Faculty of Engineering, Gunma University, Tenjin-cho, Kiryu, Gunma 376

(Received October 3, 1973)

The photochemical reaction of [2.2]metacyclophane at 2537 Å has been studied spectrophotometrically. Photocyclization took place to give 4,5,9,10-tetrahydropyrene not only in aerated but also in degassed solutions. The quantum yields for the reaction were independent of the irradiation time, concentration of starting material, light intensity, and addition of piperylene. However, the reaction quantum yields increased with temperature rise. The quantum yields in the aerated system were somewhat larger than those in the degassed system. Radiationless deactivation in $S_1(\pi\pi^*)$ was very efficient, whose quantum yield was assumed to be ~0.99, judging from the small reaction quantum yield (less than 0.01) and the lack of fluorescence and phosphorescence. It is proposed that the photocyclization of the molecule originates from $S_1(\pi\pi^*)$ to give intermediate M which is subsequently convreted into the product or the starting material. Activation energies in these processes were estimated.

The photochemical behavior of [2.2]metacyclophane (MCP) is of interest from the viewpoint of the interaction between the two benzene rings adjacent to each other.[3] The transannular interaction would affect the photochemical and photophysical processes in MCP. In the case of [2.2]paracyclophane, the intramolecular excimer formation (the excimer fluorescence at 3350 Å)[4] and the photochemical cleavage[5] have been reported. The photochemical reactions of MCP in the presence of iodine have been carried out by Sato *et al.*[6,7] and Hayashi and Sato[7] who proposed that the photocyclization of MCP proceeds *via* the CT-complex formation between MCP and I_2. However, no photochemical reaction of MCP without oxidant has been reported.

The photocyclizations of compounds such as *cis*-stilbene[8,9] and diphenylamines[10-14] have been carried out. The bond formation between the proper atoms takes place *via* the lowest excited singlet state $S_1(\pi\pi^*)$ for the former[8,9] and *via* the lowest triplet state $T_1(\pi\pi^*)$ for the latter,[11,13] the intermediate with the central two hydrogen atoms having *trans*- and *cis*-form, respectively, being produced. The photocyclization of the former needs an oxidant such as oxygen. However, the reaction of the latter proceeds with and without oxygen.

This paper reports the photochemical reaction of MCP in degassed and aerated solutions in detail.

Experimental

[2.2]Metacyclophane (MCP) was supplied by Dr. T. Sato of Tokyo Metropolitan University. The starting material, after sublimation, was purified by column chromatography (Al_2O_3 and *n*-hexane) and by repeated recrystallizations. Cyclohexane and methylcyclohexane (G. R. grade, Tokyo Kasei Co., Ltd.) were purified by passing through silica gel column and by distillation. 4,5,9,10-Tetrahydropyrene (4HP) was prepared by the irradiation of MCP solution at 2537 Å and purified by column chromatography and repeated recrystallizations. 4HP was identified by means of NMR, IR, UV, mp and elemental analyses.

A low pressure mercury lamp with a Vycor glass filter was used as the 2537 Å radiation source. A xenon lamp, equipped with a diffraction grating, was used as the 2800 Å radiation source. Actinometry was carried out using a ferric oxalate solution.[15] The quantum yields for the reaction were performed by spectrophotometry. No difference in quantum yield was observed at 20 °C for cyclohexane and methylcyclohexane. Thus methylcyclohexane was used in the temperature range 213—288 K. For the measurement of temperature effect on the quantum yield, a quartz Dewar flask designed for spectrometry was used as a reaction cell which controlled the temperature to within ±2 °C. In the measurements on degassed samples, the solutions were thoroughly degassed on a high-vacuum line by the freeze-pump-thaw-method. Emission spectra were measured with a Hitachi MPF-2 spectrofluorimeter. The conventional μ-s flash apparatus described previously[16] was used.

* To whom correspondence should be addressed.

Results

Figure 1(a) shows the spectral change of cyclohexane solution of [2.2]metacyclophane (MCP) during the course of photolysis at 2537 Å at 20 °C in the degassed system. This change indicates that the reaction product was 4,5,9,10-tetrahydropyrene (4HP). The photoproduct was identified by means of NMR, IR, UV, mp, and elemental analyses.[17] The spectral change of the aerated solution of MCP was similar to that in the degassed system (Fig. 2). However, after long irradiation, a new absorption band appeared in the 320—335 nm range in the aerated system. The

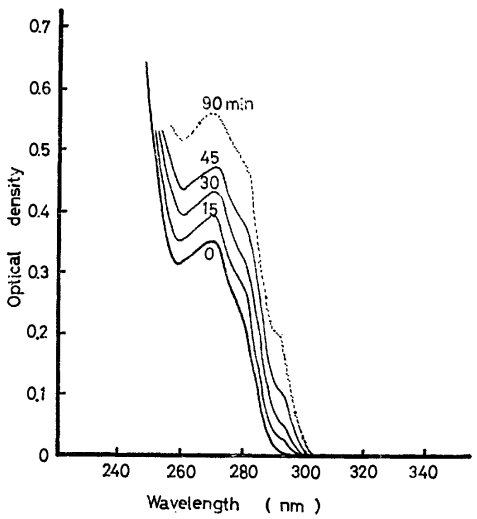

Fig. 1(a). Spectral change of MCP in degassed cyclohexane at 2537 Å and 20 °C. Numbers refer to time at measurement in minutes.

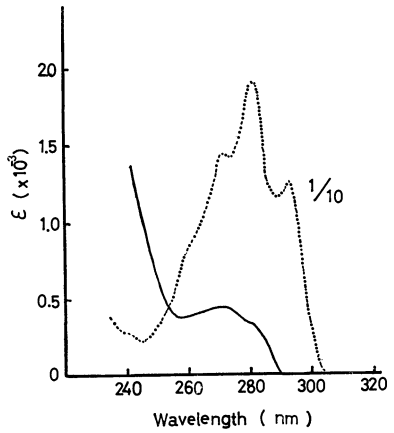

Fig. 1(b). UV absorption spectra of MCP and the photoproduct (4HP) in cyclohexane: line and broken line denote those in MCP and 4HP, respectively.

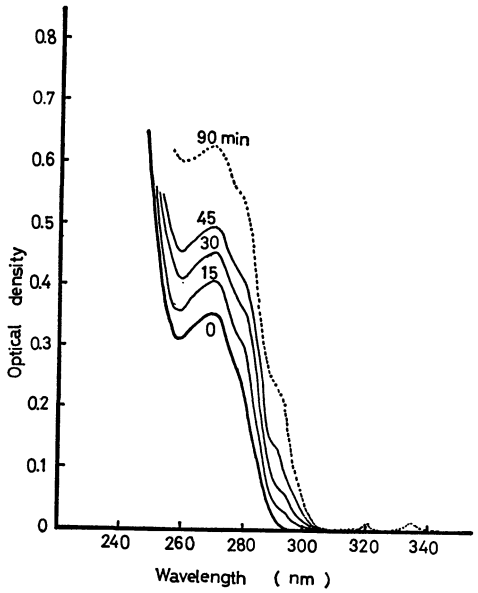

Fig. 2. Spectral change of MCP in aerated cyclohexane at 2537 Å and 20 °C.

band was assigned to that of pyrene, which was photochemically produced in the aerated solution.[17]

The molar extinction coefficients of MCP and 4HP in cyclohexane are given in Table 1. The quantum yields for the photocyclization of MCP were measured from the increase in the optical density at 293 nm, where there is a characteristic absorption band in the product. The quantum yields for the reaction were measured under various conditions at 20 °C. The results are shown in Fig. 3. The quantum yields for the product formation in cyclohexane at 2537 Å did not change with irradiation time (≤40 min), initial concentration of the starting material ($\leq 3\times10^{-2}$ M), light intensity (10^{14}—10^{15} photons s^{-1} ml^{-1}), and addition of piperylene as a triplet quencher ($\leq 7\times10^{-3}$ M). The quantum yields in degassed and aerated solutions at 2537 Å and 20 °C were $(1.7\pm0.2)\times10^{-3}$ and $(2.3\pm0.2)\times10^{-3}$, respectively. No wavelength effect on the reaction quantum yields at 2537 nad 2800 Å at 20 °C in cyclohexane was observed, but the temperature effect was significant, as shown in Fig. 4. The quantum yields in degassed and aerated conditions increased with temperature rise. A similar tendency to the temperature effect on the yields was observed both in

Table 1. Molar extinction coefficients of MCP and 4HP in cyclohexane at 20 °C

Compound	λ_{max} (nm)	ε (M^{-1} cm^{-1})
MCP	272	4.4×10^{2}
4HP	271	1.46×10^{4}
	281	1.80×10^{4}
	293	1.30×10^{4}

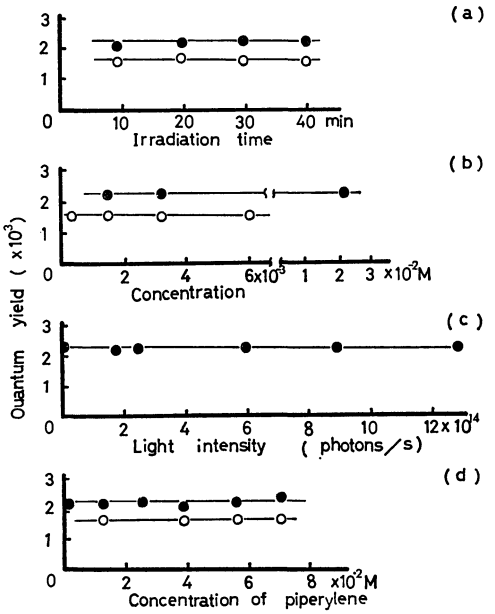

Fig. 3. Dependence of quantum yield for the product formation in cyclohexane at 2537 Å and 20 °C.
(a) On irradiation time with initial concentration of 3.2×10^{-3} M. (b) On concentration of MCP. (c) On light intensity. (d) On addition of piperylene. ○: in degassed cyclohexane. ●: in aerated cyclohexane.

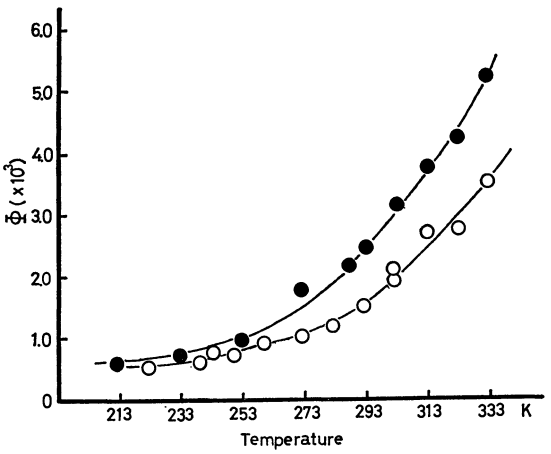

Fig. 4. Dependence of the reaction quantum yield on temperature.
○: in degassed condition, ●: in aerated condition.

degassed and aerated solutions. Although the quantum yields for product formation were very small ($\leq 10^{-2}$) as shown in Fig. 4, neither fluorescence in cyclohexane at 20 °C nor phosphorescence in a MP matrix at 77 K was observed. The long-lived intermediate could not be observed by means of conventional μs flash photolysis.

Discussion

The photocyclization of MCP in the degassed system is an intramolecular reaction, since no concentration effect of the starting matrial was observed on the quantum yields (Fig. 3b). The possibility for the charge transfer formation between MCP and dissolved oxygen in the ground state is unlikely, judging from their UV spectra and the concentration effect on the quantum yields. It seems that the photocyclization originates from the lowest excited singlet state $S_1(\pi\pi^*)$, since the addition of piperylene as a triplet quencher (E_T=2.48 eV) did not affect the quantum yields in the concentration range $10^{-4}-7\times10^{-3}$ M (Fig. 3d), dissolved oxygen (2.3×10^{-3} M)[14] increased the quantum yields for the reaction compared with those in the absence of oxygen (Figs. 3 and 4), and no excitation wavelength was observed on the yields.

The experimental results can be accounted for the following scheme, which is simplified in the processes of internal conversion and intersystem crossing.

$$S_0 + h\nu \longrightarrow S_1 \quad (0)$$

$$S_1 \longrightarrow S_0 \quad (1)$$

$$S_1 + O_2 \longrightarrow S_0 + O_2 \quad (1q)$$

$$S_1 \longrightarrow M \quad (2)$$

$$M \longrightarrow P + (H_2) \quad (3)$$

$$M \longrightarrow S_0 \quad (4)$$

$$M + O_2 \longrightarrow P + (HO_2,\ H_2O_2) \quad (5)$$

where S_0 and S_1 are the ground and the lowest excited singlet states of MCP, respectively, M is the intermediate and P is the photoproduct (4HP). The quantum yields for the product formation Φ_0 and Φ in degassed and aerated conditions, respectively, can be expressed by the following equations, using the steady-state approximation.

$$\Phi_0 = \frac{k_2}{k_1+k_2}\cdot\frac{k_3}{k_3+k_4} \quad (6)$$

and

$$\Phi = \frac{k_2}{k_1+k_{1q}[O_2]+k_2}\cdot\frac{k_3+k_5[O_2]}{k_3+k_4+k_5[O_2]} \quad (7)$$

where $k_1 \gg k_2+k_{1q}[O_2]$, because of very small quantum yields for the reaction ($<10^{-2}$) and the lack of fluorescence and phosphorescence. From Eqs. (6) and (7), we obtain

$$\frac{\Phi}{\Phi_0} = \left(1+\frac{k_4}{k_3}\right)\left(\frac{k_3+k_5[O_2]}{k_3+k_4+k_5[O_2]}\right) \quad (8)$$

If $k_3+k_5[O_2] \gg k_4$, we have

$$\frac{\Phi-\Phi_0}{\Phi_0} = \frac{k_4}{k_3} \quad (9)$$

If the rate constants k_3 and k_4 have activation energies E_3 and E_4 and frequency factors A_3 and A_4 respectively, we get the following equation from (9).

$$\log\left(\frac{\Phi-\Phi_0}{\Phi_0}\right) = \log\left(\frac{A_4}{A_3}\right) - \frac{E_4-E_3}{2.3RT} \quad (10)$$

We have no exact data of the E_3 value. However, the value of the activation energy E_3 in the molecular dehydrogenation process is assumed to be smaller than that of E_4, considering a similar process in diphenylamines.[14] Figure 5 shows the plot of $\log\{(\Phi-\Phi_0)/\Phi_0\}$ as a function of T^{-1}. The reason why the plot is bent at about 285 K (Fig. 5) is due to the fact that the relation $k_3+k_5[O_2] \gg k_4$ does not hold at temperatures higher than 285 K where the value of k_4 becomes appreciable in comparison with that of k_3 and $k_5[O_2]$. From the slope of the plot ($T \leq 285$ K) in Fig. 5, we obtain $E_4 = E_3 + 4$ kcal/mol.

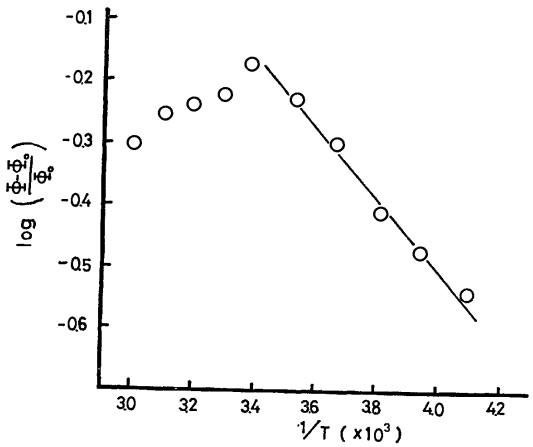

Fig. 5. Plot of $\log\{(\Phi-\Phi_0)/\Phi_0\}$ *vs.* T^{-1}

In the low temperature range ($213 \leq T \leq 285$ K), Eq. (7) is simplified as

$$\Phi = \frac{k_2}{k_1} \quad (7')$$

If the rate constant k_2 has an activation energy E_2 and frequency factor A_2, and the value of k_1 is almost constant in the temperatures ($213 \leq T \leq 285$ K), we obtain the following equation from Eq. 7'.

$$\log\Phi = \log\left(\frac{A_2}{k_1}\right) - \frac{E_2}{2.3RT} \quad (11)$$

Figure 6 shows the plots of $\log\Phi$ *vs.* T^{-1} and of $\log\Phi_0$ *vs.* T^{-1}.

From the slope of the plots, the value of E_2 can be estimated to be about 2 kcal mol^{-1} both in aerated and degassed solutions. This indicates that $k_3 \gg k_4$ in Eq. (6) at low temperatures, and the values of the quantum yields Φ in the aerated system become close to those in the degassed system with the fall of temperature (Fig. 4). Activation energy E_2 in the ring clousre process from S_1 to M is almost the same as that of *cis*-stilbene (2.6 kcal mol^{-1}).[9] MCP undergoes photocyclization to give the cyclized product even in the degassed system. However, in the case of *cis*-stilbene, dissolved oxidant is necessary to yield to corresponding photoproduct. The difference in their reactivities might be due to the intermediate structure: whether the *cis*-form or the *trans*-form of the two central hydrogen atoms in the intermediate would control the mole-

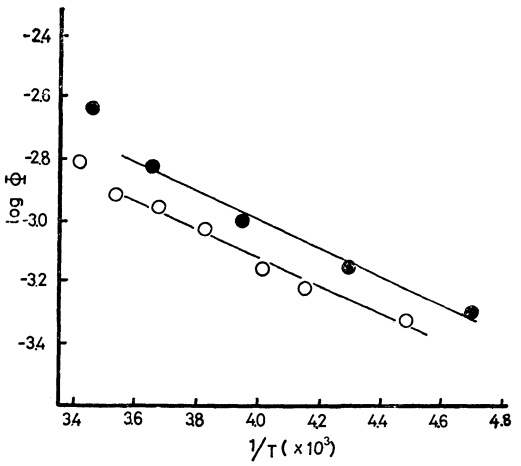

Fig. 6. Plot of $\log \Phi$ (or $\log \Phi_0$) *vs.* T^{-1}
○: $\log \Phi_0$, ●: $\log \Phi$.

cular dehydrogenation process (Eq. (3)). If the intermediate has a *cis*-form, it will thermally split into a cyclized product plus a hydrogen molecule. The photocyclization of MCP corresponds to this case, although we could not observe any transient by means of the conventional μs flash photolysis. It seems that the following structure is probable for the intermediate M.

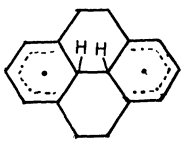

M

Radiationless deactivation (Eq. 1) is the main process in the excited singlet state of MCP, whose quantum yield is assumed to be ~0.99, on the basis of very low quantum yields for the product formation (>0.01) and the lack of fluorescence and phosphorescence. A small π-electronic interaction between the two benzene rings in the ground state is known, since the lowest transition in the molecule (λ_{max} 272 nm, $\varepsilon=4.4\times10^2$) corresponds to the $^1B_{2u}\leftarrow{}^1A_{1g}$ transition in benzene (λ_{max} 256 nm, $\varepsilon=2.2\times10^2$). It is obvious that the transannular interaction due to the proximity of two benzene rings in MCP causes the large radiationless deactivation and the very small ring-closure in the $S_1(\pi\pi^*)$ state. One explanation for the large deactivation is that the molecular structure of MCP probably promotes the internal conversion in Eq. (1), due to the vibronic coupling between S_1 and S_0 states. Another possibility is that a chemical energy wasting process such as reversible isomerization might be involved in Eq. 1, and responsible for the radiationless deactivation in S_1. The lifetime of S_1 is very short judging from the present results. A similar large radiationless deactivation is known in the case of biphenylene. Lack of photoluminescence of biphenylene has been observed,[18] the first singlet excited state being responsible for the main nonradiative channel on the basis of its lifetime (~10 ps).[19]

The abnormal shifts in the UV spectrum of [2.2] paracyclophane shows a large π-electronic interaction between the parallel planes of two benzene rings in the molecule.[20] An excimer fluorescence in [2.2]paracyclophane at 3550 Å indicates the charge transfer interaction in the emitting state.[4] The photochemical ring-opening reactions of [2.2]paracyclophane take place, which depend upon the excitation wavelengths.[5] The electronic and steric features in these isomers would cause the difference in photochemical and photophysical processes.

The proposed mechanism of the photocyclization of MCP in degassed and aerated cyclohexane is shown in Eqs. 0—5.

The authors wish to thank Dr. Takeo Sato, Tokyo Metropolitan University, for the supply of [2.2]metacyclophane and for valuable discussions.

Reference

1) This work was presented at the 24th Annual Meeting of the Chemical Society of Japan, Osaka, April, 1971.

2) Present address: Department of Physical Biochemistry, Institute of Endocrinology, Gunma University, Maebashi, Gunma.

3) Reviews: R. W. Griffin, Jr., *Chem. Rev.*, **63**, 45 (1963); T. Sato, *Kagaku no Ryoiki*, **23**, 672, 765 (1962); T. Sato *Nippon Kagaku Zasshi*, **92**, 277 (1971).

4) M. T. Vala, Jr., J. Haebig, and S. A. Rice, *J. Chem. Phys.*, **43**, 886 (1965).

5) R. C. Helgeson and D. J. Cram, *J. Amer. Chem. Soc.*, **88**, 509 (1966).

6) T. Sato, E. Yamada, Y. Okamura, T. Amada, and K. Hata, This Bulletin, **38**, 1049 (1969); T. Sato, M. Wakabayashi, S. Hayashi, and K. Hata, *ibid.*, **42**, 773 (1969).

7) S. Hayashi and T. Sato, *ibid.*, **45**, 2360 (1972).

8) F. B. Mallory, C. S. Wood, and J. T. Gordon, *J. Amer. Chem. Soc.*, **84**, 4361 (1962); *ibid.*, **85**, 828 (1963); *ibid.*, **86**, 3094 (1964); W. M. Moore, D. D. Morgan, F. R. Stermitz, *ibid.*, **85**, 829 (1963); G. S. Hammond, T. Saltiel, A. Lamola, N. J. Turro, J. S. Bradshow, D. O. Cowan, R. C. Counsell, V. Vogt, and C. Dalton, *ibid.*, **85**, 3197 (1964).

9) K. A. Muszkat and E. Fischer, *J. Chem. Soc., B*, 662 (1967).

10) E. J. Bowen and J. H. D. Eland, *Proc. Chem. Soc., London*, 202 (1963).

11) K. H. Grellmann, G. M. Sherman, and H. Linschitz, *J. Amer. Chem. Soc.*, **85**, 1881 (1963); H. Linschitz and K. H. Grellmann, *ibid.*, **86**, 303 (1964); E. W. Forster, K. H. Grellmann, and H. Linschitz, *ibid.*, **95**, 3108 (1973).

12) G. C. Terry, V. E. Uffindell, and F. W. Willetz, *Nature (London)*, **223**, 1050 (1969).

13) H. Shizuka, Y. Takayama, I. Tanaka, and T. Morita, *J. Amer. Chem. Soc.*, **92**, 7270 (1970).

14) H. Shizuka, Y. Takayama, T. Morita, and I. Tanaka, *ibid.*, **93**, 5987 (1971).

15) C. G. Hatchard and C. A. Parker, *Proc. Roy. Soc., Ser. A*, **235**, 518 (1956).

16) H. Shizuka, This Bulletin, **42**, 57 (1969).

17) H. Shizuka, K. Sorimachi, T. Morita, K. Nishiyama, and T. Sato, *ibid.*, **44**, 1983 (1971).

18) R. M. Hochstrasser and R. D. McApine, *J. Chem. Phys.*, **44**, 3325 (1966).

19) P. M. Rentzepis and C. J. Mitschele, *Anal. Chem.*, **42**, 20A (1970).

20) D. J. Cram, N. L. Allinger, and H. Steinberg, *J. Amer. Chem. Soc.*, **76**, 6132 (1954).
As for theoretical treatments of the spectra, see the following references: L. L. Ingraham, *J. Chem. Phys.*, **18**, 988 (1957); J. Koutecky and J. Paldus, *Tetrahedron*, **19**, Suppl. 2, 201 (1963); M. T. Vala, Jr., I. H. Hiller, S. A. Rice, and J. Jortner, *J. Chem. Phys.*, **44**, 23 (1966).

Photochemistry of the Electron Donor-Acceptor System. I. Exciplex Fluorescence and the Fluorescence of the Charge-Transfer Complex in the Aromatic Hydrocarbon–Fumaronitrile System

Yasuhiko SHIROTA, Isamu TSUSHI, and Hiroshi MIKAWA

Department of Applied Chemistry, Faculty of Engineering, Osaka University, Yamadakami, Suita, Osaka 565

(Received October 8, 1973)

The fluorescence of a series of aromatic hydrocarbons was quenched by the addition of fumaronitrile, which is consistent with the charge-transfer or electron-transfer mechanism. The fluorescence quenching was accompanied by the appearance of a new, broad structureless emission band attributed to the fluorescence from the exciplex in non-polar or slightly polar solvents. In highly polar solvents only quenching of the fluorescence occurred. The energies of the band maxima of the exciplex fluorescences and the magnitude of the ionization potentials of a series of fluorescers showed a good correlation with each other. Solvent and temperature dependence of the exciplex fluorescence was examined and discussed. The present aromatic hydrocarbon–fumaronitrile system also formed a charge-transfer complex in their ground states at relatively high concentrations of each component. The selective excitation of the ground state charge-transfer complex gave rise to the fluorescence emission in a fluid solution at room temperature at the same wavelength region as observed for the exciplex fluorescence. It was susgested that the electronic structure of the fluorescent state of the exciplex and the excited charge-transfer complex is the same.

Since the works by Leonhardt and Weller it has been established that the charge-transfer or electron-transfer process is an important mechanism for the quenching of fluorescence.[1] Detailed studies have since been made, particularly on the mechanism of the electron-transfer process in the excited state in relation to the fluorescence quenching.[2–4] Fluorescence quenching is often accompanied by the appearance of a new fluorescence emission attributed to the exciplex in non-poalr or weakly polar solvents, while in strongly polar solvents only quenching of the fluorescence takes place. The fluorescence emission from the exciplex has so far been observed mostly in the polynuclear aromatic hydrocarbons–aromatic amines systems, where the fluorescer acts as an electron acceptor and the quencher as an electron donor.[1,5,6] The opposite case in which the fluorescer acts as an electron donor and the quencher as an electron acceptor has also been observed in a few systems, *e.g.*, *N*,*N*-dimethyl-β-naphthylamine–methyl benzoate or dimethyl isophthalate systems[7] or *N*-vinylcarbazole–fumaronitrile or diethyl fumarate systems.[8] An examination of the effects of solvent and temperature on the exciplex fluorescence was expected to provide information on the electronic structure of exciplex. Studies from this viewpoint were made by Mataga *et al.*[5] and Beens *et al.*[6] in the polynuclear aromatic hydrocarbon–*N*,*N*-dialkylaniline system, and a dipolar nature of the exciplex with a large dipole moment of more than 10 D was indicated. However, only a few clear-cut experimental data are available.

We have found that the fluorescence of a series of aromatic hydrocarbons is quenched by the addition of fumaronitrile, the fluorescent exciplex being formed between the fluorescer which acts as an electron donor and the quencher which acts as an electron acceptor in non-polar or weakly polar solvents. The effects of solvent and temperature on the exciplex fluorescence were examined. It was found that the present aromatic hydrocarbon–fumaronitrile system shows a charge-transfer interaction in their ground states at a relatively high concentration of each component and that the excited charge-transfer complex formed by the selective excitation of the ground state charge-transfer complex emits the fluorescence in a fluid solution at room temperature. Observation of both the intermolecular exciplex fluorescence and the fluorescence of the charge-transfer complex in the same system enabled us to make a direct comparison of the electronic structures of the exciplex and the excited charge-transfer complex.

Experimental

Materials. Fumaronitrile (*trans*-1,2-dicyanoethylene) of pure grade was recrystallized three times from pure benzene, fractionally sublimed twice *in vacuo*, stored and vacuum-sublimed once more immediately before use. Extra pure grade naphthalene, phenanthrene, acenaphthene, fluorene and anthracene were recrystallized from methanol, chromatographed on an activated alumina column with benzene as an eluent, recrystallized from methanol several times, and then fractionally sublimed twice *in vacuo*. Pyrene of pure grade was recrystallized twice from ethanol and benzene, chromatographed on alumina and then silica gel columns, recrystallized from ethanol several times and then fractionally sublimed twice *in vacuo*. Benzene was purified and dried in the usual way, and then refluxed with metallic sodium for a long time, and distilled from it immediately before use. Chloroform and dichloromethane were shaken with concd. sulfuric acid, water, and 5% sodium hydroxide solution, and washed with water repeatedly, dried over calcium chloride, refluxed with calcium hydride and distilled from it immediately before use. Tetrahydrofuran and α-methyltetrahydrofuran were refluxed with solid potassium hydroxide for a long time, distilled from it, and again distilled from lithium aluminum hydride immediately before use. Acetonitrile was refluxed with phosphorus pentoxide for a long time and distilled twice from it, and then refluxed with anhydrous potassium carbonate and distilled twice from it immediately before use.

Apparatus and Measurements. The ultraviolet and visible absorption spectra were measured with a Hitachi 124 spectrophotometer. The fluorescence emission and excitation spectra were measured with a Hitachi MPF-3 spectrophotofluorometer equipped with a constant-temperature cell holder. Emission measurements were made at 77

and 196 K using a Pyrex tube of about 3.5 mm diameter in a quartz Dewar containing liquid nitrogen and dry ice-methanol, respectively, as a refrigerant. The system used for the measurement was not degassed.

Results and Discussion

The fluorescence of a series of aromatic hydrocarbons, *e.g.*, naphthalene, phenanthrene, fluorene, acenaphthene pyrene, and anthracene, was found to be quenched by the addition of fumaronitrile, new broad structureless fluorescence emissions being observed in non-polar or slightly polar solvents with maxima in the range 21100—17400 cm^{-1}. The intensity of the new emissions increased with quencher concentration with an isoemissive point in each system. The excitation spectra for the new fluorescence were the same as those for the fluorescence of the aromatic hydrocarbons, being in good agreement with the absorption spectra of the corresponding aromatic hydrocarbons. New emissions were, therefore, attributed to the fluorescence from the exciplexes formed between the excited singlet aromatic hydrocarbons which act as electron donors and the ground state fumaronitrile which acts as an electron

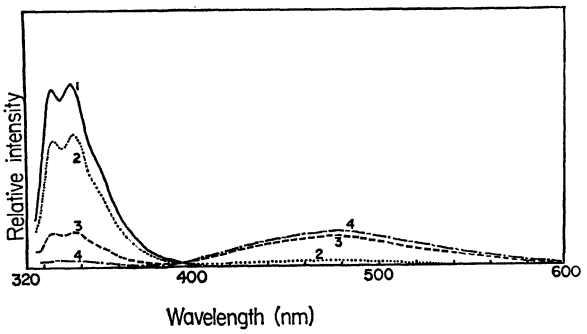

Fig. 1. Corrected fluorescence spectra of the naphthalene-fumaronitrile system in benzene at room temperature.
Excitation wavelength, 312 nm. [naphthalene]=3×10^{-3} M. [fumaronitrile]: 1)——0; 2)····· 1×10^{-3} M; 3)---- 1×10^{-2} M; 4)—·— 5×10^{-2} M.

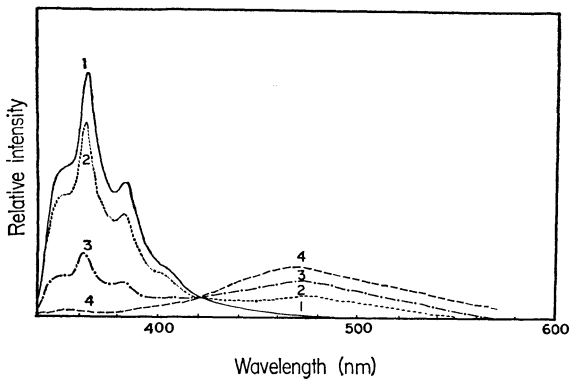

Fig. 2. Corrected fluorescence spectra of the phenanthrene-fumaronitrile system in benzene at room temperature.
Excitation wavelength, 331 nm. [phenanthrene]=3×10^{-3} M. [fumaronitrile]: 1)—— 0; 2)····· 1×10^{-3} M; 3)—·— 1×10^{-2} M; 4)---- 1×10^{-1} M.

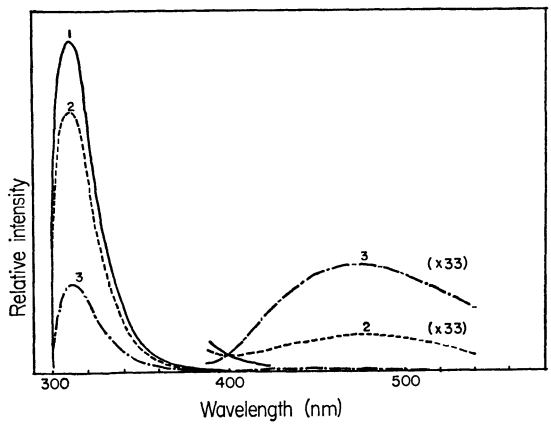

Fig. 3. Corrected fluorescence spectra of the fluorene-fumaronitrile system in benzene at room temperature.
Excitation wavelength, 301 nm. [fluorene]=1×10^{-4} M. [fumaronitrile]: 1)—— 0; 2)---- 1×10^{-3} M; 3)—·— 1×10^{-2} M.

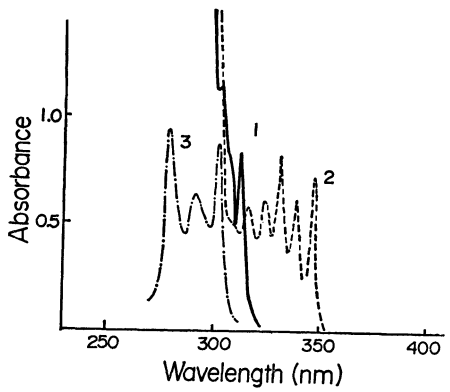

Fig. 4. The absorption spectra of naphthalene, phenanthrene, and fluorene.
Solvent, tetrahydrofuran, 1)—— naphthalene (3×10^{-3} M); 2)---- phenanthrene (3×10^{-3} M); 3)—·— fluorene (1×10^{-4} M).

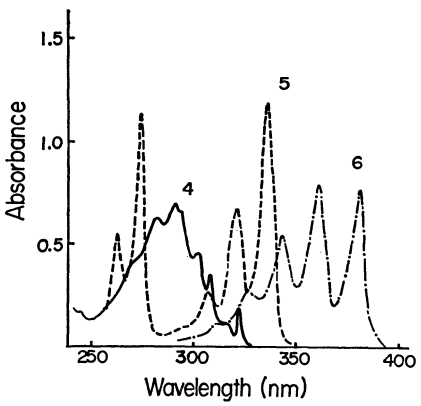

Fig. 5. The absorption spectra of acenaphthene, pyrene, and anthracene.
Solvent, tetrahydrofuran, 4)—— acenaphthene (1×10^{-4} M); 5)---- pyrene (1×10^{-5} M); 6)—·— anthracene (1×10^{-4} M).

Table 1. Wave numbers (cm^{-1}) of the band maxima of the exciplex fluorescence emission in the aromatic hydrocarbon–fumaronitrile system measured in solvents of different polarity at room temperature[a)]

Aromatic hydrocarbon	I_p(eV)[b)]	Solvent (dielectric constant)				
		Benzene (2.27)	$CHCl_3$ (4.70)	THF (7.39)	CH_2Cl_2 (8.90)	CH_3CN (37.5)
Naphthalene	8.10	21,100 (22,200)	20,200 (21,500)	20,000 (21,300)	18,900 (20,800)	—[c)]
Phenanthrene	8.09	21,100 (22,200)	19,800 (20,800)	19,600 (20,800)	18,700 (20,400)	—[c)]
Fluorene	7.99	20,800 (22,200)	19,800 (20,800)	19,400 (20,600)	18,700 (20,200)	—[c)]
Acenaphthene	7.66	19,000 (20,600)	18,500 (19,200)	18,300 (19,000)	—[c)]	—[c)]
Pyrene	7.55	18,700 (19,800)	17,900 (18,500)	17,700 (18,300)	—[c)]	—[c)]
Anthracene	7.40	18,000 (19,200)	17,400 (18,200)	—[c)]	—[c)]	—[c)]

a) Corrected values within $\pm 200\,cm^{-1}$ errors; non-corrected values in parentheses. b) Ionization potential determined from the charge-transfer absorption band.[14a)] c) No exciplex fluorescence emission detected.

acceptor. The corrected fluorescence emission spectra of a few aromatic hydrocarbon–fumaronitrile systems measured in benzene are shown in Figs. 1—3. The emissivity of the exciplex formed in the anthracene–fumaronitrile system was much weaker than that in other systems. The absorption spectra of a series of aromatic hydrocarbons (concentration was the same as that for the measurement of fluorescence emission) are shown in Figs. 4 and 5.

Appearance of the exciplex fluorescence depends on the magnitude of the ionization potential of the aromatic hydrocarbon as well as solvent polarity. Thus, as the polarity of the solvent increased from benzene (dielectric constant 2.27 at 25 °C) to dichloromethane (dielectric constant 8.9 at 25 °C), the exciplex fluorescence was no longer observed with respect to acenaphthene, pyrene and anthracene which possess relatively low ionization potentials (Table 1). In strongly polar solvent like acetonitrile (dielectric constant 37.5 at 20 °C) no exciplex fluorescence was detected, only quenching of the fluorescence of the aromatic hydrocarbon occurring. The wave number of the exciplex fluorescence maximum became smaller with the decrease of the ionization potential of the electron donor. A nearly linear relationship was found between the energies corresponding to the exciplex fluorescence maxima and the magnitude of the ionization potentials of a series of electron donors (Fig. 6).

A remarkable effect of solvent polarity was observed on the exciplex fluorescence maximum. With the increase in the polarity of solvent, the exciplex fluorescence maximum shifted toward the red region accompanied by the decrease in the emission intensity, and the energies corresponding to the exciplex fluorescence maxima were roughly correlated with the static dielectric constant of the solvent (Table 1 and Fig. 7). As the temperature was lowered from 298 K to 196 K, the exciplex fluorescence maximum also showed a red shift accompanied by the decrease in the exciplex fluorescence intensity and the increase in the fluorescence

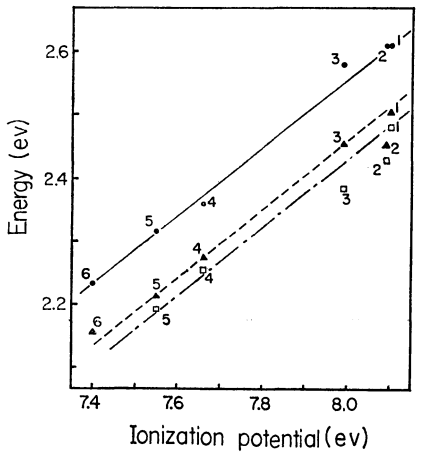

Fig. 6. Correlation between the energy of the exciplex fluorescence maximum in the aromatic hydrocarbon-fumaronitrile system and the ionization potential of the aromatic hydrocarbon in solvents of different polarity.
Solvent: —— benzene; ---- chloroform; —·— tetrahydrofuran.
1 naphthalene; 2 phenanthrene; 3 fluorene; 4 acenaphthene; 5 pyrene; 6 anthracene.

intensity of the aromatic hydrocarbon (Table 2). In α-methyltetrahydrofuran matrix at 77 K neither the production of the exciplex fluorescence emission nor the quenching of the fluorescence of the aromatic hydrocarbon occurred.[9,10)]

The Stern-Volmer plots of F_0/F against the concentration of the quencher were linear up to *ca.* 5×10^{-2} M concentration of the quencher, where F_0 and F represent the fluorescence intensity of the aromatic hydrocarbon in the absence and presence of the quencher, respectively. When the concentration of the quencher exceeded *ca.* 5×10^{-2} M, the plots deviated upward from the linear relation in all the systems except anthracene probably due to the occurrence of the photoabsorption

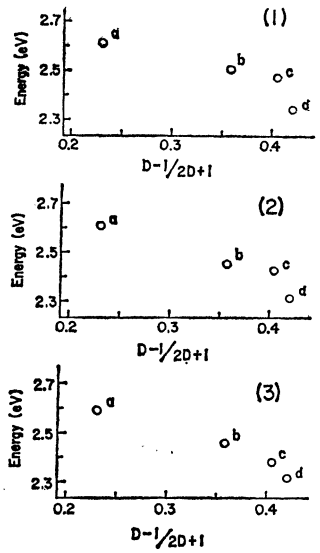

Fig. 7. Correlation between the energy of the exciplex fluorescence maximum in the aromatic hydrocarbon-fumaronitrile system and the dielectric constant of the solvent. (1) naphthalene-fumaronitrile system; (2) phenanthrene-fumaronitrile system; (3) fluorene-fumaronitrile system. a benzene; b chloroform; c tetrahydrofuran; d dichloromethane.

TABLE 2. WAVE NUMBERS (cm^{-1}) OF THE BAND MAXIMA OF THE EXCIPLEX FLUORESCENCE EMISSION IN THE AROMATIC HYDROCARBON–FUMARONITRILE SYSTEM MEASURED IN α-METHYLTETRAHYDROFURAN AT 298, 196, AND 77 K[a)]

Aromatic hydrocarbon	Temperature		
	298 K	196 K	77 K
Naphthalene	20,000	18,500	—[b)]
Phenanthrene	19,600	18,500	—[b)]
Fluorene	19,600	18,200	—[b)]
Acenaphthene	18,300	17,700	—[b)]
Pyrene	18,000	17,200	—[b)]
Anthracene	—[b)]	—[b)]	—[b)]

a) Corrected values within $\pm 200\ cm^{-1}$ errors. b) No exciplex emission detected.

TABLE 3. QUENCHING CONSTANTS AND APPROXIMATE QUENCHING RATE CONSTANTS OF THE FLUORESCENCE OF AROMATIC HYDROCARBONS BY FUMARONITRILE IN BENZENE AT 298 K

Aromatic hydrocarbon	(τ_0)[a)]	Quenching constant (M^{-1})	Quenching rate constant ($M^{-1}s^{-1}$)
Phenanthrene	(60)	185	3.1×10^9
Acenaphthene	(46)	269	5.9×10^9
Pyrene	(~400)	329	8.2×10^8
Anthracene	(4.1)	64	15.5×10^9

a) Fluorescence lifetime (nano second) of the aromatic hydrocarbon.[14b)]

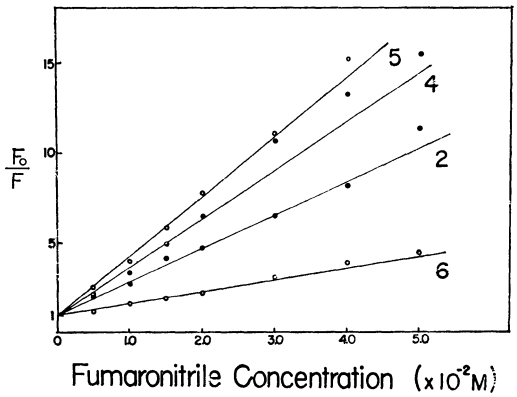

Fig. 8. Stern-Volmer plots of F_0/F against the quencher concentration measured in benzene at 298 K.
2 phenanthrene-fumaronitrile system; 4 acenaphthene-fumaronitrile system; 5 pyrene-fumaronitrile system; 6 anthracene-fumaronitrile system.

by the quencher molecule, since the tail absorption band of fumaronitrile of the concentration above *ca.* 5×10^{-2} M covers the wavelength of the exciting light. This tendency was conspicuous with respect to naphthalene and fluorene since excitation was carried out at a shorter wavelength than with the other aromatic hydrocarbon systems, the deviation occurring at the quencher concentration below 5×10^{-2} M. Some results are shown in Fig. 8. The quenching constants obtained from the slope of the Stern-Volmer plots and the approximate quenching rate constants γk_1 ($\gamma=k_3/(k_2+k_3)$ in Scheme 1) at 298 K in benzene calculated by using the known values of τ_0 (fluorescence lifetime) are summarized in Table 3.

The features of the fluorescence quenching of a series of aromatic hydrocarbons by fumaronitrile are consistent with the charge-transfer or electron-transfer mechanism in the excited state. The present results led to the following conclusions on the exciplex, which are essentially in good agreement with the conception as regards the exciplex formed in the aromatic hydrocarbon–aromatic amine system.[5,6,11)] (a) The exciplex which is stable only in the excited state is produced by the molecular motion of the electron donor and acceptor molecules during the lifetime of the excited state of the fluorescer (here the excited singlet state). Thus, no exciplex formation takes place in the rigid matrix at 77 K in which the molecular motion is restricted. (b) Just as the energies of the exciplex fluorescence maxima are correlated with the magnitude of the electron affinities of the aromatic hydrocarbons for a given aromatic amine,[6b,11)] they are correlated with the magnitude of the ionization potentials of the aromatic hydrocarbons in the present systems where the fluorescers act as electron donors. (c) The electronic structure of the exciplex in the equilibrium state is very polar, and the orientation of the solvent molecules takes place during the lifetime of the exciplex. The red shift of the exciplex fluorescence maximum observed when the temperature is lowered may be explained to be due to the increase in the polarity of the solvent at low temperatures. (d) It is suggested that as the solvent polarity increases the exciplex dis-

sociates into ions to produce solvated ion pairs with no emissivity, and that in strongly polar solvents the electron transfer occurs from the encounter complex.[2-4]

The present aromatic hydrocarbons–fumaronitrile systems also showed a weak charge-transfer interaction in their ground states at relatively high concentrations of each component (*ca.* 10^{-1} M or above), as evidenced from the electronic absorption spectra. Although no distinct charge-transfer bands separated from the component absorptions were observed, the absorption spectra of the aromatic hydrocarbons–furmaronitrile systems shifted to the red region as compared with the sum of the absorptions of each component of the same concentration. It was found that selective excitation of the ground state charge-transfer complex gave rise to the fluorescence emission in a non-polar fluid solution at room temperature in the same wavelength region as observed for the exciplex fluorescence. As an example, the absorption and the fluorescence emission spectra of the charge-transfer complex in the acenaphthene–fumaronitrile system measured at 298 K are shown in Fig. 9. The result is consistent with the known characteristic features of the fluorescence of the charge-transfer complex, *viz.*, a large Stokes shift is observed in a room temperature fluorescence in a fluid solution (the maximum wavelength of the charge-transfer absorption band is shorter than 400 nm). That the emission is not the exciplex fluorescence produced by the local excitation of the tail band of the aromatic hydrocarbon, but the so-called charge-transfer fluorescence from the excited charge-transfer complex, was further confirmed by the measurement at 77 K where no exciplex fluorescence was produced. The fluorescence emission was likewise observed at 77 K by the selective excitation of the ground state charge-transfer complex,

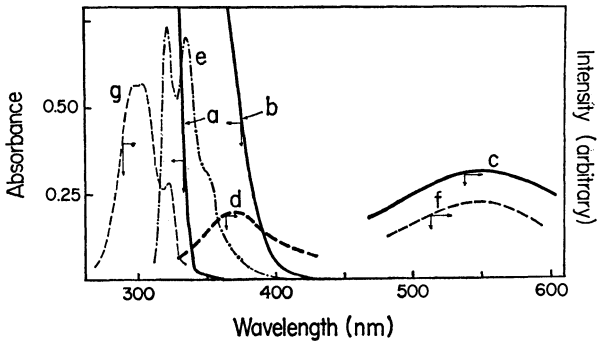

Fig. 9. The absorption and fluorescence emission and excitation spectra of the acenaphthene-fumaronitrile charge-transfer complex measured in α-methyltetrahydrofuran at 298 K. (a) absorption spectrum of acenaphthene(0.1 M); (b) absorption spectrum of the acenaphthene(0.1 M)-fumaronitrile(0.1 M) system; (c) the fluorescence spectrum of the charge-transfer complex produced by the excitation in the charge-transfer band at 370 nm in the above system; (d) excitation spectrum for the charge-transfer fluorescence(c); (e,f) fluorescence spectrum of acenaphthene and exciplex fluorescence spectrum produced by the excitation of acenaphthene (1×10^{-4} M) at 321 nm in the presence of fumaronitrile (2.5×10^{-2} M). (g) excitation spectrum for the fluorescence emissions (e) and (f).

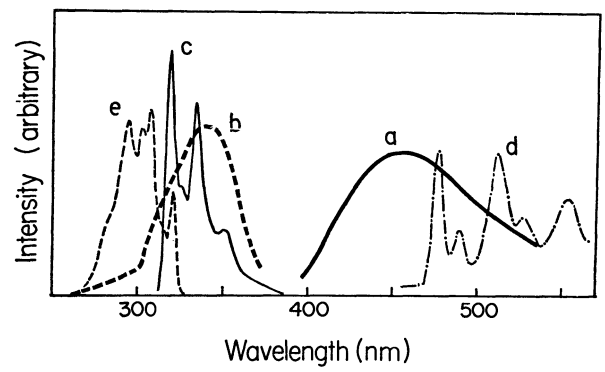

Fig. 10. The charge-transfer fluorescence and excitation spectra of the acenaphthene-fumaronitrile charge-transfer complex measured in α-methyltetrahydrofuran at 77 K. (a) the fluorescence spectrum of the charge-transfer complex produced by the excitation in the charge-transfer band at 370 nm in the acenaphthene-(0.1 M)-fumaronitrile(0.1 M) system; (b) excitation spectrum for the charge-transfer fluorescence (a); (c) fluorescence spectrum of acenaphthene produced by the excitation of acenaphthene (1×10^{-4} M) at 321 nm in the presence of fumaronitrile (2.5×10^{-2} M); (d) phosphorescence spectrum of acenaphthene produced simultaneously with the fluorescence (c); (e) excitation spectrum for the emissions (c) and (d).

but at a shorter wavelength than that observed at 298 K (Fig. 10). This is understandable since the fluorescence in a rigid medium takes place from the lowest point reached from the excited Franck-Condon state and the fluorescence in a fluid solution from the excited equilibrium state, which is stabilized due to the reorientation of the solute and the solvent molecules.[12d] Measurement of the correct excitation spectrum was difficult due to the effect of the reabsorption of the emission. The fluorescence of the charge-transfer complex was also dependent on the polarity of the solvent: the fluorescence wavelength maximum shifted to the red region accompanied by the decrease in the emission intensity as the polarity of the solvent increased; no fluorescence emission was detected in a strongly polar solvent such as acetonitrile. Observation of a room temperature fluorescence of a charge-transfer complex in a fluid solution has so far been reported only in a few systems.[11,12] Hardley any examples bave been reported except the *s*-tetracyanobenzene–α-methylstyrene system[13] in which both the exciplex fluorescence and the fluorescence of the charge-transfer complex stable in the ground state are observed in the same system. A direct comparison of the exciplex fluorescence and the charge-transfer fluorescence emissions in the same system enabled us to obtain information on the comparable electronic structure or the geometry of the exciplex and the excited charge-transfer complex. In the *s*-tetracyanobenzene–α-methylstyrene system the fluorescence from the excited charge-transfer complex, very weak in its intensity, appears at a different wavelength from the exciplex fluorescence, and different geometries have been suggested for the exciplex and the excited charge-transfer complex. The present result in which the exciplex fluorescence and the charge-

transfer fluorescence emissions were observed at the same wavelength region in a few solvents of different polarity suggests that the electronic structure of the fluorescent state of the exciplex and the excited charge-transfer complex is the same. We have also obtained the same result in the *N*-vinylcarbazole–fumaronitrile system.[8] The photochemical primary processes of the aromatic hydrocarbon–fumaronitrile system are shown in Scheme 1.

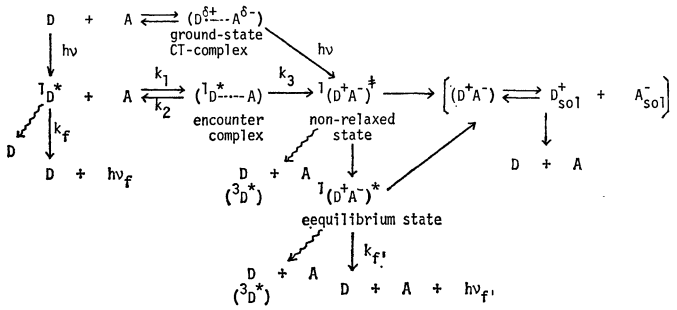

Scheme 1. The photochemical primary processes in the aromatic hydrocarbon-fumaronitrile system.

References

1) H. Leonhardt and A. Weller, *Z. Phys. Chem. N. F.*, **29**, 277 (1961); *Ber. Bunsenges. Phys. Chem.*, **67**, 791 (1963).

2) a) H. Knibbe, K. Rollig, F. P. Schaffer, and A. Weller, *J. Chem. Phys.*, **47**, 1184 (1967). b) H. Knibbe, D. Rehm, and A. Weller, *Ber. Bunsenges. Phys. Chem.*, **72**, 257 (1968).

3) a) N. Mataga, K. Ezumi, and K. Takahashi, *Z. Phys. Chem. N. F.*, **44**, 250 (1965). b) T. Okada, H. Ohari, and N. Mataga, This Bulletin, **43**, 2750 (1970). c) Y. Taniguchi, Y. Nishina, and N. Mataga, *ibid.*, **45**, 764 (1972).

4) H. Yamashita, H. Kokubun, and M. Koizumi, *ibid.*, **41**, 2312 (1968).

5) a) N. Mataga, K. Ezumi, and T. Okada, *Mol. Phys.*, **10**, 201 (1966). b) N. Mataga, T. Okada, and K. Ezumi, *ibid.*, **10**, 203 (1966). c) N. Mataga, T. Okada, and N. Yamamoto, This Bulletin, **39**, 2562 (1966). d) N. Mataga, T. Okada, and H. Ohari, *ibid.*, **39**, 2563 (1966).

6) a) H. Beens, H. Knibbe, and A. Weller, *J. Chem. Phys.*, **47**, 1183 (1967). b) D. Rehm and A. Weller, *Z. Phys. Chem. N. F.*, **69**, 183 (1970).

7) K. Kaneta and M. Koizumi, This Bulletin, **40**, 2254 (1967).

8) K. Tada, Y. Shirota, and H. Mikawa, *J. Poly. Sci, Part B*, **10**, 691 (1972).

9) The phosphorescence emission of each aromatic hydrocarbon was observed at 77 K.

10) Concerning the temperature effect on the exciplex fluorescence, it has been reported that in the pyrene-aromtic amine system the exciplex fluorescence is observed even in the rigid matrix owing to the very long lifetime of the fluorescence state of pyrene.[5a,d]

11) N. Mataga and Y. Murata, *J. Amer. Chem. Soc.*, **91**, 3144 (1969).

12) a) H. M. Rosenberg and E. C. Eimutis, *J. Phys. Chem.*, **70**, 3494 (1966). b) G. D. Short and C. A. Parker, *Spectrochim. Acta*, **23A**, 2487 (1967). c) J. Prochroow and R. Siegoczynski, *Chem. Phys. Lett.*, **3**, 635 (1969). d) T. Kobayashi, K. Yoshihara, and S. Nagakura, This Bulletin, **44**, 2603 (1971).

13) M. Irie, S. Tomimoto, and K. Hayashi, *J. Phys. Chem.*, **76**, 1419 (1972).

14) (a) J. B. Birks, "Photophysics of Aromatic Molecules," Wiley-Interscience (1969), p. 475. (b) *ibid.*, p. 122.

The Gas Chromatographic Determination of Selenium in Plant Material with 4-Nitro-*o*-phenylenediamine

Yasuaki SHIMOISHI*

Department of Chemistry, Faculty of Science, Okayama University, Tsushima, Okayama-shi 700

(Received July 16, 1973)

Selenium(IV) reacts with 4-nitro-*o*-phenylenediamine to form 5-nitropiaselenol, which is detected by means of a gas chromatograph equipped with an electron-capture detector. By this highly sensitive method, the determination of very small amounts of selenium in plant materials has been investigated. Fuming nitric acid digests the plant sample completely, and the selenium is converted to the quadrivalent state. No loss of selenium can be found by this treatment. A method is proposed for the determination of selenium in plant materials at levels as low as 0.005 μg/g in dried material.

In earlier studies of the determination of selenium contained in plant material, the interest of research workers has been directed toward the investigation of selenium toxicity for farm animals. In these studies, it was enough that the method could determine only the ppm levels of selenium in dried samples.

Recently, many investigators have demonstrated that selenium is an important micronutrient for farm animals. Scott[1] and Kubota *et al.*[2] have pointed out that the critical level for the deficiency of selenium for farm animal diets is 0.01—0.04 ppm. Therefore, it is necessary to have a method of analysis to determine amounts of selenium as low as 0.01 ppm with reasonable accuracy and reproducibility. To fulfill these requirements, a fluorometric method involving the use of 3,3′-diaminobenzidine[3,4] or 2,3-diaminonaphthalene[5,6] has been widely used in studies of animal nutrition. The neutron-activation[7] and isotope-dilution methods[8] have also been used to check the former method.

On the other hand, it is important to digest the plant material without any loss of selenium, because selenium is volatile. By the low-temperature ashing method, selenium could not be recovered completely.[9] In the oxygen-flask combustion method, selenium is obtained as an elemental state with a small amount of charred tissues in the platinum vessel, and the residue could not be dissolved completely by a bromine-bromide solution. Thus, the wet-digestion method was employed in the following experiments.

The author has recently proposed a far more sensitive method for determining selenium in pure sulfuric acid,[10] pure tellurium,[11] and sea water[12] by means of a gas chromatograph equipped with an electron-capture detector using 4-nitro-*o*-phenylenediamine. The present paper will describe an investigation of the determination of very small amounts of selenium in plant material.

Materials and Method

Reagents. 4-nitro-*o*-phenylenediamine hydrochloride solution: 1 g of the reagent was dissolved in 100 ml of 1 M hydrochloric acid. This solution is so stable that the solution can be used after standing for more than 1 week at room temperature.

Selenium(IV) stock solution: 351.3 mg of selenium dioxide was dissolved in 250 ml of distilled water (1 mg Se/ml). Working solutions were prepared by dilution. Selenium(0) stock solution: About 5 mg of elemental selenium was dissolved in 50 ml of carbon disulfide. The concentration is determined by gas chromatography[10] as 90 μg/ml. Working solutions were prepared by dilution. 7.5 M Hydrochloric acid solution: The acid solution was prepared each time before washing the toluene extract. The other reagents were of an analytical reagent grade.

Apparatus. A Shimadzu Model GC-3AE gas chromatograph equipped with an electron-capture detector was used. A glass column (1 m long, 4 mm bore) was packed with 15% SE-30 on 60—80 mesh Chromosorb W. The column and the detector temperature were maintained at 200 °C. The nitrogen flow-rate was 53 ml/min. A Shimadzu Model 250A recorder was used at a chart speed of 5 mm/min.

Standard Procedure. The whole digestion procedure must be carried out in a fume hood with an efficient extractor fan.

A tenth to 1 g portions of dried samples are put into a 100-ml conical flask. 5 ml of fuming nitric acid is added, and the mixture is heated on a sand bath (130—140 °C) in a fume hood. Vigorous oxidation reactions take place soon thereafter, and a copious brown vapor is evolved. After a few minutes, the main reaction comes to an end and the solution soon becomes clear (a few suspended particle of silicate are often observed). The solution is then heated further with frequent shaking until the white solid separates off and the volume is reduced to about 0.1—0.2 ml. During this procedure the temperature of the sand bath must be raised to 170—180 °C and maintained until the digestion is finished. At this time, if any charred material appears, erroneous results may be obtained. Therefore, special care has to be exercised to prevent the formation of a charred material by frequent shaking. If more than 0.5 g of a plant sample is needed for the determination, the digestion is not complete with the use of 5 ml of fuming nitric acid. Consequently, another 5 ml of fuming nitric acid is added and the digestion procedure has to be repeated. Digestion is usually completed by heating for about 1.5 hr. The flask is then removed and allowed to stand for 3 min. After redissolving the precipitate with 10 ml of distilled water, 2 ml of 1 M urea is added and the mixture is heated on the sand bath for 10 min to decompose the oxides of nitrogen. After cooling, the content is transferred into a 100-ml separatory funnel and the flask is rinsed with 10 ml of distilled water into the funnel. When the selenium content was too much, an aliquot containing 0.01—0.1 μg of selenium was used. Five ml of concentrated hydrochloric acid and 5 ml of toluene are added, and the toluene-soluble material is extracted with vigorous shaking for 5 min.

* Present address: School for X-ray Technicians, Faculty of Medicine, Okayama University, Shikatacho, Okayama-shi.

After standing for 2 hr, the aqueous phase is transferred into another 100-ml separatory funnel, and the initial separatory funnel is rinsed with 10 ml of distilled water into the latter. The color of the solution is pale yellow or colorless. Two milliliters of a 1% 4-nitro-*o*-phenylenediamine solution are added, and the solution is allowed to stand for 2 hr. Then, the 5-nitropiaselenol formed is extracted into 1 ml of toluene by shaking for 5 min; the toluene extract is washed, first with 5 ml of 0.2 M sodium hydroxide and subsequently with 2 ml of 7.5 M hydrochloric acid, by shaking for a minute. Five microliters of the toluene extract are injected into the gas chromatograph and the peak height is measured.

Results and Discussion

Digestion of the Plant Material. A mixture of nitric and sulfuric acids or nitric and perchloric acids is usually used in the digestion method. Gorsuch[13] suggested in his detailed study that a considerable loss of selenium at the 1 ppm level was found when using the former mixture, whereas he obtained a 100% recovery with the latter one. In recent publications, when the digestion mixture containing a catalyst such as dichromate,[14] molybdate[15] or vanadate[16] was used, vigorous bumping was observed in the reactions.

Hall and Gupta[6] used nitric acid, hydrogen peroxide, and perchloric acid in the digestion of the plant samples. They stated that the selenium loss often occurred when the temperature rose too far as a result of the use of perchloric acid. Moreover, when the plant sample was digested with only fuming nitric acid or a mixed solution of fuming nitric and perchloric acids, the recovery of the above two methods showed the same value. Thus, fuming nitric acid was used for the digestion of the plant material.

0.2 g filter paper (Toyo Roshi No. 5B) was impregnated with carbon disulfide containing 0.045 μg elemental selenium and then dried. The filter paper was digested by various amounts of fuming nitric acid. On the other hand, the same filter paper and a 0.2 g stem of wheat containing less than 0.005 μg/g selenium were digested together. Figure 1 shows that more than 4 ml of fuming nitric acid can digest the filter paper and stem of wheat completely, and a good recovery is observed.

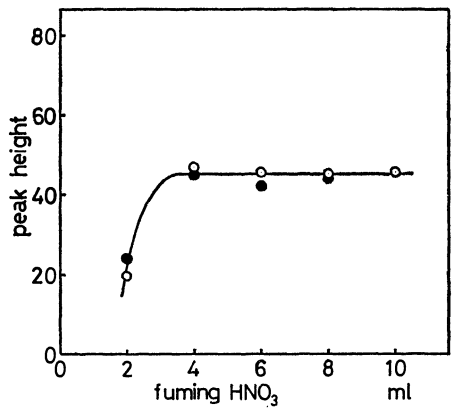

Fig. 1. Effect of the volume of fuming nitric acid.
-○- 0·045 μg selenium(0) permeated in filter paper
-●- 0.045 μg selenium(0) + 0.2 g stem of wheat (selenium content below 0.005 μg/g)

Five ml of fuming nitric acid digest 0.2 g filter paper containing 0.027 μg selenium and a wheat stem which contains less than 0.005 μg Se/g. When a larger amount of wheat is to be digested, the digestion is repeated by the use of another five ml of fuming nitric acid. If charred materials do not appear during the digestion, the determination may be undertaken. The results are shown in Fig. 2. When more than 0.5 g of a sample is digested by 5 ml of fuming nitric acid, the background of gas chromatogram becomes larger. However, this trouble is overcome by further digestion with 5 ml of fuming nitric acid without any loss of selenium.

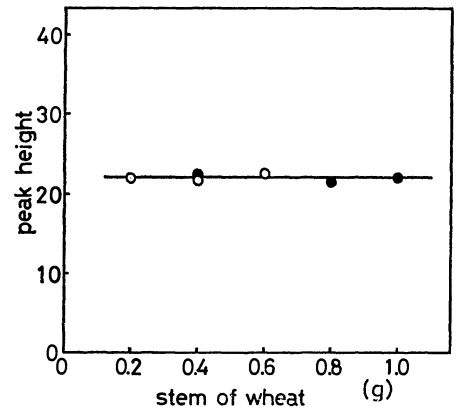

Fig. 2. The amount of the plant sample digested by 5 ml of fuming nitric acid.
-○- 0.027 μg selenium(0) + stem of wheat (selenium content below 0.005 μg/g) digested by 5 ml of fuming nitric acid.
-●- the same sample digested twice another 5 ml of fuming nitric acid

The digestion temperature is examined by the use of 0.2 g filter paper containing 0.045 μg of elemental selenium at 100—110, 160—180, and 210—220 °C (sand bath temperature). At 100—110 °C, the digestion is not enough, and at 210—220 °C the sample is sometimes charred, at which time selenium is lost. When a sample is heated at 160—180 °C for 80 min, digestion is complete. The heating is continued at this temperature till the volume of the digestion liquid reaches 0.1—0.2 ml; the smaller the volume of the liquid is, the better the result becomes. The whole digestion requires about one and half an hour.

In the digestion procedure, a small amount of undecomposed materials such as hydrocarbon constituents remains unchanged; it should be removed before gas chromatography. Five milliliters of toluene are used to eliminate any interfering substances. Selenium is not transferred into toluene by this procedure. Though a major part of the toluene-soluble substances can be eliminated by this treatment, the very small amount of interfering substances remaining disturbs the determination, because the sensitivity of the electron-capture detector is extremely high for the unknown impurities as well as for 5-nitropiaselenol. Thus, 1 ml of the toluene extract after the formation of 5-nitro-

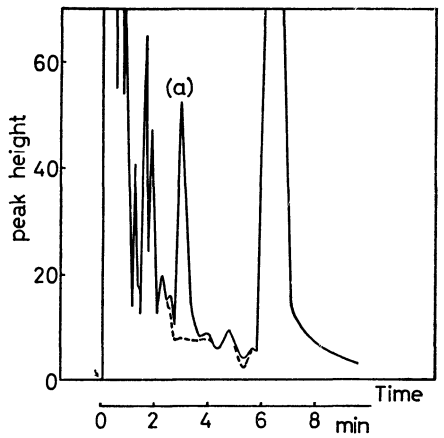

Fig. 3. Gas chromatogram of 5-nitropiaselenol.
---- 0.2 g stem of wheat.
—— 0.2 g stem of wheat + 0.045 μg selenium(0)
(a) 5-nitropiaselenol
Column: 15% SE-30/Chromosorb W, Carrier gas: N_2 (53 ml/min), Temperature: 200 °C, Range: 0.1 V, Sample: 5 μl.

piaselenol should be washed again with 5 ml of 0.2 M sodium hydroxide and then 2 ml of 7.5 M hydrochloric acid. Figure 3 shows the ECD gas chromatogram obtained by the use of the above-mentioned procedure.

Recovery Test. The recovery test by the standard procedure is carried out by the use of two samples: one is a mixed sample of 0.2 g filter paper containing 0.045 μg elemental selenium and 0.2 g of wheat stem which contains less than 0.005 μg Se/g, while the other is foliage leaves of wheat cultivated in a pot. The results, shown in Tables 1 and 2, indicate that fairly good results are obtained by this procedure.

Table 1. Recovery of the selenium added to stem of wheat

Stem of wheat[a] (g)	Added selenium(0) (μg)	Peak height	Selenium determined (μg)	Recovery (%)
0.200	none	2.0	0	
0.200	0.045	41.0	0.043	96
0.200	0.045	45.0	0.047	104
0.200	0.045	42.0	0.044	98
0.200	0.045	44.0	0.046	102

a) Containing less than 0.005 μg Se/g.

Table 2. Reproducibility of selenium in foliage of wheat

Foliage of wheat[a] (g)	Added selenium (μg)	Peak height	Selenium determined (μg/g)
0.200		3.5	0.020
0.200		4.5	0.025
0.500		12.0	0.026
0.500		12.0	0.026
0.500	0.027	35.0	0.024

a) Cultivated in the pot which contains the soil added no selenium.

Selenium(VI) in Plant. The oxidation number of the selenium contained in the plant sample should be −2, 0, or +4. The selenium in these oxidation states can be determined by the above-mentioned procedure. If selenium(VI) is present in the plant, it cannot be determined by the standard procedure as it stands. If selenium(VI) was contained in the plant, it would be reduced to the IV state by heating with 4 M hydrochloric acid on a sand bath for 10 min at about 100 °C, after the addition of 1 M urea to decompose oxides of nitrogen. By this procedure, selenium of the VI state could not be detected in the samples used in the experiment.

Effect of Chloride Ion. No loss of selenium was found during the reduction of selenium(VI) with 4 M hydrochloric acid for 10 min at about 100 °C. When the chloride ion is present together with selenium for a long digestion at 160—180 °C, selenium(VI) volatilizes to form its chloride. Even if the digestion procedure is carried out in the presence of 10 mg of sodium chloride, no loss of selenium is found.

Calibration Curves. The calibration curves are made by the use of four standard samples. The first is made from an acidic solution containing a known amount of selenium(IV). The second is prepared by treating filter paper containing selenium(IV) by the standard procedure. The third is made from filter paper containing elemental selenium. The fourth is made from a mixed sample of filter paper containing a known amount of elemental selenium and a wheat stem containing no selenium. The curves obtained are shown in Fig. 4. These are quite consistent with each other. This fact also shows that no loss of selenium is found in the standard procedure adopted.

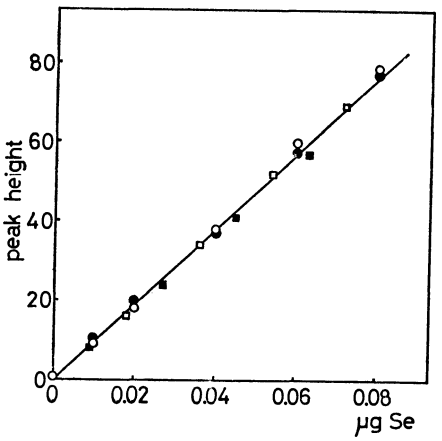

Fig. 4. Calibration curve.
-○- selenium(IV) in hydrochloric acid (no digestion)
-●- selenium(IV) permeated in filter paper
-⊟- selenium(0) permeated in filter paper
-■- selenium(0) + 0.2 g of stem of wheat (selenium content below 0.005 μg/g)

Determination of Selenium in Plant Material. The determination of the selenium involved in the plant material was carried out for cabbage, Chinese cabbage, wheat, and rice plants. The cabbages and Chinese cabbages were harvested from an ordinary field. The wheats and rice plants were obtained as follows: a seed-

TABLE 3. SELENIUM CONTENT OF PLANT MATERIALS

		Selenium content in soil[a] (ppm)	Plant sample (g)	Selenium added (μg)	Dilution	Selenium determined (μg)	Selenium content (μg/g)
Cabbage	Foliage	none	0.500			0	<0.005
		none	0.500			0	<0.005
		none	1.000			0	<0.005
		none	1.000	0.027		0.026	<0.005
	Average						<0.005
Chinese	Foliage	none	0.500			0.005	0.010
Cabbage		none	0.500			0.009	0.018
		none	0.500	0.027		0.026	<0.005
		none	1.000			0.004	0.004
		none	1.000			0.004	0.004
		none	1.000	0.027		0.024	<0.005
	Average						0.006
Wheat	Stem	none	0.400			0	<0.005
		none	0.400			0	<0.005
		none	0.800	0.027		0.025	<0.005
		none	1.000	0.027		0.026	<0.005
	Average						<0.005
	Foliage	none	0.200			0.004	0.020
		none	0.200			0.005	0.025
		none	0.500			0.013	0.026
		none	0.500			0.013	0.026
		none	0.500	0.027		0.039	0.024
	Average						0.024
	Ear	none	0.781			0	<0.005
		none	1.252			0	<0.005
		none	0.416	0.027		0.025	<0.005
		none	0.944	0.027		0.026	<0.005
	Average						<0.005
	Stem	5	0.100			0.018	0.18
		5	0.100	0.027		0.032	0.05
		5	0.200			0.038	0.19
		5	0.200			0.042	0.21
	Average						0.17
	Foliage	5	0.100			0.032	0.32
		5	0.100	0.027		0.052	0.25
		5	0.200			0.068	0.34
		5	0.200			0.066	0.33
	Average						0.31
	Ear	5	0.327			0.056	0.17
		5	0.547			0.196	0.36
		5	0.237	0.027		0.081	0.23
		5	0.320			0.066	0.21
	Average						0.24
	Stem	10	0.100		20/50[b]	0.022	0.55
		10	0.100	0.045	20/50	0.034	0.40
		10	0.200		20/50	0.048	0.60
		10	0.200		20/50	0.048	0.60
	Average						0.54
	Foliage	10	0.100		20/50	0.038	0.95
		10	0.100	0.045	20/50	0.053	0.88
		10	0.200		20/50	0.077	0.94
		10	0.200		20/50	0.086	1.08
	Average						0.97
	Ear	10	0.281		20/50	0.063	0.56
		10	0.548		20/50	0.165	0.75

TABLE 3. Continued

		Selenium content in soil[a] (ppm)	Plant sample (g)	Selenium added (μg)	Dilution	Selenium determined (μg)	Selenium content (μg/g)
		10	0.218	0.045	20/50	0.086	0.78
		10	0.403		20/50	0.084	0.52
	Average						0.65
	Stem	20	0.100		10/50	0.044	2.20
		20	0.100		10/50	0.052	2.60
		20	0.100		10/50	0.059	2.95
		20	0.100	0.18	5/50	0.047	2.90
	Average						2.7
	Foliage	20	0.100		10/50	0.077	3.85
		20	0.100		10/50	0.074	3.70
		20	0.100		10/50	0.075	3.75
		20	0.100	0.18	5/50	0.057	3.90
	Average						3.8
	Ear	20	0.174		5/50	0.037	2.13
		20	0.150	0.18	5/50	0.065	3.13
		20	0.163		5/50	0.032	1.96
		20	0.286		5/50	0.059	2.06
	Average						2.3
	Stem	50	0.100		5/50	0.034	3.40
		50	0.100		5/50	0.030	3.00
		50	0.100		5/50	0.036	3.60
		50	0.100	0.18	5/50	0.053	3.50
	Average						3.4
	Foliage	50	0.100		5/50	0.050	5.00
		50	0.100		5/50	0.057	5.70
		50	0.100		5/50	0.054	5.40
		50	0.100	0.18	5/50	0.068	5.00
	Average						5.3
	Ear	50	0.113		5/50	0.069	6.11
		50	0.112	0.18	5/50	0.057	3.48
		50	0.152		5/50	0.050	3.29
		50	0.164		5/50	0.052	3.17
	Average						4.0
	Stem	100	0.100		5/50	0.040	4.00
		100	0.100		5/50	0.042	4.20
		100	0.100		5/50	0.051	5.10
		100	0.100	0.18	5/50	0.062	4.40
	Average						4.4
	Foliage	100	0.100		5/50	0.078	7.80
		100	0.100		5/50	0.070	7.00
		100	0.100		5/50	0.074	7.40
		100	0.100	0.18	5/50	0.082	6.40
	Average						7.2
	Ear	100	0.126		5/50	0.104	8.25
		100	0.165	0.18	5/50	0.132	6.91
		100	0.139		5/50	0.069	4.96
		100	0.137		5/50	0.056	4.09
	Average						6.1
Rice plant	Mixture[c]	none	0.500			0.027	0.054
		none	0.500			0.032	0.064
		none	0.500	0.027		0.058	0.062
		none	0.500	0.027		0.070	0.086
	Average						0.067
	Stem	20	0.100		3/50	0.060	10.0
		20	0.100		3/50	0.064	10.7

TABLE 3. Continued

	Selenium content in soil[a] (ppm)	Plant sample (g)	Selenium added (μg)	Dilution	Selenium determined (μg)	Selenium content (μg/g)
	20	0.100		3/50	0.076	12.7
	20	0.100	0.27	3/50	0.077	10.2
Average						11
Foliage	20	0.100		3/50	0.109	18.2
	20	0.100		3/50	0.098	16.3
	20	0.100		3/50	0.106	17.7
	20	0.100	0.27	3/50	0.115	16.5
Average						17
Stem	50	0.100		1/50	0.039	19.5
	50	0.100		1/50	0.046	23.0
	50	0.100		1/50	0.039	19.5
	50	0.100		1/50	0.039	19.5
Average						21
Foliage	50	0.100		1/100	0.062	62.0
	50	0.100		1/100	0.057	57.0
	50	0.100		1/100	0.059	59.0
	50	0.100		1/100	0.065	65.0
	50	0.100		1/100	0.056	56.0
Average						60
Stem	100	0.100		1/50	0.043	21.5
	100	0.100		1/50	0.040	20.0
	100	0.100		1/50	0.042	21.0
	100	0.100		1/50	0.048	24.0
	100	0.100		1/50	0.046	23.0
Average						22
Foliage	100	0.100		1/100	0.067	67.0
	100	0.100		1/100	0.061	61.0
	100	0.100		1/100	0.079	79.0
	100	0.100		1/100	0.070	70.0
	100	0.100		1/100	0.066	66.0
Average						69

a) Planted soil (added as SeO_2). b) The example, indicates that the solution digested is diluted to 50 ml and 20 ml of it is used. c) A mixture of foliage and stem.

ling grown to 10 cm was transplanted into pots which had 3 kg of soil containing 0, 5, 10, 50, and 100 ppm selenium respectively (added as SeO_2). These plants were harvested after maturity. They were dried in a ventilated oven at 80 °C for 2 day. Subsequently, the dried sample was cut with scissors into portions about 1 mm long and mixed well. The selenium in 0.1—1 g of plant materials was determined by the procedure described above; also, the same sample containing 0.018—0.027 μg of selenium as the elemental form was used for the determination. As the added amount of selenium is always obtained by deducing the former values from the latter values, this method is proved to be usable for the determination of selenium in plant material. The results are shown in Table 3.

Since the sensitivity of an electron-capture detector varies during operation, a series of experiments should be carried out successively and an unknown content of selenium should be determined along with standard samples which contain similar amounts of selenium. The outstanding features are that it is simple, highly sensitive, and rapid, and no special skill is necessary to perform this method.

The author wishes to thank Professor Kyoji Tôei for his encouragement and helpful discussion throughout the work and Professors Shigeo Yoneda and Noboru Shimose for supplying the plant samples.

References

1) M. L. Scott, "Mineral Metabolism 2," Part B, Academic Press, New York, (1962), p. 543.
2) J. Kubota, W. H. Allaway, D. L. Carler, E. E. Cary, and V. A. Lazar, *J. Agr. Food Chem.*, **15**, 448 (1967).
3) F. B. Cousins and I. M. Cairney, *Aust. J. Agr. Res.*, **12**, 927 (1961).
4) J. H. Watkinson, *Anal. Chem.*, **32**, 981 (1960).
5) C. A. Parker and L. G. Harvey, *Analyst*, **87**, 558 (1962).
6) R. J. Hall and P. L. Gupta, *ibid.*, **94**, 292 (1969).
7) H. J. M. Bowen and P. A. Cawse, *ibid.*, **88**, 721 (1963).
8) W. J. Kelleher and M. J. Johnson, *Anal. Chem.*, **33**, 1429 (1961).
9) H. Nakashima, private communication.
10) Y. Shimoishi and K. Toei, *Talanta*, **17**, 165 (1970).
11) Y. Shimoishi, This Bulletin, **44**, 3370 (1971).
12) Y. Shimoishi, *Anal. Chim. Acta*, **64**, 465 (1973).
13) T. T. Gorsuch, *Analyst*, **84**, 135 (1959).
14) P. Lindberg, *Acta Vet. Scand.*, Supp. 23 (1968).
15) L. M. Cummins, J. I. Martin, G. W. Maag, and D. D. Maag, *Anal. Chem.*, **36**, 382 (1964).
16) J. S. McNulty, *ibid.*, **19**, 809 (1947).

Copper(II) Complexes of Histidine and Its Related Compounds in Aqueous Solutions

Hiroji AIBA, Akira YOKOYAMA, and Hisashi TANAKA

Faculty of Pharmaceutical Sciences, Kyoto University, Yoshida, Sakyo-ku, Kyoto 606

(Received November 1, 1973)

The copper(II) complexes of histidine and its related compounds in aqueous solution were investigated by potentiometric, spectrophotometric, and magnetic methods. The presence of a diolated binuclear copper(II) complex was indicated in the 1 : 1 histamine-copper(II) system by quantitative analysis of the titration data and the antiferromagnetic character of the complex. The titration data could not be quantitatively interpreted owing to precipitation, but the formation of a similar diolated copper(II) complex was also shown in the 1 : 1 histidine-copper(II) system by the magnetic properties of the complex. From a comparison of the spectral properties of the pertinent complexes, it was shown for the neutral 2 : 1 histidine-copper(II) complex that histidine binds to copper-(II) through the amino and imidazole groups in the chelate plane and through the carboxyl group in the apical position. In the copper(II) complexes of histidine and histamine, it was shown that ionization of the pyrrole nitrogen of the imidazole ring is promoted, causing a spectral blue shift.

Elucidation of the complex formation between copper-(II) and histidine in the aqueous solution is not easy, since histidine involves a bulkyl imidazole ring and has three or four coordination sites, and copper(II) requires a tetragonal coordination. This and the biological significance of histidine residue as a metal binding site in protein have prompted many workers to investigate copper(II)-histidine complexes. The presence of various complex species, *viz.*, protonated, normal and hydroxo complexes, has been found to be dependent on pH of medium and histidine-to-copper(II) ratio.[1-6] However, the structures of the complexes have not been completely elucidated. The coordinating groups which occupy four positions in the square coordination sp-here are not elucidated in the ligand to metal ratio 2 : 1 normal complex. In this connection, a weak coordination from the apical direction has been the subject of debate. Questions on the structure of the hydroxo complex formed in the 1 : 1 system remain undetermined and structural changes in the complexes in alkaline solution have not been fully discussed. For the purpose of obtaining further information on the structures of various complexes which may be formed in the reaction of histidine with copper(II) under various conditions, we studied the copper(II) complexes of histidine and its related compounds in aqueous solution by potentiometric, visible spectrophotometric, and magnetic methods.

Experimental

Materials. L-Histidylglycine was synthesized according to the method described previously.[7] Commercial ligands and reagents were used.

Methods. Potentiometric titration was carried out on a solution (10 ml) containing a ligand (10^{-2} M) and copper(II) (10^{-2} M or 0.5×10^{-2} M). Visible spectrophotometric measurements were made on solutions with copper(II) concentrations 4×10^{-3} M—1×10^{-2} M. Details of experimental conditions and method have been described.[7,8] The magnetic susceptibilities of the solutions containing a ligand (10^{-1} M) and copper (10^{-1} M) were measured by the Gouy method at room temperature. The molar susceptibility and magnetic moment of copper(II) in each system was calculated, with the correction of the diamagnetism of water, ligand and other ions present.

Results

Potentiometric Titration. Figure 1 shows the titration curves of L-histidine, histamine, and L-3-benzylhistidine in the presence of equimolar $CuCl_2$. In each 1 : 1 system a pH inflection is observed at $a=2$, followed by an additional deprotonation in neutral region, where a represents moles of KOH added per diprotonated ligand.

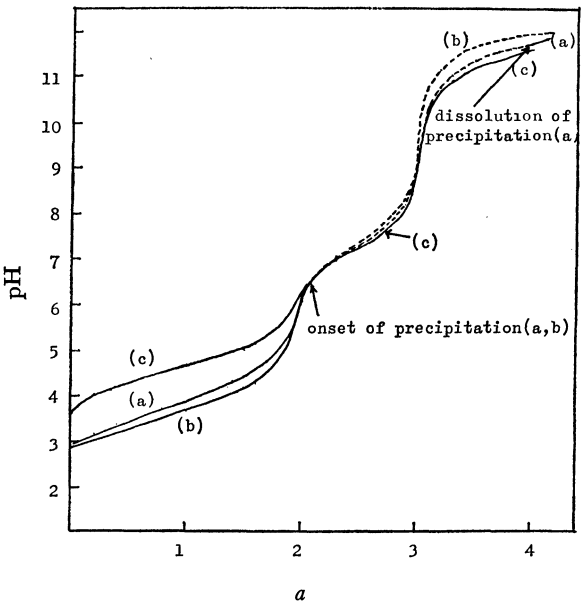

Fig. 1. Titration curves of L-histidine, L-3-benzylhistidine and histamine in the presence of equimolar $CuCl_2$:
(a) histidine, (b) 3-benzylhistidine, (c) histamine, [ligand]=[Cu(II)]=10^{-2} M (at $a=0$).
The dotted line indicates precipitation.

The 1 : 1 complex (CuL'^{2+}) is regarded as the main species in the region, where a value is about 2 in the 1 : 1 histamine-copper(II) system.[1] The following equation was assumed for the deprotonation between $a=2$ and 3 in the histamine-copper(II) system, the equilibrium constant pK_c^1 being calculated at each reaction point:

$$CuL'^{2+} \rightleftharpoons CuL'(OH)^{+} + H^{+}$$

$$K_c^1 = \frac{[CuL'(OH)^{+}][H^{+}]}{[CuL'^{2+}]} \quad (1)$$

where L' represents the neutral species of histamine.

The results given in Table 1 show that the equation does not hold, since the calculated values of pK_c^1 decrease with the increase in a value. The formation of a diolated binuclear complex might be expected with the dissociation of a proton from the complex CuL'^{2+}.[3,9] Thus the followiug reaction was assumed and the equilibrium constant pK_c^2 was calculated at each point.

$$2CuL'^{2+} \rightleftharpoons Cu_2L'_2(OH)_2^{2+} + 2H^{+}$$

$$K_c^2 = \frac{[Cu_2L_2'(OH)_2^{2+}][H^{+}]^2}{[CuL'^{2+}]^2} \quad (2)$$

The values of pK_c^2 (Table 1) remain constant irrespective of a values. In contrast, the values of pK_c^3, pK_c^4, and pK_c^5 which correspond to the formations of the trimer, tetramer, and pentamer respectively increase with the increase in a value in the region a= 2.1—2.7. This suggests the formation of a dimer with the deprotonation between a=2 and 3.

In the histidine-copper(II) 1 : 1 system, the complex precipitates immediately when the solution of KOH was added beyond a=2. The amount of precipitate increased with a value up to a=3, decreased gradually and then dissolved completely at a=4. Precipitation also occurred in the 3-benzylhistidine-copper(II) system, but in this case the precipitate did not dissolve at a=4. Due to precipitation titration data between a=2 and 3 in the histidine-copper(II) and 3-benzylhistidine-copper(II) systems were not interpretated quantitatively. In the 1 : 1 histidine-copper(II) and 1 : 1 histamine-copper(II) systems, pH in the region a=3—4 was lower than that in the systems of the ligand itself,[7] whereas in the 1 : 1 3-benzylhistidine-copper(II) system, no fall in pH was observed. The results suggest further deprotonation between a=3 and 4 in the former two systems. Similar falls of pH were also observed in the region a=2—3 in the 2 : 1 histidine-copper(II) and 2 : 1 histamine-copper(II) systems respectively.

Table 1. Quantitative analysis of the titration curve in the region a=2—3 in the 1:1 histamine-copper(II) system

a value	pH	pK_c^1	pK_c^2	pK_c^3	pK_c^4	pK_c^5
2.1	6.58	7.53	12.02	16.39	20.71	24.99
2.2	6.82	7.42	12.10	16.65	21.15	25.63
2.3	6.96	7.33	12.09	16.72	21.30	25.85
2.4	7.08	7.26	12.07	16.75	21.38	25.99
2.5	7.22	7.22	12.09	16.83	21.52	26.19
2.6	7.36	7.18	12.09	16.88	21.61	26.31
2.7	7.53	7.16	12.11	16.94	21.72	26.47
2.8	7.70	7.10	12.04	16.86	21.63	26.37
2.9	7.98	7.03	11.95	16.75	21.49	26.21

Visible Absorption Spectra. Spectral characteristics of the systems containing a ligand and copper(II) with the molar ratios of 1 : 1 and 2 : 1 are given in Table 2. Each a value corresponds to that in the titration. In the 1 : 1 histamine-copper(II) system, the spectrum at a=2 exhibited an absorption maximum at 665 nm (ε=38). Addition of equimolar KOH caused a significant blue shift (665 nm→615 nm). Addition of equimolar KOH caused another blue shift to show an absorption maximum at 590 nm. In the 1 : 1 histidine-copper(II) system, similar spectral changes were observed, although the spectrum of the solution at a=3 could not be measured owing to the precipitation. The spectrum at a=4 exhibited an absorption maximum at 605 nm. The spectra of the 1 : 1 3-benzylhistidine-copper(II) system in the region a=3—4 could not be measured owing to the precipitation. In the 2 : 1 histamine-copper(II) and 2 : 1 histidine-copper(II) systems, blue shifts were observed in the region a=2—3 by the addition of KOH. No spectral change was observed by the addition of KOH in the 2 : 1 3-benzylhistidine-copper(II) system.

The spectra of the 2 : 1 normal complexes of copper(II) with some related compounds of histidine are shown in Fig. 2, together with those of some 1 : 1 : 1 mixed ligand complexes of these ligands. The charac-

Table 2. Visible absorption characteristics of 1:1 and 2:1 copper(II) complexes

System	a value	Main species	λ_{max} (nm)	ε_{max} ($cm^{-1}M^{-1}$)[b]
Histidine·HCl+Cu(II)	2	CuL^{+}	665	38
	3[a]	$Cu_2L_2(OH)_2$	—	—
	4	$Cu_2X_2(OH)_2^{2-}$	605	62
Histamine·2HCl+Cu(II)	2	CuL'^{2+}	665	38
	3	$Cu_2L_2'(OH)_2^{2+}$	615	52
	4	$Cu_2X_2'(OH)_2$	590	64
3-Benzylhistidine+HCl+Cu(II)	2	CuL^{+}	670	36
	3[a]	$Cu_2L_2(OH)_2$	—	—
	4[a]	$Cu_2L_2(OH)_2$	—	—
Histidine·HCl+$^1/_2$Cu(II)	2	CuL_2	640	84
	3	CuX_2^{2-}	625	96
Histamine·2HCl+$^1/_2$Cu(II)	2	CuL'^{2+}	601	82
	3	CuX_2'	580	91
3-Benzylhistidine+HCl+$^1/_2$Cu(II)	2	CuL_2	642	88
	3	CuL_2	642	88

a) Complex precipitated. b) Molar absorptivity is expressed per gram atom of copper(II).

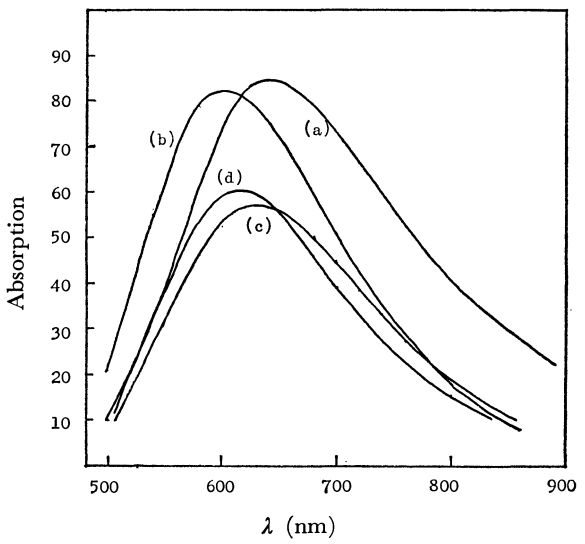

Fig. 2. Visible absorption spectra of normal 2 : 1 copper(II) complexes of histidine related compounds: (a) histidine, (b) histamine, (c) 1-methylhistidine, (d) histidine+1-methylhistidine (1 : 1): The absorbance is expressed on a molar copper(II) basis.

Table 3. Visible absorption characteristics of 2: 1 normal copper(II) complexes

	λ_{max} (nm)	ε_{max} ($cm^{-1}M^{-1}$)	$\Delta\lambda_{1/2}$ (nm)[a]
Histidine	640	84	250
3-Benzylhistidine	642	88	246
Histidylglycine	636	88	237
Histidine methyl ester	629	85	228
Histidine+Histamine (1: 1)	628	83	220
Histamine	601	82	200
1-Methylhistidine	628	57	193
Histidine+1-Methyl-histidine(1: 1)	615	60	194

a) $\Delta\lambda_{1/2}$ represents the width at the half-height of the spectra.

teristics of these spectra are given in Table 3. The molar absorptivities do not differ much from each other among the copper(II) complexes of histidine, 3-benzylhistidine, histidine methyl ester, histidylglycine and histamine. On the other hand, the molar absorptivities 2 : 1 1-methylhistidine-copper(III) and 1 : 1 : 1 1-methylhistidine-copper(II)-histidine complexes are smaller than the molar absorptivity of 2 : 1 histidine-copper (II) complex.

The order of the wavelength of the absorption maximum in the 2 : 1 complexes is : histamine histidine methyl ester, histidylglycine, histidine and 3-benzylhistidine (from shorter to longer wavelength). The width at the half-height of the spectral band increases in the same order. The broadening of the band was observed in the longer wavelength region than the absorption maximum.

Magnetic Moment. The molar susceptibilities and the magnetic moments of the copper(II) in the 1 : 1 ligand-copper(II) systems are shown in Table 4. The magnetic data at $a=3$ in the histidine-copper(II) and at $a=4$ in the histamine-copper(II) were not measured in aqueous solution owing to the precipitation. The magnetic moment decreases with the increase in a value in each system, but the values are always normal in the glycylglycine-copper(II) system. The subnormal values were obtained in the histamine-copper(II) and in the histidine-copper(II) systems when a values are 3 and 4, respectively. This suggests that antiferromagnetic interactions are present in these systems.

Table 4. Room temperature magnetic data on the copper(II) in the ligand-Cu(II) aqueous solutions

System	a value	$\chi_A \times 10^6$ c.g.s. units	T(K)	μ_{eff} (B.M.)
Histidine·HCl +Cu(II)	0	1552	296	1.87
	1	1450	293	1.82
	2	1409	293	1.82
	3[a]	not determined		
	4	1001	296	1.54
Histamine·2HCl +Cu(II)	0	1548	286	1.88
	1	1474	286	1.94
	2	1391	296	1.81
	3	1104	288	1.59
	4[a]	not determined		
Glycylglycine +Cu(II)	0[b]	1562	288	1.90
	1[b]	1457	288	1.85
	2[b]	1409	296	1.83
	3[b]	1307	296	1.76

a) Complex precipitated. b) The values represents the number of moles of KOH added per neutral (monoprotonated) glycylglycine.

Discussion

1 : 1 Hydroxo Complexes. Quantitative analysis of the titration data in the 1 : 1 histamine-copper(II) system suggests the formation of a dimer complex with the release of a proton in the region $a=2$—3. This conclusion is compatible with the results reported by Perrin and Sharma.[3,9] The source of the liberated proton is regarded as the coordinated water molecule and a dimer I is presumed to be formed by the olation between two molecules. The antiferromagnetic character of the 1 : 1 histamine-copper(II) system at

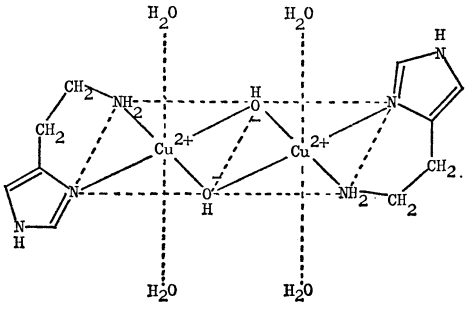

I, $Cu_2L_2'(OH)_2^{2+}$

$a=3$ is a strong evidence for the binuclear structure.[10] It is noteworthy that the formation of the diolated complex displaces the absorption maximum at a wavelength about 50 nm shorter than in the mother complex in spite of the lower position of OH^- than H_2O in the spectrochemical series.

Perrin and Sharma suggested from their quantitative analysis of the titration data that a monohydroxo complex CuL(OH), where L^- represents the anionic species of histidine, is a predominant species near $a=3$ in the 1 : 1 histidine-copper(II) system.[3] However, in the 1 : 1 histidine-copper(II) system, the titration data for the region $a=2$—3 can not be analysed quantitatively owing to precipitation, and there may be some uncertainty in their conclusion. The antiferromagnetic character of the 1 : 1 histidine-copper(II) complex at $a=4$ suggests the presence of the binuclear hydroxo complex $Cu_2L_2(OH)_2$ similar to that in the case of 1 : 1 histamine-copper(II) complex. The probable structure for the 1 : 1 histidine-copper(II) complex is shown to be II. The same diolated complex will

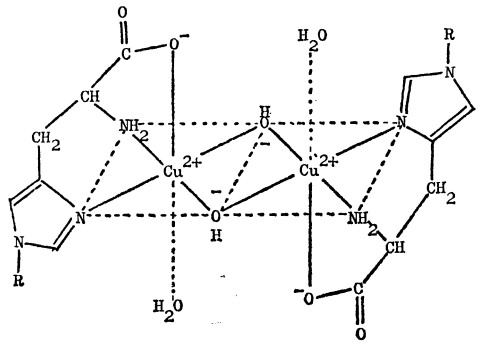

II, $Cu_2L_2(OH)_2$ R=H : histidine

R=CH_2- : 3-benzylhistidine

also be formed in the 1 : 1 3-benzylhistidine-copper(II) system. The steric requirement of the bulky imidazole group is presumed to promote the formation of the binuclear complexes in these systems.[11,12]

The dissolution of the 1 : 1 histidine-copper(II) complex accompanied by deprotonation between $a=3$ and 4 suggests the formation of an anionic complex $Cu_2X_2(OH)_2^{2-}$, where $XH^-=L^-$. The evidence that the source of this proton is imino group of the imidazole ring is given by the fact that no similar behavior was observed in the 3-benzylhistidine-copper(II) system. The structure of the 1 : 1 histidine-copper(II) anionic

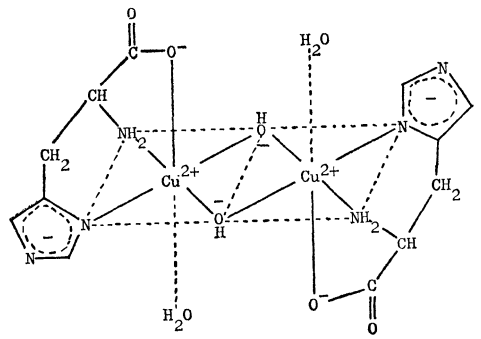

III, $Cu_2X_2(OH)_2^{2-}$

complex is shown by III. Similarly, further deprotonation accompanied by a conspicuous blue shift in absorption spectra for the region $a=3$—4 in the 1 : 1 histamine-copper(II) system suggests the dissociation of the proton from the imino group of imidazole giving a neutral complex $Cu_2X_2'(OH)_2$, where X'H=L'.

The absorption at longer wavelength at $a=4$ in the 1 : 1 histidine-copper(II) complex than in the 1 : 1 histamine-copper(II) complex can be ascribed to the relaxation of the tetragonal distortion due to the apical coordination of the carboxyl groups.[13]

2 : 1 *Complexes.* For the neutral 2 : 1 histidine-copper(II) complex, the following possibilities are taken into account for the group which occupies the four coordination positions in the copper(II) plane. (a) Two histidine molecules bind to copper(II) with the amino and imidazole groups(histamine type).[1,3,5,6,14-18] (b) Two histidine molecules bind to copper(II) with the amino and carboxyl groups (glycine type).[19-21] (c) One histidine molecule coordinates with copper(II) as in the case of histamine, and another as in the case of glycine(mixed type).[22,23]

The larger molar absorptivity of the 2 : 1 histidine-copper(II) complex than in 2 : 1 1-methylhistidine-copper(II) and 1 : 1 : 1 1-methylhistidine-copper(II)-histidine complexes suggests that the coordination is neither a glycine nor a mixed type. Possibility (a) can be accepted in view of the similarity in the molar absorptivities between the 2 : 1 complexes of histidine, 3-benzylhistidine, histidylglycine, histidine methyl ester, and histamine. The presence of the two six-membered chelate ring composed of the amino and imidazole groups in the copper(II) plane seems to give a similar absorptivity. The order of the wavelength of the absorption maximum and that of the increase of the width of the spectral band in these 2 : 1 copper(II) complexes seem to reflect the extent of tetragonal distortion of the copper(II) complexes,[13] since these orders are in agreement with the order of strength of apical coordination among the coordination groups, *viz.*, $-COO^- > \rangle C{=}O > H_2O$. This provides an evidence for apical coordination of the carboxyl group in the histidine-copper(II) and 3-benzylhistidine-copper(II) complexes. A smaller tetragonal distortion of the 2 : 1 histidine-copper(II) complex than in the 1 : 1 : 1 histamine-copper(II)-histidine complex sug-

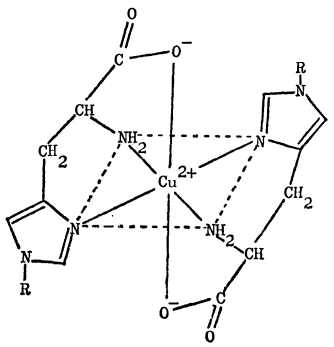

IV, CuL_2

R=H : histidine

R=CH_2- : 3-benzylhistidine

gests that both carboxyl groups coordinate to copper(II) at apical position in the former, as shown by IV.

Further deprotonation accompanied by the blue shift in the absorption spectra in the range $a=2$—3 in the 2 : 1 histamine-copper(II) and histidine-copper(II) systems, also indicates the ionization of the imino group. No deprotonation and the spectral shift in the 2 : 1 3-benzylhistidine-copper(II) system in the same condition support the conclusion. The relatively easier ionization of the imino group in the 1 : 1 and 2 : 1 copper(II) complexes of histidine and histamine would be due to the electron-withdrawing effect of copper(II) which binds to the pyridine type nitrogen.

The authors wish to express their thanks to Professer M. Kishita and Dr. W. Mori, Osaka University, for their helpful advice in magnetic measurements, and to the staff of the Kyoto University Computer Center for the use of FACOM 203—60 Computer.

References

1) R. Leberman and B. R. Rabin, *Trans. Faraday Soc.*, **55**, 1660 (1959).
2) R. H. Carlson and T. L. Brown, *Inorg. Chem.*, **5**, 268 (1966).
3) D. D. Perrin and V. S. Sharma, *J. Chem. Soc., A*, **1967**, 724.
4) H. C. Freeman and R. -P. Martin, *J. Biol. Chem.*, **244**, 4823 (1969).
5) J. L. Meyer and J. E. Bauman, Jr., *J. Amer. Chem. Soc.*, **92**, 4210 (1970).
6) D. R. Williams, *J. Chem. Soc. Dalton*, **1972**, 790.
7) A. Yokoyama, H. Aiba, and H. Tanaka, This Bulletin, **47**, 112 (1974).
8) H. Aiba, A. Yokoyama, and H. Tanaka, *ibid.*, **47**, 136 (1974).
9) D. D. Perrin and V. S. Sharma, *J. Inorg. Nucl. Chem.*, **28**, 1271 (1966).
10) M. Kato, H. B. Janassen, and J. C. Fanning, *Chem. Rev.*, **64**, 99 (1964).
11) H. Ojmia and K. Sone, This Bulletin, **35**, 298 (1962).
12) F. Basolo and R. K. Murmann, *J. Amer. Chem. Soc.*, **74**, 5343 (1952).
13) A. A. G. Tomlinson and B. J. Hathaway, *J. Chem. Soc., A*, **1968**, 1685, 1905.
14) M. A. Doran, S. Chaberek, and A. E. Martell, *J. Amer. Chem. Soc.*, **86**, 2129 (1964).
15) O. W. Urry and H. Eyring, *ibid.*, **86**, 4574 (1964).
16) E. V. Raju and H. B. Mathur, *J. Inorg. Nucl. Chem.*, **31**, 425 (1969).
17) A. Chakravorty and F. A. Cotton, *J. Phys. Chem.*, **67**, 2878 (1963).
18) H. Siegel, R. Griesser, and D. B. McCormick, *Arch. Biochem. Biophys.*, **134**, 217 (1969).
19) B. Sarkar and Y. Wigfield, *J. Biol. Chem.*, **242**, 5572 (1967).
20) B. Sarkar, M. Berson, Y. Wigfield, and T. -C. Chiang, *Can. J. Biochem.*, **46**, 595 (1968).
21) T. H. Crawford and J. O. Dalton, *Arch. Biochem. Biophys.*, **131**, 123 (1969).
22) K. M. Wellman and B. -K. Wong, *Proc. Nat. Acad. Sci.*, **64**, 824 (1969).
23) H. Siegel and D. B. McCormick, *J. Amer. Chem. Soc.*, **93**, 2041 (1971).

Cyclization Reactions of 1,2-Bis(2-cyanophenyl)propionitriles. I. Structure of the "Red Pigment" formed by the Base-catalyzed Cyclization of 1,2-Bis(2-cyano-3-methoxyphenyl)propionitrile in the Presence of Diethyl Carbonate[1]

Kazuo ANDO, Takashi TOKORO YAMA, and Takashi KUBOTA*

Faculty of Science, Osaka City University, Sugimoto-cho, Sumiyoshi-ku, Osaka 558

(Received September 7, 1973)

The reaction of 1,2-bis(2-cyano-3-methoxyphenyl)propionitrile (**1**) with diethyl carbonate and sodium ethoxide gave a red pigment **2**, $C_{22}H_{19}N_3O_4$ in 79% yield. It afforded 5-amino-4,7-dimethoxy-11*H*-indeno[1,2-*c*]-isoquinolin-11-one (**4**) on treatment with alkaline hydrogen peroxide. The "red pigment" has been confirmed to have a novel 5*H*-indeno[1,2-*c*]isoquinoline structure which transforms into colorless 11*H*-indeno-[1,2-*c*]-isoquinoline form in an acidic medium. The mechanism of the formation of **2** from **1** imparts an interesting problem as regards carbanion reactivity.

In the course of synthetic studies[1,2] of compounds related to sclerin, a plant growth hormone,[3] we happened to treat 1,2-bis(2-cyano-3-methoxyphenyl)propionitrile (**1**) with diethyl carbonate and sodium ethoxide in ethanol solution at refluxing temperature. When the brownish black reaction mixture was poured into ice-water, a red pigment **2** was obtained in 79% yield. The reaction was found to be reproducible. This led us to study the structure of **2** and investigate this reaction. In this paper we deal with the structure elucidation of **2**.

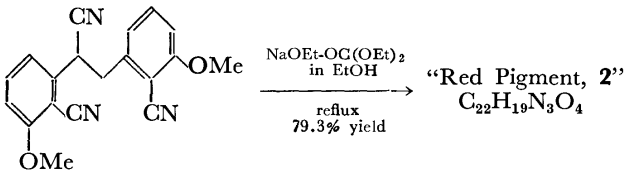

Scheme 1

The red pigment **2**, $C_{22}H_{19}N_3O_4$, is slightly soluble in chloroform and dichloromethane, and practically insoluble in other common organic solvents. It is easily soluble in strong acids such as trifluoroacetic acid or ethanolic hydrochloric acid giving a yellow solution with strong blue fluorescence. When this solution was neutralized or diluted with a large amount of water, **2** was recovered, indicating that compound **2** is a weak base. **2** is also soluble in sodium hydroxide, indicating it to be amphoteric in nature. The infrared spectrum indicates the presence of an imino or a hydroxyl group (3340 cm^{-1}), a cyano group (2166 cm^{-1}) and a carbonyl group (1705 cm^{-1}) in **2**. The imino or the hydroxyl group in **2** was found to be inactive on acetylation. It should be noted that the band due to a cyano group appears at unusually low frequency, compared to the normal range 2260—2210 cm^{-1}.[4] Because of the lack of a suitable neutral solvent, the NMR spectrum of **2** was taken in trifluoroacetic acid solution, showing the signals due to an ethoxy group, two methoxy groups and six aromatic protons. An additional signal was observed at δ 5.61 (1H). This could be tentatively assigned to be the methine proton which has a strongly deshielding environment. The results in conjunction with the molecular composition of **2** suggest that **2** is formed from **1** through a complex intramolecular cyclization, incorporating one mole of diethyl carbonate.

Upon alkaline hydrolysis under exlcusion of oxygen and the following treatment with dilute hydrochloric acid, **2** afforded a pale yellow amine hydrochloride **3**, $C_{19}H_{16}N_3O_2Cl$: ν_{max} 3300, 3080—2760 ($-NH_3^+$) and 2245 cm^{-1} (–CN); δ 4.13 ($-OCH_3$), 4.34 ($-OCH_3$) and 5.30 (1H). The IR and NMR spectra of **3** indicate that **3** is the amine hydrochloride formed by hydrolytic cleavage of the carbethoxyamide group originally present in **2**. The transformation of the cyano group in **2** was carried out using alkaline hydrogen peroxide in aqueous ethanol at 55 °C. The product **4** obtained in 92.5% yield exhibited absorption bands at 3460 3280, 3170 and 1670 cm^{-1} in the IR region, showing no band due to the cyano group. The NMR spectrum of **4** showed signals due to two methoxy groups and six aromatic protons, no signals due to ethoxy and groups being observed. In contrast to **2**, **4** was sufficiently basic to give the hydrochloride **5** and monoacetate **6**. The orange-red colored acetate **6** exhibited a UV spectrum similar to that of **4**. The peak in the IR spectrum of **6** were observed at 3330 and 1675 cm^{-1}. From the analytical values for **5** and **6**, **4** was concluded to have a molecular formula of $C_{18}H_{14}N_2O_3$ although the combustion analyses did not give a satisfactory result. This indicates that **4** is not a product of mere hydrolysis but a degraded product with the loss of one carbon, most probably corresponding to the cyano group in **2**. The formation of **5** and **6**, and the band at 3330 cm^{-1} in the IR spectrum of **6** suggest the presence of a primary amino group in **4**, though this compound is resistant to the diazotization reaction. Treatment of **4** with 6 M aqueous ethanolic potassium hydroxide solution under refluxing yielded an orange-red colored product **7**, $C_{18}H_{13}NO_4$, which no longer basic and showed IR peaks at 3380, 1690 and 1665 cm^{-1}, suggesting the presence of a lactam and an additional carbonyl group. Methylation of **7** with sodium methoxide and methyl iodide produced a monomethylation product **8**. The UV spectrum of **8** was similar to that of the strating material **7**. In the IR spectrum of **8**, the NH stretching band present in **7**

* Present address: Kinki University, Kowakae, Higashi-osaka-shi, Osaka 577.

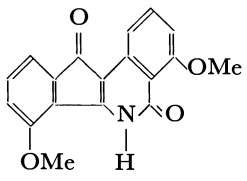

7a

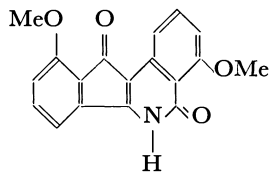

7b

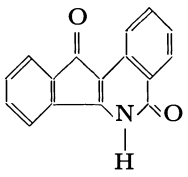

9

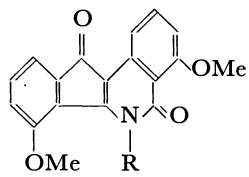

7 R=H
8 R=Me

disappeared and the carbonyl frequency was found at 1670 cm^{-1}. Three methyl singlets appeared at δ 3.92, 3.99 and 4.04 in the NMR spectrum. Thus the nitrogen atom of the lactam grouping in **7** is methylated in **8**. The only possible formula for **7**, in line with the above evidence would be **7a** or **7b**, provided that no rearrangement invoving carbon-carbon bonds occurs during the derivation of **7**. The parent compounds this ring system, 5,6-dihydro-11*H*-indeno[1,2-*c*]isoquinoline-5,11-dione (**9**), has been reported to be orange-red colored crystals but no description was of the electronic spectral data.[5] The choice **7a** or **7b** was possible by the consideration of the NH stretching band in **7**. This band was observed as a sharp peak at 3380 cm^{-1} in contrast to that of **9** as a broad band at 3226—2700 cm^{-1}. This would be interpreted by assuming that the intermolecular hydrogen bond existing in **9** becomes difficult in **7** owing to steric hindrance. Thus **7a** turned out to be the more acceptable structure for **7**. Accordingly formula **8** was assigned to the methylation product. In order to verify the structure for **7**, the reduction of the conjugated cyclopentanone group was investigated by treating with zinc dust in refluxing aqueous acetic acid. Two colorless products, **10**, $C_{18}H_{15}NO_3$ and **11**, $C_{18}H_{15}NO_4$ were obtained. When the reduction was carried out with glacial acetic acid, **10** was formed in a good yield. The UV spectra of of **10** and **11** were similar, indicating the presence of the same conjugated system in both products. The former shows the IR peaks at 3420 and 1650 cm^{-1} (lactam group), and NMR signals at δ 3.74 (>CH_2). Thus in **10** the ketonic group of **7** has been transformed into a methylene group. On the other hand **11** is found to be the product in which the ketonic group in **7** was reduced to a hydroxyl group, showing the IR peaks at 3420 (sh., -OH), 3380 (-NH) and 1654 cm^{-1} (-NHCO-). On the basis of the established structure for **7**, three formulas **4**, **4a** and **4b** are taken for the precursor **4**. When **4** was treated with zinc in glacial acetic acid in the same way as for **7**, the reduction product **12**, $C_{18}H_{16}N_2O_2$, was obtained in 70.5% yield. The IR spectrum of **12** revealed the disappearance of the carbonyl group in **4** and the NMR spectrum indicated the formation of the methylene group in **12**. Production of **12** from **4** is compatible only with the assignment of structure **4** for the latter and hence the formula for the reduction product **12**, the hydrochloride **5** and the acetylation product **6** are depicted as shown.

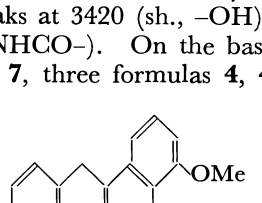

10

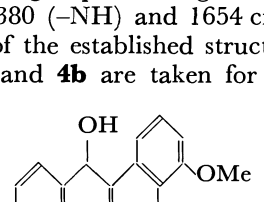

11

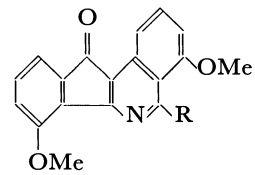

4 R=-NH_2
5 R=-$NH_3^+Cl^-$
6 R=-NHCOCH$_3$

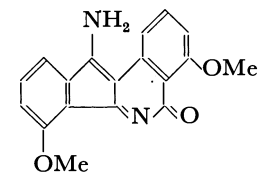

4a

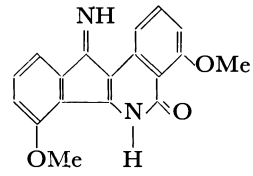

4b

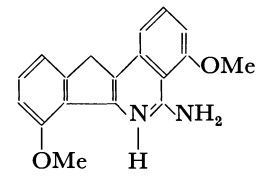

12

The disclosure of the structure for **4**[6] allows us to discuss the constitution of the "red pigment" **2**. The UV spectrum of the amine hydrochloride **3** closely resembles that of 5-amino-4,7-dimethoxy-11*H*-indeno[1,2-*c*]isoquinoline (**12**), a reduction product of **4** (Fig. 1), indicating the presence of the same chromophore in both compounds. Thus the only position available for the attachment of the cyano group in **3** would be the C-11 of 11*H*-indeno[1,2-*c*]isoquinoline nucleus, suggesting the structure **3** for the hydrochloride. When **3** was catalytically hydrogenated in the presence of palladium-on-charcoal in acetic acid containing hydrochloric acid, two products were obtained (Scheme 2). One product **13**, $C_{19}H_{18}N_2O_2$, was separated easily

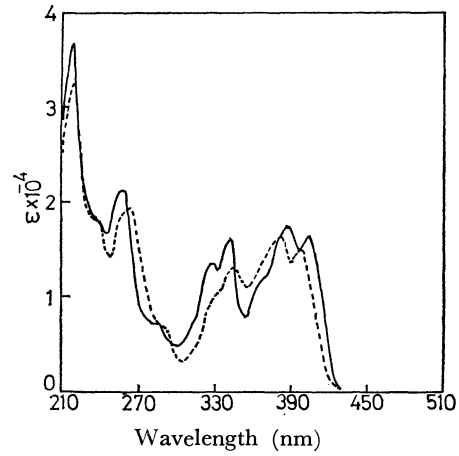

Fig. 1. Ultraviolet and visible spectra of 5-amino-4,7-dimethoxy-11*H*-indeno[1,2-*c*]isoquinoline (**12**) (——) and the hydrochloride **3** (----) in ethanol.*
* containing two drops of 1M sufuric acid per 10 ml.

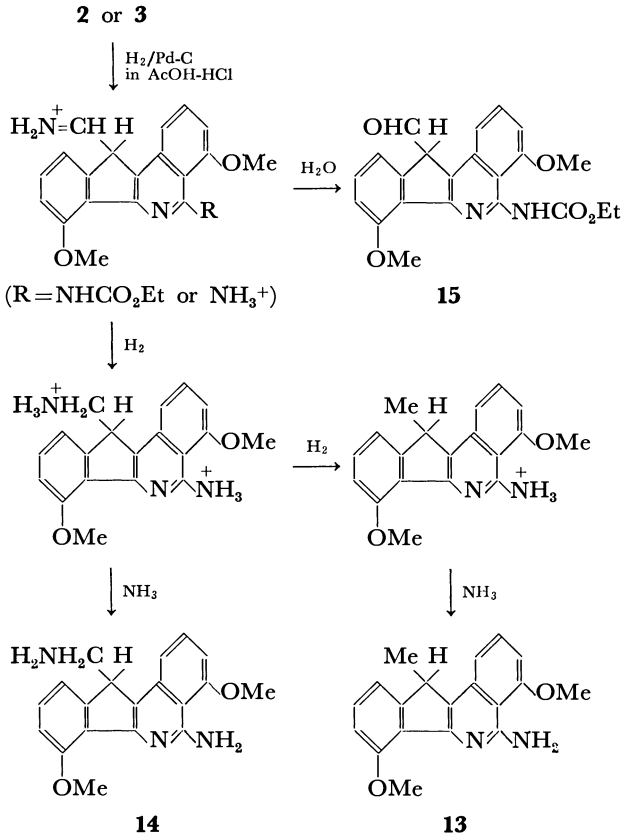

Scheme 2

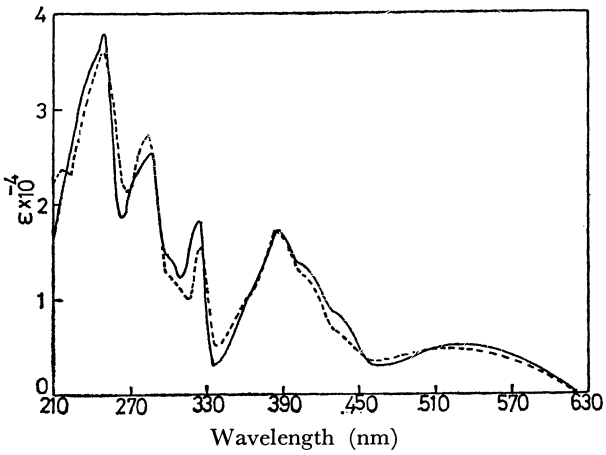

Fig. 2. Ultraviolet and visible spectra of the "red pigment" **2** and the acetate **16** in ethanol.

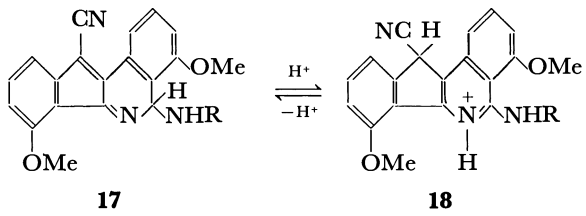

Scheme 3

from the other by treatment as hydrochloride with chloroform since only the former was soluble in this solvent. In the IR spectrum of **13** the band due to the cyano group in **3** has disappeared. A marked feature in the NMR spectrum of **13** is the appearance of the signals due to a secondary methyl groups. The UV spectrum of **13** resembles closely that of **3** and **12** (Fig. 1). This indicates that the secondary cyano group in **3** was transformed into a methyl group during the course of hydrogenation, confirming the position of the cyano group in the indenoisoquinoline skeleton of **3**. Another product obtained as an oil shows the absorption bands at 3460 and 3360 cm^{-1} in the IR spectrum. Insolubility of its hydrochloride in chloroform suggests that it could be the diamine **14** an intermediate product to **13**. Hydrogenation of **2** in the same way as **3** gives rise to the secondary aldehyde **15** though this compound could not be obtained in a pure state. Upon acetylation with acetic anhydride and concd. sulfuric acid, the hydrochloride **3** yielded a red colored acetate **16**. The UV spectrum of **16** resembles markedly that of the "red pigment" **2** (Fig. 2). This indicates that **2** and **16** have a common structure except for the acyl substituents on the primary amino group. For the sake of explanation it would be reasonable to assume that **2** and **16** have an iminoindene structure **17** which is transformed into colorless indenoisoquinoline skeleton **18** on salt formation with an acid. Thus the coloration in **2** and also in **16** is understandable.[7] In this respect the ketimine form **19** might also be taken into consideration.[8] In the IR spectrum of **2** a strong absorption band is observed at 2166 cm^{-1}, which is considerably out of the normal range for the cyano group. Although available data for the IR absorption of ketimines are very much limited, this structure appears to have the absorption band at 2040—2000 cm^{-1}.[9,10] Thus the IR peak of **2** in question would be in favor of a cyano group (conjugated). The chemical stability of the responsible group in **2** on addition reactions[9-13] precludes the ketimine structure.[14] The unusual lowering of the cyano frequency could be attributed to the contribution of the canonical formula like **20**.[15] The low-field singlets in the NMR spectra of **2** and **16** (δ 5.61 and 5.53 respectively) in the acidic conditions are assigned to the methine protons attached to the carbon atoms bearing cyano groups in the indenoisoquinoline structures. The solubility of **2** in alkali to form a light yellow solution with fluorescence is explainable by the formation of the anion **21**. In order to obtain the free amine, **3** was treated with ammonia to afford a product **22**, which has a somewhat dim red color compared to that of **2**. In the IR spectrum **22** exhibits broad bands due to the amino group at 3440 and 3300 cm^{-1} and a strong absorption due to cyano group at 2160 cm^{-1}. The product is presumed to be a tautomeric mixture of the iminoindeno derivative **22a** and the indenoisoquinoline compound **22b**. Fur-

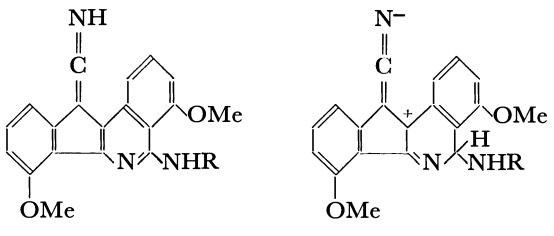

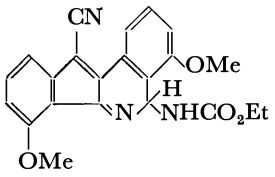

2

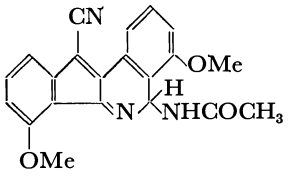

16

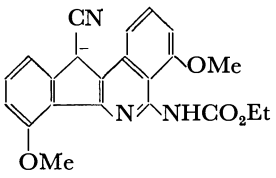

21

ther characterization was difficult since it was quite unstable in the air and converted into the same oxidation product **4** obtained from **2**.

The easy oxidative degradation of **2** by treatment with alkaline hydrogen peroxide to form **4** should be noted in terms of the established formula for **2**. In this connection Happ *et al.*[16] have reported that *N*-methyl-9-cyanoacridane **23** is oxidized by molecular oxygen in alkaline medium to afford *N*-methylacridone **24** with

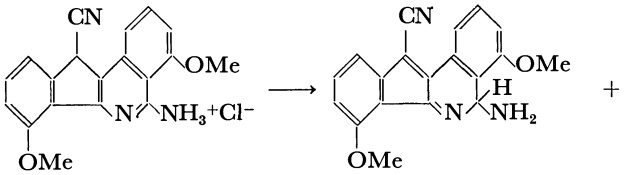

3 22a

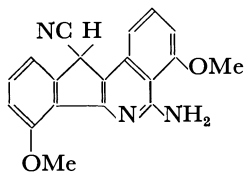

22b

Scheme 4

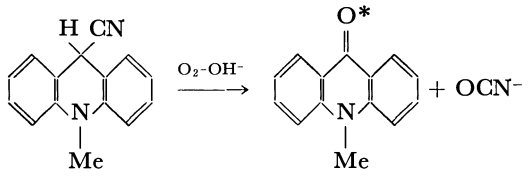

23 24

Scheme 5

chemiluminescence in which a carbanion electron transfer mechanism involving *N*-methyl-9-cyanoacridanyl radical is postulated. The reactions of **2** might proceed in the manner depicted in Scheme 6. The autoxidation of the free amine **22** to **4** could be interpreted similarly.

To our best knowledge, the 5*H*-indeno[1,2-*c*]isoquinoline system is a novel heterocycle. The relative stability of the iminoindene ring system in **2** over the tautomeric indenoisoquinoline would be a subject of interest in view of structural organic chemistry.[7]

Formation of the "red pigment" **2** from **1** provides a fascinating problem also from the side of the reaction mechanism. In the first sight the base-catalyzed reaction of **1** would be anticipated to proceed *via* a Thorp type path initiated by the anion **25**, produced by the removal of the most acidic hydrogen in **1**.[17] However the formation of **2** is accounted for only by the assumption of the path including the anion **26** (Scheme 7). The cyclization of **26** would take place involving the two cyano groups to afford the intermediate **27**, which is transformed into **2** by the redistribution of the double bonds. The reason why **26** mainly participates in the reaction instead of **25** seems to deserve further scrutiny.

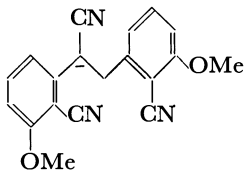

25

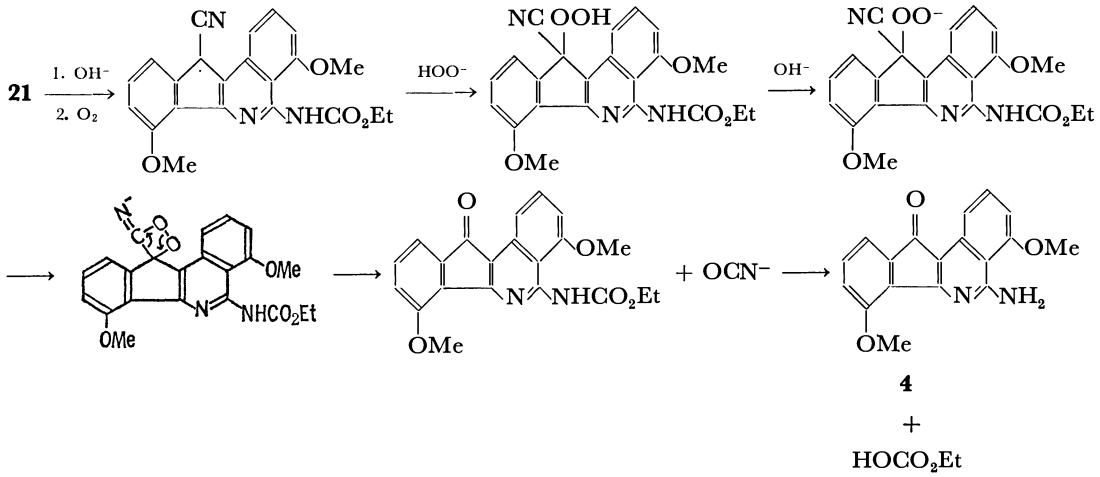

4 + $HOCO_2Et$

Scheme 6

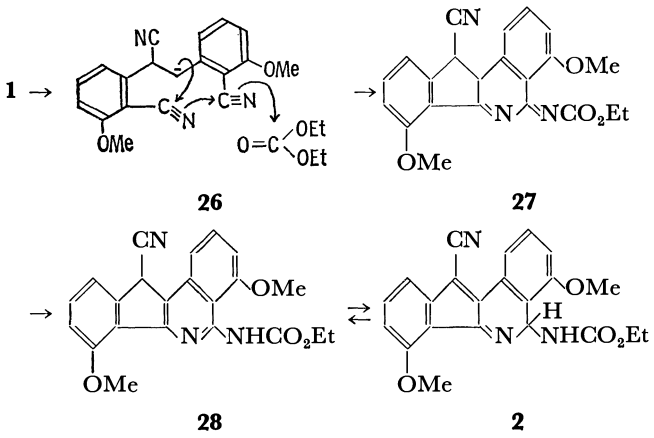

Scheme 7

Experimental

Melting points were uncorrected. The IR spectra were measured, unless specified, on Nujol mull on a Nippon Bunko IR-S spectrometer and the electronic spectra on a Hitachi EPS-2 spectrometer. Chemical shifts are reported in δ-values, using TMS as internal references.

Formation Reaction of the Red Pigment 2. A solution of sodium ethoxide in ethanol (prepared from 600 mg of sodium and 11 ml of abs. ethanol) was added to a mixture of 1,2-bis-(2-cyano-3-methoxyphenyl)propionitrile (**1**)[2] (3.6 g) and diethyl carbonate (26 ml) under stirring, and the mixture was refluxed for 2 hr. The reacting solution rapidly turned brownish black. The mixture was poured onto ice-water, providing **2** as red precipitate. Dilute acid may be added when necessary for the completion of precipitation. Recrystallization from chloroform afforded pure **2** as needles, mp 272 °C (dec.), 3.5 g (79.3% yield): λ_{max}^{EtOH} 249 (ε 37900), 283 (27100), 325 (18200), 387 (17100) and 528 nm (5200); ν_{max} 3340 (-NH), 2166(strong, -CN) and 1705 cm^{-1} (-$NHCO_2R$); $\delta(CF_3CO_2H)$, 1.57(3H, t, J=7.5 Hz, -OCH_2-CH_3), 4.33 (3H, s, -OCH_3), 4.42(3H, s, -OCH_3), 4.76(2H, q, J=7.5 Hz, -OCH_2CH_3), and 5.61(1H, s, >CH). Found: C, 67.88; H, 5.04; N, 10.76%. Calcd for $C_{22}H_{19}N_3O_4$: C, 67.85; H, 4.92; N, 10.79%.

Alkaline Hydrolysis of the Red Pigment 2. A mixture of **2** (300 mg) with sodium hydroxide (630 mg), water (12 ml) and ethanol (12 ml) was refluxed under nitrogen atmosphere for 3 hr. After cooling the reaction mixture was acidified with dil. hydrochloric acid. The solution, initially yellow, temporarily yielded a red precipitate which redissolved itself and then finally produced a white precipitate. This was filtered and washed with small amount of ethanol to afford almost pure **2**, 237 mg (87.2% yield). The analytical specimen was recrystallized from methanol: mp 249 °C (dec.); $\lambda_{max}^{H_2SO_4\text{-}EtOH}$ 220(ε 32500), 239(sh., 17400), 263(19600), 287(sh., 7050), 332(sh., 10300), 344(13200), 380(16300) and 398 nm(1500); ν_{max} 3300, 3080—2760(-NH_3^+) and 2245 cm^{-1} (-CN); $\delta(CF_3CO_2H)$, 4.13(3H, s, -OCH_3), 4.34(3H, -OCH_3), 5.30(1H, s, >CH), and 7.20—8.27(6H, m, ArH). Found: C, 64.15; H, 4.76; N, 11.72%. Calcd for $C_{19}H_{16}N_3O_2Cl$: C, 64.50; H, 4.56; N, 11.88%.

Oxidative Degradation of the Red Pigment 2 with Alkaline Hydrogen Peroxide. Hydrogen peroxide (3%) (100 ml) was added to a solution of **2**(980 mg) in ethanol (200 ml) and 10% aq. sodium hydroxide solution (10 ml) under stirring for 15 min. The reaction mixture gradually turned red and finnally gave a red precipitate, mp 288 °C(dec.), 750 mg (92.5% yield). Recrystallization from chloroform provided pure **4**, mp 289—290 °C; $\lambda_{max}^{dioxane}$ 224.5 (ε 22300), 235 (sh., 19000), 290(29700), 350(19600), 364(sh., 10800), 375 (sh., 6880), and 470 nm(3310); ν_{max} 3460, 3280, 3170 (-NH_2), and 1670 cm^{-1} (>CO); $\delta(CF_3CO_2H)$, 3.65(3H, s, -OCH_3), 3.79(3H, s, -OCH_3), and 6.72—7.94(6H, m, ArH). *Hydrochloride* **5** was prepared by stirrring a mixture of **4** (30 mg), ethanol (50 ml) and concd. hydrochloric acid (5 ml). Evaporation of the mixture to dryness and recrystallization of the residue from ethanol yielded **5**, mp 300 °C (dec.); ν_{max} 3320, 3000 (-NH_3^+), and 1705 cm^{-1} (>CO). Found: C, 63.15; H, 4.50; N, 8.16%. Calcd for $C_{18}H_{15}N_2O_3Cl$: C, 63.07; H, 4.41; N, 8.17%. Acetylation of **4** (187 mg) with acetic anhydride (50 mg) and anhyd. pyridine (25 ml) was carried out overnight at room temperature. The resulting orange red precipite (128 mg) was filtered and washed with ethanol. Recrystallization from chloroform afforded *the acetate* **6**, mp 270—273 °C; λ_{max}^{EtOH} 222(ε 21500), 275(33900), 355(19500), 368(sh., 12300), 380(sh., 6650), and 485 nm (2850); ν_{max} 3330(-NH) and 1675(-NHCO- and >CO) cm^{-1}; $\delta(CF_3CO_2H)$, 2.72(3H, s, -$COCH_3$), 4.25(3H, s, -OCH_3), 4.35(3H, s, -OCH_3), and 7.23—8.13 (6H, m, ArH).

Alkaline Hydrolysis of 4. A mixture of **4**(2.0 g), 6M potassium hydroxide solution(300 ml) and ethanol (360 ml) was refluxed for 20 hr, and filtered while hot. The filtrate, after concentration *in vacuo*, was acidified with hydrochloric acid to give almost pure **7** as a red precipitate (1.65 g, 82.% yield), which was recrystallized from ethanol: mp 295.5 °C; λ_{max}^{EtOH} 235(ε 26600), 269(33300), 291(19600), 353(18500), 372(sh., 13100), and 475 nm(3270); ν_{max} 3380 (sharp, -NH), 1690(CO), and 1665 cm^{-1} (-CONH-); $\delta(CF_3CO_2H)$, 4.16 (3H, s, -OCH_3), 4.36(3H, s, -OCH_3) and 7.26—9.00(6H, m, ArH). Found: C, 70.35; H, 4.24; N, 4.53%. Calcd for $C_{18}H_{13}NO_4$: C, 70.35; H, 4.26; N, 4.56%.

Methylation of 7. Sodium methoxide (4.05 g) and methyl iodide (5.1 ml) was alternatively added in three portions to a refluxing solution of **7** (150 mg) in abs. methanol (300 ml) for two days. After removal of most of the solvent, water was added. The red precipitate (200 mg) thus obtained was chromatographed on a column of silica gel (5 g) and the methylated product **8** (128 mg) was isolated from the chloroform eluate in 81.5% yield. Recrystallization from chloroform provided pure **8**, mp 241—242 °C; λ_{max}^{EtOH} 237 (ε 21800), 272(28900), 293(sh., 18200), 355(19500), 374 (sh., 11600) and 485 nm(1490); ν_{max} 1670 cm^{-1} (-CON< and >CO); $\delta(CDCl_3)$, 3.92, 3.99, 4.04(each 3H, s, -OCH_3) and 6.85—8.50(6H, m, ArH). Found: C, 71.06; H, 4.75; N, 4.35%. Calcd for $C_{19}H_{15}NO_4$: C, 71.02; H, 4.71; N, 4.36%.

Zinc Dust Reduction of 7. *a) In Aqeous Acetic Acid*: A mixture of **7**(1.05 g), glacial acetic acid (400 ml), water (15 ml) and zinc dust (2.1 g) was refluxed for 1.5 hr. The reaction mixture was filtered. After concentration *in vacuo*, water (700 ml) was added. The resulting white precipitate (940 mg) was chromatographed on a column of silica gel (30 g). Elution with chloroform yielded 5,6-dihydro-4,7-dimethoxy-11*H*-indeno[1,2-*c*]isoquinolin-5-one (**10**) (306 mg) and subsequent elution with 2% methanol-chloroform gave 5,6-dihydro-11-hydroxy-4,7-dimethoxy-11*H*-indeno[1,2-*c*]isoquinolin-5-one (**11**) (286 mg). **10**(from methanol), mp 275—276 °C; λ_{max}^{EtOH} 215(ε 33900), 255(21200), 274(sh., 5920), 305(sh., 5380), 325(sh., 11200), 353(14300), 369(19700) and 388 nm(16700); ν_{max} 3420(>NH) and 1650 cm^{-1}(-CONH-); $\delta(CDCl_3)$, 3.74(2H, s, $>CH_2$), 3.80(3H, s, -OCH_3) and 3.82 (3H, s, -OCH_3). Found: C, 73.57; H, 5.21; N, 4.78%. Calcd for $C_{18}H_{15}NO_3$: C, 73.70; H, 5.15; N, 4.78%. **11** (from chloroform-methanol): mp 249—250 °C(dec.); λ_{max}^{EtOH} 217(ε 26200), 258(22000), 278(sh., 5300), 312(sh., 3440),

358(14500), 376(19100) and 396 nm (16700); ν_{max} 3420(sh., -OH), 3380(>NH) and 1654 cm^{-1}(-NHCO-). Found: C, 69.46; H, 4.95; N, 4.52%. Calcd for $C_{18}H_{15}NO_4$: C, 69.89; H, 4.89; N, 4.53%.

b) In Glacial Acetic Acid: A mixture of **7**(140 mg), zinc dust (560 mg) and glacial acetic acid (14 ml) was refluxed for 30 min. After working up as above, only **10** (110 mg) was obtained in 82% yield.

Zinc Dust Reduction of 4. **4**(270 mg), zinc dust (550 mg) and glacial acetic acid (10 ml) were mixed and refluxed for 2 hr. The insoluble material was removed by filtration. Water (10 ml) was added to the filtrate, which was then made basic by the addition of ammonia solution under ice-cooling. The precipitate, mp 218—221 °C(dec.) (182 mg, 70.5% yield) was recrystallized from methanol to give pure 5-amino-4,7-dimethoxy-11*H*-indeno[1,2-*c*]isoquinoline **12**, mp 229—230 °C(dec.); $\lambda_{max}^{H_2SO_4}$ 220(ε 36900), 239(sh., 17600), 259 (21300), 289(6960), 328(13500), 342(16200), 386(17600)and 405 nm(16500); ν_{max} 3500 and 3370 cm^{-1} (each $-NH_2$); $\delta(CF_3CO_2H)$, 3.75(2H, s, $>CH_2$), 4.03(3H, s, $-OCH_3$) and 4.13(3H, s, $-OCH_3$). Found: C, 73.73; H, 5.63; N, 9.35%. Calcd for $C_{18}H_{16}N_2O_2$: C, 73.95; H, 5.52; N, 9.58%.

Ammonia Treatment of the Hydrochloride 3. When an aq. solution of 3 (72 mg) was neutralized by dropwise addition of ammonia, red precipitate **22** (52 mg), not as vivid in color as the "red pigment" was obtained. ν_{max} 3440, 3300(broad) and 2160 cm^{-1}. However, attempts to purify **22** failed since it was so unstable that it changed completely to **4** within a few days on standing in air.

Catalytic Hydrogenation of the Hydrochloride 3. A solution of the hydrochloride **3** (100 mg) in acetic acid (8 ml) was stirred for 18 hr under hydrogen atmosphere with 10% palladium-on-charcoal (150 mg) and 2M HCl (8 ml), until the starting material was consumed completely. After the removal of the catalyst by filtration, the filtrate was diluted with water and the product was extracted three times with chloroform. The organic layer was treated with ammonia. After being washed with water and dried, the solvent was evaporated to leave an oil (30 mg) which was crystallized from methanol to afford **13**, mp 189—190 °C; $\lambda_{max}^{H_2SO_4\text{-EtOH}}$ 221(ε 36600), 239(sh., 17100), 260(20500), 289 (7230), 328(13400), 387(17100) and 406 nm(16700); $\nu_{max}^{CHCl_3}$ 3460 and 3360; ν_{max}^{Nujol} 3544 and 3408 cm^{-1}; $\delta(CDCl_3)$, 1.52 (3H, d, J=7 Hz, $>CHCH_3$), 3.93(3H, s, $-OCH_3$), 3.99(1H, q, J=7 Hz, $>CHCH_3$), 4.00(3H, s, $-OCH_3$) and 6.63—7.63 (6H, m ArH). Found: C, 74.19; H, 5.93; N, 9.08%. Calcd for $C_{19}H_{18}N_2O_2$: C, 74.49; H, 5.92; N, 9.15%. The aq. layer was made alkaline by the addition of ammonia and extracted with chloroform. The evaporation of the solvent gave **14** as an oil. $\nu_{max}^{CHCl_3}$ 3460 and 3360 cm^{-1}.

Catalytic Hygrogenation of the "Red Pigment" 2. A solution of **2** (100 mg) in acetic acid (3 ml) and 1 M HCl (2 ml) was hydrogenated over 10% palladized charcoal (60 mg) for 24 hr at room temperature. After removal of the catalyst by filtration, the filtrate was treated with ammonia. The resulting precipitate (80 mg) was crystallized from chloroform to give a red colored product **15** (18 mg), mp 208 °C (dec.); ν_{max}^{Nujol} 3340 (>NH) and 1710 cm^{-1} (>CO); $\delta(CF_3CO_2H)$, 1.54(3H, t, J=7 Hz), 4.24(3H, s), 4.32(3H, s), 4.64(2H, q, J=7 Hz), 5.34(1H, d, J=3 Hz), 6.68—8.16 (6H, m) and 9.42(1H, d, J=3 Hz). The compound was contaminated with another product as revealed by the presence of smaller signals in the NMR spectrum of δ 1.57 (t, J=7 Hz), 4.06(s), 4.34(s) and 4.60(q, J=7 Hz). Attempts to separate both compounds were unsuccessful.

Acetylation of the Hydrochloride 3. To a mixture of **3** (190 mg) and acetic anhydride (15 ml) was added five drops of concd. H_2SO_4 and the total mixture was swirled until an homogeneous yellow solution was obtained. After being left to stand at room temperature overnight, the mixture was poured onto ice-water (200 g) and the resulting red precipitate was recrystallized from chloroform to yield the acetate **16**, mp 292—293 °C(dec.), 120 mg (62.2% yield): λ_{max}^{EtOH} 217(ε 23800), 250(36200), 279(sh., 24300), 286(25400), 325(15300), 384(17100) and 520 nm(4480); λ_{max}^{Nujol} 3300, 2165 and 1680 cm^{-1}; $\delta(CF_3CO_2H)$, 2.73(3H, s, $-COCH_3$), 4.27(3H, s, $-OCH_3$), 4.37(3H, s, $-OCH_3$), 5.53(1H, s, >CH) and 7.20—8.40(6H, m, ArH). Found: C, 69.84; H, 4.86; N, 11.77%. Calcd for $C_{21}H_{17}N_3O_3$: C, 70.18; H, 4.77; N, 11.69%.

References

1) A preliminary account of this work is described in T. Kubota, T. Tokoroyama, T. Kamikawa, T. Nishikawa, M. Nakatani, S. Maeda, and K. Ando, *Nippon Kagaku Zasshi*, **92**, 1053 (1971).

2) T. Tokoroyama, T. Nishikawa, K. Ando, M. Nomura, and T. Kubota, *Nippon Kagaku Kaishi*, **1974**, 136.

3) Y. Satomura and A. Sato, *Agr. Biol. Chem.*, **29**, 337 (1965).

4) K. Nakanishi, "Infrared Spectroscopy", Nankodo, Tokyo (1960), p. 34.

5) S. Wawzonek, J. K. Stowell, and R. E. Karll, *J. Org. Chem.*, **31**, 1004 (1966).

6) This structure was confirmed by a total synthesis, which constitutes the subject of Part II of this study.

7) The SCF-MO calculation on the tautomeric structure of **2** has been unertaken in collaboration with Dr. K. Nishimoto and Mr. H. Tomono of Osaka City University. The result corroborates the assignment of the iminoindene structure for **2**.

8) For references on the tautomerism between the nitrile and ketenimine forms, *cf.* J. Casanova, Jr., "The Chemistry of the Cyano Group," ed. by Z. Rappoport, Interscience, New York, N. Y. (1970), p. 894.

9) C. L. Stevens and J. C. French, *J. Amer. Chem. Soc.*, **75**, 657 (1953).

10) C. L. Stevens and J. C. French, *ibid.*, **76**, 4398 (1954).

11) C. L. Stevens, R. C. Freeman, and K. Noll, *J. Org. Chem.*, **29**, 34 (1964).

12) S. Trofimenko, E. L. Little, Jr., and H. F. Mower, *ibid.*, **27**, 433 (1962).

13) W. J. Middleton, E. L. Little, D. D. Coffman and V. A. Engelhart, *J. Amer. Chem. Soc.*, **80**, 2795 (1958).

14) For example, it has been reported[9] that, though an acetone solution of diphenylketene-*p*-tolylimine reacts only slowly with water, the hydrolysis is complete in a few seconds by the addition of a small amount of hydrochloric acid to give *N*-(*p*-tolyl)diphenylacetamide in 86% yield. The treatment of **2** with a mixture of dil. hydrochloric acid and ethanol even at refluxing temperature merely resulted in the recovery of the starting material.

15) Trofimenko has reported[12] the value 2170 cm^{-1} for the IR absorption of the cyano group in the metal salt of tricyanomethane which has the structure

$$\left[\begin{matrix}NC\\NC\end{matrix}\!\!>\!C^{-}\text{-}C\equiv N \longleftrightarrow \begin{matrix}NC\\NC\end{matrix}\!\!>\!C=C=N^{-} \quad etc.\right]M^{+}.$$

cf. also S. Trifimenko, *J. Org. Chem.* **28**, 217, 2755 (1963).

16) J. W. Happ, E. G. Janzen, and B. C. Rudy, *J. Org. Chem.*, **35**, 3382 (1970).

17) We have found that cyclization by way of this path does also occur but to a lesser extent and this subject will be dealed with in the forthcoming publications.

Cyclization Reactions of 1,2-Bis(2-cyanophenyl)propionitriles. II. Synthesis of 5-Amino-4,7-dimethoxy-11*H*-indeno[1,2-*c*]isoquinolin-11-one[1)]

Kazuo ANDO, Takashi TOKOROYAMA, and Takashi KUBOTA*

Faculty of Science, Osaka City University, Sugimoto-cho, Sumiyoshi-ku, Osaka 558

(Received September 7, 1973)

The structure of 5-amino-4,7-dimethoxy-11*H*-indeno-[1,2-*c*]isoquinolin-11-one (**2**) derived by the degradation of the "red pigment" has been confirmed by synthesis. 5,6-Dihydro-4,7-dimethoxy-11*H*-indeno[1,2-*c*]-isoquinoline-5,11-dione (**3**) obtained from **2** was used as a relay compound. This was first converted into **2** by chlorination with phosphorus oxychloride and treatment with ammonia. Subsequently **3** was synthesized from 2-(2-carboxy-3-methoxyphenyl)-4-methoxyindane-1,3-dione (**13**) *via* 4,7-dimethoxy-11*H*-indeno[1,2-*c*]isocoumarin-11-one (**12**).

In a previous paper[1)] it was reported that a red pigment **1**, $C_{22}H_{19}N_3O_4$ is obtained in a good yield by the base catalyzed cyclization of 1,2-bis(2-cyano-3-methoxyphenyl)propionitrile in the presence of diethyl carbonate, and its treatment with alkaline hydrogen peroxide leads to the formation of an oxidation product, $C_{18}H_{14}N_2O_3$. We have deduced the structure 5-amino-4,7-dimethoxy-11*H*-indeno-[1,2-*c*]isoquinolin-11-one (**2**) for this compound from spectral and chemical evidences. The crucial role of this assignment in the structure elucidation of **1** led us to confirm the structure of **2** unequivocally by synthesis.

For the synthetic route to **2** it would be reasonable to pass through 5,6-dihydro-4,7-dimethoxy-11*H*-indeno-[1,2-*c*]isoquinoline-5,11-dione (**3**), obtained from **2** by alkaline hydrolysis. Partial synthesis of **2** from **3** was studied first. Treatment of **3** with phosphorus oxychloride at refluxing temperature provided an orange-red colored substance **4**. Since its infrared spectrum revealed the disappearance of the lactam group in **3** and the retainment of the indenone carbonyl group (1705 cm^{-1}), **4** was proved to be the expected chloride, 5-chloro-4,7-dimethoxy-1*H*-indeno[1,2-*c*]isoquinolin-11-one. This was heated with ammonia in ethanol in a sealed tube at 150 °C for 14 hr. The product thus obtained was identified as **3** and the divided acetate as **2a** by comparison of their infrared spectra with those of authentic specimens, mixed thin layer chromatography and mixed melting point determination. These transformations met our first aim and at the same time verified the presumed structural relationship between **2** and **3**.[1)]

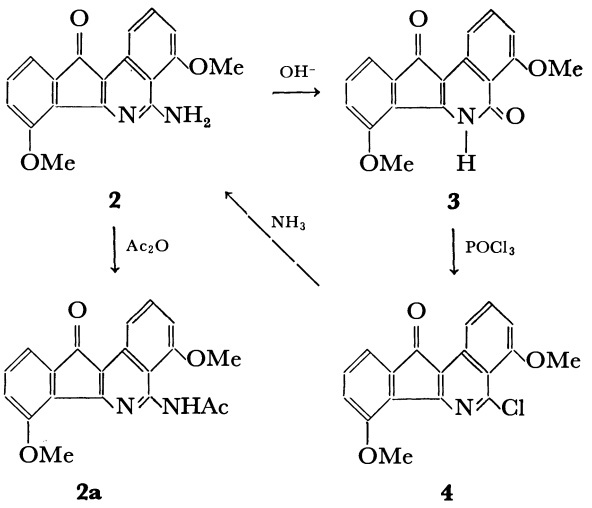

Scheme 1

In principle two ways of ring closure as depicted in **5a** and **5b** are conceivable for the construction of 5,6-dihydro-11*H*-indeno[1,2-*c*]isoquinoline-5,11-dione (**5**, X=NH) or 5,6-dihydro-11*H*-indeno[1,2-c]isocoumarin-11-one (**5**, X=O) system. The latter system is convertible to the former by treatment with ammonia.[2)]

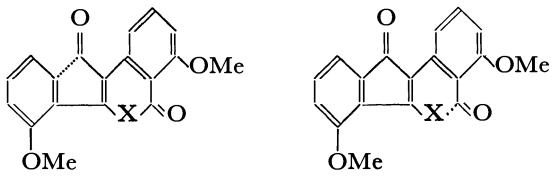

Since 4-carboxy-8-methoxy-3-(2-methoxyphenyl)isocarbostyril necessary in route **5a** seemed to be more easily accessible, the synthetic approach in this direction was investigated first. The condensation of 2-cyano-3-methoxyphenylacetonitrile (**6**)[3)] with 2-methoxybenzoyl chloride (**7**) with sodium hydride yielded the product **9**, $C_{26}H_{20}N_2O_5$. The spectral data revealed that **9** was the product, which arose through the enol-benzoylation of once-formed 1-(2-cyano-3-methoxyphenyl)-1-(2-methoxybenzoyl)acetonitrile (**8**). Thus the reaction mixture of the above condensation was directly treated with 40% hydrogen bromide in glacial acetic acid at 70 °C to provide the desired isocoumarin **10**. Treatment of **10** with ammonia at 150 °C in a sealed tube afforded the carbostyril **11**. All attempts to hydrolyse **11** to **12** including treatment with alkaline hydrogen peroxide or the refluxing with potassium hydroxide in ethylene glycol were unsuccessful. The resistance of the cyano group in **11** to hydrolysis remains unclarified.

The synthesis of **2** by way of route **5b** was investigated subsequently. We undertook to prepare 4,7-dimethoxyindenoisocoumarin-11-one (**12**) first. Indenoisocoumarin-11-one (**15**) was synthesized by the dehydrative cyclization of 2-(2-carboxyphenyl)indane-1,3-dione (**14**) by Pailer *et al.*[4)] and we examined the synthesis of **12a** by this method though the cyclizations in two directions would be possible in the intermediate, 2-(2-carboxy-3-methoxyphenyl)-4-methoxyindane-1,3-dione (**13**). The reaction of 6-methoxyphthalaldehydic acid (**16**)[5)] and 7-methoxyphthalide (**17**)[6)] with sodium

* Present address: Kinki University, Kowakae, Higashi-osaka-shi, Osaka 577

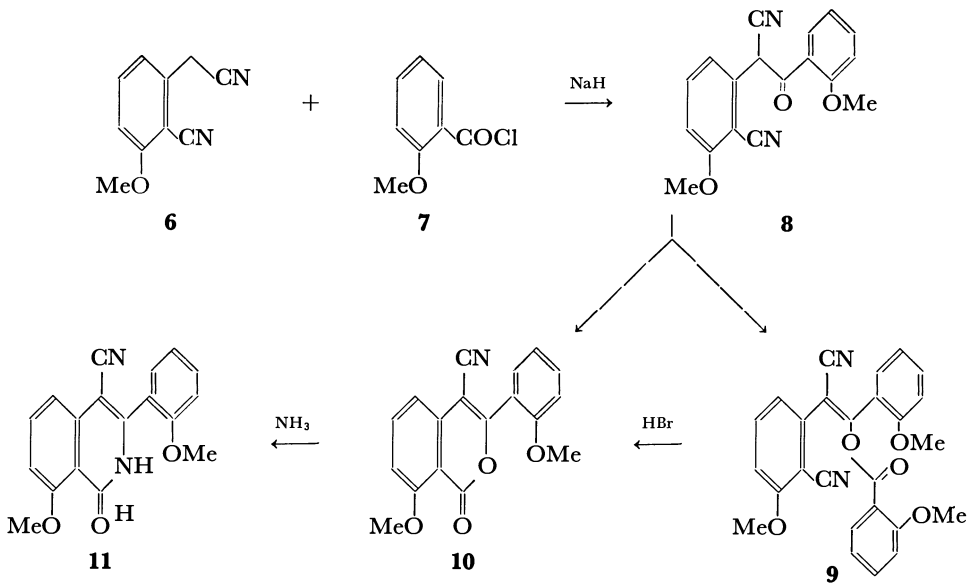

Scheme 2.

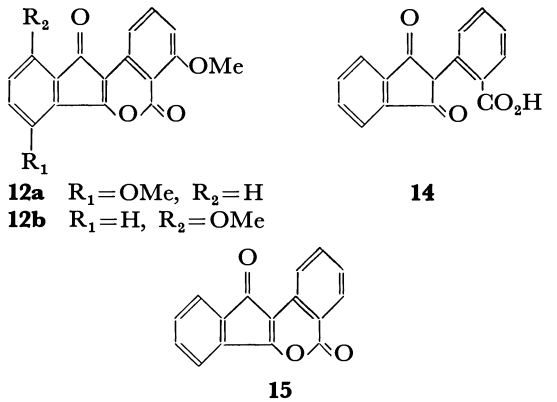

methoxide gave 2-(2-carboxy-3-methoxyphenyl)-4-methoxyindane-1,3-dione (**13**) accompanied by a mixture of the diastereomeric hydrodiphthalyls **18a** and **18b** which were separable by chromatography on a silica gel column. **18a** was more easily eluted on the chromatography than **18b**. Inspection of the models shows that the diastereomeric protons in the *dl*-form would be more susceptible to the shielding anisotropy of the β-phenyl groups in comparison to the *meso*-form in which such effect would be negligible. Thus the methine proton of **18a** resonates at lower filed than that of **18b**, and **18a** could tentatively be assigned to the

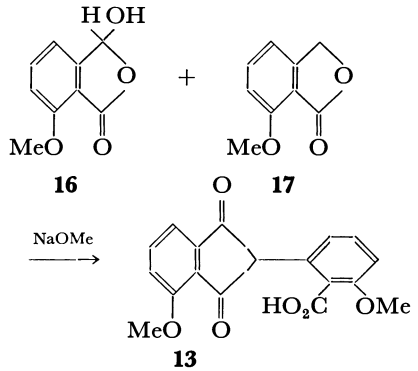

Scheme 3.

meso-form and the latter to the *dl*-form. The hydrodiphthalyls **18a** and **18b**, when treated again with excess sodium methoxide, provide the indanedione **13** which yields a red anion **13a** by treatment with base which on heating gradually turns red above 216 °C. When **13** was heated with acetic anhydride, two kinds of colored products were obtained; a reddish orange compound **12a**, mp 287 °C, ν_{max} 1770 and 1705 cm^{-1}; a yellowish orange compound **12b**, mp 247—247.5 °C, ν_{max} 1760 and 1710 cm^{-1}. Since both compounds have the same molecular composition $C_{18}H_{12}O_5$ and exhibit similar carbonyl bands due to lactonic and ketonic groups in the IR spectra, they represent the 11-oxoindenoisocoumarin isomers formed by the cyclization of **13** in two possible directions. However, it could not be said for the products which were which of the two isomers. On treatment of **12a** and **12b** with ethanolic ammonia at 120 °C for 12 hr both

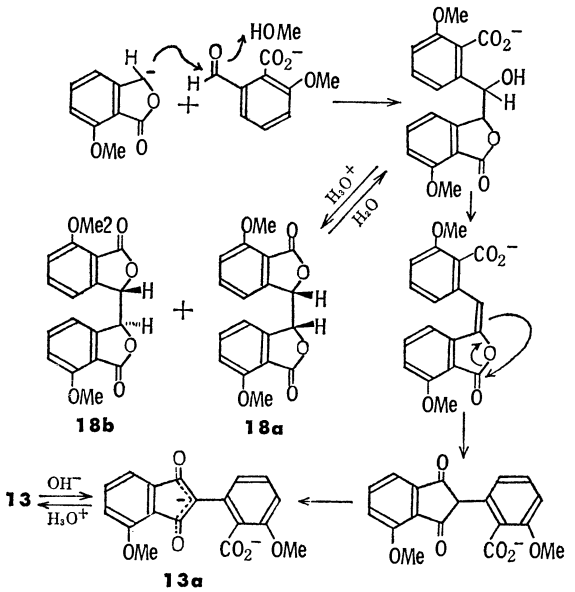

Scheme 4.

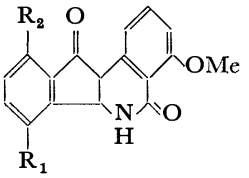

19a R=OMe, R_2=H
19b R_1=H, R_2=OMe

compounds afforded the same products **19a** and **19b** in different ratios, 2.3 : 1 and 1 : 4, respectively. The result suggests that the isocoumarins **12a** and **12b** yield mainly the corresponding isocarbostyrils **19a** and **19b** respectively, though some equilibrium may exist between the isomers during the course of reaction. Actually **19a** was found to be identical with **3** from a comparison of their IR spectra and Tlc, and the mixed melting point determination. The structure of **19b** was verified by elemental analyses and the appearance of the absorption bands at 3100—2600 (broad, lactam), 1705 (ketone) and 1650 cm^{-1} (lactam) in its IR spectrum.

Comparison of NH stretching bands of the lactam groupings in **19a** and **19b** provides important information on the differentiation of both compounds. The NH band in **19a** is observed as a sharp peak at 3380 cm^{-1} owing to the obstruction for the formation of intermolecular hydrogen bond, whereas **19b** exhibits the bonded broad absorption without such hindrance. The contrast in NH stretching bands in **19a** and **19b** rationalizes our assumption made on the assignment of structure **3** for the oxidation product of the "red pigment".[1] The structures of **19a** and **19b** are thus delineated as shown and the formulas **12a** and **12b** are given to the parent isocoumarin isomers. Thus as a matter of course **19a** has to be identical with **3** and this was found to be the case.

In conclusion, the synthesis of **2** has been accomplished using **3** as a relay compound and the structure of **2** has been determined unambiguously.

Experimental[1]

Conversion of 5,6-Dihydro-4,7-dimethoxy-11H-indeno[1,2c]isoquinoline-5,11-dione (3) into 5-Chloro-4,7-dimethoxy-11H-indeno-[1,2-c]isoquinolin-11-one (2). **3** (298 mg) was heated with phosphorus oxychloride (10 ml) under refluxing for 2 hr. After cooling the reaction mixture was poured into ice-water and the resulting reddish orange precipitate was filtered, dried and chromatographed on a silica gel column (10 g). Elution with benzene-chloroform (1 : 1) gave reddish orange crystals (105 mg) which on recrystallization from chloroform gave pure **4**, mp 266—267 °C; λ_{max}^{EtOH} 217 (ε 34700), 273(49600), 358(1820), 394(450) and 460 nm(160); ν_{max} 1705 cm^{-1} (>CO). Found: C, 66.33; H, 3.70; N, 4.26%. Calcd for $C_{18}H_{12}ClNO_3$: C, 66.37; H, 3.71; N, 4.30%.

Treatment of 5-Chloro-4,7-dimethoxy-11H-indeno[1,2-c]isoquinolin-11-one (4) with Ammonia. **4** (130 mg) was heated with saturated ethanolic ammonia solution (18 ml) in a sealed tube at 150 °C for 22 hr. The red colored product, precipitated on cooling, was collected by filtration (110 mg) and recrystallized from chloroform-ethanol to yield 5-amino-4,7-dimethoxy-11*H*-indeno[2,2-*c*]isoquinolin-11-one (**2**), mp 289—290 °C. The IR spectrum of this product was superimposable with that of an authentic sample derived from the red pigment **1**.[1] The result of mixed melting point determination and tlc also corroborated the identity of both compounds. The derived acetate **2a**, mp 270—273 °C, was found to be identical with the one obtained previously.[1]

Condensation of 2-Cyano-3-methoxyphenylacetonitrile (6) with 2-Methoxybenzoyl Chloride (7). 2-Methoxybenzoyl chloride (**7**) (9.00 g) was added to a cooled solution of sodium salt of the acetonitrile **6**, prepared by the addition of **6** (6.75 g) to a mixture of sodium hydride (50% oil-coated, 1.99 g) and dry tetrahydrofuran (200 ml) and the mixture was stirred at room temperature for 2 hr. The reaction mixture was poured into water (400 ml) and the product was extracted with benzene. The organic layer was washed successively with 5% $NaHCO_3$ and water, and then dried over anhyd. Na_2SO_4. Evaporation of the solvent left a gummy residue (*ca.* 14 g), which was then warmed with a mixture of glacial acetic acid (7 ml) and 40% hydrobromic acid (18 ml) at 70 °C for 30 min. After cooling the mixture was poured into ice-water and the product was extracted with chloroform. The extract was washed with 5% $NaHCO_3$ and dried. Evaporation of the solvent provided a solid residue (*ca.* 10 g), which, on crystallization from chloroform-methanol yielded crude 4-cyano-8-methoxy-3-(2-methoxyphenyl)isocoumarin **10**, mp 205—227 °C (3.25 g). Further recrystallization from acetic acid afforded pure **10**, mp 236—237 °C; λ_{max}^{EtOH} 212 (ε 24600), 256(13300) and 342 nm (11800); ν_{max}^{EtOH} 2230 (-CN), 1765 (>CO) and 1755 cm^{-1} (>CO); $\delta^{CF_3CO_2H}$ 4.00 (3H, s, $-OCH_3$), 4.11 (3H, s, $-OCH_3$) and 7.03—8.15 (7H, m, ArOH). Found: C, 70.12; H, 4.33; N, 4.54%. Calcd for $C_{18}H_{13}NO_4$: C, 70.35; H, 4.26; N, 4.56%. Crystallization of the gummy residue from chloroform-ether, without treatment with HBr-AcOH, gave the enol benzoate **9** as needles, mp 155—156 °C; ν_{max} 2225 (-CN) and 1745 cm^{-1} (>CO); δ^{CDCl_3} 3.53 (3H, s, $-OCH_3$), 3.85 (3H, s, $-OCH_3$), 3.90 (3H, s, $-OCH_3$) and 6.65—8.20 (11H, m, ArOH). Found: C, 70.82; H, 4.77; N, 6.39%. Calcd for $C_{26}H_{20}N_2O_5$: C, 70.90; H, 4.58; N, 6.36%.

4-Cyano-8-methoxy-3-(2-methoxyphenyl)isocarbostyril (11). The isocoumarin **10** (200 mg) was treated with saturated ethanolic ammonia solution (15 ml) in a sealed tube at 150 °C for 5 hr. The product (92 mg) precipitated on cooling was collected by filtration. Recrystallization from methanol gave **11**, mp 304—306 °C; ν_{max} 3160 (>NH), 2230 (-CN) and 1670 cm^{-1} (>CO); δ^{CDCl_3} 3.96 (3H, s, $-OCH_3$), 4.38 (3H, s, $-OCH_3$) and 7.11—8.35 (7H, m, ArOH). Found: C, 70.28; H, 4.67; N, 8.88%. Calcd for $C_{18}H_{14}N_2O_3$: C, 70.58; H, 4.61; N, 9.15%.

Condensation of 7-Methoxyphthalide (17) and 6-Methoxyphthalaldehydic Acid (16). **17** (500 mg) was dissolved in a solution of sodium methoxide in methanol (prepared from 103 mg of sodium and 25 ml of abs. methanol) and then **16** (738 mg) was added under nitrogen atmosphere. After the mixture was refluxed for 2.5 hr, the solvent was evaporated *in vacuo* from the reddish reaction mixture. The concentrated mixture was poured into ice-water (50 ml), acidified with 1M H_2SO_4 and then extracted with chloroform. Evaporation of the solvent from the washed and dried organic layer provided colorless gummy residue (1.08 g), which was treated with hot ethanol (40 ml). The insoluble material turned out to be the mixture of the diastereomers **18a** and **18b**, and was separated by chromatography on a silca gel column. Elution with benzene-chloroform (1 : 1) afforded first **18a** and then **18b** in a ratio of 1 : 1. **18a** was crystallized from a mixture of chloroform and ethanol: mp 277—278 °C (dec.); ν_{max} 1705 cm^{-1} (>CO); $\delta^{CF_3CO_2H}$ 4.00 (6H,

s, 2-OCH_3) and 6.20 (2H, s, 2-CO_2CH<). **18b** was crystallized from chloroform: mp 286—286.5 °C; ν_{max} 1770 (sh.) and 1760 cm^{-1} (>CO); $\delta^{CF_3CO_2H}$ 4.06 (6H, s, 2-OCH_3) and 6.00 (2H, s, 2-CO_2CH<). Saturated aq. $NaHCO_3$ was added to the ethanolic solution obtained in the above treatment. The red alkaline solution was, after washing with chloroform, acidified by the addition of 1M H_2SO_4 and extracted with chloroform. The organic layer was washed with water and dried. Evaporation of the solvent yielded an oil (80 mg), which on trituration with ether furnished 4-methoxy-2-(2-carboxy-3-methoxyphenyl)indane-1,3-dione (36 mg): mp 220—222 °C (from ethanol, turned red at (**13**), *ca.* 216 °C); ν_{max} 3260 (broad, -CO_2H), 1740 (weak, >CO) and 1710 cm^{-1} (strong, -CO_2H). When both **18a** (50 mg) and **18b** (50 mg) were treated with excess sodium methoxide in methanone, the indane-1,3-dione **13** was obtained in the yields of 17 mg and 38 mg, respectively.

*Dehydrative Cyclization of 4-Methoxy-2-(2-carboxy-2-methoxyphenyl)indane-1,3-dione (**13**).* The indane-1,3-dione **13** (100 mg) was heated with acetic anhydride (5 ml) on a water bath (90 °C) for 30 min. The solution became red and finally gave a reddish precipitate. The reaction mixture was poured into ice-water and the precipitated product was recrystallized from acetic acid to afford **12a** as reddish orange needles (40 mg): mp 287 °C; λ_{max}^{EtOH} 214 (ε 31800), 236 (31000), 259 (sh., 34400), 266 (44500), 278 (sh., 17300), 354 (14700) and 456 nm (3300); ν_{max} 1770 (lactone) and 1705 cm^{-1} (ketone). Found: C, 69.78; H, 4.01%. Calcd for $C_{18}H_{12}O_5$: C, 70.13; H, 3.92%. After removal of the solvent from the mother liquor of the recrystallization, the residue was recrystallized successively from benzene and acetic acid to yield **12b** as yellowish orange needles (33 mg): mp 247—247.5 °C; λ_{max}^{EtOH} 236 (ε 38700), 254 (39500), 261 (60900), 273 (sh., 18700), 352 (16800) and 430 nm (3200); ν_{max} 1760 (lactone) and 1710 cm^{-1} (ketone). Found: C, 70.10; H, 3.97%. Calcd for $C_{18}H_{12}O_5$: C, 70.13; H, 3.92%.

*Ammonia Treatment of 4,7-Dimethoxy- (**19a**) and 4,10-Dimethoxy-11H-indeno[1,2-c]isocoumarin-11-one (**19b**).* The reddish orange isomer **12a** (50 mg) was heated with saturated ethanolic ammonia in a sealed tube at 120 °C for 12 hr. After cooling the reaction mixture was poured into water and the red colored product, collected by filtration, was chromatographed on a silica gel column (2 g). Elution with chloroform afforded first the orange colored product **19a** (25 mg) and then the yellow colored isomer **19b** (11 mg). The former is more soluble in common organic solvents than the latter. When the yellow isomer **12b** was treated with ammonia in the same way as **12a**, **19a** and **19b** were obtained on fractional crystallization from chloroform in 11 mg and 44 mg yields, respectively. **19a**, mp 29.5 °C, recrystallized from a mixture of chloroform and ethanol, was identical with **3** obtained previously by the degradation of the "red pigment"[1] in the IR spectra, tlc and mixed melting point determination. Found: C, 70.15; H, 4.22; N, 4.70%. Calcd for $C_{18}H_{13}NO_4$: C, 70.35; H, 4.26; N, 4.56%. The yellow isomer **19b** was recrystallized from acetic acid: mp>300 °C; λ_{max}^{EtOH} 232 (ε 32400), 264 (36900), 290 (19700), 348 (20600), 368 (13300) and 450 nm (2500); ν_{max} 3100—2600 (broad, lactam NH), 1705 (ketone) and 1650 (lactam carbonyl) cm^{-1}. Found: C, 70.29; H, 4.33; N, 4.68%. Calcd for $C_{18}H_{13}NO_4$: C, 70.35; H, 4.26; N, 4.56%.

References

1) For Part I of this series, K. Ando, T. Tokoroyama, and T. Kubota, This Bulletin, **47**, 1008 (1974).

2) S. Warvzonek, J. Stowell, and R. E. Karil, *J. Org. Chem.*, **31**, 1004 (1966).

3) T. Tokoroyama, T. Nishikawa, K. Ando, N. Nomura, and T. Kubota, *Nippon Kagaku Zasshi*, **1974**, 136.

4) M. Pailer, H. Worther, and A. Meller, *Monatsh. Chem.*, **92**, 1037 (1961).

5) J. Blair, W. R. Logan, and G. T. Newbold, *J. Chem. Soc.*, **1956**, 2443.

6) J. Blair, J. J. Brown, and G. T. Newbold, *ibid.*, **1955**, 708.

NOTES

BULLETIN OF THE CHEMICAL SOCIETY OF JAPAN, VOL. 47(4), 1018—1019 (1974)

Photoreaction of 2,2-Diphenylvinyl Ketones

Kazuyuki MAEDA, Ichiro MORITANI, and Akio SONODA

Department of Chemistry, Faculty of Engineering Science, Osaka University, Machikaneyama, Toyonaka, Osaka 560

(Received July 4, 1973)

Synopsis. The photoreaction of 2,2-diphenylvinyl ketones leading to 1,1,4,4-tetraphenylbutadiene, which seems to formally involve α-cleavage of vinyl ketones.

Although much attention has been paid to the photochemical dimerization of unsaturated aliphatic ketones,[1-3] and (2+2) cycloaddition to olefins,[4,5] only one case has been reported on the primary photodissociation of α,β-unsaturated ketones at elevated temperature with low efficiency.[6]

We report herewith on the photoreaction of 2,2-diphenylvinyl ketones (**1**) leading to 1,1,4,4-tetraphenylbutadiene (**2**), which formally involves α-cleavage of **1** and dimerization.

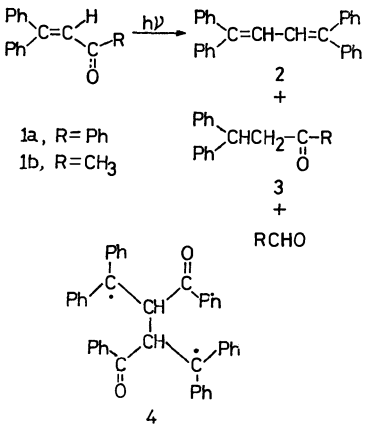

Fig. 1.

Irradiation of a solution of 1,3,3-triphenyl-2-propen-1-one (**1a**) in 2-propanol (2.9×10^{-2} mol/l) with high-pressure mercury arc was carried out for 90 hr under argon atmosphere. Removal of the resulting benzoic acid (7%) by extraction with the base followed by chromatography on Al_2O_3 gave the butadiene **2** (37%) and 1,3,3-triphenylpropan-1-one (**3a**) (27%). The structural assignment of these products was established by comparison of their spectral data with those of the authentic samples. Analogous photoreaction of 4,4-diphenyl-3-buten-2-one (**1b**) in 2-propanol afforded the butadiene **2** (18%) and 4,4-diphenylbutan-2-one (**3b**) (5%).

A probable pathway involves the initial coupling of **1** at the α-position leading to **4**, the most stable biradical of three possible intermediate species. Subsequent cleavage of Norrish Type I of **4** would lead to the butadiene **2** and two benzoyl radicals. Hydrogen abstraction of the latter followed by autoxidation during the work-up may lead to benzoic acid. Although a number of photodimers of unsaturated aliphatic ketones,[2] carboxylic acid,[1] and esters[3] have been isolated, no photodimer could be detected in this photoreaction probably because of extraordinary stability of the biradical **4**.

An alternative mechanism which includes α-cleavage of the ketones **1** affording 2,2-diphenylvinyl radical and subsequent coupling to give **2** seems unlikely, since facile hydrogen abstraction of vinyl radical can overcome the coupling reaction.[7] No product such as diphenylethylene which can be derived from hydrogen abstraction of 2,2-diphenylvinyl radical could be detected during the course of photoreaction.

Ketone **3a**, derived from photoreduction of **1a**,[8,9] could be obtained only in 2-propanol among various solvents as shown in Table 1.[10]

Table 1. Solvent effect of photoreaction of **1a** under nitrogen (30 hr)

Solvent	Conversion (%)	Yield of **2** (%)	Yield of **3a** (%)
2-Propanol	74	26	26
Cyclohexane	28	25	0
Benzene	26	17	0

Experimental

*Irradiation of 1,3,3-Triphenyl-2-propen-1-one (**1a**) in 2-Propanol.* A solution of **1a** (8.25 g), mp 87.5—88.7 °C (lit,[11] mp 84—87 °C), in 2-propanol (1000 ml) was irradiated under argon. The reaction was monitored periodically (UV analysis and tlc technique). After 90 hr irradiation, the solvent was evaporated, and the residue was dissolved in CH_2Cl_2. Extraction of the CH_2Cl_2 solution with a $NaHCO_3$ solution followed by acidification gave benzoic acid (0.20 g). The neutral products were subjected to alumina chromatography (400 g of alumina). Elution with *n*-hexane gave butadiene **2** (1.65 g, 37%), which was identified by comparison with an authentic specimen, mp 201—202 °C (lit,[12] mp 204—205 °C), Found: C, 94.04; H, 6.20%. Calcd for $C_{28}H_{22}$: C, 93.81; H, 6.19%). NMR (CCl_4, δ): 6.65 (2H, s, vinyl), 7.10 (10H, s) and 7.20—7.40 (10H, broad d). Further elution with benzene afforded a yellow oil, which upon fractional distillation under reduced pressure gave **3a** (1.93 g, 27%), bp 205—207 °C/2 mmHg, and recovered **1a** (1.22 g). The structure of **3a** was established by comparison with an authentic sample and mixed mp. Mp 92.8—93.5 °C (lit,[13] 91—92 °C). IR (nujol mull): 1670 cm^{-1} (C=O). NMR (CCl_4, δ): 3.53—3.70 (2H, d), 4.70—4.90 (1H, t) and 7.05—7.95 (15H, m). Finally, elution with ether gave a trace of a crystalline compound (mp 250—254 °C, mol wt. 554) and a tarry material.

Irradiation of ***1a*** *in the Presence of Oxygen.* A solution **1a** (16.50 g) in 2-propanol (1000 ml) was irradiated under a slow stream of dry air for 45 hr. The treatment as described above gave benzoic acid (0.17 g, 3%). An alumina chromatography of the neutral products gave the butadiene **2** (2.26 g, 27%), benzophenone (5.61 g, 66%), acetophenone (2.26 g, 46%), and recovered **1a** (1.10 g) in addition to tarry materials.

*Irradiation of 4,4-Dipheny-3-buten-2-one (**1b**) in 2-Propanol.* A solution of **1b** (2.96 g), bp 168—170 °C/7 mmHg, mp 33.5—34.5 °C (lit,[14] bp 195—205 °C/15 mmHg), in 2-propanol (500 ml) was irradiated for 50 hr under nitrogen. The resulting mixture was subjected to alumina chromatography. Petroleum ether–benzene eluted **2** (0.39 g, 18%). Elution with benzene gave benzoic acid (0.013 g, 1%) and the ketone **3b** (0.11 g, 5%). Mp 47.0—48.0 °C (lit,[15] mp 47.5 °C). IR (nujol mull): 1710 cm^{-1} (C=O). NMR (CS_2, δ): 1.93 (3H, s), 3.01 (2H, d, J=7.5 Hz), 4.44 (1H, t, J=7.5 Hz), 6.90—7.95 (10H, m).

References

1) J. Corse, B. J. Finkel, and R. E. Lundin, *Tetrahedron Lett.*, **1961**, 1.
2) G. Montaudo and S. Caccamese, *J. Org. Chem.*, **38**, 710 (1973); references cited therein.
3) H. Stobbe, *Ber.*, **45**, 3396 (1912).
4) E. J. Corey, J. D. Bass, R. LeMahieu, and R. B. Mitra, *J. Amer. Chem. Soc.*, **86**, 5570 (1964).
5) P. E. Eaton, *Accounts Chem. Res.*, **1**, 50 (1968).
6) J. N. Pitts, Jr., and J. K. S. Wan, "The Chemistry of the Carbonyl Group," Vol. I, ed. by S. Patai, John Wiley & Sons, Inc., New York, N. Y. (1966), p. 870; references cited therein.
7) J. K. Haynes, Jr., and J. A. Kampmeire, *J. Org. Chem.*, **37**, 4167 (1972).
8) H. M. Rosenberg and P. Sarve, *J. Amer. Chem. Soc.*, **92**, 4746 (1970).
9) M. J. Jorgenson and N. C. Yang, *ibid.*, **85**, 1698 (1963); idem, *Tetrahedron Lett.*, **1203** (1964).
10) Irradiation of **1a** in 2-propanol under slow stream of oxygen gave **2** (27%), benzoic acid (3%), benzophenone (66%), and acetophenone (46%).
11) H. K. Hess W. Weltzien, *Ber.*, **54**, 2511 (1921); K. H. Meyer and K. Schuster, *ibid.*, **55**, 819 (1922).
12) G. Wittig and F. v. Lupin, *ibid.*, **61**, 1627 (1928).
13) P. R. Shildneck, "Organic Syntheses," Coll, Vol. II, p. 236 (1943).
14) W. Wilson and Zu-Young Kyi, *J. Chem. Soc.*, **1321** (1952).
15) G. G. Henderson and M. A. Parker, *ibid.*, **71**, 676 (1897).

BULLETIN OF THE CHEMICAL SOCIETY OF JAPAN, VOL. 47(4), 1020—1021 (1974)

Charge-transfer and Proton-transfer in the Formation of Molecular Complexes. VIII.[1] Benzidine–2,4-Dinitrophenol Complexes

Gunzi SAITO* and Yoshio MATSUNAGA**

Department of Chemistry, Faculty of Science, Hokkaido University, Sapporo 060

(Received July 17, 1973)

Synopsis. The simultaneous operation of charge-transfer and proton-transfer interactions was demonstrated in the orange complex and also in the brown complex of a 3 : 2 composition. The former one quickly becomes the yellow monohydrate of the 1 : 1 salt upon exposure to air.

Buehler and Heap have reported that the benzidine–2,4-dinitrophenol (1 : 1) complex is brown when it is prepared in absolute ethanol, while it is yellow when 95% ethanol is employed as the solvent.[2] The latter complex contains 1 mol of water. As the first pK_a value of the diamine is higher than the value of the dinitrophenol (namely, 4.95 *vs.* 4.09), it does not seem likely that the brown-colored complex is of the charge-transfer (CT) type.[3] We can also eliminate the possibility that this "1 : 1 complex" is of the same type as the brick red-colored *o*-tolidine–picric acid (1 : 1) complex previously described by us.[4] If the brown benzidine–dinitrophenol complex belongs to Case 1 of CPT complexes as defined in a previous paper, a part of the diamine molecule acts as a proton-acceptor, while the other part has a CT interaction with the dinitrophenolate anion. The electron-donor strength of the monoprotonated benzidine can be essentially determined from that of the unprotonated part. By analogy with the case of the picrate anion,[4-7] the acceptor strength of the dinitrophenolate anion can be expected to be close to that of *m*-dinitrobenzene; therefore, the color of the 1 : 1 complex cannot be deeper than that of the aniline–*m*-dinitrobenzene complex. The observation the above-mentioned workers is undoubtedly in disagreement with this expectation.

By mixing equimolar amounts of the component compounds separately dissolved in hot chloroform which contains 0.05% of water according to the manufacturer, a yellow complex was obtained. Calcd for $C_{12}H_{12}N_2 \cdot C_6H_4N_2O_5 \cdot H_2O$: C, 55.96; H, 4.66; N, 14.51%. Found: C, 56.06; H, 4.70; N, 14.37%. When the solvent was dried with calcium chloride and the mixture was kept in a refrigerator, an orange-colored complex appeared. This complex quickly turned yellow upon exposure to air. After the color change, the composition was in good agreement with that of the monohydrate of the 1 : 1 complex. Found: C, 56.06; H, 4.84%. The brown complex was isolated at room temperature from a dried chloroform solution containing the diamine in excess and also from an absolute ethanol solution as has been reported by Buehler and Heap. Calcd for $3C_{12}H_{12}N_2 \cdot 2C_6H_4N_2O_5$: C, 61.69; H, 4.78; N, 15.22%. Found: C, 61.96; H, 4.95% (from chloroform) and C, 62.61; H, 4.78; N, 15.20% (from ethanol).

The vibrational spectrum of the yellow monohydrate clearly indicates the presence of water by a band at

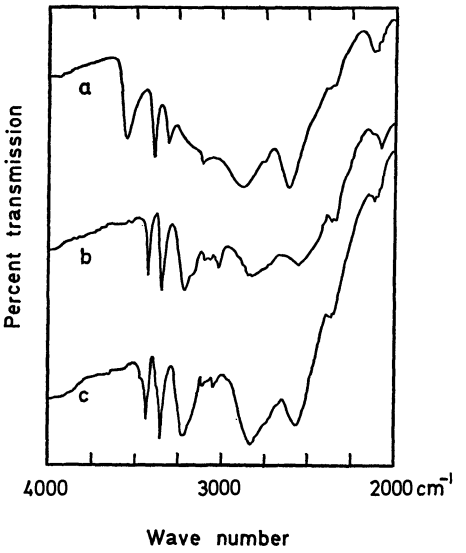

Fig. 1. Vibrational spectra, a) the yellow benzidine–2,4-dinitrophenol complex, b) the orange complex, and c) the brown complex.

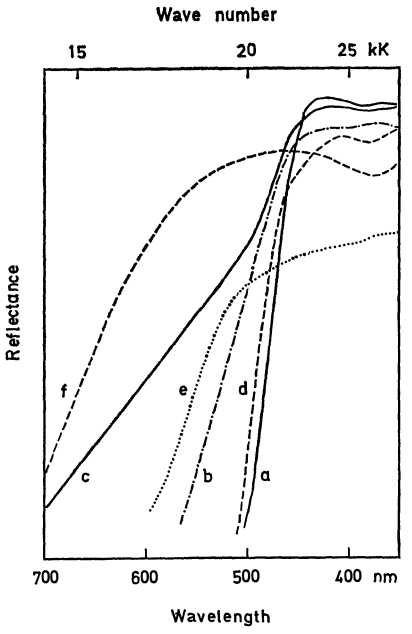

Fig. 2. Reflectance spectra, a) the yellow benzidine–2,4-dinitrophenol complex, b) the orange complex, c) the brown complex, d) sodium 2,4-dinitrophenolate, e) the aniline–*m*-dinitrobenzene complex, and f) the benzidine–*m*-dinitrobenzene complex.

* Present address: Department of Chemistry, Emory University, Atlanta, Georgia, 30322, U.S.A.

** To whom inquiries may be addressed.

3550 cm^{-1}, that of the NH_2 group by bands at 3320 and 3395 cm^{-1}, and that of the NH_3^+ group by those in the region from 2500 to 3000 cm^{-1}. As is shown by the spectrum in Fig. 1, the newly-found orange complex is undoubtedly free from water. In accordance with the composition, bands assignable to both the NH_2 and NH_3^+ groups are also detected in the orange- and brown-colored complexes.

The diffuse reflectance spectrum of the yellow complex is similar to that of sodium dinitrophenolate. Therefore, it may be concluded that the monohydrate is a salt formed by means of the proton-transfer from the phenol to the diamine. The orange complex exhibits an additional absorption band located close to the CT band in the aniline–*m*-dinitrobenzene complex (see Fig. 2). On the other hand, the location of the additional absorption band appearing in the brown 3 : 2 complex can be well compared with that of the CT band in the benzidine–*m*-dinitrobenzene complex. On the basis of these spectroscopic observations, we may conclude that the deeply-colored complexes are of the CPT type, but belong to different cases.[4] In both complexes, the electron-acceptor is the dinitrophenolate anion. The electron-donor in the orange complex is the monoprotonated benzidine cation, while that in the brown complex is the diamine molecule.

Buehler and Heap have concluded the composition of the brown complex to be 1 : 1 on the basis of the nitrogen content, which does not depend much on the mole ratio. Their results, 14.94 and 14.92%, seem not to be inconsistent with the newly-assigned composition, for which N is 15.22%.

References

1) Part VII: N. Inoue and Y. Matsunaga, This Bulletin, **46**, 3345 (1973).
2) C. A. Buehler and A. G. Heap, *J. Amer. Chem. Soc.*, **48**, 3168 (1926).
3) N. Inoue and Y. Matsunaga, This Bulletin, **45**, 3478 (1972).
4) G. Saito and Y. Matsunaga, *ibid.*, **46**, 714 (1973).
5) Y. Matsunaga and G. Saito, *ibid.*, **45**, 963 (1972).
6) G. Saito and Y. Matsunaga, *ibid.*, **45**, 2214 (1972).
7) Y. Matsunaga, *ibid.*, **46**, 998 (1973).

BULLETIN OF THE CHEMICAL SOCIETY OF JAPAN, VOL. 47(4), 1022—1023 (1974)

Dielectric Relaxation and Molecular Structure. XII. Dipole Moments and Dielectric Relaxation Times of Rigid Molecules in Solutions

Tohru NAGAI, Yoshinori KOGA, Hiroaki TAKAHASHI, and Keniti HIGASI
School of Science and Engineering, Waseda University, Shinjuku, Tokyo 160

(Received January 9, 1974)

Synopsis. Dielectric constants and losses of anthrone, xanthone, fluorenone and ten other rigid and almost rigid organic molecules were measured at the frequency of about 100 GHz in benzene at 25 °C. The dielectric relaxation times $\tau(1)$ and $\tau(2)$ and the dipole moments μ of these molecules were obtained and discussed.

Two sets of dielectric relaxation times for thirteen rigid molecules were obtained in benzene from measurements at the frequency of 96.5 GHz at 25 °C and discussion is presented on the results.

Experimental

Dielectric measurements at the frequency of 96.5 GHz were made by use of the apparatus and techniques described previously.[1] Symbols employed in this note have the same definition as that given in the preceding paper.[2]

Purchased materials of the best grade (for solutes) were purified by the usual method. Benzene for solvent was carefully purified in the usual way. All the experimental data are collected in Table 1 including those for optical and dielectric (static) measurements.

TABLE 1. SLOPES a', a'' (100 GHz), a_0 (STATIC) AND a_D (OPTICAL) IN BENZENE, 25 °C

Compound	a'	a''	a_0	a_D
Anthrone	0.847	0.551	7.877	0.417
Xanthone	0.843	0.357	5.373	0.421
Benzophenone	0.852	0.444	5.780	0.277
Fluorenone	0.766	0.549	7.181	0.362
Acetone	4.144	4.932	13.736	−0.473
Methyl ethyl ketone	2.623	3.489	10.973	−0.415
Nitrobenzene	1.077	1.805	14.194	0.109
Chlorobenzene	0.298	0.433	2.465	0.066
Dibenzofuran	0.390	0.046	0.768	0.331
Dibenzothiophene	0.495	0.037	0.803	0.434
Toluene	−0.011	0.030	0.127	−0.036
o-Xylene	0.021	0.057	0.322	0.006
m-Xylene	−0.009	0.021	0.105	−0.025

Discussion

Two dielectric relaxation times $\tau(1)$ and $\tau(2)$ were calculated from

$$\tau(1) = \frac{1}{\omega}\frac{a''}{a'-a_\infty} \quad (1)$$

$$\tau(2) = \frac{1}{\omega}\frac{a_0-a'}{a''} \quad (2)$$

(See Table 2). The first relaxation times $\tau(1)$ calculated on the assumption $a_\infty = a_D$ are found to be much smaller than the second ones $\tau(2)$. This is partly due to the neglect of atomic polarization; a_∞ is expected to be larger than a_D. Besides, the dielectric system considered here is possibly of multi-relaxation times rather than of a single relaxation time. For instance, it was found by Hassel and Walker[3] that even toluene has two relaxation times in cyclohexane. If these molecules in benzene solution are provided with a small but appreciable absorption* in the extremely

TABLE 2. DIPOLE MOMENTS μ (UNITS: 10^{-30} C m) AND RELAXATION TIMES $\tau(1)$ AND $\tau(2)$ (UNITS: ps) 25° C

Compound	μ	$\tau(1)$	$\tau(2)$	τ(lit.)
Anthrone	12.17	2.1	21.0	24.8*[a]
Xanthone	9.96	1.4	21.0	—
Benzophenone	10.12	1.3	18.3	20.4[b,**e]; 17.4*[d]
Fluorenone	11.21	2.2	19.3	19.9*[a]
Acetone	9.18	1.8	3.2	3.2***[e]; 3.3**[c]; 3.3***[f]
Methyl ethyl ketone	9.16	1.9	3.9	3.7*****[k]
Nitrobenzene	13.31	3.1	12.0	12.0[b,g]; 14.9[h]
Chlorobenzene	5.25	3.1	8.3	8.3*[i,*d]; 9.7[h]
Dibenzofuran	2.74	1.3	13.5	—
Dibenzothiophene	2.63	1.0	13.6	—
Toluene	1.24	2.0	7.5	7.58****[j]; 5.6[l]
o-Xylene	1.85	6.4	8.7	—
m-Xylene	1.18	2.1	9.0	—

a) D. A. Pitt and C. P. Smyth, *J. Amer. Chem. Soc.*, **80**, 1061 (1958). b) K. Chitoku and K. Higasi, This Bulletin, **36**, 1064 (1963). c) E. Fischer, *Z. Naturforsch.*, **4a**, 707 (1949). d) D. H. Whiffen, *Trans. Faraday Soc.*, **46**, 130 (1950). e) D. H. Whiffen, *Trans. Faraday Soc.*, **42A**, 114 (1946). f) W. Jackson and J. G. Powles, *Trans. Faraday Soc.*, **42A**, 101 (1946). g) H. Spengler, *Physik. Z.*, **42**, 134 (1941). h) H. Hase, *Z. Naturforsch.*, *A*, **8**, 695 (1953). i) S. K. Garg, H. Kilp, and C. P. Smyth, *J. Chem. Phys.*, **43**, 2341 (1965). j) F. J. Cripwell and G. B. B. M. Sutherland, *Trans. Faraday Soc.*, **42A**, 149 (1946). k) Arvind Vyas and H. N. Srivastava, *J. Sci. Ind. Res.*, **18B**, 399 (1959). l) C. W. Cumper, A. Melnikoff, and R. F. Rossiter, *Trans. Faraday Soc.*, **65**, 2892 (1969).

* 20 °C ** 23 °C *** 19 °C **** 18.5 °C ***** 30 °C

* The above-mentioned absorption includes the Poley absorption[5] which differs from the real relaxation phenomenon. We shall assume this small absorption to have a pseudo-relaxation time in order to examine the present dielectric system by use of the method of analysis for the system with two Debye dispersions.[6]

high frequency region[4,5] (for submillimeter wavelengths) and a large and dominant absorption in the lower frequency range, $\tau(1)$ and $\tau(2)$ will give average values with different weights of the two relaxation times. An analysis in the preceding paper[6] shows that the second relaxation times $\tau(2)$ will be fairly close to the relaxation times for the main absorption of molecular rotation.[6] In fact, the literature values obtained from lower frequency measurements compare favorably with $\tau(2)$. Exception may occur, however, if the molecule has a very small polarity.

The dipole moment μ is calculated from $\mu=B(a_0-a_D)^{1/2}$ and $B=(0.3197\times10^{-30}\ \mathrm{Cm})M_2^{1/2}$ in benzene at 25 °C[2], in which a_0 and a_D are slopes for concentrations expressed in weight fraction[2] and M_2 is the molecular weight of the solute. The results of calculation are shown in Table 2. The dipole moment for dibenzofuran is probably a new value and those for the other molecules compare favorably with literature values.[7]

Literature

1) K. Chitoku, K. Higasi, M. Nakamura, Y. Koga, and H. Takahashi, This Bulletin, **44**, 992 (1971).
2) Y. Koga, H. Takahashi, and K. Higasi, *ibid.*, **46**, 3359 (1973).
3) W. F. Hassel and S. Walker, *Trans. Faraday Soc.*, **62**, 861 (1966).
4) G. D. Martin and S. Walker, *Can. J. Chem.*, **50**, 707 (1972).
5) K. Higasi, R. Minami, H. Takahashi, and A. Ohno, *J. Chem. Soc. Faraday II*, **69**, 1579 (1973).
6) K. Higasi, Y. Koga and M. Nakamura, This Bulletin, **44**, 988 (1971).
7) A. L. McClellan, "Tables of Experimental Dipole Moments," W. H. Freeman and Company, San Farncisco, (1963).

BULLETIN OF THE CHEMICAL SOCIETY OF JAPAN, VOL. 47(4), 1024—1025 (1974)

X-Ray Photoelectron Spectroscopy of Oxine-Metal Chelates

Tooru YOSHIDA and Shigemasa SAWADA

Osaka Prefectural Industrial Research Institute, Enokojima, Nishi-ku, Osaka 550

(Received January 25, 1974)

Synopsis. Photoelectron spectra of oxine-metal chelates were measured. The chemical shifts of the N(1s) electron binding energy were smaller than 0.7 eV. There were nearly linear relations between the chemical shifts and the electronegativities of metals or the partial ionic characters of the nitrogen-metal bonds of chelates.

X-Ray photoelectron spectroscopy (ESCA) is rapidly becoming an established method in chemical research. The technique provides a sensitive probe of the electronic environment of atoms in molecule. A number of studies by ESCA have shown that the inner level electron binding energies (B. E.) of an atom are sensitive to the over-all charge on an atom.

The use of the ESCA to determine the effect of coordination on the electron density of a ligand is based on the fact that change in the electron density about an atom is reflected in changes in the binding energies of the core electrons.

It is the aim of this study to determine whether it will be possible to correlate the electronegativity of a metal or the partial ionic character of the bond between a metal and a ligand with the chemical shift of N(1s) binding energy in oxine-metal chelates.

Experimental

The photoelectron spectra were measured using an AEI ES100 electrostatic electron spectrometer under the control of a DS100/32 computer data processing system. The aluminum K_αX-ray line (1486.6 eV) and magnesium K_αX-ray line (1253.6 eV) were used for photoelectron excitation. All the oxine metal chelates, which have 1 : 2 ratio of metal and oxine, were prepared by ordinary procedures. All samples except free oxine were run at room temperature as powder dusted onto double sided adhesive tape under the vacuum of about 10^{-6} Torr. In the case of free oxine a freezing technique was used because of its high volatility.

To compensate for any sample charging effects, the calibration of the spectra was done using the C(1s) electron line from the carbons present in the samples. Its binding energy was taken to be 285.0 eV throughout this study.

Results and Discussion

Figure 1 showed the C(1s) and N(1s) photoelectron spectra of free oxine. The spectra of chelates showed the profiles similar to those of free oxine. All measured binding energy values were given in Table 1. In the table, ΔE is the chemical shift which is the difference between the N(1s) binding energies of free oxine and each chelate compounds, pK the common logarithm of the stability constant of a chelate which is available in the text book,[1] χ the Pauling electronegativity of a metal, I the partial ionic character ($I=1-\exp\{-0.25(\chi_N-\chi_M)^2\}$) of the bond between nitrogen and

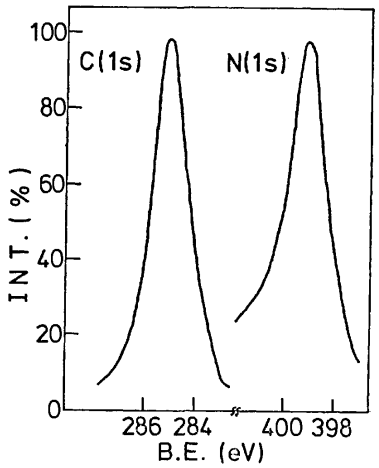

Fig. 1. C(1s) and N(1s) photoelectron spectra of oxine.

TABLE 1. N(1s) BINDING ENERGY VALUES

Compound	B.E. of N(1s) (eV)	ΔE[a] (eV)	pK[b]	χ[c]	I[d] (%)
C_9H_7NO	399.1				
$(C_9H_6NO)_2Ca$	399.1	0	3.2	1.0	63
$(C_9H_6NO)_2Mg$	399.3	0.2	11.7	1.2	55
$(C_9H_6NO)_2Mn$	399.4	0.3	15.3	1.5	43
$(C_9H_6NO)_2Zn$	399.5	0.4	18.8	1.6	39
$(C_9H_6NO)_2Pb$	399.4	0.3	18.7	1.8	30
$(C_9H_6NO)_2Co$	399.5	0.4	19.6	1.8	30
$(C_9H_6NO)_2Ni$	399.5	0.4	21.3	1.8	30
$(C_9H_6NO)_2Cu$	399.7	0.6	26.1	1.9	26

a) The differences between the N(1s) binding energies of chelates ($(C_9H_6NO)_2M$) and the ligand (C_9H_7NO). b) The common logarithms of the stability constants of chelates. c) The electronegativities of metals(M). d) The partial ionic characters in the N-M bond between a metal and a ligand.

metal given by Pauling[2] in which χ_N and χ_M are the electronegativities of nitrogen and metal.

Fig. 2 showed the nearly linear relation between the measured chemical shift (ΔE) and the electronegativity (χ). The increase of the N(1s) chemical shift of chelates with the increase of an electronegativity of a metal could be observed. The chemical shifts of the N(1s) binding energy in all chelates on the complex formation were considered to be due to the decrease of the electron density on the nitrogen atoms caused by the co-ordination of lone-pair electrons of the nitrogen atoms to the metal.

In the charge-potential model,[3] the chemical shift can be expressed in terms of the charge on the atom (Q) and the coulomb potential energy (V) of an electron due to the other atoms of the molecule. Thus:

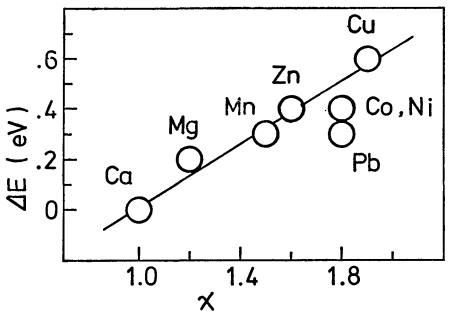

Fig. 2. Relation between the chemical shift of N(1s) binding energy (ΔE) and the electronegativity (χ).

$$\Delta E = k_1 Q + V + k_2 \quad (k_1,\ k_2;\ \text{constants}).$$

In an ionic compound, V includes the contribution from other neighboring ions, that corresponds to a Madelung term. In general, the neglect of V may cause serious error for ionic compounds but for the covalent compound studied here the chemical shift should be dominated by the charge (Q) on the atom concerned.

Here, applying the correlation, $Q=q+\Sigma I$ (Q; charge on an atom, q; formal charge of a concerned atom, ΣI; summation of partial ionic characters of all bonds) proposed by Nordberg *et al.*[4] to the case of oxine chelates, the equation, $Q=I_{C-N}+I_{C=N}+I_{N-M}$, was roughly obtained since q on the nitrogen is zero. Assuming that the summation of the first and second terms of right-hand side in the above equation was constant and V was negligible throughout all the oxine chelates studied here, then the equation, $\Delta E=k_1 I_{N-M}+K$ (K; constant), could be derived.

In practice, it was observed that this relation approximately held in this study. Figure 3 showed a linear relation between the measured chemical shift (ΔE) of the N(ls) binding energy and the calculated partial ionic character (I_{N-M}) of the bond between nitrogen and metal atoms. This indicated that the increase of the ionic character in the bond, or the decrease of the covalent character leads to the smaller chemical shift.

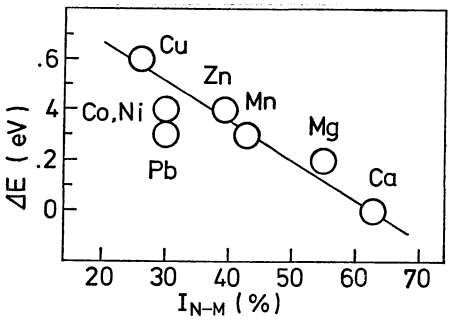

Fig. 3. Relation between the chemical shift of N(1s) binding energy (ΔE) and the partial ionic character ($I=1-\exp\{-0.25(\chi_N-\chi_M)^2\}$).

Thus it was found that the shift of an inner electron binding energy in ESCA, though it is small, give some important knowledge (ionic or covalent character) for the bonds in co-ordination compounds.

Another point, which may be important in analytical chemistry, obtained in this experiment was that there was some relation between the chemical shift (ΔE) measured in solid state and pK value determined in solution; the higher was the stability of a chelate, the larger was the chemical shift of it.

The authors wish to thank Mr. Taichiro Hirohara for the elemental analyses of all samples.

References

1) K. Ueno and T. Sakaguchi, "Kinzoku Kireito," Vol. 3, Nankodo Co., Ltd. Tokyo (1967), p. 65.

2) L. Pauling, "The Nature of the Chemical Bond," 3rd ed., Cornel University Press, Ithaca, N. Y. (1960), p. 98.

3) K. Siegbahn, C. Nordling, A. Fahlman, K. Nordberg, K. Hamrin, J. Hedman, J. Johansson, T. Bergmark, S. E. Karlson, I. Lindgren, and B. Lindberg, "ESCA Applied to Free Molecules," North Holland, Amsterdam (1969).

4) R. Nordberg, R. G. Albridge, T. Bergmark, U. Ericson, J. Hedman, C. Nordling, K. Siegbahn, and B. J. Lindberg, *Ark. Kemi*, **28**, 257 (1967).

BULLETIN OF THE CHEMICAL SOCIETY OF JAPAN, VOL. 47(4), 1026—1027 (1974)

Preparation and Properties of Dimeric Dialkoxo-bridged Chromium(III) Complexes with 3-Bromo-2,4-pentanedione

Kuninobu KASUGA, Tsunao ITOU, and Yasuo YAMAMOTO

Department of Chemistry, Faculty of Literature and Science, Shimane University, Nishikawatsu-cho, Matsue 690

(Recieved November 14, 1973)

Synopsis. μ,μ'-Dialkoxotetraquis(3-bromo-3,4-pentanedionato)dichromium(III), where alkoxo is methoxo, ethoxo, *n*-propoxo or *n*-butoxo, has been prepared. These complexes have been identified by means of the elementary analysis, determination of molecular weight and the spectrometry.

The dimeric dimethoxo bridged copper(II) complex with 2,4-pentanedione has been reported by Bertrand and Kaplan,[1] and dimeric dialkoxo bridged iron(III) complexes with 2,4-pentanedione and 2,2,4,6-tetramethylheptane have been synthesized by Wu, Rossman, Gray, Hammond, and Schugar.[2] In the course of our studies of the substitution reaction of 3-bromo-2,4-pentanedione complexes, we have found the formation of such dimeric dialkoxo bridged chromium(III) complexes as the methoxo, exthoxo, *n*-propoxo and *n*-butoxo dimers.

Experimental

Materials. Tris(3-bromo-2,4-pentanedionato)chromium(III) was refluxed in methyl alcohol for a few days. The dark green precipitates thus formed were recrystallized from benzene. The product(1) consisted of yellowish-green needles. By the same procedure, ethyl, *n*-propyl and *n*-butyl alcohol give similar precipitates. The precipitates in ethyl alcohol were recrystallized from ethanol-dichloromethane, thus giving green crystals(2). Both (3) (the product with *n*-propyl alcohol) and (4) (that with *n*-butyl alcohol) were recrystallized from heptane. These four products show a similar green colour, but of a little different shade. These products are soluble in dichloromethane and chloroform, and a little soluble in alcohol, but insoluble in water. The molecular weights and analytical data of the products are summarized in Table 1.

Measurements. The infrared spectra were measured on a Hitachi 215-type spectrophotometer using KBr pellets. The electronic spectra were measured on a Hitachi 124-type spectrophotometer. The data of the molecular weights were obtained with a Hitachi 115 vapour-pressure osmometer, using chloroform as the solvent. The molecular weight of the methoxo dimer was also measured on a Hitachi Perkin-Elmer RMS-4 single focussing mass spectrometer.

Results and Discussion

In addition to these molecular weights and analytical results, the dimeric forms were identified on the basis of the following facts.

Infrared Spectra. The bands which are not observed for the starting material are shown in Table 2. The bridging alkoxo group is said to have a band at 1040—1070 cm^{-1} which can be assigned to its C–O stretching vibration.[3] The band at 1064 cm^{-1} of (1) should be that of the methoxo group, in view of the IR results on dimeric dimethoxo 2,4-pentanedionato complexes of copper(II)[1] and iron(III).[2] The copper(II) complex shows a band at 1018 cm^{-1} and the iron(III) complex at 1050 cm^{-1}, both of which have been assigned to the C–O stretching of the bridging methoxo group. The similar ethoxo-bridged complex of iron(III) has also been reported to have bands at 1091, 1048 and 885 cm^{-1}, one of which, 1048 cm^{-1}, is assigned to C–O stretching of the ethoxo group.[2] The bands of (2), as shown in Table 2, correspond to these data. By a similar inference, it might be said that the bands at 1095, 1070 and 975 cm^{-1} of (3) as well as 1070 and 970 cm^{-1} of (4) may be attributed to the existence of the bridging propoxo and

Table 1. Molecular weight and analytical data

Compound		Mol. wt. Found	Mol. wt. Calcd	Analysis (%) Found C	Found H	Calcd C	Calcd H
(1)	$[(BrP)_2CrOCH_3]_2$	913, 876*	878.2	30.20	3.60	30.10	3.40
(2)	$[(BrP)_2CrOC_2H_5]_2$	925	906.3	32.10	3.90	31.80	3.80
(3)	$[(BrP)_2CrOC_3H_7]_2$	919	934.3	33.65	4.19	33.42	4.07
(4)	$[(BrP)_2CrOC_4H_9]_2$	974	962.4	35.40	4.65	34.94	4.41

* Datum of mass spectrometry. BrP=3-bromo-2,4-pentanedione

Table 2. Infrared spectra (cm^{-1})

(1)	$[(BrP)_2CrOCH_3]_2$		1064	
(2)	$[(BrP)_2CrOC_2H_5]_2$	1095	1064	895
(3)	$[(BrP)_2CrOC_3H_7]_2$	1095^{sh}	1070	975^{sh}
(4)	$[(BrP)_2CrOC_4H_9]_2$		1070	970^{sh}

sh=shoulder

Table 3. Electronic spectra λ_{max} (nm) (log ε)

	$(BrP)_3Cr$	560(1.95)	410^{sh} (2.80)	358(4.10)	275(4.27)	
(1)	$[(BrP)_2CrOCH_3]_2$	580(2.14)	405^{sh} (2.77)	352(4.24)	290^{sh} (4.05)	267(4.14)
(2)	$[(BrP)_2CrOC_2H_5]_2$	580(2.13)	410^{sh} (2.78)	352(4.33)	290^{sh} (4.19)	267(4.21)
(3)	$[(BrP)_2CrOC_3H_7]_2$	577(2.18)	410^{sh} (2.91)	352(4.33)	290^{sh} (4.19)	267(4.21)
(4)	$[(BrP)_2CrOC_4H_9]_2$	577(2.10)	410^{sh} (2.81)	351(4.26)	290^{sh} (4.11)	267(4.20)

butoxo groups respectively.

Electronic Spectra. As is shown in Table 3, the somewhat lower energies of the d-d bands($^4A_{2g}$—$^4T_{2g}$) of the products as compared to those of the starting material are probably due to the decreased ligand-field splitting by the replaced group. In the case of iron(III) with the same environment, the energies of the dimer d-d bands are higher than those of the monomer.[2] Therefore, the inter-electronic repulsion terms should also be considered in these cases.

While the dialkoxo bridged complex was obtained by the reaction of the 3-bromo-2,4-pentanedionato chromium(III) complex with alcohol, the reflux of the 2,4-pentanedionato chromium(III) complex in ethyl alcohol did not show any change even after a month. The bond between the central metal and carbonyl oxygen might be weaker for the 3-bromo-2,4-pentanedionato complex than for the 2,4-pentanedionato complex. Thus, the bond formation between central metal of the bromo compound and the oxygen atoms of alcohol may be promoted as compared with the case of the nonbrominated compound. Therefore, alcohol molecules react more easily with the central metal of the bromo compound.

The authors are grateful to Dr. Mitsuru Nakayama, Hiroshima University, for determining the molecular weights by means of mass spectrometry.

References

1) J. A. Bertrand and R. I. kaplan, *Inorg. Chem.*, **4**, 1657 (1965).

2) C. S. Wu, G. R. Rossman, H. B. Gray, G. S. Hammond, and H. J. Schugar, *Inorg. Chem.*, **11**, 990 (1972).

3) T. Inazu, H. Okawa, T. Inazu and T. Yoshino, This Bulletin, **42**, 2291 (1969).

BULLETIN OF THE CHEMICAL SOCIETY OF JAPAN, VOL. 47(4), 1028—1029 (1974)

Triisopropoxy Boroxine as a Reducing Agent for Substituted Benzaldehydes

Hirotada IIDA, Hironori KITAMURA, Ken SEITA, and Kazutoshi YAMADA

Department of Synthetic Chemistry, Faculty of Engineering, Chiba University, Yayoi-cho, Chiba 280

(Received June 5, 1973)

Synopsis. Substituted benzaldehydes could be reduced to corresponding benzyl alcohols in fairly good yield at 130 °C, using triisopropoxy boroxine as a reducing agent. The rates of the reduction of benzaldehyde with triisopropoxy boroxine were about ten times as large as those with triisopropyl borate at 110—130 °C.

The reducing action of various metallic alkoxides on aldehydes and ketones has been examined by Meerwein and his co-workers.[1] Under their reaction conditions, boron alkoxides were ineffective as reducing agents. However, when the reaction temperatures were rasied to 150—170 °C, aromatic aldehydes were reduced to the corresponding alcohols by triisopropyl borate.[2]

The ring structure of trialkoxy boroxines was confirmed in 1951,[3] and a convenient synthesis of trialkoxy boroxines was published in 1966,[4] but their reactivities as reducing agents have not yet been studied.

This paper will report the results of an investigation of the reducing activity of triisopropoxy boroxine toward substituted benzaldehydes and some aromatic ketones, compared with that of triisopropyl borate.

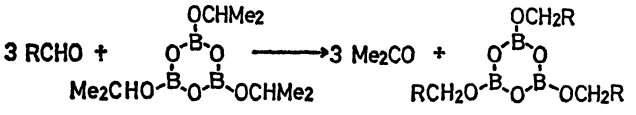

Triisopropoxy boroxine

TABLE 1. REDUCTIONS OF SUBSTITUTED BENZALDEHYDES WITH TRIISOPROPOXY BOROXINE IN XYLENE AT 130 °C FOR 22 hr

RCHO	RCH_2OH (%)
4-Nitrobenzaldehyde	90
Benzaldehyde	64
4-Chlorobenzaldehyde	63
4-Methoxybenzaldehyde	12

Table 1 shows the results obtained from the reductions of substituted benzaldehydes with triisopropoxy boroxine. The yields of alcohols in Table 1 are better than those of the reduction with triisopropyl borate,[2] although they are somewhat lower than those in the Meerwein-Ponndorf-Verley reduction.[5] Neither of the ketones investigated (acetophenone and *p*-nitroacetophenone) was reduced by triisopropoxy boroxine.

The effect of the reaction temperature on this reduction is remarkable. At 80 °C, the usual temperature in the Meerwein-Ponndorf-Verley reduction, practically no reduction occurred with triisopropoxy boroxine.

In order to compare the reducing activity of triisopropoxy boroxine with that of triisopropyl borate, we

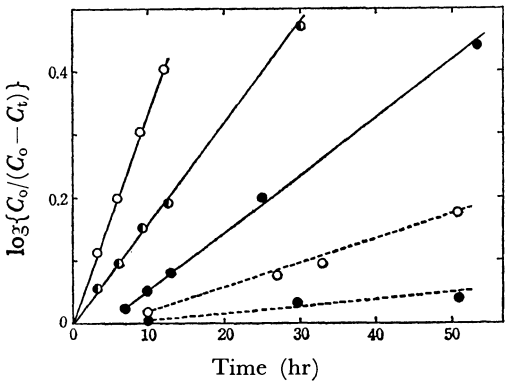

Fig. 1. Pseudo first-order rate plots for the reduction of 0.5 M benzaldehyde with 1.5 M triisopropoxy boroxine or triisopropyl borate in diglyme at these temperature: ●, 110°; ◐, 120°; ○, 130°: solid line, reduction with boroxine; dotted line, reduction with borate.

TABLE 2. THE RATE OF REDUCTION OF BENZALDEHYDE WITH TRIISOPROPOXY BOROXINE OR TRIISOPROPYL BORATE IN DIGLYME

Temp. (°C)	Rate constant, k (hr^{-1})	
	Boroxine	Borate
110	0.020	0.0020
120	0.037	
130	0.076	0.0086

measured the rate of the reduction of benzaldehyde in a diglyme solution under nitrogen, using both reducing reagents separately. A diglyme solution of benzaldehyde and an excess of triisopropoxy boroxine or triisopropyl borate was allowed to react at a constant temperature. The course of the reaction was followed by removing aliquots at appropriate intervals and by measuring the benzyl alcohol and benzaldehyde after hydrolysis by means of gas chromatography. The results are shown in Fig. 1, where C_0 is the concentration of benzaldehyde at time zero and where C_t is that of benzyl alcohol at time t (hr). The plots follow the pseudo first-order reaction for benzaldehyde. An induction period was observed in the reductions with triisopropoxy boroxine at 110 °C and with triisopropyl borate at 110 and 130 °C. The induction period may be due to the establishment of a coordination equilibrium between benzaldehyde and boroxine or borate in the same way as in the Meerwein-Ponndorf-Verley reduction.[6] The psudo first-order rate constants are given in Table 2. The activation energies obtained from the Arrhenius plots were 22.6 and 20.0 kcal/mol for reductions with triisopropyl borate and with triisopro-

poxy boroxine respectively. From these results, it is clear that triisopropoxy boroxine is more effective than triisopropyl borate as a reducing agent.

Experimental

Materials. Triisopropoxy boroxine was prepared according to the literature[4]; mp 51—52 °C (lit, 52 °C).

Triisopropyl borate was prepared by a method modified from the literature[2] as follows: Boric anhydride (0.15 mol) and isopropyl alcohol (1 mol) were mixed in a Soxhlet extracter. In its cylindrical filter paper, calcium oxide (50 g) was placed; the mixture was refluxed for 24 hr and then distilled to obtain the borate (bp 139.5—140.5 °C).

Substituted benzaldehydes were purified by the usual method.

Reduction of Substituted Benzaldehydes. Aldehyde (0.02 mol), triisopropoxy boroxine (0.023 mol), and a solvent (25 ml) were placed in a three-necked, round-bottomed flask (50 ml) fitted with a thermometer, a nitrogen-inlet tube, and a gas-outlet tube. The mixture was heated at 130 °C for 22 hr under an atmosphere of dry nitrogen, while the acetone formed was distilled off through the gas-outlet tube. The acetone was condensed in a spiral tube cooled with an acetone–dry ice mixture and was analyzed by means of gas chromatography. After cooling, the mixture was poured into 100 ml of a 1% aqueous solution of sodium hydrogen carbonate and extracted with 400 ml of ether, after which the ethereal extract was dried over sodium sulfate. The ether was distilled off, and the product was analyzed quantitatively by means of gas chromatography.

Reaction of Ketones and Triisopropoxy Boroxine. Acetophenone (0.1 mol) and triisopropoxy boroxine (0.033 mol) were treated for 14 hr at 110 °C, and *p*-nitroacetophenone was treated similarly at 110 and 125 °C, but no reaction occurred in any case.

Kinetic Procedure. A 60-ml portion of a diglyme solution containing benzaldehyde (0.03 mol) and triisopropoxy boroxine or triisopropyl borate (0.09 mol) was placed in a four-necked, round-bottomed flask (100 ml) and the reaction was carried out as has been described above at a constant temperature. From time to time, 4-ml aliquots were removed, poured into 15 ml of a 1% aqueous solution of sodium hydrogen carbonate, and extracted with 40 ml of ether; the concentrations of benzyl alcohol and benzaldehyde were determined by means of gas chromatography.

References

1) H. Meerwein, V. Bock, Br. Kirschnik, W. Lenz, and A. Migge, *J. Prakt. Chem.*, **147**, 211 (1936).

2) H. G. Kuivila, S. C. Slack, and P. K. Siiteri, *J. Amer. Chem. Soc.*, **73**, 123 (1951).

3) J. Goubeau and H. Keller, *Z. Anorg. Chem.*, **267**, 1 (1951).

4) T. Yamaguchi, K. Sonobe, and T. Shimizu, Japan, 6751 (1966); *Chem. Abstr.*, **65**, 7058 (1966).

5) A. L. Wilds, "Organic Reactions," Vol. 2, John Wiley & Sons, New York, N. Y. (1944), pp. 178, 223.

6) L. M. Jackman and A. K. Macbeth, *J. Chem. Soc.*, **1952**, 3252.

BULLETIN OF THE CHEMICAL SOCIETY OF JAPAN, VOL. 47(4), 1030—1031 (1974)

Stereospecific Reductions of Isoilludin S and M on Alumina Chromatography

Akitami ICHIHARA* and Takeshi MATSUMOTO

Department of Chemistry, Faculty of Science, Hokkaido University, Sapporo 060

(Received September 4, 1973)

Synopsis. Alumina column chromatography with ethanol as solvent converted planar α-ketols, illudin S and illudin M, to the dihydroxy compounds. The stereospecific reduction was discussed mechanistically as one of the Meerwein-Ponndorf-Verley reduction.

Though a number of reactions caused by alumina are known, very little has been recorded of the reduction of ketones on alumina chromatography.[1] This note describes the Meerwein-Ponndorf-Verley reduction of planar α-ketols, isoilludin S(**3**) and M(**4**), to dihydro compounds **6** and **7** on active alumina with alcohol as solvent.

In the course of structural investigations of illudin S(**1**), it was found that, when illudin S was adsorbed on alumina (Wako, 300 mesh) with ethyl acetate as solvent, only isomerised isoilludin S (**3**) was obtained.[2] However, on being adsorbed on alumina column for two days using ethanol instead of ethyl acetate, isomerized isoilludin S (**3**) was converted into a compound whose IR spectrum indicates the absence of the carbonyl group, the NMR spectrum showing a newly produced signal at τ 6.62 due to α proton to a hydroxyl group. From the results and correlation with the reduction product of isoilludin S with sodium borohydride, the compound was assigned to be dihydroisoilludin S (**6**). This suggests that isoilludin S is reduced to dihydroisoilludin S(**6**) on active alumina.

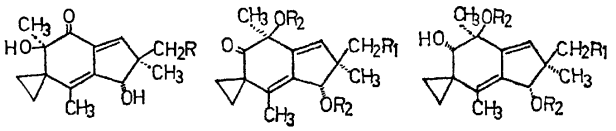

1 R=OH
2 R=H

3 R_1=OH, R_2=H
4 R_1=H, R_2=H
5 R_1=OAc, R_2=Ac

6 R_1=OH, R_2=H
7 R_1=H, R_2=H
8 R_1=H, R_2=Ac

The same kind of reduction on alumina column (Woelm, basic grade I) was observed with isoilludin M(**4**), which was obtained by isomerization of illudin M(**2**) on alumina column (Wako) using benzene, to give dihydroisoilludin M (**7**) in 64% yield. The stereochemistry of C-2 in compounds **6** and **7** was determined to be of *R* configuration since the proton signals due to equatorially oriented hydrogen in dihydro compounds **6** and **7** appear at τ 6.62 and 6.50 respectively, shielded effectively by neighboring cyclopropane ring.[3] This indicates that reduction of the ketols proceeded stereoselectively.

The same treatment on other ketols and ketones, *i.e.*, 3β-acetoxy-5α-hydroxycholestan-6-one (**9**), grayanotoxin derivative (**10**), cyclohexanone (**11**), tri-

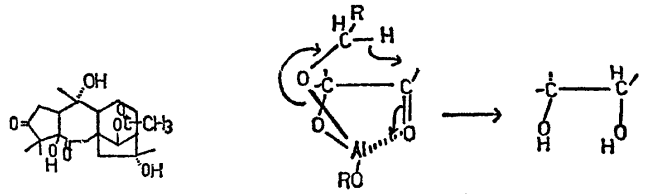

(**10**) a

acetylisoilludin S (**5**), benzoin (**12**), was attempted but only the starting material was recovered. This might be due to the difficulty to form the intermediate (a) in the following surface process of the Meerwein-Ponndorf-Verley reduction. In compounds **9** and **10**, the carbonyl and vicinal hydroxyl groups are not planar, since the hydroxyl group is oriented axially in the plane containing the carbonyl group. Since compounds **3** and **4** have a moiety of planar ketols supported by the presence of a strong intramolecular hydrogen bond between the hydroxyl and carbonyl groups (see Experimental), the formation of planar intermediate (a) is possible. In compounds **11** and **5** which have no α hydroxyl group, it is unfavorable to combine with alumina surface. The intermediate arising from benzoin might have a fairly large steric repulsion between the two phenyl groups to cause recovery of the starting material.

Experimental

Reduction of Isoilludin S (3) with Aluminum Oxide. A solution of 50 mg of isoilludin S (**3**) in 1 ml of ethanol and 2 ml of chloroform was adsorbed on a 5 g of aluminum oxide (Wako, neutral 300 mesh) column and allowed to stand for 2 days at room temperature. The column was eluted with methanol and the eluate was evaporated *in vacuo* to give a crystalline material which was recrystallized from ethyl acetate to give 22 mg of dihydroisoilludin S (**6**), m.p. 198.5—199 °C. IR (cm^{-1}, Nujol) 3250, 1745 ($CH_3COOC_2H_5$), 1653, 1033: NMR (D_2O) after heating at 130 °C: τ 8.93 (3H, s, C–CH_3), 8.45 (3H, s, =C–CH_3), 6.62 (1H, s, H
C–OH), 4.27 (1H, s, =C–H).

Found: C, 66.08; H, 8.31%. Calcd for $C_{15}H_{22}O_4$ (1/2 $CH_3COOC_2H_5$); C, 65.78; H, 8.44%.

Reduction of Isoilludin S (3) with Sodium Borohydride. A solution of 100 mg of isoilludin S (**3**) in 3 ml of ethanol was treated with 50 mg of sodium borohydride and allowed to stand for 3 hr at room temperature. The reaction mixture was taken up into ethyl acetate and the extracts were filtered. The filtrate was dissolved in ethyl acetate and again filtered. The filtrate was concentrated *in vacuo* to give an amorphous solid. The solid was dissolved in ethanol and chromatographed on 2 g of aluminum oxide and eluted with ethanol. The eluate was concentrated and the residue was recrystallized from ethyl acetate to give a crystalline

* Present address: Department of Agricultural Chemistry, Faculty of Agriculture, Hokkaido University, Sapporo.

compound, mp 197—198 °C. The IR spectrum was identical with that of dihydroilludin S.

*Isomerization of Illudin M (**2**).* A solution of 50 mg of illudin M in benzene was adsorbed on 2.5 g of alumina (Wako) and allowed to stand for 2 days. The reaction product was eluted with methanol and the eluate was evaporated *in vacuo*. The residue was recrystallized from *n*-hexane-ether. mp 133—134.5 °C. IR (cm^{-1}, Nujol): 3450, 1705, 1605, 1608. NMR ($CDCl_3$) τ 8.97, 8.83, 8.52, 8.34 (each 3H, s, C–CH_3). 5.73 (1H, s, –C(H)–OH). 4.21 (1H, s, =C(H)–).

Found: C, 72.53; H, 8.11%. Calcd for $C_{15}H_{20}O_3$; C, 72.55; H, 8.12%.

*Reduction of Isoilludin M (**4**) with Aluminum Oxide.* A solution of 22 mg of isoilludin M in chloroform containing a small amount of ethanol as stabilizer was adsorbed on 2 g of aluminum oxide for 2 days. The column was eluted with chloroform and 6 mg of unchanged isoilludin M was recovered. Further elution with methanol gave 14 mg of dihydroisoilludin M (**7**). mp 193 °C. IR (cm^{-1}, Nujol) 3480, 1648, 1030. NMR ($CDCl_3$) τ 8.98, 8.87, 8.69, 8.41 (each 3H, s, C–CH_3), 6.50 (1H, s, –C(H)OH), 5.71 (1H, s, –C(H)OH), 4.34 (1H, s, =C(H)–).

*Acetylation of Dihydroisoilludin M (**7**).* A solution of 24 mg of dihydroisoilludin M with 0.5 ml of acetic anhydride 0.5 ml of dry pyridine was allowed to stand overnight at room temperature. The reaction mixture was poured into water, extracted with ether and dried over anhydrous sodium sulfate. The solvent was evaporated *in vacuo* to give 28 mg of oily acetate. IR (cm^{-1}, film) 3480, 1740, 1648, 1235. NMR ($CDCl_3$) τ 9.00, 8.74, 8.68, 8.60 (each 3H, s, C–CH_3), 7.92 (6H, s, OAc), 5.12 (1H, s, –C(H)–OAc), 4.42 (1H, s, C(H)–OAc), 4.33 (1H, s, =C(H)–H).

*Treatment of Compounds **5**, **11**, **12**, **13** and **14** with Aluminum Oxide.* The compounds were treated under the conditions described above but none were reduced.

Thanks are due to Dr. M. Anchel, New York Botanical Garden, for her generous gift of natural illudin M.

References

1) For the reduction of benzaldehyde to benzylalcohol, see V. J. Hruby. *Proc. Nat. Acad. Sci.*, **16**, 12 (1962). For vapor phase reduction of ketones, see R. V. Ramana and C. N. Pillai *Can. J. Chem.*, **57**, 3705 (1969). L. H. Klem and D. R. Taylor *J. Org. Chem.*, **35**, 3216 (1970). Examples are given in the references.

2) H. Shirahama, Y. Fukuoka, and T. Matsumoto, *Nippon Kagaku Zasssi*, **83**, 1289 (1962). T. Matsumoto, H. Shirahama, A. Ichihara, Y. Fukuoka, T. Takahashi, Y. Mori, and M. Watanabe. *Tetrahedron*, **21**, 2671 (1965).

3) For the same kind of shielding effect on equatorial methyl group by neighboring carbonyl group, see A. Ichihara, H. Shirahama, and T. Matsumoto, *Tetrahedron Lett.*, **1969**, 3965.

BULLETIN OF THE CHEMICAL SOCIETY OF JAPAN, VOL. 47(4), 1032 (1974)

Charge-transfer Complex of Sydnones

Akiko CHINONE and Masaki OHTA

Department of Chemistry, Faculty of Science, Tokyo Institute of Technology, Ookayama, Meguro-ku, Tokyo 152

(Received September 17, 1973)

Synopsis. The complex formation of 3-methylsydnone, 3-phenylsydnone, and 3,4-diphenylsydnone with TCNE was described. From the electronic absorption spectra of the complexes, ionization potentials of sydnones are estimated.

Due to their unique mesoionic character, sydnones have been the subject of continued study since their discovery in 1935.[1] It was reported[2] that sydnones formed complexes with Friedel-Crafts catalysts, and in all cases the bonding occurred through the exocyclic oxygen atom, which was deduced from the shift of carbonyl absorption in IR spectra. The mole ratio of sydnone to metal chloride was reported to be 1 : 1. It was also reported[3] that 3-phenylsydnone formed a loose complex with iodine in acetonitrile but the complex was not isolated. In this report we describe the complex formation study of sydnone with π-acid.

The electronic-absorption spectrum of a solution of 3-methylsydnone and tetracyanoethylene (TCNE) in dichloromethane showed absorption muximum at 405 nm, which cannot be attributed to the starting materials but to a new molecular species. We assume that the absorption band in this region is due to the presence of 3-methylsydnone–TCNE charge-transfer complex. 3-Phenylsydnone and 3,4-diphenylsydnone also formed charge-transfer complex with TCNE, showing characteristic absorption bands as shown in Table. The concentration dependence of the electronic absorption spectra of these complexes was analyzed by method of Benesi-Hildebrand.[4] From the result, the molar ratio in the complex is assumed to be 1 : 1 as in the case of 3-phenylsydnone–iodine complex.[3]

Ionization potentials (I_p) of sydnones are estimated from the empirical relationship:[5]

$$\tilde{\nu}_{max} = 0.487 I_p - 1.30 \text{ (eV)}$$

as shown in Table 1.

TABLE 1. COMPLEXES FORMED BETWEEN SYDNONES AND TCNE (solvent, CH_2Cl_2; temperature, about 20 °C)

π-Base	λ_{max} (nm)	I_p (eV)
3-Methylsydnone	405	9.0
3-Phenylsydnone	405	9.0
3,4-Diphenylsydnone	495	7.8

The IR spectra of sydnone–TCNE complexes in dichloromethane did not show appreciable differences in comparison with that of each component. These complexes were not isolated as a crystal but dissociated to each component when the solvent was evaporated in a vacuum.

References

1) J. C. Earl and A. W. Mackney, *J. Chem. Soc.*, **1935**, 899.

2) a) T. S. L. Mao, *Dissertation Abstr.*, **25**, 1602 (1964). b) P. S. Gentile and T. S. L. Mao, *J. Inorg. Nucl. Chem.*, **27**, 867 (1965). c) T. S. L. Mao, U. S. At. Energy Comm. TID 20068 (1963); *Chem. Abstr.* **62**, 2488 (1965).

3) H. Yamada and K. Kozima, *J. Amer. Chem. Soc.*, **82**, 1543 (1960).

4) H. A. Benesi and J. H. Hildebrand, *ibid.*, **71**, 2703 (1949).

5) R. E. Merrifield and W. D. Phillips, *ibid.*, **80**, 2778 (1958).

BULLETIN OF THE CHEMICAL SOCIETY OF JAPAN, VOL. 47(4), 1033—1034 (1974)

Iminodithiocarbonates. VI.[1] Reaction of Sulfur-substituted Carbonium Ion with Sodium Azide

Yoshio UENO and Makoto OKAWARA

Research Laboratory of Resources Utilization, Tokyo Institute of Technology, Ookayama, Meguro-ku, Tokyo 152

(Received September, 29, 1973)

Synopsis. The reaction of 2-methylthio-1,3-dithiolan-2-ylium iodide **1** with sodium azide gave 2-methylthioimino-1,3-dithiolane **4**. Thiooxime **4** reacted with chloramine T and dimethyl sulfate to give sulfilimine **9** and sulfonium salt **10**, respectively.

In a previous paper we reported on the reaction of 2-methylthio-1,3-dithiolan-2-ylium iodide **1** with ethyleneimine to produce 2-(β-iodoethylimino)-1,3-dithiolane **2**, which is easily converted into the conjugated *N*-vinyl monomer **3**.[2]

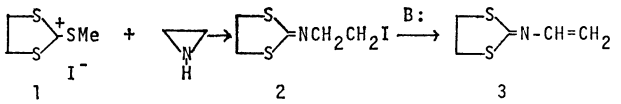

In this paper we wish to report on the reaction of the cation **1** with sodium azide as nitrogen-nucleophile. Cation **1** reacted with sodium azide in DMF at room temperature with evolution of nitrogen gas to give the thiooxime derivative **4** in 49% yield.

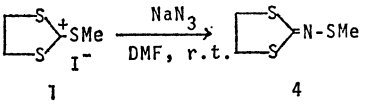

The structure of **4** was confirmed by elemental analysis and spectroscopic data. The NMR spectrum of **4** exibited a singlet peak at δ 2.40 (SMe, 3H) and multiplet peaks centered at δ 3.4 (SCH_2CH_2S, 4H). The IR absorption band due to $\nu C{=}N$ appeared at 1542 cm^{-1}. It is noteworthy that nitrogen gas evolution occurred even at room temperature, since ordinary organic azides do not decompose at such a low temperature. For the sake of explanation we postulate the sulfide participation which could accelerate the elimination of nitrogen gas: The methylthio group interacts with the negative charge on nitrogen atom by means of the vacant d-orbitals and the facile C–S bond cleavage takes place concertedly with the elimination of nitrogen molecule to produce the final product **4** as follows.

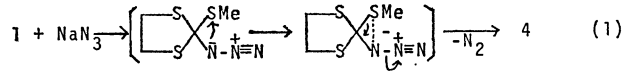

(1)

A similar explanation has been employed for the following transformation by Sudo *et al.*.[3]

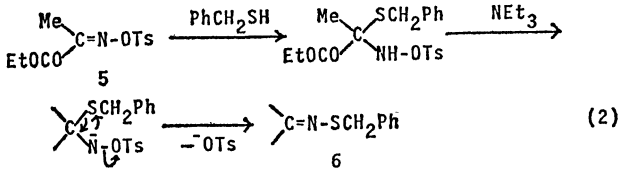

(2)

We see a similarity between the reactions (1) and (2). Thus the nitrogen gas in (1) corresponds to ^-OTs in (2) as eliminating group. 2-Dimethylamino substituted cation **7**, which would not have effective participation toward azide, did not react with sodium azide and was recovered. Participation by a ring-sulfur atom would not be involved due to the steric requirement presumed to be unfavorable.

An alternative scheme for the formation of **4** may be one involving the triazene intermediate **8**.

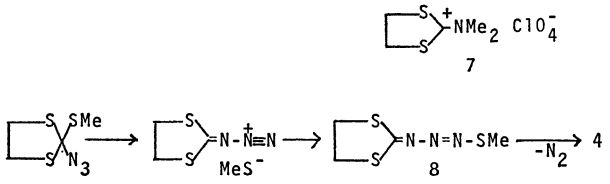

Reactions of thiooxime **4** newly obtained with chloramine T and dimethyl sulfate were undertaken, and **4** was found to react with chloramine T to give the sulfilimine **9** in 34% yield.

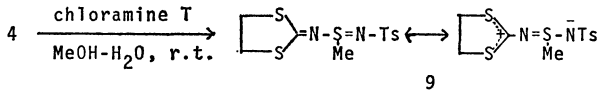

The IR absorption bands of **9** appeared at 1478 cm^{-1} (C=N) and at 955 cm^{-1} (S=N). The value due to $\nu C{=}N$ highly shifted to a lower wave number indicating a strong conjugation between the C=N and S=N groups as formulated above. This was supported by the NMR of **9**. Thus the ring methylene protons shifted from δ 3.40 to 3.67 accompanied by the conversion of **4** into **9**.

Thiooxime **4** reacted with dimethyl sulfate at 40—50 °C to give *S*-methylated sulfonium salt **10** in 50% yield. It is surprising that the methylation occurred at S and not at N atom, since ordinary 2-alkylimino-1,3-dithiolanes such as **11** are alkylated at N atom.[4]

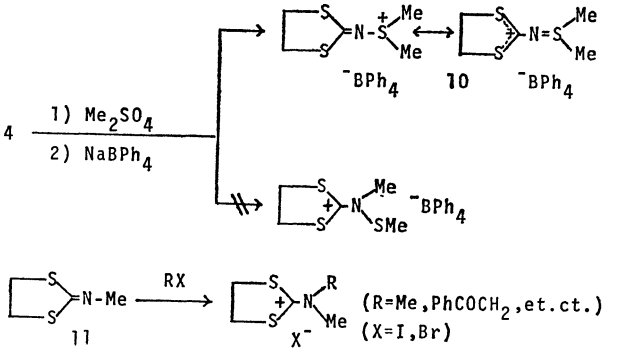

The NMR spectrum of **10** exhibited a singlet peak at δ 3.17 (SMe, 6H) and multiplet peaks centered at δ 3.66 (SCH_2CH_2S, 4H) and at δ 6.83(Ph, 20H). The presence of two equivalent methyl group supports *S*-methylation and excludes *N*-methylation. Sulfonium salt **10** is considered to be stabilized by delocalization of its positive charge into 1,3-dithiolane ring as formulated above.

Experimental

2-Methylthioimino-1,3-dithiolane ***4***. To a suspension of 11.2 g (0.04 mol) of 2-methylthio-1,3-dithiolan-2-ylium iodide[5] in 70 ml of DMF was added 2.6 g (0.04 mol) of sodium azide with stirring. Nitrogen gas was evolved and a brown suspension turned into a homogeneous solution. Sodium iodide was then precipitated as white needles. After being left to stand over-night, the solvent was removed under a reduced pressure under nitrogen atmosphere and the residue was poured into water and extracted with ether, dried over $MgSO_4$. Evaporation of ether and distillation gave 3.3 g (49%) of **4**; bp 111—113 °C (1 mmHg), IR: 1541 cm^{-1} (νC=N)„ UV λ_{max}^{EtOH} 231, 295.5, 275(sh), and 448 nm, NMR (see text) Found[6]: C, 28.61; H, 4.23; S, 57.72%. Calcd for $C_4H_7NS_3$: C, 29.10; H, 4.27; S, 58.14%.

Sulfilimine ***9***. 2.3 g (0.014 mol) of thiooxime **4** was added to a solution of 3.4 g (0.012 mol) of chloramine T in (30 ml)–MeOH (20 ml). Acetonitrile (20 ml) was added to the reaction mixture in order to crystallize the oily substance separated. Stirring was continued for 2 hr. Filtration followed by evaporation of the filtrates gave oily residues which were crystallized by washing with ether. **9** (1.24 g, 34%) was obtained as colourless prisms: mp 181—182 °C (recrystallized from ethanol), IR: 1478 cm^{-1} (νC=N), 1279, 1139 cm^{-1} (νSO_2), 955 cm^{-1} (νS=N), 1082 cm^{-1}. NMR (DMSO-d_6) δ: 2.30(Me, s, 3H), 2.45 (SMe, s, 3H), 3.67 (SCH_2CH_2S, m, 4H), 7.50 (Ar, m, 2H), and 7.97 (Ar, m, 2H).

Methylation of Thiooxime ***4***. 0.8 g (4.8 mmol) of **4** and 0.6 g (4.8 mmol) of dimethyl sulfate were heated at 40—50 °C for 1.5 hr. After the mixture was cooled, aq. solution of sodium tetraphenylborate (1.7 g in 50 ml H_2O) was added to give 1.2 g (50%) of **10**: mp, 199—201 °C (recrystallized from acetone-ether), IR; 710 and 740 cm^{-1}, NMR (DMSO-d_6) δ: 3.17 (SMe, s, 6H), 3.66 (SCH_2CH_2S, m, 4H), and 6.83 (Ph, m, 20H), Found: C, 70.09; H, 6.14; N, 2.76; S, 18.73%. Calcd. for $C_{29}H_{30}BNS_3$: C, 69.76; H, 6.06; N, 2.81; S, 19.23%.

References

1) Part V; Y. Ueno and M. Okawara, This Bulletin, **45**, 1797 (1972).
2) Y. Ueno and M. Okawara, *J. Polym. Sci. Part B*, **10**, 11 (1972).
3) R. Sudo, A. Kaneda, and N. Furuya, This Bulletin, **42**, 1380 (1969).
4) Y. Ueno, T. Nakai, and M. Okawara, *ibid.*, **44**, 1933 (1971).
5) R. Mayer and K. Schafer, *J. Prakt. Chem.*, [4] **26**, 270 (1964).
6) Contamination of a small amount of 1,3-dithiolan-2-one[5] after repeated distillation precluded the preparation of an analytically pure sample. Formation of 1,3-dithiolan-2-one might take place by the hydrolysis of cation **1** with water present in the solvent.[5]

BULLETIN OF THE CHEMICAL SOCIETY OF JAPAN, VOL. 47(4), 1035—1036 (1974)

Aromatic Substitution of Olefins. XXI.* Reaction of *o*-Alkylstyrenes with Benzene in the Presence of Palladium(II) Acetate

Morio WATANABE, Masaaki YAMAMURA, Ichiro MORITANI, Yuzo FUJIWARA, and Akio SONODA

Department of Chemistry, Faculty of Engineering Science, Osaka University, Toyonaka, Osaka 560

(Recieved October 29, 1973)

Synopsis. In aromatic substitution of olefins, steric factor of *o*-alkyl substituents of styrene was investigated. The formation of arylated products was found to be decreased by introduction of alkyl groups to *ortho* position of styrene.

In previous papers we reported on a new method for the synthesis of stilbene derivatives by the substitution of aromatics for vinylic hydrogen of styrenes in the presence of palladium(II) salts.[1] It was demonstrated that a steric factor plays an important role. The phenylation reactivity was thus found to diminish markedly in the reactions of diphenylethylene and triphenylethylene with benzene as compared with the reaction of styrene with benzene.[1]

In order to elucidate the steric factor in the arylation reaction, we have investigated the reaction of some *ortho*-alkylstyrenes with benzene as well as the reactions of styrene with some alkylbenzenes.

The arylation reactions of *o*-alkylstyrenes with benzene (Reaction(1)) were carried out under normalized conditions.[1] The results are summarized in Table 1. The reactions of *o*-methylstyrene(**1b**), 2,4,6-trimethylstyrene(**1c**), and 2,5-di-*tert*-butylstyrene(**1d**) with benzene gave **2b**, **2c**, and **2d**, respectively, as the usual phenylated products besides small amounts of 1,1-diarylethylenes, **3b** and **3c**.[2] Introduction of alkyl groups into the *ortho* positions of styrene caused a decrease in the yield of arylation products. However, it does not seem likely that the second methyl substituent has any further effect on the arylation from a comparison of the reactions of **1b** and **1c**.

On the other hand, in the reaction of styrene with methyl substituted benzenes (Reaction(2)), the depressing effect on an additional methyl group was found to be more evident. The reaction of mesitylene with styrene was found to be more than five times slower than that of *p*-xylene with styrene (Table 2). It should be noted that a small amount of 1,1-diarylethylene was formed in the reaction of mesitylene as well.

A remarkable contrast is observed between the two similar reactions (1) and (2) which lead to the same reaction product **2c**; arylation reaction of styrene with mesitylene appeared to be five times slower than that of **1c** with benzene.

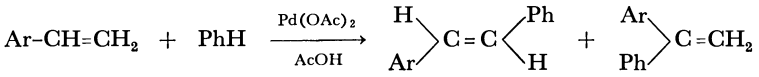

(1)

1a-d **2a-d** **3a-d**

a, Ar=Phenyl **b**, Ar=*o*-Tolyl **c**, Ar=Mesityl **d**, Ar=2,5-Di-Bu^t

TABLE 1. REACTION OF ALKYLSTYRENES WITH BENZENE

1a-d	Products and Yield %[b]	NMR δ in CCl_4	UV λ_{max}(log ε)
1a[a]	**2a**, 95		295(4.40)
	3a, ND[c]		
1b	**2b**, 50	2.41(s, 3H), 7.18(m, 11H)	294(4.35)
	3b, 3	1.97(s, 3H), 5.08(d, 1H), 5.62(d, 1H), 7.10(m, 9H)	247(4.05)
1c	**2c**, 55	2.20(s, 3H), 2.26(s, 6H), 6.40(d, 1H), 6.99(d, 1H), 6.71(s, 2H), 7.25(m, 5H)	280(4.32)
	3c, 5	2.07(s, 6H), 2.27(s, 3H), 4.99(d, 1H), 5.87(d, 1H), 6.76(s, 2H), 7.15(s, 5H)	243(4.13)
1d	**2d**, 36	1.35(s, 9H), 1.45(s, 9H), 6.62(d, 1H), 7.17(m, 3H), 7.35(m, 5H), 7.69(d, 1H)	285(4.30)
	3d, ND		

a) Ref. 1. b) based on $Pd(OAc)_2$ used. c) none detected.

* Part XX; R. Asano, I. Moritani, Y. Fujiwara, and S. Teranishi, This Bulletin, **46**, 2910 (1973).

This part presented at The Symposium of Organometallic Chemistry, Nagoya, 16, October, 1971.

$$Ph\text{-}CH{=}CH_2 + Ar'H \xrightarrow[AcOH]{Pd(OAc)_2} \underset{Ph}{\overset{H}{\diagdown}}C{=}C\underset{H}{\overset{Ar'}{\diagup}} \qquad (2)$$

4a-c **5a-c**

TABLE 2. REACTION OF STYRENE WITH ALKYLBENZENES

Ar'H		Products and Yield %[b]
Toluene	**4a**[a]	**5a**, 61
p-Xylene	**4b**[a]	**5b**, 47
Mesitylene	**4c**	**5c**, 9 (0.5) [c]

a) Ref. 1. b) based pn $Pd(OAc)_2$ used. c) 1-Phenyl-1-mesitylethylene **3c** formed.

The results suggest that there is a greater steric hindrance at the site of the arylating species in the transition state involving a palladium-carbon σ bond.[3]

Experimental

The IR and UV spectra were measured with Hitachi EPI-S2 and Hitachi EPS-2U spectrophotometers, respectively. The NMR spectra were recorded on a JEOL Co. C-60HL spectrometer with TMS as an internal standard. Vpc analyses were carried out with a JEOL JGC-20K gas chromatograph.

Starting olefins **1b**, **1c**, and **1d** were prepared by known methods.[4]

The arylation reactions were performed under normalized conditions: A mixed solution of olefin (50 mmol), palladium-(II) acetate (50 mmol), benzene (445 ml), and acetic acid (100 ml) was heated under reflux for 8 hr. After the usual work-up,[1] the product mixture was subjected to vpc analysis, (SE-30, Microwax). Samples for spectral measurement and elemental analysis were collected by means of a preparative vpc. The spectral data of these products are summarized in Table 1. The compounds showed satisfactory elemental analyses.

References

1) Y. Fujiwara, I. Moritani, S. Danno, R. Asano, and S. Teranishi, *J. Amer. Chem. Soc.*, **91**, 7166 (1969).

2) Compounds **3b** and **3c** were identified by comparison of authentic samples prepared by the reaction of acetophenone with corresponding arylmagnesium bromide followed by dehydration; L. I. Smith, "Organic Syntheses," Coll. Vol. II, p. 95 (1943); R. C. Fason, M. D. Armstrong, W. E. Wallance, and J. W. Kneisley, *J. Amer. Chem. Soc.*, **66**, 681 (1944).

3) S. Danno, I. Moriatni, and Y. Fujiwara, *Tetrahedron*, **25**, 4819 (1969).

4) C. G. Overberger and J. H. Saunders, "Organic Syntheses," Coll. Vol. III, p. 204 (1955); Hirschberg, *J. Amer. Chem. Soc.*, **71**, 3241 (1949); Eisenlahr and Schluz, *Ber.*, **57**, 1816 (1924).

BULLETIN OF THE CHEMICAL SOCIETY OF JAPAN, VOL. 47(4), 1037—1038 (1974)

Synthesis of Alkoxycyclopropane Derivatives, Intermediates in the Synthesis of Hirsutic Acid[1]

Fujio SAKAN, Emiko SUGIURA, Takeshi MATSUMOTO,* Haruhisa SHIRAHAMA,* and Hisanobu HASHIMOTO*

Chemical Laboratory, Faculty of Education, Fukui University, Fukui 910

**Department of Chemistry, Faculty of Science, Hokkaido University, Sapporo 060*

(Received November 1, 1973)

Synopsis. The addition of several alkoxycarbenes on *cis*-bicyclo[3,3,0]octane derivative (**2**) was tried. The bulkier reagent gave the better stereoselectivity and *exo* adducts were obtained more predominantly.

Recently we achieved the total synthesis of methyl hirsutate (**1**),[2] a sesquiterpene derived from a biogenetic intermediate, protoilludane.[3] A carboxylic function correctly oriented was constructed with a certain stereoselectivity by the predominant *exo* attack of methoxycarbene on *cis*-bicyclo[3,3,0]octane derivative (**2**). This paper describes the procedure of the addition of several alkoxycarbenes on *exo* methylene compound **2** and shows how the ratio of *exo* to *endo* adduct varies with alkyl group of alkoxycarbene.

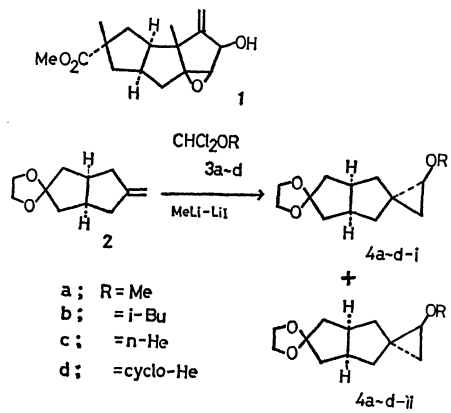

Compound **2** was obtained from known *cis*-bicyclo[3,3,0]octadione.[2a] Addition of alkoxycarbenes, prepared from dichloromethyl alkyl ethers (**3a**—**3d**) and methyllithium–lithium iodide in ether at −20——15 °C,[4] to **2** afforded epimeric mixtures of alkoxycyclopropane derivatives (**4**). The reaction was carried out with four different sizes of alkoxycarbene. Yields and ratios of *exo* to *endo* adduct are listed in Table 1. In the NMR spectra of **4**, signals due to three cyclopropyl protons appeared as typical ABX systems.[5] The configurations were assigned by taking account of the steric course of the reaction.[2b,6]

TABLE 1. RESULTS OF THE ADDITION OF ALKOXYCARBENES ON **2**

Products	Yields (%)[a]	Ratios of *exo* (**i**) to *endo* adduct (**ii**)[b]
4a (R=methyl)	75	2.2
4b (R=isobutyl)	83	2.5
4c (R=*n*-hexyl)	77	2.2
4d (R=cyclohexyl)	73	2.9

a) Isolated yield, not optimized. b) Determined by glc (see Expeeimental).

The results obtained show that the bulkier reagent clearly gave the better stereoselectivity. However, the steric course of the reaction was not so markedly effected by the bulkiness of alkoxycarbene, since the bulky alkyl group might not be close enough to the attacking point of the reagent.

Experimental

NMR spectra were measured at 100 MHz on a JEOL Co. Model PS-100 spectrometer using TMS as an internal standard. IR spectra were taken on a Hitachi Model EPI-G3 with NaCl optics. Glc were carried out on a Yanaco G8-TEP and an Aerograph Autoprep 700.

*3,3-Methoxyethano-7,7-ethylenedioxy-*cis*-bicyclo[3,3,0]octane (**4a**)* A typical procedure for carbene addition. To a solution of **2** (200 mg) and dichloromethyl methyl ether **3a**[7] (1 g) in dry ether (10 ml) was added 0.8 N ether solution of methyllithium–lithium iodide (30 ml) under stirring in an ice-salt bath (−20——15 °C). Addition was completed in 1 hr and the mixture was stirred at −20——15 °C for further 1 hr. Water was added to the resulting mixture and products were taken up with ether. The extracts were washed with brine, dried and evaporated to leave crude material which on chromatography (silica gel, 10% ethyl acetate–*n*-hexane elution) gave a mixture of methoxycyclopropane derivatives (**4a-i**) and (**4a-ii**) (188 mg, 75% yield, *exo* adduct **4a-i**/*endo* adduct **4a-ii**=2.2 by glc). Further purification by preparative glc (5% DC-550 column at 150 °C) gave pure **4a-i** and **4a-ii** as colorless oils. **4a-i**: IR (neat) 3060 cm^{-1}; NMR δ (CCl_4) 0.44, 0.55 and 2.78 (each 1H, ABX with J_{AB}=5.6, J_{AX}=6.1 and J_{BX}=3.8 Hz, CH_2 and CH–O on cyclopropane), 3.22 (3H, s., CH_2–O) and 3.77 (4H, s, O–CH_2CH_2–O); Found: C, 69.42; H, 8.85%. Calcd for $C_{13}H_{20}O_3$: C, 69.61; H, 8.99%. **4a-ii**: IR (neat) 3060 cm^{-1}; NMR δ (CCl_4) 0.27, 0.44 and 2.95 (each 1H, ABX with J_{AB}=5.8, J_{AX}=6.0 and J_{BX}=3.4 Hz, CH_2 and CH–O on cyclopropane), 3.28 (3H, s, CH_3O) and 3.77 (4H, s, O–CH_2CH_2–O); Found: C, 69.71; H, 8.93%. Calcd for $C_{13}H_{20}O_3$: C, 69.61; H, 8.99%.

*3,3-Isobutoxyethano-7,7-ethylenedioxy-*cis*-bicyclo[3,3,0]octane (**4b**).* Crude product from **2** (200 mg), dichloromethyl isobutyl ether **3b**[7] (1.4 g) and 0.8 N methyllithium–lithium iodide ether solution (30 ml) gave a mixture of isobutoxy cyclo derivatives (**4b-i**) and (**4b-ii**) (245 mg, 83% yield, *exo* adduct **4b-i**/*endo* adduct **4b-ii**=2.5 by glc) on chromatography. Preparative glc (5% QF-1 column at 165 °C) afforded pure **4b-i** and **4b-ii** as colorless oils. *Exo* adduct **4b-i**: IR (neat) 3054 cm^{-1}; NMR δ (CCl_4) 0.46, 0.58 and 2.81 (each 1H, ABX with J_{AB}=5.7, J_{AX}=6.5 and J_{BX}=3.4 Hz, CH_2 and CH–O on cyclopropane), 0.86 (6H, d with J=6.0 Hz, $CH(C\underline{H}_3)_2$), 3.10 (2H, AB part of ABX,

O–CH$_2$CH) and 3.78 (4H, s, O–CH$_2$CH$_2$–O); Found: C, 72.43; H, 9.57%. Calcd for $C_{16}H_{26}O_3$: C, 72.14; H, 9.84%. *Endo* adduct **4b-ii**: IR (neat) 3040 cm^{-1}; NMR δ(CCl_4) 0.28, 0.42 and 2.96 (each 1H, ABX with J_{AB}= 5.3, J_{AX}=6.2 and J_{BX}=3.1 Hz CH_2 and CH–O on cyclopropane), 0.87 (6H, d with J=6.0 Hz, CH(C$\underline{H}_3$)$_2$), 3.16 (2H, AB part of ABX, O–C$\underline{H}_2$CH) and 3.72 (4H, s, O–CH$_2$CH$_2$–O); Found: C, 72.38; H, 9.86%. Calcd for $C_{16}H_{26}O_3$: C, 72.14; H, 9.84%.

*3,3 - n -Hexoxylthano - 7,7-ethylenedioxy - cis - bicyclo[3,3,0]octane (**4c**).* Epimeric mixture of *n*-hexoxycyclopropane derivatives (**4c-i**) and (**4c-ii**) (248 mg, 77% yield, *exo* adduct **4c-i**/*endo* adduct **4c-ii**=2.2 by glc) was obtained from the reaction of **2** (200 mg), dichloromethyl *n*-hexyl ether **3c**[7] (1.6 g) and 0.8 N methyllithium–lithium iodide ether solution (30 ml). Preparative glc (5% QF-1 column at 180 °C) gave pure **4c-i** and **4c-ii** as colorless oils. *Exo* adduct **4c-i**: IR (neat) 3047 cm^{-1}; NMR δ(CCl_4) 0.46, 0.58 and 2.82 (each 1H, ABX with J_{AB}=5.7, J_{AX}=6.3 and J_{BX}=3.5 Hz, CH_2 and CH–O on cyclopropane), 0.89 (3H, destorted t., $CH_2C\underline{H}_3$), 3.33 (2H, destorted t, O–C$\underline{H}_2$CH$_2$) and 3.78 (4H, s, O–CH$_2$CH$_2$–O); Found: C, 73.55; H, 10.37%. Calcd for $C_{18}H_{30}O_3$: C, 73.43; H, 10.27%. *Endo* adduct **4c-ii**: IR (neat) 3042 cm^{-1}; NMR δ(CCl_4) 0.30, 0.44 and 2.96 (each 1H, ABX with J_{AB}=5.3, J_{AX}=6.9 and J_{BX}=2.7 Hz, CH_2 and O–CH on cyclopropane), 0.87 (3H, destorted t, $CH_2C\underline{H}_3$), 3.38 (2H, m, O–C$\underline{H}_2$CH$_2$) and 3.74 (4H, s, O–CH$_2$CH$_2$–O); Found: C, 73.17; H, 10.49%. Calcd for $C_{18}H_{30}O_3$: C, 73.43; H, 10.27%.

*3,3 - Cyclohexoxyethano - 7,7-ethylenedioxy - cis - bicyclo[3,3,0]octane (**4d**).* **2** (150 mg) and dichloromethyl cyclohexyl ether **3d**[7] (1g), was treated with 0.8 N methyllithium–lithium iodide ether solution (30 ml), gave an epimeric mixture of cyclohexoxycyclopropane derivatives (**4d-i**) and (**4d-ii**) (175 mg, 73% yield, *exo* adduct **4d-i**/*endo* adduct **4d-ii**=2.9 by glc). Pure **4d-i** and **4d-ii** were obtained from this mixture by preparative glc (5% DC-550 at 200 °C) as colorless oils. *Exo* adduct **4d-i**: IR (neat) 3045 cm^{-1}; NMR δ(CCl_4) 0.46, 0.58 and 2.92 (each 1H, ABX with J_{AB}= 5.4, J_{AX}=5.7 and J_{BX}=4.1, CH_2 and CH–O on cyclopropane), 3.20 (1H, m, O–C$\underline{H}$(CH$_2$–)$_2$) and 3.75 (4H, s, O–CH$_2$CH$_2$–O); Found: C, 73.91; H, 9.63%. Calcd for $C_{18}H_{28}O_3$: C, 73.93; H, 9.65%. *Endo* adduct **4d-ii**: IR (neat) 3045 cm^{-1}; NMR δ (CCl_4) 0.32, 0.44 and 3.06 (each 1H, ABX with J_{AB}=5.3, J_{AX}=6.1 and J_{BX}=3.4 Hz, CH_2 and CH–O on cyclopropane), 3.32 (1H, m, O–C$\underline{H}$(CH$_2$–)$_2$) and 3.72 (4H, s, O–CH$_2$CH$_2$–O); Found: C, 73.75; H, 9.61%. Calcd for $C_{18}H_{28}O_3$: C, 73.93; H, 9.65%.

References and Notes

1) Most of this work appeared in: E. Sugiura, Graduation Thesis, Fukui Univ., 1972.

2) a) H. Hashimoto, F. Sakan, K. Tsuzuki, H. Shirahama, and T. Matsumoto, 17th Symposium on the Chemistry of Natural Products, Tokyo, Oct. 17—19, 1973, Symposium Papers, p. 33. b) Synthesis of Skeleton; F. Sakan, H. Hashimoto, A. Ichihara, H. Shirahama, and T. Matsumoto, *Tetrahedron Lett.*, **1971**, 3703.

3) We completed the total synthesis of the following three sesquiterpenes of the protoilludane family: illudin M; T. Matsumoto, H. Shirahama, A. Ichihara, H. Shin, S. Kagawa, F. Sakan, S. Matsumoto, and S. Nishida, *J. Am. Chem. Soc.*, **90**, 3286 (1968), illudin S; T. Matsumoto, H. Shirahama, A. Ichihara, H. Shin. S. Kagawa, F. Sakan, and K. Miyano, *Tetrahedron Lett.*, **1971**, 2049, illudol; T. Matsumoto, K. Miyano, S. Kagawa, S. Yō, J. Ogawa, and A. Ichihara, *Tetrahedron Lett.*, **1971**, 3521.

4) U. Schöllkopf and J. Paust, *Angew. Chem.*, **75** 670 (1963).

5) U. Schöllkopf, A. Lerch, and J. Paust, *Chem. Ber.*, **96**, 2266 (1963).

6) Completion of the synthesis of methyl hirsutate shows these configurational assignments to be correct.

7) H. Gross, A. Rieche, and E. Höft, *Chem. Ber.*, **94**, 544 (1961).

BULLETIN OF THE CHEMICAL SOCIETY OF JAPAN, VOL. 47(4), 1039—1040 (1974)

Some Substituted 1*H*,4*H*- and 1*H*,5*H*-Pyrazolo[4,3-*c*]pyrazoles. Syntheses and Properties

Joung Hee LEE, Akira MATSUMOTO, Masayuki YOSHIDA, and Osamu SIMAMURA

Department of Chemistry, Faculty of Science, Tokyo University, Hongo, Tokyo 113

(Received November 27, 1973)

Syonpsis. 1,4-Dimethyl-3,6-diphenyl-, 1,5-dimethyl-3,3-diphenyl-, and 4-methyl-2,3,6-triphenyl-pyrazolo[4,3-*c*]-pyrazoles(IV, V, and VIII) were prepared and their structures were established on the basis of their spectral data.

Syntheses of 2,3,5,6-tetra-aryl-1,2,4,5-tetra-azapentalenes, meso-ionic heterocycles, have recently been described.[1] These compounds contain four aryl substituents on the 2*H*,5*H*-pyrazolo[4,3-*c*]pyrazole ring. This paper presents the syntheses and properties of substituted 1*H*,4*H*- and 1*H*,5*H*-pyrazolo[4,3-*c*]pyrazoles.

Condensation of 1,4-diphenyl-2-phenylazobutane-1,3-dione[2] with methylhydrazine in ethanol gave 5-benzyl-1-methyl-3-phenyl-4-phenylazopyrazole(I), mp 151—152 °C, whereas treatment of the silver salt of 3-benzyl-5-phenyl-4-phenylazopyrazole[3] with excess of methyl iodide in boiling benzene afforded a mixture of the above-mentioned pyrazole (I) and its isomer, 3-benzyl 1-methyl-5-phenyl-4-phenylazopyrazole (II), mp 89—91 °C. The structures of these pyrazoles were deduced on the basis of their mass spectra and are consistent with the experimental results described below.

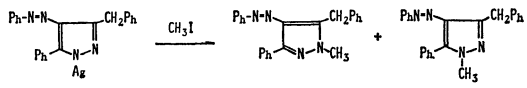

I II

Reduction of compound I with disodium dithionite and diazotization of the resulting amine by means of sodium nitrite in acetic acid followed by treatment with aqueous sodium bicarbonate yielded 3,6-diphenyl-1-methyl-4*H*-pyrazolo[4,3-*c*]pyrazole(III), mp 233—234 °C, which afforded, with excess of methyl iodide and sodium ethoxide in boiling ethanol, two mono-methylated products, 1,4-dimethyl-3,6-diphenylpyrazolo[4,3-*c*]pyrazole (IV), mp 202—204 °C, and the 1,5-dimethyl isomer (V), mp 169—171 °C, the structures being established on the basis of their mass and NMR spectra described in the experimental part.

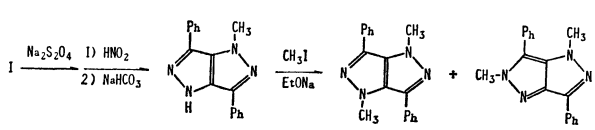

III IV V

If the structure of compound I were 3-benzyl-1-methyl-5-phenyl-4-phenylazopyrazole, the structure of compound III would be 3,6-diphenyl-2-methyl-4*H*-pyrazolo[4,3-*c*]pyrazole (III′) and, consequently, the structure of compound IV, which shows a sharp singlet proton signal from two equivalent methyl groups, would have to be 2,5-dimethyl-3,6-diphenylpyrazolo[4,3-*c*]-pyrazole (IV′); this structure, however, is ruled out, being inconsistent with the observed mass spectrum for compound IV (presence of a peak at *m/e* 82 due to $CH_3NCCNCH_3$). Thus, the structures of compounds I and II are confirmed.

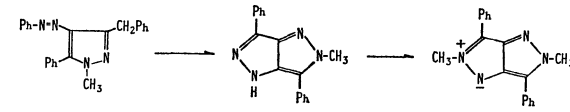

II III′ IV′

3-Benzyl-1,5-diphenyl-4-phenylazopyrazole (VI) prepared by condensation of 1,4-diphenyl-2-phenylazobutane-1,3-dione with phenylhydrazine was similarly cyclized to 2,3,6-triphenyl-4*H*-pyrazolo[4,3-*c*]pyrazole (VII), mp 277—279 °C, which was converted into a mono-methylated product (VIII), mp 191—192 °C. The mass spectrum of compound VIII (presence of a peak at *m/e* 180 due to $C_6H_5CNC_6H_5$) rules out an alternative structure of 5-benzyl-1,3-diphenyl-4-phenylazopyrazole for compound VI, in which the position of the *N*-phenyl group was uncertain in the original literature.[2]

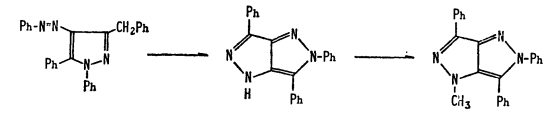

VI VII VIII

The NMR spectrum of compound VIII exhibits two multiplets centered at τ 1.75 (2H) and 2.65 (13H) due to aromatic protons, and this fact indicates that one phenyl ring (τ 1.75, *o*-2H) is coplanar with the nucleus, because Finar and Rackham showed a similar deshielding of the *ortho* protons of 1-phenyl substituted aza-aromatic compounds due to a large electric field associated with the lone pair of electrons of the nitrogen atom at position 2, this effect being operative only when both rings are coplanar.[4] Thus, to compound VIII is assigned the structure of 4-methyl-2,3,6-triphenyl-pyrazolo[4,3-*c*]pyrazole and not that of isomeric 5-methyl-2,3,5-triphenylpyrazolo[4,3-*c*]pyrazole, in which no coplanar phenyl is possible because of steric hindrance. This result is in contrast to the finding that the silver salt of 2-phenyl-4*H*-*v*-triazolo[4,5-*d*]-*v*-triazole affords both 4- and 5-methyl-2-phenyl-*v*-triazolo[4,5-*d*]-*v*-triazoles.[5]

Experimental

5-Benzyl-1-methyl-3-phenyl-4-phenylazopyrazole (I). This compound (Found: C, 78.55; H, 5.77; N, 15.81%; M^+,

352. Calcd for $C_{23}H_{20}N_4$: C, 78.38; H, 5.72; N, 15.90%; M, 352), mp 151—152 °C (from ethanol), *m/e* 352(M^+), 274($M-C_6H_5-H$), 259 ($M-PhCH_2-2H$), 103(PhCN), and 91($PhCH_2$), was prepared according to the directions given for the preparation of 3-benzyl-1,5-diphenyl-4-phenylazopyrazole[2] (VI).

3-Benzyl-1-methyl-5-phenyl-4-phenylazopyrazole (II). The silver salt (0.48 g) prepared from 3-benzyl-5-phenyl-4-phenylazopyrazole (0.36 g) and silver nitrate (1.0 g) in the usual way was heated in a mixture of benzene (15 ml) and methyl iodide (2 ml) under reflux overnight. On cooling, the precipitate was removed by filtration, and the filtrate was concentrated to yield 0.40 g of orange red solid. This crude material was subjected to purification by preparative thin layer chromatography on silica gel. Development with benzene afforded two contiguous bands with R_f lying between 0.32 and 0.47. The band with the larger R_f gave 0.10 g (26%) of compound I, and the one with the smaller R_f 0.06 g (16%) of compound II (Found: C, 78.27; H, 5.48; N, 15.92%. Calcd for $C_{23}H_{20}N_4$: C, 78.38; H, 5.72; N, 15.90%), mp 89—91 °C, *m/e* 352 (M^+), 275 ($M-C_6H_5$), 206 (PhNNCCPh), 179 (PhCHCPh), 118 ($PhCNCH_3$), and 91 ($PhCH_2$).

3,6-Diphenyl-1-methyl-4H-pyrazolo[4,3-c]pyrazole (III). To a suspension of compound I (4.0 g) in 80 ml of boiling 80% ethanol was added powdered disodium dithionite in small portions until the mixture became homogeneous. The mixture was then steam-distilled to remove aniline and ethanol. The remaining crystalline solid was collected and recrystallized from ethanol to yield the starting material (I; 1.08 g). The ethanolic filtrate was concentrated to dryness under reduced pressure. The residue was dissolved in 30 ml of acetic acid and diazotized with sodium nitrite (0.65 g) at 0—5 °C. The mixture was stirred for 15 min at this temperature and poured into cold dilute aqueous sodium bicarbonate. Organic materials were extracted with dichloromethane, and the extract was evaporated under reduced pressure. The residue was dissolved in a small amount of acetic acid and the solution was heated on a water bath for 15 min. On evaporation of the solvent, it gave 0.80 g (34%) of compound III (Found: C, 74.40; H, 5.01; N, 20.46%. Calcd for $C_{17}H_{14}N_4$: C, 74.43; H, 5.14; N, 20.43 %), mp 233—234 °C (white crystals from benzene).

1,4- and 1,5-Dimethyl-3,6-diphenylpyrazolo[4,3-c]pyrazoles (IV and V). Compound III (0.50 g) and methyl iodide (4 ml) were added to ethanolic sodium ethoxide solution prepared from 1 g of sodium and 45 ml of ethanol, and the mixture was heated under reflux overnight. The solvent was evaporated under reduced pressure, and the residue was washed with water and dried to yield 0.67 g of a solid. This crude product (0.50 g) was subjected to purification by preparative thin layer chromatography on silica gel using benzene-ether (10 : 1) as eluent. The band with R_f 0.45—0.53 gave 0.08 g (21%) of the 1,4-dimethyl isomer (IV) (Found: C, 75.14; H, 5.54; N, 19.54%. Calcd for $C_{18}H_{16}N_4$: C, 74.97; H, 5.59; N, 19.43%), mp 202—204 °C (from ethanol), τ 6.00 (6H, s, $2CH_3$), 2.65(6H, multiplet, aromatic), and 2.36(4H, multiplet, aromatic), *m/e* 288 (M^+), 103(PhCN), and 82($CH_3NCCNCH_3$). The band with R_f 0.38—0.44 yielded 0.09 g (23%) of the 1,5-dimethyl isomer (V) (Found: C, 75.11; H, 5.60; N, 19.64%. Calcd for $C_{18}H_{16}N_4$: C, 74.97; H, 5.59; N, 19.43%), mp 169—171 °C (from ethanol), τ 6.20(3H, s, CH_3), 5.95 (3H, s, CH_3), 2.53(8H, multiplet, aromatic), and 1.80(2H, multiplet, aromatic), *m/e* 288(M^+) and 118($PhCNCH_3$).

2,3,6-Triphenyl-4H-pyrazolo[4,3-c]pyrazole (VII). 3-Benzyl-1,5-diphenyl-4-phenylazopyrazole[2] (VI), treated similarly to the preparation of compound III, afforded compound VII (Found: C, 78.75; H, 4.60; N, 16.74%. Calcd for $C_{22}H_{16}N_4$: C, 78.55; H, 4.79; N, 16.66%), mp 277—279 °C (from ethanol).

4-Methyl-2,3,6-triphenylpyrazolo[4,3-c]pyrazole (VIII). Compound VII prepared above was methylated in the same way as in the preparation of compounds IV and V to yield compound VIII (Found: C, 78.56; H, 4.88; N, 16.29%. Calcd for $C_{23}H_{18}N_4$: C, 78.83; H, 5.18; N, 15.99%), mp 191—192 °C (from ethanol), *m/e* 350(M^+), 246($M-PhCNH$), and 180(PhCNPh), τ 6.15(3H, s, CH_3), 2.65(13H, multiplet, aromatic), and 1.75(2H, multiplet, aromatic).

References

1) J. H. Lee, A. Matsumoto, O. Simamura, and M. Yoshida, *Chem. Commun.*, **1969**, 1393.
2) C. Bülow and H. Grotowsky, *Ber.*, **34**, 1479 (1901).
3) D. G. Farnum and P. Yates, *J. Amer. Chem. Soc.*, **84**, 1399 (1962).
4) I. L. Finar and D. M. Rackham, *J. Chem. Soc. B*, **1968**, 211.
5) M. Yoshida, A. Matsumoto, and O. Simamura, This Bulletin, **43**, 3587 (1970).

BULLETIN OF THE CHEMICAL SOCIETY OF JAPAN, VOL. 47(4), 1041—1042 (1974)

Cycloaddition Reaction of Troponoids with Dimethyl Maleate

Hitoshi TAKESHITA*, Yoshikazu SHOJI and Shô ITÔ**

Department of Chemistry, Tohoku University, Aramaki-Aoba, Sendai 980

(Received December 3, 1973)

Synopsis. Thermal cycloaddition reaction of methyl maleate with tropone, 2-chloro-, 2-methoxytropone and tropolone was investigated. Each reaction yielded [4+2] type adducts with high peri- and stereospecificities but with less regioselectivity.

In a series of our studies on the Diels-Alder reaction of troponoids, it was shown[1,2] that maleic anhydride (I), a cyclic dienophile with symmetrical structure, yielded the *endo-cis*-adducts except in the case of tropolone(II), while acrylonitrile, an acyclic dienophile with unsymmetrical structure, yielded a mixture of *regio-* and *stereo* isomeric compounds.[3] The contrasting results there observed prompted us to investigate the reaction with another type of dienophiles, an acylic one with symmetrical structure. Thus, we have carried out the reactions with dimethyl maleate(III) for comparison.

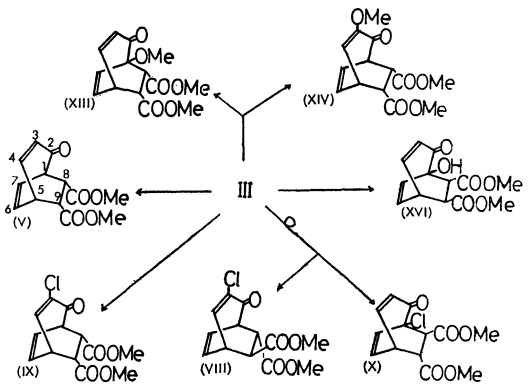

When III was heated with tropone(IV), a single product, V, was obtained in 80% yield and its structure was established by direct comparison with the dimethyl ester of the hydrolysate of the adduct(VI) obtained from I and IV.[1]

The reaction of III with 2-chlorotropone(VII) afforded three 1 : 1-adducts, VIII, IX and X in 7, 11 and 7% yield, respectively. IX was shown to be identical with the corresponding dimethyl ester of the adduct(XI) derived from I and VII.[4] VIII exhibits three vinyl proton signals in its NMR spectrum (Table 1), indicating it be a 3-chloro-derivative. The configuration of the substituents was deduced as 8α, 9β-orientation on the basis of the observed coupling constants, $J_{1,8}=1.5$, and $J_{8,9}=6.0$ Hz.[5] Similarly X was identified as 1-chloro-8β,9α-isomer by the NMR evidences (four vinylic hydrogens (Table 1 and $J_{5,9}=2.0$, $J_{8,9}=4.5$ Hz).

Heating of III with 2-methoxytropone(XII), afforded two products, XIII and XIV, in 17 and 6% yield, respectively.[6] Since XIII was chemically correlated with the adduct(XV) obtained from I and XII,[2a] its structure was established to be 1-methoxy-8α,9α-derivative. On the other hand, XIV, having three vinyl proton signals and the coupling constants, $J_{1,8}=0$, $J_{8,9}=10.0$ Hz, in the NMR spectrum, was shown to be 3-methoxy-8α,9α-derivative.

TABLE 1. NMR CHEMICAL SHIFTS OF THE ADDUCTS[5]

	H_1	H_3	H_4	H_5	H_6	H_7
V	3.95	5.80	7.05	3.70	6.53	6.22
VIII	4.10	Cl	7.27	3.4—3.8	6.27	6.17
IX	3.4—4.1	Cl	7.40	3.4—4.1	6.62	6.27
X	Cl	6.05	7.03	3.77	6.53	6.13
XIII	OMe	5.88	7.22	3.97	6.75	6.25
XIV	4.13	OMe	6.02	~3.9	6.52	6.22
XVI	OH	5.98	7.32	3.9—3.5	6.53	6.15

	$H_{8\alpha}$	$H_{8\beta}$	$H_{9\alpha}$	$H_{9\beta}$	Me
V	COOMe	3.32	COOMe	3.60	3.61, 3.65
VIII	COOMe	3.4—3.8	3.4—3.8	COOMe	3.75, 3.75
IX	COOMe	3.4—4.1	COOMe	3.4—4.1	3.69, 3.72
X	4.03	COOMe	COOMe	3.40	3.73, 3.77
XIII	COOMe	3.35	COOMe	3.5—3.7	3.53, 3.61, 3.65
XIV	COOMe	3.33	COOMe	~3.5	3.51, 3.65, 3.67
XVI	3.5—3.9	COOMe	3.45	COOMe	3.65, 3.63

* Present Address: Research Institute of Industrial Science, Kyushu University, Hakozaki, Fukuoka 812.

** To whom all the correspondences should be addressed.

The reaction of III with II was somewhat complicated yielding a mixture, and only the adduct XVI was isolated in 10% yield after the extensive silica-gel column chromatography. The NMR spectrum of XVI revealed the presence of four vinylic hydrogens and *exo-cis*-orientation for the ester groups.[7]

The present result revealed that the reaction of III with troponoids proceeded stereospecifically: All the adduct are free from their stereoisomers with opposite orientation of ester groups. This control of stereoselectivity of substituents on tropone ring is remarkable. Thus, the transition states leading to the *endo-cis* adducts are stabilized more than those to *exo-cis* products. The formation of *exo-cis* product XVI can be rationalized as the result of *endo* addition, followed by an isomerization, which are previously observed in the cycloaddition of tropolone.[2] In spite of the high stereospecificity, the regiospecificity is somewhat reduced: The formation of XIV as a minor adduct contrasts the case of maleic anhydride[1] and resembles with the case of acrylonitrile.[3]

The *trans*-adducts, VIII and X, whose formation apparently conflicts with the general rule of concerted cycloaddition, should be regarded as the adducts of not III but dimethyl fumarate (XVII), since the recovered unsaturated ester fraction in this particular case was consisted of XVII and no trace of III was detected. Some amounts of hydrogen chloride liberated by the decomposition of VII should be sufficient for this isomerization.[8,9]

Experimental

The Reaction of Dimethyl Maleate (III) with Tropone(IV). Formation of endo-cis-*Adduct(V).* IV(2 g) and III (4 g) were heated in a sealed tube(glass) for 18 hr at 130—140 °C. From the reaction mixture, III was removed by distillation *in vacuo*, and the residual mass was sublimed on a cold finger at 120 °C/2 mmHg to give V (3.6 g), colorless crystals, mp 86—88 °C(lit,[1] 83—87 °C), whose identity was confirmed by a direct comparison with the authentic sample.

*The Reaction of III with 2-Chlorotropone (VII). Formation of 3-Chloro-*endo-cis-*adduct(IX), 3-Chloro-8α,9β-*trans-*adduct (VIII) and 1-Chloro-8β,9α-*trans-*adduct(X).* VII(415 mg) and III(1.10 g) were heated in a similar manner for 20 hr at 150 °C. The reaction mixture was sublimed on a cold finger at 70 °C/2 mmHg to separate dimethyl fumarate (XVII), 870 mg. The residue was further distilled at higher temperature(120—140 °C/2 mmHg) to give a colorless liquid, 230 mg, which was then chromatographed on silica gel column to obtain VIII(a colorless liquid, 50 mg) (Found: C, 58.94; H, 4.46%. Calcd for $C_{13}H_{13}O_5Cl$: C, 58.87; H, 4.60%. ν: 1740, 1640, 1610 cm^{-1}), IX (colorless crystals, mp 172—173 °C (lit,[4] mp 172—173 °C), 90 mg, ν 1740, 1642, 1612 cm^{-1}), and X (colorless crystals, mp 177—179 °C, 50 mg) (Found: C, 59.01; H, 4.70%. ν: 1745, 1690 cm^{-1}).

*The Reaction of III with 2-Methoxytropone(XII). Formation of 1-Methoxy-*endo-cis-*adduct(XIII) and 3-Methoxy-*endo-cis-*adduct(XIV).* XII(400 mg) and III(1.0 g) were heated in a similar manner as the above for 15 hr at 150 °C. The reaction mixture was distilled *in vacuo* to remove unreacted III (620 mg). The residue was then distilled on a cold finger to give a colorless semi-soild, from which, a major component, XIII, was obtained by a filtration as colorless crystals (140 mg, mp 148—149 °C) (Found: C, 60.11; H, 5.67%. Calcd for $C_{14}H_{16}O_6$: C, 59.99; H, 5.75%. ν: 1750, 1675 cm^{-1}). The mother liquor of the above was then chromatographed on silica gel to give XIV (colorless crystals, mp 141—142 °C, 50 mg) (Found: C, 60.37; H, 5.60%. ν: 1747, 1680, 1635, 1617 cm^{-1}).

*The Derivation of 1-Methoxy-*endo-cis-*Adduct(XIII) from the adduct(XV) of I and XII.* XV (75 mg) was suspended in distilled water (3 ml) and heated for 30 min at 95—100 °C. After coling, separated colorless crystals were collected by filtration. Weight; 60 mg, mp 184—184.5 °C (Found: C, 57.16; H, 4.84%. Calcd for $C_{12}H_{12}O_6$: C, 57.14; H, 4.80%). The esterification of this specimen by diazomethane gave colorless crystals (mp 148—149 °C, 40 mg), whose identity with XIII has been established by a direct comparison.

*The Reaction of III with Tropolone(II). Isolation of 1-Hydroxy-*exo-cis-*Adduct(XVI).* II(400 mg) and III (1.0 g) were heated in a sealed tube for 15 hr at 145 °C and the reaction mixture was then distilled *in vacuo* to remove the unreacted III. The residue was fractionated by repeated column chromatography to yield XVI, colorless crystals, mp 95—101 °C, 45 mg (Found: C, 58.54; H, 5.22%. Calcd for $C_{13}H_{14}O_6$: C, 58.64; H, 5.30%. ν: 3450, 1745, 1685 cm^{-1}).

References and Footnotes

1) a) T. Nozoe, T. Mukai, T. Nagase, and Y. Toyooka, This Bulletin, **33**, 1147 (1960). b) S. Itô, H. Takeshita, Y. Shoji, Y. Toyooka, and T. Nozoe, *Tetrahedron Lett.*, **1968**, 3215.

2) S. Itô, A. Mori, Y. Shoji, and H. Takeshita, *ibid.*, **1972**, 2685.

3) S. Itô, H. Takeshita and Y. Shoji, *ibid.*, **1969**, 1815.

4) T. Nozoe and Y. Toyooka, This Bulletin, **34**, 623 (1961).

5) All NMR spectra were determined in deuteriochloroform solutions and parameters were obtained by first-order analysis.

6) The formation of third product was recognized, but due to a limited quantity available, no characterization was made.

7) Chemical correlation of XVI with the *exo-cis*-adduct of I and II was not attempted, since the latter is known to cause lactonization under a hydrolysis condition. see Ref. 1b.

8) A. Kekule and O. Strecker, *Ann. Chem.*, **183**, 170 (1884).

9) The reaction of XVII with the troponoids is a subject of the independent paper which will be published in due course.

BULLETIN OF THE CHEMICAL SOCIETY OF JAPAN, VOL. 47 (4), 1043—1044 (1974)

Spectral Difference of the A and B Forms of Deoxyribonucleic Acid

Yoshifumi NISHIMURA, Kosuke MORIKAWA, and Masamichi TSUBOI

Faculty of Pharmaceutical Sciences, University of Tokyo, Hongo, Bunkyo-ku, Tokyo 113

(Received November 19, 1973)

Synopsis. Infrared absorption spectrum of an oriented film of deoxyribonucleic acid from *Micrococcus lysodeikticus* has been examined in its A and B forms. In the A form a weak band was observed at 807 cm^{-1}, while in the B form this is absent and a broad and weak band appears at 832 cm^{-1}.

The primary purpose of this note is to report on some differences in the infrared absorption spectra in the 1000—750 cm^{-1} region of the A and B forms of deoxyribonucleic acid (DNA). Our experiment was directed by two reports,[1,2] which recently appeared. Erfurth, Kiser, and Peticolas[1] showed that in the Raman spectrum of calf thymus DNA in the A form there is a strong Raman line at 807 cm^{-1}, while in the B form this line is absent and a new line appears at 835 cm^{-1}. For characterizing these frequencies, it is desirable to examine infrared absorption spectra of the A and B forms of DNA in this frequency region, because the selection rule (or intensity rule) in the Raman effect and infrared absorption are different. Pilet and Brahms[2] made a detailed investigation on the infrared spectra of A and B forms of DNA's with various base compositions, and found a marked difference between the two forms in the dichroic properties of the 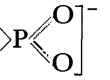 antisymmetric and symmetric stretching bands (at about 1230 and 1090 cm^{-1}, respectively). They did not show, however, any bands in the frequency region lower than 1000 cm^{-1}.

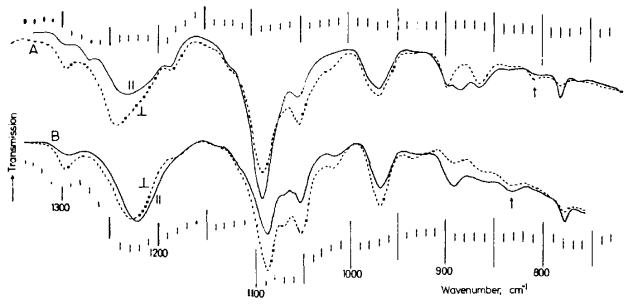

Fig. 1. Infrared absorption curves of oriented films of DNA from *Micrococcus lysodeikticus* in its A and B forms, observed with the polarized radiation. Full line, electric vector of the incident radiation is parallel to the fiber axis. Broken line, electric vector is perpendicular to the fiber axis.

Figure 1 shows the infrared spectra of an oriented DNA film from *Micrococcus lysodeikticus* in its A and B forms observed with the polarized radiation. The film was prepared from an aqueous solution of DNA with 10^{-5} M NaCl onto an AgCl plate. This film was soaked overnight in 73% ethanol with 0.1 M NaCl to add a proper amount of NaCl, and then washed only once by 80% ethanol. The spectrum A was obtained on keeping the film in the air of 75% humidity for a long time, and the spectrum B at 92% humidity. The A—B conversion readily takes place, but for regaining the spectrum A we need to keep the film in the air of 75% humidity for a week or so.

In the 1300—1000 cm^{-1} region, we have observed almost exactly what Pilet and Brahms reported:[2] in the A form the 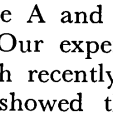 antisymmetric stretching band (whose // component is at 1230 cm^{-1} and $\perp$ component at 1243 cm^{-1}) shows a perpendicular dichroism and the symmetric stretching band (both // and $\perp$ components are at 1092 cm^{-1}) a parallel dichromism, whereas in the B form the antisymmetric stretching band (// at 1220 cm^{-1} and $\perp$ at 1230 cm^{-1}) is almost non-dichroic and the symmetric stretching band (both // and $\perp$ are at 1088 cm^{-1}) shows a perpendicular dichroism. In the 800—700 cm^{-1} region, we found practically the same frequencies with what Erfurth *et al.*[1] observed in the Raman spectra both for the A and B forms, but with greatly different relative intensities. Thus, in the A form a weak band is observed at 807 cm^{-1}, while in the B form this is absent and a broad and weak band appears at 832 cm^{-1}. The former shows a perpendicular dichroism whereas the latter is almost non-dichroic.

The Raman or infrared frequency, 807 cm^{-1} of the A form or 832 cm^{-1} of the B form, is probably caused by a vibration in which mainly P–O single-bond stretching takes place, because of the following bases:

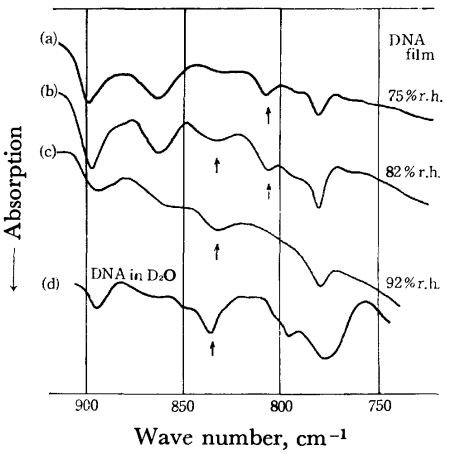

Fig. 2. Infrared absorption spectra in the 920—750 cm^{-1} region with unpolarized radiation. (a) Film of DNA from *M. lysodeikticus* at relative humidity (r.h.) 75%. (b) The same film at 82% r.h. (c) The same film at 92% r.h. (d) Calf thymus DNA in D_2O solution, pD=6 (observed with a Digilab FTS-14 Fourier Transform Infrared Spectrometer).

(1) The Raman line of nucleic acids at about 810 cm^{-1} is in general very strong and its appearence and absence are so sensitive to the mainchain conformation that it is not probable to be caused by a vibration of a base residue.[1,3]

(2) The 807 and 832 cm^{-1} bands of DNA are found to remain almost unchanged when the film is exposed to D_2O vapor. Many other data[3] indicate that the frequency now in question is insensitive to the deuteration of the amino and hydroxy groups of the nucleic acid.

We have conducted a number of experiments in an attempt to establish a correlation (if any) between the P–O stretching frequency and the conformation around this bond in the C–O–[PO_2^-]–O–C system. Unfortunately, however, what was attempted has not so far come out in any neat form. Nevertheless, this band may be useful for finding a gross mainchain-conformation around the phosphate group in a given sample of nucleic acid; it is favorable that we only need to find the position of the band and do not need to examine infrared dichroism here. As seen in Fig. 2 (b), the *M. lysodeikticus* DNA film shows both of the 807 and 832 cm^{-1} bands in the air of 82% humidity. It may be concluded, therefore, that such a film contains both of the A and B forms. This conclusion is reached in a less ambiguous manner than that from a dichroic measurement in the 1250—1000 cm^{-1} region. On the other hand, calf thymus DNA in neutral D_2O solution shows a well-defined band at 840 cm^{-1} but not at 807 cm^{-1} (Fig. 2 (d)), and this fact supports the idea that the DNA molecule is in the B-form in its aqueous solution.

It may be pointed out here that each of the double-helical ribonucleic acid (RNA)[4] and DNA-RNA hybrid[5] shows a medium intensity perpendicular band at 810 cm^{-1} but not at 832 cm^{-1}. By X-ray diffraction studies[5] both of these are known to have structures similar to that of DNA A form, but quite different from the B form. The 810 cm^{-1} band of RNA was once assigned to a nearly symmetrical stretching vibration of the $\begin{matrix}C\\C\end{matrix}>C-O$ structure at the position 2′ of the ribose residue.[6] We now consider that at least a part of this band is caused by the P–O single bond stretching mode. It is not yet excluded, however, that the band due to the ribose vibration is superposed here. Perhaps it is worthwhile to mention here our Raman spectrum of RNA from cytoplasmic polyhedrosis virus (CPV) of silk worm in comparison with that of DNA in their aqueous solutions. CPV RNA is a natural RNA with a complete double-helical structure. As may be seen in Fig. 3, CPV RNA shows a srtong and sharp Raman line at 810 cm^{-1} while DNA does not. This line is insensitive to deuteration. This fact suggests that this RNA has, in its aqueous solution, a structure similar to that of DNA A form.

Lastly, a few comments are to be added on some other band observed in the A- and B-forms of DNA.

In the 900—880 cm^{-1} region, there is another marked difference found between the A and B forms. In the A form, there is a medium intensity band at 881 cm^{-1}

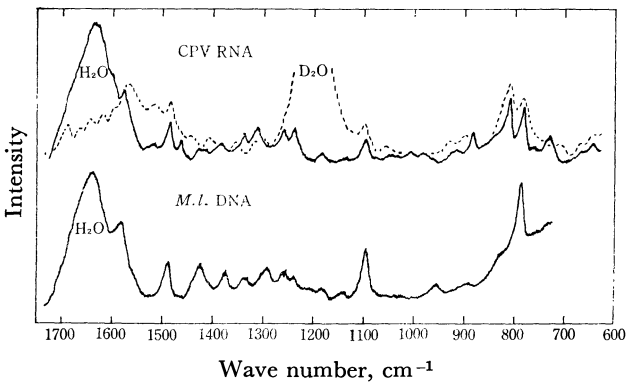

Fig. 3. Upper: Raman spectra of CPV RNA, excited by the 514.5 nm beam of an Ar^+ laser (Coherent Radiation, 52G-A) and observed with a JRS-Ul Raman spectrophotometer of Japan Electron Optics Laboratory, Company (JEOL). — in H_2O, --- in D_2O. The RNA sample was prepared under the direction of Dr. K. Miura, National Institute of Genetics. We thank Dr. Miura for his guidance. We also thank Mr. S. Muraishi, JEOL, for his kindness in the spectroscopic measurements.
Lower: Raman spectrum of DNA from *Micrococcus lysodeikticus* (GC 72%) in H_2O solution (0.02M Tris+ 0.1M NaCl, pH 7.6). The spectrum was observed by the use of a JRS-UlS Raman spectrophotometer of JEOL and 488.0 nm beam of an Ar^+ laser of coherent radiation (52G-A).

which is strongly polarized along the parallel direction with the fiber axis (Fig. 1). This is missing in the B-form; instead, there is a parallel band at 891 cm^{-1}. This is also unaffected by deuteration, and is assignable to another mainchain stretching vibration.

The strong Raman line at 780 cm^{-1} and the medium-intensity infrared band at 780 cm^{-1} should be assigned to different vibrations, in spite of the coincidence in their frequency values. The Raman line is assignable to the ring breathing vibration of the pyrimidine base residues. While, the infrared band which shows a strong parallel dichroism is assignable to an out-of-plane vibration in some base-residues.

A strong band at 1120 cm^{-1} of RNA, which was assigned to the $\begin{matrix}C\\C\end{matrix}>C-O$ "degenerate" stretching,[6] is absent in DNA even in its A form (see Fig. 1). Therefore, the assignment of this band in RNA has been supported by our present work.

References

1) S. C. Erfurth, E. J. Kiser, and W. L. Peticolas, *Proc. Nat. Acad. Sci. U.S.A.*, **69**, 938 (1972).

2) J. Pilet and J. Brahms, *Nature New Biology*, **236**, 100 (1972); *Biopolymers*, **12**, 387 (1973).

3) E. W. Small and W. L. Peticolas, *Biopolymers*, **10**, 1377 (1971).

4) T. Sato, Y. Kyogoku, S. Higuchi, Y. Mitsui, Y. Iitaka, M. Tsuboi, and K. Miura, *J. Mol. Biol.*, **16**, 180 (1966).

5) S. Higuchi, M. Tsuboi, and Y. Iitaka, *Biopolymers*, **7**, 909 (1969).

6) M. Tsuboi, K. Matsuo, T. Shimanouchi, and Y. Kyogoku, *Spectrochim. Acta*, **19**, 1617 (1963).

BULLETIN OF THE CHEMICAL SOCIETY OF JAPAN, VOL. 47(4), 1045—1046 (1974)

Nonideality of Ammonia Solutions in *N,N*-Dimethylformamide

Rabindranath PATNAIK* and William G. LLOYD

Department of Chemistry, Western Kentucky University, Bowling Green, KY 42101, USA

(Received January 6, 1973)

Synopsis. Solutions of ammonia at 0—40 °C and 0.2—1.2 atm in *N,N*-dimethylformamide exhibit negative deviations from Raoult's Law and marked departures from Henry's Law. This behavior is shown to be consistent with predictions of a simple model for solute-solute hydrogen bonding.

At moderate temperatures and partial pressures ammonia exhibits a negative deviation from Raoult's Law and a marked departure from Henry's Law solubility in *N,N*-dimethylformamide.

Materials and Methods

Anhydrous ammonia was obtained from Matheson Gas Products Corp. and *N,N*-dimethylformamide (DMF) from Matheson Coleman & Bell Corp. Purities were verified by gas chromatographic analysis. Solubility data were obtained manometrically at 0—40 °C and at 0—1.2 atm. As a check on apparatus and procedures, similar solubility data were obtained with acetylene.

Results and Discussion

The solubility data for acetylene are in the expected good accord with Henry's Law:

$$C_a = k \cdot P_a \quad (1)$$

For this system the pressure-solubility curves are linear with an average correlation coefficient of 0.997. The indicated heat of solution, −4.6 (±0.5) kcal, is in excellent agreement with Ryutani's estimate of 3—5 kcal at higher pressures.[1]

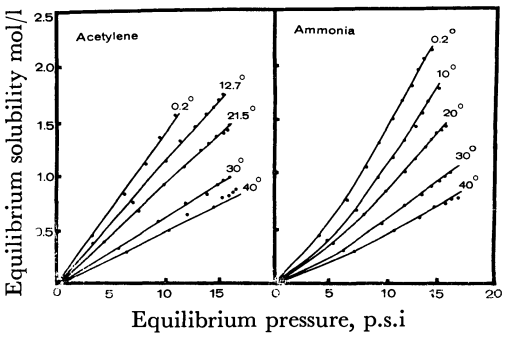

Fig. 1. Solubilities of acetylene and ammonia in *N,N*-dimethylformamide.

The corresponding data for ammonia describe a family of nonlinear curves (Fig. 1) inconsistent with Eq. (1). Under these conditions van der Waals corrections are very small. These data can be explained in terms of hydrogen bonding between solute ammonia molecules:

$$NH_{3(solute)} + NH_{3(solute)} \overset{K_d}{\rightleftharpoons} (NH_3)_{2(solute)} \quad (2)$$

Other calculations indicate a small amount of hydrogen-bonding dimerization in the gas phase;[2] the strength of the bridging bond is estimated to be 2.7—3.7 kcal.[3-5]

DMF, a very weak base,[6] is unlikely to be directly involved. A weak 1:1 ammonia–DMF complex has been detected in the solid state, but above its mp of −87 °C this is substantially dissociated.[7] Also this system shows a negative deviation from Raoult's Law, while ammonia at 0 °C shows marked positive deviations with hydrogen-bonding solvents.[8]

Taking dimerization as a simple model for solute-solute association, the total concentration of solute ammonia is:

$$\sum C = C_a + 2C_d \quad (3)$$

where C_a and C_d are the concentrations of ammonia and of ammonia dimer, respectively. From reaction 2,

$$C_d = K_d \cdot C_a^2 \quad (4)$$

Hence, by Eqs. (1), (3), and (4):

$$\sum C = k \cdot P_a + 2K_d \cdot k \cdot P_a^2 \quad (5)$$

This argument is supported by the good linearity of plots of $\sum C/P_a$ *vs.* P_a. The Henry's Law constant k is evaluated by the intercept of $\sum C/P_a$ at $P_a=0$. Estimates of k are shown in Table 1. The indicated heat of solution, 3.7 (±0.2) kcal, is consistent with those found for ammonia and the polar aprotic solvents adiponitrile (3.4 kcal)[9] and tributyl phosphate (2.5 kcal).[10]

Table 1. Equilibrium constants in *N,N*-dimethylformamide at 0.2—40.0 °C

T, °C	Henry's Law constant			Dimerization constant	
	k	stand. dev.	smoothed k[b,c]	K_d	smoothed K_d[b,d]
0.2	1.346	0.020 (8 df)	1.36	0.500	0.54
10.0	1.058	0.017 (8 df)	1.07	0.557	0.52
20.0	0.893	0.022 (8 df)	0.86	0.530	0.50
30.0	0.701	0.006 (6 df)	0.70	0.460	0.49
40.0	0.558	0.005 (5 df)	0.57	0.474	0.48

a) Calculated by the method of least squares from Eq. (5); k is in units of mol l^{-1} atm^{-1}; K_d is in units of 1 mol^{-1}.
b) By arithmetic average of five estimates using the least-squares temperature dependency.
c) The estimate of ΔH_{soln} from these data is −3.70 (±0.16) kcal.
d) The estimate of $\Delta G_{dimerization}$ from these data is −0.50(±0.40) kcal.

Under these conditions $K_d \simeq 0.5$ l mol^{-1}. Crudely, $\Delta G_{dimerization} \simeq -0.5$ (±0.4) kcal. We believe this to be the first showing of solute ammonia dimerization

at ambient temperatures and pressures.

This work was generously supported by an Air Reduction Co. fellowship.

References

* Present address: Biochemistry Research Division, Department of Medicine, Sinai Hospital, Baltimore, Md., USA.

1) B. Ryutani, *Nippon Kagaku Zasshi*, **82**, 513 (1961).
2) A. N. Roy and A. D. Gupta, *Indian J. Phys.*, **40**, 404 (1966).
3) P. A. Kollman and L. C. Allen, *J. Amer. Chem. Soc.*, **92**, 753 (1970).
4) P. A. Kollman and L. C. Allen, *ibid.*, **93**, 4991 (1971).
5) J. G. G. M. van Duijneveldt-van de Rijdt and F. B. van Duijneveldt, *ibid.*, **93**, 5644 (1971).
6) E. M. Arnett, L. Joris, E. Mitchell, T. S. S. R. Murty, T. M. Gorrie, and P. von R. Schleyer, *ibid.*, **92**, 2365 (1970).
7) B. Becker and A. W. Davidson, *ibid.*, **85**, 159 (1963).
8) W. Gerrard and V. K. Maladkar, *Chem. Ind.*, **1970**, 925.
9) G. D. Efremova and R. O. Pryanikova, *Zh. Fiz. Khim.*, **38**, 686 (1964).
10) J. Hala and D. G. Tuck, *J. Chem. Soc., A*, **1970**, 3242.

Faraday Parameters of the Magnetic Circular Dichroism of Praseodymium Trichloride and Thulium Trichloride in Poly(vinyl alcohol) Film

Yoshifumi KATO and Kyusaku NISHIOKA

Department of Chemistry, Faculty of Science, Kobe University, Nada-ku, Kobe 657

(Received July 16, 1973)

The magnetic circular dichroism and absorption spectra of $PrCl_3$ and $TmCl_3$ in polyvinylalcohol film are measured in the range of 300—700 nm. The absorption bands observed are five for $PrCl_3$, the transitions from the ground state, $^3H_4$, to the excited states, $^1D_2$, $^3P_0$, $^3P_1$, $^1I_6$, and $^3P_2$, of Pr^{3+}, and four for $TmCl_3$, the transitions from the ground state, $^3H_6$, to the excited states, $^3F_3$, $^3F_2$, $^1G_4$, and $^1D_2$, of Tm^{3+}. In order to separate the *C* term of the Faraday parameters, the temperature variation of the spectra is carried out at room temperature to 77 K. The Faraday parameters are derived from the experiment by the use of three methods; the method of moments, the graphical method, and curve fitting. The characteristics of these methods are discussed, and the uncertainty of the parameters obtained is estimated to be 30% or more. A group-theoretical consideration is applied for the interpretation of the results; this consideration fairly well explains the sign of the *C* terms obtained for $PrCl_3$, but not for $TmCl_3$.

Since the general review of Buckingham and Stephens[1] with respect to the magnetic optical activity, there have been published a number of articles[2] on the magnetic circular dichroism (MCD) with the pervasion of instruments and the utilization of a superconducting magnet. From the results obtained, it has been demonstrated that this technique gives valuable information on the electronic structure of molecules, especially the assignments of the absorption spectra and the magnetic properties of the ground and excited states.

In general, since the spin-orbit coupling of rare-earth ions is much stronger than the crystal field, these ions have appreciable orbital magnetic moments and thus strong MCD spectra may be expected, even under a weak magnetic field. Rare-earth salt is, therefore, considered to be a material favorable to the investigation by MCD; even when direct observation of the Zeeman-effect for a transition is prevented by the absorption band-width, MCD measurement makes it possible to study the effect of a magnetic field on a transition. Since the states of rare-earth ions in a salt are a little affected by the surrounding crystal field, the absorption spectra can be easily assigned by comparing these with the results established by the emission spectra of free ions and the absorption, fluorescence, and Zeeman-spectra of single crystals. However, the MCD study is still useful in confirming the spectral assignment obtained incompletely by various other methods.

Several MCD measurements for the compounds involving Pr^{3+} have already been given. Foss and McCarville[3] and Briat *et al.*[4] separately measured the MCD of $PrCl_3$ in an aqueous solution at room temperature. The former estimated the magnitude of the Zeeman-splitting from the experiment. Ferre *et al.*[5] carried out a detailed MCD measurement of Pr^{3+} diluted in an $AlLaO_3$ crystal at 300—100 K. They obtained a number of spectroscopic splitting factors, together with other information, and made a theoretical argument for the results. There have, however, been no studies of the MCD for the salts involving Tm^{3+}.

In this paper, we will present the MCD and absorption spectra of $PrCl_3$ and $TmCl_3$ dispersed into a polyvinyl alcohol (PVA) film measured in the range of room temperature to 77 K. So far as we know, the MCD measurement in a PVA film was first attempted for $Fe(CN)_6^{3-}$ by Kobayashi *et al.*[6] Since the MCD spectra in a PVA film are very similar to those in an aqueous solution, this technique is considered to be appropriate for observing the temperature variation of the MCD for a soluble salt in water. The Faraday parameters of the MCD spectra are derived from the experiment by the use of several methods proposed by previous authors,[7,8] and some discussion is given of the methods used and of the accuracy of the parameters obtained. A group-theoretical consideration is also attempted for the interpretation of the parameters.

Experimental

Materials. A PVA film of samples was obtained by the addition of an aqueous solution of $PrCl_3 \cdot 7H_2O$ or $TmCl_3 \cdot 6H_2O$ into that of PVA and by allowing it to evaporate to dryness on a glass plate. Several PVA films with different concentrations were prepared for the purpose of the measurement with an appropriate absorption strength. The concentration of a sample was determined from the interpolation in the comparison of the absorption strength of a PVA film with that of the corresponding aqueous solution.

Spectral Measurements. All the measurements were carried out by the use of a JASCO model J-10 instrument with a permanent magnet, which had a pole gap of 12 mm and which produced a magnetic field of 4.6 kG on the average. For the measurement at lower temperatures, a sample film about 1 mm thick was directly immersed in liquid nitrogen or in a mixture of liquid and solid methanol placed in a special quartz Dewar vessel which could be closely inserted between magnetic poles. The bubbles produced in the Dewar vessel were removed skilfully not to disturb the measurements. The temperature was determined within an accuracy of ± 1 K by using a copper-constantan thermocouple in contact with a PVA film. The magnitudes of the MCD bands were calibrated with an aqueous solution of *d*-camphor sulfonic acid.

Method of Analysis

Theoretical. The theoretical expression of the MCD for an absorption band has been formulated by Buckingham and Stephens[1] and used to analyze the experiments by most investigators.[2,3] The ellipticity in an isotropic solution accompanied by an electronic transition, $a \rightarrow j$, is given by;[1,9]

$$\theta = -\frac{8\pi^2 H_z N}{3ch}[f_1 A + f_2(B + C/kT)], \tag{1}$$

$$A = \frac{3}{d_a}\sum_{a,j}[\langle j|\mu_z|j\rangle - \langle a|\mu_z|a\rangle]Im\{\langle a|m_x|j\rangle\langle j|m_y|a\rangle\},$$

$$B = \frac{3}{d_a}\sum_{a,j}\mathrm{Im}\{\sum_{k\neq a}[\langle k|\mu_z|a\rangle/\Delta E_{ka}][\langle a|m_x|j\rangle\langle j|m_y|k\rangle - \langle a|m_y|j\rangle\langle j|m_x|k\rangle] + \sum_{k\neq j}[\langle j|\mu_z|k\rangle/\Delta E_{kj}] \times [\langle a|m_x|j\rangle\langle k|m_y|a\rangle - \langle a|m_y|j\rangle\langle k|m_x|a\rangle]\},$$

$$C = \frac{3}{d_a}\sum_{a,j}\langle a|m_z|a\rangle \mathrm{Im}\{\langle a|m_x|j\rangle\langle j|m_y|a\rangle\}. \tag{2}$$

Here, f_1 and f_2 express the frequency functions defining the band shape, N is the total number of absorption centers per unit of volume in the ground state, a, d_a is the degeneracy of this state, and $\boldsymbol{m}=e\sum_i \boldsymbol{r}_i$ and $\boldsymbol{\mu}=-\beta\sum_i(\boldsymbol{l}_i+2\boldsymbol{s}_i)$ are the electric and magnetic dipole-moment operators respectively. The summations are over all the states degenerate with $a \rightarrow j$. In the conventional units used by previous authors,[2a,9] the molar ellipticity, θ_M, per unit of magnetic field is in units of the degree deciliter decimeter^{-1} mol^{-1}, A in D$^2\beta$, and B and C/kT in D$^2\beta$/cm^{-1} (β=Bohr magneton, D=Debye unit). Then, the coefficient of Eq. (1) becomes -21.346. The A, B, and C Faraday parameters arise from the Zeeman-splitting of $a \rightarrow j$, the mixing of a and j with the other states, k, due to a magnetic field, and the change in the population of the Zeeman-components of the a state respectively. As may be seen in Eq. (2), the C term can arise only when the ground state, a, is degenerate, because the expectation value of μ_z must otherwise be zero; similarly, the A term arises when the ground state, a, and/or the excited state, j, are degenerate. On the other hand, the B term, consisting of an infinite summation about the other states, k, can exist always, although the contribution of the B term to the total θ_M may not be sizable for paramagnetic substances. It is apparent that the MCD of $PrCl_3$ and $TmCl_3$ should have the contributions from all the Faraday parameters, since the ground state of Pr^{3+} is a degenerate state, $^3H_4$, and that of Tm^{3+} is $^3H_6$. In Eq. (1), a dielectric correction is ignored, but this problem is avoided by expressing our results as the ratio of the Faraday parameters to the electric dipole strength, $D(D=(3/d_a)\sum|\langle a|m_x|j\rangle|^2)$. In order to obtain valuable information from the measurement, it is first necessary to extract the values of the Faraday parameters. We have applied the following three methods previously proposed; the method of moments,[7] the graphical method[8] and curve fitting.

Method of Moments. This method was first introduced by Henry, Schnatterly, and Slichter[10] in interpreting the MCD of a color center; later the generalization and application to other types of absorption systems was done by Stephens *et al.*[7,11] The moment of molar extinction coefficient, ε, and of molar ellipticity, θ_M, about the average absorption frequency, ν, are defined as:[7,11a]

$$\langle\varepsilon\rangle_n = \int_{band}(\varepsilon/\nu)(\nu-\bar{\nu})^n d\nu, \quad \langle\theta_M\rangle_n = \int_{band}(\theta_M/\nu)(\nu-\bar{\nu})^n d\nu. \tag{3}$$

With the assumption of the rigid shift model, the zero-th and first-order moments for an isotropic solution of noninteracting molecules are approximated as;

$$\langle\varepsilon\rangle_0 = 108.9D, \quad \langle\varepsilon\rangle_1 = 0, \quad \text{(definition of } \bar{\nu}) \tag{4}$$

$$\langle\theta_M\rangle_0 = -33.53(B + C/kT), \quad \langle\theta_M\rangle_1 = 33.53A. \tag{5}$$

Using these equations, one can evaluate the Faraday parameters from the moments obtained by numerical integrations through the absorption and MCD curves. This method, therefore, does not require any assumption of band shape, position or width, or any model for the vibronic structure of the states.

Graphical Method. This method, proposed by Badoz *et al.*,[8] starts from a special assumption regarding a band shape. If the shape function is taken as a Gaussian form, f_G, the expressions for ε/ν and θ_M/ν are given under the rigid shift model as;

$$\varepsilon/\nu = 108.9Df_G \equiv Y, \tag{6}$$

$$\theta_M/\nu = -33.53[Af_G' + (B + C/kT)f_G] \equiv \Delta Y,$$

where;

$$f_G = 1/(\sqrt{\pi}\delta)\exp[-(\nu-\nu_0)^2/\delta^2]. \tag{7}$$

Now, it can easily be shown from Eq. (6) that;

$$Y'/Y = -(2/\delta^2)(\nu-\nu_0),$$

$$\Delta Y/Y = \theta_M/\varepsilon = 0.3080[(2/\delta^2)(\nu-\nu_0)A/D - (B + C/kT)/D]. \tag{8}$$

Since the values of the left side in Eq. (8) obtained from the experiment are linearly related to the frequency, ν, one can obtain graphically the half-width, δ, at $1/e$ and the frequency, ν_0, of the maximum absorption and the Faraday parameters divided by D. In this procedure, there is no further assumption except for a band-shape function if the derivative of the absorption curve can be obtained accurately.

Curve Fitting. The molar ellipticity, θ_M, is a function involving the Faraday parameters, the frequency of maximum absorption, and the half-width as parameters, P. By assuming a shape function for a band, one can fit an explicit expression of θ_M to an experimental curve. When θ_M is expanded to the first order in terms of these parameters and a least-squares procedure is applied, the final equation to be solved is reduced to be following matrix form;

$$\tilde{\boldsymbol{J}}\boldsymbol{J}\Delta\boldsymbol{P} = \tilde{\boldsymbol{J}}\Delta\boldsymbol{\theta}_M \tag{9}$$

$$\boldsymbol{J} \equiv \partial(\theta_{M1}, \cdots\cdots, \theta_{Mn})/\partial(P_1, \cdots\cdots, P_m), \tag{10}$$

where $\boldsymbol{J}$ and $\tilde{\boldsymbol{J}}$ are the Jacobi and its transposed matrix respectively, n and m being the number of θ_M measured and that of the parameters used respectively. From Eq. (9), the parameter correction, $\Delta\boldsymbol{P}$, to be revised can be evaluated iteratively from the difference, $\Delta\boldsymbol{\theta}_M$, between the measured and calculated ellipticity. This method is already familiar from other spectral analyses.[12]

Throughout all the methods, the separation of the C term has been done by means of the temperature variation of θ_M; the Faraday parameters were derived by means of a FACOM 230-35 computer in Kobe University.

Results and Discussion

Results and the Faraday Parameters. The absorption and MCD spectra observed are given in Fig. 1 for $PrCl_3$ and in Fig. 2 for $TmCl_3$. As may be seen in Figs. 1 and 2, at lower temperatures the widths of the absorption bands generally become more sharp and some bands evidently split into two bands or disappear due to the change in the population of the ground crystal-field levels, while the MCD spectra also exhibit a large temperature dependence.

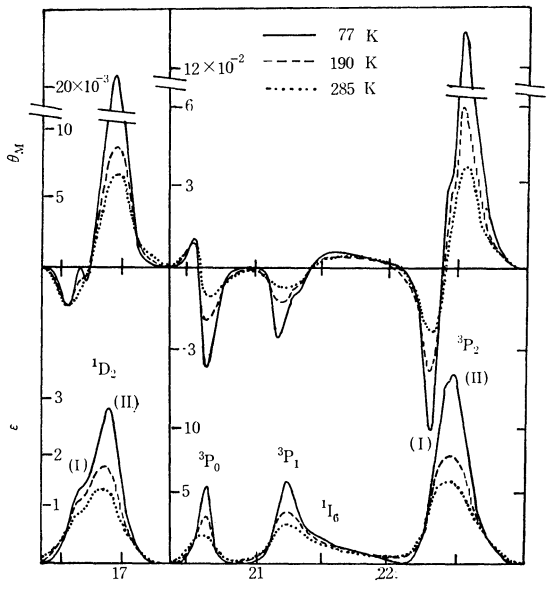

Fig. 1. Temperature variations of the absorption and MCD spectra of $PrCl_3$ in PVA film. θ_M and ε are the MCD in molar ellipticity units (degree deciliter decimeter^{-1} mol^{-1}) per unit Gauss and the molar extinction coefficient, respectively.

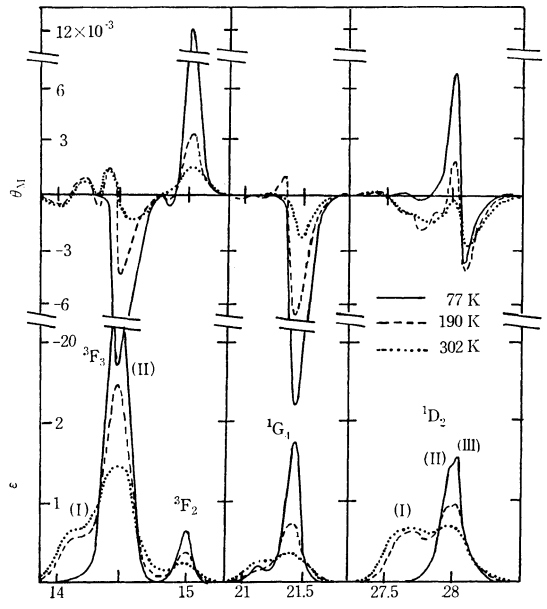

Fig. 2. Temperature variations of the absorption and MCD spectra of $TmCl_3$ in PVA film. Notations and units are the same as Fig. 1.

There are 13 electronic levels for the $4f^2$ configuration of Pr^{3+} as well as for the $4f^{12}$ configuration of Tm^{3+}; the latter being the complementary configuration of the former. Since the energy levels of several single crystals involving Pr^{3+} or Tm^{3+} have been well established,[13] it is easy to assign the absorption bands in PVA by comparison with those of single crystals; the bands of $PrCl_3$ at 16800, 20600, 21400, and 22400 cm^{-1} are identified as transitions from the ground state, $^3H_4$, to the excited states, $^1D_2$, $^3P_0$, $^3P_1$, and $^3P_2$, of Pr^{3+} respectively, the bands of $TmCl_3$ at 14400, 15000, 21300, and 27900 cm^{-1} being the transitions from the ground state, $^3H_6$, to the excited states, $^3F_3$, $^3F_2$, $^1G_4$, and $^1D_2$, of Tm^{3+} respectively. The absorption bands in the ultra-violet region are excluded from present analysis because of the disturbance due to the absorption of PVA itself in this region. (Hereafter, an absorption band will be designated with the relevant excited state.) It is certain that a weak shoulder band on the large-wave number side of the $^3P_1$ band in $PrCl_3$ is the $^1I_6$ band, because of the clear appearance of the small, positive θ_M at the corresponding position of the MCD curve. This assignment is also in agreement with that of Pr^{3+} in $LaCl_3$[14] and of the free ion.[15] Details of the derivation for the Faraday parameters of $PrCl_3$ by the moment analysis and graphical method are given in Tables 1 and 2 respectively. The absorption and MCD curve in PVA and in an aqueous solution for $PrCl_3$ at room temperature are given in Fig. 3, together with the results of the curve fitting. The corresponding tables and figures for $TmCl_3$ are abbreviated. The mean derivation $(\sum_i(\theta_M^{cald})_i/(\theta_M^{obsd})_i \times 100/n)$ for all the curve fittings were within 2%. As may be seen in Fig. 3, in both the absorption and MCD spectra, the spectral wave numbers in PVA commonly shift to a smaller side within 50 cm^{-1} of those

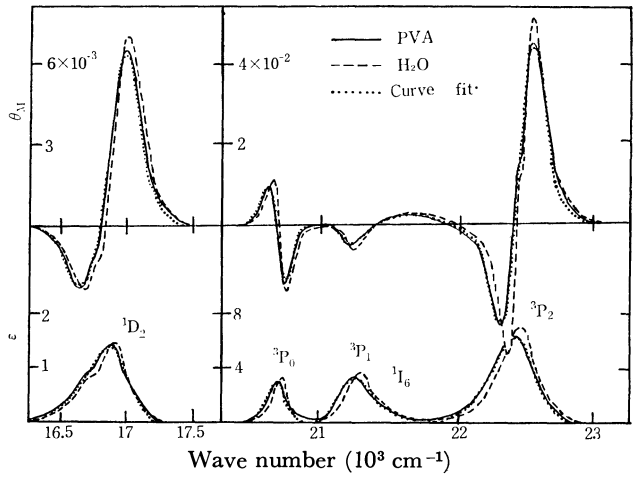

Fig. 3. Absorption and MCD spectra of $PrCl_3$ in PVA film and an aqueous solution at a room temperature, together with the results of the curve fitting. Notations and units are the same as in Fig. 1.

TABLE 1. PARAMETER VALUES FOR $PrCl_3$ IN PVA FILM BY THE MOMENT ANALYSIS

Excited state	T (K)	$\bar{\nu}$ (cm^{-1})	D ($10^{-4}D^2$)	A/D (β)	$(B+C/kT)/D$ ($10^{-3}\beta$/cm^{-1})
$^1D_2$	77	16870	5.241	2.054	−15.432
	188	16840	3.917	2.198	−6.481
	285	16830	3.529	2.262	−4.395
	289[a]	16870	3.330	2.319	−5.153
$^3P_0$	77	20650	3.184	−0.952	11.852
	190	20640	2.540	−1.073	5.891
	285	20630	2.295	−1.228	3.201
	292[a]	20680	2.361	−1.084	2.514
$^3P_1(^1I_6)$	77	21420	9.220	2.372	3.905
	190	21380	6.680	1.021	15.527
	285	21370	5.713	0.752	9.188
	292[a]	21400	6.049	0.824	8.168
$^3P_2$	77	22460	16.64	2.998	−15.071
	191	22440	12.73	2.785	−7.651
	285	22420	11.07	3.078	−6.084
	289[a]	22470	11.01	2.876	−6.431

a) Data in an aqueous solution.

TABLE 2. PARAMETER VALUES FOR $PrCl_3$ IN PVA FILM BY THE GRAPHICAL METHOD

Excited state	T (K)	ν_0 (cm^{-1})	δ[b] (cm^{-1})	A/D (β)	$(B+C/kT)/D$ ($10^{-3}\beta$/cm^{-1})
$^1D_2$(I)	77	16700	99.1	1.365	−9.870
	188	16720	164.6	1.386	2.240
	285	16730	181.4	1.143	5.325
	289[a]	16730	125.6	0.866	6.334
$^1D_2$(II)	77	16890	167.4	2.119	−17.341
	188	16880	202.1	2.518	−9.740
	285	16880	226.7	2.764	−7.468
	289[a]	16910	161.2	1.813	−8.377
$^3P_0$	77	20650	57.3	−0.960	16.494
	190	20660	60.1	−0.805	9.026
	285	20660	80.8	−1.284	6.429
	292[a]	20700	72.6	−1.187	3.961
$^3P_1$	77	21220	84.1	−0.385	17.858
	190	21240	115.8	−0.311	11.012
	285	21240	138.2	−0.369	7.503
	292[a]	21270	111.9	−0.231	7.213
$^3P_2$(I)	77	22400	143.4	5.083	−5.841
	191	22410	146.5	3.202	−2.790
	285	22410	166.8	2.829	1.362
	289[a]	22460	150.4	3.025	1.655
$^3P_2$(II)	77	22470	151.2	4.254	−2.113
	191	22470	164.2	3.432	−1.272
	285	22460	191.9	4.571	−0.461
	289[a]	22480	165.9	3.208	−0.755

a) Data in an aqueous solution. b) The half-width at $1/e$ of maximum absorption.

in aqueous solution, but the band shapes in PVA are almost identical with those in an aqueous solution. This fact shows that the electronic environment about a rare-earth ion in PVA is like that in an aqueous solution. Consequently, the site symmetry of a rare-earth ion in PVA could be considered to be C_{3v}.

The plots of $(B+C/kT)/D$ to $1/kT$ obtained by the moment method, graphical method and curve fitting are given in Figs. 4—6 for $PrCl_3$ and in Figs. 7—9 for $TmCl_3$. In these figures, the linear relations are,

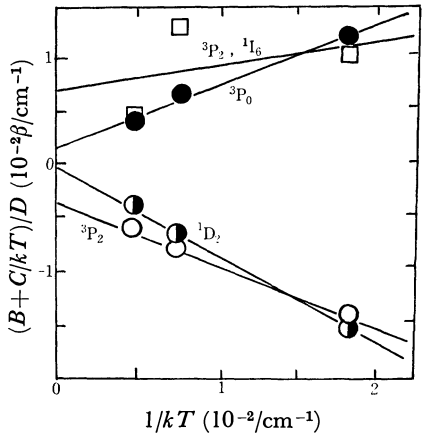

Fig. 4. Temperature dependence of $(B+C/kT)/D$ of $PrCl_3$ by the moment analysis.

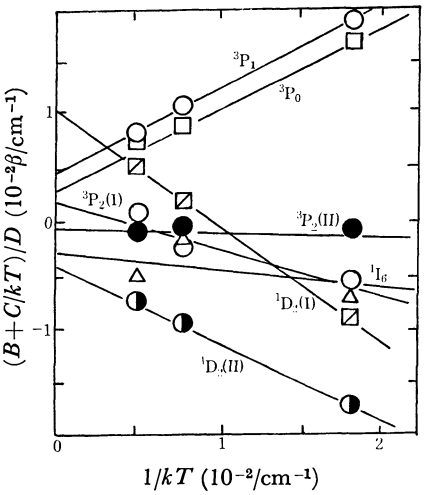

Fig. 5. Temperature dependence of $(B+C/kT)/D$ of $PrCl_3$ by the graphical method.

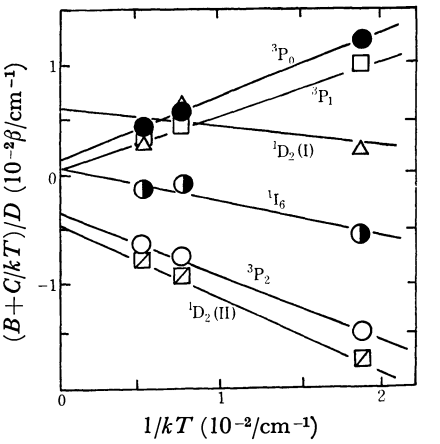

Fig. 6. Temperature dependence of $(B+C/kT)/D$ of $PrCl_3$ by the curve fitting.

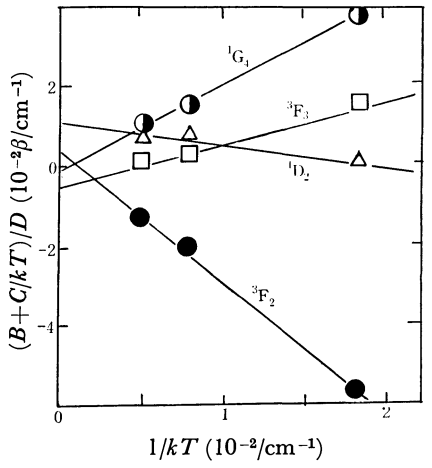

Fig. 7. Temperature dependence of $(B+C/kT)/D$ of $TmCl_3$ by the moment analysis.

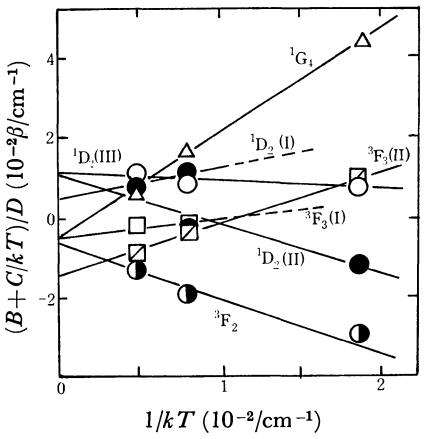

Fig. 8. Temperature dependence of $(B+C/kT)/D$ of $TmCl_3$ by the graphical method.

in general, well retained except for a few cases. The summaries of the Faraday parameters obtained are shown in Table 3 for $PrCl_3$ and in Table 4 for $TmCl_3$, where the values in parentheses are considered to be less reliable. The values of the B terms for all the bands are considerably smaller than those of the C terms. The ratio of C to B is approximately $\Delta E: kT$, as estimated by others.[1,9] Since ΔE, the order of magnitude of the energy difference between electronic states, is assumed to be $\sim$5000 cm^{-1}, and since kT is

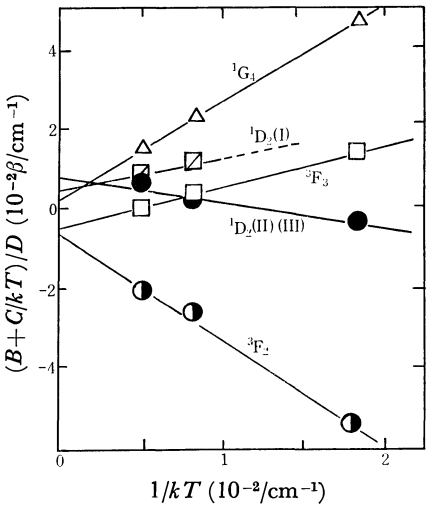

Fig. 9. Temperature dependence of $(B+C/kT)/D$ of $TmCl_3$ by the curve fitting.

$\sim$200 cm^{-1} at room temperature, this ratio becomes larger than 25; thus, the B term can be neglected at lower temperatures. The Faraday parameters obtained by means of the three methods are in fairly good agreement with one another in reliable cases.

The three methods used have some individual characteristics. The moment method may be the most powerful and general technique. In actual application, there is, however, an arbitrariness in the separation of an overlapping band; furthermore, the inclusion of higher-order moments complicates the analysis. The graphical method makes it possible to separate an overlapping band straightforwardly, as has already been pointed out by Badoz *et al.*,[8] but we could not always place trust in the numerical evaluation of the derivative of an absorption band. In the curve fitting, there is no assurance of any definite convergence by an iterative procedure using an assumed formula; in fact, some parameters may be very sensitive to the intial trial values used.

As to the accuracy of the Faraday parameters, it is possible to estimate for the transition to the non-degenerate excited state, $^3P_0$, of $PrCl_3$. In this case, the magnitude of the A/D should be, in principle, equal in absolute value and reverse in sign to that of the C/D, as may be seen in Eq. (2). This fact is not fully satisfied in any of the methods. As may be seen

Table 3. Values of the Faraday parameters of $PrCl_3$ by various methods
Units of A/D and C/D are in β, and those of B/D in 10^{-2} β/cm^{-1}.
Values in parentheses are less reliable.

Excited state	Moment analysis			Graphical method			Curve fitting			Theor. estimate of C/D
	A/D	B/D	C/D	A/D	B/D	C/D	A/D	B/D	C/D	
$^1D_2$(I)	2.17	−0.03	−0.81	1.30	1.08	−1.11	1.32	(0.60)	(−0.17)	negative
$^1D_2$(II)				2.47	−0.40	−0.71	1.75	−0.31	−0.73	
$^3P_0$	−0.98	0.06	0.63	−1.02	0.31	0.74	−0.89	0.17	0.56	positive
$^3P_1$	(1.72)	(0.71)	(0.29)	0.36	0.44	0.76	0.14	0.09	0.46	negative
$^1I_6$				(0.98)	(−0.21)	(−0.22)	(1.57)	(0.08)	(−0.35)	negative
$^3P_2$(I)	2.95	−0.32	−0.68	(3.70)	(0.27)	(−0.53)	2.65	−0.24	−0.62	negative
$^3P_2$(II)				(4.08)	(−0.02)	(−0.10)				

TABLE 4. VALUES OF THE FARADAY PARAMETERS OF $TmCl_3$ BY VARIOUS METHODS
Units of A/D and C/D are in β, and those of B/D in $10^{-2}\ \beta/cm^{-1}$.
Values in parentheses are less reliable.

Excited state	Moment analysis			Graphical method			Curve fitting			Theor. estimate of C/D
	A/D	B/D	C/D	A/D	B/D	C/D	A/D	B/D	C/D	
$^3F_3$(I)	−0.51	−0.50	1.08	(1.28)	(−0.48)	(0.44)	−0.45	−0.48	1.06	positive
$^3F_3$(II)				−1.15	−1.16	1.34				
$^3F_2$	1.86	0.41	−3.18	2.09	−0.60	−1.22	1.93	−0.60	−2.67	positive
$^1G_4$	−2.66	−0.13	1.97	−1.91	−0.42	2.55	−1.70	0.18	2.43	positive
$^1D_2$(I)				(−1.36)	(0.45)	(0.70)	(0.12)	(0.33)	(0.93)	
$^1D_2$(II)	−0.94	1.24	−0.62	(1.56)	(0.81)	(−1.32)	(−0.53)	(0.70)	(−1.07)	positive
$^1D_2$(III)				(−1.74)	(0.85)	(−0.10)				

in Table 3, the ratios of the absolute value of the A/D to that of the C/D are 0.6—0.7. Thus, the uncertainty in the parameters obtained is estimated to be 30% or more. It seems plausible, as Stephens[7a] has deduced, that 30% is the limit of the uncertainty of the parameters by the moment analysis. It is hazardous to conclude simply which method is superior to the others without a further detailed study of a favorable case. It may be pointed out that a careful consideration is necessary to obtain quantitative information on the basis of the experimental Faraday parameters.

Group-Theoretical Consideration. MCD results could be interpreted by considering the split in energy levels due to C_{3v} crystal symmetry. We will treat the A and C terms in terms of group theory, because the B term is considerably smaller than the others and there is difficulty in arriving of an infinite sum. A free-ion level including spin-orbit interaction splits into the sum of several irreducible representations of C_{3v} symmetry, as is shown in Table 5.[16] Since the species of μ_z and that of m_x and m_y in this symmetry are A_2 and E respectively, we can reduce the values of C/D and A/D according to the Wigner-Eckart theorem.[17] The expressions C/D and A/D for the transitions among crystal levels are given in Table 6, where μ_g and μ_e are a reduced matrix element $\langle E||\mu||E\rangle$ of the E species in the ground and excited states respectively.

TABLE 5. IRREDUCIBLE REPRESENTATIONS OF ION LEVELS UNDER C_{3v} SYMMETRY

Ion level	C_{3v} symmetry
$^3P_0$	A_1
$^3P_1$	A_2+E
$^1D_2$, $^3F_2$, $^3P_2$	A_1+2E
$^3F_3$	$2A_1+A_2+2E$
$^1G_4$, $^3H_4$	$2A_1+A_2+3E$
$^1I_6$, $^3H_6$	$3A_1+2A+4E$

TABLE 6. THEORETICAL REDUCTION OF THE VALUES OF C/D AND A/D FOR THE TRANSITIONS AMONG EACH SPECIES OF C_{3v} SYMMETRY

Transition	$C/D(\beta)$	$A/D(\beta)$
$E\rightarrow A_1$	$(i/\sqrt{2})\mu_g$	$-(i/\sqrt{2})\mu_g$
$E\rightarrow A_2$	$-(i/\sqrt{2})\mu_g$	$(i/\sqrt{2})\mu_g$
$E\rightarrow E$	$-(i/\sqrt{2})\mu_g$	$-(i/\sqrt{2})(\mu_e-\mu_g)$
$A_1\rightarrow E$	0	$(i/\sqrt{2})\mu_e$
$A_2\rightarrow E$	0	$-(i/\sqrt{2})\mu_e$

If we assume that the E species of the ground state consist of only f electrons, the value of μ_g comes to be $-\sqrt{2}\,i$ for Pr^{3+} and $i/\sqrt{2}$ for Tm^{3+} (see Appendix). The absorption bands observed are not due to the transitions between crystal levels, but to overall transitions. However, by assuming that the populations of all the E species in ground state are equal, we can estimate the signs of C/D, which are given in the last column in Tables 3 and 4. As may be seen in these tables, the experimental signs of the C/D for $PrCl_3$ are fairly well explained by such a simple consideration, but those for $TmCl_3$, not so well. This seems to arise from the fact that the assumption of equal populations for the four ground E species of $TmCl_3$ is not adequate, because the total splitting due to the crystal field in $TmCl_3\cdot 6H_2O$ crystal is 460 cm^{-1} (Olsen *et al.*);[18] this is twice or more as large as that of $PrCl_3\cdot 7H_2O$.[14] The further application of such a simplified treatment to the estimate of A/D is not appropriate because it involves several approximations.

Although the values of C/D and $(A+C)/D$ obtained are closely related to a weighted sum of the g-factors of the crystal levels in the ground and excited states concerned respectively, it is difficult to compare these values directly with the results obtained by other experiments because of the lack of accurate knowledge of the splitting crystal levels. From this point of view, it will be desirable to investigate the MCD of single crystals involving a rare-earth ion in order to advance further in the field of quantitative treatment.[19]

This work has been supported in part by the Ministry of Education of Japan.

Appendix

It is well known that the $4f^N$ configurations of rare-earth ions can be described satisfactorily in terms of intermediate coupling. In this case, only J and M_J become good quantum numbers and the wavefunction is a linear combination of LS functions with a constant J. If 305.4, 51.88, 5.321, and 729.5 cm^{-1}, values obtained by Margolis from the energy calculation of $PrCl_3$,[20] are taken as the values of the Slater parameters, F_2, F_4, and F_6, and the spin-orbit coupling constant, ζ, the ground state wavefunction, $\psi(J,M_J)$, of Pr^{3+} is given as;

$$\psi(J, M_J) = 0.9873\psi(^3H_4) + 0.1564\psi(^1G_4) - 0.0288\psi(^3F_4). \quad \text{(A1)}$$

Since the mixing among the LS functions is quite small, we

assume that the ground-state wavefunction of Pr^{3+} consists of only the $^3H_4$ state. When this state is put into the crystal field of C_{3v} symmetry, the eigenfunctions $\psi(L,S,J,M_J)$ for the species of C_{3v} become as follows:[16]

$$\begin{aligned} &A_1 \text{ species} \quad \psi(5,1,4,0),\\ &\qquad 1/\sqrt{2}\,[\psi(5,1,4,3)-\psi(5,1,4,-3)],\\ &A_2 \text{ species} \quad 1/\sqrt{2}\,[\psi(5,1,4,3)+\psi(5,1,4,-3)],\\ &E \text{ species} \quad \psi(5,1,4,\pm 4),\ \psi(5,1,4,\pm 1),\\ &\qquad \psi(5,1,4,\mp 2). \end{aligned} \tag{A2}$$

The expectation value of the magnetic dipole-moment operator, $\mu_z=-\beta(L_z+2S_z)$, with respect to a wavefunction, $\psi(L,S,J,M_J)$, is given as;

$$\langle\psi(L,S,J,M_J)|\mu_z|\psi(L,S,J,M_J)\rangle = -M_J g, \quad \text{(in units of } \beta) \tag{A3}$$

where g is a Landé g-factor. Although the value of g varies with the quantum numbers, J, L, and S, we assume it to be ~ 1 for the sake of simplicity, because the order of magnitude of g is about one. This approximation is equivalent to neglecting the contribution from the spin part of μ_z in Eq. (A3). Thus, the expectation values of μ_z for the three E species of the $^3H_4$ state are ∓ 4, ∓ 1, and ± 2 respectively.

On the other hand, when Griffith's coupling coefficient[17] are used, the matrix elements of μ_z with respect to the $E_{\pm 1}$ species are reduced to;

$$\begin{aligned} \langle E_{\pm 1}|\mu_z|E_{\pm 1}\rangle &= V\begin{pmatrix} E & E & A_2 \\ \mp 1 & \pm 1 & \alpha \end{pmatrix}\langle E\|\mu\|E\rangle \\ &= \pm i/\sqrt{2}\,\langle E\|\mu\|E\rangle. \end{aligned} \tag{A4}$$

Noticing that the E_{+1} state corresponds to the $\psi(5,1,4,-4)$, $\psi(5,1,4,-1)$ or $\psi(5,1,4,+2)$ function from their transformations under the symmetry operations of C_{3v}, and that the value of Eq. (A4) should be equal to the mean value of the three direct estimates by Eq. (A3) because the transitions from these three E species of the $^3H_4$ state can not be separated in our observations, we obtain $\langle E||\mu||E\rangle=-\sqrt{2}\,i$ for the $^3H_4$ state of Pr^{3+}; then, $\langle E||\mu||E\rangle=i/\sqrt{2}$ is obtained for the $^3H_6$ state of Tm^{3+} from similar considerations.

References

1) A. D. Buckingham and P. J. Stephens, *Ann. Rev. Phys. Chem.*, **17**, 399 (1966).

2) For references up to 1970, see the tables cited in: (a) P. N. Schatz and A. J. McCaffery, *Quart. Rev.*, **23**, 552 (1969); *ibid.*, **24**, 329 (1970); (b) D. Caldwell, J. M. Thorne, and H. Eyring, *Ann. Rev. Phys. Chem.*, **22**, 259 (1971).

3) J. G. Foss and M. E. McCarville, *J. Amer. Chem. Soc.*, **87**, 228 (1965).

4) B. Briat, *C. R. Acad. Sci. Paris*, **260**, 853 (1965); B. Briat, M. Billardon, J. Badoz, and J. Lorier, *Anal. Chim. Acta*, **34**, 465 (1966).

5) J. Ferre, A. C. Boccara, and B. Briat, *J. Phys.*, **31**, 631 (1970).

6) H. Kobayashi, M. Shimizu, and Y. Kaizu, This Bulletin, **43**, 2321 (1970).

7) (a) P. J. Stephens, *Chem. Phys. Lett.*, **2**, 241 (1968); (b) P. J. Stephens, *J. Chem. Phys.*, **52**, 3489 (1970).

8) J. Badoz, M. Billardon, A. C. Boccara, and B. Briat, *Symp. Faraday Soc.*, **3**, 27 (1969).

9) P. N. Schatz, A. J. McCaffery, W. Suetaka, G. N. Henning, A. B. Ritchie, and P. J. Stephens, *J. Chem. Phys.*, **45**, 722 (1966).

10) C. H. Henry, S. E. Schnatterly, and C. P. Slichter, *Phys. Rev.*, **137**, A583 (1965).

11) (a) P. J. Stephens, R. L. Mowery, and P. N. Schatz, *J. Chem. Phys.*, **55**, 224 (1971); (b) G. A. Osborne and P. J. Stephens, *ibid.*, **56**, 609 (1972).

12) (a) D. E. Mann, T. Shimanouchi, J. H. Meal, and L. Fano, *J. Chem. Phys.*, **27**, 43 (1957); (b) R. A. Hoffman, *ibid.*, **33**, 1256 (1960); S. Castellano and A. A. Bothner-By, *ibid.*, **41**, 3863 (1964); Y. Kato and A. Saika, *ibid.*, **44**, 2824 (1966).

13) G. H. Dieke, "Spectra and Energy Levels of Rare Earth Ion in Crystals," Interscience Publishers, New York (1968), p. 193.

14) R. Sarup and M. H. Crozier, *J. Chem. Phys.*, **42**, 371 (1965); G. H. Dieke and R. Sarup, *ibid.*, **29**, 741 (1958).

15) J. Sugar, *Phys. Rev. Lett.*, **14**, 731 (1965); J. Sugar, *J. Opt. Soc. Amer.*, **55**, 1058 (1965); H. M. Crosswhite, G. H. Dieke, and W. J. Carter, *J. Chem. Phys.*, **43**, 2047 (1965).

16) B. G. Wybourne, "Spectroscopic Properties of Rare Earths," John Wiley & Sons, Inc., New York (1965), chap. 6.

17) J. S. Griffith, "The Irreducible Tensor Method for Molecular Symmetry Group," Prentice-Hall, Inc., Englewood Cliffs, New Jersey (1962), p. 112.

18) D. N. Olsen and J. B. Gruber, *J. Chem. Phys.*, **54**, 2077 (1971).

19) Recently, we have measured the MCD spectra of rare-earth ethylsulfate crystals, $R(C_2H_5SO_4)_3\cdot 9H_2O$ (R=Pr, Nd, Er, and Tm), at liquid helium temperature. The results will be presented in the near future.

20) J. S. Margolis, *J. Chem. Phys.*, **35**, 1367 (1961).

Thermodynamic Properties of Moderately-concentrated Poly(γ-benzyl-L-glutamate) Solutions

Akio OKAMOTO,* Kenji KUBO, and Kazuyoshi OGINO

Department of Pure and Applied Sciences, College of General Education, The University of Tokyo, Meguro-ku, Tokyo 153

(Received August 2, 1973)

The osmotic pressures for poly(γ-benzyl-L-glutamate) solutions in ethylene dichloride and chloroform were measured at 29 °C in the concentration range of 2—15 vol % polymer. The osmotic pressures increased monotonously with an increase in the concentration. No evidence was found for the coexistence of two phases. The results are compared with the theory of the solutions of rodlike molecules. The values of the thermodynamic interaction parameter, χ, for the systems were found to be 0.44—0.47 in the concentration range lower than 6.5 vol% polymer, where the solutions must be isotropic.

Poly(γ-benzyl-L-glutamate) (PBLG) is in the state of a random coil when it is dissolved at low concentrations in dichloroacetic or trifluoroacetic acid. In other solvents, such as chloroform, ethylene dichloride (EDC), and *N*,*N*-dimethylformamide (DMF), the polymer is α-helical. Below a critical concentration (A-point), these solutions are isotropic, while above another concentration (B-point) they are anisotropic. The coexistence of these isotropic and anisotro ic hases occurs in the intermediate concentration range, and these critical concentrations depend on the temperature.

The equilibrium properties of solutions of rodlike molecules have been treated theoretically by Onsager,[1] Isihara,[2] and Flory.[3] These theories predict that, above a critical concentration, rodlike molecules will be packed closely and will all be aligned in one direction, without requiring attraction forces, thus forming a nematic liquid crystal. The molecular distribution methods of Onsager and Isihara have been given for dilute solutions. Flory's lattice theory, however, is regarded as being free from any restriction on the concentration range.

In Flory's theory the enthalpy term in the free energy of mixing is assumed to be of the Van-Laar type and to be characterized by a parameter χ, which is also used in the statistical theory of solutions of randomly-coiled polymers. The phase diagrams are shown for axial ratios of $r=50$ and 100 in Fig. 1. The differences in the two concentrations corresponding to the A- and B-points are small for $\chi<ca.$ 0.1. In the range of $\chi>ca.$ 0.1 for $r=100$, and $\chi>ca.$ 0.25 for $r=50$, the concentrations of the solute in the isotropic phases become extremely low, while the volume fractions of the solute in the anisotropic phase approach unity.

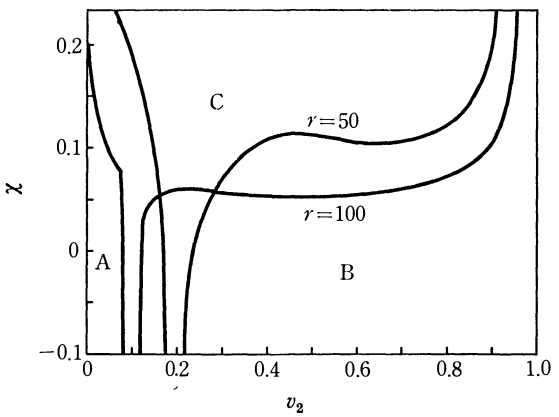

Fig. 1. Phase diagrams for solutions of rodlike molecules: region A, isotropic; B, anisotropic; C, coexistence region; axial ratio (r)=50 and 100.

Robinson *et al.*[4] found the A-point and the B-point for PBLG solutions in methylene chloride and dioxane by polarizing microscope measurements. The molecular-weight dependences of the concentrations of these points were in semiquantitative agreement with Flory's lattice theory, provided the value of χ is sufficiently small. Hermans[5] found the A-point for PBLG solutions in *m*-cresol from the viscosity methods. Nakajima *et al.*[6] discussed the phase diagrams obtained by the observation of the turbidity for the three-component system of the PBLG–DMF–poor solvent, in which the addition of a poor solvent to the polymer-solvent system caused an increase in the thermodynamic parameter, χ. Further, Wee and Miller[7] observed the A-point and the B-point as a function of the temperature by polarizing microscope and NMR spectrum measurements respectively; thus they obtained the phase diagram. These diagrams were in semiquantitative agreement with the prediction of Flory's theory. No direct values of χ, however, were given in these experiments.

The thermodynamic properties of the PBLG–pyridine, PBLG–EDC, and poly(β-benzyl-L-asparatate)–chloroform systems investigated by Flory and Leonard[8] in the concentration range of 60—100 vol% polymer. Their data could not be explained on the basis of Flory's lattice theory, but they could be explained if the mixing of a flexible side chain of the polymer with a solvent was considered. Their data were found to fit reasonably well a modified lattice model if χ_s values of 0.35, 0.20, and zero were assumed for the PBLG–pyridine, PBLG–EDC, and poly(β-benzyl-L-glutamate)–chloroform systems respectively, in which χ_s is a thermodynamic interaction parameter between the solvent and the side chain of the polymer.

There have been reported only a few studies aimed at evaluating the χ parameter in PBLG solutions from thermodynamic experiments. Goebel and Miller[9] obtained 0.5 for χ in dilute solutions of PBLG in DMF

* Present address: Insititute of Space and Aeronautical Science, The University of Tokyo, Meguro-ku, Tokyo 153.

at 22 °C from osmotic-pressure measurements. Rai and Miller[10] obtained 0.8 for χ in the same system in the concentration range of 0—30 vol% polymer from differential scanning calorimetric measurements on the assumption that χ is independent of whether the system is an isotropic or an anisotropic phase, and of the composition.

In this report, we will discuss the results of osmotic-pressure measurements on the PBLG–chloroform and PBLG–EDC systems in moderately concentrated regions and will attempt to obtain A- and B-points thermodynamically and to determine the χ value directly. The results are compared with those of Flory's theory.

Experimental

Materials. Three samples of PBLG (PBLG-A, -B, and -C) different in molecular weight were used. These were prepared by polymerzing γ-benzyl-L-glutamate-*N*-carboxy anhydride in dioxane, with triethylamine as an initiator. The molecular weights of PBLG-A, -B, and -C were found to be 1.88×10^5, 1.78×10^5, and 0.98×10^5 respectively by osmometry in DMF solutions. A high-speed membrane osmometer (Hewlett-Packard Co., Model 501) was employed. The axial ratios of PBLG-A, -B, and -C are 85, 81, and 45 respectively. After DMF was dried over $MgSO_4$ for 2 or 3 days, it was purified by vacuum distillation. The chloroform and EDC were dried over $CaCl_2$ and then distilled.

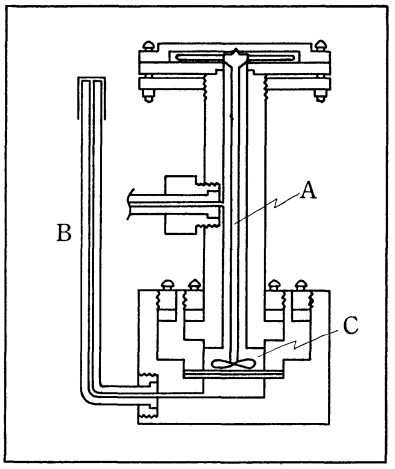

Fig. 2. Osmometer: A, stirrer; B, capillary; C, solution cell.

Osmotic-pressure Measurements. A high-pressure osmometer of the Flory[11]-Kuwahara[12] type was constructed (Fig. 2). It was designed so that highly viscous polymer solutions were stirred thoroughly without a leak in the applied pressure. The stirrer, A, was rotated by means of the outer magnet.

The osmotic pressures were measured at 29 °C by a compensation method. The solution was stirred in an Erlenmeyer flask for 24 hr; then it was put into a solution cell. After the solution had been stirred for 4—6 hr, it took 4—6 hr more until the equilibrium pressure was attained. No significant drift in this pressure was observed for a period of 24 hr. It was found that the polymer did not measurably leak into the solvent cell. In a few instances the pressure was reduced slightly after 30—40 hr; then leakages of the polymer were observed. The concentration of the polymer was estimated after each run. The volume fraction of the polymer, v_2, was obtained on the assumption that no volume change occurred on mixing. The semipermeable membranes used were degenerated cellulose membranes (Schleicher & Schuell Co., Type 08).

Results and Discussion

Table 1 shows the results of the osmotic-pressure measurements. In Fig. 3 the dependence of the osmotic pressure on the concentration is shown for PBLG-A in EDC. No data in the concentration region higher

Table 1. Osmotic pressure data and values of χ

$10^2 v_2$	π(g/cm^2)	χ
PBLG-A in EDC		
2.09	18	
3.47	36	0.44
4.90	58	0.45
7.62	138	0.46
7.82	130	0.47
PBLG-A in chloroform		
2.25	24	
4.90	49	0.46
5.67	70	0.46
5.74	76	0.46
8.88	110	0.49
10.50	158	0.498
PBLG-B in chloroform		
2.29	16	0.44
4.42	41	0.46
5.23	64	0.46
6.44	99	0.46
7.43	120	0.47
9.57	193	0.474
14.36	425	0.493
PBLG-C in chloroform		
3.11	26	0.46
3.96	40	0.46
5.71	70	0.47
7.52	120	0.47
9.95	200	0.483
11.13	279	0.479
15.17	533	0.491

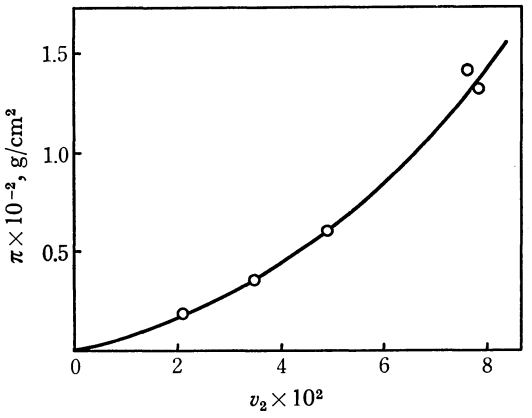

Fig. 3. Experimental values of π plotted against v_2 for solutions of PBLG-A in EDC at 29 °C.

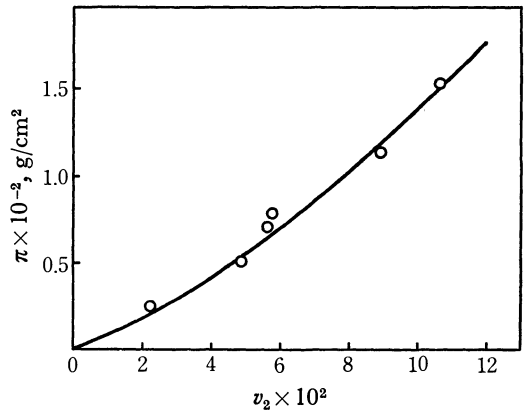

Fig. 4. Experimental values of π plotted against v_2 for solutions of PBLG-A in chloroform at 29 °C.

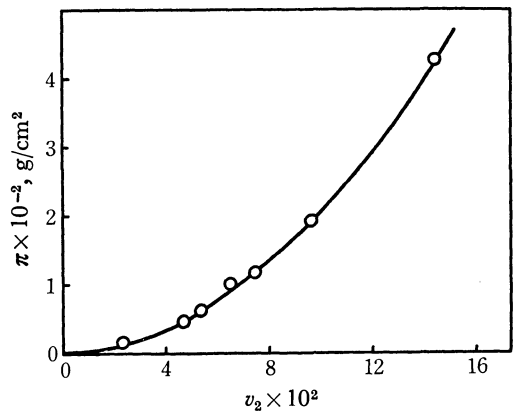

Fig. 5. Experimental values of π plotted against v_2 for solutions of PBLG-B in chloroform at 29 °C.

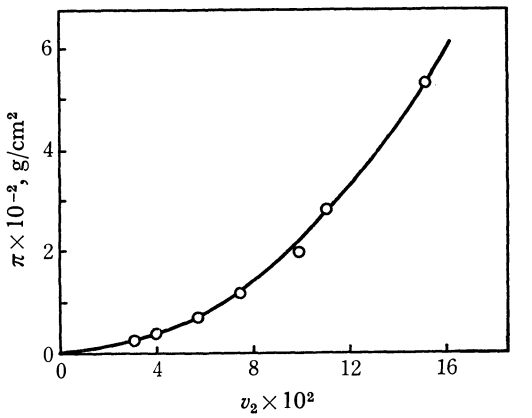

Fig. 6. Experimental values of π plotted against v_2 for solutions of PBLG-C in chloroform at 29 °C.

than the concentration of 8 vol% polymer were obtained, because this system causes gelation at higher concentrations before the attainment of the equilibrium pressure. The data for PBLG-A, -B, and -C in chloroform are shown in Figs. 4, 5, and 6 respectively.

According to the lattice theory of Flory,[3] the free energy of mixing ΔG_m for the system consisting of n_1 mol of a solvent and n_2 mol of a rodlike polymer with an axial ratio, r, is given by:

$$\Delta G_m/RT = n_1 \ln v_1 + n_2 \ln v_2 - (n_1+yn_2) \times \ln\{1-v_2(1-y/r)\} - n_2\{\ln(ry^2)-y+1\} + \chi r n_2 v_1 \quad (1)$$

where v_1 and v_2 are the volume fractions of the solvent and the polymer respectively, and y is a orientation parameter. This equation gives the chemical potentials of the solvent both in the isotropic phase and in the anisotropic phase. The relation for the isotropic phase is:

$$(\mu_1-\mu_1^0)/RT = \ln(1-v_2) + (1-1/r)v_2 + \chi v_2^2 \quad (2)$$

and that for the anisotropic is:

$$(\mu_1-\mu_1^0)/RT = \ln(1-v_2) + \{(y-1)/r\}v_2 + 2/y + \chi v_2^2 \quad (3)$$

where y is given as the solution of the following equation:

$$v_2 = \{r/(r-y)\}\{1-\exp(-2/y)\} \quad (4)$$

The plots of $\Delta\mu_1(=\mu_1-\mu_1^0)$ *versus* v_2, as calculated from Eqs. (1)—(4) for $\chi=0$ with $r=45$ and 85, are shown in Fig. 7. The straight lines parallel to the absissa show that there is no net change in $\Delta\mu_1$ when the isotropic and anisotropic phases co-exist. The rate of change in the chemical potential for the anisotropic phase is much less than for the isotropic phase.

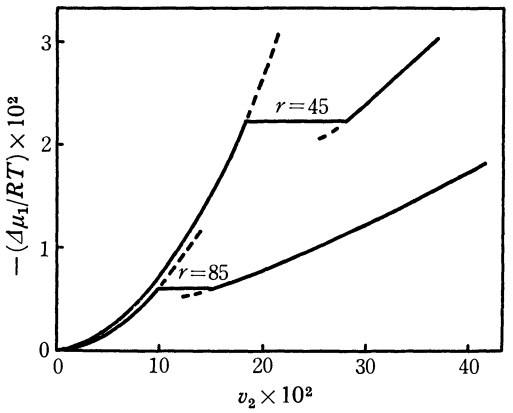

Fig. 7. Calculated curves of $\Delta\mu_1/RT$ plotted against v_2 for solutions of rodlike molecules: axial ratio $(r)=45$ and 85; thermodynamic parameter $(\chi)=0$.

The chemical potential, μ_1, of the solvent is related to the osmotic pressure, π, of the solution by:

$$\mu_1 - \mu_1^0 = -\pi V_1 \quad (5)$$

where V_1 is the molar volume of the solvent. Therefore, Fig. 7 also represents the relation between π and v_2.

In Flory's lattice theory of solutions of rodlike molecules, the concentrations corresponding to A-points for $r=45$ and 85 are respectively given as $v_2=0.18$ and 0.095 for $\chi=0$, as are shown in Fig. 7. The experimental investigations of Robinson *et al.*[4] for the PBLG–methylene chloride and PBLG–dioxane systems showed that the concentrations observed as the A-points are lower than the predicted concentrations when they are compared on the same axial ratios, provided a value of χ is sufficiently small. The concentrations of the A-points corresponding to the axial ratios of the samples used in this work are obtained on the basis of their

data as follows:

	PBLG–methylene chloride	PBLG–dioxane
	$v_2 \times 10^2$	
$r = 45$	9	8
$r = 81$	8	8
$r = 85$	8	8

It was shown in our previous paper[13] that the PBLG-A (r=85)–chloroform system separated into phases at equilibrium in the concentration 8 vol% polymer and at 30 °C.

In the concentration range where a solution is biphasic, some parts of the sample transmit light when placed between crossed polars, while others do not. Although it was difficult to determine clearly the point when no light parts remained in an Erlenmeyer flask, the A-points for the solutions of PBLG-B (r=81) and -C (r=45) in chloroform were found to be at $v_2 \approx$ 0.065—0.070 at 29 °C. The A-points are satisfactorily within the range of the present osmotic-pressure measurements except for the measurements of the PBLG-A solutions in EDC (see Figs. 3—6).

The osmotic pressures for the solutions of PBLG in EDC and chloroform increase monotonously with an increase in the concentration, as are shown in Figs. 3—6. The existence of explicit phase boundaries was not found from the dependence of the osmotic pressure on the concentration.** The reason for this may be considered to be as follows. Since the biphasic region was too narrow to be detected experimentally, and since the difference between the chemical potentials for the isotropic and the anisotropic states was not so much as that predicted by Flory's theory (see Fig. 7), we might have drawn a smooth curve over the region of the two phases in the osmotic *vs.* concentration diagram.

For isotropic solutions, the values of χ are calculated by the substitution of the osmotic-pressure data into these two relations:

$$\chi = -\{\pi V_1/RT + \ln(1-v_2) + (1-1/x)v_2\}/v_2^2 \qquad (6)$$

and:

$$x = V_2/V_1$$

where V_1 and V_2 are the molar volumes of the solvent and the solute respectively. Equation (6) is derived from Eqs. (2) and (5) by replacing r by x. The x thus defined allows the theory to be applied to actual solutions. An idealization adopted in the Flory model for theoretical derivation stipulates that the solvent molecule should be of such a diameter as to be replaceable by a segment of the rodlike solute. This condition is not fulfilled in general; hence, we adopt the definition of x given above in order to permit application to actual solutions. By the use of x, the chemical potential of a solvent at an infinitely dilute solution is of an acceptable form. If we assume that Eq. (2) can also be used in the high concentration region, the values of χ can be similarly obtained from Eq. (6).

The results are shown in Table 1. The values of χ in the concentration range lower than 6.5 vol% polymer, where the solution is isotropic, are found to be 0.44—0.47 for either EDC or chloroform. The values of χ in the concentration range higher than 6.5 vol% polymer are found to be 0.46—0.50. The set of the latter values is slightly larger than that of the former values, on the average. The experimental values of χ for solutions of randomly-coiled polymers have been found to be dependent on the concentration.[11,12,14,15] The assumption of a χ value independent of the concentration is not justified in general for polymer solutions. Therefore, it can not be concluded on the basis of the χ values that the higher concentration region with the slightly larger values of χ is not an isotropic phase.

Flory's lattice theory predicts that a system with a large value of χ will be biphasic at extremely low concentrations. The concentration corresponding to the A-point is given as $v_2 \approx 5 \times 10^{-4}$ for r=45 and χ=0.45; the polymer concentration becomes even lower for higher axial ratios. Since the experimental results are very different from the predictions, it can not be assumed that the phase separation of solutions of rodlike molecules occurs primarily because of the entropic contribution originating from an extremely assymmetric shape of the molecules. We are forced, therefore, to conclude that it is necessary to modify the lattice theory of rodlike molecules.

The authors thank the Ministry of Education for Grant-in-Aid.

** The biphasic region for the PBLG-A–chloroform system is lying near the concentration of 8 vol% polymer. Although the osmotic pressures, as are shown in Fig. 4, were not measured for the concentration range of 6—9 vol% polymer in this experiment, we dared to draw the smoothed curve over the entire region of the measurements for the system.

References

1) L. Onsager, *Ann. N. Y. Acad. Sci.*, **51**, 627 (1949).
2) A. Isihara, *J. Chem. Phys.*, **19**, 1142 (1951).
3) P. J. Flory, *Proc. Roy. Soc., Ser. A*, **234**, 73 (1956).
4) C. Robinson, J. C. Ward, and R. B. Beevers, *Discuss. Faraday Soc.*, **25**, 29 (1958).
5) J. Hermans, Jr., *J. Colloid Sci.*, **17**, 638 (1962).
6) A. Nakajima, T. Hayashi, and M. Ohmori, *Biopolymers*, **6**, 973 (1968).
7) E. L. Wee and W. G. Miller, *J. Phys. Chem.*, **75**, 1446 (1971).
8) P. J. Flory and W. J. Leonard, Jr., *J. Amer. Chem. Soc.*, **87**, 2102 (1965).
9) K. D. Goevel and W. G. Miller, *Macromolecules*, **3**, 64 (1970).
10) J. H. Rai and W. J. Miller, *J. Phys. Chem.*, **76**, 1081 (1972).
11) P. J. Flory and H. Daust, *J. Polym. Sci.*, **25**, 429 (1957).
12) N. Kuwahara, T. Okazawa, and M. Kaneko, *ibid.*, **C23**, 543 (1968).
13) K. Kubo, S. Hiraga, and K. Ogino, *Japan. J. Appl. Phys.*, **11**, 427 (1972).
14) P. J. Flory, *Discuss. Faraday Soc.*, **49**, 7 (1970).
15) P. J. Flory and H. Shih, *Macromolecules*, **5**, 761 (1972).

Isotopic Study of Water Gas Reaction Catalyzed by Platinum

Makihiko MASUDA and Koshiro MIYAHARA
Research Institute for Catalysis, Hokkaido University, Sapporo 060
(Received August 10, 1973)

By the use of ^{13}C- and ^{18}O-labelled carbon dioxide and D_2 gas, water gas reaction over an evaporated Pt film was studied at temperatures 380—450 °C under constant elimination of water vapor with cold traps. The reaction of CO_2 and H_2 was as rapid as that of CO_2 and D_2, the mixture of H_2 and D_2 changing rapidly into an equilibrium mixture of H_2, HD, and D_2 in the course of the reaction with CO_2. The mixture of $C^{18}O_2$ and CO_2 was also rapidly equilibrated by the reaction with H_2. The exchange reactions of ^{18}O and ^{13}C between CO_2 and CO in the course of the water gas reaction were similarly observed. The theory of the stoichiometric number on the rate-determining step was applied to the results. From the results and the observed rate equation of the water gas reaction, $V=k[CO_2]^{0.6}[H_2]^{0.5}[CO]^{-0.5}$, the reaction was supposed to be caused by the sequence of steps, $CO_2 \rightleftarrows CO_2(a)$, $H_2 \rightleftarrows 2H(a)$, $CO_2(a)+H(a) \rightleftarrows X(a)$, $X(a) \rightleftarrows CO(a)+OH(a)$, $CO(a) \rightleftarrows CO$, and $OH(a)+H(a) \rightleftarrows H_2O$, and to be rate-controlled by the third and fourth steps, where (a) denotes the adsorbed state and X(a) is an intermediate to rule out the direct conversion of $CO_2(a)+H(a)$ into $CO(a)+OH(a)$.

The kinetics of water gas reaction,

$$CO_2 + H_2 = CO + H_2O, \quad (1)$$

catalyzed by platinum was observed by Prichard and Hinshelwood[1] and the rate equation was given[2] as

$$V = kP_1P_2/(1+K_1P_1+K_2P_2)^2, \quad (2)$$

where P_1 and P_2 are the partial pressures of CO_2 and H_2, respectively, and k, K_1 and K_2 constants. In this experiment the rate was followed by the total pressure change caused by absorption of formed water vapor by sulfuric acid kept in the reaction vessel. This equation was considered[2] to be a prototype of the so-called Langmuir-Hinshelwood mechanism of catalysis, which assumes the rate of reaction (1) to be determined by a surface reaction of adsorbed CO_2 and adsorbed H_2. However, according to the method of Horiuti *et al.*[3] of estimating the number N^* of active centers on a catalyst surface, Eq. (2) gave an enormous value of N^*, *ca.* 10^{32} cm^{-2}.[3] In a previous work[4] the kinetics was reexamined by the use of a conventional closed circulation apparatus under constant elimination of water vapor, as in the case of Prichard and Hinshelwood, by cold traps:

$$V = k_pP_1^{0.6}P_2^{0.5}P_3^{-0.5}. \quad (3)$$

This differs from Eq. (2) especially with regard to the dependence on P_3, *i.e.*, the partial pressure of CO, and gave[4] the value of N^* at 7.3×10^{14} cm^{-2}, which is of a reasonable order of magnitude as the number of metal atoms exposed on catalyst surface. As regards such a difference in kinetics, Eq. (3) suggests the possibility that the mechanism of (1) differs from those proposed.[1,5] We have followed the redistribution of ^{13}C and/or ^{18}O atoms between carbon dioxide and monoxide, and that of deuterium atoms in hydrogen gas in the course of reaction. The results were analyzed in reference to the theory of the stoichiometric number[6,7] and an appropriate reaction mechanism was proposed.

Experimental

Materials. Pure carbon dioxide (Takachiho Chemical Industrial Co., Ltd.) was purified further by repeated distillation in a vacuum., Pure carbon monoxide (*ibid.*) was purified by being passed through copper gauge heated at *ca.* 300 °C and then a trap cooled by liquid nitrogen. Hydrogen and deuterium gas from cylinders were purified by being passed through heated Pd–Ag thimbles.

Carbon dioxide labelled by ^{13}C (Merck Sharp and Dohme Co., Ltd., Canada) was purified by repeated distillation in a vacuum. Carbon dioxide labelled by ^{18}O (Yeda Research and Development Co., Ltd., Israel) and that supplied by a reaction at *ca.* 300 °C of heavy oxygen gas of *ca.* 90 ^{18}O-atomic percents with active carbon supporting platinum were used. They were purified by distillation in a vacuum. Catalysts were platinum films evaporated on the inner surface of a reaction vessel immersed in an ice water bath and preliminarily sintered in a vacuum at 480 °C for 30 min and then 410 °C for 2 hr.

Procedure and Results. The apparatus was similar to that used in a previous work,[4] *viz.*, a conventional closed circulation system equipped with a mercury manometer and two dry ice traps on both sides of the reaction vessel. The whole apparatus was made of Pyrex glass.

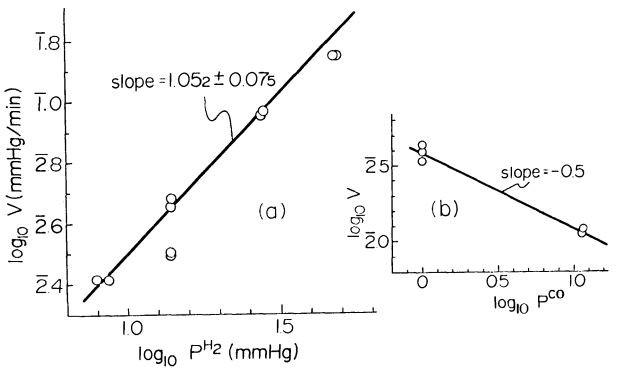

Fig. 1. Pressure dependence of the reaction rate.
(a), $\log_{10} V$ (mmHg/min) *vs.* $\log_{10} P_2$ (H_2, mmHg) at 410 °C: P_1 (CO_2)$=P_2$, P_3 (CO)$=1.0\pm0.04$ mmHg.
(b), $\log_{10} V$ *vs.* $\log_{10} P_3$ at 410 °C: $P_1=P_2=14.9\pm0.1$ mmHg.

1. Rate Equation: Rate Eq. (3) was confirmed by two series of experiments with a 1:1 mixture of CO_2 and H_2. The results of the first series are shown in Fig. 1(a) where the rate was observed at $P_3=1$ mmHg. The rate is proportional to $P_2^{1.1}$ in conformity with Eq. (3). In the second series the dependence of the rate on P_3 was examined by addition of 10 mmHg CO to a 1:1 mixture of CO_2 and H_2.

The results are shown in Fig. 1(b) which also confirms Eq. (3).

2. Kinetic Isotope Effect with Respect to Hydrogen and H_2–D_2 Equilibration: By the use of a 1:1 mixture of CO_2 and H_2 or D_2, it was found that the isotope effect on the rate was absent at temperatures 386—459 °C (Fig. 2).

In the course of reaction of a mixture of 18.2 mmHg CO_2, 18.2 mmHg H_2, and 10.8 mmHg D_2 at 410 °C, the equilibration reaction $H_2+D_2=2HD$ was completed in the first 6 minutes, whereas as little as 0.3 mmHg of the total pressure decrease had proceeded in reaction (1).

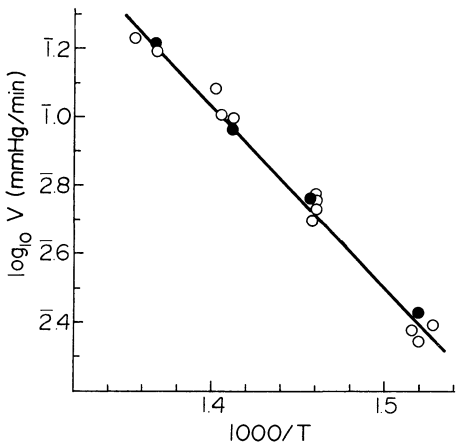

Fig. 2. Kinetic isotope effect of hydrogen:
●, reaction of CO_2 and D_2 at P_1 $(CO_2)=P_2$ $(D_2)=13.90\pm0.08$ mmHg, P_3 $(CO)=1.0\pm0.04$ mmHg; ○, reaction of CO_2 and H_2 at $P_1=P_2$ $(H_2)=13.89\pm0.11$ mmHg, $P_3=1.0\pm0.04$ mmHg.

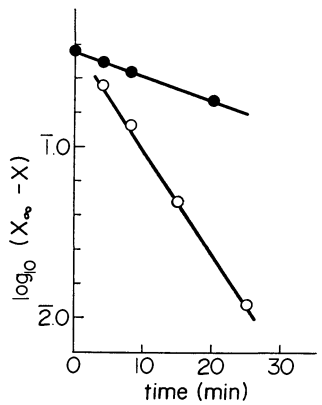

Fig. 3. The equilibration, $C^{18}O_2+CO_2=2CO^{18}O$, at 410 °C:
○, in the presence of Pt at $P_1(CO_2)=21.5\pm1$ mmHg, $P_2(H_2)=24\pm1$ mmHg, $P_3(CO)=3.5\pm0.2$ mmHg; ●, in the absence of catalyst at $P_1=19.3$ mmHg, $P_2=19.1$ mmHg, $P_3=5.5$ mmHg.

3. Equilibration of Oxygen Isotope in CO_2 Gas: Equilibration $C^{18}O_2+CO_2=2CO^{18}O$ was observed by addition of 8 mmHg ^{18}O-labelled CO_2 (79.8% $C^{18}O_2$, 19.0% $CO^{18}O$, and 1.2% CO_2) to a mixture of 25.0 mmHg H_2, 14.5 mmHg CO_2, and 3.3 mmHg CO. The result is shown in Fig. 3 where X is the mole fraction of $CO^{18}O$ in carbon dioxide and X_∞ the equilibrium value of X. The rate V_e of the equilibration was evaluated by the equation

$$N dX/dt = V_e(X_\infty - X), \qquad (4)$$

where N is the number of carbon dioxide molecules in the reaction system. This equation, being correct in the absence of reaction (1), is applicable to the present case where the decrease of P_1 was as small as 0.6 mmHg and the atomic fraction of ^{18}O in carbon dioxide was kept constant at 0.358 ± 0.001. Equilibration took place without catalyst as seen in Fig. 3 and was enhanced by the platinum catalyst by as much as 3.6×10^{17} molecules/s; the rate is far greater than that of reaction (1) which was estimated at 2.8×10^{15} molecules/s just before the introduction of ^{18}O-labelled CO_2.

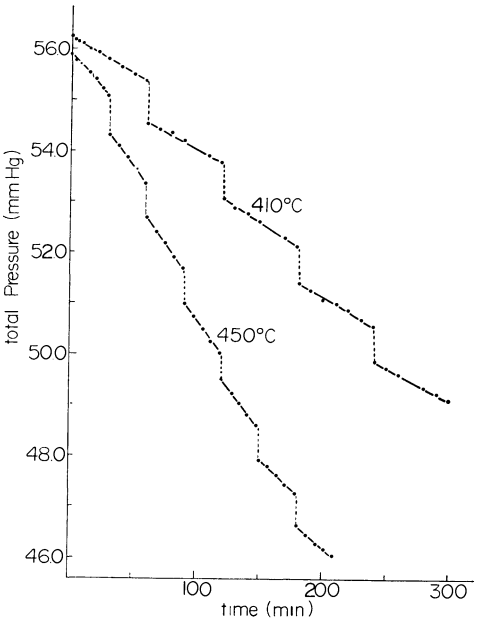

Fig. 4. Time courses of the reaction at 410 °C (runs V.6) and 450 °C (V.8).

4. Exchanges of ^{18}O and ^{13}C between CO_2 and CO: In order to see the effect of trapped water on the exchange reactions, several runs of reaction of a 1:1 mixture of normal CO_2 and H_2 were conducted at 410 °C and the formed water vapor amounting to *ca.* 9 mmHg was trapped. The exchange reaction was then observed with a mixture of 15 mmHg CO, 21 mmHg H_2, and 21 mmHg labelled CO_2. Typical time courses of the total pressure at 410 and 450 °C are shown in Fig. 4, where steep decreases of the total pressure were caused by samplings of the reacting gas. Sampled gas was analyzed mass spectrometrically for the atomic fractions of ^{18}O, (Z_1 and Z_3), and those of ^{13}C, (Y_1 and Y_3), in CO_2 and CO, respectively. In Fig. 5 Z_1 and Z_3 were plotted

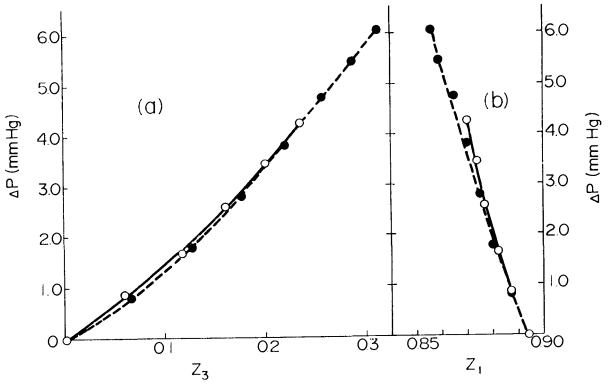

Fig. 5. Exchange reaction of ^{18}O between CO_2 and CO. (a), ΔP(mmHg) *vs.* Z_3 and (b), ΔP *vs.* Z_1: ○, 410 °C (runs V.6); ●, 450 °C (V.8).

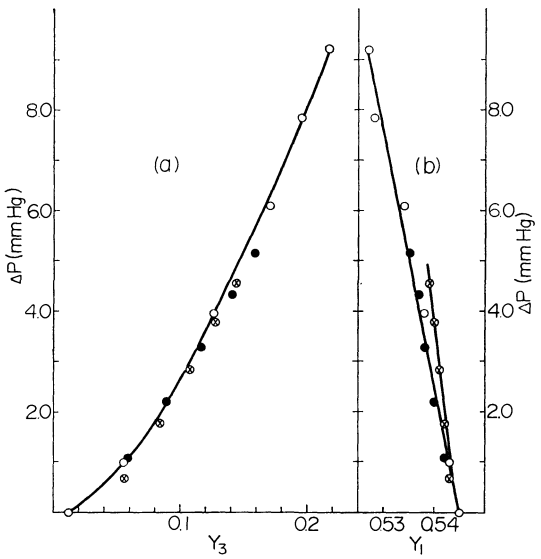

Fig. 6. Exchange reaction of ^{13}C between CO_2 and CO.
(a), ΔP (mmHg) *vs.* Y_3 and (b), ΔP *vs.* Y_1: ⊗, 410 °C (V.31); ●, 450 °C (V.32); ○, 450 °C (V.34).

TABLE 1. EQUILIBRATION $^{13}C^{18}O+CO=^{13}CO+C^{18}O$

Runs	Reaction time (min)	Mole fraction of CO (x_1)	^{13}CO (x_2)	$C^{18}O$ (x_3)	$^{13}C^{18}O$ (x_4)	$\frac{x_1x_4}{x_2x_3}$
VI. 7	0	0.985	0.011	0.004	0.000	
(410 °C)	360	0.910	0.042	0.038	0.010	5.7
	660	0.870	0.060	0.055	0.015	4.0
	1030	0.831	0.077	0.073	0.019	2.8
	1330	0.811	0.087	0.082	0.020	2.3
	1750	0.787	0.097	0.094	0.022	1.9
VI. 9	0	0.984	0.011	0.005	0.000	
(450 °C)	180	0.914	0.041	0.035	0.010	6.4
	360	0.865	0.062	0.056	0.017	4.2
	540	0.835	0.074	0.069	0.022	3.6
	720	0.810	0.086	0.080	0.024	2.8
	900	0.791	0.094	0.088	0.027	2.6

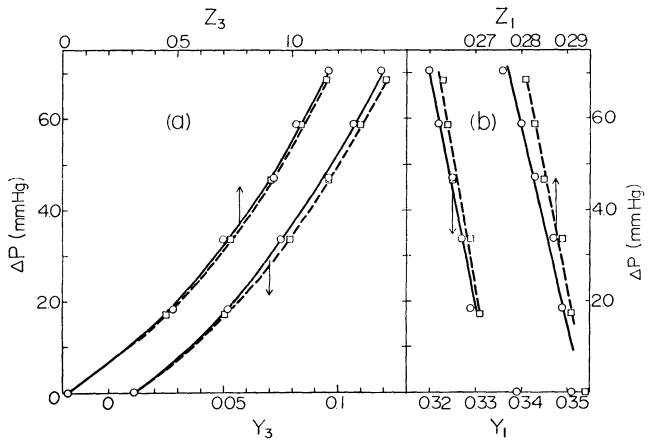

Fig. 7. Simultaneous exchange reactions of ^{13}C and ^{18}O between CO_2 and CO.
(a), ΔP (mmHg) *vs.* Y_3 or Z_3 and (b), ΔP *vs.* Y_1 or Z_1: ○, 410 °C (runs VI.7); □, 450 °C (VI.9).

against ΔP, *i.e.*, the sum of the total pressure decrements caused by the progress of reaction (1) but not by sampling. Figure 6 shows the changes of Y_1 and Y_3 with ΔP.

The exchange of ^{13}C as well as of ^{18}O between CO_2 and CO in the course of reaction (1) were followed simultaneously by the use of a mixture of ^{13}C- and ^{18}O-labelled CO_2. The results are shown in Fig. 7. In this case an equilibration, $CO+{}^{13}C^{18}O={}^{13}CO+C^{18}O$, of isotopes in CO took place additionally (Table 1), which was far slower than the equilibration of isotopes in CO_2 (Table 2).

5. Hydrogen Exchange between D_2 and H_2O: A mixture of 22.0 mmHg CO_2, 15.1 mmHg CO, and 22.1 mmHg D_2 was introduced on the catalyst successively to the runs described above. During reaction (1) which gave rise to 8.7 mmHg of the total pressure decrease, D atomic fraction of D_2 gas changed from 0.991 to 0.974, that is, dilution of D_2 by protium from condensed water was slight.

Discussion

Application of the Theory of Stoichiometric Number. The theory of stoichiometric number[6,7] assumes that all the reaction routes[8] of reaction (1) and accompanying exchanges of ^{13}C and ^{18}O are single. The stoichiometric number $\nu(s)$ of step s is the number of acts of step s necessary to complete one act of the overall reaction, *i.e.*, (1). The forward or the backward unidirectional rate of exchange is defined by the formation rate, V_{+C} or V_{-C}, of ^{13}CO or CO_2, respectively, in the reaction between pure $^{13}CO_2$ and CO, *viz.*, a particular case with $Y_1=1$ and $Y_3=0$. According to mass balance of carbon atoms irrespective of isotopic difference, it follows that

$$V = -dP_1/dt = dP_3/dt = V_{+c}-V_{-c}, \quad (5)$$

and the mass balance of ^{13}C gives

$$-d(Y_1P_1)/dt = Y_1V_{+c}-Y_3V_{-c} = d(Y_3P_3)/dt. \quad (6)$$

Solving these equations with respect to V_{+C} and V_{-C}, we have

$$V_{+c}/V_{-c} = 1 + (Y_1-Y_3)(dP_1/dY_1)/P_1 \quad (7a)$$

or

$$V_{+c}/V_{-c} = 1/[1-(Y_1-Y_3)(dP_3/dY_3)/P_3]. \quad (7b)$$

When step r in the single route of the exchange reaction is so slow as to be rate-determining for reaction (1), V_{+C} or V_{-C} might be equal to the forward or backward unidirectional rate, V_+ or V_-, of reaction (1), respectively. The stoichiometric number $\nu(r)$ of step r is then given by[6]

$$\nu(r) = -\Delta G/[RT\ln(V_+/V_-)], \quad (8)$$

where $-\Delta G$ is the affinity of reaction (1) given by

$$-\Delta G = RT\ln(K_pP_1P_2/P_3P_4). \quad (9)$$

K_p is the equilibrium constant of reaction (1) and P_4 the partial pressure of water. On the other hand, when the exchange reaction takes place without step r, V_{+C} and V_{-C} may be far larger than V_+ and V_-, and the value of V_{+C}/V_{-C} might be close to unity. Accordingly, ν_{ex} defined by

$$\nu_{ex} = -\Delta G/[RT\ln(V_{+c}/V_{-c})].$$

becomes infinitely large in this case.[9]

For the exchange of ^{18}O, similar equations are derived as

$$V = dP_3/dt = V_{+o} - V_{-o} \quad (10)$$

and

$$d(Z_3P_3)/dt = Z_1V_{+o} - Z_3V_{-o}, \quad (11)$$

where it is noteworthy that the exchange of ^{18}O between carbon monoxide and water was assumed not to take place at all. It follows from Eqs. (10) and (11) that

$$V_{+o}/V_{-o} = 1/[1-(Z_1-Z_3)(dP_3/dZ_3)/P_3]. \quad (12)$$

To evaluate the ratios of V_{+C}/V_{-C} and V_{+o}/V_{-o}, the terms dP_1/dY_1, dP_3/dY_3, and dP_3/dZ_3 in Eqs. (7a), (7b), and (12) were approximated by $-d\Delta P/dY_1$, $d\Delta P/dY_3$, and $d\Delta P/dZ_3$, respectively, which can be determined by Figs. 5, 6, and 7. The values of V_{+o}/V_{-o} given in Figs. 8 and 9 considerably fluctuate due to the large errors of estimation of terms, dP_3/dZ_3 *etc.*

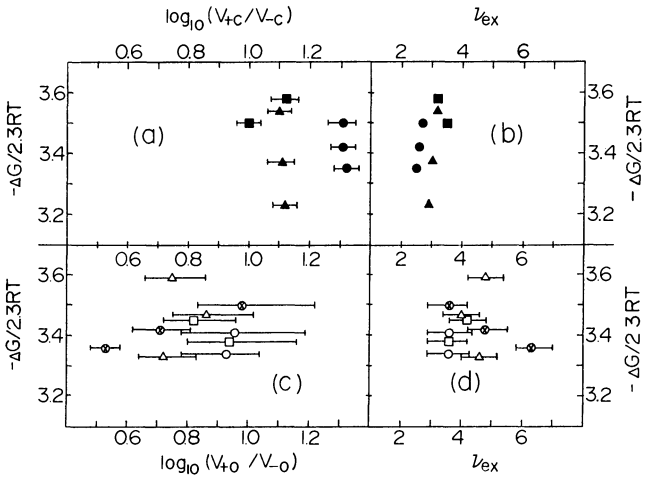

Fig. 8. $\log_{10}(V_{+C}/V_{-C})$, $\log_{10}(V_{+o}/V_{-o})$ and ν_{ex} *vs.* $-\Delta G/2.3RT$.
(a), $\log_{10}(V_{+C}/V_{-C})$ *vs.* $-\Delta G/2.3\ RT$. V_{+C}/V_{-C} was evaluated according to Eq. (7a). ●, 410 °C (runs V.31); ■, 450 °C (V.32); ▲, 450 °C (V.34)
(b), ν_{ex} (calculated from the data (a)) *vs.* $-\Delta G/2.3RT$.
(c), $\log_{10}(V_{+o}/V_{-o})$ *vs.* $-\Delta G/2.3RT$: ○, 410 °C (V.6); ⊗, 450 °C (V.8); □, 410 °C (V.29); △, 450 °C (V.35).
(d), ν_{ex} (calculated from the data (c)) *vs.* $-\Delta G/2.3RT$.

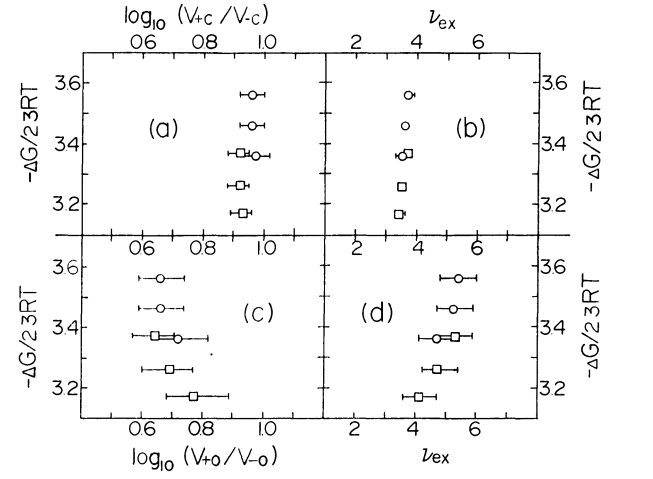

Fig. 9. $\log_{10}(V_{+C}/V_{-C})$, $\log_{10}(V_{+o}/V_{-o})$ and ν_{ex} *vs.* $-\Delta G/2.3RT$: ○, 410 °C (runs VI.7); □, 450 °C (VI.9).
(a), $\log_{10}(V_{+C}/V_{-C})$ *vs.* $-\Delta G/2.3RT$. V_{+C}/V_{-C} was evaluated according to Eq. (7a).
(b), ν_{ex} (calculated from data (a)) *vs.* $-\Delta G/2.3RT$.
(c), $\log_{10}(V_{+o}/V_{-o})$ *vs.* $-\Delta G/2.3RT$.
(d), ν_{ex} (calculated from the data (c)) *vs.* $-\Delta G/2.3RT$.

Applying the present method of analysis to the experimental result of hydrogen exchange between D_2 and H_2O, the ratio of the forward unidirectional rate V_{+H} of this exchange to the reverse one, V_{-H}, was estimated to be *ca.* 32.

Adsorption of Gaseous Components. The steps of adsorption of CO_2 and H_2 and desorption of CO and H_2O are discussed first in connection with the mechanism of reaction (1).

A large number of studies on hydrogen adsorption on platinum[10] confirm a rapid and reversible chemisorption to form adsorbed hydrogen atoms. The present results of rapid equilibration of deuterium in hydrogen gas and the fact that V was proportional to $P_2^{0.5}$ suggest that chemisorption of hydrogen is so rapid as to be nearly in equilibrium and reaction (1) is rate-determined by a surface reaction of an adsorbed hydrogen atom.

Carbon dioxide has been reported[10] to be hardly chemisorbed on platinum, but one of the authors (M.M.) observed[11] that adsorption of CO_2 on platinum film was perceptibly enhanced by the presence of equimolar hydrogen gas at temperatures above room temperature.

Adsorption of CO on platinum was found to take place reversibly and as rapidly as hydrogen[12] and, furthermore, it may be so strong as to retard reaction (1) by occupying active sites on platinum surface according to the fact that V was proportional to $P_3^{-0.5}$.

In the case where CO_2 adsorption is dissociative to form adsorbed CO, ^{13}C or ^{18}O might be exchanged between CO_2 and CO much faster than in reaction (1) on account of the rapid and reversible adsorption of CO_2 and CO and, accordingly, the ratios V_{+o}/V_{-o} and V_{+C}/V_{-C} might be close to unity against the observed results. The dissociative adsorption of CO_2 to form adsorbed CO is, thus, ruled out. The fact that the randomization of ^{18}O in CO_2 took place in the absence of platinum catalyst (Fig. 3) suggests that CO_2 adsorbed on glass surface may interact with OH groups to give an intermediate of oxygen exchange such as bicarbonate ion. However, such an intermediate is not considered to be effective for reaction (1) and isotope exchange between CO_2 and CO, since the decomposition of bicarbonate ion to CO is not plausible, and these reactions were far slower than the randomization of ^{18}O in CO_2 (Table 2).

The value of V_{+H}/V_{-H} estimated to be *ca.* 32 indicates that the step of H_2O desorption is practically irreversible in the course of reaction (1) carried out with cold traps. The adsorbed state of H_2O may be dissociative to result in the observed though slight hydrogen exchange.

Reaction Scheme and Relative Rates of Constituent Steps. According to the above discussions the water gas reaction consists of three rapid and reversible adsorption steps,

$$CO_2 \overset{1}{\longleftrightarrow} CO_2(a), \quad (13\cdot1)$$

$$H_2 \overset{2}{\longleftrightarrow} 2H(a), \quad (13\cdot2)$$

TABLE 2. REDISTRIBUTION OF ^{13}C AND ^{18}O IN CO_2

Runs	Reaction time (min)	Mole fraction of CO_2	$^{13}CO_2$	^{18}COO	$^{13}C^{18}OO$	$C^{18}O_2$	$^{13}C^{18}O_2$	Y_1	Z_1
VI. 7 (410 °C)	0	0.321	0.325	0.115	0.012	0.225	0.002	0.339	0.291
		(0.332	0.170	0.273	0.140	0.056	0.029)		
	360	0.339	0.167	0.275	0.135	0.057	0.027	0.329	0.289
		(0.339	0.166	0.276	0.135	0.056	0.027)		
VI. 8 (450 °C)	0	0.319	0.324	0.115	0.012	0.227	0.003	0.339	0.293
		(0.330	0.169	0.274	0.140	0.057	0.029)		
	180	0.336	0.167	0.276	0.136	0.057	0.028	0.331	0.291
		(0.336	0.166	0.276	0.136	0.057	0.028)		

Values in parentheses are those in equilibrium at the observed values of Y_1 and Z_1 of CO_2.

and

$$CO \overset{3}{\longleftrightarrow} CO(a), \tag{13·3}$$

and desorption of H_2O as

$$OH(a) + H(a) \overset{4}{\longleftrightarrow} H_2O, \tag{13·4}$$

which may be practically irreversible on account of constant condensation of H_2O vapor. $CO_2(a)$ is now assumed, as the simplest case, to be directly converted into CO(a) by the step

$$CO_2(a) + H(a) \overset{5'}{\longleftrightarrow} CO(a) + OH(a). \tag{13·5'}$$

The relative rates of the above steps and the propriety of step 5′ are now discussed by applying the theory of the stoichiometric number[6] on the results of the present experiments.

The ratio V_+/V_- with respect to reaction (1) is given by

$$V_+/V_- = \prod_s (v_{+s}/v_{-s}), \quad (s=1, 2, 3, 4 \text{ and } 5') \tag{14}$$

where v_{+s} and v_{-s}, respectively, are the forward and the backward unidirectional rates of constituent steps s's. Similarly we have

$$V_{+c}/V_{-c} = \prod_s (v_{+s}/v_{-s}), \quad (s=1, 3 \text{ and } 5') \tag{15}$$

for the ^{13}C-exchange between CO_2 and CO. If ^{18}O-exchange between CO and H_2O were negligible as compared with that between CO_2 and CO, the latter exchange consists of steps 1, 3, and 5′ and it follows that

$$V_{+o}/V_{-o} = V_{+c}/V_{-c}. \tag{16}$$

However, the results given in Figs. 8 and 9 are not the case, hence ^{18}O-exchange between CO and H_2O is not negligible.

It follows from Eqs. (14) and (15) that

$$V_+/V_- = (V_{+c}/V_{-c})(v_{+2}/v_{-2})(v_{+4}/v_{-4}),$$

where

$$v_{+2}/v_{-2} \cong 1$$

on account of step 2 being nearly in equilibrium. Each act of the present five steps results in one act of reaction (1), *viz.*, $\nu(r)$ of Eq. (8) is unity, whatever the rate-determining step is. We have thus

$$-\Delta G/2.3RT = \log_{10}[(V_{+c}/V_{-c})(v_{+4}/v_{-4})] \tag{17}$$

The value of $\log_{10}(V_{+c}/V_{-c})$ varied from 0.9 to 1.3 for $-\Delta G/2.3RT$=3.2—3.6 as shown in Figs. 8 and 9 and, accordingly, it follows from Eq. (17) that

$$v_{+4}/v_{-4} \cong 10^2. \tag{18}$$

This shows the practical irreversibility of step 4 and, consequently, that the irreversible transfer of ^{18}O from CO to H_2O affects the ^{18}O-exchange between CO_2 and CO.

The propriety of step 5′ is now investigated. From Eq. (15) it follows that

$$V_{+c}/V_{-c} = v_{+5'}/v_{-5'},$$

taking account of the equilibria of steps 1 and 3, *viz.*,

$$v_{+1}/v_{-1} \cong 1 \cong v_{+3}/v_{-3}. \tag{20}$$

In reference to the steady state condition of reaction (1)

$$V = v_{+1} - v_{-1} = v_{+5'} - v_{-5'},$$

and the value 8 to 20 of V_{+c}/V_{-c}, it follows from Eqs. (19) and (20) that

$$v_{-1} \gg v_{+5'},$$

which indicates that the ^{18}O-exchange between CO and H_2O is negligibly slower than that between CO and CO_2. Consequently, Eq. (16) might contradict the observed result. The next simplest set of steps to fit the experimental results in place of step 5′ is

$$CO_2(a) + H(a) \overset{5}{\longleftrightarrow} X(a) \tag{13·5}$$

and

$$X(a) \overset{6}{\longleftrightarrow} CO(a) + OH(a), \tag{13·6}$$

where X(a) is an intermediate like formate ion in its composition. In this case the effect of the ^{18}O-exchange between CO and H_2O on the rate of that between CO and CO_2 depends on how far reaction (1) is rate-controlled by steps 5 and 6. Taking account of X(a) decomposing into CO(a)+OH(a) by a rate of v_{+6} and into $CO_2(a)$+H(a) by v_{-5}, ^{18}O transfer from CO(a) to H_2O might affect the ^{18}O-exchange between CO_2 and CO in a case where v_{+6} is not negligibly smaller than v_{-5}. Furthermore, taking account of the steady state condition

$$V = v_{+5} - v_{-5} = v_{+6} - v_{-6},$$

step 6 is concluded to be the slowest in conformity with the observed slow randomization of ^{18}O and ^{13}C in CO gas (Table 1).

The simplest scheme applicable to reaction (1) catalyzed by platinum is thus concluded to be

$$\begin{array}{l} CO_2 \overset{1}{\longleftrightarrow} CO_2(a) \\ H_2 \overset{2}{\longleftrightarrow} \begin{cases} H(a) \\ H(a) \end{cases} \end{array} \Bigg\} \overset{5}{\longleftrightarrow} X(a) \overset{6}{\longleftrightarrow} \begin{cases} CO(a) \overset{3}{\longleftrightarrow} CO \\ OH(a) \end{cases} \overset{4}{\longleftrightarrow} H_2O,$$

where steps 1, 2, and 3 are so fast as to be nearly in equilibria, step 4 is practically irreversible, and the reaction is rate-controlled by step 5 and a slower step 6.

References

1) C. R. Prichard and N. Hinshelwood, *J. Chem. Soc.*, **127**, 806 (1925).

2) *e.g.*, K. J. Laidler, "Catalysis," Vol. 1, ed. by P. H. Emmett, Reinhold Publishing Corp., New York (1954), p. 119.

3) J. Horiuti, K. Miyahara, and I. Toyoshima, *J. Res. Inst. Catal., Hokkaido Univ.* (Sapporo), **14**, 59 (1966).

4) M. Masuda, *ibid.*, **14**, 85 (1966).

5) K. Kaneko and S. Oki, *ibid.*, **13**, 169 (1965); **15**, 185 (1967).

6) J. Horiuti and T. Nakamura, *Advan. Catal.*, **17**, 1 (1967).

7) J. Horiuti and M. Ikushima, *Proc. Imp. Acad. Sci.* (Tokyo), **15**, 39 (1939); J. Horiuti, *J. Res. Inst. Catal., Hokkaido Univ.* (Sapporo), **1**, 8 (1948—1951); **5**, 1 (1957), *etc.*

8) "Reaction route" of reaction (1) implies a linearly independent combination of constituent steps giving (1) as an overall reaction. For instance, the number of routes of the simple hydrogen electrode reaction, $2H^+ + 2e = H_2$, is single if it consists of steps $H^+ + e \rightleftharpoons H(a)$ and $2H(a) \rightleftharpoons H_2$, whereas two when another independent step, $H^+ + H(a) + e \rightleftharpoons H_2$, takes place additionally (*cf.* Ref. 6). H^+, e, and H(a) are proton in liquid phase, free electron in electrode metal and hydrogen atom adsorbed on electrode surface, respectively.

9) A. Matsuda and J. Horiuti, *J. Res. Inst. Catal., Hokkaido Univ.* (Sapporo), **10**, 14 (1962).

10) D. O. Hayward and B. M. W. Trapnell, "Chemisorption", Butterworths, London (1964), p. 75.

11) M. Masuda, unpublished.

A New Hypothesis Regarding the Surface Acidity of Binary Metal Oxides[1]

Kozo Tanabe, Takashi Sumiyoshi, Katsue Shibata,*
Tadamitsu Kiyoura,* and Jun Kitagawa*

Department of Chemistry, Faculty of Science, Hokkaido University, Sapporo 060
**Central Research Laboratory, Mitsui Toatsu Chemicals, Inc., Totsuka-ku, Yokohama 247*

(Received August 16, 1973)

We have proposed a new hypothesis that the acid sites on binary metal oxides are formed by an excess of a negative or positive charge in the mixed oxides and that whether the charge is excess or not, and whether it is positive or negative, are determined by the coordination numbers and valences of the positive and negative elements in the model structures pictured according to two postulates. The validity of the hypothesis is, in fact, 90% for the 31 kinds of binary oxides tested, much higher than the validity (48%) of Thomas' hypothesis. The hypothesis explains well the mechanism of the acidity generation of binary oxides and predicts whether the acid sites will be of the Brönsted or the Lewis type.

Binary metal oxides, such as SiO_2–Al_2O_3, SiO_2–MgO, SiO_2–ZrO_2, and Al_2O_3–B_2O_3, are well-known to have surface acidity and have been used as solid acid catalysts for a long time.[2] It was only very recently, though, that TiO_2–ZnO,[3] SiO_2–ZnO,[4] SiO_2–TiO_2,[5] TiO_2–ZrO_2,[6,7] ZnO–Bi_2O_3,[7] Al_2O_3–MgO[7] *etc.* have been found to show an acidic property. Thus, many other binary metal oxides may also be expected to exhibit an acidic property. However, no one can predict what kinds of binary oxides will show an acidic property. An old but popular hypothesis proposed by Thomas,[8] which gave an interpretation of the acidity generation of five species of binary oxides that were known in 1949, has been found to fail in explaining the acidity generation of recently-found binary oxides. Therefore, we have developed a new hypothesis which is well applicable to many new kinds of binary oxides.

The Hypothesis

The acidity generation of binary oxides can generally be explained by the present hypothesis that the acidity generation is caused by an excess of a negative or positive charge in a model structure of a binary oxide. The model structure is pictured according to the following two postulates:

i) The coordination number of a positive element of a metal oxide, C_1, and that of a second metal oxide, C_2, are maintained even when mixed.

ii) The coordination number of a negative element (oxygen) of a major component oxide is retained for all the oxygens in a binary oxide.

For example, the structure of TiO_2–SiO_2, where TiO_2 is the major component oxide, and that of SiO_2–TiO_2, where SiO_2 is the major component oxide, are shown in Figs. 1a and 1b. In Figs. 1a and 1b, the coordination numbers of the positive elements in the component single oxides remain 4 for Si and 6 for Ti when they are mixed, whereas those of the negative elements should be 3 and 2 respectively, according to Postulates i) and ii). In the case of Fig. 1a, the four positive charges of the silicon atom are distributed to four bonds, *i.e.*, a positive charge is distributed to each bond, while the two negative charges of oxygen atom are distributed to three bonds, *i.e.*, $-2/3$ of a valence

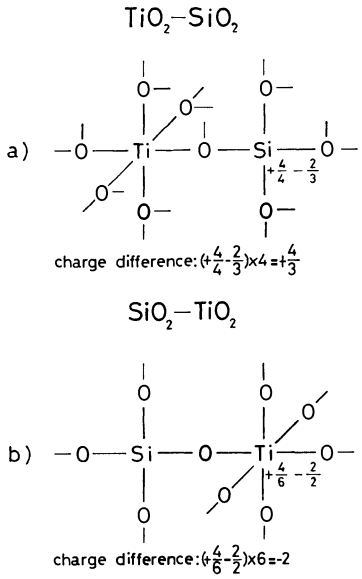

Fig. 1. Model structures of TiO_2–SiO_2 pictured according to postulates i) and ii). a): when TiO_2 is major oxide, b): when SiO_2 is major oxide.

unit is distributed to each bond. The difference in charge for one bond is $+1-2/3=+1/3$, and for all the bonds the valence unit of $+1/3\times4=+4/3$ is excess. In this case, the Lewis acidity is assumed to appear upon the presence of an excess of the positive charge. In Fig. 1b, four positive charges of the titanium atom are distributed to six bonds, *i.e.*, +4/6 of a valence unit to each bond, while two negative charges of the oxygen atom are distributed to two bonds, *i.e.*, a negative charge to each bond. The charge difference for each bond is $+4/6-1=-1/3$, and for all the bonds the valence unit of $-1/3\times6=-2$ is excess. In this case, the Brönsted acidity is assumed to appear, because two protons are considered to associate with six oxygens to keep the electric neutrality. In any case, TiO_2–SiO_2 is expected to show an acidic property because of the excess of a positive or negative charge. In fact, it exhibited a very high acidity.[5]

Let us examine another example. In ZnO–Sb_2O_3, there is no excess charge in any part of its composition according to our model structure written by Postulates

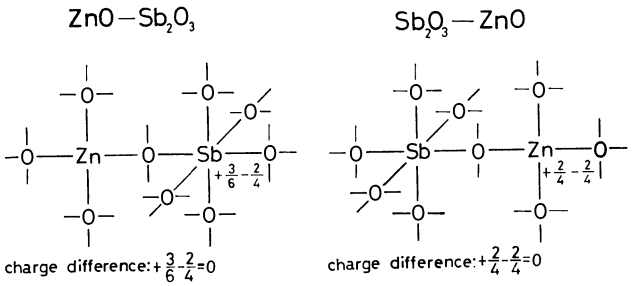

Fig. 2. Model structure of $ZnO–Sb_2O_3$ pictured according to postulates i) and ii). a): when ZnO is major oxide, b): when Sb_2O_3 is major oxide.

i) and ii), as is illustrated in Fig. 2. Therefore, the binary oxide is not expected to show any acidic property. This prediction agreed with an experimental result that $ZnO–Sb_2O_3$ did not show any acidity larger than the sum of the acidities of the component oxides.[7]

The Validity of the Hypothesis

The validity of our hypothesis was examined for 31 kinds of binary oxides. The case where the hypothesis predicts that a binary oxide should generate acidity is marked by an open circle in the fifth column of Table 1. On the other hand, the case where a binary oxide should not generate acidity is shown by a cross in the same column. The experimental results cited from the literature are shown in the next column, where open circles mark when the acid amount at a certain acid strength per unit surface area of any binary oxides is larger than the sum of the acid amounts at the same acid strength divided by the sum of the surface areas of the component single oxides, while crosses mark when no acidity is generated. The results indicate that new acid sites which differ from those of single oxides are created on the surface of 25 species of binary

Table 1. Validity of hypotheses

V: valence of positive element, C: coordniation number of positive element

Mixed-Oxides 1	2	$\alpha = V/C$ α_1	α_2	Acidity increase: Hypotheses Thomas	Ours	Experimental results	No. of references	Validity of hypotheses: Thomas	Ours
TiO_2	CuO	4/6	2/4	×	○	○	10	×	○
TiO_2	MgO		2/6	○	○	○	7	○	○
TiO_2	ZnO		2/4	×	○	○	3	×	○
TiO_2	CdO		2/6	○	○	○	7	○	○
TiO_2	Al_2O_3		3/6	○	○	○	7	○	○
TiO_2	SiO_2		4/4	×	○	○	5,7	×	○
TiO_2	ZrO_2		4/8	×	○	○	6,7	×	○
TiO_2	PbO		2/8	×	○	○	10	×	○
TiO_2	Bi_2O_3		3/6	○	○	○	7	○	○
TiO_2	Fe_2O_3		3/6	○	○	○	10	○	○
ZnO	MgO	2/4	2/6	×	○	○	7	×	○
ZnO	Al_2O_3		3/6	×	×	○	7	×	×
ZnO	SiO_2		4/4	○	○	○	7	○	○
ZnO	ZrO_2		4/8	○	×	×	7	×	○
ZnO	PbO		2/8	○	○	×	7	×	×
ZnO	Sb_2O_3		3/6	×	×	×	7	○	○
ZnO	Bi_2O_3		3/6	×	×	×	7	○	○
Al_2O_3	MgO	3/6	2/6	○	○	○	10	○	○
Al_2O_3	B_2O_3		3/3	○	○	○	11	○	○
Al_2O_3	ZrO_2		4/8	×	×	○	7	×	×
Al_2O_3	Sb_2O_3		3/6	×	×	×	7	○	○
Al_2O_3	Bi_2O_3		3/6	×	×	×	7	○	○
SiO_2	BeO	4/4	2/4	○	○	○	12	○	○
SiO_2	MgO		2/6	×	○	○	13,14	×	○
SiO_2	CaO		2/6	×	○	○	15	×	○
SiO_2	SrO		2/6	×	○	?	15	?	?
SiO_2	BaO		2/6	×	○	?	15	?	?
SiO_2	Ga_2O_3		3/6	×	○	○	12	×	○
SiO_2	Al_2O_3		3/4,3/6	○	○	○	14	○	○
SiO_2	Y_2O_3		3/6	×	○	○	12	×	○
SiO_2	La_2O_3		3/6	×	○	○	12	×	○
SiO_2	ZrO_2		4/8	○	○	○	14	○	○
ZrO_2	CdO	4/8	2/6	×	○	○	7	×	○

Thomas' hypothesis 15/31=48%
Our hypothesis 28/31=90%

oxides. Cases where the result predicted by the hypothesis agrees with the experimental result is marked by open circles in the last column of Table 1, and cases of disagreement, by a cross. As may be seen in the table, an agreement of the prediction of our hypothesis with the experimental results was found for 28 of the 31 kinds of binary oxides. Thus, the validity of our hypothesis is 90%.

Thomas[8] proposed that the acidities of binary oxides are generated when $C_1=C_2$ and $V_1<V_2$ or when $C_1=2C_2$, where C_1 and C_2 are the coordination numbers of a positive element and a second one and where V_1 and V_2 are the valences of the respective positive elements. The validity of his hypothesis is only 48%, as is shown in Table 1. Therefore, it has been verified that our hypothesis is much better. It should also be noted that the validity of his hypothesis is low despite the fact that the coordination number of oxygen is taken as arbitrary so as to fit the experimental results.

The binary oxides which are predicted to generate surface acidity according to our hypothesis, but not according to Thomas' hypothesis, are the following thirteen species: TiO_2–CuO, TiO_2–ZnO, TiO_2–SiO_2, TiO_2–ZrO_2, TiO_2–PbO, ZnO–MgO, ZnO–ZrO_2, SiO_2–MgO, SiO_2–CaO, SiO_2–Ga_2O_3, SiO_2–Y_2O_3, SiO_2–La_2O_3, and ZrO_2–CdO. It was verified by experiments that all of the binary oxides showed a distinct acidity increase. In particular, TiO_2–SiO_2 showed a higher acidity and catalytic activity than the well-known SiO_2–Al_2O_3 catalyst.[5] TiO_2–ZnO, whose acidity was much higher than that of each component oxide, showed a surprisingly high activity for the hydration of ethylene.[3]

Though Thomas' hypothesis cannot be applied to Lewis acids,[8] our hypothesis also predicts the type of acid sites (Brönsted or Lewis), as has been mentioned above. According to our hypothesis, TiO_2–ZnO should show Brönsted acidity when TiO_2 is a major component oxide and Lewis acidity when ZnO is a major component oxide. An infrared study of pyridine adsorbed on the binary oxide revealed that TiO_2 including 5% of ZnO exhibited Brönsted acidity alone, while ZnO including 5% of TiO_2 exhibited Lewis acidity alone.[3]

Limitations of the Hypothesis

As may be seen in the model structures (Figs. 1 and 2) pictured according to Postulates i) and ii), the present hypothesis is applicable to chemically-mixed binary oxides, but not to mechanically-mixed oxides. Since the binary oxides given in Table 1 were prepared by calcining mixtures of co-precipitated hydroxides at a high temperature (500 °C), they are not mechanically-mixed oxides. The X-ray diffraction diagrams of the binary oxides showed no or weak diffraction lines, and almost all of them were assumed to be amorphous.[3,6,7,10] Thus, the structures are different from those of the component single oxides.

The present hypothesis predicts which combinations of oxides in the periodic table will generate acidity and at what compositions the Brönsted or Lewis acidity will appear, but it does not predict the acid strength. The prediction of the acid strength was reported in a foregoing paper,[7] which demonstrated a good correlation between the acid strength and the average electronegativities of metal ions of binary oxides, though the prediction is not based on any hypothesis, but on a generalization.

References

1) The present work was presented at the Gordon Research Conference, New England, N. H., 15 June, 1972.
2) K. Tanabe, "Solid Acids and Bases," Kodansha, Tokyo, Academic Press, New York, London (1970), p. 58.
3) K. Tanabe, C. Ishiya, I. Matsuzaki, I. Ichikawa, and H. Hattori, This Bulletin, **45**, 47 (1972).
4) K. Tanabe, T. Sumiyoshi, and H. Hattori, *Chem. Lett.*, **1972**, 723.
5) K. Tanabe, M. Ito, and M. Sato, *Chem. Commun.*, **1973**, 676.
6) K. Shibata and T. Kiyoura, *J. Res. Inst. Catal., Hokkaido Univ.*, **19**, 35 (1971).
7) K. Shibata, T. Kiyoura, J. Kitagawa, T. Sumiyoshi, and K. Tanabe, This Bulletin, **46**, 2985 (1973).
8) C. L. Thomas, *Ind. Eng. Chem.*, **41**, 2564 (1949).
9) K. Shibata, T. Kiyoura, and K. Tanabe, *J. Res. Inst. Catal., Hokkaido Univ.*, **18**, 189 (1970).
10) S. Miyata, T. Kumura, H. Hattori, and K. Tanabe, *Nippon Kagaku Zasshi*, **92**, 514 (1971).
11) T. Aonuma, M. Sato, and T. Shiba, *Shokubai*, **5**, 274 (1963).
12) L. G. Karakchiev, *Kinet. Katal.*, **9**, 282 (1968).
13) H. Bremer and K. H. Steinberg, 4th Intern. Congr. Catalysis, Moscow, Preprints of Papers, No. 76 (1968).
14) V. A. Dzisko, Proc. 3rd Intern. Congr. Catalysis, Amsterdam, I. No. 19 (1964).
15) H. Niiyama and E. Echigoya, *Shokubai*, **10**, 129 (1968).

Properties of Ampholytic Surfactant, *N*-Alkyl-β-alanine

Takeo Okumura,* Kazuo Tajima, and Tsunetaka Sasaki

Department of Chemistry, Faculty of Science, Tokyo Metropolitan University, Setagaya-ku, Tokyo 158

(Received August 27, 1973)

Ampholytic surfactant, *N*-alkyl-β-alanine, was synthesized and its infrared absorption spectra, surface tension, isoelectric points and critical micelle concentrations of aqueous solutions were measured at various electrolyte concentrations, pH and temperature. The measurements of isoelectric points and infrared spectra confirmed a zwitterionic sructure of *N*-alkyl-β-alanine. The critical micelle concentrations determined by surface tension measurements are 1.3×10^{-2} and 9×10^{-4} mol/l respectively for the decyl and dodecyl homologs at 30 °C, the values decreasing with the increase in pH, electrolyte concentration and temperature.

Although considerable information is available concerning the properties of aqueous solutions of ionic and nonionic surfactants, little is known about those of ampholytic surfactants. Studies on *C*-alkyl betaine[1] and *N*-alkyl betaine[2-4] give information on the ampholytic surfactant. Properties of a number of other ampholytic surfactants have been investigated by Herrmann.[5] However, only a few papers have appeared on ampholytic *N*-alkyl-β-alanines.[6-8]

We have studied the effect of pH, temperature and electrolyte concentration on the critical micelle concentration (CMC) of *N*-alkyl-β-alanine by surface tension measurements. Zwitterion formation and micelle formation were discussed. A phase diagram was constructed in order to study the phase transition.

Experimental

Materials. *N*-Alkyl-β-alanine was prepared by the reaction of *n*-alkylamine with β-propiolactone in acetonitrile at 25—30 °C for one hour according to the method of Gresham *et al.*[9] The purity of *n*-alkylamine was better than 99.5% as confirmed by gas chromatography. A crude product was purified by repeated recrystallization from a mixture of acetone and ethanol (1 : 1) followed by drying in a vacuum. Thin layer chromatography confirmed the absence of unreacted materials in the purified sample. The result of elementary analysis agreed with the theoretical composition within experimental error.

Surface Tension Measurements. The surface tension was measured by a drop-weight method in a thermostated air-bath and the CMC value was determined from the surface tension *vs.* log concentration curve at different pH and temperature.

Phase Diagram. A phase diagram was constructed for the binary system consisting of surfactant and water, covering the concentration range 0—0.7 by weight fraction of the surfactant and the temperature range 0—100 °C. The transition temperature was determined by observing visually or microscopically the phase change caused by heating or cooling the sealed test-tubes containing the solutions of known concentration in a water bath.

Infrared and Proton Magnetic Resonance Spectrometry. Infrared (IR) spectra were measured with a Hitachi EPI-2 infrared spectrometer. The proton magnetic resonance (PMR) spectra in deuteriochloroform solutions were measured with a Nihon Denshi JNM PS-100 spectrometer at 100 MHz, and the chemical shifts are given by ppm, using tetramethylsilane as an external standard.

* Household Goods Research Laboratories, Kao Soap Co., Ltd., Sumida-ku, Tokyo 131.

Results and Discussion

IR and PMR Spectrometry. IR spectra of the decyl homolog in aqueous solutions are given in Table 1. The absorption bands due to COO^- and N^+H_2 in a neutral solution (pH=6) confirm the zwitterionic structure of *N*-decyl-β-alanine. The IR spectra in an acid solution (pH=1) give the absorption bands due to COOH and the characteristics of the quaternary ammonium salts. This confirms the cationic structure in an acid solution. The spectra in an alkaline medium (pH=12) lack the absorption bands due to N^+H_2 but retain the bands due to COO^-, indicating the anionic structure. Similar results have also been obtained for the dodecyl homolog.

Table 1. IR spectra of *N*-decyl-β-alanine in aqueous solutions

N-Decyl-β-alanine	COOH	COO^-	N^+H_2[a]	N^+H_2[b]
in neutral (pH 6)	—	1560 cm^{-1} 1400	2300 cm^{-1} 1650	—
in acid (pH 1)	1740 cm^{-1}	—	—	2400–2800 cm^{-1}
in alkaline (pH 12)	—	1560 cm^{-1}	—	—

a) zwitterion b) quaternary ammonium ion

The numbers of protons obtained from the measurements of PMR spectra are in agreement with those expected from the molecular structure. Thus PMR spectra also confirm the zwitterionic structure of *N*-alkyl-β-alanine.

Isoelectric Points. Isoelectric point (pH_i) of ampholytic surfactants was determined from pH titration[10] and dissociation constant measurements. The titration curves of 0.1 M hydrochloric acid solution with 0.1 M sodium hydroxide solution were plotted in the presence and also in the absence of surfactant. The common point of intersection was obtained for three such curves which gave pH_i's 7.0—7.2 and 6.8—7.0 for the decyl and dodecyl homologs, respectively.

Dissociation constant as a weak acid or base is calculated from the pH change of an acid or alkaline solution caused by the addition of a given amount of the ampholyte. The values of pK_a and pK_b thus determined for *N*-decyl-β-alanine are 3.3—3.5 and 3.1—3.2, respectively. The pH_i calculated from pK_a and pK_b for the decyl homolog is 7.0—7.2 agreeing with

Table 2. CMC values of several ampholytic surfactants in aqueous solutions

(mmol/l)

Surfactant	Decyl	Dodecyl	Reference
N-alkyl-*β*-alanine	13(30 °C)	0.9(30 °C)	Present work
C-alkyl betaine	13(30 °C)	1.3(27 °C)	1
N-alkylbetaine	18(23 °C)	1.8(23 °C)	3
trimethylamino-alkaneimide	—	1.3(25 °C)	11

those determined by pH titration.

Critical Micelle Concentrations. The CMC values determined from the plot surface tension *vs.* log concentration at 30 °C are given in Table 2 together with those of other ampholytic surfactants.[1,3,11] We see that the CMC values of *N*-alkyl-*β*-alanines are nearly equal to those of the same alkyl chain length.

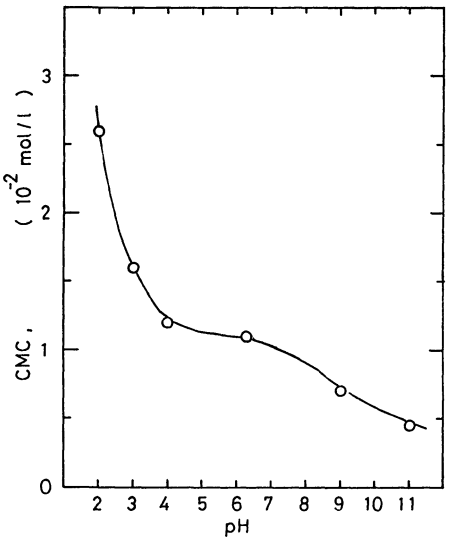

Fig. 1. Effect of pH on the CMC of *N*-alkyl-*β*-alanine at 30 °C.

The effect of pH on the CMC of *N*-decyl-*β*-alanine in 0.1 M sodium chloride solution is shown in Fig. 1. The CMC values decrease with increasing pH of the solution. The decrease is rapid in acid region, slow in alkaline side and imperceptible around pH 5—7. Corkill *et al.*[11] reported that CMC of *N,N,N*-trimethylaminododecaneimide decreased with increasing pH of the solution. This is due to the suppression of ionization of amino group, which can explain the rapid decrease of CMC of the decyl homolog in acid region but not the slow decrease of CMC in alkaline side since the enhanced dissociation of carboxyl group prevents the micelle formation. The position of the ionized group would be taken into account to explain the phenomena.

As is evident from the molecular structure, cationic ionization takes place in the inner position, while anionic ionization occurs at the end of the molecule. Thus the steric hindrance against micellization is less for the latter which acts to decrease the CMC with increasing pH. Such a steric hindrance has been studied in detail by Hartley.[12] The high CMC values in acid region show the instability of micelles in a low pH region.

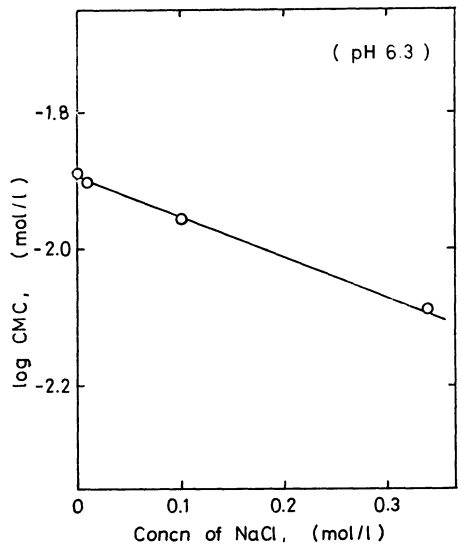

Fig. 2. Effect of electrolyte on the CMC of *N*-decyl-*β*-alanine at 30 °C.

The effect of sodium chloride on the CMC of *N*-decyl-*β*-alanine in a nearly neutral solution (pH=6.3) at 30 °C is shown in Fig. 2. The logarithm of the CMC decreases linearly with increasing concentration of added salt as in the case of nonionic surfactants.[13] In the case of ionic surfactants the plot log-log instead of that semi-log proves to be linear.[14] The difference can be explained by the zwitterionic property of *N*-alkyl-*β*-alanine in the isoelectric region where the ionic charges are neutralized in a molecule and the surfactant is considered to be nonionic.

In the plot of log CMC against $1/T$ at various pH for the decyl homolog (Fig. 3), at pH 11 the CMC increases slightly with increasing temperature in accordance with other ionic surfactants, while at pH 6.3, it decreases with increasing temperature as in the case of nonionic surfactant.[15] At pH 2, the CMC remains unchanged with temperature.

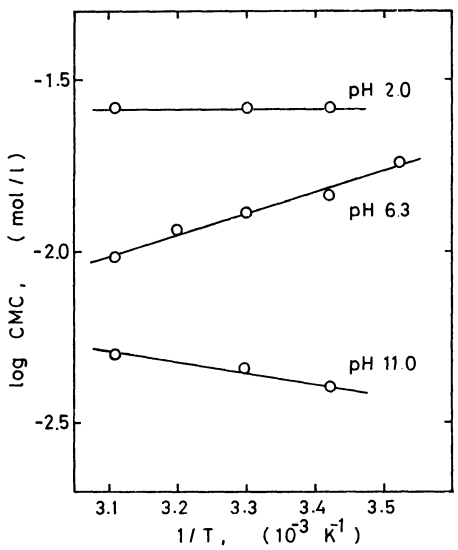

Fig. 3. Effect of temperature on the CMC of *N*-decyl-*β*-alanine

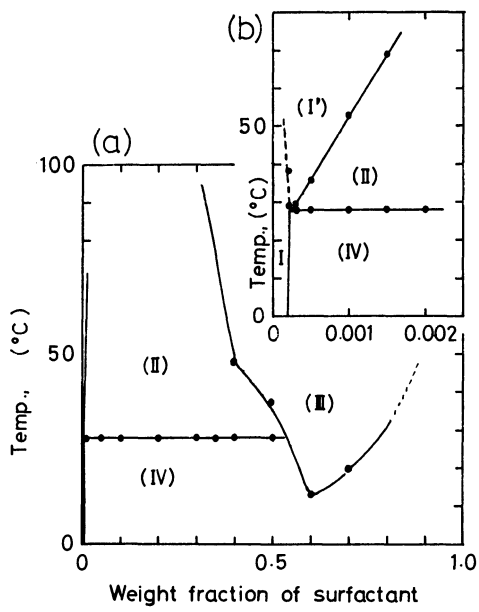

Fig. 4. Phase diagram of *N*-dodecyl-*β*-alanine/water system.
(a) system as a whole, (b) system in a dilute surfactant region; (I), (III): homogeneous region; (II), (IV): heterogeneous region.

Phase Diagram. The phase diagram of *N*-dodecyl-*β*-alanine/water system in (a) isoelectric region as a whole and (b) dilute surfactant region is shown in Fig. 4. (I) is a clear and homogeneous isotropic liquid phase consisting of surfactant monomers and water, (I') a similar phase consisting of surfactant monomers, micelles and water, (II) a region of the heterogeneous system which separates into two clear liquid phases when left standing, one rich and the other poor in surfactant, (III) a clear and homogeneous liquid phase, and (IV) a region of heterogeneous suspension consisting of a so called hydrated solid surfactant, dilute surfactant solution and (III). The line separating regions (I) and (I') shows the temperature dependence of CMC. The line separating regions (II) and (IV) is parallel to the composition axis showing the melting point of the hydrated solid surfactant determined by the differential scanning calorimetry. The cloud points usually observed in the nonionic surfactant could not be detected in the aqueous solution of *N*-decyl- and *N*-dodecyl-*β*-alanine in isoelectric region at temperatures 0—100 °C. The phase diagram for the decyl homolog and water system was also constructed for the concentrations 0—0.5 (weight fraction of surfactant) and temperatures 0—100 °C. Only one isotropic liquid phase without phase change was observed.

References

1) K. Tori and T. Nakagawa, *Kolloid-Z.*, **187**, 44 (1963); *ibid.*, **188**, 47 (1963); *ibid.*, **189**, 50 (1963); *ibid.*, **191**, 42 (1963); *ibid.*, **191**, 48 (1963).
2) S. Sakakibara, N. Kurata, and S. Komori, *Kogyo Kagaku Zasshi*, **60**, 1294 (1957).
3) A. H. Beckett and R. J. Woodward, *J. Pharm. Pharmcol.*, **15**, 422 (1963).
4) P. Molyneux, C. T. Rhodes, and J. Swarbrick, *Trans. Faraday Soc.*, **61**, 1043 (1965); J. Swarbrick and J. Daruwala, *J. Phys. Chem.*, **74**, 2627 (1969); *ibid.*, **74**, 1293 (1970).
5) K. W. Herrmann, *ibid.* **66**, 295 (1962).
6) H. B. Klevens, *J. Amer. Oil Chem. Soc.*, **30**, 74 (1953).
7) K. Durham, 3rd Int. Congr. Surface Activity, Collogne, **B**/1/3,130 (1960).
8) F. Tokiwa and K. Ohki, *J. Phys. Chem.*, **71**, 1824 (1967).
9) T. L. Gresham, J. E. Jansen, F. W. Shaver, R. A. Bankert, and F. T. Fiedorek, *J. Amer. Chem. Soc.*, **73**, 3168 (1951).
10) M. Hiraki, *J. Biochem.*, **15**, 345 (1932).
11) J. M. Corkill, K. W. Gemmel, J. F. Goodman, and T. Walker *Trans. Faraday Soc.*, **66**, 1817 (1970).
12) G. S. Hartley, *ibid.*, **37**, 130 (1941).
13) K. Shinoda, T. Yamaguchi, and R. Hori, This Bulletin, **34**, 237 (1961).
14) K. Shinoda, *J. Phys. Chem.*, **59**, 432 (1955).
15) T. Nakagawa, K. Kuriyama, and H. Inoue, Symposium on Colloid Chem. (Chem. Soc. Japan), 12th Symposium, p. 29 (1959).

Mechanism of High-energy-induced Luminescence of Solid 2,3-Dimethylbutane Containing Toluene at 77 K

Tetsuo MIYAZAKI, Yoshiteru FUJITANI, and Zen-ichiro KURI

Department of Synthetic Chemistry, Faculty of Engineering, Nagoya University, Chikusa-ku, Nagoya 464

(Received August 31, 1973)

The luminescence from 2,3-dimethylbutane (23DMB) containing a small amount of toluene (To) has been observed in the solid phase at 77 K during γ-irradiation or by ns pulse irradiation with X-rays. The emission spectrum from 23DMB–To (2 mol%) during γ-irradiation at 77 K consists of the fluorescence from the singlet-excited toluene and the phosphorescence from the triplet-excited toluene. Both the singlet- and triplet-excited toluenes are formed by the energy transfer from the irradiated 23DMB to toluene. When nitrous oxide or propylene is added to the 23DMB–To mixture, the emission spectrum is changed and becomes very similar to that from the 23DMB–To mixture during illumination with UV lights at 77 K. The spectrum, which disappears upon the addition of nitrous oxide or propylene, consists mainly of phosphorescence. It is concluded that the triplet-excited toluene may be formed by the migration of a hole and an electron. The effects of electron scavengers, such as nitrous oxide and carbon dioxide, or hole scavengers, such as propylene or tetramethylethylene, on the fluorescence have been studied by nsec-pulse irradiation. Since the fluorescence is not appreciably affected by the addition of these scavengers, the singlet-excited toluene may be formed by the excitation transfer.

We have previously studied the radiolysis of hydrocarbons in the solid phase in order to elucidate the primary process and in order to obtain information about the reaction kinetics in the solid phase. One of the most important primary processes is the migration of the short-lived entities produced by the γ-irradiation of the solid. Studies by Miyazaki *et al.* have suggested the importance of the non-ionic energy transfer in the radiolysis of solid hydrocarbons. The formation of the solvent radical and hydrogen which are formed by the fragmentation of the excited molecule is suppressed by the addition of toluene or CCl_4 in the radiolysis of solid isobutane. The phenomenon has been explained in terms of excitation transfer.[1] If toluene is an efficient acceptor of the excitation energy in the radiolysis of solid alkane, the luminescence from the excited toluene may be expected. Recently we have studied the luminescence from alkane containing a small amount of toluene during γ-irradiation at 77 K.[2] A strong emission from the excited toluene formed by the energy transfer from the irradiated alkane has been observed. The study of the luminescence gives us useful information on the energy transfer. Luminescence studies previously undertaken in radiation chemistry have been mostly concerned with the thermoluminescence or the photo-induced luminescence of γ-irradiated samples, or with the luminescence in the liquid phase during γ-irradiation.

In order to study the mechanism of the luminescence from solid 2,3-dimethylbutane containing toluene, we have here examined the effects of electron or hole scavengers on the luminescence upon irradiation with γ-rays or ns pulse X-rays.

Experimental

The 2,3-dimethylbutane(23DMB) and toluene(To) were the same as those used before.[2] They were passed through a 50 cm column packed with activated alumina and were used after distillation on a vacuum line. Nitrous oxide, carbon dioxide, and propylene, supplied by the Takachiho Shoji Co., were of a high purity and were used without further purification. The tetramethylethylene(TME), supplied by the Tokyo Kagaku Seiki Co., was more than 99.0% pure.

The errors in the measurement of the luminescence at 77 K were about 10%. Each experimental plot is an average of two or more runs.

The measurement of the luminescence during γ-irradiation was the same as that used before. The photomultiplier (Hamamatsu TV Co. R-136) can detect the light from 200 to 650 nm; its sensitivity depends upon the wavelength. It was expected that the brightness of the Shimadzu-Bausch-Lomb monochromator may depend also upon the wavelength of the lights. The sensitivity of the photomultiplier and the brightness of the monochromator were checked by using a standard tungsten lamp. The brightness of the monochromator, however, did not depend appreciably upon the wavelength of the lights. Therefore, the measured emission spectrum was corrected by considering only the sensitivity of the photomultiplier.

The pulse irradiation was done at 77 K with X-rays from Febetron 707. The maximum energy of the X-rays is 2 MeV, and the duration of a pulse is 20 ns. An apparatus for measuring the luminescence by pulse irradiation consists of a monochromator (Shimadzu GE-100), a photomultiplier (EMI-6256B), and a synchroscope (Iwatsu Electric Co., SS-112). A schematic diagram of the apparatus is given

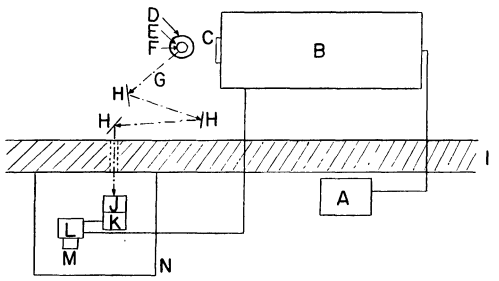

Fig. 1. Schematic diagram of the measurement of luminescence by the ns pulse irradiation at 77 K. A: Panel for operating Febetron, B: Febetron 707, C: Tungsten plate, D: Dewar flask, E: Liquid nitrogen, F: Sample, G: Emission, H: Mirror, I: Concrete wall, J: Monochrometer, K: Photomultiplier, L: Synchroscope, M: Polaroid camera, N: Dark room.

in Fig. 1. The experiment was done under condition suitable for obtaining ns time resolution.

Results

Figure 2 shows the effect of toluene on the formation of the solvent radical[2] and the luminescence from toluene in the 23DMB at 77 K. The maximum

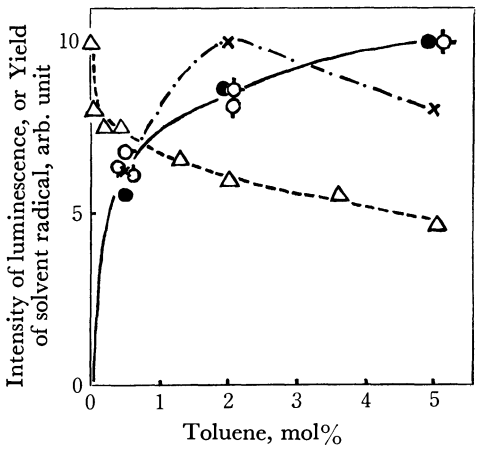

Fig. 2. Yields of solvent radical and emission from toluene in the irradiation of 23DMB at 77 K against concentration of toluene.
△: Yields of solvent radical at the dose of 9.6×10^{18} eV/g.
●: Intensity of fluorescence during γ-irradiation.
ⴱ,ⴱ,ⴱ: Intensity of fluorescence at 20 ns, 60 ns, and 180 ns after the irradiation with ns pulse X-ray respectively.
×: Intensity of phosphorescence during γ-irradiation.

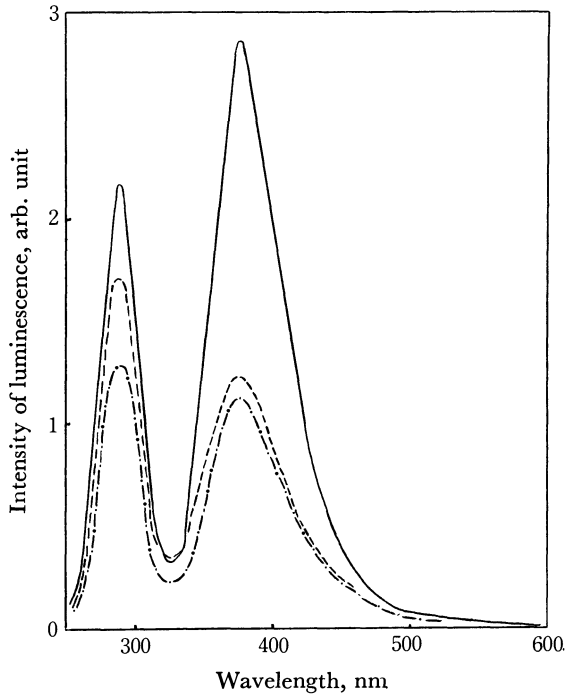

Fig. 3. Emission spectra from 23DMB-To (2 mol%) system in the solid phase during γ-irradiation at 77 K.
——: Spectrum from 23DMB–To
------: Spectrum from 23DMB–To–C_3H_6 (2 mol%)
-·-·-: Spectrum from 23DMB–To–N_2O (2 mol%)

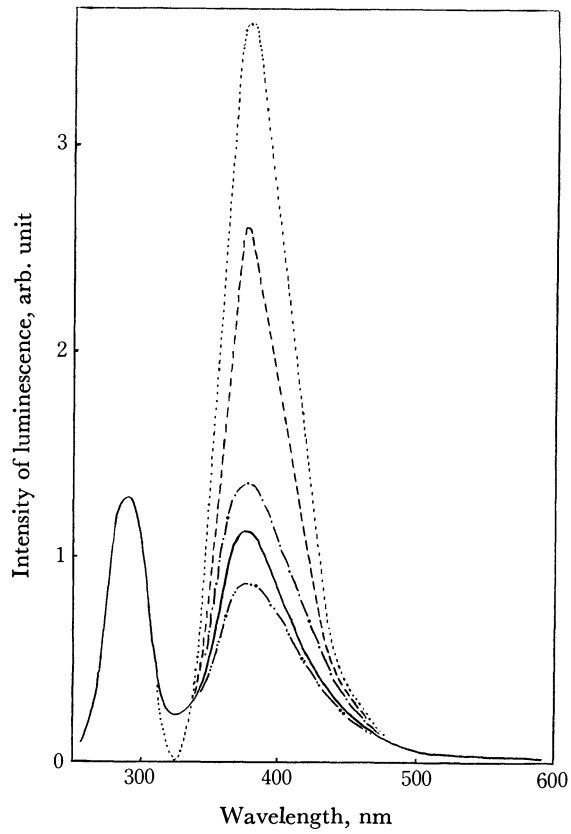

Fig. 4. Emission spectra from 23DMB–To (2 mol%) system in the solid phase at 77 K.
——: Spectrum from 23DMB–To–N_2O (2 mol%) during γ-irradiation.
-·-·-: Spectrum from 23DMB–To–C_3H_6 (2 mol%) during γ-irradiation.
------: Spectrum obtained by subtracting the spectrum of 23DMB–To–N_2O (2 mol%) from that of 23DMB–To.
·····: Spectrum obtained by subtracting the spectrum of 23DMB–To–C_3H_6 (2 mol%) from that of 23DMB–To.
-·-·-: Spectrum from 23DMB–To during UV illumination.[4]
The intensity of the fluorescence was normalized to the same peak intensity as that of 23DMB–To–N_2O (2 mol%).

intensities of the fluorescence and the phosphorescence are normalized to 10. The fluorescence was measured at 20, 60, and 180 ns after the pulse irradiation with Febetron and during γ-irradiation. The phosphorescence was measured during γ-irradiation. The fluorescences at different times show approximately the same dependence on the concentration of toluene.

The emission spectrum from 23DMB–To(2 mol%) during γ-irradiation at 77 K is shown in Fig. 3.[3] The spectrum consists of two peaks, with emission maxima near 280 and 390 nm. They are due to the fluorescence from the singlet-excited toluene and the phosphorescence from the triplet-excited toluene respectively. When nitrous oxide or propylene is added to the 23DMB–To(2 mol%), the emission spectrum is changed.

The spectrum which disappears upon the addition of nitrous oxide or propylene is obtained by subtracting

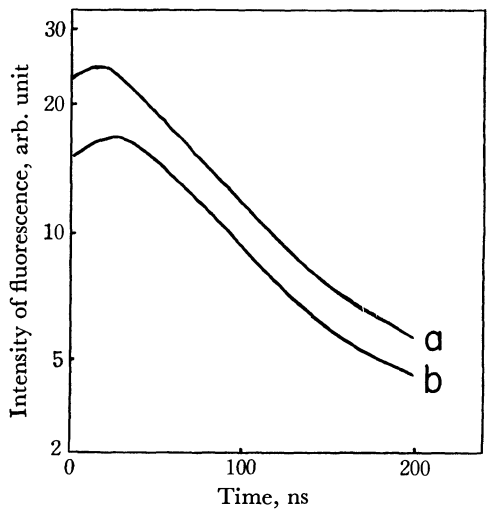

Fig. 5. Time dependence of the fluorescence intensity from toluene in the 23DMB matrix at 77 K.
a: 23DMB–To (2 mol%).
b: 23DMB–To (0.5 mol%).

the spectrum of 23DMB–To(2 mol%)–N_2O(2 mol%) or C_3H_6(2 mol%) from that of 23DMB–To(2 mol%). The intensities of the fluorescence are normalized to the same peak intensity as that of 23DMB–To(2 mol%)–N_2O(2 mol%) (Fig. 4). The emission spectrum from 23DMB–To(2 mol%) during the illumination with ultraviolet light at 77 K is also shown there.[4]

Figure 5 shows the time dependence of the fluorescence of the excited toluene formed by the ns-pulse irradiation of 23DMB containing toluene at 77 K. The rise in the fluorescence before 20 ns is due to the duration of the pulse.

Figure 6 shows the effects of electron scavengers, such as N_2O and CO_2, and hole scavengers, such as C_3H_6 and TME, on the fluorescence at 60 ns after the pulse irradiation at 77 K. Similar results are obtained also 20 and 180 ns after the pulse irradiation. The intensity of the fluorescence in the 23DMB–To(2 mol%) is taken as 10.

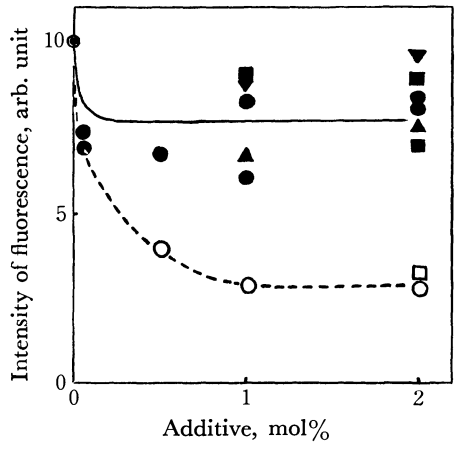

Fig. 6. Effect of additives on the fluorescence intensity from toluene at 60 ns after the ns pulse irradiation of 23DMB–To (2 mol%).
●: N_2O in the solid phase at 77 K.
■: CO_2 in the solid phase at 77 K.
▲: C_3H_6 in the solid phase at 77 K.
▼: TME in the solid phase at 77 K.
○: N_2O in the liquid phase at room temperature.
□: CO_2 in the liquid phase at room temperature.

Discussion

Energy Transfer from Irradiated 23DMB to Toluene at 77 K. There are two possibilities with regard to the formation of the excited toluene in the irradiated 23DMB matrix. One is that it results from energy transfer from the irradiated 23DMB. The other is that it results from the direct absorption of the radiation energy by the solute toluene. The following results support the former possibility: (1) As is shown in Fig. 2, the intensity of the fluorescence increases sharply with an increase in the concentration of toluene, and then gradually increases beyond 2 mol% of toluene. The intensity of the phosphorescence increases sharply and then gradually decreases beyond 2 mol% of toluene. If the luminescence is due to the direct absorption of the radiation energy by the solute toluene, the intensity should increase linearly with an increase in the concentration of toluene.

(2) The yields of the solvent radical in the radiolysis of 23DMB at 77 K decrease upon the addition of toluene; the decrease coincides complementally with the increase in the fluorescence from toluene (Fig. 2). The results suggest that the energy which ruptures the C–H bond of the irradiated 23DMB migrates to toluene to form the excited toluene.

(3) The yields of the fluorescence from toluene in the irradiated alkanes by γ-rays or pulse X-rays at 77 K depend appreciably upon the kinds of alkanes. The yield of the fluorescence in 23DMB–To(2 mol%) is about 3—4 times as large as that in *neo*-C_5H_{12}–To(2 mol%). If the fluorescence is due to the direct absorption of the radiation energy by the solute toluene, the intensity does not depend upon the kind of alkanes, but only upon the amount of toluene.

(4) The addition of CCl_4, which is an efficient energy acceptor,[1] suppresses both the fluorescence and phosphorescence from the irradiated 23DMB–To(2 mol%) at 77 K.

(5) The intensities of the fluorescence from pure solid toluene during γ-irradiation are about 4—7 times stronger than those from 23DMB–To(2 mol%). The fluorescence due to the direct absorption of the radiation energy by toluene itself may be expected to amount to, at most, 8—15% and 3—6% of the total fluorescence from 23DMB–To(2 mol%) and –To(0.5 mol%) respectively.

The time dependence of the fluorescence from 23DMB–To(2 mol%) is similar to that from 23DMB–To(0.5 mol%) (Fig. 5). Since the fluorescence of toluene appears immediately after the ns pulse irradiation,[5] the formation of the excited toluene in the irradiated 23DMB is not due to the secondary reaction of the products, such as a trapped cation, or a trapped electron, but to the rapid energy transfer in a time period less than 10 ns.

Emission Spectrum. The rapid energy transfer in

the 23DMB matrix at 77 K cannot be ascribed to the molecular diffusion of active species, although this diffusion is the most important process in the liquid phase. A mobile entity in the solid phase is an exciton (DMB*),[6] a hole (DMB^+_m),[7] or an electron. For the formation of the excited toluene by energy transfer from the irradiated 23DMB, two processes are possible. One is that the exciton migrates to toluene. The other is that the hole and the electron encounter on the same toluene molecule, even if they travel freely through the matrix.

Figure 3 shows the effects of the addition of an electron scavenger (N_2O) or a hole scavenger (C_3H_6) on the emission spectrum of 23DMB–To during γ-irradiation at 77 K. It was found that propylene reacts efficiently with a hole by means of the following ion-molecule reaction at 77 K:[8]

$$DMB^+_m + C_3H_6 \longrightarrow C_6H_{12}{}^+ + C_3H_8 \quad (1)$$

The intensities of the phosphorescence decrease clearly upon the addition of N_2O or C_3H_6, while those of fluorescence decrease a little. The emission spectra from 23DMB–To(2 mol%)–N_2O(2 mol%) or 23DMB–To(2 mol%)–C_3H_6(2 mol%) during γ-irradiation are very similar to that from 23DMB–To(2 mol%) during the illumination with UV light (Fig. 4). The singlet-excited toluene is formed even in the presence of N_2O or C_3H_6. An excitation transfer forms a singlet-excited toluene, while an energy transfer *via* the ionic process, followed by a neutralization, favors the formation of a triplet-excited toluene. Therefore, it seems that the fluorescence may be due to the excitation transfer. This process will be discussed in more detail in connection with pulse irradiation in the next section.

On the contrary, the spectra which disappear upon the addition of N_2O or C_3H_6 are quite different from the spectrum obtained from 23DMB–To(2 mol%) during the illumination with UV light (Fig. 4). The phosphorescence is much stronger than the fluorescence in these spectra. The formation of the triplet-excited toluene is suppressed remarkably by the addition of an electron scavenger or a hole scavenger. The mechanism of the formation of the triplet-excited toluene may be represented as follows:

$$23DMB \rightsquigarrow DMB^+_m + e^- \quad (2)$$

$$DMB^+_m + To \longrightarrow 23DMB + To^+ \quad (3)$$

$$e^- + To^+ \longrightarrow To^3 \quad (4)$$

$$e^- + To \longrightarrow To^- \quad (5)$$

$$DMB^+_m + To^- \longrightarrow 23DMB + To^3 \quad (6)$$

$$To^3 \longrightarrow To + h\nu \text{ (phosphorescence)} \quad (7)$$

where To^3 represents a triplet-excited toluene. The hole and the electron produced by the irradiation (Reaction (2)) migrate to toluene (Reactions (3) and (5)). Then, the neutralization reaction (Reactions (4) and (6)) produces a triplet-excited toluene. Since N_2O may capture an electron, it disturbs Reactions (4) and (5). The suppression of Reaction (5) by the addition of N_2O was demonstrated by ESR spectroscopy in the radiolysis of 23DMB–To(2 mol%)–N_2O(2 mol%) at 77 K.[2] C_3H_6 disturbs Reactions (3) and (6) by the ion-molecule reaction with DMB^+_m (Reaction (1)). Since the amount of To^- does not correspond at all to the intensity of phosphorescence,[2] Reaction (6) may play a minor role.

Therefore, it may be concluded that the energy transfer in the 23DMB matrix consists of two processes: one forms singlet-excited toluene, and the other forms mainly triplet-excited toluene. Since the efficiencies of the emissions from the two excited states of toluene are not known in the 23DMB matrix at 77 K, the extents of the two processes cannot be determined as yet.

Effect of Scavengers on the Fluorescence. The singlet-excited toluene is formed immediately after the pulse-irradiation. Since the fluorescence in the liquid phase is suppressed by the addition of the electron scavengers (Fig. 6), ionic processes may be important in the formation of the singlet-excited toluene in the liquid phase, as has been reported previously.[9–11]

On the contrary, the fluorescence in the solid phase at 77 K is not affected appreciably by the addition of electron scavengers, such as N_2O and CO_2, or hole scavengers, such as C_3H_6 and tetramethylethylene (TME). There is a possibility that these additives may not act efficiently in the 23DMB matrix at 77 K.

In the radiolysis of 23DMB–To(2 mol%)–CO_2(2 mol%) at 77 K, CO_2 captures an electron to form CO_2^-, which is clearly detected by ESR spectroscopy, and $G(CO_2^-)$ is about 0.8.[12] When 23DMB–To(2 mol%) is γ-irradiated at 77 K, a toluene anion is formed in an appreciable amount. The formation of the toluene anion is completely suppressed by the addition of N_2O, while a toluene cation is clearly observed by ESR spectroscopy in the radiolysis of 23DMB–To(2 mol%)–N_2O(2 mol%) at 77 K. The amount of electrons captured by N_2O seems to be equal to the yield of the toluene cations (*i.e.*, $G\sim1.7$). Since the G-values of the ionization in the gas and liquid phases are about 4, there is some suspicion that the ionic reaction which is not disturbed by N_2O amounts to 2.3 G-unit. Although the yields of the ionization in the gas phase, in which a free electron and a cation are produced, and about 4 G-unit, we cannot expect that, in the crystal, the yields of holes and electrons will be 4 G-unit, for if a hole and an electron are bound by their mutual Coulomb force, they may be considered as an exciton.[6] It has been reported by several investigators that the yields of the electrons which can be captured by electron scavengers are 1.5—2.0 G-unit in the radiolysis of solid alkanes at 77 K. They used biphenyl,[13] alkyl disulfide,[14] benzene,[15] iodobenzene,[16] and nitrous oxide[16] as electron scavengers. The yields were determined by different analytical methods, such as optical or ESR spectroscopy, or gas chromatography. Therefore, the amount of electrons captured by N_2O in the 23DMB matrix ($G\sim1.7$) is near the maximum yields of electrons in the irradiated solid alkane. There is a possibility that N_2O does not directly capture a mobile electron, but that it captures an electron from a toluene anion by tunneling.[17] It can be expected from the tunneling hypothesis that the yield of the toluene cation

is not affected by the addition of N_2O. The yield of the toluene cation, however, increases remarkably upon the addition of N_2O.[2] Therefore, N_2O captures a mobile electron, disturbing the neutralization reaction between the electron and the toluene cation. TME captures a hole to produce the TME^+ cation, which is observed in the irradiated 23DMB–To(2 mol%)–TME(2 mol%) by ESR spectroscopy.[12]

Therefore, it may be considered that the reactions due to electrons or holes are suppressed by the addition of the electron scavengers (N_2O or CO_2) or the hole scavengers (C_3H_6 or TME). Figure 6 shows that the fluorescence is not appreciably affected by the addition of N_2O, CO_2, C_3H_6, or TME at 77 K. It may be concluded that the formation of the fluorescence, *i.e.*, the formation of the singlet-excited toluene, is not due to the reactions of the hole and the electron, but to a non-ionic process, such as the migration of the exciton:

$$23DMB \rightsquigarrow DMB^* \quad (8)$$

$$DMB^* + To \longrightarrow DMB^* + To^1 \quad (9)$$

$$To^1 \longrightarrow To + h\nu(\text{fluorescence}) \quad (10)$$

$$\searrow\ To^3 \quad (11)$$

$$To^3 \longrightarrow To + h\nu\ (\text{phosphorescence}) \quad (7)$$

$$DMB^* \longrightarrow C_6H_{13} + H \quad (12)$$

where To^1 represents a singlet-excited toluene. The exciton produced by irradiation migrates to the toluene, this forming the singlet-excited toluene, which emits fluorescence and phosphorescence by intersystem crossing. DMB* indicates a Frenkel exciton, a Mott-Wannier exciton, or a mobile ion-pair. Reaction (9) implies also the possibility that toluene accepts energy directly from the excited 23DMB molecule, which itself absorbs the radiation energy. It is interesting to note that the C–H bond rupture in the radiolysis of solid isobutane, whose chemical structure is similar to 23DMB, is due to the fragmentation of the excited molecule,[1] and that the formation of the singlet-excited toluene in the 23DMB–To system at 77 K competes with the formation of the solvent radical (Fig. 2).

The authors wish to thank Dr. Hiroshi Masuhara of Osaka University for his measurement of the emission during illumination with UV light. They wish also to thank Dr. Masahiro Saido of Nagoya University for his help in performing the pulse-irradiation.

References

1) a) T. Wakayama, T. Kimura, T. Miyazaki, K. Fueki, and Z. Kuri, This Bulletin, **43**, 1017 (1970). b) T. Miyazaki, T. Yamada, T. Wakayama, K. Fueki, and Z. Kuri, *ibid.*, **44**, 934 (1971).

2) T. Miyazaki, Y. Saitake, Z. Kuri, and S. Sakai, *ibid.*, **46**, 70 (1973).

3) The emission spectrum is different from the previously-reported one (Ref. 2). When the sample is irradiated, some product which absorbs the light near 280 nm may be formed, thus decreasing the emission intensity at 280 nm. Therefore, the spectra in Fig. 3 are those from a freshly-sealed sample.

4) The spectrum of 23DMB–To (2 mol%) during UV illumination with light of 250 nm at 77 K was measured by Dr. Hiroshi Masuhara.

5) The initial rise in the fluorescence before 20 ns is due to the duration of the pulse. The values at 0 ns contain larger errors than those at other times.

6) It would be useful to define the technical terms used in this paper. Such terms as "ionization", "cation", "electron", and "excited molecule" are commonly used in radiation chemistry. Though they can be clearly defined in the gas phase, where each molecule exists independently, it is difficult to do so in the crystal where the character of a molecular aggregate becomes remarkable. Since there have been very few studies of the primary process in the radiolysis of organic crystals, it is impossible to give terms suitable for the radiation chemistry in the crystal. Therefore, we adopt the terms for the mobile entities which are used in solid state physics. An electron in the conduction band and a hole can travel freely and independently through the crystal. An exciton is a neutral, excited mobile state of a crystal; an exciton can travel through the crystal, but it is electrically neutral. The exciton may be classified into two different limiting approximations. One is the Frenkel exciton, which is considered to be tightly bound, while the other is the Mott-Wannier exciton, which is weakly bound by Coulomb force, having an electron-hole interparticle distance large in comparison with the atomic radius. In this paper, we do not discriminate between the two types of excitons (*cf.* C. Kittel, "Introduction to Solid State Physics," John Wiley & Sons, New York, (1956)).

7) J. B. Gallivan and W. H. Hamill, *J. Chem. Phys.*, **44**, 2378 (1966).

8) Y. Saitake, T. Miyazaki, and Z. Kuri, *J. Phys. Chem.*, **77**, 2418 (1973).

9) T. Saito, K. Takahashi, and S. Sato, This Bulletin, **41**, 2603 (1968).

10) R. R. Hentz and R. J. Knight, *J. Phys. Chem.*, **72**, 1783 (1968).

11) P. K. Ludwig and M. M. Hugue, *J. Chem. Phys.*, **49**, 805 (1968).

12) Y. Saitake, T. Miyazaki, and Z. Kuri, unpublished results.

13) J. P Guarino and W. H Hamill, *J. Amer. Chem. Soc.*, **86**, 777 (1964).

14) T. Shida, *J. Phys. Chem.*, **74**, 3055 (1970).

15) T. Wakayama, T. Miyazaki, K. Fueki, and Z. Kuri, This Bulletin, **43**, 3761 (1970).

16) T. Kimura, T. Miyazaki, K. Fueki, and Z. Kuri, *ibid.*, **41**, 2861 (1968).

17) J. R. Miller, *J. Chem. Phys.*, **56**, 5173 (1972).

The Raman Spectra and Molecular Conformations of Surfactants in Aqueous Solution and Crystalline States

Hirofumi Okabayashi, Masataka Okuyama, Teizo Kitagawa,* and Tatsuo Miyazawa*

Department of Engineering Chemistry, Nagoya Institute of Technology, Gokiso, Nagoya 466
**Institute for Protein Research, Osaka University, Yamada-kami, Suita, Osaka 565*

(Received September 4, 1973)

The Raman spectra were measured for sodium alkyl sulfates and potassium aliphatic carboxylates in the solid state and aqueous solutions. Vibrational assignments of Raman lines were made, and characteristic Raman lines of the alkyl sulfate ion were identified. The ethyl sulfate ion in the aqueous solution was found to exist predominantly as the *trans* form about the CH_2–O bond. For higher alkyl sulfate ions in aqueous solutions, Raman lines due to rotational isomers with *gauche* CH_2–CH_2 bonds were observed. Longitudinal accordion frequencies of the solid state and aqueous solutions were compared in order to discuss the conformations of hydrocarbon chains in solution.

The physicochemical properties of aqueous solutions of surfactants have been extensively studied. For more detailed investigations of surfactants, conformation studies of surfactant molecules in aqueous solutions are highly desirable. Laser Raman spectroscopy is useful for conformation studies of molecules, especially in aqueous solutions. However, the Raman spectra of surfactants in aqueous solutions have not been reported on.

In the Raman spectra of long-chain *n*-paraffins in the crystalline state, very strong Raman lines due to "accordion" vibrations have been observed; the frequencies of these accordion vibrations have been found to be inversely proportional to the number of carbon atoms.[1,2] Accordion vibrations of *n*-paraffins have also been observed in solution, and molecular conformations in solution have been discussed.[1,3,4]

In the present study, the Raman spectra of a homologous series of sodium alkyl sulfates and of potassium aliphatic carboxylates were measured. The characteristic Raman lines of alkyl sulfate groups were identified. Raman lines due to accordion vibrations were observed in order to study molecular conformations in aqueous solutions.

Experimental

The samples of sodium methyl sulfate (SMS), sodium dodecyl sulfate (SDS), and potassium aliphatic carboxylates ($C_{n-1}H_{2n-1}CO_2K$, $n=3$, 4, 6, 8, 10, and 12) were obtained from the Tokyo Kasei Co. and were purified by recrystallization. However, the samples of sodium ethyl sulfate (SES), sodium *n*-propyl sulfate (SPS), sodium *n*-butyl sulfate (SBS), sodium *n*-hexyl sulfate (SHS), sodium *n*-octyl sulfate (SOS), and sodium *n*-decyl sulfate (SDeS) were prepared from sulfuric acid, *n*-alkyl alcohol, and sodium hydroxide.[5]

The Raman spectra of sodium alkyl sulfates and potassium aliphatic carboxylates in the crystalline state and in an aqueous solution at room temperature were measured with a JEOL Raman spectrometer (JRS-O2AS, argon ion laser, 488.0 nm). The sodium alkyl sulfates were dissolved (30—50 wt%) in water, but the potassium aliphatic carboxylates were dissolved (30—50 wt%) in a 0.1 M KOH solution.

Results and Discussion

The Raman spectra of SDS, SDeS, SOS, SHS, SBS, and SPS in aqueous solutions are shown in Fig. 1. In the Raman spectra of surfactants (SDS, SDeS, and SOS), common Raman lines are observed at 890

Table 1. Raman frequencies (cm^{-1}), relative intensities,[a] and vibrational assignments of PMS (potassium methyl sulfate), SMS and SES in the solid state and aqueous solution and of the series from SPS to SDS in aqueous solution

PMS[b] soln	SMS soln	SMS solid	SES soln	SES solid	SPS–SDS soln	Assignments
273 w	272 w	271 w		263 w		C–O–S deform.
			345 s	350 m		C–C–O deform.
413 m 438 m	415 m 435 m	411 m 444 m	421 m	423 m	417—420 m	$-SO_3$ rock.
559 m	561 m	566 m	574 m	578 m	580—584 m	$-SO_3$ sym. deform.
615 m	591 w 617 m	593 w 614 m	622 w	590 w 623 w	619—625 w	$-SO_3$ asym. deform.
781 s	785 s	763 s 799 m	795 s	793 s 816 s	822—839 s	RO–SO_3 stretch.
			913 w	933 w		CH_3–CH_2 stretch.
1006 s	1004 s	1016 m				CH_3–O stretch.
			1013 s	1010 w		CH_2–O stretch.
1063 vs	1063 vs	1081 vs	1063 vs	1079 vs	1062—1065 vs	$-SO_3$ sym. stretch.

a) vs: very strong, s: strong, m: medium, w: weak. b) Ref. 7.

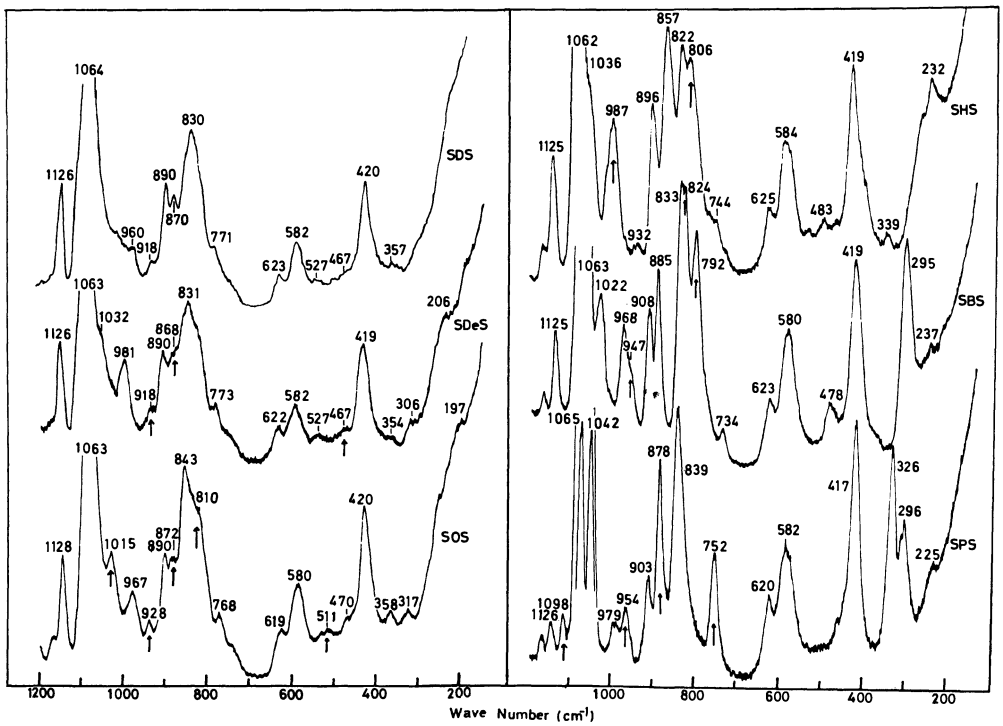

Fig. 1. Raman spectra of SDS (30 wt %), SDeS (35 wt %), SOS (40 wt %), SHS (45 wt %), SBS (50 wt %), and SPS (50 wt %) in aqueous solution at room temperature. Excited with an argon ion laser (488.0 nm). Raman lines marked with arrows are not observed in the crystalline state.

and 1131 cm^{-1}; these lines correspond to the Raman lines of long-chain *n*-paraffins[1] at about 900 and 1135 cm^{-1} and are thus assigned to the terminal-methyl rocking vibration and C–C stretching vibrations[6] respectively. For the series from SPS to SDS, common Raman lines are also observed at 417—420, 580—584, 619—625, 822—839, and 1062—1065 cm^{-1} (see Fig. 1 and Table 1). The assignment of these Raman lines was made with reference to the Raman spectra of PMS (potassium methyl sulfate)[7] and SMS.

Sodium Methyl Sulfate. The Raman frequencies of SMS in an aqueous solution are listed in Table 1, together with the Raman frequencies (and vibrational assignments) of PMS[7] in an aqueous solution. The band of PMS at 615 cm^{-1} was resolved into two components (591 and 617 cm^{-1}) in the Raman spectra of SMS. In other respects, the Raman lines of SMS closely correspond to the Raman lines of PMS; accordingly, the vibrational assignments of SMS were made following those of PMS.[7] The Raman lines due to the rocking (or asym. deform.) modes are split into two components, since there are two modes, symmetric or antisymmetric, with respect to the CH_3–O–S plane. There are two strong Raman lines at 1063 and 1004 cm^{-1}. However, the line at 1063 cm^{-1} is characteristic of alkyl sulfates; accordingly, the line at 1004 cm^{-1} is assigned to the stretching vibration of the CH_3–O bond. The weak broad line at 272 cm^{-1} can reasonably be assigned to the C–O–S deformation vibration.

The Raman line of solid SMS at about 781 cm^{-1} is split into two components. In other respects, the Raman lines of SMS in an aqueous solution closely correspond to the Raman lines in the solid state, indicating that the molecular structures of SMS in solution and in the solid state are similar.

Sodium Ethyl Sulfate. The crystal structure of SES was analyzed by the X-ray diffraction method. The ethyl sulfate ion (CH_3–CH_2–O–SO_3^-) was found to take the *trans* form in the crystalline state.[8] In solution, the *gauche* form may well be expected to appear. However, the steric repulsion between the terminal CH_3 group and oxygen atoms of the $-SO_3^-$ group possibly makes the *gauche* form much less stable than the *trans* form. In fact, the Raman spectra of the aqueous solution and the solid were found to be much the same except for the splitting of the Raman lines at about 810 and 610 cm^{-1} in the solid state, and no new lines appeared when the solid was dissolved in water. Accordingly, the ethyl sulfate ion in an aqueous solution may be concluded to exist primarily in the *trans* form.

The Raman spectra of SES were compared with those of SMS (Table 1) for vibrational assignments. The Raman lines of SES at 913 and 345 cm^{-1} were readily assigned to the CH_3–CH_2 stretching and C–C–O deformation vibrations respectively.

Sodium Propyl Sulfate. The Raman lines of SPS at 903 and 1042 cm^{-1} (Fig. 1) correspond to the infrared bands of propane at 899 and 1049 cm^{-1}, and are assigned to the methyl rocking and C–C stretching vibrations[9] respectively. The three lines of the aqueous solution at 752, 878, and 954 cm^{-1} are not observed in the solid state and are assigned to the *gauche* form about the CH_2–CH_2 bond.

Sodium Butyl Sulfate. The Raman lines of SBS

Table 2. Accordion frequencies (cm^{-1}) of sodium alkyl sulfates (SAS), potassium aliphatic carboxylates (PAC) in the solid state and aqueous solutions and of *n*-paraffins

Number of carbon atoms	SAS		PAC		*n*-Paraffin[a]	
	soln	solid	soln	solid	liquid	solid
3	326	340	496	496		
4	295	315	349	353	429	425
6	232	236	327	325	370	373
8	197	196	254	248	279	283
10	206	169	243	208	250	231
12			222	181	239	194

a) Ref. 1.

at 792 and 947 cm^{-1} disappear in the solid state. These lines closely correspond to those of the *gauche* isomer of *n*-butane at 788 and 956 cm^{-1}, and are assigned to the methylene rocking and C–C stretching vibrations[9] respectively.

Sodium Alkyl Sulfate. The Raman lines of SHS at 806 and 987 cm^{-1} disappear in the solid state; accordingly, they must be due to rotational isomers having *gauche* CH_2–CH_2 bonds. The Raman intensities of these lines relative to other lines were found to be concentration-dependent. This observation allows some detailed studies of the molecular conformations of surfactant molecules in solution (to be reported separately).

For SOS and SDeS, the Raman lines shown with arrows in Fig. 1 disappear in the solid state and are due to rotational isomers other than the all-*trans* form.

Accordion Vibrations. The accordion frequencies of sodium alkyl sulfates and potassium aliphatic carboxylates are listed in Table 2, together with those of *n*-paraffins. For the example of $n=6$, the accordion frequencies become lower in the order of: $CH_3(CH_2)_4$–CH_3 > $CH_3(CH_2)_4$–CO_2^- > $CH_3(CH_2)_4$–CH_2–OSO_3^-. These frequency differences are possibly due to the greater mass of the terminal groups of aliphatic carboxylates and alkyl sulfate ions.

For the accordion vibrations of sodium alkyl sulfate ($n \geq 4$) and potassium aliphatic carboxylate ($n \geq 6$), there are linear relations, as is shown in Fig. 2, between the reciprocal number ($1/n$) of carbon atoms and the accordion frequencies in the solid state. However,

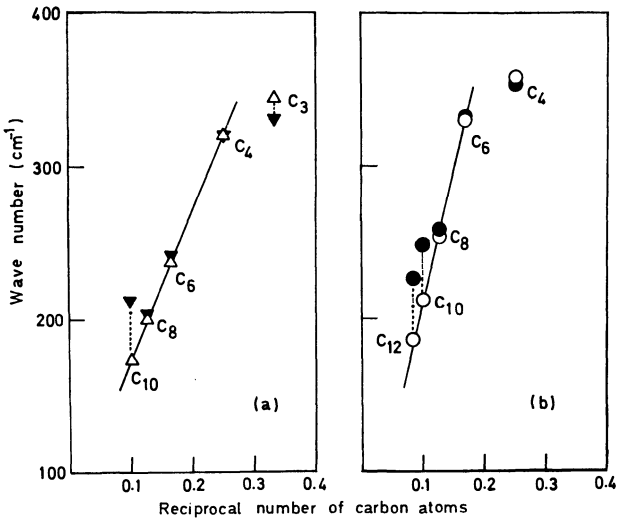

Fig. 2. Number of carbon atoms and accordion frequencies of (a) sodium *n*-alkyl sulfates (R–O–SO_3Na) and (b) potassium aliphatic carboxylates in the crystalline state (open mark) and aqueous solution (full mark).

for $n>8$, the accordion frequencies in an aqueous solution are apparently higher than those in the solid state. Similar observations were previously made of *n*-paraffins in the liquid and solid states.[3,4] Observations of these higher-frequency accordion vibrations indicate that the randomness of *n*-alkyl hydrocarbon chains is increased with the number of carbon atoms.

References

1) S. Mizushima and T. Shimanouchi, *J. Amer. Chem. Soc.*, **71**, 1320 (1949).
2) R. F. Schaufele and T. Shimanouchi, *J. Chem. Phys.*, **47**, 3605 (1967).
3) R. F. Schaufele, *ibid.*, **49**, 4168 (1968).
4) T. Fujiyama, M. Tasumi, and T. Shimanouchi, Symposium on High Polymers, Kyoto, Oct. 1970, paper 20D09.
5) R. Goto and T. Sugano, "Jikken Kagaku Koza," Vol. 7, ed. by Chem. Soc. of Japan, (1956), p. 131.
6) J. H. Schachtschneider and R. G. Snyder, *Spectrochim. Acta*, **19**, 117 (1963).
7) V. H. Siebert, *Z. Anorg. Allg. Chem.*, **289**, 15 (1957).
8) J. A. J. Jarvis, *Acta Crystallogr.*, **6**, 327 (1953).
9) R. G. Snyder, *J. Chem. Phys.*, **47**, 1316 (1967).

Electronic Excited States of the Intramolecular Exciplex and Charge-transfer Complex in (9,10-Dicyanoanthracene)-$(CH_2)_3$-(Naphthalene)

Michiya Itoh,* Tsutomu Mimura, and Toshihiko Okamoto

Faculty of Pharmaceutical Sciences, The University of Tokyo, Bunkyo-ku, Tokyo 113

(Received September 5, 1973)

In the previous paper two kinds of fluorescences due to the intramolecular exciplex (above ~200 K) and the charge-transfer complex (below ~160 K) were reported in a nonpolar solution of the (9,10-dicyanoanthracene)-$(CH_2)_3$-(naphthalene) systems. The fluorescence quantum yields as well as the fluorescence lifetimes of the exciplex and CT complex determined at several temperatures show a discontinuous change from room temperature to 77 K. The radiative and nonradiative decay constants of these fluorescent states suggest that the radiative decay in the exciplex is comparable with the nonradiative decay, while the nonradiative process is predominant in the excited state of the CT complex.

The binding energy of the exciplex has been attributed to the charge-transfer (CT) interaction between the electron donor and acceptor.[1] The CT character in the exciplex has been emphasized by the determination of the ($S_n \leftarrow S_1$) absorption spectra.[2,3] However, there has been no information available about the difference in the properties and relationship between the exciplex and the excited state of the CT complex. The present authors previously reported that the intramolecular exciplex fluorescence was observed in the (9,10-dicyanoanthracene)-$(CH_2)_3$-(naphthalene) systems in both polar and nonpolar solvents.[4] Only in the nonpolar solvent, the intramolecular CT-complex fluorescence (λ_{max} 540 nm) was observed below ~160 K in the wavelength region longer than the exciplex fluorescence (λ_{max} 500—510 nm). The fluorescence lifetimes of the exciplex and the CT complex at various temperatures were reported to be almost independent of the temperature, and different from each other. The appreciable differences in the fluorescence lifetimes and maxima between the exciplex and CT complex suggested that there were two different excited states in the potential energy surface of the electronic interaction between the electron-donor-acceptor moieties in this compound.

Therefore, in order to elucidate the properties of these fluorescent states of the intramolecular exciplex and CT complex, we determined the fluorescence quantum yields and the radiative and nonradiative rate constants of these excited states.

Experimental

The synthesis and purification of (9,10-dicyanoanthracene)-$(CH_2)_3$-(naphthalene) (abreviated as $\beta\alpha'$- and $\beta\beta'$-DCAN) and the determination of the absorption and fluorescence spectra were reported in a previous paper.[4] The fluorescence quantum yields were measured essentially in the way described by Parker and Rees,[5] where the solution of anthracene was used as the standard. In the determination of the quantum yields of the CT complex, the intensity of the absorption spectrum at a certain wavelength (an excitation light) corresponding to the CT complex at a certain temperature (~150—77 K) was obtained by the aid of an equilibrium constant which was estimated from a straight line of $\log \varepsilon/(\varepsilon_c-\varepsilon)$ against $1/T$ mentioned in the previous paper. The fluorescence lifetimes were determined by using a coaxial-type nitrogen gas laser as an exciting light source (30 kW peak intensity at 337 nm and 3 ns duration).[6]

* To whom all correspondence should be addressed.

Results and Discussion

The mechanism for the exciplex and CT-complex formations and decay processes can be expressed as follows:

$$\begin{array}{ccccc} D + A^* & \underset{k_4}{\overset{k_3}{\rightleftharpoons}} & (DA)^* & & (DA)_c^* \\ & k_1 \downarrow \{ k_2 & & k_5 \downarrow \{ k_6 & k_7 \downarrow \{ k_8 \\ D + A & \cdots\cdots\cdots\cdots\cdots\cdots\rightarrow & (DA)_c & & \end{array}$$

Here, D and A are the electron donor and acceptor respectively; and (DA)* and $(DA)_c$* are the exciplex and an excited state of the CT complex respectively. The CT complex in the ground state is expressed by $(DA)_c$.

Birks *et al.* made an extensive study of the rise and decay kinetics of the pyrene excimer and determined the rate constants.[7] Recently, Yoshihara *et al.* determined the rate constants of the exciplex formation and of the decay process in the exciplex of the pyrene–*N,N*-dimethylaniline system.[8] They obtained the rate constant of k_3 from the concentration dependence of the intermolecular exciplex, and also evaluated k_4 and (k_5+k_6) from an analysis of the time-dependent exciplex concentration. The value of k_4 in the literature are negligible compared with those of k_3.[1,7-9] However, no determination of the k_4 in the intramolecular exciplex has ever been reported. In this paper, it is noteworthy that the intramolecular exciplex formation is independent of the concentration. Furthermore, no rise-time of the exciplex fluorescence from which k_4 might be evaluated was observed. Therefore, k_4 was assumed to be negligible compared with k_3 in this stage, and also subsequent attempts were made to study the intramolecular exciplex formation and decay process.

The fluorescence quantum yields and lifetimes of 9,10-dicyanoanthracene as determined in several solvents are shown in Table 1. Table 1 suggests that the nonradiative rate constant, k_2, in a nonpolar solvent

Table 1. Fluorescence lifetimes and quantum yields of 9,10-dicyanoanthracene in various solvents

Solvent	τ (ns)	ϕ
MP	15.2	0.9
2-Methyl THF	15.8	0.52
Acetone	18.0	0.19
Acetonitrile	19.5	0.21

such as MP may be negligible compared with k_1. This assumption is not valid in a polar solvent, though, since the quantum yield shows a remarkable decrease in the polar solvent. In DCAN, the fluorescence quantum yield and lifetime of the 9,10-dicyanoanthracene moiety are expressed as follows:

$$\phi' = k_1(k_1+k_2+k_3)^{-1} \text{ and } \tau' = (k_1+k_2+k_3)^{-1}.$$

The results obtained here at 300 K are summarized in Table 2. If k_2 was neglected in an MP solution of DCAN, as mentioned above, the rate constant of the intramolecular exciplex formation, k_3, was directly estimated to be 1.1×10^8 s^{-1} for $\beta\alpha'$-DCAN and 1.2×10^8 s^{-1} for $\beta\beta'$-DCAN at this temperature from ϕ' and τ' respectively, both shown in Table 2. The value of k_3 can not be compared with those of the rate constants of the intermolecular exciplex formations in the literature,[8-10] because the former obeys different kinetics from those of the latter. Furthermore, the rate constants, k_3, at several temperatures were evaluated from the value of k_3 at 300 K and from the activation energy of the exciplex formation reported in previous papers,[4,11] where we assumed that there was no change in the entropy factor in this temperature region.

Table 2. Fluorescence lifetimes and quantum yields of DCAN's in MP

DCAN	DCA moiety[a]		Exciplex[a]		CT-Complex[d]	
	τ'(ns)	ϕ'	τ_e(ns)	ϕ_e[c]	τ_c(ns)	ϕ_c
$\beta\alpha'$-	8.0	0.097	63	0.25	127	0.13
$\beta\beta'$-	8.0	0.069	40.8	0.20	150	0.11

a) Determined at 300 K. b) Determined at 77 K.
c) Apparent quantum yields mentioned in the text.

The apparent fluorescence quantum yield of the exciplex, ϕ_e, can be expressed by the following equation:[8]

$$\phi_e = \phi_e'\frac{k_3\tau}{1+k_4\cdot\tau_e'}\left\{1+\frac{k_3\tau}{1+k_4\cdot\tau_e'}\right\}^{-1} = \phi_e'\cdot f.$$

Here, $\tau=(k_1+k_2)^{-1}$, $\tau_e'=(k_5+k_6)^{-1}$ and $\phi_e'=k_5\cdot\tau_e'$. Since k_4 was neglected, as has been mentioned above, f, k_5 and k_6 can be estimated by the aid of the τ, τ_e', k_3 and ϕ_e obtained in an MP solution of DCAN. These results, as determined at 300 K, are summarized in Table 3. These quantum yields, and the radiative and nonradiative rate constants of the exciplex at several temperatures, were determined in an MP solution of $\beta\beta'$-DCAN; the results are shown in Fig. 1.

On the other hand, the fluorescence quantum yields of the CT complex in an MP solution of $\beta\beta'$-DCAN at several temperatures below ~150 K were determined by the method described in the experimental section.

Table 3. Radiative and nonradiative rate constants (in units of s^{-1}), and fluorescence quantum yields in DCAN's (in MP)

DCAN	DCA moiety[a]		Exciplex[a]			CT-complex	
	$k_1\times10^{-7}$	$(k_2+k_3)\times10^{-8}$	ϕ'_e[c]	$k_5\times10^{-6}$	$k_6\times10^{-6}$	$k_7\times10^{-6}$	$k_8\times10^{-6}$
$\beta\alpha'$-	1.2	1.13	0.54	8.3	7.5	1.05	6.8
$\beta\beta'$-	0.86	1.2	0.42	10.4	14	0.7	5.9

a) Results evaluated from the data at 300 K.
b) Results evaluated from the data at 77 K.
c) Estimated quantum yields of the exciplex mentioned in the text.

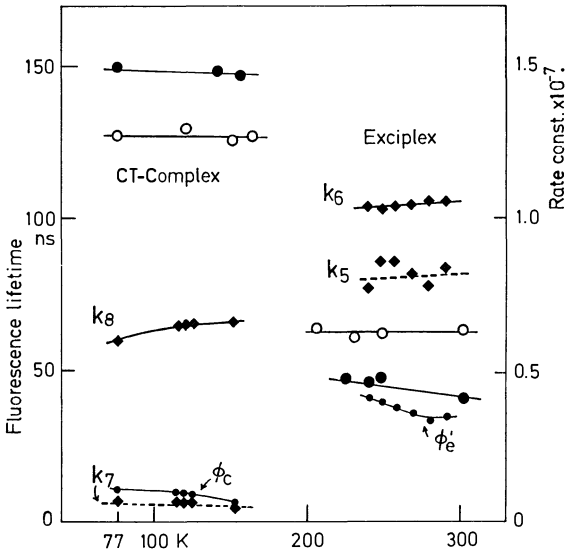

Fig. 1. Temperature dependence of the fluorescence lifetimes determined at 560 nm, —○—○— and —●—●— are $\beta\alpha'$-, and $\beta\beta'$-DCAN, respectively, and of the fluorescence quantum yields, and the radiative and nonradiative rate constants of the exciplex and the CT-complex in an MP solution. Concentrations are approximately 10^{-6}M. An unit of an ordinate for the decay rate constants is 10^7s^{-1}.

These results and the decay rate constants of the CT complex of $\beta\beta'$-DCAN at several temperatures are shown in Fig. 1. These quantum yields and the rate constants of the exciplex and the CT complex are both almost temperature-independent. It is unlikely that the quantum yield and also the rate constant can continuously change from the exciplex to the CT complex in the temperature region of ~200—160 K, as is shown in Fig. 1, where the fluorescence in the 500—550 nm region was almost quenched and was indistinguishable between the exciplex and the CT complex. This is because the solvent (MP) used here shows no steep change in viscosity in this temperature region.

Recently it has been suggested that the fluorescent state of the exciplex is identical with that of the corresponding CT complex, though no comparison of the exciplex fluorescence with that of the CT complex was made in the same electron-donor-acceptor system. Very recently, Itoh and Mimura reported experimental evidence for an identical fluorescent state of the inter-

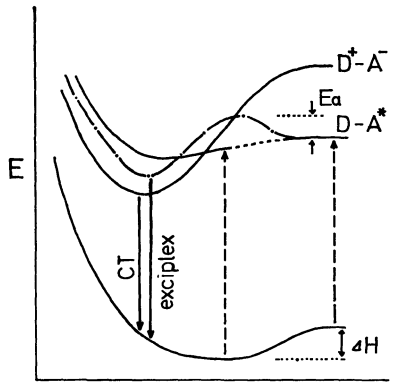

Fig. 2. The potential energy curves of the exciplex and the CT-complex.

molecular exciplex and CT complex in the 9,10-dicyanoanthracene–2-methylnaphthalene system.[12] The experimental behaviors of the intramolecular exciplex and CT complex reported here and also in the previous paper[4] demonstrate that these two fluorescences are from individual fluorescent states, as is illustrated in Fig. 2. Mataga *et al.*[13] reported the radiative and nonradiative rate constants in the exciplex of the pyrene–*N*,*N*-dimethylaniline system in the nonpolar solvent to be 2.4×10^{6} s^{-1} and 2.6×10^{6} s^{-1} respectively. Kobayashi *et al.*[14] made an extensive study of the CT complex of tetracyanobenzene and reported the radiative and nonradiative rate constants of the CT complex in a nonpolar solvent to be 10^{4-5} s^{-1} and 10^{6-7} s^{-1} respectively. As is shown in Fig. 1 and in Table 3, the radiative and nonradiative rate constants in the exciplex are comparable to each other, while the latter seems to be the main process in the CT complex. The decay constants from room temperature to 77 K obtained here are further confirmation of our arguments that the fluorescence above ~200 K is to be ascribed to the exciplex, and those below ~160 K, to the CT complex, and that there are two different fluorescent states in the intramolecular electronic interaction between the electron donor and acceptor moieties. These electronic interactions leading to the difference in the excited fluorescent states of the exciplex and the CT complex can be understood by the argument that the internal or geometrical conversion from their respective Franck-Condon excited states to the identical fluorescent state, which may be allowed in the intermolecular interaction,[12] is forbidden in these chain compounds by the steric factor concerned with the trimethylene chain.

The authors are indebted to Dr. Keitaro Yoshihara of the Institute of Physical and Chemical Research for the determination of the fluorescence lifetime and for valuable discussions.

References

1) H. Knibbe, D. Rehm, and A. Weller, *Ber. Bunsenges. Phys. Chem.*, **73**, 839 (1969), and references therein.
2) M. Ottolenghi, *Accounts Chem. Res.*, **6**, 153 (1973), and references therein.
3) T. Okada, T. Fujita, M. Kubota, S. Masaki, N. Mataga, R. Ide, Y. Sakata, and S. Misumi, *Chem. Phys. Lett.*, **14**, 563 (1972).
4) M. Itoh, T. Mimura, H. Usui, and T. Okamoto, *J. Amer. Chem. Soc.*, **95**, 4388 (1973).
5) C. A. Parker and W. T. Rees, *Analyst* (London), **85**, 587 (1960).
6) The fluorescence lifetimes were determined at the Institute of Physical and Chemical Research, Wako-shi, Saitama.
7) J. B. Birks, D. J. Dyson, and I. H. Munro, *Proc. Roy. Soc. Ser. A*, **275**, 575 (1963).
8) K. Yoshihara, T. Kasuya, A. Inoue, and S. Nagakura, *Chem. Phys. Lett.*, **9**, 469 (1971).
9) W. Ware and H. P. Richter, *J. Chem. Phys.*, **48**, 1595 (1968).
10) N. Mataga, T. Okada, and N. Yamamoto, *Chem. Phys. Lett.*, **1**, 119 (1967).
11) Although an assumption, $k_{ef}\gg k_{q}$, was made in the previous paper (Ref. 4), k_{ef} ($=k_5$ in this paper) was evaluated to be comparable with k_q ($=k_6$) as will be mentioned later. However, the activation energies of the exciplex formation reported there are correct, because $k_5/(k_5+k_6)$ does not depend appreciably on the temperature.
12) M. Itoh and T. Mimura, *Chem. Phys. Lett.*, **24**, 551 (1974).
13) N. Mataga, T. Okada, and K. Ezumi, *Mol. Phys.*, **10**, 203 (1966).
14) T. Kobayashi, K. Yoshihara, and S. Nagakura, This Bulletin, **44**, 2603 (1971).

The Crystal Structure of the 1:1 Complex of Pyromellitic Dianhydride with *trans*-Stilbene

Toshiko KODAMA and Shigekazu KUMAKURA*

The Institute of Industrial Science, The University of Tokyo, Roppongi, Minato-ku, Tokyo 106
**Department of Chemistry, Faculty of Science and Engineering, Saitama University, Shimookubo, Urawa-shi, Saitama 338*

(Received September 11, 1973)

The 1: 1 complex of pyromellitic dianhydride with *trans*-stilbene crystallizes in the space group $P2_1/c$ with two pairs of the component molecules in a unit cell with dimensions of $a=12.48$, $b=6.33$, $c=13.17$ Å, and $\beta=111.6°$. The structure was solved from a three-dimensional $|E|^2$ Patterson synthesis and refined by a block-diagonal least-squares method to a final R value of 0.12 for 1635 reflections. In the *trans*-stilbene molecule, the plane containing the central ethylene group makes an angle of 11.5° with the phenyl plane. The non-planarity of the *trans*-stilbene molecule seems to be largely due to a steric repulsion between the hydrogen atom attached to the ethylene moiety and that at the 6 and 6′ position in the phenyl group. The pyromellitic dianhydride molecule is approximately planar. The component molecules are stacked alternately in infinite columns along the a axis. The average spacing between the phenyl plane of *trans*-stilbene and the molecular plane of pyromellitic dianhydride is 3.59 Å, and these palnes make an angle of 4.8° with each other. The relative arrangement of the component molecules in the crystal differs from that observed in the crystal of the anthracene, pyrene, or perylene complex with pyromellitic dianhydride. The van der Waals forces are considered to be more important than the charge transfer force in determining the relative arrangement of the component molecules in this crystal.

The charge transfer (CT) complex of *trans*-stilbene (STB) with pyromellitic dianhydride (PMDA) crystallizes with a 1: 1 molecular ratio, whereas the CT complex of *trans*-4-methylstilbene crystallizes with a 2: 1 molecular ratio.[1] The crystal structure analysis of the former complex was carried out in order to study the molecular interaction between the donor and acceptor molecules.

Experimental

Crystals of the complex were kindly supplied by Professor Matsuo of Kyushu University. They were in the form of bright red thin plates. The cell constants were determined from zero-layer back-reflection Weissenberg photographs around the b and c axes. The crystal data are listed in Table 1. The specimens used for the intensity measurements had dimensions of $0.24\times0.24\times0.05$ mm and $0.23\times0.21\times0.05$ mm. Multiple film equi-inclination Weissenberg photographs were taken around the b axis up to the fifth layer and around the c axis up to the tenth layer. The intensities of 1635 independent reflections were estimated visually by comparison with a standard scale. The usual Lorentz, polarization, and spot-shape corrections were applied; however, no correction was made for the absorption in view of the small size of the specimens.

TABLE 1. CRYSTAL DATA

Chemical formula: $C_{10}H_2O_6\cdot C_{14}H_{12}$
M.W.=398.4
Crystal system: Monoclinic
$a=12.48\pm0.01$Å
$b=6.33\pm0.01$Å
$c=13.17\pm0.02$Å
$\beta=111.56\pm0.07°$
$V=967.6$Å^3
Space group: $P2_1/c$
$D_x=1.37$ g·cm^{-3}
$D_m=1.38$ g·cm^{-3}
$Z=2$

Structure Determination

A Patterson synthesis sharpened by the $\exp(B\sin^2\theta/\lambda^2)$ factor was calculated using the complete set of observed data, but it could not be interpreted satisfactorily because of the severe overlapping of peaks. The structure was, however, solved by an $|E|^2$ Patterson synthesis. From the peaks around the point of origin, the orientations of the benzene rings in the component molecules could be fixed. The molecular orientations and the relative arrangement of the component molecules were assumed so as to account for the characteristic distribution of the prominent peaks. The structure factors were calculated on the basis of the trial model thus obtained by assuming the isotropic temperature factors of all the atoms. The R value was 0.46. The atomic coordinates and isotropic temperature factors were refined by means of the block-diagonal least-squares procedures using a program written by Dr. Ashida. After five cycles of refinement, anisotropic temperature factors were introduced. The positions of the hydrogen atoms were supplied by calculation; they were not refined. The temperature factors of the hydrogen atoms were assumed to be isotropic and were given the same values as those of the atoms to which the hydrogen atoms were attached. The following weighting scheme was employed for the least squares refinement:

$$1.0 \text{ for } |F_o| \geq 5.0$$

and:

$$0.7 \text{ for } |F_o| < 5.0$$

The final R value was 0.12. The topography of the final differential synthesis was flat within the range of ±0.3eÅ^{-3}. The final atomic and thermal parameters are listed in Table 2. A complete list of the observed and calculated structure factors is preserved by the Chemical Society of Japan.[2] Atomic scattering curves taken from the International Tables for X-ray Crystallography were used throughout.

TABLE 2. FINAL ATOMIC COORDINATES AND THERMAL PARAMETERS

(Estimated standard deviations are shown in parentheses ($\times 10^4$). Thermal parameters are in the form of $\exp[-(h^2\beta_{11}+k^2\beta_{22}+l^2\beta_{33}+hk\beta_{12}+hl\beta_{13}+kl\beta_{23})]$.)

Atom	$x/a\times10^4$	$y/b\times10^4$	$z/c\times10^4$	$\beta_{11}\times10^4$	$\beta_{22}\times10^4$	$\beta_{33}\times10^4$	$\beta_{12}\times10^4$	$\beta_{13}\times10^4$	$\beta_{23}\times10^4$
STB									
C (1)	4056 (6)	1914 (14)	1659 (6)	0056	0242	0070	−0007	0078	−0032
C (2)	3477 (7)	1612 (15)	2362 (7)	0069	0309	0077	0006	0099	−0065
C (3)	2913 (7)	−0322 (14)	2335 (6)	0063	0296	0065	−0002	0087	−0016
C (4)	2929 (6)	−1893 (14)	1604 (6)	0061	0236	0070	−0043	0075	−0023
C (5)	3521 (6)	−1594 (14)	0903 (6)	0056	0250	0058	−0021	0057	−0023
C (6)	4121 (6)	0336 (13)	0944 (6)	0050	0248	0057	0011	0065	0009
C (7)	4847 (6)	0693 (14)	0286 (6)	0050	0264	0056	−0026	0065	0005
PMDA									
C (11)	0338 (6)	1972 (11)	0646 (5)	0054	0114	0046	−0032	0068	−0017
C (12)	−0674 (5)	−1496 (11)	0216 (5)	0042	0147	0042	−0016	0053	0001
C (13)	−0386 (5)	0384 (11)	0825 (5)	0047	0160	0035	0012	0060	0004
C (14)	−1380 (6)	−2754 (12)	0669 (6)	0052	0184	0056	−0027	0075	0015
C (15)	−0902 (6)	0329 (12)	1670 (5)	0051	0216	0047	0019	0069	0006
O (11)	−1769 (5)	−4469 (10)	0454 (5)	0090	0246	0088	−0113	0114	−0003
O (12)	−1533 (4)	−1566 (09)	1505 (4)	0060	0244	0056	−0052	0093	−0014
O (13)	−0851 (4)	1514 (10)	2385 (4)	0066	0340	0051	−0005	0083	−0057

Description and Discussion of the Structure

The bond lengths and angles of the PMDA and STB molecules are shown in Fig. 1 and are listed in Table 3. The standard deviations are also included in the Table. Both PMDA and STB molecules have a center of symmetry. The phenyl plane of the PMDA molecule is given by this equation:

$$0.621x - 0.452y + 0.640z = 0.000, \quad (1)$$

where x, y, and z are the coordinates in Å units referred to the a, b, and c crystal axes. The maximum deviation of the atoms from this plane is 0.010 Å. The carbonyl oxygen atoms in this molecule are significantly deviated outwards by 0.061 and 0.128 Å from this plane. The plane through C(14), O(11), C(15), and O(13) is expressed as;

$$0.723x - 0.395y + 0.567z = -0.322 \quad (2)$$

and makes an angle of 7.9° with the plane given by Eq. (1). The maximum deviation of the atoms from this plane given by Eq. (2) is 0.003 Å. Similar deviations of the carbonyl groups in the PMDA molecules were observed by Herbstein *et al.* in the complexes of PMDA with perylene[3] and pyrene.[4]

The C–C bond lengths in the benzene ring of PMDA agree with the normal value within 2σ. All the bond angles of the benzene ring deviate significantly from

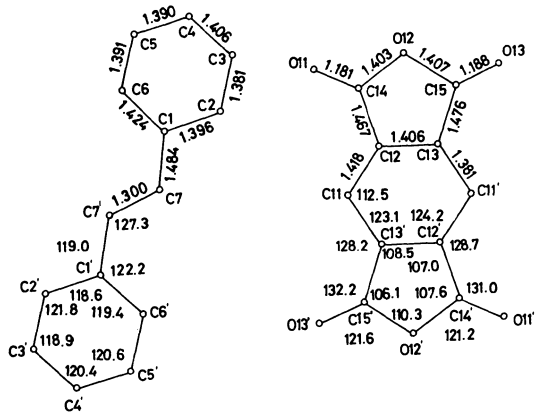

Fig. 1. Bond lengths and angles.

TABLE 3. BOND LENGTHS AND ANGLES WITH THEIR STANDARD DEVIATIONS

STB				PMDA			
C(1)–C(2)	1.396(0.012)Å	C(2)–C(1)–C(6)	118.7(0.7)°	C(11)–C(12)	1.418(0.010)Å	C(13)–C(11)–C(12)	112.6(0.4)°
C(1)–C(6)	1.424(0.012)	C(2)–C(1)–C(7)	119.0(0.5)	C(11)–C(13′)	1.381(0.011)	C(11)–C(12)–C(13)	124.2(0.5)
C(2)–C(3)	1.381(0.014)	C(6)–C(1)–C(7)	122.3(0.6)	C(12)–C(13)	1.406(0.009)	C(11)–C(12)–C(14)	128.7(0.5)
C(3)–C(4)	1.406(0.013)	C(1)–C(2)–C(3)	121.9(0.6)	C(12)–C(14)	1.467(0.011)	C(13)–C(12)–C(14)	107.1(0.6)
C(4)–C(5)	1.390(0.013)	C(2)–C(3)–C(4)	119.0(0.6)	C(13)–C(15)	1.476(0.011)	C(12)–C(13)–C(11′)	123.1(0.6)
C(5)–C(6)	1.391(0.013)	C(3)–C(4)–C(5)	120.4(0.7)	C(14)–O(11)	1.181(0.009)	C(12)–C(13)–C(15)	108.6(0.5)
C(1)–C(7)	1.484(0.012)	C(4)–C(5)–C(6)	120.6(0.6)	C(14)–O(12)	1.403(0.011)	C(11′)–C(13)–C(15)	128.2(0.5)
C(7)–C(7′)	1.300(0.012)	C(1)–C(6)–C(5)	119.5(0.6)	C(15)–O(12)	1.407(0.009)	C(12)–C(14)–O(11)	131.0(0.7)
		C(1)–C(7)–C(7′)	127.4(0.5)	C(15)–O(13)	1.188(0.009)	C(12)–C(14)–O(12)	107.7(0.4)
						O(11)–C(14)–O(12)	121.3(0.7)
						C(13)–C(15)–O(12)	106.2(0.5)
						C(13)–C(15)–O(13)	132.2(0.6)
						O(12)–C(15)–O(13)	121.6(0.7)
						C(14)–O(12)–C(15)	110.4(0.5)

the normal value of 120.0°, as in the complexes with pyrene and perylene. Such strong deviations that cause the benzene ring to destroy the six-fold symmetry were not observed even in the TCNQ and the TCNB CT complexes, but are comparable with those of the *p*-nitroaniline molecule. The bond lengths and angles in the five-membered ring of this molecule are also in accordance with those of the related complexes. The STB molecule is non-planar. The ethylene reference plane and the benzene ring plane are given by the following equations:

$$0.564x - 0.213y + 0.798z = 3.521 \quad (3)$$

and:

$$0.616x - 0.375y + 0.693z = 3.591 \quad (4)$$

respectively. The maximum deviation of the atoms from the (4) plane is 0.018 Å. The planes given by Eqs. (3) and (4) make an angle of 11.5° with each other. Robertson *et al.*[5] found that the crystal of *trans*-stilbene is composed of two kinds of STB molecules, with torsional angles of about 3° and 10° formed between the ethylene and the benzene-ring planes. The torsional angle of 11.5° observed in the STB molecule in the present complex agrees with the latter value. The H(6)···H(7′) distance of 2.1 Å coincides with the usual van der Waals contact (2.2 Å). The C(6)–C(1)–C(7) angle is significantly larger than the C(2)–C(1)–C(7) angle. This might indicate that the repulsion between hydrogen atoms plays an important role in determining the torsional angle of the molecule. The C–C bond lengths in the benzene ring of STB except for C(1)–C(6) agree with the normal value within 2σ.

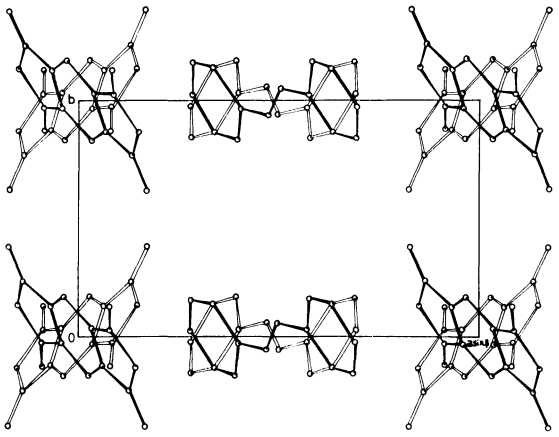

Fig. 2. The structure viewed along the c axis.

The projection of the structure viewed along the c axis is shown in Fig. 2. The crystal is composed of infinite columns in which the component molecules are alternately stacked, plane to plane, along the a axis. Each molecule is surrounded by six others in a quasi-hexagonally close-packed array. The shortest C···C, C···O, and O···O approaches between stacks are 3.64, 3.05, and 3.05 Å respectively, indicating that there are only van der Waals contacts between the stacks. In the column, one of the benzene rings of the STB molecule overlaps with the PMDA molecule related to the first by a unit translation along the *a* axis. The intermolecular contacts in the column are shown in Fig. 3. The mean plane of the PMDA molecule is given by the equation:

$$0.633x - 0.438y + 0.639z = 0.000, \quad (5)$$

and is inclined to the stack axis at an angle of 39.3°. The dihedral angle between the phenyl plane of STB and the molecular plane of PMDA is 4.8°. The average interplanar distance of 3.59 Å agrees with that observed in the crystal of the TCNB–hexamethylbenzene complex (3.54 Å)[6] and is longer than that in the crystal of graphite (3.35 Å). The shortest intermolecular contact of 3.49 Å in the stack occurs between C(4) and C(11′).

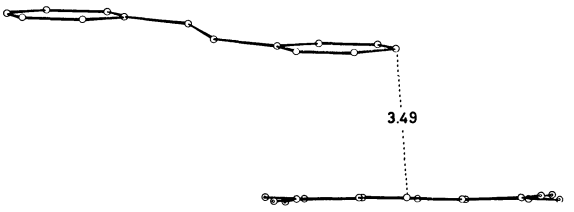

Fig. 3. Intermolecular contacts between PMDA and STB.

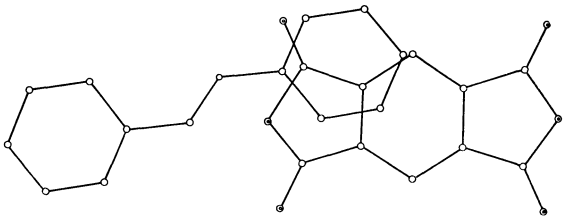

Fig. 4. The projection of STB on the molecular plane of PMDA.

A projection of the STB molecule on the molecular plane of PMDA is shown in Fig. 4. The center of the C(12′)–C(13′) bond in PMDA is superimposed on one of the C–C bonds in the phenyl group of STB adjacent to it in the stack. This relative arrangement is an interesting contrast to that observed in the crystal of the anthracene, pyrene, or perylene complexes with PMDA, in which the center of the C(12′)–C(13′) bond in PMDA is approximately superimposed on the center of the phenyl ring in the aromatic donor. The arrangements of the component molecules in these complexes seem to favor the π-π interaction between the molecules in support of the theoretical study with regard to the related complexes involving maleic anhydride as an accepter.[7] The relative arrangement observed in the present complex seems to be unfavorable for the CT interaction between the STB and the PMDA molecules. Accordingly, it may be concluded that the relative arrangment of the STB and the PMDA molecules in the crystal is mainly determined by the van der Waals interaction rather than by the CT interaction.

The authors are grateful to Professor T. Matsuo for kindly suppling the specimens. They wish also to express their sincere thanks to Professor Y. Saito, the University of Tokyo, and Professor F. Marumo, Tokyo Institute of Technology, for their helpful discussions.

The calculations were carried out on a FACOM 202 computer at the Institute for Solid State Physics and on a HITAC 5020 computer at the Computer Center of the University of Tokyo.

References

1) H. Shosenji and T. Matsuo, *Nippon Kagaku Zasshi*, **87**, 802 (1966).

2) The complete data of the F_o-F_c table are kept as document at the office of the Bulletin of the Chemical Society of Japan. (Document No. 7409)

3) J. C. A. Boeyens and F. H. Herbstein, *J. Phys. Chem.*, **69**, 2160 (1965).

4) F. H. Herbstein and J. A. Snyman, *Phil. Trans. Roy. Soc.* (London), **A264**, 635 (1969).

5) J. M. Robertson and I. Woodward, *Proc. Roy. Soc., Ser. A*, **162**, 568 (1937).

6) N. Niimura, Y. Ohashi, and Y. Saito, This Bulletin. **41**, 1815 (1968).

7) T. Kobayashi, S. Iwata, and S. Nagakura, *ibid.*, **43**, 713 (1970).

The Electronic Structures of Cu(II) Complexes as Determined by Means of the Configurational Interaction Method

Shunsuke KOBINATA

Research Laboratory of Resources Utilization, Tokyo Institute of Technology, Meguro-ku, Tokyo 152

(Received September 14, 1973)

The electronic structures of Cu(II) complexes with D_{4h} effective molecular symmetry have been investigated by means of the configurational interaction method. The locally-excited configurations of the central metal ion and the charge-transfer configurations corresponding to an electron transfer from the ligand system to the central metal ion have been taken into account. A correspondence with the crystal-field treatment has been obtained using the partitioning technique of solving the secular equation. The energies of the charge-transfer configurations, the resonance integrals, and the electrostatic contribution, D_S^{ion}, were determined so as to fit the observed d-d spectra.

There have been a number of theoretical and experimental investigations of the electronic states of transition-metal complexes. The crystal-field (CF) theory has generally been successful in the spectral assignment of the low-lying d-d spectra.[1] This method is based on an electrostatic model. On the other hand, there is much experimental evidence showing the presence of covalency between the central metal ion and the ligands.[1,2] The effect of covalency on the d-d spectra has been discussed with success in terms of a semi-empirical molecular orbital treatment based on the angular overlap model.[3,4] However, few investigations by means of the configurational interaction (CI) method have been carried out.[5] The CI method is expected to give some valuable and complemental information in this respect.

In this study the electronic structures of Cu(II) complexes with D_{4h} local symmetry were treated by means of the CI method. The physical content of the CF parameters and the nature of the bonding in these Cu(II) complexes were investigated.

Method

In the treatment of the CI method, a Cu(II) complex, CuX_4Y_2, is considered to be a composite of two component groups: a copper ion and a ligand system composed of the equatorially-coordinated ligand, X_4, and the axial ligands, Y_2. The total electronic state is described as a super-position of the various configurational wave functions:[6] the ionic configurations and the charge-transfer (CT) configurations. The ionic configurations are defined as those configurations in which the copper ion has nine valence electrons, *i.e.*, Cu^{2+}. Of the various ionic configurations, we take into account only the locally-excited configurations of the Cu^{2+} ion, which arise from the rearrangement of d-electrons, because we are primarily interested in the d-d transitions.

The wave function of an ionic configuration, which belongs to an irreducible representation, Γ, of the symmetry group D_{4h}, is given as:

$$\Phi^{ion}(\Gamma) = A\Phi_L^{ion}\Phi_M^{ion}(\Gamma) \quad (1)$$

where Φ_L^{ion} and $\Phi_M^{ion}(\Gamma)$ are the determinantal wave functions of the ligand system and the Cu(II) ion. The Φ_L^{ion} is given as:

$$\Phi_L^{ion} = |(x_1\bar{x}_1\cdots x_6\bar{x}_6)(y_1\bar{y}_1\cdots y_6\bar{y}_6)(z_1\bar{z}_1\cdots z_6\bar{z}_6)| \quad (2)$$

where x_i, y_i, and z_i are the np_x, np_y, and np_z a.o.'s of the i-th coordinated atom. The numbering of atoms and the coordinated system are shown in Fig. 1. The ns a.o. of the coordinated atom was omitted for the sake of simplicity.[7] A is the antisymmetrizer for the exchange of electrons between the ligand system and the Cu(II) ion. The energies of the ionic configurations are given, measured from the center of gravity of the $^2D(d^9)$ state of the Cu(II) ion,[8] by:

$$\begin{aligned}
&\Phi^{ion}(B_{1g}):\ E^{ion}(B_{1g}) = -2D_s^{ion} - 6D_q^{ion} + D_t^{ion}\\
&\Phi^{ion}(A_{1g}):\ E^{ion}(A_{1g}) = 2D_s^{ion} - 6D_q^{ion} + 6D_t^{ion}\\
&\Phi^{ion}(B_{2g}):\ E^{ion}(B_{2g}) = -2D_s^{ion} + 4D_q^{ion} + D_t^{ion}\\
&\Phi^{ion}(E_g):\ E^{ion}(E_g) = D_s^{ion} + 4D_q^{ion} - 4D_t^{ion}
\end{aligned} \quad (3)$$

In the CF treatment, the CF parameters, D_S^{ion}, D_q^{ion}, and D_t^{ion}, are usually determined so as to fit the observed d-d spectra, independent of their physical content. Here, they are considered to be the quantities which arise only from the effect of the ionic configurations. They are given, in the point-charge model, as:[8]

$$\begin{aligned}
D_s^{ion} &= (2/7)\langle r^2\rangle(q_e/R_e^3 - q_a/R_a^3)\\
D_q^{ion} &= (1/6)\langle r^4\rangle q_e/R_e^5\\
D_t^{ion} &= (2/21)\langle r^4\rangle(q_e/R_e^5 - q_a/R_a^5)
\end{aligned} \quad (4)$$

where q_e and q_a are the charges on the equatorially and axially coordinated atoms. R_e and R_a is the

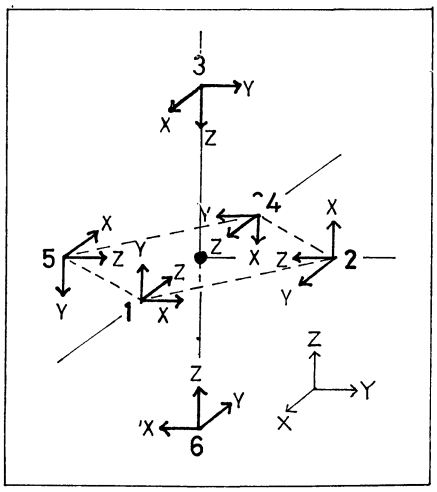

Fig. 1. Numbering and coordinate of Cu(II) complexes

distance of these atoms from the Cu(II) ion.

As to the CT configurations, we considered first those configurations which are formed by an electron transfer from the ligand system to the 3d a.o. of the Cu(II) ion (3d-CT). In these 3d-CT configurations, the copper ion has a completely filled 3d-shell. The wave function and the energy of a 3d-CT configuration, which belong to the irreducible representation of the D_{4h} symmetry group, is represented as:

$$\Phi^{CT}_{a.\delta}(\Gamma) = A\Phi^{CT}_{L.a\delta}(\Gamma)\Phi^{CT}_{M};\ E^{CT}_{a\delta}(\Gamma) \tag{5}$$

Φ^{CT}_{M} is the determinantal wave function of the copper ion of the $3d^{10}$ configuration. $\Phi^{CT}_{L.a\delta}(\Gamma)$ is the symmetry-adapted wave function of the ligand system in the 3d-CT configuration. The α and δ denote the α type of ligand and the δ type of a.o. from which an electron is transferred to the central metal ion. (α= e,a for the equatorially and axially coordinated ligand. $\delta=\sigma,\pi$ for np_z, and for np_x, np_y a.o.'s respectively) The relevant $\Phi^{CT}_{L.a\delta}(\Gamma)$'s are represented as follows:

$$\begin{aligned}
\Phi^{CT}_{L.e\sigma}(B_{1g}) &= (1/2)(z_1-z_2+z_4-z_5)\\
\Phi^{CT}_{L.a\sigma}(A_{1g}) &= (1/\sqrt{2})(z_3+z_6)\\
\Phi^{CT}_{L.e\sigma}(A_{1g}) &= (1/2)(z_1+z_2+z_4+z_5)\\
\Phi^{CT}_{L.a\pi}(E_g) &= (1/\sqrt{2})(y_3+x_6)\\
\Phi^{CT}_{L.e\pi}(E_g) &= (1/\sqrt{2})(x_2+y_5)
\end{aligned} \tag{6}$$

where z_i indicates the determinantal wave function, in which the z_i a.o. is deleted from the expression of the Φ^{ion}_{L} of Eq. (2).

The off-diagonal matrix elements between the $\Phi^{ion}_{M}(\Gamma)$ and $\Phi^{CT}_{a\delta}(\Gamma)$ are calculated by the method of Longuett-Higgins and Murrell.[6] They are expressed in terms of the diatomic resonance integrals, $\beta_{a\delta}$, between the ligand a.o. located at α position and the δ-type d-a.o. of the copper ion. They are tabulated in Table 1.

TABLE 1. OFF-DIAGONAL MATRIX ELEMENTS BETWEEN Φ^{ion} AND Φ^{CT}

$\Phi^{ion}(\Gamma)$	$\Phi^{CT}_{a\delta}(\Gamma)$	$\langle\Phi^{ion}(\Gamma)\|\mathcal{H}\|\Phi^{CT}_{a\delta}(\Gamma)\rangle$
$\Phi^{ion}(A_{1g})$	$\Phi^{CT}_{a\sigma}(A_{1g})$	$\sqrt{2}\beta_{a\sigma}$
	$\Phi^{CT}_{e\sigma}(A_{1g})$	$-\beta_{e\sigma}$
$\Phi^{ion}(B_{1g})$	$\Phi^{CT}_{e\sigma}(B_{1g})$	$\sqrt{3}\beta_{e\sigma}$
$\Phi^{ion}(B_{2g})$	$\Phi^{CT}_{e\pi}(B_{2g})$	$2\beta^{in}_{e\pi}$
$\Phi^{ion}(E_g)$	$\Phi^{CT}_{a\pi}(E_g)$	$\sqrt{2}\beta_{a\pi}$
	$\Phi^{CT}_{e\pi}(E_g)$	$\sqrt{2}\beta^{out}_{e\pi}$

The CT configurations formed by an electron transfer to 4s or 4p a.o. of the Cu(II) ion (4s-CT or 4p-CT) have the resonance interaction with all the ionic configurations of Eq. (3). It can easily be shown that these resonance interactions result in a uniform energy stabilization of the low-lying ionic configurations. Hence, these 4s-CT and 4p-CT configurations do not affect the d-a.o. splittings in a higher approximation.[5a] Therefore, we did not take the 4s-CT and 4p-CT configurations into account explicitly, for we were mainly interested in the splittings of the 3d-levels. In order to see the relationship between the CI treatment described above and the CF treatment, it is necessary first to transform the basis of the CI method (ionic and CT configurations) to the ionic configurations which appear in the CF treatment. By means of the partitioning technique,[9] the secular equation in the CI treatment is transformed to:

$$\left\{\langle\Phi^{ion}|\mathcal{H}|\Phi^{ion}\rangle - \sum_{a\delta}\frac{\langle\Phi^{ion}|\mathcal{H}|\Phi^{CT}_{a\delta}\rangle\langle\Phi^{CT}_{a\delta}|\mathcal{H}|\Phi^{ion}\rangle}{\langle\Phi^{CT}_{a\delta}|\mathcal{H}|\Phi^{CT}_{a\delta}\rangle - E(\Gamma)}\right\}c^{ion} = E(\Gamma)c^{ion} \tag{7}$$

where c^{ion} is the mixing coefficient for $\Phi^{ion}(\Gamma)$. The secular equation obtained above is different from the ordinary one in the presence of the eigenvalue, E, in the denominator. It is usually solved by an iterational procedure. When the low-lying eigenvalues, $E(\Gamma)$'s, are located in a much smaller range of energy compared with $\langle\Phi^{CT}_{a\delta}|\mathcal{H}|\Phi^{CT}_{a\delta}\rangle$, *i.e.*, when the breadth of the d-d transition energies are much smaller than the energy of the CT configurations, it can be shown that the replacement of E in the denominator of Eq. (7) by an appropriate constant, $\bar{E}$, reproduces the low-lying eigenvalues of Eq. (7) with a good accuracy. The $\bar{E}$ constant has the meaning of an averaged stabilization energy and is approximately equal to the ground-state stabilization energy. The approximation is better for larger $\bar{E}$ values, *i.e.*, for a larger covalency, if the other circumstances are same. As will be shown in the next section, the quite large value of $E^{CT}_{a\delta}-\bar{E}$ estimated by the CI treatment confirms that these conditions are fullfilled. Furthermore, the success of the CF treatment itself implies that this replacement is a good approximation.

With this replacement, the expressions of the eigenvalues are obtained as;

$$\begin{aligned}
E(B_{1g}) &= -3\gamma_{e\sigma} - 2D^{ion}_{s} - 6D^{ion}_{q} + D^{ion}_{t}\\
E(A_{1g}) &= -\gamma_{e\sigma} - 2\gamma_{a\sigma} + 2D^{ion}_{s} - 6D^{ion}_{q} + 6D^{ion}_{t}\\
E(B_{2g}) &= -4\gamma^{in}_{e\pi} - 2D^{ion}_{s} + 4D^{ion}_{q} + D^{ion}_{t}\\
E(E_g) &= -2\gamma^{out}_{e\pi} - 2\gamma_{a\pi} + D^{ion}_{s} + 4D^{ion}_{q} - 4D^{ion}_{t}
\end{aligned} \tag{8}$$

where:

$$\gamma_{a\delta} = \beta^2_{a\delta}/(E^{CT}_{a\delta}-\bar{E}) \tag{9}$$

The $\gamma^{in}_{e\pi}$ and $\gamma^{out}_{e\pi}$ are related to in-plane and out-of-plane π-bondings respectively.

When we estimate the energy splittings, a constant,

$$(4/5)\gamma_{e\sigma} + (2/5)\gamma_{a\sigma} + (4/5)\gamma^{in}_{e\pi} + (4/5)\gamma^{out}_{e\pi} + (4/5)\gamma_{a\pi} \tag{10}$$

may be added to the energy expressions of Eq. (8) so as to satisfy the center-of-gravity rule.[1b] Then, we obtain exactly the same form of energy expressions as those obtained in the CF treatment (Eq. (3)) by using the following definitions:

$$\begin{aligned}
D_s &= D^{cov}_{s} + D^{ion}_{s} = (2/7)(\gamma_{e\sigma}-\gamma_{a\sigma}) + (2/7)(2\gamma^{in}_{e\pi}-\gamma^{out}_{e\pi}-\gamma_{a\pi}) + D^{ion}_{s}\\
D_q &= D^{cov}_{q} + D^{ion}_{q} = (3/10)\gamma_{e\sigma} - (2/5)\gamma^{in}_{e\pi} + D^{ion}_{q}\\
D_t &= D^{cov}_{t} + D^{ion}_{t} = (6/35)(\gamma_{e\sigma}-\gamma_{a\sigma}) - (8/35)(2\gamma^{in}_{e\pi}-\gamma^{out}_{e\pi}-\gamma_{a\pi}) + D^{ion}_{t}
\end{aligned} \tag{11}$$

The only differences are the replacement of the D^{ion}_{s}, D^{ion}_{q}, and D^{ion}_{t} of the CF treatment by the D_q, D_s, and D_t obtained above. These differences lose all their meanings when the CF quantities are considered as parameters to be determined from the observed d-d spectra. This implies that the CF parameter treatment

gives results approximately equivalent with the CI treatment with respect to the d-d transition energies. Hence, the CF treatment is valid even in the presence of a considerable covalency.

Discussion

In the square-planar Cu(II) complexes with an *N*-coordinated ligand, such as ethylenediamine and ammonia, the effect of the axial ligand and the π-bonding of the equatorial ligand can be neglected, $\gamma_{a\sigma}=\gamma_{a\pi}=\gamma_{e\pi}^{in}=\gamma_{e\pi}^{out}=0$ in Eqs. (8) and (11). Therefore, it is apparent from Eq. (8) that $E(B_{1g})$ is the lowest energy level and $E(E_g)$ is the highest. Thus, we have obtained the same expressions of the d-d transition energies as those of Smith,[7] if $(1/5)\gamma_{e\sigma}$ in the CI treatment is replaced by the covalence parameter, σ^*, of the angular overlap model. We have studied the electronic structures of these complexes in a somewhat different manner from that of Smith.

In the case of the square-planar complexes, the $D_t^{ion}/D_q^{ion}=4/7$ and $D_t^{cov}/D_q^{cov}=4/7$ relationship hold, as may be seen from Eqs. (4) and (8) respectively. Hence, the following relationship must hold:

$$D_t/D_q = 4/7 \tag{12}$$

or, equivalently:

$$4\omega_3 = 2\omega_2 + 3\omega_1 \tag{13}$$

where ω_1, ω_2, and ω_3 are the transition frequencies from the B_{1g} ground state to the A_{1g}, B_{2g}, and E_g excited states respectively. Conversely, this relationship may be used as a criterion in the spectral assignment of the square-planar Cu(II) complexes.

In Table 2, the d-d spectra of the $Cu(NH_3)_4X_2$ and $Cu(en)_2X_2$ complexes are listed,[11] along with the D_t/D_q and D_q/D_s ratios. In these complexes the axially-ligated atom lies at a distance about 0.5—0.6 Å longer than the sum of the covalent radii of the Cu(II) ion and the ligated atom, *i.e.*, at the distance of semi-coordination.[11] However, as may be seen from Table 2, the D_t/D_q ratio for these complexes lies very near to the value, 0.57, which is expected for the square-planar complexes. This indicates that the effects of the axial covalency, $\gamma_{a\sigma}$ and $\gamma_{a\pi}$, are considerably smaller than that of the equatorial σ-bonding, $\gamma_{e\sigma}$.

To see the degree of the electrostatic and the covalent contribution to the crystal field parameters, D_s, D_q, and D_t, the D_q/D_s ratio was studied. The D_q^{ion}/D_s^{ion} ratio was estimated to be about 0.1, using in Eq. (4) the value of $\langle r^2\rangle=1.1485a_0^2$ and $\langle r^4\rangle=4.1481a_0^4$ obtained from the 3d radial function of Cu^{2+}, tabulated by Richardson *et al.*[12] The D_q^{cov}/D_s^{cov} ratio is 21/20 from Eq. (11). Hence, the D_q/D_s ratio is expected to be of the order of 0.1 or 1.05, depending on whether the electrostabic or the covalent part is the main factor in determining the values of D_q and D_s. As is shown in Table 2, the experimentally-obtained D_q/D_s ratio lies near 0.73 for *N*-coordinated complexes. This value indicates that D_s^{ion} makes a rather large contribution to D_s, because D_q^{ion} is known to be much smaller than D_q^{cov}.

CI Calculation. To make the situation clear, we investigated the $Cu(en)_2(SCN)_2$ complex as a typical example by means of the CI method. Because this complex has a rather long axial distance (R_e=2.00 Å and R_a=3.27 Å),[11] the effect of axial covalency can be neglected; *i.e.*, $\beta_{a\sigma}=\beta_{a\pi}=0$. The D_q^{ion}/D_s^{ion} and D_t^{ion}/D_q^{ion} ratios were assumed to be equal to 0.1 and 0.57 respectively, following the discussion of the preceding subsection. With these approximation, the number of the unknown CI parameters is reduced to three, $\beta_{e\sigma}$, $E_{e\sigma}^{CT}$, and D_s^{ion}. These three CI parameters were determined so as to reproduce the three observed d-d spectra. The results are shown in Table 3. As is shown in Table 3, the contribution of D_q^{ion} and D_t^{ion} to D_q and D_t is rather small. This seems reasonable because, in octahedral complexes, it is generally recognized that the CF splitting, $10D_q$, is mainly caused by the effect of the covalency.[13]

Table 3. The result of the CI calculation on $Cu(en)_2(NCS)_2$.

	Obsd	Calcd
$\omega_1(A_{1g}\leftarrow B_{1g})$	14.7 kK	14.7 kK
$\omega_2(B_{2g}\leftarrow B_{1g})$	17.2 kK	17.2 kK
$\omega_3(E_g\leftarrow B_{1g})$	20.3 kK	20.3 kK
		$\beta_{e\sigma}=-3.00$ eV
		$E_{e\sigma}^{CT}=11.17$ eV
	$D_s=2.54$ kK	$D_s^{ion}=1.12$ kK
	$D_q=1.72$	$D_q^{ion}=0.11$
	$D_t=0.91$	$D_t^{ion}=0.06$

On the other hand, the contribution of $D_s^{ion}=1.12$ kK to $D_s=2.54$ kK is large and comparable with that of $D_s^{cov}=1.42$ kK, as was expected in the preceding subsection. Smith has obtained the value of $D_s^{ion}=0.72$ for $Cu(NH_3)_4(SCN)_2$ by estimating the effective charges q_e, of Eq. (4).[7] Our method of estimation seems to be superior to that of Smith in that it does not make use of q_e.

As to the energy of the charge-transfer configuration, the value of $E_{e\sigma}^{CT}=11.17$ eV was obtained. This suggests,

Table 2. The d-d transition frequencies and the ratios D_t/D_q and D_q/D_s. (Unit of R_a and ω_i is Å and kK respectively)

		R_a	ω_1	ω_2	ω_3	D_t/D_q	D_q/D_s
1	$Cu(en)_2H_g(NCS)_2$	N-2.58	13.5	16.8	17.9	0.68	0.80
2	$Cu(en)_2(NO_3)_2$	O-2.59	14.1	17.9	19.7	0.56	0.78
3	$Cu(en)_2(NCS)_2$	S-3.27	14.7	17.2	20.3	0.53	0.68
4	$Cu(en)_2(BF_4)_2$	F-2.56	16.8	18.0	20.1	0.67	0.67
5	$Cu(NH_3)_4(NO_3)_2$	N-2.65	13.4	16.2	17.1	0.65	0.79
6	$Cu(NH_3)_4(SCN)_2$	S-3.00	14.3	15.7	17.5	0.65	0.68

TABLE 4. THE d-d TRANSITION FREQUENCIES AND THE RATIOS D_t/D_q AND D_q/D_s OF SOME *O*-COORDINATED COMPLEXES

		R_a	ω_1	ω_2	ω_3	D_t/D_q	D_q/D_s
1	$Na_2Cu(SO_4)_2 2H_2O$	O-2.41	10.3	10.3	12.7	0.59	0.57
2	$Pb_2Cu(OH)_4Cl_2$	Cl-2.75	10.9	10.9	14.6	0.47	0.52
3	$Cu(UO_2)_2(AsO_4)_2 8H_2O$	O-2.55	13.0	12.0	15.0	0.64	0.52
4	$Cu(SO_4)5H_2O$	O-2.40	10.5	10.5	13.0	0.58	0.56
5	$BaCuSi_4O_{10}$	Cu-7.56	18.8	12.9	15.8	1.00	0.41

that the CT state is the state of the strong mixing of CT and the appropriate locally-excited configurations, because the CT band can be expected at about 6—7 eV.[13]

As to the diatomic resonance integral, $\beta_{e\sigma}$, the value of −3.00 eV was obtained. In the Wolfsberg-Helmholz approximation,[18] $\beta_{e\sigma}$ is estimated to be:

$$\beta_{e\sigma} = -(1/2)F_\sigma S_{e\sigma}(I(Cu^{2+})+I(N)) \qquad (14)$$

where $S_{e\sigma}$ is the diatomic overlap integral between $3d_{x^2-y^2}$ a.o. and $2p_z$ a.o. of the ligand atom. $I(Cu^{2+})$ and $I(N)$ are the valence-state ionization potentials of the Cu^{2+} ion and nitrogen respectively. The F_σ constant is usually assumed to be 1.67.[18] Then, Eq. (14) gives $\beta_{e\sigma}=-3.54$ eV, using $S_{e\sigma}=0.0826$,[7] $I(Cu^{2+})=36.8$ eV, and $I(N)=14.5$ eV.

Using the values tabulated in Table 3 in Eq. (9), we obtain $\bar{E}=-3.44$ eV. Hence, $E_{e\sigma}^{CT}-\bar{E}$ amounts to 14.61 eV. This large value of $E_{e\sigma}^{CT}-\bar{E}$ compared with that of the d-d transition energies guarantees the validity of the replacement, $\bar{E}$, in the energy denominator to a constant, $\bar{E}$, obtained in the preceding section (Eq. (9)).

π-Bonding. In the case of Cu(II) complexes with the ligand which has a potency of the π-bonding, the treatment is complicated by the fact that we can no longer neglect $\gamma_{e\pi}^{in}$ and $\gamma_{e\pi}^{out}$ of Eqs. (8) and (11).

When the $\gamma_{e\pi}^{in}=\gamma_{e\pi}^{out}=\gamma_{e\pi}$ and $\gamma_{a\sigma}=\gamma_{a\pi}=0$ relations hold, as in $Pt(NH_3)_4CuCl_4$, Eq. (8) give same energy expressions as those of Smith by equating the covalency factors, σ* and π*, of the angular overlap model with $(1/5)\gamma_{e\sigma}$ and $(1/5)\gamma_{e\pi}$ respectively.[14] It is shown Eqs. (12) and (13) should also hold in this case. For $Pt(NH_3)_4CuCl_4$, we obtain $D_t/D_q=0.67$ and $D_q/D_s=0.43$ or $D_t/D_q=0.60$ and $D_q/D_s=0.75$, according to whether we use the assignment of Smith ($\omega_2<\omega_1<\omega_3$) or that of Hatfield and Piper ($\omega_1<\omega_2<\omega_3$)[15] respectively. The D_t/D_q ratio lies in the range of errors of Eq. (12) for both assignments. We can estimate $\gamma_{e\sigma}=(1/4)\gamma_{e\pi}$,[14] because the Wolfsberg-Helmholz relation holds approximately, as has been seen in the preceding subsection. Therefore, the D_q/D_s ratio can be expected from Eq. (11) to lie in the 0.1—0.6 range. It seems that the assignment of Smith is more reliable.

In Table 4, the d-d transition frequencies and the D_t/D_q and D_q/D_s ratios of the *O*-coordinated complexes with known crystal structures are listed. These complexes have distance longer by over 0.4 Å for the axial ligand than for the equatorial ligands.[11,16] As may be seen from Table 4, the $D_t/D_s=0.55\pm0.08$ ratios for these complexes coincide approximately with the value, 0.57, which is expected for the square-planar case, except in the case of $BaCuSi_4O_{10}$. The D_q/D_s ratio is 0.59 ± 0.08, somewhat smaller than the value for *N*-coordinated complexes, $D_q/D_s=0.73\pm0.06$. This indicates the presence of π-bonding, according to Eq. (11).

For the silicate $BaCuSi_4O_{10}$, the $D_t/D_q=1.0$ ratio was obtained following to the assignment of Clark and Burns[17] (Table 4). This high value seems unreasonable, because this complex has a complete square-planar structure ($R_e=1.91$ Å, $R_a=7.56$ Å), and because the *g*-tensor of this complex does not exhibit any abnormality compared with other complexes.[11,16] Hence, The $D_t/D_q=0.57$ ratio of square-planar complex can be expected to be fulfilled. The assignment of Clark and Burns does not seem to be very conclusive, however, because it has been made without a complete analysis of the polarized single-crystal spectrum. Another possible set of assignments which fulfills the relation of Eq. (12) is $\omega_1=15.8$ kK (or 12.9 kK), $\omega_2=12.9$ kK (or 15.8 kK), and $\omega_3=18.8$ kK. This assignment results in $D_t/D_q=0.53$ (or 0.48) and $D_q/D_s=0.42$ (or 0.70).

References

1) a) C. J. Ballhausen, "Introduction to Ligand Field Theory" McGraw-Hill, London-New York, 1962. b) H. I. Schläfer and G. Glieman, "Basic Principles of Ligand Field Theory," Wiley-Interscience, 1966.

2) J. Owen, *Proc. Roy. Soc., Ser. A*, **227**, 183 (1955).

3) C. K. Jørgensen, R. Pappalardo, and H. H. Schmidtke, *J. Chem. Phys.*, **39**, 1422, (1963).

4) C. E. Schäffer and C. K. Jφrgensen, *Mol. Phys.*, **9**, 401 (1965).

5) a) J. Hubbard, D. E. Rimmer, and F. R. A. Hopgood, *Proc. Phys. Soc.*, **88**, 13 (1966). b) I. Hanazaki, F. Hanazaki, S. Nagakura, *J. Chem. Phys.*, **50**, 265 (1969).

6) H. C. Lönguett-Higgins and Murrell, *Proc. Phys. Soc.*, **68A**, 601 (1955).

7) D. W. Smith, *J. Chem. Soc., A*, 1708 (1969).

8) Ref. 1-b, p. 343.

9) P. O. Löwdin, *J. Mol. Spectry*, **10**, 12 (1963) and *J. Math. Phys.*, **3**, 969 (1962).

10) A. B. P. Lever, *Coord. Chem. Rev.*, **3**, 117 (1968).

11) B. J. Hathaway and D. E. Billing, *ibid.*, **5**, 143 (1970).

12) J. W. Richardson, W. C. Nieuwpoort, and W. F. Edgell, *J. Chem. Phys.*, **36**, 1057 (1962).

13) C. K. Jφrgensen, "Orbitals in Atoms and Molecules" Academic Press, London-New York (1962).

14) D. W. Smith, *J. Chem. Soc., A*, **1969**, 2529.

15) D. W. Hatfield and T. S. Piper, *Inorg. Chem.*, **3**, 841 (1964).

16) D. E. Billing, B. J. Hathaway, and P. Nicholls, *J. Chem. Soc., A*, **1969**, 316.

17) M. G. Clark and R. G. Burns, *ibid.*, **1967**, 1034.

18) M. Wolfsberg and L. Helmholz, *J. Chem. Phys.*, **20**, 837 (1952).

Mechanisms of Hydrogenation and Hydrogen Exchange of Propylene over the Electron Donor-Acceptor Complexes of Polynaphthoquinones with Potassium

Yasuhiro IWASAWA, Sadao OGASAWARA, Takaharu ONISHI,* and Kenzi TAMARU*

Department of Applied Chemistry, Yokohama National University, Ooka-cho, Minami-ku, Yokohama 233

**Department of Chemistry, the University of Tokyo, Hongo, Bunkyo-ku, Tokyo 113*

(Received September 25, 1973)

The mechanisms of the deuterium addition to propylene and the propylene-deuterium exchange reaction over the electron donor-acceptor (EDA) complex of polynaphthoquinone with potassium were investigated by means of mass and microwave spectrometry and gas chromatography in the range from room temperature to 200 °C. The hydrogenation as well as the exchange reaction proceeded *via* the half-hydrogenated state of propylene formed from the adsorbed propylene and the dissociatively-adsorbed deuterium atom on the EDA complex. However, the rate of the exchange reaction decreased upon the Fe addition to the complex, while the hydrogenation was markedly accelerated. The intermediate of the propylene-deuterium exchange reaction was determined to be the half-hydrogenated isopropyl species, whereas the deuterium addition to propylene was suggested to occur *via* another half-hydrogenated state, the *n*-propyl species.

The electron donor-acceptor (EDA) complex of the polynaphthoquinone with potassium exhibits high activities for various catalytic reactions, such as the H_2–D_2 exchange reaction, the isomerization of butene, and the synthesis of ammonia from a mixture of nitrogen and hydrogen, as was reported in a previous paper.[1] The EDA complex also readily catalyzes the hydrogen exchange of propylene with deuterium. It was concluded[1,2] by means of the microwave technique[3] that the half-hydrogenated state of propylene, the isopropyl species, is the reaction intermediate in the propylene-deuterium exchange reaction. The rate of the hydrogenation of propylene with hydrogen was expressed by the following equation: $v=k(\text{propylene})(H_2)^{1/2}$, indicating that the half-hydrogenated state may also be the reaction intermediate in the hydrogenation reaction.

However, it does not follow that the hydrogenation or deuterogenation of propylene also proceeds through the half-hydrogenated state of isopropyl species. In other words, the reaction intermediates of the hydrogenation and the exhange reaction are not necessarily the same half-hydrogenated state, even if both reactions will follow the same rate equation.

In the present experiment, the mechanisms of the deuterium addition to propylene and the exchange reaction of propylene with deuterium over the EDA complex of potassium with the polynaphthoquinone were investigated in detail, and the intermediates of the deuterium addition to propylene were examined by means of mass and microwave spectrometries and gas chromatography.

Experimental

The polynaphthoquinone employed was obtained by oxidizing 1,7-naphthalenediol with nitric acid in air, followed by treating at 350 °C for 12 hr, as was reported in a previous paper.[4] The polynaphthoquinone containing $FeCl_3$ was prepared by mixing metal-free polynaphthoquinone and $FeCl_3$ (15 wt% against polynaphthoquinone) in ethyl alcohol and then evaporating the solvent. The polynaphthoquinones thus obtained were treated at 350 °C for 6 hr *in vacuo* before use. The EDA catalysts were prepared by adding potassium vapour to the polynaphthoquinones in the absence of air. The composition of the EDA complex was found to be one potassium monomer to three naphthoquinone monomers.

The reactions were carried out over the EDA complex including 0.1 g of the polynaphthoquinone in a closed circulating system (175 cm^3). The rate of the propane formation by the hydrogenation of propylene was determined by gas chromatography, while the deuterated propylene formed by the exchange reaction of propylene with deuterium was quantatively analyzed by mass and microwave spectroscopy. The mass spectroscopy was also used for analyzing the deuterated propane.

Results and Discussion

The Mechanism of the Propylene-deuterium Exchange Reaction. The exchange reaction of propylene with deuterium over the EDA complex of potassium with the polynaphthoquinone was studied by means of the microwave technique in the range from room temperature to 200 °C. The rate of the formation of deuteriopropylene was determined by mass spectrometry. The formation of deuteriopropylene is plotted against the reaction time in Fig. 1; the figure shows that hydrogen in propylene successively exchanges with deuterium over the EDA catalyst.

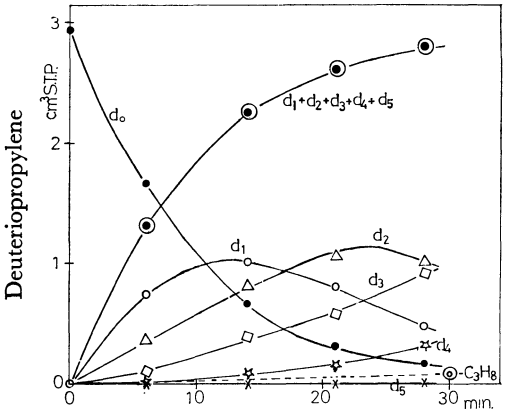

Fig. 1. Amounts of deuteriopropylenes, produced by the hydrogen exchange of propylene (1.4 cmHg) with deuterium (3.4 cmHg), against reaction time at 95 °C.

According to microwave spectrometry, three kinds of monodeuteriopropylenes, CHD=CH–CH_3(*cis*-1-d_1 and *trans*-1-d_1) and CH_2=CH–CH_2D(propylene-3-d_1), were produced in an approximate ratio of 1 : 1 : 3, and the propylene-d_2 species formed were 1,1-d_2, 3,3-d_2, and 1,3-d_2, in the approximate ratio of 1 : 3 : 6. It is concluded from these results[2] that the half-hydrogenated isopropyl species is the main reaction intermediate of the hydrogen exchange reaction over the EDA complex in the range from room temperature to 200 °C.

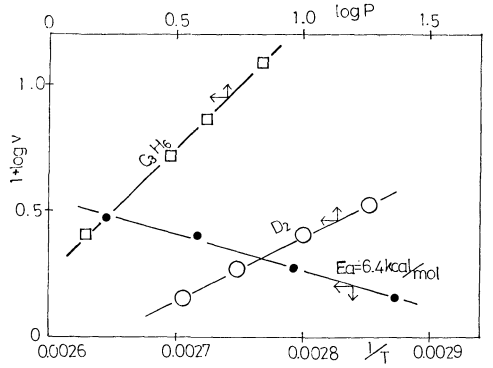

Fig. 2. Dependence of the rate of the exchange reaction upon the pressures of propylene and deuterium at 75 °C and the activation energy of the reaction.

The rate of the propylene-d_1 formation was found to be of the first-order with respect to the partial pressure of propylene and half-order with respect to the deuterium pressure as is shown in Fig. 2, where the activation energy is also given as 6.4 kcal/mol. A very small amount of propylene was reversibly adsorbed on the 1.0 g EDA complex, while the adsorption of deuterium was not appreciable under similar conditions. It was indicated in a previous paper[2] that HD in the H_2–D_2 exchange reaction was produced from hydrogen and deuterium atoms dissociated from each of the gases on the catalyst surface. The half-hydrogenated state of the isopropyl species, as the reaction intermediate, may be formed from the surface reaction of the adsorbed propylene with the deuterium atom dissociatively adsorbed on the EDA catalyst.

Consequently, the scheme of the propylene-deuterium exchange reaction may be expressed as follows;

$$C_3H_6(g) \overset{K_1}{\rightleftharpoons} C_3H_6(ad) \quad (1)$$

$$D_2(g) \overset{K_2}{\rightleftharpoons} 2D(ad) \quad (2)$$

$$C_3H_6(ad) + D(ad) \underset{k_3'}{\overset{k_3}{\rightleftharpoons}} CH_2D\text{–}\overset{*}{C}H\text{–}CH_3 \quad (3)$$

$$CH_2D\text{–}\overset{*}{C}H\text{–}CH_3 \xrightarrow{k_4} \underline{C_3H_5D}(ad) + H(ad) \quad (4)$$

where $CH_2D\text{–}\overset{*}{C}H\text{–}CH_3$ and C_3H_5D represent the half-hydrogenated state of the isopropyl species and monodeuteriopropylene(*cis*-1-d_1, *trans*-1-d_1 or 3-d_1) respectively.

The rate in the initial stage of the hydrogen exchange reaction is given as follows in the steady state according to the ordinary procedures:

provided $(C_3H_6)_{ad}=K_1(C_3H_6)_g$ and $(D)_{ad}=K_2^{1/2}(D_2)_g^{1/2}$, where $(C_3H_6)_{ad}$ and $(D)_{ad}$ were very small in amount,

$$d(CH_2D\text{–}\overset{*}{C}H\text{–}CH_3)/dt = k_3(C_3H_6)_{ad}(D)_{ad} - k_3'(CH_2D\text{–}\overset{*}{C}H\text{–}CH_3) - k_4(CH_2D\text{–}\overset{*}{C}H\text{–}CH_3) = 0,$$

$$\therefore\ (CH_2D\text{–}\overset{*}{C}H\text{–}CH_3) = (k_3/(k_3'+k_4))(C_3H_6)_{ad}(D)_{ad},$$

$$v_{ex} = d(C_3H_5D)/dt = k_4(CH_2D\text{–}\overset{*}{C}H\text{–}CH_3) = (k_3k_4/(k_3'+k_4))(C_3H_6)_{ad}(D)_{ad} = \frac{k_3k_4}{k_3'+k_4}K_1K_2^{1/2}(C_3H_6)_g(D_2)_g^{1/2} = k_{ex}(C_3H_6)_g(D_2)_g^{1/2}.$$

The rate constant for the exchange reaction, k_{ex}, is, consequently, equal to $k_3k_4K_1K_2^{1/2}/(k_3'+k_4)$.

Therefore, the exchange reaction between propylene and deuterium may be interpreted as proceeding between the adsorbed propylene and the dissociatively-adsorbed deuterium *via* the half-hydrogenated state, the isopropyl species, as the reaction intermediate, as is shown in Steps (3) and (4).

The Mechanism and the Reaction Intermediate of the Hydrogenation of Propylene. The hydrogenation of propylene to form propane proceeded over the EDA complex of potassium with the polynaphthoquinone in the temperature range from 70 to 200 °C. As is shown in Fig. 3, the rate of the deuterogenation was found to be proportional to the partial pressure of propylene and to be half-order with respect to the deuterium pressure: $d(propane)/dt=k_d(propylene)_g(D_2)_g^{1/2}$. Accordingly, the overall reaction may be expressed as follows:

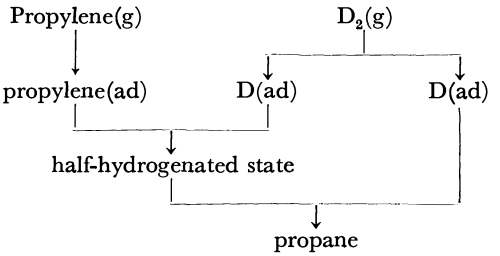

The hydrogenation of propylene to propane proceeded with hydrogen more easily by a factor of about 1.4 than with deuterium at 140 °C. The activation energy

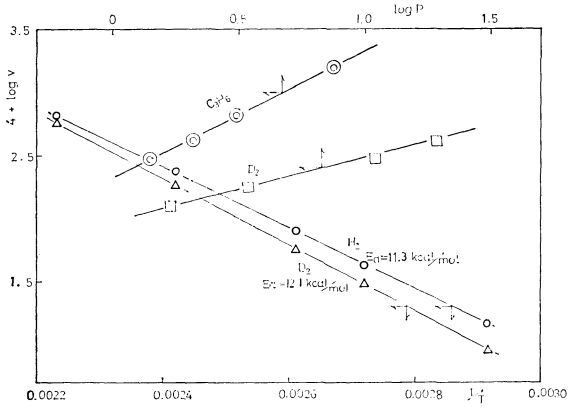

Fig. 3. Dependence of the deuterogenation upon pressures of propylene and deuterium at 140 °C and the activation energies of the reactions.

Table 1. The rates and the activation energies of reactions over the EDA catalysts

EDA catalysts[a)]	Initial rate of the monodeuterio-propylene formation (1-d_1 and 3-d_1) at 95 °C (cm^3/min)	Activation energy (kcal/mol)	Initial rate of the propane formation[c)] at 140 °C (cm^3/min)	Activation energy (kcal/mol)	Initial rate of the propylene-2-d_1 formation[c)] at 140 °C (cm^3/min)
Q–K complex	0.40	6.4	0.027	12.1	0.010
Q–$FeCl_3$–K complex	0.20	6.6	0.123	4.7	0.010

a) Q: polynaphthoquinone. b) propylene=1.4 cmHg, D_2=10 cmHg. c) propylene=1.4 cmHg, D_2=5.6 cmHg.

for the hydrogenation reaction was found to be 11.3 kcal/mol, as is given in Fig. 3.

It was confirmed in Section (1) that the half-hydrogenated state (isopropyl species) is the reaction intermediate in the hydrogen-exchange reaction of propylene with deuterium. When the deuterium addition to propylene also proceeds through the same reaction intermediate, propane will be produced by the following process (5):

$$CH_2D\text{–}\underset{*}{CH}\text{–}CH_3 + D(ad) \xrightarrow{k_5} C_3H_6D_2 \qquad (5)$$

When propane is formed by the deuterium-atom addition to the half-hydrogenated isopropyl species in Eq. (5), the rate equation in the initial stage of the reaction may be expressed as follows:

In the steady state;

$$d(CH_2D\text{–}\underset{*}{CH}\text{–}CH_3)/dt = k_3(C_3H_6)_{ad}(D)_{ad} - (k_3'+k_4)(CH_2D\text{–}\underset{*}{CH}\text{–}CH_3) - k_5(CH_2D\text{–}\underset{*}{CH}\text{–}CH_3)(D)_{ad} = 0,$$

$$(CH_2D\text{–}\underset{*}{CH}\text{–}CH_3) = \frac{k_3(C_3H_6)_{ad}(D)_{ad}}{k_3'+k_4+k_5(D)_{ad}},$$

Accordingly,

$$d(C_3H_6D_2)/dt = k_5(CH_2D\text{–}\underset{*}{CH}\text{–}CH_3)(D)_{ad} = \frac{k_3k_5(C_3H_6)_{ad}(D)_{ad}^2}{k_3'+k_4+k_5(D)_{ad}}.$$

The propylene-deuterium exchange reaction proceeded much more rapidly than the deuterogenation, as is shown in Fig. 1; that is, $k_4 \gg k_5(D)_{ad}$, or $k_3'+k_4 \gg k_5(D)_{ad}$. Accordingly, the rate of the formation of propane, $d(C_3H_6D_2)/dt$, is reduced to $(k_3k_5/(k_3'+k_4))(C_3H_6)_{ad}(D)_{ad}^2$. For $(C_3H_6)_{ad}=K_1(C_3H_6)_g$ and $(D)_{ad}=K_2^{1/2}(D_2)_g^{1/2}$, the rate is given by $(k_3k_5/(k_3'+k_4))K_1K_2(C_3H_6)_g(D_2)_g$ or, accordingly, $k'(C_3H_6)_g(D_2)_g$, where k' is equal to $(k_3k_5/(k_3'+k_4))K_1K_2$. However, the rate equation thus obtained is in disagreement with the experimental results given in Fig. 3, where the initial rate of the propane formation is first-order with respect to propylene and half-order with respect to the deuterium pressure, which excludes the mechanism of the deuterium addition through the half-hydrogenated isopropyl species in Reaction Step (5).

Though the hydrogen-exchange reaction of propylene with deuterium took place through the half-hydrogenated state, the isopropyl species, propylene-2-d_1 (CH_2=CD–CH_2) could also be observed in the temperature range higher than 70 °C. Table 1 shows the results on the EDA complexes of potassium with the polynaphthoquinone both with and without $FeCl_3$, exhibiting that another half-hydrogenated state, the normal propyl species, is present on the surface of the EDA catalyst throughout the reaction.

If the half-hydrogenated state of the normal propyl species is the reaction intermediate in the deuterogenation of propylene, the scheme of the reaction may be expressed as follows:

$$C_3H_6(ad) + D(ad) \underset{k_6'}{\overset{k_6}{\rightleftharpoons}} \underset{*}{CH_2}\text{–}CHD\text{–}CH_3 \qquad (6)$$

$$\underset{*}{CH_2}\text{–}CHD\text{–}CH_3 \xrightarrow{k_7} CH_2\text{=}CD\text{–}CH_3(ad) + H(ad) \qquad (7)$$

$$\underset{*}{CH_2}\text{–}CHD\text{–}CH_3 + D(ad) \xrightarrow{k_8} \underline{C_3H_6D_2} \qquad (8)$$

$$2\underset{*}{CH_2}\text{–}CHD\text{–}CH_3 \xrightarrow{k_9} \underline{C_3H_6D_2} + CH_2\text{=}CH\text{–}CH_3 \quad \underline{C_3H_7D} + CH_2\text{=}CD\text{–}CH_3 \qquad (9)$$

where $\underset{*}{CH_2}$–CHD–CH_3 represents the half-hydrogenated state of the normal propyl species adsorbed on the EDA catalyst. Step (8) shows that propane is produced successively from the half-hydrogenated normal propyl species and the adsorbed deuterium atom, while the propane formation by the disproportionation of the normal propyl species adsorbed on the EDA catalyst is given in Step (9).

When propane is produced successively *via* Reaction Steps (6) and (8) through the half-hydrogenated normal propyl species under the condition of a negligible hydrogen exchange, propane-d_2 ($C_3H_6D_2$) should be the only product in the deuterogenation of propylene (C_3H_6) and the formation of propane-d_1 (C_3H_7D) will not be appreciable. Propylene-d_5 (CD_2=CH–CD_3) was employed to examine clearly the deuterium content in the deuterated propane, where CD_2=CH–CD_3 remained unchanged by the rapid exchange reaction with deuterium through the isopropyl species and where the amount of the CD_2=CD–CD_3 formation through the normal propyl species was small under the present reaction conditions. The main product in the deu-

Table 2. The formation of deuterated propane in the deuterogenation of C_3HD_5 at 140 °C

EDA catalysts	The relative ratio in deuterated propane		
	$C_3H_2D_6$ (propane-d_1)	C_3HD_7 (propane-d_2)	C_3D_8 (propane-d_3)
Q–K complex	2%	81%	17%
Q–$FeCl_3$–K complex	2%	92%	6%

terium addition to CD_2=CH–CD_3(C_3HD_5) was found to be C_3HD_7, as is shown in Table 2; a small amount of C_3D_8 was also produced from the deuterium addition to CD_2=CD–CD_3, CD_2=CD–CD_3 being formed by the propylene-d_5—deuterium exchange reaction *via* the normal propyl species. Reaction Process (9) may, consequently, be excluded.

Accordingly, the initial rate of the formation of propane may be given by the following equation:

In the steady state, the *n*-propyl species on the surface stays constant,

$$\mathrm{d}(\overset{*}{\mathrm{CH_2}}\text{–CHD–}\mathrm{CH_3})/\mathrm{d}t = k_6(\mathrm{C_3H_6})_{\mathrm{ad}}(\mathrm{D})_{\mathrm{ad}} - (k_6'+k_7)(\overset{*}{\mathrm{CH_2}}\text{–CHD–}\mathrm{CH_3}) - k_8(\overset{*}{\mathrm{CH_2}}\text{–CHD–}\mathrm{CH_3})(\mathrm{D})_{\mathrm{ad}} = 0,$$

$$\therefore\ (\overset{*}{\mathrm{CH_2}}\text{–CHD–}\mathrm{CH_3}) = \frac{k_6(\mathrm{C_3H_6})_{\mathrm{ad}}(\mathrm{D})_{\mathrm{ad}}}{k_6'+k_7+k_8(\mathrm{D})_{\mathrm{ad}}},$$

$$v_{\mathrm{d}} = \mathrm{d}(\mathrm{C_3H_6D_2})/\mathrm{d}t = k_8(\overset{*}{\mathrm{CH_2}}\text{–CHD–}\mathrm{CH_3})(\mathrm{D})_{\mathrm{ad}} = \frac{k_6k_8(\mathrm{C_3H_6})_{\mathrm{ad}}(\mathrm{D})_{\mathrm{ad}}^2}{k_6'+k_7+k_8(\mathrm{D})_{\mathrm{ad}}}.$$

The rates of the deuterogenation were found to be larger than those of the propylene-2-d_1 formation by a factor of 2.7 on the Fe-free complex (Q–K complex) and by one of 12.3 over the Fe-containing complex (Q–$FeCl_3$–K complex), as is shown in Table 1. The difference in the values of k'_6 and k_7 corresponds to the isotope effect, and k_6' seems to be smaller than k_7. These observations lead to the $(k_6'+k_7)<k_8(\mathrm{D})_{\mathrm{ad}}$ relation. Accordingly, the rate equation is reduced as follows:

$$v_{\mathrm{d}} = k_6(\mathrm{C_3H_6})_{\mathrm{ad}}(\mathrm{D})_{\mathrm{ad}} = k_6K_1K_2^{1/2}(\mathrm{C_3H_6})_{\mathrm{g}}(\mathrm{D_2})_{\mathrm{g}}^{1/2},$$

$$\text{provided}\ (\mathrm{C_3H_6})_{\mathrm{ad}} = K_1(\mathrm{C_3H_6})_{\mathrm{g}}\ \text{and}\ (\mathrm{D})_{\mathrm{ad}} = K_2^{1/2}(\mathrm{D_2})_{\mathrm{g}}^{1/2}.$$

The rate equation is in agreement with the results, suggesting that the formation of propane occurs *via* the half-hydrogenated normal propyl species in Reaction Steps (6) and (8).

On the Fe-containing complex as well as over the Fe-free complex the half-hydrogenated state of propylene, the isopropyl species, was found to be the reaction intermediate of the propylene-deuterium exchange. As is given in Table 1, the activation energy of the exchange reaction was much less affected by the Fe addition to the complex. However, the activation energy of the deuterogenation markedly decreased upon the Fe addition. The value, 4.7 kcal/mol, for the deuterogenation of propylene was also smaller than that for the propylene-deuterium exchange reaction. The rate of the deuterium addition to propylene, $v_{\mathrm{d}}'=k_{\mathrm{d}}'(\mathrm{propylene})_{\mathrm{g}}(\mathrm{D_2})_{\mathrm{g}}^{1/2}$, was markedly accelerated by the Fe addition to the complex. Consequently, the difference in the effect of the Fe addition on the propylene-deuterium exchange and the deuterium addition to propylene was observed, also suggesting that the hydrogenation and the hydrogen exchange of propylene over the EDA complexes of the polynaphthoquinones proceed through different half-hydrogenated states of propylene.

Consequently, the hydrogen-exchange reaction of propylene with deuterium proceeded through the half-hydrogenated state of isopropyl species, while the half-hydrogenated state of normal propyl species was indicated to be the reaction intermediate in the hydrogenation of propylene. It is of interest to note that the half-hydrogenated state is the reaction intermediate in both the propylene-deuterium exchange and the deuterogenation of propylene over the EDA complexes of potassium with the polynaphthoquinones, but that the former reaction proceeds through the half-hydrogenated state, the isopropyl species, and the latter, through another half-hydrogenated state, the normal propyl species.

The authors wish to thank Mr. T. Kondo for his advice on and discussion of the microwave and mass spectroscopies, and Dr. K. Fukuda for his advice on the mass spectroscopy.

References

1) Y. Iwasawa, T. Onishi, and K. Tamaru, *Chem. Commun.*, **1972**, 1051.
2) Y. Iwasawa, H. Fujitsu, T. Onishi, and K. Tamaru, *J. Chem. Soc. Faraday Trans. I*, **70**, 202 (1974).
3) K. Tamaru, *Ann. N. Y. Acad. Sci.*, **213**, 161 (1973).
4) Y. Iwasawa, M. Soma, T. Onishi, and K. Tamaru, *J. Chem. Soc. Faraday Trans. I*, **68**, 1617 (1972).

Polarographic Studies of Dispersed Dyes Solubilized in Surfactant Solutions. I. Kinetics of Orange OT Solubilized in Surfactant Solutions

Hajime SUZUKI, Noriko SHINOZUKA, and Shigeo HAYANO
Institute of Industrial Science, The University of Tokyo, Roppongi, Minato-ku, Tokyo 106
(Received October 13, 1973)

Orange OT (1-*o*-tolyl-azo-2-naphthol) dissolved in an aqueous ethanol solution and solubilized in various surfactant solutions, containing a citric acid-disodium hydrogen phosphate buffer, showed well-defined irreversible polarographic waves. The anionic, cationic, and nonionic surfactants used were sodium dodecyl sulfate (SDS) and sodium dodecylbenzenesulfonate (SDBS), dodecyltrimethylammonium chloride (DTMAC), and polyoxyethylene nonylphenyl ether (NP-$\overline{10}$) respectively. The values multiplying the transfer coefficient by the number of electrons involved in the activation step, (αn_a), were calculated from the semilogarithmic plot of the wave. The plots of αn_a against the half-wave potential of Orange OT for each solution showed that a marked surfactant electric-charge dependence of αn_a was observed with a variety of surfactant solutions; *i.e.*, the electric-charges of the surfactant molecules or micelles remarkably affected the electrode kinetics of the solubilized Orange OT. No matter what Orange OT is an uncharged species, Orange OT solubilized in the anionic surfactant solutions seemed to behave in the electrode process as if it were an anionic species, and when solubilized in the cationic and nonionic surfactant solutions it seemed to behave as a cationic species.

The electrochemistry of dispersed dyes solubilized in several surfactant solutions has been described in previous papers,[1-3] mainly with regard to the mass-transfer of the micelle. Many electrochemical studies[4-6] of surfactant solutions have been published, but in most of them the surfactant concentration has usually been below the critical micelle concentration (CMC); few papers have reported concentrations above the CMC.[1-3,7] The surfactant solution may be regarded as a new solvent taking the place of aqueous and nonaqueous solvents in the sense that it has characteristics of both in electrochemistry. The solubilized system in actuality is heterogeneous, in spite of its homogeneous appearance. An electrode process of a surfactant solution, however, involves many problems: 1) the adsorption state and equilibrium of surfactant molecules or micelles on an electrode; 2) the diffusion of an electroactive substance through bulk and adsorption phases at the electrode;[8,9] 3) an electroactive species adsorbing or not adsorbing in the adsorption phase; 4) the charge in the electric double layer affecting the electrode processes; 5) the electric-charge of a surfactant affecting the double layer, *etc.* The present paper will deal with experimental results on a few of the above problems and will discuss various possible interpretations.

The reason for using Orange OT is that this dye is water-insoluble[10] and electroactive.

Determination of αn_a, *m, and* $k^0_{f,h}$. Generally, the reaction occurring at the electrode for a totally irreversible wave may be described by the equation:

$$O + ne \longrightarrow R \qquad (1)$$

where O and R are the oxidized and reduced forms of a substance respectively. The cathodic current, i, that results from the reduction of O at any potential is described by the equation:

$$i = nFAC_o{}^0k^0_{f,h} \exp[-\alpha nF(E-E^0)/RT] \qquad (2)$$

where n is the number of electrons involved in the overall reaction; F, the Faraday constant; A, the area of the electrode; $C_O{}^0$, the concentration of O at the surface of the electrode; $k^0_{f,h}$, the heterogeneous rate constant at 0 V *vs.* N.H.E.; α, the transfer coefficient; E, the electrode potential reffered to the S.C.E.; E^0, the formal potential; R, the gas constant; and T, the absolute temperature. For couples whose formal potentials are unknown or even unmeasurable (as is the case with many totally irreversible couples), however, a convenient and interpretable potential instead of the formal potential is 0 V *vs.* N.H.E. (−0.246 V *vs.* S.C.E. at 25 °C).

Taking into account the variation in the $C_O{}^0$ with the current, Koutecký *et al.*[11] calculated the values of the $F(\chi)$ for the mean current:[12]

$$\bar{i}_{irrev} = \bar{i}_{rev}\bar{F}(\chi) \qquad (3)$$

where

$$\chi = (12/7)^{1/2}k_{f,h}t^{1/2}/D_o{}^{1/2}, \qquad (4)$$

where $k_{f,h}$ varies with the electrode potential given by:

$$k_{f,h} = k^0_{f,h} \exp[-\alpha n_a F(E+0.246)/RT] \qquad (5)$$

and where i is the mean current; t, the drop time; D_O, the diffusion coefficient of the oxidized form, and n_a, the number of electrons involved in the activation step. For a totally irreversible process, $\bar{i}_{rev}$ may be said to be equal to the mean diffusion current.

The mean current was measured instead of the instantaneous maximum current because the concentration of the solubilizable dye was very low.

Many organic compounds can generally be reduced as;[12-14]

$$O + mH^+ \rightleftharpoons O' \quad \text{(fast)} \qquad (6a)$$

$$O' + n_ae \longrightarrow I \quad \text{(rate-determining)} \qquad (6b)$$

$$I + (n-n_a)e \longrightarrow R \quad \text{(fast)} \qquad (6c)$$

where m is the number of hydrogen ions, and I, the intermediate. To describe the cathodic mean current, $\bar{i}$, resulting from the above reaction, one writes this equation:

$$\bar{i} = nF\bar{A}C^0_o k^0_{f,h} \exp[-\alpha n_a F(E+0.246)/RT] \qquad (7)$$

where A is the mean surface area of the dropping mercury electrode. If the solution is well buffered,

the combination of Eq. (7) with

$$K = C_{o'}^{0}/C_{o}^{0}C_{H^+}^{m} \quad (8)$$

for the equilibrium constant, K, of Eq. (6a) yields:

$$\bar{i} = nF\bar{A}C_{o}^{0}k_{f,h}^{0}KC_{H^+}^{m} \exp\left[-\alpha n_a F(E+0.246)/RT\right] \quad (9)$$

where C_{H^+} is the concentration of hydrogen ions at the electrode surface; the $k_{f,h}^{0}$ in Eq. (9) is the one for a first-order reaction. The essential equations, as solved by Koutecký[15] for the whole rising portion of the wave, are:

$$E = -0.246 + \frac{RT}{\alpha n_a F}\ln\frac{0.886k_{f,h}^{0}Kt^{1/2}}{D_o^{1/2}}C_{H^+}^{m} - \frac{RT}{\alpha n_a F}\ln\frac{\bar{i}}{\bar{i}_d - \bar{i}} \quad (10)$$

$$E_{1/2} = -0.246 + \frac{RT}{\alpha n_a F}\ln\frac{0.886k_{f,h}^{0}Kt^{1/2}}{D_o^{1/2}} - \frac{2.303RT}{\alpha n_a F}m(\mathrm{pH}) \quad (11)$$

$$E_{1/2}^{0} = -0.246 + \frac{RT}{\alpha n_a F}\ln\frac{0.886k_{f,h}^{0}K}{D_o^{1/2}} - \frac{2.303RT}{\alpha n_a F}m(\mathrm{pH}) \quad (12)$$

Hence,

$$\frac{dE_{1/2}^{0}}{d(\mathrm{pH})} = -\frac{2.303RT}{\alpha n_a F}m \quad (13)$$

is obtained from Eq. (12) for the estimation of m and $k_{f,h}^{0}$ at a constant value of αn_a. αn_a and m are calculated from Eqs. (10) and (13) respectively. $k_{f,h}$ is evaluated from Eq. (11) or (12) if the K value is known.

αn_a and $k_{f,h}^{0}$ are evaluated by an alternative method. By multiplying both sides of Eq. (5) by $KC_{H^+}^{m}$, we obtain:

$$\log KC_{H^+}^{m}k_{f,h} = \frac{\alpha n_a F}{2.303RT}E + \log Kk_{f,h}^{0} - m(\mathrm{pH}) - \frac{0.246\alpha n_a F}{2.303RT} \quad (14)$$

for $KC_{H^+}{}^{m}k_{f,h}$ based on Eq. (4), Eq. (8), Ilkovič's equation, and the table of χ values calculated by Weber *et al.*[11] Similarly, $Kk_{f,h}^{0}$ and αn_a are calculated from Eqs. (13) and (14).

Experimental

Materials. 1-*o*-Tolyl-azo-2-naphthol (Orange OT) was recrystallized twice from ethanol. E.P.-grade sodium dodecyl sulfate (SDS) was purified by two recrystallizations from ethanol after extraction with ethyl ether for 50 hr. A sample of sodium dodecylbenzenesulfonate (SDBS; the CMC based on the polarographic method[16] was 3.2×10^{-3} M at 30 °C), kindly supplied by Lion Oil and Fats Co. was recrystallized from petroleum ether. C.P.-grade dodecyltrimethylammonium chloride (DTMAC) was purified by recrystallization from acetone. A sample of polyoxyethylene nonylphenyl ether (NP-$\bar{1}0$) was also obtained by courtesy of the Meisei Chemical Works. Ltd., and was used without further purification. Citric acid-disodium hydrogen phosphate buffers (McIlvaine's buffer solution) were prepared from G.R.-grade reagents without purification.

Solutions. Orange OT was dissolved in 6.8 M aqueous ethanol (about 40 vol%) and solubilized in anionic, cationic, and nonionic surfactant solutions, the concentrations of which were: 2×10^{-2} M SDS, 2×10^{-2} M SDBS, 5×10^{-2} M DTMAC, and 4×10^{-2} M NP-$\bar{1}0$ respectively, buffered at various pH values. Also, the dye concentrations were 5×10^{-5} M in the aqueous ethanol, 5×10^{-5} M in the SDS, 2×10^{-5} M in the SDBS, 5×10^{-5} M in the DTMAC, and 1×10^{-4} M in the NP-$\bar{1}0$ solution.

The solutions of the solubilized dye in the surfactant solutions were prepared with shaking and warming to a desired temperature for several days and were measured by polarography after the solubilization equilibrium.

The pH was measured with a Toa Dempa Model HM-5A pH meter. In the case of aqueous ethanol solutions, the apparent pH values were measured.

Polarography. Polarographic measurements were carried out by using a PAR Model 170 (Princeton Applied Research Co.). The characteristic σ value of the dropping mercury electrode was 1.74 mg s^{-1} (the height of the mercury column h=87.15 cm) in all solutions except the DTMAC solution, in which σ=1.72 mg s^{-1} (h=87.05 cm). The potential of a polarograph was recorded against the S.C.E. The solutions were deaerated by bubbling pure nitrogen gas through them for an hour and by then allowing its overflow to cover the surfaces of the solutions during measurement. The SDBS solutions were measured at 45±0.1 °C, while the other solutions were measured at 25±0.1 °C corresponding to their Krafft points.

Results

The polarographic behavior of Orange OT has already been mentioned[3] in detail in surfactant solutions with a constant pH value. The present paper, however, will be concerned with solutions of various pH values. The relation of the limiting current to the square-root of the height of the mercury head in all the solutions shows a linear line. The lmiting current, therefore, is proved to be the diffusion-controlled current.

A maximum of the first kind in the aqueous ethanol solution containing dissolved Orange OT was appreciably observed in pH 2.78 and 5.30 solutions (it was not observed between pH 2.78 and 5.30), and it increased with an increase in the pH value.

Since the reduction wave of Orange OT solubilized in the SDS solution overlapped the reorientation wave of SDS molecules on the mercury electrode[17] at pH 4.95 and 5.88, the current of the reduction wave was not analyzed.

The potential due to the reorientation of surfactant molecules shifted unwaveringly to a negative potential with an increase in the pH in the basic solution without Orange OT, while the reorientation potential-pH relation showed a curve with a minimum at pH 4.95 in

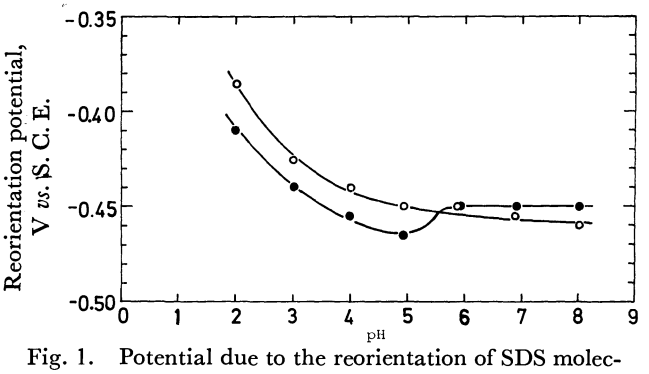

Fig. 1. Potential due to the reorientation of SDS molecules with pH: ○, SDS basic solution; ●, solution solubilizing Orange OT.

the solution solubilizing Orange OT (Fig. 1).

The reduction wave of Orange OT solubilized in the SDBS solution overlapped the tensametric wave of SDBS at pH<3.00 and could not be analyzed. The polarograph, therefore, was measured in solutions at pH>3.00.

The fine reduction wave in the DTMAC solution solubilizing Orange OT was obtained over the range of pH 1.92 to 7.99.

Two waves in the NP-$\bar{1}0$ solution solubilizing Orange OT were obtained in each pH solution. The first wave was the reduction wave of Orange OT, as the wave height linearly increased with the concentration of the dye; the second wave showed a maximum wave at −0.760 V. For a more basic solution, only the first wave shifted to the negative potential. The two waves overlapped at pH 5.88, and complicated waves were observed at pH 6.89 and 8.01 (Fig. 2).

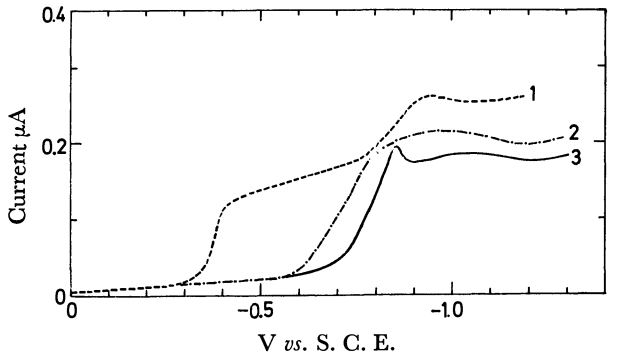

Fig. 2. Polarograms of solubilized Orange OT in NP-$\bar{1}0$ solution: (1) ------, pH 3.00; (2) -·-·-, 5.88; (3) ——, 8.01.

Discussion

$E_{1/2}$—pH. The relation of the corrected half-wave potential to the pH value in each solution is shown in Fig. 3, in which the slope of each straight line is different. The equations calculated by the least-squares procedures of each relation are shown in Table 1. The slope of each straight line is different because m and αn_a are different in the variety of solutions, as will be described below. In the SDBS solution, two straight lines are obtained; they have not yet been explained.

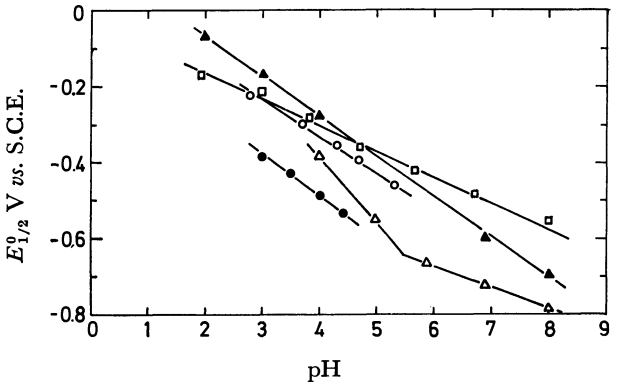

Fig. 3. $E^0_{1/2}$-pH plots: ○, aqueous ethanol; ▲, SDS, △, SDBS; □, DTMAC; and ●, NP-10 solutions.

Table 1. Relation of corrected half-wave potential against pH in each solution

Solution	Relation of $E^0_{1/2}$—pH
C_2H_5OH	$E^0_{1/2}=-0.094$ pH$+0.047$
SDS	$E^0_{1/2}=-0.107$ pH$+0.150$
SDBS	$E^0_{1/2}=-0.178$ pH$+0.329$[a]
	$E^0_{1/2}=-0.055$ pH-0.343[b]
DTMAC	$E^0_{1/2}=-0.066$ pH-0.036
NP-$\bar{1}0$	$E^0_{1/2}=-0.108$ pH-0.055

a) Left branch b) Right branch

$E_{1/2}$—log t. According to Eq. (11), the half-wave potential shifts to less negative potentials in all the solutions with an increase in the drop time. It is found that Orange OT dissolved in an aqueous ethanol solution and solubilized in each surfactant solution is an irreversible species under the conditions investigated.

The slope of $E_{1/2}$—log t in the solution of each pH value is different, mainly because of the difference in αn_a; *e.g.*, in the DTMAC solution the slopes at the pH values of pH 3.83 and 4.70 smaller than the others, which is reasonable because the (αn_a)'s of the former are larger than those of the latter (Fig. 4).

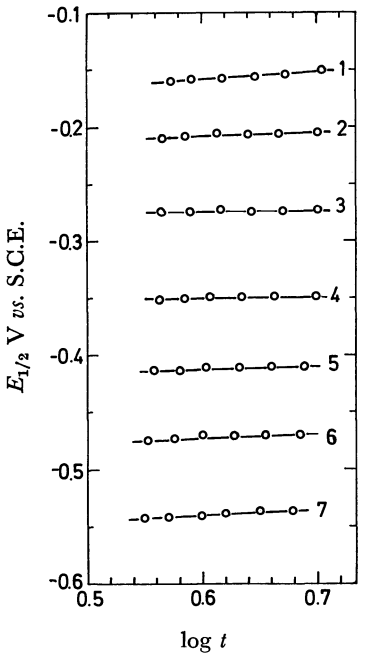

Fig. 4. $E_{1/2}$—log t plots in DTMAC solution: (1) pH 1.92; (2) 2.96; (3) 3.83; (4) 4.70; (5) 5.67; (6) 6.71; (7) 7.99.

αn_a—$E_{1/2}$. In discussing the electrode process, especially the effect of the double-layer structure on the electrode process,[18] the reaction of αn_a—$E_{1/2}$ is very important. However, the apparent value of $(\alpha n_a)_{app}$ found directly from the semilogarithmic plot of the wave, or that of the rate constant mentioned above, is markedly different from its true value.[19] The relationship between the observed value and the true value of αn_a is generally expressed by:[20,21]

$$(\alpha n_a)_{app} = \alpha n_a + (z-\alpha n_a)(\partial \Psi_1/\partial \phi)_{E_{1/2}} \quad (15)$$

where z is the electric-charge on the reacting species; Ψ_1, the potential of the outer Helmholtz plane, and

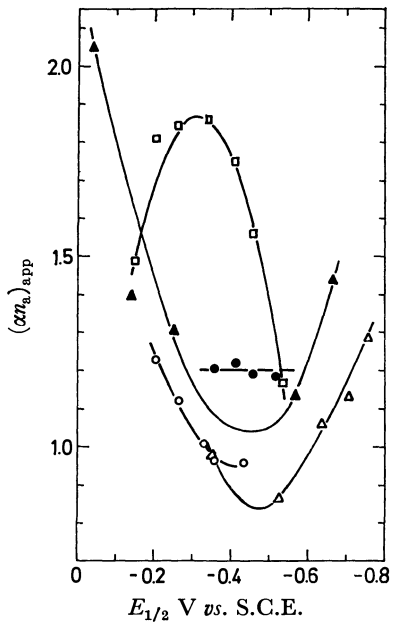

Fig. 5. Variation of $(\alpha n_a)_{app}$ with $E_{1/2}$ from semilogarithmic plot of wave: ○, aqueous ethanol; ▲, SDS; △, SDBS; □, DTMAC; and ●, NP-$\bar{1}0$ solutions.

ϕ, the potential difference between the electrode potential and the potential of the zero charge. However, most of the solutions are micellized solutions. The surfactant molecules strongly adsorb on the mercury electrode, so that the potential of zero charge can not be measured; *i.e.*, $(\partial\Psi_1/\partial\phi)_{E_{1/2}}$ can not be calculated, and the true value of αn_a can not be obtained. Therefore, only the apparent values of αn_a are shown here (Fig. 5).

In calculating $(\alpha n_a)_{app}$, the above two methods, *i.e.*, $\log i/(i_d-i)-E$ and $\log KC_H^m+k_{f,h}-E$, are applied. The difference between the values obtained by the two methods is very small.

The relation of $(\alpha n_a)_{app}$ to $E_{1/2}$ shows the curve passing through a minimum in the anionic surfactant solutions, and a maximum in the cationic surfactant solution. The $(\alpha n_a)_{app}$ in the nonionic surfactant and the aqueous ethanol solutions remains constant and decreases, respectively, with shift of the $E_{1/2}$ to the negative potential.

These results show that the electric-charge of the surfactant at the mercury electrode affects the electrode reaction of Orange OT. Though Orange OT itself is an uncharged species, when solubilized in ionic micelles it seems to behave in the electrode process as if it were an ionic species. In the cationic surfactant solution, $(z-\alpha n_a)$ becomes a positive value, judging from the fact that the plot of $\alpha n_a-E_{1/2}$ indicates a maximum; therefore, the electric-charge of the cationic surfactant micelle is not less than two.[22]

Most of the αn_a values obtained are larger than one, and the value of n_a seems to be 2 rather than one.

In the case of the aqueous ethanol and ionic surfactant solutions, the value of m is not obtained because αn_a varies with the half-wave potential and $k^0_{f,h}$ can not be calculated.

m and $Kk^0_{f,h}$ of Orange OT Solubilized in an NP-$\bar{1}0$

Table 2. Heterogeneous rate constant of Orange OT solubilized in NP-$\bar{1}0$ solution

pH	$(Kk^0_{f,h})^{a)}$ (cm l^2 mol^{-2} s^{-1})	$(Kk^0_{f,h})^{b)}$ (cm l^2 mol^{-2} s^{-1})
3.00	3.4	4.3
3.49	5.7	3.3
4.00	3.7	3.0
4.40	2.2	1.8

a) From Eq. (11). b) From Eq. (14).

Solution. In the case of Orange OT solubilized in NP-$\bar{1}0$, αn_a does not vary with the half-wave potential in the potential range. The value of m from Eq. (13) is calculated to be 2; this value is reasonable. $Kk^0_{f,h}$ is calculated from Eq. (10) or (14) as the values of αn_a and m are obtained, but K is not known. The values of $Kk^0_{f,h}$ are tabulated in Table 2.

$(z-\alpha n_a)$ in Eq. (15) becomes zero because the value of αn_a is constant in a variety of half-wave potentials. Orange OT, which is essentially an uncharged species, seems to behave as the ionic species of the unit electric-charge, because the value of αn_a is nearly equal to one.

References

1) S. Hayano and N. Shinozuka, This Bulletin, **42**, 1469 (1969).
2) S. Hayano and N. Shinozuka, *ibid.*, **43**, 2083 (1970).
3) S. Hayano and N. Shinozuka, *ibid.*, **44**, 1503 (1971).
4) R. W. Schmid and C. N. Reilley, *J. Amer. Chem. Soc.*, **80**, 2087 (1958).
5) R. G. Barradas and F. M. Kimmerle, *J. Electroanal. Chem.*, **11**, 128 (1966).
6) M. Jhring and A. Weiß, *Tenside*, **6**, 251 (1969).
7) P. G. Westmoreland, R. A. Day, and A. L. Underwood *Anal. Chem.*, **44**, 737 (1972).
8) I. R. Miller, *J. Phys. Chem.*, **69**, 2740 (1965).
9) Y. F. Frei and I. R. Miller, *ibid.*, **69**, 3018 (1965).
10) H. Schott, *ibid.*, **68**, 3612 (1964).
11) J. Weber and J. Koutecký, *Coll. Czech. Chem. Commun.*, **20**, 980 (1955).
12) J. Heyrovsky and J. Kůta, "Principles of Polarography," Academic Press, New York, (1966), Chap. 14.
13) L. Meites, "Polarographic Techniques," Interscience, New York, (1965), Chap. 4.
14) A. A. Humffray, "Modern Aspects of Electrochemistry," vol. 8, ed. by Bockris and Conway, Plenum Press, New York (1972), Chap. 3.
15) J. Koutecký, *Coll. Czech. Chem. Commun.*, **18**, 597 (1953).
16) N. Shinozuka, H. Suzuki, and S. Hayano, *Kolloid-Z. Z. Polym.*, **248**, 959 (1971).
17) K. Eda, *Nippon Kagaku Zasshi*, **80**, 349 (1959).
18) W. H. Reinmuth, L. B. Rogers, and L. E. I. Hummelstedt, *J. Amer. Chem. Soc.*, **81**, 2947 (1959).
19) R. Parsons, "Advance in Electrochemistry and Electrochemical Engineering," Vol. 1, ed. by P. Delahay, Interscience, New York, (1961), Chap. 1.
20) P. Delahay, "Double Layer and Electrode Kinetics," Interscience, New York, (1966).
21) S. G. Miranovskii, "Progress in Polarography," Vol. 3, ed. Zuman, Meites and Kolthoff, Wiley-Interscience, (1972), Chap. 5.
22) R. D. Geer, E. H. Eylar, and E. W. Anacker, *J. Phys. Chem.*, **75**, 369 (1971).

Theoretical Calculation of the Carbon-13 Chemical Shifts of Some Normal Alkanes by the Linear Combination of Gauge Invariant Atomic Orbitals-Molecular Orbital Theory Using INDO and MINDO/2 Methods

Isao ANDO, Atsuo NISHIOKA, and Masahiro KONDO

Department of Polymer Chemistry, Tokyo Institute of Technology, Ookayama, Meguro-ku, Tokyo 152

(Received August 7, 1973)

The ^{13}C chemical shifts of several *n*-alkanes (CH_4, C_2H_6, C_3H_8, C_4H_{10}, C_5H_{12}, C_6H_{14}, and C_7H_{16}) were calculated using a linear combination of the gauge invariant atomic orbitals-molecular orbital theory of Pople and the INDO and MINDO/2 methods, and the results were compared with the experimental data reported by Grant *et al.* The calculated chemical-shift differences among the carbons in these molecules were found to agree with the observed data except in some cases, whereas the observed order of the chemical shift of the carbons in *n*-alkanes, which have more than two magnetically nonequivalent carbons, cannot be interpreted by means of the average excitation energy (ΔE) approximation. Histograms showing the distribution of the excitation energies from the occupied to unoccupied orbitals were obtained and compared with ΔE.

The carbon-13(^{13}C) NMR spectra of normal(*n*-) and branched alkanes were at first studied in detail by Paul and Grant.[1] These data were summarized by the so-called "Grant's empirical additivity rule". An early attempt to interpret these data theoretically was reported by Yonezawa *et al.* using the average excitation energy(ΔE) approximation for the paramagnetic term governing the ^{13}C chemical shift(σ) of *n*- and branched alkanes,[2] but their results agree only roughly with the observed data. Recently they have tried to use various values of ΔE among the individual carbons in alkanes and have suggested that the experimental data were better explained by their method than by the usual method of using a common value of ΔE for all the carbons in an alkane molecule.[3] Although the practical utility is large, this method has an ambiguity in its theoretical basis from the point of view of molecular orbital theory. Therefore it is important to consider the ΔE approximation by means of another method without this approximation. In this paper we attempt to calculate precisely the ^{13}C chemical shifts of *n*-alkanes (CH_4, C_2H_6, C_3H_8, C_4H_{10}, C_5H_{12}, C_6H_{14}, and C_7H_{16}) in which the large molecules still have not been treated except for CH_4 and C_2H_6, by a method based on molecular orbital theory considering only the valence-electron system, in place of the ΔE approximation, and attempt to interpret theoretically the observed ^{13}C chemical shifts of large *n*-alkanes, which have not been interpreted by the ΔE approximation. For this purpose, we use Pople's consideration[4] that σ may be estimated as the sum of three terms—the diamagnetic and paramagnetic contributions, and the contribution from electrons on the other atoms in the molecule. The ^{13}C chemical shift is predominantly contributed, by the second term.[4] Pople[5] has derived the so-called linear combination of gauge invariant atomic orbitals-molecular orbital (LCGI-MO) theory for Ramsey's paramagnetic shielding tensor[6] based on a series of approximations, commonly in linear combination of atomic orbitals (LCAO-MO) theory. This approach enables us to calculate the σ values approximately for large molecules. Our calculations have been done using two different parametric self-consistent field (SCF) MO theories, that is, the MINDO/2[7] and INDO methods[8] modified for calculating the electronic excitation energies of organic compounds by Yamaguchi *et al.*[9] The major difference between these two methods is in the separation in orbital energies, which have a large effect on the ^{13}C chemical shift. As for the two MO theories, the MINDO/2 method is said to interpret better the excitation energy for π-system molecules without taking the configuration interaction (CI) into account, but for the electron density distribution, the latter may give better results than the former. Thus, in this paper the results of the two methods will be compared with each other.

Theoretical

According to Pople,[4] the chemical shielding, σ_A, of the nucleus, A, is written as;

$$\sigma_A = \sigma_d + \sigma_p + \sum_{B \neq A} \sigma_{AB} \quad (1)$$

where σ_d is the diamagnetic term, σ_p, the paramagnetic term, and σ_{AB}, the neighbour anisotropy term. The dominant factor usually governing ^{13}C chemical shielding is the paramagnetic term, whereas σ_d does not contribute predominantly. The neighbour anisotropy term can be neglected because it is unlikely to exceed a few ppm, as has been described by Pople.[10]

The diamagnetic term was calculated as:[2]

$$\sigma_d = 4.45(3.25 - 0.35(q_A - 4.0))q_A \quad (2)$$

in which q_A is the σ-electron density on the carbon, A.

According to Pople's LCGI-MO theory,[5] the paramagnetic shielding is written as:

$$\sigma_p = -2N^{-1}\chi_p^A \langle r^{-3} \rangle_{2p} \quad (3)$$

where χ_p^A is the paramagnetic contribution of the A atom to the susceptibility tensor; N, the Avogadro number, and $\langle r^{-3} \rangle_{2p}$, the mean value of r^{-3} with respect to the 2p orbital (r: the distance between the electron and nucleus). χ_p^A is written by averaging over the diagonal elements of the tensor as;

$$\chi_p^A = \frac{1}{3}\{(\chi_p^A)_{xx} + (\chi_p^A)_{yy} + (\chi_p^A)_{zz}\} \quad (4)$$

where;

$$(\chi_p^A)_{xx} = (Ne^2\hbar^2/m^2c^2)\sum_i^{occ}\sum_{k(\neq i)}^{unocc}(\Delta E_{k-i})^{-1}(c_{iy_A}c_{kz_A} - c_{iz_A}c_{ky_A}) \times \sum_B(c_{iy_B}c_{kz_B} - c_{iz_B}c_{ky_B}) \quad (5\text{-}1)$$

$$(\chi_p^A)_{yy} = (Ne^2\hbar^2/m^2c^2)\sum_i^{occ}\sum_{k(\neq i)}^{unocc}(\Delta E_{k-i})^{-1}(c_{iz_A}c_{kx_A} - c_{ix_A}c_{kz_A}) \times \sum_B(c_{iz_B}c_{kx_B} - c_{ix_B}c_{kz_B}) \quad (5\text{-}2)$$

$$(\chi_p^A)_{zz} = (Ne^2\hbar^2/m^2c^2)\sum_i^{occ}\sum_{k(\neq i)}^{unocc}(\Delta E_{k-i})^{-1}(c_{ix_A}c_{ky_A} - c_{iy_A}c_{kx_A}) \times \sum_B(c_{ix_B}c_{ky_B} - c_{iy_B}c_{kx_B}) \quad (5\text{-}3)$$

Here, c_{ixA} is the coefficient of the $2p_x$ atomic orbital on the atom of the i-th molecular orbital in the LCAO-MO theory; $\sum_i^{occ}$ and $\sum_{k(\neq i)}^{unocc}$ are the summations over the occupied and unoccoupied orbitals; $\sum_B$ runs over all the atoms in the molecule (including A), and ΔE_{k-i} is the singlet-singlet excitation energy between the i-th occupied orbital and the k-th unoccupied one. ΔE_{k-i} is expressed as follows:

$$\Delta E_{k-i} = \varepsilon_k - \varepsilon_i - J_{ki} + 2K_{ki} \quad (6)$$

where ε_k and ε_i are the unoccupied and occupied orbital energies and where J_{ki} and K_{ki} are the two-electron Coulomb and exchange integrals. $\langle r^{-3}\rangle_{2p}$ in Eq. (3) for the Slater 2p orbital of the A atom depends primarily on the local electron density on the carbon atom ($-q'_A$ e is the net charge) and is given as;[10]

$$\langle r^{-3}\rangle_{2p} = 34.33a_0^{-3}(1-0.323q_A')/24 \quad (7)$$

where a_0 is the Bohr radius. From the expressions described above, the ^{13}C chemical shieldings of n-alkanes were estimated by the INDO and MINDO/2 methods for the valence-electron system.

Here, the C–C and C–H bond lengths used are set at 1.54 and 1.10 Å respectively, and all the C–C–C, C–C–H, and H–C–H bond angles are set at 109°28′.[11]

The calculations were carried out by means of the HITAC-8800 computer of the Computer Centre of the University of Tokyo.

Results and Discussion

Before calculating the ^{13}C chemical shift of n-alkanes, it would be helpful in understanding it to discuss the electron density distributions, the orbital energies, the excitation energies, and the ionization potentials as calculated by the INDO and MINDO/2 methods. Here, although n-alkane molecules with more than three carbon atoms can take conformations containing the *gauche* form other than the *trans* form in the liquid state, only the *trans* form, which is the major conformation among the possible conformations, is involved except for n-butane and n-pentane. The total electron density and 2p electron density distributions in seven kinds of n-alkanes, as calculated by the INDO and MINDO/2 methods, are shown in Fig. 1, where the latter is given in brakets. The total and 2p electron densities on the carbon atoms as calculated by the INDO method were found to give slightly larger values than those calculated by the MINDO/2 method. Because $\langle r^{-3}\rangle_{2p}$ decreases with an increase in the total electron density, the MINDO/2 method is found to lead to a somewhat larger contribution of the paramagnetic shielding than does the INDO method. Next, let us examine the orbital energies of n-alkanes. The values calculated by both methods are shown in Fig. 2. It is found that the separations between the occupied and unoccupied orbital energies calculated by the MINDO/2 method are smaller than between those calculated by the INDO method. Therefore, the MINDO/2 method will give somewhat larger contribution to the paramagnetic shielding than will the INDO method. Further, it will become a measure of the magnitude of the paramagnetic contribution to show the histograms of the singlet-singlet transitions from occupied to unoccupied orbitals in alkanes. Therefore, they are shown in Fig. 3, where the vertical axis of the histogram indicates the number of transitions from occupied to unoccupied orbitals and where the interval of the excitation energy is 1 eV. (Such histograms for molecules with π-electrons—for example, ethylene and benzene, may not be appropriate, since the π-π^* transition of the transitions from occupied to unoccupied orbitals does not contribute to the paramagnetic shielding because of the orbital symmetry; therefore, the vertical axis of the histogram should include the weight of each transition in computing the contribution to the chemical shift. However, in the molecules considered here, a σ-electron system, such histograms may be useful in seeing the tendency of the distribution of the excitation energy of n-alkanes without the weight.) As is shown in Fig. 3, the excitation energies giving maximum values in the histograms of the transitions calculated by the MINDO/2 and INDO methods shift to higher energies with an increase in the number of carbon atoms; their exicitation energies are about 9—10 and 14—15 eV respectively, except for CH_4 and C_2H_6. Thus, the MINDO/2 method gives a value about 5 eV lower than does the INDO method. The former may be therefore expected to make a larger paramagnetic contribution than the latter.

Table 1. The calculated and observed ionization potentials of n-alkanes (eV)

	Calculated		Observed[a]
	INDO method	MINDO/2 method	
CH_4	16.71	13.15	12.95
C_2H_6	14.15	11.48	11.65
C_3H_8	12.91	10.88	11.08
C_4H_{10}	12.09	10.32	10.65
C_5H_{12}	11.52	9.96	10.33
C_6H_{14}	11.20	9.73	10.17
C_7H_{16}	10.94	9.55	10.06

a) From Ref. 12.

Before concerning with the present purpose, we will concern with the average excitation energy approximation. Our calculated results of the excitation energies showing maximum values in the histograms by the

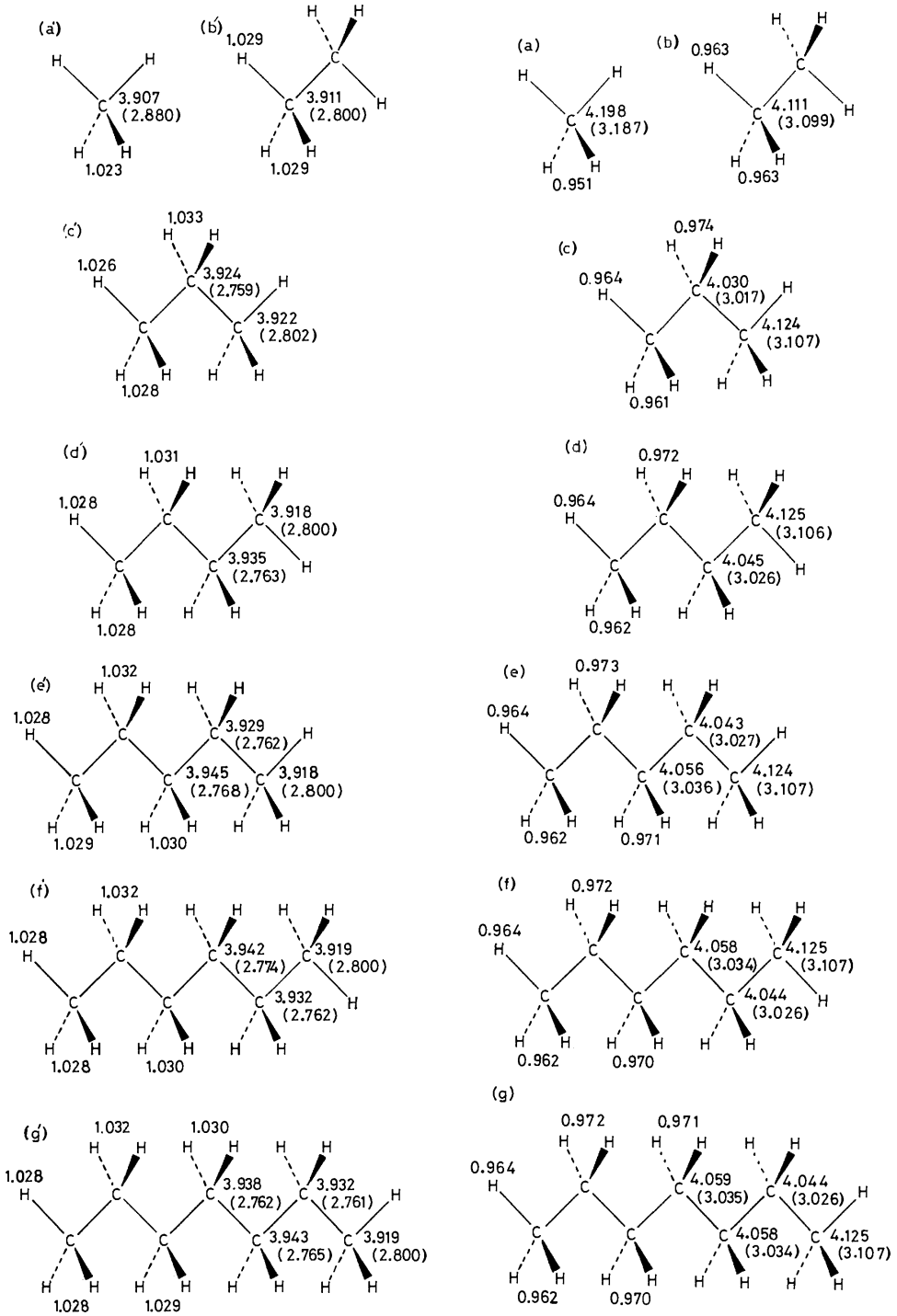

Fig. 1. Total electron density and 2p electron density (with brackets) distributions of *n*-alkanes calculated by INDO and MINDO/2 methods
a), a') CH_4; b), b') C_2H_6; c), c') C_3H_8; d), d') C_4H_{10}. e), e') C_5H_{12}; f), f') C_6H_{14}; g), g') C_7H_{16}. The prime indicates the electron density by MINDO method and other by INDO method. All the conformations are *trans* form.

MINDO/2 method are found to be near to the value of ΔE in the average excitation energy approximation, proposed by Pople[10] for the σ-system carbon atom. These may become roughly one of the measures of the value of ΔE, when the distribution of the histograms is not broad. (According to this viewpoint, the ionization potential may also become a measure of it. As for the ionization potential, the results calculated by the MINDO/2 method are somewhat lower values than those calculated by the INDO method as shown in Table 1. This corresponds to the above-obtained result for the maximum value in the histogram.) Now, let us particularly consider the large *n*-alkanes, and, as an example, let us consider *n*-pentane by the following ΔE approximation, with three magnetically non-equivalent carbon atoms:

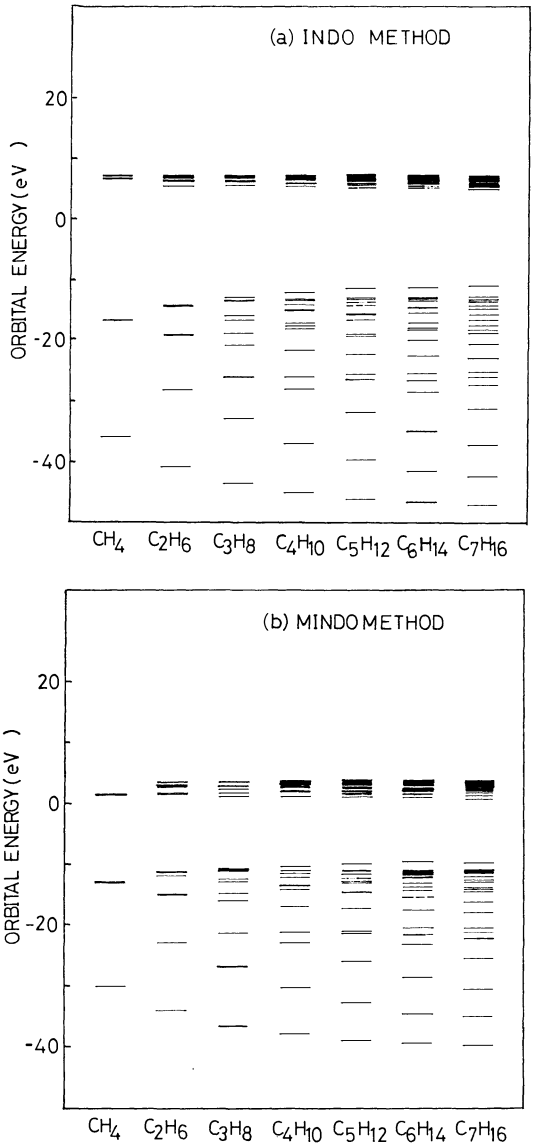

Fig. 2. Orbital energies of *n*-alkanes calculated by INDO (a) and MINDO/2 (b) methods.

$$\sigma_p = -(e^2\hbar^2/2m^2c^2\Delta E)\langle r^{-3}\rangle_{2p}\sum_{B(=A)} Q_{AB} \tag{8}$$

where;

$$Q_{AB} = \frac{3}{4}\delta_{AB}(p_{x_Ax_B}+p_{y_Ay_B}+p_{z_Az_B}) - \frac{2}{3}(p_{y_Ay_B}p_{z_Az_B}+p_{z_Az_B}p_{x_Ax_B}+p_{x_Ax_B}p_{y_Ay_B}) + \frac{2}{3}(p_{y_Az_B}p_{z_Ay_B}+p_{z_Ax_B}p_{x_Az_B}+p_{x_Ay_B}p_{y_Ax_B}) \tag{9}$$

In these formulas, $\sum_{B(=A)}$ is a summation over all the atoms; δ_{AB}, the Kronecker symbol, and p_{XAXB}, the element of the matrix for the $2p_x$ atomic orbitals on the A and B atoms. When A=B, it is the charge density in $2p_x$ on the A atom, and when A≠B, it is the bond order between the two atomic orbitals. The ^{13}C chemical shifts of *n*-pentane, as calculated by the use of the ΔE approximation using the INDO and MINDO/2 methods, are shown in Table 2, where 10 eV is used as the value of ΔE. It is shown that

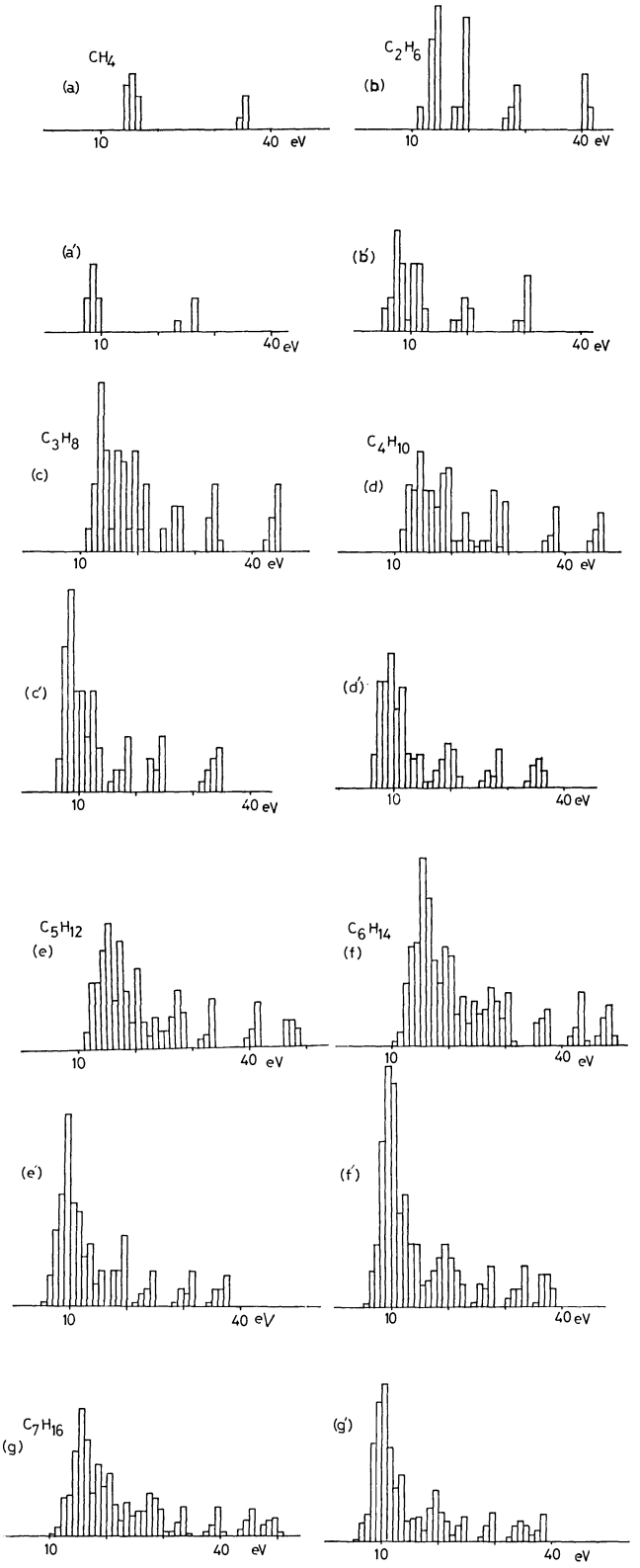

Fig. 3. Histograms of number of the excitation from occupied to unoccupied orbitals against the singlet–singlet excitation energies of *n*-alkanes calculated by INDO and MINDO/2 methods.
a), a') CH_4; b), b') C_2H_6; c), c') C_3H_8; d), d') C_4H_{10}; e), e') C_5H_{12}; f), f') C_6H_{14}; g), g') C_7H_{16}. The prime indicates the electron density by MINDO/2 method and other by INDO method. All the conformations are *trans* form.

TABLE 2. THE ^{13}C CHEMICAL SHIFTS OF *n*-PENTANE CALCULATED BY THE ΔE APPROXIMATION USING THE INDO AND MINDO/2 METHODS[a] AND THE OBSERVED ONES (ppm)

	INDO method				MINDO/2 method				Observed[d]	
	σ_d	σ_p	σ	$\Delta\sigma$[b]	σ_d	σ_p	σ	$\Delta\sigma$	σ[c]	$\Delta\sigma$[b]
$CH_3(1)$	58.85	−206.68	−147.83	0	57.17	−225.75	−168.58	0	114.97	0
$CH_2(2)$	58.20	−222.21	−164.01	−16.18	57.26	−238.42	−181.16	−12.58	106.13	−8.84
$CH_2(3)$	58.31	−221.74	−163.43	−15.60	57.39	−239.57	−182.18	−13.60	94.17	−20.80

a) The conformation is the TT form. b) The CH carbon is the reference. c) The reference is benzene.
d) From Ref. 1.

TABLE 3. THE ^{13}C CHEMICAL SHIFTS OF *n*-ALKANES CALCULATED BY THE LCGI-MO THEORY USING THE INDO AND MINDO/2 METHODS AND THE OBSERVED ONES[a] (ppm)

	INDO method[d]				MINDO/2 method[d]				Observed	
	σ_d	σ_p	σ	$\Delta\sigma$[b]	σ_d	σ_p	σ	$\Delta\sigma$[b]	σ[c]	$\Delta\sigma$[b]
CH_4	59.42	−129.24	−69.82		57.07	−248.63	−191.56		130.8	
CH_3CH_3	58.74	−132.24	−73.50		57.12	−234.05	−176.93		122.8	
$CH_3CH_2CH_3$										
$CH_3(1)$	58.85	−125.60	−66.75	0	57.20	−219.57	−162.37	0	113.10	0
$CH_2(2)$	58.10	−137.32	−79.22	−12.47	57.21	−227.31	−170.10	−7.73	112.62	−0.48
$CH_3CH_2CH_2CH_3$										
$CH_3(1)$	58.86	−120.69	−61.83	0	57.17	−206.55	−149.38	0	115.48	0
$CH_2(2)$	58.21	−133.73	−75.52	−13.69	57.31	−222.36	−165.05	−15.67	103.68	−11.80
$CH_3CH_2CH_2CH_2CH_3$										
$CH_3(1)$	58.85	−117.31	−58.46	0	57.17	−198.94	−141.77	0	114.97	0
$CH_2(2)$	58.20	−129.27	−71.07	−12.51	57.26	−211.42	−154.16	−12.39	106.13	−8.84
$CH_2(3)$	58.31	−130.87	−72.56	−14.10	57.39	−218.61	−161.22	−19.45	94.17	−20.80
$CH_3CH_2CH_2CH_2CH_2CH_3$										
$CH_3(1)$	58.85	−114.50	−55.65	0	57.18	−191.53	−134.35	0	114.82	0
$CH_2(2)$	58.21	−125.86	−67.65	−12.00	57.28	−203.94	−146.66	−12.31	105.78	−9.04
$CH_2(3)$	58.32	−128.03	−69.71	−14.06	57.37	−210.50	−153.13	−18.78	96.66	−18.16
$CH_3CH_2CH_2CH_2CH_2CH_2CH_3$										
$CH_3(1)$	58.85	−112.31	−53.46	0	57.18	−186.06	−128.88	0	114.75	0
$CH_2(2)$	58.21	−123.38	−65.17	−11.71	57.28	−196.33	−139.05	−10.17	105.70	−9.05
$CH_2(3)$	58.32	−124.83	−66.51	−13.05	57.37	−203.71	−146.34	−17.46	96.30	−18.45
$CH_2(4)$	58.33	−125.26	−66.93	−13.47	57.37	−204.77	−147.40	−18.52	99.23	−15.52

a) From Ref. 1. b) The CH_3 carbon in a molecule is the reference. c) The reference is benzene.
d) The conformation is the TT form.

the chemical-shift difference between the $CH_3(1)$ and $CH_2(2)$ carbons* agrees roughly with the experimental value, but that between the $CH_2(2)$ and central $CH_2(3)$ carbons does not agree with the experimental value (in the INDO method the order of the $CH_2(2)$ and $CH_2(3)$ carbons is opposite to that in the experimental results.) Therefore, it is difficult to interpret the ^{13}C chemical shift of long *n*-alkane by means of the ΔE approximation. When *n*-alkanes have a broad distribution of the exicitation energy, as is shown in Fig. 3, it may be seen not to be plausible to estimate the ^{13}C chemical shifts using a definite common value of ΔE.

Next, let us discuss the ^{13}C chemical shift of the *n*-alkanes calculated by means of the LCGI-MO theory using the INDO and MINDO/2 methods. The calculated results are shown in Table 3. As has been described above, the magnitudes of the paramagnetic contribution as calculated by means of the MINDO/2 method are found to give larger values than those calculated by means of the INDO method. We will first discuss the chemical shifts of the carbons in each *n*-alkane having more than two magnetically non-equivalent carbon atoms. In the case of *n*-propane calculated by the INDO and MINDO/2 methods, the order of the CH_3 and CH_2 carbons in their chemical shifts agrees qualitatively with the observed order, but for the difference between the two carbons the calculated value are too much larger than the observed value. In the case of *n*-butane, the INDO method gives a fairly good agreement with the observed results, better than the MINDO/2 method. In the case of *n*-pentane, although, as has been mentioned above, we could not interpret the observed chemical-shift difference between the $CH_2(2)$ and $CH_2(3)$ carbons when we used the ΔE approximation, the LCGI-MO theory using the MINDO/2 method gives good agreement between the calculated and observed results, while the INDO method does not give good results quantita-

* The representation of *n*-pentane is as follows; $CH_3(1)$-$CH_2(2)$-$CH_2(3)$-$CH_2(2)$-$CH_3(1)$. The representations of the other *n*-alkanes are the same as this.

tively, for the chemical-shift difference between the $CH_2(2)$ and $CH_2(3)$ carbons, although the qualitative orders of the carbons agree with each other. In the case of *n*-hexane, the MINDO/2's calculation agrees well with the observed results, but the INDO's calculation does not give good results for the chemical-shift difference between the $CH_2(2)$ and $CH_2(3)$ carbons as well as in the case of *n*-pentane. In the case of *n*-heptane, the observed four signals of the carbon atoms are assigned in order of the $CH_3(1)$, $CH_2(2)$, $CH_2(4)$, and $CH_2(3)$ carbons from the high field (the chemical-shift difference between the $CH_2(3)$ and $CH_2(4)$ is small). In the MINDO/2 method, the chemical shifts of the $CH_3(1)$, $CH_2(2)$, and $CH_2(3)$ carbons agree with the observed ones, but the $CH_2(4)$ carbon appears at a slightly lower field than the $CH_2(3)$ carbon. In the INDO method the chemical shifts of the other carbons except for the chemical-shift difference between the $CH_3(1)$ and $CH_2(2)$ carbons disagree with the observed results.

As may seen be from Table 3, the observed values of the ^{13}C chemical shifts in a molecule could be better explained by the MINDO/2 method than by the INDO method, although one of the causes of some discrepancies may be the simple *trans* planar form.

Next, with respect to *n*-butane and *n*-pentane, we will discuss the effect of possible rotational isomers on the chemical shift. Here the MINDO/2 method was used, because it gives better results than the INDO method in the TT form of *n*-pentane. The electron-density distributions and the orbital energies of the G form in *n*-butane and of the TG and GG forms in *n*-pentane are shown in Figs. 4 and 5 respectively. The latter is shown together with the *trans* forms. Histograms of the number of the excitation against

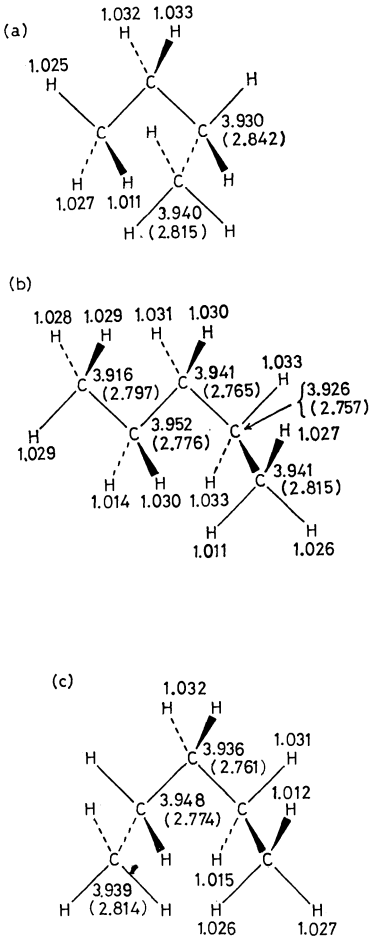

Fig. 4. Total electron density and 2p electron density distributions of the G form in *n*-butane (a), and of the TG (b) and GG (c) forms in *n*-pentane calculated by MINDO/2 method.

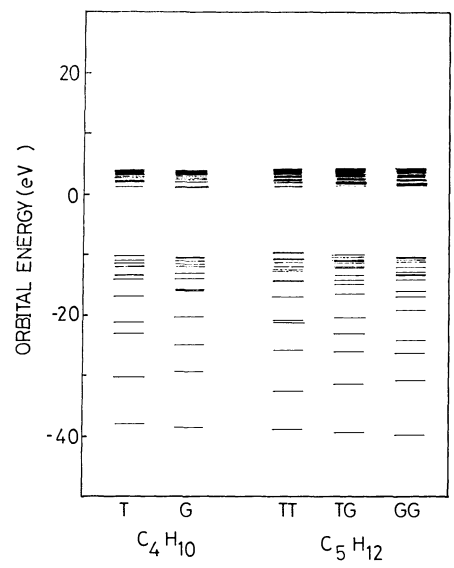

Fig. 5. Orbital energies of the T and G forms in *n*-butane and of the TT, TG and GG forms in *n*-pentane calculated by MINDO/2 method.

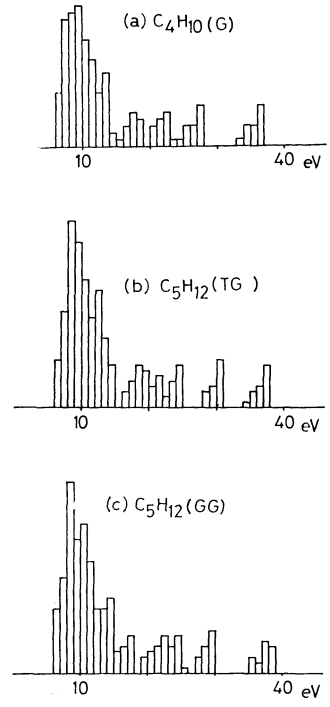

Fig. 6. Histograms of number of the excitation from occupied to unoccupied orbitals against the singlet-singlet excitation energies of the G form in *n*-butane (a), and of the TG, GG forms in *n*-pentane calculated by MINDO/2 method.

TABLE 4. THE ^{13}C CHEMICAL SHIFTS OF *n*-BUTANE AND *n*-PENTANE CALCULATED BY THE LCGI-MO THEORY USING THE MINDO/2 METHOD FOR THEIR PREFERRED ISOMERS AND STATISTICALLY AVERAGED STATES AT 300 K, USING 570 cal/mol AS ΔE_g

		^{13}C chemical shifts (ppm)			
		σ_d	σ_p	σ	$\Delta\sigma$[a]
$CH_3CH_2CH_2CH_3$					
T	$CH_3(1)$	57.17	−206.55	−149.38	0
	$CH_2(2)$	57.31	−222.36	−165.05	−15.67
G	$CH_3(1)$	57.35	−209.37	−152.02	0
	$CH_2(2)$	57.27	−221.11	−163.84	−11.82
$CH_3CH_2CH_2CH_2CH_3$					
TT	$CH_3(1)$	57.17	−198.94	−141.77	0
	$CH_2(2)$	57.26	−211.42	−154.16	−12.39
	$CH_2(3)$	57.39	−218.61	−161.22	−19.45
TG	$CH_3(1)$	57.15	−199.40	−142.25	0
	$CH_2(2)$	57.45	−212.61	−155.16	−12.91
	$CH_2(3)$	57.36	−214.14	−156.78	−14.53
	$CH_2(4)$	57.24	−209.27	−152.03	−9.78
	$CH_3(5)$	57.36	−201.01	−143.65	−1.40
GG	$CH_3(1)$	57.34	−203.36	−146.02	0
	$CH_2(2)$	57.42	−211.31	−153.89	−7.87
	$CH_2(3)$	57.32	−214.32	−157.00	−10.98
Averaged $CH_3CH_2CH_2CH_3$[b]					
	$CH_3(1)$	57.25	−207.77	−150.52	0
	$CH_2(2)$	57.29	−221.82	−164.53	−14.01
$CH_3CH_2CH_2CH_2CH_3$[c]					
	$CH_3(1)$	57.25	−200.17	−142.92	0
	$CH_2(2)$	57.32	−211.14	−153.82	−10.90
	$CH_2(3)$	57.36	−215.72	−158.36	−15.44

a) The $CH_3(1)$ carbon in a molecule is the reference. b) *n*-Butane: averaged over the T, G, and G′ isomers. c) *n*-Pentane: averaged over the TT, TG, TG′, GT, G′T, GG, and G′G′ isomers.

their singlet-singlet excitation energies are also shown in Fig. 6. These results do not differ greatly from those of the *trans* forms shown in Fig. 3. The difference in the electron density among the carbons in the conformation containing the *gauche* form is shown to be smaller than that in the *trans* form. On the other hand, the separation of the occupied and unoccupied orbital energy levels in the conformation containing the *gauche* form is shown to be somewhat larger than that in the *trans* form. Therefore, these results predict that the conformations containing the *gauche* form may give a smaller chemical-shift difference among the carbons than does the *trans* form. These calculated results are tabulated in Table 4. As has been predicted, in the conformations containing the *gauche* form their chemical-shift differences between the $CH_3(1)$ and $CH_2(2)$ carbons in *n*-butane, and between the $CH_2(2)$ and $CH_2(3)$ carbons in *n*-pentane, are somewhat smaller than the corresponding values in the *trans* forms. The observed results should be compared with the calculated results averaged over all the possible conformations (T, G, and G′ for *n*-butane; TT, TG, TG′, GT, G′T, GG, and G′G′ for *n*-pentane) using the following equation:[13]

$$\sigma_{AV} = \sum_i^n X_i \sigma_i \qquad (10)$$

where;

$$X_i = e^{-\Delta E_i/RT} / \sum_i^n e^{-\Delta E_i/RT}$$

in which X_i and σ_i are the fraction and the chemical shift of the *i*-th isomer respectively. R is the gas constant; T, the absolute temperature, and E_i, the energy difference between the *trans* form and the *i*-th isomer. Here, 570 cal/mol[14] is used as the value of the energy difference between the *trans* and *gauche* forms, and 300 K is used as the temperature. These results are also tabulated in Table 4, where the chemical shifts of the carbons in the G and G′ forms of *n*-butane are equal to each other; also, those of the carbons in the TG and TG′, the GT and G′T, and the GG and G′G′ forms of *n*-pentane are equal to each other. These agree relatively well with the observed results. Furthermore, from the results of the chemical-shift difference between the CH_3 and CH_2 carbons in the conformations containing the *gauche* form of *n*-butane and *n*-pentane, the difference is predicted to decrease with an increase in the temperature. However, the observed results of *n*-butane[15] and *n*-pentane[16] in neat liquid are opposite to the calculated ones. The reason for this is that the chemical-shift difference between the CH_3 and CH_2 carbons of the conformation containing the *gauche* form is too small compared with that of the *trans* form.

As has been mentioned above, the LCGI-MO theory was found to interpret well the tendencies of the chemical shift of the carbons in a molecule. However, Table 4 shows that the quantitative agreement between the calculated and observed chemical shifts of the carbons among the molecules is not satisfactory. This discrepancy arises partly from the MO theories, which do not strictly estimate the singlet-singlet excitation energies among the *n*-alkanes considered. Further, some other factors may be pointed out. A molecular orbital approximation cannot give an exact value for the energy of a molecule because it usually neglects the electron correlation due to the mutual Coulomb repulsion of the electrons. Some approximations are made for this in both the INDO and MINDO/2 treatments by the adjustment of the parameter, but there is a limit to this kind of adjustment. Thus, to improve our calculation it will be necessary to take the configuration interaction into account in the future.

References

1) E. G. Paul and D. M. Grant, *J. Amer. Chem. Soc.*, **85**, **1701** (1963); *ibid.*, **86**, 2984 (1964).
2) T. Yonezawa, I. Morishima, and H. Kato, This Bulletin, **36**, 1398 (1966).
3) K. Okada, I. Morishima, and T. Yonezawa, The Preprint of the 10th NMR symposium, p. 8 (1971) Tokyo.
4) J. A. Pople, *Proc. Roy. Soc., Ser. A*, **239**, 541 (1957).
5) J. A. Pople, *J. Chem. Phys.*, **37**, 53 (1962).
6) N. F. Ramsey, *Phys. Rev.*, **78**, 699 (1950).
7) M. J. S. Dewar and E. Haselbach, *J. Amer. Chem. Soc.*, **92**, 3854 (1970).
8) J. A. Pople, D. L. Beveridge, and P. A. Dobosh, *J.*

Chem. Phys., **47**, 2026 (1967).
9) K. Yamaguchi and T. Fueno, This Bulletin, **44**, 43 (1971).
10) J. A. Pople, *Mol. Phys.*, **7**, 301 (1964).
11) L. Pauling, "The Nature of the Chemical Bond," Cornell University Press, Ithaca (1960).
12) D. W. Turner, "Advances in Physical Organic Chemistry," vol. 4, Academic Press (1966), p. 31.
13) H. S. Gutowsky, *J. Chem. Phys.*, **37**, 2196 (1962).
14) I. Ando and A. Nishioka, This Bulletin, **46**, 1040 (1973).
15) I. Ando and A. Nishioka, *ibid.*, **46**, 706 (1973).
16) I. Ando, A. Nishioka, and M. Kondo, Unpublished data.

The Optically-active Vibration and Elastic Constant of Soda-niter[1]

Akio YAMAMOTO, Yuji SHIRO,* and Hiromu MURATA

Department of Chemistry, Faculty of Science, Hiroshima University, Higashisenda-machi, Hiroshima 730
**Shinonome Branch School, Faculty of Education, Hiroshima University, Shinonome-3-chome, Hiroshima 734*

(Received November 29, 1973)

A force field which reproduces satisfactorily both the observed vibrational frequencies and the elastic constants has been determined for the sodium nitrate crystal using the short-range interaction model. In addition to the short-range interactions, the long-range interactions of the vibrationally-induced dipoles were also taken into consideration on the basis of the rigid-ion model; those effective charges which explain fairly well the observed TO–LO frequency splittings were obtained. The distribution of the effective charges on each atom was examined; the best set of effective charges has been found to be $Z_{Na}=0.87\ e$, $Z_N=0.17\ e$, and $Z_O=-0.35\ e$.

The crystal vibration of soda-niter ($NaNO_3$)[2] has been extensively studied in connection with that of the isomorphic crystals having the calcite structure. However, previous investigations[2] have dealt almost exclusively with the short-range interaction model, and little attention has been paid to long-range Coulomb interactions. In the present paper, we wish to call further attention to the effect of the charge distribution on the TO–LO frequency splittings.

First, the short-range interactions are taken into consideration, and the force constants are refined so as to reproduce both the observed vibrational frequencies[2] and the elastic constants.[3] Secondly, a detailed normal coordinate treatment is performed for the optically-active crystal vibration on the basis of the rigid-ion model.[4] The basic formulation of this model was mainly established by Born and his co-workers.[4] As is implied by the name, the interactions of vibrationally-induced dipoles are taken into account as those of rigid point dipoles; any influence of the electronic polarizability of the constituent atoms is implicitly neglected. This model was first applied to the vibrational analysis of relatively simple crystals, such as alkali-halide crystals.[5] The assumptions implicit in this model are, however, considered to be untolerably drastic in a sense; as a consequence, the reproducibility of the frequency dispersion relations, in particular, is found to be poor.[6] For rather complicated crystals, even rigid-ion analyses have been scarcely performed yet because of the long and tedious procedures required, together with the experimental limitations. In the course of a survey of the vibrational properties of complex crystals,[7] in the present study the rigid-ion model is applied to the normal coordinate analysis of the optically-active vibration (wave vector $\boldsymbol{y}=\boldsymbol{0}$), regarding all the atoms as ionizable.

Method of Calculation

Crystal Structure. Sodium nitrate crystallizes in the calcite structure. As is shown in Fig. 1, this structure is most easily visualized as a sodium chloride lattice distorted by the introduction of the disk-shaped nitrate groups. Although the calcite structure is also considered to be a hexagonal lattice, the primitive unit cell is trigonal and contains two formula units of $NaNO_3$. The space group of the trigonal cell is D_{3d}^6—$R\bar{3}c$, and the cell constants[8] are found to be

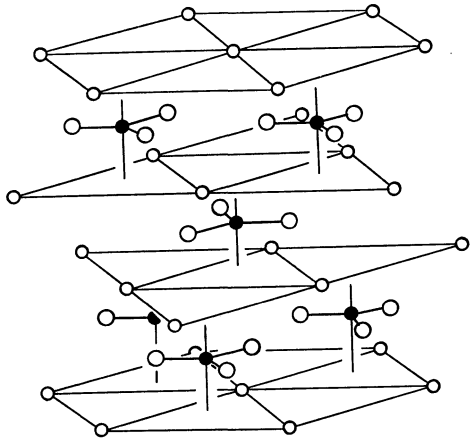

Fig. 1. Crystal structure of soda-niter.
○, Sodium; ●, Nitrogen; ◯, Oxygen.

$a_{rh}=6.3247$ Å and $\alpha=47°16'$. Each sodium atom is coordinated with six oxygen atoms of different nitrate groups, and each such oxygen atom is bound to two sodium atoms.

Normal Coordinate Treatments. In the present study, the normal coordinate treatments were performed in two steps, those based on the short-range interaction model and on the rigid-ion model.

Short-range Interaction Model: The application of Wilson's *GF*-matrix method to the analysis of the optically-active crystal vibration was previously reported by Shimanouchi *et al.*[9] In this study, the modified Urey-Bradley force field[10] was applied to the intramolecular vibrations of the nitrate groups, the correction terms of which were the bond interaction term, p, for the adjacent N–O bond pairs and the angle interaction term, n, for the adjacent O–N–O angle pairs in a single nitrate group. On the other hand, the central force field was used for the intermolecular (lattice) vibrations. With respect to the latter, only the pairs that lie within 3.5 Å were taken into consideration as effective short-range interatomic interactions. As Fig. 2 illustrates, there are six different kinds of pairs in this crystal. The corresponding interatomic distances are listed in Table 1. The dynamical matrix due to these short-range interactions will be designated as $\boldsymbol{D}^s$ hereafter.

Rigid-ion Model: In addition to the short-range interactions mentioned above, the long-range Coulomb interactions of vibrationally-induced dipoles are taken

TABLE 1. FORCE CONSTANTS (mdyn/Å) AND EFFECTIVE CHARGES (electron unit) OF SODA-NITER

FC	Coord.	NO	Pair	Dist.[a]	I $Z=0$	II $x=-1$	III $x=-1/2$	IV $x=-1/5$	V $x=0$	VI $x=+1/5$	VII $x=+1/2$	VIII $x=+3/4$
K	R	6	N O	1.2175	5.656	5.572	5.457	5.450	5.544	5.680	5.863	5.696
H[b]	θ	6	O N O	(120°)	0.581							
F[b]			O O		1.645							
α	ϕ	2	NO_3		0.485	0.492	0.513	0.509	0.493	0.469	0.438	0.428
p					−0.036	0.068	0.037	0.027	0.018	0.017	0.039	0.060
n[c]					0.145	0.107	0.110	0.107	0.130	0.150	0.170	0.184
f_1	q_1	12	Na N	3.2458	0.055	0.043	0.029	0.025	0.023	0.016	0.022	0.019
f_2	q_2	12	Na O	2.4178	0.118	0.162	0.188	0.172	0.191	0.211	0.210	0.204
f_3	q_3	12	Na O	3.4258	0.000[b]	0.000[b]	0.000[b]	0.006	0.008	0.007	0.007	0.005
f_4	q_4	6	O O	3.1638	0.054	0.026	0.028	0.076	0.068	0.052	0.036	0.030
f_5	q_5	12	O O	3.4116	0.050	0.003	0.014	0.014	0.004	−0.012	−0.033	−0.040
f_6	q_6	12	O O	3.4258	0.036	0.025	0.031	0.019	0.007	−0.008	−0.027	−0.031
Z_{Na}		2				0.77	0.74	0.86	0.90	0.87	0.74	0.62
Z_N		2				−0.77	−0.37	−0.17	0.00	0.17	0.37	0.46
Z_O		6				0.00	−0.12	−0.23	−0.30	−0.35	−0.37	−0.36

a) Unit of distance is Å. b) Fixed force constants. c) Unit of n is mdyn·Å.

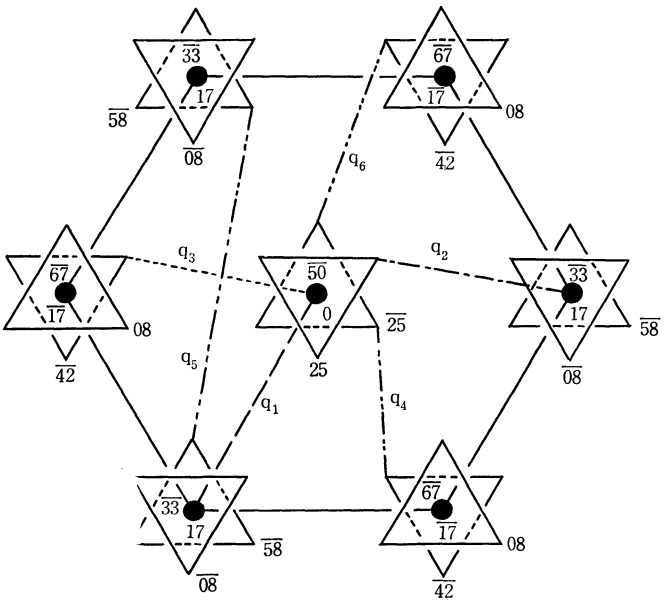

Fig. 2. Short-range interactions in soda-niter, projected on a plane perpendicular to the z axis of the hexagonal cell. The heights of atoms or nitrate groups are expressed in units of $100/c_0$.
(— —), Na···N; (·····), N···O; (—·—), Na···O; (—··—), O···O.

into account in this model. The additional interactions are considered to play an important role, especially in predominantly ionic crystals, and the frequency splitting between LO- and TO-frequencies is brought about through the interactions.[4]

According to Born and Huang,[4] the Coulomb part, $\boldsymbol{D}^c$, in the dynamical matrix near the Γ point is given by:

$$D^c_{ij}(k, k'; \boldsymbol{y}\to\boldsymbol{0}) = Z_k e^2 (m_k m_{k'})^{-1/2}\{4\pi v^{-1} \lim_{\boldsymbol{y}\to 0} (y_i y_j/|\boldsymbol{y}|^2) - Z_{k'} Q_{ij}(k, k'; \boldsymbol{y}\to\boldsymbol{0}) + \delta_{kk'}\sum(k'') Z_{k''} Q_{ij}(k, k''; \boldsymbol{y}\to\boldsymbol{0})\},$$

where $\mathbf{y}$ is the wave vector; Z_k, the effective charge of the k-th atom in terms of electronic charge, e; m_k, the mass of the k-th atom, and v, the unit cell volume. The $Q_{ij}(k, k')$ is a tensor of the second rank for the wave vector zero; it is most easily visualized as the tensor representing the gradient of the Coulomb field at the k site, which is spanned by the point dipoles at the k' site over the trigonal lattice. The numerical evaluation of the tensor elements can be carried out straight-forwardly by the Ewald method.[11] The summations were performed with the PEG0 computer program.[12] The values are constant for a fixed wave vector in the same lattice; therefore, it is sufficient to calculate the sums once for each crystal.

The overall dynamical matrix of the model is now obtained by superposing the Coulomb part, $\boldsymbol{D}^c$, on the short-range part, $\boldsymbol{D}^s$, *viz.*:

$$\boldsymbol{D} = \boldsymbol{D}^s + \boldsymbol{D}^c.$$

Since this crystal contains nitrate groups, there is another serious problem to be elucidated: the distribution of the effective charges on the groups cannot be known in advance. As is shown in Fig. 3, we have inevitably assumed several trial sets of charge distribution under electrically neutral conditions in the whole crystal. In this figure, x stands for the distribution parameter and Z denotes the magnitude of the effective

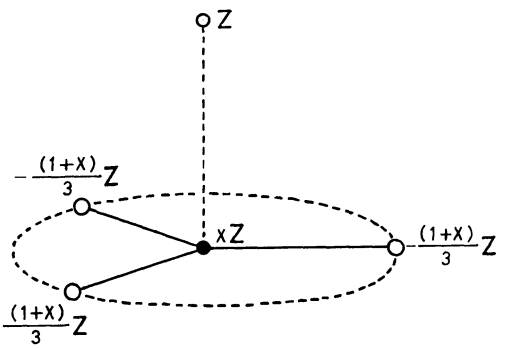

Fig. 3. Charge distribution of $NaNO_3$.
○, Oxygen; ○, Sodium; ●, Nitrogen;
z, magnitude of effective charge in terms of electronic charge e; x, distribution parameter.

charges. Supposing this distribution model, the distribution parameter, x, and the magnitude, Z, enter as independent parameters to be adjusted appropriately. Varying the parameter, x, little by little, both the magnitude, Z, and the short-range force constants were refined in order to obtain the best fit between the observed[2] and calculated frequencies, both ν_t and ν_l, by the least-squares method.[13]

If group theoretical analysis is performed on the basis of the crystal symmetry, much useful information can be obtained beforehand for the vibrational analysis. Generally, one must make the "k-group analysis" [14] based on the symmetry of the wave vector. In the case of the vibration near the center of the Brillouin zone, however, the k-group analysis is reduced to the usual factor-group analysis.[2b]

Refinement of Force Constants. As has been mentioned above, the Jacobians with respect to the frequency[13] and to the elastic constant[15] were obtained independently from the treatments of the short-range interaction model. Taking both Jacobians into consideration, the refinement of the short-range force constants was performed by the use of the following expression:

$$\Delta \boldsymbol{K} = (\tilde{\boldsymbol{J}}_h^{\nu} \boldsymbol{W}_{\nu} \boldsymbol{J}_h^{\nu} + \tilde{\boldsymbol{J}}_h^{E} \boldsymbol{W}_E \boldsymbol{J}_h^{E})^{-1} \times (\tilde{\boldsymbol{J}}_h^{\nu} \boldsymbol{W}_{\nu} \Delta \boldsymbol{\nu} + \tilde{\boldsymbol{J}}_h^{E} \boldsymbol{W}_E \Delta \boldsymbol{E}),$$

where the suffixes ν and E attached to some matrices denote those which are related to the vibrational and the elastic properties respectively. The $\boldsymbol{W}$ matrices are the relative weight matrices of the observed vibrational frequencies or elastic constants. The $\Delta\boldsymbol{\nu}$ and $\Delta\boldsymbol{E}$ are the deviation column-matrices of the calculated eigenfrequencies and elastic constants respectively from their observed values.

In the case of the rigid-ion model, both the short-range force constants and the magnitude, Z, of the effective charges were adjusted with reference to the observed ν_t and ν_l values.

The actual calculation was carried out on a TOSBAC 3400 MODEL 41 electronic computer at the Computing Center of Hiroshima University.

Results and Discussion

Optically-active Vibration. According to the rigid-ion model, certain interactions are found to be brought about between the macroscopic field and the induced dipoles if any dipole moment is induced as a whole unit cell through the vibration of fictitious charged particles. Only the A_{2u} and E_u symmetric modes of the vibration are those which give rise to the polarization. Any vibrational frequencies, ν_l, of the longitudinal wave are higher than the corresponding frequencies, ν_t, of the transverse wave. The reason for the difference in the frequencies of the longitudinal and transverse waves is obvious: in a transverse wave, the

Table 2. Dipole lattice sum, $Q_{ij}(k,k')$,[a] of soda-niter

(1_x)	0.0427								
(1_y)	0.0000	0.0427							
(1_z)	0.0000	0.0000	0.0152						
(2_x)	0.0188	0.0000	0.0000	0.0427					
(2_y)	0.0000	0.0188	0.0000	0.0000	0.0427				
(2_z)	0.0000	0.0000	0.0630	0.0000	0.0000	0.0152			
(3_x)	1.1583	0.0000	0.0000	0.0031	0.0000	0.0000	0.0427		
(3_y)	0.0000	−0.5118	0.0004	0.0000	0.0150	−0.0221	0.0000	0.0427	
(3_z)	0.0000	0.0004	−0.5458	0.0000	−0.0221	0.0825	0.0000	0.0000	0.0152
(4_x)	−0.0943	−0.7232	−0.0004	0.0120	0.0052	0.0191	0.1812	−0.1269	−0.0004
(4_y)	−0.7232	0.7407	−0.0002	0.0052	0.0061	0.0110	−0.1269	0.0346	0.0002
(4_z)	−0.0004	−0.0002	−0.5458	0.0191	0.0110	0.0825	−0.0004	0.0002	−0.1151
(5_x)	−0.0943	0.7232	0.0004	0.0120	−0.0052	−0.0191	0.1812	0.1269	0.0004
(5_y)	0.7232	0.7407	−0.0002	−0.0052	0.0061	0.0110	0.1269	0.0346	0.0002
(5_z)	0.0004	−0.0002	−0.5458	−0.0191	0.0110	0.0825	0.0004	0.0002	−0.1151
(6_x)	0.0031	0.0000	0.0000	1.1583	0.0000	0.0000	−0.0223	0.0000	0.0000
(6_y)	0.0000	0.0150	−0.0221	0.0000	−0.5118	0.0004	0.0000	0.0121	−0.0502
(6_z)	0.0000	−0.0221	0.0825	0.0000	0.0004	−0.5458	0.0000	−0.0502	0.1109
(7_x)	0.0120	0.0052	0.0191	−0.0943	−0.7232	−0.0004	0.0120	−0.0052	−0.0191
(7_y)	0.0052	0.0061	0.0110	−0.7232	0.7407	−0.0002	−0.0052	0.0061	0.0110
(7_z)	0.0191	0.0110	0.0825	−0.0004	−0.0002	−0.5458	−0.0191	0.0110	0.0825
(8_x)	0.0120	−0.0052	−0.0191	−0.0943	0.7232	0.0004	0.0120	0.0052	0.0191
(8_y)	−0.0052	0.0061	0.0110	0.7232	0.7407	−0.0002	0.0052	0.0061	0.0110
(8_z)	−0.0191	0.0110	0.0825	0.0004	−0.0002	−0.5458	0.0191	0.0110	0.0825
(9_x)	0.0422	0.0000	0.0000	0.0422	0.0000	0.0000	0.0209	−0.0730	−0.0545
(9_y)	0.0000	0.0422	0.0000	0.0000	0.0422	0.0000	−0.0730	0.0506	0.0529
(9_z)	0.0000	0.0000	0.0162	0.0000	0.0000	0.0162	−0.0545	0.0529	0.0292
(10_x)	0.0422	0.0000	0.0000	0.0422	0.0000	0.0000	0.0209	0.0730	0.0545
(10_y)	0.0000	0.0422	0.0000	0.0000	0.0422	0.0000	0.0730	0.0506	0.0529
(10_z)	0.0000	0.0000	0.0162	0.0000	0.0000	0.0162	0.0545	0.0529	0.0292
	(1_x)	(1_y)	(1_z)	(2_x)	(2_y)	(2_z)	(3_x)	(3_y)	(3_z)

Table 2. (Continued)

(4_x)	0.0427								
(4_y)	0.0000	0.0427							
(4_z)	0.0000	0.0000	0.0152						
(5_x)	−0.0386	0.0000	0.0000	0.0427					
(5_y)	0.0000	0.2544	−0.0005	0.0000	0.0427				
(5_z)	0.0000	−0.0005	−0.1151	0.0000	0.0000	0.0152			
(6_x)	0.0120	−0.0052	−0.0191	0.0120	0.0052	0.0191	0.0427		
(6_y)	−0.0052	0.0061	0.0110	0.0052	0.0061	0.0110	0.0000	0.0427	
(6_z)	−0.0191	0.0110	0.0825	0.0191	0.0110	0.0825	0.0000	0.0000	0.0152
(7_x)	0.0035	0.0149	0.0435	0.0031	0.0000	0.0000	0.1812	−0.1269	−0.0004
(7_y)	0.0149	−0.0137	0.0251	0.0000	0.0150	−0.0221	−0.1269	0.0346	0.0002
(7_z)	0.0435	0.0251	0.1109	0.0000	−0.0221	0.0825	−0.0004	0.0002	−0.1151
(8_x)	0.0031	0.0000	0.0000	0.0035	−0.0149	−0.0435	0.1812	0.1269	0.0004
(8_y)	0.0000	0.0150	−0.0221	−0.0149	−0.0137	0.0251	0.1269	0.0346	0.0002
(8_z)	0.0000	−0.0221	0.0825	−0.0435	0.0251	0.1109	0.0004	0.0002	−0.1151
(9_x)	−0.0200	0.0493	−0.0186	0.1063	0.0236	0.0731	0.0209	−0.0730	−0.0545
(9_y)	0.0493	0.0915	−0.0737	0.0236	−0.0349	0.0207	−0.0730	0.0506	0.0529
(9_z)	−0.0186	−0.0737	0.0292	0.0731	0.0207	0.0292	−0.0545	0.0529	0.0292
(10_x)	0.1063	−0.0236	−0.0731	−0.0200	−0.0493	0.0186	0.0209	0.0730	0.0545
(10_y)	−0.0236	−0.0349	0.0207	−0.0493	0.0915	−0.0737	0.0730	0.0506	0.0529
(10_z)	−0.0731	0.0207	0.0292	0.0186	−0.0737	0.0292	0.0545	0.0529	0.0292
	(4_x)	(4_y)	(4_z)	(5_x)	(5_y)	(5_z)	(6_x)	(6_y)	(6_z)

(7_x)	0.0427											
(7_y)	0.0000	0.0427										
(7_z)	0.0000	0.0000	0.0152									
(8_x)	−0.0386	0.0000	0.0000	0.0427								
(8_y)	0.0000	0.2544	−0.0005	0.0000	0.0427							
(8_z)	0.0000	−0.0005	−0.1151	0.0000	0.0000	0.0152						
(9_x)	−0.0200	0.0493	−0.0186	0.1063	0.0236	0.0731	0.0427					
(9_y)	0.0493	0.0918	−0.0737	0.0236	−0.0349	0.0207	0.0000	0.0427				
(9_z)	−0.0186	−0.0737	0.0292	0.0731	0.0207	0.0292	0.0000	0.0000	0.0152			
(10_x)	0.1063	−0.0236	−0.0731	−0.0200	−0.0493	0.0186	0.0188	0.0000	0.0000	0.0427		
(10_y)	−0.0236	−0.0349	0.0207	−0.0493	0.0915	−0.0737	0.0000	0.0188	0.0000	0.0000	0.0427	
(10_z)	−0.0731	0.0207	0.0292	0.0186	−0.0737	0.0292	0.0000	0.0000	0.0630	0.0000	0.0000	0.0152
	(7_x)	(7_y)	(7_z)	(8_x)	(8_y)	(8_z)	(9_x)	(9_y)	(9_z)	(10_x)	(10_y)	(10_z)

a) Unit of $Q_{ij}(k, k')$ is Å^{-3}. In this table, $i, j = x, y$ or z, and k and k' specify the particles in the primitive cell. Atom numbering is as follows:
1 N(1/4, 1/4, 1/4); 2 N(−1/4, −1/4, −1/4); 3 O(1/3−u, 1/4, u); 4 O(u, 1/2−u, 1/4); 5 O(1/4, u, 1/2−u); 6 O(u−1/2, −1/4, −u); 7 O(−u, u−1/2, −1/4); 8 O(−1/4, −u, u−1/2); 9 Na(1/2, 1/2, 1/2); 10 Na(0, 0, 0); u=0.4901.

vibrationally-induced dipole gives rise to the direction normal to the applying macroscopic field, while in a longitudinal wave, the dipole is induced parallel to the field; therefore, this field contributes an additional restoring force. A frequency splitting between ν_l and ν_t is called a "TO-LO splitting"; the splitting width depends entirely on the long-range Coulomb interactions.

The numerical values of the diagonal elements of the dipole lattice sums were examined by the use of the following relation:

$$\sum_{1}^{3}(i)Q_{ii}(k, k'; \boldsymbol{y}\rightarrow\boldsymbol{0}) = 4\pi/v,$$

where v denotes the unit cell volume, where $i=x$, y, or z, and where k and k' specify the particles in the primitive unit cell. The calculated lattice sums are listed in Table 2. When the charges are distributed spherically or tetrahedrally, the tensor, $\boldsymbol{Q}$, becomes scalar and has the well-known value of $4\pi/3v$ (in Å^{-3}), like that of the Lorentz field.

Intramolecular Vibration: Factor-group analysis[2b] predicts that the intramolecular modes near the center of the Brillouin zone will have the irreducible representation:

$$\Gamma_n = A_{1g} + A_{2g} + 2E_g + A_{1u} + A_{2u} + 2E_u.$$

The A_{1g} and E_g branches are Raman-active, and the A_{2u} and E_u branches are infrared-active, while the A_{1u} and A_{2g} branches are optically-inactive in both infrared absorption and Raman effect.

For the short-range interaction model, the observed[2] and calculated frequencies and the tentative assignments are listed in Table 3. The results for the rigid-ion model are given in Table 4. The corresponding force constants and effective charges are also shown in Table 1. Each distribution parameter, x, is listed at the top of Table 1. Model I corresponds to the short-range interaction model, while Model II and below are based on the rigid-ion model. Apparently, the

Table 3. Observed and calculated vibrational frequencies (cm^{-1}) of soda-niter

Sym.		Obsd[a]	Calcd	Assignment[b]
A_{1g}	ν_{11}	1068	1067	NO str.
A_{2g}	ν_{21}		836	NO_3 out-of-plane def.
	ν_{22}		200	NO_3 transl(z).
	ν_{23}		174	NO_3 rot(z).
E_g	ν_{31}	1385	1392	NO str.
	ν_{32}	727	726	ONO def.
	ν_{22}	184	178	NO_3 rot (x,y).
	ν_{34}	98	124	NO_3 transl (x,y).
A_{1u}	ν_{41}		1069	NO str.
	ν_{42}		148	Na transl(z).
A_{2u}	ν_{51}	831	831	NO out-of-plane def.
	ν_{52}	217	212	Na, NO_3 transl (z).
	ν_{53}	89	124	NO_3 rot (z).
E_u	ν_{61}	1405	1392	NO str.
	ν_{62}	692	725	ONO def.
	ν_{63}	214	209	Na, NO_3 transl(x,y).
	ν_{64}	173	173	Na transl(x,y).
	ν_{65}	145	118	NO_3 rot(x,y).

a) Ref. 2(f). b) str., stretching; def., angle deformation; rot., rotational lattice mode; transl., translational lattice mode.

vibrationally-induced dipoles are seen not to exert a critical effect on the intra-molecular vibration. Thus, the observed large frequency splittings between E_g and E_u symmetric N–O stretching modes were again poorly explained as in Model I. The rigid-ion model may, therefore, be considered not to be suitable for the vibration of strongly interacting systems, such as those coupled firmly with a co-valent bond. An analysis which is based on some models of a higher order might be essential for a satisfactory explanation of these experimental facts. These subjects have been discussed in part by Decius *et al.*;[16] however, apart from their background polarization model, the point dipole approximation may be unsuitable for the intramolecular vibration.

Lattice Vibration: The lattice modes of the crystal have the irreducible representation of:[2b]

$$\Gamma_l = A_{1u} + 2A_{2g} + 2A_{2u} + 2E_g + 3E_u.$$

Group theory reveals five distinct infrared-active frequencies, two of the A_{2u} symmetry and three of the E_u symmetry. There are also two Raman-active modes with the E_g symmetry. The observed[2] and calculated frequencies are given in Tables 3 and 4, together with the intramolecular ones. The contribution (%) of each

Table 5. Contribution (%) of potential terms to each normal frequency[a]

Sym.		K	f_1	f_2	f_3	f_4	f_5	f_6	H	F	α	p	n
A_{1g}	ν_{11}	53	0	1	0	0	1	0	0	46	0	−1	0
A_{2g}	ν_{21}	0	1	0	0	1	0	0	0	0	98	0	0
	ν_{22}	0	3	35	0	9	12	39	0	0	1	0	0
	ν_{23}	0	2	5	0	47	42	4	0	0	0	0	0
E_g	ν_{31}	83	0	1	0	0	0	0	14	5	0	1	−3
	ν_{32}	5	0	2	0	1	3	0	46	53	0	0	−9
	ν_{33}	0	0	33	0	47	0	20	0	0	0	0	0
	ν_{34}	0	23	29	0	30	0	18	0	0	0	0	0
A_{1u}	ν_{41}	53	0	1	0	0	1	0	0	46	0	−1	0
	ν_{42}	0	21	79	0	0	0	0	0	0	0	0	0
A_{2u}	ν_{51}	0	1	0	0	0	0	0	0	0	99	0	0
	ν_{52}	0	7	70	0	0	20	4	0	0	0	0	0
	ν_{53}	0	20	11	0	0	58	11	0	0	0	0	0
E_u	ν_{61}	83	1	0	0	0	0	0	14	5	0	1	−3
	ν_{62}	5	0	2	0	0	3	1	46	53	0	0	−9
	ν_{63}	0	22	68	0	0	0	9	0	0	0	0	0
	ν_{64}	0	32	62	0	0	0	5	0	0	0	0	0
	ν_{65}	0	29	2	0	0	0	69	0	0	0	0	0

a) Notations are the same as those in Tables 1 and 3.

Table 4. Observed and calculated longitudinal and transverse frequencies (cm^{-1}) of soda-niter

Sym.	Observed		II		III		IV		V		VI		VII		VIII	
	ν_t	ν_l	ν_t	ν_l	ν_t	ν_l	ν_t	ν_l	ν_t	ν_l	ν_t	ν_l	ν_t	ν_l	ν_t	ν_l
A_{1g}	1068		1068		1069		1068		1069		1068		1068		1069	
A_{1u}			1069		1070		1070		1070		1069		1068		1070	
			192		194		192		199		202		195		186	
A_{2g}			847		844		843		842		842		843		845	
			191		199		215		205		179		139		126	
			110		107		123		117		117		113		103	
A_{2u}	838	843	834	850	839	841	840	840	839	841	837	844	835	846	835	851
	205	251	216	262	217	262	188	257	190	266	198	267	205	254	211	243
	51	89	50	90	52	85	52	80	53	76	53	75	53	73	53	72
E_g	1385		1377		1377		1376		1377		1376		1375		1376	
	727		727		725		728		727		728		728		727	
	186		166		157		183		184		185		187		188	
	98		101		101		115		110		104		98		95	
E_u	1357	1419	1375	1383	1377	1377	1376	1376	1377	1378	1376	1380	1375	1382	1376	1385
	727		727	729	726	726	726	726	725	725	726	726	726	727	725	726
	204	271	210	254	212	256	183	254	187	264	196	267	208	258	213	247
	175	185	167	180	175	183	161	166	169	171	175	178	182	184	183	185
	87	97	86	102	88	102	80	92	82	93	85	95	88	95	89	96

TABLE 6. CONTRIBUTION (%) OF POTENTIAL TERMS TO EACH NORMAL FREQUENCY; DISTRIBUTION PARAMETER $x=-1$[a]

Sym.	Mode[b]	K	f_1	f_2	f_3	f_4	f_5	f_6	H	F	α	p	n	Z[c]
A_{1g}	ν_{11}	52	0	1	0	0	0	0	0	46	0	1	0	0
E_g	ν_{31}	83	0	0	0	0	0	0	14	5	0	−1	−2	0
	ν_{32}	6	0	2	0	0	0	0	44	53	0	0	−5	0
	ν_{33}	0	2	61	0	18	0	19	0	0	0	0	0	−1
	ν_{34}	0	23	33	0	48	0	10	0	0	0	0	0	−14
A_{2u}	ν_{51}(t)	0	1	0	0	0	0	0	0	0	100	0	0	−1
	ν_{51}(l)	0	1	0	0	0	0	0	0	0	96	0	0	3
	ν_{52}(t)	0	8	97	0	0	1	2	0	0	0	0	0	−7
	ν_{52}(l)	0	6	65	0	0	0	0	0	0	1	0	0	28
	ν_{53}(t)	0	58	2	0	0	29	65	0	0	0	0	0	−54
	ν_{53}(l)	0	7	18	0	0	11	26	0	0	2	0	0	35
E_u	ν_{61}(t)	83	0	0	0	0	0	0	14	5	0	−1	−2	−1
	ν_{61}(l)	82	0	0	0	0	0	0	14	5	0	−1	−2	1
	ν_{62}(t)	6	0	2	0	0	0	1	44	53	0	0	−5	0
	ν_{62}(l)	6	0	2	0	0	0	0	43	53	0	0	−5	0
	ν_{63}(t)	0	14	90	0	0	0	9	1	1	0	0	0	−15
	ν_{63}(l)	0	14	62	0	0	0	2	0	0	0	0	0	22
	ν_{64}(t)	0	30	92	0	0	0	1	0	1	0	0	0	−24
	ν_{64}(l)	0	19	78	0	0	0	7	1	1	0	0	0	−7
	ν_{65}(t)	0	51	9	0	0	0	87	0	0	0	0	0	−47
	ν_{65}(l)	0	27	11	0	0	0	66	0	0	0	0	0	−5

a) Notations are the same as those in Tables 1 and 3. b) t, transverse; l, longitudinal. c) Coulomb term.

TABLE 7. CONTRIBUTION (%) OF POTENTIAL TERMS TO EACH NORMAL FREQUENCY; DISTRIBUTION PARAMETER $x=+0.2$[a]

Sym.	Mode[b]	K	f_1	f_2	f_3	f_4	f_5	f_6	H	F	α	p	n	Z[c]
A_{1g}	ν_{11}	53	0	1	0	0	0	0	0	46	0	0	0	0
E_g	ν_{31}	85	0	0	0	0	0	0	14	5	0	0	−2	−2
	ν_{32}	6	0	3	0	1	−1	0	44	53	0	0	−8	2
	ν_{33}	0	0	37	3	55	0	−3	0	0	0	0	0	8
	ν_{34}	0	10	132	6	6	0	−11	0	0	0	0	0	−42
A_{2u}	ν_{51}(t)	0	0	1	1	0	0	0	0	0	94	0	0	4
	ν_{51}(l)	0	0	1	1	0	0	0	0	0	93	0	0	6
	ν_{52}(t)	0	4	149	0	0	−2	0	0	0	0	0	0	−51
	ν_{52}(l)	0	3	72	0	0	0	0	0	0	1	0	0	24
	ν_{53}(t)	0	10	50	9	0	−133	−27	0	0	0	0	0	191
	ν_{53}(l)	0	1	128	5	0	−73	−15	0	0	0	0	0	54
E_u	ν_{61}(t)	85	0	0	0	0	0	0	14	5	0	0	−2	−2
	ν_{61}(l)	84	0	0	0	0	0	0	14	5	0	0	−2	−1
	ν_{62}(t)	6	0	3	0	0	−1	0	44	53	0	0	−8	2
	ν_{62}(l)	6	0	3	0	0	−1	0	44	53	0	0	−8	2
	ν_{63}(t)	0	9	140	0	0	0	−1	0	0	0	0	0	−48
	ν_{63}(l)	0	6	66	0	0	0	0	0	0	0	0	0	28
	ν_{64}(t)	0	10	110	0	0	0	0	0	0	0	0	0	−19
	ν_{64}(l)	0	9	115	0	0	0	−1	0	0	0	0	0	−23
	ν_{65}(t)	0	8	20	12	0	0	−46	0	0	0	0	0	106
	ν_{65}(l)	0	3	48	11	0	0	−40	0	0	0	0	0	78

a) Notations are the same as those in Tables 1 and 3. b) t, transverse; l, longitudinal. c) Coulomb term.

potential parameter to the frequencies was calculated for Model I; the results are shown in Table 5. Similar results were obtained for the rigid-ion model; examples are given in Tables 6 and 7 for only two distribution models. Note how the Coulomb term contributes to each lattice mode. Table 4 suggests that a good agreement is obtained over a wide range of charge distributions. Unlike the intramolecular vibration, the lattice vibration is mainly concerned with the relative motion of considerably separated groups; therefore, even with the point dipole approximation the dynamical properties of the system are described satisfactorily well.

Normal coordinate treatments have been made by several groups of authors[17] using the short-range interaction model. In addition to these, both the interaction of the vibrating dipoles and the influence of the electronic polarizability were taken into account respectively as the rigid-ion model and the shell model[18]

by Plihal *et al.*[19] They regarded the nitrate group as one bulky ion, the charge of which is located at the center of the goup, and analyzed the optically-active vibrations of three crystals of the calcite structure. Their rigid-ion calculations essentially correspond to those of Model II in this study. If one assumes this charge distribution, the influence of the long-range Coulomb interactions appears mainly in the translational lattice modes, and as is illustrated in Figs. 4 and 5, the Z-dependence of the vibrational frequencies is found to be monotonic. In spite of their rather crude approximation, a good agreement was obtained between the calculated and experimental results in the same manner as in the present investigation.

As is shown in Table 1, certain short-range force constants gradually changed; however, the magnitude, Z, of the effective charges was seen to fall into the range from 0.8 e to 0.9 e, regardless of the distribution parameter, x. Though the calculated TO–LO splittings appear to depend critically on Z rather than on x under these circumstances, the x-dependence of the calculated frequencies differs slightly from model to model. Some typical behavior is illustrated in Figs. 4 and 5. As far as the present investigation is concerned, the charge distribution model of $x=+1/5$ has given the best results. In this distribution, the effective charges on the atoms are $Z_{Na}=0.87\ e$, $Z_C=0.17\ e$, and $Z_O=-0.35\ e$. Those distribution models which have

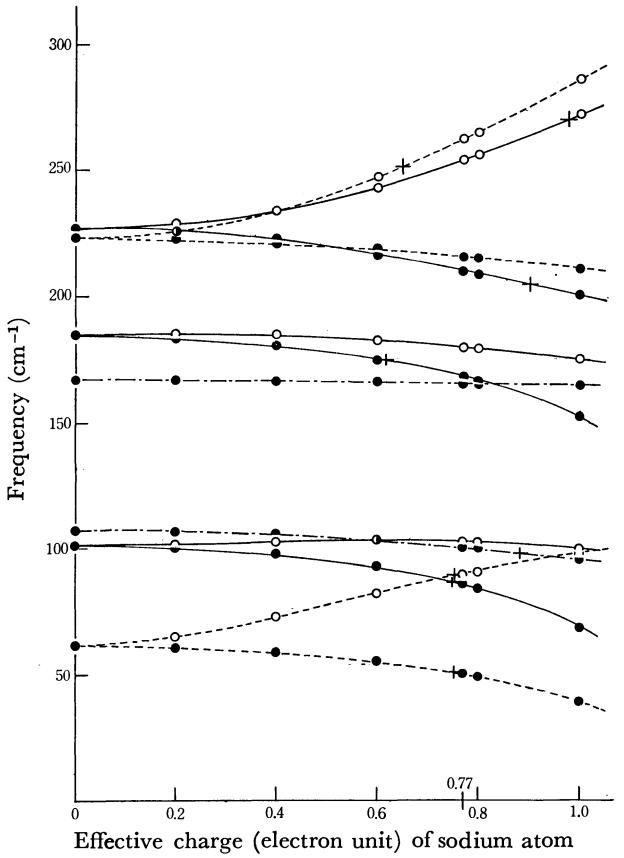

Fig. 4. Z-Dependence of optically-active lattice vibrations for $x=-1$.
(------), A_{2u}; (—·—), E_g; (——), E_u; ●, transverse mode; ○, longitudinal mode; +, observed frequency.

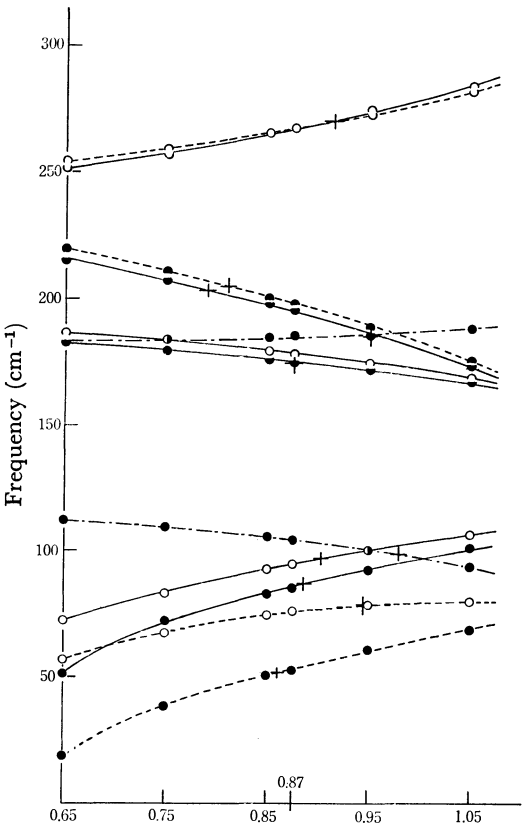

Fig. 5. Z-Dependence of optically-active lattice vibrations for $x=+1/5$. Other descriptions are the same as those in Fig. 4.

larger values of the x parameter than unity were found to give poorer results in this work. Though the above distribution is considered to be the best in this rigid-ion treatment, both the distribution parameter, x, and the magnitude, Z, might be altered in the higher-order models.

As to the short-range force constants, they have been considered in previous short-range interaction treatments to arise from the repulsive force; therefore, they must have positive values inherently. Because account was taken separately of the long-range Coulomb interactions in addition to the short-range ones, they do not necessarily have positive values. Therefore, the physical meaning of the force constants is considered to be essentially different from those in the previous treatments.

The charge distributions of various groups have been estimated from the studies of cohesive energy[20] and of electronegativity;[21] however, the results differ considerably both with the methods and with the investigators. Those obtained are, by nature, statical properties; consequently, they need not always coincide with those of the present dynamically-effective charges.

We wish to conclude this section by pointing out the following relation:

$$\sum_1^n(i)\omega_{i0}^2 = \sum_1^n(i)\omega_i^2(\boldsymbol{y}\to\boldsymbol{0}),$$

where the left and right sides are concerned with the frequencies of the equilibrium crystal field[16] and of the

TABLE 8. OBSERVED AND CALCULATED ELASTIC CONSTANTS (10^{10} dyn/cm^2) OF SODA-NITER

	Obsd[a]	Calcd	Sym.
C_{11}	86.7	81.5	A_{1g}, E_g
C_{21}	16.3	25.5	A_{1g}, E_g
C_{31}	16.0	23.0	A_{1g}
C_{33}	37.0	43.1	A_{1g}
C_{41}	8.2	8.4	E_g
C_{44}	21.3	15.6	E_g

a) Ref. 3.

TABLE 9. CONTRIBUTION (%) OF POTENTIAL TERMS TO EACH ELASTIC CONSTANT IN SODA-NITER[a]

	C_{11}	C_{21}	C_{31}	C_{33}	C_{41}	C_{44}
K	1	1	1	0	0	0
f_1	17	17	18	4	52	27
f_2	23	35	44	17	47	31
f_3	0	0	0	0	0	0
f_4	1	0	10	36	14	23
f_5	51	49	−1	0	−2	0
f_6	6	−1	27	42	−14	19
H	0	−1	0	0	1	0
F	1	0	1	0	1	0
α	0	0	0	0	0	0
p	0	0	0	0	0	0
n	0	0	0	0	0	0

a) Notations are the same as those in Table 1.

rigid-ion approximation respectively, and where n is the number of the vibrational degrees of freedom.

Elastic Constant. The elastic constants of this crystal were determined long ago; the data of Bhimasenachar[3] have been most commonly referred to. Since the space group of the crystal belongs to D_{3d}^6, the independent non-zero elements are the following terms; C_{11}, C_{21}, C_{31}, C_{33}, C_{41}, and C_{44}.[22] Few attempts have been performed to make a theoretical calculation of the elastic constants of this crystal except for that by Shiro.[17c] The calculated and observed elastic constants are compared in Table 8. The contribution of the potential parameters was also calculated; it is given in Table 9. This table suggests that the predominantly contributing terms to each element are in the following manner: C_{11} and C_{21}, f_5; C_{31}, f_2; C_{33}, f_6; C_{41}, f_1 and f_2; C_{44}, f_2. It is thus verified, by the way, that weakly-interacting parts are greatly responsible for the elastic properties of the crystalline state.

Since the mode of contribution to the elastic properties is considered to be essentially independent of that to the vibrational properties, the more reliable force constants are to be obtained with reference to the two types of properties complementarily.

Finally, the resulting elastic constants are identified as the mechanical part, because all interactions except for the short-range ones were neglected in this treatment. Therefore, further work will be required to take the contributions from the other interactions[4] into consideration.

The authors wish to express their gratitude to Mr. Masaru Ohsaku of Hiroshima University for his critical reading of the preliminary manuscript and valuable suggestions, and also to Mr. Tamaki Utida of Hiroshima University for permitting them to use his program PEG0 and for his useful discussions and advice.

References

1) Presented in part at the 28th Annual Meeting of the Chemical Society of Japan, Tokyo, April, 1973.
2) a) P. Pattabhiramayya, *Proc. Ind. Acad. Sci.*, **7A**, 229 (1938); b) S. Bhagavantam and T. Venkatarayudu, *ibid.*, **9A**, 224 (1939); c) A. K. Ramdas, *ibid.*, **37A**, 441 (1953); d) J. R. Ferraro and A. Walker, *J. Chem. Phys.*, **42**, 1273 (1965); e) D. L. Rousseau and R. E. Miller, *ibid.*, **48**, 3409 (1968); f) I. Nakagawa and J. L. Walter, *ibid.*, **51**, 1389 (1969); g) P. J. Ring, *Infrared Phys.*, **12**, 237 (1972).
3) J. Bhimasenachar, *Proc. Ind. Acad. Sci.*, **22A**, 199 (1954).
4) M. Born and K. Huang, "Dynamical Theory of Crystal Lattices," Oxford University Press, London (1954).
5) See, for example, E. W. Kellermann, *Phil. Trans. Roy. Soc.*, **238**, 513 (1940).
6) See, for example, T. Toya, *Bussei*, **6**, 121 (1966) or B. G. Dick, "Lattice Dynamics," ed., by R. F. Wallis Pergamon Press, Oxford (1965).
7) A. Yamamoto, Y. Shiro, and H. Murata, This Bulletin, **47**, 265 (1974).
8) R. L. Sass, R. Vidale, and J. Donohue, *Acta Crystallogr.*, **10**, 567 (1957).
9) T. Shimanouchi, M. Tsuboi, and T. Miyazawa, *J. Chem. Phys.*, **35**, 1597 (1961).
10) T. Shimanouchi, *Pure Appl. Chem.*, **7**, 131 (1963).
11) a) P. P. Ewald, *Ann. Phys.*, **54**, 519 (1917); b) P. P. Ewald, *ibid.*, **64**, 253 (1921).
12) The computer program PEG0 was originally written by Mr. Tamaki Utida of our laboratory for the calculation of the dipole lattice sum which appears in the long-range Coulomb part of the dynamical matrix.
13) T. Miyazawa, *Nippon Kagaku Zasshi*, **76**, 1132 (1955).
14) O. V. Kovalev, "Irreducible Representations of the Space Groups," Science Publ., New York (1964).
15) Y. Shiro and T. Miyazawa, This Bulletin, **44**, 2371 (1971).
16) a) J. C. Decius, *J. Chem. Phys.*, **49**, 1387 (1968); b) R. Frech and J. C. Decius, *ibid.*, **51**, 1536 (1969); c) R. Frech and J. C. Decius, *ibid.*, **51**, 5315 (1969); d) R. Frech and J. C. Decius, *ibid.*, **54**, 2374 (1971).
17) a) K. Venkateswarlu and K. Ramaswamy, *Indian J. Pure Appl. Phys.*, **2**, 209 (1964); b) S. C. Wait, A. T. Ward, and G. J. Janz, *J. Chem. Phys.*, **45**, 133 (1966); c) Y. Shiro, *J. Sci. Hiroshima University, Ser. A-II*, **32**, 77 (1968); d) See Ref. 2(f).
18) See, for example, R. A. Cowley, *Proc. Roy. Soc., Ser. A*, **268**, 109 (1962).
19) a) K. H. Hellwege, W. Lesch, M. Plihal, and G. Schaack, *Solid State Commun.*, **7**, 185 (1969); b) K. H. Hellwege, W. Lesch, M. Plihal, and G. Schaack, *Z. Phys.*, **232**, 61 (1970); c) M. Plihal and G. Schaack, *Phys. Stat. Sol.*, **42**, 485 (1970).
20) H. D. P. Jenkins and T. C. Waddington, *J. Inorg. Nucl. Chem.*, **34**, 2465 (1972).
21) S. S. Batsnov, *Zh. Neorg. Khim.*, **9**, 1323 (1964).
22) J. F. Nye, "Physical Properties of Crystals," Oxford University Press, London (1957).

Radiation Chemical Studies with Cyclotron Beams. III. The Heavy-ion Radiolysis of Liquid Aliphatic Ketones

Masao MATSUI and Masashi IMAMURA

The Institute of Physical and Chemical Research, Wako, Saitama 351

(Received December 6, 1973)

The liquid-phase radiolysis of acetone, methyl ethyl ketone, and diethyl ketone with ^{4}He–, ^{12}C–, and ^{14}N–ions was carried out with the intention of discovering the specific reactions taking place in a very high LET region. The heavy ions were accelerated at various energies with an IPCR cyclotron, the LET of which was up to 80 eV/Å. The radiolytic yields of the main gaseous products, hydrogen and carbon monoxide, were found to increase appreciably with an increase in the LET and to reach the maximum values in the LET region between 50 and 70 eV/Å. The ratios of the two yields, $G(H_2)/G(CO)$, also increase substantially with an increase in the LET. These results, as well as the variations in the yields of saturated and unsaturated hydrocarbons, appear to indicate a thermal-spike effect which may bring about the thermal decomposition of free radicals, giving rise to the enhanced $G(H_2)$ and $G(CO)$ values in the high LET region.

We have been studying the radiolysis with heavy charged particles, helium, carbon, and nitrogen ions, accelerated with an IPCR 160 cm cyclotorn, the LET of which was in the range up to 80 eV/Å. In previous papers[1,2] the results of the heavy-ion radiolysis of aerated aqueous solutions of ferrous sulfate (Fricke solution) have been reported. The same procedures have also been applied to some neat organic liquids.

The aim of the present experiments is to elucidate the specific reactions induced by the interaction of energetic heavy ions with matter. Although no systematic studies of radiolysis with heavy ions have been reported, some unique results seem to reflect the specific reactions going on in the high LET region. For instance, as we[3] and other investigators[4,5] have found, the radiolytic yields of hydrogen from several organic liquids increase significantly in the high LET region, above several tens of eV/Å, irrespective of the variation in the yields in the lower LET region.[4,5]

These characteristic increases in the hydrogen yields seem not to be explainable solely on the basis of the spur-diffusion model nor the specific interaction near the end of the heavy-ion tracks.[4] Burns and his colleagues[5a] explained the increases in the decomposition yield of liquid benzene as being due to the bimolecular reaction between excited molecules which becomes important with an increase in the LET. This may be a reasonable explanation for the radiolysis in a medium LET region. On the basis of Burns' hypothesis, Voltz[6] explained a complementary correlation of the LET dependences of the radioluminescence and the radiolytic yield of liquid toluene.

In a very high LET region, the production of the energetic electrons by the knock-on collision of heavy ions may also affect the chemistry, as was suggested by Mozumder *et al.*[7] This effect has been demonstrated by us[3] to be effective in the interpretation of the discontinuities of the LET-dependence curves of $G(Fe^{3+})$ for the radiolysis of a Fricke solution with different kinds of heavy ions.

Another important effect which has been assumed, but not been definitely demonstrated, in the liquid-phase radiolysis with high LET radiations is the thermal-spike effect.[8] This effect, in fact, has occasionally been assumed in interpreting significant LET effects on the radiolysis of liquid aromatic compounds[9] and polycrystalline alkali nitrates,[10a] sodium chlorate,[10b] amino acids, and proteins.[11]

In γ radiolysis, the temperature at the center of a spur is assumed to be approximately 50—100° above the ambient temperature, and the duration of the heat may be less than 10^{-9} s, according to Magee,[12] who calculated using macroscopic parameters for the heat conductivity and the specific heat.

In a similar manner, Burns and Barker[13] estimated the temperature rise not only in a spherical spur but also in a cylindrical track, suggesting substantial thermal effects on the reactions in the very high LET region.

In this paper, we will report the results of our product analysis for the radiolysis of liquid acetone, methyl ethyl ketone, and diethyl ketone with carbon and nitrogen ions; these results suggest that the thermal-spike effect plays a role in the very high LET region.

Experimental

Materials. Reagent-grade acetone (Wako Pure Chem. Ind.), methyl ethyl ketone (Junsei Pure Chem. Co.), and diethyl ketone (Koso Chem. Co.) were dried and purified by distillation in the presence of $CaSO_4$ using a 50 cm stainless steel helix-packed column. Since a trace of water has been shown to affect the product yields,[14–16] meticulous care was taken to remove the water as completely as possible. The purified ketones were degassed thoroughly and distilled into a storage bulb through a tube filled with Molecular Sieve 4A.

Irradiation Cells. The irradiation cell shown in Fig. 1 was made of Pyrex glass and had a thin aluminum-foil (13—70 μ) window for heavy-ion irradiation which was fixed in place with a screwed brass keeper. A platinum lead was connected to the ground through a current integrator. The sample was then placed in the reservoir side of the cell by distillation *in vacuo* and was then further degassed by conventional freezing-pumping-thawing cycles before being transferred into the cell. For ^{60}Co-γ irradiation, Pyrex glass tubes (1.0 cm in O.D. and 20 cm high) were used.

Irradiation. The irradiation arrangement and the experimental procedure for the cyclotron experiments were essentially the same as those described previously.[2,3] The charged particles used were helium, carbon, and nitrogen ions accelerated with the IPCR 160 cm cyclotron. The energies of these particles entering the samples were:[17]

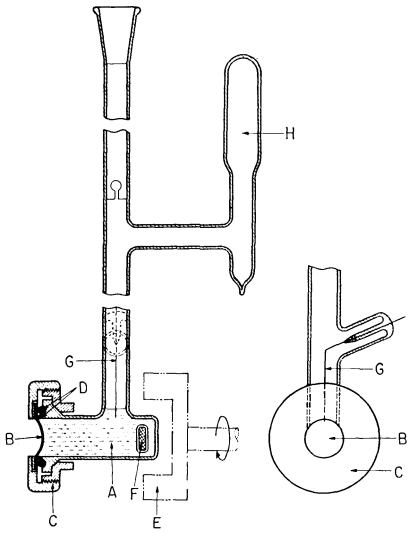

Fig. 1. Irradiation cell. A: Sample, B: Aluminum-foil window, C: Screwed brass keeper, D: Teflon rings, E: Rotating magnet, F: Stirrer, G: Platinum lead, H: Reservoir.

6.9—21.3 MeV for helium ions, 22.0—67.3 MeV for carbon ions, and 18.0—68.0 MeV for nitrogen ions, corresponding to the initial LET between 6—80 eV/Å. The current intensities were usually ~1 nA, and the total doses were in the range of $(3—10)\times10^{19}$ eV. The samples were stirred vigorously during irradiation by means of a magnetic stirrer. The ambient temperature was ~22 °C.

γ-Irradiation was carried out using a 10 kCi ^{60}Co source at a dose rate of 4.66×10^{17} eV/g min and at a total dose of up to 4.5×10^{19} eV/g.

Analysis. Gaseous products from irradiated samples were collected by using a Toepler pump. Since the hydrocarbons were found not to be degassed completely from the irradiated samples by conventional freezing-pumping-thawing cycles, we used a micro-refluxing column cooled with ice, through which the hydrocarbons were pumped out. Gas chromatographic analyses were applied to the gaseous products, H_2, CO, CH_4, C_2H_4, C_2H_6, C_3H_6, C_3H_8, and n-C_4H_{10}; analyses of the liquid products were not performed.

Energy-loss Parameter. In the present paper, the product yields are represented as a function of the energy-loss parameter, z, defined as:

$$z = \frac{1}{E}\int_0^E \left(-\frac{dE}{dx}\right) dE$$

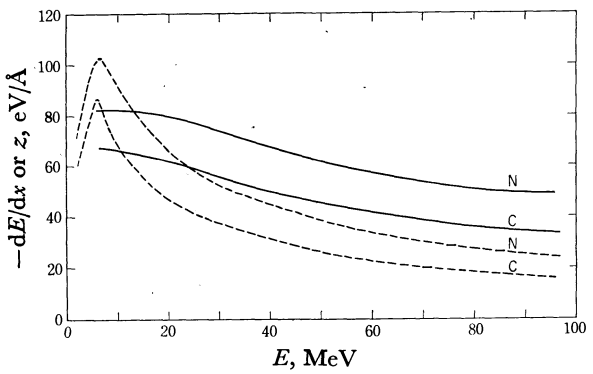

Fig. 2. Instantaneous LET (broken lines) and energy-loss parameter, z, (solid lines) for liquid acetone (20 °C) as a function of particle energy.

The values of the stopping power, $-dE/dx$, for ketones were obtained by multiplying those for water calculated by Northcliffe[18,19] by the densities of the ketones. The integration was carried out graphically; examples of z as a function of the particle energy are shown in Fig. 2.

Results

Some typical data of the product yields determined for the helium, carbon, and nitrogen ions are listed in Table 1, along with those for γ rays. The yields of the two main products, H_2 and CO, from three γ-radiolyzed ketones are reduced by 20 and 10% respectively in the presence of $I_2(10^{-2}$ M). These results, consistent with the results obtained by other workers,[15,20a] indicate that H_2 and CO are formed principally within the γ-ray spurs; therefore, in the radiolysis with carbon and nitrogen ions of high LET's, they may reasonably be assumed to be formed mostly within dense ionization tracks.

In the γ radiolysis, neither a dose nor a dose-rate

Table 1. Typical data of the product yields for aliphatic ketones

(a) Acetone

Radiation	^{60}Co-γ		He-ions		C-ions	N-ions
E, MeV			6.9	11.0	67	65.7
z, eV/Å	0.02		13.1	9.25	39	55.3
$[I_2]$, M	0	8×10^{-3}	0	1.5×10^{-2}	0	0
$G(H_2)$	0.96	0.79	1.47	1.19	2.36	2.71
G(CO)	0.56	0.48	0.80	0.73	1.05	1.22
$G(CH_4)$	1.76	0.35	0.97	0.56	0.99	0.96
$G(C_2H_6)$	0.30	0.27	0.50	0.35	0.56	0.64
$G(C_2H_2)$	0.02	0.03	—	—	—	—
$G(C_2H_4)$	0.04	0.06	0.12	0.08	0.21	0.24

(b) Methyl ethyl ketone

Radiation	^{60}Co-γ		He-ions		C-ions	N-ions
E, MeV			7.8	12.0	46.5	29.9
z, eV/Å	0.02		10.8	8.6	46.2	72.8
$[I_2]$, M	1.5×10^{-2}	0	7×10^{-3}	0	0	
$G(H_2)$	1.23	1.86	1.86	3.36	3.41	
G(CO)	0.67	0.92	0.82	1.26	1.31	
$G(CH_4)$	0.23	0.52	0.36	0.60	0.55	
$G(C_2H_6)$	0.26	0.65	0.44	0.66	0.54	
$G(C_3H_8)$	0.24	0.34	0.30	0.39	—	
$G(C_2H_2)$	0.03	0.11	0.09	0.38	—	
$G(C_2H_4)$	0.51	0.76	0.70	1.11	0.77	

(c) Diethyl ketone

Radiation	^{60}Co-γ		He-ions		C-ions	N-ions
E, MeV			22	22	53.5	36.0
z, eV/Å	0.02		6.2	6.2	46.0	71.2
$[I_2]$, M	0	$(3.5—7)\times10^{-3}$	0	7×10^{-3}	0	0
$G(H_2)$	1.18	1.07	1.48	1.45	2.61	4.01
G(CO)	0.94	0.95	1.09	0.92	1.62	2.27
$G(CH_4)$	—	0.05	0.08	0.04	0.18	0.21
$G(C_2H_6)$	—	0.22	0.52	0.26	0.36	0.80
$G(C_3H_8)$	—	0.01	—	0.03	—	—
$G(C_2H_2)$	—	0.05	—	0.09	—	—
$G(C_2H_4)$	—	0.44	0.67	0.46	0.75	1.22

dependence was observed in the ranges under study for any ketone. A detectable dose-rate dependence was not observed at intensities between 1 and 3 nA in the heavy-ion radiolysis, either.

The γ-radiolytic yields of H_2 and CH_4 from acetone containing a small amount of water were found to be substantially higher than those for dried acetone reported here, in agreement with those obtained by Barker and Noble;[14] the detailed results over a wide LET range will be communicated elsewhere.

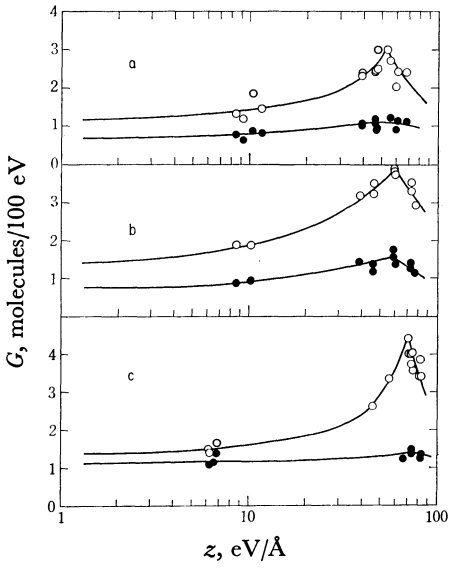

Fig. 3. Variations of $G(H_2)$ and $G(CO)$ with z. Open circles: H_2, closed circles: CO. a: acetone, b: methyl ethyl ketone, c: diethyl ketone. Yields in the vicinity of 10 eV/Å obtained with He-ions and those in the higher region with C- and N-ions.

Figure 3 shows the dependences with z of the yields of H_2 and CO for the three ketones. The yields for the γ and helim-ion radiolysis are those obtained with iodine solutions ($(3.5—7.0)\times10^{-3}$ M) in ketones; all the other yields are those with neat ketones. It should be noted that the maximum yields of H_2 and CO appear for every ketone in the very high LET region.

Discussion

Radiolysis studies of liquid acetone have been carried out by many workers,[14-16,20-25] and the ionic and the free-radical reaction mechanisms have been pointed out to be of importance. For higher ketones, one can expect reactions analogous to those of acetone.[24] Based on the reaction mechanisms proposed so far, one can reasonably assume the pathways producing hydrogen and carbon monoxide to be as follows.

A large portion of these main gaseous products are apparently formed, as may be seen from the results described above, *via* "molecular" mechanisms, even in the γ radiolysis; that is, they are formed in the spur or track region without any influence of radical scavengers. Hydrogen is presumably produced by the abstraction reaction of the hot and/or thermal hydrogen atoms which are formed by the fragmentation of the excited ketone molecules and excited ionic species resulting from the ion-molecule reactions. As will be mentioned below, hydrogen atoms are considered to be produced also by the decomposition of free radicals inside the tracks of the high LET radiations.

According to the results of photochemical studies of acetone, the excited states dissociate by these reactions:[26]

$$CH_3COCH_3^* \longrightarrow CH_3CO + CH_3 \quad (1)$$
$$CH_3COCH_3^* \longrightarrow 2CH_3 + CO \quad (2)$$
$$CH_3COCH_3^* \longrightarrow CH_2COCH_3 + H \quad (3)$$

Carbon monoxide may also be produced if acetyl radicals undergo dissociation:

$$CH_3CO \longrightarrow CH_3 + CO \quad (4)$$

Reaction (4), however, will proceed only at high temperatures because of its relatively high activation energy (13—18 kcal mol^{-1} [27,28]). Ionic reaction mechanisms producing carbon monoxide have not yet been elucidated.

As is shown in Fig. 3, both $G(H_2)$ and $G(CO)$ increase with an increase in z, reaching their maximum values at z=50, 60, and 70 eV/Å respectively for acetone, methyl ethyl ketone, and diethyl ketone. The increases in $G(H_2)$ and $G(CO)$ below the peak z's may be explained at least partly in terms of the increasing contributions of the reactions between excited ketone molecules in the dense radiation tracks, which have been proposed by Burns and his co-workers[5] for the radiolysis of benzene with high LET radiations. It should, however, be noted that, in the present study, the ratios of $G(H_2)$ to $G(CO)$ also increase from about 2(at z= 10—20 eV/Å) to about 3(at z=70—80 eV/Å) with an increase in z for the three ketones investigated. This result cannot be explained completely by the spur-diffusion model, which is based on a simple competition between the diffusion and the reaction of radicals or excited ketone molecules formed in an LET-independent step.

In order to find clues for the explanation of these significant results, the values of $G(H_2)\times z$ and $G(CO)\times z$ are plotted as a function of z in Fig. 4. The $G\times z$-value gives a measure of the number of molecules produced per 100 Å of a radiation track (G is the number of molecules produced per an absorbed energy of 100 eV). Figure 4 apparently indicates that the values of $G(CO)\times z$ almost level off above the given z's for the three ketones, whereas those of $G(H_2)\times z$ do not do so. The plateau values for $G(CO)\times z$ are estimated to be 100 ± 20.

The number of CO molecules produced should obviously not exceed the number of ketone molecules decomposed. In the γ radiolysis of liquid acetone, some oxygen-containing compounds other than carbon monoxide are produced, and their yields are greatly reduced in the presence of a radical scavenger (I_2),[15] indicating that these products are formed in the bulk. In the higher LET region, the yields of these compounds must decrease, and presumably carbon monoxide will be the main oxygen-containing product.

If this assumption is accepted, the number of CO molecules produced in the very high LET region can be said to be approximately equal to the number of

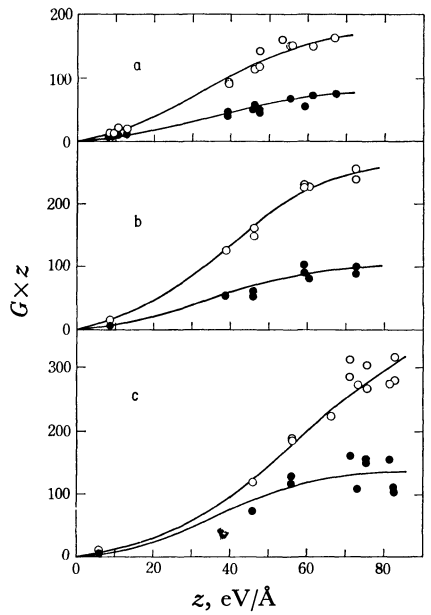

Fig. 4. Plots of $G \times z$ *vs.* z. Symbols have the same meaning as for Fig. 3.

ketone molecules decomposed. The nearly saturated curves of $G(CO) \times z$ in Fig. 4 thus indicate that the numbers of ketone molecules decomposed are limited above the given z-values: *ca.* one molecule of ketone per Å of a radiation track. The appearance of the maximum $G(CO)$ and $G(H_2)$ in Fig. 3 may be explained on the basis of such a saturation phenomenon, which has not been observed for other compounds.

The different behavior of the $G(H_2) \times z$-curves from that of $G(CO) \times z$ in Fig. 4 implies that the formation of hydrogen is still taking place more or less even after the decomposition producing carbon monoxide is "saturated." The fact that the $G(H_2)/G(CO)$ ratios increase steadily with an increase in z may support the above arguments.

Although we have not yet reached a definite conclusion, the thermal decomposition of alkyl radicals in the high temperature zones within the tracks (thermal spikes) or the formation of highly excited states of ketone molecules, thus giving rise to more hydrogen, seems to account for the increases in $G(H_2)/G(CO)$ in the high LET region.

In fact, the activation energies of the decomposition of alkyl radicals ($C_nH_{2n+1} \rightarrow C_nH_{2n}+H$) are known to be $\sim$30 kcal mol^{-1},[28] much higher than those of $C_nH_{2n+1}CO$ ($\rightarrow C_nH_{2n+1}+CO$). Therefore, the decomposition of alkyl radicals, if any, should be expected to take place only in the very high LET region where excess energies are dissipated as heat, giving rise to the formation of more hydrogen as well as that of unsaturated hydrocarbons.

The alternative explanation is the probable formation of highly (vibrationally or electronically) excited states which may form in the very high LET region and may decompose differently from the lower excited states produced in the lower LET region. The present results do not provide decisive information which can distinguish between these two proposed mechanisms; further studies are, therefore, in progress along these lines.

The authors wish to express their thanks to Dr. Takashi Karasawa for his useful suggestions throughout this study and to Messrs. Toshi Kumagaya and Yutaka Oshiro for their assistance. Thanks are also due to the members of the IPCR cyclotron operation group.

References

1) M. Matsui, H. Seki, T. Karasawa, and M. Imamura. *J. Nucl. Sci. Tech.*, **7**, 97 (1970).
2) M. Imamura, M. Matsui, and T. Karasawa, This Bulletin, **43**, 2745 (1970).
3) Unpublished results except for those reported in this paper.
4) R. H. Schuler, *Trans. Faraday Soc.*, **61**, 100 (1965).
5) (a) W. G. Burns and W. R. Marsh, *ibid.*, **64**, 2375 (1968). (b) W. G. Burns and C. R. V. Reed, *ibid.*, **66**, 2159 (1970); W. G. Burns, M. J. Hopper, and C. R. V. Reed, *ibid.*, **66**, 2182 (1970); W. G. Burns and C. R. V. Reed, *ibid.*, **68**, 67 (5972).
6) R. Voltz, Proc. Int. Discussion on Progress and Problems in Contemporary Radiation Chemistry, Prague, **1**, 45 (1971).
7) (a) A. Mozumder, A. Chatterjee, and J. L. Magee, *Adv. Chem. Ser.*, **81**, 27 (1968); (b) A. Mozumder, *Adv. Radiat. Chem.*, **1**, 1 (1969).
8) A. Norman, *Radiat. Res. Suppl.*, **7**, 33 (1967).
9) (a) R. B. Ingalls, P. Spiegler, and A. Norman, *J. Chem. Phys.*, **41**, 837 (1964); (b) J. Y. Yang, J. D. Strong, and J. G. Burr, *J. Phys. Chem.*, **69**, 1157 (1965).
10) (a) C. J. Hochanadel, *Radiat. Res.*, **16**, 286 (1962); (b) C. J. Hochanadel, *J. Phys. Chem.*, **67**, 2229 (1963).
11) T. Henriksen, P. K. Horan, and W. Snipes, *Radiat, Res.*, **43**, 1 (1970).
12) J. L. Magee, *Ann. Rev. Phys. Chem.*, **12**, 389 (1961); J. L. Magee, K. Funabashi, and A. Mozumder, Proc. 6th Conf. Radioisotopes, Tokyo (1964), p. 755.
13) W. G. Burns and R. Barker, in "Aspects of Hydrocarbon Radiolysis," ed. T. Gaumann and J. Hoigne, Academic Press, London (1968), p. 33.
14) R. Barker and C. M. Nobble, *J. Chem. Soc., A*, **1969**, 717.
15) R. Barker, *Trans. Faraday Soc.*, **59**, 375 (1963).
16) J. Kučera, *Coll. Czech. Chem. Commun.*, **31**, 355 (1966).
17) These energies were calculated from the incident energies and their losses by passing through the exit window (15 μ Al), air layer (11 mm), and cell window (13—70 μ Al) as described in the previous paper.[2]
18) L. C. Northcliffe and R. F. Schilling, *Nuclear Data Tables*, **A7**, 233 (1970).
19) These values are in good agreement with those calculated by the equations presented previously by us[2] except for minor disagreements in the low energy regions.
20) (a) P. Ausloos and J. F. Paulson, *J. Amer. Chem. Soc.*, **80**, 5117 (1958); (b) P. Ausloos, *ibid.*, **83**, 1056 (1961).
21) J. D. Strong and J. G. Burr, *ibid.*, **81**, 775 (1959).
22) R. Barker, *Nature*, **192**, 62 (1961).
23) J. Kučera, *Coll. Czech. Chem. Commun.*, **28**, 1162 (1963).
24) J. Teplý, *Radiat. Res. Rev.*, **1**, 361 (1969).
25) L. W. Sieck and P. Ausloos, *Radiat. Res.*, **52**, 47 (1972).
26) A. G. Leiga and H. A. Taylor, *J. Chem. Phys.*, **41**, 1247 (1964).
27) W. A. Noyes, Jr., G. B. Porter, and J. E. Jolley, *Chem. Rev.*, **56**, 49 (1956).
28) J. A. Kerr and A. C. Lloyd, *Quart. Rev.*, **22**, 549 (1968).

The Crystal Structure of (±)-1-Benzyl-5-phenyl-1-azacycloheptan-4-one Hydrochloride, $C_{19}H_{21}NO \cdot HCl$

Keiichi FUKUYAMA,* Shozo SHIMIZU, Setsuo KASHINO, and Masao HAISA

Department of Chemistry, Faculty of Science, Okayama University, Tsushima, Okayama 700

(Received December 6, 1973)

The crystal structure of (±)-1-benzyl-5-phenyl-1-azacycloheptan-4-one hydrochloride has been determined by the heavy-atom method from three-dimensional X-ray data. The crystals are monoclinic, space group $P2_1/c$, with four formula units in a unit cell of dimensions: $a=5.967(8)$, $b=11.20(1)$, $c=25.96(2)$ Å, and $\beta=93.8(3)°$. The structure was refined by the block-diagonal least-squares method to an R index of 0.076 for 1299 independent observed reflections. The benzyl and phenyl groups are bonded equatorially to the azacycloheptanone ring which takes a chair-like conformation. The chloride ion is hydrogen-bonded to the ring nitrogen atom at a distance of 3.075(4) Å.

The title compound $C_{19}H_{21}NO \cdot HCl$ has been prepared by Morosawa[1] at this Department as an intermediate material in the course of synthetic study of seven-membered azacyclic compounds. It is of our interest to compare the conformation of the azacycloheptanone ring with that of the azacyclic six-membered rings, say, piperidine[2] and piperazine.[3] The existence of N–H···Cl hydrogen bond is of additional interest in this work.

Experimental

The crystals supplied by Dr. Shiro Morosawa were thin transparent plates having well developed {001}. Cell constants were obtained from the rotation and Weissenberg photographs taken with Cu$K\alpha$ radiation ($\lambda=1.5418$ Å).

Crystal data:

(±)-1-Benzyl-5-phenyl-1-azacycloheptan-4-one hydrochloride $C_{19}H_{21}NO \cdot HCl$ F.W. 315.8, Mp 225 °C (decomposed)[1] Monoclinic, space group $P2_1/c$.

Systematic absences; $h0l$ when l odd, $0k0$ when k odd.

$a=5.967(8)$, $b=11.20(1)$, $c=25.96(2)$ Å, $\beta=93.8(3)°$

$V=1731$ Å^3, $Z=4$, $D_c=1.21$, $D_m=1.22$ g/cm^3 (by flotation)

μ (for Cu$K\alpha$) $=19.7$ cm^{-1}, $F(000)=672$.

The reflections were collected with Cu$K\alpha$ radiation by means of equi-inclination Weissenberg techniques for the layers from $0kl$ to $4kl$. The intensities of 1299 independent reflections were measured visually and corrected for the Lorentz and polarization factors and for spot shape. No corrections were made for absorption.

Structure Determination and Refinement

The coordinates of the chloride ion were deduced from a three-dimensional Patterson map. All the remaining non-hydrogen atoms were located in a subsequent heavy-atom Fourier map. The structure was refined by the block-diagonal least-squares method,[4] with anisotropic temperature factors for the chloride ion, to the conventional R index of 0.121. Excluding the reflections, 021, 111, 121, and 13$\bar{1}$, which were considered to suffer from extinction effect, the difference map revealed all the twenty-two hydrogen atoms.

Further least-squares refinement with anisotropic temperature factors for the non-hydrogen and with isotropic ones for the hydrogen atoms was carried out by using the weighting scheme:

$$w = 0.0 \quad \text{for } F_o < F_{min} \ (=3.6)$$

$$w = 1.0 \quad \text{for } F_{min} \leq F_o \leq F_{max} \ (=18.0)$$

and

$$w = (F_{max}/F_o)^2 \quad \text{for } F_{max} < F_o$$

The final R index was 0.076 for 1299 observed reflections.

The atomic scattering factors were taken from International Tables for X-Ray Crystallography.[5] The computations were performed on a NEAC 2200-700 computer at the Computation Center of Osaka University and on a NEAC 2200-500 computer at the Okayama University Computer Center.

Results and Discussion

The observed and calculated structure factors are given in Table 1. The final positional and thermal parameters together with their estimated standard deviations are given in Tables 2 and 3. Bond lengths and angles are shown in Fig. 1 and the stereoconfiguration drawn by the plotting program ORTEP[6] is illustrated in Fig. 2. The aromatic C–C bond lengths in the benzyl (B) and phenyl (C) groups are normal, their average values being 1.384 and 1.382 Å with maximum deviations of 0.020 and 0.038 Å, respectively. It should be noted that the bond angles of the C(sp^3) in the azacycloheptanone ring (A) range from 113.4 to 115.4° and are significantly larger than those found in piperidinium p-hydroxybenzoate (109.5 to 110.7°)[2] and in piperazinium terephthalate (110.1 to 111.0°).[3] The average C(sp^3)–C(sp^3) bond length in the ring A is 1.537 Å with maximum deviation of 0.005 Å. The C–N bond lengths, 1.494 and 1.506 Å, are close to those found in the piperidinium (1.494, 1.501 Å) and in the piperazinium (1.486, 1.494 Å) ions, but slightly differ from those in azacyclododecane hydrochloride (1.529, 1.536 Å)[7] and in 2,2,6,6-tetramethyl-4-piperidone hydrochloride (1.504, 1.533; 1.523, 1.526 Å).[8] Geometry of the carbonyl group is compared with that in some saturated cycloketones in Table 4. In the present compound, the C(4) atom deviates only by 0.02 Å from the plane through the C(3), C(5), and O(8) atoms and the C(3)–C(4)–C(5) bond angle is

* Present address: Faculty of Engineering, Tottori University, Koyama-cho, Tottori 680.

TABLE 1. OBSERVED AND CALCULATED STRUCTURE FACTORS ($\times 10$)

TABLE 2. FINAL ATOMIC PARAMETERS AND e.s.d.'s ($\times 10^4$) FOR NON-HYDROGEN ATOMS

The anisotropic temperature factor is defined as: $\exp(-\beta_{11}h^2-\beta_{22}k^2-\beta_{33}l^2-\beta_{12}hk-\beta_{13}hl-\beta_{23}kl)$.

	x	y	z	β_{11}	β_{22}	β_{33}	β_{12}	β_{13}	β_{23}
Cl	1561(2)	1696(1)	2404(1)	193(5)	58(1)	23(0)	−24(4)	12(2)	2(1)
N(1)	4586(6)	3828(3)	2725(1)	171(15)	61(3)	12(1)	15(10)	3(4)	3(2)
C(2)	3295(8)	4905(4)	2537(2)	195(19)	70(4)	15(1)	32(14)	9(6)	0(3)
C(3)	2328(8)	4802(5)	1974(2)	154(18)	83(5)	15(1)	42(14)	12(6)	2(3)
C(4)	3986(8)	5127(4)	1585(2)	298(21)	61(4)	13(1)	−2(14)	4(6)	−1(3)
C(5)	5953(9)	4305(4)	1496(2)	230(20)	75(5)	15(1)	−18(14)	15(6)	0(3)
C(6)	6246(8)	3252(4)	1875(2)	213(20)	69(4)	14(1)	34(14)	1(6)	3(3)
C(7)	6671(9)	3594(4)	2444(2)	223(21)	69(5)	18(1)	28(14)	−5(6)	2(3)
O(8)	3825(8)	6071(4)	1353(2)	640(21)	83(4)	22(1)	139(14)	81(6)	28(3)
C(9)	5275(9)	3929(5)	3301(2)	235(20)	103(5)	13(1)	−18(16)	−11(6)	9(4)
C(10)	3331(9)	4122(5)	3638(2)	275(21)	84(5)	12(1)	−2(15)	−5(6)	1(3)
C(11)	1857(9)	3206(5)	3724(2)	320(24)	112(6)	13(1)	−17(18)	2(7)	4(4)
C(12)	144(10)	3378(6)	4062(2)	339(25)	162(8)	15(1)	−22(21)	7(7)	17(5)
C(13)	−107(12)	4464(7)	4291(2)	440(30)	207(10)	14(1)	107(26)	18(8)	−8(5)
C(14)	1382(14)	5384(7)	4218(3)	738(39)	160(9)	20(1)	60(29)	69(11)	−35(5)
C(15)	3076(12)	5202(6)	3881(2)	549(30)	105(6)	20(1)	−51(21)	44(9)	−6(4)
C(16)	5747(9)	3862(5)	935(2)	269(22)	94(5)	14(1)	5(16)	32(6)	2(3)
C(17)	7362(11)	4165(6)	594(2)	399(28)	144(7)	17(1)	−2(21)	62(8)	1(4)
C(18)	7124(14)	3760(7)	83(3)	614(36)	190(10)	19(1)	113(29)	113(10)	8(6)
C(19)	5393(14)	3061(7)	−84(3)	625(36)	165(9)	18(1)	129(27)	50(10)	−3(5)
C(20)	3768(12)	2756(7)	251(3)	537(31)	141(8)	18(1)	−5(24)	−9(9)	−14(5)
C(21)	3964(10)	3159(6)	758(2)	347(25)	133(7)	15(1)	−17(20)	−2(7)	−15(4)

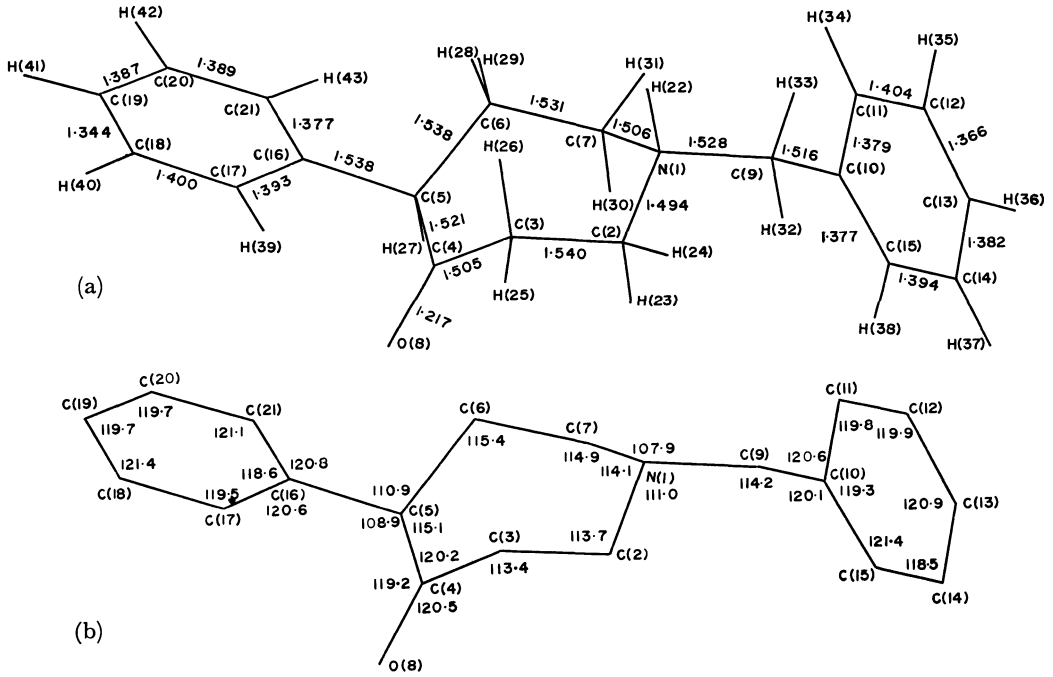

Fig. 1. (a) Bond lengths (Å) and numbering of atoms. (b) Bond angles (°). The estimated standard deviations for the bond lengths and angles are about 0.009 Å and 0.4°, respectively.

Table 3. Final fractional coordinates ($\times 10^3$) and isotropic temperature factors (Å^2) for hydrogen atoms

The e.s.d.'s are given in parentheses.

	x	y	z	B
H (22)	366 (9)	311 (5)	266 (2)	3.4 (1.3)
H (23)	435 (8)	562 (4)	258 (2)	2.2 (1.2)
H (24)	202 (8)	505 (5)	276 (2)	2.6 (1.2)
H (25)	107 (8)	533 (5)	194 (2)	2.1 (1.1)
H (26)	189 (9)	389 (5)	193 (2)	2.5 (1.2)
H (27)	722 (8)	481 (5)	155 (2)	2.7 (1.2)
H (28)	753 (10)	273 (5)	180 (2)	4.4 (1.4)
H (29)	487 (8)	270 (5)	181 (2)	2.1 (1.1)
H (30)	759 (9)	429 (5)	248 (2)	2.4 (1.2)
H (31)	749 (10)	291 (5)	265 (2)	4.2 (1.4)
H (32)	623 (9)	463 (5)	334 (2)	3.6 (1.3)
H (33)	614 (8)	317 (4)	342 (2)	1.6 (1.1)
H (34)	214 (9)	241 (5)	357 (2)	3.9 (1.4)
H (35)	−93 (11)	269 (6)	413 (2)	6.0 (1.7)
H (36)	−130 (14)	461 (7)	452 (3)	9.1 (2.3)
H (37)	108 (13)	619 (7)	439 (3)	7.5 (2.0)
H (38)	419 (9)	584 (5)	381 (2)	3.2 (1.3)
H (39)	866 (10)	469 (6)	73 (2)	5.5 (1.7)
H (40)	829 (13)	396 (7)	−14 (3)	7.4 (1.9)
H (41)	520 (12)	280 (7)	−47 (3)	7.0 (1.9)
H (42)	247 (12)	220 (6)	16 (3)	6.2 (1.7)
H (43)	280 (8)	293 (4)	102 (2)	1.3 (1.1)

120.2°, being closer to trigonal sp^2-hybrid angle than those in the six-membered cycloketones. The bond lengths of C(3)–C(4) and C(4)–C(5) are in accordance with the value, 1.505 Å, expected for C(sp^3)–C(sp^2) bond[13] and that of the C(4)=O(8) is close to the value of 1.216 Å found in acetaldehyde[14] from microwave spectra.

The least-squares planes through the ring atoms of

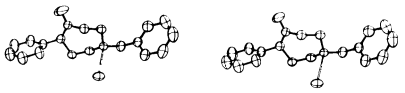

Fig. 2. Stereoconfiguration of (±)-1-benzyl-5-phenyl-1-azacycloheptan-4-one hydrochloride. The thermal ellipsoids are drawn at the 50% probability. Open bond represents hydrogen bond.

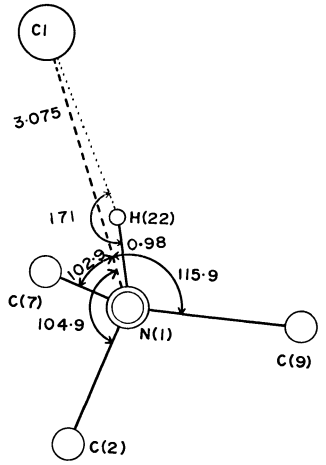

Fig. 3. Coordination of the N(1) atom.

the benzyl and phenyl groups are expressed as:

$$0.5544X - 0.3137Y + 0.7709Z + 6.5723 = 0 \quad (1)$$

and

$$0.5075X - 0.8186Y + 0.2689Z - 1.2316 = 0 \quad (2)$$

where X, Y, and Z are in Å with respect to the a, b, and c^* axes, respectively. The maximum deviations of the ring atoms from the planes (1) and (2) are 0.017 and 0.008 Å, respectively. The C(2), C(3), C(6), and C(7) atoms in the azacycloheptanone ring A give a plane,

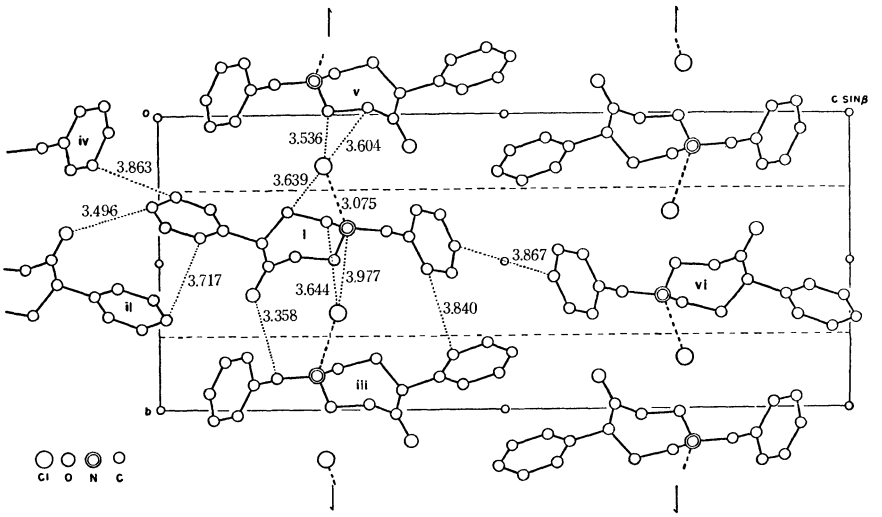

Fig. 4. The projection of the crystal structure viewed along the *a* axis. Hydrogen bonds are shown by broken lines and intermolecular contacts by dotted lines. Key to molecules; i: x, y, z. ii: $1-x, 1-y, -z$. iii: $1-x, 1/2+y, 1/2-z$. iv: $x, 1/2-y, -1/2+z$. v: $-x, -1/2+y, 1/2-z$. vi: $-x, 1-y, 1-z$.

TABLE 4. COMPARISON OF GEOMETRY OF THE CARBONYL GROUP OF THE RELATED COMPOUNDS

Compound	Bond length (Å)			Bond angle (°)
	C=O	C–C	C–C	C–C–C
1-Benzyl-5-phenyl-1-azacycloheptan-4-one[a)]	1.217	1.505	1.521	120.2
Delnudine hydrochloride[9)]	1.199	1.504	1.517	114.6
3-Chloro-2-decalone[10)]	1.20	1.50	1.52	112.8
2,2,6,6-Tetramethyl-4-piperidone hydrochloride[8)]	1.201	1.486	1.503	113.3
cis-2-Chloro-4-*t*-butylcyclohexanone[11)]	1.213	1.501	1.520	112.8
2,2,6,6-Tetramethyl-4-piperidone hydrochloride[8)]	1.221	1.490	1.508	113.3
3-Bromo-2-decalone[12)]	1.25	1.48	1.52	113.4

a) This work.

$$0.5517X + 0.7942Y - 0.2546Z + 3.5414 = 0 \quad (3)$$

with maximum deviation of 0.008 Å. The ring A takes a chair-like conformation, the N(1) atom deviating by +0.682 Å, C(5) −1.119 Å and C(4) −1.135 Å from the plane (3). The N(1) and C(5) atoms are bound equatorially to the benzyl and phenyl groups, respectively. The C(9) atom of benzyl group deviates by 0.068 Å out of the plane (1).

The chloride ion is hydrogen-bonded to the N(1) atom (N(1)···Cl=3.075(4) Å) which exhibits a nearly tetrahedral hybridization, as shown in Fig. 3. Such short hydrogen bonds have also been reported for methixene hydrochloride monohydrate (3.051 Å),[15)] azacyclododecane hydrochloride (3.061 and 3.069 Å),[7)] lidocaine hydrochloride monohydrate (3.07 Å),[16)] 1-(1-phenylcyclohexyl)piperidine hydrochloride (3.088 Å),[17)] 1-methylcytosine hydrochloride (3.1 Å),[18)] and triethylammonium tetrachlorocuprate (3.11 Å).[19)]

The projection of the crystal structure viewed along the a axis is shown in Fig. 4, together with some short contacts between the molecules. The enantiomorphs occur through the medial center of symmetry. The environment around the chloride ion is shown in Fig. 5, in which the C(12^{i})···C(9^{vii}) distance 3.460 Å is the shortest C···C contact. The bulky azacycloheptanone cations and the chloride anions may be held together mainly by Coulombic interactions and hydrogen bonding to form the sheets parallel to the *ab* plane. The sheets are stacked along the *c* axis by van der Waals forces. These are in accordance with relatively high melting point and morphology of the crystal.

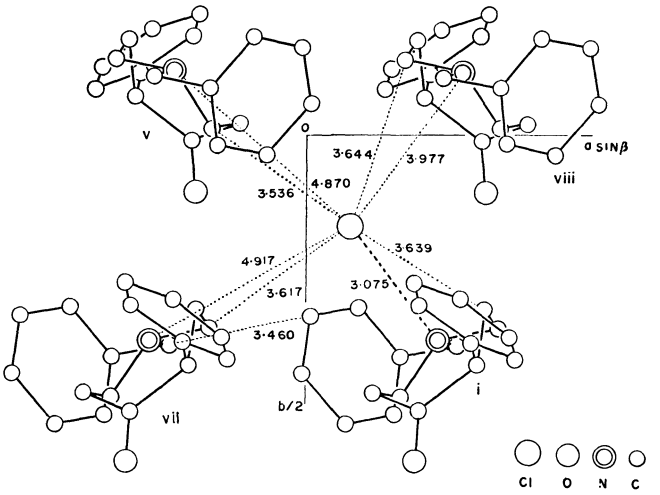

Fig. 5. The environments around the chloride ion. The estimated standard deviations of the distances are of the order of 0.005 Å.
Key to molecules. i: x, y, z. v: $-x, -1/2+y, 1/2-z$. vii: $-1+x, y, z$. viii: $1-x, -1/2+y, 1/2-z$.

References

1) S. Morosawa, private communication (1971).

2) K. Fukuyama, S. Kashino, and M. Haisa, *Acta Crystallogr.*, **B29**, 2713 (1973).
3) S. Kashino, M. Sasaki, and M. Haisa, This Bulletin, **46**, 1375 (1973).
4) T. Ashida, "HBLS IV, The Universal Crystallographic Computing System (I)," The Crystallographic Society of Japan, Tokyo (1967), p. 65.
5) "International Tables for X-Ray Crystallography," Vol. III, The Kynoch Press, Birmingham (1962), p. 210.
6) C. K. Johnson, ORTEP, Report ORNL-3794, Oak Ridge National Laboratory, Tennessee (1965).
7) J. D. Dunitz and H. P. Weber, *Helv. Chim. Acta*, **47**, 1138 (1964).
8) B. Rees and R. Weiss, *Acta Crystallogr.*, **B27**, 932 (1971).
9) K. B. Birnbaum, *ibid.*, **B27**, 1169 (1971).
10) J. Lapasset and J. Falgueirettes, *ibid.*, **B27**, 108 (1971).
11) R. A. G. de Graaff, M. Th. Giesen, E. W. M. Rutten, and C. Romers, *ibid.*, **B28**, 1576 (1972).
12) J. Lapasset and J. Falgueirettes, *ibid.*, **B27**, 624 (1971).
13) M. G. Brown, *Trans. Faraday Soc.*, **55**, 694 (1959).
14) R. W. Kilb, C. C. Lin, and E. B. Wilson, Jr., *J. Chem. Phys.*, **26**, 1695 (1957).
15) S. S. C. Chu, *Acta Crystallogr.*, **B28**, 3625 (1972).
16) A. W. Hanson and M. Röhrl, *ibid.*, **B28**, 3567 (1972).
17) P. Argos, R. E. Barr, and A. H. Weber, *ibid.*, **B26**, 53 (1970).
18) B. L. Trus and R. E. Marsh, *ibid.*, **B28**, 1834 (1972).
19) J. Lamotte-Brasseur, L. Dupont, and O. Dideberg, *ibid.*, **B29**, 241 (1973).

Counterion Effect on the Titration Behavior of Poly(itaconic acid)

Nobuhiko MUTO

Department of Polymer Science, Faculty of Science, Hokkaido University, Sapporo 060

(Received November 26, 1973)

The effect of counterions on the titration behavior of poly(itaconic acid) (PIA) was studied by titrating PIA in aqueous solutions containing alkali metal salts and a tetramethylammonium salt at 25 °C. The acidity of the primary carboxylic groups of PIA increases in the order $(CH_3)_4N^+<Li^+<Na^+<K^+$, whereas that of the secondary carboxylic groups increases with the decrease in the crystallographical radii of the counterions, in the order $(CH_3)_4N^+<K^+<Na^+<Li^+$, in agreement with the results for ordinary polycarboxylic acids. The order $K^+>Na^+>Li^+$ on the binding strength to the primary carboxylate groups in the first dissociation step is interpreted in terms of the radii of the hydrated cations; it can be ascribed to the stable ring structure of the monoanion of the itaconic acid residue, resulting from the hydrogen bonding between two adjacent carboxylate groups. In apparent complete dissociation, about 80, 60, and 40% of the itaconate residues bind to Li^+, Na^+, and K^+ ions, respectively, when it is assumed that no $(CH_3)_4N^+$ ions are bound to the carboxylate groups.

The specific effect of counterions on the titration behavior of weak polyelectrolytes is of interest in connection with the selective accumulation of specific ions in biological systems. This can be ascribed to the counterion binding by the polyion with an enormously high electrostatic potential. For polycarboxylic acids, the counterion effect has been studied extensively.[1-7] Gregor and Frederick,[1] and Kagawa and Gregor[2] demonstrated that the acidity of ordinary polycarboxylic acids, *e.g.*, poly(acrylic acid) and poly(methacrylic acid), decreases with the increase in the counterion size; that is, the alkali metal ions are bound to the polyanions in the affinity order $Li^+>Na^+>K^+$. Similar phenomena have been observed with viscosity,[3] conductivity,[3,4] counterion activity,[5] counterion mobility,[6] and dilatometry[7] in alkali metal polycarboxylate systems.

Recently, some investigators[7,8] have dealt with the specific binding of the alkali metal ions with the anions of maleic acid copolymers. The counterion binding for polydicarboxylic acids, however, has not yet been clarified. From a study of the effect of the counterions on the titration behavior of poly(maleic acid), it was found that the binding strength of the alkali metal ions to the primary carboxylate groups decreases in the order $K^+>Na^+>Li^+$, whereas that to the secondary ones $Li^+>Na^+>K^+$.[9] The latter finding agrees with those for ordinary polycarboxylic acids. On the other hand, the affinity order in the first dissociation step is interpreted in terms of the radii of the hydrated cations; it can be attributed to the hydrogen-bonded ring structure of the monoanion of the maleic acid residue.[9]

The present study is concerned with poly(itaconic acid) (PIA):

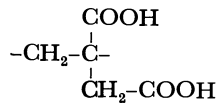

The number of carbon atoms between two adjacent carboxylic groups in the itaconic acid residue is equal to that in the maleic acid group. The author has synthesized PIA and carried out potentiometric titrations in aqueous solutions containing salts. The effect of Li^+, Na^+, K^+, and tetramethylammonium ions $(CH_3)_4N^+$, on the titration behavior of PIA, in particular the binding of the alkali metal ions to the primary and secondary carboxylate groups of PIA, is reported herewith.

Experimental

Materials. The PIA sample was prepared by the procedures of Marvel and Shepherd,[10] and Sakurada *et al.*[11] as follows. Itaconic acid was recrystallized in water[12] twice before use. The itaconic acid was polymerized in a 0.5 mol/l HCl solution containing 20 wt% monomer and 0.1 wt% potassium peroxysulfate at 50 °C for 140 hr under a nitrogen atmosphere. The reaction mixture was then added slowly dropwise to acetone to precipitate the polymer. The PIA was separated by filtration, redissolved in water, reprecipitated in acetone, and dried *in vacuo* at 35 °C. white powdery product was obtained in a 20% yield. Found: C, 45.08; H, 4.86%. Calcd for $(C_5H_6O_4)_n$: C, 46.16; H, 4.65%. The polymer seems to be slightly hydrated.[10] Figure 1 shows the dependence of the reduced viscosity of aqueous PIA solutions on polymer concentration. The molecular weight of the present PIA sample may be estimated to be about 10^5, by comparison with the viscosity data of

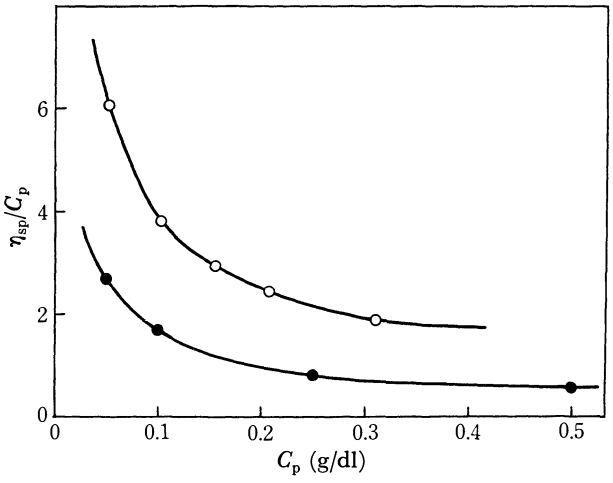

Fig. 1. The dependence of the reduced viscosity (η_{sp}/C_p) of aqueous PIA solutions on polymer concentration (C_p) at 25.0 °C. ○: present PIA and ●: PIA by Marvel and Shepherd.[10]

the PIA sample obtained by Marvel and Shepherd[10] who estimated it to be about 5×10^4. A concentrated aqueous PIA solution (*ca.* 1 wt%) was stored in a polyethylene container at 5 °C.

Carbonate-free titrants, NaOH and LiOH solutions, were prepared. The neutral salts added, $LiNO_3$, $NaNO_3$, KNO_3, and tetramethylammonium chloride, $(CH_3)_4NCl$, were thoroughly dried at 110 °C or *in vacuo* prior to weighing. All the chemicals used were of a guaranteed reagent grade. All the aqueous solutions were prepared by the use of deionized water.

Potentiometric Titrations. The pH values were measured with a Yokogawa KPH-51A pH meter equipped with Toadenpa HG-4005 glass and HC-205 calomel electrodes separated by a saturated KCl-agar salt bridge. The titrations were carried out in a special titration vessel maintained at 25.0±0.05 °C under a nitrogen atmosphere. It was found that the acid-base equilibrium was not immediately attained in the region around the half-neutralization point of PIA. The tendency was more pronounced in the case of the PIA solution without added salts. Similar phenomena have been observed in the cases of poly(maleic acid)[9] and other polyacids.[13,14] In this region, the solutions were stirred for 15 min—1 hr after each addition of a certain amount of the base until the pH readings became constant. The repeated titration curves were reproducible to within±0.01 pH unit.

Results and Discussion

pH Titration Curves. The pH titration curves of PIA with NaOH in 0.1 mol/l solutions of four kinds of 1-1 salts are shown in Fig. 2, where α' is the degree of the neutralization of the carboxylic groups of PIA (originally proportional to the gram equivalent numbers of the added base). Each titration curve has an inflection point at the same degree of neutralization ($\alpha'=1.0$), which corresponds to the equivalence point

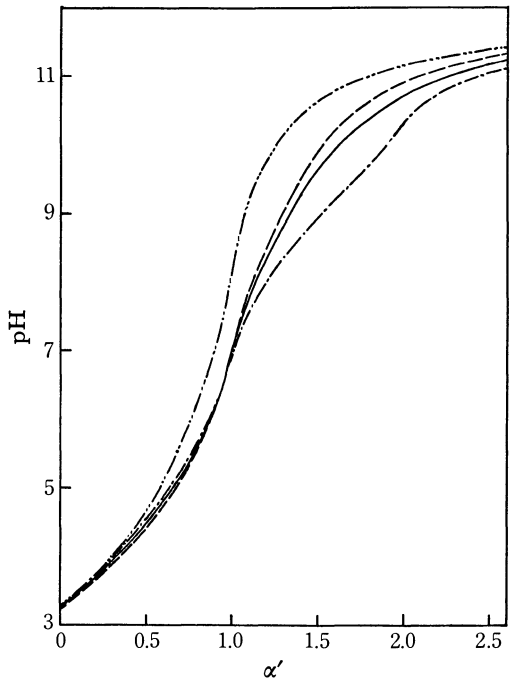

Fig. 2. The pH titration curves of 3.79×10^{-3} monomol/l PIA with NaOH in 0.1 mol/l $LiNO_3$ (·····), $NaNO_3$ (——), KNO_3 (------), and $(CH_3)_4NCl$ (-·-·-·-).

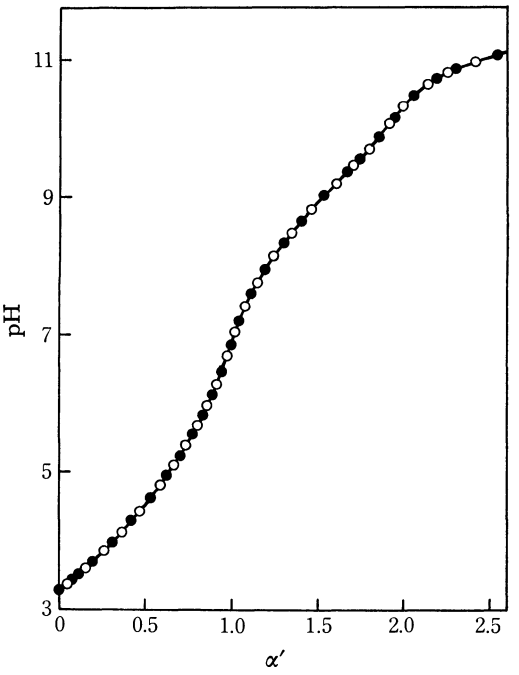

Fig. 3. The pH titration curves of 3.79×10^{-3} monomol/l PIA in 0.1 mol/l $LiNO_3$ with LiOH (○) and with NaOH (●).

of the primary carboxylic groups of PIA. The end point of the secondary ones ($\alpha'=2.0$) lies in a high pH region. Thus, no definite inflection points are observed, though a somewhat obscure inflection point is noticed in the PIA–$LiNO_3$ system (Figs. 2 and 3). It has been found that the carboxylic groups of PIA dissociate in two distinct steps,[11,15] whereas the titration curve of monomeric itaconic acid has an inflection point only at $\alpha'=2.0$.

The precise concentration of PIA, expressed in monomol/l (one monomole contains one itaconic acid residue), was determined from the gram equivalent numbers of the base added up to the first inflection point, already designated in $\alpha'=1.0$. This concentration was in fair agreement with that predicted from gravimetry of the aqueous stock solution of PIA. It has been confirmed that the PIA obtained by radical polymerization in an aqueous HCl solution has a linear chain structure consisting of repeated itaconic acid units.[10,11,16,17] Thus, in the later analysis of the dissociation behavior of PIA, it could be assumed that the amount of the secondary carboxylic groups is equal to that of the primary ones in the present PIA sample.

The added salt concentration (0.1 mol/l) is much higher than that of polyacid (*ca.* 10^{-3} monomol/l) (Fig. 2). Thus, the dissociation behavior of PIA must be substantially influenced by the cations of added salts, in spite of the use of NaOH as a titrant. For the sake of confirmation, the PIA solution in 0.1 mol/l $LiNO_3$ was titrated with LiOH as well. The titration curves with NaOH and with LiOH in 0.1 mol/l $LiNO_3$ are both in excellent agreement, as shown in Fig. 3. Such a titration procedure with NaOH in solutions containing different added salts is useful for examination of the

counterion effect, since preparing different bases so that they are carbonate-free and at approximately the same concentration is troublesome.

The effect of the four cations in the first dissociation step of PIA seems to differ from that in the second one (Fig. 2). In the second step ($\alpha' \geq 1.0$), the pH values at a given α' decrease obviously in the order $(CH_3)_4N^+ > K^+ > Na^+ > Li^+$, in agreement with the cases of ordinary polycarboxylic acids.[1,2] On the other hand, in the first step a peculiar effect of the alkali metal ions is observed; the pH values decrease in the order $(CH_3)_4N^+ > Li^+ > Na^+ > K^+$. The present findings are entirely analogous to those in the first and second dissociation steps of poly(maleic acid).[9]

Apparent Dissociation Constants. In order to characterize the counterion effect on the titration behavior of PIA, the apparent acid-dissociation constants (K_1 and K_2) of the primary and secondary carboxylic groups were calculated from the curves in Fig. 2, by the following equations:

$$pK_1 = pH + \log \frac{1-\alpha_1}{\alpha_1} \quad (1)$$

$$pK_2 = pH + \log \frac{1-\alpha_2}{\alpha_2} \quad (2)$$

where α_1 and α_2 are the degrees of dissociation of the primary and secondary carboxylic groups, respectively. The α_1 and α_2 values were determined on the basis of the electroneutrality and conservation conditions in acidic and alkaline solutions, respectively;

$$\alpha_1 = \frac{[NaOH]+[H^+]}{[A_t]} = \alpha' + \frac{[H^+]}{[A_t]} \quad (3)$$

$$\alpha_2 = \frac{[NaOH]-[A_t]-[OH^-]}{[A_t]} = \alpha' - 1 - \frac{[OH^-]}{[A_t]} \quad (4)$$

where [NaOH] is the molarity of the added titrant diluted in test solutions, and $[A_t]$ the total concentration of the itaconic acid residues, expressed in monomol/l; $[H^+]$ and $[OH^-]$ are values calculated from the measured pH values and the ionization constant of water,[18] with corrections for the activity coefficients ($y_{H^+}=0.83$ and $y_{OH^-}=0.76$ at the ionic strength of 0.1[19]). It is well-known that the apparent dissociation constants for weak polyacids continuously decrease with the increase in the degree of dissociation, that is, the increase in the charge on a polymer chain.[20]

Figures 4 and 5 show the pK_1 *vs.* α_1 and pK_2 *vs.* α_2 curves, respectively. The plots were omitted in the regions of $\alpha_1 \geq 0.9$ and $\alpha_2 \leq 0.1$ around the half-neutralization point of PIA, where Eqs. (1) and (2) hardly hold. The pK_1 values at a given α_1 are seen to decrease in the order $(CH_3)_4N^+ > Li^+ > Na^+ > K^+$, and the pK_1 curves in the presence of the alkali metal ions deviate to a greater extent from each other in the region of $0.3 \leq \alpha_1 \leq 0.6$ (Fig. 4). On the other hand, the pK_2 values at a given α_2 decrease in the order $(CH_3)_4N^+ > K^+ > Na^+ > Li^+$, the differences in the pK_2 values with the counterions being much greater than in the pK_1 values, and the effect of the alkali cations increasing with the increase in α_2 (Fig. 5).

Table 1 gives the average dissociation constants ($pK_{1,av}$ and $pK_{2,av}$) with the dffierent counterions;

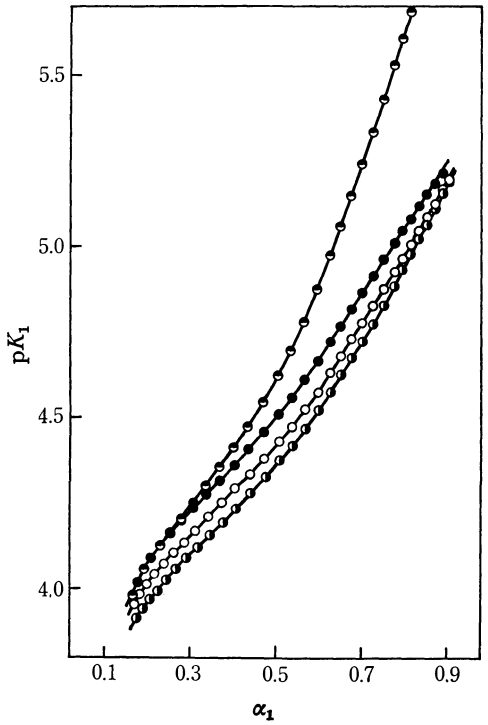

Fig. 4. The dependence of pK_1 on α_1, calculated from the curves in Fig. 2. ●: $LiNO_3$, ○: $NaNO_3$, ◑: KNO_3, and ◓: $(CH_3)_4NCl$.

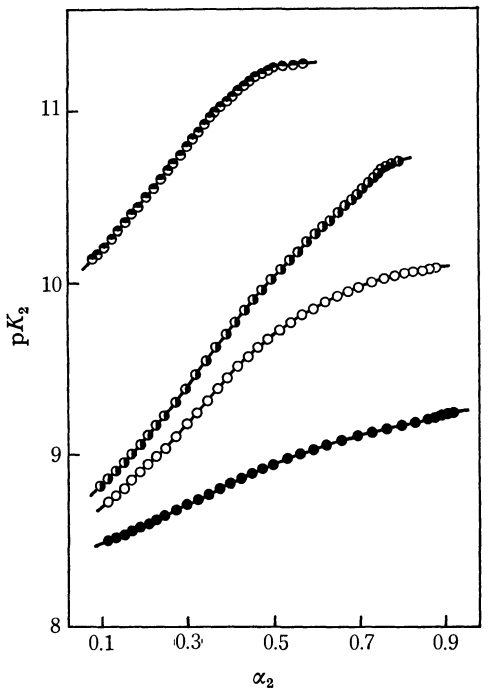

Fig. 5. The dependence of pK_2 on α_2, calculated from the curves in Fig. 2. ●: $LiNO_3$, ○: $NaNO_3$, ◑: KNO_3, and ◓: $(CH_3)_4NCl$.

the pK_1 values at $\alpha_1=0.5$ and pK_2 values at $\alpha_2=0.5$, respectively, were determined in Figs. 4 and 5. The differences in $pK_{1,av}$ with the counterions (0.06—0.12) are sufficiently larger than the estimated accuracy of pK (0.02), and hence the order of the decrease in the $pK_{1,av}$ is regarded as significant. On the other hand,

Table 1. Average dissociation constants of the primary and secondary carboxylic groups of PIA[a] in 0.1 mol/l added salts

Counterion	$pK_{1,av}$	$pK_{2,av}$
Li^+	4.50	8.95
Na^+	4.42	9.70
K^+	4.36	10.04
$(CH_3)_4N^+$	4.62	11.26

a) 3.79×10^{-3} monomol/l

such marked differences in $pK_{2,av}$ with the counterions (*e.g.*, 1.22 between K^+ and $(CH_3)_4N^+$ ions) are not known for other polycarboxylic acids. For example, the difference in pK_{av} between K^+ and $(CH_3)_4N^+$ ions for poly(acrylic acid) is 0.33 under the same conditions as the ionic strength of 0.1.[1] As for monomeric itaconic acid, the two dissociation constants have been reported to be $pK_{a,1}=3.68$ and $pK_{a,2}=5.14$ at the ionic strength of 0.1 ($NaClO_4$) at 25.0 °C.[21] Because of the increasing difficulty in the removal of protons from polyions with an enormously high electrostatic potential, the pK_{av} values of polyacids are higher than the pK_a values of the corresponding monomeric acids. Even if the effect is taken into account, the $pK_{2,av}$ values are considerably higher than the $pK_{a,2}$ of itaconic acid. Consequently, it is presumed that the protons of the secondary carboxylic groups of PIA tend to be bound to the adjacent primary carboxylate groups in each itaconic acid residue. Similar findings have been presented for poly(maleic acid).[9]

In order to support this presumption, the dependence of the titration behavior of PIA on the ionic strength in aqueous solutions was examined. Figure 6 shows the pK_1 *vs.* α_1 curves of PIA in water and in the presence of $NaNO_3$ (0.01 and 0.1 mol/l), derived from the corresponding pH titration curves according to Eqs. (1) and (3). In the cases of ordinary weak polyacids which are free from a conformational transition with the dissociation, the dependence of the apparent dissociation constant (pK) on the degree of dissociation can be represented by a second-degree polynomial.[22] The dependence in the first dissociation step, however, appears to be represented by an at least third-degree polynomial (Fig. 6). Similar findings have been presented for the primary carboxylic groups of poly(maleic acid)[23] and for poly(acrylic acid) of a relatively high molecular weight (*ca.* 10^6) without added salts.[22,24] This can be attributed to the intramolecular hydrogen bonding by the ionizable groups, in particular between the adjacent carboxylic groups.[23,24] In the absence of added salts, the portion of the pK_1 *vs.* α_1 curve in the lower α_1 region is more convex upward; hence, the structure resulting from the cooperative hydrogen bonding between two adjacent carboxylate groups in each itaconic acid residue seems to be more stable.

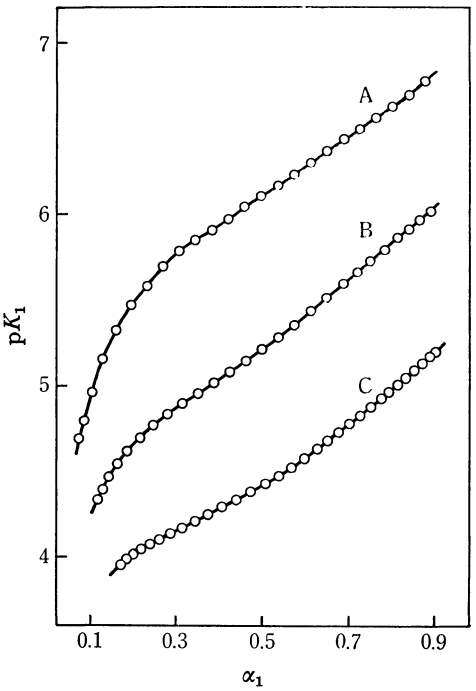

Fig. 6. The pK_1 *vs.* α_1 curves of 3.79×10^{-3} monomol/l PIA in water (curve A) and in the presence of $NaNO_3$ at 0.01 mol/l (B) and 0.1 mol/l (C).

Binding of Alkali Metal Ions. We see from Figs. 4 and 5 that the acidity of the primary carboxylic groups of PIA increases in the order $(CH_3)_4N^+<Li^+<Na^+<K^+$, and that of the secondary ones $(CH_3)_4N^+<K^+<Na^+<Li^+$. In such a case, the increment in acidity gives a measure of the interaction between carboxylic groups and counterions. Thus, the alkali metal ions are bound to the carboxylate groups of PIA in a certain way.

The carboxylic groups of PIA dissociate in the following two steps:

$$-CH_2-C(COOH)-CH_2-COOH \overset{K_1}{\rightleftharpoons} -CH_2-C(COOH)-CH_2-COO^- + H^+ \quad (5)$$

$$-CH_2-C(COOH)-CH_2-COO^- \overset{K_2}{\rightleftharpoons} -CH_2-C(COO^-)-CH_2-COO^- + H^+ \quad (6)$$

These equilibria are represented by the following simplified expressions:

$$H_2A \rightleftharpoons HA^- + H^+ \quad (7)$$

$$HA^- \rightleftharpoons A^{2-} + H^+ \quad (8)$$

On the assumption that no $(CH_3)_4N^+$ ions are bound to the carboxylate groups in the PIA–$(CH_3)_4NCl$ system, the degree of binding (θ) of the alkali metal ions (M^+) with the monoanion (HA^-) and dianion (A^{2-}) of the itaconic acid residue was calculated from the titration curves. The θ value is defined as the average number of the alkali metal ions bound to each itaconic acid residue. In the first dissociation step, MHA must be the only species of the primary carboxylate groups binding to M^+ ions. Therefore, θ can be calculated by the use of the scheme described previously.[9] In the second step, however, the scheme cannot be applied because of the presence of various species (*e.g.*, MHA, MA^-, and M_2A) as a mixture.

Thus, θ throughout the first and second steps is expressed by the equation:

$$\theta = \frac{[ML]}{[A_t]} = \frac{[L_t]-[HL]-[L^-]}{[A_t]} \quad (9)$$

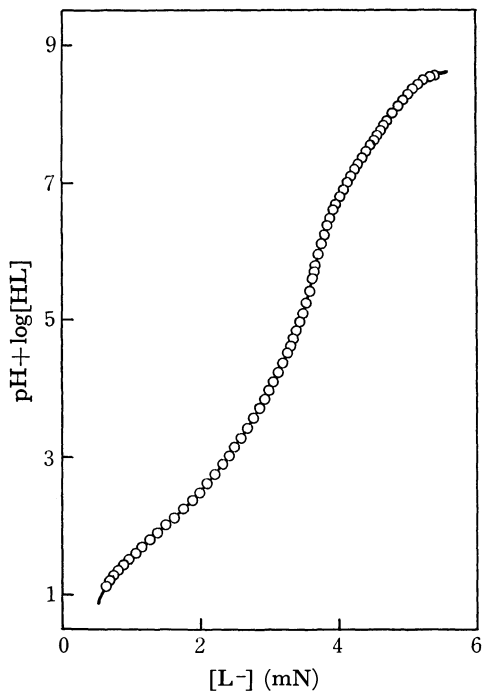

Fig. 7. The reference plot of 3.79×10^{-3} monomol/l PIA in 0.1 mol/l $(CH_3)_4NCl$, for calculation of θ.

where $[L_t]$ is the total concentration of the carboxylic groups without differentiation between the primary and secondary carboxylic groups (*i.e.*, $[L_t]=2[A_t]$), and [ML] is that of the primary and/or secondary carboxylate groups combined with M^+ ions. The [HL] related to undissociated carboxylic groups is found to be:

$$[HL] = [L_t] - [NaOH] - [H^+] + [OH^-] \qquad (10)$$

from the conservation and electroneutrality conditions. The $[L^-]$ value related to free carboxylate groups in the 0.1 mol/l MNO_3 solutions is calculated by the use of a reference plot for the 0.1 mol/l $(CH_3)_4NCl$ solution of PIA (Fig. 7).[9] After the determination of (pH+log[HL]) values for the 0.1 mol/l MNO_3 solutions of PIA, the appropriate $[L^-]$ values in the MNO_3 solutions can be found in the reference curve for the $(CH_3)_4NCl$ solution. Such a scheme with the reference plot has been devised by Mandel and Leyte.[25]

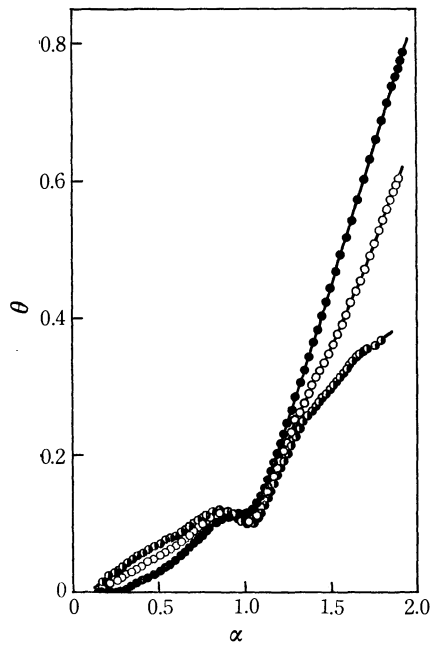

Fig. 8. The dependence of θ on α, calculated from the curves in Fig. 2. ●: Li^+, ○: Na^+, and ◑: K^+.

Figure 8 shows the dependence of θ on α, where α is the total apparent degree of dissociation of the itaconic acid groups; $\alpha=\alpha_1$ or $=1+\alpha_2$, and hence $\alpha=2$ at the apparent complete dissociation. According to the assumption on the calculation of θ, we have $\theta=0$ for $(CH_3)_4N^+$ ions over the whole α range. In the first dissociation step ($\alpha\leq1.0$), the θ values at a given α decrease in the order $K^+>Na^+>Li^+$, whereas in the second step the order of the binding strength is completely reversed. With the increase in α, the θ values in the first step gradually increase and then become practically constant (0.11—0.12) in the region near $\alpha=0.9$. The θ values in the region beyond $\alpha=1.0$ increase steeply with α, linearly for Li^+ ions. Those around $\alpha=1.0$ for Na^+ and K^+ ions appear to decrease slightly with α. However, this is not definite because of the increase in the errors inherent in the scheme with the reference plot near the half-neutralization point.

We see from Fig. 8 that when α approaches 2, about 80, 60, and 40% of the itaconic acid residues bind to Li^+, Na^+, and K^+ ions, respectively. For polyacrylate and copolymers of maleate, the binding fractions with the alkali metal ions have been evaluated from such various measurements as of counterion mobility,[6,26,27] counterion activity,[28] conductivity,[4] viscosity,[29] and apparent molal volumes[8] in the polyelectrolyte systems. The present values for polyitaconate seem to be comparable in magnitude to those for the above polycarboxylates. However, such marked differences in the θ values with the alkali cations for polyitaconate have not been found for ordinary polycarboxylates.[4,8]

The order $Li^+>Na^+>K^+$ on binding strength in the second dissociation step of PIA agrees with the results for polymonocarboxylates[1,4] and for the second step of maleic acid polymers.[7,9] These results can be explained in terms of the crystallographical ionic radii of alkali metals;[2] the smallest Li^+ ion is bound to the largest extent. This contact binding between the alkali metal ions and the carboxylate groups in these polyelectrolyte systems resembles the so-called contact ion-pairs for weak electrolytes.

It is noteworthy that, in the first dissociation step, the binding strength of the alkali metal ions to the primary carboxylate groups is in the order $K^+>Na^+>Li^+$. This can be explained in terms of the radii of the hydrated alkali cations, which increase in the order $K^+<Na^+<Li^+$. The so-called solvent-separated ion-pairs between the hydrated cations and the carboxylate groups are predominant in the first step. The same affinity sequence of the alkali metal ions has been found for polysulfonates.[4,30] For polycarboxylates, however, it has been reported only in the case of the

primary carboxylate groups of poly(maleic acid).[9]

Interpretation on Specific Counterion Binding. A common structural feature to PIA and poly(maleic acid) is that the local density of ionizable groups along the polymer chain is much higher than that for polymonocarboxylic acids; hence, the interaction between neighboring groups must be considerable. Since the binding behavior of the counterions for PIA is quite analogous to that for poly(maleic acid),[9] a similar interpretation on the specific counterion binding in the first dissociation step is given as follows.

The monoanion of the itaconic acid residue is considered to have the structure:

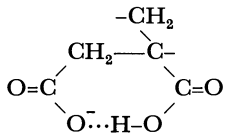

involving cooperative hydrogen bonding by two adjacent carboxylate groups; hence, a single electronic charge is distributed by resonance over a wide range. Tate, who examined the titration behavior of PIA, has proposed the same structure.[15] The stability of the seven-membered ring is comparable to that of six-membered ones because of the very small volume of the hydrogen-bonded proton. Similar hydrogen-bonded seven-membered rings have been confirmed for the monoanion of maleic acid copolymers[7,31] and for the hydrogen maleate anion.[32,33] Although no sufficient evidence has been presented, it is expected that the formation of the structure leads to a rather compact conformation of the PIA chain.

Such a stable ring structure resulting from the hydrogen bonding should be effective at least in the first dissociation step. Thus, the primary carboxylate groups, which would bind to the alkali metal ions by nature, are more tightly bound to the protons of the secondary carboxylic groups. The present findings that hydrated alkali cations are more loosely bound to the primary carboxylate groups can be ascribed to such a chelation of a proton with two adjacent carboxylate groups. The intramolecular hydrogen bonding is gradually broken up with the increase in α. This results in a conformational change from a compact form to an extended form of the PIA chain. In the absence of added salts, the compact form resulting from the hydrogen-bonded structure is more stable; the pK_1 values in the lower α_1 region are fairly high (Fig. 6).

In the second dissociation step, the contact binding between the alkali metal ions and the carboxylate groups, which is much stronger than the solvent-separated binding with the hydrated cations, is predominant. Even if part of the monoanions assume the hydrogen-bonded structure, the effect should be negligible in comparison with that of the contact binding by the dianions or the carboxylate groups free from the hydrogen-bonded protons. Incidentally, the Li^+ ion is considerably smaller than the Na^+ and K^+ ions. In the high pH region, therefore, it is presumed that the Li^+ ions are more favorably located than the others in the place of the hydrogen-bonded protons. Such a chelation of a Li^+ ion with two adjacent carboxylate groups results in the higher θ values at high α. A similar structure has been proposed for the poly(maleic acid)-LiCl system in connection with the precipitation from the concentrated solution at higher α.[34]

In conclusion, we can safely say that the counterion binding for PIA is affected throughout by the interaction between the vicinal carboxylic groups.

The author wishes to thank Prof. Tsurutaro Nakagawa and Prof. Tsuyoshi Komatsu for helpful suggestions and discussion. The present work was supported in part by a Grant for Scientific Research from the Ministry of Education.

References

1) H. P. Gregor and M. Frederick, *J. Polym. Sci.*, **23**, 451 (1957).
2) I. Kagawa and H. P. Gregor, *ibid.*, **23**, 477 (1957).
3) H. P. Gregor, D. H. Gold, and M. Frederick, *ibid.*, **23**, 467 (1957).
4) K. Tamaki, M. Ozaki, M. Ogiwara, and I. Takemura, *Nippon Kagaku Zasshi*, **88**, 711 (1967).
5) I. Kagawa and K. Katsuura, *J. Polym. Sci.*, **17**, 365 (1955).
6) G. V. Ferry and S. J. Gill, *J. Phys. Chem.*, **66**, 999 (1962).
7) A. J. Begala and U. P. Strauss, *ibid.*, **76**, 254 (1972).
8) C. Tondre and R. Zana, *ibid.*, **76**, 3451 (1972).
9) N. Muto, T. Komatsu, and T. Nakagawa, This Bulletin, **46**, 2711 (1973).
10) C. S. Marvel and T. H. Shepherd, *J. Org. Chem.*, **24**, 599 (1959).
11) I. Sakurada, Y. Sakaguchi, S. Hōrin, and H. Ueda, *Kobunshi Kagaku*, **27**, 74 (1970).
12) R. G. Fordyce and G. E. Ham, *J. Amer. Chem. Soc.*, **69**, 695 (1947).
13) H. P. Gregor, L. B. Luttinger, and E. M. Loebl, *J. Phys. Chem.*, **59**, 34 (1955).
14) N. Muto, T. Komatsu, and T. Nakagawa, *Nippon Kagaku Zasshi*, **92**, 43 (1971).
15) B. E. Tate, *Adv. Polym. Sci.*, **5**, 214 (1967).
16) S. Nagai and K. Yoshida, *Kobunshi Kagaku*, **17**, 748 (1960).
17) S. Nagai and F. Fujiwara, *Polym. Lett.*, **7**, 177 (1969).
18) H. S. Harned and B. B. Owen, "The Physical Chemistry of Electrolytic Solutions," 3rd ed., Reinhold, New York (1958), p. 638.
19) J. Kielland, *J. Amer. Chem. Soc.*, **59**, 1675 (1937).
20) J. Th. G. Overbeek, *Bull. Soc. Chim. Belges*, **57**, 252 (1948).
21) M. Yasuda, K. Yamasaki, and H. Ohtaki, This Bulletin, **33**, 1067 (1960).
22) M. Mandel, *Europ. Polym. J.*, **6**, 807 (1970).
23) N. Muto, T. Komatsu, and T. Nakagawa, *Repts. Progr. Polym. Phys. Japan*, **15**, 75 (1972).
24) A. R. Mathieson and J. V. McLaren, *J. Polym. Sci., Ser. A*, **3**, 2555 (1965).
25) M. Mandel and J. C. Leyte, *ibid., Ser. A*, **2**, 2883 (1964).
26) J. R. Huizenga, P. F. Grieger, and F. T. Wall, *J. Amer. Chem. Soc.*, **72**, 2636, 4228 (1950).
27) M. Nagasawa and S. A. Rice, *ibid.*, **82**, 5070 (1960).
28) J. W. Lyons and L. Kotin, *ibid.*, **87**, 1670 (1965).
29) H. Terayama and F. T. Wall, *J. Polym. Sci.*, **16**, 357 (1955).

30) H. Eisenberg and R. Mohan, *J. Phys. Chem.*, **63**, 671 (1959).
31) B. J. Felber and N. Purdie, *ibid.*, **75**, 1136 (1971).
32) S. Nagakura, *J. Chim. Phys.*, **61**, 217 (1964).
33) J. J. Christensen, R. M. Izatt, and L. D. Hansen, *J. Amer. Chem. Soc.*, **89**, 213 (1967).
34) J. L. Lang, W. A. Pavelich, and H. D. Clarey, *J. Polym. Sci., Ser. A*, **1**, 1123 (1963).

Conformations of Prolyl Residues in Oligopeptides

Tamaichi ASHIDA and Masao KAKUDO
Institute for Protein Research, Osaka University, Suita, Osaka 565

(Received December 18, 1973)

The structures of the prolyl residues as found in the crystals of various oligopeptides were studied, and a few interesting structural features were found. (i) The C^{α}–C′–N angle of the peptide group formed by the N atom of the pyrrolidine ring and the C^{α} and C′ atoms of the preceding residue is widened to about 118° from the usual value of 114° due to the steric repulsion between the C^{α} and the two hydrogen atoms bonded to the C^{δ} atom of the pyrrolidine ring. (ii) The C^{γ} atoms of some pyrrolidine rings have some sort of disorder, and the C^{β}–C^{γ} and C^{γ}–C^{δ} bonds seem to be shortened and the C^{β}–C^{γ}–C^{δ} angles seem to be widened than usual. (iii) Almost half of the pyrrolidine rings have an approximate C_2 (half-chair) symmetry, the twofold axis passing through the N atom and the midpoint of the C^{β}–C^{γ} bond. The others have an approximate C_s (envelope) symmetry, the mirror plane passing through either the C^{β} or C^{γ} atom with equal probabilities. In this case the $NC^{\alpha}C^{\gamma}C^{\delta}$ or $NC^{\alpha}C^{\beta}C^{\delta}$ groups are almost planar, respectively. (iv) The conformation of C^{γ}-*exo* against the C′ atom bonded to the C^{α} atom is mainly found in the residues having the α-helix type torsion angles, while the C^{γ}-*endo* is in those having the collagen type torsion angles.

Proline is a unique imino acid which imposes a certain restriction on the conformations of proteins. The restriction is due to the formation of the pyrrolidine ring, and also to the bulky methylene group linked to the imino nitrogen atom, to which only a hydrogen atom is linked in all the other amino acids. The conformations of the pyrrolidine rings as observed in crystal structures were reviewed by Balasubramanian *et al.*,[1] however, they could include in the review only five examples of the prolyl residues in peptides. Recently, the structures of seven prolyl residues in three oligopeptides were established in our laboratory. The present paper deals with the conformations and the dimensions of ten prolyl and one hydroxyprolyl residues in six crystals.

Residues **1′** *and* **1″**: Pyrrolidine rings of C(4) C(5) C(6′) C(7) N(2) and C(4) C(5) C(6″) C(7) N(2) of L-Leu-L-Pro-Gly, numbering as in the original report.[2] R=12.9, mean e.s.d. of the bond distances σ=0.015 Å.

Residues **2** *and* **3**: Pro and Hyp of tosyl-L-Pro-L-Hyp.[3] R=9.3, σ=0.016 Å.

Residue **4**: Pro of *p*-bromo-Z-Gly-L-Pro-L-Leu-Gly.[4,5] R=4.3, σ=0.02 Å.

Residues **5** *and* **6**: Pro(1) and (2) of *o*-bromo-Z-Gly-L-Pro(1)-L-Leu-Gly-L-Pro(2).[6] R=11.6, σ=0.03 Å.

Residues **7** *and* **8**: Pro(1) and (2) of Z-Gly-L-Pro(1)-L-Leu-Gly-L-Pro(2).[7] R=5.8, σ=0.008 Å.

Residues **9**, **10**, *and* **11**: Pro(1), (2), and (3) of Aoc-L-Pro(1)-L-Pro(2)-L-Pro(3).[8] R=6.0, σ=0.008 Å.

Bond Lengths and Angles

The nomenclature and the definition of the atoms, bonds and torsion angles[9] are given in Fig. 1, and the bond lengths and angles are summarized in Table 1. In Fig. 2 their mean values of the peptide groups are compared with the standard values for the usual peptide groups given by Corey and Pauling[10] and by Marsh and Donohue.[11] The torsion angles of the peptide main chain are listed in Table 2. All these values were recalculated from the published coordinates of the crystal structures.

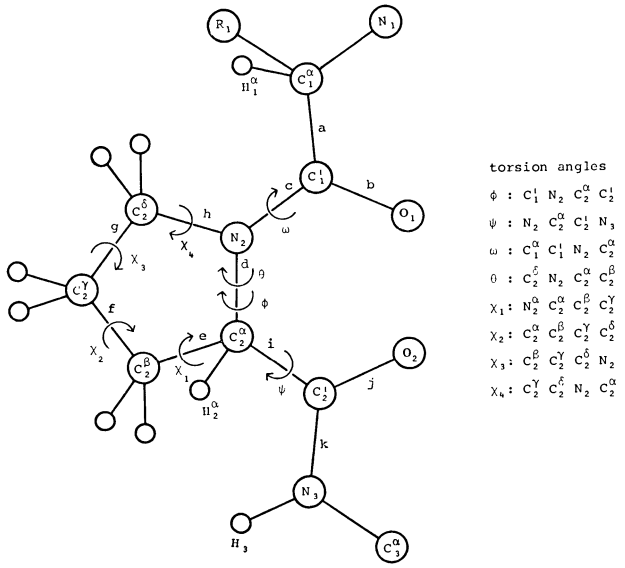

Fig. 1. The nomenclature and the definition of the atoms, bonds and torsion angles. The convention given by IUPAC-IUB Commission on Biochemical Nomenclature[9] is adopted.

Peptide Groups. The mean C^{α}–C′–N angle (ac) of 118° is significantly larger than 114° given by Corey and Pauling[10] and 116° by Marsh and Donohue.[11] While the O–C′–N (bc) of 120.5° is less than 125° or 123.5°, respectively. This is certainly due to the steric repulsion between the C^{α} atom of the preceding residue and the bulky C^{δ} methylene group of the pyrrolidine ring, in particular two hydrogen atoms bonded to the C^{δ} atom. In the cases of **4** to **8** the preceding residues are glycines, but the same tendency is observed. Thus this discrepancy from the standard values is not affected by the sizes of the side groups of the preceding residues.

A similar tendency is also found in the bond angles of C^{α}–C′–N (ik) and O–C′–N (jk) of the peptide groups between the prolyl and the following residues. However, if the residues **2**, **9**, and **10**, which are followed by prolyl residues, are not taken into account, the mean value of the C^{α}–C′–N angles of 116° is quite close to the standard value. Thus the presence of the pyr-

1′ and **1″** now discussed in this paper. On the other hand in *p*-bromo-Z–Gly–Pro–Leu–Gly,[5] Z–Gly–Pro–Leu–Gly–Pro,[7] and Aoc–$(Pro)_3$,[8] the C^γ atoms of the residues **4**, **7**, and **10** gave unusually large vibrational amplitudes in the direction perpendicular to the pyrrolidine planes, but no anomalies were found in the vicinities of the C^γ sites in the difference electron density maps. Although the possibilities of the disordered structure as postulated for Leu–Pro–Gly should be taken into account, the refinements employing usual anisotropic temperature factors seemed to be reasonably converged. The models thus obtained give the shorter bond lengths of C^β–C^γ and C^γ–C^δ and the wider C^β–C^γ–C^δ angles than the true values. DL-Proline HCl shows also a similar tendency.[12]

Puckering of Pyrrolidine Ring

The torsion angles of all the five bonds of the pyrrolidine ring are listed in Table 3. Balasubramanian *et al.* classified the proline ring structures into two classes, A and B.[1] Conformation A is characterized by negative χ_1, and C′ and C^γ are on opposite side of the roughly planar $NC^\alpha C^\beta C^\gamma$ plane (C^γ-*exo*), while conformation B has positive χ_1, and the two atoms are on the same side of the plane (C^γ-*endo*).

Among newly determined structures of the pyrrolidine rings in peptides, several residues, such as **5**, **9**, and **10**, are reported to have more planar $NC^\alpha C^\gamma C^\delta$ groups rather than $NC^\alpha C^\beta C^\delta$. Also in two of four rings in tetra-proline[13] the C^β atoms are displaced mostly from the ring planes. Therefore, a further study of the puckering of the rings is made from a slightly different viewpoint from that of Balasubramanian *et al.*[1]

The structures viewed along the C′–N bonds of the peptide linkages, more strictly, along the bisectors of the C^α–N–C^δ angles are presented in Fig. 3. It is clearly shown that almost half of the structures have roughly a C_2 (half-chair) symmetry[14] with the twofold axis passing through the N atom and the midpoint of the C^β–C^γ bond. In this structure neither the $NC^\alpha C^\beta C^\delta$ nor $NC^\alpha C^\gamma C^\delta$ groups are planar. This structure may be designated as C_2-C^γ-*exo* (C^β-*endo*) or C_2-C^γ-*endo* (C^β-*exo*) depending on whether C^γ is displaced on the same side as C′ or on the opposite side of the $NC^\alpha C^\delta$ plane. Both of these structures have been actually found so far. The others have an approximate C_s (envelope) symmetry, the mirror plane passing through either the

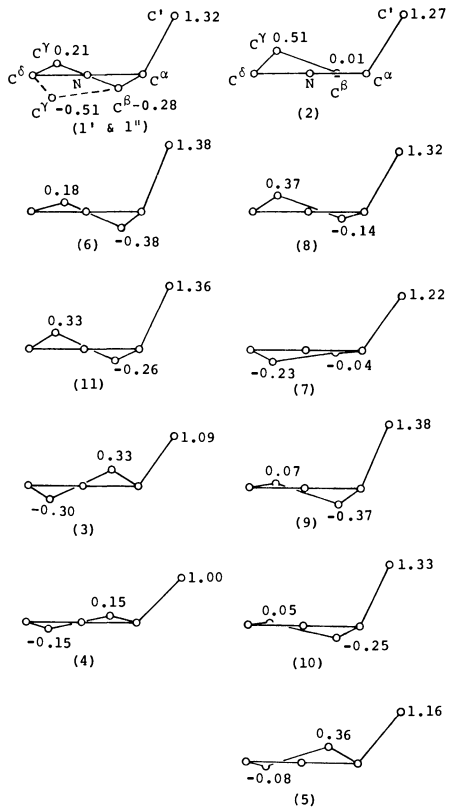

Fig. 3. The conformations of the pyrrolidine rings viewed along the bisectors of the $C^\alpha NC^\delta$ angles. The displacements of the atoms from the $NC^\alpha C^\delta$ planes are shown in Å unit. *left*: the rings of approximate C_2 symmetry, *right*: the rings of approximate C_s symmetry.

Table 3. The conformations of the pyrrolidine rings in the oligopeptides

Residue	Conformation	Shift (Å) from $NC^\alpha C^\delta$-plane			Torsion angles (degrees)				
		C^β	C^γ	C′	θ	χ_1	χ_2	χ_3	χ_4
	C^β-*endo*, C^γ-*exo*, (C^δ-*endo*) (conformation A)								
1″	C_s-C^δ-*endo*	−0.28	−0.51	1.32	−11	−3	16	−22	21
3	C_2-C^γ-*exo*	0.33	−0.30	1.09	13	−31	37	−30	12
4	C_2-C^γ-*exo*	0.15	−0.15	1.00	6	−16	21	−17	6
5	C_s-C^β-*endo*	0.36	−0.08	1.16	13	−24	27	−19	3
7	C_s-C^γ-*exo*	−0.04	−0.23	1.22	−2	−7	14	−14	9
	C^β-*exo*, C^γ-*endo* (conformation B)								
1′	C_2-C^γ-*endo*	−0.28	0.21	1.32	−11	26	−31	24	−8
2	C_s-C^γ-*endo*	0.01	0.51	1.27	0	21	−32	31	−20
6	C_2-C^γ-*endo*	−0.38	0.18	1.38	−15	32	−38	27	−7
8	C_s-C^γ-*endo*	−0.14	0.37	1.32	−5	24	−33	29	−14
9	C_s-C^β-*exo*	−0.37	0.07	1.38	−14	25	−27	19	−3
10	C_s-C^β-*exo*	−0.25	0.05	1.33	−10	17	−20	14	−2
11	C_2-C^γ-*endo*	−0.26	0.33	1.36	−10	29	−38	31	−13

The conformation of **6** is an intermediate of C_2-C^γ-*endo* and C_s-C^β-*exo*.
The conformation of **8** is an intermediate of C_s-C^γ-*endo* and C_2-C^γ-*endo*.

C^β or C^γ atoms. If the mirror plane passes through C^β, χ_4 is close to zero and the atoms $C^\alpha C^\gamma C^\delta N$ are coplanar. This structure may be designated as C_s-C^β-*endo* or C_s-C^β-*exo* depending on the direction of the displacement of the C^β atom from the $NC^\alpha C^\gamma C^\delta$ plane. If the C^γ atom is on the mirror plane, θ is close to zero, the four atoms $C^\alpha C^\beta C^\delta N$ are coplanar, and the structure may well be characterized by C_s-C^γ-*exo* or C_s-C^γ-*endo*. All the four C_s structures have also been found so far. In Fig. 3 it is clearly shown that notwithstanding the approximate symmetry the displacement of the C′ atom from the $NC^\alpha C^\delta$ plane is larger for C^γ-*endo* (C^β-*exo*) than for C^γ-*exo* (C^β-*endo*) due to a steric requirement.

The above discussion shows that the displacement alone of the C^γ atom from the $NC^\alpha C^\beta C^\delta$ plane is not necessarily appropriate to describe the conformation of the pyrrolidine ring. The five torsion angles or the displacements of the C^β and C^γ atoms from the $NC^\alpha C^\delta$ plane are the necessary informations to describe the structure. The notation suggested in this report, such as C_2-C^γ-*endo*, gives more directly an approximate picture of the prolyl ring. The conformations of the prolyl residues in peptides classified on these lines are summarized in Table 3, where the displacements of the C^β and C^γ atoms and the five torsion angles are also listed. Among these examples residue **6** is an intermediate of C_2-C^γ-*endo* and C_s-C^β-*exo*, and residue **8** is an intermediate of C_s-C^γ-*endo* and C_2-C^γ-*endo*. Residue **1″** cannot be classified into anyone of these structures, but is a unique example of C_s-C^δ-*endo*. According to the classification by Balasubramanian *et al.*,[1] conformation A includes C^β-*endo* and/or C^γ-*exo* irrespective of the symmetry of the ring, and B includes C^β-*exo* and/or C^γ-*endo*.

The pyrrolidine rings in crystals of amino acids are also classified in this way; L-proline[15] is C_2-C^γ-*endo*, L-hydroxyproline[16] and proline in copper DL-proline dihydrate[17] are C_s-C^γ-*exo*, and the pyrrolidine ring in acetyl-L-proline-*N*-methylamide[18] is an intermediate of C_2-C^γ-*endo* and C_s-C^γ-*endo*. The pyrrolidine ring of DL-proline HCl[12] might be termed C_s-C^α-*exo*, really a rare example.

A theoretical treatment of the conformations of the pyrrolidine rings by a potential energy calculation showed that C^γ-*endo* is somewhat stabler than C^γ-*exo*, but the energy difference between the two conformations is only marginal, and may not be so decisive in determining the conformations.[19,20] Among 12 examples, 7 are C^γ-*endo*, while 5 are C^γ-*exo*.

In such discussions the rotation of the C^α–C′ bond should be taken into consideration.[21] The prolyl residues are classified into two groups according to the rotation angle ϕ as shown in Table 2. One is the collagen type with large positive ϕ (residues **1**, **2**, **9**, **10**), and the other is the α-helix type with small negative ϕ (residues **4**, **5**, **7**). A model building shows easily that in the α-helix type the NH group of the following residue is in contact with the H atoms bonded to the C^γ and C^δ atoms of the ring, and the contact may be too close if the C^γ atom is in *endo* against the C′ atom. Each of the three residues of this type is C^γ-*exo* (conformation A). While in collagen type, since all the four residues are C^γ-*endo* or C^β-*exo*, the O atom of the following peptide group may be in appropriate nonbonding (van der Waals) contact with the ring atoms of conformation B. Thus, although the number of examples may not be large enough, it may be concluded that the α-helix type residues take conformation A while the collagen type residues take conformation B. The relation, however, may not be so explicit, since a simple molecule of acetyl-L-proline-*N*-methylamide[18] is an α-helix type with $\phi = -16°$, but C^γ is in the *endo* position. The intermolecular interactions may play a key role in this structure rather than the intramolecular interactions mentioned above.

The last point is that the disordered C^γ atom mentioned earlier has another effect on the shape of the pyrrolidine ring, that is, the ring having a disordered C^γ atom, such as residues **4**, **7**, and **10**, is significantly more planar than the others. All the torsion angles of the bonds of the ring are close to zero, and the displacements of the C^β and C^γ atoms from the $NC^\alpha C^\delta$ plane are smaller than the others. The C^γ atom has usually two stereochemically possible sites on each side of the ring, if the rest of the ring is fixed. For instance, in residue **10** the distance between the two possible sites is about 0.8 Å. The actually located site of the C^γ atom in this residue is on the midway of the line joining the two possible sites, 0.2 Å to the closer site and 0.6 Å to the other. Thus, the actually located site is significantly closer to the plane of the pyrrolidine ring than the stereochemically ideal one.

References

1) R. Balasubramanian, A. V. Lakshminarayanan, M. N. Sabesan, G. Tegoni, K. Venkatesan, and G. N. Ramachandran, *Int. J. Protein Res.*, **3**, 25 (1971).

2) Y. C. Leung and R. E. Marsh, *Acta Crystallogr.*, **11**, 17 (1958).

3) M. N. Sabesan and K. Venkatesan, *ibid.*, **B27**, 1879 (1971).

4) Abbreviations: Z, benzyloxycarbonyl; Aoc, *t*-amyloxycarbonyl.

5) T. Ueki, T. Ashida, M. Kakudo, Y. Sasada, and Y. Katsube, *Acta Crystallogr.*, **B25**, 1840 (1969).

6) T. Ueki, S. Bando, T. Ashida, and M. Kakudo, *ibid.*, **B27**, 2219 (1971).

7) S. Bando, N. Tanaka, T. Ashida, and M. Kakudo, The Annual Meeting of the Crystallographic Society of Japan, Osaka, 1973.

8) G. Kartha, T. Ashida, and M. Kakudo, to be published.

9) IUPAC-IUB Commission on Biochemical Nomenclature, *J. Mol. Biol.*, **52**, 1 (1970).

10) R. B. Corey and L. Pauling, *Proc. Roy. Soc., Ser. B*, **141**, 10 (1953).

11) R. E. Marsh and J. Donohue, *J. Adv. Protein Chem.*, **22**, 235 (1967).

12) Y. Mitsui, M. Tsuboi, and Y. Iitaka, *Acta Crystallogr.*, **B25**, 2182 (1969).

13) T. Matsuzaki, *ibid.*, **A28**, S38 (1972).

14) K. S. Pitzer and W. E. Donath, *J. Amer. Chem. Soc.*, **81**, 3213 (1959).

15) R. I. Kayushina and B. K. Vainshtein, *Soviet Phys.*

Cryst., **10**, 698 (1966).
16) J. Donohue and K. N. Trueblood, *Acta Crystallogr.*, **5**, 419 (1952).
17) A. McL. Mathieson and H. K. Welsh, *ibid.*, **5**, 599 (1952).
18) T. Matsuzaki and Y. Iitaka, *ibid.*, **B27**, 507 (1971).
19) G. N. Ramachandran, A. V. Lakshminarayanan, R. Balasubramanian, and G. Tegoni, *Biochim. Biophys. Acta*, **221**, 165 (1970).
20) In Ref. 1 it is reported inconsistently that C^{γ}-*exo* is stabler than C^{γ}-*endo*.
21) The possibility of a relation between ψ and the ring conformation is suggested by a referee, to whom the authors' thanks are due.

Vibration-Rotation Spectrum of Methyl Fluoride II. Analysis of $\nu_3+\nu_6$ Band

Jun NAKAGAWA, Isao SUZUKI,* Takehiko SHIMANOUCHI, and Tsunetake FUJIYAMA**

Department of Chemistry, Faculty of Science, The University of Tokyo, Bunkyo-ku, Tokyo 113

**Educational Computer Centre, The University of Tokyo, Bunkyo-ku, Tokyo 113*

***Department of Chemistry, Faculty of Science, Tokyo Metropolitan University, Setagaya-ku, Tokyo 158*

(Received December 28, 1973)

The $\nu_3+\nu_6$ band of methyl fluoride has been measured with a high-resolution infrared spectrometer. The molecular constants are obtained with the least-squares method. The effect of the x,y-type Coriolis interaction is discussed and the theoretical spectra are compared with the observed spectrum.

In a previous paper[1] (hereafter referred to as I), we have reported the analysis of the $2\nu_3$ band of CH_3F under high resolution. As mentioned in I, the $2\nu_3$ band is expected to have the x,y-type Coriolis interaction with the $\nu_3+\nu_6$ band similar to that observed in the ν_3 and ν_6 fundamentals.[2,3] The effect of this interaction may be seen more clearly in the weaker $\nu_3+\nu_6$ band and the result of the analysis is reported in the present paper.

Since the vibration-rotation energy levels for both the $2\nu_3$ and $\nu_3+\nu_6$ bands have been accurately determined, more precise scheme may be drawn for the x,y-type Coriolis interaction between the two levels. As mentioned in I, the band centers of these two bands are separated by about 140 cm^{-1}; the shifts of vibration-rotation levels are relatively small and may be treated in the conventional way. The effect of the perturbation would be more profound in the intensity of the $\nu_3+\nu_6$ band. The $\nu_3+\nu_6$ band may further couple with the $(2\nu_6)^0$ and $(2\nu_6)^2$ bands through the same ζ^y_{36} term. These bands occur at higher frequency side of the $\nu_3+\nu_6$ band and are extremely weak, and their effects on the $\nu_3+\nu_6$ band are negligible for the intensity wise.

Experimental

The sample was purchased from PCR Inc. of USA with the stated purity of 99% and used without further purification.

The spectra were measured with a 2500 mm focal length Littrow-McCubbin type instrument at the University of Tokyo,[1,4] in the 12th and 13th orders of a 31.6 lines/mm grating. An InSb detector was used at liquid nitrogen temperature. A White type long-path cell was used and its path length was kept 6 m. The sample pressure was *ca.* 45 mmHg and the resolving power was better than 0.06 cm^{-1}.

The frequencies of the observed lines were calibrated against the standard lines of CO.[5] In the region where the CO lines overlap with CH_3F lines, the suitable lines of $D^{35}Cl$ and $D^{37}Cl$ were used as the secondary standard, the frequencies of which had been calibrated against the CO lines. The standard deviation of the fitted lines was 0.007 cm^{-1} and, therefore, the accuracy of the observed lines was believed to be better than $\pm$0.01 cm^{-1}.

Spectral Features and Assignment of the Observed Bands

The rapidly scanned spectra ($\Delta\nu\simeq$0.10 cm^{-1}) of P- and R-branch sides are shown in Figs. 1 and 2, the 12th and 13th orders of grating being used respectively. Since each Q-branch is resolved into its J-components, the Q-branches cannot be distinguished from P- and R-branches. Near the band center, however, the Q-branches appear fairly clearly, because there is no overlapping with the strong ^RR- and ^PP-branches. Many of the P- and R-branch lines in the subbands are seen to be resolved into the individual components. Furthermore, the spectrum of R-branch side shows the clear series of the ^RR-branches which begin by about 2270 and 2291 cm^{-1}, while no obvious series are found in the P-branch side.

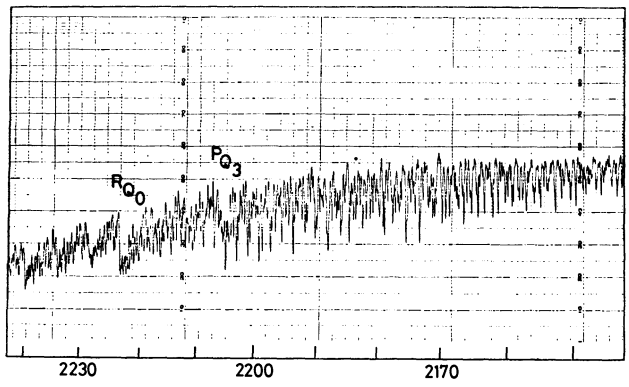

Fig. 1. The rapid scan spectrum of the $\nu_3+\nu_6$ band of CH_3F. P-branch side. Grating order=12th. Path length=6 m. Pressure=45 mmHg. Resolution=0.10 cm^{-1}.

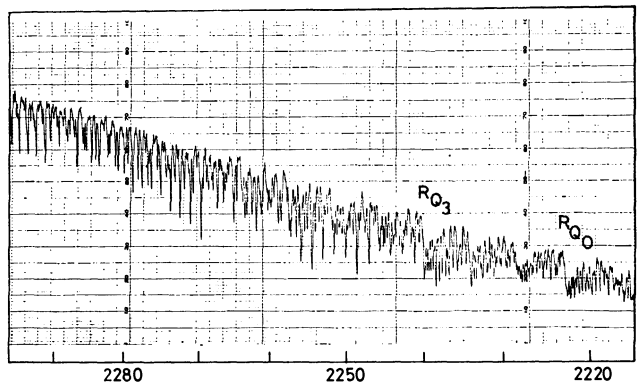

Fig. 2. The rapid scan spectrum of the $\nu_3+\nu_6$ band of CH_3F. R-branch side. Grating order=13th. Path length=6 m. Pressure=45 mmHg. Resolution=0.10 cm^{-1}.

Although the assignment of the observed lines is complicated by the fact that the Q-branches are resolved into its J-components, we can assign the lines by the following way.

(1) Since no strong ^{R}R-branch and ^{P}P-branch lines occur near the band center, the most prominent Q-branch line can be assigned to the $^{R}Q_0$. (2) The lines of the $^{R}Q_1$, $^{R}Q_2$, $^{R}Q_3$, $^{P}Q_1$, $^{P}Q_2$, and $^{P}Q_3$ branches are easily identified, because they show usual intensity alternation due to the three fold symmetry. The J-components of each Q-branch are determined graphically. (3) ^{R}R-branches are assigned in consideration of the statistical weights and the missing lines ($J \geqq K$).

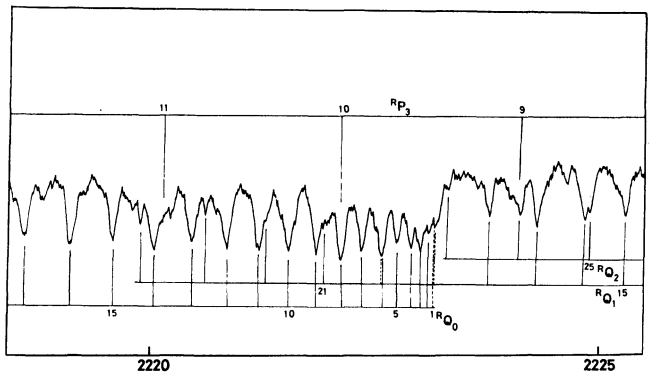

Fig. 3. The band center of the $\nu_3+\nu_6$ band. The $^{R}Q_0$-branch is mainly seen. Resolution=0.06 cm^{-1}.

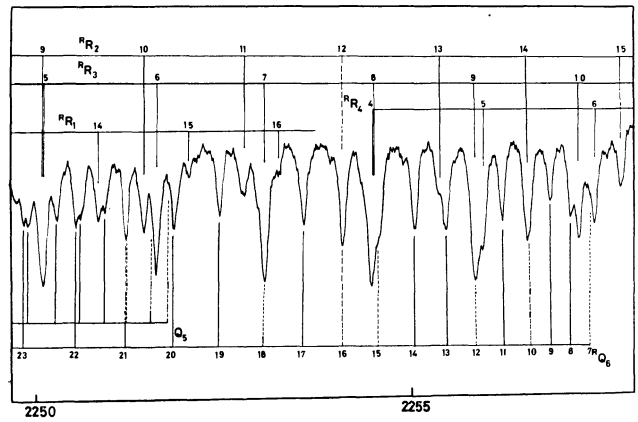

Fig. 4. The $^{P}Q_6$-branch of the $\nu_3+\nu_6$ band. Unassigned stronger bands are mainly from $^{P}P_1$- and $^{P}P_2$-branches.

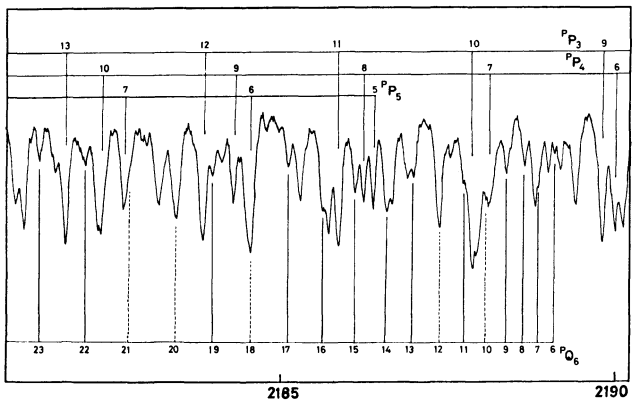

Fig. 5. The $^{R}Q_6$-branch of the $\nu_3+\nu_6$ band.

(4) The assignments of the ^{P}P-branches are made by the use of the parameters obtained from the analysis of the ^{R}R-branches and from the microwave study.[6] A few of the ^{R}P- and ^{P}R-branches are observed.

In Fig. 3 the spectrum of $^{R}Q_0$ branch is shown with the assignment of several lines. The spectra near the $^{P}Q_6$- and $^{R}Q_6$-branches are shown in Figs. 4 and 5, respectively; the P-branch side is more complex and less intense.

Determination of the Molecular Constants

The vibration-rotation energy of a symmetric top in an E-vibrational state can be written in the form

$$\begin{aligned} T_{v,l}(J,k) = {} & G(v,l) + B_v J(J+1) + (A_v - B_v)k^2 \\ & - 2A_v\zeta_v kl - D_J^v[J(J+1)]^2 \\ & - D_{JK}^v J(J+1)k^2 - D_K^v \cdot k^4 \\ & + \eta_J^v J(J+1)kl + \mu_K^v k^3 l, \end{aligned} \quad (1)$$

where $G(v,l)$ is the vibrational energy, A_v and B_v are the rotational constants, and D_J^v, D_{JK}^v, D_K^v, η_J^v, and η_K^v are the centrifugal distorsion constants and ζ_v is Coriolis coupling constant.

From the selection rules for a perpendicular band ($\Delta k=+1$, $\Delta l=+1$, and $\Delta J=0$, ± 1, or $\Delta k=-1$, $\Delta l=-1$, and $\Delta J=0$, ± 1), the transition frequencies can be calculated as the differences between the energy levels of the upper and lower states. Some of the parameters, however, cannot be determined from the analysis of this band alone. The A'' value is obtained from the ζ-sum rule,[2] the D_k'' value is calculated from the harmonic force field,[7] and the D_{JK}'' value is obtained by the microwave study.[6] The molecular constants which are obtained from the least-squares method are listed in Table 1 together with the microwave values. A part of the observed frequencies are listed in Table 2 with their assignments and the calculated frequencies.[8] The lines which are not fully resolved are given zero or smaller weights.

Table 1. Molecular constants obtained from $\nu_3+\nu_6$ band of CH_3F (cm^{-1} except ζ)

	$\nu_3+\nu_6$ Present work	Ground state	
		Present work	Winton[6]
ν_0	2221.705 (12)[a]		
A	5.0879 (2)	5.081[b]	
B	0.83657 (13)	0.85170 (12)	0.851794
α^A	−0.0069 (2)		
α^B	0.01513 (3)		
ζ	0.274 (1)		
D_J	1.84×10^{-6} (15)	1.91×10^{-6} (14)	1.997×10^{-6}
D_{JK}	1.76×10^{-5} (2)	1.47×10^{-5}[b]	1.47×10^{-5}
D_K	7.9×10^{-5} (1)	8.0×10^{-5}[b]	
η_J	3.4×10^{-5} (2)		
η_K	1.3×10^{-4} (1)		

a) The numbers in parentheses represent twice of the standard errors to be attached to the last significant figures. b) Assumed.

TABLE 2. ^{R}R-BRANCH OF THE $\nu_3+\nu_6$ BAND OF CH_3F (cm^{-1})

$J\backslash K$	1		2		3		4	
	Obsd	$\Delta\nu$	Obsd	$\Delta\nu$	Obsd	$\Delta\nu$	Obsd	$\Delta\nu$
1	2232.178[a]	−40						
2	2233.829	−2	2239.642[a]	34				
3	2235.404	−9	2241.203	13	2247.014	5		
4	2236.958	−7	2242.746	4	2248.577	17	2254.432	13
5	2238.506	20	2244.272	9	2250.080	−1	2255.920	−19
6	2239.987	10	2245.748	−6	2251.579	8	2257.423	−6
7	2241.442	5	2247.210	−4	2253.011	−20	2258.875	−13
8	2242.860	−7	2248.677[a]	34	2254.432	−28	2260.299	−18
9	2244.272	5	2250.080[a]	37	2255.840	−19	2261.719	4
10	2245.652	17	2251.416	5	2257.205	−22	2263.088	6

$\Delta\nu$: (Obsd−Calcd)×1000 cm^{-1}. a) blended lines, weight zero.

x,y-Type Coriolis Interaction

As mentioned earlier, the $\nu_3+\nu_6$ band has Coriolis interaction with $2\nu_3$, $(2\nu_6)^0$ and $(2\nu_6)^2$ bands. In this section, the influence of this interaction to the $\nu_3+\nu_6$ band will be discussed.

Since the selection rules for this type of interaction is $\Delta J=0$, $\Delta k=+1$, and $\Delta l=+1$ or $\Delta J=0$, $\Delta k=-1$, and $\Delta l=-1$, the analyses of the $2\nu_3$ and $\nu_3+\nu_6$ bands show that the levels which interact with each other are closest at $k=26$ or 27 and the effects are hardly observed for the levels of relatively small k values. In this work, assignment can be done to the $k=12$ lines for R-branch and the $k=10$ lines for P-branch. If there is any strong local interaction, the effect will be seen as the difference of the effective rotational constant B'_{eff} for each subband. In Fig. 6, the B'_{eff} values are plotted against the upper state quantum numbers $k'l'$. These B'_{eff} values agree each other within the experimental errors and no systematic variations are found. This means the interaction does not affect any particular rotational levels strongly, but the contribution of the interaction will be included as a whole in the parameters of Eq. (1).

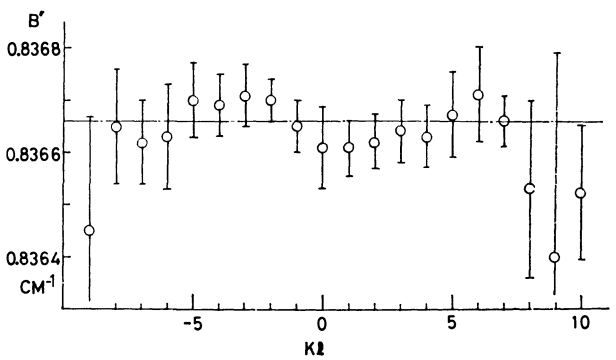

Fig. 6. The effective rotational constants plotted against the upper state quantum number $k'l'$.

The influence to the intensity is qualitatively shown in the fact that the R-branch structure is much simpler than that of the P-branch and the series of lines can be seen more clearly in the R-branch. The maximum J-values which we can assign are about 35 for the P-branch and 25 for the R-branch. For Q-branches, the ^{R}Q-branch is stronger than the ^{P}Q-branch. If the influence of the x,y-type Coriolis interaction is only seen as the anomaly of the intensity, the contribution from the weak $2\nu_6$ band can safely be neglected. Then we consider only the interaction between the $2\nu_3$ and $\nu_3+\nu_6$ bands.

The calculation of the intensity perturbation was given by di Lauro and Mills[3] in detail, the Hamiltonian matrix of this interaction can be written as

$$\begin{array}{l} |1,1^{+1};J,k+1\rangle \quad |2,0;J,k\rangle \quad\quad |1,1^{-1};J,k-1\rangle \\ \begin{bmatrix} \nu_{36}+F'(J,k,l) & +2B_e\Omega\zeta^y_{36}f(J,k) & 0 \\ & \nu_{33}+F''(J,k) & -2B_e\Omega\zeta^y_{36}f(J,k-1) \\ \text{(Hermitian)} & & \nu_{36}+F'(J,k-1,-l) \end{bmatrix} \end{array} \tag{2}$$

where ν_{36} and ν_{33} denote the vibrational energies of the $\nu_3+\nu_6$ and $2\nu_3$ levels, respectively. $F'(J,k,l)$ and $F''(J,k)$ are the rotational energy levels $T_{v,l}(J,k)-G(v,l)$ in Eq. (1),

$$\Omega = \frac{1}{2}[(\omega_3/\omega_6)^{1/2}+(\omega_6/\omega_3)^{1/2}]$$

and
$$f(J,k) = [J(J+1)-k(k+1)]^{1/2} \tag{3}$$

Perturbed energy can be obtained by diagonalizing the Hamiltonian matrix (2). Perturbed line intensities depend upon the mixing of the wave functions and the vibrational transition moments of these two bands, M_{33} and M_{36}. According to the calculations of di Lauro and Mills,[3] the enhancement or the depletion of the particular line intensity depends upon the sign of the product of $M_{33}\times M_{36}\times\zeta^y_{36}$. If this sign is positive, ^{P}P-, ^{R}P-, and ^{R}Q-branches of $\nu_3+\nu_6$ band are enhanced and ^{R}R-, ^{P}R-, and ^{R}Q-branches are depleted. This is called as 'positive' perturbation. The situation is reversed when the sign of the above product is negative.

If the unperturbed energy of the interaction levels, the intensity ratio M_{33}/M_{36}, and the Coriolis coupling constant, ζ^y_{36} are known, the theoretical spectrum can be calculated. A computer program for x,y-Coriolis interaction is written in Fortran IV for a HITAC 8800/8700 system in the University of Tokyo, and simulated spectra may be obtained with the aid of a Calcomp x,y-plotter. This program is used to judge whether the perturbation is 'positive' or 'negative'.

Discussion

The analysis of the ν_6 fundamental band[2] gave the Coriolis coupling constant ζ_6^z as 0.284, which agrees fairly well with our present result, 0.274. The vibration-rotation constants for this band are given as $(B_0-B_{36})=0.0151$ and $(A_0-A_{36})=-0.0069$ cm^{-1}. From the preceding analyses, the vibration-rotation constants of the fundamental bands have been obtained as $\alpha_3^B=0.01134$,[2] $\alpha_6^B=0.0043$,[2] $\alpha_3^A=0.00977$,[1] and $\alpha_6^A=-0.013$ cm^{-1}.[2] From these constants, the rotational constants of $\nu_3+\nu_6$ band are expected to be $(B_0-B_{36})=0.0156$ and $(A_0-A_{36})=-0.0033$ cm^{-1}. The constant for B agrees well with the observed value, while for A the agreement is poor. This is almost certainly due to the rather large experimental error of the α_6^A constant, since the unresolved ^PP-branches and the ambiguities of the J-values of Q-branch maxima make the subband origins of the ν_6 band uncertain. We believe that the value of the $2\nu_3$ and $\nu_3+\nu_6$ bands is more reliable. Since the ^RR-branches were fully resolved, the α_6^B value was obtained with smaller experimental errors.

Table 3. 'Corrected' molecular constants of $2\nu_3$ and $\nu_3+\nu_6$ bands of CH_3F (in cm^{-1} except ζ)

	$2\nu_3$ band	$\nu_3+\nu_6$ band	Ground state[6]
ν_0	2081.382	2221.705	
A	5.06170	5.08779	5.081[b]
B	0.83553	0.83369	0.851794
D_J	1.96×10^{-6}	1.82×10^{-6}	1.997×10^{-6}
D_{JK}	1.0×10^{-5}	2.26×10^{-5}	1.47×10^{-5}
D_K	8.2×10^{-5}	7.91×10^{-5}	8.0×10^{-5} [a]
ζ		0.274	
η_J		1.34×10^{-4}	
η_K		1.0×10^{-5}	
	$\lvert\zeta_{36}^y\rvert=0.38$[a]		
	$[M_{36}/M_{33}]^2=0.05$.[b]		

a) Calculated from the Harmonic force field.[7]
b) Assumed.

Since the vibration-rotation levels of both the $2\nu_3$ and $\nu_3+\nu_6$ bands are known, we can estimate the rotational and centrifugal distortion constants corrected for the perturbation between these two levels. If the value of $|\zeta_{36}^y|$ is fixed to 0.38 which has been obtained from the harmonic force field in Ref. 7, we obtain the 'corrected' constants listed in Table 3. Recently Betrencourt[9] reported the analysis of the $2\nu_3$ band which is consistent with our previous results (I). He also gave the unperturbed constants for the $2\nu_3$ level which are slightly different from ours. The differences arise mainly from the fact that somewhat different values are used for the energy levels of the $\nu_3+\nu_6$ band and for ζ_{36}^y.

If the ratio of the transition moments, M_{36}/M_{33}, is further assumed, the simulated spectra can be drawn by the program mentioned earlier. In Fig. 7, the calculated spectra are shown for the cases of the positive and negative perturbations. From the comparison with the observed spectrum, the Coriolis perturbation between the $2\nu_3$ and $\nu_3+\nu_6$ bands is concluded to be 'positive'.

So far we have ignored the effect of the $(2\nu_6)^0$ or $(2\nu_6)^2$ band. The consideration of these two bands would hardly affect the spectroscopic constants in the $2\nu_3$ band from which they are apart by about 280 cm^{-1}, but the effect may be significant on the $\nu_3+\nu_6$ band. It was shown[3] that the x,y-Coriolis interaction affects in different way on the $^RQ_0$-branch, on $^RR_0$- and $^RP_0$-branches, and on the remaining other branches, and that there are three effective rotational constants B'_{eff}. In our measurement, the effective rotational constant which is obtained from $^RQ_0$-branch is 0.83672 ± 0.00007 and the constant obtained from $^RR_0$- and $^RP_0$-branches is 0.83661 ± 0.00005, while the constant obtained from the remaining branches is 0.83667 ± 0.00002 cm^{-1}. In these calculations, the ground state constants are fixed to the microwave values, and for the calculation of $^RQ_0$- and $^RR,P_0$-branches, the upper state constants except B' and D_J' are assumed to be the same as the values obtained from

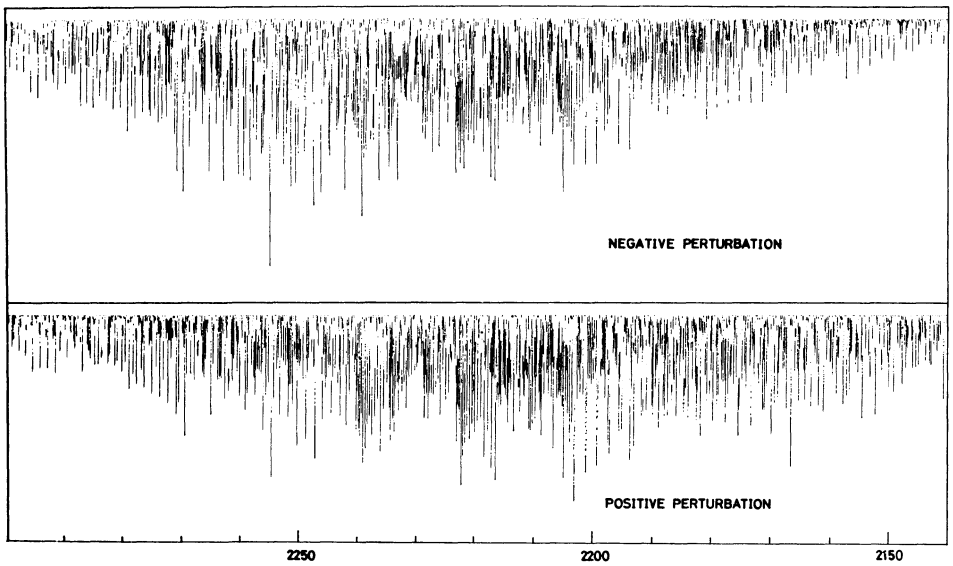

Fig. 7. Simulated spectra of the $\nu_3+\nu_6$ band.

all the other data.

If we consider the four way Coriolis interaction among the $2\nu_3$, $\nu_3+\nu_6$, $(2\nu_6)^0$, and $(2\nu_6)^2$ bands as well as the l-type doubling, the effective rotational constants of the $\nu_3+\nu_6$ band are given as

$$B'_{\text{eff}} = B'_{\text{unp}} - 4B_e^2\zeta^2\Omega^2/\Delta E'' - q/2 \quad (\text{for } {}^{R}Q_0\text{-branch}) \tag{4}$$

$$B'_{\text{eff}} = B'_{\text{unp}} + 8B_e^2\zeta^2\Omega^2/\Delta E - 4B_e^2\zeta^2\Omega^2/\Delta E' - 4B_e^2\zeta^2\Omega^2/\Delta E'' + q/2 \quad (\text{for } {}^{R}R,P_0\text{-branches}) \tag{5}$$

$$B'_{\text{eff}} = B'_{\text{unp}} + 4B_e^2\zeta^2\Omega^2/\Delta E - 2B_e^2\zeta^2\Omega^2/\Delta E' - 4B_e^2\zeta^2\Omega^2/\Delta E'' \quad (\text{for other branches}) \tag{6}$$

where $\Delta E=(\nu_3+\nu_6)-2\nu_3$, $\Delta E'=(2\nu_6)^0-(\nu_3+\nu_6)$, $\Delta E''=(2\nu_6)^2-(\nu_3+\nu_6)$, and q denotes the l-type doubling constant. The above equations are further reduced, if we assume $\Delta E=\Delta E'=\Delta E''$.

$$B'_{\text{eff}} = B'_{\text{unp}} - 4B_e^2\zeta^2\Omega^2/\Delta E - q/2 \quad (\text{for } {}^{R}Q_0\text{-branch}) \tag{7}$$

$$B'_{\text{eff}} = B'_{\text{unp}} + q/2 \quad (\text{for } {}^{R}R,P_0\text{-branches}) \tag{8}$$

$$B'_{\text{eff}} = B'_{\text{unp}} - 2B_e^2\zeta^2\Omega^2/\Delta E \quad (\text{for other branches}) \tag{9}$$

It is interesting to note that B'_{eff} for the ${}^{R}R_0$- and ${}^{R}P_0$-branches is *unperturbed* in contrast to the case of the two way Coriolis interaction originally treated by di Lauro and Mills.[3] If we use $|\zeta_{36}^{y}|=0.38$, $B_e=0.8518\ \text{cm}^{-1}$, and $\Delta E=140\ \text{cm}^{-1}$, these corrections are calculated as -0.00298, 0, and $-0.00149\ \text{cm}^{-1}$ for the above three kinds of branches. From the experimental value, l-type doubling constant can be roughly estimated as $-0.003\ \text{cm}^{-1}$.

This research has been supported by the grant from the Ministry of Education.

References

1) J. Nakagawa, I. Suzuki, T. Shimanouchi, and T. Fujiyama, This Bulletin, **46**, 3399 (1973).
2) W. L. Smith and I. M. Mills, *J. Mol. Spectrosc.* **11**, 11 (1963).
3) C. di Lauro and I. M. Mills, *ibid.*, **21**, 386 (1966).
4) T. Fujiyama, J. Nakagawa, I. Suzuki, I. Nakagawa, and T. Shimanouchi, to be published.
5) K. N. Rao, C. J. Humphreys, and D. H. Rank, "Wavelength Standards in the Infrared," Academic Press, New York (1966).
6) R. S. Winton and W. Gordy, *Phys. Lett.*, **32A**, 219 (1970).
7) T. Shimanouchi, "Molecular Force Field," in "Physical Chemistry," Vol. **4**, ed. by H. Eyring, D. Henderson, and W. Jost, Academic press, New York (1970), p. 290.
8) Numerical data of the observed and calculated frequencies and their assignments have been deposited with the Chemical Society of Japan (Document No. 7410).
9) M. Betrencourt, *J. Mol. Spectrosc.*, **47**, 275 (1973).

Electrical Properties of Ferric Oxyhydroxides

Katsumi KANEKO and Katsuya INOUYE

Department of Chemistry, Faculty of Science, Chiba University, Yayoi-cho, Chiba 280

(Received January 9, 1974)

The electrical conductivity of α-FeOOH, β-FeOOH, and γ-FeOOH was measured in dry air at room temperature in the frequency range of dc to 10 MHz under various pressures of 9—150 kg/cm². The logarithm of conductivity, log σ, shows a linear relationship with the ratio of true density to apparent density, d_0/d', of the samples compressed at different pressures. σ_1 at 7 MHz, determined by extrapolating the log σ *vs.* d_0/d' plots to unity of d_0/d', is proportional to the number of the nearest iron atoms with identical spin. The conductivity increases with increasing frequency f. The ac conductivity σ_{ac} which equals σ minus σ_{dc}, where σ_{dc} is the dc conductivity, is proportional to f^s ($0.6<s<0.8$) in the lower frequencies than 1 MHz. This behavior is presumed to be due to the hopping of a *d*-electron in the t_{2g}-orbital of Fe^{2+} to the t_{2g}-orbital of adjacent Fe^{3+}, through a slight overlapping of t_{2g}-orbitals of Fe^{2+} and Fe^{3+}.

The oxide film formed on transition metal surfaces in atmospheric environments consists of minute crystals of particular oxides and oxyhydroxides together with some amorphous polynuclear complexes. The mechanism of oxide formation under ambient atmospheric conditions has not been sufficiently established. The corrosion process of iron could be better understood if one investigates the correlation between the structure and the physico-chemical properties of the constituent substances of the oxide film. Information on the electrical conductivity of these oxides and oxyhydroxides is desirable, since it is apparent that the transport of electrons and ions plays an important role in the formation of oxide film. Although the electrical conductivity of pure iron oxides such as α-Fe_2O_3, Fe_3O_4, and FeO has been studied to a certain extent, the study on ferric oxyhydroxides (iron hydroxide oxides) is insufficient, possibly because of the difficulty to eliminate the contact resistance between oxyhydroxide crystals by means of sintering at a high temperature, since ferric oxyhydroxides unavoidably decompose around 300 °C.[1] Okamoto, Furuich, and Sato[2] measured the electrical conductivity of hydrous ferric oxides, so-called ferric hydroxides, by compressing at 1 kg/cm² with the dc-method, but not that of pure ferric oxyhydroxides, which is necessary.

In the preceding paper[3] the frequency dependence of the conductivity of unignited fine crystals of α-Fe_2O_3 was reported in the frequency range of dc to 30 MHz under various pressures of 9—150 kg/cm², and the results were discussed from the viewpoint that the electrical conductivity variations with respect to pressure and frequency reflect the intrinsic structure and imperfection of α-Fe_2O_3. The experimental procedures proposed appear to enable elimination of the contact resistance between fine crystals in general.

The same method has been applied to three forms of ferric oxyhydroxide known, α-FeOOH, β-FeOOH, and γ-FeOOH, which occur widely in the atmospheric corrosion products of iron. The relationship between structure and electrical conductivity of these three types of ferric oxyhydroxide is discussed.

Experimental

Samples. α-FeOOH was prepared by hydrolyzing 0.6 M ferric sulfate solution at 50 °C for 30 hr, the pH being adjusted to 13.6 with 0.1 M KOH solution. α-FeOOH filtered was washed with water until no sulfate ion was detected and dried at 100 °C for 3 hr.[4] β-FeOOH was prepared by the following procedure. One liter of 0.1 M $FeCl_3$ containing 60 g urea was heated to 98 °C within 1 hr and kept at this temperature for additional 5 hr. The filtered precipitates were washed with water until no Cl^- was detected and dried at 100 °C for 3 hr.[5] γ-FeOOH was obtained by warming at 60 °C for 50 min a mixed solution of 500 ml 0.2 M $FeCl_2$, 100 ml 2 M hexamethylenetetramine, 13.5 ml concentrated HCl, and 100 ml 1 M sodium nitrite. Preparation of γ-FeOOH was performed in a stream of nitrogen. The precipitates obtained were washed with water until no Cl^- was detected and dried at 60 °C for about 10 hr.[6]

Examination of Samples. The X-ray diffraction patterns were obtained by the powder method with an automatic diffractometer (Geigerflex 2001, Rigaku Denki Co.) by use of Mn-filtered FeK_α (30 kV, 10 mA). The BET surface-area was determined with a Shibata Surafce-area meter using N_2 adsorption at liquid nitrogen temperature.

The ferrous ion content was determined by titration with 0.005 N cerium sulfate solution in the presence of ferroin as an indicator, after the samples had been dissolved in hydrochloric acid by heating in a stream of carbon dioxide. The total iron content in β-FeOOH was determined by titration with 0.05 N $K_2Cr_2O_7$ solution. The chlorine content in β-FeOOH was determined by the Volhard method. The amount of cation impurities was determined by emission spectroscopy.

Electrical Measurements. Electrical conductivity in the frequency range of dc to 10 MHz under various pressures 9—150 kg/cm² at room temperature was measured by the method described in the preceding paper[3] in air dried with silica gel. Samples were dried at 100 °C for 1 hr prior to conductivity determination. The conductivity change with the adsorption of water on α-FeOOH and γ-FeOOH was negligible during the measurements but an increase of approximately 10% in conductivity was observed for β-FeOOH. The conduction was found to be approximately ohmic with applied voltage in the range ~200—~4000 V/cm.

The sign of Seebeck voltage of compressed samples dried at 100 °C for 1 hr was measured in air with a μV-meter (Oyo Denki Co.) in order to determine the sign of the predominant charge carrier.

Results

Properties of Samples. Each sample prepared gave X-ray diffraction patterns of crystalline α-FeOOH,

β-FeOOH, and γ-FeOOH, structures of which have been reported elsewhere.[7-9] In Table 1 are given the crystallite size calculated by the Scherrer formula for the half-value width of the principal lines, the specific surface area (S_{N_2}) and the ratio of iron atoms exposed to crystal surface to the total iron atoms, which was estimated by assuming that only the developed face area of crystals contributes to the specific surface area. The instrumental broadening in diffraction lines was subtracted by use of patterns of magnetite crystals. The ratio of chlorine to iron for β-FeOOH was found to be 9.5 atomic%. The content of cation impurities is given in Table 2. The amount of ferrous iron, providing the carrier, was found to be 0.06 wt% for all samples. The Fe^{2+}/Fe ratio was hence calculated as approximately 0.1 atomic%.

TABLE 1. PROPERTIES OF SAMPLES

	Crystallite size (Å)	S_{N2} (m^2/g)	Surface Fe (%)
α-FeOOH	210	65	13
β-FeOOH	470	34	6
γ-FeOOH	63	124	32

TABLE 2. CATION IMPURITIES OF SAMPLES (wt%)

Cation	α-FeOOH	β-FeOOH	γ-FeOOH
Ferrous iron	0.06	0.06	0.06
Ca	0.002	0.001	0.001
Co	<0.005	<0.005	<0.005
Cr	0.01	0.001	<0.001
Cu	0.001	0.006	0.002
Mg	0.002	0.001	0.001
Mn	0.2	<0.005	<0.005
Mo	<0.01	<0.01	<0.01
Ni	0.05	0.004	0.001
Al	0.01	0.002	0.001
Si	0.3	0.1	0.001
Sn	<0.002	<0.002	<0.002
Ti	0.005	0.005	0.001
Zr	<0.005	<0.005	<0.005
Nb	<0.005	<0.005	<0.005
V	0.005	0.005	0.001

Electrical Conductivity and Compression of Powder Sample. The logarithm of electrical conductivity log σ and the ratio of the true density to the apparent density d_0/d' of the compressed specimen show linear relationships as in the case of α-Fe_2O_3.[3] The relationships for α-FeOOH, β-FeOOH, and γ-FeOOH at different measuring frequencies are shown in Figs. 1 and 2.

The values of σ_i at dc and 7 MHz, determined by extrapolating the linear relationship between log σ and d_0/d', are shown in Table 3. The density values found in literature were used for the calculation: α-FeOOH, 4.28;[10] β-FeOOH, 3.0;[8] and γ-FeOOH, 4.07.[9]

Frequency Dependence. The frequency dependence of conductivity and dielectric constant of α-FeOOH as the representative of three forms of oxyhydroxide is shown in Fig. 3. β-FeOOH and γ-FeOOH gave a frequency dependence similar to that of α-FeOOH. The frequency dependence of σ_i is also shown in Fig. 3. The dielectric constant decreases with the frequency below 10 kHz and becomes constant above 10 kHz. It increases slightly with pressure in the whole frequency range. The electrical conductivity increases with fre-

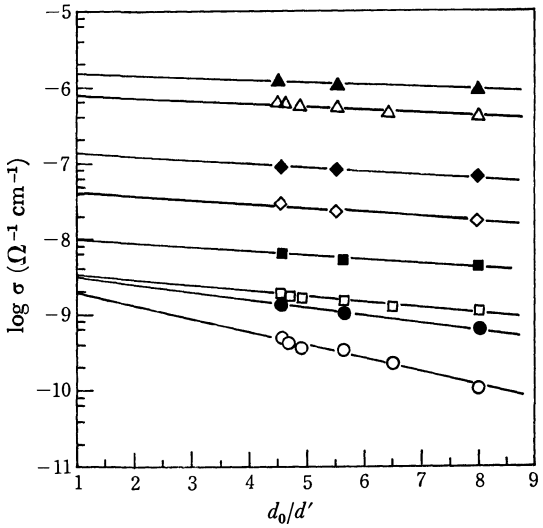

Fig. 1. Changes of conductivity with the ratio of the true density d_0 to the apparent density d' for α-FeOOH. ○: dc, ●: 400 Hz, □: 1 kHz, ■: 10 kHz, ◇: 100 kHz, ◆: 900 kHz, △: 7 MHz, ▲: 10 MHz.

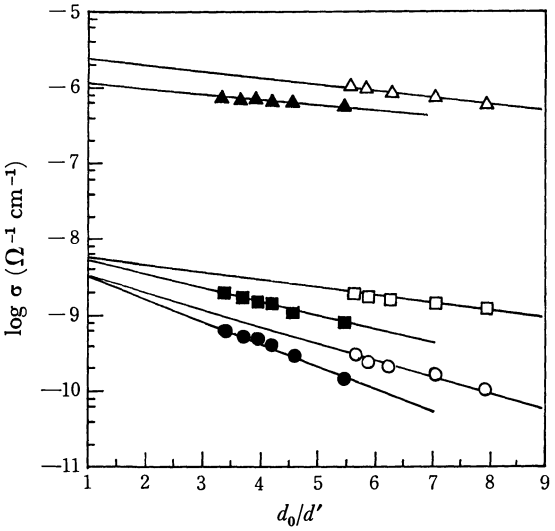

Fig. 2. Changes of conductivity with the ratio of the true density d_0 to the apparent density d'. Filled symbols denote the changes for β-FeOOH and open symbols denote the changes for γ-FeOOH. (●,○): dc, (■,□): 1 kHz, (▲,△): 7 MHz.

TABLE 3. σ_i AND z

	α-FeOOH	β-FeOOH	γ-FeOOH
σ_i at dc $\Omega^{-1}cm^{-1}$	2×10^{-9}	3×10^{-9}	3×10^{-9}
σ_i at 7 MHz $\Omega^{-1}cm^{-1}$	8×10^{-7}	1.5×10^{-6}	2.3×10^{-6}
z	2	4	6

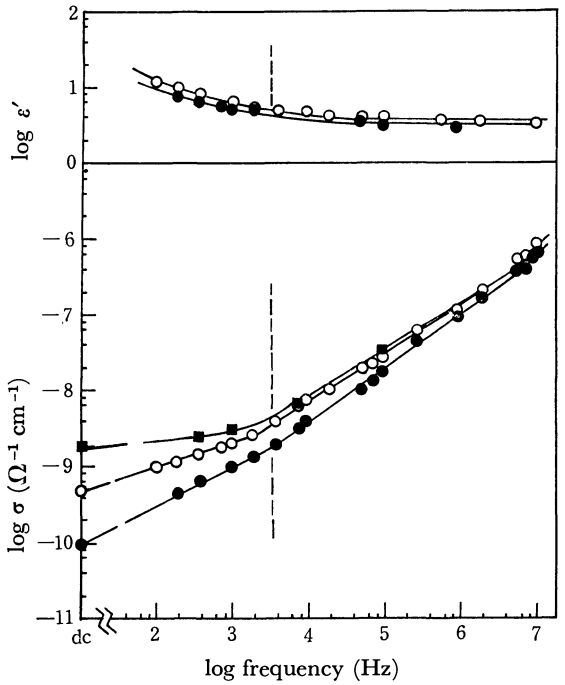

Fig. 3. Frequency dependence of conductivity σ and dielectric constant ε' for α-FeOOH compressed at 9 kg/cm² (●) and 150 kg/cm² (○). The frequency dependence of σ_i is denoted by ■.

quency in the frequency range below 10 kHz and more steeply above 10 kHz. The dispersion of electrical conductivity in the lower frequency range becomes less recognizable with the increase of pressure and is influenced by humidity. On the other hand, the dispersion in the higher frequency range is slightly affected by compression.

In the frequency range below 1 MHz, the ac conductivity (σ_{ac}) which equals σ minus σ_{dc}, where σ_{dc} is the dc conductivity, has the relation with frequency (f) as given by,

$$\sigma_{ac} \propto f^s. \quad (1)$$

The exponents s range from 0.6 to 0.8 and are almost independent of the pressure (Table 4).

The steepest increase of conductivity was observed with the frequency above 1 MHz.

Table 4. Exponents (s)

	At 9 kg/cm²	At 150 kg/cm²	σ_i
α-FeOOH	0.7	0.7	0.7
β-FeOOH	—	~ 1k 0.5	—
		2k ~ 1M 0.8	
γ-FeOOH	0.7	0.6	0.7

Sign of Carriers. The sign of carriers in both α-FeOOH and γ-FeOOH is presumed to be negative, judging from the sign of the cold probe due to the Seebeck voltage observed in the preliminary experiments. The adsorption of water molecules on crystals made it difficult to conclude the exact carrier sign for β-FeOOH, but it appears to be also negative.

Discussion

Frequency Dependence. The frequency dependence of electrical conductivity in the lower frequency range greatly depends on the pressure. The dispersion observed in the lower frequency range seems to be ascribed to the heterogeneity in the specimen, namely the intergranular gaps. The frequency dependence of dielectric constant agrees with that of the two-layer condenser which consists of two admittances in series.[11] Each layer consists of a resistance and a capacitance in parallel. The conductivity above 10 kHz does not become constant but exhibits a pronounced dispersion, though the two-layer condenser consisting of the frequency-independent admittance of crystals and that of gaps suggests that the conductivity of the system should be invariable with respect to the frequency in the frequency range above 10 kHz where the dielectric constant is unchangeable. The dispersion of conductivity occurs in both cases of 150 kg/cm² and σ_i. The dispersion seems to be due to the frequency-dependent conductivity of crystals. The two-layer condenser model could be extended to the inhomogeneous system consisting of the crystals with frequency-dependent conductivity and of the intergranular gaps as in the case of α-Fe_2O_3.[3] The frequency-dependent conductivity in the frequency range above 10 kHz is much higher than σ_{dc} and almost equals σ_{ac}. The ac conductivity given by Eq. (1), in which s is 0.8, was obtained by Pollack and Geballe[12] for the impurity conduction due to hopping processes in doped silicon at low temperature. The chemical analysis indicates that all ferric oxyhydroxides examined are non-stoichiometric having a general composition of $Fe^{II}_{3\delta}$ $Fe^{III}_{1-2\delta}$ OOH where δ is much smaller than 1. In view of the fact that the sign of carriers by the Seebeck voltage measurement is negative, the electrical conduction in ferric oxyhydroxides is attributed to the hopping of excessive d-electrons in Fe^{2+} to Fe^{3+} rather than to that of protons. Fe^{2+} ions are randomly distributed spatially and have an energy differing by about kT. The hopping occurs mainly between a pair of Fe^{2+} and the adjacent Fe^{3+}. Thus the electrical conductivity of ferric oxyhydroxides exhibits a frequency-dependence similar to the impurity conduction at low

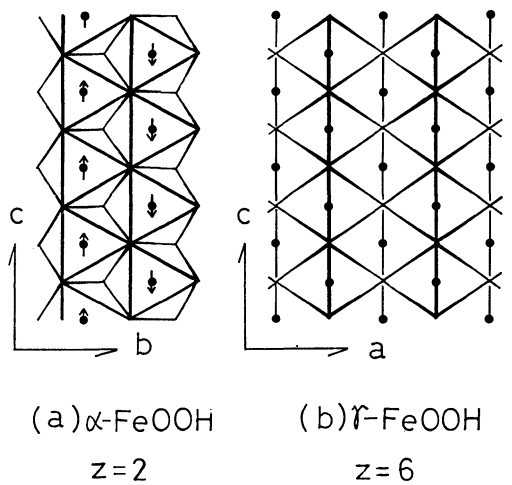

Fig. 4. Crystal structure of α-FeOOH (a) and γ-FeOOH (b). Filled circles denote iron ions and arrows the spin direction of iron ions. O and OH ions are located at the corners of octahedrons.

temperature.

The increase of conductivity with the frequency observed above 1 MHz may be due to the hopping processes with the different mechanism from the above-mentioned processes.

Structure and Hopping Conduction. In ferric oxyhydroxides, Fe^{3+} ions are surrounded octahedrally by six oxygen atoms. These octahedral units form a binuclear complex by sharing edges. In α-FeOOH[13,14] and β-FeOOH,[8,15] the dimers are stacked parallel to the c-axis and the strings are further joined by sharing corners and by hydrogen bonds, as illustrated in Fig. 4(a). In γ-FeOOH, on the other hand, the dimers form layers parallel to the ac-plane by sharing edges (Fig. 4(b)) and each layer links together with hydrogen bonds.[9] It is characteristic of β-FeOOH to embrace chlorine in tunnels parallel to c-axis. The Fe–Fe distance between the nearest neighbors is about 3 Å for each form of oxyhydroxides and there seems no appreciable interaction among iron atoms except nearest neighbors. The distortion at the surface of fine crystals is so predominant as to disturb the periodic potential and to give more localized d-electrons, since much surface Fe exists as shown in Table 1. The state of d-electrons in ferric oxyhydroxide crystals may be regarded approximately as that of "octahedral complex molecules." The d-electron level of a central metal splits into t_{2g} having a small contribution of the $2p_\pi$ orbital of oxygen and e_g having a small contribution of the sp-hybrid orbital of oxygen in molecular orbital of an octahedral complex.[16]

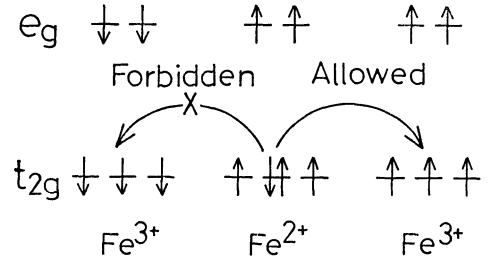

Fig. 5. Electron configurations on the occasion of the hopping of a d-electron in Fe^{2+} to Fe^{3+}.

A charge transfer occurs by the mechanism where a d-electron in the t_{2g}-orbital of Fe^{2+} hops to the adjacent site, t_{2g}-orbital of Fe^{3+}, through a slight overlapping of t_{2g}-orbitals of Fe^{2+} and Fe^{3+}. So long as no magnetic perturbation is present, the spin state of an electron before hopping must be in accord with that of an electron after hopping[17] (Fig. 5). Consequently the transfer probability is proportional to the number z of the nearest iron atoms in the same spin state. In the case of slight interactions among the partners, the transfer probability under an oriented electric field would also be proportional to z for the powdery crystals in various directions. It is noteworthy that the value of σ_i at 7 MHz is proportional to that of z at room temperature (Table 3). The preceding paper[3] showed that the σ_i at 7 MHz reflects the inner structure. This proportionality seems to be caused by the difference in the number of the nearest hopping-partners, since the amount of Fe^{2+} for each form of oxyhydroxide is equal.

All oxyhydroxides are antiferromagnetic and their Néel temperatures T_N found in previous works are as follows: β-FeOOH, 270 K;[18] γ-FeOOH, 50 K[18] or 70 K.[19] For α-FeOOH, different values ranging from 330 to 403 K have been reported.[14,20] The value of z at room temperature (Table 3) was estimated on the assumption that spins can be converted freely above T_N.

State of Chlorine in β-FeOOH. The sample of β-FeOOH examined in this work contains 9.5 atomic % chlorine which cannot be removed by washing with abundant distilled water until no Cl^- was detected with $AgNO_3$ solution. The presence of free chlorine ions would result generally in an increase of conductivity. The results obtained, however, indicate that the influence of chlorine is not remarkable and that chlorine may be immobile and does not seriously distort the electronic structure of iron. For a more definitive discussion on the chlorine effect the β-FeOOH samples with different contents of chlorine should be examined.

The authors express hearty thanks to Dr. R. Matsumoto (Fundamental Res. Inst., Nippon Steel Corp.) for emission spectroscopic analyses.

This research was partly supported by the Science Research Fund of the Ministry of Education.

References

1) T. Ishikawa and K. Inouye, This Bulletin, **45**, 2350 (1972).
2) G. Okamoto, R. Furuichi, and N. Sato, *Electrochim. Acta*, **12**, 1287 (1967).
3) K. Kaneko and K. Inouye, *Nippon Kagaku Kaishi*, **1973**, 1075.
4) W. Feitknecht, A. Wyttenbach, and W. Bunser, "Reactivity of Solids," ed. by J. H. de Boer, Elsevier Publishing Co., Amsterdam (1961), p. 1234.
5) E. R. Nightingale Jr. and R. E. Benck, *Anal. Chem.*, **32**, 566 (1960).
6) O. Baudisch and W. H. Albrecht, *J. Amer. Chem. Soc.*, **54**, 943 (1932).
7) ASTM X-ray Powder Data File No. 8—97 (1969).
8) A. L. Mackay, *Miner. Mag.*, **32**, 545 (1960).
9) F. J. Ewing, *J. Chem. Phys.*, **3**, 420 (1935).
10) R. F. Conley, *J. Amer. Ceram. Soc.*, **50**, 124 (1967).
11) J. Volger, *Prog. Semicond.*, **4**, 205 (1960).
12) M. Pollack and T. H. Geballe, *Phys. Rev.*, **122**, 1742 (1961).
13) F. J. Ewing, *J. Chem. Phys.*, **3**, 203 (1935).
14) J. B. Forsyth, I. G. Hedley, and C. E. Johnson, *J. Phys. Chem. (Solid State Phys.)*, **1**, 179 (1968).
15) A. Szytula, M. Balanda, and Ž. Dimitrijević, *Phys. Stat. Sol.* (a), **3**, 1033 (1970).
16) C. J. Ballhausen and H. B. Gray, "Molecular Orbital Theory," Benjamin, Inc., New York, (1965), p. 103.
17) J. Yamashita and T. Kurosawa, *J. Phys. Soc. Japan*, **15**, 802 (1960).
18) T. Takada, M. Kiyama, and Y. Bando, *Bull. Inst. Chem. Res., Kyoto Univ.*, **47**, 298 (1969).
19) C. E. Johnson, *J. Phys. C. (Solid State. Phys.)*, **2**, 1996 (1969).
20) A. Szytula, A. Burewicz, K. Dyrek, A. Hrynkiewicz, D. Kulgawczuk, Z. Obuszko, H. Rżany, and A. Wanic, *Phys. Stat. Sol.*, **15**, K195 (1966).

Brillouin Scattering and Elastic Constants of Tetragonal Pentaerythritol

Hiroatsu MATSUURA* and Tatsuo MIYAZAWA**

Institute for Protein Research, Osaka University, Yamada-kami, Suita, Osaka 565

(Received January 17, 1974)

The Brillouin scattering from tetragonal pentaerythritol crystals was measured by using a helium–neon laser and a pressure-scanned Fabry-Perot interferometer. The Brillouin components from the longitudinal acoustic mode and the transverse acoustic mode polarized parallel to the scattering plane were observed for various crystal directions with the scattering vector in the (001) and (010) planes. From the observed Brillouin shifts, the frequencies and velocities of sound waves with the wavelength of 290 nm were obtained, and the elastic constants were determined, in units of 10^{11} dyn/cm^2, as $C_{11}=3.94\pm0.01$, $C_{13}=0.76\pm0.03$, $C_{16}=0.00\pm0.05$, $C_{33}=1.33\pm0.02$, $C_{44}=0.44\pm0.03$, and $2C_{66}+C_{12}=5.13\pm0.03$. The present hypersonic values of the elastic constants were compared with previous values by the ultrasonic technique.

Brillouin scattering is one of the experimental techniques for determining elastic constants of solid materials. This method has become particularly useful since the development of lasers as monochromatic light sources and of high-resolution interferometers. In Brillouin-scattering measurements, velocities of thermally excited sound waves are observed and accordingly no external acoustic excitation is necessary. Furthermore, only one crystal specimen suffices for determining elastic constants, unlike the ultrasonic technique which generally requires many crystal specimens with particular faces.

In our previous study,[1] the Brillouin scattering from a cubic crystal of potassium bromide was measured and the three elastic constants were determined. The Brillouin measurement was extended, in the present study, to a molecular crystal of tetragonal pentaerythritol $C(CH_2OH)_4$, and the elastic constants were compared with previous results of an ultrasonic study on this crystal.[2]

Experimental

The experimental arrangement for the observation of Brillouin scattering was essentially the same as that was used in our previous study.[1] The light source was a helium–neon gas laser in the fundamental transverse mode, giving radiation at 632.8 nm with an output of about 50 mW. The light scattered from the sample at 90° away from the incident-beam direction was analyzed by a pressure-scanned Fabry-Perot interferometer. In the present measurements, the incident laser beam was focused by a lens inserted just before the sample, so that the beam in the crystal had an appropriately narrow width which allowed the efficient collection of the scattered light. This light-focusing system is particularly important for measuring Brillouin scattering from small crystal specimens. The spacer between the interferometer etalons had a thickness of 6.075 mm, giving the free spectral range of 24.674 GHz.

Crystal specimens of pentaerythritol were generously supplied to us by Dr. H. Yamada.[3] The crystal with dimensions of $5\times3.5\times2.5$ mm^3 was immersed in liquid anethole, which had nearly the same refractive index as that of pentaerythritol. This technique was found to be useful in reducing a large amount of unwanted light scattered from rough crystal surfaces. The sample was supported by a rotatable holder, the same apparatus that was used in the previous study on potassium bromide,[1] which allowed the crystal to be rotated about an axis perpendicular to the scattering plane. Accordingly, any direction in a crystal plane parallel to the scattering plane could be chosen as the direction of the scattering vector. The Brillouin scattering was measured for the scattering vector in two crystal planes, the (001) and (010) planes. The measurements were made at 23 ± 1°C at least five times for each orientation of the crystal. For certain crystal directions, Brillouin shifts were expected to be larger than the half of the free spectral range with the spacer of ~6 mm. Accordingly, auxiliary measurements were also made with a spacer of the 3 mm thickness so that the free spectral range was made as large as ~50 GHz.

The crystal structure of pentaerythritol at room temperature belongs to the tetragonal system with the space group of S^2_4–$I\bar{4}$.[4] The c axis was readily identified, since the crystal was cleaved very easily perpendicular to this axis. This axis was determined by the X-ray diffraction technique.

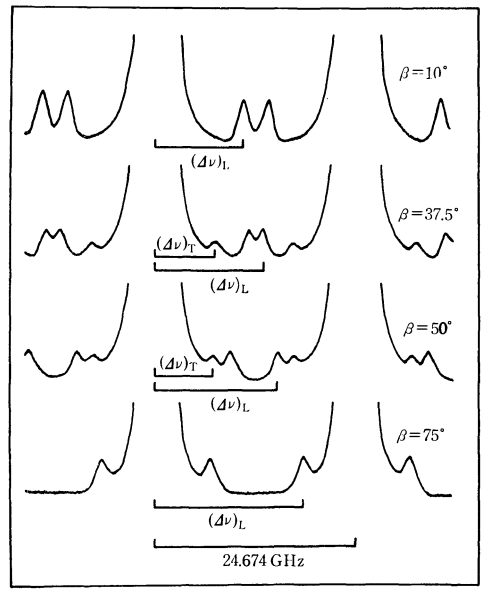

Fig. 1. Brillouin spectra of tetragonal pentaerythritol in Measurement II. $(\Delta\nu)_L$ and $(\Delta\nu)_T$ are the longitudinal and in-plane transverse Brillouin shifts, respectively.

* Present address: Department of Chemistry, Faculty of Science, The University of Tokyo, Hongo, Tokyo 113.

** Present address: Department of Biophysics and Biochemistry, Faculty of Science, The University of Tokyo,Hongo, Tokyo 113.

TABLE 1. FREQUENCIES AND VELOCITIES OF SOUND WAVES AS A FUNCTION OF PROPAGATION DIRECTION IN THE (001) PLANE IN TETRAGONAL PENTAERYTHRITOL (MEASUREMENT I)

Angle α[a] (deg)	Longitudinal mode	
	Frequency[b] (GHz)	Velocity[b] (km/s)
0	17.860(14)	5.289(4)
5	17.939(15)	5.313(4)
10	18.114(12)	5.365(3)
15	18.309(15)	5.423(5)
20	18.512(12)	5.482(3)
25	18.718(12)	5.544(3)
30	18.898(19)	5.597(5)
35	19.051(21)	5.642(6)
40	19.181(22)	5.681(7)
45	19.233(14)	5.696(4)

a) Angle between the scattering vector and the [100] direction in the (001) plane. The experimental error in α was estimated to be $\pm 1°$. b) The experimental error is given in parentheses for the last digits.

TABLE 2. FREQUENCIES AND VELOCITIES OF SOUND WAVES AS A FUNCTION OF PROPAGATION DIRECTION IN THE (010) PLANE IN TETRAGONAL PENTAERYTHRITOL (MEASUREMENT II)

Angle β[a] (deg)	Longitudinal mode		Transverse mode	
	Frequency[b] (GHz)	Velocity[b] (km/s)	Frequency[b] (GHz)	Velocity[b] (km/s)
0	10.738(15)	3.092(4)		
5	10.773(08)	3.103(2)		
10	10.855(10)	3.126(3)		
15	10.954(17)	3.155(5)		
20	11.222(13)	3.232(4)		
22.5	11.437(22)	3.294(6)		
25	11.716(20)	3.374(6)		
27.5			7.550(07)	2.174(2)
30			7.617(06)	2.194(2)
32.5			7.662(11)	2.207(3)
35			7.726(20)	2.225(6)
37.5	13.209(13)	3.804(4)	7.665(08)	2.208(2)
40	13.652(11)	3.932(3)	7.613(09)	2.193(3)
45	14.460(14)	4.165(4)	7.529(24)	2.168(7)
50	15.239(06)	4.389(2)	7.335(25)	2.112(7)
55	15.898(23)	4.579(7)	7.188(15)	2.070(4)
60	16.663(20)	4.799(6)		
65	17.259(11)	4.971(3)		
70	17.682(14)	5.092(4)		
75	17.967(08)	5.174(2)		
80	18.193(12)	5.240(4)		
85	18.309(08)	5.273(2)		
90	18.368(11)	5.290(3)		

a) Angle between the scattering vector and the [001] direction in the (010) plane. The experimental error in β was estimated to be $\pm 1°$. b) The experimental error is given in parentheses for the last digits.

Some typical examples of the observed Brillouin spectra are shown in Fig. 1, and the observed frequency shifts and sound velocities are listed in Tables 1 and 2.

Analysis of Brillouin Spectra

The frequency shift in Brillouin scattering, $\Delta\nu$, is related to the velocity of elastic waves in the medium, v, by[5]

$$\Delta\nu/\nu_i = \pm(v/c)(n_i^2+n_s^2-2n_in_s\cos\theta)^{1/2}, \quad (1)$$

where ν_i is the frequency of the incident light wave, c is the velocity of light in vacuum, n_i and n_s are the refractive indices of the medium for the incident and scattered directions, and θ is the angle of scattering. In a crystal, there are three modes of elastic waves, one longitudinal and two transverse modes, propagating with different velocities.[6] Accordingly, observation of three pairs of Brillouin components with different frequency shifts is expected for any crystal, unless double refraction is taken into account. However, the Brillouin scattering from one of the transverse modes polarized perpendicular to the scattering plane (out-of-plane transverse mode) is usually not observable, since this mode gives in general much weaker Brillouin intensities than the longitudinal mode or the other transverse mode polarized parallel to the scattering plane (in-plane transverse mode). The longitudinal and in-plane transverse modes are mixed with each other for general crystal directions.

The tetragonal pentaerythritol crystal is uniaxial, and accordingly has the optical property of double refraction. In uniaxial crystals, two refractive indices of n' and n'' for ordinary and extraordinary rays, respectively, are related, by the following equations, to the principal refractive indices of $n_a=n_b$ and n_c, where the suffixes represent the principal crystal axes,

$$n' = n_a \quad (2)$$

and

$$n'' = n_an_c/(n_a^2\sin^2\phi+n_c^2\cos^2\phi)^{1/2}, \quad (3)$$

where ϕ is the angle between the c axis and the direction of the wave vector of light. In the present measurements, the Brillouin scattering was observed for the scattering vector in the (001) plane (Measurement I) and the (010) plane (Measurement II). Since the crystal was rotated about an axis perpendicular to the scattering plane, the incident and scattered lights were also in the (001) plane or the (010) plane. For Measurement I, $\phi=90°$ for both incident and scattered lights, and accordingly the refractive indices of the ordinary and extraordinary rays are given by

$$n_i' = n_s' = n_a \quad (4)$$

and

$$n_i'' = n_s'' = n_c. \quad (5)$$

For Measurement II,

$$n_i' = n_s' = n_a, \quad (6)$$

$$n_i'' = n_an_c/(n_a^2\sin^2\phi_i+n_c^2\cos^2\phi_i)^{1/2}, \quad (7)$$

and

$$n_s'' = n_an_c/(n_a^2\sin^2\phi_s+n_c^2\cos^2\phi_s)^{1/2}. \quad (8)$$

The ordinary and extraordinary rays are polarized lights whose electric vectors are perpendicular and parallel, respectively, to the plane determined by the wave vector of light and the optical axis of the crystal

(c axis in tetragonal crystals). Hence, it may be more convenient to give the refractive indices according to the polarization of the incident and scattered lights. The refractive indices for the incident light with the vertical (V) and horizontal (H) electric vectors and for the scattered light with the vertical (v) and horizontal (h) electric vectors (the scattering plane being horizontal) are given by; for Measurement I

$$n_V = n_v = n_c \text{ (extraordinary ray)} \quad (9)$$

and

$$n_H = n_h = n_a; \text{ (ordinary ray)} \quad (10)$$

and for Measurement II

$$n_V = n_v = n_a, \text{ (ordinary ray)} \quad (11)$$

$$n_H = n_a n_c/(n_a^2 \sin^2 \phi_i + n_c^2 \cos^2 \phi_i)^{1/2}, \text{ (extraordinary ray)} \quad (12)$$

and

$$n_h = n_a n_c/(n_a^2 \sin^2 \phi_s + n_c^2 \cos^2 \phi_s)^{1/2}. \text{ (extraordinary ray)} \quad (13)$$

The Brillouin measurements were attempted in the present study with the incident laser beam with vertical (V) and horizontal (H) electric vectors. The vertically polarized light gave a pair of Brillouin components in Measurements I and II, with an additional pair for certain crystal directions in Measurement II, but the horizontally polarized light gave no detectable Brillouin components. The Brillouin spectra reported here are, accordingly, those observed by the incident light with a vertical polarization (V). The polarization of the observed scattered light was found to be vertical (v). Hence, the refractive indices for Measurement I are $n_V=n_v=n_c$, and for Measurement II, $n_V=n_v=n_a$. Equation (1) is now reduced, under the present experimental condition, to the following equations; for Measurement I

$$\Delta\nu/\nu_i = \pm 2(v/c)n_c \sin(\theta/2), \quad (14)$$

and for Measurement II

$$\Delta\nu/\nu_i = \pm 2(v/c)n_a \sin(\theta/2). \quad (15)$$

The refractive-index values of $n_a=1.5537$ and $n_c=1.5109$ (for 659 nm)[7] were used in the present analysis of Brillouin spectra of tetragonal pentaerythritol. From the polarization of the incident and scattered lights and the intensities, the observed Brillouin components were assigned to the acoustic mode almost entirely longitudinal with admixture of the transverse mode. The additional weaker components observed in Measurement II were assigned to the mode primarily in-plane transverse mixed with the longitudinal mode. The polarization of the acoustic waves were confirmed by examining eigenvectors of the Christoffel-equation matrix as will be mentioned later.

Since the Brillouin-scattering measurements were made for the scattering angle $\theta=90°$, the wavelength of the scattering sound wave, λ_s, is given by; for Measurement I

$$\lambda_s = \lambda_i/(\sqrt{2}\, n_c), \quad (16)$$

and for Measurement II

$$\lambda_s = \lambda_i/(\sqrt{2}\, n_a), \quad (17)$$

where λ_i is the wavelength of the incident light in a vacuum. By substituting $\lambda_i=632.8$ nm for a helium–neon laser, the wavelength of the sound wave is obtained as $\lambda_s=296.2$ nm for Measurement I and $\lambda_s=288.0$ nm for Measurement II.

The crystallographic a axis was determined by the X-ray diffraction technique with experimental error less than $\pm 1°$. The observed sound velocities were obtained by Eqs. (14) and (15), and are listed in Tables 1 and 2. The direction of the scattering vector, which is equivalent to the propagation direction of the sound wave responsible for Brillouin scattering, is described in Table 1 by the angles α and β for Measurements I and II, respectively. α is the angle between the scattering vector and the [100] direction in the (001) plane, and β is the angle between the scattering vector and the [001] direction in the (010) plane.

Calculation of Elastic Constants

The crystal structure of pentaerythritol at room temperature belongs to the tetragonal system with the space group of S_4^2–$I\bar{4}$.[4] Accordingly, the number of independent elastic constants is reduced to seven; namely $C_{11}=C_{22}$, C_{33}, $C_{44}=C_{55}$, C_{66}, C_{12}, $C_{13}=C_{23}$, and $C_{16}=-C_{26}$ (other elastic constants vanish by symmetry). Hence, the Christoffel equation,[8] which relates the elastic constants and elastic-wave velocities, v, is given for this crystal by

$$\begin{vmatrix} \lambda_{11}-\rho v^2 & \lambda_{12} & \lambda_{13} \\ \lambda_{12} & \lambda_{22}-\rho v^2 & \lambda_{23} \\ \lambda_{13} & \lambda_{23} & \lambda_{33}-\rho v^2 \end{vmatrix} = 0, \quad (18)$$

where $\lambda_{11}=l^2C_{11}+m^2C_{66}+n^2C_{44}+2lmC_{16}$, $\lambda_{22}=l^2C_{66}+m^2C_{11}+n^2C_{44}-2lmC_{16}$, $\lambda_{33}=(l^2+m^2)C_{44}+n^2C_{33}$, $\lambda_{12}=(l^2-m^2)C_{16}+lm(C_{66}+C_{12})$, $\lambda_{13}=nl(C_{44}+C_{13})$, $\lambda_{23}=mn(C_{44}+C_{13})$, l, m, and n are the direction cosines of the propagation direction of the sound waves, and ρ is the mass density. It is more convenient to express λ's in terms of the angle α or β. For Measurement I ($l=\cos\alpha$, $m=\sin\alpha$, and $n=0$), $\lambda_{11}=C_{11}\cos^2\alpha+C_{66}\sin^2\alpha+2C_{16}\cos\alpha\sin\alpha$, $\lambda_{22}=C_{11}\sin^2\alpha+C_{66}\cos^2\alpha-2C_{16}\cos\alpha\sin\alpha$, $\lambda_{33}=C_{44}$, $\lambda_{12}=(C_{12}+C_{66})\cos\alpha\sin\alpha+C_{16}(\cos^2\alpha-\sin^2\alpha)$, and $\lambda_{13}=\lambda_{23}=0$, and for Measurement II ($l=\sin\beta$, $m=0$ and $n=\cos\beta$), $\lambda_{11}=C_{11}\sin^2\beta+C_{44}\cos^2\beta$, $\lambda_{22}=C_{66}\sin^2\beta+C_{44}\cos^2\beta$, $\lambda_{33}=C_{33}\cos^2\beta+C_{44}\sin^2\beta$, $\lambda_{12}=C_{16}\sin^2\beta$, $\lambda_{13}=(C_{44}+C_{13})\cos\beta\sin\beta$, and $\lambda_{23}=0$.

Table 3. Elastic constants of tetragonal pentaerythritol at room temperature, in units of 10^{11} dyn/cm^2

	Ultrasonic[a]	Present study (Brillouin scattering)
C_{11}	4.05±0.04	3.94±0.01
C_{12}	2.66±0.21	...
C_{13}	1.05±0.03	0.76±0.03
C_{16}	0.31±0.24	0.00±0.05
C_{33}	1.39±0.01	1.33±0.02
C_{44}	0.274±0.003	0.44±0.03
C_{66}	0.252±0.003	...
$2C_{66}+C_{12}$	3.16±0.22	5.13±0.03

a) Ref. 2.

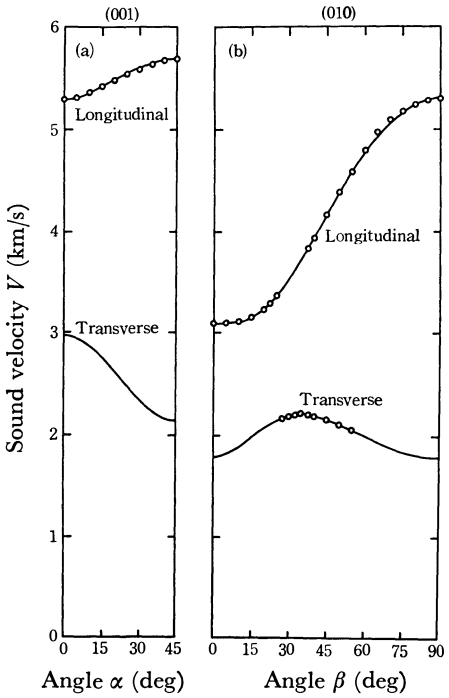

Fig. 2. Sound velocity of the longitudinal and in-plane transverse modes in tetragonal pentaerythritol, in Measurement I (a) and Measurement II (b). The sound velocity of the in-plane transverse mode in Measurement I was calculated by assuming $C_{12}=2.66\times10^{11}$ and $C_{66}=1.24\times10^{11}$ dyn/cm^2. ○: observed value; ——: calculated value.

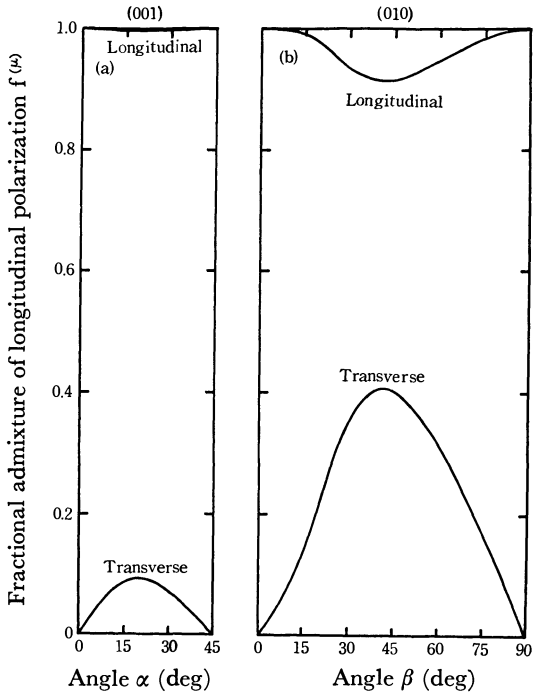

Fig. 3. Fractional admixture of longitudinal polarization for the longitudinal and in-plane transverse modes in tetragonal pentaerythritol, in Measurement I (a) and Measurement II (b).

The elastic constants of tetragonal pentaerythritol were determined, by solving Eq. (18), from 38 observed values for the sound velocity by the least-squares method. The mass density[2] of $\rho=1.398$ g/cm^3 was used in the calculations. In the least-squares adjustment of the elastic constants, the values of C_{12} and C_{66} were hardly settled, but a combination of $2C_{66}+C_{12}$ was determined fairly accurately. The determined values of the elastic constants are listed in Table 3, in comparison with values obtained previously by the ultrasonic technique.[2] The observed and calculated sound velocities are shown in Fig. 2. Figure 3 shows the fractional admixture of longitudinal polarization $f^{(\mu)}$ for the longitudinal and in-plane transverse modes, defined by

$$f^{(\mu)} = \boldsymbol{e}_{\mathrm{pol}}^{(\mu)}\cdot\boldsymbol{e}_{\mathrm{prop}}, \tag{19}$$

where μ is an index for the acoustic modes, $\boldsymbol{e}_{\mathrm{pol}}^{(\mu)}$ is a unit vector in the polarization direction of the mode μ of the sound wave [corresponding to the eigenvector of Eq. (18) for the mode μ], and $\boldsymbol{e}_{\mathrm{prop}}$ is a unit vector in the propagation direction of the sound wave [corresponding to the direction cosines l, m, and n appearing in Eq. (18)].

Discussion

The elastic constants of tetragonal pentaerythritol determined in the present study may be compared with values obtained by the ultrasonic pulse technique with a frequency of 5 MHz.[2] The Brillouin values of C_{11} and C_{33} are in excellent agreement with the ultrasonic values. Also, the agreement for C_{13} and C_{44} is almost satisfactory, considering experimental errors involved. The discrepancy in values of elastic constants may also be attributable in part to the dispersion of the sound velocities for the hypersonic and ultrasonic regions. However, the Brillouin value of $2C_{66}+C_{12}$ is much larger than the ultrasonic value. Indeterminacy of separate values for C_{12} and C_{66} in the present study does not allow further discussion on this discrepancy. The C_{11} value of pentaerythritol (3.9×10^{11} dyn/cm^2) is very close to the values of the corresponding constant for alkali halides [$(3—4)\times10^{11}$ dyn/cm^2].[1,9] The intermolecular hydrogen bonds formed in planes parallel to the (001) plane are, at least in part, responsible for the C_{11} value comparable to those of ionic crystals.

In the present study, the longitudinal Brillouin components were observed in both Measurements I and II, but the in-plane transverse components were observed only for $\beta=27.5—55°$ in Measurement II. It is evident from Fig. 3 that the appreciable mixing with the longitudinal mode allowed the observation of the transverse Brillouin components for these crystal directions. On the contrary, in Measurement I, the mixing is too small to enhance the transverse Brillouin intensities.

In Brillouin-scattering measurements, only one crystal specimen suffices for determining elastic constants, unlike the ultrasonic technique which generally requires many crystal specimens with particular faces. Accordingly, the Brillouin scattering technique is free from experimental errors arising in the process of cutting and polishing crystal specimens. This is one of the

advantages of the Brillouin-scattering method over the ultrasonic method. Also, in the Brillouin scattering, measurements of sound velocities are possible for any desired crystal direction, once the crystallographic axes are determined. However, the Brillouin scattering from the three acoustic modes, one longitudinal and two transverse modes, are generally not all observed in the spectra. This disadvantage is compensated in part by measuring sound velocities of the observable modes for many crystal directions. However, this experimental limitation sometimes makes it difficult to determine all of independent elastic constants. In the present study, separate values for C_{12} and C_{66} could not be determined uniquely because of the lack of experimental sound velocities for the in-plane transverse mode in Measurement I. The present study has nevertheless indicated that the Brillouin-scattering technique, using a laser and a high-resolution interferometer, is useful in determining elastic constants of crystals. So far only a few molecular crystals have been reported,[10-12] whose elastic constants were determined by this method, but it is expected that an increasing number of crystals will be studied by the Brillouin-scattering technique.

Numerical calculations in the present study were carried out with a NEAC 2200-700 computer at the Computer Center of Osaka University. The authors wish to thank Dr. Haruka Yamada of Kwansei Gakuin University for supplying them with crystal specimens of pentaerythritol, and Professor Masao Kakudo and Dr. Nobuo Tanaka of Osaka University for measuring X-ray diffraction of the sample.

References

1) H. Matsuura and T. Miyazawa, This Bulletin, **46**, 3031 (1973).

2) H. Nomura, K. Higuchi, S. Kato, and Y. Miyahara, *Japan. J. Appl. Phys.*, **11**, 304 (1972). The elastic constants of pentaerythritol have also been determined by the method of diffuse X-ray reflection [R. C. Srivastava and S. C. Chakraborty *J. Phys. Soc. Japan*, **17**, 1767 (1962)]. However this method is not very accurate and the values determined do not agree with the ones by the ultrasonic or Brillouin-scattering method.

3) K. Tsuji, H. Yamada, K. Suzuki, and I. Nitta, *Spectrochim. Acta*, **26A**, 475 (1970).

4) I. Nitta and T. Watanabé, *Nature*, **140**, 365 (1937); I. Nitta and T. Watanabé, *Sci. Papers Inst. Phys. Chem. Res., Tokyo*, **34**, 1669 (1938); F. J. Llewellyn, E. G. Cox, and T. H. Goodwin, *J. Chem. Soc.*, **1937**, 883; R. Shiono, D. W. J. Cruickshank, and E. G. Cox, *Acta Crystallogr.*, **11**, 389 (1958).

5) V. Chandrasekharan, *Current Sci. India*, **19**, 371 (1951); V. Chandrasekharan, *Proc. Indian Acad. Sci.*, **A33**, 183 (1951).

6) Each of the three modes is not purely longitudinal or transverse for general crystal directions. The terms of *longitudinal mode* and *transverse mode* are used in this paper to describe the quasi-longitudinal mode and the quasi-transverse mode, respectively.

7) R. Kiriyama, S. Yabumoto, and I. Nitta, This Bulletin, **27**, 115 (1954).

8) M. J. P. Musgrave, *Proc. Roy. Soc. Ser. A*, **A226**, 339 (1954).

9) G. B. Benedek and K. Fritsch, *Phys. Rev.*, **149**, 647 (1966).

10) R. Vacher, L. Boyer, and W. Longueville, *C. R. Acad. Sci. Paris*, **274**, 1383 (1972).

11) M. J. Bird, D. A. Jackson, and J. G. Powles, *Mol. Phys.*, **25**, 1051 (1973).

12) D. L. Swanson and D. A. Dows, *Chem. Phys. Lett.*, **23**, 430 (1973).

Temperature Dependence of the Lattice Vibrations of Triglycine Sulfate

Norio KANEKO, Hiroaki TAKAHASHI, and Keniti HIGASI

Department of Chemistry, School of Science and Engineering, Waseda University, Tokyo 160

(Received January 18, 1974)

Far infrared spectra from 400 to 30 cm^{-1} of triglycine sulfate and its deuterated analogue were measured and the bands due to the librational modes of glycine molecules were identified. Polarized Raman spectra below 300 cm^{-1} of triglycine sulfate single crystals were measured and the symmetry species of the observed lattice vibrations were determined. Temperature dependence of the lattice vibrations was examined. Significant changes were detected in both infrared and Raman spectra on crossing the Curie temperature, indicating a flipping motion of glycine I in the paraelectric phase and suggesting the ferroelectric transition in triglycine sulfate to be of an order-disorder type.

Triglycine sulfate (TGS) is one of the few crystals which exhibit ferroelectricity at room temperature. Since its discovery in 1956 by Matthias *et al.*,[1] the crystal structure as well as ferroelectric transition have been extensively studied.

A detailed crystal structure was reported by Hoshino *et al.*[2] and recently by Itoh and Mitsui.[3] Hoshino *et al.* proposed an order-disorder type theory of the ferroelectric transition based on their X-ray diffraction data. They explained the dipole switching mechanism in the ferroelectric phase in terms of the flipping of the $NH_3^+CH_2COOH$ glycinium ion (glycine I) between two equivalent orientations in the crystal, plus the tunneling of the hydrogen bonded proton between the $NH_3^+CH_2COO^-$ zwitter-ion (glycine II) and the other $NH_3^+CH_2COOH$ ion (glycine III).

The theory was supported by critical X-ray scattering study.[4] However, deuteron magnetic resonance studies[5,6] cast some doubt about the proposed dipole reversal mechanism and the order-disorder nature of the ferroelectric transition.

Infrared and Raman studies on TGS have been carried out by several investigators. Dodd[7] measured polarized infrared spectra from 4000 to 625 cm^{-1} and concluded that TGS, unlike crystalline glycine, was not in the zwitter-ion form. She further reported that heating the crystal above the Curie temperature (48 °C) produced no appreciable changes in the infrared spectra. Khanna *et al.*[8] investigated the infrared spectra of TGS and its deuterated analogue at room temperature and liquid N_2 temperature and found the bands due to the zwitter-ion as well as glycinium ion. Recent investigation by Raman spectra[9] supported the presence of the zwitter-ion in TGS crystals.

Barker and Tinkham[10] measured polarized infrared reflection spectra down to 14 cm^{-1}, but no soft mode was observed. Sato[11] measured infrared spectra at various temperatures and found that the band at 575 cm^{-1} markedly decreased in intensity with temperature rise of the crystal, disappearing above the Curie temperature. Quilichini *et al.*[12] measured polarized Raman spectra below 200 cm^{-1} at various temperatures, but failed to reveal significant spectral changes due to ferroelectric transition.

The purpose of this paper is two-fold; to determine symmetry species of the lattice vibrations by polarized Raman spectra, and to detect changes in the infrared and Raman spectra by temperature variation and thereby giving additional information on the mechanism of the ferroelectric transition in TGS.

Experimental

Single crystals of TGS were grown from an aqueous solution containing glycine and sulfuric acid in proper molar proportions. The composition of the crystals were checked by titrating a small amount of the sample with a standard NaOH solution. The crystals were in the form of thick plates (about 7 mm × 7 mm × 3 mm) with a broad face parallel to the b-axis (two-fold axis) and a cleavage plane perpendicular to the b-axis.

The far infrared spectra (400—30 cm^{-1}) of TGS and its *N*-deuterated powder suspended in Nujol were recorded with a Hitachi FIS-3 spectrophotometer. The *N*-deuterated analogue was prepared by recrystallizing the sample several times from heavy water solutions.

The Raman spectra were recorded with a Shimadzu R-2D double monochrometer. The 5145 Å line of an Ar^+ laser was used as the excitation wave-length with 700 mW power output. For the polarized Raman spectra, single crystals with three facets each respectively parallel to the cleavage plane (010), the optic plane ($\bar{1}02$) and the plane perpendicular to both planes was used. The third facet was almost parallel to the (100) plane, the angle between them being less than 3°. A polarization scrambler, a quartz wedge, was placed between the analyser and slit to correct preferential sensitivity of the monochrometer to the polarization of the scattered light. The spectra were recorded by photon counting detection and the wave numbers of the Raman bands were calibrated using spontaneous emission lines from the laser.

The temperature variation of the infrared and Raman-spectra were measured using high and low temperature cells. For the infrared spectra a double chopping method was employed to eliminate the effect of the radiation from the sample and the reference. The temperature of the crystal was measured and controlled within ±1°C by means of a copper-constantan thermocouple in the range −190 −25 °C and an alumel-chromel thermocouple in the range above 25 °C.

Results and Discussion

The crystal structure of TGS is monoclinic; the space group is C_2^2–$P2_1$ in the ferroelectric phase and C_{2h}^2–$P2_1/m$ in the paraelectric phase.[2,13] In either phase, the Bravais unit cell contains two units of the formula $NH_3^+CH_2COO^-(NH_3^+CH_2COOH)_2SO_4^{2-}$. The crys-

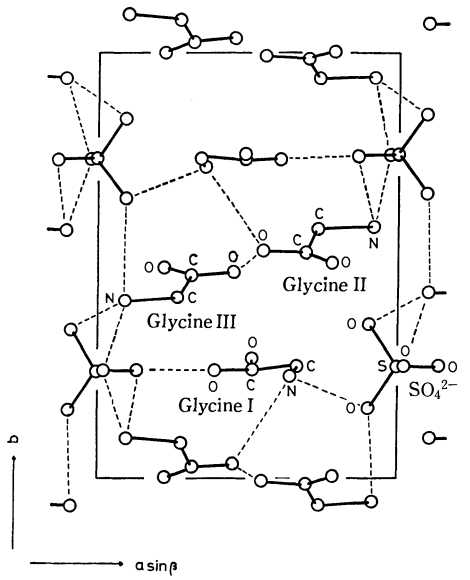

Fig. 1. Projection of the crystal structure of TGS on the ab-plane (ferroelectric phase). Positions of hydrogen atoms are not given. Hydrogen bonds are indicated by dotted lines.

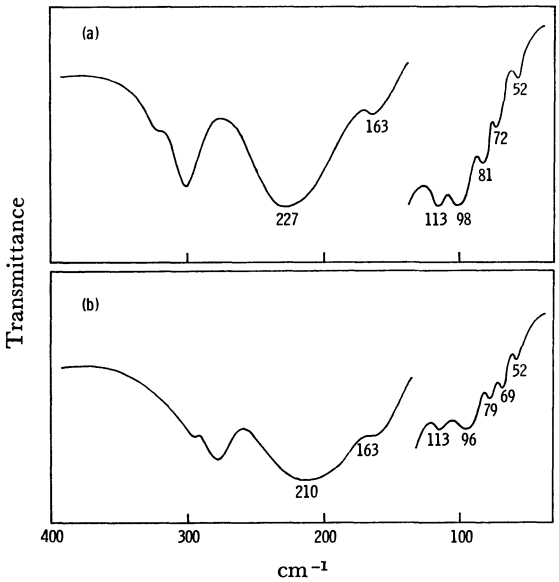

Fig. 2. Far infrared spectra of TGS and its deuterated powder suspended in Nujol.
(a) $NH_3^+CH_2COO^-(NH_3^+CH_2COOH)_2SO_4^{2-}$
(b) $ND_3^+CH_2COO^-(ND_3^+CH_2COOD)_2SO_4^{2-}$

tal structure in the ferroelectric phase is shown in Fig. 1. The lattice constants are: $a=9.417$, $b=12.643$, $c=5.735$ Å, and $\beta=110°23'$. The monoprotonated glycinium ions are denoted by glycine I and III, and the zwitter-ion by glycine II. The molecular plane of glycine I is tilted 12.5° with respect to the ac-plane. The transition from the ferroelectric to the paraelectric phase might be due to a statistical disorder in the orientation of the glycine I ions with respect to the ac-plane (y=1/4 and 3/4), *i.e.* above the Curie point, these planes become the mirror planes in a statistical sense.[3)]

Assignment of Lattice Vibrations. The 45 optically active lattice modes can be classified by the usual group theoretical method as 23A+22B in the ferroelectric phase and $12A_g+12B_g+11A_u+10B_u$ in the paraelectric phase. Classification of the lattice vibrations is given in Table 1 together with the activities in the infrared and Raman spectra.

Table 1. Classification of lattice vibrations of TGS

	(1) Ferroelectric Phase (C_2^2–$P2_1$)			
	Trans	Lib.	IR	Raman
A	11	12(3)	M_z	α_{xx} α_{yy} α_{zz} α_{xy}
B	10	12(3)	M_x M_y	α_{xz} α_{yz}

	(2) Paraelectric Phase (C_{2h}^2–$P2_1/m$)			
	Trans	Lib.	IR	Raman
A_g	6	6(1)	ia	α_{xx} α_{yy} α_{zz} α_{xy}
B_g	6	6(2)	ia	α_{xz} α_{yz}
A_u	5	6(2)	M_z	ia
B_u	4	6(1)	M_x M_y	ia

Figures in parentheses donate the number of librational modes of SO_4^{2-}.

The far infrared spectra from 400 to 30 cm^{-1} of TGS and its deuterated analogue are given in Fig. 2. Lattice vibrations are observed at 52, 72, 81, 98, 113, 163, and 227 cm^{-1}. The bands at 72, 81, 98, and 227 cm^{-1} shift respectively to 69, 79, 96, and 210 cm^{-1} by deuteration of the NH_3^+ group, while those at 52, 113, and 163 cm^{-1} remain unchanged. Accordingly, the bands at 72, 81, and 98 cm^{-1} can be assigned to the librational modes of the glycine molecules, and the band at 227 cm^{-1} being atrributable to the lattice mode associated with hydrogen bonds. The shift of the band at 227 cm^{-1} is slightly greater than that expected from the change of the moment of inertia. However, this band is undoubtedly overlapped by more than one band and its peak shift can not be determined accurately. The bands at 52, 113, and 163 cm^{-1} could be assigned either to librational modes of SO_4^{2-} or to translational modes.

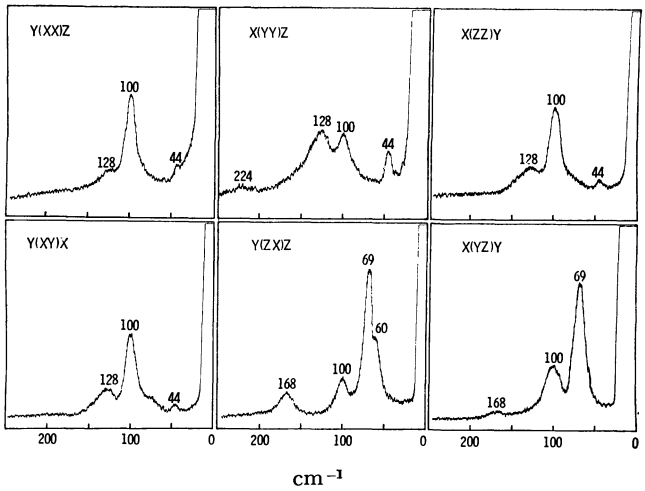

Fig. 3. Polarized Raman spectra of TGS single crystals. The Raman tensor components are expressed according to Porto's notation.

The polarized Raman spectra of TGS single crystals are shown in Fig. 3. The Raman tensor components are expressed in terms of the notation of Damen *et al.*[14] The lattice vibrations are detected at 44, 60, 69, 100, 128, 168, and 224 cm^{-1}. The frequencies agree with the values in literatures.[15-17] We see from Fig. 3 that the bands at 44, 128, and 224 cm^{-1} belong to symmetry species A and those at 60, 69, and 168 cm^{-1} to species B. The band at 100 cm^{-1} is overlapped by lattice modes belonging to species A and B. In the spectrum at liquid N_2 temperature, the band splits into three bands at 93, 101, and 111 cm^{-1}.

TABLE 2. FREQUENCIES (cm^{-1}) OF LATTICE VIBRATIONS OF TGS AND ASSIGNMENTS

IR (powder)	Raman (single crystal)	Symmetry species	Assignment
	44	A	
52			
	60	B	
72	69	B	Lib.(glycine)
81			Lib.(glycine)
98	100	A+B	Lib.(glycine)
113			
	128	A	
163	168	B	
227	224	A	H-bonds[a]

a) A lattice mode associated with hydrogen bonds.

The frequencies of the lattice modes observed in the infrared and Raman spectra are summarized in Table 2 along with some of their general assignments. The Raman spectra of TGS crystals cut at 45° to the b-axis were also measured in order to identify the longitudinal modes. However, no TO–LO splitting was observed.

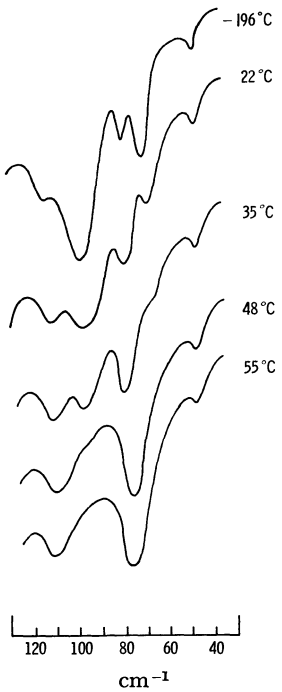

Fig. 4. Temperature dependence of the infrared bands of TGS powder.

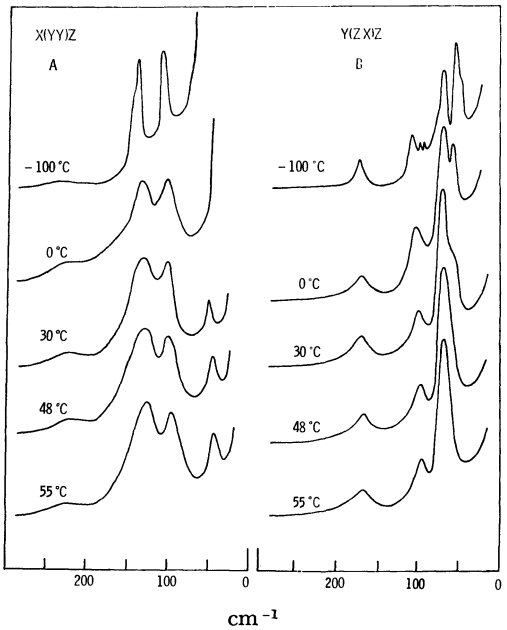

Fig. 5. Temperature dependence of the Raman bands of TGS single crystals.

Temperature Variation. The far infrared spectra from 130 to 30 cm^{-1} at liquid N_2 temperature and elevated temperatures are shown in Fig. 4. The band at 98 cm^{-1} gradually decreases in intensity with the rise in temperature of the crystal disappearing completely in the paraelectric phase (above 48 °C). The band at 72 cm^{-1} also seems to disappear above the Curie temperature, although it is probably masked by the near-by band at 81 cm^{-1} which gradually shifts to lower frequencies and become more intense and broad with the rise in temperature. The polarized Raman spectra below 250 cm^{-1} at various temperatures are reproduced in Fig. 5. It is seen that the band at 60 cm^{-1} which belongs to B symmetry species gradually decreases in intensity as the temperature rises and fades away above the Curie temperature.

As the crystal changes from non-centrosymmetric structure C_2^2 to centrosymmetric structure C_{2h}^2 at the Curie point when the crystal is heated, it is possible that the disappearance of the infrared and Raman bands is caused by the difference in the selection rule. If this is the case, the lattice vibration corresponding to the infrared band at 98 cm^{-1} should become a "gerade" mode in the paraelectric phase, intensity enhancement of the Raman band arising from this lattice mode thus being expected. Further, the lattice vibration corresponding to the Raman band at 60 cm^{-1} should be an "ungerade" mode in the paraelectric phase, giving rise to a strong band in the infrared spectrum. However, the Raman band at 100 cm^{-1} does not seem to exhibit appreciable intensity changes by temperature variation, and the band corresponding to the Raman band at 60 cm^{-1} can not be detected in the infrared spectrum.

The disappearance of the infrared band at 98 cm^{-1} and the Raman band at 60 cm^{-1} can be explained satisfactorily if we assume that these bands arise from

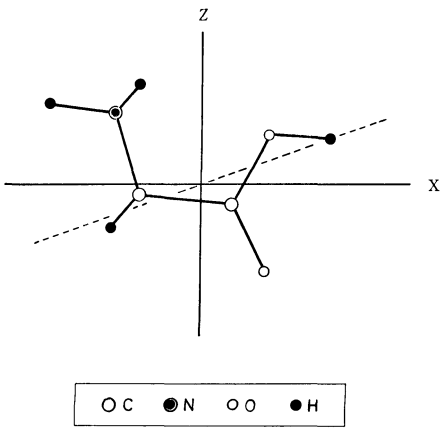

Fig. 6. Principal axes of the monoprotonated glycinium ion. The direction of the dipole moment is also shown by a dotted line.

the librational mode around the z axis of glycine I (Fig. 6). According to the crystal structure proposed by Hoshino *et al.*,[2] the molecular plane of glycine I makes an angle of 12.5° with the ac-plane in the ferroelectric phase, while in the paraelectric phase, glycine I performs a flipping motion between the two equivalent tilted positions with respect to the ac-plane. Because of this flipping motion, the infrared and Raman bands due to the librational modes of glycine I ions around the z axis might be smeared over the spectrum and their peaks would not be detected above the Curie temperature (48 °C). We see from Figs. 4 and 5 that the intensity decrease of the bands at 98 and 60 cm^{-1} starts at a temperature much lower than the Curie point. This is probably because the flipping motion of glycine I in the ferroelectric phase does not abruptly 'freeze in' at the Curie point but persists to some extent in the ferroelectric phase.

It is interesting to see that the intensity of the infrared band at 81 cm^{-1} gradually increases as the temperature of the crystal increases. The band can be assigned to the librational mode in which glycines II and III librate out-of-phase. In the paraelectric phase, TGS crystals have a center of symmetry between glycines II and III and hence glycines II and III must be in the same configuration, implying that one proton tunnels between them. Thus, the dipole moment of these two molecules in the paraelectric phase might differ from that in the ferroelectric phase and the intensity enhancement of the infrared band at 81 cm^{-1} is attributable to the change in the dipole moment.

Savatinova and Simova[18] carried out temperature variation of the low frequency Raman spectra of TGS powder using a mercury lamp as the exciting source and concluded that the frequency of the band at 70 cm^{-1} decreases to zero near the temperature of the phase transition. However, their conclusion is inconclusive since this band is heavily overlapped by the band at 60 cm^{-1} and moreover, these two bands are masked by the exciting line of the mercury lamp and the behavior of the band in their experiment is not clear in detail. We see in Fig. 5 that the band at 69 cm^{-1} in fact shifts somewhat to lower frequencies as the temperature rises. However, the frequency of this band does not go to zero even in the paraelectric phase.

Expenses incurred in the experiments were defrayed from the Kawakami Foundation.

References

1) B. T. Matthias, C. E. Miller, and J. P. Remeika, *Phys. Rev.*, **104**, 849 (1956).
2) S. Hoshino, Y. Okaya, and R. Pepinsky, *ibid.*, **115**, 323 (1959).
3) K. Itoh and T. Mitsui, Intl. Union of Crystallography 9th General Assembly and Intl. Congress, Kyoto, Japan, August-September, (1972).
4) I. Shibuya and T. Mitsui, *J. Phys. Soc. Jap.*, **16**, 479 (1961).
5) J. L. Bjorkstam, *Phys. Rev.*, **153**, 599 (1967).
6) R. Blinc, M. Pintar, and I. Zupančič, *J. Phys. Chem. Solids*, **28**, 405 (1967).
7) D. M. Dodd, *Spectrochim. Acta*, **12**, 1072 (1959).
8) R. K. Khanna, M. Horak, and E. R. Lippincott, *ibid.*, **22**, 1801 (1966).
9) A. Galustian, *Spectry. Lett.*, **6**, 347 (1973).
10) A. S. Barker and M. Tinkham, *J. Chem. Phys.*, **38**, 2257 (1963).
11) Y. Sato, *ibid.*, **45**, 275 (1966).
12) M. Quilichini, M. Krauzman, and H. Poulet, *C. R. Acad. Sci. Paris, Ser. B*, **269**, 774 (1969).
13) E. A. Wood and A. N. Holden, *Acta Crystallogr.*, **10**, 145 (1957).
14) T. C. Damen, S. P. S. Porto, and B. Tell, *Phys. Rev.*, **142**, 570 (1966).
15) L. Tauel, M. C. Delain, and C. Guerin, *Compt. Rend.*, **246**, 3042 (1958).
16) R. S. Krishnan and K. Balasubramanian, *Proc. Indian Acad. Sci., Sect. A*, **48**, 138 (1958).
17) A. N. Arbatskaya, I. S. Zheludev, U. A. Zirgit, and M. M. Sushchinskii, *Kristallografiya*, **10**, 335 (1965).
18) I. Savatinova and P. Simova, *Opt. Spectrosc.*, **24**, 111 (1967).

Interactions of β-Naphthol and β-Naphthylamine in Their Excited Singlet States with Triethylamine

Akiyoshi MATSUZAKI,* Saburo NAGAKURA,*,** and Keitaro YOSHIHARA**

*The Institute for Solid State Physics, The University of Tokyo, Roppongi, Minato, Tokyo 160

**The Institute of Physical and Chemical Research, Wako, Saitama 351

(Received January 24, 1974)

Proton donor-acceptor interactions in excited states were studied by measuring mainly time-resolved fluorescence spectra for β-naphthol–TEA in toluene and in acetonitrile, and for β-naphthylamine–TEA in nonpolar mixed solvents. The Stern-Volmer relation was found to be satisfied for β-naphthol–TEA in toluene. The rate constant and activation energy of hydrogen bond formation in the excited state of this system were obtained to be 2.2×10^9 M^{-1} s^{-1} at 30 °C and 1.6 kcal/mol, respectively, indicating that the process is diffusion-controlled. The time dependences of the intensities of the fluorescence bands due to the free and complexed β-naphthol were measured with the solutions containing various concentrations of triethylamine in acetonitrile. From the analysis of the result, it is shown that this system is led to the ion-pair formation *via* the hydrogen-bonded species in the excited state. For β-naphthylamine–TEA in nonpolar mixed solvents, the bands due to hydrogen-bonded species in the ground and excited states were observed at 370 and ~390 nm in the absorption and fluorescence spectra, respectively.

One of the present authors (S.N.) and Gouterman[1] studied the hydrogen bonding effect upon the electronic absorption spectra of α- and β-naphthols and obtained the results that the hydrogen bonding has the chargetransfer character to some extent. Förster[2] found ion-pair formation in the excited states of β-naphthol and other compounds through proton transfer. Weller *et al.*[3–5] and Stryer[6] have studied the proton-transfer reaction in the excited state of β-naphthol in aqueous solution by measuring its fluorescence and have determined several kinetic and thermodynamic constants. Mataga *et al.*[7–9] measured the fluorescence spectra of ternary solutions containing β-naphthol or other proton donors and acceptors in organic solvents. They showed that a hydrogen-bonded complex and an ion-pair exist in the excited state of the system containing β-naphthol and triethylamine in benzene. Baba *et al.*[10,11] measured fluorescence and excitation-polarization spectra with some hydrogen bonding systems including α-naphthol as proton donor and discussed the nature of their lowest excited singlet states. Hirota[12] investigated the behaviors of 3-hydroxy-2-naphthoic acid and its derivatives in their excited states by measuring relative fluorescence intensities of the free and hydrogen-bonded species as a function of temperature.

The above-mentioned studies have been made by measuring mainly fluorescence spectra, excitation polarization spectra, and quantum yields. In other words, they have been done under steady-state conditions. Recently, however, the fast transient technique has been applied to the study of proton transfer in the excited state. Ware[13] studied the intramolecular proton transfer of 2-hydroxy-3-naphthoic acid in the excited state by measuring the fluorescence decay. Furthermore, Ofran and Feitelson[14] studied the proton dissociation of β-naphthol in the excited state with the aid of fluorescence decay measurements.

In the present study, we have undertaken to study the interaction of β-naphthol or β-naphthylamine in the excited state with triethylamine by measuring nanosecond time-resolved fluorescence spectra and by analyzing the decays of fluorescence bands due to the free and complexed proton donors.

Experimental

β-Naphthol and β-naphthylamine were purified by vacuum sublimation after repeated recrystallizations from water. Triethylamine (TEA) was refluxed with acetic anhydride and thereafter distilled under reduced pressure. The purified TEA was degassed and stored in a refrigerator. Spectrograde toluene was distilled from sodium. Methylcyclohexane and isopentane were distilled after passing through a 1 m silica gel column. Acetonitrile was distilled from phosphorus pentoxide and thereafter from calcium hydride.

Samples used for fluorescence measurements were degassed by the freeze-thaw method. In order to protect them from moisture, they were prepared in a dry-box filled with dry nitrogen gas.

Absorption spectra were measured with a Cary recording spectrophotometer model 14. Fluorescence spectra were measured with a Spex 0.75 m grating monochromator, excitation being effected by an Ushio USH-102D high pressure mercury lamp and an EMI 9558QB photomultiplier being used as a detector. β-Naphthol and β-naphthylamine were excited at 313 nm by using an aqueous solution of $NiSO_4\cdot6H_2O$–$CoSO_4\cdot7H_2O$ as a solution-filter. The monochromator was used with a slit width of $\lesssim$0.5 mm. Fluorescence lifetimes and nanosecond time-resolved spectra were measured by the method described previously[15] which used a coaxial nitrogen gas laser as an excitation source.

Results and Discussion

Hydrogen Bond Formation between β-Naphthol and TEA in Toluene. Time-resolved fluorescence spectra observed with the β-naphthol–TEA–toluene system are shown in Fig. 1. The steady-excitation fluorescence spectrum of β-naphthol in toluene is also shown in this figure for the purpose of comparison. The time-resolved fluorescence spectrum measured with the ternary system immediately after excitation ($t=0$) has a new band at 410 nm in addition to the band due to the free β-naphthol molecule at 355 nm. The former corresponds to the band found in the steady-excitation fluorescence spectrum of the β-naphthol–TEA–benzene system and ascribed to the ion-pair by Mataga and

temperature coefficient of the viscosity.[18]

The k_3 value obtained by the present authors is very close to that obtained by Weller *et al.*[4,5] ($k_3=2\sim3\times10^9$ M^{-1} s^{-1}) for the systems containing β-naphthol and several carboxylate ions from the analysis of the fluorescence quantum yield. Furthermore, the value obtained is reasonable in view of the fact that k_3 is calculated to be $3\sim8\times10^9$ M^{-1} s^{-1} with the help of Smoluchowski's equation:[19,20]

$$k_3=\frac{4\pi R_0(D_A+D_B)}{R_0\int_{R_0}^{\infty}e^{U(r)/kT}\frac{dr}{r^2}}\frac{N_A}{1000}=4\pi R_0(D_A+D_B)\left(\frac{N_A}{1000}\right) \quad [M^{-1}\ s^{-1}] \qquad (4)$$

Here, R_0, the sum of collision radii is taken to be 3 Å,[21] D_A and D_B are individual diffusion coefficients, N_A is Avogadro's number, and $U(r)$ is the interaction energy between the reactants. The k_3 value was evaluated to be $3\sim8\times10^9$ M^{-1} s^{-1} by taking $U(r)$ to be zero or $-kT$.

Here let us turn to the time dependence of fluorescence of the hydrogen-bonded species measured at 410 nm for the β-naphthol–TEA–toluene system. The rise process was not observed since the rise time is too fast to be observed by the present detecting system. The decay process is almost single exponential and the fluorescence decay time of the hydrogen-bonding system decreases from ~6 to ~4 ns with the increasing concentration of TEA from 10^{-2} to 10^{-1} M.

Judging from the K_{eq} value, which is 60 M^{-1} in benzene at room temperature,[7] the concentrations of D and (DA) are almost equal to each other in the ground state for the concentrations used. Therefore the direct excitation of (DA) to (DA)* must be taken into account in addition to the process D*+A→(DA)*. In this case, the time dependence of the fluorescence due to (DA)* is represented by Eq. (5).

$$[(DA)^*]=\frac{k_3[A][D^*]_0}{(k_5+k_6)-(k_1+k_2+k_3[A])}\left(e^{-(k_1+k_2+k_3[A])t}-e^{-(k_5+k_6)t}\right)+[(DA)^*]_0e^{-(k_5+k_6)t}. \qquad (5)$$

Here, $[(DA)^*]$ and $[(DA)^*]_0$ represent the concentrations of the complexed species in the excited state at $t=t$ and $t=0$, respectively. As is expected from the experimental results, the pre-exponential factor of the first term on the right-hand side of Eq. (5) is positive. Therefore, Eq. (5) shows that the decay lifetime of (DA)* is determined by the two terms $1/(k_5+k_6)$ and $1/(k_1+k_2+k_3[A])$. This is a reason why the observed decay lifetime is slightly dependent on [A].

Hydrogen Bond Formation between β-Naphthol and TEA in Acetonitrile. The absorption spectra were measured for acetonitrile solutions containing a fixed concentration of β-naphthol and various concentrations of TEA, with the result shown in Fig. 4. The equilibrium constant, K_{eq}, in the ground state at 25 °C was obtained to be 19 M^{-1} by analyzing the dependence of the absorption intensity at a fixed wavelength upon the TEA concentration.[1]

Figure 5 shows the fluorescence spectra measured for an acetonitrile solution containing β-naphthol and TEA with steady-state excitation, the intensities of which are normalized at 340 nm. From this figure, it is revealed

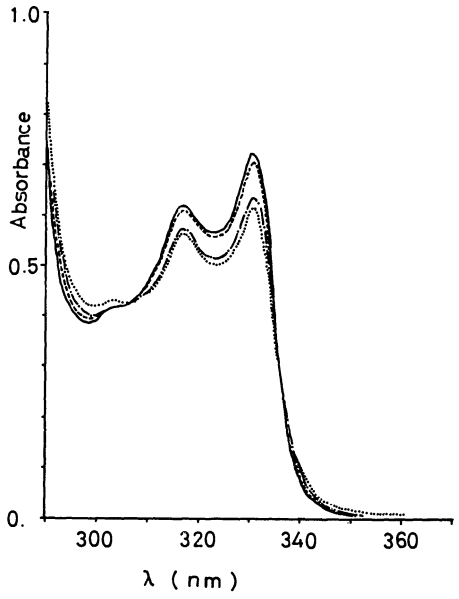

Fig. 4. Absorption spectra of the β-naphthol–TEA system in acetonitrile at 25 °C. The concentrations of TEA are 0, 0.705×10^{-2}, 2.11×10^{-2}, and 2.82×10^{-2}M for curves ——, ------, -·-·, and ·····, respectively. The concentrations of β-naphthol are commonly 3.46×10^{-4}M.

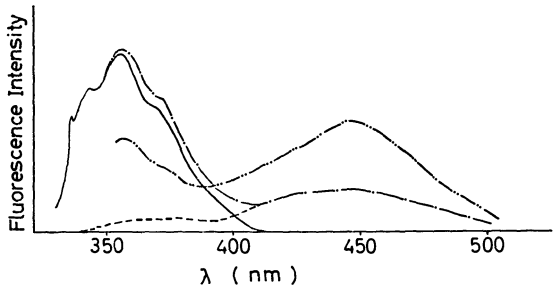

Fig. 5. The fluorescence spectra of the β-naphthol-TEA system in acetonitrile at 25 °C. The concentrations of TEA are 0, 0.705×10^{-2}, and 3.52×10^{-2}M for curves ——, -·-, and -··-, respectively. Curve —— is a difference between curves —— and -·- normalized at 340 nm. The scattering of the excitation light prevented us from measuring the spectrum for the solution containing 3.52×10^{-2}M TEA below 355 nm.

that, besides the fluorescence band at 355 nm due to the free β-naphthol molecule, two bands appear at ~370 and ~450 nm and increase their intensities with the increasing concentration of TEA, though the latter two bands are weak compared with the former band. The band at ~370 nm can be ascribed to hydrogen bonded β-naphthol[8] and the largely redshifted band at 450 nm to either of the ion pair or the β-naphtholate ion.

The above-mentioned spectral data show the existence of two different kinds of hydrogen-bonded or complexed species, $(DA)^*_{CN}$ and $(DA)^{**}_{CN}$, in the excited state of the system involving β-naphthol and TEA in acetonitrile. Therefore the following scheme may be applied to this system:

$$\begin{array}{ccccc} D^* + A & \underset{k_4}{\overset{k_3}{\rightleftharpoons}} & (DA)^*_{CN} & \underset{k_8}{\overset{k_7}{\rightleftharpoons}} & (DA)^{**}_{CN} \\ I_D \uparrow k_1 \downarrow \{k_2 & & I_{DA} \uparrow\downarrow k_5 \{k_6 & & k_9 \downarrow \{k_{10} \\ D + A & \underset{}{\overset{K_{eq}}{\rightleftharpoons}} & (DA) & & \end{array}$$

Scheme 2.

According to Scheme (2), the following equations can be obtained:

$$\frac{d[D^*]}{dt} = -(k_1+k_2+k_3[A])[D^*] + k_4[(DA)^*_{CN}] \quad (6.1)$$

$$\frac{d[(DA)^*_{CN}]}{dt} = k_3[A][D^*] - (k_4+k_5+k_6+k_7)[(DA)^*_{CN}] + k_8[(DA)^{**}_{CN}] \quad (6.2)$$

$$\frac{d[(DA)^{**}_{CN}]}{dt} = k_7[(DA)^*_{CN}] - (k_8+k_9+k_{10})[(DA)^{**}_{CN}] \quad (6.3)$$

These equations are solved as follows:

$$[D^*] = \sum_{i=1}^{3} a_i e^{-\mu_i t} \quad (7.1)$$

$$[(DA)^*_{CN}] = \sum_{i=1}^{3} b_i e^{-\mu_i t} \quad (7.2)$$

$$[(DA)^{**}_{CN}] = \sum_{i=1}^{3} c_i e^{-\mu_i t} \quad (7.3)$$

The pre-exponential factors are related with each other by

$$a_i = \frac{k_4}{K_1-\mu_i} b_i \quad (8.1)$$

$$c_i = \frac{k_7}{K_3-\mu_i} b_i \quad (8.2)$$

$-\mu_i$'s (i=1,2,3) are roots of the following cubic equation:

$$\mu^3 + \alpha\mu^2 + \beta\mu + \gamma = 0 \quad (9)$$

where

$$\alpha = K_1 + K_2 + K_3 \quad (10.1)$$

$$\beta = K_1K_2 + K_2K_3 + K_3K_1 - k_3k_4[A] - k_7k_8 \quad (10.2)$$

$$\gamma = K_1K_2K_3 - k_3k_4[A]K_3 - k_7k_8K_1 \quad (10.3)$$

$$K_1 = k_1 + k_2 + k_3[A] \quad (11.1)$$

$$K_2 = k_4 + k_5 + k_6 + k_7 \quad (11.2)$$

$$K_3 = k_8 + k_9 + k_{10} \quad (11.3).$$

According to the above scheme, the time dependences of [D*], $[(DA)^*_{CN}]$, and $[(DA)^{**}_{CN}]$ can be represented by the sum of three exponential terms with time constants of $\tau_1=1/\mu_1$, $\tau_2=1/\mu_2$, and $\tau_3=1/\mu_3$.

In order to check experimentally the above consideration, the fluorescence lifetimes of free β-naphthol and $(DA)^{**}_{CN}$ were measured at 360 and 450 nm, respectively. The measurement of the lifetime for $(DA)^*_{CN}$ was complicated by the overlapping of the fluorescence band of D*. Furthermore, it was found that the Stern-Volmer relation concerning the effect of the TEA concentration upon the fluorescence lifetime of free β-naphthol was not satisfied. This means that the dissociation reaction of the hydrogen-bonded species $(DA)^*_{CN}$ into free β-naphthol and TEA must be taken into account for this system.

The decay curves observed at 450 nm for the systems

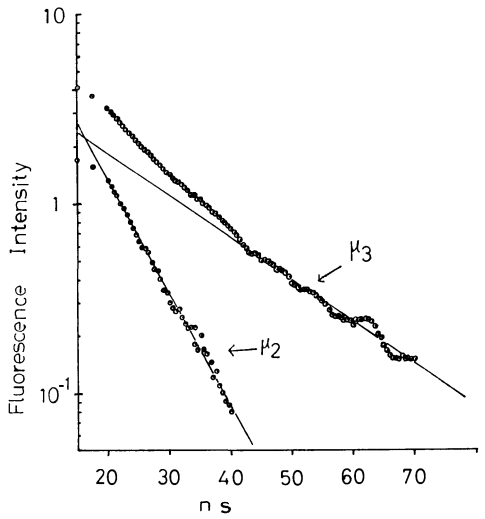

Fig. 6. Semilogarithmic plot of fluorescence intensity $I(t)$ observed at 450 nm *vs.* time for the system containing 3.46×10^{-4}M β-naphthol and 3.52×10^{-2}M TEA in acetonitrile. N_2 gas laser pulse starts at time t=0.

with various concentrations of TEA consists of two singlet exponential curves, as is clearly seen in Fig. 6 which shows an example of the observed curves. This may be explained by considering that the exponential component with the greatest μ_i, say μ_1, rises too fast to be observed. Thus the greater and smaller decay components observed at 450 nm correspond to μ_2 and μ_3, respectively.

Let us turn to the fluorescence decay at 360 nm. The decay curve at 360 nm observed for each solution is separated into two components which are assigned to μ_1 and μ_3, or μ_2 and μ_3.[22] Thus the μ_1, μ_2, and μ_3 values were obtained from the decay curves observed

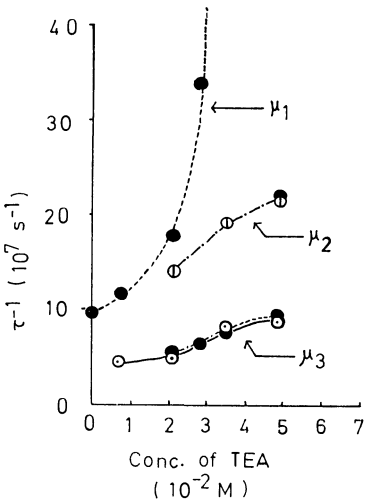

Fig. 7. Plots of the decay rates observed at 360 and 450 nm *vs.* the concentration of TEA for the β-naphthol–TEA system in acetonitrile at 30 °C. The concentration of β-naphthol is 3.45×10^{-4}M. ●, observed at 360 nm; ⊙ and ◑ are the faster and slower decay rates, respectively, observed at 450 nm. The μ_1 value at 2.8×10^{-2}M TEA was measured with the single photon counting method.[22]

at 450 and 360 nm for the solutions containing a fixed concentration of β-naphthol and various concentrations of TEA. The results are summarized in Fig. 7.

Figure 7 shows that the μ_2 or μ_3 values obtained at both wavelengths agree well with each other for the respective solutions and therefore the decay curve observed with each of the solutions consists of the three exponential components. This gives experimental evidence for the validity of Eq. (7) and therefore an experimental support for the reaction mechanism shown by scheme (2) that $(DA)^{**}_{CN}$ is produced *via* $(DA)^{*}_{CN}$.[23]

The fluorescence peak of $(DA)^{**}_{CN}$ appears at 450 nm and is far removed from that of D* (355 nm). This indicates that $(DA)^{**}_{CN}$ is an ion-pair

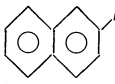

or a solvated β-naphtholate ion. In view of the fact that process 8 in reaction scheme (2), namely, the back reaction from $(DA)^{*}_{CN}$ to $(DA)^{**}_{CN}$, can not be disregarded,[24] $(DA)^{*}_{CN}$ is regarded as the ion-pair. This is because the process from the solvated β-naphtholate ion to $(DA)^{*}_{CN}$ is too slow to occur within the lifetime of $(DA)^{**}_{CN}$.[25]

Hydrogen Bond Formation between β-Naphthylamine and TEA. The hydrogen bond formation was studied for the solution containing β-naphthylamine and TEA in the 1:1 mixed solvent of isopentane and methylcyclohexane (PM). The absorption spectra observed with the system at room temperature changed only slightly with an increase in the concentration of TEA. At −30 °C, as is seen in Fig. 8, the absorption spectra change somewhat remarkably owing to the hydrogen bond formation and exhibit an isosbestic point. From the observed spectra, the equilibrium constant was found to be 7 M^{-1} at −30 °C. Thus it is obvious that at low temperature a hydrogen bond is formed between β-naphthylamine and TEA in the mixed solvent. At room temperature the spectrum of β-naphthylamine is not changed by the addition of TEA and hydrogen bond formation is negligibly small.

Fluorescence spectra observed with the β-naphthylamine–TEA system at 25 °C and −50 °C are shown in Fig. 9. They are insensitive to the concentration of TEA until it becomes 0.0705 M at which condition a remarkable change occurs in the spectra. This implies that, at this concentration of TEA, k_3[A] is comparable with the intrinsic decay rate constant of excited β-naphthylamine and hydrogen bond formation occurs within its lifetime. From this consideration, the order of magnitude of k_3 was obtained to be 10^9 M^{-1} s^{-1} by taking the critical value of [A] to be 0.1 M. This k_3 value seems to be reasonable.

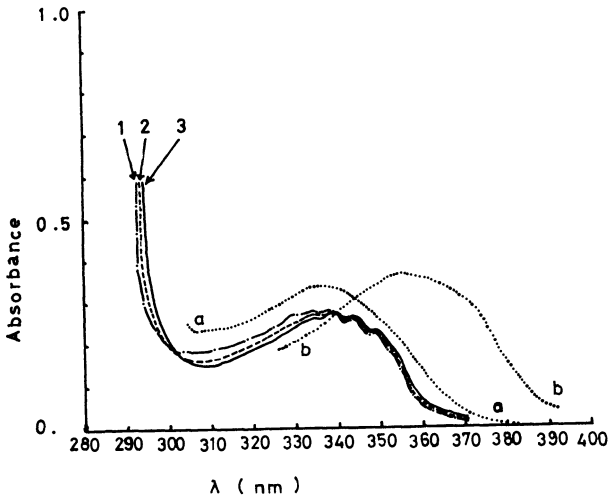

Fig. 8. Absorption spectra of β-naphthylamine in a 1:1 mixed solvent of methylcyclohexane and isopentane. Curves 1, 2, and 3 were measured at −30 °C, for solutions with the TEA concentrations of 0, 0.705×10^{-1}, and 1.41×10^{-1}M, respectively. Curves a and b were measured at 77 K for solutions with the TEA concentrations of 0 and 0.705×10^{-1}M, respectively. The concentrations of β-naphthylamine are 1.04×10^{-4}M and 0.92×10^{-4}M for curves 1∼3 and curves a∼b, respectively.

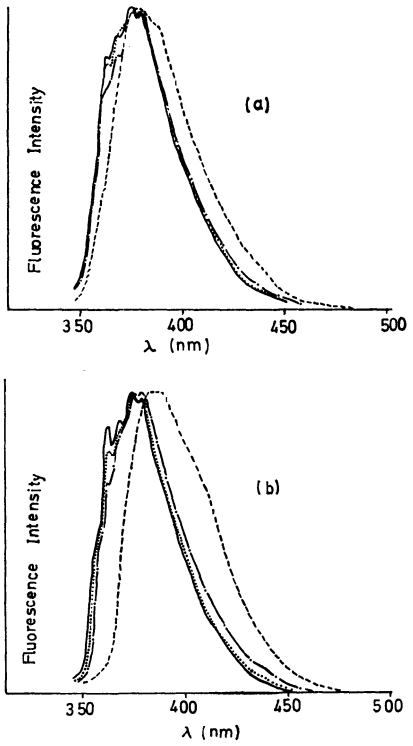

Fig. 9. Fluorescence spectra of β-naphthylamine in the 1:1 mixed solvent of methylcyclohexane and isopentane. The concentrations of TEA are 0, 0.705×10^{-4}, 0.705×10^{-2}, and 0.705×10^{-1}M for curves (1) ——, (2) ·····, (3) -·-·, and (4) ------, respectively. The concentration of β-naphthylamine is 0.92×10^{-4}M. (a) at 25 °C, (b) at −50 °C.

Fluorescence decay curves were measured at room temperature for the β-naphthylamine solutions containing various concentrations of TEA and single exponential curves were obtained. The lifetimes obtained at 360 and 420 nm are 15∼14 ns for the solutions containing $0\sim0.7\times10^{-1}$ M TEA. Hence they are almost independent of the concentration of TEA. One of the reasons for this is that the ratio of the hydrogen-bonded β-naphthylamine molecule in the excited state to the total excited molecules is small, as revealed from the observed fluorescence spectra shown in Fig. 9.

We should like to express their thanks to Professor E. Lippert, Technical University of Berlin, Professor Ichiro Hanazaki, Osaka University and Dr. Takayoshi Kobayashi, The Institute of Physical and Chemical Research for their helpful discussions.

References and Notes

1) S. Nagakura and M. Gouterman, *J. Chem. Phys.*, **26**, 881 (1957).
2) Th. Förster, *Z. Elektrochem.*, **54**, 42, 531 (1950).
3) A. Weller, *Z. Phys. Chem. N. F.*, **3**, 238 (1955); H. Beens, K. H. Grellmann, M. Gurr, and A. H. Weller, *Discuss. Faraday Soc.*, **39**, 183 (1965).
4) A. Weller, *Z. Phys. Chem. N. F.*, **17**, 224 (1958).
5) A. Weller, *Z. Elektrochem.*, **64**, 55 (1957).
6) L. Stryer, *J. Amer. Chem. Soc.*, **88**, 5708 (1966).
7) N. Mataga and Y. Kaifu, *J. Chem. Phys.*, **36**, 2804 (1962); *Mol. Phys.*, **7**, 137 (1963).
8) N. Mataga, Y. Kawasaki, and Y. Torihashi, *Theoret. Chim. Acta*, **2**, 168 (1964).
9) N. Mataga, Y. Torihashi, and Y. Kaifu, *Z. Phys. Chem. N. F.*, **34**, 377 (1962).
10) A. Matsuyama and H. Baba, This Bulletin, **44**, 1162 (1971).
11) S. Suzuki and H. Baba, *ibid.*, **40**, 2199 (1967).
12) K. Z. Hirota, *Z. Phys. Chem. N. F.*, **35**, 222 (1962).
13) W. R. Ware, P. R. Shukla, P. J. Sullivan, and R. V. Bremphis, *J. Chem. Phys.*, **55**, 4048 (1971).
14) M. Ofran and J. Feitelson, *Chem. Phys. Lett.*, **19**, 427 (1973).
15) A. Inoue, K. Yoshihara, T. Kasuya, and S. Nagakura, This Bulletin, **45**, 720 (1972).
16) The present study does not exclude the possibility that there exist some precursors to (DA)*, which decay too fast to be observed by the present time-resolving fluorescence technique.
17) O. Stern and M. Volmer, *Phys. Z.*, **20**, 183 (1919).
18) "Handbook of Chemistry and Physics," ed. by C. Hodgmon, Chemical Rubber, Cleveland, Ohio (1962), pp. 2258—2264.
19) M. V. Smoluchowski, *Z. Phys. Chem.*, (Leipzig), **92**, 129 (1917).
20) W. R. Ware and J. S. Novros, *J. Phys. Chem.*, **70**, 3246 (1966).
21) This value seems to be reasonable in view of the fact that N—O distances of hydrogen-bonded systems are usually 2.6—2.9 Å.
22) We are indebted to Dr. Nobuyuki Wakayama, Mitsubishi-Kasei Institute of Life Sciences for his kindness in measureing the decay time constant, μ_1, with the aid of the single photon counting method.
23) Another possible mechanism for the formation of $(DA)^*_{CN}$ and $(DA)^{**}_{CN}$ is the following competitive one:

$$(DA)^{**}_{CN} \underset{k_7}{\overset{k_8}{\rightleftharpoons}} D^* + A \underset{k_4}{\overset{k_3}{\rightleftharpoons}} (DA)^*_{CN}$$
$$k_9 \downarrow \lessgtr k_{10} \qquad k_1 \downarrow \lessgtr k_2 \qquad k_5 \downarrow \lessgtr k_6$$

Scheme 3.

This process can be disregarded from the concentration of the observed dependence of μ_i's upon the concentration of TEA.

As is seen in Fig. 7, the observed rises and decays are represented by $\sum_{i=1}^{3} a_i e^{-\mu_i t}$ and $\sum_{i=1}^{3} c_i e^{-\mu_i t}$ for D* and $(DA)^{**}_{CN}$, respectively. The pre-exponential factors a_1, a_3, and a_2 successively become more predominant with the increasing concentration of TEA. From this observation the following relation is obtained:

$$\Delta a_2 > \Delta a_3 > \Delta a_1 \qquad \text{relation (1)}$$

A similar relation is obtained concerning the pre-exponential factors c_i's; among these c_1 is the factor for the rise component:

$$\Delta c_2 > \Delta c_3 \qquad \text{relation (2)}$$

Here, Δ means the increment of the corresponding quantity due to the increase in the concentration of TEA. Furthermore, the relation, $\Delta\mu_1 > \Delta K_1 \gtrsim \Delta\mu_2 > \Delta\mu_3$ can be obtained from the experimental result shown in Fig. 7 and Eq. (11.1). From this relation and initial conditions of Eq. (6), say

$$\sum_{i=1}^{3} a_i = [D^*]_0, \sum_{i=1}^{3} b_i = [(DA)^*_{CN}]_0 \sim 0, \text{ and } \sum_{i=1}^{3} c_i = [(DA)^{**}_{CN}]_0 \sim 0,$$

the following relation concerning b_i's can be derived for scheme (2):

$$\Delta b_1 < \Delta b_2 < \Delta b_3 \qquad \text{relation (3)}$$

Similarly, relation (3) is also obtained for scheme (3).

According to the process shown by scheme (2), the pre-exponential factors for the decay and rise components are expressed by Eq. (8). Since a_1, a_2, a_3, b_2, b_3, c_2, and c_3 are positive and b_1 and c_1 are negative, the relation $\mu_3 < \mu_2 < K_1 < \mu_1 < K_3$ is obtained, and Δa_i's are represented by $\Delta a_1 = \{1/\Delta(\mu_1 - K_1)\} \times (-\Delta b_1)$, $\Delta a_2 = \{1/\Delta(K_1 - \mu_2)\} \times (\Delta b_2)$, and $\Delta a_3 = \{1/\Delta(K_1 - \mu_3)\} \times (\Delta b_3)$. Therefore, relation (3) is consistent with relations (1) and (2) only for the case of $1/\Delta(K_1 - \mu_2) > 1/\Delta(K_1 - \mu_3)$ and $1/\Delta(K_3 - \mu_2) > 1/\Delta(K_3 - \mu_3)$, respectively. These relations on $\Delta\mu_i$'s and ΔK_1 are satisfied. Thus, the observed dependence of the pre-exponential factors on the concentration of TEA can be explained in term of Scheme (2).

According to Scheme (3), the pre-exponential factors are expressed as follows:

$$a_i = \frac{k_4(c-\mu_i)}{(a-\mu_i)(c-\mu_i) - k_7 k_8 [A]} b_i, \text{ and}$$

$$c_i = \frac{k_7 k_8 [A]}{(a-\mu_i)(c-\mu_i) - k_7 k_8 [A]} b_i,$$

where $\mu_1 > c > \mu_2 > \mu_3$ or $\mu_1 > a > \mu_2 > \mu_3$ in this case. Furthermore, $\Delta a_1 = (\Delta Q_1) \times (-\Delta b_1)$ and $\Delta a_{2,3} = (-\Delta Q_{2,3}) \times (\Delta b_{2,3})$, and $\Delta c_{2,3} = (\Delta R_{2,3}) \times (\Delta b_{2,3})$ For this case, relation (3) is consistent with relations (1) and (2) only when $\Delta Q_2 > \Delta Q_3$ and $\Delta R_2 > \Delta R_3$ hold. In actuality, however, the examination of $\Delta\mu_i$'s and Δa_i shows that the reverse is the case. Thus, scheme (3) can safely be disregarded.

24) On the assumption of disregarding process 8, the fluorescense of D* and $(DA)^{**}_{CN}$ are to be represented by decay curves with the two time constants of λ_1^{-1} and λ_2^{-1} and of λ_2^{-1} and $(k_9+k_{10})^{-1}$, respectively, where $\lambda_{1,2} = 1/2\{(K_1+K_2) \pm \sqrt{(K_1-K_2)^2 + 4k_3k_4[A]}\}$. The expectation conflicts with the findings that the fluorescence decay of D* is repesented by three time constants and that the two decay constants obtained for $(DA)^{**}_{CN}$ are dependent on the concentration of TEA.

25) From the rate constant of the association between solvated ions, $10^{10}\ M^{-1}s^{-1}$, and the concentration of proton ($<10^{-4}$M), it is revealed that the association reaction between the solvated β-naphtholate ion and triethylammonium ion possibly proceeds with a rate smaller than $10^6\ s^{-1}$ and is too slow to occur within the intrinsic lifetime of a solvated β-naphtholate ion (*e.g.* $10^8\ s^{-1}$ in aqueous solution).[4,14]

X-Ray Photoelectron Spectroscopy of *p*-Benzoquinone, Hydroquinone and Their Halogen-Substituted Derivatives

Toshiaki OHTA, Masamichi YAMADA, and Haruo KURODA

Department of Chemistry, Faculty of Science, The University of Tokyo, Hongo, Tokyo 113

(Received February 6, 1974)

X-Ray photoelectron spectra of *p*-benzoquinone, chloranil, bromanil, iodanil, hydroquinone, tetrachlorohydroquinone and chloranilic acid were observed by using the samples freshly deposited in the high vacuum of the spectrometer. The chemical shifts of C ls and O ls levels determined from the XPS spectra are compared with the chemical shifts predicted according to the electrostatic potential model by use of the charge distributions calculated by CNDO/2 method. The charge distributions in the quinone derivatives are successfully estimated by using the observed binding energies of C ls and O ls levels.

X-Ray photoelectron spectroscopy (XPS) shows promise as a tool to investigate the electronic structures of molecules. From XPS spectra, we can determine the binding energies of core-electron levels, which are known to vary more or less depending on the chemical bonds. This chemical shift of a core-electron level exhibits a rather simple correlation with the charge distribution in the molecule. It was shown by Siegbahn and his collaborators[1] that the chemical shifts of C ls levels determined from the gas-phase XPS spectra of simple organic molecules can be successfully predicted from the charge distributions obtained by CNDO calculations, by using the electrostatic potential model.

For investigating the electronic structure of molecule, it is naturally desirable to observe the gas-phase XPS spectrum. However, this is not easy to do in the case of the organic compound which is a solid of low vapor pressure at room temperature. In such a case, the XPS spectrum is usually measured with a powder specimen, but the C ls and O ls spectra thus obtained are often affected significantly by the presence of chemical species containing carbon and/or oxygen, adsorbed on the sample surface.

This paper reports the XPS spectra of *p*-benzoquinone, hydroquinone and their halogen-substituted derivatives, which were observed with the films freshly deposited in the high vacuum of the spectrometer to avoid the contamination effects. The purpose of this study is to elucidate the effect of halogen substitution on the binding energies of C ls and O ls levels.

Experimental

The XPS spectra were measured with McPherson ESCA 36 electron spectrometer by employing AlK_α (1486.6 eV). The sample was deposited on the surface of the variable-temperature sample holder which was kept at about −50 °C by using dry ice–acetone mixture, in the 10^{-6} Torr vacuum of the spectrometer. Only in the case of iodanil, we carried out both the preparation of the film and the measurement of XPS spectra at the room temperature, since its vapor pressure is sufficiently low. For calibrating binding energies, we deposited a small amount of gold onto the sample surface, and used Au $4f_{7/2}$ (84.0 eV) as the reference,[2] the core levels of halogen being used as subsidiary references. With this method, binding energies were obtained with the accuracy better than ±0.2 eV.

All the compounds except bromanil and iodanil were commercially obtained and purified by sublimation *in vacuo*. The crystal of chloranilic acid usually contains water of crystallization but the powder which we obtained by sublimation, was found to be the water-free modification. Bromanil and iodanil were synthesized in our laboratory, and purified by sublimation.

Results

The C ls spectra of chloranil, bromanil and iodanil are shown in Fig. 1. Each of them exhibits a C ls spectrum with a shoulder in the high binding-energy side of the main peak, indicating clearly that the spectrum is composed of two bands, namely, a strong band at lower energy and a weak band at higher energy. In each case, we resolved the observed C ls spectrum into two components by means of the following procedure. First, we determined the standard profile of a single band by examining the shape of Au $4f_{7/2}$ spectrum of an evaporated gold film and that of F ls spectrum of Teflon. Then, assuming this standard profile for each constituent band, we adjusted the splitting and intensities so that the composite spectrum well reproduced the observed spectrum. The results are shown in Fig. 1 by solid lines. In these cases, we were able

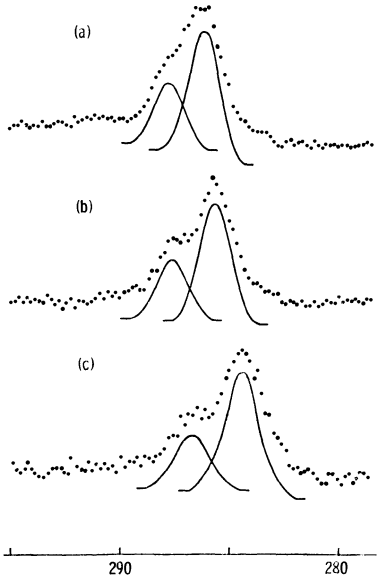

Fig. 1. Carbon 1s spectra.
(a): chloranil, (b): bromanil, (c): iodanil.

to resolve the observed C ls spectrum into two components with the intensity ratio nearly 2: 1.

The situation was slightly complicated in the case of *p*-benzoquinone, where it was not possible to obtain the C ls spectrum completely free from the contamination effect. Figure 2 shows the spectra measured respectively 10 and 20 min after preparation of the evaporated film. We can see that the profile of the spectrum appreciably changed with time. It is not clear why such phenomenon occurred only in the case of *p*-benzoquinone. Possibly it is connected in some way with the relatively high vapor pressure of this compound. As shown in Fig. 2, we can resolve the C ls spectrum of *p*-benzoquinone into three components, of which binding energies are respectively 283.4, 284.3, and 286.0 eV. Among them, we can attribute the one at 284.3 eV to the C ls band associated with the contamination carbon.

Like quinone derivatives, hydroquinone exhibited the C ls spectrum with a shoulder, which was able to be resolved into two components with intensity ratio 2: 1 as shown in Fig. 3. However, the C ls spectrum of tetrachlorohydroquinone exhibits no shoulder. Seemingly, the splitting is quite small in this case. It should be noted that there is an extra band separated by 6—7 eV from the main peak in the C ls spectrum of hydroquinone as well as in that of tetrachlorohydroquinone. The corresponding extra bands were observed very weakly also in their O ls spectra. It is most likely that these extra bands are the shake-up satellites associated with the excitations of valence electrons.[3]

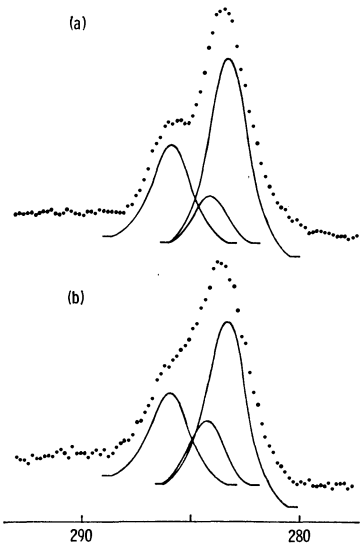

Fig. 2. Carbon 1s spectra of *p*-benzoquinone measured respectively (a) 10 min and (b) 20 min after preparation of the evaporated film.

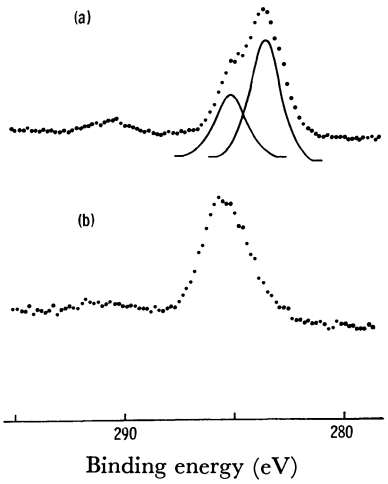

Fig. 3. Carbon 1s spectra.
(a): hydroquinone, (b): tetrachlorohydroquinone.

In the case of chloranilic acid, the O ls spectrum appeared as a very broad band with a width of about 3 eV. This spectrum was able to be resolved into two components of equal intensity. Although we can expect that the C ls spectrum of this compound is composed of three components, we could not resolve the observed C ls spectrum to the corresponding bands.

The binding energies of core levels determined from the XPS spectra are summarized in Table 1.

Table 1. Binding energies of core levels (unit; eV)

Compound	C ls		O ls	
	C_1	C_2		
Chloranil	287.7	286.1	531.5	
Bromanil	287.5	285.6	531.4	
Iodanil	286.7	284.4	531.0	
p-Benzoquinone	286.0	283.4	530.8	
Hydroquinone	285.1	283.5	532.2	
Tetrachlorohydroquinone	285.5		532.5	
Chloranilic acid	286.2		533.1	531.7

Compound	Cl 2p	Cl 2s	Br $3p_{3/2}$	Br 3d	I $3d_{5/2}$	I 4s	I 4p	I 4d
Chloranil	200.2	270.9						
Tetrachlorohydroquinone	200.0	270.7						
Chloranilic acid	200.1	271.2						
Bromanil			183.4	70.1				
Iodanil					619.8	187.2	123.0	50.1

Discussion

Chemical Shifts in C 1s and O 1s Levels. According to the electrostatic potential model, the binding energy of a core level can be correlated with the charge distribution in the molecule by Eq. (1);

$$E_i = E_A^0 + k_A q_i + \sum_j q_j/R_{ij} \quad (1)$$

where q_i is the charge on the i-th atom, q_j is that on the j-th atom, R_{ij} is the interatomic distance given in atomic units, and E_A^0 and k_A are the empirical constants characteristic of the kind of atom. This relation was originally proposed by Siegbahn *et al.*[4] on the basis of classical electrostatic theory. For the charge densities calculated by CNDO method, they gave the k_A values as follows; k_C=21.9 for C ls and k_O=25.8 for O ls (unit; eV/unit charge).[1] The quantum mechanical meaning of Eq. (1) was critically discussed by Schwartz, Switalski, and Stronski,[5] who gave theoretically the following k_A values; k_C=22.108 and k_O=30.951 (eV/unit charge).

When we are interested only in the chemical shift, we can use the energy change expression given as follows;

$$\Delta E_i = k_A q_i + \sum_j q_j/R_{ij} \quad (2)$$

We carried out CNDO/2 calculations on *p*-benzoquinone, hydroquinone, chloranil, tetrachlorohydroquinone and chloranilic acid, assuming the molecular geometries based on the crystal structure data.[6] Figure 4 shows the charge densities of the first two compounds. Due to the molecular symmetry, we can classify the six carbon atoms into two groups, namely the two carbon atoms forming bond with oxygen and the other four carbon atoms. We will denote these two types of carbon atom as C_1 and C_2, respectively. Since the charge density is considerably different between these two kinds of carbon atom, we can expect a splitting between their C ls levels.

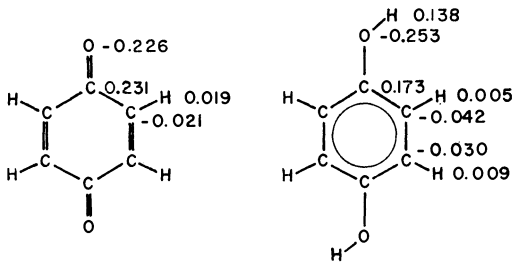

(a) *p*-Benzoquinone (b) Hydroquinone

Fig. 4. Charge densities obtained from CNDO/2 calculations.

From the charge densities obtained by CNDO/2 calculations, we calculated ΔE according to Eq. (2) with the assumption that k_C=21.9 eV/(unit charge). The results are given in Table 2. These results suggest that, in the cases of *p*-benzoquinone, hydroquinone and chloranil, the C ls spectrum will split into two bands separated by 1—2 eV. Since the intensity of each band is to be proportional to the number of atoms

Table 2. Calculated chemical shifts, ΔE (unit; eV)

Compound	C ls		O ls
	C_1	C_2	
p-Benzoquinone	2.5	0.9	−3.0
Chloranil	4.1	2.6	−1.6
Hydroquinone[a]	1.5	0.1, 0.2	−3.0
Tetrachlorohydroquinone	3.3	2.1, 2.1	−1.6

Compound	C ls			O ls	
	C_1	C_2	C_3	O_1	O_2
Chloranilic acid[b]	3.4	3.5	1.2	−2.4	−1.1

a) The C ls levels of C_2 carbons split into two depending on the orientation of OH group. b) C_1, C_2, and C_3 correspond to C(=O), C(–OH), C(–Cl) respectively, and O_1 and O_2 to (C=O, O(–H) respectively.

responsible for it, the intensity of the low-energy band will be twice of that of the high-energy band. This is in accord with the observations, consequently, we can assign without ambiguity the two bands obtained by resolving the C ls spectrum of each of these compounds to the two levels predicted by the above calculations. In the case of chloranilic acid, the calculation predicts the presence of three C ls bands of equal intensity, but we were not able to resolve its C ls spectrum to the components corresponding to these predicted bands.

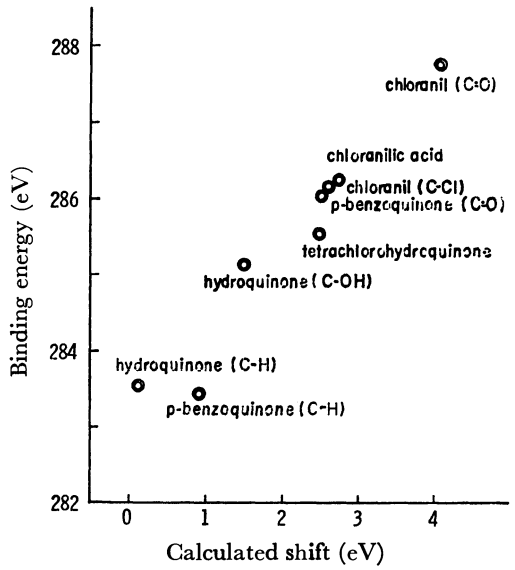

Fig. 5. Measured binding energy shifts of carbon 1s electrons versus shifts calculated with the electrostatic potential model.

Figure 5 demonstrates the good correlation between the observed binding energies of C ls level and the calculated values of ΔE. The data well fit on a straight line which makes an angle of 45 degree with the abscissa.

The correlation between the observed and calculated chemical shifts of O ls level is shown in Fig. 6, where we assumed that k_O=25.8 eV/(unit charge). The correlation is less satisfactory in this case as compared with the case of C ls level.

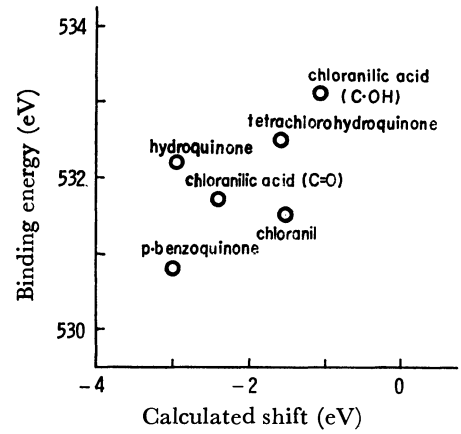

Fig. 6. Measured binding energy shifts of oxygen 1s electrons *versus* shifts calculated with the electrostatic potential model.

We can rewrite Eq. (1) in the following form:

$$E_i - \sum_j (q_j/R_{ij}) = E_A^0 + k_A q_i \quad (3)$$

Thus, if we plot $E_i - \sum_j (q_j/R_{ij})$ against q_i, we will obtain a straight line, and we can determine k_A from its inclination and E_A^0 by extrapolating it to $q_i=0$. Since the data were limited, we were not able to determine the k_A value with sufficient accuracy. Therefore, we assumed the k_A values proposed by Siegbahn *et al.*, and determined E_A^0 by the extrapolation. By this way, we found the $E_C^0=283.3\pm0.2$ eV for $k_C=21.9$ eV/(unit charge) and $E_O^0=534.0\pm0.5$ eV for $k_O=25.8$ eV/(unit charge).[7]

Charge Distributions in the Quinone Derivatives. As we can see in Table 1, the C 1s and O 1s levels of the halogen-substituted quinones are systematically shifted with the electronegativity of halogen. In these molecules, we need to know only four quantities in order to specify the charge distribution. Those are the charge densities on oxygen, halogen and two non-equivalent carbon atoms, C_1 and C_2, which we will denote as q_O, q_X, q_{C_1}, and q_{C_2}, respectively. These quantities must satisfy the condition of the electrical neutrality of molecule, consequently, one of them can be derived from other three quantities. By using the relation given by Eq. (1) for the O 1s level and the C 1s levels of the two kinds of carbon atom, we obtain three equations relating the observed binding energies to the charge densities. We solved such equations for the E_A and k_A values which we have determined in the preceeding section. The results are given in Table 3.

Table 3. Charge densities estimated from XPS spectra of quinone derivatives

Compound	C_1	C_2	O	X
Chloranil	0.29_5	0.05_3	-0.24_4	-0.07_9
Bromanil	0.29_8	0.02_8	-0.24_3	-0.05_6
Iodanil	0.29_2	-0.02_0	-0.24_6	-0.00_2
p-Benzoquinone	0.28_7	-0.08_4	-0.24_5	0.06_3

The validity of the above procedure could be questioned when we consider the approximate nature of Eq. (1), and the limited reliability of the empirical values of E_A^0 and k_A. Nevertheless, the results given in Table 3 seem to be quite satisfactory. The charge densities on carbon and oxygen atoms in C=O group are little affected by the substituted halogen. The charge density on the carbon atom directly bounded with halogen and that on the halogen atom systematically change with the electronegativity of the substituted halogen. These are in accord with the chemical intuitions.

References

1) K. Siegbahn, C. Nordling, G. Johansson, J. Hedman, P. F. Hedén, K. Hamrin, U. Gelius, T. Bergmark, L. O. Werme, R. Manne, and Y. Baer, "ESCA applied to free molecules," North-Holland, Amsterdam, (1969).

2) This method of calibration could not be used in the case of *p*-benzoquinone, where the C 1s peak of the contamination carbon (284.3 eV) was used as a subsidiary standard.

3) See for example, I. Ikemoto, J. M. Thomas, and H. Kuroda, *Faraday Discuss. Chem. Soc.*, **54**, 208 (1972).

4) K. Siegbahn, C. Nordling, A. Fahlman, R. Nordberg, K. Hamrin, J. Hedman, G. Johansson, T. Bergmark, S.-E. Karlsson, I. Lindgren, and B. Lindberg, "ESCA-Atomic, Molecular and Solid State Structure Studied by Means of Electron Spectroscopy," Almqvist and Wiksells, Uppsala, (1967).

5) M. E. Schwartz, J. D. Switalski, and R. E. Stronski, "Electron Spectroscopy," ed. by D. A. Shirley, North-Holland, Amsterdam (1972), p. 605.

6) The literatures for the crystal structure data of these molecules are as follows: *p*-benzoquinone: J. Trotter, *Acta Crystallogr.*, **13**, 86 (1960); hydroquinone: K. Maartmann-Moe, *ibid.*, **21**, 979 (1966); chloranil: S.S.C. Chu, G. A. Jeffrey, and T. Sakurai, *ibid.*, **15**, 661 (1962); tetrachlorohydroquinone: S. K. Sikka and R. Chidambaram, *ibid.*, **23**, 107 (1967); chloranilic acid: E. K. Andersen, *ibid.*, **22**, 188 (1967).

7) It is to be noted that E_C^0 and E_O^0 for the solid XPS spectra are different from the values for the gas-phase XPS spectra.

The Decomposition of Hydrogen Peroxide with Metal Complexes. I. The Catalytic Decomposition of Hydrogen Peroxide by the Ammine-Copper(II) Complex Ions in an Aqueous Solution

Katumitu HAYAKAWA and Sumio NAKAMURA

Department of Chemistry, Faculty of Science, Kagoshima University, Kamoike-cho, Kagoshima 890

(Received July 23, 1973)

The catalytic decomposition of hydrogen peroxide by the ammine-copper(II) complex ions has been studied using kinetic measurements, UV and visible spectroscopy, electron-spin resonance spectroscopy, and polarography. It was found that there were two reaction paths in the catalytic decomposition of hydrogen peroxide. In the first case, a linear part was observed in the plot of the amount of oxygen evolved *vs.* time. In this case, a brown intermediate was formed which was later found to be a diamagnetic peroxo-copper complex and to contain some of the stable oxygen anion radical just after the mixing of the reactants. The activation energy of the reaction was found to be 23 ± 1 kcal mol^{-1}. In the second case, no linear part was observed in the kinetic curve. In this case, the reaction had a reaction order in hydrogen peroxide varying from the first- to the second-order depending on the initial concentrations of the reactants. The nature of the brown compound and the active species of the reaction is discussed.

Since it was learned that the transition metal-ammine complexes have an enzyme-like activity in the decomposition of hydrogen peroxide,[1] many kinetic studies of the catalytic decomposition of hydrogen peroxide have been made for many transition-metal complexes.[2-10] On the other hand, electron spin resonance (ESR) studies have clarified the formation of complexed radical species in the reactions of the Ti^{III}–H_2O_2 system,[11-13] the Ce^{IV}–H_2O_2 system,[14] and the VO^{2+}–H_2O_2 system.[15] However, in the catalytic decomposition of hydrogen peroxide by the ammine-copper(II) complex ions, there is little information regarding such a radical intermediate and the rate of the reaction.[8,10]

The object of this paper is to clarify the nature and role of the brown intermediate formed in the catalytic decomposition of hydrogen peroxide by the ammine-copper(II) complex ions and to report a new reaction path without the brown intermediate. The active species of the ammine-copper(II) complex ions in the decomposition of hydrogen peroxide and the composition of the brown intermediate are discussed.

Experimental

Materials. Stabilized 30% hydrogen peroxide (GR) obtained from the Mitsubishi Gas Kagaku Co. was purified by distillation under reduced pressure. A solution of hydrogen peroxide was titrated with standard potassium permanganate just before use. The ammonia solution (28%, GR) was purified by distillation and was titrated with standard hydrochloric acid. The copper(II) sulfate (GR) was purified by recrystallization, after which the solution was titrated with standard ethylenediaminetetraacetic acid. The other chemicals (all GR) were used without further purification.

Measurements. The rates were determined by measuring the volume of oxygen evolved by the decomposition of hydrogen peroxide with a gas buret. The volume of the evolved oxygen agreed with the calculated volume from the initial concentration of hydrogen peroxide within an error of 2%. In order to clarify the composition of the brown compound formed during the reaction, the brown precipitate was prepared by the use of the reactants on a large scale without stirring and was analyzed after the decomposition of the precipitate by 3 M H_2SO_4. The absorption spectra of the reaction mixtures were recorded using a Shimadzu SV-50 Spectrophotometer. Polarograms of the reaction mixtures were recorded using a Yanagimoto PS-52 Polarograph and a PR-2 Polarorecorder. The potassium chloride was used as a supporting salt in the reaction mixtures. The ESR spectra were recorded using an X-band spectrometer with a 455 kHz field modulation. To obtain the ESR signal in the reaction mixture, a continuous-flow technique and a quenching technique were used.[13] The luminol test[16] was made using a solution of luminol (100 mg) in a 7 M ammonia solution (100 ml).

Results and Discussion

Kinetics. The effect of the concentration of ammonia is shown in Fig. 1. In the cases of 1, 2, and

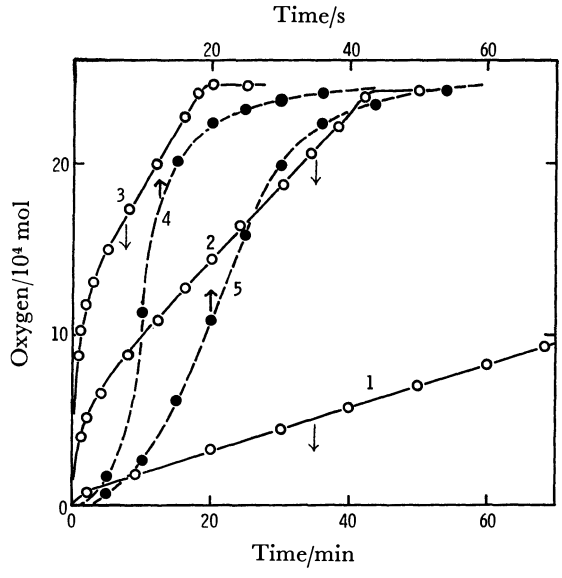

Fig. 1. Kinetic curves. The effect of the concentration of ammonia: 1. 0.04 M, 2. 0.08 M, 3. 0.10 M, 4. 0.20 M, 5. 0.50 M NH_3; 0.87×10^{-4}M $CuSO_4$; 0.125 M H_2O_2. The solid line indicates Path A and the broken line indicates Path B.

Table 1. Rate constants
Temperature 30 °C

The initial concentration of				Rate constant[a]	Order in H_2O_2	Reaction path
H_2O_2 (10^3M)	NH_3 (10^2M)	$CuSO_4$ (10^4M)	$(NH_4)_2SO_4$ (M)			
37	3.0	4.4	—	0.93	linear	A
75	3.0	4.4	—	0.73	linear	A
151	3.0	4.4	—	0.68	linear	A
34	4.0	4.4	—	1.75	linear	A
71	4.0	4.4	—	1.14	linear	A
145	4.0	4.4	—	0.85	linear	A
34	5.0	4.4	—	2.80	linear	A
49	5.0	4.4	—	1.84	linear	A
71	5.0	4.4	—	1.26	linear	A
141	5.0	4.4	—	1.08	linear	A
32	6.0	4.4	—	5.50	linear	A
67	6.0	4.4	—	1.70	linear	A
137	6.0	4.4	—	1.35	linear	A
125	4.0	0.9	—	0.62	linear	A
125	6.0	0.9	—	1.11	linear	A
125	8.0	0.9	—	2.2	linear	A
125	10	0.9	—	3.5	linear	A
20—142	2.0	2.2	0.2	0.51±0.03	1.4	B
21—141	1.0	2.2	0.3	0.31±0.02	1.5	B
71—159	3.0	16	0.5	6.54±0.40	1.6	B
33—137	1.0	8.0	0.5	2.70±0.19	1.7	B
81	0.5	9.1	1.5	1.1	1.8	B
81	1.0	9.1	1.5	2.3	1.7	B
81	1.2	9.1	1.5	1.7	1.7	B
81	2.0	9.1	1.5	1.6	1.7	B
81	3.9	9.1	1.5	0.77	1.6	B
44	0.5	9.1	0.11	9.3	1.7	B
44	0.5	9.1	0.13	11.3	1.7	B
44	0.5	9.1	0.20	7.1	1.7	B
44	0.5	9.1	0.40	1.3	1.7	B
44	0.5	9.1	0.53	0.51	1.7	B

a) 10^3 M min^{-1} for the reaction through Path A and M^{1-n} min^{-1} for the n-th-order reaction.

3 in Fig. 1, the reaction solution became brown and a linear part was observed in the kinetic curves (the plot of the amount of oxygen evolved *vs.* time). This is termed Path A (the solid line). In the cases of 4 and 5 in Fig. 1, no linear part is observed (termed Path B, the broken line). As the concentration of ammonia or the ammonium salt increases to some extent, the rate increases. The reaction path changes from Path A to Path B with the increase in the ammonia. With a further increase in the concentration of ammonia or the ammonium salt, the rate decreases and the reaction has an induction period. Path A appears at a high concentration of hydrogen peroxide and at low concentrations of the ammonia and the ammonium salt.

In Path A, the rate in the linear part, k_0, increased with an increase in the initial concentration of ammonia or the copper(II) ion and decreased with an increase in the initial concentration of hydrogen peroxide (Table 2). However, no simple relationship between the rate and the initial concentrations of three components was found. The rate was independent of the concentration of the brown intermediate, which was estimated by the optical density at 360 nm

Table 2. The rates of linear part, k_0, *versus* the optical density at 360 nm
Temperature 30 °C

The initial concentrations of			$D_{360\ nm}$	k_0 (10^3M min^{-1})
H_2O_2 (10^3M)	NH_3 (10^2M)	$CuSO_4$ (10M)		
45	5.8	3.0	0.52	2.6
45	5.8	4.4	0.74	3.4
45	5.8	5.9	1.00	4.0
20	4.8	4.6	0.47	3.6
31	4.8	4.6	0.49	2.4
42	4.8	4.6	0.51	1.8
46	4.9	3.0	0.52	1.6
46	5.9	3.0	0.52	2.0
46	7.4	3.0	0.53	3.4

(Table 2). The activation energy, which was obtained from the dependence of k_0 on the temperature (15—45 °C) at $[H_2O_2]_0$=0.04—0.09 M, $[CuSO_4]_0$=0.25—0.44 mM, and $[NH_3]_0$=0.13—0.045 M, was found to be 23±1 kcal mol^{-1}.

Path B had an order of reaction in hydrogen per-

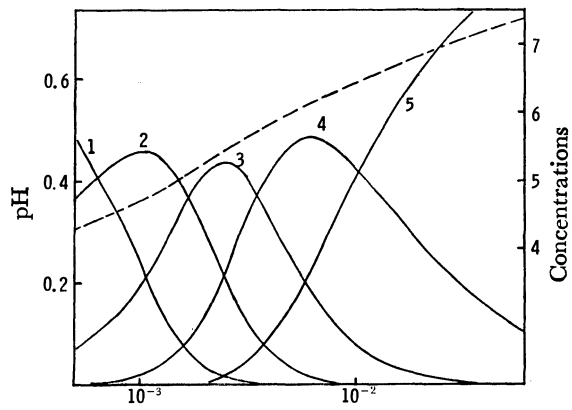

Fig. 2. The distribution of the ammine-copper(II) complex ions at the concentrations of 0.49 mM $CuSO_4$ and 1.5 M $(NH_4)_2SO_4$; 1. aquo-complex ion, 2. mono-ammine-, 3. diammine-, 4. triammine-, 5. tetra-ammine-complex ion. The broken line indicates the pH. This distribution was calculated by use of the formation constants of the ammine-copper(II) complex ions (L. G. Sillén and A. E. Martell, "Stability Constants of Metal-Ion Complexes," The Chemical Society, London (1964), p. 152).

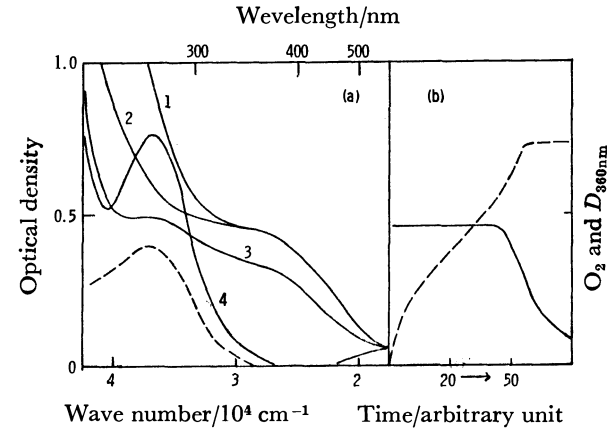

Fig. 3. (a) Spectra of the reaction mixtures: 1. 1 min, 2. 35 min, 3. 48 min, 4. 217 min. The broken line indicates a spectrum of the supernatant solution of the copper(II) sulfate-dilute ammonia mixture. (b) Schematic diagram of the relationship between the optical density at 360 nm (solid line) and the kinetic curve in the case of Path A (broken line).

oxide varying from the first- to the second-order, depending on the initial concentrations of the four components (Table 1). The order was determined by adjusting n to get an optimum linear plot of $[H_2O_2]^{-n+1}$ *vs.* time. The latter fourteen runs, given in Table 1, had a linear part in the plot of $[H_2O_2]^{-n+1}$ *vs.* time, at least in the region of an extent of reaction between 15 and 90% for each kinetic run.

For the 1.5 M ammonium sulfate, the maximum rate was observed (the 23rd row in Table 1) when the concentrations of the triammine- and tetraammine-copper(II) complex ions were much larger than those of the other ammine-copper(II) complex ions (Fig. 2). When the concentration of ammonia increases further, the concentration of $[Cu(NH_3)_4]^{2+}$ increases and the rate decreases. The maximum rate is observed when the pH is higher than that at which the concentration of the triammine-copper(II) complex ion is at its maximum (the broken line in Fig. 2). Therefore, it may be supposed that the active species is the hydroxo-triammine-copper(II) complex ion. It has been reported that the hydroxo-type complex is the active species in the catalytic decomposition of hydrogen peroxide by the triethylenetetramineiron(III) complex ion,[3,17] the citrato-copper(II) complex ion,[18] and the ammine-copper(II) complex ion.[10] The activation energy was found to be 15 ± 1 kcal mol^{-1} in one of the reactions through Path B (1.4-order rate constant), in which $[H_2O_2]_0$ is 0.04 M, $[CuSO_4]_0$ is 0.3 mM, and $[NH_3]_0$ is 0.27 M.

The Brown Compound. The brown solution has a broad absorption band in the region from 500 nm to UV (1 and 2 in Fig. 3-a), and the optical density at 360 nm was constant until the final period of the reaction (Fig. 3-b). The band with a peak at 267 nm after the termination of the reaction (4 in Fig. 3-a) is considered to be caused by the hydroxo-copper(II) complex because of the agreement with the absorption band of the supernatant solution of the mixture between the copper(II) ion and the dilute ammonia solution (the broken line). At high concentrations of the ammonium salt or ammonia, the brown compound was not observed. From the easy formation of the brown compound at a high pH and/or at a low concentration of ammonia and ammonium ion, and from the appearance of the hydroxo-copper(II) complex ion after the decomposition of the brown compound, it is supposed that the brown compound is formed from a hydroxo-copper(II) complex.

To characterize the brown compound formed in the reaction mixture, the brown precipitate was prepared by the use of the reactants on a large scale without stirring and was then separated from the reaction mixture. We could not obtain the spectrum of the solid because it was bulky like the hydroxide. The visible spectrum of the aqueous solution of the solid agreed with that of the brown intermediate. The

Table 3. Analysis of the brown precipitate

Time of reaction	Ratio of moles		
	H_2O_2/Cu	O_2/Cu	$(H_2O_2+2O_2)/Cu$
0 day	0.59	0.05	0.69
	(0)	(0.33)	(0.66)
1 day	0.16	0.02	0.20
	(0)	(0.09)	(0.18)
2 days	0.01	0.04	0.09
	(0)	(0.04)	(0.08)
10 days	0.00	0.02	0.04
	(0)	(0.02)	(0.04)
2 min[a]	0.83	0.00	0.83
30 min[a]	0.70	0.04	0.78
120 min[a]	0.81	0.00	0.81

a) The sample was separated from the solution in which the reaction was undergoing. b) ( ) self-decomposition.

peroxide and copper in the precipitate were analyzed, and the volume of the oxygen gas, which was liberated by the decomposition of the precipitate by acid or on standing for 12 hr, was measured by means of a gas buret (Table 3). When the precipitate was decomposed by acid immediately after separation from the reaction solution and washing, *ca.* 10^{-5} mol of oxygen gas evolved. Therefore, it may be supposed that a part of the oxygen which was adsorbed on the precipitate after the self-decomposition was liberated by the acid treatment. The fact that the molar ratio of $(H_2O_2+2O_2)/Cu$ in the case of decomposition by the acid treatment agreed with the molar ratio of $2O_2/Cu$ in the case of the self-decomposition (shown in the fourth column in Table 3) indicates that the hydrogen peroxide coordinates to the copper ion with a molar ratio of 1 : 1. Ammonia was detected in the brown precipitate, but the quantity was too small for us to obtain the NH_3/Cu ratio.

Thus, the brown compound is found to be a peroxo-copper complex and to decompose with the evolution of oxygen on standing. The brown peroxo-copper complex changed to a green compound on standing for several hours and to a sky-blue compound on standing for several days.

ESR. The ESR signal obtained using a quenching technique and the ESR signal of the free O_2^- radical obtained by the UV irradiation of an alkaline hydrogen peroxide aqueous solution are shown in Figs. 4-a and 4-b respectively (measured at 77 K). The S_1 signal in Fig. 4-a is assigned to the O_2^- radical. The S_2 signal is consistent with the perpendicular component of the anisotropic signal of the tetraammine-copper(II) complex ion, as is shown in Fig. 4-c. The copper(II) complex ion is considered to be present in a very small amount because of the weak intensity of the signal as compared with the signal of the copper(II) ion of the original concentration.

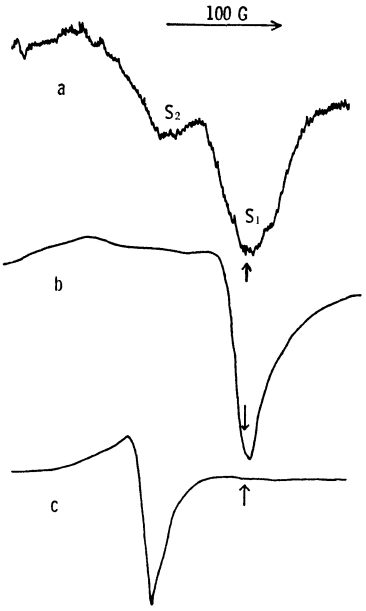

Fig. 4. ESR spectra of the quenched sample of the reaction mixture (a), the oxygen anion radical, O_2^-, (b), and the ammine-copper(II) complex ions (c) measured at 77 K.

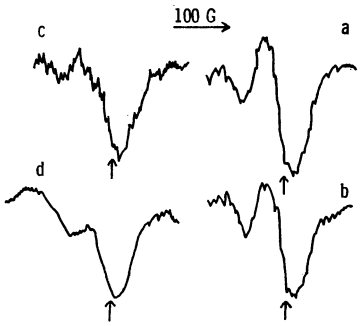

Fig. 5. Dependence of the signal of the quenched sample on the temperature: a. 108 K, b. 149 K, c. 217 K, and d. 77 K after the melting treatment for two minutes.

The dependence of the S_1 signal on the temperature is shown in Fig. 5. The S_1 signal was observed at 232 K and was also observable at 77 K after the melting treatment of the quenched sample for two minutes at *ca.* 0 °C. The signal of the free O_2^- radical obtained by the UV irradiation was not as stable as the S_1 signal; *e.g.*, it had already disappeared at 194 K.

Sometimes no signal was observed in the range of the magnetic field between 0 and 4300 gauss at 77 K in the brown quenched sample at a high concentration of hydrogen peroxide or a small rate of mixing; therefore, it may be concluded that the copper ion in the brown intermediate is a diamagnetic species.

From these facts, the increased stability of the O_2^- radical, and the lack of the copper(II) ion, the O_2^- radical which coordinates to any diamagnetic copper complex ion can be tentatively proposed as the origin of S_1, even without any direct evidence such as the hyperfine structure due to the copper nucleus. It may be supposed that the observation of the resolved hyperfine structure in the sample of the polycrystalline state is fairly difficult as compared with the case of the Ti^{III}–H_2O_2 system[19] or the VO^{2+}–H_2O_2 system,[15,20] where the ESR signal was detected by means of a flow technique.

It is known that the free radical resulting from hydrogen peroxide coordinates with the oxidized form of the metal ion in the reactions of the Ti^{III}–H_2O_2 system[11-13,21] and the VO^{2+}–H_2O_2 system[15,21] and with the reduced from of the metal ion in the reaction of the Ce^{IV}–H_2O_2 system.[14,21] The free radical is stabilized by the coordination with the metal ion.

The diamagnetic copper(III) ion in the D_{4h} symmetry has a vacant $d(x^2-y^2)$ orbital which does not overlap with the π^*-orbital of the O_2^- radical. Therefore, the electron transfer from the unpaired π^*-orbital to the vacant $d(x^2-y^2)$ orbital is difficult. For this reason, it is considered that the free radical coordinated to the copper(III) ion is stabilized. The complexed radical compound has been considered to be formed in a by-path of the catalytic decomposition of hydrogen peroxide because of the increased stability of the compound compared to that of the original free radical.[12,13,21]

About the copper(III) compound, it has been re-

ported that a colloidal copper(III) oxide is formed in the reaction between hydrogen peroxide and the ammine-copper(II) complex.[22,23]

Luminol Test. When an alkaline luminol reagent was added to a mixture of hydrogen peroxide and hemin, a chemiluminescence was observed.[24] The ammoniacal luminol reagent was here added to the brown precipitate, a mixture of hydrogen peroxide and the copper(II) ion, a hydrogen peroxide solution, and a copper(II) sulfate solution. Chemiluminescence was observed in the brown precipitate and the mixture of hydrogen peroxide and the copper(II) ion. This fact suggests that the decomposition of hydrogen peroxide by the ammine-copper(II) complex ions and that of the brown compound by the ammonia solution proceeds with the formation of a free radical, because the chemiluminescence is observed in the reaction between the luminol reagent and the free radical resulting from hydrogen peroxide.[16]

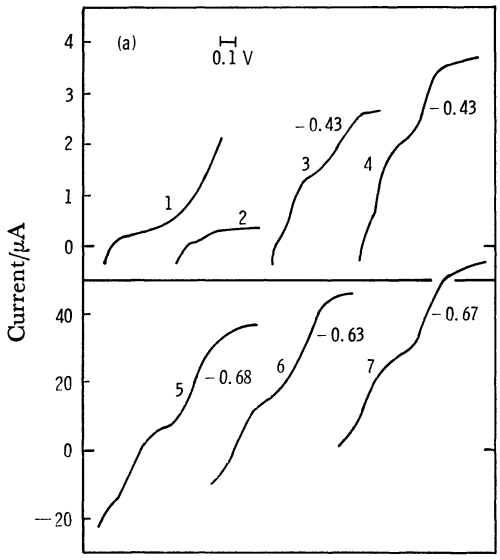

Fig. 6. Polarograms of the reaction mixture (a) and the copper(I) chloride-ammonia mixture (b); 1. 40 min, 2. 130 min, 3. 300 min, 4. 310 min after mixing of the reactants; 5. 10 min, 6. 22 min, 7. 45 min after mixing of copper(I) chloride and ammonia. The 1 M KCl and 1.5 M ammonium sulfate were used for (a) and (b) as the supporting salt respectively. The fractional values in this figure indicate a half-wave potential *vs.* SCE.

Polarography. Polarograms of the reaction mixture and the mixture of the copper(I) ion and ammonia are shown in Fig. 6. In the reaction mixture, the wave-height of the mixture of the ammine-copper(II) complex ions (3 and 4 in Fig. 6-a, the two-step wave) increased with the decrease in the brown intermediate after the disappearance of the wave of hydrogen peroxide (1 and 2 in Fig. 6-a). In the mixture of the copper(I) ion and ammonia, the first wave (*ca.* −0.25 volt *vs.* SCE) resulting from Cu(II)⇌Cu(I) shifted from a negative current to a positive current with the increase in the copper(II) ion by air-oxidation (Fig. 6-b). The shift was also observed in a mixture of a reductant and an oxidant.[25] The difference in the half-wave potential between the reaction mixture and the mixture of the copper(I) ion and ammonia is a result of the difference in the concentrations of ammonia and the supporting salt (1 M KCl for the reaction mixture and 1.5 M $(NH_4)_2SO_4$ for the mixture of the copper(I) ion and ammonia). The rate of the formation of the ammine-copper(II) complex ions by the addition of concd ammonia to the brown compound was very rapid as compared with that by the addition of concd ammonia to the copper(I) chloride, which was tested by the rate of blue coloration. These facts suggest that the copper ion in the brown intermediate is not a univalent ion.

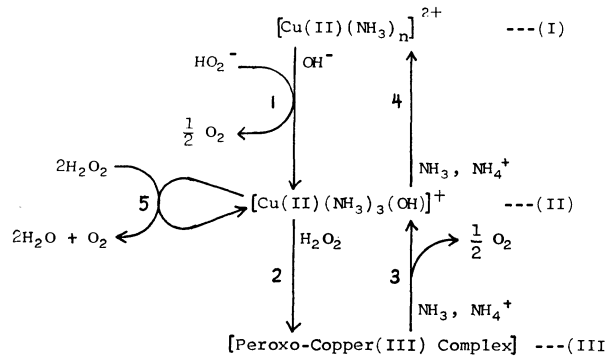

Fig. 7. Reaction scheme of the catalytic decomposition of hydrogen peroxide by the ammine-copper(II) complex ions.

Reaction Scheme. From the preceding discussions, it may be assumed that the path of the catalytic decomposition of hydrogen peroxide by the ammine-copper(II) complex ions is as is shown schematically in Fig. 7. In the reaction scheme, Reaction 1 is very slow compared with the other reactions. Reaction 2 depends on the concentrations of hydrogen peroxide and the hydroxide ion. Reaction 3 depends on the concentration of ammonia or the ammonium ion. The rate of the evolution of oxygen in Reaction 5 is much larger than that in Reaction 3.

In Path A, the rate of Reaction 2 is much larger than that of Reaction 3, so the copper compound in the reaction mixture is almost entirely Compound III (brown intermediate) during the reaction. The rate of the evolution of oxygen is the sum of the rates of Reactions 3 and 5. In the initial stage of Path A, Reaction 5 is predominant, so the rate of the evolution of oxygen is large (see the solid lines in Fig. 1). In the final stage of Path A, the concentration of Compound II increases because of the small rate of Reaction 2 resulting from the low concentration of hydrogen peroxide, so the rate of the evolution of oxygen increases because of the increase in Reaction 5 (2 and 3 in Fig. 1). The linear part can be attributed to the steady concentration of Compounds III and II. Also, the fact that the rate in the linear part is not proportional to the concentration of the brown Compound III suggests that the rate is determined by the concentrations of ammonia and Compounds II and III.

In Path B, the rate of Reaction 2 is very small compared with the rates of Reactions 3 and 4, so Com-

pound III is not observed. The increase in the ammonia or the ammonium salt decreases the active species, II, and the rate of the decomposition of hydrogen peroxide. The induction period is caused by Reaction 1. The mechanism of Reaction 5 was not found owing to the complicated rate equation.

The difference in the activation energy between the two reaction paths, A and B, suggests that their mechanisms of the evolution of oxygen gas are different.

The authors wish to express their thanks to Professor Keiji Kuwata and Professor Kozo Hirota, Osaka University, for kindly putting the ESR spectrometer at their disposal and for their valuable advice.

References

1) Y. Shibata and H. Kaneko, *Nippon Kagaku Zasshi*, **44**, 166 (1923).
2) M. Bobtelsky and A. E. Simchen, *J. Amer. Chem. Soc.*, **64**, 2492 (1942).
3) R. C. Jarnagin and J. H. Wang, *ibid.*, **80**, 6477 (1958).
4) G. Wada, T. Nakamura, K. Terauchi, and T. Nakai, This Bulletin, **37**, 447 (1964).
5) H. Brintzinger and H. Erlenmeyer, *Helv. Chim. Acta*, **48**, 826 (1965).
6) T. Kaden and H. Sigel, *ibid.*, **51**, 947 (1968).
7) R. Grieser, B. Prijs, and H. Sigel, *J. Amer. Chem. Soc.*, **91**, 7758 (1969).
8) T. Kawaguchi, *Tokyo Gakugei Daigaku Kiyo* (*Part* **4**), **20**, 67 (1968).
9) T. Kawaguchi and H. Yoshida, *ibid.*, **21**, 70 (1969).
10) B. Kirson, *Bull. Soc. Chim. Fr.*, **1952**, 957.
11) W. T. Dixon and R. O. C. Norman, *J. Chem. Soc.*, **1963**, 3119.
12) Y. S. Chiang, J. Craddock, D. Mickewich, and J. Turckevich, *J. Phys. Chem.*, **70**, 3509 (1966).
13) Y. Shimizu, T. Shiga, and K. Kuwata, *ibid.*, **74**, 2929 (1970).
14) E. Saito and B. H. J. Bielski, *J. Amer. Chem. Soc.*, **83**, 4467 (1961).
15) T. Ozawa, Y. Kirino, M. Setaka, and T. Kwan, *Nippon Kagaku Zasshi*, **92**, 304 (1971); *J. Catal.*, **15**, 209 (1969).
16) R. D. Gillard and A. Spencer, *J. Chem. Soc., A*, **1970**, 1761.
17) J. H. Wang, *J. Amer. Chem. Soc.*, **77**, 4715 (1955).
18) A. Glasner, *J. Chem. Soc.*, **1951**, 904.
19) H. Fisher, *Ber. Bunsenges. Phys. Chem.*, **71**, 685 (1967).
20) A. Samuni and G. Czapski, *J. Phys. Chem.*, **74**, 4592 (1970).
21) A. Samuni, *ibid.*, **76**, 2207 (1972).
22) I. S. Teletov and A. D. Veleshinetz, *Ukrainskii Khem. Zhur.*, **4**, 463 (1929); *ibid.*, **6**, 53 (1931); *Chem. Abstr.*, **24**, 5248 (1930); **25**, 5633 (1931).
23) T. P. Vorobeva, B. M. Berdnikov, and A. P. Purmalis, *Kinet. Katal.*, **11**, 100 (1970).
24) W. Langenbeck and U. Ruge, *Ber.*, **70**, 367 (1937).
25) I. Tachi, "Polarography," Iwanami Shoten, Tokyo (1954), p. 31.

Change from Metastable Cubic to Stable Tetragonal Form of Submicron Barium Titanate

Shigeharu NAKA, Fumihiko NAKAKITA, Yoshiko SUWA, and Michio INAGAKI

Faculty of Engineering, Nagoya University, Chikusa-ku, Nagoya 464

(Received September 27, 1973)

The change from metastable cubic to stable tetragonal form was investigated on the submicron $BaTiO_3$ which was prepared by the hydrolysis of titanium tetraisopropoxide in barium hydroxide solution and by crystallization in the glass of BaO–TiO_2–SiO_2–Al_2O_3 system. The precipitated $BaTiO_3$ was found to be the aggregates of minute grains of about 100 Å, to have large amount of strain and to absorb about 6% of OH and alcoholic radicals, some of them absorbed chemically. It is in a metastable cubic form. After the heating above 800 °C, it changed to stable tetragonal form in association with weight loss and decrease in lattice strain. The samples heated at 800—900 °C did not show the Curie point on the DTA curve although they were tetragonal. The samples heated at 1300 °C had the Curie point about 122 °C. The glass-devitrified $BaTiO_3$ was also cubic and had large lattice strain. In order to change to tetragonal form, the heating above 1000 °C was needed. The metastable cubic form of submicron $BaTiO_3$ seemed to be stabilized by the absorbants on the surface which balanced with large amount of strain in the lattice.

As the raw materials for the preparation of high-density sintered ceramic bodies, as the catalysts and as the filler materials, high-purity submicron oxide powders have been studied. On these oxide powders, some structural anomalies have been observed. For example, ZrO_2 prepared from zirconium tetra-tertiary butoxide by thermal decomposition was found to have cubic form,[1] and that precipitated from alkaline aqueous solution and calcined at low temperature was tetragonal,[2] although the monoclinic form was stable at room temperature. $BaTiO_3$, of which stable form at room temperature was tetragonal, was cubic when it was prepared by pyrolysis of barium titanyl oxalate or by simultaneous hydrolysis of barium bis-isopropoxide and titanium tetrakis-tertiary amyloxide.[3,4] The appearance of these metastable forms of oxides were discussed mainly in relation to their small crystallite sizes.

On the $BaTiO_3$ ceramics, the dependence of dielectric constant on particle size has been studied in detail. The ceramics with fine particle size of about 1 μ was found to have very different temperature dependence of dielectric constant from that with coarse particles (about 50 μ), the latter having a similar behavior to the single crystal, and the former showing very diffuse transition from tetragonal to cubic form and having large dielectric constant at room temperature.[5,6] The maximum of dielectric constant at the particle size of about 1 μ was reported on the $BaTiO_3$ which was crystallized in the glass.[7] The decrease of dielectric constant with the decrease of particle size was also shown on the pure, unsintered and pressed $BaTiO_3$.[8] These experimental results were discussed on the basis of internal strain of the crystallite, many faults in the lattice or nonferroelectric surface layer of the particle.

In the present work, the change of $BaTiO_3$ from the metastable cubic to the stable tetragonal form was investigated, in relation to lattice strain, on the submicron $BaTiO_3$ powders.

Experimental

Preparation of Submicron $BaTiO_3$ Powder. The submicron $BaTiO_3$ powders were prepared in the same way as Kiss *et al.*[3] In the 0.41—0.48 N aqueous solution of barium hydroxide (reagent grade) with pH of 11—13, the isopropyl-alcohol solution of the equivalent molar weight of titanium tetra-isopropoxide (CP grade) was hydrolyzed and the precipitates were obtained. During the reaction, the solution was stirred violently and kept at 90 °C in the N_2 atmosphere. After aging the precipitates in the solution at 90 °C, it was filtered, washed by water and then dried in a vacuum. The stoichiometry of the prepared samples was known by the fact that any additional phases, such as Ba_2TiO_4, $BaTi_2O_5$, and TiO_2, were not identified by X-ray after the heating at 1100 °C. The non-stoichiometry of the precipitates occurred from the lowering of pH during the reaction could be avoided by the addition of KOH in the $Ba(OH)_2$ solution to keep the pH-value constant.

The samples thus prepared were heated at various temperatures from 120 °C to 1300 °C in air and studied by X-ray diffraction techniques, electron microscopy, thermal analyses (DTA and TGA), and infrared absorption spectra.

Crystallization of $BaTiO_3$ in the Glass. The crystallization of $BaTiO_3$ in the glass was performed according to Herczog.[7] The glass was prepared from the mixture of 42.9 mol% $BaCO_3$, 35.8% TiO_2, 14.2% SiO_2, and 7.1% Al_2O_3 by melting at 1480 °C for 2 hr, after 1200 °C pre-heating, in the platinum crucible and quenched into water.

The glass samples thus prepared were heated at 800 °—1200 °C in air and the precipitated microcrystalline $BaTiO_3$ was studied by X-ray.

Results and Discussion

X-Ray Diffraction Studies. X-Ray diffraction patterns of submicron $BaTiO_3$ are shown in Fig. 1. After heating at 120 °C for 24 hr, X-ray pattern of the sample is indexed by the cubic system, which have to be the high-temperature modification of $BaTiO_3$. After heating at 1300 °C for 5 hr, however, the sample is tetragonal, of which X-ray pattern is not differentiated from the crystal prepared by solid state reaction.

In the BaO–TiO_2–SiO_2–Al_2O_3 system glass, $BaTiO_3$ crystals were precipitated by the heating above 800 °C. The crystals precipitated after heating at 800 °C for 5 hr were also cubic and those after heating at 1200 °C were tetragonal, which coexisted with small amount of hexagonal feldspar $BaAl_2Si_2O_8$.

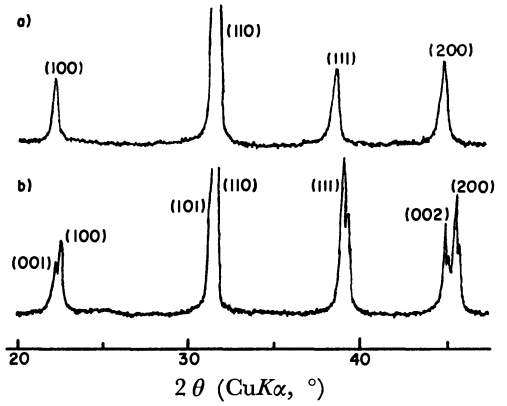

Fig. 1. X-ray diffraction patterns of submicron $BaTiO_3$ heated at 120 °C for 24 hr (a) and at 1300 °C for 5 hr (b)

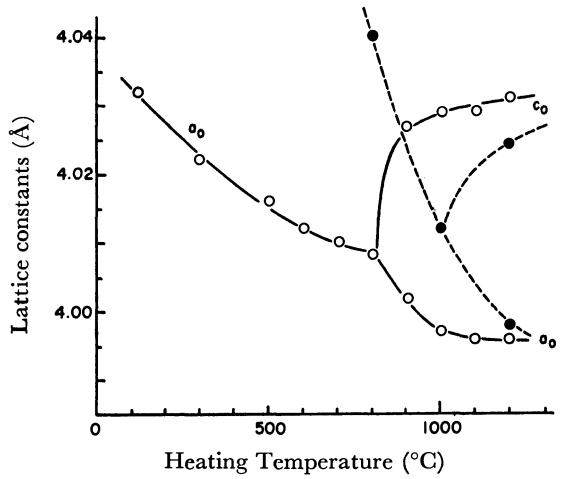

Fig. 2. Changes of lattice constants a_0 and c_0 with heating temperature for the constant heating time of 5 hr
○: precipitated, ●: glass-devitrified

On both precipitated and glass-devitrified $BaTiO_3$ samples, the changes of lattice constants a_0 and c_0, which are determined by using (111), (002), and (200) diffraction lines, with heating temperature are shown in Fig. 2. The transition temperature from the metastable cubic to the stable tetragonal form is at about 800 °C for the precipitated sample and at about 1000 °C for the glass-devitrified. At low heating temperature, the unit cell of the samples is relatively large. This might suggest the existence of large amounts and many kinds of lattice defects.

In Fig. 3, the half widths of (111) and (002) diffraction line profiles are plotted as a function of heating temperature on the precipitated $BaTiO_3$ heated at each temperature for 5 hr. The half width of (111) line decreases with the increase in heating temperature and this corresponds to the crystallite growth and the decrease in strain. However, the observed half width of (002) line shows an increase above 700 °C. This is caused from splitting of the cubic (002) line to the tetragonal (002) and (200) lines and shows consistency with the changes of lattice constants.

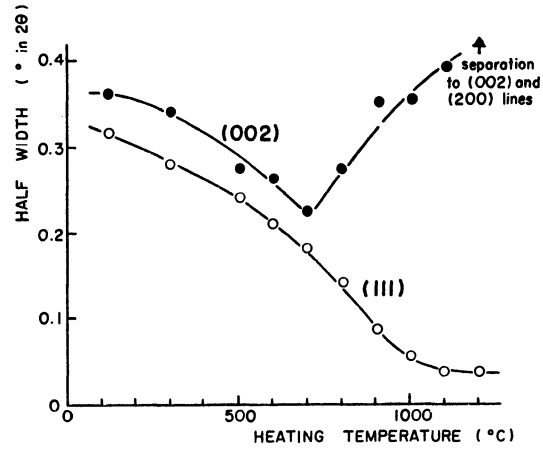

Fig. 3. Changes of half width of (111) and (002) diffraction lines with heating temperature for the constant heating time of 5 hr.

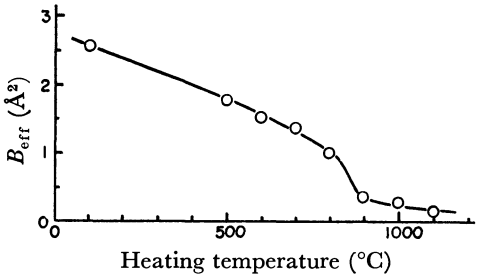

Fig. 4. Change of effective Debye parameter B_{eff} with heating temperature for the constant heating time of 5 hr.

On the same precipitated samples, the effective Debye parameter B_{eff} was measured, which was a measure of lattice strain in the powders.[9] The change of B_{eff} with heating temperature is shown in Fig. 4. With the increase of heating temperature, the value of B_{eff}, that is, lattice strain, decreases rapidly. The step-wise decrease between 800 and 900 °C corresponds to the structural change from cubic to tetragonal form.

On the metastable cubic $BaTiO_3$ devitrified in the glass, large value of B_{eff}, that is, large amount of lattice strain, was observed.

Electron Microscopic Observations. The precipitates heated at 120 °C for 24 hr, consisted of the polyhedral

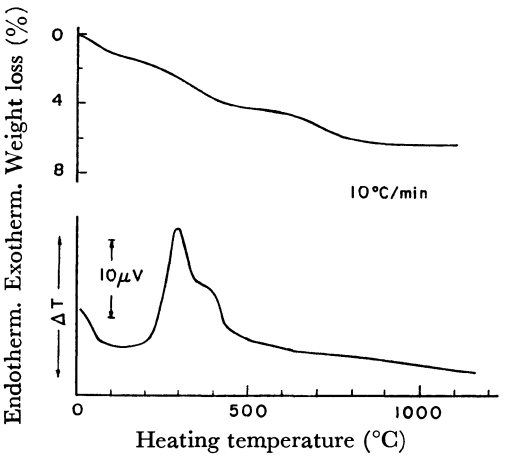

Fig. 5. TGA and DTA curves for the precipitated $BaTiO_3$.

particles with the apparent dimension of about 500 Å and these polyhedra seemed to be the aggregates of minute grains of about 100 Å. These particles grew up with the increase in heating temperature, to 0.1—1 μ in dimension after the heating at 1100 °C for 5 hr.

Thermal Analysis Studies. The results of thermogravimetric and differential thermal analyses (TGA and DTA) are shown in Fig. 5 on the precipitates heated at 120 °C for 24 hr. At 290 and 375 °C, two exothermic peaks are observed on the DTA curve. However, the weight loss occurs in two steps, though very diffuse, up to about 450 °C and to about 800 °C. The first step of weight loss corresponds to the exothermic peaks. The chemical species which cause the weight loss are supposed to be the absorbed OH and isopropoxy groups from the infrared absorption spectra for the samples quenched from different temperatures. Most of the absorbants which have been absorbed on the surfaces of submicron $BaTiO_3$ particles during their preparation, are desorbed up to 450 °C and are responsible to the exothermic peaks. Some of the absorbants remained above 450 °C and desorbed gradually up to about 800 °C. The experimental fact that one of the absorbants on the $BaTiO_3$ surfaces is OH groups, may be due to the basic nature of barium.[10]

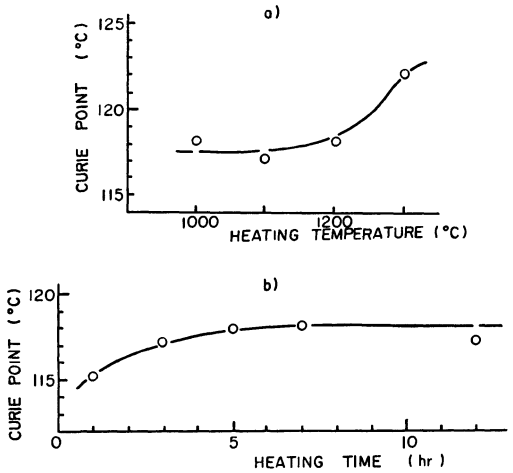

Fig. 6. Changes of Curie point with heating temperature for the constant heating time of 5 hr (a) and with heating time at 1000 °C (b)

On the precipitated $BaTiO_3$ heated above 1000 °C and transformed to the tetragonal form, the Curie point, the reversible transition point from tetragonal to cubic, was measured with DTA. In Fig. 6a, the relation between the Curie point and heating temperature for a constant heating time of 5 hr is shown. The observed Curie point is plotted as a function of heating time at 1000 °C, in Fig. 6b. With the increase of heating temperature, the Curie point increases to 122 °C. This Curie point corresponds to the value of 123 °C for the $BaTiO_3$ ceramics with coarse grain (—100 μ) reported by Jonker.[5] At 1000 °C, however, the lattice strain in the precipitates seems not to be annealed out and consequently the Curie point observed is about 118 °C even after the annealing for 12 hr. The sample heated at 900 °C was tetragonal, but Curie point was difficult to be detected on their DTA curves.

On the precipitated $BaTiO_3$ heated below 900 °C, the Curie point was not detected at low temperatures down to the liquid nitrogen temperature. This fact suggests that the Curie point disappears, not shifts to low temperatures, probably because of the presence of strain.

The measurement of dielectric constant was carried out on the pressed specimens of the precipitated $BaTiO_3$. However, the reliable value of dielectric constant was difficult to obtain because of the lack of the sufficiently dense specimens.

On the Formation of Metastable Cubic Form. The submicron $BaTiO_3$, precipitated from titanium-alkoxide and barium hydroxide solution, and precipitated in the glass matrix, had the cubic form which was metastable thermodynamically. This metastable cubic form changed to the stable tetragonal form only after heating above 800 °C for the precipitated and above 1000 °C for the glass-devitrified $BaTiO_3$. The latter needed higher temperature than the former, which might be caused from the clamping effect[11] of glass matrix. The decrease of lattice strain with heating corresponded to the change from the metastable cubic to the stable tetragonal form. Phenomenological similarity was found between the present results and the irradiation-induced transition,[12] in which the introduction of defects by irradiation resulted in the change from the tetragonal to cubic form. An amount of lattice strain remained in the tetragonal submicron $BaTiO_3$ and it caused the disappearance of the Curie point. The Curie point of $BaTiO_3$ was reported to be smeared out by grinding and compression[13] and also to disappear by the irradiation in the amount of 2.1×10^{20} nvt.[14]

As shown in the TGA and DTA curves, the submicron precipitates absorbed OH and isopropoxy groups on their surfaces, some amount of radicals being absorbed chemically. The space charge layer, which has been supposed to be present on the surface of ferroelectric solids,[15] did not appeared to exist in the present submicron $BaTiO_3$ because the charges, if they existed, might be diverged or cancelled out by the absorption of OH and alcoholic radicals. The cubic form was assumed to be stabilized, though metastably, by the absorbants which might balance with large strain in the metastable lattice structure. Above 800 °C at which almost all absorbants disappear, the submicron $BaTiO_3$ transformed to tetragonal form. On ZrO_2, the tetragonal form (hightemperature form) has been known to appear metastably at room temperature by bonding the small amounts of OH groups.[16]

The large lattice strain of the metastable cubic form of $BaTiO_3$ seemed to be related to the small particle size. According to Goswami,[8] the strained surface layer of $BaTiO_3$ particles is non-ferroelectric. The particle size of the present submicron $BaTiO_3$ is much smaller than the reported values of surface layer thickness.[8] In other words, all of the submicron particles have the characteristics of the surface layer, large strain and non-ferroelectric.

References

1) K. S. Mazdiyasni, C. T. Lynch, and J. S. Smith, *J. Amer. Ceram. Soc.*, **48**, 372 (1965).
2) R. C. Garvie, *J. Phys. Chem.*, **69**, 1238 (1965).
3) K. Kiss, J. Magder, M. S. Vukasovich, and R. J. Lockhart, *J. Amer. Ceram. Soc.*, **49**, 291 (1966).
4) K. S. Mazdiyasni, R. T. Dolloff, and J. S. Smith II, *ibid.*, **52**, 523 (1969).
5) G. H. Jonker, *Philips Tech. Rev.*, **17**[5], 129 (1955).
6) G. H. Jonker and W. Noorlander, "Science of Ceramics," Vol. 1, ed. by G. H. Stewart, Academic Press, London and New York (1962), p. 255.
7) A. Herczog, *J. Amer. Ceram. Soc.*, **47**, 107 (1964).
8) A. K. Goswami, *J. Appl. Phys.*, **40**, 619 (1969).
9) M. Inagaki, H. Furuhashi, T. Ozeki, H. Mugishima, and S. Naka, *J. Mater. Sci.*, **6**, 1520 (1971).
10) Y. Suwa and S. Naka, (to be published)
11) D. G. Grossman and J. O. Isard, *J. Mater. Sci.*, **4**, 1059 (1969).
12) M. C. Wittels and F. A. Sherrill, *J. Appl. Phys.*, **28**, 606 (1957).
13) H. Bogardus and R. Roy, *J. Amer. Ceram. Soc.*, **48**, 205 (1965).
14) F. T. Rogers, Jr., *J. Appl. Phys.*, **27**, 1066 (1956).
15) W. Känzig, *Phys. Rev.*, **98**, 549 (1955).
16) R. Cypres, R. Wollast, and J. Rancq, *Ber. Deut. Keram. Ges.*, **40**, 527 (1963).

Polarographic Studies of the Associated Ion-pairs of Polyphosphate with the Hexaamminecobalt(III) Ion

Niro MATSUURA, Kisaburo UMEMOTO, Masao TAKIZAWA,* and Yukio Sasaki*

Department of Pure and Applied Science, College of General Education, The University of Tokyo, Komaba, Meguro-ku, Tokyo 153

**Tokyo Institute of Photographic Technology, Iiyama, Atsugi, Kanagawa 243-02*

(Received October 2, 1973)

The polarographic behavior of the hexaamminecobalt(III) ion was studied in solutions of polyphosphate with different numbers of chains. The decrease in the diffusion current, i_d, with an increase in the phosphate (C_p)-to-hexaamminecobalt(III) (C_{Co}) mole ratio was found to be proportional to 1/4 the power of the molecular weight, M, of the $Co(NH_3)_6^{3+}$-polyphosphate. This fact shows the associated ions between $Co(NH_3)_6^{3+}$ ions and polyphosphate anions are transported to the electrode by diffusion at a rate depending on the square root of the molecular weight of the diffusion depolarizer. From the shift of the half-wave potential in the presence of excess polyphosphate, the chemical compositions of the associated ion-pairs were determined as a function of log C_p/C_{Co}.

The association of hexaamminecobalt(III) ions with sulfate, iodide, and several other halide ions has been evidenced by the spectrophotometric studies in aqueous media.[1-4] Hexaamminecobalt(III) ($Co(NH_3)_6^{3+}$) cations form precipitates with pyrophosphate and polyphosphate anions, but the precipitate of $Co(NH_3)_6^{3+}$-polyphosphate dissolves in an excess of polyphosphate. Laitinen *et al.*[5,6] reported the amperometric determination of pyrophosphate and triphosphate, with hexaamminecobalt(III) or tris-ethylenediamminecobalt(III) as the titrant. For completing the precipitation of $Co(NH_3)_6^{3+}$-triphosphate, the addition of some alcohol is indispensable. Since $Co(NH_3)_6^{3+}$ is highly stable and inert to ligand substitution, it is interesting to study in detail the type and the strength of the interaction exerted between $Co(NH_3)_6^{3+}$ ions and polyphosphate ions. The present work will deal with the diffusion currents and the half-wave potentials of $Co(NH_3)_6^{3+}$ in solutions of the polyphosphate with different numbers of chains.

Experimental

Apparatus. A Yanagimoto polarograph of the P8-D was employed for recording the DC polarograms. The potential was calibrated by means of potentiometer to within 1 mV. For the measurement, an H-type cell was used, the SCE being isolated from the solution by a bridge of saturated KCl with ultrafine sintered-glass membranes. The internal resistance was about 3 kΩ. The capillary used had an m value of 2.355 mg/s and a drop time of 3.57 s at a mercury height of 78.8 cm in distilled water at open circuit and at 25 °C.

Reagents. For obtaining sodium triphosphate of a high purity, a commercial triphosphate product containing more than 80% of triphosphate was used as the starting material. The purification was carried out by recrystallization, and the recrystallization was carried out by the use of 20% ethanol. When recrystallization was repeated five times, the product was the hydrate crystal of $Na_5P_3O_{10}\cdot 6H_2O$ (99.9% purity, according to our anion-exchange chromatographic analysis).[7] For preparing polyphosphate, the sodium dihydrogenphosphate (NaH_2PO_4) of the guaranteed reagent was dehydrated and melted at 800 °C for 3 hr. Vitreous oligomer phosphate with an average number of 100 chains was obtained by pouring the molten salt on a cold brass plate. The hexaamminecobalt(III) chloride was prepared according to the method described in the literature,[8] recrystallization from 60% alcohol and a 0.5 M hydrochloric acid solution was repeated two times. For the polarographic measurements, polyacrylamide was used as the maximum suppressor. All the other reagents used were guaranteed reagents. Triply-distilled water was used for test solutions throughout the experiments.

Results and Discussion

Precipitation. Hexaamminecobalt(III)-oligomer phosphate, including pyrophosphate, was precipitated either from a 0.1 M $NaClO_4$ solution of pH 5.95 or from a 0.1 M $NH_3\cdot NH_4Cl$ buffer solution of pH 9.98. The precipitate of hexaamminecobalt(III) pyrophosphate was not dissolved by increasing the pyrophosphate concentration. The precipitate of hexaamminecobalt(III) polyphosphate was formed within a C_p/C_{Co} mole ratio of about 10; the precipitate dissolved again in excess of polyphosphate. Polarograms of $Co(NH_3)_6^{3+}$ upon the addition of polyphosphate are shown in Fig. 1. The precipitate formation of hexaamminecobalt(III) polyphosphate results in a sharp decrease in the diffusion currents, as is shown in Fig. 2. Curves a and b in Fig. 2 correspond to the precipitations

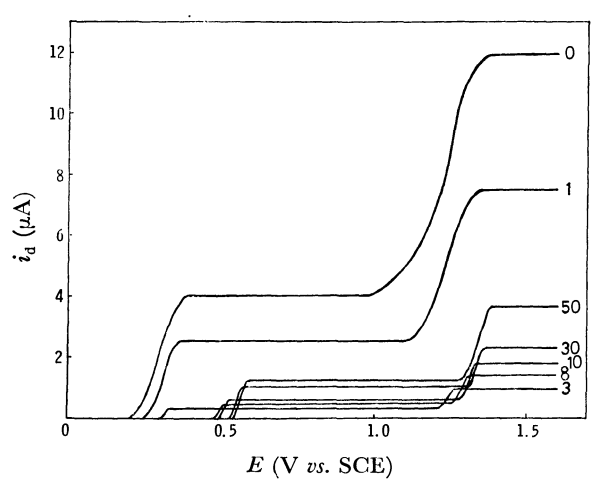

Fig. 1. Polarograms of $Co(NH_3)_6^{3+}$ with addition of polyphosphate. The numerical values show the C_p/C_{Co} mole ratio.

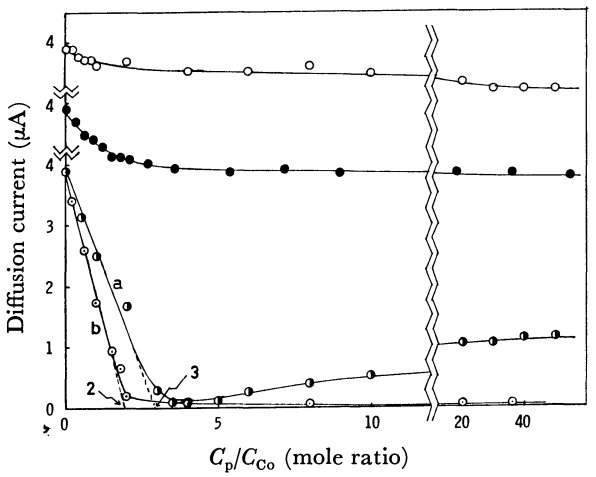

Fig. 2. Diffusion currents for reduction of 1×10^{-3} M $Co(NH_3)_6^{3+}$ ion (first wave) in 0.1 M $NaClO_4$ with 0.007% polyacrylamide.
(○) orthophosphate (◉) pyrophosphate
(●) triphosphate (◑) polyphosphate

of polyphosphate and pyrophosphate respectively. Curve a has a minimum at a C_p/C_{Co} mole ratio of about 3, which could be estimated by the extrapolation of the straight line a to the intercept on the abscissa. The diffusion current attains a constant value at a polyphosphate concentration of about 2×10^{-2} M, equal to a C_p/C_{Co} ratio of about 20. Curve b in Fig. 2 show an equivalent point, C_p/C_{Co}, equal to 2 on the abscissa, which agrees with the precipitation of hexaamminecobalt(III) pyrophosphate in a one-to-one mole ratio with respect to the concentrations of pyrophosphate and hexaamminecobalt(III). If one mole of $Co(NH_3)_6^{3+}$ and one mole of $P_2O_7^{4-}$ precipitate, then one mole of the univalent cation is required to neutralize the excess charge. From flame photometric analysis of the sodium content in the precipitate of hexaamminecobalt(III) pyrophosphate, the C_{Na}/C_{Co} mole ratio was found to be unity. From these finding, the composition of the hexaamminecobalt(III) pyrophosphate precipitate is shown to be $Na[Co(NH_3)_6]$-P_2O_7, in agreement with the formula proposed by Laitinen and McCune.[5,6] Curve a in Fig. 3 shows the decrease in the diffusion current for $Co(NH_3)_6^{3+}$ in presence of polyphosphate at various C_p/C_{Co} mole ratio. Curve b in Fig. 3 is the result of the unprecipitated phosphate concentration obtained by the molybdenum-blue method of colorimetric analysis for the phosphate after the polyphosphate form has been converted into the monomer form by acid hydrolysis.[9] Curves a and b in Fig. 3 show the equivalent point at C_p/C_{Co} mole ratio of 3 corresponding to the concentrations of 7.78×10^{-4} M and 2×10^{-4} M for $Co(NH_3)_6^{3+}$ and phosphate respectively. From these data, the apparent solubility product, K'_{sp}, can be calculated by:

$$K'_{sp} = (7.78\times10^{-4}) \times (2\times10^{-4})^3 = 6.22 \times 10^{-15}$$

for the precipitation reaction expressed by (1):

$$Co(NH_3)_6^{3+} + 3(PO_3^-) = Co(NH_3)_6(PO_3)_3 \quad (1)$$

The polyphosphate anion, $(PO_3^-)_n$, is a linear-chain oligomer with an average number of chains of about 100 and has a single negative charge per chain-like molecule, PO_3. A single PO_3^- unit produces an ionic bond with one-third of the trivalent hexaamminecobalt-(III) ion. The precipitation reaction (1) is a reasonable assumption when the PO_3^- unit in the polymer chain behaves like a monomer free ion.

Diffusion Current. The curves in Fig. 2 show that the diffusion currents due to the reduction of Co(III) to Co(II) for a fixed $Co(NH_3)_6^{3+}$ concentration of 1×10^{-3} M in a concentration range of a large C_p/C_{Co} ratio such as 20: 1 are 3.35, 2.85, and 1.05 μA for orthophosphate, triphosphate, and oligomer phosphate with an average number of chains of 100 respectively. It appears likely that the diffusion current depends on the polyphosphate species. In this respect, synthetic oligomer phosphates with numbers of chains of 6, 10, and 20 are employed for measuring the diffusion currents at the C_p/C_{Co} ratio of 50. The results are represented in Fig. 4 by plotting log i_d against log M

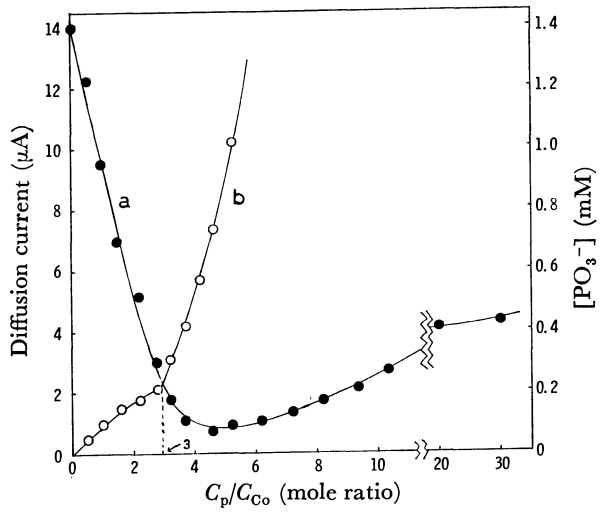

Fig. 3. Variation of diffusion current with $Co(NH_3)_6^{3+}$ concentration of 3.6×10^{-3} M (curve a) and phosphate ion concentration (curve b) with increasing C_p/C_{Co} mole ratio.

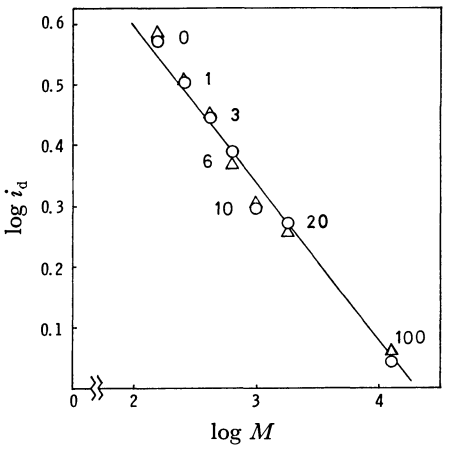

Fig. 4. The relationship between log i_d for the first wave and log M. The numerical values show the number of chains.
(○) 0.1 M NH_3—0.1 M NH_4Cl
(△) 0.1 M $NaClO_4$

Table 1. Variation of diffusion currents of hexaamminecobalt(III) with polyphosphate of different number of chains

Electrochemically active species[a]	Molecular weight, M	Current (μA) at $C_p/C_{Co}=50$			
		First wave $i_d(1)\cdot M^{1/4}$		Second wave $i_d(2)\cdot M^{1/4}$	
		NH_3[b]	$NaClO_4$[c]	NH_3[b]	$NaClO_4$[c]
Co(III) alone	161	13.46	13.96	25.95	27.06
Co(III)-monomer	257	12.95	12.97	25.38	25.94
Co(III)-trimer	416	12.55	12.73	23.21	23.71
Co(III)-polymer $n=6$	651	12.42	11.72	23.44	21.67
Co(III)-polymer $n=10$	967	11.17	11.49	21.30	22.14
Co(III)-polymer $n=20$	1757	12.04	12.04	24.41	23.43
Co(III)-polymer $n=100$	13034	11.75	12.06	29.06	26.82
Mean		12.33	12.50	24.69	24.39
Deviation: $\pm$(%)		5.74	6.34	9.24	8.38

a) Co(III): $Co(NH_3)_6^{3+}$, n: number of chains. b) 0.1 M NH_3—0.1 M NH_4Cl(pH: 9.98).
c) 0.1 M $NaClO_4$ (pH: 5.95).

in order to establish a quantitative relation between the diffusion current, i_d, and the molecular weight, M, of the $Co(NH_3)_6^{3+}$-oligomer phosphate. Since the influence of the viscosity was observed only when there were 100 chains, the corrected value of i_d was used for that. The straight line drawn for $\log i_d - \log M$ plots in Fig. 4 has a slope approximately equal to $-1/4$. This fact can be explained as follows. Since the diffusion current, i_d, is proportional to the square root of the diffusion coefficient, D, in the relation known as the Ilkovic equation, and since the diffusion coefficient, D, is inversely proportional to the square root of the molecular weight, M, of the diffusion species,[10] the diffusion current, i_d, is inversely proportional to 1/4 the power of the molecular weight, M, of $Co(NH_3)_6^{3+}$ polyphosphate. This is a reasonable assumption for associated ion-pairs with respect to $Co(NH_3)_6^{3+}$ polyphosphate when the decrease in the diffusion current is due to the diffusion coefficient. The constancy of $i_d \times M^{1/4}$ holds well for all the oligomer phosphates with different numbers of chains, as is shown in Table 1. It is worthwhile noting this application of the $i_d \times M^{1/4}$ rule that the molecular weight of an oligomer phosphate can be determined by measuring the diffusion current of the reduction containing an excess amount of the oligomer phosphate in question.

Half-wave Potential. The variation in the half-wave potentials with the increasing C_p/C_{Co} ratio is illustrated in Fig. 5 for the hexaamminecobalt(III)

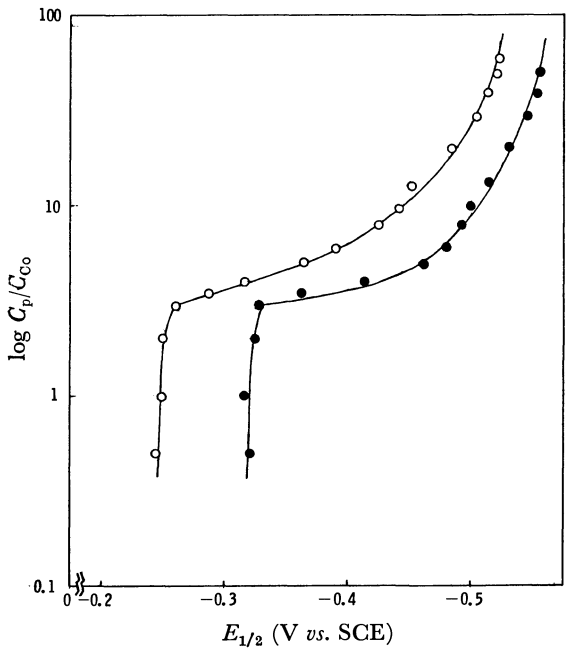

Fig. 5. Variation of half-wave potentials for polyphosphate with increasing the logarithmic function of C_p/C_{Co} ratio for the first wave.
(○) 0.1 M NH_3—0.1 M NH_4Cl
(●) 0.1 M $NaClO_4$

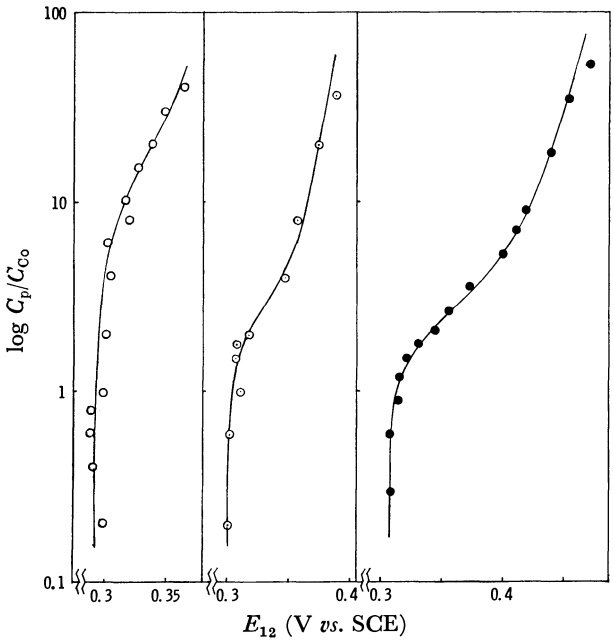

Fig. 6. Variation of half-wave potentials for orthophosphate, pyrophosphate and triphosphate with increasing the logarithmic function of C_p/C_{Co} ratio for the first wave in 0.1 M $NaClO_4$.
(○) orthophosphate (⊙) pyrophosphate
(●) triphosphate

Table 2. The half-wave potentials of the associated ion-pairs of hexaamminecobalt(III) in presence of excess phosphate at 25 °C.

First wave half-wave potentials $E_{1/2}$ in absence of phosphate are -0.251_7 V (*vs.* SCE) in 0.1 M NH_3—0.1 M NH_4Cl at pH 9.98 and -0.301_4 V (*vs.* SCE) in 0.1 M $NaClO_4$ at pH 5.95. $\Delta E_{1/2}$ is the difference in half-wave potentials between free $Co(NH_3)_6^{3+}$ and ion-pairs of $Co(NH_3)_6^{3+}$-phosphate.

Hexaamminecobalt(III) 10^{-3} M

Phosphate 5×10^{-2} M

Phosphate	$-E_{1/2}$		$-\Delta E_{1/2}$		α	
	NH_3[a]	$NaClO_4$[b]	NH_3[a]	$NaClO_4$[b]	NH_3[a]	$NaClO_4$[b]
Orthophosphate	0.344_9	0.354_3	0.093_2	0.052_9	0.48	0.66
Pyrophosphate	0.369_6	0.386_9	0.117_9	0.085_5	0.58	0.67
Triphosphate	0.418_5	0.474_5	0.166_8	0.173_1	0.54	0.80
Polyphosphate	0.522_3	0.556_2	0.270_7	0.254_8	0.97	0.85

a) 0.1 M NH_3—0.1 M NH_4Cl. b) 0.1 M $NaClO_4$.

polyphosphate system in two media with different pH values. The influence of the adsorption on the electrode surface of polyphosphate was checked by measuring the electrocapillary curve; this influence is rarely observed. The negative shifts of the half-wave potentials observed in the range of C_p/C_{Co} ratios from 3 to 6 are larger than the shifts observed at C_p/C_{Co} ratios beyond 6. This fact indicates that the soluble and stable ion-pairs were formed in the vicinity of C_p/C_{Co} ratios of about 6. The maximum value of the potential shift amounts to some hundred millivolts on the negative side at the C_p/C_{Co} ratio of 50. In Fig. 6 similar curves for the variation in half-wave potentials are illustrated for orthophosphate, pyrophosphate, and triphosphate respectively. The negative shifts of their potentials are not so large as compared with the shifts caused by the higher-oligomer phosphate. It can be seen that the larger the number of chains of phosphate, the more the negative shifts of the half-wave potentials. The final values of the half-wave potentials at the C_p/C_{Co} ratio of 50 are represented in Table 2, where all the electrochemically active species of hexaamminecobalt(III) are presented in the form of ion-pairs produced between $Co(NH_3)_6^{3+}$ and oligomer phosphate anions. The transfer coefficients, α, shown in the third column of Table 2 were obtained from the plots of $\log[i/(i_d-i)]$ against E at the C_p/C_{Co} ratio of 50.

References

1) B. E. Mironov, *Zh. Fiz. Khim.*, **44**, 416 (1970).
2) H. Yokoyama and H. Yamatera, This Bulletin, **44**, 1725 (1971).
3) M. G. Evans and G. H. Nancollas, *Trans. Faraday Soc.*, **49**, 363 (1935).
4) N. Tanaka, K. Ogino, and G. Sato, This Bulletin, **39**, 366 (1966); N. Tanaka, K. Kobayashi, and M. Kamada, *ibid.*, **40**, 2839 (1967).
5) H. A. Laitinen and L. W. Burdet, *Anal. Chem.*, **23**, 1265 (1951).
6) H. W. McCune and G. J. Argutte, *ibid.*, **27**, 401 (1955).
7) N. Matsuura, T. K. Lin, and Y. Kobayashi, This Bulletin, **43**, 2850 (1970).
8) J. Bjerrum and J. P. MacReynolds, "Inorganic Syntheses," Vol. 2, McGraw-Hill, New York (1964), p. 216.
9) N. Matsuura, M. Yoshimura, M. Takizawa, and Y. Sasaki, This Bulletin, **44**, 1027 (1971).
10) W. J. Moore, "Physical Chemistry," 3rd. edition, Maruzen (1966), pp. 216—228.

Synergism in the Liquid-Liquid Extraction and the Extraction Chromatography of Manganese(II), Cobalt(II), and Zinc(II) in the Thenoyltrifluoroacetone-Trioctylphosphine Oxide-Cyclohexane Extraction System

Takaharu Honjo, Masanobu Horiuchi, and Toshiyasu Kiba

Department of Chemistry, Faculty of Science, Kanazawa University, Marunouchi, Kanazawa 920

(Received October 15, 1973)

The synergism appearing in the liquid-liquid extraction and the extraction chromatography of trace amounts of manganese(II), cobalt(II), and zinc(II) has been investigated with TTA (thenoyltrifluoroacetone) in various solvents with or without TOPO (tri-*n*-octylphosphine oxide). For example, the $pH_{1/2}$ of the extraction of Co(TTA)$_2$ differed with the solvent used; it was, for example, 4.1 for nitrobenzene, 4.6 for cyclohexane, and 5.2 for benzene, when examined with 0.1 M TTA. When 0.01 M TOPO was present under the same conditions, the above values became 3.3, 2.4, and 3.1 respectively. The synergism was thus found to become more effective as a less polar solvent was used. The extraction constants of the three metals with only 0.1 M TTA–cyclohexane increases in the order of Mn(II)–Zn(II)–Co(II); however, when 0.001 or 0.01 M TOPO was present, all the extraction curves of the three metals became identical, even in the acidic region of pH 1—4. The overall stability constants of the adducts, M(TTA)$_2$–(TOPO)$_n$, increased in the order of Zn(II)–Co(II)–Mn(II), unlike the case of M(TTA)$_2$. The adducts were found to have two TOPO for Mn(II) and Co(II), but only one for Zn(II). The extraction equilibria were found to be attained within two minutes. Unlike as in the batch extraction, the column-extraction chromatography gave a dissimilar order of the extractability of three metals (Zn(II)–Mn(II)–Co(II)) when 0.1 M TTA–cyclohexane was the stationary phase on Kel-F in the presence of TOPO. The mutual separation could not be achieved among these metals in the presence of TOPO, and the synergism was found to be rather unfavorable for the separation of metals. The relation between the batch extraction and the extraction chromatography was also discussed briefly on the basis of the distribution data obtained.

The synergistic effect has been known to bring about a considerable enhancement of the extractability of metals in the liquid-liquid extraction of metal-β-diketonates in the presence of TOPO (tri-*n*-octylphosphine oxide); this effect can be attributed to the adduct formation between the metal chelates and TOPO.[1-5] Under the synergism, metal ions can usually be extracted quantitatively even in a lower pH region, but the distribution ratios of individual ions become so close to each other that the attempt of the mutual separation of metals by the batch extraction ends in failure. The extraction chromatography of inorganic compounds involving the metal chelates has recently been developed as a powerful separation technique,[6-8] in it the extraction and the back-extraction are repeated many times on so-called theoretical plates. A delicate separation can be expected through the use of this process. Taking advantage of this technique, Cvjetićanin studied the synergism appearing in the reversed-phase partition (extraction) chromatography of Am(III), Ce(III), and La(III) on paper treated with TTA and TOPO;[9] he found the adduct formation of M(TTA)$_3$(TOPO)$_2$, which appeared also in the liquid-liquid extraction of the same metal-chelate-solvent system. Aly and Raieh investigated the synergism in the extraction chromatography of the TTA-DBDECP-(Celite) system and clarified the factors affecting the column performance for separating Eu(III) from Sm(III) and Cm from Cf.[10] Since the same extraction process is generally used in both batch and column extractions, the extraction mechanism can be elucidated from both of the above techniques, as has been described by the present authors in connection with the system of Zn(II), Hg(II), and Co(II)–STTA–cyclohexane-(Kel-F),[11] and that of Ag(I), Bi(III), Cd(II), and Zn(II)–TOA–carbon tetrachloride(Kel-F).[12]

In the present paper we will describe the behavior of trace amounts of Mn(II), Co(II), and Zn(II) in the liquid-liquid extraction as well as in the extraction chromatography with TTA in the presence or the absence of TOPO, and will compare the results obtained by the two methods. The utility of the synergism in the extraction chromatography, the mutual separation of the metals, and the mechanism of the adduct formation will then be discussed further.

Experimental

Apparatus. Hitachi-Horiba M-3 and M-4 pH meters; a shaking machine, Type V-S, of the Iwaki Co.; a centrifuge machine of the Kubota Co.; a well-type scintillation counter of the Kobe Kogyo Co.; a 200-channel pulse-height analyzer, type EDS-34208A, of the same company; a chromatographic glass tube, 10×300 mm, with a fritted glass filter; a fraction collector, Toyo SF-200 A.

Materials. The radioisotopes, ^{54}Mn, ^{60}Co, and ^{65}Zn as chloride in a hydrochloric acid solution, were supplied by the New England Nuclear Corp. and the Radio Chemical Center, and were used as the tracers. The purity of each tracer was checked from its γ-spectra (^{60}Co: 1.17, 1.33; ^{65}Zn: 1.12; ^{54}Mn: 0.85 MeV) by the 200-channel pulse-height analyzer. TTA (thenoyltrifluoroacetone) and TOPO (tri-*n*-octylphosphine oxide), GR-grade reagents, were purchased from the Dojindo Co. Kel-F 300 moulding powder, the trade name of polytrifluorochloroethylene, was obtained from the Daikin Kogyo Co. The cyclohexane, benzene, and nitrobenzene were all purified by distillation. All the other reagents were of a GR grade and were employed without further purification.

Extraction and Back Extraction. The experimental procedure was the same as has previously been described.[2-5,11,12]

To a 10 ml portion of an aqueous solution containing a few ppm of metals, sodium acetate (0.1 M) (for the acidic region) or boric acid (0.1 M) (for the basic region) were added, after which the pH of the solution was adjusted to a desired value. A 10 or 30 ml portions of an organic solvent containing TTA (0.1 M) and varying amounts of TOPO were then added. Both phases were placed in a 50 ml glass-stoppered centrifuge tube and agitated by the shaking machine for from one to three hours at 20 °C. After centrifugation a 2 ml portion of each phase was pipetted out into a test tube, and the γ-activity of each portion was measured with the NaI(Tl) well-type scintillation counter. The distribution ratio of the metals was calculated from the counting rate of both phases. The pH of the aqueous phase was checked again after the extraction. The back extraction was carried out by shaking a 5 ml or 10 ml portions of the organic phase containing the extracted metal chelates with an aqueous solution of the desired acidity. Then a 1 or 3 ml portion was pipetted out of both phases into a test tube and the back distribution ratio was determined as in the case of the extraction.

Extraction Chromatography. All the aqueous solutions and organic solvents containing TTA should be pre-equilibrated before use. A 150 ml portion of 0.1 M sodium acetate solution which had been adjusted to pH 4.5 was shaken with a 20—30 ml portion of 0.1 M TTA–TOPO–cyclohexane for an hour. After discarding the organic solution, a 20 ml portion of the aqueous solution was taken out and was agitated with 30 ml of a new 0.1 M TTA–TOPO–cyclohexane solution for an hour. Then 20 ml of the organic solution was taken out, poured onto 5 g Kel-F powder (42—80 mesh), and allowed to stand for two hours. On the other hand, 200—250 ml of a 0.1 M sodium acetate solution, adjusted to the desired pH, was agitated with 30—40 ml of 0.1 M TTA–TOPO–cyclohexane for an hour to prepare the eluting solution. The procedure for preparing the column was the same as has previously been described.[11,12] A buffer solution of pH 4.5 was placed in the column tube, and 1—2 ml of the 0.1 M TTA–TOPO–cyclohexane was poured in. A slurry of TTA–TOPO–cyclohexane–Kel-F powder was then dropped into the tube in small portions. After every addition the slurry in the column tube was stirred with a sharp-pointed glass rod and gently pressed with the other, flat end of the same rod under a slow flow of the eluting solution. The stop-cock was then closed, and the column was filled again with the eluting solution. This operation was repeated about ten times until all the slurry made from 5 g Kel-F had been poured into the tube. Thereafter, a separating funnel was fitted at the top of the column tube; from it 100 ml of a buffer solution of pH 4.5 was passed through to wash down the excess unabsorbed organic solvent through the completely opened cock at the bottom of the tube.

The column bed thus prepared was 10×200 mm. The fraction collector was placed below the column tube and operated so as to collect each 10 ml portion of the eluate.

When the liquid surface came to the upper surface of the column bed, 1 ml of the sample solution was poured onto the bed. The sample solution containing a radioactive tracer had been buffered to pH 4.5. Then, 2—3 ml of the buffer solution was repeatedly poured onto the column and flowed through the column. By this treatment, all the metal ions could be completely retained on the column. A separating funnel containing a buffer solution with pH 4.5 was fitted on the column tube, and the column was washed with 100 ml of the solution. The eluting solution was then passed through from another separating funnel newly-fitted on the tube at the rate of 0.5 ml/min. From each 10 ml fraction of the eluate, a 3 ml portion was pipetted out in a test tube and the radioactivity was measured by means of the well-type scintillation.

Theoretical

Liquid-Liquid Extraction. The extraction constant of a metal chelate, K; the pH of the half extraction, $pH_{1/2}$, and the stability constant of the metal chelate adduct, β_n, can be calculated from the data obtained by the following equations:

$$D = (MR_2)_0/(M^{2+}) \quad (1)$$

$$K = (MR_2)_0(H^+)^2/(M^{2+})(HR)_0^2 \quad (2)$$

$$\log K = \log D - 2\log (HR)_0 - 2pH \quad (3)$$

$$pH_{1/2} = -\log K/2 - \log (HR)_0 \quad (4)$$

$$D^* = \{(MR_2)_0 + \sum_1^n (MR_2L_n)_0\}/(M^{2+}) \quad (5)$$

$$\beta_n = (MR_2L_n)_0/(MR_2)_0(L)_0^n \quad (6)$$

$$\log D^*/D = \log (1+\beta_n(L)_0^n) \quad (7)$$

where D and D^* are the distribution ratios in the absence and in the presence of the organic base, TOPO; M stands for metal, HR for β-diketone, and L for TOPO; the parentheses designate the concentration of the chemical species in the aqueous phase and in the organic phase with the suffix 0.

Extraction Chromatography. The distribution of metals can be derived from the data obtained by the column-extraction chromatography by employing the following equations:

$$D = (V_m - V^*)/V \quad (8)$$

$$D^* = (V_m^* - V^*)/V \quad (9)$$

$$\log D^*/D = \log (V_m^* - V^*)/(V_m - V^*) \quad (10)$$

where V_m and V_m^* are the volumes of the effluent necessary to reach the maximum concentration of the eluted metal ion in the absence and in the presence of TOPO; V^* is the volume of the mobile phase in the column, and V that of the stationary phase.

Results and Discussion

Liquid-Liquid Extraction in the TTA–TOPO–Solvent System. The liquid-liquid extraction was carried out for a trace amount of Co(II) with 0.1 M TTA in various solvents *i.e.* cyclohexane, benzene, and nitrobenzene, in the presence of 0.01 M TOPO as well as in the absence of the base. The results are shown in Fig. 1.

From the figure it can be seen that the $pH_{1/2}$ of cobalt extraction differs among the solvents, from 4.1 for nitrobenzene, and 4.6 for cyclohexane to 5.2 for benzene. All the straight lines with a slope of about 2 also show that the extractions proceed almost ideally, but a slight deviation from the integer suggests the formation of some water-soluble complexes in the extraction process.

On the other hand, when the same extraction was carried out in the presence of 0.01 M TOPO, the extractability of the metals is remarkably enhanced by the adduct formation and the $pH_{1/2}$ shifts lower with

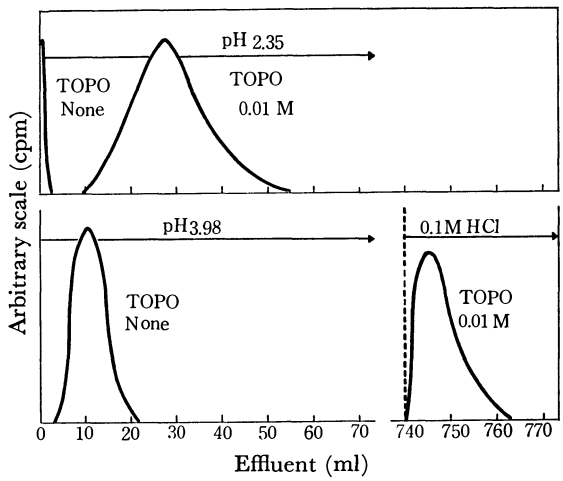

Fig. 4. Chromatograms of a trace amount of Co(II) on 0.1 M TTA–cyclohexane (Kel-F) column in the presence and in the absence of 0.01 M TOPO.

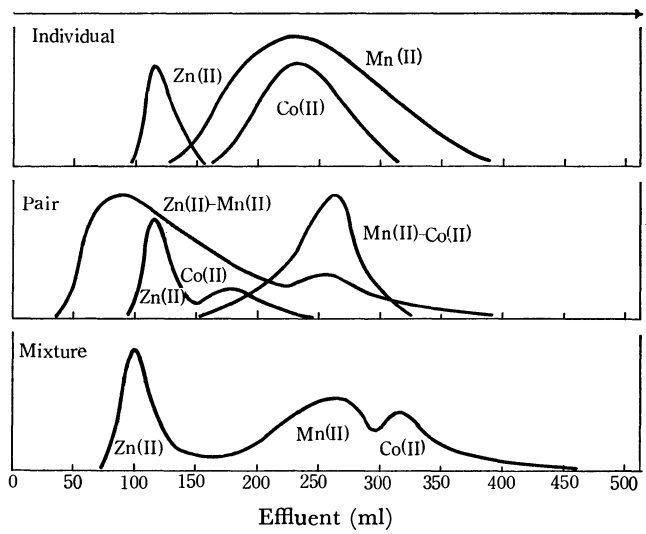

Fig. 5. Chromatograms of a trace amount of Mn(II), Co(II), and Zn(II) on 0.1 M TTA–cyclohexane (Kel-F) column in the presence of 0.01 M TOPO. pH=3.6.

on Kel-F was washed down by passing 20—30 ml of acetone through the column; the washings were received in a 200 ml measuring flask, 50—60 ml of distilled water was added, and the content was shaken by hand. After standing for a day, the separated cyclohexane solution was transferred into a graduated cylinder, and its volume was measured after every experiment. 5.8 ml was obtained as the mean value of the stationary-phase volume. The volume of the mobile phase on the column was determined as follows: one drop of 0.1 M hydrochloric acid containing a ^{60}Co tracer (20000 cpm/ml) was put on the top of the column bed and much water pre-equilibrated with a TTA–TOPO–cyclohexane solution was passed through the column at the flow rate of 0.5 ml/min; each 0.31 ml fraction of the effluent was taken in a test tube, and the γ-activity was counted; the elution curve was prepared for the counting rate against the effluent volume; the volume required to reach the maximum counting rate was estimated as the volume of the mobile phase (2.7 ml was obtained in this case). In order to investigate how to make the synergistic effect appear in extraction chromatography, the Co(II)–TTA–cyclohexane system was first tested with and without TOPO, since the synergistic effect had been known to depend on the concentration of the organic base.[1] The results are shown in Fig. 4 as the elution curves from the 0.1 M TTA–cyclohexane(Kel-F) column as well as from the 0.1 M TTA–0.01 M TOPO–cyclohexane(Kel-F) column, with eluting solutions of various pH's. When a sample solution of pH 4.5 was passed through the column, the Co(II) was retained completely on the column in both cases and was then eluted by eluting solutions. Without TOPO, Co(II) could be eluted instantly with the eluting solution of pH 2.35 into the first fraction of 2.3 ml; nevertheless, with the eluting solution of pH 4.0 it was eluted somewhat later, as its elution peak appeared around 10 ml of the effluent. On the other hand, with TOPO the elution feature changed remarkably, as the elution peak with the eluting solution of pH 2.35 appeared around 30 ml of the effluent, while with the eluting solution of pH 4.0 Co(II) did not appear in the effluent after as much as 740 ml of the eluting solution had been passed through the column.

Therefore, Co(II) had to be released from the column by passing 0.1 M hydrochloric acid through. The extraction chromatography was examined with a column of 0.1 M TTA–0.01 M TOPO–cyclohexane–(Kel-F) for Mn(II), Co(II), and Zn(II) individually, and also for mixtures of them. After the metals had been retained on the column by passing through sample solutions of pH 4.5, the metals were eluted with the eluting solution of pH 3.6. In Fig. 5, the chromatograms of the individual metal ions, of the mixtures of two ions, and of a mixture of three ions are illustrated. As some overlap of the elution curves can be seen for Mn(II) and Co(II), even in the case of the independent tests, the separation of each metal ion seems to be difficult except for that of Zn(II) from the mixture.

Table 2. Comparison of the distribution ratio, D^*, obtained by batch and chromatographic extraction

Ions		D*	
		Extraction chromatography	Batch extraction
	Mn	40.9 (98.9)	499 (99.8)
	Co	40.9 (98.9)	322 (99.7)
	Zn	15.9 (97.2)	81 (98.8)
Mn–Co	Mn	44.4 (99.0)	
	Co	44.4 (99.0)	
Mn–Zn	Mn	40.1 (98.9)	
	Zn	15.1 (97.0)	
Co–Zn	Co	29.7 (98.5)	
	Zn	19.4 (97.7)	
Mn–Co–Zn			
	Mn	45.2 (99.0)	
	Co	54.7 (99.2)	
	Zn	17.6 (97.4)	

The values in the blacket are the percent extraction, % E, of metals.

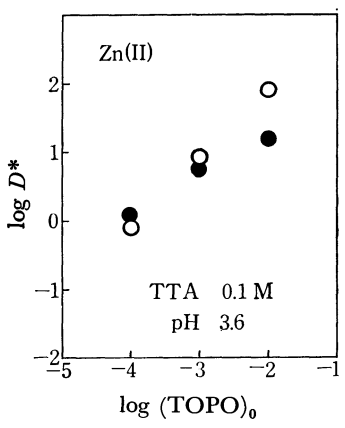

Fig. 6. Distribution ratio of a trace amount of Zn(II) with 0.1 M TTA in cyclohexane as a function of TOPO concentration obtained by batch and chromatographic extraction.
Batch extraction: —○—
Extraction chromatography: —●—

Moreover, it can also be seen that the elution peaks of the ions do not always coincide, especially when there is a wide gap between the individual ion-peak and that obtained in the mixture of two ions. The delayed appearance of the peaks of Mn(II) and Co(II) from the mixture of the three metals seems to be due to the competition of the chelate formation among metals or to some kinetic disposition of each chelate. In coclution, the synergistic effect is not favorable to the separation of metals.

Relation between Extraction Chromatography and the Liquid-Liquid Extraction. The distribution ratios of the three metals are summarized in Table 2 in the case of both the batch extraction and the extraction chromatography; some discrepancy can be noticed. The effect of the TOPO concentration on the Zn(II)–TTA–TOPO–cyclohexane system is shown in Fig. 6, in which the distribution is found to increase with the concentration of TOPO; the values are in quite good agreement with each other, whether they are determined by batch extraction or by extraction chromatography. If some discrepancy seems to exist between them, it might be caused by the difference in the process between the batch extraction and the chromatography; in the former the equilibrium could be reached after shaking the two phases, but in the chromatography the contact time of the two phases and the kinetic properties of the complex formation, as well as the rate of the release from the organic phase, back-extraction, might be an important factors in providing an elution curve.

References

1) T. Honjo and T. Shigematsu, *Kagaku* (Kyoto), **23**, 708 (1968).
2) T. Honjo, This Bulletin, **42**, 995 (1969).
3) T. Shigematsu and T. Honjo, *Bunseki Kagaku*, **18**, 68 (1969).
4) T. Shigematsu, T. Honjo, M. Tabuchi, and M. Matsui, This Bulletin, **43**, 793 (1970).
5) T. Shigematsu and T. Honjo, *ibid.*, **43**, 796 (1970).
6) E. Cerrai and G. Ghersini, "Advances in Chromatography," Vol. 9, Marcel Dekker Inc., New York (1970), p. 1.
7) T. Kiba and I. Akaza, *Kagaku* (Kyoto), **19**, 984 (1964).
8) T. Kiba, *Bunseki Kagaku*, **15**, 991 (1965).
9) N. Cvjetićanin, *J. Chromatogr.*, **34**, 520 (1968).
10) H. F. Aly and M. Raieh, *Anal. Chim. Acta*, **54**, 171 (1971).
11) T. Honjo and T. Kiba, This Bulletin, **46**, 1694 (1973).
12) T. Honjo, S. Ushijima, and T. Kiba, *ibid.*, **46**, 3764 (1973).
13) H. M. N. H. Irving and D. N. Edgington, *J. Inorg. Nucl. Chem.*, **27**, 1359 (1965).

Classification of Polarographic Current-Potential Curves of Inorganic Anions as a Function of Reduction Potentials

Yoshio UMEZAWA, Michio HIROTA, and Shizuo FUJIWARA

Department of Chemistry, Faculty of Science, The University of Tokyo, Hongo, Bunkyo-ku, Tokyo 113

(Received November 12, 1973)

DC polarographic behaviors of a variety of inorganic anions are examined systematically. Irrespective of chemical species, the shapes of current-potential curves are classified into three groups as a function of reduction potentials: i) $E_{1/2}>0$ V(SCE); The so-called minima cannot be observed beyond the ecm potentials. ii) 0 V$>E_{1/2}>$ecm; The minima can be observed. iii) $E_{1/2}<$ecm; The distortion at the rising portion of the DC polarograms can always be observed. These results suggest that whether the minima can be observed or not is due to the difference in the relative position of half-wave potentials with respect to the ecm potential. Furthermore, it is likely that the distortion at the rising portion of the DC polarogram of Group iii) is similar in origin to that of the minima of Group ii). The present results are discussed in terms of the electron density and electronic energy level of electrons in the metal electrode. The discussion based on the phenomenological equation of Butler was also given for the sake of comparison to explain the observed phenomena.

The electrochemical method is one of the most important techniques for the study of electron transfer reactions in solution. The characteristic features of the electrode reaction are i) electronic energy level of one of the reactants, *i.e.*, the electrode, is varied artificially by means of applied potentials—"quantum mechanical effect",[1,2] and ii) due to the large charge density of the double layer, electrostatic interaction between the electrode and the charged depolarizer may be much larger than that of the other types of redox reactions—"electrostatic effect".[3]

The purpose of this paper is to demonstrate experimentally the contribution of the above two effects separately in polarography. Polarographic behaviors of a variety of inorganic anions are examined systematically. It is shown that the pattern of the DC polarogram of inorganic anions is classified into three types as a function of reduction potentials. The results are discussed in terms of the quantum mechanical and electrostatic effects as mentioned above. The results of the present study will be useful to clarify the structure of the double layer and to understand the mechanism of the electrode reaction.

Experimental

DC polarograms were taken with a Yanagimoto Model P-8 Polarograph. A Yanagimoto Model MRP was used as the reference electrode (SCE). Capillaries with drop times of 3—4 s in 1 M KCl solution at a mercury height of 70 cm (open circuit) were used. Sample solutions in the cell were deaerated by bubbling purified nitrogen gas before and throughout the measurements. Gelatin was added to the sample solutions as maximum suppressor. All chemicals used were of analytical reagent grade and metal complexes used were prepared according to the usual methods. Half-wave potentials were evaluated directly from the polarograms.

Results

It is found that the shapes of DC polarograms of a variety of anion depolarizers are roughly divided into three groups A, B, C, in the decreasing order of reduction potentials. The results are cited schematically in Fig. 1. Typical DC polarograms which belong to these groups are shown in Figs. 2 and 3. For the systems of Group A, the half-wave potentials, $E_{1/2}$, are relatively more positive than those of Group B. For the system of Group C, $E_{1/2}$ is situated more negative than the electrocapillary maximum (ecm) potential.

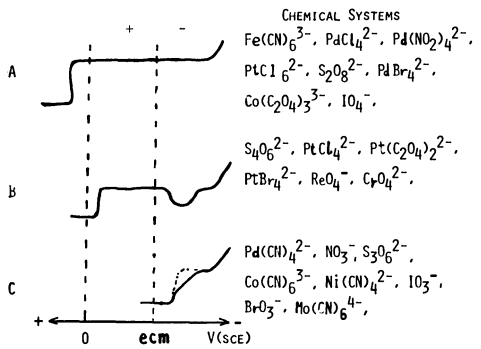

Fig. 1. Typical DC polarographic pattern of inorganic anions as a function of reduction potentials, $E_{1/2}$.
A: $E_{1/2}>0$, B: $0>E_{1/2}>$ecm potential, C: $E_{1/2}<$ecm potential, Supporting electrolyte: 0.1—1 M alkali halide (KCl), Without surface-active substances.

Dependence on Chemical Systems. As shown in Fig. 1, the chemical systems are classified into two types

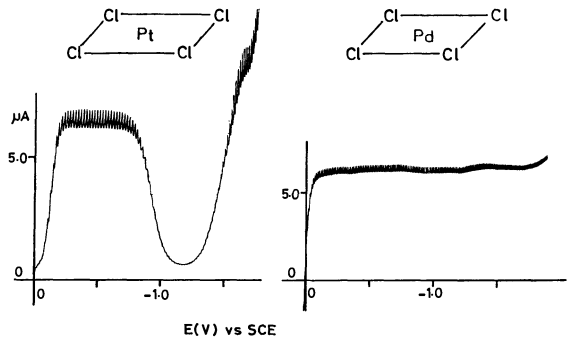

Fig. 2. Typical examples of DC polarograms which belong to Group A and B in Fig. 1.
Right: 1 mM $PdCl_4^{2-}$, 1.0 M KCl, 0.01% gelatin (Group A).
Left: 1 mM $PtCl_4^{2-}$, 1.0 M KCl, 0.01% gelatin (Group B).

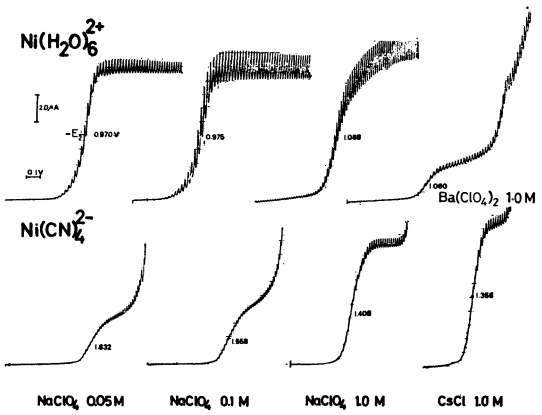

Fig. 3. Typical examples of DC polarograms which belong to Group C in Fig. 1.
Systems: 1 mM $Ni(CN)_4^{2-}$ with different kinds of supporting electrolytes, where polarograms of $Ni(H_2O)_6^{2+}$ with the same kinds of supporting electrolytes are also cited for comparison.

according to whether they do (B) or do not show (A) the decrease in the limiting diffusion current (the minimum) beyond the ecm. This classification is non-specific for the type of chemical species such as metal complexes, metal oxides, and oxo acids of halogens, but is only attributed to the difference of the relative position of the half-wave potentials between the two groups.

Effect of Supporting Electrolyte. For the systems of Group A, the decrease in the limiting diffusion current beyond the ecm (the minimum) can be observed in the absence of supporting electrolyte, but it is completely eliminated by suitable amount of supporting electrolyte. The minimum of Group B does not disappear on addition of supporting electrolyte; it merely decreases and becomes narrower in the order of $Cs^+ > Rb^+ > K^+ > Na^+ > Li^+$ and $CN^- > I^- > Cl^- > ClO_4^-$, for the cation and the anion of the supporting electrolyte, respectively. In the case of Group C, the rising portion of the DC polarogram is distorted, which is recovered by added salts in the similar way as the minimum of Group B (Fig. 3).

Effect of Surface-active Substances. The effect of surface-active substances on the shapes of the current-potential curves are also examined systematically. For Group A upon adding suitable amount of gelatin, the decrease in the limiting diffusion current beyond the ecm can be observed even in the presence of supporting electrolyte. This is shown in Fig. 4 taking $Pd(NO_2)_4^{2-}$ ion as an example. Similarly, the minimum of Group B and the distortion of the polarogram of Group C are much pronounced by the addition of gelatin. These situations are represented schematically in Fig. 5.

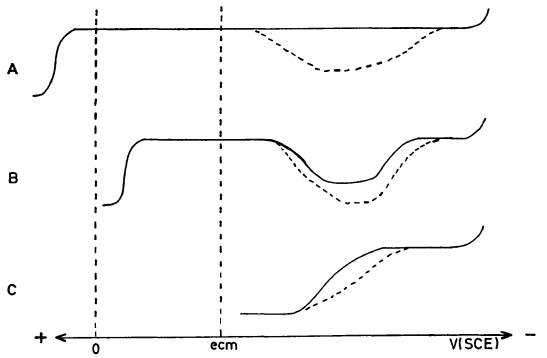

Fig. 5. Effect of surface-active substances on the shapes of $i-E$ curves of Groups A—C in Fig. 1.
Solid line: without surface-active substances
Dotted line: 0.01% surface-active substances(gelatin) added

Discussion

Electrostatic Effect. It has been well-accepted[3,4] that the electrostatic repulsion of anion depolarizers from negatively charged electrode is the dominant origin of the minimum phenomena. However, quite different behavior between Groups A and B in Fig. 1 cannot be elucidated solely by the simple electrostatic model.[4] The distortion of the DC polarogram of Group C (see Figs. 1 and 3) is generally referred to as the irreversible wave.[3] Results of Fig. 1 imply that the irreversible wave of Group C is similar in origin to that of the minimum of Group B.

At a negative potential E_n beyond the ecm, all the anions are more or less subject to electrostatic repulsion from the negatively charged electrode surface, which

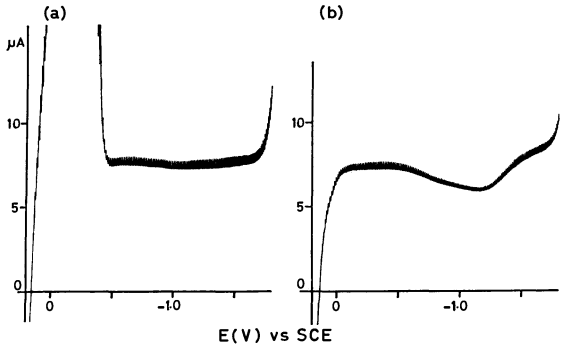

Fig. 4. Effect of surface-active substances on the i—E curve of Group A in Fig. 1.
System: 1 mM $Pd(NO_2)_4^{2-}$ in 0.1 M KNO_2
(a) without gelatin (b) 0.01% gelatin added

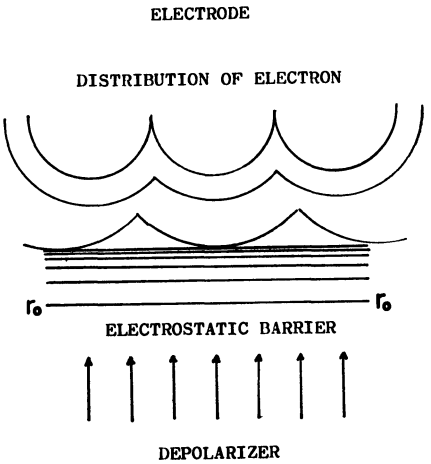

Fig. 6. Distribution of electron cloud of the metal electrode at the interface (See Text)

is non-specific for Group A, B, or C. Because the electron in the metal electrode is represented by a wave function, it will not vanish at the surface of the metal, but will die away exponentially into the remote from the electrode.[1] In Fig. 6 is drawn the distribution of the electron density of the metal electrode at the interface, where r_0 denotes the mean distance of the nearest approach of an anion against the coulombic field at the potential E_n. In the presence of the electrostatic repulsion, the anion cannot go within r_0 resulting in the small probability of electron transfer at r_0 in comparison with that at the surface of the metal. This is probably the important origin of the minimum for the systems of Groups A and B, and the distortion at the rising portion of the polarogram for the systems of Group C.

Electronic Level of the Electrode. The highest occupied electronic energy level of the metal electrode can be represented as:[1,5]

$$\phi = E_F + V \quad (1)$$

where E_F is the Fermi level of the metal electrode in contact with the electrolyte solution at open circuit, V the applied potential *vs.* the SCE. Because the current density at the dropping mercury cathode is small in polarography, the potential of the anode is made constant by the SCE. Equation (1) indicates that the effect of an electrode potential of 1 V is to raise the highest occupied level at the cathode, ϕ, by 1 eV. This situation is shown in Fig. 7. It is also seen in Fig. 7 that the number of electrons (electron density)

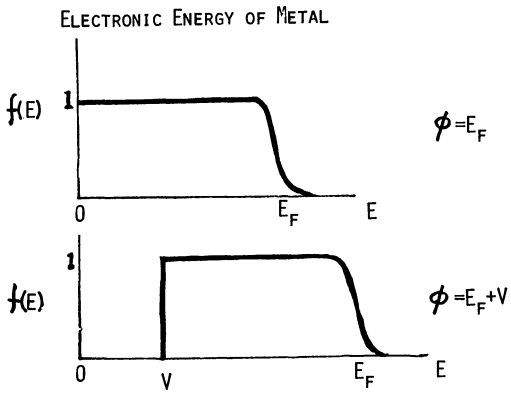

Fig. 7. Electronic energy level of the metal cathode as a function of applied potential, V.
ϕ: Highest occupied level of the metal cathode in contact with the electrolyte solution
E_F: Fermi level of the electrode in contact with the electrolyte solution
$f(E)$: Fermi distribution function

in the metal cathode whose energy is higher than any given value is increased with increasing applied negative potentials. Among a great number of electrons in the metal cathode, only the electrons that have any energy higher than the half-wave potential of depolarizers can participate in the electrochemical reduction process. As shown in Fig. 1, the half-wave potential of the system of Group B, $(E_{1/2})_b$, is always more negative than that of Group A, $(E_{1/2})_a$,

$$(E_{1/2})_a > (E_{1/2})_b > E_n \quad (2)$$

where E_n is a negative potential beyond the ecm, where the minima appear. From the above considerations, it may be concluded that in the metal cathode at the potential E_n, numbers of electrons which can participate in the electrochemical reduction for Group A is greater than that for Group B. Therefore, it appears that the different behavior of the minimum between Groups A and B is due to the difference in the numbers of electrons as mentioned above, resulting from the difference in the half-wave potential between two Groups.

In the case of the minimum of Group B, the increase of the current at rather negative potentials can be observed (Figs. 1 and 2). Furthermore, in the case of Group C, the distortion of the polarogram at the rising portion is recovered with increasing applied negative potentials until the limiting diffusion current is attained (Figs. 1 and 3). These two phenomena can also be explained in terms of the increase with increasing applied negative potentials in the numbers of electrons which can participate in the electrochemical reduction.

The effect of gelatin in Figs. 4 and 5 can be explained as being due to the enhancement by gelatin of repulsion of anions from the electrode surface (see Fig. 6).

Phenomenological Equation. According to the phenomenological equation of the irreversible electrode reaction, the current much smaller than the limiting diffusion current can be written as:[3]

$$i = nFqk_e^0[Me^{n+}]_s \exp\left\{-\frac{\alpha nF(E-E^0)-W}{RT}\right\} \quad (3)$$

$$[Me^{n+}]_s = [Me^{n+}] \exp(-zFW/RT) \quad (4)$$

where n, F, q, and R are as usual, k_e^0 the heterogeneous rate constant at the standard potential E^0, α the transfer coefficient, W the mean electrostatic potential at the distance of an ionic radius from the surface of the electrode, $[Me^{n+}]_s$ the surface concentration of depolarizers. In the above equations, it is assumed that the electrode process involves only ions in direct contact with the electrode and that electron transfer to more distant ion is hardly likely.[3] The increment of applied negative potentials beyond the ecm influences upon the observed current intensity through different two terms in Eq. (3), *i.e.*, i) $[Me^{n+}]_s$ and ii) the exponential term. Of these two, $[Me^{n+}]_s$ decreases in a similar way both in Groups A and B, which is due to the electrostatic repulsion of anions from the negatively charged electrode surface. As shown in Fig. 1 the half-wave potential of Groups A is always more positive than that of Group B. Therefore, it appears that in the case of Group A appreciable increase beyond the ecm potential in the exponential term of Eq. (3) prevents the appearance of the minima. This conclusion is to be compared with the discussion given in the previous section (*Electronic Level of the Electrode*).

References

1) R. W. Gurney, *Proc. Roy. Soc., Ser. A*, **134**, 137 (1931).
2) J. O.M. Bockris, *J. Chem. Educ.*, **48**, 352 (1971).
3) J. Heyrovsky and J. Kuta, "Principles of Polarography," Academic Press, New York and London (1966).
4) A. N. Frumkin, *Trans. Faraday Soc.*, **55**, 156 (1959).
5) R. M. Rose, L. A. Shepard, and J. Wulff, "Electronic Properties," John Wiley & Sons, Inc., New York (1966).

Stereochemical Studies of *N*-Methyl-(*S*)-alaninatocobalt(III) Complexes with Chiral Tetramines. II.[1] Cobalt(III)-*N*-Methyl-(*S*)- and (*R*)-alaninate-*N*,*N*′-Bis(β-aminoethyl)-1(*R*), 2(*R*)-diaminocyclohexane Systems

Masahiko SABURI and Sadao YOSHIKAWA

Department of Synthetic Chemistry, Faculty of Engineering, The University of Tokyo, Hongo, Bunkyo-ku, Tokyo 113

(Received January 9, 1974)

The preparation and structural assignments of *N*-methyl-(*S*)- and -(*R*)-alaninatocobalt(III) complexes with *N*,*N*′-bis(β-aminoethyl)-1(*R*),2(*R*)-diaminocyclohexane (abbreviated as (*R*)-baetchxn) are described. The *Λ*-β_2-(*SSR*) isomer has been obtained for Co(*N*-Me-(*S*)-ala)((*R*)-baetchxn)$^{2+}$ ion. The two isomers, which have been found for the Co(*N*-Me-(*R*)-ala)((*R*)-baetchxn)$^{2+}$ ion under equilibrium condition at pH 7, are assigned as the *Λ*-β_2(*SSR*) and *Λ*-β_2(*SSS*) configurations, taking into account the stereospecific coordination of the (*R*)-baetchxn. The stereoisomerism of *Δ*-β_2-Co(*N*-Me-(*S*)-ala)(trien)$^{2+}$ ion is also discussed. The structures of two species observed in the PMR measurements of Co(*N*-Me-(*R*)-ala)((*R*)-baetchxn)$^{2+}$ ion and assigned to *Λ*-β_2(*SSR*) and *Λ*-β_2-(*SSS*) configurations, respectively, are determined, based on the chemical shifts of α-methine protons of *N*-methyl-alaninate moieties.

The presence of three diastereoisomers has been proved for the β_2-Co(*N*-Me-(*S*)-ala)(trien)$^{2+}$ ion (*N*-Me-(*S*)-ala=*N*-methyl-(*S*)-alaninate ion). These isomers were assigned to the *Λ*-β_2(*SSR*) *Δ*-β_2(*RRS*), and *Δ*-β_2-(*RSS*) configurations by Buckingham and coworkers.[2,3] In a previous report, we examined the adequacy of these assignments by the use of 5(*S*)-methyl-1,4,7,10-tetraazadecane (abbreviated as 5(*S*)-metrien) in place of trien. The 5(*S*)-metrien, one of chiral trien derivatives, coordinates stereospecifically with the *Δ-cis-β*(*RR*) configuration.

The two diastereoisomers of the *Δ*-β_2-Co(*N*-Me-(*S*)-ala)(5(*S*)-metrien)$^{2+}$ ion detected by the proton magnetic resonance (PMR) measurements were assigned to the *Δ*-β_2(*RRS*) and *Δ*-β_2(*RRR*) configurations. Further, the remarkable similarities observed between the PMR and circular dichroism (CD) behaviors of the *Δ*-β_2-Co(*N*-Me-(*S*)-ala)(trien)$^{2+}$ and *Δ*-β_2-Co(*N*-Me(*S*)-ala)(5-(*S*)-metrien)$^{2+}$ isomers in equilibria in neutral aqueous solution (pH 6.5—7.0) led to the conclusion that one of the *Δ*-β_2 isomers of the trien complex has the (*RRR*) configuration, instead of the (*RSS*) configuration.[1] This conclusion interpreted consistently the difference of stabilities between the *Δ*-β_2(*RRS*) and *Δ*-β_2-(*RSS*) configurations of Co(*N*-Me-(*S*)-ala)(trien)$^{2+}$ ion expected from a strain energy minimization study (the former is 3.2 kcal/mol in favor of the latter).[2]

However, it is difficult to neglect completely the possibility of the inversion at the "planar" secondary N atom for the 5(*S*)-metrien complexes. *N*,*N*′-Bis(β-aminoethyl)-1(*R*),2(*R*)-diaminocyclohexane (abbreviated as (*R*)-baetchxn) is one of chiral trien derivatives, which has been demonstrated to adopt stereospecifically the *Λ-cis-β*(*SS*) configuration upon coordination. Further, it is significant that for the coordinated (*R*)-baetchxn there is no possibility of conformational inversion with respect to the central diamine linkage, since the 1(*R*),2(*R*)-diaminocyclohexane moiety takes solely the λ conformation due to its cyclic structure. The conformational inversion at the central diamine linkage is necessary for the isomerization from the *Λ-β*(*SS*) to *Λ-β*(*SR*) configuration. In order to confirm the conclusions on the *Δ*-β_2-Co(*N*-Me-(*S*)-ala)(5(*S*)-metrien)$^{2+}$ complexes, *N*-Me-(*S*)- and *N*-Me-(*R*)-ala (*N*-Me-(*R*)-ala=*N*-methyl-(*R*)-alaninate ion) complexes with (*R*)-baetchxn have been examined, the results of which will be reported in this paper.

Experimental

N-Methyl-(*S*)-alanine and *N*-Methyl-(*R*)-alanine were prepared by the method of Quitt, Hellerbach, and Vogler,[5] using (*S*)- and (*R*)-alanine, respectively, as the starting amino acids. Commercially available 1,2-diaminocyclohexane (Tokyo Kasei Kogyo) was resolved with *d*-tartaric acid, according to the method of Asperger and Liu.[6] *N*,*N*′-Bis(β-aminoethyl)-1(*R*),2(*R*)-diaminocyclohexane was prepared as follows.

N,N′-*Bis(chloroacetyl)-1*(R),*2*(R)-*diaminocyclohexane.* 1(*R*),2(*R*)-diaminocyclohexane dihydrochloride (14.0) was dissolved in 150 ml of water, containing 18 g of sodium hydroxide. Tothis solution cooled in an ice bath to 10°C was added a solution of chloroacetyl chloride (22.6 g) in benzene (80 ml) drop by drop with vigorous stirring by means of a blender. After the addition had been completed, the stirring was continued for 10 more min. The resultant white solid mass was filtered off, and washed with water. Yield, 28 g. The crude product was recrystallized from methanol by adding ether. Found: C, 44.71; H, 5.98; N, 11.11%. Calcd for $C_{10}H_{16}N_2O_2Cl_2$: C, 44.29; H, 5.95; N, 10.33%.

N,N′-*Bis(glycyl)-1*(R),*2*(R)-*diaminocyclohexane Dihydrochloride.* *N*,*N*′-Bis(chloroacetyl)-1(*R*),2(*R*)-diaminocyclohexane (14.0 g) dissolved in 200 ml of hot methanol was mixed with 300 ml of aqueous ammonia (28%) and ammonium carbonate (50 g). The mixture was left to stand at room temperature for 7 days, and the resultant solution was evaporated to dryness on a rotary evaporator under reduced pressure. The white precipitates, which remained, were collected, washed with ethanol and ether, and dried under vaccuum. Yield, 12.0 g. The crude product was recrystallized from methanol–ethanol mixture (1:2). Found: C, 39.83; H, 7.24; N, 18.73%. Calcd for $C_{10}H_{22}N_4O_2Cl_2$: C, 39.35; H, 7.27; N, 18.36%.

N,N′-*Bis(β-aminoethyl)-1*(R),*2*(R)-*diaminocyclohexane Tetrahydrochloride.* To a suspension of lithium aluminium

hydride (10.8 g) in anhydrous tetrahydrofuran (250 ml) was added *N,N'*-bis(glycyl)-1(*R*),2(*R*)-diaminocyclohexane dihydrochloride (14.0 g) in small portions. The mixture was then stirred and heated under reflux for 24 hr, and cooled to room temperature. The subsequent treatments were the same as those described in a previous paper.[4]

Δ-cis-*β*-*Dichloro(*N,N'-*bis(β-aminoethyl)-1*(R),*2*(R)-*diaminocyclohexane)cobalt(III) Chloride Hemihydrate* (*Δ*-cis-*β*-[$CoCl_2$(R)-*baetchxn*)]$Cl \cdot 0.5H_2O$) was also prepared according to the method reported previously.[4]

Δ-β_2(SSR)-[*Co*(N-*Me*-(S)-*ala*)(R)-*baetchxn*)]$(ClO_4)_2$. *Δ*-*cis*-*β*-[$CoCl_2$((*R*)-baetchxn)]$Cl \cdot 0.5H_2O$ (1.15 g) was dissolved in 5 ml of water, followed by 0.126 g of $LiOH \cdot H_2O$. To the solution were added 0.31 g of *N*-methyl-(*S*)-alanine and 0.5 g of active charcoal, successively. The solution was then warmed to 70 °C on a water bath for 30 min. The active charcoal was filtered off and washed with a small volume of water. The filtrate and washings were combined and concentrated to a volume of 2 ml on a water bath below 70 °C. Then, 1.5 g of solid $LiClO_4$ were added, and cooled in an ice bath for 2 hr. The orange-red crystals, which separated, were collected, washed with cold water and ethanol, and air-dried. Yield, 1.30 g. The product was recrystallized from hot water. Found: C, 27.83; H, 5.80; N, 12.77%. Calcd for $[Co(C_{10}H_{24}N_4)(C_4H_8NO_2)](ClO_4)_2$: C, 27.42; H, 5.98; N, 12.97%.

Δ-β_2-[*Co*(N-*Me*-(R)-*ala*)((R)-*baetchxn*)]I_2, *A Mixture of Δ*-β_2(SSR) *and Δ*-β_2(SSS) *Isomeres.* *Δ*-*cis*-*β*-[$CoCl_2$((*R*)-baetchxn)]$Cl \cdot 0.5H_2O$ (0.57 g) was dissolved in 5 ml of water, followed by 0.063 g of $LiOH \cdot H_2O$. The solution was warmed to 70 °C on a water bath, and 0.155 g of *N*-methyl-(*R*)-alanine and 0.2 g of active charcoal were added, successively. The resultant solution was warmed to 70°C for 15 min. The active charcoal was then filtered off, and washed with a small volume of water. The filtrate and washings were combined and concentrated to a volume of 3 ml on a water bath below 60 °C. To the solution were added 0.7 g of NaI dissolved in a minimum volume of water, and cooled in an ice bath overnight. The red crystals, which separated, were collected, washed with dilute NaI solution and ethanol, and air-dried. Yield, 0.52 g. Found: C, 27.85; H, 5.38; N, 10.83%. Calcd for $[Co(C_{10}H_{24}N_4)(C_4H_8NO_2)]I_2$: C, 27.33; H, 5.24; N, 11.39%.

Δ-β_2(SSR)-[*Co*(N-*Me*-(R)-*ala*)((R)-*baetchxn*)]$(ZnCl_4)$. The filtrate obtained after the removal of active charcoal as described above was concentrated to a volume of 7 ml on a water bath below 60 °C. The solution was, then, diluted with 20 ml of ethanol, and 1.5 g of NaI dissolved in a minimum volume of water was added. The solution was cooled in an ice bath overnight, and the orange-rad crystals, which appeared, were filtered off, washed with ethanol, and air-dried. Yield, 1.27 g. This compound, which contains the ethanol of crystallization, was added in 10 ml of 0.1 M HCl, containing an excess amounts of freshly prepared AgCl. All the contents were mixed thoroughly until the complexes dissolved completely. Silver salts were filtered off, and washed well with water. The filtrate and washings were combined, and zinc chloride (1.4 g) was added, followed by 1 ml of concentrated HCl. The resultant solution was cooled in a refrigerator overnight, and the orange crystals, which appeared, were collected, washed with cold water and ethanol, and air-dried. Yield, 0.65 g. A further crop of crystals was obtained from the filtrate after the concentration. Found: C, 28.72; H, 5.58; N, 12.05%. Calcd for $[Co(C_4H_8NO_2)(C_{10}H_{24}N_4)](ZnCl_4)$: C, 29.57; H, 5.67: N, 12.32%.

Measurements. Visible absorption spectra were measured with a Shimadzu MPS-50L recording spectrophotometer. Circular dichroism curves were obtained with a JASCO J-20 automatic recording spectropolarimeter. 100-MHz proton magnetic resonance spectra were obtained using a JEOL PS-100 spectrometer using sodium 2,2-dimethyl-2-silapentane-5-sulfonate (DSS) as an internal standard reference. For the PMR measurements, perchlorate salt (about 50 mg sample) suspended in the solvent (0.01 M DCl or D_2O, 0.5—0.7 ml) was treated with twice the molar amounts of tetraphenylarsonium chloride. The white precipitates were removed by filtration, and the filtrate was employed for PMR measurement. Iodide salts (about 60 mg samples) suspended in the solvent (0.5—0.7 ml) were treated with twice the molar amounts of silver nitrate. The precipitated AgI were removed by filtration, and the PMR spectra of the filtrates were recorded.

60 MHz PMR spectra were obtained with a Hitachi R-20B spectrometer.

Results and Discussion

The 100 MHz PMR spectra of the Co(*N*-Me-(*S*)-ala)((*R*)-baetchxn)$^{2+}$ ion, obtained in 0.01N DCl and D_2O solutions, are shown in Fig. 1(a) and (b), respectively. In 0.01 M DCl, the deuterium exchange of *N*-bonded protons is retarded sufficiently so that the *N*-methyl proton signal is observed as the doublet at 2.58 ppm (standard, DSS). In D_2O solution, the *N*-bonded protons have exchanged with solvent D_2O, and the *N*-methyl signal has collapsed to a singlet. In both spectra ((a) and (b)), the C-methyl signals were observed as the single doublet at 1.50 ppm. It is apparent from these observations that the Co(*N*-Me-(*S*)-ala)((*R*)-baetchxn)$^{2+}$ ion is composed of the single species. Further, the PMR spectrum obtained in 0.01N DCl (Fig. 1(a)) corresponds well to that of the *Δ*-β_2(*SSR*)-Co(*N*-Me-(*S*)-ala)(trien)$^{2+}$ ion reported earlier,[2] except that complicated broad peaks are found in 1.0—2.0 and 2.0—2.5 ppm regions for the (*R*)-baetchxn complex. These broad peaks should be ascribed to the signals for protons of the cyclohexane ring of (*R*)-baetchxn.

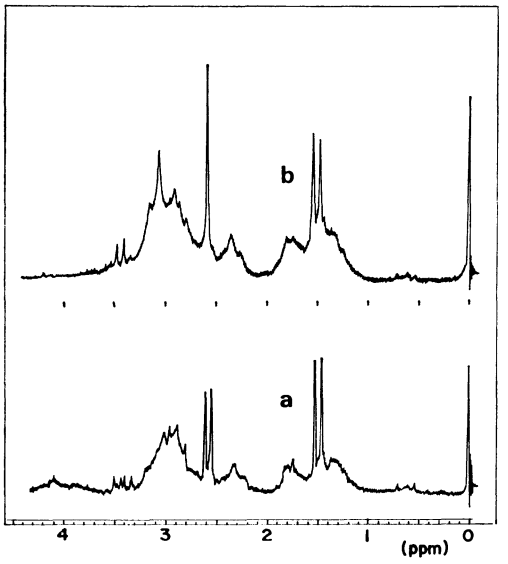

Fig. 1. 100 MHz PMR spectra of *Δ*-β_2-(*SSR*)-[Co(*N*-Me-(*S*)-ala)((*R*)-baetchxn)]$^{2+}$ ion; (a) in 0.01 M DCl, and (b) in D_2O.

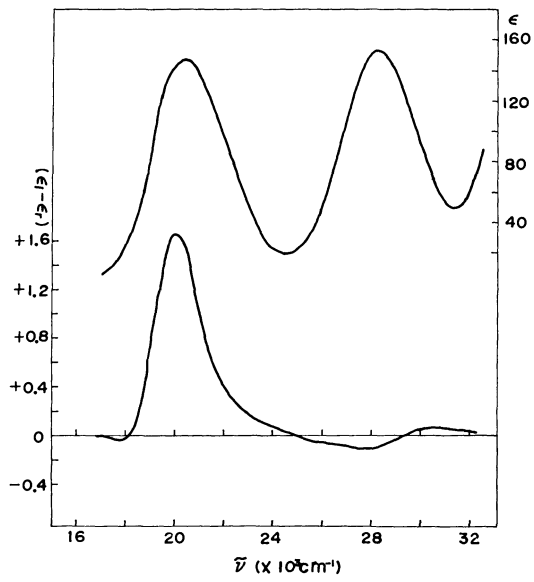

Fig. 2. Visible absorption and CD spectra of Λ-β_2-(*SSR*)-[Co(*N*-Me-(*S*)-ala) ((*R*)-baetchxn)]$^{2+}$ ion.

The Co(*N*-Me-(*S*)-ala)((R)-baetchxn)$^{2+}$ ion shows the visible absorption and CD spectra shown in Fig. 2. These curves resembles closely to the corresponding curves of the Λ-β_2(*SSR*) isomers of Co(*N*-Me-(*S*)-ala)-(trien)$^{2+}$ and Co(*N*-Me-(*S*)-ala)(5(*R*)-metrien)$^{2+}$ ions. Therefore, the present (*R*)-baetchxn complex can be assigned to the Λ-β_2(*SSR*)(*S*)[3] configuration.

It was found previously that the Δ-β_2-Co(*N*-Me-(*S*)-ala)(5(*S*)-metrien)$^{2+}$ complex arised in the single species as the iodide, whereas the same complex ion gave rise to a mixture of two isomeric forms as the perchlorate.[1] Similarly, the Δ-β_2-Co(*N*-Me-(*S*)-ala)(trien)$^{2+}$ ion could be isolated in the pure state as the iodide form.[2] On these bases, we tried to obtain the Co(*N*-Me-(*R*)-ala)((*R*)-baetchxn)$^{2+}$ ion, which should appear in the Λ-β_2 configuration and in the enantiomeric relation to the above Λ-β_2 isomers with *N*-Me-(*S*)-ala group, as the iodide form.

However, [Co(*N*-Me-(*R*)-ala)((*R*)-baetchxn)]I_2 isolated from an aqueous solution, was found to be an isomeric mixture of two species, though the complex ions had the Λ absolute configuration as expected. The PMR spectra of this complex obtained in 0.01 M DCl and D_2O solutions are shown in Fig. 3(a) and (b), respectively. The spectrum in 0.01 M DCl shows two *N*-methyl doublets at 2.40 and 2.57 ppm, indicating the presence of two isomers in the crystalline state. The *C*-methyl signals, which appeared as three peaks in the vicinity of 1.5 ppm, can be regarded as an overlap of two doublets.

It was found unexpectedly that one of the isomers of Λ-β_2-Co(*N*-Me-(*R*)-ala)((*R*)-baetchxn)$^{2+}$ ion crystallized out from an aqueous ethanol in the single isomeric form. The PMR spectrum of this orange-red needle-like crystals measured in 0.01 M DCl is shown in Fig. 3(c). This spectrum exhibits only one doublet for the *N*-methyl signal (2.40 ppm). The *C*-methyl signal is also observed as the single double (1.43 ppm). These findings indicate that the present complex is largely composed of the single species. Furthermore, the presence of ethanol in the crystal is obviously demonstrated by the triplet and quartet centered at 1.14 and 3.60 ppm, respectively. However, the elemental analysis data for this complex could not provide any sufficient results. Hence, we turned this compound to the tetrachlorozincate salt, which gave the consistent analysis data.

The PMR spectrum of the above complex obtained in 0.01 M DCl (Fig. 3(d)) was found to be identical with that shown in Fig. 3(c), except for the signals of ethanol appeared additionally in the latter case. The spectrum of this complex obtained in D_2O was also identical with that of Fig. 3(b). The PMR spectral changes caused by the variation of the pH of solvent

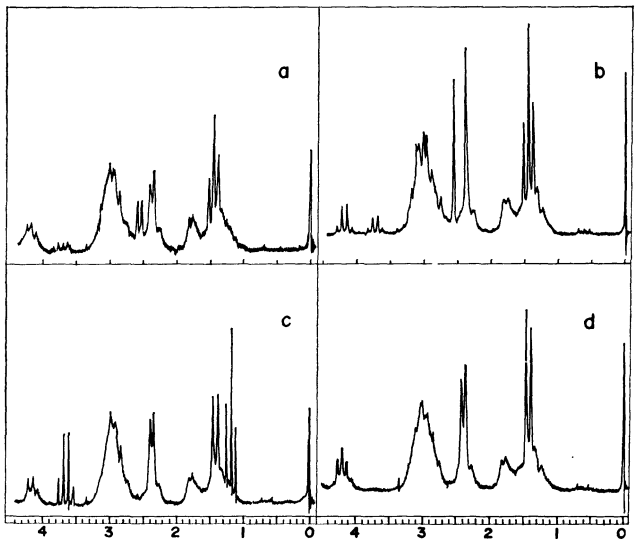

Fig. 3. 100 MHz PMR spectra of Λ-β_2-[Co(*N*-Me-(*R*)-ala) ((*R*) baetchxn)]$^{2+}$ ion; (a) Λ-β_2-(*SSR*)+Λ-β_2-(*SSS*) in 0.01 M DCl, (b) Λ-β_2-(*SSR*)+Λ-β_2-(*SSS*) in D_2O (pD=6.8), (c) Λ-β_2-(*SSR*) containing ethanol in 0.01M DCl, (d) Λ-β_2-(*SSR*), ($ZnCl_4$) salt in 0.01 M DCl.

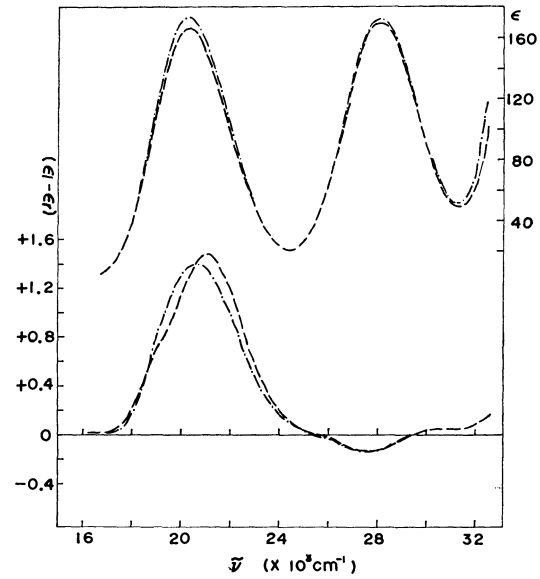

Fig. 4. Visible absorption and CD spectra of Λ-β_2-[Co-(*N*-Me-(*R*)-ala)-((*R*)-baetchxn)] ($ZnCl_4$) in 0.1 M $HClO_4$ (----), and in H_2O (pH 7) (-·-·).

are analogous to those observed for the Δ-β_2-[Co(*N*-Me-(*S*)-ala)(trien)]I_2[2] and for the Δ-β_2-[Co(*N*-Me-(*S*)-ala)(5(*S*)-metrien)]I_2. Corresponding to these PMR changes, the visible absorption and CD spectral changes were noticed for the trien and 5(*S*)-metrien complexes in acidic and neutral aqueous solutions. The CD and visible absorption curves of Λ-β_2-[Co(*N*-Me-(*R*)-ala)-((*R*)-baetchxn)]($ZnCl_4$) also changed in a similar way through the variation of the solvents, as shown in Fig. 4.

Buckingham and coworkers have supposed that the isomerization of the isolated Δ-β_2-Co(*N*-Me-(*S*)-ala)-(trien)$^{2+}$ ion at pH 6.5—7.0 may be caused by the inversion at an asymmetric secondary N center, and that two possibilities exist for scuh isomerization; inversion at the *N*-methyl group or at the "planar" secondary N center of β-trien skeleton. The latter possibility has been adopted by Buckingham *et al.*, and the equilibrium between the Δ-β_2-(*RRS*)(*S*) and Δ-β_2-(*RSS*)(*S*) configurations has been postulated.[2]

In the case of (*R*)-baetchxn complex with Λ-β configuration, the possibility of the conformational inversion of the central chelate ring can be thoroughly excluded, since the conformation of the 1(*R*),2(*R*)-diaminocyclohexane chelate ring is solely restricted in the *λ-gauche* form. Hence, the possibility of the inversion at the "planar" secondary N center which must accompany the conformational inversion of the central chelate ring can also be ruled out for the (*R*)-baetchxn complex. Therefore, the two isomers observed for the Λ-β_2-Co(*N*-Me(*R*)-ala)((*R*)-baetchxn)$^{2+}$ ion should be arisen from a source of asymmetry other than the "planar" secondary N center of trien moiety. The inversion at the *N*-methyl group can be regarded as the relevant origin of the isomerization mentioned above. Consequently, the two species detected in the PMR spectrum (Fig. 3(b)) should be assigned to the Λ-β_2(*SSR*)(*R*) and Λ-β_2(*SSS*)(*R*) configurations.

The complex ions, Λ-β_2-Co(*N*-Me-(*R*)-ala)((*R*)-baetchxn)$^{2+}$ and Δ-β_2-Co(*N*-Me-(*S*)-ala)(trien)$^{2+}$, are in the enantiomeric relation with regard to every chiral center: the absolute configuration around the Co(III) ion, those of the secondary N centers of trien skeleton and of *N*-methyl groups, and those of the asymmetric α-C atom of *N*-methylalanine moiety. Therefore, the stereoisomerism noticed for the restricted Λ-β(*SS*) framework of (*R*)-baetchxn complexes must be applicable to the Δ-β_2-Co(*N*-Me-(*S*)-ala)(trien)$^{2+}$ ion, even though the possibility of the inversion at the "planar" secondary N center would be retained for the trien complex.

The PMR spectrum of Λ-β_2-Co(*N*-Me-(*R*)-ala)((*R*)-baetchxn)$^{2+}$ ion (Fig. 3(b)) indicates that the relative intensities of *N*-methyl signals of the Λ-β_2(*SSR*)(*R*) fand Λ-β_2(*SSS*)(*R*) isomers are approximately equal. This means that these isomers have the comparable stabilities with each other. The Δ-β_2(*RRS*) and Δ-β_2(*RRR*) isomers of Co(*N*-Me-(*S*)-ala)(trien)$^{2+}$ ion must also have the nearly equal stabilities, even if the other isomer, Δ-β_2(*RSS*) form, would be sufficiently stable in comparison with the Δ-β_2(*RRS*) form, as expected by Buckingham *et al.*[2] In practice, however, only two species have been detected in the PMR spectrum of the Δ-β_2-Co(*N*-Me-(*S*)-ala)(trien)$^{2+}$ ion equilibrated at pH 7.[2] Further, the PMR spectral features of these isomers are entirely analogous to those of the Λ-β_2-Co(*N*-Me-(*R*)-ala)((*R*)-baetchxn)$^{2+}$ ion, especially in the regions of the *N*-methyl and *C*-methyl signals. Accordingly, the two detectable species of Δ-β_2-Co(*N*-Me-(*S*)-ala)(trien)$^{2+}$ ion should be assigned as the (*RRS*) and (*RRR*) isomers, instead of the (*RSS*) isomer. This conclusion is in accordance with that obtained in a previous paper, using the 5(*S*)-metrien.[1]

It has been considered to be difficult to make individual structural assignments for the two isomers of Δ-β_2-Co(*N*-Me-(*S*)-ala)(trien)$^{2+}$ ion.[2] We have tentatively assigned these isomers to the Δ-β_2(*RRS*) and Δ-β_2-(*RRR*) configurations, respectively, on the ground of the chemical shifts of *N*-methyl groups of the two isomers. To make sure these assignments, we have examined the PMR spectra of Λ-β_2-Co(*N*-Me-(*R*)-ala)-((*R*)-baetchxn)$^{2+}$ isomers, and obtained interesting findings.

In the spectrum of Fig. 3(b), two small quartets are observed at 3.73 and 4.19 ppm. These signals can be assigned to the methine protons of *N*-Me-(*R*)-ala moieties of the Λ-β_2(*SSR*) and Λ-β_2(*SSS*) isomers, respectively. For the corresponding *N*-Me-(*S*)-ala complex ion, the methine quartet is detected at 3.44 ppm in the spectrum of Fig. 1(b), though the same signal can not be recognized in Fig. 1(a) due probably to the overlap of N–H resonance. Similarly, it is rather difficult to find definitely the methine quartet in the spectrum of Fig. 3(a) because of the appearance of broad N–H peaks in the region of 4.0—4.5 ppm.

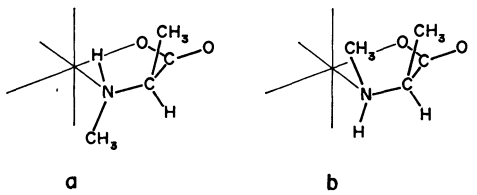

Fig. 5. Structures of coordinated *N*-Me-(*R*)-ala moiety; (a) *trans* and (b) *cis*.

The relative orientations of the *N*-methyl and C-methyl groups should be the most significant structural factor which affects the chemical shift of the methine proton of *N*-methylalaninate group. As illustrated for the *N*-Me-(*R*)-ala chelate rings in Fig. 5, the two adjacent methyl groups are *trans* (Fig. 5(a)) or *cis* (Fig. 5(b)) to each other. In the *trans* form, the *N*-methyl is *cis* with respect to the methine proton, and, therefore, the methine should be strongly affected by the magnetic anisotropy of the C–N bond of the *N*-methyl group. It is anticipated that the C–N bond anisotropy will appear in a similar manner as that for the C–C single bond, and that the methine proton in the *trans* form (Fig. 5(a)) will show the high-field shift compared to the methine in the *cis* form (Fig. 5(b)), because the C–N bond anisotropy should no longer have any significant effects to the methine proton in the latter case.

The *N*- and *C*-methyl groups are in the *trans* con-

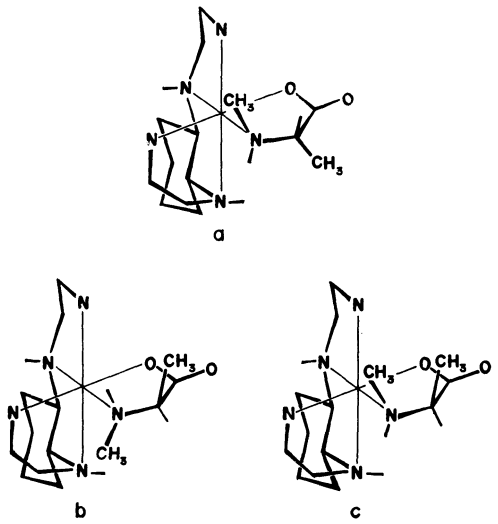

Fig. 6. Structures of (*R*)-baetchxn complexes: (a) *Λ*-β_2-(*SSR*)(*S*), (b) *Λ*-β_2-(*SSS*)(*R*), and (c) *Λ*-β_2-(*SSR*)(*R*).

figuration for the *Λ*-β_2(*SSR*)(*S*) and *Λ*-β_2(*SSS*)(*R*) isomers, while these are *cis* in the *Λ*-β_2(*SSR*)(*R*) isomer of the (*R*)-baetchxn complexs, as shown in Fig. 6(a)—(c). The methine resonance of *Λ*-β_2(*SSR*)(*S*) isomer, with the *trans* configuration, is found at 3.44 ppm as described previously. Taking account of the C–N bond anisotropy, the quartets observed at 3.73 and 4.19 ppm in Fig. 3(b) should be assigned to the *trans* and the *cis* configuration, or to the *Λ*-β_2(*SSS*)(*R*) and the *Λ*-β_2-(*SSR*)(*R*) configuration, respectively.

It was found that the *Λ*-Co((*S*)-ala)$(en)_2^{2+}$ and -Co-((*R*)-ala)$(en)_2^{2+}$ ions ((*S*)-ala and (*R*)-ala=(*S*)- and (*R*)-alaninate) show their methine quartets at about 3.98 and 4.15 ppm, respectively.[7,8] Both these complexes are free from the C–N bond anisotropy under consideration. It is interesting to note that the chemical shifts of methine protons of the (*R*)-ala complex coincide well with that of the *Λ*-β_2(*SSR*)-Co(*N*-Me-(*R*)-ala)((*R*)-baetchxn)$^{2+}$ ion (4.19 ppm), in which there are no influences of the C–N anisotropy. The difference of the chemical shifts (0.17 ppm) between the above (*S*)- and (*R*)-alanine complexes should be ascribed to the difference of the absolute configuration of the α-C atom of alaniate group. The methine signal of the *Λ*-β_2-(*SSS*)(*R*) isomer, having the *trans* configuration with respect to the *N*- and C-methyl groups, appeared in the higher field relative to that of the *Λ*-β_2(*SSR*)(*R*) isomer with the *cis* configuration, but in the lower field than that of the *Λ*-β_2(*SSR*)(*S*) isomer with the *trans* configuration. The difference in the chemical shifts of the methine signals between the (*SSR*)(*S*) and (*SSS*)(*R*) isomers (0.29 ppm), both of which take the *trans* configuration with regard to the *C*- and *N*-methyl groups, seem to be analogous to that found in the above alanine complexes.[7,8]

The determination of the *C*-methyl groups of *Λ*-β_2-(*SSR*) and *Λ*-β_2(*SSS*) isomers of Co(*N*-Me-(*R*)-ala)((*R*)-baetchxn)$^{2+}$ ion has been achieved by the spin-decoupling method. Since a 60 MHz spectrometer has been employed for these measurements, the two *C*-methyl signals have appeared separately as two doublets

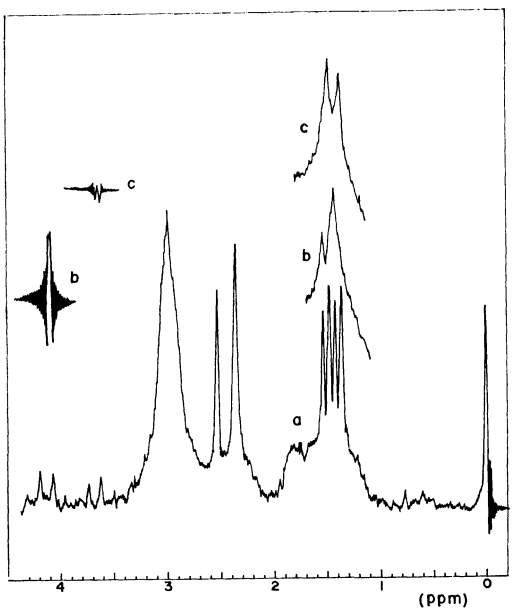

Fig. 7. 60 MHz PMR spectra of mixture of *Λ*-β_2-(*SSR*)- and *Λ*-β_2-(*SSS*)-[Co(*N*-Me-(*R*)-ala)((*R*)-baetchxn)]$^{2+}$ ion; (a) in D_2O, (b) the spectrum irradiated at 4.19 ppm, (c) the spectrum irradiated at 3.73 ppm.

as shown in Fig. 7. The irradiation of the quartet at 4.19 ppm has caused the collapse of the doublet in the higher field (1.43 ppm) to the singlet, and the irradiation of the quartet at 3.73 ppm has produced the collapse of the doublet at 1.51 ppm to the singlet, as indicated in Fig. 7. From these results, the isolated isomer of the *Λ*-β_2-Co(*N*-Me-(*R*)-ala)((*R*)-baetchxn)$^{2+}$ ion which shows the *C*-methyl doublet at 1.43 ppm (Fig. 3(d)) can be decided as the (*SSR*)(*R*) configuration. The PMR spectral data of the (*R*)-baetchxn and related complexes are summarized in Table 1.

Table 1. Assignments of proton resonance shifts[a] of *N*-methylalanine moieties

	C–CH_3	N–CH_3	C–H
Λ-β_2(*SSR*)-Co(*N*-Me-(*S*)-ala)-((*R*)-baetchxn)$^{2+}$	1.50	2.58	3.44
Λ-β_2(*SSR*)-Co(*N*-Me-(*R*)-ala)-((*R*)-baetchxn)$^{2+}$	1.43	2.40	4.19
Λ-β_2(*SSS*)-Co(*N*-Me-(*R*)-ala)-((*R*)-baetchxn)$^{2+}$	1.51	2.57	3.73
Λ-β_2(*SSR*)-Co(*N*-Me-(*S*)-ala)-(5(*R*)-metrien)$^{2+}$	1.53	2.61	3.52[b]
Λ-β_2(*RRS*)-Co(*N*-Me-(*S*)-ala)-(5-(*S*)-metrien)$^{2+}$	1.42	2.38	4.06
Λ-β_2(*RRR*)-Co(*N*-Me-(*S*)-ala)-(5(*S*)-metrien)$^{2+}$	1.50	2.58	3.80[b]
Co(*N*-Me-(*S*)-laa)$(NH_3)_4^{2+}$	1.48	2.48	3.54
Λ-Co(*N*-Me-(*S*)-ala)$(en)_2^{2+}$	1.49	2.53	3.55

a) ppm from DSS. b) Determined by the spin decoupling method, using a 60 MHz spectrometer.

No attention has been turned to the methine signals of the *N*-methylalanine group in former studies.[1,2] This may be due to the fact that the complicated methylene (and methine) proton signals of trien,[2] 5(*R*)- or 5(*S*)-metrien,[1] which appear in the region of 3.3—

3.8 ppm, obscure the methine quartets in question. However, one of the methine quartets is clearly noticed at 4.06 ppm in the PMR spectrum of the Δ-β_2-Co(*N*-Me-(*S*)-ala)(5(*S*)-metrien)$^{2+}$ isomers in D_2O.[1] The corresponding quartet can be acknowledged in the PMR spectrum of the Δ-β_2-Co(*N*-Me-(*S*)-ala)(trien)$^{2+}$ isomers reported by Buckingham *et al.*[2] We have sought the hidden methine signals of 5(*R*)- and 5(*S*)-metrien complexes by the decoupling method. The most appropriate position of the irradiation which produces the collapse of the *C*-methyl doublet to a singlet has been determined as the center of the methine signal. The data are given in Table 1. The assignments of the two isomers of Δ-β_2-Co(*N*-Me-(*S*)-ala)-(5(*S*)-metrien)$^{2+}$ ion is consistent with those made from the chemical shifts of the *N*-methyl group in a previous paper.[1] The same arguments should be applicable to the Co(*N*-Me-(*S*)-ala)(trien)$^{2+}$ system, though the adequecy has not been examined in this study.

References

1) Part I. M. Saburi, M. Homma, and S. Yoshikawa, *Inorg. Chem.*, **12**, 1250 (1973).

2) D. A. Buckingham, I. E. Maxwell, and A. M. Sargeson, *ibid.*, **9**, 2663 (1970).

3) Nomenclature: The *RS* representations of the asymmetric N atoms of trien and its derivatives and of *N*-methylalanine and the asymmetric α-C atoms of amino acids follow that by Buckingham *et al. cf.* Ref. (2). The use of β,β_1 and β_2 follows that used by L. G. Marzilli, and D. A. Buckingham, *Inorg. Chem.*, **6**, 1042 (1967). The absolute configuration about the cobalt(III) center is indicated by the prefix Λ or Δ: *Inorg. Chem.*, **9**, 1 (1970).

4) M. Goto, M. Saburi, and S. Yoshikawa, *Inorg. Chem.*, **8**, 358 (1969).

5) P. Quitt, J. Hellerbach, and K. Vogler, *Helv. Chim. Acta*, **46**, 327 (1963).

6) R. G. Asperger and C. F. Liu, *Inorg. Chem.*, **4**, 1492 (1965).

7) D. A. Buckingham, L. Durham, and A. M. Sargeson, *Aust. J. Chem.*, **20**, 257 (1967).

8) D. A. Buckingham, L. G. Marzilli, and A. M. Sargeson, *J. Amer. Chem. Soc.*, **89**, 5133 (1967).

Studies on Amino-hexoses. XVIII. A Simplified Method of Preparing 2-Amino-3-*O*-(D-1′-carboxyethyl)-2-deoxy-D-glucose 6-(Dihydrogen Phosphate) (Muramic Acid 6-Phosphate)

Sumihiro HASE and Yoshio MATSUSHIMA

The Department of Chemistry, Osaka University College of Science, Toyonaka 560

(Received July 23, 1973)

Muramic acid 6-phosphate was prepared from benzyl 2-acetamido-2-deoxy-3-*O*-[D-1′(methoxycarbonyl)-ethyl]-α-D-glucopyranoside *via* two reaction stages: diphenylphosphorylation under restricted conditions, followed by hydrolysis. When the reaction mixture was chromatographed on a Dowex 1×8 (formate form) column, the product was obtained as fine needles. Among the periodate oxidation products of the compound, glycolaldehyde phosphate was detected, while formaldehyde was not. Equimolar amounts of muramic acid and inorganic phosphate were produced by an alkaline phosphatase. The physical data are consistent with those of authentic muramic acid 6-phosphate.

The first synthetic muramic acid 6-phosphate was reported by Konami, Osawa, and Jeanloz[1] to be identical with the muramic acid phosphate obtained from bacterial cell walls, thus establishing the structure of the natural compound. We tried more or less to simplify the preparation of the compound and the estimation of a phosphate group at the 6 position of muramic acid. The route of the reactions is shown in Scheme 1. We simplified the synthesis of muramic acid 6-phosphate in a better yield (25%) to two reaction stages; selective phosphorylation and acid hydrolysis, whereas the previously reported method used 6 reaction stages. The physical constants of the synthesized compound (mp, $[\alpha]_D$, infrared spectrum, and R_{GlcNAc}) are consistent with those reported.[1] It has been reported that[2] a primary hydroxyl could be phosphorylated preferentially with a limiting amount of the reagent. For example, D-glucosamine 6-phosphate[3] was synthesized by selective diphenylphosphorylation under restricted conditions. In addition, the introduction of the bulky diphenylphosphate group at the C-4 hydroxyl of the muramic acid derivative seemed to be interfered by the lactyl group on C-3. The resulting compound was hydrolyzed with strong acid to remove the blocking groups. It seemed that phosphate migration did not occur, because a phosphate group on C-6 was more stable than that on C-4, as it was reported that D-glucosamine 4-phosphate was converted to D-glucosamine 6-phosphate during acid hydrolysis.[4] The hydrolysate of the diphenylphosphate of the muramic acid derivative showed, besides muramic acid and its 6-phosphate (main product), two minor spots on tlc. The main peak was isolated by Dowex 1×4 (formate form) column chromatography. The physical data were identical with those of the authentic compound, so the phosphate group might be at C-6. In the course of the reactions, hydrolysis by strong acid was used; therfore, the possibility of the migration of the phosphate group could not be excluded. The position of the phosphate group at muramic acid was thus estimated in the following way. Periodate oxidation study was performed by the previously reported method.[5] The periodate oxidation products of muramic acid 6-phosphate or muramicitol 6-phosphate gave a peak of glycolaldehyde phosphate which was positive for organic phosphate and diphenylamine reactions (Fig. 1). This fact indicates the 6-phosphate of muramic acid. The absorbtion spectrum of the fraction developed by diphenylamine was the same as that obtained from the reference compounds (Fig. 2). Formaldehyde was not detected in the periodate oxidation products; this is further evidence of the presence of the phosphate group at C-6 (Table 3). The infrared spectrum of the muramic acid-6-phosphate synthesized agreed well with the reported data.

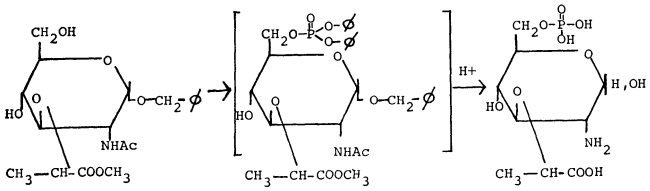

Scheme 1.

Experimental

Abbreviations used: Glc, glucose; Mur, muramic acid; Mur 6-P, muramic acid 6-(dihydrogen phosphate); GlcN, glucosamine; GlcNAc, N-acetyl-glucosamine.

The diphenylphosphorochloridate was purchased from Merck Co. and was used without purification. The muramic acid was synthesized by the reported method.[6] The glucosamine 6-phosphate sodium salt and α-DL-glycerophosphate disodium salt were commercial specimens from the Sigma Chem. Co. Avicel SF (microcrystalline cellulose) was purchased from the Funacoshi, Co. Ltd., and the Kiesel Gel F_{254} from the Merck Co. The calf mucosa alkaline phosphatase (grade II, 10 mg/ml) [EC 3.1.3.1] was purchased from Boehringer Mannheim.

2-Amino-3-O-(D-1′-carboxyethyl)-2-deoxy-D-glucose 6-(Dihydrogen Phosphate). Benzyl 2-acetamido-2-deoxy-3-*O*-[D-1′-(methoxycarbonyl)ethyl]-α-D-glucopyranoside[7] (1.0 g) was dissolved in 30 ml of pyridine, after which the solution was cooled in a dry ice-acetone bath. To this solution was added 0.65 ml of diphenylphosphorochloridate. After the reaction mixture had been maintained at −20 °C for 16 hr, 1.0 ml of water was added to this solution. The solution was then allowed to stand for 30 min and was concentrated. The residue was dissolved in chloroform. The solution was washed with water, concentrated, and placed on a silicic acid column. The conditions were as follows: a column (2.5×20 cm; 52 g

silicic acid activated overnight at 150 °C) was eluted with ethyl acetate: toluene (5:2 v/v) and 8 ml fractions were collected. The main peak appeared at the 14—21 fractions. The main fraction was concentrated to give a colorless sirup which gave a single spot on a thin-layer chromatogram (Merck Kiesel Gel F_{254}, ethyl acetate: toluene=5:2 v/v, R_f=0.37).

To the sirup we then added 20 ml of 3 M hydrochloric acid, and the solution was heated for 6 hr at 100 °C.[1] The water-soluble fraction of the hydrolysate was concentrated and placed on a Dowex 1×4 column (100—200 mesh, formate form), which was then eluted with 0.5 M formic acid.[8] Ten-ml fractions were collected, and the main peak appeared at tubes number 10—16. The main fraction was concentrated, and the residue gave fine needles in ethanol-water in a refrigerator. Yield, 230 mg (25% of theory). mp 170.5—171.5 °C (dec.); reported mp 170—172 °C (dec.).[1] Found: C, 31.29; H, 6.20; N, 4.10; P, 9.11%. Calcd for $C_9H_{18}O_{10}NP\cdot H_2O$: C, 30.95; H, 5.77; N, 4.01; P, 8.87%. Mol wt. 349.2. $[\alpha]_D^{22}$ +107.7°→+104.1° (8 min)→+90.2° (3 hr)→+90.2±7.5° (at equilibrium; *c* 0.194, water). Reported $[\alpha]_D$ +106° (8 min)→+79° (at equilibrium).[1]

Table 1. Paper and thin layer chromatography of muramic acid 6-phosphate

Relative mobilities to glucosamine or *N*-acetyl-glucosamine were shown.

Solvent	GlcN	GlcNAc	Mur	Mur 6-P
Ethylacetate: Acetic acid: Pyridine: Water (5:1:5:3) (Whatman No. 1)[a]	—	1.00	0.60	0.15
Butanol: Acetic acid: Water (5:3:2) (Whatman No. 1)[a]	—	1.00	1.13	0.67
Butanol: Acetic acid: Water (2:1:1) (Avicel SF)[b]	1.00	—	1.84	1.22
Butanol: Acetic acid: Water (2:1:1) (Kiesel Gel F_{254})[c]	1.00	—	1.12	0.45

Spots were detected. a) by silver nitrate reagent[9]. b) by ninhydrin reagent. c) by sulfuric acid.

Analyses of Muramic Acid 6-Phosphate Synthesized. The compound gave one spot on paper and thin-layer chromatograms. The results are summarized in Table 1. On a paper electrophoretogram the compound gave a single spot with $M_{\text{gluconic acid}}$=1.0 at 700 V/15 cm for 35 min in an acetic acid pyridine buffer (pH 3.5).

Periodate Oxidation of Muramic Acid 6-Phosphate. As a reference, α-DL-glycerophosphate or D-glucosamine 6-phosphate (4.1 and 5.0 μmol each) in 0.5 ml of water was treated with 9.5 μmoles of sodium periodate in 0.5 ml at pH 5. The reaction mixture was allowed to stand at 25 °C for 48 hr in the dark. It was then placed on a Dowex 1×4 column (200—400 mesh, chloride form, 0.9×10 cm); the column was eluted first with 20 ml of 0.052 M hydrochloric acid and then with 0.05 M hydrochloric acid.[5] One and a half-ml fractions were collected and the aliquots were analyzed for organic phosphate[10] and diphenylamine-positive substances[11] (Fig. 1, A, B). Muramic acid 6-phosphate (4.9 μmol) was treated in the same way, and the oxidation was continued for 62 hr (Fig. 1, C). Muramic acid 6-phosphate was reduced with sodium borohydride and then treated in the same way (Fig. 1, D). The absorbtion spectra of the color developed by diphenylamine[5] with peak fractions at tubes number 24—26 are shown in Fig. 2.

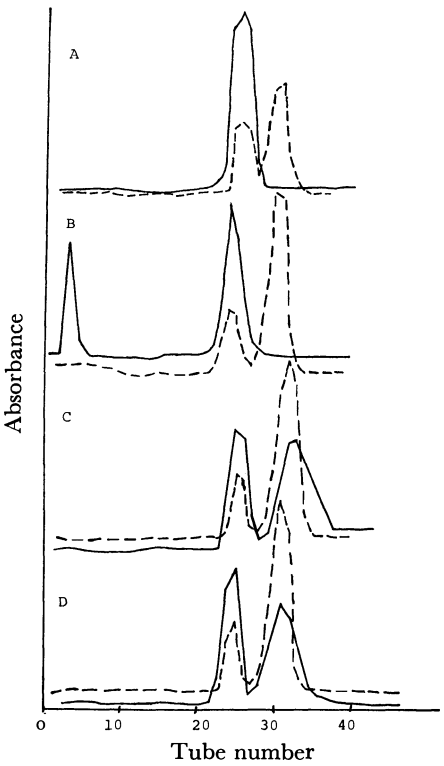

Fig. 1. Column chromatography of the periodate oxidation products of muramic acid 6-phosphate and standard samples.
A: α-glycerophosphate, B: Glucosamine 6-phosphate, C: Muramic acid 6-phosphate, D: Muramic acid 6-phosphate reduced with sodium borohydride. ——, Organic phosphate at 820 mμ. ----, Color at 660 mμ developed by diphenylamine reaction.

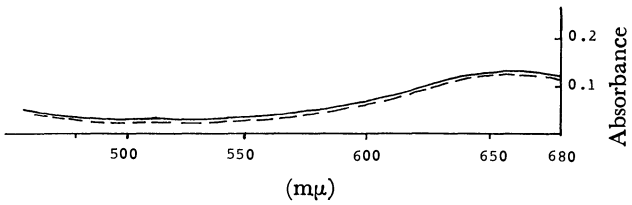

Fig. 2. Absorbtion spectra of the color developed by diphenylamine with peak fractions appeared at tube number 24—26 shown in Fig. 1.
Muramic acid 6-phosphate or reduced muramic acid 6-phosphate ----; glucosamine 6-phosphate or α-glycerophosphate ——.

Table 2. Analyses by the alkaline phosphatase of muramic acid 6-phosphate

	Recovery		
	with the enzyme	without the enzyme	incubation time (hr)
Mur 6-P	<1.0%	83%	4
Mur produced from Mur 6-P	103%	<2.5%	4
Inorganic phosphate	101%	<1%	1

Analyses by Alkaline Phosphatase. To a 0.2 ml solution of 0.40 μmole of muramic acid 6-phosphate, was added 0.4 ml of water and 0.2 ml of a 0.1 M ethanolamine–HCl buffer (pH 9.5, containing 0.005 M $MgCl_2$). To this solution 2 μl of the enzyme solution was added, after which the mixture was incubated at 37 °C.[12] Aliquots were analyzed for inorganic phosphate, and aminosugars were determined by means of an automatic amino acid analyzer (Hitachi KLA 3B). The results are shown in Table 2.

Detection of Formaldehyde in Periodate Oxidation Products. The pH of a sample solution (0.8 μmol in 0.08 ml of water) was adjusted to 5 if necessary. The oxidation was carried out with 4.3 μmol of sodium periodate in 0.02 ml at 25 °C for 48 hr. The excess periodate was decomposed with arsenite, and chromotropic acid was used for the determination of formaldehyde.[13] When glucose was used as an standard, 0.04 mol of formaldehyde was detected from one mole of muramic acid 6-phosphate, and 0.91 mol from one mol of muramic acid.

References

1) Y. Konami, T. Osawa, and R. W. Jeanloz, *Biochemistry*, **10**, 192 (1971).
2) C. E. Ballou and D. L. MacDonald, "Methods in Cabohydrate Chemistry," Vol. 2, (1963), p. 270.
3) F. Maley and H. A. Lardy, *J. Amer. Chem. Soc.*, **78**, 1393 (1956).
4) A. Nowotny, *ibid.*, **83**, 501 (1961).
5) T. Y. Liu and E. C. Gotschlich, *J. Biol. Chem.*, **242**, 471 (1967).
6) Y. Matsushima and J. T. Park, *J. Org. Chem.*, **27**, 3581 (1962).
7) H. M. Flowers and R. W. Jeanloz, *ibid.*, **28**, 2983 (1963).
8) G. Ågren and C. H. Verdier, *Acta Chem. Scand.*, **12**, 1927 (1958).
9) W. E. Trevelyan, D. P. Procter, and J. S. Harrison, *Nature*, **166**, 444 (1950).
10) P. S. Chen, T. Y. Toribara, and H. Warner, *Anal. Chem.*, **28**, 1756 (1956).
11) Z. Dische and E. Borenfreund, *J. Biol. Chem*,, **180**, 1297 (1949).
12) L. A. Heppel, "Methods in Enzymology," Vol. 2, (1955), p. 530.
13) D. A. MacFadyen, *J. Biol. Chem.*, **158**, 107 (1945).

The Formation of Ethers from Borneol and Isoborneol in the Presence of Boron Trifluoride Etherate

Kimiko NAGAI, Mitsuru NAKAYAMA, Akihiko MATSUO, Shizuko EGUCHI, and Shûichi HAYASHI

Department of Chemistry, Faculty of Science, Hiroshima University, Higashisenda-machi, Hiroshima 730

(Received August 25, 1973)

dl-Borneol and *dl*-isoborneol, when separately submitted to the action of boron trifluoride etherate at room temperature, gave different ethers; the one from borneol was characterized as bornyl isobornyl ether, and the other from isoborneol, as diisobornyl ether. The ethers were also obtained from borneol and isoborneol in the reaction with zinc chloride. When *d*-borneol was used, an optically-active bornyl isobornyl ether was obtained.

In connection with a previous communication on the formation of cyclodiethers from 6-methyl-5-hepten-2-ol and citronellol,[1] the action of boron trifluoride etherate on borneol and isoborneol was examined in the present work; two kinds of ethers were obtained, whose structures were characterized as bornyl isobornyl and diisobornyl ethers.

Long years ago Ikeda obtained a condensation product in the reaction of borneol with zinc chloride; he described it as dibornyl ether. However, he did not attempt the reaction of isoborneol with zinc chloride, for this alcohol was more sensitive than borneol. Besides, in his work the structural characterization was not thoroughgoing enough; indeed, no consideration has yet been made[2] of the formation mechanism. In the present work, then, the reactions of borneol and isoborneol with zinc chloride were reexamined, and the reaction of borneol with camphene was examined in the presence of boron trifluoride etherate.

Results and Discussion

Reactions of dl-*Borneol and* dl-*Isoborneol with Boron Trifluoride Etherate.* *dl*-Borneol (I) and *dl*-isoborneol (II) were separately submitted to the action of boron trifluoride etherate under such conditions as are shown in Table 1. The reaction mixtures were subjected to fractional distillation followed by elution chromatography to separate individual components, which were characterized as tricyclene (III), camphene (IV), and C_{20}-hydrocarbons, together with the following two ethers.

dl-*Bornyl Isobornyl Ether (V)*: In the reaction of *dl*-borneol with boron trifluoride etherate (Experiment 3), the compound was isolated as feather-like crystals (mp 42.5—43.5 °C, $[\alpha]_D^{20}$ ±0° ($CHCl_3$)) in a 14% yield. The molecular formula of this compound was determined to be $C_{20}H_{34}O$ from the molecular ion, *m/e* 290, and the molecular weight, 288, as taken by the Rast method. The IR spectrum showed characteristic ether bands at 1117, 1087, and 1078 cm^{-1}, while the NMR spectrum revealed the presence of two oxygen-carrying methine groups on the proton signals at δ 3.18 (1H, t) and 3.50 (1H, dq), but there was no indication of the presence of unsaturated bonds; the mass spectrum with characteristic ions at *m/e* 153 (8%, $C_{10}H_{17}O$), 152 (23, $C_{10}H_{16}O$), and 137 (base, $C_{10}H_{17}$) were reasonably explained as that of a di-monoterpene ether. Accordingly, the compound may be thought to be an ether consisting of two saturated bicyclic monoterpenes.

Together with the above signals, the NMR spectrum taken in a $CDCl_3$ solution showed methyl signals at δ 0.80, 0.90, 1.01 (each 3H, s) and 0.85 (9H, s). Among these, the first three were close to the separating methyl signals in the NMR spectrum of isoborneol (δ 0.81, 0.91 and 1.02; each 3H, s), while the last agreed with a combined methyl signal seen in the spectrum of borneol (δ 0.85, 9H, s). Regarding the NMR spectrum taken in a C_5D_5N solution, also, the methyl signals (δ 0.85, 9H, s; 0.95, 0.98, 1.09, each 3H, s) could be connected with those of borneol (δ 0.87, 6H, s; 0.98, 3H, s) and isoborneol (δ 0.85, 1.07, 1.28, each 3H, s), although the methyl signals to be assigned to the isobornyl moiety of the ether showed field shifts slightly higher than those of free isoborneol. These facts indicate that the compound is bornyl isobornyl ether.

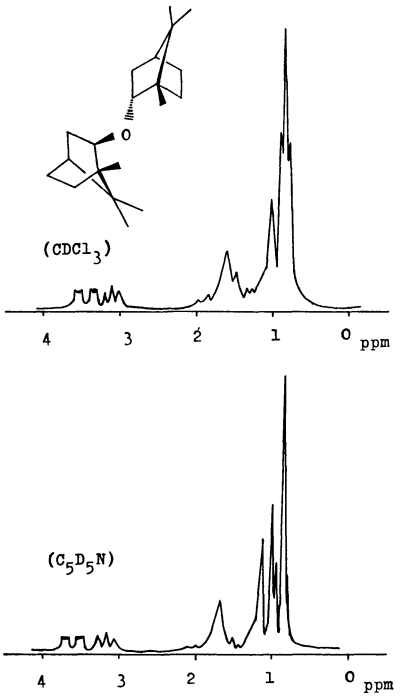

Fig. 1. NMR spectra of bornyl isobornyl ether (V).

This characterization of the ether was further supported by the signal patterns of the oxygen-carrying methine groups: according to Flautt[3] and Tori,[4] who have investigated in detail the NMR spectra of 2-substituted bornane derivatives, the α-methine proton of

the *endo*-substituted isomer (proton *exo*) appears as a quartet of two characteristic spacings split by a much smaller spacing, whereas that of the *exo*-substituted isomer (proton *endo*) appears as a triplet or a near triplet without any additional splitting; this difference gives a good test for the identification of the *exo* and *endo* isomers. The NMR spectrum taken in $CDCl_3$ showed two signals attributable to α-methine protons. That is, the one appeared as a quartet (δ 3.50) with a small splitting, and the other, as a triplet (δ 3.18). When the NMR spectrum taken in a C_5D_5N solution was compared with that in $CDCl_3$, both the α-methine signals were retained with nearly the same patterns, although the chemical shifts showed a slight down-field shift.

Thus, it is certain that the compound is optically-inactive bornyl isobornyl ether.

dl-*Diisobornyl Ether (VI)*: The compound was obtained as feather-like crystals (mp 87—88 °C, $[\alpha]_D^{20}$ ±0° ($CHCl_3$)) in a 21% yield by the reaction of *dl*-isoborneol with boron trifluoride etherate at room temperature (Experiment 10). The molecular formula, $C_{20}H_{34}O$, was the same as that of bornyl isobornyl ether (V) discussed above, and the IR and mass spectra of the two compounds were nearly superimposable upon each other. In addition, the NMR spectrum was constituted of methyl, methylene, and α-methine signals with the same relative intensity as that of the above bornyl isobornyl ether, although these proton signals differed fairly much in pattern. Accordingly, this evidence seems to indicate that the compound is a stereo-isomer of bornyl isobornyl ether (V).

The proton signals of the two α-methine groups were overlapped as a triplet centering at δ 3.18 in a $CDCl_3$ solution, and as a near triplet centering at δ 3.20 in a C_5D_5N solution. Besides, the chemical shifts of the α-methine signals were in agreement with those in $CDCl_3$ and C_5D_5N solutions respectively of the α-methine proton belonging to the isobornyl moiety of bornyl isobornyl ether (V). Such proton signals of the α-methine group indicate that the ether-linkage of this compound is in the *exo-exo* conformation. Thus, the ether was characterized as diisobornyl ether (VI).

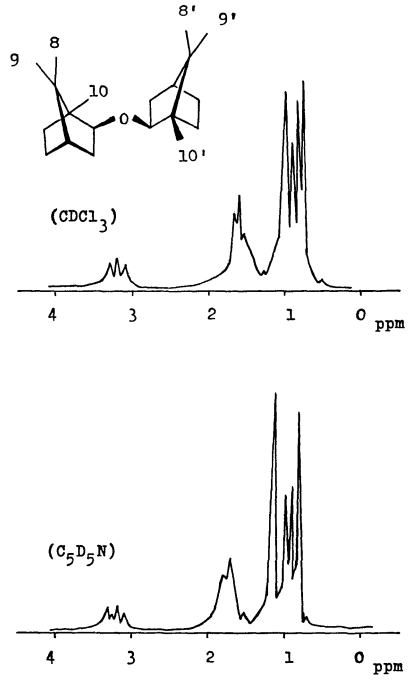

Fig. 2. NMR spectra of diisobornyl ether (VI).

The methyl signals in $CDCl_3$ and C_5D_5N solutions of the ether were also reasonably connected with those of diisobornyl ether in comparison with the methyl signals of isoborneol[4] and the isobornyl moiety of bornyl isobornyl ether; besides, according to Tori's assignments for isoborneol, the methyl signals of δ 0.85 (6H, s, $C_{(9)}$ and $C_{(9')}$) and 1.02 (6H, s, $C_{(8)}$ and $C_{(8')}$) in $CDCl_3$ and of δ 0.81 (6H, s, $C_{(9)}$ and $C_{(9')}$) and 1.09 (6H, s, $C_{(8)}$ and $C_{(8')}$) in C_5D_5N were assigned to the two gem-dimethyls, and the methyl signals of δ 0.90 and 0.95 (each 3H, s) in $CDCl_3$ and of δ 0.91 and 0.95 (each 3H, s) in C_5D_5N, to $C_{(10)}$- and $C_{(10')}$-methyls.

Reactions of Borneol and Isoborneol with Zinc Chloride. When the structural elucidation was carried out on the products of the reaction with boron trifluoride etherate, we were especially interested in a *d*-dibornyl ether which had been obtained by Ikeda in the reaction of *d*-borneol with zinc chloride,[2] for its melting point agreed with that of our bornyl isobornyl ether and dibornyl ether was not obtained in our experiment.

The reaction of *dl*-borneol with zinc chloride was thus traced, and feather-like crystals whose melting point agreed with that reported by Ikeda were obtained. This compound, however, was identical with our *dl*-bornyl isobornyl ether in the IR, NMR, and mass spectra and in a gas-chromatographic comparison. Therefore, it was confirmed that Ikeda's ether was not dibornyl ether, but bornyl isobornyl ether.

Ikeda did not examine the reaction of isoborneol with zinc chloride. We tried this reaction under similar conditions and obtained diisobornyl ether. Thus, zinc chloride also acts similarly on borneol and isoborneol as boron trifluoride etherate.

Formation Mechanism of Bornyl Isobornyl and Diisobornyl Ethers. As has been mentioned above, camphene and tricyclene were detected in the monoterpene fraction of each reaction product in the reaction of borneol and isoborneol with boron trifluoride etherate. These compounds are thought to be produced *via* a non-

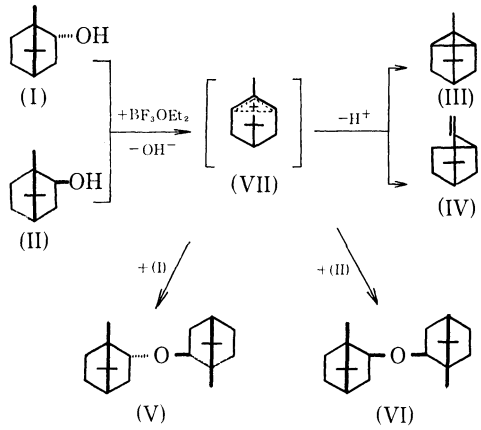

Scheme 1.

classical carbonium ion (VII): a molecule of borneol or isoborneol undergoes the elimination of the hydroxyl group, followed by deprotonation, to give camphene or tricyclene.

The formation of the bornyl isobornyl and diisobornyl ethers mentioned above may be explained in terms of the nucleophilic attack of each molecule of borneol and isoborneol on the common carbonium ion (VII), in which the alcohol molecule approaches stereospecifically from the *exo*-side because of the steric hindrance and the asymmetric influence of the molecule. By the formation mechanism, the following experimental results can also be explained. When the *d*-borneol was submitted to the action of boron trifluoride etherate, we obtained optically-active bornyl isobornyl ether, $[\alpha]_D^{20}$ +53.8° ($CHCl_3$). Next, the reaction of *dl*-borneol or *d*-borneol with *d*-camphene was attempted in the presence of boron trifluoride etherate, because it has been established that camphene produces the carbonium ion in the acid-catalyzed reaction; from the reaction of *dl*-borneol and *d*-camphene, *dl*-bornyl isobornyl ether was obtained, while from that of *d*-borneol with *d*-camphene, we obtained optically-active bornyl isobornyl ether, $[\alpha]_D^{20}$ +54.6° ($CHCl_3$), whose specific rotation was equal to that of the above optically-active ether obtained in the reaction of *d*-borneol itself.

Experimental

Apparatus. For the analyses and preparative glc of monoterpenic hydrocarbons, a Shimadzu glc-apparatus was used: column temperature, 100 °C; stainless-steel separating column (3 m×3 mm) packed with Carbowax 6000 (30%) on Celite 545 (60—80 mesh); flow rate of the helium carrier, 60 ml/min. The mass spectra were taken on a Hitachi RMS-4 spectrometer at an ionization voltage of 80 eV, an ion-accelerating voltage of 1800 eV, and an ionization chamber temperature of 150 °C, or on a Hitachi-7L high-resolution spectrometer under the same conditions.

Materials. Commercial *dl*- and *d*-borneol and *dl*-isoborneol[5] were purified through repeated recrystallizations from benzene. They each showed one peak in glc; *dl*-Borneol mp 210 °C, $[\alpha]_D^{25}$ ±0° ($CHCl_3$); *d*-borneol: mp 205—206 °C, $[\alpha]_D^{22}$ +21.4° ($CHCl_3$). *dl*-Isoborneol: mp 212.0—212.3 °C, $[\alpha]_D^{25}$ ±0° ($CHCl_3$).

Commercial *d*-camphene was purified: mp 48.5—49.5 °C, $[\alpha]_D^{20}$ +5.3° ($CHCl_3$).

The chemical grade of boron trifluoride etherate (BF_3 47%) was used without any purification.

The zinc chloride was freshly dehydrated by fusion just before the experiment.

Reactions of Borneol and Isoborneol with Boron Trifluoride Etherate. To *dl*-borneol or *dl*-isoborneol, boron trifluoride etherate was added, drop by drop, in ether or with no solvent, as is shown in Table 1; the mixtures were then allowed to stand for a period from 7 min to 10 day at temperatures from 25 °C to 80 °C. The reaction mixtures were washed with a saturated aqueous solution of sodium carbonate and then with water, dried over anhydrous sodium sulfate, and fractionated under reduced pressure into a lower-boiling (bp 30—100 °C/4 mmHg) fraction, a higher-boiling (bp 100—150 °C/4 mmHg) fraction, and a residue.

Characterization of Monoterpene Compounds. The lower-boiling fractions from Experiments (1)—(5) and (7)—(10) showed two components except for the reactant in tlc using silica gel and hexane (R_f 0.91 and 0.78) and in glc (T_R 11.7 and 16.8). The components were isolated by means of preparative glc.

Tricyclene: The compound showing one peak with T_R 11.7 in glc and one spot with R_f 0.91 in tlc was isolated as colorless and pleasant odor crystals; mp 67.3—67.9 °C. The IR,[6] mass[7] spectra and gas chromatographic behavior coincided with those of tricyclene.

dl-*Camphene*: The compound showing one peak with T_R 16.8 in glc and one spot with R_f 0.78 on tlc was isolated as colorless and camphor-like-smelling crystals; mp 51.0—51.5 °C (lit,[8] 49—51 °C), $[\alpha]_D^{20}$ ±0° ($CHCl_3$). The IR[6] and mass spectra[7,9] with those of camphene, and the compound was gas-chromatographically identical with the authentic specimen.

Characterization of Dimerized Compounds. The higher-boiling fractions of the reaction products from borneol showed one or two components with T_R 10.9 and 18.8 on glc with the SE-30 column, while those from isoborneol showed such components with T_R 10.5 and 18.1. These components were isolated through elution chromatography with silica gel–benzene and then characterized.

C_{20}-*Hydrocarbon from* dl-*Borneol*: A colorless, viscous oil showing one peak with T_R 10.9 was isolated from the reaction mixture of *dl*-borneol. From the molecular ion (*m/e* 272) and the molecular weight (275) taken by the Rast method, the molecular formula of this compound was determined as $C_{20}H_{32}$. Although the mass spectrum showed abundant ions at *m/e*

Table 1. Reactions of borneol and isoborneol with boron trifluoride etherate

	Borneol[a]						Isoborneol[a]				
No. of experiment	1	2	3	4	5	6	7	8	9	10	11
BF_3OEt_2 (ml)	5.0	5.0	5.0	5.0	5.0	5.0	2.5	5.0	2.5	5.0	5.0
Et_2O (ml)	10	—	—	—	—	—	10	10	10	—	—
Reaction temp. (°C)	30	30	25	60	80	80	30	30	60	20	30
Reaction period (hr)	24	24	240	1	0.12	1	168	24	1	7	24
Unreacted alcohol (%)[b]	98.7	98.5	85.0	98.1	8.0	—	34.0	30.0	26.0	1.0	—
Tricyclene (%)	0.1	trace	—	0.1	6.0	—	8.0	6.0	2.0	1.0	—
Camphene (%)	1.2	1.5	1.0	1.8	21.0	—	58.0	64.0	72.0	19.0	—
$C_{20}H_{32}$ (%)	—	—	—	—	65.0	65.0	—	—	—	58.0	72.0
Bornyl isobornyl ether (%)	—	—	14.0	—	—	—	—	—	—	—	—
Diisobornyl ether (%)	—	—	—	—	—	—	—	—	—	21.0	—
Residue (%)	—	—	—	—	—	35.0	—	—	—	—	28.0

a) Five grams of the alcohol were used in each experiment. b) Relative amounts of reaction products were determined with the aid of gas chromatography.

257 (M^+-15, 4%), 229 (M^+-43, 10), 109 (31), 95 (base), 81 (57), and 41 (56), no further structural information was obtained from any of the mass, IR, or NMR spectra.

C_{20}-Hydrocarbon from dl-*Isoborneol*: The compound (T_R 10.5) was isolated from the reaction mixture of *dl*-isoborneol as a colorless, viscous oil. The hydrocarbon was determined to have the same molecular formula, $C_{20}H_{32}$, as that from the reaction mixture of borneol, and it had the same molecular ion (*m/e* 272) and the same molecular weight (270, Rast method), but a difference was observed between the IR and NMR spectra of the two hydrocarbons. The mass spectrum showed abundant ions at *m/e* 257 (M^+-15, 12%), 229 (M^+-43, 23), 162 (M^+-110, base), 147 (42), 109 (55), and 95 (66).

dl-*Bornyl Isobornyl Ether from* dl-*Borneol*: Colorless feather-like crystals, mp 42.5—43.5 °C, $[\alpha]_D^{20}$ ±0° ($CHCl_3$), showing a peak with T_R 18.8 was obtained in a yield of 14% from a reaction mixture of *dl*-borneol. Found: C, 82.94; H, 11.92%. Calcd for $C_{20}H_{34}O$: C, 82.69; H, 11.80%. The mass spectrum showed ions at *m/e* 290 (M^+, 4%), 272 (M^+-18, 10), 153 ($C_{10}H_{17}O$, 8), 152 ($C_{10}H_{16}O$, 13), 137 ($C_{10}H_{17}$, base), 95 (C_7H_{11}, 29), 81 (C_6H_9, 90), 69 (27), 67 (30), 55 (28), and 41 (42).

d-*Bornyl Isobornyl Ether from* d-*Borneol*: *d*-Borneol was subjected to a reaction with boron trifluoride etherate under the same conditions as in Experiment (3) to give *d*-bornyl isobornyl ether as colorless feather-like crystals; mp 42.0—42.8 °C, $[\alpha]_D^{20}$ +53.8° ($CHCl_3$). The IR, NMR, and mass spectra were in good agreement with those of *dl*-bornyl isobornyl ether, and the compound was confirmed to be identical with the *dl*-ether in gas chromatography.

dl-*Diisobornyl Ether from* dl-*Isoborneol*: A crystalline portion of the reaction mixture from isoborneol was dried on a porous plate to separate colorless feather-like crystals in a yield of 21%, mp 87—88 °C, $[\alpha]_D^{20}$ ±0° ($CHCl_3$). Found: C, 82.93; H, 11.91%. Calcd for $C_{20}H_{34}O$: C, 82.69; H, 11.80%. The IR and mass spectra were nearly superimposable on those of *dl*-bornyl isobornyl ether, but the NMR spectra were different between the two ethers.

Reactions of Borneol and Isoborneol with Zinc Chloride. dl-*Bornyl Isobornyl Ether*: *dl*-Borneol was submitted to a reaction with zinc chloride under conditions similar to those in Ikeda's report,[2] that is, 5 g of borneol were mixed with 2.5 g of zinc chloride in dried benzene (4 ml), and the mixture was boiled for 3 hr. The reaction mixture was then washed with 2M hydrochloric acid and water, dried over anhydrous sodium sulfate, and then chromatographed over a silica-gel column with a mixed solvent of hexane and ethyl acetate (95: 5) to isolate colorless crystals in a 25% yield; mp 42.5—53.0 °C, $[\alpha]_D^{20}$ ±0° ($CHCl_3$). The IR, NMR, and mass spectra were superimposable on those of the *dl*-bornyl isobornyl ether obtained from the reaction of *dl*-borneol with boron trifluoride etherate, and their mixed-melting-point determination showed no depression.

d-*Bornyl Isobornyl Ether*: *d*-Borneol was also subjected to the reaction; we thus obtained *d*-bornyl isobornyl ether, which was identified by comparison with *d*-bornyl isobornyl ether obtained in the reaction of *d*-borneol with boron trifluoride etherate.

dl-*Diisobornyl Ether*: *dl*-Isoborneol was mixed with zinc chloride in dried benzene in the same ratio as in the case of borneol, and the mixture was then boiled for 50 min. Colorless crystals were obtained in a 16% yield; mp 87—88 °C, $[\alpha]_D^{20}$ ±0° ($CHCl_3$). This compound was identical in melting point and in the IR and NMR spectra with the *dl*-diisobornyl ether obtained from *dl*-isoborneol in the presence of boron trifluoride etherate.

Reaction of Borneol with Camphene in the Presence of Boron Trifluoride Etherate. dl-*Bornyl Isobornyl Ether*: To a mixed solution of *dl*-borneol (5 g) and *d*-camphene (5 g) in dried ether (20 ml), boron trifluoride etherate (2.5 ml) was added, drop by drop; the mixture was then allowed to stand at room temperature for 24 hr. The reaction mixture was treated with the usual procedure to give colorless crystals in a 30% yield; mp 42.5—43.5 °C; $[\alpha]_D^{20}$ ±0° ($CHCl_3$). This compound was identical with the ether drived by the above-described method.

d-*Bornyl Isobornyl Ether*: A mixed solution of *d*-borneol and *d*-camphene was treated with boron trifluoride etherate as has been described above; a colorless crystalline product was thus obtained; mp 42.0—42.8 °C, $[\alpha]_D^{20}$ +54.6° ($CHCl_3$). This compound was identical with the ether obtained in the reaction of *d*-borneol with boron trifluoride etherate.

References

1) K. Nagai, M. Nakayama, and S. Hayashi, *Chem. Lett.*, **1973**, 665.
2) T. Ikeda, *Sci. Pap. Inst. Phys. Chem. Res.* (Tokyo), **7**, 47 (1927).
3) T. J. Flautt and W. F. Erman, *J. Amer. Chem. Soc.*, **85**, 3212 (1963).
4) K. Tori, Y. Hamashima, and A. Takamizawa, *Chem. Pharm. Bull.*, (Tokyo), **12**, 924 (1964).
5) T. Takeshita and M. Kitajima, *Nippon Kagaku Zasshi*, **78**, 993 (1957).
6) R. T. Óconnor and L. A. Goldblatt, *Anal. Chem.*, **26**, 1726 (1954).
7) A. Thomas and B. Willhalm, *Helv. Chim. Acta*, **47**, 475 (1964).
8) O. Aschan, *Ann. Chem.*, **383**, 39 (1911).
9) R. Ruhage and E. von Sydow, *Acta Chem. Scand.*, **17**, 2125 (1963).

Synthetic Studies of Carbohydrate Derivatives with Photochemical Reactions. X.[1] An Unusual Photo-induced Addition of Lactonitrile to Some Enoses

Kazuo MATSUURA, Kazuo SENNA, Younosuke ARAKI, and Yoshiharu ISHIDO

Department of Chemistry, Faculty of Science, Tokyo Institute of Technology, O-okayama, Meguro-ku, Tokyo 152

(Received September 7, 1973)

The photochemical addition of lactonitrile to 3,4,6-tri-*O*-acetyl-D-glucal, 2,3,4,6-tetra-*O*-acetyl-2-hydroxy-D-glucal, methyl 4,6-di-*O*-acetyl-2,3-dideoxy-α-D-*erythro*-hex-2-enopyranoside, and methyl 5-deoxy-2,3-*O*-isorpopylidene-β-D-*erythro*-pent-4-enofuranoside afforded 1′-cyanoethyl 4,6-di-*O*-acetyl-2,3-dideoxy-α-(**6a**) and -β-D-*erythro*-hex-2-enopyranoside(**6b**), 1′-cyanoethyl 2,4,6-tri-*O*-acetyl-3-deoxy-α- and -β-D-*erythro*-hex-2-enopyranoside, **6a** and **6b**, and 1′-cyanoethyl [methyl (4*R*)-5-deoxy-2,3-*O*-isopropylidene-β-D-*erythro*-pentofuranosid]-4-uloside respectively, all in good yields. These facts can be explained by assuming the catalytic effect of a certain acidic species which might extricated from lactonitrile during the irradiation.

As part of this series of investigations, the photochemical addition of secondary alcohols to enoses has been reported briefly; in it the corresponding tertiary alcohols were obtained through the addition of α-*C*-radicals of secondary alcohols to enoses.[2] On the other hand, in contrast with the case of these secondary alcohols, the photochemical behavior of lactonitrile(**1**) was found to be unusual in such reaction; it gives the corresponding adducts, which have the 1′-cyanoethyl ether structure.[3] In this article, the detailed results of an investigation of the unusual photo-induced reaction of **1** with 3,4,6-tri-*O*-acetyl-D-glucal(**2**), 2,3,4,6-tetra-*O*-acetyl-2-hydroxy-D-glucal(**3**), methyl 4,6-di-*O*-acetyl-2,3-dideoxy-α-D-*erythro*-hex-2-enopyranoside(**4**), and methyl 5-deoxy-2,3-*O*-isopropylidene-β-D-*erythro*-pent-4-enofuranoside(**5**) will be described.

Results and Discussion

The irradiation of a solution of **2** in **1** was carried out by the use of a low-pressure mercury lamp under a nitrogen atmosphere at room temperature. The resultant reaction mixture was, after concentration *in vacuo* to a sirup, subjected to chromatographic separation to afford 1′-cyanoethyl 4,6-di-*O*-acetyl-2,3-dideoxy-α-D-*erythro*-hex-2-enopyranoside(**6a**) and the corresponding β-anomer(**6b**) in 37 and 47% yields[4] respectively. Moreover, 1′-cyanoethyl 2,4,6-tri-*O*-acetyl-3-deoxy-α-D-*erythro*-hex-2-enopyranoside(**7a**) and its β-anomer(**7b**) were similarly obtained from **1** and **3** in 40 and 40% yields respectively. The structural assignment of these products was successfully accomplished by the use of the NMR and mass spectroscopic data (Table 1 and Fig. 1 respectively). The signals of the anomeric protons of 2,3-dideoxy- and 3-deoxy-α-D-*erythro*-hex-2-enopyranosides have been shown by Ferrier *et al.*[5,6]

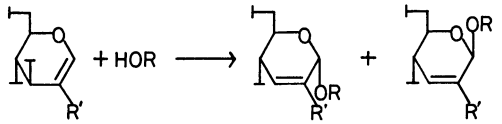

2, R′=H　　Me
3, R′=OAC　　R = CH
CN

6a, R′=H　**6b**, R′=H
7a, R′=OAc　**7b**, R′=OAc

(|— =OAc)

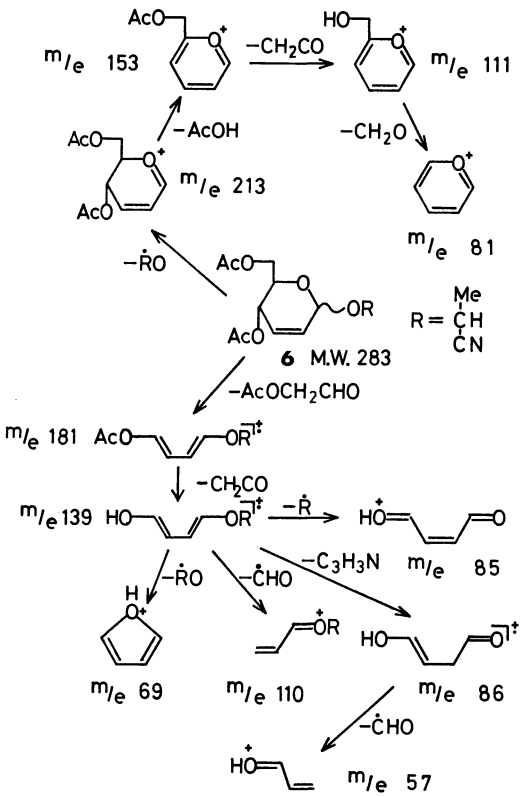

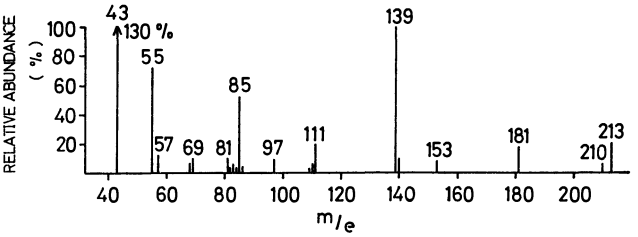

Fig. 1. Mass spectrum of **6**

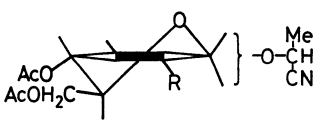

Fig. 2. **8** H1 conformation

TABLE 1. NMR DATA OF **6a**, **6b**, **7a**, AND **7b**

Protons	Chemical shifts			
	6a	**6b**	**7a**	**7b**
H-1′	4.47	4.72	4.47	4.68
H-1	5.23	5.34	5.30	5.34
H-2	6.06	6.05	—	—
H-3	5.85	5.89	5.87	5.89
H-4	5.44	5.40	5.57	5.55
H-5	4.23	4.09	4.23	4.16
H-6,6′	4.3—4.5	4.2—4.3	4.3—4.4	4.2—4.3
C-CH_3	1.63	1.64	1.66	1.66
O-$COCH_3$	2.13, 2.13	2.11, 2.11	2.13, 2.13, 2.19	2.12, 2.12, 2.24
Coupling constants				
H-1—H-2	1>	0.5>	—	—
H-1—H-3	2.5	1>		
H-2—H-3	10	10.5	—	—
H-2—H-4	1>	1>	—	—
H-3—H-4	1.5	2	2.3	2.0
H-4—H-5	9.5	9.5	9.5	10
H-5—H-6	2.5	2.2		1>
H-5—H-6′	3.5	3.5		3.5
H-1′—CH_3	7.0	7.0	7.0	7.0

All the chemical shifts in this table are expressed by δ value in ppm, and the coupling constants are expressed in Hz.

to appear at a field higher than those of the corresponding β-anomers. The signals of **6a**, **6b**, **7a**, and **7b** were observed at δ 5.23, 5.34, 5.30, and 5.34 ppm respectively; those products were thus concluded to occupy the α-, β-, α-, and β-anomeric configurations respectively. Incidentally, the chromatographic behavior of **6a** and **6b** in glc, tlc, and column chromatography was in full accordance with that of **7a** and **7b** respectively. A further comparison of their NMR data with those[5a] of 2-enopyranosides led us to the conclusion that all the D-*erythro*-hex-2-enopyranosides described herein adopted the H1 conformation(**8**) with the $J_{3,4}$ and $J_{4,5}$ values of *ca.* 2 and *ca.* 10 Hz respectively, indicative of the quasi-axial and axial protons at *C*-4 and *C*-5 respectively. Moreover, the mass spectra of **6a** and **6b** showed the same spectral pattern and supported the expected structures; such typical fragment peaks as *m/e* 213, 181, and 139 were apparently detected in their spectra, and were found to agree with the results of Ferrier *et al.*[7]

The present reaction was thus confirmed to afford neither sugar derivatives with the tertiary alcohol substituents, in contrast with the reactions of ordinary secondary alcohols to enoses,[2] nor those with an ether linkage at *C*-2, but the 2-enopyranosides.

The irradiation of a solution of **4** in **1**, followed by

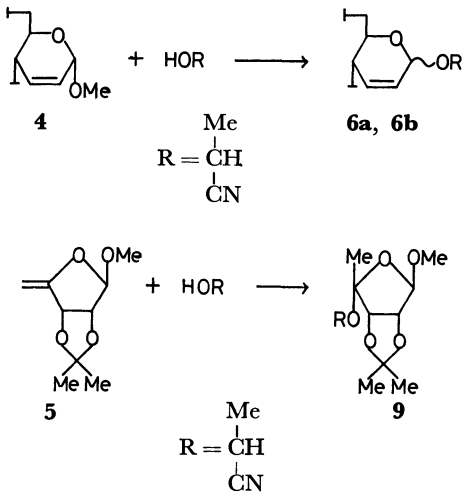

chromatographic separation, was subsequently carried out; it was found to involve a transglycosidation reaction giving **6a** and **6b** in 40 and 47% yields respectively.

Subsequently, the addition of **1** to 4-enofuranosyl derivatives such as **5**, which have an exocyclic double bond, was studied in the expectation that their higher reactivity could be proved in comparison with those having an endocyclic double bond.[1] 1′-Cyanoethyl

TABLE 2. NMR DATA OF **9**

Protons	H-1	H-2	H-3	H-1′	CH_3-1′	CH_3-4	O-CH_3	O C_3H / O CH_3
Chemical shifts, δ	4.92	4.63	4.45	4.58	1.47	1.61	3.37	1.45 1.31
Coupling constants, Hz		H-1—H-2 0.5		H-2—H-3 6.0		H-1′—CH_3 7.0		

[methyl (4*R*)-5-deoxy-2,3-*O*-isopropylidene-β-D-*erythro*-pentofuranosid]-4-uloside(**9**) was afforded in a 60% yield by the irradiation of **5** in **1**, followed by chromatographic separation. The NMR evidence for its structural determination is presented in Table 2. Two new *C*-methyl signals appeared at δ 1.61 (Me-4) and 1.47 (doublet, J_{CH-CH_3}=7.0 Hz, Me-1′) ppm besides those of the isopropylidene group. Moreover, 12% of the NOE was observed in the *H*-3 signal (δ 4.45 ppm) on irradiation at the methyl signal at δ 1.61 ppm.[8] From these data, the chirality at *C*-4 was thus established to be *R*. In the mass spectrum of this product, the peaks of *m/e* 242 (M^+-CH_3) and 226 (M^+-OCH_3) were observed as well as that of *m/e* 54 ($NC-C^+H-CH_3$), although no molecular ion peak was observed.

In order to elucidate the mechanism of these unusual photochemical reactions, the following examinations were carried out by the use of **3** as the model compound of the enoses to **1**. Each 10 mg portion of **3** was dissolved in **1** (0.5 ml) and treated under the following conditions, after which it was analyzed by glc. The dark reaction of the solution afforded no product, but resulted in a quantitative recovery of **3**. However, the treatment of **3** under dark conditions in **1**, which had previously been irradiated with a low-pressure mercury lamp for 30 hr afforded **7a** and **7b**, whose peaks were apparently observed in the glc of this reaction mixture in the same ratio as has been presented before. The peak of neither **3** nor of any other product could be detected in the chromatogram. An examination of the separately-photoirradiated **1** by ESR proved it to involve no radical species; however, the dark reaction with **3** in this **1** still afforded **7a** and **7b**. It is of interest, on the other hand, that the addition of an appropriate amount of liquid hydrogen cyanide to the system of the dark reaction resulted in the same results as were obtained in the photoinduced reaction of **3** in **1**. In view of the results reported by Ferrier *et al.*,[5a,9] boron trifluoride was also used in the above dark reaction in place of liquid hydrogen cyanide. It was, however, found to be too effective to give a mixture of the above products and a considerable amount of by-products, in spite of a short reaction period such as within 10 min.[10] In any case, the photochemical process conceivably takes place in the process of liberating a certain acidic species such as hydrogen cyanide from **1**, in considering that **1** is known to be equilibrated with a system of acetaldehyde and hydrogen cyanide in an aqueous solution.[11] Therefore, these reactions can be explained as the acid-catalyzed reactions of the enoses with **1**. The acid-catalyzed reaction of **2** or **3** with alcohols has already been shown to give the corresponding 2-enopyranosides.[5a,9] Either the formations of **6a** and **6b** or of **7a** and **7b** are thus conceivably brought about by a similar reaction process, and **4** may be interpreted to give **6a** and **6b** in terms of an acid-catalyzed *trans*-glycosidation reaction. Moreover, **5** can also be explained to afford **9** by such an acid-catalyzed reaction selectively; the sole formation of **9** can be assumed to arise from the stereochemical requirement of the carbonium ion, which was produced by the protonation on *C*-5 of **5**, which has a slightly pyramidal conformation of its quasi-*ribo* structure because of the potential repulsion with the endo-methyl group of the isopropylidene ring.

Experimental

Irradiations were carried out with a low-pressure mercury lamp (30 W) of the Riko Kagaku Co., Ltd. in a quartz-glass test tube at a distance of about 5 cm. Tlc's were carried out by the use of Wakogel B-5 and the solvent system of benzene–methanol (9: 1 v/v) for the development. The NMR spectra were taken with a Varian XL-100 appratus in deuterochloroform, using tetramethylsilane (TMS) as the internal standard. Glc was carried out with a Hitachi K-53 apparatus; column: 10% SE-30 on Chromosorb W (60—80 mesh); carrier gas: nitrogen under 1.5 Atm unless otherwise noticed; oven temperature: 200 °C, and injection temperature: 300 °C. The mass spectra were taken with a Hitachi RMU-6E appratus. The ESR spectrum was taken with a JOEL JEP-1X EPR spectrometer.

*1′-Cyanoethyl 4,6-Di-O-acetyl-2,3-dideoxy-α-(***6a***) and -β-*D-erythro-*hex-2-enopyranoside (***6b***).* *A*) A solution of 3,4,6-tri-*O*-acetyl-D-glucal (**2**) (1.00 g) in lactonitrile (**1**) (12 ml) was irradiated with the UV lamp under a nitrogen atmosphere at room temperature for 27 hr, after which the volatiles were evaporated *in vacuo*. The residue was subsequently chromatographed on a silica gel (Mallinckrodt Silica Gel, 100 mesh) column, using benzene–acetone (49: 1 v/v) as an eluting solvent system; **6b** (485 mg, 47%) and **6a** (380 mg, 37%) were in turn eluted out separately. The retention volumes of **2**, **6b**, and **6a** in glc were, respectively, 1 (=1.1 min), 1.7, and 2.1. Specific rotations: **6a**: $[\alpha]_D^{22}$ +49.4° (*c* 1.0, Me_2CO), **6b**: $[\alpha]_D^{22}$ +78.2° (*c* 1.0, Me_2CO). Found: C, 54.87 (**6a**) and 55.32 (**6b**); H, 5.81 (**6a**) and 6.18 (**6b**); N, 4.98 (**6a**) and 4.73 (**6b**) %. Calcd for $C_{13}H_{17}O_6N$: C, 55.12; H, 6.05; N, 4.95%. The NMR data of **6a** and **6b** are presented in Table 1. Their mass spectral data are presented in Fig 1.

B) A solution of methyl 4,6-di-*O*-acetyl-2,3-dideoxy-α-D-*erythro*-hex-2-enopyranoside (**4**) (1.00 g) in **1** (12 ml) was irradiated with the UV lamp under the same conditions as have been described above for 27 hr; the resultant solution was treated as in the previous experiment to afford **4** (30 mg, 3% recovery), **6b** (560 mg, 47%) and **6a** (480 mg, 40%).

*1′-Cyanoethyl 2,4,6-Tri-O-acetyl-3-deoxy-α-(***7a***) and -β-*D-erythro-*hex-2-enopyranoside (***7b***).* A solution of 2,3,4,6-tetra-*O*-acetyl-2-hydroxy-D-glucal (**3**) (500 mg) in **1** (12 ml) was irradiated with the UV lamp under the same conditions for 27 hr, and the resultant solution was evaporated *in vacuo*.

The residual sirup was subjected to chromatographic separation in the way described previously to afford **7b** (205 mg, 40%) and **7a** (205 mg, 40%). The retention volumes of **3**, **7b**, and **7a** in glc were, respectively, 2.1, 4.7, and 4.8. Specific rotations; **7a**: $[\alpha]_D^{22}$ +95.2° (*c* 1.0, Me_2CO) and **7b**: $[\alpha]_D^{22}$ +25.0° (*c* 1.0, Me_2CO). Found: C, 52.50 (**7a**) and 52.80 (**7b**); H, 5.91 (**7a**) and 5.40 (**7b**); N, 3.86 (**7a**) and 4.27 (**7b**) %. Calcd for $C_{15}H_{19}O_8N$: C, 52.78; H, 5.61; N, 4.10%.

The NMR spectral data of **7a** and **7b** are presented in Table 1.

*1′-Cyanoethyl [Methyl (4*R*)-5-Deoxy-2,3-*O*-isopropylidene-β-*D-erythro-*pentofuranosid]-4-uloside (***9***).* A solution of methyl 5-deoxy-2,3-*O*-isopropylidene-β-D-*erythro*-pent-4-enofuranoside (**5**) (1.00 g) in **1** (15 ml) was irradiated with the UV lamp under a nitrogen atmosphere at room temperature for 41 hr; the resultant solution was then subjected to column chromatography after its concentration *in vacuo* to give **9** (840 mg, 60%). Its retention volume in glc was 2.5 with reference to that of **5**

(1.0) under 0.8 Atm of nitrogen gas. $[\alpha]_D^{22}$ +24.0° (*c* 1.0, Me_2CO). Found: C, 55.55; H, 7.42; N, 5.29%. Calcd for $C_{12}H_{19}O_5N$: C, 56.02; H, 7.44; N, 5.44%. The NMR spectral data of this product are presented in Table 2. Mass spectral data of this product: *m/e* 242 (M^+–Me), 226 (M^+–OMe), 187 (M^+–OCH(Me)CN), 54 (C^+H(Me)CN), and so on.

Reactions of 2,3,4,6-Tetra-O-acetyl-2-hydroxy-D-glucal (3) with Lactonitrile (1) under Dark Conditions. *A*) A solution of **3** (10 mg) in **1** (0.5 ml) was allowed to stand for 100 hr at room temperature in the dark under a nitrogen atmosphere.

In the gas chromatogram of the resultant mixture, there are no detectable peaks except that of **3**.

B) Lactonitrile (**1**) (0.5 ml) was irradiated with the UV lamp for 30 hr at room temperature under a nitrogen atmosphere, and then **3** (10 mg) was dissolved in this **1**. The solution was allowed to stand for 30 hr under the same conditions as in the previous Experiment A. In the gas chromatogram of the resultant mixture, there are two peaks of the **7a** and **7b** products, but no peak of **3**.

C) Lactonitrile (**1**) (5 ml) was irradiated with the UV lamp much as has been described in the previous Experiment B, and then the resultant **1** was examined by ESR spectrometry.

No radical species were detected in variable measurements, even with the sensitivity of 10^{13} molecules. After these examinations, **3** (10 mg) was added to 0.5 ml of the recovered **1** and the solution was allowed to stand for 30 hr under the same conditions as in Experiment A. The gas chromatogram of the resultant mixture has the same pattern as that of Experiment B.

D) A solution of **3** (10 mg) in **1** (0.5 ml) containing a drop of liquid hydrogen cyanide was allowed to stand for 10 hr under the same conditions as above. In the gas chromatogram of the resultant mixture, there are two peaks of **7a** and **7b**, and a small peak of **3**. In another experiment involving three drops of liquid hydrogen cyanide, its gas chromatogram has only the peaks of **7a** and **7b** in the same reaction time.

E) A solution of **3** (10 mg) in **1** (0.5 ml) containing a drop of trifluoroboron-diethyl etherate (BF_3: OEt_2) was allowed to stand for 10 min under the same conditions as above. In the gas chromatogram of the resultant mixture, there are two peaks of by-products, two peaks of **7a** and **7b**, and no peak of **3**. In a reaction time of 1 hr, only the peaks of the by-products were detected. The retention volumes of the by-products in glc were 1.1 and crossed soon after (*cf.* **3**=2.1, **7a**=4.8, and **7b**=4.7). The conversion of **7a** and **7b** into the by-products was also confirmed by adding a drop of BF_3: OEt_2 to the solution of **7a** and **7b** in **1** (those substances had been obtained in Experiment B) and by then allowing the mixture to stand for 1 hr under the same conditions.

The authors are grateful to Dr. Masatsune Kainosho, Ajinomoto Co., Inc., and Mr. Katsuhiko Kushida, Nippon Electric Varian, for the measurement and analysis of the NMR spectra, and to Mr. Asao Murai, Ajinomoto Co., Inc., for the measurement of the mass spectra. They are also grateful to Associate Professor Shin Sato, Tokyo Institute of Technology, for the measurement of the ESR spectrum and its analysis, and to the members of the Laboratory of Organic Analysis, Tokyo Institute of Technology, for the elemental analysis.

References

1) Part IX: K. Matsuura, K. Nishiyama, K. Yamada, Y. Araki, and Y. Ishido, This Bulletin, **46**, 2538 (1973).

2) K. Matsuura, Y. Araki, Y. Ishido, and S. Sato, *Chem. Lett.*, **1972**, 849.

3) K. Matsuura, Y. Araki, Y. Ishido, and M. Kainosho, *ibid.*, **1972**, 853.

4) Almost the same ratio (45: 55) was obtained in glc determination with respect to the resultant reaction mixture.

5) a) R. J. Ferrier, N. Prasad, and G. H. Sankey, *J. Chem. Soc. C*, **1969**, 587 and preceding papers; b) R. J. Ferrier and M. M. Ponpipon, *ibid.*, **1971**, 560; c) R. U. Lemieux and R. J. Bose, *Can. J. Chem.*, **44**, 1855 (1960).

6) The anomeric configuration of 2,3-dideoxy- or 3-deoxy-2-enopyranosides have been shown in the reference 5b to be impossible to determine merely by means of their specific rotations.

7) R. J. Ferrier, N. Vethaviyasar, O. S. Chizov, V. I. Kadentsev, and B. M. Zolotarev, *Carbohyd. Res.*, **13**, 269 (1970).

8) The value of NOE was obtained under non-degassed conditions. Configurations of methyl substitutents on some 1,3-dioxolane and homologous rings have been shown to be confirmed by examining whether they show NOE or long-range coupling with vicinal protons [K. Nakanishi, D. A. Schooley, M. Koreeda, and I. Miura, *J. Amer. Chem. Soc*, **94**, 2866 (1972)].

9) R. J. Ferrier and N. Prasad, *J. Chem. Soc. C*, **1969**, 570.

10) In a reaction time of 1 hr, only the by-products were detected by glc. The isolations and the structuralassignments of these by-products were now in progress in our laboratory.

11) a) WM. F. Yates and R. L. Heider, *J. Amer. Chem. Soc.*, **74**, 4153 (1952). b) W. J. Svirbely and J. F. Roth, *ibid.*, **75**, 3106 (1953).

Dehydrogenation of 2-(1-Cyclohexenyl)cyclohexanone with Palladium Catalyst

Kimiaki IMAFUKU, Junko ODA,* Kenshi ITOH,** and Hisashi MATSUMURA

Department of Chemistry, Faculty of Science, Kumamoto University, 2–39–1, Kurokami, Kumamoto 860

(Received September 10, 1973)

The dehydrogenation reaction of 2-(1-cyclohexenyl)cyclohexanone was carried out in the presence of 5% palladium-on-charcoal at temperatures 280, 300, and 320 °C, the reaction time being 1/2—8 hr. *o*-Cyclohexylphenol and *o*-phenylphenol were obtained as dehydrogenation products, and dibenzofuran as the cyclization product *via* *o*-phenylphenol. In a short reaction time, 2-cyclohexylcyclohexanone was formed together with the dehydrogenation products. The compound disappeared, the amount of two phenols and dibenzofuran increasing with reaction time. The dehydrogenation process is discussed.

Many investigations have been made on the dehydrogenation of alicyclic compounds. In order to obtain *o*-phenylphenol, we carried out the dehydrogenation of *o*-cyclohexylphenol with palladium-on-charcoal and found that various rearranged products were obtained together with the desired *o*-phenylphenol.[1]

The present communication deals with the dehydrogenation of 2-(1-cyclohexenyl)cyclohexanone (I), which was unknown up to now, in the presence of the same catalyst under various conditions. Four products obtained in this procedure were confirmed to be 2-Cyclohexylcyclohexanone (II), *o*-cyclohexylphenol (III), *o*-phenylphenol (IV), and dibenzofuran (V).

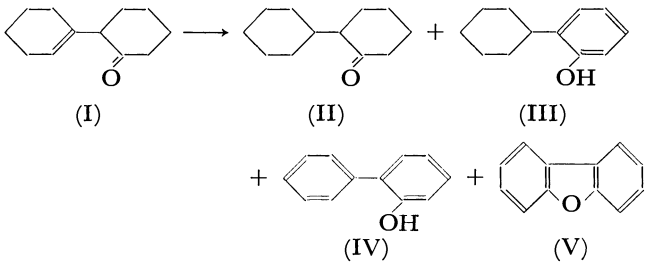

(I) (II) (III) (IV) (V)

Experimental

Materials. *5% Palladium-on-charcoal*: The palladium catalyst was prepared by the method of Mozingo.[2]

2-(1-Cyclohexenyl)cyclohexanone (I): 2-(1-Cyclohexenyl)-cyclohexanone (I) was prepared[3] by the self-condensation of cyclohexanone with phosphorus pentoxide, and was purified by distillation: bp 103—104 °C/1 mmHg [bp 114—116 °C/3.5 mmHg[4]]; oxime: mp 157—159 °C [mp 155 °C[5]].

2-Cyclohexylcyclohexanone(II): 2-Cyclohexylcyclohexanone (II) was obtained by catalytic hydrogenation of I in the presence of palladium chloride in methanol,[6] and was distilled; bp 145—147 °C/19 mmHg [bp 135 °C/11 mmHg[6]]; oxime: mp 100—102 °C [mp 102 °C[7]]; semicarbazone: mp 176—178 °C [mp 174—177 °C[8]].

Others: *o*-Cyclohexylphenol (III) and *o*-phenylphenol (IV) were supplied by Sanko Chemical Co. Ltd. Commercial dibenzofuran (V) (Tokyo Kasei Kogyo Co. Ltd.) was used.

Dehydrogenation of 2-(1-Cyclohexenyl)cyclohexanone. A mixture of I (2 g) and 5% palladium catalyst (400 mg) was heated at 280, 300, 320 °C under nitrogen atmosphere. At appropriate intervals of time, aliquots taken from the reaction mixtures were dissolved in benzene, and the catalyst was filtered off. The filtrates were analyzed gas chromatographically for determination of the reaction products.

Determination of Products. Quantitative determination of the products was performed gas chromatographically on a Shimadzu Model GC-1C gas chromatograph (column: 3% XE-60/Chromosorb W, 3 mmϕ × 150 cm; temperature 180 °C).

Measurements of Spectra. The IR spectra were recorded on a JASCO Model IRA-1 spectrophotometer in chloroform. The NMR spectra were taken on a Hitachi-Perkin-Elmer Model R-24 (60 MHz) spectrometer, using carbon tetrachloride and tetramethylsilane as the solvent and internal reference, respectively.

Results and Discussion

Dehydrogenation Products. 2-(1-Cyclohexenyl)-cyclohexanone (I) was treated with 5% palladium catalyst at 300 °C for 4 hr under nitrogen atmosphere. The gas chromatogram of the reaction mixture is shown

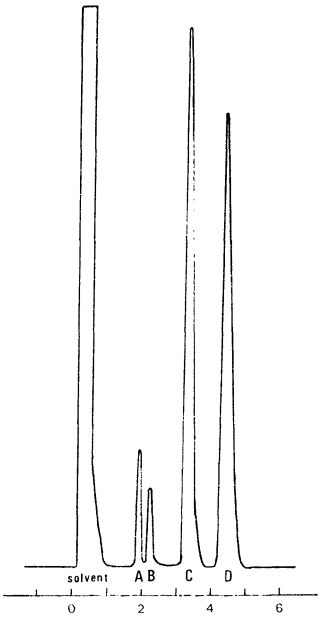

Fig. 1. Gas chromatogram of dehydrogenation products (300 °C, 4 hr).
Column: 3% XE-60/Chromosorb W, 3 mmϕ × 150 cm
temperature: 180 °C, carrier: H_2 32.1 ml/min

* Present address: Department of Industrial Chemistry, Faculty of Engineering, Kumamoto University, Kurokami, Kumamoto 860.

** Present address: Nihon Shokuhin Kako Co., Ltd., Mishima-shi, Shizuoka.

in Fig. 1. The mixture was found to contain four components. It was found that components B, C, and D are identical with dibenzofuran (V), *o*-phenylphenol (IV), and *o*-cyclohexylphenol (III), respectively, in comparison with authentic materials. V was also obtained in the dehydrogenation of III with the same catalyst.[1]

Component A was separated gas chromatographically (column: 3% XE-60/chromosorb W, 10 mmϕ × 75 cm, 150 °C); semicarbazone: mp 175—177 °C. The spectral data for this compound are given in Table 1, together with those of I and II, which were obtained[6] by catalytic hydrogenation of I.

Table 1. Spectral data

Compound	Mp of semicarbazone (°C)	IR (cm^{-1}) $\nu_{C=O}$	IR (cm^{-1}) δ_{CH_2}	NMR δ(ppm)
I	185—187	1734	1450	1.3—3.0 5.28
II	176—178	1730	1450	0.6—2.9
A	175—177	1730	1450	0.6—2.8

Thus, component A was confirmed to be 2-cyclohexylcyclohexanone.

A similar compound, 2,6-dicyclohexylcyclohexanone, was obtained in the dehydrogenation of 2,6-di(1-cyclohexenyl)cyclohexanone.[9,10]

Effects of Reaction Time and Temperature. The dehydrogenation of I was investigated in detail in the presence of 5% palladium-on-charcoal at temperatures 280, 300, and 320 °C for reaction time 1/2—8 hr. The changes in the amount of products obtained at temperatures 300 and 320 °C are shown in Figs. 2 and 3, respectively.

In all cases, increase in the reaction time caused a decrease in the yield of II and an increase in the amount of the phenols (III and IV). The change was remarkable at higher temperature. In particular, at 320 °C, II disappeared rapidly and V increased (47.3% after 8 hr).

Reaction Process. Since II hydrogenated was produced together with III and IV within 30 min, it is thought that dehydrogenation and hydrogenation take place competitively in an initial stage. Subsequently, II was dehydrogenated into III and IV.* The dehydrogenation occurs more readily in the cyclohexanone ring than in the cyclohexene ring.

III was also dehydrogenated into IV. This process has been reported.[1] It is thought that V was formed *via* IV, since it was produced in the dehydrogenation of III and in the cyclization of IV in the presence of palladium catalyst.[1]

* The dehydrogenation of 2-cyclohexylcyclohexanone is in progress. The process was found to give *o*-cyclohexylphenol, *o*-phenylphenol, and dibenzofuran.

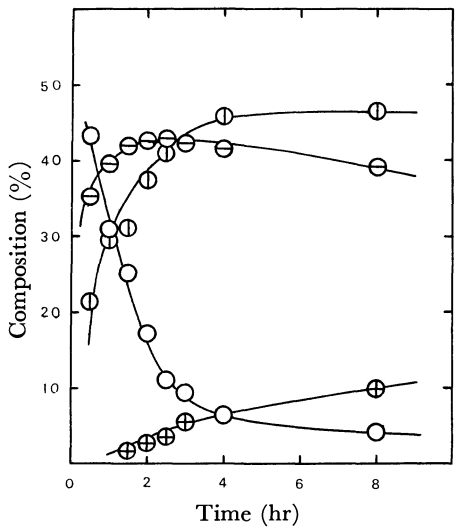

Fig. 2. Dehydrogenation at 300 °C.
○: II, ⊖: III, ⓘ: IV, ⊕: V

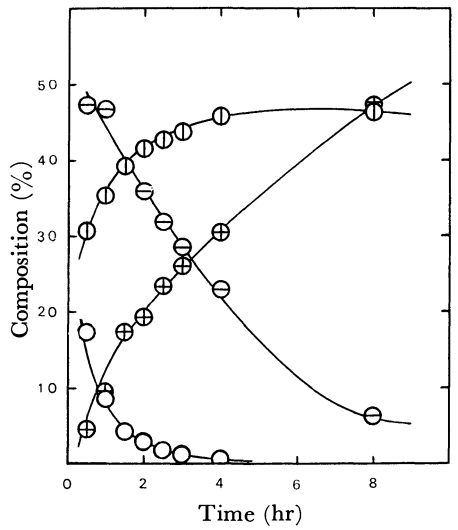

Fig. 3. Dehydrogenation at 320 °C
○: II, ⊖: III, ⓘ: IV, ⊕: V

The authors are grateful to Sanko Chemical Co. Ltd. for the supply of *o*-cyclohexyl- and *o*-phenylphenols.

References

1) H. Matsumura, K. Imafuku, I. Takano, and S. Matsuura, This Bulletin, **44**, 567 (1971).
2) R. Mozingo, "Organic Syntheses," Coll. Vol. III, p. 685 (1955).
3) K. K. Kelly and J. S. Mathews, *J. Chem. Eng. Data*, **14**, 276 (1969).
4) E. Wenkert, S. K. Bhattacharya, and E. M. Wilson, *J. Chem. Soc.*, **1964**, 5617.
5) A. Haller, *Ann. Chim.*, [10], **1**, 295 (1924).
6) J. V. Braun and H. Ritter, *Ber.*, **55**, 3792 (1922).
7) M. Guerbet, *C. R. Acad. Sci. Paris*, **155**, 1158 (1912).
8) W. Hückel and O. Neunhoeffer, *Ann.*, **477**, 120 (1930).
9) J. Plesek, *Collect. Czech. Chem. Commun.*, **21**, 375 (1956).
10) J. Kahovec and J. Pospisil, *ibid.*, **34**, 3170 (1969).

Catalytic Hydrogenation of Cyclic Olefins on Nickel Catalysts*

Masatsugu KAJITANI, Yoshiaki SASAKI, Junko OKADA, Kazuo OHMURA, Akira SUGIMORI, and (the late) Yoshiyuki URUSHIBARA

Department of Chemistry, Faculty of Science and Technology, Sophia University, Kioi-cho, Chiyoda-ku, Tokyo 102

(Received October 23, 1973)

The catalytic hydrogenation of cyclic olefins was investigated over various nickel catalysts. The hydrogenation of cyclohexene was promoted by basic reaction conditions and depressed by acidic ones, the hydrogenation of cyclooctene being only slightly influenced by the acidity. The results of competitive hydrogenation indicate that cyclooctene is adsorbed more strongly on nickel catalysts than cyclohexene. The external olefinic bond is preferentially hydrogenated to the internal olefinic bond.

Cycloalkenes show different reactivities in catalytic hydrogenation, depending on the ring size. Jardine and McQuillin found that, over a Pd-charcoal catalyst, the rate of hydrogenation is linear with respect to the heat of hydrogenation, the rates of hydrogenation being of the order: cyclohexene>cyclopentene>cyclooctene.[1] In the case of nickel catalysts, Brown[2] and Brown and Brown[3] reported the order to be: cyclopentene>cyclohexene>cyclooctene (over R-Ni catalyst), cyclopentene>cyclooctene>cyclohexene (over P-1 Nickel Boride catalyst, abbreviated to P-1 Ni_2B).

We have investigated the hydrogenation of cycloalkenes with Urushibara type nickel catalysts, the preparation conditions of which are widely variable. We also studied the effects of added alkali and acid, and the competitive hydrogenation of cycloalkenes. The results were compared with those of other nickel catalysts.

They might provide some insight into the nature of catalysts and the behavior of cycloalkenes in catalytic hydrogenation.

Experimental

Materials. Commercial cyclohexene (Tokyo Kasei, Reagent Grade) and cyclooctene (Wako Pure Chemical Industry, Reagent Grade) were distilled at 83.5 °C and 63 °C/62 mmHg. Reagent Grade cyclopentene, 4-vinylcyclohexene, 1-methylcyclohexene, 3-methylcyclohexene, and 4-methylcyclohexene (Wako Pure Chemical Industry) were used without further purification.

The samples were proved to be pure by gas-chromatography. Trace amounts of methylcyclohexene contaminants were detected by gas-chromatography.

Commercial ethanol was carefully distilled and used as the solvent of hydrogenation.

Catalysts. Urushibara type nickel catalysts were prepared by simplified methods[4] Ppt-Ni was easily prepared by adding 4.04 g of powdered nickel chloride ($NiCl_2 \cdot 6H_2O$) to 10 g of zinc dust suspended in 4 ml of distilled water under vigorous stirring. This was filtered off, washed with about 200 ml of hot distilled water previously degassed by boiling and then with EtOH.

U-Ni-N catalyst was prepared by refluxing ppt-Ni with 30 ml of isopropyl alcohol for two hours under stirring.[5]

Urushibara type nickel catalysts prepared by simplified methods are usually distinguished from ordinary catalysts by the bracketed letter (s) [U-Ni-A (s) or U-Ni-B (s)].[4,6] However, (s) has been omitted in this paper.

R-Ni(W-7 type) catalyst was prepared by the method of Adkins and Billica.[7]

Nickel Boride catalyst (Ni_2B) was prepared as reported by Paul *et al.*, by reducing nickel chloride with sodium borohydride in aqueous solution.[8]

After these catalysts had been subjected to hydrogenation, they were washed throughly with distilled water to completely remove alkali or acid, and several times with ethanol to remove contamination in the water. In particular, U-Ni-B, R-Ni and Ni_2B were sufficiently washed with water until the washings were neutral to phenolphthalein.

The catalysts thus prepared contain about 1 g of Ni.

Hydrogenation. The substrate (0.01 mol) was hydrogenated with various nickel catalysts in 20 ml of ethanol at 30 °C and atmospheric pressure in a glass bottle shaker at 300—350 strokes per minute.

Addition of alkali or acid was carried out before the catalyst was saturated with hydrogen gas. The amounts of alkali and acid added were 0.3 ml of 10% NaOH and 0.5 ml of 13% CH_3COOH, respectively. The amount of alkali added to U-Ni-A was so chosen as to make the solution faintly alkaline to phenolphthalein, as reported by Nishimura.[9]

The rate of hydrogenation was expressed in terms of the initial rate of hydrogen uptake in the region of 0 to about 20% hydrogenation, in which the hydrogen uptake curve was approximately linear.

Analysis of Reaction Mixture. The reaction mixture resulting from the competitive hydrogenation of a mixture of cyclohexene (0.01 mol) and cyclooctene (0.01 mol) was collected at about 100 ml of hydrogen uptake, and subjected to gas-chromatographic analysis as soon as possible. A column of 20% PEG 20M on Celite 545 (column temperature: 56 °C) was used.

Results and Discussion

Effect of Ring Size. In order to investigate the characteristics of nickel catalysts prepared by various methods, the hydrogenation of cyclopentene, cyclohexene, and cyclooctene was carried out at 30 °C under atmospheric pressure. The results are summarized in Table 1. The activities of the catalysts used were compared in terms of the initial rate of hydrogen uptake.

The rates of hydrogenation with U-Ni-A, U-Ni-B, and ppt-Ni were found to be in the order: cyclopentene>cyclohexene>cyclooctene (Nos. 1, 4, and 6,

* A part of the present work was presented at the 27th Annual Meeting of the Chemical Society of Japan, Nagoya, October 12th, 1972. Abstract of Paper, Vol. 2, p. 359.

TABLE 1. HYDROGENATION OF CYCLOOLEFINS OVER VARIOUS NICKEL CATALYSTS AT 30°C UNDER ATMOSPHERIC PRESSURE

Amount of samples; 0.01 mol, solvent; EtOH 20 ml, Ni content of catalysts; U-Ni-A, U-Ni-B, U-Ni-N, R-Ni, and Ni_2B, 1 g, ppt-Ni 2 g

Entry No.	Catalyst	Initial rate of H_2 uptake (ml/min)			Rate ratio (c-6/c-8)[a]
		Cyclopentene	Cyclohexene	Cyclooctene	
1	U-Ni-A	54	27	15	1.8
2	U-Ni-A+A[b]		7	11	0.6
3	U-Ni-A+B[c]		32	10	3.3
4	U-Ni-B	70	55	16	3.4
5	U-Ni-N(*i*-PrOH)[d]		24	4	6.0
6	ppt-Ni	8	8	2	4.0
7	ppt-Ni(Ni, 1g)		4	1	4.0
8	R-Ni(W-7)		84	46	1.7
9	R-Ni(W-7)+B[c]		45	20	2.2
10	Ni_2B		44	45	0.98
11	Ni_2B+A[b]		14	38	0.37
12	Ni_2B+B[c]		49	44	1.1

a) r_1=(rate of cyclohexene/rate of cyclooctene). b) A: 0.5 ml of 13% CH_3COOH. c) B: 0.3 ml of 10% NaOH. d) Prepared by refluxing ppt-Ni with *i*-PrOH (30 ml) for 2 hr.

Table 1). The order is the same as that with Raney nickel catalyst.[2,3] However, the relative reactivities varied depending on the method of preparation. When the hydrogenation is performed over U-Ni-B, the difference in reactivities is the greatest, while hydrogenation over ppt-Ni gives a rate of hydrogenation of cyclohexene similar to that of cyclopentene.

This could be explained by the change of the catalyst surface by acid and alkali. U-Ni-A catalyst can be subjected to hydrogenation under practically neutral conditions since acetic acid adsorbed on U-Ni-A can be removed easily by washing. On the other hand, sodium hydroxide adsorbed on U-Ni-B cannot be removed completely by washing with water, even if washing is repeated as often as necessary until the washings are no longer alkaline to phenolphthalein.

In order to confirm the role of acid and alkali, the effects of added alkali or acid on the rates of hydrogenation of cyclohexene and cyclooctene were investigated in detail. It was found that the rate of hydrogenation of cyclohexene is remarkably influenced by added acid or alkali, while the hydrogenation of cyclooctene is influenced to a lesser extent (Nos. 2 and 3, Talbe 1). U-Ni-B of basic character exhibited higher activity for cyclohexene than U-Ni-A of neutral character. On the other hand, cyclooctene was hydrogenated by U-Ni-A and U-Ni-B at a comparable rate.

The ratio of the rate of hydrogenation of cyclohexene to that of cyclooctene over U-Ni-A added alkali (abbreviated to U-Ni-A+B) is 3.3, and the value is similar to that of U-Ni-B. This suggests that the behavior of the U-Ni-B catalyst is due to the presence of sodium hydroxide used as the digesting agent. In the case of U-Ni-A added acid (abbreviated to U-Ni-A+A), cyclooctene was hydrogenated more easily than cyclohexene (an inversion in reactivity). Ppt-Ni, the precursor of the Urushibara nickel catalyst, behaves similarly to U-Ni-B. The U-Ni-N catalyst prepared by refluxing ppt-Ni with *i*-PrOH exhibited also a high reactivity to cyclohexene.[5]

R-Ni(W-7 type), which was well washed until the washings were no longer alkaline to phenolphthalein, behaved similarly to U-Ni-A. With R-Ni, the effect of added alkali was similar to that with U-Ni-A catalyst.

Nickel boride catalyst (Ni_2B), prepared according to Paul *et al.*[8] by reducing nickel chloride with sodium borohydride in aqueous solution and then washing until the washings were no longer alkaline to phenolphthalein, exhibited approximately the same catalytic activity in the hydrogenation of cyclohexene and cyclooctene.

It was confirmed that the effects of alkali or acid on the rate of hydrogenation of cyclohexene and cyclooctene were the same for Ni_2B as for the U-Ni-A catalyst.

As regards hydrogenation performed over various types of nickel catalysts, the activity for hydrogenation of cyclohexene is promoted by alkali and inhibited by acid, while the hydrogenation of cyclooctene is influenced slightly by alkali or acid.

Apparent Activation Energy. The rates of hydrogenation of cyclohexene and cyclooctene (Table 1) are comparable with the apparent activation energies of the hydrogenation of cyclohexene and cyclooctene in the presence of U-Ni-A, U-Ni-B, and ppt-Ni (Table 2).

TABLE 2. APPARENT ACTIVATION ENERGIES OF HYDROGENATION OF CYCLOHEXENE AND CYCLOOCTENE

Cyclohexene; 0.01 mol, cyclooctene; 0.01 mol, solvent; EtOH 20 ml, Ni content of catalysts; U-Ni-A and U-Ni-B 1 g, ppt-Ni 2 g, hydrogenation temperature; 30—50 °C

Catalyst	E_a (kcal/mol)	
	Cyclohexene	Cyclooctene
U-Ni-A	2.3	2.1
U-Ni-B	1.8	7.6
ppt-Ni	6.9	22.6

The activation energies in the hydrogenation of cyclohexene and cyclooctene over U-Ni-A were practically the same. However, in the presence of U-Ni-B or

Table 3. Competitive hydrogenation of mixture of cyclohexene and cyclooctene with various nickel catalysts at 30 °C under atmospheric pressure

Amount of samples; cyclohexene (0.01 mol)+cyclooctene (0.01 mol), solvent; EtOH 20 ml, Ni content of catalysts; 1 g

Entry No.	Catalyst	Yield (%)[a]		Product ratio	
		Cyclohexane	Cyclooctane	(c-6/c-8)=r_2[b]	(r_2/r_1)[c]
1	U-Ni-A	16.6	22.3	0.74	0.41
2	U-Ni-A+A[d]	6.1	20.0	0.31	0.52
3	U-Ni-A+B[e]	18.8	13.1	1.4	0.42
4	U-Ni-B	24.7	18.3	1.4	0.41
5	U-Ni-N(*i*-PrOH)[f]	11.9	12.7	0.94	0.15
6	ppt-Ni(Ni, 2 g)	21.4	20.3	1.1	0.28
7	R-Ni(W-7)	23.9	25.2	0.95	0.56
8	Ni_2B	16.3	43.8	0.37	0.38
9	Ni_2B+A[d]	4.8	38.1	0.13	0.35
10	Ni_2B+B[e]	18.4	33.2	0.55	0.50

a) yield of hydrogenation products at about 20% of hydrogen uptake. b) r_2=(yield of cyclohexane/yield of cyclooctane). c) [product ratio (r_2)/rate ratio (r_1)]. d) A: 0.5 ml of 13% CH_3-COOH. e) B: 0.3 ml of 10% NaOH. f) prepared by refluxing ppt-Ni with *i*-PrOH (30ml) for 1 hr.

ppt-Ni, cyclooctene gave a greater activation energy than cyclohexene. In the case of U-Ni-B, the presence of a small amount of alkali can lower the activation energy of the hydrogenation of cyclohexene. U-Ni-B and U-Ni-N have a similar behavior toward cyclohexene and cyclooctene as regards the rate and activation energy. This suggests a resemblance in the surface character of the catalysts.

Competitive Hydrogenation. The competitive hydrogenation of a mixture of cyclohexene and cyclooctene with various nickel catalysts was carried out in order to obtain further information on the selectivities of catalysts.

Competitive hydrogenation has been reported on olefins[11] and nitrobenzenes,[12] the results of which give information on the selectivity in adsorption.

The selectivity in the competitive reaction was obtained by comparing the product ratio (r_2), that is, yield of cyclohexane/yield of cyclooctane, at about 20% of hydrogen uptake,[13] with the rate ratio (r_1) obtained in individual hydrogenation. The value (product ratio/rate ratio; r_2/r_1) is used as a measure for the strength of adsorption. The results are summarized in Table 3.

We see that cyclooctene is more slowly hydrogenated than cyclohexene (No. 1, Table 1). However, in competitive hydrogenation, cyclooctene which is more strongly adsorbed on the catalyst is preferentially hydrogenated.

Though the rates of hydrogenation of cyclohexene and cyclooctene are dependent upon the catalysts and the addition of acid or alkali, it was found that the values (r_2/r_1) in the adsorption of cyclohexene and cyclooctene is approximately equal in all cases except U-Ni-N. Cyclooctene is twice as strongly adsorbed as cyclohexene. The character of U-Ni-N, which exhibits a different selectivity of adsorption from other catalysts, showed lower double bond migration in the hydrogenation of 1-octene.[5]

Hydrogenation of Methylcyclohexenes. The hydrogenation of methylcyclohexenes was studied in some detail (Table 4).

Table 4. Hydrogenation of methylcyclohexenes (0.01 mol) at 30 °C under atmospheric pressure

Solvent: EtOH 20 ml, Ni content of catalyst: 1 g

	Initial rate of H_2 uptake (ml/min)			
	(Cyclohexene)	4-Me	3-Me	1-Me
U-Ni-A	27	12	8	2
U-Ni-A+A[a]	7	5	3	1
U-Ni-A+B[b]	32	21	20	2
U-Ni-B	55	36		4

a) 0.5 ml of 13% CH_3COOH. b) 0.3 ml of 10% NaOH.

The rate of hydrogenation of cyclohexene was depressed by introducing methyl groups. The effect was in the order: 4-methyl<3-methyl≪1-methyl. 1-Methylcyclohexene could be hydrogenated only at a very small rate. This is probably explained by steric hindrance in the adsorption.

It was found that the rates of hydrogenation of 4-methylcyclohexene and 3-methylcyclohexene are accelerated by added alkali and inhibited strongly by added acid.

Hydrogenation of 4-Vinylcyclohexene (Fig. 1). The difference in reactivity between the internal olefin (cyclohexene ring) and the external olefin (vinyl group) was investigated in the hydrogenation of 4-vinylcyclohexene.

The hydrogen uptake curves at 30 °C under atmospheric pressure are shown in Fig. 1.

Hydrogenation of 4-vinylcyclohexene proceeds stepwise as follows:

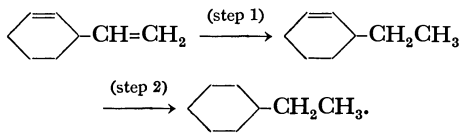

The hydrogen uptake curve exhibits a break at an

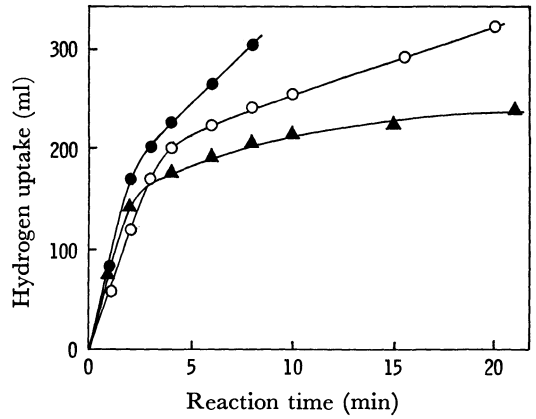

Fig. 1. Hydrogenation of 4-vinylcyclohexene (1 ml) over Urushibara type catalysts in EtOH (20 ml) at 30 °C under atmospheric pressure. Ni content of catalysts: 1 g ●: U-Ni-B, ▲: U-Ni-A, ○: ppt-Ni

uptake of 1.0 mol of hydrogen. After the uptake of 1.0 mol of hydrogen, glc analysis showed that the vinyl group had been almost completely hydrogenated. Brown has reported that the selective hydrogenation of 4-vinylcyclohexene takes palce with the P-1 Ni_2B catalyst.[2)]

The rates of hydrogenation at each step are as follows: step 1, U-Ni-B>U-Ni-A>ppt-Ni; step 2, U-Ni-B>ppt-Ni>U-Ni-A.

It is noted that ppt-Ni catalyst differs from U-Ni-A catalyst in the rate of hydrogenation at step 2, *viz.*, at the hydrogenation of cyclohexene ring. The above facts suggest that ppt-Ni exhibits characteristics similar to those of U-Ni-B which exhibits a high activity for cyclohexene owing to its basic character, as is expected from the results of cyclohexene hydrogenation and the apparent activation energy.

The authors wish to thank Dr. Shigeo Nishimura, Tokyo University of Agriculture and Technology, for his valuable suggestions.

References

1) I. Jardine and F. J. McQuillin, *J. Chem. Soc., C*, **1966**, 458.
2) C. A. Brown, *J. Org. Chem.*, **35**, 1900 (1970).
3) C. A. Brown and H. C. Brown, *J. Amer. Chem. Soc.*, **85**, 1003, 1005 (1963).
4) S. Taira, This Bulletin, **34**, 1294 (1961).
5) M. Kajitani, J. Okada, T. Ueda, A. Sugimori, and the late Y. Urushibara, *Chem. Lett.*, **1973**, 777.
6) Y. Urushibara, This Bulletin, **25**, 280 (1952); Y. Urushibara and S. Nishimura, *ibid.*, **27**, 480 (1954); Y. Urushibara, S. Nishimura, and H. Uehara, *ibid.*, **28**, 446 (1955). [see K. Hata, "Urushibara Catalysts," Univ. of Tokyo Press (1971).]
7) H. Adkins and H. R. Billica, *J. Amer. Chem. Soc.*, **70**, 695 (1948).
8) R. Paul, P. Buisson, and N. Joseph, *Ind. Eng. Chem.*, **44**, 1006 (1952).
9) S. Nishimura, *Nippon Kagaku Zasshi*, **79**, 56 (1958).
10) In X-ray diffraction studies, ppt-Ni contains zinc, zinc oxide, and zinc hydroxide chloride. In U-Ni-B and U-Ni-N, the X-ray diffraction patterns show only lines due to zinc and zinc oxide, and the lines of zinc hydroxide chloride disapper.
11) L. M. Berkowitz and P. N. Rylander, *J. Org. Chem.*, **24**, 708 (1959). G. V. Smith and R. L. Burwell, Jr., *J. Amer. Chem. Soc.*, **84**, 925 (1960). A. W. Weitkamp, *J. Catal.*, **6**, 431 (1966). N. A. Dobson, G. Eglinton, K. A. Raphael, and R. C. Wils, *Tetrahedron*, **16**, 16 (1961).
12) A. Sugimori, This Bulletin, **34**, 407 (1961).
13) It seems that the variation of the conversion at about 20% of hydrogen uptake may be due to the difference in the amount of hydrogen on the catalysts.

Regio- and Stereo-selectivities in the Epoxidations of Limonene, *endo*-Dicyclopentadiene, and *exo*-Dicyclopentadiene

Tadashi SATO and Eigoro MURAYAMA

Department of Applied Chemistry, Waseda University, Shinjuku-ku, Tokyo 160

(Received November 2, 1973)

The regio- and stereo-selectivities were observed in the radical and peracid epoxidations of limonene, *endo*-, and *exo*-dicyclopentadienes. The observations were considered in view of the proposed mechanisms for these reactions.

It has been believed that the epoxidation by molecular oxygen of olefin induced by a radical initiator proceeds through a peroxy-radical attack to open the double bond,[1] while the epoxidation by peracid proceeds through an electrophilic attack of the peracid oxygen to make a three-membered cyclic transition state.[2] In our experiments connected with studies of the unsensitized photooxidations of limonene and dicyclopentadienes,[3] we observed substantial regio- and stereo-selectivities in the radical and peracid epoxidations. These observations were then considered in the light of the proposed mechanisms.

Results

Limonene (**1**), *endo*-dicyclopentadiene (**2**), and *exo*-dicyclopentadiene (**3**) were oxidized with molecular oxygen at 40—60 °C (Ox I) and with peracid (Ox II). The epoxides **4**—**10** were isolated in pure states by preparative gas chromatography, and the product identification was carried out spectroscopically (see Experimental Section). The ratios of the regioisomers in each case were calculated; they are shown in Table 1.

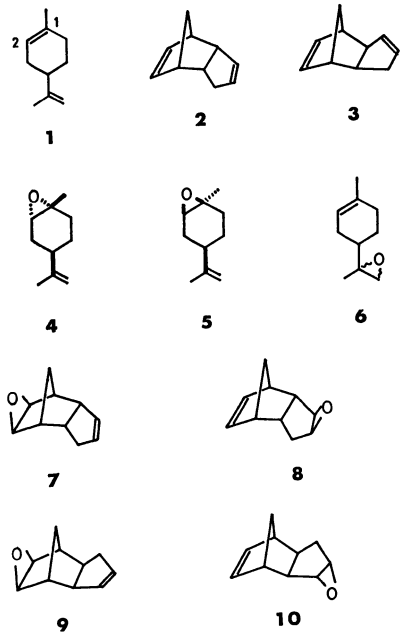

Table 1. Product ratios in the epoxidations of **1**–**3**

	(4+5)/6	7/8	9/10
Ox I	4.8	7.0	7.4
Ox II	14.0	1.3	3.7

Discussion

It was found that the 1,2-epoxidation of **1** by the radical-initiated oxidation proceeds in quite a stereoselective manner, affording mainly the *trans*-isomer **4**.* This result should be contrasted with that of the peracid epoxidation, where a 1 : 1 mixture of *trans*- and *cis*-isomers (**4** and **5**) has been obtained.[6] This observation can now be interpreted in terms of the general pattern of radical attack on 4-substituted cyclohexene.[7]

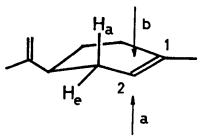

Fig. 1.

Presumably, the initial attack of the peroxy radical occurs at C-2 rather than at C-1 in view of Markownikov's principle (Fig. 1). The a-attack (*trans* to isopropenyl) at C-2 would be preferable to the alternative b-attack, since the b-attack creates a larger energy by its interference with the neighboring quasi-axial hydrogen (H_a), thus leading to the more unfavorable twisted-boat transition state. This type of attack can reasonably be said to lead to the preferential formation of **4** over **5**, as has actually been observed.

As is revealed by Table 1, the relative reactivity of each double bond in **1**—**3** was characteristic of the oxidation method. With **1**, the regioselectivity was observed in Ox II, while with **2** and **3**, the selectivity was observed to a larger extent in Ox I. These observations can be explained by the following consideration. The epoxidation with peracid has been interpreted as proceeding by an electrophilic attack of peracid oxygen on the double bond, thus producing a three-membered cyclic transition state.[2] It has generally been accepted that, in the reactions proceeding through a four-, five-, or six-membered cyclic transition state, the reactivity of a strained double bond is greatly enhanced as compared with that of a strain-free double bond, because a great deal of strain-energy release is expected in the transition state, while in the reaction proceeding through a three-membered cyclic transition state, scarcely any strain-energy release is expected in the transition state, and the strain present in the double bond can not play a very important role

* A previous experiment dealing with this problem has not led to any definite result.[4] A non-stereospecific radical epoxidation has, however, been reported with α-terpineol.[5]

in the reactivity.[8] Evidently, each double bond in **1** is characterized mostly by its electron density rather than by its strain energy, while the situation is reversed with **2** and **3**, since the double bond in the norbornene moiety is confined under strained circumstances. In the Ox II of **1**, where the reactivity of the double bond is determined mostly by the electron density, three-substituted olefin would be epoxidized preferentially over the two-substituted olefin, and a high selectivity should result. The selectivity would be reduced with Ox I, since there is little difference in strain energy between the two double bonds in **1**. The minor preference for the formation of **4** and **5** over **6** is probably a reflection of the electrophilic nature of the radical reaction.[9]

Contrary to the results with **1**, we observed a substantial regio selectivity in Ox I with **2** and **3**. Evidently the radical epoxidation *via* double-bond opening proceeds much faster with a double bond of strained norbornene. In Ox II, however, there was little selectivity between the two double bonds. A slight preference in the reactivity of norbornene double bond, particularly with **3**, induces us to picturize the transition state as involving a *loose* three-membered cyclic ring, thus affording an additional, although small, energy of strain release. The extreme low **7**/**8** ratio with **2** may be considered as a consequence of π-interaction through the space between the two double bonds in **2**, which interaction is evidently lacking in **3**.[10]

Experimental

Only experiments which do not overlap with those reported in our previous paper[3] are described here.

Starting Material. **3**: Prepared according to the method reported by Bartlett.[11]

Peracid Oxidation. Olefin (0.5 g) and perbenzoic acid (0.5 g) were dissolved in chloroform (6 ml) and stirred for 12 hr at 0 °C.

Product Identification. **5**: IR; Identical with the reported.[6] NMR; δ 1.25 (3H, s), 1.67 (3H, s), 2.85 (1H, d), and 4.65 (2H, s). **9**: IR; 1620 and 850 cm^{-1}. NMR; δ: 1.75 (2H, ABq, *endo*-methylene with an anisotropic effect by the epoxy ring), 2.96 (2H, s), and 5.43 (2H, m). **10**: IR; 1572 and 840 cm^{-1}. NMR; δ 1.40 (2H, b.s, *endo*-methylene), 3.10 (1H, d), 3.43 (1H, t), and 6.06 (2H, b.s).

References

1) S. J. Moss and H. Steiner, *J. Chem. Soc.*, **1965**, 2372, and the references cited therein.
2) D. Swern, "Organic Peroxides," Vol. II, ed. by D. Swern, Wiley-Interscience, New York, N. Y. (1971), p. 472.
3) T. Sato and E. Murayama, This Bulletin, **47**, 715 (1974).
4) G. O. Schenck, O.-A. Neumüller, G. Ohloff, and S. Schroeter, *Ann. Chem.*, **687**, 26 (1965).
5) J. P. Bain, W. Y. Gary, and E. A. Klein, US 3014047 (1961). Glidden Co. (*Chem. Abst.*, **57**, 12557 (1962)).
6) W. F. Newhall, *J. Org. Chem.*, **29**, 185 (1964).
7) O. Simamura, "Topics in Stereochemistry," Vol. 4, ed. by E. L. Eliel and N. L. Allinger, Wiley-Interscience, New York, N. Y. (1969), p. 1.
8) A. K. Awasthy and J. Rocek, *J. Amer. Chem. Soc.*, **91**, 991 (1969); K. B. Sharpless, J. M. Townsend, and D. R. Williams, *ibid.*, **94**, 295 (1972); T. Sato, T. Mori, and J. Shinoda, This Bulletin, **46**, 1833 (1973).
9) J. I. G. Cadogan and M. J. Perkins, "The Chemistry of Alkenes," Vol. 1, ed. by S. Patai, Interscience Publishers, London (1964), p. 585.
10) T. Yamazaki, N. Muto, T. Shimoda, and S. Fujiki, Abstracts of papers presented at the 23rd meeting of the Chemical Society of Japan, Tokyo, April, 1970, Vol. III, p. 1683.
11) P. D. Bartlett, *J. Amer. Chem. Soc.*, **69**, 2553 (1947).

The Photo-Fries Rearrangement of Aryloxy-1,3,5-triazines

Yukio OHTO, Haruo SHIZUKA, Shizen SEKIGUCHI, and Kohji MATSUI

Department of Chemistry, Faculty of Engineering, Gunma University, Tenjincho, Kiryu, Gunma 376

(Received November 2, 1973)

Aryloxy-*s*-triazines gave *o*- and/or *p*-hydroxyaryl-*s*-triazines upon irradiation; however, from arylamino- and arylthio-*s*-triazines, no photo-rearrangement product was obtained. The *p*-CH_3, *p*-Cl, and *p*-OCH_3 groups in the phenoxy moiety did not prevent the photoreaction of aryloxy-*s*-triazines; however, the *p*-CHO, *p*-$COCH_3$, *p*-$COOC_2H_5$, and *p*-NO_2 groups prevented the photoreaction. As to substituents in the *s*-triazine moiety, such groups as –Cl, $-OCH_3$, $-OC_6H_5$, and $-CH_3$ did not prevent the photoreaction; however, C_6H_5 and amino groups prevented the reaction. In the photolysis of 2,4-dimethoxy-6-(1-naphthyloxy)-*s*-triazine, 1-hydroxy-2-naphthyl- and 4-hydroxy-1-naphthyl-*s*-triazines were obtained, with the preferential formation of the former. On the other hand, from 2,4-dimethoxy-6-(2-naphthyloxy)-*s*-triazine, 2-hydroxy-1-naphthyl-*s*-triazine was obtained upon irradiation. In a similar manner, 2- and 4-acetyl-1-naphthols were obtained from 1-naphthyl acetate, and 1-acetyl-2-naphthol was isolated from 2-naphthyl acetate.

The photo-Fries rearrangement has been extensively investigated; the mechanism of the reaction and some of the substituent effects have been revealed with the reactions of *O*-acyl-phenols and *N*-acyl-anilines.

Recently, we have reported that aryloxy-dimethoxy-*s*-triazines rearrange photochemically to give the corresponding *o*- and/or *p*-hydroxyaryl-*s*-triazines.[1] The reaction had been found to proceed *via* a radical process. However, the characteristics of the *s*-triazinyl moiety as a migrating group and the relations between the chemical constitutions and the photoreactivities have not been revealed. In addition, aryloxy-*s*-triazines containing various substituents in the aryloxy and *s*-triazine moieties are readily available by the condensation of aryloxy-halo-*s*-triazines with nucleophiles or by the reaction of halo-*s*-triazines with phenolates. Therefore, if the photo-Fries rearrangement of aryloxy-*s*-triazines takes place regardless of substituents in the aryloxy and *s*-triazine moieties, this photoreaction may provide a useful and convenient route for the syntheses of various hydroxyaryl-*s*-triazines. This paper will report the substituent effects on the photo-Fries rearrangement of phenoxy-*s*-traizines and naphthyloxy-*s*-triazines; the function of the *s*-triazinyl group for the reaction will also be discussed.

Experimental

Materials. Aryloxy-*s*-triazines were prepared by the condensation of phenolates with cyanuric chloride in the usual way,[2] followed by treatment with nucleophiles. The compounds thus obtained are listed in Table 1.

The experimental procedure and solvents were almost the same as those previously described.[1] A low-pressure mercury lamp was used as the 254 nm radiation source. After long irradiation at 254 nm, the reaction mixture was concentrated and the photo-products were separated and purified by column chromatography.

The identification of the photo-products was performed by means of their NMR, IR, UV, and MS spectra, by elemental analyses, and by studying the solubility in an alkaline solution.

Results and Discussion

Scope of the Photo-Fries Rearrangement of s-*Triazine Derivatives.* It is well known that not only *O*-acyl-phenols,[3] but also *N*-acyl-anilines,[4] rearrange photochemically to yield the corresponding ketones. Thus, in the cases of *s*-triazine derivatives, the photolysis was investigated not only with aryloxy-*s*-triazines, but also with arylamino- and arylthio-*s*-triazines. However, such an attempt with arylamino-*s*-triazines was unsuccessful, regardless of the substituents in the *s*-triazine and aniline moieties; ordinary arylamino-*s*-triazines are stable on irradiation with UV light. On the other hand, dimethoxy-phenylthio-*s*-triazine showed a complex spectral change on irradiation, and it had no isosbestic point. Thus, it may be said that, among the arylamino-, aryloxy-, and arylthio-*s*-triazines, the aryloxy derivative is the sole *s*-triazine compound capable of yielding photo-rearrangement products.

*Effects of Substituents on the Photo-Fries Rearrangement of Phenoxy-*s*-triazines.* As preliminary experiments, the reactivities for the photoreaction of all the phenoxy-*s*-triazines listed in Table 1 were checked by measuring their spectral change with the lapse of time at 254 nm in cyclohexane and ethanol. As a result, the progress of the photoreaction of aryloxy-*s*-triazines was found to depend significantly upon the substituents in the aryloxy and *s*-triazinyl groups.[5] The *p*-CH_3, *p*-Cl, and *p*-OCH_3 groups in the phenoxy moiety did not prevent the progress of the photoreaction; however, when electron-withdrawing groups such as *p*-CHO, *p*-$COCH_3$, *p*-$COOC_2H_5$, and *p*-NO_2 were introduced into the phenoxy moiety, the photoreaction did not take place.

As for substituents in the *s*-triazine nucleus, although the overall effect varied with the combination of two substituents, such substituents as –Cl, $-OCH_3$, $-OC_6H_5$, and $-CH_3$ did not prevent the photoreaction. Thus, any aryloxy-*s*-triazines containing any two of these substituents underwent the photo-rearrangement readily. It is known[6] that the derivatives of halo-*s*-triazine dissociate into the halogen atom and the *s*-triazinyl radical in benzene to give *s*-triazinylbenzene on irradiation. However, *s*-triazine derivatives containing both chloro and aryloxy substituents are preferentially rearranged photochemically to give hydroxyaryl-chloro-*s*-triazines. On the other hand, the phenyl group and such substituents as $-NH_2$, $-NHCH_3$, $-N(CH_3)_2$, and $-NHC_6H_5$ prevented the reaction very much.

In order to make clear the effects of the substituents

Table 1. Aryloxy-*s*-triazines

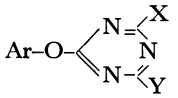

No.	Ar	X	Y	Mp (°C)	Solvent for recrystallization	Analysis (%) Found C	Found H	Calcd C	Calcd H
1	Phenyl	$-OCH_3$	$-OCH_3$	102—102.5[a]	Ligroin			—	
2	*o*-Tolyl	$-OCH_3$	$-OCH_3$	87.5—88.5	Ligroin	58.52	5.39	58.29	5.30
3	*p*-Tolyl	$-OCH_3$	$-OCH_3$	89—90.5[a]	Ligroin			—	
4	*p*-Chlorophenyl	$-OCH_3$	$-OCH_3$	86—87.5[a]	Ligroin			—	
5	*p*-Methoxyphenyl	$-OCH_3$	$-OCH_3$	80—81[a]	Ligroin			—	
6	*p*-Formylphenyl	$-OCH_3$	$-OCH_3$	146—147	Benzene	55.39	4.29	55.17	4.24
7	*p*-Acetylphenyl	$-OCH_3$	$-OCH_3$	119—120	Benzene	56.78	4.62	56.72	4.76
8	*p*-Ethoxycarbonylphenyl	$-OCH_3$	$-OCH_3$	122.6—123	Benzene	54.91	5.00	55.08	4.97
9	*p*-Nitrophenyl	$-OCH_3$	$-OCH_3$	136—136.5[b]	Benzene			—	
10	α-Naphthyl	$-OCH_3$	$-OCH_3$	87.5—88.5	Ligroin	58.62	5.39	58.29	5.30
11	β-Naphthyl	$-OCH_3$	$-OCH_3$	117—118	Benzene	63.54	4.57	63.60	4.63
12	1-Methyl-2-naphthyl	$-OCH_3$	$-OCH_3$	114—115	Ligroin	64.78	5.17	64.64	5.09
13	Phenyl	$-OCH_3$	$-Cl$	128—129	Ligroin	50.21	3.37	50.54	3.49
14	Phenyl	$-OCH_3$	$-OC_6H_5$	150—151	Benzene–Ligroin	63.78	4.76	63.60	4.63
15	Phenyl	$-OCH_3$	$-SCH_3$	112—114	Ligroin	52.89	4.36	53.21	4.47
16	Phenyl	$-OCH_3$	$-NH_2$	225—226	Benzene	55.24	4.68	55.04	4.62
17	Phenyl	$-OCH_3$	$-NHCH_3$	140.5—141.5	Benzene–Ligroin	58.88	5.52	58.53	5.72
18	Phenyl	$-OCH_3$	$-N(CH_3)_2$	94—95	Ligroin	60.03	6.01	60.46	5.46
19	Phenyl	$-OCH_3$	$-NHC_6H_5$	133—134	Benzene–Ligroin	58.18	5.52	58.53	5.73
20	Phenyl	$-OC_6H_5$	$-C_6H_5$	114—115	Ligroin	73.55	4.35	73.88	4.42
21	Phenyl	$-OC_6H_5$	$-OC_6H_5$	235—236[c]	Benzene			—	
22	Phenyl	$-OC_6H_5$	$-N(CH_3)_2$	145—146	Benzene	66.54	5.07	66.22	5.23
23	Phenyl	$-SCH_3$	$-Cl$	80.5—82.5	Ligroin	47.58	3.16	47.34	3.58
24	Phenyl	$-SCH_3$	$-SCH_3$	93—94	Ligroin	49.58	4.15	49.79	4.17
25	Phenyl	$-SCH_3$	$-N(CH_3)_2$	66—67	Ligroin	55.35	5.65	54.94	5.37
26	Phenyl	$-Cl$	$-Cl$	112—113[d]	Ligroin			—	
27	Phenyl	$-Cl$	$-NH_2$	231—232	Methanol	48.85	2.87	48.55	3.17
28	Phenyl	$-Cl$	$-NHCH_3$	148—149	Methanol–H_2O	50.35	3.85	50.75	3.83
29	Phenyl	$-Cl$	$-N(CH_3)_2$	139.5—140	Benzene–Ligroin	52.41	4.29	52.66	4.42
30	Phenyl	$-Cl$	$-NHC_6H_5$	102—104	Benzene–Ligroin	60.43	4.02	60.31	3.71
31	Phenyl	$-NHCH_3$	$-N(CH_3)_2$	136—137	Methanol–H_2O	56.90	5.54	57.13	5.66
32	Phenyl	$-N(CH_3)_2$	$-N(CH_3)_2$	106—107	Ligroin	60.49	6.54	60.22	6.60
33	Phenyl	$-NHC_6H_5$	$-NHC_6H_5$	185.5—187	Benzene	70.57	4.67	70.91	4.81
34	*p*-Tolyl	$-OCH_3$	$-OC_6H_4CH_3(p)$	96—97	Ligroin	67.06	5.51	66.86	5.30
35	*p*-Tolyl	$-OCH_3$	$-N(CH_2)_2$	87—88	Ligroin	60.34	6.50	59.97	6.20
36	*p*-Tolyl	$-Cl$	$-Cl$	90—91	Ligroin	47.27	2.90	46.90	2.75
37	*p*-Tolyl	$-OC_6H_4CH_3(p)$	$-OC_6H_4CH_3(p)$	216—217	Benzene	72.45	4.96	72.17	5.30
38	*p*-Tolyl	$-N(CH_3)_2$	$-N(CH_3)_2$	109—110	Ligroin	61.74	7.27	61.52	7.01
39	Phenylthio*	$-OCH_3$	$-OCH_3$	69—69.5	Ligroin	54.44	4.45	54.00	4.45
40	Anilino*	$-OCH_3$	$-OCH_3$	128—129[e]	Ligroin			—	
41	Anilino*	$-Cl$	$-Cl$	135.5—136.5[f]	Benzene			—	
42	Anilino*	$-N(C_2H_5)_2$	$-N(C_2H_5)_2$	87—89[g]	Ligroin			—	
43	*p*-Chloroanilino*	$-N(C_2H_5)_2$	$-N(C_2H_5)_2$	134—135[g]	Ligroin			—	
44	*N*-methylanilino*	$-OCH_3$	$-OCH_3$	51—52[h]	Aq. Methanol			—	

* Indicates that the substituent combines with the *s*-triazine nucleus in place of aryloxy group.

a) H. Shizuka, K. Matsui, *et al.*, *Tetrahedron*, **27**, 4021 (1971). b) T. Harayama, K. Matsui, *et al.*, *J. Heterocycl. Chem.*, **7**, 981 (1970). c) A. Hofmann, *Ber.*, **19**, 2063 (1886). d) R. Hirt and H. Nidecker, *Helv. Chim. Acta*, **33**, 1365 (1950). e) A. F. Crowther and F. H. S. Curd, *J. Chem. Soc.*, **1948**, 1636. f) J. T. Thurston *et al.*, *J. Amer. Chem. Soc.*, **73**, 2981 (1951). g) D. Walker, Y. L'Italien, W. Pearlman, and C. Banks, *J. Amer. Pharm. Assoc.*, **39**, 383 (1950). h) J. R. Dudley, J. T. Thurston *et al.*, *J. Amer. Chem. Soc.*, **73**, 2986 (1951).

TABLE 2. MOLAR EXTINCTION COEFFICIENTS AND QUANTUM YIELDS FOR THE PRODUCT FORMATION AT 254 nm IN CYCLOHEXANE

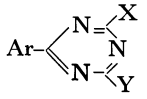

Ar	X	Y	λmax (nm)	ε	Φ	ΣΦ	$\sigma_mX+\sigma_mY$
HO-C_6H_4-(*o*)	$-OC_6H_5$	$-OC_6H_5$	270	2.25×10^4	0.21_1		
HO-C_6H_4-(*p*)	$-OC_6H_5$	$-OC_6H_5$	288	2.03×10^4	0.16_6	0.37_7	+0.504
HO-C_6H_4-(*o*)	$-OC_6H_5$	$-OCH_3$	268	1.95×10^4	0.17_3		
HO-C_6H_4-(*p*)	$-OC_6H_5$	$-OCH_3$	287	1.90×10^4	0.13_0	0.30_3	+0.367
HO-C_6H_4-(*o*)	$-OCH_3$	$-OCH_3$	267	1.67×10^4	0.14_6		
HO-C_6H_4-(*p*)	$-OCH_3$	$-OCH_3$	282	2.28×10^4	0.12_0	0.26_6	+0.230
HO-C_6H_4-(*o*)	$-OC_6H_5$	$-N(CH_3)_2$	261	1.69×10^4			
HO-C_6H_4-(*p*)	$-OC_6H_5$	$-N(CH_3)_2$	278	2.22×10^4			+0.041
HO-C_6H_4-(*o*)	$-N(CH_3)_2$	$-N(CH_3)_2$	256	1.85×10^4	0.002		
HO-C_6H_4-(*p*)	$-N(CH_3)_2$	$-N(CH_3)_2$	264	2.39×10^4	0.001	0.003	−0.422
(HO-)$(CH_3-)C_6H_3$-(2,5-)	$-OCH_3$	$-OCH_3$	268	1.85×10^4	0.13_4		+0.230
(HO-)$(CH_3-)C_6H_3$-(2,5-)	$-OCH_3$	$-N(CH_3)_2$	262	1.90×10^4	0.097		−0.096
(HO-)$(CH_3-)C_6H_3$-(2,5-)	$-N(CH_3)_2$	$-N(CH_3)_2$	257	2.18×10^4	0.002		−0.422
(HO-)$(CH_3-)C_6H_3$-(2,5-)	$-OC_6H_4-CH_3$(*p*)	$-OCH_3$	271	2.11×10^4	0.20_7		——
(HO-)$(CH_3-)C_6H_3$-(2,5-)		$-OC_6H_4-CH_3$(*p*)	273	2.29×10^4	0.23_5		——

in the *s*-triazine nucleus quantitatively, the quantum yields for the product formation were measured with several aryloxy-*s*-triazines. The results are shown in Table 2. From Table 2 it is obvious that the introduction of amino groups into the *s*-triazine nucleus hinders the photoreaction; in the experimental results it can be seen that, regardless of the substituents, the more positive the $\sigma_mX+\sigma_mY$ value in Table 2 becomes, the larger the quantum yield for the product formation becomes. These facts indicate that the progress of the photo-rearrangement depends mainly upon the electron-attracting ability of the *s*-triazine moiety. However, this apparent relation does not hold in every case; aryloxy-phenyl-*s*-triazine did not rearrange photochemically even though the phenyl group ($\sigma_m=+0.06$) is an electron-attractive substituent. If the reaction mechanism of the photo-Fries rearrangement is kept in mind, the question of the substituent effects may be solved. In general, the photo-Fries rearrangement occurs *via* the predissociation originated from $S_1(\pi\pi^*)$ $^1B_2$ (or ^1L_b), involving the β-bond fission of benzene derivatives.[1,7] The photochemical primary process of aryloxy-*s*-triazine originates from the lowest excited singlet state, $^1B_2$, which corresponds to the $^1B_{2u}$ state of benzene.[1] The reactivity in the photo-Fries rearrangement is dependent upon the electronic character of the lowest excited singlet state in a benzene derivative. The absorption spectrum of aryloxy-phenyl-*s*-triazine is very close to that of 2,4-dimethoxy-6-phenyl-*s*-triazine. Thus, the lowest absorption band of the molecule may be assigned to $^1L_a\leftarrow{}^1A$ (not to $^1L_b\leftarrow{}^1A$), considering the structureless band at 255 nm with $\varepsilon=2.25\times10^4$, just like that of biphenyl.[8] This band ($^1L_a\leftarrow{}^1A$) masks the photoreactive band ($^1B_2\leftarrow{}^1A_1$), and the $^1B_2$ state is not the lowest $\pi\rightarrow\pi^*$ singlet state, resulting in the significant decrease in the β-bond fission.

The introduction of electron-donating substituents such as amino groups into the *s*-triazine nucleus results in a bathochromic shift of the $\pi\rightarrow\pi^*$ band in *s*-triazine and a slight hypsochromic shift of the $n\rightarrow\pi^*$ band.[9a] The amino substituent increases the intensity of the lowest singlet $\pi\rightarrow\pi^*$ band in *s*-triazine, whose transition is symmetry-forbidden.[9b] Furthermore, the $^1A_1\leftarrow{}^1A_1$ band in aryloxy-*s*-triazine, with an amino group in the *s*-triazine nucleus, is assumed to be large enough to overlap the $^1B_2\leftarrow{}^1A_1$ band of the aryloxy group.[5] In fact, the vibrational structure in the $^1B_2\leftarrow{}^1A_1$ band disappears, in contrast to that of 2,4-dimethoxy-6-

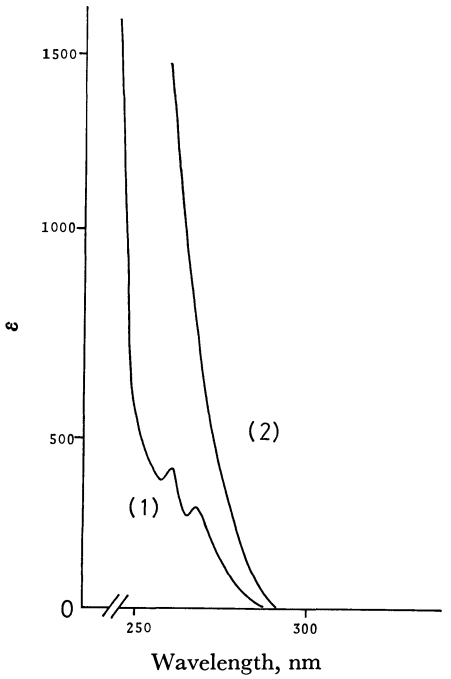

Fig. 1. UV spectra of 2,4-dimethoxy-6-phenoxy-*s*-triazine (1) and 2,4-bis(dimethylamine)-6-phenoxy-*s*-triazine (2).

phenoxy-*s*-triazine, as is shown in Fig. 1. Thus, the amino substituent in the *s*-triazine nucleus considerably lowers the quantum yield, as is shown in Table 2.

As has been mentioned above, the presence of an electron-withdrawing group such as *p*-NO_2, *p*-$COCH_3$, *p*-CHO, or *p*-$COOC_2H_5$, in the phenoxy moiety prevented the photo-rearrangement almost completely; it may be said that the predissociation at a β-band is difficult, because the $n\pi^*$ singlet state, which corresponds to the excitation from the non-bonding orbital in these substituents to the π^* molecular orbital, is the lowest excited singlet state in these cases (except for *p*-$COOC_2H_5$).

When more than two aryloxy groups are present in an *s*-triazine nucleus, the reaction stops at the stage of the rearrangement of one of the aryloxy groups, as in the photoreaction of tris(*p*-tolyloxy)-*s*-triazine to give 2-(5-methyl-2-hydroxyphenyl)-4,6-bis(*p*-tolyloxy)-*s*-triazine; *o*-hydroxyaryl-*s*-triazines are generally very stable on irradiation,[10] and *s*-triazine derivatives containing more than two *o*-hydroxyaryl groups could not be obtained by this photo-reaction.

Since *o*- and/or *p*-hydroxyaryl-chloro-*s*-triazines can be obtained in good yields by the photolysis of aryloxy-chloro-*s*-triazines, from these compounds a number of *o*- and *p*-hydroxyaryl-*s*-triazines including compounds which can not be obtained by the direct photolysis of the corresponding aryloxy-*s*-triazines were prepared by treatment with nucleophiles. There are several methods for the preparation of *o*- and *p*-hydroxyaryl-*s*-triazines.[10] Among these methods, the Friedel-Crafts *s*-triazinylation of phenols is assumed to be the most convenient; however, there are some limitations. For example, by the reaction with halo-*s*-triazines in the presence of aluminium chloride, only phenols with high reactivities towards electrophiles condense to give the desired products.[11] Therefore, the photo-Fries rearrangement of aryloxy-chloro-*s*-triazines, followed by treatment with nucleophiles, may be a novel and general convenient method for the preparation of various hydroxyaryl-*s*-triazines. Table 3 lists the *o*- and *p*-hydroxyaryl-*s*-triazines prepared directly or indirectly by the photo-Fries rearrangement.

Photo-rearrangements of Naphthyloxy-s-triazines. From the standpoint of studying the effect of the aryloxy moiety on the photo-rearrangement of aryloxy-*s*-triazines, some photo-reactions of naphthyloxy-*s*-triazines have been carried out. There have been many studies

Table 3. 2- and 4-hydroxyaryl-*s*-triazines

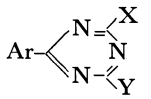

Ar	X	Y	Mp (°C)	Solvent for recrystallization	Anal. (%) Found C	Found H	Calcd C	Calcd H
HO-C_6H_4-(*o*)	$-OC_6H_5$	$-OC_6H_5$	164—165	Ligroin	70.64	4.42	70.58	4.23
HO-C_6H_4-(*p*)	$-OC_6H_5$	$-OC_6H_5$	237—238	Acetone	70.25	4.02	70.58	4.23
HO-C_6H_4-(*o*)	$-OCH_3$	$-OC_6H_5$	150—151	Ligroin	63.48	4.43	63.60	4.63
HO-C_6H_4-(*p*)	$-OCH_3$	$-OC_6H_5$	235—236	Acetone	63.78	4.51	63.60	4.63
HO-C_6H_4-(*o*)	$-N(CH_3)_2$	$-OC_6H_5$	147—148	Ligroin	65.88	4.96	66.22	5.23
HO-C_6H_4-(*p*)	$-N(CH_3)_2$	$-OC_6H_5$	238—239	Acetone	66.62	5.54	66.22	5.23
HO-C_6H_4-(*o*)	$-N(CH_3)_2$	$-N(CH_3)_2$	145—146	Ligroin	60.48	6.92	60.22	6.60
HO-C_6H_4-(*p*)	$-N(CH_3)_2$	$-N(CH_3)_2$	213—214	Acetone	60.58	6.98	60.22	6.60
(HO-)(CH_3-)C_6H_3-(2,5-)	$-OCH_3$	$-N(CH_3)_2$	137—138	Ligroin	60.28	6.47	59.97	6.20
(HO-)(CH_3-)C_6H_3-(2,5-)	$-N(CH_3)_2$	$-N(CH_3)_2$	162—163	Ligroin	61.74	7.09	61.52	7.01
(HO-)(CH_3-)C_6H_3-(2,5-)	$-OCH_3$	$-OC_6H_4-CH_3$(*p*)	131—132	Ligroin	66.50	5.49	66.86	5.30
(HO-)(CH_3-)C_6H_3-(2,5-)	$-OC_6H_4-CH_3$(*p*)	$-OC_6H_4-CH_3$(*p*)	158—159	Ligroin	71.89	5.50	72.17	5.30

Table 4. Photo-products of naphthyloxy-*s*-triazines and quantum yields for the product formation at 254 nm

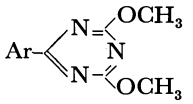

Ar	Yield[a] (%)	*o*/*p*	λmax (ε)[b] (nm)	Φ[b,c]
1-Hydroxy-2-naphthyl-(*o*-)	48	1.8	248(1.85×10^4), 325(1.07×10^4), 365(1.07×10^4)	0.12
4-Hydroxy-1-naphthyl-(*p*-)	27		236(1.21×10^4), 329(5.21×10^3)	0.09
(1-Naphthol)	18			—
2-Hydroxy-1-naphthyl-	67		301(1.67×10^4), 369(1.16×10^4)	0.17
(2-Naphthol)	17			—

a) Chemical yield in ethanol after irradiation with a 10-W low-pressure mercury lamp for 70 hr.
b) Measured in cyclohexane. c) Quantum yield for the product formation.

Table 5. Photo-products of 2,4-dimethoxy-6-naphthyloxy-*s*-triazines

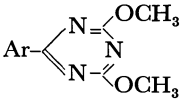

Ar	Mp °C	Solvent for recryst-allization	Anal. % Found C	Found H	Calcd C	Calcd H
HO-$C_{10}H_6$-(1,2-)	189—190	Ligroin	63.28	4.45	63.60	4.63
HO-$C_{10}H_6$-(4,1-)	203.5—204.5	Benzene	63.73	4.35	63.60	4.63
HO-$C_{10}H_6$-(2,1-)	147—148	Ligroin	63.52	4.86	63.60	4.63

of the Fries-rearrangement of *O*-acyl-naphthols;[12] however, little is known about their photo-reactions. Recently, the photolysis of 2-naphthyl ester with a high-pressure mercury lamp to give 2-naphthol[13] and the γ-radiolysis of 2-naphthyl acetate to give 1-, 6-, and 8-acetyl-2-naphthols and 2-naphthol[14] have been reported. However, no photo-Fries rearrangement of *O*-*s*-triazinyl-naphthols has been reported.

In the photolysis of 2,4-dimethoxy-6-(1-naphthyloxy)-*s*-triazine at 254 nm in ethanol, 2,4-dimethoxy-6-(1-hydroxy-2-naphthyl)-*s*-triazine, 2,4-dimethoxy-6-(4-hydroxy-1-naphthyl)-*s*-triazine, and α-naphthol were obtained, while only 2,4-dimethoxy-6-(2-hydroxy-1-naphthyl)-*s*-triazine was obtained as a rearrangement product, together with β-naphthol, from 2,4-dimethoxy-6-(2-naphthyloxy)-*s*-triazine, as is shown in Tables 4 and 5.

As has been mentioned in a previous paper,[1] in the photo-Fries rearrangement of 2,4-dimethoxy-6-phenoxy-*s*-triazine the quantum yields for the product formation are parallel to the odd π electron densities of the phenoxy radical, as is shown below, where Φ_o and Φ_p denote the quantum yields for the formation of *o*- and *p*-hydroxyphenyl derivatives and where ρ_o and ρ_p denote the odd π electron densities on the *ortho* and *para* positions in the phenoxy radical

$$0.5\Phi_o/\Phi_p = \rho_o/\rho_p \approx 0.5$$

The values of ρ_p and ρ_o are 0.125 and 0.25 respectively, as reported by Muller *et al.*[15]

In Fig. 2 are shown the calculated values of the odd π electron densities of the 1- and 2-naphthyloxy radicals

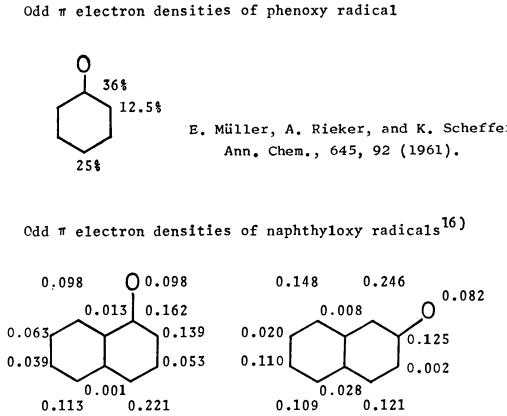

Fig. 2. Odd π electron densities of phenoxy radical and odd π electron densities of naphthyloxy radicals.[16]

obtained using the semi-empirical SCF-MO method.[16] From these values, the formation of 2-, 4-, and 5-*s*-triazinyl derivatives from 1-naphthyloxy-*s*-triazine and the formation of 1-, 6-, and 8-*s*-triazinyl derivatives from 2-naphthyloxy-*s*-triazine may be expected. However, the photoproducts from 1-naphthyloxy-*s*-triazine were the 2- and 4-*s*-triazinyl derivatives, while in the case of the 2-naphthyloxy derivative, 1-*s*-triazinyl derivative was obtained as the sole photo-rearrangement product. The result of these reactions tempted us to check the photoreaction of ordinary naphthyl esters. In a similar manner, in the photoreactions of 1-naphthyl acetate, 2- and 4-acetyl-1-naphthols were obtained, while 1-acetyl-2-naphthol was isolated from 2-naphthyl acetate. Thus, in the cases of naphthyloxy-*s*-triazines and naphthyl esters, the experimental results on isomer distribution did not agree with the calculated values of the odd π electron densities of naphthyloxy radicals; in addition, no acyl or *s*-triazinyl derivative of the adjacent aromatic nucleus was obtained, unlike the case of the ordinary Fries rearrangement of *O*-acetyl-2-naphthol to give 1- and 6-acetyl-2-naphthols.[17] When the 1-position of *O*-*s*-triazinyl-2-naphthol was occupied by another substituent, such as the methyl group, only a small amount of 1-methyl-2-naphthol was formed upon irradiation; most of the starting material was recovered, in spite of the expectation that *s*-triazinylated products at remote positions of high odd π electron densities of 2-naphthol would be formed.

Table 6. Yields of photo-products on irradiation of ethanol solutions of naphthyl acetates with a 10-W low-pressure mercury lamp for 25 hr

	Yield %	*o*/*p*
1-Naphthyl acetate	—	
1-Hydroxy-2-acetylnaphthalene (*o*-)	41	1.5
4-Hydroxy-1-acetylnaphthalene (*p*-)	27	
(1-Naphthol)	18	
2-Naphthyl acetate	—	
2-Hydroxy-1-acetylnaphthalene	67	
(2-Naphtol)	20	

In Table 4 the quantum yields for the product formation in the reactions of naphthyloxy-*s*-triazines are listed. From these results, it is obvious that, in the photoreaction of 1-naphthyloxy-*s*-triazine, the ratio

of the quantum yields for the *ortho* and *para* rearrangements [Φ_O/Φ_P (1.3)] differs considerably from that of the odd π electron densities of the 1-naphthyloxy radical [ρ_O/ρ_P (0.63)]; in the case of the 1-naphthyloxy radical, even though the calculated value of the odd π electron density at the 4-position is larger than that at the 2-position, the quantum yield for the rearrangement to the latter was larger than that to the former. A similar relation was also observed in the photoreaction of *O*-acetyl-1-naphthol, suggesting that the preferential formation of the *ortho* isomer generally holds in the photo-rearrangement of derivatives of the *O*-acyl-1-naphthol type. The preferential formation of the *ortho* isomer in these cases is of interest from the viewpoint of the synthesis of the 2-isomer, because, in the ordinary electrophilic reactions of 1-naphthol in the dark, the formation of the 4-isomer always predominates and the yield of the 2-isomer is quite low.

Thus, in the photo-rearrangement of *O*-acyl or *O*-*s*-triazinyl-naphthols the distance of the migration is considered to be also important, although the acyl or *s*-triazinyl group migrated to the positions of the high odd π electron densities; the migration of the acyl or *s*-triazinyl group to an adjacent position occurred readily, as in the cases of phenol derivatives, but it was difficult for any migration to a remote position to take place. These facts are consistent with the findings that the viscosity of a solvent scarcely affects the *ortho*-rearrangement, but does affect the *para*-rearrangement considerably.[1] A similar difficulty of the rearrangement to a remote position is also observed in the ordinary Fries rearrangement of *O*-acyl-1-naphthols. In this case, with an increase in the size of the acyl group, the rate of the formation of the 4-acyl-1-naphthols falls off to such an extent that the method is of little value in their preparation.[18] Generally, *s*-triazinyl group is a bulky substituent; therfore, in the cases of *O*-*s*-triazinyl-1-naphthols, the steric hindrance caused by the adjacent benzene nucleus, which is assumed to be the reason for the difficulty of the rearrangement to the 4-position, may be more significant than in the cases of ordinary acyl derivatives. However, the difference in steric hindrance between the *s*-triazinyl and acetyl groups seems to be small, as may be seen from a comparison of the values of the *o*/*p* ratio in these cases. On the other hand, in the photoreactions of naphthol derivatives, the formation of considerable quantities of naphthols was observed as compared with the cases of phenol derivatives. This difference between phenol and naphthol derivatives may be explained by a difference in the odd π electron densities at the oxygen atoms of the phenoxy and naphthyloxy radicals. Because of the low odd π electron densities at the oxygen atoms of naphthyloxy radicals, the probabilities of the back reactions with *s*-triazinyl radical to give the starting materials may be low, and naphthyloxy radicals are assumed to escape relatively readily from the solvent cage and to abstract a hydrogen atom from the solvent molecule to yield the respective naphthols in fairly good yields.

References

1) H. Shizuka, T. Kanai, T. Morita, Y. Ohto, and K. Matsui, *Tetrahedron*, **27**, 4021 (1971).

2) R. Hirt, H. Nidecker, and R. Berchtold, *Helv. Chim. Acta*, **33**, 1365 (1950).

3) For example, J. C. Anderson, and C. B. Reese, *Proc. Chem. Soc.*, **1960**, 217; *J. Chem. Soc.*, **1963**, 1781; H. Kobsa, *J. Org. Chem.*, **27**, 2293 (1962).

4) For examples, D. Elad, *Tetrahedron Lett.*, **1963**, 873; D. Elad, D. V. Rao, and V. I. Stenberg, *J. Org. Chem.*, **30**, 3252 (1965).

5) As for theoretical aspects, details will be published elsewhere.

6) H. Yamada, H. Shizuka, S. Sekiguchi, and K. Matsui, This Bulletin, **47**, 238 (1974).

7) H. Shizuka and I. Tanaka, *ibid.*, **41**, 2343 (1968); **42**, 909 (1969); H. Shizuka, *ibid.*, **42**, 52, 57 (1969); H. Shizuka, T. Morita, Y. Mori, and I. Tanaka, *ibid.*, **42**, 1831 (1969). H. Shizuka, M. Kato, T. Ochiai, K. Matsui, and T. Morita, *ibid.*, **43**, 67 (1970). H. Shizuka, H. Kayoiji, and T. Morita, *Mol. Photochem.*, **2**, 165 (1970).

8) H. H. Jaffé and M. Orchin, "Theory and Applications of Ultraviolet Spectroscopy," John Wiley & Sons, Inc., (1966), p. 273.

9) a) R. C. Hirt and D. J. Salley, *J. Chem. Phys.*, **21**, 1181 (1953). b) Eg. J. S. Brinen and L. Goodman, *ibid.*, **31**, 482 (1959).

10) H. Brunetti and C. E. Lüthi, *Helv. Chim. Acta*, **55**, 1566 (1972).

11) Y. Horikoshi, Y. Ohto, S. Sekiguchi, and K. Matsui, submitted to *Nippon Kagaku Kaishi*.

12) For example, A. H. Blatt, "Organic Reaction," Vol. 1, John Wiley & Sons Inc., (1942), p. 342.

13) D. H. R. Barton, Y. L. Chow, *J. Chem. Soc.*, **1965**, 3571.

14) D. Bellus, K. Schaffner, *Helv. Chim. Acta*, **51**, 1980 (1968).

15) E. Muller, A. Rieker, and K. Scheffer, *Ann. Chem.*, **645**, 92 (1961).

16) Details of the method of calculation were the same as those described in the previous paper; H. Shizuka, N. Maeno, and K. Matsui, *Mol. Photochem.*, **4**, 335 (1972). The odd π electron densities of these molecules were obtained from the square of the coefficient of the atomic orbital in the highest-occupied molecular orbital.

17) O. N. Witt and O. Braun, *Ber.*, **47**, 3216 (1914).

18) H. Lederer, *J. Prakt. Chem.*, **135**, 49 (1932); R. W. Stoughton, *J. Amer. Chem. Soc.*, **57**, 202 (1935).

Addition of Methanesulfenyl Chloride and Sulfur Chloride to 1,4-Dimethyl-3,6-dimethylene-2,5-piperazinedione and Substitution of the Adducts

Juji Yoshimura, Yuichi Sugiyama, Kenji Matsunari,* and Hiroshi Nakamura

Laboratory of Chemistry for Natural Products, Faculty of Science, Tokyo Institute of Technology Ookayama, Meguro-ku, Tokyo 152

(Received November 5, 1973)

Addition of methanesulfenyl chloride or sulfur chloride to 3,6-dimethylene-(**1a**) and 3,6-dibenzylidene-1,4-dimethyl-2,5-piperazinediones (**1b**) gave the Markownikoff products. The addition of methanesulfenyl chloride to **1a** proceeded stepwise within 1 hr, and gave a mixture of (*Z,Z*)-, (*Z,E*)-, and (*E,E*)-isomers of the corresponding 3,6-bis(methylthiomethylene) derivative, accompanied by gradual elimination of hydrogen chloride. 3,6-Dichloro groups of the adduct were substituted with water, ethanethiol and ethanol to give the corresponding hydroxy, ethylthio, and ethoxy derivatives, respectively. A similar substitution with ethanedithiol and hydrogen sulfide followed by aeration gave 7,9-dimethyl-1,6-bis(methylthiomethyl)-8,10-dioxo-2,5-dithia-7,9-diazabicyclo[4,2,2]-decane and the corresponding 3,6-epitetrathio derivative, respectively. The same mode of reaction of sulfur chloride with **1a** and **1b** gave a few 1,6-disubstituted-7,9-dimethyl-8,10-dioxo-3,4-dithia-7,9-diazabicyclo[4,2,2]-decanes. Mass fragmentations of new compounds were also described.

It was found that bromination of 1,3,4,6-tetramethyl-2,5-piperazinedione with bromine was accompanied by elimination of hydrogen bromide and re-addition of bromine gave the corresponding 3,6-dibromo-3,6-bis-(bromomethyl) derivative, and that tetrabromide was successfully substituted with water or methanol to give the corresponding 3,6-disubstituted derivatives, while that substituted with sulfur-containing nucleophiles gave only 1,4-dimethyl-3,6-dimethylene-2,5-piperazinedione (**1a**) and sulfur.[1] The latter elimination seems to proceed through the formation of the spiro-thiiranium ion of the substitued compounds, in participation with the bromine atom of bromomethyl groups. In order to extend the synthetic pathway of 3,6-epidithio-2,5-piperazinediones by substitution of 3,6-dihalogeno groups with mercapto groups and the subsequent oxidative disulfide-ring formation,[2] addition of methanesulfenyl chloride to **1a** was examined. Schmidt and Csizmadia[3] reported that the relative amount of Markownikoff and anti-Markownikoff adducts formed in the addition of 4-chlorobenzenesulfenyl chloride to *cis*- and *trans*-1-phenylpropene are strongly dependent upon the solvent and reaction temperature. Concurrent anti-Markownikoff addition of sulfur chloride to two olefinic functions of **1a** and 3,6-dibenzylidene-1,4-dimethyl-2,5-piperazinedione (**1b**)[4] was also examined with the expectation that it would give directly the 3,6-epidithio derivative. In both additions, only Markownikoff adduct was formed.

Results and Discussion

NMR analysis of the addition of methanesulfenyl chloride[5] to **1a** in chloroform (Fig. 1) showed that the first (b) and second (c) additions proceed stepwise during 10 min and 1 hr, respectively, followed by gradual elimination of hydrogen chloride (d) when the reaction mixture was kept at room temperature for a week. The elimination was accelerated by refluxing the reaction mixture for several hours to give the corresponding 3,6-bis(methylthiomethylene) derivative (**2**) in a good yield. This indicates that the addition occurs in the Markownikoff mode, and the adduct

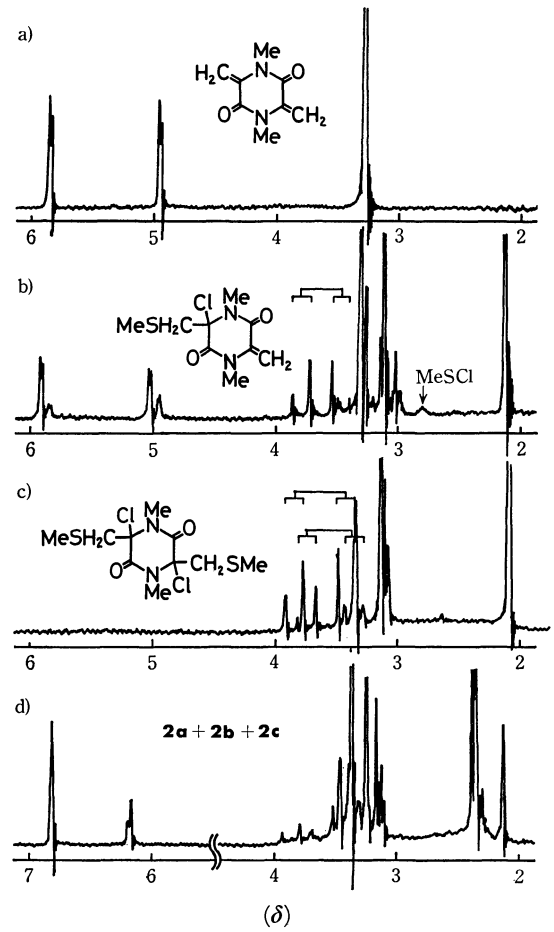

Fig. 1. A progressive change of the NMR spectrum in the addition of methanesulfenyl chloride to **1a** at room temperature.
a) before the reaction; b) after 10 min; c) after 1 hr; d) after 1 week

* Present address: Central Research Laboratory of Kumiai Chemical Industry Co. Ltd., Shibukawa, Shimizu.

does not turn into the spiro-thiiranium ion, as was observed previously.[1] Separation of **2** on tlc gave the possible three isomers in the ratio 4(**2a**): 3(**2b**): 1(**2c**). From the chemical shifts of vinyl protons (Table 1), their configurations were assigned to (*Z,Z*), (*Z,E*), and (*E,E*), respectively, the vinyl proton in *Z*-configuration being deshielded about 0.55 ppm by the neighboring carbonyl group.[6] It is worth noting that irradiation of (*E,E*)-isomer in chloroform with high-pressure mercury light for 20 hr gave a mixture of **2a**, **2b**, and **2c** in the ratio 1 : 2 : 1.

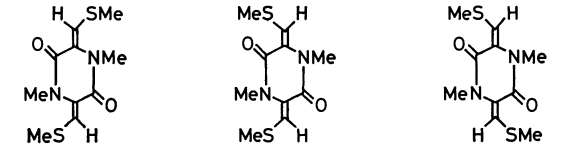

(**2a**) (**2b**) (**2c**)

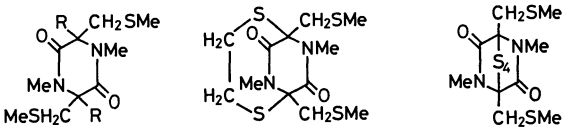

(**3a**) R=OH
(**3b**) R=SEt
(**3c**) R=OEt

(**4**) (**5**)

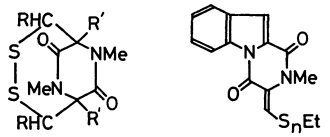

(**6a**) R=H, R′=OH
(**6b**) R=Ph, R′=OH
(**6c**) R=H, R′=OAc

(**7a**) *n*=2
(**7b**) *n*=3

Table 1. Proton chemical shifts (δ) of geometrical isomers of **2**

Compound	Olefinic Protons	NMe	SMe
2a	6.81	3.36	2.43
2b	6.80; 6.15	3.45; 3.22	2.41; 2.34
2c	6.15	3.23	2.34

Since the Markownikoff adduct was fairly stable, though it could not be isolated in a pure state, substitution of its 3,6-dichloro groups was attempted. Treatment of the adduct, obtained by evaporating the reaction mixture, with dioxane–water at room temperature overnight gave 3,6-dihydroxy-1,4-dimethyl-3,6-bis(methylthiomethyl)-2,5-piperazinedione (**3a**) in 42% yield. 3,6-Bis(ethylthio) (**3b**) and 3,6-diethoxy (**3c**) derivatives were obtained similarly by treatment with excess ethanethiol and ethanol in chloroform, respectively. A similar substitution with ethanedithiol in a dilute solution gave the bicyclic compound; 7,9-dimethyl-1,6-bis(methylthiomethyl)-8,10-dioxo-2,5-dithia-7,9-diazabicyclo[4,2,2]decane (**4**) in 18% yield. However, treatment of the adduct with sodium thioacetate or sodium tetrasulfide induced the elimination reaction to give **2** as the predominant product, even at lower temperatures with less than stoichiometric amount of nucleophiles, while that with hydrogen sulfide gave the corresponding epitetrathio derivative (**5**). In the latter case, another product which seemed to be the corresponding dimercapto derivative was detected on tlc. However, the compound polymerized easily to give an intractable sirup, compound **5** being isolated in 34% yield by aeration of the reaction mixture in a large amount of chloroform. Hydrogenation of **5** with sodium borohydride again gave the unstable dimercapto derivative, though it could not be isolated in a pure state.

Though the steric configuration of **3** could not be determined, the NMR spectra indicated that **3b** is composed of a *ca.* 1 : 3 mixture of *cis* and *trans* isomers, and the others only of one isomer. In general, mass spectra of these new compounds show intense fragment peaks of $(M-SCH_3)^+$ and $(M-CH_2SCH_3)^+$; for example, the base peak of **3a** at *m/e* 233 $(M-CH_2SCH_3)^+$ strongly supports the structure. In the case of **5**, the parent peak could not be observed, but the first fragmentation stage $M^{\ddagger}\rightarrow(M-4S)^{\ddagger}$ was deduced from a metastable ion peak, *m/e* 174.5. In the fragmentation pattern of **4** (Fig. 2) deduced from metastable ion peaks (*m/e* 221, 192, 186, 174.5, and 129.5), the *m/e* 260 $(M-C_2H_4S_2)^{\ddagger}$ peak shows the structure unambiguously.

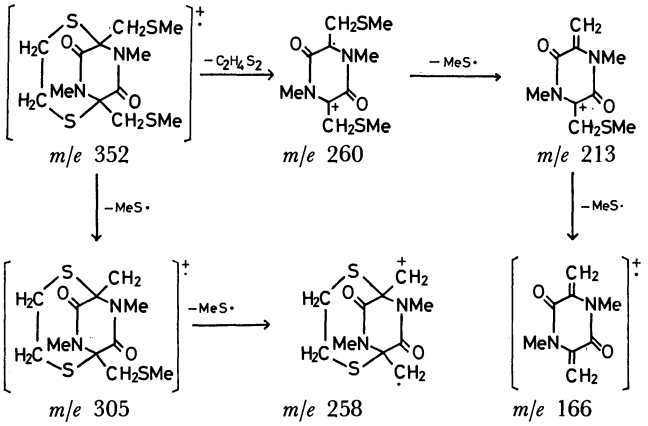

m/e 352 *m/e* 260 *m/e* 213

m/e 305 *m/e* 258 *m/e* 166

Fig. 2. The major fragmentation pathways of **4**.

NMR analysis of the addition reaction of sulfur chloride to **1a** gave similar information to that for methanesulfenyl chloride. However, isolation of the adduct was very difficult in high concentration of reactants, since its bifunctionality causes polymerization due to the intermolecular addition reaction. Examination of the effect of concentration on the relative amount of polymeric and monomeric adducts (Fig. 3) indicates that 0.0125 M solution was the best for the formation of the monomeric adduct, which was isolated as 1,6-dihydroxy-7,9-dimethyl-8,10-dioxo-3,4-dithia-7,9-diazabicyclo[4,2,2]decane (**6a**) by treatment of the reaction mixture with water. In the mass fragmentation pattern of **6a** (Fig. 4; metastable ion peaks, *m/e* 143.3, 136, 120.5, and 115.5), the peak at *m/e* 218 $(M-CH_2S)^{\ddagger}$ proves its characteristic structure. Formation of **6a** also indicates that the addition proceeded in the Markownikoff mode. Addition of sulfur chloride to **1b** proceeds very slowly in dioxane in the presence of zinc chloride, and does not proceed in tetrahydrofuran or chloroform. Consequently, the addition in dioxane

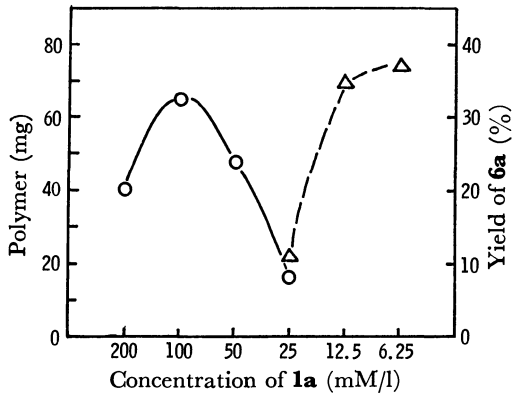

Fig. 3. The effect of concentration on the products in the addition of equimolar amount of sulfur chloride to 100 mg of **1a**.
○—○: Polymer, △—△: **6a**

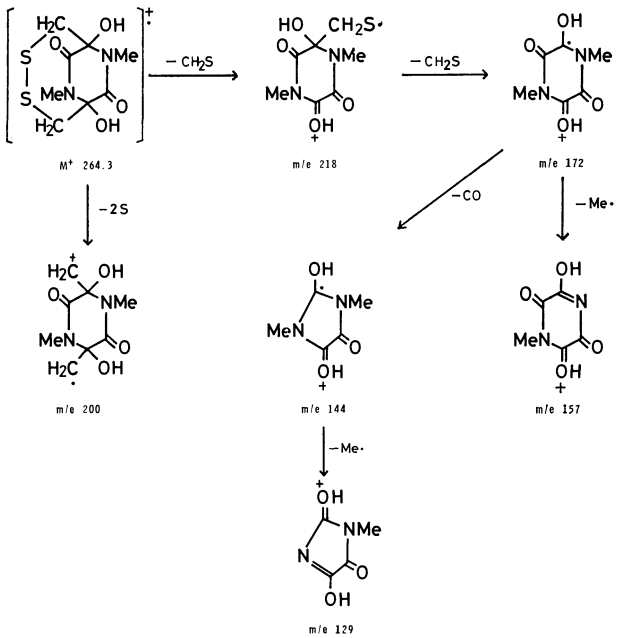

Fig. 4. The major fragmentation pathways of **6a**.

was easily subjected to side-reactions such as elimination, polymerization, and disproportionation of sulfur, making the yield of monomeric adduct (**6b**) very low. Acetylation of **6a** with acetic anhydride in pyridine gave the corresponding diacetate (**6c**).

Addition of sulfur chloride to 1,2,3,4-tetrahydro-2-methyl-3-methylene-1,4-dioxopyrazino[1,2-*a*]indole[7] gave only intractable products. However, the prevention of side-reactions by fixation of the terminal chlorodithio group of the corresponding adduct with ethanethiol gave 3-ethyldithiomethylene (**7a**) and 3-ethyltrithiomethylene derivative (**7b**) in 11% and 13% yield, respectivly.

Experimental

All the melting points are uncorrected. The solutions were evaporated under reduced pressure at a bath temperature not exceeding 60 °C. The infrared spectra were measured in KBr disks, and the NMR spectra were obtained at 100 MHz with a JNM-100H spectrometer in deuteriochloroform unless otherwise stated, using TMS as an internal reference. The mass spectra were obtained on a GEOL JNS-01S mass spectrometer, using a direct inlet and an ionization energy of 70 eV. Chemical shifts and coupling constants were recorded in δ and Hz units, respectively, and frequencies in cm^{-1}.

1,4-Dimethyl-3,6-bis(methylthiomethylene)-2,5-piperazinedione (2a, 2b, and 2c). To a solution of 1,4-dimethyl-3,6-dimethylene-2,5-piperazinedione (0.2 g, 1.2 mmol) in chloroform (20 ml) was added dropwise methanesulfenyl chloride (0.6 g, 7.2 mmol), and the resulting solution was evaporated, after being left to stand for 1 hr at room temperature. A solution of the residual sirup in chloroform (20 ml) was refluxed for 8 hr, and evaporated to give crystals (0.17 g, 56%) from ether, which were separated into three isomers (R_f= a; 0.38, b; 0.25, c; 0.2) on a preparative tlc, using benzene–ethyl acetate (5: 1) as the developing solvent. **4a**: mp 138—139 °C; yield, 0.08 g (26%), **4b**: mp 172—174 °C; yield, 0.06 g (19%), **4c**: mp 275 °C (sublime); yield, 0.02 g (6.4%).

Found: **4a**: C, 46.69; H, 5.51; N, 10.86; S, 24.58%. **4b**: C, 46.67; H, 5.46; N, 10.72; S, 24.61%. **4c**: C, 46.37; H, 5.25; N, 10.71; S, 24.72%. Calcd for $C_{12}H_{22}N_2O_2S_2$: C, 46.49; H, 5.46; N, 10.84; S, 24.82%.

These compounds show the characteristic olefinic double bond absorption at *ca.* 1570 cm^{-1}.

3,6-Dihydroxy-1,4-dimethyl-3,6-bis(methylthiomethyl)-2,5-piperazinedione (3a). Methanesulfenyl chloride (0.6 g, 7.2 mmol) was added to a solution of 1,4-dimethyl-3,6-dimethylene-2,5-piperazinedione (0.2 g, 1.2 mmol) in dry chloroform (10 ml). The mixture was allowed to stand at room temperature for 1 hr, and then evaporated to give a sirup. A solution of the sirup in dioxane–water was left to stand at room temperature overnight and evaporated to give amorphous solid (200 mg) which was recrystallized from acetone. Yield, 180 mg (42%). Mp 193—195 °C, IR: 3260 (OH), 1625 (amide); NMR (DMSO): 6.80 (OH), 3.13 and 2.95 (SCH_2; ABq, J=13.8), 2.78 (NMe), 1.92 (SMe).

Found: C, 40.99; H, 5.69; N, 9.46%. Calcd for $C_{10}H_{18}N_2O_4S_2$: C, 40.79; H, 6.16; N, 9.51%.

3,6-Bis(ethylthio)-1,4-dimethyl-3,6-bis(methylthiomethyl)-2,5-piperazinedione (3b). Excess ethanethiol (20 ml) was added to a solution of the same addition product in chloroform as for **3a** and the mixture was evaporated, after being left to stand overnight at room temperature. The sirup obtained was purified on a preparative tlc, using benzene–ethyl acetate (5: 1) as the developing solvent. The portion of R_f=0.75 (0.2 g, 43%) was collected, and recrystallized from petroleum ether. Mp 72—73 °C; IR: 1640 (amide); NMR of the main isomer in the mixture of 3: 1: 3.65 and 3.09 (CH_2S; ABq, J=15), 3.07 (NMe), 2.17 (SMe), 2.65—3.00 (CH_2S; q), 1.20 (CH_3; t, J=7.5).

Found: C, 43.64; H, 6.45; N, 7.18; S, 33.55%. Calcd for $C_{14}H_{26}N_2O_2S_4$: C, 43.97; H, 6.85; N, 7.33; S, 33.48%.

3,6-Diethoxy-1,4-dimethyl-3,6-bis(methylthiomethyl)-2,5-piperazinedione (3c). Ethanol (20 ml) was added to a solution of the same addition product in chloroform (40 ml) as for **3b**, and the resulting solution was left to stand at room temperature overnight. Evaporation of the reaction mixture gave a sirup which was purified on a preparative tlc, using benzene–ethyl acetate (10: 1) as the developing solvent. The portion of R_f=0.42 was recrystallized from ether. Mp 135—136 °C, yield, 100 mg (23%); IR: 1645 (amide), 1045 (C–O–C). NMR: 3.60 (OCH_2; q), 3.35 and 3.05 (CH_2S; ABq, J=14), 2.98 (NMe), 2.07 (SMe), 1.19 (CH_3; t, J=7.5).

Found: C, 47.99; H, 7.49; N, 8.05; S, 18.21%. Calcd for $C_{14}H_{26}N_2O_4S_2$: C, 47.99; H, 7.48; N, 8.00; S, 18.27%.

7,9-Dimethyl-1,6-bis(methylthiomethyl)-8,10-dioxo-2,5-dithia-7,9-diazabicyclo[4,2,2]decane (4). Ethanedithiol (113 mg, 1.2

mmol) was added to a solution of the same addition product in dioxane (30 ml) as for **3c**, and the resulting solution was then evaporated, after being left to stand overnight at room temperature. The residual sirup was purified on a preparative tlc, using benzene–ethyl acetate (5: 1) as the developing solvent (R_f=0.35) to give crystals which were recrystallized from methanol. Mp 170—171 °C, yield, 80 mg (18%), IR: 1650 (amide); NMR: 3.63 and 2.99 (CH_2; ABq, J=14), 3.14 (NMe), 2.14 (SMe), 1.55 (SCH_2CH_2S; s).

Found: C, 40.92; H, 5.87; N, 7.89; S, 36.41%. Calcd for $C_{12}H_{20}N_2O_2S_4$: C, 40.92; H, 5.72; N, 7.95; S, 36.38%.

1,4-Dimethyl-3,6-bis(methylthiomethyl)-3,6-epitetrathio-2,5-piperazinedione (5). To a solution of excess hydrogen sulfide in chloroform (30 ml) was added a solution of the same addition product in chloroform (20 ml) as for **4**, and the resulting solution was left to stand at room temperature overnight, and then evaporated. The solution of the residual sirup in chloroform (300 ml) was oxidized by airing for 1 day and evaporated. The residue was purified on a preparative tlc using benzene–ethyl acetate (5: 1) as the developing soluent (R_f= 0.7), to give crystals (160 mg, 34%) which were recrystallized from methanol. Mp 183—184 °C; IR: 1650 (amide); NMR: 3.63 and 3.13 (CH_2; ABq, J=14), 3.08 (NMe), 2.18 (SMe).

Found: C, 30.75; H, 4.05; N, 7.25; S, 49.39%. Calcd for $C_{10}H_{16}N_2O_2S_6$: C, 30.91; H, 4.15; N, 7.21; S, 49.50%.

1,6-Dihydroxy-7,9-dimethyl-8,10-dioxo-3,4-dithia-7,9-diazabicyclo[4,2,2]decane (6a). To a solution of **1a** (100 mg, 0.6 mmol) in dry dioxane (48 ml) was added sulfur chloride (80 mg, 0.59 mmol) and a catalytic amount of zinc chloride, and the mixture was allowed to stand at room temperature for 1 day. After addition of water (10 ml) to the solution, the mixed solution was evaporated and the residue was treated with acetone (100 ml). Insoluble materials were filtered off, and the filtrate was treated with active carbon and concentrated to 5 ml volume to give crystals (55 mg, 35%). Recrystallization from acetone gave white needles. Mp *ca.* 260 °C (sublime). IR: 3325 (OH), 1650 (amide). NMR (DMSO): 3.18 and 3.46 (CH_2; ABq, J=14), 2.82 (NMe).

Found: C, 36.08; H, 4.50; N, 10.96; S, 24.45%. Calcd for $C_8H_{12}N_2O_4S_2$: C, 36.35; H, 4.58; N, 10.60; S, 24.26%.

1,6-Dihydroxy-7,9-dimethyl-2,5-diphenyl-8,10-dioxo-3,4-dithia-7,9-diazabicyclo[4,2,2]decane (6b). A solution of 3,6-dibenzylidene-1,4-dimethyl-2,5-piperazinedione (630 mg, 1.9 mmol), sulfur chloride (370 mg, 2.7 mmol) and a small amount of zinc chloride in dioxane (20 ml) was allowed to stand for 48 hr at room temperature. The reaction mixture was extracted with chloroform (100 ml), and the extract was washed twice with water (100 ml), and evaporated to give a white powder which was recrystallized from chloroform to give white crystals (20 mg, 2.5%). Mp 229 °C (decomp.). IR: 3350 (OH), 1640 (amide).

Found: C, 75.72; H, 4.60; N, 6.37; S, 15.61%. Calcd for $C_{20}H_{20}N_2O_4S_2$: C, 57.67; H, 4.84; N, 6.73; S, 15.40%.

1,6-Diacetoxy-7,9-dimethyl-8,10-dioxo-3,4-dithia-7,9-diazabicyclo-[4,2,2]decane (6c). A solution of **6a** (50 mg, 0.19 mmol) in pyridine (10 ml) and acetic anhydride (5 ml) was allowed to stand at room temperature for 3 hr, evaporated, and the residue was treated with chloroform–ethanol to give white crystals (34 mg, 52%) which were recrystallized from chloroform–ethanol. Mp 268—271 °C. IR: 1760 (OAc), 1670 (amide). NMR: 3.85 and 3.15 (CH_2; ABq, J=15), 2.88 (NMe), 2.13 (OAc).

Found: C, 41.78; H, 4.61; N, 8.12%. Calcd. for $C_{12}H_{16}N_2O_6S_2$: C, 41.37; H, 4.63; N, 8.04%.

3-Ethyldithiomethylene- (7a) and 3-Ethyltrithiomethylene-1,2,3,4-tetrahydro-2-methyl-1,4-dioxopyrazino[1,2-a]-indole (7b). A solution of 1,2,3,4-tetrahydro-2-methyl-3-methylene-1,4-dioxopyrazino[1,2-*a*]indole (0.4 g, 1.8 mmol), sulfur chloride (2.0 g, 15 mmol) and a small amount of zinc chloride in dioxane (16 ml) was allowed to stand for 20 min. A solution of ethanethiol (4.4 g, 71 mmol) in chloroform (100 ml) was added to the reaction mixture which was left to stand for 20 min. The solution was washed with water, evaporated, and the residue was fractionated on a C-200 silicic acid column, using benzene and benzene–ethyl acetate (6: 1) as an effluent. The latter fraction was evaporated, and then the residue was again fractionated on a C-200 silicic acid column, being eluted with benzene–ethyl acetate (20: 1) to give **7b** (80 mg, 13%) and **7a** (60 mg, 11%). They were recrystallized from chloroform–ligroin to give orange and yellow needles, respectively Mp **7a**; 136 °C, **7b**; 148 °C. IR: **7a**; 1660 (amide), **7b**; 1650 (amide). NMR: **7a**; 1.40 and 2.94 (SEt; J=7.5), 3.43 (NCH_3), 7.0 (=CHSS), 8.51 (H_6: $J_{6,7}$=7.5), **7b**; 1.42 and 2.97 (SC_2H_5; J=7.5), 3.43 (NCH_3), 7.07 (=CHSSS), 8.41 (H_6; $J_{6,7}$=7.5).

7a: Found: C, 56.38; H, 4.20; N, 8.60%. Calcd for $C_{15}H_{14}N_2O_2S_2$: C, 56.58; H, 4.43; N, 8.80%.

7b: Found: C, 51.47; H, 3.74; N, 7.76%. Calcd for $C_{15}H_{14}N_2O_2S_3$: C, 51.40; H, 4.03; N, 7.99%.

The authors are indebted to the members of the Laboratory of Organic Analysis for microanalysis, to Mr. H. Matsumoto for NMR measurements, and to the members of Analytical Center of Kitasato University for mass spectral measurements.

References

1) J. Yoshimura, Y. Sugiyama, and H. Nakamura, This Bulletin, **46**, 2850 (1973).

2) P. W. Trown, *Biochem. Biophys. Res. Commun.*, **33**, 402 (1968); H. Poisel and U. Schmidt, *Chem. Ber.*, **104**, 1714 (1971); S. G. Svokos and R. B. Angier, Ger., 2029305 (1971).

3) G. H. Schmidt and V. M. Csizmadia, *Can. J. Chem.*, **50**, 2457, 2465 (1972).

4) M. O. Foster and W. B. Saville, *J. Chem. Soc.*, **121**, 816 (1922).

5) H. Brintziger, K. Pfannstiel, H. Koddebusch, and K. Kling, *Chem. Ber.*, **83**, 87 (1950).

6) A. E. A. Porter and P. G. Sammes, *J. Chem. Soc., C*, **1970**, 2530; K. W. Blake and P. G. Sammes, *ibid.*, **1970**, 980.

7) M. S. Ali, J. S. Shnnon, and A. Tayler, *idib.*, **1968**, 2044.

Aminosugars. XXII. Syntheses and Properties of 6-Deoxy-6- and 3-Deoxy-3-guanidino-D-hexoses[1]

Juji YOSHIMURA, Tetsuo SEKIYA, and Yoshio OGURA

Laboratory of Chemistry for Natural Products, Faculty of Science, Tokyo Institute of Technology Ookayama, Meguro-ku, Tokyo 152

(Received November 9, 1973)

Methyl 6-deoxy-6-guanidino-α-D-glucopyranoside, 6-deoxy-6-guanidino-D-galactose, 3-deoxy-3-guanidino-D-allose (**7**), and 3-deoxy-3-guanidino-D-glucose were synthesized by guanidination of the corresponding aminosugars. The acetate of **7** was proved to exist in a bicyclic structure; 2′,4′,6′-tri-*O*-acetyl-D-allopyrano[1′,2′,3′;4,5,6]-2-acetylimino-1,3-diacetyl-perhydropyrimidine, whereas others exist as the usual pyranoses. Properties of the new compounds and the synthetic methods were examined.

During the last decade, the syntheses and properties of aldoses having an amino or a mercapto group at *C*-4, *C*-5, or *C*-6 position have been extensively studied. It was clarified that the former two exist in various tautomeric mixtures involving five- and six-membered hemiacetal formation with functional groups at *C*-4 and *C*-5 positions, while the latter involve the corresponding septanose and bicyclic 1,6-anhydrosugar, in addition to the usual pyranose.[2] In a previous paper of this series,[3] we disclosed that 2-deoxy-2-guanidino-D-glucose exists mainly in a new bicyclic structure, α-D-glucofurano[1′,2′;4,5]-2-imino-imidazolidine, under acidic conditions, which isomerizes into 2-amino-4-(D-*arabino*-tetrahydroxybutyl)imidazole *via* the corresponding 2-imino-imidazoline-4 structure in an alkaline solution. The results stimulated us to examine the structure of 6-deoxy-6- and 3-deoxy-3-guanidino-hexoses.

Syntheses of guanidino-sugars have not been studied extensively. However, 6-deoxy-guanidino-1,2-*O*-isopropylidene-α-D-glucofuranose[4] and methyl 3-deoxy-4,6-*O*-benzylidene-3-nitroguanidino-α-D-allopyranoside[5] were synthesized by the cyanamide method. Formation of 2-deoxy-2-guanidino-D-glucopyranosyl thiol and -D-galactopyranosyl thiol through the S→N migration of amidino group in the corresponding 1-thiopseudourea derivatives was indicated by Wolfrom *et al.*[6] Glycosylguanidines could not be obtained in a pure state by direct condensation of aldoses with free guanidine,[7] but they were synthesized through glycosylisothioureas.[8] 2-Deoxy-2-guanidino-α-D-altropyranoside was obtained by the reaction of the corresponding 2,3-epoxide with guanidine, but substitution of 3-*O*- or 6-*O*-tosyl-hexoside with guanidine was unsuccessful.[9]

In this paper the syntheses and properties of several 6-deoxy-6- and 3-deoxy-3-guanidino-D-hexoses are reported.

Results and Discussion

6-Deoxy-6-guanidino-D-hexoses. Reaction of methyl 6-amino-6-deoxy-α-D-glucopyranoside[10] with 1.5 equivalent of cyanamide in water at 60 °C with an adjusted pH of 8.2—8.6 gave the corresponding 6-guanidino derivative (**1**) as crystalline flavianate, in 26 and 50% yield for 9 hr and 1 day, respectively. When the pH of the reaction mixture was not adjusted, it increased beyond 10 with the progress of guanidination, a di-*O*-carbamoyl-mono-*O*-amidino derivative (**2**) of **1** being obtained in 73% yield based on cyanamide. The compound showed characteristic absorptions of carbamoyl (1742 and 1588 cm^{-1}) and guanidino groups (1680 and 1615 cm^{-1}) in the IR spectrum, and ring proton signals of α-D-glucopyranose in the NMR spectrum. The position of three *O*-substituents was not determined definitely. However, the *C*-2 position was considered to be the most reasonable for the *O*-amidino group, since 3- and 4-*O*-amidino groups once formed seem to be hydrolyzed to *O*-carbamoyl groups by the intramolecular catalytic action of 6-guanidino group. Acetylation of **1** with acetic anhydride in pyridine gave methyl 2,3,4-tri-*O*-acetyl-6-deoxy-6-diacetylguanidino-α-D-glucopyranoside (**3**) in 31% yield, together with 6-monoacetylguanidino derivative. The former showed characteristic absorptions of diacetylguanidino group [λ_{max}^{EtOH} (nm), 221 (ε 8.35×10^3), 255 (ε 1.58×10^4); ν_{max} 1698, 1620, and 1555 cm^{-1}]. It is worth noting that *N*-acetyl groups in diacetylguanidino moiety of **3** are very labile,[11] whereas *O*-glycosidic linkage in **1** strongly resisted acid hydrolysis. De-*O*-acetylation of **3** in methanol with a small amount of sodium methoxide at room temperature caused the shift of λ_{max}^{EtOH} to 234 nm, indicating the elimination of one *N*-acetyl group. **3** was easily converted into **1** only by refluxing in methanol for 14 hr. This means that the alkalinity of 6-guanidino group arose from diacetylguanidino group[12] catalyzed de-*O*-acetylation by the ester-exchange reaction. Treatment of **1** with 6 M hydrochloric acid at 80 °C for 1 day gave no hydrolyzed product, indicating that the protonation of 6-guanidino group prevents the approach of other protons to *C*-1 position, as was observed in the case of 2-amino-2-deoxy-hexosides.[13]

For comparison of synthetic methods, synthesis of **1** by the *S*-methylisothiourea method in ammonia solution[14] was examined. This method gave nearly the same yield as the former (Table 1), but the use of hydrochloride of the aminosugar and diluted ammonia within 10% gave a better yield. This indicates that a suitable buffer action is desirable in this reaction, and that highly concentrated ammonia may consume *S*-methylisothiourea by its conversion into free guanidine.

In order to obtain a 6-guanidino derivative having no protecting group at *C*-1, 6-amino-6-deoxy-1,2;3,4-di-*O*-isopropylidene-α-D-galactose[15] was treated with *S*-methylisothiourea under the best conditions (Table 1), to give 6-guanidino derivative (**4**) as flavianate in

35% yield. Hydrolysis of **4** with flavianic acid gave de-*O*-isopropylidenated product (**5**) as flavianate in 65% yield, which was also obtained in 59% yield by successive guanidination and hydrolysis without isolation of **4**. An attempted substitution of 1,2;3,4-di-*O*-isopropylidene-6-*O*-tosyl-α-D-galactose[16] with guanidine in butanol or in dimethylformamide gave unsuccessful results, similarly to those reported by Danilov and Lishanskii.[9] Acetylation of **5** with acetic anhydride in pyridine gave a sirupy hexaacetate (**6**) in 28% yield, which showed characteristic absorptions of diacetylguanidines. Ring-proton signals of the NMR spectrum of **6** (Fig. 1) confirmed by simulation proved completely its structure to be 1,2,3,4-tetra-*O*-acetyl-6-deoxy-6-diacetylguanidino-β-D-galactopyranose.

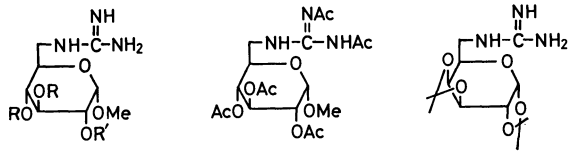

(**1**) R=R′=H (**3**) (**4**)
(**2**) R=CONH$_2$, R′=C(NH)NH$_2$

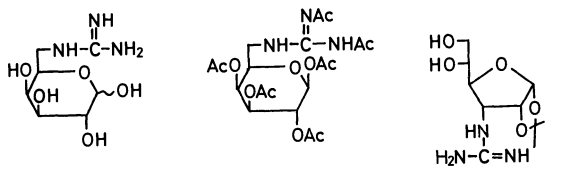

(**5**) (**6**) (**7**)

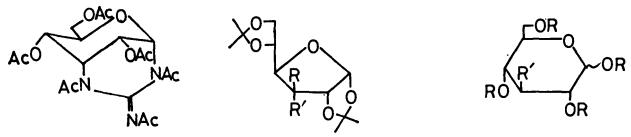

(**8**)

(**9**) R=H, R′=NHCN
(**10**) R=H, R′=NHCONH$_2$
(**11**) R=H, R′=NHCSNH$_2$
(**12**) R=NHC(NH)-NH$_2$, R′=H
(**13**) R=H, R′=NHC(NH)NH$_2$
(**14**) R=Ac, R′=NHC(NAc)-NHAc

Table 1. Guanidination of methyl 6-amino-6-deoxy-α-D-glucopyranoside with *S*-methylisothiourea sulfate in aqueous ammonia[a]

Molar ratio[b]	Concentration of ammonia (%)	Reaction time (days)	Yield (%)
1.5	0	4	40
1.5	9	1	35
1.5	5	4	48
1.5	9	4	48
1.5	10	4	51[c]
1.5	28	4	28
1.5	28	4	40[c]
1.2	0	1/3[d]	18
1.5	0	1[d]	31

a) 5 mmol of aminosugar in a 20 ml solution, at room temperature unless otherwise stated. b) *S*-methylisothiourea to the aminosugar. c) aminosugar used as the hydrochloride. d) reaction temperature 80 °C.

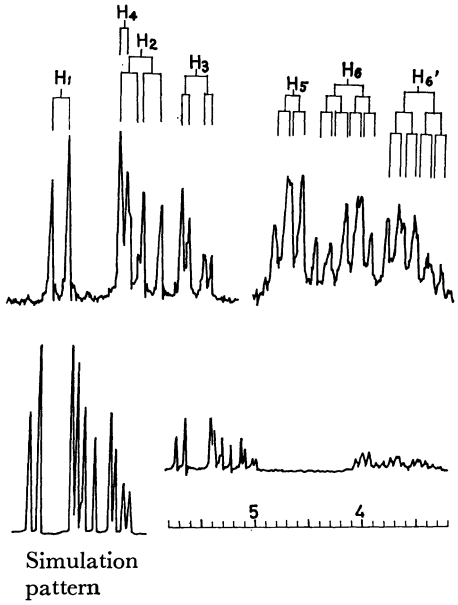

Fig. 1. Ring-proton signals in the NMR spectrum of **6**.

Although the 6-guanidino group in **1** clearly showed the electrostatic effect on the *C*-1 position, the fact that **5** showed positive Sakaguchi reaction after removal of flavianic acid, and that it was converted into **6** suggests that the nucleophilicity of guanidino group is not so strong as to make the septanose or an additional seven-membered aminal ring by surmounting new non-bonded interactions, which will arise by change of the conformation.

*3-Deoxy-3-guanidino-*D*-hexoses.* Guanidination of 3-amino-3-deoxy-1,2;5,6-di-*O*-isopropylidene-α-D-allofuranose[17] by *S*-methylisothiourea method was unsuccessful, and that with cyanamide in water gave a Sakaguchi-reaction positive product. However, it could not be isolated in a pure state. The fusion method[18] of the aminosugar hydrochloride with 1.5 equivalent of cyanamide at 130 °C for 40 min gave the de-5,6-*O*-isopropylidenated 3-guanidino derivative (**7**) as crystalline picrate in 57% yield. When the free aminosugar was used cyanamide dimerized rapidly to biguanide, no product being obtained. Hydrolysis of **7** with 2 M hydrochloric acid gave 3-deoxy-3-guanidino-D-allose as a hygroscopic sirup which is negative to both the Sakaguchi and Fehling reactions. Acetylation of this sirup with acetic anhydride in pyridine gave a sirupy hexaacetate (**8**), UV absorption of which (λ_{max}^{EtOH} 217 nm) differs from that of **3** and **6**. NMR spectrum of **8** (Fig. 2) showed the presence of α-D-allopyranose ring from the long-range coupling between H_1 and H_3 (J=1.9 Hz) and a *trans*-diaxial coupling ($J_{4,5}$=10.6 Hz). Although 1,2,4,6-tetra-*O*-acetyl-3-deoxy-3-diacetylguanidino-α-D-allopyranose structure is possible, **8** was determined to be 2′,4′,6′-tri-*O*-acetyl-α-D-allopyrano[1′,2′,3′;4,5,6]-2-acetylimino-1,3-diacetyl-perhydropyrimidine from the absence of diacetylguanidino moiety in UV spectrum, negative Sakaguchi and Fehling reaction of 3-deoxy-3-guanidino-D-allose, and the presence of lower-shifted acetylimino proton signal (δ 2.52) in the NMR spectrum, as observed in that of 3′,5′,6′-tri-*O*-acetyl-α-D-glucofurano[1′,2′;4,5]-2-acetyl-

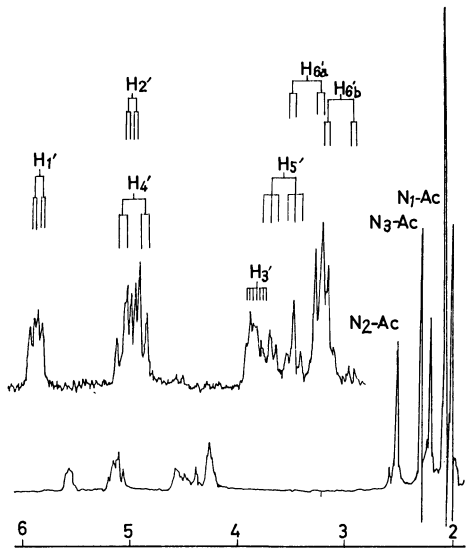

Fig. 2. The NMR spectrum of **8**.

imino-1,3-diacetylimidazolidine.[3]

For the sake of comparison, synthesis of **7** by indirect guanidination was attempted. Reaction of 3-amino-3-deoxy-1,2;5,6-di-*O*-isopropylidene-α-D-allofuranose with cyanogen bromide or with potassium cyanate gave the corresponding 3-cyanamido (**9**) and 3-ureido derivative (**10**) in 89 and 73% yields, respectively. Dehydration of **10** with methanesulfonyl chloride gave **9** in 50% yield. Reaction of **9** with methanolic ammonia at 90 °C in a sealed tube or with hydrogen sulfide in pyridine gave **8** or the corresponding 3-thioureido derivative (**11**) in 26 and 20% yields, respectively. Direct conversion of the aminosugar into **11** by the reaction with potassium thiocyanate gave only the de-5,6-*O*-isopropylidenated product, which was confirmed as the corresponding 5,6-di-*O*-acetyl derivative.[19] These results indicate that the fusion method is the best for synthesis of **7**.

In order to examine whether 3-deoxy-3-guanidino-D-glucose can make an additional aminal-ring, synthesis was carried out as follows. Though the reason is not clear, guanidination of 3-amino-3-deoxy-1,2;5,6-di-*O*-isopropylidene-α-D-glucofuranose[20] with cyanamide by the fusion method was unsuccessful. Thus an indirect method was adopted. Reaction of the aminosugar with cyanogen bromide in ether gave the corresponding 3-cyanamide as a sirup, which was then treated with methanolic ammonia in a sealed tube at 80—90 °C for 20 hr to give the corresponding 3-guanidino derivative (**12**) as the crystalline flavianate. Hydrolysis of **12** with flavianic acid gave 3-deoxy-3-guanidino-D-glucose (**13**) also as crystalline flavianate, which is positive to the Sakaguchi and Fehling tests. Base-catalyzed acetylation of **13** gave a sirup containing three products, from which a hexaacetate (**14**) was isolated with a preparative tlc.

The NMR spectrum of **14** indicated that it is composed of α- (H_1: δ 6.31, $J_{1,2}$=3.5 Hz) and β-anomers (H_1: δ 5.71, $J_{1,2}$=8.0 Hz) in the ratio 3:1. The relative amount of the α-anomer increased with reaction time, but both anomers could not be separated. Chemical shifts of ring-protons were different only in that of H_1 and H_2, and irradiation of amino-proton (δ 8.11, $J_{N,3}$=9.0 Hz) caused H_3 proton signal from quartet to triplet (δ 4.79, $J_{2,3}$=$J_{3,4}$=9.7 Hz). Consequently, **14** was determined to be 1,2,4,6-tetra-*O*-acetyl-3-deoxy-3-diacetylguanidino-α,β-D-gluco-pyranose.

The result suggests again that **13** could not make additional intramolecular aminal-ring, probably due to strong nonbonded interactions for the inversion of the conformation from *C*1 to 1*C*, as observed in the case of **6**.

Experimental

All melting points are uncorrected. The solutions were evaporated under reduced pressure at a bath temperature not exceeding 45 °C. Specific rotations were measured in a 0.5 dm tube, with a Carl Zeiss LEP-Al Polarimeter. The IR spectra were recorded in KBr discs with a Hitachi Model EPI-GS grating IR spectrophotomeser. The NMR spectra were taken with a JMN-4H-100 MHz Spectrometer in deuteriochloroform unless otherwise stated, using tetramethylsilane as an internal standard. Chemical shifts and coupling constants were recorded in δ and Hz units, and IR frequencies in cm^{-1}.

Methyl 6-Deoxy-6-guanidino-α-D-glucopyranoside (1) Dihydrochloride. i) Cyanamide Method: a) A solution of methyl 6-amino-6-deoxy-α-D-glucopyranoside hydrochloride[10] (1.15 g, 5 mmol), cyanamide (0.32 g, 7.5 mmol) and 1 M sodium hydroxide (1 ml, 1 mmol) in water (10 ml) was kept at 80 °C for 17 hr. The pH of the solution which changed to 10.0 was adjusted with 2 M hydrogen chloride to 5.0, and the solution was evaporated to give a sirup. The sirup was dissolved in ethanol (20 ml), filtered, and the filtrate was left to stand overnight in a refrigerator after addition of acetone, to give white crystals (**2**) (0.6 g, 73% based on cyanamide). Mp 183 °C, $[\alpha]_D^{23}$ +69.8° (*c* 1.0, H_2O); IR: 1742 and 1588 (urethane), 1680 and 1665 (guanidino group), 1615 (guanyl).

Found: C, 30.73; H, 6.27; N, 23.71; Cl, 17.42%. Calcd. for $C_{11}H_{23}N_7O_7Cl_2$: C, 30.28; H, 5.81; N, 23.48; Cl, 17.25%.

b) In a reaction similar to the above experiment, the pH of the solution was adjusted to 8.2 at the beginning and maintained at 8.0—8.6 during the course of reaction at 60 °C. The reaction mixture was treated with Amberlite IRA-410 (3 ml), and filtered. The solute was absorbed on a column of Amberlite CG-50 (15 ml), and the column was washed successively with deionized water (200 ml), 5% aqueous ammonia (200 ml), and water (200 ml), and then eluted with 0.5 M hydrogen chloride. The neutral effluent was evaporated, and the residue was extracted with ethanol. The extract was evaporated, and the residual sirup was dissolved in water (20 ml), deionized with Amberlite IRA-410 (3 ml), and the solution was evaporated to give a sirup. From a mixed solution of the sirup in water (0.5 ml) and flavianic acid (1.5 g) in ethanol (10 ml), yellow flavianate (**1**, 1.045 g) was obtained as crystals. The second crop (0.245 g) was obtained from the mother liquor. Yield, 1.29 g (50%); mp 155 °C (dec.); $[\alpha]_D^{23}$ +43.5° (*c* 2.0, H_2O); IR: 1673 and 1655 (sh) (mono substituted guanidine).

Found: C, 38.62; H, 4.38; N, 12.58; S, 6.02%. Calcd for $C_{18}H_{23}N_5O_{13}S$: C, 38.60; H, 4.14; N, 12.52; S, 5.73%.

ii) S-Methylisothiourea Method: A solution of methyl 6-amino-6-deoxy-α-D-glucopyranoside[10] (0.69 g, 3 mmol) and *S*-methylisothiourea sulfate (0.62 g, 4.5 mmol) in ammonia (10%, 10 ml) was left to stand at room temperature for 4 days, treated with Amberlite IRA-410 (3 ml) to remove sulfate ion, and then filtered. The filtrate was passed through an Amber-

lite CG-50-I column, and treated as above to give **1** in 51% (0.86 g) yield.

Methyl 2,3,4-Tri-O-acetyl-6-deoxy-6-diacetylguanidino-α-D-glucopyranoside (3). To a cold solution of **1** (8.34 g, 15 mmol) in pyridine (5 ml) was added dropwise acetic anhydride (15 ml, 150 mmol) for 30 min with stirring. The resulting solution was kept at room temperature for 2 day, poured into ice-water (200 ml), and then extracted with chloroform (50 ml ×4). The extract was successively washed with 2 M hydrochloric acid (40 ml×4), saturated sodium bicarbonate (40 ml ×4) and water, dried, and evaporated. The residue was fractionated on a silica-gel column (Kiesel Gel 60) with methanol–benzene (0.5—1.0% methanol), into **3** (2.04 g, 31%) and a mixture of methyl 6-monoacetylguanidino-6-deoxy-2,3,4-tri-*O*-acetyl-α-D-glucopyranoside and another unknown compound (0.62 g). $[\alpha]_D^{23}$ +71.5° (*c* 1.98, $CHCl_3$), +86.9° (*c* 0.84, EtOH); IR: 1750 (OAc), 1705, 1616, and 1555 (diacetylguanidine); λ_{max}^{EtOH} (nm) 221 (ε 8.35×10^3) and 254.7 (1.58×10^4); NMR: 4.97 (H_1: d, $J_{1,2}$=3.2), 4.87 (H_2; q, $J_{2,3}$=9.5), 5.49 (H_3; t, $J_{3,4}$=9.5), 3.95 (H_5; m, $J_{5,6}$=7.0, $J_{5,6'}$=3.4), 3.55—3.80 (H_6 and H_6'), 3.44 (OMe), 2.21, 2.12, 2.09 and 2.02 (5×Ac).

Found: C, 48.13; H, 5.90; N, 9.53%. Calcd for $C_{18}H_{27}N_3O_{10}$: C, 48.54; H, 6.11; N, 9.44%.

When a solution of **3** (305 mg, 0.69 mmol) in ethanol (20 ml) was refluxed for 14 hr, it became positive to the Sakaguchi reaction, and showed one spot on paper chromatography (Toyoroshi No. 50), using ethyl acetate–pyridine–acetic acid–water (5: 5: 1: 3) as developing solvent, of which R_f value (0.36) consists with that of **1**. Addition of flavianic acid (288 mg) in ethanol (5 ml) to the product gave the flavianate of **1**. Yield, 260 mg (69%).

6-Deoxy-6-guanidino-1,2; 3,4-di-O-isopropylidene-α-D-galactopyranose (4) Flavianate. A solution of 6-amino-6-deoxy-1,2; 3,4-di-*O*-isopropylidene-α-D-galactopyranose[15] (1.56 g, 6 mmol) and *S*-methylisothiourea sulfate (1.25 g, 9 mmol) in 10% ammonia (15 ml) was left to stand at room temperature for 4 day and then evaporated. The residue was dissolved in water (8 ml). The solution was treated with Amberlite IRA-410, and the solute was absorbed on an Amberlite CG-50-I (15 ml) column. The column was eluted with deionized water, aqueous ammonia (5%, 200 ml), and then 0.5 M hydrochloric acid. The last effluent was evaporated, and the residue was extracted with ethanol (20 ml). The ethanol solution was diluted with water (20 ml), treated with Amberlite IRA-410 (4 ml), and then evaporated to give a sirup (0.8 g). A solution of the sirup and flavianic acid (1.05 g) in ethanol (20 ml) was left to stand in a refrigerator for one day to give yellow crystals. Yield, 1.29 g (35%); mp 135 °C; $[\alpha]_D^{23}$ −20.6° (*c* 1.0, EtOH): IR: 1668 and 1650 (monosubstituted guanidine).

Found: C, 44.51; H, 4.85; N, 10.89; S, 5.38%. Calcd for $C_{23}H_{29}N_5O_{13}S$: C, 44.87; H, 4.75; N, 11.38; S, 5.21%.

6-Deoxy-6-guanidino-D-galactose (5) Flavianate. a) A solution of the flavianate of **4** (123 mg, 0.2 mmol) and flavianic acid (35 mg, 0.1 mmol) in water (5 ml) was kept at 65 °C for 2 hr, and then evaporated. From the residue, excess flavianic acid was removed with ethanol to give yellow crystals. Yield, 70 mg (65%); mp 200 °C (dec.); $[\alpha]_D^{23}$ +14.3°⟶+18.5° (*c* 0.7, H_2O); IR: 1675 and 1645 (monosubstituted guanidine).

Found: C, 38.61; H, 4.30; N, 12.79; S, 5.97%. Calcd for $C_{17}H_{21}N_5O_{13}S$: C, 38.13; H, 3.95; N, 13.08; S, 5.99%.

This compound was positive to the Fehling test, and to the Sakaguchi reaction after removal of flavianic acid with IRA-410.

b) A solution of 6-amino-6-deoxy-1,2; 3,4-di-*O*-isopropylidene-α-D-galactopyranose (1.30 g, 5 mmol) and *S*-methylisothiourea sulfate (1.04 g, 7.5 mmol) in aqueous ammonia (10%, 8 ml) was treated as above, without isolation of **4**. Yellow crystals (**5**). identical with those described above, were obtained in 59% (1.58 g) yield.

1,2,3,4-Tetra-O-acetyl-6-deoxy-6-diacetylguanidino-β-D-galactopyranose (6). To a cold solution of the flavianate of **5** (5.36 g, 0.01 mmol) in pyridine (30 ml) was added dropwise acetic anhydride (10 ml, 100 mmol), and the resulting solution was left to stand at room temperature for 2 day, and then poured into ice–water (500 ml). The aqueous solution was extracted with chloroform (100 ml×5), and the extract was washed 2 M hydrochloric acid, saturated bicarbonate and water. with Evaporation of the extract gave a sirup (3.4 g) which was fractionated on a silica-gel column (Kiesel Gel 60), using benzene–acetone (5: 1) as effluent. The first fraction gave a pure sirupy hexaacetate (1.2 g, 27.3%). $[\alpha]_D^{23}$ +16.5° (*c* 1.17, EtOH); IR: 1745 (OAc), 1694, 1600, and 1555 (diacetylguanidine); λ_{max}^{EtOH} (nm) 254 (ε 1.73×10^4), 221 (8.94×10^3); NMR: 13.04 and 9.15 (2×NH), 5.69 (H_1; d, $J_{1,2}$=7.9), 5.33 (H_2; q, $J_{2,3}$=10.0), 5.07 (H_3; q, $J_{3,4}$=3.7), 5.40 (H_4; q, $J_{4,5}$=0.5), 4.00 (H_5; q, $J_{5,6}$=8.0, $J_{5,6'}$=5.0), 3.74 (H_6; dq, $J_{6,6'}$=14.0, $J_{6,NH}$=8.0), 3.41 ($H_{6'}$; dq, $J_{6',NH}$=5.0), 1.95, 2.00, 2.09, 2.13, and 2.15 (6×Ac).

Found: C, 47.82; H, 5.66; N, 8.75%. Calcd for $C_{19}H_{27}N_3O_{11}$: C, 48.18; H, 5.75; N, 8.88%.

3-Deoxy-3-guanidino-1,2-O-isopropylidene-α-D-allofuranose (7) picrate. a) A homogeneous solution of 3-amino-3-deoxy-1,2; 5,6-di-*O*-isopropylidene-α-D-allofuranose hydrochloride[17] (296 mg, 1 mmol) and cyanamide (64 mg, 1.5 mmol) in water (10 ml) was evaporated and the residue was heated at 130—133 °C for 40 min on a silicone-oil bath. The cooled reaction mixture was dissolved in water (6 ml), treated with Amberlite IRA-410 (3 ml), and evaporated to one-third volume. Addition of picric acid (276 mg) in methanol (4 ml) to the remaining solution gave yellow crystals (295 mg, 56.6%) which were recrystallized from water. Mp 193—193.5 °C, $[\alpha]_D^{23}$ +47.9° (*c* 1.09, MeOH), IR: 1645 (monosubstituted guanidine), the Sakaguchi reaction; positive.

Found: C, 37.41; H, 4.51; N, 17.02%. Calcd for $C_{16}H_{22}N_6O_{12}$–H_2O: C, 37.21; H, 4.76; N, 16.52%.

b) A solution of **9** (100 mg, 0.35 mmol) in saturated methanolic ammonia (15 ml) was heated in a sealed tube at 80 °C for 15 hr, and then evaporated to give a sirup. From the sirup and picric acid (100 mg) in methanol–water (4 ml, 50%), yellow crystals, identical with **7**, were obtained (46 mg, 26%).

2′,4′,6′-Tri-O-acetyl-α-D-allopyrano[1′,2′,3′; 4,5,6]-2-acetylimino-1,3-diacetyl-perhydropyrimidine (8). A solution of **7** (254 mg, 0.5 mmol) in 2 M hydrochloric acid was heated at 70 °C for 6 hr, and picric acid deposited was filtered off. The water layer was extracted with ether (10 ml×5) and then evaporated to give a sirup (135 mg). The sirup was acetylated with acetic anhydride (0.5 ml) in pyridine (2 ml), and the reaction mixture was poured into ice–water and extracted with chloroform (20 ml×5). The extract was successively washed with 2 M hydrochloric acid, saturated sodium bicarbonate and water, and then evaporated to give a sirup (165 mg). This sirup showed three spots on tlc (MeOH: pyridine=9: 1), and was fractionated into a mixture (122 mg) of spot I and spot II (main), and spot III (46 mg). From the mixture, sirupy spot II (35 mg, 15%) was obtained in a pure state by fractionation on a silica-gel column (Wakogel C-200) using benzene–ethyl acetate (4: 1) as effluent, which was crystallized from ether. Mp 134 °C, $[\alpha]_D^{23}$ +188° (*c* 0.235, EtOH), IR: 1725 (OAc), 1700 (=NAc), 1635 (NAc). λ_{max}^{EtOH} 216 nm, NMR: 5.57 ($H_{1'}$; q, $J_{1',2'}$=3.4, $J_{1',3'}$=1.9), 5.17 ($H_{2'}$; q, $J_{2',3'}$=2.5), 5.12 ($H_{4'}$; q, $J_{4',5'}$=10.6), 4.59

($H_{3'}$; m, $J_{3',4'}=3.9$), 4.46 ($H_{5'}$; sex, $J_{5',6'_a}=3.5$, $J_{5',6'_b}=3.0$), 4.34 ($H_{6'_a}$; q, $J_{6'_a,6'_b}=12.0$), 4.24 ($H_{6'_b}$; q), 2.52 (=NAc), 2.30 and 2.22 (NAc), 2.09 and 2.02 (3×OAc).

Found: C, 49.51; H, 5.51; N, 9.21%. Calcd for $C_{19}H_{25}N_3O_{10}$: C, 50.11; H, 5.53; N, 9.23%.

3-Cyanamido-3-deoxy-1,2; 5,6-di-O-isopropylidene-α-D-allofuranose (9). a) To a solution of 3-amino-3-deoxy-1,2; 5,6-di-*O*-isopropylidene-α-D-allofuranose[17] (130 mg, 0.5 mmol) in ether (5 ml) was added portionwise cyanogen bromide (27 mg, 0.25 mmol) in ether (3 ml) with stirring, and the resulting solution was left to stand at room temperature for 4 hr. A white precipitate (67 mg) deposited was filtered off, and the filtrate was evaporated. The residue was extracted with benzene, and the extract was again evaporated to give colorless sirup (62.3 mg, 89%) which was purified on a silica-gel column. This sirup crystallized on standing. Mp 83—84 °C, $[\alpha]_D^{23}$ +76.1° (*c* 1.80, EtOH), IR: 2220 (CN).

Found: C, 54.89; H, 7.07; N, 9.56%. Calcd for $C_{13}H_{20}N_2O_5$: C, 54.92; H, 7.09; N, 9.85%.

b) A solution of **10** (151 mg, 0.5 mmol) and methanesulfonyl chloride (58 ml, 0.75 mmol) in pyridine (4 ml) was left to stand at room temperature for one day, poured into ice-water (30 ml), and then extracted to give a sirup (112 mg, 79%) which was purified on a silica-gel column as above. Yield, 96 mg (68%).

3-Deoxy-1,2; 5,6-di-O-isopropylidene-3-ureido-α-D-allofuranose (10). A solution of 3-amino-3-deoxy-1,2; 5,6-di-*O*-isopropylidene-α-D-allofuranose (259 mg, 1 mmol), potassium cyanate (122 mg, 1.5 mmol), and acetic acid (0.06 ml, 1 mmol) in water (5 ml) was heated at 100 °C for 90 min, and treated with Amberlite IRA-410 (2 ml) for one day and then with Amberlite CG-50-I to remove potassium ion and unreacted starting material. The effluent was evaporated to give a sirup (258 mg, 85.5%) which crystallized from ether. Yield, 220 mg (73%), mp 164 °C, $[\alpha]_D^{23}$ +87.4° (*c* 1.0, EtOH), IR: 1675 (ureido).

Found: C, 51.18; H, 7.27; N, 9.52%. Calcd for $C_{13}H_{22}N_2O_6$: C, 51.64; H, 7.34; N, 9.27%.

3-Deoxy-1,2; 5,6-di-O-isopropylidene-3-thioureido-α-D-allofuranose (11). To a solution of **9** (177 mg, 0.62 mmol) in pyridine (5 ml) was passed hydrogen sulfide at room temperature for 5 hr. The solution was then evaporated to give a sirup which crystallized from ethanol (40 mg, 20%). Recrystallization from methanol gave fine needles. Mp 219—220 °C, $[\alpha]_D^{23}$ +108.4° (*c* 0.5, EtOH), IR: 3430, 3360, and 3330 (NH), 1532 (thioureido).

Found: C, 48.64; H, 7.00, N, 9.00; S, 9.83%. Calcd for $C_{13}H_{22}N_2O_5S$: C, 49.04; H, 6.97; N, 8.79; S, 10.07%.

3-Deoxy-3-guanidino-1,2; 5,6-di-O-isopropylidene-α-D-glucofuranose (12) Flavianate. To a cold solution of 3-amino-3-deoxy-1,2; 5,6-di-*O*-isopropylidene-α-D-glucofuranose[20] (2.5 g, 9.7 mmol) in ether (60 ml) was added with stirring 0.5 equivalent of cyanogen bromide in ether (40 ml), and the resulting solution was left to stand at room temperature for 6 hr, the hydrobromide of the aminosugar then being filtered. The sirupy product obtained by evaporation of the filtrate was purified on a silica-gel column with benzene–ethyl acetate (8: 1) as effluent. The cyanamido derivative (1.11 g, 81.5% based on cyanogen bromide) showed the characteristic absorption of nitrile (2200 cm^{-1}) in IR spectrum. A solution of the cyanamide in methanol (50 ml) saturated with ammonia was heated in a sealed tube at 80—90 °C for 20 hr, and then evaporated. Addition of flavianic acid (1.4 g, 3.8 mmol) in ethanol to a suspension of the resulting sirup in a small amount of water gave the flavianate of **12** as yellow crystals, which were recrystallized from aqueous acetone. Mp 185—190 °C (decomp.), yield, 39% based on the cyanamide; $[\alpha]_D^{23}$ −22.4° (*c* 1.0, pyridine).

Found: C, 44.77; H, 4.73; N, 11.47; S, 5.58%. Calcd for $C_{23}H_{29}N_5O_{13}S$: C, 44.87; H, 4.74; N, 11.37; S, 5.21%.

3-Deoxy-3-guanidino-D-glucose (13) Flavianate. A suspension of the flavianate of **12** (500 mg, 0.81 mmol) and flavianic acid (200 mg, 0.51 mmol) in water (60 ml) was heated at 80 °C for 4 hr to give a homogeneous solution, and the solution was then evaporated. The residue was washed with ethanol to give **13** quantitatively as flavianate. For elemental analyses. a portion of it was recrystallized from methanol. Mp 210 °C (decomp.); $[\alpha]_D^{23}$ +17.2→+23.8° (in H_2O, after 48 hr).

Found: C, 38.65; H, 4.01; N, 13.41%. Calcd for $C_{17}H_{21}N_5O_{13}S$: C, 38.13; H, 3.95; N, 13.08%.

This compound was positive in the Sakaguchi and Fehling reactions.

1,2,3,4-Tetra-O-acetyl-3-deoxy-3-diacetylguanidino-α,β-D-glucopyranose (14). Acetylation of **13** (300 mg, 0.56 mmol) with acetic anhydride (620 mg, 6.08 mmol) in pyridine gave sirupy product which showed three spots (R_f=0.66, 0.52 and 0.12) on a preparative tlc with benzene–ethyl acetate (1: 1) as developing solvent. The portion R_f=0.52 was extracted with acetone to give **14** (50 mg, 19%) as a sirup. $[\alpha]_D^{23}$ +35.8° (*c* 1.21, $CHCl_3$); λ_{max}^{EtOH} 256 and 220 nm.

Found: C, 48.52; H, 5.82; N, 8.32%. Calcd for $C_{19}H_{27}N_3O_{11}$: C, 48.19; H, 5.74; N, 8.87%.

The authors are greatful to Mr. H. Matsumoto for measurement of NMR spectra, and to members of the Laboratory of Organic Analysis for elemental analysis.

References

1) Part XXI: M. Iwakawa and J. Yoshimura, This Bulletin, **46**, 1525 (1973).
2) H. Paulsen and K. Todt, *Adv. Carbohyd. Chem.*, **23**, 116 (1968).
3) J. Yoshimura, T. Sekiya, and T. Iida, This Bulletin, **45**, 1227 (1972).
4) S. N. Danilov and I. S. Lishanskii, *Zh. Obshch. Khim.*, **21**, 366 (1951).
5) B. R. Baker and T. Neilson, *J. Org. Chem.*, **29**, 1047 (1964).
6) M. L. Wolfrom, D. Horton, and D. H. Hutson, *ibid.*, **28**, 845 (1963); M. L. Wolfrom, W. A. Cramp, and D. Horton, *ibid.*, **29**, 2302 (1964).
7) R. S. Morrell and A. E. Bellars, *J. Chem. Soc.*, **91**, 1010 (1907).
8) H. Dorn and M. Schütt, *Chem. Ber.*, **97**, 3256 (1964).
9) S. N. Danilov and I. S. Lishanskii, *Zh. Obshch. Khim.*, **25**, 2106 (1955).
10) M. J. Cron, O. B. Fardig, D. L. Johnson, H. Schmitz, D. F. Whitehead, I. R. Hooper, and R. U. Lemieux, *J. Amer. Chem. Soc.*, **80**, 2342 (1958).
11) R. Greenhalgh and R. A. B. Bannard, *Can. J. Chem.*, **37**, 1810 (1959).
12) R. Greenhalgh and R. A. B. Bannard, *ibid.*, **39**, 1017 (1961).
13) A. B. Foster, D. Horton, and M. Stacey, *J. Chem. Soc.*, **1957**, 81.
14) E. Schütte, *Z. Physiol. Chem.*, **279**, 52 (1943).
15) K. Freudenberg and A. Doser, *Ber.*, **58**, 294 (1925).
16) K. Freudenberg and R. M. Hixson, *ibid.*, **56**, 2123 (1923).
17) M. L. Wolfrom, F. Shafizadeh, and R. K. Armstrong, *J. Amer. Chem. Soc.*, **80**, 4885 (1958).
18) K. Sugino, K. Shirai, and K. Aoyagi, This Bulletin, **17**, 126 (1942).
19) B. Coxon and L. Hough, *J. Chem. Soc.*, **1961**, 1643.
20) W. Meyer, *Angrew. Chem. Int. Ed. Engl.*, **5**, 967 (1966).

Solvent Effects in Diazo-coupling Reactions

Yōji HASHIDA, Hiroki ISHIDA, Shizen SEKIGUCHI, and Kohji MATSUI
Department of Chemistry, Faculty of Engineering, Gunma University, Tenjincho, Kiryu, Gunma 376
(Received November 26, 1973)

The kinetics of the diazo-coupling reactions of benzenediazonium fluoroborates with 1,3,5-trimethoxybenzene and 2-naphthol have been studied in non-aqueous media including both protic and dipolar aprotic solvents. In the case of the reaction with 1,3,5-trimethoxybenzene, no significant solvent effect on the reaction rate was observed. However, in the case of the reaction with 2-naphthol, the reaction rate was affected markedly by the solvent; in dipolar aprotic solvents, the reaction proceeded much faster than in protic solvents. The observed results are interpreted in terms of the difference in solvation toward the naphtholate ion.

Generally, diazo-coupling reactions are carried out in an aqueous medium. The mechanisms of these reactions and the reactivities of the reactants have been extensively studied kinetically.[1] However, little is known about the solvent effects on the reaction rate. Recently, a kinetic study of the coupling reactions of *N,N*-dimethylaniline in several dipolar aprotic solvents (nitromethane, acetonitrile, and sulfolane) has been reported by Penton *et al.*,[2] who showed that no significant solvent effect was observed.

In this paper, we wish to report the solvent effects on the reactions of diazonium salts with 1,3,5-trimethoxybenzene and 2-naphthol.

Experimental

Reagents. Commerical 1,3,5-trimethoxybenzene and 2-naphthol were recrystallized from ethanol and water respectively. *m*-Nitrobenzenediazonium fluoroborate and benzenediazonium fluoroborate were prepared by the usual method[3] and dried under a vacuum over phosphorus pentoxide in the dark.

Solvents. The methanol was dried with calcium oxide and fractionally distilled. The formic acid was twice fractionally distilled. The acetic acid was purified according to the method of MacInnes *et al.*[4] The propionic acid was dried over anhydrous sodium sulfate and fractionally distilled. The nitromethane and acetonitrile were purified by drying over phosphorus pentoxide and fractionally distilled. The dimethyl sulfoxide was purified by distillation on sodium hydroxide. The dimethylformamide was purified according to the method of Clare.[5]

Kinetic Measurements. The rates were measured by following the increase in the optical density of the azo compound formed with the lapse of time using a Hitachi 124-type spectrophotometer thermostated at 20 °C. As a large excess of the substrate was always present, the reactions followed a pseudo-first-order relationship (1):

$$k't = \ln \frac{E_\infty}{E_\infty - E_t} \quad (1)$$

where E_∞ and E_t denote the optical densities at an infinite time and at time t respectively. The rate constants thus obtained were constant up to more than 80% of the reaction.

Reaction with 1,3,5-Trimethoxybenzeme: To 100 ml of a solution of 1,3,5-trimethoxybenzene (2×10^{-3}M), was added 1 ml of a solution of *m*-nitrobenzenediazonium salt (4×10^{-3}M). Aliquots of the reaction mixture were pipetted into a thermostated spectrophotometric cell at 20 °C, and the optical density was measured at the absorption maximum of the azo compound.

Reaction with 2-Naphthol: Because of the dependence of the apparent rate constant (k') on the solvent acidity, all the kinetic measurements were carried out in appropriate buffer solutions. A reaction mixture containing 2-naphthol ($1—5\times10^{-3}$M) and appropriate buffer reagents was divided into two parts. One of the parts was used for the kinetic measurement in a manner similar to that described in the reaction of 1,3,5-trimethoxybenzene. The 475 mμ wavelength was monitored for an increase in the optical density of the azo compound. The other part was used for the measurement of the acidity function (H_-) using Eq. (2), by adding an appropriate indicator; the ionization ratio of an indicator was measured spectrophotometrically.

$$H_- = \mathrm{p}K_a + \log \mathrm{R} \quad (2)$$

$\mathrm{p}K_a$: Ionization constant of an indicator in a given solvent
R: Ionization ratio for an indicator in a given solvent

Table 1 lists the indicators employed and their $\mathrm{p}K_a$ values. The kinetic results are summarized in Tables 2, 3, 4, and 5.

In an aqueous medium, the rates were measured as follows: bacause of the low solubility of the azo compound, 10 ml portions of the sample solution were withdrawn from the reaction mixture at definite time intervals and added to 5 ml of a 2 M HCl solution in order to stop the reaction. The solution was then diluted to 25 ml with methanol, and the extinction was measured.

$\mathrm{p}K_a$ *Measurements.* The $\mathrm{p}K_a$ values of 2-naphthol in organic solvent were determined by the indicator method using Eq. (3);[6] the ratio of the acidic to the basic form of an indicator and 2-naphthol was determined spectrophotometrically.

$$\mathrm{p}K_a = \mathrm{p}K_I + \log \frac{C_{Ib}\times C_{Na}}{C_{Ia}\times C_{Nb}} \quad (3)$$

$\mathrm{p}K_a$: $\mathrm{p}K_a$ value of 2-naphthol

Table 1. $\mathrm{p}K_a$ VALUES OF INDICATORS

Indicator	Neutral red	Brom cresol green	Brom cresol green	Brom phenol blue
Solvent	Acetonitrile	Dimethyl sulfoxide	Dimethylformamide	Methanol
$\mathrm{p}K_a$	15.6[a]	7.4[b]	8.3[c]	8.9[d]

a) I. M. Kolthoff, M. K. Chantoni, Jr., and S. Bhowmik, *Anal. Chem.*, **39**, 315(1967). b) I. M. Kolthoff and T. B. Reddy, *Inorg. Chem.*, **1**, 189 (1962). c) Ref. (5). d) I. M. Kolthoff, *J. Amer. Chem. Soc.*, **60**, 2516 (1938).

Table 2. Apparent rate constants for the reaction of benzenediazonium fluoroborate with 2-naphthol in methanol at 20 °C
($Ar-\overset{+}{N}_2$: 3×10^{-5} M, Ar–OH: 2.5×10^{-3} M)

Buffer	AA(0.007M)–AAS(0.007M)[a]	AA(0.02M)–AAS(0.01M)	NBA(0.01M)–NBAS(0.01M)[b]
H_-	9.24	8.79	8.43
$k'(min^{-1})$	3.48	1.58	0.708

a) AA and AAS denote acetic acid and its sodium slat respectively. b) NBA and NBAS denote *p*-nitrobenzoic acid and its sodium salt respectively.

Table 3. Apparent rate constants for the reaction of benzenediazonium fluoroborate with 2-naphthol in dimethylformamide at 20 °C
($Ar-\overset{+}{N}_2$: 3×10^{-5} M, Ar–OH: 3.2×10^{-3} M)

Buffer	NB(0.004M)–NBS(0.001M)[a]	NB(0.008M)–NBS(0.002M)	DNB(0.002M)–DNBS(0.002M)[b]	DNB(0.004M)–DNBS(0.002M)
H_-	9.02	8.72	8.07	7.80
$k'(min^{-1})$	1.71	0.781	0.178	0.0762

a) NB and NBS denote *p*-nitrobenzoic acid and its sodium salt respectively. b) DNB and DNBS denote 3,5-dinitrobenzoic acid and its sodium salt respectively.

Table 4. Apparent rate constants for the reaction of benzenediazonium fluoroborate with 2-naphthol in dimethyl sulfoxide at 20 °C
($Ar-\overset{+}{N}_2$: 3×10^{-5} M Ar–OH: 2.5×10^{-3} M)

Buffer	DNB(0.004M)–DNBS(0.01M)[a]	DNB(0.01M)–DNBS(0.01M)	DNB(0.01M)–DNBS(0.005M)	DMB(0.01M)–DMBS(0.004M)	DNB(0.01M)–DNBS(0.002M)
H^-	8.20	7.63	7.26	7.15	6.77
$k'(min^{-1})$	0.117	0.0495	0.0247	0.0194	0.0109

a) DNB and DNBS denote 3,5-dinitrobenzoic acid and its sodium salt respectively.

Table 5. Apparent rate constants for the reaction of benzenediazonium fluoroborate with 2-naphthol in acetonitrile at 20 °C ($Ar-\overset{+}{N}_2$: 3×10^{-5} M Ar–OH: 1.25×10^{-3} M)

Buffer	DNB(0.003M)–DNBT(0.002M)[a]	DNB(0.0035M)–DNBT(0.002M)	DNB(0.005M)–DNBT(0.002M)	DNB(0.007M)–DNBT(0.002M)
H_-	16.06	15.67	15.29	15.04
$k'(min^{-1})$	0.928	0.331	0.154	0.0795

a) DNB and DNBT denote 3,5-dinitrobenzoic acid and its tetrabutylammonium salt respectively.

Table 6. pK_a values for phenol and 2-naphthol at 20 °C

Acid	$pK_a(H_2O)$	pK_a(MeOH)	pK_a(DMF)	pK_a(DMSO)	pK_a(MeCN)
Phenol	—	14.3 (14.2)[a]	—	16.4 (16.4)[b]	(27.2)[b]
2-Naphthol	9.51	13.8	14.5	16.2	27.0
Indicator	—	14.0[c] (Thymol blue)	13.85[d] (*m*-Nitrophenol)	15.3[b] (Thymol blue)	27.2[b] (Thymol blue)

a) B. D. England and D. A. House, *J. Chem. Soc.*, **1962**, 4421. b) I. M. Kolthoff and M. K. Chantonni, *J. Amer. Chem. Soc.*, **90**, 23 (1968). c) I. M. Kolthoff, *ibid.*, **60**, 2516 (1938). d) S. M. Petrov and Yu. I. Umanskii, *Zh. Fiz. Khim.*, **41**, 1374 (1967).

pK_I: pK_a value of an indicator

C_{Ia}, C_{Ib}: Concentrations of the acidic and basic forms of an indicator respectively.

C_{Na}, C_{Nb}: Concentrations of the acidic and dissociated forms of naphthol respectively

The results obtained are summarized in Table 6.

As a check of the method described above, the pK_a value of phenol was also measured. As is evident from Table 6, there is no disagreement between the pK_a values of phenol in the present work and the reference.

Results and Discussion

Reaction with 1,3,5-Trimethoxybenzene. The first-order dependence of the reaction rate on the concentration of a diazonium salt may be apparent from the applicability of Eq. (1) to this reaction; the reaction rate (k') also showed a first-order dependence on the substrate concentration. Thus, the reaction rate can be expressed by Eq. (6), showing that this is a reaction

between a cation and an uncharged molecule:

$$\text{Rate} = k_2(\text{Ar}-\overset{+}{\text{N}}_2)\left(\begin{array}{l}\text{MeO}\\ \\ \text{MeO}\end{array}\!\!\!

must be small, because this reaction is a cation-anion combination reaction and in the transition state the charge is considered to have almost disappeared.[1] Therefore, the rate change shown in Table 9 is considered to depend mainly on the difference in solvation energy toward the naphtholate ion.

It is well known that an anion is solvated in protic solvents by the general hydrogen-bonding interaction;[7] consequently, the substrate is stabilized and the rate is slow in the hydroxylic solvents, as can be seen in Table 9. The increase in the rate on transfer from water to methanol may be understood from the difference in the hydrogen-bonding capacity of these solvents.[12] On the other hand, the fact that anions are poorly solvated in dipolar aprotic solvents[7] is considered to be responsible for the rapid reactions in these solvents.

It is interesting that, despite the similar physical properties of dimethyl sulfoxide and acetonitrile, a large difference was observed between the rate constants of the reactions in these solvents; the reactivity sequence in Table 9 is in accord with the order of the pK_a values of naphthol (Table 6) in these solvents. The results suggest that a naphthol generates a reactive naphtholate ion in a solvent in which it indicates a high pK_a value. However, a detailed discussion of these results must wait until later.

References

1) H. Zollinger, "Azo and Diazo Chemistry," Interscience Publishers, New York (1961), p. 211.

2) J. R. Penton and H. Zollinger, *Helv. Chim. Acta*, **54**, 573 (1971).

3) R. Putter, "Methoden der Organischen Chemie (Houben-weyl)," Band X/3 (Stickstoffverbindungen I), George Thieme Verlag., Stuttgart (1965), p. 37.

4) D. A. MacInnes and T. Schedlovsky, *J. Amer. Chem. Soc.*, **54**, 1429 (1932).

5) B. W. Clare, D. Cook, E. C. F. Ko, Y. C. Mac, and A. J. Parker, *ibid.*, **88**, 1911 (1966).

6) In a given solvent, the acidity functions are expressed by Eqs. (4) and (5):

$$H_- = pK_I + \log \frac{C_{Ib}}{C_{Ia}} \quad (4)$$

$$H_- = pK_a + \log \frac{C_{Nb}}{C_{Na}} \quad (5)$$

Eq. (3) is obtained by taking Eqs. (4) and (5) as equal.

7) For recent reviews, see, a) A. J. Parker, *Quart. Rev.* (London), **1962** 163 b) A. J. Parker, *Chem. Rev.*, **69**, 1 (1969); c) A. J. Parker, "Advances in Physical Organic Chemistry," Vol. 5, ed. by V. Gold, Academic Press, New York (1967), p. 173. d) C. D. Ritchie, *Accounts Chem. Res.* **5**, 348 (1972).

8) E. D. Hughes and D. J. Whitingham, *J. Chem. Soc.*, **1960**, 806

9) In the case of dimethyl sulfoxide, the slope of the line is 0.85. This small deviation from unit, however, may be ascribed to the change of the ionic strength of the reaction medium.

10) H. Zollinger, *Helv. Chim. Acta.*, **36**, 1723 (1953).

11) H. Zollinger, *ibid.*, **39**, 1600 (1956).

12) N. Kornblum, N. P. J. Berrigan, and W. J. le Noble, *J. Amer. Chem. Soc.*, **85**, 1141 (1963).

Oxytocin Analogues Containing No Disulfide Bond. III. The Synthesis of Three Analogues of 1,6-Aminosuberic Acid-Oxytocin

Tsutomu YAMANAKA* and Shumpei SAKAKIBARA**
Peptide Institute, Protein Research Foundation, Ina, Minoh, Osaka 562
(Received November 26, 1973)

[Asu^{1,6}]-oxytocin, an analogue of deamino-oxytocin in which the disulfide bond is replaced by an ethylene linkage, is completely resistant to deterioration during storage under concentrated conditions. In the present study, three new analogues of this material, [Phe^3, Asu^{1,6}]-oxytocin, [Val^4, Asu^{1,6}]-oxytocin, and [Gly^7, Asu^{1,6}]-oxytocin, were synthesized to find out a hormonal compound possessing a specifically higher uterotonic activity. Among them, the [Gly^7]-analogue was found to be the most promising compound; it showed a relatively higher uterotonic activity (245 IU/mg) in the rat, with a faint antidiuretic activity (0.02 IU/mg) and a weak depressor activity.

Deamino-oxytocin, which has a β-mercaptopropionyl residue in place of the cysteinyl residue in the 1 position of oxytocin, exhibits a higher oxytocic activity than the original oxytocin.[2] This fact indicates that the free amino group of oxytocin is not essential for the hormonal function. One or both sulfur atoms of the disulfide bridge in the deamino-oxytocin can also be replaced by one or two methylene groups respectively without any conspicuous loss of the hormonal activities.[3–5] In the first paper of this series,[5] we introduced an efficient procedure for the synthesis of such an analogue of deamino-oxytocin, [Asu^{1,6}]-oxytocin, in which the disulfide bond is replaced by an ethylene linkage, as is shown in Fig. 1.[5] The compound synthesized by the new procedure showed a much higher oxytocic potency than the reported value[4] for the compound. Then, the procedure was applied to the syntheses of [Asu^{1,6}]-vasopressins and vasotocins. These new derivatives were also confirmed to be biologically active, as had been expected.[6–8] Thus, it was concluded that the disulfide bridge itself in neurohypophyseal hormones in not required, in general, for the exhibition of their hormonal activities.[8] Later, the [Asu^{1,6}]-oxytocin synthesized by our procedure was found to be crystallized from water,[9] and the crystallized compound showed a higher uterotonic activity (160 IU/mg) than the highest value (134 IU/mg),[9] so far reported for the amorphous compounds.

Both natural and synthetic neurohypophyseal hormones are known to be reduced in their potency in the course of such common procedures for isolation as concentration and lyophilization. The Asu-derivatives, however, are completely resistant to inactivation during those procedures, even in the presence of triethylamine.[8,9]

Therefore, if we can find an analog of the Asu-oxytocin, which has a sufficiently higher potency in oxytocic activity, with negligibly lower potencies in pressor and antidiuretic activities, the use of such a compound as a drug for labor induction should be much more advantageous than that of natural oxytocin.

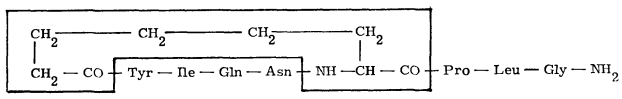

Fig. 1. Structure of [Asu^{1,6}]-Oxytocin.

In the present study, we have synthesized three new analogues of the Asu-oxytocin, [Phe^3, Asu^{1,6}]-oxytocin, [Val^4, Asu^{1,6}]-oxytocin, and [Gly^7, Asu^{1,6}]-oxytocin, and their hormonal activities have been compared in order to find a promising compound for use as an oxytocic hormone. Their parent compounds, [Phe^3]-oxytocin,[10] [Val^4]-oxytocin,[11] and [Gly^7]-oxytocin,[12] are already known to exhibit specific spectra in their biological activities (See Table 1).

The syntheses were carried out by the stepwise elongation technique,[13] as is shown in Charts 1, 2, and 3. Two different procedures, which had previously

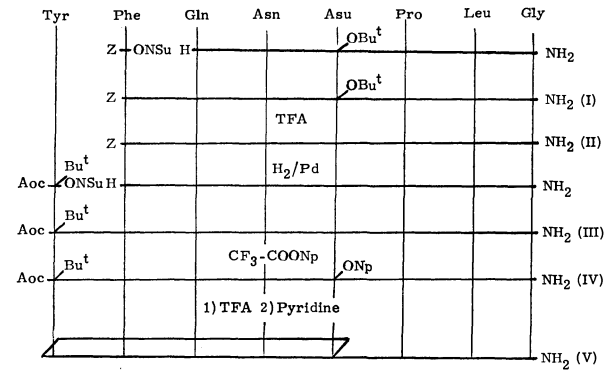

Chart 1. Synthesis of [Phe^3, Asu^{1,6}]-Oxytocin.

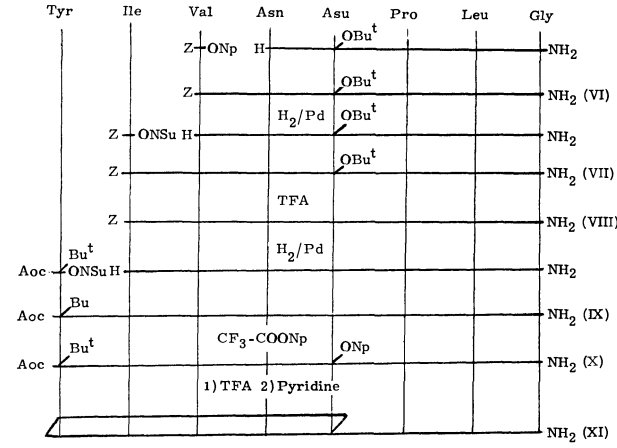

Chart 2. Synthesis of [Val^4, Asu^{1,6}]-Oxytocin.

* Present address: Research Laboratories, Yoshitomi Pharmaceutical Industries, Ltd., Yoshitomi-cho, Chikujo-gun, Fukuoka-ken.

** To whom correspondence should be addressed.

Table 1. Biological potencies of oxytocin analogues

Compound	Oxytocic (rat)	Depressor (fowl)	Pressor (rat)	Antidiuretic (rat)
[Phe^3, Asu^{1,6}]-Oxytocin(V)	21.6	—	<0.1	—
[Val^4, Asu^{1,6}]-Oxytocin(XI)	14.9	—	<0.25	—
[Gly^7, Asu^{1,6}]-Oxytocin(XX)	244.7	4.6	Weak depressor	0.02
[Phe^3]-Oxytocin[b]	20	45	3	—
[Val^4]-Oxytocin[c]	139±5	230 ±14	<0.005	0.5
[Gly^7]-Oxytocin[d]	330	—	—	0.01
Oxytocin[e]	450±30	450 ±30	5±1	5±1
Deaminooxytocin[f]	803±36	975 ±24	1.44±0.06	19
[Asu^{1,6}]-Oxytocin[g]	160±4.4	44 ±1.7	0.10±0.02	4.7±0.3

a) Expressed in IU/mg. Determined by T. Okada *et al.* of Yoshitomi Pharmaceutical Industries, Ltd. Details will be published elsewhere. b) Cited from Ref. 10. c) Cited from Ref. 11. d) Cited from Ref. 12. e) R. A. Boissonnas, S. Guttmann, B. Berde, and H. Konzett, *Experientia*, **17**, 377 (1961). f) B. M. Ferrier, D. Jarvis, and V. du Vigneaud, *J. Biol. Chem.*, **240**, 4264 (1965). g) Cited from Ref. 9.

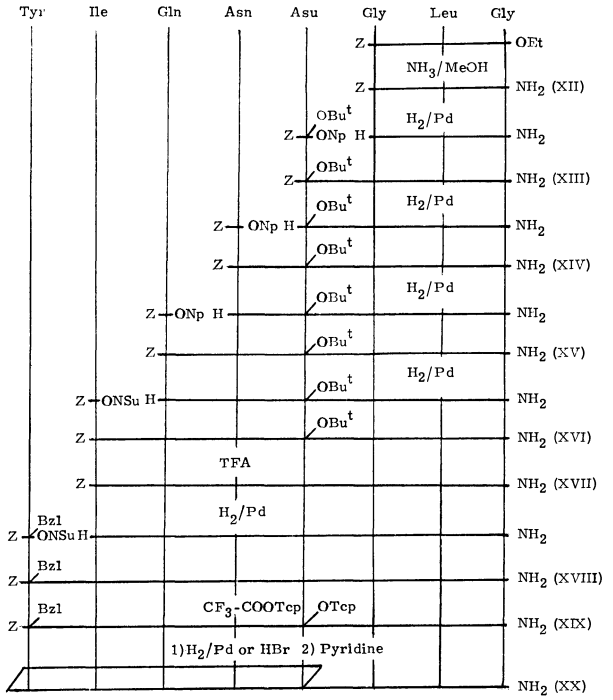

Chart 3. Synthesis of [Gly^7, Asu^{1,6}]-oxytocin.

been used for the synthesis of Asu-oxytocin[5] and Asu-vasopressins,[8] were applied to the cyclization of these linear peptides in order to compare the efficiency of the respective procedures. Consequently, no particular difference was found between these two procedures in terms of the yield.

The biological activities of the products were determined by the Yoshitomi Pharmaceutical Industry; the data are shown in Table 1. For comparison, the reported values for the original compounds are also included in the Table. In the cases of Phe- and Val-analogues, no significant changes were observed in their biological activities. However, the Gly-analogue was considered to be one of the promising compounds as an oxytocic hormone; its uterotonic activity was much more potent than that of the original Asu-oxytocin, and the ratios of the pressor and antidiuretic activity to the uterotonic activity were both sufficiently lower than those of the original compounds.

Experimental[14]

All the melting points were determined by the capillary method, and are given as uncorrected values. The products were dried over phosphorus pentoxide *in vacuo* at room temperature, unless otherwise noted. The solvent systems used for chromatography were: I, Chloroform: methanol: acetic acid (95: 5: 3 v/v); II, *n*-butanol: acetic acid: water (4: 1: 1 v/v); III, *n*-butanol: pyridine: water (4: 1: 1 v/v).

General Procedure for the Removal of Benzyloxycarbonyl or Benzyl Groups by Catalytic Hydrogenolysis. Hydrogen was gently bubbled through a solution or suspension of a benzyloxycarbonyl or benzyl derivative at room temperature, in which palladium black or palladium charcoal had previously been added as the catalyst. The progress of the reaction was monitored by thin-layer chromatography using Merck's Silica-gel G. After the completion of the reaction had been confirmed by thin-layer chromatography, the catalyst was removed by filtration, the filtrate was concentrated under reduced pressure, and the residue was subjected to the next step.

Benzyloxycarbonyl-L-phenylalanyl-L-glutaminyl-L-asparaginyl-ω-t-butyl-L-α-aminosuberyl-L-prolyl-L-leucylglycine Amide (I).

Benzyloxycarbonyl-L-glutaminyl-L-asparaginyl-ω-*t*-butyl-L-α-aminosubery-L-prolyl-L-leucylglycine amide[5] (4.0 g, 4.41 mmol) was subjected to catalytic hydrogenolysis in a mixture of dioxane–water (3: 1 v/v, 80 ml), and the product was dissolved in DMF (20 ml). The benzyloxycarbonyl-L-phenylalanine *N*-hydroxysuccinimide ester[15] (2.8 g, 7.06 mmol) was then added to the solution, and the mixture was allowed to react for 3 days at room temperature. Ethyl acetate was added to the reaction mixture to precipitate the product, which was collected by filtration and recrystallized from 90% aqueous ethanol; wt. 3.79 g (81.5%); mp 184—186 °C, $[\alpha]_D^{17}$ −42.7° (*c* 0.95, DMF).

Found: C, 57.95; H, 7.28; N, 13.47%. Calcd for $C_{51}H_{74}O_{13}N_{10}\cdot H_2O$: C, 58.16; H, 7.27; N, 13.30%.

Benzyloxycarbonyl-L-phenylalanyl-L-glutaminyl-L-asparaginyl-L-α-aminosuberyl-L-prolyl-L-leucylglycine Amide (II). Compound I (3.71 g, 3.5 mmol) was dissolved in TFA (50 ml), and the solution was kept for an hour at room temperature. Then, the TFA was removed under reduced pressure and the oily residue was solidified by trituration with ether. The product was reprecipitated from 90% ethanol, washed with ethanol, and dried; wt. 2.85 g (80.7%); mp 182.5—185 °C (decomp.), $[\alpha]_D^{18}$ −45.9° (*c* 0.91, DMF).

Found: C, 56.14; H, 6.90; N, 13.57%. Calcd for $C_{47}H_{66}O_{13}N_{10}\cdot 1.5H_2O$: C, 56.10; H, 6.91; N, 13.92%.

t-Amyloxycarbonyl-O-t-butyl-L-tyrosyl-L-phenylalanyl-L-glutaminyl-L-asparaginyl-L-α-aminosuberyl-L-prolyl-L-leucylglycine Amide (III). Compound II (4.5 g, 4.4 mmol) was subjected to catalytic hydrogenolysis in a mixture of dioxane–water (4: 1 v/v, 100 ml). Then the heptapeptide amide thus formed was treated with the *t*-amyloxycarbonyl-*O*-*t*-butyl-L-tyrosine *N*-hydroxysuccinimide ester[8] (4.0 g, 8.9 mmol) in DMF (20 ml) at room temperature for 24 hr. The product was precipitated by the addition of ethyl acetate, and the precipitates were collected by filtration, washed well with hot ethyl acetate, and then reprecipitated from 33% aqueous ethanol; wt. 2.17 g (41.3%); mp 197.5—198.5 °C (decomp.), $[\alpha]_D^{23}$ −37.7° (*c* 1.0, DMF).

Found: C, 58.09; H, 7.40; N, 12.74%. Calcd for $C_{58}H_{87}O_{15}N_{11}\cdot H_2O$: C, 58.22; H, 7.50; N, 12.88%.

t-Amyloxycarbonyl-O-t-butyl-L-tyrosyl-L-phenylalanyl-L-glutaminyl-L-asparaginyl-ω-p-nitrophenyl-L-α-aminosuberyl-L-prolyl-L-leucylglycine Amide (IV). Compound III (1.33 g, 1.11 mmol) was treated with *p*-nitrophenyl trifluoroacetate[5,16] (2.8 g, 11.9 mmol) in a mixture of DMF (25 ml) and pyridine (6.2 ml) for 3 hr at 50 °C. The product was precipitated with ether, collected by filtration, and washed well with ether. The washed material was reprecipitated from 40% aqueous ethanol; wt. 1.08 g (74%); mp 198—199 °C (decomp.), $[\alpha]_D^{23}$ −32.9° (*c* 0.75, DMF).

Found: C, 58.34; H, 7.19; N, 12.42%. Calcd for $C_{64}H_{90}O_{17}N_{12}\cdot H_2O$: C, 58.34; H, 7.04; N, 12.76%.

Lactam of L-Tyrosyl-L-phenylalanyl-L-glutaminyl-L-asparaginyl-L-α-aminosuberyl-L-prolyl-L-leucylglycine Amide (V): [Phe³, Asu¹,⁶]-Oxytocin. Compound IV (616 mg, 0.47 mmol) was dissolved in TFA (6 ml), and the solution was allowed to react for 1.5 hr at room temperature. Then, the TFA was evaporated out under reduced pressure, and the residue was dissolved in DMF (10 ml). The solution was stirred into pyridine (300 ml), drop by drop, at 40 °C. After the addition, the mixture was kept overnight at room temperature, and then concentrated to a residue under reduced pressure, and the residue was treated with ether to obtain the product as a powder. The powdered material was dissolved in a minimum amount of methanol and charged on the top of a column of Sephadex LH-20 (1.5×45.5 cm). The column was eluted with methanol, 1.5 g fractions were collected, and peptides were detected by means of the UV absorption at 280 nm. The effluents in tubes No. 21 to 27 were pooled and concentrated. The product was applied to 7 thin-layer plates of Silica-gel GF 254 (5×16 cm each) and developed by the solvent system II. The locations of the separated materials were detected by UV-irradiation, and the major band on each plate was collected by scraping. The material adsorbed on the pooled silica-gel was extracted with methanol and further applied to a column of CM-Sephadex C-25 (H^+ form) (1.5×27 cm). The column was eluted with 50% aqueous methanol, and 3 g fractions were collected. The effluents in tubes No. 15 to 24 were pooled and concentrated, and the residue was lyophilized from water; wt. 47 mg (overall 18%), $[\alpha]_D^{17}$ −68.1° (*c* 0.36, methanol).

Ratio of amino acids in an acid hydrolyzate (6 M HCl, 48 hr at 105 °C): Tyr, 1.00; Phe, 1.00; Glu, 1.03; Asp, 1.00; Asu, 0.97; Pro, 0.94; Leu, 0.97; Gly, 0.97. The average recovery was 93%.

Found: C, 51.58; H, 7.01; N, 13.08%. Calcd for $C_{45}H_{67}O_{12}N_{11}\cdot 7H_2O$: C, 51.65; H, 7.31; N, 13.08%.

This material was confirmed to be homogeneous by thin-layer chromatography (Silica-gel G, Solvent II) and by paper electrophoresis (Toyo, No. 514, pH 4.8 pyridine-acetic acid buffer). The R_f-values on paper chromatography (Toyo, No. 51) were 0.74 for Solvent II and 0.55 for Solvent III. These chromatograms were located with Pauly's reagent.

Benzyloxycarbonyl-L-valyl-L-asparaginyl-ω-t-butyl-L-α-aminosuberyl-L-prolyl-L-leucylglycine Amide (VI). Benzyloxycarbonyl-L-asparaginyl-*ω*-*t*-butyl-L-α-aminosuberyl-L-prolyl-L-leucylglycine amide[5] (3.5 g, 4.6 mmol) was subjected to catalytic hydrogenolysis in a dioxane–water mixture (3: 1 v/v, 80 ml), and the resulting material was allowed to react with the benzyloxycarbonyl-L-valine *p*-nitrophenyl ester[17] (2.25 g, 6.0 mmol) in DMF (16 ml) for 2 days at room temperature. Excess ethyl acetate was added to the reaction mixture to precipitate the product, which was then collected by filtration and washed with ethyl acetate. The filtrate was recrystallized from 90% aqueous ethanol; wt. 3.4 g (86%); mp 222—223 °C (decomp.), $[\alpha]_D^{26}$ −46.5° (*c* 0.79, DMF).

Found: C, 59.02; H, 7.94; N, 12.61%. Calcd for $C_{42}H_{66}O_{11}N_8$: C, 58.72; H, 7.75; N, 13.02%.

Benzyloxycarbonyl-L-valyl-L-asparaginyl-ω-t-butyl-L-α-aminosuberyl-L-leucylglycine Amide (VII). Compound VI (3.15 g, 3.67 mmol) was suspended in a mixture of dioxane and water (2: 1 v/v, 75 ml), and the mixture was subjected to catalytic hydrogenolysis as has been shown above. During the course of the hydrogenolysis, the insoluble material went into a solution. After the removal of the catalyst, the solution was concentrated under reduced pressure, the residue was dissolved in 30 ml of DMF, and then the benzyloxycarbonyl-L-isoleucine *N*-hydroxysuccinimide ester[15] (2.0 g, 5.5 mmol) was added to the solution. The mixture was allowed to react for one day at room temperature. Then, ethyl acetate was added to the reaction mixture, the precipitated product was collected by filtration, and it was reprecipitated from 90% aqueous ethanol; wt. 2.45 g (67.5%); mp 240—240.5 °C (decomp.), $[\alpha]_D^{17}$ −40.6° (*c* 0.85, DMF).

Found: C, 58.18; H, 8.06; N, 12.48%. Calcd for $C_{48}H_{77}O_{12}N_9\cdot H_2O$: C, 58.22; H, 8.04; N, 12.73%.

Benzyloxycarbonyl-L-isoleucyl-L-valyl-L-asparaginyl-L-α-aminosuberyl-L-prolyl-L-leucylglycine Amide (VIII). Compound (VII) (2.17 g, 2.16 mmol) was dissolved in TFA (25 ml) and the solution was kept for one hour at room temperature. Then, the TFA was removed under reduced pressure, and an oily residue was solidified by trituration with ether. The product was reprecipitated from 90% aqueous ethanol, collected by filtration, washed with ethanol, and dried; wt. 1.63 g (80.1%); mp 224—226 °C (sintered) and 236—238 °C (decomp.), $[\alpha]_D^{23}$ −44.9° (*c* 0.84, DMF).

Found: C, 55.88; H, 7.46; N, 13.08%. Calcd for $C_{44}H_{59}O_{12}N_9\cdot 1.5H_2O$: C, 56.03; H, 7.70; N, 13.37%.

t-Amyloxycarbonyl-O-t-butyl-L-tyrosyl-L-isoleucyl-L-valyl-L-asparaginyl-L-α-aminosuberyl-L-prolyl-L-leucylglycine Amide (IX).

Compound VIII (1.57 g, 1.68 mmol) was subjected to catalytic hydrogenolysis in dioxane–water (3: 1 v/v) as has been described above. The catalyst was filtered off, the filtrate was concentrated under reduced pressure, and the resulting peptide amide was dissolved in DMF (60 ml). The *t*-amyloxycarbonyl-*O*-*t*-butyl-L-tyrosine *N*-hydroxysuccinimide ester[8] (1.29 g, 2.88 mmol) was then added to the solution, and the mixture was allowed to react for 2 days at room temperature; the pH of the solution was kept at 7—8 throughout the period using *N*-ethylmorpholine. Then, the product was precipitated by the addition of ethyl acetate, collected by filtration, and washed well with ethyl acetate. Finally, the washed product was reprecipitated from 90% aqueous ethanol; wt. 0.93 g (49%); mp 229—230 °C (decomp.), $[\alpha]_D^{25}$ −43.1° (*c* 0.77, DMF). Ratio of amino acids in an acid hydrolyzate (6 M HCl, 48 hr at 105 °C): Tyr, 1.29; Ile+Asu, 2.17; Val, 0.84; Asp, 0.97; Pro, 1.00; Leu, 1.19;

Gly, 0.97.

Found: C, 58.27; H, 8.36; N, 12.08%. Calcd for $C_{55}H_{90}O_{14}N_{10}\cdot H_2O$: C, 58.28; H, 8.18; N, 12.36%.

t-Amyloxycarbonyl-O-t-butyl-L-tyrosyl-L-isoleucyl-L-valyl-L-asparaginyl-ω-p-nitrophenyl-L-α-aminosuberyl-L-prolyl-L-leucylglycine Amide (X). The protected octapeptide amide (IX) (871.7 mg, 0.77 mmol) was treated with *p*-nitrophenyl trifluoroacetate[5,16] (2.8 g, 11.9 mmol) for 3 hr at 50 °C in a mixture of DMF (25 ml) and pyridine (6.2 ml). Then, the product was precipitated with ether, collected by filtration, and washed well with ether. The product was purified by reprecipitation from DMF–ether; wt. 0.60 g (62%); mp 251—252 °C (decomp.), $[\alpha]_D^{27}$ −37.0° (*c* 0.73, DMF).

Found: C, 58.67; H, 7.78; N, 12.09%. Calcd for $C_{61}H_{93}O_{16}N_{11}\cdot H_2O$: C, 58.40; H, 7.63; N, 12.28%.

Lactam of L-Tyrosyl-L-isoleucyl-L-valyl-L-asparaginyl-L-α-aminosuberyl-L-prolyl-L-leucylglycine Amide (XI): [Val⁴, Asu¹·⁶]-Oxytocin. Compound X (0.67 g, 0.53 mmol) was dissolved in TFA (6 ml), and the mixture was allowed to react for 1.5 hr at room temperature. Then, the TFA was evaporated out under reduced pressure and the residue was dissolved in DMF (10 ml). The solution was stirred into pyridine (300 ml), drop by drop, at 40 °C. After standing overnight at room temperature, the pyridine solution was concentrated to a residue under reduced pressure, the residue was triturated with ether, and the separated material was collected. The product was dissolved in water (15 ml), and the solution was passed through a column of Amberlite IR-45 (OH^- form, 1×10 cm) and a column of CM-Sephadex C-25 (H^+ form, 1×10 cm) successively. The effluents were monitored by means of the UV absorption at 280 nm, and the fractions containing a major peak were pooled and lyophilized to obtain the final product; wt. 99.5 mg (24.8%); $[\alpha]_D^{20}$ −101° (*c* 0.47, water). The homogeneity of the product was confirmed by thin-layer chromatography on Silica gel G using the solvent system II (single spot, with R_f 0.58 as located by exposure to iodine vapor) and by paper electrophoresis (Toyo No. 514), using a pyridine–acetic acid buffer pH 4.8 (50V/cm, 60 min, located by a Pauly reagent). Ratio of amino acids in an acid hydrolyzate (6 M HCl, 48 hr at 105 °C): Tyr, 0.95; Ile, 1.00; Val, 0.98; Asp, 1.04; Asu, 1.05; Pro, 1.04; Leu, 1.03; Gly, 0.98. The average recovery was 85%.

Found: C, 53.89; H, 8.00; N, 13.86%. Calcd for $C_{45}H_{70}O_{11}N_{10}\cdot 4H_2O$: C, 54.09; H, 7.87; N, 14.02%.

Benzyloxycarbonyl-glycyl-L-leucylglycine Amide (XII). Benzyloxycarbonyl-glycyl-L-leucylglycine ethyl ester[18] (26.0 g) was dissolved in methanol (340 ml), and the solution was saturated with ammonia at 0 °C. After having been kept for 72 hr at room temperature, the solution was concentrated under reduced pressure and the residue was recrystallized from ethanol –*n*-hexane; wt. 19.6 g (81.3%); mp 123—125 °C, $[\alpha]_D^{16}$ −15.2° (*c* 1.1, DMF). lit[12], mp 113—115°C, $[\alpha]_D^{28}$ −15.3° (*c* 1, DMF).

Found: C, 56.49; H, 7.11; N, 14.69%. Calcd for $C_{18}H_{26}O_5N_4\cdot 1/4H_2O$: C, 56.46; H, 6.98; N, 1D.63%.

Benzyloxycarbonyl-ω-t-butyl-L-α-aminosuberyglycyl-L-leucylglycine Amide (XIII). Compound XII (8.2 g, 22 mmol), was subjected to catalytic hydrogenolysis in ethanol, and the glycyl-L-leucylglycine amide thus obtained was coupled with the benzyloxycarbonyl-ω-*t*-butyl-L-α-aminosuberic acid α-*p*-nitrophenyl ester[5] (8.4 g, 16.8 mmol) in DMF (12 ml) for 24 hr at room temperature. Water was added to the reaction mixture to precipitate the product, which was then taken up with ethyl acetate. The solution was washed thoroughly with 1 M aqueous ammonia until no yellow color was detectable in the washing; then the solution was washed once with 0.6 M hydrochloric acid and dried over sodium sulfate. The dried solution was concentrated under reduced pressure, and the residue was recrystallized from ethyl acetate–ethanol; wt. 9.1 g (88.1%); mp 144—146 °C, $[\alpha]_D^{22}$ −10.8° (*c* 0.98, DMF).

Found: C, 59.01; H, 8.13; N, 11.11%. Calcd for $C_{30}H_{47}O_8N_5\cdot 1/4H_2O$: C, 59.04; H, 7.85; N, 11.48%.

Benzyloxycarbonyl-L-asparaginyl-ω-t-butyl-L-α-aminosuberyglycyl-L-leucylglycine Amide (XIV). Compound XIII (9.3 g, 15.4 mmol) was subjected to hydrogenolysis in ethanol, and the product was allowed to react with the benzyloxycarbonyl-L-asparagine *p*-nitrophenyl ester[13] (6.3 g, 16.2 mmol) in DMF (20 ml) for 2 days at room temperature. The product was precipitated by dilution with ethyl acetate and collected by filtration; the collected material was washed with ethyl acetate and acetone, and recrystallized from 90% aqueous ethanol; wt. 9.8 g (86.3%); mp 223—224.5 °C (decomp.), $[\alpha]_D^{22}$ −13.1° (*c* 0.96, DMF).

Found: C, 55.59; H, 7.52; N, 13.09%. Calcd for $C_{34}H_{53}O_{10}N_7\cdot H_2O$: C, 55.34; H, 7.51; N, 13.29%.

Benzyloxycarbonyl-L-glutaminyl-L-asparaginyl-ω-t-butyl-L-α-aminosuberylglycyl-L-leucylglycine Amide (XV). The benzyloxycarbonyl group of Compound XIV (9.8 g, 13.3 mmol) was removed by catalytic hydrogenolysis, and the product was coupled with the benzyloxycarbonyl-L-glutamine *p*-nitrophenyl ester[13] (5.6 g, 14 mmol) as above. The product was precipitated from the reaction mixture, collected by filtration, and boiled in 90% aqueous ethanol to extract the soluble materials. The remaining insoluble material was collected by filtration and dried; wt. 9.8 g (85.9%); mp 244.5—245 °C (decomp.), $[\alpha]_D^{25}$ −30.7° (*c* 0.75, acetic acid). Ratio of amino acids in an acid hydrolyzate (6 M HCl, 48 hr at 105 °C): Glu, 1.08; Asp, 1.00; Asu, 0.94; Gly, 2.03; Leu, 1.00; The average recovery was 97%.

Found: C, 54.76; H, 7.35; N, 14.92%. Calcd for $C_{39}H_{61}O_{12}N_9\cdot 1/2H_2O$: C, 54.66; H, 7.29; N, 14.71%.

Benzyloxycarbonyl-L-isoleucyl-L-glutaminyl-L-asparaginyl-ω-t-butyl-L-α-aminosuberylglycyl-L-leucylglycine Amide (XVI). The benzyloxycarbonyl group of Compound XV (9.8 g, 11.4 mmol) was removed by catalytic hydrogenolysis, and the product was coupled with the benzyloxycarbonyl-L-isoleucine *N*-hydroxysuccinimide ester[15] (5.5 g, 15.2 mmol) in DMF (90 ml), as in the case of Compound VII. Ethyl acetate was added to the reaction mixture, and the precipitate was reprecipitated from DMF–ethyl acetate; wt. 8.1 g (73.3%); mp 248—249 °C (decomp.), $[\alpha]_D^{25}$ −39.4° (*c* 0.83, acetic acid).

Found: C, 55.69; H, 7.72; N, 14.50%. Calcd for $C_{45}H_{72}O_{13}H_{10}\cdot 1/2H_2O$: C, 55.71; H, 7.58; N, 14.44%.

Benzyloxycarbonyl-L-isoleucyl-L-glutaminyl-L-asparaginyl-L-α-aminosuberylglycyl-L-leucylglycine Amide (XVII). Compound XVI (7.9 g, 8.14 mmol) was treated with TFA (80 ml) as in the case of the synthesis of compound VIII. The product was reprecipitated from 90% aqueous ethanol; wt. 7.55 g (98.6%); mp 239—240 °C (decomp.), $[\alpha]_D^{23}$ −33.3° (*c* 1.0, acetic acid).

Found: C, 52.57; H, 7.22; N, 14.88%. Calcd for $C_{41}H_{64}O_{13}N_{10}\cdot 2H_2O$: C, 52.33; H, 7.28; N, 14.89%.

Benzyloxycarbonyl-O-benzyl-L-tyrosyl-L-isoleucyl-L-glutaminyl-L-asparaginyl-L-α-aminosuberylglycyl-L-leucylglycine Amide (XVIII). Compound XVII (7.45 g, 7.9 mmol) was subjected to hydrogenolysis in an ethanol–water–acetic acid mixture (5: 5: 2 v/v, 100 ml), and the free heptapeptide amide thus obtained was treated with the benzyloxycarbonyl-*O*-benzyl-L-tyrosine *N*-hydroxysuccinimide ester[19] (7.0 g, 13.9 mmol) in a mixture of dimethyl sulfoxide (250 ml) and DMF (50 ml) for 2 days at room temperature. The reaction mixture was kept at pH 6—7 with *N*-ethylmorpholine throughout the period. Excess ethyl acetate was added to the reaction mixture, and the precipitate was collected by filtration and boiled in 80%

aqueous ethanol (400 ml). The remaining material was collected by filtration at room temperature and washed well with ethanol; wt. 8.0 g, (86.5%); mp 251—252 °C (decomp.), $[\alpha]_D^{25}$ −15.2° (*c* 0.63, dimethylsulfoxide). Ratio of amino acids in an acid hydrolyzate (6 M HCl, 48 hr at 105 °C): Tyr, 0.90; Ile, 1.10; Glu, 1.00; Asp, 0.98; Asu, 1.03; Gly, 1.90; Leu, 0.98. The average recovery was 98%.

Found: C, 58.67; H, 6.97; N, 13.15%. Calcd for $C_{57}H_{79}O_{15}N_{11}\cdot 1/2H_2O$: C, 58.65; H, 6.91; N, 13.20%.

Benzyloxycarbonyl-O-benzyl-L-tyrosyl-L-isoleucyl-L-glutaminyl-L-asparaginyl-ω-2,4,5-trichlorophenyl-L-α-aminosuberylglycyl-L-leucylglycine Amide (XIX). Compound XVIII (4.3 g, 3.68 mmol) was suspended as a fine powder in a mixture of DMF (80 ml) and pyridine (29 ml), and 2,4,5-trichlorophenyl trifluoroacetate[5,16] (10.7 g, 36.4 mmol) was added to the suspension. The mixture was stirred for 7 hr at 50 °C, and then the product was precipitated by the addition of ether, collected by filtration, and dried; wt. 4.64 g (93.7%); mp 253—254 °C (decomp.), $[\alpha]_D^{25}$ −21.4° (*c* 0.42, dimethyl sulfoxide).

Found: C, 56.20; H, 6.37; N, 11.63; Cl, 8.37%. Calcd for $C_{63}H_{80}O_{15}N_{11}Cl_3\cdot 1/2H_2O$: C, 56.18; H, 6.06; N, 11.44; Cl, 7.90%.

Lactam of L-Tyrosyl-L-isoleucyl-L-glutaminyl-L-asparaginyl-L-α-aminosuberylglycyl-L-leucylglycine Amide (XX): [Gly,[7] Asu[1,6]]-Oxytocin. a) Compound XIX (1.31 g, 0.97 mmol) was subjected to catalytic hydrogenolysis using palladium black in DMF (350 ml). After 40 hr at room temperature, the catalyst was removed by filtration and the filtrate was concentrated under reduced pressure. The residue was triturated with ether to obtain a hygroscopic powder, which was then extracted with water (15 ml×2). The extract was passed through a column of Amberlite IR-45 (OH^- form, 3×11.5 cm), which was then eluted with water. The fractions of the effluents which showed an optical density of >2.0 at 280 nm were collected and passed through another column of CM-Sephadex C-25 (H^+ form, 3×12.5 cm). The effluent and washing of the latter column were pooled and lyophilized to obtain a crude product; wt. 504 mg (52.5%). A portion (240 mg) of this material was further purified by silica-gel column chromatography (Merck's Silica-gel for column chro matography, 70—325 mesh, 2.0×22.5 cm) using the solvent system. II Fractions of 6 g were collected, and the presence of peptides was monitored by means of the UV absorption at 280 nm. The effluents in tubes No. 57 to 63 were collected and concentrated under reduced pressure. The residue was passed through a column of CM-Sephadex C-25 (H^+ form, 3×8.5 cm). The effluents in fractions corresponding to the volume from 75 to 110 ml were pooled and lyophilized to obtain the final product; wt. 164 mg (recovery 68.3%); $[\alpha]_D^{25}$ −44.0° (*c* 0.55, water). The homogeneity of the purified product was confirmed by thin-layer chromatography, as in the case of compound XI. The R_f-values on paper chromatography (Toyo No. 51) were 0.65 for the solvent system II, 0.59 for the solvent system, III and 0.76 for a solvent system of *n*-butanol: acetic acid: pyridine: water (15: 3: 10: 6 v/v). This peptide was Pauly-positive and ninhydrin-negative. Ratio of amino acids in an acid hydrolyzate (6 M HCl, 48 hr at 105 °C): Tyr, 1.00; Ile+Asu, 2.00; Glu, 1.02; Asp, 1.00; Gly, 1.98; Leu, 0.96. The average recovery was almost quantitative.

Found: C, 51.22; H, 7.31; N, 15.31%. Calcd for $C_{42}H_{65}O_{12}N_{11}\cdot 4H_2O$: C, 51.05; H, 7.45; N, 15.60%.

b) Compound XIX (20.0 g, 14.8 mmol) was dissolved in TFA (150 ml) together with anisole (50 ml), and HBr gas was introduced gently into the solution for 90 min at room temperature. Then, the mixture was concentrated under reduced pressure, and the residue was washed with ether and dried. The dried compound was dissolved in 150 ml of DMF, and the solution was stirred into pyridine (31), drop by drop, at 50 °C over a 4 hr period. After standing overnight at room temperature, the solution was concentrated under reduced pressures (lower than 45 °C), the residue was treated with columns of Amberlite IR-45 and CM-Sephadex C-25 successively, as in the case of a), and the crude lactam was obtained as an amorphous powder; wt. 3.0 g (21%). This material was subjected to further purification as has been shown above to obtain the final product; wt. 2.2 g (recovery 73%).

The authors wish to express their thanks to Dr. Tadao Okada of the Yoshitomi Pharmaceutical Ind. for determining the biological activities of the synthetic peptides.

References

1) A part of this work was presented at the 7th Symposium on Peptide Chemistry, Tokyo, November 21, (1969). Part II in this series is Ref. 7.

2) V. du Vigneaud, G. Winestock, V. V. S. Murti, D. B. Hope, and R. D. Kimbrough, Jr., *J. Biol. Chem.*, **235**, PC 64 (1960); D. B. Hope, V. V. S. Murti, and V. du Vigneaud, *ibid.*, **237**, 1563 (1962).

3) J. Rudinger and K. Jošt, *Experientia*, **20**, 570 (1964).

4) K. Jošt and J. Rudinger, *Collect. Czech. Chem. Commun.*, **32**, 1229 (1967).

5) A. Kobayashi, S. Hase, R. Kiyoi, and S. Sakakibara, This Bulletin, **42**, 3491 (1969).

6) S. Sakakibara and S. Hase, *ibid.*, **41**, 2816 (1968).

7) S. Hase, T. Morikawa, and S. Sakakibara, *Experientia*, **25**, 1239 (1969).

8) S. Hase, S. Sakakibara, M. Wahrenburg, M. Kirchberger, I. L. Schwartz, and R. Walter, *J. Amer. Chem. Soc.*, **94**, 3590 (1972).

9) T. Yamanaka, S. Hase, S. Sakakibara, I. L. Schwartz, B. M. Dubois, and R. Walter, *Mol. Pharmacol.*, **6**, 474 (1970).

10) R. A. Boissonnas, S. Guttmann, P. A. Jaquenoud, and J. P. Waller, *Helv. Chim. Acta*, **39**, 1421 (1956); P. G. Katsoyannis, *J. Amer. Chem. Soc.*, **79**, 109 (1957).

11) V. du Vigneaud, G. Flouret, and R. Walter, *J. Biol. Chem.*, **241**, 2093 (1966); G. Flouret and V. du Vigneaud, *J. Med. Chem.*, **12**, 1035 (1969).

12) M. Bodanszky and R. J. Bath, *Chem. Commun.*, **1968**, 766.

13) M. Bodanszky and V. du Vigneaud, *J. Amer. Chem. Soc.*, **81**, 5688 (1959).

14) The special abbreviations used in the text are: Asu, α-aminosuberic acid residue; HONSu, *N*-hydroxysuccinimide; HOTcp, 2,4,5-trichlorophenol; Aoc, *t*-amyloxycarbonyl; TFA, trifluoroacetic acid; DMF, *N,N*-dimethylformamide.

15) G. W. Anderson, J. E. Zimmerman, and F. M. Callahan, *J. Amer. Chem. Soc.*, **86**, 1839 (1964).

16) S. Sakakibara and N. Inukai, This Bulletin, **38**, 1979 (1965); *ibid.*, **39**, 1567 (1966).

17) B. Iselin, W. Rittel, P. Sieber, and R. Schwyzer, *Helv. Chim. Acta*, **40**, 373 (1957).

18) R. W. Young, K. H. Wood, R. J. Joyce, and G. W. Anderson, *J. Amer. Chem. Soc.*, **78**, 2126 (1956).

19) M. Löw and L. Kisfaludy, *Acta Chim. Hung.*, **44**, 61 (1965).

Superacids and Their Derivatives. III.[1] Kinetics of the Oxonium Ion Formation from Superacid Esters and Tetrahydropyran. Oxonium-Ester Equilibria

Shiro KOBAYASHI, Tadashi ASHIDA, and Takeo SAEGUSA

Department of Synthetic Chemistry, Faculty of Engineering, Kyoto University, Sakyo-ku, Kyoto, 606

(Received December 20, 1973)

Kinetic studies on the oxonium formation reaction between superacid esters ($ROSO_2X$) and tetrahydropyran (THP) were carried out by means of NMR spectroscopy. The reaction was found to be an equilibrium process.

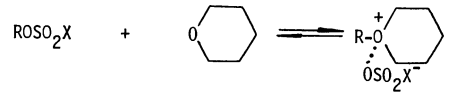

The rate constant (k) of S_N2 reaction and the equilibrium constant ($1/K=k/k'$) were determined. The solvent effect was examined and k was found to be in the order: nitrobenzene>chlorobenzene≈CH_2Cl_2>liquid SO_2. The effects of R and X in $ROSO_2X$ were studied. Relative reactivities of primary alkyl series in the reaction of $ROSO_2Cl$ with THP were: Me: Et: *n*-Pr=4.63: 1.0: 0.294 in CH_2Cl_2 and Me: Et: *n*-Pr=3.19: 1.0: 0.452 in nitrobenzene. The effect of X on k was in the order Cl≈CF_3>F, the $1/K$ value being also extremely low when X=F. The result was discussed in relation to the kinetics of the polymerization of tetrahydrofuran (THF) by $ROSO_2X$.

We have found that superacid esters[2] and anhydrides[1] are very effective initiators for the cationic ring-opening polymerization of tetrahydrofuran (THF). Kinetic studies on the THF polymerization with a superacid ester initiator revealed that the propagating species was predominanantly a cyclic oxonium one (**1**), and that the concentration of ester type species (**2**) was very small although the latter might be in equilibration with the former species under the polymerization conditions as shown in the following. In fact, **2** could not be detected during the THF polymerization in CH_2Cl_2 by means of high resolution NMR spec-

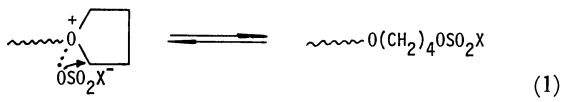

(1)

1 2

(X=Cl, F, CF_3)

troscopy.[2] Thus it is importantto examine the oxonium-ester equilibrium in more detail by independent reactions. Although it is known that a superacid ester such as ethyl fluorosulfate ($EtOSO_2F$) reacts with ether to form an oxonium ion,[3] no quantitative study on the oxonium formation reactions from superacid esters has been carried out so far.[4]

In the present study reactions of superacid esters with tetrahydropyran (THP) were examined as a model system, as shown in the following. Superacid esters examined were primary alkyl esters of chlorosulfonic ($ROSO_2Cl$), fluorosulfonic ($ROSO_2F$) and trifluoromethanesulfonic ($ROSO_2CF_3$) acids.

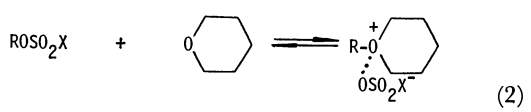

(2)

R=primary alkyl THP

X=Cl, F, CF_3

THP was employed as an ether component since THP is an ether of high basicity[5] and has no ring-opening polymerizability.[6] The reaction corresponds to the initiation of the cyclic ether polymerizations by superacid ester initiators.[2] Kinetic analysis was carried out by direct determination of the instantaneous concentrations of THP and the product oxonium ion by means of NMR spectroscopy. Thus, the reaction was found to be characterized by a reversible reaction, *i.e.*, the ester and oxonium species are in equilibration. We have also studied the effects of the nature of R and X in $ROSO_2X$ as well as those of solvents on the reaction rate (k) and equilibrium constant ($1/K$).

Results and Discussion

Determination of Reaction Rates. Figure 1 shows an NMR spectrum of the reaction system of $EtOSO_2Cl$ with THP in CH_2Cl_2 at a reaction time of 124 min at 35 °C. Signal assignments are given in Table 1.

The following relationships are given for the concentration of the respective component:

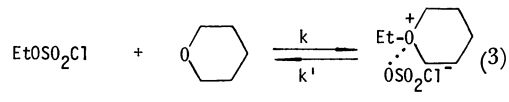

(3)

3

at time 0	$[E]_0$	$[T]_0$	—
at time t	$[E]_0-[Ox]$	$[T]_0-[Ox]$	$[Ox]$

where $[E]_0$ and $[T]_0$ denote the initial concentrations of $EtOSO_2Cl$ and THP, respectively, [Ox] denotes the concentration of the product, cyclic oxonium, and k and k' denote the rate constants of the oxonium formation reaction and the reverse reaction, respectively. The stoichiometry of (3) was shown to be valid by the areas of the respective peaks on the basis of that of the internal standard $CHCl_3$ (Table 1). From the signal (peak D) of the β-methylene protons of the cylic oxonium, the [Ox] *vs.* time relationship was obtained (Fig. 2). The rate equation of the oxonium formation of (3) is given by

TABLE 1. SIGNAL ASSIGNMENTS IN THE REACTION OF $EtOSO_2Cl$ WITH THP IN CH_2Cl_2 AT 35 °C AND INTEGRAL VALUES

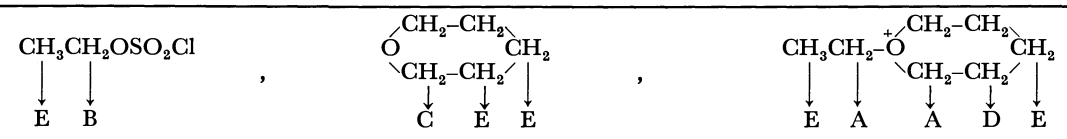

Signal	Chemical shifts in ppm[a)]	Integral value
A	4.9—4.7 (m)	$6Ox+2(E_0-Ox)=2E_0+4Ox$
B	4.60 (q)	
C	3.6 (m)	$4(T_0-Ox)=4T_0-4Ox$
D	2.0 (m)	$4Ox$
E	1.8—1.3 (m)	$3(E_0-Ox)+6(T_0-Ox)+5Ox=3E_0+6T_0-4Ox$
$CHCl_3$	7.30 (s)	S_0

a) Calculated from the chemical shift of $CHCl_3$ as δ 7.30. Multiplicity: m=multiplet, q=quartet and s=singlet

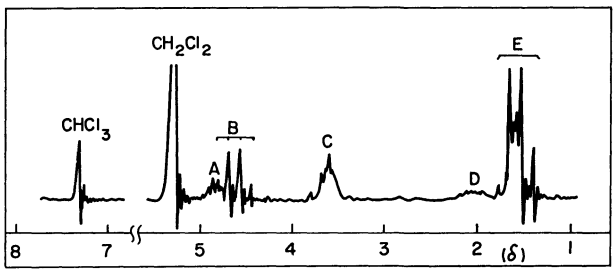

Fig. 1. NMR spectrum of the reaction system of $EtOSO_2Cl$ with THP in CH_2Cl_2 after 124 min at 35 °C. $[E]_0=0.822$ mol/l, $[T]_0=0.835$ mol/l, $CHCl_3$: an internal standard.

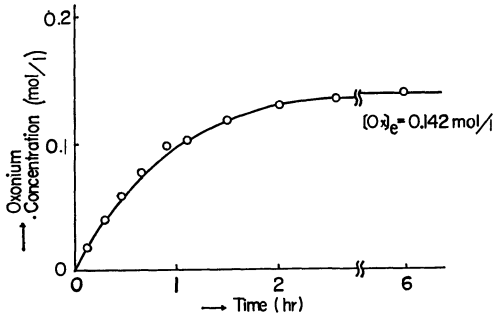

Fig. 2. Time-conversion curve of the reaction of $EtOSO_2Cl$ with THP at 35 °C in CH_2Cl_2. $[E]_0=0.822$ mol/l, $[T]_0=0.835$ mol/l.

$$\frac{d[Ox]}{dt} = k([E]_0-[Ox])([T]_0-[Ox]) - k'[Ox], \quad (4)$$

and the equilibrium constant of (3), $1/K$, is defined by

$$\frac{1}{K} = \frac{k}{k'} = \frac{[Ox]_e}{([E]_0-[Ox]_e)([T]_0-[Ox]_e)} \quad (5)$$

where $[Ox]_e$ is the concentration of the cyclic oxonium at equilibrium which can be obtained from Fig. 2. Equation (4) is then transformed by using Eq. (5) into

$$\frac{d[Ox]}{dt} = k\{[Ox]^2-(K+[E]_0+[T]_0)[Ox]+[E]_0[T]_0\} \quad (6)$$

By introducing α and β, which are two roots of the equation $X^2-(K+[E]_0+[T]_0)X+[E]_0[T]_0=0$, Eq. (6) becomes

$$\frac{d[Ox]}{dt} = k([Ox]-\alpha)([Ox]-\beta) \quad (7)$$

where

$$\alpha = \frac{1}{2}\left\{K+[E]_0+[T]_0+\sqrt{(K+[E]_0+[T]_0)^2-4[E]_0[T]_0}\right\}$$
$$\beta = \frac{1}{2}\left\{K+[E]_0+[T]_0-\sqrt{(K+[E]_0+[T]_0)^2-4[E]_0[T]_0}\right\} \quad (8)$$

Integrating (7) from t_1 to t_2 and $[Ox]_1$ to $[Ox]_2$, we have

$$k = \frac{2.303}{(\alpha-\beta)(t_2-t_1)} \log \frac{(\beta-[Ox]_1)(\alpha-[Ox]_2)}{(\alpha-[Ox]_1)(\beta-[Ox]_2)} \quad (9)$$

The $1/K$ value could be obtained from $[Ox]_e$ value (Fig. 2) according to Eq. (5). Thus the values of α and β of Eq. (8) were calculated. In the $EtOSO_2Cl$–THP system at 35 °C in CH_2Cl_2, $1/K$ value was 0.301 l/mol, and k was then obtained by Eq. (9): $k=7.80\times10^{-5}$ l/mol·s at 35 °C in CH_2Cl_2.

Similarly, kinetic analysis was carried out with other superacid esters in CH_2Cl_2 and liquid sulfur dioxide (SO_2) solvents. In nitrobenzene and chlorobenzene solvents, however, no internal standard was used; instead, these solvents were used as standards for integration. The reactions in these four solvents were homogeneous throughout the kinetic runs. Kinetic runs were carried out at 35 °C and dataare summarized in Table 2.

Reaction Mechanism. The reaction of THP with superacid esters (Eq. (2)) is a dipole-dipole reaction to produce an onium salt. It is interesting to compare Eq. (2) with the Menschutkin reaction, which is also a dipole-dipole reaction between amine and alkyl halide to produce an ammonium salt (Eq. (10)).

$$RY + R_3'N \longrightarrow RR_3'\overset{+}{N}\overset{-}{Y} \quad (10)$$

Since the Menschutkin reaction is not reversible[9] the present reaction of (2) is characterized by equilibrium process.

Kinetic runs of the $EtOSO_2Cl$–THP reaction (3) were carried out in CH_2Cl_2 and nitrobenzene at various temperatures. Arrhenius plots were linear in both cases, and activation parameters were obtained (Table 3). The reaction was faster in nitrobenzene than in CH_2Cl_2. ΔH^* values 14.4 and 15.2 kcal/mol are relatively low for a bimolecular reaction (favorable for k), whereas ΔS^* values, −31 and −26 e.u., are also low (unfavorable for k). It is typical for a dipole-dipole reaction to form ionic species. These values of activation

Table 2. Kinetic data of the reactions of THP with superacid esters at 35 °C

Run No.	$ROSO_2X$ X	R	Solvent (ε)[a]	$1/K$ (1/mol)	$10^5 \cdot k$ (l/mol·s)
1	Cl	Me	CH_2Cl_2 (8.93)[b]	2.68	36.1
2	Cl	Et	CH_2Cl_2	0.301	7.80
3	Cl	*n*-Pr	CH_2Cl_2	0.258	2.29
4	Cl	Me	$C_6H_5NO_2$ (34.8)	5.29	79.0
5	Cl	Et	$C_6H_5NO_2$	1.40	24.8
6	Cl	*n*-Pr	$C_6H_5NO_2$	0.756	11.2
7	Cl	Et	C_6H_5Cl (5.94)[b]	0.480	9.37
8	Cl	Et	SO_2 (12.4)[c]	2.15[d]	1.22[d]
9	F	Me	CH_2Cl_2	0.412	12.4
10	F	Et	CH_2Cl_2	0.070	2.43
11	F	Me	$C_6H_5NO_2$	3.60	70.1
12	F	Et	$C_6H_5NO_2$	0.805	24.1
13	CF_3	Et	CH_2Cl_2	0.177	6.10
14	CF_3	Et	$C_6H_5NO_2$	0.733	27.3

a) Dielectric constant at 25 °C. b) Taken from Ref. 7. c) Taken from Ref. 8. d) Data at 20 °C.

Table 3. Kinetic data and activation parameters in the reaction of $EtOSO_2Cl$ with THP[a]

	In CH_2Cl_2	In nitrobenzene
$10^5 \cdot k$(l/mol·s)	2.51 ($1/K$=0.595, 20 °C)	6.01($1/K$=1.70, 18 °C)
	5.56 ($1/K$=0.476, 30 °C)	10.9 ($1/K$=1.60, 29 °C)
	7.80 ($1/K$=0.301, 35 °C)	24.8 ($1/K$=1.40, 35 °C)
	17.0 ($1/K$=0.175, 42 °C)	55.9 ($1/K$=1.08, 44 °C)
$\Delta H^{\ddagger}$ (kcal/mol)	14.4	15.2
$\Delta S^{\ddagger}$ (e.u.)	−31	−26

a) $1/K$ in l/mol.

parameters are very close to those of the Menschutkin reaction, *e.g.*, $\Delta H^{\ddagger}$=13.0 kcal/mol and $\Delta S^{\ddagger}$=−29 e.u. in the reaction of pyridine with methyl iodide in nitrobenzene.[10]

(11)

Thus the transition state of Eq. (2) may be formulated in a similar way to the Menschutkin reaction.[9]

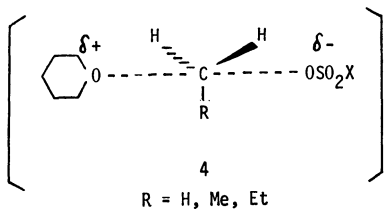

4

R = H, Me, Et

In the reaction of $EtOSO_2Cl$ with THP, $1/K<1$ in CH_2Cl_2 but $1/K<1$ in nitrobenzene in the temperature range examined (Table 3). The temperature rise led to a decrease in $1/K$ values, *i.e.*, oxonium formation is thermodynamically favored at lower temperatures. It should be added that no side reactions were observed in all the kinetic runs.

Solvent Effects. As seen from Tables 2 and 3 the rates (k) were in the order nitrobenzene>chlorobenzene≈CH_2Cl_2>liquid SO_2. This order can not be simply explained by the solvent polarity because it is not in line with the order of dielectric constants (Table 2): nitrobenzene>liquid SO_2>CH_2Cl_2>chlorobenzene. Since the solvents are of different character they may have complicated effects. It can be said that the reaction is faster in more polar solvents as in the case of the Menschutkin reaction.[7] In aromatic solvents, k in nitrobenzene is 2.6 times as high as that in chlorobenzene at 35 °C. This can be compared with the reactivity in the Menschutkin reaction of Eq. (11), in which the rate was 9.3 times as high as that in chlorobenzene.[10]

In liquid SO_2 at 20 °C, k was 5.3 times smaller than in nitrobenzene (calculated value of $k=6.50\times10^{-5}$ l/mol·s at 20 °C). A similar observation was also noted in the above Menschutkin reaction.[11] A decreased reactivity in liquid SO_2 may be attributed to the solvation of THP at the initial state (**5**) as an interaction of amine with liquid SO_2.[11] The complex formation of **5** is not unreasonable, because it is known that equilibrium constants are significantly large in the formation of complexes between SO_2 and alcohol.[12]

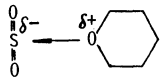

5

It may be significant to compare activation parameters of the $EtOSO_2Cl$–THP reaction in CH_2Cl_2 and in nitrobenzene. Although k was larger in nitrobenzene, the $\Delta H^{\ddagger}$ value was also larger in it, *i.e.*, an increased reactivity is ascribed to the more favorable entropy factor in nitrobenzene. A similar result was observed in the Menschutkin reaction of Eq. (11), in

TABLE 4. SOLVENT EFFECTS ON Eqs. (2) AND (11)

Solvent	$10^5 \cdot k$ (l/mol·s)	$\Delta H^{\ddagger}$ (kcal/mol)	$\Delta S^{\ddagger}$(e.u.)
C_2HCl_2	7.80[a]	14.4	−31
C_6H_5Cl	9.37[a]	—	—
$C_6H_5NO_2$	24.8[a]	15.2	−26
C_6H_6	141[b]	13.4	−34
$CHCl_3$	335[b]	12.5	−35
C_6H_5Cl	398[b]	13.2	−33
$C_6H_5OCH_3$	676[b]	12.5	−34
$C_6H_5NO_2$	3720[b]	13.0	−29

a) Present work of the reaction of Eq. (2). Data at 35 °C. b) Taken from Ref. 10. Data at 100 °C in the Menschutkin reaction of Eq. (11).

which an entropy factor ($\Delta S^{\ddagger}$) determines the reaction rate in various solvents irrespective of a slight change in $\Delta H^{\ddagger}$ values.[10] These solvent effects are compared and summarized in Table 4.

As to $1/K$ values of Eq. (2) the order of magnitude is roughly proportional to that of dielectric constants. The product oxonium ion is highly stabilized in solvents of high polarity. Among the solvents examined, liquid SO_2 is probably unique in the sense that it stabilizes the oxonium ion by electrophilic solvation of the counter-anion.[11]

Effects of R and X in $ROSO_2X$. The rate of Eq. (2) depends upon the nature of R in $ROSO_2X$ (Table 2). The order of reactivities is Me>Et>*n*-Pr as seen in the other series of S_N2 reactions.[13] This order agrees with that of $1/K$ values in both CH_2Cl_2 and nitrobenzene.

Table 5 shows relative rates (Et=1.0) in several S_N2 reactions of dipole-dipole reactions (Nos. 1—5) like Eq. (2) and dipole-ion reactions (Nos. 6 and 7). The change of solvent (CH_2Cl_2 and nitrobenzene) had little effect on the relative reactivities (Nos. 1 and 2). A close resemblance of the relative rates, especially between reactions of Nos. 1, 2, 3, and 7, seems to indicate that the reactions proceed *via* a similar mechanism. The nature of X in $ROSO_2X$ also affects the rate. In the $EtOSO_2X$–THP reaction at 35 °C the order of reactivities is Cl≈CF_3>F in both CH_2Cl_2 and nitrobenzene solvents (Table 2). It should be noted that $1/K$ values are extremely low in the case of $ROSO_2F$.

Comparison of Eq. (2) with the THF Polymerization. It would be worth while to compare the reaction (2) with the THF polymerization initiated by superacid esters.[2] The equilibrium of Eq. (1) resembles rather the reverse reaction of Eq. (2) as given by Eq. (12).

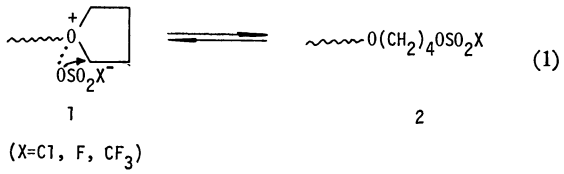

(1)

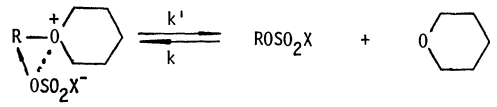

(12)

Both processes Eqs. (1) and (12) are intramolecular ones to produce ester type species. The products, however, are entirely different. In Eq. (1), the counter-anion of OSO_2X^- attacks the α-carbon of THF ring in the oxonium **1** to cause the ring-opening of THF. On the other hand, in Eq. (12) the counter-anion attacks alkyl group rather than α-carbon of the THP ring. In the propagation process of the THF polymerization (Eq. (13)), THF monomer attacks intermolecularly the α-carbon of THF ring in **1** instead of the intramolecular attack of the counter-anion of OSO_2X^-.

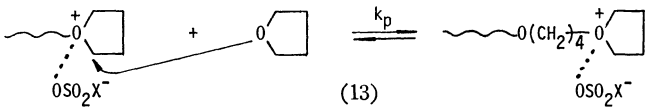

(13)

The existence of the oxonium-ester type equilibrium of Eq. (2) (or Eq. (12)) strongly suggests that the same type of equilibration (Eq. (1)) actually takes place during the course of THF polymerization. Such equilibration is very likely dependent upon the solvent since the present results of the solvent effect show remarkable changes of k and $1/K$ values of Eq. (2).

In a very recent presentation by Matyjaszewski *et al.*[19] the oxonium-ester equilibrium (Eq. (1)) has been discussed in the kinetic study of the THF polymerization by $EtOSO_2CF_3$ initiator. With a variation of polymerization solvents a wide range of apparent k_p values ($2.0—23.0 \times 10^{-3}$ l/mol·s, at 25 °C) have been obtained. They claimed that low apparent k_p values in non-polar solvents were due to a larger fraction of

TABLE 5. RELATIVE RATES OF SOME PRIMARY COMPOUNDS IN S_N2 REACTIONS

Reaction		Relative rate			Ref.
		Me	Et	*n*-Pr	
1. $ROSO_2Cl$+	in CH_2Cl_2 (35 °C)	4.63	1.0	0.294	This work
2. $ROSO_2Cl$+	in $C_6H_5NO_2$ (35 °C)	3.19	1.0	0.452	This work
3. $ROSO_2Cl+H_2O$	in dioxane (25 °C)	2.93	1.0	0.555	14)
4. $RI+Et_3N$	in acetone (100 °C)	11.4	1.0	0.19	15)
5. RI+	in $C_6H_5NO_2$ (25 °C)	18.7	1.0	—	16)
6. $RBr+EtO^-$	in ethanol (55 °C)	17.6	1.0	0.281	17)
7. $RI+PhO^-$	in ethanol (42.5 °C)	4.84	1.0	0.386	18)

the ester type **2** concentrations. However, no concentrations of oxonium **1** and ester **2** were determined in their kinetics.[19] For a quantitative argument further study of the oxonium-ester equilibria in detail is required.

Experimental

Materials. All the reagents were distilled under nitrogen. Methyl ($MeOSO_2Cl$), ethyl ($EtOSO_2Cl$) and *n*-propyl (*n*-$PrOSO_2Cl$) chlorosulfates were prepared by the reactions of sulfuryl chloride with the corresponding alcohols,[14] bp, $MeOSO_2Cl$, 51—52 °C/25 mmHg (lit.[14] 40 °C/14 mmHg), $EtOSO_2Cl$, 58 °C/25 mmHg (lit.[14] 42 °C/10 mmHg) and *n*-$PrOSO_2Cl$, 61 °C/20 mmHg (lit.[14] 52 °C/10 mmHg). $EtOSO_2F$ and $EtOSO_2CF_3$ were obtained in the same manner as reported.[2] $MeOSO_2F$ was prepared by the reaction of dimethyl sulfate with FSO_3H,[2] bp 92—94 °C. THP was dried on sodium metal and distilled. This procedure was repeated twice. Purification of CH_2Cl_2 was carried out in the same way as in the previous work.[2] Nitrobenzene was dried on phosphorus pentoxide and distilled *in vacuo*.[7] Chlorobenzene and $CHCl_3$ (an internal standard) were dried on Molecular Seives and distilled before use. Liquid SO_2 was obtained by condensation of gaseous SO_2 (Seitetsu Kagaku Co., Ltd).

Kinetic Procedures. Kinetic reactions were carried out under nitrogen. A typical run is as follows. Into an NMR sample tube containing 0.752 ml of CH_2Cl_2, 0.088 ml (0.822 mmol) of $EtOSO_2Cl$, 0.081 ml (0.835 mmol) of THP, and 0.080 ml (1.00 mmol) of $CHCl_3$ were introduced with a microsyringe, giving the initial concentrations of $[E]_0=0.822$ mol/l and $[T]_0=0.835$ mol/l. During the sample preparation the NMR sample tube was cooled in a Dry Ice–acetone bath. The tube was sealed, and inserted into the probe of the NMR spectrometer (Hitachi R-20B). Up to this step the extent of the reaction was negligible. The reaction was then followed by taking spectra several time at the desired temperature. For the determination of equilibrium concentration, the sample tube was kept at the same temperature until the reaction no longer proceeded. The NMR spectrum was then recorded. The oxonium concentration of the spectrum was taken to be an $[Ox]_e$ value. The reaction temperature was kept constant within ± 1 °C and the experimental error of the integration was within $\pm 2\%$.

References

1) Part II; S. Kobayashi, T. Saegusa, and Y. Tanaka, This Bulletin, **46**, 3220 (1973).
2) S. Kobayashi, H. Danda, and T. Saegusa, *ibid.*, **46**, 3214 (1973).
3) M. G. Ahmed, R. W. Alder, G. H. James, M. L. Sinnott, and M. C. Whiting, *Chem. Commun.*, **1968**, 1533.
4) a) H. Perst, "Oxonium Ions in Organic Chemistry," Verlag Chemie and Academic Press (1971). b) S. Kobayashi, *Yuki Gosei Kagaku Kyokai Shi*, **31**, 935 (1973).
5) E. M. Arnett and C. Y. Wu, *J. Amer. Chem. Soc.*, **84**, 1684 (1962).
6) F. S. Dainton, T. R. E. Devlin, and P. A. Small, *Trans. Faraday Soc.*, **51**, 1710 (1955).
7) J. A. Riddick and W. B. Bunger "Organic Solvents," Wiley-Interscience (1970).
8) A. L. Vierk, *Z. Anorg. Allg. Chem.*, **261**, 279 (1950).
9) K. B. Wiberg, "Physical Organic Chemistry," John Wiley & Sons, Inc., New York (1963), p. 379.
10) N. J. T. Pickles and C. N. Hinshelwood, *J. Chem. Soc.*, **1936**, 1353.
11) N. Tokura and Y. Kondo, This Bulletin, **37**, 133, (1964).
12) P.A.D. de Maine, *J. Chem. Phys.*, **26**, 1036 (1957).
13) C. K. Ingold, "Structure and Mechanism in Organic Chemistry," 2nd Ed., Cornell University Press (1969),Chapter VII.
14) E. Buncel and J. P. Millington, *Can. J. Chem.*, **43**, 556, (1965).
15) N. Menschutkin, *Z. Phys. Chem.*, **5**, 589 (1890).
16) H. C. Brown and A. Cahn, *J. Amer. Chem. Soc.*, **77**, 1715 (1955).
17) I. Dostrovsky and E. D. Hughes, *J. Chem. Soc.*, **1946**, 157.
18) D. Segaller, *ibid.*, **105**, 106 (1914).
19) K. Matyjaszewski, P. Kubisa, and S. Penczek, Presented at the "International Symposium on Cationic Polymerization" September, 1973, Rouen, France.

A Macrocyclic Enzyme Model System. Acyl Transfer from *p*-Nitrophenyl Carboxylates to Paracyclophane Oxime[1]

Yukito MURAKAMI, Junzo SUNAMOTO,* and Koji KANO

Department of Organic Synthesis, Faculty of Engineering, Kyushu University, Hakozaki, Higashi-ku, Fukuoka 812

(Received January 8, 1974)

The deacylation reactions of *p*-nitrophenyl carboxylates by 10-hydroxy-11-hydroxyimino[20]paracyclophane (Oxime-I) have been investigated in an alkaline aqueous acetone. Oxime-I was acylated by *p*-nitrophenyl laurate (PNPL) and decanoate (PNPD), but was not affected by *p*-nitrophenyl acetate (PNPA) and hexanoate (PNPH). Meanwhile, 2-hydroxycyclodecanone oxime (Oxime-II) and acetoxime (Oxime-III) did not undergo any reaction with all of the present carboxylic esters under the same conditions. These results suggest that the acylation reactions of Oxime-I with PNPD and PNPL proceed primarily through incorporation of the substrates into the cyclic oxime cavity. The formation of an intra-complex was also suggested by an evidence that the copper(II) ion markedly retarded the reaction rate of PNPL with Oxime-I below the catalyst-absence level. The binding constant for PNPL with Oxime-I was considerably large in comparison with the usual micelle-substrate or synthetic polymer-substrate complexes. On the basis of thermodynamic parameters for the binding and the subsequent acylation, the driving force for the incorporation and the geometry of the intra-complex have been discussed.

The three kinds of esterase model systems have been widely developed to establish some new catalytic systems for organic synthesis as well as to understand the enzymatic mechanisms from the bioorganic viewpoints: these are micellar surfactants,[2] synthetic polymers,[3] and macrocyclic compounds.[4] Micellar surfactants and synthetic polymers have been known to construct the hydrophobic field through micelle formation and aggregation, respectively. The hydrophobic interaction between these enzyme models and substrates resulted in the formation of intra-complexes to provide the proximity effects due to plausible orientation and to raise the local concentrations of the attacking nucleophiles. The formation of hydrophobic binding sites in these cases is, however, in dynamic equilibria with the bulk phase and subject to the external medium effects consequently.[5] Thus, these mobile structures may provide a limited substrate specificity. On the other hand, macrocyclic compounds may exhibit several novel and unique characters primarily due to the following effects.

1) The macrocyclic cavity provides a steady binding site due to a characteristic ring conformation of hydrophobic nature. This binding site can be little affected by the external factors such as temperature, hydrogen ion concentration, ionic strength, dielectric constant, and other medium properties.

2) A high substrate specificity can be brought about by the geometric requirements for binding of substrates into these macrocyclic cavities as well as by spatial geometries of substrate molecules incorporated into these cavities on the other. Utilization of cycloamyloses,[4a] cyclic peptides,[4b] and cyclic *N*-methylhydroxamic acid[4c] have provided much fruitful results though they need to be further investigated.

In this work, we prepared a sizable cyclic compound, 10-hydroxy-11-hydroxyimino[20]paracyclophane (Oxime-I), and studied the acyl transfer from *p*-nitrophenyl carboxylates to the cyclic oxime. Oxime-I provides an appropriate hydrophobic binding site with the paracyclophane skeleton and one nucleophilic function with the oxime group. In reference to the Stuart molecular models shown in Fig. 1, Oxime-I has an inner diameter of about 6.5 Å and a depth of about 4.5 Å. 2-Hydroxycyclodecanone oxime (Oxime-II) and

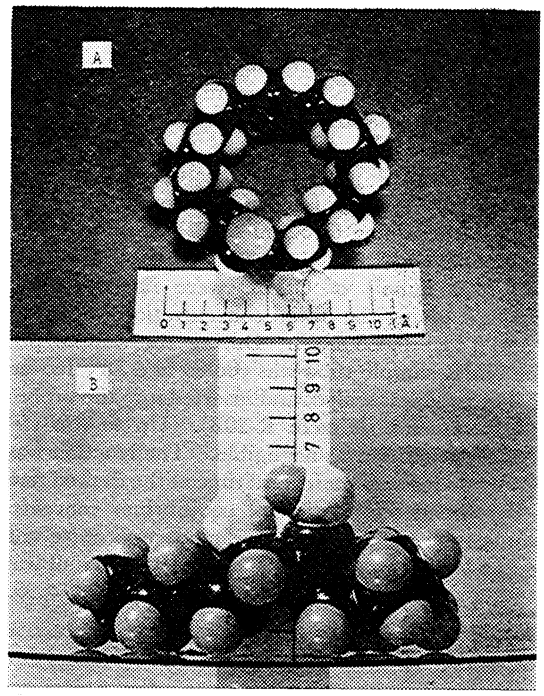

Fig. 1. Stuart molecular models of Oxime-I with scale: A, top view showing an inner diameter of *ca.* 6.5 Å; B, side view showing a depth of *ca.* 4.5 Å.

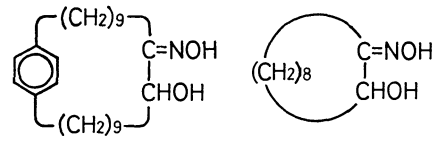

Oxime-I Oxime-II

* Present address: Department of Industrial Chemistry, Faculty of Engineering, Nagasaki University, Nagasaki 852.

acetoxime were also used in order to characterize the catalytic ability of Oxime-I.

Experimental

Spectroscopic measurements were run on a JASCO DS-403G grating IR spectrophotometer, a Varian A60 NMR spectrometer, a JEOL JMS-01SG mass spectrometer, and a Hitachi EPS-2 recording spectrophotometer. pH measurements were carried out with a TOA HM-9A pH-meter equipped with a Metrohm EA-125 combined electrode.

Acetoxime of reagent grade was commercially obtained (Nakarai) and used without further purification.

p-Nitrophenyl Carboxylates. *p*-Nitrophenyl acetate (PNPA), hexanoate (PNPH), decanoate (PNPD), and laurate (PNPL) were respectively prepared by the reaction of the corresponding carbonyl chlorides with *p*-nitrophenol in ether in the presence of pyridine. The crude esters were further purified and identified by elemental analyses and spectroscopic measurements before use.

The synthetic steps for Oxime-I are shown in Scheme 1.

Ethyl ω-Phenyldecanoate (1). Ethyl ω-phenyldecanoate was prepared by the esterification of ω-phenyldecanoic acid, which was synthesized according to the procedures described in the literature,[6] and purified by distillation *in vacuo*: bp 140—142 °C/0.075 mmHg, yield 82.3%.

1-(9-Carbethoxynonanyl)-4-(9-carbethoxy-1-oxononanyl) benzene (2). In a 100-ml three-necked flask was placed a mixture of 2.76 g (0.01 mol) of **1**, 4.0 g (0.03 mol) of anhydrous aluminum chloride, and 20 ml of carbon disulfide and the reaction flask was cooled in an ice bath with vigorous stirring. Then, 2.48 g (0.01 mol) of ω-carbethoxypelargonoyl chloride was added dropwise into the mixture in about 15 min. The reaction mixture was stirred for 30 min at room temperature and 3 hr under reflux, and then allowed to stand overnight at room temperature. The red oil obtained was treated with hydrochloric acid at ice-cooled temperature and extracted with carbon disulfide. The organic layer was separated, washed with water, and dried over sodium sulfate. After removal of the solvent, the pale yellow residue was recrystallized from petroleum ether (bp 30—70 °C): mp 56—58.5 °C, yield 2.4 g (49%).

Found: C, 73.74; H, 9.87%. Calcd for $C_{30}H_{18}O_5$: C, 73.73; H, 9.90%.

p-Bis(9-carboxynonanyl)benzene (3). A mixture of 6.0 g (0.012 mol) of **2**, 8.4 g (0.15 mol) of potassium hydroxide, 9.0 g (0.13 mol) of hydrazine hydrate, and 50 ml of diethylene glycol was heated under reflux for 3 hr. After removal of hydrazine and water, the mixture was refluxed for additional 10 hr. Into the resulting solution cooled to room temperature was added about 250 ml of water. This solution was neutralized with hydrochloric acid. The precipitates were recovered, washed with water, and recrystallized from methanol: mp 124—128.5 °C, yield 3.2 g (64%).

Found: C, 74.35; H, 10.16%. Calcd for $C_{26}H_{42}O_4$: C, 74.58; H, 10.13%.

p-Bis(9-carbomethoxynonanyl)benzene (4). A mixture of 4.5 g (0.011 mol) of **3**, 5 ml of concentrated sulfuric acid, and 150 ml of methanol was heated under reflux for 12 hr. A half volume of methanol was distilled off. The residue was diluted with water and extracted with ether. The ethereal solution was washed with water and dried over sodium sulfate. After removal of ether, the crude material was recrystallized from methanol: mp 61—66.4 °C, yield 3.5 g (71.2%). NMR (CCl_4, TMS as an internal reference): δ 1.27—2.63 (36H, m, methylene envelope), 3.58 (6H, s, $-C\underline{H}_3$), and 6.96 (4H, br., $-C_6\underline{H}_4-$).

Found: C, 75.35; H, 10.31%. Calcd for $C_{28}H_{46}O_4$: C, 75.27; H, 10.39%.

10-Hydroxy-11-oxo[20]paracyclophane (5). A 3-liter creased flask of three-necked round-bottom was equipped with a mechanical vacuum stirrer of stainless steel and a reflux condenser, the top of which was connected to a dropping funnel furnished with a needle valve. In the flask were placed 500 ml of xylene and 1.0 g (0.043 g atom) of crust-free sodium metal. It was refluxed for 15 min with vigorous stirring under nitrogen atmosphere. Gaseous nitrogen was streamed throughout the apparatus during the course of reaction. Then, 3.0 g (6.7 mmol) of **4** dissolved in 250 ml of xylene was added dropwise for a period of 20 hr. Reflux was continued for additional 30 min after the complete addition of **4**. The reaction flask was then cooled in an ice bath. Glacial acetic acid (4 ml) dissolved in 6 ml of xylene was added dropwise in about 30 min while cooling and stirring were continued. The resulting mixture was transferred into a 2-liter separatory funnel together with 25 ml of water. The xylene layer was separated, washed with water, and dried over active calcium sulfate. After rapid removal of xylene, the crude material was recrystallized from *n*-pentane as white granular crystals: mp 46—51 °C, yield 1.4 g (53.7%). IR (KBr disk): ν_{OH}, 3400; $\nu_{C=O}$, 1704 cm^{-1}.

Found: C, 81.57; H, 11.48%; M^+, 386. Calcd for $C_{26}H_{42}O_2$: C, 80.75; H, 10.97%; mol wt, 386.68.

10-Hydroxy-11-hydroxyimino[20]paracyclophane (Oxime-I). Into a mixture of 500 mg (1.29 mmol) of **5**, 300 mg (4.32 mmol) of hydroxylamine hydrochloride, and 10 ml of methanol

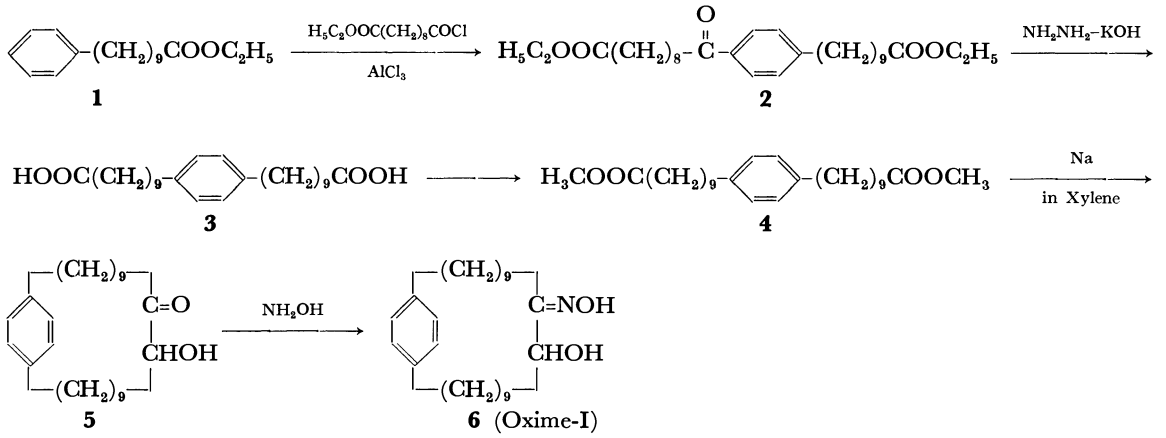

Scheme 1. Synthesis of Oxime-I.

containing a small amount of water was added gradually 530 mg (13 mmol) of sodium hydroxide powder. The mixture was heated under reflux for 10 min, neutralized with dilute aqueous hydrochloric acid, and then extracted with about 200 ml of *n*-pentane. The organic layer was separated, washed with water, and dried over sodium sulfate. After a half volume of *n*-pentane was distilled off, the residue was cooled to about −10 °C. The colorless needles were recovered: mp 91.5—93 °C, yield 440 mg (84.8%). IR (KBr disk): ν_{OH}, 3300; $\nu_{C=N}$, 1650 cm^{-1}.

Found: C, 77.70; H, 11.28; N, 3.20%; M^+, 401. Calcd for $C_{26}H_{43}NO_2$: C, 77.73; H, 10.81; N, 3.49%; mol wt, 401.70.

2-Hydroxycyclodecanone (sebacoin). 2-Hydroxycyclodecanone was prepared according to the procedures described in the literature:[7] mp 36.5—39 °C (lit,[7] 38—39 °C), yield 47.3%.

2-Hydroxycyclodecanone Oxime (Oxime-II). Sebacoin oxime was prepared by a method similar to that used for the preparation of Oxime-I. The crude Oxime-II (mp 86—96 °C) was purified by means of column chromatographic technique with the combination of active alumina and absolute methanol: mp 101—103 °C, yield 1.2 g (50%). IR (KBr disk): ν_{OH}, 3220; $\nu_{C=N}$, 1650 cm^{-1}.

Found: C, 64.92; H, 10.58; N, 7.30%; M^+, 185. Calcd for $C_{10}H_{19}NO_2$: C, 64.81; H, 10.36; N, 7.56%; mol wt, 185.30.

Kinetic Measurements. The rate of formation of *p*-nitrophenoxide ion was measured at 400 nm. Reactions were initiated by the addition of 30 μl of 1×10^{-3}M *p*-nitrophenyl carboxylate in acetone to 3.0 ml of a reaction solution which was pre-equilibrated at an appropriate temperature in the thermostatted cell set in a Hitachi 124 recording spectrophotometer. The reaction solution was prepared in a 10 ml volumetric flask by placing 1.0 ml of $1-7\times10^{-4}$M Oxime-I in acetone–water (1: 1 by volume), 0.5 ml of acetone, 0.9 ml of 1.0 M aqueous potassium chloride, and an appropriate amount of 0.1 M sodium hydroxide to adjust the pH-value of medium in this order, and subsequently by filling up with distilled and deioninized water to the mark. The overall concentrations of *p*-nitrophenyl esters and the oxime in the reaction mixture were 1×10^{-5}M and $2-15\times10^{-6}$M, respectively. The acetone content in the above reaction mixture was about 10% of the total volume, and also varied in a 10—30% (v/v) range. The temperature of a reaction mixture was maintained constant with an accuracy of ±0.1 °C. A buffer system, sodium carbonate–sodium borate, was used for reactions at pH 10.

Product Analysis. *p*-Nitrophenyl laurate (82.9 mg, 0.26 mmol) underwent reaction at 20 °C with Oxime-I (98.8 mg, 0.24 mmol) in 50 ml of acetone–water (1: 5 by volume) containing 2.6 ml of 0.1 M sodium hydroxide. After the complete decomposition of the ester, the reaction mixture was extracted with *n*-hexane. The aqueous alkaline layer remained was carefully neutralized with dilute hydrochloric acid and extracted with ether. Upon evaporation of the ethereal layer, *p*-nitrophenol and lauric acid were detected by tlc as well as by UV and IR spectroscopy. On the other hand, tlc of the mixture obtained from *n*-hexane extracts showed the existence of three components. Two of them were identified as the unreacted Oxime-I and its hydrolyzate, 10-hydroxy-11-oxo[20]paracyclophane (**5**), though both were only in a trace amount. The third component, which was isolated from the mixture, showed a strong IR absorption band at 1710 cm^{-1} ($\nu_{C=O}$) and a UV spectrum having absorption maxima at 213, 220, 260, 267, and 274 nm in methanol. These results indicate that Oxime-I was acylated by *p*-nitrophenyl laurate (Eq. (1)) in a manner as seen for the acylation of aryl-oxime with *p*-nitrophenyl carboxylates.[8]

$$\text{>C=N-OH} + \text{Ph-O-C(O)-R} \longrightarrow \text{>C=N-O-C(O)-R} + \text{Ph-OH} \quad (1)$$

Meanwhile, Oxime-I was hydrolyzed to give the parent ketocyclophane (**5**) to an insignificant extent under the same reaction conditions. In addition, the degradation of Oxime-I did not show any meaningful effect on the reaction kinetics.

Results and Discussion

In the alkaline hydrolyses of PNPD and PNPL, pseudo-first-order plots deviated positively after 25—30% conversion of the esters. This phenomenon has been attributed to the self-aggregation of the substrates.[9] Meanwhile, in the presence of Oxime-I the rate of *p*-nitrophenol release from the esters started to deviate gradually downward from the first-order plot in the same conversion range. Therefore, a pseudo-first-order rate constant k_{obs} was obtained from the linear portion at the initial stage of reaction. Oxime-I did not, however, provide any effect on the *p*-nitrophenol release from esters of smaller alkyl chains, PNPA and PNPH (Table 1). Similarly, smaller cyclic oxime (Oxime-II) as well as acetoxime also did not show any effect on the reaction rate of all the substrates studied (Table 1). In the reaction of Oxime-I either with PNPD or PNPL, the usual saturation-type kinetics have been observed as illustrated for the PNPL–Oxime-I system in Fig. 2. These kinetic evidences and the product analysis suggest that there proceed two competetive reactions, the hydrolysis of an uncomplexed substrate and the acyl transfer reaction *via* an intra-complex formed between Oxime-I and either PNPD or PNPL, as shown by Eq. (2).

$$\begin{array}{ccc} S + \text{Oxime-I} & \overset{K}{\rightleftharpoons} & \text{S-Oxime-I} \\ \downarrow k_{hyd} & & \downarrow k_{acyl} \\ P_1 & & P_2 \end{array} \quad (2)$$

where k_{hyd} and k_{acyl} stand respectively for the rate

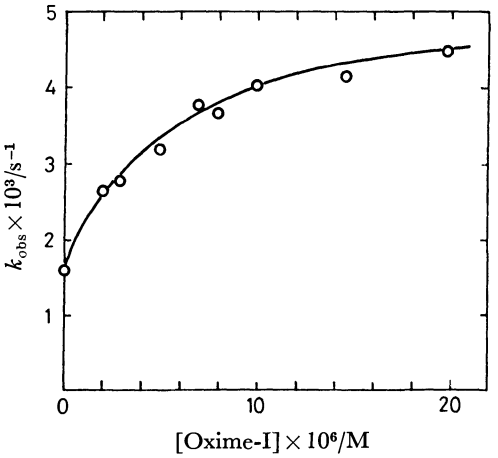

Fig. 2. Saturation-type kinetics for the reaction of PNPL (9.90×10^{-6}M) with Oxime-I in 10.9% (v/v) aqueous acetone at 34.1 °C, μ=0.10 (KCl), and pH 12.3 (1.00×10^{-2}M sodium hydroxide).

Table 1. First-order rate constants for the *p*-nitrophenol release from *p*-nitrophenyl carboxylates in the presence of oxime-I, -II, and acetoxime (oxime-III)

Carboxylate Species: 10^{-5}M	Oxime Species: M	NaOH, 10^{-2}M	Acetone content, % (v/v)	Ionic strength (KCl), M	Temp., °C	k_{obs}, $10^{-3}s^{-1}$
PNPA: 5.00	None	0.50	30.0	0.05	25.0	26.5
PNPA: 5.00	I: 1.00×10^{-4}	0.50	30.0	0.05	25.0	26.5
PNPH: 5.00	None	0.50	30.0	0.05	25.0	20.7
PNPH: 5.00	I: 1.00×10^{-4}	0.50	30.0	0.05	25.0	20.2
PNPH: 4.76	None	1.00	26.7	0.01	19.6	20.9
PNPH: 4.76	I: 4.76×10^{-5}	1.00	26.7	0.01	19.6	19.7
PNPH: 4.76	II: 4.76×10^{-5}	1.00	26.7	0.01	19.6	20.9
PNPD: 4.76	None	1.00	26.7	0.01	19.6	7.05
PNPD: 4.76	I: 4.76×10^{-5}	1.00	26.7	0.01	19.6	5.57
PNPD: 4.76	II: 4.76×10^{-5}	1.00	26.7	0.01	19.6	7.55
PNPD: 0.99	None	1.00	10.9	0.10	20.3	3.59
PNPD: 0.99	I: 9.90×10^{-6}	1.00	10.9	0.10	20.3	4.26
PNPL: 0.99	None	1.00	10.9	0.10	20.0	0.31
PNPL: 0.99	I: 9.90×10^{-6}	1.00	10.9	0.10	20.0	2.25
PNPL: 0.99	II: 9.90×10^{-6}	1.00	10.9	0.10	20.0	0.33
PNPL: 0.99	III:9.90×10^{-6}	1.00	10.9	0.10	20.0	0.33

Table 2. Kinetic parameters for the reactions of *p*-nitrophenyl decanoate and laurate with oxime-I at μ=0.10 (KCl)

Carboxylate [a,b]	Temp., °C	Acetone content, % (v/v)	pH	$k_{hyd}\times10^4$, s^{-1}	$k_{acyl}\times10^4$, s^{-1}	$K\times10^{-5}$, M^{-1}
PNPD	20.3	10.9	12.3	35.9	43.0	3.8
	30.3	10.0	9.3	0.88	3.42	14.6
	30.3	10.0	9.9	2.71	7.29	6.4
	30.3	10.0	11.0	20.9	44.1	5.4
PNPL	15.2	10.9	12.3	2.1	13.8	4.8
	24.5	10.9	12.3	5.1	33.7	1.5
	34.1	10.9	12.3	16.1	58.7	1.3
	42.1	10.9	12.3	37.1	137	0.6
	33.9	10.9	10.4	0.3	4.4	1.3
	43.1	10.9	10.4	1.4	8.9	1.3
	20.0	10.9	12.3	3.1	20.0	2.6
	20.1	20.8	12.5	14.1	54.9	1.2

a) Total initial concentration: PNPD, 1.03×10^{-5}M; PNPL, 9.90×10^{-6}M. b) Total initial concentration of Oxime-I: with PNPD, $6.03-48.2\times10^{-6}$M; with PNPL, $1.98-19.80\times10^{-6}$M.

constant of hydrolysis in the bulk phase and that of acylation due to the intra-complex; S and S–Oxime-I represent the substrate and the substrate—Oxime-I complex, respectively, and K is the binding constant. The observed pseudo-first-order rate constant k_{obs} is given by Eq. (3)

$$k_{obs} = (k_{hyd}+k_{acyl}K[\text{Oxime-I}])/(1+K[\text{Oxime-I}]) \quad (3)$$

which can be rearranged to

$$1/(k_{hyd}-k_{obs}) = 1/(k_{hyd}-k_{acyl}) + 1/(k_{hyd}-k_{acyl})K[\text{Oxime-I}] \quad (4)$$

A good linear relationship has been obtained by plotting the left-hand side of Eq. (4) against the reciprocal concentration of Oxime-I, as typically seen in Fig. 3. We calculated the rate constant for acylation and the binding constant from the intercept and the slope, respectively. Kinetic results are summarized in Table 2.

It is interesting to examine the difference in reactivity in terms of the correlations between the ring size of

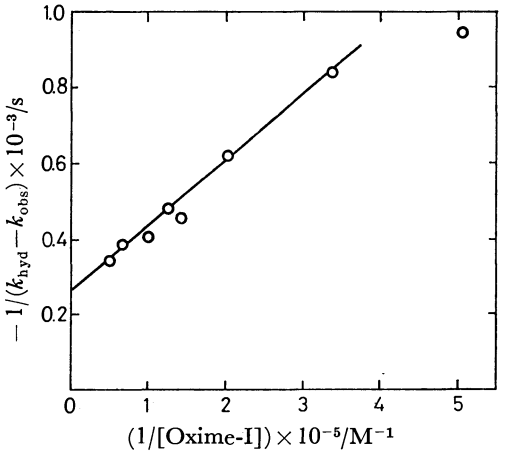

Fig. 3. Analysis of kinetic data (given in Fig. 2) for the decomposition of PNPL in the presence of Oxime-I by means of Eq. (4).

cyclic oximes and the molecular size (or geometry) of substrates. Table 1 shows that Oxime-I was acylated only by the esters having a long alkyl chain residue and not by the smaller esters such as PNPA or PNPH, while Oxime-II and acetoxime could not be acylated even by longer esters. It may be, therefore, reasonable to assume that the present acyl transfer reactions from PNPL and PNPD to Oxime-I must proceed through the intra-complex formation, which would be caused by an incorporation of a substrate into the cyclic cavity of Oxime-I and not by a simple hydrophobic entanglement.

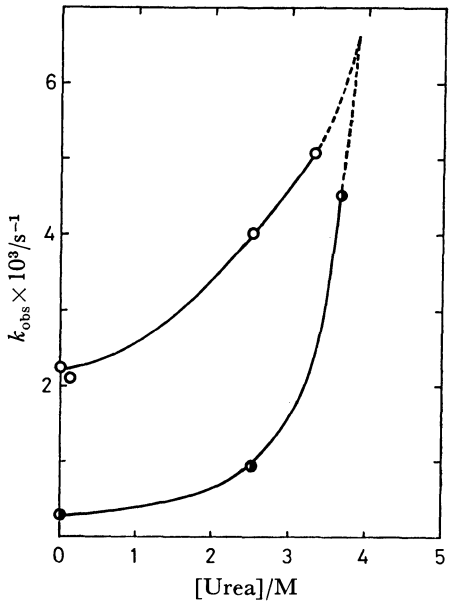

Fig. 4. Effects of added urea on the decomposition of PNPL (9.90×10^{-6}M) in 10.9% (v/v) aqueous acetone at 20.0 °C, μ=0.10 (KCl), and pH 12.3 (1.00×10^{-2}M sodium hydroxide): ○, with Oxime-I (9.90×10^{-6}M); ◑, without Oxime-I.

Driving Force for Incorporation. The increase in concentration of acetone appeared to decrease the incorporation of the substrate into the cyclic cavity of Oxime-I significantly (Table 2). Similar results have been obtained for the cycloamylose—phenyl acetate system,[4a] where the effect of acetonitrile content was examined. Moreover, Fig. 4 shows that the addition of urea to the reaction system also reduces the incorporation: as the concentration of urea increases, the overall pseudo-first-order rate constant (k_{obs}) and the rate constant for spontaneous hydrolysis increase and finally both become equal. Consequently, a driving force for the incorporation of a substrate into the cavity of Oxime-I should be attributed to the hydrophobicity of a substrate and the oxime as well. These results suggest that the self-aggregation of the substrate acts in favor of the incorporation but the resulting hindered nucleophilic center provides a steric effect against attacking hydroxide ion. The Stuart molecular model shows, in fact, that the folded substrate molecule can be inserted tightly into the Oxime-I cavity. If the elongated substrate molecule could be incorporated, PNPA and PNPH, having molecular head and tail similar to PNPD and PNPL, would also undergo the acyl transfer reaction with Oxime-I. It should be noted in the present study that urea or an organic solvent perturbs the hydrophobicity of the substrate esters only and not the cyclic oxime cavity.

Effect of the Copper(II) Ion. Oxime-I has three donor atoms, one nitrogen and two oxygens. It is expected that an appropriate metal ion may show somewhat a unique effect on the reactivity of Oxime-I. The copper(II) ion, which was used as nitrate, did not give any effect on the reaction of PNPL in the absence of Oxime-I, while it profoundly retarded the *p*-nitrophenol release in the presence of the oxime. Upon addition of over equimolar amount of copper ion relative to the ester and the oxime, the reaction rate was reduced below the Oxime-I absence level (Fig. 5). These results suggest that Oxime-I deactivated by the coordination of the copper(II) ion still holds a large ability of substrate-incorporation and consequently the ester decomposition becomes largely decelerated. Thus, we can say that the effect of copper(II) provides another evidence for the incorporation. Hershfield and Bender investigated the hydrolysis of PNPL catalyzed by a macrocyclic hydroxamic acid. Although the reaction rate was markedly accelerated upon addition of copper(II), they did not give any plausible elucidation for the catalytic mechanism.[4c] The copper-concerned reactions in both cases apparently proceed through somewhat different mechanisms.

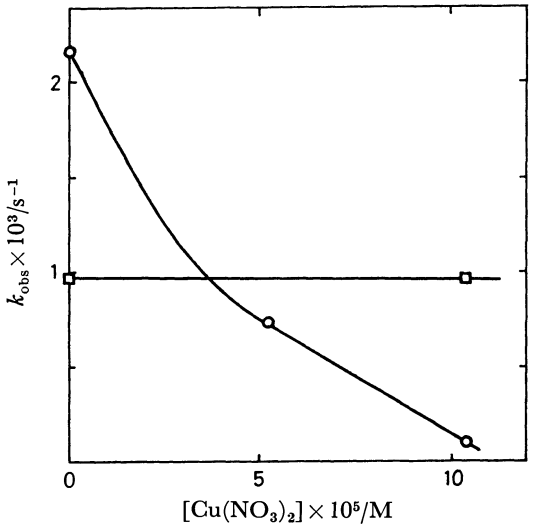

Fig. 5. Effects of added copper(II) ion on the decomposition of PNPL (4.76×10^{-5}M) in 26.7% (v/v) aqueous acetone at 20.0 °C and pH 12.3 (1.00×10^{-2}M sodium hydroxide): ○, with Oxime-I (4.76×10^{-5}M); □, without Oxime-I.

Catalytic Effect and Substrate Specificity. Oxime-II and acetoxime did not show any meaningful effect on the decomposition of PNPD and PNPL. This means that these two oximes undergo no acyl transfer reaction at least under the present conditions. It has been well known that acetoxime (pK_a 12.4) shows exceedingly large nucleophilicity due to α-effect.[10] Our present cyclic oximes, Oxime-I and -II, must have approximately the same nucleophilicity as that of acetoxime as

far as the oxime moiety concerns. The large reactivity of Oxime-I, therefore, can be attributed to the incorporation which brings about the proximity effect for the reaction. This effect is analogous to the cases of intramolecular catalysis. The inertness of Oxime-II, on the other hand, seems to be ascribed to its small ring size which inhibits such an incorporation.

Table 3. Catalytic specificity of oxime-I in the reactions with *p*-nitrophenyl carboxylates

Carboxylate	$k_{obs(Oxime-I)}/k_{obs(Oxime-II)}$	k_{acyl}/k_{hyd}
PNPA	*ca.* 1[a]	—
PNPH	*ca.* 1[a]	—
PNPD	0.7[b]; 1.2[c]	2.4[c]
PNPL	2.3[b]; 7.4[c]	14.7[c]

a) At 25.0 °C in 30% (v/v) aqueous acetone with pH 11.5. b) At 19.6 °C in 26.7% (v/v) aqueous acetone with pH 12. c) At 20.0 °C in 10.9% (v/v) aqueous acetone with pH 10.

Clearly from the preceding comments, the overall rate constant in the presence of Oxime-II, $k_{obs(Oxime-II)}$, is nearly equal to the rate constant for spontaneous hydrolysis of esters. We define the catalysis specificity of Oxime-I in terms of either $k_{obs(Oxime-I)}/k_{obs(Oxime-II)}$ or $k_{obs(Oxime-I)}/k_{hyd}$, each rate constant being obtained under the same conditions. These are listed in Table 3, along with the specific rate ratio, k_{acyl}/k_{hyd}. The specificity of Oxime-I further increased at lower pH region where the nucleophilicity of the oxime group must become smaller. This fact, as well as the product analysis, suggests that the acyl transfer reaction in the intra-complex may proceed through the direct nucleophilic attack of the oxime to the carbonyl carbon, not through the general base catalysis. In addition, the acylation exhibits the linear dependence on pH in a 9—12 pH range (Fig. 6). This is consistent with a mechanism shown by Eq. (5). Deceleration of the decomposition rate of PNPD in the presence of Oxime-I at higher pH (Table 3) is not clear at

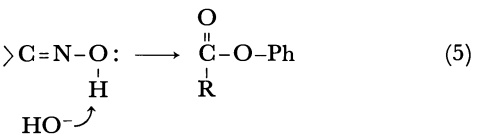

(5)

present. However, this is predictive of the presence of substrate specificity for Oxime-I. Our results are, therefore, apparently different from those obtained by Hershfield and Bender,[4c] in which the rate enhancement was gained only by the extension of alkyl-chain length without substrate specificity. They did not indicate clearly which effect, simple entanglement or

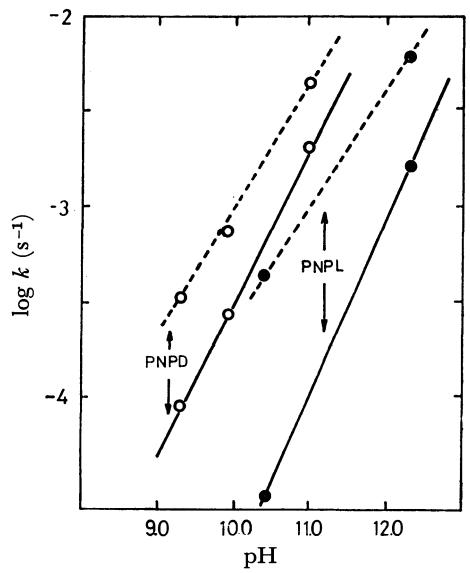

Fig. 6. pH-rate correlations for alkaline hydrolyses (solid lines) of PNPD (1.00×10^{-5}M, ○) in 10.0% (v/v) aqueous acetone with μ=0.10 (KCl) at 30.0 °C and PNPL (9.90×10^{-6}M, ●) in 10.9% (v/v) aqueous acetone with μ=0.10 (KCl) at 33.9 °C; and acyl transfer reactions of these carboxylates (broken lines) with an equimolar concentration of Oxime-I under the same conditions employed for the corresponding alkaline hydrolyses.

incorporation, contributed to the interaction of the cyclic compound with substrates.

Binding Property. Table 2 shows that the binding constants for the incorporation of PNPD and PNPL into Oxime-I are considerably larger ($K\approx10^5$ M^{-1}) than those for phenyl acetates into cycloamyloses ($K\approx10^3$ M^{-1}).[11] In the present study, it became clear that large hydrophobic guest molecules lead to the formation of relatively stable inclusion complexes and the interior of the cyclic oxime provides a better hydrophobic binding site. In order to understand the nature of incorporation, the temperature dependency of binding constant for PNPL–Oxime-I was examined using kinetic method. Thermodynamic parameters were obtained from a plot of $\ln K$ *vs.* $1/T$(K) by the least-squares method: $\Delta G°$(307.3 K) = −7.2 kcal mol^{-1}, $\Delta H°$ = −9.4 kcal mol^{-1}, and $\Delta S°$ = −7.3 e.u. at pH 12 in 10.9 vol% aqueous acetone. The binding constant is comparatively temperature dependent in a similar trend as observed for the combination of *m*-ethylphenyl acetate and cyclohexaamylose.[11a] The thermodynamic data apparently show that the stabilization due to binding is mostly caused by a favorable enthalpy change. Bender and his co-workers have proposed

Table 4. Activation parameters for alkaline hydrolysis and acylation reaction of PNPL[a]

Reaction	E_a kcal mol^{-1}	$\Delta S^{\ddagger}$ e.u.	$\Delta H^{\ddagger}$ kcal mol^{-1}	$\Delta G^{\ddagger}$ kcal mol^{-1}
Hydrolysis	18.5±0.7	−13.2±2.3	17.9±0.7	22.0±1.5
Acylation	14.9±0.3	−22.5±0.8	14.3±0.3	21.3±0.6

a) Experimental conditions: pH, 12.3; μ, 0.10 (KCl); temp., 307.3 K; medium, 10.9% (v/v) acetone–water.

that the sizable enthalpy change in the formation of cycloamylose complex was brought about by liberating water molecules, which were loosely bound to the cycloamylose cavity through hydrogen bonding, upon inclusion of a guest molecule.[11a] In the paracyclophane cavity, however, the van der Waals forces would provide such a favorable enthalpy effect. Further investigation is in progress in our laboratories.

Activation Parameters for Hydrolysis and Acyl Transfer Reactions. Activation parameters for the hydrolysis of PNPL and the acylation of Oxime-I with the same ester are listed in Table 4. A decrease of activation enthalpy ($\Delta\Delta H^{\ddagger}=4$ kcal mol^{-1}), which plays the major role in the stabilization of transition state, may be caused by the difference in nucleophilicity between hydroxide ion and oximate. Furthermore, the proximity effect brought about by the intra-complex formation seems to be responsible for such a smaller activation enthalpy. A much larger loss of activation entropy ($\Delta\Delta S^{\ddagger}=-10$ e.u.) for the acyl transfer reaction would be rather unexpected: the intramolecular catalysis is entropically favored.[12] This fact suggests that the base-catalyzed nucleophilic reaction results in the formation of a polar transition state and consequently the hydrophobic interaction is partly destroyed.

Conclusion

The sizable paracyclophane oxime demonstrated several unique behaviors as expected. An appropriate cavity size can give out the substrate specificity: this is associated with bulkiness, geometry, and molecular volume of a substrate as well as hydrophobicity of both substrate and paracyclophane. Most significantly, the incorporation of a substrate, having an appropriate geometrical character, into the cyclic cavity was confirmed by the kinetic method. It has been also shown that Oxime-I has a large binding ability toward *p*-nitrophenyl decanoate and laurate, as can be compared to some native enzyme systems.[13] The present study provides a rare and unique example among the enzyme model systems so far studied,[2-5] and may be predictive of the possibility for preparation of a more reactive esterase models. Upon substitution with appropriate functional groups, the paracyclophane skeleton may be modified to yield higher deacylation ability.

Thanks are due to Miss Chieko Gondo for her assistance in part of the rate measurements, and also to the Research Institute of Yoshitomi Pharmaceutical Co., Ltd. for the mass spectral measurements.

References

1) Contribution No. 318 from the Department of Organic Synthesis, Faculty of Engineering, Kyushu University. Preliminary communication: Y. Murakami, J. Sunamoto, and K. Kano, *Chem. Lett.*, **1973**, 223.

2) E. J. Fendler and J. H. Fendler, "Advances in Physical Organic Chemistry," Vol. 8, ed. by V. Gold, Academic Press, New York, N. Y. (1970), p. 271.

3) M. L. Bender, "Mechanisms of Homogeneous Catalysis from Protons to Proteins," Wiley-Interscience of John Wiley & Sons, Inc., New York, N. Y. (1971), pp. 382—390.

4) a) Ref. 3, pp. 373—382; b) J. C. Sheehan, G. B. Bennett, and J. A. Schneider, *J. Amer. Chem. Soc.*, **88**, 3455 (1966); K. Nakajima and K. Okawa, This Bulletin, **46**, 1811 (1973); c) R. Hershfield and M. L. Bender, *J. Amer. Chem. Soc.*, **94**, 1376 (1972).

5) E. Cordes, Ed., "Reaction Kinetics in Micelles," Plenum Press, New York, N. Y. (1973).

6) R. Huisgen, W. Rapp, I. Ugi, H. Walz, and I. Glogger, *Ann. Chem.*, **586**, 52 (1954).

7) N. L. Allinger, "Organic Syntheses," Coll. Vol. IV, p. 840 (1963).

8) A. K. Yatsimirski, K. Martinek, and I. V. Berezin, *Tetrahedron*, **27**, 2855 (1971).

9) F. M. Menger and C. E. Portnoy, *J. Amer. Chem. Soc.*, **90**, 1875 (1968).

10) J. O. Edwards and R. G. Pearson, *ibid.*, **84**, 16 (1962).

11) a) R. L. VanEtten, J. F. Sebastian, G. A. Clowes, and M. L. Bender, *ibid.*, **89**, 3242 (1967); b) R. L. VanEtten, G. A. Clowes, J. F. Sebastian, and M. L. Bender, *ibid.*, **89**, 3253 (1967).

12) T. C. Bruice and S. J. Benkovic, "Bioorganic Mechanisms," Vol. 1, W. A. Benjamin, Inc., New York, N. Y. (1966), Chapt. 1.

13) D. M. Chipman and N. Sharon, *Science*, **165**, 454 (1969).

Table 1. NMR-spectra of ethylnicotinic acid and its derivatives
(Expressed in δ-value)

	4-Ethylnicotinic acid	Ethyl 6-ethyl-nicotinate	6-Ethyl-3-cyano-pyridine
H at 2-position	8.95 (d)	8.97 (d)	8.85 (d)
H at 4-position	—	8.05 (dd)	7.88 (dd)
H at 5-position	6.93 (d)	7.12 (d)	7.30 (d)
H at 6-position	8.60 (dd)	—	—
CH_2	3.07 (q)	2.83 (q)	2.95 (q)
CH_3	1.33 (t)	1.28 (t)	1.35 (t)

N, 23.03%.

2-Hydroxynicotinamide. Found: C, 50.14; H, 4.56; N, 19.43%.

Photo-products from the UV-irradiation in Acidic Ethanol Solutions: Ethylated nicotinic acid and its derivatives were identified mainly on the basis of NMR-spectra (Table 1). 4-Ethylnicotinic acid (mp 137—138 °C), λ_{max} 268 nm. Found: C, 61.85; H, 5.82; N, 9.15%.

Photo-ethylation product from 3-cyanopyridine was a mixture consisted of 6-ethyl- and 4,6-diethyl-3-cyanopyridines. These compounds could not be separated by column chromatography. Identification was made only on the basis of NMR-spectra.

Photo-products from the UV-irradiation of Nicotinic Acid in Aqueous Solutions: UV-irradiation of nicotinic acid in aqueous solution (without adding acid or alkali) brought about the increase in absorption at 284 nm. The photo-product (mp 229—230 °C, decomp.) was identified as 2-(3-pyridyl)pyridine-5-carboxylic acid from the following ground. Equivalent as an acid (by titration with sodium hydroxide), 188; Calcd,

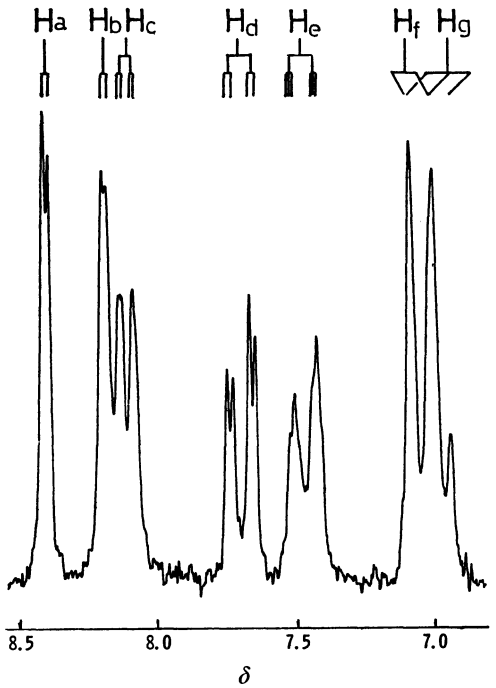

Fig. 1. NMR spectrum of 2-(3-pyridyl)pyridine-5-carboxylic acid

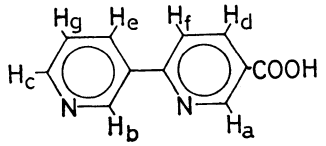

200. The NMR-spectrum was assigned as shown in Fig. 1. The assignment was confirmed by double resonance technique.

Found: C, 65.32; H, 3.87; N, 13.96%. Calcd for $C_{11}H_8N_2O_2$: C, 65.99; H, 4.03; N, 13.99%.

Photo-products from the UV-irradiation in Ethanol Solutions: 3-Cyano-6-(1-hydroxyethyl)pyridine (liquid) and ethyl 6-(1-hydroxyethyl)nicotinate (liquid) were identified on the basis of UV, IR, and NMR spectra.

3-Cyano-6-(1-hydroxyethyl)pyridine: UV; λ_{max}, 268 nm; IR, 3400 (OH), 2980 (aliph. CH), 1480, 1380 (CH_3) and 2240 cm^{-1} (CN). The assignment of NMR-spectra is shown in Table 2.

Ethyl 6-(1-hydroxyethyl)nicotinate: UV; λ_{max}, 266 nm; IR, 3340 (OH), 1720 (C=O), 2960, 1470 and 1370 cm^{-1} (aliph. CH); NMR, Table 2.

Table 2. NMR-spectra of (1-hydroxyethyl)-nicotinic acid derivatives
(Expressed in δ-value)

	Ethyl 6-(1-hydroxy-ethyl)nicotinate	3-Cyano-6-(1-hydroxy-ethyl)pyridine
H at 2-position	9.00 (d)	8.86 (d)
H at 4-position	8.19 (dd)	8.10 (dd)
H at 5-position	7.42 (d)	7.66 (d)
OH -CH-CH_3	4.84 (q)	5.00 (q)
OH -CH-CH_3	1.43 (d)	1.55 (d)
OH	~4.3	~4.1

Photo-products from the UV-irradiation in Alkaline Ethanol Solution: The photo-product in the irradiation of nicotinic acid in alkaline ethanol solution was not trapped by anion exchange resin. The UV spectra (λ_{max}, 266 and 251 nm) and the effects of acid and alkali on UV spectra agreed with those of pyridine. They were different from those of ethylpyridine, another candidate of the photo-product.

Results and Discussion

Photoreactions in Acidic Solutions. Nicotinic acid and its derivatives show a similar UV spectral change on irradiation with 254 nm light in acidic aqueous solutions. An example of nicotinic acid is shown in Fig. 2. The absorption at ~320 nm brought about by UV irradiation corresponds to the introduction of hydroxyl group at the 2-position of pyridine nucleus. This type of UV spectral change was also observed in the irradiation of 3-cyanopyridine and nicotinamide in acidic aqueous solutions. The results of the product

Table 3. Photoreactions of nicotinic acid and 3-cyanopyridine in acidic aqueous solutions (pH: 0—1)

Compound	Reaction condition	Product	
Nicotinic acid	5×10^{-4} mol/l	2-Hydroxynicotinic acid	40%
	LP[a)]-17 W	Recovered	0%
	120 min		
3-Cyanopyridine	5×10^{-4} mol/l	2-Hydroxy-3-cyano-	
	LP-17 W	pyridine	60%
	25 min	Recovered	0%

a) LP: Low pressure mercury lamp

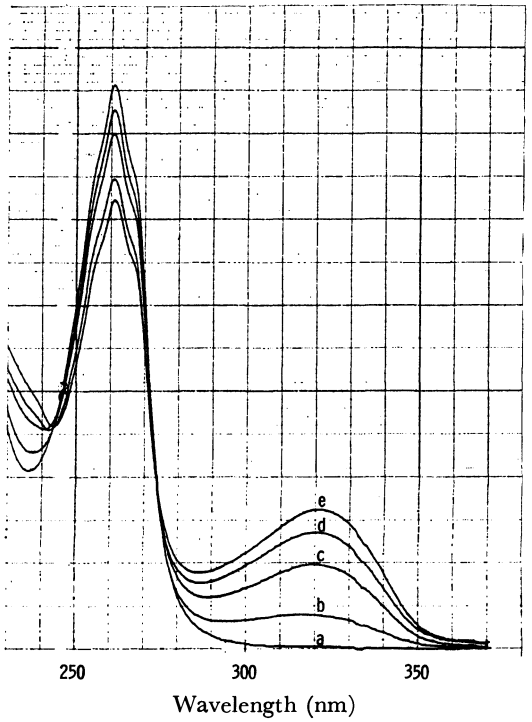

Fig. 2. Change of UV-spectra during the irradiation of nicotinic acid in acidic aqueous solution.
(5×10^{-4} mol/l solution saturated with nitrogen)
a: before irradiation, b: 30 min, c: 60 min, d: 90 min, e: 120 min.

analysis are shown in Table 3. 2-Hydroxynicotinamide was identified in the photo-product from nicotinamide, but the rate of its formation was much smaller compared with 2-hydroxy-3-cyanopyridine and 2-hydroxynicotinic acid.

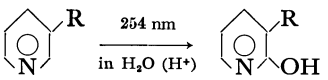

R=COOH, CN, $CONH_2$

The photo-hydroxylation of nicotinic acid was quenched by oxygen. Oxygen not only inhibited the formation of 2-hydroxynicotinic acid, but also diminished remarkably the transformation of nicotinic acid. This indicates that the photoreaction is ascribed to the triplet state.

In order to obtain further information on the photo-hydroxylation, the pH dependence of the reaction was investigated on nicotinic acid and 3-cyanopyridine (Figs. 3 and 4). In addition, is shown the pH dependence of either λ_{max} of UV-absorption (for nicotinic acid) or the molecular extinction coefficient (for 3-cyanopyridine) of the starting materials. They inform of the form of the substances in solutions. In both

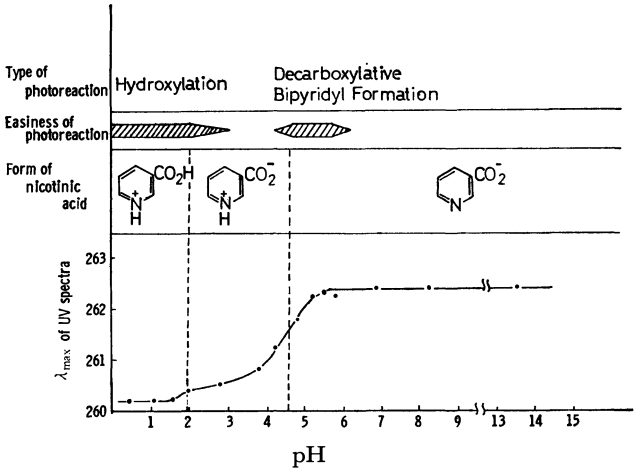

Fig. 3. pH dependence of the photoreaction and λ_{max} of nicotinic acid in aqueous solutions

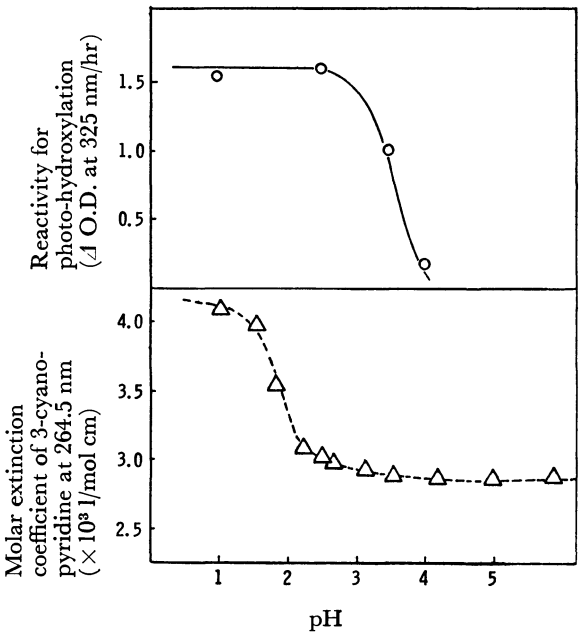

Fig. 4. pH dependence of the reactivity for photo-hydroxylation and the molar extinction coefficient (at 264.5 nm) of 3-cyanopyridine
UV-Irradiation: 5×10^{-4} mol/l under nitrogen
Measurement of UV-absorption: 10 fold dilution

Table 4. Photoreactions of nicotinic acid and its derivatives in acidic ethanol solutions
(Concentration of HCl, 0.1 mol/l)

Compound	Reaction Condition	Product	Yield
Nicotinic acid	5×10^{-4} mol/l	4-Ethylnicotinic acid	85%
	LP[a])-17 W	Recovered starting	
	10 min	material	0%
3-Cyanopyridine	10^{-2} mol/l	6-Ethyl-3-cyanopyridine	10%
	LP-100 W	4,6-Diethyl-3-cyanopyridine	6%
	15 hr	Ethyl nicotinate	5%
		Recovered starting material	13%
Ethyl nicotinate	10^{-2} mol/l	Ethyl 6-ethylnicotinate	30%
	LP-170 W	Recovered starting material	34%
	3 hr		

a) LP: Low pressure mercury lamp

cases, the change of chemical form correlates well to that of photoreactivity. Since pK_a value of the protonated nicotinic acid is 2.07, photo-hydroxylation is considered to occur in pyridinium form.

It has been reported that in several pyridine derivatives such as quinoline and acridine, the basicity of the lowest singlet excited state differes by 10^5 from that of the ground state, whereas the basicity of the lowest triplet state is similar to that of the ground state.[8,9] If the photo-hydroxylation derives from the excited singlet state and the lifetime of the excited state is long enough to permit the proton transfer before reaction, the pH range for the photo-hydroxylation should be much wider than our results indicate. This fact also supports that the triplet state is responsible for the photo-hydroxylation. The photo-hydroxylation is thus characteristic for the triplet state of the cationic form of nicotinic acid and its derivatives.

For photo-hydroxylation, the electron attracting group at the pyridine nucleus is essential. Pyridine and the zwitterion form of 3-carboxy-1-methylpyridinium do not undergo photo-hydroxylation.[2] 2-Pyridinecarboxylic acid also shows similar photoreactivity.[1a]

The photoreaction of nicotinic acid and its derivatives in acidic ethanol solutions are summarized in Table 4. The dominant photoreaction of the cationic form of nicotinic acid and its derivatives is the substitution on the pyridine nucleus introducing an ethyl group.

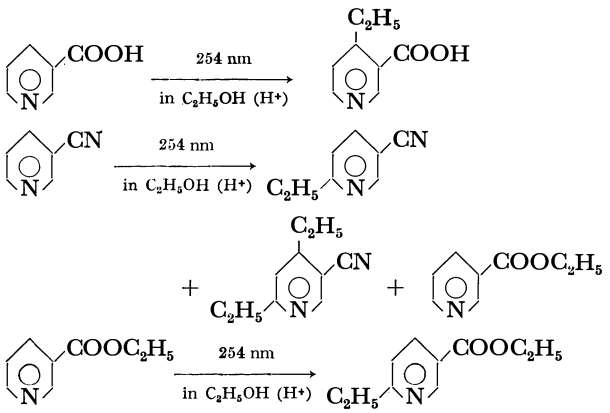

The position of substitution is dependent on the functional group attached to the pyridine nucleus. Nicotinic acid gives 4-ethylnicotinic acid, while ethyl nicotinate is ethylated at 6-position. The UV-irradiation of 3-cyanopyridine yields 6-ethyl- and 4,6-diethyl-3-cyanopyridines. In the photo-ethylation of 3-cyanopyridine, ethylation at 6-position is the initial photoreaction, because at lower conversion, 6-ethyl-3-cyanopyridine was the dominant ethylation product. In the prolonged UV-irradiation of nicotinic acid in acidic methanol, 4-methyl- and 4,6-dimethylnicotinic acids were obtained.

Photo-ethanolysis of nitrile was observed in 3-cyanopyridine. In our reaction condition, ethyl nicotinate was not formed without UV-irradiation.

Photo-alkylation has been reported for several *N*-heteroaromatic compounds such as pyridine,[10] quinoline,[11,12] phenanthridine,[13] and pyrimidine.[14] Similarly to other *N*-heteroaromatic compounds, photo-ethylation of nicotinic acid and its derivatives would be initiated by the hydrogen abstraction from ethanol by N atom of the π-π^* excited state of nicotinic acid, followed by the combination of monohydrogenated nicotinic acid and 1-hydroxyethyl radicals and finally dehydration by acid.

In neutral ethanol solution, 3-cyanopyridine and ethyl nicotinate gave 6-(1-hydroxyethyl) derivative in UV-irradiation, but in lower yield, in comparison with in photo-ethylation in acidic solution. Natsume *et al.* obtained only addition product in UV-irradiation in methanol.[3] We identified the aromatized product. This behavior is similar to that of quinoline reported by Stermitz *et al.*[12]

Photoreactions in Alkaline Solutions. The high photo-stability of nicotinic acid and its derivatives in strongly alkaline aqueous solutions is remarkable. Nicotinic acid and nicotinamide were satisfactorily recovered after comparatively long irradiation (Table 6). 3-Cyanopyridine is also resistant to UV-irradiation, but a part of it is hydrolyzed thermally to nicotinamide.

In contrast to the behavior in aqueous solutions, nocitinic acid undergoes photo-decarboxylation in basic ethanol solution.

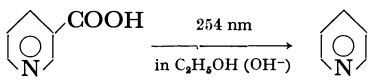

The corresponding photoreaction in aqueous solution would be the decarboxylative bipyridyl formation accompanying the formation of a trace of pyridine in

Table 5. Photoreactions of nicotinic acid derivatives in ethanol solutions

Compound	Reaction condition	Product	Yield
3-Cyanopyridine	10^{-2} mol/l	6-(1-Hydroxyethyl)-	
	LP-[a] 17 W	3-cyanopyridine	16%
	15 hr	Recovered starting material	10%
Ethyl nicotinate	7×10^{-3} mol/l	Ethyl 6-(1-hydroxyethyl)-	
	LP-17 W	nicotinate	8%
	2 hr	Recovered starting material	53%

a) LP: Low pressure mercury lamp

Table 6. Photoreactions of nicotinic acid and its derivatives in alkaline aqueous solutions (pH: 13—14)

Compound	Reaction condition	Recovery
Nicotinic acid	5×10^{-4} mol/l	82%
	LP[a]-17 W	
	200 min	
3-Cyanopyridine	5×10^{-4} mol/l	77%
	LP-17 W	
	120 min	
Nicotinamide	5×10^{-4} mol/l	90%
	LP-17 W	
	120 min	

a) LP: Low pressure mercury lamp

the comparatively small pH range from 4 to 6 (Fig. 3).

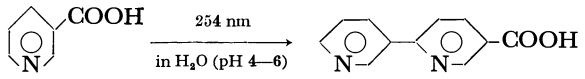

The pH dependence of the photochemical bipyridyl formation indicates that the reaction is initiated by the excitation of the anionic form of nicotinic acid (pK_a value of nicotinic acid is 4.81 at 25 °C). This photoreaction involves probably the attack of pyridyl carbanions formed by the decarboxylation of nicotinate ions to the positively charged 6-position of the ground state nicotinate ions.

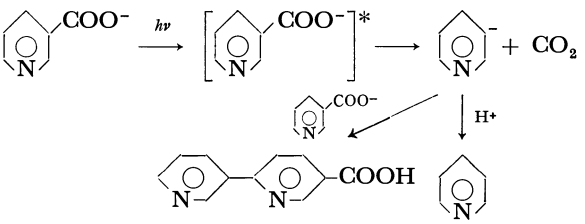

CNDO/2 Considerations of the Photoreactivity. Some of the photoreactivities of nicotinic acid can be reasoned on the basis of CNDO/2 consideration.

Electronic State of the Cationic Form of Nicotinic Acid. The electronic configurations of π-orbitals near highest occupied and lowest vacant levels as well as the total electron density of π-π^* state of the cationic form of nicotinic acid are shown in Fig. 5. Photo-hydroxylation occurs at 2-position with the greatest positive charge in π-π^* state. This suggests that the photosubstitution proceeds *via* nucleophilic attack of water toward the positively charged 2-position of excited nicotinic acid, although the mechanism of photohydroxylation has not yet been elucidated.

Photo-ethylation is considered to be initiated by the

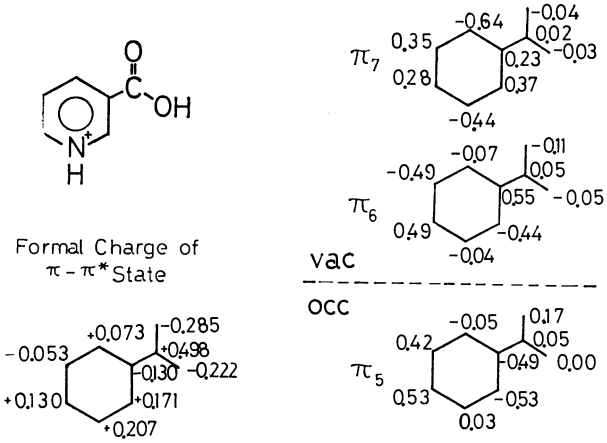

Fig. 5. Electronic states of nicotinic acid in pyridinium form

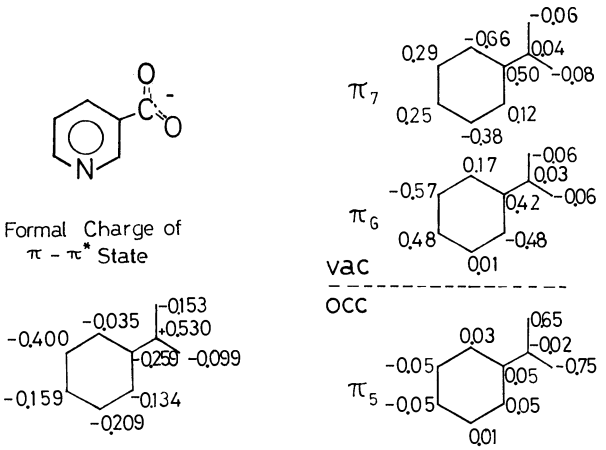

Fig. 6. Electronic states of nicotinic acid in anionic form

hydrogen abstraction by the N atom of excited nicotinic acid. This behavior can not be reasoned by the CNDO/2 calculation, because the free valence of nicotinic acid cation at N atom is not large.[15]

Electronic State of Anionic Form of Nicotinic Acid. The electronic configurations of π-orbitals (π_5, π_6, and π_7) are shown in Fig. 6. In this case, it is remarkable that one electron localized at carboxylate group in highest occupied level is promoted to π_7, where the electron is localized only in the pyridine ring. This electronic promotion could be schematically expressed in the following way;

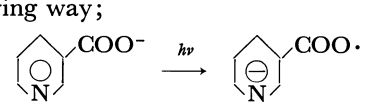

In analogy with benzoyloxy radicals, the excited

nicotinate anion would be easily decarboxylated.

The photo-decarboxylation of nicotinic acid in alkaline ethanol solution and the decarboxylative bipyridyl formation can be interpreted well in terms of CNDO/2 calculation.

Concerning the photoreactivity of the excited nicotinate anion, the following problems remain unsolved:

i) Why does the excited nicotinate anion become photo-resistant in strongly alkaline aqueous solution?

ii) Why does the excited nicotinate anion give bipyridyl derivative instead of pyridine in aqueous solution, in which the protonation of pyridyl carbanion is more favorable than in ethanol solution?

The authors wish to thank Mr. Humitaka Miyazawa and Miss Harumi Nakazawa for their experimental assistance. They are grateful to Prof. Shigeo Nishimura and Mrs. Michiko Tsuchimoto for the measurement of NMR spectra and to Nihon Denshi Co. for the careful measurement of double resonance spectra.

References

1) a) Part III: H. Kurokawa, T. Furihata, F. Takeuchi, and A. Sugimori, *Tetrahedron Lett.*, **1973**, 2623. b) Preliminary report; F. Takeuchi, T. Fujimori, and A. Sugimori, This Bulletin, **43**, 3637 (1970).

2) S. Y. Wang, *Biochemistry*, **7**, 3740 (1968).

3) M. Natsume and M. Wada, *Tetrahedron Lett.*, **1971**, 4503.

4) C. Azuma and A. Sugimori, *Kogyo Kagaku Zasshi*, **72**, 239 (1969).

5) E. C. Taylor and A. J. Crovetti, *J. Org. Chem.*, **19**, 1633 (1954).

6) H. L. Bradlow and C. A. V. Werf, *ibid.*, **14**, 509 (1949).

7) W. G. Robinson and R. H. Hook, *J. Biol. Chem.*, **239**, 4257 (1964).

8) G. Jackson and G. Porter, *Proc. Roy. Soc. Ser. A*, **260**, 13 (1961).

9) A. Weller, *Z. Elektrochem.*, **61**, 1956 (1957).

10) E. F. Travecedo and V. I. Sternberg, *Chem. Commun.*, **1970**, 609.

11) F. R. Stermitz, C. C. Wei, and W. H. Huang, *ibid.*, **1968**, 482.

12) F. R. Stermitz, C. C. Wei, and C. M. O'Donnell, *J. Amer. Chem. Soc.*, **92**, 2745 (1970).

13) F. R. Stermitz, R. P. Seiber, and D. E. Nicoden, *J. Org. Chem.*, **33**, 1136 (1968).

14) M. Ochiai, E. Mizuta, Y. Asahi, and K. Morita, *Tetrahedron*, **24**, 5861 (1968).

15) The contribution of π_7 state to the character of excited nicotinic acid (in pyridinium form) can explain the photoreactivity of nicotinic acid both in aqueous and in ethanol solutions. In π_7 state, the electron density at 2-position is low and the partial free valence at N is large.

Photochemistry of Heterocyclic Compounds. VI. The Photochemical Behavior of Phenazine in Hydroxylic Solvents[1]

Shigeo WAKE, Yoshio OTSUJI, and Eiji IMOTO

Department of Applied Chemistry, College of Engineering, University of Osaka Prefecture, Sakai-shi, Osaka 591

(Received January 21, 1974)

The photochemical behavior of phenazine in acidified hydroxylic solvents varied with the concentration of acids present in the solutions. Irradiation of phenazine in an aqueous phosphoric acid afforded a 1 : 1 mixture of phenazinium and 1-hydroxyphenazinium cation radicals which were converted to a mixture of phenazine and 1-hydroxyphenazine. Irradiation in moderately strongly acidified alcohols (0.1—1.0 M HCl in alcohols) or in acetic acid containing 0.1 M *p*-toluenesulfonic acid yielded a 1 : 1 mixture of phenazine and the corresponding 1-alkoxyphenazines or 1-acetoxyphenazine after work-up of the reaction mixture. On the other hand, irradiation in a very strongly acidified methanol (5.6—9.6 M HCl in methanol) gave only the phenazinium cation radical. Mechanistic studies revealed that in the moderately strongly acidified media the reaction proceeds through a solvent-addition to the excited singlet phenazinium monocation, and in the very strongly acidified methanol the reaction proceeds through an electron transfer from the solvent to the excited singlet phenazinium dication.

The photochemistry of phenazine has received considerable attention. Toromanoff[2] has shown that irradiation of phenazine in deaerated alcohols gives 5,10-dihydrophenazine. Koizumi and co-workers[3] have proposed that the photoreduction of phenazine in alcohols occurs through a hydrogen abstraction from the higher n, π^* triplet state. However, Davis and co-workers[4] have presented evidence that a reactive state of the photoreduction is the n, π^* singlet state.

Recently, Bailey, Roe, and Hercules[5] have studied the photochemistry of phenazine in acidified methanol. They have concluded on the basis of spectroscopic evidence that in very weakly acidified media (acetate buffers in methanol), phenazine is reduced to 5,10-dihydrophenazine through the lowest n, π^* singlet state. They have also shown that in moderately strongly acidified media (0.1—1.0 M HCl in methanol), phenazine gives the green phenazinium cation radical, which is produced by the reaction of 5,10-dihydrophenazine with phenazinium cation, through the lowest excited singlet state. However, the structure of the photoproducts was deduced only from electronic and ESR spectra of the reaction mixtures, and no unequivocal evidence for the structures was given in their investigation.

We have recently investigated the photochemistry of phenazine in detail and have found that the photochemical behavior of phenazine in hydroxylic solvents is strongly dependent on the concentration of acids present in the solutions. For example, we obtained a mixture of phenazinium and 1-methoxyphenazinium cation radicals upon irradiation of phenazine in moderately strongly acidified methanol (0.1—1.0 M HCl in methanol). However, in the photoreaction in very strongly acidified methanol (5.6—9.7 M HCl in methanol), the photoreduction took place to give the phenazinium cation radical. In this paper, the results accumulated so for are summarized and the mechanisms are proposed on the basis of informations obtained from kinetic studies of these photochemical reactions.

Results

Photoreactions in Moderately Strongly Acidified Solutions. When a 2.8×10^{-3} M solution of phenazine (I) in 2 M aqueous phosphoric acid was irradiated with a high-pressure mercury lamp under nitrogen atmosphere, a green solution containing green precipitates was produced. Oxidation of the green reaction mixture with air or other oxidizing agents, followed by neutralization of the resulting solution, gave 1-hydroxyphenazine (IIa) accompanied by the starting material. Irradiation of I in various alcohols acidified with 0.1 M *p*-toluenesulfonic acid and similar work-up of the reaction mixture afforded a mixture of I and the corresponding 1-alkoxyphenazines (IIb—IId). Similarly, the photoreaction of I in acetic acid containing *p*-toluenesulfonic acid yielded 1-acetoxyphenazine (IIe). These photochemical solvent-addition reactions were not observed upon irradiation in the absence of acids. The results are summarized in Table 1.

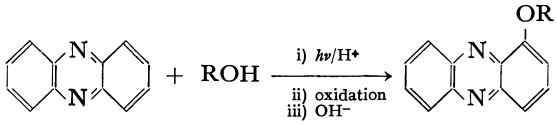

IIa, R=H
b, R=CH_3
c, R=C_2H_5
d, R=i-C_3H_7
e, R=CH_3CO

The structure of the photoproducts was confirmed by comparison with the respective authentic samples or by the spectroscopic data.

Quantitative studies of these photoreactions were then preformed. When I was irradiated in 2 M phosphoric acid, the yield of IIa increased with increasing irradiation time.

However, the molar ratio of IIa to I in the reaction mixture reached a plateau, which was very close to unity, upon prolonged irradiation under nitrogen atmosphere as shown in Table 1. Irradiation under air brought about a decrease in the recovery of I (14%) and an increase in the yield of IIa (81%). IIa was surprisingly stable under the reaction conditions; ir-

TABLE 1. PHOTOCHEMICAL ADDITION OF SOLVENTS[a]

Solvents	ml	Irrad. time, hr	Recovered starting material, %	Compd.	Products yield,[b] %	Ratio[c]
H_2O, 2M H_3PO_4	200	7	52	IIa	45	0.9
H_2O, 2M H_3PO_4	200	48	53	IIa	47	0.9
H_2O, 2M HCl	50	7	76	IIa	19	0.3
MeOH, 0.1M TsOH[d]	50	7	65	IIb	26	0.4
MeOH, 0.1M HCl	50	7	57	IIb	32[e]	0.6
EtOH, 0.1M TsOH[d]	50	7	70	IIc	16	0.2
i-PrOH 0.1M TsOH[d]	100	7	82	IId	4	0.05
AcOH, 0.1M TsOH[d]	50	7	75	IIe	19[f]	0.2

a) A 100 mg of phenazine was irradiated under N_2 atmosphere. b) Based on total amount of the starting material. c) The molar ratio of the product to phenazine found in the reaction mixture. d) *p*-Toluenesulfonic acid. e) Irradiation was carried out in the presence of air. f) The yield of IIe was estimated as that of IIa obtained by hydrolysis.

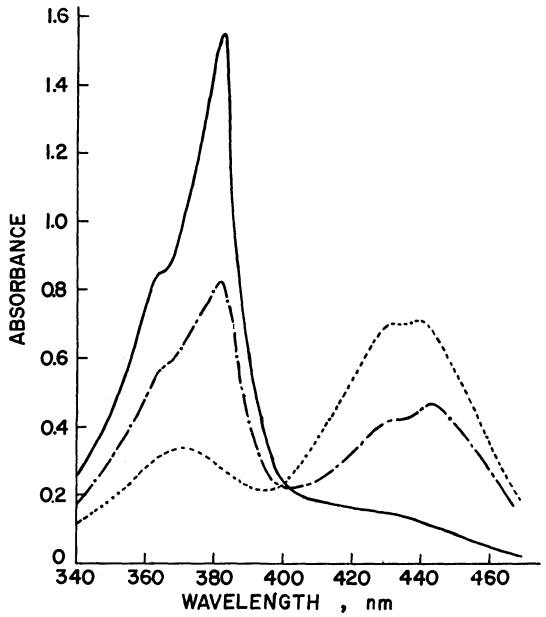

Fig. 1. Spectral change during irradiation of 7.0×10^{-5}M solution of phenazine in 2 M H_3PO_4: ——, before irradiation; ·····, irradiation for 20 min; ------, irradiation for 1.5 hr.

radiation of IIa in 2 M phosphoric acid for 7 hr under air resulted in the recovery of the starting material in a quantitative yield.

The change in the absorption spectrum during the photoreaction was also examined. A solution of I in 2 M phosphoric acid in a quartz cell was irradiated after degassing by a freeze-pump-thaw cycle method. The result is shown in Fig. 1. The spectral change almost ceased after irradiation for 1.5 hr. The spectrum recorded after irradiation for 1.5 hr was identical in shape with that of phenazinium cation radical (III) prepared by the method similar to that of Fellion and Uebersfeld.[6] Furthermore, the green precipitates obtained by the photoreaction displayed the same IR and electronic spectra as those of the green species which was produced by treatment of a mixture of I and IIa in dioxane containing 2 M phosphoric acid with an aqueous solution of sodium hydrosulfite (the green species produced by this treatment in the dark gave a mixture of I and IIa after oxidation and neutralization).

The ESR spectrum of the green precipitate obtained by the photoreaction exhibited the same *g*-value (2.003) as that of the known ESR spectrum of III previously reported.[7]

These observations strongly suggest that the product primarily formed by the photoreaction of I in 2 M phosphoric acid consists of a 1:1 mixture of III and 1-hydroxyphenazinium cation radical (IV), which affords I and IIa upon oxidation and neutralization. The green species, the primary products, obtained by the photoreactions of I in solvents other than water are therefore supposed to be a 1:1 mixture of III and the respective 1-alkoxyphenazinium cation radicals (V) or 1-acetoxyphenazinium cation radical (VI).

Photoreactions in Very Strongly Acidified Solutions. When I was irradiated in HCl-saturated methanol, the green solution was obtained. The absorption spectrum of this green solution was very similar to that obtained by the photoreaction of I in 0.1 M HCl–methanol. However, work-up of this green solution resulted in a complete recovery of the starting material and no IIb could be detected. These results indicate that in HCl-saturated methanol, the photoreduction of I to give III takes place preferentially over the photochemical solvent-addition reaction.

Mechanistic Studies. Deoxygenated solutions of I in water or methanol containing various concentrations of acids in a 1 cm optical cell were irradiated with a high-pressure mercury lamp fitted with a cut-off filter which transmitted >310 nm light. At appropriate time intervals, the spectra of the solutions were recorded.

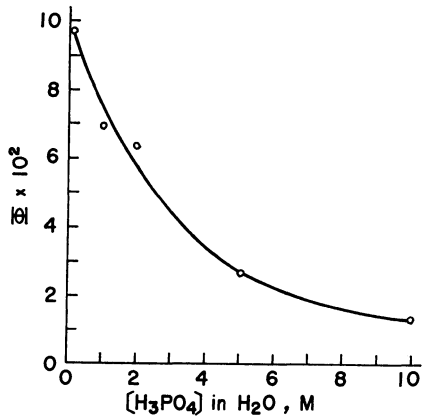

Fig. 2. Quantum yields for the formation of a 1:1 mixture of III and IV as a function of the acid concentrations upon irradiation of I in aqueous phosphoric acid. Initial concentrations of I were 7.22×10^{-5}—6.07×10^{-5}M. The quantum yield at 7.0×10^{-5}M of I in 0.1 M H_3PO_4 was estimated by using the relationship of Eq. (9), coupled with the quantum yields in Table 2 (Φ=0.08 at 4.21×10^{-5}M of I and Φ=0.071 at 3.25×10^{-5}M of I).

For each reaction the 380 nm band of I decayed with production of the 430 nm band as has been shown in Fig. 1. For calculations of the rates of formations of the products, it was considered that the 430 nm band was of a mixture of the cation radicals (III+IV or III+V) or of the single phenazinium cation radical (III) depending on the concentration of acids. The rates were then converted to the quantum yields by use of the potassium ferrioxalate actinometer.[8]

Photoreactions in Aqueous Media. Variation of the quantum yields for the formation of a mixture of the cation radicals III and IV with the concentrations of phosphoric acid was investigated. The quantum yields decreased with increase of the concentrations of acid in a fashion depicted in Fig. 2. Dependence of the quantum yields on the concentrations of I in 2 M phosphoric acid was also studied. The results are summarized in Table 2. A plot of reciprocal quantum yields *vs.* reciprocal concentrations of I gave a straight

Table 2. Quantum yields for hte formation of a 1:1 mixture of the cation radicals III and IV upon irradiation of I in aqueous phosphoric acid

Concn. of I, M	Concn. of H_3PO_4, M	Quantum yield
4.21×10^{-5}	0.1	0.080
3.25×10^{-5}	0.1	0.071
7.22×10^{-5}	1.0	0.069
7.67×10^{-5}	2.0	0.065
7.00×10^{-5}	2.0	0.063
7.00×10^{-5}	2.0	0.062
5.15×10^{-5}	2.0	0.056
2.85×10^{-5}	2.0	0.049
6.07×10^{-5}	5.0	0.027
6.80×10^{-5}	10.0	0.013
6.07×10^{-5}[a]	10.0	0.013

a) Irradiation was carried out in the presence of air.

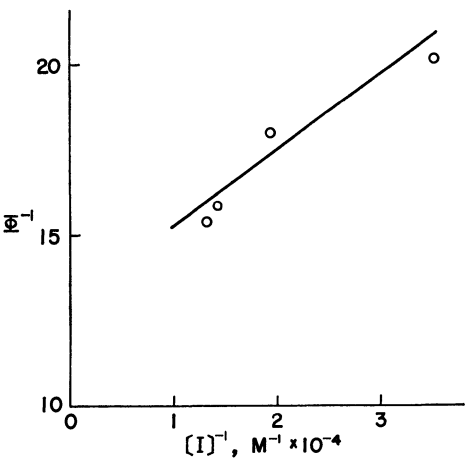

Fig. 3. Dependence of the quantum yields for the formation of a 1:1 mixture of III and IV on the concentrations of I in 2 M H_3PO_4.

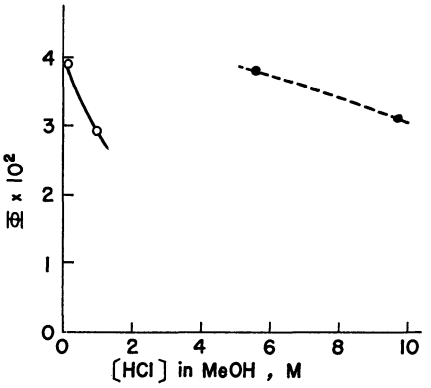

Fig. 4. Quantum yields for the product formation as a fuction of the acid concentrations upon irradiation of I in HCl–methanol: ——, the product is a 1:1 mixture of III and Va; ------, the product is III.

line as shown in Fig. 3. No quenching was observed with air under a wide variety of reaction conditions (Table 2).[9]

Photoreactions in Acidified Methanol. The quantum yields for the formation of the cation radicals were measured as a function of the concentrations of HCl. The result is shown in Fig. 4. The quantum yields varied with variation of the acid concentrations in such

Table 3. Quantum yields for the formation of the photoproducts upon irradiation of I in acidified methanol

Concn. of I, M	Concn. of HCl, M	Additive, M	Quantum yield
6.22×10^{-5}	0.1		0.039[a]
7.56×10^{-5}	0.1	1,2-DBE,[c] 0.01	0.041[a]
6.36×10^{-5}	1.0		0.029[a]
6.36×10^{-5}	1.0	1,2-DBE,[c] 0.01	0.029[a]
6.73×10^{-5}	5.6		0.038[b]
3.66×10^{-5}	5.6		0.047[b]
6.42×10^{-5}	9.7		0.031[b]
6.11×10^{-5}	9.7	1,2-DBE,[c] 0.01	0.032[b]

a) The product is a 1:1 mixture of the cation radicals III and Va. b) The product is phenazinium cation radical III. c) 1,2-DBE represents 1,2-dibromoethane.

a manner that a minimum is produced at an intermediate concentration of the acid. Furthermore, the quantum yields for the formation of III at the high concentration of the acid (5.6 M HCl in methanol) decreased with increase of the concentrations of I as shown in Table 3. This result is in sharp contrast with the result of the photoreactions in 2 M phosphoric acid, where the photoproduct was the mixed cation radicals and the quantum yields for their formation increased with increase of the concentrations of I.

Quenching experiments employing 1,2-dibromoethane as a quencher were also performed. Essentially no quenching was observed as recognized from the results shown in Table 3.

Discussion

Phenazine (I) undergoes the solvent-addition reaction or the reduction reaction, depending on the concentration of acids, upon irradiation in acidified hydroxylic solvents.

$$P + H^+ \xrightarrow{h\nu,\ k_1} {}^1PH^{+*} \text{ (excitation and protonation)} \quad (1)$$

$$PH^+ \xrightarrow{h\nu,\ k_2} {}^1PH^{+*} \text{ (excitation)} \quad (2)$$

$${}^1PH^{+*} + H^+ \xrightarrow{k_3} {}^1PH_2^{2+*} \text{ (excited state protonation)} \quad (3)$$

$${}^1PH^{+*} + ROH \xrightarrow{k_4} PHOR + H^+ \text{ (photoreaction; solvent-addition)} \quad (4)$$

$$PHOR + P \xrightarrow{k_5} PH\cdot + POR\cdot \text{ (radical formation)} \quad (5)$$

$$PHOR + PH^+ \xrightarrow{k_6} PH\cdot + POR\cdot + H^+ \text{ (radical formation)} \quad (6)$$

$$PH\cdot + H^+ \xrightarrow{k_7} PH_2^+\cdot \text{ (radical protonation)} \quad (7)$$

$$ROR\cdot + H^+ \xrightarrow{k_8} PHOR^+\cdot \text{ (radical protonation)} \quad (8)$$

where P = 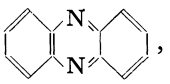 , I

PH^+ = 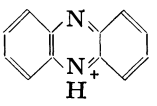 ,

PH_2^{2+} = 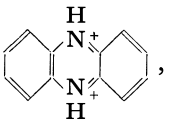 ,

PHOH = 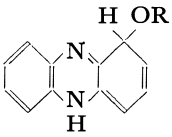 or 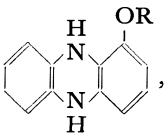 ,

$PH\cdot$ = 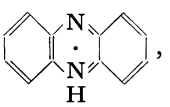 , $POR\cdot$ = 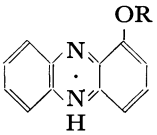 ,

$PH_2^+\cdot$ = 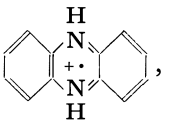 , III; $PHOR^+\cdot$ = 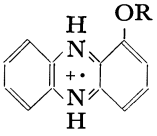 , IV, V or VI

Scheme 1.

Photoreactions in Moderately Strongly Acidified Media. The pathway represented in Scheme 1 is proposed for the photochemical solvent-addition reactions which occur upon irradiation of I in moderately strongly acidified hydroxylic solvents (in Scheme 1, all the intersystem crossing and radiationless deactivation processes of excited species, which have no immediate relation to the chemical reactions, are omitted).

The pK_a of the ground state of I has been reported to be 1.23 in water[10] and to be 4.5 in methanol.[5] Thus, in aqueous phosphoric acid (the first pK_a of phosphoric acid in water is 1.04 at 18 °C), I exists either in the neutral form or in the form of monoprotonated phenazinium cation (PH^+). In acidified methanol containing HCl more than 0.1 M, I exists almost exclusively in the form of PH^+.

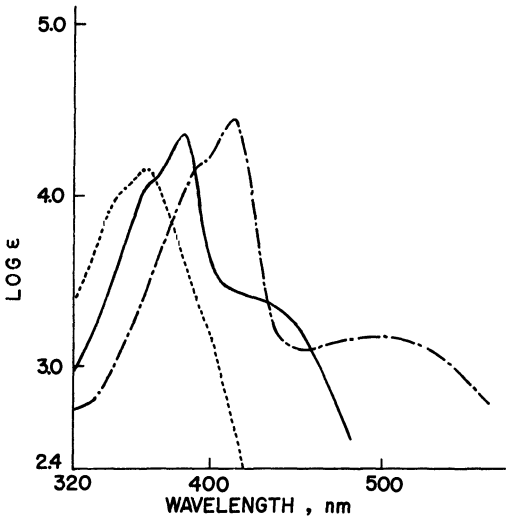

Fig. 5. Absorption spectra of phenazine: ------, in methanol; ——, in aqueous 10 M phosphoric acid; -·-·-, in concentrated sulfuric acid.

The pK_a^* of the lowest excited singlet state of I is expected to be much higher than the corresponding ground state pK_a judging from the fact that the absorption spectrum of I shifts to longer wavelength in acidified media than in neutral media as shown in Fig. 5. It is therefore reasonable to suppose that in the excited singlet state I exists predominantly in the form of phenazinium cation even in relatively weakly acidified media.[11]

We thus propose that the excited monoprotonated phenazinium cation (PH^{+*}) is a reactive species for the photochemical solvent-addition reactions to I. This proposal was derived further from the following arguments.

Firstly, the nonprotonated species is immediately disqualified as a reactive species from the fact that the solvent-addition reactions did not take place in neutral media. Secondly, let's consider variation of proportion of PH^{+*} as a function of the acid concentration. The proportion of PH^{+*} will decrease with increasing the proportion of the excited diprotonated species (PH_2^{2+*}) which would presumably be produced in the presence of the higher concentrations of acids (see also later). Therefore, if PH^{+*} is the reactive species, the quantum

yield for the formation of a mixture of the cation radicals, $PHOR^{+}\cdot$ and $PH_2^{+}\cdot$, is expected to decrease at such higher concentrations of acids as to bring the formation of $PH_2^{2+}*$ predominant. This is exactly the results shown in Figs. 2 and 4. Quenching experiments performed by employing 1,2-dibromoethane and air as quenchers (Tables 2 and 3) suggest that the excited singlet is the reactive state, which is consistent with the conclusion reached by Bailey and co-workers[5] for the photoreactions of I in acidified methanol. An application of the steady state assumption regarding the transient species, $^1PH^{*1}$, $^1PH_2^{2+*}$, PHOR, $PH\cdot$, and $POR\cdot$, in Scheme 1 leads to the relationship of Eq. (9) under the conditions where the concentration of acids is constant:

$$1/\Phi = A/[P] + B \quad (9)$$

where [P] is the concentration of I present in the reaction mixture, which will be roughly equal to the concentration of I initially added, and the coefficients, A and B, are of constant values. The relationship depicted in Fig. 3 is in accordance with this equation.

Photoreactions in Very Strongly Acidified Media. The photoreaction of I in methanol containing HCl more than 5.6 M gave only phenazinium cation radical, $PH_2^{+}\cdot$. A proposed mechanism for this photoreduction is shown in Scheme 2 (in this scheme, all the intersystem crossing and deactivation processes of the excited species, which have no immediate relation to the chemical reactions, are also omitted, as does in Scheme 1).

$$PH^{+} \xrightarrow{h\nu,\, k_1} {}^1PH^{+}* \text{ (excitation)} \quad (2)$$

$$^1PH^{+}* + H^{+} \xrightarrow{k_3} {}^1PH_2^{2+}* \text{ (excited state protonation)} \quad (3)$$

$$^1PH_2^{2+}* + PH^{+} \xrightarrow{k_{10}} 2PH^{+} + H^{+}$$
(quenching of the excited protonated species) (10)

$$^1PH_2^{2+}* + CH_3OH \xrightarrow{k_{11}} PH_2^{+}\cdot + CH_3OH^{+}\cdot$$
(photoreaction; electron transfer) (11)

where all symbols are the same as those in Scheme 1.

Scheme 2.

The absorption spectrum of I in methanol containing 9.7 M HCl indicated that a predominant form of I in its ground state in this medium was PH^{+}. But the pK_a* for the second protonation at the excited singlet state to form the excited diprotonated phenazinium dication ($PH_2^{2+}*$) is again expected to be much higher than the corresponding second pK_a at the ground state judging from the magnitude of the spectral shift observed in the concentrated sulfuric acid (see Fig. 5). Therefore, the excited phenazine may possibly exist in the form of $PH_2^{2+}*$ at higher concentrations of acids.

The electron transfer reaction to $PH_2^{2+}*$ from solvent would produce phenazinium cation radical ($PH_2^{+}\cdot$) as represented in the reaction (11) of Scheme 1. The observation that in the presence of higher concentrations of acids, $PH_2^{+}\cdot$ was produced only in methanol but not in water strongly supports this electron transfer mechanism; the electron transfer from water to the substrate would be unfavorable under the reaction conditions. Noteworthy is in this connection the behavior of diazaheteroaromatic diquaternary salts. Curphey[13] has reported that 1,4-diethylpyrazinium difluoroborate is converted to its cation radical upon dissolving in ethanol. This observation implies that dications of diazaheteroaromatic compounds possess enough ability to abstract an electron from an alcohol even in the dark owing to their high electron deficiency caused by an accumulation of two positive charges.

The result that the quantum yields for the formation of $PH_2^{+}\cdot$ increased with decrease of the initial concentrations of I suggests that $PH_2^{2+}*$ may effectively be quenched by PH^{+}.

Lack of quenching by 1,2-dibromoethane again suggests that the excited singlet state ($^1PH_2^{2+}*$) is a reactive state for the photochemical reduction of I in very strongly acidified methanol.

Experimental

Unless otherwise indicated, irradiations were carried out with a Taika 100 W high-pressure immersion mercury lamp at room temperature.

Materials. Phenazine (I) was prepared by the method of Wohl and Aue.[14] Purification was performed by column chromatography on acidic alumina using benzene as an eluent, followed by recrystallization from EtOH, mp 171—172 °C.

All other chemicals were of commercial origin and were usually used after purification by distillation or recrystallization. Water was purified by redistillation of deionized water.

Preparation of the Authentic Samples. 1-Hydroxyphenazine (IIa), mp 156—158 °C, and 1-methoxyphenazine (IIb), mp 166—167 °C, were prepared by the method of Surrey.[15] 1-Acetoxyphenazine (IIe) was prepared by the reaction of IIa and acetic anhydride in pyridine, and purified by recrystallization from MeOH, mp 119—120 °C; NMR ($CDCl_3$) δ 2.58 (s, 3H, $-CH_3$), 7.50—8.38 (m, 7H, aromatic H).

The structure of the photoproducts was identified by the mixed melting point test and by the comparison of IR spectra of the products with those of the corresponding authentic samples unless otherwise indicated.

Irradiation of I in Aqueous 2 M H_3PO_4 Solution. I (100 mg, 0.56 mmol) in aqueous 2 M H_3PO_4 solution (200 ml) was placed in a quartz vessel and N_2 was bubbled for 20 min. Irradiation was then carried out for 7 hr with bubbling N_2. Green solid (A) deposited was collected by filtration. The filtrate was allowed to stand overnight under air, while the color of the solution turned from green to red. The solution was then neutralized with Na_2CO_3 and extracted with ether. The ether solution was extracted with 10% NaOH until no more purple color moved to aqueous layer, and then the ether layer was dried over Na_2SO_4. Distillation of the ether gave 17 mg of the unchanged I. The combined aqueous extracts were made faintly acid with dilute HCl, and again extracted with ether. The ether extract was dried over Na_2SO_4, and then concentrated by distillation to give 34 mg of IIa which was recrystallized from EtOH–H_2O, mp 156—158 °C. The green solid A was dispersed in aqueous EtOH and oxidized with $K_3Fe(CN)_6$. Work-up of the resulting solution by the procedure similar to that described above gave 35 mg of I and 15 mg of IIa.

Irradiation of I in Acidified Methanol. A mixture of I (100 mg, 0.56 mmol) and *p*-toluenesulfonic acid monohydrate

(1 g, 5.3 mmol) in dry MeOH (50 ml) was placed in a quartz vessel, and N_2 was bubbled for 20 min. After irradiation for 7 hr under N_2, $K_3Fe(CN)_6$ in H_2O was added until the solution turned into yellow. The solution was evaporated to dryness under reduced pressure. The residue was neutralized with 5% Na_2CO_3 and then extracted with ether. The extract was dried over Na_2SO_4, and the ether was removed by distillation The residue was chromatographed on alumina. Elution with benzene yielded 65 mg (65%) of unchanged I. Elution with benzene–EtOH (10: 1) yielded 30 mg (26%) of IIb, which was recrystallized from EtOH–H_2O to give the analytical sample, mp 166—167.5 °C.

I (100 mg, 0.56 mmol) in dry MeOH (50 ml) containing 0.1 M HCl was also irradiated for 7 hr under air. Similar work-up of the reaction mixture gave 57 mg (57%) of I and 37 mg (32%) of IIb.

Irradiation of I in Acidified Ethanol. A mixture of I (100 mg, 0.56 mmol) and *p*-toluenesulfonic acid monohydrate (1 g, 5.3 mmol) in dry EtOH (50 ml) was irradiated under N_2 for 7 hr. Work-up of the reaction mixture by the method similar to that described above gave 70 mg (70%) of I and 20 mg (16%) of 1-ethoxyphenazine (IIc) which was recrystallized from EtOH–H_2O to give the analytical sample, mp 126—127 °C (lit,[16] mp 130 °C); picrate, mp 188—190 °C (lit,[16] mp 195 °C). Found: C, 75.10; H, 5.32; N, 12.57%. Calcd for $C_{14}H_{12}N_2O$: C, 74.99; H, 5.38; N, 12.49%.

Irradiation of I in Acidified 2-Propanol. A mixture of I (100 mg, 0.56 mmol) and *p*-toluenesulfonic acid monohydrate (2 g, 10.6 mmol) in dry i-PrOH (100 ml) was irradiated under N_2 for 7 hr. Work-up of the reaction mixture similar to that described above gave 82 mg (82%) of I and 5 mg (4%) of 1-isopropoxyphenazine (IId) which was recrystallized from EtOH–H_2O to give the analytical sample, mp 83—85 °C; NMR (CCl_4) δ 1.58 (d, 6H, J=6 Hz, $-CH_3$), 4.70—5.30 (m, 1H, $>CH$), 7.72—8.58 (m, 7H, aromatic H); mass spectrum (80 eV) *m/e* 238, 223, 196, 180, 168. Found: C, 75.42; H, 5.70; N, 11.56%. Calcd for $C_{15}H_{14}N_2O$: C, 75.60; H, 5.92; N, 11.76.

Irradiation of I in Acetic Acid. A mixture of I (100 mg, 0.56 mmol) and *p*-toluenesulfonic acid monohydrate (1 g, 5.3 mmol) in dry AcOH (50 ml) was irradiated under N_2 for 7 hr. After irradiation, $FeCl_3$ was added to the reaction mixture until the solution turned into yellow. The solution was then evaporated to dryness under reduced pressure, and an aqueous Na_2CO_3 was added to the residue until the neutralized solution was obtained. The neutralized solution was extracted with ether. After the ether extracts were dried over Na_2SO_4, the ether was removed by distillation. The residue was subjected to tlc (silica gel, DMF: AcOH: H_2O= 10: 1: 1). The upper spot was extracted with $CHCl_3$, then the solvent was evaporated to dryness. IR and NMR spectra of the residue were identical with those of the authentic sample of IIe. Quantitative analyses of I and IIe were performed by converting IIe to IIa by treatment with an aqueous NaOH: the residue obtained upon irradiation was dissolved in a mixture of EtOH (5 ml) and 10% NaOH solution (5 ml), and the mixture was kept at 40 °C for 1 hr. A 10% NaOH solution (20 ml) was added to the mixture, and the alkaline solution thus obtained was extracted with ether. Work-up of the ether and aqueous layers gave 75 mg (75%) of I and 20 mg (19%) of IIa.

Irradiation of IIa in 2 M H_3PO_4 Solution. IIa (100 mg, 0.51 mmol) in aqueous 2 M H_3PO_4 (80 ml) was irradiated under air for 7 hr. The solution was neutralized with Na_2CO_3 and extracted with ether. Work-up of the ether extracts resulted in a quantitative recovery of IIa.

Quantum Yield Determinations. A 5 ml of reactant solution was degassed under vacuum by four freeze-pump-thaw cycles in a side arm through which a 1 cm quartz cell was connected. Then the quartz cell and the side arm were closed under vacuum and the solution was transfered into the quartz cell. The absorption spectrum of the reactant solution was recorded, and irradiation was then started. During the course of the photoreactions, additional complete spectra (6—8 times) were taken. Optical densities at 380 nm band of the reactant and at 430 nm band of the product were monitored and the simultaneous equations were used to determine the amount of product formed. A plot of the amount of the product formed *vs.* total quanta absorbed was prepared, and the quantum yield was determined from the slope of the straight line. The photoreaction was never carried out beyond the point where 20% of I has been photolyzed. All studies were made at room temperature. After the photoreaction was ceased, the solution was oxidized by exposing it to air, and the analysis of IIa or IIb was performed by taking absorption spectrum.

A Toshiba SHL-100 UV high-pressure mercury lamp was used as a light source. Light was filtered through a Toshiba UV 31 filter glass. The filter glass permitted to pass the light with the following wavelength distribution: 3% 3130 Å, 18% 3660 Å, 16% 4045 Å, 28% 4358 Å, 28% 5461 Å, 6% 5780 Å. Potassium ferrioxalate actinometer[8] was used for measuring the light intensity. Reproducible output rates of 8.7×10^{16} quanta min^{-1} were recorded.

References

1) Part V, S. Wake, H. Inoue, Y. Otsuji, and E. Imoto, *Tetrahedron Lett.*, **1970**, 2415.
2) E. Toromanoff, *Ann. Chim* (Paris), **1**, 115 (1956).
3) T. Iwaoka, S. Nizuma, and M. Koizumi, This Bulletin, **43**, 2786 (1970).
4) G. A. Davis, J. D. Gresser, and P. A. Carapellucci, *J. Amer. Chem. Soc.*, **93**, 2179 (1971).
5) D. N. Bailey, D. K. Roe, and D. M. Hercules, *ibid.*, **90**, 6291 (1968).
6) Y. Fellion and J. Uebersfeld, *Arch. Sci., (Geneva)*, **9**, 89 (1956); *Chem. Abstr.*, **50**, 12645 (1956).
7) A. N. Holden, W. A. Yager, and F. R. Merritt, *J. Chem. Phys.*, **19**, 1319 (1951).
8) C. G. Hatchard and C. A. Parker, *Proc. Roy. Soc. Ser. A*, **235**, 518 (1956).
9) The rates of formation of the photoproducts, the cation radicals, upon irradiation in the presence of air gradually decreased after about 10% completion of the reaction. This diminution of the rates was found to be due to the oxidation of the cation radicals to their oxidized forms by air.
10) A. Albert, R. Goldacre, and J. Phillips, *J. Chem. Soc.*, **1948**, 2240.
11) The pK_a* of I is unknown. However, the estimation[12] by means of the Forster cycle from a spectral shift on protonation (about -1500 cm^{-1} both in water and methanol) predicts that the pK_a* would be about 3 units higher than the ground state pK_a. The predicted value of pK_a* by this method (pK_a*$\sim$4 in water) implies that I exists almost exclusively in the form of phenazinium cation (PH^+) even in 0.1 M phosphoric acid.
12) H. H. Jaffé, D. L. Beveridge, and H. L. Jones, *J. Amer. Chem. Soc.*, **86**, 2932 (1964).
13) T. J. Curphey, *ibid.*, **87**, 2063 (1965).
14) A. Wohl and W. Aue, *Ber.*, **34**, 2442 (1901).
15) A. R. Surrey, "Organic Syntheses," Coll. Vol. 3, p. 753 (1955).
16) S. B. Serebryani, *Zh. Obshch. Khim.*, **20**, 1629 (1950); *Chem. Abstr.*, **45**, 2009 (1951).

Photochemistry of Heterocyclic Compounds. VII. The Photochemical Behavior of Phthalazine and Quinoxaline in Acidified Alcohols

Shigeo WAKE, Yuichi TAKAYAMA, Yoshio OTSUJI, and Eiji IMOTO

Department of Applied Chemistry, College of Engineering, University of Osaka Prefecture, Sakai-shi, Osaka 591

(Received January 23, 1974)

Irradiation of phthalazine (**1**) and quinoxaline (**2**) in acidified methanol yielded 1-methylphthalazine (**3a**) and 2-methylquinoxaline (**4**), respectively. The quantum yields for the formation of 1-alkylphthalazines, which were obtained upon irradiation of **1** in acidified alcohols, varied with the sort of alcohols used and decreased in the order of methanol>ethanol≫2-propanol. When a mixture of **1** and 2,6-di-*t*-butylphenol (**6**) was irradiated in benzene containing trifluoroacetic acid under evacuated conditions, the oxidation of **6** occurred to form 3,5,3′,5′-tetra-*t*-butyldiphenoquinone (**7**) without destruction of **1**. Detailed mechanistic studies suggest that the photoalkylations of **1** and **2** in acidified alcohols proceed through an electron-transfer from solvents to an excited state of the protonated diazines.

In the previous communication,[1] we have reported that phenazine undergoes an ionic solvent-addition reaction to form 1-hydroxy- or 1-alkoxyphenazines upon irradiation in water or alcohols in the presence of protic acids. However, other studies on the photoreactions of nitrogen heteroaromatic compounds in acidified alcohols have indicated that the photoalkylation, rather than the solvent-addition, appears to be a general reaction for this class of compounds.[2-3] These two distinct observations led us to study the photochemical behaviors of phthalazine and quinoxaline, both of which belong to the class of diazine similar to phenazine.

In contrast to phenazine, phthalazine and quinoxaline underwent the photoalkylation reaction upon irradiation in acidified alcohols. Detailed mechanistic studies on the photoreaction of phthalazine suggested that the photoalkylation proceeded through the pathway involving an electron-transfer from alcohols to the excited protonated phthalazine. The details are presented in this paper.

Results

Photo-products. Irradiation of dilute solutions of phthalazine (**1**) in methanol and ethanol containing HCl with a low-pressure Hg lamp under nitrogen atmosphere afforded 1-methyl and 1-ethylphthalazines (**3a** and **3b**), respectively. Irradiation of quinoxaline (**2**) in acidified methanol under similar conditions gave 2-methylquinoxaline (**4**). The results are summarized in Table 1. *p*-Toluenesulfonic acid was also effective as an acid-catalyst for these photoalkylations. On the other hand, when a 0.01 M solution of **1** in methanol was irradiated for 3 hr in the absence of acid, **3a** was not obtained. However, treatment of the resulting reaction mixture with HCl gave **3a** in an 11% yield.

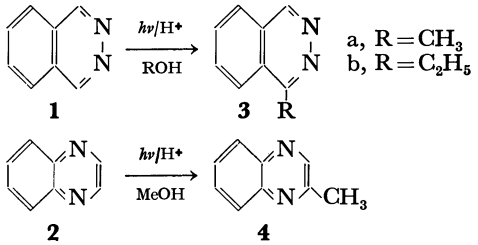

Reaction temperature influenced remarkably on the yields of the products, *i.e.*, irradiation of the solutions of **1** and **2** in acidified methanol at their reflux temperatures raised the yields of the products as shown in Table 1. No reactions took place upon irradiation of aqueous solutions of **1** and **2** both in the presence and absence of acids.

In contrast to the above photoreactions, irradiation of **1** in 2-propanol containing *p*-toluenesulfonic acid gave only a small amount of tarry material. Vpc analysis of the reaction mixture did not show any indication for the presence of the photoalkylation products. Vpc analysis also showed that the rate of disappearance of **1** was faster in methanol than in 2-propanol. Thus, irradiation of **1** in 2-propanol containing 0.1 M *p*-toluenesulfonic acid for 3 hr resulted in a 77% recovery of **1**, while a similar irradiation of **1** in methanol resulted in a 51% recovery of the starting material (see Table 1).

Irradiation of **1** in 2-propanol without added acid afforded a reductive dimerization product (**5**). The structure of **5** was established by a combination of the elemental analysis and spectral data (see Experimental section). The dimer was not obtained by the irradiation in methanol.

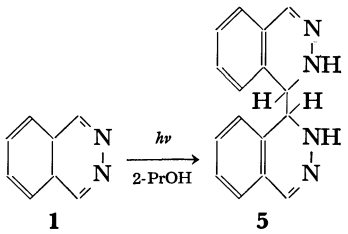

Photoreaction of 2,6-Di-t-butylphenol (6) in the Presence of 1 in an Acidic Medium. When irradiation of an equimolar mixture of **1** and **6** in benzene containing trifluoroacetic acid was carried out under evacuated conditions, 3,5,3′,5′-tetra-*t*-butyldiphenoquinone (**7**) was obtained together with a small amount of unidentified tarry material. The yield of **7** increased with increase of irradiation time, and in every case **1** was recovered

TABLE 1. PHOTOREACTIONS OF **1** AND **2**

Compd.[a]	Solvent	Irrad. conditions		Recovered starting material, %	Product	
		Temp., °C	Time, hr		Compd.	Yield[b] %
1	MeOH 0.08 M HCl	20	3	28	**3a**	30
1	EtOH 0.08 M HCl	20	3	74	**3b**	5
1	MeOH 0.08 M HCl	reflux	3	9	**3a**	50
1	MeOH 0.1 M TsOH[c]	20	3	51	**3a**	32
1	2-PrOH	20	3	83	**5**	8
1	2-PrOH 0.1 M TsOH[c]	20	3	77	—	—
2	MeOH 0.08 M HCl	20	1	64	**4**	trace
2	MeOH 0.08 M HCl	reflux	1	54	**4**	10

a) The 0.01 M solutions of **1** and **2** were irradiated under nitrogen atmosphere. b) The yields are based on the amount of the starting material used. c) TsOH represents *p*-toluenesulfonic acid.

TABLE 2. IRRADIATION OF A MIXTURE OF **1** AND **6** IN AN ACIDIC MEDIUM[a]

Irrad. time, hr	Recovered starting materials, %		Yield of **7**,[b] %
	1	**6**	
12	88	83	9
24	80	71	11
50	74	47	18

a) A mixture of 0.5 mmol of **1** and 0.5 mmol of **6** in 50 ml of benzene containing trifluoroacetic acid (0.1 M) was irradiated under evacuated conditions.
b) The yields of **7** were calculated on the basis of the amount of **6** used.

in a high yield. The results are shown in Table 2. However, **7** could not be detected in the reaction mixture when the irradiation was conducted without added acid or in the absence of **1**. In these cases, the starting materials were recovered unchanged. No reaction also took place without irradiation.

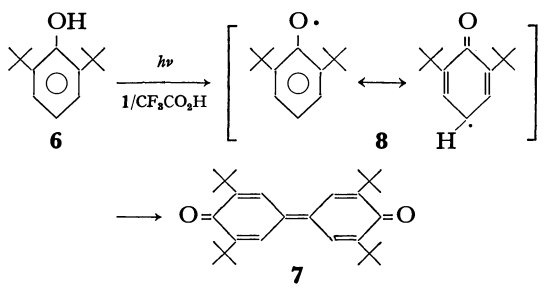

Quantum Yields. The quantum yields for the formation of alkylated products obtained by irradiation of **1** in various acidified alcohols were measured. The results are shown in Table 3. The quantum

TABLE 3. THE QUANTUM YIELDS FOR THE FORMATION OF 1-ALKYLPHTHALAZINES[a]

Solvent	Product	Φ
MeOH, 0.1 M HCl	**3a**	0.026
EtOH, 0.1 M HCl	**3b**	0.0055
2-PrOH, 0.1 M HCl	—[b]	0

a) The 0.01 M solutions of **1** in acidified alcohols were irradiated for 4 hr, and then the products were analyzed to determine the quantum yields.
b) No alkylated product was detected in the reaction mixture.

yields decreased in the order of methylation>ethylation≫propylation.

The quantum yields for the formation of **3a** from **1** were also determined in the presence of various amounts of HCl. The results are depicted in Fig. 1. The

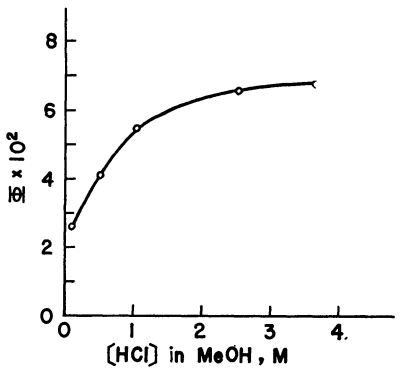

Fig. 1. Effect of HCl concentrations on the quantum yields for the formation of **3** upon irradiation of **1** in acidified methanol. A 0.01 M solution of **1** was irradiated.

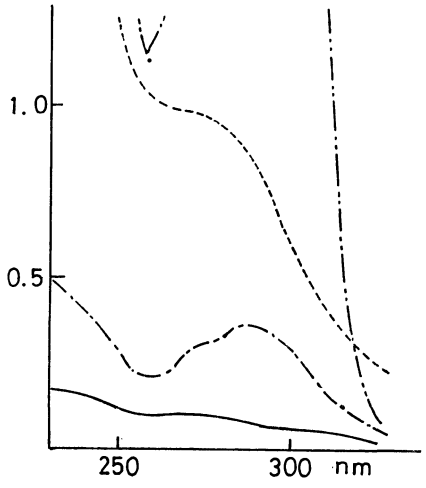

Fig. 2. UV spectra of acidified alcohols: ——, methanol containing of 1 M HCl; ------, methanol containing 5 M HCl; -·-·-, ethanol containing 1 M HCl; —·—, ethanol containing 5 M HCl.

quantum yields increased with increase of the concentration of the acid present. However, when the irradiation was carried out in the presence of 7.2 M HCl, it was found that the quantum yield for the formation of **3a** decreased to a half of the value that was obtained upon irradiation in the presence of 3.6 M HCl. However, spectral examination (Fig. 2) demonstrated that in the presence of higher concentrations of acids, methanol itself absorbed much of the light at 245 nm which was also a main effective light for the photoreaction. Therefore, decrease in the quantum yield for the formation of **3a** in the presence of 7.2 M HCl does not necessarily mean that the quantum efficiency for the reaction decreases at higher concentrations of the acid, but it may merely due to the decrease in number of quanta absorbed by **1**.

To evaluate effects of air on the quantum efficiency of the photoreaction, irradiation of **1** in 0.1 M HCl–MeOH was carried out under evacuated conditions. Quenching experiment employing 1,2-dibromoethane as a quencher was also performed. The results are summarized in Table 4.

Table 4. Irradiation of **1** in acidified methanol[a)]

Quencher	Quantum yield for disappearance of **1**	Quantum yield for the formation of **3a**
None	0.102	0.080
Air	0.072	0.026
1,2-DBE,[b)] 0.19 M	0.121	0.073

a) A 0.01 M solution of 1 in methanol containing 0.1 M HCl was irradiated. b) 1, 2-DBE represents 1,2-dibromoethane.

Absorption Spectra. The absorption spectra of **1** and *N*-methylphthalazinium iodide were studied. The absorption spectra of **1** in MeOH, EtOH, and 2-PrOH were essentially identical. A red shift was observed upon an addition of acid. The spectra of **1** in methanol containing 0.1—1.0 M HCl were very similar in shape to the spectrum of *N*-methylphthalazinium iodide in methanol as shown in Fig. 3.

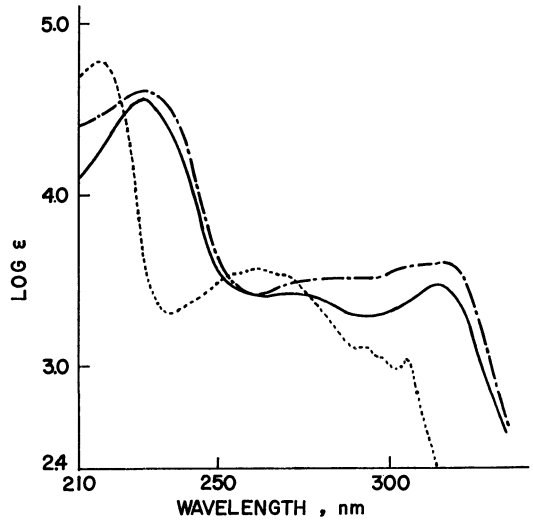

Fig. 3. UV spectra of **1** and *N*-methylphthalazinium iodide: ------, **1** in methanol; ——, **1** in methanol containing 1.0 M HCl; -·-·-, *N*-methylphthalazinium iodide in methanol.

Discussion

A proposed mechanism for the photoalkylation of azaaromatic compounds is illustrated in Scheme 1 taking an example of the photomethylation of **1** in acidified methanol.

Absorption spectra shown in Fig. 3 strongly suggest that **1** exists at its ground state predominantly in the

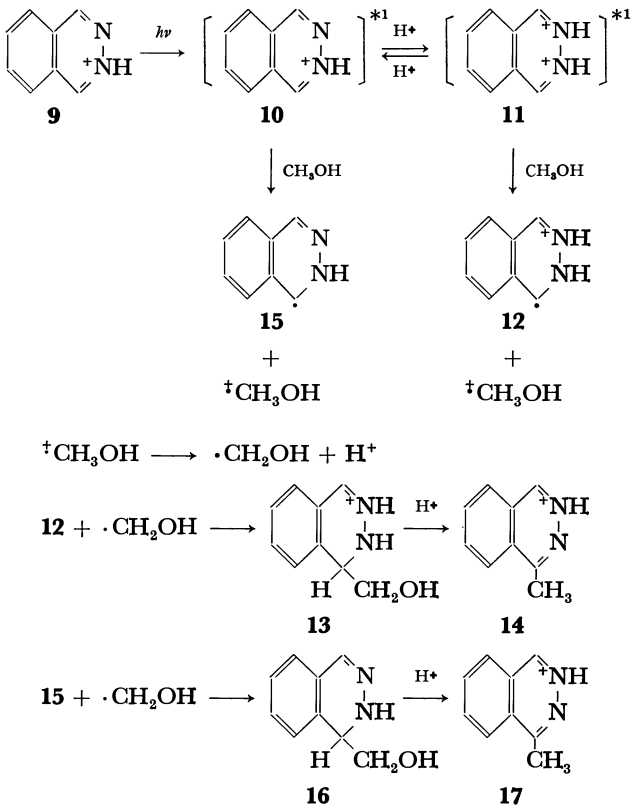

Scheme 1.

form of monoprotonated phthalazinium cation (**9**) in methanol containing 0.1—1.0 M HCl. However, at the excited state **1** may exist either in the excited monoprotonated form (**10**) or in the excited diprotonated form (**11**) in acidified methanol.[4]

The excited diprotonated species **11** picks up an electron from methanol to form the cation radical **12** and the cation radical of methanol, $^{\ddagger}CH_3OH$, which is converted to hydroxymethyl radical. A coupling of **12** with hydroxymethyl radical produces the intermediate **13**. The reaction of **13** with a proton affords the monoprotonated 1-methylphthalazinium cation (**14**).

The result of Fig. 1 can be explained by assuming that the reactive species is **11**, since the proportion of **11** in the reaction mixture would increase with increase of the acid concentrations.[5]

A striking feature of the proposed mechanism is the electron transfer from alcohols to the excited protonated azines. This mechanism was derived from the following considerations. Firstly, the electron affinity of **11** is supposed to be high enough to take up an electron from alcohols. An increased electron affinity of the dication of diazines has been recognized by Curphey,[6] who observed that *N,N'*-diethylpyradinium difluoroborate is reduced to the corresponding cation radical upon dissolving it in ethanol even in the dark. Secondly, the solvent effects on the photoreaction of **1** are consistent with the electron transfer mechanism. We observed that the quantum yields of the photoalkylations of **1** in acidified alcohols varied with the sort of alcohols used and decreased in the order of methanol>ethanol≫2-propanol (Table 1). Furthermore, the results of Table 1 indicate that the rate of disapperance of **1** decreases also in the above order. If the photoreaction is initiated *via* a hydrogen abstraction from alcohols by **10** or **11**, the reversed solvent effects must be observed. Absorption spectra shown in Fig. 2 suggest that alcohols may be transformed to their oxonium ions in the presence of higher concentrations of HCl (HCl and alcohols themselves have no absorptions at 220—250 nm where the acidified alcohols exhibited strong absorptions). If this is the case, it is reasonable to assume that the formation of oxonium ions in acidified alcohols would become favorable in more basic 2-propanol than in more acidic ethanol or methanol. An electron abstraction from the oxonium ions would be more difficult than from the free alcohols. Thus, it is supposed that the photoreactivity varies in the observed order, if the photoreaction is initiated *via* the electron transfer from acidified alcohols to **11**. Thirdly, an evidence supporting the electron transfer mechansim was provided by the result that the irradiation of a mixture of **1** and **6** in benzene in the presence of acid brought about the oxidation of **6** to **7** without destruction of **1**. This photooxidation can be best explained in terms of the mechanism involving the electron transfer from **6** to **11** to form the phenoxy radical **8**.[7] Finally, further supporting data for the mechanism were found in the literature. 1) Ochiai and co-workers[8] have found that the photomethylation of pyrimidine derivatives in acidified methanol is favored by the electron-withdrawing substituents attached to the pyrimidine ring, and they have also observed the $\cdot CH_2OH$ radical. 2) Castellano and co-workers[9] have recently detected the cation radicals of **2**, pyrazine, and phenazine in the reaction mixtures by ESR spectroscopy upon irradiation of their acidified methanolic solutions. These results are in accordance with the mechanism shown in Scheme 1.

It must be noted here that the photoreactions of azaaromatic compounds in the absence of acids may proceed through a hydrogen abstraction from alcohols by the excited azaaromatics.[3]

1,2-Dibromoethane caused essentially no quenching effect on the quantum yield for the formation of **3a**. This result suggest that the photoreaction of **1** proceeds from a singlet excited state. A decrease in the quantum yield of the photoalkylation of **1** in the presence of air is explainable on the basis of the assumption that oxygen reacts with the intermediate radical species (**12** or hydroxymethyl radical, or both) to quench further reactions. The effect of temperature on the yields of **3a** and **4** in the photolyses of **1** and **2** may be attributed to the acid-catalyzed dehydration reaction of the type **13**→**14** in the dark. However, a more work has to be done before the final conclusion can be reached.

Experimental

Melting points are uncorrected. UV spectra were recorded with a Hitachi EPS-3T recording spectrophotometer. IR spectra were obtained with a Hitachi model 215 infrared spectrophotometer. NMR spectra were obtained with a Hitachi H-60 high resolution NMR spectrometer, using TMS as an internal standard. Microanalyses were performed with a Yanagimoto MT-1 CHN corder. Mass spectra were obtained with a Hitachi RMU-6E mass spectrometer. Vpc analyses were performed with a Hitachi K-23 gas chromatograph, using a column packed with 30% Silicone grease on Celite 545. Unless otherwise noted, irradiations were carried out with a Taika 15 W low-pressure mercury lamp in an immersion-type apparatus.

Materials. Phthalazine (**1**) was prepared by the method of Gabriel and Muller[10] and purified by recrystallization from ether, mp 89—91 °C. Quinoxaline (**2**) was prepared by the method of Jones and McLaughlin[11] and purified by distillation, bp 109.5—111 °C/15 mmHg. All other chemicals were of commercial origin and were usually used after purification by distillation or recrystallization.

Preparation of the Authentic Samples. 1-Methylphthalazine (**3**) was prepared by the method of Popp and Wefer;[12] NMR (CCl_4) δ 2.87 (3H, s, $-CH_3$), 7.55—8.00 (4H, m, benzoaromatic H), and 9.12 ppm (1H, s, $-CH{=}N-$); picrate, mp 201—203 °C (lit,[13] mp 205 °C). 2-Methylquinoxaline (**4**) was prepared by the method of Bottcher,[14] bp 121—125 °C/19 mmHg; NMR (CCl_4) δ 2.66 (3H, s, $-CH_3$), 7.25—7.95 (4H, m, benzoaromatic H), and 8.49 ppm (1H, s, $-N{=}CH-$). 3,5,3',5'-Tetra-*t*-butyldiphenoquinone (**7**) was prepared by the method of Cook, English, and Wilson,[7] mp 232—234 °C.

Photoreaction of 1. (A) Irradiation in Acidified Methanol: A solution of 130 mg (1 mmol) of **1** in 100 ml of an anhydrous methanol containing 0.08 M dry HCl or 0.1 M *p*-toluensulfonic acid was placed in a cylindrical quartz vessel and nitrogen was passed into the solution for 20 min. Irradiation was then carried out at room temperature or at refluxing tempera-

ture of the solvent. After irradiation for an appropriate period of time, the irradiated solution was evaporated to dryness under reduced pressure. The residue was neutralized with 10% aqueous Na_2CO_3, and the aqueous mixture was extracted with benzene by means of a liquid extractor. The benzene extract was dried over Na_2SO_4 and then evaporated. The NMR, IR and vpc examinations showed that the residue consisted of a mixture of **1** and **3**. The quantitative analysis of the residue was performed by vpc, employing quinaldine as an internal standard.

(B) Irradiation in Methanol without Added Acid: A solution of 130 mg (1 mmol) of **1** in 100 ml of an anhydrous methanol was irradiated at room temperature as described above. A concentrated HCl (1 ml) was then added to the reaction mixture, and the resulting mixture was refluxed for 1 hr. The mixture was then worked up as described above.

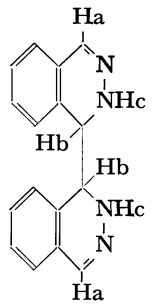

5

(C) Irradiation in 2-Propanol. A solution of 130 mg (1 mmol) of **1** in 100 ml of an anhydrous 2-propanol was irradiated for 3 hr as described above. The solution was concentrated to 5 ml under reduced pressure. The crystals precipitated were collected by filtration and washed with 2-propanol, then with ether. The crystals (10 mg, 8%) were recrystallized from ethanol to give an analytical sample, mp 225—227 °C (decomp.), which was identified as the dimer **5**; NMR (CF_3COOH) δ 5.15 (2H, s, Hb), 7.09—7.21 (2H, broad m, Hc), 7.68—8.08 (8H, m, benzoaromatic H), and 8.6 ppm (2H, s, Ha); MS (50 eV) *m/e* 262 (M^+), 236, 230, 131, and 130. UV (EtOH) λ_{max} 245 (ε 2.56×10^4) and 345 nm (ε 5.63×10^3); IR (KBr) 3300, 3050, 1490 and 1420 cm^{-1}.

Found: C, 73.02; H, 5.59, N, 21.13%. Calcd for $C_{10}H_{14}N_4$: C, 73.26; H, 5.38; N, 21.36%.

The filtrate and washings obtained above were evaporated under reduced pressure and the residue was subjected to vpc analysis. The analysis indicated that the starting material was recovered in an 83% yield.

Photoreaction of **2**. A solution of 130 mg (1 mmol) of **2** in 100 ml of an anhydrous methanol containing 0.08 M dry HCl was irradiated at room temperature or at refluxing temperature of the solvent, in the same manner as previously described for the photolysis of **1**. After irradiation, the irradiated solution was evaporated to dryness under reduced pressure. The residue was neutralized with 10% aqueous Na_2CO_3, and the neutralized solution was extracted with benzene by means of a liquid extractor. The benzene extract was dried over Na_2SO_4 and then evaporated. Examinations of the residue by NMR, IR and vpc revealed that the residue consisted of a mixture of **2** and **4**. The quantitative analysis was performed by vpc with diphenyl ether as an internal standard.

Photoreaction of a Mixture of **1** *and* **6**. A mixture of 65 mg (0.5 mmol) of **1** and 103 mg (0.5 mmol) of **6** in a dry benzene containing 0.1 M trifluoroacetic acid was placed in a cylindrical quartz vessel and degassed by four or five freeze-pump-thaw cycles. Irradiation was then carried out from the outside of the reaction vessel at room temperature for 12 hr. The irradiated solution was extracted with 1 M HCl. The benzene layer was dried over Na_2SO_4 and then evaporated under reduced pressure. The residue was separated by preparative tlc on silica using CCl_4 as an eluent. Extraction of the first spot (R_f 0.3) with $CHCl_3$ and evaporation of the solvent gave 85 mg (83%) of unreacted **6**. Extraction of the second spot (R_f 0.5) with $CHCl_3$ and evaporation of the solvent gave 9 mg (9%) of **7** which melted at 231—233 °C after recrystallization from ethanol and was identical with the authentic sample in every respect. There were other few spots, from which 8 mg of unidentified materials were obtained.

On the other hand, the aqueous acid solution was made to pH 8 with Na_2CO_3 and filtered. The filtrate was extracted with benzene by means of a liquid extractor. The benzene extract was dried over Na_2SO_4 and then evaporated to give 57 mg (88%) of **1**.

Quantum Yield Determinations. A reactant solution (20 ml) in a quartz vessel was irradiated after degassing by four freeze-thaw cycles or under air with a Taika 15 W low-pressure mercury lamp. Although filter was not employed, the spectral examination of the radiation showed that the light source radiated the light with the following wavelength distribution: 74% 2537 Å, 4% 3130 Å, 4% 3660 Å, 4% 4055 Å, and 14% 4358 Å. All studies were made at room temperature. Potassium ferrioxalate actinometer[15] was used for measuring the light intensity. Reproducible output rates of 3.4×10^{18} quanta min^{-1} were recorded. After irradiation for 4 hr, the solution was neutralized with Na_2CO_3 and evaporated to dryness under reduced pressure. The residue was extracted with benzene, and the benzene extract was subjected to vpc analysis.

References

1) S. Wake, H. Inoue, Y. Otsuji, and E. Imoto, *Tetrahedron Lett.*, **1970**, 2415.

2) E. F. Travecedo and V. I. Stenberg, *Chem. Commun.* **1970**, 609.

3) F. R. Stermitz, C. C. Wei, and C. M. O'Donnell, *J. Amer. Chem. Soc.*, **92**, 2745 (1970), and references cited therein.

4) It is well known that pK_a's in the lowest excited singlet state of azaaromatic compounds are much higher than the corresponding ground state pK_a's. (E. V. Donckt, "Progress in Reaction Kinetics," ed. by G. Porter, Pergamon Press, Oxford, Vol. 5 (1970), p. 273.)

5) The possibility remaines that the excited monoprotonated phthalazinium cation (**10**) may also pick up an electron from methanol to form the radical **15** and $^{\ddagger}CH_3OH$. However, it is reasonable to assume that the diprotonated species (**11**) more effectively picks up an electron than does **10**.

6) T. J. Curphey, *J. Amer. Chem. Soc.*, **87**, 2063 (1965).

7) It has been well established that a one-electron oxidation of **6** gives **7** through the intermediate **8** (C. D. Cook, E. S. English, and B. J. Wilson, *J. Org. Chem.*, **23**, 755 (1958)).

8) M. Ochiai, E. Mizuta, Y. Asahi, and K. Morita, *Tetrahedron*, **24**, 5861 (1968).

9) A. Castellano, J.-P. Catteau, and A. Lablache-Combier, *Chem. Commun.*, **1972**, 1207.

10) S. Gabriel and F. Muller, *Ber.*, **28**, 1830 (1895).

11) R. G. Jones and K. C. McLaughlin, "Organic Syntheses," Coll. Vol. 4, p. 824 (1963).
12) F. D. Popp and J. M. Wefer, *Chem. Commun.*, **1967**, 59.
13) S. Gabriel and G. Eschenbach, *Ber.*, **30**, 3022 (1897).
14) K. A. Bottcher, *ibid.*, **46**, 3084 (1913).
15) C. G. Hatchard and C. A. Parker, *Proc. Roy. Soc., Ser. A*, **235**, 518 (1956).

Substituent Effects in the Benzofuran System. I. Proton and Carbon-13 Chemical Shifts

Tadashi OKUYAMA and Takayuki FUENO

Department of Chemistry, Faculty of Engineering Science, Osaka University, Toyonaka, Osaka 560

(Received August 7, 1973)

PMR and CMR spectra of benzofuran and its derivatives (2-CH_3, 3-CH_3, 5-CH_3, 6-CH_3, 5-CH_3O, 6-CH_3O, and 5-Cl) have been measured. The chemical shifts of 2-H and 2-C of 5- and 6-substituted derivatives obeyed a modified Hammett equation, $\delta=\rho_1\sigma_1+\rho_2\sigma_2+\delta_0$. Electronic effects were found to be transmitted mainly through the bond 8—3. It was concluded that the ground-state electronic structure is similar to that of styrene rather than phenyl vinyl ether.

A great number of reaction rates and ground-state properties of benzene derivatives have been treated in terms of the Hammett $\rho\sigma$ relationship.[1] Much less is known of its application to fused ring systems which have two transmission paths of substituent effects. Such an application was first undertaken by Jaffé[2a] with the use of a modified Hammett equation.

$$\log (k/k_0) = \rho_1\sigma_1 + \rho_2\sigma_2 \quad (1)$$

The treatment has successfully been applied to the phthalide system.[2a] These treatments on heteroaromatic fused rings have been summarized in a review.[2b] Some examples of the benzofuran system are included but full accounts are not available. Noyce and Nichols[3] have recently treated the solvolysis rates of 2- and 3-benzofuryl derivatives in terms of the σ_{ij} constants with the modified Dewar-Grisdale equation.[4]

Because of our continuing interest in the chemica properties of aromatic olefins as well as enol ethers, we have studied the substituent effects observable in the benzofuran system. Benzofuran (BF) is structurally analogous to both styrene (ST) and phenyl vinyl ether (PVE).

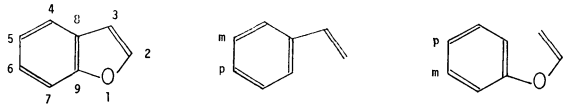

BF ST PVE

Accordingly, its chemical behavior should be dual in its character. First, in the present communication, we will analyze the ground-state electronic structure of BF on the basis of ^1H and ^{13}C NMR observations. In the following two papers, the chemical reactivities will be treated for the bromination[5a] and the cationic polymerization.[5b]

Results

PMR Spectra. The proton magnetic resonance (PMR) spectra of BF and its derivatives have been recorded at a frequency of 100 MHz with a 10% solution in carbon tetrachloride using tetramethylsilane as internal standard. Measurements are accurate within 0.05 Hz. Assignment of signals has been made based on their coupling mode. Spectral feature of unsubstituted phenylene ring is too complicated for simple analysis and was not subjected to further attempts of analysis. Chemical shifts and coupling constants are summarized in Table 1.

CMR Spectra. The ^{13}C NMR spectra of BF derivatives have been obtained usually with a 50% solution in carbon disulfide. The complete proton noise decoupled spectrum of BF gave eight sharp singlets. The signals responsible for quaternary carbon atoms are easily characterized by a partial proton decoupling technique, remaining as singlet. All the signals have been assigned empirically by using the additivity rule.[6] The 6-methoxy derivative, proton spectrum of which is well separated, was subjected to single-frequency decoupling to aid the assignment. The chemical shifts are given in Table 2 as expressed in ppm downfield from TMS. For closely-spaced signals, however, some uncertainties were inevitable and such chemical shifts are presented with parentheses in Table 2.

TABLE 1. THE CHEMICAL SHIFTS AND COUPLING CONSTANTS FOR THE PMR SPECTRA OF SUBSTITUTED BENZOFURANS[a]

Substituent	Chemical shift, ppm						Coupling constant, Hz					
	H-2	H-3	H-4	H-5	H-6	H-7	J_{23}	J_{37}	J_{45}	J_{67}	J_{57}	J_{46}
H	7.507	6.623					2.3	1.0				
2-CH_3	(2.39)	6.21					(1.0)	1.0				
3-CH_3	7.291	(2.20)					(1.1)					
5-CH_3	7.463	6.532	7.24	(2.425)	7.28	6.96	2.2	0.8		8.4		
6-CH_3	7.439	6.564	7.343	6.93	(2.42)	7.209	2.2	0.9	8.1			
5-CH_3O	7.476	6.544	6.888	(3.745)	6.566	7.280	2.3	0.9		8.9		2.6
6-CH_3O	7.423	6.562	7.324	6.754	(3.747)	6.92	2.2	0.9	8.4		2.2	
5-Cl	7.544	6.586	7.476	—	7.158	7.343		0.9		9.0		2.0

a) The values in parentheses show those concerning methyl protons.

Table 2. The ^{13}C chemical shifts[a] of substituted benzofurans

Subst.	C-2	C-3	C-4	C-5	C-6	C-7	C-8	C-9	CH_3
H	145.1	106.9	121.6	123.2	124.6	111.8	127.9	155.5	—
2-CH_3	(155.9)	104.0	121.2	123.5	124.2	111.7	130.2	(155.7)	14.7
3-CH_3[b]	141.6	116.0	119.8	122.7	124.5	111.7	129.4	155.8	7.4
5-CH_3	145.4	107.1	121.9	132.5	126.4	111.7	128.4	154.1	22.0
6-CH_3	144.8	107.2	121.5	125.1	134.8	112.5	125.6	156.0	22.7
5-CH_3O	146.2	107.6	104.2	156.8	112.6	114.1	128.8	150.6	55.9
6-CH_3O	144.4	106.9	121.7	112.6	158.7	95.8	121.2	156.6	55.1
5-Cl	146.8	107.1	121.7	(129.7)	125.4	110.9	(129.4)	154.0	—

a) In ppm downfield from TMS. Measured with a 50% solution in CS_2. b) Measured with a neat sample.

Discussion

Spectral Characterization. PMR spectra of various methyl-substituted BF's have previously been measured, and the results on the 2- and 3-protons reported.[7] The present results on these derivatives coincide satisfactorily with those reported data.[7] A long-range coupling between the 3- and 7-protons of *ca.* 1 Hz observed here conforms also to the earlier results.[7]

The CMR spectrum of BF has recently been measured.[8] Assignment of signals has been made in analogy to that for indoles.[9] The assignment of C-4, C-5, and C-6 reported contradicts that presented in Table 2. Although the signals responsible for these carbons are very close, a comparison of these signals among various 5- and 6-substituted BF's coupled with the empirical additivity rule[6] permits us to assign them with confidence. Since *ortho*-methyl substitution usually effects a small downfield shift,[6] a signal at 121.6 ppm of BF should be assigned to C-4. It is noticeable by comparing the results on a pair of 5- and 6-substituted derivatives that the chemical shift of C-6 is greater than that of C-5 for both the methyl and methoxy derivatives. Hence, it might be reasonable that the signals at 123.2 and 124.6 ppm should be assigned to C-5 and C-6 of BF, respectively. These assignments are consistent for all the derivatives from the viewpoint of the additivity rule.

Substituent Effects on the Chemical Shifts. A variety of proton and carbon chemical shifts (δ_H and δ_C) of benzene derivatives have been treated in terms of a Hammett-type equation.[1b] They reflect the ground-state electronic structure. The effects of 5- and 6-substituents on δ_H and δ_C at the 2- and 3-positions of BF may be treated in a similar way. Because of two transmitting paths of electronic effects, they should be expressed by an equation similar to Eq. (1):

$$\delta = \rho_1\sigma_1 + \rho_2\sigma_2 + \delta_0 \qquad (2)$$

where ρ_1 and ρ_2 are defined as sensitivity constants through the bonds 8–3 and 9–1–2, respectively.

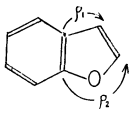

The constants σ_1 and σ_2 refer correspondingly to the Hammett σ values of substituent relative to carbons 8 and 9, respectively. The value δ_0 is the chemical shift for the parent BF.

Table 3. Sensitivity constants for the effects of 5- and 6-substituents on the proton and carbon chemical shifts of benzofuran

	H-2	H-3	C-2	C-3
ρ_1	0.175	0.017	4.08	0.53
$S_{\rho 1}$	0.041	0.070	0.41	0.33
ρ_2	0.036	0.094	−0.88	−1.04
$S_{\rho 2}$	0.051	0.087	0.51	0.42
δ_0	7.477	6.571	145.43	107.11
$S_{\delta 0}$	0.008	0.014	0.08	0.07
S_δ	0.020	0.035	0.20	0.16

The values ρ_1, ρ_2, and δ_0 were calculated by the least-squares method and are given in Table 3. Noticeable in Table 3 is that both δ_H and δ_C at the 3-position receive virtually no effect or at least no simple electronic effect (with a large standard deviation) by substitution. By contrast, δ_H and δ_C at the 2-position reflect normal electronic effects of ring substituents. Linearities between the calculated values (Eq. (2)) and the observed δ_H and δ_C are illustrated in Figs. 1 and 2. The greater magnitude of ρ_1 as compared with ρ_2 for the 2-position indicates that the electronic effects of substituents are transmitted to C-2 mainly through the bond 8–3, ST-type. A similar tendency was previously observed for the acid dissociation of coumarilic acid.[2b]

As a whole, the electronic structure of the 2–3 double bond of BF system seems to be similar to that of the

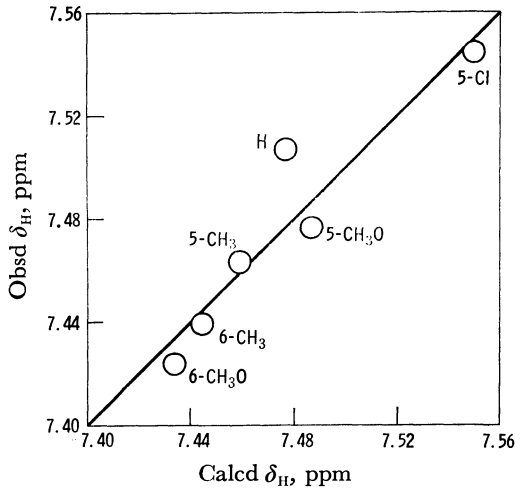

Fig. 1. Plots of the calculated and the observed chemical shifts of H-2 of substituted benzofurans.

Table 4. Boiling points and elemental analysis data of substituted benzofuran

Substuent	Mp[a] (°C)	Bp (°C/mmHg(lit.))	Calcd(%) C	Calcd(%) H	Found(%) C	Found(%) H
H	191.5	54.0/13(66.5/22)[b]	81.33	5.11	81.06	5.08
2-CH_3	—	87—88/20(81/14)[c]	81.78	6.11	81.84	6.14
3-CH_3	192—193	75.2/15(90/23)[c]	81.78	6.11	81.69	6.12
5-CH_3	234.8	88.0/18(86/20)[c]	81.78	6.11	81.64	6.04
6-CH_3	200	80.0/22(88/23)[c]	81.78	6.11	81.67	6.17
5-CH_3O[d]	211	123/30(119—120/25)[e]	72.95	5.44	73.08	5.48
6-CH_3O	211—213	103—104/10(99—100/10)[f]	72.95	5.44	73.05	5.51
5-Cl[g]	190—193	91.5/20(56/2)[h]	62.97	3.31	63.00	3.29

a) Mp of coumarilic acid. b) Ref. 13a. c) Ref.7. d) Mp of BF was 32—33 °C (lit,[e] 33—34.5 °C). e) S. D. Darling and K. D. Wills, *J. Org. Chem.*, **32**, 2794 (1967). f) R. L. Shriner and J. Anderson, *J. Amer. Chem. Soc.*, **60**, 1418 (1938). g) Cl: Calcd, 23.23; Found, 23.28%. h) E. N. Givens, L. G. Alexakos, and P. B. Venuto, *Tetrahedron*, **25**, 2407 (1969).

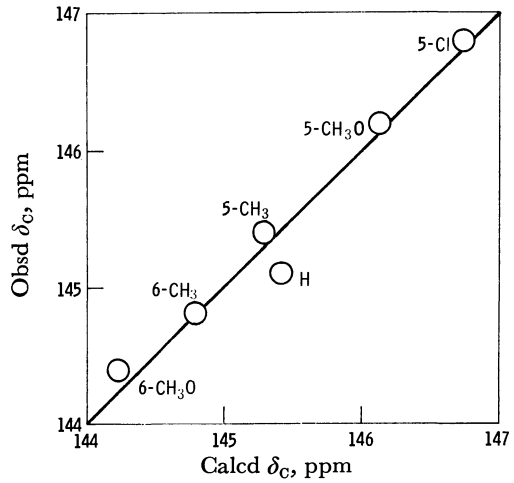

Fig. 2. Plots of the calculated and the observed chemical shifts of C-2 of substituted benzofurans.

extracyclic double bond of ST rather than PVE. However, the ρ_I values are relatively small (markedly for δ_H) as compared with the ρ values for the terminal chemical shifts of styrene, 0.325 (δ_H)[10] and 4.73 (δ_C)[11] ppm/σ. This may probably be due to the substantial difference in the structure; the 2–3 bond is a part of aromatic ring of BF.

Experimental

Materials. Benzofuran (BF) and its 5- and 6-substituted derivatives were prepared from an appropriate salicylaldehyde and diethyl bromomalonate[12] *via* coumarilic acid according to the procedure of Nakazaki.[13] Methyl- and methoxysalicylaldehydes were obtained by the Reimer-Tiemann reaction.[14] 5-Chlorosalicylaldehyde was prepared by the chlorination of salicylaldehyde.[15] Treatments of a salicylaldehyde and bromomalonate by Nakazaki's procedure gave 50—30% of a coumarilic acid which was decarboxylated to give a benzofuran. Bp and elemental analysis data are given in Table 4.

2- and 3-Methylbenzofurans were prepared according to the literature.[16,17] Boiling points and analysis data are included in Table 4.

NMR Measurements. The PMR spectra were obtained on a JNM-4H-100 spectrometer operating at a frequency of 100 MHz at room temperature (*ca.* 22 °C). A 10% solution of a sample in CCl_4 was applied to the measurement and the chemical shifts did not vary within the experimental error of 0.05 Hz by dilution. TMS was used as an internal standard.

The CMR spectra were recorded at *ca.* 24 °C on a JEOL C-60HL spectrometer with a 15.09 MHz RF unit. Samples of neat liquid or 50% solution in CS_2 were used. The signal-to-noise ratio of the spectra was enhanced by the ^{13}C–H noise decoupling. The chemical shift measurements were performed with a nuclear-resonance single-side-band technique, being accurate within 0.2 ppm. CS_2 was used as an external standard. The chemical shifts are given in PPM downfield from TMS by using the chemical shift of CS_2 of 192.8 ppm.

The authors wish to thank Messers. Y. Terawaki and H. Okuda for recording the spectra.

References

1) a) H. H. Jaffé, *Chem. Rev.*, **53**, 191 (1953); b) Y. Yukawa and Y. Tsuno, "Bunkokagaku 168-B," ed. by Y. Morino, T. Shimanouchi, and M. Ōki, Nankodo, Tokyo (1968), pp. 87—112.

2) a) H. H. Jaffé, *J. Amer. Chem. Soc.*, **76**, 4261 (1954); b) H. H. Jaffé and H. L. Jones, *Adv. Heterocyclic Chem.*, **3**, 209 (1964).

3) D. S. Noyce and R. W. Nichols, *J. Org. Chem.*, **37**, 4306, 4311 (1972).

4) M. J. S. Dewar and P. J. Grisdale, *J. Amer. Chem. Soc.*, **84**, 3539 (1962).

5) a) Part II: T. Okuyama, K. Kunugiza, and T. Fueno, This Bulletin, **47**, 1267 (1974); b) Part III: T. Okuyama, K. Kunugiza, and T. Fueno, *ibid.*, **47**, 1271 (1974).

6) a) P. C. Lauterbur, *J. Amer. Chem. Soc.*, **83**, 1846 (1961); b) G. C. Levy and G. L. Nelson, "Carbon-13 Nuclear Magnetic Resonance for Organic Chemists," Wiley-Interscience, New York, N. Y., (1972), p. 81.

7) J. A. Elvidge and R. G. Foster, *J. Chem. Soc.*, **1963**, 590; *ibid.*, **1964**, 981.

8) R. J. Abraham, D. F. Wileman, G. R. Bedford, and D. Greatbanks, *J. Chem. Soc., Perkin II*, **1972**, 1733.

9) R. G. Parker and J. D. Roberts, *J. Org. Chem.*, **35**, 996 (1970).

10) T. Fueno, O. Kajimoto, K. Izawa, and M. Masago, This Bulletin, **46**, 1418 (1973).

11) K. S. Dhami and J. B. Stothers, *Can. J. Chem.*, **43**, 510 (1965).

12) C. S. Palmer and P. W. McWherter, "Organic Syntheses," Coll. Vol. 1, p. 245 (1932).
13) a) M. Nakazaki, *Yuki Gosei Kagaku Kyokai Shi*, **8**, 32 (1956); b) Y. Takeda, Y. Hayakawa, T. Fueno, and J. Furukawa, *Makromol. Chem.*, **83**, 234 (1965)
14) K. Reimer and F. Tiemann, *Ber.*, **9**, 824 (1876); L. Gattermann and T. Wieland, "Die Praxis des organischen Chemikers," Walter de Gruyter & Co., Berlin, (1961), p. 206.
15) H. Biltz and K. Stepf, *Ber.*, **37**, 4024 (1904).
16) R. Adams and R. E. Rindfusz, *J. Amer. Chem. Soc.*, **41**, 648 (1919).
17) W. R. Boehme, "Organic Syntheses," Coll. Vol. IV, p. 590 (1963).

Substituent Effects in the Benzofuran System. II.[1] Electrophilic Bromination

Tadashi OKUYAMA, Kiyomitsu KUNUGIZA, and Takayuki FUENO

Department of Chemistry, Faculty of Engineering Science, Osaka University, Toyonaka, Osaka 560

(Received August 7, 1973)

Bromination of benzofuran (BF) and its derivatives (5-CH_3, 6-CH_3, 5-CH_3O, and 5-Cl) has been studied kinetically in acetic acid and by product analysis under various conditions. Product analysis revealed that bromine adds to BF in *trans* fashion, electrophilic bromine attacking at the 2-position. Analysis of substituent effects on the rate of bromination showed that the electronic effects are transmitted through both the bond 8—3 and the bonds 9–1–2 by a comparable magnitude. The transition state of the reaction was concluded to closely resemble a cyclic bromonium ion intermediate.

Benzofuran (BF) is a class of heterocyclic compounds which shows a dual character in its reactivity. One type of reactions is the electrophilic substitution as an aromatic compound, resulting in the substitution of the 2-hydrogen. The other is the electrophilic addition to the 2–3 bond as an olefin.[2]

As an olefin, BF can be taken as an analog of either styrene (ST) or phenyl vinyl ether (PVE).

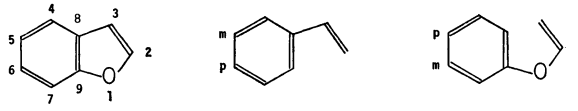

BF ST PVE

BF is often considered as a vinyl ether analog[2] implicitly assuming the 3-attack of an electrophile in addition reaction. However, substitution occurs at the 2-position and, moreover, it was found that the ground-state electronic structure of BF is rather close to ST.[1] Thus, it seems more likely that BF would behave as an ST analog in the addition reaction, an electrophile attacking at the 2-position.

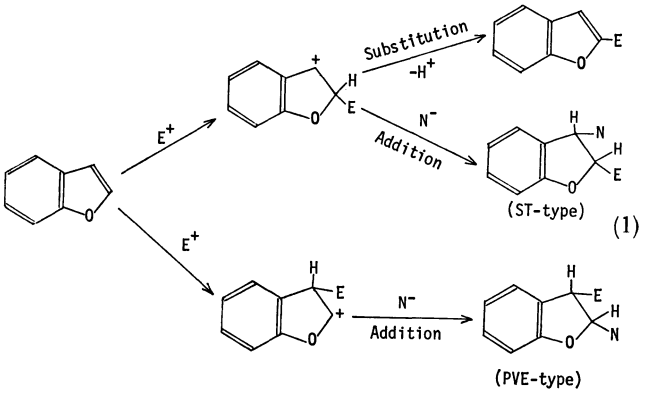

The above confusion arises from the unknown orientation of the addition reaction of BF. The halogenation[3] and the cationic polymerization[4] are the only known electrophilic addition reactions of BF.[2] Product analysis of neither of the two reactions provides any information with regard to the orientation of addition owing to the structural identity of the electrophilic and nucleophilic fragments of the reactions.

The present and the following papers are concerned first with this orientation problem in these reactions. The other purpose of the present investigations is to obtain useful information on the nature of the transition state of the reaction by analyzing the cross-ring transmission of substituent effects.

It is generally accepted that the electrophilic addition of bromine to alkenes proceeds through an intermediate cyclic bromonium ion.[5] However, intermediacy of the cyclic bromonium ion has recently been questioned for some conjugated olefins from the stereochemical studies.[5] Several investigations of the bromination of aryl-substituted olefins have been undertaken, resulting in the above conclusion.[6–9]

The effects of 5- and 6-substituents on the reactivity of BF would be transmitted through both the C–C (8–3) and C–O–C (9–1–2) bonds. This cross-ring transmission of substituent effects can be compared with the effects of *m*- and *p*-substituents of ST and *p*- and *m*-substituents of PVE. Thus, a possible symmetric character of the activated complex like I can be judged by this comparison.

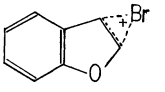

I

Results and Discussion

Product Analysis. Bromination of BF in carbon disulfide gave quantitatively 2,3-dibromo-2,3-dihydrobenzofuran. In attempts to obtain unsymmetric adducts, the reaction was carried out in nucleophilic solvents. Bromination in acetic acid resulted in essentially the dibromide along with a small amount of acetate. On the other hand, the reaction in methanol initially gave a mixture of several adducts which changed quantitatively into a single product, 2,3-dimethoxy-2,3-dihydrobenzofuran, in 3 hr. The dimethoxide is considered to be a substitution product of the initially formed adducts. The products of the reaction time of 15 min contained about 50% of dibromide, 10% of dimethoxide, and probably two kinds of bromomethoxide by the NMR analysis of the mixture. Thus, it was difficult to know the unambiguous orientation of addition from these products.

Under these circumstances, we have undertaken the addition of an unsymmetric reagent, bromine azide. To the methylene chloride solution of BrN_3 prepared by the method of Hassner *et al.*[9] was added BF. The

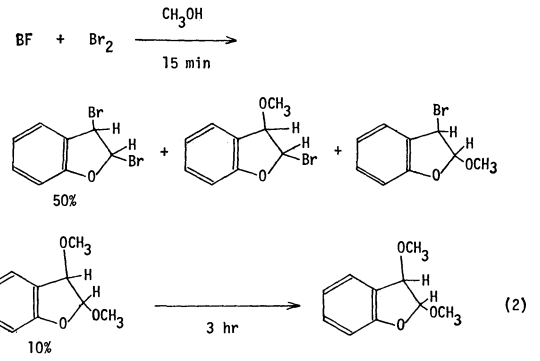

3 hr reaction yielded quantitatively 2-Bromo-3-azido-2,3-dihydrobenzofuran. The structure of the bromoazide was determined by the transformation shown in Eq. (3).

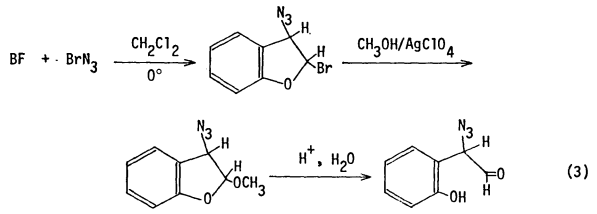

This result clearly shows that the electrophilic bromine adds at the 2-position. That is, the orientation is of the ST-type.

The stereochemistry of the products deserves some comment here. Both the adducts, the dibromide and the bromoazide, are isomerically pure by NMR spectrum and the spin-spin coupling between 2-H and 3-H is very small; ~0 and 1.2 Hz, respectively. Brust *et al.*[10] showed that J_{23} is smaller for the *trans* isomer than for the *cis* isomer of 2,3-dimethyl-2,3-dihydrobenzofuran derivatives; $J_{23}(trans)$ ~4 Hz and $J_{23}(cis)$ ~7 Hz. The Karplus equation[11] predicts $J_{23}(trans) = 2.3 \pm 0.7$ Hz and $J_{23}(cis) = 6.7 \pm 0.6$ Hz for the dihedral angles of $120 \pm 5°$ and $25 \pm 5°$, respectively.[10] Thus, the small coupling constants of the adducts strongly suggest their *trans* structure.

In conclusion, the addition of bromine to BF takes place in the *trans* fashion by the orientation of the ST-type.

Kinetic Measurements. Kinetic investigations of BF and its derivatives (5-CH_3, 6-CH_3, 5-CH_3O, and 5-Cl) were carried out spectrophotometrically in acetic acid at 25.0 °C. A simple second-order rate analysis by Eq. (4) did not give satisfactory results.

$$\text{rate} = k_2[\text{BF}][\text{Br}_2] \tag{4}$$

The rate equation for styrene bromination under similar conditions[6] was represented by

$$\text{rate} = k_2[\text{S}][\text{Br}_2] + k_3[\text{S}][\text{Br}_2]^2 \tag{5}$$

where [S] denotes olefin concentration. The rate analysis of the present reaction has been carried out according to Eq. (5) by a least-squares curve fitting by the aid of a computer. As is shown in Fig. 1, the values k_2 and k_3 thus obtained gave an excellent linear correlation of Eq. (6), which is derived by integration of Eq. (5).

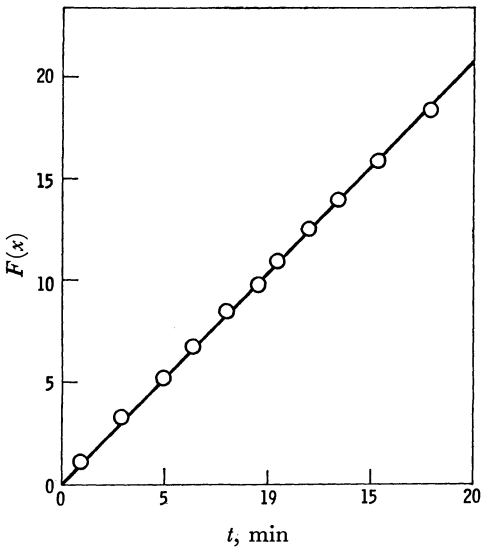

Fig. 1. Typical plots of simultaneous second- and third-order bromination rate according to Eq. (6) (5-methylbenzofuran).

$$t = \frac{\ln[(a-x)/a]}{k_3(a-b)(k_2/k_3+b-a)} + \frac{\ln[(b-x)/b]}{k_2(b-a)} + \frac{\ln[(k_2/k_3+b-x)/(k_2/k_3+b)]}{k_2(a-b-k_2/k_3)} \equiv F(x) \tag{6}$$

where a=initial concentration of BF, b=initial concentration of Br_2, and x=bromine reacted at time t.

Table 1. Rate constants for bromination of substituted benzofurans in acetic acid at 25.0 °C

Substituent	$10^2 k_2$, $M^{-1}s^{-1}$	k_3, $M^{-2}s^{-1}$
H	0.64	3.6
5-CH_3	2.96	35.9
6-CH_3	8.28	616
5-CH_3O	3.48	261
5-Cl	0.053	0.17

The rate constants, k_2 and k_3, for BF and its derivatives are summarized in Table 1. The constants k_2 and k_3 are roughly parallel to each other but analysis of substituent effects will be conducted only on the k_2 values because of lower precision of k_3 determination.

The cross-ring substituent effects can be analyzed by the Jaffé equation.[1,12]

$$\log k = \rho_1\sigma_1 + \rho_2\sigma_2 + \log k_0 \tag{7}$$

where suffixes 1 and 2 correspond to the values concerning the transmitting routes 8-3 (ST-type) and 9-1-2 (PVE-type), respectively. The least-squares treatment of k_2 according to Eq. (7) gave the values with standard deviations: $\rho_1 = -2.21 \pm 0.41$, $\rho_2 = -2.23 \pm 0.53$, and $\log k_0 = -2.01 \pm 0.08$. For the present analysis, the σ^+ values were used for σ_1. Linearity of the calculated and the observed values of $\log k_2$ is illustrated in Fig. 2.

Equality of ρ_1 and ρ_2 ($\rho_2/\rho_1 = 1.01$) is rather un-

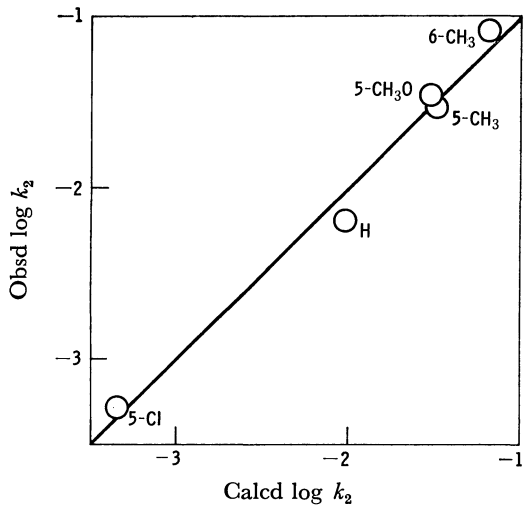

Fig. 2. Linearity of the observed and the calculated log k_2 values (Eq. (7)).

expected because we concluded that both the ground-state electronic structure[1] and the orientation of addition of BF are of the ST-type but not of the PVE-type. The present observation is explainable only by assuming the symmetric transition state closely resembling the intermediate I; the transmission of electronic effects through the route 9–1–2 (PVE-type) cna become effective.

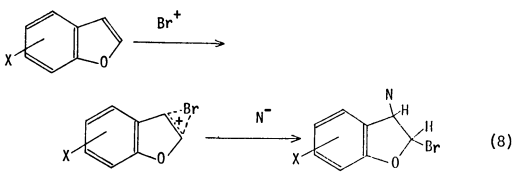

The value of $\rho_2/\rho_1=1.01$ is very close to the relative ρ values of PVE and ST observed for the silver-ion π-complex formation ($\rho_{PVE}/\rho_{ST}=1.03$).[13]

The kinetic observations also show that the electronic effects on the ionic reactivity operate predominantly at the transition state and the ground-state electronic structure seems to have virtually no effect. The ρ_1 value of −2.21 is a reasonable magnitude which is close to the ρ value (−2.24)[6] for the bromination of styrenes bearing an electron-attracting substituent.[15] The latter reaction is assumed to involve a cyclic bromonium ion intermediate.[6]

In conclusion, the assumption of a symmetric cyclic bromonium ion mediating in the bromination of BF is confirmative. The stereochemistry of addition, exclusively *trans*, conforms to this assumption.

Experimental

Materials. The preparation of benzofuran (BF) derivatives was described previously.[1] Acetic acid was refluxed overnight over triacetyl borate and distilled. Bromine and sodium azide were of the best grade commercially available.

Bromination in CS_2. The solutions of BF and Br_2 in CS_2 were prepared separately (*ca.* 1 M) and mixed together at room temperature. Color of Br_2 faded in 1 hr. The reaction mixture was washed with aqueous sodium thiosulfate (0.01 N) and then water. Drying with anhydrous sodium sulfate and evaporation of the solvent left white solid. Recrystallization from petroleum ether gave 2,3-dibromo-2,3-dihydrobenzofuran melting at 86 °C (lit,[16] 86—87 °C). NMR (CCl_4); δ 5.67 (s, 1, 3-H), 6.81 (s, 1, 2-H), and 7—7.5 (m, 4, aromatic H).

Bromination in Acetic Acid. Reaction of equimolar BF and Br_2 (1 M) was carried out in the same way as above. The ethereal extract was dried (Na_2SO_4) and concentrated *in vacuo* leaving an oily product. NMR spectrum of the product was essentially the same as that of the dibromide obtained in CS_2 with indication of the formation of a small amount of acetate (~10%); NMR (CCl_4), δ 2.0 (s, $OCOCH_3$).

Bromination in Methanol. The solutions of 1 M Br_2 in methanol and 1 M BF in methanol were mixed together at room temperature. The color of Br_2 faded essentially in 15 min. The reaction mixture was withdrawn by a syringe at appropriate time intervals, added to 0.01 N sodium thiosulfate, and shaken with ether. The ethereal layer was washed with water, dried over sodium sulfate, and evaporated to dryness leaving an oily product, which was applied to NMR analysis. The final product after 3 hr reaction was 2,3-dimethoxy-2,3-dihydrobenzofuran, which was isolated by distillation in 60% yield, boiling at 130—132 °C (5 mm). NMR (CCl_4); δ 3.31 (s, 3, 3-CH_3O), 3.48 (s, 3, 2-CH_3O), 4.53 (broad s, 1, 3-H), 5.26 (d, J=1.4 Hz, 1, 2-H), and 6.6—7.3 (m, 4, aromatic H).

Reaction with Bromine Azide. A solution of BrN_3 in CH_2Cl_2 was prepared according to the method of Hassner *et al.*[9] To this solution, an equimolar amount of BF was added under stirring at 0 °C and left to stand for 3 hr. The solvent was evaporated under reduced pressure to yield an oil. This crude oil was applied to spectral analyses. NMR spectrum showed that the product is essentially pure bromoazide. NMR (CCl_4); δ 5.03 (broad s, 1, 3-H), 6.03 (d, J=1.2 Hz, 1, 2-H), and 6.9—7.5 (m, 4, aromatic H).

The reaction of the bromoazide with methanol in the presence of $AgClO_4$ gave quantitatively a methoxyazide (an oil), which is a mixture of two isomers (1/2) by NMR spectrum. NMR (CCl_4); δ 3.28 (s, 1, CH_3O), 4.46 (broad s, 0.3, 3-H), 5.66 (d, J=1.2 Hz, 0.3 2-H), 3.47 (s, 2, CH_3O), 4.71 (d, J=5.8 Hz, 0.7) 5.17 (d, J=5.8 Hz, 0.7), and 6.7—7.3 (m, 4, aromatic H). IR (thin film); 2130 cm^{-1} (N_3).

The methoxyazide obtained above (1 g) was hydrolyzed at room temperature in acidic 50% aqueous dioxane (0.2 M HCl). After 5 hr of reaction, the reaction mixture was extracted with ether. The ethereal layer was then shaken with 0.1 M NaOH. The aqueous layer was acidified with 0.1 M HCl and extracted with ether again. The ether extract was washed with water, dried ($MgSO_4$), and evaporated under reduced pressure to leave an oil (0.2 g). IR (thin film); 3300 (broad, OH), 2110 (N_3), and 1675 cm^{-1} (C=O). The product was not pure but further attempts of purification was given up because of its high lability. It is considered from its IR spectrum and acidic character to be mainly *o*-hydroxyphenylazidoacetaldehyde.

Kinetic Measurements. The rate of bromine addition was followed spectrophotometrically at the bromine maximum of 395 nm (ε=200) with use of a Cary Model 15 spectrophotometer. Bromine concentration of a stock solution (10^{-2}—10^{-3} M in acetic acid) was determined by titration with standard thiosulfate. Ten ml of a bromine solution and 10 ml of a benzofuran solution in acetic acid were respectively thermally equilibrated at 25.0 °C, mixed together and placed in a stoppered quartz cuvette inserted in a water-

jacketed cell holder. The decrease of bromine absorption was followed.

Footnotes

1) Part I: T. Okuyama and T. Fueno, This Bulletin, the preceding paper.

2) L. A. Paquette, "Principles of Modern Heterocyclic Chemistry," W. A. Benjamin, Inc., New York, N. Y., (1968), Chapt. 5.

3) R. Stroermer, *Ann.*, **312**, 237 (1900).

4) G. Kraemer and A. Spilker, *Ber.*, **23**, 78 (1890).

5) For reviews, see a) P. B. D. de la Mare and R. Bolton, "Electrophilic Additions to Unsaturated Systems," Elsevier, Amsterdam, (1966), Chapt. 7; b) R. C. Fahey, *Top. Stereochem.*, **3**, 237 (1968).

6) K. Yates and W. V. Wright, *Can. J. Chem.*, **45**, 167 (1967).

7) R. C. Fahey and H.-J. Schneider, *J. Amer. Chem. Soc.*, **90**, 4429 (1968).

8) J. H. Rolston and K. Yates, *ibid.*, **91**, 1469, 1477, 1483 (1969).

9) A. Hassner, F. P. Boerwinkle, and A. B. Levy, *ibid.*, **92**, 4879 (1970).

10) D. P. Brust, D. S. Tarbell, S. M. Hecht, E. C. Hayward, and L. D. Colebrook, *J. Org. Chem.*, **31**, 2192 (1966).

11) M. Karplus, *J. Amer. Chem. Soc.*, **85**, 2870 (1963).

12) H. H. Jaffé, *ibid.*, **76**, 4261 (1954). Noyce and Nichols (*J. Org. Chem.*, **37**, 4306, 4311 (1972)) have recently treated the solvolysis rates of 2- and 3-benzofuryl derivatives in terms of the σ_{ij} parameters. However, such treatments are not adequate to the reactions such as those concerned here, during which the aromatic skeleton is partly broken by the addition.

13) T. Fueno, T. Okuyama, T. Deguchi, and J. Furukawa, *J. Amer. Chem. Soc.*, **87**, 170 (1965); O. Kajimoto, Doctorate thesis, Osaka University, 1971. See further Ref. 14 for the comparisons of ρ's like this.

14) T. Fueno, T. Okuyama, I. Matsumura, and J. Furukawa, *J. Polym. Sci. A-1*, **7**, 1447 (1969).

15) Rolston and Yates[8] have reported $\rho^+ \simeq -4.5$ for the bromination of reactive styrene derivatives. The reaction of these styrene derivatives is considered to involve highly unsymmetric (α-carbonium ion-like) transition state.

16) B. B. Corson, H. E. Tiefenthal, J. E. Nickels, and W. J. Heintzelman, *J. Amer. Chem. Soc.*, **77**, 5428 (1955).

Substituent Effects in the Benzofuran System. III.[1] Cationic Polymerization

Tadashi OKUYAMA, Kiyomitsu KUNUGIZA, and Takayuki FUENO

Department of Chemistry, Faculty of Engineering Science, Osaka University, Toyonaka, Osaka 560

(Received August 7, 1973)

Cationic copolymerizations of various pairs of benzofuran derivatives have been carried out in CH_2Cl_2 using $SnCl_4$–CCl_3CO_2H (2: 1) as catalyst at 0 °C. Effects of 2- and 3-methyl substitutions on the monomer reactivity ratio suggested that the polymeric cation adds at the 2-carbon of benzofuran. Analysis of the effects of 5- and 6-substituents on the reactivity revealed that the transmission efficiency of electronic effects through the two paths, the bonds 8–3 and 9–1–2, is comparable in magnitude. It was concluded that the transition state of the propagation step closely resembles a bridged carbonium ion intermediate.

The bromination of benzofuran (BF) was treated in the preceding paper[1] as a typical example of electrophilic addition reactions. Cationic polymerization includes chain reactions of addition of a polymeric carbonium ion and can be classified as an electrophilic addition reaction.

Cationic polymerizability of BF has long been known since Kraemer and Spilker[2] noted the resinification upon treating BF with sulfuric acid. More recently, BF has attracted the attention of polymer chemists because of its possible formation of optically active polymers.[3] However, the orientation of the reaction is not established, being considered as styrene(ST)-type[4] or vinyl ether(VE)-type.[3b]

On the other hand, we have concluded, by a series of investigations on the structure-reactivity relationship of α,β-unsaturated ethers,[5] that the transition state in the carbonium-ion attack (propagation step) in the cationic polymerization closely resembles a symmetric cyclic carbonium ion like I.

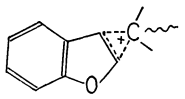

I

This possible symmetric nature of the transition state can be judged by the analysis of the cross-ring transmission of the electronic effects of 5- and 6-substituents on the polymerizability of BF.

Thus, the present investigation concerns with the orientation of polymerization and the substituent effects on the reactivity of BF.

Results

Cationic copolymerizations of various pairs of BF derivatives were carried out in methylene chloride at 0 °C with the use of stannic chloride–trichloroacetic acid (2: 1) as catalyst. The reaction proceeds easily under these conditions; *e.g.*, *ca.* 30% conversion in 1 hr for the 1: 1 pair of BF and the 5-methyl derivative.

The monomer reactivity ratios calculated with the aid of the integral form of the Mayo-Lewis copolymerization equation[6] are given in Table 1. The table includes values of r_1r_2 and $(r_2/r_1)^{1/2}$. The products r_1r_2 provide information about the nature of an attacking polymeric cation and the values $(r_2/r_1)^{1/2}$ are considered to be the best estimation of relative polymerizability of M_2 and M_1.[6,7]

The 6-methoxy and 5-chloro derivatives showed reactivities greatly different from those of other derivatives, and accurate evaluation of the monomer reactivity ratios for the systems involving these derivatives has hardly been achieved. Hence, the reactivities of these derivatives have been estimated by the log-log method, which was conveniently used for the styryl ether system.[7] The relative polymerizability, r, of M_2 and M_1 is expressed as

Table 2. The relative polymerizability, R, of benzofuran derivatives

Substituent	R[a]
H	(1.00)[b]
5-CH_3	4.81 ± 0.70
6-CH_3	6.03 ± 0.21
5-CH_3O	12.9 ± 0.9
6-CH_3O	241 ±24
5-Cl	0.017± 0.002

a) Shown with standard deviation.
b) Reference value.

Table 1. Monomer reactivity ratios[a] for the cationic copolymerization of benzofuran derivatives

Substituent M_1	Substituent M_2	r_1	r_2	r_1r_2	$(r_2/r_1)^{1/2}$
H	2-CH_3	0.25±0.06	0.74±0.01	0.19	1.72±0.24
H	3-CH_3	0.12±0.18	0.50±0.08	0.06	2.04±1.54
H	5-CH_3	0.21±0.06	4.86±0.24	1.02	4.81±0.70
H	5-CH_3O	0.16±0.01	5.83±0.17	0.93	6.03±0.21
5-CH_3O	6-CH_3	0.63±0.05	2.89±0.27	1.82	2.14±0.13
6-CH_3	6-CH_3O				18.7 ±1.3[b]
5-Cl	H				60.5 ±7.3[b]

a) Shown with standard deviation. b) Estimated by the log-log treatment.

$$r = \frac{\log [M_2]/[M_2]_0}{\log [M_1]/[M_1]_0} \quad (2)$$

The results are included in Table 1.

From $(r_2/r_1)^{1/2}$ and r values given in Table 1, the polymerizabilities, R, relative to the unsubstituted BF were calculated and summarized in Table 2. All the methyl and methoxy derivatives are more reactive than the parent BF. The 6-methoxy substitution greatly enhances the reactivity of BF. The 5-chloro derivative is *ca.* 1/60 as reactive as BF.

Discussion

Effect of the 2- and 3-Methyl Groups. As is seen in Table 1, the product r_1r_2 is much less than unity for the system comprising BF (M_1) and the 2- or 3-methyl derivative (M_2), implying the difference in the nature of attacking cations, M_1^+ and M_2^+. The methyl substitution at either of the 2- and 3-positions enhances the reactivity of BF toward $M_1^+(r_1<1)$, whereas the methyl substitution reduces the reactivity of BF toward $M_2^+(r_2<1)$. The reduction in the reactivity must be attributed to the steric effect of the methyl group close to the reaction center. This steric effect is greater for the 3-methyl than for the 2-methyl group, suggesting the formation of 3-cation. That is, the orientation of the ST-type in polymerization is very probable, in accord with the results of bromination.[1]

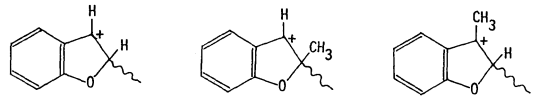

The enhancement in reactivity toward M_1^+ by either 2- or 3-methyl substitution (4 or 8 times) may be reasonably explained by assuming a cyclic onium-type transition state.[8]

Cross-ring Substituent Effects. The effects of 5- and 6-substituents on the polymerizability of BF given in Table 2 can be analyzed by the Jaffé equation;[9]

$$\log R = \rho_1\sigma_1 + \rho_2\sigma_2 \quad (3)$$

where suffixes 1 and 2 refer to the values concerning the transmitting routes 8–3 (ST-type) and 9–1–2 (PVE-type), respectively.

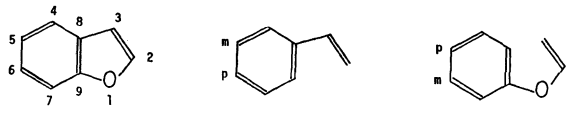

BF ST PVE

The least-squares treatment of R according to Eq. (3) gave $\rho_1=-3.39\pm0.19$ and $\rho_2=-2.79\pm0.34$. Brown-Okamoto's σ^+ values were used for σ_1. Linearity of the calculated and the observed values of $\log R$ is illustrated in Fig. 1.

The contribution of the PVE-type transmission to the observed substituent effects is nearly as great as that of the ST-type in spite of the orientation of addition of the ST-type. This situation is similar to that of bromination.[1] These observations can be considered to be characteristic of symmetric transition state resembling a cyclic onium ion like I and seem to be

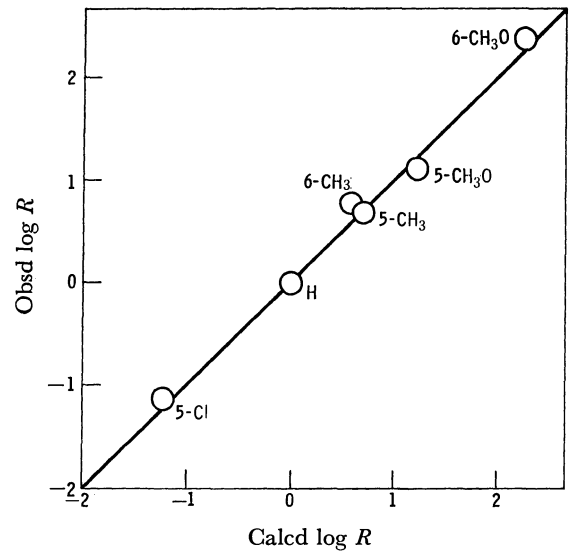

Fig. 1. Linearity of the observed and the calculated log R values (Eq. (3)).

explainable only by this assumption. Thus, the course of polymerization is represented by

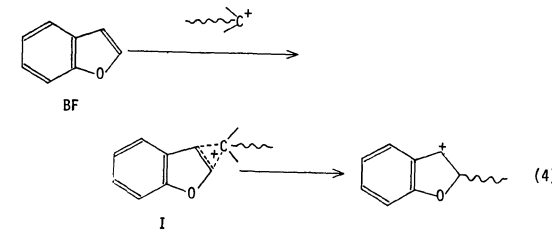

BF I (4)

The possibility of symmetric transition state like I has already been suggested by us for the cationic polymerization of vinyl monomers on the basis of various sources of evidence.[5] The present results provide additional confirmative evidence to support our earlier suggestion.[5]

The values ρ_1 and ρ_2 are compared with those for the cationic polymerization of ST and PVE; $\rho_{ST}^+=-2.03$[10] and $\rho_{PVE}=-1.76$.[11] Both ρ_1 and ρ_2 are appreciably greater in magnitude than ρ_{ST} and ρ_{PVE}, respectively. However, relative magnitude, $\rho_2/\rho_1=0.82$, is close to $\rho_{PVE}/\rho_{ST}=0.87$. The transmission efficiency through oxygen atom in cyclic compound, BF, is close to that in acyclic system, PVE.

All the observations in the BF polymerization conforms to the symmetric cyclic transition state which structurally resembles I.

Experimental

Materials. Benzofuran (BF) and its derivatives were obtained as described previously.[12] Methylene chloride was dried and distilled from calcium hydride. Tetralin and stannic chloride were purchased and distilled. Trichloroacetic acid was of the best grade commercially available.

Polymerization. Cationic copolymerization was carried out in methylene chloride under a nitrogen atmosphere at 0 °C by using stannic chloride–trichloroacetic acid (2:1) as catalyst. Monomer and catalyst concentrations were usually

7 vol% and 0.03 M, respectively. The detailed procedure was the same as described before.[6] Monomer reactivity ratios were calculated with the aid of the integral form of the Mayo-Lewis copolymerization equation by the least-squares method based on the VPC analysis as described previously.[6] The relative polymerizability of a great magnitude was estimated by the relative monomer consumption method (the log-log treatment).[7]

Roferences

1) Part II. T. Okuyama, K. Kunugiza, and T. Fueno, This Bulletin, the preceding paper.

2) G. Kraemer and A. Spilker, *Ber.*, **23**, 78 (1890).

3) (a) G. Natta, M. Farina, M. Peraldo, and G. Bressan, *Makromol. Chem.*, **43**, 68 (1961); (b) Y. Takeda, Y. Hayakawa, T. Fueno, and J. Furukawa, *ibid.*, **83**, 234 (1965); (c) Y. Hayakawa, T. Fueno, and J. Furukawa, *J. Polym. Sci. A-1*, **5**, 2099 (1967).

4) A. Mizote, T. Tanaka, T. Higashimura, and S. Okamura, *J. Polym. Sci. A-1*, **4**, 869 (1966).

5) See for a review, T. Okuyama and T. Fueno, *Kobunshi Kagaku*, **28**, 369 (1971).

6) T. Okuyama, T. Fueno, and J. Furukawa, *J. Polym. Sci. A-1*, **6**, 993 (1968).

7) T. Okuyama, N. Asami, and T. Fueno, This Bulletin, **43**, 3549 (1970).

8) G. M. Beverly and D. R. Hogg, *J. Chem. Soc. B*, **1971**, 175; R. C. Fahey and H. J. Schneider, *J. Amer. Chem. Soc.*, **90**, 4429 (1968).

9) H. H. Jaffé, *ibid.*, **76**, 4261 (1954).

10) J. P. Kennedy, in "Copolymerization," G. E. Ham, Ed., Interscience, New York, N. Y., 1964, p. 308.

11) T. Fueno, T. Okuyama, I. Matsumura, and J. Furukawa, *J. Polym. Sci. A-1*, **7**, 1447 (1969).

12) T. Okuyama and T. Fueno, This Bulletin, **47**, 1263 (1974).

Perkin Synthesis of Bromobenzalphthalides. Their Reactions with Amines and Hydrazine

A. M. Islam, A. M. Khalil, and A. A. El-Maghraby
Department of Chemistry, Al-Mansoura Faculty of Science, Al-Mansoura, A.R.E., Egypt
(Received February 28, 1973)

The isomeric 5-bromo- and 6-bromo-3-benzalphthalides were prepared by condensation of 4-bromophthalic anhydride with phenylacetic acids. The reaction of such isomeric bromobenzalphthalides with primary aromatic amines give the corresponding bromobenzalphthalimidines. Bromophthalazinone derivatives were obtained in good yields by the reatcion of bromobenzalphthalides with hydrazine hydrate.

It has been reported[1-4] that symmetric anhydrides react with phenylacetic acids in the presence of sodium or potassium acetate to give the corresponding monobenzal derivatives. The interaction of asymmetric anhydrides with phenylacetic acids in the Perkin reaction should lead to the formation of structural isomers.

The condensation of naphthalene-1,2-dicarboxylic[2] and 1-phenylnaphthalene-2,3-dicarboxylic anhydrides[3-4] with phenylacetic acid was reported to give only one isomer (I and II).

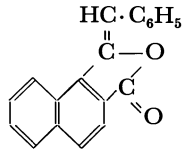

I

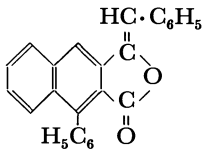

II

On the other hand, there are a few instances which report the isolation of two structural isomers from a Perkin condensation of phenylacetic acid with 3-nitrophthalic[5] and 4-nitrophthalic anhydrides,[6-7] though Zelmens and Vanages[8] isolated only one isomer (III) in the former case.

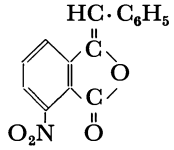

III

Recently, however, Islam[9] found that the condensation of 3-nitrophthalic anhydride with phenylacetic acid gives actually a mixture of the two structural isomers 4-nitro- and 7-nitro-3-benzalphthalides.

In the present investigation, we report that the condensation of 4-bromophthalic anhydride with phenylacetic or *p*-nitrophenylacetic acid gave isomeric bromobenzalphthalides (IVa—b) and (Va—b).

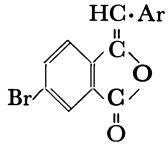

IV

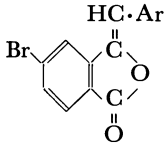

V

a: Ar=C_6H_5; b: Ar=$C_6H_4\cdot NO_2$-*p*

These products (IV—V) showed stretching frequency at 1780 cm^{-1} characteristic for benzalphthalides.[10]

The isomeric nature of these products was proved unequivocally by the fact that both (IVa) and (Va) were readily rearranged under the influence of sodium methoxide, to 5-bromo-2-phenylindan-1,3-dione (VIa). Similarly, both (IVb) and (Vb) were rearranged to 5-bromo-2-(*p*-nitrophenyl)indan-1,3-dione (VIb).

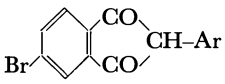

VI

a: Ar=C_6H_5; b: Ar=$C_6H_4\cdot NO_2$-*p*

The compounds (VI) showed stretching frequency at 1690—1655 cm^{-1} characteristic for the 1,3-dione group.[10]

Unequivocal chemical evidence for these structural isomers IVa, IVb, Va, and Vb was achieved by the direct synthesis of particular isomers.

Condensation of 6-bromophthalide with benzaldehyde in the presence of catalytic amounts of piperidine gave a product, mp 139 °C, identical with the product IVa. On this basis, the isomer IVa was identified as 3-benzal-6-bromophthalide, while the second isomer of high melting point 180 °C was tentatively given structure Va as 3-benzal-5-bromophthalide.

Similarly, condensation of 6-bromophthalide with *p*-nitrobenzaldehyde gave a product, mp 160 °C, identical with (IVb). The high melting isomer (mp 220 °C) was tentatively given structure (Vb).

It is worth to note that in this series, the benzalphthalides substituted at position 6 always possess lower melting points than the corresponding 5-substituted analogues.

In agreement with the previous work,[11] reaction of bromobenzalphthalides (IV) and (V) with amines gave the corresponding bromobenzalphthalimidines.

Thus, 3-benzal-6-bromophthalides (IVa—b) reacted readily with primary aromatic amines such as aniline,

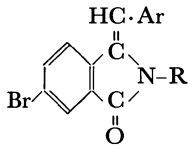

VII

a: Ar=C_6H_5; R=C_6H_5
b: Ar=C_6H_5; R=$C_6H_4\cdot CH_3$-*o*
c: Ar=C_6H_5; R=$C_6H_4\cdot CH_3$-*m*
d: Ar=C_6H_5; R=$C_6H_4\cdot CH_3$-*p*
e: Ar=C_6H_5; R=$C_6H_4\cdot NO_2$-*p*
f: Ar=$C_6H_4\cdot NO_2$-*p*; R=C_6H_5

o-toluidine, *m*-toluidine, *p*-toluidine, and *p*-nitroaniline to give the corresponding 2-aryl-3-benzal-6-bromophthalimidines (VIIa—f).

Similarly 3-benzal-5-bromophthalides (Va—b) reacted with the same amines to give the corresponding 2-aryl-3-benzal-5-bromophthalimidines (VIIIa—h).

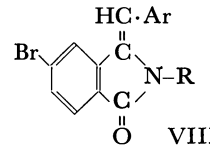

VIII

a: Ar=C_6H_5; R=C_6H_5
b: Ar=C_6H_5; R=$C_6H_4\cdot CH_3$-*o*
c: Ar=C_6H_5; R=$C_6H_4\cdot CH_3$-*m*
d: Ar=C_6H_5; R=$C_6H_4\cdot CH_3$-*p*
e: Ar=C_6H_5: R=$C_6H_4\cdot NO_2$-*p*
f: Ar=$C_6H_4\cdot NO_2$-*p*; R=C_6H_5
g: Ar=$C_6H_4\cdot NO_2$-*p*; R=$C_6H_4\cdot CH_3$-*p*
h: Ar=$C_6H_4\cdot NO_2$-*p*; R=$C_6H_4\cdot NO_2$-*p*

In agreement with the finding of Ephraim[12] and Islam,[9] the isomeric bromobenzalphthalides (IV, V) reacted readily with hydrazine hydrate in alcohol solution to give 4-arylmethyl-7-bromophthalazin-1-ones (IXa—b) and 4-arylmethyl-6-bromophthalazin-1-ones (Xa—b).

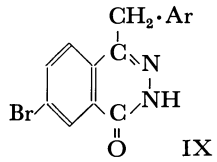

IX

a: Ar=C_6H_5
b: Ar=$C_6H_4\cdot NO_2$-*p*

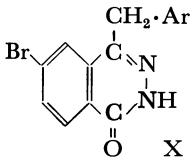

X

a: Ar=C_6H_5
b: Ar=$C_6H_4\cdot NO_2$-*p*

Experimental

Analytical data were determined in the microanalytical unit at Cairo University, Infra-red spectra were recorded on SP 1200 a Pye-Unicam Spectrophotometer. Melting points are uncorrected.

Condensation of 4-Bromophthalic Anhydride with Phenylacetic Acid. A mixture of 4-bromophthalic anhydride (22.7 g), phenylacetic acid (13.6 g) and freshly fused sodium acetate (2.0 g) was fused together at 180—200 °C for one hour. The cold reaction mass was washed with dilute sodium carbonate solution (100 ml) to remove unreacted materials. The remaining solid (15 g, 50%) was extracted with boiling ethanol (100 ml), which on crystallization gave 3-benzal-6-bromophthalide (IVa) (9.0 g, 30%) as yellow powder, mp 139—141 °C. Found: C, 60.26; H, 3.38; Br, 27.0%. Calcd for $C_{15}H_9O_2Br$: C, 59.80; H, 3.00; Br, 26.58%.

The alcohol-insoluble residue was recrystallized from acetic acid to give 3-benzal-5-bromophthalide (Va), (4.5 g, 15%) as pale yellow crystals, mp 180—182 °C. Found: C, 59.67; H, 3.22; Br, 26.9%. Calcd for $C_{15}H_9O_2Br$: C, 59.80; H, 3.00; Br, 26.58%.

5-Bromo-2-phenylindan-1,3-dione (VIa). A solution of (IVa) (3 g) in methanol (80 ml) was treated with sodium methoxide solution (100 ml) and the mixture was heated under reflux for 1 hr. The cold mixture was diluted with water and acidified with cold dilute sulphuric acid. Recrystallization of the obtained brown solid from methanol gave (VIa) (1.4 g, 46.4%) as reddish-brown prisms, mp 164—165 °C. Found: C, 60.15; H, 3.44%. Calcd for $C_{15}H_9O_2Br$: C, 59.80; H, 3.00%.

Similarly, (Va) (3 g) gave the same product (VIa) (1.2 g, 40%).

Condensation of 4-Bromophthalic Anhydride with p-*Nitrophenyl-*

Table 1. Reaction of bromobenzalphthalides with amines

Bromobenzal-phthalide	Amine	Product	Solv. of crystn.	Colour	Mp (°C)	Yield (%)	Analysis %: Calcd / Found C	H	N
IVa	Aniline	VIIa	AcOH	Creamy	188	65	67.02	3.72	3.72
							67.23	3.65	3.32
IVa	*o*-Toluidine	VIIb	EtOH	Colourless	167	92	67.69	4.10	3.58
							66.54	4.03	3.12
IVa	*m*-Toluidine	VIIc	AcOH	White	175	72	67.69	4.10	3.58
							67.28	3.82	3.43
IVa	*p*-Toluidine	VIId	EtOH	Pale yellow	149	82	67.69	4.10	3.58
							66.94	4.62	3.42
IVa	*p*-Nitroaniline	VIIe	AcOH	Yellow	195	66	59.85	3.08	6.65
							59.32	2.94	6.55
IVb	Aniline	VIIf	AcOH	Yellow	184	63	59.85	3.08	6.65
							59.63	3.11	6.30
IVa	Aniline	VIIIa	AcOH	White	192	59	67.02	3.72	3.72
							67.08	3.63	3.43
IVa	*o*-Toluidine	VIIIb	EtOH	Colourless	198	92	67.69	4.10	3.58
							66.99	3.92	3.33
Va	*m*-Toluidine	VIIIc	AcOH	White	205	82	67.69	4.10	3.58
							67.41	3.71	3.35
Va	*p*-Toluidine	VIIId	EtOH	Cream	176	77	67.69	4.10	3.58
							67.04	3.63	3.64
Va	*p*-Nitroaniline	VIIIe	AcOH	Pale yellow	212	74	59.85	3.08	6.65
							59.08	3.12	6.86
Va	Aniline	VIIIf	EtOH	Yellow	224	76	59.85	3.08	6.65
							59.71	2.88	6.55
Vb	*p*-Toluidine	VIIIg	EtOH	Yellow orange	241	69	60.68	3.44	6.43
							60.51	3.30	6.86
Vb	*p*-Nitroaniline	VIIIh	AcOH	Yellow	205	76	54.07	2.57	9.01
							54.00	2.41	8.78

acetic Acid. A mixture of 4-bromophthalic anhydride (22.7 g), *p*-nitrophenylacetic acid (18.1 g) and freshly fused sodium acetate (2 g) was fused together at 220—240 °C for one hour. The cold mass was washed with dilute sodium carbonate solution, boiled with acetic acid, and cooled. The insoluble part was recrystallized from acetic acid to give 5-bromo-3-(*p*-nitrobenzal)-phthalide (Vb) (8.1 g, 23%) as yellow crystals, mp 219—221 °C. Found: C, 51.94; H, 2.19; N, 3.92%. Calcd for $C_{15}H_8NO_4Br$: C, 52.02; H, 2.31; N, 4.04%.

The mother-liquor gave, on concentration and addition of ethanol, a dark yellow solid which was recrystallized from dilute acetic acid to give 3-(*p*-nitrobenzal)-6-bromophthalide (IVb) (2.7 g, 8%) as yellow crystals, mp 159—161 °C. Found: C, 51.87; H, 2.41; N, 4.23%. Calcd for $C_{15}H_8NO_4Br$: C, 52.02; H, 2.31; N, 4.04%.

*5-Bromo-2-(*p*-nitrophenyl)-indan-1,3-dione* (VI*b*). A mixture of (IVb) (3.4 g) and methanol (100 ml) was heated with sodium methoxide solution (100 ml) under reflux for one hour. The cold reaction mixture was diluted with water (100 ml) and acidified with cold dilute sulphuric acid. Recrystallization of the reddish brown solid obtained from acetic acid gave (VIb) (2.1 g, 63%) as reddish brown needles, mp 199—200 °C. Found: C, 51.73; H, 1.98; N, 4.12%. Calcd for $C_{15}H_8NO_4Br$: C, 52.02; H, 2.31; N, 4.04%.

Similarly, (Vb) (3.4 g) gave the same compound (VIb) (1.9 g, 65%), mp 199—200 °C.

3-Benzal-6-bromophthalide (IVa). A mixture of 6-bromo phthalide (2.2 g), benzaldehyde (1 g) and 3 drops of piperidine was fused at 220—240 °C for 3 hr. After being cooled, the obtained solid was recrystallized from ethanol to give (IVa), mp 139—141 °C (1.4 g, 47%) as yellow crystals. The melting point did not depress when mixed with a sample of (IVa) obtained from 4-bromophthalic anhydride.

*3-(*p*-Nitrobenzal)-6-bromophthalide (IVb).* A mixture of 6-bromophthalide (2.2 g), *p*-nitrobenzaldehyde (1.5 g) was treated similarly. The obtained solid was recrystallized from acetic acid to give (IVb) (2.1 g, 61%) as pale yellow crystals, mp 159—161 °C. The melting point did not depress when mixed with a sample of (IVb) obtained from 4-bromophthalic anhydride.

Bromobenzalphthalimidine (VII—VIII). A mixture of the bromobenzalphthalides (0.1 mol) and appropriate amine (0.12 mol) in acetic acid (30 ml) containing freshly fused sodium acetate (0.1 g) was heated under reflux for 36 hr.

Table 2. Reaction of bromobenzalphthalides with hydrazine

Bromobenzal-phthalide	Product	Mp (°C)	Yield (%)	Analysis %: Calcd / Found C	H	N
IVa	IXa	175—177	66	57.14	3.49	8.88
				57.01	3.32	8.90
IVb	IXb	175—177	55	50.00	2.77	11.66
				49.72	2.61	11.91
Va	Xa	196—198	79	57.14	3.49	8.88
				57.11	3.22	8.71
Vb	Xb	235—236	77	50.00	2.77	11.66
				49.91	2.53	12.01

The reaction mixture was decomposed with dilute hydrochloric acid. Recrystallization of the product gave the corresponding bromobenzalphthalimidines (*cf.* Table 1).

Bromophthalazones (IX—X). A mixture of bromobenzalphthalides (0.1 mol) and hydrazine hydrate (3 ml, excess) in ethanol (30 ml) was heated under reflux for 20 min. The cold solution was diluted with water (70 ml). Recrystallization of the obtained solid from ethanol gave the corresponding bromophthalazones as colourless crystals (*cf.* Table 2).

References

1) S. Gabriel, *Ber.*, **18**, 3470 (1885).
2) C. F. Keolsch, *J. Org. Chem.*, **10**, 366 (1945).
3) O. M. Aly, W. I. Awad, and A. M. Islam, *ibid.*, **22**, 517 (1957).
4) O. M. Aly, W. I. Awad, and A. M. Islam, *ibid.*, **23**, 1624 (1958).
5) P. Hrnciar and D. Joniak, *Chem. Zvest.*, **20**,(5) 336 (1966).
6) E. Leupold, *Ber.*, **34**, 2836 (1901).
7) J. Klosa, *Pharmazie*, **9**, 682 (1945).
8) V. Zelmens and G. Vanages, *Dokl. Akad. Nauk S.S.S.R.*, **109**, 535–536 (1956).
9) A. M. Islam, *et al.*, unpublished work.
10) L. J. Bellamy, "The Infra-red Spectra of Complex Molecules," John Wiley, N.Y. (1959), p. 214.
11) I. B. Hannout, S. A. Hassan, A. M. Islam, and I. M. Ismail, *U.A.R. J. Chem.*, **13**, (2), 199 (1970).
12) J. Ephraim, *Ber.*, **26**, 1376 (1893).

Bitter Principles of *Isodon umbrosus* HARA. The Structures of Umbrosin A and B

Isao KUBO, Tadao KAMIKAWA, Takahiko ISOBE,* and Takashi KUBOTA**

Faculty of Science, Osaka City University, Sugimoto, Sumiyoshi, Osaka 558

(Received November 15, 1973)

Two new *ent*-kaurene derivatives have been isolated from *Isodon umbrosus* HARA and formulated by spectroscopic and chemical evidence as structures (**1**) and (**2**), respectively. Antimicrobial activity has been tested.

Our continuing investigation of the bitter principles of various *Isodon* species (Labiatae) has led to the isolation of several new diterpenes, which have been assumed to possess enmein or kaurene type skeletons on the basis of spectral and chemical evidence.[1]

We should now like to report the structures of umbrosin A (**1**), $C_{20}H_{30}O_4$, mp 225—228 °C(decomp.), $[\alpha]_D$ −126° (c=1.0, pyridine), and umbrosin B (**2**), $C_{20}H_{28}O_4$, mp 262—265 °C (decomp.), $[\alpha]_D$ −150° (c=1.0, pyridine). Both compounds display a highly specific antibacterial activity against gram positive bacteria.[2]

Results and Discussion

The main bitter principle, umbrosin A (**1**) exhibits a UV absorption at 233 nm (ε 8400), IR bands at 1730 and 1640 cm^{-1}, and NMR signals at 5.25 and 6.13 δ (1H, broad singlets), typical for a five-membered ring ketone conjugated with an exocyclic methylene group, as exemplified by the D-ring of enmein[3] and oridonin.[4] Its environment was confirmed by spin decoupling, thus: the irradiation of the H_c proton at 3.05 δ (1H), collapsed the broad singlets of the H_a and H_b protons to sharp singlets, showing the removal of allylic coupling. The other broad singlet of the H_d proton at 4.90 δ (1H) also collapsed to a sharp singlet. The appearance of a broad singlet for the H_d proton indicates the dihedral angle between the protons H_c and H_d to be roughly 90°.

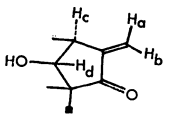

1_A

In addition, the IR spectrum shows the presence of hydroxyl groups at 3300 cm^{-1}, and the NMR spectrum exhibits evidence for three tertiary methyl groups at 0.85, 0.90, and 1.04 δ (3H, singlets), and for two other methine protons on oxygenated carbons at 3.96 and 4.45 δ (discussed later).

Umbrosin A forms a triacetate (**3**), $C_{26}H_{36}O_7$, mp 187—189 °C, of which IR spectrum shows no hydroxyl group, indicating that three oxygen atoms in umbrosin A are unhindered hydroxyl groups. These data and the analogy with congeners isolated from *Isodon* species support a tetracyclic diterpene structure with the *ent*-kaurene type skeleton for umbrosin A, in which the partial structure $\mathbf{1}_A$ would form the D-ring and the hydroxyl group should be situated at C_{14} and α-oriented.

Catalytic hydrogenation of umbrosin A, followed by oxidation with Jones' reagent, gave a diketone (**4**), $C_{20}H_{30}O_4$, of which IR spectrum still shows the presence of hydroxyl groups at 3300 cm^{-1} and a newly produced band due to a six-membered ring ketone at 1710 cm^{-1}. The latter compound yielded a diacetate (**5**), $C_{24}H_{34}O_6$ which exhibits in the NMR spectrum the signals of two acetoxyl groups, indicating that one hydroxyl group was oxidised and the other two were resistant to Jones' oxidative condition. This can be rationalized by assuming an intramolecular hydrogen bond between the two hydroxyl groups, which suggests, in turn, the O—O distance in the –O–H···O–H group is within 3 Å.[5] This assumption is also supported by the formation of an acetonide (**6**), $C_{23}H_{34}O_4$ and a phenylboronate (**7**),[6] $C_{26}H_{33}O_4B$ of umbrosin A, respectively.

In the NMR spectrum of **4**, the signals at 4.34 δ (1H, doublet of doublets, $J_{ax\text{-}ax}$=13 and $J_{ax\text{-}eq}$=5 Hz) and 4.93 δ (1H, broad singlet) were assigned to the protons on carbons bearing hydroxyl group. The appearance of a broad singlet for the latter signal shows that the $C_{14\beta}$ proton still remains in **4** and the coupling constant of the former signal is evidence of the axial nature. An examination of Dreiding model indicates that only when a second hydroxyl group is located at C_7 and β-oriented in the assumed skeleton are the above data explicable. The structure of umbrosin A can therefore be represented by $\mathbf{1}_B$, in which the position and configuration of the third secondary hydroxyl group remain to be settled.

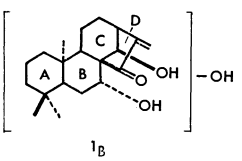

1_B

The mass spectrum of umbrosin A allows the possibility of the existence of the hydroxyl group on the A-ring. Thus, it shows a molecular ion at m/e 334 and intense fragment ions at m/e 316, 301, 298, 283, 194, 176, 140, 122, and 107. The most prominent peaks belong to the fragments formed by cleavage of the B-ring; this can be initiated by α-cleavage of the C_{15} ketonic carbonyl group producing the m/e 194 radical ion **a**. The formation of the ion **a** affords a

* Present address: Hyogo College of Medicine, Mukogawa, Nishinomiya, Hyogo 663

** Present address: Kinki University, Kowakae, Higashi-osaka, Osaka 577

TABLE 1. NMR SPECTRA OF UMBROSIN A AND B, AND SOME DERIVATIVES (in ppm)[a)]

Compounds	CH_3–C	COC=CH_2	$C_{2\alpha}H$–OH	$C_{7\beta}H$–OH	$C_{14\alpha}H$–OH
1	0.85(s) 0.90(s) 1.04(s)	5.25(bs) 6.13(bs)	3.97(tt, $J_{ax-ax}=12$, $J_{ax-eq}=4$)	4.45(dd, $J_{ax-eq}=13$, $J_{ax-eq}=5$)	4.90(bs)
2	0.85(s) 1.05(s) 1.20(s)	5.45(bs) 6.30(bs)		4.65(dd, $J_{ax-ax}=14$, $J_{ax-eq}=5$)	4.95(bs)
3	0.94(s) 0.96(s) 1.30(s)	5.36(bs) 6.12(bs)	5.07(tt, $J_{ax-ax}=12$, $J_{ax-eq}=4$)	5.20(dd, $J_{ax-ax}=14$, $J_{ax-eq}=5$)	6.00(bs)
6	0.87(s) 0.94(s) 1.06(s) 1.20(s) 1.54(s)	5.35(bs) 6.25(bs)	3.83(tt, $J_{ax-ax}=12$, $J_{ax-eq}=4$)	4.16(dd, $J_{ax-ax}=14$, $J_{ax-eq}=5$)	4.53(d, $J=2$)
4	0.86(s) 1.05(s) 1.13(s)			4.34(dd, $J_{ax-ax}=14$, $J_{ax-eq}=5$)	4.93(bs)

a) Determind in C_5D_5N (**1**, **2** and **4**) or in $CDCl_3$ (**3** and **6**) at 100 MHz. Coupling constants are expressed in Hz. s: singlet, bs: broad singlet, dd: doublet of doublets, tt: triplet of triplets.

convenient means of locating the remaining hydroxyl group in **1B**.

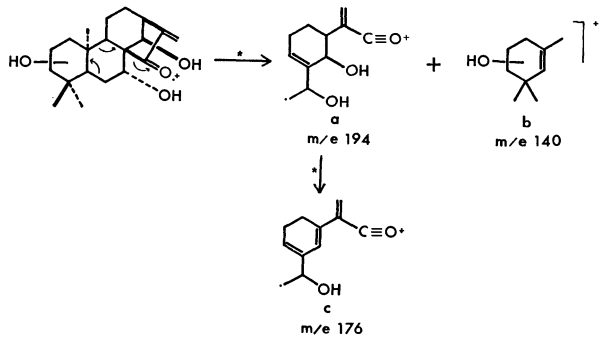

On the other hand, the NMR spectrum of umbrosin A indicates a signal at 3.97 δ (1H, triplet of triplets, $J_{ax-ax}=12$ and $J_{ax-eq}=4$ Hz) which disappeared on oxidation. The multiplicity and coupling constants of the signal can only arise by interaction of an axial proton with two neibouring axial and two equatorial protons. Hence the third secondary hydroxyl group must be placed at C_2 and α-oriented. The splitting pattern of this proton is quite similar to that of the $C_{2\beta}$ proton of creticoside A isolated from *Pteris cretica* L.[7,8)]

Finally the structure was confirmed by correlation with mebadonin (**8**)[9)] isolated from *Isodon kameba* OKUYAMA, whose structure was determined by X-ray analysis. Catalytic hydrogenation of mebadonin, followed by oxidation with Jones' reagent, gave the same diketone (**4**), and therefore umbrosin A must be represented by **1**, that is *ent*-15-oxokaur-16-ene-2α, 7β,14α-triol. It was also found in *Isodon kameba* OKUYAMA.

A minor bitter principle, umbrosin B (**2**) isolated from a less polar fraction, differs from umbrosin A by having two fewer hydrogens, and shows the presence of a six-membered ring ketone at 1710 cm^{-1} in the IR spectrum. It exhibits the similar NMR to that of umbrosin A, with the exception of lack $C_{2\beta}$ proton at 3.97 δ present in the latter. This suggests that the structure of umbrosin B is *ent*-2,15-dioxokaur-16-ene-7β,14α-diol. Its correlation with umbrosin A was carried out by catalytic hydrogenation of umbrosin B, which yielded **4** in good yield.

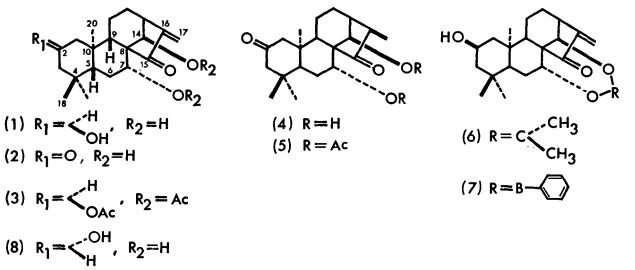

Experimental

NMR spectra were determined at 100 MHz using a JEOL PS-100 spectrometer. Mass spectra were measured with a Hitachi RMU-6 spectrometer, high resolution spectra being obtained with a JEOL JMS-D100 instrument. IR spectra were recorded on Nujol mull with a JASCO IRA-1 spectrophotometer. UV data were measured with a Hitachi EPS-2 spectrometer. A Rex Optical Works model NEP-2 was used to measure the optical rotations. Column chromatography was performed on Mallinckrodt silicic acid. Mps were taken in glass capillaries and uncorrected.

Isolation. The dried leaves (1.5 kg) of *Isodon umbrosus* HARA collected near Mt. Amagi (Shizuoka) were extracted with ether (20.5 l). The crude extract was treated with activated charcoal (50 g), concentrated and left to cool overnight. Then a solid (11.4 g) was filtrated off. The filtrate was chromatographed on silicic acid (250 g). Elution with 3% methanol in chloroform gave umbrosin B and A in this order.

Umbrosin A (1). The crude fractions (1.56 g) were recrystallized from ethanol to give pure umbrosin A, as fine needles, mp 225—228° (decomp.), $[\alpha]_D$ −126° ($c=1.0$, pyridine), UV (ethanol) 233 nm (ε 8000), IR (Nujol) 3250, 1730, 1640, 1080 and 1040 cm^{-1}, NMR (see Table 1), Mass *m/e* 334 (M^+), 316 ($M-H_2O$), 298 ($M-2H_2O$), 283 ($M-2H_2O-CH_3$), 194, 176, 149, 122, 107 and 105. (Found: C, 71.34; H, 9.52%. Calcd for $C_{20}H_{30}O_4$: C, 71.82; H, 9.04%),

High resolution mass: 334.2168. $C_{20}H_{30}O_4$ requires: 334.2144.

Umbrosin B (2). The less polar fractions (23 mg) were recrystallized from ethanol to give pure umbrosin B, as needles, mp 262—265° (decomp.), $[\alpha]_D$ −150° (c=1.0, pyridine), UV (ethanol) 232.5 nm (ε 8700), IR (Nujol) 3430, 3200, 1730, 1710, and 1080 cm^{-1}, NMR (see Table 1), Mass m/e 332 (M^+), 314 ($M-H_2O$), 194 and 176. (Found: C, 72.16; H, 8.80%. Calcd for $C_{20}H_{28}O_4$: C, 72.26; H, 8.49%).

Triacetylumbrosin A (3). A solution of umbrosin A (82 mg) in acetic anhydride (1 ml) and pyridine (0.5 ml) was treated as usual manner and recrystallized from acetone–hexane to give the triacetylumbrosin A (**3**), (74 mg), as fine needles, mp 187—189°, IR (Nujol) 1720, 1640 and 1230 cm^{-1}, NMR (see Table 1) also 1.93, 2.00, and 2.05 δ (3H, singlets, $OCOCH_3$), (Found: C, 67.62; H, 8.35%. Calcd for $C_{26}H_{36}O_7$: C, 67.80; H, 7.88%).

Bisdehydrodihydroumbrosin A (4). Umbrosin A (190 mg) in ethanol (10 ml) was hydrogenated over 10% Pd-C (20 mg) for 3 hr. The catalyst was removed by filtration. Then the filtrate was evaporated and crystallized from ethanol to yield the dihydroumbrosin A (185 mg), as rods, mp 239—243 °C (decomp.), IR (Nujol) 3300, 3080, and 1740 cm^{-1}, (Found: C, 71.05; H, 9.43%. Calcd for $C_{20}H_{32}O_4$: C, 71.39; H, 9.59%). To a solution of dihydroumbrosin A (100 mg) in acetone (25 ml) was added Jones' reagent (1 ml) dropwise with stirring and ice cooling. The reaction was complete within 10 min, the mixture was stirred for further 10 min, then worked up by dilution with water (25 ml) and concentrated *in vacuo* to remove acetone. The white precipitate was filtered off and chromatographed on silicic acid (1 g). Elution with chloroform gave the bisdehydrodihydroumbrosin A (83 mg) which was recrystallized from ethanol to give the pure compound, as needles, mp 254—259° (decomp.), $[\alpha]_D$ −126° (c=1.0, pyridine) IR (nujol) 3450, 3200, 1740, and 1710 cm^{-1}, NMR (see Table 1), strongly positive Zimmermann test, (Found: C, 71.95; H, 9.13%. Calcd for $C_{20}H_{30}O_4$: 71.82; H, 9.04%).

Acetylbisdehydrodihydroumbrosin A (5). Bisdehydrodihydroumbrosin A (45 mg) was treated as described above to yield the acetylbisdehydrodihydroumbrosin A (37 mg), as needles, mp 178—179 °C, IR (Nujol) 1740, 1710, and 1260 cm^{-1}, NMR ($CDCl_3$) 1.90 and 2.00 δ (3H, singlets, $OCOCH_3$).

Isopropylideneumbrosin A (6). To a solution of umbrosin A (150 mg) in acetone (25 ml) was added concd sulfuric acid (2 drops). The mixture was left at room temperature for 6 days and then extracted with chloroform (200 ml). The extract was washed with sodium bicarbonate solution and water, dried over magnesium sulfate and evaporated to dryness. The residue was chromatographed on silicic acid, elution with chloroform gave the isopropylideneumbrosin A (51 mg), which was recrystallized from acetone–hexane to yield the pure material, as needles, mp 200—201 °C, IR (Nujol) 3320, 1730, 1645, 1115, and 1030 cm^{-1}, NMR (see Table 1), (Found: C, 73.65; H, 9.35%. Calcd for $C_{23}H_{36}O_4$: C, 73.36; H, 9.64%).

Umbrosin A-phenylboronate (7). Umbrosin A (105 mg) was treated in boiling benzene (25 ml) with phenylboronic acid (55 mg); water was removed with molecular sieves. Removal of the main part of the benzene and addition of ethanol caused the crystallization of the product; almost quantitative yield was obtained. Recrystallization from ethanol gave the umbrosin A phenylboronate (134 mg), as plates, mp 218—219 °C, IR (Nujol) 3550, 1730, 1640, 1600, and 1300 cm^{-1}, Mass m/e 420 (M^+).

Bisdehydrodihydromebadonin (4). Mebadonin (88 mg) was treated as described above to give the bisdehydrodihydromebadonin (**4**) which was identified by mixed mp., IR, and NMR comparison with the bisdehydrodihydroumbrosin A.

Dihydroumbrosin B (4). Umbrosin B (85 mg) was hydrogenated as described above to give the dihydroumbrosin B (**4**), which was identified by mixed mp., IR, and NMR comparison with the bisdehydrodihydroumbrosin A.

We are grateful to Dr. F. McDonald, University of Oklahoma, for recording the mass spectra and Mr. M. Taniguchi, Osaka City University, for carring out the antimicrobial activity tests.

References

1) T. Isobe, T. Kamikawa, and T. Kubota, *Nippon Kagaku Kaishi*, 2143 (1972).

2) The results of antimicrobial activity test will be detailed else where.

3) T. Kubota, T. Matsuura, T. Tsutsui, S. Uyeo, H. Irie, A. Numata, T. Fujita, and T. Suzuki, *Tetrahedron*, **22**, 1659 (1966).

4) E. Fujita, T. Fujita, H. Katayama, M. Shibuya, and T. Shingu, *J. Chem. Soc. C*, **1970**, 1674.

5) P. A. Kollman and L. C. Allen, *Chem. Rev.*, **72**, 283 (1972), and references cited therein.

6) R. J. Ferrier, D. Prasad, A. Rudowski, and I. Sangster, *J. Chem. Soc.*, **1964**, 3330.

7) C. M. Chen and T. Murakami, *Tetrahedron Lett.*, 1121 (1971).

8) C. M. Chen and T. Murakami, *Chem. Pharm. Bull.* (Tokyo), **19**, 1495 (1971).

9) K. Hirotsu, T. Kamikawa, T. Kubota, A. Shimada, and T. Isobe, *Chem. Lett.*, **1973**, 255.

Study in Some Heterochelates. III. Cu(II), Ni(II), Zn(II) or Cd(II)+Histidine or Ethylenediaminetetraacetic Acid+Polyphenols Systems

I. P. MAVANI, C. R. JEJURKAR, and P. K. BHATTACHARYA
Department of Chemistry, M.S. University of Baroda, Baroda-2, India
(Received June 27, 1972)

An extension of Irving-Rossotti technique has been applied to study the formation constant of mixed ligand complexes as follows:

$$[MA] + [L] \rightleftharpoons [MAL]$$

where M=Cu(II), Ni(II), Zn(II), and Cd(II), A=histidine or ethylenediaminetetraacetic acid and LH_2= catechol, pyrogallol or 2,3-dihydroxynaphthalene. The values obtained for the mixed ligand formation constants K_{MAL} are found to be less than the first formation constant K_{ML}, in the binary systems.

The oxidation of mono and diphenols in biological systems by the enzyme phenol oxidases is considered to proceed through the formation of ternary complex.[1] The enzyme is a Cu-protein complex. In the mixed ligand intermediate, copper gets bound with both protein and the substrate phenol. This leads to oxidation of phenol to quinonoid form and Cu(II) gets reduced to Cu(I). This has led us to study the possibility of the formation of similar mixed ligand complexes MAL where M=Cu(II), Ni(II), Zn(II), and Cd(II), A=histidine or ethylenediaminetetraacetic acid, L=catechol, pyrogallol or 2,3-dihydroxynaphthalene. Systems MAL where A=NTA have been reported by us earlier.[2]

Histidine and EDTA are known to form complexes with several metal ions.[3-6] Histidine exhibits bi- or ter-dentate character,[7] coordination taking place from COO^- and from nitrogen of the imidazole or two nitrogens from both imidazole and amino groups. EDTA mostly exhibits quadridentate character,[8] coordination taking place from two nitrogen atoms and two COO^-.

In case of 1:1 histidine or EDTA complexes of metal ions with high coordination numbers, the vacant positions are occupied by water molecules or hydroxyl ions. On addition to this of a bidentate ligand coordinating with metal ion at higher pH, vacant positions around the metal ion are occupied by the secondary ligand, resulting in the formation of the mixed ligand complexes of the type M·histidine·L or M·EDTA·L. The copper complexes retain blue colour and do not indicate reduction to Cu(I). This may be because of the difference between the proteins in the enzymes and the polycarboxylic amino acids used in the present work. The reaction can be represented as follows:

$$[MA] + [L] \rightleftharpoons [MAL]$$

$$K_{MAL} = \frac{[MAL]}{[MA][L]}$$

A=histidine or EDTA.

The charges have been avoided for the sake of generalisation. The formation constants K_{MAL} corresponding to the association of polyhydroxy phenol, with M·Histidine or M·EDTA have been determined by the modified form of Irving-Rossotti technique.[9,10]

Experimental

Disodium salt of EDTA (Riedel-Haens), histidine, polyhydroxy aromatic ligand (A.R. quality), $NaClO_4$ (A.R. Fluka), perchloric acid (Baker analysed), sodium hydroxide (Chamapol, Czechoslovakia) were used. In order to avoid complexing tendency of anion, metal perchlorates were prepared in solution and their metal contents were determined. All solutions were prepared in doubly distilled water.

Metrohm pH meter type E350A (accuracy ±0.05) was employed for all the pH measurements. Titrations were carried out at 30 °C, using a constant temperature bath (±0.1 °C).

The ionic strength of the solution was raised to 0.2 M. Fifty milliliters of each sample wa titrated against 0.2 M NaOH. Nitrogen gas was passed through the solutions to avoid oxidation of the aromatic ligands. The pH titration curves for systems Ni-histidine-catechol and Ni-EDTA-catechol are represented in Figs. 1 and 2. Similar curves are obtained in other systems of Cu^{2+}, Zn^{2+}, and Cd^{2+}.

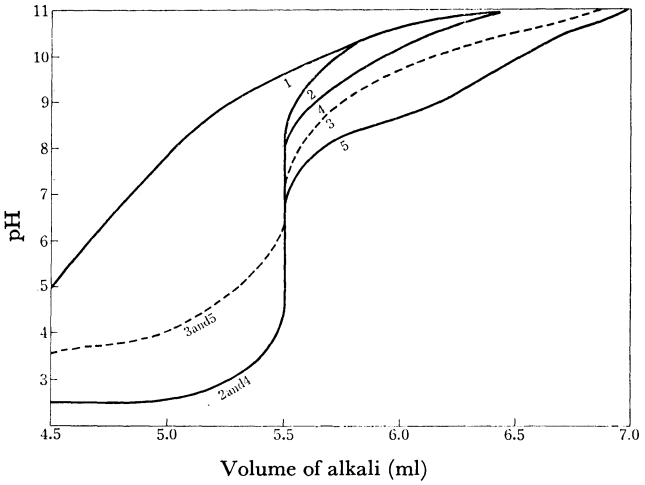

Fig. 1. Ni·histidine·catechol.
1: 0.02 M perchloric acid, 0.002 M histidine, 0.178 M sodium perchlorate.
2: 0.022 M perchloric acid, 0.178 M sodium perchlorate.
3: 0.02 M perchloric acid, 0.002 M histidine, 0.002 M metal perchlorate, 0.176 M sodium perchlorate.
4: 0.022 M perchloric acid, 0.002 M secondary ligand, 0.176 M sodium perchlorate.
5: 0.02 M perchloric acid, 0.002 M histidine, 0.002 M metal perchlorate, 0.002 M secondary ligand, 0.174 M sodium perchlorate.

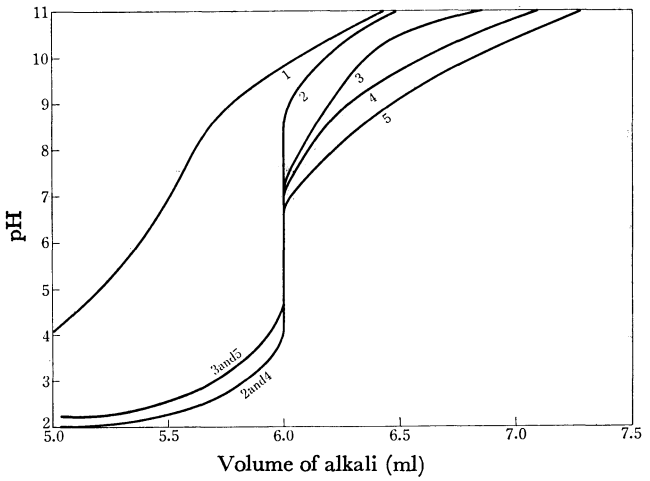

Fig. 2. Ni·EDTA·catechol.
1: 0.02 M perchloric acid, 0.002 M EDTA, 0.178 M sodium perchlorate.
2: 0.024 M perchloric acid, 0.176 M sodium perchlorate.
3: 0.02 M perchloric acid, 0.002 M EDTA, 0.002 M metal perchlorate, 0.176 M sodium perchlorate.
4: 0.024 M perchloric acid, 0.002 M secondary ligand, 0.174 M sodium perchlorate.
5: 0.02 M perchloric acid, 0.002 M EDTA, 0.002 M metal perchlorate, 0.002 M secondary ligand, 0.174 M sodium perchlorate.

Discussion

It is evident from curves (1) and (3) that 1:1 complex of histidine and EDTA with Cu^{2+}, Ni^{2+}, Zn^{2+}, and Cd^{2+} are formed at lower pH and are stable at higher pH. The separation between two curves starts at low pH and reaches maximum at pH ~5 in histidine and at pH ~4.2 in EDTA. This shows that 1:1 complex formation is complete at lower pH. At higher pH, the curves converge showing absence of hydrolysis or hydroxy complex formation. M+histidine or EDTA+secondary ligand (catechol, pyrogallol, 2,3-dihydroxynaphthalene) curve (5) is not below the M+histidine or EDTA curve (3), in the lower pH range. This is an evidence that in this range where M^{2+} and histidine or EDTA 1:1 complexation takes place, the polyhydroxy phenols do not combine with metal ion. In the polyhydroxy phenols curve (4) one and two equivalents of extra perchloric acid (where primary ligand is histidine or disodium salt of EDTA respectively) have been added to compensate for hydrogen ions liberated by the combination of M^{2+} with histidine or EDTA, in the M+primary ligand+secondary ligand solutions. Below pH 5.5 in histidine and 4.5 in EDTA, the curve (5) is not overlapping curve (4) but it is slightly above it. This is due to the fact that in the lower pH range amino acids take up hydrogen ion

Table 1. Stability constants of mixed ligand chelates (30 °C)

Ligand	$\log K^{Ni\cdot Hist}_{Ni\cdot Hist\cdot L}$	$\log K^{Zn\cdot His}_{Zn\cdot His\cdot L}$	$\log K^{Cd\cdot Hist}_{Cd\cdot Hist\cdot L}$
Catechol	6.82	7.24	5.76
Pyrogallol	5.69	6.84	—
2,3-Dihydroxy-naphthalene	8.53	—	7.74

from the solution and exist as a mixture of species $CH_2NH_3^+\cdot COOH$ and $CH_2NH_3^+\cdot COO^-$. After pH 6 curve (5) goes below the curve (4). This confirms that in this range coordination of secondary ligand with M·histidine or M·EDTA takes place resulting in the liberation of extra hydrogen ions. Reactions can be represented as follows:

$$M^{2+} + \text{Histidine} \rightleftharpoons [M\ Hist]^+ + H^+$$

$$[M\ Hist]^+ + C_6H_4(OH)_2 \rightleftharpoons [M\ Hist(C_6H_4O_2)]^- + 2H^+$$

and in case of EDTA, (disodium salt),

$$M^{2+} + Na_2H_2\ EDTA \rightleftharpoons [MEDTA]^{2-} + 2Na^+ + 2H^+$$

$$[MEDTA]^{2-} + C_6H_4(OH)_2 \rightleftharpoons [MEDTA(C_6H_4O_2)]^{4-} + 2H^+$$

From the horizontal distance between curve (4) and curve (5), $\bar{n}$ values have been calculated. pL has been calculated using known equation.[9] The precise values of mixed complex formation constants have been worked out as done in earlier communication.[10] The values have been reported below:

Table 2. Stabliity constants of mixed ligand chelates (30°C)

Ligand	$\log K^{Cu\cdot EDTA}_{Cu\cdot EDTA\cdot L}$	$\log K^{Zn\cdot EDTA}_{Zn\cdot EDTA\cdot L}$	$\log K^{Ni\cdot EDTA}_{Ni\cdot EDTA\cdot L}$	$\log K^{Cd\cdot EDTA}_{Cd\cdot EDTA\cdot L}$
Catechol	7.01	3.73	4.44	3.53
Pyrogallol	6.13	—	—	—
2,3-Dihydroxy-naphthalene	7.73	5.25	5.38	4.96

In case of Cu·Hist·L system and also Zn·Hist·2,3-dihydroxynaphthalene the method could not be applied because the coordination of secondary ligand starts before the formation of M·histidine 1:1 complex is complete. In the system M·EDTA·pyrogallol, where (M=Zn, Ni, or Cd) calculations could not be possible because the separation between curves (4) and curve (5) is very small. In the system Cd·Hist·Pyrogallol, there is a precipitation after pH 6 onwards and hence calculation was not carried out.

It is observed that in all cases K_{MAL} has lower value than K_{ML}. The value of $K^{M\cdot EDTA}_{M\cdot EDTAL}$ is less than K^{M}_{ML} (where L=polyhydroxy aromatic ligands) by about 3 to 4.5 log unit, and $K^{M\cdot Hist}_{M\cdot HistL}$ is less than K^{M}_{ML} by about 1 to 1.2 log unit. This can be explained to be due to electrostatic repulsion between the incoming charged ligand and already existing charged ion histidine or EDTA. The values of K_{MAL} are higher where A=histidine. This is because histidine has one negative charge and hence exerts lesser repulsion on the incoming ligand than EDTA with four negative charges.

The order of the stability constants of the complexes with different metal ion is as follows:

2,3-dihydroxynaphthalene > catechol > pyrogallol

This is in accordance with their basicities. It is also observed that the difference $K^{Cu\cdot EDTA}_{Cu\cdot EDTA\cdot L} - K^{Cu}_{CuL_1}$ is more than $K^{Ni\cdot EDTA}_{Ni\cdot EDTA\cdot L} - K^{Ni}_{Ni\cdot L_2}$. This can be explained by the

consideration of Jahn-Teller effect in case of copper complexes as done earlier.[11,12]

Thanks are due to Prof. S. M. Sethna, Head, Chemistry Department, M. S. University of Baroda, Baroda-2 for providing necessary laboratory facilities. The authors also thank University Grant Commission, New Delhi for the award of Junior Research Fellowship to I.P.M. and C.R.J.

References

1) J. C. Bailar, Jr., "The Chemistry of Coordination Compounds," Reinhold, New York (1956), p. 723.
2) I. P. Mavani, C. R. Jejurkar, and P. K. Bhattacharya, *Ind. J. Chem.*, **10**, 742 (1972).
3) G. Weitzel, W. Schaeg, and F. Schneider, *Ann.*, **632**, 124 (1960).
4) A. Chakraverty and F. A. Cotton, *J. Phys. Chem.*, **68**, 2878 (1963).
5) Y. J. Israeli, *Nature*, **201**, 389 (1964).
6) M. Kopanica and T. C. Huyen, *J. Electroanal. Chem., Interfacial Electrochem.*, **20**, 457 (1969).
7) T. Nortia, *Suomen Kemistillehti*, **33B**, 161 (1960).
8) D. H. Busch and J. C. Bailar, Jr., *J. Amer. Chem. Soc.*, **78**, 716 (1956).
9) H. M. Irving and H. S. Rossotti, *J. Chem. Soc.*, **1954**, 2904.
10) M. V. Chidambaram and P. K. Bhattacharya, *J. Inorg. Nucl. Chem.*, **32**, 3271 (1970).
11) D. Hopgood and R. J. Angelici, *J. Amer. Chem. Soc.*, **90**, 2508 (1968).
12) M. T. Beck, "Chemistry of Complex Equilibria," Van Nostrand Reinhold Company, London (1970), p. 249.

NOTES

BULLETIN OF THE CHEMICAL SOCIETY OF JAPAN, VOL. 47(5), 1283—1284 (1974)

ESR Spectra of Quadridentate Salicylaldehyde Schiff Base Complexes of Cobalt(II) and Copper(II) in Chloroform and in Dichloromethane

Makoto CHIKIRA, Toshio KAWAKITA, and Taro ISOBE

Chemical Research Institute of Non-Aqueous Solutions, Tohoku University, Katahira, Sendai 980

(Received December 4, 1973)

Synopsis. ESR parameters for the titled complexes have been obtained from the spectra of "powders of frozen solutions." The spectra of "not crushed frozen solutions" indicated that the axes of g_3 (3.23—3.68) of the cobalt complexes are in the molecular planes.

Chloroform has been frequently used as a solvent for ESR measurements of many metal chelate complexes. However, chloroform does not form good glass at 77 K, and therefore, the typical ESR patterns of frozen solutions cannot be observed for some metal chelate complexes in chloroform. This phenomenon had been explained by Fierz and von Zelewsky for frozen chloroform solutions of bis(1,3-diphenyl-1,3-propanedionato)copper(II) as follows:[1] When the sample tube of the chloroform solution was cooled directly with liquid nitrogen, some metal complexes are aligned in certain orientations in considerably large grains of chloroform crystals. We have observed the same phenomena for salicylaldehyde Schiff base complexes of cobalt(II) and of copper(II) both in chloroform and in dichloromethane. In order to obtain correct ESR parameters of these complexes in these solvents, we measured the ESR spectra of the "powders of the frozen solutions" by the method as explained below.

The dewar and sample tube system is set as shown in Fig. 1. A stream of dry nitrogen is passed through the upper part of the sample tube during the measurement to prevent the condensation of oxygen or moisture into the sample tube. After both the dewar and sample tube were filled with liquid nitrogen, a chloroform solution is added dropwise into the sample tube from the capillary. When the spectra of cobalt(II) complexes were measured, the capillary filled with dry nitrogen or dry argon was used. The solid sample deposited at the bottom of the tube should be further crushed to fine powders by a bamboo rod.

The ESR spectra of *N,N'*-ethylene-bis(5-methoxysalicylideneiminato)copper(II) (Cu(5MeOSalen)) in chloroform measured by the two different methods are shown in Fig. 2, where (a) is measured by simply freezing the solution as usual, while (b) is measured by the above-mentioned method. As figure 2 shows, the spectra obtained by the usual method did not show any structures due to $g_{//}$ and $A_{//}$. These phenomena were also observed for commercially obtained chloroform which contains about 1% ethanol. These spectra clearly indicate that when the chloroform solution is rapidly frozen in the sample tube by liquid nitrogen, the chloroform crystal has a tendency to grow toward a certain direction with respect to the sample tube and to align the coordination plane of the complex perpendicular to the direction of the sample tube. The same phenomena were also observed in the case of the other quadridentate salicylaldehyde Schiff base complexes of copper(II). The ESR spectra of *N,N'*-ethylene-bis(salicylideneiminato)cobalt(II) (Co(Salen)) in chloroform are shown in Fig. 3. In this case, the intensities of the spectra in the field range

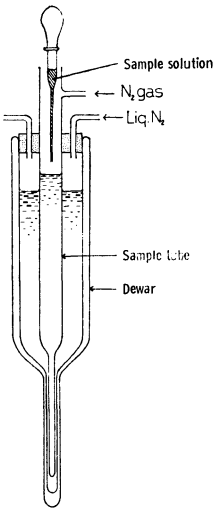

Fig. 1. Dewar and sample tube system.

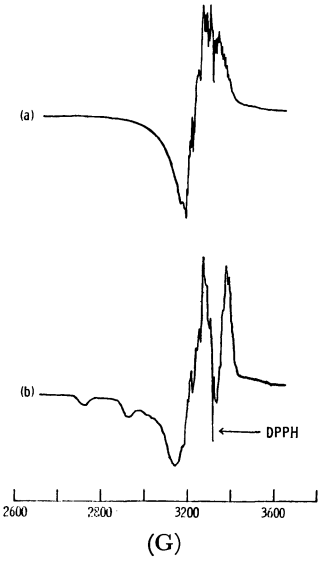

Fig. 2. ESR spectra of Cu(5MeOSalen) in chloroform measured by a), simply freezing the sample solution as usual, and b), improved method.

Table 1. Magnetic parameters

Complex	Solvent	g_1	g_2	g_3			A_1[a]	A_2[a]	A_3[a]		
Co(Salen)	$CHCl_3$	—	—	3.34	3.28	3.23	—	—	153	141	125
	CH_2Cl_2	1.91	1.96		3.32		38	34		149	
Co(Salbn)[b]	$CHCl_3$	—	—	3.61	3.35	3.28	—	—	223	164	142
	CH_2Cl_2	—	—		3.32					147	
Co(Salibn)[c]	$CHCl_3$	—	—	3.68	3.59		—	—	250	221	
	CH_2Cl_2	1.85	1.89		3.64		48	48		233	
Co(Salstn)[d]	$CHCl_3$	—	—	3.66	3.42		—	—	234	177	
	CH_2Cl_2	1.91	1.98		3.30		35	36		146	

a) $\times 10^4$ cm^{-1}. b) *N,N'*-Bis(salicylidene)-2,3-butylenediaminocobalt(II) (*racemic*). c) *N,N'*-Bis(salicylidene)-isobutylenediaminocobalt(II). d) *N,N'*-Bis(salicylidene)stilbenediaminocobalt(II) (*meso*).

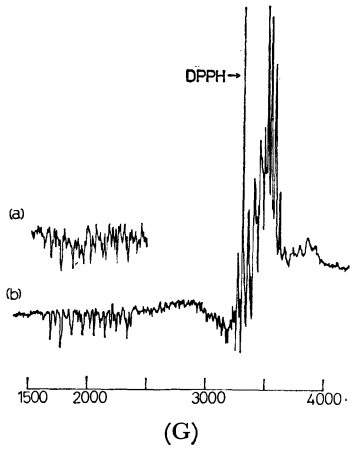

Fig. 3. ESR spectra of Co(Salen) in chloroform measured by a), simply freezing the sample solution as usual, and b), improved method.

between 1600 and 2400 gauss measured by the usual method did not decrease so much as that of the $g_{//}$ component of Cu(5MeOSalen) did, though the patterns of the spectra in this region became very complicated. It is naturally supposed that the orientation of Co(Salen) in rapidly frozen solutions is similar to those of Cu(5MeOSalen) in chloroform crystals. Therefore, if the principal axis of the g tensor corresponding to the progressions between 1600 and 2400 gauss had directed perpendicular to the molecular planes of the cobalt complexes, similar decrease in the intensity of these progressions could have been observed. These experimental results suggest that the peaks observed in this region are not due to the component of the g tensor perpendicular to the molecular plane. The ESR spectrum of Co(Salen) in chloroform indicates that more than 3 kinds of paramagnetic centers exist in the chloroform crystals. The observed ESR parameters were slightly different from those reported by Busset, *et al.* for the ESR spectra measured at 113 K.[2] Though they have reported the time development of the signals, we could not observe such phenomena but always observed the reproducible spectra. Similar phenomena due to the crystallizations of the solvents were observed for the dichloromethane solutions of cobalt(II) complexes. In the case of dichloromethane solutions, the peaks due only to one paramagnetic centers were more intensely observed than those of any other centers, so that various magnetic parameters could be estimated. This is the first report that the high field part of the ESR spectra of the low spin planar salicylaldehyde Schiff base complexes of cobalt(II) in the non-coordinating solvent like dichloromethane could be clearly analysed.

In Table 1, the magnetic parameters of various quadridentate salicylaldehyde Schiff base complexes of cobalt(II) in chloroform and in dichloromethane are shown. It should be noted that the g_2 values obtained in this experiment are considerably smaller than those reported for Co(Salen) in chloroform by Busset, *et al.*[2] All the attempts to correlate these parameters to the possible ground electronic configurations of these complexes by the usual second-order perturbation calculations[2–4] have failed. It seems necessary to calculate the g values by diagonalizing the spin orbit interactions for several possible electronic configurations.

Experimental

The salicylaldehyde Schiff base complexes of cobalt(II) and copper(II) were obtained according to the literature.[5] Chloroform and dichloromethane were purified by the usual methods.[6] Deoxygenated solutions of cobalt(II) complexes were prepared with a vaccum line and transfered into the sample tube in an atmosphere of dry argon. ESR spectra at X-band were measured with a Hitachi 771 spectrometer. The resonance fields were calibrated with that of powders of DPPH.

References

1) H. Fierz and A. von Zelewsky, *Inorg. Chem.*, **10**, 1556 (1971).

2) C. Busset, F. Cariati, A. Fusi, M. Gulloti, F. Morazzoni, A. Pasini, R. Ugo, and V. Valenti, *J. Chem. Soc., A*, **1973**, 754.

3) A. H. Maki, N. Edelstein, A. Davison, and R. H. Holm, *J. Amer. Chem. Soc.*, **86**, 4580 (1964).

4) Y. Nishida and S. Kida, *Chem. Lett.*, **1973**, 57.

5) T. Tanaka, This Bulletin, **33**, 259 (1960); H. Nishikawa and S. Yamada, *ibid.*, **37**, 8 (1964).

6) "Techniques of Chemistry, Organic Solvents," 3rd ed. by J. A. Riddick and W. B. Bunger, John Wiley & Sons, Inc., (1970), Chapter V.

BULLETIN OF THE CHEMICAL SOCIETY OF JAPAN, VOL. 47(5), 1285—1286 (1974)

Solubility Studies of Ion-pairs in Organic Solvents

Takejiro TAKAMATSU

Department of Chemistry, Faculty of Science, Kyoto University, Sakyo-ku, Kyoto 606

(Received June 26, 1973)

Synopsis. The solubilities of several types of ion-pairs were measured in many organic solvents at 25 °C. A good correlation holds between the logarithmic solubilities and the solubility parameters of solvents over the whole range of polarity.

In the previous paper,[1] the extraction behavior of ion-pairs of the $Ru(phen)_3A_2$ type was studied from the viewpoint of the ionic equilibrium involved in the extraction system. However, no clear discussion was given of the distribution ratio in connection with the physical parameter of the extraction solvent. The distribution ratio is generally determined as the ratio of the solubilities of the solute in the two phases. Therefore, the solubility measurement of the ion-pairs in the organic solvents seems to be useful in order to elucidate the solvent characters, which mainly govern the distribution ratio.

In this paper, the solubilities of several types of ion-pairs, such as $Ru(phen)_3A_2$ and MA will be measured; M refers to the alkali metal ions, and A, to the chloride ion, the perchlorate ion, and the tetraphenylborate ion. The results obtained will be discussed with respect to the two characteristic parameters of solvents, *i.e.*, the solubility parameter and the dielectric constant.

Experimental

Reagents. The organic solvents used here were purified several times by using a 1 m distillation column packed with helical steel wire, as was recommended in the literature.[2] The $Ru(phen)_3A_2$ salts were prepared as follows: 200 mg of $RuCl_3 \cdot H_2O$, 526 mg of *o*-phenanthroline, and 218 mg of hydroxylammonium sulfate were dissolved in 50 ml of an ethanol–water (1: 1) solution and the pH of the solution was adjusted to 6 with a saturated $Ba(OH)_2$ solution. After refluxing for two days at 100 °C, the $BaSO_4$ was filtered out and the excess *o*-phenanthroline was removed by washing the solution several times with chloroform and then with *n*-hexane. After the resulting solution had been dried *in vacuo*, the residue was dissolved with a minimum volume of acetonitrile and any undissolved precipitates present were filtered out. $Ru(phen)_3Cl_2$ could be crystallized by adding chloroform to the filtrate. $Ru(phen)_3(ClO_4)_2$ was obtained by adding a large excess of sodium perchlorate to a slightly acidic solution of $Ru(phen)_3Cl_2$. $Ru(phen)_3(B(C_6H_5)_4)_2$ (abbreviated as $Ru(phen)_3(BPh_4)_2$) was prepared by adding a slight excess of sodium tetraphenylborate to an aqueous solution of $Ru(phen)_3Cl_2$. The addition of sodium tetraphenylborate should be restricted to a minimum; otherwise, contamination with the excessive tetraphenylborate ions takes place. All the precipitates were dried for two days *in vacuo*. (Calcd for $Ru(phen)_3Cl_2$: C: N: Cl, 6.10: 1.19: 1.0; Found: 6.09: 1.17: 1.0, Calcd for $Ru(phen)_3(BPh_4)_2$: H, 5.03; C, 78.81; N, 6.56%; Found: H, 4.81; C, 78.78; N, 6.60%.) The $KBPh_4$ and $CsBPh_4$ were prepared by adding small excesses of KCl and CsCl respectively to an aqueous sodium tetraphenylborate solution. After the precipitates had been washed several times with water, they were dried for two days *in vacuo*. The other reagents were purchased with reagent-grade purities.

Solubility. The solubility measurements were carried out as follows. After the $Ru(phen)_3A_2$ and $MBPh_4$ had been added to approximately 10-ml portions of pure solvents in test tubes equipped with ground stoppers, the equilibration was performed in a thermostat at 25 °C by shaking the solution

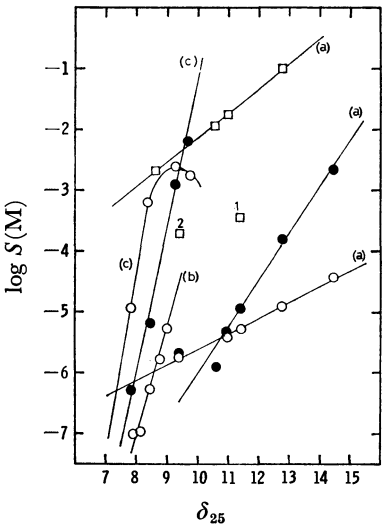

Fig. 1. The relations between the solubilities of $Ru(phen)_3A_2$ and the solubility parameters of solvents.
(a): alcohols, (b): esters, (c): ketones.
(○): $Ru(phen)_3(BPh_4)_2$, (●): $Ru(phen)_3(ClO_4)_2$,
(□): $Ru(phen)_3Cl_2$ (1): 2-propanol, (2): 2-butanol

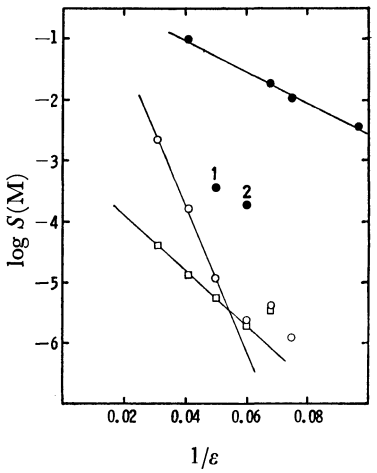

Fig. 2. The relations between the solubilities of $Ru(phen)_3A_2$ and $1/\varepsilon$ of alcohols.
(□): $Ru(phen)_3(BPh_4)_2$, (○): $Ru(phen)_3(ClO_4)_2$,
(●): $Ru(phen)_3Cl_2$
(1): 2-propanol, (2): 2-butanol

Table 1. Solubilities of $Ru(phen)_3A_2$ in organic solvents
M represents $Ru(II)(phen)_3$ here

Solvent	δ_{25}	ε	$M(B(C_6H_5)_4)_2$	$M(ClO_4)_2$	MCl_2
Methanol	14.5	32.7	3.84×10^{-5}	2.16×10^{-3}	
Ethanol	12.9	24.6	1.30×10^{-5}	1.60×10^{-4}	1.00×10^{-1}
2-Propanol	11.5	19.9	5.41×10^{-6}	1.20×10^{-5}	3.62×10^{-4}
Isoamyl alcohol	11.0(10.8)[a]	14.7	3.78×10^{-6}	4.11×10^{-6}	1.83×10^{-2}
2-Butanol	9.4(11.1)[a]	16.6	2.05×10^{-6}	2.32×10^{-6}	1.88×10^{-4}
1-Hexanol	10.7	13.3		1.19×10^{-6}	1.04×10^{-2}
1-Octanol	8.7(10.2)[a]				1.96×10^{-3}
Benzyl alcohol	12.1	13.1	2.68×10^{-4}	3.43×10^{-3}	
Acetone	9.8	20.7	2.02×10^{-3}	6.81×10^{-3}	1.60×10^{-4}
Methyl ethyl ketone	9.3	18.5	2.45×10^{-3}	1.39×10^{-3}	2.89×10^{-4}
Methyl isobutyl ketone	8.4	13.1	6.92×10^{-4}	5.59×10^{-6}	$<10^{-7}$
Diisobutyl ketone	7.8		1.19×10^{-5}	5.40×10^{-7}	$<10^{-7}$
Tetrahydrofuran	9.3	7.6	6.03×10^{-4}		
Isopropyl ether	7.0		4.32×10^{-7}		
Methyl acetate		6.7		1.21×10^{-5}	$<10^{-7}$
Ethyl acetate	9.1	6.0	5.41×10^{-6}	$<10^{-7}$	$<10^{-7}$
n-Propyl acetate	8.8	6.0	1.62×10^{-6}	$<10^{-7}$	$<10^{-7}$
n-Butyl acetate	8.5	5.0	5.94×10^{-7}	$<10^{-7}$	$<10^{-7}$
Isobutyl acetate	8.3	5.3	1.08×10^{-7}	$<10^{-7}$	$<10^{-7}$
Isoamyl acetate	8.1		$\sim10^{-7}$	$<10^{-7}$	$<10^{-7}$
Chloroform	9.2	4.8	1.29×10^{-4}		9.7×10^{-5}
1,2-Dichloroethane	9.9	10.4	4.18×10^{-4}		
Monochlorobenzene	9.5	5.6	7.03×10^{-6}		$<10^{-7}$
o-Dichlorobenzene		9.9			$<10^{-7}$
1-Nitropropane	10.5	23.2	4.22×10^{-3}		7.29×10^{-4}
Bis(2-chloroethyl) ether		21.2	1.26×10^{-2}		2.90×10^{-3}

a) The value calculated according to the Hildebrand rule using ΔH_{25} in the literature.[2]

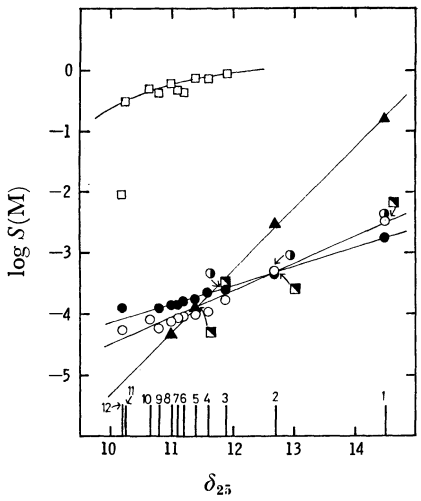

Fig. 3. The relations between the solubilities of some other salts and the solubility parameters of alcohols.
(□): $NaBPh_4$, (○): $KBPh_4$, (●): $CsBPh_4$, (◑): $CsClO_4$, (—): $RbClO_4$, (▲): CsCl.
(1): methanol, (2): ethanol, (3): 1-propanol, (4): 2-propanol, (5): 1-butanol, (6): isobutyl alcohol, (7): 2-butanol, (8): 1-pentanol, (9): isoamy lalcohol, (10): 1-hexanol, (11): 1-octanol, (12): *tert*-amyl alcohol

for 7—8 days. The absorbance of the equilibrated solution was measured at 448 nm for $Ru(phen)_3A_2$ and at 274 nm for $MBPh_4$, from the molar absorptivities, 18500[1] and 1950 respectively. The solubilities of the other salts were measured gravimetrically.

Results

The observed solubilities of $Ru(phen)_3A_2$ in various solvents are listed in Table 1, together with the characteristic parameters of the solvents. The logarithmic solubilities ($\log S$) are shown as a function of the solubility parameters (δ) of the solvents (Fig. 1) and of the reciprocal of the dielectric constants ($1/\varepsilon$) of the solvents (Fig. 2). In Fig. 3, the solubilities of the other salts are plotted against δ values of the solvents.

As a result, a good correlation can be obtained between $\log S$ and δ in the solvents of the same sort, although the slopes of the plots are different from one sort of solvent to another. No clear relation, however, could be drawn between the dielectric constants and the solubilities in the low-polarity range.

References

1) T. Takamatsu, This Bulletin, **47**, 118 (1974).
2) J. A. Riddick and W. B. Bunger, "Techniques of Chemistry, 2, Organic Solvents," Wiley-Interscience., New York (1970).

BULLETIN OF THE CHEMICAL SOCIETY OF JAPAN, VOL. 47(5), 1287—1288 (1974)

The Application of the Regular Solution Theory to the Ion-pair Systems

Takejiro TAKAMATSU

Department of Chemistry, Faculty of Science, Kyoto University, Sakyo-ku, Kyoto 606

(Received November 6, 1973)

Synopsis. The solubilities of these ion-pairs, KCl, KBr, and KI, were measured in alcohols. The logarithmic solubilities could be well correlated with the solubility parameters of the solvents.

In the previous paper,[1] the solubilities of such ion-pairs as chloride, perchlorate, and tetraphenylborate salts of alkali metals and Ru(II)(phen)$_3$ could be well correlated to the solubility parameters of solvents.

In this study, the solubilities of the typical ion-pairs, KCl, KBr, and KI, were measured in alcohols. By using the solubility parameters of the ion-pairs (δ_1) calculated from the lattice energies of the ionic crystals, a better application of the regular solution theory to the ion-pair systems will be suggested.

Experimental

All the reagents used here were purchased as reagent-grade pure. The alcohols were purified by distillation as has been described before.[1] The solubility measurements were performed gravimetrically at 25 °C in a fashion similar to that previously described.[1]

Results and Discussion

The solubilities of KCl, KBr, and KI in alcohols are shown in Fig. 1 as a function of the solubility parameters of the solvents (δ_2), which were calculated according to Eq. (1) by using the heat of vaporization

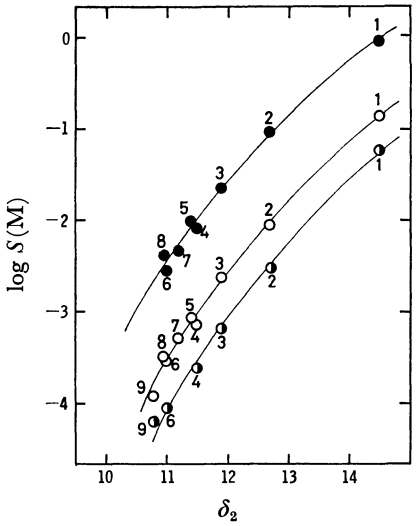

Fig. 1. The relation between log S and δ_2.
In all the figures, (◑): KCl, (○): KBr, (●): KI
(1): methanol, (2): ethanol, (3): 1-propanol, (4): 2-propanol, (5): 1-butanol, (6): 2-butanol, (7): isobutyl acohol, (8): 1-amyl alcohol, (9): isoamyl alcohol

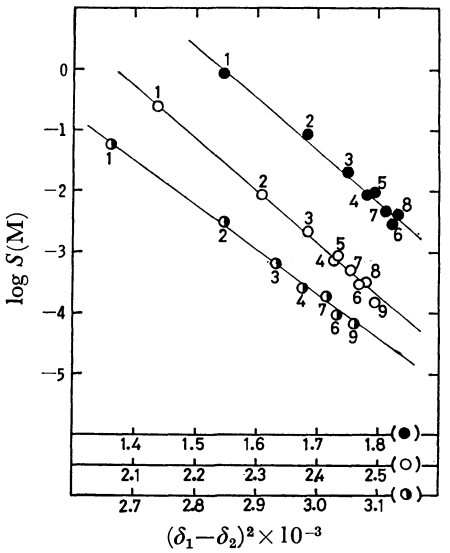

Fig. 2. The relation between log S and $(\delta_1-\delta_2)^2$

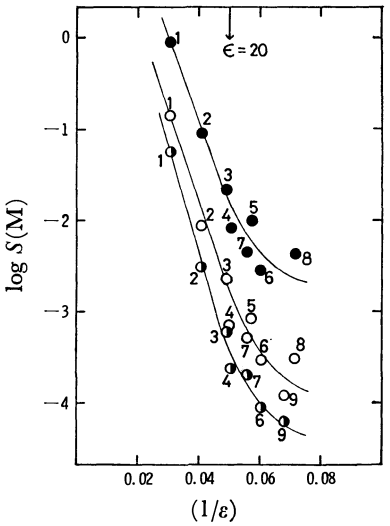

Fig. 3. The relation between log S and $1/\varepsilon$

Table 1. The calculated δ_1 values of ion-pairs

	r_c+r_a (Å)	U (kcal/mol)	V (ml^3)	δ_1
KCl	3.14	162.78	37.29	66.11
KBr	3.28	156.64	42.50	60.75
KI	3.49	148.25	51.20	53.76

at 25 °C (ΔH_{25}) cited from the literature.[2]

$$\delta_2 = \left(\frac{\Delta H_{25}-RT}{V}\right)^{1/2} \quad (1)$$

Although smooth correlations are obtained between the solubilities of the ion-pairs and δ_2, a slight bending is observed for all the systems, as is shown in Fig. 1.

Therefore, the solubility parameters of the ion-pairs (δ_1) were estimated from the square root of the lattice energy density, $(U/V)^{1/2}$, where the lattice energy, U, was approximated from Eq. (2), which was derived by Kapustinskii,[3] and the molar volume, V, from Eq. (3):

$$U = 574.4\left(\frac{z_1 z_2}{r_c + r_a}\right)\left(1 - \frac{0.345}{r_c + r_a}\right) \quad (2)$$

$$V = 2N(r_c + r_a)^3 \quad (3)$$

where r_c and r_a refer to the ionic radii of the cation and the anion respectively at the sixth coordination, and N, the Avogadro's number. In Table 1, the calculated values are shown. The relations between the logarithmic solubilities ($\log S$) and $(\delta_1 - \delta_2)^2$ are demonstrated in Fig. 2. As is shown in Fig. 2, these plots give an excellent straight line.

In Fig. 3, the plots between $\log S$ and the reciprocal of the dielectric constants ($1/\varepsilon$) are shown for comparison. Although a fairly good correlation is observed in the range of high polarity, no relationship holds in the low-polarity range.

In conclusion, the regular solution theory could be applied to the ion-pair systems by estimating the δ_1 values from the lattice energies of the ionic crystal. However, the slopes of the plots could not be discussed here because of the lack of data.

References

1) T. Takamatsu, This Bulletin, **47**, 1285 (1974).

2) J. A. Riddick and W. B. Bunger, "Techniques of Chemistry, 2, Organic Solvents," Wiley-Interscience, New York (1970).

3) R. B. Heslop and P. L. Robinson, "Inorganic Chemistry," Elsevier Publishing Co., Amsterdam (1960), p. 92.

BULLETIN OF THE CHEMICAL SOCIETY OF JAPAN, VOL. 47(5), 1289—1290 (1974)

The Reaction of α-Ethoxybenzyl *t*-Butyl Peroxide with Grignard Reagents

Masao Ōkubo, Hiroshi Saitō, and Toshiaki Tomiyoshi

Department of Chemistry, Faculty of Science and Engineering, Saga University, Honsho-cho, Saga 840

(Received May 25, 1973)

Synopsis. Effect of the ethoxyl group of the peroxide in the title was examined. Reactivities of some peroxides having oxygen- and nitrogen-atom adjacent to O-O linkage against magnesium compounds and alkali iodide were compared, and effect of the coordination of heteroatoms to the cationic species was discussed.

It was previously found that di-*t*-butyl peroxide (I) did not react with phenyl-[1] and methyl-[2]magnesium bromide (PhMgBr and MeMgBr) in tetrahydrofuran (THF) at 60 °C. Peroxide I reacts with Grignard reagents prepared from primary and secondary alkyl halides,[3] but the formation of *t*-butanol and olefins, both of which may be the result of "the reducing action of the β-hydrogen atom" of alkyl groups of reagents,[4] has been reported. These are excluded in this work to avoid complication of the reaction products. On the other hand, benzoyl peroxide (II) and *t*-butyl perbenzoate (III) reacts rapidly with PhMgBr in THF at 0 °C.[1] In these cases, the acceptance of the electron by peroxidic linkage[5] can probably be facilitated by the coordination of the neighboring carbonyl-oxygen to the Mg-atom of PhMgBr. Thus, the authors desired to see the effect of neighboring heteroatoms on the reactivity of peroxides with PhMgBr. α-Ethoxybenzyl *t*-butyl peroxide (IV)[6] was chosen as a model compound with neighboring ethereal oxygen.

Table 1. Molar ratio and extent of reaction (in THF, at 60 °C, 7 hr, under N_2)

Purity of peroxide (wgt %)	[PhMgBr]/[P.O.]	P.O. reacted (%)	Yield of Ph–O–*t*-Bu (%)
70.7	1.8	38.1	67.1
70.7	3.1	68.9	59.1
70.7	4.5	97.4	69.9
85.6	2.0	65.3	
85.6	3.0	85.2	63—70
85.6	4.8	100	

A 85.6%-pure sample of IV was obtained by the repeated treatments of benzaldehyde diethylacetal with *t*-BuOOH at 80 °C.[6] The main products of the reaction of IV with PhMgBr after hydrolysis were benzhydrol and phenyl *t*-butyl ether. The reaction proceeds moderately at 60 °C in THF under an N_2-atmosphere, but the final extent of the reaction varies with the molar ratio of the reactants, as is shown in Table 1. It may be seen that about 4 mol of PhMgBr are necessary for the complete decomposition of IV. The products and their yields obtained using 4.8 molar PhMgBr will now be given. Benzhydrol was obtained quantitatively based on the reacted peroxide. The yield of phenyl *t*-butyl ether was 63—70%, almost independent of the purity (Table 1). *t*-Butanol was about 25%. Ethanol was found to have a 36—50% yield; however, it must really be much higher, as this product is readily lost in treating the reaction mixture. Small amounts of by-products were triphenylmethane and benzhydryl ethyl ether, both of which came from benzaldehyde diethylacetal, the sole contaminant in the sample of IV.

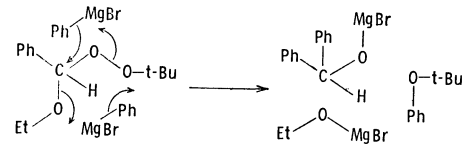

The mechanism of the reaction can be suggested on the basis of these results (Formula 1). Ethereal oxygen coordinates to the Mg-atom, and the ethoxyl anion is withdrawn from the aldehyde-carbon, thus facilitating the attack of the phenyl anion of the other Grignard molecule to produce benzhydrol. One more phenyl anion attacks the butoxyl-oxygen (*t*-Bu—O(—O–+Ph—)MgBr) to produce phenyl *t*-butyl ether. These are the main reactions. The considerable yield of *t*-butanol suggests the possibility of inverse heterolysis (*t*-Bu—O—)O–+Ph—)MgBr). As 4 mol of Grignard reagent are needed to complete the reaction, PhMgBr in Formula 1 should be written as dimers and thus takes a structural configuration favoring the attack of the cationic Mg-atom on the butoxyl-oxygen. Another mechanism in which Grignard molecule directly attacks the O–O linkage, can be rejected because 35 and 15% of peroxide remained unreacted after heating the reaction mixture for more than 7 hr even with two and three molar PhMgBr respectively. Probably, the dimerization process of PhMgBr($2PhMg\text{-}Br \rightleftharpoons Ph_2Mg \cdot MgBr_2 \rightleftharpoons Ph_2Mg + MgBr_2$) favors the release of the phenyl anion. Though there are some uncertainities, the initial abstraction of the ethoxy group has at least been ascertained.

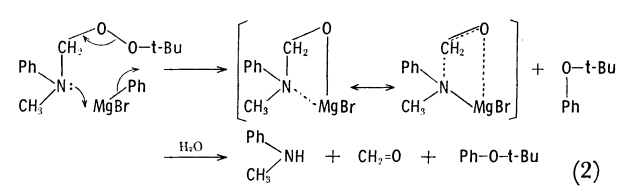

N-Methyl-*N*-phenylaminomethyl *t*-butyl peroxide (V),[9] which has neighboring nitrogen atom, was also examined. Peroxide V decomposed completely with an equimolar PhMgBr at 60 °C in about 7 hr and formed *N*-methylaniline (73%) and phenyl *t*-butyl ether (81%) (Formula 2). Formaldehyde was detected as 2,4-dinitrophenylhydrazone. α-Cyanodiphenylmethyl *t*-butyl peroxide (VI)[10] was unchanged after having been treated with two molar PhMgBr at 60 °C for 7 hr. Around the O–O linkages peroxide VI structurally resembles triphenylmethyl *t*-butyl peroxide,

which is stable to PhMgBr, but it is uncertain why the nitrile group itself does not react. Although these heteroatom-containing peroxides are not crowded to the same extent sterically around the O–O linkages, the adjacent oxygen and/or nitrogen, which can coordinate to the Mg-atom, seems to play an important part in reactions with PhMgBr.

Table 2. Correlation of reactivity

	Structure of P.O.	Mg-reagents: PhMgBr	Mg-reagents: $MgBr_2$ + ⟨⟩	Iodometry (a)	Iodometry (b)	Iodometry (c)
II	Ph–C(=O)–O–O–C(=O)–Ph	±	+	○	—	—
III	Ph–C(=O)–O–O–C$(CH_3)_3$	±	−	×	○	—
I	$(CH_3)_3$C–O–O–C$(CH_3)_3$	−	−	×	×	○
V	CH_2(Ph)HC_3–N–O–O–C$(CH_3)_3$	+	+	○	−	−
IV	Ph–CH(Et–O)–O–O–C$(CH_3)_3$	+	−	×	○	—
VI	Ph_2–C(N≡C)–O–O–C$(CH_3)_3$	−	−	×	×	○

Concerning the reaction of Grignard reagents with organic peroxides, we found that $MgBr_2$ and II in THF form an orange-colored complex, which acts as a moderate reagent for the bromine-addition to olefins, especially easily to cyclohexene, at room temperature.[11] In this colored complex, the carbonyl-oxygen of II is considered to coordinate to the Mg-atom and to induce a positive charge on the bromine atom. Thus, the combination of $MgBr_2$ and cyclohexene may be regarded as a magnesium reagent, based on the mechanistic resemblance. Peroxide V slowly afforded 1,2-dibromocyclohexane at 60 °C, but the IV and VI peroxides did not react at the same temperature. The reactivities to these two magnesium reagents of some peroxides containing and not containing adjacent heteroatoms are classified in Table 2. The methods of iodometry used are also included in the table. Method a), using a saturated KI solution and acetic acid, is applied to "highly reactive" peroxides, such as II and *t*-BuOOH.[12] Method b) is applied to "moderately reactive" peroxides such as III,[7] which reacts with alkali iodide alone in acetic acid, but so slowly that a catalytic amount of ferric ion is necessary for iodometry. Method c) is used to titrate "stable" peroxides such as I, which can be decomposed only in refluxing acetic acid.[13]

As Table 2 shows, diacyl-type (II) and *N*-containing (V) peroxides, both of which react with two magnesium reagents, are titrated by Method a). Perester-type (III) and *O*-containing (IV) peroxides, both of which react only with PhMgBr, are titrated by Method b). Di-*t*-alkyl-type (I) and *CN*-containing (VI) peroxides cannot react with both of the two magnesium reagents; they are titrated only by Method c). This correlation of reactivities seems reasonable when it is taken into account that Grignard reagents behave as ion-pairs and that alkali iodide is also known to exist as ion-pairs at a high concentration in a low dielectric solvent such as acetic acid.[14] The diminution of the rate of reaction of alkali iodide with acyl peroxides in ethanol by adding water,[15] which is a highly dielectric solvent, may thus be the result of the degree of association of the ion-pairs becoming lower and the participation of the counter cation being retarded. The higher reactivity of V than IV may be at least in part due to the higher coordinating ability of nitrogen. The non-reactivity of I and di-triphenylmethyl peroxide to PhMgBr has been ascribed to steric hindrance,[16] but the absence of adjacent heteroatom is probably another important factor.

Experimental

The purity of the IV peroxide was determined by integrating the NMR spectrum of aldehyde-protons of unreacted acetal (5.5 ppm) and of IV (5.8 ppm). In the iodometry, ferric chloride was used as a catalyst;[7] the amount of it was determined so as to obtain the same value as that found by the NMR method.

To a filtered solution of PhMgBr (prepared from 2.9 g of bromobenzene and excess Mg-turnings in 30 ml of THF), 1.0 g of IV (85.6% pure) in 20 ml of THF was added all at once under an N_2-stream. The reaction flask was transferred into a water bath (60 °C) and stirred gently. After 7 hr, the peroxide-content became nearly zero. The reaction products were analyzed by glc.

References

1) M. Ōkubo, K. Maruyama, and J. Ōsugi, This Bulletin, **44**, 125 (1971).

2) Methyl *t*-butyl ether was not detected, and the peroxide was recovered.

3) T. W. Campbell, W. Burney, and T. L. Jacobs, *J. Amer. Chem. Soc.*, **72**, 2735 (1950).

4) H. S. Mosher and E. L. Combe, *ibid.*, **72**, 3944 (1950).

5) K. Tokumaru and O. Simamura, This Bulletin, **36**, 333 (1963).

6) A. Rieche and C. Bischoff, *Chem. Ber.*, **94**, 2457 (1961).

7) L. S. Silbert and D. Swern, *Anal. Chem.*, **30**, 385 (1958).

8) A. E. Tschitschibabin and S. A. Jelgasin, *Ber.*, **47**, 48 (1914).

9) M. S. Kharasch and A. Fono, *J. Org. Chem.*, **24**, 72 (1959).

10) M. S. Kharasch and G. Sosnovsky, *Tetrahedron*, **3**, 105 (1958).

11) M. Ōkubo, H. Kusakabe, T. Hiwatashi, and K. Kishida, This Bulletin, **47**, 860 (1974).

12) J. P. Wibaut, H. B. van Leewen, and B. van der Wal, *Rec. Trav. Chim. Pays-Bas*, **73**, 1033 (1954).

13) R. D. Mair and J. Graupner, *Anal. Chem.*, **36**, 194 (1964).

14) R. A. Robinson and R. H. Stokes, "Electrolytic Solution," Butterworth, London (1959), p. 401.

15) G. Tsuchihashi, S. Miyajima, T. Ōtsu, and O. Simamura, *Tetrahedron*, **21**, 1039 (1965).

16) G. A. Baramki, H. S. Chang, and J. T. Edward, *Can. J. Chem.*, **40**, 333 (1963).

BULLETIN OF THE CHEMICAL SOCIETY OF JAPAN, VOL. 47(5), 1291—1292 (1974)

The Preparation of 5,8-Quinolinediol and 1,4-Acridinediol Derivatives[1)]

Shōshichi OGUCHI

Department of Chemistry, Faculty of Education, The Tokyo Gakugei University, Koganei, Tokyo 184

(Received September 8, 1973)

Synopsis. Compounds of 6,7-di X substituted 5,8-quinolinediol (X=$COOC_2H_5$; CN; $COCH_3$) have been prepared from diethyl pyridine-2,3-dicarboxylate and the respective active methylene compounds. Similarly, 2,3-di X substituted 1,4-acridinediol (X=$COOC_2H_5$) has been prepared.

In previous papers, it was reported that ethyl pyrazine-2,3-dicarboxylate and quinoxaline-2,3-dicarboxylate condensed with ethyl succinate to form 5,8-dihydroxyquinoxaline[2)] and 1,4-dihydroxyphenazine derivatives respectively. The condensation of pyridine 2,3-dicarboxylate or quinoline 2,3-dicarboxylate with a compound which has two adjacent active methylenes like ethyl succinate would lead to the formation of the analogous rings. Both 5,8-quinolinediol[3)] and 1,4-acridinediol derivatives contain an oxine-type structure and are expected to form a metal chelate.[4)] Quinolino-5,8-quinone and its dioxime are also interesting in their bacteriostatic properties.[5)]

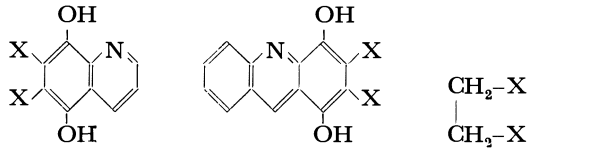

I: X=$COOC_2H_5$ IV: X=$COOC_2H_5$ V: X=$COOC_2H_5$
II: X=CN VI: X=CN
III: X=$COCH_3$ VII: X=$COCH_3$

Thus, 6,7-di X substituted 5,8-quinolinediols (I: X=$COOC_2H_5$, II: X=CN, III: X=$COCH_3$) have been prepared from diethylpyridine 2,3-dicarboxylate and the respective active methylene compounds (V, VI, VII) by procedure analogous to that previously reported.[2)] Similarly, the condensation of diethyl quinoline-2,3-dicarboxylate with ethyl succinate gave diethyl 1,4-dihydroxyacridine-2,3-dicarboxylate (IV: X=$COOC_2H_5$). However, the analogous compounds of IV, X=CN and X=$COCH_3$, were not obtained under similar conditions. The oxidation of I and IV with silver oxide gave the corresponding quinoline 5,8-quinone and acridino-1,4-quinone respectively.

Experimental

Diethyl 5,8-dihydroxyquinoline-6,7-dicarboxylate (I). Procedure A: A mixture of 2.23 g (0.010 mol) of diethyl pyridine-2,3-dicarboxylate, 1.92 g (0.011 mol) of diethyl succinate, and 0.50 g (0.022 mol) of powdered sodium in 6 ml of xylene was heated at 110 °C under stirring and with moisture excluded. If the reaction did not start within ten minutes after stirring, a few drops of ethanol were added; then the reaction definitely began and the solution turned reddish brown and viscous. After an hour the solution was cooled and most of the unreacted sodium was destroyed by the addition of ethanol; then the mixture was acidified with hydrochloric or acetic acid. The mixture was extracted twice with 10 ml portions of xylene, and the solvent was removed by steam distillation. The residue from steam distillation was filtered and washed with water. Yield, 2.2 g (73.7%). Pale yellow needles (from methanol); mp 112.5—113 °C. It forms reddish precipitates in concentrated aqueous sodium hydroxide and turns yellow with concentrated sulfuric acid. Found: C, 58.58; H, 4.95; N, 4.63%. Calcd for $C_{15}H_{15}O_6N$ (I): C, 59.01; H, 4.95; N, 4.59%. IR: (KBr) ~3420 (OH), 1730 (C=O) cm^{-1}.

Diacetate of I: mp 162.5—163 °C. Colorless pillows (from ethanol); Found: N, 3.62%. Calcd for $C_{19}H_{19}O_8N$: N, 3.60% IR: 1775 (OAc), 1725 (C=O) cm^{-1}. *Dibenzoate of I*: mp 183—183.5 °C. Colorless needles (from ethanol); Found: N, 2.73%; Calcd for $C_{29}H_{23}O_8N$: N, 2.78%.

Oxidation of I. I (0.2 g) in benzene was shaken with silver oxide (prepared from 1 g of silver nitrate) for two hours. The precipitate which was subsequently filtered out was extracted with ethyl acetate. The extract from the ethyl acetate was recrystallized from chloroform and petroleum ether. Yield, 0.04 g. Yellowish crystals, mp 176 °C (decomp.). Found: C, 59.22; H, 4.30; N, 4.59%. Calcd for $C_{15}H_{13}O_6N$ (Quinone of I): C, 59.40; H, 4.32; N, 4.62%. IR: (KBr) 1742, 1690 cm^{-1}.

6,7-Dicyanoquinoline-5,8-diol (II). Procedure B: A mixture of 2.23 g of diethyl pyridinedicarboxylate (0.01 mol), 0.80 g of succinonitrile (0.01 mol) and 0.88 g of powdered metal potssium (0.022 mol) in 5 ml of xylene was stirred, with moisture excluded for half an hour at room temperature. By the same treatment of the product as with I, 0.64 g (30%) of pale yellowish crystals (from ethanol) was obtained. mp> 320 °C. Found: C, 62.53; H, 2.50; N, 19.73%: Calcd for $C_{11}H_5O_2N_3$ (II): C, 62.45; H, 2.55; N, 19.87%. IR: (KBr) ~3200 (OH), 2200 cm^{-1} (CN). *Monoacetate*: Colorless plates (from ethanol) mp 232 °C. Found: C, 61.09; H, 2.86; N, 16.48%. Calcd for $C_{13}H_7O_3N_5$ (Monoacetate of II): C, 61.66; H, 2.79; N, 16.60%. IR: (KBr) ~3200 (OH), 2490 (CN), 1788 cm^{-1} (OAc).

6,7-Diacetylquinoline-5,8-diol (III). By Procedure A, III was prepared by the condensation of diethyl 2,3-pyridinedicarboxylate with acetonylacetone. Yield, 36%; mp 243 °C (decomp.). Yellowish crystals (from aqueous ethanol). Found: C, 63.24; H, 4.48; N, 5.71%. Calcd for $C_{13}H_{11}O_4N$ (III): C, 63.67; H, 4.52; N, 5.71%. IR: (KBr) ~3220 (OH), 1682 cm^{-1} (C=O).

Diethyl 1,4-dihydroxyacridine-2,3-dicarboxylate (IV). By Procedure A IV was prepared from diethyl quinoline-2,3-dicarboxylate, ethyl succinate, and sodium metal. Recrystallization from ethanol gave 43% of pale yellowish needles (mp 177 °C). Found: C, 63.91; H, 5.05; N, 4.04%. Calcd for $C_{19}H_{17}O_6N$ (IV): C, 64.22; H, 4.82; N, 3.94%. IR: (KBr) ~3350 (OH), 1690 (C=O), 1660 cm^{-1} (C=O). NMR: (δ in $CDCl_3$) 1.43 (t, 6H, CH_3–), 4.41 (quart, 4H, $-CH_2-$), 7.5—8.4 (m, 5H, aromatic), 9.24 (s, 2H, –OH). *Diacetate*: mp 149—150 °C (from ethanol) Pale yellowish pillows. Found: C, 62.59; H, 5.05; N, 3.30%: Calcd for $C_{23}H_{21}O_8N$:

C 62.86; H 4.82; N, 3.19%. IR: (KBr) ~1780 (OAc) 1730 cm^{-1} (C=O). NMR: (δ in $CDCl_3$) 1.32 (t, 6H, CH_3–), 2.32 (s, 6H, $COCH_3$), 4.30 (quart, 4H, –CH_2–), 7.3—8.3 (m, 5H, aromatic).

Oxidation of IV. By a procedure analogous to that described before, IV (0.1 g) in an ether solution was oxidized to the corresponding quinone (0.07 g) with silver oxide. The quinone was yellowish needles. Mp 184 °C (from ether). Found: C, 64.23; H, 4.20; N, 3.95%. Calcd for $C_{19}H_{15}O_6N$ (quinone of IV) C, 64.58; H, 4.28; N, 3.96%. IR: (KBr) 1762, 1685 cm^{-1}.

References.

1) Studies of Chelating Reagents Containing *N*-Heterocycles. Part VI; for Part V, see This Bulletin, **41**, 980 (1968).

2) S. Kawai, M. Torigoe, S. Fujiki, S. Odaki, N. Sakakibara, and S. Oguchi, *Nippon Kagaku Zasshi* **80**, 788 (1959); *Chem. Abstr.* **55**, 3597 (1961); S. Oguchi, *Nippon Kagaku Zasshi*, **86**, 435 (1965); *Chem. Abstr.*, **63**, 7011 (1965).

3) R. G. W. Hollingshead, "Oxine and its Derivatives," Vol. I, Butterworths Scientific Publications, London (1956), p. 969.

4) H. Diehl and F. H. Lohman, *Proc. Iowa Acad. Sci.* **61**, (1954) 255; *Chem. Abstr.*, **49**, 2929 (1955).

5) a) R. Long, and K. Schofield, *J. Chem. Soc.* **1953**, 3161. b) T. Urbanski, *Roczniki Chem.* **25**, 297 (1951); *Chem. Abstr.*, **48**, 4546 (1954).

BULLETIN OF THE CHEMICAL SOCIETY OF JAPAN, VOL. 47(5), 1293—1294 (1974)

Lilac Aldehydes

Seiji WAKAYAMA and Satoshi NAMBA

Chemical Laboratory, Hokkaido University of Education, Sapporo 064

(Received November 8, 1973)

Synopsis. New odorous aldehydes, diastereomers, have been found in lilac flower oil and named lilac aldehydes. The structure was established to be 2-(1'-formyl)ethyl-5-methyl-5-vinyl tetrahydrofuran. Absolute configurations have also been inferred.

Odorous ingredients of lilac flower oil[1] and lilac alcohols,[2] naturally occurring odorous components, were previously reported.

This paper describes the isolation of aldehydic components having an excellent green tone and their identification as diastereomeric 2-(1'-formyl)ethyl-5-vinyltetrahydrofuran (I) by combined gas chromatography-mass spectometry.*

In the gas chromatogram (Fig. 1) three unidentified peaks subsequent to number 13 peak of linalool were the aldehydes having R_t 6.6, 7.3, and 8.5 min.

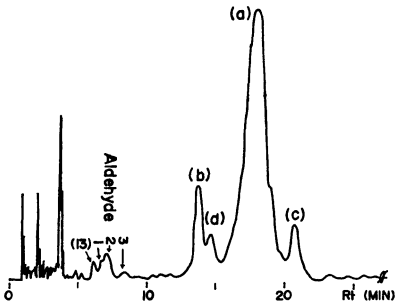

Fig. 1. Gas chromatogram of the lilac flower oil.
Column: 20% DEGS, 3 mm×3 m, Carrier Gas: He 30 ml/min, Oven Temp.: 120 °C, TCD

The mass spectra of the aldehydes are shown in Fig. 2; *m/e* 168 M^+, 153 $(M-CH_3)^+$, 141 $[M-(CH=CH_2)]^+$, 111 $[M-(CH\langle^{CH_3}_{CHO})]^+$, 55 $(CH_2=CH-C\equiv O)^+$, 43 $(CH_3-CO)^+$, 29 $(CHO)^+$. These fragments suggest structure (I) for the aldehydes.

In agreement with this formulation, R_t and mass spectra of the aldehydes synthesized from *d*-linalyl acetate were identical with those of natural aldehydes.

The structure of the aldehydes is comfirmed to be (I).

The aldehydes had been synthesized as intermediates for synthesizing lilac alcohols, but occurrence in nature has not yet been recorded. We wish to call them lilac aldehydes.

We intended to comfirm the absolute configurations

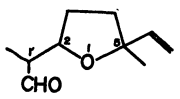

(I)

* Hitachi RM 50 GC, Ionization voltage 70 eV.

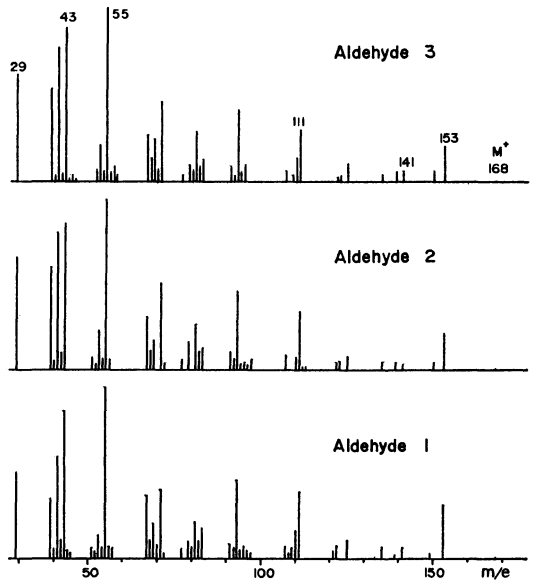

Fig. 2. Mass spectra of the lilac aldehydes.

of lilac aldehydes by converting them by reduction into lilac alcohols whose absolute configurations are comfirmed.** The gas chromatogram of the synthetic lilac aldehydes is shown in Fig. 3. Fractions corresponding to each peak were separated by repeated gas chromatography (PEG 20 M, 6 mm×5 m, 165 °C, He 45 ml/min). 2.4, 7.3, and 9.7 mg of d-2, d-3, and d-4 aldehydes, respectively, were reduced with $LiAlH_4$ to give the alcohols. The gas chromatograms of the alcohols are shown in Fig. 4. Judging from R_t and mass spectra, the alcohols were confirmed to consist of lilac alcohol-a, -b, -c, and -d.

Natural lilac aldehyde fraction exhibiting three peaks in gas chromatogram were reduced in the same manner as in synthetic aldehydes. The derived alcohols were also a mixture of the four diastereomeric lilac alcohols (Fig. 4).

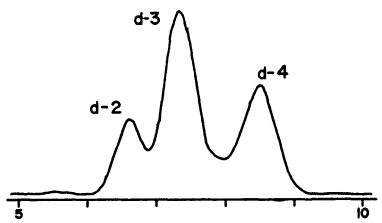

Fig. 3. Gas chromatogram of the synthetic *d*-lilac aldehydes.
Columun: 20% DEGS, 3 mm×3 m, carrier gas: He 30 ml/min, oven temp.: 120 °C, TCD.

** Since *d*-lilac alcohols in lilac flower oil amount to 70 per cent, lilac aldehydes would be *d*-series in view of biogenesis.[2] Due to too small amount of available natural aldehydes, measurements of $[\alpha]_D$ have not been carried out.

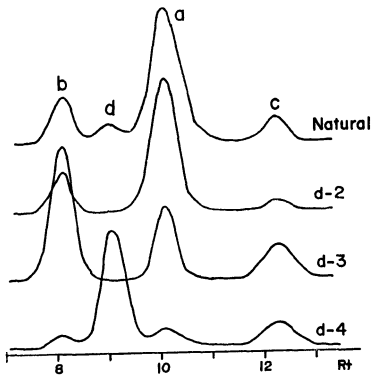

Fig. 4. Gas chromatograms of the reduced alcohols of natural and synthetic aldehydes.
Column: 15% DEGS, 3 mm×2 m, carrier gas: He 30 ml/min, oven temp.: 130 °C, TCD.

Although synthetic as well as natural lilac aldehydes showed only three peaks in gaschromatograms due to too small difference of R_t in two isomers, they were found to be a mixture of four diastereomers just as in lilac alcohols.

In the process of separation by liquid chromatography on alumina, it is interesting that natural lilac aldehydes were eluted in ether fraction, while synthetic lilac aldehydes were eluted in benzene–hexane (1: 1) fraction in the same manner as usual carbonyl compounds. Such an anomaly in natural lilac aldehydes seems to be due to an interaction between lilac aldehydes and abundantly existent lilac alcohols.

The characteristic greenish tone of the lilac flower seems to be duplicated by adding lilac aldehydes to lilac alcohols. This might also be ascribed to the interaction between the alcohols and the aldehydes.

References

1) S. Wakayama, S. Namba, and M. Ohno, *Nippon Kagaku Zasshi*, **92**, 256 (1971).
2) S. Wakayama, S. Namba, and M. Ohno, This Bulletin, **43**, 3319 (1970); S. Wakayama, S. Namba, K. Hosoi, and M. Ohno, *ibid.*, **44**, 875 (1971); **46**, 3183 (1973).

BULLETIN OF THE CHEMICAL SOCIETY OF JAPAN, VOL. 47(5), 1295—1296 (1974)

Synthetic Studies of Amino Acids by the Use of Copper(II) Complexes. V.[1] The Preparation of Hydroxy Amino Acids by a Set of Improved Procedures

Shohji OHDAN, Tetsuya ICHIKAWA, Younosuke ARAKI, and Yoshiharu ISHIDO

Department of Chemistry, Faculty of Science, Tokyo Institute of Technology, O-okayama, Meguro-ku, Tokyo 152

(Received December 7, 1973)

Synopsis. A variety of hydroxy amino acids were prepared by a brief treatment of a resulting mixture, which was obtained by a base-catalyzed condensation reaction of *N*-pyruvylideneglycinatoaquocopper(II) with aldehydes, on a column of Amberlite IR-120B (H form) resin.

The base-catalyzed condensation reaction of *N*-pyruvylideneglycinatoaquocopper(II) (**1**) with aldehydes has been shown[2c,d] to be especially useful in the preparation of 2-amino-2-deoxyaldonic acids from aldehydo sugar derivatives, in contrast with the reaction of bisglycinatocopper(II) *etc.* And it has recently been confirmed that glycine can be isolated from some of the corresponding copper(II) complexes in fairly good yields merely by treating the solution of the complexes on a column of Amberlite IR-120B (H form), even in the case of the solution in aqueous DMF.[1] In order to establish a more effective and facile method of preparing hydroxy amino acids, the present authors undertook an investigation of the preparation of hydroxy amino acids by a set of improved procedures—*i.e.*, the base-catalyzed condensation reaction of **1** with aldehydes[2] and the facile isolating procedure of amino acids.[1]

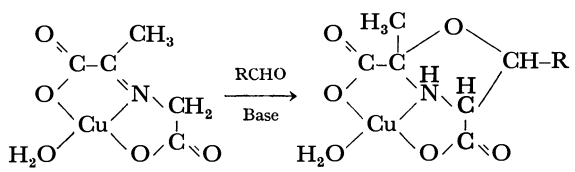

1

R–CH(OH)–CH(NH_2)–COOH

Base-catalyzed condensation reactions of **1** with acetaldehyde (**2**), propionaldehyde (**3**), *n*-butyraldehyde (**4**), benzaldehyde (**5**), 2,4-*O*-ethylidene-*al*-D-erythrose (**6**), and 2,3;4,5-di-*O*-isopropylidene-*al*-D-arabinose (**7**) were carried out. Each resulting reaction mixture was then divided into two aliquots for the subsequent treatment after adjusting the pH to 4.5 with an aqueous acetic acid solution; one was directly adsorbed on a column of IR-120B (H form), followed by elution with an aqueous ammoniacal solution after washing with water (A procedure); while the other was treated on a column of the ion-exchange resin after the removal of the copper(II) ion by treating it with hydrogen sulfide gas, as has been done traditionally (B procedure), for comparison with the A procedure. The reaction conditions and yields of the corresponding hydroxy amino acids obtained by both A and B procedures are summarized in Table 1. It is possible to discuss the comparative merits of the two procedures directly on the basis of these results because their samples came from the same source. The expected superiority of the A procedure to the B procedure is apparently exhibited in the cases of **2**, **3**, and **6**, which were found to give the corresponding hydroxy amino acid copper(II) complexes easily soluble in water; however, the yields of hydroxy amino acids were not so much improved in the cases of **4**, **5**, and **7**, which were found

Table 1. An examination of the comparative merit of A and B procedure[a]

Run	Aldehydes (R–CHO)	R–CHO/**1**	Reaction period (min)	Yields (%) of the corresponding hydroxy amino acids obtained by	
				A procedure[b]	B procedure[c]
1	Me– (**2**)[d]	1.5	120	87.6	71.7
2	Et– (**3**)[e]	3.0	240	90.1	70.0
3	*n*-Pr– (**4**)[e]	3.0	240	60.8	57.7
4	Ph– (**5**)[e]	3.0	540	61.2	65.5
5	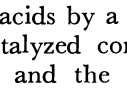 (**6**)[d]	1.1	45	79.7[f]	52.1[f]
6	(**7**)[d]	1.1	90	40.1[f]	34.0[f]

a) All the reactions were carried out by the use of **1** (5.200 g, 20 mmol) and divided into two aliquots after the treatments as described in d and e. b) The one aliquot was directly adsorbed on a column (3×9 cm) of Amberlite IR-120B (H form), and the column was eluted with 0.5 M aqueous ammoniacal solution (2000 ml) after washing with distilled water (5000 ml). c) The other aliquot was treated with hydrogen sulfide gas, and was successively treated on the column of the ion exchange resin as described in b after the filtration of the resulting copper sufide through the filter-cell. d) The condensation reaction was carried out in an aqueous solution (distilled water: 100 ml) at pH 9.5—9.8 at room temperature, and the resulting mixture was then acidified with 5 M aqueous acetic acid (pH 4.5). The procedure of d and b is termed as A-1 procedure. e) The condensation reaction was carried out in a mixture of methanol (60 ml) and 1 M methanolic sodium methoxide solution (14 ml) at room temperature under nitrogen atmosphere. To the resultant mixture, was added 5 ml of a 5 M aqueous acetic acid solution, and the mixture was diluted with distilled water to a volume of 200 ml. The procedure of e and b is termed as A-2 procedure. f) These products were isolated as the corresponding deblocked derivatives.

to give the corresponding copper(II) complexes less soluble in water. This defficiency in the procedure in the latter cases was, as will be described later, overcome by carrying out treatment with the ion-exchange resin batchwise or by the use of aqueous *N,N*-dimethylformamide as the solvent for the condensation reaction and/or as a dissolution-assisting agent prior to treatment on the column of the resin. Consequently, it can be expected that a variety of hydroxy amino acids can be effectively prepared by this set of improved procedures and that, in addition, the copper(II) ion can be recovered by a subsequent washing of the column with an appropriate eluent.

Table 2. Preparations of hydroxy amino acids by the treatment of A procedure[a)]

Run	Aldehydes (R–CHO)	R–CHO/**1**	Solvent systems	Reaction period (hr)	Yields of hydroxy amino acids obtained by the A procedure (%)[b)]
1	Me– (**2**)	1.5	A-1 (pH 9.8)	3.0	87.6 (61[2c)])
2	Et– (**3**)	3.0	A-2	4.0	90.1 (77[2c)])
3	*n*-Pr– (**4**)	3.0	A-2	4.0	81.2 (75[2c)])
4	**4**	3.0	A-6	2.0	84.4
5	*i*-Pr–	3.0	A-2	7.0	73.3 (75[2c)])
6	*i*-Pr–	3.0	A-6	2.0	65.6
7	**5**	3.0	A-2	9.0	61.2 (67[2c)])
8	**5**	3.0	A-3	9.0	62.3
9	**5**	3.0	A-5	9.0	64.5
10	**5**	3.0	A-6	2.0	69.3
11	*p*-Me–Ph–	3.0	A-3	15.0	46.6 (41[2c)])
12	*p*-Me–Ph–	3.0	A-6	2.5	52.8
13	*p*-O_2N–Ph–	1.0	A-4 (pH 9.0)	2.0	81.3 (80[2c)])
14	*p*-O_2N–Ph–	1.0	A-6	2.0	72.2
15	*o*-O_2N–Ph–	1.0	A-4 (pH 9.0)	0.5	52.7 (66[2c)])
16	*o*-O_2N–Ph–	1.0	A-6	0.5	50.4
17	*p*-Cl–Ph–	3.0	A-3	10.0	61.3 (44[2c)])
18	*p*-Cl–Ph–	3.0	A-6	2.0	75.9
19	**6**	1.1	A-1 (pH 9.5)	0.75	79.7[c)] (60[2d)])
20	**6**	1.1	A-7 (pH 9.5)	0.75	77.5[2d)]
21	**7**	1.2	A-1 (pH 9.5)	1.5	63.2[c)] (65[2d)])
22	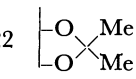	1.1	A-1 (pH 9.5)	1.5	45.4[c)] (22[2d)])

a) All the reactions were carried out by the use of **1** (2.600 g, 10 mmol). b) The yields shown in parentheses correspond to those obtained by the B procedure. c) These products were isolated as the corresponding deblocked derivatives.

A-3: The resultant mixture treated in such a way as in A procedure was stirred with the amount of the ion-exchange resin corresponding to that of being packed in a column of 3×9 cm in water to adsorb the corresponding product (batchwise operation), after which the resin was transfered into a column and the column was washed and eluted successively in the same way as has been described in A procedures. A-4: The condensation reaction was carried out in aqueous methanol (50 ml+50 ml), and the resultant mixture was treated as has been described in A-3. A-5: Prior to the admixture with aqueous acetic acid in A-2 procedure, the resultant reaction mixture was mixed with 50 ml of *N,N*-dimethylformamide. A-6: In place of methanol in A-2 procedure, aqueous *N,N*-dimethylformamide (50 ml+50 ml) was used as the solvent for the condensation. A-7: The volume of water (5000 ml) for washing in A-1 procedure was reduced to 1000 ml.

In the above connection, an extension of the A procedure was, with some modifications, attempted with respect to a variety of aldehydes; the reaction conditions, the details of the A procedures, and the yields of the hydroxy amino acids are summarized in Table 2. To homogenize the reaction systems, aqueous methanol, methanol, aqueous DMF, and DMF were used as solvents for the condensation reactions besides water. Moreover, a batchwise operation was found to be effective for the cases affording corresponding copper(II) complexes less soluble in water in order to adsorb the corresponding hydroxy amino acids on the ion-exchange resin. Furthermore, the addition of DMF to the resulting mixture prior to its treatment on the column of the resin was found to be more advantageous than the batchwise operation, and the use of DMF as the solvent for the condensation reaction was found to be exceedingly advantageous because of its eminent shortening effect in the reaction period. Thus, the set of improved procedure was confirmed to be sufficiently applicable to the preparation of a variety of hydroxy amino acids.

Experimental

All the hydroxy amino acids obtained herewith were respectively identified with the corresponding authentic specimens.[2c,d)] The preparation of DL-threonine will be described as a representative of the set of improved procedures.

DL-*Threonine.* A mixture of *N*-pyruvylideneglycinatoaquocopper(II) (**1**) (2.600 g, 10 mmol) and acetaldehyde (0.85 ml, 15 mmol) in water (50 ml) was stirred at pH 9.8 at room temperature for 2 hr. After the reaction, the pH of the resultant reaction mixture was adjusted to 4.5 with a 5 M aqueous acetic acid solution.

The resultant solution was then treated by the A-1 procedure and poured onto a column (3×9 cm) of Amberlite IR-120B (H form). The column was washed with distilled water (5000 ml) and successively eluted with a 0.5 M aqueous ammoniacal solution (2000 ml). The effluent was concentrated *in vacuo* almost to dryness, and the residue was treated with ethanol (10 ml) to give white crystals of DL-threonine (1.042 g, 87.6%). Mp 216 °C (dec) [lit,[2c)] 216 °C (dec)].

References

1) Part IV. S. Ohdan, T. Ichikawa, Y. Araki, and Y. Ishido, This Bulletin, **46**, 1019 (1973).

2) a) T. Ichikawa, S. Maeda, Y. Araki, and Y. Ishido, *J. Amer. Chem. Soc.*, **92**, 5514 (1970); b) T. Ichikawa, T. Okamoto, S. Maeda, S. Ohdan, Y. Araki, and Y. Ishido, *Tetrahedron Lett.*, **1971**, 79; c) T. Ichikawa, S. Maeda, T. Okamoto, Y. Araki, and Y. Ishido, This Bulletin, **44**, 2779 (1971); d) S. Ohdan, T. Okamoto, S. Maeda, T. Ichikawa, Y. Araki, and Y. Ishido, *ibid.*, **46**, 981 (1973).

BULLETIN OF THE CHEMICAL SOCIETY OF JAPAN, VOL. 47(5), 1297—1298 (1974)

Reaction of *N*-Nitroso-1,2,3,4-tetrahydroisoquinolines with Base. A New Method for the Conversion of 1,2,3,4-Tetrahydroisoquinolines into 3,4-Dihydroisoquinolines

Kazuo SAKANE, Ken-ichi TERAYAMA, Eiichi HARUKI, Yoshio OTSUJI, and Eiji IMOTO

Department of Applied Chemistry, College of Engineering, University of Osaka Prefecture, Sakai-shi, Osaka 591

(Received December 27, 1973)

Synopsis. Treatment of *N*-nitroso-1,2,3,4-tetrahydroisoquinoline (**2a**) and its 1-methyl derivative (**2b**) with base gave the corresponding 3,4-dihydroisoquinolines (**3a** and **3b**). However, similar treatment of *N*-nitroso-1,2,3,4-tetrahydroisoquinoline-1-acetic acid (**2c**) gave a mixture of **3b** and 1,2,3,4-tetrahydroisoquinoline-1-(α-hydroxyimino)acetic acid (**4**).

Reaction for the preparation of 3,4-dihydroisoquinolines from 1,2,3,4-tetrahydroisoquinolines can be classified into two types: direct dehydrogenation using oxidizing agents such as Hg(II)-EDTA[1] and potassium ferrate (VI),[2] and the elimination of a substituent attached to *N*-heteroatom and a hydrogen at the 1-position of tetrahydroisoquinolines, such as the base-induced elimination of hydrogen halide from *N*-halogeno-1,2,3,4-tetrahydroisoquinolines,[3,4] and the photochemically induced elimination of *p*-toluenesulfinic acid from *N*-tosyl-1,2,3,4-tetrahydroisoquinolines in the presence of base.[5] . We report here a new method belonging to the latter.

N-Nitroso-1,2,3,4-tetrahydroisoquinolines derived from 1,2,3,4-tetrahydroisoquinolines were converted into 3,4-dihydroisoquinolines with base. The sequence of the reactions employed is outlined in Chart 1. The procedure is simple and the yields are generally good.

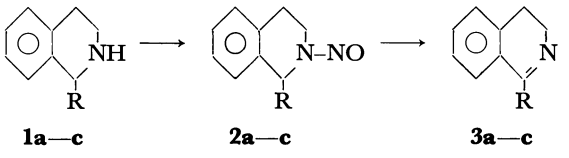

1a—c **2a—c** **3a—c**

a, R=H; b, R=CH_3; c, R=CH_2CO_2H.

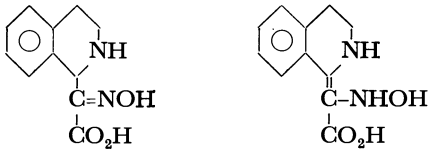

4a **4b**

Chart 1.

N-Nitroso-1,2,3,4-tetrahydroisoquinolines (**2a—c**) were prepared by the nitrosation of the corresponding 1,2,3,4-tetrahydroisoquinolines (**1a, b**) or the hydrochloride (**1c**) with isoamyl nitrite or sodium nitrite in hydrochloric acid. Treatment of **2a** and **2b** with aqueous sodium hydroxide resulted in the formation of the corresponding 3,4-dihydroisoquinolines in high yields, no other products being detected in the reaction mixture. Total yields of **3a** and **3b** from **1a** and **1b** were 70 and 80%, respectively. It is almost certain that **3a** and **3b** are produced by the base-induced elimination of hydrogen hyponitrite from *N*-nitroso compounds, although the reaction of this type has scarcely been reported. Daeniker[6] noted that *N*-nitroso-*N*-benzylaniline undergoes the elimination of hydrogen hyponitrite on being treated with a base.

However, a similar treatment of **2c** with sodium hydroxide afforded two products, **3b** and 1,2,3,4-tetrahydroisoquinoline-1-(α-hydroxyimino)acetic acid (**4**). The yields of **3b** and **4** from **2c** were 20 and 70%, respectively. Compound **3b** probably arises by the decarboxylation of **3c**, a primary product of the reaction of **2c** with base. On the other hand, the base-induced migration of the nitroso group from nitrogen to the carbon adjacent to the carboxyl group in **2c** accounts for the production of **4**. The migration of nitroso group of this kind, *viz.*, migration of nitroso group from nitrogen to an active methylene, has been observed in the reaction of *N*-nitroso amino acid.[6]

The structure of the compounds were confirmed by means of analytical and spectral data or by comparison with the respective authentic samples. The spectral data suggested that **4** exists in the form of **4a** or **4b**, or in equilibrium between **4a** and **4b**.

Experimental

*3,4-Dihydroisoquinoline (**3a**) from 1,2,3,4-Tetrahydroisoquinoline (**1a**).* A mixture of 1.3 g (0.01 mol) of **1a** and 4.6 g (0.04 mol) of isoamyl nitrite was allowed to stand at room temperature for 1 hr, and the excess isoamyl nitrite was evaporated. The residue dissolved in benzene was passed through a column of alumina using *n*-hexane–benzene mixture as an eluent to give 1.5 g (90%) of *N*-nitroso-1,2,3,4-tetrahydroisoquinoline (**2a**) as yellow solids: IR (KBr) 2920, 1420, 1355, 1330, 1160, 1100, 1040, 920, 805, and 750 cm^{-1}; NMR ($CDCl_3$) δ 2.84 (t, J=6.4 Hz, 2/3H), 2.99 (t, J=5.9 Hz, 4/3H), 3.76 (t, J=6.4 Hz, 2/3H), 4.42 (t, J=5.9 Hz, 4/3H), 4.71 (s, 4/3H), 5.27 (s, 2/3H), and 7.10 ppm (m, 4H). The NMR spectrum exhibited the same pattern as that reported by Chow and Colon[7] for **2a** indicating that **2a** exists in a pair of *syn* and *anti* conformers along the axis of the N–N partial double bond in the ratio 2: 1.

Compound **2a** thus obtained was used without further purification for the preparation of **3a**. A mixture of 1.5 g (0.009 mol) of **2a** in 20 ml of ethanol and 10 ml of 20% aqueous NaOH was refluxed for 10 hr, cooled, diluted with water and then taken up in CH_2Cl_2. The CH_2Cl_2 solution was extracted with 3 M HCl. The aqueous extract was made basic with 10% NaOH and extracted with CH_2Cl_2.

The extract was washed with water and dried over Na_2SO_4. Removal of CH_2Cl_2 left an oil, which was dissolved in benzene and passed through a column of alumina with benzene to give 0.9 g (70%) of **3a**. The IR spectrum (film) showed an absorption at 1630 cm^{-1} (C=N) and was identical with that of the authentic sample prepared by the method of Snyder and Werber.[8] The picrate, mp 172—175 °C, showed no depression in the mixed melting point test with the picrate from the authentic sample of **3a**.

*1-Methyl-3,4-dihydroisoquinoline (**3b**) from 1-Methyl-1,2,3,4-tetrahydroisoquinoline (**1b**).* *N*-Nitroso-1,2,3,4-tetrahydroisoquinoline (**2b**) was prepared from 1.5 g (0.01 mol) of **1b** and 4.6 g (0.04 mol) of isoamyl nitrite by a method similar to that described above. A solution of the crude product in benzene was chromatographed on alumina. Elution with *n*-hexane–benzene gave 1.5 g (85%) of **2b** as a yellow viscous oil: IR (film) 2970, 2930, 2860, 1495, 1430, 1360, 1315, 1295, 1150, 1110, and 760 cm^{-1}; NMR ($CDCl_3$) δ 1.47 (d, J=7.3 Hz, 3/2H), 1.72 (d, J=7.3 Hz, 3/2H), 2.80—3.30 (m, 2H), 3.40—5.10 (m, 2H), 5.91 (q, J=7.3 Hz, 1H), and 7.17—7.50 ppm (m, 4H, aromatic).

The oil **2b** was used without further purification for preparation of **3b**. A 1.5 g (0.0085 mol) sample of **2b** in 20 ml of ethanol was treated with 10 ml of 20% NaOH. Work-up of the reaction mixture yielded an oil, which upon distillation gave 1.1 g (92%) of **3b** as a colorless oil, bp 127—138 °C/20 mmHg: IR (film) 1630 cm^{-1} (C=N). The IR spectrum of this compound was identical with that of the authentic sample prepared by the method of Lora-Tamayo, Madronero, and Munoz.[9] The picrate, mp 187—190 °C, showed no depression in the mixed melting point test with the authentic specimen.

*1,2,3,4-Tetrahydroisoquinoline-1-acetic Acid (**1c**) Hydrochloride.* A mixture of 17 g (0.078 mol) of ethyl 1,2,3,4-tetrahydroisoquinoline-1-acetate[10-12] in 50 ml of 3 M HCl was refluxed for 1 hr. A half of water was removed under atmospheric pressure at 130—140 °C (oil bath temperature) left solids. The solids were extracted with 30 ml of boiling acetone, and the insoluble material (HCl salt of **1c**) was separated by filtration. The filtrate was evaporated to dryness, and the residue (unhydrolyzed ester) was repeatedly hydrolyzed. The solids obtained by hydrolysis were combined and recrystallized from dioxane–methanol to give 17 g (quantitative) of the hydrochloride of **1c** as white crystals; mp 183—184 °C: IR (KBr) 3500—2400 (OH), and 1720 cm^{-1} (C=O). Found: C, 58.44; H, 5.91; N, 6.42%. Calcd for $C_{11}H_{14}NO_2Cl$: C, 58.02; H, 6.15; N, 6.15%.

*N-Nitroso-1,2,3,4-tetrahydroisoquinoline-1-acetic Acid (**2c**).* To a solution of 2.0 g (0.0088 mol) of the hydrochloride of **1c** in 20 ml of 3 M HCl was added 20 ml of 10% sodium nitrite under cooling in an ice–water bath. The mixture was stirred for 1 hr under cooling. The resulting solids were filtered, and recrystallized from aqueous ethanol to give 1.7 g (90%) of **2c** as white needles, mp 167—169 °C: IR (KBr) 3100—2300 (OH) and 1720 cm^{-1}. Found: C, 59.71; H, 5.50; N, 12.48%. Calcd for $C_{11}H_{12}N_2O_3$: C, 59.99; H, 5.49; N, 12.72%.

*Reaction of **2c** with Aqueous Sodium Hydroxide.* A mixture of 3.0 g (0.014 mol) of **2c**, 50 ml of ethanol and 30 ml of 20% NaOH was refluxed for 10 hr. The precipitates were occasionally filtered. Additional precipitates obtained upon cooling the mixture were separated by filtration. The filtrate was extracted with CH_2Cl_2. The extract was washed with water, dried over Na_2SO_4, and then evaporated. The residue was chromatographed on a column of alumina. Elution with CH_2Cl_2 gave 0.4 g (20%) of **3b**. The IR spectrum of this compound was identical with the authentic sample.

The precipitates were combined and dissolved in water. The solution was acidified with concd HCl and allowed to stand for 2 hr. The resulting precipitates were filtered, and recrystallized from aqueous ethanol to give 2.1 g (70%) of 1,2,3,4-tetrahydroisoquinoline-1-(α-hydroxyimino) acetic acid (**4**) as white needles, mp 145—146 °C: IR (KBr) 3520, 3350, 2900—2200, and 1680 cm^{-1} (C=O); UV (EtOH) λ_{max} (log ε) 212 (3.90) and 294 nm (3.87); NMR (CF_3COOH) δ 3.10—3.70 (m, 4H), 4.17—5.10 (m, 2H), 6.15—6.70 (m, 1H), and 7.56 ppm (m, 4H, aromatic). Found: C, 59.90; H, 5.50; N, 12.45%. Calcd for $C_{11}H_{12}N_2O_3$: C, 59.99; H, 5.49; N, 12.72%.

References

1) J. Knabe and G. Grund, *Arch. Pharmz.*, **296**, 820 (1963).
2) R. J. Audette, J. W. Quail, and P. J. Smith, *Tetrahedron Lett.* **1971**, 279.
3) N. Whittaker, U. S. 3135759; *Chem. Abstr.*, **61**, 5710g (1964).
4) E. Eckhart, *Magy. Kem. Folyoirat*, **70**, 296 (1964); *Chem. Abstr.*, **61**, 13355e (1964).
5) B. Umezawa, O. Hoshino, and S. Sawaki, *Chem. Pharm. Bull.* (Tokyo), **17**, 1115 (1969).
6) von H. U. Daeniker, *Helv. Chim. Acta*, **47**, 33 (1964).
7) Y. L. Chow and C. J. Colon, *Can. J. Chem.*, **46**, 2827 (1968).
8) H. R. Snyder and F. X. Werber, *J. Amer. Chem. Soc.*, **72**, 2962 (1950).
9) M. Lora-Tamayo, R. Madronero, and G. G. Munoz, *Chem. Ber.*, **93**, 289 (1960).
10) S. G. Agbalyan, A. O. Nshanyan, and L. A. Nersesyan, *Izv. Akad. Nauk Arm. SSR, Khim. Nauki*, **16**, 77 (1963); *Chem. Abstr.*, **59**, 5132c (1964).
11) W. Sobotka, W. N. Beverung, G. G. Munoz, J. C. Sircar, and A. I. Meyers, *J. Org. Chem.*, **30**, 3667 (1965).
12) G. Van Binst and J. C. Nouls, *J. Chem. Soc. C*, **1970**, 150.

BULLETIN OF THE CHEMICAL SOCIETY OF JAPAN, VOL. 47(5), 1299—1300 (1974)

Pyrolysis of Tris(2,3-dibromopropyl) Phosphate and Its Related Compounds

Yoshiki OKAMOTO, Norio KIMURA, and Hiroshi SAKURAI

The Institute of Scientific and Industrial Research, Osaka University, Yamada-kami, Suita-shi, Osaka 565

(Received Junuary 18, 1974)

Synopsis. The main product obtained by the pyrolysis of halogenated alkyl phosphate was found to be alkyl halide. The phosphoryl group was substituted for the halogen atom, olefins being minor products.

In a previous paper, we reported that the products obtained by the pyrolysis of *n*-hexyl phosphates were the mixtures of hexene isomers, the acid having a conspicuous influence on the isomer distribution.[1)]

Tris(2,3-dibromopropyl) phosphate (I) is wellknown as an effective fire retardant for synthetic polymers, but its behavior in pyrolysis has not yet been studied.

We have investigated the pyrolysis of I and its related compounds as regards the behavior of halogen atom.

Tris(2,3-dichloropropyl) phosphate (II)[2)] and trihexyl phosphate (III) were prepared by the reaction of phosphorus oxychloride with 2,3-dichloropropyl alcohol and hexyl alcohol, respectively.

Tris(2-chloroethyl) phosphate (IV),[2)] tris(1-methyl-2-chloroethyl) phosphate (V)[2)] and tris(1-chloromethyl-2-chloroethyl) phosphate (VI)[2)] were prepared by the addition of phosphorus oxychloride to ethylene oxide, propylene oxide and epichlorohydrin, respectively.

I and diethyl 2,3-dibromopropyl phosphate (VII)[2)] were prepared by the addition of bromine to the corresponding allyl phosphates at −15 °C. After they had been treated with a cation exchange resin column chromatography to remove trace of free acid, they were dried *in vacuo*.

In each run of pyrolysis, 0.1 mol of the phosphate was decomposed in a 20 ml-distilling flask heated (250—260 °C) with a metal bath at reduced pressure (3 mmHg).

The decomposition was over in a few minutes. The pyrolysis products were trapped in a tube cooled with liquid nitrogen. They were analyzed with glc on a 3 m×3 mmϕ column, packed with Ucon LB 550X on Chromosorb W (60—80 mesh) at column temperature of 160 °C, using nitrogen gas as the carrier. The glc peaks were identified by comparing their retention times with those of authentic samples, or by analysis of NMR and mass spectra of the fractions obtained by preparative glc.

The results of the pyrolysis of several halogenated alkyl phosphates are given in Table 1.

In the pyrolysis of I, 1,2,3-tribromopropane as the main product, *cis*- and *trans*-1,3-dibromopropene, 2,3-dibromopropene-1 and 3-bromopropene-1 were given as distillable products. No free bromine and a trace amount of hydrogen bromide could be detected. The residue was halogen-containing polymerized alkyl phosphate, the structure of which is still unidentified. II gave a mixture of 1,2,3-trichloropropane as a major product, 2,3-dichloropropene-1, 1,3-dichloropropene and a trace amount of 3-chloropropene-1. IV gave 1,2-dichloroethane as a major product and a small amount of vinyl chloride. In the pyrolysis of VII, 87% ethyl bromide was obtained but only a trace amount of 1,2,3-tribromopropane. In the case of the equimolar mixture of I and III, 50% hexyl bromide was obtained but only a trace amount of 1,2,3-bromopropane. In the case of the equimolar mixture of II and III, 21% hexyl chloride was obtained, which was less than the corresponding hexyl bromide from the mixture of I and III. In the case of the equimolar mixture of I and II, 49% of 1-bromo-2,3-dichloropropane and 35% of 1,2,3-tribromopropane, formed

TABLE 1. YIELDS AND COMPOMENTS OF THE PRODUCTS OBTAINED BY THE PYROLYSIS OF TRIS(2,3-DIBROMOPROPYL) PHOSPHATE AND ITS RELATED COMPOUNDS

Phosphate	Yield (wt%)	Components (relative ratio, mol%)
I	55	CH_2=$CHCH_2Br$ (12), CH_2BrCH=$CHBr$ (*trans*-: 5.7, *cis*-: 13), CH_2BrCBr=CH_2 (2.3), $CH_2BrCHBrCH_2Br$ (67)
II	30	CH_2=$CHCH_2Cl$ (t), CH_2ClCH=$CHCl$ (*trans*-: 5, *cis*-: 8), CH_2ClCCl=CH_2 (12), $CH_2ClCHClCH_2Cl$ (75)
IV	23	CH_2=$CHCl$ (5), CH_2ClCH_2Cl (95)
VII	41	C_2H_5Br (84.7), CH_2=$CHCH_2Br$ (10.3), CH_2=$CBrCH_2Br$ (4.2), CH_2BrCH=$CHBr$ (*trans*-: t, *cis*: 0.8), $CH_2BrCHBrCH_2Br$ (t)
I+III	45	CH_2=$CHCH_2Br$ (t), CH_2BrCH=$CHBr$ (t), CH_2BrCBr=CH_2 (t), $CH_2BrCHBrCH_2Br$ (t), C_6H_{12} (50), $C_6H_{13}Br$ (50)
II+III	44	CH_2=$CHCH_2Cl$ (t), CH_2ClCH=$CHCl$ (*trans*-: 1.3, *cis*-: 0.7), CH_2ClCCl=CH_2 (t), $CH_2ClCHClCH_2Cl$ (3), C_6H_{12} (77), $C_6H_{13}Cl$ (18)
V	43	CH_2=$CHCH_2Cl$ (45.5), CH_3CH=$CHCl$ (45.5), $CH_3CHClCH_2Cl$ (9)
VI	60	C_2HClCH=$CHCl$ (*trans*-: 26.7, *cis*-: 36.0), $CH_2ClCHClCH_2Cl$ (34.4), CH_2=CH-CH_2Cl (2.9)

Table 2. Effects of additives on the pyrolysis of I

Additive[a]	Yield (wt%)	Component (relative ratio, mol%)				
		$CH_2=CHCH_2Br$	$CH_2=CBrCH_2Br$	$CHBr=CHCH_2Br$		$CH_2BrCHBrCH_2Br$
				cis	*trans*	
$H_4P_2O_7$	53	23	1	21	3	52
NaH_2PO_4	55	12	14	10	4	60
Na_2HPO_4	58	17	23	6	5	49
$Na_4P_2O_7$	56	12	23	5	4	56
$Ca_3(PO_4)_2$	59	22	15	8	3	52
CH_3COONa	60	9	68	16	2	5
Sb_2O_3	55	83	1	1	1	14

a) 25 wt%

by the transfer of bromine, and 5% of 1,2,3-trichloropropane and 4% of 1,2-dibromo-3-chloropropane, formed by the transfer of chlorine, were obtained.

The main products obtained by the pyrolysis of the halogenated alkyl phosphates were alkyl halides (95—67%), and olefins were minor products, different from the behaviors of unsubstituted alkyl phosphates in the pyrolysis.[1] This suggests that the formation process of alkyl halide involves intermolecular transfer of halogen atom, and the transfer of bromine atom occurred more easily than that of chlorine atom. The halogen substitution occurred more readily at the carbon atom having no halogen atom in the neighboring position. The following mechanism is suggested to account for the behavior.

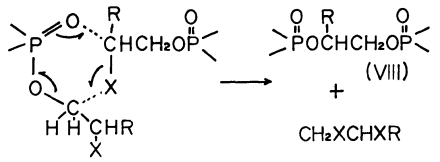

The formation of 2,3-dibromopropene-1 or 2,3-dichloropropene-1 might proceed through a six-membered ring transition intermediate as in the pyrolysis of alkyl carboxylate.[3]

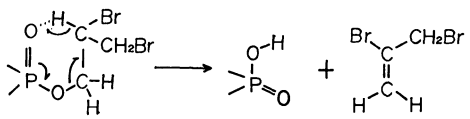

1,3-Dibromopropene or 1,3-dichloropropene might be given through the isomerization of 2,3-dihalopropyl cation which was formed by acid catalyzed pyrolysis, into 1-halomethyl-2-haloethyl cation, followed by the elimination of a proton as follows.

3-Bromopropene-1 can be obtained from further decomposition of VIII.

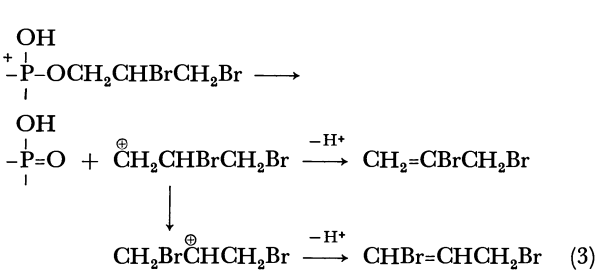

Secondary alkyl phosphates V and VI gave more olefinic products than the halogen substituted products. This decomposition may proceed preferentially through reaction (2) or (3).

The effects of additives on the pyrolysis of I were studied. The results are given in Table 2.

Addition of sodium phosphates to I induced the substantial change in the yields of 2,3-dibromopropene-1 and *cis*-1,3-dibromopropene, which might be formed *via* reaction (2) or (3), in the same manner as the case of the pyrolysis of III.[1] However, the formation of alcohol could not be observed. Addition of phosphoric acid increased 3-bromopropene-1 and 1,3-dibromopropene, but decreased 1,2,3-tribromopropane. It was observed that by the addition of sodium acetate 2,3-dibromopropane markedly increased, whereas 1,2,3-tribromopropane decreased. Antimonous trioxide is also known to be an effective fire retardant when it is used with halogen-containing material. It was found that its addition caused serious changes of the composition of the products.

References

1) Y. Okamoto, N. Kimura, and H. Sakurai, This Bulletin, **47**, 491 (1974).

2) K. Sasse, "Methoden der Organischen Chemie XII/2 Organische Phosphorverbindungen," ed. by E. Muller, Georg Thieme Verlag, Stuttgart (1964).

3) H. E. Baumgarten and R. A. Setterquist, *J. Amer. Chem. Soc.*, **79**, 2605 (1957).

BULLETIN OF THE CHEMICAL SOCIETY OF JAPAN, VOL. 47(5), 1301—1302 (1974)

Effects of Substituents on pK_a and τ_{OH} Values of Hydroxyaryl-1,3,5-triazines; σ_p^- Values of 1,3,5-Triazinyl Groups.

Yukio OHTO, Yōji HASHIDA, Shizen SEKIGUCHI, and Kohji MATSUI

Department of Chemistry, Faculty of Engineering, Gunma University, Tenjin-cho, Kiryu, Gunma 376

(Received January 25, 1974)

Synopsis. Regular relations were found between substituents in the *s*-triazine nucleus and pK_a values, τ_{OH} values of *o*- and *p*-hydroxyphenyl-*s*-triazines, and stabilities of chelation of the *o*-isomers. The substituent constants (σ_p^-) for some *s*-triazinyl groups were also found.

No detailed information has been given on the relation between chemical constitutions of 2-(*o*-hydroxyaryl)-nitrogen heteroaromatics and their stability of chelation because of the difficulty of obtaining a series of 2-(*o*-hydroxyaryl)-nitrogen heteroaromatics. However, a number of hydroxyaryl-*s*-triazines are readily available by the photolysis of aryloxy-chloro-*s*-triazines followed by treatment with nucleophiles.[1] These *s*-triazine derivatives can provide an appropriate series of 2-(*o*-hydroxyaryl)-nitrogen heteroaromatic for studying the substituent effects on the strength of chelation. This paper deals with the effects of substituents in the *s*-triazine nucleus on pK_a value and ^{1}H chemical shift of phenolic proton of hydroxyaryl-*s*-triazine giving substituent constants for the *s*-triazine nucleus.

Experimental

The NMR spectra were recorded on a Varian A-60D spectrometer in DMSO-d_6 with tetramethylsilane as an internal standard, and the pK_a values were measured spectrophotometrically in water at 25 °C.

Materials. Hydroxyaryl-*s*-triazines were synthesized by the method described previously.[1]

Results and Discussion

pK_a *Values of Hydroxyaryl-s-triazines.* In the ordinary chelated phenols the stabilities of chelation are regularly correlated with their pK_a values. Thus, the stabilities of chelation of *o*-hydroxyaryl-*s*-triazines were discussed in connection with their pK_a values. The pK_a values of various hydroxyaryl-*s*-triazines are given in Table 1.

We see that the pK_a values of *o*-hydroxyphenyl-*s*-triazines are higher than those of the corresponding *p*-isomers, suggesting that chelate ring formation takes place in each *o*-hydroxyphenyl-*s*-triazine. The pK_a values of *o*- and *p*-hydroxyphenyl-*s*-triazines vary regularly with two substituents in the *s*-triazine nucleus [$pK_a(o) = -0.890\ \Sigma\sigma_m + 11.37$, where $\Sigma\sigma_m$ denotes a summation of σ_m values of two substituents in the *s*-triazine nucleus]. However, the pK_a values of *p*-hydroxyphenyl-*s*-triazines were affected to a lesser extent than the *o*-isomers by the substituents in the *s*-triazine nucleus; the relatively large difference in pK_a value between the *o*-hydroxyaryl-*s*-triazines is considered

TABLE 1. pK_a VALUES AND ^{1}H CHEMICAL SHIFTS OF PHENOLIC PROTONS OF HYDROXYARYL-*s*-TRIAZINES

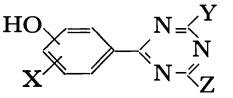

No.	HO–	X	Y	Z	pK_a	τ_{OH}
1	*o*-OH	H	$-OC_6H_5$	$-OC_6H_5$	10.92	−1.57
2	*o*-OH	H	$-OC_6H_5$	$-OCH_3$	11.06	−1.93
3	*o*-OH	H	$-OCH_3$	$-OCH_3$	11.17[a]	−2.52[a]
4	*o*-OH	H	$-OC_6H_5$	$-N(CH_3)_2$	11.29	−2.57
5	*o*-OH	H	$-N(CH_3)_2$	$-N(CH_3)_2$	11.76	−3.75
6	2-OH	5-CH_3	$-OC_6H_4-CH_3(p)$	$-OC_6H_4-CH_3(p)$	11.45	−1.37
7	2-OH	5-CH_3	$-OC_6H_4-CH_3(p)$	$-OCH_3$	11.61	−1.77
8	2-OH	5-CH_3	$-OCH_3$	$-OCH_3$	11.71[a]	−2.31[a]
9	2-OH	5-CH_3	$-OCH_3$	$-N(CH_3)_2$	11.94	−2.92
10	2-OH	5-CH_3	$-N(CH_3)_2$	$-N(CH_3)_2$	12.23	−3.13
11	*p*-OH	H	$-OC_6H_5$	$-OC_6H_5$	—	−0.35
12	*p*-OH	H	$-OC_6H_5$	$-OCH_3$	8.37	−0.27
13	*p*-OH	H	$-OCH_3$	$-OCH_3$	8.46[a]	−0.18[a]
14	*p*-OH	H	$-OC_6H_5$	$-N(CH_3)_2$	8.55	−0.10
15	*p*-OH	H	$-OCH_3$	$-N(CH_3)_2$	8.65	−0.07
16	*p*-OH	H	$-N(CH_3)_2$	$-N(CH_3)_2$	8.88	+0.12
17	2-OH	5-Cl	$-OCH_3$	$-OCH_3$	10.39[a]	−2.64[a]
18	2-OH	6-H	$-OCH_3$	$-OCH_3$	11.17[a]	−2.52[a]
19	2-OH	6-OCH_3	$-OCH_3$	$-OCH_3$	11.97[a]	−2.10[a]

a) reported in the previous paper.[1]

to be due not only to the difference in the original acidity of *s*-triazinyl-phenol but also to the difference in stability of the chelation. If steric requirements in all the *o*-hydroxyaryl-*s*-triazines are similar in magnitude as might be anticipated in these cases, the relative strength of intramolecular hydrogen bond can be evaluated by means of the difference in pK_a value between *o*- and corresponding *p*-hydroxyaryl-*s*-triazines [$\Delta pK_a = pK_a(o) - pK_a(p)$]. When ΔpK_a values are plotted against the $\sum\sigma_m$ values, a straight line of negative slope ($\Delta pK_a = -0.248 \sum\sigma_m + 2.77$) was obtained, suggesting that the stability of chelation varies with the substituents in the *s*-triazine nucleus, although the substituent effect is small. Similar relations were also observed in the case of 5-methyl-2-hydroxyphenyl-*s*-triazines, showing that the greater the electron-donating tendency of the two substituents in the *s*-triazine nucleus, the higher the pK_a value owing to the formation of stronger chelated ring due to an increase in electron density at the ring nitrogen atom. Thus, among the *o*-hydroxyaryl-*s*-triazines of the same phenol moiety the relative stability of chelation can be represented by the summation of σ_m values of two substituents in the *s*-triazine ring.

Chemical Shifts of Hydroxyl Protons of Hydroxyaryl-s-triazines. Substituent effects on the chemical shifts of hydroxyl protons of hydroxyaryl-*s*-triazines were investigated. Effects of substituents on the NMR signals of phenolic protons have been studied with many substituted phenols;[2] in each case a good correlation holds between the substituents in the *meta* and *para* positions and ^1H chemical shifts of phenolic protons. ^1H Chemical shifts (in τ) of phenolic protons of hydroxyaryl-*s*-triazines are given in Table 1. In this case also the difference in τ_{OH} value between *p*-*s*-triazinylphenols is relatively small [$\tau_{OH}(p) = -0.487 \sum\sigma_m - 0.091$]; the large difference in τ_{OH} value between *o*-isomers [$\tau_{OH}(o) = 2.27 \sum\sigma_m - 2.79$] being ascribed to the difference in the strength of chelation. A linear relation holds between the $\Delta\tau_{OH}$[$\Delta\tau_{OH} = \tau_{OH}(o) - \tau_{OH}(p)$] and $\sum\sigma_m$ values ($\Delta\tau_{OH} = -2.77 \sum\sigma_m + 2.71$). Similar relations are also observed in the case of 5-methyl-2-hydroxyphenyl-*s*-triazines. Thus, among the *o*-hydroxyaryl-*s*-triazines of the same phenol and different *s*-triazine moieties, not only the ΔpK_a and $\Delta\tau_{OH}$ values but also the $\sum\sigma_m$ values of two substituents in the *s*-triazine nucleus can be utilized as a measure for the relative stability of chelation.

Substituent Constants of s-*Triazinyl Groups.* The *s*-triazinyl group is known as an electron-attracting substituent. However, so far there has been no quantitative evaluation for the electron-withdrawing powers of common *s*-triazinyl groups. In the *p*-hydroxyphenyl-*s*-triazines, each pK_a value was smaller than that of phenol, indicating that the *s*-triazinyl group is electron-attracting regardless of two substituents in the *s*-triazine nucleus. However, the pK_a value of this series also varies regularly with the $\sum\sigma_m$ value [$pK_a(p) = -0.635 \sum\sigma_m + 8.60$].

Since a good linear relation holds between the substituent and dissociation constants of phenols ($pK_a = -2.23\sigma + 9.92$),[3] substituent constants for the *s*-triazinyl groups of σ_p^- character can be obtained from the pK_a values of *p*-*s*-triazinylphenols. The results are given in Table 2. When these σ_p^- values are plotted against the $\sum\sigma_m$ values, a straight line with a positive slope of 0.30 is obtained, indicating that the substituents in the *s*-triazine nucleus affect the electron-attracting power of *s*-triazine nucleus only to a minor extent.

In the case of τ_{OH} value, a linear correlation is also observed between the $\sum\sigma_m$ and τ_{OH} values of *p*-hydroxyphenyl-*s*-triazines. Substituent constants attributable to *s*-triazinyl groups were also obtained from τ_{OH} values using an equation obtained by plotting τ_{OH} values of substituted phenols[2] against the substituent constants σ_p^-.

The σ_p^- values of the two series agree fairly well. $\sum\sigma_m$ was found to become zero at $\sigma_p^- = 0.61$, indicating the *s*-triazinyl group itself to be a fairly electron-attracting substituent. The bis(dimethylamino)- and dichloro-*s*-triazinyl groups were found to have the smallest and greatest σ_p^- values of the common *s*-triazinyl groups, being 0.47 and 0.85, respectively. This shows that the electron-attracting powers of the common *s*-triazinyl groups are comparable to those of ordinary acyl and other related groups.

TABLE 2. σ_p^- VALUES OF *s*-TRIAZINYL GROUPS

Y	Z	$\sum\sigma_m$ (σ_mY+σ_mZ)	σ_p^- (a)	(b)	(d)
-Cl	-Cl	0.747	(0.82)[c]	(0.88)[c]	0.85
$-OC_6H_5$	$-OC_6H_5$	0.504	—	0.80	0.80
$-OC_6H_5$	$-OCH_3$	0.367	0.71	0.75	0.73
$-OCH_3$	$-OCH_3$	0.230	0.66	0.70	0.68
$-OC_6H_5$	$-N(CH_3)_2$	0.041	0.61	0.63	0.62
-H	-H	0	(0.60)[c]	(0.62)[c]	0.61
$-OCH_3$	$-N(CH_3)_2$	−0.096	0.57	0.59	0.59
$-N(CH_3)_2$	$-N(CH_3)_2$	−0.422	0.47	0.47	0.47

a) obtained from pK_a values using the Hammett equation of Biggs and Robinson.[3] ($pK_a = 9.92 - 2.23\sigma_p^-$). b) obtained from τ_{OH} values using the Hammett equation of Quellette[2] ($\tau_{OH} = 0.774 - 1.40\sigma_p^-$). This equation was obtained using the results of Quellette by the method of least squares. c) obtained using correlation equations between σ_p^- and $\sum\sigma_m$ values; in the case of (a) series, $\sigma_p^- = 0.30\sum\sigma_m + 0.60$; in the case of (b) series, $\sigma_p^- = 0.35\sum\sigma_m + 0.62$. d) mean value of σ_p^-.

References

1) Y. Ohto, H. Shizuka, S. Sekiguchi, and K. Matsui, This Bulletin, in press.

2) R. J. Quellette, *Can. J. Chem.*, **43**, 707 (1965); L. A. Cohen and W. M. Jones, *J. Amer. Chem. Soc.*, **85**, 3402 (1963).

3) A. I. Biggs and R. A. Robinson, *J. Chem. Soc.*, **1961**, 388.

BULLETIN OF THE CHEMICAL SOCIETY OF JAPAN, VOL. 47(5), 1303—1304 (1974)

Photo-induced Condensation Reaction of *p*-Quinones with Aldehydes

Kazuhiro MARUYAMA and Yo MIYAGI

Department of Chemistry, Faculty of Science, Kyoto University, Sakyo-ku, Kyoto 606

(Received December 27, 1973)

Synopsis. The quantum yield of a photo-induced condensation product between a *p*-quinone and an aldehyde was determined, the reaction course being investigated by CIDNP technique.

Quantum Yield of the Reaction. Qualitative inspection on photo-induced reaction of *p*-quinones with aldehydes has been reported by Bruce and Cutts.[1] Their conditions for the reaction were unusual; a quinone dissolved in an aldehyde was subjected to irradiation to yield acylated hydroquinone derivatives. In the present investigation a more dilute mixture of *p*-quinone and aldehyde in a suitable solvent was irradiated by Xenon arc lamp. The quantum yields of major products, 2-acylated hydroquinones, are given in Tables 1—3 for several combinations of *p*-quinones and aldehydes.

Monochromatic light of 445 nm was used in the reaction of *p*-benzoquinone, and that of 425 nm in the reaction of 1,4-naphthoquinone. Each absorption band corresponds to the n→π^* excitation band of the respective carbonyl groups.

TABLE 1. YIELDS OF 2-ACETYLHYDROQUINONE(**7**) IN THE PHOTOCHEMICAL REACTION OF *p*-BENZOQUINONE AND ACETALDEHYDE[a]
(monochromatic light: 445 nm, solvent: acetonitrile)

Time (min)	Yield of **7** (%)[b]	Yield of **7** per hour (%/hr)	Quantum yield
0	—	—	
30	1.44	2.8_6	
65	3.09	2.8_9	
95	4.60	2.9_0	0.55_9
125	5.82	2.7_9	
155	7.12	2.7_6	
185	8.32	2.7_6	

a) Initial concentrations of *p*-benzoquinone and acetaldehyde were 0.01 and 0.1 mol/l. b) Determined by absorption at 360 nm.

TABLE 2. YIELDS OF 2-PROPIONYL-1,4-NAPHTHOHYDROQUINONE(**8**) IN THE PHOTOCHEMICAL REACTION OF 1,4-NAPHTHOQUINONE AND PROPANAL[a]
(monochromatic light: 425 nm, solvent: acetonitrile)

Time (min)	Yield of **8** (%)[b]	Yield of **8** per hour (%/hr)	Quantum yield
30	2.7_2	5.4_3	0.51_8
60	4.9_0	4.9_0	0.47_8
90	6.6_7	4.4_4	0.42_4
120	8.4_0	4.2_0	0.40_1
150	9.8_3	3.9_3	0.37_6

a) Initial concentrations of 1,4-naphthoquinone and propanal were 0.005 and 0.05 mol/l. b) Determined by absorption at 390 nm.

TABLE 3. QUANTUM YIELDS OF 2-ACYL- OR 2-AROYL-HYDROQUINONES IN THE PHOTOCHEMICAL REACTION OF *p*-BENZOQUINONE AND ALDEHYDES
(monochromatic light: 445 nm, solvent: acetonitrile)

Aldehyde	$[BQ]_0$[a] : [RCHO]	Quantum yield[b]
CH_3CHO	1 : 100	0.78_5
CH_3CHO	1 : 50	0.69_9
CH_3CHO	1 : 10	0.55_9[c]
CH_3CHO	1 : 4	0.56_7
C_2H_5CHO	1 : 5	0.55_4
C_3H_7CHO	1 : 10	0.57_4
C_6H_5CHO	1 : 10	0.54_7

a) Initial concentration of *p*-benzoquinone, $[BQ]_0$, was 0.01 mol/l. b) Mean quantum yield during 90 min reaction. The yields were determined by absorption at 360 nm. c) Mean quantum yield during 95 min reaction.

The mean quantum yields estimated in the duration of every 30 min remain constant in the reaction of *p*-benzoquinone with aldehydes, but they change with time in the reaction of 1,4-naphthoquinone with propanal. This can be ascribed to the quenching effect by the major product, 2-acyl-1,4-naphthohydroquinone, accumulated in the reacting solution. The following indirect evidence deduced from the investigation of the reaction by means of CIDNP would support the view. The fresh solution of 1,4-naphthoquinone and an aldehyde dissolved in carbon tetrachloride showed fairly strong polarized PMR signals during the course of irradiation, but the intensity is strongly depressed without exception when the corresponding 2-acyl-1,4-naphthohydroquinones were added to the solutions.

Reaction Mechanism. Thus, 2-acylated hydroquinone was obtained from *p*-quinone and aldehyde in a free form or in the form of quinhydrone addition compound.[2] On the mechanism of these condensation reactions, Bruce and Cutts included the addition of acyl radical to the quinone followed by subsequent enolization of the primary adduct.[1] In the reaction of *p*-benzoquinone with acetaldehyde they obtained the scavenged product (**1**) of the reactive intermediate radical by 1,1-diphenylethylene added in the reaction system.

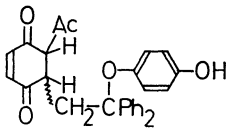

(**1**)

According to this mechanism the reaction should proceed as follows.

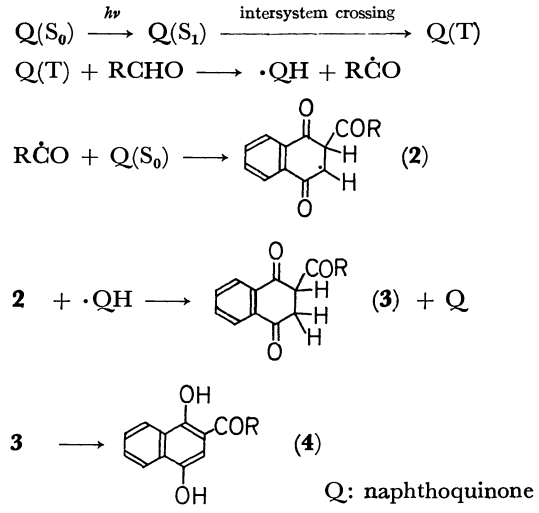

Scheme 1.

The reaction could proceed in part through the above reaction scheme, but our investigation by CIDNP technique revealed a modified aspect. The polarized PMR signal (multiplet, emission and absorption) observed in the region δ=3.70—4.30 and the polarized signal (emission) due to 2,3-protons of naphthoquinone can be interpreted by this mechanism. However, both the strongly polarized signals (emission) in the region δ=6.25—6.45 and the strongest polarized alkyl proton signal or signals (absorption) of acyl group suggest the concomitant generation of **5** or **6** through direct recombination of the radical pair in an original solvent cage[3] (Fig. 1), (Scheme 2). The polarized emission signals observed in the region δ=6.25—6.45 can be reasonably interpreted by taking account of the olefinic protons of **5** and **6**. No evolution of carbon monoxide during the course of irradiation supports our scheme.

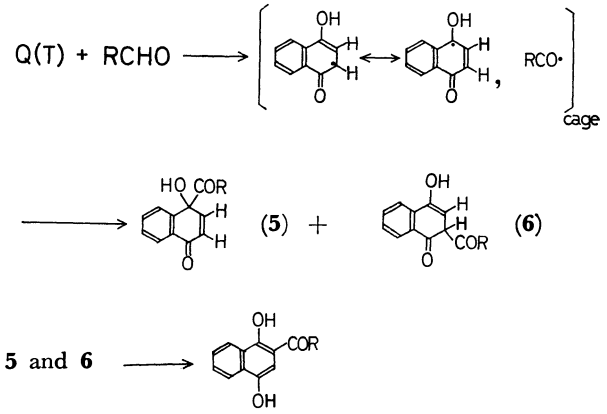

Scheme 2.

Experimental

Quantum yields were determined by the use of ferrous succinate as an actinometer. Monochromatic light was attained with a Shimadzu RF-501 spectrophotometer. CIDNP examinations were carried out with a JEOL 60 MHz NMR spectrometer (solvent; CCl_4). Details are described elsewhere.[4]

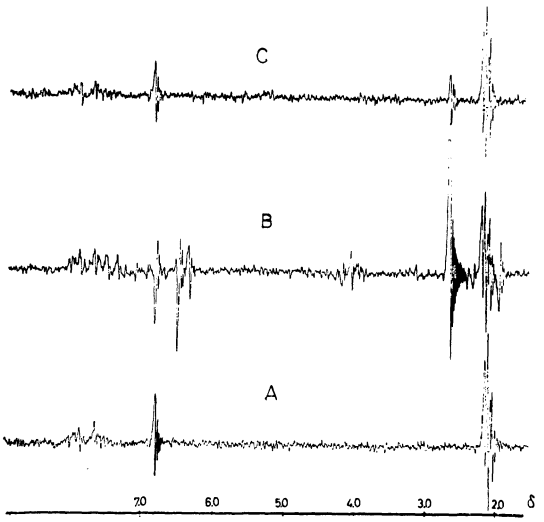

Fig. 1 a. Polarized PMR signals observed in the photochemical reaction of 1,4-naphthoquinone and acetaldehyde.
A: Before irradiation, B: During irradiation, C: After irradiation.

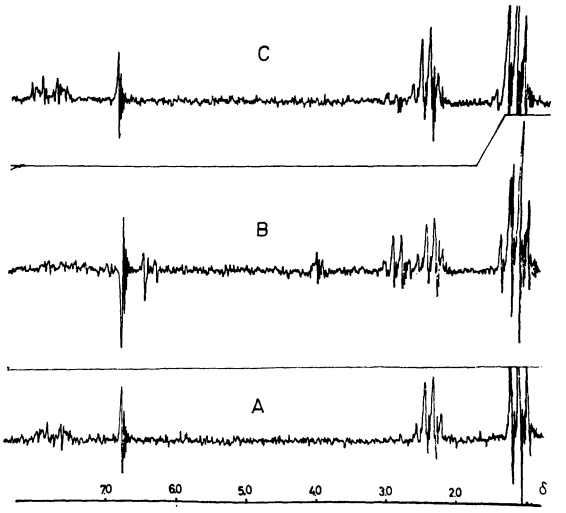

Fig. 1b. Polarized PMR signals observed in the photochemical reaction of 1,4-naphthoquinone and propanal.
A: Before irradiation, B: During irradiation, C: After irradiation.

References

1) J. M. Bruce and E. Cutts, *J. Chem. Soc., C*, **1966**, 449.
2) No 2-acylated hydroquinone was obtained in the photochemical reaction of *p*-quinone with *p*-nitrobenzaldehyde, the so-called 1,4-addition compound, hydroquinone monoester, being the sole product (*cf.* 1)).
3) In the photochemical reaction between *p*-quinones and *p*-nitrobenzaldehyde no polarized PMR signal could be observed in the region δ=3.50—6.0.
4) K. Maruyama, T. Otsuki, A. Takuwa, and S. Arakawa, This Bulletin, **46**, 2470 (1973).

BULLETIN OF THE CHEMICAL SOCIETY OF JAPAN, VOL. 47 (5), 1305 (1974)

Synthesis of (4-Pyridyl)-1,2-ethanediol

Herbert S. AARON and Jacob I. MILLER

Chemical Research Division, Edgewood Arsenal, Aberdeen Proving Ground, Maryland, 21010 USA

(Received August 13, 1973)

Synopsis. A conflict in the literature regarding the physical properties of 4-(pyridyl)-1,2-ethanediol has been resolved. The melting point and solubility data of this compound are correct as reported in *J. Org. Chem.*, **30**, 1331 (1965).

Furuyama, Mori, and Wakasa[1] recently modified our procedure[2] for the synthesis of (4-pyridyl)-1,2-ethanediol (I) and obtained a liquid product reported to be insoluble in acetone, and which seemed to dissolve only in solvents with a Hildebrand solubility parameter greater than 12.7. Although no analytical data was offered to establish the purity of their product, they suggested that the melting point and solubility we reported for I were in error. However, their claim that Haas *et al.*[3] also indicated a similar doubt with respect to our results is incorrect. Actually, our paper was uncited by Haas *et al.*, and was probably unknown to them, since it appeared only shortly before their own publication. The fact that Haas *et al.* obtained I as a pasty mass that could not be readily purified (by unspecified means) does not disprove our results. Indeed, these workers recrystallized the corresponding 2-pyridylglycol from methylene chloride, which has a solubility parameter of only 9.8.[4]

In view of the claim[1] that I was insoluble in acetone, we ran the reaction as described by Furuyama *et al.*, in order to evaluate their product. The solubility discrepancy is apparently resolved from the fact that the crude product thus obtained did give an initial appearance of being insoluble in acetone, but only because it contained about 18% of a mixture of acetone-insoluble magnesium and potassium salts of isonicotinic acid. In our hands, the modified procedure[1] gave a 54% yield of crude I (unrecrystallized), after separation from these salts. By our original procedure, a 35% yield of the purified product had been obtained.[2]

Experimental

(4-Pyridyl)-1,2-ethanediol (I) was obtained as a clear, viscous, yellow oil (22 g); as described.[1] A less-than-theoretical yield was signalled by the strong odor of 4-vinylpyridine on the inorganic filter cake. The crude product appeared, initially, to be insoluble in acetone. However, when a 1.1 g portion was stirred into 6 ml of acetone, it formed an opaque gum, which slowly dissolved, and left an insoluble, tan, solid residue II, 0.15 g, mp 265—320 °C. Combustion, NMR (in D_2O) and atomic absorption analysis (for K and Mg) indicated II was a mixture of inorganic salts of isonicotinic acid, consistent with a composition of four parts $C_5H_4NCOOK \cdot 1/2H_2O$ (IIA) and one part $C_5H_4NCOO(Mg)OH \cdot 1/2H_2O$ (IIB).

Found: C, 42.0; H, 3.0; N, 7.9; O, 25.2; Mg, 2.5; K, 19.3%. Calcd for 4/1 mixture of IIA/IIB: C, 42.4; H, 3.1; N, 8.2; O, 25.3; Mg, 2.8; K, 18.5%.

After II had been filtered off, the acetone solution was allowed to stand overnight, and an additional 0.03 g of solid precipitated. This material shriveled in a capillary tube at about 290 °C, but did not melt, even when heated to 340 °C; it was not further characterized. The acetone solution was then concentrated under reduced pressure to give 0.8 g of I as an oil, which slowly crystallized, when seeded.[2] A larger batch (14.5 g) of the initial liquid product (I), above, was similarly treated (60 ml of acetone, 10 min stirring) to give 2.3 and 0.4 g of insoluble salts, respectively, and 11.8 g (54%) of crude I, as a tacky, orange solid. The NMR spectrum of I, mp 69—71 °C (from CH_2Cl_2), was recorded in deuteroacetone, on a Varian A-60D Spectrometer (60 MHz, internal TMS reference, ambient probe temperature of 33 °C): δ 3.65, $2H_{(a)}$ m; 3.90, $2H_{(b)}$ s; 4.76, $H_{(c)}$ ~t; 7.40, $2H_{(d)}$ ~d; 8.48, $2H_{(e)}$ broad m. In D_2O, unless heated,[1] the $H_{(b)}$ and $H_{(c)}$ signals overlapped at about δ 4.88.

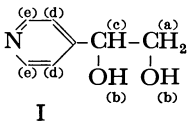

I

We thank Mr. Donald Hench, Mrs. Marjorie Buckles and Mr. John Corliss and staff for the analytical results, and Mrs. Linda Szafraniec for the NMR data.

References

1) T. Furuyama, K. Mori, and R. Wakasa, This Bulletin, **45**, 1924 (1972).

2) H. S. Aaron, O. O. Owens, P. D. Rosenstock, S. Leonard, S. Elkin, and J. I. Miller, *J. Org. Chem.*, **30**, 1331 (1965).

3) H. C. Haas, H. S. Kolesinski, and N. W. Schuler, *J. Polym. Sci. Part B*, **3**, 879 (1965).

4) J. H. Hildebrand and R. L. Scott, "Regular Solutions," Prentice Hall, Inc., Englewood Cliffs, N.J. (1962), p. 172.

Corrections

Volume 46, 1973

S. Takeuchi: A Kinetic Study on the Decomposition of Benzyl *N*-(Hydroxymethyl)carbamate in Alkaline Solution.
Transfer the figures of Fig. 3 and Fig. 4 in p. 1497 to those of Fig. 4, Fig. 3, respectively, keeping the factors in the both axes of the figures and the figure captions at the original locations.

K. NAKAMURA: The Structure of Ordered β V_2D as Determined by Means of the Deuteron Magnetic Resonance.
Page 2589. In col. 1, line 10, for "$(e^2qQ/h)^{\beta}_{oct}$ and $(e^2qQ/h)^{\beta}_{oct}$" read "$(e^2qQ/h)^{\beta}_{oct}$ and $(e^2qQ/h)^{\beta}_{tet}$."

A. SERA, C. YAMAGAMI, and K. MARUYAMA: Effect of Pressure on the Rate of Solvolysis. Formolysis and Methanolysis of Secondary Alkyl Tosylates.
Page 3867. In experimental part, line 7, for "1-*t*-Butylethyl tosylate(8)" read "Di-*t*-butylmethyl tosylate(8)."

A Study of Catalysis by Metal Phosphates. II.[1] A Kinetic Study of the Dehydrogenation of 2-Propanol over the Cadmium Phosphate Catalyst and an Investigation of the Acid-base Character of the Catalyst

Fumio Nozaki and Haruo Ohta

Department of Industrial Chemistry, Faculty of Engineering, Chiba University, Yayoi-cho, Chiba 280

(Received April 12, 1973)

The dehydrogenation of 2-propanol over the *ortho* cadmium phosphate catalyst has been investigated by means of a conventional tubular-flow reactor operating at atmospheric pressure. The adequate temperature for the calcination of catalyst was about 400 °C. The reaction-rate data were approximately arranged by Eq. (3), using the Langmuir-type expression described in the text. The catalytic activity for dehydrogenation to acetone was completely poisoned by the addition of a small amount of CCl_3COOH during the course of the reaction, whereas the activity for dehydration to propylene was greatly enhanced. The behavior of $CH_2ClCOOH$ and C_6H_5COOH as poisons was also investigated. C_5H_5N had no effect on the catalytic reaction. It has been concluded that the cadmium phosphate is to be characterized as a basic catalyst.

A preliminary study of various *ortho* metal phosphate catalysts revealed that two phosphates, $Ca_3(PO_4)_2$ and $Cd_3(PO_4)_2$, had a high and selective activity for the dehydrogenation of 2-propanol to acetone; in this they strongly contrasted with the other phosphates which generally catalyzed the dehydration for propylene formation.[2]

Ishiguro and Ohtsuka[3] have already reported that the cadmium phosphate catalyst selectively promotes the dehydrogenation of 2-propanol; however, they have not presented the detailed reaction kinetics or a characterization of the catalyst.

In this paper, we will describe a further study of the cadmium phosphate catalyst.

Experimental

Materials. The cadmium phosphate catalyst was prepared from $Cd(NO_3)_2$ and Na_3PO_4 according to the method of Ishiguro and Ohtsuka.[3] The catalyst was calcined at the prescribed temperatures between 300 and 600 °C for 4 hr in an air stream. In all cases, the catalysts were white in color.

The N_2 and 2-propanol used in the catalytic tests were the highest pure grade of reagent.

Procedures. The apparatus and procedure for the measurements of the catalytic reaction were the same as those described in the previous report.[1] The experimental data of the catalytic reactions were represented by the total conversion of 2-propanol (x) and the selectivity to acetone (S).[4]

In order to reveal the acid-base character of the catalyst during the course of reaction, the effects of pyridine (C_5H_5N), trichloroacetic acid (CCl_3COOH), monochloroacetic acid ($CH_2ClCOOH$), and benzoic acid (C_6H_5COOH) on the catalytic reaction were investigated by means of the following procedure: 2-propanol with the additive of 0.067 mol/l was prepared for the tests. After we have ascertained that the catalytic reaction for 2-propanol without the additive proceeds at a stationary state, we exchange the feed instaneously with 2-propanol containing the additive and then follow the change in the catalytic activity and in the selectivity.

Results and Discussion

Effect of Reaction Conditions on the Catalytic Activity and Selectivity. The changes in the catalytic activity and in the selectivity with the calcination temperature of the catalyst are shown in Fig. 1. The catalytic activity increased with an increase in the calcination temperature, passed through a maximum at about 400 °C, and then almost disappeared above 500 °C. The catalyst, even when it was calcined at the low temperature of 300 °C, exceeds 80% in selectivity for dehydrogenation to acetone. The selectivity to acetone over the catalyst calcined at 400 °C displayed only a slight decrease of up to 5%, depending on the reaction temperature and the time factor (W/F). Thus, the dehydration of 2-propanol to propylene was negligible in amount under appropriate reaction conditions.

Reaction Rates and Rate Equation. The kinetic studies have been made over the catalyst calcined at 400 °C, wherein the selectivity to acetone was excellent and the activity was almost unchanged throughout the time of the reaction.

In the low range of W/F up to 4 g-cat·hr/mol, the observed conversion of 2-propanol was approximately proportional to W/F, without regard to the reaction temperature. Therefore, one may assume the differential

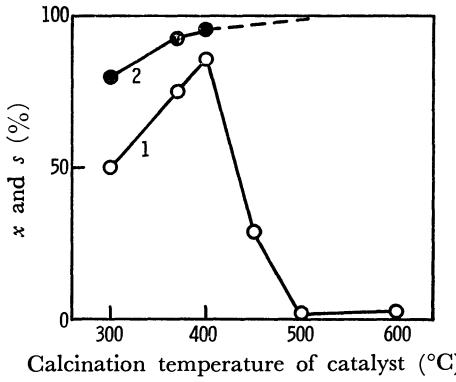

Fig. 1. Effect of the calcination temperature of catalyst on the reaction.
1: Conversion of 2-propanol, x
2: Selectivity to acetone, S
Reaction temperature: 295 °C, Catalyst weight (W): 1.5 g, Feed rate of 2-propanol and N_2 (F): 0.23 mol/hr, Mol-fraction of 2-propanol in feed $\left(y_0 = \frac{IPA}{IPA+N_2}\right)$: 0.26

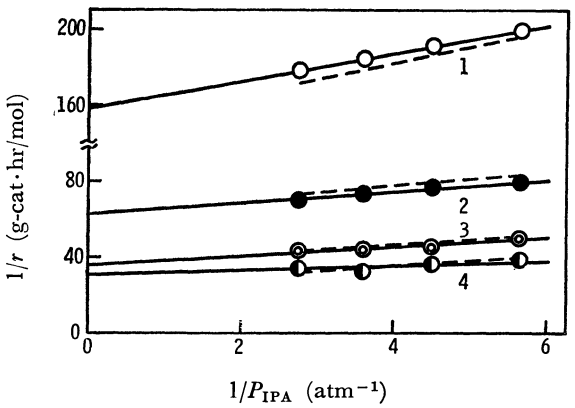

Fig. 2. $1/r$ *vs.* $1/P_{IPA}$ plots.
1: 220 °C, 2: 245 °C, 3: 260 °C, 4: 270 °C
The dotted lines show the correlation between $1/r_{calc}$ and $1/P_{IPA}$, where r_{calc} is the reaction rate computed from Eq. (3).

reactor, in which the reaction rates, $r(=y_0x/(W/F)$ mol/g-cat·hr), can be obtained from the slopes of the linear relationships between y_0x (y_0: mol-fraction of 2-propanol at the inlet of reactor) and W/F.

The observed reaction rates are illustrated in Fig. 2, plotted as reciprocal relations between r and P_{IPA}.

A plot of $1/r$ *vs.* $1/P_{IPA}$ gives a straight line for each of the reaction temperatures. The following equation can be derived and rearranged to the conventional form of the Langmuir-type rate expression:

$$\frac{1}{r} = \frac{1}{k} + \frac{1}{kK}\frac{1}{P_{IPA}} \tag{1}$$

or:

$$r = k\frac{KP_{IPA}}{1+KP_{IPA}} \tag{2}$$

where k is the rate constant (mol/g-cat·hr) and where K is the adsorption equilibrium constant for 2-propanol (atm^{-1}). The intercepts to the ordinate and the slopes of the straight lines give the values of k and K shown in Fig. 3.

Both $\log k$ and $\log K$ are correlated to $1/T$ by straight lines, with slopes of $(-E/R)$ and (Q/R) respectively,

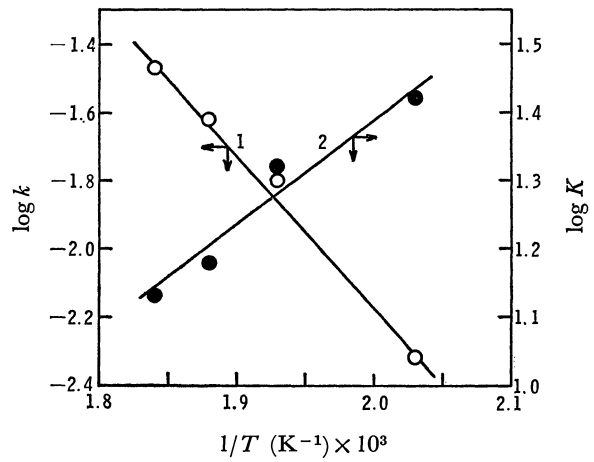

Fig. 3. Arrhenius plots for k and K.
1: $\log k$ *vs.* $1/T$, 2: $\log K$ *vs.* $1/T$

where E is the activation energy for the reaction and where Q is the adsorption heat of 2-propanol. We obtained approximately $E=19$ kcal/mol and $Q=6.7$ kcal/mol. By substituting these values into Eq. (2) and by evaluating the pre-exponential factors of k and K, we obtain:

$$r = 1.84\times10^{-2}\exp\left(\frac{-19000}{RT}\right)\frac{2.3\times10^{-2}P_{IPA}\exp\left(\frac{6700}{RT}\right)}{1+2.3\times10^{-2}P_{IPA}\exp\left(\frac{6700}{RT}\right)} \tag{3}$$

Considering the stoichiometry of the reaction and using Eq. (2) for the rate expression, we obtain Eq. (4) as a conventional integral form for the ideal tubular reactor:[5]

$$W/F = y_0\int_0^x \frac{dx}{r} = \frac{y_0}{k}\left[\frac{1}{K}\left(1+\frac{1}{y_0}\right)\ln\frac{1}{1-x}+x\left(1-\frac{1}{K}\right)\right] \tag{4}$$

At a constant temperature of 260 °C, a series of the conversion data was obtained under conditions in which W/F varied widely from 1.5 to 22.3, and y_0, from 0.183 to 0.383. Fig. 4 shows a plot of W/F *vs.* $y_0[\{(1+1/y_0)/K\}\ln(1/1-x))+x(1-1/K)]$ for $K=13.0$, which is evaluated from Eq. (3) for K at 260 °C. A good linear correlation is shown in Fig. 4. Consequently, it can be concluded that Eq. (3) is satisfactory for the rate equation under all the present experimental conditions.

When comparing 2-propanol which contained much acetone and 2-propanol without acetone for the feed of the reaction, no essential differences in reaction rates could be detected. Thus, the retardation effect of acetone on the reaction rate was found to be negligible.

Acid-base Character of the Catalyst. The coexistence of C_5H_5N in the reactant flow had no effect on the catalytic reaction within the limits of experimental error, whereas CCl_3COOH showed a remarkable influence on the catalyst activity, as is shown in Fig. 5. Dehydrogenation to acetone was retarded rapidly and was poisoned completely after the reaction had been continued for about 30 min by using 2-propanol with 0.067 mol/l CCl_3COOH. In contrast, dehydration to

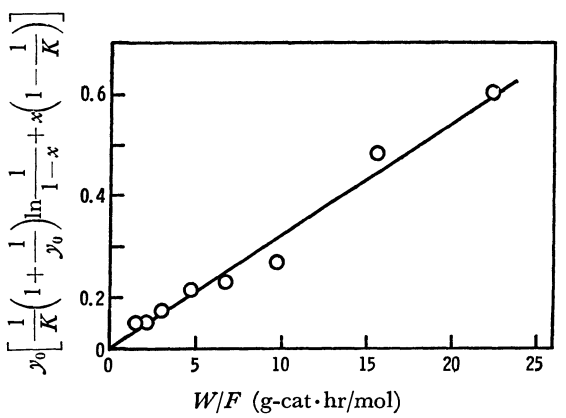

Fig. 4. Test of the Langmuir-type rate equation by integral method.
Reaction temperature: 260 °C, y_0: 0.183~0.383

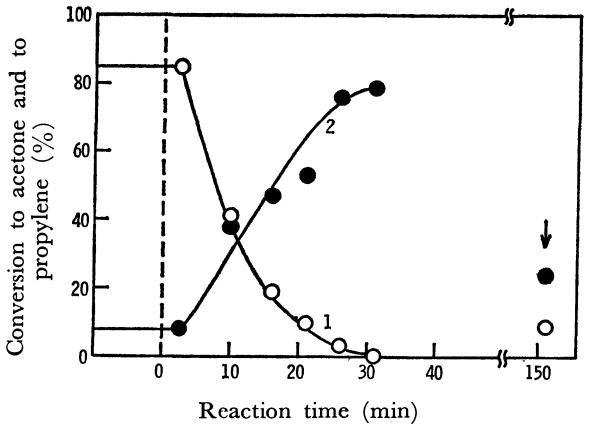

Fig. 5. Influence of CCl_3COOH addition on the catalytic reaction.
1: Conversion to acetone
2: Conversion to propylene
Reaction temperature: 305 °C, Concentration of CCl_3COOH in the feed of 2-propanol: 0.067 mol/l, The other reaction conditions are the same as noted in Fig. 1. The dotted line shows the time when the feed of 2-propanol without the additive was exchanged with 2-propanol containing CCl_3COOH. The data marked by an arrow show the result after the catalyst has been reactivated by passing through N_2 at 350 °C for 2 hours.

propylene increased remarkably, as CCl_3COOH had been accumulated on the catalyst surface. The disappearance of the dehydrogenation activity upon the addition of a small amount of CCl_3COOH to the catalyst indicates that the active sites of the catalyst contributing to the dehydrogenation reaction are basic. The required quantity of CCl_3COOH which completely poisoned the dehydrogenation activity of the catalyst was almost unchanged with the change in the reaction temperature or in the concentration of CCl_3COOH; it was estimated to be about 0.05 mmol/g-cat from the results shown in Fig. 5. However, it was difficult to determine the exact amount of CCl_3COOH for the complete poisoning because of the presence of poison

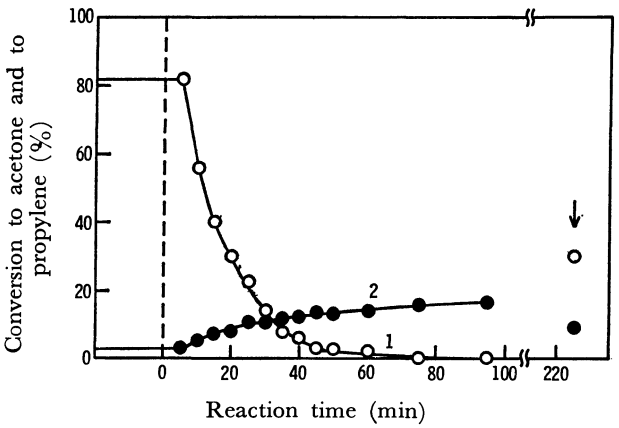

Fig. 6. Influence of $CH_2ClCOOH$ addition on the catalytic reaction.
Reaction temperature: 300 °C, The other reaction conditions and the notes are the same as described in Fig. 5.

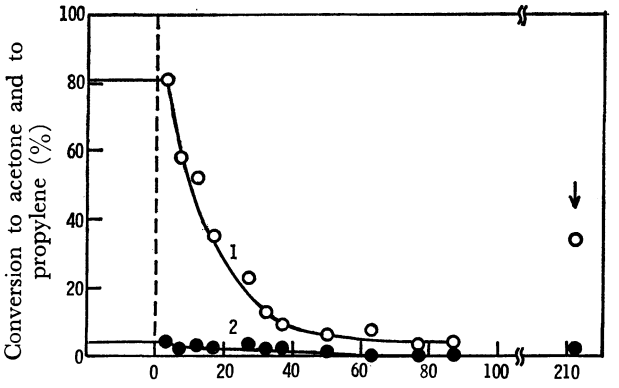

Fig. 7. Influence of C_6H_5COOH addition on the catalytic reaction.
Reaction temperature: 300 °C, The other reaction conditions and the notes are the same as described in Fig. 5.

adsorbed on the sties which are not active for the catalytic reaction.

To make sure that the catalyst can be characterized as basic, the influences of $CH_2ClCOOH$ and C_6H_5COOH on the catalytic reaction were also investigated. As is shown in Figs. 6 and 7, the dehydrogenation to acetone was explicitly poisoned by the addition of the organic acids, although their rates of poisoning the dehydrogenation and also their degree of enhancing the dehydration are somewhat different from that of CCl_3COOH.

None of the catalysts poisoned with CCl_3COOH, $CH_2ClCOOH$, or C_6H_5COOH regained their catalytic activity for dehydrogenation when the catalytic reaction of 2-propanol without the additive was continued at the reaction temperature of 300 °C for two hours, or when it was passed through N_2 at 300 °C for two hours. By passing it through N_2 at such a slightly higher temperature as 350 °C, however, some of the catalytic activity for dehydrogenation was restored, although the degree of the recovery depended primarily on the species of the poisons, as is shown in Figs. 5—7. The enhanced dehydration activity directly attributable to the addition of CCl_3COOH or $CH_2ClCOOH$ readily disappeared when it was passed through N_2; in contrast, the recovery of dehydrogenation activity was rather difficult. The detailed role of CCl_3COOH or $CH_2ClCOOH$ in the appearance of dehydration activity during the poisoning test is not yet clear. However, a feasible and tentative explanation is that Brönsted acid molecules adsorbed on the catalyst surface catalyze the dehydration to propylene. The reason for this is that the decreasing order of dehydration activity of the catalysts poisoned with the organic acids is as follows: $CCl_3COOH > CH_2ClCOOH > C_6H_5COOH$; this order is in accord with expectations based on the acid strength. Since the acid molecules adsorbed on the catalyst surface other than basic sites would be rapidly desorbed, the ready recovery of dehydration activity is understandable, as has been described above.

The effect of H_2O on the catalytic reaction was not observable under the same conditions as those studied for the poisoning of CCl_3COOH, except that the concentration of H_2O varied over a wide range between 0.098 and 0.65 mol/l.

On the basis of the observations presented above, it appears clear that the cadmium phosphate is intrinsically a basic catalyst. However, the catalyst structure which causes this basic character must remain the subject for a future study.

References

1) Part I of this series: F. Nozaki, T. Itoh, and S. Ueda, *Nippon Kagaku Kaishi*, **1973**, 674.
2) Unpublished work.
3) T. Ishiguro and A. Ohtsuka, *Yakugaku Zasshi*, **78**, 1383 (1958).
4) Selectivity to acetone=Conversion to acetone/Total conversion of 2-propanol (x).
5) At the point in the reactor where the conversion is x, P_{IPA} may be written as $P_{IPA}=y_0(1-x)/(1+y_0x)$.

The Microwave Spectra and r_0, r_s, and r_m Structures of Ethylene Oxide

Chiaki HIROSE

Laboratory of Molecular Spectroscopy, Tokyo Institute of Technology, O-okayama, Meguro-ku, Tokyo 152

(Received April 23, 1973)

The rotational spectra of ten isotopic species of ethylene oxide, $^{12}C_2H_4{}^{16}O$, $^{12}C^{13}CH_4{}^{16}O$, $^{12}C_2H_4{}^{18}O$, $^{12}C_2H_3D^{16}O$, *cis*- and *trans*-$^{12}C_2H_2D_2{}^{16}O$, $^{12}C^{13}CH_2D_2{}^{16}O$, and $^{12}C_2H_2D_2{}^{18}O$ were observed. A least-squares fit including centrifugal distortion effect to the first order was made to derive the effective values of the A′, B′, C′, τ'_{aaaa}, τ'_{bbbb}, τ'_{cccc}, and τ'_{aabb} parameters and their correlation factors; τ'_{bbcc} and τ'_{aacc} were found to be insignificant. The rotational constants were used to determine the r_0, r_s, and r_m structures. The structural parameters were derived as:

$r_0(CC)=1.470\pm0.003$, $r_s(CC)=1.466\pm0.002$, $r_m(CC)=1.462\pm0.003$,

$r_0(CH)=1.085\pm0.004$, $r_s(CH)=1.085\pm0.001$, $r_m(CH)=1.086\pm0.004$,

$r_0(CO)=1.434\pm0.002$, $r_s(CO)=1.431\pm0.001$, $r_m(CO)=1.428\pm0.002$,

$\angle_0HCH=116.28\pm0.69$, $\angle_sHCH=116.61\pm0.09$, $\angle_mHCH=116.92\pm0.69$,

$\theta_0=22.34\pm0.46$, $\theta_s=21.99\pm0.11$, $\theta_m=21.63\pm0.48$ in units of Å and degrees; θ represents the angle of the H_2C plane to the CC bond. The indicated error limits are 2.5 times the variances.

Ethylene oxide is one of the molecules for which bent bonds can be expected.[1] Cunningham *et al.* first investigated the r_0 structure on the basis of the microwave spectra of several isotopic species and showed both C-C and C-O distances were considerably different from those in aliphatic hydrocarbons and ethers.[2] Turner and Howe carried out a computer calculation of the r_0 structure which uses the rotational constants obtained by Cunningham *et al.* to improve the structural parameters:[3]

The rotational spectra of ethylene oxide in the ground and excited vibrational states were observed in the present study in order to get further information on the molecular structure and the vibrational modes. The present paper will report on the microwave spectra of ten isotopic species in their ground vibrational states. The rotational and centrifugal distortion constants were determined by a least-squares fit. Effective parameters were obtained by assuming some of the centrifugal distortion constants.

The structural parameters, r_0, r_s, and r_m, were derived from the rotational constants by taking into account correlations among the rotational constants.

Experimental

The species studied in the present work are normal ethylene oxide, *cis*- and *trans*-dideutero ethylene oxide, monodeutero ethylene oxide, and the ^{13}C- and ^{18}O-substituted species. Normal ethylene oxide was purchased from the Matheson Co., the *cis*- and *trans*-dideutero species were provided by Mr. Masahiro Kawasaki of the Tokyo Institute of Technology, monodeutero ethylene oxide was present in the dideutero species as an impurity, and the ^{13}C- and ^{18}O-isotopic species were used in their natural abundance.

The microwave spectrum was observed using a conventional Stark modulation spectrometer with a waveguide cell cooled with dry ice. Since the vibrational frequencies are higher than 600 cm^{-1}, the rotational spectra of ^{13}C- and ^{18}O-species were assigned by comparing the change in spectral intensity at room temperature and at the temperature of dry ice. The observed frequencies and their assignments are listed in Table 1.

Analysis of Data

Since the analysis showed effects of centrifugal distortion of as much as 30 MHz for the $J=8$—8 transition of normal ethylene oxide, a least-squares fit including centrifugal distortion to the first order was carried out.

The parameters describing the transition frequencies are expressed as follows:[4]

$$\begin{aligned} A' &= A - \hbar^4(3\tau_{bcbc}-2\tau_{acac}-2\tau_{abab})/4, \\ B' &= B - \hbar^4(3\tau_{acac}-2\tau_{abab}-2\tau_{bcbc})/4, \\ C' &= C - \hbar^4(3\tau_{abab}-2\tau_{bcbc}-2\tau_{acac})/4, \\ \tau'_{aaaa} &= \hbar^4\tau_{aaaa}, \\ \tau'_{aa\beta\beta} &= \hbar^4(\tau_{aa\beta\beta}+2\tau_{aa\beta\beta}), \quad (\alpha\neq\beta) \end{aligned} \tag{1}$$

where α and β stand for a, b, or c. As has been pointed out by Watson,[5] when the centrifugal distortion is treated by the first-order perturbation, at most eight parameters (three effective rotational constants, τ'_{aaaa}, τ'_{bbbb}, τ'_{cccc}, and the two linear combinations of τ'_{aabb}, τ'_{bbcc}, and τ'_{aacc}) can be experimentally determined. A detailed analysis of the correlation among the parameters showed that the observed spectra contained sufficient information to determine only four centrifugal terms with statistical significance. Since τ'_{aacc} and τ'_{bbcc} were estimated to be indistinguishable from zero by preliminary calculations where one of the two parameters was put equal to zero to give the other the stated value, they were both tentatively set equal to zero in the present analysis. The same situations were encountered in all the isotopes. Table 2 lists the converged values of the parameters.*

* The listed values should be understood as effective ones which are enough to account for the frequencies listed in Table 1. Systematic errors can be introduced from the assumption that $\tau'_{aacc}=\tau'_{bbcc}=0$, the shortages in observation of high-J transitions and R-type transitions, and perhaps even from the lack of transitions of the a- or c-type. A preliminary analysis of the millimeter-wave spectrum of normal species indicates that the inclusion of high-J transitions gives τ'_{cccc} a negative value, as is expected from the theory of centrifugal distortion.

Table 1. Observed frequencies and their deviations from calculated frequencies (in MHz)

Transition	$^{12}C_2H_4{}^{16}O$			$^{12}C^{13}CH_4{}^{16}O$		
	Obsd[a]	Δ(cent)[b]	Δ[c]	Obsd[a]	Δ(cent)[b]	Δ[c]
$1_{11}\leftarrow 0_{00}$	39581.64*	−0.05	+0.18	39117.71*	−0.07	+0.14
$1_{10}\leftarrow 1_{01}$	11386.05	−0.14	+0.11	11466.11	−0.12	+0.09
$2_{12}\leftarrow 1_{01}$	67777.40	−0.02	−0.09	66768.56	−0.31	−0.27
$2_{02}\leftarrow 1_{11}$	63558.67	+0.07	+0.00	—	—	—
$2_{11}\leftarrow 2_{02}$	24923.69*	−0.67	−0.01	24351.97*	−0.39	+0.18
$2_{20}\leftarrow 2_{11}$	15603.90	−0.73	+0.30	16195.69	−0.76	+0.07
$2_{21}\leftarrow 2_{12}$	34157.04*	−1.16	−0.02	34397.53*	−0.91	+0.02
$3_{21}\leftarrow 3_{12}$	23610.42*	−1.64	+0.00	23278.44*	−1.41	+0.10
$3_{30}\leftarrow 3_{21}$	23134.16*	−2.52	−0.10	24667.66	−2.67	−0.09
$3_{31}\leftarrow 3_{22}$	39680.05*	−3.43	−0.11	40513.89	−3.33	+0.11
$4_{22}\leftarrow 4_{13}$	41579.46*	−3.75	−0.04	40166.73	−2.61	−0.17
$4_{31}\leftarrow 4_{22}$	24834.30*	−3.56	+0.00	25247.76*	−3.48	−0.05
$4_{40}\leftarrow 4_{31}$	34147.76*	−6.64	−0.01	36859.03	−7.06	−0.04
$5_{23}\leftarrow 5_{14}$	63538.10	−8.22	+0.04	—	—	—
$5_{32}\leftarrow 5_{23}$	37780.74*	−5.64	+0.01	36462.89	−4.76	−0.13
$5_{41}\leftarrow 5_{32}$	29687.08*	−7.78	+0.02	31407.24	−8.02	−0.17
$6_{42}\leftarrow 6_{33}$	35790.57*	−8.99	+0.01	35337.94	−8.66	−0.13
$6_{51}\leftarrow 6_{42}$	38701.05*	−16.15	−0.01	42134.12	−16.84	+0.03
$6_{61}\leftarrow 6_{52}$	66648.16	−25.16	+0.06	—	—	—
$7_{52}\leftarrow 7_{43}$	37328.78*	−16.05	−0.01	38541.78	−16.65	+0.12
$8_{62}\leftarrow 8_{53}$	43398.00*	−29.67	+0.65	—	—	—
$9_{54}\leftarrow 9_{45}$	—	—	—	67840.89	−20.52	+0.11

Transition	$^{12}C_2H_4{}^{18}O$			$^{12}C_2H_3D^{16}O$		
	Obsd[a]	Δ(cent)[b]	Δ[c]	Obsd[a]	Δ(cent)[b]	Δ[c]
$1_{11}\leftarrow 0_{00}$	37620.59	−0.02	−0.78	37580.17	−0.04	+0.34
$1_{10}\leftarrow 1_{01}$	10364.10	−0.14	−0.03	10925.00	−0.11	+0.04
$2_{02}\leftarrow 1_{11}$	62732.60	+0.31	+1.53	58336.18	+0.12	−0.67
$2_{11}\leftarrow 2_{02}$	25754.59	−0.87	−0.10	21284.05	−0.53	−0.05
$2_{20}\leftarrow 2_{11}$	12511.59	−0.62	+0.19	16822.39	−0.61	−0.01
$2_{21}\leftarrow 2_{12}$	31091.52	−1.26	−0.03	32774.05	−0.98	−0.18
$3_{12}\leftarrow 3_{03}$	—	—	—	38190.67	−1.72	+0.17
$3_{21}\leftarrow 3_{12}$	24202.90	−1.67	+0.09	21212.88	−1.26	−0.02
$3_{30}\leftarrow 3_{21}$	—	—	—	27356.03	−2.21	+0.04
$3_{31}\leftarrow 3_{22}$	34058.27	−3.13	+0.02	40137.71	−2.88	+0.02
$4_{22}\leftarrow 4_{13}$	—	—	—	33890.10	−2.88	+0.09
$4_{23}\rightarrow 4_{14}$	—	—	—	59363.97	−4.38	−0.93
$4_{31}\leftarrow 4_{22}$	23342.08	−2.99	−0.03	25443.48	−2.92	−0.01
$4_{40}\leftarrow 4_{31}$	21764.68	−5.16	+0.09	41664.47	−5.89	−0.03
$4_{41}\leftarrow 4_{32}$	38064.99	−6.48	−0.04	—	—	—
$5_{32}\leftarrow 5_{23}$	41912.03	−6.03	+0.21	31522.22	−4.48	−0.01
$5_{41}\leftarrow 5_{32}$	23839.29	−5.73	−0.14	35048.15	−6.79	+0.05
$5_{50}\leftarrow 5_{41}$	29262.73	−11.30	+0.11	—	—	—
$6_{42}\leftarrow 6_{33}$	39058.16	−7.31	−0.03	33776.67	−7.82	+0.02
$6_{51}\leftarrow 6_{42}$	26191.58	−11.37	+0.01	—	—	—
$6_{60}\leftarrow 6_{51}$	38315.34	−21.22	−0.20	—	—	—
$7_{43}\leftarrow 7_{34}$	—	—	—	42232.50	−10.63	+0.07
$7_{52}\leftarrow 7_{43}$	36599.93	−9.89	−0.04	42052.25	−14.89	−0.08
$7_{61}\leftarrow 7_{52}$	30733.70	−21.87	−0.26	—	—	—
$8_{53}\leftarrow 8_{44}$	—	—	—	42246.24	−15.96	−0.09
$8_{71}\leftarrow 8_{62}$	37573.58	−39.10	−0.02	—	—	—
$8_{62}\leftarrow 8_{53}$	35395.60	−16.15	−0.01	—	—	—
$9_{72}\leftarrow 9_{63}$	36144.65	−29.11	+0.10	—	—	—

Table 1. (continued)

Transition	*trans*-$^{12}C_2H_2D_2{}^{16}O$			*trans*-$^{12}C^{13}CH_2D_2{}^{16}O$		
	Obsd[a]	Δ(cent)[b]	Δ[c]	Obsd[a]	Δ(cent)[b]	Δ[c]
$1_{11}\leftarrow 0_{00}$	35528.55+	−0.04	+0.13	35164.55	−0.04	+0.25
$1_{10}\leftarrow 1_{01}$	10357.87	−0.09	+0.04	10409.28	−0.09	+0.03
$2_{12}\leftarrow 1_{01}$	60698.73	+0.01	−0.28	59918.84	−0.01	−0.49
$2_{11}\leftarrow 2_{02}$	18829.50+	−0.38	−0.06	18577.22	−0.37	−0.12
$2_{20}\leftarrow 2_{11}$	17092.35+	−0.57	−0.05	17499.89	−0.55	−0.03
$2_{21}\leftarrow 2_{12}$	31072.93+	−0.84	+0.01	31227.11	−0.81	−0.10
$3_{12}\leftarrow 3_{03}$	33196.82+	−1.21	+0.05	32549.29	−1.17	+0.16
$3_{21}\leftarrow 3_{12}$	19742.85+	−0.98	−0.04	19794.69	−0.99	−0.06
$3_{22}\leftarrow 3_{13}$	40992.29+	−1.68	+0.04	40857.24	−1.61	−0.09
$3_{30}\leftarrow 3_{21}$	28947.35+	−2.20	+0.01	29903.69	−2.09	+0.03
$3_{31}\leftarrow 3_{22}$	39254.25+	−2.67	−0.05	39776.08	−2.56	−0.05
$4_{22}\leftarrow 4_{13}$	29191.80+	−2.06	−0.03	28623.67	−2.10	−0.05
$4_{31}\leftarrow 4_{22}$	25859.61	−2.60	−0.02	—	—	—
$5_{32}\leftarrow 5_{23}$	28611.88+	−3.49	+0.08	28592.74	−3.54	−0.01
$5_{41}\leftarrow 5_{32}$	37879.62+	−6.51	+0.11	39386.60	−6.20	+0.04
$5_{50}\leftarrow 5_{41}$	59941.84	−12.51	+0.08	—	—	—
$6_{33}\leftarrow 6_{24}$	39274.01+	−5.80	−0.03	38268.18	−5.99	+0.08
$6_{42}\leftarrow 6_{33}$	34017.64+	−6.93	+0.00	34985.04	−6.81	+0.02
$6_{43}\leftarrow 6_{34}$	58775.94	−10.63	−0.31	58987.79	−10·47	−0.62
$7_{43}\leftarrow 7_{34}$	37235.33+	−8.27	−0.03	37060.07	−8.51	−0.03
$8_{53}\leftarrow 8_{44}$	41800.99	−14.28	+0.04	—	—	—

Transition	*trans*-$^{12}C_2H_2D_2{}^{18}O$			*cis*-$^{12}C_2H_2D_2{}^{16}O$		
	Obsd[a]	Δ(cent)[b]	Δ[c]	Obsd[a]	Δ(cent)[b]	Δ[c]
$1_{11}\leftarrow 0_{00}$	33833.37	−0.03	−0.00	35350.40+	−0.04	−0.05
$1_{10}\leftarrow 1_{01}$	9459.80	−0.08	−0.20	10050.36	−0.08	+0.11
$2_{12}\leftarrow 1_{01}$	—	—	—	60650.68	−0.06	+0.09
$2_{11}\leftarrow 2_{02}$	19157.03	−0.37	−0.02	18741.21+	−0.31	+0.09
$2_{20}\leftarrow 2_{11}$	—	—	—	16168.23+	−0.58	−0.04
$2_{21}\leftarrow 2_{12}$	28379.49	−0.72	−0.03	30150.23+	−0.80	+0.04
$3_{12}\leftarrow 3_{03}$	34581.47	−1.19	−0.02	33290.15+	−0.95	+0.11
$3_{21}\leftarrow 3_{12}$	18684.45	−0.93	+0.05	19252.90+	−0.92	+0.03
$3_{22}\leftarrow 3_{13}$	39298.85	−1.54	+0.00	40230.90+	−1.38	−0.01
$3_{30}\leftarrow 3_{21}$	22176.30	−1.68	+0.18	27008.93+	−2.27	+0.21
$3_{31}\leftarrow 3_{22}$	—	—	—	37656.90+	−2.72	−0.10
$4_{22}\leftarrow 4_{13}$	30996.24	−2.10	+0.35	29325.75+	−1.88	−0.24
$4_{31}\leftarrow 4_{22}$	21381.52	−2.16	−0.25	24407.96	−2.49	−0.11
$4_{40}\leftarrow 4_{31}$	33574.31	−4.51	−0.03	41241.83	−6.20	+0.12
$5_{32}\leftarrow 5_{23}$	28366.27	−3.25	−0.09	28096.93+	−3.25	−0.01
$5_{41}\leftarrow 5_{32}$	28218.20	−5.02	+0.13	35040.32+	−6.33	−0.27
$5_{50}\leftarrow 5_{41}$	—	—	—	—	—	—
$6_{33}\leftarrow 6_{24}$	—	—	—	39828.92+	−5.46	+0.06
$6_{42}\leftarrow 6_{33}$	—	—	—	32116.27+	−6.44	+0.09
$6_{43}\leftarrow 6_{34}$	—	—	—	—	—	—
$6_{52}\leftarrow 6_{43}$	—	—	—	59627.63	−14.77	−0.05
$6_{51}\leftarrow 6_{42}$	39123.20	−10.61	+0.00	—	—	—
$7_{43}\leftarrow 7_{34}$	38859.46	−7.65	−0.09	36874.07+	−7.70	−0.06
$7_{52}\leftarrow 7_{43}$	33947.92	−10.71	−0.11	42337.10	−13.38	−0.00
$8_{53}\leftarrow 8_{44}$	37039.15	−11.16	+0.25	39567.17+	−13.01	+0.08

Table 1. (continued)

Transition	*cis*-$^{12}C^{13}CH_2D_2{}^{16}O$			*cis*-$^{12}C_2H_2D_2{}^{18}O$		
	Obsd[a]	Δ(cent)[b]	Δ[c]	Obsd[a]	Δ(cent)[b]	Δ[c]
$1_{11}\leftarrow 0_{00}$	34994.35	−0.04	−0.07	33667.52	−0.03	+0.07
$1_{10}\leftarrow 1_{01}$	10116.74	−0.08	+0.06	—	—	—
$2_{12}\leftarrow 1_{01}$	59872.17	−0.11	+0.12	58154.31	+0.05	−0.12
$2_{11}\leftarrow 2_{02}$	18479.78	−0.28	+0.15	19142.06	−0.41	−0.10
$2_{20}\leftarrow 2_{11}$	16614.63	−0.54	+0.02	13208.26	−0.44	−0.03
$2_{21}\leftarrow 2_{12}$	30349.66	−0.71	+0.09	—	—	—
$3_{12}\leftarrow 3_{03}$	32629.38	−0.78	+0.07	34650.75	−1.40	−0.08
$3_{21}\leftarrow 3_{12}$	19298.48	−0.91	+0.06	18425.51	−0.93	−0.03
$3_{22}\leftarrow 3_{13}$	40124.32	−1.18	−0.02	38645.13	−1.69	+0.09
$3_{30}\leftarrow 3_{21}$	28068.41	−2.04	−0.02	20429.47	−1.59	−0.19
$3_{31}\leftarrow 3_{22}$	38258.30	−2.48	+0.02	32710.84	−2.16	+0.12
$4_{22}\leftarrow 4_{13}$	28697.60	−1.83	−0.19	31344.38	−2.31	+0.20
$4_{31}\leftarrow 4_{22}$	25122.36	−2.39	−0.01	20389.44	−2.03	−0.03
$4_{32}\leftarrow 4_{23}$	—	—	—	40801.46	−3.60	−0.04
$4_{40}\leftarrow 4_{31}$	—	—	—	30707.86	−4.29	+0.19
$4_{41}\leftarrow 4_{32}$	—	—	—	39615.30	−4.87	−0.02
$5_{41}\leftarrow 5_{32}$	36668.79	−5.82	+0.03	25968.08	−4.59	+0.14
$5_{50}\leftarrow 5_{41}$	58187.61	−11.58	−0.04	—	—	—
$6_{33}\leftarrow 6_{24}$	38676.12	−5.43	+0.10	—	—	—
$6_{42}\leftarrow 6_{33}$	33041.21	−6.30	−0.12	—	—	—
$7_{43}\leftarrow 7_{34}$	36486.33	−7.90	+0.03	39728.02	−8.11	−0.17
$8_{53}\leftarrow 8_{44}$	40608.35	−12.95	+0.13	36911.87	−10.68	+0.07
$8_{62}\leftarrow 8_{53}$	—	—	—	39371.86	−17.83	+0.21
$5_{32}\leftarrow 5_{23}$	27998.56	−3.28	−0.09	—	—	—

a) Values marked by * and + agree essentially with previous measurements in Ref. 2 and in R. J. Myers and W. D. Gwinn, cited in NBS Monograph 70 "Microwave Spectral Tables", Vol. IV, p. 197 (1968) issued by U. S. Department of Commerce respectively. One of the latter values for 8_{53}—8_{44} of *cis*-$^{12}C_2H_2D_2{}^{16}O$ seems to be a typographical error. b) Correction due to centrifugal distortion. c) $\Delta=\nu$(obsd)$-\nu$(calcd), where ν(calc)'s are obtained by use of the parameters given in Table 2.

Within the quoted uncertainties, we can assert that the values of A', B', and C' are equal to those of A, B, and C respectively. The B values for the ^{16}O- and ^{18}O-species have appreciable differences both in the normal and the *trans*-dideutero species. Since the oxygen atom is on the b axis, this is due to the effect of zero-point vibration. The correlation matrix for the rotational constants has appreciable off-diagonal elements.** These correlations were taken into account when these rotational constants were used in the calculation of the structural parameters.[6]

Calculation of Structurel Parameters

By the use of the rotational constants of the ten isotopic molecules, it was possible to apply the method of r_s(Costain)[7] and r_m(Watson).[8] Since the rotational constants are indirect observations,[6,9] nondiagonal weight matrices, which took correlations into account, were used in the calculation.

Equation (1) shows that the values of $\tau_{\alpha\beta\alpha\beta}$'s are needed to obtain the rotational constants, whereas only a combination of $\tau_{\alpha\alpha\beta\beta}$ and $\tau_{\alpha\beta\alpha\beta}$ is determined when the centrifugal distortion is treated to the first order. However, as the $\tau_{\alpha\beta\alpha\beta}$'s are expected to be small and as their isotopic differences are even smaller, the effective rotational constants, A', B', and C', were used without corrections for the calculation of the structural parameters.***

Because of the C_{2v} symmetry, there are four independent structural parameters to be determined.

The r_0 Structure. The r_0 structure was derived by a least-squares fitting of all the observed rotational constants. The weight matrix, **W**, was calculated as:

$$\mathbf{W}=\begin{pmatrix}\mathbf{D}_1^{-1} & & & \\ & \mathbf{D}_2^{-1} & & \mathbf{0} \\ & & \ddots & \\ & \mathbf{0} & & \mathbf{D}_{10}^{-1}\end{pmatrix} \quad (2)$$

where the suffixes are for each isotopic species and where

** For example, suppose that 1_{10}—1_{01}, 1_{11}—0_{00}, and 2_{12}—1_{01} transitions are observed with equal accuracy. In the rigid rotor approximation, their frequencies are $A-C$, $A+C$, and $A+3C$ respectively. The correlation factor between A and C is calculated to be −0.5222.

*** The rotational constants corrected for $\tau_{\alpha\beta\alpha\beta}$ and their isotopic differences should be used for the calculation of the r_0 and r_s structures respectively, if we were to be in strict accordance with the original definitions. Thus, the structures derived in the present study contain systematic errors introduced by the neglect of the corrections, but they may be assumed to be within the reliability intervals of the structural parameters.

Table 2. Converged values and their variances of effective parameters (in MHz)[a]

	$^{12}C_2H_4{}^{16}O$	v_i[b]	$^{12}C^{13}CH_4{}^{16}$	v_i[b]	$^{12}C_2H_4{}^{18}O$	v_i[b]
A'	25483.79	0.028	25291.89	0.055	23992.83	0.112
B'	22120.76	0.031	21597.77	0.058	22121.58	0.117
C'	14097.71	0.026	13825.75	0.056	13628.56	0.126
τ'_{aaaa}	−0.2186	0.002	−0.2301	0.013	−0.1843	0.009
τ'_{bbbb}	−0.0730	0.002	−0.0750	0.006	−0.0700	0.005
τ'_{cccc}	+0.0294	0.008	−0.0483	0.032	0.0952	0.064
τ'_{aabb}	−0.1534	0.002	−0.1520	0.004	−0.1407	0.004
σ^2 [c]	0.0129		0.0205		0.0916	

	t-$^{12}C_2H_2D_2{}^{16}O$	v_i[b]	t-$^{12}C^{13}CH_2D_2{}^{16}O$	v_i[b]	t-$^{12}C_2H_2D_2{}^{18}O$	v_i[b]
A'	22943.19	0.030	22786.84	0.061	21646.74	0.092
B'	18198.47	0.032	17852.32	0.072	18202.46	0.099
C'	12585.27	0.030	12377.50	0.060	12186.66	0.093
τ'_{aaaa}	−0.1667	0.003	−0.1617	0.015	−0.1377	0.009
τ'_{bbbb}	−0.0358	0.001	−0.0379	0.004	−0.0385	0.003
τ'_{cccc}	0.0251	0.007	0.0201	0.017	0.0214	0.022
τ'_{aabb}	−0.0815	0.001	−0.0842	0.003	−0.0817	0.002
σ^2 [c]	0.0064		0.0261		0.0321	

	c-$^{12}C_2H_2D_2{}^{16}O$	v_i[b]	c-$^{12}C^{13}CH_2D_2{}^{16}O$	v_i[b]	c-$^{12}C_2H_2D_2{}^{18}O$	v_i[b]
A'	22700.41	0.050	22555.61	0.037	21424.03	0.047
B'	18318.39	0.054	17963.42	0.040	18317.20	0.050
C'	12650.08	0.051	12438.85	0.038	12243.45	0.048
τ'_{aaaa}	−0.1754	0.006	−0.1627	0.004	−0.1336	0.005
τ'_{bbbb}	−0.0401	0.002	−0.0432	0.002	−0.0413	0.002
τ'_{cccc}	0.0061	0.013	−0.0067	0.010	0.0334	0.013
τ'_{aabb}	−0.0768	0.002	−0.0817	0.002	−0.0776	0.002
σ^2 [c]	0.0184		0.0100		0.0157	

	$^{12}C_2H_3D^{16}O$	v_i[b]
A'	24252.47	0.058
B'	19905.34	0.057
C'	13327.40	0.056
τ'_{aaaa}	−0.1791	0.008
τ'_{bbbb}	−0.0486	0.002
τ'_{cccc}	0.0390	0.010
τ'_{aabb}	−0.1095	0.002
σ^2 [c]	0.0229	

a) Both τ'_{bbcc} and τ'_{aacc} are assumed to be zero. b) Variance of parameter. 2.5 times v_i indicates a reliability intervals of the corresponding parameter. c) The standard deviation of transition frequencies is represented by σ.

$\mathbf{D}_i^{-1}$ are the 3×3 submatrices corresponding to the rotational constants A, B, and C. The method for estimating this weight matrix has been described in a separate paper.[6]

The bond length, r_0(CH), was assumed to be longer than r_0(CD) by about 0.002 Å.[10] In order to verify this difference, four parameter sets were investigated; besides r(CO) and r(CC) and the angle, θ, between H_2C plane and CC bond, which were taken as variables, the following assumptions were made for r(CD), ∠HCH, and ∠DCH:

Set 1) $r(CH)=r(CD)$, $\angle HCH=\angle DCH$,

Set 2) $r(CH)\neq r(CD)$, $\angle HCH=\angle DCH$,

Set 3) $r(CH)=r(CD)$, $\angle HCH\neq\angle DCH$, and

Set 4) $r(CH)\neq r(CD)$, $\angle HCH\neq\angle DCH$.

The analysis led to the following conclusions: a) The most proper set of parameters in the r_0 structure is set 1, since higher correlations emerge among the parameters in the other sets, and b) the isotope effects on r_0(CH) and ∠HCH cannot be detected. The resulting parameters, summarized in Table 4, agree with those reported in previous papers.[2,3]

The r_s Structure Obtained from Kraitchman's Formula. The structure of ethylene oxide was derived from the conventional Kraitchman method;[11] the coordinates of each atom were first calculated by solving an equation

in a matrix form as:

$$\begin{bmatrix} P_{aa}P_{ab}P_{ac} \\ P_{ba}P_{bb}P_{bc} \\ P_{ca}P_{cb}P_{cc} \end{bmatrix} = \mu \begin{bmatrix} P_{ab}P_{ac} & P_{ac}P_{aa} & P_{aa}P_{ab} \\ P_{bb}P_{dc} & P_{bc}P_{ba} & P_{ca}P_{bb} \\ P_{cb}P_{cc} & P_{cc}P_{ca} & P_{ca}P_{cb} \end{bmatrix} \cdot \begin{bmatrix} a_s^2 \\ b_s^2 \\ c_s^2 \end{bmatrix} \quad (3)$$

where:

$$P_{\alpha\beta} = P_\alpha' - P_\beta, \quad (4)$$

$$P_\alpha = (-I_\alpha + I_\beta + I_\gamma)/2, \quad (5a)$$

$$P_\alpha' = (-I_\alpha' + I_\beta' + I_\gamma')/2, \quad (5b)$$

$(\alpha, \beta, \gamma = \text{a, b, or c})$

and

$$\mu = M\Delta m/(M+\Delta m).$$

The I_a, I_b, I_c quatities are the principal moments of inertia of one of the reference species (normal, *trans*-D_2 and *cis*-D_2- ethylene oxide), and the primed quantities, I_a'"s, are the principal moments of inertia of one of the species in which one of the atoms in the reference molecule is replaced by an isotope. M is the molecular weight of the reference species, Δm is the change in the molecular weight caused by the isotopic substitution, and a_s, b_s, and c_s are the coordinates of the substituted atom referred to the principal axis system of the reference species.

A direct substitution of the observed values into Eq. (3) gave imaginary values to those coordinates which are expected to be equal to or close to zero. Hence, the following conditions were imposed: 1) The values of P_a' for the ^{18}O species of normal, *trans*-D_2-, and *cis*-D_2- ethylene oxides were set equal to P_a. The observed values of $P_a'-P_a$ were taken into account in the error analysis of the results by the use of the law of the propagation of errors.[6] 2) The values of P_c' for the ^{18}O species of the normal and the *trans*-D_2-ethylene oxide were set equal to P_c, with the observed values of $P_c'-P_c$ treated in the same manner as $P_a'-P_a$.

The calculations were carried out for the sets of isotopic species (the normal ^{18}O-, ^{13}C-, and D_1-ethylene oxides), *trans*-D_2-, *trans*-D_2-^{18}O-, *trans*-D_2-^{13}C-, and D_1-ethylene oxides), and (*cis*-D_2-, *cis*-D_2-^{18}O-, *cis*-D_2-^{13}C-, and D_1-ethylene oxides), taking the first species in each set as the reference molecule. The principal axis coordinates of the O, C, and H atoms for the normal *trans*-D_2-, and *cis*-D_2- species thus calculated are shown in Table 3. The coordinates of the H atoms in the deuteroethylene oxides which are not replaced by D could not be determined by the present method; even the use of the first-moment equation provided only the b and c coordinates of the hydrogen atoms in the *cis*-D_2 molecule. The values thus derived are shown in parentheses in Table 3. The remaining coordinates, the a and c coordinates of the *trans*-D_2 and the c coordinates of the *cis*-D_2 species, could not be obtained by the first-moment equation or by setting the cross products of inertia at zero. The structural parameters calculated from the coordinates are also summarized in Table 3, along with their estimated error limits. The r_s(CH) derived for the normal species is longer than that for the dideutero species by about 0.003 Å, but they overlap in their reliability intervals.

Table 3. Atomic coordinates and structural parameters[a]

	Nomal	*trans*-D_2	*cis*-D_2
a_s(O)	0.00000(363)	0.00000(322)	0.00000(286)
b_s(O)	0.80226(204)	0.82883(108)	0.83079(88)
c_s(O)	0.00000(337)	0.00000(313)	0.01945(197)
a_s(C)	0.73239(79)	0.72581(65)	0.73202(62)
b_s(C)	0.42741(113)	0.39915(102)	0.39348(98)
c_s(C)	0.00000(271)	0.09115(391)	0.07163(470)
a_s(H)[b]	1.26235(81)	—	—
b_s(H)	0.64112(117)	0.61247(78)	(0.5251)[c]
c_s(H)	0.92344(64)	—	(0.9458)[c]
a_s(D)[c]	—	1.37277(60)	1.26203(76)
b_s(D)	—	0.61247(78)	0.69174(91)
c_s(D)	—	0.74997(56)	0.82280(66)
r(CO)	1.4313(31)	1.4294(24)	1.4293(38)
r(CC)	1.4648(16)	1.4630(23)	1.4640(12)
r(CH)	1.0859(18)	1.0824(34)	1.0816(56)
∠HCH	116.50(43)	—	—
θ[b]	21.59(28)	—	—
∠OCC	59.21(13)	59.21(13)	59.18(11)

a) Coordinates and bond lengths are in Å and angles are in degreees with reliability intervals indicated in parentheses. b) Rotational constants of the D_1 species species were used to derive the coordinates of the H or D atoms. c) Calculated by the first moment equation. d) Angle of the C-C bond to the H_2C plane.

The value of c_s(C) of the *trans*-D_2 species combined with the r(CC) indicates that the principal axis system of the species is obtained by the rotation of 7.15° around the b-axis, following the displacement of the origin of that of the normal species. For the *cis*-D_2-species, the rotation angle of 4.25° around the a-aixs is derived from the c_s(C), c_s(O), r(CC), and r(CO) values. A μ_s value of 0.14 D can be expected for the latter species if one assumes that the total dipole moment of 1.88 D of the normal species is unchanged and lies along the symmetry axis of the ring.

The r_s Structure Derived by a Least-squares Fit. The r_s parameters were also derived from a least-squares fit of the changes caused by isotope substitutions in the principal moments of inertia. The analysis was based on either a diagonal or a nondiagonal weight matrix.[6] The converged parameters were not significantly different, but the correlation factors obtained for a nondiagonal weight matrix were somewhat smaller. This tendency is contrary to that observed for the r_0 structure. The parameters derived from the non-diagonal weight matrix are shown in Table 4. Strong correlations were observed between r_s(CH) and r_s(CD) and between $\angle_s$HCH and $\angle_s$DCH, but the other parameters were not affected. No significant differences were observed between r_s(CH) and r_s(CD) or between $\angle_s$HCH and $\angle_s$DCH.

The r_m Structure. The r_m structure was derived from an approximate equation: $I_e = 2I_s - I_0$ as proposed by Watson for estimating the equilibrium structure.[8] He pointed out that one of the disadvantages of the r_m structure is that the equation is not sufficiently

Table 4. Structural parameters of ethylene oxide[a,e]

	r_0	r_s	r_m	r_0[b]	r_0[c]
r(CC)	1.470(3)	1.466(2)	1.462(3)	1.472	1.470(3)
r(CH)	1.085(4)	1.085(1)	1.086(4)	1.082	1.084(5)
r(CO)	1.434(2)	1.431(1)	1.428(2)	1.436	1.435(3)
∠HCH	116.3(7)	116.6(1)	116.9(7)	116.7	116.3(11)
θ[d]	22.3(5)	22.0(1)	21.6(5)	21.9	21.9(11)
∠COC	61.67	61.64	61.62	61.24	61.61
φ[f]	7.24	7.60	7.97	7.66	7.70

a) Bond lengths are in Å and bond angles are in degrees. b) Ref. 2. No error limits are given in the reference. c) Ref. 3. Error limits indicated in the original paper are multiplied by 2.5 to make them consistent with others. d) Angle of the C-C bond to the H_2C plane. e) Values in parentheses indicate the reliability intervals. f) $\varphi = \angle OCC/2 - \theta$.

Table 5. Comparison of structures of three-membered rings[a]

	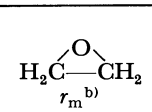 r_m[b]	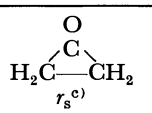 r_s[c]	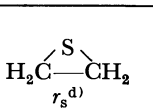 r_s[d]	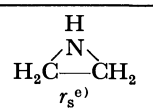 r_s[e]
r(CC)	1.462(3)	1.575(12)	1.484(6)	1.481
r(CH)	1.086(4)	1.086(25)	1.083(10)	1.084
r(CX)	1.428(2)	1.475(17)	1.815(14)	1.475
∠HCH	116.9(7)	114.1(20)	115.8	115.72
θ[i]	21.6(5)	29.1(20)	28.2	—
∠CXC	61.62	64.60	48.27	60.25
φ[j]	7.97	−0.26	5.28	—

	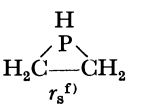 r_s[f]	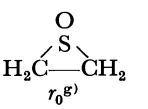 r_0[g]	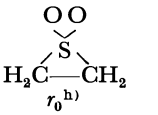 r_0[h]	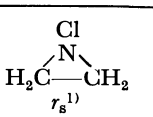 r_s[l]
r(CC)	1.502	1.504(3)	1.590(11)	1.484
r(CH)	1.093	(1.078)[k]	(1.078)[k]	1.093
r(CX)	1.867	1.822(3)	1.731(6)	1.488
∠HCH	114.4	(116.0)[k]	(116.0)[k]	117.1
θ[i]	30.5	(28.3)[k]	(28.3)[k]	—
∠CXC	47.4	48.77(16)	54.40(25)	59.80
φ[j]	2.65	4.5	3.1	—

a) Bond lengths are in Å and bond angles are in degrees. Reliability intervals are shown in parentheses. Note that r(CC) for propane, $(CH_3)_2CH_2$, is 1.526±0.002 Å (Ref. 13). b) Present study. c) J. M. Pochan, J. E. Baldwin, and W. H. Flygare, *J. Amer. Chem. Soc.*, **91**, 1896 (1969). d) K. Okiye, C. Hirose, D. Lister, and J. Sheridan, *Chem. Phys. Lett.*, **24**, 111 (1974). e) B. Bak and S. Skaarup, *J. Mol. Struct.* **10**, 385 (1971). f) M. T. Bowers, R. A. Beaudet, H. Goldwhite, and R. Tang, *J. Amer. Chem. Soc.*, **91**, 17 (1969). g) S. Saito, This Bulletin, **42**, 663 (1969). h) Y. Nakano, S. Saito, and Y. Morino, *ibid.*, **43**, 368 (1970). i) Dihedral angle of the C-C bond and the H_2C plane. j) $\varphi = \angle OCC/2 - \theta$, the positive value of φ corresponds to the case when the H_2C plane is pushed toward another H_2C plane from the plane bisecting the OCC angle. k) assumed values. l) B. Bak and S. Skaarup, *J. Mol. Struct.* **12**, 259 (1972). The CH_2 groups are reported to be twisted.

Table 6. Comparison of C-X bond lengths in three-membered rings and dimethyl compounds (in Å)

	X=O	X=CO	X=NH	X=PH	X=S	X=SO	X=SO_2
$(CH_2)_2X$[a]	1.428(2)	1.475(17)	1.475	1.867	1.815(14)	1.822(3)	1.731(6)
$(CH_3)_2X$	1.410(3)[b]	1.507(3)[c]	1.462(5)[d]	1.848(3)[e]	1.802(2)[f]	1.799(5)[g]	1.777(6)[h]

a) As for the references on structures of the ring compounds, see footnotes of Table 5. b) U. Blukis, P. H. Kasai and R. J. Myers, *J. Chem. Phys.*, **38**, 2753 (1963). c) R. Nelson and L. Pierce, *J. Mol. Spectrosc.*, **18**, 344 (1965). d) J. E. Wollab and V. W. Laurie, *J. Chem. Phys.*, **48**, 5058 (1968). e) R. Nelson, *ibid.*, **39**, 2382 (1963). f) L. Pierce and M. Hayashi, *ibid.*, **35**, 479 (1961). g) W. Feder, H. Dreizler, H. D. Rudolph, and V. Typke, *Z. Naturforsch.*, **24A**, 266 (1969). h) S. Saito and F. Makino, This Bulletin, **45**, 92 (1972).

accurate for the hydrogen-deuterium isotope effects.

The calculation of the r_m structure followed the derivation of the r_0 structure, with I_0 replaced by $I_m = 2I_s - I_0$. The weight matrix used in the derivation of the r_0 structure was used. Typical r_m parameters obtained with a nondiagonal weight matrix are listed in Table 4.

Discussion

In calculating the structural parameters, the rotational constants were treated as indirect observations. In other words, the rotational constants were derived by a least-squares fit of directly-observed transition frequencies. The correlations found among the rotational constants were accounted for by the use of nondiagonal weight matrices. The use of a nondiagonal weight matrix for the analysis of mutually-correlated data was first done by Morino *et al.* in their study of gas-phase electron diffraction.[9] As Kirchhoff suggested,[12] similar situations are often encountered in microwave spectroscopy. The present study is an application of this method with a slight modification (see Ref. 6 for details). A comparison of the present results with those derived assuming a mutual independence of rotational constants led to the following conclusions:

a) The parameters converged to slightly different values, although the reliability intervals estimated from a 2.5-fold variance covered the differences.

b) The correlation factors among the parameters were also different.

c) No general statement can be made as to whether a conventional use of a diagonal weight in the calculation gives smaller variances and less correlations than that of a nondiagonal weight.

The r_s structure derived from Kraitchman's method is consistent with that derived statistically within the estimated error limits (Tables 3 and 4). Therefore, the apparent isotopic differences in the parameters obtained by Kraitchman's formula (Table 3) are artifacts, as has been indicated by the present statistical analysis.

A comparison of the structural parameters of three-membered ring compounds is presented in Table 5. The CX bond lengths of these compounds are compared with those of $(CH_3)_2X$ in Table 6. The CC bond length in $(CH_3)_2CH_2$ is reported to be 1.526± 0.002 Å.[13] An inspection of Tables 5 and 6 shows that, in three-membered rings of the $H_2C\text{-}X\text{-}CH_2$ type, the CC length is shortened for X=O, S, NH, PH, and SO, whereas the CX lengths are longer than their typical values by about 0.02 Å. The angles, φ, of the H_2C plane to the line bisecting the CCX plane are significantly different from zero. Since φ is expected to be equal or very close to zero in normal chemical bonds, the departure from zero in the three-membered rings is an indication of strain in the bonding.

The author is grateful to Professor Kunio Kozima for his help and encouragement and to Mr. Masahiro Kawasaki, whose sample of dideuteroethylene oxides were vital in the present study. Grateful acknowledgements also go to Professor Yonezo Morino, Professor Kozo Kuchitsu, Dr. Takeshi Oka, and Dr. Charles D. LeCroix for their helpful comments on the manuscript.

References

1) C. A. Coulson, "Valence," Oxford University Press, New York, 2nd Ed. (1961), Chap. viii.
2) G. L. Cunningham, A. W. Boyd, R. J. Myers, W. D. Gwinn, and W. J. LeVan, *J. Chem. Phys.*, **19**, 676 (1951).
3) T. E. Turner and J. A. Howe, *ibid.*, **24**, 924 (1956).
4) D. Kivelson and E. B. Wilson, Jr., *ibid.*, **20**, 1575 (1952).
5) J. K. G. Watson, *ibid*, **48**, 181 (1968).
6) C. Hirose, This Bulletin, **47**. 976 (1974).
7) C. C. Costain, *J. Chem. Phys.*, **29**, 864 (1958).
8) J. K. G. Watson, *J. Mol. Spectrosc.*, **48**, 479 (1973).
9) Y. Morino, K. Kuchitsu, and Y. Murata, *Acta Cryst.*, **18**, 549 (1965).
10) V. W. Laurie and D. R. Herschbach, *J. Chem. Phys.*, **37**, 1687 (1962).
11) J. Kraitchman, *Amer. J. Phys.*, **21**, 17 (1966).
12) W. H. Kirchhoff, *J. Mol. Spectrosc.*, **41**, 333 (1972).
13) D. R. Lide, *J. Chem. Phys.*, **33**, 514 (1960).

Chemical Behavior of Intermediates Produced in Sulfuric Acid Glass by Gamma Irradiation. II. Yield of Trapped Hydrogen Atoms in the System Containing Metallic Ions

Teikichi SASAKI

Chemistry Division, Japan Atomic Energy Research Institute, Tokai-mura, Ibaraki-ken 319-11

(Received May 24, 1973)

The yield of trapped hydrogen atoms, H_t, in gamma-irradiated sulfuric acid glass is remarkably increased by adding a small amount, 10^{-2} M, of metallic ions. The increase is followed with a slow decrease at the higher solute concentrations. The efficiency of the formation depends on the kind of cationic solute. The largest $G(H_t)$ is observed in a system containing Co^{2+} ions; it amounts to 8.7. These findings can be explained by a mechanism in which not only mobile electrons produced by the initial ionic processes, but also excited states of the matrix molecule, contribute to the H_t formation. The excitation energy is transferred from the matrix molecule to the solute, which consequently undergoes ionization; the resulting electron causes the H_t formation. This mechanism seems to be supported by the observation that the yield of H_t increases with a decrease in the charge-transfer energy of the solute in the rigid matrix.

The photochemical production of hydrogen atom in an aqueous acidic solution containing Fe^{2+} ions was first found by Weiss *et al.*[1] Afterwards, it was proposed that its primary process is the formation of an excited state of the Fe^{2+} ion, from which an electron is transferred to the water molecule of the surrounding hydration shell.[2,3] This explanation was also given for the photochemical reaction in other frozen solutions.[3,4]

On the other hand, it has been considered that H_t in the gamma-irradiated acidic frozen solution is produced only through ionic processes. In their spectrophotometric study of irradiated glasses containing transition metals, Brown and Dainton[5] have found that some kinds of solutes are reduced according to:

$$M^{n+} + e_m^- \longrightarrow M^{(n-1)+} \qquad (1)$$

where $M^{n+}=Mn^{2+}$, Ni^{2+} *etc.* Since the mobile electron is considered to be a precursor of H_t in the acidic matrix, a decrease in the H_t yield can be anticipated for these systems containing cationic solutes.

In the present systematic study, however, a remarkable increase in the H_t yield was observed only upon the addition of a small amount of the transition-metal ion to the sulfuric acid glass. The yield curves always have maxima and their trends are analogous to those obtained photochemically by Moorthy and Weiss.[3] The largest G value amounts to 8.7, which is much larger than the value reported for H_t formation through ionic processes in the pure matrix: $G(H_t)\simeq 1.2$.[6] Although the primary processes are somewhat different from those in the photochemical production, excited states of the water molecule seem to play an important role in the formation. In the gamma irradiation, a secondary electron excites the matrix molecule during the slowing-down processes. Then an excitation energy seems to be transferred from the molecule to the solute, which consequently undergoes ionization.

Experimental

Sample Preparation. The water was redistilled. The sulfuric acid and all the chemicals from the Kanto Kagaku Co., Ltd. were of an analytical reagent grade. A small amount of cationic sulfate was added to an aqueous solution of 6 M sulfuric acid, after which the solution was cooled to 77 K.

The samples for ESR measurements were prepared as has previously been described.[7] On the other hand, the samples for gas-chromatographic analysis were degassed and then sealed in Pyrex cells with breakable seals. The sample volume was constantly 10 ml.

Irradiation and Measurement. The gamma irradiations were carried out by means of a 45 kCi ^{60}Co source at the dose rate of 6.4×10^{18} eV g^{-1} hr^{-1}. The dose absorbed was determined by Fricke dosimetry. The sample was usually exposed in the dark at 77 K for one hr.

The ESR spectra were obtained with an X-band Hitachi 771-type spectrometer equipped with 100 kHz modulator and were scanned without power saturation. The absolute H_t yields were determined by comparison with the signal intensity of a calibrated amount of the DPPH radical in a tetrahyrdofuran solution frozen at 77 K. The relative H_t yields were obtained from the signal intensity of the higher field. The SO_4^- yield was relatively determined from the signal height in the central part of the spectrum where its anisotropic singlet appeared. For the measurements of the H_2 yield, the irradiated sample was melted and the H_2 gas was recovered with a Toepler pump. The gas analyses were performed with a Yanagimoto G-8-type gas chromatograph, and the yield was determined absolutely by comparison with a standard volume of pure H_2 gas.

Results

The bright brown color due to the SO_4^- radical was not observed for the irradiated samples containing a large amount of the cationic solute.

The ESR spectrum of the irradiated sulfuric acid glass consisted of a doublet splitting by 510 G and a singlet centered at 3288 G. These have been ascribed to the H_t and SO_4^- radicals respectively.[8] A power saturation of the H_t signal in the samples containing a paramagnetic cation was observed to begin at approximately 3×10^{-2} mW. This observation agrees with the results obtained previously for H_t power saturations in the sulfuric acid glasses.[9] The intensity ratios of the low-field line to the high-field line in the H_t signal were measured for the following systems; 6M sulfuric acid glass and the glasses containing the 0.04 M Co^{2+} ion and the 0.5 M Co^{2+} ion. For all

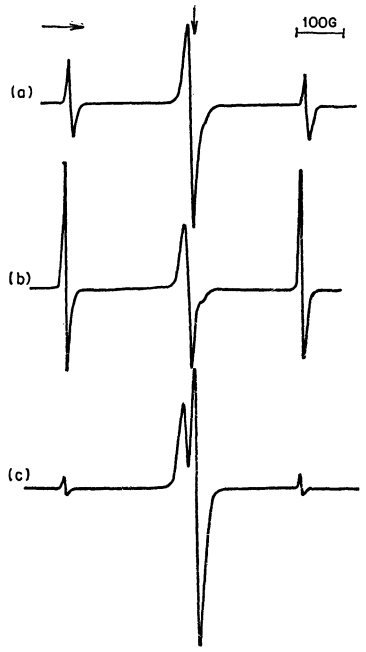

Fig. 1. ESR spectra of the samples irradiated at 77 K. A vertical arrow indicates a signal position of DPPH radical.
(a) 6M sulfuric acid glass.
(b) 6M sulfuric acid glass containing 5×10^{-2} M Ni^{2+} ion.
(c) 6M sulfuric acid glass containing 5×10^{-2} M Ni^{2+} and 0.1 M TeO_4^{2-} ions.

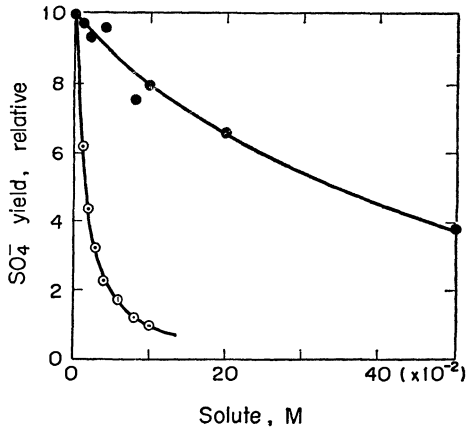

Fig. 2. Positive hole scavenging in the 6 M sulfuric acid glass by Ni^{2+} and Fe^{2+} ions.
●: Ni^{2+}, ⊙: Fe^{2+}

the above systems, the ratios were 1.1 ± 0.1 under the microwave power employed.

The addition of the Ni^{2+} ion resulted in an abrupt increase in the H_t yield, as is shown in Fig. 1(b). As the intense H_t signal declines in the presence of a strong electron scavenger, TeO_4^{2-}, as may be seen in Fig. 1(c), it is considered that a mobile electron contributes to a reaction of the H_t formation. On the other hand, the SO_4^- yield decreases upon the addition of the cationic solute. The details for the systems containing Fe^{2+} and Ni^{2+} ions are shown in Fig. 2. For the other systems, it was difficult to obtain analogous scavenger

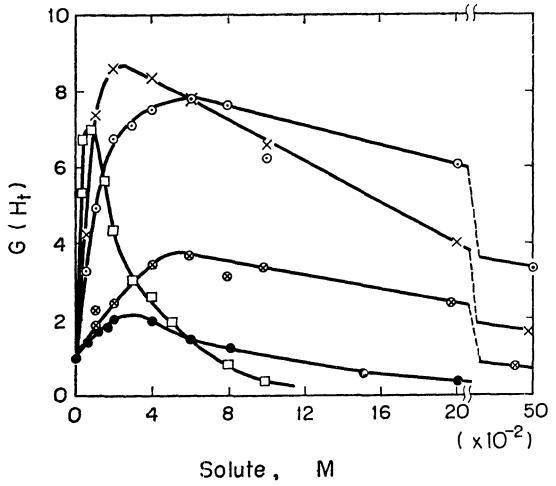

Fig. 3. $G(H_t)$ for the 6 M sulfuric acid glass containing various kinds of cationic solute.
●: VO^{2+}, ⊗: Ni^{2+}, ⊙: Fe^{2+}, ×: Co^{2+}, □: Mn^{2+}

Table 1. Maximum $G(H_t)$ in 6M sulfuric acid glass containing various kinds of cationic solute

Solute	Max. $G(H_t)$	Solute concentration $\times10^{-2}$ M
none	1.0	—
VO^{2+}	2.1	2.5
Ni^{2+}	3.7	5.5
Fe^{2+}	7.8	6.0
Co^{2+}	8.7	2.5
Mn^{2+}	6.5	0.8

curves because of the complexity in the central part of the ESR spectra. The decrease in the SO_4^- yield has been also previously observed for the system containing the Fe^{2+} ion and ascribed to a hole scavenging by the solute.[10] The present monotonous decreases suggest that the G value for initial ionic processes is almost constant, even in the presence of the solutes.

Figure 3 shows the curves of the H_t yield in the systems containing the cationic solute. The curves have two principal characteristics. The first is a remarkable increase in the H_t yields, followed by a slow decrease. Especially in the system containing the Co^{2+} ion, the maximum G value amounts to 8.7, which is much larger than yield of H_t in the pure matrix ($G(H_t)=1.0$). At the higher solute concentration, the $G(H_t)$ becomes less than 1.0 because of Reaction (1). It is noteworthy that these cationic solutes can scavenge mobile electrons as well as positive holes. The second is that the slope of the increasing curve and the maximum H_t concentration depend on a kind of solute. The maximum $G(H_t)$ are summarized in Table 1, together with the solute concentrations. In all the systems, the G value reaches its maximum at the solute concentrations of 0.8×10^{-2}—6×10^{-2} M.

The decreases at the higher solute concentrations suggest that the excited states of the solute also participate in the H_t formation, as has been observed in the photochemical production.[3] To confirm this presumption the second solute effect on the H_t formation

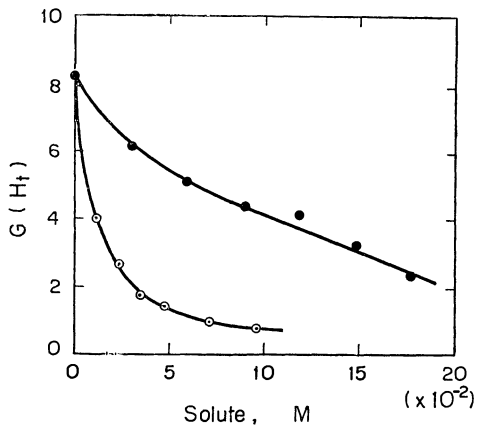

Fig. 4. Second solute effect on the H_t formation in the 6 M sulfuric acid glass containing 4×10^{-2} Co^{2+} ion. ●: Ni^{2+}, ⊙: TeO_4^{2-}

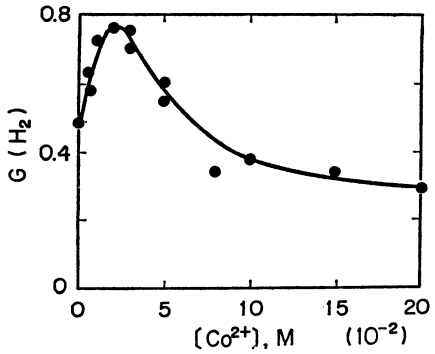

Fig. 5. $G(H_2)$ values determined after melting the irradiated 6 M sulfuric acid glass containing Co^{2+} ion.

was studied. Monotonous decreases in the H_t yield with an increase in the solute concentration were observed; the results are shown in Fig. 4. The depression of the H_t formation seems to be easily attained by the addition of the TeO_4^{2-} ion, which acts not only as an electron scavenger but also probably as a quencher for excited states of the Co^{2+} ion.

The $G(H_2)$ value for the pure matrix was determined to be 0.48 which is almost a half of the H_t yield. The H_2 yield for the system containing the Co^{2+} ion is shown in Fig. 5. Although the yield increases about 1.5 times upon the addition of 2.5×10^{-2} M of the Co^{2+} ion, the absolute value is incompatible with the results of the H_t yield. This discrepancy may arise from the complex reactions during the melting procedures.

Discussion

The primary processes in the radiation effects on matter are ionization and the formation of various excited states of the matrix molecule:

$$S \longrightarrow S^+ + e^- \text{ (or } e_m^-) \quad (2)$$

$$S \longrightarrow S^* \quad (3)$$

According to the following reactions, the mobile electron in the 6 M sulfuric acid glass produces H_t at almost the same rates:[7,11]

$$e_m^- + H^+ \longrightarrow H\ (\rightarrow H_t) \quad (4)$$

$$e_m^- + HSO_4^- \longrightarrow H\ (\rightarrow H_t) + SO_4^{2-} \quad (5)$$

Assuming that H in the acidic glasses is produced only through Reactions (4) and (5), the yield could not exceed $G\simeq4$, which is the ultimate yield of the ionic processes in the aqueous solution at 293 K.[12]

On the other hand, the behavior of the excited states of the water molecule in an aqueous solution is scarcely known, while triplet formation through energy transfer from the excited matrix molecule to the solute have been observed in several organic systems[13] and energy-transfer processes in scintillator systems have been well established.[14] In the liquid water, the probability of energy transfer from the excited states to the solute would be very small, because the excited singlets are quenched in the time of a single vibration, 10^{-13} s, and the excited triplets are unknown.[15] However, in the vapor phase, isotope exchange experiments gave $G\simeq12$ for the total activated water[16] and $G\simeq8$ for the total H-atom formation.[17] Moreover, in the frozen system of an ethylene glycol-water mixture containing a small amount of triptophane, Steen has obtained $G\simeq10$ for the total light emission from its singlet and triplet states.[18] Because the $G(e_t^-)$ has been determined to be approximately 3,[19] the last observation indicates that an excitation energy is efficiently transferred from the excited matrix molecule to the solute. Moorthy *et al.*[3] have elucidated that the excited states of the solute bring about the H_t production by exposing an acidic frozen solution containing the Fe^{2+} ion or the I^- ion to 2537 Å light. In these cases, the H_t yield increases with an increase in the solute concentration and reaches maximum at $[I^-]\simeq0.01$ M for the polycrystalline specimen and at $[Fe^{2+}]\simeq0.2$ M for the glassy specimen. For these observation, a mechanism was proposed that a primary process is a direct excitation of the solute, followed by electron detachment from the excited state, which causes the H_t production by means of Reactions (4) and (5).

As regards the present results, it seems impossible to interpret the large $G(H_t)$ on the basis of the ionic processes alone. Though more direct evidence on the reaction processes is necessary, the following mechanism would, however, account for the yield curves in Fig. 3.

In the present systems, it may be considered that the excitation energy of the matrix molecule is efficiently transferred to the solute, which is consequently excited to its metastable states. The energy of the lowest electronic excited state of the isolated water molecule is *ca.* 7.5 eV, while its ionization energy is 12.6 eV.[20] On the other hand, as regards the solute, *e.g.*, the Fe^{2+} ion, the lowest charge-transfer energy in the rigid matrix is 4.7 eV.[21] These data indicate that the excited states of the water molecule can be converted to those of the Fe^{2+} ion. Hydration ligands surrounding the Fe^{2+} ion and hydrogen bondings probably facilitate energy transfer:

$$S^* + Fe^{2+} \longrightarrow S + Fe^{2+*} \quad (6)$$

Because the energy transferred exceeds its ionization energy, the Fe^{2+*} ion undergoes ionization or, in some cases, is competitively deactivated by light emissions

and radiationless transitions:

$$Fe^{2+*} \longrightarrow Fe^{3+} + e^- \text{ (or } e_m^-) \quad (7)$$

$$Fe^{2+*} \longrightarrow Fe^{2+} \quad (8)$$

The resulting mobile electron is converted to H_t through Reactions (4) and (5). There is no difference in the physicochemical properties of the mobile electrons formed through the two reactions, (2) and (7).

At lower solute concentrations the mechanism described above predicts the promotion of the H_t formation with a decrease in the ionization energy of the solute. As is listed in Table 2, the initial increase in the rate of the H_t formation, *i.e.*, $dG(H_t)/d[S]$ is closely related to the decline in the charge transfer energy, E_{ct}, of the solute. Especially, the excitation energy is most efficiently utilized for the H_t formation in the system containing the Co^{2+} ion, and the maximum $G(H_t)$ amounts to 8.7.

Table 2. Efficiencies of the H_t formation in the sulfuric acid glass containing cationic solute

Solute	$dG(H_t)/d[S]$[a] $\times 10^{-2}\,M^{-1}$	E_{ct}[b] eV	Ref.
VO^{2+}	0.68	5.2	22)
Ni^{2+}	0.85	5.2	23)
Fe^{2+}	3.9	4.7	21)
Co^{2+}	6.5	4.6	24)
Mn^{2+}	17.1	4.5	23)

a) The values were taken from the initial slopes in Fig. 3.
b) E_{ct} denotes an absorption edge of charge transfer band in the optical spectrum and was taken from the UV spectrum in the rigid matrix.

On the other hand, the decrease in the H yield at higher solute concentrations must be due to Reaction (1) and the deactivation of the excited states. The latter process may be caused by a resonance energy transfer between the excited and the ground states of the solute, as is found in the system of the liquid scintillator.[25]

Here, it is worthwhile to interpret on the basis of the present mechanism the results obtained at 77 K by Dainton *et al.*[5] They have observed the hyper-reduced ion in the gamma-irradiated sulfuric acid glasses containing transition-metal ions. The solute concentrations were 0.12 M Mn^{2+} and 0.5 M Ni^{2+} ions where the $G(H_t)$ were less than 1.0, as is seen in Fig. 3. Therefore, the observations may be attributed to a predominant contribution from Reaction (1). On the contrary, they could not observe the reduced form in the system containing the 0.01 M Fe^{2+} ion. This may be due not only to the hole scavenging by the solute, but also to the predominance of Reaction (7) over the competitive reaction (1) at that solute concentration where $G(H_t)$ amounts to 5.0. This presumption is also consistent with their results, which have revealed the absence of the reduced species.

The author is grateful to Dr. Shin-ichi Ohno for his helpful discussions and encouragement. He also wishes to thank Dr. Akihisa Sakumoto for his making available the gas chromatograph.

References

1) J. J. Weiss, *Nature*, **137**, 71(1936); R. H. Poterill, O. J. Walker, and J. J. Weiss, *Proc. Roy. Soc., Ser. A.*, **156**, 561 (1936).
2) E. Hayon and J. J. Weiss, *J. Chem. Soc.*, **1960**, 3866.
3) P. N. Moorthy and J. J. Weiss, *J. Chem. Phys.*, **42**, 3121 (1965).
4) J. J. Weiss, *Trans. Faraday Soc.*, **37**, 463 (1941).
5) D. M. Brown and F. S. Dainton, *ibid.*, **62**, 1139 (1966).
6) R. Livingston and A. J. Weinberger, *J. Chem. Phys.*, **33**, 499 (1960).
7) T. Sasaki, This Bulletin, **47**, 529 (1974).
8) P. N. Moorthy and J. J. Weiss, *J. Chem. Phys.*, **42**, 3127 (1965).
9) J. Zimbrick and L. Kevan, *ibid.*, **47**, 5000 (1967); S. K. Wong and J. K. S. Won, *ibid.*, **55**, 4940 (1971).
10) P. N. Moorthy and J. J. Weiss, *Advan. Chem. Ser.*, **50**, 180 (1965).
11) L. Kevan, P. N. Moorthy, and J. J. Weiss, *J. Amer. Chem. Soc.*, **86**, 771 (1964); L. Kevan, "Radiation Chemistry of Aqueous Systems," ed. by G. Stein, The Weizman Science Press of Israel, Jerusalem(1968), p. 21.
12) F. S. Dainton and D. B. Peterson, *Proc. Roy. Soc., Ser. A*, **267**, 443 (1962).
13) For example, R. Cooper and J. K. Thomas, *J. Chem. Phys.*, **48**, 5103 (1968).
14) M. Burton, K. Funabashi, R. R. Hentz, P. K. Ludwig, J. L. Magee, and A. Mozumder, "Transfer and Strage Energy by Molecules," Vol. 1, ed. by G. M. Burnett and A. M. North, John Wiley & Sons, Ltd., London(1969), p. 161.
15) G. Stein, "The Chemistry of Ionization and Excitation," ed. by G. R. A. Johnson and G. Scholes, Taylor and Francis, Ltd., London(1967), p. 25; "Radiation Chemistry of Aqueous Systems," ed. by G. Stein, The Weizman Science Press of Isreal, Jerusalem(1968), p. 83.
16) R. W. Firestone, *J. Amer. Chem. Soc.*, **79**, 5593 (1957).
17) J. H. Baxendale and G. P. Gilvert, *Discuss. Faraday Soc.*, **36**, 186 (1963).
18) H. B. Steen, *Photochem. Photobiol.*, **6**, 803 (1967).
19) T. Sasaki and S. Ohno, This Bulletin, **44**, 2626 (1971).
20) K. Watanabe and M. Zerikoff, *J. Opt. Soc. Amer.*, **43**, 753 (1953); K. Watanabe and J. Jurse, *J. Chem. Phys.*, **41**, 1650 (1964); D. W. Turner and C. R. Brundle, *Proc. Roy. Soc., Ser. A.*, **307**, 27 (1968).
21) O. G. Holmes and D. S. McClure, *J. Chem. Phys.*, **26**, 1686 (1957).
22) C. J. Ballhausen and H. B. Gray, *Inorg. Chem.*, **1**, 1111 (1962).
23) G. Kuwabara and K. Aoyagi, *Japan. J. Appl. Phys.*, **4**, *Suppl.*, I, 627 (1965).
24) A. Mehra, *ibid.*, **6**, 1030 (1967).
25) The probability of resonance energy transfer in liquid scintillator is equal to that of deactivation through all the other processes(emission, internal conversion *etc.*) when separated from each other by 15—20 Å. R. Voltz, J. Klein, F. Heisel, H. Lauri, G. Laustriat, and A. Coche, *J. Chim. Phys.*, **63**, 1259 (1966).

Vibrational Spectra and Normal Coordinate Analysis of Bis(methylthio)mercury

Noriko IWASAKI, Jo TOMOOKA*, and Koichi TOYODA
Department of Chemistry, Faculty of Science, Kumamoto University, Kumamoto 860

(Received July 23, 1973)

The IR and Raman spectra of bis(methylthio)mercury and methyl(methylthio)mercury were studied. Fundamental vibrations were assigned as follows: frequencies 698, 330, 530 and 174 cm^{-1} to C–S stretching, S–Hg stretching, C–Hg stretching and C–S–Hg bending vibrations, respectively. The fundamental vibrations were confirmed by normal coordinate analysis. The force constants of S–C and S–Hg stretching vibrations were estimated to be 2.16 and 1.5 md/Å, respectively.

Irukayama *et al.*[1] reported on the IR spectra of ethyl(methyl)mercury, bis(ethylmercury)sulfide, and bis(ethylthio)mercury in NaCl region. Since sulfur atoms greatly contribute to formation of complexes between mercury and proteins such as cystine in a living body, it seems important to find also in the biochemical field vibrational bands characteristic of S–Hg and C–Hg linkages. We have carried out spectroscopic studies on a series of alkylmercury compounds containing sulfur.

Assignment of the IR and Raman spectra of bis(methylthio)mercury $(MeS)_2Hg$ and methyl(methylthio)-mercury MeHgSMe was made in order to get information on S–Hg and C–Hg bond vibrations. Molecular structure was discussed. Bradley and Kuncher[2] determined the geometry of $(MeS)_2Hg$ by X-ray diffraction. They concluded that a skeletal S–Hg–S bond was linear in form and methyl groups at both ends were oriented in *trans* around S–Hg–S bond, but the conformations of hydrogens could not be determined. We have confirmed the assignment by normal coordinate analysis.

Experiment

$(MeS)_2Hg$ and MeHgSMe were prepared by the methods of Wertheim[3] and Kondo,[4] respectively. The mp and IR spectra were in good agreement with those given by them.

Instruments used for IR measurements were a JASCO-DS 403G grating infrared spectrophotometer from 4000 to 250 cm^{-1} and a FIS-3 Hitachi far infrared spectrophotometer from 400 to 30 cm^{-1}. IR spectra of $(MeS)_2Hg$ were measured by the KBr disk method in the region 4000—400 cm^{-1} and Nujol method in the far IR region. Raman spectrum was measured in powder state. Measurements of IR and Raman spectra of MeHgSMe were carried out in liquid state(mp 25 °C).

Assignment

Band assignments were made by comparing the spectra of $(MeS)_2Hg$ with those of MeHgSMe and Me_2Hg. It was assumed that the structure of MeHgSMe belongs to the C_s point group. Assignment of Me_2Hg was made in reference to Gutowsky's investigation.[7] The vibrational modes of Me group and the remaining skeleton were discussed. Observed vibrational spectra are shown in Figs. 1—5.

* Present address: Prefectural Institute of Public Health and Environmental Pollution, 4-33 Minamisendanbata, Kumamoto 860.

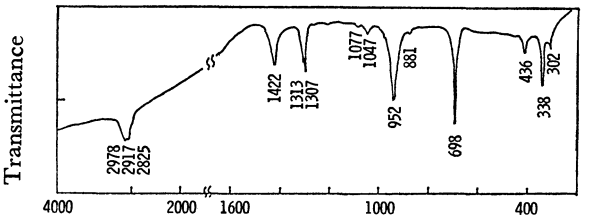

Fig. 1. Observed infrared spectrum in the 4000—300 cm^{-1} region for $(MeS)_2Hg$.

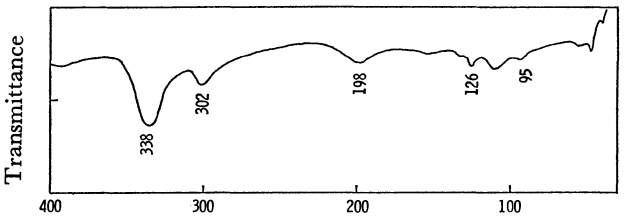

Fig. 2. Observed far-infrared spectrum for $(MeS)_2Hg$.

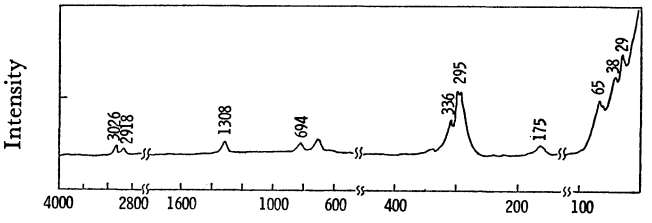

Fig. 3. Observed Raman spectrum of $(MeS)_2Hg$.

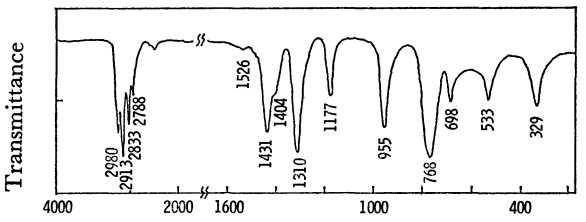

Fig. 4 Observed infrared spectrum for MeHgSMe.

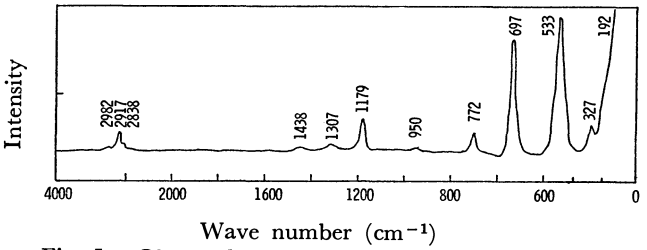

Fig. 5. Observed Raman spectrum of MeHgSMe.

Methyl Group Fundamental Frequencies. Assignment of degenerate and symmetric stretching frequencies of Me group is straightforward. It is well-known that the bands of Me group deformation vibrations occur near 1400, 1300 and 1000 cm^{-1}. It can be predicted that the bands observed for both $(MeS)_2Hg$ and MeHgSMe are due to the Me group attached to sulfur atom (Me–S) and those for both MeHgSMe and Me_2Hg are due to the Me group attached to mercury atom (Me–Hg).

The frequencies of 1422, 1313 and 952 cm^{-1} in $(MeS)_2Hg$ were thus assigned to degenerate deformation, symmetric deformation and rocking vibrations of the former, respectively. The frequencies are in good correspondence with the frequencies 1432, 1307 and 950 cm^{-1} in dimethyldisulfide[5] and 1432, 1322 and 964 cm^{-1} in methylmercaptane.[6] Similarly, IR bands at 1404, 1177 and 768 cm^{-1} in MeHgSMe were assigned to the deformation vibrations of the latter. The splitting was observed at the symmetric deformation band of Me–S in $(MeS)_2Hg$ as in Me_2GeO, the reason not being known.

Skeletal Fundamental Frequencies. The band at 698 cm^{-1} in $(MeS)_2Hg$ and MeHgSMe can be assigned to C–S stretching vibration.

Gutowsky[7] suggested that C–Hg stretching frequency was 550 cm^{-1} in IR and 515 cm^{-1} in Raman spectra of Me_2Hg. Goggin and Woodward[8] also observed C–Hg stretching bands at 538—546 cm^{-1} and Cl–Hg stretching band at 313 cm^{-1} in IR spectra of MeHgX (X=Cl, Br and I). The results indicate that S–Hg stretching bands might appear in the range 500—200 cm^{-1}. Strong bands are observed near 330 cm^{-1} for $(MeS)_2Hg$ and MeHgSMe but not Me_2Hg. $(MeS)_2Hg$ exhibits anti-symmetric(B_u) and symmetric(A_g) stretching vibrations of S–Hg–S bond at 338 cm^{-1} in IR and 295 cm^{-1} in Raman spectra. The weak bands at 336 cm^{-1} in Raman and 302 cm^{-1} in IR seem to be essentially forbidden, since their frequencies are very close to the allowed ones.

Similarly the IR absorption band at 198 cm^{-1} and Raman shift of 175 cm^{-1} in $(MeS)_2Hg$ are assigned to anti-symmetric(B_u) and symmetric(A_g) C–S–Hg bending vibrations, respectively. In the region below 150 cm^{-1}, frequencies 126 and 95 cm^{-1} (Fig. 2) are regarded to be the fundamental bands of S–Hg–S bending vibrations(A_u and B_u), since their combinations are most consistent with the observed values 1077 and 1047 cm^{-1}. It is assumed that the Raman shifts of 65, 38 and 29 cm^{-1} (Fig. 3) are assigned to the torsional vibration of methyl group around S–Hg–S axis or lattice vibrations.

Results and Discussion

Normal coordinate treatment for $(MeS)_2Hg$ was performed using the molecular geometry shown in Fig. 6 (C_{2h}). Normal vibrations of species constitute

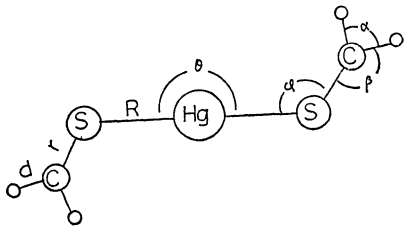

Fig. 6. Molecular geometry of $(CH_3S)_2Hg$ (C_{2h}).

$8A_g+6A_u+4B_g+9B_u$. Molecular parameters of skeleton were taken from results of X-ray diffraction.[2] The methyl group was regarded to be tetrahedral.[10] Thus, bond distances(Å): Hg–S, 2.36; S–C 1.70; C–H 1.09, bond angles(degree): S–Hg–S 180; Hg–S–C 111; S–C–H 109.5; H–C–H 109.5.

The internal rotations of Me groups and the torsional vibrations about S–Hg–S axis were neglected since they possessed frequencies low enough to be separated. A computer program by Shimanouchi[11] and modified for this work was used for carrying out the numerical calculations with the GF matrix method. The potential function employed was based on a modified Urey-Bradley force field. It was necessary to introduce an intramolecular tension term[12] to bring the calculated frequencies close to the observed ones. Repulsive force between non-bonded S and S atoms was ignored.

Table 1. Modified Urey-Bradley force constants for bis(methylthio)mercury (md/Å)

	I	II		III		IV		V	
		FC	ϕ	FC	ϕ	FC	ϕ	FC	ϕ
K(CH)	4.56	4.566	0.003	*		4.566	0.004	*	
K(SC)	2.17	2.159	0.016	*		2.170	0.017	*	
K(SHg)	1.50	1.492	0.030	*		1.587	0.022	*	
H(HCH)	0.389	0.389	0.001	*		0.390	0.001	*	
H(HCS)	0.246	0.247	0.001	*		0.248	0.001	*	
H(CSHg)	0.140	0.127	0.005	*		0.109	0.005	*	
H(SHgS)	0.122					0.122	0.005	*	
F(H:H)	0.085	*		0.086	0.002	*		0.087	0.002
F(H:S)	0.298	*		0.304	0.004	*		0.304	0.006
F(C:Hg)	0.130	*		0.104	0.010	*		0.071	0.012
Kappa**	−0.057	*		−0.058	0.002	*		−0.058	0.003

ϕ) dispersion. I) starting values; II), III) refined for A_g and B_g species; IV), V) refined for A_u and B_u species. * As in column I. ** md·Å.

At first contributions of the force constants concerned with mercury atom to the calculated frequencies were estimated. Final adjustments of all the force constants were accomplished by the Jacobian matrix.[11]

The MUBF constants given in Table 1 fall in a reasonable range, *e.g.*, for alkyl sulfide[13] K(C–S)=1.75, H(HCS)=0.17, K(C–H)=4.250, and H(HCH)=0.37 md/A.

K(Hg–S) in question is evaluated to be 1.5 md/Å. Cooney and Hall[14] measured the Raman spectra of sodium sulfide mercury Na_2HgS_2, in which only a single line was observed at 352 cm^{-1}. The data and the result of X-ray investigation suggest that the ion HgS_2^{2-} is linear in form. For a linear XYX-type molecule, the symmetric stretching frequency is approximately given by

$$\nu = 1303.16[(K+2F)/\mu N]^{1/2}$$

where K and F are stretching and repulsive force constants, respectively. Substituting 352 cm^{-1} into ν, we obtain 2.02 md/Å for the value of $K+2F$, which is slightly greater than 1.5 md/Å in Table 1.

In the Gordy rule,[15] which is simple and applicable to various molecules,

$$K_G = 1.67N(x_A x_B/d^2)^{3/4} + 0.30$$

where N is the bond order, x_A and x_B are the electronegativities of bonded atoms A and B, respectively, d is bond distance at equilibrium and K_G is the stretching force constant. Since potential energy distribution(PED) for Hg-S and S-C stretching coordinates are nearly 100% (Table 2), the evaluation of K_G(Hg–S) and K_G(S–C) was attempted, the results being 1.22 and 3.35 md/Å, respectively, for the values 1.5 and 2.17 md/Å in Table 2.

Table 2. Calculated and observed vibrational frequencies (cm^{-1})

Calcd	Obsd	Assignment
A_g species		
2978	2978	C-H asym str
2917	2917	C-H sym str
1422	1422	Me deg deform
1310	1308	Me sym deform
954	952	Me rock
694	694	S-C str
295	295	Hg-S str
175	175	C-S-Hg bend
A_u species		
2978	2978	C-H asym str
1422	1422	Me deg deform
949	952	Me rock
130	126	S-Hg-S out-of-plane bend
B_g spcies		
2978	2978	C-H asym str
1421	1422	S-C str
948	952	Me rock
B_u species		
2977	2978	C-H asym str
2917	2917	C-H sym str
1422	1422	Me deg deform
1311	1310	Me sym deform
954	952	Me rock
698	698	S-C str
338	338	Hg-str
198	198	C-S-Hg bend
88	95	S-Hg-S in-plane bend

The calculated frequencies are in good agreement with those observed within experimental error (Table 2). Repeated calculations showed a reproducible tendency for A_g frequency to be lower than B_u for Hg–S stretching vibrations and A_u frequency higher than B_u for S–Hg–S bending vibrations. The frequency 126 cm^{-1} was thus assigned to A_u rather B_u. Ambiguity in assignment near 100 cm^{-1} region did not affect the resulting values of force constants so much.

Each PED located to one symmetry coordinate is given in Table 2. It is also possible to employ a local symmetry force field instead of MUBFF. Some normal coordinates which mix two kinds of symmetry coordinate indicate total PED exceeding 100%. This is due to negligence of the negative PED contributions or cross terms.

The selection rules indicate that methyl groups at both ends have *trans* conformation with respect to the S–Hg–S bond. Normal coordinate analysis of $(MeS)_2Hg$ was made on the basis of C_{2h} point group. Using MUBFF, K(S–Hg), H(CSHg) and H(SHgS) were evaluated to be 1.5, 0.11 and 0.122 md/Å, respectively. Separation into group vibrations was satisfactory.

This work was partly supported by a grant of the Ministry of Education of Japan. We wish to thank Prof. Tatsuo Mizayawa, Osaka University, for the use of Raman and far IR spectrometers. Thanks are also due to JASCO Co., Ltd. and JEOL Co., Ltd. for the measurement of Raman spectra, and to Mr. Fumitsugu Muraoka for his assistance. Numerical computations were carried out with FACOM 230–60 computer system of Kyushu University.

References

1) W. Irukayama, M. Fujiki, T. Kondo, and F. Kai, *Jap. J. Hyg.*, **19**, 238 (1964).
2) D. C. Bradley and N. R. Kuncher, *J. Chem. Phys.*, **40**, 2258 (1964).
3) E. Wertheim, *J. Amer. Chem. Soc.*, **51**, 3661 (1929).
4) T. Kondo, *Yakugaku Zasshi*, **84**, 173 (1963).
5) D. W. Scott and H. L. Finke, *J. Amer. Chem. Soc.*, **22**, 2424 (1950).
6) I. W. May and E. L. Pace, *Spectrochim. Acta*, **24A**, 1605 (1968).
7) H. S. Gutowsky, *J. Chem. Phys.*, **17**, 128 (1949).
8) P. L. Goggin and L. A. Woodward, *Trans. Faraday Soc.*, **62**, 1423 (1966).
9) R. A. Nyquist and J. R. Mann, *Spectrochim. Acta*, **28A**, 511 (1972).
10) T. Kojima, *J. Phys. Soc. Jap.*, **15**, 1248 (1960).
11) T. Shimanouchi, "Computer Programs for Normal Coordianate Treatment of Polyatomic Molecules," p. 82 and p. 186 (The Univ. of Tokyo).
12) T. Shimanouchi, *J. Chem. Phys.*, **17**, 245 (1949).
13) M. Ohsaku, Y. Shiro, and H. Murata, this Bulletin, **46**, 1399 (1973).
14) R. P. J. Cooney and J. R. Hall, *Aust. J. Chem.*, **19**, 2179 (1966).
15) W. Gordy, *J. Chem. Phys.*, **14**, 305 (1946).

A Photo-selection Study of the Charge-transfer Phosphorescence

Takako AMANO* and Yoshiya KANDA

Department of Chemistry, Faculty of Science, Kyushu University, Hakozaki, Higashi-ku, Fukuoka 812

(Received August 18, 1973)

The polarization of the charge-transfer phosphorescence has been studied by the method of photo-selection. It has been measured relative to the electric vector of the excitation light corresponding to the charge-transfer band in wavelength for the complexes of tetracyanobenzene, *o*-, *m*-, and *p*-dicyanobenzenes, tetrachlorophthalic anhydride, and phthalic anhydride as electron acceptors, and methyl-substituted benzenes as electron donors, in organic glass at 77 K. It has been shown that the degree of polarization through excitation into the charge-transfer band is almost constant in the phosphorescence region, while it gradually decreases as the ionization potential of the donor increases for any of the acceptors. These observations can reasonably be interpreted in terms of a model in which the charge-transfer phosphorescence is polarized normal to the molecular plane, irrespective of the complex, and in which the change in the polarization degree of the charge-transfer phosphorescence is responsible for the change in the direction of the transition moment of the charge-transfer absorption band.

Phosphorescences of molecular complexes different from those of the constituent molecules themselves were observed by Iwata *et al.* for the complexes containing tetracyanobenzene (TCNB), phthalic anhydride (PA), tetrachlorophthalic anhydride (TCPA), and pyromellitic dianhydride as electron acceptors and methyl-substituted benzenes as electron donors.[1] These phosphorescences were ascribed to the phosphorescence from the lowest triplet state of the complex with the charge-transfer character. Hayashi *et al.* observed the ESR spectra of the phosphorescent triplet states of the TCNB, *o*-dicyanobenzene(*o*-DCNB), *m*-DCNB, and *p*-DCNB complexes and determined the contribution of the charge-transfer character in the lowest triplet states from an analysis of the observed fine structure constants.[2-4]

It seemed that it would be interesting to clarify the S-T mixing mechanism in the triplet states of these complexes. Kobayashi *et al.* studied energy-transfer processes involving the triplet states of TCNB complexes and estimated the contribution of the phosphorescence state from the phosphorescence radiative rate constant.[5] Tsujino *et al.* confirmed that the TCNB complexes in the phosphorescent state are produced directly from the excited Franck-Condon state.[6] We ourselves tried to apply the photo-selection method to the charge-transfer phosphorescence in order to obtain some information on this problem. In this paper the experimental results of the polarization of the charge-transfer phosphorescence will be presented, and the nature of the charge-transfer triplet state of these complexes and also that of the lowest excited charge-transfer singlet state will be discussed.

Experimental

The phosphorescence spectra and their polarizations were measured by means of an apparatus described previously.[7] The degree of polarization was calculated using this formula:

$$P = \frac{I_{//} - I_{\perp}}{I_{//} + I_{\perp}}$$

in which $I_{//}$ and $I_{\perp}$ refer to the intensities of the emitted light polarized parallel to and perpendicular to the exciting light respectively.

All the measurements were carried out at 77 K in an ether-isopentane(EP) (1 : 1 volume ratio) or an ethanol glass solution, the concentrations of the samples being 10^{-2}—10^{-4} M of the donor and 10^{-3}—10^{-5} M of the acceptor. The sample was transferred into a Pyrex cell, degassed, and sealed off.

The absorption spectra were measured at room temperature by a Shimadzu MPS-50L spectrophotometer.

Benzene, *p*-xylene, and mesitylene were of a reagent grade and were purified further through distillation under reduced pressure. Durene of an u.p. grade supplied by the Tokyo Kasei Co. was used without purification. Hexamethylbenzene(HMB), TCPA, PA, *o*-DCNB, *m*-DCNB, and *p*-DCNB were repeatedly recrystallized from ethanol and sublimed *in vacuo*. TCNB was prepared according to Lawton *et al.*[8] and was purified through recrystallization from ethanol several times. Ether, isopentane, and ethanol were carefully purified by modifications of methods described in a book by Kuwata.[9]

Results

The phosphorescence spectra of the TCNB-HMB complex in ethanol obtained by the excitation of the Hg 405 nm and TCNB obtained by the excitation of the Hg 313 nm line are shown in Fig. 1, together with the absorption spectra of TCNB, HMB, and the TCNB-HMB complex in an ethanol solution. Figure 2 illustrates the degree of polarization, P, of the phosphorescence of the TCNB-HMB complex analyzed at 540 nm plotted as a function of the excitation wavelength. It is shown that the polarization measured in the charge-transfer absorption region is nearly constant within the limits of experimental error. The P values of the phosphorescence excited in the local excitation region are smaller than those excited in the charge-transfer band. Figure 3 shows that the polarization degree measured by the excitations at 436, 365, and 313 nm depends upon the wavelength of the phosphorescence spectrum. It is found that the polarization is roughly constant throughout the region of the phosphorescence spectrum obtained by excitation with the charge-transfer band. It may be concluded from Figs. 2 and 3 that the degree of polarization relative to the charge-transfer band is about 0.4. This value indicates that the transition moment of the phosphorescence is nearly parallel to that of the charge-transfer

* Present Address: Fujitsu Limited, 1015 Kamikodanaka, Nakahara-ku, Kawasaki

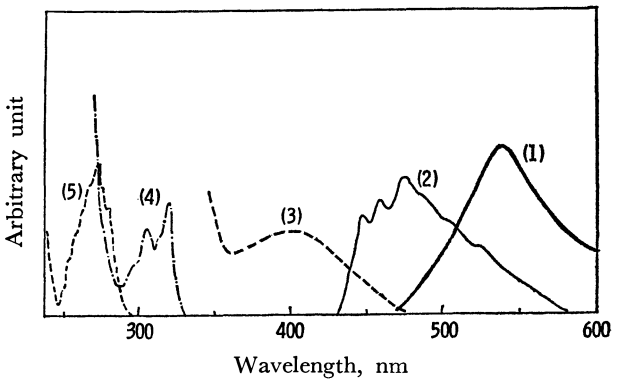

Fig. 1. Phosphorescence and absorption spectra of TCNB, HMB and TCNB-HMB complex in ethanol solution: (1) Phosphorescence spectrum of TCNB-HMB complex at 77 K (uncorrected to photomultiplier sensitivity); (2) Phosphorescence spectrum of TCNB at 77 K (uncorrected to photomultiplier sensitivity); (3) Charge-transfer absorption band; (4) Absorption Spectrum of TCNB; (5) Absorption spectrum of HMB.

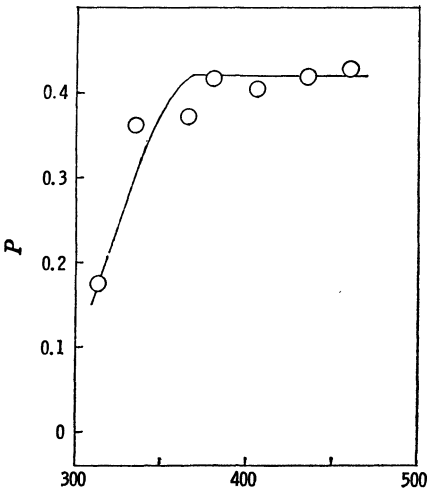

Fig. 2. Variation of the degree of polarization of TCNB complex analyzed at 540 nm with the wavelength of excitation.

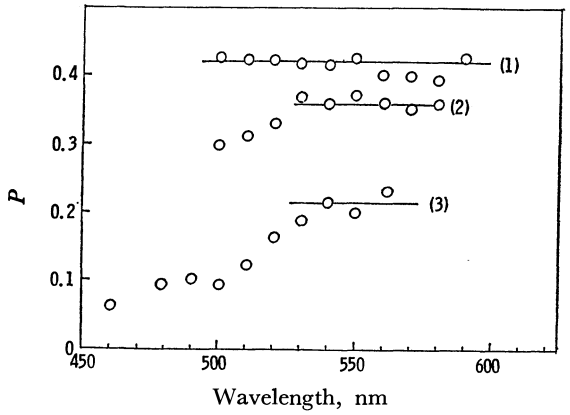

Fig. 3. Phosphorescence polarization of TCNB-HMB complex as obtained by excitation at various wavelengths: (1) 436 nm; (2) 365 nm; (3) 313 nm.

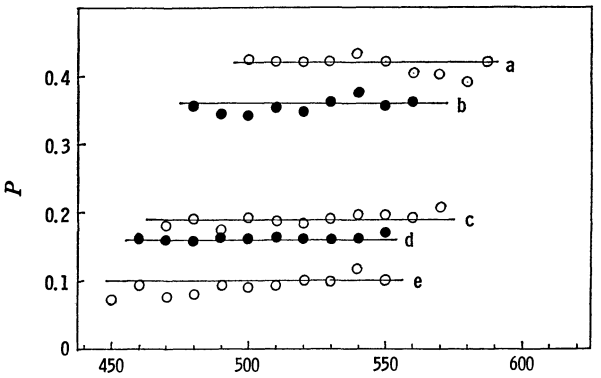

Fig. 4. Phosphorescence polarization of TCNB complexes with excitation into the charge-transfer band; (a) TCNB-HMB, (b) TCNB-durene, (c) TCNB-mesitylene, (d) TCNB-*p*-xylene, and (e) TCNB-benzene.

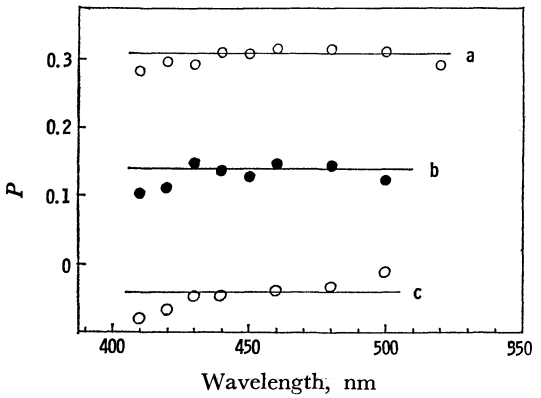

Fig. 5. Phosphorescence polarization of *o*-DCNB complexes; (a) *o*-DCNB-HMB, (b) *o*-DCNB-durene, and (c) *o*-DCNB-mesitylene.

band and that the phosphorescence is, therefore, polarized mostly perpendicular to the molecular plane. Being influenced by the uncomplexed TCNB molecules and/or some other impurities, the *P* values gradually decrease in the shorter-wavelength region of the phosphorescence obtained by excitation at 365 and at 313 nm, as is shown in Fig. 3. Similar behavior of the phosphorescence polarization was also observed for all the other complexes upon excitation into the S-S transition region of the constituent molecules.

Figure 4 compares the polarization of the phosphorescences of the TCNB complexes with HMB, durene, mesitylene, *p*-xylene, and benzene in an ethanol solution relative to the excitation of the molecule to the charge-transfer band. The polarizations were found to be nearly constant throughout the phosphorescence region for any of the complexes. Furthermore, it is apparent that the degree of polarization increases as the number of the CH_3-radical of the donor increases from benzene to HMB.

Similar results were also obtained for the *o*-DCNB, *m*-DCNB, *p*-DCNB, TCPA, and PA complexes with methylated benzenes; they are shown in Figs. 5—9

Table 1. Polarization degrees of TCNB complexes and ionization potentials of donors

Donor	P						I_p (eV)
	TCNB	*o*-DCNB	*m*-DCNB	*p*-DCNB	TCPA	PA	
HMB	0.4_2	0.3_1	0.2_6	0.2_2	0.1_8	0.3_2	7.85
Durene	0.3_6	0.1_4	0.1_2	0.1_1	0.1_6	0.1_0	8.03
Mesitylene	0.1_9	-0.0_4	-0.0_4	-0.0_3	0.0_5	0.0_5	8.39
p-Xylene	0.1_6				0.0_4		8.445
Benzene	0.1_0						9.245

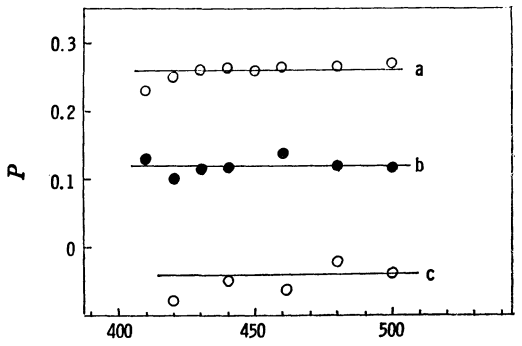

Fig. 6. Phosphorescence polarization of *m*-DCNB complexes; (a) *m*-DCNB-HMB, (b) *m*-DCNB-durene, and (c) *m*-DCNB-mesitylene.

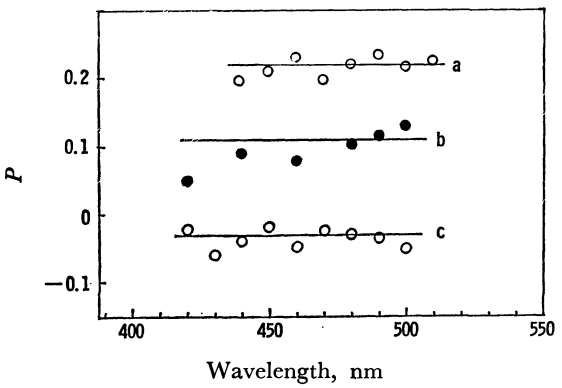

Fig. 7. Phosphorescence polarization of *p*-DCNB complexes; (a) *p*-DCNB-HMB, (b) *p*-DCNB-durene, and (c) *p*-DCNB-mesitylene.

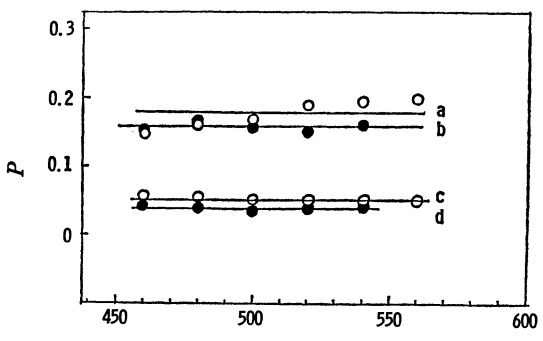

Fig. 8. Phosphorescence polarization of TCPA complexes; (a) TCPA-HMB, (b) TCPA-durene, (c) TCPA-mesitylene, and (d) TCPA-*p*-xylene.

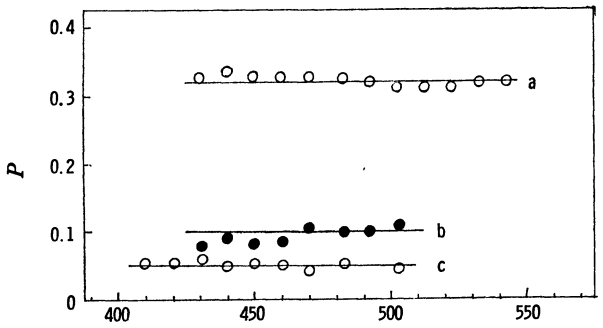

Fig. 9. Phosphorescence polarization of PA complexes; (a) PA-HMB, (b) PA-durene, and (c) PA-mesitylene.

respectively.

Table 1 summarizes and compares the polarization degrees of the charge-transfer phosphorescences of the complexes and the ionization potentials of the corresponding donor molecules.

Discussion

The experimental results described in the previous section are seemingly similar to those of the fluorescence polarization experiment with TCNE complexes with benzene, toluene, *p*-xylene, and *o*-xylene studied by Prochorow *et al.*[10] They interpreted the change in the polarization relative to the charge-transfer band by means of a model of a partially disoriented complex. According to this model, the P values would decrease with a decrease in the stability of a complex (with an increase in the amount of the disoriented forms). It seems inadequate to apply this model to the phosphorescence polarization, however, since the previous experimental and theoretical studies of TCNB-methyl-substituted benzene complexes show that the lowest triplet states differ considerably from each other in electronic structure, while the lowest charge-transfer singlet states of TCNE complexes, rather, resemble each other.[3]

The transition moment between the ground state, $|G\rangle$, and the lowest triplet state, $|T\rangle$, is roughly given by[11]:

$$\mu_{TG} = \frac{\langle T|H_{so}|S_k\rangle}{|E_T - E_{S_k}|}\mu_{S_kG}$$

where $|S_k\rangle$ represents the perturbing singlet state and where E_T and E_{sk} denote the energies of $|T\rangle$ and $|S_k\rangle$ respectively. No *a priori* information about the perturbing singlet state is available. The lowest

triplet state of the TCNB complex is approximately expressed as[3]:

$$|T\rangle = \alpha|^3CT\rangle + \beta|^3DA^*\rangle$$

where $|^3CT\rangle$ and $|^3DA^*\rangle$ represent the lowest charge-transfer triplet configuration and the lowest excited triplet configuration respectively, and where $|\alpha|^2+|\beta|^2=1$. For example, $|\alpha|^2$ equals 0.95 for the TCNB-HMB complex and $|\alpha|^2$ equals 0.07 for the TCNB-benzene complex.[3]

Let us extend this relation to such an extreme case as $|\alpha|^2=0$, so that the phosphorescence of an acceptor itself can be discussed along the same lines as that of its complex compound, since the position of the phosphorescence shifts towards shorter wavelengths as the donor changes from HMB to benzene, and since the phosphorescence spectrum of TCNB itself is located at a little higher energy than that of the TCNB-benzene complex. Therefore, it may be expected that the polarization of the phosphorescence derived from the locally-excited configuration is analogous to that of TCNB itself.

Along these lines, the polarization degree of the shortest wavelength band, presumably including the 0–0 band of the phosphorescence spectrum of TCNB relative to the first and second absorption bands, was measured; negative values were obtained for both bands. This indicates that the phosphorescence of TCNB is predominantly polarized perpendicular to the molecular plane. The transition borrows its intensity from the $(\sigma\pi^*)$ transition, as in the case of aromatic hydrocarbon.[11] It then follows that $|^3DA^*\rangle$ couples with $\pi\sigma^*$ or $\sigma\pi^*$ state of TCNB through spin-orbit interaction and that the transition between $|G\rangle$ and $|^3DA^*\rangle$ is polarized alomst normal to the molecular plane.

It is easily derived, as is illustrated schematically in Fig. 10, that $|^3CT\rangle$ couples with a higher charge-transfer transition from a π donor-orbital to a σ acceptor-orbital in a way similar to that in which $|^3DA^*\rangle$ couples with the $\pi\sigma^*$ transition in the acceptor as far as one-electron spin-orbit Hamiltonian is concerned. Such a higher charge-transfer transition should also be polarized along the direction connecting the donor with the acceptor nearly perpendicular to the molecular plane. If the other terms can be neglected, the polarization of the phosphorescence can be expressed as a linear combination of the polarizations of the locally-excited transition and the charge-transfer transition described above. It may, therefore, be safely concluded that the phosphorescence is polarized nearly perpendicular to the molecular plane, irrespective of the complex. The validity of this conclusion seems to be verified by the fact that the polarization degree of the TCNB-HMB complex, in which the contribution of $|^3CT\rangle$ to $|T\rangle$ is very large, is about 0.4 relative to excitation into the charge-transfer absorption band, which is polarized nearly normal to the molecular plane.

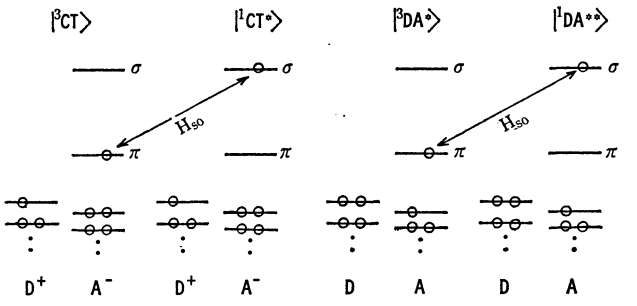

Fig. 10. Schematic diagram of one-electron spin-orbit interaction in donor-acceptor system.

It then follows that the experimental change in the values of the TCNB complexes can be determined not by the change in the phosphorescence polarization, but by the change in the transition moment of the charge-transfer absorption band. The wavefunctions of the TCNB complex in the ground and excited states are generally given by:[13]

$$\Psi_G = a^0\Phi_G + \sum b_i^0\Phi_i(D^+A^-) + \sum c_i^0\Phi_i(DA^*)$$
$$\Psi_E = a\Phi_G + \sum b_i\Phi_i(D^+A^-) + \sum c_i\Phi_i(DA^*)$$

where Ψ_G and Ψ_E represent the ground and excited state wavefunctions respectively. The transition moment is approximately expressed as:

$$\langle\Psi_G|\mu|\Psi_E\rangle \simeq \sum b_i^0 b_i\langle\Phi_i(D^+A^-)|\mu|\Phi_i(D^+A^-)\rangle + \sum (a^0c_i+c_i^0a)\langle\Phi_i(DA^*)|\mu|\Phi(DA)\rangle + \sum (a^0b_i+b_i^0a)\langle\Phi_i(D^+A^-)|\mu|\Phi(DA)\rangle.$$

In the case of TCNB complexes, $|a^0| \gg \sum|b_i^0|$, $\sum|c_i^0|$, and $|a| \ll 1$. For the sake of simplicity, we assume that $a^0=1$, $b_i^0=c_i^0=0$, and $a=0$ and that the lowest charge-transfer state mainly consists of the lowest charge-transfer singlet configuration, $\Phi(D^+A^-)$, and the lowest locally-excited singlet configuration, $\Phi(DA^*)$. The transition moment of the charge-transfer absorption band is approximately given by:

$$\mu_{S_1G} = a\mu_{CT} + b\mu_{DA^*} \quad (1)$$

where:

$$\mu_{CT} \equiv \langle\Phi(D^+A^-)|\mu|\phi(DA)\rangle$$
$$\mu_{DA}{}^* \equiv \langle\Phi(DA^*)|\mu|\Phi(DA\rangle$$
$$a \equiv b_1 \quad \text{and} \quad b \equiv c_1.$$

The polarization of μ_{CT} is nearly normal to the molecular plane, while that of μ_{DA^*} is parallel to it. As the donor changes from benzene to HMB, the charge-transfer singlet configuration increases its contribution and the in-plane character of the direction of the transition moment decreases, but the out-of-plane character increases. The above considerations may similarly be applied to the *o*-DCNB, *m*-DCNB, and *p*-DCNB com-

Table 2. Coefficients and contribution of charge-transfer character in the lowest charge-transfer singlet state of TCNB complexes calculated from degree of polarization.

Donor	*a*	*b*	CT(%)
HMB	0.94	0.35	88
Durene	0.89	0.46	79
Mesitylene	0.75	0.66	56
p-Xylene	0.72	0.70	52
Benzene	0.67	0.74	45

Table 3. Coefficient of charge-transfer singlet configuration in the lowest charge-transfer singlet state calculated from degree of polarization.

	TCNB	*o*-DCNB	*m*-DCNB	*p*-DCNB	TCPA	PA
HMB	0.94	0.85	0.80	0.77	0.74	0.85
Durene	0.89	0.71	0.69	0.68	0.72	0.67
Mesitylene	0.75	0.54	0.54	0.55	0.62	0.62
p-Xylene	0.72				0.62	
Benzene	0.67					

plexes and may also be applied to the TCPA and PA complexes.

The *a* and *b* coefficients can be estimated from Equation (1) using the *P* values. By the use of the values, $|\mu_{CT}| \approx 0.3$ Å and $|\mu_{DA^*}| \approx 0.3$ Å, obtained from the experimental values of the oscillator strengths, 0.02 and 0.03 respectively, and assuming that the transition moments, μ_{CT} and μ_{TG}, are polarized normal to the molecular plane and that the μ_{DA^*} moment is polarized in the molecular plane, one can make a rough estimation of the *a* and *b* coefficients and the charge-transfer character in the lowest charge-transfer singlet state of the TCNB complexes. Table 2 summarizes the results. It can be said that these results coincide considerably well with those reported by Iwata *et al.*[12] Table 3 shows the contributions of the charge-transfer character in the lowest charge-transfer singlet states of the complexes calculated under an assumption of the same values of the transition moments as those of the TCNB complexes and using the same assumptions described above.

The authors wish to express their deep gratitude to Dr. Yasuhiko Gondo and Dr. Nobuyuki Nishi for their helpful discussions.

References

1) S. Iwata, J. Tanaka, and S. Nagakura, *J. Chem. Phys.*, **47**, 2203 (1967).
2) H. Hayashi, S. Nagakura, and S. Iwata, *Mol. Phys.*, **13**, 489 (1967).
3) H. Hayashi, S. Iwata, and S. Nagakura, *J. Chem. Phys.*, **50**, 993 (1969).
4) H. Hayashi, Preprint Symp. Electronic Processes in Molecules, Fukuoka, Japan, 1969, p. 81.
5) T. Kobayashi and S. Nagakura, This Bulletin, **45**, 987 (1972).
6) N. Tsujino, H. Masuhara, and N. Mataga, *Chem. Phys. Letters*, **15**, 357 (1972).
7) Y. Murakami, R. Shimada, and Y. Kanda, "Molecular Luminescence," ed. by E. C. Lim, Benjamin, New York (1969), p. 119.
8) E. A. Lawton and D. D. McLitchie, *J. Org. Chem.*, **24**, 26 (1959).
9) T. Kuwata, "Yobai", Maruzen, Tokyo (1940).
10) J. Prochorow and A. Tramer, *J. Chem. Phys.*, **47**, 775 (1967).
11) For example, (a) S. P. McGlynn, T. Azumi, and M. Kinoshita, "Molecular Spectroscopy of The Triplet State", Prentice-Hall. Inc., N. J. (1969). (b) H. F. Hameka, "Advanced Quantum Chemistry", Addison-Wesley, Massachusetts (1965).
12) S. Iwata, J. Tanaka, and S. Nagakura, *J. Amer. Chem. Soc.*, **88**, 894 (1966).

A Study of Quenching of Triplets by Ferrocene

Masae KIKUCHI,* Koichi KIKUCHI,** and Hiroshi KOKUBUN**

**The Research Institute for Iron, Steel and other Metals, Tohoku University, Katahira, Sendai 980*

***Department of Chemistry, Faculty of Science, Tohoku University, Aoba, Aramaki, Sendai 980*

(Received September 11, 1973)

Rate constants for quenching of several triplets by ferrocene have been determined in ethanol. Most triplets have been found to be deactivated by ferrocene, yielding no observable transient absorption. The rate constant increases with increasing triplet energy in the range 8000—17000 cm^{-1}. The quenching mechanism has been discussed, the lowest triplet level of ferrocene being estimated to be 15000±1000 cm^{-1}.

It is well-known that ferrocene is an excellent quencher for many triplets of organic compounds.[1-3] Fry *et al.*[1] investigated the quenching of typical triplets by ferrocene and found that all triplets whose levels are located between 14000 and 23800 cm^{-1} are quenched by ferrocene at about a diffusion-controlled rate. However, they found no evidence for the formation of excited states of ferrocene, and could not account for the quenching mechanism.

Scott and Becker[4] observed an S→T absorption of ferrocene at 18940 cm^{-1} and a long-lived emission interpreted to be phosphorescence in EPA at 77 K, since the location corresponds to the band assigned to S→T absorption. Armstrong *et al.*[5] observed S→T absorption bands of ferrocene at 14000, 16500 and 18500 cm^{-1}, but no emission in EPA at 77 K. Smith and Meyer[6] observed phosphorescence at 20 K which has an emission peak at 21500 cm^{-1} in argon and at 20000 cm^{-1} in methane matrix. Information on the triplet of ferrocene is very conflicting and the lowest triplet level of ferrocene cannot be estimated exactly. However, it seems certain that the triplet level is higher than 14000 cm^{-1}.

All the triplet levels of the compounds studied by Fry *et al.* are higher than 14000 cm^{-1}. Thus a study of quenching by ferrocene for triplets having energy levels lower than 14000 cm^{-1} is expected to clarify, whether it is a triplet energy transfer or not. A triplet with energy level lower than 14000 cm^{-1} can not be quenched if the quenching is due to triplet energy transfer, but can be quenched if it is due to another mechanism. We have determined accurately the rate constants of quenching of several triplets whose levels are located between 8000 and 23800 cm^{-1}.

Experimental

Materials. Ferrocene (G. R. grade, Tokyo Kasei) was purified by recrystallization from benzene, zone refining twice, and sublimation twice. Pentacene and tetracene (G. R. grade, Tokyo Kasei) were used without further purification, but confirmed by measuring absorption and fluorescence spectra. Ethanol (G. R. grade, Wako Junyaku) was used without further purification. All other reagents were purified by standard methods.

Apparatus and Procedure. The flash energy was usually about 130 J, its half duration being about 10 μs. A Hoya-U2 or Toshiba V-051 filter was used for excitation. All measurements were made at room temperature. Ethanol solutions were degassed by repeating bulb to trap distillation in vacuum. Benzene solutions were degassed by freeze-pump-thaw method.

Results and Discussion

The dependence of decay curves of triplets upon the concentration of ferrocene has been studied. The observed first-order rate constants, k_{obs}, of perylene and anthracene are plotted against the ferrocene concentration in Fig. 1 as a typical example. From the plots the quenching rate constant k_q is obtained, since the observed first-order rate constant is given by

$$k_{obs} = k_t + k_q\,[\text{Ferrocene}] \qquad (1)$$

where k_t is the pseudo-first order rate constant of triplet deactivation in the absence of ferrocene.

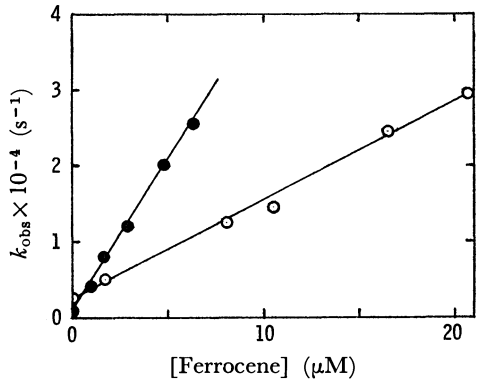

Fig. 1. The dependence of the decay rate of triplet upon the concentration of ferrocene.
○: Perylene, 8×10^{-5} M
●: Anthracene, 1×10^{-4} M

TABLE 1. RATE CONSTANTS FOR QUENCHING OF TRIPLETS BY FERROCENE AND ΔG-VALUES

Compound	Triplet level (cm^{-1})	Quenching rate constant ($M^{-1}s^{-1}$)	ΔG (kcal/mol)
Triphenylene	23800	$(6.5\pm0.5)\times10^9$	−6.2
Naphthalene	21300	$(7.0\pm1.5)\times10^9$	2.1
β-Acetonaphthone	20700	$(6.0\pm0.5)\times10^9$	
1,2,5,6-Dibenzanthracene	18300	$(5.0\pm1.0)\times10^9$	
Pyrene	16800	$(6.0\pm0.5)\times10^9$	5.5
Phenazine	15250	$(4.6\pm0.5)\times10^9$	
Eosine	14800	$(3.5\pm0.5)\times10^9$	
Anthracene	14700	$(3.5\pm0.5)\times10^9$	8.2
Perylene	12600	$(1.3\pm0.1)\times10^9$	7.1
Tetracene	10250	$(4.6\pm0.5)\times10^7$	10.8
Pentacene[a]	8000	$\ll10^7$	

a) In benzene.

The quenching rate constants in ethanol are summarized in Table 1. It is apparent that triplets having higher energy than 16000 cm^{-1} are quenched by ferrocene at about a diffusion-controlled rate* in accordance with the result of Fry *et al.*, but the quenching rate decreases with lowering triplet level between 8000 and 15000 cm^{-1}, and finally pentacene triplet, 8000 cm^{-1}, is scarcely quenched at all.

It is well-known that the rate of triplet energy transfer becomes slower owing to the reversible energy transfer when triplet levels of donor and acceptor are close to each other.[7-9] Sandros[8] studied the reversible energy transfer between biacetyl and many aromatic hydrocarbons, and found that the rate constant of energy transfer, k, is related to the difference of triplet levels of donor and acceptor, ΔE_T, as follows:

$$k = k_D \cdot \frac{1}{1+\exp(-\Delta E_T/RT)} \qquad (2)$$

where k_D is the diffusion-controlled rate constant, R is the gas constant and $\Delta E_T = E_T(\text{Donor}) - E_T(\text{Acceptor})$. Since $k \simeq k_D$ when $\Delta E_T \gg RT \simeq 200$ cm^{-1}, $k = \frac{1}{2} k_D$ when $\Delta E_T = 0$ cm^{-1}, and $k < k_D/140$ when $\Delta E_T < -1000$ cm^{-1}, the rate constant of the energy transfer decreases about two orders of magnitude as compared with the diffusion-controlled rate constant when the triplet level of acceptor (quencher) is higher than that of donor by 1000 cm^{-1}. Irrespective of the triplet level of ferrocene, it is obvious that the dependence of the quenching rate constant on the triplet level (Table 1) is too small as compared with the case of the energy transfer. Thus the results cannot be explained by energy transfer only.

It has been reported that the triplet level of ferrocene is higher than 14000 cm^{-1}, but it is necessary i) to confirm by kinetic study that triplet of tetracene is quenched not by energy transfer but by another mechanism, and ii) to clarify the reason why no transient absorption of ferrocene can be observed. We carried out the kinetic study of i) by examining the data given in Table 1. Assuming that tetracene triplet is quenched by energy transfer from tetracene triplet to ferrocene, we can calculate the triplet level of ferrocene by Eq. (2). From the values $k_D = 6 \times 10^9$ M^{-1} s^{-1} and $k = 4.6 \times 10^7$ M^{-1} s^{-1}, $\Delta E_T = E_T(\text{tetracene}) - E_T(\text{ferrocene}) = -990$ cm^{-1} was obtained. Thus the triplet level of ferrocene is estimated to be 11240 cm^{-1}. If this is the case, all the triplets having levels higher than about 12000 cm^{-1} should be quenched by ferrocene at the diffusion-controlled rate. However, this is inconsistent with the results (Table 1). Thus we could conclude that the quenching of tetracene triplet is not due to energy transfer, and that the triplet level of ferrocene is higher than 12000 cm^{-1}, which is in line with earlier reports.[4-6] For ii) we carried out an energy transfer experiment for a mixed system of eosin (D), tetracene (A) and ferrocene (F), in which eosin is at first irradiated selectively by a flash, the triplet eosin acting as an energy donor. The reaction scheme is described as follows.

* Most published rate constants for triplet quenching are about 5×10^9 M^{-1} s^{-1}.

$$(0)\quad D \xrightarrow{\phi_{ST} I_{ab}} {}^3D$$
$$(1)\quad {}^3D \longrightarrow D$$
$$(2)\quad {}^3D + F \longrightarrow D + {}^3F$$
$$(3)\quad {}^3D + A \longrightarrow D + {}^3A$$
$$(4)\quad {}^3F + A \longrightarrow F + {}^3A$$
$$(5)\quad {}^3F \longrightarrow F$$
$$(6)\quad {}^3A \longrightarrow A$$
$$(7)\quad {}^3A + F \longrightarrow A + {}^3F$$

If the rate of deactivation of tetracene triplet is negligibly small in comparison with that of other triplets, the concentration of tetracene triplet immediately after flashing is given by

$$[{}^3A]_0 = \frac{1}{k_1 + k_2[F] + k_3[A]} \cdot \left(k_3[A] + \frac{k_4[A]}{k_4[A] + k_5} \cdot k_2[F] \right) \cdot \phi_{ST} I_{ab} . \qquad (3)$$

When $[F] = 0$, we have

$$[{}^3A]_0^0 = \frac{k_3[A]}{k_1 + k_3[A]} \cdot \phi_{ST} I_{ab} . \qquad (4)$$

From Eqs. (3) and (4) we get

$$\frac{[{}^3A]_0^0}{[{}^3A]_0} = 1 + \frac{k_2[F]}{k_1 + k_3[A]} - \frac{[{}^3A]_0^0}{[{}^3A]_0} \cdot \frac{k_4[A]}{k_4[A] + k_5} \cdot \frac{k_2[F]}{k_3[A]} \qquad (5)$$

Figure 2 shows the plot of $[{}^3A]_0^0/[{}^3A]_0$ *vs.* [F] for $[D] = 6.3 \times 10^{-6}$ M and $[A] = 5.0 \times 10^{-5}$ M. A straight line was obtained. This implies that the third term of the right-hand side of Eq. (5) is negligibly small as compared with the first and the second terms. Thus, $k_5 \gg k_4$ [A] or $k_4 \approx 0$. But it is obvious that $k_5 \gg k_4[A]$, because $k_4 \approx 0$ is very unlikely. Eq. (5) can thus be written as

$$\frac{[{}^3A]_0^0}{[{}^3A]_0} = 1 + \frac{k_2[F]}{k_1 + k_3[A]}, \qquad (6)$$

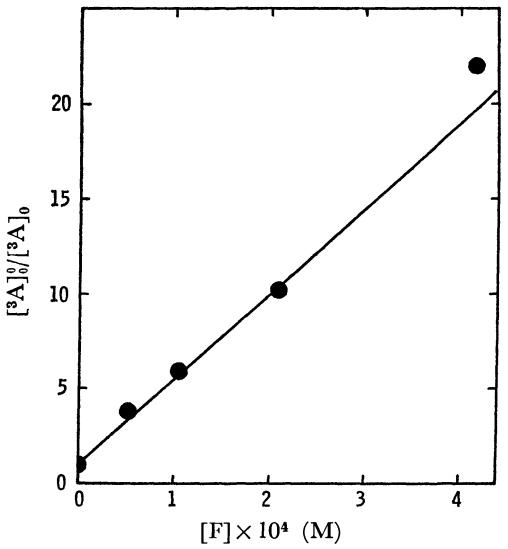

Fig. 2. The plot of $[{}^3A]_0^0/[{}^3A]_0$ *vs.* [F].
Straight line was calculated according to Eq. (6) by using independent data.

where $[A]=5.0\times10^{-5}$ M**. The slope, $k_2/(k_1+k_3[A])$, agrees with the calculated value using $k_1=1.0\times10^3$ s^{-1}, $k_2=3.5\times10^9$ M^{-1} s^{-1}, and $k_3=1.5\times10^9$ M^{-1} s^{-1}, which have been obtained by other independent flash experiments. $k_5\gg k_4[A]$ implies that the energy transfer from ferrocene triplet to tetracene is inefficient. This is attributable to the fast deactivation of ferrocene triplet, because $k_5\gg10^5$ s^{-1} if k_4 is of the order of the diffusion-controlled rate constant. This is consistent with the fact that no transient absorption owing to ferrocene has been observed by the conventional flash technique.

The triplet level of ferrocene can be estimated as 15000 ± 1000 cm^{-1} by the following considerations; 1) it has been reported that the triplet level of ferrocene is higher than 14000 cm^{-1}, 2) all triplets having a level higher than 16000 cm^{-1} are quenched with the diffusion-controlled rate, 3) the quenching rates of anthracene and eosin triplet are nearly one-half of the diffusion-controlled rate, 4) the quenching of tetracene triplet by energy transfer to ferrocene is highly improbable, 5) the rate constant of energy transfer decreases by about two orders of magnitude as compared with the diffusion-controlled rate constant when the triplet level of acceptor is higher than that of donor by 1000 cm^{-1}, and is practically the diffusion-controlled rate constant when the triplet level of donor is higher than that of acceptor by 500 cm^{-1}, 6) the reversible energy transfer is very inefficient because the lifetime of ferrocene triplet may be very short,7) as the rate of energy transfer depends on ΔE_T predominantly and other factors, it would be suitable to estimate the error as ±1000 cm^{-1}.

Rosenblum *et al.*[10] have reported that ferrocene forms a charge transfer complex with tetracyanoethylene owing to low ionization potential of ferrocene. The quenching of fluorescence due to charge transfer interaction between fluorescer and quencher is widely known.[11] Thus it is necessary to examine the possibility of triplet quenching by charge-transfer interaction, although quenching of triplet by charge transfer interaction has scarcely been reported at all. The changes of free enthalpy (ΔG) involved in the electron transfer reactions[11] are calculated approximately and listed in Table 1. It seems that a qualitative correlation between the rate constant and ΔG is satisfactory. This strongly suggests that charge transfer interaction is involved in the quenching.

If the triplet quenching by ferrocene is exclusively attributed to the electron transfer reaction, detection of anion originating in the triplet might be expected. However, no additional transient absorption was observed by the addition of ferrocene. Triphenylene which is most expected to produce anion was also examined in acetonitorile, but no additional transient absorption was observed. If the quenching is due to the charge transfer interaction, it seems most likely that the lifetime of charge transfer complex is extremely short.

Porter and Wright[12] studied the quenching action of various metal ions to naphthalene triplet in water and in ethylene glycol, and found that paramagnetic metal ions of first transition series deactivate the triplet at the rate constant, $k_q\approx5\times10^7$ M^{-1} s^{-1}. As the rate constant of quenching for tetracene triplet is 4.6×10^7 M^{-1} s^{-1}, the quenching ability of ferrocene for tetracene triplet is similar to that of Fe^{2+} and Fe^{3+}. However, pentacene triplet has not been quenched by ferrocene in benzene, and paramagnetic quenching cannot be considered, since ferrocene is diamagnetic. It thus seems that the iron atom in ferrocene does not contribute directly to the quenching.

If several compounds with triplet levels between 8000 and 15000 cm^{-1} are contained simultaneously in ferrocene as impurities, the results might be interpreted as those given in Table 1. But quenching by such impurities is improbable since no emissoin due to impurities has been observed in concentrated solution of ferrocene. The result in Fig. 2 denies the existence of such impurities.

Consequently, it seems that the quenching of triplet by ferrocene might occur according to the following mechanisms. As the triplet level of ferrocene has been estimated as 15000 ± 1000 cm^{-1}, a triplet with a level higher than 15000 cm^{-1} would be quenched mainly by the energy transfer, but a triplet with a level lower than 13000 cm^{-1} would be quenched by another mechanism. The most probable mechanism would be the instantaneous formation of charge transfer complex with an extremely short lifetime.

The authors wish to express their thanks to Professor Masao Honma for his kind guidance and encouragement in the course of the work. H. K. and K. K. wish to thank the Mitsubishi Foundation for financial support.

** Eq. (6) is also satisfied when $k_4[A]+k_5\ll k_6+k_7[F]$, where $[A]=5\times10^{-5}$ M, $k_6=1.2\times10^3$ s^{-1} and $k_7=4.6\times10^7$ M^{-1} s^{-1}. However, this assumption is improbable, since the triplet level of ferrocene is higher than that of tetracene.

References

1) A. J. Fry, R. S. H. Liu, and G. S. Hammond, *J. Amer. Chem. Soc.*, **88**, 4781 (1966).
2) M. L. Bhaumik and M. A. El-Sayed, *J. Phys. Chem.*, **69**, 275 (1965).
3) R. B. Cundall, G. B. Evans, and E. J. Land, *ibid.*, **73**, 3982 (1969).
4) D. R. Scott and R. S. Becker, *J. Amer. Chem. Soc.*, **35**, 516 (1961).
5) A. T. Armstrong, F. Smith, E. Elder, and S. P. McGlynn, *J. Chem. Phys.*, **46**, 4321 (1967).
6) J. J. Smith and B. Meyer, *ibid.*, **48**, 5436 (1968).
7) H. L. J. Bäckström and K. Sandros, *Acta Chem. Scand.*, **16**, 958 (1962).
8) K. Sandros, *ibid.*, **18**, 2355 (1964).
9) K. Kikuchi, H. Kokubun, and M. Koizumi, This Bulletin, **43**, 2732 (1970).
10) M. Rosenblum, R. W. Fish, and C. Bennett, *J. Amer. Chem. Soc.*, **86**, 5166 (1964).
11) D. Rehm and A. Weller, *Ber. Bunsenges. Physik. Chem.*, **73**, 834 (1969).
12) G. Porter and M. R. Wright, *Discuss. Faraday Soc.*, **27**, 18 (1957).

Medium Effects for Single Ions in Dimethyl Sulfoxide, *N,N'*-Dimethylformamide, and Propylene Carbonate

Niro MATSUURA and Kisaburo UMEMOTO

Department of Pure and Applied Sciences, College of General Education, The University of Tokyo, Komaba, Meguro-ku, Tokyo 153

(Received September 27, 1973)

The solubility products of thallium halides were measured in dimethyl sulfoxide, *N,N'*-Dimethylformamide, and propylene carbonate for the purpose of obtaining the values of the medium effect for these electrolytes on transfer from water to these solvents. The medium effects for cations were estimated from the standard potentials of metal/ion couples obtained by the method of the corrected rubidium scale. The medium effects for halide ions were calculated from the medium effects for thallium halides and the thallium ion. A comparison of extrathermodynamic assumptions was made for the values of the medium effect for the silver ion as estimated by various methods; the method of the corrected rubidium scale was found to give a reasonable result.

The significance of the medium effect in non-aqueous solution chemistry and the current status of the extrathermodynamic assumptions needed to estimate the medium effect for single ion have been reviewed in several recent, stimulating works.[1-8]

The medium effect, $\log {}_m\gamma$, is defined as a measure of the difference between the free energy of a solute, i, in its aqueous (${}_wG_i^\circ$) and non-aqueous (${}_sG_i^\circ$) standard states:

$$ {}_sG_i^\circ - {}_wG_i^\circ = RT \ln {}_m\gamma_i \quad (1) $$

For the 1 : 1 electrolyte:

$$ \ln {}_m\gamma_i = \ln {}_m\gamma_\pm{}^2 = \ln {}_m\gamma_+ + \ln {}_m\gamma_- \quad (2) $$

where ${}_m\gamma_+$, ${}_m\gamma_-$, and ${}_m\gamma_i$ are the medium effects for the cation, the ainon, and the electrolyte respectively. Therefore, the solubility products of the AB salt in the solvent, S, K_s^s, are related to the solubility product in water, K_s^w, through:

$$ K_s^w = K_s^s({}_m\gamma_+)({}_m\gamma_-) \quad (3) $$

Expressions like Eq. (3) relate the constants for a variety of equilibria in a solvent, S, to the equilibrium constants in water. A knowledge of the medium effect for any one ion would render accessible such knowledge for all other ions in the same solvent on the basis of the thermodynamic data for the complete electrolytes. The knowledge of the medium effects for single ions enables us to express any ionic activity and electromotive force series on a single scale, referred to the aqueous standard state.

The medium effects for single ions can not be determined exactly by rigorous thermodynamic methods. In spite of the limitations imposed by extract thermodynamics, though, many investigators have estimated at least approximate values for the medium effect for single ions with the aid of extrathermodynamic assumptions. One of the methods used is based on the "normalized potential scale" method originated by Pleskov.[9] In this method, the standard potential of the rubidium electrode is assumed to be a solvent-independent reference point for a universal series of standard electrode potentials(Rubidium Scale). Pleskov's method of the rubidium scale has been proved by estimating the change in the solvation energy of the rubidium ion with the solvent by the application of a modified Born equation(Corrected Rubidium Scale).[6,10,11] Other than the rubidium-rubidium ion, ferrocene-ferricinium[12] and iron(II-III) complexes of *o*-phenanthlorine[13] have been proposed as reference redox couples. Another way of estimating the medium effect is the "reference electrolyte" method.[1-5] This method is based on the assumption that the medium effect for an ideal reference electrolyte—composed of very large symmetrical ions as similar in size and structure as possible—can be divided equally between the anion and the cation. The number of proposed extrathermodynamic solutions has multiplied, and some discrepancies have been observed among the results obtained by various methods.

The objective of the present paper is, first, to estimate the medium effects for alkali metal, thallium, silver, halide, and perchlorate ions in dimethyl sulfoxide (DMSO), *N,N'*-Dimethylformamide(DMF), and propylene carbonate(PC) on the basis of the normalized potential scale which was previously determined on the assumption of the corrected rubidium scale method.[11] Then, the medium effects for the silver ion obtained in this work were compared with those estimated by other various extrathermodynamic methods in order to verify the applicability of the method of the corrected rubidium scale.

Experimental

Solvents and Electrolytes. The purification of solvents, the preparation and purification of tetraethylammonium iodide(TEAI) and thallium perchlorate, and the preparation of the thallium amalgam electrode have been described elsewhere.[11,14] The tetraethylammonium chloride(TEACl) and tetraethylammonium bromide(TEABr) were obtained commercially and were purified by recrystallization from an ethyl alcohol-ethyl acetate mixture. The electrolytes were dried in a vacuum oven for several tens of hours at 60—70 °C.

Procedure. The solubilities of thallium halides in DMF and PC were determined by potentiometric titration. A 0.002 M solution of thallium perchlorate was titrated with a 0.01 M solution of tetraethylammonium halide(TEAX). The indicator electrode was the thallium amalgam electrode, and the reference electrode was an aqueous saturated calomel electrode(SCE) equipped with a non-aqueous salt bridge.[11] Nitrogen gas was bubbled through the solution before and during the run of the titration. The potential of the cell was measured by means of Yokogawa Hewlett-Paccard Model 2727 potentiometer. The temperature was kept at 25±0.05 °C.

Table 1. Solubility products K_s ($mol^2 l^{-2}$) of thallium halides at 25 °C[a)]

	DMSO			DMF			PC		
	solubility $\times 10^3$	$f_\pm$	$K_s \times 10^6$	solubility $\times 10^5$	$f_\pm$	$K_s \times 10^9$	solubility $\times 10^6$	$f_\pm$	$K_s \times 10^{12}$
TlCl	1.99	0.89	3.16	5.25	0.97	2.62	2.24	1.00	5.01
TlBr	2.74	0.88	5.78	8.91	0.97	7.37	3.31	1.00	11.0
TlI	5.32	0.84	19.8	31.6	0.93	87.1	12.0	1.00	144.0

a) Solubilities are in mol l^{-1}. $f_\pm$ is salt activity coefficient. The values of solubility in DMF and PC were determined by potentiometric titration and those values in DMSO by polarographic amperometry.

The solubility of thallium halides in DMSO were rather high, and they could not be determined accurately by potentiometric titration. They were, however, determined by polarographic amperometry. The thallium halides were shaken with DMSO for twenty hours at 30 °C and then for ten hours at 25 °C. Pure DMSO and 0.1 M of tetraethylammonium perchlorate were added to the DMSO solution saturated with thallium halide, and then the polarogram was recorded. The concentration of thallium halide was determined from the magnitude of the diffusion current by using a predetermined calibration curve. The solubilities of thallium halides in DMF were also determined by polarographic amperometry in order to obtain auxiliary data.

Results and Discussion

The Determination of the Solubility Products of Thallium Halides. The potentiometric measurements for thallium salt were made with the following cell:

$$\text{aqueous SCE} \left| \begin{matrix}\text{salt}\\ \text{bridge}\end{matrix} \right| \text{TlClO}_4 \quad 0.002\,\text{M} \left| \text{Tl(Hg)} \right. \quad \text{(A)}$$

For the thallium amalgam electrode, it was found that the Nernst equation was nearly obeyed in all the solvents containing thallium perchlorate in the concentration range from 1×10^{-4} to 2×10^{-3} M as is shown in Fig. 1.

The titrations of thallium perchlorate with tetraethylammonium halides were carried out in the right-hand-half cell of Cell A. The titration curve shown in Fig. 2 is typical of the curves when 0.002 M $TlClO_4$ was titrated with 0.01 M TEAX in PC and DMF at 25 °C. In all the titration curves, we found one well-defined end point of titration corresponding to this rection:

$$Tl^+ + X^- = TlX\downarrow \qquad (4)$$

The precipitation of TlX appeared soon after the titration started. The solubilities of TlX were calculated from the titration curves by using the Nernst equation; the results are given in Table 1. No further complex formation of the thallium ion with the halide ion was observed in these solvents, even in the presence of an excess concentration of the halide ion. In the presence of an excess concentration of the halide ion, the potential of the thallium amalgam electrode was found to be very stable. This electrode would be useful as a reference electrode of the second kind for electromotive force measurements in these solvents.

For the calculation of the solubility products of thallium halides, the complete dissociation of the salts was assumed, since the association between the perchlorate anion and metal ions has been found to be negligibly small in these solvents at the concentrations below 10^{-2} M.[15] The salt activity coefficient, f, was calculated by means of the Debye-Hückel equation:

$$\log f_\pm = -\frac{A\sqrt{\mu}}{1+Ba\sqrt{\mu}} \qquad (5)$$

where A and B are constants and were calculated to

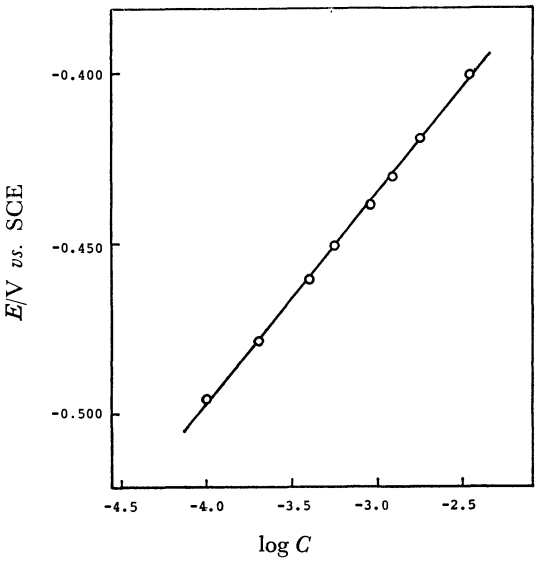

Fig. 1. Relation between the potential of the thallium amalgam electrode and the concentration of thallium perchlorate in PC at 25 °C.

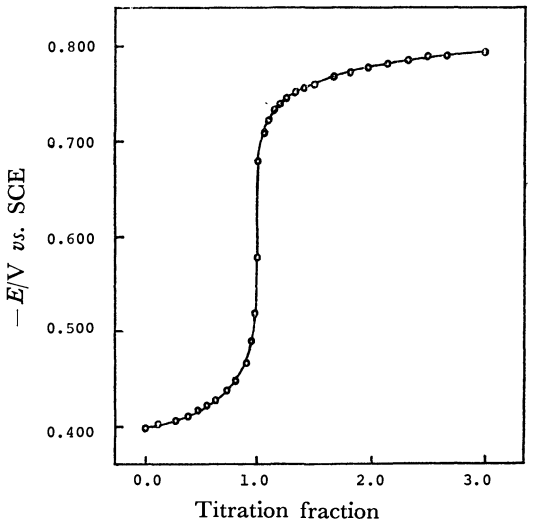

Fig. 2. The titration curve of 0.002 M $TlClO_4$ with 0.01 M TEACl in PC at 25 °C.

Table 2. Solubility products pK_s (molality) and medium effects for electrolytes

	DMSO		DMF		PC		Water
	pK_s	ΔpK_s[a]	pK_s	ΔpK_s[a]	pK_s	ΔpK_s[a]	pK_s
TlCl	5.58	1.82	8.53	4.77	11.45	7.69	3.76[b]
TlBr	5.32	−0.15	8.08	2.61	11.11	5.64	3.62[b]
TlI	4.78	−2.41	7.01	−0.18	9.99	2.80	7.19[b]
$KClO_4$	−0.72[c]	−2.38	0.05[d]	−1.61	e)		1.7[d]

a) $\Delta pK_s = pK_s^s - pK_s^w$. b) Ref. 6. c) R. Alexander, E. C. F. Ko, Y. C. Mac, and A. J. Parker, *J. Amer. Chem. Soc.*, **89**, 3703 (1967). Correction for solvent molality was made. d) Ref. 4. Correction for solvent molality was made. e) not determined.

be respectively, 1.18 and 0.435 for DMSO, 1.73 and 0.493 for DMF, and 0.717 and 0.368 for PC by using the dielectric constants of these solvents. The ion-size parameter, *a*, has been determined to be 3.6 for DMSO, 5.0 for DMF, and 0.0 for PC.[14] The activity coefficients and solubility products of thallium halides are given in Table 1.

The solubility products of TlX in DMF as determined by polarographic amperometry were different by 10 per cent from the solubility products as determined by potentiometric titration. Accordingly, the values given in Table 1 must involve an uncertainty of this order.

In Table 2, the solubility products of thallium halides, pK_s, are listed in the molality scale, along with those of potassium perchlorate available in the literature. To convert from molar to molal pK_s, the solvent density of these solvents was used.

The medium effects for thallium halides, $\log {}_m\gamma_{TlX}$ were calculated by means of the following equation:

$$\log {}_m\gamma_{TlX} = \Delta pK_s = pK_s^s - pK_s^w \quad (6)$$

The results are listed in Table 2. Equation (6) is strictly valid only when no crystal solvates are formed. We assumed an absence of solvates in all these solvent-solute combinations.

Estimation of the Medium Effects for Single Ions. The medium effects for alkali metal, thallium, and silver ions were calculated from the difference between the standard potentials of the metal electrode in an aqueous solution, $E_w°$, and in a non-aqueous solution, $E_s°$, estimated on the basis of the corrected rubidium scale:[14]

$$\log {}_m\gamma_{M^+} = (E_s° - E_w°)/0.05916 \quad (7)$$

The medium effects for halide ions were calculated from:

$$\log {}_m\gamma_{X^-} = \log {}_m\gamma_{TlX} - \log {}_m\gamma_{Tl^+} \quad (8)$$

where, X=Cl, Br, I. The medium effect for perchlorate was calculated from $\log {}_m\gamma_{KClO_4}$ and $\log {}_m\gamma_{K^+}$ in the same manner. The medium effects for individual ions thus estimated are summarized in Table 3. A positive value of a medium effect means a lower solvation energy (tighter solvation) in water than in other solvents. This is the case for most small anions. The solvation of halide ions depends on strong hydrogen bonding, which is available in water but not in DMSO, DMF, and PC. The tighter solvation of cations in DMSO and DMF is characterized by the solvent structure, especially by the strong Lewis basicity of these solvents. PC is a weaker Lewis base; accordingly, the cationic solvation of PC is weaker than that of water.

Table 3. Medium effects for single ions (Molality scale). Reference solvent is water

	DMSO	DMF	PC
Li^+	−1.49	−0.24	+5.53
Na^+	−1.10	+0.05	+3.82
K^+	−1.20	−0.37	+2.15
Rb^+	−0.58	+0.08	+2.52
Cs^+	−0.61	−0.08	+2.42
Tl^+	−3.16	−1.74	+2.53
Ag^+	−5.11	−2.30	+3.77
Cl^-	+4.98	+6.51	+5.36
Br^-	+3.01	+4.35	+3.31
I^-	+0.75	+1.56	+0.47
ClO_4^-	−1.18	−1.24	a)

a) not determined.

A Comparison of Extrathermodynamic Assumptions. It will now be interesting to compare the values of the medium effect for the single ions estimated in this work with those values estimated on the basis of other extrathermodynamic assumptions. For this purpose, the medium effect for the silver ion was examined, since, among the ions studied in this work, the silver ion has been studied most extensively by various methods.

In Fig. 3 we have plotted the medium effects for the silver ion in DMSO, DMF, PC, and acetonitrile (ACN). The classification of Assumptions 1–5 and the values of the medium effect estimated by these assumptions were taken from Ref. 3. The values from the rubidium scale method are denoted by R, and those from the corrected rubidium scale method, by B.

Each individual assumption has its own inherent limitations.[1] Assumption 1, which equates the medium effect for the tetraphenylarsonium cation with that for the tetraphenylboride anion, $\log {}_m\gamma_{Ph_4As^+} = \log {}_m\gamma_{Ph_4B^-}$, involves difficulty in dividing the medium effect for the reference electrolyte equally among the component cation and anion; moreover, the accuracy of the determined solubility products of the reference electrolyte is not sufficient. In Assumptions 2 and 3, the electrostatic interaction of solvent with very large anions, which were formed in the transition states for the S_N2 or S_NAr reaction, is assumed to be unchanged, $\log {}_m\gamma_{ArF} = \log {}_m\gamma_{ArN_3F^-}$ or $\log {}_m\gamma_{CH_3I} = \log$

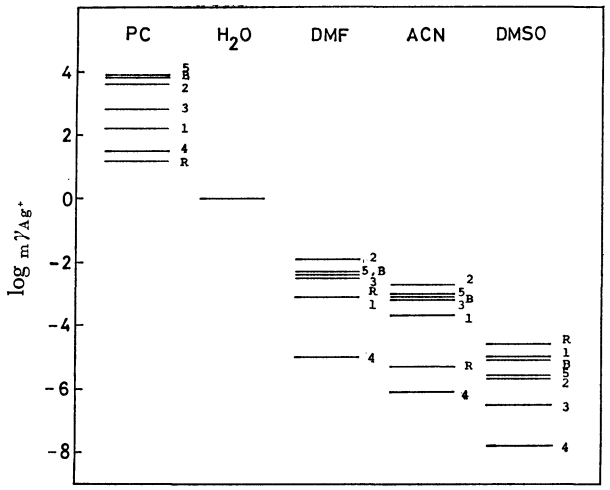

Fig. 3. A comparison of extrathermodynamic assumptions, leading to the medium effect for silver ion for transfer from water to other solvents at 25 °C. The assumptions are (1) $\log {}_m\gamma_{Ph_4As^+} = \log {}_m\gamma_{Ph_4B^-}$; (2) $\log {}_m\gamma_{ArF} = \log {}_m\gamma_{ArN_3F^-*}$; (3) $\log {}_m\gamma_{CH_3I} = \log {}_m\gamma_{NCSCH_3I^-*}$; (4) $\log {}_m\gamma_{Fe(C_5H_5)_2} = \log {}_m\gamma_{Fe(C_5H_5)_2^+}$; (5) Negligible liquid junction potential; (B) Corrected rubidium scale; (R) Rubidium scale.

${}_m\gamma_{NCSCH_3I^-*}$, but the large anions have a large polarizability and the electrostatic interaction of these anions with solvents must be affected by the solvent polarity. Assumption 4 equates the medium effect for ferrocene with that for the ferricinium cation, $\log {}_m\gamma_{Fe(C_5H_5)_2} = \log {}_m\gamma_{Fe(C_5H_5)_2^+}$. This assumption must be criticized in view of the large increase in the solubility of ferrocene on transfer from water to organic solvents, which would result in a serious change in the medium effect for ferrocene. Moreover, the electrostatic interaction of the ferricinium ion with solvent must be affected by the solvent polarity. Assumption 5 neglects the liquid junction potential in a cell composed of silver wire in a silver perchlorate solution connected by a proper non-aqueous salt bridge of tetraethylammonium picrate: the liquid junction potential of the aqueous and non-aqueous interface would not be completely eliminated. Assumption R neglects the change in the electrostatic interaction of the rubidium ion with solvents of different dielectric properties. Assumption B simplifies too much the change in the solvation energy of the rubidium ion with solvents mainly electrostatic in nature.

At this time we have no reason to defend any one assumption with confidence. However, it seems reasonable to support assumptions which give focusing values for the medium effect.

As is shown in Fig. 3, the internal coherency of the values of the medium effect as estimated by individual assumptions for different solvents is excellent except for the method of the rubidium scale; the magnitudes of the medium effect for the silver ion estimated by individual assumptions lie in this order; PC>H_2O>DMF>ACN>DMSO; only the values of the medium effect estimated by the method of the rubidium scale for DMSO and ACN are in an inverse order. Accordingly, the method of the rubidium scale is considered to be unfavourable as a universally-applicable method for these solvents. In this connection, the limitation of the assumption of rubidium scale must be overcome by the method of the corrected rubidium scale. Most values of the medium effect for the silver ion lie in ranges between 3 and 4 in PC, −2 and −3 in DMF, −3 and −4 in ACN, −5 and −6 in DMSO. The values of the medium effect for the silver ion, as estimated by the method of the corrected rubidium scale, lie in these ranges for all the solvents. Accordingly, it would be reasonable to say that the method of the corrected rubidium scale is one of the most reliable methods of estimating the medium effect for single ions.

It is quite interesting that the assumption of the negligible liquid junction potential seems reasonable, since the values of the medium effect estimated by this assumption lie in the focusing ranges. The method of the negligible liquid junction potential determines directly, unlike the other extrathermodynamic assumptions, the medium effect for the ion from the electrode potential measured against a silver-silver perchlorate electrode in the reference solvent. The practical procedure is very easy to comprehend.[3] Therefore, this method would throw light on the urgent problem in the non-aqueous electrochemistry of normalizing the potential of a given redox system directly to the water scale by measuring the cell potential.

The authors wish to express their thanks to Mr. Zen'ichi Takeuchi for his cooperation in the experimental work.

References

1) O. Popovych, *Crit. Rev. Anal. Chem.*, **1**, 73 (1970).
2) D. H. Bern and O. Popovych, *Anal. Chem.*, **44**, 817 (1972).
3) R. Alexander, A. J. Parker, J. H. Sharp, and W. E. Waghorne, *J. Amer. Chem. Soc.*, **94**, 1148 (1972).
4) A. J. Parker and R. Alexander, *ibid.*, **90**, 3313 (1968).
5) E. Grundwald, G. Baugham, and G. Kohnstam, *ibid.*, **82**, 5801 (1960).
6) J. F. Coetzee and J. J. Champion, *ibid.*, **89**, 2513, 2517 (1967).
7) R. G. Bates, "The Chemistry of Non-Aqueous Solvents," ed. by J. J. Lagowski, Academic Press, New York and London (1966), Chap. 3.
8) H. Strehlow, *ibid.*, Chap. 4.
9) V. A. Pleskov, *Usp. Khim.*, **16**, 254 (1947).
10) J. F. Coetzee, J. M. Simon, and R. J. Bertozzi, *Anal. Chem.*, **41**, 766 (1969).
11) N. Matsuura, K. Umemoto, M. Waki, Z. Takeuchi, and M. Omoto, This Bulletin, **47**, 806 (1974).
12) H. M. Koepp, H. Wendt, and H. Strehlow, *Z. Elektrochem.*, **64**, 483 (1960).
13) I. M. Kolthoff and F. G. Thomas, *J. Phys. Chem.*, **69**, 3049 (1965).
14) N. Matsuura, K. Umemoto, and Z. Takeuchi, This Bulletin, **47**, 813 (1974).
15) N. Matsuura, K. Umemoto, and Y. Takeda, to be published.

Solvent Effects on the Formation of Aromatic Hydrocarbon Ions and Mo^{5+} on the Surface of Al_2O_3–MoO_3

Hisashi UEDA

National Chemical Laboratory for Industry, 2-19-19 Mita, Meguro-ku, Tokyo 153

(Received October 3, 1973)

The formation of two aromatic hydrocarbon ions on the surface of Al_2O_3–MoO_3 has already been postulated. The concentrations of these paramagnetic species were measured for various solvents by using DPPH single crystals as the reference standard. The formation of two different aromatic ions on the surface of Al_2O_3–MoO_3 could also be confirmed by the solvent dependence. The intensity of microwave magnetic field H_1 and the modulation width were considered in this measurement. Without solvent molecules such as benzene on the oxide surface, an ESR signal without cation hyperfine structure was almost exclusively observed. The intensities and intensity ratio between the two components of the ESR absorption at $g=2.00$, with and without hyperfine structure, change with solvent. The results indicated that solvent molecules, when adsorbed on the oxide surface, form a surface structure or a surface system which makes the charge transfer from the oxide surface to the solute hydrocarbon easier.

The electron spin resonance (ESR) method is used in studies of catalysis for various purposes, being (1) to know the orbital function of the unpaired electron spin or the crystal field in the bulk or on the surface of solid catalysts,[1] and (2) to detect the reaction intermediates (molecular or atomic) in a stable or in a semi-stable state.[2] As another application, the interaction among the system components can also be analysed if the mixture (catalyst, reaction-substrate, reaction-intermediates, reaction products, and reaction-byproducts) is considered as a reaction system consisting of these system components.[3] If such a system is treated as a reaction system, some additive added to the system, or the solvent used to dissolve the substrate should also be treated as a system component. For this reason, a study of solvent effects on the formation of the paramagnetic species is expected to clarify some facts important for the study of catalysis. In order to see some of the dynamic aspects of the system, quantitative measurements and processings of the concentrations of the system components are necessary. As intermediates paramagnetic species were chosen and quantitative ESR method was used to find the solvent effects on the perylene– (or anthracene)–Al_2O_3–MoO_3 system.

Experimental

Quantitative ESR Measurement. Quantitative ESR measurements normally employ several reference standards with which comparisons are made between these references and the samples to be measured.[4] If DPPH is used as a reference, it is diluted in the form of a solution or a solid mixture to obtain the unpaired electron concentration almost equal to that of the sample.[5] However, decomposition of DPPH during the course of dilution or storage is inevitable and an accurate and consistent measurement is not easy. Thus a single crystal of DPPH has been used as a reference. The maximum measurable number of unpaired electron spins obtained with the ESR instrument used, a JES-3BX, under the usual adjustment conditions of detector and amplifier, changes with input microwave power and modulation width. At 10 μW and 2.0 G modulation width at 100 kHz, 2×10^{19} unpaired electron spin gives a final first derivative output voltage of 10 mV on the recording device. A 10 mg single crystal contains 1.5216×10^{19} molecules and if weighed by a microbalance, 10.00 mg is obtained as effective figures. The number of unpaired electron spins contained in a (10.00 ± 0.005) mg crystal is $(1.5216\pm0.0008)\times10^{19}$ or 1.521×10^{19}.

The dependence of the ESR signal on the input microwave power should also be considered.[6] The magnitude of the microwave magnetic field H_1 is determined by the incident power to the resonant cavity, P, and the "Q" of the cavity. Therefore, the Q value for each sample should be known to estimate the relative H_1 value. The ESR absorption energy is proportional to H_1.[2,7] If we denote the Q value of an empty resonant cavity by Q_0, and the H_1 value by H_{10}, we have $H_{10}^2=k\cdot P\cdot Q_0$ where k is a constant. If a sample is placed in the cavity, we have $H_1^2=k\cdot P\cdot Q$. From these two relations we get $H_1^2=H_{10}^2\cdot Q/Q_0$. Q/Q_0 is estimated by the intensity of an Mn^{2+} line from the $MnSO_3$/MgO sample fixed in the cavity. The microwave circuit is so adjusted as to give the strongest signal amplitude.

Modulation width should be taken into consideration in order to analyze an ESR spectrum having two spectral components.[8] If one of the components has a hyperfine structure (hfs), the modulation width should be small enough to observe the hfs. Since the first derivative absorption function is obtained experimentally as a function of the magnetic field H, $f(H)=f_1(H)+f_2(H)$, the integral absorption function $F(H)=F_1(H)+F_2(H)$ must be derived from $f(H)$. If the amplitude of $f(H)$, A_1, is plotted against the modulation width, h, it is proportional to h until h reaches h_{max}, after which A_1 shows a decreasing tendency. A_1 is directly proportional to $F_1(H_c, h_{max})$, which is the height of $F_1(H)$ observed by h_{max} modulation width, where H_c is the value of the magnetic field for the peak point of the absorption curve. The height of $F_2(H)$ is $F_2(H_c, h'_{max})$, where h'_{max} differs from h_{max}. If the relation between the amplitude of $f_1(H)$ (or $f_2(H)$) observed with a modulation width h and $F_1(H_c, h_{max})$ (or $F_2(H_c, h'_{max})$) is known, the latter value can be estimated from A_1 or (A_2). From these quantities the spin concentration, y, was calculated as $y=N_2/M$, where M is the weight of the sample placed in the 45 mm × 5.0 mm ϕ cylindrical section the sample tube where microwave magnetic field is the strongest, and N_2 is the total number of the paramagnetic species contained in the same space. N_2 is determined by the relation

$$N_2=\frac{N_1}{I_1}\times\frac{S(\text{sample})}{S(\text{DPPH})}\times\frac{I(P')}{J(P')},$$

where N_1 is the number of molecules in the DPPH single crystal, $I(P')$ is the intensity of $F_1(H)$ or $F_2(H)$ at P' (dimension, mV G), I_1 is that for the DPPH single crystal at 1 μW,

and $J(P')$ is equal to $I(P')/I(1\ \mu W)$ determined by the power dependence curves. S(sample) or S(DPPH) is equal to

$$\int_{H=0}^{H=+\infty} h(H-H_0)\mathrm{d}H/h(0)$$

where $h(H-H_0)$ is the spectrum function written in H(dimension, mV) and the integral value is obtained by a double integration of the first derivative absorption curve. The values of S observed for DPPH (single crystal sealed in a vacuum), perylene cation, R^+O^{*2-}, and Mo^{5+} are 2.8488, 6.61, 13.75, and 108.18 G, respectively.

Preparation of Sample. If the amount of MoO_3 supported on Al_2O_3 is small, (1—3%), the amount of cation formation after contact with a hydrocarbon solution is also small.[9] A fairly large number of cations are formed when the wt% of MoO_3 is above 5%. For this reason, 8.5% of MoO_3 was supported on γ-alumina. The method of preparation is the same as that given in a previous paper.[10] The solvent well shaken with concentrated sulfuric acid, distilled twice, and then distilled into the vessel in which perylene crystals had been placed. After dissolving perylene this solution was mixed with the Al_2O_3–MoO_3 which had been evacuated to 10^{-4} mmHg in a vacuum line. Immediately after contact of the perylene solution a certain amount of perylene cation was formed, gradually increasing as shown in Fig. 2. The first spectrum was recorded at 10—12.5 min after contact of the solution and the subsequent measurements were made at 1, 2, 3, and 6 hr, 1, 2, 3 day, and so on.

It seems that the solvent molecules are working as something more than a simple dispersing medium of perylene molecules.[11] The following experiment was made to see the solvent effect. An aromatic compound was adsorbed on the surface of Al_2O_3–MoO_3, to which the solvent vapor was introduced. For this purpose, anthracene, whose vapor pressure is higher than that of perylene, is more suitable. 0.5 g of Al_2O_3–MoO_3 and 50 mg of anthracene was mixed well and placed in a sample tube, which was placed in the microwave resonant cavity and connected to the vacuum line. During evacuation, the anthracene vapor was adsorbed by the oxide and ESR absorption without hyperfine structure was gradually built up. The notation R^+O^{*2-} was used for this species.[12] Here R denotes anthracene, O^{*2-} the oxygen anion located at some particular points on the oxide surface at which the p-orbitals of an O^{2-} ion might be expected to overlap with the π-orbitals of the aromatic compound adsorbed more easily than at other positions. Various solvent vapors were introduced into the sample and the ESR spectrum after vapor introduction was recorded.

Results

The ESR spectrum obtained by perylene–Al_2O_3–MoO_3–solvent system is shown as "total" in Fig. 1. The total spectrum can be analyzed to consist of Component-1 and Component-2. The amplitude of the strongest hyperfine line A (or the central line) was read from the total spectrum. Using ΔH_{msl} of each hyperfine component line, amplitude A, and combination coefficients ${}_8C_r/70$, the first derivative hyperfine spectrum which represents a pure perylene cation on a solid surface was drawn (Component-2, Fig. 1). The difference between total and Component-2 is Component-1. Component-2 is due to perylene cation, R^+, and Component-1 to R^+O^{*2-}.[10,11,12] The absorption intensity of ESR spectrum (Fig. 1) changes with time after the formation of the paramagnetic species as

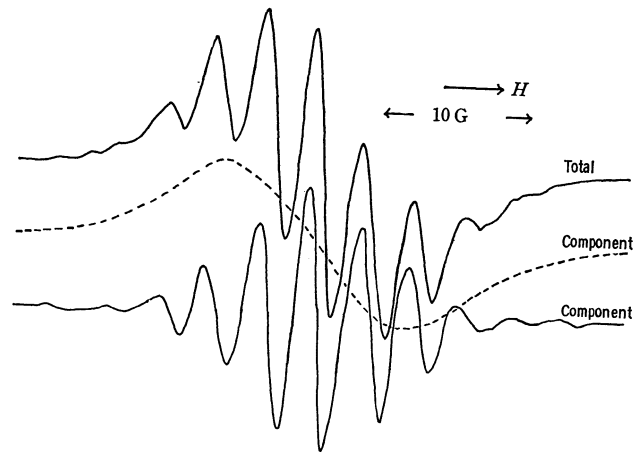

Fig. 1. The two component spectra, Component-1 and Component-2, contained in the observed spectrum, total.

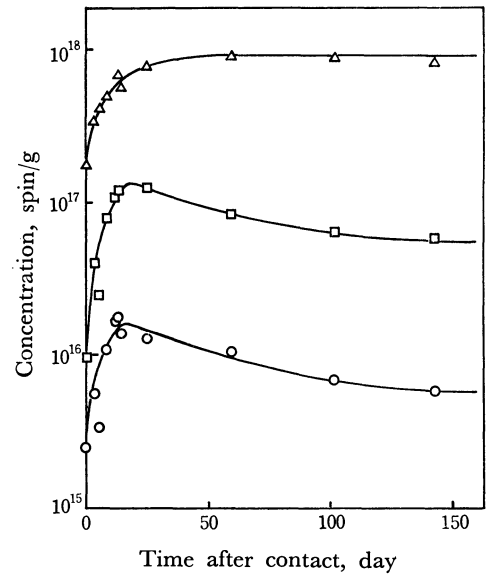

Fig. 2. The time dependence of the concentrations of the paramagnetic species observed.
△: Mo^{5+}, □: R^+O^{*2-}, ○: R^+

shown in Fig. 2. The temperature of storage and that of the measurements was 20 °C. The results in Table 1 were calculated so as to give the values which would be obtained under the conditions, $Q=Q_0$ and input power of 1 μW, or obtained with H_{10} for 1 μW. All the data were calculated as if they were obtained with the same H_1 value and without any power saturation. The change in the ESR spectra of anthracene–Al_2O_3–MoO_3 system when a solvent vapor was introduced is shown in Fig. 3. The temperature of measurement was 20 °C. The modulation width, microwave imput power and signal amplification factors were 20 mG, 1.0 mW, 5×10^2; 32 mG, 1.0 mW, 1×10^3; 50 mG, 0.1 mW, 2×10^3; 50 mG, 0.1 mW, 2×10^3; 25 mG, 1.0 mW, 1×10^3; 10 mG, 0.1 mW, 1×10^3. Solvents used have different structures. However, they were added into the sample tube in vapor phase in small amounts making the difference in Q which was slightly affected by different solvent vapor negligibly.

TABLE 1. SOLVENT EFFECT ON THE FORMATION OF R^+, R^+O^{*2-}, AND Mo^{5+} a)

Solvent	R^+ b)	R^+O^{*2-} c)	Mo^{5+} d)
n-Hexane	.59	.95	.86
Cyclohexane	1.5	3.2	.58
Benzene	1.1	2.7	8.5
Toluene	2.0	4.7	1.6
Ethylbenzene	1.0	3.4	1.5
n-Propylbene	.70	2.9	.90
Cumene	.94	3.2	1.3
t-Butylbenzene	.36	2.6	.86
p-Xylene	2.3	4.9	1.7
o-Xylene	1.1	2.0	.88
m-Xylene	.68	2.7	.70
1,2,3-Trimethylbenzene	10.8	25.5	11.7
1,2,4-Trimethylbenzene	2.4	6.6	2.6
1,3,5-Trimethylbenzene	.90	4.1	1.4
Mixtures of benzene-cyclohexane			
BZ/CH 3:1	.36	2.9	.67
BZ/CH 1:1	1.2	4.2	1.3

a) Measured 143 day after preparation.
b) $\times 10^{15}$/g. c) $\times 10^{16}$/g. d) $\times 10^{17}$/g.

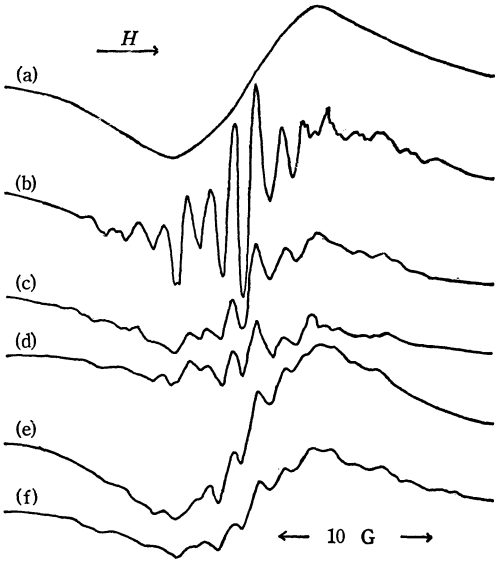

Fig. 3. The change in the ESR spectra from anthracene-Al_2O_3-MoO_3 after vapor of various solvents is introduced.
(a): Before solvent in, (b): C_6H_6 80 mmHg, (c): C_6H_{12} 70 mmHg, (d): CCl_4 20 mmHg, (e): *t*-Butylbenzene 3 mmHg, (f): Aniline <1 mmHg

Discussion

Formation of Two Paramagnetic Species. Evidence to show the formation of two paramagnetic species, R^+ and R^+O^{*2-}, has been given in a few cases. The reactivity of R^+ with H_2O is higher than that of R^+O^{*2-} and with use of this R^+O^{*2-} was separated from R^+.[11] The ESR microwave saturation factor of R^+ is larger than that of R^+O^{*2-} which makes the shape of the ESR spectrum of the mixture of these two paramagnetic species strongly power dependent.[13] The experimental results were analysed assuming the presence of two paramagnetic hydrocarbon species. The following assumption was found to be correct: if Component-1 is a spurious signal formed by a broadening of Component-2, the ratio between Component-1 and Compontne-2 should be the same for all the solvents used provided that the measurements are made under the same conditions, *i. e.*, the same H_1 value, and the same modulation width. However, the results (Table 1) show that the ratio greatly depends on the solvent, *viz.* 15 for *n*-hexane, 70 for *t*-butyl benzene, and 46 for 1,3,5-trimethyl benzene. Thus, the solvent effects give evidence to conclude that Component-1 and Component-2 are due to chemically different paramagnetic species.

Necessity of a Solvent in a Cation Formation. The effect of introduced benzene vapor on the ESR of Al_2O_3-MoO_3-anthracene system indicates that solvent molecules are necessary for observing an ESR spectrum having hfs of the anthracene cation. However, a perylene cation might give an ESR spectrum without a hyperfine structure if trapped on a solid surface. The hyperfine structure in the ESR of a hydrocarbon cation is given by two spin Hamiltonian terms, anisotropic which depends on the direction of the external magnetic field, and isotropic which does not. In solution the anisotropic term cannot be observed since it is averaged out by the tumbling motion of the molecule.[14] On a solid catalyst surface the hfs can only be partly observed because of the restricted motions.[15] However, if the sample is cooled to liquid nitrogen temperature, the hfs almost vanishes.[15] Thus, the appearance of a hfs in the ESR upon introduction of a solvent can be due to either (A) formation of the cation by the action of the solvent vapor, or (B) change of the cation, which existed but whose ESR spectrum did not show a hfs, to one which shows a hfs in the spectrum. If (B) is the case it would only be explained as motions of the cation on the surface of the oxide, which have been frozen, resume their activities because the solvent molecules defreeze them. Such defreezing should be due to a partial dissolution of the cation by the solvent molecules on the oxide surface. However, such a partial dissolution will disappear if the solvent is removed from the sample. The hfs in the ESR spectrum once formed does not change when the sample is evacuated subsequently.[11] Thus, case (B) is ruled out. It is concluded that the solvent molecule is necessary for the formation of an aromatic cation on the oxide surface.

Role of the Solvent Molecule in the Cation Formation. If solvent molecules are indispensable to the formation of a hydrocarbon cation, the question arises as to how a "solvent" molecule differs from a "solute" molecule. The solvent dealt with is a substance which is liquid at room temperature and can dissolve aromatic hydrocarbons. This indicates that the solvent molecule can move freely and occupy the oxide surface continuously, cover the narrower places like small pores, and move from one place to another on the surface. The following three roles are possible for solvents. (A) The solvent dissolves the solute and

carries it to the micropores where the parent cation (or the positive electric charge source) lies. (B) The solvent molecule accepts a positive charge from the parent cation and delivers it to the solute molecule by thermal molecular motions. (C) The oxide surface combined with a certain arrangement of the adsorbed solvent molecules, as a whole, promotes the charge transfer process. In this case the aromatic cation formation occurs if an aromatic compound and a positive charge exist on both ends of this surface and solvent arrangement. The possibility for (A) will be excluded because a small amount of solvent (contact pressure <10 mmHg) can cause the formation of anthracene cation. It is hard to distinguish (B) from (C). An experiment carried out with mixed solvents of benzene and cyclohexane (Table 1) seems to exclude (B). If (B) holds, the total formation of the solute cation will be the sum of its formations due to benzene and cyclohexane. If (C) is correct, a small number of cyclohexane present in the surface arrangement of benzene molecules would weaken the function of this surface–benzene system and a linear relation between the composition of the mixed solvent and the cation formation could not be expected. If the solvent or the third component is a liquid at 20 °C, (B) should be more probable. However, when naphthalene which is solid at 20 °C was added as a third component, 10 mg of naphthalene to 30 mg of anthracene, a strong ESR signal of anthracene cation was observed.[16] Thus (C) is more probable.

The results obtained by alkylated benzenes are shown in Table 1. The results shown for toluene to cumene are similar. In the case of dimethylbenzenes, the formation of the paramagnetic species decreases in the order *p*-, *o*-, and *m*-. In the case of trimethyl derivatives, the formation of the paramagnetic species decreases in the order 1,2,3-trimethyl benzene (TMB), 1,2,4-TMB, and 1,3,5-TMB. It is desirable to analyze the results and know what physical factors of the solvent molecules are responsible for the difference. The results from trimethyl benzenes (Table 1) indicate that the molecule with a lower molecular symmetry produces more cation, indicating that a higher dielectric constant favors cation formation. The effect of ionization potential may be studied by computing the energy eigen-values of the molecular orbitals in the methyl substituted benzene cation molecules. The steric effects may also be seen in the series of toluene, ethyl benzene, propyl benzene, and butyl benzene, the formation of perylene cation decreasing in this order.

Paramagnetic Species other than R^+, R^+O^{*2-}, and Mo^{5+}. ESR absorption which is not due to any of these three species is always found in the spectra obtained by Al_2O_3–MoO_3 and has not been interpreted.[3,10] The observed concentration of Mo^{5+} is far greater than the sum of R^+ and R^+O^{*2-}. If benzene is used as a solvent, $(Mo^{5+})=8.5\times10^{17}$ spin/g, while the sum $((R^+)+(R^+O^{*2-}))=2.86\times10^{16}$ spin/g, and is 8.2×10^{17} spin/g less than the former. This indicates that at least this amount of static electricity is compensated by some positively charged species, T^+. Though R^+ and R^+O^{*2-}, both having net positive electric charge, decrease with time, the concentration of Mo^{5+}, having a net negative charge, increases with time. This seems to indicate that the neutralization of R^+ and R^+O^{*2-} takes place not by Mo^{5+} but by some other negatively charged species, T^-. Thus, if the Al_2O_3–MoO_3–hydrocarbon catalytic reaction system is analyzed, T^+ and T^- should be included in the system components.

References

1) G. E. Pake, "Paramagnetic Resonance," W. A. Benjamin, Inc., New York (1962), p. 48.
2) D. J. E. Ingram, "Free Radicals as Studied by Electron Spin Resonance," Butterworths Scientific Publications, London (1958), p. 135.
3) H. Ueda and N. Todo, *J. Catal.*, **27**, 281 (1972).
4) M. Bersohn and J. C. Baird, "An Introduction to Electron Paramagnetic Resonance," W. A. Benjamin, Inc., New York (1966), p. 73.
5) p. 97 of Ref. (2).
6) A. J. Nanassy, *J. Appl. Polym. Sci.*, **16**, 2577 (1972).
7) P. B. Ayscough, "Electron Spin Resonance in Chemistry," Methuen and Co., Ltd., London (1967), p. 127.
8) p. 206 of Ref. (4).
9) C. Nacchache, J. Bandiera, and M. Dufaux, *J. Catal.*, **25**, 334 (1972).
10) H. Ueda and N. Todo, This Bulletin, **43**, 3698 (1970).
11) H. Ueda and N. Todo, *Can. J. Chem.*, **51**, 885 (1973).
12) H. Ueda, This Bulletin, **43**, 319 (1970).
13) H. Ueda, unpublished results.
14) p. 97 of Ref. (1).
15) G. M. Muha, *J. Phys. Chem.*, **71**, 633 (1967).
16) H. Ueda, unpublished results.

The Diffusion of Gases at High Pressures. V. The Diffusion of CTH_3 in the CO_2–Ar System

Shinji TAKAHASHI

Chemical Research Institute of Non-aqueous Solutions, Tohoku University, Katahira, Sendai 980

(Received October 5, 1973)

The diffusion coefficients of radioactive methane (CTH_3) in argon and in mixtures of carbon dioxide with argon(0.719, 0.497, and 0.245 mol fractions of argon) were measured at the temperatures of 25, 50, and 75 °C in the 15~250 atm pressure range. The measurements were made through a plug of porous bronze in the diffusion cell by using the radioactive tracer technique. The diffusion coefficient-density products, $D\rho$, for the CTH_3-argon system increased slightly with the density in the region below 5 mol/l, and decreased slightly in the region above 5 mol/l. The $D\rho$ for the CTH_3-mixture systems decreased slightly with the density over the whole range studied here. The density dependence of $D\rho$-values at high densities could not be predicted by Enskog-Thorne's theory.

This investigation is a part of a continuing research project into the diffusion coefficients of gases at high pressures. The previous investigations were made for the diffusion coefficients of $^{14}CO_2$ in the CO_2–Ar[1,2] and CO_2–CH_4 system[3] and for those of CTH_3 in the CH_4–CO_2 system.[4] This paper will present the diffusion coefficients of CTH_3 in the CO_2–Ar system. Measurements were made at the temperatures of 25, 50, and 75 °C in the 15~250 atm pressure range. The mole fractions of argon in the mixtures were 0.719, 0.497, and 0.245.

Experimental

The apparatus and the experimental procedure were the same as those described previously.[1] The diffusion path in the cell was porous bronze plug with pores of about 10 μ. Radioactive methane (CTH_3), obtained from the New England Nuclear Corp., was diluted with non-radioactive methane to a specific activity of about 450 μCi/mmol. The purities of the carbon dioxide and argon used in this investigation were 99.9%. Mixtures of carbon dioxide with argon were prepared in the cylinders. The exact compositions were determined by absorbing carbon dioxide from samples into a potassium hydroxide solution. Under the conditions studied, the mixtures were not in a liquid state.[5]

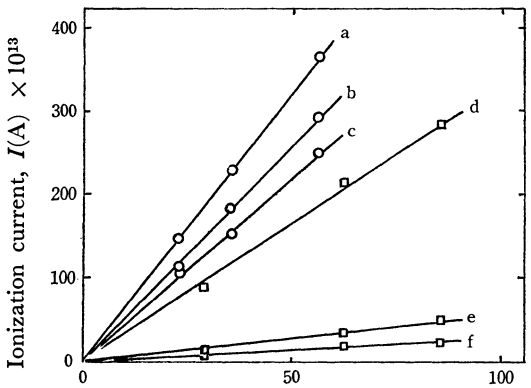

Fig. 1. Relations between the amounts of radioactive methane and the ionization currents at 50 °C.
○: for pure argon, □: for the mixture of 0.497 mol fraction of argon. Pressure(atm) — a, d: 14.55; b, e: 97.8; c: 243.0; f: 194.6

The proportionality between the concentration of radioactive methane and the ionization current, essential for a quantitative treatment of the diffusion data, was confirmed experimentally for pure argon and for mixtures. As examples, the results for pure argon and for the mixture of the 0.497 mol fraction of argon at 50 °C are shown in Fig. 1.

Results and Discussion

In Table 1, showing the experimental results, D is the diffusion coefficients of radioactive methane (CTH_3) in argon and in mixtures. The densities of argon were calculated from the compressibility factors obtained by Michels *et al.*[6] The densities of carbon dioxide–argon mixtures were calculated by using the compressibility chart described in a previous paper.[2] In Fig. 2 the diffusion coefficient-density products, $D\rho$, are plotted against the densities. Curves a, b, c, and d are drawn through the experimental points for the systems where the mole fractions of argon, x_3, are 1.000, 0.719, 0.497, and 0.245. Curve e has been obtained in a previous investigation[4] for the diffusion of CTH_3 with carbon dioxide; it is shown for the sake of comparison. The D at $x_3=1.000$ is the diffusion coefficient of radioactive methane with argon, D_{13}, where the subscripts 1 and 3 denote radioactive methane and argon respectively. The values of $D_{13}\rho$ increase slightly with the density in the region below 5 mol/l, and decrease slightly in the region above 5 mol/l.

The extrapolation of $D\rho$ *vs.* ρ curves to 1 atm provides a basis for comparison with published low-pressure experimental results and with theoretical values. Applying the mass correction[7] to the binary diffusion coefficient of normal methane with argon, D_{43}, which was measured by Carswell[8] at only 25 °C, the binary diffusion coefficient of radioactive methane with argon, D_{13}, was obtained. On the other hand, theoretical values of D_{13} at 1 atm were obtained by applying the mass correction to the binary diffusion coefficients of normal methane with argon, D_{43}, given by:[9]

$$(D_{43})^\circ = 0.002628\frac{\sqrt{T^3(M_4+M_3)/2M_4M_3}}{p\sigma_{43}^2\Omega_{43}^{(1,1)*}}$$

Here, $(D_{43})^\circ$ is the first approximation to diffusion coefficient of normal methane with argon (cm^2/s); T, the temperature (K); M, the molecular weight;

TABLE 1. EXPERIMENTAL RESULTS

P atm	ρ mol·l^{-1}	$D\times10^3$ cm^2·s^{-1}	$D\rho\times10^3$ cm^2·mol·s^{-1}·l^{-1}
		25 °C	
		$x_3=1.000$	
14.45	0.5953	15.8	9.41
14.47	0.5961	15.2	9.06
14.58	0.6007	14.9	8.95
48.9	2.0534	4.53	9.30
49.7	2.0876	4.51	9.42
50.9	2.1393	4.44	9.50
101.5	4.3480	2.23	9.70
109.0	4.6791	2.05	9.60
144.3	6.2262	1.49	9.28
196.4	8.4359	1.12	9.45
245.6	10.3753	0.885	9.18
		$x_3=0.719$	
14.37	0.5990	14.24	8.53
14.41	0.6007	13.7	8.23
49.9	2.1781	3.83	8.34
50.9	2.2159	3.94	8.73
100.0	4.6435	1.82	8.45
147.1	7.1057	1.16	8.24
184.6	9.0550	0.934	8.46
219.8	10.7418	0.721	7.74
		$x_3=0.497$	
14.32	0.6074	12.3	7.47
14.41	0.6113	13.0	7.95
50.3	2.3394	3.34	7.81
50.4	2.3444	3.29	7.71
101.0	5.3565	1.41	7.55
101.5	5.3900	1.49	8.03
149.2	8.6154	0.904	7.38
202.5	12.1441	0.601	7.48
		$x_3=0.245$	
14.37	0.6198	11.2	6.94
14.40	0.6212	11.3	7.02
50.0	2.5426	2.79	7.09
68.6	3.7330	1.89	7.06
82.3	5.2595	1.43	7.52
84.3	5.4868	1.24	6.80
99.9	7.5693	0.914	6.92
122.4	10.9569	0.650	6.84
		50 °C	
		$x_3=1.000$	
14.41	0.5462	17.1	9.34
14.41	0.5462	17.1	9.34
14.41	0.5462	17.0	9.26
14.44	0.5473	17.1	9.36
50.1	1.9209	4.91	9.43
50.9	1.9655	4.71	9.26
99.2	3.8405	2.54	9.75
101.8	3.9325	2.48	9.78
149.8	5.8045	1.61	9.35
200.4	7.6976	1.21	9.31
201.8	7.7481	1.19	9.22
235.8	8.9572	1.08	9.67
253.5	9.5604	0.974	9.31
		$x_3=0.719$	
50.1	1.9821	4.40	8.72
50.3	1.9903	4.42	8.80
101.2	4.1708	2.11	8.80
151.2	6.3936	1.31	8.38
200.9	8.5362	0.982	8.38
		$x_3=0.497$	
14.37	0.5556	14.2	7.89
14.50	0.5606	13.8	7.75
49.8	2.0423	3.83	7.82
99.3	4.4457	1.68	7.47
148.6	7.0861	1.09	7.72
247.0	12.0139	0.593	7.12
		$x_3=0.245$	
13.82	0.5416	13.8	7.47
14.41	0.5657	12.8	7.24
50.2	2.2125	3.32	7.35
100.5	5.4049	1.32	7.13
148.2	9.2849	0.727	6.75
		75 °C	
		$x_3=1.000$	
14.41	0.5057	19.6	9.91
14.41	0.5057	19.7	9.96
50.0	1.7654	5.76	10.17
101.8	3.6060	2.66	9.59
151.0	5.3286	1.88	10.02
202.6	7.0695	1.33	9.40
247.1	8.4947	1.17	9.94
		$x_3=0.719$	
14.37	0.5082	18.5	9.40
14.39	0.5089	18.1	9.21
50.4	1.8284	4.86	8.89
50.9	1.8480	4.90	9.06
51.4	1.8662	4.98	9.29
97.8	3.6454	2.46	8.97
122.6	4.6160	1.92	8.86
152.5	5.7884	1.54	8.91
201.7	7.6493	1.13	8.64
250.0	9.3874	0.890	8.35
		$x_3=0.497$	
14.41	0.5133	16.5	8.47
14.41	0.5133	16.7	8.57
14.41	0.5133	17.0	8.73
50.4	1.8772	4.56	8.56
50.6	1.8848	4.52	8.52
101.0	4.0034	2.12	8.49
101.8	4.0392	2.08	8.40
149.6	6.1655	1.39	8.50
197.8	8.3520	0.965	8.06
		$x_3=0.245$	
14.37	0.5187	15.6	8.09
14.31	0.5165	15.2	7.85
51.0	2.0052	3.96	7.94
96.8	4.2627	1.83	7.80
126.3	5.9224	1.32	7.82
150.3	7.3604	0.991	7.29
193.0	9.8887	0.746	7.38

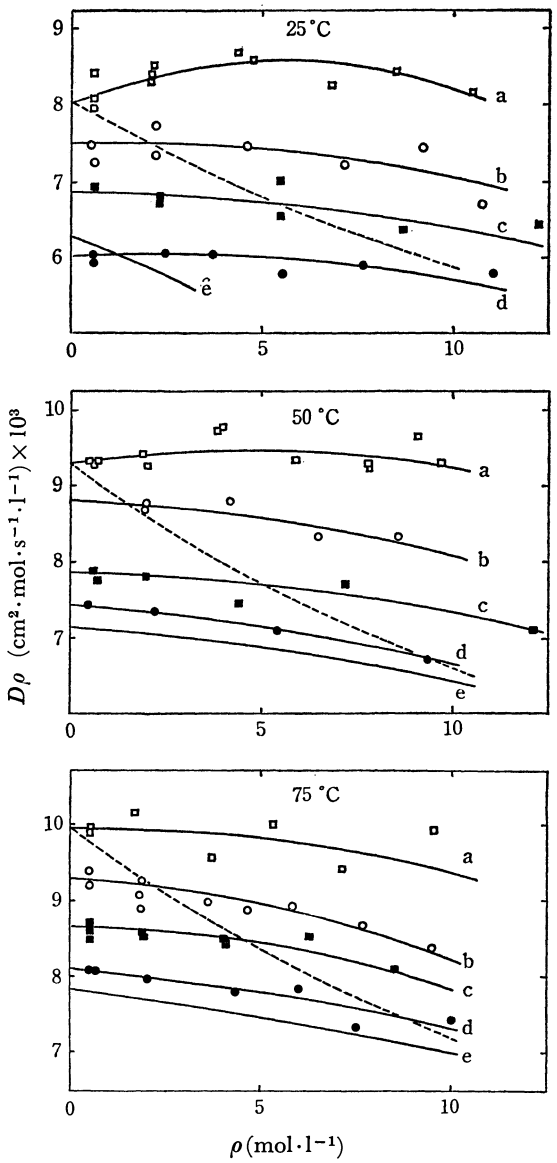

Fig. 2. Variation of $D\rho$ with density.
□, ○, ■, and ● are the experimental points obtained in the present investigation and the mole fraction of argon (x_3) are as follows; □: 1.000, ○: 0.719, ■: 0.497, ●: 0.245. Solid lines (a~d) are the smoothed curves for the experimental points; a: $x_3=1.000$, b: $x_3=0.719$, c: $x_3=0.497$, d: $x_3=0.245$. Solid lines(e) are the smoothed curves obtained in the previous investigation for $x_3=0.000$. Dashed lines are the theoretical curves for $D_{13}\rho$.

p, the pressure (atm); σ_{43}, the potential parameter (A); $\Omega_{43}^{(1,1)*}$, the reduced collision integral. The subscripts 3 and 4 denote argon and normal methane respectively. The values obtained by Carswell and the theoretical values are compared with those extrapolated in this investigation in Table 2. The deviation of the value obtained by Carswell from that extrapolated is not small, but the deviation of the theoretical values are −5~−10%, consistent with those of the values observed for other systems.[10]

According to Enskog-Thorne's theory,[11] which is the only theoretical treatment offering any practical application, the binary diffusion coefficient at high pressures is given by:

$$D_{13}\rho = (D_{13})^{\circ}\rho/\chi_{13} \quad (2)$$

Here, $(D_{13})^{\circ}$ is the binary diffusion coefficient calculated on the basis of the low-density kinetic theory; it is obtained by applying the mass correction to the values given, for example, by Eq. (1). χ_{13} is a correction factor depending on the density of gas; it is given by:

$$\chi_{13} = 1 + 0.2618 n_1 \sigma_1^3 (8 - 3\sigma_1/\sigma_{13}) + 0.2618 n_3 \sigma_3^3 (8 - 3\sigma_3/\sigma_{13}) + \cdots\cdots \quad (3)$$

where n_1 and n_3 are the numbers of molecules per unit volume (cm^{-3}) and where σ_1 and σ_3 are the collision diameters (cm). σ_{13} is $(\sigma_1+\sigma_3)/2$ according to an empirical combining rule. Since radioactive methane is present as only a trace in this investigation, the second term on the right-hand side of Eq. (3) may be neglected. In the calculation of $D_{13}\rho$ at high pressures by means of Eqs. (2) and (3), the extrapolated values of $D_{13}\rho$ at 1 atm were used in place of $(D_{13})^{\circ}\rho$; σ_1 and σ_3 are approximated by the parameters for the Lennard-Jones (12-6) model—3.882 Å for normal methane and 3.418 Å for argon.[12] As is shown in Fig. 2, the theoretical values of $D_{13}\rho$ decrease with the density; they are about 26% lower than those obtained in the present experiment at $\rho=5$ mol/l. Such discrepancies, which have been found for many systems,[13] seem to result from the fact that, in the derivation of Eq. (3), the rigid-sphere model was assumed and the properties of real gases were not taken into consideration. Therefore, it may be expected that the agreement between the theory and the experiment will be better if χ_{13} is evaluated from the P-V-T relations of real gases according to Enskog's suggestion. The results obtained by applying his suggestion will be reported later.

The diffusion coefficients of radioactive methane in mixtures, D_{1m}, at 1 atm may be calculated by using Wilke's equation:[14]

$$1/D_{1m} = x_2/D_{12} + x_3/D_{13} \quad (4)$$

Here, x_2 and x_3 are the mole fractions of carbon dioxide and argon, D_{12} and D_{13} are the binary diffusion coefficients of radioactive methane with carbon dioxide and with argon, and $x_2+x_3\fallingdotseq 1$. In Table 3 the values of D_{1m} at 1 atm given by Eq. (4) are compared with

Table 2. Comparison of the extrapolated values (D_{extra}) of the binary diffusion coefficients at 1 atm with the theoretical values (D_{theor}) and with that reported by Carswell (D_{obs})

CTH_3-Ar system

Temp. °C	D_{extra} $cm^2\cdot s^{-1}$	D_{theor} $cm^2\cdot s^{-1}$	D_{obs} $cm^2\cdot s^{-1}$	Dev.[a] %
25	0.220		0.194	−11.8
25		0.198		−10.0
50	0.247	0.229		−7.3
75	0.277	0.263		−5.1

a) Dev. (%)$=(D_{theor}-D_{extra})\times 100/D_{extra}$ or $(D_{obs}-D_{extra})\times 100/D_{extra}$

Table 3. Comparison of the extrapolated values of the diffusion coefficients of the trace-component (CTH_3) in the mixtures ($D_{1m,extra}$) with those calculated using Wilke's equation ($D_{1m,calc}$)

Temp. °C	CTH_3(trace)-(CO_2+Ar) system $D_{1m,extra}$ $cm^2 \cdot s^{-1}$	$D_{1m,calc}$ $cm^2 \cdot s^{-1}$	Dev.[a] %
	x_3(mole fraction of argon)=0.719		
25	0.205	0.210	+2.7
50	0.234	0.228	−2.6
75	0.266	0.259	−2.6
	x_3=0.497		
25	0.193	0.199	−3.1
50	0.209	0.214	+2.4
75	0.248	0.246	−0.8
	x_3=0.245		
25	0.173	0.188	+8.7
50	0.196	0.200	+2.0
75	0.232	0.233	+0.4
		average[b]	2.8

a) Dev. (%)=$(D_{1m,calc}-D_{1m,extra}) \times 100/D_{1m,extra}$. b) average of the absolute values of Dev.

those extrapolated. In the calculation of D_{1m} at 1 atm by using Eq. (4), the values extrapolated in this investigation were used for D_{12} and those extrapolated in the previous paper[4] were used for D_{13}. As is shown in Table 3, the deviation is 2.8% on the average; therefore, Eq. (4) seems to be approximately valid.

As Enskog-Thorne's theory has not yet been extended to ternary systems, the prediction of $D_{1m}\rho$ at high pressures was made by using Eq. (5), derived from Eq. (4):

$$1/D_{1m}\rho = x_2/D_{12}\rho + x_3/D_{13}\rho \quad (5)$$

where D_{1m}, D_{12}, and D_{13} are the values at the same density, ρ(mol/l), and where $x_2+x_3 \fallingdotseq 1$. According to Eq. (5) $D_{1m}=D_{12}$ at $x_3=0$, $D_{1m}=D_{13}$ at $x_3=1$, and $1/D_{1m}\rho$ should vary linearly with x_3. By using the values of $D_{1m}\rho$ read from the smoothed curves in Fig. 2, the values of $1/D_{1m}\rho$ were plotted against the mole fractions of argon, x_3, at ρ=2, 4, 6, 8, and 10 mol/l in Fig. 3. Although the plots do not give very good straight lines, the deviation of the values given by Eq. (5) from the smoothed values obtained in Fig. 2 is 2.1% on the average; therefore, Eq. (5) seems to be approximately valid also at high pressures in the present system.

The author wishes to express his deep gratitude to Professor Hiroji Iwasaki for his kind direction and encouragement throughout this work.

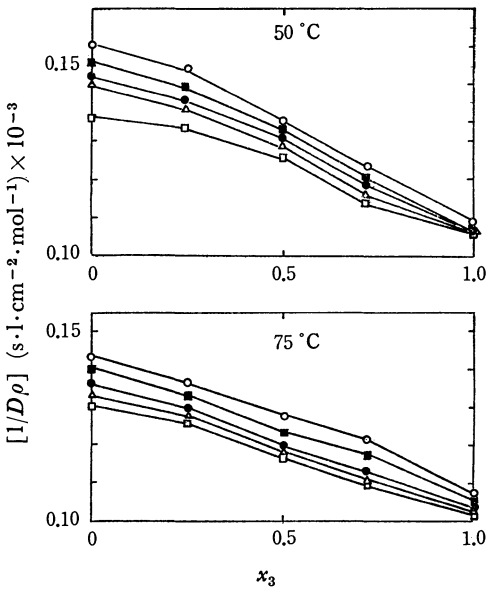

Fig. 3. Variation of $1/D\rho$ with composition. Density (mol·l^{-1}); □: 2, △: 4, ●: 6, ■: 8, ○: 10

References

1) S. Takahashi and H. Iwasaki, This Bulletin, **39**, 2105 (1966).
2) S. Takahashi, This Bulletin, **41**, 1573 (1968).
3) S. Takahashi and H. Iwasaki, *Rev. Phys. Chem. Japan*, **38**, 28 (1968).
4) S. Takahashi, This Bulletin, **45**, 2074 (1972).
5) G. Kaminishi, Y. Arai, S. Saito, and S. Maeda, *J. Chem. Eng. Japan*, **1**, 109 (1968).
6) A. Michels, Hub. Wijker, and H.K. Wijker, *Physica*, **15**, 2074 (1949).
7) F. Hutchinson, *J. Chem. Phys.*, **17**, 1081 (1949).
8) A. T. Carswell and J. C. Stryland, *Can. J. Phys.*, **41**, 708 (1963).
9) J. O. Hirschfelder, C. F. Curtiss, and R. B. Bird, "Molecular Theory of Gases and Liquids," John Wiley & Sons, Inc., New York (1954), p. 539.
10) R. C. Reid and T. K. Sherwood, "The Properties of Gases and Liquids," McGraw-Hill Book Company, Inc., New York (1958), p. 274.
11) S. Chapman and T. G. Cowling, "The Mathematical Theory of Non-uniform Gases," Cambridge Univ. Press, London (1960), p. 292.
12) Ref. 9, p. 1110.
13) For example, L. Durbin and R. Kobayashi, *J. Chem. Phys.*, **37**, 1643 (1962).
14) C. R. Wilke, *Chem. Eng. Progress*, **46**, 95 (1950).

The Crystal Structure of Acridinium Bis(7,7,8,8-Tetracyanoquinodimethanide), $ARD^+(TCNQ)_2^-$ and Some Remarks on the Possibility of a Peierls Distortion of a Linear Chain of TCNQ

Hayao KOBAYASHI

Department of Chemistry, Faculty of Science, Toho University, Narashino, Chiba 275

(Received December 10, 1973)

Crystals of acridinium-TCNQ(ARD(TCNQ)$_2$) are triclinic, space group $P\bar{1}$ with $a=3.841(2)$, $b=13.018(6)$, $c=18.370(12)$ Å, $\alpha=114.32(5)$, $\beta=119.31(4)$, $\gamma=90.57(7)°$ and $Z=1$. ARD and TCNQ are separately stacked to form columns along the a axis. Each ARD column is surrounded by six TCNQ columns. The orientation of ARD is disordered. Intermolecular distance between adjacent TCNQs is 3.246 Å and that between adjacent ARDs is 3.418 Å. The possibility of a Peierls distortion of TCNQ columns was discussed on the basis of the model of one-dimensional distorted lattice. Calculations of free energy show that alternation of intermolecular spacing disappears at Peierls transition temperature, T_p of about 200 K. For $T>T_p$, the one-dimensional band is not split (metallic), while it is split below T_p(semiconductive). The specific heat curve shows a peak at about 180 K and the heat of transition is calculated to be about 130 cal/mol.

The recent reports on the extraordinarily high conductivity of TTF–TCNQ[1] ($\sigma>10^4(\Omega\ cm)^{-1}$(60 K)) shed light on the physical basis of the conduction mechanism of TCNQ salts. Besides TTF–TCNQ, three TCNQ salts have been known, whose temperature dependence of the electrical conductivities shows their metallic nature. They are *N*-methylphenazinium-TCNQ (NMP–TCNQ)[2], quinolinium–$TCNQ_2$ (Q(TCNQ)$_2$) and acridinium–$TCNQ_2$(ARD(TCNQ)$_2$)[3,4].

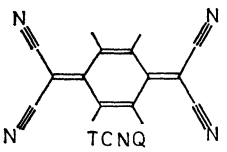

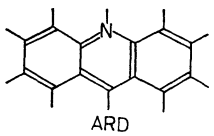

Crystals of ARD(TCNQ)$_2$ were subjected to X-ray crystal structure analysis to obtain structural information. A simple calculation was made to examine the possibility of a Peierls distortion of TCNQ columns.

Experimental

The crystals of ARD(TCNQ)$_2$ were prepared by a diffusion method, an acetonitrile solution of acridinium hydrochloride and an aqueous solution of Li-TCNQ and LiI being used. The black needles were obtained after a month. The crystals are triclinic. The crystal data are: $(C_{13}H_{10}N)^+(C_{12}H_4N_4)_2^-$, F. W. 588.6; $a=3.841(2)$, $b=13.018(6)$, $c=18.370$ (12) Å, $\alpha=114.32(5)$, $\beta=119.31(4)$, $\gamma=90.57(7)$, Space group, $P1$ or $P\bar{1}$; $U=703.5$ Å^3; $D_m=1.389$ g/cm^3, $D_x=1.389$ g/cm^3; $Z=1$

The intensity data were collected on an automated Rigaku four-circle diffractometer with Mo$K\alpha$ radiation monochromated by a graphite crystal. The $\omega-2\theta$ scan technique was employed. Among the 3149 accessible reflections ($2\theta\leqq55°$), 900 non-zero reflections were observed.

Structure Determination

The trial atomic coordinates were easily deduced from the three-dimensional Patterson synthesis and were refined isotropically by the block-diagonal least-squares method. The space group $P\bar{1}$ was assumed. The nine hydrogen atoms were found on the difference synthesis. Further refinements were carried out in anisotropic mode, however, the thermal parameters of the hydrogen atoms were assumed to be isotropic. The R-value converged to 0.087. The shifts of the parameters were about one fifth of their standard deviations. The weighting scheme adopted was: $w=1$ for $|F_o|\geq5.5$ and $w=0.32$ for $|F_o|<5.5$. The atomic scattering factors were taken from International Tables for X-ray Crystallography.[5] Because the orientation of ARD is disordered, the atomic scattering factor of CN(Table 1) was assumed to be $(f_C+f_N)/2$.

The final positional and thermal parameters are listed in Table 1. The calculated structure amplitudes are compared with the observed values in Table 2.*

Description of the Structure and Discussion

An ARD cation lie at (0,1/2,0) whose site symmetry is $\bar{1}$. Therefore, the orientation of ARD must be disordered because ARD is not centrosymmetric. Similar orientational disorder of cations has been frequently observed in the crystals of highly conducting salts(NMP–TCNQ[6] and Q(TCNQ)$_2$[7]). Fig. 1 shows that TCNQ and ARD are stacked along the a axis to form infinite columns. Each column of cations is surrounded by six columns of TCNQ as found in the crystals of Q(TCNQ)$_2$, which is a so-called complex salt (TCNQ/cation=2). The intermolecular distances of TCNQ and ARD are 3.246 and 3.418 Å, respectively. The least-squares planes and the displacement of the atoms from them are listed in Table 3. The mode of overlap of TCNQ is ring-external bond type as illustrated in Fig. 2. The similar type of overlapping of TCNQ is also found in NMP–TCNQ, Q(TCNQ)$_2$, Rb–TCNQ II,[8] ditoluenechromium (TCNQ)$_2$[9] and TTF–TCNQ[10]. All of them contain columns of monadic units of TCNQ, which indicates that this type of overlapping is common to the salts with monadic units of TCNQ. Short intermolecular contacts are listed in Table 4. A close approach distance of 3.15 Å occurs between the nitrogen atom of

* Table 2 have been deposited with the Chemical Society of Japan (Document No. 7413).

TABLE 1. ATOMIC PARAMETERS

Positional and thermal parameters of the non-hydrogen atoms, with their standard deviations in parantheses. The B_{ij}'s are defined by:

$$\exp[-(h^2B_{11}+k^2B_{22}+l^2B_{33}+2hkB_{12}+2hlB_{13}+2klB_{23})]$$

	x $\times 10^3$	y $\times 10^4$	z $\times 10^4$	B_{11} $\times 10^4$	B_{22} $\times 10^4$	B_{33} $\times 10^4$	B_{12} $\times 10^3$	B_{13} $\times 10^3$	B_{23} $\times 10^4$
C(1)	−415(3)	2879(9)	636(7)	63(11)	65(9)	48(7)	5(3)	10(2)	32(7)
C(2)	−217(3)	2269(8)	1134(7)	82(12)	41(8)	46(6)	4(3)	9(2)	22(6)
C(3)	173(3)	2783(8)	1941(7)	64(11)	57(9)	49(7)	2(3)	5(2)	36(7)
C(4)	358(3)	3984(8)	2330(7)	59(11)	54(8)	40(6)	2(2)	5(2)	26(6)
C(5)	157(3)	4603(8)	1840(7)	87(12)	47(9)	54(7)	3(3)	9(2)	31(7)
C(6)	−229(3)	4073(8)	1027(7)	88(12)	57(9)	54(7)	7(3)	11(3)	34(7)
C(7)	−828(3)	2336(9)	−209(7)	88(13)	67(9)	48(7)	7(3)	11(3)	34(7)
C(8)	760(3)	4528(8)	3165(7)	115(14)	47(8)	50(7)	7(3)	12(3)	34(7)
C(9)	−1035(3)	1149(8)	−623(7)	69(11)	60(8)	31(6)	5(3)	6(2)	23(6)
C(10)	−1045(3)	2924(9)	−717(7)	86(12)	57(9)	43(6)	4(3)	6(2)	25(7)
C(11)	977(3)	3967(9)	3698(7)	85(13)	56(10)	53(7)	1(3)	8(3)	20(7)
C(12)	966(3)	5699(9)	3538(7)	82(12)	61(9)	39(6)	3(3)	7(3)	24(7)
C(13)	−204(3)	578(8)	4478(7)	84(12)	62(9)	41(6)	10(3)	12(2)	30(7)
C(14)	−401(3)	1182(10)	3971(8)	110(14)	84(11)	58(7)	11(3)	17(3)	43(8)
C(15)	−776(3)	564(10)	3110(8)	146(17)	113(13)	62(8)	19(3)	19(3)	58(9)
C(16)	−934(3)	−638(10)	2732(8)	127(16)	90(12)	49(8)	7(3)	11(3)	23(8)
C(17)	−755(3)	−1238(9)	3216(7)	82(13)	82(11)	40(7)	3(3)	6(3)	25(8)
C(18)	−369(3)	−615(8)	4130(7)	75(12)	57(9)	47(6)	4(3)	14(2)	25(6)
N(1)	−1192(3)	181(8)	−982(6)	130(13)	73(9)	54(6)	0(3)	4(2)	29(7)
N(2)	−1221(3)	3410(8)	−1107(7)	132(13)	99(10)	68(7)	9(3)	10(3)	54(7)
N(3)	1141(3)	3498(8)	4128(7)	144(14)	91(10)	73(7)	2(3)	2(3)	51(7)
N(4)	1131(3)	6634(7)	3809(6)	163(15)	40(7)	40(6)	−4(3)	3(3)	13(6)
CN	175(3)	1157(7)	5357(6)	85(11)	47(7)	49(6)	4(3)	10(2)	30(6)

Positional parameters of the hydrogen atoms ($\times 10^3$)
The mean isotropic temperature factor is 1.3 Å^2.

	x	y	z		x	y	z
H(1)	−328(23)	144(7)	82(5)	H(6)	−891(27)	107(8)	279(6)
H(2)	304(24)	221(7)	218(5)	H(7)	−1251(34)	−88(10)	232(7)
H(3)	256(24)	542(7)	208(5)	H(8)	−851(24)	298(5)	298(5)
H(4)	−393(23)	449(7)	72(5)	H(9)	264(23)	196(7)	554(5)
H(5)	−270(29)	218(8)	430(7)				

TABLE 3. LEAST-SQUARES PLANES

Direction cosines of the normal of the plane with respect to:

		a		b		c
TCNQ		0.8453		−0.0539		−0.5315
ARD		0.8899		−0.0325		−0.4550
Deviation (Å)						
TCNQ	C(1)	0.03	C(2)	−0.00	C(3)	0.04
	C(4)	−0.03	C(5)	−0.01	C(6)	−0.03
	C(7)	−0.02	C(8)	0.01	C(9)	0.01
	C(10)	−0.03	C(11)	−0.03	N(1)	0.10
	N(2)	−0.07	N(3)	−0.09	N(4)	0.10
ARD	C(13)	−0.01	C(14)	0.01	C(15)	−0.03
	C(16)	0.03	C(17)	−0.01	C(18)	−0.01
	CN	0.01				

TABLE 4. INTERATOMIC DISTANCES

(i)	x	y	z	(ii)	$2-x$	$1-y$	$1-z$
(iii)	$-1-x$	$-y$	$-z$	(iv)	$-1+x$	y	z
(v)	$-2+x$	y	z	(vi)	$1-x$	$1-y$	$1-z$

Atom in unit (i)	To atom	In unit	d (Å)
N(4)	CN	ii	3.15
N(4)	H(9)	ii	2.36
N(1)	H(2)	iii	2.85
C(2)	C(3)	iv	3.28
C(4)	C(8)	iv	3.27
C(5)	C(12)	iv	3.30
C(6)	C(5)	iv	3.30
C(7)	C(1)	iv	3.25
H(5)	N(3)	v	2.83
N(4)	CN	vi	3.19
N(4)	H(9)	vi	2.66

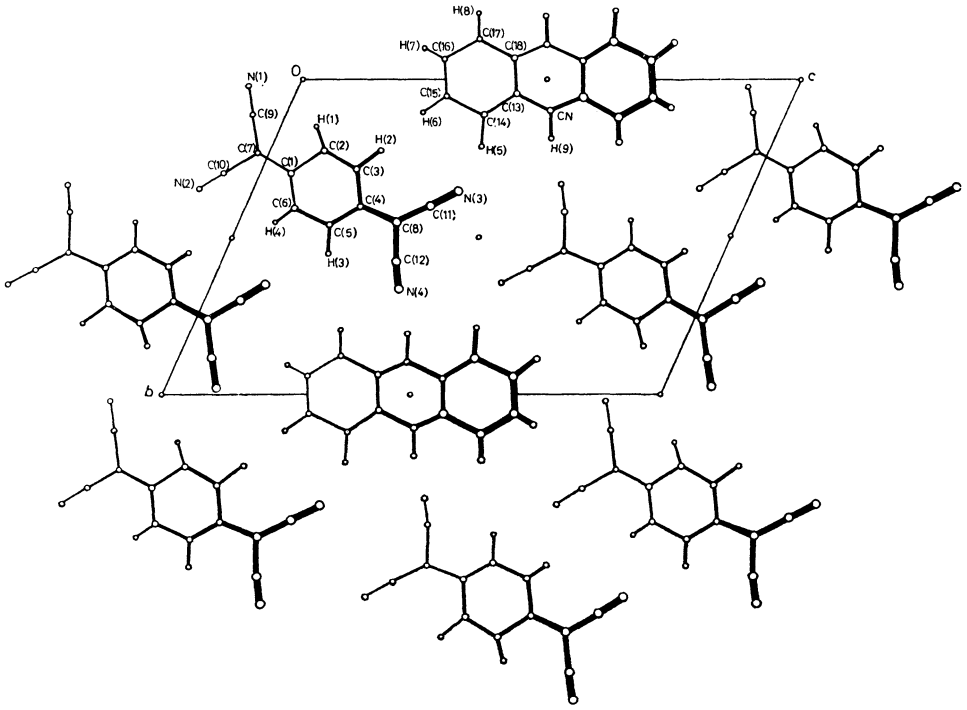

Fig. 1. The structure viewed along the *a* axis.

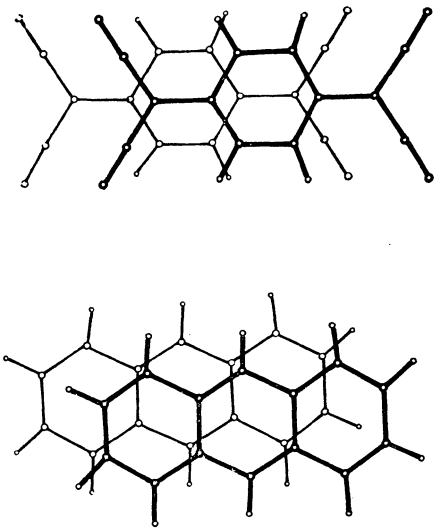

Fig. 2. Nearest neighbor overlap of TCNQ and that of ARD.

the cyano group of TCNQ and the CN atom(Table 1) of ARD cation. This indicates the possibility of the existence of the hydrogen bond of N–H···N type. Similar contact has been observed in the crystals of $Q(TCNQ)_2$ (3.13 Å).

TCNQ is almost planar but the cyano groups are rotated by about 2.4° around C=C bond from the molecular plane. Interplanar distance of ARD is approximately equal to the normal van der Waals distance.

The bond lengths and angles are shown in Fig. 3. The molecular geometry of TCNQ is that of $TCNQ^{-1/2}$ because only one TCNQ is crystallographycally independent. However, it dose not seem to be practicable to compare the bond lengths with those of $TCNQ^0$ and $TCNQ^-$ because of their large standard deviations.[11] Some rigid-body parameters are given in

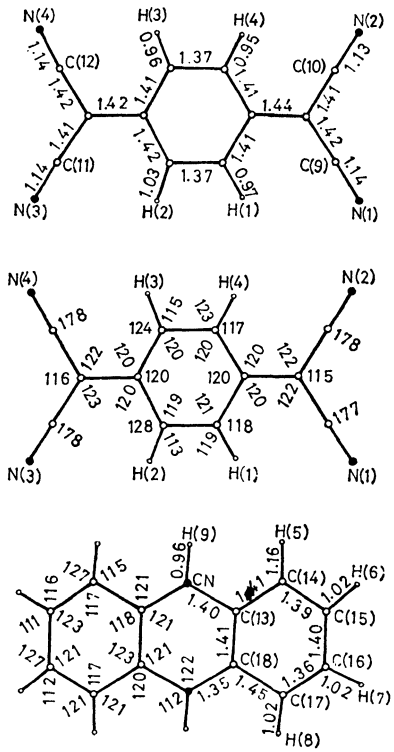

Fig. 3. Bond lengths (Å) and angles (°).
Estimated standard deviations for C–C(N) and C(N)–H bonds are about 0.018 and 0.10 Å, respectively. Those for C–C(N)–C(N) and C–C(N)–H angles are 1.1° and 5°, respectively.

Table 5. Rigid-body parameters of TCNQ

Principal axes in the form: **La**+**Mb**+**Nc**

axis	L	M	N
1	0.2808	0.0391	0.0600
2	0.0045	−0.0737	0.0050
3	−0.1308	0.0268	0.0378

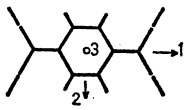

Molecular vibrational tensors

$$\mathbf{T}\times 10^4/419\begin{pmatrix} 8 & -19 \\ 280 & 7 \\ & 404 \end{pmatrix}\text{Å}^2 \qquad \boldsymbol{\omega}\times 10/465\begin{pmatrix} -14 & 10 \\ 20 & 7 \\ & 29 \end{pmatrix}\text{deg}^2$$

Principal axes of the **T** and $\boldsymbol{\omega}$ tensors relative to the molecular axes

R.m.s. amplitude	Direction cosines		
0.17 Å	−0.063	0.996	−0.064
0.20	−0.555	−0.088	−0.829
0.21	0.831	0.016	−0.556
1.2°	0.038	0.874	−0.485
1.8	0.003	−0.485	−0.874
6.8	0.999	−0.032	0.021

Table 6. Intermolecular distances and the temperatures showing the maximum electrical conductivities of some highly conducting TCNQ salts

	intermolecular distance		$T^{2-4)}$
	TCNQ	cation	
TTF-TCNQ[10]	3.17 Å	3.47 Å	60 K
NMP-TCNQ[6]	3.26	3.36	200
Q(TCNQ)$_2$[7]	3.22	3.50	240
ARD(TCNQ)$_2$	3.25	3.42	150

Table 5. Interplanar distances in columns of highly conducting salts are listed in Table 6.

Classification of Columnar Structures of TCNQ. The magnetic susceptibility of alkali metal–TCNQ can be understood on the basis of the one-dimensional band model.[12] The extraordinarily large conductivity of TTF–TCNQ seems to suggest that the band gap produced by the deformation of a linear chain of TCNQ is important for the electrical properties of this salt. Thus it may be useful to make an attempt to interpret the physical properties of TCNQ salts on the basis of one-dimensional band picture. Table 7 shows the relationship between the columnar structures and the electrical conductivities of some TCNQ salts of known crystal structure. The columns composed of monadic, diadic, triadic and tetradic units of TCNQ have been reported. The salts with triadic and diadic units are

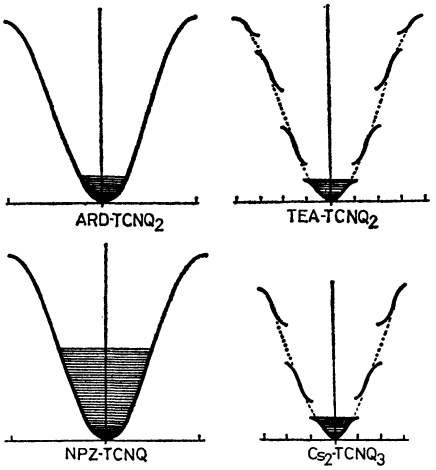

Fig. 4. Band structures for some types of TCNQ columns.

Table 7. Columnar structures and electrical resistivities of some TCNQ salts

	Cation : TCNQ	periodic unit	log $R^{a)}$	E_a(eV)$^{a)}$	Group
Rb-TCNQ I[b]	1:1	2	5	0.5	i
Cs_2TCNQ_3	2:3	3	4	0.3	i
$Morp_2TCNQ_3$	2:3	3	4	—	i
TEA(TCNQ)$_2$	1:2	4	1	0.13	ii
Meϕ_3P(TCNQ)$_2$	1:2	4	3	0.3	ii
Meϕ_3As(TCNQ)$_2$	1:2	4	3	0.3	ii
NproQ(TCNQ)$_2$	1:2	4	0	—	ii
Q(TCNQ)$_2$	1:2	1	−2	0.023[c]	iii
ARD(TCNQ)$_2$	1:2	1	−2	0.022[c]	iii
Rb-TCNQ II[b]	1:1	1	2	0.17	iii'[d]
NMP-TCNQ	1:1	1	−2	0.037[c]	iii
TTF-TCNQ	1:1	1	−4	0.006[c]	iii

Morp: Morpholinium, TEA: Triethylammonium, Meϕ_3P: Methyltriphenylphosphonium, Meϕ_3As: Methyltriphenyltriphenylarsonium, NproQ: *N*-(*n*-propyl)quinolinium.

a) Anisotropy of R(Ωcm at R.T.) is neglected. E_a is activation energy.[1-3,13,20] b) Rb-TCNQ I and RbTCNQ II are monoclinic and triclinic modification, respectively. c) Activation energy is that of low temperature region. d) The columnar structure of Rb-TCNQ II is similar to that of the salts of group (iii) but Rb-TCNQ I was not classified into group (iii) for convenience, because of its high resistivity. However, attention should be called to the fact that the conductivity of this modification is 10^3 times larger than that of the monoclinic modification.

low conductive(Cs_2TCNQ_3,[14] morpholinium$_2$TCNQ$_3$,[15] Rb-TCNQ I[16]). The salts with tetradic units are intermediately conductive(TEA(TCNQ)$_2$,[17] methyl triphenylphosphonium(TCNQ)$_2$, methyltriphenylarsonium(TCNQ)$_2$,[18] *N*-(*n*-propyl)quinolinium-(TCNQ)$_2$[19]). These facts indicate that the salts which contain two excess electrons in a repeating unit of TCNQ(2e/3TCNQ(Cs_2TCNQ_3), 2e/4TCNQ(TEA-(TCNQ)$_2$) are not highly conductive. Among these salts, those with tetradic units are more conductive. The high conductive salts are constructed from monadic units of TCNQ. The activation energy of the electrical conductivity of semiconductive region is less than 0.04 eV.[1-3,20] This small value suggests that the electrical conduction is not due to hopping process of excess electrons accompanying the deformation of TCNQ skeletons because such a process needs the activation energy more than 0.05 eV ($TCNQ_1^0 + TCNQ_2^- \rightarrow TCNQ_1^- + TCNQ_2^0, E > 0.05$ eV[17]) (a simple consideration is presented in Appendix). This seems to be one example showing the validity of the band picture. According to the band picture, the salts of groups (i) and (ii) (Table 7) are not metallic because they have filled bands (Fig. 4). Whereas, the salts of group (iii) with unfilled bands seem to be metallic and large electrical conductivity can be expected, which is consistent with the large conductivities of these salts. Thus, it may be useful to classify the columnar structure by the band picture.

Some Remarks on the Possibility of a Peierls Distortion of a Linear Chain of TCNQ. Although the columnar structures of the high conducting TCNQ salts indicate that these salts are metallic, they are semiconductive at low temperature. It may be of interest to see why they are not metallic at low temperature. The main reasons seem to be as follows:

(1) Owing to the Coulombic repulsion between two electrons on the same TCNQ site the antiferromagnetic state is considered to be more stable than the paramagnetic state, so that a simple band picture does not seem to be appropriate.[21] The metal-insulator transition of NMP–TCNQ has been analyzed in detail from this point of view.

(2) At low temperature, one-dimensional metallic lattice is unstable and the lattice seems to be distorted periodically with the wave vector of $2k_F$ (Peierls instability of one-dimensional lattice). Therefore, the metallic state may not be realized.[22]

A simple calculation was made in order to examine the possibility of a Peierls distortion of TCNQ columns.

If Peierls transition is realized at T_p, the following situations may result:

(1) At low temperature($T < T_p$), the electronic energy is lowered by the lattice distortion which produces the band gap at $k = k_F$.

(2) As temperature increases($T > T_p$), the free energy of the metallic state(columns with monadic units of TCNQ) becomes lower than that of semiconductive state(distorted columns) because the entropy of the metallic state increases. Accordingly the stabilization energy due to the lattice deformation will not be important.

Figure 5 shows a model of one-dimensional lattice

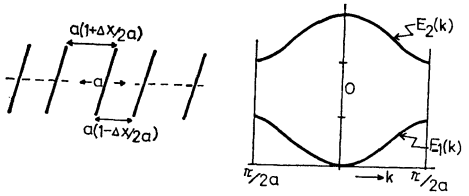

Fig. 5. A model of one-dimensional lattice of TCNQ and its split-band. a is assumed to be 3.25 Å.

of TCNQ. The two interplanar spacings $a(1+\Delta x/2a)$ and $a(1-\Delta x/2a)$ appear alternately. Each TCNQ is assumed to have one excess electron as in the case of NMP–TCNQ, which is usually called as a simple salt. Similar analysis may be applied to complex salts but the mode of alternation of lattice spacing will be more complicated. Δx is a parameter indicating the magnitude of the distortion of the lattice. Of course, real lattices are not one-dimensional, so that Δx may be regarded as a parameter representing a longitudinal modulation of a three-dimensional lattice. The tight-binding model of the band structure was adopted. The band structure is given by[12]

$$E_1(k) = -E_c(g^2 + \cos^2 ak)$$
$$E_2(k) = -E_1(k) \qquad (1)$$

where $E_c = 2(h_1h_2)^{1/2}$ and $g = E_g/E_c$ ($E_g = |h_1| - |h_2|$, h_1 and h_2 are transfer integrals ($|h_1| > |h_2|$)). The transfer integral is estimated from Eq. (2).

$$h = h_0 \exp(-p\Delta x) \qquad (2)$$

where $\Delta x = R - 3.16$ and $h_0 (= 1878$ K) and $p (= 3.91)$ are evaluated using the values employed by Vegter *et al.*[12] ($h(3.48$ Å$) = 538$ K, $h(3.16$ Å$) = 1878$ K). If $\Delta x \neq 0$, band gap is produced by lattice distortion at $k = k_F (= \pi/2a)$. The energy of lattice deformation is $\beta(\Delta x/2)^2/2$ per TCNQ(β=force const.). Free energy is written as

$$F = N\mu - k_B T \sum_\tau \log(1 + \exp(-(\varepsilon_\tau - \mu)/k_B T) + N\beta(\Delta x/2)^2/2 \qquad (3)$$

where $\varepsilon_\tau = E_1(k)$ or $E_2(k)$ and chemical potential μ is determined by,

$$N = \sum_\tau (\exp((\varepsilon_\tau - \mu)/k_B T) + 1)^{-1} \qquad (4)$$

By employing this simple model, Δx which minimizes free energy was obtained numerically at various temperatures. When $\beta = 1.2 \times 10^5$ dyn/cm, the transition indicating Peierls instability was obtained at about 200 K(T_p). Considering the stiffness of the columns of TCNQ, this value does not seem to be unreasonable. The temperature dependence of Δx is shown in Fig. 6a. Δx decreases to zero as temperature increases up to T_p and it is zero when $T > T_p$. Figure 6b shows the specific heat of the electrons which is calculated by use of the values of Δx shown in Fig. 6a. A peak accompanied by Peierls instability is obtained around the temperature about 20 K below T_p. The heat of the transition is about 130 cal/mol. The magnetic susceptibility (Fig. 6c) is temperature independent above T_p($\chi = 9.0 \times 10^{-5}$ emu), indicating the Pauli spin susceptibility.

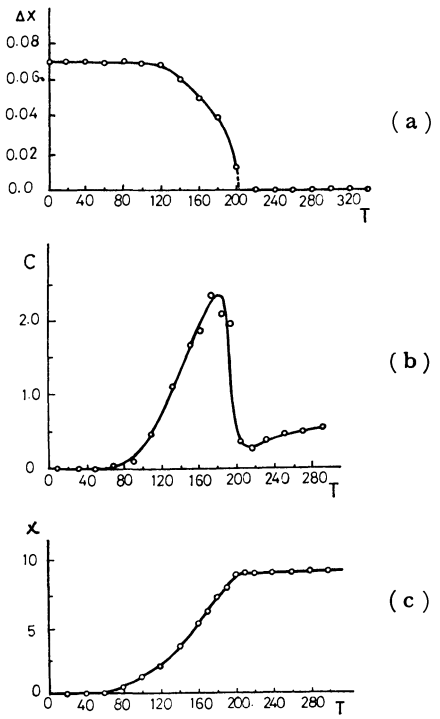

Fig. 6. (a) The temperature dependence of Δx(Å). (b) Specific heat. C is in $0.05k_B$ unit. (c) Magnetic susceptibility ($\chi \times 10^5$).

Thermal expansion of the intermolecular spacing was neglected in this model. Although this model seems to be oversim lified, it may be reasonable to consider that it shows the possibility of a Peierls distortion of high conducting TCNQ salts. Recently, Rice and Strässler have presented an interesting theory of Peierls distortion and Peierls soft mode of a quasi-one-dimensional band-conductor. Starting from a Fröhlich electron-phonon Hamiltonian, they show "how the giant Kohn anomaly in a higher-temperature metallic state can be the precusor of a second-order phase transition to a lower-temperature insulating phase (Peierls insulator)".[23] Zeller *et al.* showed that the evidence of Peierls instability or Kohn anomaly in one-dimensional conductors of type $K_2Pt(CN)_4Br_{0.30}\cdot xH_2O$.[24] The coherence length of the modulated chains is found to be larger than 400 Å. Anomaly in the longitudinal acoustic phonon branch of $K_2Pt(CN)_4Br_{0.3}\cdot 3H_2O$ was observed by inelastic neutron scattering.[25]

The calculations were performed on the HITAC 8700/8800 computer at the Computer Centre of Tokyo University.

The author would like to express his thanks to Professor Yoshihiko Saito for his keen interest and for his kind permission to use the four-circle diffractometer. He also thanks to Dr. Ichimin Shirotani for valuable discussions.

Appendix

The molecular geometry of TCNQ°(neutral molecule) is different from that of TCNQ$^-$.[11,26] The magnitude of the change in bond lengths corresponds to the change in their bond orders. It is the purpose of this Appendix to see a role of molecular deformation on a hopping motion of an excess electron TCNQ columns.

Table 8. Bond lengths and force constants

	TCNQ°	TCNQ$^-$	$\lvert\Delta r\rvert$	k[30]	m
1	1.344 Å	1.356 Å	0.012 Å	5.7 mdyn/Å	4
2	1.446	1.425	0.021	3.6	8
3	1.371	1.401	0.030	4.8	4
4	1.434	1.417	0.017	4.9	8
5	1.140	1.155	0.015	16.7	8

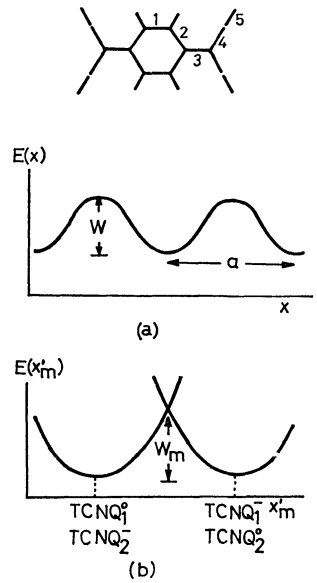

Fig. 7. (a) Potential energy-configuration diagram. (b) The deformation energy of TCNQs for one-electron transfer.

Because the frequency of hopping motion of an excess electron ($\nu_0 \simeq 10^{12}$ s^{-1})[27] is considered to be less than that of molecular vibrations ($\nu_m \simeq 10^{13}$ s^{-1}), the hopping motion of the excess electron may be accompanied by the molecular deformation. Consider an excess electron moving on an adiabatic potential surface $E(x)$ (see § 4 in Ref. 28). $E(x)$ is a periodic potential with a period of a Å. By a simple consideration, following equation can be obtained.[28,29]

$$\sigma = \nu_0 e^{-W/kT} Nne^2a^2/kT \qquad \text{(A1)}$$

where σ is the electrical conductivity, N is the number of chains of TCNQ per unit cross sectional area and n is the electron density on the chain. If $W=0$, Eq. (A1) is identical to that derived by Bloch *et al.* (Einstein equation).[27] σ is maximum when $T=W/k$ (Eq. (A1) is not accurate when $kT \geqq W$ but it may be useful for qualitative discussion). The activation energy may be written as

$$W = W_l + W_m, \qquad \text{(A2)}$$

where W_l and W_m are deformation energies due to lattice and molecular distortions, induced by the excess electron respectively. In most cases, W_m may be approximately equal to the energy of deformation of TCNQ and can be estimated using molecular geometries obtained by X-ray crystal structure analyses (Table 8 and Fig. 7)

$$W_m = \sum_i m_i k_i (\Delta r_i/2)^2/2 \qquad \text{(A3)}$$

where k_i is the force constant of the i-th bond, Δr_i is the change of bond length and m_i is the multiplicity of the i-th bond per

two TCNQs.

W_m is calculated to be 0.059 eV. Therefore, $W(=W_1+W_m)>W_m\simeq 0.06$ eV. Considering that W is larger than kT (=0.025 eV at R. T.), the molecular distortion seems to play important role when an excess electron moves between strongly localized states. Of course, the situation is more complicated in real crystals. Electron-electron interaction may be important. However, concerning the interaction between molecular vibrations and excess electrons, the situation would be similar to that of this simple model to some extent. From this point of view, it may be unlikely that the electric conduction of the highly conductive TCNQ salts is due to the simple hopping mechanism because the activation energies are less than 0.04 eV.[1-3,20]

References

1) L. B. Coleman, M. J. Cohen, D. J. Sandman, F. G. Yamagishi, A. F. Galito, and A. J. Heeger, *Solid State Column.*, **12**, 1125 (1973). J. Ferraris, D. O. Cowan, V. Walatka, and J. H. Perlstein, *J. Amer. Chem. Soc.*, **95**, 948 (1973). P. M. Chaikin, J. F. Kwak, T. E. Jones, A. F. Galito, and A. J. Heeger, *Phys. Rev. Lett.*, **31**, 601 (1973). J. Bardeen, *Solid State Commun.*, **13**, 357 (1973). A. A. Bright, A. F. Galito, and A. J. Heeger, *ibid.*, **13**, 943 (1973).
A. N. Bloch, J. F. Ferrais, D. O. Cowan, and T. O. Poehler, *ibid.*, **13**, 753 (1973). P. W. Anderson, P. A. Lee, and M. Saitoh, *ibid.*, **13**, 595 (1973). P. A. Lee, T. M. Rice, and P. W. Anderson, *Phys. Rev. Lett.*, **31**, 462 (1973).

2) A. J. Epstein, S. Etemad, A. F. Galito, and A. J. Heeger, *Phys. Rev., B*, **5**, 952 (1971). L. B. Coleman, J. A. Cohen, A. F. Galito, and A. J. Heeger, *ibid., B*, **7**, 2122 (1973).

3) V. Walatka and J. H. Perlstein, *Mol. Cryst. Liq. Cryst.*, **15**, 269 (1971).

4) L. I. Bravov, D. N. Fedutin, and I. F. Shchegolve, *Sov. Phys. JETP*, **32** 612 (1971).

5) "International Tables for X-ray Crystallography," (1962). Vol III, Birmingham: Kynoch Press. References therein.

6) C. J. Fritchie, *Acta Crystallogr.*, **20**, 892 (1966).

7) H. Kobayashi, F. Marumo and Y. Saito, *ibid., B*, **27**, 373 (1971).

8) I. Shirotani and H. Kobayashi, This Bulletin, **46**, 2595 (1973).

9) R. P., Shibaeva, L. O. Atovmyan, and M. N. Orfanova, *Chem. Commun.*, **1969**, 1494.

10) T. E. Philips, T. J. Kistenmacher, J. P. Ferrais and D. O. Cowan *ibid.*, **1973**, 471.

11) H. Kobayashi, This Bulletin, **46**, 2945 (1973).

12) J. G. Vegter, J. Kommandeur, and P. A. Fedders, *Phys. Rev., B*, **7**, 2929 (1973).

13) L. R. Melby, R. J. Harder, W. R. Hertler, W. Mahler, R. E. Benson, and W. E. Mochel, *J. Amer. Chem. Soc.*, **84**, 3374 (1962). W. J. Siemons, P. E. Biersted, and R. G. Kepler, *J. Chem. Phys.*, **39**, 3523 (1963).

14) C. J. Fritchie and P. Arthur, *Acta Crystallogr.*, **21**, 139 (1966).

15) T. Sundaresan and S. C. Wallwork, *ibid., B*, **28**, 491 (1972).

16) A. Hoekstra, T. Spoelder, and A. Vos, *ibid., B*, **28**, 14 (1972).

17) H. Kobayashi, Y. Ohashi, F. Muramo, and Y. Saito, *ibid., B*, **26** 459 (1970).

18) A. T. McPhail, G. M. Semeniuk, and D. B. Chesnut, *J. Chem. Soc., A*, **1971**, 2174.

19) T. Sundaresan nad S. C. Wallwork, *Acta Crystallogr., B* **28**, 1163 (1972).

20) I. F. Shchegolev, *Phys. Stat. Sol., A*, **12**, 9 (1972).

21) H. Shiba, *Bussei*, **13**, 615 (1972). D. Adler, *Solid State Phys.*, **21**, 1 (1968). B. Johansson and K. F. Berggren, *Phys. Rev.*, **181**, 855 (1969).

22) R. E. Peierls, "Quantum Theory of Solids," Oxford U. P., London (1955), D. Adler and H. Brooks, *Phys. Rev.*, **155**, 826 (1967).

23) M. J. Rice and S. Strässler, *Solid State Commun.*, **13**, 125 (1973).

24) R. Comes, M. Lambert, H. Launois, and H. R. Zeller, *Phys. Rev., B*, **8**, 571 (1973).

25) B. Renker, H. Rietschel, L. Pintschovius, W. Gläser, P. Brüesch, D. Kuse, and M. J. Rice, *Phys. Rev. Lett.*, **30**, 1144 (1973).

26) F. H. Herbstein, "Perspectives in Structural Chemistry," eds. J. D. Dunitz and J. A. Ibers, Vol. IV, (1971).

27) A. N. Bloch, R. B. Weisman, and C. M. Verma, *Phys. Rev. Lett.*, **28**, 753 (1972).

28) J. Yamashita and T. Kurosawa, *J. Phys. Soc. Japan*, **15**, 802 (1960).

29) H. Fröhlich, "Theory of Dielectrics," Clarendon Press, Oxford (1958).

30) T. Takenaka, General Symposium on Molecular Structure and Spectroscopy, Fukuoka, Oct. 1969.

Some Environmental Effects on the shf Lines in the ESR Spectra of Vanadyl Tetraphenylporphin

Mitsuo SATO and Takao KWAN

Faculty of Pharmaceutical Sciences, The University of Tokyo, Bunkyo-ku, Tokyo 113

(Received October 8, 1973)

The ESR spectra of vanadyl tetraphenylporphin (VOTPP) have been studied in a number of organic matrices, with special attention paid to the resolution of the nitrogen shf lines. The matrices were classified into three groups according to their effects on the resolutions of the vanadium hf lines and of the nitrogen shf lines. In the A-group matrices, the spectra of VOTPP displayed well-resolved hf lines, accompanied by shf splittings; in the B-group matrices, the spectra gave rise to well-resolved hf lines, but without shf splittings, and in the C-group matrices, the hf lines were resolved only poorly. It is suggested that a high dispersion of VOTPP molecules is required for the higher resolution of spectra.

The ESR spectra of vanadyl porphyrin complexes have been studied by many workers,[1-4] but superhyperfine (shf) splittings due to the ligand nitrogen nuclei($I=1$) have been only poorly characterized.

For example, it was shown by O'Reilly[1] and Roberts *et al.*[2] that each of the vanadyl complexes of etioporphyrin, I and II, the mesoporphyrin IX dimethylester, and the deuteroporphyrin IX dimethylester gave the hyperfine (hf) structure due to the vanadium nucleus ($I=7/2$), but none had any observable shf splittings. Kivelson *et al.*,[3] however, found that nitrogen shf lines could be resolved when vanadyl tetraphenylporphin (VOTPP) was diluted in the frozen matrices of $CHCl_3$ and CS_2 although the spectra of VOTPP in other matrices failed to yield any evidence of shf splittings. On the contrary, Assour[4] shortly afterward reported that VOTPP did not display the shf splittings even in the $CHCl_3$ and CS_2 matrices.

More recently, the present authors,[5] studying the spectra of vanadyl phthalocyanine (VOPc) diluted in the matrices of conc. H_2SO_4, α-chloronaphthalene, quinoline, metal-free phthalocyanine, and zinc phthalocyanine,[6] found that the spectra of VOPc can give rise to nitrogen shf splittings in all the matrices investigated. This result was in contrast with those of previous studies of vanadyl porphyrin complex, and stimulated us to reinvestigate the spectra of VOTPP diluted in many kinds of organic matrices, with special attention being paid to the effects of matrix states on the resolution of the shf lines. As a result, we found, contrary to the previous authors,[3,4] that shf lines could be easily detected in almost all the matrices and that their resolution is associated with the homogeneity of the matrix environment of VOTPP. The present paper will report the results of such investigations.

Experimental

Materials. *Vanadyl Tetraphenylporphin (VOTPP)*: Tetraphenylporphin (H_2TPP) and its vanadyl complex (VOTPP) were prepared according to the procedure in the literature[7] and were purified by recrystallization from benzene. The thin-layer chromatograph[8] showed few impurities to be present.

Organic Matrices: The various organic solvents and crystals used as diluents for VOTPP are listed in Table 1. These were all commercial samples either of a reagent grade or of an extra pure grade; all of them except α- and β-methylnapthalene, *o*-dichlorobenzene, triphenylphosphate, and triphenylmethane were further purified, either by distillation or by recrystallization.

Preparation of Diluted VOTPP Samples. *VOTPP in Frozen Organic Solvents*: The VOTPP was dissolved in various organic solvents in a concentration of $1-5\times10^{-3}$ mol/l at room temperature. Each solution was then subjected to rapid cooling with liquid nitrogen to form either a polycrystalline or glassy matrix. In the present paper, the expression "polycrystalline state" will arbitrarily be used to signify the matrix state accompanied by polycrystals which scatter light strongly, while the term "glassy state" indicates the transparent matrix state. The two states were easily distinguishable from one another with the naked eye. The matrix states for the respective frozen solutions are shown in Table 1 in terms of "p" (polycrystalline state) and "g" (glassy state) respectively.

VOTPP in Organic Crystals: The VOTPP samples diluted in organic crystals were prepared in the following way otherwise stated. After the VOTPP had been dissolved in 100—500 times their weight of melts of organic crystals which had been kept at a temperature 50—60 °C above their melting points, the melts were suddenly cooled to 77 K with liquid nitrogen. Although most of the samples formed excellent glasses at this stage, they were later warmed to room temperature. This procedure generally gave finely polycrystalline matrices.

VOTPP in H_2TPP: A chloroform solution containing VOTPP and H_2TPP in a weight ratio of 1 : 200 was poured into a large amount of methanol, causing finely-dispersed precipitates to separate out. The precipitates thus obtained were washed with methanol and dried. The powder was then heat-treated in a vacuum at 300 °C.

Measurements of the ESR Spectra. The ESR spectra were recorded with a JEOL spectrometer, Model JES P-10 (X-band), using 100 KHz field modulation. The magnetic field was calibrated with an ESR marker, MgO: Mn^{2+} powder, supplied by JEOL. The *g*-values were determined using powdered DPPH, with $g=2.0036$ as the standard.

The VOTPP samples diluted in frozen organic solvents were measured at 77 K, while those in organic crystals were measured mainly at room temperature. Degassing was not carried out for all the samples, since the effect of oxygen on the linewidths was preliminarily found to be negligible for VOTPP in the $CHCl_3$, toluene, H_2TPP, and triphenylphosphine matrices.

Results and Discussion

As is summarized in Table 1, the organic solvents and crystals employed as the diluents of VOTPP were

Table 1. Resolution of hf and shf lines in ESR spectra of VOTPP diluted in various organic matrices

	Matrices		Vanadium hf lines	Nitrogen shf lines	Diluted states of VOTPP
	Frozen organic solvent[a]	Organic crystals			
A-Group	Toluene(g) *o*-Xylene(p) *m*-Xylene(p) Xylene(g)[b] α-Methylnaphthalene(g) $CHCl_3$(p) CH_2Cl_2(p) Quinoline(g) α-Chloronaphthalene(p) *o*-Dichlorobenzene(p) *o*-Fluorotoluene(p)	H_2TPP Triphenylmethane *sym*-Triphenylbenzene Triphenylphosphine Triphenylphosphate[d]	well resolved	resolved	well dispersed (homogeneous environment)
B-Group	*p*-Xylene(p) CS_2(p)[c] Tetrahydrofuran(p) α-Methyltetrahydrofuran(g) Pyridine(p) Isoquinoline(p)		well resolved	unresolved	well dispersed (inhomogeneous environment)
C-Group	Benzene(p) CCl_4(p)	Naphthalene β-Methylnaphthalene	poorly resolved	unresolved	aggregated

a) (g): "glassy state", (p): "polycrystalline state". b) A commercial mixture of three isomeric xylenes. c) Many attempts to obtain an evidence of shf splittings in the CS_2 matrix were unsuccessful. This agreed with the result by Assour[4] rather than that by Kivelson *et al.*[3] d) See text.

classified conventionally into three groups according to their effects on the resolutions of the vanadium hf lines and the nitrogen shf lines. In the "A group" matrices, the spectra of VOTPP gave rise to well-resolved vanadium hf lines, accompanied by nitrogen shf splittings; in the "B-group" matrices, the spectra gave rise to well-resolved hf lines, but without any evidence of shf splittings, and finally, in the "C-group" matrices, only poorly-resolved hf lines were observed.

Vanadium hf Lines. As has been reported in the literature,[3,4] the spectra of VOTPP showed, in general, eight hf lines due to the vanadium nuclei ($I=7/2$) in the matrices employed. The present work also showed such a characteristic. However, the apparent linewidth of hf lines was found to depend upon the kind of matrix species, hence causing the degree of hf resolution to differ from one matrix to the other. The linewidths observed in the A-group and B-group matrices were much smaller than those observed in the C-group matrices. Some representative spectra are illustrated in Figs. 1 and 2.

The interpretation of these spectra follows closely the method developed by Sands[9] and Bleaney.[10] The spin Hamiltonian used in the one reflecting the axial symmetry:

$$\mathcal{H} = \beta[g_{//}H_zS_z + g_\perp(H_xS_x+H_yS_y)] + A_{//}I_zS_z + A_\perp(I_xS_x+I_yS_y) \quad (1)$$
$$S = 1/2, \quad I = 7/2$$

where $A_{//}$ and $A_\perp$ are the vanadium hf coupling constants and where the other symbols have their usual meanings. The spectrum shown in Fig. 1 is composed of two distinct set of hf lines that correspond to $g_{//}$ and $g_\perp$; the two weak peaks at the low-field peaks

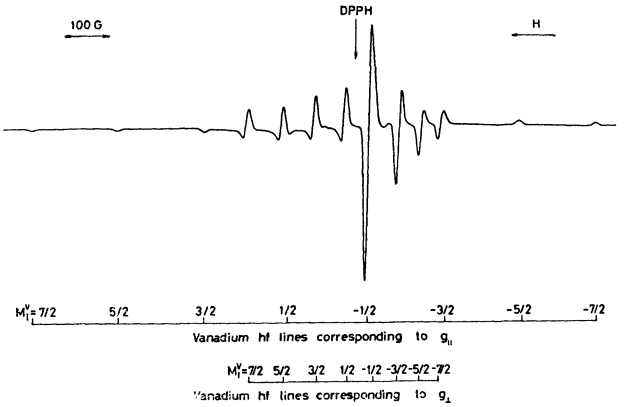

Fig. 1. ESR spectrum typical for VOTPP diluted in the A-group and B-group matrices.
Matrix: Toluene, Concentration of VOTPP: [VOTPP]$=2.9\times10^{-3}$ M, Temperature: $T=77$ K.
(Two sets of vanadium hf lines that correspond to $g_{||}$ and $g_\perp$ are indicated at the bottom of the figure. M_I^V refers to the nuclear-spin quantum number of the vanadium atom and is assigned on the basis of the negative values of hf constants.)

and the three high-field peaks correspond to $g_{//}$, while the strong central peaks are associated with $g_\perp$. However, such a spectral feature is rather obscure in the spectrum shown in Fig. 2 because of its larger linewidth. The spin Hamiltonian parameters obtained from some of the A-group and B-group matrices are summarized in Table 2.

Since a smaller linewidth is usually taken to imply smaller magnetic interaction between the neighboring VOTPP molecules, it may be suggested that VOTPP

TABLE 2. ELECTRON SPIN RESONANCE DATA OF VOTPP DILUTED IN ORGANIC MATRICES

Matrices	$g_{//}$	$g_{\perp}$	$A_{//}$ ($\times 10^{-4}$ cm^{-1})	$A_{\perp}$ ($\times 10^{-4}$ cm^{-1})	Average separation of shf multiplets (G)
Toluene	1.960	1.985	160	56	~2.8
$CHCl_3$	1.962	1.986	159	55	2.7~2.9
CH_2Cl_2	1.984	1.984	156	54	2.7~3.0
α-Methyltetrahydrofuran	1.963	1.984	157	55	unresolved
Pyridine	1.964	1.984	157	54	unresolved
H_2TPP	1.961	1.986	160	57	2.6~2.8
Triphenylphosphine	1.960	1.985	159	57	~2.8

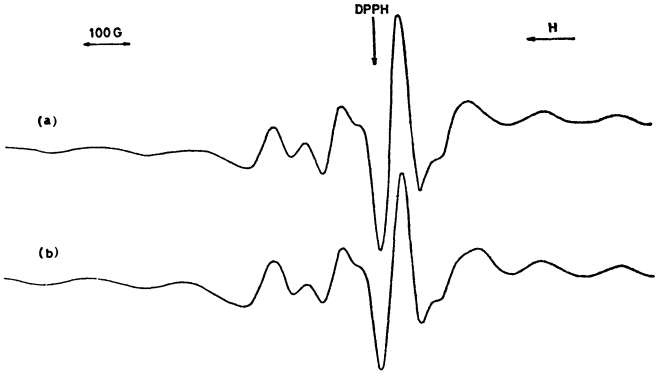

Fig. 2. ESR spectrum typical for VOTPP diluted in the C-group matrices and that obtained from the polycrystalline VOTPP samples.
(a) Matrix: Benzene, [VOTPP]$=1.5\times10^{-3}$ M, $T=$ 77 K. (b) Polycrystalline VOTPP, $T=77$ K.

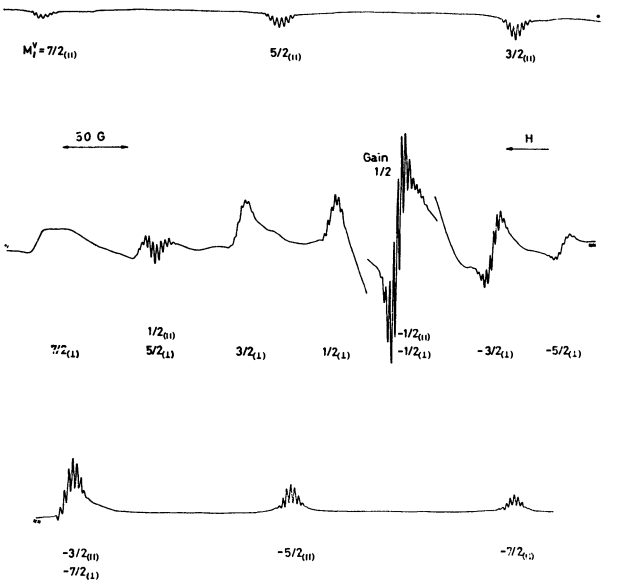

Fig. 3. Nitrogen shf splittings recorded for VOTPP diluted in the $CHCl_3$ matrix. [VOTPP]$=2.9\times10^{-3}$ M, $T=77$ K.

molecules are highly dispersed in the A-group and B-group matrices, without any intermolecular interactions such as association and aggregation. It is interesting to note that the apparent hf linewidth observed in the A-group matrices did not differ much from that observed in the B-group matrices, irrespective of their different effects on the shf resolutions. This aspect will be discussed below.

On the other hand, the spectra observed in the C-group matrices displayed an extraordinarily large linewidth, indicating that strong magnetic interactions between neighboring VOTPP molecules exist in these matrices. Moreover, the spectral line shape was quite similar to that observed for the polycrystalline VOTPP sample, as is shown in Fig. 2. It can, therefore, be presumed that VOTPP molecules are present in either a crystalline or an aggregated form in the C-group matrices. Probably, the aggregation of the VOTPP molecules proceeded during the course of cooling with liquid nitrogen. Actually, microcrystals of VOTPP were observed in the frozen matrix of benzene. Moreover, some finely-dispersed precipitates of VOTPP were perceptible when the frozen CCl_4, naphthalene, and β-methylnaphthalene solutions were thawed.

Nitrogen shf Lines. When ESR spectra were recorded with a small amplitude of the field modulation such as 0.5 G, some of the vanadium hf lines were further split into shf lines due to the magnetic interaction between the V^{4+} electron and the pyrrole nitrogens. Typical examples are illustrated in Figs. 3 and 4. The matrices which gave rise to shf splittings are listed in Table 1, where it is apparent that the great majority belong to the A-group. This result might be compared with the previous results[3,4] which showed that the spectra of VOTPP seldom gave rise to shf splittings.

Judging from the spectral features of the vanadium hf lines in various matrices, it seems very likely that a high dispersion of VOTPP molecules through the matrices is essential for the resolution of shf lines, although the state of dispersion alone would not be sufficient to meet the requirements.

In the A-group matrices, the best resolution of shf lines was recorded from the $CHCl_3$ matrix. It can be seen from Fig. 3 that each of the hf lines is further split into shf multiplets, which are apparently composed of nine equally-spaced lines of varying intensities. Their average separations were 2.9 and 2.7 gauss for the parallel and perpendicular hf components respectively, indicating that the nitrogen shf interaction is nearly isotropic.

The shf Hamiltonian ($\mathscr{H}_{shf}$) describing the system of this sort can generally be expressed as.[11]

$$\mathscr{H}_{shf} = \boldsymbol{S}\cdot\sum_{n}\boldsymbol{A}_n\cdot\boldsymbol{I}_n \qquad (2)$$

where $\boldsymbol{A}_n$ and $\boldsymbol{I}_n$ refer to the shf tensor and the nuclear

spin operator for the ligating nitrogen atom, n, respectively. Since the shf tensors, $\boldsymbol{A}_n$, have different functional forms for different nitrogen atoms in terms of the molecular coordinates (x,y,z), it is a rather complicated problem to derive the resonance field from Eq. (2). However, if one assumes that the shf tensors are isotropic and that the four nitrogen ligands are magnetically equivalent, Eq. (2) can simply be rewritten as:

$$\mathscr{H}_{\text{shf}} = a^{\text{N}}(S_z I_z^{\text{N}} + S_x I_x^{\text{N}} + S_y I_y^{\text{N}}) \quad (3)$$

where a^{N} represents the isotropic shf constant and where I_z^{N}, I_x^{N}, and I_y^{N} are the sums of the nitrogen nuclear-spin components in the z, x, and y directions respectively.

One can, then readily obtain the predicted spectrum in which each of the vanadium hf lines is split into 9 shf components, with an equal separation of a^{N} and with the intensity ratio of 1 : 4 : 10 : 16 : 19 : 16 : 10 : 4 : 1. The shf multiplets observed on the hf components other than that corresponding to $M_{\text{I}}^{\text{V}}=-1/2$ are, in fact, consistent with this expectation, with the isotropic shf constant being approximated as $a^{\text{N}}=2.8$ G. The observation of at least 13 shf components on the $M_{\text{I}}^{\text{V}}=-1/2$ hf line is not in conflict with the above prediction either, since the $M_{\text{I}}^{\text{V}}=-1/2$ hf line exhibits a "polycrystalline anomalous line" which has previously been discussed.[12]

It was noted that the resolution of the shf multiplets is rather poor except for the $CHCl_3$ matrix in the A-group matrices. In these matrices, the M_{I}^{V} values of the hf components with resolved shf multiplets were also found to differ from those observed in the $CHCl_3$ matrix. As can be seen from Fig. 4, the shf multiplets have a tendency to be resolved not on the parallel hf components but the perpendicular hf components.

Although the accurate determination of the shf constant was difficult due to its poor resolution, the average separation of the shf lines was estimated to range from 2.6 to 3.0 G in the matrices of toluene, xylene, H_2TPP, CH_2Cl_2, and triphenylphosphine. If Eq. (3) is valid in these cases, the above values of 2.6—3.0 G can be regarded as a^{N}, in agreement with the the shf constant, $a^{\text{N}}=2.8$ G, obtained for the $CHCl_3$ matrix.

It follows from the above arguments that the matrices have little effect on the magnitude of the shf constant, while they play a significant role in the resolution of shf multiplets.

Environmental Effect on the Resolution of shf Lines.

While the solution of $CHCl_3$ or CH_2Cl_2 was polycrystalline by itself at 77 K, the mixed solution of $CHCl_3$–CH_2Cl_2 (1 : 1 volume ratio) exhibited an excellent glassy state when it was subjected to rapid cooling with liquid nitrogen. The shf lines observed in these different matrix states are compared in Fig. 5. It can clearly be seen from Fig. 5 that the mixed $CHCl_3$–CH_2Cl_2 solution gives no appreciable shf splittings, while both solutions show well-resolved shf lines.

It might be considered, therefore, that VOTPP molecules in the $CHCl_3$–CH_2Cl_2 glass have slightly different g-values and hf coupling constants, hence causing the apparent absence of shf splittings in the observed spectrum.

Triphenylphosphine formed an excellent glass at 77 K when the molten sample was subjected to sudden

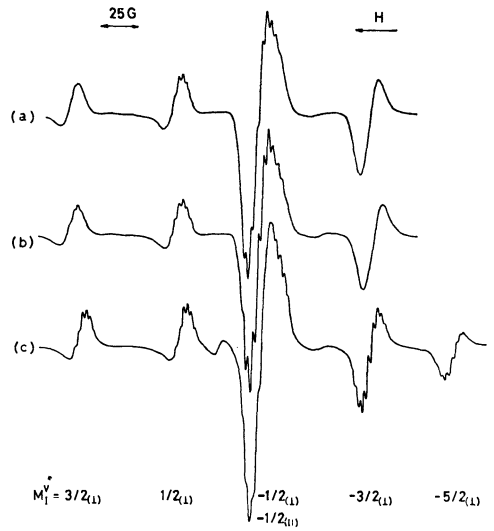

Fig. 4. Nitrogen shf splittings recorded for VOTPP diluted in some of the A-group matrices. (Only the central field portion of the spectra are reproduced in the figure.)
(a) Matrix: Toluene, [VOTPP]=4.4×10^{-3} M, T= 77 K. (b) Matrix: Xylene (commercial mixture of the three isomeric xylenes), [VOTPP]=4.4×10^{-3} M, T=77 K. (c) Matrix: H_2TPP, Weight ratio of VOTPP/H_2TPP; about 1/200, T=room temp.

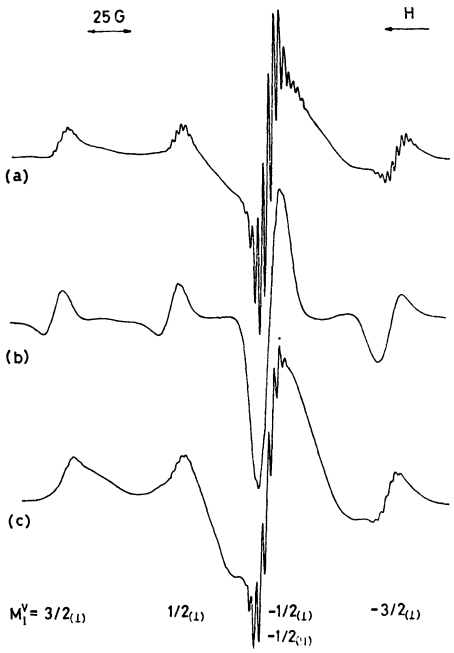

Fig. 5. Effect of matrix states on the resolution of nitrogen shf lines.
VOTPP diluted in the "polycrystalline" $CHCl_3$ matrix (a), in the "glassy" $CHCl_3$–CH_2Cl_2 (volume ratio, 1:1) matrix (b), and in the "polycrystalline" CH_2Cl_2 matrix (c). [VOTPP]=$2.9-3.2\times10^{-3}$ M, T=77 K.

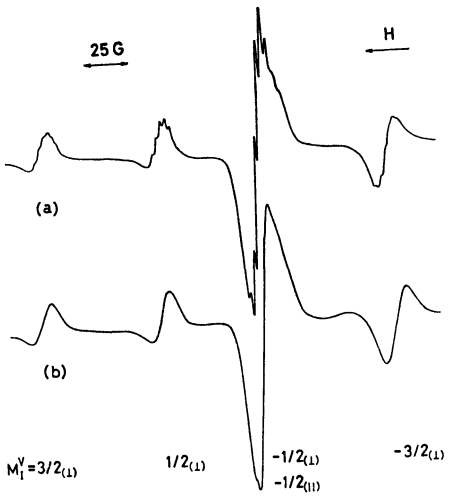

Fig. 6. Effect of matrix states on the resolution of nitrogen shf lines.
VOTPP diluted in the "polycrystalline" triphenylphosphine matrix (a) and in the "glassy" triphenylphosphine matrix (b). Weight ratio of VOTPP/triphenylphosphine: 1/250, $T=77$ K.

cooling with liquid nitrogen; the resulting glassy matrix was, however, converted into a polycrystalline one on warming to room temperature. Such a polycrystalline matrix was also formed upon cooling the molten triphenylphosphine slowly to room temperature. The ESR spectra obtained in these glassy and polycrystalline matrices are illustrated in Fig. 6, from which it can also be seen that the shf lines are resolved in the polycrystalline matrix rather than in the glassy one.

On the other hand, a commercial mixture of three isomeric xylenes was frozen in a glassy state at 77 K, each of the *o*-, *m*-, and *p*-xylenes was polycrystalline at 77 K. The order of the increasing resolution of the shf lines in these matrices was; xylene (mixture of the three isomers) > *o*-xylene $\simeq$ *m*-xylene > *p*-xylene. This is in marked contrast with the $CHCl_3$-CH_2Cl_2 systems.

For triphenylphosphate, both the glassy and polycrystalline samples were prepared in the same manner as triphenylphosphine. In this case, however, the resolution of the shf lines in the polycrystalline matrices was found to depend upon the method of sample preparation. When the polycrystalline matrix was prepared by cooling the molten triphenylphosphate to room temperature, the spectrum of VOTPP exhibited poorly-resolved hf lines without any shf splittings like that shown in Fig. 2. This indicates that the aggregation of VOTPP molecules takes place in the course of slow cooling. On the other hand, in the polycrystalline matrix obtained by warming the frozen glassy sample to room temperature, the shf lines were clearly detected. However, this spectrum changed from a well-resolved type into a poorly-resolved one with the lapse of time, suggesting that VOTPP molecules can diffuse through the polycrystalline triphenylphosphate matrix to form an aggregated state.

To summarize briefly, there is much evidence to show the importance of environments in the ESR spectra of VOTPP. A homogeneous dispersion of VOTPP molecules in a given matrix usually yields a highly-resolved spectrum. However, the method of obtaining such a dispersed state sensitively depends on the kind of matrix species and the mode of sample preparation.

References

1) D. E. O'Reilly, *J. Chem. Phys.*, **29**, 1188 (1958).
2) E. M. Roberts, W. S. Koski, and W. S. Caughey, *ibid.*, **32**, 591 (1961).
3) D. Kivelson and S. K. Lee, *ibid.*, **21**, 1896 (1964).
4) J. M. Assour, *ibid.*, **43**, 2477 (1965).
5) M. Sato and T. Kwan, *ibid.*, **50**. 558 (1969).
6) M. Sato and T. Kwan, unpublished work.
7) J. T. Horeczy, B. N. Hill, A. E. Walters, H. G. Schutze, and W. H. Bonner, *Anal. Chem.*, **27**, 1899 (1955).
8) M. Sato and T. Kwan, *Chem. Pharm. Bull.* (Tokyo), **20**, 840 (1972).
9) R. H. Sands, *Phys. Rev.*, **99**, 1222 (1955).
10) G. Bleaney, *Phil. Mag.*, **42**, 441 (1951).
11) M. Abkowitz, I. Chen, and J. H. Sharp, *J. Chem. Phys.*, **48**, 4561 (1968).
12) R. Neimen and D. Kivelson, *ibid.*, **35**, 156 (1961); H. R. Gersmann and J. D. Swalen, *ibid.*, **36**, 3221 (1962).

Studies of the ESR Spectra of Semiquinone Anions of Xanthene Dyes. Variation in the Linewidth of the Phloxine Semiquinone Anion with the Temperature and the Viscosity in Protic Solvents

Kazuie KIMURA and Masashi IMAMURA

The Institute of Physical and Chemical Research, Wako, Saitama 351

(Received October 13, 1973)

The ESR linewidths of semiquinone anions of xanthene dyes in alkaline protic solvents were studied as functions of the temperature and the viscosity. It was found that the linewidths of phloxine semiquinone, the ESR spectra of which show three hyperfine lines due to two equivalent protons, decrease with a decrease in the temperature or an increase in the viscosity of the solvents, and vary unimolecularly. Such a variation can not be explained either by a usual "chemical exchange" process between different states or by intramolecular motion. We propose that the linewidths may be due to the modulation of the hyperfine coupling constants of H atoms; the modulation results from the dissociation and/or distortion of the hydrogen bonds.

We previously reported the formation of stable semiquinone anions of xanthene dyes by the γ-irradiation of degassed alkaline alcoholic solutions, and the photo-dehalogenation reaction of the halogenated ones.[1]

In the course of ESR studies of these semiquinone anions, we have found that the linewidths of the ESR spectra of some of them, *e. g.*, phloxine semiquinone (X=Br and Y=Cl, in Fig. 1), decrease without any further splitting of their three lines with a decrease in the temperature or an increase in the viscosity of solutions, and that the process of sharpening is pseudo-unimolecular.

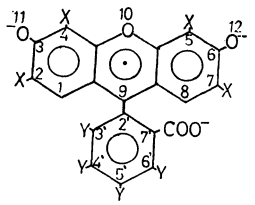

Fig. 1. Structure of xanthene-dye semiquinone anion.

The linewidth variation can not be explained in terms of a "chemical exchange" process between different states or the relaxation matrix theory developed by Freed *et al.*[2]

The present results seem to suggest that hydrogen bonding between semiquinone anions and solvent molecules plays an important role in the variation of linewidths. This paper will describe the results obtained with phloxine semiquinone and the discussion leading to the conclusion put forward above.

Experimental

Materials. The xanthene dyes were recrystallized three times from slightly alkaline methanolic solutions. The alcohols and water were purified by distillation as has been described previously.[1] The glycerol was distilled *in vacuo*. Extra pure lithium, sodium, and potassium hydroxides were used without further purification.

Preparation of Semiquinone Solutions. Xanthene semiquinones (S) were prepared by the ^{60}Co γ-irradiation of degassed alkaline solutions of xanthene dyes (D) in alcohols or in water containing small amounts of methanol at room temperature. The reduction of D proceeds by these reactions:

$$RCH_2OH \xleftarrow{r\text{-}\wedge\!\vee\!\wedge} e^-_{sol}, \dot{H}, \dot{R}CHOH$$

$$D + e^-_{sol} \longrightarrow S$$

$$D + \dot{H} \xrightarrow{OH^-} S + H_2O$$

$$D + \dot{R}CHOH \xrightarrow{OH^-} S + RCHO + H_2O$$

This method gives S in a higher yield and with fewer by-products than other methods, such as chemical or photochemical reduction. The concentration of S produced was adjustable by controlling the initial concentration of the dye and the γ-ray dose, and was determined spectrophotometrically. The semiquinone solutions were so stable in the dark that no detectable change in the concentration was found during ESR measurements.

The ESR spectra were recorded by using a JEOL JES-X spectrometer at various temperatures between -100 and 60 °C with an accuracy of $\pm$0.5 °C. The temperature of the cavity was carefully kept constant by circulating thermostated water through a pipe around the cavity. The magnetic field was calibrated by means of proton resonance.

Results

The Lineshape and Temperature Dependence of the Linewidth. Phloxine semiquinone gives three well-resolved hyperfine lines with an intensity ratio of 1 : 2 : 1 in the temperature range of -80—$+60$ °C. They have the Lorentzian shape and equal linewidths, independent of the total nuclear spin quantum number, M_1, in the temperature range of -50—$+5$ °C. Below -60 °C, the lines were broadened heterogeneously and were dependent on M_1, indicating "anisotropic broadening."

On the other hand, as is shown in Fig. 2, the linewidth of 1.02$\pm$0.02 gauss at 23 °C in methanolic solutions (T/η=510 K/cp) decreases with a decrease in the temperature to attain a minimum of 0.4$\pm$0.02 gauss at -58 °C (T/η=80 K/cp). No such a variation in the linewidth has been previously reported, and so detailed experiments were focused on this point.

Effects of Solutes. If alkali metal ions play an important role in some such a manner as ion-pair formation or any "chemical exchanges," the concentration and the kind of metal ion should affect the linewidth variation with the temperature. However, no

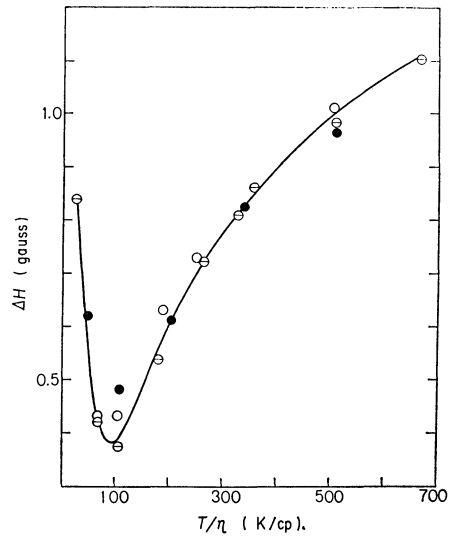

Fig. 2. Temperature dependence of the linewidth of phloxine semiquinone anion in alkaline methanolic solutions: Concentrations of the semiquinone and unreduced phloxine are: ⊖ [2.9×10^{-4}, 6.4×10^{-5} M; ○ 4.2×10^{-5}, 1.4×10^{-5} M; ● 1.3×10^{-3}, 5×10^{-3} M. [KOH], 0.1 M.

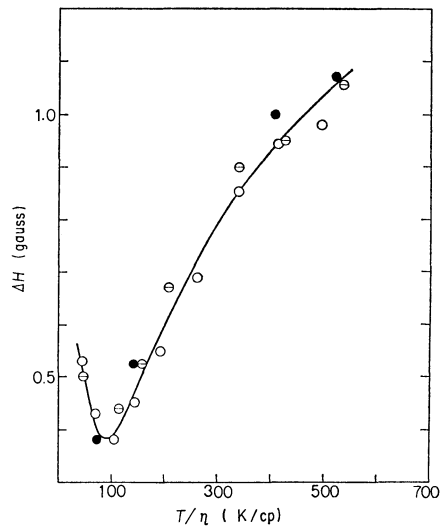

Fig. 3. Variation of linewidth with T/η at various concentrations of KOH in methanol: ○ 0.2 M, ⊖ 0.04 M, ● 0.005 M. Concentration of the semiquinone is about 1.5×10^{-4} M.

essential change in the curve was observed over a range of KOH concentrations (Fig. 3). The variation in the linewidth with T/η was compared for LiOH, KOH, and NaOH solutions, but no detectable differences were observed among these systems, as is shown in Fig. 4. Therefore, it may be concluded that the effect of the metal ions on the linewidth is negligible in the present case; any effect on the linewidths by protons is also ruled out.

Neither the dependence of the semiquinone concentration on the linewidth up to 1.3×10^{-3} M, nor the effects of unreduced parent phloxide $D(5\times10^{-5}$—5×10^{-3} M) on the linewidth of the semiquinone (10^{-4} M), were observed between 35 and −75 °C. (Fig. 2).

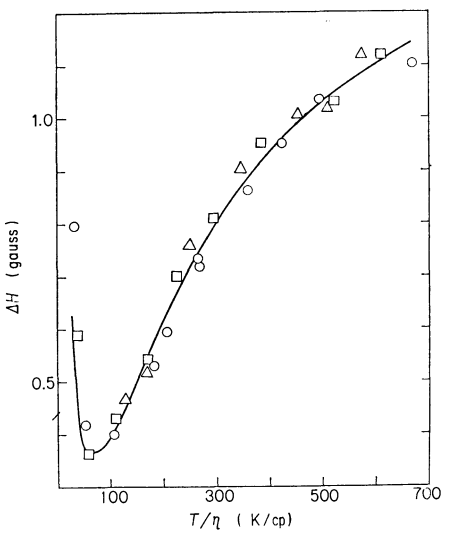

Fig. 4. Variation of linewidth with T/η in the 0.05 M solutions of KOH (○), NaOH (□), and LiOH (△).

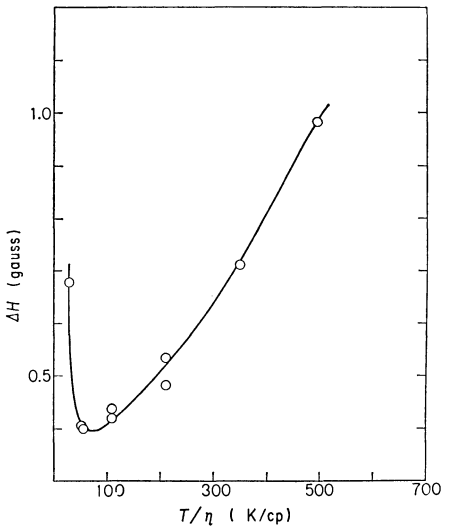

Fig. 5. Dependence of linewidth on solvent viscosity at 22°C. The viscosity was varied by changing the concentration of glycerol (10, 20, 30, 40, and 50 vol%) in methanolic solutions.

It is apparent, therefore, that the variation in the linewidth proceeds unimolecularly.

Dependence of the Linewidth on the Viscosity of a Solvent. Since the viscosity of the solution varies with the temperature, measurements were made of the net viscosity effect on the linewidth, using solutions of various compositions of glycerol in methanol at room temperature. The linewidths at 22 °C are shown in Fig. 5 as a function of T/η for mixtures containing 10, 20, 30, 40, and 50 vol% glycerol in methanol, where the concentration of the semiquinone was kept constant in the range of 7.2×10^{-5}—1.42×10^{-4} M. Figure 5 shows that the increase in viscosity caused a decrease in the linewidth of about 0.6 G, which is the same amount of variation as when the temperature was lowered; it also shows that the linewidth has a minimum value of

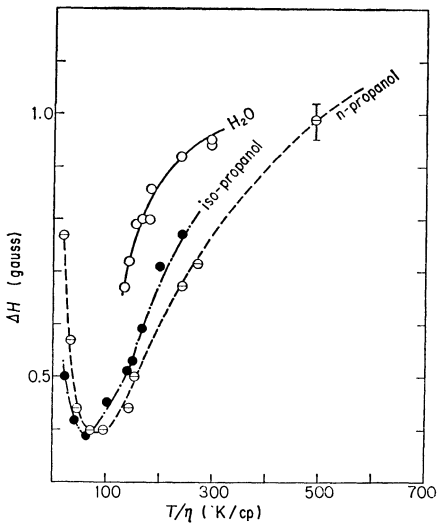

Fig. 6. Variation of linewidth with T/η in 1-propanol (⊖), 2-propanol (●), and aqueous solutions. (○).

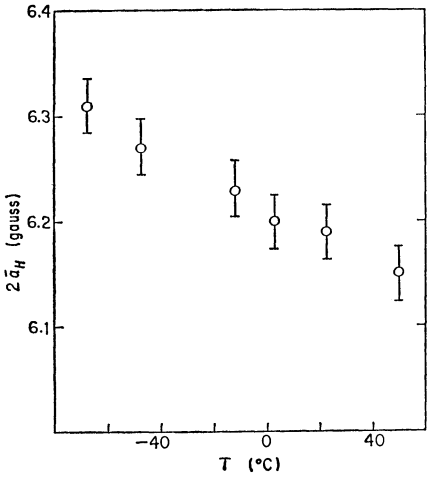

Fig. 7. Temperature dependence of hyperfine coupling constants of protons. The $2a_H$ means the sum of the coupling constants of two equivalent protons.

about 0.4 Gauss at T/η=80 K/cp. These results indicate that the linewidth is strongly dependent on the viscosity of the solvent, or that the linewidth variation is due to the motion of the solvent molecules. The temperature dependence of the linewidth mentioned above may also be explained as being due to the motion of solvent molecules rather than to an intramolecular motion of the semiquinone.

Effect of Solvents. The ESR spectra of the phloxine semiquinone were also taken in other protic solvents: 1-propanol, 2-propanol, and water. The linewidths in three solvents were 0.46, 0.51, and 0.96 Gauss respectively at room temperature. However, the plots of the linewidth against T/η are similar to that in the methanolic solution except for slight differences in curvatures, as is shown in Fig. 6. Since semiquinones were found to be very unstable in aprotic solvents or even in alcoholic solutions containing only a few tens vol% of aprotic solvents, no experiment has been carried out.

Dependence on the Temperature of Hyperfine Coupling Constants of Two Protons in Xanthyl Ring. In Fig. 7 is shown the temperature dependence of a sum of the hyperfine coupling constants of two protons (2a in Fig. 7) in a methanolic solution. For the other solvents mentioned above, a similar dependence was also obtained within the range of experimental errors.

Measurements at the Q-band were also carried out at room temperature, but no difference from the above results at X-band was observed in either the linewidth or the line-shape. Therefore, it may be concluded that the linewidth is not dependent on the static magnetic field, H_0.

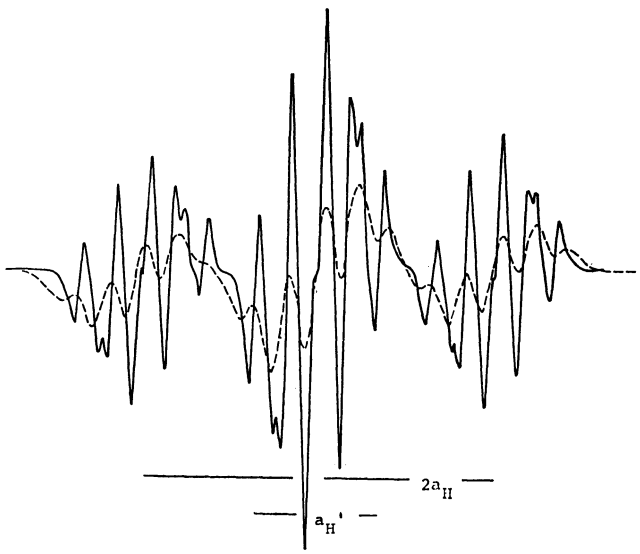

Fig. 8. ESR spectra of eosine semiquinone anion: ——, 24 °C; ----, −54 °C.

ESR Spectra of Eosine Semiquinone. The linewidths of eosine semiquinone (X=Br and Y=H) increase with a decrease in the temperature, while the total hyperfine coupling constants of the four hydrogen atoms on the 9-phenyl ring increase slightly (Fig. 8 and Table 1). From the spectral simulation, it was found that large three groups with an intensity ratio of 1 : 2 : 1 are ascribed to two equivalent protons at the 1- and 8-positions on the xanthyl ring. Each group is further split into lines with an intensity ratio of 1 : 1 : 3 : 3 : 3 : 3 : 1 : 1 by three nearly-equivalent protons with hyperfine coupling constants of 0.3 and by one proton

TABLE 1. TEMPERATURE DEPENDENCE OF HYPERFINE COUPLING CONSTANTS OF EOSINE SEMIQUINONE

Temp. (°C)	24.0	4.0	−17.0	−31.0	−43.3	−54.4
a_H' (G)	2.3_0	2.3_0	2.3_4	2.3_7	2.4_0	2.4_9
$2a_H$ (G)	6.4_4	6.4_4	6.5_2	6.6_0	6.4_7	6.5_2

of 0.2 G on the 9-phenyl ring.[1]

However, the MO calculation shows that the spin densities at the 3′- and 5′-positions on the 9-phenyl ring are much larger than those at the 4′- and 6′-positions, and that the latter two are nearly equivalent. These discrepancies must be due to the calculation being made for a fixed molecular structure. Therefore, the observed coupling constants are thought to be the averaged ones under the hindered rotation of the 9-phenyl ring.

Discussion

The experimental results on the linewidths of phloxine semiquinone may be summarized as follows. The linewidth decreases with a decrease in the temperature or an increase in the solvent viscosity, while no further splitting of the lines is observed and their Lorentzian shapes are kept. The variation in the linewidth is unimolecular, strongly dependent on the motion of the solvent molecules and independent of the H_0.

The linewidth variation has mostly been explained by a usual "chemical exchange" process. However, this process can not be applied to the present results as will be described below. According to the simple exchange process between two different states, A and B, when the exchanging rate is high, the lines of a Lorentzian shape should appear between each pair of A and B. As the rate is slowed down, however, the lines are broadened, deviate from Lorentzian, and finally separate into Lorentzian lines intrinsic to A and B, the linewidths of which decrease. Similar behavior may be expected when there are three or four different states.[3]

Other processes which are worth further consideration may be (1) Orbach effects,[4] (2) the spin-rotational coupling,[5] (3) the collapsing of hyperfine lines of Cl atoms, and (4) the modulation of the hyperfine coupling constants of H atoms by interaction with the solvent molecules.

For the (1) process to be appreciable, the phloxine semiquinone should have energy levels adjacent to and above the ground Zeeman levels. However, its electronic absorption band at 415 nm is sharp, indicating that the (1) process does not apply.

The (2) process does not apply either, because the linewidth calculated by Kivelson's equations[5] is only about 5×10^{-6} gauss.[6]

According to the (3) process, the linewidth should be dependent on the spin density on the 9-phenyl ring. It may be plausible that, with an increase in the temperature, the xanthyl and the 9-phenyl rings of phloxine semiquinone may approach a coplanar structure and that, therefore, the spin density on the latter ring may increase. This might not be inconsistent with the linewidth variation in the present results. However, the roughly estimated linewidth of the collapsed hyperfine lines of four Cl atoms is about 0.18 gauss at room temperature,[7] six times smaller than the observed value, indicating that the (3) process is not appropriate for explaining the results. It is also noted that the linewidth caused by the quadrupole effects of Cl atoms is generally smaller in a liquid state, and that the effects of the temperature and the viscosity are opposite to the present results.[9]

Now, therefore, we should like tentatively to propose the (4) process as the most plausible explanation for the present results. The semiquinone anion of xanthene dye must form hydrogen bonds at the anionic oxygen atoms ($-O^-$) of the 11- and 12-positions. This induces the variation in the spin densities, especially at the 1- and 8-positions, which has been demonstrated experimentally[10] and from the MO calculation.[11] Therefore, in view of the fact that the linewidth is strongly dependent on the motion of the solvent molecules, it seems plausible that the modulation of hydrogen bonds is a source of the linewidth.

As the temperature increases, the frequency of (a) the dissociation and/or (b) the ligand exchange of hydrogen bonds will increase. Suppose that, in the case of (a), the hyperfine coupling constants of the hydrogen-bonded form are modulated by its dissociation that the dissociated (anionic) form has no sufficient lifetime to be observable in ESR. Then the transverse relaxation time, $T_{2,\mathrm{obs}}$, may be given as below, intuitively by analogy with the lifetime broadening or by solving the modified Bloch equations by assuming that the dissociated form has a short lifetime:

$$T_{2,\mathrm{obs}}^{-1} = T_2^{-1} + \tau^{-1} \tag{1}$$

where τ is the lifetime of the hydrogen-bonded semiquinone and where T_2 is the transverse relaxation time when no dissociation of hydrogen bonds occurs. If, on the other hand, the lifetime of the dissociated form is long, the process may be regarded as a usual "chemical exchange" process, which has already been ruled out.

In the case of (b), a simple exchange of solvent molecules in the ligand causes neither line broadening nor sharpening, since no difference in the spin state is expected before and after the exchange. Therefore, we assume that, in the ligand exchange of the hydrogen-bonded form, there is an exchange intermediate which coordinates with excess solvent molecules. Such an intermediate may have a very short transverse relaxation time, since it is easily and frequently distorted by the collisions of solvent molecules. Therefore, the relaxation time in the hydrogen-bonded form is given by the same equation as has been given above from the modified Bloch equations. This equation is based on a similar one reported by McConnell[12] and Johnson, Jr.[13] for the linewidth of the broad-line NMR of diamagnetic ions undergoing electron-exchange reactions with their paramagnetic ions.

The temperature effect of the linewidth being sharpened with a decrease in the temperature without any further splitting can be explained by Eq. (1).

The decrease in the linewidths with a decrease in the temperature, which does not affect the Lorentzian shape and which proceeds unimolecularly, implies that the relaxation time can be represented by this equation:

$$\Delta H = \hbar(\sqrt{3}g\beta T_2)^{-1} \propto \tau^{-1}$$

The τ^{-1} may be given by $\tau^{-1}=A\exp(\Delta E/RT)$; therefore, as is obvious from Eq. (1), $T_{2,\mathrm{obs}}^{-1}$ may also be given by a similar equation when T_2 can be neglected. In fact, the plots of $\ln T_{2,\mathrm{obs}}^{-1}$ *vs.* $1/T$ are linear, from which

activation energies of 2.1, 3.1, and 2.4 kcal/mol were obtained for methanol, 2-propanol, and aqueous solutions. Each of these values is very close to the activation energy of the self-diffusion of each solvent, suggesting a strong dependence of the linewidth upon the viscosity of the solvent.

The lack of nuclear-spin dependence of the linewidth may be explained on the basis of the fact that the formation of hydrogen bonds at the two $-O^-$ sites should be at random, so the spin densities on the 1- and 8-positions are occasionally in "uncorrelated conditions".[2] (*Cf.* Ref. 11)

On the other hand, it is noted that, in the eosine semiquinone, the 9-phenyl ring undergoes a hindered rotation, and the resulting modulation of the hyperfine coupling constants of the H atoms on the 9-phenyl ring is perhaps a principal source of the linewidth, for the modulation must be much larger than in the cases of (a) and (b).

The authors are grateful to Professor Keiji Kuwata, Professor Shunichi Ohnishi, Dr. Masamoto Iwaizumi, and Dr. Tadamasa Shida for many helpful discussions and suggestions. They also wish to express their thanks to Dr. Suehiro Iwata for the use of his computer programs for the MO calculations.

References

1) K. Kimura, T. Miwa, and M. Imamura, This Bulletin, **43**, 1329, 1337 (1970).
2) J. H. Freed, P. H. Rieger, and G. K. Fraenkel, *J. Chem. Phys.*, **37**, 1881 (1962).
3) P. F. C. Claridge, B. M. Peake, and R. M. Golding, *J. Magn. Resonance*, **6**, 29 (1972).
4) D. Kivelson, *J. Chem. Phys.*, **45**, 1324 (1966).
5) R. E. D. McClung and D. Kivelson, *J. Chem. Phys.*, **49**, 3380 (1968).
6) In these calculations, the following values were used: moments of inertia, $I_{XX}=1.05\times10^{-36}$, $I_{YY}=2.22\times10^{-36}$, $I_{ZZ}=2.60\times10^{-36}$ g cm^2. The deviation of the average g value from that of the free electron, $\Delta g=-6\times10^{-4}$, was used for the deviation of the principal values of the g tensor. Another piece of evidence is that the value of Δg ($=0.03$) necessary to give the observed linewidth is too large to be acceptable in a π-radical of an aromatic molecule.
7) The linewidth of the *p*-chloranil anion is known to be about 1 G at room temperature.[8] The sum of the spin densities on the four carbon atoms with Cl atoms was assumed to be 0.38, which is the observed value for the *p*-benzosemiquinone anion. Similarly, the corresponding sum of the 9-phenyl ring of the phloxine semiquinone anion was assumed from the data of the eosine semiquinone anion to be 0.09. Therefore, $1\times0.09/0.38=0.2$
8) J. E. Wertz and J. L. Vivo, *J. Chem. Phys.*, **23**, 2441 (1955).
9) E. F. Ullman and L. Call, *J. Amer. Chem. Soc.*, **92**, 7211 (1970).
10) I. H. Leaver, *Aust. J. Chem.*, **24**, 753 (1971).
11) According to the ASMO SCF CI calculation of the uranine semiquinone (X=Y=H in Fig. 1) protonated at the 12-position, the spin density increases by 0.04 at the 8-position and decreases by 0.02 at the 1-position. The uranine semiquinone protonated at the 11-position shows the opposite change. In the case of the diprotonated one, the spin densities at the 1- and 8-positions increase by about 0.01.
12) H. M. McConnell, *J. Chem. Phys.*, **25**, 307 (1956).
13) C. S. Johnson, Jr., "Advances in Magnetic Resonance," Vol. 1, ed. by J. S. Waugh, Academic Press, (1965), p. 79.

Anomalous Light Scattering by Poly(2-vinylpyridine) in Methanol

Noriyuki SAKAMOTO, Masafumi YOSHIDA*, and Shizuo ARICHI*

Department of Chemistry, Faculty of Literature and Science, Shimane University, Nishikawatsu-cho, Matsue 690

**Chemical Laboratory, Department of General Education, Kumamoto University, Kurokami-2-chome, Kumamoto 860*

(Received October 15, 1973)

The light scattering of a poly(2-vinylpyridine) solution was measured under various conditions. In solvents such as methanol, ethanol, 2-propanol, 2-butanone, and pyridine, anomalous Zimm plots with an upward inflection at lower angles were observed. This anomaly was especially striking in methanol, in which the dissymmetry coefficient was frequently less than unity. Systematic investigations carried out with methanol as a solvent revealed that; (1) the anomaly does not depend appreciably on the concentration or tacticity of the polymer, the temperature, or the wavelength of the incident light; (2) the anomaly diminishes with an increase in the molecular weight of the polymer; (3) the anomaly disappears upon the addition of dry ammonia of 10^{-2} mol/l or more in methanol, and (4) similar perturbed Zimm plots are realized by the addition of a trace amount of hydrochloric acid or sulfuric acid in a methanol solution of a higher-molecular-weight fraction which showed a normal Zimm plot in pure methanol. The anomaly can not be explained in terms of the effects of the optical anisotropy of the polymer segment, but the external interference arising from the non-random arrangement of the polymer in solution may contribute to it.

Recently several reports on the anomalous light-scattering behavior of solutions of vinylpyridine polymers have been published. Miura *et al.*[1] reported an anomaly with poly(2-methyl-5-vinylpyridine) in methanol; Cashin,[2] with poly(2-vinylpyridine) in nitromethane, and Fuoss *et al.*[3] suggested the existence of some trouble in the measurement of the light scattering of poly(4-vinylpyridine) in absolute ethanol. In the course of studies of the poly(2-vinylpyridine) solution one of the present authors[4] showed in brief the existence of the anomaly in several solvents. More recently, Seely[5] reported on the anomaly with poly(4-vinylpyridine) in nitromethane. However, no reasonable explanation of the origin of the anomaly of the light scattering of the poly(vinylpyridine) solution has yet been given. On the other hand, the similar anomaly of the light-scattering behavior of several other polymers has been clarified by some theoretical considerations.[6–10] In this paper we will present the results of our experimental investigation of the light-scattering behavior of the poly(2-vinylpyridine) solution, especially when the measurement is carried out in methanol. The results will be discussed in terms of the theories proposed for the other polymers.

Experimental

Atactic Poly(2-vinylpyridine). The polymerization, fractionation, and characterization of atactic poly(2-vinylpyridine), our sample number A-2 ($M_w=3.4\times10^4$), E-2 (1.20×10^5), G-2 (2.19×10^5) and I-2 (3.11×10^5), were described in a previous paper.[4] Three other higher-molecular-weight fractions, P-4 (1.1×10^6), P-3 (1.6×10^6), and P-2 (4.0×10^6), were obtained by redox polymerization using potassium persulfate and sodium bisulfite in an acidic aqueous solution of the monomer[11] and by subsequent fractionation.[12] The $2U_0$ sample (3.30×10^5) was obtained by thermal polymerization in an ampoule without any initiator or diluents, and was then purified by repeated precipitation.

Isotactic Poly(2-vinylpyridine). The polymerization and purification of isotactic poly(2-vinylpyridine) were carried out in the same way as in a previous paper.[13] The polymres were fractionated by the precipitation method, using the benzene-ligroin system. The tacticity was checked by the methods of X-ray diffraction, IR spectrum, melting point, and insolubility in hot acetone.[13] The fourth fraction, S4F-4 (3.25×10^5), was mainly used in this study.

Solvent. All the solvents used in this study were dried by the standard methods[14] and were fractionally distilled before use. The middle fractions of each solvent were retained for use in the experiment described below.

Light-scattering and Viscosity. All the apparatus and procedure for the measurements of the light scattering and viscosity were approximately the same as those previously described by one of the present authors.[4] Measurements were made of the intensity of scattered light in eleven different directions, ranging from 30° to 150° with unpolarized or polarized blue light (436 mμ) or green light (546 mμ) of Hg. The correction for the backward reflection was applied throughout the measurements.[15] The solutions were ordinarily optically purified by filtering the solution by means of double membranes of "mittel" or "fein" supplied by the Sartorius Co., Göttingen, West Germany.

Results and Discussion

The fundamental equation of the light scattering of the polymer solution is expressed,[16] as is well known, by:

$$Kc/R(\theta) = 1/[M_wP(\theta)] + 2A_2c$$
$$= 1/M_w + (16\pi^2/3\lambda^2M_w)\langle s^2\rangle\sin^2(\theta/2) + 2A_2c$$

where K is the optical constant; c the concentration expressed by g/ml; $R(\theta)$, the reduced intensity of scattering at the angle θ; M_w, the molecular weight of the polymer; $P(\theta)$, the factor arising from the internal interference of scattered light in the polymer molecule; A_2, the second virial coefficient; λ, the wavelength of the incident light, and $\langle s^2\rangle$, the mean square of the radius of gyration of the polymer chain.

For random coils of linear polymers, straight lines are obtained to a good approximation if $Kc/R(\theta)$ is plotted against $\sin^2(\theta/2)$; therefore, in the so-called Zimm plots (plots of $Kc/R(\theta)$ *vs.* $\sin^2(\theta/2)+kc$, where k is the arbitrary constant) the initial slope of the extrapolated straight line at $c=0$ corresponds to the radius

In addition, the Zimm plots of the light scattering of the standard polystyrene, MS–I,[17] in benzene was a normal one, from which no inflection of lines for $Kc/R(\theta)$ *vs.* $\sin^2(\theta/2)$ is observed; the molecular weight as estimated from the plots is 2.20×10^5, which is in accord with the average value of 2.53×10^5 reported in the literature.[17] Furthermore, the results of our measurements of the absolute scattering intensity of a polystyrene solution of the identical sample showed no particular defect in our apparatus or procedure.[18]

Concerning the optical purification of the solution, similar results were obtained even if the solution of the G-2 sample in methanol was ultra-centrifugated at 2×10^4 *G* for 2 hr. The effect of fluorescence from the polymer was checked and found to have no considerable effect in methanol.

Recently theoretical investigations of similar anomalies in light scattering have been reported for other polymer-solvent systems as well. According to those results, the anomaly can be explained in some cases by the effects of the optical anisotropy of segments,[7-9] while in the other cases it can be explained by the effects of intermolecular interference arising from a non-random arrangement of the solute molecules in solution.[6,10] Some qualitative examinations of our results with regard to these theories were carried out as follows.

The Effect of the Optical Anisotropy of the Polymer. Uchiyama and Kurata[7,8] have shown that the unusual Zimm plots obtained by Ehrlich and Doty[19] for aqueous solutions close to the isoionic point of a copolymer consisting of approximately equal amounts of methacrylic acid and 2-dimethylaminoethylmethacrylate, and also obtained by Uchiyama and Kurata themselves for the monochlorobenzene solution of isotactic polystyrene can be explained by the effects of the large optical anisotropy of the polymer. In such cases they proposed primarily to use polarized incident light and to correct the effects of anisotropy by subtracting four-

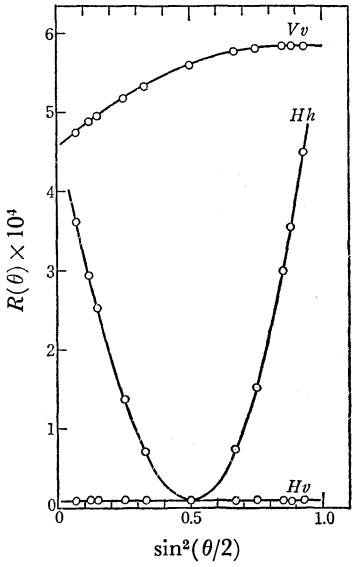

Fig. 4. The angular variation of each component of the scattered intensity of a fraction of isotactic poly-(2-vinylpyridine), S4F-4, in methanol at 25 °C. $\lambda=$ 436 mμ and $c=2.00\times10^{-3}$ g/ml.

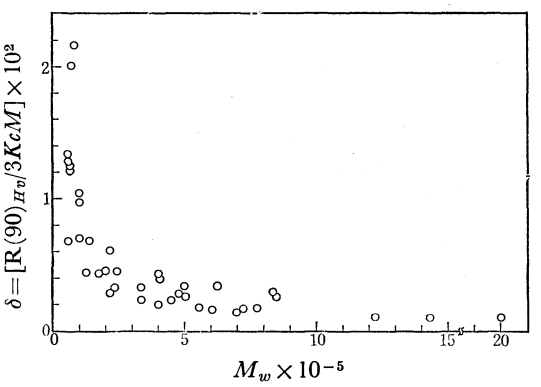

Fig. 5. Dependence of the values of optical anisotropy parameter, $\delta=R(90)_{Hv}/3K_cM$, of isotactic poly(2-vinylpyridine) in methanol at 25 °C on molecular weight of the polymers.

thirds of the amount of the *Vh* or *Hv* component of the scattered light from that of the *Vv* component at each scattering angle. Schurz *et al.*[20] found that the anomaly they observed with solutions of vinyon N (copolymer of 40% acrylonitrile and 60% vinylchloride) in dimethylformamide disappeared when they used verticallypolarized light.

The results of the measurements of all the components of scattered light with vertically-polarized incident light are given in Fig. 4 for the fraction of isotactic poly(2-vinylpyridine) S4F-4 in methanol. As is illustrated by the figure, the intensity of the *Hv* component and, consequently, the effects of depolarization for this polymer in methanol are, in general, comparatively small, and the anomaly can not be corrected by subtracting $(4/3)R_{Hv}$ from R_{Vv}. This situation was further confirmed by additional experiments carried out with a series of fractions whose molecular weights covered a wide range. In Fig. 5 the values of the optical anisotropy parameter, δ, defined[7] by:

$$\delta = R_{Hv}/3KcM$$

for a series of isotactic poly(2-vinylpyridine) in methanol are plotted as a function of the molecular weight of the polymers. The amounts of depolarization are not very large, and the values of δ are, in general, in the order of 10^{-3} except for very-low-molecular-weight fractions.

Secondly, when the measurements were carried out with unpolarized incident light in methanol, the values of the dissymmetry coefficient were often smaller than unity; consequently, the application of the data to the equations proposed by Uchiyama and Kurata for the correction of the effect of optical anisotropy was impossible. Even in the solvents other than methanol, where the application of the data to the equations is possible, the effects of the correction were not appreciable. In conclusion, the anomaly in Zimm plots can not be explained by the effect of the optical anisotropy of polymer segments.

The Effect of Order in Solution. It was first reported by Doty and Steiner[6] in the case of bovine serum albumin, and later by Oth and Doty[21] in the case of polyelectrolytes in the absence of added electrolytes,

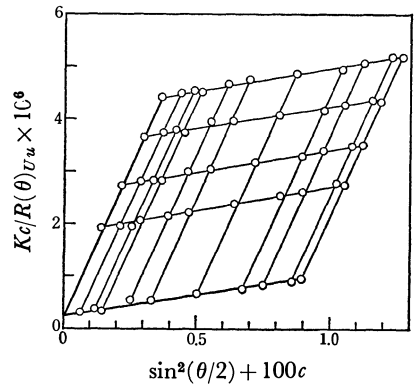

Fig. 6-1. Effects of the concentration, c, of added hydrogen chloride in methanol at 25 °C on the inflection in Zimm plots for atactic poly-(2-vinylpyridine), P-2 ($M_w=4.0\times10^6$). $\lambda=436$ mμ, unpolarized light. $c=0$ mol/l.

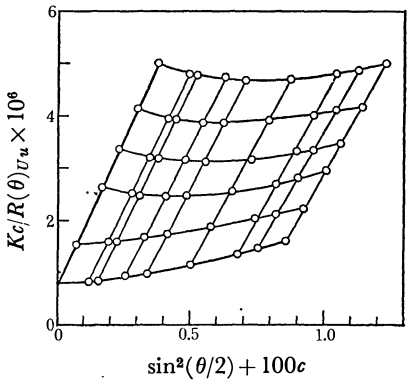

Fig. 6-2. $c=10^{-8}$ mol/l.

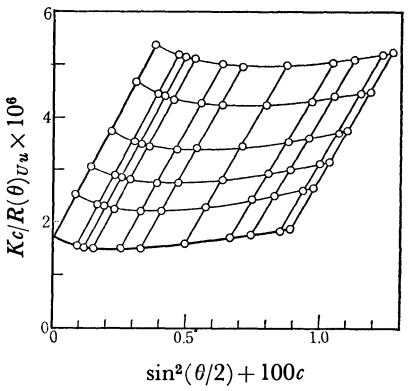

Fig. 6-3. $c=10^{-6}$ mol/l.

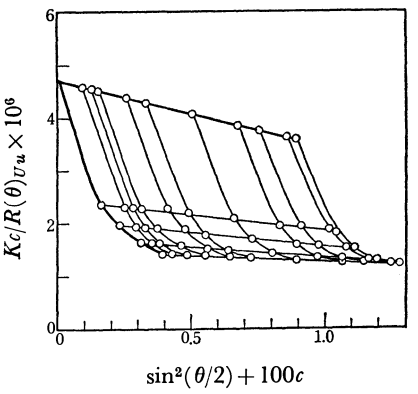

Fig. 6-4. $c=10^{-4}$ mol/l.

that unusual light scattering was caused by the external interference arising from non-random rearrangements of the polymer, the so-called "order" in solution. More recently, Burchard[10] has explained an anomalous light-sattering behavior like ours for poly(vinylcarbanilate) in diethyl ketone in terms of the influence of order arising from a certain strong solvation due to hydrogen bonding in solution.

According to Burchard, the ordering rearrangements of polymer coils in solution are perhaps caused by the effects of; (1) electrostatic repulsion force, (2) the formation of an intramolecular-bond-forming wire netting, and (3) a certain strong solvation.

First, we tried to check for the possible ionization of our polymer at nitrogen atoms in solution. Figures 6-1—6-4 demonstrate several Zimm plots observed for a fraction of atactic poly(2-vinylpyridine), P-2, in methanol, to which were added increasing amounts of hydrochloric acid. The light-scattering behavior for this fraction in pure methanol is normal, as is shown in Fig. 6-1. A similar perturbation as observed for lower-molecular-weight fractions in pure methanol appeared when the fraction was partially ionized by the addition of hydrochloric acid to methanol until the concentration reaches 10^{-8}—10^{-6} mol/l; the degree of anomaly increased with the concentration of hydrochloric acid, as is shown in Figs. 6-2 and 6-3. The pattern of the Zimm diagram at the concentration of 10^{-4} mol/l shows some similarities to the one reported for a polyampholite based on methacrylate by Ehrlich and Doty.[19]

The results of viscometric measurements for the same fraction in the solvents used above are shown in Fig. 7. The curves for these systems are typical for polyelectrolytes in a medium with a low ionic strength.

Similar results of light-scattering measurements were obtained when a trace amount of sulfuric acid was added to methanol used as a solvent until the con-

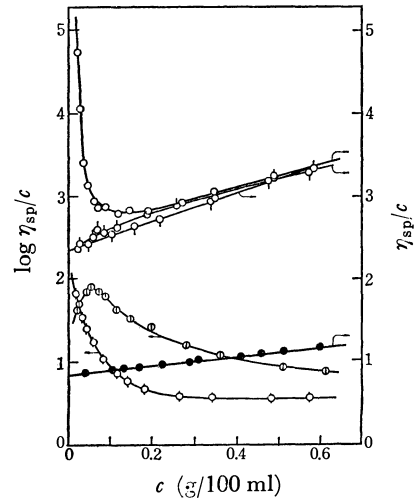

Fig. 7. Effects of the concentration, c, of added hydrogen chloride in methanol at 25 °C on the reduced viscosity number for fractions of atactic poly-(2-vinylpyridine) P-2 [○ ($c=0$ mol/l), ○ (10^{-8}), ○ (10^{-6}), ○ (10^{-4}), ⊙ (10^{-3})] and G-2 [● (0)].

centration reaches 10^{-8}—10^{-4} mol/l. From these results, it may be concluded that the anomaly in these cases depends on the effects of electrostatic interaction between ionized groups of the polymer.

We then considered whether the anomaly was affected by the same origin in the case of lower-molecular-weight-fractions. We have repeatedly measured the reduced viscosity numbers of many fractions of poly(2-vinylpyridine) in pure methanol and have always obtained normal viscosity curves typical of non-electrolytic polymers, as is shown in Fig. 7 for the G-2 fraction as an example.

On the other hand, the results of light scattering and viscosity in pure methanol for the $2U_0$ sample, which had been prepared with particular care taken to diminish any possibility of contamination by electrolytes, were the same as those of other fractions. Judging from these results, the explanation of the anomaly in terms of ionization in methanol may not be possible.

Secondly, the occurrence of strong solvation by means of hydrogen bonding between poly(vinylpyridine) homologues and alcohols has been ascertained by the large value of the Flory constant,[22,23] defined by:

$$K = 6^{3/2}\Phi_0(\langle s^2\rangle_0/M)^{3/2}$$

where Φ_0 is the universal constant and $\langle s^2\rangle_0$ the unperturbed radius of the gyration of the polymer chain, and by the large negative values of the parameters of excess enthalpy and entropy for dilution, as evaluated by measurements of the temperature coefficient of the intrinsic viscosity and the osmotic second virial coefficient.[24] The results of the direct calorimetric determination of the heat of solution equally support the possibility of hydrogen-bonding formation in these systems.[25]

Judging from these facts, it may be supposed that the anomalous light-scattering behavior with poly(2-vinylpyridine) in methanol was caused by strong fixation due to hydrogen bonds between the nitrogen atoms in the pyridine residue and the –OH groups of the methanol, as in the case of poly(vinylcarbanilate) in diethyl ketone.[10] Such a coil may have a weakly elastic repulsive potential and might resist the overlapping of the segment clouds.

The molecular-weight dependence of the degree of inflection of the light-scattering curves shown in Fig. 2 may be explained by the masking of the external interference by the internal one for larger particules, as was pointed out by Doty and Steiner.[6]

It may be supposed that the influence of added ammonia on the anomalous light scattering for methanol solutions is due to the diminution of solvation rather than some possible dissociation of the polymer. This may be supposed on the basis of the facts that the values of the intrinsic viscosity number and those of the Flory constant decrease considerably with an increase in the amount of added ammonia in methanol and ethanol, as has previously been shown by one of the present authours.[22]

In conclusion, it seems probable that anomalous behavior of light scattering such as is reported here is caused by the effect of order in solution, arising from a strong solvation.

References

1) M. Miura, Y. Kubota, and T. Masuzukawa, This Bulletin, **38**, 316 (1965).
2) W. M. Cashin, *J. Colloid Sci.*, **6**, 271 (1951).
3) J. B. Berkowits, M. Yamin, and R. M. Fuoss, *J. Polym. Sci.*, **28**, 69 (1958).
4) S. Arichi, This Bulletin, **39**, 439 (1966).
5) G. R. Seely, *Macromolecules*, **2**, 302 (1969).
6) P. Doty and F. Steiner, *J. Chem. Phys.*, **20**, 85 (1952).
7) H. Uchiyama and M. Kurata, *Bull. Inst. Chem. Research, Kyoto Univ.*, **42**, 128 (1964).
8) H. Uchiyama, *J. Phys. Chem.*, **69**, 4138 (1965).
9) M. Nakagaki, This Bulletin, **34**, 834 (1961).
10) W. Burchard, *Polymer*, **9**, 29 (1968).
11) J. M. Pritchard, M. H. Opheim, and P. H. Moyer, *Ind. Eng. Chem.*, **47**, 863 (1955).
12) S. Arichi, S. Mitsuta, N. Sakamoto, and H. Murata, This Bulletin, **39**, 428 (1966).
13) S. Arichi, *ibid.*, **21**, 244 (1967).
14) J. A. Riddick and W. B. Bunger, "Techniques of Chemistry, Vol. II Organic Solvents," Third Edition, Edited by A. Weissberger, Wiley-Interscience (1970).
15) J. P. Kratohvil, *J. Colloid Interface Sci.*, **21**, 498 (1966).
16) B. H. Zimm, *J. Chem. Phys.*, **16**, 1093 (1948).
17) The Committee on Molecular Weight and Molecular Weight Distribution of the Society of Polymer Science, Japan, *Report. Prog. Polymer Phys., Japan*, **4**, 141 (1961).
18) The Committee on Molecular Weight and Molecular Weight Distribution of the Society of Polymer Science, Japan, *Rept, Prog. Polymer Phys., Japan*, **14**, Appendix 1 (1971).
19) G. Ehrlich and P. Doty, *J. Amer. Chem. Soc.*, **76**, 3764 (1954).
20) J. Schurz, G. Warnecke, and Th. Steiner, *Monatsh. Chem.*, **91**, 561 (1960).
21) A. Oth and P. Doty, *J. Phys. Chem.*, **56**, 43 (1952).
22) S. Arichi, This Bulletin, **41**, 548 (1968).
23) A. Dondos, *Makromol. Chem.*, **135**, 181 (1970).
24) S. Arichi, Y. Tanimoto, and H. Murata, This Bulletin, **41**, 1296 (1968).
25) Unpublished Data.

Gel Filtration of Starch–Iodine System

Makoto KODAMA* and Tsunetaka SASAKI

Department of Chemistry, Faculty of Science, Tokyo Metropolitan University, Fukazawa, Tokyo 158

(Received November 8, 1973)

The well-known starch-iodine reaction was taken up to study the applicability of gel filtration to the problem of physical chemistry. Gel filtration by the frontal analysis was carried out, the following results being obtained. (1) Soluble starch- and amylose-iodine systems give elution volumes of iodine containing constituents (V_{si} and V_{ai}, respectively) distinctly smaller than that of iodine, which decrease with increasing concentration of iodine, C, and starch, approaching the elution volume of starch. This is a direct experimental evidence of starch-iodine complex formation. (2) An equation derived for V_{si} *vs.* C and V_{ai} *vs.* C relations holds satisfactorily. The concentration of free iodine in equilibrium with the complex is calculated by the equation. (3) Presence of iodide ion facilitates the complex formation, but its decomposition is instantaneous when it is isolated from free iodine. (4) Some iodide ions are found to be incorporated in the complex. (5) Amylopectin also forms a complex with iodine, but the amount of iodide incorporated is not large. (6) Potentiometric titration of starch with iodine exhibits a similar behavior to the gel filtration measurement.

A number of studies have been made on starch–iodine complex formation by various methods such as potentiometry,[1] spectrophotometry,[2] electrophoresis[3] and X-ray diffraction,[4] but there do not seem to be many on the direct experimental confirmation of the binding between starch and iodine. The gel filtration method is suitable for such a measurement, since it enables us not only to identify the independent solute species as in the usual analytical procedure but also to study the solutes mutually in a rapid equilibrium such as

$$mA \rightleftharpoons A_m \text{ (a) or } A + B \rightleftharpoons AB \text{ (b)}$$

Case (a) has been reported for the system of aqueous solution of sodium dodecyl sulfate[5] and case (b) for polyvinylacetate–sodium dodecyl sulfate system.[6] The starch–iodine system belongs to the latter case, for which the gel filtration method is expected to give direct information on the formation of a starch–iodine complex.

Experimental

Material. Starch used included soluble starch, amylose and amylopectin. Commercial soluble starch (Wako Pure Chemicals Industries, Co., Ltd.) was used without further purification. Amylose and amylopectin were prepared from potato starch by selective precipitation with *n*-amyl and methyl alcohols.[7] Amylose and amylopectin solutions were prepared by dissolving purified sample in aqueous potassium hydroxide solution (0.5 M), neutralizing with dilute hydrochloric acid and desalting by gel filtration. Iodine was purified by repeated sublimation. Other reagents were of the commercial purest grade and were used without further purification. The gel used was Sephadex G-50 fine.

Apparatus. The apparatus used for gel filtration was similar to that described in a preceding report,[5] except for the flow cell for measuring the absorbance of blue starch-iodine mixture in place of the conductance cell. Absorbance was conventionally measured using a light source of an ordinary 40 W lamp without filter, the intensity being recorded as an electrical output of a photocell. The gel column used was Sephadex column K 15/30 (colorless) or brown glass column. The former, 1.5 cm in diameter, 30 cm long, and containing gel 11.4 cm in height, was used for the soluble starch-iodine system, and the latter, 1.1 cm in diameter, 30 cm long, and containing gel 20.0 cm in height, was used used for the amylose-iodine and amylopectin-iodine systems. The latter column was equipped with a water jacket thermostated at 30.0±0.05 °C. Soluble starch-iodine system was studied at room temperature (*ca.* 18 °C).

Method. The gel column was previously equilibrated with distilled water or 0.004 mol/l potassium iodide solution. A starch–iodine mixture of varying concentrations of starch and iodine as listed in each figure, and a constant iodide concentration of 0.004 or 0.025 mol/l was charged on top of the gel column. In order to carry out elution, the sample solution was charged in sufficient amount to ensure a wide plateau in the elution curve. The elution volume of starch, V_s, is determined by a slight depression appearing in the elution curve of soluble starch–iodine system shown in Fig. 2. The slight depression observed is further confirmed to be V_s since the outer volume of the gel as determined by blue dextran is in agreement with V_s obtained above, which would be expected from the gel used. This serves for the determination of the elution volume of amylose where the slight depression is lacking in the elution curve. The elution volume of free iodine, V_i, is determined by detecting yellow iodine eluted by the photocell. All experiments were carried out in a dark room to protect a light sensitive iodine–iodide solution.

Theoretical

When a sufficient amount of starch–iodine solution is subjected to gel filtration using an appropriate gel, a starch and starch–iodine complex, if any, moves faster than free iodine in the gel column. However, a part of starch–iodine complexes eluted in advance of free iodine decomposes and liberates starch and iodine at the front. Equilibrium is established between these substance and the remaining complexes, provided that decomposition is sufficienly rapid. As a result, starch is eluted first, followed by starch-iodine complexes and iodine. The behavior is shown schematically in Fig. 1. An imaginary elution front of starch–iodine complexes moves from left to right without decomposition (Fig. 1(A)). In this figure, □ACDH and □HDEG respectively represent the outer (or void) and inner

* Present address: Research Institute for Polymers and Textiles, Sawatari, Kanagawa-ku, Yokohama, 221.

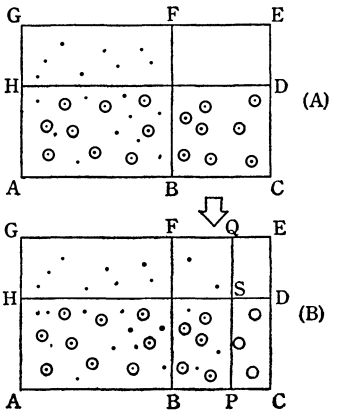

Fig. 1. Elution diagram of starch-iodine complex.
(A): Imaginary elution diagram without decomposition of starch-iodine complex
(B): Actual elution diagram
• Iodine, ⊙ Starch-iodine complex, ○ Starch
GH: Cross section area of inner space
HA: Cross section area of outer space

spaces of the gel column, AG and CE the upper and lower ends of the gel, AH and GH the cross sections of outer and inner gel spaces, CE and FB the imaginary elution fronts of starch-iodine complexes (⊙) and iodine (•). The actual front where the decomposition of the complexes takes place is shown in Fig. 1(B). The line CE indicates the front of starch (○) and PQ that of starch-iodine and iodine. The starch-iodine complexes in □SPCD decompose to liberate iodine of a constant equilibrium concentration to fill the space □FBPQ.

Such a decomposition is similar in nature to the case of the elution of sodium dodecyl sulfate above the critical micelle concentration, where the decomposition of micelles occur at the elution front.[5] Thus we obtain the equation

$$\frac{1}{V_{si}-V_s} = -\frac{1-\alpha}{(V_i-V_s)a} + \frac{C}{(V_i-V_s)a\alpha} \qquad (1)$$

from Eq. (8) for the micelle decomposition[5] by substituting $1/V_s$, $1/V_i$ and $1/V_{si}$ for R_f^m, R_f^s and R_f respectively. V_{si}, corresponding to the line PQ, represents the elution volumes of starch-iodine, V_s corresponding to EC the elution volume of starch, V_i corresponding to FB the elution volume of iodine, a the concentration of free iodine in equilibrium with starch-iodine complexes and α the rate parameter of the decomposition of starch-iodine complexes. $\alpha=1$ indicates that the decomposition of the isolated complexes is faster than the rate of elution and $\alpha=0$ no decomposition.[5] According to Eq. (1), V_{si} approaches V_s when C becomes large and C *vs.* $1/(V_{si}-V_s)$ plots are linear provided that a is constant. If the linear part of the plot when extrapolated passes the origin, we have $\alpha=1$ and decomposition of the complexes is rapid.

Results and Discussion

(1) Soluble starch. Elution volumes were determined by the sharp rise (V_{si}) and slight depression (V_s) of the elution curve shown in Fig. 2. In Fig. 3,

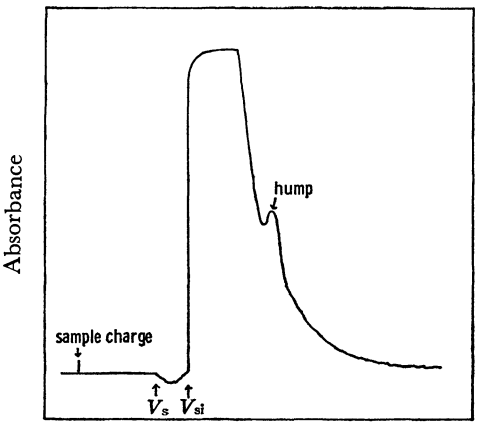

Fig. 2. The elution pattern of soluble-starch-iodine system.

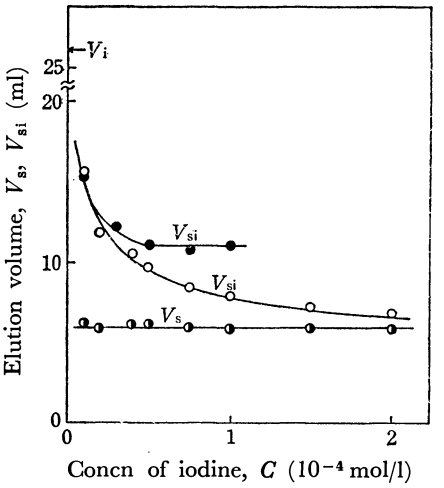

Fig. 3. V_s *vs.* C and V_{si} *vs.* C plots for soluble starch-iodine systems.
Sample solution: Concn of KI 0.025 mol/l
Concn of soluble starch ○ 0.5%, ● 0.05%
Gel column: Concn of KI 0 mol/l

V_{si} and V_s obtained are plotted against iodine concentration C. Here, the value V_s is constant (5.91 ml) as might be expected. The value V_{si}, being smaller than V_i (26.16 ml), decreases with C and approaches a constant for sufficiently large value of C. The constant is still a function of the concentration of soluble starch and approaches V_s for sufficiently high concentration as shown in Fig. 3.

The appearance of blue iodine front, V_{si}, moving faster than free iodine front is direct indication of the formation of large solute particles containing iodine, namely starch-iodine complexes. The tendency of V_{si} to approach a constant value distinctly larger than V_s for smaller starch concentration and larger iodine concentration as shown in the upper V_{si} *vs.* C curve of Fig. 3 indicates the saturation or a limit of binding capacity of iodine for starch.

The applicability of Eq. (1) was tested by plotting C against $1/(V_{si}-V_s)$. Figure 4 shows the results for soluble starch-iodine system. A straight line passing through the origin with a deviation in dilute and

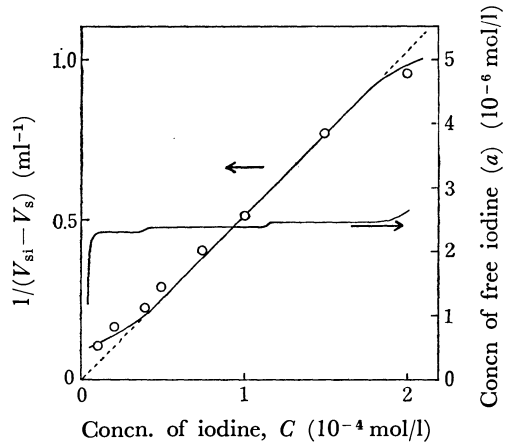

Fig. 4. $1/(V_{si}-V_s)$ *vs.* C plots and the potentiometric titration curve for soluble starch-iodine systems.
Gel filtration: Concn of KI 0.025 mol/l, V_s and V_{si} same as in Fig. 3
Potentiometry: Concn of KI 0.025 mol/l

concentrated iodine regions was obtained. The linear part shows the constancy of the concentration of free iodine in equilibrium with the complexes (a) and $\alpha=1$ obtained proves a rapid decomposition of the complexes at the elution front. From the inclination of the linear part of the plot and the values of V_s and V_i, a was calculated to be 9.6×10^{-6} mol/l.

The potentiometric titration of soluble starch (0.5%) with iodine in 0.025 mol/l KI solution was carried out for comparison. The results are shown in Fig. 4. Since soluble starch contains several hydrolysis products, the plateau part of the titration curve consists of several flat steps. The presence of hydrolysis products is also indicated in the elution curve as a hump in Fig. 2.

It is evident from Fig. 4 that the linear part of the gel filtration curve corresponding as a whole to the plateau part of the titration curve shows a constant value of a while the initial and final deviations from the linearity of the gel filtration curve indicate a smaller and larger concentration, respectively, of free iodine than a. The latter deviation also corresponds to the saturation of iodine in starch. A detailed potentiometric titration confirmed the value a to be *ca.* 2.5×10^{-6} mol/l. The smaller value as compared with the value obtained from gel filtration may be due to the absence of KI in the gel column in the former system as mentioned later.

(2) Amylose. The iodide concentration was kept constant to 0.004 mol/l, which was the largest possible concentration without the formation of amylose–iodine precipitate at high iodine concentration (2.0×10^{-4} mol/l). The gel column is equilibrated with distilled water as in the case of soluble starch. Elution curves obtained (not shown) lack the hump due to hydrolysis product shown in Fig. 2. Plots of the elution volume of blue amylose–iodine solution, V_{ai} and $1/(V_{ai}-V_a)$ against C shown in Figs. 5 and 6 respectively (called system II) resemble those of soluble starch. The observed V_a value of 4.50 ml was used. It is seen from Fig. 6 that $1/(V_{ai}-V_a)$ *vs.* C plots for different amylose concentration fall on a common straight line passing through the origin with similar deviations to

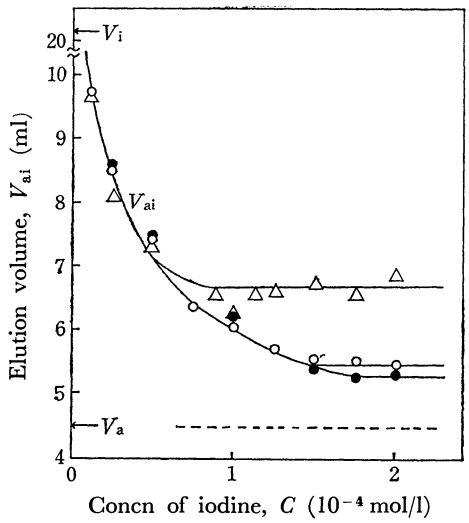

Fig. 5. V_{ai} *vs.* C plots for amylose-iodine systems.
Sample solution: Concn of KI 0.004 mol/l
Conc. of amylose 0.08%, 0.12%, 0.02%
Gel column: Concn of KI 0 mol/l

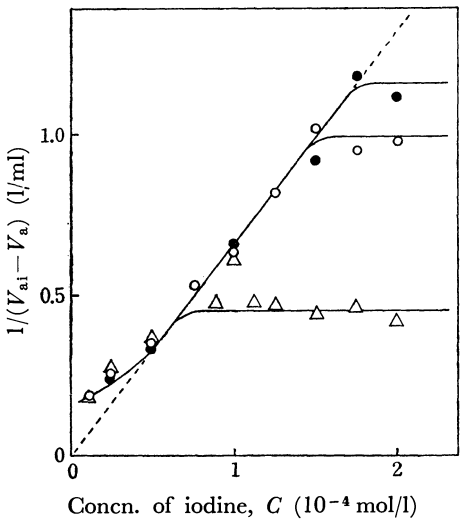

Fig. 6. $1/(V_{ai}-V_a)$ *vs.* C plots for amylose-iodine systems.
Sample solution: same as in Fig. 5
Gel column: same as in Fig. 5

those in Fig. 3.

From Fig. 5 it is clear that the constant V_{ai} for large C depends on the concentration of amylose. Such a tendency and similar behavior appearing in the potentiometric titration curve (not shown) also indicate the saturation of iodine in amylose as in the case of soluble starch. The value a calculated from Eq. (1) using the values $V_s(=V_a=4.50$ ml) and $V_i(21.17$ ml) is 9.1×10^{-6} mol/l.

While the binding of iodine with soluble starch or amylose is well accepted, the state of iodide ion in the solution has been precisely studied only in a few reports.[1,2] Although the blue amylose–iodine complexes are believed to form in the presence of iodide ions in the solution,[8] amylose–iodine complexes can be prepared without the addition of potassium iodide, *viz.*, as a solution almost free from iodide ions. Using

Table 1. Effects of iodide ion in amylose-iodine complex

System	Iodine species in solution	Gel matrix	a (mol/l)	V_{ai} at $C=1.0\times10^{-4}$ mol/l (ml)	Mol I_2 bound per g amylose at $C=1.0\times10^{-4}$ mol/l
I	I_2	—	19×10^{-6}	8.8	1.0×10^{-4}
II	I_2, I^-	—	9.1×10^{-6}	6.0	1.1×10^{-4}
III	I_2, I^-	I^-	1.1×10^{-6}	4.7	1.2×10^{-4}

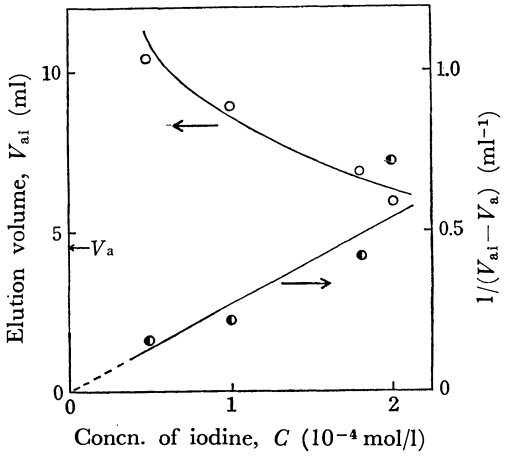

Fig. 7. V_{ai} and $1/(V_{ai}-V_a)$ *vs.* C plots for amylose-iodine systems.
Sample solution: Concn of KI 0 mol/l
Concn of amylose 0.08%
Gel column: Concn of KI 0 mol/l

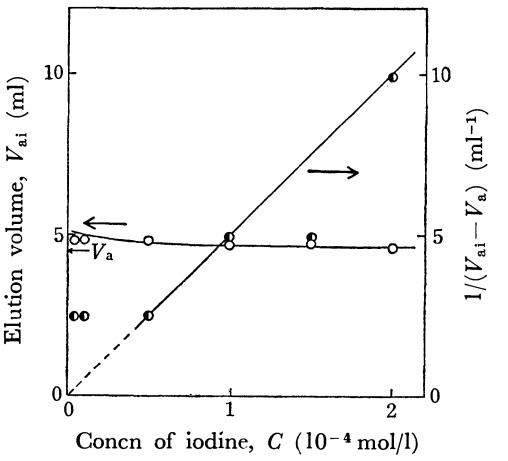

Fig. 8. V_{ai} and $1/(V_{ai}-V_a)$ *vs.* C plots for amylose-iodine systems.
Sample solution: Concn of KI 0.004 mol/l
Concn. of amylose 0.08%
Gel column: Concn of KI 0.004 mol/l

such an iodide free solution, gel filtration of 0.08% amylose was carried out under the same conditions as in system II. The result is shown in Fig. 7 (system I). The value a was calculated to be 19×10^{-6} mol/l. We further made the gel filtration of 0.08% amylose which is similar to system II except that the gel column was filled with aqueous potassium iodide solution of the same concentration as that for system II. The results are shown in Fig. 8 (system III). The value a was also calculated from the $1/(V_{ai}-V_a)$ *vs.* C plots to be 1.1×10^{-6} mol/l. As seen in Figs. 7 and 8, the plots scatter about a straight line and the value a calculated are not accurate. However, it might be certain from V_{ai} of system II that the value a of system III is smaller than that of system II.

Potentiometric determination of a was also carried out for system III, giving 1.6×10^{-6} mol/l which is in agreement with the result of gel filtration. This may be expected since the titration system resembles the gel filtration system for system III more closely than the other two systems as regards the addition of iodide ions. The results obtained from Figs. 5, 7 and 8 are summarized in Table 1. The effect of iodide ions in the solution and in the gel matrix on gel filtration of the amylose-iodide system is compared. It is seen that the values a and V_{ai} decrease as the iodide ions added becomes distributed over the solution and gel matrix. In the region of constant a, mol of iodine bound per g of amylose at a given concentration C is equal to $(C-a)/0.8$ for $C=1.0\times10^{-4}$ mol/l. We see from Table 1 that in order to obtain a nearly equal amount of iodine bound to amylose, 19×10^{-6} mol/l free iodine is

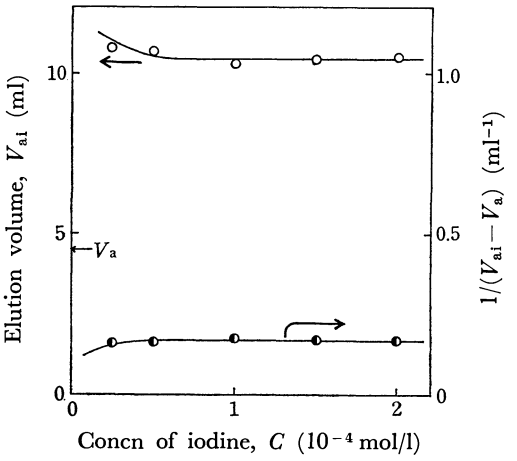

Fig. 9. V_{ai} and $1/(V_{ai}-V_a)$ *vs.* C plots for amylopectin-iodine systems
Sample solution: Concn of KI 0.004 mol/l
Concn. of amylopectin 0.08%
Gel column: Concn of KI 0 mol/l

necessary for system I and 9.1×10^{-6} mol/l for system II, but only 1.1×10^{-6} mol/l is sufficient for system III. Thus, iodide ions seem to favor the complex formation.

Iodide ions are bound to amylose in addition to iodine molecules. If amylose-iodine complexes of system II (Table 1) do not bind iodide ions, its elution front, which is in advance of the free iodide ions and is therefore exposed to the iodide free medium, is in the same condition as that elution front of the system I, and the value a should be equal to that of system I.

This, however, is not the case. Incorporation of iodide ions into amylose molecule increases iodide ions at the front and gives a lower a value compared with that of system I. Thus, iodide ions can be explained as bound to to amylose molecule.

(3) Amylopectin. Amylopectin, another component of starch, was further used for gel filtration. The result is shown in Fig. 9. For a wide range of iodine concentration, elution volume of amylopectin–iodine complexes, V_{ai} is nearly constant and is very large compared with the elution volume of amylopectin, V_a and amylose–iodine complexes V_{ai} for the same concentration of iodine. Plots $1/(V_{ai}-V_a)$ *vs.* C show a straight line. However, the nearly zero inclination of this straight line as well as the large V_{ai} value might give a large a value, and this in turn indicates the instability of amylopectin–iodine binding. The potentiometric titration curve (not shown), showing no plateau, is also in accordance with this. All these facts are in agreement with the general view that amylopectin–iodine binding is not so strong as soluble starch- and amylose–iodine binding.[6]

References

1) G. A. Gilbert and J. V. R. Marriott, *Trans. Faraday Soc.*, **44**, 84 (1948). K. Kuge and S. Ono, This Bulletin, **33**, 1273 (1960).
2) T. Kuge and S. Ono, This Bulletin, **33**, 1269 (1960).
3) D. L. Mould and R. L. M. Synge, *Biochem. J.*, **58**, 585 (1954).
4) R. E. Rundle and D. French, *J. Amer. Chem. Soc.*, **65**, 554 (1943).
5) H. Suzuki and T. Sasaki, This Bulletin, **44**, 2630 (1971).
6) K. Tanaka and T. Sasaki, Proc. VIth Int. Congress of Surface Active Substances, Zurich (1972), in press.
7) S. Lansky, M. Kooi, and T. J. Schoch, *J. Amer. Chem. Soc.*, **71**, 4066 (1949).
8) J. A. Thoma and D. French, *ibid.*, **82**, 4144 (1960).

Mass Spectrometric Study of the Primary Processes in Photochemical Reactions. II. Mass Spectra of Methyl and Ethyl Radicals

Shigeru YAMASHITA

Department of Chemistry, Faculty of Liberal Arts and Sciences, University of Osaka Prefecture, Mozu-Umemachi, Sakai, Osaka 591

(Received December 12, 1973)

The mass spectra of methyl and ethyl radicals have been determined by the photolyses of methyl and ethyl iodide using a high intensity light beam and a collision-free photochemical reactor incorporated in the ion-source of a mass spectrometer. The parent ion peak was the most intense in the mass spectra of methyl and of ethyl radicals. Fair agreement was found between the present work and the result obtained by previous workers for pyrolytically produced methyl radicals.

In a previous work, the primary processes in 1,1′-azopropane photolysis were studied with a collision-free reactor incorporated in the ion source of a mass spectrometer.[1] The photofragments produced were ionized by electron impact without their undergoing secondary processes and estimation of the primary processes was thus facilitated as compared with the conventional procedure of analysis of final reaction-products.

The primary step of the photolysis of 1,1′-azopropane was found to be composed of three competitive processes:

$$CH_3CH_2CH_2N_2CH_2CH_2CH_3 + h\nu \longrightarrow CH_3CH_2CH_2N_2CH_2 + CH_2CH_3 \quad (1)$$

$$CH_3CH_2CH_2N_2CH_2CH_2CH_3 + h\nu \longrightarrow CH_3CH_2CH_2N_2 + CH_2CH_2CH_3 \quad (2)$$

$$CH_3CH_2CH_2N_2CH_2CH_2CH_3 + h\nu \longrightarrow 2CH_3CH_2CH_2N \quad (3)$$

As many as five kinds of photofragment radicals were formed in the primary step, and their assignments had to be made from the recorded mass spectrum of the photolyte mixture without any information on their cracking patterns. It is known that a large number of photochemical reactions consist of several competitive primary processes as in the case of 1,1′-azopropane. For analysis of the recorded mass spectrum of the photolyte mixture of photofragment radicals, it is desirable that the cracking patterns of the expected radicals are known before the experiment.

The mass spectra of free radicals have been measured only in a few cases.[2] Only the parent-ion peaks of a number of free radicals were observed with the use of several kinds of reactors connected to the ion sources of mass spectrometers in the studies of free radicals produced by pyrolyses[3-6] and of photochemical reactions.[7-9]. It was thought to be worthwhile and of theoretical interest to measure the mass spectra of some frequently-appearing free radicals such as simple alkyl radicals, since several theoretical treatment have been reported for explaining the cracking pattern of the stable molecules.[10,11] The theory could be extended to free radicals provided that suitable parameters are chosen for calculation.

In the present work, alkyl iodides were used for producing the corresponding alkyl radicals by photolyses. Since the C–I bond dissociation energies of alkyl iodides are much smaller than those of the C–C and C–H bonds,[12] only the C–I bond rupture is expected in the primary step of the alkyl iodide photolysis.

Experimental

Methyl iodide and ethyl iodide(guaranteed-reagent grade, Tokyo Kasei Kogyo Co.) were purified by vacuum distillation.

The apparatus and method of operation were reported previously.[1] The molecular flow of the reactant gas was supplied from a 5-l reservoir kept in the dark into the reactor zone of the ion source through an orifice and a Pyrex glass gas-lead. The light source was a USH-500D 500W high-pressure mercury lamp(Ushio Electric Co.) and the light output was collimated in a housing fitted with a condensing lens system and a spherical mirror to obtain maximum intensity. The light flux was focused on the molecular flow of the reactant in the reactor through a quartz window fixed on a side-hole of the ion source of a Hitachi RMU-5 mass spectrometer. Considering the absorption spectra of methyl iodide and ethyl iodide in gas phase[13] and the transmission of the Pyrex glass of the apparatus, the effective wavelength for the photolyses was estimated to be in the range 290—320 nm of the mercury-lamp output.

The mass spectrum obtained at 50 eV for each run was a superposition of the cracking patterns of the photofragments and that of unreacted alkyl iodide. The mass spectrum of the photofragment mixture was obtained after subtracting the contribution from unreacted alkyl iodide.

Results and Discussion

Mass spectrum of a photofragment mixture from the recorded mass spectrum is given in Table 1. By subtracting the contribution from unreacted methyl iodide from the recorded peak height, the residue Δ was obtained as the sum of the mass spectrum of each photofragment. Subtraction was done by normalizing at the mass number 142, the parent-ion peak of methyl iodide. Since all peaks can be attributed to CH_3 and I, it would be evident that only one primary process

Table 1. Mass spectrum of the photolyte flow of methyl iodide at 50 eV (in arbitrary units)

m/e	Peak height	Methyl iodide contribution	Δ	Assignment
12	1.1	0.8	0.3	CH_3
13	2.1	1.5	0.6	
14	5.3	3.6	1.7	
15	55.0	48.5	6.5	
127	60.5	55.2	5.3	I
142	150.5	150.5	—	methyl iodide

(4) is possible under the present conditions.

$$CH_3I + h\nu \longrightarrow CH_3 + I \quad (4)$$

The mass spectrum of methyl radical obtained by averaging the results of nineteen runs is given in Table 2. The results of the present work are compared with those of Osberghaus and Taubert.[2] In both cases, the parent-ion peak was found to be the most intense and a fair agreement is obtained in relative abundance of the peaks at each mass number except for *m/e* 14. The discrepancy at *m/e* 14 might be caused by the difference between the procedure for methyl radical formation in the present work and that of Osberghaus and Taubert. In the latter, methyl radicals were produced by the pyrolysis of tetramethyl lead at 900 °C.

TABLE 2. MASS SPECTRUM OF METHYL RADICAL

m/e		12	13	14	15
Relative abundance	This work	5±2	11±6	25±8	100
	Osberghaus and Taubert	3	10	54	100

TABLE 3. MASS SPECTRUM OF THE PHOTOLYTE FLOW OF ETHYL IODIDE AT 50 eV (in arbitrary units)

m/e	Peak height	Ethyl iodide contribution	*Δ*	Assignment
15	0.6	0.6	—	C_2H_5
25	0.5	0.4	0.1	
26	5.5	5.0	0.5	
27	30.0	24.9	5.1	
28	12.0	10.1	1.9	
29	39.0	33.7	5.3	
127	13.9	12.2	1.7	I
156	41.0	41.0	—	ethyl iodide

The mass spectrum of the photolyte flow of ethyl iodide is shown in Table 3. It can be seen that the procedure for obtaining it is the same as in the case of methyl iodide. Since the peak height at *m/e* 128 was found negligible in the residue *Δ* of each run, the process

$$C_2H_5I + h\nu \longrightarrow C_2H_4 + HI$$

could be neglected. Thus, only the following process is possible under the present experimental conditions.

$$C_2H_5I + h\nu \longrightarrow C_2H_5 + I \quad (5)$$

The mass spectrum of ethyl radical obtained by averaging the results of twelve runs is shown in Table 4. In the mass spectrometric study of argon-ion bombardment on the ethylated surface of germanium,[14] occurrence of the fragment-ion from the liberated ethyl radicals by electron impact was suggested although the relative abundance of fragment-ion peak in the mass spectrum of ethyl radical was not determined because of the coexistence of other species emitted from the surface.

The peaks at *m/e* 12~15 were not detected, indicating a negligible contribution of C–C bond rupture by electron impact of ethyl radical (Table 4).

Thus the results of the present work suggest that all the significant fragment-ions are produced solely by C–H bond rupture resulting from the electron bombardment at 50 eV both in the case of methyl and ethyl radicals. It is seen that the relative abundance of the fragment-ion is larger in the mass spectrum of C_2H_5 than in that of CH_3. The difference might be caused by the difference of excess energy partition in C_2H_5 and CH_3.

TABLE 4. MASS SPECTRUM OF ETHYL RADICAL

m/e	25	26	27	28	29
Relative abundance	1±1	13±3	82±12	44±10	100

The excess energy E_{exc} is expressed by the following equation:

$$\begin{aligned} E_{exc} &= h\nu + E^{P}_{int} - D(\text{C–I}) \\ &= E_{tr} + E_{int} \\ &= (E^{R}_{tr} + E^{I}_{tr}) + (E^{R}_{int} + E^{I}_{int}) \end{aligned} \quad (6)$$

where, $h\nu$ is the photon energy, E^{P}_{int} the initial parent molecule internal energy which is small, and D(C–I) the dissociation energy of the C–I bond. The excess energy is distributed in the total translational energy E_{tr} of alkyl radical R and iodine atom I and in the total internal energy E_{int} of both fragments.

In their photofragment spectroscopic study of the photodissociation of alkyl iodides, Riley and Wilson[15] pointed out that the ratio of E^{R}_{int} appearing as the energy for alkyl-fragment internal excitation to the total energy E^{R}_{tot} (translational and internal) given to alkyl fragment was found to be three times larger in C_2H_5 than in CH_3. It is plausible that the higher fraction of internal excitation can be one cause for the larger relative abundance of fragment-ion in the mass spectrum of ethyl radical as compared with methyl radical.

The author is grateful to Professor Teruo Hayakawa for encouragement and discussion. The work was supported in part by a grant of the Ministry of Education.

References

1) S. Yamashita and T. Hayakawa, This Bulletin, **46**, 2290 (1973).
2) O. Osberghaus and R. Taubert, *Z. Phys. Chem.*, **4**, 264 (1955).
3) G. C. Eltenton, *J. Chem. Phys.*, **10**, 403 (1942).
4) F. P. Lossing and A. W. Tickner, *ibid.*, **20**, 907 (1952).
5) A. J. B. Robertson, *Proc. Roy. Soc., Ser. A*, **199**, 394 (1949).
6) P. LeGoff, *J. Chim. Phys.*, **53**, 269 (1956).
7) R. F. Pottie, A. G. Harrison, and F. P. Lossing, *Can. J. Chem.*, **39**, 102 (1961).
8) A. Jones, S. Yamashita, and F. P. Lossing, *ibid.*, **46**, 833 (1968).
9) K. O. MacFadden and C. L. Currie, *J. Chem. Phys.*, **58**, 1213 (1973).
10) H. M. Rosenstock, M. B. Wallenstein, A. L. Wahrhaftig, and H. Eyring, *Proc. Nat. Acad. Sci. U. S.*, **38**, 667 (1952).
11) K. Hirota, *Nippon Kagaku Zasshi*, **89**, 327 (1967).
12) V. I. Vedeneyev, L. V. Gurvich, V. N. Kondratyev, V. A. Medvedev, and Ye. L. Frankevich, "Bond Energies, Ionization Potentials and Electron Affinities," St. Martin's Press, New York (1966), p. 63.
13) D. Porret and C. F. Goodeve, *Proc. Roy. Soc., Ser. A*, **165**, 31 (1938).
14) J. A. Amick, G. W. Cullen, and D. Gerlich, *J. Electrochem. Soc.*, **109**, 124 (1962).
15) S. J. Riley and K. R. Wilson, *Discuss. Faraday Soc.*, **53**, 132 (1972).

Solution Properties of Phycocyanin. I. Studies of Dissociation-Association by Sedimentation Measurement*

Takahide SAITO, Naomichi ISO, and Haruo MIZUNO

Department of Food Science and Technology, Tokyo University of Fisheries, Konan, Minato-ku, Tokyo 108

(Received December 28, 1973)

The dissociation-association properties of phycocyanin, isolated from the red algae, "*Porphyra tenera*," have been investigated by sedimentation velocity measurements at pH 6.8 and 5.4 and at the ionic strengths of 0.1 and 0.2. The sedimentation coefficient data indicated that the predominant component in the phycocyanin solution was a trimer at pH 6.8 and a hexamer at pH 5.4. The concentration dependence of the sedimentation coefficient for various hypothetic systems of the dissociation-association equilibrium of phycocyanin was simulated by a computer model. It was reasonable to consider, from the simulation, that the dissociation-association system of phycocyanin was trimer$\rightleftarrows$monomer at pH 6.8 and hexamer$\rightleftarrows$monomer at pH 5.4. The dissociation constant was calculated for each system. The value of the dissociation constant was 0.15×10^{-4} (g/dl)^2 at pH 6.8 and an ionic strength of 0.1; 0.13×10^{-4} (g/dl)^2 at pH 6.8 and an ionic strength of 0.2; 0.5×10^{-13} (g/dl)^5 at pH 5.4 and an ionic strength of 0.1 and 0.1×10^{-13} (g/dl)^5 at pH 5.4 and an ionic strength of 0.2. The dissociation constants decrease with an increase in the ionic strength in solution.

Phycocyanin is an accessory photosynthetic chromoprotein obtained from red- and blue-green algae. The properties of phycocyanin have been studied by many investigators. Svedberg and Katsurai[1] and Svedberg and Eriksson[2] measured the molecular weight of the protein under various pH conditions by the sedimentation equilibrium method; they found that the molecular weight of phycocyanin changed reversibly according to the pH change of the solution. Recently, Hattori and Fujita[3] and Berns *et al.*[4] confirmed this phenomenon by ultracentrifugation and spectrometry. It was showen that the reversible aggregation of this protein depended upon the ionic strength and the temperature of the solution.[5-7] It has also been reported by Berns *et al.*[8] that phycocyanin decomposed into many smaller units in the presence of urea or sodium dodecyl sulfate, and that the minimum molecular weight of phycocyanin was 30000. Scott and Berns.[7] claimed that the molecular weight of the phycocyanin aggregates were 90000, 180000, or 360000. From these observations, it has been presumed that the aggregates of phycocyanin are a trimer, a hexamer and a dodecamer, and also that the dissociation-association equilibrium was attained between these higher aggregates and lower aggregates or a monomer in the solution.

Hattori *et al.*[6] obtained the equilibrium constant from their measurements of the concentration dependence of the extinction coefficient of the phycocyanin solution. Scott and Berns[7] observed two or more peaks in the schlieren patterns obtained by the sedimentation velocity measurement of phycocyanin from *Plectonema calothricoides*, and calculated the equilibrium constant using the relative areas under these peaks.

Adams *et al.*[9-12] have published a theory of the association-dissociation of molecules in an ultracentrifugal field and have derived a method for evaluating the equilibrium constant from the sedimentation equilibrium experiment. They applied this theory to the study of the self-association of β-lactoglobulin B in an acid solution[13] and showed that the experimental results could easily be explained by this theory.

In order to investigate the molecular shape and size of phycocyanin, which undergoes the dissociation-association reaction according to the environmental changes in the solution, it is necessary to estimate the dissociation-association constant of this protein. Adams' method is not always a convenient one for obtaining such preliminary knowledge as described above. If it is possible to estimate the equilibrium constant for the dissociation-association of phycocyanin by using the sedimentation transport method, such an experiment would, however, be quite useful.

In this paper we will attempt to estimate the equilibrium constant by using the sedimentation velocity method, and also to presume the state of the equilibrium of phycocyanin in solution. Moreover, we wish to contribute to the knowledge about the solution properties of the phycocyanin.

Experimental

Preparation. The phycocyanin used in this study was obtained from dried *Porphyra tenera* by repeating the precipitation with ammonium sulfate. The details of this preparation were reported by Fujiwara.[14] The outline of this procedure is presented in Fig. 1. The purity of phycocyanin was ascertained by measurements of its electrophoretic behavior, while the absorption spectra of this protein solution were measured at pH 6.8 and at an ionic strength of 0.1. As is shown in Fig. 2, the ratio of extinction at 620 nm and 280 nm was greater than 4.0. This value agreed with that obtained by earlier investigators[3,15,16] for pure phycocyanin. The purified phycocyanin was stored at 5 °C under 40% saturated ammonium sulfate. The sample of phycocyanin was dissolved in water and dialyzed against a phosphate or acetate buffer at 5 °C. Dialysis was continued for at least 48 hr, with an occasional change of the external solution.

Determination of Concentration. The protein concentrations were determined by weighing the substances after they had been dried at 105 °C for 24 hr; they were also determined by the semi-micro-Kjeldahl method. The value of the concentrations obtained by the different methods

* Some of the experimental results in this paper were presented at the 27th Annual Meeting of The Chemical Society of Japan, Nagoya, October 12, 1972, and at the 22nd Annual Meeting of The Society of Polymer Science, Japan, Kyoto, May 30, 1973.

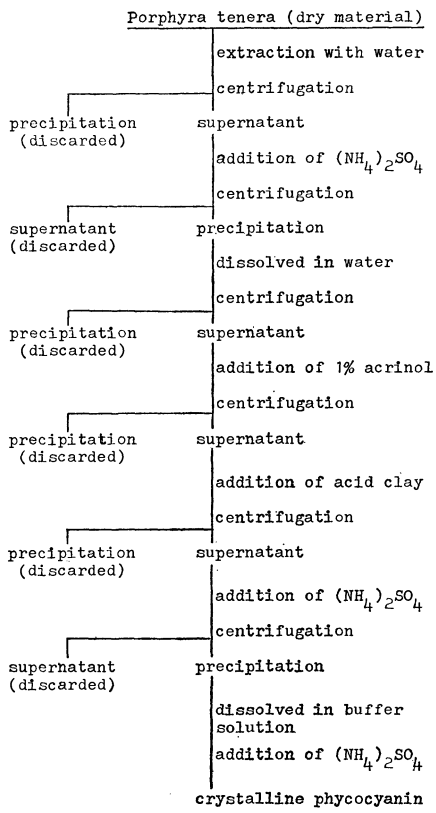

Fig. 1. Flow-sheet of preparation of phycocyanin.

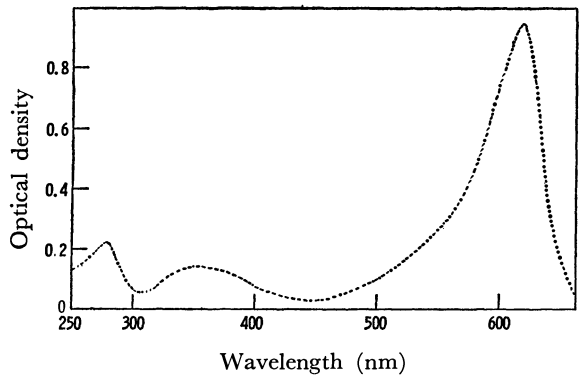

Fig. 2. Absorption spectrum of aqueous solution of phycocyanin.

agreed with each other within the limits of experimental error.

Ultracentrifugation. The sedimentation velocity experiments were performed with a Hitachi Model UCA-1 ultracentrifuge with a schlieren optical system; double sectorial cells were used. In all runs the rotor speed was set at 47,300 rpm, and the temperature was maintained at 25 °C.

The sedimentation coefficient, s, is represented by the following equation:

$$s = \frac{\ln(r_p/r_m)}{\omega^2(t-t_0)},$$

where r_p is the boundary position measured from the second moment of the refractive index gradient; r_m, the position of the meniscus; ω, the angular velocity; t, the time, and t_0, the initial time correction. In general, if the shape of the schlieren pattern is of a Gaussian type, $r_p=r_h$, where r_h is the position of the maximum of the refractive index gradient. In our experiment, the schlieren patterns were satisfactorily considered to be Gaussian, as is shown in Fig. 3; the position of the maximum of the refractive index gradient dose not differ significantly from the boundary position obtained. For example, the calculated values of r_p and r_h were 6.362 cm and 6.363 cm respectively 30 min after reaching a constant speed of 47300 rpm, in the sedimentation velocity measurement of phycocyanin at pH 6.8 and at I (ionic strength) of 0.1. The position of the maximum of the refractive index gradient was, then, used in place of the boundary position for the evaluation of the sedimentation coefficient throughout this study. The position of maximum of the refractive index was measured using a Sinko-VF-12 projector.

Estimation of the Equilibrium Constant for Dissociation-Association Reactions. The sedimentation coefficient for a system containing many species is represented by the following equation:

$$s = \frac{\sum s_i c_i}{\sum c_i}. \quad (1)$$

where c_i and s_i are the weight concentration(g/dl) and the sedimentation constant for the i-th species respectively. The equilibrium constant for the i-mer$\rightleftarrows$monomer($M_i \rightleftarrows iM_1$) system, K_i, is defined by using the mass-action equation:

$$K_i = \frac{{c_1}^i}{c_i}. \quad (2)$$

The total concentration, c, is given by the following equation:

$$c = \sum c_i. \quad (3)$$

Thus, Equation (1) is rewritten in the form:

$$s = \frac{\sum ({c_1}^i/K_i)s_i}{c}. \quad (4)$$

The concentration dependence of the sedimentation coefficient is usually shown as follows:

$$s_i^* = s_i^0(1-\alpha_i), \quad (5)$$

$$s^* = \frac{\sum ({c_1}^i/K_i)s_i^0(1-\alpha_i)}{c}, \quad (6)$$

where s^* is an apparent sedimentation coefficient and s^0, the sedimentation coefficient at an infinite dilution. Moreover α_i is $k_{s_i}c_i$, where k_{s_i} is the concentration-dependence coefficient of the i-th species. Now, by assuming that α_i is constant for all species, the following equation is obtained from Eq. (6):

$$s^* = \left[\frac{\sum ({c_1}^i/K_i)s_i^0}{c}\right](1-k_s c). \quad (7)$$

Thus the equilibrium constant, K_i, can be evaluated if the values of s_i^0, c_1, s^*, and k_s are known.

The sedimentation coefficient of the phycocyanin aggregates, s_i^0, was determined by extrapolating the linear plot over a limited region at higher concentrations to an infinite dilution, while the concentration-dependence coefficient, k_s, was determined from the slope according to Eq. (5). The sedimentation coefficient of the monomer, s_i^0, was assumed to be 3.2 S, a value reported by Hattori *et al.*[6] Then K_i can be computed by assuming the value of c_1. In practice, the value of the right-hand side of Eq. (7) are calculated by assuming both the values of c_1 and K_i, and then compared with the s^* obtained experimentally. The values of c_1 and K_i were systematically changed, and the most probable value of K_i was decided according to where the standard deviation of the difference between the calculated s^* and the observed s^k reaches its minimum. The TOSBAC-3400 computer was used for the calculations.

Results and Discussion

Some investigators[6,7,15-17] have observed two or more peaks in the sedimentation patterns of a phycocyanin solution under various values of pH and the ionic sterngth. However, all of our sedimentation patterns showed a single peaks, as is shown in Fig. 3. This discrepancy seems to be caused by the sources of phycocyanin being different from one another.

Scott and Berns[7] estimated the equilibrium constant using the relative areas under the peaks of the schlieren patterns, but in our experiments this procedure is inapplicable to the estimation of the equilibrium constant. Therefore, the following treatment was necessary for the estimation of the equilibrium constant.

Figures 4—7 show the sedimentation coefficients of phycocyanin as a function of the protein concentration at pH 6.8 and 5.4 and at I values of 0.1 and 0.2. In these figures, the calculatted lines for the dissociation-association equilibria are given. The variation of s^* with the concentration shows a tendency to increase with a decrease in the concentration in the higher-concentration region, while it tends to decrease near a zero concentration. These results show that the protein molecules associate in the higher-concentration region. This behavior is similar to that of β-lactoglobulin or γ-G-globulin.[18]

Figure 4 shows the results at pH 6.8 and at $I=0.1$. From the plots in Fig. 4, the s_i^0 of 6.3 S and the k_s of 0.30 were obtained. Since the s_i^0 value agreed with the value reported for the trimer,[6,17] we assumed that this dissociation-association equilibrium was the trimer$\rightleftarrows$monomer ($M_3\rightleftarrows 3M_1$) system. The calculated line A is that for the $M_3\rightleftarrows 3M_1$ system. In order to know whether or not the hexamer species exist in the solution, the (hexamer+trimer)$\rightleftarrows$monomer($M_6+M_3\rightleftarrows 9M_1$) system was calculated as a trial. Line B is that calculated for the system. As is shown in Fig. 4, the experimental results can be well represented by the calculated line A. The hexamer could not be considered to exist in the solution. The equilibrium constant for the $M_3\rightleftarrows 3M_1$ system, K_3, was decided to be 0.15×10^{-4} (g/dl)^2.

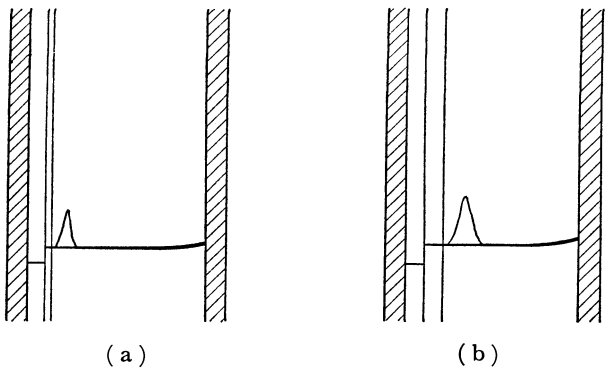

(a) (b)

Fig. 3. Sedimentation patterns of phycocyanin.
(a): at pH 6.8, ionic strength 0.1; phosphate buffer, 26 min after reaching constant speed, (b): at pH 5.4, ionic strength 0.1; acetate buffer, 28 min after reaching constant speed.

The results at pH 5.4 and $I=0.1$ are shown in Fig. 5; values of 10.8 S for s_i^0 and 0.30 for k_s were obtained from the results. The s_i^0 value agreed with the value which was reported for the hexamer.[6,7,15,16] This result shows clearly that the state of the dissociation-association equilibrium of the protein is closely related to the pH change in the solution. It was assumed that this dissociation-association equilibrium was the hexamer$\rightleftarrows$monomer($M_6\rightleftarrows 6M_1$), hexamer$\rightleftarrows$trimer($M_6\rightleftarrows 2M_3$), or $M_6+M_3\rightleftarrows 9M_1$ system. The calculated line C is that for the $M_6\rightleftarrows 6M_1$ system; line D, that for the $M_6+M_3\rightleftarrows 9M_1$ system, and line E, that for the $M_6\rightleftarrows 2M_3$ system. It is shown in this figure that the calculated line C for the $M_6\rightleftarrows 6M_1$ system almost coincides with the experimental points, while the other two lines show a larger deviation from the results obtained experimentally. The value of 0.5×10^{-13} (g/dl)^5

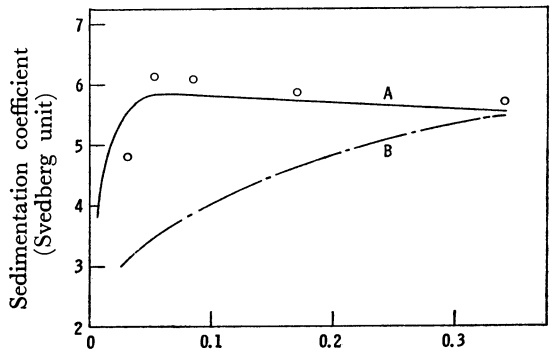

Fig. 4. Plots of sedimentation coefficients *versus* phycocyanin. Concentration in phosphate buffer solution at pH 6.8 and ionic strength 0.1, and calculated lines for the assumed equilibrium systems.
○: experimental points, line A: for the trimer$\rightleftarrows$monomer system, line B: for the (hexamer+trimer)$\rightleftarrows$monomer system.

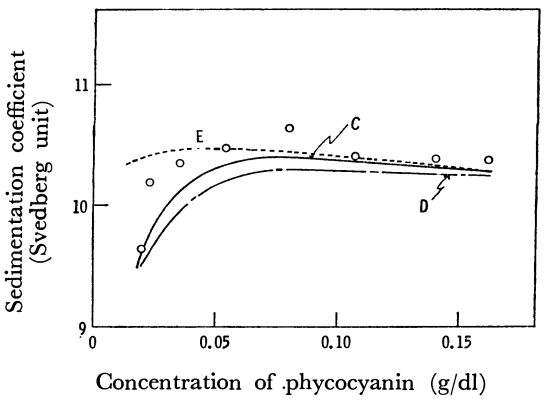

Fig. 5. Plots of sedimentation coefficients *versus* phycocyanin. Concentration in acetate buffer solution at pH 5.4 and ionic strength 0.1, and calculated lines for the assumed equilibrium systems.
○: experimental points, line C: for the hexamer$\rightleftarrows$monomer system, line D: for the (hexamer+trimer)$\rightleftarrows$monomer system, line E: for the hexamer$\rightleftarrows$trimer system.

for the $M_6 \rightleftarrows 6M_1$ dissociation constant, K_6, was obtained.

In order to determine the effect of the ionic strength on the dissociation-association, sedimentation-velocity experiments were also carried out at $I=0.2$ under the same pH condition as before. Some investigations with regard to the effect of the ionic strength on the dissociation-association of phycocyanin have been reported by several authors,[6,7] and it has been found that the quantity of aggregates increased with an increase in the ionic strength of the solution. However, these studies have been done in the lower ionic strength region.

Figure 6 shows the results at pH 6.8 and at $I=0.2$. From the results, the s_i^0 of 6.5S and k_s of 0.16 were obtained. This s_i^0 value agreed with that obtained $I=0.1$ and pH 6.8 in this work. It seemed reasonable to assume that the dissociation-association equilibrium was the $M_3 \rightleftarrows 3M_1$ or the $M_6+M_3 \rightleftarrows 9M_1$ system. This assumption was clearly the same as that at pH 6.8 and at $I=0.1$. The calculated line F is that for the $M_3 \rightleftarrows 3M_1$ system, while line G is that for the $M_6+M_3 \rightleftarrows 9M_1$ system. As is shown in Fig. 6, it was clear that the hexamer did not exist in the solution. The equilibrium constant for the $M_3 \rightleftarrows 3M_1$ system, K_3, was decided to be 0.13×10^{-4} (g/dl)^2. At the same pH, K_3 of 0.4×10^{-4} (g/dl)^2, which acts for the dissociation of phycocyanin in the 0.01 M phosphate buffer solution ($I=0.04$), and K_3 of 1.0×10^{-4} (g/dl)^2 in the 0.001 M phosphate buffer solution(I 0.004) were reported by Hattori *et al.*[6], using an absorption method. As has been described above, K_3 of 0.15×10^{-4} (g/dl)^2 for the phycocyanin solution was obtained in this work at the same pH and at $I=0.1$. These four values for K_3 under the different conditions of ionic strength show a tendency for the equilibrium constant to decrease with an increase in the ionic strength.

Figure 7 shows the results at pH 5.4 and at I=0.2; the s_i^0 of 11.3 S and the k_s of 0.24 were obtained. The s_i^0 value agrees with s_i^0 of 10.8 S which was obtained at $I=0.1$ and at pH 5.4 in this work. As before, this dissociation-association equilibrium was assumed to be $M_6 \rightleftarrows 6M_1$, $M_6+M_3 \rightleftarrows 9M_1$, or $M_6 \rightleftarrows 2M_3$ system. The calculated line H is that for the $M_6 \rightleftarrows 6M_1$ system, line I, that for the $M_6+M_3 \rightleftarrows 9M_1$ system, and line J, that for the $M_6 \rightleftarrows 2M_3$ system. Figure 7 shows that both the H and I calculated lines seem to be in satisfactory agreement with the experimental points. However, the concentration of the trimer, which was calculated in the process of the computation of K_i on the assumption of the $M_6+M_3 \rightleftarrows 9M_1$ system, was negligibly small. Therefore, it seems reasonable to say that the $M_6 \rightleftarrows 6M_1$ equilibrium was attained in the solution at pH 5.4 and at $I=0.2$. The equilibrium constant for the $M_6 \rightleftarrows 6M_1$ system, K_6, was decided to be 0.1×10^{-13} (g/dl)^5. The value is smaller than that obtained in this work at pH 5.4 and at I=0.1. It is found that the increase in the ionic strength relates to the decrease in the equilibrium constant; this result is identical with that obtained at pH 6.8. Hattori *et al.*[6] have explained that an increase in ionic strength results in a reduction of the electrostatic repulsive force of phycocyanin particles, and that this leads to the association of the monomer. The experimental results obtained in this study support their conclusion.

The association-dissociation equilibrium system of phycocyanin was suggested to be either the $6M_1 \rightleftarrows 2M_3 \rightleftarrows M_6$ system or two parallel reactions, that is, the $3M_1 \rightleftarrows M_3$ and the $6M_1 \rightleftarrows M_6$ system.[6,7] Berns *et al.*[19] proposed that the equilibrium system involved three parallel reactions, that is, the $3M_1 \rightleftarrows M_3$, the $6M_1 \rightleftarrows M_6$, and the $2M_3 \rightleftarrows M_6$ systems. In our experiments, the value of the equilibrium constant was small under the pH conditions of 6.8 and 5.4. Thus, it seems reasonable to assume that the dissociation-association equilibrium of phycocyanin under the conditions in this study inclines toward an one-side extreme (aggregate).

The concentration-dependence coefficients, k_s, of these solutions were found to be 0.30 (pH 6.8, $I=0.1$),

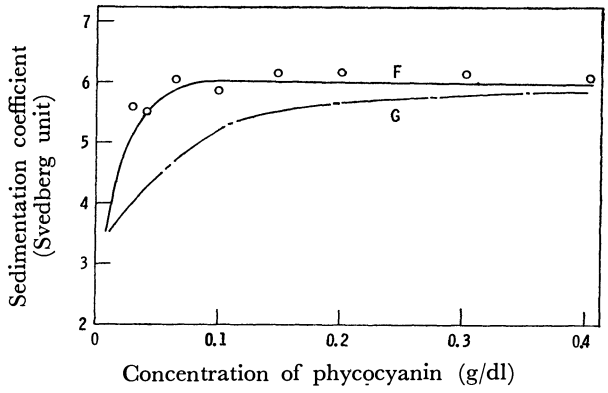

Fig. 6. Plots of sedimentation coefficients *versus* phycocyanin. Concentration in phosphate buffer solution at pH 6.8 and ionic strength 0.2, and calculated lines for the assumed equilibrium systems.
○: Experimental points, line F: for the trimer⇌monomer system, line G: for the (hexamer+trimer)⇌monomer system.

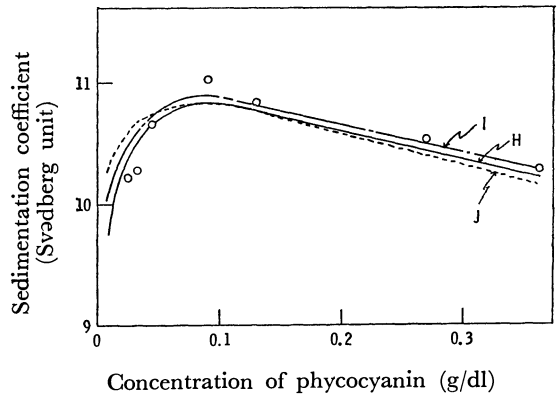

Fig. 7. Plots of sedimentation coefficients *versus* phycocyanin. Concentration in acetate buffer solution at pH 5.4 and ionic strength 0.2, and calculated lines for the assumed equilibrium systems.
○: experimental points, line H: for the hexamer⇌monomer, line I: for the (hexamer+trimer)⇌monomer system, line J: for the hexamer⇌trimer system.

0.30 (pH 5.4, I=0.1), 0.16 (pH 6.8, I=0.2), and 0.24 (pH 5.4, I=0.2). As with the k_s values of many other proteins, these values were small. Weirich *et al.*[20] have published a basic theory of the sedimentation coefficient of self-association species and described a method of estimating the sedimentation coefficient using the equilibrium constant, K_i, and the monomer concentration, c_1, obtained from sedimentation-equilibrium, light-scattering, or osmotic-pressure experiments on the same self-associating solute. Our study was aimed at estimating the equilibrium constant of the dissociation-association equilibrium system from the results of the sedimentation-velocity experiment. Since a sedimentation coefficient is not an equilibrium quantity, the equilibrium constant derived in this study should be considered to be only approximate values. Nonetheless, the dissociation constants obtained in this work are in fair agreement with those constants previously reported.[6] In view of the fact that the sedimentation-velocity measuement requires only a short time, it can be said that the procedure in this paper is a convenient method for the study of the dissociation-association system of a protein.

References

1) T. Svedberg and T. Katsurai, *J. Amer. Chem. Soc.*, **51**, 3573 (1929).
2) T. Svedberg and I. B. Eriksson, *ibid.*, **54**, 3998 (1932).
3) A. Hattori and Y. Fujita, *J. Biochem.* (Tokyo), **46**, 633 (1959).
4) D. S. Berns, H. L. Crespi, and J. J. Katz, *J. Amer. Chem. Soc.*, **85**, 8 (1963).
5) D. S. Berns and M. R. Edward, *Arch. Biochem. Biophys.*, **110**, 511 (1965).
6) A. Hattori, H. L. Crespi, and J. J. Katz, *Biochemistry*, **4**, 1225 (1965).
7) E. Scott and D. S. Berns, *ibid*, **4**, 2597 (1965).
8) D. S. Berns, E. Scott, and K. T. O'Reilly, *Science*, **145**, 1054 (1964).
9) E. T. Adams, Jr. and H. Fujita, "Ultracentrifugal Analysis in Theory and Experiment," ed. by J. W. Williams, Academic Press, Inc., New York (1963), p. 119.
10) E. T. Adams, Jr. and J. W. Williams, *J. Amer. Chem. Soc.*, **86**, 3454 (1964).
11) E. T. Adams, Jr., *Biochemistry*, **4**, 1646 (1965).
12) E. T. Adams, Jr. and D. L. Filmer, *ibid.*, **5**, 2971 (1966).
13) J. Visser, R. C. Deonier, E. T. Adams, Jr., and J. W. Williams, *ibid.*, **11**, 2634 (1972).
14) T. Fujiwara, *J. Biochem.* (Tokyo), **42**, 411 (1955).
15) J. J. Lee and D. S. Berns, *Biochem. J.*, **110**, 457 (1968).
16) J. J. Lee and D. S. Berns, *ibid.*, **110**, 465 (1968).
17) R. MacColl, J. J. Lee, and D. S. Berns, *ibid.*, **122**, 421 (1971).
18) J. W. Williams, "Ultracentrifugation of Macromolecules," Academic Press, New York (1972), p. 39.
19) D. S. Berns and A. Morgenstern, *Biochemistry*, **5**, 2985 (1966).
20) C. A. Weirich, E. T. Adams, Jr., and G. H. Barlow, *Biophys. Chem.*, **1**, 35 (1973).

Three Methods to Look at Walsh-type Diagrams Including Nuclear Repulsions*+

Yuuzi TAKAHATA† and Robert G. PARR

Department of Chemistry, The Johns Hopkins University, Baltimore, Maryland 21218, U.S.A.

(Received October 21, 1973)

Energy correlation diagrams for molecules of type AH_2 are examined by three different methods: (1) the quantum-mechanical virial theorem, (2) the method of median partition, (3) the integral Hellmann-Feynman theorem. Nuclear-nuclear repulsions are included. The formula for the first method takes the form $W=-\sum t_i$, where t_i is an orbital kinetic energy. The theory is applied to H_2O, CH_2, and BeH_2. Negative-kinetic-energies-*versus*-angle diagrams for these molecules are presented. The pattern of the diagrams is quite different from the usual Walsh diagram. With this resolution non-bonding electrons play a significant role in determining bond angles. In the second method the resolution of the total energy takes the form $W=\sum_i[e_i+V_n(i)]$, where e_i is a median electronic energy and $V_n(i)$ is a resolved nuclear repulsion energy calculated from an expression derived from ideas of population analysis. The energies-*versus*-angle diagram thus obtained for H_2O is similar to the one obtained by the first method. For the third method, the integral Hellmann-Feynman formula for the electronic energy change on bending is written in terms of corresponding orbital contributions, $\Delta E_l=\sum_i \Delta E_l(i)$, and nuclear-nuclear repulsion is added in a resolved form. For H_2O the ΔE_l resemble Walsh diagrams closely, both with and without the nuclear-nuclear repulsion increments. Wave functions used throughout are LCAO-SCF functions built from medium-size Gaussian basis sets.

Much effort has been dedicated to elucidate numerical rules governing molecular shapes, since Walsh first pointed out the existence of such rules for large number of simple polyatomic molecules.[1] There are two schools of thought in explaining the rules, valence bond theory and molecular orbital theory. It has been shown that the valence-shell electron pair repulsion theory (VSEPR) can explain Walsh's rules.[2] More recently it has been argued that closed shells on terminal atoms play an important role in the bending process, and a model has been given which predicts Walsh's magic numbers.[3,4] Connections between the model and the crystal field theory were noted.

Most quantum mechanical explanations of Walsh's rules have followed the lines laid by Mulliken[5] and Walsh.[1] Molecular orbital theory has been extensively applied giving "Walsh Diagrams."[6] United-atom approaches have also been applied producing Walsh-type diagrams.[7] It has remained a matter of argument, however, whether one should use the LCAO-MO-SCF orbital energies or some other one-electron MO energy quantities which genuinely add to give the total electronic energy in order to identify the Walsh ordinate.[8] There is another difficulty in the MO approach; Nuclear-nuclear repulsion has almost always been left out of consideration in calculating a Walsh diagram or at most added at the end.

In the present paper we explore the possibilities of obtaining method which enable one to partition the *total* molecular orbital energy of a molecule into one-electron energy quantities which are genuinely additive. Three schemes are employed for this purpose. They are the quantum-mechanical virial theorem, the method of median partition, and the integral Hellmann-Feynman theorem. The first method has already been applied by us to the H_2O molecule.[9] The energy correlation diagram obtained differed very much from the Walsh diagram. In Section II numerical results of further calculations on H_2O are presented, and the theorem is also applied to CH_2 and BeH_2. The second method follows closely the work of Coulson and Neilson[10] except that nuclear-nuclear repulsion energy is divided and included in the individual orbital components. The third method is of interest since it parallels the analysis of the same problem with the Hellmann-Feynman theorem, by Coulson and Deb.[8]

I. Wave Functions

Throughout this work we use single-determinantal linear combinations of Gaussian-type orbitals (LCGTO) SCF wave functions. A medium-size Gaussian basis set $(53/3)^{11a)}$ is employed for H_2O, while basis sets $(73/3)^{11b)}$ and $(53/3)^{11c)}$ are used for CH_2 and BeH_2 respectively. Gaussian exponents are tabulated in Table 1. LCGTO-SCF calculations are carried out at various bond angles and bond distances. The calculated equilibrium geometry H_2O has bond length 1.85 a.u. and bond angle of 112°, the corresponding experimental values being 1.8103 a.u. and 105°.

In the calculations reported in Section II below, the variation of bond distances with bond angle are considered, as described there. In the diagrams in Sections III and IV, on the other hand, the bond distances are held constant with change in bond angle.

II. Correlation Diagrams from the Quantum-mechanical Virial Theorem

It has already been pointed out that the polyatomic virial theorem in the form given by Nelander[12] gives theoretically rigorous correlation diagrams.[9] The central result of the Nelander theorem is that the relation $W=-T$ holds between the total energy W

* Aided by research grants to The Johns Hopkins University from the National Institutes of Health and the Pertroleum Research Fund of the American Chemical Socity.

+ Based on a thesis submitted by Yuuzi Takahata in partial fulfillment of the requirements for the degree of Doctor of Philosophy, The Johns Hopkins University, 1970.

† Present address: Department of Material Science, University of Electro-Communications, 1-5-1, Chofugaoka, Chofu-shi, Tokyo, Japan.

Table 1. Gaussian basis set for H_2O, CH_2, and BeH_2

Molecule	Center	Type	Exponents
	O	S	378.00
			74.5
			14.7
			2.89
			0.57
H_2O			
		P	9.38
			1.81
			0.35
	H	S	4.24
			0.658
			0.148
	C	S	994.9
			160.6
			39.91
			11.82
			3.698
			0.6026
			0.1817
CH_2			
		P	4.279
			0.8669
			0.2036
	H	S	6.4805
			0.9810
			0.2180
	Be	S	78.615
			15.524
			3.054
			0.600
			0.118
BeH_2		P	
			0.384
			0.074
	H	S	5.740
			0.775
			0.159

and the total kinetic energy T not only at the equilibrium geometry of a polyatomic molecule, but also for bond angles distorted from equilibrium, if the bond distances are optimum for each set of angles. Since kinetic energy is a one-electron quantity in the Hartree-Fock scheme, the total energy may be expressed as a sum of negative orbital kinetic energies:

$$W = \sum_i(-t_i). \quad (1)$$

This seems to be the only known theory which makes it possible to partition the total energy (including nuclear-nuclear repulsion) into genuinely additive one-electron componets. No nuclear-nuclear repulsion or electron-electron terms appear in the expression.

For approximate wave functions, the virial theorem as just stated does not hold unless the wave functions are scaled. The scaling procedure for polyatomic molecules may be patterned after Löwdin's treatment for diatomic molecules.[13]

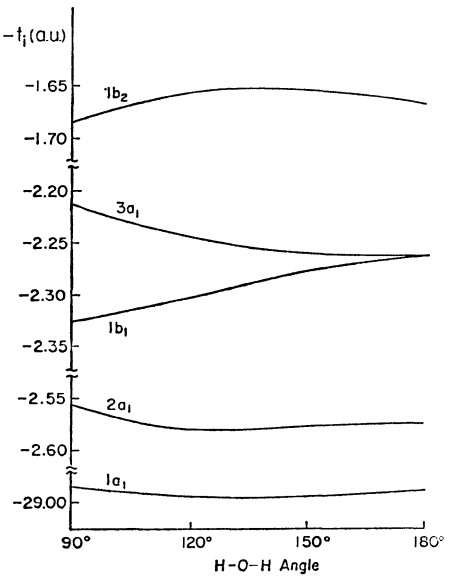

Fig. 1. Negative kinetic energies of the molecular orbitals of H_2O, as a function of H-O-H angle. See text.

In Table 2 are shown scaling factors (η), equilibrium bond lengths (R_e), kinetic (T), potential ($V=V_{ne}+V_{ee}$), nuclear repulsion (V_{nn}), and total (W) energies at various bond angles for H_2O. Note that the total energies are indeed equal to negative kinetic energies. The kinetic energies partitioned into one-electron components are listed in Table 3. These are plotted in Fig. 1 as a function of HOH angle.[9]

Figure 1 differs from a conventional Walsh diagram in two respects; (1) The order of the top three orbitals: $(1b_2)>(3a_1)>(1b_1)$, *versus* $(1b_1)>(3a_1)>(1b_2)$ in the conventional Walsh diagram, (2) The trends in changes of orbital energies differ. The $3a_1$ orbital energy component, for example, decreases with increasing apex angle in our diagram, whereas it increases in Walsh's.[1] The $1b_1$ orbital energy increases in Fig. 1, it remains constant in the Walsh diagram; *etc.*

We may note that the kinetic-energy-*versus*-angle diagram in Fig. 1 appears almost identical qualitatively with that of Coulson and Neilson,[10] who obtained their diagram by an entirely different method; see Section III below.

Earlier we argued,[9] by considering the diagram corresponding to Fig. 1 which is obtained by a certain unitary transformation of the orbitals, that lone-pair kinetic energies dominate the determination of geometry. The previously given evidence was basis-set dependent, but the conclusion may survive with accurate molecular orbitals if one makes an appropriate definition of the localization process—we do not know.

We next consider the molecule CH_2, in its $^1A_1$ state. This species has six valence electrons, and according to the Walsh rules it should be bent. In Fig. 2 are plotted the negative kinetic energies of CH_2 as functions of the HCH angle. If the figure is compared with the corresponding diagram for H_2O, Fig. 1, it can be seen that the same order of orbital (negative) kinetic energies prevails: $1b_2>3a_1>2a_1>1a_1$. However,

TABLE 2. SCALED QUANTITIES FOR H_2O

Scaling factors η, equilibrium bond distances R_e, scaled electronic kinetic (T), potential (V) energies, nuclear repulsion energies V_{nn}, total energies W.

θ	η	R_e	T	$V=V_{ne}+V_{ee}$	V_{nn}	W
90°	1.0015	1.8651	75.5373	−151.0747	8.9577	−75.5373
105°	1.0016	1.8442	75.5508	−151.1016	9.0176	−75.5507
130°	1.0017	1.8189	75.5458	−151.0916	9.0840	−75.5458
150°	1.0018	1.8034	75.5301	−151.0603	9.1590	−75.5301
180°	1.0018	1.7811	75.5171	−151.0342	9.2639	−75.5171

TABLE 3. MOLECULAR ORBITAL KINETIC ENERGIES t_i FOR H_2O

θ	Orbital					Total
	$1a_1$	$2a_1$	$3a_1$	$1b_2$	$1b_1$	
90°	28.9852	2.5551	2.2146	1.6871	2.3267	75.5378
105°	28.9913	2.5709	2.2311	1.6661	2.3159	75.5506
130°	28.9949	2.5789	2.2510	1.6541	2.2942	75.5458
150°	28.9963	2.5765	2.2605	1.6551	2.2766	75.5302
180°	28.9893	2.5731	2.2632	1.6697	2.2632	75.5170

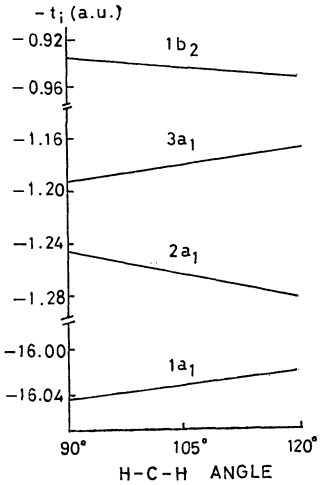

Fig. 2. Negative kinetic energies of the molecular orbitals of CH_2.

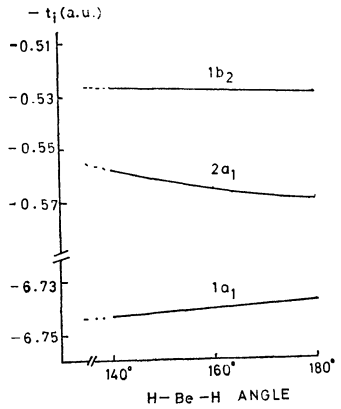

Fig. 3. Negative kinetic energies of the molecular orbitals of BeH_2.

energy changes with angle of individual orbitals are not the same in the two cases.

In Fig. 3 are plotted the corresponding orbital kinetic energies for BeH_2. The two top curves show minima at 180°, which may be regarded as showing how the four valence electrons drive the molecule linear.. This could be considered to be an explanation of one of the Walsh rules, which states that AH_2 molecules containing four valence electrons are linear. In the Figure it is seen that, indeed, the two bonding orbitals, $1b_2$ and $2a_1$, favor a linear conformation. This kinetic energy correlation diagram accounts for the shape of BeH_2. The orbital which contributes most in determining the molecular shape is $2a_1$.

Comparisons among the kinetic energy diagrams of H_2O, CH_2, and BeH_2 reveal that the kinetic diagram varies from one molecule to another—there seems to be no universal kinetic energy diagram. However, the kinetic diagrams do contain information about the roles played by the various orbitals, and they certainly do correspond to a rigorous resolution of the energy into components.

III. Correlation Diagrams from the Method of Median Partition

A true energy-angle correlation diagram must take into account all effects which occur on changing bond-angles, including nuclear-nuclear repulsion changes. The application of the virial theorem is an *indirect* method to include the nuclear repulsion energy; in this section we search for a possibility of including nuclear-nuclear repulsion directly. The question is how the total energy W can be resolved into additive parts $w(i)$ such that $W=\sum_i w(i)$. With $W=E+V_{nn}$, the problem is to find methods which partition both E and V_{nn} into additive parts.

First we consider the partition of the electronic energy E. In the Hartree-Fock approximation the additive resolution of E was discussed as early as 1951 in connection with semi-empirical calculations with the LACO-MO method; namely,

$$E = \sum_{\text{occupied MO's}}(\varepsilon_i + I_i) = 2\sum_i m_i \tag{2}$$

where I_i is the core integral $\int \phi_i^* H_{\text{core}} \phi_i d\tau'$ of the molecular orbital ϕ_i, and

$$m_i = 1/2(\varepsilon_i + I_i) = 1/2e_i. \tag{3}$$

The quantity m_i has been called the *median one-electron energy* or simply median energy.[14]

In 1963 Coulson and Neilson suggested the use of the median energies m_i in obtaining Walsh diagrams.[10] They rejected the use of the Hartree-Fock orbital energies ε_i for that purpose on the basis that ε_i are not truly additive. The Walsh diagram of median energies for the water molecule H_2O reported by Coulson and Neilson differs significantly from the diagram of orbital energies. Since then the use of the median energies m_i for a Walsh diagram has been a matter of controversy. Yet Eq. (2) is a resolution, which is truly additive of the total electronic energy, and we will use this in this section.

The task left is how to partition V_{nn} into additive parts. Coulson and Neilson did not address this problem.

Consider a diatomic molecule AB with nuclear charges Z_A and Z_B. Let N_A and N_B be gross atomic populations according to Mulliken's definition,[15] on atoms A and B, respectively. $N(i, A)$ and $N(i, B)$ are subtotal populations in molecular orbital ϕ_i on A and B, and related to N_A and N_B by $N_A = \sum_i N(i,A)$, and $N_B = \sum_i N(i, B)$. The nuclear-nuclear repulsion energy V_{nn} of AB is exactly $V_{nn} = Z_A Z_B/R$, where R is the bond length of the molecule. V_{nn} is related to N_A and N_B by the formula

$$\begin{aligned} V_{nn} &= \frac{1}{R}[(Z_A - N_A)(Z_B - N_B) + (Z_A N_B + Z_B N_A) - N_A N_B] \\ &= \frac{1}{R}[(Z_B - 1/2N_B)N_A + (Z_A - 1/2N_A)N_B] \\ &\quad + \frac{1}{R}(Z_A - N_A)(Z_B - N_B). \end{aligned} \tag{4}$$

Let us assume that the second term of Eq. (4) is much smaller than the first term, call it Δ. Then V_{nn} is given by,

$$\begin{aligned} V_{nn} &= \frac{1}{R}[(Z_B - 1/2N_B)N_A + (Z_A - 1/2N_A)N_B] + \Delta \\ &= \sum_i \frac{1}{R}[(Z_B - 1/2N_B)N(i,A) + (Z_A - 1/2N_A)N(i,B)] + \Delta \\ &= \sum_i \left[V_n'(i) + \frac{V_n'(i)}{\sum_i V_n'(i)}\Delta \right] = \sum_i V_n(i) \end{aligned} \tag{5}$$

where

$$V_n'(i) = \frac{1}{R}[(Z_B - 1/2N_B)N(i,A) + (Z_A - 1/2N_A)N(i,B)]. \tag{6}$$

The quantity Δ vanishes when $Z_A = N_A$ or $Z_B = N_B$. This happens whenever $Z_A = Z_B$. The quantity in the bracket of Eq. (5),

$$V_n(i) = V_n'(i) + \frac{V_n'(i)}{\sum_i V_n'(i)}\Delta, \tag{7}$$

defines the i-th component of the partitioned V_{nn}.

For polyatomic molecules, the foregoing partitioning method may be applied to each contribution to the nuclear repulsion energy. For instance the nuclear repulsion energy of a molecule AH_2 is the sum of two terms as follows,

$$\begin{aligned} V_{nn} &= 2\frac{Z_A Z_H}{R_{AH}} + \frac{Z_H^2}{R_H} \\ &= 2\sum_i \frac{1}{R_{AH}}[(Z_H - 1/2N_H)N(i,A) + (Z_A - 1/2N_A)N(i,H)] \\ &\quad + \sum_i \frac{1}{R_H}[(Z_H - 1/2N_H)N(i,H) \\ &\quad + (Z_H - 1/2N_H)N(i,H)] + \Delta \\ &= \sum_i [2V_{AH}'(i) + V_{HH}'(i)] + \Delta \\ &= \sum_i \left[V_n'(i) + \frac{V_n'(i)}{\sum V_n'(i)}\Delta \right] = \sum_i V_n(i), \end{aligned} \tag{8}$$

where

$$V_{AH}'(i) = \frac{1}{R_{AH}}[(Z_H - 1/2N_H)N(i,A) + (Z_A - 1/2N_A)N(i,H)], \tag{9}$$

$$V_{HH}'(i) = \frac{2}{R_H}(Z_H - 1/2N_H)N(i,H), \tag{10}$$

and

$$V_n(i) = 2V_{AH}'(i) + V_{HH}'(i) + \frac{V_n'(i)}{\sum V_n'(i)}\Delta. \tag{11}$$

For the total energy, from Eq. (2) and Eq. (8) we have a rigorous partitioning,

$$W = E + V_{nn} = \sum_{\text{occupied MO's}} [\varepsilon_i + I_i + V_n(i)] = \sum_i w(i) \tag{12}$$

where

$$w(i) \doteq \varepsilon_i + I_i + V_n(i). \tag{13}$$

The partitioned nuclear energies in H_2O are tabulated in Table 4. In Table 5 are presented the quantities $w(i)$. The sum $\sum w(i)$ in Table 5 does not necessarily agree with W in Table 3, since the bond distances are fixed to 1.8103 in Table 5 whereas in Table 2 they are varied to satisfy Eq. (1).

In Fig. 4 is given the correlation diagram obtained

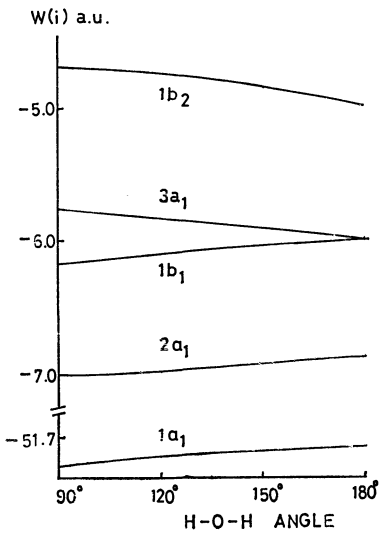

Fig. 4. Energy components for the different molecular orbitals in H_2O — Eqs. (12) and (13) of text.

Table 4. Partitioned nuclear repulsion energies $V_n(i)$ for H_2O

θ	$V_n(i)$					$\sum V_n(i)$
	$1a_1$	$2a_1$	$3a_1$	$1b_2$	$1b_1$	
90°	1.43267	2.10801	1.74001	2.51846	1.42977	9.22892
105°	1.44428	2.08528	1.67666	2.53868	1.44155	9.18645
110°	1.44890	2.08218	1.65972	2.53847	1.44623	9.17549
130°	1.47407	2.08421	1.60254	2.51059	1.47164	9.14306
150°	1.50721	2.09869	1.55957	2.45382	1.50496	9.12424
180°	1.53645	2.11302	1.53434	2.39635	1.53434	9.11450

Table 5. Partitioned total energy components $w(i)$ for H_2O

θ	$w(i)$					$\sum w(i)$
	$1a_1$	$2a_1$	$3a_1$	$1b_2$	$1b_1$	
90°	−51.9021	−7.03109	−5.75927	−4.67812	−6.16456	−75.5351
105°	−51.8810	−7.02489	−5.80927	−4.69610	−6.13834	−75.5496
110°	−51.8727	−7.01751	−5.82285	−4.71020	−6.12806	−75.5513
130°	−51.8303	−6.97196	−5.87446	−4.79132	−6.0773	−75.5453
150°	−51.7791	−6.91668	−5.9264	−4.89046	−6.01703	−75.5297
180°	−51.7356	−6.87195	−5.96618	−4.97592	−5.96618	−75.5159

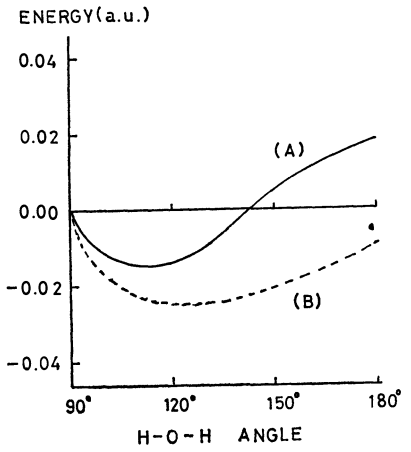

Fig. 5. (A) Total relative energy of H_2O. (B) Lone pair relative energies in H_2O. See text.

by plotting $w(i)$ *versus* bond angle. If Fig. 4 is compared with Fig. 1, it is noticed that the order and the patterns of the curves are similar in the two figures. The coincidences prevailing among the figures are remarkable because they are obtained by entirely different methods of partition.

It is interesting to see how the "lone pair" energies $[w(3a_1)+w(1b_1)]$ change with θ. In Fig. 5 are plotted the relative lone pair energies and the total energy with the reference angle $\theta=90°$. The "lone pair" energies are seen to monitor the total energy W. We previously found a similar result when the quantum-mechanical virial theorem was applied for partitioning W.[9] The implication again is that lone pair electrons may control the equilibrium bond angle in H_2O. Further investigation along this line is required.

The partitioned nuclear-nuclear repulsion components are relatively small in comparison with the electronic energy components, as seen in Tables 4 and 5. This implies that inclusion of the partitioned nuclear repulsion energies does not alter general appearance of correlation diagrams obtained without including nuclear repulsion.

It would be interesting to extend the present method of partitioning W to various diatomic molecules as well as to other polyatomic molecules, and to compare the correlation energy diagrams so obtained—energy-*versus*-bond length for diatomic molecules, energy-*versus*-bond angle for polyatomic molecules—with the traditional ones.

IV. Correlation Diagrams from Integral Hellmann-Feynman Theorem

An energy difference ΔW_i between two isoelectronic states X and Y may be obtained from the integral Helmann-Feynman Theorem (IHF):[16]

$$\Delta W_i = \int \Psi_X H' \Psi_Y d\tau \Big/ \int \Psi_X \Psi_Y d\tau \qquad (14)$$

where H' is the difference of the two Hamiltonian operators of states X and Y. If one defines the transition density between the two states X and Y by

$$\rho_{XY}(1) = \frac{N}{S} \int \Psi_X(12\cdots N)\ \Psi_Y(12\cdots N)\ d\tau(23\cdots N) \qquad (15)$$

then Eq. (14) becomes

$$\Delta W_i = \int \rho_{xy}(1) h(1) d\tau(1) + \Delta V_{nn}, \qquad (16)$$

where $h(1)$ is the change in the nuclear-electron attraction operator. This equation shows that the electronic energy difference is directly related to the transition density. Hence the IHF theorem admits a classical interpretation of an energy change.

If approximate wavefunctions Ψ_X and $\tilde{\Psi}_Y$ for states X and Y are specified as single Slater determinants built from one-electron orbitals ϕ_X and ϕ_Y, it is always

Table 6. Orbital contributions to the changes of total electronic energies of H_2O

θ	$[1a_1]$	$[2a_1]$	$[3a_1]$	$[1b_2]$	ΔE_i
105°	−0.00003	−0.02185	0.05925	−0.02704	0.020667
110°	−0.00004	−0.03025	0.07948	−0.03547	0.027443
130°	−0.00010	−0.06959	0.16357	−0.06652	0.054727
150°	−0.00013	−0.11969	0.25221	−0.08998	0.084818
180°	−0.00014	−0.08844	0.25470	−0.10122	0.129805

a) Energies relative to 90° bond angle. Bond distance 1.8103 Å.

Table 7. Resolved nuclear repulsion energy changes for H_2O[a)]

θ	$-\Delta V(1a_1)$	$-\Delta V(2a_1)$	$-\Delta V(3a_1)$	$-\Delta V(1b_2)$	$-\Delta V_{\text{total}}$
105°	0.00002	0.00143	0.01876	0.02219	0.04246
110°	0.00002	0.00166	0.02378	0.02787	0.05343
130°	0.00005	0.00192	0.0393	0.04426	0.08585
150°	0.00059	0.00215	0.0486	0.05308	0.10466
180°	0.00060	0.02000	0.03608	0.0567	0.11440

a) Relative to the 90° configuration.

Table 8. Resolved total energy changes for H_2O[a)]

θ	$\Delta W(1a_1)$	$\Delta W(2a_1)$	$\Delta W(3a_1)$	$\Delta W(1b_2)$	$\Delta W(1b_1)$	$\Delta W_i^{\text{total}}$
105°	−0.00005	−0.02328	0.04049	−0.04923	0	−0.02179
110°	−0.00006	−0.03191	0.05570	−0.06334	0	−0.02599
130°	−0.00015	−0.07151	0.12427	−0.11078	0	−0.03112
150°	−0.00072	−0.12184	0.20361	−0.14306	0	−0.01984
180°	−0.00074	−0.10844	0.2187	−0.15792	0	0.01541

a) Relative to the 90° configuration.

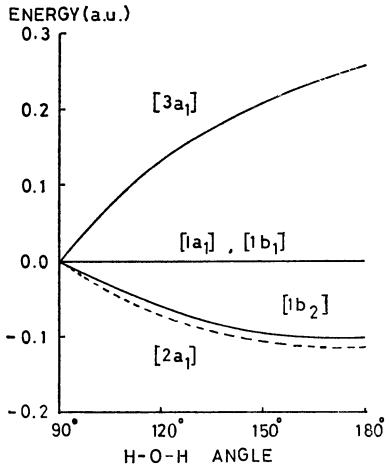

Fig. 6. Correlation diagram for H_2O obtained by the IHF theorem. Nuclear-nuclear repulsion is not included.

possible to find $\tilde{\Psi}'_X$ and $\tilde{\Psi}'_Y$ which diagonalize the transition density matrix by unitary transformations of $\tilde{\Psi}_X$ and $\tilde{\Psi}_Y$. It can be shown that Eq. (16) may be written[17)]

$$\Delta W_l = 2\sum_{k}^{N/2} \frac{\langle \hat{\phi}_k^X | h(1) | \hat{\phi}_k^Y \rangle}{\langle \hat{\phi}_k^X | \hat{\phi}_k^Y \rangle} + \Delta V_{nn} \qquad (17)$$

where $\hat{\phi}_k$'s are molecular orbitals from which Ψ''s are built. They are called corresponding orbitals. Equation (17) shows that the change of the total electronic energy ΔE_l can be expressed as a sum of the partitioned quantities $\Delta E(i) \equiv 2\langle \hat{\phi}_i^X | h(1) | \hat{\phi}_i^Y \rangle / \langle \hat{\phi}_i^X | \hat{\phi}_i^Y \rangle$. This is an equation which we may make use of to obtain energy-angle correlation diagrams for polyatomic molecules by plotting $\Delta E(i)$ as a function of bond angle.

Integral Hellmann-Ferynman calculations were carried out for the molecule H_2O to compute energy changes with changes of bond angles. In Table 6 are presented the results, for the symmetric bent in which two hydrogen atoms are moved symmetrically. They are plotted in Fig. 6 as functions of HOH angles. This is a *relative correlation* diagram because only relative electronic energies to that of HOH angle 90° are plotted.

From Fig. 6 we can see which orbital components favor linear conformations and which favor bent conformations, and so on. For instance $[3a_1]$ strongly favors the bent conformation for H_2O, whereas both $[1b_2]$ and $[2a_1]$ favor the linear conformation. The rest, $[1a_1]$ and $[1b_1]$, have little effect in determining the shape of the molecule. Thus the bent shape of H_2O may be attributed to the specific character of $[3a_1]$. This is in accord with Walsh's statement of the role played by the $3a_1$ orbital from the point of view of binding energy.[1)] If Fig. 6 is compared with the energy diagram of Walsh, an interesting feature is noticed: The *trends* of energy changes of individual orbital components coincide completely. In both diagrams $1a_1$ and $1b_1$ remain constant, $3a_1$ increases, $2a_1$

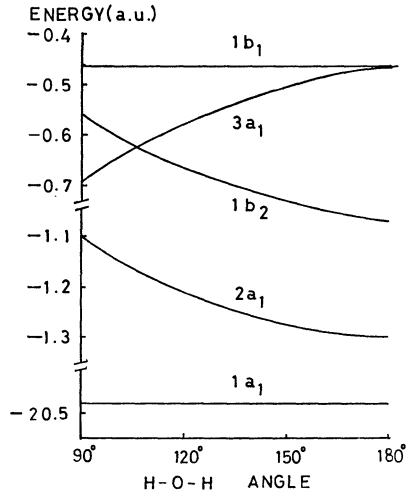

Fig. 7. Energy correlation diagram for H_2O including nuclear repulsion energies.

and $1b_2$ decrease as the bond angle increases from 90° to 180°.

Instead of using the IHF theorem, Coulson and Deb used the ordinary Hellmann-Feynman theorem, giving a new interpretation of the ordinate in the Walsh diagram.[8] Their force diagram looks similar to our IHF diagram except that $2a_1$ contribution rises in force diagram while it goes down in our diagram, as the bond angle increases.

So far the nuclear repulsion energies ΔV_{nn} have been left out, although clearly they should be taken into account in dealing with the problem of total energy change with conformational change. Resolution of ΔV_{nn} may be achieved in an analogous manner to the way V_{nn} was resolved in orbital components in Section III using corresponding orbitals and the method of population analysis of Mulliken with modifications. Because of close analogy between the two, detailed descriptions will not be given here. The resolved nuclear repulsion energies $\Delta V(i)$ are presented in Table 7.

The $\Delta V(i)$ may be divided into two classes: One is $\{[1a_1], [2a_1]$, and $[1b_1]\}$, the other is $\{[3a_1]$ and $[1b_2]\}$. The first class remains nearly constant with variations of bond angles, whereas the second changes very much more. The resolved nuclear energies $\Delta V(i)$ were added to the corresponding part of the electronic energies ΔE (i) to give total energy changes; these are listed in Table 8.

A *relative* correlation diagram such as Fig. 6 is useful when relative energy changes are concerned. However, it is desirable to have absolute correlation diagrams that show which orbital is higher in energy, and one comes next, and so on in treating Walsh's rules. If we assume a one to one correspondence between a Hartree-Fock molecular orbital and a corresponding orbital CMO in the IHF theory, $(1a_1)_{MO}$ *vs.* $[1a_1]_{CMO}$, $(2a_1)_{MO}$ *vs.* $[2a_1]_{CMO}$, $(3a_1)_{MO}$ *vs.* $[3a_1]_{CMO}$ *etc.*, and, assume that they have the same orbital energies at H–O–H angle 180°, an aboslute correlation diagram may be obtained, as in Fig. 7. If the correlation diagram in Fig. 7 is compared with the Walsh original diagram, a parallelism between the two figures is seen. Walsh's rules can be explained exactly as by Walsh if Fig. 7 is used.

The general trends of changes of one electron component stay more or less the same before and after inclusions of ΔV_{nn} terms, as seen in Figs. 6 and 7. This is another implication that *qualitative* Walsh-diagram may be obtained without taking ΔV_{nn} into consideration.

References

1) A. D. Walsh, *J. Chem. Soc.*, **1953**, 2260, 2266, 2288, 2296, 2301.
2) H. F. Thompson, *J. Amer. Chem. Soc.*, **93**, 4609 (1971).
3) Y. Takahata, G. Schnuelle, and R. G. Parr, *ibid.*, **93**, 784 (1971).
4) G. W. Schnuelle and R. G. Parr, *ibid.*, **94**, 8974 (1972).
5) R. S. Mulliken, *Rev. Mod. Phys.*, **14**, 204 (1942).
6) For example, S. D. Peyerimhoff, R. J. Buenker, and L. C. Allen, *J. Chem. Phys.*, **45**, 734 (1966 .
7) C. E. Wulfman, *ibid.*, **31**, 381 (1959).
8) C. A. Coulson and B. M. Deb, *Int. J. Quant. Chem.*, **V**, 411 (1971).
9) Y. Takahata and R. G. Parr, *Chem. Phys. Lett.*, **4**, 109 (1969).
10) C. A. Coulson and A. H. Neilson, *Discuss. Faraday Soc.*, **35**, 71 (1963).
11) (a) J. W. Moscowitz and M. C. Harrison, *J. Chem. Phys.*, **43**, 3550 (1965); (b) D. R. Whitman, and C. J. Hornback, *ibid.*, **51**, 398 (1969); (c) M. C. Harrison and I. G. Csizmadia, MIT SSMTG, QPR, July 15, 1963.
12) B. Nelander, *J. Chem. Phys.*, **51**, 469 (1969).
13) P. O. Löwdin, *J. Mol. Spectrosc.*, **3**, 46 (1959).
14) R. G. Parr, *J. Chem. Phys.*, **19**, 799 (1951).
15) R. S. Mulliken, *ibid.*, **23**, 1833 (1955).
16) R. G. Parr, *ibid.*, **40**, 3726 (1964).
17) H. F. King, R. E. Stanton, H. Kim, R. F. Wyatt, and R. G. Parr, *ibid.*, **47**, 1936 (1967).

The Structure and Reactivity of Organic Ions in Gas-phase Radiolysis. VIII. The $C_7H_7^+$ Ion from Toluene and Ethylbenzene

Nobuo SAGI, Yukio YAMAMOTO, Kenji NAGAOKA, Setsuo TAKAMUKU, and Hiroshi SAKURAI

The Institute of Scientific and Industrial Research, Osaka University, Yamadakami, Suita, Osaka 565

(Received November 19, 1973)

The gas-phase radiolysis of a mixture of toluene or ethylbenzene and dimethylamine has been studied at room temperature as a function of the dimethylamine pressure in order to investigate the structure and reactivity of the $C_7H_7^+$ ion. The structure of the $C_7H_7^+$ ion which takes part in the subsequent ion-molecule reaction was suggested to be the benzyl type on the basis of the reaction products. The radiolyses of toluene-α-d_3 and ethylbenzene-α-d_2 in the presence and in the absence of dimethylamine have been investigated, and the following information has been obtained: (i) the $C_7H_7^+$ ion formed from toluene and ethylbenzene mainly consists of the benzyl ion, retaining its original structure; (ii) two types of scrambling processes may be involved in the $C_7H_7^+$ ion formation, one of which, especially important in the case of toluene, includes the ring expansion of the original molecular ion, while the other consists of repeated rapid isomerization between the benzyl ion and the tropylium ion. These results were compared with those of mass spectrometric studies, which indicate that an almost complete isotope scrambling occurs, hence supporting the symmetrical tropylium structure for the $C_7H_7^+$ ion.

The structure of the $C_7H_7^+$ ion formed by the electron impact of toluene and higher alkylbenzenes has been the subject of numerous mass spectrometric investigations.[1] Extensive labeling experiments indicate the $C_7H_7^+$ ion, which further decomposes to the $C_5H_5^+$ ion, is a symetrical tropylium ion rather than a benzyl ion.[2] For example, the isotope retentions in the $C_7H_7^+$ ions from deuterated toluenes indicate that the eight hydrogen atoms are almost completely scrambled in the molecular ion. On the basis of this evidence and energetic considerations, Meyerson concluded that the toluene molecular ion rearranges to a cycloheptatriene-like structure of an even higher symmetry.[3] Harrison proposed instead an irreversible isomerization of the molecular ion to the cycloheptatriene isomer involving a transfer of an α-hydrogen to the adjacent ring carbon atom, followed by the insertion of the methylene group at random between any two ring carbon atoms.[4] This random insertion, leading to carbon scrambling, has been supported by studies using di-^{13}C-labeled toluene.[5,6]

Furthermore, Harrison's postulation has been supported by Howe and McLafferty.[7] They have also reported that the degree of scrambling decreases with an increase in the internal energy; hence, in the case of toluene some part of the $C_7H_7^+$ ion is formed by the direct dissociation of α-hydrogen before the scrambling of the hydrogen atoms occurs. For ethylbenzene, the tropylium structure has been again assigned to the $C_7H_7^+$ ion, although the formation process has not been clarified.[2]

More recently, Dunbar[8] has investigated the photoexcitation of toluene parent ions by ion-cyclotron resonance and shown that the photodissociation occurs with a complete hydrogen scrambling and a strong isotope effect. The energy dependence agrees with that determined for dissociative electron-impact ionization by Howe and McLafferty.[7] However, it has been also shown that non-dissociating $C_7H_8^+$ ions from toluene and cycloheptatriene are non-interconverting and that there is no important degree of interconversion among the toluene, cycloheptatriene, and norbornadiene molecular ions or conversion to a common structure, as determined on the basis of different photodissociation curves of these compounds.[9] This behavior is also in accord with the conclusion drawn from the ion-molecule reaction of $C_7H_8^+$ ions with nitrate by Hoffman and Bursey.[10]

On the other hand, during the course of our investigations of the gas-phase radiolysis it has been found that the $C_7H_7^+$ ions from toluene, ethylbenzene, xylenes, and cycloheptatriene react with aromatics to produce benzylated compounds; the reaction has been regarded as an electrophilic substitution reaction, which is well-known in solution chemistry.[11,12] Such a reactivity of the $C_7H_7^+$ ion with aromatics, as well as the structures of the products, seemed to suggest that the $C_7H_7^+$ formed in the gas-phase radiolysis of these compounds is a benzyl ion with a positive-charged center rather than a tropylium ion in which the positive charge is distributed equally among the seven carbon atoms. However, the question has been raised whether a tropylium ion is produced, since such a less electrophilic ion can hardly react with aromatics even if formed.

In connection with these problems, we have investigated the gas-phase radiolysis of alkylbenzene–dimethylamine (DMA) mixture. DMA has a higher basicity than aromatics and, therefore, would be expected to react with the tropylium ion.[13] Moreover, we have also investigated the gas-phase radiolysis of toluene-α-d_3 and ethylbenzene-α-d_2 in order to obtain information about the formation process of the $C_7H_7^+$ ion. The present paper will describe the structure and formation process of the ion from toluene and ethylbenzene on the basis of more evidence than in the preceding communications.[14]

Experimental

Materials. Toluene and ethylbenzene obtained from the Wako Pure Chemicals Industries Co. were fractionated through a spinning-band column after the usual purification. The purity, as determined gas-chromatographically, was more than 99.9%. The xylene isomers were purified in the same way; the purities were more than 99.1%. Cycloheptatriene prepared by the pyrolysis of 7,7-dichloronorcarane was purified by preparative gas chromatography. Norbornadiene obtained from the Aldrich Chemical Company, Inc. was purified by preparative gas chromatography. The DMA was

evolved by heating an aqueous dimethylamine solution obtained from the Wako Pure Chemicals Industries Co., dried by being passed through a KOH column twice, and stored in a storage bulb. Oxygen obtained from the Awao Industrial Co. was dried by means of a P_2O_5 column and was then used without further purification.

The toluene-α-d_3 was prepared by the method given in the literature,[15] and the deuterium content of the methyl group was determined to be more than 93.5% by NMR analysis. Ethylbenzene-α-d_2 was prepared by means of the following paths:

$$C_6H_5COCH_3 \xrightarrow{LiAlD_4} C_6H_5CD(OH)CH_3 \xrightarrow{SOCl_2}$$

$$C_6H_5CDClCH_3 \xrightarrow{LiAlD_4} C_6H_5CD_2CH_3$$

The isotopic purity was found by NMR analysis to be better than 99%. *N,N*-Dimethylbenzylamine-α-d_2, a standard authentic sample for analytical purposes, was prepared by the reduction of *N,N*-dimethylbenzamide with $LiAlD_4$ under THF reflux conditions. The isotopic purity was found to be better than 99% by NMR analysis.

Procedures. The experimental procedures were almost the same as those reported previously[11b] With the exception of the labeled experiments, all the irradiations were carried out in Pyrex cylinders approximately 110 ml in volume with γ-rays from a 5000 Ci ^{60}Co source at room temperature. The dosimetry was based on $G(C_2H_4 \rightarrow H_2) = 1.28$,[16] assuming that the energy distribution was proportional to the electron density of the sample. The dose rates in the present experiments were 3.0×10^{15} eV/hr·μmol for toluene, cycloheptatriene, and norbornadiene, and 3.47×10^{15} eV/hr·μmol for ethylbenzene and xylenes. The *G*-values in the runs were calculated on the basis of the energy absorbed by alkylbenzene, cycloheptatriene, or norbornadiene alone. The identification of the products was carried out by gas-chromatographic comparison with authentic samples using several columns (Apieson L—KOH, 6 m at 80 °C or 140 °C and Amine 3 m at 80 °C).[17] The yields of the products were determined by a comparison of the peak areas with those of known amounts of benzene, which were submitted to gas chromatography before each analysis. The calibration of the sensitivity for a flame-ionization detector was also carried out.

For the labeled experiments, spherical cells approximately 5 l in volume were used. Irradiation was carried out with a 3000 or 7000-Ci ^{60}Co source. The irradiated samples were collected in a glass tube by trap distillation. The reaction products, *N,N*-dimethylbenzylamine or diphenylmethanes, were isolated by preparative gas chromatography (Apiezon L-KOH, 3 m at 105 °C and Thermol 2 m at 190 °C respectively). The product isolated in a trap was dissolved with CCl_4 for NMR measurements and then submitted to NMR spectrometry (Hitachi Perkin-Elmer R-20 spectrometer), using CAT and a gas chromatography-mass spectrometry combination (Hitachi RMS-4).

Results and Discussion

The Reaction of the $C_7H_7^+$ Ion with DMA. Toluene-DMA mixtures were irradiated with ^{60}Co γ-rays to a dose of 8.4×10^{18} eV at 10 mmHg of toluene at room temperature. The formation of *N,N*-dimethylbenzylamine (DMBA) and a trace amount of an unknown product were observed, along with such products as benzene, ethylbenzene, xylenes, bibenzyl, and methyldiphenylmethanes(MDPM), which are known as radiolysis products of toluene. Figure 1 shows the correlation between the yields of DMBA and MDPM from toluene irradiated in the presence of varying amounts of DMA. The yields of these products were not affected by oxygen added as a radical scavenger. Quite similar relationships between DMBA and ethyldiphenylmethanes (EDPM) were also observed in the radiolysis of ethylbenzene–DMA mixtures, as is shown in Fig. 2. In this case, the formation of a small amount of *N,N*-dimethyl-α-phenethylamine was observed in addition to that of DMBA. Furthermore, in the radiolysis of xylenes, cycloheptatriene, and norbornadiene in the presence of DMA, the formation of DMBA was observed and the yields were not affected by the addition of oxygen (Table 1). These hydrocarbons are known to produce a similar $C_7H_7^+$ ion by electron impact.[18,19] Thus, the results suggest the formation of a common $C_7H_7^+$ ion as a precursor of both alkyldiphenylmethanes and DMBA, as is shown in Eqs. (1)—(3).

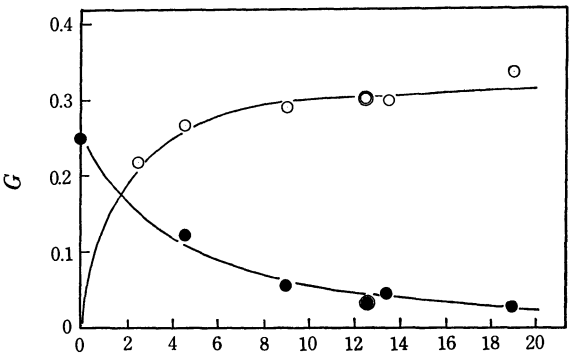

Fig. 1. Variations of the yields of methyldiphenylmethanes (MDPM, ●) and *N,N*-dimethylbenzylamine (DMBA, ○) as a function of the dimethylamine pressure in the radiolysis of toluene vapor (10 mm); ◉, ◎, when 10 mol% of oxygen was added.

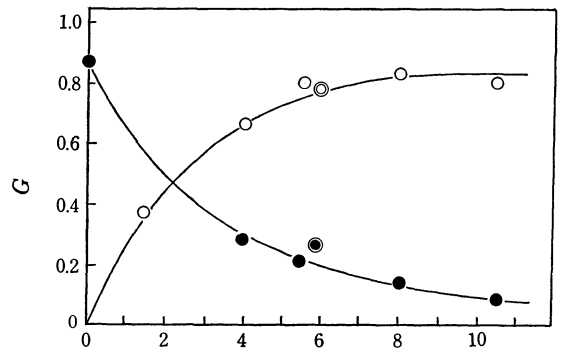

Fig. 2. Variations of the yields of ethyldiphenylmethanes (EDPM, ●) and *N,N*-dimethylbenzylamine (DMBA, ○) as a function of the dimethylamine pressure in the radiolysis of ethylbenzene vapor (4 mm); ◉, ◎, when 10 mol% of oxygen was added.

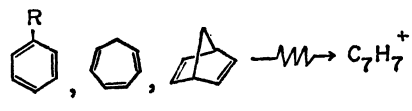

(1)

Table 1. The yields of DMBA produced in the gas-phase radiolysis of hydrocarbon–dimethylamine mixtures

Hydrocarbon	Pressure, mmHg	Dimethylamine, mmHg	G(DMBA)	G(DMBA) with O_2[a]
Toluene	10	13.5	0.30	0.30
Ethylbenzene	4	5.5	0.82	0.78
o-Xylene	4	6	0.24	0.26
m-Xylene	4	6	0.21	0.22
p-Xylene	4	6	0.23	0.25
Cycloheptatriene	10	14	0.19	0.26
Norbornadiene	11	14	0.22	0.21

a) Oxygen was added up to about 10 mol%.

Table 2. The NMR data of D-labeled products in the radiolysis of ethylbenzene-α-d_2 and toluene-α-d_3.

Reactant (mmHg)	Product	H_{CH_2}/H_{Ph}[a]		Scrambling (%)
		Calculated (Complete scrambling)	Observed	
Ethylbenzene-α-d_2(2.2)-DMA(3.8)	DMBA	0.40	0	0
Ethylbenzene-α-d_2(1.0)-DMA(1.7)	DMBA	0.40	0.084	27.2
Ethylbenzene-α-d_2(5)	EDPM	0.189	0.024	14.5
Ethylbenzene-α-d_3(3)	EDPM	0.189	0.028	17.4
Ethylbenzene-α-d_3(1)	EDPM	0.189	0.045	27.1
Ethylbenzene-α-d_3(0.4)	EDPM	0.189	0.063	37.5
Toluene-α-d_3(8)-DMA(12)	DMBA	0.40	0.14	36～39
Toluene-α-d_3(19)	MDPM	0.24	0.062	31～33

a) DMBA, H_{Ph}, τ 2.7—2.9, H_{CH_2}, τ 6.6; MDPM, H_{Ph}, τ 2.9—3.1, H_{CH_2}, τ 6.1; EDPM, H_{Ph}, τ 2.7—3.1, H_{CH_2}, τ 6.1

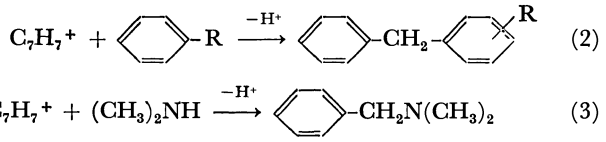

From the data shown in Figs. 1 and 2, the relative reactivities of the $C_7H_7^+$ ion with DMA, ethylbenzene, and toluene were calculated to be 5.7, 2.1, and 1.0 respectively.

However, *N*,*N*-dimethyltropylamine, which is expected to be formed by the reaction of a tropylium ion with DMA, was not detected among the products under these experimental conditions except for the case of the cycloheptatriene–DMA mixture.[20]

$C_7H_7^+$ Ion from Ethylbenzene. Although a tropylium ion was not captured in the gas-phase radiolysis of alkylbenzenes, the possibility still remains that a tropylium ion is formed as an intermediate and that it reacts with the substrate after being rearranged to a benzyl ion. Since the deuterium-labeling study would be expected to present instructive information in this respect, ethylbenzene-α-d_2 and toluene-α-d_3 were irradiated in the presence and in the absence of DMA, and the NMR and mass spectra of the DMBA, EDPM, and MDPM thus produced were measured. The results obtained from these measurements are shown in Table 2 and Fig. 3.

The mass spectra of the DMBA formed in the gas-phase radiolysis of an ethylbenzene-α-d_2–DMA mixture agreed very closely with that of authentic *N*,*N*-dimethylbenzylamine-α-d_2, suggesting that the precursor

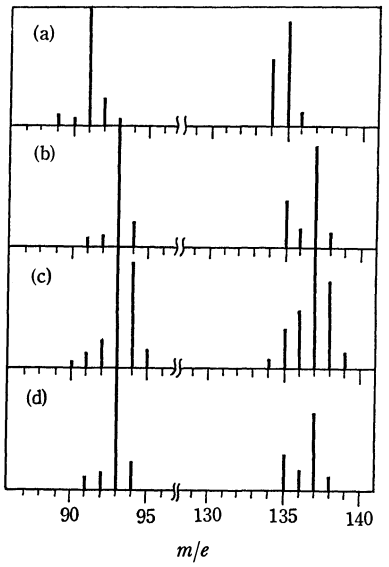

Fig. 3. Partial mass spectra of (a) authentic DMBA-d_0, (b) authentic DMBA-α-d_2, (c) DMBA formed in the gas-phase radiolysis of a toluene-α-d_3–dimethylamine mixture, and (d) DMBA formed in the gas-phase radiolysis of an ethylbenzene-α-d_2–dimethylamine mixture.

ion for this product is the $C_7H_5D_2^+$ ion formed by the loss of β-methyl from the original molecular ion without involving any isotopic mixing between β-methyl and benzyl groups (Fig. 3). Although the mass spectra of the EDPM formed in the gas-phase radiolysis of

pure ethylbenzene-α-d_2 were not analyzed because of its complexity resulting from the scrambling of this compound in the mass spectrometer, it seems reasonable to conclude on the basis of Eqs. (1)—(3) that the precursor ion for this product is also the $C_7H_5D_2^+$ ion.

The NMR data provide an important clue to the information on the isotopic distribution in these products. The ratios of the methylene protium atoms to the total phenyl protium atoms in DMBA and EDPM were determined and converted into the ratio of the methylene protium atoms to phenyl protium atoms of the benzyl group originating from the $C_7H_5D_2^+$ ion. If the $C_7H_5D_2^+$ ion took a symmetrical structure, that of a tropylium ion or another possible ion, the protium and deuterium atoms of the benzyl group of both products would be statistically distributed between the methylene and phenyl units and the H_{CH_2}/H_{Ph} ratio would be 0.40. On the other hand, if the $C_7H_5D_2^+$ ion were the benzyl ion retaining the original structure, no protium atoms would be introduced to the methylene group of either product. Since the observed H_{CH_2}/H_{Ph} ratios are between these two values except for one case (ethylbenzene-α-d_2 2.2 mmHg, DMA 3.8 mmHg), it may be suggested that a partial hydrogen scrambling occurs in the $C_7H_5D_2^+$ ion. The degree of scrambling calculated is also shown in Table 2.

On the other hand, in the mass spectrometric studies of ethylbenzene it has been proposed that the $C_7H_7^+$ ion, which undergoes further decomposition, is a tropylium ion, though the timing when ring expansion occurs is obscure, as is shown in Scheme 1.[21]

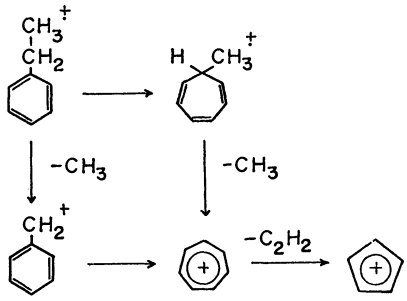

Scheme 1.

On the basis of the present observation, however, it seems reasonable to conclude that the $C_7H_7^+$ ion is formed as a benzyl ion by a loss of β-methyl from the ethylbenzene molecular ion before the ring expansion of the molecular ion. The benzyl ion thus formed reacts rapidly with DMA to produce DMBA without involving hydrogen scrambling when DMA is present at a higher pressure. When, in the absence of DMA, the $C_7H_7^+$ ion reacts with ethylbenzene, which has a lower reactivity to the ion, a hydrogen scrambling of the $C_7H_7^+$ ion may come to compete with the product formation. Such a hydrogen scrambling may occur *via* a tropylium ion, as has been suggested by the mass-spectrometric studies. For each experiment, the extent of scrambling was determined and plotted against the pressure of ethylbenzene, as is shown in Fig. 4. The extent of scrambling depends on the reaction

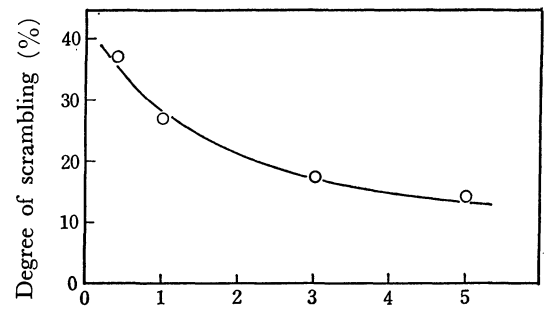

Fig. 4. Pressure effect on scrambling of EDPM formed in the gas-phase radiolysis of ethylbenzene-α-d_2.

system; the scrambling becomes more remarkable as the pressure of ethylbenzene decreases, while the scrambling is completely depressed in the presence of enough DMA (3.8 mm) in the reaction system.

It is likely that the mechanism described above is also supported by the formation of a product derived from the $C_8H_9^+$ ion from ethylbenzene. It has been suggested in the mass-spectrometric investigations[22] that the $C_8H_9^+$ ion from ethylbenzene undergoes an extensive scrambling of the ring and α-hydrogen atoms, and that this scrambling is caused by a ring expansion from the ethylbenzene ion to the methylcycloheptatriene ion, followed by hydrogen shift, before the loss of the hydrogen (Scheme 2).

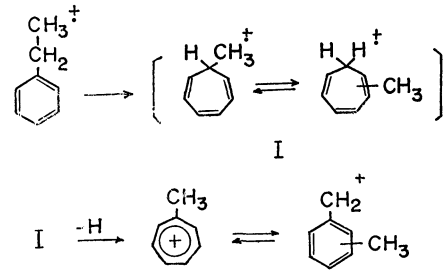

Scheme 2.

If the methyltropylium ion were formed in this manner in the gas-phase radiolysis of ethylbenzene, this ion would be expected to rearrange to the xylyl ion,[23] which would react with DMA to produce *N,N*-dimethylxylylamines. However, no *N,N*-dimethylxylylamines were detected among the reaction products; *N,N*-dimethyl-α-phenetylamine was observed instead. The precursor ion for *N,N*-dimethyl-α-phenetylamine is presumably the α-phenetyl ion, which is formed either by a hydrogen loss from the ethylbenzene ion or by a hydride transfer from ethylbenzene to any primary ion, and which does not rearrange to the methyltropylium ion nor to xylyl ions. Therefore, it may be concluded that the rearrangement from the ethylbenzene ion to the methylcycloheptatriene ion does not occur, at least not under the present radiolytic conditions.

$C_7H_7^+$ Ion from Toluene. As is shown in Fig. 3, the mass spectra of the DMBA formed in the gas-phase radiolysis of a toluene-α-d_3–DMA mixture is different

from that of authentic *N,N*-dimethylbenzylamine-α-d_2, indicating that both DMBA-d_2 and DMBA-d_3 are formed. The ratio of DMBA-d_2 to DMBA-d_3 was calculated to be 1.2 from relative intensities of the ions in the molecular ion region and the region corresponding to the $C_7H_7^+$ ion. This ratio also indicates that of $C_7H_5D_2^+$ to $C_7H_4D_3^+$. From the NMR spectrum, the ratio of the methylene protium atoms to the phenyl protium atoms was determined to be 0.14. The observed value suggests that a partial isotope scrambling occurs in the precursor ions of DMBA. The results can be explained by assuming the following scheme:

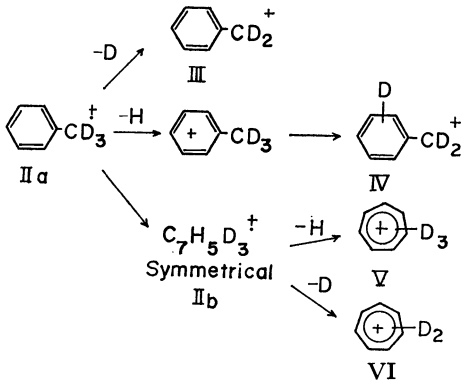

Scheme 3.

The benzyl ions, III and IV, are formed by the direct dissociations of D and H respectively from the molecular ion, IIa; the second dissociation is followed by a rapid intramolecular D^- transfer from the methyl to the phenyl group. These ions rapidly react with DMA to produce DMBA before the isomerization to tropylium ions occurs, since the concentration of DMA is high enough (12 mmHg). On the other hand, the tropylium ions, V and VI, are formed by the loss of H and D respectively *via* the symmetrical intermediate, IIb, as has previously been proposed by Meyerson. These tropylium ions also produce the DMBA, in which the deuterium atoms are statistically distributed in the benzyl groups *via* the isomerization to the benzyl ions. The benzyl ions, III and IV, produce DMBA containing five and four H_{Ph} respectively and no H_{CH_2} in the benzyl group. When i represents the isotope effect (k_H/k_D) on the hydrogen loss from the symmetrical intermediate, IIb, the ratio of V to VI is $3/5i$; the numbers of H_{Ph} and H_{CH_2} in the benzyl group of the DMBA originating from these ions are given by $5[(5\times 3)+(4\times 5i)]/7(5i+3)$ and $2[(5\times 3)+(4\times 5i)]/7(5i+3)$ respectively. On the other hand, the experimental values for H_{Ph} and H_{CH_2} in the benzyl group of the DMBA formed in the gas-phase radiolysis of a toluene-α-d_3-DMA mixture were calculated to be 4.0 and 0.56 respectively on the basis of the NMR and mass spectra. On the assumption of the wide range of i, 1~4, the relative contributions of III, IV, and V and VI to the DMBA formation were calculated to be 28~33, 33~31, and 39~36% respectively by correcting for the isotopic impurity in toluene-α-d_3.

The results for the MDPM formed in the gas-phase radiolysis of toluene-α-d_3 in the absence of DMA were treated in a similar manner; the relative contributions of III, IV, and V and VI to the MDPM formation were thus calculated to be 30~37, 39~29, and 33~31% respectively.

Aspects of the Mechanism. In the radiolysis of toluene, the degree of scrambling estimated from the DMBA formation agreed approximately with that from MDPM as described above; about one-third of the $C_7H_7^+$ ion leading to the product formation is a scrambled ion. This coincidence might be attributed to the fact that scrambling occurs only by a ring expansion from the toluene molecular ion to a symmetrical cycloheptatriene-like intermediate, not by isomerization from the benzyl ion to the tropylium ion. The reason for this is that, in the radiolysis of ethylbenzene-α-d_2, the benzyl ion formed by direct dissociation was trapped without involving as much isomerization in the presence of DMA as in the radiolysis of the toluene system. If the isomerization of the benzyl ion to a tropylium ion occurs, some differences in the degree of scrambling should be observed between the DMBA and MDPM formation, since this scrambling process competes with product formation, in which the reactivities of the $C_7H_7^+$ ion to DMA and toluene are different, as has been shown previously.

However, the scrambling is, generally, not so significant in the gas-phase radiolysis of toluene and ethylbenzene as in the mass spectrometry. As reasons why such a disagreement is observed, two factors may be considered; (i) the difference in the magnitude of the internal energy of the molecular ion, and (ii) the difference in such conditions as the pressure; these factors are both concerned with the lifetime of the ion. As for (i), in the fields of mass spectrometry Howe and McLafferty[7] have repoted that the degree of scrambling decreases with an increase in the internal energy; thus, in the case of toluene the direct dissociation of α-hydrogen becomes significant compared with the scrambling process. Assuming that the molecular ion fromed in the gas-phase radiolysis posseses greater internal energy, the question seems to be answered in a satisfying manner. Furthermore, with regard to (ii), the benzyl ion formed by such a direct dissociation comes to isomerize to a tropylium ion when the pressure of the substrate is low (Fig. 4) or when the rate of the product formation is slow (trapping by aromatics). These possibilities may become large under the conditions in a mass spectrometer.

Finally, a distinction between toluene and ethylbenzene in the $C_7H_7^+$-ion-formation process may be considered; the ethylbenzene ion does not rearrange to a symmetrical molecular ion, while a part of the toluene ion does. This difference can be explained in terms of the lifetimes of molecular ions. Since the ethylbenzene ion, in which the β C–C bond fission occurs with greater facility,[24] is probably more short-lived than the toluene ion, the scrambling path cannot compete with the direct dissociation. The benzyl ion thus formed is rapidly trapped by the successive ion-molecule reaction with ethylbenzene or DMA, without involving any significant unimolecular isomerization when enough of these trapping agents are present in the reaction system.

We wish to thank Dr. Seung Geon Kim for his advice on the preparation of toluene-α-d_3 and ethylbenzene-α-d_2. Thanks are also due to Mr. Yoshio Takai and Mr. Norio Kimura for their measurements of the NMR and mass spectra respectively, and Mr. Tomikazu Sawai and Mr. Tamotsu Yamamoto for the γ irradiations.

References

1) H. M. Grubb and S. Meyerson, "Mass Spectrometry of Organic Ions", ed., by F. W. McLafferty, Academic Press, New York, N. Y. (1963), Chapter 10.
2) P. N. Rylander, S. Meyerson, and H. M. Grubb, *J. Amer. Chem. Soc.*, **79**, 842 (1957).
3) S. Meyerson, *ibid.*, **85**, 3340 (1963).
4) F. Meyer and A. G. Harrison, *ibid.*, **86**, 4757 (1964).
5) K. L. Rinehart, Jr., A. C. Buchholz, G. E. Van Lear, and H. L. Cantrill, *ibid.*, **90**, 2983 (1968).
6) A. S. Siegel, *ibid.*, **92**, 5277 (1970).
7) I. Howe and F. W. McLafferty, *ibid.*, **93**, 99 (1971).
8) R. C. Dunbar, *ibid.*, **95**, 472 (1973).
9) R. C. Dunbar and E. W. Fu, *ibid.*, **95**, 2716 (1973).
10) M. K. Hoffman and M. M. Bursey, *Tetrahedron Lett.*, **1971**, 2539.
11) Y. Yamamoto, S. Takamuku, and H. Sakurai, (a) *J. Amer. Chem. Soc.*, **91**, 7192 (1969), (b) *J. Phys. Chem.*, **74**, 3325 (1970), (c) This Bulletin, **44**, 574 (1971), (d) *ibid.*, **44**, 2104 (1971).
12) S. Takamuku, K. Nakamura, K. Nagaoka, and H. Sakurai, *Chem. Lett.* **1973**, 1303.
13) It has been reported that tropylium ion reacts with dimethylamine to produce *N,N*-dimethyltropylamine in liquid phase (W. E. von Doering and L. H. Knox, *J. Amer. Chem. Soc.*, **79**, 352 (1957)).
14) (a) Y. Yamamoto, S. Takamuku, and H. Sakurai, *J. Amer. Chem. Soc.*, **94**, 661 (1972). (b) S. Takamuku, N. Sagi, K. Nagaoka, and H. Sakurai, *ibid.*, **94**, 6217 (1972).
15) R. Renaud and L. C. Leitch, *Can. J. Chem.*, **34**, 98 (1956).
16) R. A. Back, T. W. Woodward, and K. A. McLauchlan, *ibid.*, **40**, 1380 (1962).
17) Especially, *N,N*-dimethylbenzylamine was also identified by a comparison of NMR and mass spectra with those of an authentic sample.
18) S. Meyerson and P. N. Rylander, *J. Chem. Phys.*, **27**, 901 (1957).
19) S. Meyerson, J. D. McCollum, and P. N. Rylander, *J. Amer. Chem. Soc.*, **83**, 1401 (1961).
20) The formation of *N,N*-dimethyltropylamine was also observed in the gas-phase radiolysis of 7-methylcycloheptatriene–DMA mixture. These results will be described in a separated paper.
21) P. Brown, *Org. Mass Spectrom.*, **2**, 1317 (1969).
22) S. Meyerson and P. N. Rylander, *J. Amer. Chem. Soc.*, **79**, 1058 (1957).
23) This rearrangement is analogous to that from tropylium ion to benzyl ion, and it was also observed in the radiolysis of xylene–DMA mixtures.
24) This correlation is compatible with the relative intensities of M^+ to $C_7H_7^+$ in the mass spectra of both compounds; the ratio in ethylbenzene (0.32) is smaller than that in toluene (0.74), indicating that the ethylbenzene ion decomposes more rapidly to $C_7H_7^+$ ion than toluene ion does.

Molecular Structure of Tungsten Oxide Tetrachloride by Gas Electron Diffraction

Kinya IIJIMA and Shuzo SHIBATA

Department of Chemistry, Faculty of Science, Shizuoka University, Oya, Shizuoka 420

(Received October 13, 1973)

The molecular structure of tungsten oxide tetrachloride was determined by the sector-microphotometer method of gas electron diffraction. The molecule was found to have a square-pyramidal structure, and the following molecular parameters were obtained by a least-squares method; r_g(W–Cl)=2.281±0.003 Å, r_g(W–O)=1.686±0.011 Å, and r_g(Cl···Cl(s))=3.151±0.015 Å. The OWCl angle, 102.4±1.3°, is much larger than the corresponding angles found in other square-pyramidal molecules such as $XeOF_4$ and IF_5.

The geometrical structures of five-coordinated molecules can be divided into trigonal bipyramid and square pyramid. The former type was reported, for example, for PCl_5[1] and SOF_4,[2,3] though SOF_4 was found to be slightly distorted from a regular trigonal bipyramid. The latter type was reported for ClF_5,[4] BrF_5,[4] IF_5,[4] and $XeOF_4$.[4,5] The possibility of these structures can be explained in terms of the valence-shell electron-pair repulsion theory of Gillespie.[6] The electron configurations in the outermost shell of neutral tungsten and sulfur atoms are $(5d)^4(6s)^2$ and $(3s)^2(3p)^4$, respectively, and hence, the numbers of valence electrons in $WOCl_4$ and SOF_4 are equal to each other. Therefore, the structure of $WOCl_4$ should essentially be the same as that reported for SOF_4. From spectroscopic studies of $WOCl_4$ in the gas phase,[7,8] where the molecule is monomeric, however, the molecular structure is predicted to be square pyramidal. It is therefore interesting to determine the gas-phase structure of $WOCl_4$ by means of electron diffraction.* On the other hand, an X-ray diffraction study[9] has shown that the $WOCl_4$ molecule has C_{4v} symmetry in the crystal state by formation of –O–W–O– linkages.

Experimental and Analysis

The sample was prepared by the method described in Ref. 10 and was purified by repeated sublimations *in vacuo*. Since the sample was very reactive with moisture, it was loaded in a high-temperature nozzle in a dry box. The sample was vaporized at 65 °C, and electron-diffraction photographs were taken with an r^3-sector at a camera length of 144.08 mm. The accelerating voltage was about 40 kV, the exposure times were 30~40 sec, and the electron-beam current was 0.6 μA. Diffraction patterns of gold, the lattice constant of which was calibrated by means of X-ray diffraction, were used in order to measure the electron wavelength. Photographs were recorded on Fuji process hard plates, and the photographic densities of two plates were measured with a digital microphotometer at intervals of 0.4 mm. Intensities in a range of q=17~102 Å^{-1} were obtained and leveled by a theoretical background, which was calculated by using the elastic scattering factors of Kimura *et al.*[11] and the inelastic scattering factors of Tavard[12] for chlorine and oxygen and that of Bewilogua[13] for tungsten.

The radial distribution function was calculated by the use of the method of Bartell[14] because of the large differences in the atomic numbers. The corresponding correction terms for the radial distribution function are

$$\Delta M(q) = R\sum_{i\neq l}\sum C_{ij}(N_{ij}-\mu_{ij})\cos(\Delta\eta_{ij}) \times \sin[(\pi q/10)\{r_{a_{ij}}-\kappa(\pi q/10)^2\}] \times \exp\{-l_{ij}^2(\pi q/10)^2/2\}/(\pi q/10)r_{a_{ij}},$$

where R is the index of resolution, and

$$C_{ij} = Z_{ij}/\sum_k (Z_k^2+Z_k),$$

$$\mu_{ij} = |\dot{F}_i||F_j|/C_{ij}\sum_k (|F_k|^2+S_k),$$

$$N_{ij} = a_{ij} + b_{ij}\exp(-c_{ij}q^2),$$

$$|F_k| = h^2(\pi q/10)^2|f_k|/8\pi^2 me^2.$$

Other notations follow Refs. 14 and 15. N_{ij} was determined as follows so as to fit μ_{ij} in the whole range of the scattering angle:

$$N_{W\text{-}Cl} = 1.200$$

$$N_{W\text{-}O} = 1.205 + 0.289\exp(-0.00040\,q^2)$$

$$N_{Cl\cdots Cl} = 1.695 + 0.531\exp(-0.00029\,q^2)$$

$$N_{Cl\cdots O} = 1.762 + 1.049\exp(-0.00046\,q^2)$$

The parameters μ_{ij} and N_{ij} and the radial distribution curve are shown in Figs. 1 and 2, respectively. By inspection of the radial distribution curve and by comparison of the observed molecular intensities with those calculated on the assumption of C_{2v}, C_{3v}, and C_{4v} models, it was concluded that the molecular structure of $WOCl_4$ is a square pyramid, C_{4v}.

In order to refine the structure parameters, least-squares analyses based on the smooth-background method[16] by use of a polynomial of 7th degree were carried out. When the molecule was assumed to be a trigonal bipyramid like SOF_4, several parameters did not converge even after the 10th cycle of refinement. All the parameters carried large standard deviations, and the equatorial and polar W–Cl distances converged to the same value within the limit of error. The C_{3v} model was not tested in the least-squares calculation. On the other hand, when the molecule was assumed to be a square pyramid, all the parameters converged after several iterations. Thus the above-mentioned conclusion was confirmed by the least-squares analysis.

The index of resolution, r(W···Cl), r(W···O), r(Cl···Cl(s)), and five root-mean-square amplitudes l(W···Cl), l(W···O), l(Cl···Cl(s)), l(Cl···Cl(1)), and l(Cl···O) were determined by the least-squares analysis. The asymmetry parameters for bonded distances were estimated by a diatomic-molecule

* Preliminary results were reported in *Chem. Lett.*, **1972**, 1033. Spiridonov *et al.* have also reported the molecular structure of gaseous $WOCl_4$ by electron diffraction (V. P. Spiridonov, E. Z. Zasorin, I. M. Zharskii, and G. I. Novikov, *Zh. Strukt. Khim.*, **13**, 511 (1972)). The configuration reported by them is the same as that determined in the present study, but their bond lengths are much larger than those determined in the present study. The origin of the discrepancies, which exceed the limits of error, is unknown.

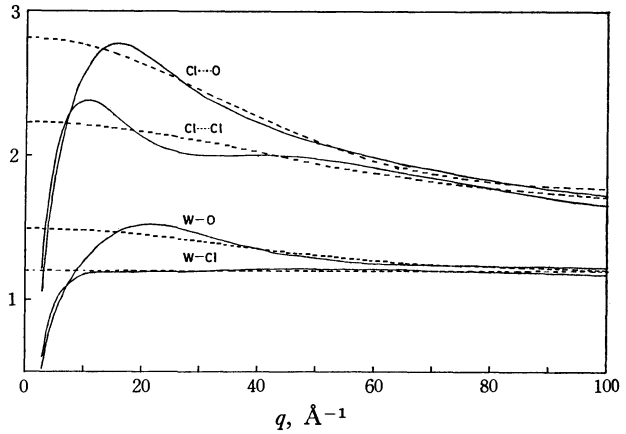

Fig. 1. μ_{ij} (solid lines) and N_{ij} (dashed lines) for $WOCl_4$.

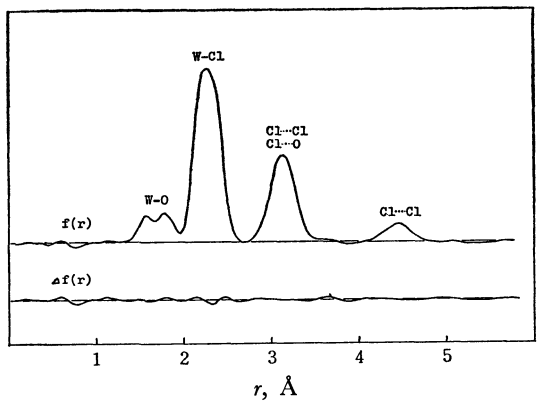

Fig. 2. Radial distribution for $WOCl_4$, $f(r)$, and the difference between observed and theoretical ones, $\Delta f(r)$.

approximation.[17] The parameter in the Morse function, a, was assumed to be 2.0 $Å^{-1}$, and the frequencies of ν_{W-O} and ν_{W-Cl} were taken to be 1027 and 402 cm^{-1}, respectively.[8] The assymmetry parameters thus obtained were 0.5×10^{-6} $Å^3$ for W–O and 4.0×10^{-6} $Å^3$ for W–Cl, and those for non-bonded distances were assumed to be zero. These asymmetry parameters were fixed throughout the least-squares analysis.

In the first stage, it was discovered that the correlation between the Cl···Cl(s) and Cl···O amplitudes was very large. This is probably because of the small difference between the distances, as observed by Jacob *et al.* in the analysis of $XeOF_4$.[5] In the analyses, where no constraint was set on the l(Cl···Cl(s)) and l(Cl···O), the difference between them was estimated to be about 0.03 Å, as listed in Table 1.

Since the results obtained from two independent intensity data are in good agreement with each other, as shown in Table 1, random errors were estimated as 2.5 σ_1 from the standard errors in least-squares calculations.[18] Systematic errors were estimated as follows. The error associated with the calibration of the lattice constant of gold was 0.06%, and the errors in the measurements of the diffraction patterns of the gold foil and the camera length were 0.08 and 0.04%, respectively. Then the total error of the wavelength was estimated to be 0.11% from the square root of the squared sum of the individual errors. The error in the q values was estimated from those in the electron wavelength and the camera length. The total errors in the bond distances were evaluated from the systematic errors (0.12%) and the random errors. The uncertainties in the atomic scatterign factor, f, and the phase angle, η, of tungsten were estimated** to have negligible effect on the systematic error in the atomic distances, but the systematic errors from this origin were found to be about 0.01 Å for l(Cl···Cl(s)) and l(Cl···O).

Table 1. Results of the least-squares analysis (in Å units)

	Plate 1	Plate 2	Average	σ_1
r_a(W–Cl)	2.2793	2.2800	2.2797	0.0007
r_a(W–O)	1.6847	1.6841	1.6844	0.0043
r_a(Cl···Cl(s))	3.1427	3.1493	3.1460	0.0057
l(W–Cl)	0.0523	0.0520	0.0522	0.0015
l(W–O)	0.0456	0.0439	0.0448	0.0043
l(Cl···Cl(s))	0.1220	0.1214	0.1217	0.0102
l(Cl···Cl(l))	0.1160	0.1202	0.1181	0.0078
l(Cl···O)	0.1002	0.0903	0.0953	0.0148
R	0.9232	0.9226	0.9229	0.0071

Table 2. Distances and mean amplitudes

r_g(W–Cl)	2.281±0.003 Å
r_g(W–O)	1.686±0.011
r_g(Cl···Cl(s))	3.151±0.015
r_g(Cl···Cl(l))	4.452±0.021
r_g(Cl···O)	3.120±0.026
l(W–Cl)	0.052±0.004
l(W–O)	0.045±0.011
l(Cl···Cl(s))	0.122±0.028
l(Cl···Cl(l))	0.118±0.020
l(Cl···O)	0.095±0.038
∠OWCl	102.4±1.3°
∠ClWCl	87.3±0.5°

The final results of the analysis are given in Table 2, where r_g parameters were calculated from r_a parameters by $r_g = r_a + l^2/r_a$. The correlation matrix[19] is given in Table 3, and the best-fit theoretical intensity curve is shown in Fig. 3.*** The least-squares computations were carried out by the use of a FACOM 230—60 at Nagoya University Computing Center.

Discussion

The square-pyramidal structure of $WOCl_4$ in the gas phase is in accord with that derived from infrared and Raman spectroscopy.[7,8] Although the structure of $WOCl_4$ in the gas phase is essentially the same as those of IF_5, ICl_5, IBr_5, and $XeOF_4$, the XMY angle in an MXY_4 molecule of C_{4v} symmetry is found to be remarkably different. The OWCl angle is 102.4± 1.3°, whereas the corresponding angles in IF_5, ICl_5, IBr_5, and $XeOF_4$ are about 90° or less. Moreover,

** A least-squares calculation, where the f and η values for platinum were used in place of those for tungsten, was carried out, and the changes in the parameter values were used for the estimation of their errors. The choice of platinum was inferred from a comparison of the observed cut-off point with the calculated ones.

*** Numerical experimental data of the leveled total intensity and the background have been deposited with the Chemical Society of Japan (Document No. 7411).

TABLE 3. CORRELATION MATRIX FOR MOLECULAR PARAMETERS OF $WOCl_4$[a)]

	r_{W-Cl}	r_{W-O}	$r_{Cl\cdots Cl(s)}$	l_{W-Cl}	l_{W-O}	$l_{Cl\cdots Cl(s)}$	$l_{Cl\cdots Cl(l)}$	$l_{Cl\cdots O}$	R
r_{W-Cl}	1.0	−0.235	0.053	−0.006	0.191	0.210	0.043	−0.223	−0.027
r_{W-O}		1.0	0.097	−0.106	−0.085	0.288	0.065	−0.287	0.171
$r_{Cl\cdots Cl(s)}$			1.0	−0.003	−0.009	−0.286	−0.007	0.201	0.003
l_{W-Cl}				1.0	−0.013	0.095	0.087	−0.015	0.608
l_{W-O}					1.0	0.046	0.032	−0.037	0.001
$l_{Cl\cdots Cl(s)}$						1.0	0.094	−0.955	0.312
$l_{Cl\cdots Cl(l)}$							1.0	−0.056	0.166
$l_{Cl\cdots O}$								1.0	−0.167
R									1.0

a) The elements are defined as $\rho_{ij}=B^{-1}{}_{ij}/(B^{-1}{}_{ii}\times B^{-1}{}_{jj})^{1/2}$.

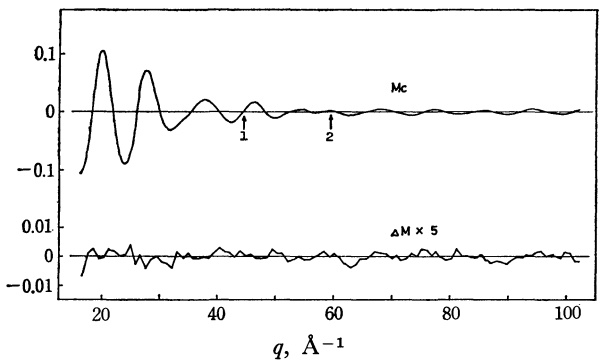

Fig, 3. Calculated molecular intensities, M_c, and the difference between observed and calculated ones, ΔM. The arrows 1 and 2 indicate the theoretical cut-off points due to the atomic pairs of W-O and W-Cl, respectively.

the OWCl angle in $WOCl_4$ is nearly equal to the OTiCl angle in $TiOCl_4^{2-}$ (102°) in crystalline $[N(C_2H_5)_4]_2$-$TiOCl_4$.[20] $TiOCl_4^{2-}$ has approximate C_{4v} symmetry in the crystalline state, and the Ti–O distance is 1.79 Å and the Ti–Cl distances are 2.32 and 2.34 Å. The shortening of the W–Cl distances of $WOCl_4$ in comparison with the Ti–Cl distance of $TiOCl_4^{2-}$ is consistent with the fact that the ionic radius of W^{6+} is about 0.06 Å shorter than that of Ti^{4+}.

The W–Cl distance found in the gaseous $WOCl_4$ molecule is equal to that in the crystal (2.28 Å), whereas the W–O distance in the vapor is considerably shorter than those in the crystal (1.8 and 2.2 Å).[9] The lengthening of the W–O distance in the crystal is apparently due to the decrease in the double bond character by the formation of –O–W–O– linkage.

Available data of infrared and Raman spectra are not sufficient to calculate the mean amplitudes of vibration of the atomic pairs in $WOCl_4$. However, if fundamental frequencies, ν_{W-O} and ν_{W-Cl}, are estimated to be 1027 and 402 cm^{-1}, respectively,[8] l(W–O) and l(W–Cl) can be estimated by a diatomic-molecule approximation to be 0.034 and 0.049 Å, respectively, in essential agreement with the results from the electron diffraction analysis.

We are pleased to acknowledge a grant from the Ministry of Education.

References

1) G. V. Romanov and V. P. Spiridonov, *Zh. Strukt. Khim.*, **8**, 159 (1967).
2) K. Kimura and S. H. Bauer, *J. Chem. Phys.*, **39**, 3172 (1963).
3) J. L. Hencher, D. W. J. Cruikshank, and S. H. Bauer, *ibid.*, **48**, 518 (1968).
4) G. M. Begun, W. H. Fletcher, and D. F. Smith, *ibid.*, **42**, 2236 (1965).
5) E. J. Jacob, H. B. Thompson, and L. S. Bartell, *J. Mol. Struct.*, **8**, 383 (1971).
6) R. J. Gillespie, *J. Chem. Educ.*, **40**, 295 (1963); *J. Amer. Chem. Soc.*, **85**, 4672 (1963).
7) B. G. Ward and F. E. Stafford, *Inorg. Chem.*, **7**, 2569 (1968).
8) I. R. Beattie, K. M. S. Livingston, D. J. Reynolds, and G. A. Ozin, *J. Chem. Soc., A*, **1970**, 1210.
9) H. Hess and H. Hartung, *Z. Anorg. Allgem. Chem.*, **344**, 157 (1966).
10) S. E. Feil, S. Y. Tyree, and F. N. Collier, Inorganic Syntheses, Vol. 9, p. 123 (1967).
11) M. Kimura, S. Konaka, and M. Ogasawara, *J. Chem. Phys.*, **46**, 2559 (1967); M. Ogasawara, S. Konaka, and M. Kimura, *ibid.*, **50**, 1488 (1969).
12) C. Tavard, D. Nicolas, and M. Rouault, *J. Chim. Phys.*, **64**, 540 (1967).
13) L. Bewilogua, *Physik. Z.*, **32**, 740 (1931).
14) R. M. Gavin and L. S. Bartell, *J. Chem. Phys.*, **48**, 2460 (1968).
15) S. Konaka, Y. Murata, K. Kuchitsu, and Y. Morino, This Bulletin, **39**, 1134 (1966).
16) S. Shibata, *ibid.*, **45**, 1631 (1972).
17) K. Kuchitsu, *ibid.*, **40**, 505 (1967).
18) Y. Morino, K. Kuchitsu, and Y. Murata, *Acta Crystallogr.*, **18**, 549 (1965).
19) O. Bastiansen, L. Hedberg, and K. Hedberg, *J. Chem. Phys.*, **27**, 1311 (1957).
20) W. Haase and H. Hoppe, *Acta Crystallogr., B*, **24**, 282 (1968).

On the EPR Emission Spectrum of Transient Naphthosemiquinone Radical

Hiroshi YOSHIDA, Junkichi SOHMA, and Tetsuo WARASHINA*

Faculty of Engineering, Hokkaido University, Kita-ku, Sapporo 060

**Research Reactor Institute, Kyoto University, Kumatori-cho, Osaka 590-04*

(Received November 5, 1973)

EPR spectrum in emission mode at the low-field hyperfine lines was observed for 1,4-naphthosemiquinone radical formed by the steady-state photolysis of solution of corresponding quinone in ethanol flowing through the cavity. Observed behavior of this spectrum was analyzed by a phenomenological way. The results support the view that the anomalous electron spin polarization is generated in the radical formation process. The conclusion was compared with the results of intermittent photolysis.

Since the first observation of EPR emission spectrum (more precisely emission-absorption combined spectrum) for H radical during the radiolysis of alkanes,[1] chemically induced dynamic electron spin polarization (CIDEP) in short-lived free radicals has been reported[2] and also generated theoretical interests.[3] Among several theoretical attempts to interpret the anomalous spin polarization, the most promising mechanism at present seems to be a formation of radical pair, in which nonequilibrium populations of the spin levels arises from the combined effects of an exchange interaction between a radical pair and differences in the Larmor frequencies between the two radicals in the pair. This mechanism leads to the spin polarization which produces the EPR spectra composed of hyperfine lines both in emission and in enhanced absorption at such high field as 3000G. Fessenden applied this radical pair mechanism to interpret the anomalous spectra of H radical[1c] and others[4] and attained the conclusion that the nonequilibrium population was generated during the decay of the radicals by mutual recombination. This was the reason why the emission-absorption spectrum could be observed during the steady-state radiolysis, though the spin-lattice relaxation time should be much shorter than the chemical lifetime.

However, the radical pair mechanism does not seem to be a general and exclusive one for all CIDEP phenomena, because some photochemically generated transient free radicals were found to give EPR spectra entirely in emission. Among them, Wong and Wan studied the inversion from emission to absorption for 1,4-naphthosemiquinone radical formed in a solution of naphthoquinone in 2-propanol by intermittent photolysis, and found the time constant of about 300 μs for this inversion process.[5] They mentioned also that all hyperfine lines of the radical exhibited the same behavior. They proposed, to interpret this observation, a mechanism where the spin polarization occurs in photoexcited naphthoquinone during the course of intersystem crossing from singlet to triplet state and it is retained when the triplet-excited naphthoquinone abstracts a hydrogen atom from solute.[2e]

During the course of EPR study of short-lived free radicals under the steady-state photolysis of the solutions of quinones in ethanol, the present authors (H.Y. and T.W.) found an anomalous behavior of the spectrum due to 1,4-naphthosemiquinone radical which was recorded as a combination of emission and absorption.[6] This appeared different from the results obtained by Wong and Wan under the intermittent photolysis. Therefore, the study is extended to elucidate the behavior of the spectrum under the steady-state photolysis and the difference between two different photolysis conditions and to understand fully the spin polarization mechanism in this particular free radical.

Experimental

The apparatus used has been described in detail elsewhere.[7] EPR measurements were carried out with a conventional X-band spectrometer (Varian, E-3) during photolysis of flowing solution of 1,4-naphthoquinone (3.8 mM) in ethanol with unfiltered light from a super-high pressure mercury arc (Philips, SP 500). The effective volume of a quartz flat cell was $7\times0.2\times32$ mm). Ethanol and naphthoquinone were of analytical grade and were used without further purification. The solution was purged with helium gas before use to remove dissolved oxygen.

Results

Typical examples of the observed spectra are shown in Fig. 1. Although the photochemical reactions involved and the observed hyperfine structures were reported previously,[6] they are summarized here briefly. In a neutral solution, naphthosemiquinone anions and naphthosemiquinone radicals are formed simultaneously as shown in Fig. 1a. Their hyperfine structures are illustrated by the stick-spectra. The coupling constants for the anions are 3.25, 0.64 and 0.51 G (two equivalent protons for all three values), which agree with those reported by Wenkataraman *et al.*[8] The radical spectrum is identified by referring to the spectrum observed

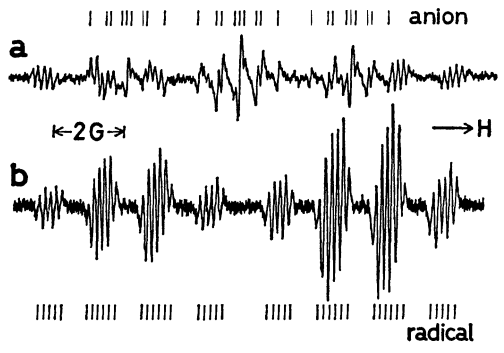

Fig. 1. EPR spectra observed during photolysis of 1,4-naphthoquinone (3.8 mM) (a) in ethanol at the residence time of the solution in the cell 0.07 s and (b) in ethanol with acetic acid (30 mM) at the residence time of 1.2 s.

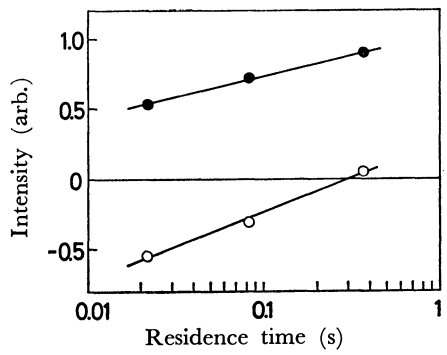

Fig. 2. Dependence of spectral line intensity of the naphthosemiquinone radical formed during the photolysis of naphthoquinone (3.8 mM) solution in ethanol on the residence time of the flowing solution in the cell at 20 °±3 °C, (○) average intensity of the second and fourth hyperfine lines from the low-field extreme and (●) that of the second and fourth lines from the high-field extreme.

when the solution is acidified with acetic acid (Fig. 1b). Its hyperfine coupling constants are temperature dependent and determined to be 6.80, 1.63 (2 protons), 1.50, 0.37 and 0.17 G (2 protons) at 34 °C.

The remarkable feature of the radical spectrum is that the intensity ratio of hyperfine lines depends very much on the flow rate of the solution. At the highest flow rate examined, a half of the spectrum at the low field is recorded as emission lines, whereas the high field half is in absorption (see Fig. 1a). The central part is too weak to be observed clearly. When the flow rate decreases, the emission lines gradually revert to normal absorption. The reversion of the spectrum is illustrated in Fig. 2 by the observed intensity of the second and fourth hyperfine lines from the low field end and those from the high field end as a function of the residence time of the solution in the cell (flow rate/cell volume) with other experimental conditions unchanged. It is surprising that the emission lines are observed not only under the intermittent photolysis condition[5] but also the steady-state photolysis condition. However, the spectrum is not entirely in emission in the latter case.

The chemical lifetime of the radical was estimated by means of a boxcar integrator and a rotating sector (11 cps) at the residence time of 1 s. The free radicals are thought to disappear by following a second-order kinetics, so that the lifetime may depend on the average concentration. However, the observed curve of radical formation and decay gives a rough estimate of the lifetime, 10 ms in the present photolysis condition.

Discussion

Normal steady-state photolysis is not a pertinent method to study the CIDEP phenomena in detail, because the observed spectra provide the information of spin populations in Zeeman sublevels averaged over the chemical lifetime of the free radical in question. However the steady-state photolysis method has some advantages, because the stability and sensitivity of the measurements are generally better than the time-resolved EPR measurement with flash (or intermittent) photolysis. Therefore, the anomalous behavior of the EPR spectra observed by this method indicates unequivocally, though qualitatively, something about CIDEP. In this discussion, we shall not go into the mechanism of spin polarization in detail but try to interpret phenomenologically the present observations.

Emission-absorption spectra are observed by the steady-state photolysis at high flow rates, but the chemical lifetime of free radicals as well as the residence time of the solution is very much longer than the spin-lattice relaxation time of the free radicals. This seems to indicate that the anomalous spin population is not generated in the radical formation process but by a continuous "pumping" during the decay of the radicals. For simplicity, let us consider a model radical with single proton. According to Fessenden's treatment based on the radical pair theory,[4] the spin populations are well approximated by the following differential equations:

$$\mathrm{d}(n_2-n_1)/\mathrm{d}t = -\{[(n_2-n_1)-\beta(n/4)]/T_1\} - f_{\mathrm{R}}k''(n/4)^2 \quad (1)$$

$$\mathrm{d}(n_4-n_3)/\mathrm{d}t = -\{[(n_4-n_3)-\beta(n/4)]/T_1\} + f_{\mathrm{R}}k''(n/4)^2 \quad (2)$$

where the subscripts 1,2,3 and 4 indicate the Zeeman sublevels (α_e, α_N), (β_e, α_N), (α_e, β_N) and (β_e, β_N), β the Boltzmann factor given by $h\nu/kT$, f_{R} the fractional degree of polarization induced by the recombination reaction, and k'' the second-order decay constant. For the steady-state photolysis of flowing solution, the number of total spin n changes as the following function of photolysis time, t,

$$n = (c/2k'')^{1/2}\tanh\{(2k''c)^{1/2}t\} \quad (3)$$

when the free radicals in question disappear by a second-order reaction, which should be additionally taken into account. c is the rate of radical formation. The observed intensity of the low-field hyperfine line is proportional to $\tau^{-1}\int_0^{\tau}(n_2-n_1)\mathrm{d}t$, where τ represents the residence time of solution in the cell.[9] Although the integration cannot be given analytically, Eqs. (1) and (2) indicate the qualitative nature of the low-field emission line. For the emission line to be observed, (n_2-n_1) should be negative, which turns out that $\mathrm{d}(n_2-n_1)/\mathrm{d}t$ should be negative in an appropriate range of time. Under proper conditions (strictly speaking, when $\beta<k''f_{\mathrm{R}}T_1(n''_s/4)$), the emission line develops in $\tau\approx 1/k''n''_s$ and its intensity reaches $\beta(n''_s/4)\{1-f_{\mathrm{R}}k''T_1(n''_s/4)/\beta\}$ at $\tau=\infty$ where n''_s is the steady-state value of $n(=\sqrt{c/2k''})$. The observation that the emission lines are recorded only for big flow rate, or short residence time τ (see Fig. 2) is just contrary to what is theoretically expected on the basis of the phenomenological analysis and excludes the possibility of generation of the anomalous spin population during the decay of radicals.

An alternative approach is that the CIDEP phenomena observed in steady-state photolysis and intermittent photolysis experiments are from the same origin, that is, the anomalous spin polarization generated at

the moment of radical formation when, no matter what the operative mechanism is, both (α_e, α_N) and (α_e, β_N) sublevels are overpopulated. Then Eqs. (1) and (2) are modified as follows,

$$d(n_2-n_1)/dt = -\{[(n_2-n_1)-\beta(n/4)]/T_1\} - f_F(c/2) \quad (4)$$

$$d(n_4-n_3)/dt = -\{[(n_3-n_4)-\beta(n/4)]/T_1\} - f_F(c/2) \quad (5)$$

under the assumption that the radical lifetime is much longer than T_1, where f_F represents the fractional degree of polarization induced in the radical formation process. The steady-state treatment can be applied to Eq. (4) except for the small time interval $t \lesssim T_1$, and the approximate relation

$$n_2 - n_1 = \beta(n/4) - f_F(c/2)T_1 \quad (6)$$

is obtained.

For simplicity, let us assume at first that the radical disappears in the following first-order decay:

$$n = (c/k')\{1-\exp(-k't)\}, \quad (7)$$

where k' represents the first-order decay rate constant. From (6) and (7), the line intensity is derived as

$$\frac{1}{\tau}\int_0^\tau (n_2-n_1)dt = \beta(n'_s/4)\{[1-(2f_Fk'T_1/\beta)] - (1/k'\tau)[1-\exp(-k'\tau)]\}, \quad (8)$$

where n'_s represents the steady-state value of n, c/k'. If $2f_Fk'T_1>\beta$, the emission line is observed regardless of the residence time τ. Even if $2f_Fk'T_1$ is smaller than β but not very much, the line can be in emission at such a low flow rate as $\tau\sim 1/k'$, as shown in Fig. 3. In this case, the line reverts from emission to absorption with increasing τ. If one takes values 1.48×10^{-3} for Boltzmann factor β for 9300 MHz at room temperature, 10^2 s^{-1} for k' and, arbitrarily 10^{-5} s for T_1, $f_F=0.7$ well develops the emission line. This f_F value turns out that the enhancement factor $f_F/2\beta$ of 250, which is compared with the value of 313 estimated by Wong *et al.* for naphthosemiquinone radical based on the intersystem crossing mechanism.[3e]

For the second-order decay, the line intensity is

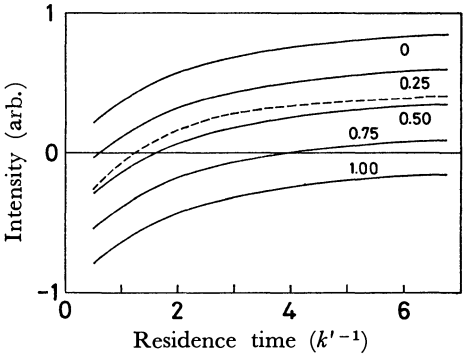

Fig. 3. Dependence of line intensity on the residence time of flowing solution expected from Eq. (8) for the first-order decay of radical. The value of parameter $2f_Fk'T_1/\beta$ for each curve is shown in the figure. The dependence for the second-order decay based on Eq. (9) is shown only for $2f_F\sqrt{2k''c}\cdot T_1=0.5$ by a dashed line. The intensity 1.0 corresponds to the Boltzmann distribution and negative intensities represent spectral lines in emission.

derived from equations (3) and (6) and expressed by a somewhat complex form as

$$\frac{1}{\tau}\int_0^\tau (n_2-n_1)dt = \beta(n_s''/4)\{(\sqrt{2k''c}\cdot\tau)^{-1} \times \ln[\cosh(\sqrt{2k''c}\cdot\tau)] - 2f_F\sqrt{2k''c}\cdot T_1/\beta\} \quad (9)$$

The intensity increases from negative to positive value and approaches to the limiting value of $\beta(n''s/4)\{1-2f_F\cdot\sqrt{2k''c}\cdot T_1/\beta\}$ in similar manner as that for the first-order decay. The difference in the dependence of the intensity upon τ is not significant between the second-order decay and the first-order one, as shown in Fig. 3 representatively for $2f_F\sqrt{2k''c}\cdot T_1/\beta=0.5$. Therefore, behavior of the spectrum is not seriously affected by the mode of radical decay except for unrealistically small values of τ.

It is most crucial to test whether the totally emissive spectrum immediately after the photolysis with pulsed light can be recorded as the emission-absorption spectrum under the steady-state photolysis. Really it can if f_F and/or T_1 are dependent on the nuclear spin state (in the simplified single proton model radical, dependent on the state α_N or β_N) as shown in Fig. 3. Assuming that the value of $2f_F\sqrt{2k''c}\cdot T_1$ is slightly smaller for the high field lines in naphthosemiquinone radical spectrum, they revert to absorption, as a function of τ, much quicker than the low field lines do.

Paramagnetic relaxation times were tried to be measured from the cw saturation and the line width. They were estimated as $T_1\sim T_2\sim10^{-6}$ s and their dependence on hyperfine lines could not be observed. However, the relaxation times based on the cw saturation may not be reliable enough to be involved in the present discussion of CIDEP. In addition, it was claimed by Atkins *et al.*[10] that a simple T_1 determination using the saturation properties of an emission is invalid.

In conclusion, the latter approach is reasonable to interpret the emission-absorption spectrum of naphthosemiquinone radical observed during steady-state photolysis of the flowing solution of naphthoquinone in ethanol. Although the flow rate is very slow compared with T_1, the anomalous spin polarization observed is generated at the radical formation rather than at the radical recombination. It was shown that the emission-absorption spectrum in the present study can be consistent, by choosing proper parameters, with the totally emissive spectrum previously observed by the intermittent photolysis. However, to attain the rigid conclusion, it is essentially desirable to examine the behavior of the emission lines of this particular radical by a time-resolved EPR measurements for a long time duration after a photolysis pulse, even though it may be difficult experimentally because of weak signal intensities.

Finally, it should be noted that the hyperfine lines at the high field of the naphthosemiquinone radical spectrum are in reduced absorption, as the population difference between electronic Zeeman sublevels is smaller than that in Boltzmann distribution as illustrated in Fig. 3. This feature is in contrast to the enhanced absorption observed for the high-field line of the H

radical spectrum in which the radical pair mechanism is operative at the radical disappearance. The present investigation suggests that the reduced absorption may sometimes occur for the electron paramagnetic resonance of short-lived free radicals which are known to give asymmetric EPR spectra very often.

References

1) (a) R. W. Fessenden and R. H. Schuler, *J. Chem. Phys.*, **39**, 2147 (1963). (b) K. Eiben and R. W. Fessenden, *J. Phys. Chem.*, **75**, 1186 (1971). (c) N. C. Verma and R. W. Fessenden, *J. Chem. Phys.*, **58**, 2501 (1973).

2) (a) P. W. Atkins, I. C. Buchanan, R. C. Gurd, K. A. McLauchlan, and A. F. Simpson, *Chem. Commun.*, **1970**, 513. (b) B. Smaller, E. C. Avery, and J. R. Remenko, *J. Chem. Phys.*, **55**, 2414 (1971). (c) R. Livingstone and H. Zeldes, *J. Magn. Resonance*, **9**, 331 (1973). (d) S. K. Wong, D. A. Hutchinson, and J. K. S. Wan, *J. Amer. Chem. Soc.*, **95**, 622 (1973), and previous papers cited therein.

3) (a) R. Kaptein and J. L. Oosterhoff, *Chem. Phys. Lett.*, **4**, 195 (1969). (b) H. Fischer and M. Lehning, *J. Phys. Chem.*, **75**, 3410 (1971). (c) F. J. Adrian, *J. Chem. Phys.*, **57**, 5107 (1972). (d) J. B. Pedersen and J. H. Freed, *ibid.*, **58**, 2746 (1973). (e) S. K. Wong, D. A. Hutchinson, and J. K. S. Wan, *ibid.*, **58**, 985 (1973), and papers cited therein.

4) R. W. Fessenden, *ibid.*, **58**, 2489 (1973).

5) S. K. Wong and J. K. S. Wan, *J. Amer. Chem. Soc.*, **94**, 7197 (1972).

6) H. Yoshida, K. Hayashi, and T. Warashina, This Bulletin, **45**, 3515 (1972).

7) H. Yoshida and T. Warahsina, This Bulletin, **44**, 2950 (1971).

8) B. Venkataraman, B. G. Segel, and G. K. Fraenkel, *J. Chem. Phys.*, **30**, 1006 (1959).

9) The intensity observed under the steady-state photolysis of flowing solution is proportional to $I=S\int_0^l (n_2-n_1)\mathrm{d}l$, where S and l are the cross-section and effective length of the cell, respectively. Because the velocity of the flowing solution is $v=\mathrm{d}l/\mathrm{d}t=l/\tau$, I is rewritten as $(lS/\tau)\int_0^\tau (n_2-n_1)\mathrm{d}t$.

10) P. W. Atkins, K. A. McLauchlan and P. W. Percival, *Mol. Phys.*, **25**, 281 (1973).

ESR Study on Transient Radicals in Plastic Crystals under Electron Irradiation

Hirotsugu SHIRAISHI, Hajime KADOI, Kenichi HASEGAWA, Yoneho TABATA, and Keichi OSHIMA

Department of Nuclear Engineering, Faculty of Engineering, The University of Tokyo, Bunkyo-ku, Tokyo 113

(Received December 21, 1973)

An apparatus was constructed for ESR measurements during electron irradiation, and the behavior of transient radicals in the plastic crystals of cyclohexane (CyH) and 2,2,3,3-tetramethylbutane (TMB) was investigated. It was found from the experiment that cyclohexyl radical produced by irradiation of CyH decays with a rate constant of 2×10^{-8} exp $(-7.9$ kcal$/RT)$ cm^3/s. The rate constant is in good agreement with the results reported by Buben *et al.* On the other hand, radicals formed in irradiated TMB were assigned to be

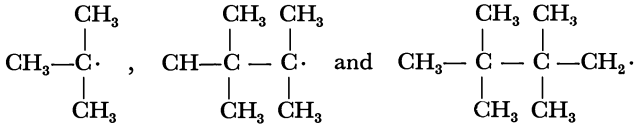

from the present results. It was shown from the results that the assignment made by Marx *et al.* before should be corrected to some extent. In the plastic crystals of CyH and TMB, it was suggested that the decay reactions of the observed radicals are controlled by the diffusional migration of the radicals. The analysis of radiolytic products of TMB was also made, and the results were compared with the results of ESR observation.

In order to study early stages of radiation chemical processes, it is very important to follow the dynamical behavior of transient species. The method of pulse radiolysis has been used with great success in the optical measurement of various kinds of transient species. ESR methods have been employed to give useful information about radicals produced by irradiation, but most studies were made by trapping of radicals in solids at low temperatures.

The ESR measurement of short-lived radicals under electron irradiation was first reported by Molin and his coworkers,[1] and an extensive study has been made by Fessenden and Schuler.[2] Recently a pulsed irradiation method in ESR spectroscopy has been developed by Smaller and his co-workers.[3] In the present paper, we report on apparatus for ESR measurements during electron irradiation and on some recent experimental results. Since there is much to be learned about the transient behavior of radicals in solids, the experiments using the apparatus are primarily aimed at such transient species. As the first step we have tried to measure transient radicals in cyclohexane (CyH) and in 2,2,3,3-tetramethylbutane (TMB), which are known to be typical of plastic crystals. It is known that radicals produced in a plastic crystal exhibit a well-resolved ESR spectrum due to motional narrowing and that they disappear rapidly far below the melting point of the crystal. Radicals formed in irradiated cyclohexane in its plastic crystal phase have been studied by previous investigators.[4-6]

The products formed in the radiolysis of TMB in its plastic crystal phase were analyzed chromatographically, and the results were correlated with radicals observed by ESR spectroscopy.

Experimental

Figure 1 illustrates the schematic diagram of the irradiation system. A Dynamitron accelerator was used as the irradiation source, and it was usually operated at 1.2 MeV with the beam current of 10—200 μA for ESR measurements. The focusing of an electron beam was at first difficult because of the long distance from the accelerator to the ESR cavity; the latter was located at the end of beam duct which penetrated through one of the pole pieces of ESR magnet. Several focusing magnets and a coil for the compensation of terrestrial magnetism were located along the beam duct to get a stable electron beam. When a sample of 3 mm in diameter and 7 mm in length was irradiated with an electron beam of 0.05 μA, the dose rate was about 1.5×10^8 R/hr. The dose rate was determined by the method developed by Tamura *et al.*,[7] that is, by measuring peroxy radicals formed in irradiated

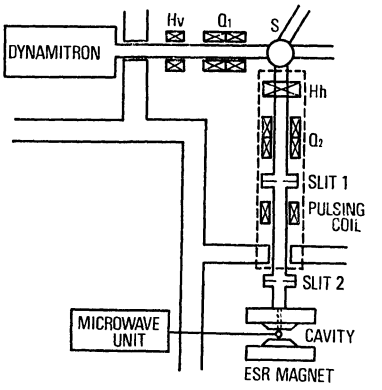

Fig. 1. Irradiation system.
Hv, Hh: Helmholtz coils for vertical and horizontal deflection. S: Switching magnet. Q_1, Q_2: Quadrupole magnets for focusing. Broken line: Coil for compensation of terrestrial magnetism.

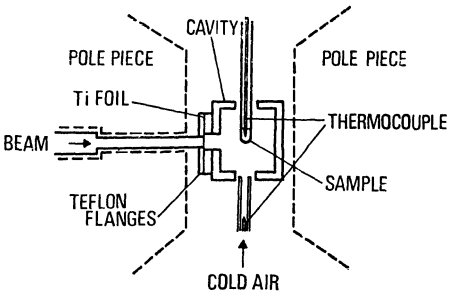

Fig. 2. ESR magnet and cavity.

polytetrafluoroethylene.

The ESR spectrometer used is a conventional X-band system with 100 kHz field modulation, and with cylindrical TE-011 mode cavity. The cavity has a 5 mm-diam. circular aperture on the wall to let an electron beam pass through it. Figure 2 is a sketch around the ESR magnet.

Dry air cooled by liquid nitrogen is used to control the temperature of the samples. Oxygen in air rapidly captures free electrons produced in the cavity and reduces their steady state concentration during irradiation. Oxygen, therefore, serves to suppress fluctuations of the resonant frequency of the cavity which would occur due to the presence of conduction electrons in the irradiated cavity if pure nitrogen was used as the coolant.

Commercial grade CyH and TMB (both above 99.9% purity) were used without further purification. Samples were degassed by a usual freeze-pump-thaw method, and were sealed off in thin-walled tubes of Spectrosil quartz.

The analysis of radiolytic products of TMB was made by a conventional gas-phase chromatograph with a flame ionization detector. Columns of squalane and of Apiezone L were used.

Results and Discussion

CyH exists in a plastic crystal phase between the transition point of −87.1 °C and the melting point of 6.3 °C. ESR studies on radicals formed in the plastic crystal of CyH under electron irradiation were already carried out by Buben *et al.*[4] and by Fessenden *et al.*,[5] and the radicals were assigned to cyclohexyl radicals. This decay was also studied by Buben *et al.*[6]

The decay characteristic of cyclohexyl radicals after the cessation of irradiation was studied more precisely in the plastic crystal phase by using our apparatus. The plots of reciprocal of radical concentration *versus* time obtained from the decay curves at different temperatures are shown in Fig. 3, where for convenience the reciprocal of each initial concentration is subtracted for each series of plots. All curves represent good fit to linear plots at the early stage of the decay. This implies that the decay is dominated by the second-order reaction, as was indicated by Buben *et al.* From the analysis of Fig. 3, the rate constant is estimated to be 2×10^{-8} exp(−7.9 kcal/RT) cm³/s, which is a little smaller than the value of 3×10^{-8} exp(−8 kcal/RT) cm³/s obtained by Buben *et al.*

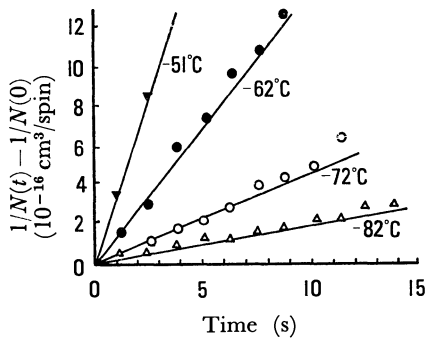

Fig. 3. Second-order plots of the decay of cyclohexyl radicals.
$1/N(t)$, $1/N(0)$: Reciprocal radical concentration at time t and zero, respectively.

As pointed out in their previous study, both the abrupt change in the rate of the decay at the transition point of −87 °C and the coincidence of the activation energy with that of self-diffusion in the plastic crystal phase, 8 kcal/mol,[8] seem to support the view that the decay reaction is controlled by the diffusional migration of the radicals. But the rate constant obtained, though smaller than the value of Buben *et al.*, seems too large compared with the one expected from Smoluchowsky equation of diffusion-controlled reaction, 2.5×10^{-9} exp(−8 kcal/RT) cm³/s, assuming a diffusion constant of 2×10^{-3} exp(−8 kcal/RT) cm²/s[9] and a reaction radius of 5 Å. Since it is not probable that the radicals observed are distributed homogeneously, the above-mentioned fact may indicate that the radicals are able to diffuse more easily than ordinary molecules in the crystalline matrix.

TMB (2,2,3,3-tetramethylbutane) is in the plastic crystal phase between the transition point of −120.6 °C and the melting point of 100.6 °C. The ESR spectrum of γ-irradiated TMB was recently reported by Marx *et al.*,[10] but the present study led us to different assignments of the radicals. Figure 4a is the ESR spectrum of TMB at −113 °C, which was taken after electron irradiation, since the decay is very slow at this temperature. Marx *et al.* obtained a similar spectrum, but they seem to have been unaware of two outermost lines, which are small due to the corresponding binominal coefficient. They analyzed the spectrum as having 15 lines, and attributed the spectrum to radical A of 15 lines and B of three lines, where radical A was considered to be formed by isomerization of

[R_A]

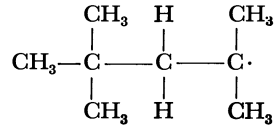

[R_B]

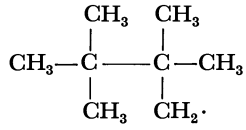

radical B. But in fact there are 17 lines, and it is plausible that the spectrum consists of sets of ten and of seven equally spaced lines, both exhibiting the same hyperfine splitting of 23.4±0.2 G and about the same g-factor; 2.0026±0.0002 for the 10 lines, and 2.0025±0.0002 for the seven lines. The line width is about 2.5 G at this temperature. The observed ratio of the relative intensities of the ten lines is 1 : 10 : 65 : 201 : 377 : 361 : 194 : 62 : 9.5 : 1 in the order of increasing magnetic field. The 10 lines are attributable to the *tert*-butyl radical R_I, though a considerable contribution from other radicals may be inferred from the observed ratio, which should be 1 : 9 : 36 : 84 : 126 : 126 : 84 : 36 : 9 : 1 in case of the *tert*-butyl radical alone. The fact that the ratio of the

[R_I]

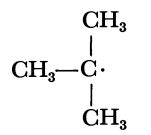

[R_{II}]

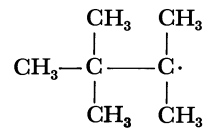

$$[R_{III}] \quad CH_3-\overset{\overset{CH_3}{|}}{\underset{\underset{CH_3}{|}}{C}}-\overset{\overset{CH_3}{|}}{\underset{\underset{CH_3}{|}}{C}}-CH_2\cdot$$

line next to the outermost is close to 9 : 1 indicates radical R_A contributes little to the spectrum. Moreover, it is improbable that the rate of the decay of R_A is greater than that of R_B, which must be assumed to explain the spectrum at the higher temperature. The discrepancy between the observed central part of the ratio and that expected for R_I cannot be ascribed to a definite primary radical. Part of this discrepancy may be explained by the isobutyl radical which must be formed by an addition of a hydrogen atom to R_I. The presence of this secondary addition process is also presumed from the results of the analysis of the radiolytic products, as described later. The ratio of the relative intensities of the 7 lines is 1 : 6.5 : 21 : 41 : 23 : 6.5 : 1 in the order of increasing magnetic field, and the 7 lines are attributable to the overlapping of R_{II} of seven lines and R_{III} of three lines that have about the same hyperfine coupling constant; the ratio of the concentration of the former to the latter is about 2.3 : 1.

Figure 4b is the spectrum obtained at −40 °C under electron irradiation, and it shows that the intensity of *tert*-butyl radical became smaller relative to radicals of R_{II} and R_{III}. Correspondingly the measured decay rate of the former was larger than that of the latter at the higher temperature. This seems to imply that in this case also the reaction is diffusion-controlled and that the activation energy of the diffusion of *tert*-butyl radical is smaller.

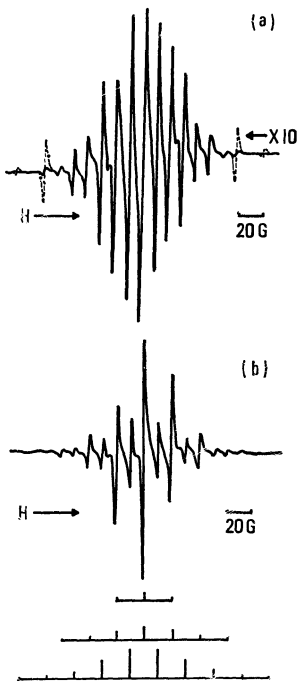

Fig. 4. ESR spectra of electron-irradiated TMB.
(a): at −113 °C after irradiation.
(b): at −40 °C during irradiation.

Table 1. Radiolysis of TMB[a] *G*-values[b]

Products	Irradiation −50 °C	Temperature −10 °C
Isobutane	0.80	1.18
Isobutene	0.30	0.17
Neopentane	0.02	0.02
2-methylbutane	0.01	0.02
2,3,3-trimethyl-1-butene	0.07	0.06
2,2,3-trimethylbutane	0.16	0.23
2,2,4-trimethylpentane	0.25	0.30
2,2,3-trimethylpentane	0.03	0.03
2,3,3-trimethylpentane	0.03	0.02

a) The dose rate was about 2 Mrad/min and samples were irradiated to about 60 Mrad. b) The absolute *G*-values may have errors of ±20% due mainly to possible errors in the dose rate measurements, but the relative *G*-values in each series are accurate with errors of ±5%.

Quantitative analysis of the decay curve was not made because of the complication brought about by the coexistence of three kinds of radicals and by the presence of secondary reactions during irradiation; these are discussed in the next section.

Table 1 shows analysis of products in the range C_4 to C_8[11] formed in samples irradiated at −50 and −10 °C. The irradiation was carried out under the same conditions as the ESR experiments.

The major products of the radiolysis are isobutane, isobutene, 2,2,3-trimethylbutane and 2,3,3-trimethyl-1-butene. These products are considered to be formed by the disproportionation reactions of R_I and R_{II}, respectively. But the ratios of the unsaturated to the saturated products are less than unity for both C_4 and C_8 products. This indicates that secondary addition reaction must have occurred during irradiation. This interpretation is consistent with the fact that the lower the temperature of irradiation, the closer the ratio approaches unity.

It must be noted that the ratio of C_4 to C_8 products is far larger than expected from the ratio of the *G*-values of R_I to R_{II}, which were estimated to be about 0.5 from the ESR measurements. This implies that a considerable fraction of C_4 products is formed by processes other than the radical mechanism.

A large *G*-value of 2,2,4-trimethylpentane is not expected directly from the assigned radicals but its presence is reasonably explained by the recombination of R_I with isobutyl radical that is thought to be formed by the addition of a hydrogen atom to isobutene. The isobutyl radical is not clearly recognized in the ESR spectrum, although the presence of such a radical is inferred from the consideration of relative intensities of the lines, as mentioned earlier.

As for products larger than C_8, two were found to have *G*-values of about 0.1∼0.2. These products are presumably related to the assigned R_{III} radical, but their exact identification is difficult.

The authors wish to thank Mr. M. Onoue and Mr. T. Kawanishi for their help in the experimental setup and for operating the accelerator.

References

1) Yu. N. Molin, A. T. Koritskii, N. Ya. Buben, and V. V. Voyevodskii, *Dokl. Akad. Nauk SSSR*, **123**, 882 (1958); Yu. N. Molin, A. T. Koritskii, N. Ya. Buben, and V. N. Shamshev, *Priborii i Tekhn. Eksperim.*, **6**, 73 (1960).

2) R. W. Fessenden and R. H. Schuler, *J. Chem. Phys.*, **39**, 2147 (1963).

3) B. Smaller, J. R. Remko, and E. C. Avery, *ibid.*, **48**, 5174 (1968); E. C. Avery, J. R. Remko, and B. Smaller, *ibid.*, **49**, 951 (1968).

4) N. Ya. Buben, Yu. N. Molin, A. I. Pristupa, and V. N. Shamshev, *Dokl. Akad. Nauk SSSR*, **152**, 352 (1963).

5) Ref. 2 and S. Ogawa and R. W. Fessenden, *J. Chem. Phys.*, **41**, 99 (1964).

6) N. Ya. Buben, A. I. Pristupa, and V. N. Shamshev, *Kinetika Katal.*, **5**, 190 (1964).

7) N. Tamura, Y. Oshima, K. Yotsumoto, and H. Sunaga, *Japan. J. Appl. Phys.*, **9**, 1148 (1970).

8) E. R. Andrew and R. G. Eades, *Proc. Roy. Soc.*, **216**, 398 (1953).

9) Estimated from the jumping rate f in the Ref. 8, using the relation $D=f\gamma^2/6$, where γ is a unit jump length, assumed to be 5 Å. For the lack of percise knowledge on the diffusion constant the above statement may seem somewhat ambiguous.

10) J. Gerola, B. Lamotte, and R. Marx, *J. Chim. Phys. Physicochim. Biol.*, **66**, 216 (1969).

11) Hydrogen, methane and ethane are considered to be formed in relatively high G-values, but quantitative analysis was not made.

The Crystal Structure of *dl*-1,2,3,4,5,6-Hexahydro-6,11,12,12-tetramethyl-2,6-methano-3,11-propano-3-benzazocine Hydrochloride Monohydrate

Michio KIMURA, Takesi NAKAJIMA, Shigeho INABA, and Hisao YAMAMOTO

Takarazuka Research Laboratories, Sumitomo Chemical Co., Ltd., Takatsukasa, Takarazuka, Hyogo 665

(Received December 26, 1973)

The structure of the title crystal ($C_{19}H_{27}N \cdot HCl \cdot H_2O$) has been determined by X-ray diffraction method. The racemate crystallizes in monoclinic, space group $P2_1/c$ with $a=14.30$, $b=15.74$, $c=7.79$ Å, $\beta=98°58'$ and $Z=4$. The reflection intensities were measured visually from equi-inclination integrating Weissenberg photographs taken with Cu$K\alpha$ radiation. The structure was solved by the direct method of phase determination. The final R factor was 0.113. The molecules are linked in endless chains along c-axis by $N^+ \cdots Cl^-$ and $Cl^- \cdots H_2O \cdots Cl^-$ hydrogen bonds. Two piperidine rings in the molecule have the chair conformation. This product which shows analgesic activity has a new molecular structure having a four-ring system, part of which is a benzomorphan nucleus.

In several synthetic studies of 6,7-benzomorphan derivatives,[1] it has been reported that the cyclization of 1-allyl-1,2,5,6-tetrahydro-2-benzyl-3,4-dimethylpyridine or the corresponding 1-(3′-methylallyl) derivatives with Lewis acid gives the 6,7-benzomorphan derivatives. We have discovered that cyclization of 1-(3′,3′-dimethylallyl) derivatives [I] with P_2O_5-85% H_3PO_4 does not give 3-(3′,3′-dimethylallyl)-1,2,3,4,5,6-hexahydro-6,11-dimethyl-2,6-methano-3-benzazocine [II], but another product in high yield, which shows analgesic activity. We failed to determine the molecular structure of the product by NMR, IR and Mass spectra. An X-ray diffraction investigation for its hydrochloride has been undertaken, and the chemical structure of the product established is [III].

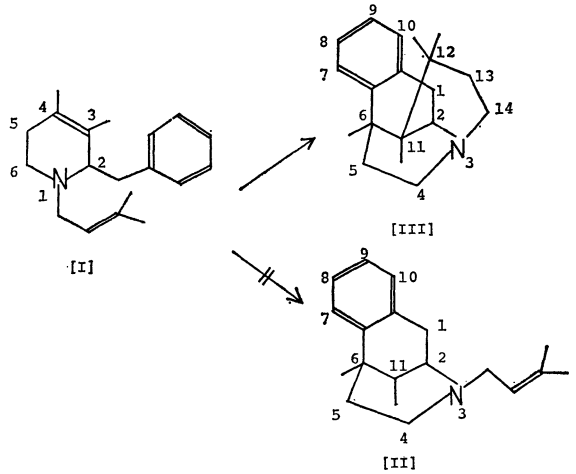

Experimental

Preparation of 1,2,3,4,5,6-Hexahydro-6,11,12,12-tetramethyl-2,6-methano-3,11-propano-3-benzazocine[III]. A mixture of 40 g of [I], 262 g of phosphorus pentoxide and 329 g of 85%-phosphoric acid was kept at 135~140 °C (bath temperature 150~160 °C) for 20 hours under nitrogen atmosphere, cooled, poured into 500 ml of ice-water and basified with concentrated ammonium hydroxide. The oily product was extracted three times by 500 ml of ether and dried over anhydrous sodium sulfate. After removal of ether, the residue was distilled under reduced pressure. Bp: 144~147 °C (0.25~0.28 mmHg); Mp: 72~74 °C (uncorr.). Anal. Calcd for $C_{19}H_{27}N$: C(84.70); H(10.10); N(5.20%). Found: C (84.65); H(9.97); N(5.16%). IR: ν_{max}^{Neat} 2850~3050, 1600, 1580, 1480, 1440, 760, 740, 710, 700 cm^{-1}. NMR ($CDCl_3$);

Table 1. Crystal data

Crystal system	monoclinic
Systematic absence	$h0l$ with odd l, $0k0$ with odd k
Space group	$P2_1/c$
a	14.30±0.08 Å
b	15.74±0.09
c	7.79±0.06
β	98°58′±45′
V	1731.0 Å^3
Z	4
ρ_c	1.257 g/cm^3
ρ_o	1.251

Table 2. Initial set

H	$\lvert E_h \rvert$	sign or symbol
2 2 7	3.88	+
3 11 3	3.42	+
11 2 1	3.25	+
5 8 4	2.87	a
$\bar{2}$ 0 6	2.85	b
$\bar{3}$ 6 3	2.77	c
$\bar{7}$ 6 5	2.78	d

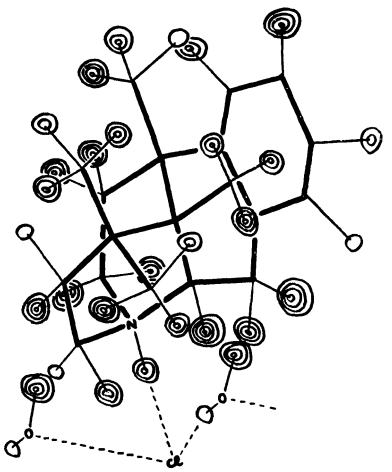

Fig. 1. Difference map projected along the b axis. The contours are drawn at equal intervals on an arbitrary scale.

Table 3. Final atomic parameters with their standard deviations (in parentheses).

(a) Atomic coordinates ($\times 10^4$) for non-hydrogen atoms

Atom	x/a	y/b	z/c	Atom	x/a	y/b	z/c
Cl	5392(6)	8702(6)	2959(12)	C (9)	2248(22)	474(20)	3192(40)
N	3512(19)	9613(18)	2087(34)	C (10)	1503(21)	9752(20)	2758(39)
O	4557(30)	6944(30)	4238(54)	C (11)	1753(24)	9243(23)	1218(41)
C (1)	1557(21)	9140(20)	4289(38)	C (12)	2795(25)	8949(24)	1460(43)
C (2)	754(24)	8668(23)	4557(47)	C (13)	3717(27)	229(26)	742(47)
C (3)	795(27)	8098(24)	5911(52)	C (14)	2857(28)	778(26)	216(47)
C (4)	1653(31)	7990(26)	7000(49)	C (15)	2383(25)	1143(23)	1754(47)
C (5)	2476(29)	8436(24)	6722(44)	C (16)	1997(26)	930(24)	4816(44)
C (6)	2417(23)	9011(21)	5370(38)	C (14)	454(25)	57(25)	2344(49)
C (7)	3319(24)	9491(23)	5202(42)	C (18)	1447(30)	1581(28)	910(62)
C (8)	3251(22)	68(21)	3662(39)	C (19)	3056(31)	1844(25)	2534(59)

(b) Anisotropic temperature factors ($\times 10^4$) for non-hydrogen atoms in the form of $\exp\{-(B_{11}h^2+B_{22}k^2+B_{33}l^2+B_{12}hk+B_{13}hl+B_{23}kl)\}$

Atom	B_{11}	B_{22}	B_{33}	B_{12}	B_{13}	B_{23}
Cl	34(1)	29(1)	158(2)	6(1)	−1(1)	−6(1)
N	29(2)	24(2)	86(6)	2(1)	14(2)	2(2)
O	96(4)	95(3)	264(13)	−44(3)	−36(6)	52(6)
C (1)	29(2)	18(1)	86(6)	1(1)	19(3)	−6(3)
C (2)	41(2)	22(2)	165(9)	−2(2)	31(3)	−3(4)
C (3)	55(3)	19(2)	198(10)	−2(2)	58(4)	0(4)
C (4)	70(3)	25(2)	134(9)	5(2)	50(4)	8(4)
C (5)	62(3)	24(2)	96(7)	2(2)	19(4)	6(3)
C (6)	37(2)	20(1)	68(6)	2(1)	10(3)	1(3)
C (7)	34(2)	28(2)	91(7)	0(2)	−3(3)	8(3)
C (8)	28(2)	24(2)	84(7)	1(1)	9(3)	2(3)
C (9)	27(2)	19(1)	91(7)	0(1)	7(3)	−2(3)
C (10)	26(2)	19(1)	86(7)	0(1)	8(3)	−5(3)
C (11)	35(2)	29(2)	82(7)	−1(2)	8(3)	−14(3)
C (12)	37(2)	30(2)	104(8)	0(2)	12(3)	−22(3)
C (13)	52(3)	36(2)	128(8)	4(2)	35(4)	19(4)
C (14)	49(3)	36(2)	118(8)	1(2)	20(4)	21(4)
C (15)	37(2)	21(2)	134(8)	0(2)	11(4)	11(3)
C (16)	43(2)	25(2)	106(8)	−1(2)	19(4)	−16(3)
C (17)	26(2)	31(2)	149(9)	4(2)	−1(4)	−3(4)
C (18)	43(3)	32(2)	222(13)	12(2)	9(5)	32(5)
C (19)	56(3)	23(2)	210(12)	−9(2)	10(5)	5(4)

δ 7.0～7.4(m, 4H, aromatic); 1.7～3.4 (m, 11H, methylene); 1.6 (s, 3H, methyl); 1.2 (s, 3H, methyl); 1.1 (s, 3H, methyl); 0.8(s, 3H, methyl).

Preparation of the Hydrochloride of III. To the ethereal solution of III was bubbled anhydrous hydrogen chloride gas at 0～5 °C for 10 minutes. The resulting crystals were filtered and recrystallized from acetone at room temperature. Colorless prisms, $C_{19}H_{27}N\cdot HCl\cdot H_2O$. Mp: 243.5～244.5 °C (uncorr.). Anal. Calc. for ($C_{19}H_{30}ONCl$): C(70.43); H (9.35); N(4.32); Cl(10.95%). Found: C(70.40); H(9.31); N(4.30); Cl(10.91%). IR: ν_{max}^{Nujol} 3500, 3450, 2500, 1640, 780, 740 cm^{-1}. $[\alpha]_D^{20°}$: 0°(c=1.316, MeOH).

The thermogravimetric analysis(TGA) scan showed a 5.20 % weight loss in the temperature region 65—149 °C (in comparison with 5.562% calculated for one water molecule of the monohydrate).

X-Ray Analysis of $C_{19}H_{27}N\cdot HCl\cdot H_2O$. Single crystals suitable for X-ray analysis were shaped to rectangular prism elongated along the c axis, by dissolving with methanol. The unit cell dimensions were calibrated with NaCl powder patterns superposed on Weissenberg photographs. The density was measured by flotation in a mixture of benzene and carbon tetrachloride. Crystal data was listed in Table 1. Crystal specimens of dimensions $0.44\times0.40\times0.51$ mm and $0.24\times0.29\times0.52$ mm were selected for data collection around the b and c axes respectively. Weissenberg photographs for layers of $h0l$-$h121$ and $hk0$-$hk5$ were taken with nickel-filtered Cu$K\alpha$ radiation. Intensities were esitmated visually, and corrected for Lorentz and polarization factors and for absorption. But no correction for spot shapes was applied. An absolute scale and overall temperature factor (B=3.122 Å^2) were determined by Wilson plot[2] and a total of 3211 independent reflections were obtained.

Solution and Refinement of the Structure

A symbolic addition procedure[3,4] was used to solve the phase problem. Normalized structure factors, $|E_h|$

TABLE 4. BOND DISTANCES AND ANGLES IN [III]

(a) Bond distances

	Distance (Å)		Distance (Å)		Distance (Å)		Distance (Å)
C (1)-C (2)	1.409	C (11)-C (12)	1.544	C (6)-C (7)	1.520	C (15)-C (9)	1.572
C (2)-C (3)	1.379	C (12)-N	1.491	C (7)-C (8)	1.495	C (9)-C (16)	1.545
C (3)-C (4)	1.388	N-C (8)	1.516	C (8)-C (9)	1.560	C (10)-C (17)	1.558
C (4)-C (5)	1.417	N-C (13)	1.491	C (9)-C (10)	1.558	C (15)-C (18)	1.558
C (5)-C (6)	1.381	C (13)-C (14)	1.505	C (10)-C (1)	1.526	C (15)-C (19)	1.526
C (6)-C (1)	1.393	C (14)-C (15)	1.575	C (10)-C (11)	1.530		

(b) Bond angles

	Angle (deg.)		Angle (deg.)
C (2)-C (1)-C (6)	119.8	C (8)-C (9)-C (16)	108.7
C (2)-C (1)-C (10)	120.4	C (16)-C (9)-C (15)	110.0
C (6)-C (1)-C (10)	119.8	C (16)-C (9)-C (10)	106.1
C (1)-C (2)-C (3)	121.2	C (10)-C (9)-C (15)	119.4
C (2)-C (3)-C (4)	118.4	C (8)-C (9)-C (15)	103.3
C (3)-C (4)-C (5)	121.5	C (9)-C (10)-C (1)	109.9
C (4)-C (5)-C (6)	119.1	C (1)-C (10)-C (17)	106.6
C (5)-C (6)-C (1)	120.0	C (17)-C (10)-C (11)	109.5
C (5)-C (6)-C (7)	116.1	C (11)-C (10)-C (9)	108.4
C (1)-C (6)-C (7)	123.9	C (9)-C (10)-C (17)	111.2
C (6)-C (7)-C (8)	114.9	C (1)-C (10)-C (11)	107.0
C (7)-C (18)-C (9)	112.3	C (10)-C (11)-C (12)	113.7
C (7)-C (8)-N	111.6	C (11)-C (12)-N	115.4
C (9)-C (8)-N	109.7	C (12)-N-C (8)	110.8
C (9)-C (8)-N	109.7	C (12)-N-C (8)	110.8
C (8)-C (9)-C (10)	109.1	C (12)-N-C (13)	115.2
C (8)-N-C (13)	111.1	C (18)-C (15)-C (9)	113.8
N-C (13)-C (14)	108.9	C (9)-C (15)-C (19)	109.9
C (13)-C (14)-C (15)	115.6	C (19)-C (15)-C (14)	104.4
C (14)-C (15)-C (18)	106.5	C (14)-C (15)-C (9)	111.4
C (19)-C (15)-C (18)	107.3		

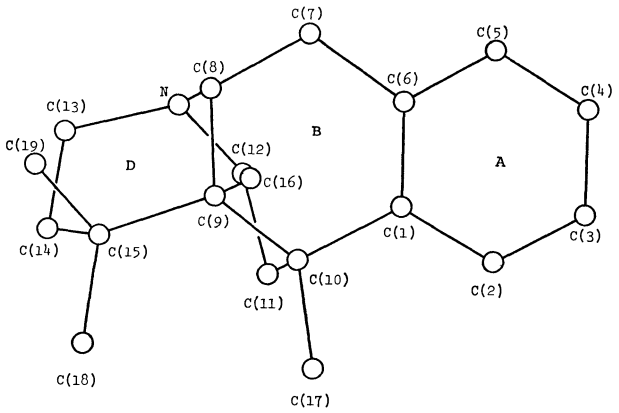

Fig. 2. The molecule viewed normal to the benzene ring plane.

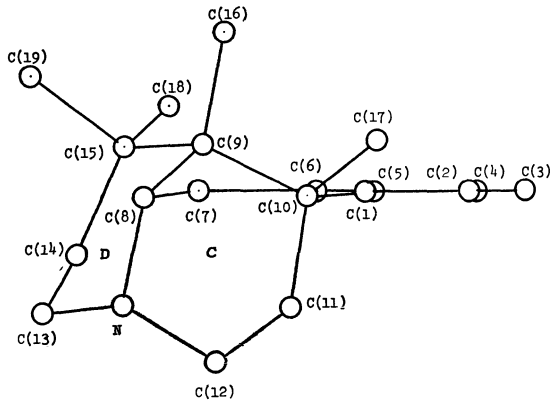

Fig. 3. The molecule viewed along the benzene ring plane.

were calculated and a set of Σ_2 relationships was tabulated. Three origin defining reflections and four reflections given symbols were selected by consideration of the magnitudes of the $|E_h|$ and the number of high probability Σ_2 relationships for each reflection, shown as in Table 2. The signs or symbols of 293 reflections out of 486 with $|E_h| \geq 1.4$ were determined by Σ_2 relationships. An E map was calculated based on these 293 signed E's with a=d=(+) and b=c=(−), and 21 of the 22 non-hydrogen atoms were located. The oxgen atom of water was revealed on a subsequent difference Fourier map. The R value, $\Sigma||F_o|-$

$|F_c|/\Sigma|F_0|$, at this stage was 0.469 with all 22 atoms assumed as carbon atoms. Refinement of the structure was done first by diagonal and then block-diagonal least-squares until $R=0.134$. A difference Fourier map using all reflections, indicated the positions of all 30 hydrogen atoms, which is shown in Fig. 1. The hydrogen atom coordinates used in further refinement, however, were calculated from geometrical considerations and were not refined. All hydrogen atoms were given isotropic temperature factors which were those of the atoms to which they are attached. The final R was 0.113 for all observed reflections. The final atomic parameters are shown in Table 3. Atomic scattering factors were taken from "International Tables for X-ray Crystallography".[5]

A list of the observed and calculated structure factors is kept by the office of the Chemical Society of Japan, (Document No. 7415). All calculations were done on a CDC 3600 and IBM 370 computers using the UNICS programs and those written by the present authors.

Results and Discussion

The molecule [III] consists of a four-ring system, the rings being named as A, B, C and D in Figs. 2 and 3. The molecular structure shown in Figures is one of the racemic paires. The bond distances and angles are shown in Table 4. The standard deviations in the distances and angles are estimated to be 0.049 Å and 2.8° respectively. The molecule of [III] is a new molecular skeleton, but it can be considered as a segment of morphine molecule,[6] since the corresponding parts (rings A, B and C) have the same configuration as the latter. The bond distances and angles are in good agreement with those in cyclazocine,[7] 2-allyl-2'-hydroxy-5,9-dimethyl-6,7-benzomorphan (AHDB).[8] The product [III] has analgesic activity as well as AHDB and cyclazocine. The averages of the aromatic C–C, saturated C–C and C–N bonds are 1.395, 1.541, and 1.499 Å respectively. The ring B attached to the benzene ring has a slightly distorted half-chair conformation with C(9) lying 0.66 Å above the benzene ring plane (Table 5). Two piperidine rings (C and D) assume a nearly regular chair form, and the conformations about the ten single bonds in C and D are staggered. The methyl groups C(16), C(17) and C(18) are in equatorial positions with re-

Table 5. The deviation of individual atoms from least-squares plane of the benzene ring

$(-0.334X+0.727Y+0.600Z=11.856)$

Where X, Y, and Z in Å are referred to the axes a*, b, c respectively.

Atom	Distance (Å)	Atom	Distance (Å)
C (1)	0.01	C (6)	0.00
C (2)	0.01	C (7)	0.03
C (3)	0.00	C (8)	0.05
C (4)	0.01	C (9)	0.66
C (5)	0.01	C (10)	0.03

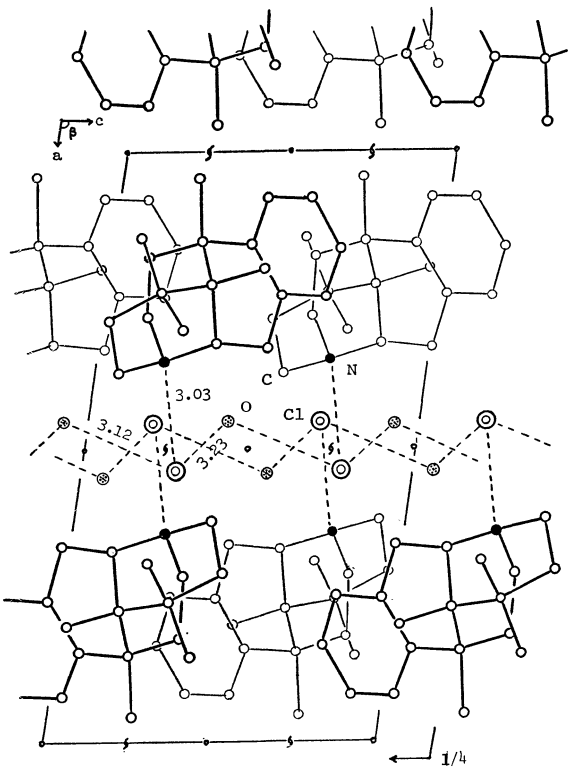

Fig. 4. Projection of the structure along the b axis.

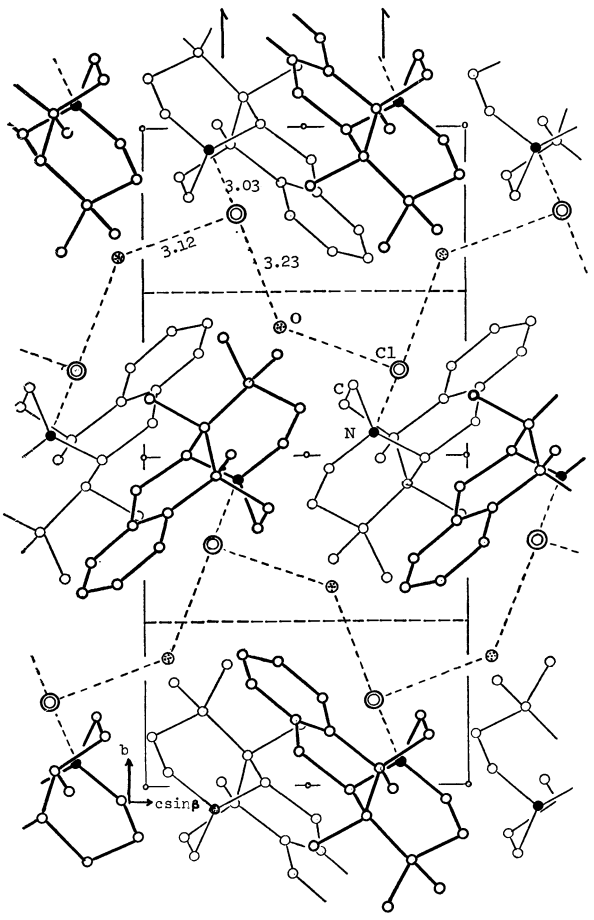

Fig. 5. Projection of the structure along the c axis.

TABLE 6. INTERMOLECULAR DISTANCES (<4 Å).

		Distance (Å)			Distance (Å)
C (2) ··· C (17)	d	3.76	C (17) ··· C (2)	d	3.76
C (3) ··· C (2)	b	3.98	C (17) ··· C (3)	d	3.77
C (3) ··· C (11)	b	3.93	C (19) ··· Cl	c	3.94
C (3) ··· C (17)	d	3.77	C (19) ··· O	f	3.88
C (4) ··· C (1)	b	3.81	Cl ····· C (7)	c	3.57
C (4) ··· C (2)	b	3.64	Cl ····· C (8)	c	3.59
C (4) ··· C (3)	b	3.86	Cl ····· C (16)	c	3.91
C (4) ··· C (11)	b	3.57	Cl ····· C (19)	e	3.94
C (4) ··· C (12)	b	3.52	Cl ····· C (13)	f	3.73
C (5) ··· C (12)	b	3.79	Cl ····· C (14)	f	3.87
C (7) ··· Cl	c	3.57	Cl ····· O	b	3.23
C (8) ··· Cl	c	3.59	O ····· C (13)	f	3.66
C (13) ··· Cl	f	3.73	O ····· C (19)	f	3.88
C (13) ··· O	f	3.66	N ····· Cl	a	3.03
C (14) ··· Cl	f	3.87	O ····· Cl	a	3.12
C (16) ··· Cl	c	3.91			

Symmetry code	Symmetry operation		
a	x	y	z
b	x	$\frac{3}{2}-y$	$\frac{1}{2}+z$
c	$1-x$	$2-y$	$1-z$
d	$-x$	$2-y$	$1-z$
e	$1-x$	$-\frac{1}{2}+y$	$\frac{1}{2}-z$
f	$1-x$	$2-y$	$-z$

spect to the piperdine ring C and/or D. C(19) is in axial positions with respect to D. Figures 2 and 3 show the molecule viewed normal to and parallel to the benzene ring plane respectively. These figures show that the benzomorphan nucleus is approximately shaped. Intermolecular distances (<4 Å) are shown in Table 6. Hydrogen bonds exist between the N^+ and Cl^- ions and between the Cl^- ion and the water molecule, so that endless chains along c-axis are formed as seen from Figs. 4 and 5.

The authors wish to express their thanks to professor Kenji Osaki of the Pharmaceutical Department of Kyoto Univ. for discussions about this manuscript and to the staffs of Sumitomo Chemical Computer Center for computing.

References

1) T. Kametani and K. Kigasawa, *Yuki Gosei Kagaku Kyokai Shi* **29**, 227 (1971), T. Kametani *et al.*, *J. Heterocyclic Chem.* **6**, 43 (1969), N. F. Albertson and W. F. Wetterau, *J. Med. Chem.* **13**, 302 (1970), T. Kametani *et al.*, *ibid.*, **12**, 694 (1969), Sumitomokagaku, Jap. Pat. 45—31664 (1970), Ger. Pat. 1,927,724 (1970), T. Kametani *et al.*, *J. Heterocyclic Chem.* **9**, 1057, 1065 (1972), **8**, 769 (1971).

2) A. J. C. Wilson, *Nature*, **50**, 151 (1942).

3) I. L. Karle and J. Karle, *Acta Crystallogr.*, **16**, 969 (1963), **21**, 894 (1966).

4) W. H. Zachariasen, *ibid.*, **5**, 68 (1952).

5) "International Tables for X-ray Crystallography", vol. III, Kynoch Press, Birmingham (1962), pp. 202—203.

6) M. MacKay and D. C. Hodgkin, *J. Chem. Soc.*, **1955** 3261.

7) I. L. Karle, R. D. Gilardi, A. V. Fratini, and J. Karle, *Acta Crystallogr.*, **B25**, 1469 (1969).

8) W. Fedeli, G. Giacomello, S. Cerrini, and A. Vaicago, *J. Chem. Soc., B*, **1970**, 1190.

The Crystal Structure of Pyrazinic Acid

Fusao TAKUSAGAWA, Taiichi HIGUCHI, Akira SHIMADA,†
Chihiro TAMURA,* and Yoshio SASADA**

Department of Chemistry, Faculty of Science, Osaka City University, Sugimoto-cho, Sumiyoshi-ku, Osaka 558
**Central Research Laboratories, Sankyo Co., Ltd., Hiromachi, Shinagawa-ku, Tokyo 140*
***Laboratory of Chemistry for Natural Products, Tokyo Institute of Technology, Ookayama, Meguro-ku, Tokyo 152*

(Received December 27, 1973)

The crystal structure of pyrazinic acid has been determined by X-ray diffraction method. The crystal is orthorhombic, space group $Pna2_1$, $a=11.352$, $b=7.363$, $c=6.454$ Å, and $Z=4$. The structure was solved by inspecting the sharpened Patterson map. The final R value is 6.4% for all observed reflections. The molecule does not take a zwitter ion, but a neutral form. The dimensions of the pyrazine ring are close to those of pyrazine. Each molecule is joined, through the O–H···N hydrogen bond with distance of 2.669 Å, to two neighboring molecules forming the chain. These chains are linked by the weak C–H···O hydrogen bond to form the sheet parallel to the (0 0 1) plane. This hydrogen bonding scheme is quite similar to that of nicotinic acid. The hydrogen bonding type found in nicotinic acid is considered energetically favored more than that found in picolinic acid.

This work is a part of serial studies on the O–H···N hydrogen bonding in solids. The crystal structures of picolinic acid (I)[1] and nicotinic acid (II)[2] are quite different from each other. Each picolinic acid molecule is joined by two kinds of hydrogen bonds,

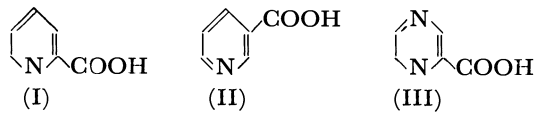

(I) (II) (III)

O—H—O and N—H—N, to two neighboring molecules forming the chain. On the other hand, the O–H···N hydrogen bonds between the carboxyl group and the pyridine ring link the nicotinic acid molecules to form an endless chain.

Pyrazinic acid(III) has a similar framework and isoelectronic structure to both of (I) and (II) and hence might form either types of hydrogen bonds mentioned above. The crystal data of (III),[3] however, indicate that it is isomorphous with neither of crystals (I) nor (II). Therefore, elucidation of the effect of nitrogen atoms on the hydrogen bond formation in solids should be interesting.

Experimental

The crystals were obtained in the form of light yellow prisms by recrystallization from a mixed solution of water and ethanol. Weissenberg photographs showed that the space group is $Pna2_1$ or Pnam(absent spectra: $0kl$ when $k+l$ is odd, $h0l$ when h is odd). The cell dimensions were measured from zero-layer photographs taken with a double radius Weissenberg camera($R=57.296$ mm). They are given, along with other crystal data, in Table 1. One of the crystals was shaped to a sphere with an average diameter of 0.4 mm. The intensity data were collected for the 0—6 layers around the c axis and for the 0—5 layers around the b axis using the equi-inclination integrating Weissenberg technique, with Cu$K\alpha$ radiation. The intensities were estimated visually by comparison with an intensity scale; 662 independent reflections were obtained. Absorption and extinction corrections were not applied.

† Deceased August 5, 1973.

Table 1. Crystal data for pyrazinic acid

Molecular formula	$C_5H_4N_2O_2$
Molecular weight	124.04
Crystal system	Orthorhombic
Space group	$Pna2_1$
Cell dimensions:	$a=11.352\pm0.001$ Å
	$b=7.363\pm0.001$
	$c=6.454\pm0.001$
	$V=539.43$ Å^3
Z	4
Density(calcd)	1.528 g/cm^3
Density(obsd)	1.53
$F(000)$	256
Radiation	Cu$K\alpha$($\lambda=1.5418$ Å)
Linear absorption coefficient	12.01
Number of independent reflections	662

Structure Determination and Refinement

The structure was solved by inspecting the sharpened Patterson map. Successful solution of the structure led to assignment of $Pna2_1$ as the appropriate space group. All the hydrogen atoms were found in a difference Fourier map. The structural parameters of the atoms including isotropic hydrogen were refined by a full-matrix least-squares, minimizing the function $\Sigma w(F_o-F_c)^2$, where

$$w = 1.0/[10(|F_o|-2.0)^2 + 1.0] \text{ for } |F_o| \leqq 2.0$$

and

$$w = 1.0/[(|F_o|-2.0)^2 + 1.0] \text{ for } |F_o| \geqq 2.0$$

The final agreement factors were:

$$R = \Sigma||F_o|-|F_c||/\Sigma|F_o| = 0.064$$
$$R_w = [\Sigma w(|F_o|-|F_c|)^2/\Sigma w|F_o|^2]^{1/2} = 0.090.$$

The atomic scattering factors used were those listed in the International Tables for X-ray Crystallography[4] for C, N, and O atoms, and those of Stewart *et al.*[5] for H atom. The observed and calculated structure factors are listed in Table 2.*** The fractional co-

*** Table 2 has been submitted to, and is kept by the office of the Chemical Society of Japan, 1-5, Kanda-Surugadai, Chiyoda-ku, Tokyo (Document No. 7412).

Table 3. The final parameters and their estimated standard deviations (in parentheses)

The coordinates of the non-hydrogen atoms have been multiplied by 10^4; those of the hydrogen atoms, by 10^3. The anisotropic thermal factors of non-hydrogen atoms are of the form of $\exp(-B_{11}h^2\cdots-B_{12}hl\cdots)$, and have been multiplied by 10^4. For the hydrogen atoms, the values are isotropic thermal factors B(Å^2).

Atom	x	y	z	B_{11}	B_{22}	B_{33}	B_{12}	B_{13}	B_{23}
N(1)	4360(2)	3485(3)	0(10)	64(2)	129(4)	173(5)	8(4)	20(11)	−6(15)
C(2)	4209(2)	5288(3)	130(10)	54(2)	129(4)	108(5)	−2(4)	15(10)	−17(15)
C(3)	3091(2)	6066(4)	89(14)	52(2)	132(4)	165(6)	1(4)	39(13)	55(16)
N(4)	2119(2)	5039(3)	119(10)	53(2)	146(5)	227(7)	−10(4)	−58(11)	−60(16)
C(5)	2270(2)	3237(4)	45(11)	70(2)	138(5)	205(7)	−23(5)	9(15)	34(21)
C(6)	3385(3)	2471(4)	97(14)	73(2)	132(4)	229(7)	−15(4)	−29(14)	121(18)
C(7)	5294(2)	6434(4)	21(12)	51(2)	143(5)	145(6)	8(4)	8(11)	−102(18)
O(1)	6275(2)	5782(2)	124(13)	51(1)	143(4)	245(6)	8(3)	37(11)	54(12)
O(2)	5068(2)	8191(3)	41(10)	57(2)	115(4)	364(7)	1(3)	−21(14)	−43(18)
H(1)	301(3)	735(4)	−56(6)	2.5(7)					
H(2)	163(4)	243(5)	−46(7)	3.2(9)					
H(3)	352(3)	111(5)	59(6)	1.9(7)					
H(4)	569(4)	896(5)	69(8)	3.6(9)					

ordinates and thermal parameters are listed in Table 3.

Results and Discussion

Molecular Structure. Figure 1 shows the difference Fourier map viewed along the c axis, in which there is no high peaks except for those due to the hydrogen atoms. Figure 2 shows the thermal ellipsoids of atoms, drawn with the 74% probability level. The bond lengths and angles are given in Fig. 3.

The pyrazinic acid molecule can take either of the following three forms;

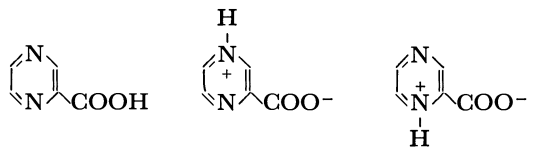

(A) (B) (C)

From the position of the hydrogen atom in the difference Fourier map, however, it is evident that the molecule takes the neutral form (A) in the crystal. This is also concluded from the difference of 0.104(3) Å between the C(7)–O(1) and C(7)–O(2) bond lengths and the C(3)–N(4)–C(5) bond angle of 117.0(2)° (the values in parentheses denote the e.s.d.'s in the last digits).

A pyrazinic acid molecule is approximately planar with a maximum deviation of 0.044 Å, but close examination reveals that the pyrazine ring takes a chair form; the planes of C(2), N(1) and C(6) and of C(3), N(4) and C(5) make the dihedral angles of 7.2° and C(3), respectively, with the least-squares plane of C(2), 4.0°, C(5) and C(6). The least-squares planes and displacements of the atoms from them are given in Table 4.

The dimensions of the pyrazine ring are close to those of pyrazine.[7] The substitution of a carboxyl group at the C(2) atom may cause the small differences between the N(1)–C(2) and N(1)–C(6) bond lengths and between the C(2)–C(3) and C(5)–C(6) bond lengths. They are quite compatible with the difference in the π-bond orders calculated by the CNDO/2 method,[6] shown in Fig. 4. A small difference between the C(2)–N(1)–C(6) and C(3)–N(4)–C(5) bond angles may be

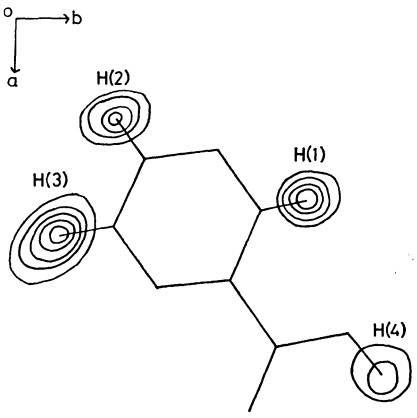

Fig. 1. A composite drawing of the electron density associated with the hydrogen atoms. The contours are at intervals of 0.1 e·Å^{-3}, beginning with the 0.2 e·Å^{-3}.

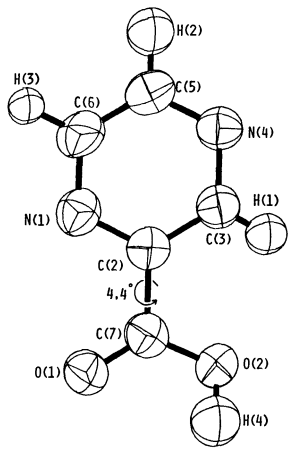

Fig. 2. The thermal ellipsoids of atoms.
The numeral indicates the dihedral angle between the planes of the pyrazine ring and the carboxyl group.

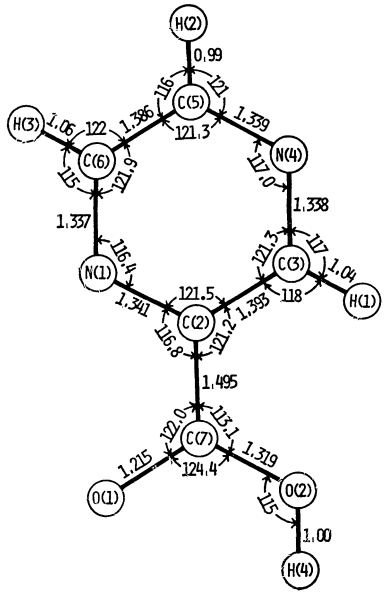

Fig. 3. Dimensions of pyrazinic acid molecule.
The estimated standard deviations are as follows: X-X=0.003~0.004 Å, X-H=0.03~0.04 Å, X-X-X=0.2°, X-X-H=2, where X and H represent the non-hydrogen atom and the hydrogen atom, respectively.

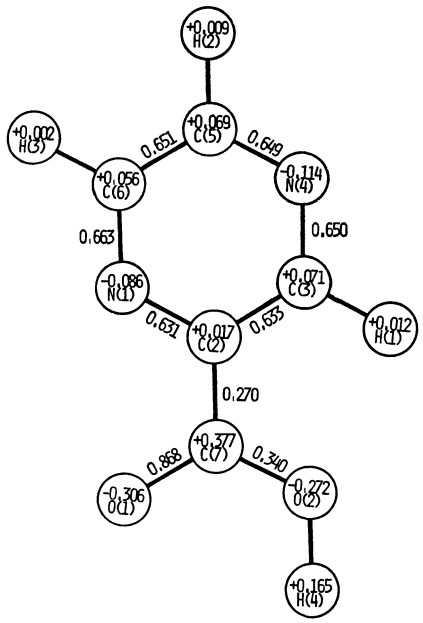

Fig. 4. The π-bond orders and net charges calculated by the CNDO/2 method.

explained by the fact that the N(4) atom participates in a hydrogen bond, while the N(1) atom does not. The 4.4(2)° difference between the N(1)–C(2)–C(7) and C(3)–C(2)–C(7) bond angles is significant judging from their estimated standard deviations. Similar differences are found in dipicolinic acid[8] and orotic acid.[9] When the hydroxyl oxygen of the carboxyl group at α-position of pyridine, pyrazine or pyrimidine ring is *s-cis* to the nitrogen atom in the ring, these two bond angles are approximately equal to each other,

Table 4. Deviations (Å) from the least-sequares planes

Plane (I) defined by six non-hydrogen atoms of a pyrazine ring

$$0.0058X-0.0146Y+0.9999Z=0.0271$$

Plane (II) defined by four carbon atoms of a pyrazine ring

$$-0.0242X-0.0011Y+0.9997Z=-0.0342$$

where X, Y, and Z are in Å.

Atom	(I)	(II)	Atom	(I)	(II)
N(1)	−0.036	−0.088	O(1)	0.032	−0.063
C(2)	0.028	−0.002	O(2)	−0.055	−0.085
C(3)	−0.015	0.002	H(1)	−0.45	−0.42
N(4)	0.009	0.049	H(2)	−0.40	−0.31
C(5)	−0.018	−0.002	H(3)	0.37	0.32
C(6)	−0.031	0.002	H(4)	0.36	0.32
C(7)	−0.048	−0.103			

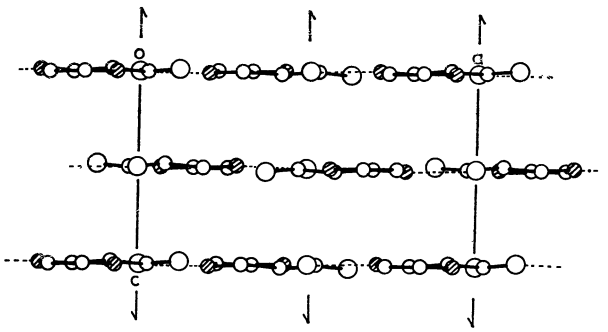

Fig. 5. A view of the crystal structure down the *b* axis. The hydrogen bonds are shown by broken lines.

but when it is *s-trans*, they are significantly different from each other.[1,8-11] The dihedral angle between the planes of the pyrazine ring and the carboxyl group is 4.4° and its direction is shown in Fig. 2.

Molecular Arrangement and Hydrogen-bond System. Figures 5 and 6 show the molecular arrangement viewed along the *b* and *c* axes, respectively. The molecules are arranged in layers parallel to the (001) plane with a spacing of 3.227 Å. The zig-zag chains along the *c* axis, consisting of the molecules linked by the O–H···N hydrogen bonds, on the same plane are joined by the weak C–H···O hydrogen bonds to form a sheet. There is no hydrogen bond between the sheets, but they are packed only by the van der Waals forces. This hydrogen bonding scheme is quite similar to that of nicotinic acid and the distance of the hydrogen bond of 2.669(3) Å is approximately equal to the 2.665 Å of nicotinic acid. Although the positions of hydrogen atoms are not determined in the crystal structure analysis of nicotinic acid, the difference between the two C–O bond lengths of the carboxyl group and the C–N–C bond angle of the pyridine ring suggest the existence of O–H···N hydrogen bond. However, the stacking of the pyrazinic acid molecule is considerably different from that of nicotinic acid, as shown in Fig. 7. There are two short contacts, 3.238(5) and 3.265(5)

Table 5. Distances of hydrogen bonds and short contacts

a) Closest contact between the layers (symmetry operation applied is given in parentheses)

Pyrazinc acid		Nicotinic acid	
N(1)···C(7)	$(1-x, 1-y, 1/2+z)$ 3.265(5) Å	C(6)···O(2)	3.405 Å
N(1)···C(7)	$(1-x, 1-y, -1/2+z)$ 3.238(5)	C(7)···N(4)	3.413
N(1)···O(1)	$(1-x, 1-y, -1/2+z)$ 3.273(5)		

b) Within a layer

Pyrazinc acid		Nicotinic acid
X—H···Y	X···Y	X···Y
O(2)-H(4)···N(4)	2.669(3) Å	2.665 Å
C(3)-H(1)···O(1)	3.104(3)	3.265
C(5)-H(2)···O(1)	3.168(3)	3.259

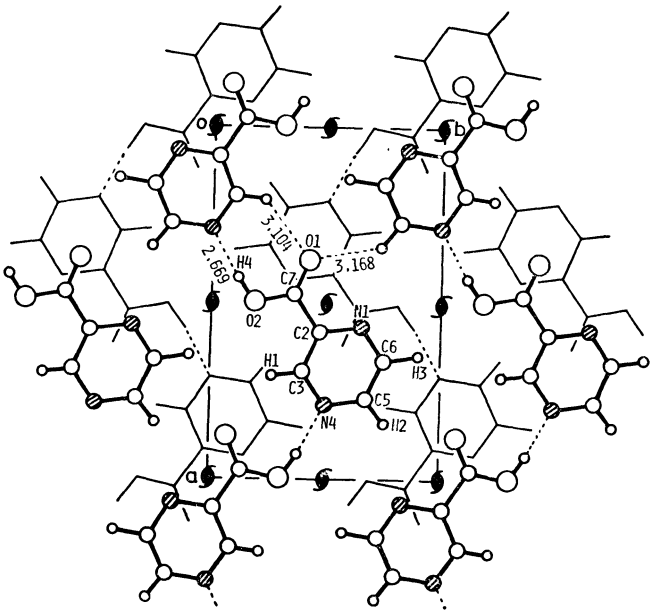

Fig. 6. A view of the crystal structure down the *c* axis, showing the relative orientation of the molecules in two adjacent layers parallel to the (001) plane. The hydrogen bonds are shown by broken lines.

Å, between the N(1) and C(7) atoms in the different sheets. The net charges on the N(1) and C(7) atoms are −0.086 and +0.377, respectively; these values indicate some electrostatic attractive-forces between them. On the other hand, nicotinic acid molecule does not contain such electronegative atom. The closest interlayer contacts of pyrazinic acid are listed, along with those of nicotinic acid, in Table 5.

As for the hydrogen bond between the carboxyl group and the nitrogen atom in the pyridine ring, the $\overset{+}{N}$–H···$\bar{O}$ hydrogen bond is found in all the crystal structures of pyridine-carboxylic acids.[11-13] As mentioned above, hydrogen bonding types of pyrazinic acid and nicotinic acid are not the $\overset{+}{N}$–H···$\bar{O}$, but the O–H···N. This fact may be explained as follows: The carbonyl oxygen atom O(1) is surrounded with two hydrogen atoms, H(1) and H(2), as illustrated in Fig. 8. The distances and angles are: O(1)···H(1)=2.44(4) Å, O(1)···H(2)=2.43(4) Å, C(7)=O(1)···H(1)=120(2)°, C(7)=O(1)···H(2)=

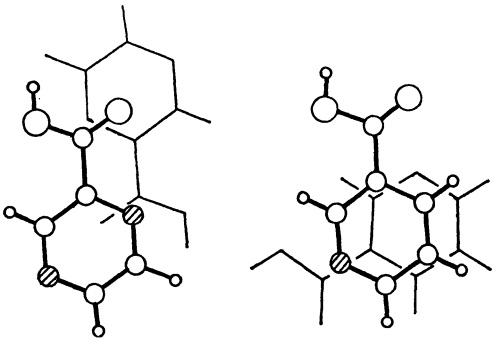

(I) Pyrazinic acid (II) Nicotinic acid

Fig. 7. Stackings of pyrazinic acid and nicotinic acid molecules.

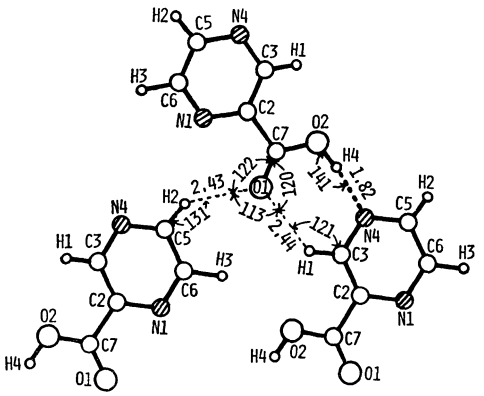

Fig. 8. Short intermolecular contacts within a molecular layer. The O-H···N and C-H···O hydrogen bonds are illustrated by heavy and thin broken lines, respectively.

122(2)°, and H(1)···O(1)···H(2)=113(5)°. These angles indicate that the H(1), H(2), O(1), and C(7) atoms are nearly on a plane. Since the O(1) atom takes the sp^2 hybrid orbitals, the two lone pairs of O(1) atom will interact with the H(1) and H(2) atoms. These may be considered as the weak C–H···O hydrogen bonds. If the H(4) atom moves from the O(2) atom to the N(4) atom, the O(1) atom no longer would take the sp^2 hybrid orbitals and the lone pairs would not be directed toward H(1) and H(2), so that the C–H···O hydrogen bonds are not formed. Therefore,

the C–H···O hydrogen bond formation and protonation on the nitrogen atom are competitive. The crystal structures of pyrazinic acid and nicotinic acid suggest that the formation of the two weak C–H···O hydrogen bonds is energetically favored more than the formation of zwitter ion.

The N(4) atom takes part in the hydrogen bond, while the N(1) atom is free from it. This may be explained by the facts that the N(4) atom is more electronegative than the N(1) atom, and that the N(1) atom is shielded by the carboxyl group from the donor group for the hydrogen bond. The melting point of nicotinic acid is higher than that of picolinic acid. These two experimental facts indicate that the hydrogen bonding type found in nicotinic acid is energetically favored more than that found in picolinic acid.

Computer Programs. All the calculations were performed on a FACOM 270–30 computer at the Computer Center of Osaka City University, using the UNICS[14] programs, SCALE(film factor, Lp and layer scaling),[15] BOND(bond length, bond angle and least-squares plane),[16] TE-I(thermal ellipsoid),[17] and CNINDO (CNDO and INDO calculations).[6]

The authors are greatly indebted to Dr. Kichisuke Nishimoto and to Mr. Ken Hirotsu of Osaka City University for their useful advice on the theoretical calculation and their valuable discussions and suggestions during this investigation.

References

1) F. Takusagawa and A. Shimade, *Chem. Lett.*, **1973**, 1089.
2) W. B. Wright and G. S. D. King, *Acta Crystallogr.*, **6**, 305 (1953).
3) C. Tamura, H. Kuwano, and Y. Sasada, *ibid.*, **14**, 693 (1961).
4) "International Tables for X-ray Crystallograpy," Vol. III, Kynoch Press, Birmingham (1962).
5) R. F. Stewart, E. R. Davidson, and W. T. Simpson, *J. Chem. Phys.*, **42**, 3175 (1965).
6) J. A. Pople and D. L. Bereridge, "Approximate Molecular Orbital Theory," McGraw-Hill Book Co., New York (1970).
7) P. J. Wheatley, *Acta Crystallogr.*, **10**, 182 (1957).
8) F. Takusagawa, K. Hirotsu, and A. Shimada, This Bulletin, **46**, 2020 (1973).
9) F. Takusagawa and A. Shimada, *ibid.*, **46**, 2011 (1973).
10) F. Takusagawa and A. Shimada, *Chem. Lett.*, **1973**, 1121.
11) F. Takusagawa, K. Hirotsu and A. Shimada, This Bulletin, **46**, 2372 (1973).
12) F. Takusagawa, K. Hirotsu, and A. Shimada, *ibid.*, **46**, 2292 (1973).
13) F. Takusagawa, K. Hirotsu, and A. Shimada, *ibid.*, **46**, 2669 (1973).
14) "The Universal Crystallographic Computing System-(I)," ed. by T. Sakurai, The Crystallographic Society of Japan (1967).
15) H. Yoshioka, K. Hirotsu, and F. Takusagawa, unpublished work.
16) H. Yoshioka, unpublished work.
17) F. Takusagawa, unpublished work.

Studies of Ruthenium Complexes. VII.[1] Photochemical Reactions of *cis*-Dihalogenotetraammineruthenium(III) Complexes in Aqueous Solutions

Akira OHYOSHI, Noriyuki TAKEBAYASHI, Yutaka HIROSHIMA, Kenichiro YOSHIKUNI, and Kazuhiko TSUJI

Department of Industrial Chemistry, Faculty of Engineering, Kumamoto University, Kumamoto 860

(Received September 13, 1973)

Studies have been made of the photochemistry of *cis*-dihalogenotetraammineruthenium(III) in aqueous solutions. For the *cis*-dichlorocomplex, no photochemical reaction has been observed by the irradiation of the visible light region. For *cis*-dibromo- and *cis*-diiodo-complexes, a simple aquation of halide ligand seems to occur in a solution with a pH lower than 2.5. The typical values of the quantum yields for the *cis*-$[RuX_2(NH_3)_4]^+ + H_2O \xrightarrow{h\nu}$ *cis*-$[RuX(OH_2)(NH_3)_4]^{2+} + X^-$ reaction were 0.27×10^{-2} (382 nm light) and 0.82×10^{-2}(408 nm light) for dibromo- and dichloro-complexes respectively. The quantum yield was dependent on the wavelength of light, but was independent of the concentrations of halide and hydrogen ions. The quantum yield seems to depend on the oxidizability of the ligand or on probability of the deactivation process in the primary excited state. In accounting for the low quantum yield, it seems most probable that the photoexcited complex species is converted to the ground state by non-radiative transitions.

Although there have been many studies of the photochemistry of 3d metal complexes,[2-7] those of 4d metal analogs, in particular of the ruthenium complexes, are scarce. A recent photochemical study of hexaammine- and chloropentaammineruthenium(III)[8] has demonstrated that both of the complex ions are largely unreactive when their ultraviolet absorption bands are irradiated and that the photoinduced aquation of the ammine ligand can be established for each complex with a low quantum yield ($\phi<0.1$). The detectable photoredox process has not been observed by the irradiation of light in the region of charge transfer from ligand to metal(CTTM-band). Qualitatively, it might be expected that absorption in the region of an electron-transfer band would lead to the oxidation-reduction process, while the absorption in the region of a ligand-field band would cause a substitution reaction of the ligand. This photochemical inertness of the t_{2g}^6 ruthenium(III) complexes has been interpreted on the assumption of a small distortion at the excited states with a t_{2g}^5 electronic configuration and on the assumption that the CTTM states are lower in energy than those of the d-d excited states.

In the present study, the photoaquation rates of *cis*-dihalogenotetraammineruthenium(III) complexes were determined as a function of the hydrogen and halide ion concentrations, and the dependence of the quantum yield on the wavelength of the incident radiation was investigated. The results were then discussed in comparison with those of the hexaammine and chloropentaammine complexes of ruthenium(III) and with those of the analogous complexes of cobalt(III) and chromium(III).

Experimental

Materials. All the chemicals used were of a reagent grade. The *cis*-dihalogenotetraammineruthenium(III) halogenides were prepared by the method of Gleu and Breuel.[9] These compounds were analyzed by the usual elemental analysis and were confirmed by means of their spectra.

Photolysis Procedures. The photolyses were performed using a JASCO CRM-FA spectral irradiator equipped with a 2 kW Xenon arc lamp. A known volume of a sample solution in a rectangular quartz cell with a 1-cm light path length was kept at 25 °C; purified argon gas was passed through the solution during irradiation to avoid an appreciable secondary photolysis or inner filter effects. The solution was then irradiated for a preset time period by monitoring the light flux using a JASCO RMI-1 integrating radiometer equipped with a thermopile. The absorbed light intensities (I_a) were determined using a ferrioxalate actinometer[10] ($\lambda<400$ nm) and a reineckate actinometer[11] ($\lambda>400$ nm). The concentration of the reactant was determined from the absorbance of the first absorption band at 352 nm (*cis*-dichlorocomplex), 441 nm (*cis*-dibromocomplex), and 646 nm (*cis*-diiodocomplex) using a Hitachi 124 spectrophotometer. The pseudo first-order plot gave a straight line for about 120 min at an irradiation rate of 2.5×10^3 photons l^{-1} min^{-1}. The initial slope of this plot was used to calculate the initial rate of complex decomposition. This rate was used along with the I_a values to calculate the quantum yield.

Results and Discussion

Qualitative Observation of Photoreaction. The progressive changes in the absorption spectrum are shown in Figs. 1 and 2 for two kinds of complexes in acidic and neutral solutions. The two absorption bands in the spectra for the original complexes can be assigned to the charge-transfer absorptions from ligand to metal ($\pi\rightarrow t_{2g}$)[12] from the facts that; (1) their molar absorption coefficients take large values (10^3 M^{-1} cm^{-1}); (2) the plot of the wave number (ν_{max}) of the CT band from ligand to metal *vs.* the redox potential value of the coordinated halide ligand indicates a linear relationship (Fig. 3); and (3) the ν_{max} values obtained from the electronic spectra of the complexes are in agreement with those calculated by Jørgensen's empirical formula.[13]

The changes in the absorption spectra in the neutral solution appear to be different from those in the acidic solutions. The first and second bands of the complexes decrease, and a new peak appears in the UV region. The wavelength of this peak (291 nm) is very close to that of the hydroxo-complex (293 nm) resulting from the base hydrolysis of the corresponding initial complex. Thus, the photochemical reactions presumably proceed as follows:

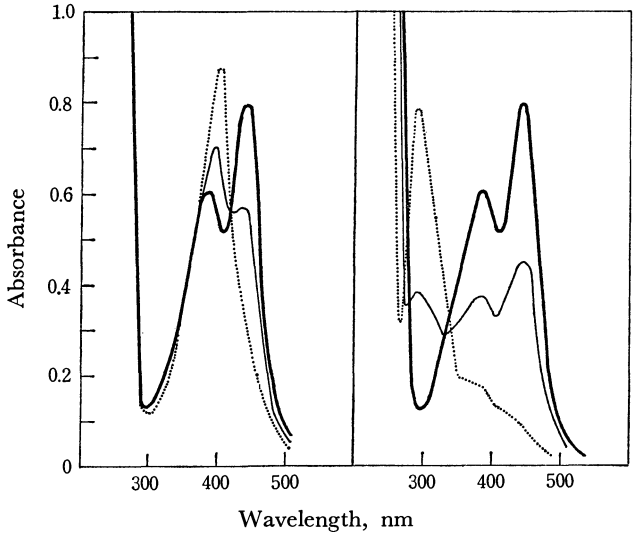

Fig. 1. Spectral change of *cis*-dibromotetraammineruthenium(III) in the photochemical reaction, at pH 2.0 (left), 7.0 (right), 434 nm light irradiation (2.5×10^3 photons l^{-1} min^{-1}), 25 °C.
——: initial, ——: intermediate (60 min), ·····: final (300 min). [complex]: 5×10^{-4} M, temp: 25 °C.

$$[RuX_2(NH_3)_4]^+ + 2OH^- \xrightarrow{h\nu} [Ru(OH)_2(NH_3)_4]^+ + 2X^- \quad (1)$$

On the other hand, the changes in the spectra in acidic solutions differ from those in the above case, *i.e.*, the first band decreases with the increase in the second band with the shift toward the longer wavelength as the reaction proceeds. The final spectra (Figs. 1 and 2) show a new peak different from those of the initial complex. In separate experiments where the acid hydrolysis of *cis*-dihalogenotetraammineruthenium(III) were carried out in the dark, similar changes in the absorption spectra were observed throughout the reactions. Similar observations have been reported in the aquation of dichlorobisethylenediammineruthenium(III),[14] and in the study of the preparation of dichlorotetraammine- and chloroaquotetraammineruthenium(II) complexes.[15] All the observations of the changes in the absorption spectrum gave evidence for the formation of a partially-aquated ruthenium(III) complex species, *cis*-$[RuX(OH_2)(NH_3)_4]^{2+}$. Thus, we concluded that the photoreaction took place mainly *via* the aquation process in the acidic solution:

$$cis\text{-}[RuX_2(NH_3)_4]^+ + H_2O \xrightarrow{h\nu} cis\text{-}[RuX(OH_2)(NH_3)_4]^{2+} + X^- \quad (2)$$

Determination of the Variables Affecting the Photoreaction Rate. Several experiments with various reaction parameters of the photolysis system were carried out in order to investigate their effects on the reaction rate or the quantum yield. The photoreaction rates were determined by measuring the decrease in the absorbance at the first absorption band of the respective complexes under different conditions of light irradiation. The plots of log C_t/C_0 *vs.* the reaction time are exemplified in Fig. 4, where C_t and C_0 denote the con-

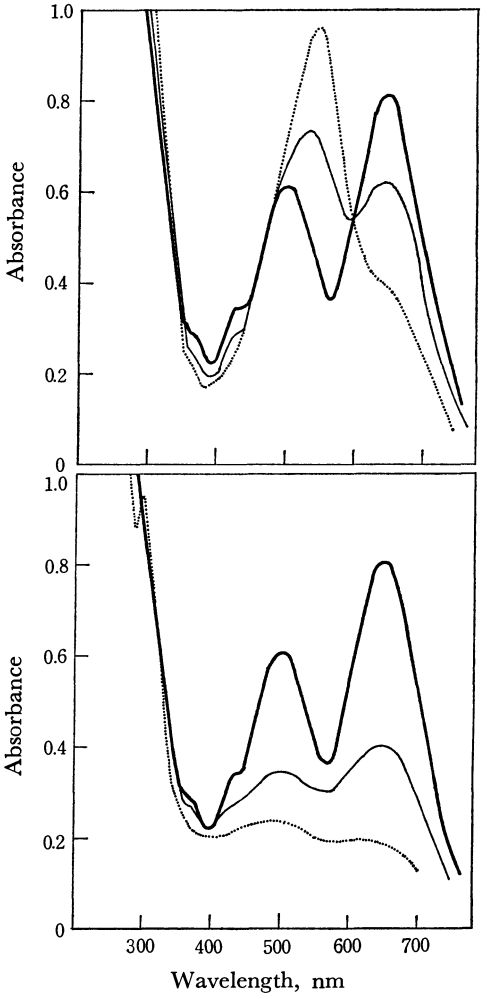

Fig. 2. Spectral change of *cis*-diiodotetraammineruthenium(III) in the photochemical reaction, at pH 2.0 (upper), 7.0 (bottom), 512 nm light irradiation (2.5×10^3 photons l^{-1} min^{-1}), 25°C.
——: initial, ——: intermediate (60 min), ·····: final (300 min).

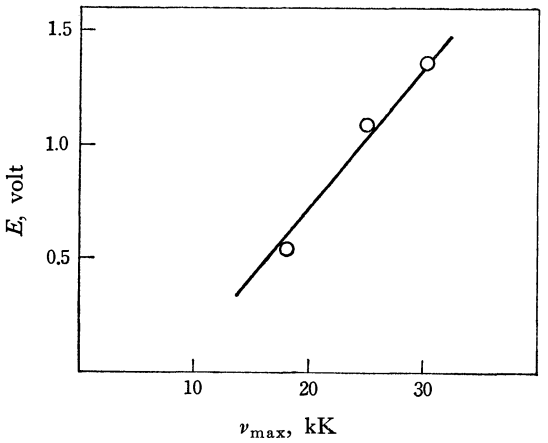

Fig. 3. Relationship between ν_{max} and oxidation potential for halide ligand.

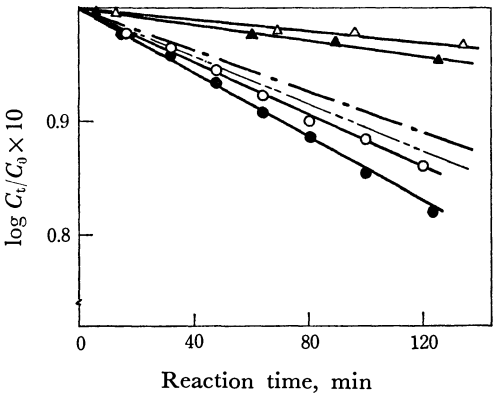

Fig. 4. Plots of $\log C_t/C_0$ *vs.* reaction time at 25 °C, pH 2.2, C_0: initial concentration of complex (5.0×10^{-4} M), C_t: concentration at the reaction time, t. [Complex]: 5×10^{-4} M, temp: 25 °C
cis-Dibromotetraammine complex, at 434 nm light irradiation
●: apparent reaction, ▲: thermal reaction
———: net photoreaction
cis-Diiodotetraammine complex, at 512 nm light irradiation
○: apparent reaction, △: thermal reaction
——: net reaction

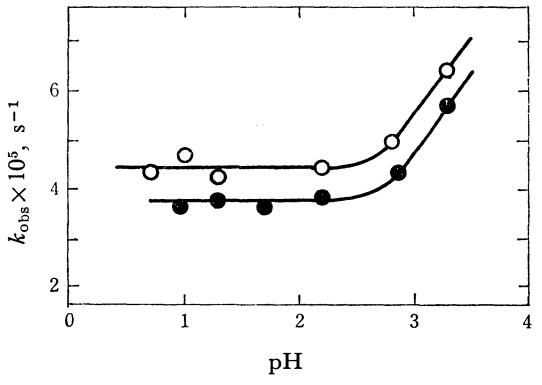

Fig. 5. Effect of pH on the photoreaction rate constant at 434 nm (dibromo-complex) and at 512 nm (diiodo-complex) light irradiation, 25 °C, [complex]: 5.0×10^{-4} M.
-○- dibromo-complex, -●- diiodo-complex

centrations of the reactant complex at the reaction time t and at zero, respectively. The straight lines indicate that the photoaquation and thermal reaction are both first-order with respect to the complex concentration under given reaction conditions. The thermal reactions are somewhat observed at 25 °C; therefore, the net photoreaction rates were determined by subtracting these contributions. The photoreaction of the *cis*-dichlorotetraammine complex was found only in the case of ultraviolet light irradiation.

No effects of the halide-ion concentration or of the ionic strength on the reaction rate have been observed in acidic solutions. Three facts indicate that neither the halide ion nor a charged particle is concerned with the rate-determining step.

As is shown in Fig. 5, the effect of pH on the reaction rate has not been observed in a pH range lower than 2.2, while higher than 2.2, the apparent reaction rate increased with an increase in the pH values. Although this fact has not yet been investigated in detail, it may be considered that the base hydrolysis participates to some extent in the aquation reaction. The spectral observations provide evidence for this consideration (Figs. 1 and 2).

Quantum Yield for the Photochemical Aquation Reaction. The quantum yield for the photochemical aquation was determined with different light wavelengths. The results are given in Table 1, along with those of analogous and reference reactions and along with the available data on the thermal aquation reaction rates. The quantum yields for the photoaquation of *cis*-dihalogenotetraammineruthenium(III) complexes are dependent on the light wavelength and are small compared with those for the ammine ligand aquation of the hexaammine- and chloropentaammineruthenium-(III).[8] It was also found that the *cis*-dichlorotetraammine complex was photochemically unreactive and that *cis*-diiodotetraammine was more photosensitive than *cis*-dibromotetraammine in the wavelength region of visible light; for example, the quantum yield was 0.82×10^{-2} (at 408 nm) for the former and 0.27×10^{-2} (at 382 nm) for the latter complex, The relatively high yield observed at shorter wavelengths can be regarded as indicating a CTTM excited state with a different electronic configuration, for it is more populous than that produced by the light irradiation with longer wavelengths. The dependence of the irradiation wavelength on the quantum yield can be interpreted by the mechanism proposed by Adamson and Sporer,[3] which postulated that the first chemical consequence of light absorption is a homolytic bond fission of the metal-ligand bond. When a considerable excessive energy is available, the net quantum yield would be increased by the ease of nascent radicals in escaping their solvent cage. Thus, high quantum yields can be predicted to be favored by the use of the shorter-wavelength light. The homolytic bond fission of the metal ligand may be essentially different from that in the thermally-excited state, because there is no correlation between the photoreactivity and the instability towards thermal aquation as expressed by the rate constants (Table 1). The photoreactivity is rather correlated with the ease of the oxidation of the halide ligand and, hence, with the thermodynamic instability of the complexes towards redox reaction. A similar trend is more evidently observed in the photoreaction of the halogenopentaamminecobalt(III) complexes.[16] The oxidation potential of the halide ligand seems to play the dominant role in determining the photolytic behavior of the halogenoammine complex.

As is shown in Table 1, most studies of the photochemistry of ammine complex ions have dealt with the cobalt(III), chromium(III), and ruthenium(III) systems. These metal complexes differ from each other in photochemical behavior; the photoreactions of cobalt(III) complexes can be either substitution reactions or redox reactions, whereas for chromium(III) and ruthenium(III) complexes only substitution reactions are observed. Although there is no direct comparison of complexes with the same

TABLE 1. PHOTOCHEMICAL REACTIONS OF RUTHENIUM(III) AND OTHER TRANSITION METAL COMPLEXES

Complex	Wavelength Irrad., nm	Product	Quantum yield 10^{-2}	Hydrolysis rate constant, k 10^{-4}, s^{-1}
cis-$RuCl_2(NH_3)_4^+$	330—492	no reaction	— [a]	8.68 [b]
cis-$RuBr_2(NH_3)_4^+$	320	$RuBr(OH_2)(NH_3)_4^{2+}$	0.56	7.98
	382		0.27	
	434		0.14	
	492		0.00	
cis-$RuI_2(NH_3)_4^+$	408	$RuI(OH_2)(NH_3)_4^{2+}$	0.82	3.24
	463		0.33	
	512		0.10	
	642		0.00	
$Ru(NH_3)_6^{3+}$	254	$Ru(OH_2)NH_3)_5^{3+}$	7 [c]	
		NH_4^+	5	
	321	$Ru(OH_2)(NH_3)^{3+}$	1	
$RuCl(NH_3)_5^{2+}$	230	NH_4^+	1.7	3.28 [d]
	254	disappearance	6	
		NH_4^+	3.2	
		Cl^-	2.9	
	321	disappearance	4 [e]	
	321	disappearance	0.8 [f]	
		NH_4^+	2.0	
$Co(NH_3)_6^{3+}$	370, 550	disappearance	0.2 [g]	
$CoCl(NH_3)_5^{2+}$	370	$Co(OH_2)(NH_3)_5^{3+}$	1.1	0.017 [h]
	550		0.1	
$CoBr(NH_3)_5^{2+}$	370	$Co(OH_2)(NH_3)_5^{3+}$	21	0.063
		Co(II)	21	
	550	$Co(OH_2)(NH_3)_5^{3+}$	0.13	
$CoI(NH_3)_5^{2+}$	370	Co(II), I_2	66	0.083
	550	Co(II), I_2	10	
$Cr(NH_3)_6^{3+}$	254	$Cr(OH_2)(NH_3)_5^{3+}$	49 [i]	0.001
$Cr(OH_2)(NH_3)_5^{3+}$	320—600	$Cr(OH_2)_2(NH_3)_4^{3+}$	25	
$Cr(OH_2)_2(NH_3)_4^{3+}$	320—700	$Cr(OH_2)_3(NH_3)_3^{3+}$	16	

a) [Complex] $=5.0\times10^{-4}$ M, $I_0=2.5\times10^3$ photons l^{-1} min^{-1}, 25±1 °C, pH 2.0. b) Ref. 14, values for $[RuX_2(en)_2]^+$ at 54.5 °C, $[H^+]=0.1$ M. c) Ref. 8, 25 °C, pH 3. d) Ref. 15, at 80.1 °C. e) 0.5 M C_3H_7OH solution. f) 0.1 M NaCl, 0.5 M C_3H_7OH solution. g) Ref. 17, 25 °C, pH 4. h) Ref. 18. i) Ref. 19, $[H^+]=1-0.05$ M.

ligand, the photoreaction type of the ruthenium(III) complex is the same as that of the chromium(III) complex except that the quantum yield depends on the light wavelength. These differences are presumably due to the greater difficulty of reduction from the trivalent to the divalent state or to the greater instability of the divalent state metal complex.

Photoreaction Mechanism of the cis-*dihalogenotetraammineruthenium(III) Complex.* According to the three-stage mechanism proposed by Adamson and Sporer,[3] the present photochemical reactions can be well interpreted. The first stage is homolytic-bond-breaking:

$$Ru^{III}X_2(NH_3)_4 \xrightarrow{h\nu} Ru^{II}X(NH_3)_4\cdot X^{\cdot} \quad (3)$$

and

$$Ru^{III}X_2(NH_3)_4 \xrightarrow{h\nu} Ru^{I}(NH_3)_4\cdot X_2^{\cdot\cdot} \quad (4)$$

where X denotes the halide ligand. These intermediate products have not yet been confirmed in our experiment; however, they can react in one of two ways. They can return to the ground state:

$$Ru^{II}X(NH_3)_4\cdot X^{\cdot} \rightarrow Ru^{III}X_2(NH_3)_4 \quad (5)$$

or

$$Ru^{I}(NH_3)_4\cdot X_2^{\cdot\cdot} \rightarrow Ru^{II}X(NH_3)_4\cdot X^{\cdot} \rightarrow Ru^{III}X_2(NH_3)_4 \quad (6)$$

In another path, they can react with a water molecule in an acidic solution or with the hydroxide ion in neutral and basic solutions:

$$Ru^{II}X(NH_3)_4\cdot X^{\cdot} \begin{cases} \rightarrow + H_2O \rightarrow \\ \quad Ru^{II}X(OH_2)(NH_3)_4\cdot X^{\cdot} \quad (7) \\ \rightarrow + OH^- \rightarrow \\ \quad Ru^{II}X(OH)(NH_3)_4\cdot X^{\cdot} \quad (8) \end{cases}$$

$$Ru^{I}(NH_3)_4\cdot X_2^{\cdot\cdot} \begin{cases} \rightarrow + 2H_2O \rightarrow \\ \quad Ru^{I}(OH_2)_2(NH_3)_4\cdot X_2^{\cdot\cdot} \quad (9) \\ \rightarrow + 2OH^- \rightarrow \\ \quad Ru^{I}(OH)_2(NH_3)_4\cdot X_2^{\cdot\cdot} \quad (10) \end{cases}$$

The species formed in Reactions (7), (8), and (9), (10) may be ruthenium(II) and ruthenium(I) complexes respectively, with an $X^{\cdot}$ radical in the second coordination sphere; however, the formation of the latter complexes may be difficult in view of the coordination ability of ruthenium(I). If the electron transfer from ruthenium(II) to X is energetically favorable, aquation or base hydrolysis proceeds:

$$Ru^{II}X(OH_2)(NH_3)_4 \cdot X^{\cdot} \rightarrow Ru^{III}X(OH_2)(NH_3)_4 + X^- \quad (11)$$

$$Ru^{II}X(OH)(NH_3)_4 \cdot X^{\cdot} \rightarrow Ru^{III}X(OH)(NH_3)_4 + X^- \quad (12)$$

Wells and Endicott[8] reported that the quantum yield for the photoaquation of the chloropentaammineruthenium(III) is independent of the wavelength. This has been interpreted by assuming that the over-all reaction rate is controlled by the step of ligand-exchange reaction in the lowest-energy excited state formed by the CTTM-band irradiation.

To account for the variation in the quantum yield with the wavelength in our results, it may be reasonable to assume that the probability of the deactivation process (5), (6) of the primary excited state increases with the decrease in the excitation energy, unless the probability of the primary excitation (3), (4) decreases with a decrease in the excitation energy. In particular, the fact that the low quantum yields are different from those for the other metal complexes may be supported by the instability of the radical containing ruthenium-(II) or (I) in the deactivation processes (5) and (6).

References

1) Part VI of this series: A. Ohyoshi, S. Hiraki, and H. Kawasaki, This Bulletin, **47**, 841 (1974).
2) A. Linhard and M. Weigel, *Z. Anorg. Allg. Chem.*, **266**, 49 (1951).
3) A. W. Adamson and A. H. Sporer, *J. Amer. Chem. Soc.*, **80**, 3865 (1958).
4) J. F. Endicott and M. Z. Hoffman, *ibid.*, **87**, 3348 (1965).
5) G. Caspari, R. G. Hughes, J. F. Endicott, and M. Z. Hoffman, *ibid.*, **92**, 6801 (1970).
6) J. F. Endicott, M. Z. Hoffman, and L. S. Beres, *J. Phys. Chem.*, **74**, 1021 (1970).
7) T. L. Kelly and J. F. Endicott, *J. Amer. Chem. Soc.*, **92**, 5733 (1970).
8) W. L. Wells and J. F. Endicott, *J. Phys. Chem.*, **75**, 3075 (1971).
9) K. Gleu and W. Breuel, *Z. Anorg. Allg. Chem.*, **237**, 335 (1938).
10) C. A. Parker, *Proc. Roy. Soc., Ser. A*, **220**, 104 (1953).
11) E. E. Wegner and A. W. Adamson, *J. Amer. Chem. Soc.*, **88**, 399 (1966).
12) H. Hartmann and C. Buschbeck, *Z. Phys. Chem. (N. F.)*, **11**, 120 (1957).
13) C. K. Jørgensen, *Mol. Phys.*, **2**, 309 (1959).
14) J. A. Broomhead and L. A. P. Kane-Maguire, *Inorg. Chem.*, **7**, 2519 (1968).
15) W. G. Movius and R. G. Linck, *J. Amer. Chem. Soc.*, **92**, 2677 (1970).
16) G. B. Schmidt, *Z. Phys. Chem. (N. F.)*, **41**, 26 (1964).
17) A. W. Adamson, *Discuss. Faraday Soc.*, **29**, 163 (1960).
18) F. Basolo and R. G. Pearson, "Mechanisms of Inorganic Reactions," John Willey and Sons, New York (1967), p. 164.
19) M. R. Edelson and R. A. Plane, *Inorg. Chem.*, **3**, 231 (1964).

A Solubility Study of Coacervates of Magnesium, Calcium and Aluminum Highpolyphosphates in Acid Solutions

Takafumi KANAZAWA, Takao UMEGAKI, Yōzō KITAJIMA, and Takeshi OGAWA

Department of Industrial Chemistry, Faculty of Technology, Tokyo Metropolitan University, Fukazawa, Setagaya-ku, Tokyo, 158

(Received October 9, 1973)

Dissolution of the highpolyphosphate coacervates of magnesium, calcium and aluminum was studied in order to understand the conformational feature of polyphosphate chains in the coacervates. Electrical conductivity and viscosity of the coacervate solutions were measured. Paper chromatographic technique was employed for the analysis of the solutions. It was concluded that the polyphosphates dissolve into acid solvents without cleavage of phosphate chains, the degree in the extension of the chains being considerably small. Dissolution processes of the three coacervates were compared. Optimum conditions on the syntheses of the threadforming coacervates are given.

Magesium highpolyphosphate coacervate (MPC), calcium highpolyphosphate coacervate (CPC) and aluminum highpolyphosphate coacervate (APC) with high viscosity (10—10^3 poise) and transparency were prepared from mixed solutions of sodium highpolyphosphate and metal chlorides.

The main purpose of this study was to clarify the dissolution processes of the three coacervates from the results of electrical conductivity and viscosity. Paper chromatography was utilized to examine whether cleavage of the chain phosphate anions occurred during the course or after the completion of the dissolution process.

The degradation of some highpolyphosphates has been investigated by Thilo and Wieker[1,2] and Gill and Riaz.[3] However, a detailed study of the dissolution process of polyphosphates into acid solvents does not seem to have been dealt with.

The synthetic conditions of CPC and APC are briefly described in the present report. The preparation of MPC and its thermal change were discussed in previous papers.[4–6]

Experimental

Materials. The synthetic conditions for CPC and APC were partly the same as those for MPC.[4] CPC was obtained from a mixture of 15% sodium highpolyphosphate solution (400 parts) and 20% calcium chloride solution (166 parts) by the addition of ethyl alcohol. In the synthesis of APC, the threadforming property of the coacervates changes with the molar ratio of P to aluminum ion. Acids such as HCl (0.05%, 0.1%) and citric acid (H_3Cit) (2%, 10%) were used as solvents.

Measurements. Viscosities of the coacervate solutions were measured with an Ostwald capillary viscometer with efflux time of ca. 120 s for distilled water. The conductivities of the coacervate solutions of various concentrations were measured with an apparatus consisting of an alternating current bridge and a conductivity cell. All the measurements of viscosities and conductivities were carried out in a bath maintained at 30±0.02 °C.

Paper chromatography. Each strip of filter paper (Toyo Roshi No. 51A) on which 25 μl of sample solution was spotted was immersed in Kolloff solvent No. 92-D5.[7] The filter paper was left at about 5 °C for 7—10 hr during which time the solvent rose 10—15 cm.

TABLE 1. SPINNABILITY AND RATIO OF METAL ION(M) TO P IN THE MIXED SOLUTIONS

Coacervate	M : P(mole ratio)	Note
MPC	1 : 2	spinnability
CPC	1 : 2	spinnability
APC	1 : 3	no spinnability
APC	1 : 6	
APC	1 : 12	spinnability

Results and Discussion

A comparison of spinnability among the three coacervates is given in Table 1. Threadforming MPC and CPC were obtained when the metal chloride solution and the sodium highpolyphosphate solution were mixed in the molar ratio P : metal=2 : 1. Threadforming APC formed from the mixture with a lower ratio of aluminum chloride to sodium polyphosphate. The optimum conditions for the synthesis of threadforming coacervate seem to be related to the acidity of the mixtures and the content of sodium ion in the coacervates.

No cleavage of highpolyphosphates occurred in the course of dissolution since such short chain phosphates as orthophosphates, pyrophosphates and tripolyphosphates were not detected by the paper chromatography. In a few hours after the complete dissolution of APC, orthophosphate ions were formed in the APC solution by the hydrolysis of polyphosphates, which was accelerated by the hydrogen ion and aluminum ion[1,2] in the coacervate solution. Consequently, all the

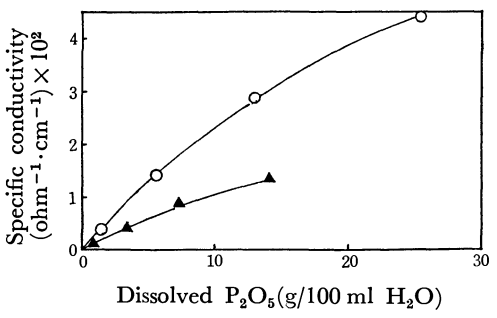

Fig. 1. Conductivity of aqueous solutions of polyphosphates.
○: sodium metaphosphate, ▲: MPC

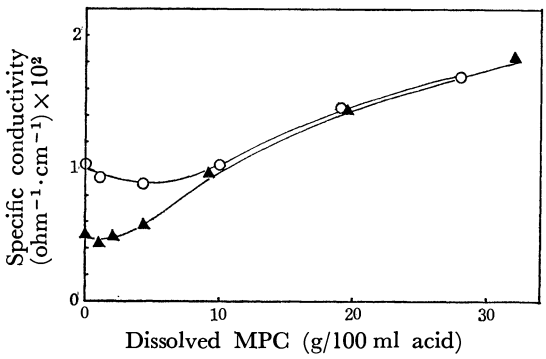

Fig. 2. Conductivity of MPC-HCl systems.
○: 0.1% HCl, ▲: 0.05% HCl

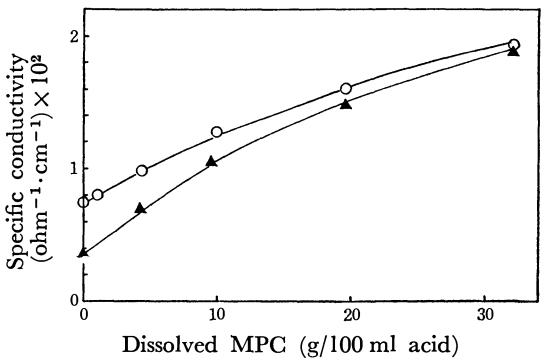

Fig. 3. Conductivity of MPC-H_3Cit systems.
○: 10% H_3Cit, ▲: 2% H_3Cit

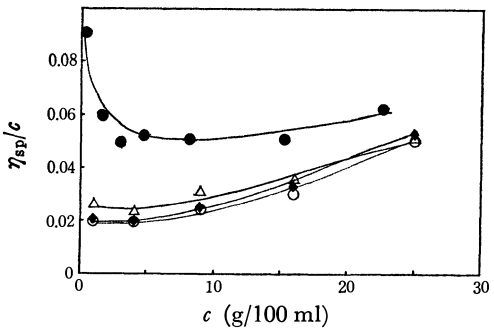

Fig. 4. Viscosity of MPC solutions.
●: sodium metaphosphate-H_2O, △: MPC-H_2O,
○: MPC-0.1% HCl, ◆: MPC-10% H_3Cit,

highpolyphosphates of magnesium, calcium and aluminum dissolved without degradation.

Figure 1 shows the electrical conductivity-concentration curves of the aqueous solutions of MPC and sodium highpolyphosphate used as a starting material of the coacervates. The coordination of magnesium ions to polyphosphate chains seems to depress the ionic dissociation of MPC. The conductivities of MPC solution were lower than those of the sodium highpolyphosphate solution. Figures 2 and 3 show the electrical conductivity *versus* concentration curves of the acid solutions of MPC. The conductivities of the citric acid solutions of MPC increased monotonically and the conductivity-concentration curves nearly coincide in the same manner as in the case of the HCl solution of MPC.

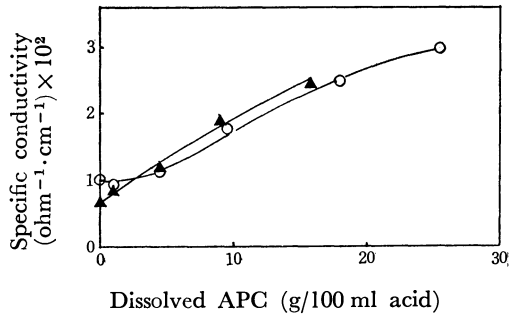

Fig. 5. Conductivity of APC solutions.
○: 0.1% HCl, ▲: 10% H_3Cit

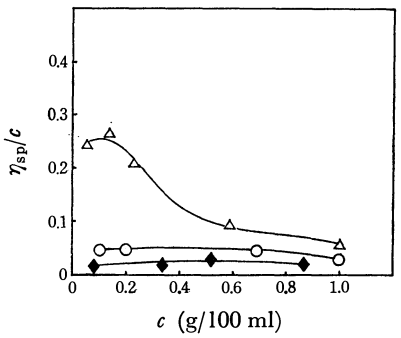

Fig. 6. Viscosity of APC solutions.
△: H_2O, ○: 0.1% HCl, ◆: 10% H_3Cit.

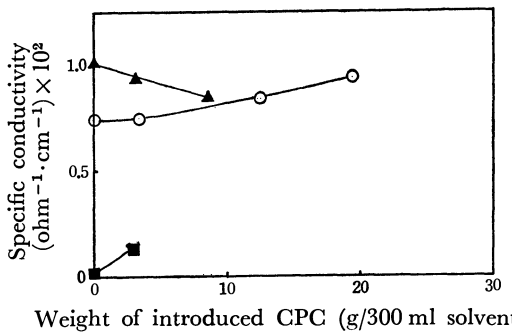

Fig. 7. Conductivity change of CPC solutions with amount of introduced CPC.
■: H_2O, ▲: 0.1% HCl, ○: 10% H_3Cit

The electrical conduction by hydrogen ion was predominant in the dilute HCl solutions of MPC. The bonding between the hydrogen ions in the HCl solution and the polyphosphate ions from the dissolved MPC caused a decrease of the hydrogen ions in the MPC solution, the conductivities decreasing with the concentration of MPC. The citrate ions in the citric acid solutions of MPC acted as a buffer and enhanced the concentration of hydrogen ion when the polyphosphate ion linked with the hydrogen ions in the acid solvent. Thus no conductivity decrease was observed at low concentrations of MPC in the case of citric acid. On both acid solvents the contribution of the dissolved ions to the conductivity increased with concentration of the MPC, the convergence of the conductivities to one curve occurring when the effect of the hydrogen ions in the acid solvents almost disappeared.

With the decrease in the concentration of polyelectrolyte the net charge on a polymer ion increases due to the increase of the ionic dissociation of the polyelectrolyte, and polymer chains extend owing to the intermolecular repulsive force among the charges with equal sign. Then the reduced viscosity of the polyelectrolyte solutions at low concentration often exhibits a curve considerably concave upward.[8]

Figure 4 gives a plot of the reduced viscosity of the MPC solution against concentration c. We see that the reduced viscosity of the MPC solution at low concentration does not increase with dilution although some curves indicate a slight extention of polymer coils of polyphosphates. Most of the polyphosphate chains of the MPC solutions were to some extent tightly coiled since the intermolecular repulsion was restricted owing to the neutralization of the charges on the chains by such cations as Mg^{2+}, H^{+} and Na^{+}. The results of the viscosity measurement confirmed the conclusion from the conductivity measurement that the initial conductivity lowering of the HCl solution of MPC (Fig. 2) was caused not by the extention of the polymer chains but by the depression in the ionic dissociation of hydrogen. The changes in the conductivity and the viscosity of the acid solutions of threadforming APC were similar to those of the MPC solution (Figs. 5 and 6). The electrical conductivity change of the CPC solutions (Fig. 7) was also similar to that of the MPC solutions indicating that the more CPC was introduced into a solvent, the more electrolytes dissolved. However, a very small amount of viscous substance remains undissolved in the solution at a concentration of about 0.5 g/100 ml. CPC might contain some undissolved species, none of which was identified in the present study.

From the results obtained so far it was concluded that MPC, APC and soluble part of CPC dissolved without degradation of polyphosphate chains, which do not extend so much in the solutions. The polyphosphate ions in the coacervates seem to be more tightly coiled than those in the solutions of the coacervates since polyphosphates and some other electrolytes were much more concentrated as compared with those in the coacervate solutions.

Hydration of such cations as Mg^{2+}, Al^{3+}, Ca^{2+} and Na^{+} and the coordination of these ions to polyphosphate ions should be clarified for more detailed discussion on the dissolution of the coacervates.

Some of the data in this report was cited from Ref. 4.

The work was supported by a grant from the Asahi Glass Foundation for Contribution to Industrial Technology.

References

1) E. Thilo and W. Wieker, *Z. Anorg. Allgem. Chem.*, **291**, 164 (1957).
2) E. Thilo and W. Wieker, *J. Polym. Sci.*, **53**, 55 (1961).
3) J. B. Gill and S. A. Riaz, *J. Chem. Soc., A*, **1969**, 183.
4) T. Kanazawa, T. Umegaki, and H. Kawazoe, *Asahi Garasu Kogyo Gijutsu Shorei-Kai Kenkyu Hokoku*, **21**, 81 (1972).
5) T. Kanazawa, H. Kawazoe, and T. Matsubara, *Kogyo Kagaku Zasshi*, **74**, 1784 (1971).
6) T. Umegaki and T. Kanazawa, This Bulletin, **46**, 3587 (1973).
7) R. H. Kolloff, *Anal. Chem.*, **33**, 373 (1961).
8) M. Kato, T. Nakagawa, and H. Akamatsu, This Bulletin, **33**, 322 (1960).

Electron Transfer Reaction between Thallium(I) and Thallium(III) in the Presence of Cerium(IV) in Aqueous Solution

Goro WADA and Kyoko TAMAKI

Department of Chemistry, Nara Women's University, Nara 630

(Received November 12, 1973)

The kinetics of the electron transfer reaction between Tl(I) and Tl(III) was investigated in the presence of Ce(IV) by use of a radioactive tracer ^{204}Tl. The apparent rate constant of the reaction, k_{app}, was dependent upon $[H^+]$ and [Co(IV)] ($<0.6\times10^{-3}$ M) and can be expressed by

$$k_{app} = k_A + \frac{k_B}{[H^+]} + \left(k_C + \frac{k_D}{[H^+]}\right)[Ce(IV)].$$

k_{app} is gradually saturated to a limiting value according to $[H^+]$ at higher [Ce(IV)]. The observed values are $k_A=4.70\ M^{-1}\ h^{-1}$, $k_B=2.13\ h^{-1}$, $k_C=1.30\times10^3\ M^{-2}\ h^{-1}$, and $k_D=2.61\times10^3\ M^{-1}\ h^{-1}$ at 50 °C. Since Ce(IV) is a one-electron-oxidant, Tl(I) is oxidized by one-electron transfer to produce Tl(II) as an intermediate. However, in the absence of one-electron-oxidant or -reductant, two electrons are transferred from Tl(I) to Tl(III) not through double steps of one-electron transfer but predominantly through a single step of two-electron transfer.

The electron transfer reaction between thallium(I) and thallium(III) has been investigated on the effects of hydrogen ion,[1-6] anions such as NO_3^-,[1] Cl^-,[2,7-9] CN^-,[10] SO_4^{2-},[11,12] Br^-,[13,14] and N_3^-,[15] organic acids such as acetic,[16,17] succinic,[16,17] and mono-, di-, and tri-chloroacetic acids,[18] and various organic substances[19-21] by using a radioactive isotope ^{204}Tl as a tracer. The investigations clarified the roles of the effective substances on the electron transfer reaction.

An important feature of this "thallous-thallic" redox reaction is that two electrons in total are transferred between them. The occurrence of thallium(II) has been proposed as a reaction intermediate on the basis of kinetic studies of the redox reaction between iron(II) and thallium(III)[22] and between thallium(I) and cerium(IV)[23] and on the irradiation of X-rays[24] and ultraviolet rays[25] upon the thallium(I)-thallium(III) system. Consequently, the electron transfer reaction between thallium(I) and thallium(III) in the absence of catalyst has been considered to proceed not *via* a single step of "two-electron transfer" but *via* two successive steps of "one-electron transfer" with thallium(II) as an intermediate.

Recently, the acceleration due to the addition of iron(II) to thallium(I)-thallium(III) system[26] and of iron(III) to uranium(IV)-uranium(VI) system[27] was reported, the latter being also an overall reaction with a two-electron transfer. We have investigated the thallium(I)-thallium(III) system in the presence of cerium(IV), and the functions of thallium(II) when it occurs.

Experimental

Materials. Thallium(I) perchlorate was prepared by dissolving thallium metal of 99.99% purity in warm perchloric acid, crystallized, washed by ethanol and dried. The crystal thus obtained was in anhydrous form.

Thallium(III) perchlorate was prepared by dissolving Tl_2O_3 in 4 M perchloric acid at 60—70 °C for many hours. Both thallium(I) and thallium(III) salts were confirmed to be free of chloride ion.

$Ce_2(SO_4)_3\cdot8H_2O$ and $Ce(SO_4)_2\cdot nH_2O$ were used in aqueous perchloric acid as salts of cerium(III) and cerium(IV) respectively. The sulfate ion concentration was regulated with sodium sulfate. As a radioactive tracer, ^{204}Tl obtained in the form of $TlNO_3$ was converted into $TlClO_4$ in perchloric acid. The ionic strength of the reaction solutions was adjusted with sodium perchlorate.

Pure water was made by treating tap water with ion-exchange resin, followed by distillation of the alkaline permanganate solution.

Analyses of Thallium Concentrations. Thallium(III) was determined by titration with disodium ethylenediaminetetraacetate (EDTA) by use of Xylenol Orange as an indicator at pH 4—5 and 50—55 °C. Thallium(I) was oxidized by bromine to thallium(III), most of the excess bromine being removed by heating and the rest completely removed by addition of a few drops of methanolic solution of phenol. Thallium(III) was then titrated in a similar way. A mixture of thallium(I) and (III) was titrated before and after the treatment with bromine, and the concentration of thallium (I) was determined from the difference.

Rate of Oxidation of Thallium(I) by Cerium(IV). Cerium(IV) was spectrophotometrically observed to exhibit an absorption peak at a wavelength of 320 nm, while no absorption was observed in thallium(I), (III), or cerium(III) at wavelengths greater than 300 nm in perchloric and sulfuric acid solution. Thus, the rate of oxidation of thallium(I) by cerium(IV) could be followed by virtue of the decrease in the absorbance of cerium(IV). The absorbance was measured with a Hitachi UV-VIS spectrophotometer Model 139. The oxidation rate could be also followed by measuring the increase in the radioactivity of thallium(III), when thallium(I) was labeled, by a method similar to that for the electron transfer reaction.

Rate of Electron Transfer Reaction Between Thallium(I) and Thallium(III). A reaction mixture containing $TlClO_4$, $Tl(ClO_4)_3$, $Ce(SO_4)_2$, $HClO_4$, Na_2SO_4, and $NaClO_4$ was set in a thermostat in advance. The reaction was initiated at the instant the radioactive thallium(I) was added to the solution. The concentration of sulfate ion, the ionic strength, and temperature of the reaction were always maintained at $[SO_4^{2-}]=0.02$ M, $\mu=3$ M, and 50 °C, respectively.

An aliquot of the reaction solution was taken out into a quenching solution at appropriate time intervals. The quenching solution contained EDTA and was cooled in ice-water beforehand. Ten minutes after removal of an aliquot of the reaction solution, sodium chromate was added as a precipitating reagent for thallium(I), and the pH value was adjusted to about 4—5 with ammonia and ammonium acetate solution. Fifteen minutes later, the solution was filtered,

thallium(III) being separated from thallium(I) into the filtrate. A small portion of the filtrate was gently evaporated in a stainless-steel dish with irradiation by an infrared lamp and the β-radioactivity due to thallium(III) was counted with an Aloka G-M scaler Model TDC-102.

In earlier works on thallium(I)-thallium(III) systems, cyanide ion was usually used as a masking reagent for thallium(III). However, since cyanide ion is highly poisonous, EDTA was adopted in its place. The rate of masking of thallium(III) by EDTA is slower than that by cyanide ion, and EDTA has a masking action even toward thallium(I) in an alkaline medium. Thus, EDTA sometimes induced a zero-time exchange as much as 30—40%, which could be attributed to the accelerated exchange on the interface at the moment of precipitation, whenever EDTA was added at the same time as chromate ion and ammonia. In spite of these disadvantages of EDTA, the procedure described above was found to be accurate enough.

Results and Discussion

Oxidation of Thallium(I) by Cerium (IV). The standard redox potentials of Tl^{3+}/Tl^{+} and Ce^{4+}/Ce^{3+} are 1.28 V[28] and 1.74 V[29] at 25 °C, respectively. Thus, the reaction $Tl^{+}+2Ce^{4+}\rightleftharpoons Tl^{3+}+2Ce^{3+}$ occurs almost completely towards right with an equilibrium constant $\log K=15.6$. But the rate of the reaction is very small as observed photometrically at a wavelength of 360 nm (Fig. 1). In practice, the autoreduction of cerium(IV) takes place even in the absence of thallium(I) in the air, besides the reduction by thallium(I). Consequently, the values of [Ce(IV)] at time t employed in the figure are the observed ones corrected for the autoreduction.

If the reaction proceeds *via* the following two successive paths by stepwise reductions,

$$Tl(I) + Ce(IV) \rightleftarrows Tl(II) + Ce(III) \quad (k_1,\ k_{-1}) \qquad (1)$$

$$Tl(II) + Ce(IV) \rightarrow Tl(III) + Ce(III) \quad (k_2) \qquad (2)$$

Tl(II) is produced as an intermediate species. By the method of steady state applied to Tl(II), the following rate equation is obtained, when $[Tl(I)]_0$ is much greater than $[Ce(IV)]_0$.

$$\ln\frac{[Ce(IV)]}{[Ce(IV)]_0} - \frac{k_{-1}}{k_2-k_{-1}}\left(\frac{[Ce(IV)]_0}{[Ce(IV)]}-1\right) = \frac{-2k_1k_2[Tl(I)]}{k_2-k_{-1}}t \qquad (3)$$

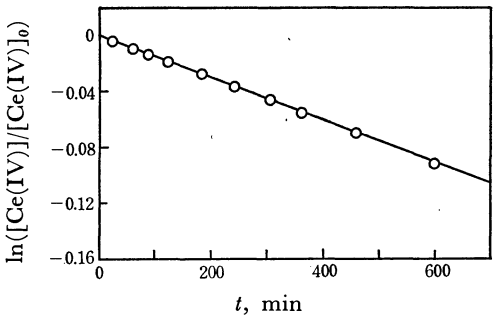

Fig. 1. Rate of oxidation of Tl(I) by Ce(IV) at $[H^+]=1.0$ M, $[SO_4^{2-}]=0.02$ M, $\mu=3$ M, and 50 °C, observed at 360 nm.
$[Tl(I)]_0=0.03$ M, $[Ce(IV)]_0=0.001$ M

Since k_{-1} is supposed to be negligibly small as compared with k_2, Eq. 3 may be simplified as follows.

$$\ln\frac{[Ce(IV)]}{[Ce(IV)]_0} = -2k_1[Tl(I)]t \qquad (4)$$

This is satisfied in Fig. 1, where the plot of $\ln([Ce(IV)]/[Ce(IV)]_0)$ against t shows a straight line, from the slope of which $k_1=0.17\ M^{-1}\ h^{-1}$ is obtained at 50 °C.

If k_{-1} were much greater than k_2, Eq. 3 would become the following equation, whose linear relationship does not hold in this case.

$$\ln\frac{[Ce(IV)]}{[Ce(IV)]_0} + \frac{[Ce(IV)]_0}{[Ce(IV)]} - 1 = \frac{2k_1k_2[Tl(I)]}{k_{-1}}t \qquad (5)$$

Electron Transfer Reaction Between Thallium(I) and Thallium(III). When $\log(x_\infty-x)$ was plotted against t, straight lines were always obtained irrespective of the presence or absence of cerium(IV), x and x_∞ being the specific radioactivities of thallium(III) in the reaction solution at time t and at time of equilibrium, respectively. Two typical plots in the absence and presence of cerium(IV) are shown in Fig. 2.

Since the reaction was very slow and it was too troublesome to determine x_∞ by observation for every kinetic run, x_∞ was estimated by calculation on the basis of statistical distribution of radioactivity between thallium(I) and thallium(III) at equilibrium as $x=x_t\cdot[Tl(III)]/([Tl(I)]+[Tl(III)])$, where x_t is the total radioactivity of ^{204}Tl.

Thus, the apparent rate constant k_{app} of the electron transfer reaction is given from McKay's relation,[30] since the reaction is of the first order with respect to both [Tl(I)] and [Tl(III)], $\text{Rate}=k_{app}[Tl(I)][Tl(III)]$.

$$k_{app} = \frac{0.693}{([Tl(I)]+[Tl(III)])t_{1/2}} \qquad (6)$$

Here $t_{1/2}$ is the half-life period of the reaction, which is easily obtained from the slope of the straight line in Fig. 2.

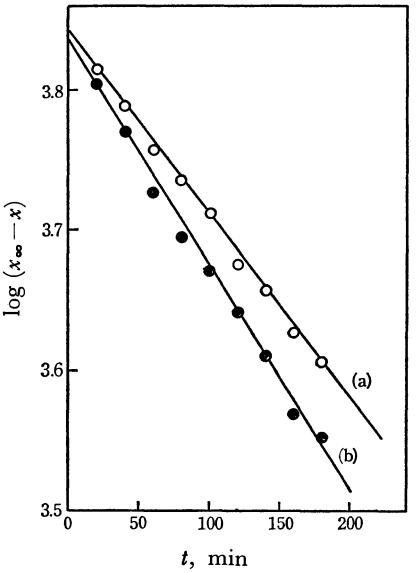

Fig. 2. McKay's plot of $\log(x_\infty-x)$ *vs.* time t at $[Tl(I)]=[Tl(III)]=0.01$ M, $[SO_4^{2-}]=0.02$ M, $[H^+]=0.50$ M, $\mu=3$ M, and 50 °C.
(a) $[Ce(IV)]=0$, (b) $[Ce(IV)]=0.001$ M

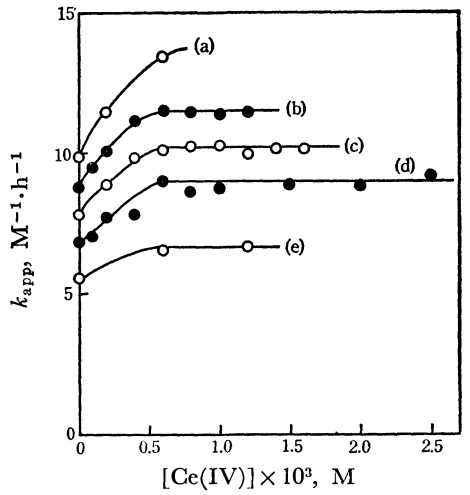

Fig. 3. Dependence of k_{app} upon [H⁺] and [Ce(IV)] at $[SO_4^{2-}]=0.02$ M, $\mu=3$ M, and 50 °C.
(a) [H⁺]=0.41 M, (b) [H⁺]=0.50 M, (c) [H⁺]=0.70 M, (d) [H⁺]=1.00 M, (e) [H⁺]=1.50 M

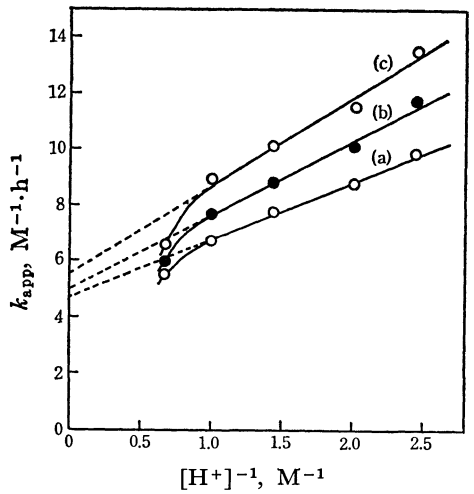

Fig. 4. Linear relationships between k_{app} and $[H^+]^{-1}$ at various [Ce(IV)] at $[SO_4^{2-}]=0.02$ M, $\mu=3$ M, and 50 °C.
(a) [Ce(IV)]=0, (b) [Ce(IV)]=0.2×10^{-3} M, (c) [Ce(IV)]=0.6×10^{-3} M

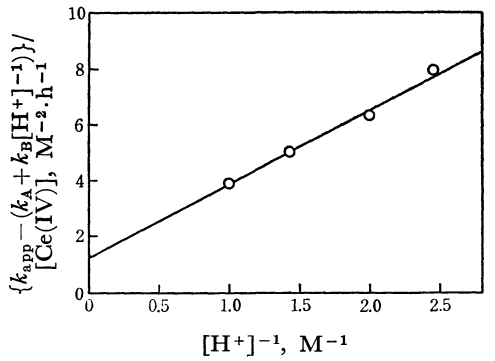

Fig. 5. Linear relationship between $\{k_{app}-(k_A+k_B/[H^+])\}/[Ce(IV)]$ and $[H^+]^{-1}$ at $[SO_4^{2-}]=0.02$ M, $\mu=3$ M, and 50 °C.

The results obtained in the concentration range [H⁺]=0.4—1.5 M and [Ce(IV)]=0—2.5×10^{-3} M are illustrated in Fig. 3. We see that k_{app} increases with decreasing [H⁺] at constant [Ce(IV)] and with increasing [Ce(IV)] at constant [H⁺] when [Ce(IV)] is less than 0.6×10^{-3} M. Above this concentration, k_{app} is saturated to a limiting value at respective [H⁺].

i. When [Ce(IV)]$\leqq0.6\times10^{-3}$ M: Linear relationships of k_{app} with $[H^+]^{-1}$ at [Ce(IV)]=0, 0.2×10^{-3}, and 0.6×10^{-3} M are shown in Fig. 4, and another linear relationship of (k_{app}-intercept in Fig. 3)/[Ce(IV)] with [H⁺] in Fig. 5. The following equation of k_{app} is thus established as functions of [H⁺] and [Ce(IV)], where k_A, k_B, k_C, and k_D are constants.

$$k_{app}=\left(k_A+\frac{k_B}{[H^+]}\right)+\left(k_C+\frac{k_D}{[H^+]}\right)[Ce(IV)] \qquad (7)$$

From the intercepts and slopes of these straight lines, the values of the individual rate constants at 50 °C can be determined as:

$$k_A = 4.70\ M^{-1}\,h^{-1}$$
$$k_B = 2.13\ h^{-1}$$
$$k_C = 1.30\times10^3\ M^{-2}\,h^{-1}$$
$$k_D = 2.61\times10^3\ M^{-1}\,h^{-1}$$

At least four sets of reactants, *viz.* oxidant, reductant, reductant, and catalyst, may be involved in parallel in the electron transfer reaction between thallium(I) and thallium(III) species; k_B and k_D may be connected with the hydrolyzed species of one of its participants. The sulfate ion is an accelerating ligand, bonding with thallium(I) and/or thallium(III).[11,12]

ii. When [Ce(IV)] exceeds 0.6×10^{-3} M: At increased cerium(IV) concentrations, k_{app} gradually deviates from the linearity in Eq. 7 but reaches a saturated value at respective acid concentrations.

According to the results of irradiation of ultraviolet rays on thallium(I)-thallium(III) system,[25] the rates of exchange of the following are very fast.

$$*Tl(I) + Tl(II) \rightleftarrows *Tl(II) + Tl(I) \qquad (k_I) \qquad (8)$$
$$*Tl(II) + Tl(III) \rightleftarrows *Tl(III) + Tl(II) \qquad (k_{III}) \qquad (9)$$

$k_I = 1.8\times10^8\ M^{-1}\,h^{-1}$ at 25°C
$k_{III} = 3.6\times10^8\ M^{-1}\,h^{-1}$ at 25°C

The acceleration of electron transfer in the thallium(I)-thallium(III) system by cerium(IV) is due to the initial occurrence of thallium(II) through Reaction 1, followed by the rapid exchanges through Reactions 8 and 9. Thus, the increased rate due to cerium(IV) might be proportional to [Tl(II)], which is approximately expressed as follows.

$$[Tl(II)]=\frac{k_1[Tl(I)][Ce(IV)]}{k_{-1}[Ce(III)]+k_2[Ce(IV)]} \qquad (10)$$

As [Ce(IV)] increases, [Tl(II)] increases at first, and attains a limiting value [Tl(II)]=(k_1/k_2)[Tl(I)]. This may qualitatively correspond to the saturation phenomenon of k_{app} at higher [Ce(IV)] as seen in Fig. 3.

How are the Two Electrons Transferred ? The two-electron transfer system between thallium(I) and thallium(III) is also known to be accelerated by the addition of a minute amount of iron(II),[22,26] which is a one-electron-reductant. In this case, the smaller

the concentration of iron(II), the larger the acceleration, as long as $[Fe(II)]>6.8\times10^{-5}$ M. A rate equation for the fact has been proposed.[26]

The reduction of thallium(III) by iron(II) was not affected by the addition of thallium(I) at all but retarded by the addition of iron(III).[22] Thus, the reduction was deduced to proceed in the following paths.

$$Tl(III) + Fe(II) \rightleftarrows Tl(II) + Fe(III) \quad (11)$$

$$Tl(II) + Fe(II) \rightarrow Tl(I) + Fe(III) \quad (12)$$

Thallium(II) is produced as an intermediate, and since Reaction 12 is rate-determining, Reaction 11 maintains partial equilibrium. It can therefore be reasonably said that the addition of iron(III) diminishes [Tl(II)] and consequently the total rate, but the addition of thallium(I) has no effect on the total rate.

It is worthwhile investigating the effect of the addition of iron(III) on the rate of thallium(I)-thallium(III) electron transfer reaction. If this electron transfer were to exactly undergo an initial production of thallium(II), as expressed by

$$Tl(I) + Tl(III) \rightleftarrows Tl(II) + Tl(II), \quad (13)$$

the addition of iron(III) should interfere with Reaction 13 on account of the promotion of the backward reaction of Reaction 11, resulting in the retardation of thallium(I)-thallium(III) electron transfer, which would have otherwise occurred through Reactions 8 and 9.

The results of addition of various metal ions to the thallium(I)-thallium(III) system are listed in Table 1. Although the concentration of iron(III) added in the reaction system seems to be high enough to interfere with the production of thallium(II) markedly, no actual retardation effect on the rate of the electron transfer but only a slight acceleration was observed. Attention should be paid to the fact that iron(III) has no ability to oxidize thallium(I) to thallium(II) and as a consequence to thallium(III), on account of its oxidation potential.

This suggests that the two electrons are transferred not through double one-electron transfer steps but mostly through a single step of two-electron transfer without thallium(II) species as the intermediate, when neither one-electron-oxidant nor one-electron-reductant exists in the thallium(I)-thallium(III) system; the chemical equation is as follows.

$$*Tl(I) + Tl(III) \rightarrow *Tl(III) + Tl(I) \quad (14)$$

A tentative check by ESR method for the occurrence of thallium(II) was negative in a mixture of thallium(I) and thallium(III) species, while thallium(II) was detected in the presence of one-electron-oxidant.[31] Since chromium exists in such oxidation states as II, III and IV, chromium(II) is known to reduce thallium(III) to thallium(I) as a two-electron-reductant, resulting in chromium(IV) which forms a binuclear complex with an unreacted chromium(II).[32,33] This supports the possibility of the direct two-electron transfer mechanism between thallium(I) and thallium(III) in the absence of one-electron catalyst.

Table 1. Effects of metal ions on the rate of Tl(I)-Tl(III) electron transfer reaction at $[Tl(I)]=[Tl(III)]=0.01$ M, $[H^+]=0.5$ M, $\mu=1.57$ M, and at 50°C

[Added ion], M	k_{app}, $M^{-1}\,h^{-1}$
None	2.77
Cu^{2+} 0.01	2.77
Fe^{3+} 0.1	2.98, 2.89, 2.65
Hg^{2+} 0.01	2.88

It might be concluded that thallium(I)-thallium(III) electron transfer reaction proceeds mainly *via* a single step of two-electron transfer in the absence of catalyst and *via* two steps of stepwise one-electron transfer in the presence of a one-electron-oxidant or a one-electron-reductant.

References

1) R. J. Prestwood and A. C. Wahl, *J. Amer. Chem. Soc.*, **71**, 3137 (1949).
2) G. Harbottle and R. W. Dodson, *ibid.*, **73**, 2442 (1951).
3) R. W. Dodson, *ibid.*, **75**, 1795 (1953).
4) E. Roig and R. W. Dodson, *J. Phys. Chem.*, **65**, 2175 (1961).
5) F. J. C. Rossotti, *J. Inorg. Nucl. Chem.*, **1**, 159 (1955).
6) H. J. Born, H. Vogg, and G. Vogt, *Z. Elektrochem.*, **66**, 372 (1962).
7) B. Baysal, *Actes Intern. Congr. Catalyse*, **1**, 559 (1960).
8) G. Nord-Waind, Proc. Symp. Coord. Chem., Tihany, Hung., (1964), p. 437.
9) A. Iandelli and A. Palenzona, *J. Less-Common Metals*, **9**, 1 (1965); A. G. Lee, "The Chemistry of Thallium," Elsevier, Amsterdam (1971), p. 302.
10) E. Penna-Franca and R. W. Dodson, *J. Amer. Chem. Soc.*, **77**, 2651 (1955).
11) C. H. Brubaker and J. P. Mickel, *J. Inorg. Nucl. Chem.*, **4**, 55 (1957).
12) D. R. Wiles, *Can. J. Chem.*, **36**, 167 (1958).
13) L. G. Carpenter, M. H. Ford-Smith, R. P. Bell, and R. W. Dodson, *Discuss. Faraday Soc.*, **29**, 92 (1960).
14) H. Schäfer, *Z. Anorg. Allgem. Chem.*, **305**, 64 (1960).
15) V. G. Vogt and H. J. Born, *Ber. Bunsenges. Phys. Chem.*, **69**, 741 (1965).
16) C. H. Brubaker and C. Andrade, *J. Amer. Chem. Soc.*, **81**, 5282 (1959).
17) T. P. Donas, *Anales Fac. Quim. Farm.*, **13**, 149 (1961).
18) R. G. Mcgregor and D. R. Wiles, *J. Chem. Soc. A*, **1970**, 325.
19) O. Farver, *Acta Chem. Scand.*, **26**, 534 (1972).
20) A. Cecal and I. A. Schneider, *J. Inorg. Nucl. Chem.*, **35**, 1565 (1973).
21) A. Cecal and I. A. Schneider, *J. Phys. Chem.*, **77**, 1904 (1973).
22) K. G. Ashurst and W. C. E. Higginson, *J. Chem. Soc.*, **1953**, 3044.
23) M. K. Dorfman and J. W. Gryder, *Inorg. Chem.*, **1**, 779 (1962).
24) G. E. Challenger and B. J. Masters, *J. Amer. Chem. Soc.*, **78**, 3012 (1956).
25) D. R. Stranks and J. K. Yandell, *J. Phys. Chem.*, **73**, 840 (1969).
26) B. Warnquist and R. W. Dodson, *Inorg. Chem.*, **10**, 2624 (1971).
27) H. Tomiyasu and H. Fukutomi, The 26th Spring Annual Meeting of Chem. Soc. Japan, Tokyo, 1972.
28) G. Biedermann, *Arkiv Kemi*, **5**, 441 (1953).
29) H. L. Conley, Ph. D. Thesis UCRL-9332 (1960).
30) H. A. C. McKay, *Nature*, **142**, 997 (1938).
31) I. A. Elson and J. K. Kochi, *J. Amer. Chem. Soc.*, **95**, 5060 (1973).
32) M. Ardon and R. A. Plane, *ibid.*, **81**, 3197 (1959).
33) J. C. Kenny and D. W. Carlyle, *Inorg. Chem.*, **12**, 1952 (1973).

Kinetic Studies of the Reactions of the Ferricyanide Ion with Cobalt(II)-Aminopolycarboxylate Complexes

Hiroshi OGINO, Masatake TAKAHASHI, and Nobuyuki TANAKA

Department of Chemistry, Faculty of Science, Tohoku University, Aoba, Aramaki, Sendai 980

(Received November 26, 1973)

Kinetic studies of the reactions of the ferricyanide ion with cobalt(II)-aminopolycarboxylate complexes were carried out. The aminopolycarboxylates used in this study were trimethylenediaminetetraacetate (TRDTA), *trans*-1,2-cyclohexanediaminetetraacetate (CyDTA), propylenediaminetetraacetate(PDTA), and *N*-hydroxyethyl ethylenediaminetriacetate(HEDTA). The first step in the reaction is the rapid formation of a binuclear complex intermediate, [(aminopolycarboxylate)$Co^{III}NCFe^{II}(CN)_5]^{n-}$ ($n=5$ for TRDTA, CyDTA and PDTA and 4 for HEDTA), followed by the dissociation of the intermediate to ferrocyanide and Co(III)-aminopolycarboxylate ions. The equilibrium constant of the formation reaction and the rate constant of the dissociation reaction of the intermediate at an ionic strength of 0.66 were 6.2×10^{2} M^{-1} and 2.0×10^{-2} s^{-1} respectively for the TRDTA system at 5 °C, 3.3×10 M^{-1} and 2.7×10^{-2} s^{-1} for the CyDTA system at 25 °C, and 2.4×10^{3} M^{-1} and 3.0×10^{-3} s^{-1} for the PDTA system at 25 °C. The rate constant of the dissociation of [hedta $Co^{III}NCFe^{II}(CN)_5]^{4-}$ was found to be smaller than 1×10^{-4} s^{-1} at 25 °C and at an ionic strength of 0.66.

It has been reported that the reaction of the ferricyanide ion with ethylenediaminetetraacetatocobaltate(II) (cobalt(II)-EDTA) produced the ferrocyanide ion and the cobalt(III)-EDTA complex as the final products:[1,2]

$$Fe^{III}(CN)_6^{3-} + Co^{II}edta^{2-} \longrightarrow Fe^{II}(CN)_6^{4-} + Co^{III}edta^{-} \quad (1)$$

This reaction proceeds through two consecutive steps. The first step is the formation reaction of a metastable binuclear intermediate, $[edtaCo^{III}NCFe^{II}(CN)_5]^{5-}$, by an inner-sphere electron-transfer reaction between ferricyanide and cobalt(II)-EDTA. The second step is the dissociation of the intermediate to ferrocyanide and cobalt(III)-EDTA. Analogous reactions of the ferricyanide ion with cobalt(II) complexes containing *trans*-1,2-cyclohexanediaminetetraacetate (CyDTA) and diethylenetriaminepentaacetate (DTPA) were investigated by Huchital and Hodges very recently.[3,4]

This paper will describe kinetic studies of the reactions between the ferricyanide ion and cobalt(II) complexes with several aminopolycarboxylates,[5] studies which have been carried out in order to ascertain how the change in the nature of aminopolycarboxylates influences the features of the reactions.

Experimental

Materials. H_4pdta,[6] H_4trdta,[7,8] K[Co pdta]·H_2O,[6] K[Co cydta]·$3H_2O$,[9] and K[Co trdta]·$2H_2O$[7] were prepared by methods described previously. The solution of Co hedta-(H_2O) was prepared in a way similar to that which has been reported for the preparation of $Co^{III}trdta^{-}$.[7] The resulting solution was passed through a cation-exchange resin column, Dowex 50W-X8 (hydrogen-ion form). The effluent was then passed through an anion-exchange resin column, Dowex 1 X-4 (acetate-ion form). The resulting solution was evaporated to a small volume with a rotating evaporator and dried over a phosphorus pentoxide desiccator. Found: C, 32.21; H, 5.27; N, 7.72%. Calcd for $[Co(C_{10}H_{15}N_2O_7)(H_2O)]\cdot H_2O$: C, 32.45; H, 5.17; N, 7.57%.

Kinetic Measurements. Kinetic measurements were made by recording the change in the absorbance at a given wavelength as a function of the time, using a Hitachi EPS-3 pen-recording spectrophotometer. The solution containing given amounts of cobalt(II) ions, aminopolycarboxylate, and an acetate buffer was placed in a quartz spectrophotometer cell, which was then sealed with a serum cap. The reaction was initiated by the addition of a potassium ferricyanide solution using a syringe. The mixing was performed by the passage of a rapid stream of nitrogen gas. The concentration of aminopolycarboxylate was kept at five to ten times that of the cobalt(II) ions. The temperature of the optical cell was controlled at 25.0 °C for the PDTA, CyDTA, and HEDTA systems and 5.0 °C for the TRDTA system. The pH of the solution was adjusted to 5.0 with the acetate buffer solution, and the ionic strength was regulated at 0.66 with sodium acetate.

Results

Spectral Change in the Reactions of the Ferricyanide Ion with Cobalt(II)-Aminopolycarboxylates. Figure 1 shows the change in the absorbance at 550 nm with the time which was obtained for the reaction of $Fe^{III}(CN)_6^{3-}$ with $Co^{II}pdta^{2-}$. The absorbance at zero time which was calculated from the initial concentrations and the molar extinction coefficients of the two reactants is 0.196. However, this calculated value was much smaller than the actual value which was obtained from the extrapolation of the absorbance-time

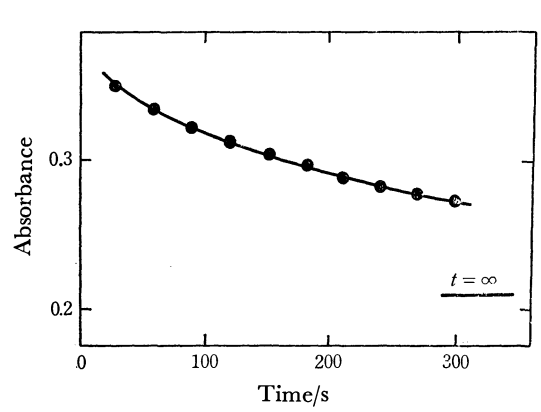

Fig. 1. Absorbance at 550 nm as a function of time obtained for the reaction of ferricyanide ion with cobalt(II)-PDTA complex. Initial concentrations are: $[Fe(CN)_6^{3-}]_{t=0}=0.500$ mM and $[Co^{II}pdta^{2-}]_{t=0}=8.63$ mM.

curve in Fig. 1 to zero time. This suggested that an intermediate was rapidly formed and then converted to the other species. The final reaction products were identified spectrophotometrically as $Fe^{II}(CN)_6^{4-}$ and $Co^{III}pdta^-$. Similar phenomena were also observed for the CyDTA and the TRDTA system. These observations mean that the reaction proceeds in a fashion similar to that of the EDTA system;[1,2] that is, it proceeds through two consecutive steps:

$$Fe^{III}(CN)_6^{3-} + Co^{II}Y^{2-} \overset{K_a}{\rightleftharpoons} YCo^{III}NCFe^{II}(CN)_5^{5-} \quad (2)$$

$$YCo^{III}NCFe^{II}(CN)_5^{5-} \overset{k}{\longrightarrow} Fe^{II}(CN)_6^{4-} + Co^{III}Y^- \quad (3)$$

where Y denotes the tetranegative anion of aminopolycarboxylates. The reaction of $Fe^{III}(CN)_6^{3-}$ with cobalt(II)-HEDTA, however, was found to be different; an intensely-colored species was formed when the reactants were mixed, and it remained unchanged for at least several hours. Figure 2 shows the spectra of the species related to the reaction of $Fe^{III}(CN)_6^{3-}$ with $Co^{II}hedta(H_2O)^-$. Curve A in Fig. 2 is the spectrum for the solution containing $Fe^{III}(CN)_6^{3-}$ and $Co^{II}hedta(H_2O)^-$. This does not coincide with the synthetic spectrum (Curve E in Fig. 2) which was calculated by assuming that the following reaction occurred:

$$Fe^{III}(CN)_6^{3-} + Co^{II}hedta(H_2O)^- \longrightarrow Fe^{II}(CN)_6^{4-} + Co^{III}hedta(H_2O) \quad (4)$$

The shape of Spectrum A is very similar to those of [edta $Co^{III}NCFe^{II}(CN)_5]^{5-}$ and [cydta $Co^{III}NCFe^{II}(CN)_5]^{5-}$.[1,3] These facts suggest that [hedta $Co^{III}NCFe^{II}(CN)_5]^{4-}$ is formed rapidly by the reaction between $Fe^{III}(CN)_6^{3-}$ and $Co^{II}hedta(H_2O)^-$ and that Spectrum A corresponds to the sum of the spectra of [hedta $Co^{III}NCFe^{II}(CN)_5]^{4-}$ and $Co^{II}hedta(H_2O)^-$, the latter of which is present in a large excess.

Kinetic Results. The dissociation of the intermediates was followed under pseudo-first order conditions. The rate constant, k_{app}, was obtained from the slope of plots of log $|D_t - D_\infty|$ *vs.* time, where D_t and D_∞ mean the absorbances at time t and at infinite, respectively. Adamson and Gonick[1] derived the following equation for k_{app} by assuming that the reaction proceeds by means of the mechanism indicated in Eqs. 2 and 3:

$$k_{app} = \frac{kK[Co^{II}Y^{2-}]}{1+K[Co^{II}Y^{2-}]} \quad (5)$$

This equation may be rewritten as:

$$\frac{1}{k_{app}} = \frac{1}{k} + \frac{1}{kK[Co^{II}Y^{2-}]} \quad (6)$$

As is shown in Fig. 3, the plots of $1/k_{app}$ *vs.* $1/[Co^{II}Y^{2-}]$ for various aminopolycarboxylate systems show linear relations which are consistent with the mechanism given in Eqs. 2 and 3. The values of k and K were obtained from the intercepts and slopes of these plots. The results are summarized in Table 1, along with the values reported previously. The values of k and K for the CyDTA system obtained in this work are in good agreement with those obtained by Huchital and Hodges.[3] In the case of the HEDTA system, only a lower limit of the rate constant could be determined.

Discussion

The rate constants of the dissociation of the intermediate, $[YCo^{III}NCFe^{II}(CN)_5]^{n-}$, were found to be

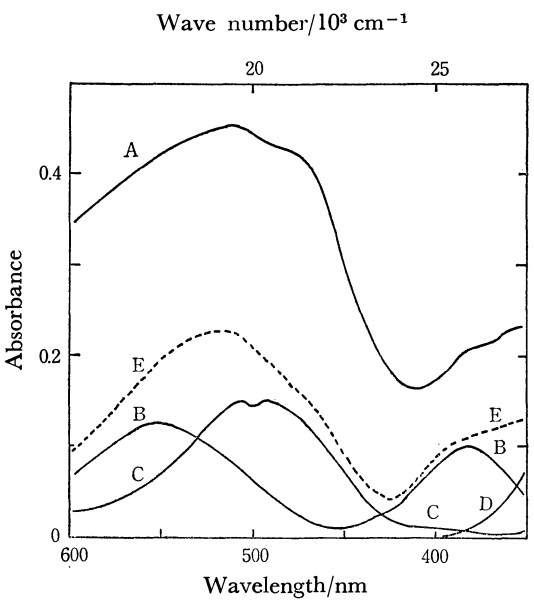

Fig. 2. Spectra of the species related to the reaction of ferricyanide ion with cobalt(II)-HEDTA.
(A) Spectrum obtained for the cobalt(II)-HEDTA solution upon the addition of ferricyanide: $[Co^{II}hedta(H_2O)^-]_{t=0}=8.63$ mM, $[Fe(CN)_6^{3-}]_{t=0}=0.500$ mM. (B) Spectrum of 0.500 mM $[Co^{III}hedta(H_2O)]$ (C) Spectrum of 8.13 mM $[Co^{II}hedta(H_2O)^-]$, (D) Spectrum of 0.500 mM $[Fe(CN)_6^{4-}]$, (E) Synthetic spectrum resulted from the sum of spectra (B), (C) and (D).

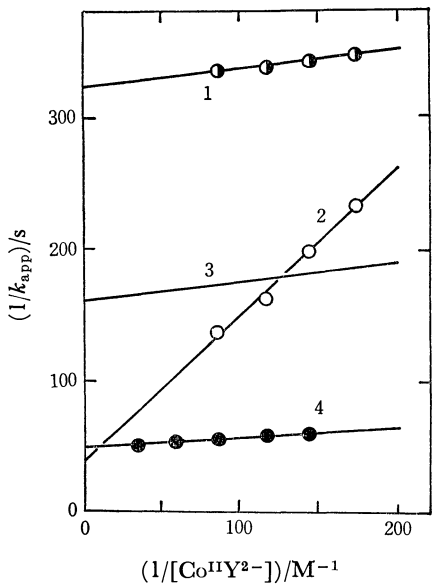

Fig. 3. Plots of reciprocal pseudo-first order rate constant as a function of reciprocal concentrations of cobalt(II)-PDTA (1), -CyDTA (2), -EDTA (3) and -TRDTA (4). Temperature: 25.0 °C for PDTA, CyDTA and EDTA systems and 5.0 °C for TRDTA system. Data for EDTA system are taken from Ref. 1.

Table 1. Equilibrium constants K of reaction (2) and rate constants k of reaction (3).

Aminopoly-carboxylate	Temp/°C	K/M^{-1}	k/s^{-1}	Ref.
TRDTA	5	6.2×10^{2}	2.0×10^{-2}	This work
CyDTA	5	4.0×10^{2} a)	1.2×10^{-3} a)	3
	25	4.4×10	2.2×10^{-2}	3
	25	3.3×10	2.7×10^{-2}	This work
EDTA	5	6.1×10^{3} a)	2.1×10^{-4} a)	3
	25	8.3×10^{2}	5.4×10^{-3}	3
PDTA	25	2.4×10^{3}	3.0×10^{-3}	This work
HEDTA	25	—	$<1\times10^{-4}$	This work
	—	$\sim5\times10^{3}$	—	4

a) The value was calculated from the data reported in Ref. 3 by the present authors.

in the following order with the natures of the aminopolycarboxylates:

$$\text{TRDTA} > \text{CyDTA} > \text{EDTA, PDTA} \gg \text{HEDTA}$$

where $n=5$ for TRDTA, CyDTA, EDTA, and PDTA, and 4 for HEDTA. This order is parallel to the tendency of aminopolycarboxylates to take a hexadentate structure in the cobalt(III) complexes. Several facts demonstrate that the hexadentate structures of the Co(III)CyDTA and Co(III)-TRDTA complexes are much more stable than the corresponding pentadentate structures, while the hexadentate structures of the Co(III)-EDTA and Co(III)-PDTA complexes are slightly more stable than the pentadentate structures. Complexes of the $Co^{III}Xedta^{2-}$ and $Co^{III}Xpdta^{2-}$ types, where X is Cl^-, Br^-, NO_2^- or OH^-, have also been prepared.[10-13] The ligand X in these complexes is slowly eliminated in a solution, and the complexes come to have the hexadentate structure.[14,15] Dwyer and Garvan observed a rapid conversion of Co^{III}-Clcydta^{2-} to $Co^{III}cydta^-$.[9] Van Saun and Douglas failed in preparing complexes in which TRDTA functions as a pentadentate ligand.[16] Therefore, the $[trdtaCo^{III}NCFe^{II}(CN)_5]^{5-}$ complex detected in this work is the first example of a complex in which TRDTA functions as a pentadentate ligand.

The equilibrium constant of the following acid dissociation reaction may also be a measure of the tendency of aminopolycarboxylates to take a hexadentate structure in cobalt(III) complexes:

$$Co^{III}HY(H_2O) \overset{K_a}{\rightleftharpoons} Co^{III}Y^- + H^+ + H_2O \qquad (7)$$

The value of K_a for the EDTA complex has been determined to be 1.31 M^{-1} at 25 °C and at an ionic strength of 2.0.[17] In this work, the K_a value for the PDTA complex was determined spectrophotometrically to be 1.04 M^{-1} at 25 °C and at an ionic strength of 2.0, this value is very close to that of the EDTA complex. The value of K_a for the CyDTA complex has not yet been reported. However, it was found in this work that $Co^{III}cydta^-$ did not show any spectral change with the increase in the hydrogen-ion concentration up to 5 M in nitric acid. This is the same result as for Co^{III} trdta$^-$.[17] Hence, the formations of $Co^{III}Hcydta(H_2O)$ and $Co^{III}Htrdta(H_2O)$ are considered to be very unfavored.

The increasing tendency to have a hexadentate structure of the CyDTA and TRDTA complexes compared with the EDTA and PDTA complexes holds also in the corresponding complexes of other metals. Both chromium(III)-EDTA[18] and PDTA[19] complexes contain one water molecule in the first coordination sphere, while both CyDTA[19] and TRDTA[20] function as hexadentate ligands in their chromium(III) complexes.

Higgison determined the proportions of several metal(II) complexes containing EDTA, PDTA, or CyDTA in the hexadentate form, the remaining part being the pentadentate form in which the sixth coordination position of the central metal(II) ion is occupied by an aqua ligand.[21] These data also show the increasing tendency to be of a hexadentate structure of the cobalt(II)-, nickel(II)- and copper(II)-CyDTA complexes compared with the corresponding EDTA and PDTA complexes.

The HEDTA system provides an extreme case in which HEDTA functions as a pentadentate ligand because of the very weak coordination ability of the *N*-hydroxyethyl group. The rate of the dissociation of $[hedta\ Co^{III}NCFe^{II}(CN)_5]^{4-}$ was very slow; this is consistent with the interpretation of the order of the dissociation rate of the intermediates presented above. Therefore, the dissociation of the intermediates, $[YCo^{III}$-$NCFe^{II}(CN)_5]^{n-}$, may be a S_N2 reaction, as has been proposed by Huchital and Hodges,[3] in which unbound carboxylate assists the elimination of $Fe^{II}(CN)_6^{4-}$ from the central cobalt(III) ion.

All the hexadentate EDTA, TRDTA, PDTA and CyDTA complexes of cobalt(III) contain two nonequivalent acetate rings. One is in the plane of the diamine chelate ring (in-plane acetate), and the other is perpendicular to the in-plane acetate rings (out-of-plane acetate). In a previous paper,[8] it was suggested that the trimethylenediamine chelate ring in Co^{III} trdta$^-$ takes a twist-boat form and that the in-plane acetate rings are more strained than the out-of-plane acetate rings. This was confirmed later by X-ray study.[22] The data revealed that the shape and size of the four acetate rings of $Co^{III}trdta^-$ are essentially identical to those of $Co^{III}edta^-$.[23] The in-plane acetate rings show considerable departure from planarity and are strained, while the out-of-plane acetate rings are nearly planar. It has been inferred that the conformational situations of acetate rings in $Co^{III}pdta^-$ and $Co^{III}cydta^-$ are similar to those in $Co^{III}edta^-$.[24,25] This may be true also for $Co^{III}hedta(H_2O)$, because HEDTA has a structure very similar to that of EDTA.

It is known that X in $Co^{III}Xedta^{2-}$ replaces an in-plane acetate.[26] Busch *et al.* investigated the reactions of ethylenediamine with $Co^{III}edta^-$ and Co^{III}-pdta$^-$ to produce the tris(ethylenediamine)cobalt(III) ion.[24,27,28] They found a satisfactory interpretation for the reaction mechanism on the assumption that the first step of the entry of ethylenediamine to the coordination sphere of the cobalt(III) ion is the replacement of an in-plane acetate group. Therefore, it is reasonable to consider that the cyano group coordinated to the

cobalt(III) ion in the intermediate given in Eq. 2 replaces an in-plane acetate group.

Huchital and Hodges reported that the higher value of k for the CyDTA complex than that for the EDTA complex was due to the steric hindrance between the methylene protons of the acetate ring and the axial proton in the 3 position of the cyclohexane ring.[3] However, this does not seem to be the cause of the higher value of k, because the acetate protons which interfere with the axial proton in the 3 position of the cyclohexane ring are out-of-plane protons. There is no steric interaction between the axial proton in the cyclohexane ring and the proton of the in-plane acetate ring which is replaced by the incoming cyano group. The molecular model for the $Co^{III}pdta^-$ complex reveals that there is a steric hindrance between the proton of the out-of-plane acetate ring and the methyl protons. This steric hindrance is similar to that between the proton of the out-of-plane acetate ring and the axial proton in the 3 position of the cyclohexane ring for the CyDTA complex. If the out-of-plane acetate group, which suffers steric hindrance from the proton of the methyl group, is replaced by a cyano group, the value of k for the PDTA system would be expected to be much different from that for the EDTA system. The results given in Table 1 show that this is not true and that the values of k for the two systems are essentially identical. Therefore, it may be concluded that the cyano group coordinated to the cobalt(III) ion in the intermediate replaces the in-plane acetate group.

The equilibrium constant of Reaction 2, K, was found to increase in the following order with the nature of the aminopolycarboxylates:

$$\text{CyDTA, TRDTA} < \text{EDTA, PDTA} < \text{HEDTA}$$

This order is not related to that of the magnitude of the oxidation-reduction potentials of the Co(III)-Y/Co(II)-Y sysetm,[29,30] but it is the reverse of the order found for the values of the rate constant, k, except for TRDTA and CyDTA. Hence, it can reasonably be concluded that the value of K becomes larger for aminopolycarboxylates, which have a stronger tendency to take a pentadentate structure.

The authors are grateful to the Ministry of Education for its financial support and to the Matsunaga Science Foundation for a grant to one of them (H. O.).

References

1) A. W. Adamson and E. Gonick, *Inorg. Chem.*, **2**, 129 (1963).
2) D. H. Huchital and R. G. Wilkins, *ibid.*, **6**, 1022 (1967).
3) D. H. Huchital and R. J. Hodges, *ibid.*, **12**, 998 (1973).
4) D. H. Huchital and R. J. Hodges, *ibid.*, 12, 1004 (1973).
5) The aminopolycarboxylates used in this study were 1,2-diaminoethane-*N*,*N*,*N*′,*N*′-tetraacetate (EDTA), *trans*-1,2-diaminocyclohexane-*N*,*N*,*N*′,*N*′-tetraacetate (CyDTA), 1,2-diaminopropane-*N*,*N*,*N*′,*N*′-tetraacetate (PDTA), 1,3-diaminopropane-*N*,*N*,*N*′,*N*′-tetraacetate (TRDTA), and *N*-hydroxy ethylethylenediamine-*N*,*N*′,*N*′-triacetate (HEDTA).
6) F. P. Dwyer and F. L. Garvan, *J. Amer. Chem. Soc.*, **81**, 2955 (1959).
7) N. Tanaka and H. Ogino, This Bulletin, **37**, 877 (1964).
8) H. Ogino, M. Takahashi, and N. Tanaka, *ibid.*, **43**, 424 (1970).
9) F. P. Dwyer and F. L. Garvan, *J. Amer. Chem. Soc.*, **83**, 2610 (1961).
10) G. Schwarzenbach, *Helv. Chim. Acta*, **32**, 839 (1949).
11) M. L. Morris and D. H. Busch, *J. Amer. Chem. Soc.*, **78**, 5178 (1956).
12) I. A. W. Shimi and W. C. E. Higginson, *J. Chem. Soc.*, **1958**, 260.
13) K. Swaminathan and D. H. Busch, *J. Inorg. Nucl. Chem.*, **20**, 159 (1961).
14) M. L. Morris and D. H. Busch, *J. Phys. Chem.*, **63**, 340 (1959).
15) K. Swaminathan and D. H. Busch, *Inorg. Chem.*, **1**, 256 (1962).
16) C. W. Van Saun and B. E. Douglas, *ibid.*, **8**, 1145 (1969).
17) H. Ogino, M. Takahashi, and N. Tanaka, This Bulletin, **46**, 178 (1973).
18) G. Schwarzenbach and W. Biedermann, *Helv. Chim. Acta*, **31**, 459 (1948).
19) N. Tanaka, K. Kanno, T. Tomita, and A. Yamada, *Inorg. Nucl. Chem. Letters*, **7**, 953 (1971).
20) J. A. Weyh and R. E. Hamm, *Inorg. Chem.*, **7**, 2431 (1968).
21) W. C. E. Higginson, *J. Chem. Soc. A*, **1970**, 1579.
22) R. Nagao, F. Marumo, and Y. Saito, *Acta Crystallogr., B*, **26**, 1852 (1972).
23) H. A. Weakliem and J. L. Hoard, *J. Amer. Chem. Soc.*, **81**, 549 (1959).
24) D. H. Busch and K. Swaminathan, *J. Inorg. Nucl. Chem.*, **23**, 150 (1961).
25) J. B. Terrill and C. N. Reilley, *Inorg. Chem.*, **5**, 1988 (1966).
26) C. W. Van Saun and B. E. Douglas, *ibid.*, **7**, 1393 (1968).
27) D. H. Busch and D. W. Cooke, *J. Inorg. Nucl. Chem.*, **23**, 145 (1961).
28) D. H. Busch, K. Swaminathan, and D. W. Cooke, *Inorg. Chem.*, **1**, 260 (1962).
29) N. Tanaka and H. Ogino, This Bulletin, **38**, 1054 (1965).
30) H. Ogino, unpublished results.

Kinetics of Multidentate Ligand Substitution Reactions. XVI. Substitution Reactions of 1,2-Cyclohexanediamine-*N*,*N*,*N*′,*N*′-tetraacetic Acid (CyDTA) with the Zinc(II)–Ethylenediaminemonoacetate (EDMA) and –Ethylenediamine-*N*,*N*′-diacetate (EDDA) Complexes and That of Ethylenediamine-*N*,*N*,*N*′,*N*′-tetraacetic Acid (EDTA) with the Nickel(II)–EDDA Complex

Mutsuo KODAMA

Department of Chemistry, College of General Education, Hirosaki University, Bunkyo, Hirosaki, Aomori 036

(Received November 26, 1973)

The kinetics of the substitution reactions of CyDTA with zinc(II)–EDMA and –EDDA complexes and that of EDTA with the nickel(II)–EDDA complex were studied systematically by using the polarographic technique. All the substitution reactions were found to be first-order with respect to the CyDTA or EDTA anion and also first-order with respect to the 1 : 1-ratio EDMA or EDDA complex. From a comparison of the observed rate constants with those estimated on the basis of the proposed reaction intermediates, the detailed reaction mechanisms were discussed. The rates of the reactions of zinc(II)–EDMA complex and nickel(II)–EDDA complex could be understood in terms of the ethylenediamine reaction mechanism, but that of the reaction of the zinc(II)–EDDA complex with the CyDTA anion could not. This discrepancy may be ascribed by the steric hindrance of the CyDTA anion to the formation of an ethylenediamine reaction intermediate in the reaction of the zinc(II)–EDDA complex.

In a previous paper,[1] the present author studied the steric effect of the cyclohexane ring on the rate of the substitution reactions of metal(II)–aminopolycarboxylate complexes. In this paper, the present author will deal with the kinetics of the substitution reactions of CyDTA with the zinc(II)–EDMA and –EDDA complexes as an extention of an earlier investigation of the steric effects of the CyDTA anion on the reaction of the metal(II)–aminopolycarboxylate complex. In order to describe more precisely the nature of the steric effect of the CyDTA anion, the substitution reaction of EDTA with the nickel(II)–EDDA complex will also be studied.

Experimental

Reagents. The preparation and standardization of zinc(II) and nickel(II) solutions were described in previous papers.[2,3] Reagent-grade EDDA, CyDTA, and glycine were recrystallized from their aqueous solutions by adding pure hydrochloric acid and ethanol. The preparation and recrystallization of EDMA were also described previously.[4] The other chemicals used in this study were of an analytical reagent-grade and were used without further purification.

Apparatus and Experimental Procedures. The apparatus and the experimental procedures were the same as those described previously.[1] In this study, all the measurements were conducted in solutions with an ionic strength of 0.30 ($NaClO_4$) at 25 °C. No buffer reagent was used, because the sample solutions always contained a large excess of uncomplexed EDMA, EDDA, or Gly, and had enough buffer capacity in the pH ranges studied ($9.50<pH<10.50$ in the EDMA system and $9.00<pH<10.20$ in the EDDA system). In the case of the zinc(II) system, the kinetic measurements were carried out in sample solutions containing large excesses of uncomplexed CyDTA and EDMA or EDDA over the complexed EDMA or EDDA. In the reaction of the nickel(II) complex, the kinetic measurements were carried out in solutions containing large excesses of complexed and uncomplexed EDDA over EDTA. Therefore, all the reactions could be treated as pseudo-first-order reactions. The rate of the substitution reaction of the zinc(II) complex was determined by measuring the change in the reduction wave-height of the zinc(II)–EDMA or –EDDA complex. On the other hand, the rate of the reaction involving the nickel(II)–EDDA complex was determined by observing the change in the dissolution wave due to the uncomplexed EDTA.

Results and Discussion

The reaction of CyDTA with the zinc(II)–EDMA complex showed the same kinetic behavior as that with the zinc(II)–*N*-(2-hydroxyethyl)iminodiacetate (HIDA) complex,[1] suggesting the following reaction mechanism (I):

$$MX_2^{(2-2m)+} \rightleftharpoons MY^{(2-m)+} + X^{m-} \quad (1_a) \text{ in a rapid equil.}$$

(I)

$$MX^{(2-m)+} + \begin{cases} HY^{3-} \overset{k_H}{\rightleftharpoons} MY^{2-} + HX^{(1-m)} & (1_b) \\ Y^{-4} \overset{k_0}{\rightleftharpoons} MY^{2-} + X^{m-} & (2_c) \end{cases} \text{ rds}$$

Therefore, the k_0 and k_H values were determined from the intercept and slope of the linear relation between $k_{ap}^{+}\cdot(1+K_2\cdot[X]_f/(\alpha_H)_x)\cdot(\alpha_H)_Y/[Y]_f$ and $[H^+]$ (Table 1). Here, all the symbols used have their usual meanings.[1] The substitution reactions of the nickel(II)–EDDA complex with EDTA was studied in sample solutions containing excess glycinate. In this reaction, the k_{ap}^{+} value determined from the slope of the linear relation between $\log(i_0/i_t)$ and t was independent of the concentration of the uncomplexed EDDA and of the initial concentration of EDTA. However, it decreased appreciably with an increase in the Glut concentration $[G]_f$, and the plot of the $[Ni(II)]/k_{ap}^{+}\cdot(\alpha_H)_Y$ against the concentration of the Glut anion, $[G]_f/(\alpha_H)_G$, gave a straight line with an intercept of a finite value (Fig. 1). This indicates the formation of a 1 : 1 : 1-ratio mixed ligand complex, MXG^-, corresponding to the following reaction mechanism (II):

$$MXG^- \rightleftharpoons MX^0 + G^- \quad (2_a) \text{ in a rapid equil.}$$

(II)

$$MX^0 + \begin{cases} HY^{3-} \overset{k_H}{\rightleftharpoons} MY^{2-} + HX^- & (2_b) \\ Y^{4-} \overset{k_0}{\rightleftharpoons} MY^{2-}. + X^{2-} & (2_c) \end{cases} \text{ rds}$$

TABLE 1. RATE CONSTANTS (μ=0.30, 25°C)

A) Ni(II) system

log K_{MX}	System	Observed rate constant		Rate constant ratio		
				Obsd		Calcd (En mechanism)
		k_0	k_H	k_0	k_H	
13.20	EDDA	7.0	3.72	1.0	1.0	1.0
10.44	EDMA[7]	1.5×10^3	3.90×10^2	$10^{2.30}$	$10^{2.02}$	$10^{2.26}$

B) Zn(II) system

log K_{MX}	System	Observed rate constant		k_0 ratio		
				Obsd	Calcd	
		k_0	k_H		En mecha.	Gly mecha.
8.02	HIDA	2.7×10^4	2.60×10^2	1.0	—	1.0
8.22	EDMA	5.6×10^2	3.20×10^1	$10^{-1.68}$	$10^{-1.74}$	—
10.79	EDDA	1.9×10^1	$6.0_0\times10^{-1}$	$10^{-3.15}$	$10^{-4.00}$	$10^{-2.77}$

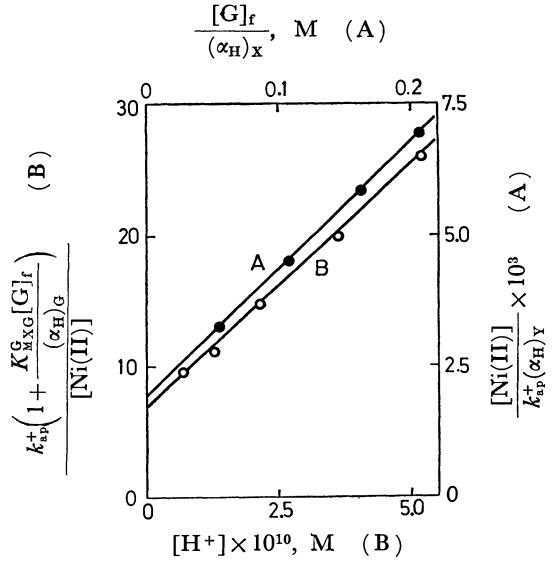

Fig. 1. The relation between $[Ni(II)]/k^+_{ap}\cdot(\alpha_H)_Y$ and $[G]_f/(\alpha_H)_G$ and that between $k^+_{ap}\cdot(\alpha_H)_Y\cdot(1+K^G_{MXG}\cdot[G]_f/(\alpha_H)_G)/[Ni(II)]$ and $[H^+]$.
μ=0.30, 25 °C
$[EDDA]_f$=28.3 mM, $[EDTA]_l$=0.566 mM
A) The relation between $[Ni(II)]/k^+_{ap}\cdot(\alpha_H)_Y$ and $[G]_f/(\alpha_H)_G$
pH=9.70, [Ni(II)]=5.66 mM
$[G]_f$ ranged from 80 to 290 mM
B) The relation between $k^+_{ap}\cdot(\alpha_H)_Y(1+K^G_{MXG}\cdot[G]_f/(\alpha_H)_G)/[Ni(II)]$ and $[H^+]$
[Ni(II)]=7.55 mM, $[G]_f$=28.3 mM
pH ranged from 9.20 to 10.20

Since the 1 : 1 : 1-ratio mixed ligand complex of the nickel(II)-ion involving the EDDA and Glut anions can be synthesized easily by mixing $NiCl_2$, EDDA, and Glut solutions and by evaporating the resulting mixture to dryness,[5] the above conclusion seems reasonable. From the ratio between the slope and the intercept of the above linear relation, the equilibrium constant, $K^G_{MXG}=[MXG^-]/[MX^0]\cdot[G^-]$, was determined to be 13.1. For the above reaction mechanism, the apparent rate constant, k^+_{ap}, is given by $[Y]_f(k_0+k_H\cdot[H^+]/K_4)/(\alpha_H)_Y\cdot(1+K^G_{MXG}\cdot[G]_f/(\alpha_H)_G)$. Therefore, the k_0 and k_H values were determined from the intercept and slope of the linear relation between $k^+_{ap}\cdot(\alpha_H)_Y\cdot(1+K^G_{MGX}\cdot[G]_f/(\alpha_H)_G)/[Y]_f$ and $[H^+]$ (Fig. 1). They are also listed in Table 1.

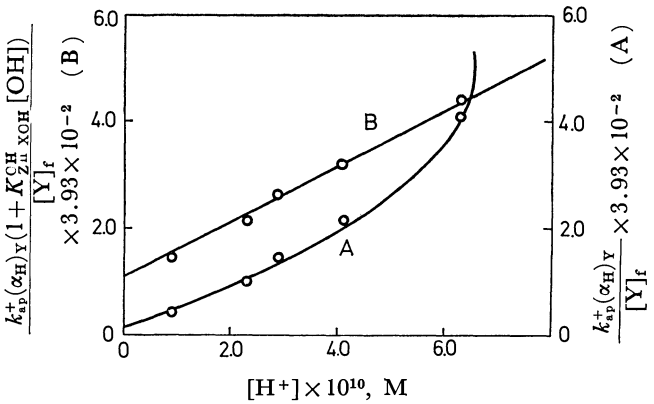

Fig. 2. The plot of $k^+_{ap}\cdot(\alpha_H)_Y/[Y]_f$ or $k^+_{ap}(\alpha_H)_Y(1+K^{OH}_{ZnX(OH)}[OH^-])/[Y]_f$ against $[H^+]$.
[Zn(II)]=1.0 mM, $[EDDA]_f$=20.0 mM
$[CyDTA]_l$=10 mM
μ=0.30, 25 °C
A) The plot of $k^+_{ap}\cdot(\alpha_H)_Y/[Y]_f$ against $[H^+]$
B) The plot of $k^+_{ap}\cdot(\alpha_H)_Y(1+K^{OH}_{ZnX(OH)}[OH^-])/[Y]_f$ against $[H^+]$

The substitution reaction of the zinc(II)-EDDA complex with CyDTA was studied in solutions not containing glycinate. As in the case of the nickel(II)-EDDA system, the k^+_{ap} value was independent of the cocentration of the uncomplexed EDDA and of the initial concentration of the zinc(II)-EDDA complex. However, the plot of k^+_{ap} multiplied by $(\alpha_H)_Y/[Y]_f$ against the hydrogen ion concentration, $[H^+]$, gave no linear relation (Fig. 2). This may suggest the formation of a mixed-ligand complex involving the hydroxide anion. Since the zinc(II)-EDDA complex forms a mixed-ligand complex, $ZnX(NCS)^-$,

with NCS^-,[6] it is natural to assume the formation of the 1 : 1 : 1-ratio mixed ligand complex, $ZnX(OH)^-$. If the slow reaction pathways, (2_b) and (2_c), are preceded by the rapid dissociation of $ZnX(OH)^-$ into ZnX^0, corresponding to the k_{ap}^+ value of $[Y]_f(k_0+k_H[H^+]/K_4)/(\alpha_H)_Y(1+K_{ZnX(OH)}^{OH}[OH^-])$, the equilibrium constant, $K_{ZnX(OH)}^{H}(=[ZnX(OH)^-]/[ZnX^0]\cdot[OH^-])$, should be given by Eq. (1):

$$k_{ZnX(OH)}^{OH}=\frac{1}{K_w}\frac{(P_1\cdot[H^+]_1-P_2\cdot[H^+]_2)([H^+]_1-[H^+]_2\cdot)-(P_1\cdot[H^+]_1-P_3\cdot[H^+]_3)\cdot([H^+]_1-[H^+]_3)}{(P_1-P_2)([H^+]_1-[H^+]_3)-(P_1-P_3)([H^+]_1-[H^+]_2)} \quad (1)$$

and the plot of $k_{ap}^+\cdot(1+K_{ZnX(OH)}^{OH}\cdot[OH^-])\cdot(\alpha_H)_Y/[Y]_f$ against $[H^+]$ should give a straight line with an intercept of a finite value. By using the $K_{ZnX(CH)}^{OH}$ value of 2×10^4 estimated with the aid of Eq. (1), the $k_{ap}^+\cdot(\alpha_H)_Y\cdot K_{ZnX(OH)}^{OH}\cdot[OH^-])/[Y]_f$ value was plotted against $[H^+]$. As is illustrated by the straight line (B) in Fig. 2, the above plot invariably gave a linear relation with an intercept of a finite value. From the intercept and the slope of the above linear relation, the k_0 and k_H values for the substitution reaction of the zinc(II)–EDDA complex with CyDTA were determined (Table 1). Previously,[1] the present author systematically studied the substitution reaction of the zinc(II)–HIDA complex with CyDTA at 0 °C and drew the conclusion that the reaction proceeds through the glycinate-reaction mechanism. In this paper, this reaction was studied at 25 °C, and the k_0 and k_H values were determined to be 2.7×10^4 and $2.6_0\times10^2$ respectively.

Previously,[7] the present author mentioned that the substitution reaction of the nickel(II)–EDMA complex with EDTA proceeds through the ethylene diamine(En)-reaction intermediate, where the leaving EDMA and entering EDTA anions are bonded to the nickel(II) ion through ethylenediamine- and glycinate-chelate rings respectively. Therefore, it is reasonable to assume the En mechanism for the substitution reaction of the nickel(II)–EDMA complex with EDTA. The relative rate constant for the reaction of the nickel(II)–EDDA complex with EDTA was calculated on the basis of the En-reaction intermediate by means of this relation; $k=k_{rds}\cdot K_L\cdot K_A\cdot K_{st}\cdot K_{elec}/K_{MX}$,[1] and was compared with the observed one (Table 1). Here, all the symbols in the above relation have their usual meanings.[1] The good agreement between the calculated and observed relative rate constants supports the above En-mechanism explanation. Since the steric hindrance to the CyDTA anion in its reaction with the zinc(II)–HIDA complex is considered to be quite the same as those of the reactions with the zinc(II)–EDMA and –EDDA complexes, one can also calculate the relative rate constants with reference to the zinc(II)–HIDA system on the basis of the proposed reaction intermediate. Since, in the substitution reaction, the zinc(II)-aminopolycarboxylate complex shows kinetic behavior very similar to that of the corresponding nickel(II) complex,[8] one can assume the En-reaction mechanism for the reactions of CyDTA with the zinc(II)–EDMA and –EDDA complexes. As is shown in Table 1, the k_0 ratio between the HIDA and EDMA systems calculated by assuming the En-reaction mechanism for the EDMA system agreed well with the observed one. However, the rate of the substitution reaction of the zinc(II)–EDDA complex with CyDTA cannot be understood by assuming the En mechanism. This discrepancy may be ascribed to the steric effect of the CyDTA anion on the reaction mechanism. The k_{rds} values for the Gly and En mechanisms were approximated by the dissociation rate constants of the 1 : 1-ratio zinc(II)–Gly and –En complexes respectively. The dissociation rate constant of the zinc(II)–Gly complex was estimated to be 1.5×10^3 from the formation rate constant, k_f, with the aid of the $K_{MX}=k_f/k_d$ relation. The k_f value was calculated by using the $k_{Zn}^{H_2O}$ value of 3.2×10^7 and the K_{os} value of 5 on the basis of the usual water-exchange mechanism.[9] The dissociation rate constant of the 1 : 1-ratio zinc(II)–En complex was evaluated as 3.0×10^2 from the dissociation constant of the 1 : 1-ratio zinc(II)–ammine complex[10] by correcting it for the rotational barrier around the C–N bond.[11] In order to explain more thoroughly the fact that the CyDTA reaction with the zinc(II)–EDMA complex proceeds through the En mechanism, whereas that with the zinc(II)–EDDA complex does not, the steric effect of the CyDTA on the formation of the reaction intermediate in the reactions of the EDMA and EDDA complexes was investigated by using the molecular model. A close molecular model examination revealed that the ethylenediamine reaction intermediate can be formed without any difficulty in the EDDA~EDTA and EDMA~CyDTA systems. However, it is almost impossible to build the En intermediate in the EDDA~CyDTA system because of the steric interaction of the CyDTA with the free carboxylate group of the EDDA anion. For this reason, the substitution reaction of CyDTA with the zinc(II)–EDDA complex could not proceed through the En reaction intermediate. As has been mentioned above, it is impossible to form the En-reaction intermediate from the EDDA and CyDTA anions. However, the glycinate reaction intermediate could be formed, although with some difficulty. The relative rate constant calculated on the basis of the Gly mechanism is also listed in Table 1 and compared with the observed one. The agreement between the two values can be regarded as satisfactory. This agreement and the conclusion obtained in the molecular-model examination suggest that the glycinate reaction mechanism can be assumed for the reaction of the zinc(II)–EDDA complex with with CyDTA.

References

1) M. Kodama and K. Hagiya, This Bulletin, **46**, 3151 (1973).
2) M. Kodama, H. Nunokawa, and N. Oyama, *ibid.*, **44**, 2849 (1971).
3) M. Kodama and N. Oyama, *ibid.*, **45**, 2169 (1972).
4) Y. Fujii, E. Kyuno, and R. Tsuchiya, *ibid.*, **43**, 786 (1970).

5) F. F. -L. Ho, L. E. Erickson, S. R. Watkins, and C. N. Reilley, *Inorg. Chem.*, **9**, 1139 (1970).
6) M. Kodama, unpublished results.
7) M. Kodama, M. Hashimoto, and T. Watanabe, This Bulletin, **45**, 2761 (1972).
8) T. J. Bydalek and D. W. Margerum, *Inorg. Chem.*, **4**, 678 (1963).
9) H. Ogino, "Formation, Substitution and Isomerization Reactions of Metal Complexes," in "Mechanisms of Inorganic Reactions," ed. by N. Tanaka, K. Tamaru, and S. Kawaguchi, Kagakudozin, Kyoto (1967), p. 5.
10) D. B. Rorabacher, *Inorg. Chem.*, **5**, 1891 (1966).
11) D. W. Margerum, D. B. Rorabacher, and J. F. G. Clarke, Jr., *ibid.*, **2**, 667 (1963).

A Polarographic Study of the Zinc(II)–Ethylenediamine-*N*,*N*′-diacetate (EDDA) and –Triethylenetetraamine (Trien) Complexes

Mutsuo KODAMA

Department of Chemistry, College of General Education, Hirosaki University, Bunkyo, Hirosaki, Aomori 036

(Received November 26, 1973)

Zinc(II)–EDDA and –Trien complexes produced kinetic waves. By conducting a systematic examination of the nature of the kinetic waves, the reaction mechanisms and the rates of the rate-determining step were determined. The kinetic wave of the zinc(II)–EDDA complex could be ascribed to the reduction of the zinc(II) aquo ion formed upon its slow dissociation at the electrode surface. From a comparison of the observed rate constant with that estimated on the basis of the proposed reaction intermediate, the dissociation of the zinc(II)–EDDA complex was found to proceed through a reaction intermediate in which the leaving EDDA anion is bonded to the zinc(II) ion through the ethylenediamine chelate ring. In the case of the Trien complex, the kinetic wave could be ascirbed to the reduction of the zinc(II)–Trien complex formed upon the slow configurational change of the tetrahedral zinc(II)–Trien complex at the electrode surface.

Previously,[1] the present author studied the dissociation reactions of zinc(II)–, lead(II)–, and cadmium(II)–aminopolycarboxylate complexes by examining the nature of the kinetic waves they gave. The zinc(II)–EDDA and –Trien complexes also produced kinetic waves. In this paper, the author will describe a systematic study of the nature of the above kinetic waves and will determine the reaction mechanism and reaction rates. The effect of the thiocyanate anion on the polarographic behavior of the zinc(II)–EDDA and –Trien complexes will also be investigated.

Experimental

Reagents. The previous paper[2] explained the preparation of a standard zinc(II) solution. An EDDA was recrystallized from its aqueous solution. Its standard solution was prepared by dissolving a known amount of recrystallized EDDA in redistilled water. The Trien was redistilled under reduced pressure. All the other chemicals were of an analytical reagent-grade and were used without further purification.

Apparatus and Experimental Procedures. The polarographs used for the measurement of the dc current-voltage cuvres were given previously.[2] The rate of the flow of mercury, m, and the drop time, t_d, of the dropping mercury electrode (DME) used in this study were 0.836 mg/s and 4.30 s respectively at a mercury height of 58.0 cm in an air-free 0.10 M sodium perchlorate solution at 0.0 V *vs.* SCE. All the other pieces of the apparatus and all the experimental procedures employed in this study were the same as those described in the previous paper.[2] For the EDDA system, an acetate buffer solution was used. In the case of the Trien system, no buffer reagent was used, because the sample solutions always contained a large excess of uncomplexed Trien and had a sufficient buffer capacity over the entire pH range covered ($6.00 < pH < 7.50$).

Results and Discussion

Under the experimental conditions where all the zinc(II) ions exist as complexes, the zinc(II) ions in EDDA and Trien solutions gave two- and one-step polarographic waves respectively. The first wave of the EDDA complex and the reduction step of the Trien complex showed a characteristic kinetic-controlled nature, while the second wave of the EDDA complex showed a diffusion-controlled nature. From the effects of the mercury pressure, the solution pH, and the uncomplexed ligand concentration on the limiting current, the second step of the EDDA complex could be ascribed to its direct reduction at the electrode surface.

As in the cases of the cobalt(II)–iminodiacetate (IDA) and –aspartate (Asp) complexes,[3] the first step of the zinc(II)–EDDA complex invariably gave a linear relation passing through the point of origin between $i_k/(i_d-i_k)$ and $(\alpha_H)_X^{1/2}$ (at a given EDDA concentration, $[X]_f$) or $[X]_f^{-1/2}$ (at a given solution pH) (Fig. 1). Here, $(\alpha_H)_X$ and i_k are, respectively, the (α_H) value of EDDA and the kinetic wave height. Provided that the other experimental conditions are kept constant, the plot of $i_k/(i_d-i_k)$ against $\beta_{Ac}^{1/2}$ $(=1+K_1^{Ac}\cdot[Ac^-]+K_1^{Ac}\cdot K_2^{Ac}\cdot[Ac^-]^2+\cdots]^{1/2})$[1] also gave a straight line which passes through the point of origin. Since the zinc(II) ion forms only a 1 : 1-ratio complex with EDDA[4], the above facts suggest that the following

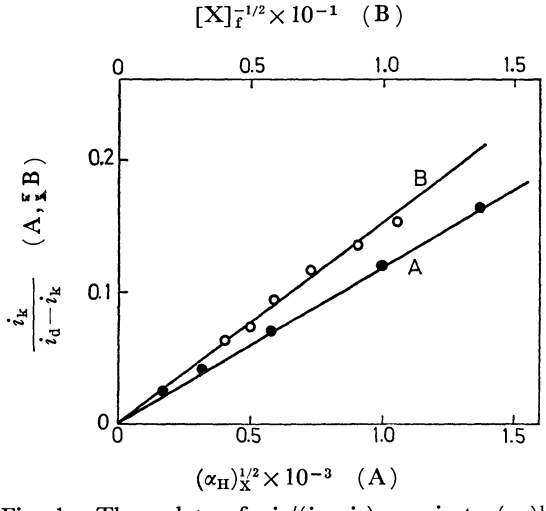

Fig. 1. The plot of $i_k/(i_d-i_k)$ against $(\alpha_H)_X^{1/2}$ or $[X]_f^{-1/2}$.
$\mu=0.30$, 25 °C
$[Zn(II)]=0.60$ mM, $]Ac]_f=0.060$ M
A) The plot of $i_k/(i_d-i_k)$ against $(\alpha)_X^{1/2}$
$[EDDA]_f=14.0$ mM
pH ranged from 4.60 to 5.90
B) The plot of $i_k/(i_d-i_k)$ against $[X]_f^{-1/2}$
$[EDDA]_f$ ranged from 9.0 to 40.0 M
pH=5.00

reaction mechanism can be assumed for the kinetic wave of the zinc(II)-EDDA complex:

$$ZnX^0 \overset{k_d}{\rightleftharpoons} Zn^{2+} + X^{2-} \quad (1)\ \text{rds}$$

$$\underbrace{Zn^{2+} + iAc^- \rightleftharpoons Zn(Ac)_i^{2-i}}_{Hg \downarrow 2e^-} \quad \text{in a rapid equil.}$$

$$Zn(Hg)$$

The k_d value was determined from the slope of the linear relation in Fig. 1; it is listed in Table 1, together with other numerical data. In the presence of the thiocyanate anion, the plot of $((i_d-i_k)/i_k)\cdot\beta_{NCS}^{1/2}$ against [NCS$^-$] gave a linear relation with an intercept of a finite value (Fig. 2). Here, β_{NCS} is defined as $1+K_1^{NCS}\cdot[NCS^-]+K_1^{NCS}\cdot K_2^{NCS}\cdot[NCS^-]^2+\cdots$, and [NCS$^-$] is the concentration of the uncomplexed thiocyanate anion. The above facts evidently suggest the formation of a mixed-ligand complex, ZnX(NCS)$^-$. Therefore, in view of the fact that the zinc(II)-thiocyanate complex is much more stable than the corresponding acetate complex, one can assume the following reaction mechanism for the kinetic wave of the zinc(II)-EDDA complex in solutions containing thiocyanate anions:

$$ZnX(NCS)^- \rightleftharpoons ZnX^0 + NCS^- \quad (2)\ \text{in a rapid equil.}$$

$$ZnX^0 \overset{k_d}{\rightleftharpoons} Zn^{2+} + X^{2-} \quad (1)\ \text{rds}$$

$$\underbrace{Zn^{2+} + jNCS^- \rightleftharpoons Zn(NCS)_j^{2-j}}_{Hg \downarrow 2e^-} \quad \text{in a rapid equil.}$$

$$Zn(Hg)$$

corresponding to Relation (1):

$$\frac{i_k}{i_d-i_k} = 0.886\cdot\sqrt{\frac{k_d\cdot t\cdot(\alpha_H)_X\cdot\beta_{NCS}}{K_{ZnX}\cdot[X]_f}}\cdot\frac{1}{1+K_{ZnX(NCS)}^{NCS}\cdot[NCS^-]} \quad (1)$$

Relation (1) was examined successfully by using some typical experimental data and the $K_{ZnX(NCS)}^{NCS}$ (=[ZnX(NCS)$^-$]/[ZnX^0]·[NCS$^-$]) value of 2.24 determined from the ratio between the intercept and the slope of the straight line (A) in Fig. 2. The good agreement of the k_d value estimated from the slope of the linear relation (B) in Fig. 2 with that determined from the slope of the straight line in Fig. 1 also supports the above explanation.

In the zinc(II)-Trien system, i_k also decreased with an increase in the solution pH, and the plot of $i_k/(i_d-i_k)$ against $K^H\cdot[H^+]^{1/2}/(1+K^H\cdot[H^+])$ gave a linear relation passing through the point of origin (Fig. 3). However, the $i_k/(i_d-i_k)$ ratio was almost independent of the concentration of the uncomplexed Trien, $[X]_f$. These facts suggest the following reaction mechanism

Table 1. Rate constants (μ=0.30, 25 °C)

Dissociation rate constant, k_d (s^{-1}), of Zn(II)-EDDA complex

Obsd	Calcd	
	En mechanism	Gly mechanism
3.5	1.0	7.7×10^{-3}

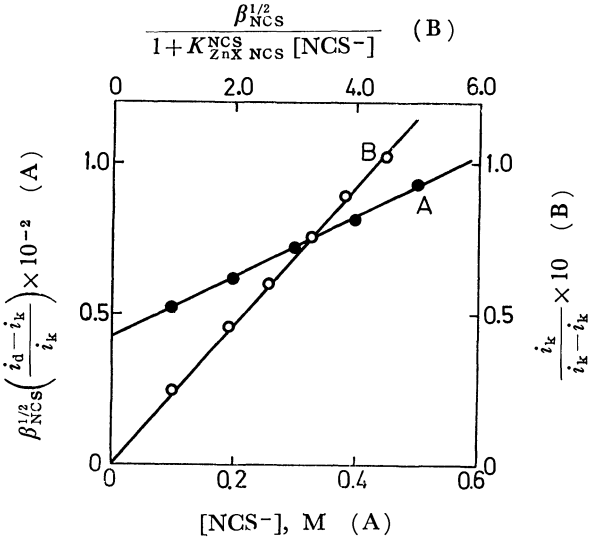

Fig. 2. The effect of NCS$^-$ on the kinetic wave of the zinc(II)-EDDA complex.
μ=0.50, 25 °C
[EDDA]$_f$=20.0 mM, [Zn(II)]=1.0 mM
[Ac]$_f$=0.06 M, pH=5.50
[NCS$^-$] ranged from 0.10 to 0.50 M
A) The plot of $((i_d-i_k)/i_k)\ \beta_{NCS}^{1/2}$ against [NCS$^-$]
B) The plot of $i_k/(i_d-i_k)$ against $\beta_{NCS}^{1/2}/(1+K_{ZnX(NCS)}^{NCS}[NCS^-])$

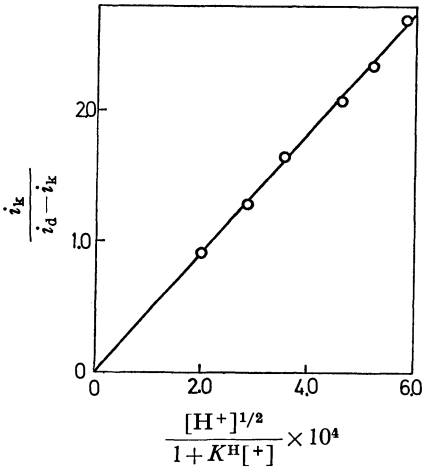

Fig. 3. The plot of $i_k/(i_d-i_k)$ against $[H^+]^{1/2}/(1+K^H(H^+])$
μ=0.30, 25 °C
[Trien]$_f$=24·0 mM, [Zn(II)]=1.0 mM
pH ranged from 6.00 to 7.30.

for the kinetic wave of the zinc(II)-Trien complex:

$$ZnX^{2+} + H^+ \rightleftharpoons ZnHX^{3+} \quad \text{in a rapid equilibrium}$$

$$ZnHX^{3+} \overset{k}{\rightleftharpoons} ZnX^{2+}* + H^+ \quad \text{rds}$$

$$ZnX^{2+}* + 2e^- + Hg \rightleftharpoons Zn(Hg) + X^\circ$$

corresponding to Relation (2):

$$\frac{i_k}{i_d-i_k} = 0.886\cdot\sqrt{\frac{k\cdot t}{K\cdot[H^+]}}\cdot\frac{K^H\cdot[H^+]}{1+K^H\cdot[H^+]} \quad (2)$$

where K^H is the protonation constant of ZnX^0, K, [ZnHX^{3+}]/[ZnX^{2+}*]·[H$^+$], and ZnX^{2+}*, the electroactive zinc(II)-Trien complex. If the above reaction mech-

TABLE 2. THE EFFECT OF pH ON THE HALF-WAVE POTENTIAL OF THE Zn(II)-Trien COMPLEX

$[Trien]_f=24.0$ mM, $[Zn(II)]=1.0$ mM
$\mu=0.30$, 25 °C

pH	$E_{1/2}$ V *vs.* SCE	$\Delta E_{1/2}$, mV	
		Obsd	Calcd
6.24	−1.120	+ 5	+4.7
6.40	−1.125	0	0
6.58	−1.130	− 5	−5.3
6.62	−1.133	− 8	−6.5
6.88	−1.145	−15	−14.2
7.28	−1.165	−25	−26.0

anism is assumed for the zinc(II)-Trien system, the half-wave potential of the kinetic wave, $(E_{1/2})_k$, should be given by:[5]

$$(E_{1/2})_k = \text{constant} + \frac{0.0591}{4\alpha}\log [H^+] \qquad (3)$$

By using the α value of 0.51, the effect of the solution pH on the half-wave potential was examined with the aid of Eq. (3). The result is given in Table 2. The shifts of the half-wave potential observed agreed well with those calculated.

As was discussed in connection with the dissociation mechanism of the zinc(II)-aminopolycarboxylate complex, the structure of the reaction intermediate in the dissociation of the zinc(II)-EDDA complex was determined by comparing the observed k_d value with that calculated on the basis of the proposed reaction intermediate. The k_d value calculated with the aid of the well-known relation; $k=k_{rds}\cdot K_{inter}\cdot K_{st}\cdot K_{elec}/K_{MX}$,[3] on the basis of the ethylenediamine reaction intermediate was 1.0. Here, $K_{inter}=10^{6.15}$, $K_{st}=1.0\times 10^2$, $k_{rds}=3.1\times 10^2$, and $K_{MX}=10.$[10.79] The k_{rds} value used in the above calculation was estimated from the dissociation rate constant of the 1 : 1-ratio zinc(II)-ammine complex by making a correction for the rotational barrier around the C-N bond.[6] The agreement between the calculated and observed rate constants can be regarded as satisfactory. The rate constants calculated on the basis of the other reaction intermediates showed no satisfactory agreement with the observed one.

In the case of the zinc(II)-Trien complex, one can not determine the k value from the slope of the linear relation in Fig. 3, because the K value is unknown. With regard to the nature of the electroactive zinc(II)-Trien complex, two explanations are possible. One is that electroactive zinc(II)-Trien complex, ZnX^{2+}*, is the species produced upon the partial dissociation of the original complex, ZnX^{2+}. The other is that ZnX^{2+}* is the Trien complex formed upon the configurational change of the original complex. Generally, protonation of a metal complex always involves a partial dissociation of the metal complex. Therefore, the fact that the rate-determining step includes the deprotonation of the protonated zinc(II)-Trien complex eliminates the former explanation. On the basis of the ΔS value of the formation reaction, Sacconi *et al.*[7] concluded that the zinc(II)-Trien complex in a solution is tetrahedral. This could be confirmed by the finding that the thiocyanate anion had practically no effect on the polarographic behavior of the zinc(II)-Trien complex. If the zinc(II)-Trien complex in solution is octahedral, the thiocyanate anion will form a mixed ligand complex with ZnX^{2+} and will have a remarkable effect on the kinetic wave. Therefore, it must be reasonable to believe that the rate-determining step in the zinc(II)-Trien system is the configurational change of the zinc(II)-Trien complex from tetrahedral to octahedral or square pyramid. In order to describe the nature of the above configurational change more precisely, a further systematic investigation should be conducted.

References

1) M. Kodama, K. Namekawa, and T. Horiuchi, This Bulletin, in press.
2) M. Kodama and N. Oyama, This Bulletin, **45**, 2169 (1972).
3) M. Kodama, *ibid.*, **46**, 3422 (1973).
4) L. G. Sillen and A. E. Martell, "Stability Constants of Metal-Ion Complexes," 2nd ed., The Chemical Society, London (1964), p. 519.
5) M. Kodama, H. Nunokawa, and N. Oyama, This Bulletin, **44**, 2387 (1971).
6) D. W. Margerum, D. B. Rorabacher, and J. F. Clarke, Jr., *Inorg. Chem.*, **2**, 667 (1963).
7) L. Sacconi, P. Paoletti, and M. Ciampolini, *J. Chem. Soc.*, **1961**, 5515.

Copper(II) Complexes of Glycyl-L-histidine, Glycyl-L-histidylglycine, and Glycylglycyl-L-histidine in Aqueous Solution

Hiroji AIBA, Akira YOKOYAMA, and Hisashi TANAKA

Faculty of Pharmaceutical Sciences, Kyoto University, Yoshida, Sakyo-ku, Kyoto 606

(Received November 29, 1973)

The complex formation of glycyl-L-histidine, glycyl-L-histidylglycine, and glycylglycyl-L-histidine with copper (II) ion in aqueous solutions containing equimolar amounts of copper(II) and the respective ligand was investigated by potentiometric and visible spectrophotometric methods. The presence of the following copper (II) complex species was assumed: $CuLH^{2+}$, CuX, and $Cu_nY_n^{n-}$ for glycyl-L-histidine-copper(II) and glycyl-L-histidylglycine-copper(II) systems, and $CuLH^{2+}$, CuY^-, and CuZ^{2-} for glycylglycyl-L-histidine-copper(II) system, where LH is the neutral species of the ligand and $LH=XH_2=YH_3=ZH_4$. The formation and ionization constants were obtained graphically, and the distribution of copper(II) among the complex species was calculated for each system. The results indicate that copper(II) ions are bound to the imidazole and carboxyl (or carbonyl) groups in $CuLH^{2+}$ and to the amino, imidazole, and deprotonated amide groups in CuX, CuY^-, and CuZ^{2-}. The spectral blue shift accompanying a deprotonation in the region from $a=4$ to 5 in the glycyl-L-histidine and glycyl-L-histidylglycine copper(II) systems indicates the formation of a polymer complex $Cu_nY_n^{n-}$ in which the imidazole ring acts as a bridge to connect copper atoms, where a represents moles of KOH added per completely protonated ligand.

In previous papers,[1,2] we discussed the complex species formed in the reaction of L-histidylglycine and L-histidylglycylglycine with copper(II) ion in an aqueous solution. Since the histidyl residue in the peptides plays an important role in their complex formation with metal ions, the position of the histidyl residue in the peptide molecule may cause remarkable differences in the modes of their complex formation. In an attempt to obtain further information on the interaction of the histidyl residue in the peptides with metal ion, the complex formation of glycyl-L-histidine, glycyl-L-histidylglycine, and glycylglycyl-L-histidine (abbreviated as GH, GHG, and GGH hereafter) with copper(II) ion was studied in aqueous solutions containing equimolar amounts of copper(II) and the ligand by potentiometric and spectrophotometric methods.

The copper(II) complexes of GH and GGH in aqueous solution have been investigated by various physico-chemical methods, and the binding sites of copper(II) have been deduced.[3-7] The structure of the neutral 1 : 1 GH-copper(II) complex was elucidated by X-ray diffraction analysis.[8] Recently, copper(II) complex of GHG was also studied in both aqueous solution and crystalline state.[9-11] However, the complex formation of these peptides with copper(II) ion in aqueous solution has not been elucidated completely, and there remain problems on the quantitative interpretation of the experimental results, the complex species formed in the reaction, and their structures.

Experimental

Materials. The preparation of the peptides were described previously.[12] Other reagents were commercial products.

Methods. The potentiometric and visible absorption spectral measurements were carried out as described previously.[1,12]

Results

Potentiometric Titration of GH-copper(II) and GHG-copper(II) Systems. The titration curves for the solutions containing $CuCl_2$ and GH or GHG (molar ratio 1 : 1) are shown in Fig. 1, together with those for the ligands in the absence of copper(II). Each curve shows the onset of pH fall at a point near $a=1$ and an extensive overlap of the ionization, giving a strong pH inflection at $a=4$, where a represents the number of moles of KOH added per completely protonated ligand. The same titration curve has been reported by Martin and Edsall,[3] and Bryce *et al.*[4] for the GH-Cu(II) system. From these titration behaviors, coordination is presumed to occur initially at the imidazole group with subsequent release of the protons from the amino and the peptide amide groups. Accordingly, the following equilibria are assumed in the region between $a=1$ and $a=4$,

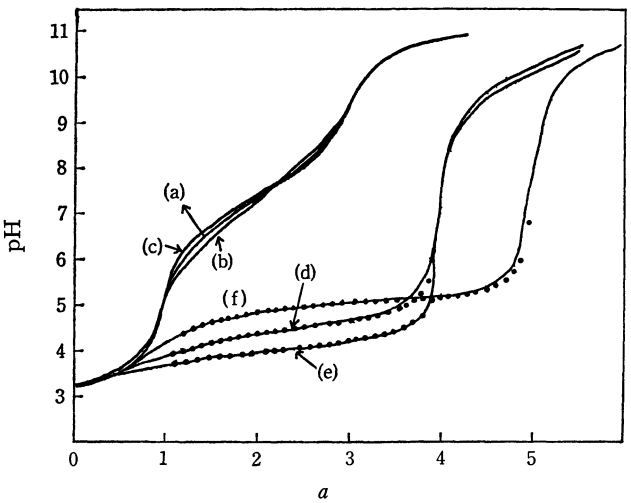

Fig. 1. Titration curves of GH, GHG, and GGH in the absence and presence of $CuCl_2$.
(a) GH+2HCl, (b) GHG+2HCl, (c) GGH+2HCl, (d) GH+2HCl+$CuCl_2$, (e) GHG+2HCl+$CuCl_2$, (f) GGH+2HCl+$CuCl_2$; ligand concentration is 10^{-3} M (at $a=0$).
The lines are experimental curves. Each point was calculated from the equilibrium constant.

TABLE 1. FORMATION AND IONIZATION CONSTANTS FOR COPPER(II)-PEPTIDE SYSTEMS

Ligand	pK_{COOH}[a)]	pK_{Im}[a)]	pK_{NH_3}[a)]	$\log K_1$	pK_{2c}	pK_{3c}	"pK_c"[b)]
GH	2.75	6.85	8.33	5.08	8.40	—	9.65
GHG	3.19	6.63	8.17	4.94	7.10	—	9.55
GGH	2.84	6.99	8.23	5.33	—	14.81	10.69

a) The acid dissociation constants of ligands were reported previouly (Ref. 12). b) The values of "pK_c" are pH values at the half-neutralization points.

$$LH_3^{2+} \rightleftharpoons LH_2^+ + H^+$$
$$K_{COOH}=[LH_2^+][H^+]/[LH_3^{2+}] \quad (1)$$
$$LH_2^+ \rightleftharpoons LH + H^+$$
$$K_{Im}=[LH][H^+]/]LH_2^+] \quad (2)$$
$$Cu^{2+} + LH \rightleftharpoons CuLH^{2+}$$
$$K_1=[CuLH^{2+}]/[Cu^{2+}][H^+] \quad (3)$$
$$CuLH^{2+} \rightleftharpoons CuX + 2H^+$$
$$K_{2c} = [CuX][H^+]^2/[CuLH^2] \quad (4)$$

where LH is the neutral species of the ligand and LH=XH_2. For the sake of electroneutrality we have

$$2[Cu^{2+}] + 2[CuLH^{2+}] + 2[LH_3^{2+}] + [LH_2^+] + [K^+] + [H^+] = [OH^-] + [Cl^-]. \quad (5)$$

The total concentrations of the ligand and the copper(II) ion are given as follows.

$$[Cu]_T = [Cu^{2+}] + [CuLH^{2+}] + CuX] \quad (6)$$
$$[L]_T = [LH_3^{2+}] + [LH_2^+] + [LH] + [CuLH^{2+}] + [CuX] \quad (7)$$

From Eq. (1)—(7), the following relationship between K_1 and K_{2c} is derived.

$$K_1 = (ABC+2\alpha B^2+ABDK_{2c})/(\gamma C^2+2\gamma CDK_{2c}+\gamma D^2K_{2c}^2) \quad (8)$$

where A, B, C, D, α, β, and γ are defined as follows.

$$A = 2\alpha + \beta$$
$$B = \alpha\gamma - A[Cu]_T$$
$$C = 2\alpha[Cu]_T - \alpha\gamma$$
$$D = -\alpha\gamma/[H^+]^2$$
$$\alpha = 1 + [H^+]/K_{Im} + [H^+]^2/K_{COOH}K_{Im}$$
$$\beta = [H^+]/K_{Im} + 2[H^+]^2/K_{COOH}K_{Im}$$
$$\gamma = [OH^-] + [Cl^-] - [H^+] - [K^+]$$

The acid dissociation constants, K_{COOH} and K_{Im}, have been reported.[12)]

The values of K_1 and K_{2c} were evaluated by the graphical method of Schwarzenbach *et al.*[13)] The results for the GH-copper(II) system are shown in Fig. 2. The equilibrium constants obtained are listed in Table 1. From the K_1 and K_{2c} values, the titration curves were recalculated and compared with those obtained experimentally in Fig. 1. In the region between $a=4$ and $a=5$, an additional deprotonation is observed. The apparent ionization constants "pK_c", which are the pH values at the half-neutralization point, are 9.65 and 9.55 for the GH-copper(II) and the GHG-copper(II) systems, respectively. The distribution of copper(II) among the complex species at various pH values was calculated. The results for the GH-copper(II) system are shown in Fig. 3.

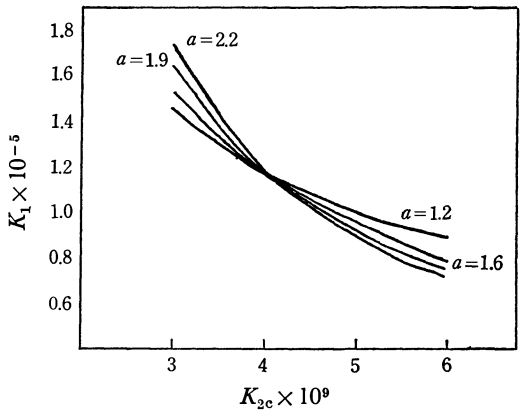

Fig. 2. Graphical calculation of K_1 and K_{2c} for GH-Cu(II) system.

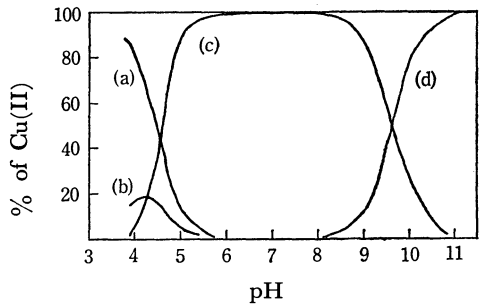

Fig. 3. Distribution of Cu(II) species for the 1 : 1 GH-Cu(II) system;
(a) Cu^{2+}, (b) $CuLH^{2+}$, (c) CuX, (d) $Cu_nY_n^{n-}$.

GGH-copper(II) System. The titration curve o the 1 : 1 GGH-copper(II) system is given in Fig. 1. The same curve has been reported by Bryce *et al.*[4)] The titration behavior in the GGH-copper(II) system is similar to that of the GH-copper(II) system, in the region between $a=1$ and $a=4$, but a remarkable pH inflection is observed at $a=5$. This indicates the deprotonation of the two amide groups of the peptide bonds. Accordingly, the following equilibria are assumed, with Eqs. (1) and (2), where LH=YH_3.

$$Cu^{2+} + LH \rightleftharpoons CuLH^{2+}$$
$$K_1 = [CuLH^{2+}]/[Cu^{2+}][LH] \quad (9)$$
$$CuLH^{2+} \rightleftharpoons CuY^- + 3H^+$$
$$K_{3c} = [CuY^-][H^+]^3/[CuLH^{2+}] \quad (10)$$

The values of K_1 and K_{3c} were calculated by the same method as in the case of GH-copper(II) system. The results are shown in Fig. 4 and Table 1. An additional deprotonation is observed in the region between $a=5$ and $a=6$, giving the apparent ionization constants 10.69. The value is a little higher than the values of

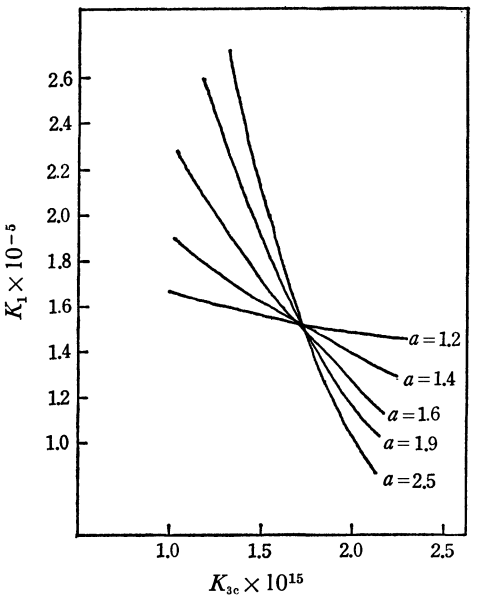

Fig. 4. Graphical calculation of K_1 and K_{3c} for GGH-Cu(II) system.

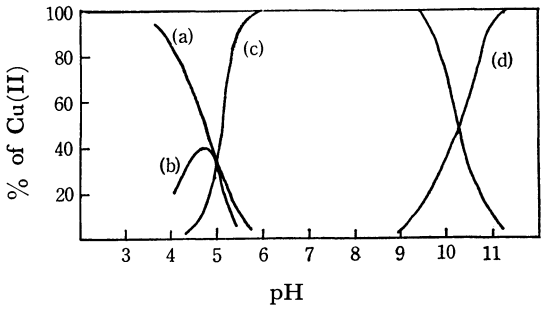

Fig. 5. Distribution of Cu(II) species for the 1 : 1 GGH-Cu(II) system;
(a) Cu^{2+}, (b) $CuLH^{2+}$, (c) CuY^-, (d) CuZ^{2-}.

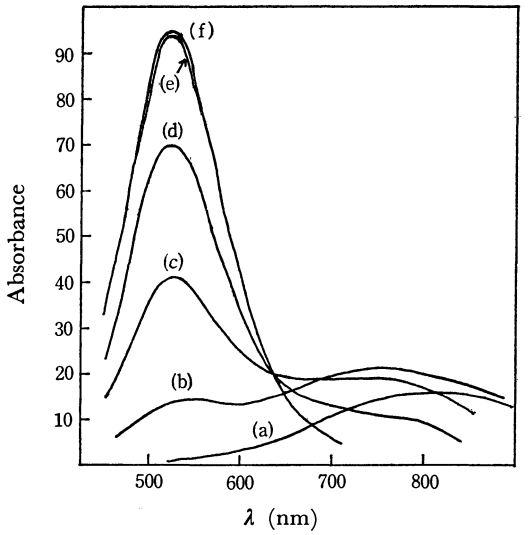

Fig. 6. Visible absorption spectra of the 1 : 1 GGH-Cu(II) system;
(a) GGH+HCl+$CuCl_2$, (b) GGH+$CuCl_2$, (c) GGH+KOH+$CuCl_2$, (d) GGH+2KOH+$CuCl_2$, (e) GGH+3KOH+$CuCl_2$, (f) GGH+4KOH+$CuCl_2$.
Absorbance is expressed per gram atom of copper(II).

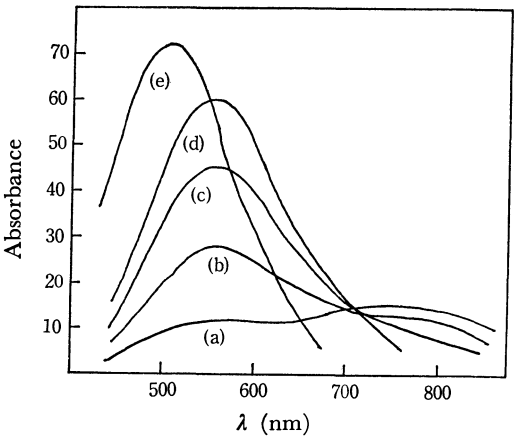

Fig. 7. Visible absorption spectra of the 1 : 1 GHG-Cu(II) system;
(a) GHG+HCl+$CuCl_2$, (b) GHG+$CuCl_2$, (c) GHG+KOH+$CuCl_2$, (d) GHG+2KOH+$CuCl_2$, (e) GHG+3KOH+$CuCl_2$.
Absorbance is expressed per gram atom of copper(II).

Table 2. Spectral characteristics of Cu(II)-peptide complexes

Ligand	*a* Value	λ_{max} (mμ)	ε ($M^{-1}cm^{-1}$)	Main species
GH	4	600	60	CuX
	5	557	70	$Cu_nY_n^{n-}$
GHG	4	602	60	CuX
	5	556	72	$Cu_nY_n^{n-}$
GGH	5	525	94	CuY^-
	6	525	95	CuZ^{2-}
GG[a)]	2	638	87	CuX
	3	641	83	$CuL(OH)^-$

a) GG=glycylglycine, and in this case *a* value represents moles of KOH added per neutral (monoprotonated) glycylglycine.

the GH-copper(II) and the GHG-copper(II) systems. The distribution of copper(II) among the complex species is shown in Fig. 5.

Absorption Spectra of the Peptide-copper(II) 1 : 1 Solutions. The characteristics of the visible absorption spectra of the GH-copper(II) and GGH-copper(II) complex has been reported,[5,6] but the relation between the absorption spectra and the pH of the solution has not been fully discussed. The spectra of the GHG-copper(II) complex has not been studied.

The spectra of the GGH-copper(II) and GHG-copper(II) systems are shown in Figs. 6 and 7, where *a* has the same meaning as those in titration. The spectra of the GH-copper(II) system are similar to those of GHG-copper(II) systems. The absorption characteristics of those spectra are given in Table 2. The spectrum at $a=2$ in the GGH-copper(II) system shows two absorption maxima at 750 nm and 525 nm. The absorption at 750 nm decreases whereas that at 524 nm increases, with the increase of *a*. The absorption maximum at 750 nm is presumed to be due to Cu^{2+} and $CuLH^{2+}$, and that at 525 nm to CuY^-. The spectral behavior corresponds reasonably to the equilibrium

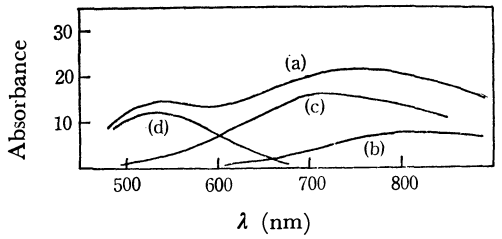

Fig. 8. Resolution of the spectrum at $a=2$ in the 1 : 1 GGH-Cu(II) system;
(a) GGH+Cu(II), (b) Cu^{2+} (45.6%), (c) $CuLH^{2+}$ (38.4%), (d) CuY^- (16.0%).

assumed from the titration curve. The spectrum at $a=2$ was resolved into three components corresponding to the three complex species by the use of the equilibrium constants. The results is shown in Fig. 8.

In the GH-copper(II) and GHG-copper(II) systems, the spectral behavior is similar to that in the GGH-copper(II) system up to $a=2$, the neutral complex CuX exhibiting a maximum at ~600 nm. However, the additional deprotonation causes a shift of the maximum to 555 nm.

Discussion

The stepwise ionization constants of GH-copper(II) and GGH-copper(II) complexes have been reported.[3,4] However, the formation constants of these complexes have not been calculated because of the complexity of the titration behavior. The assumption in Eqs. (3) and (4) (or (9) and (10)) made the quantitative interpretation of the titration data possible.

In Table 1, the log K_1 values decrease in the order GGH, GH, and GHG, which agrees with that of the basicity of the imidazole group. This suggests the presence of a bond between the imidazole group and copper(II) in the complex $CuLH^{2+}$. The copper(II) ions will also be bound to the carboxyl or the carbonyl groups. The following structures are suggested for the complexes $CuLH^{2+}$.

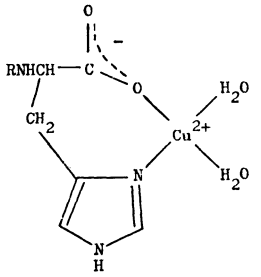

(I) $CuLH^{2+}$
R = $^+NH_3CH_2CO$: GH-Cu(II)
R = $^+NH_3CH_2$-$CONHCH_2CO$: GGH-Cu(II)

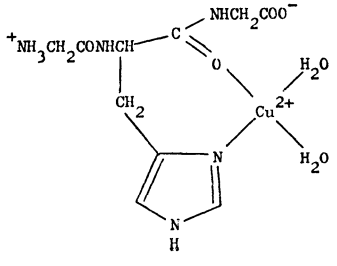

(II) $CuLH^{2+}$, GHG-Cu(II)

From the titration data it has been suggested that the copper(II) predominantly binds to the three nitrogens of the imidazole, amino, and deprotonated amide groups in the pH region 6—8 in the GH-copper(II) system. In the GH-copper(II) and GHG-copper(II) systems, the liberation of three protons and the remarkable blue shift of the absorption maxima in the region between $a=1$ and $a=4$ indicate that the copper(II) in the neutral complex CuX is bound to the three nitrogen atoms. In aqueous solutions the fourth coordination site of copper(II) is presumed to be mainly occupied by water molecule. The probable structure of CuX can be represented by III. However, the neutral chelate of the GH-copper(II) system precipitates on standing from the solution at $a=4$. Thus in the crystalline state, the fourth coordination site would be occupied by the carboxyl groups of a neighboring molecule to give a polymer Cu_nX_n as shown by IV. The structure of Cu_nX_n has been elucidated by X-ray diffraction analysis.[8] The same structure has been proposed to the GHG-copper-(II) complexes.[10,11]

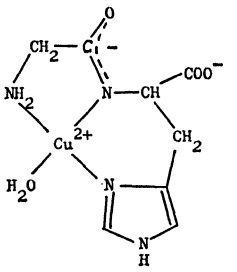

(III) CuX

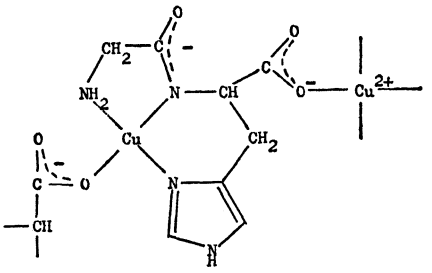

(IV) Cu_nX_n

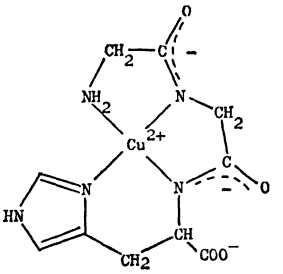

(V) CuY^-

As in the case of the GH-copper(II) system, it is apparent that the copper(II) in the anionic species CuY^- of the GGH-copper(II) complex is bound to the nitrogen atoms of the amino, imidazole, and two deprotonated amide groups as shown in V.

A further spectral blue shift caused by an additional deprotonation at $a=5$ in the GH-copper(II) and GHG-copper(II) systems suggests important changes in the coordination sphere of the copper(II) ion. The fol-

lowing three possibilities have been taken into account for the deprotonation for the GH–copper(II) system: (1) the proton dissociation of the coordinated water molecule at the fourth position,[4,5] (2) the proton dissociation from the imino nitrogen of the imidazole ring,[3] (3) the coordination of the deprotonated imino nitrogen to the fourth position of another copper(II).[6] The dissociation of the water molecule at the fourth position causes some red shift in the glycylglycine–copper(II) system, as indicated in Table 2. Deprotonation of the imino group in the GGH–copper(II) complex CuY^- does not occur below pH 10. The results exclude the possibilities (1) and (2). The most probable assumption is that a deprotonated imino nitrogen of the imidazole ring coordinates to the fourth position of another copper(II) to give a negatively charged polymer complex $Cu_nY_n^{n-}$. The structure of $Cu_nY_n^{n-}$ is shown as VI. The polymer is presumed to be a

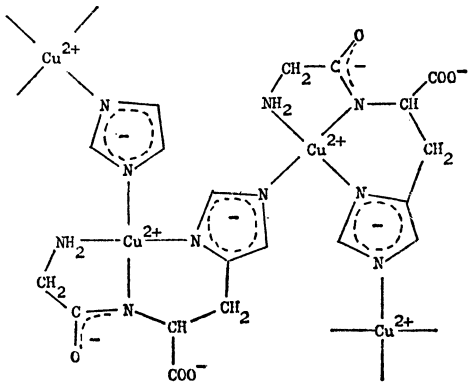

(VI) $Cu_nY_n^{n-}$

tetramer from the molecular model, as suggested by Morris and Martin[6] but no evidence was obtained from the quantitative analysis of the titration curve.

Further addition of the base to CuY^- of the GGH–copper(II) system would cause the liberation of a proton from the imino nitrogen to give a dianionic chelate CuZ^{2-} as indicated by VII, where $LH{=}YH_3{=}ZH_4$. The spectral characteristic of CuZ^{2-} is similar to that of CuY^-.

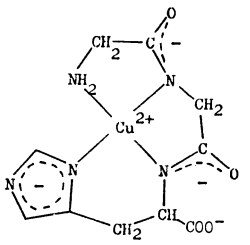

(VII) CuZ^{2-}

The authors wish to express their thanks to the staff of Kyoto University Computer Center for the use of FACOM 230—60 Computer, and to the members of the Micro Analytical Center, Kyoto University, for elemental analysis.

References

1) H. Aiba, A. Yokoyama, and H. Tanaka, This Bulletin, **47**, 136 (1974).
2) A. Yokoyama, H. Aiba, and H. Tanaka, *Chem. Lett.*, **1972**, 489.
3) R. B. Martin and J. T. Edsall, *J. Aemr. Chem. Soc.*, **82**, 1107 (1960).
4) G. F. Bryce, R. W. Roeske, and F. R. N. Gurd, *J. Biol. Chem.*, **240**, 3837 (1965).
5) G. R. Bryce and F. R. N. Gurd, *ibid.*, **241**, 122 (1966).
6) P. J. Morris and R. B. Martin, *J. Inorg. Nucl. Chem.*, **33**, 2913 (1971).
7) G. F. Bryce, *J. Phys. Chem.*, **70**, 3549 (1966).
8) J. F. Blout, K. A. Fraser, H. C. Freeman, J. T. Szymanski, and C. -H, Wang, *Acta Crystallogr.*, **22**, 96 (1967).
9) R. Österberg and B. Sjöberg, *Acta Chem. Scand.*, **22**, 689 (1968).
10) R. Österberg and B. Sjöberg, *J. Chem. Soc. Chem. Commun.*, **1972**, 983.
11) R. Österberg, B. Sjöberg, and R. Söderquist, *Acta Chem. Scand.*, **26**, 4184 (1972).
12) A. Yokoyama, H. Aiba, and H. Tanaka, This Bulletin, **47**, 112 (1974).
13) G. Schwarzenbach, A. Willi, and R. O. Bach, *Helv. Chim. Acta*, **30**, 1303 (1947).

Cobalt-59 Nuclear Magnetic Resonance Study of Cobalt(III) Complexes. Empirical Rules for the Cobalt-59 Chemical Shifts and Line Widths of $[Co^{III}(en)_x(NH_3)_{6-2x-y}L_y]$-type Complexes*

Fumikazu YAJIMA**, Yasuo KOIKE**, Akira YAMASAKI, and Shizuo FUJIWARA

Department of Chemistry, Faculty of Science, The University of Tokyo, Hongo, Tokyo 113

(Received December 15, 1973)

The cobalt-59 chemical shifts and line widths for about seventy cobalt(III) complexes of the $[Co^{III}(en)_x(NH_3)_{6-2x-y}L_y]$ (L=Cl, Br, NO_2, N_3, OH, H_2O, CO_3, and C_2O_4) type have been measured. The cobalt-59 chemical shifts of this type of complex are approximately represented by a simple relation:

$$\delta(\text{ppm}) = 360x + \sum_{i=1}^{y} \delta_i(\text{L}) \qquad (x=0,\ 1,\ \text{and}\ 2),$$

where $\delta_i(\text{L})$ is the i-th ligand shift parameter which represents the contribution of the i-th ligand, L, to the total chemical shift. Three empirical rules can be derived from experimental observations: I. The chemical shift of a *trans*-isomer is higher than that of the corresponding *cis*-isomer. II. The line width of the *trans*-CoA_4B_2 isomer is larger than that of the *cis*-CoA_4B_2 isomer. III. The line width of a *meridional* isomer is larger than that of the corresponding *facial* isomer. Illustrative examples are presented where cobalt-59 NMR is used to identify cobalt (III) complexes and to study the kinetics and equilibrium in solution.

The cobalt-59 chemical shifts and line widths have been reported for a variety of cobalt(III) complexes in solution.[1-8] However, the values of the chemical shifts of the same complexes as measured by different workers are not in good agreement with each other. This inconsistency is assumed to be due to the fact that all the works in the literature are based on one species of chemical shift standard, *i.e.*, $[Co(CN)_6]^{3-}$, which has the highest chemical shift among the cobalt(III) complexes studied so far. Hence, two other complexes ($[Co(en)_3]^{3+}$ and $[Co(acac)_3]$) have here been chosen as the standards besides $[Co(CN)_6]^{3-}$, and used as the standards of chemical shifts in the middle- and low-field regions respectively.

Experimental

Materials. Cobalt(III) complexes were synthesized by standard procedures and purified by recrystallization. Monoethylenediamine-cobalt(III) complexes of the $[Co(en)(NH_3)_2L_2]$ (L=OH, NO_2, and N_3) and $[Co(en)(NH_3)_3L]$ (L=Cl, Br, OH, NO_2, and N_3) types were prepared from $[Co(en)(NH_3)_2Cl_2]Cl$ and $[Co(en)(NH_3)_3H_2O]X_3$,[8] respectively according to the modification of the procedure for the preparation of the corresponding $[Co(NH_3)_{6-x}L_x]$ or $[Co(en)_2(NH_3)_{2-x}L_x]$ type complexes.

NMR Measurements. The cobalt-59 NMR measurements were made at 25.0 °C using a JEOL JNM-WB-20 spectrometer operating at 13.5550 MHz. Some measurements were carried out on a Varian Associates VF-16 spectrometer at several frequencies. For the chemical shift measurements, $[Co(CN)_6]^{3-}$, $[Co(en)_3]^{3+}$, and $[Co(acac)_3]$ were used as the internal or external reference in the high-, middle-, and low-field regions respectively. The difference in chemical shift between the internal and external references was less than 5 ppm. The resonant fields for the above three standards were determined separately from lithium-7 NMR of aqueous lithium chloride solutions using an autodyne oscillator. The standard deviation of the observed values of the chemical shifts was less than 0.5%. In the case of chloro-, bromo-, and aquo-complexes, the standard deviation of the chemical shifts was 2—3% for their large line widths. The line widths were obtained as the peak-to-peak intervals of the first derivatives of the absorption signals, which were recorded under a quite small amplitude of modulation at a frequency of 35 Hz.

Results and Discussion

Chemical Shift. All the cobalt(III) complexes studied were of the $[Co(en)_x(NH_3)_{6-2x-y}L_y]$ type, where L is Cl, Br, NO_2, N_3, OH, H_2O, CO_3, and C_2O_4. The chemical shifts and line widths of these complexes are listed in Table 1. The chemical shift of the $[Co(NH_3)_6]^{3+}$ ion is taken as zero in the present study. Figures 1-a—1-e show that the chemical shifts change regularly with the combination of ligands. On the basis of these results, the chemical shift of the complexes of the $[Co(en)_x(NH_3)_{6-2x-y}L_y]$ type can be approximately represented as follows:

$$\delta(\text{ppm}) = 360x + \sum_{i=1}^{y} \delta_i(\text{L}),\ (x=0,\ 1,\ \text{and}\ 2) \qquad (1)$$

where $\delta_i(\text{L})$ represents the contribution from the i-th ligand, L, to the total chemical shift. Hereafter, $\delta_i(\text{L})$ will be referred to as the i-th ligand shift parameter.

Table 1-a. Chemical shifts and line widths for $[Co(en)_x(NH_3)_{6-2x}]$ type of complexes

Complex	Chemical shift (ppm)	Line width (G)
$[Co(NH_3)_6]^{3+}$	0[a]	0.05
$[Co(en)(NH_3)_4]^{3+}$	360	0.23
trans-$[Co(en)_2(NH_3)_2]^{3+}$	760	0.43
cis-$[Co(en)_2(NH_3)_2]^{3+}$	710	0.27
$[Co(en)_3]^{3+}$	1030[b]	0.05

a) $[Co(NH_3)_6]^{3+}$ is taken as a standard for the chemical shift. b) The resonant field was determined using Li-7 NMR; 13320.2 G at 13.5550 MHz.

* Based on a part of the D. Sc. Thesis of F. Y., The University of Tokyo, 1972.

** Present address: Central Research Laboratory, Mitsubishi Chemical Industries, Ltd., Hisamoto, Takatsu-ku, Kawasaki 213.

Table 1-b. Chemical shifts and line widths for $[Co(en)_x(NH_3)_{6-2x-y}Cl_y]$ type of complexes

Complex	Chemical shift[a] (ppm)	Line width (G)
$[Co(NH_3)_5Cl]^{2+}$	−700	1.0
trans-$[Co(NH_3)_4Cl_2]^+$	−1660[b]	4.0
cis-$[Co(NH_3)_4Cl_2]^+$	−1660[b]	2.0
$[Co(en)(NH_3)_3Cl]^{2+}$	−270	2.5
cis-$[Co(en)_2(NH_3)Cl]^{2+}$	100	2.5
trans-$[Co(en)(NH_3)_2Cl_2]^+$ [c]	−1150	4.0
cis-trans-$[Co(en)(NH_3)_2Cl_2]^+$ [d]	−1170	3.0
trans-$[Co(en)_2Cl_2]^+$	−820	8.0
cis-$[Co(en)_2Cl_2]^+$	−820	4.5

a) The standard deviation of observed values of chemical shifts was 3%. b) The difference in chemical shift between *cis* and *trans* isomers could not be obtained because of their large line widths. c) *trans*-dichloro-*cis*-diammine(ethylenediamine)cobalt(III) ion. d) *cis*-dichloro-*trans*-diammine(ethylenediamine)cobalt(III) ion.

Table 1-c. Chemical shifts and line widths for $[Co(en)_x(NH_3)_{6-2x-y}Br_y]$ type of complexes

Complex	Chemical shift[a] (ppm)	Line width (G)
$[Co(NH_3)_5Br]^{2+}$	−670	1.0
$[Co(en)(NH_3)_3Br]^{2+}$	−240	2.5
trans-$[Co(en)(NH_3)_2Br_2]^+$	−1160	4.8
cis-$[Co(en)_2NH_3Br]^{2+}$	110	2.0
trans-$[Co(en)_2Br_2]^+$	−810	5.5
cis-$[Co(en)_2Br_2]^+$	−810	3.0

a) The standard deviation of observed values of chemical shifts was 3%.

Table 1-d. Chemical shifts and line widths for $[Co(en)_x(NH_3)_{6-2x-y}(NO_2)_y]$ type of complexes

Complex	Chemical shift (ppm)	Line width (G)
$[Co(NH_3)_5NO_2]^{2+}$	525	0.15
mer-$[Co(en)(NH_3)_3NO_2]^{2+}$	915	0.28
fac-$[Co(en)(NH_3)_3NO_2]^{2+}$	895	0.17
cis-$[Co(en)_2NH_3NO_2]^{2+}$	1265	0.29
trans-$[Co(NH_3)_4(NO_2)_2]^+$	960	0.28
cis-$[Co(NH_3)_4(NO_2)_2]^+$	895	0.15
trans-$[Co(en)(NH_3)_2(NO_2)_2]^+$ [a]	1275	0.50
cis-trans-$[Co(en)(NH_3)_2(NO_2)_2]^+$ [b]	1260	0.34
trans-$[Co(en)_2(NO_2)_2]^+$	1880	1.1
cis-$[Co(en)_2(NO_2)_2]^+$	1700	0.7

a) *trans*-dinitro-*cis*-diammine(ethylenediamine)cobalt(III) ion.
b) *cis*-dinitro-*trans*-diammine(ethylenediamine)cobalt(III) ion.

Table 1-e. Chemical shifts and line widths for $[Co(en)_x(NH_3)_{6-2x-y}(N_3)_y]$ type of complexes

Complex	Chemical shift (ppm)	Line width (G)
$[Co(NH_3)_5N_3]^{2+}$	−530	0.20
fac-$[Co(en)(NH_3)_3N_3]^{2+}$	−90	0.37
$[Co(en)_2NH_3N_3]^{2+}$	255	0.7
trans-$[Co(NH_3)_4(N_3)_2]^+$	−1070	0.30
cis-$[Co(NH_3)_4(N_3)_2]^+$	−1110	0.21
$[Co(en)(NH_3)_2(N_3)_2]^+$	−670	0.6
cis-$[Co(en)_2(N_3)_2]^+$	−250	0.5
mer-$[Co(NH_3)_3(N_3)_3]$	−1750[a]	0.71[a]
fac-$[Co(NH_3)_3(N_3)_3]$	−1820[a]	0.17[a]

a) NMR measurements were made in DMSO.

Table 1-f. Chemical shifts and line widths for $[Co(en)_x(NH_3)_{6-2x-y}(OH)_y]$ type of complexes

Complex	Chemical shift (ppm)	Line width (G)
$[Co(NH_3)_5OH]^{2+}$	−990	0.23
mer-$[Co(en)(NH_3)_3OH]^{2+}$	−635	0.43
fac-$[Co(en)(NH_3)_3OH]^{2+}$	−560	0.18
trans-$[Co(en)_2NH_3OH]^{2+}$	−110	0.18
cis-$[Co(en)_2NH_3OH]^{2+}$	−220	0.29
cis-$[Co(NH_3)_4(OH)_2]^+$	−1940	0.14
trans-$[Co(en)(NH_3)_2(OH)_2]^+$ [a]	−1580	0.23
cis-trans-$[Co(en)(NH_3)_2(OH_2)]^+$ [b]	−1660	0.59
cis-cis-$[Co(en)(NH_3)_2(OH)_2]^+$ [b]	−1670	0.23
trans-$[Co(en)_2(OH)_2]^+$	−1130	0.15
cis-$[Co(en)_2(OH)_2]^+$	−1150	0.23
$[Co(en)NH_3(OH)_3]$	−2710	0.20

a) *trans*-dihydroxo-*cis*-diammine(ethylenediamine)cobalt(III) ion. b) *cis*-dihydroxo-*trans*-diammine(ethylenediamine)cobalt(III) ion. c) *cis*-dihydroxo-*cis*-diammine-cobalt(III) ion.

Table 1-g. Chemical shifts and line widths for $[Co(en)_x(NH_3)_{6-2x-y}(H_2O)_y]$ type of complexes

Complex	Chemical shift[a] (ppm)	Line width (G)
$[Co(NH_3)_5H_2O]^{3+}$	−930	2.8
fac-$[Co(en)(NH_3)_3H_2O]^{3+}$	−550	5.0
mer-$[Co(en)(NH_3)_3H_2O]^{3+}$	−550	8.0
trans-$[Co(en)_2(NH_3)H_2O]^{3+}$	−100	7.3
cis-$[Co(en)_2(NH_3)H_2O]^{3+}$	−200	7.0
cis-$[Co(NH_3)_4(H_2O)_2]^{3+}$	−1810	3.0
trans-$[Co(en)_2(H_2O)_2]^{3+}$	−950	—
cis-$[Co(en)_2(H_2O)_2]^{3+}$	−1000	6.5
fac-$[Co(NH_3)_3(H_2O)_3]^{3+}$	−2630	0.20

a) The standard deviation of observed values of chemical shifts was 2%.

Table 1-h. Chemical shifts and line widths for $[Co(en)_x(NH_3)_{6-2x-2y}(CO_3)_y]$ type of complexes

Complex	Chemical shift (ppm)	Line width (G)
$[Co(NH_3)_4(CO_3)]^+$	−1580	1.1
$[Co(en)_2(CO_3)]^+$	−730	1.9
$[Co(en)NH_3)_2(CO_3)]^+$	−1180	1.9
$[Co(NH_3)_2(CO_3)_2]^-$	−3550	1.6
$[Co(en)(CO_3)_2]^-$	−2940	2.4
$[Co(CO_3)_3]^{3-}$	−5770	0.25

Table 1-i. Chemical shifts and line widths for $[Co(en)_x(NH_3)_{6-2x-2y}(C_2O_4)_y]$ type of complexes

Complex	Chemical shift (ppm)	Line width (G)
$[Co(NH_3)_4(C_2O_4)]^+$	−1850[a]	—
$[Co(en)_2(C_2O_4)]^+$	−460[b]	2.0[b]
$[Co(NH_3)_2(C_2O_4)_2]^-$	−2780	1.5
$[Co(en)(C_2O_4)_2]^-$	−2250	3.2
$[Co(C_2O_4)_3]^{3-}$	−4700	0.25

a) This signal may be ascribed to $[Co(NH_3)_4(H_2O)_2]^{3+}$ ion. b) NMR measurements were made at 45 °C.

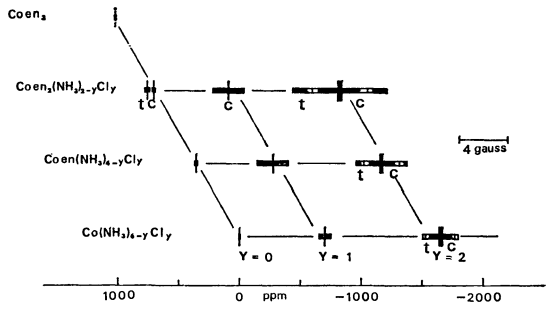

(a) $[Co(en)_x(NH_3)_{6-2x-y}Cl_y]$ type of complexes

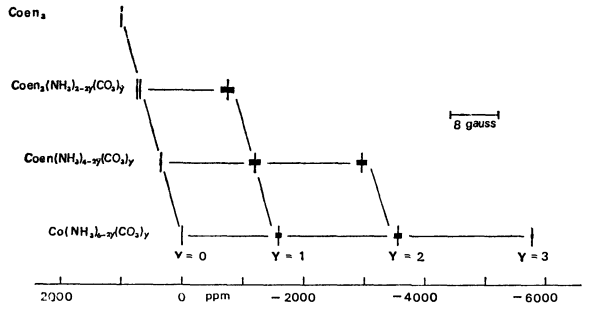

(b) $[Co(en)_x(NH_3)_{6-2x-2y}(CO_3)_y]$ type of complexes

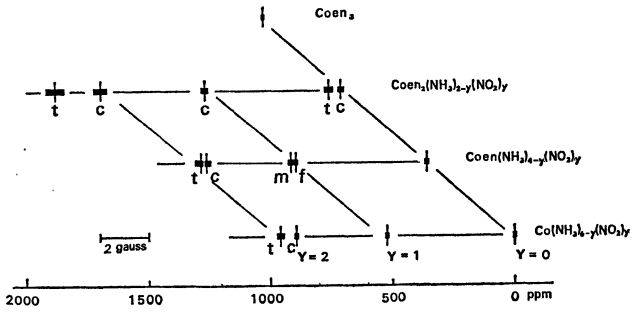

(c) $[Co(en)_x(NH_3)_{6-2x-y}(NO_2)_y]$ type complexes

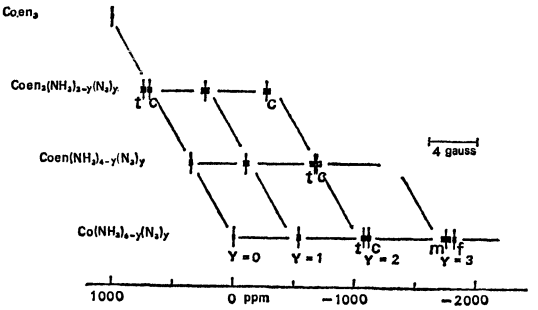

(d) $[Co(en)_x(NH_3)_{6-2x-y}(N_3)_y]$ type of complexes

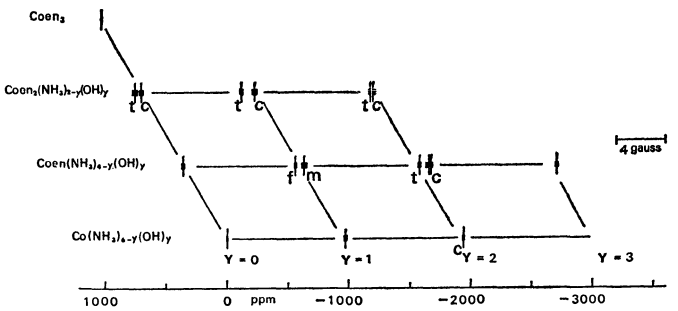

(e) $[Co(en)_x(NH_3)_{6-2x-y}(OH)_y]$ type of complexes

Fig. 1. The diagram for chemical shifts and line widths for $[Co(en)_x(NH_3)_{6-2x-y}L_y]$ type of complexes. The chemical shift and line width are represented by longitudinal and transverse bars, respectively. *Trans*, *cis*, *meridional*, and *facial* isomers are represented by t, c, m, and f, respectively.

The ligand shift parameters obtained are listed in Table 2.

The chemical shifts for ammine–ethylenediamine mixed complexes are listed in Table 1-a. The chemical shifts are proportional to the number of the ethylenediamine(or ammine) groups. The replacement of two NH_3 by one (en) results in a high-field shift of 360 ppm.

Figure 1-a shows the relation between the chemical shifts and the combinations of ligands for chloroammine complexes. From this diagram, the first and the sec-

TABLE 2. LIGAND SHIFT PARAMETER

Ligand	first (ppm)	second (ppm)	third (ppm)
NO_2^-	530± 20	420±100	—
N_3^-	−480± 50	−540± 50	−660± 50
Cl^-	−650± 50	−900± 50	—
Br^-	−620± 50	−900± 50	—
OH^-	−950±100	−950±100	−1100±100
H_2O	−900±100	−870±100	−830±100
Ligand	second (ppm)	fourth (ppm)	sixth (ppm)
CO_3^{2-}	−1500±100	−1900±100	−2200
$C_2O_4^{2-}$	−1200±100	−1500±100	−2000

ond ligand shift parameters are estimated as $\delta_1(Cl) = -(650+50)$ and $\delta_2(Cl) = -(900\pm50)$ ppm respectively. A quite similar diagram is obtained for bromoammine complexes, which show a slightly higher shift than to the chloroammine complexes.

The diagram for the carbonato species is shown in Fig. 1-b. The second, fourth, and sixth ligand shift parameters are estimated to be $-(1500\pm100)$, $-(1900\pm100)$, and -2200 ppm respectively. The absolute values for the ligand shift parameters become large with the increase in the number of substituted carbonato groups. Similar trends are observed for the Cl, Br, N_3, and C_2O_4 series. According to these results, it may be concluded that the absolute values of ligand shift parameters becomes smaller with an increase in the resonant fields of complexes. The diagrams for the NO_2 and N_3 series are shown in Figs. 1-c and 1-d respectively.

As Fig. 1-e shows, the contribution of the OH radical to the chemical shifts of cobalt-59 is additive: *i.e.*, the first, second, and third ligand shift parameters are almost equal ($\delta_1 \cong \delta_2 \cong \delta_3 \cong -(950\pm100)$ ppm). The chemical shifts of aquo-complexes also show a similar trend. The line width for aquo-complexes is much larger than that for the corresponding hydroxo-complexes: this certainly reflects the difference in the quadrupolar interactions of cobalt-59 between Co–OH and Co–OH_2 bonds.

Empirical Rules for the Chemical Shifts and Line Widths of Geometrical Isomers. The following rules have been deduced from the results of the present experiment concerning the relations between the geometrical isomers and their chemical shifts or line widths.

Rule I. The chemical shift of the trans-*isomer is higher than that of the corresponding* cis *isomer.* This rule holds for the complexes of the CoA_4B_2, $CoA_2A'_2B_2$, and CoA_4BC types, where A, B, and C refer to the different ligand atoms directly coordinate with cobalt, and where A and A′ represent the ligands of the same ligand atoms, such as NH_3 and (en). Shimura[9] presented an empirical rule for d-d absorption bands of *cis* and *trans* isomers of CoA_4B_2 type complexes: if A is in a higher rank than B in the spectroschemical series, $\nu_{max(cis)} - \nu_{max(trans)} > 0$, while if B is in a higher rank than A, $\nu_{max(cis)} - \nu_{max(trans)} < 0$. However, as has been described above, the chemical shift of a *trans* isomer, the chemical shift of a *trans* isomer is always higher than that of the corresponding *cis* isomer, regardless of the strength of the ligand fields for A and B. Simple calculation suggests that the difference in radial parameters and orbital reduction factors[10] is reponsible for the difference in chemical shifts between the *cis* and *trans* isomers.

Rule II. The line width of the trans-CoA_4B_2 *isomer is larger than that of the* cis-CoA_4B_2 *isomer.* It is well established that the cobalt-59 line widths for the species in solution are determined by quadrupolar interaction. A calculation based on a simple point-charge model has shown that the electric field gradient of a *trans* isomer is twice as that of the corresponding *cis* isomer.[6] The line widths of *cis*- and *trans*-$[Co(en)_2(NH_3)_2]^{3+}$, $[Co(en)_2(NO_2)_2]^+$, $[Co(en)_2Cl_2]^+$, $[Co(en)_2Br_2]^+$, $[Co(NH_3)_4(NO_2)_2]^+$, $[Co(NH_3)_4(N_3)_2]^+$, and $[Co(NH_3)_4Cl_2]^+$ are consistent with this rule. $[Co(en)_2(OH)_2]^+$ ion is the only exception among all the complexes studied which does not obey the general trends cited above. The relatively large line width of the *cis*-$[Co(en)_2(OH)_2]^+$ ion suggests a distortion of the field, resulting in a significant deviation from the regular octahedral structure.

Rule III. The line width of the mer-*isomer is larger than that of* fac-*isomer.* The electric field gradient at the site of the central cobalt nucleus in the *fac*-triaquotriamminecobalt(III) complex is estimated to be very small, as we see a sharp spectrum with a line width of 0.20 G. This value is in contrast to the broad spectra (about 2G) of the other aquoammine-complexes.[6] It can also be predicted from the point-charge model that *mer*-CoA_3B_2C complexes should give larger line widths than *fac*-CoA_3B_2C complexes. In fact, the line width of the *mer*-$[Co(en)(NH_3)_3NO_2]^{2+}$ ion is twice as large as that of the corresponding *fac*-isomer.

The Application of Cobalt-59 NMR to the Kinetics and Equilibria in Solution. The ligand shift parameters given in Table 2 can be used, along with the empirical rules presented above, to identify the cobalt(III) complexes and to study the kinetics and equilibria in solution. Illustrative examples will be presented and briefly discussed below.

Example 1. It is well established that the $[Co(NH_3)_5OH]^{2+}$, $[Co(NH_3)_4(OH)_2]^+$, $[Co(en)_2(NH_3)(OH)]^{2+}$, and $[Co(en)_2(OH)_2]^+$ ions exist in an alkaline solution.[11–13] However, the corresponding monoethylenediamine hydroxo-complexes, such as $[Co(en)(NH_3)_3(OH)]^{2+}$ and $[Co(en)(NH_3)_2(OH)_2]^+$ ions, have not yet been identified. In a concentrated alkaline solution, *trans*-$[Co(en)(NH_3)_2Br_2]Br$ shows two cobalt-59 NMR signals which do not coincide with that of the *trans*-$[Co(en)(NH_3)_2Br_2]^+$ ion (Fig. 2-a). The chemical shifts of these two signals are -1670 and -1580 ppm, which are very close to the value, -1540 ppm, estimated by means of Equation (1). This suggests that *trans*-$[Co(en)(NH_3)_2Br_2]^+$ is hydrolyzed to yield $[Co(en)(NH_3)_2(OH)_2]^+$ ion in an alkaline solution. On the basis of Rule I, the high- and low-field signals of the doublet can be assigned to the *trans*-dihydroxo and *cis*-dihydroxo isomers respectively. Figure 2-b shows an NMR spectrum of *trans*-$[Co(en)(NH_3)_2Br_2]$-Br dissolved in 10% aqueous ammonia and heated at 40 °C for 10 minutes. A high-field doublet in Fig. 2-b

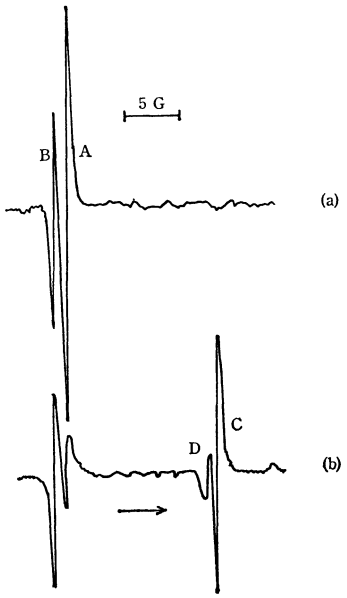

Fig. 2(a). Co-59 NMR spectra of *trans*-$[Co(en)(NH_3)_2Br_2]Br$ in concentrated ammonia solution. A and B correspond to *trans*- and *cis*-$[Co(en)(NH_3)_2(OH)_2]^+$ ions, respectively.
(b). Co-59 NMR spectra of *trans*-$[Co(en)(NH_3)_2Br_2]Br$ is ammonia solution which is heated at 40 °C for 10 minutes. C and D correspond to *fac*- and *mer*-$[Co(en)(NH_3)_3OH]^{2+}$ ions, respectively.

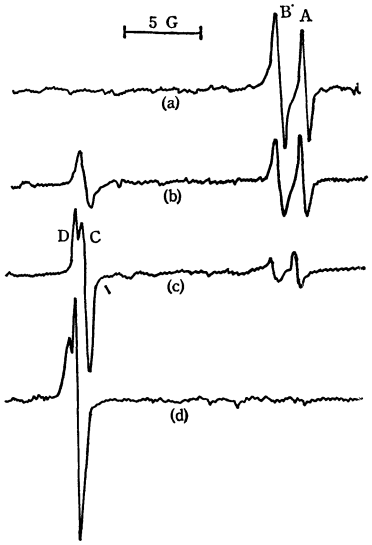

Fig. 3. Time variation of Co-59 NMR spectra of *cis*-$[Co(en)_2NH_3Br]Br_2$ in alkaline solution;
(a) at initial state, (b) after 5 min, (c) after 15 min, and (d) after 60 min.
The base hydrolysis reaction proceeded at 60 °C. NMR measurements were made at 25 °C after the reaction was quenched by cooling.
A, B, C, and D correspond to *trans*- and *cis*- $Co(en)_2NH_3OH]^{2+}$ and *trans*- and *cis*-$[Co(en)_2(OH)_2]^+$ ions, respectively.

with chemical shifts of −560 and −635 ppm is assigned to *mer*- and *fac*-$[Co(en)(NH_3)_3(OH)]^{2+}$. The chemical shift for $[Co(en)(NH_3)_3(OH)]^{2+}$ estimated from Equation (1) is −590 ppm. The broad and sharp signals of the doublet can be assigned to the *mer*- and *fac*-isomers respectively by means of Rule III.

Example 2. A doublet signal was observed in an alkaline solution of *cis*-$[Co(en)_2(NH_3)Br]Br_2$ which does not coincide with that of the *cis*-$[Co(en)_2(NH_3)Br]^{2+}$ ions itself. The high- and low-field signals of the doublet coincide with those of the *trans*- and *cis*-$[Co(en)_2(NH_3)(OH)]^{2+}$ ions respectively, suggesting that Br^- is replaced by OH^- to yield the *cis*- and *trans*-$[Co(en)_2(NH_3)(OH)]^{2+}$ ions. The fact that the initial concentrations of the *cis*- and *trans*-$[Co(en)_2(NH_3)(OH)]^{2+}$ ions (*cis* 80%, *trans* 20%) gradually change to reach the equilibrium concentrations (*cis* 70%, *trans* 30%) shows that the isomerization takes place between the *cis*- and *trans*-isomers.[8] If a large excess of the OH^- ion exists, the signal intensities of *cis*- and *trans*-$[Co(en)_2(NH_3)(OH)]^{2+}$ decrease and a new doublet corresponding to *cis*- and *trans*-$[Co(en)_2(OH)_2]^+$ appears (Fig. 3). These results clearly indicate that the *cis*- and *trans*-$[Co(en)_2(NH_3)(OH)]^{2+}$ ions are hydrolyzed to yield the *cis*- and *trans*-$[Co(en)_2(OH)_2]^+$ ions. The intensity measurements of each signal[8] would make it possible to determine the rate constants for the base hydrolysis. A quantitative treatment of this system is now under study and will be discussed in detail in a coming paper.

The authors wish to thank Prof. Yoji Arata and Prof. Takeo Yamamoto for their valuable discussions. Thanks are also due to Dr. Keikichi Nakamura, National Research Institute for Metals, for his assistance of measurement by Varian VF-16 spectrometer.

References

1) W. G. Proctor and F. C. Yu, *Phys. Rev.*, **81**, 20 (1951).
2) R. Freeman, G. R. Murray, and R. E. Richards, *Proc. Roy. Soc., Ser. A.*, **242**, 455 (1957).
3) S. S. Dharmatti and C. R. Kanekar, *J. Chem. Phys.*, **31**, 1436 (1960).
4) H. Hartmann and H. Sillescu, *Theor. Chim. Acta*, **2**, 371 (1964).
5) C. R. Kanekar, M. M. Dhingra, V. R. Marathe, and R. Nagarajan, *J. Chem. Phys.*, **46**. 2009 (1967).
6) A. Yamasaki, F. Yajima, and S. Fujiwara, *Inorg. Chim. Acta*, **2**, 39 (1968).
7) N. A. Matwiyoff and W. E. Wageman, *ibid.*, **4**, 460 (1970).
8) F. Yajima, Y. Koike, T. Sakai, and S. Fujiwara, *Inorg. Chem.*, **11**, 2054 (1972).
9) Y. Shimura, This Bulletin, **25**, 49 (1952).
10) S. Fujiwara, F. Yajima, and A. Yamasaki, *J. Magn. Resonance*, **1**, 203 (1969).
11) F. Yajima, A. Yamasaki, and S. Fujiwara, *Inorg. Chem.*, **10**, 2350 (1971).
12) W. Kruss and H. Taube, *J. Amer. Chem. Soc.*, **83**, 1280 (1961).
13) D. F. Martin and M. L. Tobe, *J. Chem. Soc.*, **1962**, 1388.

Crystal Structure of Bis(iminodiacetamide)copper(II) Perchlorate[1)]

Masao SEKIZAKI*

Department of Chemistry, Faculty of Science, Nagoya University, Chikusa, Nagoya 464

(Received July 2, 1973)

Bis(iminodiacetamide)copper(II) perchlorate was newly synthesized, and the crystal structure was determined from three-dimensional X-ray data collected on a diffractometer. The structure was refined by block-diagonal least-squares methods to give $R=0.08$ for the 950 observed reflections. The crystals are monoclinic with the space group of $P2_1/c$. There are two formula units per unit cell with $a=6.183$, $b=17.617$, $c=8.900$ Å, and $\beta=110.2°$. The complex is centrosymmetric, in which the two ligand molecules coordinate to the central copper atom through two imino nitrogen atoms and two of the four amide oxygen atoms in *trans* positions, exhibiting a square-planar coordination. The other two amide oxygen atoms are weakly bonded to the copper atom above and below this square-plane, thus completing an *s-facial* distorted (elongated) octahedral coordination. The complex cations are held together through hydrogen bonds to form infinite chains along the *a* axis. These chains are connected with one another by perchlorate ions through hydrogen bonds, thus forming three-dimensional networks.

A number of bivalent copper complexes of bidentate ligands exhibit an elongated octahedral structure of D_{2h} symmetry.[2-7)] There are some complexes of terdentate ligands in which the length of the four coordination bonds in the same plane are longer than those of the other two coordination bonds, such as $[Cu(dien)_2](NO_3)_2$ (dien=diethylenetriamine).[8)] Such an unusual structure is sometimes called a "compressed" distorted octahedral structure.[9)] The complex of the other terdentate ligand, such as $[Cu(ida)_2]^{2-}$ (ida=iminodiacetate), was, however, reported on the basis of a spectroscopic investigation, to have an elongated octahedral structure.[10)] Two of the factors that differentiate the structures of these complexes may be as follows: the iminodiacetate ion[11)] has a smaller stability constant of complex formation than diethylenetriamine,[12)] and the force constant of Cu–O is generally smaller than that of Cu–N.[13)]

Iminodiacetamide, $HN(CH_2CONH_2)_2$, (abbreviated as $idaaH_2$) can act as a terdentate ligand. It can also function as a neutral ligand, forming a cationic complex like diethylenetriamine. It can coordinate to a metal atom through two oxygen and one nitrogen atoms like the iminodiacetate ion. It is difficult to decide by the spectroscopic method whether or not the distorted octahedral coordination around the copper atom is "compressed." A copper complex of iminodiacetamide, $Cu(idaaH_2)_2(ClO_4)_2$, was subjected to X-ray crystal analysis in order to clarify this point and to facilitate the assignments of the infrared spectra.

Experimental

Preparations. Iminodiacetamide was prepared as white needles by the reaction of diethyliminodiacetate and ammonia in ethanol. The melting point, 142 °C, and the results of chemical analysis agreed with the reported values.[14)]

The complex was prepared by mixing 0.07 g of the ligand with 0.09 g of copper(II) perchlorate dissolved in water and then by concentrating the mixture *in vacuo* at room temperature. The crystals thus obtained were washed with a small amount of water. Yield, 0.06 g.

Found: C, 18.00; H, 3.46; N, 15.67; Cu, 11.90%. Calcd for $C_8H_{18}N_6O_4Cu(ClO_4)_2$: C, 18.00; H, 3.56; N, 15.75; Cu, 11.92%.

Determination of the Cell Constants and Collection of the Intensity Data. The cell constants were determined by the least-squares methods based on the 2θ values measured on a single-crystal diffractometer using Cu$K\alpha$ radiation ($\lambda=1.5418$ Å). A crystal with a diameter of about 0.2 mm was sealed in a glass capillary. The intensities were collected on a Hilger-Watts automatic four-circle diffractometer, using Ni-filtered Cu$K\alpha$ radiation. The ω-2θ step-scan technique with $\Delta\omega=0.02°$ and a counting time of 1 sec per step were used. The scan range was 0.8° in the 0—57° region and 1.2° in the 57—75° region. At each end of the scan, the backgrounds were measured for 10 sec in the $\theta\leqq57°$ region and for 15 sec in the $\theta>57°$ region. The fluctuations in intensity of the three standard reflections measured every 100 reflections were about 2% during the data collection. A total of 1600 independent reflections were measured up to $\theta=75°$; of them, 650 had an intensity less than σ's above the background. Thus, 950 independent non-zero reflections were used in the analysis. They were converted to $|F|$ by applying Lorentz and polarization corrections. No corrections were made for absorption or extinction ($\mu r=0.2$).

The crystal data are:
$Cu(C_4H_9N_3O_2)_2(ClO_4)_2$, *F.W.* 524.72, monoclinic, $a=6.183$ (2), $b=17.617(4)$, $c=8.900(2)$ Å, $\beta=110.2(1)°$, $U=908$ Å^3, $D_m=1.94$, $D_x=1.92$ g cm^{-3}, $Z=2$.
The systematic absences are $h0l$ with l odd and $0k0$ with k odd. Hence, the space group is $P2_1/c$.

Solution and Refinement of the Structure

The copper atoms must lie on a set of twofold special positions, since there are only two formula units in a unit cell. The complex must thus have a center of symmetry. The coordinates of the chlorine atoms were determined from the prominent peaks in a Patterson map; those of all the other atoms except the hydrogens were determined by a three-dimensional electron density map calculated on the basis of the copper and chlorine atoms.

The block-diagonal least-squares refinements were carried out for the 950 reflections with equal weights. After five cycles of refinement with isotropic thermal parameters, the R-value became 0.12. Further refinements with anisotropic thermal parameters finally reduced the R-value to 0.08.

The atomic scattering factors were taken from the "International Tables for X-ray Crystallography."[15)]

* Present address: College of Liberal Arts, Kanazawa University, Marunouchi, Kanazawa 920.

TABLE 2. FINAL ATOMIC PARAMETERS AND THEIR ESTIMATED STANDARD DEVIATIONS

Values are given $\times 10^4$. Positional parameters are expressed as fractions of the lattice parameters. The estimated standard deviations are in parentheses and refer to the last decimal positions of the respective values in this table and other subsequent tables.

Thermal parameters are in the form: $\exp[-(h^2\beta_{11}+k^2\beta_{22}+l^2\beta_{33}+hk\beta_{12}+hl\beta_{13}+kl\beta_{23})]$

Atom	x	y	z	β_{11}	β_{22}	β_{33}	β_{12}	β_{13}	β_{23}
Cu	0	0	0	198(1)	12(1)	85(1)	16(3)	108(2)	14(4)
Cl	2123(1)	1877(1)	4403(1)	268(1)	16(1)	113(2)	−9(3)	161(2)	−11(5)
O(1)	2212(2)	−189(1)	−1078(3)	230(.2)	8(2)	119(4)	30(8)	116(5)	17(11)
O(7)	3076(3)	−88(2)	2650(4)	262(4)	17(1)	86(2)	−44(9)	93(6)	−5(13)
O(10)	2001(3)	1637(2)	2853(4)	702(11)	47(5)	120(7)	48(17)	346(7)	−44(18)
O(11)	−225(4)	2020(2)	4285(3)	365(12)	43(5)	381(11)	99(18)	425(19)	46(24)
O(12)	3075(3)	1311(2)	5622(2)	476(8)	37(6)	187(12)	112(14)	184(17)	79(19)
O(13)	3390(3)	2557(2)	4835(2)	729(19)	38(7)	386(19)	−301(19)	309(35)	−107(26)
N(4)	453(2)	−1106(2)	638(2)	199(4)	12(1)	73(2)	20(9)	54(6)	4(13)
N(8)	4578(3)	−1089(1)	−1504(2)	192(2)	19(2)	112(3)	−0(12)	226(2)	−8(15)
N(9)	2274(3)	−505(2)	4812(2)	339(10)	43(2)	94(3)	−70(16)	194(12)	−7(19)
C(2)	3130(3)	−843(2)	−846(3)	214(7)	18(1)	87(4)	−47(11)	27(11)	−7(17)
C(3)	2528(2)	−1395(4)	296(2)	231(3)	20(3)	93(5)	6(14)	186(3)	160(18)
C(5)	691(3)	−1192(1)	2347(1)	213(8)	16(1)	57(2)	−55(12)	152(10)	−3(15)
C(6)	2086(2)	−549(2)	3282(2)	205(5)	14(2)	83(4)	−9(11)	100(5)	8(16)

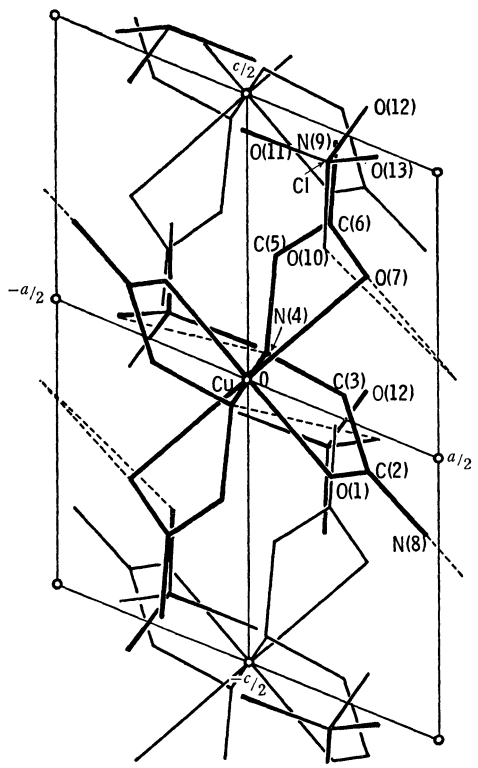

Fig. 1. Projection of the structure along the b axis. Dashed lines indicate hydrogen bonds.

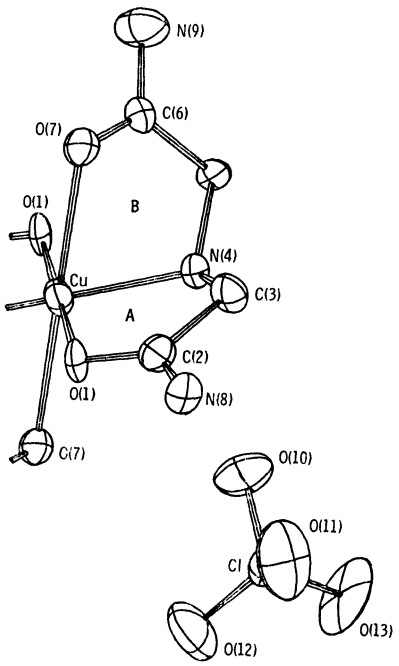

Fig. 2. Thermal ellipsoids of atoms at 50% probability level.

The calculations of the data reduction and the Fourier syntheses were carried out by means of programs written by Dr. Sasaki. The block-diagonal least-squares refinements and the calculations of the bond distances and angles were done with the HBLS-4 and DAPH programs written by Dr. Ashida. The thermal ellipsoids were drawn by means of the ORTEP program of Dr. Johnson. All the calculations were performed on a FACOM 230-60 computer at the Computation Center of Nagoya University.

The observed and calculated structure factors are listed in Table 1,** and the final atomic parameters, in Table 2.

Results and Discussion

A projection of the structure along the b axis is shown in Fig. 1. The anisotropic thermal ellipsoids of the

** Table 1 has been deposited with the Chemical Society of Japan (Document No. 7414).

Table 3. Bond distances and angles

Cu-O(1)	1.952(2) Å	O(1)-C(2)-C(3)	118.9(3)
Cu-N(4)	2.021(2)	C(2)-C(3)-N(4)	109.6(4)
Cu-O(7)	2.471(3)	C(3)-N(4)-Cu	108.3(3)
O(1)-C(2)	1.269(3)	C(5)-N(4)-Cu	110.0(2)
C(2)-C(3)	1.543(5)	C(3)-N(4)-C(5)	112.5(3)
C(3)-N(4)	1.506(5)	N(4)-C(5)-C(6)	109.1(2)
N(4)-C(5)	1.484(3)	C(5)-C(6)-O(7)	121.1(3)
C(5)-C(6)	1.492(3)	C(6)-O(7)-Cu	97.7(3)
C(6)-O(7)	1.261(4)	O(1)-C(2)-N(8)	124.6(3)
C(2)-N(8)	1.301(3)	N(8)-C(2)-C(3)	116.6(3)
C(6)-N(9)	1.328(4)	O(7)-C(6)-N(9)	122.4(3)
Cl-O(10)	1.420(3)	N(9)-C(6)-C(5)	116.5(3)
Cl-O(11)	1.441(3)	Perchlorate ion	
Cl-O(12)	1.441(2)	O(10)-Cl-O(11)	105.5(2)
Cl-O(13)	1.409(3)	O(11)-Cl-O(12)	108.3(2)
Complex ion		O(12)-Cl-O(13)	109.8(2)
O(1)-Cu-N(4)	85.5(1)°	O(13)-Cl-O(10)	110.9(2)
O(1)-Cu-O(7)	91.1(1)	O(10)-Cl-O(12)	113.3(2)
N(4)-Cu-O(7)	71.7(1)	O(11)-Cl-O(13)	108.8(2)
Cu-O(1)-C(2)	115.2(2)		

Table 4. Intermolecular contacts less than 3.5 Å

$O(13^{I})$-$O(10^{II})$	3.401(4) Å	$N(8^{I})$-$O(10^{V})$	2.933(3)
$O(11^{I})$-$C(3^{III})$	3.214(5)	$O(1^{I})$-$C(2^{V})$	3.335(3)
$O(13^{I})$-$C(5^{III})$	3.406(3)	$O(1^{I})$-$O(1^{V})$	3.381(5)
$O(11^{I})$-$C(5^{III})$	3.439(3)	$N(4^{I})$-$O(11^{VI})$	3.307(3)
$O(11^{I})$-$N(4^{III})$	3.307(3)	$N(4^{I})$-$O(13^{VI})$	3.268(3)
$O(13^{I})$-$N(4^{III})$	3.268(3)	$C(3^{I})$-$O(11^{VI})$	3.214(5)
$N(8^{I})$-$N(4^{IV})$	3.469(3)	$C(5^{I})$-$O(11^{VI})$	3.439(3)
$N(8^{I})$-$O(1^{V})$	3.337(3)	$C(5^{I})$-$O(13^{VI})$	3.406(3)
$N(8^{I})$-$O(7^{V})$	2.910(4)		

I at	x	y	z
II	x	$1/2-y$	$1/2+z$
III	$-x$	$1/2+y$	$1/2-z$
IV	$1+x$	y	z
V	$1-x$	$-y$	$-z$
VI	$-x$	$-1/2+y$	$1/2-z$

atoms are shown in Fig. 2. The bond distances and angles are listed in Table 3, and the intermolecular contacts, in Table 4.

The complex is centrosymmetric, with two ligand molecules coordinating in *trans* positions through two imino nitrogen atoms, N(4), and two of the four amide oxygen atoms, O(1). The other two amide oxygen atoms, O(7), lie above and below the plane defined by the N(4), O(1), and Cu atoms, thus completing an *s-facial* octahedral coordination.

The bond distances and angles of the two chelate rings, Cu–O(1)–N(4) (Chelate ring A in Fig. 2) and Cu–O(7)–N(4) (Chelate ring B), are shown in Fig. 3 along with those of *cis*-bis(glycinato)copper(II) monohydrate.[16] All the distances and angles except for the C(2)–O(1) double bond in the Chelate ring A agree with those of the glycinato complex. This indicates that no large influence due to terdentate coordination is introduced in the Chelate ring A.

The Cu–O(7) distance (2.47 Å) in the Chelate ring B is much longer than the Cu–O(1) distance in the ring A, indicating a weak bonding interaction, a "semi-

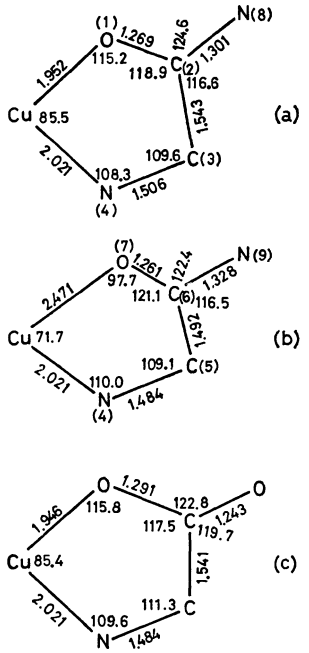

Fig. 3. Bond distances and angles of (a) Chelate ring A, (b) Chelate ring B and (c) *cis*-$Cu(H_2NCH_2COO)_2 \cdot H_2O$.[16]

coordination bond,"[6] between Cu and O(7). The O(7)–Cu–N(4) angle (71.7°) is too small to be a normal angle between the coordination bonds. Hence, the structure of the complex is not simply elongated but is distorted octahedral.

The equations of the planes defined by Cu and the coordinating atoms (coordination planes) are listed in Table 5. The Chelate rings, A and B, are not planar and show considerable deviations of carbon atoms from each of the coordination planes, while the chelate ring of the glycinato complex is almost coplanar.[16] Judging by the model, this difference may be due to the C=O double bond in these chelate rings rather than to fused-ring formation.

Table 5. Equations for the coordination planes in the chelate rings A and B, and the deviations of the atoms therefrom

Planes are expressed in the form: $DX+EY+FZ=0$, where X, Y, and Z are coordinates in Å measured along the a, b, and c^* axes respectively

Chelate ring	A	B
Atoms defining the plane	Cu, O(1), N(4)	Cu, O(7), N(4)
D	0.4911	−0.8925
E	0.2494	0.0831
F	0.8346	0.4434
Deviation of the atoms from the plane	C (2) 0.118 Å	C (5) 0.958 Å
	C (3) 0.316	C (6) 0.887

The complex cations are connected through hydrogen bonds between $N(8^{I})$ and $O(7^{V})$, forming infinite chains along the a axis. These chains are held with one another by perchlorate ions through hydrogen bonds of the N–H···O type between $O(13^{I})$ and $N(4^{III})$ and between $O(10^{I})$ and $N(8^{V})$ (Table 4). The crystal thus consists of three-dimensional networks of hydrogen bonds connecting the complex and perchlorate ions with one another.

The perchlorate ion is regularly tetrahedral, and the thermal motions of the four oxygen atoms are larger than those of the atoms in the complex ion.

The infrared and visible spectra of nickel(II) and cobalt(II) complexes of iminodiacetamide could be well assigned on the basis of the structural features of this complex. These results will be published elsewhere.[17]

The author wishes to acknowledge valuable discussions with Professor Kazuo Yamasaki of Nagoya University. He also wishes to thank Professor Jiro Tanaka, Dr. Noriyoshi Sakabe, and Dr. Kyoyu Sasaki of Nagoya University for the use of the Hilger-Watts four-circle automatic diffractometer and the computation programs. Part of the expenses were met by a grant from the Matsunaga Science Foundation, to which the author's thanks are due.

References

1) Spectroscopic and Crystallographic Investigations of the Metal Complexes of Iminodiacetamide. I.
2) M. Sekizaki and K. Yamasaki, *Revue de Chimie Minérale*, **6**, 255 (1969).
3) M. Mikami, I. Nakagawa, and T. Shimanouchi, *Spectrochim. Acta*, **25A**, 365 (1969).
4) D. H. Brown, D. R. MacSween, M. Mercer, and D. W. A. Sharp, *J. Chem. Soc., A*, **1971**, 1574.
5) M. Sekizaki, *Acta Crystallogr.*, **B29**, 327 (1973).
6) M. Sekizaki, F. Marumo, K. Yamasaki, and Y. Saito, This Bulletin, **44**, 1731 (1971).
7) Refs. 11, 12, and 13 cited in Ref. 5.
8) F. S. Stephens, *J. Chem. Soc., A*, **1969**, 883.
9) B. J. Hathaway and A. A. G. Tomlinson, *Coord. Chem. Revs.*, **5**, 1 (1970).
10) S. Laitinen and T. Nortia, *Suomen Kemistilehti*, **B43**, 61 (1970).
11) S. Chaberek, Jr. and A. E. Martell, *J. Amer. Chem. Soc.*, **74**, 5052 (1952).
12) H. B. Jonassen, R. B. LeBranc, and R. M. Rogan, *ibid.*, **72**, 4968 (1950).
13) See for example: Ref. 3; J. A. Kieft and K. Nakamoto, *Inorg. Chim. Acta*, **2**, 225 (1968); J. L. Walter, C. S. C. and R. J. Hooper, *Spectrochim. Acta*, **25A**, 647 (1969).
14) W. J. A. Jongkees, *Rec. Trav. Chim. Pays-Bas*, **27**, 300.
15) "International Tables for X-ray Crystallography," Vol. III, Kynoch Press, Birmingham (1962).
16) H. C. Freeman, M. R. Snow, I. Nitta, and K. Tomita, *Acta Crystallogr.*, **17**, 1463 (1964).
17) M. Sekizaki, Y. Yamada, and H. Takahashi, *Nippon Kagaku Kaishi*, **1974**(6), 1057.

The Reaction of *N*-Chlorocarbamoylethyl Starch with Amines in an Aqueous Alkaline Medium; Reactions of An Isocyanate Group[1]

Mitsuo HIGUCHI, Kenji TAKESHITA,* and Ryoichi SENJU

Department of Forest Products, Faculty of Agriculture, Kyushu University, Hakozaki, Higashi-ku, Fukuoka 812

**Technical Research Institute, Chuetsu Pulp Industry Co., Ltd., Ginza 2-10-6, Chuo-ku, Tokyo 104*

(Received September 12, 1973)

The reactions of *N*-chlorocarbamoylethyl starch with simple monoamines were investigated in order to elucidate the mechanism of the reaction of an isocyanate group with amines in an aqueous alkaline medium. It was confirmed that the *N*-chloroamide group reacts with amines through the formation of an isocyanate group. The reactions of the isocyanate with amines in the presence of sodium hydroxide obeyed the following equation: (rate of isocyanate–amine reaction)/(rate of isocyanate–OH^- reaction)$=k_u$[amine]/k_a[OH^-] showing no catalytic effects of reactants or products. The reactivities of most of the primary amino groups attached to primary carbon with the isocyanate are comparable to that of the hydroxide ion. The relative rates of the reactions of amines with the isocyanate are not always correlated to their basicities, even when differences in steric hindrance are not great. Both the enthalpy and entropy of activation for the isocyanate–amine reactions are smaller than those for the isocyanate–OH^- reaction.

Polymers bearing *N*-chloroamide groups are of interest because of the variety of reactions of the *N*-chloroamide groups. It is well known that *N*-haloamides in acid form (RCONHX) react as oxidizing agents or as halogenating agents,[2] and that, in salt form or in ionized form ($RCONX^-$), they produce isocyanate groups through the Hofmann rearrangement.[3]

The *N*-chlorocarbamoylethyl derivatives of polysaccharides can be readily synthesized and have some possibilities of practical use. With regard to the utilization of these derivatives, it may be most promising to exploit the reactions of the isocyanate group which is formed through the Hofmann rearrangement of the *N*-chloroamide group, leading to the syntheses of novel derivatives of polysaccharides.

On the reactions of isocyanates with active hydrogen compounds, although numerous papers have been published[4] and some papers have dealt with the reaction of water with isocyanates, nothing is yet known concerning the reactions of isocyanates in aqueous medium. Therefore, the reactions of *N*-chlorocarbamoylethyl starch with amines were investigated in an attempt to elucidate the mechanism of the reaction of the isocyanate group with amines in an aqueous alkaline medium.

Results and Discussion

Course of the Reaction of the N*-chloroamide Group with Amines.* First, as it was possible that the *N*-chloroamide would not always react with amines only through the formation of the isocyanate group, the effects of amines on the rate of decomposition of the *N*-chloroamide and the material balance in the reaction were investigated in order to make the course of the reaction clear.

It is well known that the rate of the Hofmann rearrangement of *N*-chloroamides obeys a first-order equation:[5]

$$-\mathrm{d[RCONCl^-]}/dt = k[\mathrm{RCONCl^-}] \qquad (1)$$

All the runs for various combinations of *N*-chlorocarbamoylethyl starch with amines employed in this study followed Eq. (1), and the concentration of the amines had no effect on the rate of the decomposition of *N*-chloroamide above pH 11.

The rate constants and energies of activation for the decomposition of *N*-chloroamide in the presence of amines were almost identical with those for the *N*-chloroamide–NaOH system, a typical case of Hofmann rearrangement.

Table 1 shows the material balance in the reaction of *N*-chlorocarbamoylethyl starch with methylamine. The amount of the *N*-chloroamide group decomposed is in agreement with the increase in the nitrogen content of the starch derivative and with half of the amount of methylamine consumed. This result is in accord with the following reaction sequence:

$$\mathrm{RCONHCl + R'NH_2} \xrightarrow{\text{instantaneous}} \mathrm{(RCONCl)^-(R'NH_3)^+}$$

$$\mathrm{(RCONCl)^-(R'NH_3)^+} \xrightarrow{\text{slow}} \mathrm{RN{=}C{=}O + R'NH_3{+}Cl^-}$$

$$\mathrm{RN{=}C{=}O + R'NH_2} \xrightarrow{\text{very fast}} \mathrm{RNHCONHR'} \qquad (2)$$

The results on other amine–*N*-chloroamide systems were essentially identical with this.

From the facts discussed above, it may be concluded that the *N*-chloroamide reacts with amines through the formation of an isocyanate, and that any side reactions are negligible in these systems.

Table 1. Material balance in the reaction of *N*-chlorocarbamoylethyl starch with methylamine[a]

Reaction time (min)	Relative[b] amount of *N*-chloroamide decomposed	Relative[c] amount of amine consumed	Relative[d] increase in nitrogen content
10	0.156	0.310	0.155
30	0.398	0.795	0.400
60	0.637	1.277	0.635
100	0.815	1.634	0.813
210	0.971	1.940	0.970
420	1.00	2.01	0.997

a) Initial concentrations: *N*-chloroamide 0.05 mol/l, methylamine 0.35 mol/l, temperature: 45 °C. b, c, and d) On the basis of the initial amount of the *N*-chloroamide group. d) Nitrogen content: Nitrogen content of the starch derivative obtained.

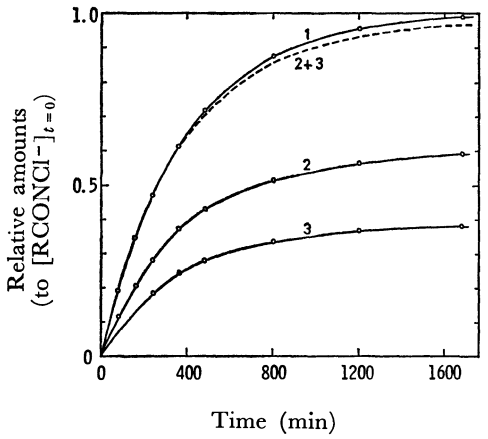

Fig. 1. A typical case of the reaction course in *N*-chloroamide-amine-NaOH system.
$[N\text{-chloroamide}]_{t=0}$: 0.05 mol/l, $[\text{Methylamine}]_{t=0}$: 0.2 mol/l, $[\text{NaOH}]_{t=0}$: 0.2 mol/l, temp: 30 °C.
1: Amount of the *N*-chloroamide group decomposed.
2: Amount of the urea derivative formed (evaluated from the increase in nitrogen content of the starch derivative).
3: Amount of the aminoethyl group formed.

Reaction of the Isocyanate Group with Amines in the Presence of Sodium Hydroxide. As can be seen from the results shown in Table 1, in the absence of caustic alkalies almost all of the reaction products consisted of the corresponding urea derivatives when more than a four-~fivefold excess of amines was employed. This fact indicates that the reactivity of H_2O with the isocyanate group is negligible in comparison with those of amines.

In the presence of sodium hydroxide, however, a considerable amount of the aminoethyl group was produced. Figure 1 shows a typical case of the reaction course. The sum of the amounts of the aminoethyl group and the urea derivative (evaluated from the increase in nitrogen content of the starch derivative) is in good agreement with the amount of the *N*-chloroamide decomposed, though a slight discrepancy appears in the late stage of the reaction. This discrepancy was significant when the concentration of amines was too low or when the reactivities of amines were too low, as in the cases of aniline and *tert*-butylamine. This may be attributed to the formation of an intramolecular urea derivative, *i. e.*, the product of the reaction of the isocyanate group with the aminoethyl group formed by the Hofmann degradation.

The relative rate of the isocyanate–amine reaction to the isocyanate–OH^- reaction, R_u/R_a, can be readily calculated from the ratio of the amount of the urea derivative to that of the aminoethyl group formed.

As Fig. 2 shows, a linear relationship was observed between R_u/R_a and [Amine]/[NaOH] when the concentrations of amine and sodium hydroxide were not too low or not too high. This result indicates that the catalytic effects of reactants or products, which have often been observed in the reactions of isocyanates in some nonaqueous media,[4] are absent in this isocyanate–amine–NaOH system, and that the reactions obey simple second-order kinetics;

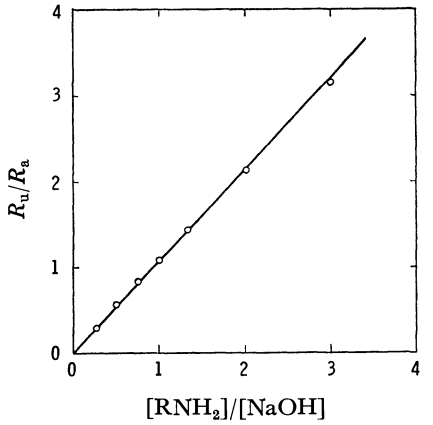

Fig. 2. Relation between R_u/R_a and $[RNH_2]/NaOH]$.
$[N\text{-chloroamide}]_{t=0}$: 0.02 mol/l, [Ethylamine]: 0.125—0.5 mol/l, [NaOH]: 0.125—0.5 mol/l, temp: 30 °C.

$$\text{d[Urea derivative]/d}t = k_u[\text{Isocyanate}][\text{Amine}] \quad (3)$$

$$\text{d[Aminoethyl group]/d}t = k_a[\text{Isocyanate}][OH^-] \quad (4)$$

$$\frac{\text{d[Urea derivative]/d}t}{\text{d[Aminoethyl group]/d}t} = \frac{R_u}{R_a} = \frac{k_u}{k_a}\frac{[\text{Amine}]}{[OH^-]} \quad (5)$$

The k_u/k_a ratio represents the relative reactivity of amine to the hydroxide ion in the reaction with the isocyanate.

The Arrhenius plots of k_u/k_a are shown in Fig. 3. The energies of activation for the isocyanate–amine reactions are smaller than that for the isocyanate–OH^- reaction.

Relative Reactivities of Amines. The rate constant ratios, k_u/k_a, at 30 °C and the derived activation parameters are summarized in Table 2. The relative reactivities of primary amines are in this order: amino groups attached to primary carbon>attached to secondary carbon>attached to tertiary carbon; this result is in agreement with the order in the extent of steric hindrance. It is noteworthy that the reactivities of most of the primary amino groups attached to primary carbon are comparable to that of the hydroxide ion, and that the

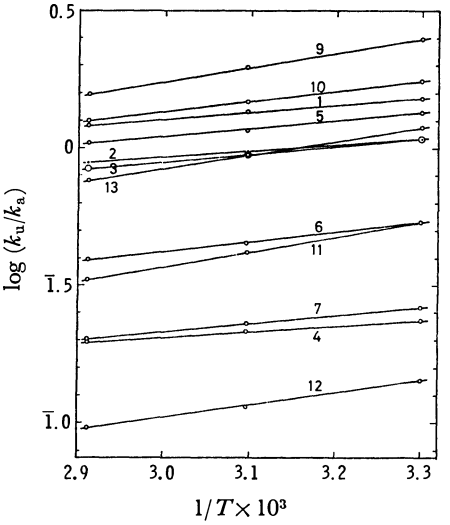

Fig. 3. Arrhenius plots of k_u/k_a.
The numbers, 1~13, denote the code numbers for amines in Table 2.

TABLE 2. RELATIVE REACTIVITIES OF AMINES IN THE REACTION WITH THE ISOCYANATE GROUP

	Amine	pK_a	k_u/k_a (30 °C)	$\Delta\Delta H^{\neq}$ a) (kcal/mol)	$\Delta\Delta S^{\neq}$ b) (cal/deg·mol)
1	Methylamine	10.62c)	1.54	−1.21±0.1	−3.1±0.3
2	Ethylamine	10.63c)	1.07	−1.09±0.1	−3.5±0.3
3	*n*-Propylamine	10.53c)	1.07	−1.33±0.1	−4.2±0.3
4	Isopropylamine	10.63c)	0.47	−0.94±0.2	−4.7±0.6
5	*n*-Butylamine	10.62c)	1.35	−1.55±0.2	−4.5±0.6
6	Isobutylamine	10.43c)	1.09	−1.63±0.2	−5.2±0.6
7	*sec*-Butylamine	10.56c)	0.52	−1.36±0.1	−5.8±0.3
8	*tert*-Butylamine	10.45c)	0.04		
9	Dimethylamine	10.87c)	2.52	−2.42±0.1	−6.1±0.3
10	Diethylamine	10.98c)	1.73	−1.68±0.1	−4.5±0.3
11	Ethyl aminoethyl ether	9.89	0.52	−2.48±0.1	−9.5±0.3
12	Ammonia	9.21c)	0.14	−2.10±0.3	−10.8±0.9
13	Benzylamine	9.34c)	1.19	−2.36±0.1	−7.4±0.3
14	Aniline	4.6c)	<0.01		

a) Calculated from the slopes of the lines for Arrhenius plots of k_u/k_a (Fig. 3). $\Delta\Delta H^{\neq} = \Delta H_u^{\neq} - \Delta H_a^{\neq} = E_u - E_a$. b) $\Delta\Delta S^{\neq} = \Delta S_u^{\neq} - \Delta S_a^{\neq} = 2.303\,R \log (k_u/k_a) + \Delta\Delta H^{\neq}/T$. c) Taken from the paper of H. K. Hall, Jr., *J. Amer. Chem. Soc.*, **79**, 5441 (1957).

relative reactivities of amines are not always in agreement with the concept, accepted for the reactions in some nonaqueous media, that the more basic amines react faster when the differences in steric hindrance are not great.

The negative values of $\Delta\Delta H^{\neq}$ and $\Delta\Delta S^{\neq}$ suggest that the hydration of the reactants plays an important role in the reaction of the isocyanate group with amines in aqueous alkaline media. It is conceivable that, in forming the transition-state complex with the isocyanate, the hydroxide ion requires a larger energy than amines do because of the greater extent of hydration, in spite of its greater basicity. The larger value of the entropy of activation for the isocyanate–OH^- reaction in comparison with those for the isocyanate–amine reactions may be attributed to the larger amount of the water molecule released on the formation of the transition-state complex. Differences in the extent of hydration of amines may also be reflected in their relative reactivities.

Experimental

Materials. Carbamoylethyl starch was prepared by means of a Michael reaction of acrylamide with corn starch; the degree of substitution was 0.9.[6]

Amines purchased from commercial sources were purified by distillation under a N_2 atmosphere. Ethyl aminoethyl ether (a model for the aminoethyl group attached to polysaccharide) was prepared by means of the Hofmann degradation of ethyl carbamoylethyl ether; $C_2H_5OC_2H_4NH_2$=89, bp 108.5 °C.

Reaction Procedure. The chlorination of carbamoylethyl starch was carried out under these conditions: amide group concentration: 0.2 mol/l; sodium hypochlorite concentration: 0.22 mol/l; temperature: 0 °C, and reaction time: 7 hr. The degree of *N*-chlorination was 99% on the basis of the amide group. After this process, acetone was added to the reaction mixture (1 vol%) in order to eliminate the excess hypochlorite.[7] After 10 hr the solution was neutralized to pH 5.5 with dilute HCl and diluted to 0.1 mol/l on the basis of the *N*-chloroamide group.

Adequate portions of this solution and an amine solution and/or a NaOH solution were mixed under cooling with ice-water, and 15-ml portions of the mixture were enclosed in 20-ml Pyrex ampoules. The ampoules were immersed in a constant-temperature bath under vigorous shaking for the desired times, then cooled with ice–water and subjected to analysis.

Analytical Methods. The *N*-chloroamide group was analyzed by iodometry. The nitrogen contents of the starch derivatives were determined by the following procedure.

A 10-ml portion of the reaction mixture was pipetted out and transferred into a 200-ml beaker containing 50 ml of methanol, 100 ml of acetone, and 1 ml of acetic acid. The mixture was then agitated by a magnetic stirrer until the starch derivative had been precipitated completely. Then the supernatant liquid was removed, and the precipitate was redissolved with 10 ml of a 1 M acetic acid aqueous solution and reprecipitated by the addition of 100 ml of acetone. After the completion of the precipitation, the supernatant liquid was removed and the precipitate was washed with ethanol and dissolved with 30 ml of 20% sulfuric acid and then subjected to Kjeldahl analysis. The complete precipitation of starch derivatives and the complete removal of the unreacted amine were confirmed by testing the samples of zero reaction time.

The amino-group contents of the starch derivatives were determined by colloid titration;[8] a 2-ml (or 5-ml) portion of the reaction mixture was pipetted out, put into 150 ml of 0.1 M acetic acid aqueous solution, and then titrated with a M/400 potassium polyvinyl sulfate solution, using toluidine blue as an indicator.

The authors wish to express their thanks to Professor Isao Sakata, Kyushu University, for his helpful suggestions.

References

1) Derivatives of Natural Polymers and Their Applications X. Part IX of this series; H. Tanaka and R. Senju, *Nippon Kagaku Kaishi*, **1974**, 359.

2) R. Filler, *Chem. Rev.*, **63**, 21 (1963),

3) E. S. Wallis and J. F. Lane, "Organic Reactions," Vol. III, John Wiley & Sons, New York (1962).
4) T. Mukaiyama, *Yuki Gosei Kagaku*, **19**, 775 (1961); J. H. Saunders and K. C. Frisch, "Polyurethanes, Chemistry and Technology," Interscience Publ., New York (1962); R. Vieweg and A. Höchtlen, "Kunststoff Handbuch," Band VII, "Polyurethane," Carl Hanser Verlag, München (1966).
5) T. Imamoto, Y. Tsuno, and Y. Yukawa, This Bulletin, **44**, 1639 (1971).
6) A 0.9 mol of the amide group/162 g of starch.
7) M. Higuchi, I. Sakata, and R. Senju, *Kogyo Kagaku Zasshi*, **73**, 421 (1970).
8) R. Senju, This Bulletin, **26**, 143 (1953); *Kobunshi*, **22**, (256), 407 (1973).

A Mechanistic Study of the Acetolyses of 3-Chloropropene Sulfide and 2-Chloroethyl Methyl Sulfide

Iwao TABUSHI,* Yoshinao TAMARU, and Zen-ichi YOSHIDA
Department of Synthetic Chemistry, Kyoto University, Yoshida, Kyoto 606
(Received September 22, 1973)

Forming a marked contrast to hydrolysis, the first-order rate constant in the acetolyses of 3-chloropropene sulfide (I) and 2-chloroethyl methyl sulfide (II) has been observed to be seriously decreased; this may be ascribed to the return to the starting material of the sulfonium intermediate (III′ or IV) by the chloride ion liberated in the course of the reaction. The reaction has substantially obeyed first-order kinetics, giving exclusively and quantitatively skeletally-rearranged 3-acetoxy-thietane (the first-order rate constant; $k_1=2.1\times10^{-5}$ s^{-1}, at 55.0 °C) and 2-acetoxyethyl methyl sulfide ($k_1=4.8\times10^{-4}$ s^{-1}, at 55.0 °C) from I and II respectively.

On the hydrolyses of 2-chloroethyl alkyl (or aryl) sulfides, the kinetics (of the profound acceleration due to sulfur participation) and mechanism (S_N1) involving the rate-determining formation of the episulfonium ion (III), followed by the facile destruction of III to alcohol, as is expressed in Eq. 1, have been well established.[1]

Making a marked contrast to the mechanistic and/or kinetic simplicities in hydrolysis, in acetolysis some complex observations have been reported.[2]

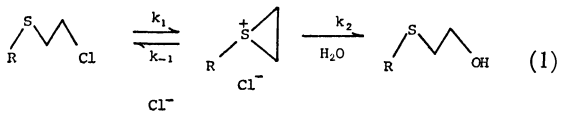

(1)

(III)

$k_2[\mathrm{III}][H_2O]>k_{-1}[\mathrm{III}][Cl^-]>k_1[RSCH_2CH_2Cl]$
R=alkyl, aryl, *etc.*

For example, one report has stated that the rate of decrease of 3-chloropropene sulfide in acetic acid follows the apparent first-order kinetics to give many kinds of unidentified products containing C–Cl bonds.[4]

Another report says that the acetolysis of 3-chloropropene sulfide gives 3-acetoxythietane only in a 33% yield.[5] Along with these intricate observations, the conspicuous mechanistic change in the acetolysis of 2-*endo*-chloro-7-thiabicyclo[2.2.1]heptane[6] (the rate-determining acetoxy ion attack on the sulfonium intermediate, S_N2) constrained us to investigate the mechanism and kinetics of the acetolysis of 3-chloroethyl alkyl sulfide, taking 3-chloropropene sulfide (I) and 2-chloroethyl methyl sulfide (II) as typical models.

Results

The acetolyses of 3-chloropropene sulfide (I) and 2-chloroethyl methyl sulfide (II) were performed in anhydrous acetic acid buffered with varying amounts of sodium acetate ([I], [II]=0.05 M, [NaOAc]=0.0, 0.065, 0.25, and 1.00 M). The rate of solvolysis was followed by means of the Volhard method for the liberated chloride ion. In several runs, the rate was also followed by means of vpc, where the amount of the acetate produced was in accord with the results of the titrimetric determination. The reuults for I and II are plotted in Figs. 1 and 2 respectively.

* Present address: Faculty of Pharmaceutical Science, Kyushu University, Katakasu, Fukuoka, 812.

The apparent first-order rate constants of I and II drifted downward, especially in the runs with low concentrations of sodium acetate. The same result was obtained for the acetolysis of II in the one-tenth concentrations involving with II and sodium acetate

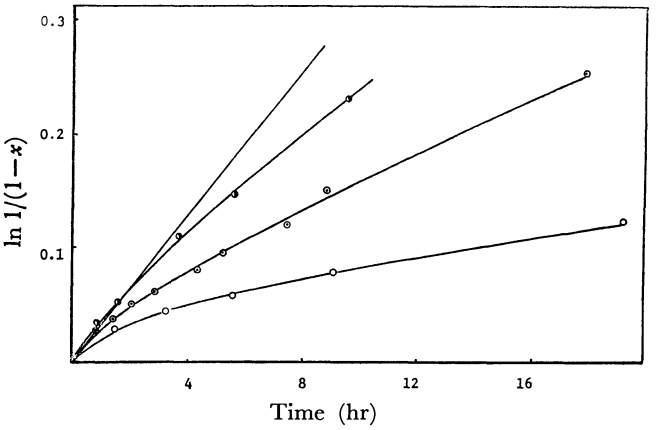

Fig. 1. Acetolysis of thiaepichlorohydrin (I) at 55.0 °C.
◑: [I]=0.05 M, [NaOAc]=1.00 M
⊙: [I]=0.05 M, [NaOAc]=0.25 M
○: [I]=0.05 M, [NaOAc]=0.065 M
Straight line was that obtained by means of numerical treatment.

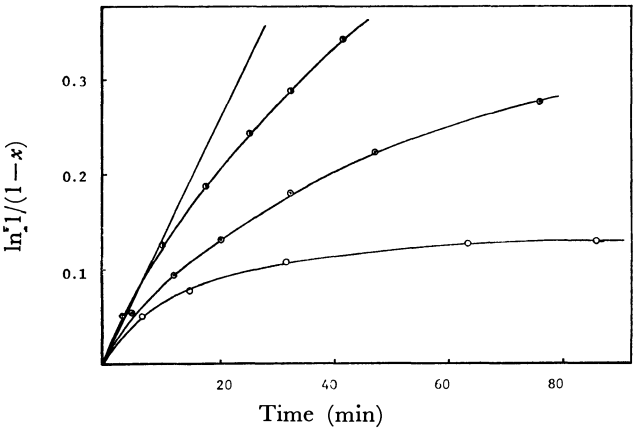

Fig. 2. Acetolysis of 2-chloroethyl methyl sulfide (II) at 55.0 °C.
◑: [II]=0.05 M, [NaOAc]=1.00 M
⊙: [II]=0.05 M, [NaOAc]=0.25 M
○: [II]=0.05 M, [NaOAc]=0.65 M
Straight line was that obtained by means of numerical treatment.

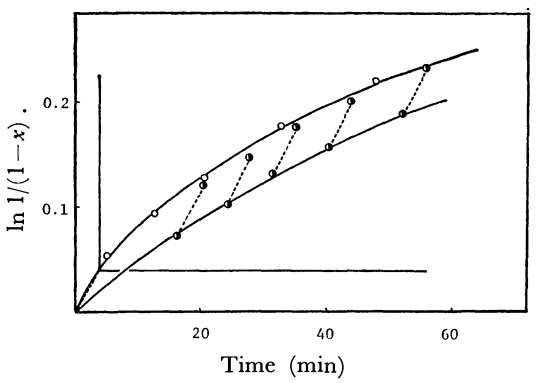

Fig. 3. Acetolysis of 2-Chloroethyl methyl sulfide (II) in the presence of added chloride ion at 55.0 °C.
○: [II[=0.05 M, [NaOAc]=0.25 M
◑: [II]=0.05 M, [NaOAc]=0.25 M, [NaCl]=0.0041 M
The plots, obtained in the presence of added chloride ion, were slided by 8.1% reaction.

([II]=0.005 M, [NaOAc]=0.0065 M).

In the absence of sodium acetate, no appreciable amount of acetate was produced or of the chloride ion was liberated within 5 hr for I and within 64 min for II at 55.0 °C, indicating that no reaction proceeded under those conditions.

The marked retardation of the reaction was observed in the presence of initially-added sodium chloride (8.1% to substrate; 0.0041 M). However, the time-conversion curve obtained in the presence of an added chloride ion could be just superimposed on the curve (at 8.1% conversion) obtained under the corresponding conditions where the chloride ion was not added (see Fig. 3).

On the basis of the vpc, NMR, and IR spectra of the reaction mixture of I, the exclusive and quantitative formation of skeletally-rearranged 3-acetoxythietane was observed, but the recovered sulfur chloride was not contaminated with the skeletally-rearranged 3-chlorothietane. From 2-chloroethyl methyl sulfide, 2-acetoxyethyl methyl sulfide was obtained in a quantitative yield (see Experimental section).

Discussion

Our observation that no appreciable amount of liberated chloride ions was detected in the absence of sodium acetate is quite in accord with the observation reported by Morita and Oae[4] that, in the absence of a base, the acetolysis (at 105 °C) of 3-chloropropene sulfide (I) gave mainly many kinds of unidentified products containing C–Cl bonds, along with small amounts of acetates (3-acetoxypropene sulfide and 3-acetoxythietane).

An examination of Fig. 2 will make it clear that, under the conditions of ([KOAc]/[II]=1.45, on a steam bath for 20 hr) which Adams *et al.*[5] employed to obtain 33% of 3-acetoxythietane, the reaction practically ceases at around a 30~40% reaction.

The result in the run of a high dilution ([II]=0.005 M, [NaOAc]=0.0065 M) indicates that the direct displacement reaction by the acetoxy ion (S_N2) is not operative.

Figures 1 and 2 indicate that, in the initial period of reaction, the reaction proceeds at practically the same rate, with a small but appreciable amount of the salt effect of sodium acetate. This seems to indicate that the reaction proceeds *via* the rate-determining formation of the carbonium ion (delocalized by sulfur, S_N1 mechanism) and that the retardation is due to the liberated chloride ion (Eq. (2)). This explanation is supported by the quantitative retardation caused by the added chloride ion (Fig. 3) and can be reconciled with the fact of no reaction in the absence of a base (Eq. (2)).

The validity of this explanation is also reflected by the numerical treatment of the data (see the section on the numerical treatment of the rate data), by which the first-order rate constants, together with the ratios of the competition factors of the chloride ion to the acetoxy ion (k Cl^-/k OAc^-, given in parentheses) were determined to be 4.8×10^{-4} s^{-1} (*ca.* 30) for II and 2.1×10^{-5} s^{-1} (*ca.* 30)[7] for I.

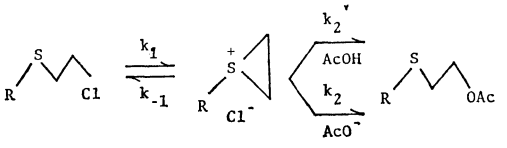

(2)

(III')

$k_{-1}[III'][Cl^-]>k_2[III'][AcO^-]>k_1[RSCH_2CH_2Cl]$

$k_{-1}[III'][Cl^-]>k_2'[III][AcOH]$

The apparent difference between the behavior in water and in acetic acid may partly be explained in terms of the differences in nucleophilicities of these solvents. Using the ratio of nucleophilicities[10] among acetic acid, water, and the chloride ion, the following relation may be drawn:

$$v_{H_2O} : v_{Cl^-} = 1 \quad : \quad 0.016 \text{ for hydrolysis} \tag{3}$$

$$v_{Cl^-} : v_{AcOH} = 1 \quad : \quad 0.0013 \text{ for acetolysis} \tag{4}$$

Thus, in a less nucleophilic solvent, as in acetic acid, the reaction seems to be governed exclusively by the chloride ion liberated, thus returning the sulfonium ion to the starting chlorosulfide (See Eqs. (2) and (4)).

The exclusive formation of the skeletally-rearranged 3-acetoxythietane and the absence of 3-acetoxypropene sulfide or 3-chlorothietane[12] in the reaction mixture (at 10% and 66% reactions), as monitored by means of vpc and NMR spectra, indicate that the acetoxy ion and the chloride ion reacted regioselectively with 1-thiabicyclo[1.1.0]butonium ion (IV) to produce 3-acetoxythietane and 3-chloropropene sulfide respectively. (See Eq. (5))

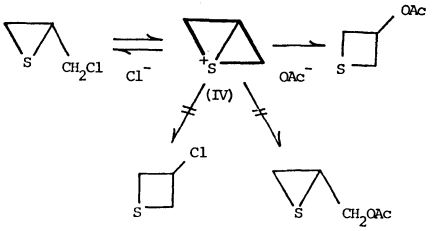

(5)

The rate of I is about seventy times the published

combined acetolysis-rearrangement constant for cyclopropylmethyl chloride.[15] This is typical of enhanced rate data supporting delocalization as the driving force for ionization. In view of the observed product, sulfur participation to form IV would seem to be a reasonable explanation for the reactivity of I. The moderately diminished reactivity of I compared with that of II may be due to the remarkable strain in the intermediate, IV, and/or to the expected poorer electron donation of episulfide.[16]

Numerical Treatment of Rate Data[17]

The most plausible reaction pathway for the acetolysis of II is illustrated in Eq. (6).

$$CH_3SCH_2CH_2Cl \underset{k_{-1}}{\overset{k_1}{\rightleftharpoons}} CH_3\overset{+}{S}\!\!\triangleleft \xrightarrow[OAc^-]{k_2} CH_3SCH_2CH_2OAc \qquad (6)$$

Cl^- Cl^-

II V

where $k_{-1}[Cl^-][V]$ and $k_2[OAc^-][V]$ are assumed to be much larger than $k_1[II]$. The rate of the disappearance of the substrate can, then, be written as:

$$-\frac{d[R\text{-}Cl]}{dt} = \frac{k_1k_2[R\text{-}Cl][OAc^-]}{k_{-1}[Cl^-]+k_2[OAc^-]} \qquad (7)$$

The substitution of 1-x for R–Cl, x for Cl^-, $a-x$ for OAc^-, and x for ROAc gives:

$$-\frac{d(1-x)}{dt} = \frac{k_1k_2(1-x)(a-x)}{k_{-1}x+k_2(a-x)} \qquad (8)$$

where x: conversion expressed in terms of the fraction.

a: molar ratio of the sodium acetate to the substrate.

Integration gives:

$$k_1t = \ln\frac{1}{1-x} + \frac{k_{-1}}{k_2(a-1)}\left(\ln\frac{1}{1-x} - a\ln\frac{a}{a-x}\right) \qquad (9)$$

The k_{-1}/k_2 term is the ratio of the competition factors of the chloride ion to the acetoxy ion. Figure 4 shows the results calculated according to Eq. (9), with the value of k_{-1}/k_2 varying from 0 to 90, in which a systematic change could be observed; when the value of k_{-1}/k_2 was overestimated, an upward derivation of the calculated k_1 with the time was observed. An underestimation of the k_{-1}/k_2 value results in downward deviations of k_1. The first-order rate constant, k_1, and the ratio of the competition factors of the chloride ion to the acetoxy ion in the acetolysis of II at 55.0 °C were determined from Fig. 4 to be $(4.8\pm0.7)\times10^{-4}$ s^{-1} and *ca.* 30 respectively. Similarly, k_1 and k_{-1}/k_2 for the acetolysis of I at 55.0 °C were determined to be $(2.1\pm0.30)\times10^{-5}$ s^{-1} and *ca.* 30 respectively (see Fig. 5).

Effect of Added Chloride Ions. The rate constant, k_1, in the presence of added chloride ions was similarly expressed as:

$$k_1t = \ln\frac{1}{1-x} + \frac{k_{-1}}{k_2(a-1)}\left\{(\alpha+1)\ln\frac{1}{1-x} + (\alpha+a)\ln\frac{a}{a-x}\right\} \qquad (10)$$

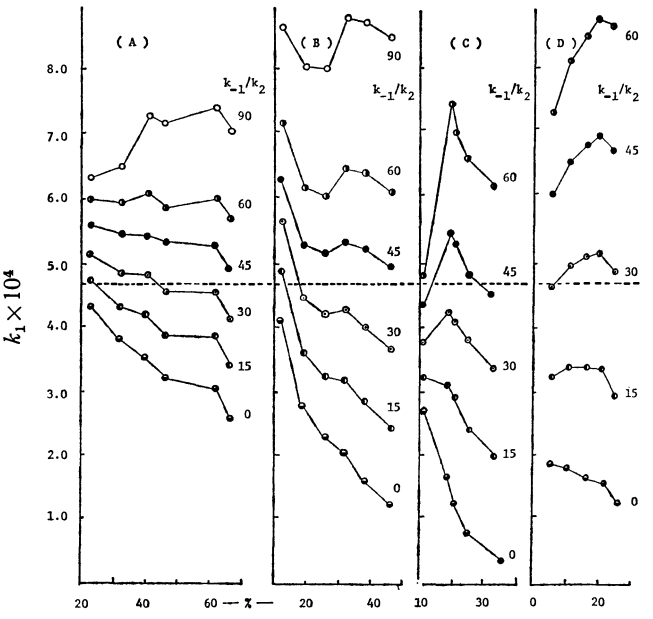

Fig. 4. Acetolysis of 2-chloroethyl methyl sulfide at 55.0 °C; The plots obtained from Eqs. (9) and (10), varying the value of k_{-1}/k_2 from 0 to 90.
(A): [NaOAc]=1.00 M, (B): [NaOAc]=0.25 M, (C): [NaOAc]=0.065 M, (D): [NaOAc]=0.25 M, [NaCl]=0.004 M.

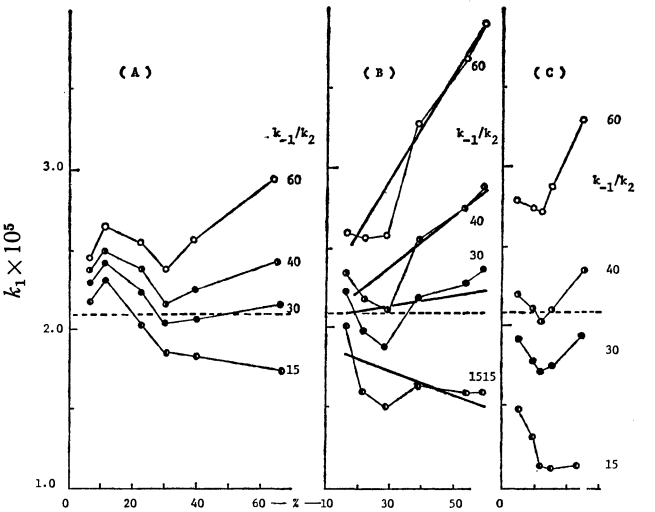

Fig. 5. Acetolysis of thiaepichlorohydrin at 55.0 °C; The plots obtained from Eqs. (9) and (10), varying the value of k_{-1}/k_2 from 0 to 60.
(A), [NaOAc]=1.00 M, (B): [NaOAc]=0.25 M, (C): [NaOAc]=0.065 M.

where α is the molar ratio of the added sodium chloride to the substrate. The k_1 value calculated on the basis of Eq. (10) is plotted in Fig. 4.

Experimental

All the boiling points are uncorrected. The NMR spectra were recorded with a Varian T 60 spectrometer, while chemical shifts were reported in δ values relative to the TMS internal standard. The infrared spectra were measured with a Hitachi Model EPI-G3 grating spectrophotometer, and

the mass spectra were recorded with a Hitachi Model RMU 6C mass spectrometer.

The acetic acid was used after distillation from a mixture containing 5% of acetic anhydride (118.0—118.3 °C). The sodium acetate was used without further purification after drying by means of Abderhalden at the toluene reflux temperature.

2-Chloroethyl Methyl Sulfide (II). Into a solution of 20.0 g of β-hydroxyethyl methyl sulfide in 100 ml of benzene we vigorously stirred dry hydrogen chloride at room temperature for 3 hr. The reaction mixture was diluted with 100 ml of pentane, and the excess hydrogen chloride was neutralized with sodium bicarbonate. After washing with saturated sodium chloride, the organic layer was dried over magnesium sulfate. After the distillation of the solvent through a 10-cm Vigreux column, II was distilled twice under reduced pressure (66.5—67.2 °C/70 mmHg, 87.0—87.8 °C/138 mmHg), 22.0 g of II was thus obtained (the yield was 82%). $\delta_{CCl_4}^{TMS}$ 3.56 (2H, triplet, J=9Hz), 2.70 (2H, triplet, J=9 Hz) and 2.08 (3H, singlet). ν_{max}^{neat} 1220 (s), 705 (s) and 680 cm^{-1} (s).

3-Chloropropene Sulfide (I). I was prepared according to the method of Culvenor.[18] Thus, into a solution of 92 g (1.0 mol) of epichlorohydrin in 300 ml of methanol, chilled with ice, 84 g (1.1 mol) of thiourea was gradually dropped as a crystalline over a period of 1 hr: the reaction mixture was then stirred at 0~5 °C for an additional 2 hr and then at room temperature for an additional 2 hr.

The reaction mixture was subsequently poured onto 2 l of ice-water and extracted with two 300-ml portions of ether. The combined ether extracts were washed twice with saturated sodium chloride and dried over calcium chloride. After the distillation of the ether through a 10-cm Vigreux column, the residue was distilled twice under reduced pressure (77.0 °C/93 mmHg, 81.0 °C/112 mmHg). Sixty grams of I were thus obtained (the yield was 55%). 3-Chloropropene sulfide should be stored in refrigerator to prevent decomposition. At room temperature, I decomposes at a moderate speed to give an amorphous white solid. $\delta_{CDCl_3}^{TMS}$ 3.9 (1H, multiplet), 3.2 (2H, multiplet), 2.6 (1H, multiplet and 2.25 (1H, multiplet). ν_{max}^{neat}, 1260 (s), 1040 (s) and 705 cm^{-1} (s).

3-Acetoxythietane. A reaction mixture consisting of 500 ml of acetic acid, 62 g (0.75 mol) of sodium acetate, and 10 g (0.093 mol) of I was heated at about 60 °C for 5 day.

The reaction mixture was then poured into 3 l of water and extracted with two 250-ml portions of petroleum ether; the combined petroleum ether extracts were washed with saturated sodium bicarbonate until the evolution of carbon dioxide had ceased and then washed with saturated sodium chloride. After the evaporation of the solvent, 3-acetoxythietane was distilled under reduced pressure (83.5 °C/23 mmHg) (the yield was 82%). $\delta_{CCl_4}^{TMS}$ 5.56 (1H, quintet, J=8 Hz), 3.46 (2H, triplet, J=8 Hz), 3.26 (2H, triplet, J=8 Hz) and 2.00 (3H, singlet). ν_{max}^{neat} 1740 (s), 1370 (m), 1240 (s), 1040 (s) and 905 cm^{-1} (w). *m/e* 132 (P^+), 89, 72 and 43.

β-Acetoxyethyl Methyl Sulfide. A mixture consisting of 50 ml of acetic acid, 2 g of II, and 10 g of sodium acetate was heated at 60 °C for 8 hr. The reaction mixture was then poured into 300 ml of water and extracted with two 50-ml portions of petroleum ether. The combined extracts were neutralized with sodium bicarbonate, washed with saturated sodium chloride, and then dried over calcium chloride. After the evaporation of the solvent, the β-acetoxyethyl methyl sulfide was distilled under reduced pressure (125 °C/133 mmHg). (Yield, *ca.* 90%). $\delta_{CCl_4}^{TMS}$ 4.20 (2H, triplet, J= 7 Hz). 2.65 (2H, triplet, J=7 Hz), 2.08 (3H, singlet) and 2.00 (3H, singlet). ν_{max}^{neat}; 1755 (s), 1396 (m), 1240 (s) and 1040 cm^{-1} (m), *m/e*; 74 (100), 61 (75), 43 (90).

Procedure for Titration. In a 25-ml measuring flask, 1.25 mmol of the substrate was dissolved with acetic acid containing some sodium acetate, heated to 55.00±0.05 °C beforehand, up to 25 ml; this flask was immersed immediately into a bath maintained constant at 55.00±0.05 °C. At desired intervals of time, 3-ml samples were measured out and dropped into a separatory funnel containing 15 ml of distilled water and 10 ml of carbon tetrachloride. After vigorous shaking, the aqueous portion was washed once more with 10 ml of carbon tetrachloride and then transferred into a flask quantitatively. (The separatory funnel was washed off with 2 ml of distilled water). To a combined aqueous layer, we then added 2.00 ml of 0.100 M of silver nitrate, two drops of fuming nitric acid, and a few drops of a saturated ferric ammonium sulfate solution, after which this solution was back-titrated with 0.116 M ammonium thiocyanate (Volhard method).

References and Notes

1) (a) G. M. Bennett and W. A. Berry, *J. Chem. Soc.* **1927**, 1626. (b) A. G. Ogston, E. R. Holiday, J. St. L. Philpot, and L. A. Stocken, *Trans. Faraday Soc.*, **44**, 45 (1948). (c) P. D. Bartlett and C. G. Swain, *J. Amer. Chem. Soc.*, **71**, 1406 (1949). (d) H. L. Goering and K. L. Howe, *ibid.*, **79**, 6542 (1957). (e) S. J. Cristol and R. P. Arganbright, *ibid.*, **79**, 3441 (1957).

2) For the acetolyses of γ- and δ-halosubstituted sulfides, normal first-order kinetics have been reported.[3]

3) (a) M. Hojo, T. Ichi, Y. Tamaru, and Z. Yoshida, *J. Amer. Chem. Soc.*, **71**, 5170 (1969). (b) L. A. Paquette, G. V. Meehan, and L. D. Wise, *ibid.*, **91**, 3231 (1969).

4) H. Morita and S. Oae, *Tetrahedron Lett.*, **1969**, 1347.

5) E. P. Adams, K. N. Agod, F. P. Doyle, D. O. Halland, W. H. Hunter, J. H. C. Nayler, and A. Queen, *J. Org. Chem*, **25**, 2665 (1960).

6) The rate of the acetolysis of 2-*endo*-chloro-7-thiabicyclo-[2.2.1]heptane was proportional to the concentration of the substrate and that of sodium acetate (S_N2 mechanism), and the product (2-*endo*-acetoxy-7-thiabicyclo[2.2.1]heptane) of the retention of the configuration was obtained exclusively and quantitatively. These results will be reported soon.

7) This value seems to be too large compared with the value (K_{Cl^-}/K_{OAc^-} = *ca.* 2) obtained in the hydrolysis of bis-β-chloroethyl sulfide,[1b,c,8] but the competition factors were found to be sensitive to substrates, the dielectric constants of solvents, and many other factors.[9]

8) E. J. Leffler and E. Grunwald, "Rates and Equilibria of Organic Reactions," John Wiley & Sons, Inc., New York and London (1963), p. 231.

9) (a) C. G. Swain, C. B. Scott, and H. L. Lohman, *J. Amer. Chem. Soc.*, **75**, 136 (1953). (b) D. Golomb, *J. Chem. Soc.*, **1959**, 1327, 1334. (c) D. Kovacevic, Z. Majerski, S. Borcic, and D. E. Sunko, *Tetrahedron*, **28**, 2469 (1972).

10) The ratio of nucleophilicities among acetic acid, water, and the chloride ion is $1 : 2.5\times10^2 : 2.5\times10^5$, obtained by Swain and Scott and Winstein and Marshall[11] for the solvolysis of methyl bromide. For Eq. 3, $[Cl^-]$=0.00089 M, the concentration of the substrate for the hydrolysis of 2-chloroethyl 2'-hydroxyethyl sulfide, was used (Ref. 1c). For Eq. (4), $[Cl^-]$=0.05 M was adopted.

11) (a) C. G. Swain and C. B. Scott, *J. Amer. Chem. Soc.*, **75**, 141 (1953). (b) S. Winstein and H. Marshall, *ibid.*, **74**, 1120 (1952).

12) 3-Chlorothietane is estimated to be less reactive than

3-chloropropene sulfide on the basis of the formolyses data of 3-chlorothietane (3.7×10^{-4} s^{-1}) and 2-chloroethyl ethyl sulfide[13] (1.21×10^{-2} s^{-1}). A similar result has been reported for nitrogen analogues; that is, in the acetolysis, 1-chloromethylaziridine reacts much faster than 3-chloroazetidine.[14]

13) H. Morita and S. Oae, 24th Annual Meeting of the Chemical Society of Japan, Osaka, April, Abstract III, 1071 (1971).

14) (a) V. R. Gaertner, *Tetrahedron Lett.*, **1968**, 5919. see also, (b) J. A. Deyrup and C. L. Moyer, *ibid.*, 6179 (1968). (c) V. R. Gaertner, *J. Org. Chem.*, **35**, 3952 (1970). (d) R. H. Higgins, F. M. Behlen, D. F. Eggli, J. H. Kreymborg, and N. H. Cromwell, *ibid.*, **37**, 524 (1972).

15) J. D. Roberts and R. H. Mazur, *J. Amer. Chem. Soc.*, **73**, 2509 (1951).

16) S. Searles, M. Tamres, and E. R. Lippincott, *ibid.*, **75**, 2775 (1953); R. E. Davis, *J. Org. Chem.*, **23**, 1380 (1958).

17) The salt effect of sodium acetate was negligibly small compared with the mass law effect of the chloride ion and was neglected for the sake of simplification.

18) C. C. J. Culvenor, *J. Chem. Soc.*, **1946**, 1050.

Photo-induced Polar Addition of Protic Solvents to Cycloalkenones. Evidence for the Ground-state *trans* Isomers as Chemically-reactive Intermediates[1]

Ryoji NOYORI and Masao KATÔ

Department of Chemistry, Nagoya University, Chikusa, Nagoya 464

(Received October 5, 1973)

The photo-induced reaction of cyclic α,β-unsaturated ketones with protic media is described. The irradiation of 2-cycloheptenone or 2-cyclooctenone in various protic solvents (alcohols, acetic acid, water, and diethylamine) results in the formation of Michael-type solvent adducts. The chemically-reactive species have been demonstrated to be the highly strained *trans* isomers in a ground state. The irradiation of *cis*-2-cyclononenone affords the stable *trans* isomer, which reacts in the dark with methyl alcohol at an elevated temperature to give 3-methoxycyclononanone. The irradiation of 2-cyclohexenone in methyl alcohol yields 3-methoxycyclohexanone in a poor yield. The possible existence of *trans*-2-cyclohexenone is discussed.

In recent decades the photochemistry of cyclic α,β-unsaturated ketones has received considerable attention.[2] Particularly interesting is the fact that the reaction course is profoundly influenced by the ring size. Diphenylcyclopropenone, the smallest cyclic enone, suffers photochemical decarbonylation to give tolan.[3] Cyclobutenone derivatives afford ketenes under electrocyclic ring opening.[4] The five- and six-membered homologs can undergo intermolecular photoreactions. 2-Cyclopentenone, upon irradiation, leads to the cyclobutane dimers in good yields,[5] while in the presence of an excess of cyclopentene [2+2] cross-cycloaddition takes place.[6] 2-Cyclohexenone shows a reactivity qualitatively parallel to that of 2-cyclopentenone in cycloaddition.[7] Certain 4,4-disubstituted 2-cyclohexenones are known to rearrange to the bicyclo[3.1.0]hexan-2-ones with group migration.[8] Throughout these intra- and intermolecular reactions, two points are noteworthy: (1) mechanistically, most of these reactions have been believed to occur in an electronically-excited state (either a singlet or a triplet), and (2) formally, the reactions are regarded as being a nonpolar (nonionic) process. In striking contrast, as will be shown below, upon irradiation seven- and eight-membered cyclenones can undergo polar (ionic) reactions arising from a highly reactive ground-state molecule. The mechanisms of the related polar reactions of 2-cyclohexenones are also a subject of our interest.

Results and Discussion

The photo-induced reactions of alcohols across a carbon—carbon double bond may be divided into the two classes depicted in Chart 1. Path *a* is a radical process and involves a fission of a weak C–H bond bearing an OH function (bond energy ~92 kcal/mol[9]). The second pathway, *b*, defined as a polar addition, involves a rupture of the stronger (~102 kcal/mol[9]), more ionic O–H bond.[10]

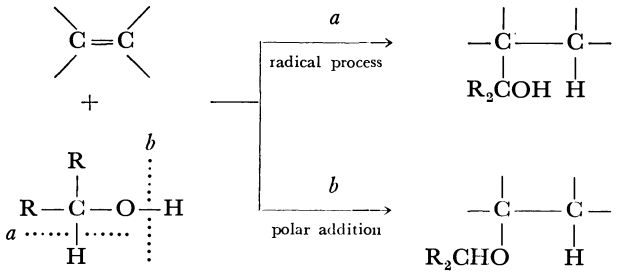

Chart 1.

The irradiation of 2-cycloheptenone (I)[11] with a high-pressure mercury arc in such protic solvents as alcohols, acetic acid, water–acetonitrile, and diethylamine at room temperature afforded the corresponding polar adducts, II. The results are given in Table 1. In certain cases, considerable amounts

Table 1. Irradiation of 2-cycloheptenone in protic solvents[a]

Solvent	Conversion %[b]	Yield of II %[b,c]
Methyl alcohol	68	86
Ethyl alcohol	66	73
Isopropyl alcohol	54	50[d]
tert-Butyl alcohol	40	3[d]
Acetic acid	34	23[d]
Water–acetonitrile (1 : 5)	61	27[d]
Diethylamine	80	55[e]

a) Irradiation was effected on 1.0% solution at room temperature for 15 min. b) Determined by glpc. c) Based on the consumed enone. d) Considerable amounts of cyclodimers were obtained.[12] Irradiation of I in cyclohexane gave cyclobutane dimers in 88% yield. e) Photolysis was performed at 0 °C and yield was determined by NMR analysis.

Table 2. Photolysis of 2-cyclooctenone in protic solvents[a]

Solvent	Irradiation time, min	Conversion %[b]	Yield of IV %[b,c]
Methyl alcohol	10	92	72
Isopropyl alcohol	150	90	43
Acetic acid	150	58	76
Water–acetonitrile (1 : 5)	75	81	25
Diethylamine	30[d]	85	66[e]

a) All photolyses were performed in a 1.0% solution at room temperature. b) Determined by glpc. c) Based on the consumed III. d) Irradiation was carried out at 0°C. e) Determined by NMR analysis.

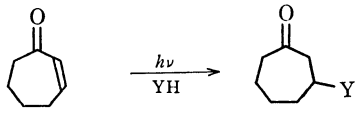

I II a: Y=OCH_3 e: Y=$OCOCH_3$
b: Y=OC_2H_5 f: Y=OH
c: Y=$OCH(CH_3)_2$ g: Y=$N(C_2H_5)_2$
d: Y=$OC(CH_3)_3$

of cyclodimers[12] were also formed. No products were obtained *via* a radical process. A similar photo-induced polar addition of protic solvents was observed for 2-cyclooctenone (III),[11] as is summarized in Table 2. The structural determination of the photoproducts was made on the basis of elemental analyses and spectral data (Table 3). The structure of the β-ketols, IIf and IVd, was confirmed by converting them to the acetates, IIe and IVc, respectively.

The photo-induced polar addition reaction of the protic solvents mentioned here provides a new synthetic means of introducing oxygen or nitrogen functions to the β position of a carbonyl group under neutral or comparatively mild reaction conditions.

The observed photo-induced reaction could be interpreted in various ways. As the product-forming species, the π,π^* triplet states of the enones[13,14] or, alternatively, the highly strained ground-state molecules derived therefrom may be involved. Oxabicyclobutanes[7b,12a,15] or enones containing a *trans* double bond[1,12,14,16] would be the candidates in the latter case (Chart 2). The

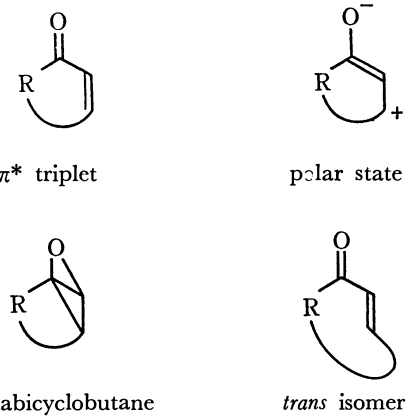

π,π^* triplet polar state

oxabicyclobutane *trans* isomer

Chart 2. Possible reactive species.

reaction could also be accounted for by assuming the intervention of the polar state, a hypothetical dipolar species first suggested by Chapman.[17] We have examined in detail the behavior of I and III and found that their *trans* isomers are the product-determining intermediates.

Eaton and Lin observed that the photolysis of the medium-sized enone III causes a *cis-trans* isomerization, thus establishing an equilibrium between III and V (*ca.* 20 : 80 ratio).[16] The moderate thermal stability of the *trans* cyclenone, V, permitted low-temperature studies of its chemical behavior. The enone III was irradiated in 2-methyltetrahydrofuran at −78 °C for 15 min. After the light source had then been turned off, the photolysate was poured into an excess of cold (−78 °C) methyl alcohol and allowed to warm up to

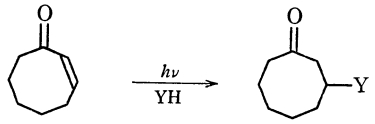

III IV a: Y=OCH_3 d: Y=OH
b: Y=$OCH(CH_3)_2$ e: Y=$N(C_2H_5)_2$
c: Y=$OCOCH_3$

room temperature in the dark, thus producing the corresponding alcohol adducts, IVa, in a 43% yield. The starting enone, III, was recovered in a 41% yield. When isopropyl alcohol was used in place of methyl alcohol, IVb was obtained in a 24% yield. The irradiation of III in isopropyl alcohol under the same conditions, followed by treatment with a large excess of methyl alcohol in the dark, gave almost exclusively the methyl alcohol adduct, IVa (80%). Only a very small amount of the isopropyl alcohol adduct, IVb (<1%), if any, was formed. Apparently the polar addition to the photo-excited states is not significant.

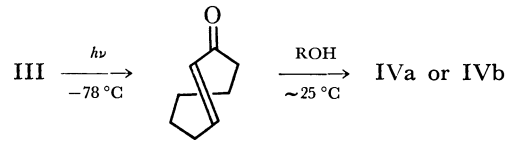

V

The more strained *trans*-2-cycloheptenone (VI) can also be generated by the irradiation of the *cis* enone I.[12] Because of the much reduced stability, however, it was difficult to demonstrate that the ground-state molecule, VI, is involved in the photo-induced polar addition of alcohols. The irradiation of I in EPA at the temperature of liquid nitrogen was followed by turning the lamp off, the addition of cold (−78 °C) methyl alcohol, and a gradual warming to room temperature. Only cyclodimers of I[12] were obtained, however. No methyl alcohol adduct could be detected in the reaction mixture. The irradiation of I in methyl alcohol at −196 °C, followed by warming up to room temperature, also failed to produce the adduct IIa. Fortunately, however, a proof was obtained using diethylamine, a more efficient nucleophile. Thus, the addition of diethylamine to the photolysate of I at −196 °C (EPA glass), followed by warming up to 0 °C, led to the formation of the Michael-type adduct IIg in a 25% yield. A control experiment showed that the *cis* enone I gives no trace of the adduct IIg under these thermal conditions.[18]

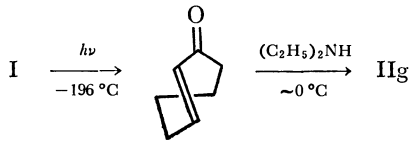

VI

The irradiation of a nine-membered cyclenone, *cis*-2-cyclononenone (VII) in methyl alcohol or cyclohexane below room temperature afforded a mixture of VII and the *trans* isomer, VIII. The latter was stable enough to be isolated by a usual work-up. The enone VIII in methyl alcohol remained unchanged at

Table 3. Spectral properties of polar addition products

Adduct	IR, cm^{-1} a) (assignment)	NMR, δ ppm from TMS b)				
		$C(2)H_2$	C(3)H	$C(4—n)H_2$	$C(n+1)H_2$	others
IIa	1700 (C=O) 1090 (COC)	2.70 m c)	3.45 m	1.6—1.9 m	2.38 m	3.30 s (CH_3)
IIb	1700 (C=O) 1085 (COC)	2.65 m c)	3.65 m	1.5—2.0 m	2.40 m	1.15 t ($CH_2\underline{CH_3}$) d) 3.47 q ($\underline{CH_2}CH_3$) d)
IIc	1700 (C=O) 1060 (COC)	2.70 m c)	3.70 m	1.5—2.0 m	2.46 m	1.15 d ($CH(\underline{CH_3})_2$) e) 3.65 m ($\underline{CH}(CH_3)_2$) e)
IId	1700 (C=O) 1050 (COC)	2.55 m c)	3.80 m	1.6—1.9 m	2.32 m	1.16 s ($C(CH_3)_3$)
IIe	1740 (OC=O) 1700 (C=O) 1240 ($OCOCH_3$)	2.68 d e)	5.00 m	1.6—1.9 m	2.40 m	2.00 s (CH_3)
IIf	3450 (OH) 1695 (C=O) 1040 (COH)	2.70 d f)	4.00 m	1.6—2.0 m	2.45 m	4.05 s (OH)
IIg g)	1695 (C=O)	2.59 m	2.80 m	1.3—2.0 m	2.35 m	1.02 t ($CH_2\underline{CH_3}$) d) 2.42 m ($\underline{CH_2}CH_3$) d)
IVa	1700 (C=O) 1095 (COC)	2.60 m c)	3.38 m	1.1—2.1 m	2.25 m	3.30 s (CH_3)
IVb	1700 (C=O) 1065 (COC)	2.61 m c)	3.47 m	1.3—2.1 m	2.25 m	1.10 d ($CH(\underline{CH_3})_2$) e) 3.69 q ($\underline{CH}(CH_3)_2$) e)
IVc	1738 (OC=O) 1700 (C=O) 1240 ($OCOCH_3$)	2.60 d d)	5.12 m	1.2—2.0 m	2.30 m	1.98 s (CH_3)
IVd	3460 (OH) 1695 (C=O) 1055 (COH)	2.62 m c)	3.92 m	1.2—2.1 m	2.32 m	3.52 s (OH)
IVe g)	1695 (C=O)	2.60 m	2.90 m	1.3—2.1 m	2.35 m	1.06 t ($CH_2\underline{CH_3}$) d) 2.55 m ($\underline{CH_2}CH_3$) d)
IX	1700 (C=O) 1095 (COC)	2.65 m c)	3.50 m	1.3—2.2 m	2.35 m	3.26 s (CH_3)
XI	1710 (C=O) 1100 (COC)	2.52 m c)	3.70 m	1.7—2.1 m	2.30 m	3.32 s (CH_3)

a) Neat liquid film. b) Taken in 5—10% CCl_4 solutions. Splitting patterns are designated as s, singlet; t, triplet; q, quartet; m, multiplet. The number n is 6 (II), 7 (III), 8 (IX), or 5 (XI). c) An AB part of ABX system. d) J=7 Hz. e) J=6 Hz. f) J=5 Hz. g) NMR spectrum was measured in $CDCl_3$ solution.

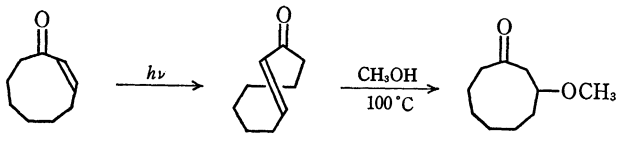

VII VIII IX

0 °C, but heating the solution at 100 °C gave rise to the adduct IX in a high yield. The spectral data are given in Table 3.

Thus, the photo-induced polar addition of cyclic enones proved to consist of two chemical reactions, *i. e.*, a prior *photochemical* isomerization to the *trans* isomers and a subsequent *thermal* reaction with nucleophilic solvents. The protic solvent addition to six-,[19] seven-,[19] and eight-membered cycloalkenes[20] under irradiation has been previously reported. The reaction was proposed to proceed by a sequence; (1) a photochemical *cis-trans* isomerization of the olefins, (2) protonation to the strained *trans* olefins to produce cycloalkyl cations, and (3) nucleophilic capture by the solvent. In the present case, however, the nucleophilic attack of the solvent takes place directly on the carbon—carbon double bond of the strained enones.

The relationship between the reactivity and the ring size of cyclic enones could be inferred from the potential energy curves of the twisted olefins (Fig. 1). The twist angle, ϕ, indicates the deviation from the normal $C(sp^2)=C(sp^2)$ plane. An electronically-excited olefin (either S_1 or T_1) should prefer a rotation about the $C(sp^2)-C(sp^2)$ single bond to afford an orthogonal geometry (ϕ=90°), thus minimizing the mutual repulsive interactions of the π and π^* electrons.[21] Decay by either internal conversion[22] or intersystem crossing leads to the *cis* or *trans* ground state, in which ϕ is 0° or 180° respectively. With rather small ring olefins,

TABLE 4. IR-, UV-, AND NMR-SPECTROSCOPIC DATA OF 2-CYCLOALKENONES

2-Cycloalkenone	IR, cm^{-1} a)		UV, nm b)		NMR, δ ppm from TMS, J in Hz c,d)			
	C=O	*trans* CH=CH	$\lambda_{max}^{\pi\to\pi^*}$ (ε)	$\lambda_{max}^{n\to\pi^*}$ (ε)	H_α	H_β	$J_{H\alpha H\beta}$	$J_{H\beta H\gamma}$
2-Cyclopentenone	1720 e)	—	217 (10, 200) d)	304 (65) d)	6.28	8.01	6.0	2.8
2-Cyclohexenone (X)	1691 e)	—	225 (13, 800) e)	— —	5.90	6.90	10.3	3.9
cis-2-Cycloheptenone (I)	1669 d)	—	227 (10, 220) f)	317 (52) f)	6.03	6.60	11.7	5.4
trans-2-Cycloheptenone (VI)	1715 g)	1010 g)	— —	— —	—	—	—	—
cis-2-Cyclooctenone (III)	1664 d)	—	230 (7, 700) h)	310 (80) h)	5.96	6.32	12.5	6.4
trans-2-Cyclooctenone (V)	1715 g)	1008 g)	— —	283 (70) g,l)	—	—	18 j)	
cis-2-Cyclononenone (VII)	1667 d)	—	231 (8, 100) d) 223 (8, 800) i,k)	318 (86) d) 332 (47) i,k)	5.95	6.20	12.5	8.6
trans-2-Cyclononenone (VIII)	1692 i,k)	980 i,k)	221 (7, 700) i,k)	327 (47) i,k)	5.95 k)	6.35 k)	16.0 k)	8.0 k)
cis-2-Cyclododecenone	1695 l)	—	228 (5, 250) l)	320 (47) l)	6.21	5.69	11.6	7.5
trans-2-Cyclododecenone	1669 l) 1695	990 l)	230 (11, 200) l)	321 (174) l)	6.22	6.65	15.9	7.0

a) Neat liquid film. b) Unless otherwise stated, UV-data were taken in C_2H_5OH. c) Taken in CCl_4. d) M. Regitz and J. Rüter, *Chem. Ber.*, **102**, 3877 (1969). e) H. N. A. Al-Jallo and E. S. Waight, *J. Chem. Soc., B*, **1966**, 73. f) See Ref. 11. g) See Ref. 12b. h) A. C. Cope, M. R. Kinter, and R. T. Keller, *J. Amer. Chem. Soc.*, **76**, 2757 (1954). i) Taken in C_6H_{12}. j) See Ref. 16. k) This work. l) See Ref. 23a.

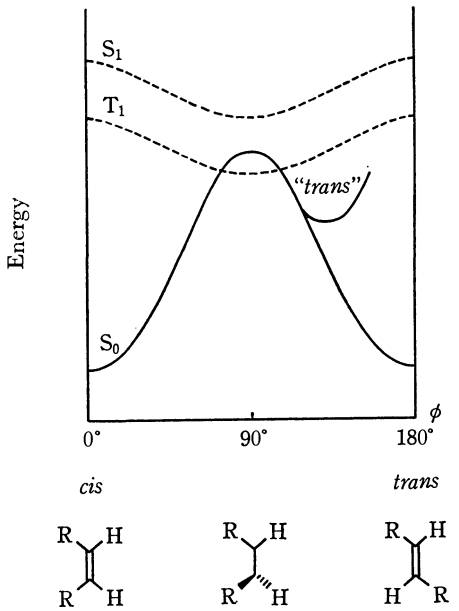

Fig. 1. Energy for the twisting of various electronic states of 1,2-disubstituted olefin. $\phi = \angle C(sp^2) - C(sp^2)$

however, a complete twisting ($\phi > 90°$) is sterically impossible; consequently, their *cis* to *trans* isomerization is precluded. In contrast, open-chain or sufficiently large-membered cyclic olefins undergo the geometrical isomerization facilely. Seven- and eight-membered cyclic olefins are located intermediate between the two extremes. Obviously, a coplanar *trans* double bond ($\phi = 180°$) could not be accommodated, but a 90°-twisted conformation can be adopted and further twisting to a ground-state isomer ($90° < \phi < 180°$) with minimized energy could occur. Such molecules are conventionally referred to as *trans* isomers. Table 4 compares the spectral data of certain *cis* and *trans* cyclenones. The degree of the conjugation of the C=C bond with the C=O group in the seven- and eight-membered *trans* enones (VI and V) is markedly decreased as compared with that of the *cis* isomers. These *trans* double bonds suffer enough torsional strain to provide effective strain-releasing reactions. Apparently the nine-membered *trans* enone VIII is sterically less constrained and, consequently, undergoes the addition of methyl alcohol under only forcing thermal conditions. Both *cis*- and *trans*-2-cyclododecenones,[23] enones free from torsional strain, were inert under these reaction conditions. Electron-deficient olefins including α,β-unsaturated ketones are susceptible to nucleophilic reagents (alcohols, water, primary and secondary amines, *etc.*) under basic conditions and afford Michael-type addition products.[24] A similar type of the addition of acids is also known.[25] Therefore, the above findings are not surprising. The *trans* cyclenones, even though torsionally strained, conform electronically to a ground-state singlet; therefore, they exhibit reactivities understandable on the basis of our knowledge of classical organic chemistry.

In principle, the reactivities of *cis* and *trans* double bonds are identical in type; they are different from each other only in a quantitative way. If this were generally the case for cyclenones, the photolysis in turn in protic solvents might serve as a probe for the chemical detection of the elusive *trans*-2-cyclohexenone. This assumption prompted us to examine the behavior of 2-cyclohexenone (X). In the dark X did not react

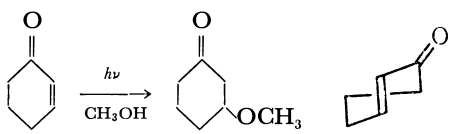

X XI XII

with freshly-distilled methyl alcohol below 100 °C. Upon the irradiation of a 0.1% solution of X in methyl alcohol at room temperature, 3-methoxycyclohexanone (XI) was obtained, though in a low yield (0.7%) (see Table 3). The major products were its cyclodimers.[7] Thus, the formation of the polar adduct, XI, may suggest the existence of *trans*-2-cyclohexenone (XII),

Table 5. Analytical data of the polar adducts[a]

Compound	Bp, °C/mmHg (mp, °C)	Molecular formula	Found (Calcd), % C	H
3-Ethoxycycloheptanone (IIb)	65/3	$C_9H_{16}O_2$	69.43 (69.19)	10.37 (10.32)
3-Isopropoxycycloheptanone (IIc)	70/3	$C_{10}H_{18}O_2$	70.47 (70.54)	10.94 (10.66)
3-*tert*-Butoxycycloheptanone (IId)	110—120/10	$C_{11}H_{20}O_2$	71.88 (71.69)	10.82 (10.94)
3-Acetoxycycloheptanone (IIe)	80/3	$C_9H_{14}O_3$	63.76 (63.51)	8.22 (8.29)
3-(*N*,*N*-Diethylamino)cycloheptanone (IIg) picrate[b]	(103—107)	$C_{17}H_{24}O_8N_4$	49.55 (49.51)	5.94 (5.86)
3-Isopropoxycyclooctanone (IVb)	70/3	$C_{11}H_{20}O_2$	71.52 (71.69)	11.10 (10.94)
3-Acetoxycyclooctanone (IVc)	105—110/3	$C_{10}H_{16}O_3$	65.27 (65.19)	8.85 (8.75)
3-(*N*,*N*-Diethylamino)cyclooctanone (IVe) picrate[b]	(102—106)	$C_{18}H_{26}O_8N_4$	50.89 (50.70)	6.07 (6.15)

a) Microanalyses were performed at the Elemental Analyses Center of Kyoto University. b) IIg (bp, 83 °C/3 mmHg) and IVe (bp, 90 °C/3 mmHg) afforded a correct molecular peak in mass spectrum at *m/e* (70 eV) 183 and 197, respectively.

though attempted low-temperature experiments had failed to demonstrate the formation of the highly-reactive enone.[12] Although Hammond showed that the photodimerization of X proceeded *via* the triplet state,[7c] the problem of whether or not the ground-state molecule, XII, can be derived therefrom has remained unsolved. In the literature, we can find various examples of a similar type of polar photoreaction: the alcohol addition to Pummerer's ketone,[26] the reaction of cyclohexenone derivatives in aqueous acetic acid,[17] the *tert*-butyl alcohol addition to 5,5-dimethyl-2-cyclohexenone,[27] and the alcohol addition to acetylcyclohexene.[14] As to the behavior of 2-cyclohexenone (X) itself, irradiation in a phosphate buffer solution forming 3-hydroxycyclohexanone has been recorded.[13] Finally, it is worth pointing out that 2-cyclopentenone reacts with alcohols photochemically *via* only a radical process (*cf.* Chart 1).[28]

Experimental

Instrumentation. The IR spectra were taken on a JASCO DS-402G or a Shimadzu IR-27-G spectrophotometer. The UV spectra were recorded on a Perkin-Elmer Model 202 spectrophotometer. The NMR spectra were measured with a Jeol JNM C-60H spectrometer, using tetramethylsilane (TMS) as the internal standard. The mass spectra were obtained with a Hitachi RMU-6C spectrometer. The gas-chromatographic analyses (glpc) were performed on a Yanagimoto Model G-8 chromatograph equipped with a column of Apiezon L on Chromosorb (10% or 30%, 2 mm × 2 m) or one of PEGS on Neosorb (5%, 2 mm × 2 m), and a flame ionization detector, using nitrogen as the carrier gas. The preparative work was done on a Yanagimoto Model GCG-3D instrument with a thermal conductivity detector and using helium as the carrier gas. Columns of Apiezon L on Chromosorb (30%, 5 mm × 2 m) and of PEGS on Neosorb (5%, 5 mm × 2 m) were employed. Analytical and preparative thin-layer chromatography (tlc) was carried out on silica-gel plates (Merck silica gel GF_{254}, buffered at pH 7; 0.25 mm and 1.00 mm thickness respectively).

Materials and Solvents. The 2-cyclohexenone, 2-cycloheptenone, and 2-cyclooctenone were prepared as has been reported by Garbisch.[11] The 2-cyclononenone[29] was obtained by the oxidation[30] of 3-hydroxycyclononene.[31] S.P.- (methyl alcohol, acetonitrile, and cyclohexane) or G.R.-grade solvents (other alcohols, acetic acid, diethylamine, and isopentane) were purchased from Nakarai Chemicals, Ltd., Kyoto, and were used for photochemical studies without further purification. The 2-methyltetrahydrofuran, ether, and water were used after distillation.

General Procedure for Preparative Scale Irradiations. A solution of the cyclic enones (3.6—15 mmol) in various solvents (10—400 ml) was placed in Pyrex tubes (15 × 180 mm), flushed with purified nitrogen for 15 min, and then irradiated externally using a 200 W high-pressure mercury arc for 0.5—24 hr at room temperature. The progress of the reaction was monitored by the glpc analysis of aliquots removed from the reaction vessel. The removal of the solvent, followed by rough distillation, gave a crude oil. Pure materials were obtained by preparative glpc (Apiezon L 30%, 150—180 °C). The spectral properties of the polar adducts are given in Table 3, while the analytical data of new compounds are summarized in Table 5. The fairly unstable adducts, IIg and IVe, were analyzed after their conversion to crystalline picrates.

The treatment of two labile hydroxy ketones, IIf and IVd (0.5—1.6 mmol), with a 1 : 3 mixture of acetic anhydride and pyridine (1.3—2.5 ml) at 100 °C for 1.5 hr, followed by a usual work-up, gave the respective acetoxy ketones, IIe and IVc; they were identified by means of the IR spectra and the retention times of glpc.

All the 3-methoxycycloalkanones were compared with authentic samples.[29b,c]

Irradiation for Analytical Purposes (Tables 1 and 2). A

1.0% solution (2.5—20 ml) of the enones was placed in a quartz tube (10×80 mm) or a Pyrex tube (15×180 mm) and irradiated externally with a 200 W high-pressure mercury lamp through a Pyrex filter at a distance of 15 mm at room temperature or 0 °C under a nitrogen atmosphere. The irradiation was continued for the stated time, and then the yield of polar adducts was determined by glpc (Apiezon L 30% or 10%).

Low-temperature Photolysis of 2-Cyclooctenone (III). *(a) In 2-Methyltetrahydrofuran*: The enone III (13.6 mg, 0.11 mmol) was dissolved in 2-methyltetrahydrofuran (1.5 ml) containing cyclododecane (14.9 mg, 0.09 mmol) as an internal standard for glpc analysis. The solution was then divided into two parts and irradiated in Pyrex tubes (10×80 mm) at −78 °C (Dry Ice–CH_3OH bath) for 15 min under nitrogen, using a 200 W high-pressure mercury arc. After the lamp had then been turned off, each photolysate was poured into methyl alcohol and isopropyl alcohol (1.0 ml), respectively, each of which had been cooled to −78 °C and flushed with dry nitrogen. The methyl alcohol solution was then allowed to warm spontaneously to room temperature in the dark. The solvent was removed *in vacuo*,. The glpc analysis of the residue showed two peaks of retention times identical with those of the starting ketone, III, (41%) and IVa (43%). A similar work-up of the isopropyl alcohol solution, followed by glpc analysis, demonstrated the existence of III (60%) and IVb (24%).

(b) In Isopropyl Alcohol: A solution of III (10.2 mg, 0.08 mmol) and cyclododecane (11.0 mg, 0.07 mmol), an internal reference for glpc analysis, in isopropyl alcohol (1.0 ml) was flushed with dry nitrogen and irradiated at −78 °C as has been described above. After 15 min, the lamp was turned off and the photolysate was treated with an excess of cold methyl alcohol (5.0 ml) in the dark. The mixture was then allowed to warm up to room temperature. Subsequent glpc analysis revealed the existence of only two components, with reaction times identical with those of III and IVa (17 and 80% yields respectively). The isopropyl alcohol adduct, IVb, could not be detected over 1%, if at all.

Low-temperature Photolysis of 2-Cycloheptenone (I). *(a) In Methyl Alcohol*: A solution of the enone I (100 mg, 0.91 mmol) in a 1 : 1 mixture of methyl alcohol and 2-methyltetrahydrofuran (10.0 ml) was irradiated at −196 °C (liq. nitrogen) for 3 hr. After the lamp had then been turned off, the reaction mixture was allowed to warm up to room temperature. The residue obtained after the removal of the solvents was analyzed by glpc and mass analyses. Although the starting material was consumed (30%), no methyl alcohol adduct was obtained.

(b) In EPA: A solution of I (142 mg, 1.29 mmol) in a 5 : 5 : 2 mixture of ether, isopentane, and ethyl alcohol (EPA) (2.0 ml) was irradiated at −196 °C for 3 hr, after which the lamp was turned off. To the cold photolysate we then quickly added diethylamine (1.8 ml) in EPA (4.0 ml) which had been chilled at −78 °C. The solution was allowed to warm to 0 °C while the vessel was caused to vibrate. The subsequent careful removal of the solvents at 0 °C *in vacuo* gave an oily residue; an NMR analysis of this residue showed that 3-(*N*,*N*-diethylamino)cycloheptanone (IIg) was afforded in a 25% yield (40%, based on the consumed enone I).

The treatmcnt of I (116 mg, 1.05 mmol) with a 1 : 10 mixture of diethylamine and EPA (11.0 ml) at 0 °C for 3 hr in the dark did not produce IIg, as ascertained by NMR analysis. The heating of I in diethylamine at 60 °C for 3 hr gave IIg in a 30% yield.

Irradiation of cis*-2-Cyclononenone (VII) in Cyclohexane.* A solution of VII (1.0 g, 7.25 mmol) in cyclohexane (100 ml) was divided into five portions, and each aliquot was irradiated in a Pyrex tube (15×180 mm) affixed to the extension of the lamp at room temperature. After 30 min, the solvent was removed at room temperature under reduced pressure. The residual oil was shown by NMR analysis to consist of the starting enone, VII, and a *trans* isomer, VIII (45 : 55 ratio). Preparative scale tlc (*n*-hexane : ether=4 : 1, three developments) afforded pure VIII. Mass spectrum: *m/e* 138 (M^+). The IR-, UV-, and NMR-spectral data are given in Table 4.

The heating of a solution of VIII (200 mg, 1.47 mmol) in methyl alcohol at 100 °C for 1 hr, followed by the evaporation of the solvent, gave 65 : 35 mixture of 3-methoxycyclononanone (IX) and the *cis* enone, VII (by glpc analysis). The IR and NMR spectra (Table 3) were identical with those of an authentic sample.[29c]

Irradiation of VII in Methyl Alcohol. A solution containing VII (42.6 mg, 0.32 mmol) in methyl alcohol (5.0 ml) was irradiated at 0 °C for 30 min. The subsequent careful removal of the solvent at 0 °C under reduced pressure gave a residue which was found, by NMR and glpc analyses, to contain no methyl alcohol adduct, IX. The oil consisted of only VII and VIII (46 : 54 ratio).

Photolysis of 2-Cyclohexenone (X) in Methyl Alcohol. A dilute solution of X (345 mg, 3.69 mmol) in freshly-distilled methyl alcohol (400 ml) was irradiated in an immersion well at room temperature under nitrogen for 3 hr. By glpc, 70% of the enone X was found to be consumed. The subsequent careful removal of methyl alcohol at 0 °C *in vacuo*, followed by distillation, afforded an oily product (45 mg). Glpc and NMR analyses showed that 3-methoxycyclohexanone (XI) was produced in a 0.7% yield. Glpc examination revealed that no trace of XI was found in the dark under the above-described conditions.

An authentic sample of XI was obtained according to the known procedure.[29c] The IR and NMR spectral data are given in Table 3.

The authors wish to thank Professor H. Nozaki for his encouragement throughout this work. They are also indebted to Mr. M. Kurita for carrying out preliminary studies with regard this investigation. Moreover thanks are due to Messrs. Y. Ohnishi and A. Watanabe for their skillful assistance. Financial support from the Kurata Science Foundation is also acknowledged.

References and Notes

1) For the preliminary communications, see a) H. Nozaki, M. Kurita, and R. Noyori, *Tetrahedron Lett.*, **1968**, 2025; b) R. Noyori, A. Watanabe, and M. Katô, *ibid.*, **1968**, 5443.

2) See, for example, R. O. Kan, "Organic Photochemistry," McGraw-Hill Book Co., Inc., New York, N. Y. (1966), Chapters 3 and 4.

3) a) G. Quinkert, K. Opitz, W. W. Wiersdorff, and J. Weinlich, *Tetrahedron Lett.*, **1963**, 1863; b) C. W. Bird and J. Hudec, *Chem. Ind.* (London), **1959**, 570.

4) a) D. H. R. Barton, *Helv. Chim. Acta*, **42**, 2604 (1959); b) J. E. Baldwin and M. C. McDaniel, *J. Amer. Chem. Soc.*, **89**, 1537 (1967); c) J. E. Baldwin and M. C. McDaniel, *ibid.*, **90**, 6118 (1968).

5) P. E. Eaton, *Accounts Chem. Res.*, **1**, 50 (1968), and other papers cited therein.

6) a) P. E. Eaton, *J. Amer. Chem. Soc.*, **84**, 2344 (1962); b) P. E. Eaton, *ibid.*, **84** 2454 (1962); c) P. E. Eaton, *Tetrahedron Lett.*, **1964**, 3695.

7) a) E. J. Corey, R. B. Mitra, and H. Uda, *J. Amer. Chem. Soc.*, **86**, 485 (1964); b) E. J. Corey, J. D. Bass, R. LeMahieu, and R. B. Mitra, *ibid.*, **86**, 5570 (1964); c) E. Y. Y. Lam, D. Valentine, and G. S. Hammond, *ibid.*, **89**, 3482 (1967).

8) a) O. L. Chapman, T. A. Rettig, A. A. Griswold, A. I. Dutton, and P. Fitton, *Tetrahedron Lett.*, **1963**, 2049; b) H. E. Zimmerman and J. W. Wilson, *J. Amer. Chem. Soc.*, **86**, 4036 (1964); c) H. E. Zimmerman, R. G. Lewis, J. J. McCullough, A. Padwa, S. Staley, and M. Semmelhack, *ibid.*, **88**, 159 (1966); d) H. E. Zimmerman, R. D. Rieke, and J. R. Scheffer, *ibid.*, **89**, 2033 (1967).

9) P. Gray, A. A. Herold, and A. Jones, *Chem. Rev.*, **71**, 247 (1971).

10) Little is known of the photochemical hydrogen abstraction from an alcoholic OH bond. For the only substantiated example (intramolecular radical process), see W. M. Moore and C. Baylor, Jr., *J. Amer. Chem. Soc.*, **88**, 5677 (1966).

11) E. W. Garbisch, Jr., *J. Org. Chem.*, **30**, 2109 (1965).

12) a) E. J. Corey, M. Tada, R. LeMahieu, and L. Libit, *J. Amer. Chem. Soc.*, **87**, 2051 (1965); b) P. E. Eaton and K. Lin, *ibid.*, **87**, 2052 (1965).

13) P. de Mayo and J. S. Wasson, *Chem. Commun.*, **1967**, 970.

14) B. J. Ramey and P. D. Gardner, *J. Amer. Chem. Soc.*, **89**, 3949 (1967).

15) L. E. Friedrich and G. B. Schuster, *ibid.*, **94**, 1193 (1972).

16) P. E. Eaton and K. Lin, *ibid.*, **86**, 2087 (1964).

17) O. L. Chapman, J. B. Sieja, and W. J. Welstead, Jr., *ibid.*, **88**, 161 (1966).

18) Thermal reactions of cyclic dienones with primary amines at room temperature are known. a) A. T. Bottini and J. Gal, *J. Org. Chem.*, **36**, 1718 (1971); b) T. Sato, K. Sato, and T. Mukai, This Bulletin, **44**, 1708 (1971).

19) a) P. J. Kropp, *Pure Appl. Chem.*, **24**, 585 (1970), and references cited therein; b) J. A. Marshall, *Science*, **170**, 137 (1970), and references cited therein.

20) H. Kato and M. Kawanisi, *Tetrahedron Lett.*, **1970**, 865.

21) For a review, see A. J. Merer and R. S. Mulliken, *Chem. Rev.*, **69**, 639 (1969).

22) G. L. Lange and E. Neidert, *Tetrahedron Lett.*, **1972**, 1349.

23) a) H. Nozaki, T. Mori, and R. Noyori, *Tetrahedron*, **22**, 1207 (1966); b) A. Marchesini, G. Pagani, and U. M. Pagnoni, *Tetrahedron Lett.*, **1973**, 1041.

24) a) H. A. Bruson, "Organic Reactions," Vol. V, ed. by R. Adams *et al.*, John Wiley & Sons, Inc., New York and London (1949), p. 79; b) J. Lichtenberger and R. E. Rusch, *Bull. Soc. Chim. Fr.*, **1962**, 254; c) J. Lichtenberger and R. E. Rusch *ibid.*, **1962**, 325.

25) M. J. S. Dewar and R. C. Fahey, *Angew. Chem. Int. Ed. Eng.*, **3**, 245 (1964).

26) T. Matsuura and K. Ogura, This Bulletin, **40**, 945 (1967).

27) W. G. Dauben, G. W. Shaffer, and N. D. Vietmeyer, *J. Org. Chem.*, **33**, 4060 (1968).

28) a) M. Pfau, R. Dulou, and M. Vilkhs, *C. R. Acad. Sci. Paris*, **254**, 1817 (1962); b) W. C. Agosta and A. B. Smith, III, *J. Amer. Chem. Soc.*, **93**, 5513 (1971). See also, c) I. A. Williams and P. Bladon, *J. Chem. Soc., C*, **1967**, 2032.

29) a) M. Santelli, M. Bertrand, and M. Ronco, *Bull. Soc. Chim. Fr.*, **1964**, 3273; b) N. Heap and G. H. Whitham, *J. Chem. Soc., B*, **1966**, 164; c) P. Chamberlain and G. H. Whitham, *ibid.*, **1969**, 1131.

30) R. K. Sharma, B. A. Shoulders, and P. D. Gardner, *J. Org. Chem.*, **32**, 241 (1967).

31) H. C. Brown and C. P. Garg, *J. Amer. Chem. Soc.*, **83**, 2952 (1961).

The Cationic Oligomerization of 2-Methylfuran and the Characteristics of the Oligomers

Akira ISHIGAKI and Toshiyuki SHONO*

Nara Technical College, Yata, Yamato-Kōriyama-shi

** Department of Applied Chemistry, Faculty of Engineering, Osaka University, Yamada-kami, Suita-shi 565*

(Received October 11, 1973)

The treatment of 2-methylfuran with phosphoric acid yields the 2,4,4-tris(5′-methyl-2′-furyl)-1-pentanol (**1**) as a tetrameric product. This product gives its acetate (**2**) on acetylation with acetic anhydride, and forms a equimolar adduct (**3**) after treatment with maleic anhydride. The structural formula of **1** is supported by the IR, UV, NMR, and mass spectral data and by the other experimental facts. The other oligomers are separated as a product (**4**) which contains tetra-, penta-, hexa-, and heptamer. The structure of these oligomers discussed, and some possible reaction mechanisms for oligomerization are suggested.

Furan and alkylfurans are polymerized to resins by the action of acidic catalysts. The structures of these polymeric substances have been the subject of a number of investigations.[1-7] However, the structures of these substances have still not been completely elucidated.

A tetramer of 2-methylfuran formed by the catalytic action of BF_3 was noted by Dunlop and Peters in 1953.[8] As the structure of this tetramer they suggested a large ring compound linked with four 5-methyl-2,5-furylene units.

In a previous paper[9] we reported the formation of 2-methylfuran tetramer by the catalytic action of phosphoric acid. We also suggested another structure for this product.

In the further investigation reported here we will present the most reliable structure of this product and will point out the presence of the other 2-methylfuran oligomers, *i.e.*, penta-, hexa-, and heptamer, in the reaction mixture. We believe that the investigation of these oligomers will provide valuable information for clarifying the structure of the 2-methylfuran polymer and the other polymeric compounds of furan and alkylfurans.

Results and Discussion

Tetramer of 2-Methylfuran and Its Related Compounds. The treatment of 2-methylfuran with phosphoric acid under reflux results in the formation of 2,4,4-tris(5′-methyl-2′-furyl)-1-pentanol **1** in a good yield. The product can be separated as a slightly colored viscous liquid by fractional distillation. Product **1** gives its acetate (**2**) after treatment with acetic anhydride in pyridine. A maleic anhydride adduct of **1** can be separated as a colorless crystalline product. Elementary analyses data indicate that this product (**3**) is an equimolar adduct of **1** and maleic anhydride.

The structural formula of **1** is based on its spectral data, elementary analyses, and other experimental facts. The elementary analysis data of **1**, **2**, and **3** correspond to their calculated values. Moreover the mass numbers of their molecular ions also correspond to their calculated molecular weights. These facts indicate that (**1**) is a tetramer of 2-methylfuran.

Several IR characteristic bands (3100, 1610, 1560, and 775 cm^{-1}) suggest the presence of a furan nucleus which reacts with a dienophile (*e.g.*, maleic anhydride).

The treatment of **1** with alkaline hydrogen peroxide results in an aqueous solution of an oxidation product mixture. This mixture contains 5-methyl-2-furoic acid as an oxidation product. This indicates the presence of 5-methyl-2-furyl groups in the structure.

The UV absorption maximum of **1** in hexane appears at 222 nm. This absorption maximum is similar to the π-π transition absorption maximum of alkylfurans (at 215 nm for 2-methylfuran and at 218 nm for 2,5-dimethylfuran in hexane). This indicates that the π electron system of the furan nucleus does not conjugate with any other π electron system in the structure of **1**.

The NMR spectrum of **1** reveals six heteroaromatic protons at τ 4.2—4.4. These protons correspond to the ring protons of three 5′-methyl-2′-furyl groups.[10]

Therefore the signals which appear as two singlets at τ 7.80 (6H) and 7.82 (3H) must correspond to the protons of three methyl groups attached to the 5′-position of the furan nucleus. The other signals correspond to the following functional groups; the methyl group attached to tertiary aliphatic carbon (τ 8.56, 3H), the hydroxyl group (τ 8.42, 1H; this signal disappears after treatment with D_2O), the methylene group attached to the hydroxyl group (τ 6.72, 2H; this signal is shifted to τ 6.10 in the spectrum of the acetate **2**), the methine group attached to the hydroxymethyl group (τ 7.30, 1H, quintet; this signal is shifted to τ 7.80 in the spectrum of **2**), and another methylene group between tertiary aliphatic carbon and the methine group (τ 7.72, 2H; this signal overlaps with the broad singlet at τ 7.80).

The mass spectrum of **1** indicates a possible fragmentation mechanism, as is shown in the following schemes. Most heterocyclic-system fragmentation occurs by means of β-fission. The fission process is initiated by the loss of one of the non-bonded electrons of the heteroatom, which induces the "*onium ion*". Therefore, it is possible to form four fragment ions (II—V) on the β-fission process from the molecular ion (I), as is shown in Scheme I. The fragment ion III is a tertiary carbonium ion which is stabilized by two furan nuclei. Therefore, it appears as a predominant peak at *m/e* 189. This fragment ion is also possibly forms by the successive fragmentation of V

Scheme I.

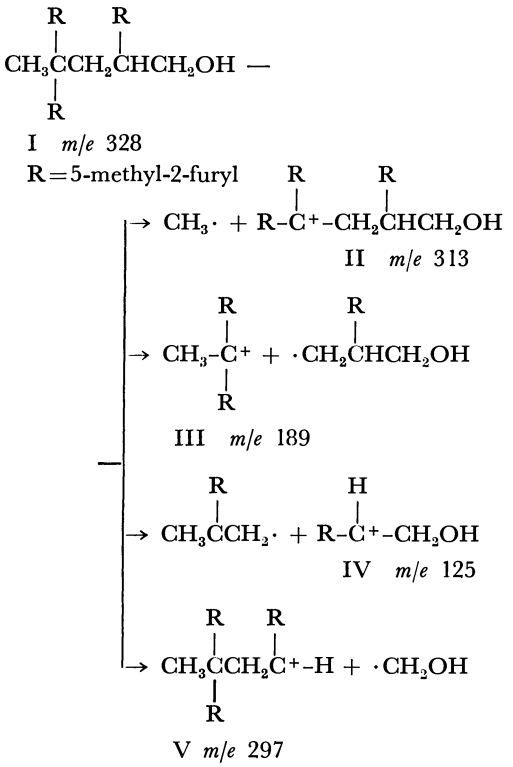

Scheme II.

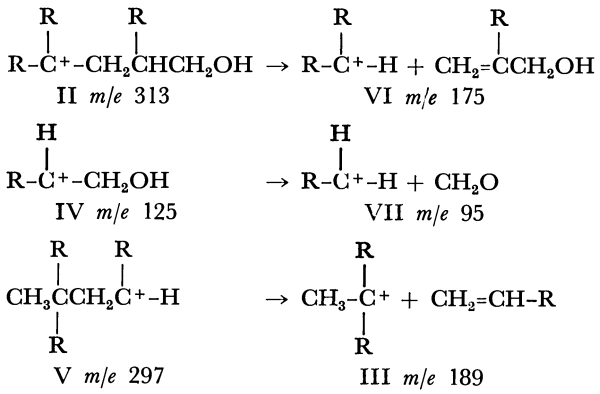

(Scheme II). The other fragment ions (II and IV) may be changed to minor fragment ions (VI and VII) with the elimination of neutral molecules (Scheme II). The mass spectrum of **1** indicates the presence of these ions (III, IV, VI and VII). The peak at *m/e* 43 may be due to CH_3CO^+, which is generally found in the mass spectra of 5-methyl-2-substituted furan compounds.

The facts presented above support the idea that the 2-methylfuran tetramer (**1**) definitely corresponds to 2,4,4-tris(5'-methyl-2'-furyl)-1-pentanol. This structure present a clue to elucidating the reaction mechanism of oligomerization.

Meisel and others reported the trimer of thiophene in 1950.[11] They indicated the structure of this compound and presented a reaction mechanism. This investigation will suggest a possible reaction mechanism to form **1** from 2-methylfuran; it is shown in Fig. 1.

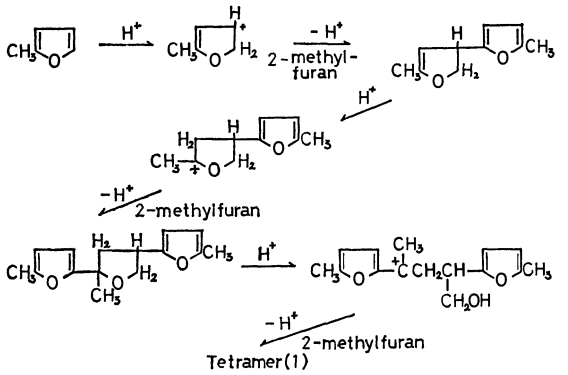

Fig. 1. A possible reaction mechanism for tetramerization.

The Other 2-Methylfuran Oligomers. The other 2-methylfuran oligomers can be separated as product **4** by the molecular distillation of the residue remaining after the removal of **1**. This product **4** is a slightly colored waxy substance. The elementary analysis data indicate that **4** correspond to the oligomer. The mass spectrum of **4** reveals the presence of a number of oligomers, *i.e.*, tetra-, penta-, hexa-, and heptamer.

Product **4** resembles **1** very closely in IR, UV, and NMR spectral patterns. These facts indicate a considerable structural resemblance between them. However, one of the appreciable differences between **1** and **4** is the ratio of the heteroaromatic proton signal intensities to the total one; **1** has a value of 6H/24H, but **4** has a value of 6H/30H. In addition, **4** has a strong IR characteristic band at 1700 cm^{-1}. This indicates the presence of a carbonyl group in the structure of **4**. These facts suggest that the pentamer is formed from **1** or another tetrameric precursor, accompanied by the ring cleavage of the furan nucleus. Some possible reaction routes illustrating this idea are shown in Fig. 2.

The structure of the tetrameric precursor is not necessarily the same as **1**. It is possible that the tetramer contained in **4** is another precursor for oligomerization. The tetramer contained in **4** could not be separated in this work. Therefore, we can not elucidate the structural difference between **1** and the tetramer in **4**. This problem is an interesting subject for investigation in the future.

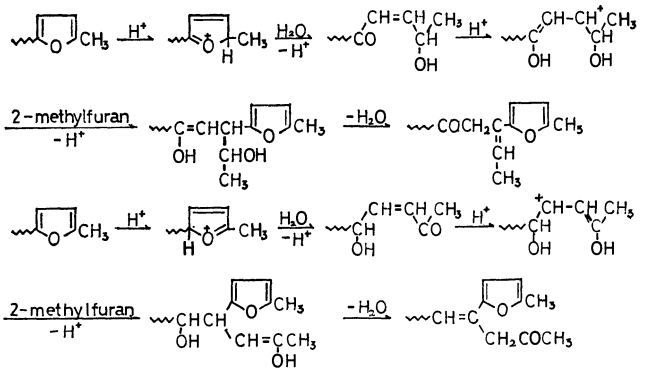

Fig. 2. Some possible propagation mechanisms for oligomerization.

Experimental

The elementary analyses were performed by the microanalytical division in the Department of Applied Chemistry of Osaka University. The infrared spectra were obtained with JASCO IR-G infracord as a neat liquid. The ultraviolet spectra were obtained with a Hitachi model 124 spectrometer. The mass spectra were obtained with a Hitachi RMU-6E spectrometer at 70 eV. The nuclear magnetic resonance spectra at 100 MHz were obtained with a Nippon Denshi JNM-P-100 instrument. The molecular distillation was carried out in a micro pot still in order to separate the oligomeric product.

The 2-methylfuran was prepared by the Wolff-Kishner reduction of 2-furaldehyde and was purified by fractional distillation; bp 62.8 °C (750 mmHg).

Oligomerization Reaction of 2-Methylfuran with Phosphoric Acid. One hundred and fifty grams of 2-methylfuran were stirred vigorously under reflux; then 8 g of phosphoric acid were added, drop by drop over a 10-minute period. The dark brown reaction mixture was stirred for an additional 30 min; then the reaction mixture was poured into a potassium carbonate solution and extracted with ether. The extract was dried over anhydrous magnesium sulfate, the ether and unchanged 2-methylfuran were removed by fractional distillation, and then it was concentrated under vacuum at room temperature. About 110 g of a brown viscous liquid was obtained as a residue.

*2,4,4-Tris(5'-methyl)-2'-furyl-1-pentanol (**1**).* The residual liquid was distilled, giving 57 g (38%) of **1** as a slightly colored viscous liquid; bp 200 °C (3 mmHg); n_D^{20} 1.5290. This product gave a satisfactory elementary analysis for **1**.

Found: C, 73.05; H, 7.35%. Calcd for $C_{20}H_{24}O_4$: C, 73.17; H, 7.31%.

UV max (hexane) 222 nm (ε 25100); IR (liquid film) 3400 (OH), 3100, 1608, 1555, and 775 cm^{-1} (a series of characteristic bands due to 2,5-disubstituted furan nuclei); NMR (CCl_4) τ 4.2—4.4 (m, 6H, β,β'-ring protons of furan nuclei), 6.68 (d, 2H, J=7 Hz, $C\underline{H}_2OH$), 7.30 (quintet, 1H, J=7 Hz, $CH_2C\underline{H}CH_2OH$), 7.72 (d, 2H, $-C\underline{C}H_2\underline{C}H-$, overlapped with a broad singlet at τ 7.80), 7.80 (s, 6H, $C\underline{H}_3$ of 5-methyl-2-furyl groups), 7.82 (s, 3H, $C\underline{H}_3$ of another 5-methyl-2-furyl group), 8.42 (s, 1H, $CH_2O\underline{H}$, washed out with D_2O) and 8.56 (s, 3H, $CH_3\underline{C}CH_2$); mass spectrum (70 eV) *m/e* (rel. intensity) 328 (9), 190 (16), 189 (100), 175 (10), 125 (5), 122 (5), 95 (7), 43 (12).

*Oxidation of the Tetramer (**1**) with Alkaline Hydrogen Peroxide.* One gram of **1** was added to a mixture of 1.2 g of potassium hydroxide and 40 ml of hydrogen peroxide (30% aqueous solution) with vigorous stirring, after which the mixture was left to stand four weeks. Then the mixture was treated with manganese (IV) oxide to decompose the excess hydrogen peroxide and filtered. The firtrate was neutralized with phosphoric acid and extracted with ether. According to thin-layer chromatographic separation (5 cm × 10 cm Wakogel UA Plate and Polyamide UA Plate; solvent: benzene: acetic acid, 40 : 1), 5-methyl-2-furoic acid was found in the extract as an oxidation product. An authentic sample of 5-methyl-2-furoic acid was prepared from 5-methyl-2-furaldehyde.

*2,4,4-Tris(5'-methyl-2'-furyl)-1-pentyl Acetate (**2**).* We dissolve 8.2 g of **1** in 50 g of pyridine and cooled in ice bath; then 36.5 g of acetic anhydride were added, and the mixture was left standing for eight days at room temperature. The reaction mixture was then treated with 1.6 liter of water and extracted with 300 ml of ether. The extract was thoroughly washed with water and distilled under reduced pressure, giving 6.4 g (70%) of **2** as a slightly colored viscous liliquid; bp 182 °C (2 mmHg); n_D^{23} 1.5135.

Found: C, 71.15; H, 7.35%. Calcd for $C_{22}H_{26}O_5$: C, 71.33; H, 7.07%.

IR (liquid film) 1725 (C=O, ester), 3100, 1608, 1555, and 775 cm^{-1} (a series of characteristic bands due to 2,5-disubstituted furan nuclei); NMR (CCl_4) τ 4.2—4.4 (m, 6H, β,β'-ring protons of furan nuclei), 6.02 (d, 2H, J=7 Hz, $C\underline{H}_2OAc$), 7.08 (quintet, 1H, J=7 Hz, $CH_2C\underline{H}CH_2OAc$), 7.72 (d, 2H, overlapped with a broad singlet at τ 7.80), 7.80 (s, 6H, $C\underline{H}_3$ of 5-methyl-2-furyl groups), 7.82 (s, 3H, $C\underline{H}_3$ of another 5-methyl-2-furyl groups), 8.10 (s, 3H, $C\underline{H}_3CO$) and 8.56 (s, 3H, $C\underline{H}_3CCH_2$); mass spectrum (70 eV) *m/e* (rel. intensity) 370 (2), 310 (2), 228 (4), 190 (15), 180 (100), 175 (4), 167 (2), 145 (3), 125 (4), 122 (2), 43 (13).

*Maleic Anhydride Adduct (**3**).* One gram of maleic anhydride and 1.0 g of **1** were dissolved in 10 ml of ether under reflux; then the solution was cooled to room temperature and left to stand for two weeks. A colorless, transparent, crystalline product was obtained; 0.13 g (10%); mp 151.7 °C.

This product gave a satisfactory elementary analysis for an equimolar adduct of **1** and maleic anhydride.

Found: C, 67.11; H, 6.10%. Calcd for $C_{24}H_{26}O_7$: C, 67.60; H, 6.10%.

Mass spectrum (70 eV) *m/e* (rel. intensity) 426 (trace), 328 (9), 190 (18), 189 (100), 175 (5), 125 (9), 98 (7), 95 (9), 54 (9), 43 (18), 28 (11), 26 (7).

This spectrum reasonably represents the superimposed spectrum of **1** and maleic anhydride (molecular weight, 98). This compound can appear from the adduct **3** as the result of the retro-Diels Alder process.

Separation of a Mixture of 2-Methylfuran Oligomers. Fifty-two grams of a hard brown brittle substance remained in the vacuum distillation flask after the removal of **1**. From 5.2 g of this substance, 2.1 g of an oligomeric product **4** was separated by molecular distillation; bp 195—200 °C (10^{-4} mmHg). The product **4** is a yellow, waxy substance and gave a satisfactory elementary analysis for the 2-methylfuran oligomers.

Found: C, 72.58; H, 7.38%. Calcd for $(C_5H_6O)_n$: C, 73.17; H, 7.31%.

UV max (methanol) 221 nm (ε 23,200); IR (thin film) 3400 (OH), 1700 (C=O), 3100, 1608, 1555, and 775 cm^{-1} (a series of characteristic bands due to 2,5-disubstituted furan nuclei); NMR (CCl_4) τ 4.1—4.4 (m, 6H, β,β'-ring protons of furan nuclei), 6.68 (d), 7.30 (quintet), 7.72, 7.80 (s), 7.82 (s), 7.85 (m), 8.60 (s) and 8.4—8.7 (m); mass spectrum (70 eV) *m/e* (rel. intensity) 328 (5), 410 (9), 492 (3), 574 (trace), 189 (100) and others.

The authors wish to thank Dr. Yoshikazu Hachihama, President of Nara Technical College, for his support of this work. (This report was present at the 28th Annual Meeting of the Chemical Society of Japan, Tokyo, April, 1973).

References

1) V. V. Korshak, A. S. Sultanov, and A. A. Abduvaliev, *Uzb. Khim. Zh.*, **4**, 39 (1959).

2) A. V. Topchiev, B. A. Krentsel, and Y. Y. Goldfarb, *Izv. Akad. Nauk SSSR, Otd. Khim. Nauk*, **369** (1959).
3) A. V. Topchiev, Y. Y. Goldfarb, and B. A. Krentsel, *Vysokomol. Soedin.*, **3**, 870 (1961).
4) K. V. Khaidarov, A. A. Abduvaliev, and A. S. Sultanov, *ibid.*, **5**, 1012 (1963).
5) A. Ishigaki, T. Shono, and Y. Hachihama, *Kogyo Kagaku Zasshi*, **66**, 119 (1963).
6) M. Armour, A. G. Davies, J. Upadhyhay, and A. Wasserman, *J. Polym. Sci., Part A-1*, **5**, 1527 (1967).
7) J. Kresta and H. Livingston, *Polymer Lett.*, **8**, 795 (1970).
8) A. P. Dunlop and F. N. Peters, "The Furans," Reinhold Publish Co., New York, N. Y. (1953), p. 65.
9) Y. Hachihama, T. Shono, and A. Ishigaki, *Technology Report of the Osaka Univ.*, **13**, 481 (1963).
10) J. B. Barr and S. B. Wallon, *J. Appl. Polym. Sci.*, **15**, 1079 (1971).
11) S. L. Meisel, G. C. Johonson, and H. D. Hartough, *J. Amer. Chem. Soc.*, **72**, 1910 (1950).

The Diazotization of 2-Aminoazulene Derivatives. The Formation of 2-Diazo-2,6-azulenoquinone Derivatives[1]

Tetsuo NOZOE,* Toyonobu ASAO,** Hiroshi SUSUMAGO,*** and Masayoshi ANDO

Department of Chemistry, Faculty of Science, Tohoku University, Aramaki, Aoba, Sendai 980

(Received October 29, 1973)

The Diazotization of 2-amino-6-bromo (or alkoxy)-azulene, with alkoxycarbonyl or cyano groups at the 1 and 3-positions, by sodium nitrite in dioxane-sulfuric acid afforded mainly the corresponding 2-diazo-2,6-azulenoquinone derivatives (**2a**, **2b**, **16**). The catalytic hydrogenation of these compounds gave 1,3-disubstituted 6-hydroxyazulenes (**4a**, **4b**, **18**), from which 1,3-disubstituted 6-alkoxy- or 6-acetoxy-azulenes were obtained. The diazotization of diethyl 2-amino-6-bromoazulene-1,3-dicarboxylate (**1a**) in dry benzene with isoamyl nitrite in the presence of hydrogen chloride afforded the 2,6-dichloroazulene derivative (**20**) and the 5-bromo-2-diazo-2,6-azulenoquinone derivative (**21**); the latter, accompanied by a bromine addition product (**22**), was also obtained by the bromination of **2a**. The diazotization of diethyl 2-aminoazulene-1,3-dicarboxylate (**25**) afforded **2a** and a deamination product (**26**). The structure and mechanism of the formation of these diazoazulenoquinones are discussed.

It has long been known that 1,3-disubstituted 2-aminoazulene derivatives easily undergo a diazo reaction similar to benzenoid amines, by way of which deamination products or 2-haloazulenes are obtained.[2]

However, it has also been found that the deamination of diethyl 2-amino-6-bromoazulene-1,3-dicarboxylate does not proceed well under the same reaction conditions.[3] We have studied the reaction for 2-aminoazulene derivatives and have found that the reaction afforded 2-diazo-2,6-azulenoquinone derivatives in good yields. The results will be reported in this paper.

Results and Discussion

When a solution of diethyl 2-amino-6-bromoazulene-1,3-dicarboxylate (**1a**)[4] in dioxane containing concentrated sulfuric acid was diazotized with sodium nitrite, Compound **2a**, with a molecular formula of $C_{16}H_{14}O_5N_2$, was obtained, besides a small amount of diethyl 6-bromoazulene-1,3-dicarboxylate (**3**).[3] We first assigned the structure of (A) (azulene diazocarboxylate derivative) to the compound **2a** formed by the intramolecular elimination of bromine by the ethoxyl group.[1] However, from the facts that diethyl 6-acetoxy- and 6-chloroazulene-1,3-dicarboxylates were formed from **2a**, as will be described below, the structure of (A) was found to be incorrect.

Compound **2a** shows a UV absorption pattern similar to those of azulene derivatives, an IR (KBr) spectrum at 2165 cm^{-1} (diazonium group), and NMR ($CDCl_3$) signals at δ 6.61 ppm (2H) and 8.29 (2H), with an A_2B_2-type pattern. When Compound **2a** was submitted to catalytic hydrogenation in the presence of 5% Pd–C, no hydrogen absorption could be observed; however, the reaction yielded an acidic compound (**4a**), $C_{16}H_{16}O_5$, which gave methyl ether (**5a**), ethyl ether (**6**), and acetate (**7**) upon reaction with diazomethane, ethyl iodide with a silver salt of **4a**, and acetic anhydride respectively. Furthermore, Compound **4a** reacted with thionyl chloride to give a 6-chloro derivative (**8**), and it has already been reported that the hydrolysis, followed by the decarboxylation of **4a** with acid, afforded 6-hydroxyazulene.[5]

Compound **6** was found to be identical with the known diethyl 6-ethoxyazulene-1,3-dicarboxylate obtained by the reaction of **3** with ethoxide;[3] therefore, Compound **2a** must be diethyl 2-diazo-2,6-azulenoquinone-1,3-dicarboxylate or its inner salt. This compound is presumably formed by the nucleophilic attack of water on the 6-position of the initially-formed diazonium compound **9**, followed by the elimination of hydrogen bromide from an intermediate **10**. The attack at the 6-position must occur easily, because the position is activated by an electron-attractive diazonium group at the 2-position and by ethoxycarbonyl groups at the 1- and 3-positions, especially under acidic conditions.

The fact that the apparent hydrogen absorption could not be observed in the catalytic hydrogenation of **2a** can be explained by the liberation of an equimolar amount of nitrogen probably through an intermediate **11** when hydrogen is absorbed.

The nucleophilic substitution of Compound **1a** afforded the corresponding azulenes, the 6-ethoxy (**12**), 6-ethylthio (**13**), and 6-*p*-tolylthio (**14**) derivatives. However, the reaction of **1a** with methoxide in methanol afforded dimethyl 2-amino-6-bromoazulene-1,3-dicarboxylate (**1b**) as insoluble precipitates.

The similar diazotization of **12** and **13** yielded the same compound **2a** in good yields. The diazotization of **1b** afforded dimethyl ester (**2b**) in a good yield. The catalytic reduction of **2b** gave the 6-hydroxyazulene derivative (**4b**), the reaction of which with diazomethane afforded the corresponding methyl ether (**5b**). The heating of these diazoazulenoquinones (**2a** and **2b**) in isopropyl alcohol in the presence of HCl or H_2SO_4 for a short time yielded the corresponding 6-hydroxyazulene derivatives (**4a** and **4b** respectively) and acetone by disproportionation, followed by the extrusion of N_2.

The diazotization of the 2-amino-6-bromo-1,3-

* Present address: No 811, 2-5-1, Kamiyoga, Setagaya-ku, Tokyo 158.

** Present address: Department of Chemistry, College of General Education, Tohoku University, Kawauchi, Sendai 980.

*** Present address: Asahi Chemical Industries Ltd., Ukishima, Kawasaki 210.

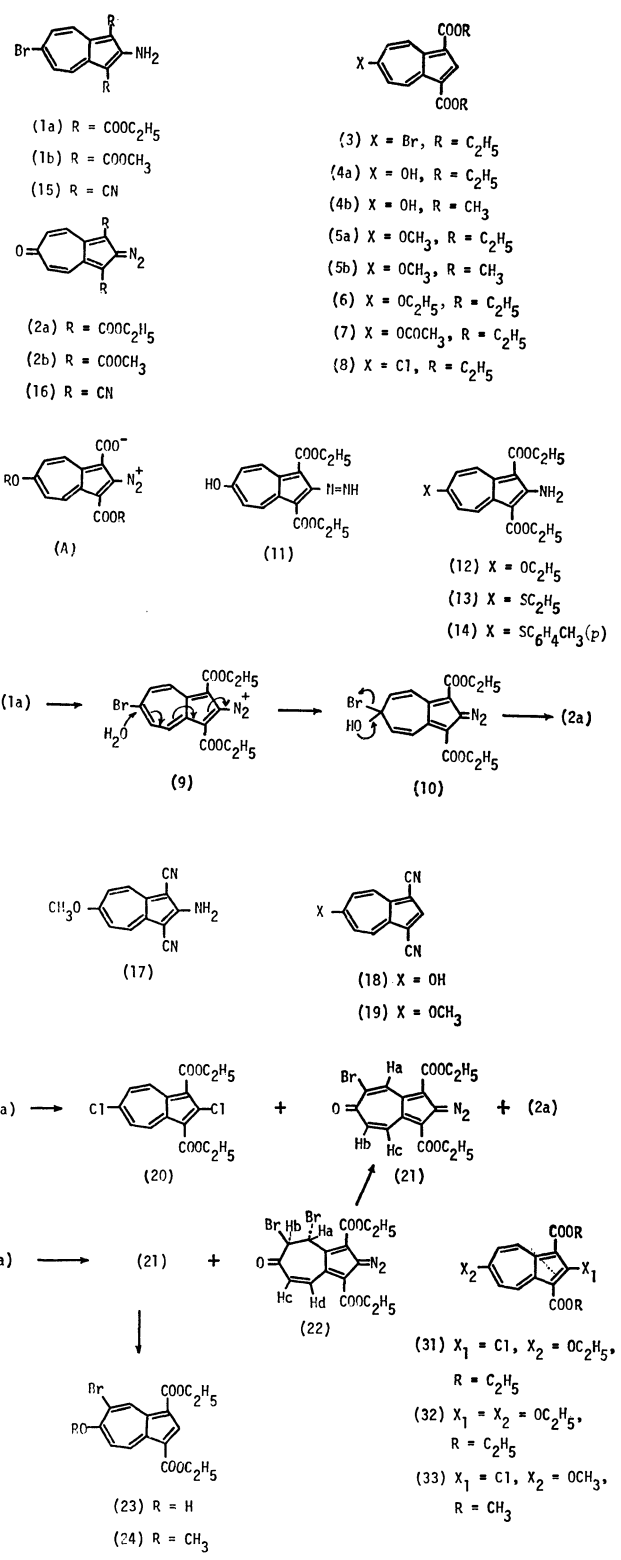

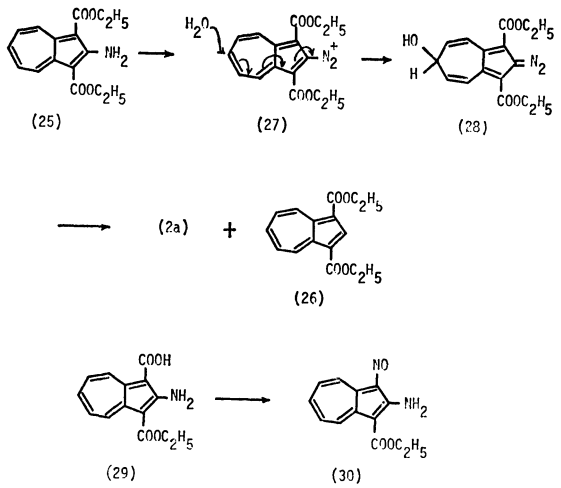

dicyanoazulene (**15**) obtained by the bromination of 2-amino-1,3-dicyanoazulene[2] in acetic acid at an elevated temperature afforded a similar diazo compound, 1,3-dicyano-2-diazo-2,6-azulenoquinone (**16**), which was also obtained by the diazotization of 2-amino-6-methoxy-1,3-dicyanoazulene (**17**). The structure of **16** was confirmed by reduction to yield unstable 6-hydroxy-1,3-dicyanoazulene (**18**), followed by methylation which gave 6-methoxy-1,3-dicyanoazulene (**19**), and by the IR spectrum of **16**, which shows a diazonium band at 2155 cm^{-1} and a cyano band at 2217 cm^{-1}.

On the other hand, when a solution of **1a** in dry benzene containing dry hydrogen chloride was diazotized with isoamyl nitrite, diethyl 2,6-dichloroazulene-1,3-dicarboxylate (**20**), a compound **21** with the molecular formula of $C_{16}H_{13}O_5N_2Br$, and a small amount of **2a** were obtained. Compound **21** shows an UV absorption curve similar to that of **2a**; IR (KBr) 2175 cm^{-1}; NMR ($CDCl_3$) δ 6.71 ppm (d, J=12.5 Hz, Hb), 8.01 (d, J=12.5 Hz, Hc), and 9.08 (s, Ha). From the above data, as well as on the basis of following reactions, Compound **21** was assumed to be diethyl 5-bromo-2-diazo-2,6-azulenoquinone-1,3-dicarboxylate, which must be formed by the bromination of the initially-formed diazoazulenoquinone (**2a**); the bromine might have been produced by the oxidation of liberated hydrogen bromide under these conditions. Therefore, it is reasonable that a similar diazotization of the 6-ethoxyazulene derivative (**12**) in benzene–HCl with isoamyl nitrite afforded only Compound **2a**.

The bromination of **2a** with bromine in $CHCl_3$ actually afforded Compound **21**, accompanied by a bromine addition product (**22**), and the treatment of **22** with triethylamine afforded **21** in a quantitative yield. The dibromide (**22**) was assumed to have the structure shown in the scheme on the basis of its derivation to **21**, the results of elemental analysis, and NMR spectrum ($CDCl_3$) δ 4.82 ppm (d, d, J=6.0, 1.8 Hz, Hb), 6.12 (d, d, J=13.0, 1.8 Hz, Hc), 6.56 (d, J=6.0 Hz, Ha), and 8.06 (d, J=13.0 Hz, Hd).

Compound **21** was catalytically hydrogenated to yield the 5-bromo-6-hydroxyazulene derivative (**23**), which was then reacted with diazomethane to give the methyl ether (**24**).

The formation of the dichloro compound (**20**) can be explained by a nucleophilic replacement of the bromine of the diazonium compound (**9**) by the chloride ion, followed by a Sandmeyer reaction at the 2-position. No change was observed in the reaction of **1a** and hydrogen chloride; therefore, it is clear that halogen exchange occurred after diazotization.

When diethyl 2-aminoazulene-1,3-dicarboxylate

(**25**)[2] was diazotized in dioxane containing sulfuric acid with sodium nitrite, diazoazulenoquinone (**2a**) and a deamination product, diethyl azulene-1,3-dicarboxylate (**26**), were unexpectedly obtained, although in low yields. This reaction may be explained as follows; at first the diazotization of **25** occurs to yield diazonium compound (**27**), which is easily attacked by water at the 6-position to give the quinol compound (**28**); then dispropotionation occurs between **27** and **28** to afford **26** and **2a** respectively.

The fact that the diazonium compound (**27**) undergoes a nucleophilic attack at the 6-position, in contrast with the reactivity of azulene itself, which preferentially occurs at the 4-position,[6] may be attributable to the steric hindrace of ethoxycarbonyl groups at the 1 and 3 positions.

The diazotization of 2-amino-3-ethoxycarbonylazulene-1-carboxylic acid (**29**) was attempted in the anticipation of obtaining a diazoazulenecarboxylate derivative; however, only a violet powder was obtained, and upon treatment with sodium carbonate it yielded ethyl 2-amino-3-nitrosoazulene-1-carboxylate (**30**), which had been synthesized by the nitrosation of ethyl 2-aminoazulene-1-carboxylate.[7]

When the dichloroazulene derivative (**20**) was treated with ethoxide in ethanol, 2-chloro-6-ethoxyazulene and 2,6-diethoxyazulene derivatives (**31** and **32**) were obtained, depending on the amount of the reagent used. The alkaline hydrolysis of **20** afforded 2-chloro-6-hydroxyazulene-1,3-dicarboxylic acid as an amorphous powder, which then gave dimethyl 2-chloro-6-methoxyazulene-1,3-dicarboxylate (**33**) upon reaction with diazomethane.

The 2-diazo-2,6-azulenoquinone derivatives obtained in this paper are very stable, with definite melting points; they are soluble in non-polar solvents such as $CHCl_3$ and benzene, less soluble in alcohol, and insoluble in water.

The electronic spectra of the diazoazulenoquinones in MeOH, acidic, and basic media (Fig. 1 and see Experimental section) show that the spectra are little changed by the solvent used and do not show any absorption maxima over 450 nm.

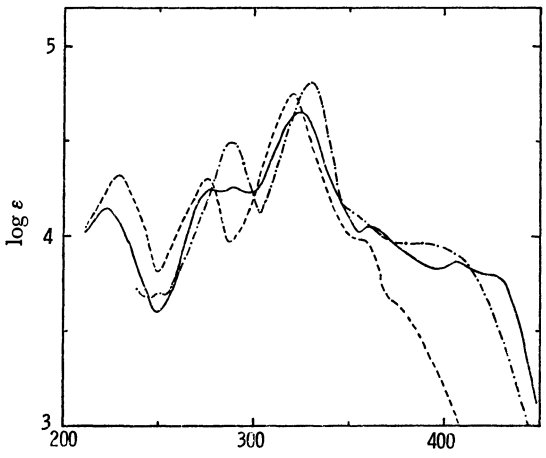

Fig. 1. UV absorption spectra of compound (**2a**) in MeOH (——), in MeOH-HCl (----) and in MeOH-NaOH (—·—·—).

The infrared spectra of the compounds show strong diazonium bands at 2155—2175 cm^{-1}, a frequency a little higher than those of *p*-diazobenzoquinone, 2100 cm^{-1},[8] and diazocyclopentadiene, 2082 cm^{-1},[9] but considerably lower than that of benzene diazonium tetrafluoroborate, 2298 cm^{-1}.[8]

These facts would indicate that the compounds exist in the following resonance hybrids:

The ultraviolet absorption spectrum of the rather stable dibromo compound (**22**) is completely different from those of azulene compounds, and the infrared spectrum shows a diazonium band at 2135 cm^{-1} and a broad carbonyl band at 1690—1655 cm^{-1}. The compound seems to be stabilized by the contribution of the following resonance forms, as is also observed in diazocyclopentadiene.[9]

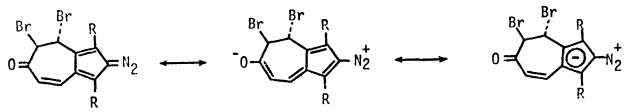

Experimental[10]

*The Diazotization of Diethyl 2-Amino-6-bromoazulene-1,3-dicarboxylate (**1a**) and Related Compounds (**1b**, **12**, **13**, **15**, and **17**).* *a) In Dioxane*: To a stirred solution of **1a** (300 mg) in purified dioxane (7 ml) and concentrated sulfuric acid (1 ml), a solution of sodium nitrite (150 mg) in water (1 ml) was added over a 3-hr period under cooling with ice. After the mixture had been stirred for 2 hr, water (20 ml) was added and the separated precipitates were collected, washed, and recrystallized from benzene to give 190 mg of diethyl 2-diazo-2,6-azulenoquinone-1,3-dicarboxylate (**2a**). The filtrate of the recrystallization was chromatographed on an alumina column and eluted with benzene. From the first effluent 10 mg of 6-bromoazulene-1,3-dicarboxylate (**3**) was obtained; it was identified by a direct comparison of the infrared spectrum with that of an authentic specimen.[3]

In a similar manner, five compounds (**1a**, **12**, **13**, **15**, and **17**) gave the corresponding 2-diazo-2,6-azulenoquinones (**2b**, **2a**, and **16**). The analytical and physical data of the products are as follows.

2a: orange needles, mp 148—149 °C (decomp.).
Found: C, 61.45; H, 4.27; N, 8.94%. Calcd for $C_{16}H_{14}O_5N_2$: C, 61.14; H, 4.49; N, 8.91%.
λ_{max}^{MeOH} nm (log ε); 223 (4.15), 277 (4.25), 289 (4.26), 324 (4.65), 360 (4.05), 406 (3.87) and 426^{sh} (3.80).
$\lambda_{max}^{MeOH-HCl}$ nm (log ε); 229 (4.32), 276 (4.30), 321 (4.75), 358^{sh} (3.98) and 373^{sh} (3.66).
$\lambda_{max}^{MeOH-NaOH}$ nm (log ε); 250 (3.84), 288 (4.39), 330 (4.81), 358^{sh} (4.14) and 390 (3.97).

2b: orange needles (from benzene), mp 173—175 °C.
Found: C, 58.66; H, 3.70; N, 9.86%. Calcd for $C_{14}H_{10}O_5N_2$: C, 58.74; H, 3.52; N, 9.79%.
λ_{max}^{MeOH} nm (log ε); 223 (4.11), 278 (4.20), 289 (4.20), 325 (4.69), 360 (3.98), 406 (3.90) and 426 (3.85).
$\lambda_{max}^{MeOH-HCl}$ nm (log ε); 228 (4.32), 275 (4.29), 320 (4.76),

359 (3.98), and 374 (3.63).
$\lambda_{max}^{MeOH-NaOH}$ nm (log ε); 250 (3.60); 287 (4.37), 329 (4.81), 360^{sh} (4.11), and 390 (3.92).

16: brown prisms (from dioxane), mp 155 °C (explosively decomp.).

Found: C, 65.17; H, 2.03; N, 25.63%. Calcd for $C_{12}H_4ON_4$: C, 65.44; H, 1.83; N, 25.44%.
λ_{max}^{MeOH} nm (log ε); 235 (3.97), 262^{sh} (3.94), 274^{sh} (4.01), 315^{sh} (4.27), 323 (4.29), 375^{sh} (3.86), and 400 (3.93).
$\lambda_{max}^{MeOH-HCl}$ nm (log ε); 225 (4.21), 265 (3.88), 315^{sh} (4.39), 319 (4.40), 374 (3.82), 396 (3.79), and 420 (3.70).
$\lambda_{max}^{MeOH-NaOH}$ nm (log ε); 246 (4.07), 262 (3.96), 271 (3.92), 324 (4.50), and 399 (3.86).

b) In dry benzene: A solution of **1a** (2 g) in dry benzene (100 ml) was saturated with dry hydrogen chloride gas under cooling with ice, and then isoamyl nitrite (1.5 ml) was added to the solution. After the mixture had been allowed to stand in an ice box overnight, benzene (100 ml) was added and the solution was washed with water five times. After the benzene solution had then been dried over anhydrous sodium sulfate, the solution was concentrated to about 30 ml under reduced pressure. The solution was submitted to column chromatography on an alumina and then eluted with benzene. From the first effluent, 300 mg of diethyl 2,6-dichloroazulene-1,3-dicarboxylate (**20**) as reddish-purple crystals (mp 160—161 °C (from benzene-cyclohexane)) were obtained.

Found: C, 56.02; H, 3.95%. Calcd for $C_{16}H_{14}O_4Cl_2$: C, 56.30; H, 4.13%.
λ_{max}^{MeOH} nm (log ε); 237 (4.31), 266 (4.05), 305 (4.54), 315 (4.60), 349^{sh} (3.68), 362 (3.77), and 500 (2.54).

The latter effluents were combined and rechromatographed on an alumina column; 1.1 g of diethyl 5-bromo-2-diazo-2,6-azulenoquinone-1,3-dicarboxylate (**21**) as orange needles (mp 166—168 °C (decomp.) (from benzene)) were thus obtained.

Found: C, 49.05; H, 3.28; N, 7.26%. Calcd for $C_{16}H_{13}O_5N_2Br$: C, 48.87; H, 3.33; N, 7.13%.
λ_{max}^{MeOH} nm (log ε); 229 (4.11), 280 (4.20), 292 (4.25), 323^{sh} (4.55), 334 (4.62), 264^{sh} (4.01), 382^{sh} (3.83) and 410^{sh} (3.42).
$\lambda_{max}^{MeOH-HCl}$ nm (log ε); 232 (4.19), 277 (4.19), 322 (4.64), 356^{sh} (3.95), 383 (3.81) and 430^{sh} (3.22).
$\lambda_{max}^{MeOH-NaOH}$ nm (log ε); 245 (4.01); 289 (4.35), 333 (4.73), 360^{sh} (4.12), and 398^{sh} (3.88).

From the latter effluent, 80 mg of Compound **2a** (mp 148 °C (decomp.)) were obtained.

A similar diazotization of Compound **12** in dry benzene afforded only **2a**.

The Diazotization of Diethyl 2-Aminoazulene-1,3-dicarboxylate (25) in Dioxane. To a solution of Compound **25** (500 mg) in dioxane (5 ml) and concentrated sulfuric acid (1.5 ml), a solution of sodium nitrite (250 mg) in water (1 ml) was added under cooling with ice. The solution was then stirred overnight, water (30 ml) was added, and the solution was extracted with benzene. The extract was washed with water, dried, and submitted to chromatography on an alumina column. From the first effluent 50 mg of reddish crystals (mp 120 °C) were obtained; their infrared spectrum was superimposable upon that of authentic diethyl azulene-1,3-dicarboxylate (**26**).[2b] From the next effluent, 70 mg of Compound **2a** were obtained. From the latter effluents, a dark brown oil was obtained; however, its structure could not be clarified.

The Reaction of 2-Amino-3-ethoxycarbonylazulene-1-carboxylic Acid (29) with Nitrous Acid. To a stirred solution of **29** (140 mg) in dioxane (5 ml) and concentrated sulfuric acid (0.5 ml), isoamyl nitrite (0.1 g) was added under cooling with ice. After the mixture had been stirred for 30 min, the resulting precipitate was filtered to give black violet crystals (mp 199—201 °C (decomp.)). The crystals were dissolved in water, and the solution was neutralized by sodium hydrogen carbonate to afford ethyl 2-amino-1-nitrosoazulene-3-carboxylate (**30**) in a quatitative yield. The infrared spectrum of Compound **30** was superimposable upon that of an authentic sample.[7]

The Hydrogenation of 2-Diazo-2,6-azulenoquinones to 6-Hydroxyazulenes. A solution of **2a** (300 mg) in ethanol (100 ml) was submitted to catalytic hydrogenation in the presence of 5% Pd–C (30 mg), after which the solution was shaken for 3 hr. Hydrogen was not takenup, to all appearances. The catalyst was then filtered off, the solvent was removed, and the residue was recrystallized from benzene to give 200 mg of diethyl 6-hydroxyazulene-1,3-dicarboxylate (**4a**) as yellow needles (mp 171—172 °C).

Found: C, 66.79; H, 5.46%. Calcd for $C_{16}H_{16}O_5$: C, 66.65; H, 5.59%.
λ_{max}^{MeOH} nm (log ε); 225 (4.33), 278 (4.42), 323 (4.75), 330^{sh} (4.67), 356^{sh} (4.12), 374 (3.90), 395^{sh} (3.56) and 464 (2.74).

A similar hydrogenation of **2b** and **21** afforded the corresponding 6-hydroxyazulenes (**4b** and **23**).

4b: yellow needles, mp 235—237 °C (decomp.).

Found: C, 64.73; H, 4.40%. Calcd for $C_{14}H_{12}O_5$: C, 64.61; H, 4.65%.

23: dark yellow needles, mp 203—205 °C (decomp.).

Found: C, 52.51; H, 4.03%. Calcd for $C_{16}H_{15}O_5Br$: C, 52.30; H, 4.12%.
λ_{max}^{MeOH} nm (log ε); 235 (4.28), 280 (4.35), 293 (4.26), 326 (4.71), 383 (4.01), 410^{sh} (3.55) and 475^{sh} (2.95).

6-Methoxyazulenes from 6-Hydroxyazulenes. Thirty mg of Compound **4a** was methylated with diazomethane in methanol. The crystals obtained by the removal of the solvent were dissolved in benzene, and the solution was passed through an alumina column and then recrystallized from a mixture of benzene and cyclohexane to give 25 mg of **5a** as reddish prisms (mp 140—141 °C).

In a similar manner, two compounds (**4b** and **23**) gave the corresponding 6-methoxyazulenes (**5b** and **24**); the hydrogenation of **16**, followed by its methylation afforded 1,3-dicyano-6-methoxyazulene (**19**). The analytical and physical data of the products are as follows.

5a: Found: C, 67.60; H, 5.78%. Calcd for $C_{17}H_{18}O_5$: C, 67.54; H, 6.00%.
λ_{max}^{MeOH} nm (log ε); 228 (4.46), 276 (4.40), 310^{sh} (4.65), 321 (4.77), 349 (4.06), 376 (3.75), and 456 (3.00).

5b: orange needles, mp 144—146 °C.

Found: C, 65.92; H, 5.31%. Calcd for $C_{15}H_{14}O_5$: C, 65.69; H, 5.15%.
λ_{max}^{MeOH} nm (log ε); 233 (4.40), 276 (4.36), 307^{sh} (4.60), 320 (4.76), 348 (4.03), 374 (3.81), and 453 (3.04).

24: reddish crystals, mp 133—134 °C.

Found: C, 53.71; H, 4.30%. Calcd for $C_{17}H_{17}O_5Br$: C, 53.56; H, 4.49%.
λ_{max}^{MeOH} nm (log ε); 237 (4.32), 270^{sh} (4.27), 279 (4.34), 312^{sh} (4.65), 325 (4.84), 355 (4.04), 386 (4.08), and 470 (3.03).

19: orange needles, mp 245 °C (decomp.).

Found: C, 74.76; H, 4.17; N, 13.17%. Calcd for $C_{13}H_8ON_2$: C, 74.99; H, 3.87; N, 13.46%.
λ_{max}^{MeOH} nm (log ε); 220 (4.38), 227 (4.38), 265 (3.94), 306^{sh} (4.55), 313^{sh} (4.68), 318 (4.71), 352 (3.96), and 460 (2.98).

6-Methoxyazulenes from 6-Haloazulenes. a): A solution of 2-amino-6-bromo-1,3-dicyanoazulene (**15**) (816 mg) in methanol (40 ml) containing 200 mg of sodium was refluxed for 5 hr. After cooling, greenish-yellow needles (640 mg) were obtained. Recrystallization from dioxane gave 2-amino-6-methoxy-1,3-dicyanoazulene (**17**) as yellow needles (mp 285 °C (decomp.)).

Found: C, 69.52; H, 4.04; N, 18.67%. Calcd for $C_{13}H_9ON_3$: C, 69.94; H, 4.06; N, 18.83%.

b): A solution of **20** (100 mg) in 50% ethanol (10 ml) containing potassium hydroxide (1 g) was refluxed for 2 hr. Water (20 ml) was then added, and the solution was acidified by the addition of 2M hydrochloric acid. A dark yellow solid was filtered off, washed with water, and dried. A suspended solution of the solid in methanol was methylated with diazomethane, the solvent was removed, and the residue was recrystallized from ethanol to give dimethyl 2-chloro-6-methoxyazulene-1,3-dicarboxylate (**33**) (30 mg) as orange needles (mp 140—142 °C).

Found: C, 58.58; H, 4.15%. Calcd for $C_{15}H_{13}O_5Cl$: C, 58.33; H, 4.23%.

λ_{max}^{MeOH} nm (log ε); 228 (4.38), 275 (4.32), 310^{sh} (4.71), 320 (4.82), 364 (4.11), and 440 (3.16).

6-Ethoxyazulenes. *a)*: A dried silver salt obtained from 130 mg of **4a** was suspended in dry benzene (20 ml), and the solution was refluxed with ethyl iodide (500 mg) for 3 hr. The black precipitate was then filtered off, and the solvent was removed from the filtrate to leave orange crystals. Recrystallization from a mixture of benzene and methanol gave 45 mg of diethyl 6-ethoxyazulene-1,3-dicarboxylate (**6**) as orange needles (mp 139—141 °C).

Found: C, 68.31; H, 6.36%. Calcd for $C_{18}H_{20}O_5$: C, 68.34; H, 6.37%.

λ_{max}^{MeOH} nm (log ε); 228 (4.41), 276 (4.37), 308^{sh} (4.62), 320 (4.78), 349 (4.07), 375 (3.85), and 454 (3.04).

b): After a solution of Compound **1a** (300 mg) in anhydrous ethanol (20 ml) containing 200 mg of sodium had been refluxed for 2 hr, orange crystals which were precipitated out by cooling the reaction mixture were recrystallized from benzene to afford diethyl 2-amino-6-ethoxyazulene-1,3-dicarboxylate (**12**) (160 mg) as yellow needles (mp 160—161 °C).

Found: C, 65.52; H, 6.11%. Calcd for $C_{18}H_{21}O_5N$: C, 65.24; H, 6.39%.

λ_{max}^{MeOH} nm (log ε); 232^{sh} (4.28), 245^{sh} (4.37), 255 (4.39), 281 (4.27), 325^{sh} (4.66), 336 (4.77), 370^{sh} (3.90), 410 (3.89) and 460 (3.86).

c): A solution of Compound **20** (100 mg) in anhydrous ethanol (10 ml) containing sodium ethoxide prepared from 7 mg of sodium was refluxed for one hour. A usual working up afforded 65 mg of diethyl 2-chloro-6-ethoxyazulene-1,3-dicarboxylate (**31**) as orange needles (from benzene) (mp 137—138 °C).

Found: C, 61.52; H, 5.30%. Calcd for $C_{18}H_{19}O_5Cl$: C, 61.63; H, 5.46%.

λ_{max}^{MeOH} nm (log ε); 229 (4.38), 276 (4.30), 311^{sh} (4.71), 321 (4.82), 365 (4.02), and 445 (3.10).

d): A solution of Compound **20** (100 mg) in anhydrous ethanol (10 ml) containing sodium ethoxide prepared from 60 mg of sodium was refluxed for 2 hr. A usual working up gave diethyl 2,6-diethoxyazulene-1,3-dicarboxylate (**32**) as orange needles (from benzene) (mp 148—149 °C).

Found: C, 66.85; H, 6.82%. Calcd for $C_{20}H_{24}O_6$: C, 66.65; H, 6.71%.

λ_{max}^{MeOH} nm (log ε); 229 (4.44), 273 (4.34), 313^{sh} (4.71), 323 (4.82), 365 (4.07), and 436 (3.10).

*Diethyl 2-Amino-6-ethylthioazulene-1,3-dicarboxylate (**13**).* A solution of **1a** (200 mg) and ethylmercaptane (45 mg) in anhydrous ethanol (5 ml) containing 14.5 mg of sodium was refluxed for one hour. The orange crystals which precipitated out were filtered, washed with water, and recrystallized from ethanol to give 170 mg of **13** as orange crystals (mp 104—105 °C).

Found: C, 62.42; H, 5.87; N, 3.95%. Calcd for $C_{18}H_{21}O_4NS$: C, 62.24; H, 6.10; N, 4.03%.

λ_{max}^{MeOH} nm (log ε); 246 (4.50), 277 (4.17), 345 (4.73), 432 (4.18), and 485 (3.66).

*Diethyl 2-Amino-6-(p-tolylthio)azulene-1,3-dicarboxylate (**14**).* The reaction of **1a** (200 mg) and *p*-thiocresol in anhydrous ethanol in the presence of sodium ethoxide afforded 190 mg of **14** as orange needles (from ethanol) (mp 129—130 °C).

Found: C, 67.57; H, 5.49; N, 3.32%. Calcd for $C_{23}H_{29}O_4NS$: C, 67.46; H, 5.66; N, 3.42%.

λ_{max}^{MeOH} nm (log ε); 246 (4.54), 277 (4.23), 344 (4.73), 433 (4.22), and 480 (3.70).

*Dimethyl 2-Amino-6-bromoazulene-1,3-dicarboxylate (**1b**).* The refluxing of a solution of Compound **1a** (300 mg) in anhydrous methanol containing 200 mg of sodium afforded orange crystals, which were subsequently purified by chromatography and recrystallization from chloroform to give **1b** (220 mg) as orange needles (mp 203—204 °C).

Found: C, 50.05; H, 3.40; N, 4.12%. Calcd for $C_{14}H_{12}O_4NBr$: C, 49.72; H, 3.57; N, 4.14%.

λ_{max}^{MeOH} nm (log ε); 244 (4.57), 276 (4.18), 320 (4.69), 333 (3.90), 404^{sh} (3.96), 416 (3.97), and 473 (3.58).

*2-Amino-6-bromo-1,3-dicyanoazulene (**15**).* A mixture of 2-amino-1,3-dicyanoazulene (1.76 g), bromine (3.5 g), and sodium acetate (1.23 g) in acetic acid (50 ml) was heated at 60 °C for 7 hr. The crystals (2.3 g) which separated out were filtered and recrystallized from dioxane to give 2-amino-6-bromo-1,3-dicyanoazulene (**15**) (2.3 g) as yellowish-brown needles (mp over 300 °C).

Found: C, 52.84; H, 2.45; N, 15.14%. Calcd for $C_{12}H_6N_3Br$: C, 52.99; H, 2.24; N, 15.45%.

λ_{max}^{MeOH} nm (log ε); 231 (4.59), 252^{sh} (4.08), 270 (3.83), 315 (4.79), 328 (4.86), 416^{sh} (4.00), and 418 (4.01).

*The Bromination of Diethyl 2-Diazo-2,6-azulenoquinone-1,3-dicarboxylate (**2a**).* To a stirred solution of Compound **2a** (200 mg) in chloroform (5 ml), a solution of bromine (105 mg) in chloroform (1 ml) was added at room temperature over a 30-min period. After having been stirred a further hour, the solution was washed with water, dried, and chromatographed on a silica gel column. The first effluent, obtained by the use of $CHCl_3$–CCl_4 (2 : 1), gave 100 mg of a dark yellow viscous oil, and the second effluent, obtained by the use of $CHCl_3$, gave 80 mg of diethyl 5-bromo-2-diazo-2,6-azulenoquinone-1,3-dicarboxylate (**21**); these substances were identified by a comparison of their infrared spectra. From the last effluent, the starting azulene (**2a**) (30 mg) was recovered. The dark yellow viscous oil obtained from the first effluent could not be crystallized; it was found to be the bromine addition compound **22** from the spectroscopic data.

Found: N, 5.64%. Calcd for $C_{16}H_{14}O_5N_2Br_2$: N, 5.91%.

λ_{max}^{MeOH} nm (log ε); 217 (4.33), 295 (4.16), 335 (4.20), and 385 (4.17). A solution of Compound **22** (70 mg) in chloroform (3 ml) was treated with 5 drops of triethylamine; the solution was thus immediately changed to dark yellow, and from it 40 mg of Compound **21** were obtained.

*Diethyl 6-Acetoxyazulene-1,3-dicarboxylate (**7**).* The acetate **7** was obtained as reddish-purple needles by the reaction of Compound **4a** with acetic anhydride in the presence of pyridine (mp 133—134 °C).

Found: C, 65.22; H, 5.60%. Calcd for $C_{18}H_{18}O_6$: C, 65.44; H, 5.49%.

λ_{max}^{MeOH} nm (log ε); 233 (4.45), 271 (4.36), 296^{sh} (4.54), 307 (4.65), 331 (4.05), 362 (3.90), 373 (3.97), and 497 (3.80).

*Diethyl 6-Chloroazulene-1,3-dicarboxylate (**8**).* A solution of Compound **4a** (480 mg) and thionyl chloride (3 ml) in anhydrous benzene (50 ml) was allowed to stand overnight and was then gently refluxed for 30 min. After the solvent

had been removed, a solution of the residue in benzene was chromatographed on an alumina column to give Compound **8** (290 mg) as reddish-purple needles (mp 200—201 °C).

Found: C, 62.76; H, 5.05%. Calcd for $C_{16}H_{15}O_4Cl$: C, 62.65; H, 4.93%.

λ_{max}^{MeOH} nm (log ε); 236 (4.54), 270 (4.29), 300 (4.69), 311 (4.81), 337^{sh} (3.88), 345 (3.93), 375 (4.00) and 510 (3.08).

This work was financially supported by grants from the Ministry of Education of Japan and the Sankyo Co., Ltd., to both of which the authors' thanks are due.

References

1) A part of this work was presented at the 15th Annual Meeting of the Chemical Society of Japan, Kyoto, April, 1962.

2) a) T. Nozoe, S. Matsumura, Y. Murase, and S. Seto, *Chem. Ind.* (London), **1955**, 1257; This Bulletin, **35**, 1179 (1962). b) T. Nozoe, S. Seto, S. Matsumura, and T. Asano, *Proc. Japan Acad.*, **32**, 339 (1956). c) T. Nozoe, S. Seto, and S. Matsumura, *Chem. Ind.* (London), **1961**, 1715. d) T. Nozoe, S. Seto, and S. Matsumura, This Bulletin, **35**, 1990 (1962). e) T. Nozoe, S. Seto, K. Takase, S. Matsumura, and T. Nakazawa, *Nippon Kagaku Zasshi*, **86**, 346 (1965).

3) T. Nozoe, K. Takase, and M. Tada, This Bulletin, **38**, 247 (1965).

4) S. Matsumura, *Chem. Pharm. Bull.* (Tokyo),, **10**, 1024 (1962).

5) K. Takase, T. Asao, Y. Takagi, and T. Nozoe, *Chem. Commun.*, **1968**, 368.

6) K. Hafner and H. Weldes, *Ann. Chem.*, **606**, 90 (1957).

7) T. Nozoe, P. W. Yang, H. Ogawa, and T. Toda, This Bulletin, **41**, 2095 (1968).

8) R. J. W. Le Fevre, J. B. Sousa, and R. L. Werner, *J. Chem. Soc.*, **1954**, 4686.

9) W. von E. Doering and C. H. Dupuy, *J. Amer. Chem. Soc.*, **75**, 5955 (1953).

10) All the melting points are uncorrected.

The Relative *cis/trans* Reactivity in the Hydrochlorination of 1-Arylpropenes

Kunisuke IZAWA, Tadashi OKUYAMA, and Takayuki FUENO

Department of Chemistry, Faculty of Engineering Science, Osaka University, Toyonaka, Osaka 560

(Received November 5, 1973)

Hydrochlorination of *cis*- and *trans*-1-phenylpropenes and their ring-substituted derivatives (*p*-CH_3O, *p*-CH_3, and *p*-Cl) has been studied in acetic acid at 16—35°C. 1-Phenylpropene gave predominantly a *cis*-adduct while the *p*-CH_3O derivative yielded a non-stereospecific product. For the *p*-CH_3O and *p*-CH_3 derivatives, the *cis* isomer was found to be more reactive than the corresponding *trans* isomer, while for the *p*-Cl derivative the opposite relative reactivity was observed. The origins of these *cis/trans* reactivities have been discussed in terms of the electronic and steric effects on stability of the solvated transition state.

The question of the relative reactivity of the geometrical isomers of an olefin in addition reactions is one of the problems remaining to be solved. We have studied the acid-catalyzed hydrolyses of various alkenyl alkyl ethers and found that all the *cis* isomers are more reactive than the corresponding *trans* isomers.[1] Since most of the *cis* ethers are thermochemically less stable than the *trans* isomers, the reactivity difference was at first ascribed to the difference in the ground-state stability.[2] A similar reasoning of the relative reactivities in some electrophilic additions was presented previously.[3] However, we have later found that *cis*-β-chlorovinyl ethyl ether[4] and *cis*-1,2-dialkoxyethylenes,[5] which are more stable than the *trans* isomers, are more reactive than the *trans* isomers. An alternative explanation for this reactivity has tentatively been presented but is not general.[4,5] Furthermore, we have found that *trans*-styryl ethyl ether is less reactive than the *cis* isomer at ordinary temperatures but the activation enthalpy for the former is smaller than that for the latter, despite the greater stability of the former at the ground state.[6] The reactivity difference in this case is controlled by the entropy term at higher temperatures and the origin of this observation is still ambiguous.

Addition reactions of various electrophiles have already been studied with *cis*- and *trans*-1-phenylpropenes (**1c** and **1t**).[7–11] The reactivity difference between **1c** and **1t** was found to be very small and vary depending on the electrophile. Thus, the *trans* isomer is slightly more reactive in bromination[7] and sulfenylation[8] but less reactive in methoxymercuration[9] and hydrobromination.[10] Results on cationic polymerization are not definite.[11]

In the present investigation, the relative reactivities of *cis* and *trans* isomeric pairs of **1c** and **1t** and their ring-substituted derivatives have been measured for their hydrochlorination in acetic acid in the temperature range of 16—35 °C. Possible origins of these reactivities are discussed.

Results

The hydrochlorination of both **1c** and **1t** in glacial acid acetic gave predominantly 1-phenylpropyl chloride (**2**) with a contamination by 1-phenylpropyl acetate (**3**).

In order to confirm the stereochemistry of the present reaction, the deuteriochlorination was carried out in acetic acid-*O*-*d*. The *cis* isomer **1c** gave predominantly an *erythro* adduct **2c** while **1t** yielded a *threo* adduct **2t**, in agreement with the results obtained in hydrobromination.[10] The most favorable conformations of **2c** and **2t** are shown below.

$$\underset{\mathbf{1}}{C_6H_5CH{=}CHCH_3} + HCl \xrightarrow[CH_3COOH]{} \underset{\mathbf{2}}{C_6H_5\overset{\displaystyle Cl}{\overset{|}{C}}H\text{-}CH_2CH_3} + \underset{\mathbf{3}}{C_6H_5\overset{\displaystyle OCOCH_3}{\overset{|}{C}}H\text{-}CH_2CH_3} \quad (1)$$

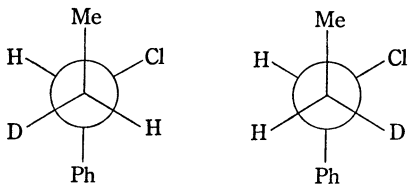

2c **2t**

The stereochemistry of the adducts was determined by NMR spectra. The vicinal H-H coupling constants were 7.5 and 4.5 Hz for **2c** and **2t**, respectively. It is known that the spin-spin coupling constant between vicinal hydrogens is greatly dependent on the dihedral angle of their bonds.[12] The coupling constant between trans protons is greater than that between gauche protons. Consequently, **2c** should have a greater coupling constant than **2t**. A similar pair of compounds, *erythro*- and *threo*-1-phenyl-2-methylaminopropyl alcohols, have $J=8.2\pm0.2$ and 4.0 ± 0.2 Hz, respectively.[13]

By contrast, the products from both the *p*-methoxy derivatives of **1c** and **1t** gave the same NMR spectrum, suggesting the formation of nonstereospecific adducts. This observation is consistent with the observation that the geometrical isomerization of *p*-CH_3O-**1c** to *p*-CH_3O-**1t** is taking place during the reaction. Other derivatives suffered little geometrical isomerization under the reaction conditions adopted here.

During the reaction of **1c**, no trace of the *trans* isomer **1t** was found by vpc. With the *p*-CH_3 derivative, the relative concentration of the *trans* isomer (*ca.* 5%) concomitant with the *cis* isomer did not increase during the reaction. But geometrical isomerization of *p*-CH_3-**1c** to *p*-CH_3-**1t** seems to take place to some extent. However, it did not affect rate-determination under low conversion.

The kinetic measurements were carried out gas-chromatographically with a pure isomer or with a

Table 1. Pseudo-first order rate constants in the hydrochlorination of substituted 1-phenylpropenes in acetic acid[a)]

Substituent	Temp., °C	$10^4 k_1$, s^{-1}	
		cis	*trans*
p-CH_3O	25	329	244
	16	188	124
p-CH_3	25	0.416	0.331

a) [Olefin]=0.45 M; [HCl]=0.65 M.

Table 2. Relative *cis/trans* reactivity of substituted 1-phenylpropenes

Substituent	Rel. reactivity[a)]			$\delta\Delta H^{\neq}$,[c)] kcal/mol	$\delta\Delta S^{\neq}$,[c)] e.u.
	16°C	25°C	35°C		
p-CH_3O	1.52[b)]	1.35[b)]		-2.2_7	-7.0_2
p-CH_3		1.25[b)]			
		1.31	1.46	$+1.9_7$	$+7.1_5$
H		0.97	1.97	$+2.3_1$	$+1.6_9$
p-Cl		0.30	0.35	$+2.8_2$	$+7.0_5$

a) By the competitive method. b) Calcd from the k_1 values listed in Table 1. c) $2.303\,R \log (k_{cis}/k_{trans}) = -\delta\Delta H^{\neq}(1/T)+\delta\Delta S^{\neq}$, $\delta\Delta H^{\neq}=\Delta H^{\neq}(cis)-\Delta H^{\neq}(trans)$ $\delta\Delta S^{\neq}=\Delta S^{\neq}(cis)-\Delta S^{\neq}(trans)$

mixture of isomeric olefins. Because of the complexity of kinetic order in [HCl],[14] the pseudo-first order rate constants were determined under low conversion (5—10 %) for isomerically pure *p*-CH_3O and *p*-CH_3 derivatives. The results are given in Table 1. Although the isomerization accompanied the reaction of *p*-CH_3O-**1c**, the rate of decay of the substrate is considered to be that of protonation and recorded as such in Table 1.

The relative rates of geometrical isomers were measured mostly by the competitive method with an isomeric mixture. The results are given in Table 2. The *cis* isomers are more reactive in the case of 1-phenylpropenes bearing an electron-donating group (*p*-CH_3O and *p*-CH_3) while the *trans* isomer of the *p*-Cl derivative is more reactive than its *cis* isomer. Unsubstituted **1c** and **1t** are similar in reactivity; relative reactivity is reversed between 25 and 35 °C.

The relative *cis/trans* reactivity tends to increase with the rise in temperature except for the *p*-CH_3O derivative. The differences in activation enthalpy $\delta\Delta H^{\neq}$ and activation entropy $\delta\Delta S^{\neq}$ between the *cis* and *trans* isomers were calculated and are listed in Table 2. The activation enthalpies of *cis* isomers are greater than those for the corresponding *trans* isomers except for the *p*-CH_3O derivative. The apparently greater reactivity of the *cis* isomer of the *p*-CH_3 derivative in the present temperature range is entropy-controlled. Negative $\delta\Delta H^{\neq}$ obtained for the *p*-CH_3O derivative implies that the *cis* isomer is energetically more reactive.

Discussion

Stereochemistry. Deuteriochlorination of **1c** and **1t** in DCl-DOAc gave mainly *erythro*- and *threo*-adducts, respectively. That is, hydrochlorination of **1c** and **1t** takes place preferentially through *syn*-addition. Similar results were obtained in the hydrobromination of **1c** and **1t** and interpreted in terms of the mechanism involving carbonium halide ion-pair intermediates.[10]

The *p*-CH_3O derivative reacts non-stereospecifically, being accompanied by geometrical isomerization. The intermediate carbonium ion, which should be stabilized by *p*-CH_3O group, would be reluctant to collapse by the attack of the chloride ion and hence could rotate freely before completion of the reaction. Thus, the isomerization accompanies the reaction of the *cis* isomer.

Relative cis/trans *Reactivities.* Relative reactivities of geometrically isomeric pairs vary depending on the ring substituent and reaction temperature. As has been described above,[7,8,11] *trans* isomers are often more reactive in styryl compounds. Similar observations were previously made for another class of styryl derivatives, styryl ethyl ether.[6] On the other hand, it was found that the *cis* isomers of α,β-unsaturated ethers are usually more reactive than the corresponding *trans* isomers toward some electrophiles, irrespective of ground-state stability.[1,2,4,5,15] Clearly, relative reactivities cannot be interpreted by the ground-state stability differences alone.

Yamaguchi *et al.*[16] have theoretically made general considerations on the origin of the *cis/trans* reactivities of olefins. It was concluded that the *cis* isomer should generally be more reactive in ionic reactions irrespective of the ground-state stability and that the Coulombic interaction in the transition state plays a predominant role in determining the greater reactivity of *cis* isomer relative to the *trans* counterpart. The observations on styryl compounds are however outside this scope, and another factor has to be taken into account to interpret the reactivities.

Relative *cis/trans* reactivity increases with increasing electron-donating character of a ring substituent as is seen in Table 2. This implies that the *cis* isomer is more sensitive to the electronic effects of ring substituents. It was suggested earlier that the diminished reactivity of **1c** is due to steric hindrance against electrophilic attack because of nonplanar conformation of **1c**.[11] This view implicitly presumes that the transition state for **1c** is less bonding (between an electrophile and the reaction site of olefin) than that for **1t**. However, this interpretation seems to contradict the present result that **1c** is more sensitive to the substituent effects than **1t**.

Alternatively, a steric effect against solvation of intermediate ion-pair in the *cis* isomers seems to account for all the results available. Effective solvation of intermediate carbonium-chloride ion-pair derived from the *trans* isomer stabilizes the transition state and hence enhances the reactivity of **1t** on one hand. Charge dispersion by solvation, on the other hand, would result in lower sensitivity of **1t** to substituent effects.[17] For very reactive derivatives like *p*-CH_3O-**1**, the electronic effects will overcome the steric effects, thus allowing the *cis* isomer to be more reactive.

In conclusion, the *cis* isomers of any olefins including styryl compounds should be intrinsically (or electro-

nically) more reactive in protonation than are the *trans* counterparts. The Coulombic interaction at the transition state contributes mainly to this reactivity. In the protonation and probably in other types of reactions also, the steric inhibition against intermediate solvation should more or less reduce the reactivity of *cis* isomers. The relative *cis/trans* reactivities experimentally observed are probably a reflection of the relative importance of these two opposing contributions.

Experimental

Materials. Preparation of *cis*- and *trans*-1-phenylpropenes (**1c** and **1t**) and their derivatives will be described elsewhere.[8]

1-Phenylpropyl chloride was prepared as an authentic sample by treatment of 1-phenylpropyl alcohol with thionyl chloride. NMR (CCl_4); δ 1.02 (3H, t, J=7.5 Hz, CH_3), 2.10 (2H, q, J=7.5 Hz, CH_2), 4.70 (1H, t, J=7.5 Hz, CH–Cl), 7.3 (5H, s, C_6H_5).

Hydrochlorination. Procedure of the reaction and the method of kinetic measurements were described previously.[18] The reaction procedure for deuteriochlorination was also described before.[19]

NMR spectra of the products were recorded on a JNM-4H-100 spectrometer. NMR (CCl_4): **2t**. δ 0.96 (3H, d, J=7 Hz, CH_3), ~2.0 (1H, m, CH–Me), 4.63 (1H, d, J=4.5 Hz, CH–Cl), ~7.25 (5H, m, C_6H_5). **2c**: δ 0.98 (3H, d, J=7 Hz, CH_3), ~2.0 (1H, m, CH–Me), 4.66 (1H, d, J=7.5 Hz, CH–Cl), ~7.22 (5H, m, C_6H_5). Product from *p*-CH_3O-**1t**; δ 0.96 (3H, d, J=7 Hz, CH_3), ~2 (1H, m, CH–Me), 3.73 (3H, s, CH_3O), 4.63 (1H, d, J=6.0 Hz, CH–Cl), 6.7—7.25 (4H, m, C_6H_4). Product from *p*-CH_3O-**1c**; δ 0.96 (3H, d, J=7 Hz, CH_3), ~2 (1H, m, CH–Me), 3.70 (3H, s, CH_3O), 4.65 (1H, d, J=6.0 Hz, CH–Cl), 6.72—7.27 (4H, m, C_6H_4).

References

1) T. Okuyama, T. Fueno, H. Nakatsuji, and J. Furukawa, *J. Amer. Chem. Soc.*, **87**, 5826 (1967).
2) T. Okuyama, T. Fueno, and J. Furukawa, *Tetrahedron*, **25**, 5409 (1969).
3) J. E. Dubois and G. Mouvier, *Tetrahedron Lett.*, **1965**, 1622.
4) T. Okuyama, T. Fueno, and J. Furukawa, *J. Polym. Sci. A-1*, **7**, 2433 (1969).
5) T. Okuyama and T. Fueno, *ibid.*, **9**, 629 (1971).
6) T. Okuyama, T. Fueno, and J. Furukawa, This Bulletin, **43**, 3256 (1970).
7) (a) R. C. Fahey and H. -J. Schneider, *J. Amer. Chem. Soc.*, **90**, 4429 (1968); (b) J. H. Rolston and K. Yates, *ibid.*, **71**, 1483 (1969).
8) K. Izawa, T. Okuyama, and T. Fueno, This Bulletin, the succeeding paper.
9) W. R. R. Park and G. F. Wright, *J. Org. Chem.*, **19**, 1435 (1954).
10) M. J. S. Dewar and R. C. Fahey, *J. Amer. Chem. Soc.*, **85**, 3645 (1963).
11) (a) C. G. Overberger, D. Tanner, and E. M. Pearce, *ibid.*, **80**, 4566 (1958); (b) A. Mizote, T. Higashimura, and S. Okamura, *J. Polym. Sci. A-1*, **6**, 1825 (1968).
12) M. Karplus, *J. Chem. Phys.*, **30**, 11 (1959).
13) J. B. Hyne, *Can. J. Chem.*, **37**, 2536 (1961).
14) R. C. Fahey and C. A. McPherson, *J. Amer. Chem. Soc.*, **91**, 3865 (1969).
15) T. Okuyama and T. Fueno, to be published.
16) K. Yamaguchi, T. Okuyama, and T. Fueno, to be published.
17) J. L. Fry, J. M. Harris, R. C. Bingham, and P. v. R. Schleyer, *J. Amer. Chem. Soc.*, **92**, 2540 (1970).
18) T. Okuyama, and K. Izawa, and T. Fueno, *ibid.*, **95**, 6749 (1973).
19) K. Izawa, T. Okuyama, T. Sakagami, and T. Fueno, *ibid.*, **95**, 6752 (1973).

The Addition of 2,4-Dinitrobenzenesulfenyl Chloride to *cis*- and *trans*-1-Arylpropenes and Some Other Olefins

Kunisuke IZAWA, Tadashi OKUYAMA, and Takayuki FUENO

Department of Chemistry, Faculty of Engineering Science, Osaka University, Toyonaka, Osaka 560

(Received November 5, 1973)

Kinetic investigations were carried out on the addition of 2,4-dinitrobenzenesulfenyl chloride to the geometrically isomeric pairs of various 1-arylpropenes as well as some related olefins. All the *trans* isomers of 1-arylpropenes were more reactive than the corresponding *cis* isomers and the Hammett correlations were observed for respective isomers with $\rho = -2.64$ (*trans*) and -2.3 (*cis*). By contrast, *cis*-alkenes were more than 10 times as reactive as the corresponding *trans* isomers. The reactivities of various unsaturated compounds in this reaction were found to be correlated with their ionization potentials constituting two lines accodring to the type of substrates. It was concluded that the greater reactivity of *trans*-1-arylpropene as compared with the *cis* isomer is ascribable to the difference in the charge-transfer interaction between the electrophile and a substrate at the transition state. The conclusion is contrasting to the generalization that the relative *cis*/*trans* reactivity of alkenes is determined mainly by the Coulombic interaction at the transition state.

The addition of sulfenyl halide to olefins is known to proceed through an episulfonium ion intermediate.[1] The influence of electronic effects on the rate of this reaction has been extensively studied with various olefins; ring-substituted styrenes,[2] cyclic olefins,[3-5] and alkenes.[6,7] However, little attention has ever been paid to the relative reactivities of geometrical isomers. Available data seem to suggest complexity of the reactivity.

cis-Alkene was found to react faster than the *trans* isomer[7] and the latter deviates from the Hammett-Taft correlation.[6] *cis*-Stilbene, on the other hand, is less reactive than *trans*-stilbene; this observation was explained in terms of the steric effects against electrophilic attack to the former.[8]

In the present study, we have investigated the reaction of 2,4-dinitrobenzenesulfenyl chloride (**1**) with *cis*- and *trans*-1-phenylpropenes (**2c** and **2t**) and their ring-substituted derivatives, *cis*- and *trans*-2-heptenes (**3c** and **3t**) and *cis*- and *trans*-4-methyl-2-pentenes (**4c** and **4t**) in order to clarify the relationship between relative *cis*/*trans* reactivities and olefin structure. The reaction rates of some other related olefins have been measured for the sake of comparison. Possible factors that influence these reactivities have been discussed.

Results

Reaction Products. The reaction of **1** with **2t** in glacial acetic acid led to a high yield of 1 : 1 adduct which was shown to be *erythro*-1-phenyl-1-chloro-2-(2,4-dinitrophenylthio)propane by NMR specroscopy. That is, the addition is specifically of Markownikoff-type and *anti* fashion. On the other hand, the reaction with **2c** under the same conditions yielded *ca.* 30% of the anti-Markownikoff isomer together with 70% the normal adduct. Both adducts were *threo*-type; the addition is, therefore, specifically *anti*. Stereochemistry of the adducts was determined by comparing the NMR spectra (see Experimental) with the compilation of spectra of related compounds.[9,10]

Kinetic Measurements. The rates of addition of **1** to **2c** and **2t** and their ring-substituted derivatives were determined in dry acetic acid solution. The reactions were followed by measuring the rates of disappearance of the sulfenyl chloride by the titration method. The rate is first order in each reactant as was found for other olefins.[2-6] Initial reactant concentrations were varied in the different rate runs but there was found no indication of deviations from the simple second-order kinetics.

The second-order rate constants k_2 for phenylpropene derivatives are summarized in Table 1. All the *trans* isomers of phenylpropenes are several times more reactive than the corresponding *cis* isomers. From the temperature dependence of k_2, activation parameters, $\Delta H^{\ddagger}$ and $\Delta S^{\ddagger}$, were calculated in a usual way. Although they may not be precise enough because of a limited range of temperature variation, they are included in Table 1 for the sake of comparison between *cis*-*trans* isomeric pairs.

The Hammett $\rho\sigma$ correlation for the reaction of the derivatives of **2c** and **2t** at 25 °C are shown in Fig. 1. The reaction constants ρ were evaluated excluding *p*-methoxy derivatives, which show apparent

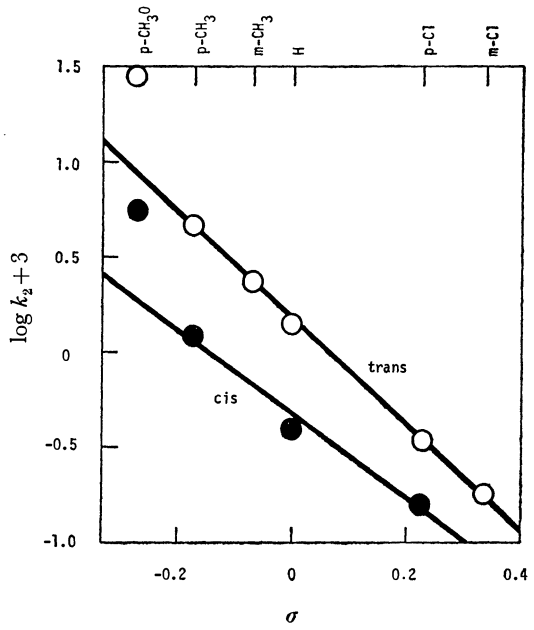

Fig. 1. The Hammett plots for the reaction of **1** with **2t** (○) and **2c** (●) in acetic acid at 25 °C.

Table 1. Second-order rate constants and activation parameters for the reaction of **1** with ring-substituted 1-phenylpropenes in acetic acid

Substituent	$10^3 k_2$, $M^{-1}s^{-1}$ 15 °C	25 °C	35 °C	45 °C	$\Delta H^{\neq}$, kcal/mol	$\Delta S^{\neq}$, e. u.
		trans-1-Phenylpropene				
p-CH_3O	16.8	28.8			8.7	−36.9
p-CH_3		4.60	8.20		10.0	−37.2
m-CH_3		2.34				
H(**2t**)		1.44	2.72	5.29	11.7	−32.8
p-Cl		0.335	0.607		10.3	−40.3
m-Cl		0.180				
		cis-1-Phenylpropene				
p-CH_3O	2.48	5.63			13.5	−23.0
p-CH_3		1.25	2.83		15.7	−19.7
H(**2c**)		0.393	1.04	2.79	17.9	−14.4
p-Cl		0.156	0.368		15.2	−25.6

Table 2. Second-order rate constants and activation parameters for the addition of **1** to some olefins

No.	Olefin	$10^3 k_2$, $M^{-1}s^{-1}$ 18 °C	25 °C	35 °C	45 °C	$\Delta H^{\neq}$ kcal/mol	$\Delta S^{\neq}$, e.u.
5	Styrene[a]		0.741				
6	Indene		0.512	1.11		13.6	−28.5
7	1-Hexene		1.32	2.49	4.67	11.4	−34.1
3t	*trans*-2-Heptene		1.59	3.03		11.2	−34.1
3c	*cis*-2-Heptene	14.7	18.8			5.5	−47.8
4t	*trans*-4-Methyl-2-pentene		0.457	1.09		15.4	−22.7
4c	*cis*-4-Methyl-2-pentene	20.0	26.9	41.4		7.1	−42.3

a) Orr and Kharasch[2] reported $0.737\times10^{-3}\,M^{-1}s^{-1}$ for k_2 value at 25 °C.

deviation from the linearities: $\rho=-2.64$ for the *trans* isomers and $\rho\sim-2.3$ for the *cis* isomers.

Listed in Table 2 are the kinetic data for styrene (**5**), indene (**6**) and some alkenes. The *cis* isomer of an alkene is significantly reactive than its *trans* isomer.

Discussion

Specific *anti*-additions of **1** to both **2c** and **2t** are explained as usual by the mechanism involving an episulfonium ion intermediate.[1] The anti-Markownikoff-type adduct was found only for the *cis* isomer (30 %). This trend was observed earlier in the addition of *p*-chlorobenzenesulfenyl chloride.[10] In this reaction, **2c** gave 66% of anti-Markownikoff product. The reduced yield of anti-Markownikoff product in the present reaction is consistent with the general observation[11] that the *ortho*-nitro substitution of sulfenyl chloride tends to increase Markownikoff adduct.

The *trans* isomers of aryl-substituted olefins were found to be more reactive than the *cis* counterparts, while *trans*-alkenes were found to be less reactive than the *cis* isomers. These results are seemingly similar to those obtained for the protonation in which *cis* isomers are more reactive in the case of aliphatic olefins but are less reactive in the case of most of 1-phenylpropene derivatives.[12]

However, the effect of ring substituents on the protonation rate of **2** is contrasting to the present results. In the hydrochlorination of **2**, the relative *cis*/*trans* reactivity increases with increasing electron-donating character of the ring substituent. That is, the ring substitution exerts more influence on the reactivity of the *cis* isomer ($|\rho_{cis}|>|\rho_{trans}|$).[12] From these observations, the reduced reactivity of the *cis* isomers was interpreted by the steric inhibition of intermediate solvation.[12] On the other hand, the substituent effects observed in the present reaction are just opposite to those observed in the hydrochlorination. The relative *cis*/*trans* reactivity tends to diminish with the increasing electron-donating character of ring substituents. Correspondingly, the magnitude of the reaction constant ρ is greater for the *trans* isomers than for the *cis* isomers (Fig. 1). Furthermore, all the values of $\Delta H^{\neq}$ are greater for the *cis* isomers. These results seem to suggest, in contrast to the hydrochlorination, that the *trans* isomers are electronically more reactive in sulfenylation of 1-phenylpropenes. If the steric factor were important to the reaction,[13] its effect would be analogous to that in the hydrochlorination.[12]

Electronic interactions controlling the reactivity may divided into two factors, Coulombic and charge-transfer interactions.[14,15] It was concluded that the former predominates in the greater reactivity of *cis* isomers in protonation.[13,14] The latter factor of charge transfer interaction seems to contribute to the greater

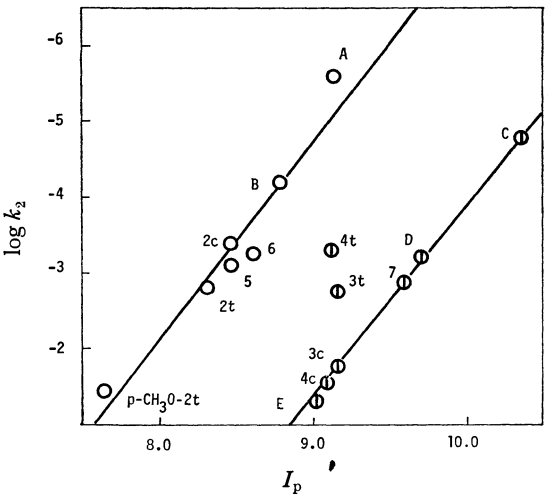

Fig. 2. Correlation of the reaction rates (k_2 for the addition of **1** in acetic acid at 25 °C) with ionization potentials. Ionization potential data are taken from Y. Morino, *et al.*, "Kagaku Binran (Handbook of Chemistry)" Ed. by Chem. Soc. Japan, Maruzen, Tokyo, 1966 and K. Yamaguchi, Doctor thesis, Osaka Univ., 1972. For Nos., see Tables 1 and 2. (A) Phenylacetylene (Ref. 8); (B) 1-phenylpropyne; (C) 1-hexyne; (D) 2-heptyne (T. Okuyama, K. Izawa, and T. Fueno, *J. Org. Chem.*, **39**, 351 (1974)); (E) cyclohexene (Ref. 4).

reactivity of the *trans* isomers in the present reaction. Importance of the charge transfer interaction is in accord with the tendency of episulfonium intermediate formation.

The charge-transfer controlled reactivity might be ascribed to the softness of electrophilic sulfur. The correlation between the reactivity of an olefin or an acetylene and its ionization potential (I_p) is substantiated in Fig. 2 as expected for the charge-transfer controlled reaction. Two classes of compounds, aromatic and aliphatic, constitute different lines. This fact might arise from the different contributions from other factors to the respective class of unsaturated compounds.

The greater reactivity of **2t** seems to reflect the lower ionization potential of **2t** as compared with **2c**. The large magnitude of the ρ value for the *trans* isomers compared with that for the *cis* isomers is consistent with the greater contribution of charge-transfer interaction to the reactivities of the former.

As for the alkene series, the difference in ionization potential is negligibly small between *cis* and *trans* isomers. Thus, the reactivity difference does not seem to reflect charge-transfer contribution. The reduced reactivity of the *trans* isomers as compared with the *cis* counterparts will be accounted for in terms of different Coulombic interaction as in the case of protonation.

The observed Hammett-Taft correlation for sulfenyl chloride addition to alkenes[6] may have some bearing on this log k_2—I_p correlation. The rate enhancement by *cis*-β-methyl substitution corresponds to the decrease in I_p (**7** and **3c**). The points for the *trans*-alkenes (**3t** and **4t**) are deviated from the line in Fig. 2. This type of deviations of *trans*-alkenes were pointed out also in the Hammett-Taft correlations not only for sulfenylation[6] but bromination.[16]

In conclusion, the contribution of charge-transfer interaction is considerably great in the reaction of "soft" reagent like sulfur with a substrate of low I_p even if the reaction is ionic. Relative *cis*/*trans* reactivities of aromatic olefins are ascribed to this factor.

Experimental

All boiling points and melting points are uncorrected. The nuclear magnetic resonance spectra were obtained on a JNM-4H-100 spectrometer operating at a frequency of 100 MHz. All vpc analyses were performed with a Shimadzu gas chromatograph Model 4APT.

Materials. Glacial acetic acid was dried according to the literature.[17] 2,4-Dinitrobenzenesulfenyl chloride (**1**) was prepared by the method of Kharasch and Langford[18] and recrystallized from carbon tetrachloride; mp 95.0—95.5 °C (lit,[18] 95.0—95.5 °C).

trans-1-Phenylpropene (**2t**) and its ring-substituted derivatives were prepared by prototropic rearrangement[19] of corresponding allylbenzenes, which were obtained by the Grignard coupling between allylbromide and bromobenzenes.[20] *cis*-1-Phenylpropene (**2c**) and its ring-substituted derivatives were prepared by decarboxylation of corresponding α-methylcinnamic acids, which were obtained by the Perkin reaction of appropriate benzaldehydes.[21] All the 1-phenylpropenes obtained were geometrically pure over 95% and were further purified by preparative vpc whenever necessary. The isomer thus purified were pure in >99%. IR spectra of **2t** and **2c** agreed well with those reported in the literature. Their boiling points and spectral data were as follows: **2t**, bp 48 °C(8 mmHg) (lit,[22] 105 °C (80 mmHg)); NMR (CCl_4) δ 1.84 (3H, d, J=6 Hz, CH_3), 5.96—6.40 (2H, m, -CH=CH-) 7.07—7.73 (5H, C_6H_5). *p*-CH_3O-**2t**, bp 108 °C (12 mmHg); NMR (CCl_4) δ 1.83 (3H, d, J=6 Hz, CH_3), 3.67 (3H, s, OCH_3), 5.8—6.33 (2H, m, -CH=CH-), 6.61—7.15 (4H, C_6H_4). *p*-CH_3-**2t**, bp 58 °C (4 mmHg); NMR (CCl_4) δ 1.83 (3H, d, J=6 Hz, CH_3), 2.27 (3H, s, CH_3), 5.85—6.37 (2H, m, -CH=CH-), 6.9—7.13 (4H, C_6H_4). *m*-CH_3-**2t**, bp 67 °C (8 mmHg); NMR (CCl_4) δ 1.85 (3H, d, J=6 Hz, CH_3) 2.30 (3H, s, CH_3), 5.95—6.38 (2H, m, -CH=CH-), 6.85—7.07 (4H, C_6H_4). *p*-Cl-**2t**, bp 79 °C (7 mmHg); NMR (CCl_4) δ 1.84 (3H, d, J=6 Hz, CH_3), 5.95—6.36 (2H, m, -CH=CH-), ~7.15 (4H, C_6H_4). *m*-Cl-**2t**, bp 80.5 °C (7 mmHg); NMR (CCl_4) δ 1.86 (3H, d, J=7 Hz, CH_3), 5.96—6.40 (2H, m, -CH=CH-), 7.05-7.15 (4H, C_6H_4). **2c**, bp 45°C (10 mmHg) (lit,[22] 95—96 °C (80 mmHg); NMR (CCl_4) δ 1.85 (3H, dd, J=7 and 1.5 Hz, CH_3), 5.5—5.85 (1H, m, =CH-Me), 6.85 (1H, dd, J=11 and 1.5 Hz, Ph-CH=), 7.1—7.2 (5H, C_6H_5). *p*-CH_3O-**2c**, bp 88 °C (10 mmHg); NMR (CCl_4) δ 1.85 (3H, dd, J=7 and 1.5 Hz, CH_3), 3.72 (3H, s, OCH_3), 5.42—5.75 (1H, m, =CH-Me), 6.29 (1H, dd, H=11 and 1.5 Hz, Ph-CH=), 6.67—7.20 (4H, C_6H_4). *p*-CH_3-**2c**, bp 66 °C (10 mmHg); NMR (CCl_4) δ 1.84 (3H, dd, J=7 and 1.5 Hz, CH_3), 2.30 (3H, s, CH_3), 5.45—5.80 (1H, m, =CH-Me), 6.83 (1H, dd, J=11 and 1.5 Hz, Ph-Ch-), ~7.06 (4H, C_6H_4). *p*-Cl-**2c**, bp 72 °C (8 mmHg); NMR (CCl_4) δ 1.84 (3H, dd, J=7 and 1.5 Hz, CH_3), 5.5—5.85 (1H, m, =CH-Me), 6.35 (1H, dd, J=11 and 1.5 Hz, Ph-CH=), 7.1—7.2 (4H, C_6H_4).

Styrene (**5**), indene (**6**), 1-hexene (**7**), *trans*- and *cis*-2-heptenes (**3t** and **3c**), and *trans*- and *cis*-4-methyl-2-pentenes

(**4t** and **4c**) were commercially obtained (Nakarai Chemicals) and distilled under nitrogen atmosphere immediately before use.

*Reaction of **1** with **2t**.* A sample of 2.50 g of **1** was mixed with 1.75 g of **2t** in 50 ml dry acetic acid and allowed to react for two days at room temperature. Yellow precipitates were separated and recrystallized from absolute alcohol to give 3.14 g of yellow prisms, mp 91° (83.5% yield as a 1 : 1 adduct). Found: C, 51.34; H, 3.57; N, 7.94; Cl, 9.94; S, 9.14. Calcd for $C_{15}H_{13}O_4N_2ClS$: C, 51.06; H, 3.72; N, 7.95; Cl, 10.06; S, 9.09. NMR ($CDCl_3$) δ 1.63 (3H, d, J=7 Hz, CH_3), 3.95 (1H, double quartet, J=7 and 8 Hz, S-CH-Me), 5.0 (1H, d, J=8 Hz, Ph-CH-Cl), 7.17—7.36 (5H, m, C_6H_5), 7.5—8.78 (3H, m, $C_6H_3(NO_2)_2$). By comparing the spectrum with those of related compounds,[9,10] the adduct was assigned to be *erythro*-1-phenyl-1-chloro-2-(2,4-dinitrophenylthio)propane.

*Reaction of **1** with **2c**.* The reaction product was obtained in the same way as in the case of **2t**. One to one adducts were isolated in *ca.* 80% yield. NMR spectrum in $CDCl_3$ showed that the product is a mixture of isomers. Two doublet signals were observed at δ=1.47 and 1.71 in an integral ratio of 7 : 3. They were attributed to the methyl groups of the *thero*-Markownikoff (δ 1.47) and the *threo*-anti-Markownikoff (δ=1.71) adducts, respectively.

Separation of isomers was carried out by liquid chromatography with silica gel column using ethanol as eluent. The Markownikoff adduct was obtained in 65% yield as yellow needles melting at 113.5 °C. Found: C, 50.95; H, 3.54; N, 8.03; Cl, 9.90; S, 9.18%. Calcd for $C_{15}H_{11}O_4N_2ClS$: C, 50.99; H, 3.68; N, 7.93; Cl, 10.21; S, 9.08%. NMR ($CDCl_3$) δ 1.47 (3H, d, J=6 Hz, CH_3), 4.10 (1H, m, Me-CH) 5.09 (1H, d, J=5 Hz, CHCl), ~7.40 (5H, m, C_6H_5), 7.56 (1H, d, J=8 Hz, 6-H of $C_6H_3(NO_2)_2$), 8.32 (1H, dd, J=8 and 2 Hz, 5-H of $C_6H_3(NO_2)_2$), 8.97 (1H, d, J=2 Hz, 3-H of $C_6H_3(NO_2)_2$).

Kinetic Measurements were made by essentially the same method as used by Orr and Kharasch.[2] Stock solutions of **1** and unsaturated compounds were respectively prepared by dissolving weighed amounts of freshly purified materials in the desired volume of dry acetic acid at the temperature of each run.

References

1) For reviews, see (a) P. B. D. de la Mare and R. Bolton, "Electrophilic Additions to Unsaturated Systems", Elsevier, New York, N. Y. (1966), pp. 166—173; (b) N. Kharasch, "Organic Sulfur Compounds," Vol. 1, Pergamon Press, New York, N. Y., 1961, pp. 375—396; (c) N. Kharasch, Z. S. Ariyan, and A. J. Havlik, *Quart. Rep. Sulfur Chem.*, **1**, 93 (1966); (d) D. R. Hogg and J. H. Smith, *ibid.*, **3**, 63 (1968); (e) R. C. Fahey, *Top. Stereochem.*, **3**, 318 (1968); (f) W. H. Mueller, *Angew. Chem. Int. Ed. Eng.*, **8**, 482 (1969).

2) W. L. Orr and N. Kharasch, *J. Amer. Chem. Soc.*, **78**, 1201 (1956).

3) H. Kwart and L. J. Miller, *ibid.*, **83**, 4552 (1961).

4) C. Brown and D. R. Hogg, *J. Chem. Soc. B*, 1262 (1968).

5) C. Brown and D. R. Hogg, *ibid.*, **1969**, 1054.

6) G. M. Beverly and D. R. Hogg, *ibid.*, **1971**, 175.

7) W. A. Thaler, *J. Org. Chem.*, **34**, 871 (1969).

8) N. Kharasch and C. N. Yiannios, *ibid.*, **29**, 1190 (1964).

9) G. H. Schmid, *Can. J. Chem.*, **46**, 3415 (1968).

10) G. H. Schmid and V. Csizmadia, *Chem. Ind.* (London), **1968**, 1811.

11) G. M. Beverly, D. R. Hogg, and J. H. Smith, *ibid.*, 1403 (1968).

12) K. Izawa, T. Okuyama, and T. Fueno, This Bulletin, the preceding paper.

13) A slightly reduced reactivity of **2c** as compared with styrene seems to reflect the steric effects arising from a non-planar *cis* structure of **2c**, even though the effects are too small to offset the relative reactivity to **2c**.

14) K. Yamaguchi, T. Okuyama, and T. Fueno, to be published.

15) G. Klopman, *J. Amer. Chem. Soc.*, **90**, 223 (1968).

16) J. E. Dubois and G. Mouvier, *Tetrahedron Lett.*, **1965**, 1629; **1963**, 1325.

17) L. F. Fieser, "Experiments in Organic Chemistry," D. C. Heath & Co., Boston, Mass. (1955).

18) N. Kharasch and R. B. Langford, "Organic Syntheses," Vol. 44, p. 47 (1964).

19) A. Schriesheim, C. A. Rowe, Jr., and L. Naslund, *J. Amer. Chem. Soc.*, **85**, 2111 (1963).

20) E. B. Hershberg, *Helv. Chim. Acta*, **17**, 352 (1934).

21) J. R. Johnson, "Organic Reactions," Vol. 1, ed. by R. Adams *et al.*, John Wiley & Sons, Inc., New York and London (1942), p. 251.

22) M. J. S. Dewar and R. C. Fahey, *J. Amer. Chem. Soc.*, **85**, 3645 (1963).

Total Syntheses of Holomycin, Thiolutin, and Aureothricin

Katsuaki HAGIO and Naoto YONEDA

Research Laboratory of Applied Biochemistry, Tanabe Seiyaku Co., Ltd., Kashima-cho, Higashiyodogawa-ku, Osaka 532

(Received November 9, 1973)

The reactions of 4-benzylthio-5-benzylthiomethyl-3-hydroxy-2-oxo-2,5-dihydrofuran with ammonia and primary amines gave 3-amino-4-benzylthio-5-benzylthiomethyl-3-pyrrolin-2-one derivatives. 3-Acylamino-4-benzylthio-5-benzylthiomethylene-3-pyrrolin-2-one derivatives, including the intermediate of the synthesis of holomycin by Büchi, were prepared by the treatment of the 3-acylaminolactams derived from the 3-aminolactams with chloranil or DDQ. Thiolutin and aureothricin were also synthesized from 3-acetamido- and 3-propionamido-4-benzylthio-5-benzylthiomethylene-1-methyl-3-pyrrolin-2-one respectively.

Holomycin (**1**),[1] thiolutin (**2**),[2] aureothricin (**3**),[2] and isobutyropyrrothine (**4**)[3] are antibiotics produced by certain *Streptomyces* species. Their structures have been shown by degradative studies to have pyrrolinonodithiole nucleus.[1,2] Furthermore, two antibiotics (**5** and **6**) bearing a formamide group at the side chain were also isolated.[4] These substances are effective against Gram-positive and Gram-negative bacteria, fungi, and ameboid parasites. The total syntheses of **1** and **2** was first reported by Schmidt and Geiger.[5] Somewhat later, an alternate total synthesis of **1** was presented by Büchi and Lukas.[6]

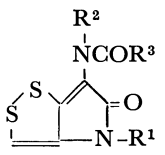

1; $R^1=R^2=H$, $R^3=CH_3$
2; $R^1=CH_3$, $R^2=H$, $R^3=CH_3$
3; $R^1=CH_3$, $R^2=H$, $R^3=CH_2CH_3$
4; $R^1=CH_3$, $R^2=H$, $R^3=CH(CH_3)_2$
5; $R^1=R^2=R^3=H$
6; $R^1=H$, $R^2=CH_3$, $R^3=H$

Scheme 1.

In the course of studies of the sulfonium ylides, we have developed a synthesis of a new lactone, 4-benzylthio-5-benzylthiomethyl-3-hydroxy-2-oxo-2,5-dihydrofuran (**7**), which is expected to be a useful intermediate for the synthesis of **1**—**3**.[7] This paper will describe how a new route for the synthesis of **1**—**3** was successfully established in three stages from **7**; this route involves the formation of five-membered lactams, dehydrogenation, and the final ring closure to the desired antibiotics.

Formation of Five-membered Lactams. The reaction of **7** with methylamine and acetic acid in refluxing ethanol gave 4-benzylthio-5-benzylthiomethyl-1-methyl-3-methylamino-3-pyrrolin-2-one (**9**) (mp 106—108 °C), which was then purified by a chromatographic separation on silica gel G. The IR spectrum showed absorptions at 3310, 1693, and 1645 cm^{-1} due to NH stretching, five-membered lactam carbonyl, and a double bond respectively. The NMR spectrum ($CDCl_3$) exhibited signals at δ 2.80 (3H, s, N-CH_3), 2.90 (2H, m, the methylene protons attached to C_5), 2.93 (3H, s, N-CH_3), 3.65 (1H, m, the methine proton at C_5), 3.64 (2H, s, S-CH_2-Ph), 3.68 (2H, s, S-CH_2-Ph), 3.9—4.6 (1H, D_2O-exchangeable, NH), 7.21 and 7.29 (two phenyl groups). By the reaction of **7** with methylamine in water or ethanol in a sealed tube at 80 °C, **9** was also obtained in a comparable yield. The prolonged reaction in the absence of acetic acid resulted in the decomposition of **7**. Similarly, 3-aminolactams (**8** and **10**—**13**) were synthesized from **7** (see Table 1).

However, the attempted isolation of 3-aminolactone (**14**), another product anticipated in this reaction, was unsuccessful.[8]

Contrary to ordinary methods for the transformation of lactones into lactams, the formation of 3-aminolactams (**8**—**13**) from **7** proceeded under relatively mild conditions. The low yield in the reaction with *p*-toluidine may be due to the low basicity or the steric

Table 1. Reactions of **7** with ammonia and primary amines

R^1NH_2	Solvent	Temp (°C)	Time (hr)	Product		
				No	yield (%)	mp (°C)
CH_3COONH_4	—	120	1	**8**	29	syrup
NH_3	EtOH	70—75	5	**8**	29	
NH_3	H_2O	80	1	**8**	22	
$CH_3COO^- \cdot CH_3NH_3^+$	EtOH	refl.	2	**9**	38	107—108
CH_3NH_2	EtOH	80	0.5	**9**	33	
CH_3NH_2	H_2O	80	0.5	**9**	31	
n-$C_3H_7NH_2$	*n*-$C_3H_7NH_2$	refl.	20	**10**	50	syrup
$C_6H_5CH_2NH_2$	Benzene	refl.	1	**11**	52	121—122
$C_6H_5CH_2NH_2$	—	90—100	1	**11**	39	
$C_6H_5CH_2CH_2NH_2$	Benzene	refl.	3	**12**	56	syrup
p-$CH_3C_6H_4NH_2$	Benzene	refl.	23	**13**	18	132—133

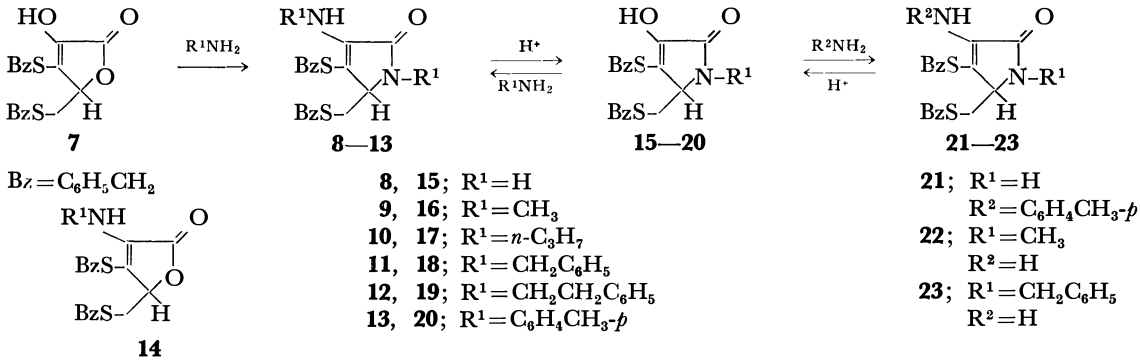

Scheme 2.

hindrance.

The treatment of **9** with hydrochloric acid in boiling ethanol afforded 4-benzylthio-5-benzylthiomethyl-3-hydroxy-3-pyrrolin-2-one (**16**) as colorless needles (mp 123—124 °C); they turned blue with ferric chloride. Under similar conditions, 3-aminolactams (**8** and **10**—**13**) were converted readily into the corresponding 3-hydroxy derivatives in good yields.

3-Hydroxy lactam (**16**) was refluxed in ethanol with ammonium acetate to give 3-amino-4-benzylthio-5-benzylthiomethyl-1-methyl-3-pyrrolin-2-one (**22**) in an 84% yield; the substance turned violet upon treatment with ninhydrin. Analogous reactions of 3-hydroxy derivatives yielded the corresponding 3-aminolactams.

Thus, the introduction of the desired substituents of 3-amino group was achieved through the hydrolysis of 3-aminolactams, followed by the condensation of the resulting 3-hydroxylactams with appropriate amines.

In contrast to the assumption that the reactivity of the 3-amino group in a conjugated system would be low, the acylation of the 3-aminolactams proceeded easily, yielding the acyl derivatives. The treatment of **22** with acetic anhydride in boiling benzene furnished 3-acetamido-4-benzylthio-5-benzylthiomethyl-1-methyl-3-pyrrolin-2-one (**25**) in an 86% yield (mp 140—142 °C). By a similar treatment of 3-aminolactams, several 3-acylamino derivatives were obtained in good yields.

Dehydrogenation. The reaction of **24** with chloranil and DDQ in refluxing benzene afforded the dehydrogenated product (**30**) as yellow needles (mp 178—179 °C) in 63 and 67% yields respectively. The melting point and the spectral properties were consistent with those of 3-acetamido-4-benzylthio-5-benzylthiomethylene-3-pyrrolin-2-one, as reported by Büchi[6] in his holomycin synthesis. On the contrary, the reaction with thionyl chloride, which had been successfully used by Büchi[6] for the dehydrogenation of the side chain of 3-acetyl-4-hydroxy-5-benzylthiomethyl-3-pyrrolin-2-one, gave **30** only in a 7% yield. The resulting product in both the reactions was a single isomer, though its geometric configuration was not clarified.

The dehydrogenation of **26** with chloranil or DDQ in boiling benzene or *t*-butyl alcohol gave a mixture of *cis* and *trans* isomers (**32a** and **32b**) as yellow microcrystals (mp 120—125 °C). Separation by preparative thin-layer chromatography on silica gel G gave **32a** (mp 154—156 °C) and **32b** (mp 128—129 °C). On the basis of the elemental analyses and spectral data (see Table 3), both of them were confirmed to be the geometric isomers with an exocyclic methylene group. Considering the deshielding effect of the phenyl groups, the lower-shifted signals of the vinylic proton and the *N*-methyl protons in the NMR spectrum of **32b** suggest that both the benzylthio groups are *trans*. From the peak areas of the vinylic and *N*-methyl protons, **32** was found to be a mixture of *cis* and *trans* isomers in the ratio of 1 : 5.

Although the interconversion of **32a** and **32b** was attempted under various conditions, no useful method for the isomerization was obtained.

Under similar conditions, **31** and **33** were obtained in good yields as mixtures of geometric isomers (see Table 2). The mixture (**31**) was treated by preparative thin-layer chromatography (silica gel G) to separate the *cis* and *trans* isomers, but attempts to sepearte

Table 2. Dehydrogenations of 3-acylamino-5-benzylthiomethyl-3-pyrrolin-2-ones

No	Reagent	Yield(%)	Mp(°C)	*cis*/*trans*[a]
30	Chloranil	62	178—179	[b]
30	DDQ	67		[b]
30	$SOCl_2$	7		[b]
31	Chloranil	82	130—135	1 : 5
31	DDQ	81		1 : 5
32	Chloranil	92	120—125	2 : 5
32	DDQ	79		2 : 5
33	Chloranil	76	149—152	1 : 2 or 2 : 1[c]
34	Chloranil	70	164—166	[b]

a) Determined by NMR spectrometric analysis of the mixture. b) The single isomer. c) The geometric configuration was not determined.

Table 3. Physical data of geometric isomers of **31** and **32**

Compd	Mp(°C)	λ_{max}^{MeOH} nm(ε)	NMR(δ, in $CDCl_3$) S-CH=	N-CH_3
31a(*cis*)	137—138	365(21000)	6.05	3.01
31b(*trans*)	132—134	363(26200)	6.28	3.37
32a(*cis*)	154—156	368(21600)	6.02	3.03
32b(*trans*)	128—129	362(26100)	6.29	3.39

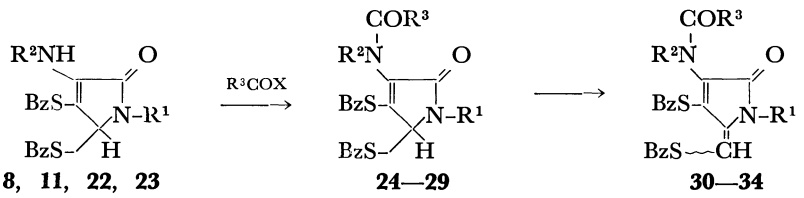

8, 11, 22, 23 **24—29** **30—34**

24, 30: $R^1=R^2=H$, $R^3=CH_3$
25, 31; $R^1=CH_3$, $R^2=H$, $R^3=CH_3$
26, 32; $R^1=CH_3$, $R^2=H$, $R^3=CH_2CH_3$
27, 33; $R^1=CH_2C_6H_5$, $R^2=H$, $R^3=CH_3$
28, 34; $R^1=CH_2C_6H_5$, $R^2=H$, $R^3=C_6H_5$
29; $R^1=R^2=CH_2C_6H_5$, $R^3=CH_3$

Scheme 3.

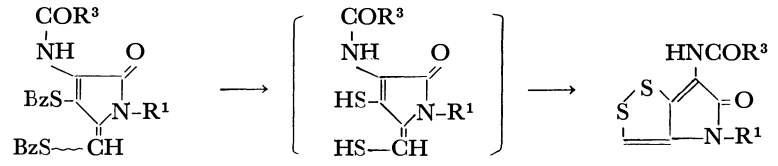

31, 32 **35, 36** **2, 3**

35; $R^1=R^2=CH_3$
36; $R^1=CH_3$, $R^2=CH_2CH_3$

Scheme 4.

the isomers (**33**) were unsuccessful.

The dehydrogenation of **28** yielded one (**34**) of the isomers, though its geometric configuration remained unclear.

Together with the interconversion between 3-aminolactams (*e. g.* **9** and **22**), the success in the dehydrogenation of the side chain with chloranil or DDQ made this synthetic line an advantageous method.

Debenzylation and Ring Closure. At the final stage of the synthesis, the reductive debenzylation of both benzylthio groups was carried out by a slight modification of Büchi's method[6] using 4 equivalent of lithium in liquid ammonia. The subsequent air-oxidation of the crude dithiol (**35**) thus obtained in aqueous methanol at pH 2 afforded aureothricin (**3**) as yellow needles (mp 260—270 °C (dec)). The similar treatment of **31** gave thiolutin (**2**) (mp 270—275 °C (dec)). The NMR spectra of **2** and **3** were consistent with the structural assignment made. The IR, UV spectra, and the thin-layer chromatographic behavior were identical with those of the natural antibiotics.

Experimental

All the melting points are uncorrected. The IR spectra were obtained on a Shimadzu IR-27G spectrophotometer. The NMR spectra were recorded on a Hitachi R-20A instrument, using TMS as the internal standard. The UV spectra were determined with a Hitachi EPS-3F spectrophotometer. The elemental analyses of the new compounds are listed in Table 8.

Preparation of 3-Amino-4-benzylthio-5-benzylthiomethyl-3-pyrrolin-2-one Derivatives (8-13). The reactions were achieved in the following two fashions. The results and spectral data are listed in Tables 1 and 4 respectively.

a) By Reaction in the Presence of Acetic Acid: To a cooled solution of **7** (10.0 g) and methylamine (8.5 g) in ethanol (50 ml) was added acetic acid (16 ml) with stirring. After refluxing for 2 hr, the reaction mixture was evaporated and the residue was extracted with ethyl acetate. The extract was washed with 1% hydrochloric acid, with a 5% sodium bicarbonate solution, and with water, and then dried over sodium sulfate. After the removal of the solvent, the tarry residue was chromatographed on silica gel G, using chloroform as the eluent, to give 4.10 g (38%) of **9** as colorless needles, (mp 106—108 °C); it was subsequently recrystallized from 2-propanol.

b) By Reaction in the Absence of Acetic Acid: A solution of **7** (3.58 g) and methylamine (0.93 g) in water (5 ml) was heated in a sealed tube for 30 min and then poured into water. The mixture was extracted with ethyl acetate, and the organic layer was worked up to afford 1.20 g (31%) of **9** by a procedure similar to that described above.

Hydrolysis of 3-Aminolactams. A solution of **9** (1.50 g) in ethanol (25 ml) was refluxed with 10% hydrochloric acid (5 ml) for 1 hr and then evaporated. The residue was extracted with ethyl acetate, and the extract was washed with water, dried over sodium sulfate, and evaporated. The recrystallization of the residue from 2-propanol gave 1.41 g (96%) of **16** as colorless needles (mp 123—124 °C).

In a similar manner, **8** and **10—13** were treated with hydrochloric acid to afford hydrolysis products: **15**, 71%, yellow syrup; **17**, 64%, mp 96—98 °C; **18**, 94%, mp 128—129 °C; **19**, 71%, mp 130—131 °C; **20**, 83%, mp 129—130 °C. The spectral data are shown in Table 5.

Conversion of 3-Hydroxylactams into 3-Aminolactams. a) By Reaction with Ammonium Acetate: A solution of **16** (4.14 g) and ammonium acetate (4.0 g) in ethanol (50 ml) was refluxed for 2 hr and then evaporated to give a syrup, which was subsequently extracted with ether. The extract was washed with water, dried and evaporated to dryness. The addition of cyclohexane to the residue, followed by recrystallization from isopropyl ether, afforded 3.05 g (84%) of **22** as colorless needles (mp 69—71 °C). The product gave a violet color with ninhydrin.

Similarly, **18** reacted with ammonium acetate to furnish **23** (mp 66—67 °C) in an 81% yield.

Table 4. Spectral data of 3-aminolactams (**8**—**13** and **21**—**23**)

No	ν_{max}^{Nujol} cm^{-1} a)	NMR(δ, in $CDCl_3$)
8	3450—3150, 1700, 1650	2.02(1H, q), 2.91(1H, q), 3.6(1H, m), 3.65(2H, s), 3.69(2H, s), 3.8(2H, broad s)c), 6.7(1H, broad s)c), 7.20(5H, s), 7.27(5H, s)
9	3310, 1693, 1645	2.80(3H, s), 2.90(2H, m), 2.93(3H, s), 3.65(1H, m), 3.64(2H, s), 3.68(2H, s), 3.9—4.6(1H)c), 7.21(5H, s), 7.29(5H, s)
10	3300, 1685, 1637	0.6—1.2(6H, m), 1.2—1.8(4H, m), 2.5—3.0(3H, m), 3.1—3.9(4H, m), 3.1—3.9(1H)c), 3.60(2H, s), 3.68(2H, s), 7.19(5H, s), 7.28(5H, s)
11	3210, 1690, 1638	2.75(2H, m), 3.30—3.55(1H, m), 3.46(2H, s), 3.51(2H, s), 3.70(1H, d), 4.3(1H, broad s)c), 4.57(2H, d), 5.08(1H, d), 6.7—7.2(20H, m)
12	3330, 1685, 1637	2.50—2.95(8H, m), 3.35—3.65(2H, m), 3.60(4H, s), 3.4—4.2(1H)c), 3.7—4.2(1H, m), 6.8—7.5(20H, m)
13	3360, 1697, 1680(sh)b)	2.34(6H, s), 2.66(1H, q), 3.00(1H, q), 3.45(2H, s), 3.48(2H, s), 6.6(1H, broad s)c), 6.8—7.4(18H, m)
21	3380, 1710, 1632, 1610	1.96(1H, q), 2.32(3H, s), 2.92(1H, q), 3.30(2H, s), 3.68(2H, s), 3.76(1H, m), 5.5—6.1(1H)c), 6.8—7.3(14H, m), 6.8—7.3(1H)c)
22	3460, 3320, 1690, 1645	2.81(3H, s), 2.76(2H, d), 3.59(1H, t), 3.61(2H, s), 3.70(2H, s), 4.08(2H, broad s)c), 7.27(5H, s), 7.23(5H, s)
23	3450, 3310, 1692, 1650	2.71(2H, d), 3.51(1H, t), 3.56(2H, s), 3.66(2H, d), 3.76(1H, d), 4.25(2H, broad s)c), 5.09(1H, d), 6.9—7.5(15H, m)

a) Syrupy substances were measured as a film. b) Sh, shoulder absorption. c) D_2O-exchangeable peak.

Table 5. Spectral data of 3-hydroxylactams(**15**—**20**)

No	ν_{max}^{Nujol} cm^{-1}	NMR(δ, in $CDCl_3$)
15	3250, 1690(broad)a)	1.87(1H, q), 2.79(1H, q), 3.5—3.8(1H, m), 3.60(2H, s), 4.05(2H, s), 5.5—6.5(1H)c), 7.17(5H, s), 7.21(5H, s), 7.4(1H, broad s)c)
16	3200, 1685, 1660	3.17(2H, m), 2.85(3H, s), 3.50—3.75(1H, m), 3.62(2H, s), 4.14(2H, s), 7.28(10H, s), 9.0(1H, broad s)c)
17	3170, 1660(broad)	0.88(3H, m), 1.1—1.7(3H, m), 2.64(2H, m), 2.95(1H, m), 3.61(2H, s), 3.4—3.9(1H, m), 4.12(2H, s), 7.25(10H, s), 8.8(1H, broad s)c)
18	3240, 1667	2.65(2H, d), 3.57(2H, s), 3.54(1H, t), 3.84(1H, d), 4.09(2H, s), 5.12(1H, d), 6.8—7.5(15H, m), 8.1—8.9(1H)c)
19	3150(broad), 1680, 1660	2.2—3.0(4H, m), 3.1—3.5(2H, m), 3.57(2H, s), 3.7—4.2(1H, m), 4.06(2H, s), 6.9—7.4(15H, m), 8.4—9.2(1H)c) .
20	3310, 1655(sh)b), 1650	2.34(3H, s), 2.73(1H, d), 2.77(1H, d), 4.25(2H, d), 4.40(1H, q), 6.9—7.5(14H, m), 8.22(1H, broad s)c)

a) Measured as a film. b) Sh, shoulder absorption. c) D_2O-exchangeable peak.

Table 6. Spectral data of 3-acylaminolactams (**24**—**29**)

No	ν_{max}^{Nujol} cm^{-1}	NMR(δ, in $CDCl_3$)
24	3200, 1680(broad)a), 1625	2.09(3H, s), 2.35(1H, q), 3.02(1H, q), 3.73(2H, s), 3.79(2H, s), 4.09(1H, q), 7.1—7.4(1H)c), 7.23(5H, s), 7.27(5H, s), 8.22(1H, s)c)
25	3160, 1690(sh)b), 1655	2.13(3H, s), 2.8(2H, m), 2.87(3H, s), 3.86(2H, s), 3.90(2H, s), 4.05(1H, m), 7.1—7.5(10H, m), 8.58(1H, s)c)
26	3150, 1685(sh)b), 1650(broad)	1.17(3H, t), 2.40(2H, q), 2.8(2H, m), 2.89(3H, s), 3.77(2H, s), 3.88(2H, s), 4.02(1H, m) 7.1—7.5(10H, s), 8.30(1H, s)c)
27	3270, 1668, 1663	2.13(3H, s), 2.80(2H, d), 3.71(2H, d), 3.77(2H, s) 4.00(1H, t), 3.85(1H, d), 5.12(1H, d), 6.8—7.5(15H, m), 8.50(1H. s)c)
28	3200(broad), 1660(broad)a)	2.86(2H, d), 3.77(2H, s), 3.82(2H, s), 3.92(1H, d), 4.02(1H, t), 5.16(1H, d), 6.9—8.1(20H, m) 8.33(1H, s)c)
29	1695, 1670	2.18(3H, s), 2.75(2H, d), 3.4—3.8(2H, m), 3.57(2H, s), 3.63(2H, s), 4.99(2H, s), 5.08(1H, d), 6.6—7.5(20H, m)

a) Measured as a film. b) Sh, shoulder absorption. c) D_2O-exchangeable peak.

b) By Reaction with Primary Amines: A solution of **18** (500 mg) and benzylamine (655 mg) in benzene (6 ml) was refluxed for 5 hr. After cooling, the reaction mixture was washed with 1% hydrochloric acid and with water, and dried. The removal of the solvent gave **11** (570 mg, 78%) (mp 121—122 °C), which was subsequently recrystallized from ethanol. In this way, **15** was allowed to react with *p*-toluidine for 7 hr to afford **21** as colorless needles in a 23% yield (mp 110—111 °C).

The spectral data are shown in Table 4.

*Preparation of 3-Acylamino-3-pyrrolin-2-one Derivatives. a) Preparation of **24***: A solution of **8** (2.12 g) and acetic anhydride (6 ml) in benzene (20 ml) was refluxed for 2 hr and evaporated to dryness. The residue was extracted with ethyl acetate, and the extract was washed with a 5% sodium bicarbonate solution and with water, and dried. The removal of the solvent left a syrup; this syrup was then chromatographed over silica gel G, using benzene–ethyl acetate (4 : 1) as the eluent, to give 1.33 g (56%) of **24** as a pale yellow syrup. The structure of **24** was confirmed by the spectral properties shown in Table 6.

*b) Preparation of **25**—**27** and **29***: A solution of **22** (2.92 g) and acetic anhydride (6 ml) in benzene (20 ml) was refluxed for 2 hr and then evaporated to give a syrup, which was subsequently crystallized by the addition of ether. Filtration and recrystallization from ethanol afforded 2.78 g (86%) of **25** as colorless needles (mp 140—142 °C). By the procedure described above, **26** (72%, mp 142—144 °C), **27** (88%, mp 128—129 °C), and **29** (88%, mp 95—96 °C) were obtained. The spectral data are listed in Table 6.

*c) Preparation of **28***: A solution of **23** (1.0 g) and benzoyl chloride (1.0 g) in benzene (5 ml) was stirred for 2 hr at room temperature. By the procedure described in the preparation of **24**, the resulting reaction mixture afforded 0.87 g (71%) of **28** as a pale yellow syrup. The structural assignment was made on the basis of spectral properties shown in Table 6.

Dehydrogenations of 3-Acylamino-5-benzylthiomethyl-3-pyrrolin-2-one Derivatives. a) With Chloranil or DDQ: A solution of **24** (0.63 g, 1.6 mmol) and chloranil (0.43 g, 1.8 mmol) in benzene (6 ml) was refluxed for 30 min and then diluted with methylene chloride. The solution was washed with 1% aqueous sodium hydroxide and with water, and dried. The removal of the solvent and recrystallization of the residue from ethanol gave 0.39 g (62%) of **30** as pale yellow needles: mp 178—179 °C; λ_{max}^{EtOH} 361 nm (ε 23500); M^+ ion at *m/e* 396. The IR and NMR spectra shown in Table 7 were consistent with the published data.[6] When DDQ was employed, **24** (0.40 g) yielded 0.27 g (67%) of **30**.

Similarly, **25**—**28** were treated with chloranil or DDQ to afford the corresponding exocyclic methlene compounds (**31**—**34**). The reactions in *t*-butanol also gave the dehydrogenated products in yields comparable to those in benzene. The results and the spectral properties are shown in Tables 2 and 7.

b) With Thionyl Chloride: Thionyl chloride (0.32 g, 3.8 mmol) was added to a cooled solution of **24** (1.50 g, 3.8 mmol) in chloroform (15 ml) with stirring. The resulting dark solution was allowed to stand overnight, and then washed with water and dried. After the evaporation of the solvent, the residue was chromatographed on silica gel G, using benzene–ethyl acetate (1 : 1) as the eluent, to give 103 mg (7%) of **30**. The reaction of 1-substituted lactams (**25**—**28**) with thionyl chloride led to the formation of unidentified products.

Separation of Geometric Isomers. The mixture (**32**, 500 mg) was treated by thin-layer chromatography (benzene–ethyl acetate, 1 : 1 on silica gel G) to give **32a** (70 mg, yellow leaflets) and **32b** (255 mg, yellow needles), which were recrystallized from 2-propanol. Similarly, the mixture (**31**, 300 mg) was separated into **31a** (60 mg, yellow leaflets) and **31b** (145 mg, yellow needles). The spectral properties are shown in Table 3.

*Thiolutin (**2**) and Aureothricin (**3**).* A solution of **31** (215 mg, 0.53 mmol) in tetrahydrofuran (2 ml) was introduced to liquid ammonia (20 ml). To the solution was added small pieces of lithium (15 mg, 2.2 mg. atom) with vigorous stirring. After 5 min, ammonium chloride (0.2 g) was added to the resulting orange-colored suspension. Evaporation left a yellow solid which was subsequently dissolved in methanol (20 ml). The solution was adjusted to pH 2 with 10% hydrochloric acid. After air was bubbled through the solution for 3 hr, evaporation gave a solid which was chromatographed on alumina, using chloroform–ethyl acetate (4 : 1), to give a yellow powder. Recrystallization from *n*-butanol afforded 13 mg (11%) of thiolutin (**2**) as yellow needles: mp 270—275 °C (dec); IR (KBr) 3270, 3060, 1670, 1640, 1605, 1550, 1235, 825 and 740 cm^{-1}; λ_{max}^{MeOH} 250, 312, 390 nm (6200, 5200, 11100); NMR (DMSO-d_6) δ

Table 7. Spectral data of 5-benzylthiomethylene-3-pyrrolin-2-ones (**30**—**34**)

No	ν_{max}^{KBr} cm^{-1}	NMR(δ, in $CDCl_3$)
30	3250, 1690, 1660	2.08(3H, s), 3.83(2H, s), 3.91(2H, s), 6.08(1H, s), 7.15(5H, m), 7.26(5H, s), 7.50(1H, broad s)[b], 8.24(1H, broad s)[b]
31a	3230, 1690, 1665	2.09(3H, s), 3.01(3H, s), 4.02(4H, s), 6.05(1H, s), 7.2(5H, m), 7.35(5H, s), 8.05(1H, s)[b]
31b	3280, 1700, 1670	2.08(3H, s), 3.37(3H, s), 3.80(2H, s), 3.93(2H, s), 6.28(1H, s), 7.2(5H, m), 7.33(5H, s), 7.91(1H, s)[b]
32a	3200, 1693, 1655	1.17(3H, t), 2.27(2H, q), 3.03(3H, s), 4.00(2H, s), 4.03(2H, s), 6.02(1H, s), 7.2(5H, m), 7.35(5H, s), 7.62(1H, s)[b]
32b	3270, 1680(broad)	1.17(3H, t), 2.35(2H, q), 3.39(3H, s), 3.80(2H, s), 3.96(2H, s), 6.29(1H, s), 7.2(5H, m), 7.36(5H, s), 8.71(1H, s)[b]
33[a]	3350, 3280, 1675(broad)	2.05(3H, s), 3.74(s), 3.82(s) and 3.94(s)(4H), 4.72(s) and 5.11(s)(2H, 2 : 1), 5.96(s) and 6.24(s)(1H, 2 : 1), 6.8—7.6(10H, m), 7.76(s)[b] and 7.81(s)[b] (1H)
34	3230, 1667, 1648	2.83(2H, s), 3.92(2H, s), 4.74(2H, s), 5.97(1H, s), 6.7—7.8(20H, m), 7.72(1H, s)[b]

a) The IR and NMR spectra of the isomeric mixture are shown. b) D_2O-exchangeable peak.

Table 8. Elemental analyses of new compounds

No	Formula	Calcd(%)				Found(%)			
		C	H	N	S	C	H	N	S
9	$C_{21}H_{24}N_2OS_2$	65.59	6.29	7.29	16.68	65.71	6.36	7.25	16.77
11	$C_{33}H_{32}N_2OS_2$	73.84	6.00	5.21	11.94	73.52	5.96	5.17	11.83
13	$C_{33}H_{32}N_2OS_2$	73.84	6.00	5.21	11.94	73.99	6.10	5.10	11.87
16	$C_{20}H_{21}NO_2S_2$	64.53	5.69	3.76	17.26	64.68	5.80	3.42	17.22
17	$C_{22}H_{25}NO_2S_2$	66.12	6.30	3.50	16.04	66.06	6.39	3.29	15.79
18	$C_{26}H_{25}NO_2S_2$	69.76	5.62	3.12	14.32	69.47	5.75	3.29	14.42
19	$C_{27}H_{27}NO_2S_2$	70.24	5.89	3.03	13.89	70.30	6.09	3.18	13.61
20	$C_{26}H_{25}NO_2S_2$	69.76	5.62	3.12	14.32	69.76	5.74	3.02	14.30
21	$C_{26}H_{26}N_2OS_2$	69.91	5.86	6.27	14.35	70.03	5.95	6.25	14.22
22	$C_{20}H_{22}N_2OS_2$	64.82	5.98	7.56	17.30	64.65	6.12	7.75	17.46
23	$C_{26}H_{26}N_2OS_2$	69.91	5.86	6.27	14.35	69.82	5.79	6.38	14.29
25	$C_{22}H_{24}N_2O_2S_2$	64.04	5.86	6.79	15.54	63.54	5.87	6.87	15.25
26	$C_{23}H_{26}N_2O_2S_2$	64.75	6.14	6.56	15.03	64.52	6.34	6.37	15.03
27	$C_{28}H_{28}N_2O_2S_2$	68.81	5.77	5.73	13.12	68.61	5.88	5.81	13.06
29	$C_{35}H_{34}N_2O_2S_2$	72.62	5.92	4.84	11.07	72.72	5.98	4.74	11.00
30	$C_{21}H_{20}N_2O_2S_2$	63.59	5.08	7.06	16.14	63.57	5.06	7.03	16.10
31a	$C_{22}H_{22}N_2O_2S_2$	64.36	5.40	6.80	15.63	64.16	5.60	7.02	15.60
31b	$C_{22}H_{22}N_2O_2S_2$	64.36	5.40	6.80	15.63	64.34	5.58	6.65	15.66
32a	$C_{23}H_{24}N_2O_2S_2$	65.06	5.70	6.60	15.10	64.81	5.79	6.64	15.03
32b	$C_{23}H_{24}N_2O_2S_2$	65.05	5.70	6.60	15.10	65.23	5.88	6.54	15.03
33	$C_{28}H_{26}N_2O_2S_2$	69.10	5.38	5.75	13.17	68.90	5.48	5.77	12.94
34	$C_{33}H_{28}N_2O_2S_2$	72.23	5.14	5.10	11.68	71.96	5.29	5.07	11.62

2.05 (3H, s), 3.92 (3H, s), 7.19 (1H, s) and 9.85 (1H, broad s).

By a similar procedure, **32** (1.04 g) yielded 37 mg (6%) of aureothricin (**3**) as yellow needles: mp 260—270 °C (dec); IR (KBr) 3250, 3050, 1670, 1640, 1605, 1545, 1230, 815 and 730 cm^{-1}; λ_{max}^{MeOH} 246, 313, 390 nm (6300, 4000, 11100); NMR (DMSO-d_6) δ 1.02 (3H, t), 2.40 (2H, q), 3.25 (3H, s), 7.28 (1H, s) and 9.8 (1H, broad s).

Both substances showed no depression on a mixed-melting-point determination with an authentic sample. The IR, UV spectra, and the thin-layer chromatographic behavior on silica gel G and alumina using benzene–ethyl acetate (1 : 1), benzene–methanol (9 : 1) and chloroform–ethyl acetate (4 : 1) could not distinguish between the synthetic and natural antibiotics (**2** and **3**).

The authors wish to thank Professor Teruaki Mukaiyama and Associate professor Hisashi Takei for their valuable suggestions. They also thank Director Dr. Ichiro Chibata and Dr. Muneji Miyoshi for their encouragement in this work.

References

1) L. Ettlinger, E. Gaümann, R. Hütter, W. Keller-Schierlein, F. Kradolfer, L. Neipp, V. Prelog, and H. Zähner, *Helv. Chim. Acta*, **42**, 563 (1959).

2) W. D. Celmer and I. A. Solomons, *J. Amer. Chem. Soc.*, **77**, 2861 (1955) and the earlier papers cited therein.

3) D. S. Bahte, R. K. Hulyalkar, and S. K. Menon, *Experientia*, **16**, 504 (1960).

4) a) W. Daehne, W. O. Godtfredson, L. Tybring, and and K. Schaumburg, *J. Antibiot.*, **22**, 233 (1969). b) B. Jensen, *ibid.*, **22**, 231 (1969).

5) U. Schmidt and F. Geiger, *Angew. Chem.*, **74**, 328 (1962); *Ann*, **664**, 168 (1963).

6) G. Büchi and G. Lukas, *J. Amer. Chem. Soc.*, **85**, 647 (1963); *ibid.*, **86**, 5654 (1964).

7) Presented at the 26th Annual Meeting of the Chemical Society of Japan, Hiratsuka, April 1st, 1972.

8) 3-Aminolactone was obtained by the reaction of 3-hydroxy-2-oxo-2,5-dihydrofuran derivative with ammonium acetate; E. Galantary, H. Engel, A. Szabo, and J. Fried, *J. Org. Chem.*, **29**, 3560 (1964).

A Polarographic Study of Aryl-substituted Tetra-aza- and Hexa-aza-pentalenes in Dimethylformamide

Akira MATSUMOTO, Joung Hee LEE, Masayuki YOSHIDA, and Osamu SIMAMURA

Department of Chemistry, Faculty of Science, Tokyo University, Hongo, Tokyo 113

(Received November 27, 1973)

The polarographic reduction potentials of aryl-substituted 1,2,4,5-tetra-aza- and 1,2,3,4,5,6-hexa-aza-pentalenes were shown to be approximately governed by the numbers of nitrogen atoms and aryl-substituents. Such effect of nitrogen atoms was discussed in terms of the orbital energies of parent azapentalenes obtained by HMO calculations.

The preparations and properties of aryl-substituted 1,2,4,5-tetra-aza- (I) as well as 1,2,3,4,5,6-hexa-aza- (V–X) pentalenes were described previously,[1,2] and these compounds were shown to be very stable. In the present work the polarographic reduction of a number of 1,2,4,5-tetra-aza- and 1,2,3,4,5,6-hexa-aza-pentalenes (including compounds I and V–X) has been studied to examine any correlation between the half-wave reduction potentials and the chemical properties.

Results and Discussion

Polarograms of polyazapentalenes in dimethylformamide containing tetra-*n*-butylammonium iodide (0.155 M) as supporting electrolyte showed two well-defined reduction waves; polarographic data are given in Table 1. Plots of polarographic potential E *versus* log $[(i_d - i)/i]$ give straight lines with a slope in good agreement with the theoretical value of 0.0585 V at 22 °C according to Heyrovsky and Ilkovic's derivation.[3] This result, therefore, indicates that these reduction waves correspond to reversible one-electron reduction of polyazapentalenes to radical anions.

A plot of the potentials for the first reduction waves ($E_{1/2}$) against the number (N) of aryl-substituents in each molecule (Fig. 1) gives two parallel straight lines, one ($E_{1/2}=0.36\,N\,-2.60$ (V)) for tetra-aza- and the other ($E_{1/2}=0.36\,N\,-1.32$(V)) for hexa-aza-pentalenes. These correlations clearly show that the number of nitrogen atoms in the azapentalene nucleus is important in determining the reduction potential. On the other hand, the fact that the slopes of the straight lines are found identical shows that the effect of an aryl substituent on the potential is additive and the same, giving rise to an elevation by 0.36 V for one substituent, irrespective of the nature of the nucleus. The effects of other factors such as the orientation of substituents or the replacement of a phenyl with a *p*-chlorophenyl group (V–VI) are small in comparison with the above major effects.

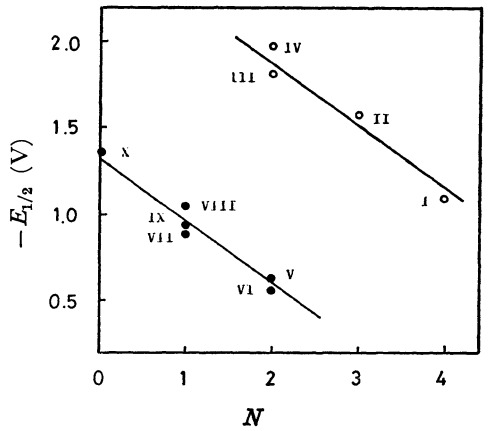

Fig. 1. Plot of the half-wave reduction potentials of the tetra-aza- and hexa-aza-pentalenes against the number (N) of aryl-substituents.
—○— Tetra-azapentalenes
—●— Hexa-azapentalenes

The plot corresponding to compound VIII does not fall on the straight line for hexa-azapentalenes; the reason is obviously the difference in the type of electronic structure, because compound VIII is not mesoionic, carrying a methyl and a phenyl group at positions 1 and 5, respectively, while the other hexa-azapentalenes examined are mesoionic carrying substituents at positions 2 and 5.

As regards the regression line for tetra-azapentalenes,

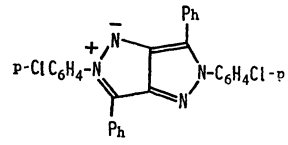

I

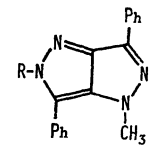

II: R = Ph
III: R = CH_3

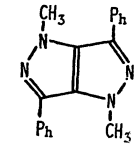

IV

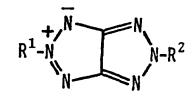

V: $R^1 = R^2 = Ph$
VI: $R^1 = Ph$, $R^2 = p\text{-}ClC_6H_4$
VII: $R^1 = Ph$, $R^2 = CH_3$
IX: $R^1 = Ph$, $R^2 = cyclo\text{-}C_6H_{11}$
X: $R^1 = R^2 = cyclo\text{-}C_6H_{11}$

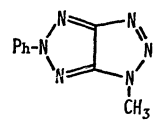

VIII

Table 1. Polarographic data of poly-azapentalenes in dimethylformamide containing tetra-*n*-butylammonium iodide at 22 °C

Compound	$E_{1/2}$	i_d/c	Slope × 10^2	$E'_{1/2}$	i'_d/c
I	−1.10	3.4	6.4		
II	−1.58	4.6	5.2		
III	−1.82	4.6	5.2		
IV	−1.98	4.1	5.6		
V	−0.62	3.2	6.5	−1.37	3.0
VI	−0.57	2.4	6.2	−1.27	2.4
VII	−0.90	3.4	5.8	−1.5	5
VIII	−1.06	4.3	5.3	−1.88	6.7
IX	−0.94	2.7	6.4	−1.47	3.5
X	−1.32	2.7	6.1	−1.7	6

$E_{1/2}$: Half-wave potential (V) *vs.* mercury pool for the first reduction wave.
Slope: Slope from plot of E *vs.* $\log[(i_d-i)/i]$.
i_d: Diffusion current in μA.
c: Concentration (mmol/l).
$E'_{1/2}$, i'_d: Half-wave potential and diffusion current for the second reduction wave, respectively.

Table 2. Energy levels ($E_m=\alpha+k_m\beta$) and total energy of π-electrons[a] of some azapentalenes calculated by HMO method[7]

	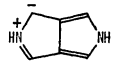	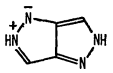	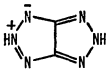		
k_m[b]	XI	XIII	XV	XII	XIV
k_8	−2.00	−1.93	−1.85	−1.67	−1.54
k_7	−1.48	−1.35	−1.17	−1.41	−1.34
k_6	−0.85	−0.68	−0.50	−1.19	−1.05
k_5	0.00	0.25	0.50	0.00	0.25
k_4	1.00	1.18	1.24	0.92	0.98
k_3	1.23	1.24	1.35	1.41	1.59
k_2	2.35	2.43	2.50	1.69	1.80
k_1	2.75	2.84	2.90	3.26	3.31
$\sum_m^{occ} k_m$	14.66	15.90	16.98	14.55	15.86

a) Values of only k_m's are shown. b) Occupied levels are distinguished from unoccupied ones by underline.

the correlation can not be regarded as excellent, as is apparent, for example, from the discrepancy between the plots for compounds III and IV. This is probably because the type of electronic structure may be slightly different in the compounds examined, the orientations of the four substituent groups being different except between compounds II and III, and furthermore, compound I is mesoionic.

If a straight line is drawn through the two points representing compounds II and III, the slope will be decreased to 0.24 V/N, indicating thus a weaker effect of the aryl substituent in this type of compounds. The reason may be attributable to non-coplanarity of the phenyl group with the azapentalene nucleus owing to the juxtaposition of substituent groups.[4]

The polarographic reduction potentials of aromatic hydrocarbons are known to be correlated linearly with the energy of their lowest vacant molecular orbitals as calculated by the simple HMO method.[5] This is found to be the case also with 2,5-disubstituted hexa-azapentalenes as is shown in Fig. 2. In the present calculations, aryl substituents were thought

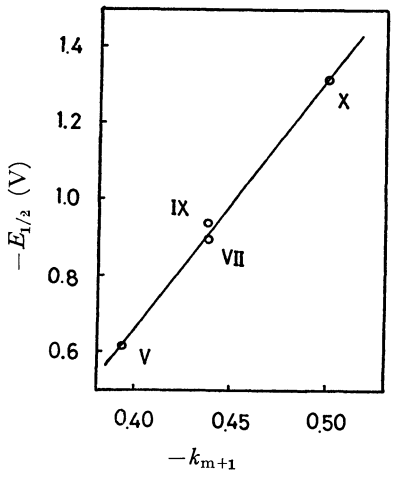

Fig. 2. Half-wave reduction potentials for hexa-azapentalenes in dimethylformamide *versus* energies of lowest vacant orbitals.
The axis of abscissa shows energy in terms of coefficient k_{m+1} in energy expression $E_{m+1}=\alpha+k_{m+1}\beta$ of lowest vacant orbital.[7]

to be coplanar with the hexa-azapentalene nucleus, as is supported by UV and NMR spectroscopic measurements.[6]

Hückel molecular orbital calculations were also carried out for some mesoionic azapentalene parent rings[7] in order to compare the effect of the number and positions of nitrogen atoms on the π-electron energy with that on the chemical behaviour. The results are summarized in Table 2. 2,5-Diaza- (XI) and 3a,6a-diaza- (XII)[8] pentalenes have an occupied non-bonding orbital, and the total π-electron energy is nearly the same for the two rings, but the lowest vacant orbital lies lower in ring XI than in ring XII. Introduction of two nitrogen atoms into these diazapentalenes to give 1,2,4,5-tetra-aza-(XIII) and 1,3a,4,6a-tetra-aza-(XIV) pentalenes results in lowering of the energies of all the orbitals, but again the energy of the highest occupied orbital and the total π-electron energy are nearly the same for (XIII) and (XIV), and the energy of the lowest vacant orbital of (XIII) is lower than that of (XIV). Introduction of two more nitrogen atoms into XIII to give 1,2,3,4,5,6-hexa-azapentalene (XV) causes further decrease in the energy of each of the molecular orbitals and hence in the total energy.

Thus, in the series of the azapentalenes, XI, XIII, and XV, the effect of the number of nitrogen atoms on the energy of the lowest vacant orbital, to which the polarographic reduction potential should be related, is in harmony with the earlier mentioned result that introduction of two more nitrogen atoms into positions 3 and 6 of the 1,2,4,5-tetra-azapentalene nucleus causes elevation of the reduction potentials by 2.60—1.32=1.28 V.

The HMO calculations also show that the energy of the highest occupied orbital and the stability of azapentalenes as judged by the total π-electron energy seem to be approximately governed by the number of nitrogen atoms, their position in the nucleus exerting insignificant influence.

Irrelevance of the position of nitrogen atoms appears to be the case also with the chemical behaviour relating to the highest occupied orbital; the reactivity of 2,3,5,6-tetra-aryl-1,2,4,5-tetra-azapentalene in reaction such as electrophilic substitution and oxidation parallels closely that reported for dibenzo-1,3a,4,6a-tetra-aza- and dibenzo-1,3a,6,6a-tetra-aza-pentalenes.[4,9]

Comparison of the energy values shown in Table 2 predicts that 1,2,3,4,5,6-hexa-azapentalene (XV) should be subjected to more facile reduction, but not to more facile oxidation than 1,2,4,5-tetra-azapentalene (XIII). This view is supported by the finding that 2,5-diphenyl-1,2,3,4,5,6-hexa-azapentalene (V) is easily reduced by sodium to the corresponding anion radical, but does not undergo any oxidation with potassium permanganate in boiling pyridine, whereas the reverse is the case with the tetra-azapentalene (I).[10]

Experimental

The syntheses of compounds I and V—X were reported previously.[1,2] Non-mesoionic tetra-azapentalenes II—IV are new compounds and their syntheses were reported in a separate paper.[4] Commercial tetra-*n*-butylammonium iodide was twice recrystallized from a mixture of ethanol and ethyl acetate and stored under nitrogen. Dimethylformamide was boiled under reflux with calcium hydride and distilled under nitrogen.

Polarographic measurements were carried out with a Yanagimoto Model P-8 apparatus. The dropping mercury electrode was operated at 60 cm pressure and had a drop-time of 4.36 sec in dimethylformamide (open circuit).

The authors are grateful to Prof. S. Fujiwara and Dr. Y. Umezawa for allowing them to use their polarographic facilities.

References

1) J. H. Lee, A. Matsumoto, O. Simamura, and M. Yoshida, *Chem. Commun.*, **1969**, 1393.

2) M. Yoshida, A. Matsumoto, and O. Simamura, This Bulletin, **43**, 3587 (1970).

3) J. Heyrovsky and D. Ilkovic, *Collect. Czech. Chem. Commun.*, **7**, 198 (1935).

4) J. H. Lee, A. Matsumoto, M. Yoshida, and O. Simamura, This Bulletin, **47**, 1039 (1974).

5) I. Bergman, *Trans. Faraday Soc.*, **50**, 829 (1954); G. J. Hoijtink, *Rec. Trav. Chim. Pays-Bas*, **74**, 1625 (1955).

6) A. Matsumoto, M. Yoshida, and O. Simamura, This Bulletin, **47**, 1493.

7) The following parameters were used for the calculation: $\alpha_N=\alpha_C+1.5\beta$ (pyrrole-like N), $\alpha_N=\alpha_C+0.5\beta$ (pyridine-like N), and all $\beta=\beta_{CC}$ (*cf.* A. Streitwieser, Jr., "Molecular Orbital Theory for Organic Chemists," John Wiley & Sons, Inc., New York, N. Y. (1961), p. 135).

8) S. Trofimenko, *J. Amer. Chem. Soc.*, **87**, 4393 (1965); T. W. G. Solomons and C. G. Voight, *ibid.*, **87**, 5256 (1965).

9) R. A. Carboni, J. C. Kauer, J. E. Castle, and H. E. Simmons, *ibid.*, **89**, 2618 (1967).

10) M. Yoshida, A. Matsumoto, and O. Simamura, unpublished results.

Preparations and Properties of 5-Phenyl-5*H*[1,2,3]-triazolo[4,5-*c*][1,2,5]-oxadiazole, -thiadiazole, and -selenadiazole

Akira MATSUMOTO, Masayuki YOSHIDA, and Osamu SIMAMURA
Department of Chemistry, Faculty of Science, Tokyo University, Hongo, Tokyo 113
(Received November 27, 1973)

The title compounds have been synthesized, and their chemical reactivities and spectroscopic properties are discussed in comparison with those of 2,5-diphenyl-*v*-triazolo[4,5-*d*]-*v*-triazole.

The preparations and properties of some meso-ionic 1,2,4,5-tetra-aza- as well as 1,2,3,4,5,6-hexa-aza-pentalenes were described previously.[1,2] These investigations and a polarographic study of azapentalenes have shown that the major factor affecting the properties of the above polyazapentalenes is the number of nitrogen atoms in the azapentalene nucleus.[3] Thus, it seemed of interest to examine the physical and chemical consequences of replacing one of the nitrogen atoms in the polyazapentalene nucleus with another electronegative atom such as oxygen, sulphur, and selenium. This paper presents the syntheses and properties of a series of new heteropentalenes, 5-phenyl-5*H*[1,2,3]-triazolo[4,5-*c*][1,2,5]-oxadiazole (I), -thiadiazole (II), and -selenadiazole (III), in which a hetero atom at position 2 contributes two π-electrons to the π-electronic system of the nucleus.

The preparative routes to these compounds are summarized in Scheme 1. The details of the synthetic procedures are given in the Experimental Part.

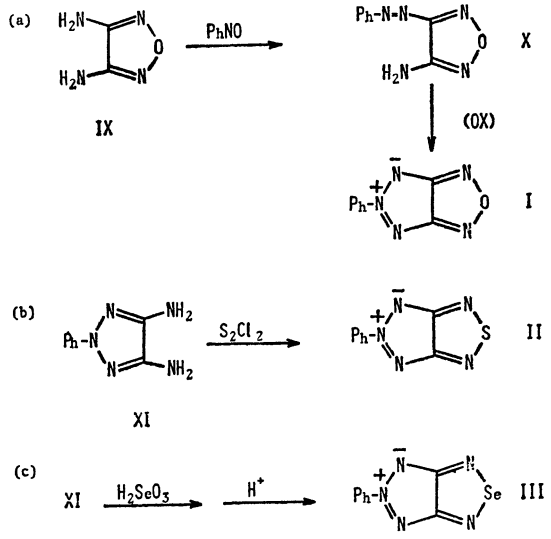

Scheme 1. The Preparative Routes to Heteropentalenes.

The behaviour of these heteropentalenes under oxidizing or reducing conditions is particularly interesting. Whereas 2,3,5,6-tetra-aryl-1,2,4,5-tetra-azapentalenes are readily oxidized or reduced with ring-opening,[1,3] 2,5-diphenyl-hexa-azapentalene (V) is entirely resistant to oxidation and is catalytically hydrogenated to yield products with the azapentalene nucleus being left intact, *viz.*, 2,5-dicyclohexyl-(VIII) and 2-cyclohexyl-5-phenyl-hexa-azapentalene (VI).[2] These results caused us to examine the reactions of the triazolothiadiazole (II) under similar conditions. It was resistant to oxidation with *m*-chloroperoxybenzoic acid in chloroform or with hydrogen peroxide in acetic acid. Heated at 95 °C for 9 hr with potassium permanganate in a mixture of pyridine and water (10 : 1), however, it underwent extensive oxidation giving no isolable compounds. On the other hand, the triazolothiadiazole (II) was not hydrogenated at 1 atm of hydrogen with platinum catalyst under acidic conditions. Possible poisoning of the catalyst by the sulphur-containing substrate was suspected, but an excess of catalyst did not effect the reduction. However, reduction with lithium aluminium hydride in tetrahydrofuran occurred readily at room temperature, giving 4,5-diamino-2-phenyl-*v*-triazole (XI) in 90% yield.

The triazolooxadiazole (I) was resistant to attack by *m*-chloroperoxybenzoic acid, a result not unexpected in view of the stability of II described above.

The ultraviolet and NMR spectral characteristics and the half-wave reduction potentials of these heteropentalenes (I–III) as well as those of phenyl-substituted hexa-azapentalenes (IV–VII) are listed in Tables 1 and 2. All of these compounds exhibit two ultraviolet absorption maxima without vibrational structure. It is noteworthy that the absorption peaks of compounds I, II, and and III show an appreciable shift to longer wavelength regions according as the atom at position 2 varies from O to S to Se; this effect is particularly pronounced with the maxima of the longer wavelength. Obviously, electronic conjugation occurs between the nitrogen-containing system and the hetero atom at position 2.

In view of the apparent similarity in reactivity observed between compounds II and V, the polarographic reduction of these compounds was examined. As shown in Table 2, the half-wave potentials of compounds II and III are strikingly higher than those of the hexa-azapentalenes, IV–VII. Apparently, the difference is attributable to the effect of a sulphur or selenium atom present in the nucleus in place of a nitrogen, although

TABLE 1. ABSORPTION MAXIMA OF PHENYL-SUBSTITUTED HETEROPENTALENES IN ETHANOL

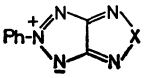
(I—V)

	X	λ_{max} in nm (log ε)
I	O	319(4.27), 234(3.59)
II	S	337(4.47), 235(3.61)
III	Se	365(4.52), 238(3.74)
IV	NCH_3	301(4.40), 226(3.79)
V	NPh	342(4.62), 231(4.11)

Table 2. Chemical shifts (τ) in $CDCl_3$ and polarographic half-wave reduction potentials (*vs.* Hg pool) for 5-phenyl-substituted heteropentalenes

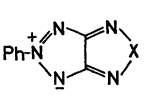

(I–VI)

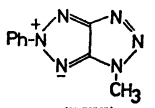

(VII)

		(*o*-H)	(*m*, *p*-H)	$-E_{1/2}$	(i_d/c)
I	O	1.51	2.32		
II	S	1.55	2.41	0.28	(3.1)
III	Se	1.44	2.37	0.21	(3.1)
IV	NCH_3	1.69	2.48	0.90	(3.4)
V	NPh	1.62	2.45	0.62	(3.2)
VI	NC_6H_{11}	1.74	2.55	0.94	(2.7)
VII		1.87	2.54	1.06	(4.3)

$E_{1/2}$: Half-wave reduction potential (V) for the first wave in dimethylformamide containing tetra-*n*-butylammonium iodide (0.155 M) as supporting electrolyte.
i_d: Diffusion current in μA.
c: Concentration (mmol/l).

nitrogen is more electronegative than sulphur.[4]

In these phenyl-substituted heteropentalenes, the phenyl group may be regarded as almost coplanar with the bicyclic nucleus, since large bathochromic shifts are observed in the ultraviolet absorption spectra of phenyl substituted hexa-azapentalenes when compared to those of the corresponding cyclohexyl derivatives.[2] This conclusion is further supported by the fact, shown in Table 2, that the NMR signals of the *ortho*-protons of the substituent phenyl group occur in lower field regions than those of the *meta*- and *para*-protons. Finar and Rackham attributed similar deshielding observed with 1-phenyl-substituted aza-aromatic compounds such as 1-phenylpyrazole to the interaction due to a large electric field associated with the lone pair of electrons of the nitrogen atom at position 2, this effect being operative only when both rings are coplanar.[5] Thus, the large difference in chemical shift (0.81—0.93 ppm) between the *o*-protons and the *m*- and *p*-protons in 5-phenyl heteropentalenes (I–VII, Table 2) can be attributed to the coplanarity of the phenyl-substituent and the presence of two lone pairs at 4- and 6-positions. Similar strong deshielding was observed with the NMR spectrum of 2-phenyl-*s*-triazolo[1,5-*a*]pyridine.[6]

Experimental

3-Amino-4-phenylazo-1,2,5-oxadiazole (X). 3,4-Diamino-1,2,5-oxadiazole (IX)[7] (2.9 g, 29 mmol) was suspended in a mixture of aqueous sodium hydroxide (50%, 60 ml) and benzene (2 ml). Nitrosobenzene (3.1 g, 29 mmol) was added in small portions to the stirred mixture kept at 60 °C over a period of 7 min, and the mixture was stirred for an additional 7 min. The solution was poured onto *ca.* 500 ml of ice-water, and the orange solid deposited was collected by filtration, washed with water, and recrystallized from benzene to give 1.5 g (27%) of X as orange crystals, mp 172.4—174.0 °C (Found: C, 50.61; H, 3.81; N, 37.07%. Calcd for $C_8H_7N_5O$: C, 50.79; H, 3.73; N, 37.02%), ν_{max} (Nujol) 3450, 3300, 1610, 1020, 770, 735, and 680 cm^{-1}, *m/e* 189 (M^+, 29%), 105(20), 91(3), 78(10), and 77(100).

5-Phenyl-5H[1,2,3]-triazolo[4,5-c][1,2,5]oxadiazole (I). 3-Amino-4-phenylazo-1,2,5-oxadiazole (X) (1.1 g, 58 mmol) was heated under reflux with 3.5 g of lead tetraacetate in 50 ml of benzene for 23 hr. After filtration of insoluble solid and evaporation of the solvent, the residue was eluted through a column of silica-gel (Wakogel C-200) with benzene. The solvent was evaporated from the eluate, and the residue recrystallized first from benzene and then from ethanol (with active charcoal) yielded 0.3 g (28%) of the triazolooxadiazole (I) as yellow crystals, mp 165.5—166.5 °C (Found: C, 51.59; H, 2.44; N, 37.59%. Calcd for $C_8H_5N_5O$: C, 51.34; H, 2.69; N, 37.42%), ν_{max} (Nujol) 1580, 1300, 1185, 1110, 1070, 930, 830, 800, 765, and 670 cm^{-1}, *m/e* 187 (M^+, 27%), 131(6), 105(13), 78(11), 77(100), and 51(33).

5-Phenyl-5H[1,2,3]-triazolo[4,5-c][1,2,5]thiadiazole (II). To a mixture of 0.57 g (3.3 mmol) of 4,5-diamino-2-phenyl-*v*-triazole[8] (XI) and 14 ml of benzene was slowly added 0.88 g (6.6 mmol) of sulphur monochloride to give a dark violet solution. The mixture was heated under reflux for 18 hr and the solvent was evaporated, yielding a brownish black solid mixture. Column chromatography on silica-gel (Wakogel C-200) in benzene gave a yellowish crystalline mixture containing sulphur. The mixture was freed from sulphur by percolating a dilute benzene solution of the mixture through a chromatographic tube packed with copper powder treated with 30% sulphuric acid at room temperature. Evaporation of the solution and recrystallization of the residue from benzene gave 0.26 g (38%) of the triazolothiadiazole (II) as yellow crystals, mp 181.0—182.5 °C (Found: C, 47.44; H, 2.21; N, 34.72%. Calcd for $C_8H_5N_5S$: C, 47.28; H, 2.48; N, 34.46%), ν_{max} (KBr) 1610, 1480, 1450, 1290, 1180, 1095, 1065, 915, 855, 800, 760, 680, and 660 cm^{-1}, *m/e* 203(M^+, 50%), 105(7), 78(5), and 77(100).

5-Phenyl-5H[1,2,3]-triazolo[4,5-c][1,2,5]selenadiazole (III). To a solution of 3.4 g (19 mmol) of 4,5-diamino-2-phenyl-*v*-triazole (XI) in 75 ml of ethanol was added 2.75 g (21 mmol) of selenous acid.[9] The solution was kept at 40 °C for 10 hr, giving black precipitate. The precipitate was collected by filtration, washed with water and then added to a mixture of 50 ml of benzene and 5 ml of concd hydrochloric acid in 100 ml of water. The mixture was heated under reflux for 4 hr, and the resulting yellow benzene layer was separated and replaced with 50 ml of fresh benzene. Heating and separation in the same way were repeated additional three times each with addition of 50 ml of benzene, and the combined benzene solutions (200 ml), on evaporation, gave 0.6 g of dark-red crystals. Recrystallization from benzene and column chromatography on silica-gel (Wakogel C-200) in benzene gave 0.35 g (7.2%) of the triazoloselenadiazole as yellow crystals, mp 203.8—204.5 °C (Found: C, 38.56; H, 2.01; N, 28.04%. Calcd for $C_8H_5N_5Se$: C, 38.42; H, 2.02; N, 28.00%), ν_{max} (Nujol) 1330, 1290, 1190, 1095, 1070, 925, 770, 750, 680, and 670 cm^{-1}, *m/e* 251 (M^+, 12%), 105(20), 78(13), 77(100), and isotopic peaks (due to the isotopes of selenium) at 253, 249, 248, and 247.

Oxidation of 5-Phenyl-5H[1,2,3]-triazolo[4,5-c][1,2,5]thiadiazole (II). *(a) With m-Chloroperoxybenzoic Acid*: Phenyltriazolothiadiazole (II) (0.102 g, 0.50 mmol) was refluxed with *m*-chloroperoxybenzoic acid (0.42 g, 2.44 mmol in 40 ml of of dichloromethane) for 18 hr. Acidic matter was removed with aqueous sodium carbonate solution and the residual solution was dried (Na_2SO_4). Removal of dichloromethane left 0.082 g (80%) of the starting material.

(b) With Hydrogen Peroxide: A mixture of 0.086 g (0.42 mmol) of II, 13 ml of hydrogen peroxide (30%), 1 ml of diluted sulphuric acid (1%), 30 ml of acetic acid, and 10 ml

of chloroform was heated at 60 °C for 20.5 hr. The mixture was neutralized with dilute sodium carbonate solution and the chloroform layer was separated, which, on evaporation, gave back 0.081 g of the starting material.

(c) With Potassium Permanganate: A mixture of 0.103 g (0.51 mmol) of II, 0.1 g of potassium permanganate and 0.50 ml of water in 5 ml of pyridine was stirred at 95 °C for 1.5 hr. Stirring was continued for a further 2 hr at 95 °C with an additional 0.1 g of potassium permanganate, but most of compound II remained unoxidized. The oxidation was complete after further heating for 5 hr with an additional 0.2 g of the oxidizing agent. The manganese dioxide was removed by filtration and the filtrate was concentrated to give only a trace amount of reddish black tarry matter.

*Reduction of 5-Phenyl-5*H[*1,2,3*]-*triazolo*[*4,5*-c][*1,2,5*]*thiadiazole (II).* *(a) Catalytic Hydrogenation*: The phenyltriazolothiadiazole (II) (0.506 g, 2.4 mmol) in 30 ml of dioxane was hydrogenated with 0.106 g of platinum oxide catalyst at 1 atm of hydrogen for 5 days. The starting material was recovered (91%) from the reaction mixture.

(b) With Lithium Aluminium Hydride (LAH): A mixture of 0.46 g (2.2 mmol) of II and 0.1 g of LAH in 30 ml of anhydrous tetrahydrofuran was stirred for 18 hr at room temperature, followed by heating under reflux for 4.3 hr with an additional 0.2 g of LAH. Water (2 ml) was added carefully to the mixture and the solvent was removed under reduced pressure. Organic products were extracted with ethanol and evaporation of the solvent from the extract gave 4,5-diamino-2-phenyl-*v*-triazole (XI) in 90% yield.

Polarographic Measurements. Polarographic measurements of the heteropentalenes (I, II, and III) were carried out in a similar manner to that described in the literature.[10] No distinct polarogram was obtained for compound I.

References

1) J. H. Lee, A. Matsumoto, O. Simamura, and M. Yoshida, *Chem. Commun.*, **1969**, 1393.
2) M. Yoshida, A. Matsumoto, and O. Simamura, This Bulletin, **43**, 3587 (1970).
3) A. Matsumoto, J. H. Lee, M. Yoshida, and O. Simamura, *ibid.*, **47**, 946, 1490 (1974).
4) L. Pauling, "The Nature of the Chemical Bond," 3rd ed., Cornell Univ. Press, Ithaca, N. Y. (1960), p. 93.
5) I. L. Finar and D. M. Rackham, *J. Chem. Soc., B*, **1968**, 211.
6) K. T. Potts, H. R. Burton, T. H. Crawford, and S. W. Thomas, *J. Org. Chem.*, **31**, 3522 (1966).
7) A. Gasco, G. Rua, E. Menziani, G. M. Nano, and G. Tappi, *J. Heterocyclic Chem.*, **6**, 769 (1969).
8) J. Thiele and K. Schleussner, *Ann. Chem.*, **295**, 129 (1897).
9) A. J. Nunn and J. T. Ralph, *J. Chem. Soc.*, **1965**, 6769.
10) S. Wawzonek and D. Wearring, *J. Amer. Chem. Soc.*, **81**, 2067 (1959).

Formation and Conformation of Benzoyloxylated Sulfur-containing Heterocycles

Tadashi SUGAWARA, Hiizu IWAMURA, and Michinori ŌKI
Department of Chemistry, Faculty of Science, The University of Tokyo, Tokyo 113
(Received December 18, 1973)

Thiane, 1,3-dithiane, and 1,3,5-trithiane were treated with *t*-butyl peroxybenzoate in the presence of cuprous chloride to yield benzoyloxylated products. Methylenes placed between two sulfur atoms were found to be more reactive than those next to one sulfur atom. Introduction of two benzoyloxy groups into 1,3,5-trithiane afforded *cis*-2,4-dibenzoyloxy-1,3,5-trithiane only. PMR spectra of benzoyloxylated products at various temperatures indicate that benzoyloxy-axial conformation is overwhelming for all the compounds investigated.

Some stereospecific reactions of anions derived from dithianes and trithianes have been reported.[1,2] As an extension of these works, it was thought of interest to study the reactions of sulfur-heterocycles taking place *via* carbonium ions. In order to carry out such studies, it is necessary to synthesize sulfur-heterocycles which carry electronegative substituents.

The synthesis of these compounds was found to be tedious halogenation of 1,3,5-trithiane under either basic or neutral conditions gave intractable materials, attempts to introduce a hydroxyl group being unsuccessful. Acyloxylation of ethers and sulfides by peroxy esters with the aid of cuprous salt is known.[3] The reaction should introduce a benzoyloxy group to the sulfur-heterocycles if *t*-butyl peroxybenzoate is used and the products could be used for the nucleophilic reactions. A benzoyloxy group itself is not a good leaving group in solvolytic reactions but the presence of sulfur atoms may enhance the reactivity of the compound. This paper concerns the benzoyloxylation of thiane, 1,3-dithiane, and 1,3,5-trithiane, the stereoselectivity of the reaction, and the conformation of the products.

Results and Discussion

Benzoyloxylation and Stereoselectivity. When 1,3,5-trithiane (**1**) was treated with *t*-butyl peroxybenzoate (**2**) in benzene, the number of benzoyloxy groups introduced into the trithiane skeleton was found to depend on the molar ratio of **1** to **2**. The results are summarized in Table 1.

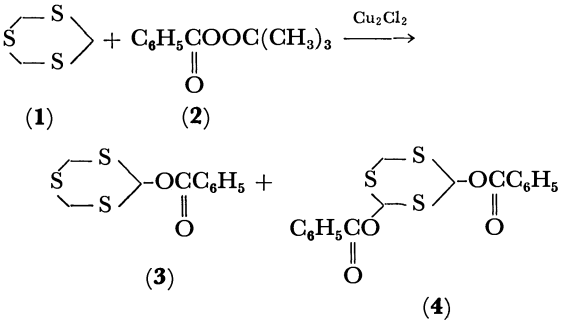

The highest yield (70—80% based on the unrecovered trithiane) of 2-benzoyloxy-1,3,5-trithiane (**3**) was obtained when 0.7 mol of the peroxy ester **2** was used per mole of **1**. When a mixture of 3.0 mol of the peroxy ester **2** and 1.0 mol of **1** was treated with cuprous chloride in benzene, *cis*-2,4-dibenzoyloxy-1,3,5-trithiane (**4**) was obtained as the main product.

TABLE 1. DISTRIBUTION OF PRODUCTS IN THE REACTION BETWEEN *t*-BUTYL PEROXYBENZOATE AND 1,3,5-TRITHIANE OR ITS DERIVATIVES

Substrate	Peroxy ester (mol/mol substrate)	Relative yield including recovery		
		1	**3**	**4**
1	0.5	1.5	1.0	—
1	0.7	0.4_5	1.0	0.1
1	1.0	1.0	1.0	0.25
1	2.0	0.01	1.0	1.5
1	3.0	—	1.0	4.0
3	1.0	—	1.0	1.2

Assignment of the stereochemistry of the product is straight-forward. The PMR spectrum of compound **4** in deuteriochloroform shows a quartet (δ 3.74 and 5.32, J=15.0 Hz) for the ring methylene group, indicating that the two protons are magnetically nonequivalent, and a singlet for the methine protons indicating that they are equivalent. The features are not significantly altered when the solution is cooled to −80 °C. If the compound were of *trans* form, the spectra would show sharp singlets for the methylene and methine protons at room temperature, and two kinds each of methylenes and methines would be observed at low temperatures as bis(phenylthio)trithiane did.[4]

The absence of 2,2-dibenzoyloxy-1,3,5-trithiane or other geminally disubstituted products and the sole formation of the *cis*-disubstituted isomer deserves special attention.[5] Benzoyloxylation with *t*-butyl peroxybenzoate has been extensively studied and the mechanism has been established as follows.[6] **2** is decomposed catalytically by cuprous ion to *t*-butoxy radical and cupric benzoate at the initial step. The *t*-butoxy radical thus formed abstracts a hydrogen from the substrate to form a radical R· and *t*-butyl alcohol. The radical R· is oxidized by cupric ion to the corresponding carbonium ion which then reacts with the benzoate ion to form a benzoate ester.

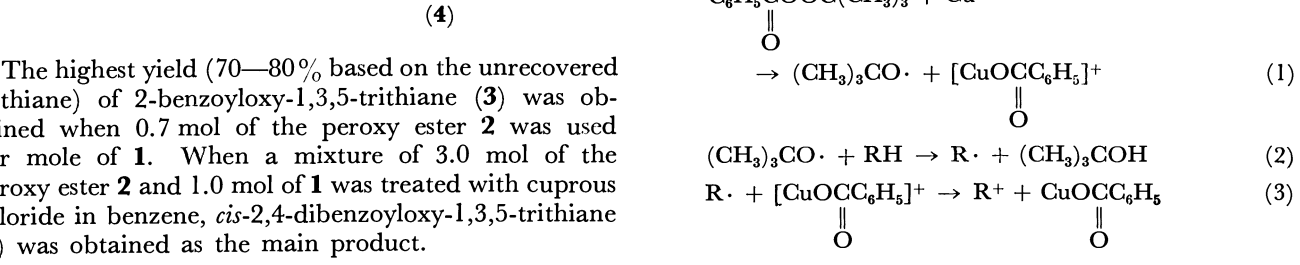

$$R^+ + CuOCC_6H_5 \rightarrow ROCC_6H_5 + Cu^+ \quad (4)$$

Although the rate-determining step is generally step 2, if the free radical formed is reluctant to release an electron, the net reaction would hardly proceed at all.[7] Thus steps 2 and 3 are important in determining whether the reaction occurs easily or with difficulty. The lack of *gem*-dibenzoyloxy compound in the product may be interpreted by assuming either a slow step 2 due to the electron-defficient hydrogen to be removed by an electron-demanding *t*-butoxy radical or a slow step 3 because of the possible instability of a carbonium ion which possesses electronegative substituents. Either case seems possible but we prefer the former for the following reasons.

Firstly, if benzoyloxytrithianyl radical (**5**) is formed easily but step 3 is very slow, **5** may abstract hydrogen from other sources. This indicates that products like **4** have a strong possibility of existing as a *cis-trans* mixture but none of the isomers of **4** was detected.[8] Secondly, the carbonium ion (**6**) to be formed may not be too unstable because of the participation of p-electrons of oxygen and sulfur atoms. Nakai and Okawara reported such stable tri-hetero-substituted carbonium ions.[9]

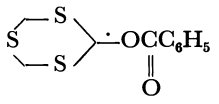

(**5**)

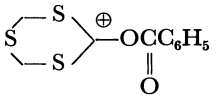

(**6**)

The stereoselectivity of the reaction may be explained on the basis of either thermodynamic or kinetic control. The thermodynamic control of the products cannot be ruled out because of the failure in an equilibration experiment. However, the authors are inclined to consider that the stereoselectivity is of the kinetic origin. The stereospecific formation of 2-methylene-*trans*-5-*t*-butylcyclohexyl benzoate (**8**) is known for the reaction between 4-*t*-butyl-1-methylenecyclohexane (**7**) and *t*-butyl peroxybenzoate and is interpreted by assuming the preferred axial-side attack with the benzoate anion on a carbonium ion produced by the oxidation of the radical.[10]

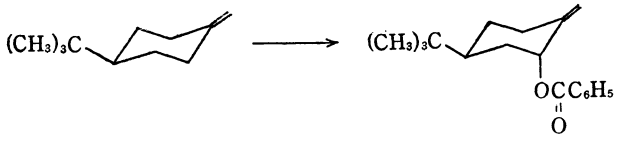

(**7**) (**8**)

Since the benzoyloxy group in 1,3,5-trithiane takes axial conformation as will be discussed later, the benzoate anion attacking from the axial side should form the *cis*-dibenzoate. It is not yet clear whether the cause for the preferred axial attack is the same in the cases of cyclohexane and trithiane series.

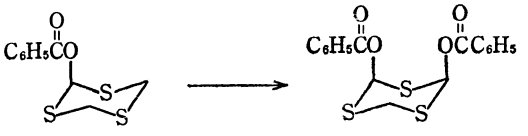

Table 2. Comparison of the reactivities of sulfides toward *t*-butyl peroxybenzoate[a]

Substrate	Total yields of benzoates (%)	Half-Lives of peroxybenzoate[b] (min)
1	70—80	2
9	70	8
12	50	75

a) Molar ratios were 0.5 and 0.07 for the peroxybenzoate and cuprous chloride, respectively, per mole of substrate. b) The half-lives were determined by iodometric titration.

Reaction of 1,3-dithiane (**9**) and thiane (**12**) with *t*-butyl peroxybenzoate was carried out as in the case of 1,3,5-trithiane. Yields and half-lives of the peroxy ester as revealed by iodometry are summarized in Table 2. It is evident that thiane is the least reactive among the compounds tested, and dithianes and trithianes react more easily. It was also noted that the reaction with thiane gave 15% methyl benzoate and 2—3% biphenyl in contrast to the absence of these by-products in the cases of dithiane and trithiane. This means that the methylene between two sulfur atoms is much more reactive than the others and the following product analysis is consistent with the idea.

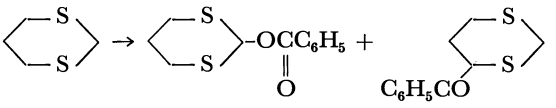

(**9**) (**10**) (**11**)

Since dithiane has three kinds of methylene groups, three kinds of mono-benzoyloxylated products are expected. The structural assignment for the isomers should be easy from the PMR spectra. 2-Benzoyloxy-1,3-dithiane (**10**) was too unstable to be isolated in the air. Thus the reaction mixture was treated with benzenethiol for conversion into 2-phenylthio-1,3-dithiane which was characterized. Identification and estimation of the yields of **10** were performed with a PMR signal at 6.68 ppm which is close to the chemical shift of the methine proton of 2-benzoyloxy-1,3,5-trithiane and thus is assigned to the proton at the foot of the benzoyloxy group. Similarly 4-benzoyloxy-1,3-dithiane was identified by a signal at 6.08 ppm; this chemical shift is close to that of the methine proton of 2-benzoyloxythiane.

The product ratio seems to reflect the reactivities of the methylenes[11] since the reverse of the final reaction, coupling of the ions, is assumed to be very slow. Thus, the relative reactivity of position 2 of 1,3-dithiane is found to be 10.0±1.0 after correction was made as regards the statistical factor, the reactivity of position 4 of 1,3-dithiane being taken as unity and that of 5 practically zero. Thus the methylene between two sulfur atoms is more reactive than the methylene next to one sulfur atom and the methylene beta to a sulfur atom is still less reactive. The smaller half-life of the peroxy ester, when mixed with trithiane, can be attributed to the presence of three methylene groups of the enhanced reactivity.

One of the reaction products from thiane (**12**) and *t*-butyl peroxybenzoate was found to be 2-benzoyloxy-

thiane (**13**) and was purified by chromatography. However, the reaction gave another product which was not identified.

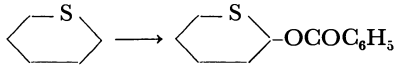

(**12**) (**13**)

Conformation of the Benzoyloxy Derivatives. The PMR spectrum of 2-benzoyloxythiane in carbon tetrachloride showed a near-triplet signal for the methine proton at position 2 at 5.98 ppm from the internal TMS. The half-band width of the signal was 7.2 Hz. These features of a methine proton in six-membered rings are characteristic of equatorially oriented ones.[12] The benzoyloxy group should be axial at least mainly at room temperature. The signal shape of the methine proton, as measured in a mixture of chloroform and carbon disulfide, was not altered even though the temperature was lowered from the ambient to −90 °C. The results are best interpreted by assuming that the conformation of 2-benzoyloxythiane is almost fixed in the benzoyloxy-axial form even at room temperature. No evidence for the presence of the benzoyloxy-equatorial form was obtained even though the spectra were determined in various solvents.

Studies were carried out on the anomeric effect in oxane derivatives. The alkoxy-equatorial form was reported by some authors to be present to the extent of 20—30%[13] but in very small amount by others.[14] The result presented here corresponds to an extreme case even in the oxane series and indicates that no significant difference is caused by replacing an oxygen atom by a sulfur in the heterocyclic system. The only report on the anomeric effect in thiane series also suggests that the alkoxy-axial form is present to the extent of *ca.* 80%.[15]

The PMR spectrum of 2-benzoyloxy-1,3,5-trithiane in deuteriochloroform at 34 °C is shown in Fig. 1 together with an expanded spectrum of the methylene region. The signals at the higher field, assigned to equatorial protons of the methyl groups,[16] appear as triplets with coupling constant of 0.9 Hz and are smaller in height than the counterparts of the AB signal. The phenomenon can be attributed to the W-letter coupling and may be taken as evidence supporting the view that this compound exists solely in the benzoyloxy-axial form, since if the ring were to invert rapidly, the small couplings would have been averaged out to disappear. Another piece of evidence for the assignment of the conformation is obtained by comparing the chemical shifts of the methylene protons: the chemical shift difference, 1.24 ppm, is much greater than that for the methylene protons of 1,3,5-trithiane, 0.76 ppm,[17] and this variation is only explainable by assuming the insertion of an axial benzoyloxy group to trithiane. Thus 2-benzoyloxy-1,3,5-trithiane is seen to exist in the benzoyloxy-axial conformation. The PMR spectrum of this compound in a mixture of deuteriochloroform and acetone-d_6 at −80 °C shows no significant variation from that at room temperature. Thus the conformation of 2-benzoyloxy-1,3,5-trithiane is almost exclusively the benzoyloxy-axial form. No evidence for the presence of the benzoyloxy-equatorial conformation was obtained.

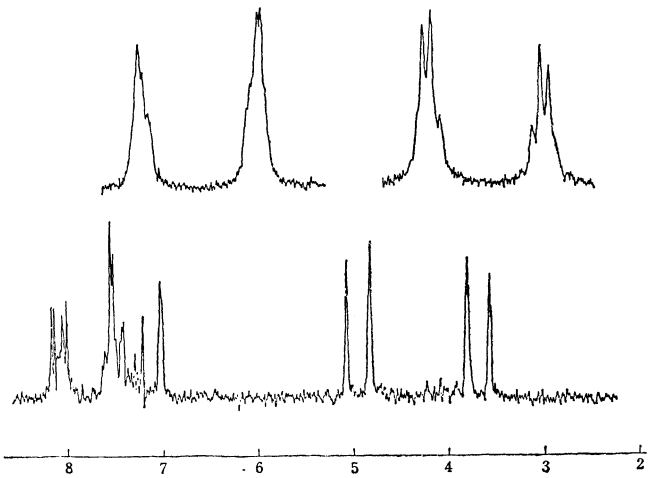

Fig. 1. Below: PMR spectrum of 2-benzoyloxy-1,3,5-trithiane in $CDCl_3$-CS_2 at 34 °C.
Above: Expanded (× 5) spectrum of the AB part for the ring methylenes.

PMR spectra of 2-benzoyloxy-1,3-dithiane in a mixture of deuteriochloroform and carbon disulfide showed a similar feature. A broad signal at 6.68 ppm, assigned to the methine proton at position 2, showed no temperature dependency. The expanded spectrum revealed that the signal was of triplet nature. These results suggest that this compound also exists in the benzoyloxy-axial conformation.

The methine proton signal of 4-benzoyloxy-1,3-dithiane appeared at 6.08 ppm as a near-triplet with a coupling constant of *ca.* 3 Hz and a half-band width of 9 Hz. These results can best be interpreted by assuming the equatorial proton at position 4. This indicates the predominance of the axial benzoyloxy group. The spectral feature was essentially unchanged, though the temperature was lowered to −80 °C.

The PMR spectrum of *cis*-2,4-dibenzoyloxy-1,3,5-trithiane showed similar features to those of the monobenzoyloxy compound. Two signals due to the equatorial proton of the methylene group showed a triplet nature, the coupling constant being estimated to be *ca.* 1 Hz. The spectrum was not significantly altered even at −80 °C. The shape of the signal was practically the same in various solvents. The difference in the chemical shift of the AB protons in deuteriochloroform was 1.58 ppm and greater than that for the methylene protons of 1,3,5-trithiane: compared with the difference between 2-benzoyloxy-1,3,5-trithiane, it almost doubles and the results are expected because two benzoyloxy groups are inserted to trithiane this time. Thus it is concluded that *cis*-2,4-dibenzoyloxy-1,3,5-trithiane exists solely in the benzoyloxy-axial form. The 1,3-diaxial conformation is strongly disfavored in cyclohexane series[18] but, in trithiane series, the diaxial interaction may be relieved to some extent because of the longer distance of the C-S than the C-C and also the strong anomeric effect.[19]

Experimental

Reaction of Cyclic Sulfides with t-Butyl Peroxybenzoate. To a refluxing solution of 0.04 mol of the substrate in 350 ml of anhydrous benzene was added an appropriate amount of a 50 vol% solution of *t*-butyl peroxybenzoate in benzene and 0.05—0.1 equivalent of cuprous chloride. The resulting mixture was heated under nitrogen. The reaction was monitored by checking the decrease in carbonyl absorption of the peroxybenzoate (1760 cm^{-1}) and was stopped when the carbonyl band disappeared. It took about 40 min for trithiane and dithiane, and about 4 hr for thiane. After the mixture had been cooled to room temperature, it was quickly filtered through a potassium carbonate layer to remove the cupric-cuprous salt and acidic materials. Evaporation of the solvent under reduced pressure below 40 °C gave a crude product which was purified by either chromatography or recrystallization.

*2-Benzoyloxy-1,3,5-trithiane (**3**)*, mp 137—138 °C, was best prepared by treating 1,3,5-trithiane with 0.7 molar peroxy ester and was purified by recrystallization from 1 : 1 benzene–hexane. Found: C, 46.49; H, 3.90; S, 37.23%. Calcd for $C_{10}H_{10}O_2S_3$: C, 46.63; H, 3.86; S, 37.06%. IR (Nujol): 1720 cm^{-1}. NMR ($CDCl_3$, δ from TMS): 3.71 and 4.95 (quartet, J=15.0 Hz, 4H), 7.05 (broad singlet, 1H), 7.30—8.20 (multiplet, 5H).

The compound slowly deteriorated in the air unless stored in a desiccator.

cis-*2,4-Dibenzoyloxy-1,3,5-trithiane (**4**)*, mp 156 °C, was best prepared by treating 1,3,5-trithiane with 3 molar peroxy ester and was purified by recrystallization from 7 : 3 benzene–hexane. Found: C, 53.92; H, 3.73%. Calcd for $C_{17}H_{14}O_4S_3$: C, 53.78; H, 3.93. IR (Nujol): 1720 cm^{-1}. NMR ($CDCl_3$, δ from TMS): 3.74 and 5.32 (quartet, J= 15.0 Hz, 2H), 7.17 (broad singlet, 2H), 7.50—8.20 (multiplet, 10H).

*2-Benzoyloxy-1,3-dithiane (**10**)* was found to be labile. It decomposed in the air with a half-life of *ca.* 5 min at 20 °C, unless prevention against moisture was provided. The reaction mixture was therefore treated under a dry atmosphere. 1,3-Dithiane was treated with an equimolar peroxybenzoate and the mixture was treated as above. After evaporation of the solvent, the mixture was heated at 60 °C under 2 mmHg pressure to remove unchanged dithiane as far as possible. Thus **10** with a purity of *ca.* 80% was obtained, the main impurity being 4-benzoyloxy-1,3-dithiane (**11**). IR (neat): 1720 cm^{-1}. NMR(CCl_4, δ from TMS): 2.0—3.6 (multiplet, 6H), 6.68 (broad singlet, 1H), 7.30—8.20 (multiplet, 5H).

*4-Benzoyloxy-1,3-dithiane (**11**)* was obtained as a by-product of the reaction between 1,3-dithiane and the peroxy ester. IR (neat): 1720 cm^{-1}. NMR (CCl_4, δ from TMS): 4.41 and 3.40 (quartet, 2H), 6.01 (triplet, 1H), 7.30—8.20 (multiplet, 5H).

Since both **10** and **11** were unstable compounds, they were converted into phenylthiodithianes for the sake of confirmation by the following procedure. Three molar excess of benzenethiol was added to a freshly prepared solution of benzoyloxylated dithianes in benzene and the mixture was heated at 80 °C for 3 hr. After removal of the solvent, the residue was chromatographed on alumina. 2-Phenylthio-1,3-dithiane, mp 59—60 °C, was eluted with 3 : 7 benzene–hexane and 4-phenylthio-1,3-dithiane, a glass, was eluted with 1 : 1 benzene–hexane. 2-Phenylthio-1,3-dithiane: Found: C, 52.31; H, 5.29; S, 41.87%. 4-Phenylthio-1,3-dithiane: Found: C, 52.86; H, 5.28; S, 41.92%. Calcd for $C_{10}H_{12}S_3$: C, 52.58; H, 5.29; S, 42.11%.

*2-Benzoyloxythiane (**13**)* was obtained as the main product when an equimolar mixture of thiane and the peroxy ester was treated as above. The compound deteriorated unless chromatography was carried out on neutral alumina at low temperature (−4∼−6 °C). Elution with 2 : 8 benzene–hexane gave the desired compound as a colorless oil. IR (neat). 1720 cm^{-1}. NMR (CCl_4, δ from TMS): 5.98 (near triplet, 1H): 1.20—1.35 (multiplet, 8H), 7.20—8.12 (multiplet, 5H).

The compound was unstable and thus was converted into 2-phenylthiothiane, an oil, by the above procedure. The following analytical data were obtained for a substance after purification by chromatography. Found: C, 63.08; H, 6.42; S, 30.33%. Calcd for $C_{11}H_{14}S_2$: C, 62.80; H, 6.71; S, 30.48%.

PMR Measurement. The PMR spectra were recorded on a Hitachi R-20B spectrometer equipped with a temperature variation accessory operating at 60 MHz. Temperature was read by the difference in chemical shift of methyl and hydroxy protons of methanol.

References

1) A. A. Hartmann and E. L. Eliel, *J. Amer. Chem. Soc.*, **93**, 2572 (1972).
2) M. Fukunaga, K. Arai, H. Iwamura, and M. Ōki, This Bulletin, **45**, 302 (1972): M. Fukunaga, T. Sugawara, and M. Ōki, *Chem. Lett.*, **1972**, 55.
3) D. J. Rawlinson and G. Sosnovsky, *Synthesis*, **1** (1972).
4) M. Ōki, T. Sugawara, K. Arai, and M. Fukunaga, presented before the fourth International Congress of Heterocyclic Chemistry, Salt Lake City, Utah, July 13, 1973, Abstract P. 209.
5) The lack of *gem*-dihalogenation is well known, an example being bromination of xylenes which gives bis(bromomethyl)benzene. However, dibenzoyloxylation under similar conditions has not been reported.
6) J. K. Kochi, *Tetrahedron*, **18**, 482 (1962).
7) J. K. Kochi and D. M. Mog, *J. Amer. Chem. Soc.*, **87**, 522 (1965).
8) There is a possibility that the *cis* isomer is thermodynamically so stable that the *trans*-form is not detected. Equilibration of *cis* and *trans* 2,4-dibenzoyloxy-1,3,5-trithiane should shed light on this problem. However, **4** is thermally unstable, giving only intractable materials on being treated with acids.
9) T. Nakai and M. Okawara, This Bulletin, **43**, 1864 (1970).
10) B. Cross and G. H. Whitham, *J. Chem. Soc.*, **1961**, 1650.
11) C. Walling, *J. Amer. Chem. Soc.*, **85**. 2084 (1963).
12) A. Hassner and C. Heathcock, *J. Org. Chem.*, **24**, 1886 (1961).
13) A. J. de Hoog, H. R. Buys, C. Altona, and E. Havinga, *Tetrahedron*, **25**, 3365 (1969).
14) E. L. Eliel and C. A. Giza, *J. Org. Chem.*, **33**, 3754 (1968).
15) N. S. Zefirov, V. S. Blagoveschensky, I. V. Kazimizchik, and O. P. Yakovleva, *Zh. Org. Khim.*, **7**, 594 (1971).
16) E. Campaigne, N. F. Chamberlian, and B. E. Edwards, *J. Org. Chem.*, **27**, 135 (1962).
17) J. E. Anderson, *J. Chem. Soc., B*, **1971**, 2030.
18) E. L. Eliel, N. L. Allinger, S. J. Angyal, and G. A. Morrison, "Conformational Analysis," John Wiley & Sons, New York (1965), p. 55.
19) M. Ōki, T. Sugawara, and H. Iwamura, *Chem. Lett.*, **1973**, 997.

Reactions of Iodocarbenoid of Zinc. II.[1] The Iodocyclopropanation of Olefins with Diethylzinc and Iodoform[2]

Sotaro MIYANO and Harukichi HASHIMOTO

Department of Applied Chemistry, Faculty of Engineering, Tohoku University, Arakami, Sendai 980

(Received December 20, 1973)

The iodocyclopropanation of olefins by the iodocarbenoid of zinc generated from diethylzinc and iodoform was investigated. When the reaction was carried out in a neat olefin, cyclohexene, 1-hexene, *cis*-2-butene, isobutene, and styrene gave the corresponding iodocyclopropanes in yields of 70, 34, 63, 55, and 44% respectively, showing that the CHI_3–Et_2Zn system is a convenient route for iodocyclopropanes. The reaction with cyclohexene was investigated in some detail. *syn*-7-Iodonorcarane easily gave 3-ethylcycloheptene upon treatment with diethyl zinc in the presence of zinc iodide.

Various carbene and carbenoid reagents are available for the cyclopropanation of olefins.[3] However, there seem to be only a few reports describing the iodocyclopropanation of olefins by iodocarbene or iodocarbenoids.[4-6] In 1971, Nishimura and Furukawa reported the formation of 7-iodonorcaranes from cyclohexene in trace amounts by a reaction with diethylzinc and iodoform in a light petroleum medium.[5] In the preceding paper,[1] we ourselves reported that, in the ring-expansion of benzene by the CHI_3–Et_2Zn system, the dilution of the substrate (benzene) with hexane caused a remarkable reduction in the yield of 7-ethyltropilidene. This was ascribed to the consumption of the iodocarbenoid reagent of zinc in the formation of propylene. These observations prompted us to examine the iodocarbenoid reaction with diethylzinc and iodoform in neat olefins; in this paper we wish to describe a convenient synthetic route for iodocyclopropanes.

Results and Discussion

Reaction of Diethylzinc and Iodoform in Neat Cyclohexene. The addition of iodoform to an equimolar quantity of diethylzinc in cyclohexene resulted in an exothermic reaction, with the precipitation of white solids. Hydrolysis with aqueous hydrogen chloride gave an organic layer which was analyzed on glc. The results are summarized in Eq. (1):

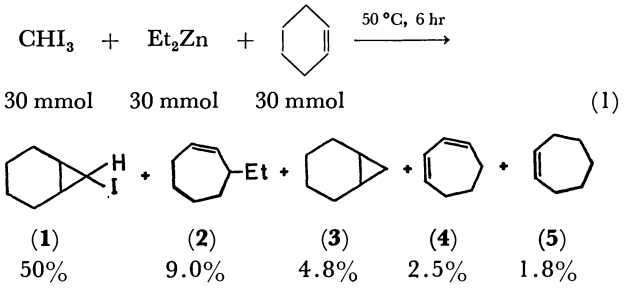

Figure 1 shows the effects of the amount of diethylzinc on the reaction. The quantitative formation of ethyl iodide and the consumption of a part of the reagents in the formation of propylene upon the treatment of diethylzinc and iodoform were reported in the previous paper.[1]

The 7-iodonorcaranes (**1**) were separated as a mixture of *syn*- and *anti*-isomer[7] after a usual work-up of the reaction mixture. The structures were confirmed by elemental analysis, by studying the NMR spectra, and by the formation of norcarane by the Na–MeOH–H_2O reduction according to the method described by Dale and Swartzentruber.[8] The *syn*- and *anti*-7-iodonorcarane were assigned on the basis of the facts that: (1) the alkylsubstituents on a cyclopropane ring would shield the *cis* H_7 more than the *trans* H_7,[9] (2) in cyclopropanes a coupling constant of vicinal-ring protons is generally $J_{cis} > J_{trans}$,[10] and (3) halocarbenoids tend to yield the more sterically-crowded *syn*-isomers.[7,11] The assignment is consistent with that for 7-bromonorcaranes reported by Seyferth *et al.*[10]

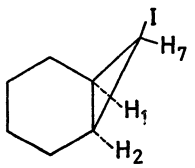

syn-**1**

H_7; $\delta = 3.05$ (triplet)
$J_{1,7}$; 7.05 Hz

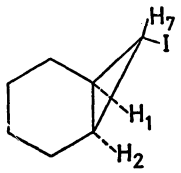

anti-**1**

H_7; $\delta = 2.05$ (triplet)
$J_{1,7}$; 4.2 Hz

Diethylzinc reacts with a 2-molar amount of iodoform in the iodocyclopropanation of cyclohexene, since when the molar ratio of diethylzinc to iodoform is less than 1/2, the molar amount **1** is greater than that of the diethylzinc used (Eq. (2)):

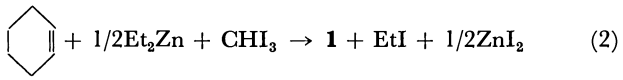

3-Ethylcycloheptene (**2**), norcarane (**3**), 1,3-cycloheptadiene (**4**), and cycloheptene (**5**) were characterized by comparing their retention times on glc and on the basis of their NMR and IR spectra. Magid *et al.* reported the stereospecific formation of 7-methylnorcarane from **1** upon treatment with methyllithium.[6a] On the contrary, **1** was almost inactive toward diethylzinc in benzene. It may be concluded, however, from the effects of the amount of diethylzinc on the product composition shown in Fig. 1 and from the following results, that the **2**, **4**, and **5** were formed in the subsequent reactions of *syn*-**1** in the presence of an excess of EtZnX (X=Et or I). Diethylzinc was allowed to react with a mixture of *syn*- and *anti*-**1** in the presence of zinc iodide in benzene at 50 °C for 5 hr. Almost all of the latter was recovered unchanged, but the former was consumed to give **2**, **4**, and **5**, **2** being the major product. These results are consistent with

Table 1. Reaction of several Olefins with Et_2Zn-CHI_3

Olefin	ml	Et_2Zn mol×10	CHI_3 mol×10	Reaction temp. (°C)	Iodocyclopropane yield (%)[a]	*Syn*/*Anti* ratio
Cyclohexene	30	0.10	0.30	50	35	53/47
	30	0.30	0.30	50	50	45/55
	30	0.45	0.30	50	38	34/66
	30	0.30	0.30	0	70[b]	66/34
n-1-Hexene	100	1.0	3.0	50	34	67/33
cis-2-Butene	20	0.20	0.30	0—20	63[b]	69/31
Isobutene	20	0.25	0.30	0—20	55[b]	
Styrene	100	1.0	3.0	50	44	

a) Based on iodoform, and determined by glc. b) Diethylzinc was added to iodoform in olefin.

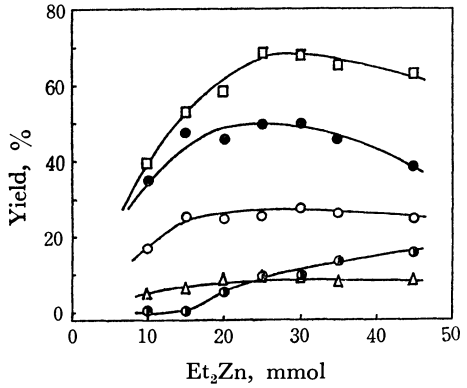

Fig. 1. Effect of the amount of Et_2Zn.
CHI_3 (30 mmol) was added over 1-hr period to a Et_2Zn in cyclohexene (30 ml) at 50 °C, and the reaction was continued for an additional 5 hr.
□: total products (**1**+**2**+**3**+**4**+**5**).
●: *syn*- and anti-7-iodonorcarane (*syn*-**1**+*anti*-**1**).
○: *anti*-7-iodonorcarane (*anti*-**1**).
◑: 3-ethylcycloheptene (**2**).
△: norcarane, 1,3-cycloheptadiene, and cycloheptene (**3**+**4**+**5**).

the assumption that, in a concerted cyclopropane ring-opening, a preferred inward rotation of *cis* groups to the leaving iodide leads to a stable allylic cation from the *syn*-**1**, as was suggested by DePuy *et al.*[12] In the *anti*-**1**, the outward rotation of the *trans* groups is prevented and a concerted ring-opening may also be forbidden (Eqs. (3) and (4)):

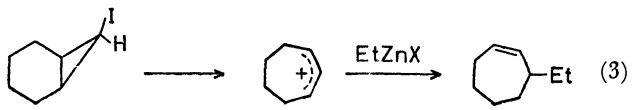

(3)

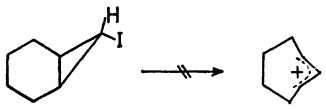

(4)

The *syn*-**1** was thermally less stable than the *anti*-isomer, and it easily gave **4** even during a glc analysis when a glc apparatus was operated at a high temperature. Ando *et al.* reported a similar transformation of *syn*-1-chloronorcarane into **4** upon treatment in quinoline at 200 °C.[13] The precise mechanism for the formation of the reduced products (**3** and **5**) is not yet clear.

Iodocyclopropanation of Several Olefins. Table 1 shows the results of the iodocyclopropanation of several olefins. Cyclohexene gave **1** in the yield of as much as 70% when diethylzinc was allowed to react with iodoform in cyclohexene at 0 °C. The reaction temperature is one of the important reaction variables; Nishimura and Furukawa reported that the yield of **1** was 10% when the reaction was carried out in refluxing cyclohexene.[5] On the other hand, when the reaction temperature was kept at —5—0 °C; 1-hexene gave the 1-iodo-2-*n*-butylcyclopropanes in only a 9.8% yield, and methylene iodide was obtained as the major product. It seems to be formed by the hydrolysis of the iodocarbenoid of zinc (Eq. (5)):

$$EtZnX + CHI_3 \xrightarrow{-EtI} I_2CHZnX \xrightarrow{H_2O} CH_2I_2 \qquad (5)$$

cis-2-Butene afforded the corresponding epimeric pair of 1-iodo-*cis*,*cis*- and 1-iodo-*trans*,*trans*-2,3-dimethylcyclopropane, and no 1-iodo-*cis*,*trans*-dimethyl isomer was detected in the reaction mixture, showing a stereospecific[14] CHI addition to *cis*-2-butene.

n-Butyl vinyl ether was polymerized vigorously upon treatment with diethylzinc and iodoform at room temperature,[15] and it failed to produce the cyclopropanated products.

When styrene was subjected to a reaction, the iodocyclopropanation of ethylene linkage preceded the ring-expansion of the benzene nucleus,[1] but it was accompanied by the formation of a large amount of polystyrene (Eq. (6)):

$$CHI_3 + Et_2Zn + PhCH{=}CH_2 \longrightarrow$$

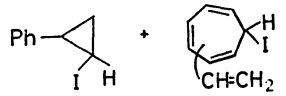

(6)

44% 8.7%

The isolated iodocyclopropanated product[16] seemed to be a mixture of *syn*- and *anti*-1-iodo-2-phenylcyclopropane, but the two isomers were not differentiated from each other because of their complex NMR spectrum.

We proposed a free-radical-chain mechanism involving the homolytic abstraction of the iodo radical from CH_2IX for the formation of a zinc-carbenoid

reagent from diethylzinc and CH_2IX (X=I, Cl).[9] It may be concluded that a similar mechanism is also applicable to the CHI_3–Et_2Zn system for the formation of iodocarbenoid of zinc, in view of the facts that the system is known to catalyze the radical polymerization of vinyl monomers, such as styrene and methyl methacrylate,[15] and that the iodide in CHI_3 seems to be more easily abstracted homolytically than that in CH_2IX.

Several methods have been reported to afford iodocycloproanes,[4-6,18-20] but where sufficient amounts of the starting olefins are available the CHI_3–Et_2Zn system is the preferred method in view of the simplicity of its reaction procedure and the easiness of the isolation of the products.

Experimental

The glc analysis was carried out on a Shimadzu GC 3AF apparatus equipped with hydrogen-flame detectors and two 3 m×3 mm stainless steel columns packed with Diasolid M coated with Silicone DC 550 and Silicone DC 410 respectively. The infrared spectra were obtained with a JASCO Model IR-E spectrophotometer. The NMR data were obtained with a Varian Associates Model A-60D instrument. All the chemical shifts are relative to an internal TMS or benzene reference (*ca.* 5 wt% solution in CCl_4 or benzene). Elemental analysis was performed at the Elemental Analysis Center, Chemical Research Institute of Nonaqueous Solutions, Tohoku University.

Materials. The diethylzinc and iodoform were purified as has been reported before.[1] The 1,3-cycloheptadiene (bp 69.3—70.2 °C/140 mmHg, lit,[21] 121—122 °C/760 mmHg), phenylcyclopropane,[9] and norcarane[9] were prepared according to the methods in the literature. Reagent-grade commercial olefins were purified by the usual methods before use. The materials were stored under nitrogen.

Reaction of Cyclohexene with Diethylzinc and Iodoform. The reaction procedure was almost analogous to that reported for the reaction of benzene with diethylzinc and iodoform.[1] For the identification of the reaction products, a controlled reaction was carried out as follows. Iodoform (40.0 g, 0.102 mol) was added, portion by portion, to a diethylzinc (10 ml, 0.10 mol) solution in cyclohexene (100 ml) over a 2-hr period at 50 °C. The reaction mixture was stirred at 50 °C for another 4 hr, and was then hydrolyzed in an ice-water bath with a dilute aqueous hydrogen chloride solution. After the usual work-up, the distillation of the organic layer gave three fractions: (1) 0.16 g, boiling range 55—56 °C/78 mmHg, (2) 0.71 g, bp 68—68.5 °C/28 mmHg, (3) 6.3 g, 65.5—71 °C/3 mmHg. Glc analysis showed that Fraction 1 was composed of almost equal amounts of cycloheptene (**5**) (NMR: δ 5.85—5.65 (m) for olefinic protons, 2.3—1.9 (br) for allylic protons, IR: 3020 cm^{-1} (>C=CH–), 1650 cm^{-1} (>C=C<)) and norcarane (**3**) (characteristic absorptions of the cyclopropane ring, IR: 3060, 1020 cm^{-1}, NMR: δ 0.8——0.2), plus a trace amount of 1,3-cycloheptadiene (**4**). The retention times of these three substances in glc increased in this order: **5**<**3**<**4** (Silicone DC 550, 110 °C). Fraction 2 was 3-ethylcycloheptene contaminated with a small amount of an unidetified material. NMR: δ 5.7—5.5 (2H, m), 2.3—1.8 (4H, br), 1.8—1.1 (7H, m), 1.1—0.3 (3H, t). IR (liq. film): 3020 cm^{-1} (>C=CH–), 1645 cm^{-1} (>C=C<).

Fraction 3 was essentially pure 7-iodonorcaranes (**1**), and redistillation gave 4.0 g of an analytical sample of a 46 : 54 mixture of *syn*- and *anti*-**1** boiling at 68.5—69.5 °C/3 mmHg. Found: C, 38.04; H, 4.90%. Calcd for $C_7H_{11}I$: C, 37.86; H, 4.99; I, 57.15%. IR (liq. film, cm^{-1}): 3000(m, sh), 2900 (s), 2850(s), 1460(m, sh), 1445 (s), 1355 (m), 1340 (m), 1270(m), 1240(s), 1205(s), 1180(w), 1155(w, sh), 1140(m), 1080(w, sh), 1070(w), 1005(m), 960(w), 950(w), 920(w), 895(w), 830(w), 765(w), 725(w). The *syn*- and *anti*-isomer ratio was determined on the basis of the NMR spectrum and the peak areas on glc (Silicone DC 410 column, 110 °C), the former giving a longer retention time than the latter. When a glc analysis was carried out on a Silicone DC 550 column operated at 170 °C, the *syn*-isomer completely disappeared, giving a new peak the retention time of which coincided with that of 1,3-cycloheptadiene.

Reduction of ***1*** *with Na–MeOH–H_2O.* A 46 : 54 mixture of *syn*- and *anti*-**1** (1.30 mmol) in wet methanol (0.5 ml of water to 10 ml of methanol) was treated with 1.0 g of sodium metal. The reaction mixture was then neutralized with hydrogen chloride and extracted with ether. Glc analysis showed the presence of 0.82 mmol of norcarane (63% based on **1**), 0.17 mmol of unchanged *syn*-**1**, and 0.25 mmol of *anti*-**1**.

The Reaction of ***1*** *with Diethylzinc in the Presence of Zinc Iodide.* To a 43 : 57 mixture of *syn*- and *anti*-**1** (2.06 mmol) and 1.03 mmol of zinc iodide in 10 ml of benzene, we added 0.50 ml of diethylzinc (5.0 mmol). The reaction mixture was then stirred at 50 °C for 5 hr. Glc analysis showed that 98.4% of the *anti*-**1** was recovered unchanged, but 50% of the *syn*-**1** reacted to leave a 27 : 73 mixture of *syn*- and *anti*-**1**, and 0.40 mmol of **2**, 0.064 mmol of **5**, and 0.022 mmol of **4** were detected in the reaction mixture. Upon the similar treatment of **1** with diethylzinc in the absence of zinc iodide, the **1** was recovered almost unchanged and trace amounts of **5** and **4** were detected after the reaction.

Reaction with Styrene. Iodoform was allowed to react with diethylzinc in styrene according to the above procedure except that the iodoform was added over a 1-hr period, after which the reaction was continued for another 5 hr. The distillation of the reaction mixture gave a portion boiling at 74.5—76 °C/6.5 mmHg (0.5 g), which was characterized as a mixture of vinyl-7-ethyltropilidenes on the basis of its NMR and IR spectra. IR (liq. film, cm^{-1}): 985, 900 (vinyl), 1630, 1613, 1595 (polyene structure). After the distillation, 20.5 g of a viscous, dark brown residue remained; this was dissolved in 10 ml of acetone and precipitated with 300 ml of methanol. The precipitate (8.2 g) gave IR absorption spectra (KBr) identical with those of polystyrene film over the wave range from 650 to 3200 cm^{-1}. The methanol solution was distilled to give 5.3 g of 1-iodo-2-phenylcyclopropane (**6**) as a slightly pale yellow liquid boiling at 100—102 °C/3 mmHg (lit,[18] bp 80—81 °C/0.4 mmHg). Found: C, 44.23; H, 3.56%. Calcd for C_9H_9I: C, 44.29; H, 3.72; I, 52.00%. IR (liq. film, cm^{-1}): 3080 (m, sh), 3060(s), 2930(m, sh), 2850(m, sh), 1605(s), 1580(w, sh), 1505(s), 1455(s), 1440(m, sh), 1370(w), 1240(s), 1220(m), 1185(w), 1165(w), 1160—1070(m), 1045(m), 1030(m), 995(m), 960(w), 915(m), 820(m), 770(m), 735(m), 700(s). NMR: δ 7.3—7.0 (5H), 3.1—1.0 (4H, m).

6 (0.40 mmol) in wet methanol (0.5 ml of water to 10 ml of methanol) was treated with 1 g of sodium metal to give phenylcyclopropane in a yield of 77%.

*1-Iodo-2-*n*-butylcyclopropanes (****7****).* Bp 68—71 °C/7 mmHg (5.0 g). Found: C, 37.02; H, 5.96%. Calcd for $C_7H_{13}I$: C, 37.52; H, 5.85; I, 56.64%. IR (liq. film, cm^{-1}): 2950(s, sh), 2925(s), 2855(s), 1460—1440(m, br), 1380(m), 1235(s), 1192(m), 1035(m), 822(m), 735(w). NMR: δ 2.8—2.4 (m, H_1 for *syn*-**7**), 2.3—1.8 (m, H_1 for *anti*-**7**).

In a separate run, diethylzinc (15 ml) was added to iodoform (60 g) in 1-hexene (100 ml) which had been kept at —5—0 °C over a 1-hr period, after which the reaction mix-

ture was kept at 0 °C for 5 hr with stirring. Glc analysis showed that the yield of **7** was reduced to 9.8%; 10.4 g of methylene iodide were recovered by distillation.

1-Iodo-2,3-dimethylcyclopropanes (8). *cis*-2-Butene (*ca.* 20 ml) was distilled into a sealed tube which contained 12 g of iodoform. From the side arm of the tube, 2 ml of diethylzinc were added to the mixture, drop by drop, over a 2-hr period with occasional cooling in an ice-water bath. The reaction mixture was then allowed to stand at room temperature for 1 hr with stirring. After the unchanged butene had been distilled off, the reaction mixture was diluted with ether and treated as usual. A portion boiling at 63—64 °C/29 mmHg was collected as a mixture of *syn*- and *anti*-**8** (2.0 g) (lit,[18] bp 50—52 °C/40 mmHg). Found: C, 29.50; H, 4.79%. Calcd for C_5H_9I: 30.63; H, 4.63; I, 64.74%. IR (liq. film, cm^{-1}): 3025(m, sh), 3000(s, sh), 2950(s), 2925(s), 2870(s, sh), 1455(s, br), 1390(s), 1240(s), 1220(s), 1165(m), 1115(s), 1060(m), 910(w), 750(s). The NMR spectrum was consistent with that of **8**[18]; H_1 for the *syn*-**8**, δ 2.85, $J_{1,3}=7.7$ Hz.

1-Iodo-2,2-dimethylcyclopropane (9). Bp 56—57 °C/51 mmHg (1.5 g) (lit,[18] bp 40—41 °C/20 mmHg). Found: C, 30.97; H, 4.23%. Calcd for C_5H_9I: C, 30.63; H, 4.63; I, 64.74%. IR (liq. film, cm^{-1}): 2950(s), 2840(s, sh), 1465(m, sh), 1450(s), 1440(s), 1380(m), 1280(m), 1195(s), 1123(w), 1086(w), 1035(m), 950(w), 900(m), 825(w). NMR spectrum was consistent with **9**.[18]

References

1) Part I: S, Miyano and H. Hashimoto, This Bulletin, **46**, 3257 (1973).

2) Presented at the 21st Symposium on Organometallic Chemistry, Japan, Sendai, October, 1973.

3) W. Kirmse, "Carbene Chemistry," 2nd ed, Academic Press, New York, N. Y., 1971.

4) a) T. Marolewski and N. C. Yang, *Chem. Commun.*, **1967**, 1225; b) N. C. Yang and T. A. Marolewski, *J. Amer. Chem. Soc.*, **90**, 5645 (1968).

5) J. Nishimura and J. Furukawa, *Chem. Commun.*, **1971**, 1375.

6) a) R. M. Magid and J. G. Welch, *ibid.*, **1967**, 518; b) R. M. Magid, S. E. Wilson, and J. G. Welch, *Tetrahedron Lett.*, **1969**, 4921; c) R. M. Magid and S. E. Wilson, *ibid.*, **1969**, 4925; d) R. M. Magid and J. G. Welch, *ibid.*, **1967**, 2619.

7) The notation follows to Fueno and Nagase's: T. Fueno and S. Nagase, *Kagaku no Ryoiki*, **26**, 441 (1972).

8) W. J. Dale and P. E. Swarzentruber, *J. Org. Chem.*, **24**, 955 (1959).

9) S. Miyano and H. Hashimoto, This Bulletin, **46**, 892 (1973).

10) D. Seyferth, H. Yamazaki, and D. L. Alleston, *J. Org. Chem.*, **28**, 703 (1963).

11) R. Hoffmann, C. C. Levin, and R. A. Moss, *J. Amer. Chem. Soc.*, **95**, 629 (1973).

12) C. H. DePuy, L. G. Schnack, and J. W. Hausser, *ibid.*, **88**, 3343 (1966).

13) T. Ando, H. Yamanaka, S. Terabe, A. Horike, and W. Funasaka, *Tetrahedron Lett.*, **1967**, 1123.

14) Ref. 3), p. 267.

15) J. Furukawa, N. Kawabata, and J. Nishimura, *Kobunshi Kagaku*, **25**, 36 (1968).

16) Nozaki *et al.* prepared (+)-*trans*-1-iodo-2-phenylcyclopropane by the iododecarboxylation of the (+)-*trans*-phenylcyclopropanecarboxylic acid.[17] But the reported NMR and IR spectral data and bp of it are rather different from those of ours.

17) T. Aratani, Y. Nakanishi, and H. Nozaki, *Tetrahedron*, **26**, 1675 (1970).

18) J. P. Oliver and U. V. Rao, *J. Org. Chem.*, **31**, 2696 (1966).

19) C. Kaiser, A. Burger, L. Zirngibl, C. S. Davis, and C. L. Zirkle, *ibid.*, **27**, 768 (1962).

20) H. M. Walborsky, F. J. Impastato, and A. E. Young, *J. Amer. Chem. Soc.*, **86**, 3283 (1964).

21) L. Hafner and W. Rellensmann, *Chem. Ber.*, **95**, 2567)1962).

Spin Trapping of Free Radicals Generated from Arylazo *p*-Tolyl Sulfones[1]

Michio KOBAYASHI, Eri AKIYAMA, Hiroshi MINATO, and Noboru KITO*

Department of Chemistry, Tokyo Metropolitan University, Fukazawa, Setagaya, Tokyo 158

**Sagami Chemical Research Center, 3100 Sagamihara, Ohnuma, Sagamihara, Kanagawa 229*

(Received December 21, 1973)

Arylazo *p*-tolyl sulfones(I) were thermolyzed or photolyzed in the presence of trapping agents such as α,*N*-diphenyl nitrone(II), α-phenyl *N*-*t*-butyl nitrone(III) and 2-methyl-2-nitrosopropane(X). ESR studies showed that phenyl radical or *p*-methoxyphenyl radical is produced from the decomposition of I and adds to II or III. The adduct of phenyl radical to II and that of *p*-methoxyphenyl radiacl to III were synthesized for comparison by separate pathways. The photolysis of phenyl *p*-tolylazo sulfone(Ia) in the presence of III yielded benzhydryl *t*-butyl nitroxide, benzoyl *t*-butyl nitroxide and *t*-butyl *p*-toluenesulfonyl nitroxide(XVI) radicals. The photolysis of Ia in the presence of X gave di-*t*-butyl nitroxide(XII) and XVI. The photolysis of phenylazotriphenylmethane in the presence of X yielded XII and *t*-butyl nitroxide radical. The mechanisms of the formation of these radicals are discussed. The formation of arenesulfonyl radicals from the decomposition of I has been proved indirectly (analyses of the products of the combination of nitroxide radicals with arenesulfonyl radicals) and directly (detection of *t*-butyl *p*-toluenesulfonyl nitroxide radical).

Arylazo *p*-tolyl sulfones(I) decompose when they are heated in neutral or weakly basic media[2] or when they are irradiated by UV light,[3] and the generation of aryl radicals has been proposed on the basis of kinetic studies[4] or product studies (orientation and partial rate factors in arylating various aromatics).[5]

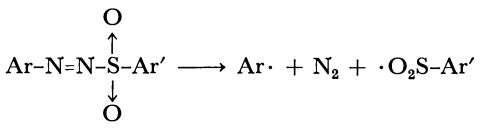

(I)

Ia: Ar=Ph, Ar′=*p*-Tolyl

Ib: Ar=*p*-MeO-C_6H_4, Ar′=*p*-Tolyl

However, no evidence has been presented indicating the formation of arenesulfonyl radicals, since they do not attack aromatics easily.[6,7] Consequently, mechanisms involving only aryl radicals (*i. e.*, not arenesulfonyl radicals) cannot be excluded. A plausible example is the following mechanism, which is similar to the diazoanhydride–acetic anhydride mechanism proposed for the decomposition of N-nitrosoacetanilide by Rüchardt *et al.*[8]

Even the formation of aryl radicals from I has not been proved by physical methods. Spin trapping of aryl and arenesulfonyl radicals has therefore been investigated, and the results are descirbed in this paper.

Results and Discussion

When benzene solutions of phenylazo *p*-tolyl sulfone (Ia) or *p*-methoxyphenylazo *p*′-tolyl sulfone (Ib) were heated or irradiated, ESR spectra did not indicate the presence of aryl radicals. The reactivities of aryl radicals are probably so great that the steady-state concentrations of aryl radicals produced are not large enough for ESR detection.

Trappings[9] of aryl radicals by reactions with α,*N*-diphenyl nitrone (II) or α-phenyl *N*-*t*-butyl nitrone (PBN) (III) were attempted. When benzene solutions of Ia and II (or Ib and II) were mixed at room temperature in the dark, ESR signals were observable. This indicates that free radicals are slowly produced by thermolysis of Ia or Ib at room temperature. When these mixtures were irradiated with a 100-W high pressure mercury lamp, very strong ESR signals composed of 40 hyperfine splittings (shown in Fig. 1a) were observed. The ESR signal patterns of the radicals produced by photolysis were the same as those observed for the radicals produced by thermolysis at room temperature. Thus, the radicals produced by photolysis and thermolysis should be the same.

The following hyperfine splitting constants were cal-

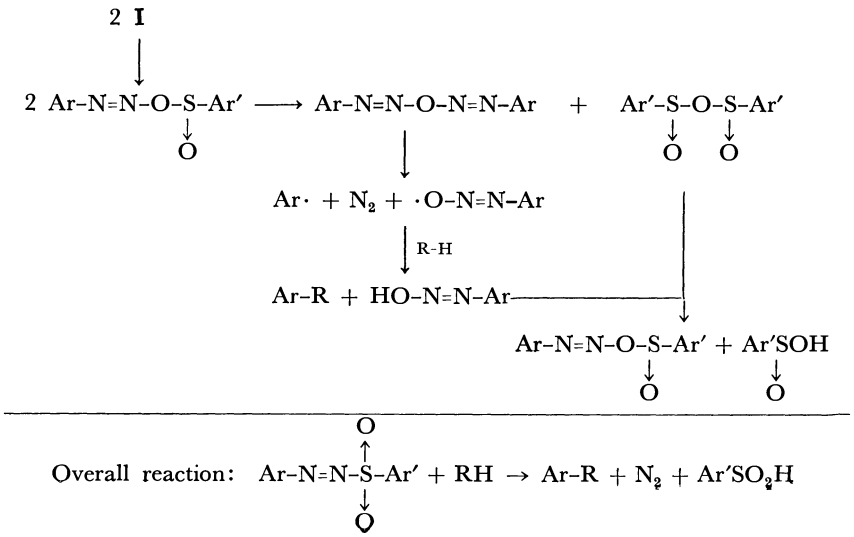

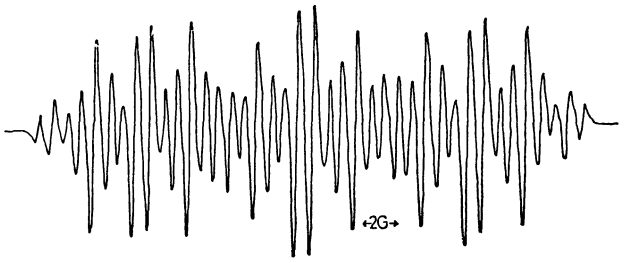

Fig. 1(a). The ESR spectrum of an irradiated mixture of *p*-$MeOC_6H_4N{=}NO_2SC_6H_4Me$-*p* and PhCH=N-Ph (O) in benzene.

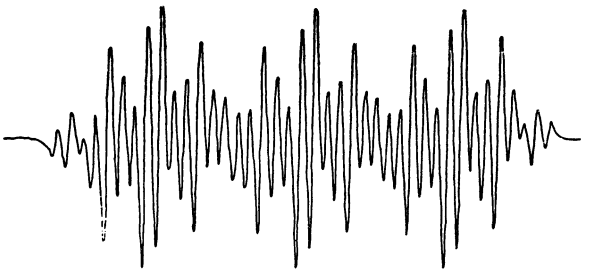

Fig. 1(b). An ESR spectrum obtained by simulation using $A_N=10.01$, $A_{\beta\text{-H}}=3.41$, $A_{o\text{-H}}=2.51$, $A_{m\text{-H}}=0.88$, and $A_{p\text{-H}}=2.51$G.

culated from analysis of the hyperfine splittings.

$A_N = 10.01$	$A_{o\text{-H}} = 2.51$
$A_{\beta\text{-CH}} = 3.41$	$A_{m\text{-H}} = 0.88$
	$A_{p\text{-H}} = 2.51$
	$g = 2.0056$

Simulation was carried out by using these hyperfine splitting constants, the result (Fig. 1b) being in excellent agreement with what was experimentally observed. Thus the radical responsible for the ESR pattern is benzhydryl phenyl nitroxide radical (IVa) shown below.

Ia ⟶ Ph·

Ph· + Ph-CH=N-Ph (O) → Ph-CH(Ph)-N-Ph (O·)

(II) (IVa)

Bluhm and Weinstein[10] trapped the phenyl radical, produced from phenylazotriphenylmethane, by the reaction with II, and the hyperfine splitting constants they reported for radical IVa are approximately the same as those described above.

When Ib was decomposed by irradiation or by heating in the presence of II, ESR signals ascribable to nitroxide radical IVb were observed. The following hyperfine splitting constants were obtained from the analysis of the ESR pattern.

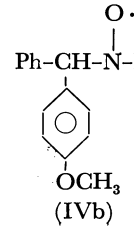

(IVb)

$A_N = 10.0$ $A_{o\text{-H}} = 2.5$

$A_{\beta\text{-H}} = 3.4$ $A_{m\text{-H}} = 0.9$

$A_{p\text{-H}} = 2.5$

When the samples were irradiated at room temperature and the ESR signals were examined after the light was turned off, they were observable for about 15 min. This indicates that radicals IVa and IVb are fairly stable.

ESR studies on the reaction between Ia and nitrone III and that between Ib and III showed the presence of nitroxide radicals Va and Vb, respectively. The following hyperfine splitting constants were obtained.

t-Bu-N=CH-Ph (O) + Ph· ⟶ t-Bu-N(Ph)-CH-Ph (O·)

(III) (Va)

t-Bu-N=CH-Ph (O) + p-MeO-C_6H_4· ⟶ t-Bu-N(·O)-CH(Ph)-C_6H_4-OMe-*p*

(Vb)

	A_N	$A_{\beta\text{-CH}}$	g
Va	13.93	2.09	
Vb	13.91	2.15	2.0061

Concerning Va, Janzen and Blackburn reported that $A_N=13.73$ and $A_{\beta\text{-CH}}=2.08$ G.[11]

In order to prove the structure of IVa, *N*-benzhydryl-*N*-phenylhydroxylamine (VIa) was synthesized from nitrone II and phenylmagnesium bromide, and was oxidized with air in a weakly alkaline (NaOH) aqueous ethanol. The ESR signals observed were exactly the same as those observed when Ia was photolyzed in the presence of II. When VIa was treated with *n*-BuLi in benzene and then irradiated with a high pressure mercury lamp in the presence of air, similar ESR signals ascribable to nitroxide radical IVa were observed.

Ph-N(OH)-$CHPh_2$ $\xrightarrow{OH^-}$ Ph-N(O⊖)-$CHPh_2$ $\xrightarrow{O_2}$ Ph-N(O·)-$CHPh_2$

(VIa) (IVa)

In a similar manner, when an alkaline ethanol solution of *N*-*t*-butyl-*N*-(phenyl-*p*-methoxyphenylmethyl)hydroxylamine (VIb) was oxidized with air or irradiated in the presence of air, nitroxide radical Vb was formed and its ESR signals were identical with those obtained from azosulfone Ib and nitrone III.

t-Bu-N(OH)-CH(Ph)-C_6H_4-OMe-*p* $\xrightarrow[\text{or } h\nu]{OH^-,\ O_2}$ t-Bu-N(O·)-CH(Ph)-C_6H_4-OMe-*p*

(VIb) (Vb)

These data obtained by means of ESR have established that aryl free radicals are formed by thermolysis or photolysis of azosulfones Ia or Ib.

In order to determine the final products from nitroxide radicals IV and V, a mixture of Ia, pyridine (3 mol/mol Ia; added in order to keep the medium weakly alkaline) and nitrone II (1.5 mol/mol Ia) was thermolyzed. Recrystallization of the products gave a compound, which appeared to be *N*-benzhydryl-*N*-phenylhydroxylamine *O*-*p*-toluenesulfonate (VII). It was very unstable, readily isomerizing to *o*- and *p*-benzhydrylaminophenyl *p*-toluenesulfonates (VIII) and (IX), when allowed to stand at room temperature. When the products of thermolysis of Ia-II-pyridine in benzene were separated by column chromatography, VII was not detected and VIII and IX were isolated in 17% and 1% yields (per 100 mol Ia), respectively.

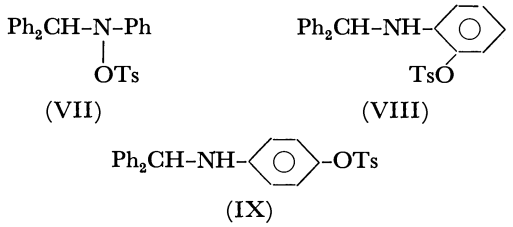

When *N*-benzhydryl-*N*-phenylhydroxylamine (VIa) was allowed to react with *p*-tosyl bromide in pyridine at room temperature, VII was not obtained; isomerization took place during the course of recrystallization and the product isolated was VIII. A similar rearrangement of hydroxylamine-O-esters has been reported.[12]

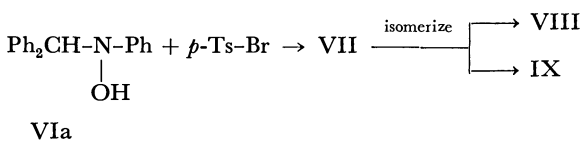

The formation of VII can be ascribed to a combination of nitroxide radical IVa and *p*-toluenesulfonyl radical.

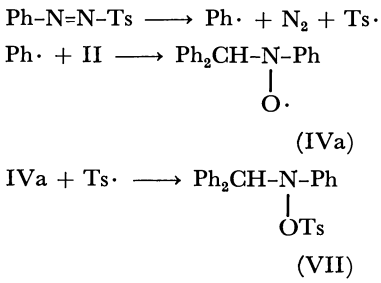

The fact that VII is formed proves indirectly that the decomposition of azosulfone Ia yields *p*-toluenesulfonyl radical in addition to phenyl radical.

In an attempt to trap *p*-tosyl radical with nitrone III, Ia was photolyzed in the presence of excess III at room temperature under various conditions. The presence of two new nitroxide radicals in addition to Va were detected by ESR; A_N=12.5 G and 7.67 G (for Va, A_N=13.93 G). Since these two radicals showed simple triplets without hyperfine splittings due to β-hydrogens, addition of radicals on some nitroso compounds containing only *t*-butyl groups was suspected. When an ethereal solution of Ia was irradiated at 366 nm in the presence of 2-methyl-2-nitrosopropane(X), ESR signals of two radicals were observed; A_N=12.5 G and 15.5 G, and g=2.0060 for both. In order to determine whether or not these radicals arose from trapping of phenyl radical, *p*-tolyl 2,4,6-trideuteriophenylazo sulfone (Ia-d_3) was photolyzed in the presence of X. Since the radicals detected were identical with those formed in the case of Ia, they cannot be the products of trapping of phenyl radical with X.

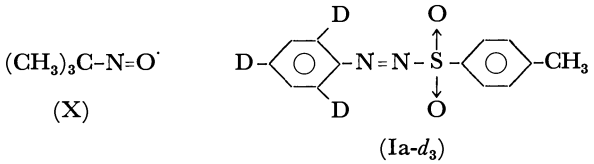

When phenylazotriphenylmethane (XI), another phenyl radical source, was photolyzed in ether in the presence of X, two radicals were detected; one with A_N=12.8 G and $A_{\beta\text{-CH}}$=2.6 G and the other with A_N=15.5 G. When X was irradiated in ether with a sodium lamp (589 nm), the ESR signals obtained were a simple triplet with A_N=15.5 G. Therefore, the radical with A =15.5 G must be di-*t*-butyl nitroxide radical (XII).

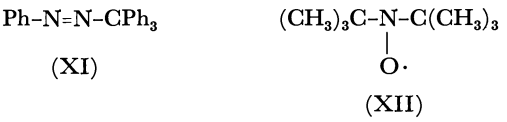

It has been reported that XII is formed by the photolysis of X; A_N=15.7 G[13] or 15.5 G,[14] and also that *t*-butyl phenyl nitroxide (XIII) formed by the trapping of phenyl radical with X shows hyperfine splittings due to *ortho* and *para* hydrogens of the benzene ring.[13,14]

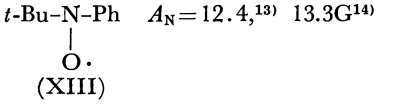

The fact that no XIII was found in the photolysis of Ia in the presence of X can be ascribed to the consumption of phenyl radical by abstraction of α-hydrogens of ether.

The radical with A_N=7.67 G formed in the photolysis of Ia in the presence of III is probably benzoyl *t*-butyl nitroxide radical[11] (XIV) produced by the photolysis of III. It has been reported[15] that upon irradiation nitrone III isomerizes to α-phenyl-*N*-*t*-butyloxazirane (XV), which then yields 2-methyl-2-nitrosopropane (X) and XIV.

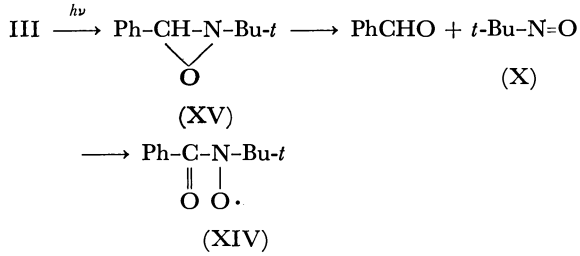

Thus, of the three radicals produced from the photolysis of Ia in the presence of III, the one with A_N=13.93G is Va, that with A_N=7.67 G is XIV, and that with A_N=12.5 G remains to be explained. If this is not XIII, the only possibility seems to be nitroxide radical XVI, which can be formed by the trapping of *p*-toluenesulfonyl radical with X. In order to confirm the

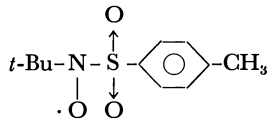

(XVI)

possibility, *p*-toluenesulfonyl iodide, another *p*-tosyl radical source, was irradiated at 589 nm in the presence of X. A nitroxide radical with $A_N=12.5$ G was observed, which is identical with that obtained in the photolysis of Ia or Ib in the presence of X.

The rate of decrease of the ESR signals of XVI was determined after light was turned off, and the nitroxide radical XVI was found to be a fairly stable radical with a half-life of 44 seconds. When an ethereal solution of X was irradiated in the absence of *p*-tosyl iodide, ESR signals observed were those of di-*t*-butyl nitroxide (XII) alone. The following reaction sequence is therefore plausible.

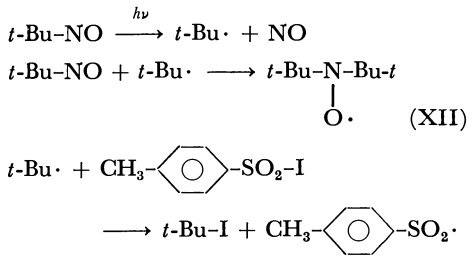

(XII)

Fig. 2(a). The ESR spectrum of an irradiated mixture of PhN=$NO_2SC_6H_4$-Me-*p* and *t*-Bu-N=CH-Ph (O) in benzene ($A_N=13.13$, $A_{\beta\text{-H}}=2.09$; $A_N=12.5$; $A_N=7.67$G).

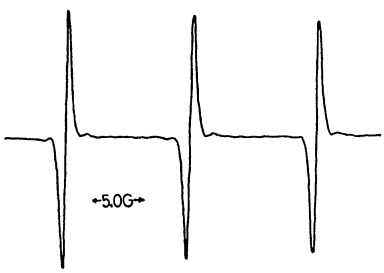

Fig. 2(b). The ESR spectrum of an irradiated solution of *t*-Bu-N=O in ether ($A_N=15.5$G).

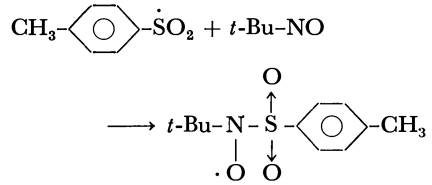

It is possible that *p*-toluenesulfonyl radical is produced by direct photolysis of *p*-toluenesulfonyl iodide itself.[6]

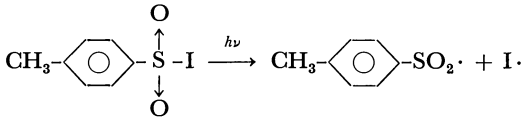

However, since X absorbs at longer wavelength region (near 589 nm), it seems more probable that the *t*-butyl radical produced by photolysis of X abstracts the iodine atom from *p*-tosyl iodide, yielding *p*-tosyl radical and *t*-butyl iodide.

When an ethereal solution of iodobenzene was irradiated in the presence of X, two sets of ESR signals were observed; a triplet with $A_N=15.5$ G and a triplet with $A_N=12.5$ G and with hyperfine splittings. The former is due to XII, and the latter can be ascribed to *t*-butyl phenyl nitroxide (XIII). The formation of XIII can be explained in terms of the following reaction steps: 1) photolysis of X gives *t*-butyl radical, 2) *t*-butyl radical abstracts the iodine atom from iodobenzene, and 3) the phenyl radical formed is trapped

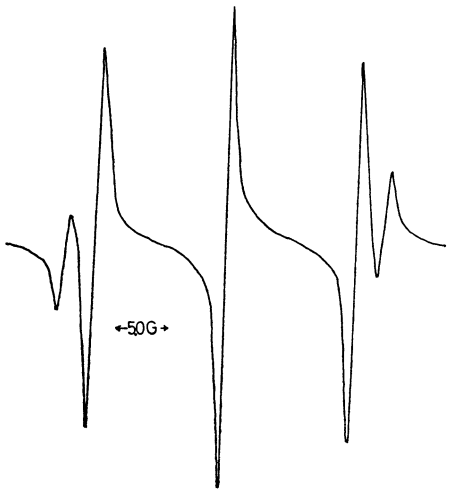

Fig. 2(c). The ESR spectrum of an irradiated mixture of PhN=$NO_2SC_6H_4$Me-*p* and *t*-Bu-N=O in ether ($A_N=12.5$, and $A_N=15.5$G).

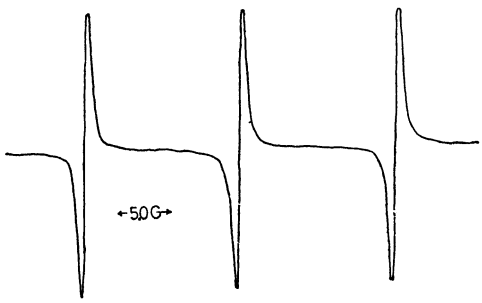

Fig. 2(d). The spectrum of an irradiated mixture of *p*-$MeC_6H_4SO_2I$ and *t*-Bu-N=O in ether ($A_N=12.5$ G).

by X. In contrast with the case of the photolysis of azosulfone Ia in the presence of X, phenyl radical was trapped by X in the photolysis of iodobenzene. In this case, iodobenzene was used in a high concentration, and therefore not all of the phenyl radicals produced were consumed by the reaction with ether.

Thus, the spin trapping experiments with nitrones II, III and 2-methyl-2-nitrosopropane (X) have proved that aryl radicals and sulfonyl radicals are produced by the thermolysis or photolysis of azosulfones Ia or Ib.

Experimental

Materials. Arylazo *p*-tolyl sulfones were synthesized by the addition of aqueous solutions of *p*-toluenesulfinate to aqueous solutions of arenediazonium salts,[4] and recrystallized from methanol. Nitrone II was produced by the condensation of phenylhydroxylamine with benzaldehyde, and recrystallized from ethanol. Nitrone III was synthesized by the following two steps; 1) H_2O_2(90%)-Ac_2O-oxidation of benzylidene-*t*-butylamine to 2-*t*-butyl-3-phenyloxaziridine and 2) isomerization of the oxaziridine by refluxing in acetonitrile for 2 days.[16] It was recrystallized from hexane; mp 76 °C.

ESR Measurements. ESR signals were observed by use of a JES-ME-1X.

Formation of Benzhydryl Phenyl Nitroxide Radical IVa. Benzhydryl bromide, phenylhydroxylamine and sodium acetate were ground in a porcelain mortar. When the mixture was washed with water and then with hexane and the residue was recrystallized from benzene-hexane, *N*-benzhydryl-*N*-phenylhydroxylamine (VIa) was obtained. This hydroxylamine was also synthesized from α,*N*-diphenyl nitrone II and phenylmagnesium bromide.

Oxidation of VIa with HgO or 2,6-dichlorophenol-indophenol sodium was attempted, but was not successful. However, when air was bubbled through a weakly alkaline (NaOH) aqueous ethanol solution of VIa, ESR signals were observed. The same ESR signals were observed when a benzene solution of VIa containing some *n*-butyl lithium was irradiated with a high pressure mercury lamp. The hyperfine splittings of the ESR signals were identical with those obtained from azosulfone Ia and nitrone II, and are ascribable to benzhydryl phenyl nitroxide radical IVa.

Formation of t-*Butyl Phenyl*-p-*methoxyphenylmethyl Nitroxide Radical IVb.* *N*-*t*-Butyl-*N*-(phenyl-*p*-methoxyphenylmethyl) hydroxylamine (VIb) was prepared from α-phenyl *N*-*t*-butyl nitrone and *p*-methoxyphenylmagnesium bromide, and was oxidized by air in a weakly alkaline (NaOH) aqueous ethanol solution. The ESR signals observed were identical with those obtained in the reaction between azosulfone Ib and nitrone III, and are ascribable to *t*-butyl phenyl-*p*-methoxyphenylmethyl nitroxide radical IVb.

Products of the Reaction between Azosulfone Ia and Nitrone II. A mixture of Ia (2.5 g), II(4.0 g), pyridine (4.0 g) and benzene (130 ml) was heated at 91 °C for 3 hr (the half-life of Ia under these conditions is 46 min). The reaction mixture was washed with water and with dilute HCl for removal of pyridine, and then concentrated. The column chromatography (Florisil) of the residue gave biphenyl 10.8, azobenzene 6.1, *o*-benzhydrylaminophenyl *p*-toluenesulfonate (VIII) 17.2 and *p*-benzhydrylaminophenyl *p*-toluenesulfonate (IX) 1.0 mol/100 mol Ia.

Synthesis of VIII. *o*-Nitrophenyl *p*-toluenesulfonate was reduced with $SnCl_2$-HCl, and the *o*-aminophenyl *p*-toluenesulfonate obtained (1.5 g) was heated with benzhydryl chloride (1.0 g) and pyridine (5 ml) at 90 °C for 3 days. The reaction mixture was washed with water and then with dilute HCl, and pyridine was distilled off under reduced pressure. Recrystallization of the residue from hexane-benzene gave VIII; mp 122—123 °C.

Synthesis of IX. A mixture of *p*-aminophenyl *p*-toluenesulfonate (1.5 g), benzhydryl chloride (1.0 g) and pyridine (5 ml) was refluxed for 13 hr and then treated in a manner similar to that described for VIII. Recrystallization from hexane-benzene gave IX; mp 133—134 °C.

Analysis:	C	H	N	M.W.
VIII (authentic)	72.38	5.37	3.13%	
VIII (from Ia and II)	72.87	5.43	3.09	419
IX (authentic)	71.21	5.31	2.99	
IX (from Ia and II)	69.85	5.31	3.41	421
Calcd.	72.8	5.4	3.3	429

Molecular weights were determined by use of the vapor pressure method with a Hitachi-Perkin Elmer Molecular Weight Apparatus 115.

Footnotes

1) Organic Sulfur Compounds. Part 50.
2) C. G. Overberger and A. J. Rosenthal, *J. Amer. Chem. Soc.*, **82**, 108, 117 (1960).
3) M. Kobayashi, S. Fujii, and H. Minato, This Bulletin, **45**, 2039 (1972).
4) M. Kojima, H. Minato, and M. Kobayashi, *ibid.*, **45** 2032 (1972).
5) M. Kobayashi, H. Minato, M. Kojima, and N. Kamigata, *ibid.*, **44**, 2501 (1971).
6) J. M. Squire and W. A. Waters, *J. Chem. Soc.*, **1962**, 2068; C. M. M. de Silva Correa, A. S. Lindsay, and W. A. Waters, *J. Chem. Soc., C.*, **1968**, 1874.
7) M. Kobayashi, K. Tanaka, and H. Minato, This Bulletin, **45**, 2906 (1972).
8) C. Rüchardt and E. Merz, *Tetrahedron Lett.*, **1964**, 2431; C. Rüchardt and B. Freudenberg, *ibid.*, **1964**, 3623.
9) For a recent review, see: G. Janzen, *Accounts Chem. Res.*, **4**, 31 (1971).
10) A. L. Bluhm and J. Weinstein, *J. Org. Chem.*, **27**, 1748 (1972).
11) E. G. Janzen and B. J. Blackburn, *J. Amer. Chem. Soc.*, **91**, 4481 (1969).
12) R. Huisgen and F. Bayerlein, *Ann. Chem.*, **630**, 138 (1960).
13) A. Mackor, Th. A. J. W. Majer, Th. J. de Boer, and J. D. W. van Voorst, *Tetrahedron Lett.*, **1966**, 2115.
14) H. Lemaire and A. Rassat, *J. Chim. Phys.*, **61**, 1580 (1964).
15) A. L. Bluhm and J. Weinstein, *J. Amer. Chem. Soc.*, **92**, 1444 (1970).
16) W. D. Emmons, *ibid.*, **79**, 5739 (1957).

The Reaction of the Hydroxamic Acid Group in Polymer with *p*-Nitrophenyl Acetate[1]

Toyoki KUNITAKE, Yoshio OKAHATA, and Reiko ANDO

Department of Organic Synthesis, Faculty of Engineering, Kyushu University, Fukuoka, 812

(Received February 12, 1974)

Water-soluble copolymers containing protected hydroxamate groups were prepared by radical copolymerization of acetyl *N*-phenylacrylohydroxamate and acrylamide, and the hydroxamic acid group (PHA) was unmasked by treating it with hydroxylamine. In acetylation with *p*-nitrophenyl acetate (1.4 v/v% CH_3CN-H_2O, 30 °C) the PHA unit was less reactive than the corresponding monomeric compound. When the PHA content was low (3 mol%), the reactivity of a given PHA anion (true reacting species) was invariant (9.1 M^{-1} s^{-1}) over a wide range of the dissociation of the PHA unit. However, in the case of the copolymer of a higher PHA content (11 mol %) the reactivity decreased as the neutralization of the PHA anion progressed. This phenomenon was attributed to the intramolecular aggregation of the undissociated PHA side chain. The deacylation rate of the acetylated PHA unit was comparable to those of the monomeric counterparts, in contrast with the acylation process. Finally, the probable role of the PHA unit as catalyst for the ester hydrolysis was discussed.

In the past several years, we have studied the catalytic hydrolysis of phenyl esters by imidazole-containing polymers.[2] Apart from a few exceptional cases,[3] the efficiency of the imidazole catalysis is limited by the rate-determining acylation step.

The hydroxamate anion is known to be highly nucleophilic toward phenyl esters,[4-9] and attempts to use it as catalyst for the hydrolysis of phenyl esters have been carried out by Bender and coworkers in small-molecule systems.[10,11] However, in polymeric systems, introduction of hydroxamic acid groups has not been necessarily straight-forward, and their nucleophilic reactivity was not examined. Thus, in the present study the hydroxamic acid group was introduced into water-soluble polymers and characterized unambiguously, and the reaction with *p*-nitrophenyl acetate(PNPA) was investigated in order to evaluate the usefulness of the hydroxamic acid group in polymer as a catalyst for the ester hydrolysis.

Experimental

All melting points are uncorrected. The UV-visible spectroscopic measurements were made with a Hitachi 124 spectrophotometer. NMR spectra were obtained with a Varian A60 instrument.

Materials. *p*-Nitrophenyl acetate was prepared by acylation of *p*-nitrophenol with acetic anhydride and recrystallized from cyclohexane, mp 78 °C (lit,[12] 81—82 °C). Acrylamide was purified by repeated recrystallizations from benzene, mp 83.5—84.5 °C.

N-Phenylacrylohydroxamic acid (**1**) was prepared according to Barda and Manole from *N*-phenylhydroxylamine and acryloyl chloride.[13] Repeated recrystallizations from cyclohexane gave pale yellow plates; yield 46—58%, mp 90—91 °C (lit,[13] 88—89 °C).

Similar procedures were employed in ether or chloroform solvent for the preparation of the following hydroxamic acids.

N-Phenylisobutyrohydroxamic acid (**2**); yield 60%, colorless plates from a cyclohexane-*n*-hexane mixture, mp 49—50 °C. Found: C, 67.01; H, 7.26; N, 7.86%. Calcd for $C_{10}H_{13}NO_2$: C, 67.02; H, 7.31; N, 7.82%.

N-Methylisobutyrohydroxamic acid (**3**); yield 45%, bp 91—95 °C/5 mmHg. Found: C, 51.18; H, 9.57; N, 11.81 %. Calcd for $C_5H_{11}NO_2$: C, 51.25; H, 9.46; N, 11.95%.

N-Methyl-α-naphthohydroxamic acid (**4**); yield 52%, colorless plates from acetone, mp 133—134 °C. Found: C, 71.52; H, 5.43; N, 6.86%. Calcd for $C_{12}H_{11}NO_2$: C, 71.53; H, 5.53; N, 6.96%.

Acetyl *N*-phenylacrylohydroxamate (**1a**); *N*-phenylacrylohydroxamic acid (38 g, 0.23 mol) and 24 g (0.24 mol) of triethylamine were dissolved in a mixture of 700 ml of ether and 100 ml of chloroform. To this solution was added dropwise 17.7 g (0.23 mol) of freshly-distilled acetyl chloride in 100 ml of ether with stirring at −10 °C over 30 min, and stirring was continued for an additional hour at room temperature. The reaction mixture was washed with 100 ml of saturated aqueous NaCl and with three 50-m*l* portions of a dilute Na_2CO_3 solution, and dried over Na_2SO_4. The solvent was evaporated and the tan-brown residue was distilled *in vccuo*. The distillate (dark yellow oil, bp 100—110 °C/0.08 mmHg) was recrystallized from petroleum ether in a dry ice-methanol bath; pale yellow oil, yield 52—65%. Found: C, 64.19; H, 5.53; N, 6.60%. Calcd for $C_{11}H_{11}NO_3$: C, 64.38; H, 5.40; N, 6.83%.

Similar procedures were applied to the preparation of the following acetyl hydroxamates.

Acetyl *N*-phenylisobutyrohydroxamate (**2a**); yield 80%. colorless plates from *n*-hexane. mp 77—78 °C. Found: C, 65.14; H, 6.31; N, 6.31%. Calcd for $C_{12}H_{15}NO_3$: C, 65.03; H, 6.83; N, 6.33%.

Acetyl *N*-methylisobutyrohydroxamate (**3a**); yield 53%. bp 95—98 °C/20 mmHg. Found: C, 52.78; H, 8.26; N, 8.81%. Calcd for $C_7H_{13}NO_3$: C, 52.82; H, 8.23; N, 8.80%.

Copolymerization. The radical copolymerization of acetyl *N*-phenylacrylohydroxamate and acrylamide was performed with azobisisobutyronitrile as an initiator in acetonitrile. The polymerization mixture was placed in an ampoule, which was sealed under nitrogen. After given polymerization periods, water was added to the reaction mixture, and the polymer was recovered by precipitation in excess methanol and dried *in vacuo*. The polymerization results are summarized in Table 1.

Deacetylation. A copolymer sample was dissolved in a small amount of water which contained a large excess of hydroxylamine, and was allowed to stand for 24 hr. The product polymer was recovered by precipitation in excess methanol, washed with methanol and dried *in vacuo*. Completion of deacylation was confirmed by disappearance of an IR peak at 1800 cm^{-1} due to the acetyl hydroxamate group ($\nu_{C=O}$). IR spectra of the copolymer before and after deacetylation are compared in Fig. 1. The corresponding spectra of the model compound are shown for comparison.

Determination of Copolymer Composition. The composition of the deacetylated copolymer was determined by NMR

TABLE 1. COPOLYMERIZATION[a]

Run No	Monomer feed		Time min	Conversion wt %	Copolymer Composition PHA unit, mol%
	PHA, M	AAm, M			
1 (PHA-AAm-1)	0.60	3.40	7	18	11.0[b] (11.1)[c]
2 (PHA-AAm-2)	0.20	3.80	10	8	3.9 (4.6)
3	0.40	3.60	7	22	(8)
4[d]	—	4.00	60	40	100

a) 70 °C, AIBN 0.02 M, CH_3CN solvent. b) Determined by the UV method. c) Data given in parentheses are obtained by the NMR method. d) 80 °C, AIBN 0.02 M, benzene solvent.

TABLE 2. TITRATION OF HYDROXAMIC ACID GROUP[a]

Hydroxamic acid	Polymer composition PHA, mol%	pK_a		n' [b]	pK_{int}[c]	k_a $M^{-1}s^{-1}$
		UV,	potentiometric			
PHA-AAm-1	11	8.69	8.64	1.35	8.58	5.31
PHA-AAm-2	3.9	8.60	—	1.04	8.56	9.12
2	—	8.81	—	—	—	25.1
3	—	9.08	9.03	—	—	32.6
4	—	8.23	8.20	—	—	10.5

a) Titration condition: 30 °C, 0.1 M KCl, 1.4 vol% CH_3CN–H_2O. b) Obtained from UV titration data. c) $pK_{int} = \lim_{\alpha \to 0} pK_{apparent}$.

TABLE 3. ELECTRONIC SPECTRA

Species	Medium	λ_{max}, nm (ε)	
PHA-AAm-1	0.01 M HCl	240 (4200)	205 (1.17×10^4)
	0.01 M NaOH	218 (9280)	275 (2200)
o-Acetyl-PHA-AAm-1	H_2O	240 (7200)	195 (2.15×10^4)
2	0.01 M HCl	240 (4200)	205 (1.10×10^4)
	0.01 M NaOH	218 (9200)	275 (2280)
2a	CH_3CN	240 (7180)	200 (2.10×10^4)

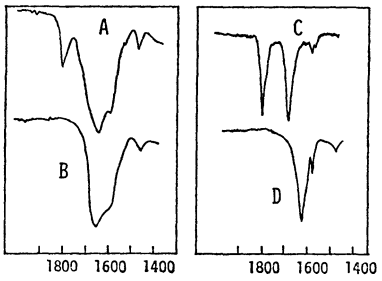

Fig. 1. Partial IR spectra (KBr disk)
A: *o*-acetyl PHA-AAm-1; before deacylation
B: PHA-AAm-1; after deacylation
C: **2a** (acetylated), D: **2** (not acetylated)

spectroscopy and by the UV titration of the hydroxamate group. In the first method, the copolymer composition was determined from the relative peak area of the phenyl protons and the methine and methylene protons. In the second method, the UV absorption characteristics of the hydroxamic acid unit (PHA) in the polymer was assumed to be the same as that of *N*-phenylisobutyrohydroxamic acid, and the copolymer composition was calculated by using the absorption of the hydroxamate anion at 300 nm (ε 1230). The PHA homopolymer prepared by radical polymerization was not utilized for this purpose because of its insolubility in water. The copolymer compositions thus determined are included in Table 1. The UV method appears to be more reliable particularly for samples of the low PHA content.

Determination of pK_a *Value.* The pK_a value of the hydroxamic acids (including the PHA unit in polymer) was determined by the UV spectroscopic and potentiometric titrations. The UV titration was conducted by using the absorbance of the hydroxamate anion at 300 nm in 1.4 vol% CH_3CN–H_2O at 30 °C (0.1 M KCl, 0.05 M Tris buffer), and the potentiometric titration was carried out in 1.4 vol% CH_3CN–H_2O at 30 °C, 0.1 M KCl. The UV titration data for the polymer hydroxamic acids were plotted according to the modified Henderson-Hasselbach equation[14]

$$pK_a = pH + n'\log\frac{1-\alpha}{\alpha} \qquad (1)$$

where α is the fraction of the dissociated hydroxamic acid group. The pK_a value corresponds to pH at the half neutralization, and the deviation of the n' value from unity is a qualitative measure of the electrostatic repulsion between the negatively-charged groups.

These titration data are summarized in Table 2. The agreement between the two methods is satisfactory.

Rate Measurements. The rate of acetylation of hydroxamic acids with *p*-nitrophenyl acetate was determined by following the increase in the absorption of the *p*-nitrophenolate anion at 401 nm. The hydrolysis of acetyl hydroxamates was followed in 1.4 vol% CH_3CN–H_2O (0.1 M KCl) at 30 °C by observing the increase in the absorption of the hydroxamate anion at 300 nm. Tris and phosphate buffers

were used. The pH of the reaction mixture was confirmed not to vary from pH measurements (Toa Digital pH Meter Model HM-15A) before and after the reaction.

Results

Electronic Spectra. Electronic spectra of the copolymer are shown in Fig. 2. The absorption of the hydroxamate anion is shifted to the longer wavelength compared with those of the acid and the acetate. The spectral characteristics are summarized in Table 3 together with those of the model compound. It is apparent that the PHA unit gives almost identical spectra with those of the model compound. These results are not inconsistent with those of other hydroxamic acids.[15]

The extinction coefficient of the PHA anion at 300 nm (ε 1250) is much greater than those of the corresponding acid or ester ($\varepsilon<100$). Therefore, the alkaline hydrolysis of acetyl hydroxamates can be followed by the use of the absorption difference at 300 nm, as mentioned above.

Reaction of Hydroxamic Acids with PNPA. The reaction of hydroxamic acids with PNPA leads to the release of *p*-nitrophenol as follows.

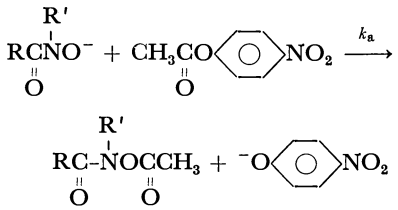

(2)

This was confirmed for the polymer hydroxamic acid employed. A solution of PHA-AAm-1 (1×10^{-3} baseM of the PHA unit) in 20 vol% EtOH–H_2O was made alkaline and treated with 0.01 M of 3-nitro-4-acetoxybenzoic acid at room temperature. After 4 hrs, the mixture was poured into excess methanol. The polymer recovered possessed an IR peak at 1800 cm^{-1} which indicated the presence of the acetyl hydroxamate group and the validity of Eq. (2) for the polymeric system.

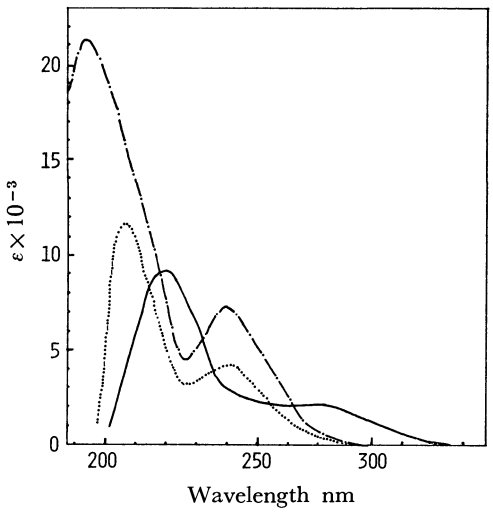

Fig. 2. Electronic spectra of the polymer.
·—· *o*-acetyl PHA-AAm-1 in CH_3CN
---- PHA-AAm-1 in 0.01 M HCl
—— PHA-AAm-1 in 0.01 M NaOH

The nitrophenol release due to spontaneous hydrolysis, v_{H_2O}, was corrected: $v_a=v_{total}-v_{H_2O}$. Figures 3 and 4 show the dependence of the rate of nitrophenol release on the concentrations of hydroxamic acid (HA) and PNPA.

$$v_a = k_{a,obs}[HA][PNPA] \quad (3)$$

When the concentrations of hydroxamic acid and PNPA are comparable as in these experiments, the reaction rate, v_a, follows the overall second-order kinetics. On the other hand, the spontaneous hydrolysis

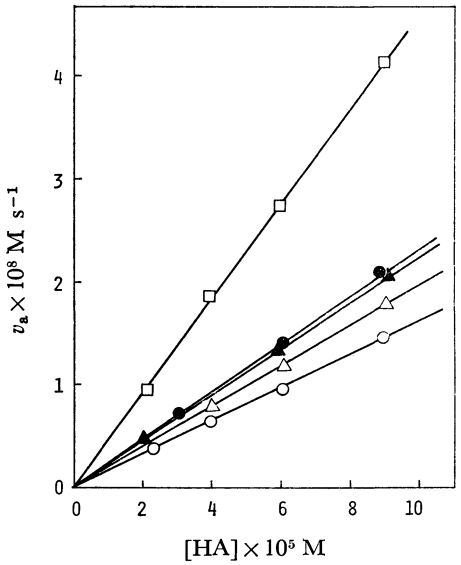

Fig. 3. Reaction of PNPA with a series of hydroxamic acids.
○: PHA-AAm-1, ● PHA-AAm-2; □ **2**, ▲ **3**, △ **4**
pH=8.57, 30 °C, 1.4 vol% CH_3CN–H_2O, 0.1 M KCl, 0.05 M Tris., [PNPA]$=5.01\times10^{-5}$ M

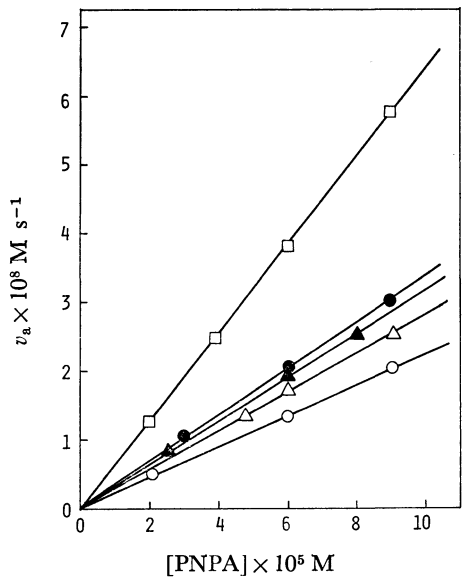

Fig. 4. Reaction of PNPA with a series of hydroxamic acids.
○ PHA-AAm-1, ● PHA-AAm-2, □ **2**, ▲ **3**, △ **4**
pH=8.57, 30 °C, 1.4vol%CH_3CN–H_2O, 0.1 M KCl, 0.05 M Tris., [HA]$=7.01\times10^{-5}$ M

Table 4. Reaction of hydroxamic acid with PNPA[a]

Hydroxamic acid	pH of the reaction medium	$k_{a,obs}$ $M^{-1}s^{-1}$	
		A[b]	B[c]
2	8.57	9.18	9.30
	8.99	14.9	15.2
3	8.57	7.35	7.40
	9.00	14.1	13.9

a) Reaction condition: 30 °C; 0.05 M Tris buffer; 0.1 M KCl; 1.4 vol% CH_3CN-H_2O. b) Obtained from the initial rate. [PNPA]$=3.15\times10^{-5}$ M. [HA]$=5.28\times10^{-5}$ M. c) Obtained from the first-order plot. [PNPA]$=3.15\times10^{-5}$ M. [HA]$=6.28\times10^{-3}$ M.

is a pseudo-first-order process. Therefore, the initial rate of the phenol release was employed for calculating $k_{a,obs}$ values from these data.

The total phenol release adheres strictly to the pseudo-first-order kinetics up to more than 90% reaction, when a large excess of the hydroxamic acid was used. In this case, the rate constant ($k_{a,obs}=k_{total}-k_{H_2O}$) was determined by the Guggenheim method.[16] In Table 4 are compared the rate constants obtained with and without large excesses of hydroxamic acids. The agreements are satisfactory. The use of excess hydroxamic acid concentrations was difficult in the polymeric system, because of the limitation in solubility.

Subsequently, the reaction of hydroxamic acids with PNPA was carried out at the pH range of 7 to 9. The apparent rate constants $k_{a,obs}$ at different pH's are plotted against α(degree of dissociation of hydroxamic acids). Linear relationships were obtained except for PHA-AAm-1, as shown in Fig. 5. An upward curvature was obtained for PHA-AAm-1. This result will be discussed later. It is clear that the hydroxamate anion is the true reacting species and that the reaction rate can be expressed as follows for the first three cases.

$$v_a = k_a\cdot\alpha\cdot[HA][PNPA] \quad (4)$$

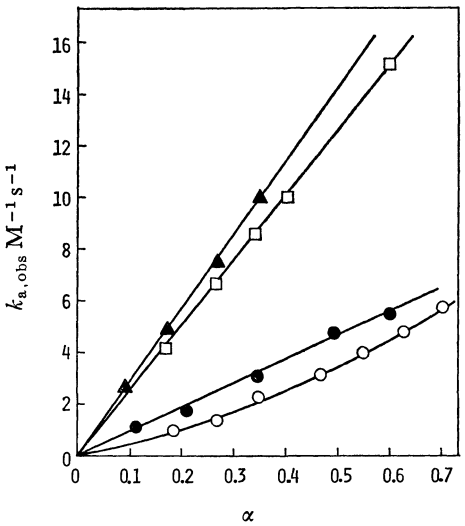

Fig. 5. Reaction of PNPA with a series of hydroxamic acids.
○ PHA-AAm-1, ● PHA-AAm-2, □ **2**, ▲ **3**
30 °C, 1.4vol%CH_3CN-H_2O, 0.1 M KCl, 0.05 M Tris.

where [HA] is the total concentration of the hydroxamic acid employed, and k_a is the true second-order rate constant of acylation.

It is to be noted that the rate of acylation of the polymeric hydroxamate anion was much smaller than that of the model compounds. The k_a value was also calculated for the PHA-AAm-1 case, from the slope at $\alpha=0$. The k_a values are summarized in Table 2.

Hydrolysis of Acetyl Hydroxamates. The hydrolyses of polymeric and monomeric acetyl hydroxamates were performed at three buffer concentrations (0.05, 0.10, 0.15 M) over the pH range between 8.8 and 9.6. The ionic strength was maintained at 0.1 by adding necessary amounts of a KCl solution. The apparent first-order rate constants were calculated by the method of Guggenheim and they were extrapolated to the zero buffer concentration, giving the observed first-order rate constant of deacetylation, $k_{d,obs}$.

$$k_{d,obs} = k_{OH}[OH^-] + k_w \quad (5)$$

The rate constants for the hydroxide and water hydrolyses were determined from the slope and intercept of the linear relationships shown in Fig. 6, and summarized in Table 5.

The k_{OH} values of acetyl *N*-methylhydroxamates were greater than those of the *N*-phenyl counterparts. It is interesting that there is not much difference in k_{OH} values between the corresponding polymeric and small-

Table 5. Hydrolysis of acetyl hydroxamates[a]

hydroxamate	pK_a of hydroxamic acid	k_{OH} $M^{-1}s^{-1}$	$10^4\cdot k_w$ s^{-1}	$10^4\cdot k_{d_0}$ at pH 7 s^{-1}
o-acetyl-PHA-AAm-1	8.58[b]	11.1	0.15	0.16
o-acetyl-PHA-AAm-2	8.56[b]	13.8	0.31	0.32
2a	8.81	9.10	0.23	0.24
3a	9.08	24.2	0.03	0.27

a) Reaction condition: 30 °C, 0.1 M KCl. b) pK_{int}.

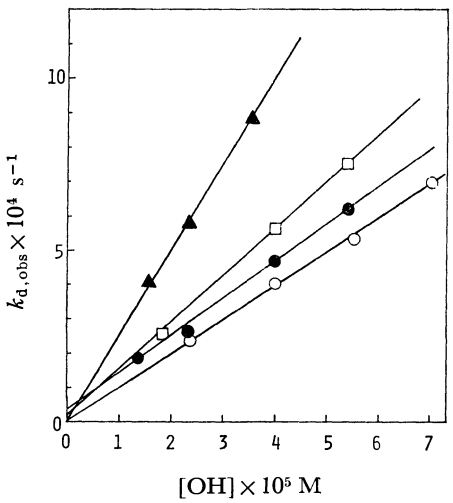

Fig. 6. Deacylation of acetyl hydroxamates.
○ *o*-acetyl PHA-AAm-1, ● *o*-acetyl PHA-AAm-2, □ **2a**, ▲ **3a**
30 °C, 1.4vol%CH_3CN-H_2O, 0.1 M KCl

molecule acetyl hydroxamates. This result is in sharp contrast with that observed in the acylation process.

Discussion

Preparation of Polymers Containing the Hydroxamic Acid Group. The introduction of the hydroxamic acid group into polymer has been investigated by several groups. For example, Reiz[17] and Hatano *et al.*[18] prepared polymers containing the hydroxamic acid group (**5**) by reaction of poly(methyl acrylate) with NH_2OH. The conversion was, however, not quantitative. Okawara and coworkers reported a quantitative conversion of the *p*-nitrophenyl ester unit to the hydroxamic acid group in a crossed-linked copolymer. However, the radical polymerization of methacrylohydroxamic acid (**6**) was not successful.[19] Previously we copolymerized a new monomer (**7**) with acrylamide. The hydroxamic acid unit was generated by hydrolysis.[20]

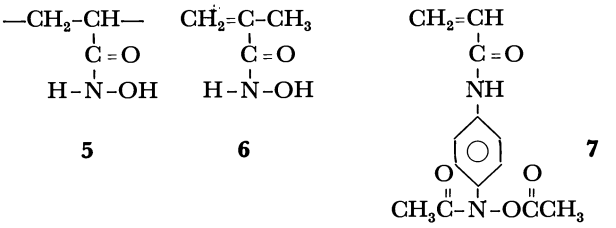

5 **6** **7**

Incorporation of the functional group by polymer reactions often leads to ambiguous results. This is particularly true for rather labile functional groups like hydroxamic acid. Therefore, we synthesized a new monomer (**1a**) which possessed the acetyl hydroxamate group. The hydroxamic acid group was regenerated by NH_2OH treatment of the original polymer.

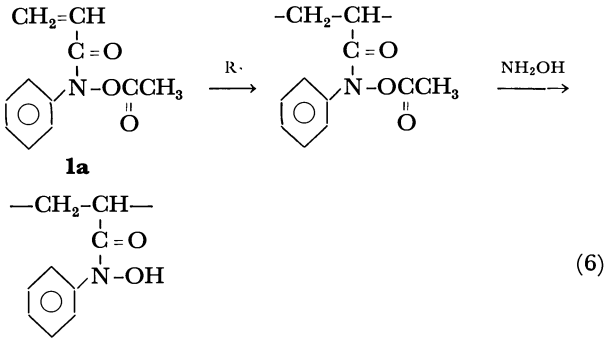

1a

PHA unit (6)

The polymerization of monomers with unprotected hydroxamic acid groups seems difficult, probably because the hydroxamic acid group is tautomeric with the nitrone structure. Nitrones are known to be very efficient trapping agents of the propagating free radical.[21]

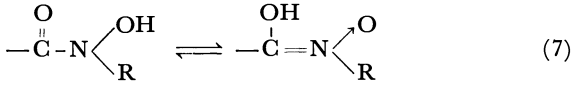

a nitrone (7)

Reactions of Hydroxamic Acids with Phenyl Esters. It has been confirmed by several research groups that the reaction of simple hydroxamate anions with phenyl esters yields acyl hydroxamates and phenols.[6,22] The acyl hydroxamate formed can undergo the Lossen rearrangement to isocyanates under strongly basic conditions if the nitrogen of the hydroxamate group is not substituted.[23,24] On the other hand, the Lossen rearrangement can be suppressed by alkyl substitution on the hydroxamic acid nitrogen, and the hydrolysis of acyl hydroxamate to regenerate hydroxamic acid occurs exclusively under basic conditions.[10,25] Thus, Bender and coworkers[10,11] employed *N*-alkylhydroxamic acids as catalysts for the hydrolysis of some phenyl esters. That the same sequence of reactions occurs for polymeric hydroxamic acids (Eqs. (8) and (9)) was established by the present study.

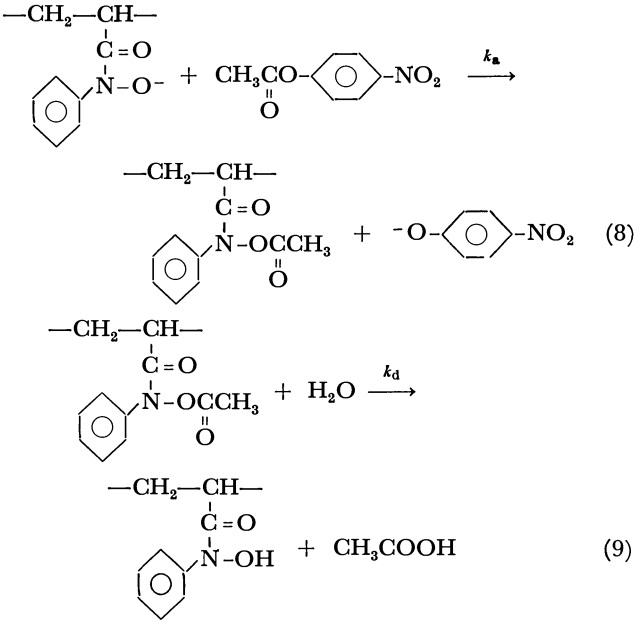

(8)

(9)

Acylation Step. As is clear from Fig. 5, the reaction of the PHA unit in polymer was much slower than that of the monomeric counterpart **2**. Furthermore, two polymer hydroxamic acids show different dependence of the acylation rate on α. This different acylation behavior is interesting. The $k_{a,obs}$ value increases linearly with the increase in α in the case of PHA-AAm-2, whereas the same relation for PHA-AAm-1 is not linear; instead a concave curve is observed. The $k_{a,obs}$ values for PHA-AAm-1 are somewhat lower than those for PHA-AAm-2 at small α values, but they become closer at higher α values.

The n' value determined by the UV titration was 1.35 for PHA-AAm-1 (PHA unit content: 11%) and 1.04 for PHA-AAm-2 (PHA unit content: 3.9%). Therefore, there must be considerable electrostatic repulsion among the hydroxamate anion when the PHA unit content is high. The electrostatic repulsion is conceivably intensified by intramolecular aggregation of the hydrophobic PHA unit. When the content of the PHA unit is small as in PHA-AAm-2, there is not observed noticeable electrostatic repulsion ($n'=1.04$): the dissociation behavior of a given PHA unit is almost the same throughout titration.

The acylation behavior of the polymer hydroxamic

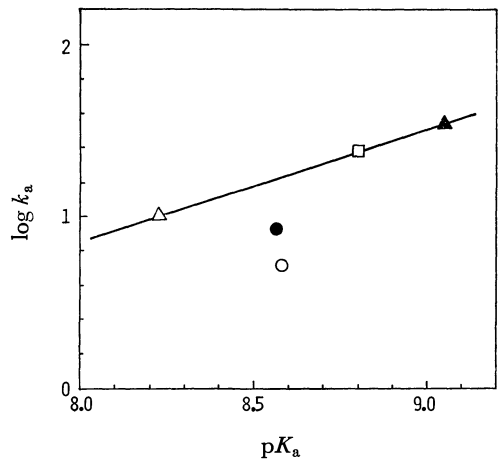

Fig. 7. Brønsted plots.
○ PHA-AAm-1, ● PHA-AAm-2, □ **2**, ▲ **3**, △ **4**
The pK_{int} value was used instead of pK_a for the polymers

acid can be explained by referring to the titration data. The reactivity of the hydroxamate anion in PHA-AAm-2 is invariant since the electrostatic interaction promoted by the side-chain aggregation is negligible. In the case of PHA-AAm-1, the reactivity of a given hydroxamate anion is lessened because of intramolecular aggregation probably with the undissociated PHA unit. As the degree of dissociation increases, the side-chain aggregation is destroyed by expansion of the polymer coil due to increasing electrostatic repulsion among the negatively-charged groups. Therefore, the reactivity of the individual hydroxamate anion increases with α, approaching that of PHA-AAm-2 at higher α values. In the latter polymer, the electrostatic interaction among the PHA unit is considered to be negligible.

The difference in the nucleophilic reactivity between the polymeric and small-molecule systems is also apparent in the Brønsted plot shown in Fig. 7. The three plots for the monomeric hydroxamic acid fall on a straight line, which is expressed by the following equation.

$$\log k_a = 0.62\, pK_a - 4.0 \qquad (10)$$

The slope of the line, the so-called β value in the Brønsted correlation, is 0.62, in fair agreement with those obtained by other workers. Dessolin, *et al.* found β=0.72 for the reaction of PNPA with series of benzohydroxamic acids and cinnamohydroxamic acids.[6] Hershfield and Bender obtained a β value of 0.68 for the reaction of PNPA with three *N*-methylhydroxamic acids.[11] Therefore, it is concluded that the structure variation in the acyl portion and in the *N*-substituent exerts simply the ordinary electronic influence on the nucleophilic reactivity of the hydroxamate group in these systems. The deviation of Brønsted plots for the PHA unit in polymer is, thus, reasonably ascribed to the steric hindrance of the polymer chain on the acylation, rather than to its electronic influence.

Deacylation. The deacylation results are contrasting with the acylation data, in that there is no polymer effect. Thus, the rate constants of deacylation k_{OH} are very similar for three acetyl hydroxamates studied. It might be expected that the hydrolysis rate would decrease with the increase in the basicity of the corresponding hydroxamic acid. However this is not the case, as is clear from the data given in Table 5. It is to be noted that the acetyl hydroxamate unit in polymer possesses a little higher k_{OH} values than the model compound, **2a**. Apparently, the polymer chain does not interfere with the hydroxide attack contrary to the acylation by PNPA. The probable electrostatic repulsion between the partially hydrolyzed O-acetyl-PHA-AAm copolymers and OH^- seemingly does not affect deacylation of the remaining acetyl hydroxamate unit, since the pseudo-first order plot holds well in the deacylation process up to at least 90% completion.

Concluding Remark. As described above, the hydroxamic acid group in polymer undergoes clean acylation and deacylation reactions, as are the monomeric counterparts.* Therefore, polymer hydroxamic acids are potential catalysts for the hydrolysis of phenyl esters. However, the deacylation process is not efficient and the acetyl intermediate is accumulated under the ordinary reaction condition. In fact, the k_{OH} value of PNPA (9.5 $M^{-1}\,s^{-1}$, 25 °C, 1.0 M KCl)[25] is in the same range as those of acetyl hydroxamates. This behavior of the hydroxamic acid is quite contrasting with that of imidazole. In the catalytic hydrolysis of PNPA with imidazole, the acylation process is rate-limiting[26] and the deacylation process is much more efficient than that of acetyl hydroxamates. Therefore, it appears that the catalytic efficiency of the hydroxamic acid can be enhanced by introduction of the intramolecular imidazole unit which assists deacylation of acetyl hydroxamates. This has been accomplished to some extent in a polymeric system.[27]

References

1) Contribution No. 325 from this department. Presented in part at the 22nd annual meeting of the Society of Polymer Science, Japan, May, 1973, Kyoto.
2) S. Shinkai and T. Kunitake, *Polymer J.* (Tokyo), **4**, 253 (1973), and papers cited therein.
3) C. G. Overberger, M. Morimoto, I. Cho, and J. C. Salamone, *J. Amer. Chem. Soc.*, **93**, 3228 (1971).
4) H. Kwart and H. Omura, *J. Org. Chem.*, **34**, 318 (1969).
5) J. D. Aubort and R. F. Hudson, *Chem. Commun.*, **1970**, 937, 938.
6) M. Dessolin, M. Laloi-Diard, and M. Vilkas, *Bull. Soc. Chim. France*, **1970**, 2573.
7) M. Dessolin and M. Laloi-Diard, *ibid.*, **1971**, 2946.
8) M. Dessolin, *Tetrahedron Lett.*, **1972**, 4585.
9) F. Filippini and R. F. Hudson, *Chem. Commun.*, **1972**, 522.
10) W. B. Gruhn and M. L. Bender, *J. Amer. Chem. Soc.*, **91**, 5883 (1969).
11) R. Hershfield and M. L. Bender, *ibid.*, **94**, 1376 (1972).
12) I. Heilbron and H. M. Bunbury, "Dictionary of Organic Compounds," Oxford Univ. Press, New York, N. Y. (1953).
13) N. A. Barda and C. F. Manole, *J. Mendeleev, All Union Chem. Soc.*, **16**, 478 (1971).
14) A. Katchalski, N. Shavit, and H. Eisenberg, *J. Polym.*

Sci., **13**, 69 (1954).
15) *Eg.*, R. E. Plapinger, *J. Org. Chem.*, **24**, 802 (1959).
16) A. A. Forst and R. G. Pearson, "Kinetics and Mechanism," 2nd. Ed., Wiley, New York, N. Y., 1961, p. 49.
17) L. Reiz, *Angew. Chem.*, **69**, 158 (1957).
18) M. Hatano, Y. Nose, T. Nozawa, and S. Kambara, *Kogyo Kagaku Zasshi*, **69**, 571 (1966).
19) M. Narita, T. Teramoto, and M. Okawara, This Bulletin, **45**, 3149 (1972).
20) T. Kunitake and S. Shinkai, Papers Presented at the 20th Polymer Symposium p. 81, Tokyo, Nov., 1971.
21) E. G. Janzen, *Accounts Chem. Res.*, **4**, 31 (1971).
22) W. P. Jencks and J. Carriuolo, *J. Amer. Chem. Soc.*, **82**, 1778 (1960).
23) C. R. Hauser and W. B. Renfrow, Jr., *ibid.*, **59**, 121 (1937); **61**, 618 (1939).
24) D. G. Hoare, A. Olson, and D. E. Koshland, Jr., *ibid.*, **90**, 1638 (1968).
25) J. F. Kirsh and W. P. Jencks, *ibid.*, **86**, 837 (1964).
26) M. L. Bender and B. W. Turnquest, *ibid.*, **79**, 1656 (1957).
27) T. Kunitake, Y. Okahata, and R. Ando, *Macromolecules*, **7**, 140 (1974).

Synthetic Study of Colchicine

Michiharu KATO, Fusao KIDO, Ming-Der WU, and Akira YOSHIKOSHI

Chemical Research Institute of Non-Aqueous Solutions, Tohoku University, Katahira, Sendai 980

(Received February 16, 1974)

An efficient route based upon solvolytic fragmentation of a cyclopentadiene-dichloroketene adduct **4c** has been investigated for the synthesis of trimethoxyphenylpropyltropolone **2b**, a synthetic intermediate of colchicine **1a**. Attempted synthesis of the corresponding unsaturated tropolones **8a** and **10** is also discussed.

Many synthetic approaches have been reported for colchicine **1a**[1] because of its characteristic biological activity on cell divisions and because of the rarely encountered tricyclic tropolone structure. The synthetic goals in many of these studies were desacetamidocolchiceine **1b** since the conversion of the latter compound into natural colchicine has been accomplished by Corrodi and Hardegger.[2] In some instances 4-substituted tropolones, **2a** and **2b**, were used as precursors for **1b**, and the formers were cyclized by intramolecular oxidative coupling[1d] or by Pschorr cyclization[1g] to tricyclic derivatives. In this paper we describe an efficient route to **2b** and attempted synthesis of the related unsaturated systems, such as **8a** and **10**.

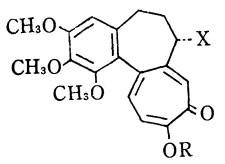

1

a, X=NHCOCH$_3$, R=CH$_3$
b, X=R=H

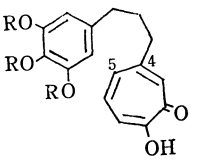

2

a, R=H
b, R=CH$_3$

Results and Dicussion

4-*t*-Butyltropolone[3a] and 4-isopropyltropolone (hinokitiol)[3b] were regiospecifically synthesized by the addition of the corresponding 1-alkylcyclopentadienes with dichloroketene followed by solvolytic fragmentation. These results imply that a similar synthetic route *via* 1-(trimethoxyphenylpropyl)cyclopentadiene **4a** and its dichloroketene adduct **4c** would be useful for the regiospecific preparation of 4-(trimethoxyphenylpropyl)tropolone **2b**, although the latter was previously synthesized in devious paths from 4-formyltropolone.[4]

Methyl *trans*-3,4,5-trimethoxycinnamate[5] **3a** was hydrogenated to he cortresponding hydrocinnamate **3b** (91% yield). Reduction of **3b** with lithium aluminum hydride gave hydrocinnamyl alcohol **3c** quantitatively. Tosylation of the alcohol in pyridine at an ice bath temperature afforded tosylate **3d**. By treatment with sodium cyclopentadienide in tetrahydrofuran, the tosylate yielded an oily product. The product showed a single spot on tlc, but it was not so sufficiently stable as to give an analytically pure sample. The NMR spectrum of the product displays an overlapped signal corresponding to three protons at δ 5.92—6.50 ppm, proposing **4a** or **4b** as the possible structure of the product. In view of the selective formation of 4-isopropyltropolone upon isopropylation of cyclopentadienylmagnesium bromide,[3b] the selected reaction conditions seemed favorable to the formation of **4a**. Without further examination of the structure, the crude product was immediately allowed to react with equimolar dichloroketene generated from dichloroacetyl chloride and triethylamine in *n*-hexane, giving an oil (42% yield from **3c**) as homogeneous product (tlc). An intense carbonyl absorption at 1805 cm^{-1} in the IR spectrum and a one-proton multiplet at 5.55 ppm in the NMR spectrum are indicative of an α,α-dichlorocyclobutanone structure and a trisubstituted double bond, respectively. The known regiospecificity in the addition reaction of ketenes with conjugated dienes[6] allows to assign the structures **4c** or **4d** to the adduct. On the basis of the known regiospecific formation of substituted tropolones upon acetolysis,[7] **4c** or **4d** should provide the desired 4-(trimethoxyphenylpropyl)tropolone (**2b**) or the corresponding 5-substituted derivative, respectively. The adduct was refluxed in aqueous acetic acid containing potassium acetate, and the tropolonic product was extracted with alkali to give **2b** (67% yield). No formation of other tropolonic products was observed. The physical data of the tropolone were identical with those reported, and the identity was finally ascertained by direct comparison with an authentic sample.[8] The results demonstrates that the aforementioned substituted cyclopentadiene and its dichloroketene adduct must be **4a** and **4c**, respectively. We thus ensured a brief route of good overall yield (25% from **3a**) for the preparation of the tropolone **2b**.

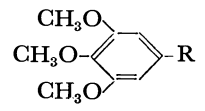

3

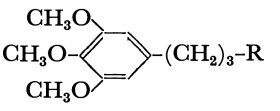

4

a: R=-CH=CH-CO$_2$CH$_3$
b: R=-(CH$_2$)$_2$-CO$_2$CH$_3$
c: R=-(CH$_2$)$_3$-OH
d: R=-(CH$_2$)$_3$-OTs
e: R=-CH=CH-CO$_2$H
f: R=-(CHBr)$_2$-CO$_2$H
g: R=-CH=CHBr
h: R=-C≡CH

a: R=

b: R=

c: R=

d: R=
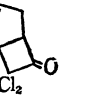

The first successful Pschorr cyclizations of aminotropolones **5a**—**5c** into tricyclic tropolones **6a**—**6c** were achieved by Nozoe *et al.*[9] Kaneko and Matsui[1g] also submitted aminotropolone **7b**, obtained from **2b** *via* azo compound **7a**, to the Pschorr cyclization leading to desacetamidocolchiceine **1b**. We followed the above results and obtained **1b** in a poor yield as reported. The product was reaffirmed by comparison with the au-

thentic compound derived from colchicine according to Eschenmoser *et al.*[1a] In Pschorr cyclization, the fixation of participated aryl groups in *cis* gives better yields of cyclization products than free-rotational systems, *e.g.*, *cis*-2-aminostilbene yielded phenanthrene in 61% yield while 1-phenyl-2-*o*-aminophenylethane gave only a trace of of 9,10-dihydrophenanthrene.[10] In our case *cis*-stilbene type derivative **8b** was presumed to give better yield in the cyclization. We then endeavored to synthesize **8b**.

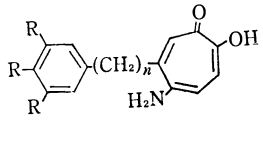

5

a: R=H, n=2
b: R=OCH_3, n=2
c: R=H, n=3

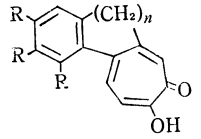

6

a: R=H, n=2
b: R=OCH_3, n=2
c: R=H, n=3

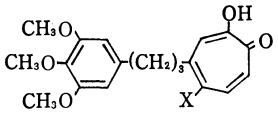

7

a: X=N=N-C_6H_4-CH_3(p)
b: X=NH_2

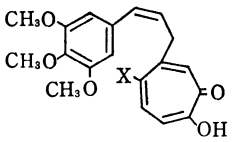

8

a: X=H
b: X=NH_2

The cinnamic acid **3e** was brominated in chloroform to give crystalline dibromo acid **3f** (95% yield). The dibromo acid was then heated with sodium bicarbonate in dry acetone yielding a mixture of *cis*- and *trans*-bromostyrenes **3g** (91% yield). The mixture showed two peaks in a ratio of 2 : 1 in glc, and the major product was separated by silver nitrate–silica gel tlc. The NMR spectrum of the major product exhibited two olefin proton signals of an AB-pattern, and their coupling constants (8.8 Hz) demonstrate, in accordance with the findings of Grovenstein and Lee,[11a] and Cristol and Norris,[11b] the major decarboxylative dehydrobromination product to be the *cis*-bromostyrene. Upon treatment with sodium amide in liquid ammonia, the mixture of the bromostyrenes **3g** produced phenylacetylene **3h** (85% yield), whose Grignard reagent was then treated with excess formaldehyde in tetrahydrofuran. The reaction afforded two products (68% yield in total), which were separated by silica gel chromatography in a ratio of 3 : 1. The major product ($C_{12}H_{14}O_4$) was identified as the desired compound **9a** by its spectra, while the minor one ($C_{13}H_{14}O_5$) exhibited a strong absorption at 1720 cm^{-1} and a one-proton triplet signal (J=1.5 Hz) at 8.15 ppm in the IR and NMR spectra, respectively. Since these spectra seemed to suggest that the compound is a formate **9b**, the minor product was hydrolyzed with aqueous alkali. The hydrolysis product was found to be identical with the major product **9a**. It was proved by decoupling experiments that the observed splitting of the formate proton signal are due to a spin-spin coupling between this proton and the propargylic methylene protons. The spin-spin coupling through two C-H and two C-O bonds of formate grouping seems to be uncommon. The formation of **9b** may be accounted for oxymethylenation of the initially formed alcoholate **9c** with formaldehyde leading to **9d**, followed by Oppenauer oxidation with excess formaldehyde. The abnormal Grignard reactions of this type have also been reported for some sterically hindered arylmagnesium bromides.[12]

The alcohol **9a** was converted into bromide **9e** with phosphorus tribromide and a catalytic amount of pyridine (83% yield). Upon treatment with sodium cyclopentadienide under conditions similar to those used for the saturated system **4a**. The bromide gave an oil after passing through a short silica gel column (66% yield), which was nearly homogeneous on tlc. The NMR signals of the product at 3.00 (a two-proton multiplet), 3.51 (a two-proton multiplet), and 6.22—6.62 ppm (a three-proton multiplet) are attributable to propargylic methylene, cyclopentadiene methylene, and olefin protons, respectively. Formula **9f** or **9g**, therefore, may be given to the product. Without further investigation on the structure, the product was allowed to react with dichloroketene leading to an oily adduct (32% yield from the substituted cyclopentadiene). The UV spectrum of the adduct (**9h** or **9i**) shows a maximum absorption at 263 nm, and no IR absorption at near 1785 cm^{-1}, a characteristic carbonyl absorption of α,α-dichlorocyclobutenone and its derivatives,[13] was observed. These spectral data demonstrate that the acetylenic bond was unaffected in the course of the addition with dichloroketene. Solvolytic fragmentation of the adduct in acetic acid containing potassium acetate gave a solid product after extraction with aqueous alkali. Despite of some characteristic IR absorptions at 3150, 1610, and 1550 cm^{-1} of the crude product, attempted separation of the desired tropolone **10** was unsuccessful. Catalytic hydrogenation of the crude product over palladium-carbon gave **2b** in only 11% yield.

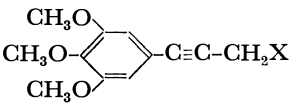

9

a: X=OH
b: X=OCHO
c: X=OMgBr
d: X=OCH_2OMgBr
e: X=Br

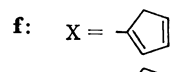

f: X=

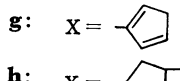

g: X=

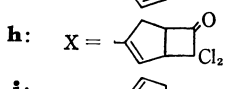

h: X=

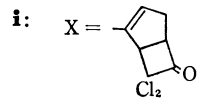

i: X=

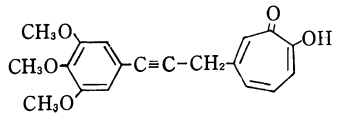

10

Since the pure tropolone **10** was unavailable, we then turned to another approach. The propargyl alcohol **9a** was hydrogenated over Lindlar catalyst to an olefinic alcohol (77% yield), whose NMR spectrum is consistent with the anticipated structure **11a**. Two olefin proton signals of an AB-pattern (J=12 Hz) at 5.80 and 6.50 indicates a cis disubstituted olefin bond. Reaction of **11a** with phosphorus tribromide yielded an unstable bromide **11b**. The crude bromide was submitted to the reaction with sodium cyclopentadienide under conditions similar to those employed for **4a** to give a substituted

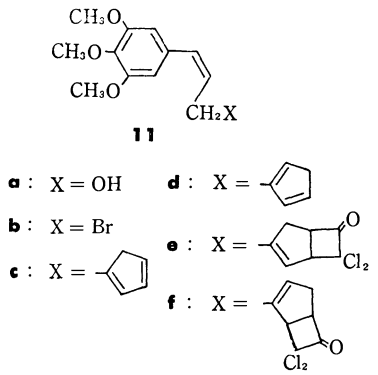

cyclopentadiene derivative (36% yield from **11a** after brief purification). The spectra is consistent with the proposed structure **11c** or **11d**. Since the product was also unstable to obtain analytically pure compound, the roughly purified product was immediately submitted to the addition reaction with dichloroketene. A homogeneous oily adduct was obtained on chromatography (5% from **11a**). A UV absorption maximum at 260 nm and an AB-patterned *cis* disubstituted ethylene protons (J=14 Hz) in the NMR spectrum, as disclosed by decoupling (*cf.* Experimental), obviously demonstrate a cis β-substituted styrene moiety. An α,α-dichlorocyclobutanone structure was shown in the IR spectrum (1807 cm^{-1}). These results are in accordance with the structure **11e** or **11f**. The solvolytic fragmentation of the adduct gave an acidic oil, which shows IR absorptions typical of tropolones at 3180, 1615, and 1550 cm^{-1}. The oil, however, was an inseparable mixture. Hydrogenation of the oil, followed by chromatography, gave **2b** in a low yield.

It has still been unclarified why, while the dichloroketene adduct **4c** smoothly yielded the desired tropolone **2a**, the solvolysis of the unsaturated systems resulted in the formation of intractable mixtures.

Experimental

All melting points and boiling points were uncorrected. The spectra were taken with the following instruments: UV, Cary Model 14 spectrophotometer; IR, Hitachi EPI-S2 spectrophotometer; NMR, JEOL Model C-60-HL (60 MHz) and JEOL Model PS-100 (100 MHz). Unless otherwise stated, NMR spectra were recorded in deuterochloroform solutions containing tetramethylsilane (δ=0 ppm) as internal standard. Coupling constants were given in Hz.

*Methyl 3-(3,4,5-Trimethoxyphenyl)-propionate (**3b**).* A solution of methyl *trans*-3,4,5-trimethoxycinnamate[5] **3a** (10 g) in methanol (250 ml) was hydrogenated over 10% palladium-carbon (0.7 g) under atmospheric pressure at room temperature. After hydrogen uptake ceased, the solution was filtered and concentrated to leave an oily **3b** (9.1 g, 91%), which was homogeneous in tlc. IR (Liquid film): 1735 cm^{-1}. NMR: 2.77 (2H, octet), 3.70 (3H, s), 3.81 (3H, s), 3.83 (6H, s), and 6.43 (2H, s).

An analytical sample was obtained by distillation *in vacuo* [bp 110 °C (bath temperature)/0.2 mmHg].

Found: C, 61.24; H, 6.72%. Calcd for $C_{13}H_{18}O_5$: C, 61.40; H, 7.14%.

*3-(3,4,5-Trimethoxyphenyl)-propyl Alcohol (**3c**).* A solution of the hydrocinnamate **3b** (20 g) in dry ether (150 ml) was added dropwise into a suspension of lithium aluminum hydride (2.3 g) in the same solvent (350 ml) over 4 hr with stirring in an ice bath. After the reaction mixture was allowed to stand overnight at room temperature, the excess reagent was destroyed by adding moist ether and then water. The organic layer was dried and evaporated to give an oily **3c** (17 g), which was homogeneous in tlc. IR (liquid film): 3300 cm^{-1}. NMR: 1.96 (2H, q, J=6), 2.70 (2H, t, J=6), 3.73 (2H, t, J=6), 3.88 (9H, s), and 6.49 (2H, s).

An analytical sample was obtained by distillation *in vacuo* [bp 120—130 °C (bath temperature)/1 mmHg (lit.[14] bp 136—139 °C/0.3 mmHg) as colorless oil.

Found: C, 63.47; H, 7.92%. Calcd for $C_{12}H_{18}O_4$: C, 63.70; H, 8.02%.

*1-[3-(3,4,5-Trimethoxyphenyl)-propyl]-cyclopentadiene (**4a**).* A solution of tosyl chloride (17.2 g) in dry pyridine (50 ml) was added dropwise to a solution of **3c** (18.5 g) in the same solvent (200 ml) over 2 hr with stirring in an ice bath. The mixture was kept in a refrigerator overnight and then filtered. The filtrate was diluted with cold ether (500 ml) and then washed with cold 10% hydrochloric acid to remove the pyridine. The organic layer was washed with water and brine, and dried. Evaporation of the solvent gave oily tosylate **3d** (27.1 g), which was homogeneous in tlc. The tosylate was used, without further purification, in the next step. IR (liquid film): 1360 and 1180 cm^{-1}.

A solution of freshly distilled cyclopentadiene (380 mg) in dry tetrahydrofuran (3 ml) was added dropwise to a stirred suspension of sodium hydride (126 mg) in the same solvent (4 ml) under nitrogen in an ice bath. After hydrogen evolution ceased, a solution of the crude tosylate (985 mg) in dry tetrahydrofuran (7 ml) was added dropwise to the above cyclopentadienide solution with stirring. Stirring was continued for an additional 3 hr, and the reaction mixture was poured into cold water. The mixture was extracted with ether, and the extracts were washed with water and brine, and dried. Removal of the solvent left a yellow oil (715 mg). The oil was chromatographed on silica gel. Petroleum ether–ether (1 : 1) eluted a small amount of an olefin fraction and then **4a** (576 mg) as a yellow oil. NMR: 1.55—3.05 (8H, m), 3.82 (3H, s), 3.86 (6H, s), 6.43 (2H, s), and 5.92—6.50 (3H, m). Further purification was attempted to obtain an analytically pure sample, but removal of a small amount of impurity from the main fraction was unsuccessful. Thus the roughly purified product was used in the next step.

*7,7-Dichloro-3-[3-(3,4,5-trimethoxyphenyl)-propyl]-bicyclo[3.2.0]-hept-2-en-6-one (**4c**).* Dichloroacetyl chloride (73 mg) was added to a stirred solution of **4a** (137 mg) in *n*-hexane (4 ml), and then the solution was cooled in an ice bath. A solution of triethylamine (60 mg) in the same solvent was added to the above solution over 2 min with stirring. The mixture was stirred for an additional 5 hr. Cold water was added, and the mixture was extracted with ether. The extracts were washed with water and brine, and dried. An oil obtained by evaporation of the solvent was chromato-

graphed on silica gel. Petroleum ether–ether eluted the unreacted **4a** (30 mg) and then the oily adduct **4c** (114 mg, 42% from **3c**). IR: 1805 and 1640 cm^{-1}. NMR: 1.5—2.8 (8H, m), 3.82 (3H, s), 3.85 (6H, s), 4.25 (1H, d.t., J= 7.5 and 2.5, assigned to the proton adjacent to carbonyl[3b]), 5.55 (1H, m), and 6.38 (2H, d, J=2.2).

Found: C, 58.94; H, 5.46%. Calcd for $C_{19}H_{22}O_4Cl_2$: C, 59.21; H, 5.75%.

*4-[3-(3,4,5-Trimethoxyphenyl)-propyl]-tropolone (**2b**).* A mixture of **4c** (4.16 g), potassium acetate (10.6 g), acetic acid (60 ml), and water (0.5 ml) was refluxed for 2 days. The reaction mixture was concentrated *in vacuo*, and the residue was diluted with water. The product was extracted with ether. The organic layer was extracted with dilute sodium hydroxide, and the aqueous layer was acidified with dilute hydrochloric acid. The precipitate was filtered and recrystallized from ethanol to give **2b** (2.40 g, 66%), mp 111—112.5 °C (lit.[1d] 113—115 °C). UV (methanol): 238 nm (log ε, 4.81) and 338 (3.93). IR (KBr): 3180, 1606, 1590, and 1540 cm^{-1}. NMR:[15] 2.00 (2H, m), 2.64 (2H, t, J=8), 2.70 (2H, t, J=8), 3.86 (3H, s), 3.88 (6H, s), 6.44 (2H, s), and 6.8—7.4 (6H, m).

The spectra were identical with those of the authentic compound[1d] provided by Professor Scott.

*4-[3-(3,4,5-Trimethoxyphenyl)-propyl]-5-p-tolylazotropolone (**7a**) and 4-[3-(3,4,5-Trimethoxyphenyl)-propyl]-5-aminotropolone (**7b**).* These compounds were prepared according to the known procedure,[1g] and similar results were obtained. The unreported NMR data of **7a** are given below. NMR of **7a**: 2.00 (2H, m), 2.45 (3H, s), 2.75 (3H, t, J=7), 3.32 (3H, t, J=7), 3.37 (3H, s), 6.43 (2H, s, assigned to the aromatic protons of trimethoxyphenyl), 7.37 and 8.20 (1H, d, J=12 each, assigned to the C-6 and C-7 tropolone protons), 7.40 nad 7.80 (1H, d, J=6 each, assigned to the aromatic protons of tolylazo group), and 7.51 (1H, s, assigned to the C-3 tropolone proton).

*Desacetamidocolchiceine (**1b**).* The cyclization reaction was performed under reaction conditions essentially identical with those described by Kaneko and Matsui,[1g] except that no copper catalyst was used in decomposition of the diazonium salt of **7b**.

Thus a solution of isoamyl nitrite (0.1 ml) in dioxane (1 ml) was added dropwise to a stirred solution of **7b** (69 mg) and sulfuric acid (0.1 ml) in dioxane (1.5 ml) at room temperature. After stirring for an additional 2 hr, the mixture was heated at 55—57 °C for 1 hr. The mixture was diluted with water and extracted with methylene chloride. After usual work-up, the crude product was chromatographed on phosphoric acid impregnated Celite. After an unidentified product was eluted with a mixture of *n*-hexane and benzene, **1b** was eluted with benzene as crystals, which was recrystallized from ethanol giving 2 mg (3%) of the pure product melting at 167—169 °C (lit. 168—169 °C,[1a] 165—167 °C[1b]). The IR and NMR spectra of the product were identical with those of an authentic sample of desacetamidocolchiceine.

*3-(3,4,5-Trimethoxyphenyl)-2,3-dibromopropionic Acid (**3f**).* A solution of bromine (176 mg) in chloroform (1 ml) was added dropwise to an ice-cooled solution of **3a** (238 mg) in the same solvent (2 ml) over 2 min with stirring. The reaction mixture was filtered to separate the precipitate after 30 min, and the filtrate was concentrated to give an additional solid. The combined solids were recrystallized from benzene–ligroin to afford colorless crystals (377 mg, 95%), mp 153—155 °C. IR(KBr): 1745 cm^{-1}. NMR (acetone-d_6): 3.80 (3H, s), 3.91 (6H, s), 5.22 and 5.52 (1H, d, J=12 each), and 7.04 (2H, s).

Found: C, 35.77; H, 3.78%. Calcd for $C_{12}H_{14}O_5Br_2$: C, 36.11; H, 3.51%.

*3,4,5-Trimethoxy-β-styrene (**3g**).* A suspension of **3f** (100 mg) and sodium bicarbonate (252 mg) in dry acetone (10 ml) was refluxed with stirring for 2 hr. The acetone was removed *in vacuo*, and water (3 ml) was added to the residue. The mixture was extracted with ether. The combined extracts were washed with water and brine, and dried. Removal of the solvent left an oil, which was distilled *in vacuo* [120—130 °C (bath temperature)/1 mmHg] giving a colorless oil (62 mg, 91%).

Found: C, 48.81; H, 4.73%. Calcd for $C_{11}H_{13}O_3Br$: C, 48.47; H, 4.79%.

The mixture of the isomers showed two peaks in glc (SE-30 column) in an approximate ratio of 1 : 2. The major isomer was separated by silver nitrate-silica gel preparative tlc. IR (liquid film): 3050 and 1615 cm^{-1}. NMR (carbon tetrachloride):[15] 3.70 (3H, s), 3.75 (6H, s), 6.35 (2H, s), and 6.55 and 6.85 (1H, d, J=8.8 each).

*3,4,5-Trimethoxyphenylacetylene (**3h**).* A solution of the isomeric mixture of **3g** (27.3 g) in dry ether (100 ml) was added dropwise to a stirred sodium amide solution, prepared from sodium (2.7 g) and liquid ammonia (500 ml), over 20 min. A vigorous reaction took place and appeared to complete when the addition finished. Stirring was continued for an additinal 30 min, and ammonium chloride was added. After removal of the liquid ammonia, water was added, and the mixture was extracted with ether. The combined extracts were washed with dilute hydrochloric acid and water, and then brine. Evaporation of the solvent left crystals, which was recrystallized from ether–petroleum ether to give colorless crystals melting at 68—68.5 °C (16.3 g, 85%). IR (KBr): 3250 cm^{-1}. NMR (carbon tetrachloride): 2.93 (1H, s), 3.81 (3H, s), 3.89 (6H, s), and 6.74 (2H, s).

Found: C, 68.79; H, 6.03%. Calcd for $C_{11}H_{12}O_3$: C, 68.73; H, 6.29%.

*3-(3,4,5-Trimethoxyphenyl)-propargyl Alcohol (**9a**) and Its Formate (**9b**).* A solution of **3h** (192 mg) in dry tetrahydrofuran (0.5 ml) was added dropwise to a Grignard reagent solution prepared from ethyl bromide (131 mg) and magnesium (29 mg) in the same solvent (0.5 ml). Excess formaldehyde vapor was passed through the above acetylenic Grignard reagent solution with stirring at room temperature, and then water was added to quench. The organic layer was separated and washed with water and brine, and dried. Evaporation of the solvent left an oil, which showed three spots in tlc. The oil was chromatographed on silica gel. Petroleum ether–ether (3 : 2) eluted the unreacted **3h** (33 mg) and then the formate **9b** (40 mg, 16%). Petroleum ether–ether (2 : 3—1 : 4) eluted **9a** (115 mg, 52%).

An analytical sample of **9a** was obtained by recrystallization from ether–petroleum ether as colorless crystals melting at 89—91 °C. IR (KBr): 3300, 2210, and 1127 cm^{-1}. NMR:[15] 3.85 (9H, s), 4.51 (2H, s), and 6.71 (2H, s).

Found: C, 64.55; H, 6.45%. Calcd for $C_{12}H_{14}O_4$: C, 64.85; H, 6.35%.

An analytical sample of **9b** was obtained by recrystallization from *n*-hexane–benzene as colorless crystals melting at 89—90 °C. IR (KBr): 2200, 1720, and 1210 cm^{-1}. NMR: 3.86 (9H, s), 5.00 (2H, d, J=1.5), 6.71 (2H, s), and 8.15 (1H, t, J=1.5). The doublet at 5.00 or the triplet at 8.15 ppm collapsed to a singlet on decoupling of the other signal.

Found: C, 62.59; H, 5.87%. Calcd for $C_{13}H_{14}O_5$: C, 62.39; H, 5.64%.

A solution of the formate **9b** (50 mg) and sodium hydroxide (16 mg) in ethanol (10 ml) was allowed to stand overnight. After evaporation of the solvent, the residue was diluted with water and extracted with chloroform. A usual work-up

gave **9a** (41 mg, 93%).

*3-(3,4,5-Trimethoxyphenyl)-propargyl Bromide (**9e**).* A solution of phosphorus tribromide (300 mg) in dry tetrahydrofuran was added dropwise to a stirred solution of **9a** (889 mg) and a catalytic amount of pyridine in the same solvent (8 ml) over a period of 10 min in an ice bath. After stirring for an additional 2 hr, the mixture was poured into cold water and extracted with ether. The combined extracts were washed with water and brine, and dried. Removal of the solvent left an oil, which was chromatographed on silica gel. Petroleum ether–ether eluted **9e** (1.14 g, 83%) as crystals, which was recrystallized from petroleum ether–ether to afford colorless crystals, mp 48—50 °C. IR (KBr): 2200 cm^{-1}. NMR (carbon tetrachloride): 3.75 (3H, s), 3.81 (6H, s), 4.11 (2H, s), and 6.60 (2H, s).

Found: C, 50.27; H, 4.58%. Calcd for $C_{12}H_{13}O_3Br$: C, 50.53; H, 4.58%.

*1-[3-(3,4,5-Trimethoxyphenyl)-2-propynyl]cyclopentadiene (**9f** or **9g**).* A solution of **9e** (550 mg) in dry tetrahydrofuran (5 ml) was added dropwise to a stirred cyclopentadienide solution, prepared from cyclopentadiene (152 mg) and sodium hydride (53 mg) in the same solvent (5 ml), over 10 min in an ice bath. Stirring was continued for an additional 3 hr, and the reaction mixture was extracted with ether. The extracts were washed with water and brine, and dried. Removal of the solvent *in vacuo* gave a yellow oil, which was chromatographed on a short silica gel column. A mixture of petroleum ether–ether eluted an oil (344 mg, *ca.* 66%), whose tlc showed it to be nearly homogeneous. Further purification, however, was unsuccessful owing to its instability. IR (liquid film): 2300 cm^{-1}. NMR:[15] 3.00 (2H, m), 3.51 (2H, m), 3.85 (9H, s), 6.22—6.62 (3H, m), and 6.65 (2H, s).

*Dichloroketene Adduct of the Propargylcyclopentadiene (**9h** or **9i**).* Dichloroacetyl chloride (888 mg) was added to a stirred solution of the above propargylcyclopentadiene (1.48 g) in *n*-hexane (40 ml), and the mixture was cooled in an ice bath. A solution of triethylamine (638 mg) in the same solvent was added to the above mixture over 5 min with stirring at the same temperature. The mixture was stirred for an additional 5 hr, and then water was added. The organic layer was washed with water and brine, and dried. Removal of the solvent gave an oil. Petroleum ether containing ether eluted an oily adduct (668 mg, 32%). UV (methanol): 218 nm (log ε, 4.60) and 263 (4.23). IR (liquid film): 1807 cm^{-1}. NMR: 2.77 (2H, m), 3.10—3.80 (2H, m), 3.85 (9H, s), 3.95—4.50 (2H, m), 5.95 (1H, m), 6.70 (1H, s), and 6.75 (1H, s).

Found: C, 59.34; H, 4.90%. Calcd for $C_{19}H_{18}O_4Cl_2$: C, 59.69; H, 4.75%.

*Solvolysis of the Adduct (**9h** or **9i**) and Hydrogenation of the Product.* A solution of the adduct (**9h** or **9i**) (215 mg), potassium acetate (320 mg), and water (2 drops) in acetic acid (5 ml) was refluxed for 2 days. The solvent was removed *in vacuo*, and the residue was diluted with water and extracted with chloroform. The combined extracts were washed with dilute sodium hydroxide solution. The aqueous layer was acidified with dilute hydrochloric acid and extracted with chloroform. The extracts were washed with water and brine. Evaporation of the solvent left a solid (72 mg), which could not be purified by recrystallization or chromatography.

The crude product (70 mg) dissolved in ethyl acetate (5 ml) was hydrogenated over 10% palladium-carbon (5 mg). After hydrogen uptake ceased, the catalyst was filtered off. The filtrate was evaporated to give a solid (61 mg), which was then dissolved in hot methanol (10 ml). The solution was filtered, and the filtrate was concentrated and cooled to give **2b** (8 mg).

*3-(3,4,5-Trimethoxyphenyl)-allyl Alcohol (**11a**).* A mixture of **9a** (66 mg), 5% palladium-barium sulfate (20 mg), quinoline (0.4 ml), and methanol (2 ml) was treated with hydrogen under atmospheric pressure at room temperature. After hydrogen uptake ceased (1 molar equivalent), the catalyst was filtetered off, and then the filtrate was passed through a 5% silver nitrate-silica gel column to remove the quinoline. The solvent was removed, and the residue was submitted to preparative tlc using petorleum ether–ether (1 : 1) as eluent. The allylic alcohol (**11a**) was obtained (51 mg, 77%) as an oil. IR (liquid film): 3400 and 1640 cm^{-1}. NMR: 3.83 (9H, s), 4.42 (2H, q, J=6 and 1.5), 5.80 (1H, d.t, J=12 and 6), 6.50 (1H, br. d, J=12), and 6.45 (2H, s).

Found: C, 64.12; H, 7.25%. Calcd for $C_{12}H_{16}O_4$: C, 64.27; H, 7.19%.

*Dichloroketene Adduct(**11e** or **11f**).* Phosphorus tribromide (1.39 g) was added dropwise to a stirred solution of **11a** (3.12 g) and pyridine (0.2 ml) in dry tetrahydrofuran (70 ml) over 5 min in an ice bath, and stirring was continued for an additional 1 hr. The mixture was poured into water and extracted with ether. The combined extracts were washed with water and brine, and dried. Removal of the solvent gave an unstable oil (4.09 g), whose IR spectrum showed no hydroxyl absorptions. The freshly prepared bromide was used, without further purification, in the next step.

A solution of the crude bromide (4.09 g) in dry tetrahydrofuran (70 ml) was added dropwise to a stirred cyclopentadienide solution, prepared from cyclopentadiene (1.06 g) and sodium hydride (370 mg) in the same solvent (70 ml), over 10 min at an ice-bath temperature. After stirring for an additional 2 hr, the mixture was poured into water and extracted with ether. A usual work-up gave a yellow oil, which was chromatographed on a short silica gel column. Petroleum ether–ether (2 : 1) eluted an oily product (1.37 g, 36% from **11a**), which was homogeneous in tlc. NMR: 3.02 (2H, m), 3.36 (2H, m), 3.87 (3H, s), 3.91 (6H, s), 6.12—6.60 (5H, m), and 6.67 (2H, s).

Owing to its instability, no analytical sample of the product was obtained.

Dichloroacetyl chloride (54 mg) was added to a stirred solution of the roughly purified product (100 mg) in *n*-hexane (5 ml) in an ice bath. A solution of triethylamine (38 mg) in the same solvent (3 ml) was added dropwise to the above mixture. After stirring for an additional 2 hr, the mixture was poured into water and extracted with ether. A usual work-up gave an oil, which was purified twice by preparative silica gel tlc using petroleum ether–ether (1 : 1) as eluent. A homogeneous product **11e** (or **11f**) (20 mg, 5% from **11a**) was obtained. UV (methanol): 260 nm (log ε, 4.22). IR (liquid film): 1807 cm^{-1}. NMR:[15] 2.67 (2H, m), 3.00 (2H, br. d, J=6), 3.81 (3H, s), 3.84 (6H, s), 3.95 (1H, m, assigned to the C-1 proton[16]), 4.25 (1H, d. t, assigned to the C-5 proton[16]), 5.48 (1H, br. s), 6.04 (1H, q, J=14 and 6), 6.32 (1H, d, J=14), and 6.45 (2H, s). On irradiation at 3.00 ppm, the quartet signal at 6.04 ppm changed into a doublet (J=14).

Found: C, 59.66; H, 4.61%. Calcd for $C_{19}H_{20}O_4Cl_2$: C, 59.31; H, 4.82%.

*Solvolysis of the Adduct (**11e** or **11f**) and Hydrogenation of the Product.* A mixture of the adduct (**11e** or **11f**) (95 mg), potassium acetate (200 mg), water (2 drops), and acetic acid (2 ml) was refluxed for 2 days. The solvent was evaporated *in vacuo*, and the residue was poured into water and extracted with ether. The extracts were washed with aqueous sodium hydroxide, and the aqueous layer was acidified with dilute hydrochloric acid. The acidic product was extracted with chloroform. The organic layer was extracted

with 85% phosphoric acid, and the phosphoric acid extracts were diluted with water. The liberated product was collected with ether. An oil (27 mg) was obtained by evaporation of the solvent. The oil was a mixture and gave no homogeneous product upon attempted purification.

A mixture of the crude solvolysis products (20 mg), 10% palladium-carbon (3 mg) and ethyl acetate (2 ml) was hydrogenated under atmospheric pressure at room temperature. After usual work-up, an oil obtained was passed through a phosphoric acid-Celite column. Benzene eluted crystals, which were recrystallized from methanol to give **2b** (4 mg), as identified by IR.

References and Notes

1) (a) J. Schreiber, W. Leimgruber, M. Pesaro, P. Schudel, and A. Eschenmoser, *Angew. Chem.*, **71**, 637 (1959); J. Schreiber, W. Leimgruber, M. Pesaro, P. Schudel, T. Threefall, and A. Eschenmoser, *Helv. Chim. Acta*, **44**, 540 (1961); b) E. E. van Tamelen, T. R. Spencer, Jr., D. S. Allen, and R. L. Orvis, *Tetrahedron*, **14**, 8 (1961); (c) T. Nakamura, Y. Murase, R. Hayashi, Y. Endo, G. Sunagawa, and J. Nakazawa, *Chem. Pharm. Bull.* (Tokyo), **10**, 281, 291, 299 (1962); (d) A. I. Scott, F. McCapra, R. L. Buchanan, A. C. Day, and D. W. Young, *Tetrahedron*, **21**, 3605 (1965); (e) R. B. Woodward, "The Harvey Lecture," Ser. 59, 31 (1963—1964), Academic Press, New York, N. Y. (1965); (f) J. Martel, E. Toromonoff, and C. Huynh, *J. Org. Chem.*, **30**, 1752 (1965); (g) S. Kaneko and M. Matsui, *Agr. Biol. Chem.*, **32**, 995 (1968); (h) S. Tobinaga and E. Kotani, Abstracts of Papers of the 12th Symposium on the Natural Products, p. 259 (1968).

2) H. Corrodi and E. Hardegger, *Helv. Chim. Acta*, **40**, 193 (1957).

3) (a) P. D. Bartlett and T. Ando, *J. Amer. Chem. Soc.*, **92**, 7518 (1970); (b) K. Tanaka and A. Yoshikoshi, *Tetrahedron*, **27**, 4889 (1971).

4) M. Matsui, K. Yamashita, K. Mori, and S. Kaneko, *Agr. Biol. Chem.*, **31**, 675 (1967).

5) H. P. Kung and W.-Y. Huang, *J. Amer. Chem. Soc.*, **71**, 1836 (1949).

6) For a review, *cf.* H. Urlich, "Cycloaddition Reactions of Heterocumulenes", Academic Press, New York, N. Y. (1967), pp. 45—50.

7) Regarding the machanisms of the solvolytic fragmentations, *cf.* T. Asao, T. Machiguchi, and Y. Kitahara, this Bulletin, **43**, 2662 (1970) and Ref. 3a. See also Ref. 3b.

8) Kindly provided by Professor A. I. Scott, whom we thank.

9) (a) For **6a**, *cf.* T. Nozoe, K. Takase, H. Matsumura "Daiyukikagaku," Vol. 13, M. Kotake, Ed., Asakura Shoten, Tokyo (1960), p. 416; (b) for **6b** and **6c**, *cf.* T. Nozoe, K. Takase, Y. Kitahara, and K. Doi, Abstracts of Papers of the 132nd National Meeting of the American Chemical Society, New York (1957), p. 47. Also refer to T. Nozoe, *Experientia*, Suppl. VII, 307 (1957) and ref. 9a, p. 417.

10) P. Ruggli and A. Staub, *Helv. Chim. Acta*, **19**, 1288 (1936). For a review, *cf.* R. A. Abramovitch, "Advances in Free-Radical Chemistry," Vol. II, G. H. Williams, Ed., Logos Press, London (1967), pp. 87—138.

11) (a) E. Grovenstein, Jr. and D. E. Lee, *J. Amer. Chem. Soc.*, **75**, 2639 (1953); (b) S. J. Cristol and W. P. Norris, *ibid.*, **75**, 2645 (1953).

12) A. Rieker, Y. Butsugan, and M. Shimizu, *Tetrahedron Lett.*, **1971**, 1905.

13) J. D. Roberts, G. B. Kline, and H. E. Simmons, Jr., *J. Amer. Chem. Soc.*, **75**, 4765 (1953).

14) H. Rapoport and J. E. Campion, *ibid.*, **73**, 2239 (1951).

15) Measured at 100 MHz.

16) See formula **4c** in the text.

The Base-induced Reactions of 2-Halogeno-1,3-diketones in a Variety of Solvents

Tadahiro WAKUI, Yoshio OTSUJI, and Eiji IMOTO

Department of Applied Chemistry, College of Engineering, University of Osaka Prefecture, Sakai-shi, Osaka 591

(Received February 20, 1974)

The reactions of 2-bromo-2-methyldimedone (**1**), 2,2-dibromodimedone (**6**), 2-bromo- and 2-chloro-2-methylcyclohexane-1,3-dione (**10a** and **10b**) and 2-acetyl-2,6-dibromocyclohexanone (**14**) with an equivalent of sodium acetate in a variety of solvents were studied. The constitutions and proportions of the products obtained by these reactions depended strongly on the structure of 2-halogeno-1,3-diketones and the solvents employed. The results were discussed in terms of the mechanisms proposed.

In a previous paper,[1] we have reported that 2-alkyl-2-bromodimedones undergo various types of reactions upon treatment with bases in aprotic solvents such as benzene and THF, and the mode of reactions strongly depends on the bases employed. This paper deals with the reactions of various 2-halogeno-1,3-diketones including 2-bromo-2-methyldimedone with a weak nucleophilic base such as sodium acetate in a variety of solvents. In this investigation, we found that the proportions of the products depended remarkably on the solvents used and also the structure of the 1,3-diketones.

Results

Effects of Solvents. The reactions of 2-bromo-2-methyldimedone (**1**) with an equivalent of sodium acetate were conducted in a variety of solvents. In these reactions, 2,4,4-trimethyl-2-cyclopenten-1-one (**2**), 2,5,5-trimethyl-3-oxo-1-cyclopentenecarboxylic acid (**3**), 2-methyldimedone (**4**), 2,5,5-trimethylcyclohexane-1,3,4-trione (**5**) and carbon monoxide were isolated, proportions of these products being strongly dependent on the solvents employed. The reactions of 2,2-dibromodimedone (**6**) with an equivalent of sodium acetate in various solvents were then examined. These reactions afforded 2,3-dibromo-4,4-dimethyl-2-cyclopenten-1-one (**7**), 2-bromo-5,5-dimethylcyclohexane-1,3,4-trione (**8**), 2-bromodimedone (**9**) and carbon monoxide, proportions of the products again depending on the solvents used.

The structures of the products **2**—**4** and **7**—**9** were assigned as previously reported,[1] and the evolution of carbon monoxide was confirmed by vpc analysis of the evolved gas collected during the reaction. The structure of **5** was established from its elemental analysis and spectral data. The IR spectrum (KBr) showed a hydrogen-bonded hydroxyl absorption at 3200 cm^{-1}, three carbonyl absorptions at 1705, 1685, and 1650 cm^{-1}, and an absorption due to the C=C bond at 1640 cm^{-1}. The NMR spectrum ($CDCl_3$) exhibited a singlet (6H, two CH_3's attached at the 5-position) at δ 1.27, a singlet (3H, CH_3 attached at the 2-position) at δ 1.92, a singlet (2H, $-CH_2-$ at the 4-position) at δ 2.73, and a broad singlet (1H, an enol proton) at δ 7.0. The mass spectrum showed a parent peak at *m/e* 168. These spectral data indicate that **5** exists essentially in the form of **5a** under the conditions where the spectra were measured. The yields of the products **2**—**9** obtained by the above reactions are summarized in Table 1.

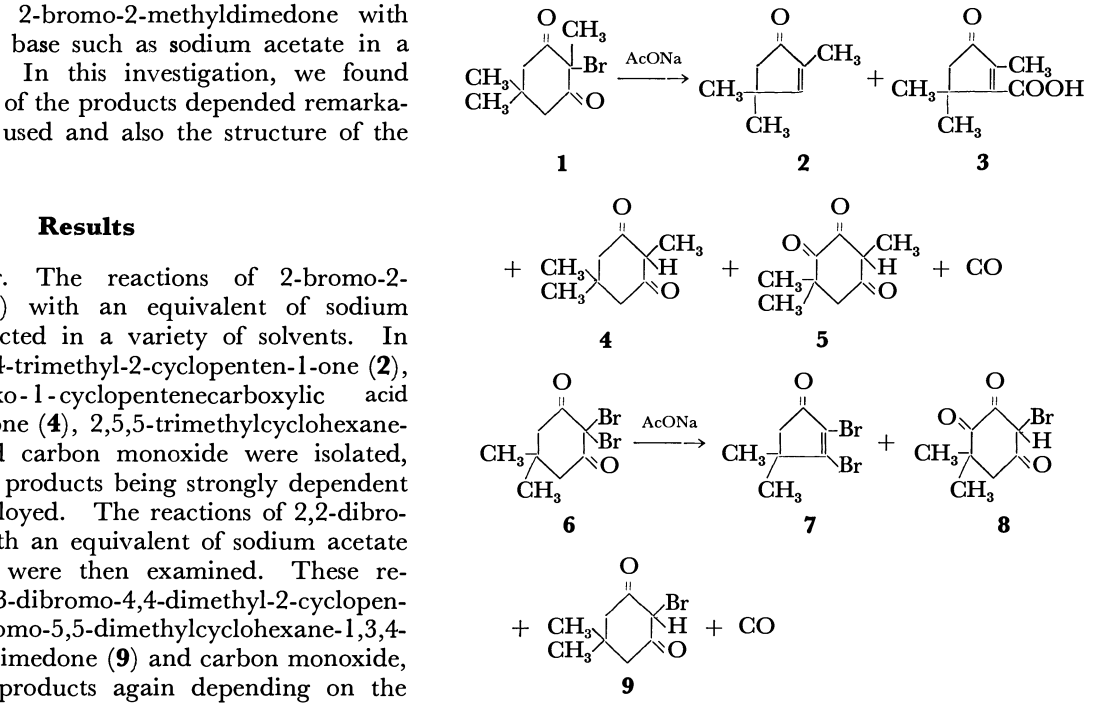

1 **2** **3** **4** **5** **6** **7** **8** **9**

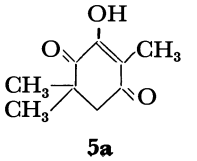

5a

Effects of the Structure of 1,3-Diketones. Treatment of 2-bromo-2-methylcyclohexane-1,3-dione (**10a**) with an equivalent of sodium acetate in THF under reflux afforded 2-methyl-3-oxo-1-cyclopentenecarboxylic acid (**11**), its mixed anhydride (**12**) and 2-methylcyclohexane-1,3-dione (**13**). Similar treatment of 2-chloro-2-methylcyclohexane-1,3-dione (**10b**) with an equivalent of sodium acetate in THF gave the same products. However, the reaction of 2-acetyl-2,6-dibromocyclohexanone (**14**) with an equivalent of sodium acetate in THF afforded a mixture of 2-acetyl-1-cyclopentenecarboxylic acid (**15**) and its mixed anhydride (**16**). The yields of the products obtained by the above reactions are summarized Table 2.

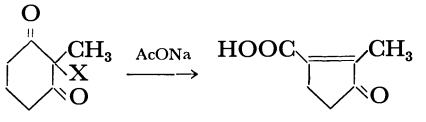

10a; X=Br
b; X=Cl

11

Table 1. Reactions of **1** and **7** with sodium acetate

Compd	Solvent	Reaction temp., °C	Time hr	Products			Recovered starting material
1	Benzene	80	5	**2**(4)	**3**(3)	**4**(Trace)	**1**(57)
1	Ether	35	5	**2**(4)		**4**(5)	**1**(42)
1	THF	65	5	**2**(20)	**3**(37)	**4**(20)	**1**(6)
1	*t*-BuOH	83	5	**2**(20)	**3**(13)	**4**(20)	
1	CH_3CN	80	5	**2**(28)	**3**(18)	**4**(8)	
1	EtOH	78	5	**2**(50)	**5**(22)	**4**(2)	
1	MeOH	65	5	**2**(58)	**5**(20)		
1	MeOH	0—5	5	**2**(20)			
1	THF-water (3 : 2)	70	5	**2**(22)	**3**(15)	**4**(15)	
1	Benzene-water (6 : 1)	80	5				**1**(88)
6	THF	65	5	**7**(25)	**8**(16)	**9**(32)	
6	THF-water (6 : 1)	70	5	**7**(12)	**8**(25)	**9**(33)	
6	DMF	80	5	**7**(3)	**8**(75)		

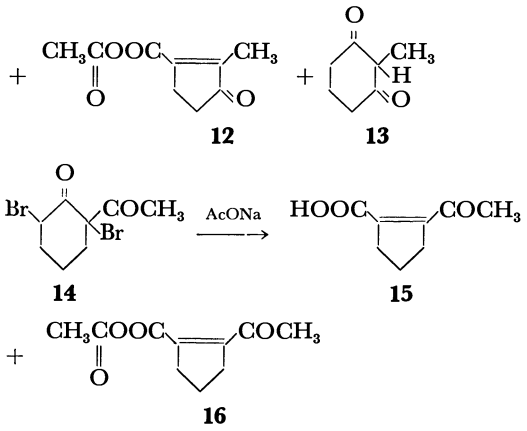

The structure of **13** was confirmed by the comparisons of IR and NMR spectral data with those of the authentic sample and also by the mixture melting-point test. The structure of **11** was assigned by its spectral data. The IR spectrum (KBr) showed multiple absorptions characteristic of a carboxyl group at 3200—2800 cm^{-1}, carbonyl absorptions at 1720 and 1670 cm^{-1}, and an absorption due to the C=C bond at 1630 cm^{-1}. The NMR spectrum ($CDCl_3$) exhibited a singlet (3H, $-CH_3$ attached at the 2-position) at δ 1.76, a multiplet (4H, $-CH_2-CH_2-$ at the 4- and 5-positions) at δ 2.1—3.0, and a singlet(1H, –COOH at the 3-position) at δ 8.37. The UV spectrum (95% ethanol) had a maximum absorption at 243 nm (ε 13000). This spectrum was similar in shape to that of 3-oxo-1-cyclopentenecarboxylic acid (λ_{max}^{EtOH} 243 nm(ε1 5000)).[2] The mass spectrum showed a parent peak at *m/e* 140. The structure of **12** was confirmed by its spectral data (see Experimental) and chemical modification; the mild treatment of **12** with sodium hydroxide solution gave **11**. The structure of **15** was also established by its spectral data. The IR spectrum showed a carbonyl absorption at 1700 cm^{-1}, a carboxyl absorption at 1690 cm^{-1}, and an absorption due to the C=C bond at 1630 cm^{-1}. The NMR spectrum ($CDCl_3$) exhibited a singlet (3H, $-COCH_3$) at δ 2.45, a multiplet (6H, $-CH_2-CH_2-CH_2-$ at the 3-, 4- and 5-positions) at δ 2.0—2.91, and a singlet (1H, –COOH) at δ 12.4. The mass spectrum showed a parent peak at *m/e* 154. The structure of **16** was deduced by its spectral data (see Experimental) and by the fact that the mild treatment of **16** with NaOH solution gave **15**.

Table 2. Reactions of various 2-halogeno-1,3-diones with sodium acetate in THF under reflux

1,3-Dione	Reaction time, hr	Products (%)		
10a	5	**11**(25)	**12**(12)	**13**(18)[a]
10b	4	**11**(18)	**12**(4)	**13**(20)[b]
14	5	**15**(40)	**16**(17)	

a) The starting material, **10a**, was recovered in 11% yield. b) The starting material, **10b**, was recovered in 15% yield.

Discussion

Effects of Solvents. A striking feature of the reaction of **1** with sodium acetate is that the proportion and constitution of the products are largely dependent on the solvents employed. The results of Table 1 indicate that the yields of the products increase with increase in the polarity of the solvents. Specifically, the use of alcohols caused pronounced effects on the constitution of the products; *i. e.*, (1) the yield of **2** increased remarkably with a marked decrease in the yields of **3** and **4**, and (2) the formation of the trione **5** was observed.

These results could be interpreted in terms of the mechanism proposed in the previous paper,[1] which is outlined in Scheme 1.

A key intermediate in the formation of **2** is the cyclopropanone **18** which is produced by an elimination of bromide ion from the carbanion **17**. The carbanion **17** reacts also with **1** to produce the dibromide **19** and the carbanion **20** which affords **4** on protonation. The dibromide **19** is converted by the semibenzylic type-rearrangement to **22** and then to **3** upon treatment with sodium acetate. The polar solvents may facilitate these ionic reactions, thus leading to an increase in the yields of the products. The use of alcohols may favor the formation of **18** by assisting the elimination of

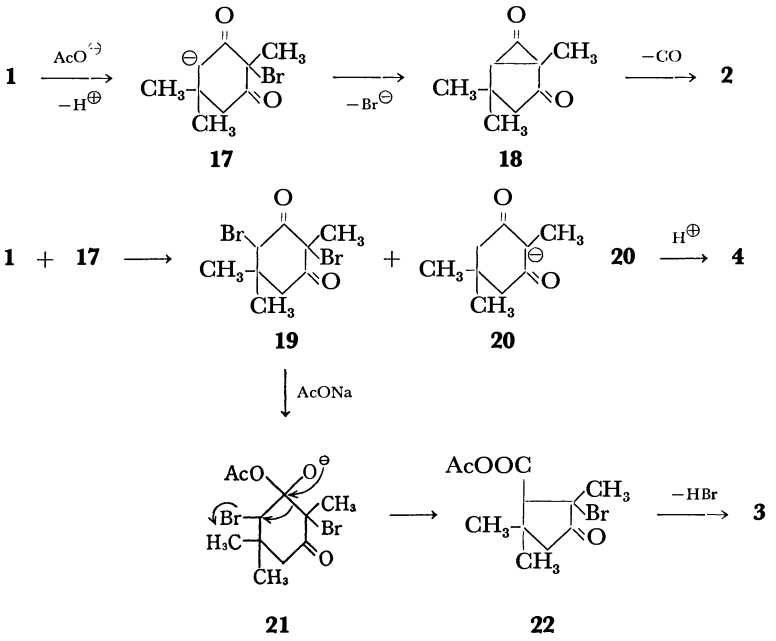

Scheme 1.

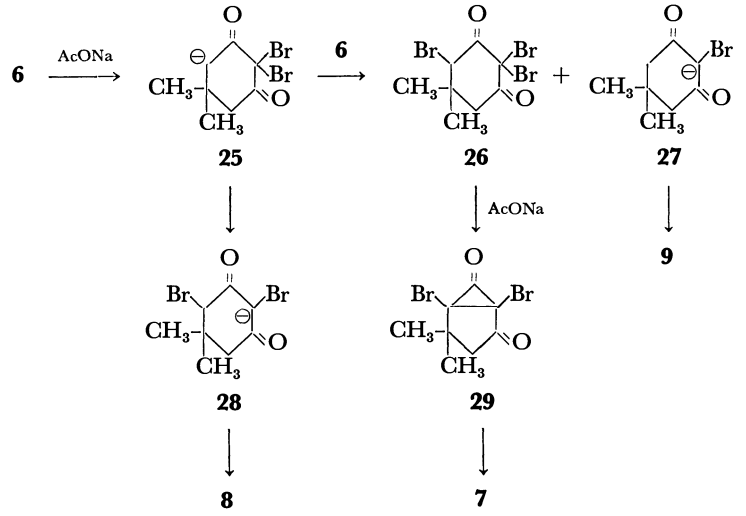

Scheme 2.

bromide ion from **17**, probably through a hydrogen bonding between the solvents and bromine, which is depicted as -Br···HOR. Thus, the reactions in alcohols result in the increase in the yield of **2**, accompanied by the decrease in the yield of other products which are produced from **17**. It is conceivable that in an alcohol **18** forms the alkyl acetal which is stable.[3] The reaction of **23** with sodium acetate may result in the formation of **5**.

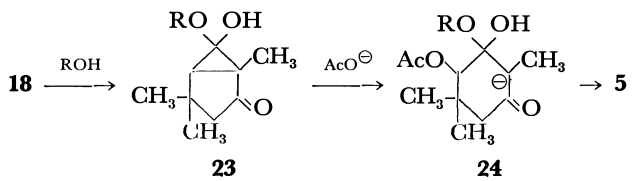

The behavior of **6** for the reaction with sodium acetate could also be explained by the mechanism proposed previously[1] (Scheme 2).

Effects of the Structure of 2-Halogeno-1,3-diketones. Another striking feature of the results of this investigation is that the mode of the reaction of 2-halogeno-1,3-diketones with sodium acetate is strongly influenced by the structure of the 1,3-diketones. The reaction of **10a** and **10b** with sodium acetate led to the formation of **11**, **12**, and **13**. However, in these reactions the cyclopentenone corresponding to **2** could not be isolated.

These results suggest that two methyl substituents attached at the 5-position of cyclohexane-1,3-dione plays an important role for the formation of the cyclopropanone intermediate. In the case of the reaction of **1**, the reaction of the carbanion **17** with **1** is more or less interfered by a steric interference caused by two methyl substituents at the 5-position, thus **17** can partly be transformed to the cyclopropanone **18** (see Scheme 1). On the other hand, in the reactions of **10a** and **10b**, the carbanion **30** is readily converted to **32** and **33** upon

the reaction with **10a, b** without the formation of the cyclopropanone **31** (see Scheme 3).

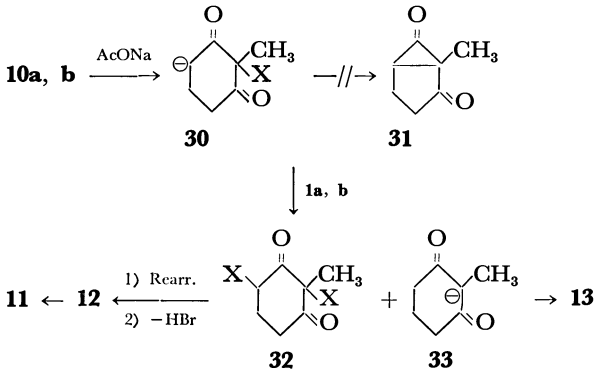

Scheme 3.

Similarly, the reaction of **14** with sodium acetate in THF lead preferentially to the formation of the rearranged products **15** and **16** in accordance with the mechanism proposed.

Experimental

2-Bromo-2-methyldimedone (**1**) and 2,2-dibromodimedone (**6**) were prepared by the methods previously reported.[1]

*Reactions of **1** with Sodium Acetate in Benzene, Ether, THF, THF–Water (3 : 2), t-Butyl Alcohol, and Acetonitrile.* A mixture of 0.5 g (2.2 mmol) of **1** and 0.2 g (2.5 mmol) of AcONa in 30 ml of a solvent was refluxed for 5 hr. The reaction mixture was poured into water, neutralized with 1M HCl, and then extracted with ether. The ether extract was washed with a 5% aqueous Na_2CO_3 solution, dried over Na_2SO_4, and evaporated to leave an oil. Distillation of the oil gave 2,4,4-trimethyl-2-cyclopenten-1-one (**2**); bp 160—165 °C. The yield of **2** was determined by vpc analysis of the reaction mixture.

The Na_2CO_3 solution was neutralized with 1 M HCl and extracted with ether. The ether extract was dried over Na_2SO_4 and evaporated. The residue was chromatographed on a silica gel with benzene–CCl_4 (1 : 3). The earlier fraction gave 2,5,5-trimethyl-3-oxo-1-cyclopentenecarboxylic acid (**3**); mp 189—191 °C. The latter fraction afforded 2-methyldimedone (**4**); mp 160—162 °C. The yields of **2**, **3** and **4** are given in Table 1.

*Reaction of **1** with Sodium Acetate in Methanol.* A mixture of 0.5 g (2.2 mmol) of **1** and 0.2 g (2.5 mmol) of AcONa in 30 ml of MeOH was refluxed for 5 hr. The reaction mixture was worked up as described above and separated into two fractions (the neutral fraction and the Na_2CO_3 soluble fraction). From the neutral fraction, crude **2** was obtained as an oil. Vpc analysis of the reaction mixture indicated that the mixture contained 0.15 g (58%) of **2**.

From the Na_2CO_3 soluble fraction, a solid was obtained. Recrystallization of the solid from $CHCl_3$ gave 0.07 g (20%) of 2,5,5-trimethylcyclohexane-1,3,4-trione (**5**); mp 161—162 °C.

Found: C, 64.35; H, 7.33%. Calcd for $C_9H_{12}O_3$: C, 64.27; H, 7.19%.

*Reaction of **6** with Sodium Acetate.* A mixture of 1.0 g (3.4 mmol) of **6** and 0.3 g (3.7 mmol) of AcONa in 50 ml of DMF was heated at 70 °C for 5 hr. The reaction mixture was poured into 50 ml of water, neutralized with 1 M HCl, and then extracted with two 30 ml portions of ether. The ether extracts were washed with 5% aqueous Na_2CO_3 solution, dried over Na_2SO_4 and evaporated to leave an oil. The oil was chromatographed on a silica gel with *n*-hexane–CCl_4 (5 : 1) to give 27 mg (3%) of 2,3-dibromo-4,4-dimethyl-2-cyclopenten-1-one (**8**); mp 85—86 °C.

The Na_2CO_3 solution was neutralized with 1M HCl and extracted with ether. The ether solution was dried over Na_2SO_4, and evaporated to give a solid. Recrystallization of the solid from CCl_4–$CHCl_3$ (1 : 3) gave 0.59 g (75%) of 2-bromo-5,5-dimethylcyclohexane-1,3,4-trione (**8**); mp 188—190 °C.

The reactions of **6** with AcONa in other solvents were carried out similarly, and the products shown in Table 1 were isolated.

*2-Bromo-2-methylcyclohexane-1,3-dione (**10a**).* To a stirred mixture of 4.5 g (36 mmol) of 2-methylcyclohexane-1,3-dione[5] and 4.2 g (36 mmol) of AcONa in 60 ml of $CHCl_3$–H_2O (6 : 1), 5.7 g (36 mmol) of bromine was added dropwise below 5 °C. After the addition, the mixture was further stirred for 1 hr, and then the $CHCl_3$ layer was separated. The aqueous layer was extracted with 30 ml of $CHCl_3$. The combined $CHCl_3$ solutions were dried over Na_2SO_4 and evaporated under reduced pressure. The residue was chromatographed on a silica gel with CCl_4 to give 4.5 g (62%) of **10a**; bp 65—66 °C/2 mmHg. IR(film): 1735 and 1710 cm^{-1}. NMR(CCl_4): δ 1.75 (s, 3H, CH_3) and 1.90—3.60 ppm (m, 6H, $-CH_2CH_2CH_2-$).

Found: C, 41.33; H, 4.68%. Calcd for $C_7H_9O_2Br$: C, 41.00; H, 4.42%.

*Reaction of **10a** with Sodium Acetate.* A mixture of 1.5 g (7.3 mmol) of **10a** and 0.6 g (7.4 mmol) of AcONa in 50 ml of THF was refluxed for 5 hr. The reaction mixture was poured into water, neutralized with 1M HCl and then extracted with two 30 ml portions of ether. The combined ether extracts were washed with 5% aqueous Na_2CO_3 solution. The ether layer was separated, dried over Na_2SO_4 and evaporated to give an oil. The oil was separated into two fractions by chromatography on a silica gel with CCl_4. The earlier fraction gave 0.16 g (12%) of acetic 1-oxo-2-methyl-2-cyclopentene-3-carboxylic anhydride (**12**). IR(film): 1770, 1720, 1680 and 1630 cm^{-1}. NMR($CDCl_3$): δ 1.56 (s, 3H, $-CH_3$), 2.18 (*s*, 3H, $-OCOCH_3$), and 1.95—2.85 ppm (m, 4H, $-CH_2CH_2-$). Mass spectrum: *m/e* 182 (M^+).

Found: C, 59.72; H, 5.83%. Calcd for $C_9H_{10}O_4$: C, 59.34; H, 5.53%.

The mild treatment of **12** with an aqueous NaOH afforded 2-methyl-3-oxo-1-cyclopentenecarboxylic acid (**11**). The latter fraction of the chromatography gave 0.2 g (13%) of **10a**.

The aqueous Na_2CO_3 solution was neutralized with 1M HCl, and then extracted with ether. The ether extract was dried over Na_2SO_4, and evaporated. The solidified residue was subjected to fractional recrystallizations from CCl_4–$CHCl_3$ (4 : 1), which afforded 0.2 g (22%) of 2-methylcyclohexane-1,3-dione (**13**); mp 200—202 °C (lit,[5] mp 204 °C and 0.26 g (25%) of 2-methyl-3-oxo-1-cyclopentenecarboxylic acid (**11**). An analytical sample of **11** was obtained by recrystallization from $CHCl_3$; mp 168—170 °C.

Found: C, 59.82; H, 5.51%. Calcd for $C_7H_8O_3$: C, 59.99; H, 5.75%.

*2-Chloro-2-methylcyclohexane-1,3-dione (**10b**).* To a stirred suspension of 3.0 g (24 mmol) of **13** in 100 ml of $CHCl_3$, 2.7 g (25 mmol) of *t*-butyl hypochlorite was added gradually under nitrogen atmosphere at −10 °C. After the addition was completed, the reaction mixture was further stirred for 2 hr at −10 °C, and washed with 20 ml of 5% aqueous Na_2CO_3 solution, then with water. The $CHCl_3$ solution was dried over Na_2SO_4 and evaporated. The residue was chromatographed on a silica gel with CCl_4 to give 2.2 g (58%)

of **10b**; bp 70—71 °C/4 mmHg. IR(film): 1740 and 1715 cm^{-1}. NMR (CCl_4): δ 1.60 (s, 3H, CH_3) and 2.00—3.60 ppm (m, 6H, $-CH_2CH_2CH_2-$).

Found: C, 52.58; H, 5.33%. Calcd for $C_7H_9O_2Cl$: C, 52.35; H, 5.65%.

*Reaction of **10b** with Sodium Acetate.* A mixture of 1.5 g (9.3 mmol) of **10b** and 0.78 g (9.5 mmol) of AcONa in 50 ml of THF was refluxed for 4 hr. The reaction mixture was worked up according to the procedures similar to those described for the reaction of **10a** with AcONa, and separated into the neutral fraction and the Na_2CO_3 soluble fraction. The oil obtained from the neutral fraction was chromatographed on a silica gel with CCl_4. The earlier fraction gave 0.07 g (4%) of **12**. The latter fraction afforded 0.23 g (15%) of the recovered starting material (**10b**). The solid obtained from the Na_2CO_3 soluble fraction was subjected to fractional recrystallizations from CCl_4–$CHCl_3$ (4 : 1), which afforded 0.24 g (18%) of **11** and 0.24 g (20%) of **13**.

*2-Acetyl-2,6-dibromocyclohexanone (**14**).* To a stirred mixture of 5.0 g (36 mmol) of 2-acetylcyclohexanone[6] in 80 ml of $CHCl_3$, 5.7 g (36 mmol) of bromine was added gradually below 5 °C. A solution of 4.9 g (36 mmol) of AcONa, and then 5.7 g (36 mmol) of bromine were added successively to the above mixture below 5 °C. After the addition was completed, the reaction mixture was stirred further for 2 hr at 5 °C, and then the $CHCl_3$ layer was separated. The $CHCl_3$ solution was washed with water, dried over Na_2SO_4 and evaporated under reduced pressure. The residual oil decomposed upon distillation, but could be chromatographed on a silica gel with CCl_4 to give (7.2 g (68%) of **14**. IR(film): 1720 and 1730 cm^{-1}. NMR (CCl_4): δ 24.2 (s, 3H. $-COCH_3$) and 1.2—4.0 (m, 7H, $-BrCH-CH_2-CH_2-CH_2-$).

Found: C, 32.56; H, 3.67%. Calcd for $C_8H_{10}O_2Br_2$: C, 32.25; H, 3.38%.

*Reaction of **14** with Sodium Acetate.* A mixture of 1.0 g (3.3 mmol) of **14** and 0.3 g (3.6 mmol) of AcONa in THF was refluxed with stirring for 5 hr. The reaction mixture was worked up as described above and separated into two fractions. An oil obtained from the neutral fraction was chromatographed on a silica gel with *n*-hexane–benzene (1 : 1) to give 82 mg (12%) of acetic 2-acetyl-1-cyclopentene-1-carboxylic anhydride (**16**); bp 85—90 °C/1 mmHg. IR(film): 1770, 1730, 1700 and 1630 cm^{-1}. Mass spectrum: *m/e* 196 (M^+).

Found: C, 61.58; H, 6.42%. Calcd for $C_{10}H_{12}O_4$: C, 61.22; H, 6.17%.

The mild treatment of **16** with an aqueous NaOH solution afforded 2-acetyl-1-carboxy-1-cyclopentene (**15**). The chromatography gave also 0.15 g of a tarry material which could not be purified.

An oily material, which was obtained from the Na_2CO_3 soluble fraction, was triturated with ice-water. A solid thus obtained was recrystallized from $CHCl_3$ to give 0.2 g (40%) of **15**; mp 75—76 °C.

Found: C, 62.31; H, 6.48%. Calcd for $C_8H_{10}O_3$: C, 62.33; H, 6.54%.

References

1) T. Wakui, Y. Otsuji, and E. Imoto, This Bulletin., submitted for publication.

2) M. Sutter and E. Schlittler, *Helv. Chim. Acta*, **32**, 1855 (1949).

3) It is well established that cyclopropanone is readily converted to the alkyl acetal upon dissolving it in alcohol.[4]

4) (a) N. J. Turro and W. B. Hammond, *J. Amer. Chem. Soc.*, **89**, 1028 (1967). (b) N. J. Turro, *Accounts Chem. Res.*, **2**, 25 (1969).

5) H. Stetter and W. Dierichs, *Chem. Ber.*, **85**, 1061 (1952).

6) R. Levine, J. A. Conroy, J. T. Adams, and C. R. Hauser, *J. Amer. Chem. Soc.*, **67**, 1516 (1945).

Fractionation of Polyvinyl Chloride Pitch by Vacuum Sublimation

Mutsukazu KAMO, Hisao KANDA, Yoichiro SATO, and Nobuo SETAKA

National Institute for Researches in Inorganic Materials, Sakura-mura, Niihari-gun, Ibaraki 300-31

(Received July 23, 1973)

Pitch prepared by heating polyvinyl chloride at 400 °C (PVC pitch) was fractionated by vacuum sublimation. The fractions were studied by means of elementary analysis, determination of molecular weight, IR spectroscopy and NMR spectroscopy. It was found that each fraction has a characteristic constituent as follows: 1) Zones 1 and 2 are composed of some aromatic nuclei with 3—4 rings and 3—5 rings linked with aliphatic chains, respectively; 2) Zones 3 and 4 are composed of condensed aromatic nuclei with 6—8 rings and 6—7 rings, respectively; 3) In zone 5, aromatic nuclei have 2—4 aromatic rings on an average, and the ratio of the aliphatic group is higher than that of other zones; 4) The sublimation residue is mainly composed of condensed aromatic nuclei, and the ratio of aromatic hydrogen to aliphatic hydrogen in the residue is the highest.

The initial stage of carbonization of pitch can be studied by chemical methods until the optically anisotropic phase insoluble in usual organic solvents develops.[1] Since pitch is a multi-component system, solvent extraction and chromatographic methods are utilized for fractionation or separation in order to study the mechanism of carbonization.

In this work, vacuum sublimation was used for fractionation. The fractionation is carried out by the difference in vapor pressure. The vapor pressure decreases with increasing molecular weight in a homologous series.

Polyvinyl chloride(PVC) pitch was chosen, since investigations of the carbonization of PVC[2-6] show it to be suitable for examining the utility of vacuum sublimation. Aromatization of aliphatic components is an important process in carbonization and PVC pitch is a typical system prepared from aliphatic compound.

Each fraction obtained by vacuum sublimation was studied by means of elementary analysis, determination of molecular weight, IR spectroscopy and NMR spectroscopy. The results are discussed as regards size of aromatic nuclei, because carbonization is considered to be a process of the growth of aromatic nuclei.

Experimental

Preparation of PVC Pitch. PVC pitch was prepared by heating commercial polyvinyl chloride (Wako Pure Chem. Ind.) under a nitrogen stream at 400 °C. Heat treatment was carried out for 5 hr at 400 °C until the weight loss became constant. The yield was 23%.

Vacuum Sublimation. The heater of the vacuum sublimation furnace consists of two parts, one for sample heating and the other for separation, both of which can be controlled independently. The sublimation column made of a Pyrex glass tube, 8 mm inner diameter and sealed at one end, is connected to a vacuum system consisting of a rotary vacuum pump and monitored by a Pirani guage. Powdered sample, 300—400 mg, was charged in each run. Sublimation was performed at 390—395 °C at $5—6\times10^{-3}$ Torr as vacuum was attained at the end of each run.

Measurement of Molecular Weight. Number-average molecular weights of sublimed fractions in chloroform were determined at 34 °C with a Hitachi 115 vapor-pressure osmometer. Zone-refined benzil (Tokyo Chemical Industry Co., Ltd.) was used as reference material. The stationary value $(\Delta R)_s$ of the difference of thermister resistance ΔR was defined to be the value when the change of ΔR with time was nearly zero ($d\Delta R/dt \simeq 0$). The change was found to be less than 1.3×10^{-2} ohm/min. The value of $\lim_{c\to0}(\Delta R)_s/c$ was estimated from the intercept of the plot of $\Delta R/c$ *versus* concentration c at zero concentration.[7] The cryoscopic method using anthracene as a solvent was employed for the original pitch and the sublimation residue, which contained chloroform-insoluble components. The number-average molecular weights obtained will henceforth be referred to as mean molecular weight.

Instruments. Infrared spectra were measured with a Hitachi spectrometer (EPI-G3) by the usual KBr-disk method. Nuclear magnetic resonance spectra were obtained with a Hitachi spectrometer (R-24) using $CDCl_3$ as a solvent.

Results and Discussion

The temperature gradient curves of the sublimation furnace and each deposition zone are given in Fig. 1. Zones 1, 2, 3, 4, and 5 are numbered with decreasing temperature. Oily deposition product was obtained in the region between temperature 5 and room temperature, but the deposition was not sufficient for analysis. The relations between the yield of each fraction and heating temperatures of samples are given in Fig. 2. Sublimation yields tend to be constant at temperatures higher than 420 °C. However, the difference (indicated by □) has a tendency to increase with temperature. This indicates the possibility of degradation of the pitch at temperatures higher than 400 °C. As

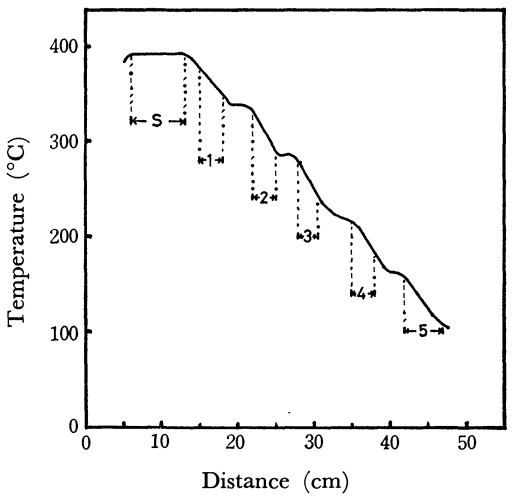

Fig. 1. Temperature gradient of sublimation furnace. S: sample, 1: 1st zone, 2: 2nd zone, 3: 3rd zone, 4: 4th zone, 5: 5th zone.

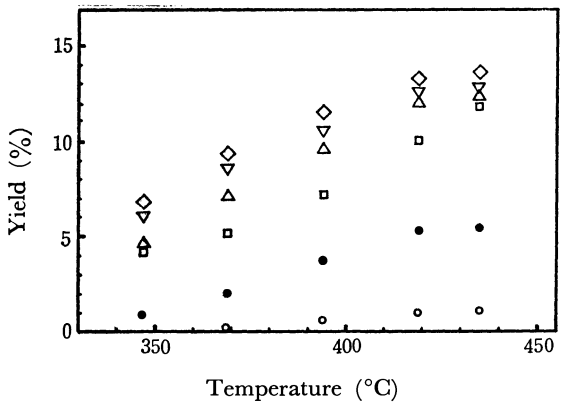

Fig. 2. Relations between yield of each zone and sample temperatures.
○: 1st zone, ●: 2nd zone, △: 3rd zone, ▽: 4th zone, ◇: 5th zone, □: difference between the sublimation yield of sample and the total of the yield of each zone from 1 to 5.

high an yield as possible is desirable, but degradation and/or reaction in pitch during sublimation should be avoided. The sublimation was therefore performed in the temperature range 390—395 °C, at a temperature lower than that of the preparation of the pitch (400 °C). The yields were 42—45%.

Sublimation of the mixture of the following eight compounds was performed: ovalene, violanthrene, decacyclene, coronene, 1,12-benzoperylene, perylene, pyrene, and anthracene. The results are given in Table 1. Each zone is divided into two parts, high temperature and low temperature except for zone 5. The high temperature side is similar to the low temperature side of the neighboring higher temperature zone. Results of elementary analysis of PVC pitch and mean molecular weights are given in Table 2. Mean molecular weights of sublimation products increase with rise in temperature of deposition zones. However, the mean molecular weight of the first zone is greater than that of the residue. This indicates the difference in structure of the main constituents.

NMR data are analyzed according to Brown *et al.*[8,9] and the results are given in Table 3. R denotes the number of condensed aromatic rings per average aromatic unit estimated from H_{aru}/C_{ar}. R′ values indicate actual numbers of aromatic rings per average aromatic unit obtained by the correction of R values with mean molecular weights and chemical formulas.

In the case of the unsubstituted aromatic hydrocarbons, vapor pressure and hydrogen content are usually lowered with increase in the number of rings, *i.e.*, with increase in molecular weight. The tendency is also observed with the aromatic compounds used in this work as seen from Table 1. In contrast, a considerable discrepancy from this trend is noted for PVC pitch fractions of zones 1 and 2.

The deposition of zone 1, though highest in molecular weight, exhibits higher H/C and smaller R than those of zones 2—4 as shown in Tables 2 and 3. It is

Table 1. Sublimation of polynuclear aromatic hydrocarbons

Zone number	Deposited hydrocarbons
2-H[a]	Violanthrene(A)[e]
2-L[b]	Ovalene, Decacyclene, Violanthrene(A)
3-H	Ovalene, Decacyclene
3-L	Ovalene, Violanthrene(B)[f]
4-H	Violanthrene(B)
4-L	Coronene
5-H	Coronene, 1,12-Benzoperylene
5-M[c]	Perylene, 1,12-Benzoperylene
5-L	Pyrene, Anthracene
6[d]	Pyrene, Anthracene

a) High temperature side. b) Low temperature side. c) Middle temperature region. d) Region between zone 5 and room temperature. e) Violanthrene A type. f) Violanthrene B type.

Table 2. Results of elementary analysis and mean molecular weights

Sample	Atomic ratio (H/C)	Molecular weight	Chemical formula
Zone 1	0.89	790	$C_{61}H_{54}$
Zone 2	0.81	600	$C_{47}H_{38}$
Zone 3	0.75	500	$C_{39}H_{29}$
Zone 4	0.76	440	$C_{34}H_{26}$
Zone 5	1.02	310	$C_{24}H_{24}$
Residue	0.60	730	$C_{58}H_{35}$
PVC pitch	0.83	570	$C_{44}H_{37}$

Table 3. Results of NMR measurements and NMR-derived parameters for each zone

Zone number	H_a/H_t	H_α/H_t	H_0/H_t	F_a	H_{aru}/C_{ar}	R	R′
1	0.39	0.32	0.30	0.72	0.68	4	3—4
2	0.40	0.32	0.29	0.75	0.61	5	3—5
3	0.38	0.34	0.28	0.77	0.54	6	6—8
4	0.37	0.34	0.30	0.76	0.54	6	6—7
5	0.36	0.31	0.32	0.67	0.76	2	2—4

H_a/H_t; Ratio of aromatic hydrogen(H_a) to the total hydrogen(H_t).
H_α/H_t; Ratio of hydrogen in saturated groups α to aromatic rings (H_α) to H_t.
H_0/H_t; Ratio of hydrogen on other saturated carbon atoms(H_0) to H_t.
F_a; Aromaticity defined as the ratio of the aromatic carbon to the total carbon.
H_{aru}/C_{ar}; The atomic hydrogen to carbon ratio of the hypothetical unsubstituted aromatic material.
R; Number of condensed aromatic rings per average aromatic unit estimated from H_{aru}/C_{ar}.
R′; Corrected value of R with mean molecular weight and chemical formula.

estimated that the average aromatic unit consists of 3—4 rings, corresponding to the unit weight of 180—220. The observed molecular weight indicates that the average molecule should contain about 4 aromatic units. Taking the chemical composition into account and allowing for the contribution of alkyl groups to the molecular weight, the average molecular structure may be described as a cluster of 3—4 aromatic units linked with aliphatic chains, each unit containing 3—4 condensed rings.

The fraction of zone 2 also shows an anomalous tendency exhibiting a smaller R than that of the fractions of zones 3 and 4 in spite of higher molecular weight. This suggests that the components of zones 1 and 2 are similar in chemical structure. The analysis shows that the average molecule consists of 2—3 aromatic units each having 3—5 fused rings on an average.

The results obtained with the fractions of zones 3 and 4 are almost the same except for molecular weight. Both fractions show lower H/C and H_{aru}/C_{ar} than those of other zones. Their molecular weights and chemical formula indicate that the average molecular structure can be described by the single aromatic unit, in contrast to the case of zones 1 and 2. The analysis shows that the average components of zones 3 and 4 are aromatic hydrocarbons containing 6—8 and 6—7 rings, respectively. NMR parameters and the molecular weights indicate that the aromatic compounds have alkyl substituents.

The deposition of zone 5 exhibits higher H/C and H_{aru}/C_{ar}, and lower F_a than those of other zones. It is estimated that the aromatic unit consists of 2—4 rings on an average. The mean molecular weight indicates that the average components are these aromatic units each having a few alkyl groups. It should be noted that the fraction is somewhat oily, which implies that it contains aliphatic compounds, since aromatic hydrocarbons with molecular weight near 300 are usually solid at room temperature.

The residue has the smallest H/C and as seen from the IR spectra (Fig. 3), the relative intensity of aromatic CH stretching (3060 cm^{-1}) to aliphatic CH stretching (2920 cm^{-1}) is the highest in all the fractions. It is thus inferred that the residue consists mainly of highly condensed aromatic compounds.

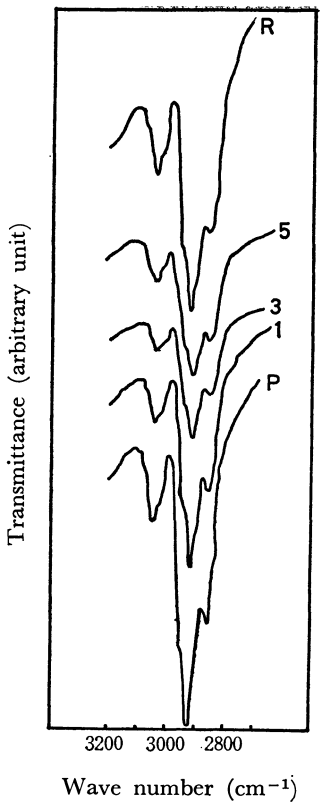

Fig. 3. IR spectra of PVC pitch, each zone and residue.
P: PVC pitch, 1: 1st zone, 3: 3rd zone, 5: 5th zone, R: sublimation residue.

References

1) J. D. Brooks and G. H. Tayler, *Carbon*, **3**, 185 (1965).
2) S. Otani, *Kogyo Kagaku Zasshi*, **61**, 447 (1958).
3) S. Otani, *ibid.*, **61**, 1324 (1958).
4) S. Otani and T. Ishikawa, *ibid.*, **65**, 1617 (1962).
5) S. Otani, *Carbon*, **3**, 31 (1965).
6) H. Marsh, J. W. Akitt, J. M. Hurley, J. Melvin and A. P. Warburton, *J. Appl. Chem. Biotechnol.*, **21**, 251 (1971).
7) "Kobunshisokuteiho," Jo, Baihukan Co., Ltd., Tokyo (1973), p. 57.
8) J. K. Brown, W. R. Ladner and N. Sheppard, *Fuel*, **39**, 79 (1960).
9) J. K. Brown and W. R. Ladner, *ibid.*, **39**, 87 (1960).

NOTES

BULLETIN OF THE CHEMICAL SOCIETY OF JAPAN, VOL. 47(6), 1530 (1974)

Synthesis of Sesquirosefuran

Satoru KUMAZAWA, Koichi NISHIHARA, Tadahiro KATO, Yoshio KITAHARA,**
Hisashi KOMAE,*,** and Nanao HAYASHI*

Department of Chemistry, Faculty of Science, Tohoku University, Sendai 980

* *Department of Chemistry, Faculty of General Education, Hiroshima University, Hiroshima 730*

(Received March 2, 1974)

Synopsis. Sesquirosefuran (I) was synthesized by the coupling of geranyl bromide with 2,2′-bis(3-methylfuryl)-mercury in 29% yield.

Quite recently, Chakravarti *et al.* reported the synthesis[1] of sesquirosefuran (I), one of the components isolated from *Actinodaphne longifolia* Nakai by two of us[2] who also established the structure of other component, longifolin (II). The Chakravarti's paper prompted us to report our own result. Although identity of both natural and synthetic sesquirosefuran (I) was ascertained,[3] the result of the synthesis was kept unpublished since our effort was then directed toward the synthesis of longifolin (II) by the similar method.

As in the case of 2-farnesyl-3-methylfuran (III),[4] coupling of geranyl bromide with 3-methylfurano moiety was achieved using 2,2′-bis(3-methylfuryl)mercury[5] in the presence of zinc-copper powder as described below. Although Chakravarti *et al.* carried out the coupling using 3-methyl-2-furyllithium in 40% yield, our trials with the same reagent gave no satisfactory results.

To an ice cooled anhydrous benzene solution (6 ml) of 2,2′-bis(3-methylfuryl)mercury (1.45 g, 4 mmol) was added 0.87 g (4 mmol) of geranyl bromide in 2 ml of anhydrous benzene. After an addition of zinc-copper powder (15 mg) to the mixture, the reaction mixture was stirred at room temperature for 15 hr, and poured into ice–water. Extraction with ether and a usual work up afforded crude product which was purified by passing through silica gel column with mixed solvents of *n*-hexane: cyclohexane (1 : 1) to give 243 mg (29%) of oily sesquirosefuran (I). IR, NMR, mass fragmentations and analysis were in accord with those of natural product.

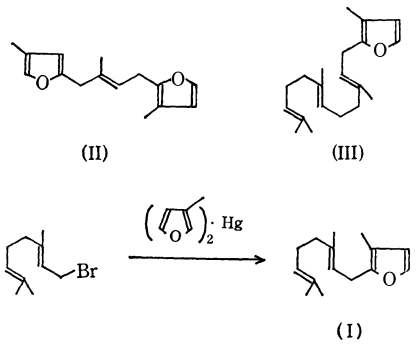

Reaction scheme

** To whom all the correspondences should be addressed.

References

1) Y. Gopichand, R. S. Prasad, and K. K. Chakravarti, *Tetrahedron Lett.*, **1973**, 5177.

2) N. Hayashi, H. Koma , S. Eguchi, M. Nakayama, S. Hayashi, and T. Sato, *Chem. Ind.* (London), **1972**, 572.

3) Thesis of Bachelor of Science of Mr. K. Nishihara at Tohoku University, Feb., 1973.

4) T. Kato, M. Tanemura, S. Kanno, T. Suzuki, and Y. Kitahara, *Bioorg. Chem.*, **1**, 84 (1971).

5) G. Büchi, E. Sz. Kovats, P. Enggist, and G. Unde, *J. Org. Chem.*, **33**, 1227 (1968).

BULLETIN OF THE CHEMICAL SOCIETY OF JAPAN, VOL. 47(6), 1531—1532 (1974)

A New Lanthanoid Double Trifluoride Compound $(Er_{0.3}Nd_{0.7})F_3$

Kiyohito OKAMURA and Seishi YAJIMA

The Oarai Branch, The Research Institute for Iron, Steel and Other Metals, Tohoku University, Oarai, Ibaraki 311-13

(Received March 30, 1973)

Synopsis: A new compound, $(Er_{0.3}Nd_{0.7})F_3$, in the ErF_3–NdF_3 system was prepared by the solid state reaction of NdF_3 (hexagonal LaF_3-type) and ErF_3 (orthorhombic YF_3-type). It was found to be of an isostructure with ErF_3 of the space group Pnma. Structural data are compared with those of ErF_3.

The lanthanoid trifluorides from LaF_3 to NdF_3 have the hexagonal phase of LaF_3-type structure in the temperature range, from room temperature to melting.[1-2] Trifluorides of elements from Sm to Lu, with orthorhombic YF_3-type structure, exhibit equilibrium dimorphic transformation at high temperatures. Compounds from SmF_3 to HoF_3 turn into the hexagonal LaF_3-type, and compounds from ErF_3 to LuF_3 into the hexagonal YF_3-type[1-2] (trifluoride with the hexagonal LaF_3-type and that with the orthorhombic YF_3-type are abbreviated as $(LnF_3)_{hex}$ and $(LnF_3)_{orth}$, respectively). The lanthanoid trifluorides of the same structure have a wide solid solubility range,[3] while the solubility of $(LnF_3)_{orth}$ in $(LnF_3)_{hex}$ differs with the lanthanoid element in $(LnF_3)_{orth}$. However, lanthanoid double trifluoride compounds, such as $(Er_x \cdot Nd_y)F_3$, are not found in the $(LnF_3)_{orth}$–$(LnF_3)_{hex}$ system.

The present work was carried out in order to find new lanthanoid double fluoride compounds consisting of components $(LnF_3)_{orth}$ and $(LnF_3)_{hex}$. Such a compound could be obtained by a solid phase reaction at high temperatures between the lanthanoid trifluorides having a similar radius of the Ln^{3+} ions. Of the $(LnF_3)_{orth}$ type compounds, ErF_3 has the highest transition temperature 1075 °C, and of the $(LnF_3)_{hex}$ compounds, the radius of Nd^{3+} is closest to that of Er^{3+} in ErF_3, compound NdF_3 having a hexagonal phase up to its melting temperature 1380 °C. Thus, ErF_3 and NdF_3 were considered to be the most suitable combination.

Experimental

Erbium and neodymium trifluorides were prepared as described previously.[4] Powders (325 mesh under) of ErF_3 and NdF_3 were mixed in various molar ratios and pressed into pellets of 10 mm diameter and 10 mm height. These were placed in a platinum boat kept in an electric furnace, heated at 1000 °C for five hours in a highly pure argon stream, and cooled slowly to room temperature. Equilibrium was considered to have been established when the X-ray diffraction patterns showed no change on further heating. The crystal structure of the heated specimen was determined from X-ray diffraction patterns taken at room temperature, using Ni-filtered Cu$K\alpha$ radiation (λ=1.5418 Å) and an NaI(Tl) counter connected to a pulse-height analyzer.

Results and Discussion

A new compound was obtained by heating a powder mixture of ErF_3 and NdF_3 with molar ratio 3 : 7. The X-ray diffraction patterns are assigned to an orthorhombic unit cell; the lattice constants are a=6.660±0.003 Å, b=7.053±0.005 Å and c=4.393±0.002 Å. Chemical analysis of the compound was made by the X-ray fluorescence method since ErF_3 and NdF_3 were found to evaporate slightly during the course of heat treatment. The analysis shows the ratio Er : Nd to be 3.06±0.10 : 6.94±0.09. The compound is represented by $(Er_{0.3}Nd_{0.7})F_3$. The crystal is isostructural with ErF_3. The relative intensities of the X-ray diffraction patterns for $(Er_{0.3}Nd_{0.7})F_3$ and ErF_3 are almost the same, but the lattice constants a and b of the former are greater by 5% and 3%, respectively, while c is greater by only 0.2%. The positional and isotropic thermal parameters of $(Er_{0.3}Nd_{0.7})F_3$ were refined by the least-squares by means of powder reflections. The initial atomic parameters of ErF_3[5] with space group Pnma were used. The occupancies of Er and Nd at the lanthanoid atomic sites (abbreviated as $\overline{Ln}$) were fixed at the ratio 3.06 : 6.94. The atomic scattering factors were corrected for the anomalous dispersion effect due to $\Delta f'$ and $\Delta f''$ values (International Tables for X-Ray Crystallography, Vol. II). The final structure is given in Table 1 with that of ErF_3. The final calculated intensities are compared with the observed values (I_0) in Table 2. The reliability factor, $R=(\sum_{hkl}|I_0-I_c|)/\sum_{hkl}I_0$, is 10.10% for the observed reflections.

The fluorine atoms are displaced to some extent from their sites in ErF_3, while the lanthanoid atoms are only slightly displaced from the erbium atom sites in ErF_3. The distances between the $\overline{Ln}$ and fluorine

Table 1. Comparison of atomic parameters of $(Er_{0.3}Nd_{0.7})F_3$(I) and ErF_3(II)

Atomic site	Position	x_j	y_j	z_j	B_j
$\overline{Ln}$ in I	4c	0.360±0.001	1/4	0.050±0.001	0.46±0.01
Er in II		0.367	1/4	0.058	
F(1) in I	4c	0.543±0.002	1/4	0.616±0.002	0.90±0.01
F(1) in II		0.528	1/4	0.601	
F(2) in I	8d	0.146±0.002	0.080±0.001	0.380±0.002	0.90±0.01
F(2) in II		0.165	0.060	0.363	

Table 2. Observed (I_o) and calculated intensities (I_c) for the X-ray powder patters of $(Er_{0.3}Nd_{0.7})F_3$

hkl	d_{cal}(Å)	d_{obsd}(Å)	I_o	I_c		*hkl*	d_{cal}(Å)	d_{obsd}(Å)	I_o	I_c	
011	3.731	3.744	40	40		232	1.446	1.447	30	31	
101	3.670	3.684	154	161		013	1.434			16	
020	3.527	3.539	175	179		322	1.428	1.430	27	3	22
111	3.225	3.265	244	274		103	1.430			3	
210	3.011	3·022	126	143		113	1.403	1.404	7	10	
201	2.655	2.662	6	5		042	1.357	1.376	15	14	
121	2.543	2.549	45	57		430	1.359	1.359	5	6	
211	2.485	2.490	5	7		142	1.347			10	
002	2.199	2.202	24	34		051	1.343	1.346	24	1	20
221	2.121	2.124	35	34		203	1.340			9	
102	2.088	2.090	5	4		402	1.327	1.326	17	11	17
112	2.002	2.004	43	47		123	1.325			6	
301	1.981	1.983	188	79	192	151	1.317			17	
131	1.980			113		341	1.317	1.317	47	25	44
230	1.921	1.923	76	84		213	1.317			2	
311	1.908	1.910	30	30		431	1.298			1	
022	1.866	1.868	24	38		332	1.300	1.299	21	3	16
122	1.797	1.798	33	27		250	1.299			12	
212	1.776	1.776	57	59		511	1.254	1.255	44	18	44
040	1.763	1.764	30	25		223	1.253			26	
321	1.728	1.728	57	58		422	1.242	1.244	25	16	21
400	1.665	1.666	19	23		033	1.243			5	
141	1.589	1.589	25	16		440	1.211	1.211	8	9	
132	1.561	1.562	10	8		521	1.199	1.199	6	2	
312	1.524	1.521	42	17	45	060	1.176	1.177	17	10	17
411	1.520			9		152	1.169			7	
331	1.515			19		432	1.156	1.156	10	2	7
420	1.506	1.506	18	17		351	1.149			5	
241	1.469	1.469	10	8		252	1.118	1.120	19	13	

atoms lie in the range 2.234 Å—2.771 Å, and those between fluorine atoms in the range 2.398 Å—3.083 Å. The corresponding distances in ErF_3 are 2.248 Å—2.589 Å, and 2.552 Å—2.846 Å. The fluctuations of the interatomic distances from the average ($\overline{Ln}$-F; 2.332 Å, F-F; 2.679 Å) are larger than the corresponding deviations from the mean values ($\overline{Ln}$-F; 2.284 Å, F-F; 2.686 Å) in ErF_3. It seems that the atomic arrangement in $(Er_{0.3}Nd_{0.7})F_3$ is more strongly distorted than that in ErF_3.

References

1) F. H. Spedding and A. H. Daane, "The Rare Earth," John Wiley & Sons, Inc., New York, N. Y. (1961), p. 78.

2) R. E. Thoma and G. D. Brunton, *Inorg. Chem.*, **5**, 1937 (1966).

3) D. A. Jones and W. A. Shand, *J. Crystal Growth*, **2**, 361 (1968).

4) K. Niihara and S. Yajima, This Bulletin, **44**, 643 (1971).

5) A. Zalkin and D. H. Templeton, *J. Amer. Chem. Soc.*, **75**, 2453 (1953).

BULLETIN OF THE CHEMICAL SOCIETY OF JAPAN, VOL. 47(6), 1533—1534 (1974)

The Direct-current Conductivity of Silica Gel†

Masa-aki MUROYA and Seiichi KONDO*

Osaka Electro-Communication University, Neyagawa-shi, Osaka 572

** Osaka University of Education, Tennoji-ku, Osaka 543*

(Received June 16, 1973)

Synopsis. The study of the effect of heat-treatment on the direct-current conductivity of silica gel showed that the conductivity changed in response to the dehydration of the adsorbed water and of various kind of silanols. The temperatures of dehydration by this experiment seems to coincide with other experiments such as IR spectroscopy.

The study of direct-current conductivity is useful in investigating the surface of a colloid such as high specific-surface-area silica, since a major part of the measured current is considered to be due to the surface current in such material[1] and, since the behavior of the charge carriers lying on its surface may play a central role in the conductivity. According to the recent studies of this material, several types of silanol groups dehydrate from the surface in various temperature ranges.[2,3] Therefore, the thermal behaivor of these silanol groups is expected to influence the conductivity of this material sensitively. Similar points of view have been presented in several investigations of the conductivity of silica gel.[4,5] In this kind of experiment, however, such impurities as alkali ions generally have a marked influence not only on the drastic thermal changes of the properties of silica gel,[6] but also on the values of the conductivity. Therefore, the thermal effect of the surface conductivity of silica gel was studied in this investigation using high-purity silica gel with high-purity gold electrodes.

Experimental

Material. Ethyl orthosilicate was hydrolyzed to silica sol and gelled on a plastic plate. When the hydrogel thus formed was dried in air, a glass-like plate about 1 mm thick and about 3 cm^2 in area was obtained. The organic substances remaining in the silica gel were oxidized by hydrogen peroxide. No alkali and alkaline earth impurities were detected within our range of experimental error (about ± 1 ppm) in the case of sodium ion. The BET N_2 specific surface area of this sample, S_A, was about 650 m^2/g, and the pore volume was 0.33 ml/g.

Conductivity Measurement. Gold films about 99.999% pure and of 10^{-5} cm thick, and 0.28 cm^2 in area were vacuum-deposited as the electrodes on the same plate which had been sufficiently preheated at about 150 °C and 10^{-5} Torr. This sample was then placed between platinum electrodes placed in a furnace, whose temperature range was from room temperature to 650 °C under a vacuum of 10^{-3} Torr. All these parts were then placed in a vacuum cell made of quartz and Pyrex glass. The applied voltage was mostly 1.000 ± 0.001 V, which was sufficiently low enough to maintain the Ohm's law, and the error of the current measurement was about $\pm 1\%$ or 10^{-3} A. More details of the experiment will be described elsewhere.[7]

According to a simple pore structure model of silica gel in which all the pores lie uniformly in the directions parallel to x, y, and z axes (the z axis is the direction of the electric field, and the x and y axes are perpendicular to the z axis), one third of the total pores in the z axis, which has one third of the total surface area, contribute to the surface conductivity. With this model, the value of the surface conductivity, σ_s, can be calculated as follows;

$$\sigma_s = \frac{l^2}{r} \cdot \frac{3}{S_A \cdot \rho \cdot v} \qquad (\text{ohm}^{-1})$$

where l is the electrode distance; r, the resistance; ρ the apparent density, and v, the volume between the electrodes. The experimental error of the relative value of the resistance was $\pm 1\%$, that of the absolute value was about $\pm 5\%$, and the minimum observable value was about 1×10^{-21} ohm^{-1}.

Results and Discussion

Figure 1 shows the relation between the surface conductivity, log σ_s, and the reciprocal temperature of the heat-treatment of silica gel. The surface conductivity increased gradually and irreversibly when the heat-treatment temperature was elevated in the range from room temperature to about 160 °C, as is shown by the white circles in the figure. When this sample was then cooled from 160 °C, the conductivity decreased linearly along a different route from the original one, as is shown by Curve *a* of this figure. With this thermal history, the conductivity change was reversible along Curve *a*. This difference seems to be caused by the desorption of adsorbed water. From

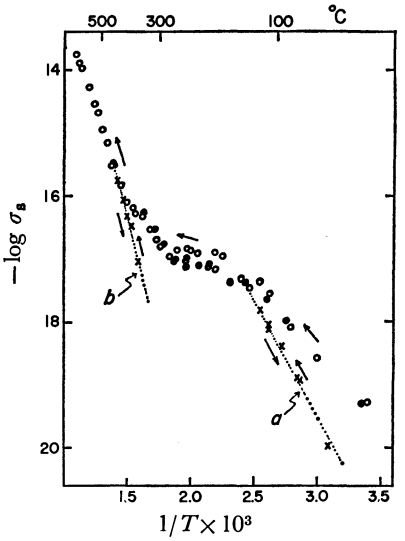

Fig. 1. Log σ_s (the surface conductivity) *versus* reciprocal temperature relation of silica gel.

† Presented at the 26th annual meeting of the Chemical Society of Japan, 1972.

about 170 °C, at which the desorption of water was completed, to about 350 °C, the conductivity curve deviated largely from linearity. As is shown by black and white circles in this figure, the conductivity in this range showed an analogous thermal behavior, but has different absolute values from sample to sample. On the other hand, the infrared study[8] revealed the existence of four types of silanols (b, c, d, and e), and the b-type silanol, whose absorption band is the largest and has the maximum at 3260 cm^{-1}, starts to decrease at 170 °C and disappears at 350 °C. Therefore, the dehydration of this b-type silanol may be responsible for the large decrease in the conductivity. From about 350 to 650 °C, the conductivity increased when the heating temperature was elevated. When the sample cooled after heating at about 450 °C, for example, the conductivity decreased with a different temperature coefficient from that of the heating curve along reversibly Curve *b* in Fig. 1, while it increased reversibly within the range of Curve *b* when the sample was heated. The reason for this difference seems to be that the c-type silanol, which has the 3470 cm^{-1} absorption band, begins to dehydrate at 350 °C. Although still more silanol groups stable at temperatures higher than 650 °C are known to exist,[2,3,8] measurements at such high temperatures in a vacuum were not possible in the present experiment.

References

1) J. J. Bikerman, "Physical Surfaces," Academic Press, New York (1970), p. 428.
2) S. Kondo, *Hyomen*, **10**, 321 (1972).
3) L. H. Little, "Infrared Spectra of Adsorbed Species," Academic Press, London (1966).
4) A. Soffer and M. Folman, *Trans. Faraday Soc.*, **62**, 3559 (1966).
5) J. H. Anderson and G. A. Parks, *J. Phys. Chem.*, **72**, 3662 (1968).
6) S. Kondo and M. Muroya, This Bulletin, **43**, 3453 (1970).
7) M. Muroya and S. Kondo, *Rept. Osaka Electro-Communication Univ.*, **10**, 1973.
8) S. Kondo, M. Muroya, and K. Fujii, This Bulletin, **47**, 553 (1974).

BULLETIN OF THE CHEMICAL SOCIETY OF JAPAN, VOL. 47(6), 1535—1536 (1974)

The Alkylation of Phenol over the $ZnO-Fe_2O_3$ Catalyst

Takeshi KOTANIGAWA and Katsuyoshi SHIMOKAWA

The Government Industrial Development Laboratory, Hokkaido, Higashi-Tsukisamu, Toyohira-ku, Sapporo 061-01

(Received September 14, 1973)

Synopsis. The highly selective alkylation at the *ortho* position of phenol was caused by the dissociative adsorption of phenol; it was discussed by taking account of the acidic and the basic properties of the $ZnO-Fe_2O_3$ catalyst.

The catalytic alkylation of phenol with alcohols by means of a vapor-phase reaction is well known. A large number of related papers have been reported. Enomoto *et al.* have studied the alkylation at the *meta* position of phenol, using a condensed phosphoric acid-Kieselguhr[1] and Al_2O_3–SiO_2[2] as catalysts. Ogata *et al.* have reported the alkylation of phenol with various types of alcohol by means of vapor-phase reactions.[3] The alkylation over solid acidic catalysts is considered to proceed *via* phenyl ether as the intermediate.

It was found in our previous work that the selective methylation at the *ortho* position of phenol over the $ZnO-Fe_2O_3$ catalyst proceeded by means of a reaction between the *ortho* position of the phenoxide surface species and the methyl cation which is formed on the surface of the catalyst.[4] In this paper, we wish to report the results of the selective alkylation of phenol with various alcohols over the $ZnO-Fe_2O_3$ catalyst.

Experimental

Materials. The phenol, ethanol, 1-propanol, 2-propanol, and *t*-butyl alcohol were also of an analytical reagent grade. These alcohols were used after one distillation.

Catalyst. The catalyst was prepared as follows: after the dissolution of 1 mol of ferric nitrate and 1 mol of zinc nitrate in 2.2 l of water, a 14% aqueous ammonium solution was added to the solution until it gave a pH value of 6.85. The coprecipitate was washed several times with water, dried at 150 °C in an oven, calcined in air at 400 °C for 3 hr, and sieved to 12-14-mesh-size particles.[5]

Acidic and Basic Properties of the Catalyst. As the catalyst was colored, the acidic and basic properties were measured by means of gas chromatography, as was illustrated in a previous work.[4] The acidity and the basicity were defined as the saturated amounts of the adsorption of pyridine and phenol respectively.

Reaction Apparatus and Conditions. A conventional flow-type reaction apparatus (reactor : Pyrex glass, i.d. 18 mm) was used. A mixture of 1 mol of phenol and 5 mol of alcohol was introduced into the vaporizer; the reaction vapors were carried by nitrogen gas onto the catalyst bed. The partial pressures of phenol, alcohol, and nitrogen gas in the reaction system was 0.058 atm 0.288 atm, and 0.654 atm respectively. The time factor, W/F, was 53.3 g-cat. h/mol-feed. The vaporizer was maintained at about 300 °C, and the temperature of the catalyst bed was controlled at 350 °C.

Analysis of Products. The reaction products were identified by means of infrared, NMR, and mass spectrometry. The content of each component was quantitatively determined by gas chromatography (column: active carbon, Silicon DC 550, and Porapak Q).

Results and Discussion

The catalyst possesses the following properties: the surface area is 26.6 m^2/g, the pore volume is 0.094 ml/g, and the component is analyzed as $ZnO-ZnFe_2O_4$ by X-ray analysis (Fe-Kα radiation). Moreover, the acidic and the basic properties of the catalyst are shown in Fig. 1. Figure 1 shows that: (1) the acidity and the basicity are 91.3 μmol/g-cat. and 98.0 μ mol/g-cat. respectively, (2) the amounts of the adsorption of pyridine on the catalyst after the saturated adsorption of phenol are 3.8 μ mol/g-cat., and (3) the amounts of the adsorption of pyridine decrease from 91.3 μmol/g-cat. to 3.8 μmol/g-cat. with an increase in the amounts of of the pre-adsorbed phenol.

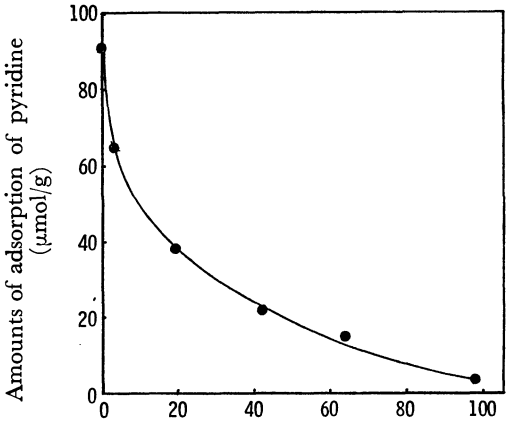

Fig. 1. Acidic and basic properties of the $ZnO-Fe_2O_3$ catalyst.

From these results, it may be considered that the adsorbed phenol lies on both the acid site and the base site. This seems to mean that a dissociative adsorption of phenol takes place on the catalyst.[4] The products of the reaction between phenol and various alcohols are shown in Table 1. The reaction may be divided into the alkylation of phenol and the decomposition of alcohols.

Alkylation of Phenol: The alkylation of phenol over such a solid acidic catalyst as alumina is said to proceed by means of the rearrangement of alkyl phenyl ether.[2] The ratio of alkylphenol to alkyl phenyl ether in the reaction products depends on the structure of the alcohol.[6] However, the alkylation of phenol over the present catalyst proceeds selectively at the *ortho* position even with various alcohols, as is shown in Table 1. Ogata *et al.* reported that phenol was not only alkylated by the rearrangement of alkyl phenyl ether, but also by the direct nuclear alkylation.[3] The present catalyst

Table 1. Products by the reaction between phenol and various types of alcohols

Alcohol	Ethanol	1-Propanol	2-Propanol	*t*-Butyl alcohol
Conversion of phenol (mol %)	33.1	23.9	12.0	trace
Yields of *o*-alkylphenol (mol %)	26.4	20.2	11.4	trace
Conversion of alc. (mol %)	100	100	100	100
Selectivity (%)				
Acetone	100	—	93.1	—
C_4H_7-CO-CH_3	—	—	1.9	—
4-me-3-Pentene-2-one	—	—	4.8	—
Pentan-3-one	—	86.0	—	—
Hexan-3-one	—	14.0	—	—
iso-Butylene	—	—	—	100
Composition of gaseous products (mol %)				
Carbon dioxide	16.8	18.5	—	—
Hydrogen	78.7	77.1	100	—
Carbon monoxide	4.5	4.5	—	—

can, therefore, be considered to catalyze the nuclear alkylation of phenol directly without the rearrangement of alkyl phenyl ether. For the nuclear alkylation, phenol must be dissociated on the surface of the catalyst. In the previous work, it was described that selective methylation at the *ortho* position of phenol was carried out by the reaction between the phenoxide surface species and the methyl cation.[4] If this mechanism is applied in this study, the alkylation of phenol with various alcohols may also be effected to take place at the *ortho* position. The high selectivity for the alkylation at the *ortho* position of phenol may be concluded to be caused by the dissociative adsorption of phenol on the acid site and the base site of the present catalyst.

Decomposition of Alcohols: The ethanol and 1-propanol decomposed to form gaseous products and ketones. The gaseous products from primary alcohols were composed of 17% of CO_2, 78% of H_2, and 4.5% of CO. From these facts, the path of the decomposition of primary alcohols may be considered to be as follows;

$$2\,RCH_2OH \longrightarrow 2\,RCHO + 2\,H_2 \quad (1)$$

$$2\,RCHO \longrightarrow \begin{matrix}R\\R\end{matrix}\!\!>\!C{=}O + CO + H_2 \quad (2)$$

$$CO + H_2O \longrightarrow CO_2 + H_2 \quad (3)$$

where R denotes a methyl or ethyl group. 2-propanol decomposed to form hydrogen, acetone, and small amounts of unsaturated ketone (C_4H_7-CO-CH_3). From these facts, the reaction may be considered to proceed as follows;

$$\begin{matrix}CH_3\\CH_3\end{matrix}\!\!>\!CHOH \longrightarrow \begin{matrix}CH_3\\CH_3\end{matrix}\!\!>\!C{=}O + H_2 \quad (4)$$

$$CH_3\text{-}CO\text{-}CH_3 + O{=}C\!<\!\begin{matrix}CH_3\\CH_3\end{matrix} \longrightarrow$$

$$CH_3\text{-}CO\text{-}CH{=}C\!<\!\begin{matrix}CH_3\\CH_3\end{matrix} + H_2O \quad (5)$$

t-butyl alcohol decomposed to form *iso*-butylene and water by dehydration, which is said to proceed in an acidic medium.

References

1) M. Inoue and S. Enomoto, *Chem. Pharm. Bull.* (Tokyo), **19**, 2518 (1971).
2) M. Inoue and S. Enomoto, *ibid.*, **20**, 232 (1972).
3) Y. Ogata, K. Sakanishi, and H. Hosoi, *Kogyo Kagaku Zasshi*, **72**, 1102 (1969).
4) T. Kotanigawa, This Bulletin, **47**, 950 (1974).
5) T. Kotanigawa, M. Yamamoto, K. Shimokawa, and Y. Yoshida, *ibid.*, **44**, 1961 (1971).
6) Kannan S. V. and Pillai C. Narayana, *Indian J. Chem.*, **8**, 1144 (1970).

BULLETIN OF THE CHEMICAL SOCIETY OF JAPAN, VOL. 47(6), 1537—1538 (1974)

The Effect of Ion Exchange on the 1,2-Epoxybutane-Isomerization Activity[1,2]

Shigemi MATSUMOTO, Masahiro NITTA, and Kazuo AOMURA
Faculty of Engineering, Hokkaido University, Sapporo 060

(Received September 27, 1973)

Synopsis. The isomerization of 1,2-epoxybutane was studied over NaA-type zeolite and its zinc-exchanged forms in a flow system. The catalytic activity increased from 31 to 92% upon the replacement of Na^+ by Zn^{2+}. This increase may be the consequence of the enlargement of the zeolite pore size and the increase in the surface acidity.

We reported previously that the synthetic A-type zeolites exchanged with various cations are effective as catalysts in 1,2-epoxybutane (EB) isomerization.[1] It was shown that the catalytic activity depends upon the surface acidity, which varies with the kind of cation. It may, then, be expected that the degree of ion exchange also has an influence on the acidity and activity.

In this paper we will deal with the effects of the degree of ion exchange on the EB isomerization activity and on acidity of zinc-exchanged A-type zeolite.

Table 1 shows various properties of A-type zeolites exchanged with the zinc ion. The X-ray diffraction patterns and specific surface areas of all the catalysts (ZnA=sample II-VIII) were similar to those of the original Linde 4A(NaA=sample I) and showed ZnA to be highly crystalline.

The products of the EB isomerization reaction were BA, CA_c, CA_t, EMK, and a small amount of *n*-butyl alcohol (NB). Sample I showed no catalytic activity under the conditions studied here. Figure 1 shows the correlation between the catalytic activity and the extent of zinc ion exchanged on ZnA. As is evident from Fig. 1, ZnA begins to show the catalytic activity slightly when the extent of exchange exceeds 30%, the activity increases rapidly as the extent of exchange exceeds 50%, and then becomes almost constant in the range above 80%. This suggests that any comparison of the catalytic activity among zeolites exchanged with various cations, which are of widely differing degrees of ion exchange, should be done with extra care. The order of activity of cation-exchanged A-type zeolites will be effective only when the degree of ion exchange is either the same or $\geq 80\%$.

Many authors have already reported on the influence of the degree of ion exchange on the activity of zeolite catalysts.[4-6] All of their studies, however, have been of X- and Y-type zeolites. Type-A zeolites have hardly been investigated at all.[7] X- and Y-type zeolites with large pores (9—10 Å) also show an activity change with the degree of ion exchange similar to that described above. Those zeolites have three kinds of cation sites.[6] When the replacement of cations at inactive sites is achieved, *i.e.*, when the degree of ion exchange exceeds *ca.* 50%, the activity increases suddenly.

In the case of the A-type, however, the effective pore size of zeolite should be considered aside from the above interpretation, because the cation sites of the A-type differ from those of the X- and Y-types and the size of the reactant molecule is close to the pore size. The molecular size of EB** is larger than the effective pore size of NaA(4.2 Å). The reactant molecules cannot, therefore, pass the pore and are not adsorbed on the internal surface(cavity of zeolite). Consequently, Samples I, II, III, and IV, which are Na-rich forms, are inactive for isomerization. The effective pore size of the A-type is determined by the number and species of cations at the 8-membered oxygen-ring sites, as has been pointed out by Breck *et al.*[8] and Takaishi and Yusa.[9] Takaishi and Yusa have proposed cation-exchange scheme as below to account for the adsorption phenomena of ZnA. The A-type zeolite has two types of cation sites; that is, there are 3 of the 8-membered oxygen ring sites and 8 of the 6-membered oxygen ring sites per unit cell. A total of 12 mon ovalent cations per unit cell are distributed among those sites (see Ref. 9). When 2 Zn ions are introduced (*i.e.*, when the Na ions at the 8-ring sites and the 2 Na ions at the 6-ring sites are replaced (4/12=33%)), the effective pore size becomes 5 Å since 2 Zn ions are located at the 6-ring sites and one of the 8-ring sites is vacant, and the adsorption of *n*-butane begins to occur.[10] At a point corresponding to the replacement of 4 Zn ions for 8 Na ions(8/12=67%) all the 8-ring sites become vacant and molecules of about 5Å size can freely

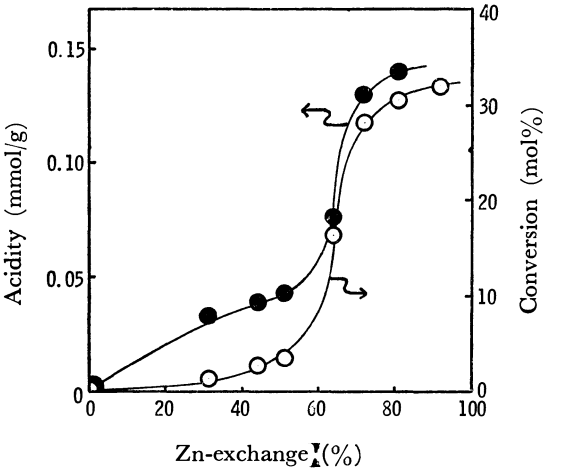

Fig. 1. Change of catalytic activity and acidity with degree of ion exchange.
○: Conversion of EB, ●: Acid amount at $H_0 \leqq +4.8$

* In our paper the "4A" zeolite, which contains only sodium as a cation, is designated as NaA, while forms in which sodium has been exchanged to even a slight degree with the zinc ion are designated "ZnA,"

** About 4.9 Å; estimated from *n*-butane: 4.89 Å; tehane: 4.2 Å; ethylene oxide: 4.2 Å.

Table 1. Various properties of ZnA type zeolites

Sample	Zn-exchanged (%)	Surface area (m^2/g)	Diffraction peak intensity[b]	ΔE_a[c] (kcal/mol)	Selectivity (BA+CA)/EMK	Acid strength[d] (H_0)
I	0	659[a]	144	0	—	$>+4.8$
II	31	—	128	11.2	39.2	-5.6
III	44	—	133	23.6	37.5	-5.6
IV	51	643	—	22.1	40.0	-5.6
V	64	—	119	—	36.5	-5.6
VI	72	—	—	—	38.0	-5.6
VII	81	619[e]	121	31.6	41.2	-5.6
VIII	92	631	124	—	42.3	-5.6

a) Using O_2; b) Sum of peak heights for (311), (321) and (410, 322) planes; c) Apparent activation energy; Reaction temp.: 180—240 °C; d) Maximum value which the catalyst shows; e) After reaction.

go in and out of the cavity. Thus, the catalytic activity of Samples V and VI increases. Beyond this point Zn ions occupy the 8-ring sites, but do not disturb the passage of molecules since one of the 8-ring sites is still vacant and since the Zn ion(ionic radius, 0.74Å) is smaller than the Na ion (0.97 Å); hence, Samples VII and VIII are highly active, much like V and VI.

The constitution of the products is almost the same in all the catalysts except I. The selectivity, (BA+CA)/EMK, is about 40; this indicates that BA is preferentially produced. This implies that the "molecular sieve action" characteristic of A-type zeolite does not change with the degree of ion exchange for this reaction.

The acidic character of the catalysts is given in Table 1. Sample I has no acidity at $H_0 \leqq 4.8$. It is known from the results of spectroscopic study that the Na-forms in X- and Y-type zeolites are also nonacidic.[11] As may be seen in Table 1, the strong acid sites as $H_0 = -5.6$ appear rapidly, as the degree of ion exchange is about 30%. When the degree of exchange rises, the total amount of acid sites increase, although the strength of the acid sites does not change further. A previous study clarified that those acid sites are the active sites for EB isomerization.[1] The inertness of Sample I (NaA) is due to both the absence of acid sites and the small pore size. The rise in activity with the growing zinc content can be explained as an increase in the total amount of acid sites and an enlargement of the effective pore size. On the low-exchanged ZnA(II, III, IV) the activity is considerably smaller than that expected from the amount of acid, as is shown in Fig. 1. This is due to the diffusion hindrance, as has been mentioned above.

The apparent activation energy changes are shown in Table 1. The apparent activation energy of EB isomerization over low-exchanged ZnA(II, III, IV) was smaller than that of the high-exchanged sample, VII. A similar dependence of the activation energy was noted by Balandin *et al.* for A-type zeolite (CoA) in a 1-butanol dehydration study.[7] The low activation energy may be a result of diffusion hindrance because of the small effective pore size; this would be in agreement with the conclusion of Balandin.

Experimental

Materials. The original sodium-form zeolite(NaA)* was Linde Molecular Sieves 4A, which is in a binder-free powder form. The zinc chloride used for ion-exchange was of a guaranteed grade. The EB was of an extra pure grade, and the heart-cut after distillation was chromatographically pure. The nitrogen deoxygenated and dehydrated was used as a carrier gas.

Ion-exchange. The ion-exchange experiment was carried out at 85 °C ±1 for 5 hr in a thermostat.

The NaA was treated as has been described in Part II.

The degree of ion exchange was determined by flame photometry after dissolution in dilute hydrochloric acid.

The X-ray powder diffraction patterns of the hydrated samples were obtained using filtered copper K_α radiation. The specific surface areas of the samples were measured by the BET method using N_2 and O_2. The crystallinity of the ion-exchanged zeolites was judged by a comparison of these results.

Reaction and Analysis. For estimating the catalytic activity, a flow reactor was used.[1] The zeolite catalysts were heat-treated at 400 °C for 3 hr in a reactor. The reaction was carried out at 220 °C in a nitrogen carrier. The activity of the catalyst was given in terms of EB conversion. The selectivity of the catalyst was expressed in terms of the mole ratio of butyraldehyde (BA) and crotyl alcohol (*cis*=CA_c, *trans*=CA_t) to ethyl methyl ketone(EMK).

Acidity. The acidic properties of the catalysts, which were heated at 400 °C for 3 hr in air, were determined by the titration method with *n*-butylamine and using a series of Hammett indicators.[3]

References

1) Studies of the Catalytic Properties of Synthetic A-Type Zeolite. Part III. Part II: M. Nitta, S. Matsumoto, and K. Aomura, *Nippon Kagaku Kaishi*, **1973**, 1839.

2) Presented at the Summer Meeting of the Hokkaido Branch of the Chemical Society of Japan, Hakodate, July, 1973.

3) O. Johnson, *J. Phys. Chem.*, **59**, 827 (1955).

4) G. M. Schwab and R. Sieb, *Z. Naturforsch, A*, **18**, 164 (1963).

5) H. Otouma and H. Ukihashi, This Bulletin, **42**, 2449 (1969).

6) K. Tsutsumi and H. Takahashi, *J. Catal.*, **24**, 1 (1972).

7) Z. V. Gryajnova, M. M. Ermilova, A. A. Balandin, G. V. Tsitsishvili, and V. I. Bashin, "Proc. 4th Internat. Congr. Catalysis,,' (Moscow, 1968), Paper 58.

8) D. W. Breck, W. G. Eversole, R. M. Milton, T. B. Read, and T. L. Thomas, *J. Amer. Chem. Soc.*, **78**, 5963 (1956); *ibid.*, **78**, 5972 (1956).

9) T. Takaishi and A. Yusa, *Shokubai*, **13**, 149 (1971).

10) T. Takaishi, A. Yusa, and Y. Yatsurugi, The 24th Annual Meeting of the Chemical Society of Japan, Osaka, April, 1971; Preprint **B**. 12342.

11) J. W. Ward, *J. Catal.*, **11**, 238 (1968).

BULLETIN OF THE CHEMICAL SOCIETY OF JAPAN, VOL. 47(6), 1539—1540 (1974)

Solid Complex Formation of Malonic Acid with Glycine

Jujiro NISHIJO

Kobe Women's College of Pharmacy, Higashinada-ku, Kobe 658

(Received October 2, 1973)

Synopsis. A solid complex in a molar ratio of 1 : 1 was inferred to be formed by means of an intermolecular hydrogen bond between the hydrogen atom of the -COOH of malonic acid and the $-COO^-$ of glycine.

As a part of a series of studies of the interaction of organic acid with amino acid, we previously reported[1] that oxalic acid forms a solid complex at a molar ratio of 1 : 1 with a large number of α-amino acids and also at a molar ratio of 1 : 2 with some of the α-amino acids. Therefore, it was presumed that the formation of the complexes was promoted by proton-transfer from the carboxyl group in oxalic acid to the carboxyl ion of amino acid in the case of the 1 : 1 complex and by the intermolecular hydrogen bond between two hydrogen atoms of the carboxyl groups in oxalic acid and the carboxyl ions of two molecules of amino acid in the case of the 1 : 2 complex. To investigate further the factors affecting the formation of a solid complex of organic acids with α-amino acid, we have chosen malonic acid, which is a weaker acid than oxalic acid and glycine, and studied it with respect to the formation of a solid complex between them.

Experimental

Preparation of the Solid Complex. A mixture of malonic acid (special-grade chemicals) and glycine (special-grade chemicals) in a molar ratio of 1 : 1 was dissolved into purified water. By evaporating the solvent at 60 °C under a pressure of 30—40 mmHg, a viscous residue was obtained. The residue gradually crystallized when left standing at room temperature. This substance will hereafter be called M_1-G_1, where M and G stand for malonic acid and glycine respectively where the subscripts refer to the molar ratio. The crystalline substance was dried at 60 °C for 10 hr, pulverized in an agate mortar, and then used as the sample. The same procedure was followed to prepare samples of different molar ratios.

Measurements. The X-ray analysis and DTA-TG were carried out using the apparatus previously reported.[1] The infrared absorption spectra were measured with a Hitachi spectrophotometer, Model EPI-G2. The Nujol-mull method was used in the measurements. The pH value was measured by means of a Toa Denpa HM-5A-type apparatus. The determination of malonic acid and glycine by X-ray diffractometry was carried out by the method reported previously.[1]

Results and Discussion

The X-ray diffraction patterns of malonic acid, γ-glycine, and M_1-G_1 are shown in Fig. 1. In the case of M_1-G_1, a new diffraction pattern, diffrent from those of the component, malonic acid, and glycine, was obtained. On the other hand, M_2-G_1, M_3-G_2, and M_4-G_3 gave patterns of M_1-G_1 and malonic acid, while

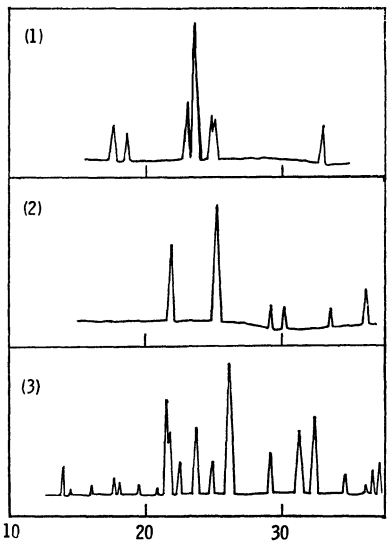

Fig. 1. X-Ray diffraction patterns of malonic acid (1), γ-glycine (2) and M_1-G_1 (3).

M_1-G_2, M_2-G_3, and M_3-G_4 gave those of M_1-G_1 and γ-glycine. The determination of the mole ratio of malonic acid to glycine in the complex was carried out by the method reported previously;[1] it was concluded that malonic acid reacts with glycine in a 1 : 1 molar ratio to produce a solid complex which gives the diffraction pattern of M_1-G_1.

The infrared spectrum of M_1-G_1 is shown in Fig. 2. For comparison, the infrared spectra of the components, malonic acid and glycine, are shown in Fig. 2. The infrared spectrum of M_1-G_1 is diffrent from the sum; this fact indicates the presence of an interaction between

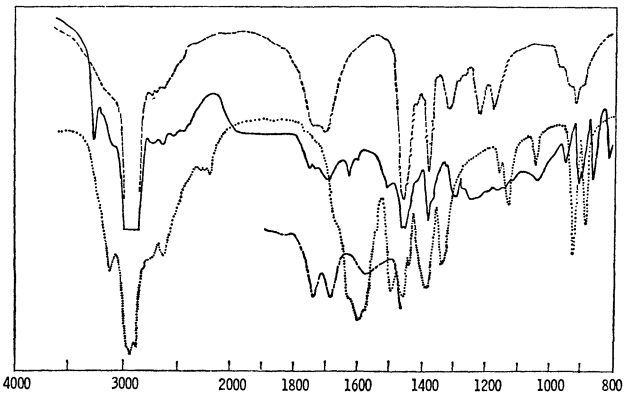

Fig. 2. Infrared absorption spectra of M_1-G_1 (——), malonic acid (----), γ-glycine (·····) and deuterated M_1-G_1 (— — — —) in Nujol.

malonic acid and glycine. The absorption bands which are observed at 3250—2300 cm^{-1}, 1620 cm^{-1}, and 1510 cm^{-1} in M_1-G_1 shift toward lower wave numbers upon deuteration. Therefore, NH_3^+ is present in M_1-G_1. An absorption band assigned to COOH is observed in the region of 1750—1695 cm^{-1}, and it is inferred from the shape of the absorption band and the wave number that there exists a COOH group of a different type of intermolecular hydrogen bond in M_1-G_1. Also, an absorption band appearing near 1575 cm^{-1} in the deuterated M_1-G_1 seems to be assignable to $-COO^-$. The X-ray diffraction pattern of M_1-G_1 was identical with that of the deuterated M_1-G_1.

The DTA-TG of M_1-G_1 and malonic acid are shown in Fig. 3. In the case of malonic acid, a small endothermic peak due to a transition and a large endothermic peak due to fusion are observed near 92 °C and 132 °C respectively. Following this sharp endothermic peak, a broad endothermic change due to the decomposition of malonic acid into acetic acid and carbon dioxide was observed. Now, in the case of M_1-G_1, a sharp, large endothermic peak due to fusion and a small but sharp exothermic peak due to the crystallization of the dissolved glycine to α-glycine were observed near 113 and 145 °C respectively. The gradually increasing endothermic change shown by M_1-G_1 after fusion is similar to that shown by malonic acid alone and is

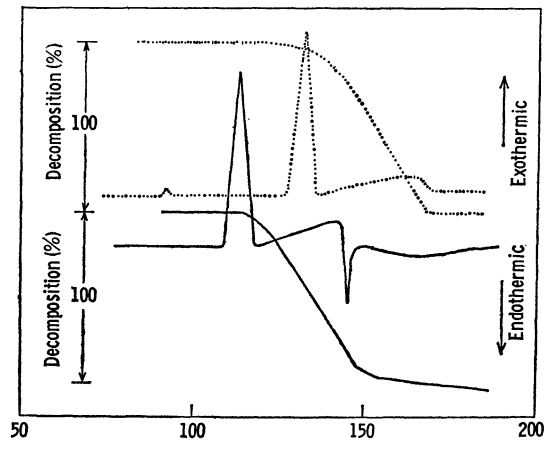

Fig. 3. DTA-TG curves of M_1-G_1 (——) and malonic acid (·····), in air. heating rate: 1.25 °C/min, sensivility: ±50 μV, reference: α-alumina powder.

considered to be the energy required for the decomposition of M_1-G_1 into glycine, acetic acid, and carbon dioxide. The slight exothermic change observed after the exothermic peak due to the crystallization to α-glycine indicates a possibility that glycine in part undergoes thermal polymerization in this temperature range.[2]

The driving force in the formation of a solid complex of malonic acid with glycine was considered. The pK_1 and pK_2 of malonic acid are 2.76 and 5.29 respectively, whereas the pK_1 of glycine is 2.35.[3] Hence, the formation of the so-called salt in aqueous solution would not be extensive. The pH of an aqueous solution of mixture of malonic acid and glycine, 0.1 mol/l in respect to each component, was 2.60 at room temperature. The ratio of $G^{\pm}(NH_3^+CH_2COO^-)$ to $G^+(NH_3^+CH_2COOH)$ in the aqueous solution was determined by means of the following equation:

$$\frac{[G^{\pm}][H^+]}{[G^+]} = 10^{-2.35}, \quad \frac{[G^{\pm}]}{[G^+]} = 1.8$$

Therefore, G^+ is about one half of $G^{\pm}$. It is known that the shape of the infrared absorption band of -COOH in M_1-G_1 differs from that of -COOH in malonic acid alone, but is similar in wave number, that the stretching vibration of NH_3^+ is shifted toward the higher wave-number side compared with that of glycine alone, that M_1-G_1 undergoes a breakdown to malonic acid and γ-glycine upon treatment with methanol or ethanol and malonic acid dissolves in an organic solvent while γ-glycine remains undissolved. On the basis of these experimental results, it is difficult to consider that the proton of -COOH of malonic acid has transferred to the $-COO^-$ of glycine in M_1-G_1. It has, hence, been inferred that the solid complex is formed as a result of formations of an intermolecular hydrogen bond between the hydrogen atom of malonic acid and the $-COO^-$ of glycine.

The author wishes to thank Professor Toshio Kinugasa, Professor Isamu Imanishi and Doctor Genzo Hashizume for their encouragement.

References

1) J. Nishijo, I. Imanishi, G. Hashizume, and T. Kinugasa, *Nippon Kagaku Kaishi*, **1973**, 442.
2) H. Watanabe and Y. Kozai, *Nippon Kagaku Zasshi*, **87**, 613 (1966).
3) T. Sakaguchi and K. Ueno, "Kinzoku Kireto," Vol. 3, Nankodo, Tokyo (1967), p. 6.

BULLETIN OF THE CHEMICAL SOCIETY OF JAPAN, VOL. 47(6), 1541—1542 (1974)

The ESR Spectra of Michler's Ketone Anion Radicals

Hideo FUJITA, Saburo KAKO, Jun YAMAUCHI*, Hiroaki OHYA-NISHIGUCHI**, and Yasuo DEGUCHI

College of Liberal Arts and Sciences, Kyoto University, Kyoto 606

** Institute for Chemical Research, Kyoto University, Uji 611*

*** Faculty of Science, Kyoto University, Kyoto 606*

(Received November 12, 1973)

Synopsis. The ESR spectra of Michler's ketone anion radicals reduced by alkali metal in solution consist of five groups of lines at +20 °C, but change into three groups of lines at −50 °C. The assigned hyperfine splitting constants are $A_H^o=3.22$, $A_H^m=0.43$, $A_N=0.72$, $A_{H^3}^{CH_3}=0.29$ gauss at +20 °C.

Since Müller[1] reported the complete 1 : 1 metal ketyl monomer fomation of Michler's ketone with counter cations on the basis of magnetic-susceptibility measurements, the cation radicals of this ketone[2] in solution have been investigated by ESR and characterized as similar to those of Wuerster's blue[3] and *N,N'*-tetramethylbenzidine[4] in the relative magnitudes of their hyperfine splitting constants among nitrogen and differrent sorts of protons. The results of the first observation of the ESR spectra of anion radicals of this ketone will be presented in this report.

Experimental

Anion radicals of Michler's ketone were prepared by the standard alkali metal reduction method.[5] The ESR spectra were measured with a JEOL X-band spectrometer equipped with 100 kHz modulation (MODEL ME-3) over the temperature range from +90 to −120 °C. Spectral simulations were carried out with a JEOL Spectral Computer (MODEL JEC-6).

Results and Discussion

The ESR spectra of the anion radicals obtained by potassium metal reduction on a mixed solvent (75%-DME and 25%-MeTHF) consisted of five groups of lines in the temperature range from 0 to +40 °C; a typical example at +20 °C is shown in Fig. 1a. Upon cooling to a lower temperature range (from −30 to −60 °C), the spectral structures were changed into those of three groups of lines with an approximate intensity ratio of 1 : 2 : 1; a representative spectrum at −50 °C is shown in Fig. 2. No appreciable line broadening has been detected in this temperature region, and the overall spectral width was constant at a value of around 21.2 gauss. The temperature dependency was found to be reproducible even when the temperature was changed to the reverse. The slightly broader linewidth on the high-field side than on the low-field side seems to be attributable to the contribution from the anisotropic *g*-tensor.[6]

A satisfactory simulation spectrum for Fig. 1a is shown in Fig. 1b, while the splitting constants used are compiled in Table 1 together with the corresponding spin densities calculated by H.M.O. procedures (using the hyperconjugation model[7] for the methyl-group

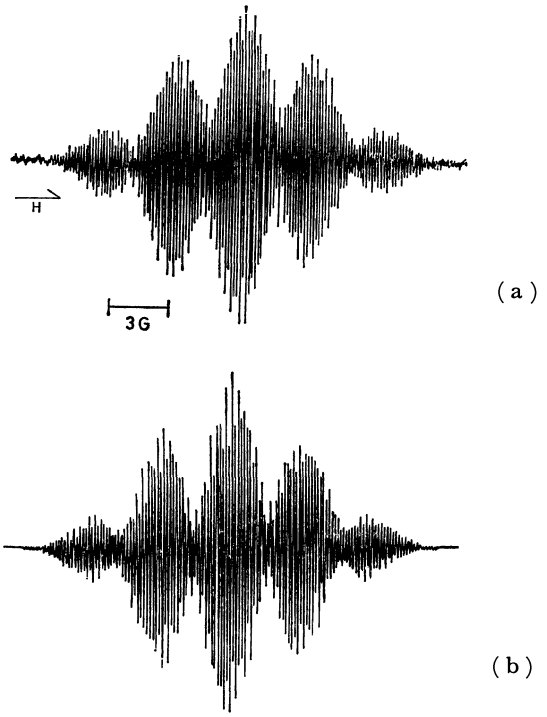

Fig. 1. The ESR spectrum of Michler's ketone anion radical in mixture of DME(75%) and MeTHF(25%) at +20 °C. The upper spectrum (a) is the experimental and the lower (b) is the simulation based on the splitting constants given in Table 1.

TABLE 1. SPIN DENSITIES AND SPLITTING CONSTANTS AT +20 °C FOR MICHLER'S KETONE ANION RADICAL

Positions	Calcd Spin Densities[a] Hückel	McLachlan	Calcd h. f. s. Const.[b] (gauss)	Obsd h. f. s. Const (gauss)
1 a	0.3012	0.4054		
1 b	0.1061	0.1204		
1	0.0051	−0.0466		
2, 6	0.0829	0.1110	2.66	3.22
3, 5	0.0012	−0.0379	0.91	0.43
4	0.0753	0.0889		
7	0.0409	0.0432	0.86	0.72
8, 10	0.0000	−0.0012		
9, 11	0.0031	0.0034	0.57	0.29

a) The parameters used for the calculation were cited from Ref. 7.

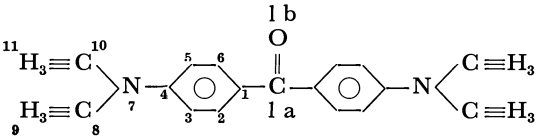

b) These values were calculated by using McLachlan spin densities in the table with Q values:
$|Q_{C-H}^H| = 24$, $|Q_{C-N}^N| = 20$, $|Q_{CH_3}^H| = 508/3$

contributions). The 3.22 gauss splitting from *o*-proton frames the characteristic five-group structure. The structure in the groups is accounted for by the contribution of the nitrogen and the other proton splittings. The potassium metal splitting constant is estimated to be less than 0.08 gauss; thus, the spectral patterns have not been affected significantly.

The change in the spectral structures around −30 °C to −60 °C has not yet been explained satisfactorily. However, the present authors assume that either a non-equivalency in a pair of *o*- or *m*-protons on the respective phenyl rings in the molecule or the presence of a linewidth alternation[8] similar to those found in the case of benzophenone[9] is responsible for this peculiar change. Many simulations for Fig. 2 have been carried out following a couple of the aforementioned mechanisms, but no statisfactory agreements have yet been found.

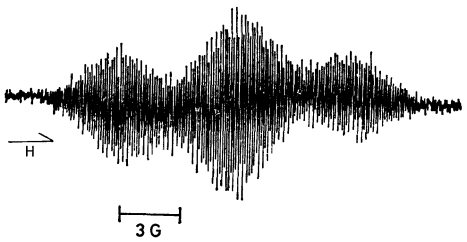

Fig. 2. The ESR spectrum of Michler's ketone anion radical in mixture of DME(75%) and MeTHF (25%) at −50 °C.

Recently the triplet-state ESR spectra of Michler's ketone ketyl have been observed; they suggest the formation of a metal ketyl similar to that of benzophenone.[10] These results will be reported in detail elsewhere.

References

1) E. Müller und W. Janke, *Z. Elektrochem.*, **45**, 380 (1939).
2) B. M. Latta and R. W. Taft, *J. Amer. Chem. Soc.*, **89**, 5172 (1967).
3) J. R. Bolton, A. Carrington, and J. D. Santos-Veiga, *Mol. Phys.*, **5**, 615 (1962).
4) J. M. Fritsch and R. N. Adams, *J. Chem. Phys.*, **43**, 1887 (1965).
5) D. E. Paul, D. Lipkin, and S. I. Weissman, *J. Amer. Chem. Soc.*, **78**, 116 (1956). H. Nishiguchi, Y. Nakai, K. Nakamura, K. Ishizu, Y. Deguchi, and H. Takaki, *J. Chem. Phys.*, **40**, 241 (1964).
6) R. D. Allendoerfer, *J. Magn. Resonance*, **9**, 140 (1973).
7) Y. Ikegami, H. Watanabe, and S. Seto, This Bulletin, **45**, 2205 (1972). A Streitwieser, Jr., "Molecular Orbital Theory for Organic Chemists," John Wiley & Sons, New York (1962), p. 135.
8) P. D. Sullivan and J. R. Bolton, "Advances in Magnetic Resonance," ed. by J. S. Waugh, Vol. 4, Academic Press, New York and London, (1970), p. 39.
9) T. Takeshita and N. Hirota, *J. Chem. Phys.*, **51**, 2146 (1969).
10) N. Hirota and S. I. Weissman, *J. Amer. Chem. Soc.*, **86**, 2538 (1964). N. Hirota, *ibid.*, **89**, 32 (1967).

BULLETIN OF THE CHEMICAL SOCIETY OF JAPAN, VOL. 47(6), 1543—1544 (1974)

Energized Vinyl Radical Formation in the Photolysis of Ethylene

Hiroshi HARA and Ikuzo TANAKA

Department of Chemistry, Tokyo Institute of Technology, Ohokayama, Meguro-ku, Tokyo 152

(Received January 31, 1974)

Synopsis. Energized vinyl radical formation was found in the primary process of the 1634 Å photolysis of ethylene in the pressure region up to about 1 atm. The energized vinyl radical either decomposes unimolecularly to give acetylene and a hydrogen atom, or is deactivated to a stable vinyl radical at collision.

The primary processes in the photolysis of ethylene had been reported to be (1) and (2) in Scheme 1.[1-4] In recent years, however, another process, vinyl radical formation (3) was found on the basis of the formation of 1-butene as a product.[5,6]

$$C_2H_4 + h\nu \longrightarrow C_2H_2 + H_2 \quad (1)$$
$$\longrightarrow C_2H_2 + 2H \quad (2)$$
$$\longrightarrow C_2H_3 + H \quad (3)$$

Scheme 1.

More detailed mechanisms of the primary processes are still open to further investigation. In the present report, the mechanism involving two kinds of vinyl radical is proposed from the photolysis of high pressure ethylene (up to about 1 atom) at 1634 Å.

Experimental

The experimental procedures used in this experiment were almost the same as described previously.[6]

Results and Discussion

Ethylene was photolyzed at 1634 Å with and without nitrogen as a deactivator. The reaction products were the same as reported previously.[6] The ratio of formation rate of 1-butene to that of *n*-butane was plotted as a function of ethylene pressure, and as a function of nitrogen pressure with a fixed ethylene pressure in Figs. 1 and 2, respectively. In each case, the ratio follows a straight line with intercept against ethylene or nitrogen pressure.

As reported previously, 1-butene and *n*-butane are formed through recombination reactions of vinyl and ethyl radicals and of two ethyl radicals, respectively.[6]

It might be also possible that 1-butene is formed through Reaction (4).

$$C_2H_4^* + C_2H_4 \longrightarrow 1\text{-}C_4H_8 \quad (4)$$

But this process is ruled out in this experiment since 1-butene could not be detected in the photolysis of 360 Torr of ethylene with 19 Torr of nitric oxide added as a free radical scavenger. Thus, 1-butene is formed only by the recombination of vinyl and ethyl radicals. The product ratio evidently shows the pressure dependence, and it strongly suggests that the formation of the vibrationally excited vinyl radical, which either

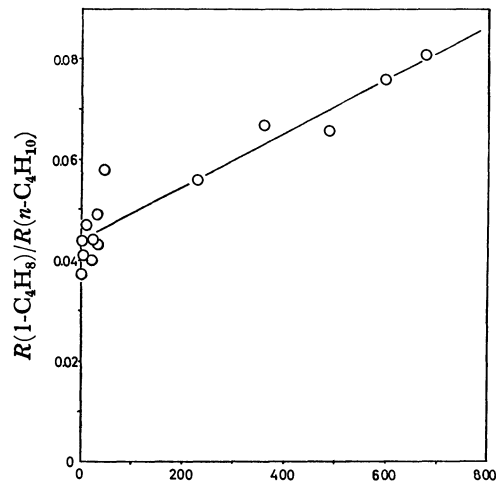

Fig. 1. $R(1\text{-}C_4H_8)/R(n\text{-}C_4H_{10})$ *vs.* the pressure of ethylene (Torr).

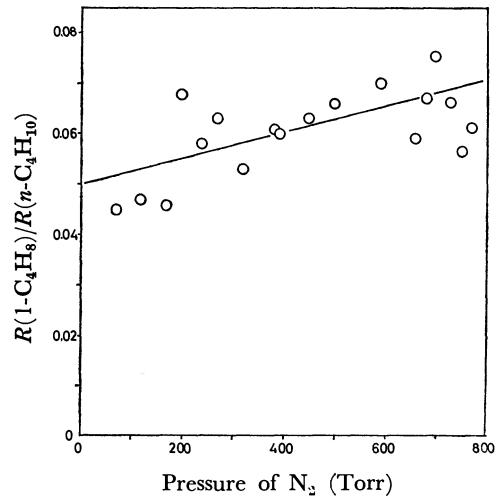

Fig. 2. $R(1\text{-}C_4H_8)/R(n\text{-}C_4H_{10})$ *vs.* the pressure of nitrogen (Torr) (C_2H_4: 25 Torr)

decomposes to give acetylene and a hydrogen atom, or is stabilized at collision to yield a stable vinyl radical. This mechanism has been proposed by Back and Griffith as follows.[4]

$$C_2H_4 + h\nu \longrightarrow H + [C_2H_3^*] \longrightarrow 2H + C_2H_2 \quad (5)$$

The details of the mechanism would be Reaction (6)

$$C_2H_4^* \longrightarrow C_2H_3^{\neq} + H \quad (6)$$

followed quickly by Reaction (7)

$$C_2H_3^{\neq} \longrightarrow C_2H_2 + H \quad (7)$$

provided the lifetime of $C_2H_3^{\neq}$ for dissociation is short enough to preclude any reactions requiring a bimolecu-

lar collision. But they have no direct evidence of the existence of the energized vinyl radicals. If this mechanism were the case, the ratio of 1-butene to *n*-butane would be extrapolated to zero at zero pressure. As seen in Figs. 1 and 2, the intercepts are, however, not zero. Thus, an additional path forming stable vinyl radicals should be considered. Namely two kinds of vinyl radicals must be formed in the primary process; one undergoes the unimolecular decomposition into acetylene and a hydrogen atom competing with collisional deactivation to a stable vinyl radical, and the other does not decompose even at very low pressures.

In the light of these arguments, the following scheme is proposed with the aid of our previous study.

$$C_2H_4 + h\nu \xrightarrow{\phi_1} C_2H_2 + H_2 \quad (8)$$

$$\xrightarrow{\phi_2} H + C_2H_3^{**} \xrightarrow{k_d} C_2H_2 + H_2 \quad (9)$$

$$\xrightarrow{\phi_3} H + C_2H_3^{*} \xrightarrow{k_s[M]} C_2H_3 \quad (10)$$

$$H + C_2H_4 \longrightarrow C_2H_5 \quad (11)$$

$$C_2H_5 + C_2H_5 \longrightarrow C_2H_4 + C_2H_6 \quad (12)$$

$$\longrightarrow n\text{-}C_4H_{10} \quad (13)$$

$$C_2H_3 + C_2H_5 \longrightarrow 2C_2H_4 \quad (14)$$

$$\longrightarrow C_2H_2 + C_2H_6 \quad (15)$$

$$\longrightarrow 1\text{-}C_4H_8 \quad (16)$$

Scheme 2.

Steady state treatment leads to the relationship

$$\frac{R(1\text{-}C_4H_8)}{R(n\text{-}C_4H_{10})} = A\left\{\frac{\phi_3}{\phi_2} + \left(1+\frac{\phi_3}{\phi_2}\right)\frac{k_s^{C_2H_4}}{k_d}[C_2H_4] + \left(1+\frac{\phi_3}{\phi_2}\right)\frac{k_s^{N_2}}{k_d}[N_2]\right\} \quad (17)$$

where $A=k_9(k_5+k_6)/k_6(k_7+k_8+k_9)$. The value of A was obtained in the previous study as 0.45 at 1634 Å.

From the intercepts and the slopes of the plots in Figs. 1 and 2, the values of ϕ_3/ϕ_2, $k_s^{C_2H_4}/k_d$ and $k_s^{N_2}/k_d$ can be determined. The results are summarized in Table 1.

Table 1. ϕ_3/ϕ_2, k_s^M/k_d, and β

M	ϕ_3/ϕ_2	k_s^M/k_d Torr^{-1}	β
C_2H_4	0.098±0.08	1.1 ±0.1	1.0
N_2	—	0.47±0.1	0.43

It is concluded that at least some portion of acetylene in Scheme 1 may be formed through $C_2H_3^{**}$ from ϕ_2 in Scheme 2.

The rate constant of stabilization, k_s, is written as follows:

$$k_s = \frac{\beta Z^{C_2H_3^{**}-M}}{[M]} \quad (18)$$

where β is the collisional deactivation efficiency and $Z^{C_2H_3^{**}-M}$ is the collision frequency between the energized vinyl radical and the deactivator, M. The latter was calculated by means of the gas kinetic theory on the assumption that the collisional diameter of vinyl radical was the same as that of ethylene. If the unit probability of energy transfer per collision is assumed for ethylene, the experimental value of $k_s^{C_2H_4}/k_d$ and the collisional frequency yield an upper limit of the dissociative rate constant, k_d, 1.0×10^{11} s^{-1}. Using this value of k_d, the collisional deactivation efficiency is obtained. These values are also shown in Table 1.

Calculation using a simple RRKM theory was carried out to compare with the dissociative rate constant obtained experimentally.

It is generally accepted that k_d corresponds to the specific rate constant k_E for the energies ranging from 50 to 80% of the maximum available energy for the decomposition. In this study, the specific rate constant for the decomposition of the vinyl radical was calculated. The computation was carried out for four models of activated complexes by the usage of the program by Akimoto *et al.*[7] The result is shown in Fig. 3. The experimental value of k_d, 1.0×10^{11} s^{-1} corresponds to the k_E at 48—57 kcal mol^{-1}, which is 70—80% of the available energy (70 kcal mol^{-1}). Thus the experimental value and our proposed mechanism are quite reasonable.

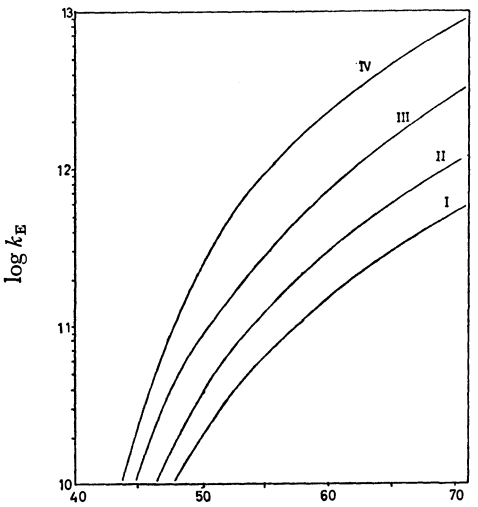

Fig. 3. log k_E *vs.* E. The numbering of the models is taken in order of rigidness.

References

1) M. C. Sauer, Jr., and L. M. Dorfman, *J. Chem. Phys.*, **35**, 497 (1961).
2) H. Okabe and J. R. McNesby, *ibid.*, **36**, 601 (1962).
3) J. R. McNesby and H. Okabe, *Advan. Photochem.*, **3**, 157 (1964).
4) R. A. Back and D. W. L. Griffiths, *J. Chem. Phys.*, **46**, 4839 (1967).
5) Y. Inel, A. Siddiqi, and G. G. Meisels, *J. Phys. Chem.*, **75**, 1317 (1971); P. Borrell, A. Cervanka, and J. W. Turner, *J. Chem. Soc., B*, **1971**, 2293; P. Potzinger, L. C. Glasgow, and G. Von Bunau, *Z. Naturforsch., A*, **27**, 628 (1972).
6) H. Hara and I. Tanaka, This Bulletin, **46**, 3012 (1973).
7) H. Akimoto, K. Obi, and I. Tanaka, *ibid.*, **46**, 2267 (1973).

BULLETIN OF THE CHEMICAL SOCIETY OF JAPAN, VOL. 47(6), 1545—1546 (1974)

Polarized Raman Spectra of $(NH_4)_2SO_4$ Single Crystals

Katsuo UCHIDA, Hiroaki TAKAHASHI, and Keniti HIGASI

Department of Chemistry, School of Science and Engineering, Waseda University, Tokyo 160

(Received February 5, 1974)

Synopsis. Polarized Raman spectra of $(NH_4)_2SO_4$ single crystals were measured at room temperature. The symmetry species of the observed Raman bands due to the internal vibrations of SO_4^{2-} as well as the lattice modes were determined.

Several articles have appeared on the vibrational spectra of $(NH_4)_2SO_4$.[1-5] In spite of the importance of this crystals as one of the improper ferroelectrics, the vibrational problem does not seem to have been solved. The most thorough study is that by Torrie *et al.*[5] who measured infrared and Raman spectra of $(NH_4)_2SO_4$ and $(ND_4)_2SO_4$ powder at temperatures above and below the Curie point (−50 °C). Their results are convincing but do not determine the symmetry species of the infrared and Raman bands.

It is the purpose of this note to report the polarized Raman spectra of $(NH_4)_2SO_4$ single crystals in the paraelectric phase and to give the symmetry species of the Raman bands.

Experimental

Single crystals of $(NH_4)_2SO_4$ were grown from an aqueous solution by slow evaporation at room temperature. The crystals were obtained as thick plates (about 10 mm × 10 mm × 3 mm) with the broad face parallel to the (010) plane and the cleavage plane perpendicular to the *a*-axis. The crystal axes were checked by X-ray oscillation photographs. The polarized Raman spectra were recorded with a Shimadzu R-2D double monochrometer using photon counting detection. The 5145 Å line of an Ar^+ laser was used as the excitation wavelength with 700 mW power output. A polarization scrambler was placed between analyzer and slit and the wave numbers of the Raman bands were calibrated using spontaneous emission lines from the laser.

Results and Discussion

The crystal structure of $(NH_4)_2SO_4$ in the paraelectric phase is orthorhombic P_{nam}-D_{2h}^{16}, with four units of $(NH_4)_2SO_4$ in a Bravais unit cell.[6] All the ions occupy the sites with C_s symmetry.

Internal vibrations of the NH_4^+ ions are expected to appear between 3100 and 1400 cm^{-1}. However, because of their weak intensities in the Raman spectrum, polarization measurements were not successful. According to the factor group analysis, the Raman-active internal vibrations of the SO_4^{2-} ions are classified as $6A_g(\nu_1, \nu_2, 2\nu_3, 2\nu_4)+6B_{1g}(\nu_1, \nu_2, 2\nu_3, 2\nu_4)+3B_{2g}(\nu_2, \nu_3, \nu_4)+3B_{3g}(\nu_2, \nu_3, \nu_4)$ and the Raman-active lattice modes as $9A_g$(6 trans., 2 NH_4^+ lib., SO_4^{2-} lib.)+$9B_{1g}$(6 trans., 2NH_4^+ lib., SO_4^{2-} lib.) + $9B_{2g}$ (3 trans., 4 NH_4^+ lib., 2 SO_4^{2-} lib.)+$9B_{3g}$(3 trans., 4 NH_4^+ lib., 2 SO_4^{2-} lib.).

Polarized Raman spectra below 1200 cm^{-1} are shown in Fig. 1. The bands which appear between 1120 and 440 cm^{-1} are undoubtedly due to the internal modes (ν_1, ν_2, ν_3 and ν_4) of the SO_4^{2-} ions. In spite of the fact that ν_1 is inactive in B_{2g} and B_{3g} species, a very weak band is observed at 976 cm^{-1} in the spectra of both species. Imperfection in the crystal or the polarizer may be responsible for this. It should be noted that the relative intensity of the same vibrational mode belonging to A_g species can vary remarkably in the polarized spectra with different Raman tensor component. As can be seen in Fig. 1, the splitting of the internal modes of the SO_4^{2-} ions is not large. This is in accord with the result of the neutron diffraction study by Schlemper and Hamilton[6] that the SO_4^{2-} ions are not much distorted from tetrahedral symmetry.

The neutron inelastic scattering study at 172 K by Rush and Taylor[7] and the infrared study at 77 K by Torrie *et al.*[5] indicate that the librational modes of the NH_4^+ ions should appear around 330 cm^{-1}. In the present work, however, no band was observed between 440 and 200 cm^{-1}. This is probably because the NH_4^+ ions are almost in free rotation at room temperature.

The liberational modes of the SO_4^{2-} ions and the

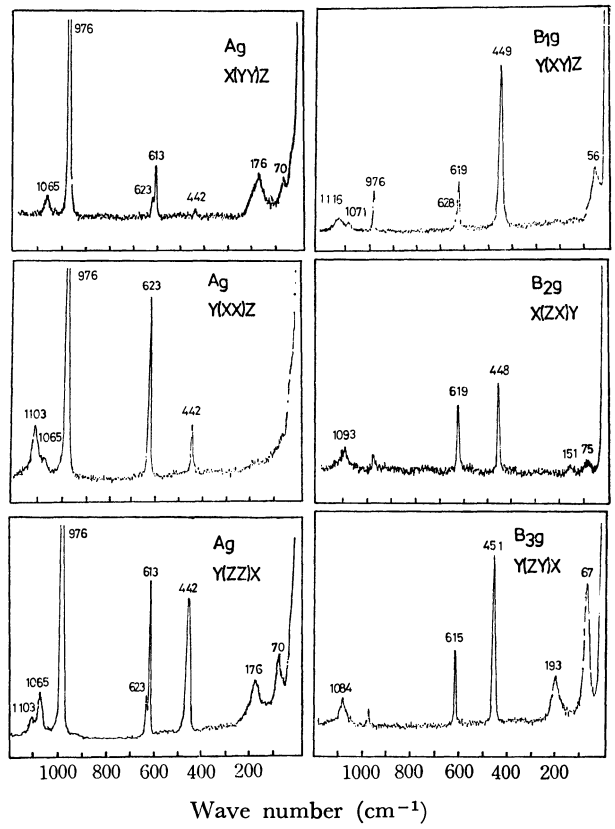

Fig. 1. Polarized Raman spectra of $(NH_4)_2SO_4$ single crystals. The Raman tensor components are expressed according to Porto's notation.[8]

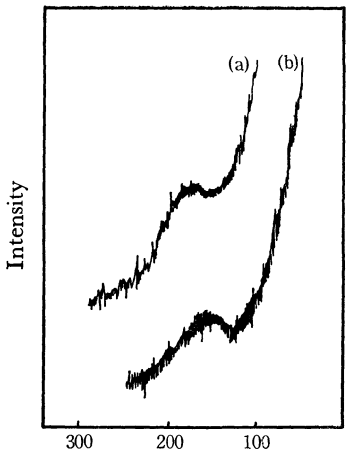

Fig. 2. Low frequency Raman spectra of (a) $(NH_4)_2SO_4$ and (b) $(ND_4)_2SO_4$ powder.

translational modes of the NH_4^+ and SO_4^{2-} ions are expected to appear below 200 cm^{-1}. The Raman spectra below 300 cm^{-1} of $(NH_4)_2SO_4$ and $(ND_4)_2SO_4$ powder are shown in Fig. 2. The band at 185 cm^{-1} of $(NH_4)_2SO_4$ shifts to 167 cm^{-1} by deuteration. The frequency ratio 185/167 is almost equal to $(22/18)^{1/2}$. This means that the band is attributed to the translational modes of the NH_4^+ ions. Thus, the bands at 176(A_g), 151(B_{2g}) and 193(B_{3g}) cm^{-1} in the polarized Raman spectra were assigned to the translational modes of the NH_4^+ ions.

Since the SO_4^{2-} ions do not differ significantly from the regular tetrahedral,[6] it is highly probable that the Raman intensity of the librational modes of the SO_4^{2-} ions is too weak to be detected. The bands at 70(A_g) 56(B_{1g}), 75(B_{2g}) and 67($B3_g$) cm^{-1} in the polarized Raman spectra were therefore assigned to the translational modes of the SO_4^{2-} ions (Table 1).

Table 1. Observed Raman frequencies (cm^{-1}) and assignment of $(NH_4)_2SO_4$

Assignment	A_g	B_{1g}	B_{2g}	B_{3g}
Lattice modes				
SO_4^{2-} trans.	70	56	75	67
NH_4^+ trans.	176		151	193
Internal modes				
ν_2	442	449	448	451
ν_4	613 623	619 628	619	615
SO_4^{2-}				
ν_1	976	976		
ν_3	1065 1103	1071 1116	1093	1084

This work was supported by the Kawakami foundation.

References

1) R. Blinc and I. Levstek, *J. Phys. Chem. Solids*, **12**, 295 (1960).
2) J. C. Thrierr, *Proc. Nat. Acad. Sci. U. S. Sci.*, **253**, 2917 (1961).
3) M. Trefler and G. R. Wilkinson, *Discuss. Faraday Soc.*, **48**, 108 (1969).
4) M. Trefler, *Can. J. Phys.*, **49**, 1694 (1971).
5) B. H. Torrie, C. C. Lin, O. S. Binbrek, and A. Anderson, *J. Phys. Chem. Solids*, **33**, 697 (1972).
6) E. O. Schlemper and W. C. Hamilton, *J. Chem. Phys.*, **44**, 4498 (1966).
7) J. J. Rush and T. I. Taylor, IAEA Symposium on Inelastic Scattering of Neutrons in Solids and Liquids, **2**, 333, (1965).
8) T. C. Damen, S. P. S. Porto, and B. Tell, *Phys. Rev.*, **142**, 570 (1966).

BULLETIN OF THE CHEMICAL SOCIETY OF JAPAN, VOL. 47(6), 1547—1548 (1974)

A Polarographic Study of the Complex Formation Equilibria of Lead(II) Ions with Glutamate and Ethylenediamine-*N*,*N*′-diacetate Anions

Mutsuo KODAMA

Department of Chemistry, College of General Education, Hirosaki University, Bunkyo, Hirosaki, Aomori 036

(Received November 26, 1973)

Synopsis. In this experiment, the complex formation equilibria of the lead(II) ions with glutamic and ethylenediamine-*N*,*N*′-diacetic acids were studied by using the polarographic method. The lead(II) ion forms 1 : 1- and 1 : 2-ratio complexes with glutamic acid, while, with ethylenediamine-*N*,*N*′-diacetic acid, it forms only a 1 : 1-ratio complex, PbX⁰.

Previously,[1] the present author reported in his polarographic study of the lead(II) ions in aspartate and iminodiacetate solutions that the lead(II) ion forms 1 : 1- and 1 : 2-ratio complexes with aspartate and iminodiacetate anions. The lead(II) ion also can form stable complexes with Glut* and EDDA* anions. However, no systematic equilibrium study of the complex formation reactions of the lead(II) ion with Glut and EDDA anions had been reported. In this connection, it seemed to be worthwhile to determine the equilibria of the lead(II) ion with Glut and EDDA anions. In this paper, the present author will determine the solution equilibria of the lead(II) ion with Glut and EDDA anions by using a polarographic technique.

Experimental

Reagents. The preparation of a lead(II) nitrate solution has been described previously.[1] The Gult and EDDA were recrystallized from their aqueous solutions. The ionic strength of the sample solution was adjusted to 0.30 by adding an appropriate amount of $NaClO_4$. The other chemicals used were of an analytical reagent-grade and were used without further purification.

Apparatus and Experimental Procedures. All the apparatus and the experimental procedures employed in this study were the same as those described previously.[1] The characteristic feature of the DME used was also described previously.[2] For the EDDA system, an acetate buffer solution was used. In the Glut system, no buffer reagent was used, because all the sample solutions contained an appropriate amount of uncomplexed Glut and had enough buffer capacity.

Results and Discussion

Lead(II) ions in Glut ($8.50<pH<9.40$) and EDDA ($3.00<pH<4.00$) solutions exhibited single reversible waves, which are diffusion-controlled in nature. In Glut solutions of pH's higher than 9.50, the 1.0 mM lead(II) ion yielded a white precipitate. Therefore, the equilibrium study of the Glut system was conducted in sample solutions containing the 0.30 mM lead(II) ion at pH's lower than 9.50. Since the Glut anion can act as a bidentate or tridentate ligand in the complexation reaction, the lead(II) ion will form 1 : 1- and 1 : 2-ratio complexes with the Glut anion. Therefore, the following relation can be derived for the lead(II)-Glut system:[1]

$$\mathrm{Antilog}\left(\frac{\Delta E_{1/2}}{0.0296}+\log\frac{k_{Pb}}{k_{PbG}}\right) = K'_{PbG}\cdot[\mathrm{Glut}]_f+K'_{PbG}\cdot K^{G'}_{PbG_2}\cdot[\mathrm{Glut}]_f^2 \quad (1)$$

where $\Delta E_{1/2}$ indicates the shift of the half-wave potential by the complex formation and where K'_{PbG} and $K^{G'}_{PbG}$ are, respectively, the conditional first and second successive formation constants of the lead(II)-Glut complex. By using the above relation, the solution equilibrium between the lead(II) ion and the Glut anion was studied. A typical result obtained is reproduced in Fig. 1. From the intercept and slope of the straight line in Fig. 1, K_{PbG} and $K^{G}_{PbG_2}$ were estimated to be 5.0×10^4 and $7.0_0\times10^2$ respectively.

The limiting current of the lead(II) ion in the EDDA solution decreased with an increase in the concentration of the uncomplexed EDDA, $[X]_f$. This decrease can be ascribed to the formation of a lead(II)–EDDA complex. If the aquo lead(II) ion coexists with the 1 : 1-ratio EDDA complex, one can derive the following equation for the conditional formation constant of a 1 : 1-ratio lead(II)-EDDA complex, K'_{PbX}, by combining the relation given by Kacena and Matousek[3] and the Ilkovic equation:

$$K'_{PbX}[X]_f=\frac{(i_d)^2_{Pb}-(i_d)_0^2}{(i_d)_0^2-(i_d)^2_{PbX}} \quad (2)$$

where $(i_d)_{PbX}$ and $(i_d)_{Pb}$ are the diffusion currents of complexed and uncomplexed lead(II) ions respectively,

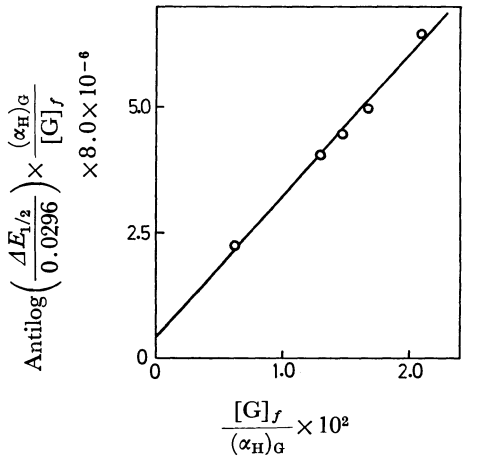

Fig. 1. Determination of formation constants of lead-(II)-Glut complex.
$\mu=0.30$, 25 °C
[Pb(II)]=0.30 mM
$[\mathrm{Glut}]_f$ ranged from 50 to 250 mM

* Glut, glutamate; EDDA, ethylenediamine-*N*,*N*′-di acetate.

BULLETIN OF THE CHEMICAL SOCIETY OF JAPAN, VOL. 47(6), 1549—1550 (1974)

Solvolytic Reactions in Dipolar Aprotic Solvents. Reaction Rates of the Tertiary Aralkyl System

Takane UCHIDA, Sumie MARUI, Yo MIYAGI,* and Kazuhiro MARUYAMA*

Department of Chemistry, Faculty of Education, Fukui University, Bunkyo, Fukui 910

**Department of Chemistry, Faculty of Science, Kyoto University, Sakyo-ku, Kyoto 606*

(Received September 14, 1973)

Synopsis. Solvolytic reaction rates of 2-aryl-2-chloropropanes in dipolar aprotic solvents were determined in order to obtain activation parameters, ρ-values, and β-deuterium effect. The results are compared with those in protic solvents.

Solvolytic reactions in protic media proceed through S_N1, El, S_N2, and E2 routes depending on the structure of substrate and the nature of solvent. In some cases several reaction routes occur concurrently, while in other cases only one appears to occur. Relative ionizing powers of protic solvents have been determined so far[1] without determination of the partitions of each route. In aprotic media most reactions can proceed through the El route because of the slight nucleophilic character of the solvents.[2] Thus the solvolytic reaction in aprotic media may reflect the characteristics of carbonium ion type intermediates more precisely than in protic media. A few such reactions have been studied for the tertiary system, such as reactions of triphenylmethyl chloride in benzene[3] and nitromethane,[4] *t*-butyl chloride in nitromethane,[5] acetonitrile[6] and dimethylformamide,[7] and *t*-butyl nitrate in acetonitrile.[8]

We have studied the reaction rates of 2-chloro-2-phenylpropanes (cumyl chlorides) in dimethyl sulfoxide (DMSO), nitromethane, acetonitrile and dimethylformamide (DMF). The reaction was carried out in the presence of pyridine and the acid liberated was titrated with methanolic sodium methoxide solution. Constant first-order rate coefficients were obtained up to 60% reaction. Rate constants (k_H) of 2-chloro-2-phenylpropane (**1**), with activation parameters, are given in Table 1, and rate constant (k_{Br}) of 2-(4'-bromophenyl)-2-chloropropane (**2**) and their rate ratios to **1** (k_{Br}/k_H) in Table 2. Rate constants (k_D) of 2-chloro-1,1,1,3,3,3-hexadeuterio-2-phenylpropane (**3**) and sixth roots of their ratios to **1** ($\sqrt[6]{k_H/k_D}$) are also shown in Table 2. The corresponding values obtained in protic media are given in Table 3.

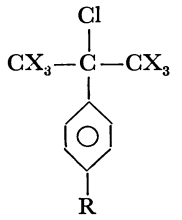

1; R=X=H
2; R=Br, X=H
3; R=H, X=D

The effect of solvents on the reaction rate of **1** is in the order, DMSO>nitromethane>acetonitrile>DMF. Paucity of substituents might give unreliable ρ-values. However, the fact that **1** shows almost the same ρ-values in aprotic solvents indicates a sufficient reliability.

If we compare the results obtained in aprotic solvents with those in protic media, characteristics observed can be summarized as follows. i) ρ-values are similar in both media, ii) although k_H/k_D-values are almost constant in both media, they are slightly larger in aprotic, iii) $\Delta S^{\neq}$-values in aprotic media are negatively larger.

Experimental

Materials. Chlorides were prepared from the corresponding alcohols by the method of Brown and Rei:[9] 2-phenyl-2-propanol,[10], bp 94—96 °C/19 mmHg; 2-(4'-bromophenyl)-2-propanol, mp 40.1 °C (lit,[11] 45.6 °C); 1,1,1,3,3,3-hexadeuterio-2-phenyl-2-propanol was prepared from acetone-d_6 and phenylmagnesium bromide,[10] bp 65 °C/2.5 mmHg, no detectable methyl H-signals in NMR. Dimethyl sulfoxide was refluxed over calcium hydride under reduced pressure and distilled (bp 48.5—50.0 °C/2.5 mmHg). Nitromethane was dried over Drierite and distilled (bp 100.5—101.8 °C). Acetonitrile was refluxed over phosphorus pentoxide and distilled (bp 80.9—82.3 °C). Dimethylformamide was distilled with benzene (about 5%) to remove impurities azeotropically. A fraction boiling at 150—152 °C was collected. Pyridine was dried over potassium hydroxide and distilled (bp 115 °C).

Rate Measurements. About 0.5 mmol of chloride was

Table 1. Rate constants and activation parameters for elimination reactions of 2-chloro-2-phenylpropane (**1**) in aprotic solvents[a]

Solvent	Rate constant, k_H[b]			$\Delta H^{\neq}$[d]	$\Delta S^{\neq}$[e]
	45.0 °C	35.0 °C	25 °C[c]		
DMSO	28.2	11.45	4.41	17.0	−21.5
Nitromethane	13.75	5.25	1.895	18.2	−19.2
Acetonitrile	3.98	1.463	0.507	18.9	−19.4
DMF	2.12	0.649	0.1853	22.5	−9.4

a) [Chloride], 0.05 M; [Pyridine]; 0.05 M. b) $\times 10^5$ s^{-1}. c) Calculated from rate constants observed at 45.0 and 35.0 °C. d) kcal/mol. e) at 25 °C, eu.

Table 2. Rate constants and derived data for elimination reaction of 2-(4′-bromophenyl)-2-chloropropane (**2**) and its D_6-derivative (**3**) in aprotic solvents[a]

Solvent	Temp (°C)	k_{Br}[b]	k_{Br}/k_H[c]	(ρ[d])	k_D[b]	$\sqrt[6]{k_H/k_D}$
DMSO	55.0	14.28	0.22	(−4.4)		
	45.0				14.55	1.12
Nitromethane	55.0	6.77	0.21	(−4.5)		
	45.0				6.68	1.13
Acetonitrile	55.0	2.07	0.20	(−4.7)		
	45.0				1.812	1.14
DMF	55.0	1.301	0.20	(−4.7)		
	45.0				0.918	1.15

a) [Chloride], 0.05 M; [Pyridine], 0.05 M. b) $\times 10^5$ s^{-1}. c) k_H at 55 °C were calculated from rate constants at 45.0 and 35.0 °C. d) Calculated from k_{Br}/k_H-value *vs.* σ^+.

Table 3. Solvolysis data of 2-chloro-2-phenylpropanes

Reaction	Temp[a]	k_1[b]	$\Delta H^{\neq}$[c]	$\Delta S^{\neq}$[d]	ρ[e]	k_H/k_D[f]
Hydrolysis[g]	35	36.1	18.8	−12.4		
(90% aq. acetone)	25	12.4			−4.54[h]	
	0	0.600				
Ethanolysis[i]	50	490				
(ab. ethanol)	25	34.4	20.3	−8.3	−4.67[j]	1.06[i]

a) °C. b) $\times 10^5$ s^{-1}. c) kcal/mol. d) eu. e) *vs.* σ^+. f) per D. g) H. C. Brown, J. D. Brady, M. Grayson, and W. H. Bouner, *J. Amer. Chem. Soc.*, **79**, 1897 (1957). h) H. C. Brown and Y. Okamoto, *ibid.*, **79**, 1913 (1957). i) S. G. Smith and D. J. W. Goon, *J. Org. Chem.*, **34**, 3127 (1969). j) R. L. Buckson and S. G. Smith, *ibid.*, **32**, 634 (1967).

weighed in a 10 ml volumetric flask and 0.05 M solution of pyridine in an aprotic solvent was added. The flask was immersed in a thrmostatt. At an appropriate interval an aliquot of 1 ml was drawn out, poured into 20 ml of acetone, and titrated with a standard solution of sodium methoxide in methanol with lacmoid as an indicator.

Products. Quantitative isolation of 2-phenylpropene (**4**) was difficult because of polymerization. In the case of acetonitrile solution, the yields of **4** determined by an ultraviolet absorption at 243 nm of diluted reaction solutions with ethanol were almost quantitative based on acid formation. The yields of **4** in the other solvents derermined by ultraviolet absorption were less reproducible.

References

1) E. Grunwald and S. Winstein, *J. Amer. Chem. Soc.*, **70**, 846 (1948). See other texts, for example, E. M. Kosower, "An Introduction to Physical Organic Chemistry," John Wiley & Sons, Inc., New York, N. Y. (1968), p. 293.

2) Y. Pocker, "Progress in Reaction Kinetics," Pergamon Press, New York, N. Y. (1961), Vol. 1, p. 218.

3) E. D. Hughes, C. K. Ingold, S. Patai, and Y. Pocker, *J. Chem. Soc.*, **1957**, 1256.

4) Y. Pocker, *ibid.*, **1958**, 240.

5) Y. Pocker, *ibid.*, **1959**, 1179, 3939, 3944.

6) a) D. N. Kevill and J. R. Dorsey, *Chem. Ind.* (London), **1967**, 2174, b) D. N. Kevill and J. R. Dorsey, *J. Org. Chem.*, **34**, 1985 (1969).

7) S. D. Ross and M. M. Labes, *J. Amer. Chem. Soc.*, **79**, 4155 (1957).

8) D. N. Kevill and R. F. Sutthoff, *J. Chem. Soc., B*, **1969**, 366.

9) H. C. Brown and M. Rei, *J. Org. Chem.*, **31**, 1090 (1966).

10) H. C. Brown, J. D. Brady, M. Grayson, and H. Bonner, *J. Amer. Chem. Soc.*, **79**, 1897 (1957).

11) H. C. Brown, Y. Okamoto, and G. Ham, *ibid.*, **79**, 1906 (1957).

BULLETIN OF THE CHEMICAL SOCIETY OF JAPAN, VOL. 47(6), 1551—1552 (1974)

Reaction Paths in the Photochemical Isomerization between *cis*-Butadiene and Cyclobutene

Osamu KIKUCHI

Department of Chemistry, Tokyo Kyoiku University, Otsuka, Tokyo 112

(Received October 29, 1973)

Synopsis. During the disrotatory process of the photoinduced cycloaddition of *cis*-butadiene, two lower symmetric states play an important role and the ground state of cyclobutene is formed directly through a radiationless transition between these two states.

One of the most important questions in photochemical reactions is the actual path along which the excited molecule travels to the product. van der Lugt and Oosterhoff[1] have proposed an interesting reaction path related to this problem. They have calculated the potential curves of the lowest and excited singlet states in the cyclo-addition of *cis*-butadiene to form cyclobutene:

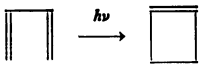

(I)

and concluded that, for the disrotatory process of (I), the generation of the excited state of cyclobutene derived from the Woodward-Hoffmann rule[2] can not be expected and that the ground state of cyclobutene is formed directly through the excited singlet state, which has a symmetric (not an anti-symmetric) property with respect to the symmetry plane. In their calculations, however, only four electrons, π electrons of butadiene, were included. In this note, the potential curves for (I) will be obtained by an all-valence-electron SCF-CI method, and the reaction processes will be discussed.

The potential curves were calculated for the ideal paths, in which the molecule has C_s and C_2 symmetries for the disrotatory and the conrotatory processes respectively. In the course of doing so, the C-C distances and bond angles were varied from the values of *cis*-butadiene to those of cyclobutene. The rotation angle of the methylene groups, θ, was varied from 0° to 90° in steps of 15°. The energies of the lowest and excited (singlet and triplet) states were calculated by the MINDO/2 method[3], followed by CI calculations in which 38 singly- and doubly-excited configurations were included. One of the deficiencies of the MINDO/2 method is its underestimation of the strain energies of small-membered cyclic compounds. This deficiency was adjusted by adding strain energy to the system which increases with the θ and which is about 1 eV[3] at $\theta=90°$, cyclobutene.

The potential curves are shown in Fig. 1. In the conrotatory process, the potential curve for the ground state has a maximum point which did not appear in the potential curve obtained by van der Lugt and Oosterhoff[1] and was not expected in the qualitative diagram of Longuest-Higgins and Abrahamson.[4] The barrier was 1.8 eV,[5] as compared with an experimental estimation, 1.4 eV,[6] and with a theoretical estimation obtained by Hsu *et al.*, 2.0 eV.[7]

In the disrotatory process, the spectroscopic excited singlet state (A″, $\pi\rightarrow\pi^*$) of *cis*-butadiene[8] crosses an excited state (A′) at $\theta\simeq30°$, and two lower singlet states have the same symmetry (A′) at $\theta\simeq45°$, in contrast with Longuet-Higgins–Abrahamson's diagram. The approach of the two lower A′ states in the intermediate of the disrotatory process is caused by the change in the lowest closed-shell electron-configuration in this area. Thus, an appreciable non-adiabatic transition caused by a finite velocity of the rotational motion of CH_2 groups can be expected from the upper A′ state to the lowest A′ state. This has been pointed out by van der Lugt and Oosterhoff.[1]

The probability, P, of the non-adiabatic transition between two states can be estimated by Zener's formula:[9]

$$P = \exp\left\{-\frac{4\pi^2}{h}\varepsilon_{12}^2\Big/\left|\frac{\mathrm{d}}{\mathrm{d}t}(\varepsilon_1-\varepsilon_2)\right|\right\}$$

where the ε's are the energies calculated with two configuration functions whose linear combinations describe the two states in question.[10] Zener's formula can be used for the system in which ε_{12} is independent of the time and in which $\varepsilon_1-\varepsilon_2$ is a linear function of time. In the region of $\theta=30°$—$60°$ of the present

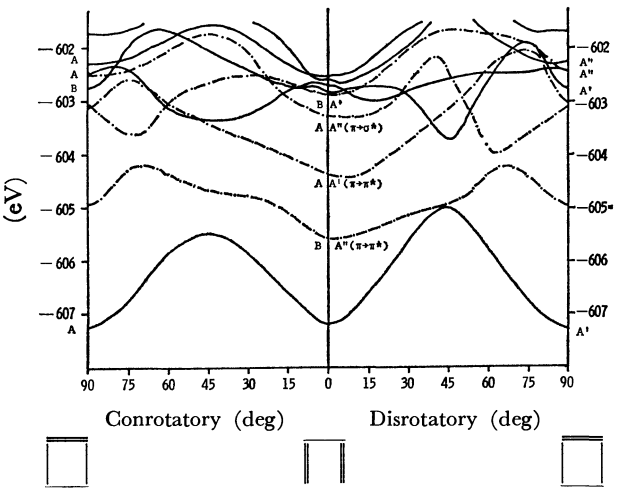

Fig. 1. Potential energy curves ploted as a function of the rotation angle θ of methylene groups.
Solid lines: Singlet states whose electronic symmetry properties are shown at both sides of the figure. The characters of excited states are given in the Ref. 8.
Broken lines: Triplet states whose electronic symmetry properties are shown at the center of the figure. The characters of excited states are given in parentheses.

disrotatory process, $\varepsilon_1-\varepsilon_2$ is approximately a linear function of θ and ε_{12} is almost constant. The probability of the non-adiabatic transition from the upper A′ singlet state to the lowest A′ one within the half-period of the oscillation was estimated as $P\simeq\exp\{-25\}$, a value which corresponds to the mean lifetime, $\simeq 10^{-3}$ s, of the upper A′ state. Between the two corresponding A states of the conrotatory process, no appreciable non-adiabatic transition can be expected because of the lack of interaction between the two A states, as in the two A′ states of the disrotatory process. We feel that the path proposed by van der Lugt and Oosterhoff is reasonable: *cis*-butadiene excited into the A″ singlet state changes its electronic symmetry property near $\theta=30°$,[12] and then the ground state of cyclobutene is formed directly through a radiationless transition at $\theta\simeq 45°$ from the upper A′ state to the lowest A′ state.

The potential curves of the triplet states indicate that the excited triplet states of *cis*-butadiene have no driving force for Reaction (I). This agrees with the experimental facts.[13] A photochemical ring opening of cyclobutene occurs from the upper excited triplet state (not the excited singlet states or the lowest triplet state) of cyclobutene.[13-14] The potential curves of the triplet states in Fig. 1 indicate that the photoinduced ring opening of cyclobutene is possible if cyclobutene is excited into the upper triplet state, T_2, and if the non-adiabatic transition from T_2 to T_1 is appreciable near $\theta=70°$. This path, however, involves the generation of the excited triplet state (A″) of *cis*-butadiene, which may be inconsistent with the experimental facts.[13] Moreover, the absence of the ring-opening path *via* the excited A″ singlet state of cyclobutene[13] can not be understood from the potential curves in Fig. 1.

The calculations were carried out on a HITAC 8700 computer at the Computer Center, The University of Tokyo. The author wishes to thank Professor K. Suzuki for his useful suggestions.

References and Notes

1) W. Th. A. M. van der Lugt and L. J. Oosterhoff, *J. Amer. Chem. Soc.*, **91**, 6042 (1969).
2) R. B. Woodward and R. Hoffmann, *ibid.*, **87**, 395 (1965).
3) N. C. Baird and M. J. S. Dewar, *J. Chem. Phys.*, **50**, 1262 (1969); M. J. S. Dewar and E. Haselbach, *J. Amer. Chem. Soc.*, **92**, 590 (1970); N. Boder, M. J. S. Dewar, A. Harget, and E. Haselbach, *ibid.*, **92**, 3854 (1970).
4) H. C. Longuet-Higgins and E. W. Abrahamson, *ibid.*, **87**, 2045 (1965).
5) This value may be reduced by including the flexibility of the rotation about the C_2-C_3 bond.
6) W. Cooper and W. D. Walter, *J. Amer. Chem. Soc.*, **80**, 4220 (1958); H. M. Frey, B. M. Pope and R. F. Skinner, *Trans. Faraday Soc.*, **63**, 1166 (1967).
7) K. Hsu, R. J. Buenker and S. D. Peyermihoff, *J. Amer. Chem. Soc.*, **93**, 2117 (1971).
8) The four lower excited singlet states of *cis*-butadiene are $\sigma\rightarrow\pi^*$(B,A′), $\sigma\rightarrow\pi^*$(A,A″), $\pi\rightarrow\pi^*$(B,A″), and $\pi\rightarrow\pi^*$(A,A′), lying in this order within the range of 4.4—4.6 eV above the ground state. At $\theta=15°$ for the disrotatory process, the lowest excited stinglet state (A″) has the $\pi\rightarrow\pi^*$ character. At $\theta=15°$ for the conrotatory process, the second excited singlet state has the $\pi\rightarrow\pi^*$ character.
9) C. Zener, *Proc. Roy. Soc., Ser. A*, **137**, 696 (1932). The limits within which Zener's formula is valid have been discussed by C. A. Coulson and K. Zalewski, *ibid., Ser. A*, **268**, 437 (1962).
10) The electron configuration functions, $\Psi_1=|\cdots(7a')^2(5a'')^0|$ and $\Psi_2=|\cdots(7a')^0(5a'')^2|$, contribute effectively to the two A′ states in $\theta=30°$—$60°$ of the disrotatory process. In this region, $d|\varepsilon_1-\varepsilon_2|/d\theta=0.5$ eV/degree and $\varepsilon_{12}=1.5$ eV.
11) $\varepsilon_1-\varepsilon_2$ is not a linear function of the time but of the θ in $\theta=30°$—$60°$, and the value of $d|\varepsilon_1-\varepsilon_2|/dt$ was estimated from the value of $d|\varepsilon_1-\varepsilon_2|/d\theta$.
12) Two states, A′ and A″, will mix with only a small distortion of the molecular symmetry property, and the non-crossing curves enable the symmetry property of the system to change from A″ to A′.
13) R. Srinivasan, *J. Amer. Chem. Soc.*, **84**, 4141(1962); **90**, 4498 (1968); **91**, 7557(1969).
14) J. Michl and J. Kolc, *ibid.*, **92**, 4148 (1970).

BULLETIN OF THE CHEMICAL SOCIETY OF JAPAN, VOL. 47(6), 1553—1554 (1974)

The Reactions of Several Carbonyl Compounds with Hexamethylphosphoric Triamide

Seiji ARIMATSU, Ryohei YAMAGUCHI, and Mituyosi KAWANISI*

Department of Indnstrial Chemistry, Faculty of Engineering, Kyoto University, Yoshida, Sakyo-ku, Kyoto 606

(Received December 19, 1973)

Synopsis. Non-enolizable carbonyl compounds were found to undergo intriguing reaction upon heating with hexamethylphosphoric triamide; benzophenone gave 1,1,2,2-tetraphenylethane and benzophenone methylimine, while fluorenone afforded 9-methylfluorene, 9-dimethylaminofluorene, and fluorene. In contrast, anthrone, an enolizable compound, was completely recovered unchanged under the the same reaction conditions.

Hexamethylphosphoric triamide (HMPT), an excellent dipolar aprotic solvent,[1] has also been widely utilized as a reagent in organic synthesis.[2] In line with this tendency, Monson and his co-workers reported an intriguing chemical process in which cycloalkanones were converted by thermal treatment with HMPT into pyridine derivatives *via* 1-dimethylaminocycloalkenes.[2g] They were successful in explaining the reaction by assuming a cationic species derived from the enamines.

With this in mind, we hoped that the reaction of non-enolizable carbonyl compounds with HMPT might lead to a yet unexplored mode of reaction, since enamine formation is unlikely in this case. This proved to be the case, and 1,1,2,2-tetraphenylethane was obtained from benzophenone, and 9-methylfluorene from fluorenone.

Upon thermal treatment with HMPT at 230—240 °C for 2 hr, benzophenone afforded 1,1,2,2-tetraphenylethane (**1**) by a formally deoxygenative condensation, together with diphenylmethane (**2**), benzhydryldimethylamine (**3**), and benzophenone methylimine (**4**), as is shown in Table 1. On the other hand, a similar treatment of fluorenone gave mainly the reduction product, fluorene (**5**), together with 9-methylfluorene (**6**) and 9-dimethylaminofluorene (**7**). All these compounds gave satisfactory spectral data, and **1**,[3] **4**,[4] and **6**[5] were identical with the authentic specimens independently prepared. In the case of benzaldehyde, a complex mixture containing at least eleven products resulted, from which bibenzyl (**8**), benzyldimethylamine (**9**), and dibenzylmethylamine (**10**) were isolated.

Furthermore, xanthone was converted to xanthene in a 47% yield, but anthrone, an enolizable compound, was completely recovered under these conditions, in accordance with the fact that phenol was converted only slightly to phenyl tetramethylphosphorodiamidate[6] by treatment with HMPT for 5 hr.

When an equimolar mixture of benzophenone and HMPT was heated at 230—240 °C for 2 hr, both the benzophenone and the HMPT were fully consumed. In this case, benzophenone methylimine (**2**) was obtained in a 49% yield after the vacuum distillation of the reaction mixture, although trace amount of **2** and **3** were included as impurities.

Additionally, as is shown in Table 1, the reaction of deoxybenzoin and benzopinacol with HMPT gave peculiar compounds (Runs 7 and 8). In both examples, a cleavage of the central C-C bond of the starting materials took place, although the detailed mechanism is yet unclear.

An inspection of the results listed in the Table (Runs 1 to 4) and the results for the corresponding alcohols[7] indicates that a mechanism similar to that of the reaction of alcohols with HMPT might operate also in the reaction of non-enolizable carbonyl compounds with HMPT, though including some different factors.

Thus, we tentatively propose Scheme 1 with regard to the first step of the reaction.

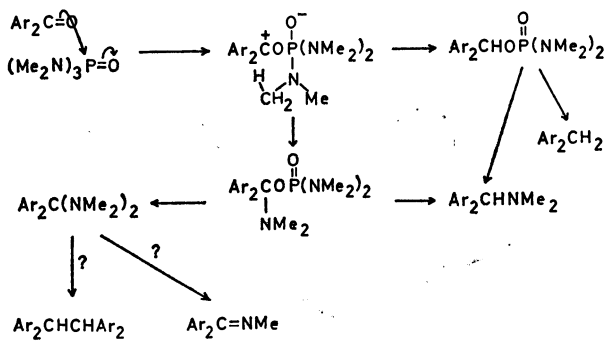

Scheme 1.

Since benzophenone methylimine (**4**) which had been independently prepared was unchanged even if it was treated with HMPT at 230—240 °C for 2 hr, **4** was the final product in this reaction. The presumed intermediate, an aminal, was prepared in the case of benzaldehyde[8] and was treated *without* a solvent at 230—240 °C, affording only a trace amount of bibenzyl, while the starting material was almost entirely recovered. The detailed mechanism for the formation of the peculiar products, such as **1**, **4**, **7**, and **8**, is not yet understood.

The formation of 2,3,5,6-tetraphenylpyridine (**11**) from deoxybenzoin was well explained by Monson's mechanism.[2g] The compound (**11**) was identical with an authentic specimen independently prepared.[9]

Finally an additional observation might be noted. Throughout Runs 1—3 and 5—7, octamethylpyrophosphoramide[10] was formed.

Experimental

All the temperatures are uncorrected. The IR spectra were obtained on a Shimadzu IR-27 spectrometer. The mass spectra were taken by using a Hitachi RMS-4 mass spectrometer. The NMR spectra were obtained on an EM-360

* To whom all correspondence should be addressed.

Table 1. The reaction with HMPT

Run	Substrate	Products (%)
1	Benzophenone	$Ph_2CHCHPh_2$(13), Ph_2CH_2(3), Ph_2CHNMe_2(9), $Ph_2C{=}NMe$(12)
2	Benzaldehyde	$PhCH_2CH_2Ph$(1), $PhCH_2NMe_2$(11), $(PhCH_2)_2NMe$(8), etc.
3	Fluorenone	fluorene(68), 9-methylfluorene(6), 9-dimethylaminofluorene(13)
4	9-Fluorenol	fluorene(11), 9-methylfluorene(1), 9-dimethylaminofluorene(35)
5	Xanthone	xanthene (47, based on unrecovered xanthone) xanthone was recovered in 52%.
6	Anthrone	no reaction
7	Deoxybenzoin	$PhCH{=}C(NMe_2)Ph$(34), $PhCONMe_2$(13), 2,3,5,6-tetraphenylpyridine(3)
8	Benzopinacol	$Ph_2CHCHPh_2$(15), Ph_2CH_2(4), Ph_2CHNMe_2(49), $Ph_2C{=}NMe$(7)

spectrometer, TMS being chosen as the internal standard.

Starting Materials. The benzophenone, benzaldehyde, fluorenone, xanthone, and anthrone were commercially-available products. The following compounds were prepared by the reported method; 9-fluorenol,[11] deoxybenzoin,[12] and benzopinacol.[13]

Hexamethylphosphoric Triamide (HMPT). Commercially-available HMPT was refluxed for 5 hr under N_2 over calcium hydride, and then distilled; bp 110—115 °C/15 mmHg.

General Procedure for the Reaction with HMPT. The substrate (0.01 mol) was dissolved in HMPT (10 ml) and heated at 230—240 °C under N_2 for 2 hr. The reaction mixture was then distilled under reduced pressure. After the HMPT had been distilled off at 110—115 °C/15 mmHg, the residue was separated to a single product by a combination of vacuum distillation, column chromatography, and preparative glc.

Preparation of Benzophenone Methylimine (4).[14] A mixture of benzophenone dichloride (6 g, 0.025 mol) and 30% aqueous methylamine (60 ml) was stirred for 4 hr. After an additional methylamine solution (20 ml) had been added and stirring had been continued for 1 hr, the organic material was extracted with ether and dried (Na_2SO_4). The removal of the ether and distillation at 133—135 °C/5 mmHg gave 4.3 g (88%) of benzophenone methylimine, which was identical with the product of the reaction of benzophenone with HMPT.

The authors wish to thank Professor Hitosi Nozaki for his valuable advice and continuous encouragement.

References

1) H. Normant, *Angew. Chem. Int. Ed. Engl.*, **6**, 1046 (1967).

2) (a) R. S. Monson, *Chem. Commun.*, **1971**, 113; (b) R. S. Monson, *Tetrahedron Lett.*, **1971**, 567; (c) J. S. Lomas, D. S. Sagatys, and J.-E. Dubois, *ibid.*, **1972**, 165; (d) R. S. Monson and D. N. Priest, *J. Org. Chem.*, **36**, 3826 (1971); (e) J. Kopecký and J. Šmejkal, *Chem. Ind.* (London), **1966**, 1529; (f) R. S. Monson and D. N. Priest, *Chem. Commun.*, **1971**, 1018; (g) R. S. Monson, D. N. Priest, and J. C. Ullrey, *Tetrahedron Lett.*, **1972**. 929; (h) M. Kawanisi, S. Arimatsu, R. Yamaguchi, and K. Kimoto, *Chem. Lett.*, **1972**, 881; (i) R. S. Monson and D. N. Priest, *Can. J. Chem.*, **49**, 2897 (1971); (j) E. B. Pedersen, N. O. Vesterager, and S.-O. Lawesson, *Synthesis*, **1972**, 547; (k) N. O. Vesterager, R. Dyrnesli, E. B. Pedersen, and S.-O. Lawesson, *ibid.*, **1972**, 548; (l) M. Kawanisi, S. Arimatsu, and R. Yamaguchi, *Chem. Lett.*, **1972**, 1031; (m) R. S. Monson and B. M. Broline, *Can. J. Chem.*, **51**, 942 (1973).

3) K. Sisido, Y. Takeda, and H. Nozaki, *J. Org. Chem.*, **27**, 2411 (1962).

4) C. R. Hauser and D. Lednicer, *ibid.*, **24**, 46 (1959).

5) E. J. Greenhow, E. N. White, and D. McNeil, *J. Chem. Soc.*, **1951**, 2848.

6) U. S. 3475536 through *Chem. Abstr.*, **72**, 24625v (1970).

7) S. Arimitsu, R. Yamaguchi, and M. Kawanisi, This Bulletin, in press.

8) S. V. Lieberman, *J. Amer. Chem. Soc.*, **77**, 1114 (1955).

9) V. J. Traynelis and R. H. Ode, *J. Org. Chem.*, **35**, 2207 (1970).

10) A. D. F. Toy and E. N. Walsh, "*Inorg. Synth.*," **7**, 73 (1963).

11) R. F. Nystrom and C. R. A. Berger, *J. Amer. Chem. Soc.*, **80**, 2896 (1958).

12) D. A. Ballard and W. M. Dehn, *ibid.*, **54**, 3969 (1932).

13) L. F. Fieser, "Experiments in Organic Chemistry," 3rd ed. Heath & Co., Boston (1955), p. 165.

14) This procedure was followed by that for the preparation of *cis-p*-chlorobenzophenone methylimine. *cf.* D. Y. Curtin and J. W. Hausser, *J. Amer. Chem. Soc.*, **83**, 3474 (1961).

BULLETIN OF THE CHEMICAL SOCIETY OF JAPAN, VOL. 47(6), 1555—1556 (1974)

Determination of Enantiomeric Purity of 1-Phenylalkanols Using a Chiral NMR Shift Reagent

Keiji YAMAMOTO, Tamio HAYASHI, and Makoto KUMADA
Department of Synthetic Chemistry, Kyoto University, Yoshida, Kyoto 606

(Received December 27, 1973)

Synopsis. Addition of tris[3-(trifluoromethylhydroxymethylene)-*d*-camphorato]europium(III) to solutions of partly active (*S*)-1-phenylalkanols caused large enantiomeric-shift differences ($\Delta\Delta\delta$) in their ^{1}H NMR spectra, which permitted a direct determination of enantiomeric compositions of these alkanols.

Recently, chiral lanthanide shift reagents[1] have been applied to the direct determination of enantiomeric purity of certain organic Lewis bases.

We wish to record a quantitative determination of enantiomeric compositions of a series of partly active 1-phenylalkanols (excess (*S*) isomer), obtained *via* catalytic asymmetric hydrosilylation of the corresponding alkyl phenyl ketones[2] (Eq. 1).

$$\begin{matrix} R \\ \diagdown \\ \quad C{=}O \\ \diagup \\ Ph \end{matrix} + Me_2PhSiH \xrightarrow[\text{catalyst}]{\text{chiral Rh}^+} RPhC^*HOSiMe_2Ph \xrightarrow{OH^-} RPhC^*HOH \qquad (1)$$

(R=Me, Et, *iso*-Pr, and *tert*-Bu)

In ^{1}H NMR spectra of the alkanols, addition of tris[3-(trifluoromethylhydroxymethylene)-*d*-camphorato]europium(III) (**1**) to the solutions examined caused large enantiomeric-shift differences ($\Delta\Delta\delta$) in the α-proton signals, as for 1-phenylethanol ($\Delta\Delta\delta$=0.30 ppm).[1b,3] The effect of this chiral shift reagent on the alkanol spectra is shown in Table 1.

It is interesting to note that a systematic decrease in the magnitude of downfield paramagnetic-induced shifts ($\Delta\delta$) of alkanol proton signals (*tert*-Bu<*iso*-Pr<Et) can reflect differences in the bulkiness of these alkanols, showing a relationship parallel to the reverse of the degree of asymmetric induction by the hydrosilylation of alkyl phenyl ketones. The fact that all the protons of (*R*)-alkanols resonate definitely at lower fields than those of (*S*)-enantiomers supports the view that the enantiomeric-shift difference can result from the difference in the stability constants of forming diastereoisomeric complexes of **1** with the alkanols[1a] rather than that in magnetic environments of the complexes.[1b,d]

The enantiomeric compositions of the respective alkanols have been determined on the basis of peak areas of completely separated signals due to their α-proton in the lanthanide-assisted spectra. The results are summarized in Table 2, showing exact agreement with those determined from maximum rotations.[4]

Experimental

Complex **1** was prepared by the reaction of 3-trifluoromethylhydroxymethylene-*d*-camphor (**2**) with europium(III) chloride according to the procedure of Goering *et al.*[1b] Diketone **2** was prepared by the following Grignard reaction of *d*-3-bromocamphor with ethyl trifluoroacetate.[5]

A mixture of 23.3 g (0.10 mol) of *d*-3-bromocamphor, 14.5 g (0.105 mol) of ethyl trifluoroacetate, and 2.56 g (0.105 g-atom) of magnesium in 230 ml of anhydrous ether was heated at reflux for 2 hr. The reaction mixture was then hydrolyzed with 10% hydrochloric acid. The organic layer was separated and the aqueous layer was extracted with ether. The combined ether solution and extracts were washed twice with saturated sodium chloride solution, and the solvent was

TABLE 1. EFFECT OF CHIRAL SHIFT REAGENT (**1**) ON THE NMR SPECTRA OF ENANTIOMERIC SECONDARY ALCOHOLS

Compound	Proton	Paramagnetic-induced shifts ($\Delta\delta$, ppm)					
		Mole ratio[a] 0.3			Mole ratio[a] 0.5		
		(*R*)	(*S*)	$\Delta\Delta\delta$[b]	(*R*)	(*S*)	$\Delta\Delta\delta$[b]
1-Phenyl-2,2-dimethyl-1-propanol	CH_3	1.20	1.15	0.05	1.69	1.64	0.05
	CH[c]	2.78	2.61	0.17	3.93	3.72	0.21
	H_{ortho}	1.36	1.29	0.07	1.93	1.83	0.10
1-Phenyl-2-methyl-1-propanol	CH_3[d]	1.53	1.44	0.09	2.35	2.24	0.11
	CH_3[d]	2.04	2.01	0.03	2.89	2.85	0.04
	CH[c]	4.32	3.98	0.34	6.25	5.81	0.44
	H_{ortho}	2.06		—	3.04		—
1-Phenyl-1-propanol	CH_3	2.05	2.03	0.02	2.44	2.42	0.02
	CH[c]		—[e]		7.50	7.21	0.29
	H_{ortho}		—[e]		3.57		—

a) **1**/alkanol: stepwise addition of **1** to a solution containing 0.2—0.3 mmol of the alkanol in 0.4 ml of CCl_4 (TMS as an internal standard). b) Differential downfield shifts in ppm. c) Used for quantitative determination of enantiomeric compositions under complete separation of signals. d) Diastereotopic methyls. e) Not measured.

Table 2. Enantiomeric purity of partly active 1-phenylalkanols

Compound	Peak ratio[a] (*S*)/(*R*)	$[\alpha]_D^{20}$, deg	Enantiomeric purity, %[b]
1-Phenyl-2,2-dimethyl-propanol	2.52	−11.20 (*c* 4.1, PhH)	43 (43.3)
1-Phenyl-2-methyl-propanol	2.28	−18.81 (*c* 7.0, Et_2O)	39 (39.4)
1-Phenylpropanol	1.89	−8.47 (neat)	31 (30.2)

a) Determined by cutting out and weighing each peak.
b) Values based on maximum rotations are indicated in parentheses.

removed by evaporation. The residue was fractionally distilled to give 18.9 g (76%) of diketone **2**;[6] bp 62.0—62.5 °C/2 mmHg; n_D^{20} 1.4520; $[\alpha]_D^{20}$ +148° (*c* 4.12, benzene).

The NMR spectra were measured on 0.50—0.75 M-solutions of partly active 1-phenylalkanols[2] in CCl_4 (TMS as an internal standard) using a Varian HA-100 (at 31.4 °C) or a Hitachi R-20B spectrometer. The chiral shift reagent (**1**) was dried *in vacuo* at 60° over phosphorus pentoxide before use. All data are given in Tables 1 and 2.

The authors are indebted to Mr. H. Fujita for the NMR measurements.

References

1) a) G. M. Whitesides and D. W. Lewis, *J. Amer. Chem. Soc.*, **92**, 6979 (1970), idem, *ibid.*, **93**, 5914 (1971); b) H. L. Goering, J. N. Eikenberry, and G. S. Koermer, *ibid.*, **93**, 5913 (1971); c) R. R. Fraser, M. A. Petit, and J. K. Saunders, *Chem. Commun.*, **1971**, 1450; d) R. R. Fraser, M. A. Petit, and M. Miskow, *J. Amer. Chem. Soc.*, **94**, 3253 (1972).

2) K. Yamamoto, T. Hayashi, and M. Kumada, *J. Organometal. Chem.*, **54**, C45 (1973).

3) Other modifications of **1**, in which the trifluoromethyl group was replaced by a *tert*-Bu or C_3F_7 have no advantage in this respect (Ref. 1c).

4) R. MacLeod, F. J. Welch, and H. S. Mosher, *J. Amer. Chem. Soc.*, **82**, 7102 (1969).

5) V. Schurig, *Inorg. Chem.*, **11**, 736 (1972).

6) Although Schurig [*Tetrahedron Lett.*, **1972**, 3297] has recommended the exchange reaction of lanthanide salts with the barium chelate of diketone **2**, the preparation of the free diketone does not seem to be tedious.

BULLETIN OF THE CHEMICAL SOCIETY OF JAPAN, VOL. 47(6), 1557—1558 (1974)

Radiation Synthesis of Methylal from Methanol Solution of Ferric Chloride

Yasumasa IKEZOE, Shoichi SATO, and Keichi OSHIMA*

Japan Atomic Energy Research Institute, Tokai-mura, Ibaraki 319-11

(Received December 28, 1973)

Synopsis. The gamma radiolysis of $FeCl_3$–CH_3OH solution was studied by measuring the *G*-values of the products. The mechanism of the selective formation of the main product methylal (G=8.3) was discussed.

The radiolysis of methanol has been studied by several workers.[1] In this paper, the γ-radiolysis of methanol solution of ferric chloride at high absorbed dose is described from the viewpoint of preparative radiation chemistry. The products of radiolysis, in the presence of ferric ion in high concentration known to act as a radical scavenger,[2-4] were analyzed in order to explain the main reaction scheme. The additive was found to act not only as a scavenger but also as a reactant.

Experimental

Preparation of Sample. Reagent grade methanol was distilled twice, first with magnesium and then with tribromobenzoic acid on a 2 m column. Anhydrous ferric chloride (E.P. grade) was dissolved without further purification in methanol under dry nitrogen atmosphere. The irradiation sample (1 ml) was sealed in a 7 ml ampoule after evacuation at liquid nitrogen temperature.

Irradiation. Samples were irradiated by a 16 kCi ^{60}Co gamma source mostly at an exposure rate of 3.2×10^5 R/hr. Before and after irradiation, the samples were kept at Dry Ice temperature to suppress thermal reactions.

Dose rates were determined by Fricke dosimetry with correction for the difference in the electron densities of water and methanol, the energy absorbed by the additive being neglected.

Analysis. The evolved gas, consisting of hydrogen, methane and carbon monoxide, was analyzed by volumetry after being passed through a liquid nitrogen trap, and by mass spectrometry. Two μl of liquid condensed in the liquid nitrogen trap was sampled and injected into a capillary column gas chromatograph with a 60 m column of PEG-400 and a 30 m column of 3,3′-iminodipropionitrile in series connection for the determination of yields of dimethyl ether, methyl chloride, and methylal (dimethoxymethane). The remaining liquid was titrated for induced acidity with 1/10 M sodium hydroxide solution, using methyl red as an indicator. 20 ml of saturated dimedone solution, with pH adjusted to 4.5, was then added to determine formaldehyde yield by precipitation. The filtrate and residue of vacuum distillation were jointly dissolved in distilled water, and the yield of ferrous ion was determined by colorimetry at 552 mμ, after the addition of α,α'-dipyridyl and sodium acetate solution for pH adjustment.

Results and Discussions

The *G*-values of products from the methanol–ferric chloride system are shown in Table 1. The selective formation of methylal[5] at high ferric chloride concentration should be noted. The mechanism could be considered as follows.

$$CH_3OH \rightsquigarrow \cdot CH_2OH,\ H,\ CH_3O\cdot,\ e_s^-,\ etc. \quad (1)$$

$$CH_3O\cdot + CH_3OH \longrightarrow \cdot CH_2OH + CH_3OH \quad (2)$$

Hydroxymethyl radical $\cdot CH_2OH$ is produced directly and indirectly, and is oxidized by ferric ion producing formaldehyde:[4]

$$\cdot CH_2OH + Fe^{3+} \longrightarrow HCHO + Fe^{2+} + H^+ \quad (3)$$

The hydroxymethyl radical, the precursor of ethylene glycol in the absence of ferric ion, is thus converted into formaldehyde, which subsequently reacts in acid solutions with methanol molecules to produce methylal. The thermal reaction between formaldehyde and methanol proceeds through hemiacetal as an intermediate:[7]

$$HCHO + CH_3OH \xrightarrow[acid]{} CH_2(OH)(OCH_3) \quad (4)$$

$$CH_2(OH)(OCH_3) + CH_3OH \longrightarrow CH_2(OCH_3)_2 + H_2O \quad (5)$$

Thus, formaldehyde and ethylene glycol are not formed in the presence of large quantities of ferric ions and methylal is obtained instead. If the above mechanism holds, G(methylal) should be equal to the sum of G(formaldehyde) and twice G(ethylene glycol) in the absence of the scavenger. G(methylal) in this experiment is 8.3, which is consistent with the sums calculated from literature values, 6.3—9.5.[1] The approximate agreement of the calculated and experimental *G*-values as well as the disappearance of formaldehyde caused

Table 1. Effect of ferric chloride concentration on *G*-values

Concn. of $FeCl_3$(wt %)	0	0.09	0.92	9.17
H_2	5.0	6.3	6.0	1.7
CH_4	0.5	0.7	0.5	0.2
CO	0.1	0.2	0.2	0.2
CH_3OCH_3	0.1	0.1	0.2	0.3
CH_3Cl	0.0	0.0	0.1	0.9
$CH_2(OCH_3)_2$	0.0	3.3	6.7	8.3
HCHO	1.3	0.2	0.0	0.0
H^+	0.1	0.2	1.5	6.5
Fe^{2+}	—	0.2[a]	1.6[a]	7.9
(H_2O)[b]	—	—	7.5	(9.7)

Irradiation at room temperature, exposure rate 3.2×10^5 R/hr, exposure 3.0×10^7 R.
a) All ferric ions were converted into ferrous ions. b) Yields by mass balance calculation with regard to carbon and oxygen.

* Present address; The University of Tokyo, Bunkyo-ku Tokyo 113.

by the increase in the amount of ferric chloride indicate that the above mechanism is satisfactory.

References

1) B. Ya Ladygin and V. V. Saraeva, *Kinet. Katal.*, **6**, 221 (1965).
2) J. H. Baxendale and R. S. Dixon, *Z. Phys. Chem.*, **43**, 161 (1964).
3) J. Teply and A. Habersbergerova, *Collect. Czech. Chem. Commun.*, **30**, 785 (1965).
4) J. H. Baxendale and F. W. Mellows, *J. Amer. Chem. Soc.*, **83**, 4720 (1961).
5) At high ferric chloride concentration, an unidentified product was found to be present from the mass balance of yields by Teply and Habersbergerova.[3] The product was identified to be methylal.
6) S. F. Dainton, I. Janovsky, and G. A Salmon, *Proc. Roy. Soc., Ser. A*, **327**, 305 (1972).
7) Kirk-Othmer "Encyclopedia of Chemical Technology," Vol. 1, Interscience Encyclopedia, Inc., New York, (1947) p. 44.

Calculation of the Carbon-13 NMR Chemical Shifts of Linear and Branched Paraffins and Saturated Cyclic Hydrocarbons

Kitsuma TAKAISHI, Isao ANDO, Masahiro KONDO, Riichirô CHÛJÔ, and Atsuo NISHIOKA

Department of Polymer Chemistry, Tokyo Institute of Technology, Ookayama, Meguro-ku, Tokyo 152

(Received September 13, 1973)

The carbon-13 NMR chemical shifts of linear and branched paraffins have been calculated by means of Pople's theory, particularly using the averaged excitation energy method. The calculation was carried out based on the CNDO/2 molecular orbital method. The values calculated by means of the averaged excitation energy method deviate extremely from the experimental ones; therefore, the energies most suitable for giving good agreement are investigated and determined for linear and branched paraffins. The suitable energies are expressed by an empirical formula, correlated to the molecular structure. The results obtained may be briefly expressed by;

$$\Delta E = 11.30 \times 1.015^a \times 0.958^b \times 1.010^c \times S$$
$$S = 1.011^d \times 1.009^e \times 1.029^f \times 1.009^g \times 1.030^h \times 1.031^i$$

(see Results and Discussion for the notations used).

This empirical averaged excitation energy expression is applied to cyclic hydrocarbons, such as cyclohexane, methylcyclohexane, and dimethylcyclohexane. Further, the γ-effect is estimated on the basis of these results.

The carbon-13 (C-13) NMR chemical shifts of saturated hydrocarbons have been studied systematically by Grant *et al.*[1-5]

Pople *et al.*[6-8] have developed a theory of the C-13 chemical shift and have calculated the C-13 shielding constants of simple hydrocarbons using an averaged excitation energy method (AEE method). It is very convenient to use the AEE method for the calculation of the C-13 shielding constants with the Pople expression. Since the AEE method is, however, a severe approximation, its use makes it difficult to obtain a suitable value for the averaged excitation energy (ΔE), and the calculated chemical shifts are not in good agreement with the experimental values. For example, when the value of 10 eV is used for the ΔE of linear and branched hydrocarbons, the calculated chemical shifts deviate from the experimental values by about 10 or 20 ppm. The C-13 chemical shifts depend on the electronic states of molecules which are influenced by their molecular structures, and the ΔE which largely contributes to the C-13 chemical shifts should be correlated to the molecular structures; *i.e.*, the values of ΔE are not equal to each other for various carbons in a molecule.

Okada *et al.*[9] proposed an empirical expression for ΔE in which ΔE was influenced by adjacent carbons until γ-carbon and by the difference in the molecule. This expression is very simple and convenient; however, it is theoretically limited because it uses an extended Hückel theory (EHT) method. The idea that one tries to determine the values of ΔE unified for various molecular structures is based on the fact that the C-13 chemical shifts depend on the molecular structure, though this is ambiguous theoretically. Nevertheless, the empirical ΔE expression is a useful method for calculating the chemical shifts of many molecules. In order to improve this method and to obtain a wider adoptability, a new empirical expression for ΔE will be proposed. This expression is based on the idea of Okada *et al.*, but the method of computation is a CNDO/2 MO one[10,11] instead of an EHT one. The expression obtained is parameterized for linear and branched paraffins, and then is applied to saturated cyclic compounds, such as cyclohexane and its derivatives. Further, the γ-effect will be estimated on the basis of these results.

Theory

The C-13 shielding constants of any specified carbon atom, A, in a molecule may be approximated as follows;[6,12,13]

$$\sigma^A = \sigma_d{}^A + \sigma_p{}^A + \sum_{B(\neq A)} \sigma^A + \sigma^A_{ring} \quad (1)$$

where $\sigma_d{}^A$ and $\sigma_p{}^A$ are the diamagnetic and paramagnetic contributions on the specified carbon atom, A, respectively, where $\sum_{B(\neq A)} \sigma^B$ is sum of the contributions from the neighbouring atoms bonded to the A atom and where σ^A_{ring} is the contribution from the ring current. Usually the effects of $\sum\sigma^B$ and σ^A_{ring} in the C-13 chemical shifts are known to be very small and contribute less than a few parts per million (ppm). With Slater atomic orbitals, the increase in $\sigma_d{}^A$ when a 2p electron is added is 14 ppm, only about 10% of the entire observed range of the C-13 chemical shifts. The differences in C-13 chemical shifts among various carbon atoms are mostly due to the difference in $\sigma_p{}^A$. In this paper, in order to discuss the C-13 chemical shifts in detail we will take $\sigma_d{}^A$ and $\sigma_p{}^A$ into account and will neglect the contributions from $\sum\sigma^B$ and σ^A_{ring}. The value of $\sigma_d{}^A$ is given by the following formula:

$$\sigma_d{}^A = \frac{e^2}{3mc^2} \sum_i \left\langle \frac{1}{r_i} \right\rangle \quad (2)$$

where $\langle r_i^{-1} \rangle$ is the mean inverse distance of the i-th electron from a nucleus, m is its mass, e is its charge, and c is the light velocity, and where the sum is taken over all the electrons on the atoms being considered.

According to the Pople theory, $\sigma_p{}^A$ is given by the following equations:

$$\sigma_p{}^A = -2N^{-1}\langle r^{-3}\rangle_A \chi_p{}^A \quad (3)$$

$$(\chi_p{}^A)_{zz} = \frac{Ne^2\hbar^2}{m^2c^2} \sum_i^{occ} \sum_j^{unocc} (E_j - E_i)^{-1} (C_{ixA}C_{jyA} - C_{iyA}C_{jxA}) \times \sum (C_{ixB}C_{jyB} - C_{iyB}C_{jxB}) \quad (4)$$

In order to calculate these equations, some approximations are introduced; therefore,[12]

$$\sigma_d^A = 4.45z^*q \tag{5}$$

where:

$$z^* = 3.25-0.35(q-4) \tag{6}$$

in which q is the total electron density around the particular carbon atom and in z^* which is the "effective nuclear charge" estimated according to Slater's rules.

$$\sigma_p^A = -\frac{e^2\hbar^2}{2m^2c^2\Delta E}\left\langle\frac{1}{r^3}\right\rangle_{2p}\sum_B Q_{AB} \tag{7}$$

where;

$$Q_{AB} = \frac{4}{3}\delta_{AB}(P_{X_AX_B}+P_{Y_AY_B}+P_{Z_AZ_B}) - \frac{2}{3}(P_{Y_AY_B}P_{Z_AZ_B}+P_{Z_AZ_B}P_{X_AX_B}+P_{X_AX_B}P_{Y_AY_B}) + \frac{2}{3}(P_{Y_AZ_B}P_{Z_AY_B}+P_{Z_AX_B}P_{X_AZ_B}+P_{X_AY_B}P_{Y_AX_B}) \tag{8}$$

$$\left\langle\frac{1}{r^3}\right\rangle_{2p} = \frac{1}{24a_0^3}\{3.25-0.35(q_{2p}-3)\}^3 \tag{9}$$

$$q_{2p} = P_{X_AX_A} + P_{Y_AY_A} + P_{Z_AZ_A} \tag{10}$$

In these formulae, ΔE is an averaged excitation energy, $\langle r^{-3}\rangle_{2p}$ is the mean inverse cube radius for carbon 2p orbitals and depends on the local electron density on the particular carbon atom, $\sum$ is a sum over all the atoms, δ_{AB} is a Kronecker symbol, and a_0 is a Bohr radius.

$P_{X_AX_B}$ is the matrix element for the $2p_X$ atomic orbitals on the A and B atoms. When A=B, it is the electron density in $2p_X$ on the A atom and when A≠B, it is the bond-order between the two atomic orbitals.

To estimate the bond-order matrix, as the molecular orbital method the CNDO/2 MO method was used.

Results and Discussion

The carbon-13 chemical shifts were calculated for linear and branched paraffins, using the Pople theory for the shielding constants by means of the AEE method and the CNDO/2 MO method.

As a result of using the value of 10 eV for ΔE, the calculated chemical shifts were found to deviate from the experimental values by more than 10 ppm for paraffins. In an *n*-pentane, for example, the experimental carbon-13 chemical shifts of two secondary carbons differ from each other by about 12 ppm, while the calculated values are almost indistinguishable from each other. The total electron densities of the two secondary carbons are nearly identical when calculated by the CNDO/2 MO method. In molecules which have π-electrons and/or lone pair electrons, such as aromatic and azine compounds, it has been reported that there is a correlation between the C-13 chemical shifts and the charge distributions.[14] Sichel *et al.*[15] have reported empirically on the apparent correlation between the C-13 chemical shifts and the electron-charge densities on the carbon atoms in hydrocarbons; they worked on the basis of the extended Hückel method. On the other hand, if the calculation is carried out by the CNDO/2 MO method, there is no obvious correlation between the C-13 chemical shifts and the electron densities for the same compounds.

In the calculation of the C-13 chemical shift of saturated hydrocarbons, one of the most important factors is the averaged excitation energy. Various values have been proposed for ΔE.[7,8,14,16] It should be noted that, in the vacuum UV spectra of *n*-paraffins the wavelengths at the most intense absorption peak become larger as the chain length increases. This suggests that the averaged excitation energies depend on the molecular structures. The tendency for the C-13 chemical shifts to increase as the carbon numbers of hydrocarbons decrease can be barely explained, using the excitation energy values from the UV spectra as ΔE.

Okada *et al.*[9] obtained an empirical averaged excitation energy expression for linear and branched paraffins using the extended Hückel method:

$$\Delta E = 10.0 \times \alpha^a \times \beta^b \times \gamma^c \times c^d \tag{9}$$

where α, β, and γ are the parameters showing the effects of α, β, and γ-carbons respectively, where a, b, and c are the numbers of α, β, and γ-carbons respectively, where c is the parameter showing the conformational effect, and where d is the number of the possible gauche conformation. The numerical values for the α, β, γ, and c parameters are 0.974, 0.960, 1.009, and 1.009 respectively. The value of 10.0 is adopted as the ΔE coefficient for all the carbons. Using this expression, the calculated C-13 chemical shifts are considerably improved. However, this expression is based on an extended Hückel method, so there is a substantial limitation. Nevertheless, this method is important because it is convenient for calculating ΔE from the structural parameters. In order to improve this expression, we proposed the new empirical one with a similar form and more structural parameters, using the CNDO/2 MO method. The new ΔE expression has the following form:

$$\Delta E = K \times \alpha^a \times \beta^b \times \gamma^c \times S \tag{10}$$

$$S = [1°(4°)]^d \times [2°(3)°]^e \times [2°(4°)]^f \times [3°(2°)]^g \times [3°(3°)]^h \times [4°(2°)]^i \tag{11}$$

where K is a coefficient and would be a ΔE of methane when there are no α, β, and γ-carbons, where S is a structural parameter [1°(4°)] showing the effect of the primary carbon adjacent to the quaternary carbon, and where d is the number of [1°(4°)] carbons. These parameters were determined for linear and branched paraffins by the least-squares multiple method.

Contrary to the modified ΔE expression given above, there is another method which represents ΔE by means of the sum of the contributions from all the carbons. Considering that these are all empirical expressions, we must choose a simplified formula.

The coefficient of this expression, K, has an important influence on the improvement of the calculated values. Instead of the value of 10 eV, we tried to adopt 9.705 eV,[17] which was obtained from a vacuum UV spectrum, for the averaged excitation energy of methane, but we did not get any improvement in the calculated values. Strong[18] got the value of 11.30 eV for the ΔE of methane by statistically averaging the excitation energies between the ground states and the excited states.

It has been found that the deviation of the calculated values from the experimental values is considerably influenced by varying the K, *i.e.*, the coefficient of the ΔE expression. Therefore, we can expect at least to get the most preferable K which makes the difference between the calculated and experimental values. The equation representing the relation between the experimental chemical shifts and the calculated ones is as follows:

$$\delta_i = \delta_c + \delta_{di} - \frac{K_i}{\Delta E_i} \qquad (12)$$

where δ_i is the experimental chemical shift of the i-th carbon, δ_{di} is a calculated diamagnetic contribution from the i-th carbon, $K_i/\Delta E_i$ is a paramagnetic one, and δ_c is a constant that is common to all the carbons. Then, the ΔE of each n-paraffin can be determined from this equation because δ_c and δ_i are known and δ_{di} and K_i can be calculated. We plotted such ΔE's for various n-paraffin's carbons against the number of carbon atoms in n-paraffins in Fig. 1. In this figure, three kinds of ΔE values are adopted as follows: (a) 10.0, (b) 9.705, and (c) 11.30eV. Comparing the curves in Fig. 1, we can conclude that the value of 11.30 eV is the most suitable for the calculation by using an empirical expression, because in Curve (c) the slopes between the nearest and second nearest carbons from an end are all equal to one another, irrespective of the increase in n, and because the ΔE's of the nearest and second nearest carbons are equal to each other when n is larger than 4. Using the above-determined ΔE, we can determine the parameters for n-paraffins having

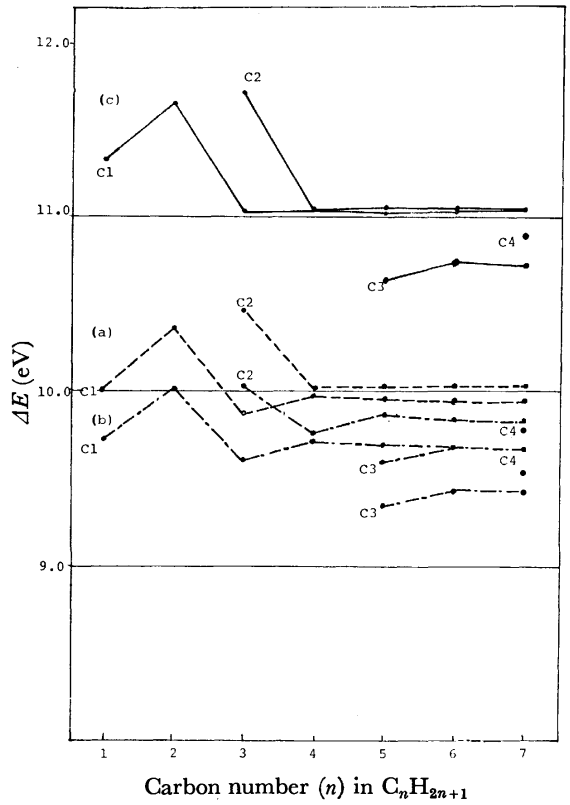

Fig. 1. The averaged excitation energies of linear paraffins when (a) 10.0, (b) 9.705, and (c) 11.30 eV are adopted as the reference values for methane.

Table 1. Calculated values of C-13 chemical shifts in linear and branched paraffins

Compound		ΔE (eV)	Error[a]	Chem. shift[b] (ppm)	Error[c]
Methane		11.30	0.0	130.8	0.0
Ethane		11.46	−0.17	119.94	−2.86
Propane	1	10.98	−0.05	112.18	−0.92
	2	11.63	−0.05	111.69	−0.93
n-Butane	1	11.09	−0.07	114.24	−1.24
	2	11.14	0.0	103.76	0.08
n-Pentane	1	11.09	−0.05	114.08	−0.89
	2	11.25	−0.02	105.70	−0.43
	3	10.67	0.05	95.29	1.12
n-Hexane	1	11.09	−0.03	114.22	−0.60
	2	11.25	0.0	105.86	0.08
	3	10.78	0.05	97.71	1.05
n-Heptane	1	11.09	−0.03	114.22	−0.53
	2	11.25	0.01	105.84	0.14
	3	10.78	0.07	97.69	1.39
	4	10.89	0.03	99.68	0.45
Isobutane	1	10.51	−0.03	103.84	−0.51
	2	11.80	0.10	105.y4	1.82
2,2-Dimethylbutane	1	10.28	0.01	99.62	−0.15
	2	11.82	0.0	98.17	−0.09
	3	10.51	0.0	92.09	0.07
	4	11.32	0.10	118.38	−1.65
Neopentane	1	10.18	0.01	97.47	0.24
	2	11.97	−0.02	100.52	−0.28
Isopentane	1	10.62	−0.03	106.0	−0.67
	2	11.40	0.0	98.78	−0.02
	3	10.-6	0.0	96.83	−0.05
	4	11.20	−0.05	116.23	−0.95
2,3-Dimethylbutane	1	10.73	−0.06	108.15	−1.20
	2	11.15	0.0	94.57	−0.03

a) (Error) = − (ΔE when calculated chemical shift coincide with observed one) + (ΔE calculated by the empirical formula) b) From benzene c) (Error) = (calculated value) − (observed value)

the carbons of from 1 to 7.

Next, using the above empirical expression, we obtain:

$$\Delta E = 11.30 \times 1.015^a \times 0.958^b \times 1.010^c \times S \qquad (13)$$

$$S = 1.011^d \times 1.009^e \times 1.029^f \times 1.009^g \times 1.030^h \times 1.031^i \qquad (14)$$

as the most suitable empirical formula for the estimation of the C-13 chemical shift in n-paraffin. We tried to calculate inversely the C-13 chemical shifts in the compounds which were used for parameterization. These results are listed in Table 1. The differences between the experimental and calculated values are extremely small for most paraffins. A considerable discrepancy was seen in ethane, isobutane, 2,2-dimethylbutane, *etc.* In the case of ethane, there is only an α-effect; it is, therefore, difficult to estimate the absolute value of the α-effect instead of a relative value. The discrepancy in ethane may be due to this circumstance. For isobutane and 2,2-dimethylbutane, the principal source for the discrepancy is probably due to their steric hindrances.

Table 2. Calculated values of C-13 chemical shifts in cyclohexane derivatives

Compound		ΔE (eV)	Chem. shift[a] (ppm)	Error[b]
Cyclohexane		10.78	96.91	−4.09
Methylcyclohexane	1	11.12	93.89	−1.11
	2, 6	10.41	89.90	−2.48
	3, 5	10.89	99.13	−2.17
	4	10.78	96.88	−4.54
	Me	10.73	108.07	2.89
1,1-Dimethyl-cyclohexane	1	11.78	98.17	0.28
	2, 6	10.46	91.37	3.30
	3, 5	11.00	101.29	−4.03
	4	10.78	96.90	−4.33
	Me	10.28	99.57	0.50
cis-1,2-Dimethyl-cyclohexane	1, 2	10.88	89.54	−3.96
	3, 6	10.51	92.01	−4.52
	4, 5	10.89	99.14	−5.28
	Me	10.84	110.20	−2.23
trans-1,2-Dimethyl-cyclohexane	1, 2	10.88	89.65	1.00
	3, 6	10.51	92.07	0.22
	4, 5	10.89	99.10	−1.85
	Me	10.84	110.18	2.25
cis-1,3-Dimethyl-cyclohexane	1, 3	11.24	96.y6	1.47
	2	10.06	82.89	−0.04
	4, 6	10.41	89.90	−2.74
	5	11.00	101.32	−0.12
	Me	10.73	108.02	2.82
trans-1,3-Dimethyl-cyclohexane	1, 3	11.24	96.16	−4.43
	2	10.06	82.63	−4.03
	4, 6	10.41	89.75	−4.23
	5	11.00	101.20	−6.00
	Me	10.73	107.99	0.48
cis-1,4-Dimethyl-cyclohexane	1, 4	11.12	93.81	−3.93
	2, 3 5, 6	10.51	92.03	−5.04
	Me	10.73	108.08	0.09
trans-1,4-Dimethyl-cyclohexane	1, 4	11.12	93.89	−1.30
	2, 3 5, 6	10.51	92.07	−0.21
	Me	10.73	108.07	2.63

a) From benzene. b) (Error) = (calculated value) − (observed value).

Further, we calculated the C-13 chemical shifts of cyclohexane and its methyl derivatives, using the above empirical expression. The cyclohexane system has the least steric hindrance among the cyclic hydrocarbons. The calculated values are listed in Table 2 and are illustrated by the schematic stick spectrum models in Fig. 2. The stick spectra calculated by Grant's additive rule are also shown in Fig. 2 for purposes of comparison. In cyclohexane, the calculated value is lower than the experimental one by 4.09 ppm. In various kinds of dimethylcyclohexane, *trans*-1,2-, *cis*-1,3-, and *trans*-1,4-dimethylcyclohexanes deviate a little from the experimental values. On the other hand, 1,1-, *cis*-1,2-, *trans*-1,3-, and *cis*-1,4-dimethylcyclohexane deviate from the experimental values by more than about 3 to 4 ppm (see Table 2). By comparing the values calculated by Pople's method using the ΔE expression and the values

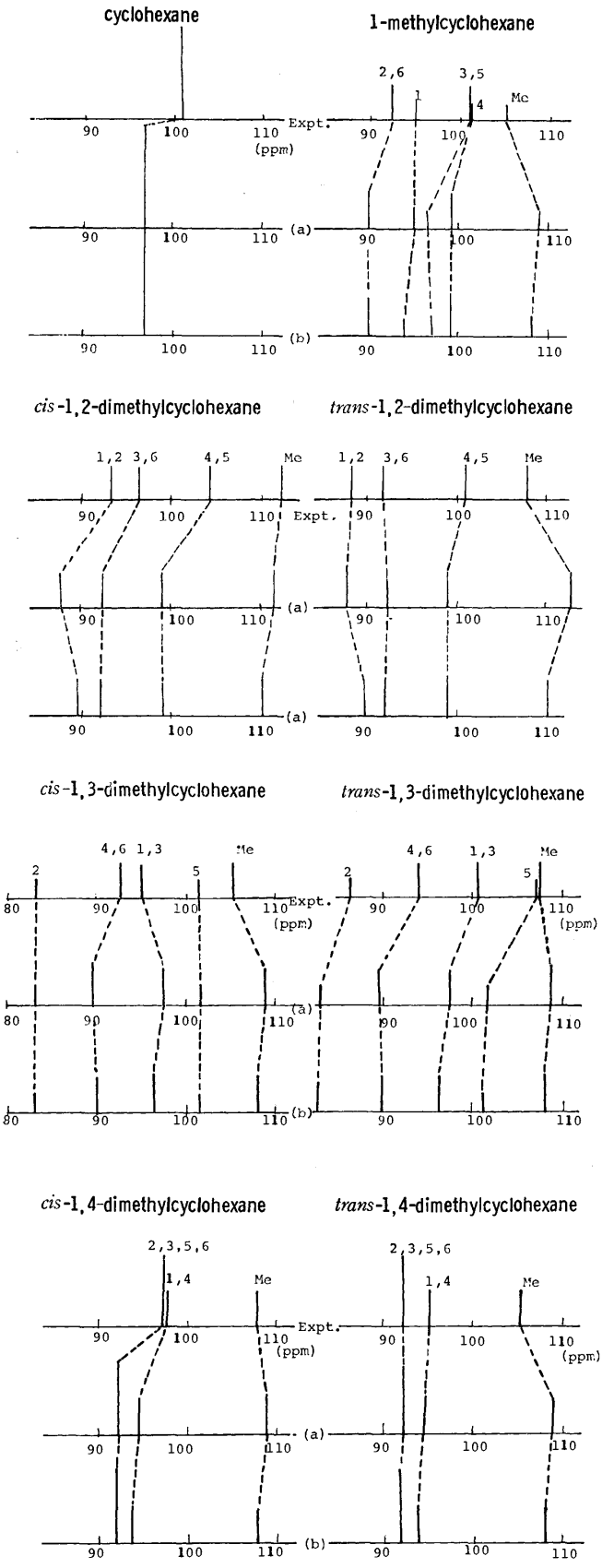

Fig. 2. Experimental and calculated C-13 chemical shifts of cyclohexane derivatives. Expt. shows the experimental values. (a) and (b) are calculated ones by Grant's additive rule and the empirical ΔE formula, respectively.

calculated by Grant's method, we find that the former are more improved than the latter in methylcyclohexane and *cis*-1,2-, *trans*-1,2-, *cis*-1,3-, and *trans*-1,4-dimethylcyclohexanes. On the other hand, the former are nearly equal to the latter in *trans*-1,3- and *cis*-1,4-dimethylcyclohexanes. In cyclohexane their values are equal to each other. Consequently, it can be said that Pople theory, in which ΔE is calculated by the empirical ΔE expression, can predict the most exact C-13 chemical shift of non-constrained cyclic saturated hydrocarbons, such as cyclohexane and its methyl derivatives.

In cyclohexane, however, the deviation of about 4 ppm suggests that the ΔE expression cannot include the steric factor. The C-13 chemical shift of cyclohexane is higher than the value of the central carbon of *n*-hexane by 4.3 ppm. Furthermore, the calculated values agree fairly with the experimental ones when both methyl groups are in equatorial positions, while the agreement is not so good when the methyl groups are in axial positions. However, if about 4 ppm is added to the values of dimethylcyclohexane of which the methyl groups are in axial positions, the results are excellently improved. We can conclude that about 4 ppm is the contribution from the steric effect in the cyclohexane system.

In the carbons of methyl groups, the deviations are about 2 to 3 ppm. This is due to the steric influence of the cyclohexane ring. This steric effect is almost thought to equal the γ effect. In a cyclohexane system, all the ring carbons are in a *gauche* conformation, the axial methyl groups are *gauche* to the γ-carbons of the cyclohexane ring. γ-Effects in *gauche* conformations are estimated by comparison with various hydrocarbons, such as norbornane,[19] its methyl derivatives, and methylcyclohexane. The correlation between the γ-effect and a dihedral angle between C_1 and C_4 carbons is illustrated in Fig. 3.

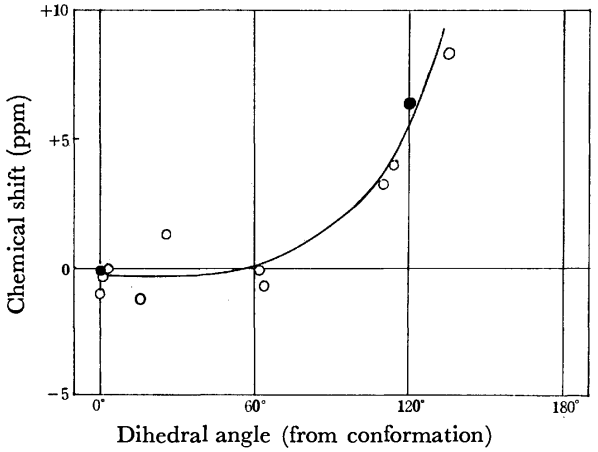

Fig. 3. Correlation between γ-effect and dihedral angle. ○ and ● correspond to the values obtained from norbornane and a methyl derivatives of cyclohexane, respectively.

As is shown in Fig. 3, the γ effect in a *trans* conformation is -0.4 ppm, and the γ-effect in which a dihedral angle is 60° is nearly zero and the γ-effect in which a dihedral angle is 120° (*gauche* conformation) is almost 6 ppm. These results show that, in equatorial methyl groups, the γ-effect are very small, while in axial methyl groups the cyclohexane ring's influence about comprises the γ-effects.

Since the ΔE expression includes the averaged γ-effect, there is no difference in the calculated C-13 chemical shifts between compounds with the same framework, such as *cis*-1,3- and *trans*-1,3-dimethylcyclohexane. By showing the improved calculated value of the C-13 chemical shift in cyclohexane and its derivatives it is proved that the empirical ΔE expression is useful for cyclics and that the C-13 chemical shift of saturated hydrocarbons may be explained with regard only to the influence of α-, β-, and γ-carbons. In the future, it will be interesting to apply this method to the cyclic strained hydrocarbons and to examine the steric effects.

References

1) D. M. Grant and E. G. Paul, *J. Amer. Chem. Soc.*, **86**, 2984 (1964).
2) W. R. Woolfenden and D. M. Grant, *ibid.*, **88**, 1496 (1966).
3) D. M. Grant and B. V. Cheney, *ibid.*, **89**, 5319 (1967).
4) D. K. Dalling and D. M. Grant, *ibid.*, **89**, 6612 (1967).
5) D. K. Dalling and D. M. Grant, *ibid.*, **94**, 5318 (1972).
6) J. A. Pople, *Mol. Phys.*, **7**, 301 (1964).
7) J. A. Pople, *J. Chem. Phys.*, **37**, 53 (1962).
8) J. A. Pople, *ibid.*, **37**, 60 (1962).
9) K. Okada, I. Morishima, and T. Yonezawa, Paper read at the 10th NMR Symposium (Tokyo, 1971).
10) J. A. Pople and G. A. Segal, *J. Chem. Phys.*, **43**, 129 (1965).
11) J. A. Pople and G. A. Segal, *ibid.*, **43**, 136 (1965).
12) T. Yonezawa, I. Morishima, and H. Kato, This Bulletin, **39**, 1398 (1966).
13) A. Saika and C. P. Slichter, *J. Chem. Phys.*, **22**, 26 (1954).
14) T. Tokuhiro and G. Fraenkel, *J. Amer. Chem. Soc.*, **91**, 5005 (1969).
15) J. M. Sichel and M. A. Whitehead, *Theor. Chem. Acta*, **5**, 35 (1966).
16) R. A. Hegstrom and W. N. Lipscomb, *J. Chem. Phys.*, **46**, 1594 (1964).
17) B. A. Lombos, P. Sauvageau, and C. Sandorfy, *J. Mol. Spectrosc.*, **24**, 253 (1967).
18) A. B. Strong, *Discuss. Abstr., Int. B*, **32** (**2**), 869 (1971).
19) J. B. Grutzner, M. Jautelat, J. B. Dence, R. A. Smith, and J. D. Roberts, *J. Amer. Chem. Soc.*, **92**, 7107 (1970).

On the Behavior of O_2^- and O^- Radicals over V_2O_5–SiO_2 Catalyst

Satohiro YOSHIDA, Tokuo MATSUZAKI, Tomonori KASHIWAZAKI, Kozo MORI, and Kimio TARAMA

Department of Hydrocarbon Chemistry, Faculty of Engineering, Kyoto University, Sakyo-ku, Kyoto 606

(Received September 20, 1973)

The behavior of oxygen, O_2^- and O^- radicals adsorbed on the partially reduced V_2O_5–SiO_2 catalysts has been investigated. Oxygen is adsorbed mainly in a molecular state at room temperature, the sum of amounts of paramagnetic adsorbed species O_2^- and O^- being less than 10% of total amount of adsorbed oxygen. High degree of reduction, high content of V_2O_5 and low pressure of oxygen at adsorption equilibrium are favorable for the formation of O^- radical. It was confirmed by the quantitative analysis of reaction products and the adsorbed species that O_2^-, not O^-, is the active species in the oxidation of propylene at room temperature. A mechanism involving an intermediate of an epoxide structure was proposed.

In the last decade, many works have been carried out mainly by ESR technique on the formation of O_2^- and/or O^- on the surface of partially reduced metal oxide. It has been established that O^- is very reactive to carbon monoxide, while O_2^- seems to be unreactive to such gases as hydrogen and carbon monoxide at room temperature.[1] In most works, zinc oxide and titanium oxide were chosen as adsorbents, which exhibit poor activity for the oxidation of hydrocarbons. No reports seem to have been given on the oxidation of hydrocarbons by O_2^- or O^- over these oxides.

Schvets *et al.*[2] and Tarama *et al.*[3] found that O_2^- and/or O^- were formed on partially reduced vanadium oxide used as a commercial catalyst for oxidation, when the oxide was supported on silica. Kazansky *et al.* have established the high reactivity of O^- to carbon monoxide and claimed that O_2^- is inactive in oxidation reactions.[4]

In a previous paper[5] a report was given on the stability and reactivity of O_2^-. It was found that propylene is oxidized to propionaldehyde by adsorbed oxygen species over this catalyst, a hypothesis being proposed that O_2^- is the active species in the reaction. Kazansky *et al.* reported that O^- was formed on the reduced vanadium oxide[4] but they gave no favorable conditions for its formation, and this could not be confirmed in the previous work. The first aim of the present work is the establishment of favorable conditions for the formation of O^-. The second aim is clarification of the active species in the oxidation of hydrocarbons. A large amount of diamagnetic oxygen species are coexistent on the surface.[5] The possibility of participation of these species can not be excluded from ESR investigation only. We attempted to solve the problem by investigation of the quantitative correlation between the amount of products and oxygen species.

Experimental

Materials. Carrier (SiO_2); Silica gel obtained from ethyl orthosilicate hydrolyzed in a water–ethanol mixture at boiling point was calcined at 500 °C for 5 hr in a dry stream of air and was ground to powder of less than 100 mesh.

Catalysts (V_2O_5–SiO_2): Silica gel impregnated with 0.3 M ammonia solution containing ammonium metavanadate was dried and calcined at 500 °C for 10 hr in dry stream of air. The amounts of vanadium oxide (V_2O_5) supported on SiO_2 were 2 and 5 wt%.

Gases: Commercial oxygen and propylene were used. Carbon monoxide was obtained by the decomposition of sodium formate. All gases were purified by vacuum distillation at a low temperature.

Apparatus and Procedure. Measurements of oxygen adsorption were carried out by the usual volumetric method. ESR spectra were recorded with a JES-3BSX type ESR spectrometer (X-band). Amounts of O_2^- were determined by means of a TE105 cavity using DPPH as a standard. Amounts of O^- were estimated from the amount of CO_2 produced by its reaction with CO at room temperature. The reaction of propylene with adsorbed oxygen was carried out in a similar manner to that described previously.[5] The reaction mixtures were recovered with a liquid N_2 trap and analyzed by a gas chromatograph with 3m column (PEG 1500 20% Celite) at 80 °C. Partial reduction of catalysts was carried out at 420 °C for a given time with CO. The degree of reduction was calculated from the amount of CO_2 produced and given in terms of the percentage of V^{4+} produced to the total V ions.

Results and Discussion

Adsorption of Oxygen. Adsorption isotherms* of oxygen on partially reduced V_2O_5(5 wt%)–SiO_2 cata-

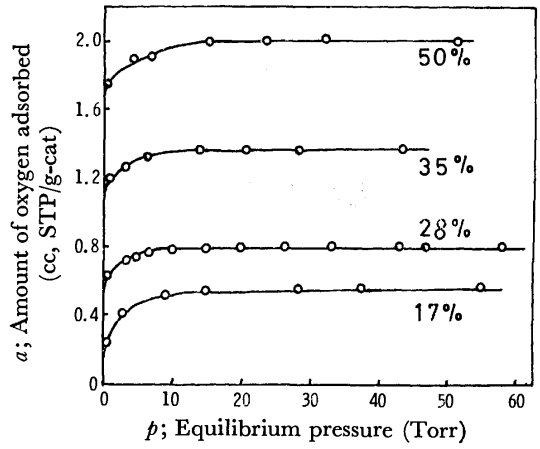

Fig. 1. Adsorption isotherms of oxygen on partially reduced V_2O_5(5 wt%)–SiO_2 (%; reduction degree)

* V_2O_5–SiO_2 catalyst before reduction adsorbed a small amount of oxygen at room temperature. The adsorbed amount of oxygen on partially reduced catalysts was corrected by subtracting the amount.

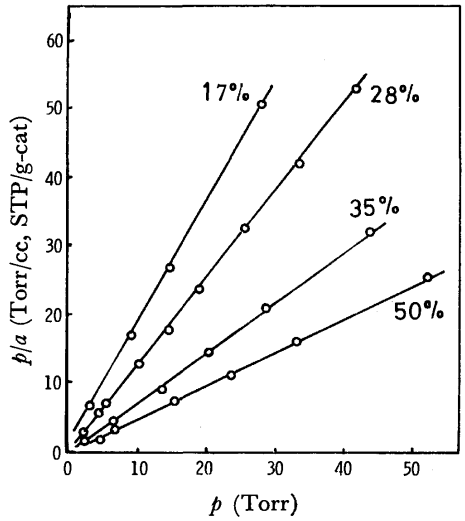

Fig. 2. Langmuir plot for oxygen adsorption isotherm (%; degree of reduction)

Table 1. Variation of a_s/V^{4+} by reduction

Degree of reduction (%)	16.7	20.0	22.1	28.5	34.7	49.6	50.1
a_s/V^{4+} (%)	26.9	23.6	27.1	22.7	32.2	25.8	33.7

a_s: Saturated adsorption amount of oxygen (mol/g-cat)
V^{4+}: Amount of V^{4+} produced by reduction (mol/g-cat)

lysts at room temperature are shown in Fig. 1. Since the Langmuir equation for non-dissociative adsorption fits the isotherms (Fig. 2), oxygen should be mainly adsorbed in a molecular state on these catalysts at room temperature. The saturated amount of adsorption of oxygen (a_S) increases with the increase in the reduction degree of the catalyst and the ratio of a_S to V^{4+} produced by reduction falls in the range 23—34% (Table 1).

ESR Spectra of Adsorbed Oxygen. Figure 3 shows the ESR spectrum of oxygen radical species adsorbed on the 17% reduced V_2O_5(5 wt%)–SiO_2 catalyst at room temperature. This spectrum with hfs of $A_{//}$= 9.3 G and $A_\perp$=5.8 G at $g_{//}$=2.022 and $g_\perp$=2.004 can

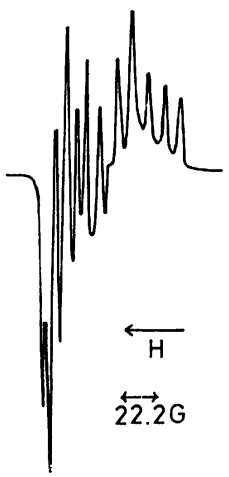

Fig. 3. ESR spectrum of oxygen adsorbed on 17% reduced V_2O_5 (5 wt%)–SiO_2.

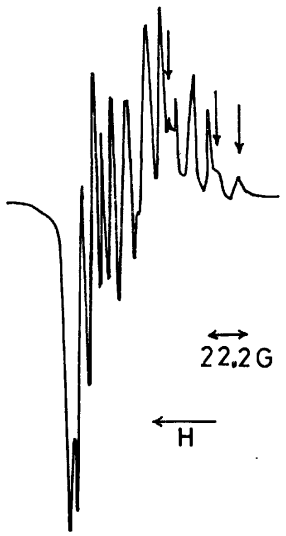

Fig. 4. ESR spectrum of oxygen adsorbed on 22% reduced V_2O_5 (5 wt%)–SiO_2.

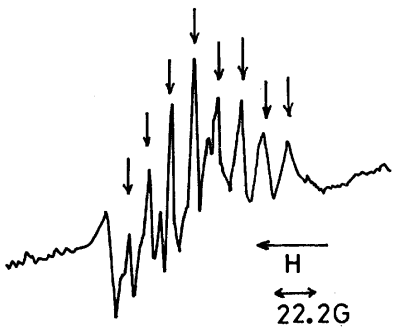

Fig. 5. ESR spectrum of oxygen adsorbed on 51% reduced V_2O_5 (5 wt%)–SiO_2.

be assigned to O_2^- radical.[2,3] Figures 4 and 5 show the ESR spectra of oxygen radical species adsorbed on the 22 and 51% reduced V_2O_5(5 wt%)–SiO_2 catalyst, respectively. In these spectra, a new signal (marked by arrows) is superimposed on the O_2^- signal. The new signal g=2.027, A=13 G corresponds to that assigned to the O^- radical by Kazansky.[4]

The signal assignable to the O^- radical was detected on catalysts more highly reduced than 20% for V_2O_5-(5 wt%)–SiO_2 and 30% for V_2O_5(2 wt%)–SiO_2, the ratio of O^-/O_2^- increasing with the increase in the reduction degree of catalysts (Fig. 6).

The influence of adsorption pressure of oxygen on the formation of oxygen radical species was investigated, the results being given in Table 2. Increase in the pressure of oxygen resulted in the increase in relative signal intensity of O_2^- and decrease in that of O^-, regardless of degree of reduction of the catalysts. This evidently shows that high degree of reduction, high content of V_2O_5 and low pressure of oxygen at equilibrium are favorable for the formation of O^- radicals.**

Both signals of O_2^- and O^- radicals are stable *in*

** In the former study,[5] the O^- radical was not detected for the catalyst of 1—45% reduction, which seems to have been due to high oxygen pressure.

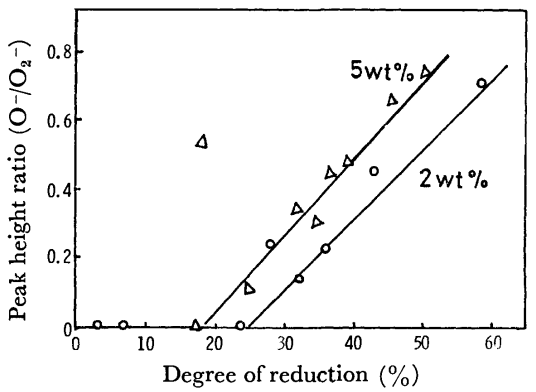

Fig. 6. Variation of O^-/O_2^- by reduction (wt%; V_2O_5 content in catalyst)

Table 2. Relative intensity of O_2^- and O^-

Catalyst	Equilibrium pressure p (Torr)	Amount of oxygen adsorbed 10^{-6} mol/g-cat	a/V^{4+}	Relative intensity of ESR signal O_2^-	O^-	O^-/O_2^-
50% reduced V_2O_5(5 wt%)-SiO_2	<0.1	63.1	22.8	29	20	0.69
	2.1	76.5	27.6	49	15	0.31
	7.5	78.0	28.2	43	11	0.26
	15.2	91.3	33.2	49	7.4	0.15
	25.3	92.7	33.7	52	4.6	0.09
35% reduced V_2O_5(5 wt%)-SiO_2	<0.1	53.8	27.6	20	6.0	0.30
	4.4	57.3	29.4	24	4.0	0.17
	10.6	60.0	30.1	29	2.0	0.07
	17.4	62.8	32.2	29	1.2	0.04

vacuo at room temperature even after 16 hr, but heating for 15 min at 150 °C caused a decrease of O_2^- by 80% and O^- by 30%. This shows that O^- is more stable than O_2^- at high temperatures in agreement with the result of Shvets *et al.*[6]

Quantitative Measurement of O_2^- and O^-. 17% reduced V_2O_5(5 wt%)-SiO_2 catalyst adsorbed 2.6×10^{-5} mol oxygen/g-cat at room temperature. The amount of O_2^- on this catalyst was determined to be 1.6×10^{-6} g ion/g-cat by the ESR method. On the other hand, both ESR signals of O_2^- and O^- were observed for 20% reduced V_2O_5(5 wt%)-SiO_2 catalyst adsorbing 2.62×10^{-5} mol oxygen/g-cat, the ratio of O^- to O_2^- being 0.59 from the relative signal intensity. Addition of CO at room temperature caused instantaneous disappearance of the ESR signal of O^- and formation of CO_2, as reported by Kazansky *et al.*[4] It was confirmed that the ESR signal intensity of O_2^- radical is not affected by either the addition of CO or the recovery of the resulting CO_2. This can be utilized for the evaluation of the amount of O^- by measuring the amount of CO_2 produced by reaction of O^- with CO. The amount of O^- radical adsorbed on 20% reduced V_2O_5(5 wt%)-SiO_2 was evaluated to be 9.6×10^{-7} g-ion/g-cat. The amount of O_2^- calculated from these values of O^- and O^-/O_2^- was 1.6×10^{-6} g-ion/g-cat. Thus, the values from the two different methods agree. In the following experiments, the amounts of O_2^- and O^- were estimated by the latter method.

Table 3. Amount of adsorbed species

Reduction degree %	V^{4+} $10^{-4}\times$ mol/g-cat	Amount of oxygen adsorbed $10^{-5}\times$ mol/g-cat	$\frac{O^-}{O_2^-}$	O^- $10^{-6}\times$ mol/g-cat	O_2^- $10^{-6}\times$ mol/g-cat	$\frac{\frac{1}{2}O^-+O_2^-}{a}$ %
17	1.12	2.60	—	—	1.6	6.2
20	1.20	2.62	0.59	0.95	1.6	7.91
35	2.0	6.13	0.04	0.13	3.	5.2
45	2.5	4.76	0.65	1.2	1.8	5.0
50	2.75	9.27	0.09	0.42	4.8	5.4

The amounts of V^{4+}, total adsorbed oxygen (a), O_2^- and O^- for several catalysts are given in Table 3. In all cases, the values of $[O_2^-+(1/2)O^-]/a$ are smaller than 10%. From the fact that paramagnetic adsorbed species are only a small part of total adsorbed oxygen and the Langmuir equation for non-dissociative adsorption fits the isotherms, a large part of oxygen seems to be adsorbed as a neutral molecule.

Reaction with Propylene. Some olefins are oxidized by adsorbed oxygen, accompanied by the simultaneous disappearance of O_2^- signal in ESR spectra.[5] Since large amounts of adsorbed oxygen besides O_2^- are existent together with O^- on the catalyst surface, it seems that the previous results can not exclude the possibility of oxidation of olefins by adsorbed oxygen species other than O_2^-. In order to specify the oxidative species unambiguously a correlation between amounts of consumed O_2^- and oxidation products of propylene was quantitatively investigated.

At room temperature, propylene was brought into contact with catalysts, on which O^- had been removed by CO treatment to exclude the possibility of oxidation by O^-. After 1 hr, the reaction mixture was recovered in a liquid N_2 trap. For the desorption of products, the catalyst was evacuated at 200 °C during the course of recovery (1 hr). The results of gas chromatographic analysis of reaction products are given in Table 4. The amounts of recovered oxidation products (p_{ox}) for the A-series experiments are in the same order as that of consumed O_2^-, the ratios of p_{ox} to O_2^- being nearly in the range 0.8—1. Case B shows the result for the 46.5% reduced V_2O_5(5 wt%)-SiO_2 catalyst, on which both O_2^- and O^- initially coexist and O^- mainly remains after heating at 150 °C for 15 min. Although both O^- and O_2^- rapidly diminish in contact with propylene, the amount of oxidation product is in the same order as that of O_2^- rather than that of O^-. This probably means that in spite of reaction of O^- with propylene, the oxidation products resists the desorption from catalyst surface,[7] where oxidation products of propylene on zinc oxide are too tightly adsorbed to remove and are recovered as CO_2 only at a higher temperature than 200 °C. The oxidation products (Table 4) can be regarded to result from the reaction of O_2^- but not from other oxygen species.

Propionaldehyde, acetaldehyde and acrolein were detected with small amounts of acetone and propylene oxide in the oxidation products. Since these products except acrolein are not expected from the allylic intermediate, it is suggested that low temperature oxidation

TABLE 4. PRODUCTS OF PROPYLENE OXIDATION ON V_2O_5 (5 wt%)-SiO_2 CATALYST

Expt. No.*)	10^{-6}mol/g-cat		Composition of product (%)						Oxygen containing product P_{ox}; $10^{-6}\times$ mol/g-cat	P_{ox}/O_2^- %
	O_2^-	O^-	C_3H_6	CH_3CHO	Propylene oxide	Propion-aldehyde	Acetone	Acroleine		
A-1	1.8	—a)	99.3	0.16	—	0.55	—	—	1.78	99
A-2	3.1	—a)	92.3	2.47	—	3.34	0.80	1.14	2.94	95
A-3	3.7	—a)	96.1	1.16	—	2.69	—	—	2.95	80
A-4	4.8	—a)	59.0	15.94	1.46	16.33	2.89	4.40	4.40	92
Bb)	0.36	0.97	99.2	0.36	—	0.34	0.13	—	0.165	47
Cc)	—	—	10.6	—	22.0	52.8	14.6	—	—	—

a) O^- was removed by reaction with CO. b) Catalyst adsorbing oxygen was heated at 150 °C for 15 min. c) 1.5×10^{-5} mol propylene oxide was introduced at room temperature on the 10% reduced V_2O_5(5 wt%)-SiO_2 and then evacuated. The reaction products were recovered by the same method as for Expt. A and B. *) Reduction degrees of catalysts in A-1, A-2, A-3, A-4 and B were 22.1, 34.7, 47.6, 50.1 and 46.5%, respectively.

of propylene with O_2^- radical occurs mainly through the intermediate of an epoxide structure as follows.

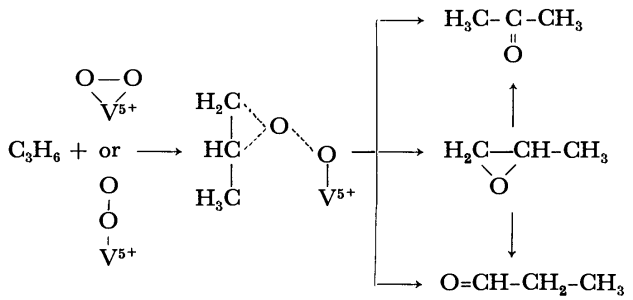

Propionaldehyde and acetone are also formed by the isomerization of propylene oxide on this catalyst. (Expt. No. C, Table 4).

The mechanism of formation of acetaldehyde is not clear, but the following mechanism might be partially cooperative with the above one.

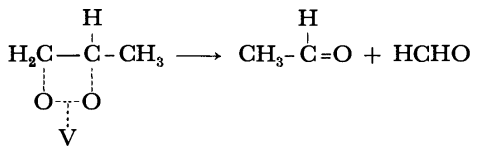

However, we could not detect any formaldehyde in reaction products, nor could be elucidate the reaction products of O^- with propylene.

In conclusion, the respective amounts of total oxygen, O_2^- and O^- adsorbed on partially reduced V_2O_5-SiO_2 catalyst were quantitatively determined. It was confirmed that O_2^- on the catalyst oxidized propylene at room temperature by a mechanism involving the intermediate of an epoxide structure.

References

1) R. J. Kokes, *J. Phys. Chem.*, **66**, 99 (1962); M. Setaka and T. Kwan, This Bulletin, **38**, 1414 (1964), *J. Catal.*, **16**, 44 (1970); K. Sancier, *ibid.*, **5**, 314 (1966); J. Lunsford, *J. Chem. Phys.*, **44**, 1487 (1966); A. I. Maschenko, V. B. Kazansky, G. B. Parinsky, and V. M. Schpapov, *Kinet. Katal.*, **8**, 853, 1363 (1967).

2) V. A. Schvets, M. E. Sarichev, and V. B. Kazansky, *J. Catal.*, **11**, 378 (1968).

3) K. Tarama, S. Yoshida, S. Ishida, and Y. Doi, This Bulletin, **42**, 1161 (1969).

4) V. B. Kazansky, V. A. Shvets, M. Ya. Kon, V. V. Nikisha, and B. N. Shelimov, "Catalysis" Proc. the Fifth Int. Cong. Catalysis, Vol. 2, edited by J. W. Hightower, North-Holland Pub. Co., Amsterdam (1973), p. 1423, and *J. Catal.*, **25**, 123 (1972).

5) S. Yoshida, T. Matsuzaki, S. Ishida, and K. Tarama, "Catalysis" in Ref. 4, Vol. 2, p. 1049 (1972).

6) V. A. Shvets, V. M. Vorotinthev, and V. B. Kazansky, *Kinet. Katal.* **10**, 356 (1969).

7) Y. Kubokawa, T. Ono, T. Tomino, and N. Yano, This Bulletin, **43**, 291 (1970).

A New Pyrochlore System, $Pb(Ti_x \cdot Sn_{1-x})O_3$, and Its Transition to a Perovskite System

Shin-ichi SHIRASAKI, Hiroshi YAMAMURA, Kunitaka MURAMATSU, and Kōichiro TAKAHASHI

National Institute for Researches in Inorganic Materials, Sakura-mura, Niihari-gun, Ibaraki, 300-31

(Received October 19, 1973)

A series of pyrochlore compounds of $Pb(Ti_x \cdot Sn_{1-x})O_3$, was aqueously prepared. They were characterized in terms of inhomogeneously distributed Ti and Sn ions in the equivalent lattice positions. In the composition range where the value x was between 0.00 and 0.45, monophasic pyrochlore was crystallized. In the composition range of $x \gtrsim 0.45$, however, the pyrochlore phase more or less coexisted with a noncrystalline substance whose composition was supposed to be Pb/(Ti+Sn) mole ratio <1.0. The process of thermal transition from the pyrochlore-type $Pb(Ti_{0.4} \cdot Sn_{0.6})O_3$ to the perovskite-type system was traced by two lines of measurements of the pyrochlore, *i.e.*, the lattice constant and the degree of fluctuation of interplanar spacings, and by measurements of the tetragonal lattice strain of the resultant perovskite. The results showed that the transition occurred preferentially at Ti-rich microregions in the matrix lattice, in which a measurable fluctuation of the Sn: Ti ratio was detected.

The pyrochlore family, like the perovskite group, draw our attention in view of its ferroelectricity and/or high permittivity. The ferroelectric properties of cadmium pyroniobate, $Cd_2Nb_2O_7$, were discovered some time ago.[1] Recently it has been reported that the anion-deficient pyrochlore $Bi_2Zn_{4/3}Ta_{2/3}O_6$ is ferroelectric below 570 °C,[2] and unusual dielectric properties have been found at low temperatures for the Pb_2BiNbO_6 pyrochlore.[3] On the other hand, numerous studies have been successful in preparing $A^{2+}B^{4+}O_3$ perovskites (A: Ba, Pb, Sr, Cd, and Ca; B: Ti, Zr, Sn, and Hf). Among them, however, no attempts to prepare any single phases with a composition of $PbSnO_3$ have yet been successful under an atmospheric pressure. In the present study, two new pyrochlore compounds, $PbSnO_3$ and $Pb(Ti_x \cdot Sn_{1-x})O_3$ were aqueously prepared with a strong expectation as to their ferroelectricity. The present interest was directed to the thermal transition from the solid-solution-type pyrochlore into the perovskite. The degree of the inhomogeneous distribution of Ti and Sn ions in the equivalent lattice positions of the pyrochlore during the transition was estimated; it could be a useful parameter for the analysis of the transition characteristics.

Experimental

Materials. $Pb(CH_3CO_2)_2 \cdot 3H_2O$ was dissolved into a 5 M NaOH solution, and then this solution was neutralized by means of a 3 M HNO_3 solution. A mixed solution of $TiCl_4$ and $SnCl_4$ with a desired mole ratio was added to the neutralized solution to obtain a white precipitate. After this mixture has stood for a while, a light yellow precipitate appeared. This precipitate was repeatedly washed with water to remove any adsorbed Na^+ and Pb^{2+} and was then oven-dried at 130 °C for 1 day. Experiments were repeated by varying the mole ratio of $TiCl_4/SnCl_4$; more than 30 types of materials were thus obtained.

Chemical Analyses. Chemical analyses for Pb and Na were undertaken for one specimen of $x=0.4$ as-dried, which was readily soluble in a dilute HCl solution. In the determination of its composition on the basis of the chemical analysis data, therefore, the presence of its adsorbed water was taken into account. The Na content in the specimen solution was analyzed using a frame photometer (type EP-3, Shimadzu Co.). The drop-by-drop addition of a 0.3 M solution of cupron (α-benzoinoxime) to the specimen solution led to the quantitative formation of a pale-yellow mixed precipitate of cupron-Ti and cupron-Sn, leaving the cupron-Pb complex solution behind. The resultant precipitate was filtered and washed with diluted acid until all the adsorbed cupron-Pb complex had been removed. The collected solution of the cupron-Pb complex was then titrated with a standard EDTA solution in order to determine the Pb content. The water content in the dried specimen was determined from the weight loss up 650 °C.

Determination of a, (c/a)-1, and $\Delta d/d$. X-Ray diffraction patterns were obtained at room temperature using a JEOL diffractometer (Nihondenshi Co.) with Cu$K\alpha$ radiation in order to determine the lattice constant of pyrochlores and the tetragonal lattice strain, (c/a)-1, of perovskites transformed from a pyrochlore. The lattice constants of the pyrochlores were calculated for typical specimens using 8 of the well-resolved diffraction lines. The result indicated that the estimated accuracy of the lattice constant was ± 0.01 Å (see Tables 2 and 3). The lattice constant for other materials was conveniently calculated using the {622} reflection. The tetragonal strain of the perovskites was determined using the {111} and (002) diffraction lines. Further experiments were designed to determine whether each composition of solid-solution-type pyrochlores was microscopically uniform. For this purpose, the magnitude of the fluctuation of the interplanar spacings, $\Delta d/d$, was calculated by observing the reflection angle, θ, and the pure diffraction line broadening, β, relative to a silicon standard according to the $\Delta d/d = \beta\cos\theta/\sin\theta$ equation; for the determination of this, 4 of the well-resolved reflection, {222}, {400}, {440}, and {622}, were chosen. The crystallite size, r, was determined simultaneously using the Walker equation: $\beta = 0.9/r \cdot \cos\theta$, with $\beta\cos\theta$ extrapolated to $\sin\theta = 0$.

Determination of Degree of Transition. A quantitative determination of the relative amounts of the pyrochlore- and perovskite-phases was made by X-ray diffraction. The perovskite {111} and pyrochlore {222} reflections were used, and their integrated intensity ratio was planimetrically determined. This was compared with the corresponding ratios for a series of pyrochlore-perovskite mixtures.

Thermogravimetry. TG was undertaken at a temperature elevation speed of about 10 °C under the sensitivities of 50 mg/full-scale (Chō Keiryoki Co.) and of 2 mg/full-scale (Rigaku Denki Co.).

Infrared Absorption. The infrared absorption in the wave number range of 1500—4000 cm^{-1} is a way to directly observing the presence of OH^- and H_2O in specimens. A

spectrometer (type EPI-S_2, Hitachi Co.) was used to record the spectra of KBr plus specimen disks which were formed after a prolonged evacuation at room temperature to eliminate water adsorbed on KBr and specimen powders.

Results and Discussion

The X-ray diffraction indicated that no crystalline phases other than the pyrochlore one were found in any of the specimens prepared by varying the Ti/(Ti+Sn) mole ratio, x, in the starting mixed solution. TG of all the dried specimens under the sensitivity of 50 mg/full-scale revealed that the majority of dehydration was completed up to about 300 °C, thereafter, no considerable weight changes occurred up to about 1000 °C, at which the temperature volatilization of PbO started (Fig. 1). The DTA profiles of the dried specimens of $x \lesssim 0.45$ gave only heat absorption due to the removal of water, whereas those of $x \gtrsim 0.45$ showed, besides the heat absorption, an exothermic peak at about 550 °C, in which its intensity increased with an increase in the value of x. The latter fact was in harmony with the fact that the intensity of the background of X-ray diffraction also increased with an increase in the value of x. These facts strongly suggest that each specimen of $x \gtrsim 0.45$ more or less involves noncrystalline material, and that its exothermic peak of interest is due to its crystallization to perovskite and/or pyrochlore. Our previous reports[4-7] indicated that in the present manner of aqueous synthesis under the condition of $x=1.0$, "pure" noncrystalline material with a composition of $Pb_{1-y}TiO_{3-y}$ ($y \lesssim 0.3$) resulted, and that this crystallized to the perovskite at about 550 °C. It is thus believed that the compositions of noncrystalline materials coexisting with the pyrochlores are all Pb/(Ti+Sn) mole ratio <1.0. No further discussion will be undertaken of the specimens of $x \gtrsim 0.45$ in the present study.

The foregoing results allow us to regard the materials of $x \lesssim 0.45$ as roughly monophasic, even if a very small amount of a noncrystalline substance coexists. The results of chemical analyses for the material of $x=0.4$ as a typical example gave $Pb_{1.05}(Ti_{0.4} \cdot Sn_{0.6})O_3$ as its composition; no measurable content of Na was detected. Thus, its $Pb/(Ti_{0.4}+Sn_{0.6})$ and hence $Pb/(Ti_x+Sn_{1-x})$

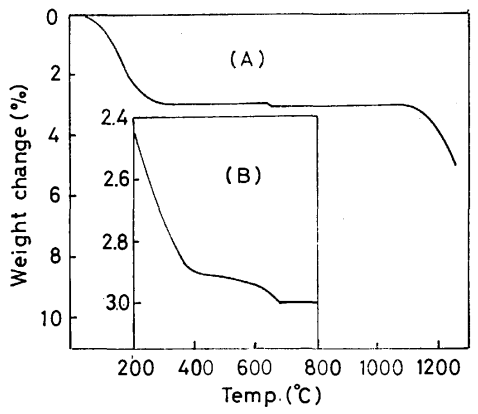

Fig. 1. Thermogravimetric trace of pyrochlore Pb $(Ti_{0.4} \cdot Sn_{0.6})O_3$ under the sensitivities of 50 mg/full-scale (A) and 2 mg/full-scale (B).

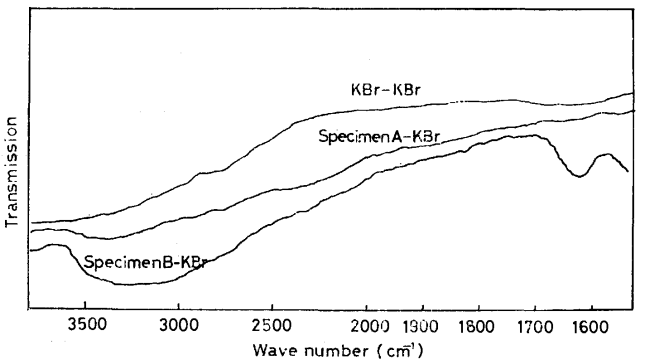

Fig. 2. Infrared absorption spectra of specimens A and B which were obtained by firing pyrochlore $Pb(Ti_{0.4} \cdot Sn_{0.6})O_3$ at 800 and 550 °C.

mole ratio in general may be taken to be unity within the limits of experimental error. Here we may need to further examine the possibility of the $Pb_2(Ti_{0.4} \cdot Sn_{0.6})_2(O,OH)_7$ composition besides $Pb(Ti_{0.4} \cdot Sn_{0.6})O_3$, since the two compositions may both lie within the accuracy of chemical analyses. Fortunately, as will be described later, the pyrochlore of $x=0.4$ was transformed to monophasic perovskite at elevated temperatures. Therefore, a composition of $Pb^{2+}(Ti_{0.4} \cdot Sn_{0.6})_2[O_5 \cdot (OH)_2]$ where the electroneutrality is maintained would be an accepted possibility, since only this composition can be transformed to the $Pb^{2+}(Ti_{0.4} \cdot Sn_{0.6})_2O_6$ by losing one molecule of water from the pyrochlore composition. A close examination was, therefore, done of the weight change at elevated temperatures using a microthermobalance. The results for a thermogravimetric trace of the specimen under the senstivity of 2 mg/full-scale is shown in Fig. 1; a slight weight change occurs over the temperature range from 300 to 620 °C. To ascertain the constituent species which causes the weight change, the infrared absorption spectra of two specimens of $x=0.4$ fired at 800 °C (Specimen A) and 550 °C (Specimen B) were recorded, (Fig. 2). For Specimen B, two kinds of absorptions, in the vicinity of 3400 cm^{-1} due to the stretching vibration mode of OH^{-1} and in the vicinity of 1600 cm^{-1} due to its bending vibration mode, are obvious. For Specimen A, whose relative mole ratio of perovskite/pyrochlore was 0.50, no absorption was detected over the wavelength range of interest. However, it should be stressed that the percent weight change in the temperature range of 300—620 °C ($\approx$0.1 wt%) was far less than the calculated H_2O percentage in $Pb_2(Ti_{0.4} \cdot Sn_{0.6})_2[O_5 \cdot (OH)_2]$ (=2.54 wt%). This fact shows the possible existence of pyrochlore with a composition of $Pb(Ti_{0.4} \cdot Sn_{0.6})O_3$ over a temperature range of at least 300—600 °C; the very small amounts of OH^- detected by the infrared absorption technique may arise from either zeolitic water or strongly-absorbed water present. Remarks will be necessary, for dehydration occurred up to $\approx$300 °C. The lattice constants of two specimens of $x=0.4$ before and after the dehydration were equal within the limits of experimental error. This fact gives negative evidence for the occurrence of pyrochlore with a composition of $Pb_2(Ti_{0.4} \cdot Sn_{0.6})_2[O_5(OH)_2]$.

Recently a number of the anion-deficient pyrochlores,

TABLE 1. COMPOSITIONS AND PHASES OF MATERIALS AT 300 AND 900°C
Compositions are indicated without taking the presence of "water" into consideration

$x=\frac{Ti}{Ti+Sn}$ (Mole fraction)	Phases present	
	Specimen fired at 300 °C	Specimen fired at 900 °C
$x<0.35$	Pyro.—$Pb(Ti_x\cdot Sn_{1-x})O_3$	$Pb_2SnO_4+SnO_2$ +Pero.—$Pb(Ti_{x'}\cdot Sn_{1-x'})O_3$
$0.35\lesssim x<0.45$	Pyro.—$Pb(Ti_x\cdot Sn_{1-x})O_3$	Pero.—$Pb(Ti_x\cdot Sn_{1-x})O_3$
$0.45\lesssim x<0.85$	Pyro.—$Pb(Ti_{x'}\cdot Sn_{1-x'})O_3$ +Noncryst.—$Pb_{1-y}(Ti_{x''}\cdot Sn_{1-x''})O_{3-y}$	Pero.—$Pb(Ti_{x'}\cdot Sn_{1-x'})O_3$ +Pero.—$Pb_{1-y}(Ti_{x''}\cdot Sn_{1-x''})O_{3-y}$
$x\gtrsim 0.85$	Noncryst.—$Pb_{1-y}(Ti_x\cdot Sn_{1-x})O_{3-y}$	Pero.—$Pb_{1-y}(Ti_x\cdot Sn_{1-x})O_{3-y}$

such as Pb_2BiNbO_6,[8] and $Bi_3A_2^{2+}TaO_9$, where A=Mg, Zn, and Ca,[8] and $Pb_2Cd_{1/2}Mn_{1/2}TaO_6$[8] and $Pb_2Sb^{3+}B^{5+}O_6$, where B=Nb and Ta,[8] have been reported. In view of the fact that many of these pyrochlores involve Pb, the existence of the oxygen-deficient pyrochlore system $Pb(Ti_x\cdot Sn_{1-x})O_3$ in the present study may be accepted. The $Pb(Ti_x\cdot Sn_{1-x})O_3$ composition in general indicates that the structure is oxygen-deficient with respect to a standard type of pyrochlore, $A_2B_2O_7$, where lattice positions available are fully occupied. In the standard pyrochlore structure, the configuration of the BO_6 octahedral is complicated, the O–B–O chains lying on a zig-zag line along the <110> direction. In this structure the seventh set of oxygen are not essential to the stability of the structure. Therefore, the number of oxygen ions in the $A_2B_2O_7$ pyrochlore may be reduced to 6. Our pyrochlores can also be such a case.

In summary, the compositions and phases of materials prepared aqueously and then fired at 300 °C are summarized in Table 1 in relation to the mole ratio, x. The X-ray diffraction data of $PbSnO_3$ and $Pb(Ti_{0.45}\cdot Sn_{0.55})O_3$, both fired at 300 °C, are listed in Table 2. It may be seen from the table that they have cubic symmetry, for which more strict proof will be presented later. Figure 3 shows the lattice constant, a, as a function of the x value. No anomaly is found in the plot. The materials precipitated aqueously and then dried were heat-treated at elevated temperatures, and then quenched in air down to room temperature. The

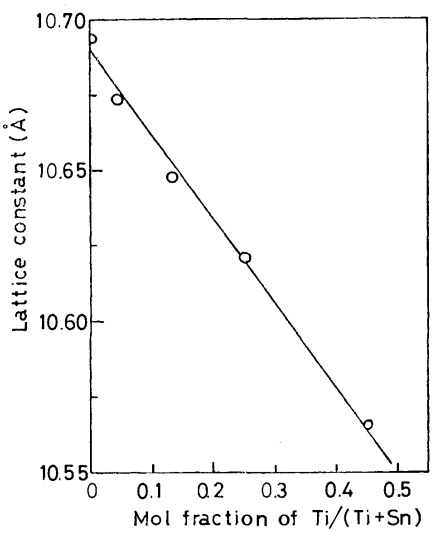

Fig. 3. Lattice constant as a function of x in pyrochlore $Pb(Ti_x\cdot Sn_{1-x})O_3$.

TABLE 2. X-RAY DIFFRACTION DATA OF PYROCHLORES $PbSnO_3$ AND $Pb(Ti_{0.45}\cdot Sn_{0.55})O_3$ FIRED AT 300°C

$PbSnO_3$			
d(Å)	I/I(%)	hkl	a(Å)
3.083	100	222	10.680
2.671	42	400	10.684
2.459	10	331	10.706
1.889	51	440	10.686
1.612	50	622	10.693
1.541	18	444	10.681
1.220	17	662	10.679
1.195	17	840	10.688
			Av. 10.682±0.013

$Pb(Ti_{0.45}\cdot Sn_{0.55})O_3$			
d(Å)	I/I(%)	hkl	a(Å)
3.056	100	222	10.565
2.639	40	400	10.556
2.427	10	331	10.579
1.860	40	440	10.573
1.590	35	622	10.573
1.525	10	444	10.566
1.213	10	662	10.574
1.182	10	840	10.572
			Av. 10.570±0.012

results of phase analyses for the materials fired at 900 °C are shown in the third column in Table 1. The pyrochlore of x=0.0, *i.e.*, $PbSnO_3$, decomposed into Pb_2SnO_4 and SnO_2 at about 800 °C. This fact indicates that if a solid-solid reaction between PbO and SnO_2 could occur in the vicinity of 800 °C, there can be no single stable phases of the $PbSnO_3$ composition. On the other hand, restricted monophasic pyrochlores of $0.35\lesssim x\lesssim 0.45$ were transformed into monophasic perovskites, the starting temperature being about 600 °C.

The $Pb(Ti_{0.4}\cdot Sn_{0.6})O_3$ composition was chosen to study the transition characterisitics of a solid-solution-type pyrochlore. The material was fired at a series of temperatures in order to measure the lattice constant of the pyrochlore phase. Table 3 gives the lattice constants of the pyrochlores fired at 720 and 870 °C, at which temperatures the extents of the transition were about 50 and 90% respectively. The pyrochlore phase held cubic symmetry during the transition. It is noticeable that the lattice constant, a, varies continuously during the transition. (Fig. 4). To ascertain the cause of such "anomalous" transition characteristics,

TABLE 3. X-RAY DIFFRACTION DATA OF MATERIALS OF PYROCHLORE-TYPE OBTAINED BY FIRING PYROCHLORE $Pb(Ti_{0.4} \cdot Sn_{0.6})O_3$ AT 720 AND 870 °C

Material fired at 720 °C		Material fired at 870 °C	
hkl	*a*(Å)	*hkl*	*a*(Å)
222	10.613	222	10.677
400	10.610	400	10.676
331	10.614	331	10.677
440	10.613	440	10.675
622	10.615	622	10.675
444	10.617	444	10.677
662	10.614	662	10.676
840	10.614	840	10.677
Av.	10.614±0.004	Av.	10.676±0.001

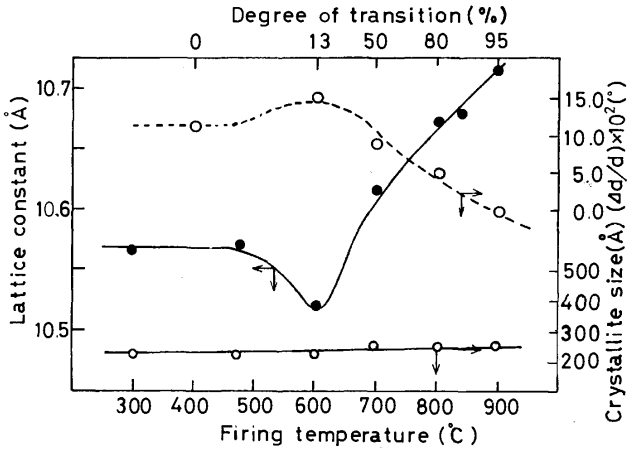

Fig. 4. Variations of $\Delta d/d$ and a of materials of pyrochlore-type obtained by firing pyrochlore $Pb(Ti_{0.4} \cdot Sn_{0.6})O_3$, with firing temperature.

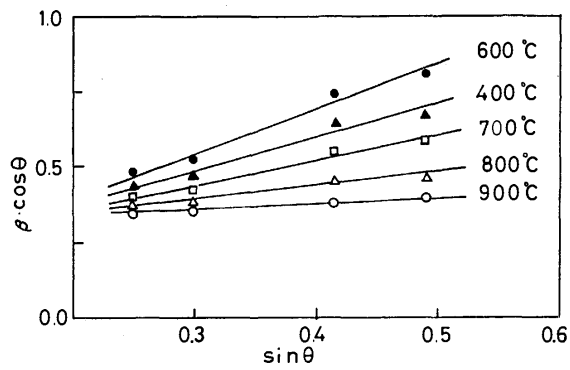

Fig. 5. Plots of $\beta cos\ \theta$ vs. $sin\ \theta$ of materials of pyrochlore-type obtained during transition from pyrochloro $Pb(Ti_{0.4} \cdot Sn_{0.6})O_3$ into perovskite one.

the magnitude of the fluctuation of the interplanar spacings and crystallite size of pyrochlores were determined. Figure 5 shows the plots of $\beta\cos\theta$ *vs.* $\sin\theta$ for the pyrochlores. The linearity of the plots is fairly good; the slopes give the $\Delta d/d$ value. Care must be taken that no diffraction line broadening due to crystallite size reduction contributes to the $\Delta d/d$ value. The $\Delta d/d$ value and the crystallite size are shown together in Fig. 4 as a function of the firing temperature. The $\Delta d/d$ value decreases continuously with the progress of the transition after a slight increase at an early stage of the transition. It should be noted that the $\Delta d/d$ value of the pyrochlore at the final stage of the transition is nearly zero, mainly because its diffraction lines are very sharp. Therefore, the interpretation of the pyrochlore fired at 870 °C in terms of cubic symmetry (Table 3) is valid. Accordingly, one might expect that all the pyrochlores treated in the present study have an exactly cubic symmetry even if their diffraction lines were unsharp in some cases.

It is very important to note that a decrease in $\Delta d/d$ follows an increase in a during the transition. There are two ways of interpreting the fluctuation of the interplanar spacings characteristic of the materials. One is based on the presence of an inhomogeneous strain, and the other, on its composition fluctuation. The literature[9,10] has indicated that the application of mechanical stress to polycrystalline solids causes an inhomogeneous strain. Throughout the formation process of the pyrochlores, however, there are not external environments enough for any residual stress or microstress to occur so as to create an inhomogeneous strain. One possibility to be considered is an internal stress stemming from a difference in the ionic radii of Ti^{4+} and Sn^{4+} ions. However such a stress, even if could be developed, may be quickly removed *via* free surfaces during the formation process of the materials. Therefore, it seems reasonable to give the interpretation in terms of composition fluctuation for $\Delta d/d$. A more rigorous proof for this will be described later. The majority of the composition fluctuation may occur as a result of the clustering of Sn ions in the B-positions of the $A_2B_2O_6$ pyrochlore in the formation process, by which an inhomogeneous distribution of Sn and Ti ions may result. The clustering tendency of Sn ions seems in harmony with the fact that an Sn-rich composition was apt to crystallize in a pyrochlore-type structure. The foregoing discussion suggests that a decrease in $\Delta d/d$ above 600 °C (see Fig. 4) occurs as a result of either Sn-rich or Ti-rich sides of the composition being missing. The accompanying increase in the lattice constant, a, above that temperature allows us to choose a preferential lack of a Ti-rich composition in the pyrochlore phase from among the two possibilities; a Sn-rich composition thus comes to predominate in the pyrochlore phase remaining. This feature of the two parameters, a and $\Delta d/d$, during the transition is also indicative of the validity of the interpretation based on composition fluctuation for $\Delta d/d$, because if the $\Delta d/d$ value is due to an inhomogeneous strain, its decrease has to proceed without varying the lattice constant. Here it is important to evaluate the actual range of the composition fluctuation of pyrochlores. The $\Delta d/d$ value was used with the data of Fig. 3 for this purpose. The composition range of, for example, $Pb(Ti_{0.4} \cdot Sn_{0.6})O_3$ fired at 300 °C was calculated as $x=0.364$—0.436 (average of $x=0.4$). In summary, it seems reasonable that the transition from the solid-solution-type pyrochlore to the perovskite occurs favorably in Ti-rich microregions. To confirm this line of thought definitely, it is useful to trace the tetragonal lattice strain, $(c/a)-1$, of the resultant

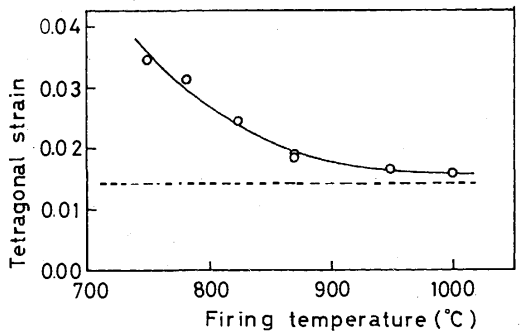

Fig. 6. Tetragonal lattice strain of materials of perovs kite-type obtained during transition from pyrochlore $Pb(Ti_{0.4}\cdot Sn_{0.6})O_3$ to perovskite one.

perovskite during the transition. Figure 6 shows the result; the dotted line shows the literature value[11] of the tetragonal strain of $Pb(Ti_{0.4}\cdot Sn_{0.6})O_3$ perovskite. As may be seen, the tetragonal strain of our perovskite lies in the vicinity of 0.04 at an early stage of the transition and then goes down to the literature value, 0.014, as the transition proceeds. This means that the composition of the resultant perovskite is Ti-richer at an early stage of the transition, thus fitting the foregoing interpretation of the transition characteristics of the solid-solution-type pyrochlore.

It is noticeable that a slight increase in $\Delta d/d$ occurs up to 600 °C, along with a slight decrease in the lattice constant, a (Fig. 4). A probable interpretation for this may be worked out by postulating that the as-dried solid solution contains a very small quantity of a noncrystalline material with a value of x slightly higher than that of the host. This line of thought may be supported by the fact that material with a high value of x is apt to become amorphous (Table 1). If this consideration is valid, and if its crystallization to pyrochlore proceeds near 500—600 °C, there can occur an increase in $\Delta d/d$ accompanying a decrease in the lattice constant, a, in the restricted temperature range of interest.

Some discussion may be needed regarding the displacement of the constituent ions, especially that of the Pb ions of the pyrochlore during the transition. Only when the displacement is "inhomogeneous", it can contribute to the $\Delta d/d$ value. Even if such a type of displacement could occur during the transition, however, the $\Delta d/d$ value has to go to a higher level than that before the transition without the lattice constant being varies. The results show in Fig. 4 and contrary to this requirement.

Further examinations were designed to trace the thermal-decomposition process of the monophasic pyrochlore $PbSnO_3$ by measurements along the same lines. These examinations may serve for checking whether the

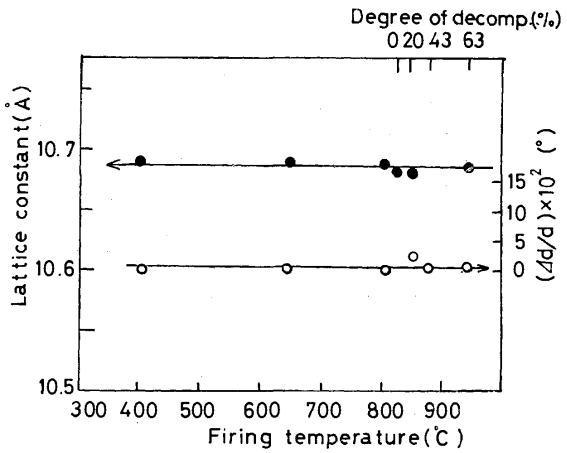

Fig. 7. Trace of $\Delta d/d$ and a of pyrochlore $PbSnO_3$ during thermal decomposition.

"anomalous" transition behavior is characteristic of the solid-solution-type pyrochlore. Figure 7 shows the two parameters, a and $\Delta d/d$, of the pyrochlore phase as a function of the firing temperature or of the extent of decomposition. No variations in the two are found up to at least 950 °C, at which temperature the extent of the decomposition reached about 63%; the $\Delta d/d$ value was zero before and throughout the transition, as had been expected. This fact can be taken as positive evidence for the foregoing way of understanding of the transition characterisitics of the solid-solution-type pyrochlore $Pb(Ti_x\cdot Sn_{1-x})O_3$ in general, and also as negative evidence for the occurrence of the displacement of the constituent ions of the pyrochlore during thetransition.

References

1) W. R. Cook and H. Jaffe, *Phys. Rev.*, **88**, 1426 (1952).
2) L. G. Nikiforov, V. M. Petrov, and Yu. N. Venevtsev, *Izv. Akad. Nauk SSSR, Ser. Fiz.*, **31**, 1074 (1967).
3) A. S. Viskov, Author's Abstract of Dissertation for Candidate's Degree, L. Ya. Kharkov Physicochemical Institute, Moscow (1966).
4) S. Shirasaki, *Solid State Commun.*, **9**, 1217 (1971).
5) S. Shirasaki, K. Takahashi, and K. Manabe, This Bulletin, **44**, 3189 (1971).
6) S. Shirasaki, K. Takahashi, and K. Kakegawa, *J. Amer. Ceram. Soc.*, **56**, 430 (1973).
7) K. Kakegawa, J. Mori, H. Yamamura, and S. Shirasaki, *Jap. J. Appl. Phys.*, **12**, 1821 (1973).
8) D. G. Demurov, L. G. Nikiforov, A. S. Viscov, and Yu. N. Venevtsev, *Fizika Tverdogo Tela*, **11**, 3674 (1969).
9) W. Cochran, *Proc. Roy. Soc. Ser., A*, **166**, 288 (1927).
10) T. Kubo and M. Kato, *Kogyo Kagaku Zasshi*, **66**, 318 (1963).
11) S. Nomura, *J. Phys. Soc. Japan*, **10**, 112 (1955).

A Study of the Thermal Degradation of Several Halogen-containing Polymers by Torsional Braid Analysis

Noboru FURUSHO, Tsuyoshi KOMATSU, and Tsurutaro NAKAGAWA

Department of Polymer Science, Faculty of Science, Hokkaido University, Sapporo 060

(Received October 20, 1973)

The thermal degradation of several halogen-containing polymers in air was studied by means of the TBA (Torsional Braid Analysis) method and IR spectroscopy. The samples were poly(vinyl chloride)(PVC), vinylidene chloride-vinyl chloride copolymer(PVdC-VC), poly(vinyl fluoride)(PVF), poly(vinylidene fluoride)(PVdF), poly(vinyl bromide)(PVB), and poly(vinylidene bromide)(PVdB). The dynamic mechanical properties of these polymers are complicated at higher temperatures because of the thermal degradation, by, for example, dehydrohalogenation. The relative shear modulus (G_r) increases and then decreases through a maximum, accompanied by changes in the logarithmic decrement. The temperatures at which the changes in G_r occur become higher in the order of PVdB<PVB<PVdC-VC<PVC<PVdF<PVF. This order agrees with that of the bond energy in carbon-halogen bonds. The apparent activation energies of these reactions were obtained from the changes in G_r and from the relative absorbance ratio of the carbon-carbon double bond with time, respectively. In general, the values estimated by these two procedures agreed well in each case.

The thermal degradation of polymers has been studied widely by various methods, by, for instance, thermogravimetric analysis and pyrolysis gas chromatography. On the other hand, relatively few studies have been carried out on the basis of measurements of the mechanical properties, which are much more sensitive to the changes in the state of the material. This situation may be attributed to the difficulties in the measurements of the mechanical properties of polymers at higher temperatures because of softening and fluidity. Gillham and Lewis[1] have established a new procedure, called the Torsional Braid Analysis (TBA) method, in which a composite system composed of a polymer and a mechanically-inactive supporting material (usually glass braids) is used.

Previously, using this TBA method, we have studied the change in the dynamic mechanical properties of several polymers during the thermal degradation and concluded that the TBA method can be used as a convenient tool for the kinetic study of the thermal degradation of polymers.[2,3]

In the present paper, we will report some results on the thermal degradation of several halogen-containing polymers: poly(vinyl halide) and poly(vinylidene halide). The halides are chloride, fluoride, and bromide. We will also report on the correlation between the changes in the dynamic mechanical behavior at higher temperatures and the chemical reactions with the aid of the results of the thermogravimetric analysis and the IR spectra.

The purpose of this work is to elucidate the effects of the various halogens and the types of substitution on the thermal stabilities of polymers on the basis of the measurements of the mechanical properties. Also, we intend to examine the applicability of these mechanical procedures to the kinetic studies by comparing the data obtained from the mechanical measurements with the values obtained from the IR spectra.

Experimental

The poly(vinyl chloride)(PVC), vinylidene chloride-vinyl chloride copolymer(PVdC-VC), poly(vinyl fluoride)(PVF), and poly(vinylidene fluoride)(PVdF) were commercial materials. The poly(vinyl bromide)(PVB) and poly(vinylidene bromide)(PVdB) were obtained as the starting materials from the 1,2-dibromoethane in the ordinary way;[4] the polymers were identified by elementary analysis and by IR spectroscopy. The known parameters relating to the molecular dimensions of the present samples are as follows. The viscosity-average molecular weights are 1.0×10^5 for PVC and 1.2×10^5 for PVB. The intrinsic viscosity in *N,N*-dimethylformamide at 20 °C is 1.8 (dl/g) for PVdF. The number-average degree of polymerization is 1000 for PVdC-VC, and the weight ratio of the components is 82: 18.

The details of the TBA method have been described elsewhere.[2] The relative shear modulus ($G_r=(T_0/T)^2$) and the logarithmic decrement ($\lambda=(1/n)\ln(A_{2n+1}/A_1)$) are obtained from the frequencies and the amplitudes of the damped oscillations. The measurements of G_r and λ are carried out under the conditions of a constant heating rate and under isothermal conditions. In the former case, the moduli at room temperatures, and in the latter case, the values 10 min after the setting of the specimen, were used as standards of the relative shear moduli. The test specimens were prepared by the impregnation of the polymer solutions into the glass braids and by the subsequent evaporation of the solvents. The frequency range is about 0.13—0.35 Hz.

The measurements of the IR spectra were carried out as follows. At first, KBr pellets with a known concentration of these polymers were prepared and then heated in air for the desired periods under isothermal conditions. The pellets were made again from those heat-treated materials and then used in the IR experiment. The relative absorbance ratios for the C–C double bond and the C–H group were calculated from the heights of the absorption peaks.

The thermogravimetric analysis(TGA) and the differential thermal analysis(DTA) were carried out in the air at a constant heating rate by using an apparatus made by the Rigaku Denki Co.

Results and Discussion

Temperature Dependence of G_r and λ. The dynamic mechanical properties of these polymers are shown in Figs. 1, 2, and 3. In these figures, the ordinates are arbitrarily shifted in order to avoid the overlapping of the curves. As is shown in Fig. 1, the G_r and λ of PVC behave in a complicated way. The curves of the

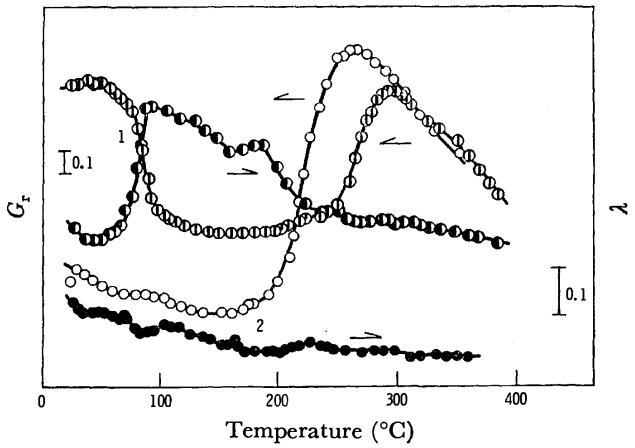

Fig. 1. G_r, λ *vs.* T plots of PVC and PVdC–VC heated in air. Heating rate: 1 °C/min. (1): PVC, (2): PVdC–VC.
① ○: G_r, ◐ ●: λ.

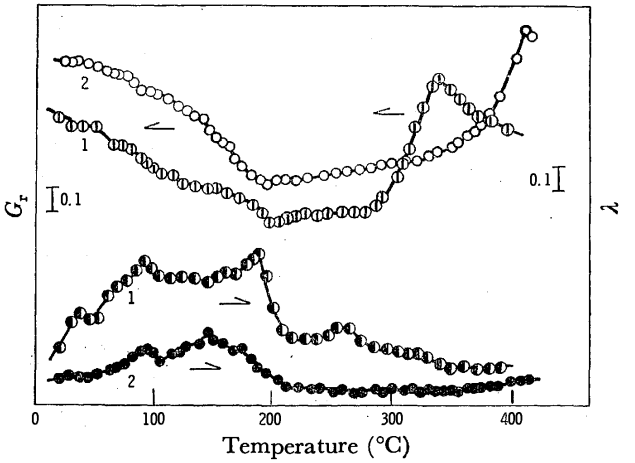

Fig. 2. G_r, λ *vs.* T plots of PVF and PVdF heated in air. Heating rate: 1 °C/min. (1): PVF, (2): PVdF.
① ○: G_r, ◐ ●: λ.

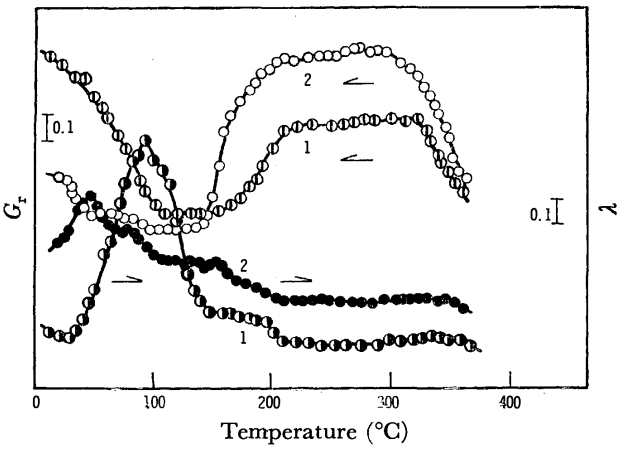

Fig. 3. G_r, λ *vs.* T plots of PVB and PVdB heated in air. Heating rate: 1 °C/min. (1): PVB, (2): PVdB.
① ○: G_r, ◑ ●: λ.

temperature dependence of G_r and λ consist of several parts. These features can be explained by assuming the following mechanism. The first abrupt decrease in G_r and the corresponding maximum of λ at about 90 °C are due to the glass transition. The gradual decrease in G_r and, presumably, the corresponding maximum of λ at about 180 °C may be due to the flow or the fusion. The successive increase in G_r (and the corresponding shoulder of λ at about 250 °C) and the last decrease in G_r through the maximum at about 300 °C may be attributed to the thermal degradation. The assumption about the last stage of the thermo-mechanical change is supported by the results of the thermogravimetric analysis shown in Fig. 4. In the case of PVC, as is shown in the figure, the weight loss accompanied by the dehydrochlorination reaction begins at about 230 °C and becomes intense between 250 and 290 °C; this temperature range is the same as that in which the values in G_r increase considerably. Considering the difference in the heating rates, it is reasonable to assume that these results correspond to each other.

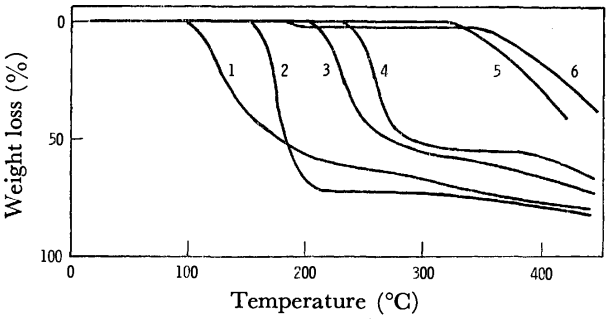

Fig. 4. TGA thermograms of halogen-containing polymers in air. Heating rate: 2.5 °C/min (1,2), 3 °C/min (3,4,5,6). (1): PVdB, (2): PVB, (3): PVdC–VC, (4): PVC, (5): PVF, (6): PVdF.

In the cases of the other polymers, the features in the dynamic mechanical properties can be also explained in the same way as in the case of PVC. For PVdC-VC, as is shown in Fig. 1, the decrease in G_r at the lower temperatures, the shoulder of λ at about 70 °C, and the successive decrease in G_r accompanied by the small peak (110 °C) and the shoulder (160 °C) of λ may be attributed to the physical relaxations. Such a situation is in agreement with the results obtained by Schmieder and Wolf.[5] The successive increase in G_r (and the corresponding small peak of λ at about 230 °C) and the last decrease in G_r through the maximum at about 270 °C are the results of the thermal degradation. It may be noticed that the values of G_r sharply decrease through a maximum in spite of the relatively slight loss of weight. Similar behavior is observed in the other systems. This result may be attributed to the destruction of the network structure by the oxidative chain scission, because the mechanical properties are very sensitive to the change in the network structure.

In the case of PVF, as is shown in Fig. 2, the decrease in G_r, the corresponding shoulder of λ at 40 °C, and the maximum of λ at 90 °C may be attributed to the molecular motions in the amorphous region and to those in the crystalline region, respectively. Considering our finding that the endothermic peak exists at about 190 °C, the small drop in G_r and the maximum of λ at 190 °C are due to the melting. These considerations

are supported by the results of Kawasaki and Hashimoto,[6] and Nielsen[7] with regard to its mechanical dispersion. The successive increase in G_r (and the corresponding shoulder of λ at about 320 °C) and the decrease in G_r through the maximum at 360 °C come from the thermal degradation. The nature of the small peak of λ at 260 °C has not been elucidated.

For PVdF (Fig. 2), the decrease in G_r and the corresponding peaks of λ at 90 and 150 °C may be attributed to the molecular motion in the crystalline region and to the melting, respectively. These assumptions are supported by the results of Kakutani[8] and Ota *et al.*[9] and by our finding that the endothermic peak exists at about 150 °C. The successive increase in G_r is due to the thermal degradation. However, the correlation between the gradual increase in G_r at about 200 °C and the chemical process is not clear at present. A slight weight loss is observed at about 180 °C. Ishii found a similar weight loss and stated that it was the result of the dehydrofluorination.[10] It should be pointed out here that the increase in G_r is greater than that to be expected from the curve of the weight loss; moreover, G_r continues to grow without showing any plateau.

For PVB (Fig. 3), the decrease in G_r and the corresponding maximum at 100 °C in λ relate to the glass transition. This agrees with the results obtained by Zutty and Whitworth.[11] The successive increase in G_r (and the corresponding shoulder of λ at 180 °C) and the decrease in G_r above 300 °C through the high plateau arise from the thermal degradation.

For PVdB (Fig. 3), the decrease in G_r, the corresponding maximum at 50 °C, and the shoulder at about 80 °C in λ are the results of the physical relaxation. The successive increase in G_r (and the corresponding shoulder of λ at 160 °C) and the decrease in G_r above 280 °C through a high plateau come from the thermal degradation. It may be noted that the values of G_r remain constant at a high plateau, irrespective of the continuous weight loss. This fact can be explained by assuming that the crosslinked network is formed at the first stage of the thermal degradation and that the so-formed polymeric structure remains unchanged in spite of the escape of small molecules, resulting in a continuous weight loss. In the case of epoxy resins during the curing process, the changes in G_r with time are similar to those of the present case (Fig. 6), and so an analogous mechanism of the formation of crosslinkage may be proposed.

These results concerning the thermal degradation are summarized in Table 1. The temperatures at which the values of G_r begin to increase become higher in the order of PVdB<PVB<PVdC-VC<PVC<PVdF<PVF. This order agrees well with that of the bond energy in the carbon-halogen bonds. Considering these features, together with the relation between the dynamic mechanical and the thermogravimetric results, and considering the appearance of the peak of the C-C double bond in the IR spectra, the increase in G_r seems to be attributable mainly to the dehydrohalogenation and the crosslinking reaction. The temperatures of the maximum of G_r become higher in the order of PVdB≈PVB<PVdC-VC<PVC<PVF<PVdF. In the cases of PVB and PVdB, those of the left-hand side of the plateau were taken as the maxima. The order of the temperatures at which G_r begins to decrease is PVdC-VC≈PVdB<PVC<PVB<PVF<PVdF.

These features are attributable to the difference in the stability of the dehydrohalogenation products against the oxidation which proceeds at the relatively higher temperatures, though the details have not been elucidated.

Time Dependence of G_r and λ. In order to study the kinetics of the thermal degradation, the G_r and λ are measured under isothermal conditions. Two typical results are shown in Figs. 5 and 6. Assuming that the

Table 1. The temperatures at which the changes in the mechanical properties and the weight loss occur

Sample	G_r (in)[a]	W (loss)	G_r (max)	G_r (de)[a]
PVC	190 °C	230 °C	300 °C	300 °C
PVdC–VC	160	210	280	280
PVF	280	310	340	340
PVdF	200	180	400	400
PVB	150	150	200—320	320
PVdB	130	100	200—280	280

a) G_r begins to increase or decrease.

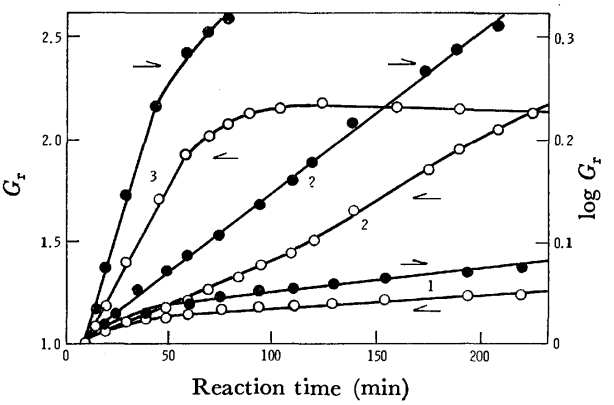

Fig. 5. G_r *vs.* t and log G_r *vs.* t plots of PVC during degradation in air at various temperatures. (1): 196 °C, (2): 221 °C, (3): 246 °C.
○: G_r, ●: log G_r.

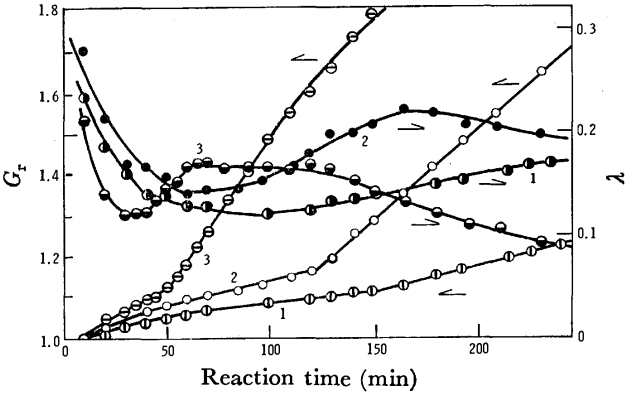

Fig. 6. G_r, λ *vs.* t plots of PVdB during degradation in air at various temperatures. (1): 102 °C, (2): 110 °C, (3): 122 °C.
⊕ ○ ⊖: G_r, ◑ ● ◒: λ.

Table 2. The apparent activation energies obtained from the several ways of analysis

Sample	Temp. range (°C)	G_r [a]	The apparent activation energies (kcal/mol)					
			From G_r	A_r	log G_r	log A_r	shift	t (λ-max)
PVC	170—250	in	24.7	26.4	29.6	12.4	29.7	
	250—340	de	21.7		28.6		21.7	
PVdC–VC	150—250	in	26.0	27.5	26.5	20.7	26.5	
	250—300	de	29.5		29.5		17.5	
PVF	190—300	in	22.7	20.7	22.3	17.0	26.3	
	270—370	de	10.8		16.0		18.0	
PVdF	250—300	in	10.6		10.0		23.5	
	300—390	in	30.2	36.6	30.5	18.2	31.1	
	350—420	de	27.9		31.6		31.1	
PVB	120—200	in	12.8	47.9	11.7	30.2	12.8	
	250—320	de	29.8		34.7		28.6	
PVdB	110—170	in	18.2	19.1	16.0	18.4	15.7	18.2
	250—300	de	17.7		21.8		21.6	

a) G_r increases or decreases.

order of the reaction is zero or first, the plots of the G_r *versus* the time and of the log G_r *versus* the time were made. In the case of PVC (Fig. 5), these two curves are linear at the initial stage. The order of the reaction has not yet been determined. At any rate, the slopes of these curves are a measure of the velocity constants, irrespective of the order of the reactions. The time dependence of λ is very slight and has been omitted from the figure. For other polymers, behavior was observed similar to that in the case of PVC. In the case of PVdB (Fig. 6), on the other hand, the curves are each composed of the two stages, and, at the same time, there exists a maximum in λ corresponding to the transition between the two stages. These phenomena have been found for polystyrene in our previous work[2] and for many cases of epoxy resins during the curing process. The time corresponding to the maximum of λ, therefore, may be regarded as a measure inversely proportional to the velocity constants.

The logarithms of the initial slopes and the time of the maximum λ were plotted against the reciprocal temperature (K^{-1}). From this analysis, the apparent activation energies are obtained as is shown in Table 2. These values agree well with those obtained by the other methods. For example, in the case of PVC, the value estimated from G_r, 24.7 kcal/mol, agrees well with 24 kcal/mol obtained by Talamini and Pezzin by TGA method.[12]

Furthermore, as was done in the previous work, a superposition procedure for the temperature dependence of G_r-reaction time curves was made. A typical composite curve is shown in Fig. 7. As was pointed out by Tobolsky[13] and shown in our previous work, the apparent activation energies can be obtained from the Arrhenius plot of the so-called shift factor in this procedure. The values are shown in Table 2. Except for a few cases, the agreement of the values estimated by various procedures is excellent; this fact confirms the validity of the analysis mentioned above.

The Changes in the Relative Absorbance Ratio. In order to substantiate the above discussion about the correlation between the changes in the dynamic mechanical properties and the chemical processes, and also

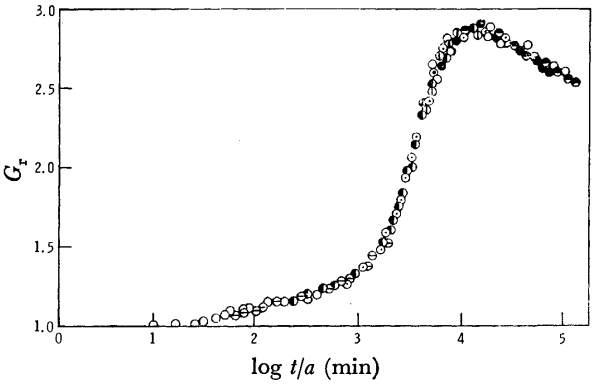

Fig. 7. Composite curve for relative shear modulus of PVC. (T_0=172 °C)
○: 172 °C, ⊖: 196 °C, ◐: 221 °C, ⊙: 246 °C, ⓘ: 271 °C, ●: 294 °C, ○: 319 °C, ◓: 343 °C.

in order to carry out the kinetic study, the IR spectra were measured. The change proceeds as follows; first, the peak of C-X bond disappears and the peak of C-C double bond appears in consequence of the dehydrohalogenation; second, the peaks of the carbonyl and ether groups resulting from the oxidation reaction appear. Otani suggested that the appearance of the peak of the ether group is the result of a crosslinking formation by the oxidation reaction.[14] These features support the considerations mentioned above of the mechano-chemical processes.

A typical example of the changes in the relative absorbance ratio (A_r) is shown in Fig. 8. A procedure of kinetic study similar to that used in the time dependence of G_r was used. The A_r *vs.* time and log A_r *vs.* time curves are linear at the initial stage. The slopes of these curves are, therefore, a measure of the velocity constant.

The logarithmic initial slopes in their curves were plotted against the reciprocal temperature (K^{-1}). From this analysis, the apparent activation energies were obtained as is shown in Table 2. These values agree well with the values obtained from the several other procedures of analysis. For example, in the case of PVdC-VC, the values are 26.0 kcal/mol from the G_r

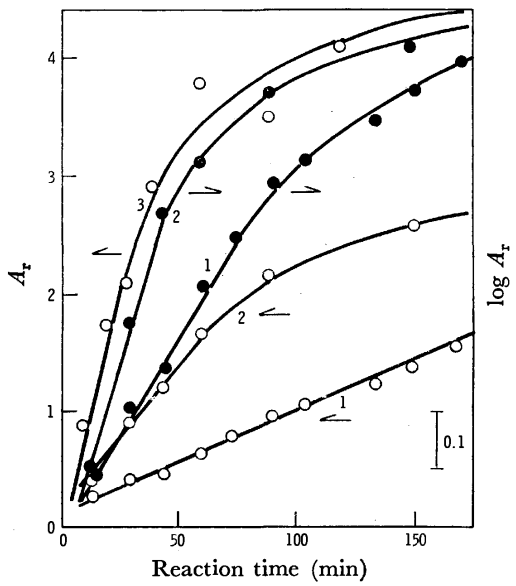

Fig. 8. A_r vs. t and log A_r vs. t plots of heat-treated PVdC–VC. (1): 184 °C, (2): 201 °C, (3): 221 °C. ○: A_r, ●: log A_r.

vs. t curves, 26.5 from log G_r *vs.* t, 26.5 from the shift factor of the composite curve, 27.5 from A_r *vs.* t curves, and 20.7 from log A_r *vs.* t. These agreements support also the considerations mentioned above of the correlation between the mechanical processes and the chemical reactions. There are, however, some deviations in several cases in the table. The problem of these deviations remains unsolved.

Conclusion

The changes in the mechanical properties at higher temperatures are associated with such chemical reactions as dehydrohalogenation, crosslinking and oxidation. The effect of the different halogen species on the thermal stability was elucidated. The stability of the polymers studied lies in the order of PVdB<PVB<PVdC-VC<PVC<PVdF<PVF.

Kinetic studies of these reactions were carried out, and the apparent activation energies were obtained by several ways of analysis. These values agree well each other except for a few cases. Finally, composite curves for the relative shear modulus were obtained for all the polymers studied.

The authors wish to thank Mr. Yoshio Takahashi (Electrotechnical Laboratory) and Associate Professor Yoshio Shibazaki (Saitama University) for affording the facilities for the use of the TGA and DTA apparatus.

References

1) J. K. Gillham and A. F. Lewis, *J. Appl. Polym. Sci.*, **7**, 685 (1963).
2) N. Furusho, T. Komatsu, and T. Nakagawa, *Nippon Kagaku Kaishi*, 1166 (1973).
3) N. Furusho, T. Komatsu, and T. Nakagawa, *Repts. Progr. Polym. Phys. Japan*, **16**, 335 (1973).
4) W. W. Korshrk and N. G. Matwejewa, *C. Zentralbl.*, **127**, 3317 (1956); G. Blauer, M. Shenblat, and A. Katchalsky, *J. Polym. Sci.*, **38**, 189 (1959).
5) K. Schmieder and K. Wolf, *Kolloid-Z.*, **134**, 149 (1953).
6) N. Kawasaki and T. Hashimoto, *J. Polym. Sci., Part A-2*, **9**, 2095 (1971).
7) L. E. Nielsen, "Mechanical Properties of Polymers," Reinhold Publishing Co., New York (1953), pp. 17, 34.
8) H. Kakutani, *J. Polym. Sci., Part A-2*, **8**, 1177 (1970).
9) M. Ota, S. Nishida, and H. Ishii, *Kobunshi Kagaku*, **27**, 785 (1970).
10) H. Ishii, *ibid.*, **27**, 858 (1970).
11) N. L. Zutty and C. J. Whitworth, *J. Polym. Sci., Part B*, **2**, 709 (1964).
12) G. Talamini and G. Pezzin, *Makromol. Chem.*, **39**, 26 (1960).
13) A. V. Tobolsky, "Properties and Structure of Polymers," John Wiley & Sons, Inc., New York (1960), p. 226.
14) S. Otani, *Kogyo Kagaku Zasshi*, **61**, 447 (1958).

A Study of the Upper and Lower Bounds of the Second-order Perturbation Energy

Tokio YAMABE, Kazuyoshi TANAKA, Shingo ISHIMARU, and Kenichi FUKUI

Department of Hydrocarbon Chemistry, Faculty of Engineering, Kyoto University, Sakyo-ku, Kyoto 606

(Received October 31, 1973)

A method of calculation for the upper and lower bounds of the second-order perturbation energy is investigated. The expression for the upper bound is based on Hylleraas's variation perturbation condition and is an improved version of that obtained by Goodisman. The lower bound is based on the Temple-type inequality and is an improved version of that by Prager and Hirschfelder. The result is numerically tested for examples of the polarizability of a hydrogen atom and the coefficients (C_6 and C_8) of the dispersion force between two separated hydrogen atoms, yielding fairly good results. Particularly, the results of the upper bound for C_8 are the best so far calculated in a non-empirical way.

The second-order perturbation energy, E_2, is given by:

$$E_2 = -\sum_{i>0}^{\infty}|H_{1i}|^2/\varepsilon_i, \tag{1}$$

where $H_{1i}=\langle\phi_0^{(i)}|H_1|\phi_0^{(0)}\rangle$ and $\varepsilon_i=E_0^{(i)}-E_0^{(0)}$, in which H_1 is the perturbation, and $\phi_0^{(i)}$ and $E_0^{(i)}$ are the i-th eigenfunction and eigenvalue of the unperturbed Hamiltonian H_0 respectively. In the following, we will denote $\phi_0^{(0)}$ and $E_0^{(i)}$ as ϕ_0 and E_0 respectively, since we will deal with only the ground state in this paper.

Generally it is difficult to calculate the summation of Eq. (1); therefore, many approximate methods have been devised. Among them, the most useful method is Hylleraas's variation condition for the second-order perturbation energy:[1]

$$\langle\tilde{\phi}_1|H_0-E_0|\tilde{\phi}_1\rangle+\langle\tilde{\phi}_1|H_1-E_1|\phi_0\rangle+\langle\phi_0|H_1-E_1|\tilde{\phi}_1\rangle \geqq E_2, \tag{2}$$

in which $\tilde{\phi}_1$ is an arbitrary function corresponding to the first-order perturbation function. One of the effective forms which have been applied for $\tilde{\phi}_1$ is that of Goodisman,[2] who, using Eq. (2), obtained the upper bound of the second-order energy for the case in which first n excited states of unperturbed system are known. On the other hand, neglecting energies of a higher order than the second-order, Prager and Hirschfelder[3] found the lower bound of the second-order energy based on the Temple principle:[4]

$$\langle(H-E^{(0)})\tilde{\Psi}|(H-E^{(1)})\tilde{\Psi}\rangle \geqq 0, \tag{3}$$

where $E^{(i)}$ is the i-th eigenvalue associated with i-th eigenfunction, $\Psi^{(i)}$, of the total Hamiltonian, $H=H_0+H_1$, and where $\tilde{\Psi}$ is a variational function for $\Psi^{(0)}$, which may be divided into $\phi_0+\tilde{\phi}_1$.

Other theories estimating the upper and lower bounds were developed by Lindner and Löwdin[5] and subsequently by Miller.[6] They utilized operator techniques in the direction of using a finite arbitrary basis set for $\tilde{\phi}_1$. Especially Miller extended the theory of Lindner and Löwdin, who treated only the second-order energy in the ground state, to a theory which can be adopted to the second-order energy in the arbitrary excited state.

It seems, however, that the form of $\tilde{\phi}_1$ used by Goodisman is rather tractable for performing the calculation. Therefore, in the present paper, we will try to improve both the upper bound of Goodisman and the lower bound of Prager and Hirschfelder by the use of a form of $\tilde{\phi}_1$ similar to that of Goodisman.

Derivation of the Upper Bound

Let us consider the following first-order variational function:

$$\tilde{\phi}_1(n,\lambda,\{\mu_i|i\geqq n+1\}) = -\sum_{i>0}^{n}H_{1i}\phi_0^{(i)}/\varepsilon_i + \lambda\sum_{i=n+1}^{\infty}\mu_i H_{1i}\phi_0^{(i)}, \tag{4}$$

where λ and each μ_i are arbitrary real parameters. Substituting this function into Hylleraas's condition in Eq. (2), one obtains:

$$E_2^{\mathrm{up}}(n,\lambda,\{\mu_i|i\geqq n+1\}) = (\sum_{i=n+1}^{\infty}\mu_i^2|H_{1i}|^2\varepsilon_i)\lambda^2 + 2(\sum_{i=n+1}^{\infty}\mu_i|H_{1i}|^2)\lambda + A_n, \tag{5}$$

where:

$$A_n = -\sum_{i>0}^{\infty}|H_{1i}|^2/\varepsilon_i. \tag{6}$$

$E_2^{\mathrm{up}}(n,\lambda,\{\mu_i|i\geqq n+1\})$ in Eq. (5) is a quadratic formula with regard to λ and takes the minimum value:

$$E_2^{\mathrm{up}}(n,\{\mu_i|i\geqq n+1\}) = A_n-(\sum_{i=n+1}^{\infty}\mu_i|H_{1i}|^2)^2/(\sum_{i=n+1}^{\infty}\mu_i^2|H_{1i}|^2\varepsilon_i), \tag{7}$$

when λ is:

$$\lambda = -(\sum_{i=n+1}^{\infty}\mu_i|H_{1i}|^2)/(\sum_{i=n+1}^{\infty}\mu_i^2|H_{1i}|^2\varepsilon_i). \tag{8}$$

After modifying μ_i into some more convenient form, as will be shown below, we can further optimize $E_2^{\mathrm{up}}(n,\{\mu_i|i\geqq n+1\})$ with respect to $\{\mu_i\}$ for each n to get the desired upper bound, $E_2^{\mathrm{up}}(n)$. If the simplest form of μ_i is chosen, *i.e.*, $\mu_i=1$ for any i, the result is just that obtained by Goodisman.

It can easily be proved that the upper bound thus obtained really satisfies the relation that $E_2^{\mathrm{up}}(n-1)\geqq E_2^{\mathrm{up}}(n)$. In order to prove this, let us calculate the following subtraction between $E_2^{\mathrm{up}}(n,\{\mu_i|i\geqq n+1\})$ and $E_2^{\mathrm{up}}(n-1,\{\mu_i|i\geqq n\})$ of Eq. (7), keeping $\{\mu_i\}$ in common for both:

$$E_2^{\mathrm{up}}(n,\{\mu_i|i\geqq n+1\}) - E_2^{\mathrm{up}}(n-1,\{\mu_i|i\geqq n\}) = -|H_{1n}|^2/\varepsilon_n-(\sum_{i=n+1}^{\infty}\mu_i|H_{1i}|^2)^2/(\sum_{i=n+1}^{\infty}\mu_i^2|H_{1i}|^2\varepsilon_i) + (\sum_{i=n}^{\infty}\mu_i|H_{1i}|^2)^2/(\sum_{i=n}^{\infty}\mu_i^2|H_{1i}|^2\varepsilon_i). \tag{9}$$

The right-hand side in Eq. (9) becomes:

$$-|H_{1n}|^2\{\sum_{i=n+1}^{\infty}\mu_i|H_{1i}|^2(\mu_i\varepsilon_i-\mu_n\varepsilon_n)\}^2/$$
$$\{\varepsilon_n(\sum_{i=n}^{\infty}\mu_i^2|H_{1i}|^2\varepsilon_i)(\sum_{i=n+1}^{\infty}\mu_i^2|H_{1i}|^2\varepsilon_i)\}\leqq 0,$$

and is always nonpositive, since all of ε_i values are nonnegative. Consequently, when n becomes infinite, $E_2^{\mathrm{up}}(n,\{\mu_i|i\geqq n+1\})$; hence, $E_2^{\mathrm{up}}(n)$ also approaches to E_2 in Eq. (1) from the upper side.

Next, we set the modified form of μ_i as $\mu_i=1+\mu E_0^{(i)}/E_0$ to get the optimal value, $E_2^{\mathrm{up}}(n)$.[7] Substituting this μ_i into Eq. (7) and optimizing with respect to μ, one gets:

$$\begin{aligned}E_2^{\mathrm{up}}(n) = {} & A_n-\{\langle\phi_0|H_1^2|\phi_0\rangle+(\mu_{\mathrm{opt}}/E_0)\langle\phi_0|H_1H_0H_1|\phi_0\rangle\\ & -\sum_{i>0}^{n}(1+\mu_{\mathrm{opt}}E_0^{(i)}/E_0)|H_{1i}|^2\}^2/\{\langle\phi_0|H_1(H_0-E_0)H_1|\phi_0\rangle\\ & +(2\mu_{\mathrm{opt}}/E_0)\langle\phi_0|H_1H_0(H_0-E_0)H_1|\varphi_0\rangle\\ & +(\mu_{\mathrm{opt}}^2/E_0^2)\langle\phi_0|H_1H_0(H_0-E_0)H_0H_1|\phi_0\rangle\\ & -\sum_{i>0}^{n}(1+\mu_{\mathrm{opt}}E_0^{(i)}/E_0)^2|H_{1i}|^2\varepsilon_i\},\end{aligned}\tag{10}$$

where:

$$\begin{aligned}\mu_{\mathrm{opt}} = {} & [-(a^2e-b^2c)-\{(a^2e-b^2c)^2\\ & -(a^2d-2abc)(2abe-b^2d)\}^{1/2}]/(a^2d-2abc)\\ = {} & (bd-2ae)/(ad-2bc),\end{aligned}\tag{11}*$$

and where:

$$\left.\begin{aligned}a &= \langle\phi_0|H_1H_0H_1|\phi_0\rangle/E_0-\sum_{i=0}^{n}(E_0^{(i)}/E_0)|H_{1i}|^2,\\ b &= \langle\phi_0|H_1^2|\phi_0\rangle-\sum_{i=0}^{n}|H_{1i}|^2,\\ c &= \langle\phi_0|H_1H_0(H_0-E_0)H_0H_1|\phi_0\rangle/E_0^2\\ &\quad -\sum_{i>0}^{n}(E_0^{(i)}/E_0)^2|H_{1i}|^2\varepsilon_i,\\ d &= 2\{\langle\phi_0|H_1H_0(H_0-E_0)H_1|\phi_0\rangle/E_0\\ &\quad -\sum_{i>0}^{n}(E_0^{(i)}/E_0)|H_{1i}|^2\varepsilon_i.\end{aligned}\right\}\tag{11'}$$

and:

$$e=\langle\phi_0|H_1(H_0-E_0)H_1|\phi_0\rangle-\sum_{i>0}^{n}|H_{1i}|^2\varepsilon_i.$$

Derivation of the Lower Bound

If the variational function $\tilde{\Psi}$, which is divided into $\phi_0+\tilde{\phi}_1$, as has previously been mentioned, is orthogonal to the first several excited eigenfunctions of the total Hamiltonian, *i.e.*:

$$\langle\tilde{\Psi}|\Psi^{(k)}\rangle=0\quad(k=1,2,\cdots,n),\tag{12}$$

the following Temple-type inequality:

$$\langle(H-E^{(0)})\tilde{\Psi}|(H-E^{(n+1)})\tilde{\Psi}\rangle\geqq 0,\tag{13}$$

is easily established and can be utilized as the base to get the lower bound. Here we try to employ the same form as in Eq. (4) for $\tilde{\phi}_1$; namely, $\tilde{\Psi}$ is:

$$\tilde{\Psi}=\phi_0+\tilde{\phi}_1=\phi_0-\sum_{i>0}^{n}H_{1i}\phi_0^{(i)}/\varepsilon_i+\lambda\sum_{i=n+1}^{\infty}\mu_iH_{1i}\phi_0^{(i)},\tag{14}$$

which satisfies Eq. (12) as far as the second-order energy is considered.[8] Substituting this $\tilde{\Psi}$ into Eq. (13) and neglecting the energies of a higher order than the second-order one, we obtain a lower bound for the second-order energy:

$$\begin{aligned}E_2 \geqq {} & \{\sum_{i=n+1}^{\infty}\mu_i^2|H_{1i}|^2\varepsilon_i(1-\varepsilon_i/\varepsilon_{n+1})\}\lambda^2\\ & +2\{\sum_{i=n+1}^{\infty}\mu_i|H_{1i}|^2(1-\varepsilon_i/\varepsilon_{n+1})\}\lambda\\ & +\{A_n-\sum_{i=n+1}^{\infty}|H_{1i}|^2/\varepsilon_{n+1}\}\\ \equiv {} & E_2^{\mathrm{low}}(n,\lambda,\{\mu_i|i\geqq n+1\}),\end{aligned}\tag{15}$$

which takes the maximum value:

$$\begin{aligned}E_2^{\mathrm{low}}(n,\{\mu_i|i\geqq n+1\}) = {} & -\{\sum_{i=n+1}^{\infty}\mu_i|H_{1i}|^2(1-\varepsilon_i/\varepsilon_{n+1})\}^2/\\ & \{\sum_{i=n+1}^{\infty}\mu_i^2|H_{1i}|^2\varepsilon_i(1-\varepsilon_i/\varepsilon_{n+1})\}+\{A_n-\sum_{i=n+1}^{\infty}|H_{1i}|^2/\varepsilon_{n+1}\},\end{aligned}\tag{16}$$

when:

$$\begin{aligned}\lambda = {} & -\{\sum_{i=n+1}^{\infty}\mu_i|H_{1i}|^2(1-\varepsilon_i/\varepsilon_{n+1})\}/\\ & \{\sum_{i=n+1}^{\infty}\mu_i^2|H_{1i}|^2\varepsilon_i(1-\varepsilon_i/\varepsilon_{n+1})\}.\end{aligned}\tag{17}$$

$E_2^{\mathrm{low}}(n,\{\mu_i|i\geqq n+1\})$ can be further optimized with regard to $\{\mu_i\}$ to obtain $E_2^{\mathrm{low}}(n)$ much as in the previous section. If $n=0$ and $\mu_i=1$, the result coincides with that obtained by Prager and Hirschfelder.

Furthermore, the relation that $E_2^{\mathrm{low}}(n)\geqq E_2^{\mathrm{low}}(n-1)$ can be proved by calculating the following subtraction with the use of Eq. (15), keeping λ and $\{\mu_i\}$ in common for both $E_2^{\mathrm{low}}(n,\lambda,\{\mu_i|i\geqq n+1\})$ and $E_2^{\mathrm{low}}(n-1,\lambda,\{\mu_i|i\geqq n\})$:

$$\begin{aligned}& E_2^{\mathrm{low}}(n,\lambda,\{\mu_i|i\geqq n+1\})-E_2^{\mathrm{low}}(n-1,\lambda,\{\mu_i|i\geqq n\})\\ & = \{(\varepsilon_{n+1}-\varepsilon_n)\sum_{i=n+1}^{\infty}\mu_i^2|H_{1i}|^2\varepsilon_i^2/\varepsilon_n\varepsilon_{n+1}\}\lambda^2\\ & \quad +2\{(\varepsilon_{n+1}-\varepsilon_n)\sum_{i=n+1}^{\infty}\mu_i|H_{1i}|^2\varepsilon_i/\varepsilon_n\varepsilon_{n+1}\}\lambda\\ & \quad +\{(\varepsilon_{n+1}-\varepsilon_n)\sum_{i=n+1}^{\infty}|H_{1i}|^2/\varepsilon_n\varepsilon_{n+1}\}.\end{aligned}\tag{18}$$

Equation (18) is a quadratic formula of λ and is always positive, since the coefficient of λ^2 is positive and since the discriminant of Eq. (18):

$$\begin{aligned}D = {} & (\varepsilon_{n+1}-\varepsilon_n)^2\{(\sum_{i=n+1}^{\infty}\mu_i|H_{1i}|^2\varepsilon_i)^2\\ & -(\sum_{i=n+1}^{\infty}\mu_i^2|H_{1i}|^2\varepsilon_i^2)(\sum_{i=n+1}^{\infty}|H_{1i}|^2)\}/(\varepsilon_{n+1}^2\varepsilon_n^2),\end{aligned}$$

is always negative, which is ensured by the Schwartz inequality. Therefore, when n becomes infinite, $E_2^{\mathrm{low}}(n,\lambda,\{\mu_i|i\geqq n+1\})$; hence, $E_2^{\mathrm{low}}(n)$ also approaches to the true E_2 value from the lower side.

As a special case, by substituting $\mu_i=1$[7] into Eq. (16) one gets the lower bound, $E_2^{\mathrm{low}}(n)$:

$$\begin{aligned}E_2^{\mathrm{low}}(n) = {} & -\{\sum_{i=n+1}^{\infty}|H_{1i}|^2(1-\varepsilon_i/\varepsilon_{n+1})\}^2/\\ & \{\sum_{i=n+1}^{\infty}|H_{1i}|^2\varepsilon_i(1-\varepsilon_i/\varepsilon_{n+1})\}+\{A_n-\sum_{i=n+1}^{\infty}|H_{1i}|^2/\varepsilon_{n+1}\},\end{aligned}\tag{19}$$

which can then be rewritten by using the a, b, d, and e defined in the previous section:

$$\begin{aligned}E_2^{\mathrm{low}}(n) = {} & -[b-(a-b)E_0/\varepsilon_{n+1}]^2/\\ & [(a-b)E_0-(d/2-2e+aE_0-bE_0)E_0/\varepsilon_{n+1}]\\ & +(A_n-b/\varepsilon_{n+1}).\end{aligned}\tag{20}$$

* We are indebted to the referee for the final result of Eq. (11).

Results and Discussion

Polarizability of a Hydrogen Atom in the Ground State. The value of the polarizability, α, is twice the absolute value of E_2 caused by the perturbation, H_1, which, in this case, is z (in a.u.), the coordinate of the direction of the electric field (we will always use the atomic unit hereafter). Then,

$$\alpha = -2E_2 = 2\sum_{i>0}^{\infty}|\langle\psi_0^{(i)}|z|\psi_0\rangle|^2/(E_0^{(i)}-E_0). \quad (21)$$

In order to examine the usefulness of the present theory for the upper and lower bounds, we must calculate Eqs. (10), (11), and (20). In the calculation, the following values of integrals are required:

$$\left.\begin{aligned}&\langle\psi_0|z|\psi_0\rangle = 0,\\ &\langle\psi_0|z^2|\psi_0\rangle = 1,\\ &\langle\psi_0|zH_0z|\psi_0\rangle = 0,\\ &\langle\psi_0|zH_0^2z|\psi_0\rangle = 1/12,\\ &\text{and}\\ &\langle\psi_0|zH_0^3z|\psi_0\rangle = 5/12,\end{aligned}\right\} \quad (22)$$

in which ψ_0 is the 1s-function of a hydrogen atom and in which E_0 is $-1/2$.

In Table 1, the results for n=0, 1, 2, 3, and 4 are shown. The values of λ and μ are also shown, since they are the parameters corresponding to $1/E_0$ and $E_0/(E_0-E_0^{(i)})$ respectively.[7] Compared with the results of the lower bounds of α reported by Goodisman (μ_i=1), the present lower bounds are fairly well improved because of the existence of the μ_i parameter; the upper bounds are also better than that reported by Prager and Hirschfelder. For both the upper and lower bounds, the improvement from n=0 to n=1 is meaningful, but for $n\geqq 2$ the improvement does not seem to be substantial.

The Dispersion Force between Two Hydrogen Atoms. When the internuclear distance, R, between two hydrogen atoms in the ground state is large enough, the overlap and, hence, the exchange are insignificant; we can take $\psi_0=\psi_A(1)\psi_B(2)$ as the unperturbed wavefunction for this system, where $\psi_A(1)$ and $\psi_B(2)$ are the isolated atomic wavefunctions of the two hydrogen atoms. Besides, the perturbation, H_1, in usual notations:[9]

$$H_1 = -1/r_{B1} - 1/r_{A2} + 1/R + 1/r_{12}, \quad (23)$$

can be expanded in an inverse power series of R, and the second-order energy is generally represented by:

$$-E_2 = C_6/R^6 + C_8/R^8 + \cdots, \quad (24)$$

where:

$$C_6 = \sum_{i>0}^{\infty}|\langle\psi_0^{(i)}|H_{dd}|\psi_0\rangle|^2/(E_0^{(i)}-E_0),$$
$$H_{dd} = x_1x_2 + y_1y_2 - 2z_1z_2, \quad (25)$$

and

$$C_8 = \sum_{i>0}^{\infty}|\langle\psi_0^{(i)}|H_{qd}|\psi_0\rangle|^2/(E_0^{(i)}-E_0),$$
$$H_{qd} = (3/2)\{r_1^2z_2 - r_2^2z_1 + (2x_1x_2+2y_1y_2-3z_1z_2)(z_1-z_2)\}. \quad (26)$$

In the calculation of the bounds for C_6, we need various kinds of integrals, which are evaluated as follows:

$$\left.\begin{aligned}&\langle\psi_0|H_{dd}|\psi_0\rangle = 0,\\ &\langle\psi_0|H_{dd}^2|\psi_0\rangle = 6,\\ &\langle\psi_0|H_{dd}H_0H_{dd}|\psi_0\rangle = 0,\\ &\langle\psi_0|H_{dd}H_0^2H_{dd}|\psi_0\rangle = 1,\\ &\text{and}\\ &\langle\psi_0|H_{dd}H_0^3H_{dd}|\psi_0\rangle = 5.\end{aligned}\right\} \quad (27)$$

In Table 2, the results for C_6 using n=0, 1, 2, 3, 4, 5, 6, and 7 are shown. As in the case of polarizability, the improvement from n=0 to n=1 is remarkable, but for $n\geqq 2$ the effect is not so large.

When calculating the bounds for C_8, the following integrals are required:

$$\left.\begin{aligned}&\langle\psi_0|H_{qd}|\psi_0\rangle = 0,\\ &\langle\psi_0|H_{qd}^2|\psi_0\rangle = 135,\\ &\langle\psi_0|H_{qd}H_0H_{qd}|\psi_0\rangle = 45/2,\\ &\langle\psi_0|H_{qd}H_0^2H_{qd}|\psi_0\rangle = 207/8,\\ &\text{and}\\ &\langle\psi_0|H_{qd}H_0^3H_{qd}|\psi_0\rangle = 12501/160.\end{aligned}\right\} \quad (28)$$

In Table 3, the results for C_8 are presented in the case of n=0 and 1. It can also be seen that the improvement of the lower bound is remarkable when variable parameters, μ_i, are used in comparison with that obtained by using a constant $\mu_i=1(\mu=0)$; moreover, the improvement for both bounds from n=0 to n=1 is appreciable. The present result for the upper bound for C_8 is the best so far calculated in a non-empirical way.

From the above numerical results, it is clear that the present treatment is very tractable because of the convenient form of the variational function used. Although the numerical results are rather inferior to those in Refs. 5 and 10, the average of the both bounds for each n gives good approximations to the exact values as may be seen in Tables 1, 2, and 3. Hence, the

TABLE 1. THE UPPER AND LOWER BOUNDS FOR POLARIZABILITY OF A HYDROGEN ATOM IN THE GROUND STATE (Exact=4.5)

n	$\alpha^{low}(n)=-2E_2^{up}(n)$ [a]	λ	μ	$\alpha^{low}(n)$ [b] ($\mu_1=1$)	$\alpha^{up}(n)=-2E_2^{low}(n)$ [a]	λ	$\{\alpha^{low}(n)+\alpha^{up}(n)\}/2$
0	4.125	−2.063	0.09091	4.0000	4.762*	−0.8571	4.444
1	4.363	−1.611	0.07286	4.3162	4.646	−0.7495	4.505
2	4.391	−1.499	0.06644	4.3636	4.623	−0.7156	4.507
3	4.415	−1.457	0.06638	4.3800	4.612	−0.7007	4.514
4	4.420	−1.435	0.06525	—	4.607	−0.6929	4.514

a) Present work (*; Ref. 3). b) Ref. 2.

Table 2. The upper and lower bounds for dispersion force constant C_6 between two hydrogen atoms in the ground state (Reliable value=6.4990267[c])

n	$C_6^{low}(n)=-E_2^{up}(n)$ [a]	λ	μ	$C_6^{low}(n)$ [b] ($\mu_i=1$)	$C_6^{up}(n)=-E_2^{low}(n)$ [a]	λ	$\{C_6^{low}(n)+C_6^{up}(n)\}/2$
0	6.171	−1.029	0.1667	6.000	6.800	−0.6000	6.486
1	6.302	−0.9393	0.1445	6.201	6.709	−0.5560	6.506
2	6.339	−0.9049	0.1365	6.256	6.684	−0.5412	6.512
3	6.345	−0.8917	0.1335	6.269	6.674	−0.5345	6.510
4	6.357	−0.8853	0.1321	6.284	6.668	−0.5310	6.513
5	6.360	−0.8817	0.1313	6.289	6.665	−0.5288	6.513
6	6.362	−0.8794	0.1308	—	6.663	−0.5274	6.513
7	6.364	−0.8779	0.1304	—	6.662	−0.5264	6.513

a) Present work. b) Ref. 2. The values are recalculated by us. c) Ref. 5.

Table 3. The upper and lower bounds for dispersion force constant C_8 between two hydrogen atoms in the ground state (Reliable value=124.3991[c])

n	$C_8^{low}(n)=-E_2^{up}(n)$ [a]	λ	μ	$C_8^{low}(n)$ [b] ($\mu_1=1$)	$C_8^{up}(n)=-E_2^{low}(n)$ [a]	λ	$\{C_8^{low}(n)+C_8^{up}(n)\}/2$
0	119.749	−0.9225	0.2306	115.714	129.837	−0.6103	124.793
1	120.035	−0.9136	0.2262	—	127.368	−0.5552	123.702

a) Present work. b) The value obtained by us. c) Ref. 10.

present treatment may be expected to be effective for larger molecular systems.

Appendix A

In deriving the upper bounds, we considered the following form of $\tilde{\phi}_1$:

$$\tilde{\phi}_1(n,\lambda,\mu) = -\sum_{i>0}^{n}(H_{1i}/\varepsilon_i)\phi_0^{(i)} + \lambda\sum_{i=n+1}^{\infty}(1+\mu E_0^{(i)}/E_0)H_{1i}\phi_0^{(i)}. \quad \text{(A-1)}$$

Now, let us refer to the first-order function derived by Lennard-Jones in order to compare it with the $\tilde{\phi}_1$ of Eq. (A-1). The function derived by Lennard-Jones is:[11]

$$\phi_1 = (H_1-E_1)\phi_0/E_0 + \sum_{i>0}^{\infty}E_0^{(i)}H_{1i}\phi_0^{(i)}/\{E_0(E_0-E_0^{(i)})\}, \quad \text{(A-2)}$$

which is reduced to:

$$\phi_1 = -\sum_{i>0}^{n}(H_{1i}/\varepsilon_i)\phi_0^{(i)} + (1/E_0)\sum_{i=n+1}^{\infty}\{1+E_0^{(i)}/(E_0-E_0^{(i)})\}H_{1i}\phi_0^{(i)}. \quad \text{(A-3)}$$

When we compare Eq. (A-1) with Eq. (A-3), it may be seen that λ and μ are taken to correspond to $1/E_0$ and the average of $E_0/(E_0-E_0^{(i)})$ respectively. If we also choose $\mu_i=1+\mu E_0^{(i)}/E_0$ for the derivation of lower bounds, there appears an integral such as $\langle\phi_0|zH_0^4z|\phi_0\rangle$ which diverges. Hence, the simplest form, $\mu_i=1$, is adopted for any i.

Appendix B

The inequality in Eq. (13) can be established not for a completely arbitrary function, but for a restricted one, under the conditions of Eq. (12). Since our variational function satisfies Eq. (12) only approximately, there remains the necessity of estimating the resulting error.

Using an arbitrary $\tilde{\Phi}$ function, Θ, which strictly satisfies the next relation:

$$\langle\Theta|\Psi^{(k)}\rangle = 0 \quad (k=1,2,\cdots,n), \quad \text{(B-1)}$$

may be rewritten as follows:

$$\Theta = \tilde{\Phi} - \sum_{i>0}^{n}\langle\Psi^{(i)}|\tilde{\Phi}\rangle\Psi^{(i)}. \quad \text{(B-2)}$$

Then, instead of Eq. (13), the inequality;

$$\langle(H-E^{(0)})\tilde{\Phi}|(H-E^{(n+1)})\tilde{\Phi}\rangle \geqq \sum_{i>0}^{n}|\langle\Psi^{(i)}|\tilde{\Phi}\rangle|^2(E^{(i)}-E^{(0)})(E^{(i)}-E^{(n+1)}), \quad \text{(B-3)}$$

may easily be obtained. Setting the exact $\Psi^{(i)}$ as:

$$\Psi^{(i)} = \phi_0^{(i)} + \phi_1^{(i)} + \cdots = \phi_0^{(i)} + \sum_{j\neq i}^{\infty}\{\langle\phi_0^{(j)}|H_1|\phi_0^{(i)}\rangle/(E_0^{(i)}-E_0^{(j)})\}\phi_0^{(j)} + \cdots, \quad \text{(B-4)}$$

ans setting $\tilde{\Phi}$ as $\tilde{\Psi}$ in Eq. (14), we obtain:

$$\langle\tilde{\Phi}|\tilde{\Psi}^{(k)}\rangle = \langle\tilde{\Psi}|\Psi^{(k)}\rangle = \langle\phi_0|\phi_0^{(k)}\rangle + \langle\phi_0|\phi_1^{(k)}\rangle + \langle\tilde{\phi}_1|\phi_0^{(k)}\rangle + \langle\tilde{\phi}_1|\phi_1^{(k)}\rangle + \cdots \quad (k=1,2,\cdots,n). \quad \text{(B-5)}$$

It can be easily seen that the first term on the right-hand side of Eq. (B-5) vanishes, and that the second and the third terms cancel each other out when we use the form of $\tilde{\phi}_1$ in Eq. (14) and that of $\phi_1^{(i)}$ in Eq. (B-4). As a result, the first non-vanishing term in Eq. (B-5) is of the second-order of the perturbation. Therefore, the value of the right-hand side of Eq. (B-3) is of the fourth-order of the perturbation and can be neglected as long as we consider the second-order energy.

References

1) E. A. Hylleraas, *Z. Phys.*, **65**, 209 (1930).
2) J. Goodisman, *J. Chem. Phys.*, **47**, 2707 (1967).
3) S. Prager and J. O. Hirschfelder, *ibid.*, **39**, 3289 (1963).
4) G. Temple, *Proc. Roy. Soc., Ser. A*, **119**, 276 (1928).
5) P. Lindner and P. O. Löwdin, *Intern. J. Quant. Chem.*, **IIs**, 161 (1968).
6) W. H. Miller, *J. Chem. Phys.*, **50**, 2758 (1969).
7) See Appendix A.
8) See Appendix B.
9) L. Pauling and E. B. Wilson, Jr., "Introduction to Quantum Mechanics with Application to Chemistry," McGraw Hill Book Co., Inc., New York (1935), p. 384.
10) W. Kołos, *Intern. J. Quant. Chem.*, **1**, 169 (1967).
11) J. E. Lennard-Jones, *Proc. Roy. Soc., Ser. A*, **129**, 598 (1930).

The Crystal Structure of the Cupric Complex with Succinimide. II. Potassium Tetrakis(succinimidato)copper(II) Hexahydrate and Lithium Tetrakis(succinimidato)copper(II) Monohydrate

Tomitake TSUKIHARA, Yukiteru KATSUBE, Kumiko FUJIMORI, Kiyoshi KAWASHIMA, and Yoshiaki KAN-NAN

Faculty of Engineering, Tottori University, Koyama 1-1, Tottori, 680

(Received November 9, 1973)

As part of a program for the study of the crystal structure of copper(II)-complex with succinimide, the crystal structures of potassium tetrakis(succinimidato) copper(II) hexahydrate and lithium tetrakis(succinimidato) copper-(II) monohydrate have been determined by means of X-ray analysis. In the potassium-salt, the copper atom has a square planar coordination and the potassium ion has a trigonal prismatic environment formed by six oxygen atoms. In the lithium-salt, the copper atom has a flattened tetrahedral coordination, and each lithiun ion is tetrahedrally surrounded by four oxygen atoms. The conformational difference between the complex anion of the potassium-salt and that of the lithium-salt seems to result from the different sizes of the alkali-metal ions.

As part of a systematic study of the crystal structures of the copper(II)-complexes, crystal structure analyses of the $M_2(Cu(sucim)_4)nH_2O$ type, where M indicates an alkalimetal, have been planned to find the conformational features around the metals that might be responsible for the difference between the crystal structures of the complexes. The first investigation in this series was the crystal structure determination of $Cs_2(Cu(sucim)_4)2H_2O$.[1] In this paper, the crystal structures of $K_2(Cu(sucim)_4)6H_2O$ and $Li_2(Cu(sucim)_4)H_2O$ will be described.

Experimental and Structure Determination

*Potassium Tetrakis(succinimidato)copper(II) Hexahydrate.** Pink-colored crystals in the form of platelets were prepared by the method described by Tschugaeff.[2] Since the crystals effloresce easily in air, the crystals were sealed in glass capillaries for the X-ray work.

Preliminary Weissenberg and oscillation photographs showed the crystals to be triclinic; the crystal data are listed in Table 1.

For the 0kl–5kl layers about the *a* axis, intensity data were collected by the equi-inclination Weissenberg method with Cu$K\alpha$ radiation. A large crystal with the approximate dimensions of $0.6\times0.6\times0.2$ mm^3 was used for the collection of the data, because the crystal of a suitable size for the X-ray work was consumed within one layer's exposure. Therefore, the data collected were not of a high degree of accuracy. A total of 1515 reflections was obtained, and the intensities were estimated visually with a standard scale. The usual Lorentz and polarization corrections were applied, but no correction was made for absorption and extinction. Corrections for variation in spot-size on the high-layer-line photographs were made by the method presented by Phillips.[3]

Table 1. Crystal data

	Potassium-salt	Lithium-salt
Molecular formula:	$K_2CuC_{16}H_{28}N_4O_{14}$	$Li_2CuC_{16}H_{18}N_4O_9$
Molecular weight:	642.71	487.77
Crystal system:	Triclinic	Monoclinic
Space group:	$P\bar{1}$	$P2_1/a$
Cell dimension:	$a=8.51\pm0.03$Å	$a=24.61\pm0.02$Å
	$b=8.50\pm0.03$	$b=9.65\pm0.03$
	$c=9.28\pm0.02$	$c=8.58\pm0.02$
	$\alpha=97.4°\pm0.3°$	$\beta=94.4°\pm0.2°$
	$\beta=100.4°\pm0.2°$	
	$\gamma=79.9°\pm0.2°$	
Chemical units per unit cell:	1	4
D(calculated):	1.64 g/cm^3	1.59 g/cm^3
D(observed):	1.63 g/cm^3	1.57 g/cm^3

The space group was initially assumed to be $P\bar{1}$, implying a center of symmetry in the complex. The copper atom was placed at the origin of the unit cell, and approximate coordinates for the remaining atoms were obtained by Patterson synthesis and successive Fourier syntheses. The atomic positions and temperature factors were refined by a block-diagonal least-squares method. After several refinement cycles, the structure converged, with an *R*-value of 16%. The refinement with the *P*1 space group did not improve the *R* value and showed no tendency to destroy the center of symmetry. Thus, the space group was confirmed to be $P\bar{1}$.

All the atomic scattering factors were taken from the "International Tables for X-ray Crystallography."[4] Those of the copper and potassium atoms were corrected for anomalous dispersion, and anisotropic temperature factors were introduced for the copper and potassium atoms.

The final composite electron density and atomic parameters are shown in Fig. 1 and Table 2 respectively. The mean estimated standard deviations of the positional para-

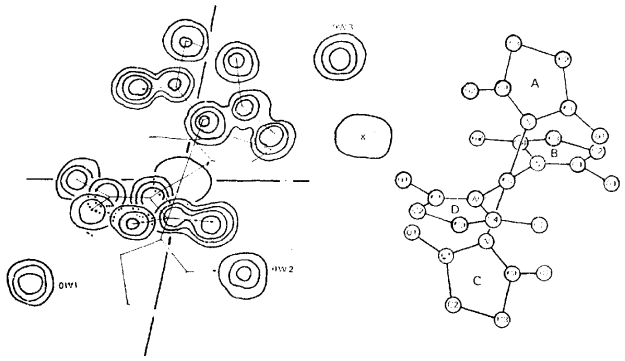

Fig. 1. The composite electron-density map and atomic numbering for $K_2(Cu(sucim)_4)6H_2O$. The contours are drawn at intervals of 2.0 e/Å^3 starting at 0.5 e/Å^3.

* The term 'potassium-salt' will be utilized in this paper to describe this complex.

Table 2. Final atomic parameters of the potassium-salt

Atom	x	y	z	B	Atom	x	y	z	B
Cu	0.0000	0.0000	0.0000		K	−0.3971	0.1481	−0.0866	
OA1	0.2882	0.1756	0.1649	3.93	OA2	−0.2128	0.3160	0.0529	2.26
OB1	0.3555	0.0035	−0.1573	4.13	OB2	−0.1317	0.1497	−0.2928	2.56
NA	0.0391	0.2081	0.0969	0.89	NB	0.0874	0.0667	−0.1927	1.03
CA1	0.1574	0.2566	0.1676	1.43	CA2	0.1034	0.4285	0.2288	1.90
CA3	−0.0677	0.4773	0.1958	1.31	CA4	−0.0828	0.3277	0.1140	1.59
CB1	0.2305	0.0623	−0.2331	2.38	CB2	0.2859	0.1081	−0.3840	2.77
CB3	0.1265	0.1552	−0.4267	2.18	CB4	0.0161	0.1261	−0.3028	1.19
OW1	0.4384	0.3551	0.3648	3.71	OW2	−0.2808	0.3367	−0.4968	5.35
OW3	0.4580	0.4261	−0.1648	4.59					

Atom	B_{11}	B_{22}	B_{33}	B_{12}	B_{13}	B_{23}
Cu	0.0042	0.0021	0.0027	−0.0014	−0.0098	0.0019
K	0.0064	0.0050	0.0067	−0.0029	−0.0107	0.0048

Temperature factor $=\exp(-(h^2B_{11}+k^2B_{22}+hl^2B_{33}+hkB_{12}+hlB_{13}+klB_{23}))$
or $=\exp(-B(\sin\theta/\lambda)^2)$

Table 3. Final atomic parameters of the lithium-salt

Atom	x	y	z	B	Atom	x	y	z	B
Cu	0.1240	0.2090	0.2258		Li1	0.0488	0.0464	−0.0449	2.93
Li2	0.1403	0.4808	0.4491	3.87	OA1	0.0687	0.4033	0.4817	3.80
OA2	0.0073	0.0629	0.1452	2.57	OB1	0.1886	0.3489	0.5324	3.60
OB2	0.1393	−0.0908	0.3990	3.14	OC1	0.1166	−0.0461	−0.0149	3.03
OC2	0.2567	0.1799	0.2426	3.37	OD1	0.0565	0.2343	−0.1258	5.05
OD2	0.1419	0.5222	0.2208	2.95	NA	0.0510	0.2250	0.3052	2.22
NB	0.1562	0.1405	0.4324	1.63	NC	0.1774	0.0943	0.1226	2.19
ND	0.1066	0.3503	0.0632	2.26	CA1	0.0382	0.3104	0.4242	2.33
CA2	−0.0159	0.2620	0.4831	2.83	CA3	−0.0375	0.1559	0.3686	2.82
CA4	0.0073	0.1436	0.2634	2.23	CB1	0.1839	0.2180	0.5392	2.89
CB2	0.2114	0.1350	0.6713	2.96	CB3	0.1947	−0.0138	0.6300	2.65
CB4	0.1583	0.0069	0.4751	1.57	CC1	0.1630	−0.0185	0.0439	2.77
CC2	0.2072	−0.1285	0.0453	3.89	CC3	0.2571	−0.0420	0.1100	3.50
CC4	0.2311	0.0891	0.1599	1.62	CD1	0.0758	0.3440	−0.0663	3.21
CD2	0.0659	0.4768	−0.1452	3.74	CD3	0.0923	0.5811	−0.0275	5.21
CD4	0.1194	0.4823	0.0946	2.93	OW	0.1524	0.6573	0.5481	2.93

Atom	B_{11}	B_{22}	B_{33}	B_{12}	B_{13}	B_{23}
Cu	0.0006	0.0029	0.0042	0.0005	−0.0006	−0.0015

meters are 0.02 Å for the carbon, nitrogen, and oxygen atoms and 0.006 Å for the potassium atom.

*Lithium Tetrakis(succinimidato)copper(II) Monohydrate.*** Blue-colored, needle-like crystals were prepared by the same procedure as was used for the potassium-salt. Since the crystals were hygroscopic, the crystals for the X-ray work were sealed in glass capillaries. The crystals were monoclinic, with a space group of $P2_1/a$; the cell dimensions are shown in Table 1.

The intensity data were collected for the crystal ($0.05\times 0.40\times 0.05$ mm^3) rotating about the c axis, allowing the observation of 1869 independent reflections ($l=0$—6). The procedure of the determination of the structure was similar to that used in the case of the potassium-salt. The position of the copper atom was deduced from Patterson synthesis; a Fourier synthesis based on the phases determined by the copper atom revealed all of the non-hydrogen atoms except the lithium ions. The positions of the lithium ions were found by a difference Fourier synthesis. The refinement was carried out by the block-diagonal least-squares method; the final R value was 13%. The final atomic parameters are shown in Table 3. The estimated standard deviations of the

** The term 'lithium-salt' will be utilized in this paper.

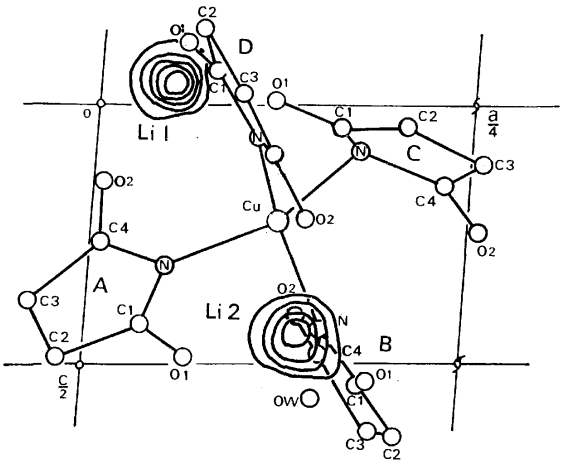

Fig. 2. The composite difference electron density map for $Li_2(Cu(sucim)_4)H_2O$. The contributions of the hydrogen atoms and lithium ions were excluded from the calculated structure factors. Two lithium ions are clearly shown in the map. The contours are drawn at intervals 0.05 e/Å^3 starting at 0.05 e/Å^3 for lithium ions, and there is no other peak higher than 1.2 e/Å^3.

positional parameters are 0.05 Å for the lithium ions, 0.02 Å for the carbon, nitrogen, and oxygen atoms and 0.003 Å for the copper atom.

Results and Discussion

Geometry of the Coordination around the Copper Atom. In the present series of complexes, each of the copper atoms is coordinated by four nitrogen atoms from four succinimides. The bond lengths and angles around the copper atoms for the potassium- and lithium-salts are shown in Fig. 3.

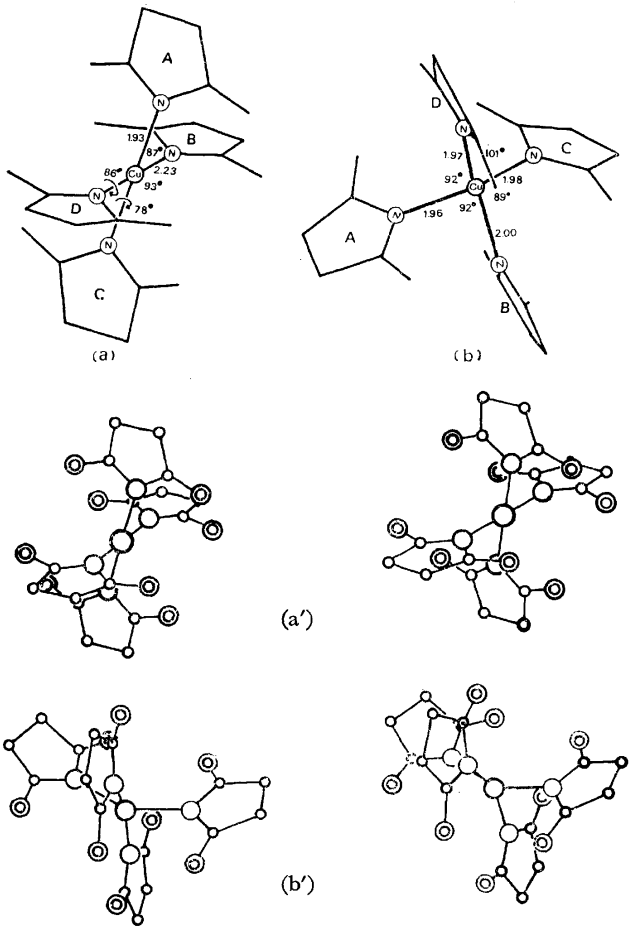

Fig. 3. The geometry around the copper atom.
(a) and (a'): Potassium-salt
(b) and (b'): Lithium-salt
(a') and (b') are the stereographic illustrations.

In the potassium-salt, the coordination around the copper atom is square planar and the complex anion is centrosymmetric. The coordination plane defined by the copper atom and four nitrogen atoms is, therefore, exactly planar. Although a distortion from an ideal square planar configuration may be evident in the different lengths of the Cu–N bonds and in the different angles of the N–Cu–N's, this can not be discussed in detail because of the low accuracy of the present analysis. Each plane of the succinimide residues is tilted by 82° to the coordination plane. Thus, the whole structure of the complex anion of the potassium-salt has a slightly distorted D_{4h} symmetry. This configuration for the anion agrees with that proposed spectroscopically by Yamada *et al.*[5]

In the lithium-salt, the coordination around the copper atom may be considered as either a distorted square planar or a distorted flattened tetrahedron. This configuration of the coordination resembles that of bis(*N*-ethyl-salicylaldiminato)copper(II) monohydrate[6] and that of 2,2'-biphenylbis(2-iminomethylenephenolato)copper(II).[7] The bond angles around the copper atoms in these complexes are listed in Table 4. Such a coordination polyhedron has generally been described as a tetrahedron distorted in the flattened form.

TABLE 4. BOND ANGLES AROUND THE COPPER ATOM

Crystal I*		Crystal II*		Crystal III*
N(A)–Cu–N(B)	92°	O–Cu–N	93°	
N(A)–Cu–N(D)	92	O'–Cu–N	91	
N(B)–Cu–N(C)	89	O–Cu–N'	93	
N(C)–Cu–N(D)	101	O'–Cu–N'	94	
Average	94		93	92°
N(A)–Cu–N(C)	148	O–Cu–O'	152	
N(B)–Cu–N(D)	155	N–Cu–N'	157	
Average	152		155	152

* Crystal I, II, and III represent lithium tetrakis(succinimidato)copper(II), monohydrate, bis(*N*-ethylsalicylaldiminato)copper(II),[6] and 2,2'-biphenylbis(2-iminomethylenephenolato)copper(II),[7] respectively.

Environment of the Alkali-metal Ion. The distances around the alkali-metal ions are shown in Fig. 4. The mean distance from the alkali-metal ion to the oxygen atom in the individual complex is in fairly good agreement with the sum of their ionic radii: 3.11 Å for Cs–O, 2.71 Å for K–O, and 1.93 Å for Li–O respectively.

In the case of the potassium-salt, each of the K^+ ions is surrounded by six oxygen atoms at the corners of a distorted trigonal prism. One of these oxygen atoms belongs to the water molecule, while the remaining

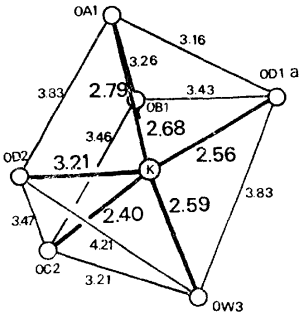

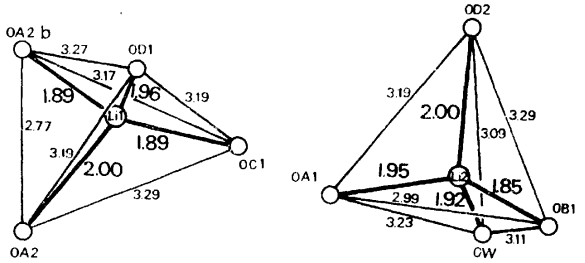

Fig. 4. The environment of the alkali-metal ion.

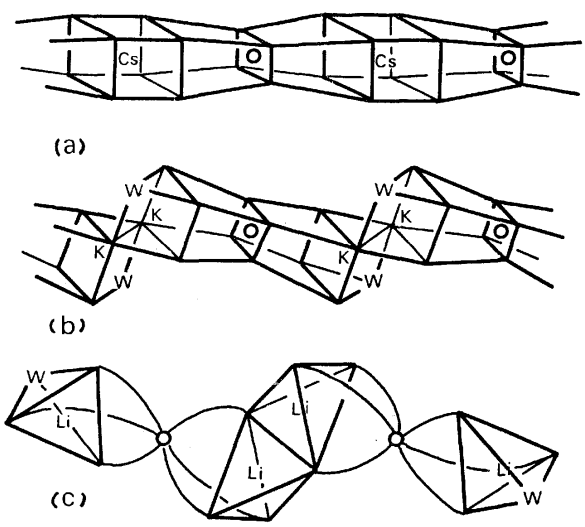

Fig. 5. The arrangements of coordination polyhedra around the alkali-metal ions in (a) cesium-salt, (b) potassium-salt and (c) lithium-salt. Circle and W represent the copper atom and the water oxygen atom, respectively.

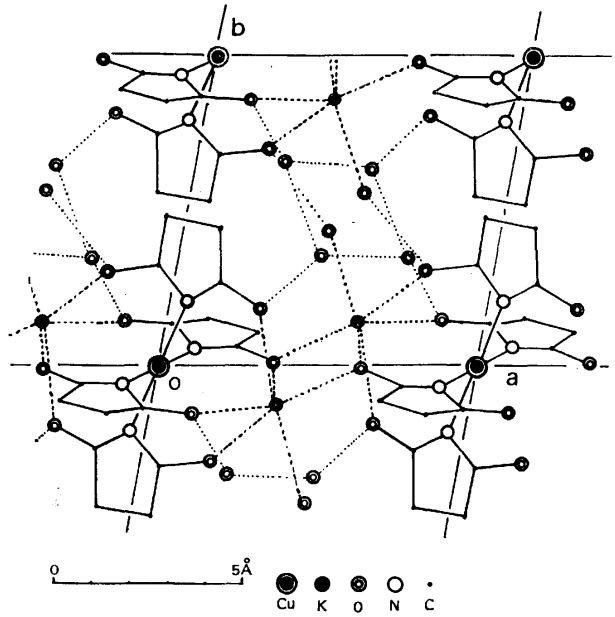

Fig. 6. The crystal structure of potassium-salt.

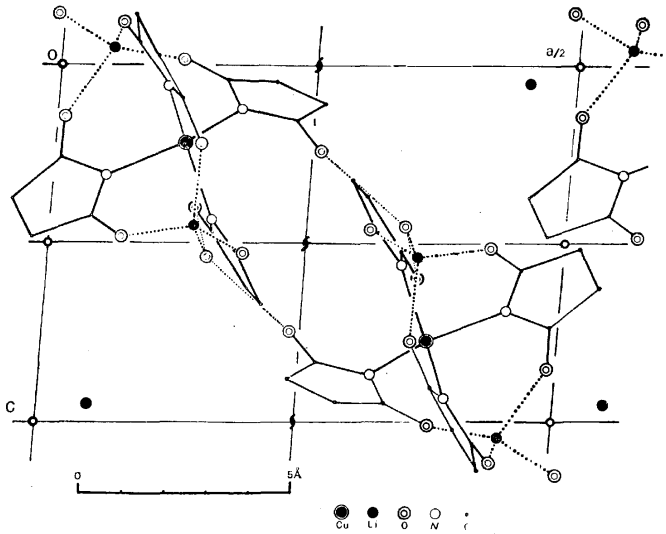

Fig. 7. The crystal structure of lithium-salt.

five are the carbonyl oxygen atoms. Of these five carbonyl oxygen atoms, the four lying on the corners of a rectangular face of the prism, OA1, OB1, OC2, and OD2, belong to the same complex anion. Two trigonal prisms related to each other by a center of symmetry share an edge. Thus, an endless chain having the –A–K·K– sequence, where A indicates the complex anion and where K·K denotes two polyhedra sharing an edge, is formed. The chain formed by electrostatic interactions between the K^+ ions and the oxygen atoms is schematically shown in Fig. 5. The crystal structure consists of these chains held together by hydrogen bonds involving the water molecules.

In the case of the lithium-salt, two independent Li^+ ions exist in the structure. Both lithium ions have tetrahedrally-distributed oxygen neighbors; $Li(1)^+$ is surrounded by four carbonyl oxygen atoms, while $Li(2)^+$ has three carbonyl oxygen atoms and one water oxygen atom as neighbors. Of the eight carbonyl oxygen atoms in the complex anion, three coordinate to $Li(1)^+$, another three coordinate to $Li(2)^+$, and the remaining two are free. Such an arrangement of the carbonyl oxygen atoms with respect to the Li^+ ions may impose a large distortion from the D_{4h} symmetry upon the structure of the complex anion. Two tetrahedra related to each other by a center of symmetry are condensed by sharing an edge. The compositions of Li–A–Li·Li–A–Li, which are formed by electrostatic interactions between the Li^+ ions and the oxygen atoms, are linked together to form an infinite chain by the hydrogen bonds between the water molecules and the carbonyl oxygen atoms which are free from the Li^+ ions.

The crystal structures and the hydrogen-bonding schemes are illustrated in Figs. 6 and 7.

Consequently, it appears that the size of the alkali-metal ion may govern the structure of the complex.

The authors wish to express their thanks to Dr. Tamaichi Ashida for permission to use his program and to Dr. Seiko Komorita for her valuable discussions and for kindly supplying the samples.

References

1) T. Tsukihara, Y. Katsube, K. Fujimori, and T. Ito, This Bulletin, **45**, 2959 (1972).
2) L. Tschugaeff, *Ber.*, **39**, 2897 (1905).
3) D. C. Phillips, *Acta Crystallogr.*, **7**, 746 (1954).
4) "International Tables for X-ray Crystallography," Vol. III, Birmingham (1962), p. 202.
5) S. Yamada and S. Miki, This Bulletin, **36**, 680 (1963).
6) C. Panattoni, G. Borbieri, and R. Graziani, *Acta Crystallogr.*, **23**, 537 (1967).
7) T. P. Cheeseman, D. Hall, and T. N. Waters, *Proc. Chem. Soc.*, **1963**, 379.

Isoelectric Point of Manganese Oxide

Tetsuo MORIMOTO and Shigeharu KITTAKA*

Department of Chemistry, Faculty of Science, Okayama University, Tsushima, Okayama 700
**Department of Chemistry, Faculty of Science, Okayama College of Science, Ridaicho, Okayama 700*

(Received December 3, 1973)

The isoelectric point (IEP) of manganese oxide is measured on samples prepared by heating β-MnO_2 and amorphous manganese oxide, $MnO_{1.75}$, at temperatures from 200 to 1400 °C. The IEP values thus obtained are characteristic of each stage of the oxidation of manganese oxide; that is, <5.1 for MnO_2, 7.6—9.0 for α-Mn_2O_3, and 3.3—5.2 for Mn_3O_4. These values can be explained by the electrostatic interaction theory introduced by Parks, in which the CFSE correction is eliminated. It is also found that manganese ions with specific valencies are responsible for the electrification of the surfaces of manganese oxide.

In order to clarify the origin of the electrification of metal oxides in aqueous media, the present authors have measured the electrokinetic potential (ζ-potential) or isoelectric point (IEP) of TiO_2,[1,2] Al_2O_3, Cr_2O_3, and Fe_2O_3[3-5] in electrolyte solutions. The results obtained indicate that the electrification of these metal oxides is generally determined by the electrostatic interaction between a metal ion on the solid surface and the H^+ ion in the surface hydroxyl group bonded to the metal ion,[4] to which the crystal structure of the oxide and the valency of the metal ion concerned are decisively responsible. A number of papers[6-8] have been published concerning the study of the IEP of metal oxides, but a very few works have related IEP to the crystal structure of a metal oxide and the valency of the component metal ion, which changes step-by-step upon heat treatment.[4,9]

The heat treatment of manganese oxide gives three types, which differ in the valency of the manganese ion, *i.e.*, MnO_2, Mn_2O_3, and Mn_3O_4. Fuerstenau *et al.*[10] have studied the electrification of manganese oxide, but only that of MnO_2. The purpose of this study is to measure the IEP of three kinds of manganese oxides which differ in composition, and to investigate the origin of the electrification of the oxides.

Experimental

Materials. Two samples of manganese oxide were used in this study. One was β-MnO_2 (MI), which was prepared by the pyrolysis of $Mn(NO_3)_2$ by heating it at 160 °C for 500 hr in air. The other was amorphous manganese oxide (MII), which was precipitated by mixing a 1 mol/l $Mn(NO_3)_2$ solution with 3 mol/l ammonia water in the presence of H_2O_2. The two samples were treated at various temperatures from 200 to 1400 °C for 3 hr in air, and then washed with distilled water until the ionic impurities in the filtrate disappeared; this resulted in the complete hydration of the surfaces.

The crystal structure of the samples was analyzed by the X-ray diffraction method, and the thermal analysis was carried out by means of the TGA method, in which the temperature was raised at the rate of 20 °C/min.

Measurement of IEP. The IEP of the samples was obtained by measuring the ζ-potential in aqueous solutions of various pH values. The ζ-potential was measured at 25.0 °C by using the streaming potential method, the Helmholtz-Smoluchowski equation being used as has been described previously.[3] The pH value was varied with HCl and NaOH. In order to keep the thickness of the electrical double layer constant and in order to eliminate the effect of surface conductance on the ζ-potential measurement,[11,12] the ionic strength was adjusted at 10^{-3} mol/l by using a NaCl solution. The deionized water used for the experiments was further purified by double distillation from an alkaline permanganate solution; prior to the measurement N_2 was bubbled in to remove any dissolved carbon dioxide.

Results and Discussion

Figure 1 shows the TGA data of the samples. It may be seen from Fig. 1 that the decomposition of MI starts at 540 °C and finishes at 650 °C to form Mn_2O_3, and that the latter decomposes at 920 °C to produce Mn_3O_4. On the other hand, the first sharp decomposition of MII occurs between 420 and 560 °C, while the second one occurs in the same temperature range as that of MI. X-Ray analysis showed that the MI sample has the structure of β-MnO_2, whereas the MII sample is amorphous; it has a nonstoichiometric composition, $MnO_{1.75}$, at room temperature, as is found by calculating from the data in Fig. 1. Furthermore, it was found that both samples represent α-Mn_2O_3 from 600 to 900 °C and Mn_3O_4 over 1000 °C, while the crystallinity of the α-Mn_2O_3 and Mn_3O_4 prepared from MII is more excellent than that prepared from MI.

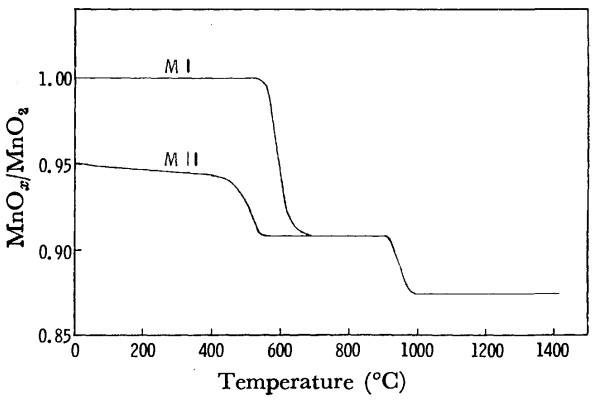

Fig. 1. TGA curve of manganese oxides.

The ζ-potential of MI is plotted against the pH value in Fig. 2. It may be seen clearly from Fig. 2 that the pH value of the zero point of charge, *i.e.*, IEP, changes remarkably with the pretreatment temperature of the samples. The IEP of MI and MII is plotted in Fig. 3 as a function of the temperature of pretreatment.

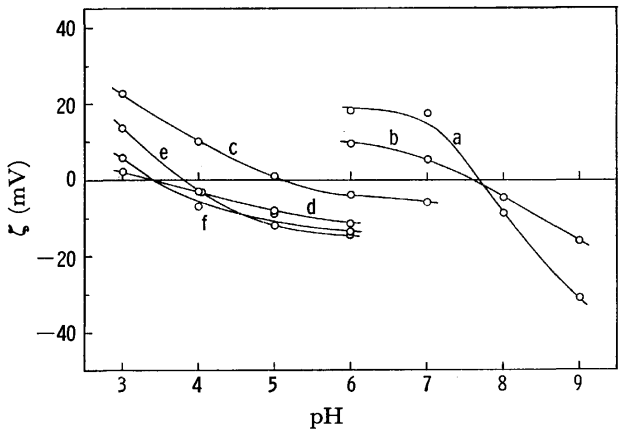

Fig. 2. ζ-potential of manganese oxide MI against pH, pretreated at a 500, b 800, c 900, d 1000, e 1200 and f 1400 °C.

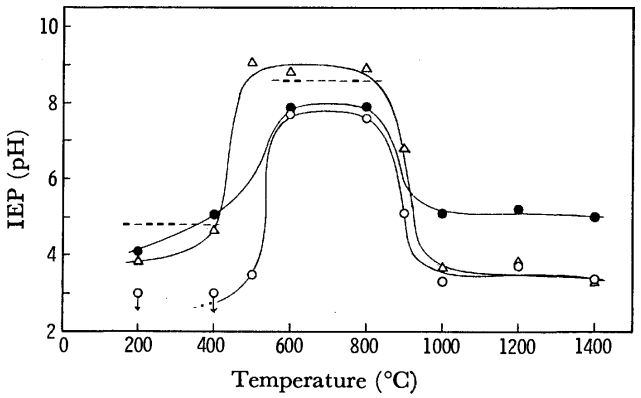

Fig. 3. IEP of manganese oxides against pretreatment temperature, ○ MI, ● crushed MI, and △ MII.

In this figure, the IEP of the samples which were obtained by crushing MI in an agate mortar is also added. Since the measurement of the ζ-potential of the samples pretreated below 400 °C (below 500 °C in the case of MI), however, was very difficult because of the high electric conductivity of the solids, the IEP in this temperature range was determined from the point where the sign of the streaming potential changed.

The comparison of the change in composition (Fig. 1) with the change in IEP (Fig. 3) makes it possible to infer that each oxidation state of manganese oxide has a characteristic value of IEP: that is, <5.1 for MnO_2, 7.6—9.0 for α-Mn_2O_3, and 3.3—5.2 for Mn_3O_4. Parks[6] has introduced a simi-empirical relation which describes the IEP of metal oxides can be expressed by this equation:

$$\text{IEP} = A - 11.5\left[\frac{Z}{R} + 0.0029a\right]. \quad (1)$$

Here, A is a constant which depends on the extent of surface hydration and the coordination number of surface metal ions, being 18.6 for fully-hydroxylated surfaces of metal oxides containing octahedrally-coordinated metal ions; Z is the valency of the metal ion. R is the distance between a surface metal ion and the H^+ ion in the surface hydroxyl group attached to the metal ion, that is, the sum of the radius of the metal ion and the diameter of the adjacent O^{2-} ion. a is the crystal-field stabilization energy for the hydration of metal ions, the second term in the bracket being the correction term for the coulombic interaction between a H^+ ion and the surface of a metal oxide. A preliminary calculation indicates that this correction is generally small in the present samples.

By introducing the crystallographic data into Eq. (1), IEP can be calculated to be 4.8 and 8.6 for β-MnO_2 and α-Mn_2O_3 respectively; they are represented as dotted lines in Fig. 3. Figure 3 shows that the observed and calculated values of IEP agree well with each other except for the data on uncrushed MI below 500 °C. It is interesting to note that IEP approaches more closely to the calculated value when the sample is crushed. This may be due to the fact that, on pyrolyzing and oxidizing the original samples at 160 °C in air, an excess of oxygens is bonded to surface metal ions, thus giving rise to a higher oxidation state of the metal ions.

As is well known, the structure of Mn_3O_4 is a spinel exhibiting the tetragonal form. The oxidation state of manganese ions and their coordination number to oxygen in Mn_3O_4, however, are subject to dispute; the formulas of $Mn^{2+}[Mn_2^{3+}]O_4$,[13] $Mn^{3+}[Mn^{2+}Mn^{3+}]O_4$,[14] and $Mn^{2+}[Mn^{2+}Mn^{4+}]O_4$[15] have been proposed, where the manganese ions in and outside the bracket are those of the coordination numbers of 6 and 4 respectively. The calculation of IEP for every type of these manganese ions according to Eq. (1) gives the values of 12.2, 9.6, and 5.8 for the octahedrally-coordinated Mn^{2+}, Mn^{3+} and Mn^{4+}, and 9.2 and 5.6 for the tetrahedrally-coordinated Mn^{2+} and Mn^{3+}, respectively. The observed value, 5.1, of IEP on the crushed MI approximates the calculated values, 5.6 and 5.8. This suggests that the octahedrally-coordinated Mn^{4+} and/or tetrahedrally-coordinated Mn^{3+} ions will determine the IEP of the samples. On the other hand, the IEP of uncrushed MI and MII are considerably smaller than these calculated values. This fact may be considered to depend on the characteristic features of the surfaces of Mn_3O_4 treated at elevated temperatures. If the Mn^{4+} ions tetrahedrally coordinated by oxygens are formed on the surfaces, then the calculated IEP will result in the value of 2.1. Thus, it may be possible to infer that the tetrahedrally-coordinated Mn^{4+} ions coexist along with tetrahedrally-coordinated Mn^{3+} and/or octahedrally-coordinated Mn^{4+} ions on the actual surface of Mn_3O_4.

References

1) T. Morimoto and M. Sakamoto, This Bulletin, **36**, 1369 (1963).
2) T. Morimoto and M. Sakamoto, *ibid.*, **37**, 719 (1964).
3) T. Morimoto and S. Kittaka, *ibid.*, **46**, 3040 (1973).
4) S. Kittaka, "Isoelectric Point of Al_2O_3, Cr_2O_3, and Fe_2O_3 I." *J. Colloid Interface Sci.*, in press.
5) S. Kittaka, "Isoelectric Point of Al_2O_3, Cr_2O_3, and Fe_2O_3 II." *J. Colloid Interface Sci.*, in press.
6) G. A. Parks, *Chem. Rev.*, **65**, 177 (1965).
7) S. M. Ahmed and D. Maksimov, *J. Colloid Interface Sci.*, **29**, 97 (1969).
8) P. H. Tewari and A. W. McLean, *ibid.*, **40**, 267 (1972).

9) V. Pravdic and S. Sotman, *Croat. Chim. Acta*, **35**, 247 (1963).
10) T. W. Healy, A. P. Herring, and D. W. Fuerstenau, *J. Colloid Interface Sci.*, **21**, 435 (1966).
11) J. Th. G. Overbeek and P. W. O. Wijga, *Rec. Trav. Chim.*, **65**, 556 (1946).
12) T. Morimoto and S. Kittaka, *J. Colloid Interface Sci.*, **44**, 289 (1973).
13) N. N. Greenwood, "Ionic Crystals, Lattice Deffects and Nonstoichiometry," p. 101 Chem. Pub. Co., New York (1968).
14) T. J. Gray, "High Temperature Oxides," Vol. 5, Part 4, ed. by A. Alper, p. 84 Academic Press (1971).
15) F. C. Romeijn, *Philips Research Rep.*, **8**, 304 (1954).

Charge-transfer and Proton-transfer in the Formation of Molecular Complexes. IX.[1] Polynitrobenzoic Acid Complexes with Aromatic Monoamines

Yoshio MATSUNAGA and Ryuzo OSAWA*

Department of Chemistry, Faculty of Science, Hokkaido University, Sapporo 060

(Received December 7, 1973)

When 2,4,6-trinitrobenzoic acid is combined with aromatic monoamines, true benzoates are mostly formed. However, not only a white true benzoate, but also a red 2: 1 complex of the CPT type, in which charge-transfer and proton-transfer interactions operate simultaneously between the component molecules, were obtained with aniline. In addition, the brown 2,4,5-trimethylaniline complex reported by Noelting and Sommerhoff was found to be of a similar nature. The phenomenon of complex isomerism was observed upon combination with *o*-chloroaniline; that is, the colorless salt isomerizes into an orange-colored charge-transfer complex at about 133 °C. Only the complexes with *p*-dimethylaminobenzaldehyde and *o*-nitroaniline, which have the lowest pK_a values among the amines examined, and those with the halogenated 2-naphthylamines are of the charge-transfer type. The 3,5-dinitrobenzoic acid complexes were also examined. Complexes of the CPT type with a 3: 2 composition were isolated with aniline and *p*-toluidine.

The combination of an aromatic amine and a polynitrophenol is known to form a true phenolate by acid-base interaction or a charge-transfer (CT) complex by electron donor-acceptor interaction. In addition, some interesting phenomena have been noted with the complexes of such bifunctional component molecules. Many years ago, Hertel demonstrated that the same components, if appropriately chosen, can form either phenolates or CT complexes, depending upon the ambient conditions.[2] This phenomenon was named "complex isomerism" by this author. Further pairs of complex isomers have been presented in a previous paper of the present series.[3] Secondly, our study of the vibrational and electronic spectra of the orange-colored 1-naphthylamine-picric acid (2: 1) complex revealed that a proton is transferred from the acid to the amine, and that the interaction between the picrate ion and the second amine molecule is capable of producing a CT absorption band.[4] For brevity, such a complex was denoted as a complex of the CPT type because of the simultaneous operation of CT and proton-transfer (PT) interactions between the component molecules. Many complexes of a similar nature, including the brick red *o*-toluidine–picric acid (1: 1), the reddish orange tryptophan picrate, and the orange-red *o*-toluidine-tetranitrobiphenyldiol (2: 1), have been prepared by us.[1,5-7]

Bifunctional component molecules are not limited to aromatic amines and polynitrophenol. The present work will be concerned with the behavior of polynitrobenzoic acids when subjected to complexation with aromatic monoamines. 2,4,6-Trinitrobenzoic acid, hereafter abbreviated as TNBA, was selected for this purpose, because not only its strength as an acid but also that as an electron acceptor are well comparable with those of picric acid.[8,9] The salts of TNBA with fourteen aromatic amines, including aniline, 2,4,5-trimethylaniline, *m*-nitroaniline, and naphthylamines, were prepared by Sudborough and his collaborators as early as the turn of the century.[10,11] They noted that all the salts become dark when heated and then melt, evolving a considerable quantity of gas and yielding a dark red oil. The melting points were observed to depend on the rate of heating. The red product was identified by Sudborough to be the corresponding *s*-trinitrobenzene (TNB) complex formed by the decarboxylation of TNBA.[12] Moreover, Noelting and Sommerhoff isolated a colorless salt by combining TNBA and 2,4,5 trimethylaniline in cold ethanol and a brown complex in warm methanol.[13] The nature of the latter was left unclarified. In addition, we studied the complexes of 3,5-dinitrobenzoic acid (DNBA) in the present investigation.

Experimental

Materials. The polynitrobenzoic acids, all the derivatives of aniline, and 1-naphthylamine used in this work were commercially obtained. The 1-chloro-2-naphthylamine was prepared by the procedure of Cleve,[14] and the 1-bromo- and 1,6-dibromo-2-naphthylamines, by those of Franzen and Eidis.[15] The complexes were precipitated by mixing the component compounds separately dissolved in ethanol.

Measurements. The vibrational spectra of the solid complexes were measured as hexachloro-1,3-butadiene mulls in the region from 2000 to 4000 cm^{-1} and as Nujol mineral oil mulls in the region from 1500 to 1800 cm^{-1} with a Jasco IR–G infrared spectrophotometer, and the electronic spectra of the powdered complexes sandwiched between two quartz plates in the visible region, with a Beckman DK-2A spectroreflectometer. The calorimetric curves were recorded on a Rigaku Denki differential scanning calorimeter, Model 8001 SL/C, at a heating rate of 3 °C/min. The heats of transition were estimated by comparing the peak areas with that for the transition in hexamethylbenzene, which is known to take place at 110.6 °C with ΔH=0.422 kcal/mol.[16]

Results and Discussion

TNBA Complexes. The solid complexes with the following twenty-three amines (arranged in the order of decreasing pK_a values) were found to be colorless or pale yellow, in accordance with the work by Lloyd and Sudborough:[10] *N,N*-diethyl-*m*-toluidine (pK_a= 7.12), *N,N*-diethylaniline (6.61), *p*-anisidine (5.31),

* Present address: Bridgestone Tire Co., Kodaira, Tokyo.

p-phenetidine (5.20), *N*-butylaniline (5.12), *N*-ethylaniline (5.12), *p*-toluidine (5.10), 2,4,5-trimethylaniline (4.96), *m*-xylidine (4.89), *N*-methylaniline (4.84), *m*-toluidine (4.69), aniline (4.60), *o*-anisidine (4.52), *o*-toluidine (4.39), *m*-aminophenol (4.3), *m*-anisidine (4.20), *p*-chloroaniline (4.15), 1-naphthylamine (3.96), *m*-chloroaniline (3.46), *o*-chloroaniline (2.65), *o*-iodoaniline (2.60), *o*-bromoaniline (2.53), and *m*-nitroaniline (2.46). As no experimental pK_a value is available for 2,4,5-trimethylaniline,[17] the value predicted by the equation of Clark and Perrin is used above.[18] The large shift of the carbonyl-stretching vibrational band clearly indicates that the expected PT from TNBA to the amines is taking place in these complexes. While TNBA exhibits a band at about 1730 cm^{-1}, the salts have a band around 1630 cm^{-1} attributable to the COO^- group. Additional evidence for the PT is provided by the replacement of an NH_2 pattern by a NH_3^+ pattern when the amines are primary. Furthermore, an examination of the vibrational spectrum revealed that the red decomposition product is essentially the corresponding TNB complex, as was noted by Sudborough and also by Noelting and Sommerhoff.[12,13] As has been demonstrated with picrates and 2,4-dinitrophenolates,[19] the phenomenon of complex isomerization by melting may be expected to be observed with the complexes with some amines with relatively low pK_a values if there is no decarboxylation.

In addition to the colorless trinitrobenzoate, a red complex with a 2:1 mole ratio was isolated with aniline by employing an excess of the donor component. Calcd for $2C_6H_7N \cdot C_7H_3N_3O_8$: C, 51.46; H, 3.83; N, 15.79%. Found: C, 51.39; H, 3.84; N, 15.86%. The vibrational spectrum has a carbonyl-stretching band at about 1630 cm^{-1}, indicating the PT from the acid to the amine and both the NH_2 and NH_3^+ patterns in the region from 2300 to 3500 cm^{-1}. Consequently, it is certain that this complex consists of anilinium trinitrobenzoate and aniline. The diffuse reflectance spectrum given in Fig. 1 is almost identical with that of the aniline-TNB complex. The absorption appearing upon the incorporation of the second aniline molecule is undoubtedly to be ascribed to a CT interaction between the amine molecule and the trinitrobenzoate ion. Therefore, this is a complex of the CPT type as defined in our previous paper.[5] As the acceptor-strength of TNBA is comparable with that of TNB,[9] the effect of the dissociation of the carboxyl group appears to be negligible. This conclusion is in accordance with that for the case of picric acid.[4,20] The brown 2,4,5-trimethylaniline complex reported by Noelting and Sommerhoff was found to be of a 3:2 composition. Calcd for $3C_9H_{13}N \cdot 2C_7H_3N_3O_8$: C, 53.54; H, 4.93; N, 13.70%. Found: C, 54.08; H, 5.15; N, 14.22%. Here again, a close similarity in the diffuse reflectance spectrum was observed between this complex and the corresponding TNB complex (see Fig. 1). It is evident that this deeply colored complex is also of the CPT type. This conclusion is supported by the presence of the NH_2, NH_3^+, and COO^- patterns in the vibrational spectrum.

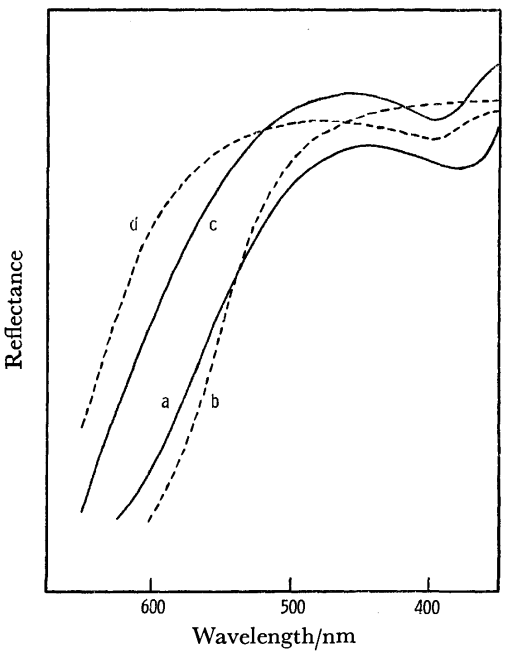

Fig. 1. Reflectance spectra of a) the aniline–TNBA (2:1) complex, b) the corresponding TNB complex, c) the 2,4,5-trimethylaniline–TNBA (3:2) complex, and d) the corresponding TNB complex.

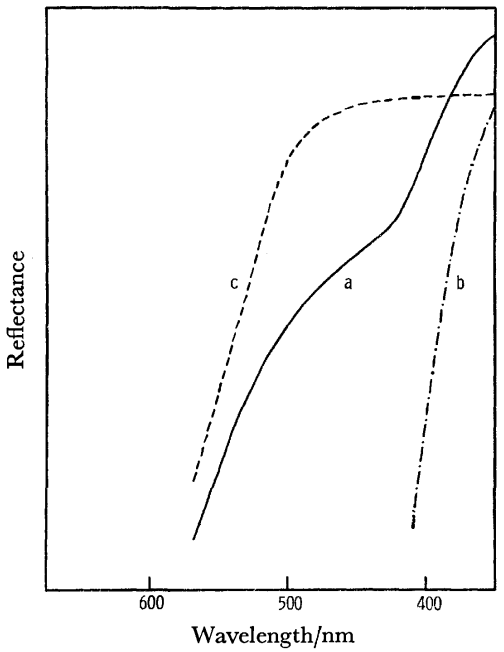

Fig. 2. Reflectance spectra of a) the orange form and b) the colorless form of the *o*-chloroaniline-TNBA complex and c) the corresponding TNB complex.

The most interesting result of the present work is the complex isomerism observed with the *o*-chloroanilinium salt. The colorless benzoate was found to turn orange at about 133 °C. Calcd for $C_6H_6NCl \cdot C_7H_3N_3O_8$: C, 40.57; H, 2.34; N, 14.56; Cl, 9.23%. Found: C, 40.41; H, 2.21; N, 14.58; Cl, 8.96%. The color change is due to the appearance of an absorption in the region from 410 to 600 nm; see Fig. 2. This location is in good agreement with that of the CT absorption in the corresponding TNB complex. The transition is accompanied by a drastic change in the

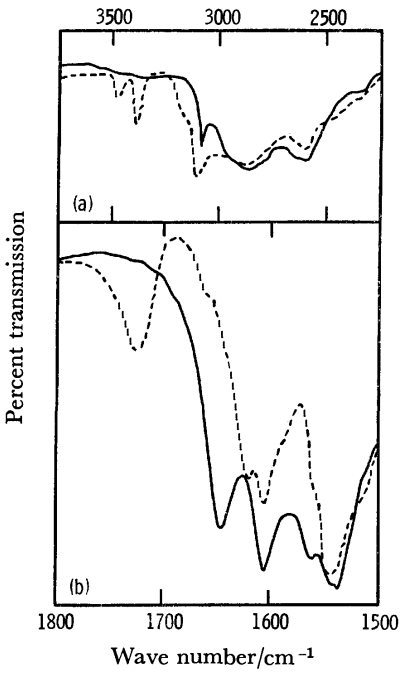

Fig. 3. Vibrational spectra of the colorless form (——) and the orange form (------) of the *o*-chloroaniline–TNBA complex.

vibrational spectrum. As is shown in Fig. 3, the appearance of an NH_2 pattern is noted above the transition temperature. Moreover, the carbonyl-stretching band located at 1650 cm^{-1} in the colorless form is replaced by the one located at 1730 cm^{-1} in the orange form. The X-ray diffraction patterns of these two forms are distinctly different from each other. The complex melts at about 145 °C. The narrow temperature difference between the transition point and the melting point did not allow us to carry out the above-mentioned measurements at high temperatures. Therefore, samples heated a little above the transition point with the differential scanning calorimeter and then cooled as quickly as possible were employed for the spectroscopic and X-ray examinations. These observations lead to the conclusion that the benzoate isomerizes into a CT complex at about 133 °C. The heat of this enantiotropic transition was estimated to be about 2.2 kcal/mol. It must be added that this value is markedly smaller than those observed with the transitions in Hertel's picric acid complexes; that is, 6—8 kcal/mol.[21] Previously it was noted that the chance of finding complex isomers is high in the salts derived from halogenated amines, especially *o*-haloanilines.[3] The newly-found pair fits into this group. As to the electron-acceptor components, it may be said that all the component compounds so far found have two nitro groups at the *ortho* positions related to the proton-donating group; namely, 2,6-dinitrophenol, picric acid and its alkyl derivatives, 3,3′,5,5′-tetranitrobiphenyl-4,4′-diol, and the present acid.[2,3,7]

The complexes with *p*-dimethylaminobenzaldehyde and *o*-nitroaniline, which have the lowest pK_a values among the amines examined (1.62 and −0.26 respectively) are deeply colored. Their vibrational spectra indicate the lack of PT; therefore, these two complexes may be supposed to be of the CT type. The pK_a value of the former amine is significantly higher than that of the acid, 0.65, suggesting that pK_a is not a good measure of the acid strength in these molecular solids or that the pK_a value of TNBA is a little too small. It must be noted that, in contrast to the case studied here, we have seen a good coincidence between the pK_a value of the acceptor component and the lower limit of the pK_a range when PT occurs in the complex formation of 2,4-dinitrophenol.[19] 1-Chloro-, 1-bromo- and 1,6-dibromo-2-naphthylamines are known to form true phenolates with picric acid which isomerize into CT complexes at the transition points.[2,22] Their TNBA complexes are as red as the TNB complexes are. Because of the deep coloration and the presence of the NH_2 and COOH patterns in the vibrational spectra, these three complexes are also considered to be of the CT type.

DNBA Complexes. Solid complexes were obtained with all the above-mentioned anilines except *m*- and *o*-nitroanilines. The fifteen anilines among the seventeen with pK_a values higher than 4.15 give colorless or pale yellow benzoates. The pK_a value of the last aniline in this group is, again, markedly higher than that of DNBA, that is, 2.82.[8] They easily lose the electron-donor component upon heating; therefore, we did not attempt to examine the possible complex isomerization by melting. However, the observation made by Ley and Grau of the diethylanilinium salt might be related to this phenomenon. This salt, with a melting point of 93 °C, was reported to turn a brownish red at 70 °C when heated under water.[23] The calorimetric measurements indicated that a transition without complex isomerization takes place at 108 °C in the pale-yellow *m*-hydroxyanilinium salt. Calcd for $C_6H_7NO \cdot C_7H_4N_2O_6$: C, 48.61; H, 3.45; N, 13.08%. Found: C, 49.75; H, 3.60; N, 13.03%. The enthalpy change is as small as 1.3 kcal/mol, reflecting the absence of complex isomerization.

p-Toluidine and aniline give deep orange-colored complexes of a 3: 2 composition. Calcd for $3C_7H_9N \cdot 2C_7H_4N_2O_6$: C, 56.39; H, 4.73; N, 13.15%. Found: C, 55.93; H, 4.72; N, 13.11%. Calcd for $3C_6H_7N \cdot 2C_7H_4N_2O_6$: C, 54.62; H, 4.15; N, 13.93%. Found: C, 54.49; H, 4.12; N, 13.98%. As may be expected from the high pK_a values of these amines, the spectroscopic examinations revealed that these two complexes are of the CPT type. Since we made no effort to prepare such complexes, their isolation may have been rather accidental and the formation of this type of complexes may not be limited to these two amines. The CT complex-forming ability of the 3,5-dinitrobenzoate ion has been known by the work of Menger and Bender on complexes in an aqueous solution with *N*-(indole-3-acryloyl)-imidazole and two more compounds, and also by the work of Colter and Grunwald on a complex in an aqueous solution with 1-naphthol.[24,25] However, no solid complex containing the anion as an electron-acceptor has been isolated. The five anilines the pK_a values of which are in the range from 3.46 to 1.62 form complexes of the CT type.

References

1) Part VIII; G. Saito and Y. Matsunaga, This Bulletin, **47**, 1020 (1974).
2) E. Hertel, *Ann.*, **451**, 179 (1926).
3) N. Inoue and Y. Matsunaga, This Bulletin, **46**, 3345 (1973).
4) Y. Matsunaga and G. Saito, *ibid.*, **45**, 963 (1972).
5) G. Saito and Y. Matsunaga, *ibid.*, **46**, 714 (1973).
6) Y. Matsunaga, *ibid.*, **46**, 998 (1973).
7) G. Saito and Y. Matsunaga, *ibid.*, **46**, 1609 (1973).
8) J. F. J. Dippy, S. R. C. Hughes, and J. W. Laxton, *J. Chem. Soc.*, **1956**, 2995.
9) J. Czekalla, G. Briegleb, W. Herre, and R. Glier, *Z. Elektrochem.*, **61**, 537 (1957).
10) L. L. Lloyd and J. J. Sudborough, *J. Chem. Soc.*, **75**, 580 (1899).
11) J. J. Sudborough and W. Roberts, *ibid.*, **85**, 234 (1904).
12) J. J. Sudborough, *ibid.*, **79**, 522 (1901).
13) E. Noelting and E. O. Sommerhoff, *Ber.*, **39**, 76 (1906).
14) P. T. Cleve, *ibid.*, **20**, 1989(1897).
15) H. Franzen and A. Eidis, *J. Prakt. Chem.* (2), **88**, 755 (1913).
16) M. E. Spaght, S. B. Thomas, and G. S. Parks, *J. Phys. Chem.*, **36**, 882 (1932).
17) D. D. Perrin, "Dissociation Constants of Organic Bases in Aqueous Solution," Butterworths, London (1965), pp. 58—91.
18) J. Clark and D. D. Perrin, *Quart. Rev.*, **18**, 295 (1964).
19) N. Inoue and Y. Matsunaga, This Bulletin, **45**, 3478 (1972).
20) G. Saito and Y. Matsunaga, *ibid.*, **45**, 2214 (1972).
21) R. Osawa, E. Osawa, and Y. Matsunaga, Paper presented at the Symposium on Molecular Structures, October 1971, Kyoto.
22) G. Briegleb and H. Delle, *Z. Elektrochem.*, **64**, 347 (1960).
23) H. Ley and R. Grau, *Z. Phys. Chem.*, **100**, 271 (1922).
24) F. M. Menger and M. L. Bender, *J. Amer. Chem. Soc.*, **88**, 131 (1966).
25) A. K. Colter and E. Grunwald, *J. Phys. Chem.*, **74**, 3637 (1970).

Dielectric Relaxation and Molecular Structure. XI. Dielectric Behavior of Various Polar Molecules in the Supercooled *o*-Terphenyl Solution

Masahiko NAKAMURA, Hiroaki TAKAHASHI, and Keniti HIGASI

Department of Chemistry, School of Science and Engineering, Waseda University, Shinjuku, Tokyo 160

(Received December 7, 1973)

The dielectric constants and losses of dilute solutions of anthrone, xanthone, phenothiazine, 9-fluorenone, benzophenone, diphenylnitrosamine, 1,8-dinitronaphthalene, *p*-nitrotoluene and *m*-nitrophenol in *o*-terphenyl have been measured in the supercooled state in the frequency range 1—100 MHz and temperature range 15—30 °C. The results have been analyzed by Davidson-Cole's skewed-arc method to calculate the relaxation times, the distribution parameters, the activation enthalpies and entropies for the dielectric relaxation processes.

Davidson and Cole[1] found that glycerol and propylene glycol in the supercooled liquid state show the skewed-arc behavior and introduced the empirical equation

$$\varepsilon' - j\varepsilon'' = \varepsilon_\infty + \frac{\varepsilon_0 - \varepsilon_\infty}{(1+j\omega\tau_0)^\beta} \quad (1)$$

where ε_0 and ε_∞ are the limiting low and high frequency dielectric constants, respectively, ω is the angular frequency, τ_0 the characteristic relaxation time and β the distribution parameter. When β is equal to unity, the locus becomes a Debye-type semicircle.

Recently Shears and Williams made dielectric measurements on various polar molecules in supercooled *o*-terphenyl solution.[2] The absorption curves were found to be unsymmetrical and broader than expected for any Debye relaxation process; large activation energies were obtained in agreement with the cooperative process.

The present study has been conducted since little information is available on the dielectric behavior of the supercooled state in this particular solvent. *o*-Terphenyl provides a medium having viscosity so high that the region of dielectric absorption is in the range 1—100 MHz at room temperature.

Experimental

Materials. Commercial chemicals were carefully purified by recrystallization before use. The melting and glass transition points of *o*-terphenyl are 58 and −29 °C, respectively. The measurements were carried out not in a glassy state, but in the state of so-called metastable equilibrium.[3] Crystallization in the solution was prevented either by examining visually or by checking its dielectric constant and loss.

Apparatus. Dielectric constants and losses were measured in the frequency range 1—100 MHz with a twin-T bridge of type DLB-1101D (Fujisoku Electric Co., Ltd.). This bridge consists essentially of a circuit for impedance measurement divised by Sinclair and Woods, the detailed description of which was given by S. Okamoto.[4] Temperature was kept constant within ±0.2 °C by thermistors.

Results and Discussion

Dielectric constants and losses are plotted against the logarithm of the frequency (*e.g.*, *cf.* Fig. 1 for anthrone in *o*-terphenyl). In all the solutions the dispersion and absorption of solute molecules were observed in the frequency range 1—100 MHz and temperature range 15—30 °C. Dielectric constants and losses are also plotted in a complex plane; normalized Davidson-Cole

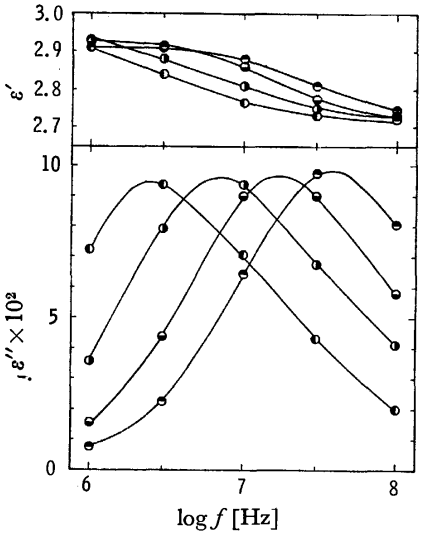

Fig. 1. Dielectric constant and loss curves for anthrone (Mole fraction, f_2=0.028) in *o*-terphenyl solution.
◐: 15 °C, ◑: 20 °C, ◒: 25 °C, ◓: 30 °C.

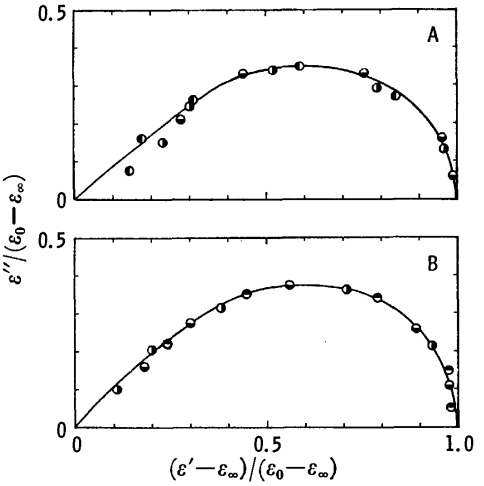

Fig. 2. Normalized Davidson-Cole plots for solutions in *o*-terphenyl.
A: Anthrone (f_2=0.028), B: 1,8-Dinitronaphthalene (f_2=0.010).
◐: 15 °C, ◑: 20 °C, ◒: 25 °C, ◓: 30 °C.

TABLE 1. VALUES OF THE CHARACTERISTIC RELAXATION TIME (τ_0)

Substance	τ_0(ns) 15°C	20°C	25°C	30°C	τ (ps) (in benzene)
Anthrone	106	41.7	18.7	11.2	24.8(20°C)[5] 18.4(40°C)
Phenothiazine	115	45.0	21.0	11.4	
Xanthone	94.9	40.0	18.2	9.1	21.0(25°C)[6]
9-Fluorenone	80.4	37.1	15.3	7.6	19.9(20°C)[5] 14.9(40°C)
Diphenyl-nitrosamine	76.4	32.8	14.2	7.1	
1,8-Dinitronaphthalene		65.0	32.0	14.6	
p-Nitrotoluene	48.4	22.7	10.1	5.6	19 (22°C)[7]
Benzophenone	52.9	24.2	12.4		16.2(20°C)[8]
m-Nitrophenol	53.4	26.2	11.7	6.3	

diagrams are shown in Fig. 2. The values of ε_0 and ε_∞ are obtained by extrapolation at each temperature.

The characteristic relaxation times τ_0 obtained in this experiment are shown in Table 1 together with literature values in benzene. The decrease in the relaxation times in benzene with a rise of 20 °C is 6.4 ps for anthrone and 5.0 ps for 9-fluorenone. In the supercooled state the decrease for 15 °C becomes almost ten times for anthrone, 9-fluorenone and other compounds.

According to Eyring the relaxation time τ_0 is expressed in terms of thermodynamic parameters as follows.

$$\tau_0 = \frac{h}{kT}\exp\left(\frac{\Delta H^*}{RT}\right)\exp\left(-\frac{\Delta S^*}{R}\right). \qquad (2)$$

where ΔH^* is the activation enthalpy, ΔS^* the activation entropy and k, h, and R are the Boltzmann, Planck and gas constants, respectively. The activation enthalpy obtained from temperature dependence of τ_0 (Table 2) is much greater than that obtained in ordinary non-polar solvents; ΔH^*s for anthrone and 9-fluorenone in benzene are 8.8 and 8.4 kJ mol^{-1}, respectively.[5] We see that ΔS^* increases with ΔH^* so that an apparently linear relationship exists between these parameters.

$$\Delta S^*(\text{J deg}^{-1}\text{ mol}^{-1}) = 3.44\Delta H^*(\text{kJ mol}^{-1}) - 106 \qquad (3)$$

Equations similar to Eq. (3) have been obtained for

TABLE 2. VALUES OF THE DISTRIBUTION PARAMETER (β), THE ACTIVATION ENTHALPY (ΔH^*) AND ENTROPY (ΔS^*)

Substance	β	ΔH^* $\left(\frac{\text{kJ}}{\text{mol}}\right)$	ΔS^* $\left(\frac{\text{J}}{\text{deg mol}}\right)$
Anthrone	0.47	122	313
Phenothiazine	0.49	119	302
Xanthone	0.49	116	293
9-Fluorenone	0.35	114	289
Diphenylnitrosamine	0.49	113	282
1,8-Dinitronaphthalene	0.52	108	261
p-Nitrotoluene	0.40	102	249
Benzophenone	0.27	101	246
m-Nitrophenol	0.29	101	245

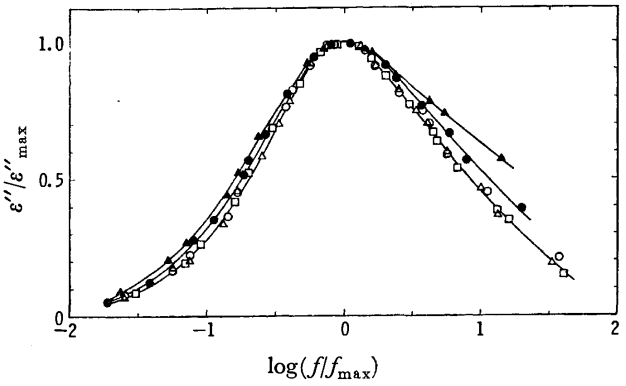

Fig. 3. Normalized plots of $\varepsilon''/\varepsilon''_{max}$ against $\log(f/f_{max})$ for solutions in *o*-terphenyl at 15°, 20°, 25°, and 30 °C.
○: Anthrone (f_2=0.028), △: Xanthone (f_2=0.028),
□: Phenothiazine (f_2=0.040),
●: 9-Fluorenone (f_2=0.028),
▲: Benzophenone (f_2=0.030).

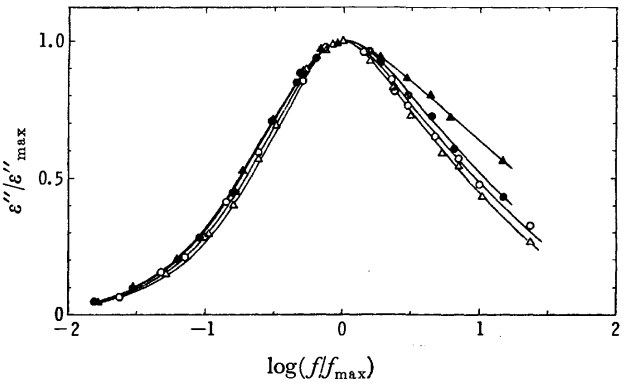

Fig. 4. Normalized plots of $\varepsilon''/\varepsilon''_{max}$ against $\log(f/f_{max})$ for solutions in *o*-terphenyl at 15°, 20°, 25°, and 30 °C.
△: 1,8-Dinitronaphthalene (f_2=0.010),
○: Diphenylnitrosamine (f_2=0.028),
●: *p*-Nitrotoluene (f_2=0.020),
▲: *m*-Nitrophenol (f_2=0.020).

other dielectric relaxation processes,[9] *e.g.*, for polar polymers[10] and for nonrigid molecules in the polystyrene matrix.[11]

Normalized absorption curves, shown in Figs. 3 and 4, are unsymmetrical in shape and broader than the pure Debye curves. All the points measured at different temperatures are reasonably close to a single curve for each sample. The above feature differs from one for polar molecules dispersed in the polystyrene matrix, where a symmetrical distribution of relaxation times occurs;[11] it also differs from that for rigid molecules in Nujol[12,13] or decalin (normal[13]) and supercooled[14] liquids), where the absorption curves become broader with decreasing temperature.

The abosorption curves of anthrone, xanthone and phenothiazine have almost the same shape with nearly the same values of β (Fig. 3 and Table 2). This might arise from the similarity in the size and shape of these molecules. The absorption curve of benzophenone (▲ in Fig. 3) is, however, broader than that of its related molecules 9-fluorenone (● in Fig. 3) in the higher frequency side. Possibly an extra absorption

occurs in the higher frequency region on account of the intramolecular rotation of the phenyl groups of benzophenone.[15]

Figure 4 shows the normalized absorption curves of four remaining molecules whose size and shape are not similar. The curve for *m*-nitrophenol (▲ in Fig. 4) is far broader in the higher frequency side than curves of other molecules. The deviation might originate from the high frequency absorption due to rotation of the OH group.

Denny[16] made skewed-arc plots for several supercooled, branched hydrocarbon halides including isobutyl bromide which is known to have a single relaxation time in the normal liquid state.[17] In order to explain the unsymmetrical distribution of relaxation times of those nonassociated molecules, Glarum[18] proposed a defect diffusion model, in which the shape of the distribution function becomes very little dependent upon temperature (Figs. 3 and 4). High activation energies obtained indicate the difficulty of diffusion of defects through solvent molecules. The results of this experiment seem to support Glarum's mechanism.

One of us (M.N.) is indebted to Professor Mansel Davies, University of Wales, for his interest and encouragement.

References

1) D. W. Davidson and R. H. Cole, *J. Chem. Phys.*, **19**, 1484 (1951).
2) M. F. Shears and G. Williams, *J. Chem. Soc. Faraday II*, **69**, 608, 1050 (1973).
3) S. Seki, *Nihon Kessho Gakkaishi*, **14**, 335 (1972).
4) S. Okamoto, *Kobunshi*, **17**, 1092 (1968).
5) D. A. Pitt and C. P. Smyth, *J. Amer. Chem. Soc.*, **80**, 1061 (1958).
6) T. Nagai, Y. Koga, H. Takahashi, and K. Higasi, This Bulletin, **47**, 1022 (1974).
7) R. J. W. Le Fevre and E. P. A. Sullivan, *J. Chem. Soc.*, **1954**, 2873.
8) K. Chitoku, K. Higasi, M. Nakamura, Y. Koga, and H. Takahashi, This Bulletin, **43**, 992 (1971).
9) K. Higasi, "Dielectric Relaxation and Molecular Structure," *Monogr. Res. Inst. Appl. Elec., Hokkaido University*, No. 9 (1961).
10) M. Davies, *Quart. Rev.*, **8**, 250 (1954).
11) M. Davies and J. Swain, *Trans. Faraday Soc.*, **67**, 1637 (1971).
12) E. N. DiCarlo and C. P. Smyth, *J. Phys. Chem.*, **66**, 1105 (1962).
13) E. L. Grubb and C. P. Smyth, *J. Amer. Chem. Soc.*, **83**, 4122 (1961).
14) G. P. Johari and C. P. Smyth, *J. Chem. Phys.*, **56**, 4411 (1972).
15) W. E. Vaughan and C. P. Smyth, *J. Phys. Chem.*, **65**, 98 (1961).
16) D. J. Denny, *J. Chem. Phys.*, **27**, 259 (1957).
17) E. J. Hennelly, W. M. Heston, Jr., and C. P. Smyth, *J. Amer. Chem. Soc.*, **70**, 4102 (1948).
18) S. H. Glarum, *J. Chem. Phys.*, **33**, 639 (1960).

Spectroscopic and Theoretical Studies on the Protonation to Xanthone Derivatives

Kimiko MIZUTANI,* Kimiko MIYAZAKI, Kimiko ISHIGAKI, and Haruo HOSOYA**

Department of Chemistry, Ochanomizu University, Bunkyo-ku, Tokyo 112

(Received December 18, 1973)

Ultraviolet absorption, fluorescence, and excitation spectra of xanthone and its hydroxyl and methoxyl derivatives were measured in sulfuric acid solutions of various acidities. The basicities (pK_a's) of these compounds were obtained from the spectral change. Variable-β type molecular orbital calculations of the π-systems were performed, assignment of the absorption spectra being made. It was confirmed that protonation occurs at the carbonyl oxygen atom. A method for obtaining the equilibrium constant without knowing the absolute intensity is proposed.

It has been established that in strong acidic media protonation occurs at the carbonyl oxygen atom of γ-pyrone and its derivatives.[1,2] As a dibenzo derivative of γ-pyrone, xanthone (or 9H-xanthen-9-one, **1**: X=H) is also expected to be protonated at the carbonyl oxygen atom forming hydroxyxanthylium ion (**2**: X=H).

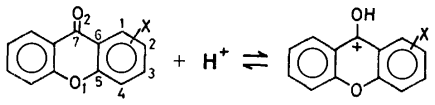

1 **2**

Actually xanthone is known to be stable in concentrated sulfuric acid showing strong emission,[3] and the basicity of xanthone has been obtained from the change of the ultraviolet absorption spectra.[4-6] The basic and emissive characters of xanthone are expected to vary with the number and positions of the substituent such as a hydroxyl group, according to reports on the features of the substitution effect on the absorption and emission of xanthone derivatives.[3,5,7] These phenomena have close resemblance to those of the hydroxyl derivatives of anthraquinone forming the alizarin dye group where electron donating power of the hydroxyl group and the competitive intramolecular hydrogen bonding are the major factors determining basic and emissive characters. It should also be noted that the emissive character of xanthone is related to that of fluorescein (**3**).

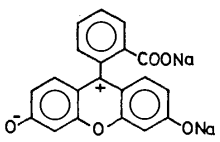

3

We have studied in detail the acidity dependence of the electronic absorption and emission spectra and the basicities of mono-hydroxyl and methoxyl derivatives of xanthone (**1**: X=OH, OCH_3) and interpreted the results with the molecular orbital calculations of the π-electronic structures.

* Present address: Department of Chemistry, College of Science and Engineering, Aoyama Gakuin University, Chitosedai, Setagaya-ku, Tokyo 157.

** To whom correspondence should be addressed.

Experimental

Materials. Commercial G.R. grade of xanthone was purified by recrystallization from ethanol. 1-, 2-, 3-, and 4-methoxyxanthones and the corresponding hydroxyxanthones were synthesized after Ullmann and Zlokasoff[8] and purified by recrystallization from aqueous ethanol. Concentrated sulfuric acid of high special grade (Wako Pure Chemical Industries, Ltd.) was used without further purification.

Measurement. A Shimadzu multiconvertible spectrophotometer D40R was used to measure the ultraviolet and visible absorption spectra with stopcocked fused quartz 1 cm cells. A Hitachi MPF-2A fluorescence spectrophotometer was used for the excitation and fluorescence spectra. Fluorescence spectra were automatically corrected with Rhodamine B by use of the spectrum correction attachment. Absorption and emission spectra were measured in ethanol and in sulfuric acid of various acidities at room temperature. All the solutions were prepared just before the measurement, the concentration of the solute being about 10^{-4}—10^{-5} M. The acid concentrations were determied by titration with a standard aqueous solution of sodium hydroxide. The value of Hammett's acidity function were taken from the table by Jørgensen and Hartter.[9] The basicities (pK_a) of the xanthone derivatives were determined from the change of the ultraviolet absorption spectra by the iterative least squares calculation for the sigmoid curve of ε-H_0 plot.[10] Although the absolute intensity of excitation spectra was not obtained, we could obtain fairly accurate values of pK_a from the relative change of the excitation spectra at two different wavelengths. Details are given in the Appendix.

Results and Discussion

Ultraviolet Absorption Spectra. Ultraviolet absorption spectra of the neutral (**1**, in EtOH) and protonated (**2**, in conc. H_2SO_4) xanthone are shown in Fig. 1 and Table 1, the former spectrum being in accordance with the previous results.[7,11,12] The spectra of the hydroxyl and methoxyl derivatives are given in Figs. 2 and 3 and Table 1. The spectra of the hydroxyl and the corresponding methoxyl derivatives, except for the 1-derivatives are so similar that the spectra of 2-,

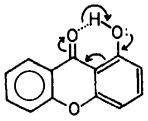

4

Table 1a. Observed and calculated absorption spectra of xanthone derivatives

X	Observed value		Calculated value		
	ΔE (eV)	f	ΔE (eV)	f	θ(°)[a]
H	3.69	0.09	4.07	0.19	00
	4.31	0.02	4.51	0.00	90
	4.38	0.02			
	4.79	0.16	4.78	0.08	90
	5.21	0.37	5.23	0.14	0
			5.25	1.46	90
	5.64	0.31	5.66	0.04	90
			5.67	0.13	0
1-OCH_3	3.60	0.11	3.91	0.19	43
	4.21	0.04	4.33	0.11	−35
	4.50	0.08	4.56	0.00	23
			4.98	0.43	−76
	5.21	0.81	5.25	0.27	54
			5.33	0.89	−80
			5.67	0.09	−9
2-OCH_3	3.44	0.09	3.80	0.23	−10
	4.16	0.05	4.35	0.11	4
			4.69	0.23	83
	4.98	0.46	5.14	0.10	−49
	5.25	0.60	5.21	0.06	77
			5.28	0.43	−75
			5.62	0.03	−5
3-OCH_3	4.08	0.32	4.08	0.14	−16
	4.63	0.14	4.48	0.05	63
			4.63	0.10	−52
			4.98	0.82	−80
	5.23	0.71	5.29	0.73	59
			5.58	0.30	−39
			5.72	0.26	−66
4-OCH_3	3.59	0.09	3.90	0.19	26
	4.28	0.03	4.36	0.09	−58
			4.65	0.03	−83
	5.01	0.66	5.08	0.58	−66
			5.26	0.82	83
			5.33	0.16	−50
			5.59	0.14	3

a) Direction of the transition moment.

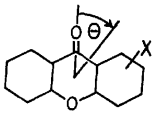

3-, and 4-hydroxyxanthones have been omitted. The spectra of 1-hydroxy- and 1-methoxyxanthones are quite different from each other indicating an intramolecular hydrogen bonding in 1-hydroxyxanthone (**4**). The n→π^* bands of these compounds were not observed in the polar solvents used in this study.[12] The spectra of the neutral compounds are generally seen to shift to the red on protonation, *viz.*, the 340 nm band of xanthone is shifted to 400 nm. The electronic structures of forms **1** and **2** of the 1-, 2-, and 4-derivatives seem very similar to those of xanthone, while those of the 3-derivatives are modified by the electron flow from the substituent etherial lone pair electrons.[7] This anomaly is also reflected in the basicity.

Table 1b. Observed and calculated absorption spectra of protonated xanthone derivatives

X	Observed value		Calculated value		
	ΔE (eV)	f	ΔE (eV)	f	θ(°)[a]
H	3.16	0.05	3.37	0.17	0
	3.71	0.31	3.84	0.48	90
			4.02	0.00	90
	4.61	0.04	4.91	0.10	0
	4.93	0.46	5.00	1.05	90
	5.69	0.39	5.34	0.06	0
			5.64	0.61	90
1-OCH_3	2.95	0.11	2.97	0.19	41
	3.79	0.23	3.75	0.30	−69
			3.95	0.07	81
	4.63	0.09	4.68	0.79	84
	4.79	0.33	4.95	0.14	−49
			5.24	0.14	62
	5.64	0.29	5.51	0.67	−75
			5.85	0.03	72
2-OCH_3	2.99	0.06	2.99	0.18	−24
	3.62	0.14	3.75	0.18	76
	3.94	0.16	3.89	0.23	−78
	4.82	0.55	4.71	0.82	82
			4.86	0.16	29
	~5.6	~0.5	5.14	0.73	82
			5.37	0.13	−80
			5.70	0.07	−84
3-OCH_3	3.52	0.37	3.41	0.28	65
	3.94	0.02	3.61	0.52	−65
			4.15	0.01	−66
	4.55	0.05	4.75	0.06	−5
	5.01	0.56	5.01	0.74	−73
			5.22	0.40	48
	~5.6	~0.3	5.61	0.69	85
4-OCH_3	2.99	0.06	2.90	0.13	31
	3.72	0.24	3.79	0.28	66
			3.91	0.03	52
	4.82	0.58	4.56	0.96	88
			4.80	0.21	−54
	~5.6	~0.3	5.25	0.14	53
			5.45	0.37	−66
			5.73	0.22	37

a) See the footnote in Table 1a.

Fluorescence and Excitation Spectra. We did not measure the phosphorescence spectra of xanthones, since a number of studies have been reported.[12-14] Fluorescence spectra of xanthone in concentrated sulfuric acid is exemplified in Fig. 1 as the most typical of the compounds studied. That the conjugate acid **2** fluoresces more strongly than the neutral compound **1** reminds one of the structure of the fluorescent form **3** of fluorescein.

For a series of the protonated xanthone derivatives the values of the Stokes shift are scattered in the range 3500—7000 cm^{-1}, revealing a drastic change in the geometry of the compounds on protonation. However, no apparent correlation was observed between the values of the Stokes shift and the basicity of the parent compound.

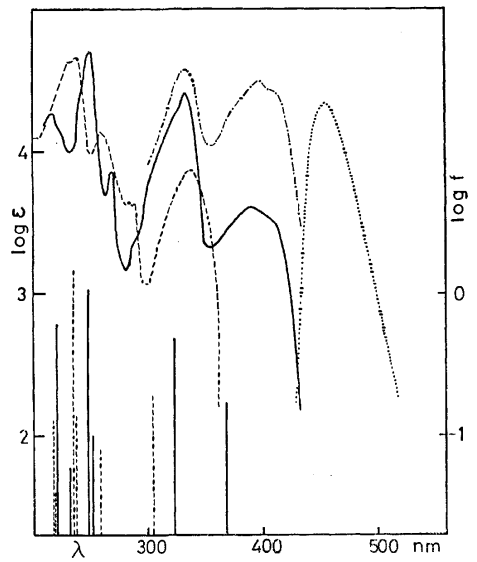

Fig. 1. Observed and calculated spectra of neutral (**1**) and protonated (**2**) xanthones
----: Absorption spectrum in EtOH and calculated transition energies of **1**, X=H.
——: Absorption spectrum in conc. H_2SO_4 and calculated transition energies of **2**, X=H.
-•-•-: Excitation spectrum of **1** (2.66×10^{-5}M) in conc. H_2SO_4. Excited at 456 nm.
·····: Fluorescence spectrum (corrected) of **1** ($\sim10^{-5}$ M) in conc. H_2SO_4. Emitted at 420 nm.

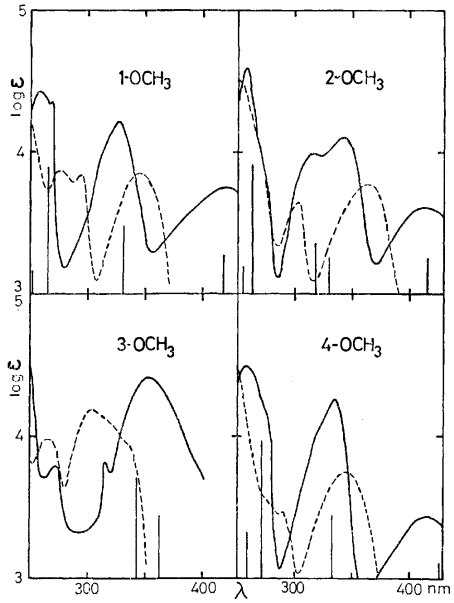

Fig. 2. Ultraviolet absorption spectra of methoxyxanthones in ethanol (----) and in concentrated sulfuric acid (——) solutions. The spectra of hydroxyxanthones are essentially the same as the corresponding methoxyl derivatives except for 1-substituted compounds (See Fig. 3). The calculated spectra of the protonated compounds are shown with solid bars.

Excitation spectrum of xanthone in concentrated sulfuric acid changes with the solute concentration as shown in Fig. 4. For the solutions with solute concentration lower than 10^{-5} M, 330 and 400 nm bands

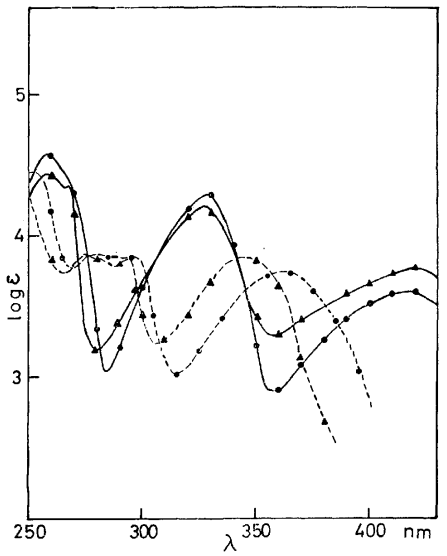

Fig. 3. Ultraviolet absorption spectra of 1-hydroxy- (●) and 1-methoxyxanthones (▲) in ethanol (----) and in concentrated sulfuric acid (——) solutions.

undoubtedly correspond to the absorption spectrum. As the solute concentration increases the relative intensities of these two bands become reversed, and reabsorption is gradually observed around 330 nm. As a result, solutions with concentration higher than 10^{-3} M give a quite different spectral shape. However, at lower concentrations no secondary change such as energy transfer seems to occur. We therefore adjusted the concentration below 10^{-4} M for the measurement of the excitation spectra for obtaining the basicities of the xanthone derivatives. The change of the excitation spectra of xanthone with the solvent acidity is shown in Fig. 5.

Basicities. The basicities (pK_a's) of xanthone and

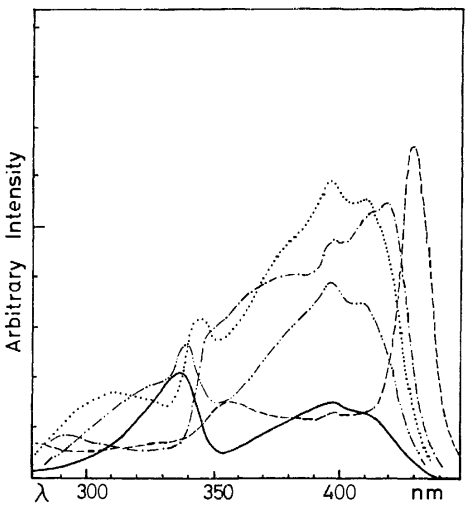

Fig. 4. Concentration dependence of the excitation spectrum of xanthone in concentrated sulfuric acid. Emitted at 452 nm.
Concentrations are
——: 2.66×10^{-5}M, -·-·-: 1.06×10^{-4}M,
·····: 2.66×10^{-4}M, -•-: 5.32×10^{-4}M,
----: 2.66×10^{-3}M.

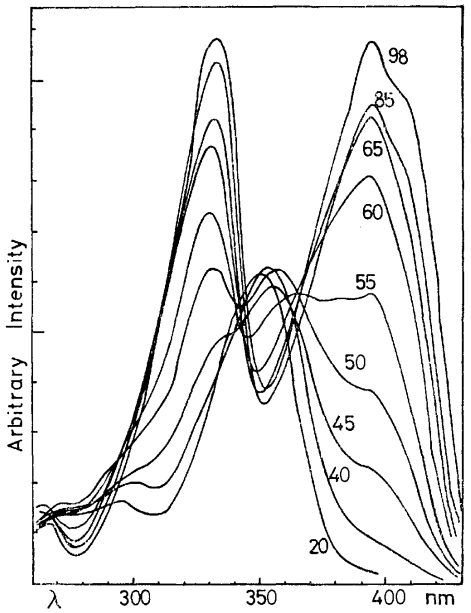

Fig. 5. Solvent acidity dependence of the excitation spectrum of xanthone in concentrated sulfuric acid. The numbers indicate the weight per cent of sulfuric acid. Excited at 452 nm.

Table 2. Basicities and π-electron densities of xanthone derivatives

X	$-pK_a$		π-Electron density	
	Absorption	Excitation	Carbonyl O	Ethereal O
H	4.1	4.0	1.425	1.772
1-OH	4.1	4.3	1.455	1.769
1-OCH_3	2.2	2.2		
2-OH	3.9	3.8	1.428	1.773
2-OCH_3	3.7	3.7		
3-OH	3.0	2.6	1.434	1.771
3-OCH_3	2.8	2.5		
4-OH	4.2	4.2	1.425	1.777
4-OCH_3	4.2	4.4		

its eight derivatives were determined both from the absorption and excitation spectra (Table 2). The values for xanthone, −4.1 (absorption) and −4.0 (excitation), are in agreement with the reported values, −4.08,[4] −4.12,[5] and −4.2,[6] all from the ultraviolet absorption measurement, but no report can be found for the derivatives studied here. Comparing these values with those for benzophenone (−6.4), anthrone (−5.0), 4,4'-dimethoxybenzophenone (−4.4), and 4,4'-dihydroxybenzophenone (−4.2),[15] we find these data suggest that protonation occurs at the carbonyl oxygen atom of xanthone. The electron donating ethereal oxygen lone pair of xanthone acts as a bridge for the conjugation of the π-electron between the two benzene rings and also an electron supplier to the carbonyl oxygen atom, placing the basicity of xanthone as high as that of dihydroxybenzophenone. All the hydroxyl and methoxyl derivatives are no less basic than xanthone.

Except for the 1-substituted derivatives the basicities of hydroxyl and the corresponding methoxyl derivatives are almost the same. The basicities of the methoxyxanthones are in the following order:

$$1 > 3 > 2 > 0\ (=\text{xanthone}) > 4.$$

Note a gap between the 3- and 2-methoxyxanthones. This can be explained by the resonance theory as in the following scheme:

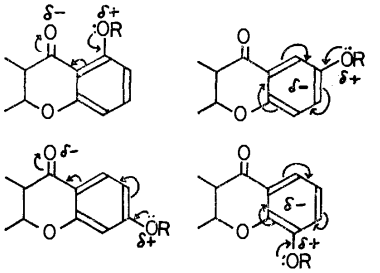

More quantitative correlation can be obtained from the molecular orbital calculation. In Table 2 the π-electron densities on the carbonyl and ethereal oxygen atoms of the xanthone derivatives are compared with the basicity data, which are correlated well with the π-electron densities on the carbonyl oxygen atom (Fig. 6) but not with the ethereal oxygen atom. Although a similar argument has been given by Efimov and Komarov for the basicities of xanthone and γ-pyrone derivatives, it is based on the Hückel molecular orbital.[16] It should be noted that for π-electron systems with many heteroatoms the Hückel method often gives unreasonable π-electron densities.[17]

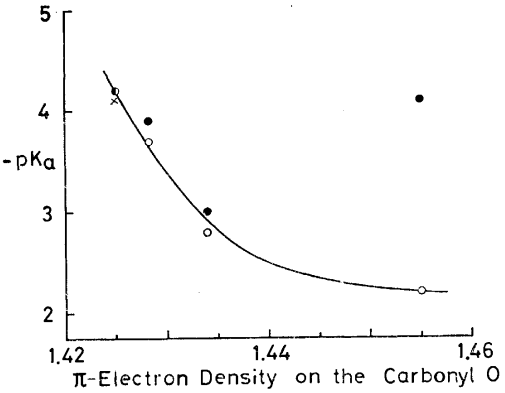

Fig. 6. Correlation between the basicities (pK_a's) and the π-electron densities on the carbonyl oxygen atom of xanthone derivatives
×: xanthone ●: hydroxyxanthone
○: methoxyxanthone
The pK_a values are taken from the UV absorption data.

On the other hand, as evident from **4** the excess π-electron on the carbonyl oxygen atom of 1-hydroxyxanthone is pulled away through the hydrogen bond, causing no net effect on the value of the basicity.

If no side-reaction intervenes in the excited states of fluorescent molecules the basicities can be obtained fairly accurately from the change of the excitation spectra.

Calculation of the π-Electronic Structures of Xanthone and Its Derivatives. In order to get theoretical support

for the mechanism of protonation to xanthone derivatives and to interpret the observed electronic spectra, the π-electronic structures of the ground and lower excited states of the neutral and protonated xanthone derivatives were calculated with the variable-β approximation proposed by Nishimoto and Forster,[21] in which the consistency of the bond order-bond length relation is attained automatically with the PPP type molecular orbital framework. No accurate geometry of a molecule is therefore necessary for the input data.[22] No distinction was taken between the hydroxyl and methoxyl derivatives. For the protonated xanthones the protonated carbonyl oxygen atom was treated simply as a hydroxyl oxygen atom. No parametrization was tried for the different electronegativities of positively charged carbon atoms. Extensive singly excited configuration interaction was carried out. The parameters and details of the calculation are after Nishimoto.[23]

Electronic Structures of Xanthone and Its Derivatives. The net π-electron charge densities and the calculated bond lengths of the two forms of xanthone (**1**,**2**: X=H) are shown in Fig. 7. In both cases the charge distribution over the central three atoms lying on the molecular axis (z-axis) is rather uneven, while electron is uniformly populated over the wing benzene moiety. For the hydroxyl and methoxyl derivatives, the π-electron densities on the carbonyl oxygen atom are found to be correlated well with their basicities (Table 2 and Fig. 6), but not the total π-electron energies of **1** and **2**.

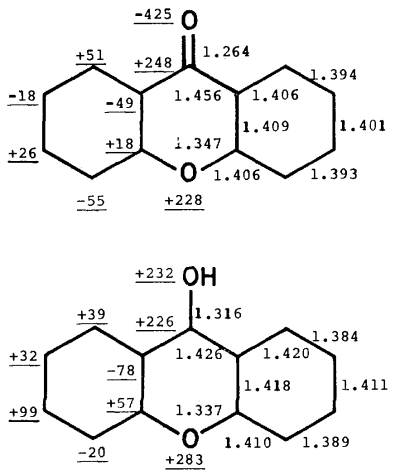

Fig. 7. The bond lengths and the net charge densities of the ground state of the neutral and protonated xanthones. The charge densities in the unit of 10^{-3} electron are underlined.

Assignment of the Electronic Spectrum of Xanthone. In order to discuss the assignment, the higher occupied and lower vacant π-molecular orbitals given in Table 3 should be considered. Both the HOMO and LUMO are symmetric (S) with respect to the plane passing through the molecular axis, and perpendicular to the molecular plane (yz-plane) to which the symmetry notations S and A will be referred unless otherwise stated. Assignment of the electronic spectra is given in Table 4. Pownall and Huber (abbreviated as PH) gave the assignment based on their phosphorescence excitation measurement.[12] There are a few discrepancies between their assignment and ours. Although σ-electron is not taken into this calculation we can expect that the lowest $^1n\rightarrow\pi^*$ transition (Band I according to PH) is roughly expressed as (n→9) and x-polarized, *i.e.*, perpendicularly to the molecular plane, as both the π-LUMO 9 and σ-HOMO n have S symmetry. That this band is observed by PH as z-polarized may be an outcome of possible vibrational perturbation. The most dominant contribution to the lowest $\pi\rightarrow\pi^*$

Table 3. Higher occupied and lower vacant π-orbitals of xanthone

AO[a]	Occupied MO		Vacant MO	
	7	8	9	10
C_1	0.3451	0.1363	−0.3050	0.1599
C_2	0.0597	0.3500	−0.0220	−0.3888
C_3	−0.2905	0.1064	0.3188	0.1872
C_4	−0.3405	−0.2773	−0.1863	0.2142
C_5	−0.0192	−0.2714	−0.1985	−0.4145
C_6	0.2961	−0.2632	0.1896	0.2656
C_7	−0.0532	−0.0288	0.4459	0.0000
O_1	0.0333	0.3930	0.1565	0.0000
O_2	−0.4171	0.3167	−0.4077	0.0000
Symmetry	S	S	S	A
Energy (eV)	−10.4359	−9.3827	−2.2098	−1.3450

a) For numberings see formula **1** in the text.

Table 4. Assignment of the electronic spectra of xanthone

Band[a]	Observed values[b]		Calculated values[b]	Polarization[c]	Assignment	
	in EtOH	in 3-Methylpentane[a]			Configuration	Character
I	—	3.37 (—)[d]	—	x (z)[a]	n→9[e]	n→π^*[f]
II	3.69 (0.09)	3.69 (0.10)	4.07 (0.19)	z (z)	8→9	CT
III	{4.31 (0.02) / 4.38 (0.02)}	4.39 (0.02)	4.51 (0.00)	y (y)	8→11 / {5→9} / 7→10	LE
IV	4.79 (0.16)	4.84 (0.10)	4.78 (0.08)	y (z)	8→10	Back CT
V	5.21 (0.37)	5.29 (0.50)	{5.23 (0.14) / 5.25 (1.46)}	z / y } (z)	{7→9 / 6→9}	LE

a) Ref. 12. b) Energies are in eV. The values in parentheses are oscillator strengths. c) Choice of axis is explained in the text. d) $\log \varepsilon_{max} \sim 0.8$.[12] e) For notations see Table 3 and the text. 5, 6, 10, and 11 are S and 7—9 are A. f) CT: Charge-transfer, LE: Locally excitation.

transition (Band II) is denoted by (8→9) and polarized along the molecular axis. Inspection of the wave functions indicates that this is a charge-transfer band, in which electron flows into the carbonyl oxygen atom from the ring moiety. The next higher band (Band III) is a mixture of several transitions with y-polarization, most of which are locally-excited in the ring moiety. In contrast to the tentative assignment by PH that Band IV is a z-polarized charge-transfer band, our calculation shows that it is a y-polarized *back*-charge-transfer band due to transition (8→10). The upper orbital 10 has A symmetry with no coefficient on the carbonyl group. The electron flow associated with the electronic transitions II, III, and IV in xanthone are shown in the diagram below, in which the two-headed arrow shows the direction of the transition moment.

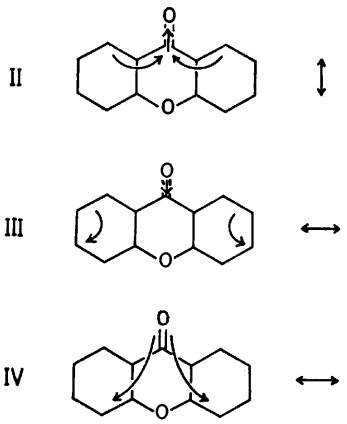

The reliability of the variable-β calculation especially for the assignment of the electronic spectra of heteroatomic systems has been tested with a number of molecules.[21,24] As evident from Figs. 1 and 2 and Table 1 this is also the case for the xanthone derivatives. Agreement between calculation and observation is generally better for the protonated xanthone derivatives than the neutral compounds.

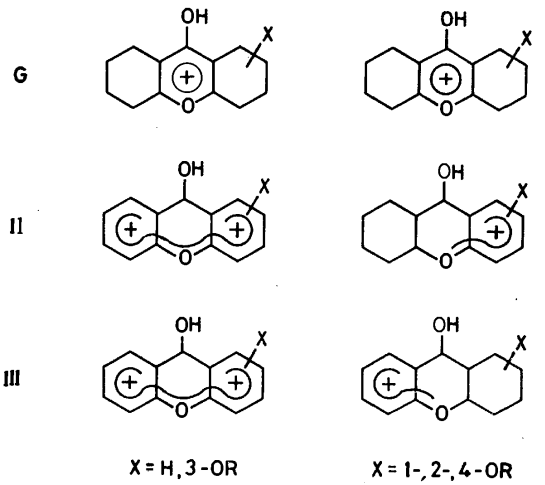

Fig. 8. Illustrative sketches of the charge densities of the ground and lower excited states of the protonated xanthone derivatives
G: Ground state II: Lowest $\pi\rightarrow\pi^*$ state
III: Second lowest $\pi\rightarrow\pi^*$ state

The 3-substituted derivatives show quite different spectral patterns, which are reproduced fairly well by the molecular orbital calculation. Charge densities of the ground and lower excited states of the protonated xanthone derivatives are given in Fig. 8. The 3-derivatives again behave quite differently from other derivatives, *viz.*, in xanthone and 3-derivatives the lowest two $\pi\rightarrow\pi^*$ excitations are delocalized all over the molecules, while in other derivatives the excitations are localized. Of the four derivatives of the protonated xanthone the 3-derivative has the lowest value of the total π-electron energy.

The authors are indebed to Dr. T. L. Kunii, the University of Tokyo, for allowing them to use the variable-β program on a Hitac 5020E computer at the Computer Centre, the University of Tokyo. Part of this study was supported by a grant from the Ministry of Education.

Appendix

Determination of the Equilibrium Constant without Knowing the Absolute Intensity. Let us assume that following acid-base equilibrium takes place.

$$B + H^+ = A, \tag{A1}$$

where B and A are, respectively, an organic base and the conjugate acid. If the analytical concentration of B is c, of wflich fraction x is protonated to form A, the dissociation constant K_a of the conjugate acid A is expressed as

$$K_a = \frac{c(1-x)h_0}{cx} = \frac{h_0(1-x)}{x}, \tag{A2}$$

where the acid concentration h_0 is related to Hammett's acidity function H_0 as

$$H_0 = -\log h_0.^{25} \tag{A3}$$

By definition the basicity of B or its pK_a value is expressed as

$$\begin{aligned} pK_a &= -\log K_a \\ &= H_0 + \log\frac{x}{1-x}, \end{aligned} \tag{A4}$$

A physical quantity Q for an equilibrated system is assumed to be additive of the components as in

$$Q = \alpha\{c(1-x)q_b + cxq_a\}, \tag{A5}$$

where q is the molar quantity of the component, such as molar extinction coefficient and the emission intensity per mole expected with a unit quantum yield, and α is a factor dependent on experimental conditions. Namely, factor α is the length of the cell in the case of electronic absorption measurement, while for emission spectra it is a function of the quantum yield, cell length, quenching mechanism, *etc.* and is usually left unknown.

Let us consider the latter case with unknown α. By choosing two different abscissae, or wavelengths, λ_1 and λ_2 (Fig. 9), we get

$$\begin{aligned} Q_1 &= \alpha\{c(1-x)q_{b1} + cxq_{a1}\} \\ Q_2 &= \alpha\{c(1-x)q_{b2} + cxq_{a2}\}. \end{aligned} \tag{A6}$$

For the ratio R, we get

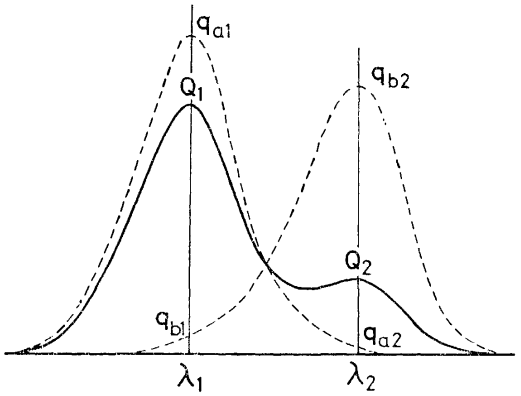

Fig. 9. Illustration for obtaining the equilibrium constant by measureing the absorbances at two different wavelengths
——: Observed spectrum
----: Spectrum of the component A
·····: Spectrum of the component B

$$R = \frac{Q_1}{Q_1+Q_2} = \frac{(1-x)q_{b1}+xq_{a1}}{(1-x)(q_{b1}+q_{b2})+x(q_{a1}+q_{a2})}$$
$$= \frac{q_{b1}+(q_{a1}-q_{b1})x}{(q_{b1}+q_{b2})+(q_{a1}+q_{a2}-q_{b1}-q_{b2})x}$$
$$= \frac{F+Gx}{D+Ex}, \qquad \text{(A7)}$$

which is a function of x (Eq. (A4)) and can be changed by varying the acidity H_0 of the solvent. By plotting R against H_0 we get a sigmoid curve whose limits are F/D and $(F+G)/(D+E)$ (Fig. 10).

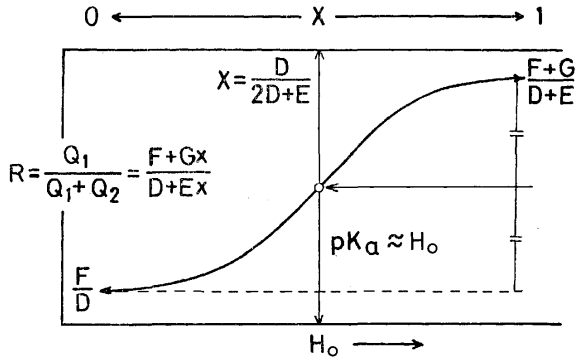

Fig. 10. Graphical method for obtaining the inflexion point of a sigmoid curve. Inflexion point is marked with ○.

Now let us find the inflexion point of this curve. By means of the relations[10]

$$\frac{dx}{dh_0} = \frac{(1-x)^2}{K_a} \qquad \text{(A8)}$$

$$\frac{dh_0}{dH_0} = -2.303h_0 \qquad \text{(A9)}$$

we get

$$\frac{dR}{dH_0} = -\frac{2.303h_0(1-x)^2(DG-EF)}{K_a(D+Ex)^2} \qquad \text{(A10)}$$

$$\frac{d^2R}{dH_0^2} = \frac{2.303^2h_0(1-x)^2(DG-EF)\{D-(2D+E)x\}}{K_a(D+Ex)^3} \qquad \text{(A11)}$$

By equating the identity (A11) to be zero, we get

$$x = \frac{D}{2D+E} = \frac{q_{b1}+q_{b2}}{(q_{b1}+q_{b2})+(q_{a1}+q_{a2})}, \qquad \text{(A12)}$$

with which the identity (A10) is not zero. Thus Eq. (A12) certifies the inflexion point. Substitution of Eq. (A12) into Eq. (A4) gives

$$pK_a = H_0 + \log\frac{q_{b1}+q_{b2}}{q_{a1}+q_{a2}}, \qquad \text{(A13)}$$

This means that if $q_{b1}+q_{b2}$ is nearly equal to $q_{a1}+q_{a2}$ the basicity pK_a is obtained as the H_0 value at the inflexion point of the curve $Q_1/(Q_1+Q_2)$ against H_0. Usually the quantities q's are unknown. However, if the maxima of Q for components A and B are of the same order of magnitude, the second term of the right hand side of Eq. (A13) would be negligible by choosing these peak wavelengths as λ_1 and λ_2 as in Fig. 9. This is shown in Table 2 for the case of xanthone derivatives, where the pK_a values estimated from the excitation spectra by using this method are very close to the values obtained from the ultraviolet absorption spectra.

When it is difficult to read the inflexion point of a sigmoid curve, the following additional relations are helpful. As evident from Eqs. (A10) and (A11), the slope of the curve R–H_0 is maximum at the inflexion point. It can easily be shown that the R value at the inflexion point is the arithmetic mean of the two asymptote readings

$$\left(F+G\frac{D}{2D+E}\right)\Big/\left(D+E\frac{D}{2D+E}\right) = \left(\frac{F}{D}+\frac{F+G}{D+E}\right)\Big/2. \qquad \text{(A14)}$$

The present method is not restricted to the case of an acid-base equilibrium (A1) and is also applicable to other types of equilibrium such as that of monomer-dimer

$$2A = A_2. \qquad \text{(A15)}$$

Analysis is straightforward.[26]

References

1) D. Cook, *Can. J. Chem.*, **41**, 505 (1963).
2) E. M. Arnett, "Progress in Physical Organic Chemistry," Vol. 1, Interscience Publishers, New York, N. Y. (1963), p. 203.
3) E. H. Rodd ed., "Chemistry of Carbon Compounds," Vol. IVB, Elsevier Publ. Co., Amsterdam (1957), p. 976.
4) A. I. Tolmachev, L. M. Shulezhko, and A. A. Kisilenko, *Russ. J. Gen. Chem.*, **35**, 1708 (1965).
5) I. Degani, R. Fochi, and G. Spunta, *Boll. Sci. Fac. Chim. Ind. Bologna*, **26**, 3 (1968).
6) E. M. Arnett, R. P. Quirk, and J. W. Larsen, *J. Amer. Chem. Soc.*, **92**, 3977 (1970).
7) A. A. L. Mesquita, D. de B. Corrêa, O. R. Gottlieb, and M. T. Magallães, *Anal. Chim. Acta*, **42**, 311 (1968).
8) F. Ullmann and M. Zlokasoff, *Ber.* **38**, 2111 (1905).
9) M. J. Jørgensen and D. R. Hartter, *J. Amer. Chem. Soc.*, **85**, 878 (1963).
10) H. Hosoya and S. Nagakura, *Spectrochim. Acta*, **17**, 324 (1961). All the last terms in Eq. (14) should be multiplied by ε.
11) R. N. Nurmuchametov, L. A. Mileshina, and D. N. Shigorin, *Opt. Spectrosc.*, **22**, 404 (1967).
12) H. J. Pownall and J. R. Huber, *J. Amer. Chem. Soc.*, **93**, 6429 (1971).
13) A. A. Efimov, R. N. Murmukhametov, I. L. Belaits, and A. I. Tolmachev, *Opt. Spectrosc.*, **30**, 337 (1971).

14) D. N. Shigorin, L. Sh. Tushishvii, N. A. Scheglova, and N. S. Dokunikhin, *Russ. J. Phys. Chem.*, **45**, 283 (1971).
15) R. Stewart, M. R. Granger, R. B. Moodie, and L. J. Muenster, *Can. J. Chem.*, **41**, 1065 (1963). The basicity scale is corrected to the H_0 scale of Jørgensen and Hartter.[9]
16) A. A. Efimov and V. M. Komarov, *Opt. Spectrosc.*, **30**, 10 (1971).
17) For example, see the large discrepancies between the π-electron densities by the Hückel[18] and more elaborated[19] methods cited in Ref. 20.
18) P. Caveng, P. B. Fischer, E. Heilbronner, A. L. Miller, and H. Zollinger, *Helv. Chim. Acta*, **50**, 848 (1967).
19) H. Hosoya, S. Hosoya, and S. Nagakura, *Theor. Chim. Acta*, **12**, 117 (1968).
20) M. J. Strauss, *Chem. Rev.*, **70**, 667 (1970).
21) K. Nishimoto and L. S. Forster, *Theor. Chim. Acta*, **4**, 155 (1966).
22) The X-ray structural analysis has been performed by S. C. Biswas and R. K. Sen, *Ind. J. Pure Appl. Phys.*, **7**, 408 (1969). However, their analysis is too rough to be compared with the theoretical bond lengths.
23) The program was written by Dr. T. L. Kunii and the computation was performed on a Hitac 5020E computer in the University of Tokyo.
24) K. Nishimoto and L. S. Forster, *J. Phys. Chem.*, **71**, 409 (1967); *ibid.*, **72**, 914 (1968); K. Nishimoto, *Theor. Chim. Acta*, **7**, 207 (1967); K. Nishimoto *et al.*, *ibid.*, **14**, 80 (1969).
25) L. P. Hammett and A. J. Deyrup, *J. Amer. Chem. Soc.*, **54**, 2721 (1932).
26) See for example H. Hosoya, J. Tanaka, and S. Nagakura, *J. Mol. Spectrosc.*, **8**, 257 (1962).

Studies of the π-π^* Absorption Bands of *p*-Quinones and *o*-Benzoquinone

Akira KUBOYAMA, Sanae MATSUZAKI, Hiroshi TAKAGI, and Hiroshi ARANO
National Chemical Laboratory for Industry, Shibuya-ku, Tokyo 151
(Received January 11, 1974)

The π—π^* absorption spectra of *p*-benzoquinone, α-naphthoquinone, anthraquinone, and their derivatives, mainly in *n*-heptane up to the vacuum UV region, were obtained. On the other hand, MO calculations of the π-electronic systems of these *p*-quinones and *o*-benzoquinone were carried out by means of the P-P-P method. The π—π^* absorption bands of these quinones could be favorably assigned on the basis of the calculated results.

As for the assignments of the $\pi \rightarrow \pi^*$ absorption bands of quinones in the ultraviolet (UV) region, many theoretical works[1-3] have been carried out. However, it is very desirable to clarify the absorption spectra in the vacuum ultraviolet (VUV) region in assigning the $\pi \rightarrow \pi^*$ absorption bands. The VUV absorption spectra of quinones have never been reported. In this work, the $\pi \rightarrow \pi^*$ absorption spectra of *p*-benzoquinone (*p*-BQ), α-naphthoquinone (α-NQ), anthraquinone(AQ), and their derivatives have been obtained up to the VUV region. On the other hand, MO calculations of the π-electronic systems of these *p*-quinones and *o*-benzoquinone have been carried out by means of the P–P–P method in order to determine the assignments of the $\pi \rightarrow \pi^*$ bands of these quinones.

Experimental

Measurements. The absorption spectra in the UV region were measured with a Cary 14 M recording spectrophotometer, and those in the VUV region, with a VUV-3 recording spectrophotometer of the Japan Spectroscopic Co., Ltd. The sample chamber and detector system of the latter apparatus have been modified as is shown in Fig. 1 after our previous work[4] on ketone vapors. Quartz cylindrical cells with 0.1, 0.5, and 1 mm paths were used; the design was similar to that used by Tsubomura *et al.*[5] *n*-Heptane and 1,1,1,3,3,3-hexafluoroisopropanol were used as solvents; they could be used up to 175 and 170 nm respectively with an 0.1 mm-path cell, but the former was mainly used. Daifloil (polymer of trifluorochloroethylene) was also used for *p*-benzoquinone in the UV region for the purpose of comparison.

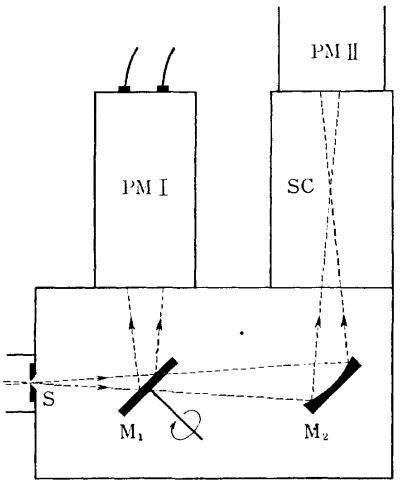

Fig. 1. The sample chamber and detector system
S: excit slit, M_1: plane rotating-sector mirror, M_2: concave mirror, SC: sample chamber, PMI and PMII: photomultiplyers (HTV R189).

Materials. *p*-BQ, 2,5-dimethyl-, and 2,5-dichloro-*p*-BQs, AQ, and 2-*t*-butyl-AQ (commercial products) were purified by sublimation. α-NQ (commercial products) was purified by vacuum sublimation at 30 °C. 2,5-Di-*t*-butyl-*p*-BQ (commercial products) was twice recrystallized from cyclo-

Table 1. Wavelengths, energies and molar absorptivities of the absorption maxima

	λ_{max} (nm)	E_{max} (eV)	ε_{max}	Solvent
p-BQ	277	4.48	338	*n*-Heptane
	240.5	5.16	20000	
	295	4.20	310	1,1,1,3,3,3-hexa-
	243	5.10	31000	fluoroisopropanol
	171.5	7.23	15500	
	296	4.19	271	Daifloil
	243.5	5.09	27800	
2,5-Dimethyl-*p*-BQ	305	4.07	291	*n*-Heptane
	256.5	4.83	20500	
	248.5	4.99	23200	
	178	6.97	19000	
2,5-Di-*t*-butyl-*p*-BQ	305	4.07	294	*n*-Heptane
	261	4.75	15100	
	253	4.90	17800	
	175.5	7.07	23600	
2,5-Dichloro-*p*-BQ	325	3.82	340	*n*-Heptane
	270	4.59	26500	
	186.5	6.65	18700	
α-NQ	328	3.78	2840	*n*-Heptane
	245.5	5.05	21300	
	239.5	5.18	19100	
	193.5	6.41	38200	
2,3-Dimethyl-α-NQ	326	3.80	2510	*n*-Heptane
	268.5	4.62	18600	
	259.5	4.78	18100	
	247.5	5.01	18000	
	242	5.12	16200	
	192	6.46	41900	
AQ	332.5	3.73	3620	*n*-Heptane
	319.5	3.88	4800	
	270.5	4.58	18000	
	250.5	4.95	56800	
	204	6.08	36800	
	181	6.85	40400	
2-*t*-Butyl-AQ	321	3.86	5380	*n*-Heptane
	273.5	4.53	21000	
	255.5	4.85	54200	
	203	6.11	35800	
	182	6.81	37500	

hexane. 2,3-Dimethyl-α-NQ was prepared according to the methods described in the literature[6] and, was purified by vacuum sublimation. The melting points of all these purified samples agreed with those reported in the literature. *n*-Heptane was treated with conc. sulfuric acid and purified by silica gel chromatography. 1,1,1,3,3,3-Hexafluoroisopropanol (Eastman Co.) and Daifloil (#1; mean molecular weight, 500; Daikin Kogyo Co.) were used without further purification.

Results. The absorption spectra obtained are shown in Figs. 2—5. In Fig. 3, the absorption bands of 2,5-di-*t*-butyl- and 2,5-dichloro-*p*-BQs near 305 and 325 nm respectively are not shown; that of the former is very similar to that of 2,5-dimethyl-*p*-BQ. The wavelength (λ_{max}), energies (E_{max}), and molar absorptivities (ε_{max}) of the absorption maxima in these spectra are shown in Table 1. Since the solubility of AQ in *n*-heptane was too poor for us to determine its concentration, the molar absorptivities of the absorption maxima of AQ in *n*-heptane were obtained by assuming that of the band near 320 nm to be 4800, considering its value (4800) in cyclohexane, obtained by Brockmann.[7]

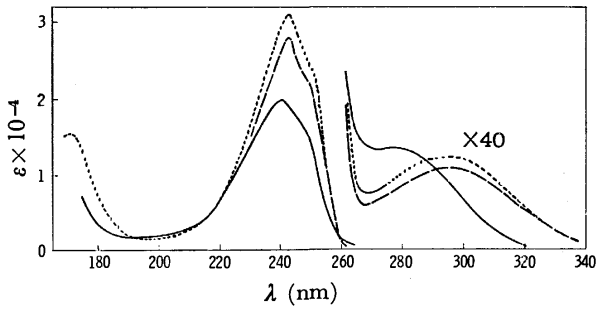

Fig. 2. Absorption spectra of *p*-benzoquinone in various solvents
——: *n*-heptane, ——: Daifloil, -----: 1,1,1,3,3,3-hexafluoroisopropanol

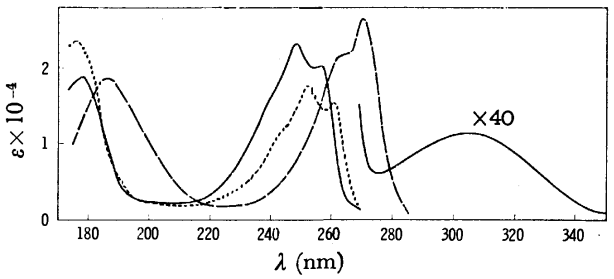

Fig. 3. Absorption spectra of *p*-benzoquinone substitutes in *n*-heptane
——: 2,5-dimethyl-, -----: 2,5-di-*t*-butyl-,
——: 2,5-dichloro-BQs

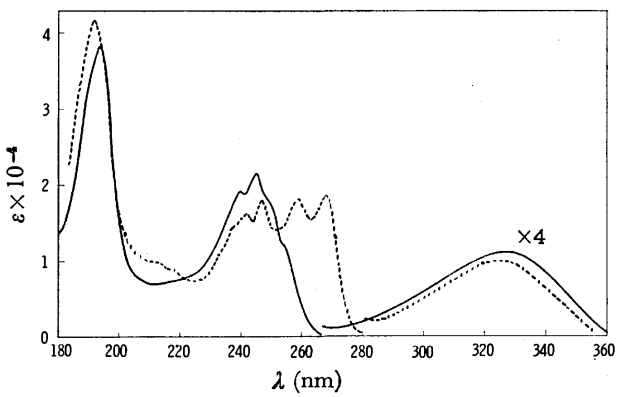

Fig. 4. Absorption spectra of α-naphthoquinones in *n*-heptane
——: α-naphthoquinone
-----: 2,3-dimethyl-α-naphthoquinone

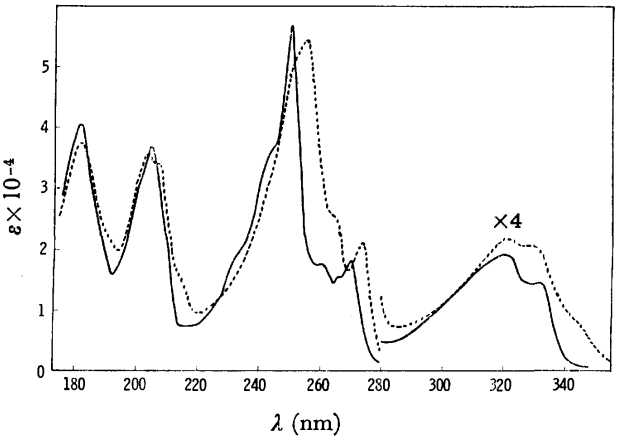

Fig. 5. Absorption spectra of anthraquinones in *n*-heptane
——: anthraquinone
-----: 2-*t*-butyl-anthraquinone

Calculations

Method. As for the electronic integral values in the P-P-P method, various kinds of integral values were tentatively used, considering the results obtained in our previous calculation[1a] on the π-electronic system of *o*-BQ. Finally, it was proved that a good agreement between the calculated and the experimental results was generally obtained using the electronic integral values shown in Table 2. In this table, the suffix letters C and O denote the carbon and oxygen atoms respectively. U_C^* denotes the U_C of the carbonyl carbon atoms, while β_{CC}, β_{CC}^*, β_{CC}^{**}, and β_{CO} denote those of the conventional C–C single, double and benzene-ring bonds, and carbonyl C–O bond respectively. The values in brackets are those for α-NQ. The value of U_C is the same as that used in Hush and Pople's paper,[9] while that of $|U_O|$ seems to be too small in view of the valence-state ionization potential of the oxygen atom (17.25 eV).[10] As has been pointed out by Sidman,[2e] however, the U-term in Pople's SCF MO method[11] should be regarded as the valence-state orbital energy corrected for the fact that the atom is no longer isolated,

Table 2. Electronic integral values (eV)

(1) One-center core integrals	
U_C	−9.50
U_C^*	−10.00
U_O	−13.00
(2) Two-center core integrals	
β_{CC}	−2.00 (−1.80)
β_{CC}^*	−2.50 (−2.70)
β_{CC}^{**}	−2.30
β_{CO}	−2.50
(3) Electronic repulsion integrals	
Nishimoto-Mataga method[8]	

but is now a part of a molecule. From this point of view, the value of U_O may not be unreasonable. The value of U_C^* was taken in view of the π-electron densities being considerably smaller than those of other carbon atoms. In order to explain theoretically the effect of methyl-group substitution on the energy of the $\pi\rightarrow\pi^*$ bands of α-NQ, the calculation of 2,3-dimethyl-α-NQ was carried out taking the U_C value of the substituted carbon atoms as −9.00 eV, considering the inductive effect of the methyl group, but without considering its resonance effect. The values of β_{CC}, β_{CC}^*, and β_{CO}, except those for α-NQ, are the same as those of Case II in our previous work[1a] on *o*-BQ and close to those used by Edwards *et al.*[3d] in the calculations of conjugated carbonyl compounds. The values of β for carbon-carbon bonds are, except those for α-NQ, far less sensitive to the variation in C–C bond distance than those generally used.

In the calculations, all the singly-excited configurations were included except in the case of AQ, where the lowest forty configurations were included. The calculations were carried out with a FACOM 270-30 computer. The dimensions of the quinones assumed are shown in Fig. 6. Those of the three *p*-quinones were assumed according to the results of the X-ray analysis.[12-14] The lengths of all the bonds in the benzene rings in α-NQ and AQ were assumed to be 1.40 A. The value for *o*-BQ was assumed on the basis of the bond orders obtained in our previous work.[1a]

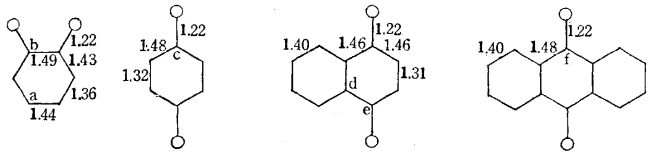

o-BQ (C_{2v}) *p*-BQ (D_{2h}) α-NQ (C_{2v}) AQ (D_{2h})

Fig. 6. Dimensions of the quinones (Å)
a: 120°, b: 121.5°, c: 117.5°, d: 118°, e: q118°, f: 117.5°

Results. The calculated excitation energies (E), oscillator strengths (f), and symmetry species[15] of the excited singlet states are shown, along with the observed results in *n*-heptane solutions, in Table 3. In this paper, the molecular planes are regarded as yz-planes, and the symmetry axes of *o*-BQ and α-NQ and the C–O bond axes of *p*-BQ and AQ are regarded as z-axes. The first column of this table indicates the numbering of the magnitude of E. In this table, the data on the higher excited states with small f-values have been omitted.

Table 3. The calculated excitation energies, oscillator strengths and symmetry species of the singlet excited states and the corresponding observed results

		Calculated		Observed	
No.	Symmetry	E(eV)	f	E(eV)	f
		(1) *o*-BQ			
1	B_2	3.716	0.234	3.5	0.05
2	A_1	5.134	0.001		
3	B_2	5.442	0.146	4.9	~0.03
4	B_2	5.994	0.014		
5	A_1	6.310	1.106	~6.2	>0.2
7	A_1	7.421	0.405		
8	B_2	7.644	0.216		
10	B_2	7.946	0.320		
		(2) *p*-BQ			
1	B_{3g}	4.223	0	4.5	<0.01
2	B_{1u}	4.489	1.031	5.2	0.54
3	B_{3g}	5.471	0		
4	A_g	5.814	0		
5	B_{2u}	6.795	0.127		
7	B_{1u}	7.146	0.194		
8	B_{1u}	7.267	1.072	~7.2	~0.5
9	B_{2u}	8.070	0.233		
		(3) α-NQ			
1	A_1	4.213	0.028	3.8	0.08
2	B_2	4.468	0.178		
3	B_2	4.850	0.549	5.1	0.40
4	A_1	5.138	0.331		
5	B_2	5.629	0.018		
6	A_1	5.809	0.026		
9	A_1	6.366	0.617	5.6	0.1
12	B_2	7.126	1.251	6.4	0.68
14	A_1	7.293	0.301		
16	B_2	7.832	0.303		
		(4) AQ			
1	A_g	4.167	0		
2	B_{2u}	4.206	0.066	3.9	0.05
3	B_{3g}	4.418	0		
4	B_{1u}	4.564	0.647	4.6	0.15
5	A_g	5.135	0		
6	B_{2u}	5.180	0.888	5.0	0.61
7	B_{3g}	5.465	0		
8	B_{1u}	5.684	0.126		
12	B_{2u}	6.111	1.251	6.1	0.46
18	B_{1u}	6.913	1.619	6.9	0.80
30	B_{1u}	8.073	0.749		

Discussion

o- *and* p-*Benzoquinones.* The absorption spectra of *o*-BQ in solutions obtained by Goldschmidt *et al.*[16] show that *o*-BQ has two $\pi\rightarrow\pi^*$ bands of a moderate intensity near 360 and 250 nm, and a strong $\pi\rightarrow\pi^*$ band near, 200 nm, or a little shorter than 200 nm.

The absorption spectra of *p*-BQ and its derivatives in Figs. 2 and 3 show that *p*-BQ has a weak $\pi\rightarrow\pi^*$ band[2f,17] near 280 nm and two strong $\pi\rightarrow\pi^*$ bands near 240 and 170 nm. It is noticeable that the absorption intensity of the band near 240 nm of *p*-BQ in 1,1,1,3,3,3-hexafluoroisopropanol and Daifloil is considerably stronger than that in *n*-heptane, and that the relative intensity of the absorption maxima of the bands near 250 and 175 nm is considerably different between 2,5-dimethyl- and 2,5-di-*t*-butyl-*p*-BQs.

In *o*- and *p*-BQs, the correspondences between the calculated and observed results are excellent, and the excited states of the $\pi\rightarrow\pi^*$ bands mentioned above could be favorably assigned, as is shown in Table 3. The theoretical and experimentally-determined[2b,18] assignments of the transitions of *p*-BQ in the UV region agree with each other. In our previous work[1a] on *o*-BQ, the assignment of the band near 250 nm was uncertain, but it could be reasonably determined in

TABLE 4. THE CHANGES OF THE CALCULATED $\pi\rightarrow\pi^*$ EXCITATION ENERGIES OF α-NQ WITH THE SUBSTITUTION OF TWO METHYL GROUPS TO ITS 2- AND 3-POSITIONS

No.	ΔE (eV)	No.	ΔE (eV)
1	+0.016	6	−0.098
2	−0.023	9	−0.013
3	−0.200	12	−0.029
4	+0.046	14	+0.082
5	+0.005	16	+0.023

this work. In *o*-BQ, two or three $\pi\rightarrow\pi^*$ bands of a moderate intensity may be expected to be found in the VUV region, judging from the calculated results shown in Table 3.

α-Naphthoquinone. As may be seen in Fig. 4, α-NQ has three distinct $\pi\rightarrow\pi^*$ bands—that is, a relatively weak band near 330 nm and two strong bands near 245 and 195 nm. Besides these three bands, α-NQ appears to have a $\pi\rightarrow\pi^*$ band of a moderate intensity between the two bands near 245 and 195 nm. Furthermore, comparing the absorption spectrum of 2,3-dimethyl-α-NQ with that of α-NQ in Fig. 4, it is clear that the band near 245 nm of α-NQ is composed of two bands the intensities of which are of comparable order, and that one of these two bands remarkably shifts toward longer wavelengths with the substitution of two methyl groups at the 2- and 3-positions of α-NQ. The changes in the calculated $\pi\rightarrow\pi^*$ excitation energies of α-NQ with this substitution are shown in Table 4.[19] As may be seen in Table 4, only the No. 3 state shows a large energy decrease with this substitution. Therefore, the No. 3 state may be assigned to the excited state of the band which largely shifts toward longer wavelengths with that substitution. On the other hand, the band near 330 nm is quite broad; this band may be composed of two $\pi\rightarrow\pi^*$ bands. Considering the above discussion, the excited states of the $\pi\rightarrow\pi^*$ bands of α-NQ can be reasonably assigned as is shown in Table 3. The assignments of the bands in the UV region agree with those made by Titz *et al.*[3e]

Anthraquinone. As may be seen in Fig. 5, AQ has five distinct $\pi\rightarrow\pi^*$ bands—that is, a relatively weak band near 320 nm, and four strong bands near 270, 250, 205, and 180 nm. As may be seen in Table 3, the correspondences between the calculated and observed results for these five bands are excellent, and the excited states of these $\pi\rightarrow\pi^*$ bands can be favorably assigned.[20] The assignments of the bands in the UV region agree with those by Nishimoto *et al.*[3a] and Titz *et al.*[3e] and are consistent with the experimental facts obtained by many authors.[21] As for the No. 30 state in Table 3, a $\pi\rightarrow\pi^*$ band corresponding to this state is expected to be found at the wavelength region shorter than 170 nm.

The authors are grateful to Dr. Fumihiko Hirota of Shizuoka University for his helpful advice in making the computer program and to Mr. Fumio Kobayashi and Mr. Teruo Kimura for their helpful co-operation in the experiments.

References and Notes

1) *o*-Benzoquinone: a) A. Kuboyama and K. Wada, This Bulletin, **38**, 1709 (1965); *Rep. Gov. Chem. Ind. Res. Inst., Tokyo*, **63**, 123 (1968); b) J.-C. Bery, *Theor. Chim. Acta*, **3**, 363 (1965); c) G. Hojer, S. Meza, and M. E. Ruiz, *Acta Chem. Scad.*, **27**, 1860 (1973).

2) *p*-Benzoquinone: a) H. Kon, This Bulletin, **28**, 275 (1955); b) L. E. Orgel, *J. Chem. Soc.*, **1955**, 121; c) M. Okuda, *J. Chem. Phys.*, **25**, 1083 (1956); d) T. Anno, I. Matsubara, and A. Sado, This Bulletin, **30**, 168 (1957); T. Anno, A. Sado, and I. Matsubara, *J. Chem. Phys.*, **26**, 967 (1957); e) J. W. Sidman, *ibid.*, **27**, 429 (1957); f) A. Sado, This Bulletin, **35**, 1514 (1962); g) A. Julg, J. C. Bery, and M. Bonnet, *Tetrahedron*, **20**, 2237 (1964); h) H. P. Trommsdorff, *J. Chem. Phys.*, **56**, 5358 (1972); i) P. E. Stevenson, *J. Phys. Chem.*, **76**, 2424 (1972); j) 1c).

3) Quinones; a) K. Nishimoto and L. S. Forster, *Theor. Chim. Acta*, **4**, 155 (1966); b) L. Leibovici and J. Deschamps, *ibid.*, **4**, 321 (1966); c) T. L. Kunii and H. Kuroda, *Rep. Compt. Cent. Univ. Tokyo*, **1**, No. 1, Apr.—Sept. (1968); d) T. G. Edwards and R. Grinter, *Mol. Phys.*, **15**, 349 (1968); e) M. Titz and M. Nepras, *Coll. Czech. Chem. Commun.*, **37**, 2674 (1972).

4) M. Ito, Y. Nogata, S. Matsuzaki, and A. Kuboyama, This Bulletin, **42**, 2453 (1969); A. Kuboyama and S. Matsuzaki, *Rep. Gov. Chem. Ind. Res. Inst., Tokyo*, **65**, 127 (1970).

5) H. Tsubomura, K. Kimura, K. Kaya, J. Tanaka, and S. Nagakura, This Bulletin, **37**, 417 (1964).

6) L. I. Smith and I. M. Webster, *ibid.*, **59**, 664 (1937).

7) DMS, "UV Atlas of Organic Compounds", Butterworths (1968), B8/10.

8) K. Nishimoto and M. Mataga, *Z. Phys. Chem.* (*N. F.*), **12**, 335 (1957).

9) N. S. Hush and J. A. Pople, *Trans. Faraday Soc.*, **51**, 600 (1955).

10) G. Pilcher and H. A. Skinner, *J. Inorg. Nucl. Chem.*, **24**, 937 (1962).

11) J. A. Pople, *Trans. Faraday Soc.*, **49**, 1375 (1953).

12) J. Trotter, *Acta Crystallogr.*, **13**, 86 (1960).

13) J. Gaultier and C. Haum, *ibid.*, **18**, 179 (1965).

14) a) B. V. R. Murty, *Z. Krist.*, **113**, 445 (1960); b) K. Lonsdale, H. J. Millege, and K. El-Sayed, *Acta Crystallogr.*, **20**, 1 (1967).

15) H. Eyring, J. Walter, and G. E. Kimball, "Quantum Chemistry," J. Wiley & Sons, New York (1944), p. 376.

16) S. Goldschmidt and F. Graef, *Ber.*, **61**, 1858 (1928).

17) This band has been assigned to a $\pi\rightarrow\pi^*$ band from the solvent effect on its position (S. Nagakura and A. Kuboyama, *Nippon Kagaku Zasshi*, **74**, 499 (1953); *J. Amer. Chem. Soc.*, **76**, 1003 (1954)).

18) a) J. C. D. Brand and T. H. Goodwin, *Trans. Faraday Soc.*, **53**, 295 (1957); b) J. W. Sidman, *J. Amer. Chem. Soc.*, **78**, 2362 (1956).

19) ΔE in Table 4 denotes the remainders where the $\pi\rightarrow\pi^*$ excitation energies of α-NQ are subtracted from the corresponding ones of 2,3-dimethyl-α-NQ.

20) In our previous work on AQ (A. Kuboyama and K. Wada, This Bulletin, **39**, 1874 (1966)), the assignments of the $\pi\rightarrow\pi^*$ bands were erroneous owing to miscalculations in the configuration interactions.

21) a) H. R. Drott and H. H. Dearman, *J. Chem. Phys.*, **47**, 1896 (1967); b) A. Kuboyama and S. Yabe, This Bulletin, **40**, 2475 (1967); c) H. Inoue, T. Hoshi, and Y. Tanizaki, *Nippon Kagaku Zasshi*, **92**, 25 (1971).

High-resolution Photoelectron Spectroscopy of Naphthacene Polycrystal by Means of Helium 21.22 eV Resonance Line

Kazuhiko SEKI, Yoshiya HARADA,* Koichi OHNO,* and Hiroo INOKUCHI

The Institute for Solid State Physics, The University of Tokyo, Roppongi, Minato-ku, Tokyo 106
**Department of Chemistry, College of General Education, The University of Tokyo, Komaba, Meguro-ku, Tokyo 153*

(Received January 28, 1974)

The photoelectron spectrum of naphthacene polycrystal was obtained with a high-resolution photoelectron spectrometer using a helium 21.22 eV light source, and the vibrational fine structures were examined. The resolution, 21 meV FWHM for the argon $P_{3/2}$ peak, became much better than that obtained by means of a retarding-potential-type electron analyzer. Broad peaks with no distinct intramolecular vibrational structure were observed, and the origin of the peak width was discussed.

Recent progress in the molecular photoelectron spectroscopy of the polycyclic aromatic hydrocarbons[1-3] has made possible a direct comparison between the photoelectron spectra of these compounds in the gaseous and solid states. From the comparison, it has been made clear that the ionization in the solid state reflects that of one molecule very well.[4,5] Until the present time, however, almost all solid-state photoelectron spectroscopic studies of these compounds[6] have been carried out by rather low-resolution retarding-potential-type electron-energy analyzers, and the precise examination of the fine structures associated with the electronic transitions was very difficult.

Considering the narrow electronic valence-band width of the molecular crystals, one might expect to find the well-seperated intramolecular vibrational levels of the ionic states by means of photoelectron spectroscopy.

Recently Kiyono *et al.*[7] studied the energy states of naphthacene polycrystal with a high-resolution photoelectron spectrometer. They suggested the existence of some intramolecular vibrational structures, but the weak intensity of the signal prevented them from drawing any definite conclusion. On the other hand, some mechanisms have been proposed which lead to the broadening of the peaks. Zagrubskii and Vilesov[8] pointed out the possibility of a Franck-Condon quantum-mechanical spread. Further, Silinsh[9] and Sworakowski[10] suggested the dispersion of the ionization potential by the lattice vibrations in the neutral state.

In this paper, we wish to report our findings regarding the high-resolution photoelectron spectrum of naphthacene polycrystal obtained using the helium 21.22 eV line.

Experimental

The photoelectron spectrometer was an electrostatic 127° co-axial cylindrical-type one which has already been reported.[11] The ionization chamber of the instrument, however, was modified for the solid sample. Naphthacene was evaporated on a copper substrate and was inserted into the ionization chamber. The resolution of the electron spectrometer was 21 meV FWHM for the argon $P_{3/2}$ peak, but it was about one-third of this FWHM value at the first ionization peak of naphthacene, since the kinetic energy of the photoelectron was scanned by the voltage between the two deflector electrodes. The contact potential difference between the sample and the deflector electrodes was hard to estimate, so in calculating the ionization potentials it was assumed to be zero.

Results and Discussion

In Figs. 1a and 2a, the full and expanded spectra of the lower ionization potential region of naphthacene polycrystal are shown. In Figs. 1b and 2b, the molecular photoelectron spectra of the corresponding regions[1] are shown for comparison. In Table 1, the numerical values of the ionization potentials for the region of Fig. 2a are listed, along with the gaseous-state values and also other photoemission results.

Figures 1a and 2a show that the resolution is much better than that of the previous retarding potential method.[5] For example, the peaks at 8.77 and 10.72 eV appeared as shoulders in the retarding potential study. The position of the small shoulder at 8.3 eV was a little less reproducible than the other peaks, so the numerical value in Table 1 is given as 0.1 eV. A comparison with the other photoemission works in Table 1 shows that the agreement is very good; this finding suggests that the contact potential difference,

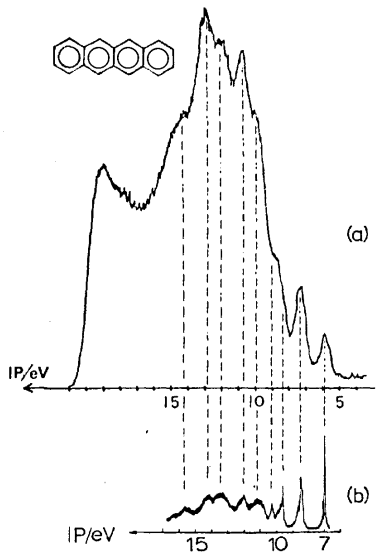

Fig. 1. (a) Photoelectron spectrum of naphthacene polycrystal (full spectrum). (b) Molecular photoelectron spectrum of naphthacene (from Ref. 1).

Table 1. Ionization potentials of the peaks in Fig. 2

	Gas[1),a)]		This work[a)]		Seki *et al.*[5),a)]		Kiyono *et al.*[7),a)]		Hirooka *et al.*[4),b)]	
	IP	ΔIP	IP	ΔIP	IP	ΔIP	IP	ΔIP	IP	ΔIP
A	7.01	0.0	5.83	0.0	5.9	0.0	5.75	0.0	5.83	0.0
B	8.41	1.41	7.31	1.48	7.3	1.4	7.27	1.52	7.28	1.45
	(8.6)	(1.5_9)								
C	9.56	2.55	(8.3)	2.5					8.29	2.46
D	(9.7)	(2.6_9)	8.77	2.94	8.7	2.8	8.64	2.89	8.70	2.87

a) $h\nu$=21.22 eV b) The average values obtained by several photon energies ($h\nu \leq 10.78$ eV).

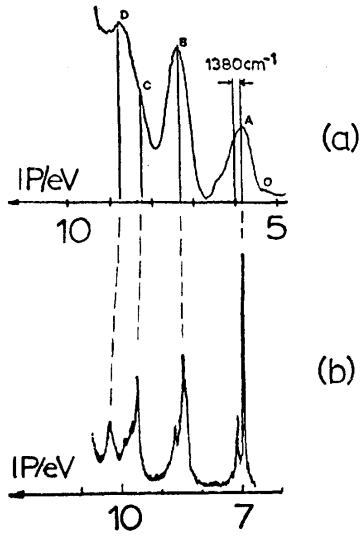

Fig. 2. (a) Expanded photoelectron spectrum of the lower ionization potential region of naphthacene polycrystal. (b) Molecular photoelectron spectrum of the region corresponding to (a) (from Ref. 1).

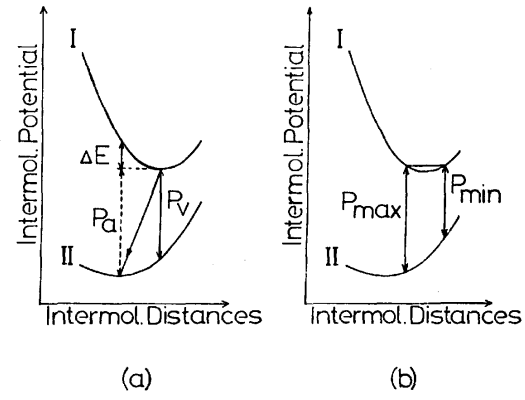

Fig. 3. Two mechanisms for the broadening of the peaks. On ionization, potential curve of the neutral state (curve I) changes to that of the ionized state (curve II) due to the polarization effect.
(a) Franck-Condon quantum-mechanical spread.
(b) Polarization energy dispersion due to the lattice vibrations in the neutral state.

ignored in this work, is really very near to zero.

The work in the gaseous state shows[1)] that the first ionization peak contains only one electronic transition, so it is appropriate for the examination of fine structures. As is shown in Fig. 2b, there is an intramolecular vibrational structure of 1380 cm^{-1} (0.17 eV) in the gas spectrum, but, at least at this stage of resolution, there is no distinct corresponding structure in the first ionization peak in the solid state and the peak width (the overall FWHM of this band is 0.64 eV) is much larger than that of the gas spectrum (*cf.* Fig. 2a).

The fact that the 0–0 transition is very strong in the gaseous state suggests that no large deformation of the molecule occurs upon ionization; therefore, it is difficult to ascribe the large peak width in the solid state to intramolecular vibrations.

Some other mechanisms which lead to the broadening of the peaks have been proposed. If these effects are large enough, and if every intramolecular vibrational level is accompanied by them, the disappearance of the fine structures may be explained. Considering the interaction of the ion as a point charge with the nearest four molecules, Zagrubskii and Vilesov[8)] estimated the Franck-Condon quantum-mechanical spread due to the local lattice deformation for anthracene and obtained a value of 0.35 eV for the difference between the adiabatic and vertical transitions (*cf.* Fig. 3a, where this difference is $P_a - P_v$). However, they took the value for the total ion-dipole and dipole-dipole interactions and neglected the energy for the lattice deformation itself (ΔE in Fig. 3a). After correction for this, the value for anthracene is only 0.08 eV. We made similar calculations for naphthacene with a mean molecular polarizability of 32.4 $Å^3$ [12)] and with a force constant of 100 cm^{-1} for the lattice deformation; we thus obtained a value of 0.17 eV. With this value, and considering the roughness of the approximation, we are not able to decide at this stage whether this mechanism can explain the large peak width or not.

Further, Silinsh[9)] and Sworakowski[10)] suggested a dispersion of the polarization energy due to the lattice vibrations in the neutral state (P_{max} to P_{max} in Fig. 3b). The FWHM expected for this mechanism amounts to about 0.3 eV (assuming σ=0.1 eV for the gaussian distribution). It seems certain that this mechanism plays some role in the broadening of the peaks.

In both mechanisms, the first peak is expected to correspond to the vertical ionization from the equilibrium position for the lattice vibrations. The fact that the ionization energies estimated for this process (5.81 eV by Sworakowski[10)] and 5.83 eV by Batley *et al.*[13)]) agree well with the value for the first peak confirms this idea.

Other possible mechanisms contributing to the peak width are as follows: (1) a variation in the ionization potential between the bulk and the surface;[14)] (2) an energy loss of the photoelectrons on the way to the surface[15)] as a result of the excitations of the intra-

molecular vibrations of the other neutral molecules (an energy loss due to the phonons is less likely because of their small energy quantum), and (3) the lifetime broadening of the photoelectrons.[16] To determine the degrees of contribution from these factors, however, further comprehensive studies, including the improvement of the resolution, will be necessary.

The authors are very grateful to Drs. I. Harada, N. Ueno, and M. Kotani for their helpful discussions and to the Nishina Memorial Foundation for its financial support. They also wish to thank to Mr. Kiyoo Tsuji for modifying the photoelectron spectrometer.

References

1) P. A. Clark, F. Brogli, and E. Heilbronner, *Helv. Chim. Acta*, **55**, 1415 (1972).
2) R. Boschi, J. N. Murrell, and W. Schmidt, *Discuss. Faraday Soc.*, **54**, 116 (1972).
3) R. Boschi and W. Schmidt, *Tetrahedron Lett.*, **1972**, 2577.
4) T. Hirooka, K. Tanaka, M. Fujihira, H. Inokuchi, Y. Harada, and K. Kuchitsu, *Chem. Phys. Lett.*, **18**, 930 (1973).
5) K. Seki, H. Inokuchi, and Y. Harada, *ibid.*, **20**, 197 (1973).
6) References 4, 5, 8, and 15 and references cited therein.
7) S. Kiyono, N. Ueno, and Y. Hayashi, *Tech. Rep. Tohoku Univ.*, **38**, 173 (1973).
8) A. A. Zagrubskii and F. I. Vilesov, *Sov. Phys. Solid State*, **13**, 1927 (1973).
9) E. A. Silinsh, *Phys. Stat. Sol.*, **3a**, 817 (1970).
10) J. Sworakowski, *ibid.*, **13a**, 381 (1972).
11) Y. Harada, K. Seki, A. Suzuki, and H. Inokuchi, *Chem. Lett.*, **1973**, 893.
12) F. Gutmann and L. E. Lyons, "Organic Semiconductors", John Wiley & Sons, New York, N.Y. (1967).
13) M. Batley, L. J. Johnstone, and L. E. Lyons, *Aust. J. Chem.*, **23**, 2397 (1970).
14) D. R. Kearns and M. Calvin, *J. Chem. Phys.*, **34**, 2026 (1961); J. Sworakowski, *Phys. Stat. Sol.*, **10b**, K89 (1972).
15) F. I. Vilesov, A. A. Zagrubskii, and D. Z. Garbuzov, *Sov. Phys. Solid State*, **5**, 1460 (1964).
16) C. N. Berglund and W. E. Spicer, *Phys. Rev.*, **136**, 1030 (1964); C. N. Berglund and W. E. Spicer, *ibid.*, **136**, 1044 (1964).

Effect of Cesium Counterion on the ESR Spectrum of Tetracyanoethylene Anion Radicals

Masaaki OGASAWARA, Seizo INABA, Hiroshi YOSHIDA, and Koichiro HAYASHI*

Faculty of Engineering, Hokkaido University, Sapporo, 060

(Received August 1, 1973)

Evidence was obtained by ESR for the ion-pair formation between the tetracyanoethylene anion radical and the cesium counterion in tetrahydrofuran. The hyperfine lines of the ESR spectrum of cesium tetracyanoethylenide were exceptionally broad at high salt concentrations in tetrahydrofuran, while they were remarkably narrowed by the addition of a small amount of DMF or triglyme (cation-solvating agents) or by replacing the counterion with the tetra-*n*-butylammonium ion. This indicates that the broad linewidth is due to the unresolved hyperfine splitting of the cesium counterion. In addition, the concentration dependence of the ESR spectrum indicates that the line broadening is to be interpreted not only in terms of the Heisenberg spin exchange, but also in terms of the equilibrium between the ion-pair and the free ion. The cesium hyperfine coupling constant was estimated by simulating the line shape to be 40 m Gauss in the ion-pair state between the tetracyanoethylene anion radical and the cesium ion in the tetrahydrofuran solution.

Since the first observation of the electron spin resonance (ESR) spectrum of the tetracyanoethylene (TCNE) anion radical by Weissman *et al.* in 1960,[1] this anion radical has been known to be very stable in many solutions at room temperature and has been known to give a simple well-resolved ESR spectrum with a hyperfine structure due to the four equivalent ^{14}N nuclei. Several workers have studied the variety of metal tetracyanoethylenide systems by ESR, but have failed to observe any metal hyperfine splittings.[1-4] Furthermore, the electronic spectra of these systems were found to depend neither on the solvent nor on the metal cation.[5]

Recently, we studied the electron-transfer reaction of the TCNE anion in ethereal solvents and found that the observed kinetical behavior could be interpreted in terms of the electrostatic interactions between anions and counterions, and also that the line shape of the ESR spectrum of cesium tetracyanoethylenide became wide and distorted as the concentration of TCNE anion increased.[6] The previous investigation will be extended here to a study of the shape of the ESR spectrum of cesium tetracyanoethylenide in tetrahydrofuran (THF) and 1,2-dimethoxyethane (DME) in more detail. Our new evidence for the ion-pair formation of the TCNE anion will be reported in the present paper.

Experimental

Materials. The cesium tetracyanoethylenide (TCNE$^-$Cs$^+$) was synthesized as follows.[7] TCNE of a guaranteed reagent grade (Tokyo Kasei Kogyo Co., Ltd.) was purified by repeated sublimations *in vacuo*. Cesium iodide of a guaranteed reagent grade (Wako Pure Chemical Ind., Ltd.) was dried *in vacuo* at 100 °C for 24 hr. The TCNE and cesium iodide were dissolved into acetonitrile *in vacuo*, and the mixture was stirred by a magnetic stirrer for 48 hr at 0 °C. The solution was filtered *in vacuo* and condensed by evaporating the solvent. After the solution had then stood overnight, a reddish-brown solid, TCNE$^-$Cs$^+$, crystallized; this was washed with acetonitrile and dried. The crystalline TCNE$^-$Cs$^+$ was stable at room temperature in a glass ampoule for more than one year. The purity of the sample, as determined by elementary analysis, was approximately 92%.

The THF and DME were carefully purified and dried as has been described previously.[6] The trimethylene glycol dimethylether (triglyme) and *N,N*-dimethylformamide (DMF) were distilled over calcium hydride at reduced pressure. The tetra-*n*-butylammonium perchlorate (Bu_4NClO_4) was synthesized and purified as has been described previously.[6]

Sample Preparation and Measurements. The sample solution was prepared by dissolving crystalline TCNE$^-$Cs$^+$ into the respective solvent *in vacuo* and was sealed into a ESR sample tube made of Pyrex glass. Triglyme or DMF was added to the sample solution, if needed, through a break seal.

The concentration of TCNE$^-$Cs$^+$ was determined from the absorption maximum at 420 nm ($\varepsilon = 7100\ cm^{-1}\cdot l\cdot mol^{-1}$)[7] in the visible spectra.

All the ESR spectra were taken with a JES-NE-2X spectrometer equipped with 100 kHz filed modulation and a variable-temperature control unit.

Results and Discussion

Effect of Additives. The ESR spectrum of the TCNE anion consists of 11 lines with a separation of 1.65 Gauss, as has been reported by Weissman *et al.*[1] Most of the alkali metal (Li^+, Na^+, K^+) salts and tetra-*n*-butylammonium(Bu_4N^+) salt give ESR spectra consisting of sharp hyperfine lines, though their width increases slightly with an increase in the salt concentration. In contrast, it was found for cesium salt that the width of the hyperfine lines increased remarkably with an increase in the concentration. Figure 1 shows a representative spectrum with broad hyperfine lines at a high concentration of cesium salt. It was also found that the line shape deviated more and more

Fig. 1. ESR spectrum of 3.0×10^{-4} M TCNE$^-$Cs$^+$ in THF at 25 °C.

* Present address: The Institute of Scientific and Industrial Research, Osaka University, Suita, Osaka, 565.

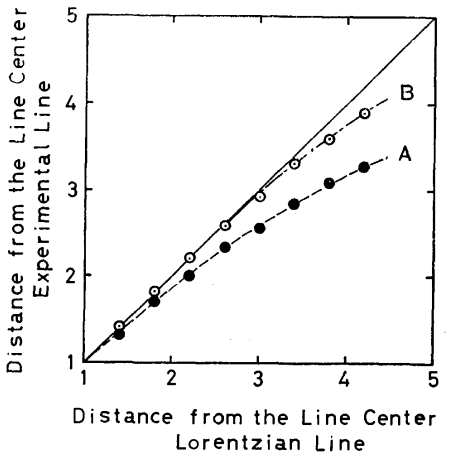

Fig. 2. Line shapes of the $\bar{M}=0$ lines in the first-derivative ESR spectra of TCNE$^-$Cs$^+$ at 25 °C. The distance in units of half the peak-to-peak width of the experimental line is plotted against the distance at which a Lorentzian line has the same relative amplitude: A, 4.2×10^{-4} M TCNE$^-$Cs$^+$ in THF; B, 4.6×10^{-4} M TCNE$^-$Cs$^+$ in THF–triglyme (2.8 mole%) mixture; solid line, a Lorentzian shape.

from a Lorentzian shape as the concentration increased. Figure 2(A) shows the deviation of the ESR spectral shape for the central hyperfine line observed at the 4.2×10^{-4} M TCNE$^-$, Cs$^+$ solution in THF from the ideal Lorentzian shape. The experimentally-observed first-derivative line shape is compared with the first-derivative line shape of a Lorentzian line having the same peak-to-peak amplitude and width as the experimental line. The distance in units of half the peak-to-peak width of the experimental line from the line center at several amplitudes is plotted against the corresponding value for the pure Lorentzian line. The solid line indicates the relation expected for a pure Lorentzian line shape. It is evident that the observed shape falls off at the tail much more rapidly than a Lorentzian shape. It has been reported that potassium tetracyanoethylenide gave a Lorentzian shape even at concentrations as high as 7×10^{-4} M.[4]

To study the effect of solvation on the ESR spectrum

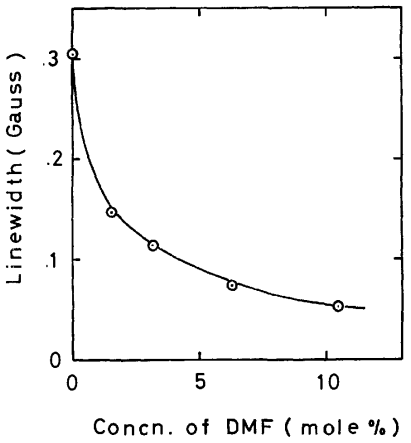

Fig. 3. Change of ESR linewidth ($\bar{M}=0$) of 3.0×10^{-4} M TCNE$^-$Cs$^+$ upon addition of DMF into THF solution at 25 °C.

of the TCNE$^-$Cs$^+$–THF system, DMF and triglyme were used as cation-solvating agents. Figure 3 shows the change in the ESR linewidth for the 3×10^{-4} M of TCNE$^-$ caused by the added DMF. The linewidth is considerably reduced by the presence of a small amount of DMF. With the increasing amount of DMF, the linewidth seems to decrease beyond the limit of measurement (—25 m Gauss). The linewidth is also reduced by the addition of triglyme. The results at several temperatures are shown in Fig. 4.

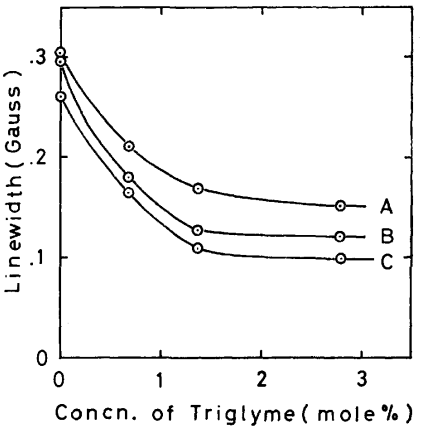

Fig. 4. Change of ESR linewidth ($\bar{M}=0$) of 3.0×10^{-4}M TCNE$^-$Cs$^+$ upon addition of triglyme into THF solution at various temperatures: A, 25 °C; B, 0 °C; C, −30 °C.

Because both additives are known to solvate preferentially the cesium ion,[8,9] the observed change of the linewidth may be interpreted by Process (1) or (2);

$$\text{TCNE}^-\text{Cs}^+ + n\text{DMF} \longrightarrow \text{TCNE}^-\text{Cs}^+(\text{DMF})_n \quad (1)$$

$$\text{TCNE}^-\text{Cs}^+ + n\text{Triglyme} \longrightarrow \text{TCNE}^-\text{Cs}^+(\text{Triglyme})_n \quad (2)$$

Here, TCNE$^-$Cs$^+$ and TCNE$^-$Cs$^+$(additive)$_n$ denote the ion-pair and the solvent-separated ion-pair respectively. Thus, the effect of cation-solvating agents strongly suggests that the abnormally broad ESR spectrum is to be attributed to unresolved cesium hyperfine splitting.

The linewidth tends to reach a plateau at high concentrations of triglyme (>2—3 mol%). The plateau value is thought to be the linewidth of the cesium-free TCNE anion at this radical concentration. On the other hand, there is no such trend for DMF, and the linewidth seems to decrease continuously. Because DMF is known to solvate not only cations but also anions, the narrower linewidth at high concentrations of DMF may be due to the coordination of DMF molecules to the TCNE anion.

Figure 5 shows the change in the linewidth of the 3.0×10^{-4} M TCNE$^-$Cs$^+$ sample caused by the addition of Bu_4NClO_4 salt. The linewidth is rapidly reduced at first and then gradually by the addition of Bu_4NClO_4. It is known that the alkali metal hyperfine splitting in the ESR spectrum of the alkali metal anthracenide–THF system disappears upon the addition of this salt, which has been interpreted in terms of the

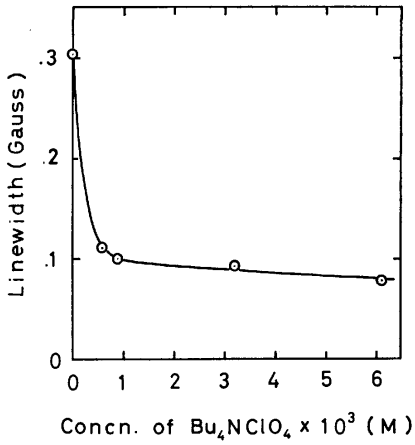

Fig. 5. Change of ESR linewidth ($\bar{M}=0$) of 3.0×10^{-4}M TCNE$^-$Cs$^+$ upon addition of tetra-*n*-butylammonium perchlorate into THF solution at 25 °C.

replacement of counterion.[10] The analogous replacement of the counterion is responsible, in this case, for the narrowing of the linewidth, as;

$$TCNE^-Cs^+ + Bu_4N^+ \longrightarrow TCNE^-Bu_4N^+ + Cs^+. \quad (3)$$

Concentration Dependence. Figure 6 shows the relation between the radical concentration and the ESR linewidth of TCNE$^-$Cs$^+$ in three different solvents; THF, DME, and THF containing 2.8 mol% of triglyme. In THF, the linewidth increases rapidly with an increase in the radical concentration up to 3×10^{-4} M and then the rate of increase is lowered. The linewidth in DME and the THF–triglyme mixture is dependent rather slightly on the radical concentration. Especially in the THF–triglyme mixture, only a small dependence was observed. The intercepts of these three curves at zero concentration were coincident with each other within the limits of experimental error.

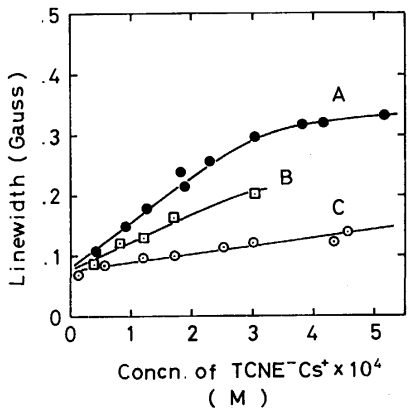

Fig. 6. Concentration dependence of ESR linewidth ($\bar{M}=0$) of TCNE$^-$Cs$^+$ in various solvents at 0 °C: A, THF; B, DME; C, THF-triglyme (2.8 mol%) mixture.

One of the possible mechanisms is the Heisenberg spin exchange between the anion radicals, which results in an increase in the linewidth with an increase in the concentration. It is well established that the effects of the Heisenberg spin exchange on the ESR spectra are identical with those of the diffusion-controlled or nearly diffusion-controlled chemical exchange.[4,11,12] In the slow exchange limit, the second-order rate constant of the spin exchange, k, is expressed for a Lorentzian line as:

$$k = \frac{\sqrt{3}}{2} f_{\bar{M}} |\gamma_e| \Delta H_{\bar{M}} / C, \quad (4)$$

where γ_e is the gyromagnetic ratio; $\Delta H_{\bar{M}}$ is the increase in linewidth due to the spin exchange; C, the concentration of paramagnetic entities in question, and $f_{\bar{M}}$, the statistical factor for the transition of the spectral index number, $\bar{M}$ ($f_0=1.306$ for the TCNE anion).[4] Assuming that the observed ESR broadening is attributable to the Heisenberg spin exchange, the second-order rate constant can be evaluated from Fig. 6 and Eq. (4). Table 1 summarizes the values calculated from the slopes of the lines in Fig. 6. Since the plots for the THF as solvent are not linear over the entire concentration range examined, the rate constant was evaluated from the slope of the line (A) in the low-concentration range (0—2×10^{-4} M).

Table 1. Spin-exchange rate constants k at 0 °C

Solvent	k($M^{-1}\cdot s^{-1}$) Experimental	Theoretical
THF	1.48×10^{10}	5.0×10^9
DME	8.9×10^9	4.9×10^9
THF–triglyme (2.8 mol%) mixture	2.7×10^9	5.0×10^9

Table 1 also includes the rate constants estimated from the simple Brownian diffusion model, in which the mean time, τ, between successive bimolecular encounters of radicals is represented by the following equation:[4]

$$\tau^{-1} = 4\pi d D \Pi \quad (5)$$

where Π refers the density of the radicals and where D is the diffusion coefficient in a Stokes-Einstein model:

$$D = kT/6\pi a\eta \quad (6)$$

determined by the molecular radius, a, the solvent viscosity, η, and the interaction distance for exchange, d (here it was assumed to be $2a$).[4] For the sake of simplicity, the effect of the charge was neglected in deriving Eq. (5). With the effect of the charge involved, the rate constant would be smaller than those given in Table 1. The viscosity of THF–triglyme was assumed to be the same as that of pure THF.

The k value derived from the observed linewidths in THF is much larger than that to be expected from the diffusion model. This leads to the recognition that the line broadening (Line A in Fig. 6) can not be explained solely by the spin-exchange mechanism. This fact, together with the effects of additives, may indicate that the strong dependence of the linewidth on the radical concentration in THF is, to a large extent, due to the ion-pair formation between the THF anion and the cesium ion. The equilibrium between the ion-pair and the free ion:

$$TCNE^-Cs^+ \rightleftarrows TCNE^- + Cs^+, \quad (7)$$

shifts to the left-hand side, and the fraction of the ion-

pair increases, when the radical concentration increases, resulting in a broadening of the ESR linewidth. The break of Line (A) at 3×10^{-4} M may be interpreted in terms of the complete ion-pair formation at this concentration.

As is shown in Fig. 6 and Table 1, the linewidth increases more slowly and the observed k is rather close to the expected k in DME than in THF. This is attributable to the high solvation of the cesium ion in DME,[13] which results in the formation of a solvent-separated ion-pair and/or increase in the free-ion fraction and, therefore, less effect of the cesium counterion on the ESR linewidth.

In the THF–triglyme mixture, the observed k is in agreement with the expected one. A more excellent agreement can be obtained if the effect of the charge and the increment in the viscosity arising from the addition of triglyme are taken into account. The activation energy evaluated from the Arrhenius plot of the observed k was found to be 3 kcal·mol^{-1}. This value is comparable with that of the diffusion-controlled chemical reaction in THF. Furthermore, the observed k agrees with that for the potassium tetracyanoethylenide–DME system reported by Freed *et al.*[4] In addition, the hyperfine lines were found to have a Lorentzian shape in this solvent within the limits of experimental error, as is shown in Fig. 2(B). These observations indicate that there is no broadening effect of the cesium ion in the THF–triglyme mixture and that the Heisenberg spin exchange solely determines the ESR linewidth in this system.

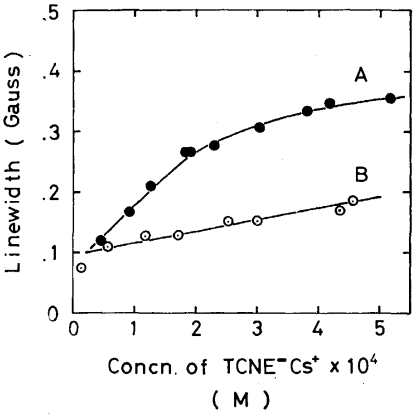

Fig. 7. Concentration dependence of ESR linewidth ($\bar{M}=0$) of TCNE$^-$Cs$^+$ in various solvents at 25 °C: A, THF; B, THF–triglyme (2.8 mol%) mixture.

Figure 7 shows the concentration dependence of the linewidth at 25 °C in THF and THF–triglyme. In comparison with the results obtained at 0 °C (Fig. 6), the break of the curve for the THF shifts toward a lower concentration. This can reasonably be interpreted in terms of the quilibrium (7). Because the dissociation reaction of the ion-pair is exothermic in a liquid, as has been suggested by Denison and Ramsay[14] and Szwarc *et al.*,[13,15] the equilibrium (7) will be shifted to the left-hand side by raising temperature. Therefore, the higher the temperature, the more readily is the ultimate formation of the ion-pair reached. Figure 7 shows the same slope for both THF and THF–triglyme, after the ultimate formation of ion-pair is reached in the former solvent. This suggests that only the Heisenberg spin exchange contributes to the ESR line-broadening in this concentration range in THF, as is the case over the entire concentration range in the THF–triglyme mixture.

Simulation of ESR Spectra. Although the behavior of the spectra indicated ion-pair formation in the TCNE$^-$Cs$^+$–THF system, as has been mentioned above, the hyperfine splitting due to the cesium ion was too small to be resolved experimentally.

Therefore, the hyperfine coupling constant was estimated by comparing the observed spectra with the simulated ones. The simulated spectra were synthesized by means of digital computer (Hokkaido University Computing Center) under the following assumptions: (1) the life-time of the cation-anion pair is long enough compared with the inverse of the cesium hyperfine splitting; (2) each of the 11 lines of the spectrum of the TCNE anion (see Fig. 1) consists of equally-spaced Lorentzian component lines due to $I=7/2$ for the cesium nuclei, and (3) the contribution from the natural abundance of ^{13}C can be ignored. Then, the first-derivative line shape was simulated for an observed line; the $\Delta H_{obs}/\Delta H_L$ ratio is numerically related to the $a_{Cs}/\Delta H_L$ ratio. Here, ΔH_{obs} is the observed peak-to-peak linewidth; ΔH_L, the peak-to-peak linewidth for the first-derivative of the component Lorentzian line, and a_{Cs}, the hyperfine coupling constant of the cesium ion. This treatment is essentially the same as that used for the ion-pair with a sodium counterion by Jones *et al.*[16] The ΔH_{obs} increases with the increasing $a_{Cs}/\Delta H_L$ ratio. When the value of $a_{Cs}/\Delta H_L$ reaches 0.8, the individual component lines begin to become resolved.

If the value of ΔH_L is known, a_{Cs} can be derived from the observed linewidth of the TCNE$^-$Cs$^+$–THF system (ΔH_{obs}) at concentrations high enough for all the anions to form ion-pairs with cesium ion. We presumed that the linewidth observed in the THF–triglyme mixture (Line B in Fig. 7) is identical with the ΔH_L in THF at the same concentration and temperature, because the anion is free from the counterion in the mixture solvent. Thus, the cesium hyperfine coupling constant, a_{Cs}, in THF at 25 °C is determined to be 40 m Gauss from the Line A in Fig. 7 at concentrations higher than 3×10^{-4} M.

References

1) W. D. Phillips, J. C. Rowel, and S. I. Weissman, *J. Chem. Phys.*, **33**, 626 (1960).
2) R. H. Rieger, I. Bernal, W. H. Reinmuth, and G. K. Fraenkel, *J. Amer. Chem. Soc.*, **85**, 683 (1963).
3) J. Gendell, J. H. Freed, and G. K. Fraenkel, *J. Chem. Phys.*, **41**, 949 (1964).
4) M. P. Eastman, P. G. Kooser, M. R. Das, and J. H. Freed, *ibid.*, **51**, 2690 (1969).
5) M. Itoh, *J. Amer. Chem. Soc.*, **92**, 886 (1970).
6) M. Ogasawara, H. Takaoka, and K. Hayashi, This Bulletin, **46**, 35 (1973).
7) O. W. Webster, W. Mahler, and R. E. Benson, *J. Amer. Chem. Soc.*, **84**, 3678 (1962).

8) B. F. Wong and N. Hirota, *ibid.*, **94**, 4419 (1972).
9) R. V. Slates and M. Szwarc, *ibid.*, **89**, 6043 (1967).
10) K. Suga and S. Aoyagi, This Bulletin, **45**, 1375 (1972).
11) T. A. Miller and R. N. Adams, *J. Amer. Chem. Soc.*, **88**, 5713 (1966).
12) M. P. Eastman, G. V. Bruno, and J. H. Freed, *J. Chem. Phys.*, **52**, 2511 (1970).
13) C. Carvajal, K. J. Tölle, J. Smid, and M. Szwarc, *J. Amer. Chem. Soc.*, **87**, 5548 (1965).
14) J. T. Denison and J. B. Ramsay, *ibid.*, **77**, 2615 (1955).
15) M. Szwarc, "Carbanions, Living Polymers, and Electron Transfer Processes," Chapter 5, John Wiley & Sons, New York (1968), p. 225.
16) M. T. Jones, M. Komarynsky, and R. D. Rataiczak, *J. Phys. Chem.*, **75**, 2769 (1971).

Molecular Orbital Study on the H_2O-HCl System

Shuzo SHIBATA, Fumihiko HIROTA, and Yukio OTA
Department of Chemistry, Shizuoka University, Oya, Shizuoka 420
(Received December 14, 1973)

The hydrogen bonded system of H_2O–HCl was studied by the CNDO/2 method. Calculation of the potential energy for the system showed that the complex of H_2O–HCl is considerably stable. The equilibrium structure of the complex and its charge distribution were also investigated.

A number of studies by molecular orbital calculations on simple hydrogen bonded systems have been reported since Clementi carried out a detailed study on ammonium chloride.[1] One of us (S.S.) determined experimentally the molecular structure of NH_4Cl in gaseous phase.[2] Structure determination of the H_2O–HCl system was undertaken for studying simple hydrogen bonded systems. Electron diffraction study was also carried out on the system in gas state. The result confirmed the existence of the molecular complex of H_3OCl. A theoretical study was made in order to see whether the H_2O–HCl molecular complex is actually stable and, if so, to confirm its geometrical structure.

According to Murthy and Rao[3] who carried out many molecular orbital calculations on various hydrogen bonded systems showed that the CNDO/2 procedure[4] can yield satisfactory results for potential energies of hydrogen bonds. Kollman and Allen,[5] and Rao and Murthy[6] recently carried out calculations for the H_2O–HF and NH_3–HF systems, respectively. However, there have been no CNDO/2 studies on hydrogen bonds containing a chlorine atom. It is well-known that the CNDO/2 method is also applicable to the system in which d orbitals contribute.[7] Thus CNDO/2 calculation was carried out on the H_2O–HCl system.

Procedure

Most calculations were performed with the use of a spd set as a basis, and some of them with a sp set. The values of the parameters used in these calculations were the same as those given by Santry and Segal[7] except for the empirical parameter K which is defined by the following relation of the resonance integral:

$$\beta_{AB} = K(\beta_A + \beta_B)/2$$

Santry and Segal suggested the use of 0.75 for K. However, this seems to be somewhat ambiguous, and other values were also used.

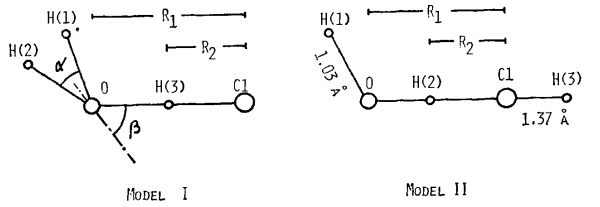

Fig. 1. Geometries of the H_2O–HCl system.
The numbering of hydrogen atoms and the notation of molecular parameters are given in the figure. The listed values of the molecular parameters were assumed in the CNDO/2 caculations.

With respect to geometries of the H_2O–HCl complex two structures, shown in Fig. 1, were taken into consideration. Both were inferred from the gas electron diffraction study. The O–Cl distance, denoted by R_1, and the H(3)–Cl distance (H(2)–Cl distance in model II), by R_2, were varied at intervals of 0.3 and 0.1 Å, respectively. In the neighbourhood of minimum of potential energy R_1 was varied at an interval of 0.1 Å. The angle H(1)OH(2), denoted by α, and the O–H distance were also varied. In the first stage of calculations α was assumed to be 105° from the experimental data for water[8] and the O–H distance was fixed as 1.05 Å obtained from the calculation where other parameters were kept in most probable values. In model I the angle between the H(1)OH(2) plane and the OH(3)Cl line, denoted by β, was also varied preserving the C_s symmetry of the complex. A planar structure was assumed for model II. In both models the hydrogen bonds of O–H–Cl were assumed to be linear. All the calculations were carried out with a FACOM 230-60 computor at Nagoya University Computing Center.

Results and Discussion

For model I, the potential energies of the system, shown in Fig. 2, were calculated as a function of R_1 with the fixed R_2. The calculations were carried out by using K=0.75, spd set, R(O–H)=1.05 Å and α=105°. A potential energy minimum was found at R_1=2.8 Å, independent of R_2. Calculations using the sp basis set also gave nearly the same equilibrium distances

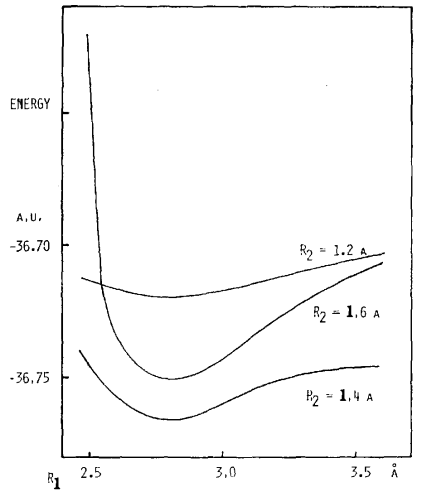

Fig. 2. The energy of the H_2O–HCl system (the model I) as a function of the O–Cl distance, R_1.

as those for the spd basis set though the total energies were considerably different. The distance of 2.8 Å seems to be reasonable in comparison with the O–Cl distance of 2.95 Å found experimentally in crystalline hydrogen chloride monohydrate H_2O–HCl.[9]

The potential curve shows no energy barrier for formation of the complex $H_2O \cdot HCl$. The dissociation energy of the complex was found to be 16 kcal/mol (Table 1). This value also seems to be reasonable in compaison with the calculated value of 10.7 kcal/mol for the H_2O–HF system.[3]

Table 1. Dissociation energies for the H_2O–HCl systems (kcal/mol)

K	Model I		Model II	
	spd	sp	spd	sp
0.75	16	19	8	−14
0.875	8		19	
1.0	5	6	40	−18

Fixed as R(O–H)=1.03 Å, α=104°.

Calculations were carried out varying β from 0 to 60°. The planar structure (β=0°) was found to be most stable. The energy difference between the planar structure and the structure with β=60° was estimated to be 4 kcal/mol. This is contrary to the expectation that the hydrogen bond would be formed toward the direction of the lone pair sp^3 hybrid orbitals of the oxygen atom. It would be understandable from the view point of dipole-dipole interaction.[10]

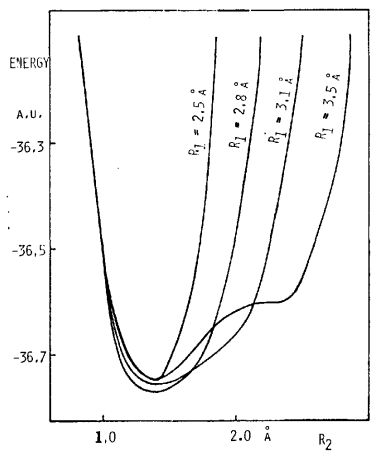

Fig. 3. The energy of the H_2O–HCl system (the model I) as a function of the H(3)–Cl distance.

Figure 3 shows potential energy calculated as a function of R_2 with the fixed R_1, using K=0.75 and spd set. The minimum of the potential energy was found at R_2=1.4 Å, nearly independent of R_1. The H(3)–Cl equilibrium distance of 1.4 Å is considerably greater than 1.27 Å found experimentally for free hydrogen chloride.[11] However, the HCl equilibrium distance calculated by the CNDO/2 method is 1.37 Å. Thus the net increment of H–Cl distance in the complex formation seems to be fairly small. On the other hand, the O–H(3) distance of 1.4 Å is much greater than the O–H(1) distance of 1.03 Å, which is the value calculated for water molecule by the CNDO/2 method. Thus the H_2O–HCl complex can be considered essentially as H_2O hydrogen bonded to HCl. It can be seen from Fig. 3 that transfer of the hydrogen atom of HCl to H_2O is very difficult.

When R_1 is smaller than 2.8 Å, there is no evidence for a double minimum potential. The potential is close to the NH_3–HF potential calculated by Rao and Murthy,[6] differing slightly from the NH_3–HCl potential calculated by Mazur and Ratajczak[12] by means of the Extended Hückel method. As R_1 becomes larger, the potential curve appears asymmetric around the minimum. For R_1=3.5 Å, which is unreasonably long, a new minimum was found around R_2=2.3 Å. In this configuration an ionic structure can be predominant because excess electronic charge on the chlorine atom is 0.67. The complex can thus be considered as hydronium chloride, $H_3O^+Cl^-$.

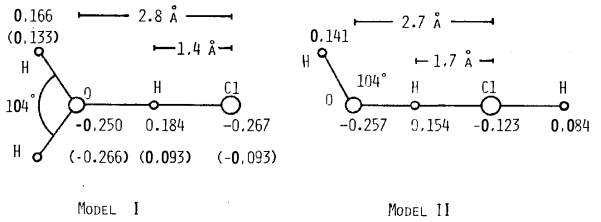

Fig. 4. The equilibrium structures and the atomic populations for the two models.

Figure 4 shows equilibrium structures and their charge distributions calculated by the use of K=0.75 and spd set. Numbers in parentheses are the charge distributions in free H_2O and HCl molecules. In the formation of the complex, H_2O donates electron to HCl, especially to the chlorine atom. However, the total amount of electrons donated to HCl is 0.08. The amount of charge transfer is almost the same as in the case of NH_3–HF system where it was estimated to be 0.05.[6] When the spd basis set was used with K=1 in the CNDO/2 calculations, the equilibrium structure and the charge distribution obtained were the same as those from K=0.75, but the dissociation energy of the complex decreased to about 5 kcal/mol.

For model II, the calculations were carried out by use of the spd basis set with K=0.75 in order to estimate the dissociation energy as well as the equilibrium structure. The dissociation energy was 8 kcal/mol (Table 1), which leads to the conclusion that model I is preferable to model II in agreement with the result for H_2O–HF system by Kollman and Allen.[5] On the other hand the use of the sp basis set showed that model II was unstable itself. From the calculation using the spd set with K=1, however, the dissociation energy was estimated to be 40 kcal/mol, which seems large as compared with the calculated value of 100 kcal/mol (experimental value of 37—58 kcal/mol) for the very strong hydrogen bonds such as HF_2^-.[13] This calculation also gives a large population in d_σ orbital of the chlorine atom, 0.2. This is caused mainly by a large overlap between d_σ orbital of the chlorine atom and 1s orbitals of the H(2) and H(3) atoms. The use of the

spd set with $K=1$ may not be correct since it gives rise to an excessive contribution of the d orbital. Santry and Segal found that good agreement of calculation with experiment is obtained for $K=0.75$.[7] These results lead us to prefer model I for the structure of the H_2O–HCl complex. However, a definite conclusion cannot be made since the stabilities of the two models are essentially dependent on the choice of the K value.

Conclusion

The CNDO/2 procedure gave the conclusion that the H_2O–HCl complex is stable in the planar structure with the equilibrium O–Cl distance of 2.8 Å. The complex can be considered to be H_2O hydrogen bonded to HCl than H_3O^+ bonded to Cl^-. The results, however, could not exclude the other structure of HOH–ClH with the O–Cl distance 2.7 Å.

References

1) E. Clementi, *J. Chem. Phys.*, **46**, 3851 (1967), *ibid.*, **47**, 2323 (1967).
2) S. Shibata, *Acta Chem. Scand.*, **24**, 705 (1970).
3) A. S. N. Murthy and C. N. R. Rao, *J. Mol. Structure*, **6**, 253 (1970).
4) J. A. Pople and G. A. Segal, *J. Chem. Phys.*, **43**, S136 (1965), *ibid.*, **44**, 3289 (1966).
5) P. A. Kollman and L. C. Allen, *J. Amer. Chem. Soc.*, **92**, 1753 (1970), *J. Chem. Phys.*, **52**, 5085 (1970).
6) C. N. R. Rao and A. S. N. Murthy, *J. Mol. Structure*, **9**, 197 (1971).
7) D. P. Santry and G. A. Segal, *J. Chem. Phys.*, **47**, 158 (1967).
8) S. Shibata and L. S. Bartell, *ibid.*, **42**, 1147 (1965).
9) Y. K. Yoon and I. Olovsson, *Acta Crystallogr.*, **12**, 17 (1959).
10) P. A. Kollman, *J. Amer. Chem. Soc.*, **94**, 1837 (1972).
11) L. E. Sutton(Editor), "Tables of Interatomic Distances and Configurations in Molecules and Ions," Chemical Society, London, 1965.
12) K. Mazur and H. Ratajczak, *J. Mol. Structure*, **11**, 201 (1972).
13) P. A. Kollman and L. C. Allen, *Chem. Rev.*, **72**, 283 (1972).

An MO Calculation of 1,3-Dipolar Cycloaddition between Ethylene and Diazomethane

Tsutomu MINATO, Shinichi YAMABE, Satoshi INAGAKI, Hiroshi FUJIMOTO, and Kenichi FUKUI

Faculty of Engineering, Kyoto University, Sakyo-ku, Kyoto 606

(Received February 1, 1974)

A semiempirical SCF MO calculation of the reaction between ethylene and diazomethane was carried out as an example of 1,3-dipolar cycloaddition. A calculation of the interaction energy and electron population by the use of the configuration interaction wave function showed that the formation of the two new bonds in this reaction is concerted but non-synchronous. This result is attributable to the extension of the highest occupied molecular orbital of diazomethane.

The molecular orbital (MO) approach can be used to interpret the chemical reactivity of organic molecules, both saturated[1] and unsaturated.[2] Most of the MO criteria for the chemical reactivity are based upon the use of various reactivity indices.[3] These indices agree fairly well with the experimental results. Therefore, the study of electronic effects appears to lead to the elucidation of the reaction mechanism. We will study 1,3-dipolar cycloaddition through calculations of the electron states of ethylene and diazomethane.

1,3-Dipolar cycloaddition is the union of a 1,3-dipole (a—b—c) with a multiple bond system (d—e), the so-called dipolarophile, to form a five-membered ring.[4,5] A 1,3-dipole a—b—c is described by a zwitterionic octet structure, *e.g.*:

$$a \equiv b^+ - c^- \longleftrightarrow a^- = b^+ = c \quad (b=N)$$

$$a = b^+ - c^- \longleftrightarrow a^- - b^+ = c \quad (b=N\text{-}R,\ O)$$

Specific classes of molecular 1,3-dipoles include diazoalkanes ($R_2C{=}N^+{=}N^-$), nitrile oxides (Ar–C≡N^+–O^-), azides (Ar–N=N^+=N^-), nitrones (Ar–CH=N^+(Me)–O^-) and nitrile amines (Ar–C≡N^+–N^-–Ar).

The concept of this reaction was first suggested by Smith.[6] The generality of the reaction was recognized by Huisgen[4] in a splendid series of researches, during which many new reactions were predicted and discovered. The picture of the reaction mechanism which Huisgen's group drew was that of a single-step, concerted cycloaddition, in which the concerted formation of the two new bonds (*i.e.*, a—d and c—e) is not necessarily synchronous.[4]

Woodward-Hoffmann rules for the conservation of orbital symmetry[7] supply the theoretical basis and, taken with most of the experimental results,[4] provide support for Huisgen's earlier predictions.[8] That is, the rules reveal that 1,3-dipolar cycloaddition is symmetry-allowed for the ground state. Recently Firestone has argued in favour of a two-step mechanism involving biradical intermediates.[9]

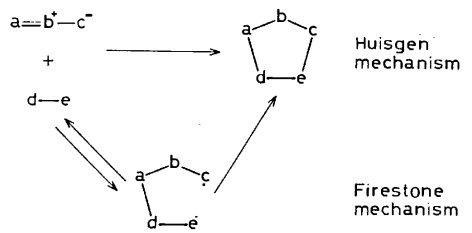

The nature of orientation in the reaction (*i.e.*, unsymmetrical dipolarophiles can add to the unsymmetrical 1,3-dipole in two directions, (I) and (II)) has not been adequately interpreted and predicted.

(I) (II)

However, Houk qualitatively discussed the regioselectivity in 1,3-dipolar cycloaddition in terms of the extension of particular MO's, and his conclusion is consistent with the experimental results.[10,11] Furthermore, he and his co-workers[11] qualitatively discussed nonsynchroneity in the formation of two new bonds; this nonsynchroneity seems to play a part in the determination of the orientation of the concerted mechanism.[12]

Considering these circumstances, we will undertake a more detailed perturbational MO calculation of the nonsynchronous formation of new bonds in the course of the 1,3-dipolar cycloaddition reaction between olefin and diazoalkane.

Here olefin (dipolarophile) and diazoalkane (1,3-dipole) will be typified by ethylene and diazomethane for the sake of simplicity of calculation.

Method of Calculation

In this paper, the means of calculation is based upon one[13] of the isolated molecule approximations that Fukui *et al.* have developed. That is, the wave function (Ψ) of a chemically-interacting state in a reaction between ethylene and diazomethane is represented by means of the configuration interaction (CI) procedure;

$$\Psi = C_0\Psi_0 + \sum_{i=1}^{6}\sum_{l=9}^{14} C_{i\to l}\Psi_{i\to l} + \sum_{k=1}^{8}\sum_{j=7}^{12} C_{k\to j}\Psi_{k\to j} + \sum_{i=1}^{6}\sum_{j=7}^{12} C_{i\to j}\Psi_{i\to j} + \sum_{k=1}^{8}\sum_{l=9}^{14} C_{k\to l}\Psi_{k\to l} \qquad (1)$$

where Ψ_0 means the adiabatically-interacting state in which all valence electrons occupy the MO's of ethylene (i) and those of diazomethane (k), both doubly-occupied in their initially-isolated state. $\Psi_{i\to l}$ implies the charge-transferred state, with one electron in the i-th occupied MO of ethylene transferred into the l-th unoccupied one of diazomethane, while $\Psi_{k\to j}$ implies a back charge-

transferred state in which one electron in the k-th occupied MO of diazomethane jumps up into the j-th unoccupied one of ethylene. $\Psi_{i\to j}$ is a locally-excited state in which an electron in the i-th MO of ethylene is excited into the j-th MO of ethylene and $\Psi_{k\to l}$ indicates a locally-excited state in diazomethane as does $\Psi_{i\to j}$ in ethylene. These wave functions are constructed by means of Slater determinants, composed of the semiempirical LCAO SCF MO's,[14] including all valence electrons and overlap integrals. C_0, $C_{i\to l}$, $C_{k\to j}$, $C_{i\to j}$, and $C_{k\to l}$ in Eq. (1) are the CI coefficients obtained by solving the usual CI secular equation.

When the CI seqular equation is expanded in the approximate sense that the interaction is not too strong, the total stabilization energy (ΔW) due to the CI effect mentioned above can be partitioned into the following four terms: Coulombic (E_Q), exchange (E_K), delocalization (D), and polarization (π) terms.[13]

$$\Delta W = E_Q + E_K - D - \pi \qquad (2)$$

E_Q is the electrostatic interaction energy between ethylene and diazomethane. E_K is the exchange repulsion energy between two closed-shell molecules[15] resulting from the overlap between the occupied MO's of two molecules; it increases unfavorably as the reaction proceeds. D is the stabilization energy due to the mixing-in of the charge-transferred states ($\Psi_{i\to l}$ and $\Psi_{k\to j}$) with the adiabatically-interacting state (Ψ_0); it works to promote the reaction. The last term in Eq. (2), π, is also the stabilization energy due to the mixing-in of local excited states ($\Psi_{i\to j}$ and $\Psi_{k\to l}$). π is usually less important than the others on the right-hand side of Eq. (2).[15]

The electron density ($\rho(1|1)$) of the interacting state (Ψ) is given by:[16]

$$\rho(1|1) = 28\int \Psi^*(1, 2, \cdots, 28)\Psi(1, 2, \cdots, 28) \times d\varepsilon_1 d\tau_2 \cdots d\tau_{28} \qquad (3)$$

where the number "28" indicates the total valence electrons in the whole system, where $d\varepsilon_1$ is the integral over the spin coordinate of the 1 electron, and where $d\tau_i$ is the integral over both the spin and space coordinates of the i electron. Furthermore, $\rho(1|1)_{C_2H_4}+\rho(1|1)_{CH_2N_2}$ signifies the simple sum of the electron density of ethylene and that of diazomethane. Of course, $\rho(1|1)$ is different from $\rho(1|1)_{C_2H_4}+\rho(1|1)_{CH_2N_2}$.

Results and Discussion

The molecular geometry of ethylene and diazomethane which we have employed comes from Herzberg[17] without any deformation, because it seems that the interaction between ethylene and diazomethane is sufficiently weak at the early stage of the reaction. Figure 1 illustrates the geometry of the assumed reaction models. M in Fig. 1 represents the center of the linear C_3–N_4–N_5 line of diazomethane. Theta (θ) in Fig. 1 represents the angle between the C_3–N_4–N_5 line and the X-axis. The restrictions adopted in the selection of the geometry in Fig. 1 are as follows. The two molecular planes (*i.e.*, two Y–Z planes) to which ethylene and diazomethane respectively belong are parallel at $\theta=90°$. The distance between the planes is 2.7 Å. M moves horizontally along the C_3–N_4–N_5 line of diazomethane from a position just above the C_1 of ethylene to one above the C_2 of ethylene in order to determine the relative position of the two parallel molecules. Therefore, the geometry of the assumed reaction model is selected in terms of the position of M which gives the lowest total energy by the CNDO/2 method.[18] This geometry ($\theta=90°$) is defined as Model 1. Furthermore, diazomethane is rotated about M by $\pm5°$; we define the geometry at $\theta=85°$ as Model 2 and the geometry at $\theta=95°$ as Model 3.

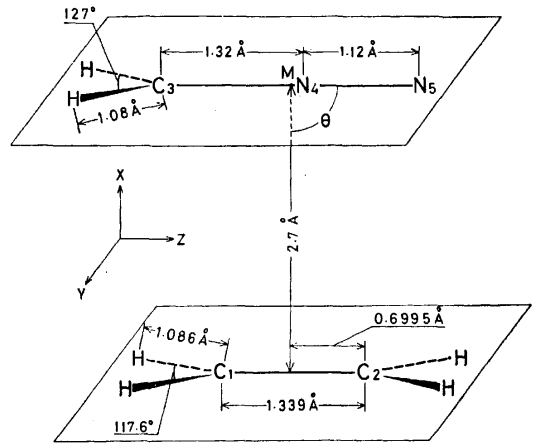

Fig. 1. Assummed interacting models between ethylene and diazomethane at the initial stage of the reaction. The former molecule holds D_{2h} symmetry and latter has C_{2v} one.

The MO energy levels of the ethylene and diazomethane obtained by the SCF procedure are given in Fig. 2.

First let us consider Model 1 at $\theta=90°$, in which

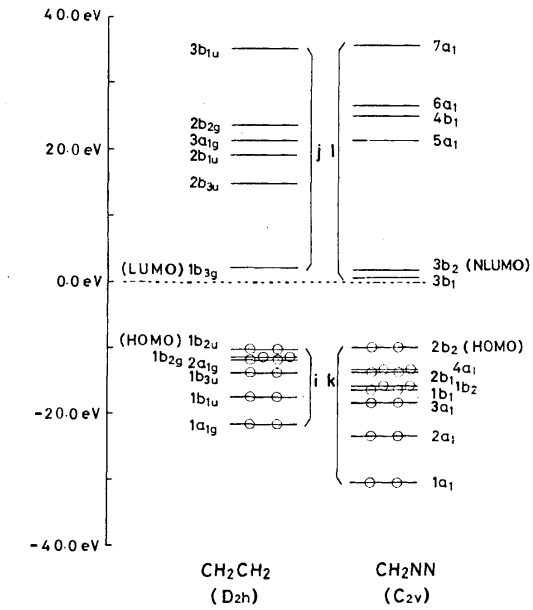

Fig. 2. Schematic presentation of MO levels of ethylene and diazomethane. NLUMO in this figure represents the next unoccupied MO of the lowest unoccupied MO.

two molecular planes are parallel. The interaction energy, ΔW, was calculated for Model 1; the results are given in Table 1. Table 1 shows that, in this reaction model, E_Q and π are small in value because the two reactants we use are *neutral* molecules. E_K and D are larger than the former two terms. E_K is found to hinder the progress of the reaction. On the other hand, D greatly stabilizes this reaction system, thus prompting the reaction.

Table 1. Interaction energies between diazomethane and ethylene

	Model 1	Model 2	Model 3
θ[a] (°)	90	85	95
E_K (eV)	2.769	2.588	3.260
E_Q (eV)	−0.015	−0.014	−0.015
D (eV)	1.325	1.141	1.958
π (eV)	0.040	0.044	0.053
ΔW (eV)	1.389	1.389	1.234

a) θ is shown in Fig. 1.

In order to seek for the CI configuration ($i \rightarrow l$ and $k \rightarrow j$ combinations) which is the most contributive to D, the calculated CI coefficients of Eq. (1) are given in Eq. (3). Here, the polarization effect is neglected because the effect is sufficiently small, as may be understood from the value of π in Table 1.

$$\Psi_{\text{Model 1}} = 0.883\Psi_0 + 0.342\Psi_{2b_2 \rightarrow 1b_{3g}} + 0.129\Psi_{2a_{1g} \rightarrow 3b_2} - 0.059\Psi_{2a_1 \rightarrow 1b_{3g}} - 0.034\Psi_{1b_{2u} \rightarrow 3b_2} \quad (3)$$

The terms with a CI coefficient whose absolute value is smaller than 0.03 are neglected. Equation (3) shows that the largest CI coefficient except C_0 (=0.883) that is contributive to D is that of the charge-transferred state from the highest occupied (HO) MO of diazomethane ($2b_2$) to the lowest unoccupied (LU) MO of ethylene ($1b_{3g}$). Therefore, there is no doubt that the charge-transfer interaction between the particular MO's, *i.e.*, the HOMO of diazomethane and the LUMO of ethylene, plays a remarkably important role in promoting the reaction.[2]

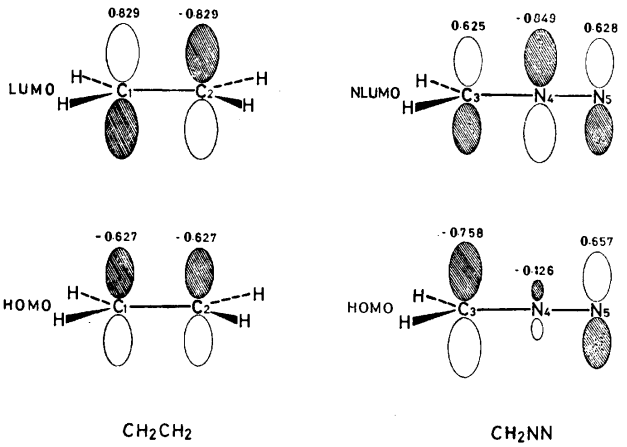

Fig. 3. The nodal property of the particular MO's in ethylene and diazomethane. The values in this figure are the AO coefficients.

The *frontier* MO's* nodal property of ethylene and diazomethane is given in Fig. 3. The values represent the atomic orbital (AO) coefficients of the *fronitier* MO's. Figure 3 shows that the AO coefficient of C_3 (−0.758) is larger than that of N_5 (0.657) in the HOMO of diazomethane.

Here, the electron-density contour maps, which make it easy to understand the new bond formation and the old bond disappearance along the reaction course, are considered at the stage of the reaction shown in Fig. 1 by the use of the CI coefficients of Eq. (3). These contour maps are given in Fig. 4 with respect to Model 1. All the electron density lines are pictured on the X-Z plane of Y=0.0.

Figure 4(a) shows the simple sum of the electron density of ethylene and diazomethane, without any interaction between them. This electron density is defined as $\rho(1|1)_{C_2H_4} + \rho(1|1)_{CH_2N_2}$.

Figure 4(b) shows the electron density with only the adiabatic interaction included; this density is defined as $\rho(1|1)_{0,0}$. It may be noted by observing the 0.1 e/Å^3 density line that the electron density in the intermolecular region, especially that between C_1 of ethylene and C_3 of diazomethane, and that between C_2 of the former molecule and N_5 of the latter, decreases as a result of the inclusion of the electron-exchange interaction in Fig. 4(b), compared with that in Fig. 4(a). This reflects the fact that E_K works repulsively between the two molecules. This is essential to the interaction between two closed-shell systems, as in the case of two helium atoms.

Figure 4(c) shows the electron density with both adiabatic interaction and charge-transfer interaction; this density is defined as $\rho(1|1)$. The comparison of the 0.1 e/Å^3 density line in Fig. 4(c) with that in Fig. 4(a) shows that the electron density between C_1 of ethylene and C_3 of diazomethane, and that between C_2 of the former and N_5 of the latter, overcome the electron density decrease caused by the electron-exchange interaction, thus resulting in an increasing electron density in the reaction zone on account of the mixing-in of the charge-transferred state. We can see that the decrease in the intermolecular electron density between N_4 of diazomethane and ethylene in Fig. 4(b) by the exchange interaction is still preserved in Fig. 4(c). As the overlap between the diazomethane HOMO on N_4 and the ethylene LUMO is small, as Fig. 3 shows, the charge-transfer effect does not appear on N_4 and ethylene. This causes the bending of 1,3-dipole which was adopted in Huisgen's model.[4] Furthermore, Fig. 4(c) also gives us the information that the electron density between C_3 and N_4 of diazomethane decreases, shown, for instance, by the 1.5 e/Å^3 density line which indicates the weakening of the C_3–N_4 bond. The electron density between C_1 and C_2 of ethylene is calculated to decrease in Fig. 4(c), but the decrease is too small to be observed in the figure. Figure 4(c) demonstrates that the electron density increases in the neighborhood of C_1 and C_2 of

* The LUMO of diazomethane is not the *frontier* MO, because it ($3b_1$) can not overlap with the HOMO of ethylene ($1b_{2u}$).

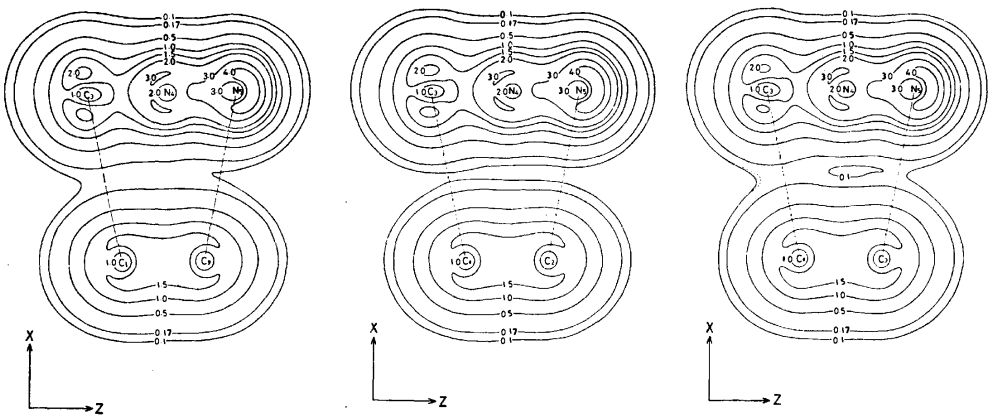

(a) (b) (c)

Fig. 4. Total electron density (in e/Å^3) of Model 1.
(a): $\rho(1|1)_{C_2H_4}+\rho(1|1)_{CH_2N_2}$, (b): $\rho(1|1)_{0,0}$,(c): $\rho(1|1)$.
The dotted line is the 0.1 e/Å^3 density line of (a).

ethylene and decreases in the neighborhood of C_3 of diazomethane. This shows that the carbon of diazomethane is *nucleophilic*.[4c]

Figure 4 shows that the formation of two intermolecular new bonds, C_1–C_3 and C_2–N_5, and the weakening of the old bonds, C_3–N_4 in diazomethane and C_1–C_2 in ethylene, can be described approximately in terms of the mixing-in of the charge-transferred state with the adiabatically-interacting one. That is, at the early stage of this reaction the two bonds are formed by the charge-transfer interaction corresponding to D in the energy expression and the N_4 atom is repulsed from ethylene by the exchange interaction (E_K). The five-membered ring can, then, be pictured by this scheme. At the same time, the HOMO–LUMO interaction is most important, as is shown by the CI coefficients in Eq. (3).

The AO coefficient of C_3 is larger than that of N_5 in the HOMO of diazomethane, as is shown in Fig. 3. To see how this difference in the values influences the reactivity, we prepared Model 2 (θ=85°) and Model 3 (θ=95°).

The interaction energy of Model 2 and that of Model 3 are evaluated, in comparison with that of Model 1 in Table 1. Here the most preferable reaction path may be defined as the model that makes ΔW the smallest.[15] Therefore, the results in Table 1 show that Model 3 is the most reasonable among the three models considered here at the early stage of this reaction.

The wave functions with respect to Model 2 and Model 3 corresponding to Eq. (3) of Model 1 are given by Eqs. (4) and (5):

$$\begin{aligned}\Psi_{\text{Model 2}} = {} & 0.898\Psi_0 + 0.310\Psi_{2b_2\to 1b_{3g}} + 0.128\Psi_{2a_{1b}\to 3b_2} \\ & - 0.058\Psi_{2a_1\to 1b_{3g}} - 0.042\Psi_{1b_{2u}\to 3b_2} \\ & + 0.039\Psi_{1b_{2g}\to 3b_1} \qquad (4)\end{aligned}$$

$$\begin{aligned}\Psi_{\text{Model 3}} = {} & 0.843\Psi_0 + 0.411\Psi_{2b_2\to 1b_{3g}} + 0.130\Psi_{2a_{1g}\to 3b_2} \\ & - 0.059\Psi_{2a_1\to 1b_{3g}} - 0.056\Psi_{1b_{1u}\to 3b_2} \\ & - 0.033\Psi_{3a_1\to 1b_{3g}} \qquad (5)\end{aligned}$$

The absolute values of the CI coefficients smaller than 0.03 are neglected, as in Eq. (3). A comparison of Eqs. (4) and (5) indicates that the charge-transfer effect works most successfully in Model 3. When C_3 which has the largest AO coefficient of the HOMO of diazomethane, approaches C_1 of ethylene, the MO overlap between the HOMO of diazomethane and the LUMO of ethylene is extended. Therefore, Model 3 is favorable to the charge-transfer interaction.

Furthermore, the contour maps are depicted for Model 2 and Model 3. Figure 5 indicates the electron density of Model 2 in the X–Z cross section. Figure 5(a) shows the sum of the electron density of ethylene and diazomethane, corresponding to Fig. 4(a) of Model 1. Figure 5(b) shows the electron density with the adiabatic and the charge-transfer interactions, corresponding to Fig. 4(c) of Model 1. Model 2 is an unfavorable reaction path, as may be understood from the interaction energy in Table 1; a comparison of Fig. 5(a) with Fig. 5(b) gives the information that the electron-density increase in the intermolecular region of Model 2 as a result of the mixing-in of the charge-transferred state with Ψ_0 is similar in appearance to that of Model 1.

Figure 6 indicates the electron density of Model 3 in the X–Z cross section. Figure 6(a) shows the sum of the electron density of ethylene and diazomethane, corresponding to Fig. 4(a) of Model 1 and Fig. 5(a)

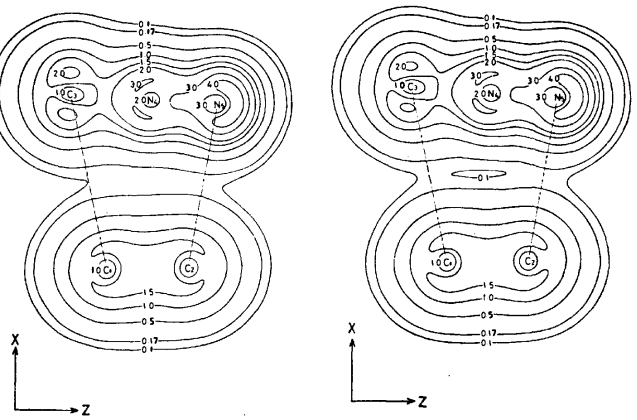

Fig. 5. Total electron density (in e/Å^3) of Model 2.
(a): $\rho(1|1)_{C_2H_4}+\rho(1|1)_{CH_2N_2}$, (b): $\rho(1|1)$.

of Model 2. Figure 6(b) shows the electron density with the adiabatic and the charge-transfer interactions, corresponding to Fig. 4(c) of Model 1 and Fig. 5(b) of Model 2. Model 3 is found, from the findings on interaction energy in Table 1, to be the most favorable reaction model. In this model, the electron density in the intermolecular region, especially C_1–C_3, shows a considerable increase as a result of a more effective mixing-in of the charge-transferred state with Ψ_0 than the others, as the comparison of the 0.17 e/Å^3 density line in Fig. 6(a) with that in Fig. 6(b) shows. Therefore, a concerted cycloaddition of diazomethane to ethylene may be expected to show an unequal progress of the bond formation, as Houk and his co-workers proposed.[11]

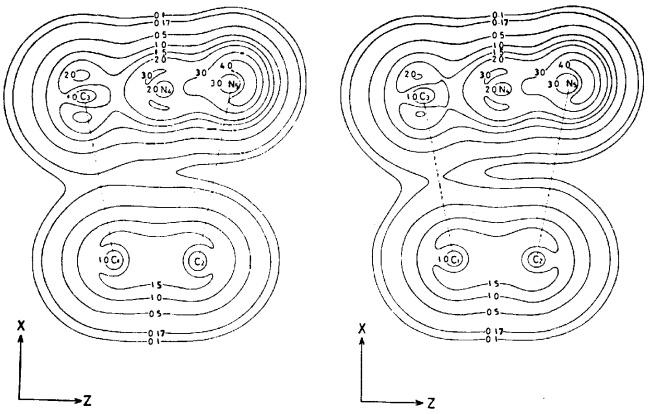

Fig. 6. Total electron density (in e/Å^3) of Model 3.
(a): $\rho(1|1)_{C_2H_4}+\rho(1|1)_{CH_2N_2}$, (b): $\rho(1|1)$.

This nonsynchroneity of the two new bond formations may be explained as follows. In ΔW, the largest stabilization comes from D; it is the charge-transfer interaction from the HOMO of diazomethane to the LUMO of ethylene that is the most contributive to D, as is shown by the comparison of the CI coefficients. Therefore, the reaction will take place along the path which maximizes the MO overlap between the HOMO and the LUMO. The HOMO of diazomethane has a larger extension on C_3 than on N_5. Therefore, it is favorable that the approach of C_3 to C_1 occurs first.

If steric complications are not considered it is reasonable to assume that, in an asymmetric dipolarophile, the largest HOMO-coefficient atom of diazomethane (*i.e.*, the carbon atom) unites with the largest LUMO-coefficient atom of the dipolarophile.[10,11,19]. Diels-Alder reactions between two dissymmetrical reagents are also most likely to be non-synchronous, as has been suggested by Woodward and Katz.[20] As Diels-Alder reactions have been shown to be under *frontier* control,[21] it seems reasonable to think that the first bond would link the largest HOMO-coefficient atom of diene and the largest LUMO-coefficient atom of dienophile.[12,22]

Conclusion

An approximate MO calculation of the 1,3-dipolar cycloaddition of diazomethane to ethylene has been carried out by a CI method. The results of the present calculation have proved nonsynchroneity in the formation of two new bonds. This result can be explained on the basis of the fact that the extension of the HOMO of diazomethane is different on different constituting atoms. Therefore, the extension of the HOMO is important in any consideration of the reaction path.

The authors wish to express their appreciation to the Data Processing Center of Kyoto University for a generous permission to use the FACOM 230-60 computer.

References

1) K. Fukui, "Modern Quantum Chemistry," Vol. I, ed. by O. Sinanoğlu, Academic Press, New York (1965), and the references cited therein.
2) K. Fukui, "Molecular Orbitals in Chemistry, Physics and Biology," ed. by P.-O. Löwdin and B. Pullman, Academic Press, New York (1964).
3) A. Streitwieser, Jr., "Molecular Orbital Theory for Organic Chemists," John Wiley & Sons, New York (1961), Chapter 11 and the references cited therein.
4) a) R. Huisgen, *Angew. Chem.*, **75**, 604, 742 (1963); b) R. Huisgen, *Proc. Chem. Soc.* (London), **1961**, 357; c) R. Huisgen, R. Grashey, and J. Sauer, "The Chemistry of Alkenes," ed. by S. Patai, Interscience, London (1964), p. 739; d) R. Huisgen, *J. Org. Chem.*, **33**, 2291 (1968).
5) G. W. Cowell and A. Ledwith, *Quart. Rev.*, **24**, 119 (1970).
6) L. I. Smith, *Chem. Rev.*, **23**, 193 (1938).
7) a) R. Hoffmann and R. B. Woodward, *J. Amer. Chem. Soc.*, **87**, 2046 (1965); b) R. Hoffmann and R. B. Woodward, *Accounts Chem. Res.*, **1**, 17 (1968).
8) A. Ledwith, *Ann. Reports (B)*, **65**, 143 (1968).
9) R. A. Firestone, *J. Org. Chem.*, **33**, 2285 (1968).
10) K. N. Houk, *J. Amer. Chem. Soc.*, **94**, 8953 (1972).
11) K. N. Houk, J. Sims, C. R. Watts, and L. J. Luskus, *J. Amer. Chem. Soc.*, **95**, 7301 (1973).
12) O. Eisenstein, J.-M. Leffour, and N. T. Anh, *Chem. Commun.*, **1971**, 969.
13) K. Fukui and H. Fujimoto, This Bulletin, **41**, 1989 (1968).
14) H. Kato, H. Konishi, H. Yamabe, and T. Yonezawa, *ibid.*, **40**, 2761 (1967).
15) H. Fujimoto, S. Yamabe, and K. Fukui, *Tetrahedron Lett.*, **1971**, 439.
16) H. Fujimoto, S. Yamabe, and K. Fukui, This Bulletin, **44**, 2936 (1971).
17) G. Herzberg, "Molecular Spectra and Molecular Structure," D. Van Nostrand Co., New York (1966).
18) J. A. Pople and D. L. Beveridge, "Approximate Molecular Orbital Theory," McGraw-Hill, New York (1970).
19) J. Bastide, N. El Grandour, and O. Henri-Rousseau, *Tetrahedron Lett.*, **1972**, 4225.
20) R. B. Woodward and T. J. Kats, *Tetrahedron*, **5**, 70 (1959).
21) a) K. Fukui, This Bulletin, **39**, 498 (1966); b) L. Salem, *J. Amer. Chem. Soc.*, **90**, 553 (1968).
22) a) A. Devaquet and L. Salem, *ibid.*, **91**, 3793 (1969); b) T. Inukai, H. Sato, and T. Kojima, This Bulletin, **45**, 891 (1972); c) N. D. Epiotis, *J. Amer. Chem. Soc.*, **95**, 5624 (1973).

Magnetic Susceptibility of Magnesium 2,2'-Dipyridylide in its THF Adducts

Tatsuo HORIBA, Ken-ichi HARA,* Motomichi INOUE, and Masaji KUBO
Department of Chemistry, Nagoya University, Chikusa, Nagoya 464
(Received February 20, 1974)

The magnetic susceptibility of magnesium 2,2'-dipyridylide has been determined in its THF (tetrahydrofuran) adducts in a temperature range of 1.6—20 K. The susceptibility of $Mg(dipy)_2 \cdot THF$ exhibits two maxima at about 3.9 and 9.5 K due to short range and long-range interactions, respectively. The observed susceptibility conforms to the alternating linear Heisenberg model above about 6 K. $Mg(dipy)_2 \cdot 3THF$ shows no definite maximum of magnetic susceptibility. The magnetic behavior of these complexes different from that of $Be(dipy)_2$ is attributable to the difference in the ionic character between Mg–N and Be–N bonds.

The magnetic susceptibility of beryllium 2,2'-dipyridylide, $Be(dipy)_2$, conforms to an equation for isolated binuclear clusters, indicating that antiferromagnetic interaction operates between two 2,2'-dipyridyl radical anions within a molecule.[1] The tetrahydrofuran adduct of magnesium 2,2'-dipyridylide, $Mg(dipy)_2 \cdot 3THF$, was found to show an effective magnetic moment of 2.73 B.M. at room temperature.[2] This value is nearly equal to $(2 \times 3)^{1/2}$ B.M. for a biradical having two independent unpaired electrons, indicating the presence of two dipyridyl ion radicals in a molecule. However, magnesium 2,2'-dipyridylide is suspected to show a magnetic property different from that of $Be(dipy)_2$ at low temperature, because beryllium and magnesium compounds differ from each other in bond nature. One may expect to obtain information about magnetic interaction by comparing the magnetic properties of the beryllium and magnesium complexes. Therefore, we have undertaken to determine the magnetic susceptibility of magnesium 2,2'-dipyridylide.

Experimental

Preparation of Materials. Excess metallic magnesium was mixed with a solution of 2,2'-dipyridyl in THF. On adding a small quantity of iodine to the solution, deep red crystalline precipitate separated. Recrystallization from THF yielded the crystals of $Mg(dipy)_2 \cdot 3THF$[2] (Calcd: Mg, 4.5%. Found: Mg, 4.4%). When the precipitate was recrystallized from benzene, deep red needle crystals were obtained. On heating in vacuum at about 90 °C, weight loss amounted to 19.2%. The liberated gas did not freeze even at dry-ice temperature, indicating that the crystals were those of a THF (mp, −108.5°) adduct, $Mg(dipy)_2 \cdot THF$, rather than a benzene adduct (Calcd: Mg, 5.9%; THF, 17.6%. Found: Mg, 5.6%; THF, 19.2%). As the compounds were very sensitive to atmospheric oxygen and moisture, they were preserved in an atmosphere of argon or helium.

Magnetic Measurement. The magnetic susceptibility was determined by means of a Hartshorn bridge operating at 90 Hz with a field strength equal to about 10 Oe. Iron(III) alum was employed as a standard. The molar susceptibility was corrected for diamagnetic contributions (10^{-6} emu/mol) from 2,2'-dipyridyl (−93) and THF (−55). The values were calculated on the basis of the observed susceptibility of pyridine and the Pascal constants.[3]

Electronic Spectra. Electronic spectra were recorded in solutions by means of a Model 323 recording spectrophotometer from Hitachi Ltd.

Results and Discussion

The magnetic susceptibility *versus* temperature curve of $Mg(dipy)_2 \cdot THF$ exhibits two maxima at about 3.9 and 9.5 K as shown in Fig. 1. The broad maximum

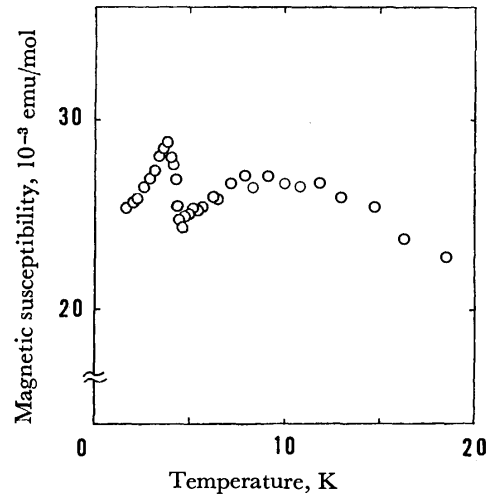

Fig. 1. Magnetic susceptibility of $Mg(dipy)_2 \cdot THF$.

at the higher temperature is undoubtedly due to a short-range magnetic interaction. An ESR study carried out on magnesium 2,2'-dipyridylide in a glassy 2-methyltetrahydrofuran matrix has indicated that each metal ion has a tetrahedral coordination comprising four nitrogen atoms from two dipyridyl ions.[4] From the result, the biradical molecules of $Mg(dipy)_2$ are expected to exist as units in the crystals of $Mg(dipy)_2 \cdot THF$. This suggests that the magnetic behavior due to a short-range interaction can be explained by the binuclear cluster model. However, the observed curve can be reproduced with difficulty by the theoretical formula for weakly coupled biradicals[5] as well as by isolated biradicals. For the coupled dimer model or the alternating linear Heisenberg model, the Hamiltonian is given by

$$\mathcal{H} = -2J\sum_{i=1}^{N/2}(\mathbf{S}_{2i-1}\cdot\mathbf{S}_{2i} + a\mathbf{S}_{2i}\cdot\mathbf{S}_{2i+1}) + g\beta\sum_{i=1}^{N}\mathbf{S}_i\cdot\mathbf{H}$$

* Present address: Central Research Laboratory, Fuji Electric Co., Ltd., Nagasaka, Yokosuka.

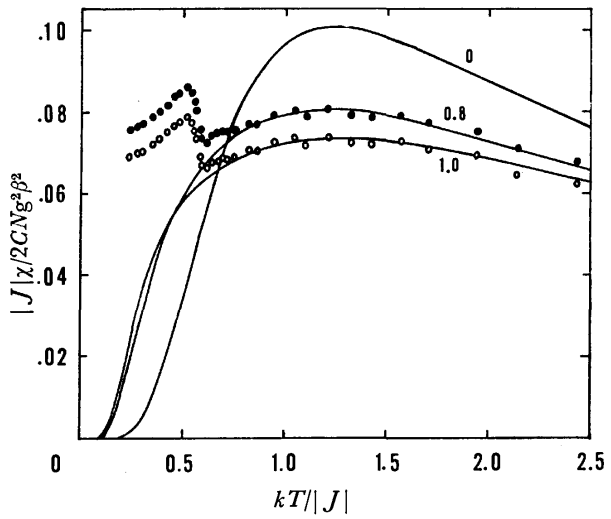

Fig. 2. Theoretical magnetic susceptibility of alternating linear chains with a=0—1 and the observed curves of Mg(dipy)$_2$·THF (○: $J/k=-7.6$ K, C=0.93; ●: $J/k=-7.6$ K, C=0.85).

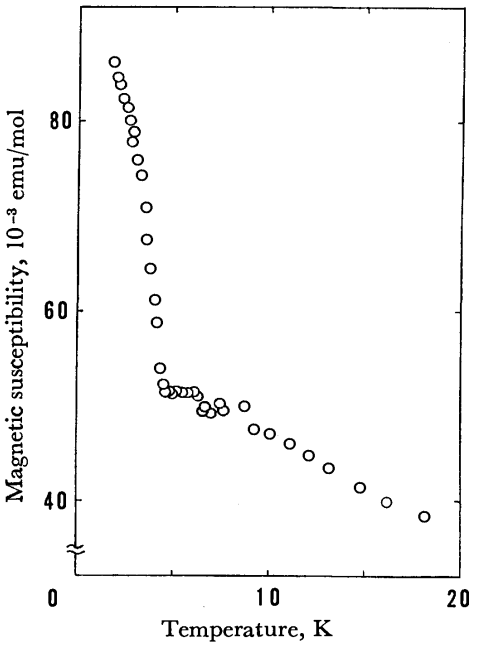

Fig. 3. Magnetic susceptibility of Mg(dipy)$_2$·3THF.

where apart from obvious notations, J denotes the exchange integral and a is the alternation parameter ($0\leq a\leq 1$). Duffy and Barr[6] have calculated the theoretical curve of $|J|\chi/Ng^2\beta^2$ *versus* $kT/|J|$ for various a values using the Hamiltonian with N=10. The result is applicable to the susceptibility of Mg(dipy)$_2$·THF, when $|J|\chi/Ng^2\beta^2$ is rewritten as $|J|\chi/2CNg^2\beta^2$ (C denotes the fractional radical concentration and g is reasonably assumed to be equal to 2.00 for organic radicals). As shown in Fig. 2, the theoretical curves with a=0.8 and 1.0 agree well with the observed data except for a region below about 6 K. The exchange integral was evaluated as $J/k=-7.6$ K. As described above, the curve for isolated binuclear clusters (a=0) does not reproduce the observed curve even in a region above the temperature of the maximum susceptibility.

The magnetic susceptibility exhibits another maximum at about 3.9 K. The appearance of the second peak in a susceptibility *versus* temperature curve has been observed for some metal complexes having one-dimensional lattices,[7,8] but no quantitative discussion has been given. Undoubtedly, the maximum at the lower temperature is due to a three-dimensional ordering existing below the temperature.

The magnetic behavior of Mg(dipy)$_2$·3THF resembles that of Mg(dipy)$_2$·THF to some extent, but no definite maxima were observed in the temperature range investigated (see Fig. 3). Below about 4.5 K, the susceptibility *versus* temperature curve shows a sharp increase and a gradual diminution of the slope with decreasing temperature, suggesting the appearance of a peak at still lower temperature. The almost constant susceptibility between 4.5 and 6 K is due to a short-range interaction. Although accurate analysis is difficult owing to the absence of any definite maximum, the susceptibility conforms to the alternating linear chain model rather than to the isolated binuclear cluster model.

From the result of an ESR study carried out on the magnesium salt in a glassy matrix,[4] the biradical molecules of Mg(dipy)$_2$ are expected to be present as crystal units. However, the observed value of the alternation parameter, a=0.8—1.0, shows that alternating linear chains rather than binuclear clusters should be regarded as magnetic units. The appearance of long-range ordering also suggests the presence of alternating linear magnetic chains interacting with one another. On the other hand, Be(dipy)$_2$ shows magnetic properties conforming to theoretical susceptibility for isolated binuclear clusters. The quite different magnetic properties are evidently due to the difference in crystal structure between the magnesium and beryllium compounds, because the electronic absorption spectrum of the magnesium salt in a diethyl ether solution bears a strong resemblance to those of the corresponding lithium and beryllium salts[1,9] (see Table 1). Beryllium occupies a unique position among group IIA elements and readily forms covalent bonds.[10] This favors the regular tetrahedral arrangement of Be–N bonds. Because Mg–N bonds are essentially ionic in the crystals of some magnesium salts, 2,2'-dipyridyl anions are presumably stacked face to face to form a one-dimensional array, which exists commonly in the crystals of

Table 1. Absorption maxima (10^{-3} cm^{-1}) in the electronic spectra of 2,2'-dipyridylides

Mg(dipy)$_2$ (in diethyl ether)	Be(dipy)$_2$ (in diethyl ether)	Li(dipy)[a] (in THF)
10.9	11.2	10.6
12.2	12.6	12.0
13.5[b]	14.3[b]	13.0
19.2	20.0	18.2
20.1	21.2	19.2
	22.5	
26.2	26.1	26.0
26.8	26.7[b]	

a) Ref. 9. b) Shoulders.

radical ion salts.[11,12] Even if a tetrahedral arrangement comprising Mg–N bonds exists in crystals, the tetrahedral coordination is suspected to be distorted to a great extent. Probably the distortion facilitates the presence of magnetic interaction between the biradicals. The magnitude of exchange interaction ($J/K=-7.6$ K) is smaller than those in $Be(dipy)_2$ (-11.6 K) and $Li(dipy)\cdot(C_2H_5)_2O$ (-80 K).[1,11] If interaction takes place through the sp^3 orbitals of the central metal in the beryllium complex, ferromagnetic interaction ($J>0$) must be dominant because the sp^3 orbitals are orthogonal to one another. This contradiction to the experimental results suggests the intervention of a more complicated mechanism. A charge-transfer mechanism proposed for Wurster's salts is applicable also to beryllium 2,2'-dipyridylide. When a charge-transfer state, $Be^0(dipy^0)_2$, interacts with the ground state, $Be^{2+}(dipy^-)_2$, to some extent, the singlet state in the degenerate ground state is stabilized, whereas the triplet state is unaffected. This mechanism leads to an antiferromagnetic interaction, which masks the ferromagnetic interaction through the sp^3 orbitals as experimental results indicate. In the magnesium salts also, only the singlet state of $Mg^{2+}(dipy^-)_2$ can interact with a charge-transfer state, $Mg^0(dipy^0)_2$ or $Mg^{2+}(dipy^0)(dipy^{2-})$. Evidently, the magnitude of exchange interaction depends on the ionization potential and the distance between radical ions.

References

1) K. Hara, M. Inoue, and M. Kubo, *Chem. Lett.*, **1972**, 839.
2) S. Herzog and R. Taube, *Z. Chem.*, **2**, 208 (1962).
3) G. Foëx, "Constantes Sélectionées, Diamagnétisme et Paramagnétisme," Masson, Paris (1957).
4) I. M. Brown, S. I. Weissman, and L. C. Snyder, *J. Chem. Phys.*, **42**, 1105 (1965).
5) K. Hara, M. Inoue, S. Emori, and M. Kubo, *J. Magn. Resonance*, **4**, 337 (1971).
6) W. Duffy, Jr., and K. P. Barr, *Phys. Rev.*, **165**, 647 (1968).
7) S. Emori, M. Inoue, M. Kishita, and M. Kubo, *Inorg. Chem.*, **8**, 1385 (1969).
8) S. Emori, M. Inoue, and M. Kubo, This Bulletin, **45**, 2259 (1972).
9) Y. Torii, T. Yazaki, Y. Kaizu, S. Murasato, and H. Kobayashi, *ibid.*, **42**, 2264 (1964).
10) L. Pauling, "The Nature of the Chemical Bond," 3rd ed., Cornell University Press, Ithaca, New York (1960), p. 102.
11) M. Inoue, K. Hara, T. Horiba, and M. Kubo, *Chem. Lett.*, **1973**, 1055.
12) P. L. Nordio, Z. G. Soos, and H. M. McConnell, *Ann. Rev. Phys. Chem.*, **17**, 237 (1966).
13) J. Tanaka, M. Inoue, M. Mizuno, and K. Horai, This Bulletin, **43**, 1998 (1970).

Topochemical Studies. III. The Crystal and Molecular Structures of Crotonic Acid, $CH_3CH=CHCOOH$, and Crotonamide, $CH_3CH=CHCONH_2$

Shozo SHIMIZU, Shinji KEKKA,* Setsuo KASHINO, and Masao HAISA

Department of Chemistry, Faculty of Science, Okayama University, Tsushima, Okayama 700

(Received March 25, 1974)

Crotonic acid crystallizes in the monoclinic space group C2/c, with $a=15.30(3)$, $b=4.06(1)$, $c=16.18(2)$ Å, $\beta=107.4(1)°$ and $Z=8$; crotonamide in the monoclinic space group $P2_1/a$, with $a=9.71(2)$, $b=6.90(2)$, $c=7.75(1)$ Å, $\beta=104.0(4)°$ and $Z=4$. The structures have been solved by the Patterson method and refined by the block-diagonal least-squares method. The final R values are 0.090 for 337 observed reflections for crotonic acid, and 0.088 for 525 observed ones for crotonamide. The configuration of the molecules of crotonic acid and crotonamide is approximately planar and of *trans*-type regarding the C=C bond. Every two centrosymmetrically related molecules form a dimer through hydrogen bonds of 2.645 Å (OH···O) for crotonic acid and 2.963 Å (NH···O) for crotonamide. In the crystals of crotonamide additional NH···O hydrogen bonds (2.862 Å) link the neighboring molecules related by the a-glide plane to form a sheet parallel to (001) plane. Distances between the C=C bonds of the nearest neighbors are 3.86 Å for crotonic acid and 3.62 and 3.88 Å for crotonamide.

In the first paper of this series[1] attention has been drawn to the crystal structure of aconitic acid as an unsaturated aliphatic acid in order to test the topochemical rule[2] and to examine the relationship between the molecular geometry and the hydrogen bond system.[3] The present paper is devoted to the examination of the degree of planarity of the molecules and the packing arrangement of the simplest α,β-unsaturated acid, crotonic acid, and its amide.

Experimental

Crotonic acid crystallized from aqueous solution as soft, colorless transparent plates elongated along the b axis and became gradually sublimate. The differential thermogram showed a weak *endo*-peak at 44 °C and the melting peak at 72 °C. Crontonamide crystallized from ethanol solution as twinned plates or as prisms elongated along the a axis. Crystals of crotonic acid were sealed in glass capillaries. Single crystals of crotonamide were obtained by cutting the twinned plates with razor. Equi-inclination Weissenberg photographs were taken by using Cu$K\alpha$ radiation, $\lambda=1.5418$ Å. Crystal data are summarized in Table 1. The space group for crotonic acid was deduced from the systematic absences to be Cc or C2/c, but the latter was assumed, and confirmed by subsequent refinement. The intensities were estimated visually, and corrected for the Lorentz and polarization factors and for spot shape.

TABLE 1. CRYSTAL DATA

	Crotonic acid	Crotonamide
Chemical formula	$CH_3CH=CHCOOH$	$CH_3CH=CHCONH_2$
Molecular weight	86.09	85.12
Melting point	72 °C	158 °C
Space group	Monoclinic, C2/c	Monoclinic, $P2_1/a$
Systematic absences	hkl for $h+k$ odd	$h0l$ for h odd
	$h0l$ for l odd	$0k0$ for k odd
Cell constants: a	15.30(3) Å	9.71(2) Å
b	4.06(1)	6.90(2)
c	16.18(2)	7.75(1)
β	107.4(1)°	104.0(4)°
Z	8	4
D_c	1.19 g/cm^3	1.12 g/cm^3
D_m	1.19	1.11
$F(000)$	368	184
μ for Cu$K\alpha$ ($\lambda=1.5418$ Å)	8.18 cm^{-1}	6.72 cm^{-1}
Dimension of crystals used	0.5×1.5×0.2 mm	0.3×0.1×0.1 mm
	0.7×0.5×0.2 mm	
Layers photographed	$h0l$ to $h2l$	$0kl$ to $7kl$
	$0kl$ to $7kl$	
Observed reflections	337	525

* Present address: Dainichi Seika Co., Ltd., Kawaguchi 332.

Structure Determination and Refinement

Crotonic Acid. Two-dimensional Patterson and Fourier maps projected along the b axis were used to obtain the trial structure. The y coordinates were estimated by tilting and shifting the planar molecular model against the b axis so that the calculated structure factors may suit to the observed ones. The trial structure gave an R value of 0.27. Three cycles of block-diagonal least-squares refinement of positional and isotropic thermal parameters reduced the R value to 0.15. The reflections $20\bar{4}$, $11\bar{3}$, and $11\bar{2}$, which were considered to suffer from extinction effect, were dropped off in subsequent refinements. Including the positions of hydrogen atoms obtained from a difference synthesis and the appropriate isotropic thermal parameters, further refinements were repeated with the weighting scheme:

$$w = (16.0/F_o)^2 \quad \text{for } |F_o| > 16.0$$

$$w = 1.0 \quad \text{for } 16.0 \geq |F_o| \geq 6.7$$

and

$$w = 0.5 \quad \text{for } 6.7 > |F_o| > 0.0.$$

The final R value was 0.090 for 337 observed reflections.

Crotonamide. The trial structure was obtained from the Patterson maps projected along the b and a axes, and corrected by the Fourier synthesis projected along the b axis. A three-dimensional Fourier map

gave the structure of the R value of 0.33. A diagonal least-squares refinement with isotropic thermal parameters reduced the R value to 0.178. A difference synthesis at this stage revealed all the seven hydrogen atoms. Excluding the reflections 012, 201, and 20$\bar{1}$, block-diagonal least-squares refinement with anisotropic thermal parameters for the non-hydrogen atoms and with isotropic ones for the hydrogen atoms was carried out by using the weighting scheme:

$$w = (4.0/F_o)^2 \quad \text{for } |F_o| > 4.0$$

$$w = 1.0 \quad \text{for } 4.0 \geq |F_o| \geq 2.2$$

and

$$w = 0.5 \quad \text{for } 2{\cdot}2 > |F_o| > 0.0.$$

The final R value was 0.088 for 525 observed reflections.

The computations were carried out on a HITAC 8800/8700 computer at the Computer Center of the University of Tokyo and on a NEAC 2200—500 computer at the Okayama University Computer Center. The main programs used were RSSFR-5, HBLS-4, RSDLS-3, RSDA-4, and RSBP-3 of the UNICS Program System.[4] The atomic scattering factors were taken from International Tables for X-ray Crystallography.[5]

TABLE 2. OBSERVED AND CALCULATED STRUCTURE FACTORS ($\times$ 10) FOR CROTONIC ACID

L	FO	FC	L	FO	FC	L	FO	FC	L	FO	FC	L	FO	FC	L	FO	FC
H,K= 0	0		10	68	-48	-3	881	1208	-6	245	-209	H,K= 11		1	1	151	131	-6	92	102
2	562	611	H,K= 8		0	-2	951	1369	-5	146	140	-16	50	50	3	54	61	-5	116	123
4	592	-722	-14	48	54	-1	311	-348	-4	172	-162	-9	93	97	3	110	102	-4	96	95
6	100	84	-12	212	197	0	393	425	-3	33	-20	-8	58	61	4	154	145	-3	86	86
8	298	291	-8	311	-310	1	487	-608	-2	394	-439	-7	90	84	5	206	198	-2	153	-124
10	284	306	-6	212	195	2	170	-184	-1	84	-74	-6	57	44	7	142	124	-1	69	-66
12	105	104	-4	417	418	3	85	74	0	391	-394	-2	179	157	9	116	132	2	72	75
14	61	66	-2	290	267	4	81	89	1	452	-445	-1	83	-82	11	58	75	3	104	110
16	81	87	0	202	195	5	169	170	2	451	-439	2	150	-154	13	92	-76	4	41	49
H,K= 2	0	4	264	-68	6	118	117	3	139	114	3	207	202	H,K= 4		2	5	59	59	
-12	185	186	6	192	185	7	288	297	4	101	-91	H,K= 15		1	-14	111	-108	H,K= 3		3
-10	255	262	14	48	45	8	154	139	5	311	309	-10	59	-77	-12	100	-120	-12	74	-83
-8	398	-352	H,K= 10		0	9	135	130	6	164	153	-9	73	92	-11	99	101	-9	152	169
-6	355	-369	-16	192	169	12	59	60	7	174	-172	-7	85	91	-9	162	165	-8	69	75
-4	1101	1348	-14	150	133	13	42	17	8	112	-112	-6	75	87	-8	70	70	-7	97	111
-2	574	598	-12	96	-101	14	99	95	9	188	-182	-5	101	-121	-6	103	-101	-6	55	-42
0	162	-133	-8	174	170	15	40	-48	10	149	-154	-4	66	-66	-5	76	81	-5	67	-61
2	45	-21	-6	305	321	H,K= 3		1	12	42	-50	-3	124	-129	-4	190	-187	-4	66	-63
4	491	-491	-4	257	253	-13	79	94	-11	117	-93	-11	83	-87	-1	147	129	-2	163	-165
6	142	-125	0	197	190	-11	117	-93	-11	83	-87	-1	147	129	-2	163	-165	1	65	64
8	42	-48	4	46	-72	-10	174	-147	-10	87	-92	0	73	-63	-1	60	-58	2	54	43
10	137	135	6	107	121	-9	69	-24	-9	192	-161	1	85	103	0	181	-168	3	67	65
12	141	148	H,K= 12		0	-8	60	-64	-6	247	-237	H,K= 15		1	1	52	43	5	68	67
14	130	-126	-6	65	60	-7	407	386	-5	195	203	-11	53	73	2	159	-158	6	40	14
16	107	-120	-4	220	189	-6	247	267	-4	55	-41	-7	91	-107	3	165	154	7	57	61
H,K= 4	0	-2	174	-162	-5	304	306	-3	227	-254	-6	91	-91	7	107	106	H,K= 5		3	
-16	47	-72	0	389	-369	-4	218	-218	-1	283	-324	H,K= 17		1	8	86	-100	-5	80	-49
-12	117	-93	4	76	78	-3	214	226	0	137	142	2	55	47	9	170	-192	-3	112	-99
-10	193	-190	H,K= 14		0	-2	258	-245	1	59	50	H,K= 0		2	10	88	-74	0	103	-101
-8	146	-142	-12	102	-111	0	67	-59	2	198	211	1	393	-428	11	87	-92	1	92	85
-6	529	-540	-8	145	136	1	229	-260	3	31	-35	2	164	160	13	49	38	2	47	35
-4	201	-199	-4	269	-282	2	360	-352	6	51	53	3	321	-338	H,K= 6		2	3	66	5
-2	87	72	-2	175	-158	3	114	99	7	88	-90	4	210	214	-8	58	54	4	67	5
0	609	-631	H,K= 16		0	4	275	-260	9	82	-90	5	216	208	-7	141	-124	5	66	-54
2	572	-612	-10	42	32	5	175	172	H,K= 9		1	6	134	134	-6	54	44	6	92	-88
4	906	-930	4	82	55	6	263	-250	-14	146	148	7	158	141	-5	123	-121	7	110	-114
6	117	-107	H,K= 18		0	7	292	295	-13	128	122	8	79	63	-4	174	-183	H,K= 7		5
8	347	338	-10	32	43	9	107	96	-12	112	112	9	82	61	-2	304	-330	-9	46	-6
10	138	-142	-2	33	38	10	110	102	-11	176	-176	13	50	53	-1	141	-144	-8	80	70
12	237	-256	0	88	86	11	189	-189	-10	81	-60	14	34	38	2	233	219	-7	135	-158
14	57	-74	H,K= 1		1	12	117	-111	-9	92	95	15	32	46	3	68	59	-6	65	59
H,K= 6		0	-18	46	59	13	69	-62	-7	153	139	16	49	49	5	164	-176	-5	65	-89
-18	57	-59	-16	43	46	14	121	-121	-6	177	157	H,K= 2		2	6	134	-116	-4	79	-93
-16	66	-66	-14	47	44	15	49	63	-5	35	-36	-10	100	-101	7	123	-141	-1	65	70
-10	223	-227	-13	38	38	H,K= 5		1	-4	244	267	-9	85	-85	H,K= 8		1	0	80	92
-8	238	-211	-12	107	105	-18	47	-44	-3	126	-113	-8	51	41	-11	116	-152	1	46	-42
-6	256	-221	-10	185	175	-16	75	-70	-2	220	214	-7	216	216	-10	115	123	3	114	-127
-4	371	-375	-9	171	-154	-14	115	-109	-1	127	-112	-6	283	280	-9	178	-193			
-2	126	127	-8	168	172	-12	60	-66	0	84	71	-5	488	480	-6	105	-102			
0	516	-548	-7	333	-357	-10	51	-59	1	107	94	-4	216	209	-2	174	172			
2	387	-359	-6	187	-187	-9	71	-63	2	203	207	-2	197	-182	2	154	149			
4	319	317	-5	389	412	-8	271	-269	4	120	113	-1	46	-44	H,K= 1		3			
6	55	41	-4	292	285	-7	116	102	7	73	55	0	142	-151	-8	52	-56			

Results and Discussion

Observed and calculated structure factors for crotonic acid are given in Table 2, and those for crotonamide in Table 3.

TABLE 3. OBSERVED AND CALCULATED STRUCTURE FACTORS ($\times$ 10) FOR CROTONAMIDE

L	FO	FC	L	FO	FC	L	FO	FC	L	FO	FC	L	FO	FC	L	FO	FC
H,K= 0	0		1	37	-33	H,K= 2	3		5	23	23	H,K= 4	3		1	73	-76	4	50	31
1	263	362	2	75	74	-8	19	-31	7	17	+16	-7	37	44	2	31	27	5	8	12
2	234	-242	3	66	50	-7	42	45	8	11	11	-5	54	-52	3	33	H,K= 6		5	
3	96	-92	4	72	70	-6	111	107	H,K= 3		4	-3	24	23	4	11	16	-4	22	26
4	169	-164	5	72	74	-5	27	-23	-7	32	-32	-2	29	-29	H,K= 8		5	-2	83	-93
5	99	-93	6	25	29	-4	29	-24	-5	80	90	-1	79	-85	-6	7	8	-1	34	-38
6	44	-43	H,K= 1		4	-2	122	-118	-4	82	87	0	28	30	-5	15	12	0	17	15
7	19	21	-8	21	21	-1	156	-160	-3	23	-30	1	118	117	-4	18	19	1	9	11
8	33	34	-6	45	-40	0	165	-163	-2	15	-15	2	45	-48	-3	16	-16	2	19	19
H,K= 0		1	-4	70	68	1	177	182	-1	27	31	3	22	-20	-2	55	-56	3	27	28
1	233	-278	-2	63	2	2	104	88	0	79	-84	4	16	19	-1	35	34	4	27	28
2	492	-739	-2	162	-150	4	24	27	1	95	-91	6	15	18	1	18	19	H,K= 6		6
3	172	-176	-1	16	-18	5	52	-53	2	9	18	H,K= 4		4	2	40	-6	-6	16	17
5	36	34	0	45	45	7	36	34	3	38	39	-5	31	-35	3	17	17	-4	13	-14
6	68	70	1	84	71	H,K= 2		4	4	18	18	-3	31	31	H,K= 5		6	-3	16	-15
H,K= 0		2	2	119	115	-5	53	-52	6	19	-19	-2	42	42	-6	6	18	0	30	36
0	275	-338	3	54	52	-4	111	-104	7	17	-17	-1	90	90	-4	31	-35	1	29	26
1	136	-135	7	39	-38	-3	47	-47	H,K= 3		5	2	11	-11	-3	37	41	2	17	15
2	200	-203	H,K= 1		5	-2	57	-58	-6	20	17	3	40	-40	-1	20	21	4	9	-9
3	140	149	-4	14	-20	-1	91	94	-5	41	-41	H,K= 4		5	2	15	12	H,K= 6		7
4	262	287	-3	36	-50	0	121	120	-2	58	-63	-4	38	41	4	16	-15	-1	11	11
6	29	-29	-2	38	-40	1	26	27	-1	14	-11	-3	102	108	H,K= 5		7	0	28	25
7	13	-19	-1	53	52	2	67	65	0	26	30	-2	23	-25	-5	25	-25	2	20	-21
8	28	-23	0	96	93	3	29	-30	1	26	29	-1	86	-87	-2	8	8	H,K= 7		1
H,K= 0		3	1	37	36	5	22	20	2	45	47	0	23	-20	-1	11	12	-6	29	29
1	64	68	2	29	-25	H,K= 2		5	3	20	26	1	33	-38	0	6	6	-4	18	-16
2	161	169	5	31	-30	-5	34	-36	4	17	-17	H,K= 5		5	1	8	9	-2	30	26
3	10	12	H,K= 1		6	-4	52	-48	5	27	-28	5	17	13	-2	8	9	-2	47	50
4	42	39	-6	37	-34	-3	104	110	H,K= 3		6	H,K= 4		6	H,K= 6		0	-1	18	17
5	67	-67	-1	46	45	-2	133	135	-5	29	-28	-5	36	37	-6	63	-60	1	23	24
6	99	-106	0	46	51	-1	26	24	-4	18	21	-3	30	-37	-5	52	-57	2	113	107
7	25	23	2	25	-20	0	29	33	-1	65	72	-2	31	-34	-4	93	89	6	7	-10
8	34	30	3	29	-25	2	21	-22	0	43	44	-1	60	-67	-3	26	25	H,K= 7		2
H,K= 0		4	4	14	-16	H,K= 2	6		1	10	-14	1	32	37	-2	42	-40	-7	18	17
0	125	137	H,K= 1		7	-5	41	35	2	27	-29	H,K= 6		4	0	92	-80	-6	24	29
1	38	-37	-4	38	31	-4	34	37	3	29	-27	-5	20	-20	1	66	62	-5	22	22
2	38	-35	-1	31	28	-2	25	29	4	26	-24	-1	18	14	2	113	107	-2	23	14
3	44	-39	0	24	23	-1	58	-63	H,K= 3		7	0	25	24	3	60	57	-1	30	-29
4	65	-66	1	34	-37	0	57	-59	0	28	-26	1	38	36	4	15	20	0	41	-42
5	23	24	2	55	-46	1	45	44	1	56	-59	3	21	-18	7	25	-26	1	8	8
6	18	18	4	19	17	H,K= 2		7	2	28	-27	H,K= 4		8	H,K= 6		1	2	12	12
7	20	21	H,K= 1		8	-6	19	20	3	19	16	2	14	-20	-6	31	31	3	31	-31
8	26	24	-1	15	-16	-5	18	-13	H,K= 3		8	H,K= 6		1	-5	20	20	4	21	-24
H,K= 0		5	0	19	-16	-3	23	-18	-2	14	-14	-9	18	17	-4	41	36	H,K= 7		3
2	69	-75	H,K= 2		0	-2	12	-13	-1	17	-16	-7	25	-25	-2	99	-101	-5	18	-17
3	54	53	-7	33	32	-1	12	13	0	12	-12	-6	21	17	-1	22	23	-4	40	-42
4	66	67	-6	92	87	1	20	25	H,K= 4		0	-5	27	24	0	104	90	-3	23	-27
H,K= 0		6	-4	69	-64	3	28	-21	-7	56	64	-4	56	-45	1	74	63	1	15	-14
0	64	-71	-3	40	-37	H,K= 2		8	-6	40	39	-3	88	-83	2	46	42	2	13	-13
1	40	40	-2	240	-235	-4	10	-11	-5	82	-84	-2	85	-84	3	17	-15	H,K= 7		4
2	48	53	-1	339	374	-3	31	24	-4	51	-45	-1	47	-47	4	23	-26	-7		-11
7	10	-11	1	292	-393	-2	28	34	-3	139	-132	0	51	46	5	34	-34	-6	14	13
H,K= 0		7	2	130	-120	3	37	-35	-2	261	-257	1	74	68	6	31	-32	-5	9	-15
1	13	-14	3	60	-66	H,K= 3		1	0	183	-174	2	11	9	H,K= 6		2	-3	28	30
2	12	18	4	114	-109	-5	46	49	1	71	-72	3	22	22	-8	28	25	-2	53	56
H,K= 0		8	5	81	-84	4	20	18	2	167	151	4	59	56	-7	20	22	-1	13	-12
2	30	-26	7	47	59	-3	36	-31	3	105	99	6	29	-32	-5	17	-20	0	46	-44
4	26	-26	H,K= 2		1	-2	112	-115	4	11	12	H,K= 5		2	-4	37	-36	1	9	9
H,K= 1		1	-6	34	-35	-1	220	-215	6	28	29	-7	8	-11	-2	9	8	2	20	-20
-4	83	-67	-5	66	-59	0	73	-75	8	23	-24	-6	48	-74	-1	39	34	5	12	12
-3	115	110	-4	172	-154	1	117	98	H,K= 4		1	-3	63	-58	0	75	79	H,K= 7		5
-2	297	334	-3	148	143	2	25	-23	-7	22	-25	-2	110	96	3	52	-50	-5	23	21
-1	17	17	-2	261	261	3	97	-104	-6	50	-51	-1	154	156	4	59	-65	-4	29	28
0	137	-147	-1	216	-204	4	14	11	-5	95	-97	0	80	82	6	21	22	-2	31	-27
1	233	261	0	27	43	5	47	50	-4	103	-96	1	53	56	H,K= 6		3	-1	18	-17
2	196	194	1	263	-282	H,K= 3		2	-3	67	64	2	53	54	-6	35	-37	0	9	-14
3	184	-192	2	221	-206	-6	24	-23	-2	34	-34	3	20	-16	-5	15	-18	2	14	11
4	146	-154	4	9	-2	-4	83	-87	-1	29	27	4	52	-53	-4	31	31	H,K= 7		6
H,K= 1		2	4	15	11	-3	233	-215	0	215	223	5	22	-25	-3	46	43	-4	29	-29
-8	35	26	5	74	71	-2	91	-79	1	100	92	H,K= 5		3	-2	32	32	-3	16	-16
-6	45	-38	6	45	-39	-1	137	138	2	86	80	-7	11	-15	-1	24	21	1	27	26
-5	37	33	9	9	-15	0	101	97	4	31	-35	-4	26	23	0	37	40	2	13	27
-4	134	123	H,K= 2		2	2	32	31	6	25	-24	-3	69	67	1	38	-40	H,K= 7		7
-3	60	49	-8	36	-41	3	30	28	H,K= 4		2	-2	94	94	2	106	-112	-1	22	22
-2	9	-18	-6	44	-37	5	17	19	-9	25	-28	-1	59	59	3	12	-12	0	19	19
-1	27	26	-5	54	-52	H,K= 3		3	-8	20	-20	0	56	-55	4	21	23			
0	56	-55	-4	150	136	-6	46	-53	-5	14	15	2	98	-108	5	8	11			
1	210	-225	-3	9	-8	-5	45	-42	-3	50	48	3	53	-56	6	10	13			
2	211	-208	-2	62	55	-3	67	74	-2	102	100	H,K= 5		4	H,K= 6		4			
3	123	-127	-1	69	-83	2	133	128	0	17	21	-7	15	-16	-4	37	39			
4	48	-41	0	155	-160	-1	87	78	1	64	-74	-6	8	12	-3	21	25			
5	51	52	1	123	-130	0	36	36	2	22	-18	-5	44	47	-1	36	-37			
6	53	54	2	102	-99	1	23	17	3	35	36	-4	16	12	0	84	-92			
H,K= 1		3	3	234	219	2	44	-43	4	73	-67	-2	37	40	1	36	-34			
-1	173	-180	4	96	-92	3	40	-39	5	35	-37	-1	19	-22	2	12	-14			
0	263	-260	5	56	-52	4	14	19	6	19	21	0	128	-137	3	8	9			

TABLE 4. FINAL ATOMIC PARAMETERS AND ESTIMATED STANDARD DEVIATIONS ($\times 10^4$) FOR NON-HYDROGEN ATOMS

The anisotropic thermal parameters are defined as: $\exp(-\beta_{11}h^2-\beta_{22}k^2-\beta_{33}l^2-\beta_{12}hk-\beta_{13}hl-\beta_{23}kl)$.

	x/a	y/b	z/c	β_{11}	β_{22}	β_{33}	β_{12}	β_{13}	β_{23}
Crotonic acid									
O(1)	1113(3)	−719(14)	72(3)	61(3)	1246(46)	52(2)	2(21)	34(4)	−154(19)
O(2)	533(3)	2121(15)	978(3)	55(3)	1437(54)	66(3)	−3(24)	37(5)	−165(21)
C(1)	3824(5)	1335(21)	1821(5)	58(4)	1151(80)	64(4)	−49(35)	17(7)	69(32)
C(2)	2874(5)	698(18)	1236(4)	63(4)	779(55)	58(3)	−5(31)	37(6)	30(26)
C(3)	2114(5)	1698(18)	1345(4)	68(4)	838(60)	51(3)	54(31)	40(6)	25(24)
C(4)	1211(4)	952(18)	753(4)	42(4)	820(56)	58(3)	−20(28)	4(6)	86(26)
Crotonamide									
O	−561(3)	2038(4)	1263(4)	120(5)	254(6)	302(7)	−11(7)	106(8)	−31(11)
N	1613(4)	1505(5)	797(5)	138(6)	252(7)	315(9)	5(9)	118(10)	−12(13)
C(1)	898(6)	7542(6)	3790(8)	281(10)	252(10)	284(11)	−68(14)	109(16)	−59(18)
C(2)	415(5)	5650(5)	2921(6)	210(8)	214(8)	226(8)	−28(12)	82(11)	31(14)
C(3)	1232(5)	4415(5)	2313(6)	172(7)	236(8)	197(8)	−53(11)	80(10)	28(13)
C(4)	668(4)	2547(5)	1419(5)	115(6)	219(8)	204(7)	8(9)	74(9)	54(12)

TABLE 5. FINAL FRACTIONAL COORDINATES ($\times 10^3$) AND ISOTROPIC THERMAL PARAMETERS (Å^2) FOR HYDROGEN ATOMS
Their estimated standard deviations are in parentheses.

	x/a	y/b	z/c	B
Crotonic acid				
H(1)	383(5)	294(22)	224(4)	6.3(2.0)
H(2)	409(4)	231(19)	147(4)	5.2(1.8)
H(3)	405(5)	−73(24)	206(5)	8.2(2.5)
H(4)	278(6)	−63(21)	78(5)	7.2(2.1)
H(5)	216(5)	329(19)	181(5)	6.0(1.9)
H(6)	−10(5)	162(20)	62(5)	6.7(2.1)
Crotonamide				
H(1)	46(6)	895(10)	308(8)	8.1(1.6)
H(2)	95(6)	764(8)	506(8)	6.1(1.3)
H(3)	196(4)	758(5)	401(6)	3.7(1.0)
H(4)	−72(5)	535(7)	268(7)	5.0(1.2)
H(5)	247(4)	456(5)	252(5)	2.7(0.8)
H(6)	138(5)	12(6)	20(6)	4.4(1.1)
H(7)	282(4)	164(7)	111(6)	4.5(1.1)

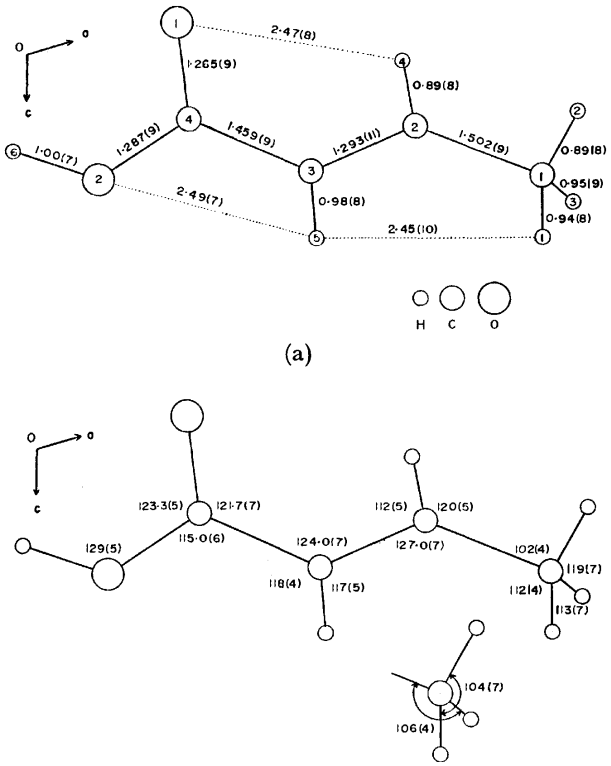

(a)

(b)

Fig. 1. The molecular structure of crotonic acid.
(a) Bond lengths (Å) and numbering of atoms.
(b) Bond angles (°). The estimated standard deviations are given in parentheses.

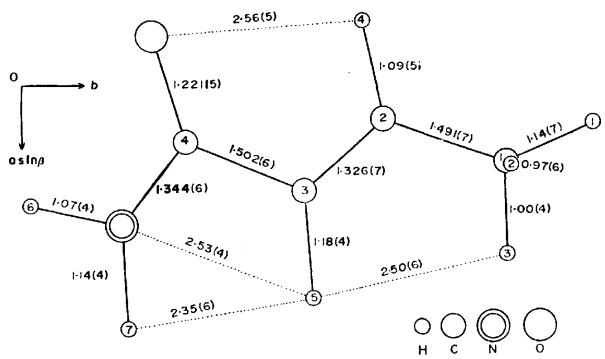

(a)

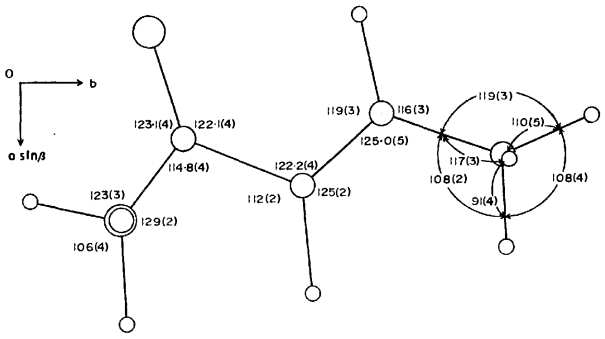

(b)

Fig. 2. The molecular structure of crotonamide.
(a) Bond lengths (Å) and numbering of atoms.
(b) Bond angles (°). The estimated standard deviations are given in parentheses.

TABLE 6. LEAST-SQUARES PLANES
Each plane is represented by $lX+mY+nZ=p$, where X, Y and Z (in Å) are referred to the crystallographic axes.

	Crotonic acid		Crotonamide	
	(1) Best plane through the ethylenic group	(2) Best plane through the carboxyl group	(1) Best plane through the ethylenic group	(2) Best plane through the amide group
l	0.2068	0.1931	0.0153	0.0597
m	0.8316	0.8390	−0.4587	−0.4781
n	−0.5536	−0.5431	0.8584	0.8358
p	0.0336	0.0208	0.1541	0.1146
Deviation (Å)				
C (1)	−0.004	O (1) 0.0002	C (1) −0.006	O −0.001
C (2)	0.004	O (2) 0.0002	C (2) 0.007	N −0.001
C (3)	0.003	C (3) 0.0002	C (3) 0.006	C (3) −0.001
C (4)	−0.004	C (4) −0.0006	C (4) −0.006	C (4) 0.003

Table 3; the final atomic parameters in Tables 4 and 5. Bond lengths and angles along with the numbering scheme for atoms are shown in Fig. 1 for crotonic acid, and in Fig. 2 for crotonamide.

Molecular Shape. The equations of best planes and the deviations of the atoms from each plane are listed in Table 6. Dihedral angle between the ethylenic and carboxylic planes of crotonic acid is only 1.0°, and that between the ethylenic and amide planes of crotonamide is 2.9°, which are rather smaller than the corresponding value (3.6°) found in *trans*-β-2-furylacrylamide.[6] Thus the configurations of both crotonic acid and crotonamide are nearly planar. The bond length C(2)=C(3) of crotonic acid is rather shorter. The difference between the bond lengths C(4)=O(1) and C(4)–O(2) in crotonic acid is very small as observed in β-methyl-*cis*-cinnamic acid and β-chloro-*cis*-cinnamic acid.[7] On the other hand, the C(4)=O and C(4)–N distances in crotonamide are very close to the values (1.225 and 1.349 Å, respectively) predicted from hybridization effect.[8] The C=O bonds of both carboxyl and amide groups adopt the *cis*-configuration with respect to the ethylenic C=C bonds. Some intramolecular contacts are shown in Figs. 1 and 2.

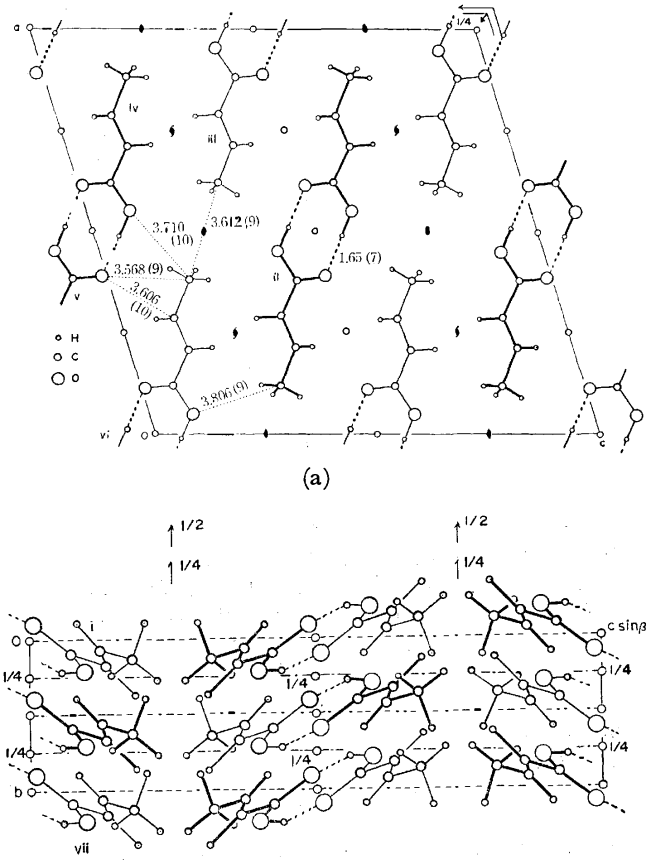

Fig. 3. Projections of the crystal structure of crotonic acid.
(a) Viewed along the b axis.
(b) Viewed along the a axis.
Broken lines show hydrogen bonds, and dotted lines intermolecular contacts.
Symmetry code: i $x/a, y/b, z/c$; ii $1/2-x/a, 1/2+y/b, 1/2-z/c$; iii $1-x/a, y/b, 1/2-z/c$; iv $1/2+x/a, 1/2+y/b, z/c$; v $1/2-x/a, 1/2-y/b, -z/c$; vi $-x/a, -y/b, -z/c$; vii $x/a, 1+y/b, z/c$.

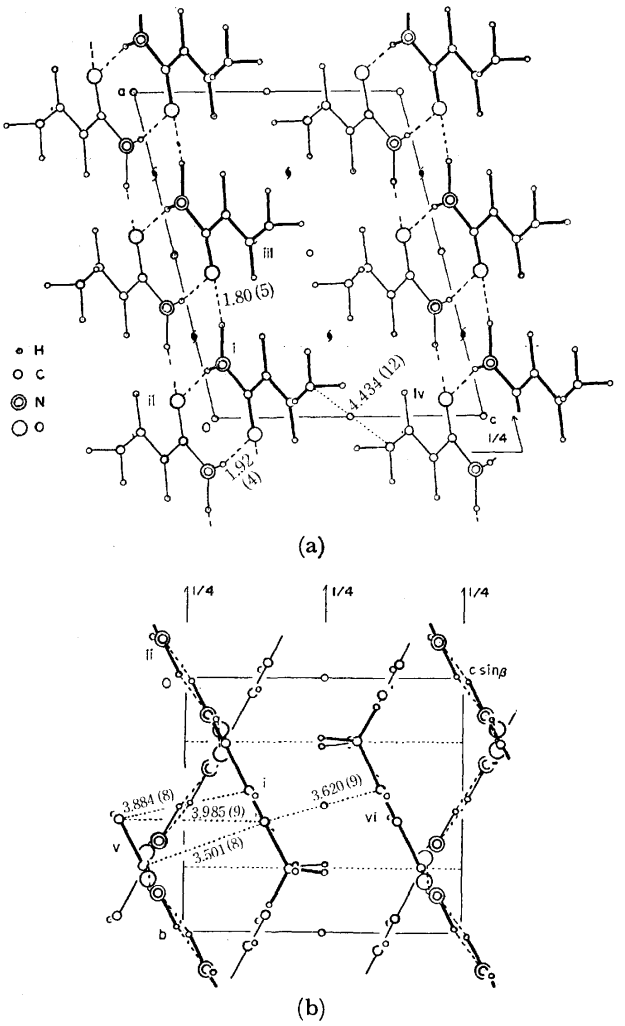

Fig. 4. Projections of the crystal structure of crotonamide.
(a) Viewed along the b axis.
(b) Viewed along the a axis.
Broken lines show hydrogen bonds, and dotted lines intermolecular contacts.
Symmetry code: i $x/a, y/b, z/c$; ii $-x/a, -y/b, -z/c$; iii $1/2+x/a, 1/2-y/b, z/c$; iv $-x/a, 2-y/b, 1-z/c$; v $-x/a, 1-y/b, -z/c$; vi $-x/a, 1-y/b, 1-z/c$.

A significant difference in the C=O bond lengths has been pointed out between the carboxyl (1.209 Å) and the amide (1.247 Å) groups in fumaramic acid,[9] but the situation has reversed in the case of crotonic acid and crotonamide.

Molecular Packing. Projections of the crystal structure of crotonic acid viewed along the b and a axes and some intermolecular contacts are shown in Fig. 3 and those of crotonamide in Fig. 4. Geometry of the hydrogen bonds is listed in Table 7. The crystal structure of crotonic acid consists of two identical stacks of centrosymmetrically hydrogen-bonded pairs of the molecules, which are held together by van der Waals interactions between the methyl groups at a distance of 3.61 Å to form infinite chains along the

TABLE 7. HYDROGEN-BOND DISTANCES (Å) AND ANGLES (°)
Symmetry code is given in Figs. 3 and 4.

Crotonic acid			
O(1)···O(2^{vi})	2.645(6)	C(4)–O(2)···O(1^{vi})	115.6(4)
O(2)–H(6)	1.00(7)	C(4)–O(2)–H(6)	129(8)
H(6)···O(1^{vi})	1.65(7)	O(2)–H(6)···O(1^{vi})	174(8)
		C(4)–O(1)···O(2^{vi})	121.1(4)
		C(4)–O(1)···H(6^{vi})	123(8)
Crotonamide			
N···O^{ii}	2.963(8)	C(4)–N···O^{ii}	117.3(3)
N–H(6)	1.07(4)	C(4)–N–H(6)	123(3)
H(6)···O^{ii}	1.92(4)	N–H(6)···O^{ii}	165(4)
		C(4)–O···N^{ii}	119.5(3)
		C(4)–O···H(6^{ii})	122(2)
N···O^{iii}	2.862(7)	C(4)–N···O^{iii}	118.9(3)
N–H(7)	1.14(4)	C(4)–N–H(7)	129(2)
H(7)···O^{iii}	1.80(5)	N–H(7)···O^{iii}	153(4)
		N···O^{iii}–C(4^{iii})	142.7(3)
		H(7)···O^{iii}–C(4^{iii})	133(2)
		O^{ii}···N···O^{iii}	123.6(2)
		H(6)–N–H(7)	106(4)

[201] direction. The corresponding contact in α-tetronic acid[10] is 3.81 Å, and that in *p*-toluic acid[11] 3.50 Å. The hydrogen-bonded carboxyl groups are not fully coplanar, being offset 0.04 Å.

Crotonamide molecules related by a center of symmetry are linked by N–H···O hydrogen bonds to form pairs at (000) and (1/2, 1/2, 0), which are held together side by side through the a-glide plane by additional N–H···O hydrogen bonds. This packing mode belongs to the glide-plane packing type.[12] The intrapair amide groups are distinctly not planar, the separation between the two corresponding parallel planes being 0.23 Å. The inclination of the amide pair to the glide plane is 61.5° and the nearest methyl-methyl distance is 4.43 Å. The interpair angles C–N···O and C=O···N are 118.9 and 142.7°, respectively, which are close to those found in furylacrylamide.[6]

The structures of crotonic acid and crotonamide show short enough distances between ethylenic groups (C(3)···C(2^{vii}) 3.86 and C(3)···C(3^{v}) 3.88 Å, respectively) to dimerize or polymerize on irradiation with ultraviolet light, and the parallel alignment of double bonds considered as a pre-requisite for cycloaddition occurs in both compounds.

References

1) K. Fukuyama, S. Kashino, and M. Haisa, *Chem. Lett.*, **1972**, 599.
2) M. D. Cohen and G. M. J. Schmidt, *J. Chem. Soc.*, **1964**, 1996.
3) M. A. Higgs and R. L. Saas, *Acta Crystallogr.*, **16**, 657 (1963).
4) "Universal Crystallographic Computation Program System," ed. by T. Sakurai, The Crystallographic Society of Japan, Tokyo (1967).
5) "International Tables for X-ray Crystallography," Vol. III, Kynoch Press, Birmingham (1962), p. 202.
6) L. Leiserowitz and D. Rabinovich, *J. Chem. Soc., Ser. A*, **1969**, 2367.
7) S. E. Fillippakis, L. Leiserowitz, D. Rabinovich, and G. M. J. Schmidt, *J. Chem. Soc., Perkin II*, **1972**, 1750.
8) M. G. Brown, *Trans. Faraday Soc.*, **55**, 694 (1959).
9) V. Benghiat, H. W. Kaufman, L. Leiserowitz, and G. M. J. Schmidt, *J. Chem. Soc., Perkin II*, **1972**, 1758.
10) V. Benghiat and L. Leiserowitz, *ibid.*, **1972**, 1763.
11) M. G. Takwale and L. M. Pant, *Acta Crystallogr.*, **B27**, 1152 (1971).
12) L. Leiserowitz and G. M. J. Schmidt, *J. Chem. Soc., Ser. A*, **1969**, 2372.

UV-Spectra of Fluorenyl Salts in the Binary Mixtures of DME and Benzene

Katsuhiko TAKAYA and Norio ISE

Department of Polymer Chemistry, Kyoto University, Kyoto 606

(Received March 28, 1974)

The temperature dependence of UV spectra of fluorenyl lithium and sodium was investigated in 30, 40, and 50 vol% dimethoxyethane (DME)–benzene mixtures. The lithium salt had two absorption peaks at 352 and 373 nm, and the sodium salt at 358 and 373 nm. The fraction of solvent-separated ion pairs for the sodium salt was much lower than that of the lithium salt, and the heat of conversion ($-\Delta H_i$) of contact-ion pairs to solvent-separated ion pairs was larger (9—11 kcal/mol) for the sodium salt than that (1—4 kcal/mol) for the lithium salt.

In our laboratory living anionic polymerizations of styrene with alkali metal gegenions were investigated in the binary mixtures of 1,2-dimethoxyethane (DME) and benzene[1-3] and in triglyme–benzene mixtures.[4] The reactivity of ion pairs in DME–benzene mixtures was higher[1-4] than that in other ethereal solvents in general.[5-9] The dissociation constants of polystyryl ion pairs in DME–benzene systems were not larger than those in other solvent systems. These tendencies suggest that the higher reactivity of the ion pair (even for the caesium salt) should be attributed to the contribution of the solvent-separated ion pairs. This is supported by the fact that lithium and sodium salts have a larger inter-charge distance a in the ion pair (6—10.5 and 9.3 Å, respectively),[2] calculated by the Fuoss equation,[10] than in THF (4.5 and 4.4 Å, respectively) and in MeTHF (3.3—3.4 Å) and in THP (3.5—3.7 Å)

$$K_d = \frac{3000}{4\pi Na^3} \cdot \exp\left(-\frac{e^2}{a\varepsilon kT}\right), \qquad (1)$$

where K_d, N, ε, and k are the dissociation constant of ion pair, the Avogadro number, the dielectric constant, and the Boltzmann constant, respectively.

It must, however, be taken into consideration in the present systems that the formation of the "cybotactic region" [11] of DME molecules or a different composition of the solvent in the vicinity of the ions and ion pairs from that in the bulk solvent system might be probable as one of the reasons for the larger a values.

It was also a question why the sodium ion pair was most reactive among the polystyryl salts in DME–benzene (50 vol%) mixture. To obtain information about the solvation of the ion pairs, we investigated UV spectra of lithium and sodium salts of fluorene as model compounds in the binary mixtures of DME and benzene between 0 and 25 °C. Smid *et al.* studied the UV spectra of the same salts in ethereal solvents.[12]

Experimental

Commercial fluorene was recrystallized several times using alcohol and dried under a high vacuum. DME, preliminarily dehydrated by metal sodium, were refluxed over CaH_2 for a week and distilled onto Na–K alloy. Then DME was subjected to deaeration-dehydration treatment on a vacuum line by cooling and degassing with stirring in the presence of Na–K alloy dispersion. Benzene, contacted with concentrated sulfuric acid for a few weeks, was fully washed with concentrated sulfuric acid, aqueous sodium hydroxide solution, and water to be neutral, then dehydrated with $CaCl_2$ and thereafter with CaH_2. This benzene was then treated in the same manner as DME.

The fluorenyl salts were prepared from solutions of the corresponding polystyryl salts in tetrahydrofuran (THF) under a high vacuum. The THF of the fluorenyl salt solution was substituted with DME–benzene mixtures.

The fluorenyl salt solutions directly prepared in the DME–benzene mixture by treating fluorene with sodium mirror did not show different spectra from those of the salts prepared from polystyryl salts. The salt solutions were stored in a freezer or in an ice-box.

Results and Discussion

In Fig. 1, the UV spectra of fluorenyl lithium in the binary mixture of DME and benzene (at DME contents of 30, 40, and 50 vol%) between 0 and 25 °C are given. The carbanions had absorption bands at 350 and 373 nm, and the absorption peak at 350 nm decreased and that at 373 nm increased when the temperature was lowered.

In Fig. 2, the UV spectra of fluorenyl sodium in the 30, 40, and 50 vol% DME–benzene mixtures between 0 and 25 °C are shown. Two peaks were observed and maxima were at 358 and 373 nm in addition to the absorptions in the visible regions.

In both salts, absorption peaks were the same as those observed in other solvent systems.[12] As new

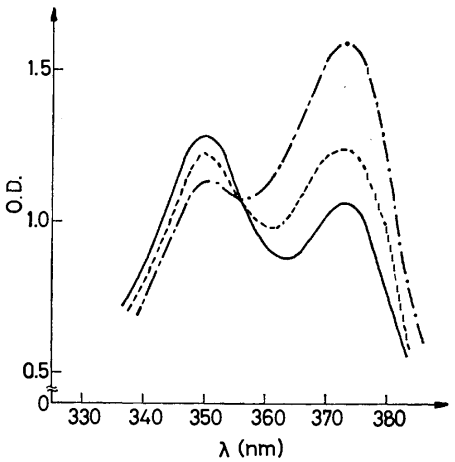

Fig. 1(a). Absorption spectra of fluorenyl lithium in DME–benzene (30: 70) mixture.
——: 25 °C, ----: 14.5 °C, ·——·: 0 °C.

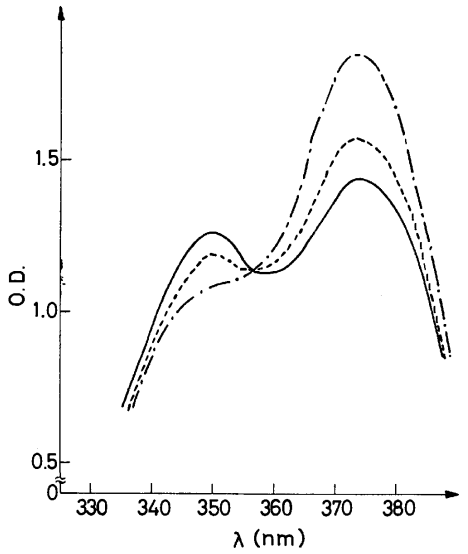

Fig. 1(b). Absorption spectra of fluorenyl lithium in DME–benzene (40: 60) mixture.
——: 25.0 °C, ----: 15.0 °C, –·–·–: 0 °C

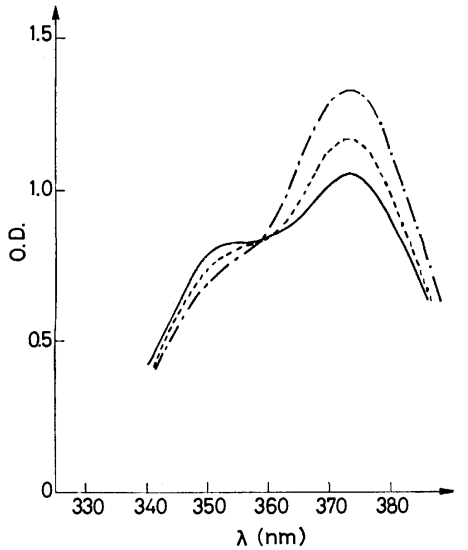

Fig. 1(c). Absorption spectra of fluorenyl lithium in DME–benzene (50: 50) mixture.
——: 25.0 °C, ----: 15.6 °C, –·–·–: 0 °C

peaks were not observed, the presence of higher aggregates in these salts than ion pairs remained unknown.[4]

The isosbestic points were observed for all cases and the relative heights of the two peaks were not affected by addition of highly dissociable tetraphenylboride as common ion salt. These facts indicate that the observed changes correspond to an equilibrium between contact ion pairs and solvent-separated ion pairs, which is sensitive to solvent, temperature, and gegenions. The peaks, which were predominant at high temperatures, are dependent on cations (*viz.* 350, and 358 nm for lithium and sodium salts, respectively, in the present system), but the peaks at 373 nm were independent of cations, as was shown by Smid *et al.*[12] The formation of the cybotactic region in the present system was suggested by the fact that the absorption peaks of the contact-ion pairs of lithium and sodium salts (F^-, M^+) were most bathochromically shifted in DME–benzene systems among the ethereal solvents and close to those in pure DME.

In Table 1, the fraction of solvent-separated ion pair $F^-//M^+$ was calculated according to Smid's method and is summarized together with other relevant data. The fraction of $F^-//M^+$ for both the lithium and sodium salts was larger than in other ethereal solvents with a similar polarity. Comparing the lithium and sodium ion pairs, the former is much richer in $F^-//Li^+$ than the latter. So the fraction of the solvent-separated ion pairs in the sodium salt of living polystyrene should be expected to be smaller than that of lithium salt, when we assume that the polystyryl anions have a structure

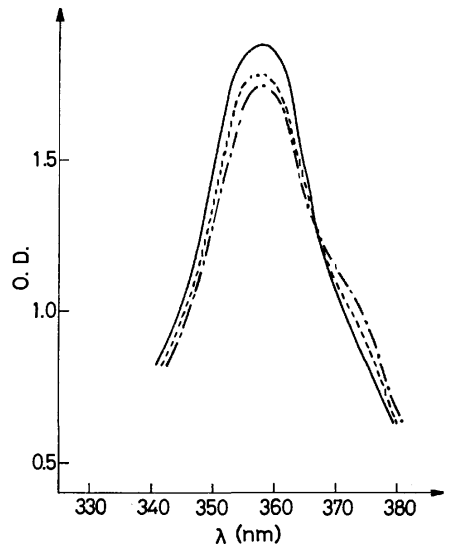

Fig. 2(a). Absorption spectra of fluorenyl sodium in DME–benzene (30: 70) mixture.
——: 25.0 °C, ----: 13.5 °C, –·–·–: 0 °C

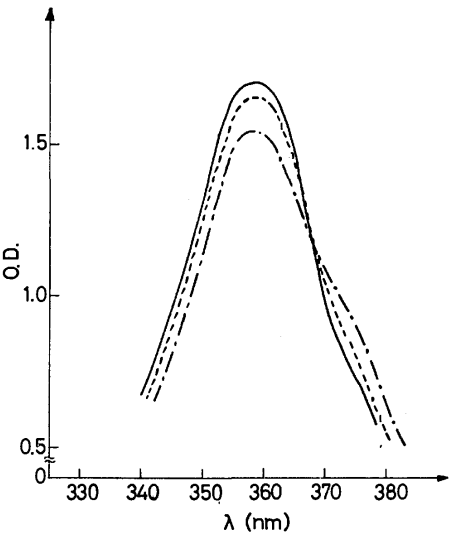

Fig. 2(b). Absorption spectra of fluorenyl sodium in DME–benzene (40: 60) mixture.
——: 24.5 °C, ----: 13.0 °C, –·–·–: 0 °C

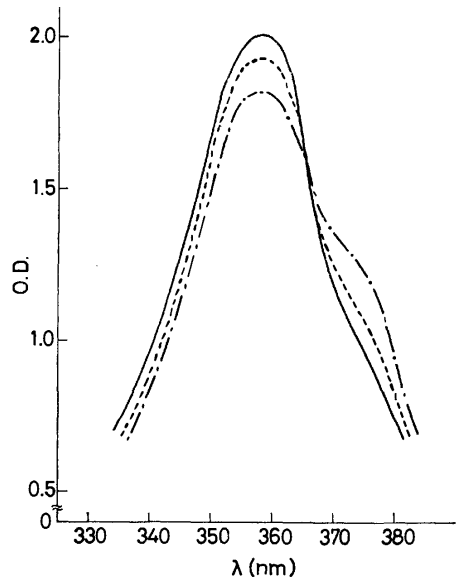

Fig. 2(c). Absorption spectra of fluorenyl sodium in DME–benzene (50: 50) mixture.
——: 24.7 °C, ----: 15.5 °C, -·--: 0 °C

TABLE 1. ABSORPTION MAXIMA OF CONTACT AND SOLVENT-SEPARATED FLUORENYL ION PAIRS IN DME–BENZENE MIXTURES

Gegenion	Fraction of DME (vol%)	Temp. (°C)	Dielectric constant ε	λ_{max} F^-,M^+ (nm)	λ_{max} $F^-//M^+$ (nm)	Fraction of $F^-//M^+$
Li^+	30	25	3.38	350	373	0.45
		0	3.60	350	373	0.60
	40	25	3.81	350	373	0.54
		0	4.07	350	373	0.64
	50	25	4.33	350	373	0.63
		0	4.67	350	373	0.72
Na^+	30	25	3.38	358	373	0
		0	3.60	358	373	0.07
	40	25	3.81	358	373	0.04
		0	4.07	358	373	0.17
	50	25	4.33	358	373	0.06
		0	4.67	358	373	0.21

relatively similar to fluorenyl anions. Therefore the difference of the ion-pair rate constant k_p' between the lithium and sodium salts in the DME–benzene systems should be attributed to the difference of the structure of the solvent-separated ion pairs of the both salts.

The equilibrium constant K between the two kinds of ion pairs should be written as

$$F^-, M^+ + n\cdot DME \overset{K}{\rightleftharpoons} F^-//M^+ \quad (2)$$

$$K = \frac{[F^-//M^+]}{[F^-, M^+]\cdot[DME]} \quad (3)$$

If the solvent is in a large excess, the ratio $[F^-//M^+]/[F^-, M^+](\equiv K_i)$ should be proportional to K. So the K_i value should be constant at a fixed temperature. The K_i values for the fluorenyl salts in the DME–benzene systems were calculated by the method by

TABLE 2. EQUILIBRIUM CONSTANT K_i FOR FLUORENYL SALTS IN DME–BENZENE MIXTURES

Gegenion	Solvent	Temp. (°C)	K_i
	DME–benzene		
Li^+	30:70	0	1.5
		14.5	1.1
		25.5	0.8
	40:60	0	1.8
		15.0	1.4
		25.0	1.2
	50:50	0	3.5
		15.6	3.0
		24.6	2.8
	DME–benzene		
Na^+	30:70	0	0.070
		13.5	0.025
		25.0	0
	40:60	0	0.21
		13.0	0.092
		24.5	0.040
	50:50	0	0.26
		15.5	0.11
		24.7	0.06

Smid *et al.*[12,13] and are given in Table 2. From the slope of $\log K_i$ *vs.* $1/T$ plot, the $-\Delta H_i$ values were given as 1.3—3.8 kcal/mol and 9.2—11 kcal/mol for the lithium and sodium ion pairs, respectively. The ΔH_i and ΔS_i values in the present systems are summarized in Table 3, together with the results in other solvents.

TABLE 3. THERMODYNAMIC QUANTITIES OF THE CONVERSION OF F^-,M^+ TO $F^-//M^+$ IN VARIOUS SOLVENTS

Group	Gegenion	Solvent (ε)	$-\Delta H_i$ (kcal/mol)	$-\Delta S_i$ (e.u.)
	DME–Benzene			
(I)	Li^+	50:50 (4.3)	1.3±1	1.0±2
		40:60 (3.8)	2.7±1	6.0±2
		30:70 (3.6)	3.8±1	13 ±2
	Na^+	50:50 (4.3)	9.2±2	38 ±8
		40:60 (3.8)	11 ±2	44 ±8
		30:70 (3.6)	(11)	(50)
(II)[a]	Na^+	THF (7.4)	7.1	33
	Li^+	THF	7.6	22
	Li^+	THP (5.6)	6.6	28
	Li^+	MeTHF (6.2)	7.5	27

a) Taken from Ref. 12.

The $-\Delta H_i$ values should be determined by a competition between the Coulombic energy between electric charges in the ion pairs and the solvation energy; the former is endothermic and the latter exothermic. If we assume that the solvation energy for ion pairs of fluorenyl lithium and sodium is nearly the same, as seen from the fact that the absorption peaks of solvent-separated ion pairs are independent of solvent, gegenions and temperature, and if we assume that the degrees of solvation in solvent-separated ion pairs and those in free ions should differ from each other, the trends of

$-\Delta H_i$ in Table 3 will be understood as follows. The smaller $-\Delta H_i$ values for the lithium salt in DME–benzene systems is reasonable because Coulombic forces in the lithium contact ion pairs are stronger than in the sodium ion pairs. In this respect, the sodium salt of 4,5-dimethyl-phenanthrene anion[14] has larger $-\Delta H_i$ and $-\Delta S_i$ values than the lithium salt (namely, $-\Delta H_i=5.0$ and 12.6 kcal/mol and $-\Delta S_i=17.0$ and 51.6 e.u. for the lithium and sodium salts, respectively, in THF, and $-\Delta H_i=3.7$ and 19.1 kcal/mol and $-\Delta S_i=10.9$ and 61.2 e.u. for the lithium and sodium salts, respectively, in DME). When we compare these values for the lithium salt between the DME–benzene system and the THF system, the larger $-\Delta H_i$ value in the latter should be attributed to the lack of the external solvation towards contact-ion pairs. The fact that the increase of DME content decreased the $-\Delta H_i$ value might be due to solvation towards the contact-ion pairs.

References

1) N. Ise, H. Hirohara, T. Makino, K. Takaya, and M. Nakayama, *J. Phys. Chem.*, **74**, 606 (1970).
2) K. Takaya, S. Yamauchi, and N. Ise, *J. Chem. Soc., Faraday I*, **70**, 1330 (1974).
3) K. Takaya and N. Ise, *ibid.*, **70**, 1338 (1974).
4) K. Takaya, H. Tatsuta, and N. Ise, *Polymer*, in press.
5) M. Szwarc, "Carbanions, Living Polymers and Electron Transfer Processes," Interscinece, N. Y. (1968).
6) M. Szwarc, *Accounts Chem. Res.*, **2**, 87 (1967).
7) L. L. Bohm, M. Chmelir, G. Lohr, B. J. Schmitt, and G. V. Schulz, *Adv. Polym. Sci.*, **9**, 1 (1972).
8) N. Ise, *ibid.*, **6**, 347 (1967).
9) H. Hirohara and N. Ise, *Macromol. Rev.*, **6**, 295 (1972).
10) R. M. Fuoss and F. Accascina, "Electrolylic Conductance," John Wiley & Sons., New York (1959), Chap. 17.
11) E. M. Kosower, "An Introduction of Physical Organic Chemistry," John Wiley & Sons., New York (1968), Chap. 2.
12) J. Smid, "Ions and Ion Pairs in Organic Reactions," ed. by M. Szwarc, Interscience, N. Y. (1972), Chap. 3.
13) T. E. Hogen-Esch and J. Smid, *J. Amer. Chem. Soc.*, **88**, 307 (1966).
14) D. Casson and B. J. Tabner, *J. Chem. Soc., Ser. B*, **1969**, 572.

Polarographic and Anodic Stripping Polarographic Studies of Aliphatic Polyamine Complexes of Several Metal Ions

Masahiro KOMATSU

National Industrial Research Institute of Kyushu, Tosu, Saga 841

(Received September 3, 1973)

The polarography of several aliphatic polyamine complexes of Pb(II), Zn(II), and Ni(II), and the anodic stripping polarography of polyamine complexes of Zn(II), Cd(II), Pb(II), and Cu(II) were studied. The aliphatic polyamines used were ethylenediamine(en), 1,3-propanediamine(1,3-pn), 1,2-propanediamine(1,2-pn), diethylenetriamine(den), and triethylenetetramine(trien). These lead(II) complexes gave a one-step reversible wave which was diffusion-controlled. The relation between the logarithm of the concentration of polyamine and the half-wave potential of the Pb(II) complex was straight, so that one species of complex ion was found to be predominant in the bulk of solution. The ionic species in the bulk of solution were found to be $Pb(en)_2^{2+}$, $Pb(1,3\text{-pn})_2^{2+}$, $Pb(1,2\text{-pn})_2^{2+}$, $Pb(den)_2^{2+}$, and $Pb(trien)^{2+}$. The stability constants of these complexes were calculated and were found to increase in the order of $Pb(1,3\text{-pn})_2^{2+} < Pb(en)_2^{2+} < Pb(1,2\text{-pn})_2^{2+} < Pb(den)_2^{2+} < Pb(trien)^{2+}$. The polarographic waves of Zn(II)-polyamine and Ni(II)-polyamine complexes were irreversible and diffusion-controlled, so the electrode reactions of these complexes were assumed using Matsuda-Ayabe's theory. All these polyamine complexes of Zn(II), Cd(II), Pb(II), and Cu(II) gave well-defined anodic stripping polarograms. 1,3-pn was the best complexing reagent among these polyamines, because it gave the best separation of the peaks of the anodic stripping polarograms of the four metal ions. Calibration curves were obtained from 0.01 to 0.10 ppm for Zn(II), Pb(II), and Cu(II), and from 0.001 to 0.010 ppm for Cd(II) in 0.4 M 1,3-pn and 0.2 M KCl media. The effects of acid and base on the anodic stripping polarograms were also studied.

It has been well known that aliphatic polyamines react with metal ions to give stable complexes in a fairly strongly alkaline medium.[1] The copper(II) and cadmium(II)-ethylenediamine(en), 1,2-propanediamine(1,2-pn), 1,3-propanediamine(1,3-pn), diethylenetriamine(den), and triethylenetetramine(trien) complexes were studied by means of a dropping mercury electrode.[2-4] Also, zinc(II) and nickel(II)-en complexes,[5] the lead(II)-trien complex[6] and the nickel(II)-1,2-pn complex[7] were studied by means of a dropping mercury electrode.

Anodic stripping polarography has been known to be a sensitive method for the analysis of the metal ions and various supporting electrolyte solutions have been used.[8] Moreover, the anodic stripping polarography of nickel(II), cobalt(II), manganese(II) has been studied in an aqueous solution of polyamine.[9] In a fairly strongly acidic solution (<pH 2), the hydrogen wave interferes with the determination of the zinc (II) ion, so it is interesting that anodic stripping polarography is carried out in an alkaline medium.

The present paper will report about the electrode reaction of lead(II), zinc(II), and nickel(II) in an aqueous solution of polyamine and about an application of these polyamine complexes to trace analysis by anodic stripping polarography.

Experimental

Materials. All the solutions of the amines, obtained from the Tokyo Kasei Co., Ltd, were standardized by 0.1 M HCl using a B.P.B. indicator. The lead(II) nitrate, zinc(II) nitrate and nickel(II) nitrate were standardized with 0.01 M EDTA. The potassium nitrate was once recrystallized and was used as a supporting electrolyte for polarography. Gelatine was used as a maximum suppressor for the zinc(II) and nickel(II) complexes. The potassium chloride was purified by extracting heavy metal ions with dithizone–chloroform system, after then having been recrystallized twice and heated at 300 °C in an electric furnace for 3 hr and it was used as the supporting electrolyte for anodic stripping polarography. The standard solution of the metal ions for anodic stripping polarography was prepared from metal chlorides. Water was deionized on a mixed-bed ion-exchange resin and was then distilled from an alkaline permanganate.

Apparatus. The polarograms were recorded with a Shimadzu polarograph, model RP-50. The initial potentials were measured with a Shimadzu potentiometer, model K-2. The span voltage was 1.0 V for lead(II), and 2.0 V for zinc-(II) and nickel(II). An H-type cell with a saturated calomel electrode was then used. The dropping mercury electrode (DME) used for lead(II) and zinc(II) had an m value of 2.47 mg/s and a drop time of 3.47 s at the mercury column height of 70 cm in a distilled water with an open circuit. The other DME used for nickel(II) had an m value of 1.75 mg/s and a drop time of 2.85 s at the mercury column height of 40 cm at the applied potential of −1.40 V *vs.* SCE. All the DC polarograms were recorded in a thermostat at 25.0± 0.1 °C.

The block diagram of anodic stripping polarograph is shown in Fig. 1. The potential-current curves were recorded with a X–Y recorder (D5–SN, Rikendenshi Co., Ltd.). The potential was driven by a sweep generator (Sanyo Denki Co., Ltd.). The scanning rate was 0.1 V/s. The initial voltage

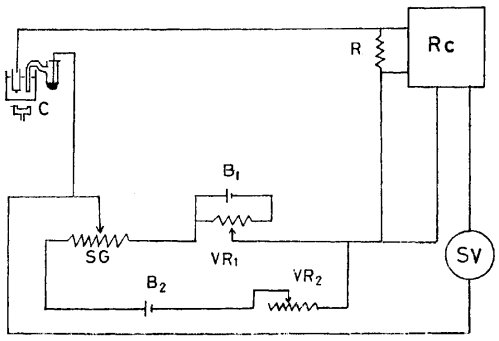

Fig. 1. Block diagram of anodic stripping polarograph. Rc, X-Y recorder; SV, standard voltage generator; C, electrolytic cell; B_1, B_2, battery; R, load resistor; SG, sweep generator; VR_1, VR_2, variable resistor

of the X–Y recorder was adjusted by a standard voltage generator (SV–12, Rikendenshi Co., Ltd.). The applied potential was controlled by B_1 and B_2. A balanced-head, stationary hanging mercury drop electrode(HMDE)[10] was used. The surface area of HMDE used was 0.028 cm^2. A saturated calomel electrode was used as the reference electrode. The cell assembly has been reported elsewhere.[11]

Procedure. The polarographic electrolyte solutions were prepared by placing a stock solution of metal(II) nitrate, potassium nitrate, polyamine and, lastly, a fresh solution of gelatine in a 25 ml flask. The anodic stripping polarographic electrolyte solutions were prepared by placing a stock solution of metal(II)-chloride, potassium chloride and polyamine in a 50 ml flask. Oxygen was removed from the electrolyte solutions by passing nitrogen gas through them for about 10—15 min, prior to the measurements of the DC polarogram and pre-electrolysis in anodic stripping polarography. The procedure of anodic stripping polarography was as follows. The electrolyte solution was stirred at 360 rpm during the pre-electrolysis with a magnetic stirrer by means of synchronous rotating motor. Following the pre-electrolysis for a certain time, the stirring was stopped for 30 s, then the potential was scanned into a positive direction in order to strip the deposited metal anodically from the mercury electrode. All the anodic stripping polarographic measurements were carried out at room temperature.

Results and Discussion

Polarography of Lead(II) Complexes. Typical DC polarogram of the lead(II)-polyamine complex is given in Fig. 2(a). The limiting current varied with the

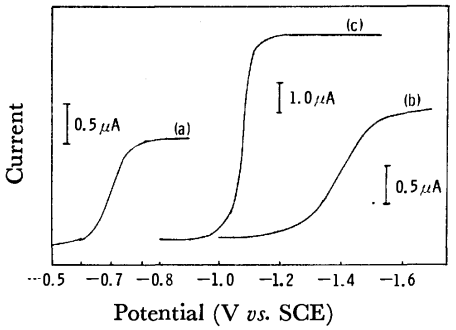

Fig. 2. Typical DC polarograms of Pb(II), Zn(II), and Ni(II) in the aqueous solution of aliphatic polyamine.
(a) 0.44 mM Pb(II) in 0.19 M ethylenediamine and 0.2 M KNO_3
(b) 0.44 mM Zn(II) in 0.10 M 1,2-propanediamine, 0.2 M KNO_3 and 0.01% gelatine
(c) 0.98 mM Ni(II) in 0.10 M 1,3-propanediamine, 0.2 M KNO_3 and 0.015% gelatine

mercury column height, while the $i_l/\sqrt{H_{corr}}$ value, where H_{corr} is the value corrected for the back pressure, was constant, this indicates that the electrode reactions were diffusion-controlled. The waves were analyzed by the log plot method from the current i at the potential of E of the dropping mercury electrode and the limiting current, i_l. The reciprocal slopes of the log plot of the lead(II) waves are given in Table 1 and these electrode reactions were reversible, two-electron reactions. The limiting current was gradually lowered with an increase in the concentration of the polyamine, because of the enhancement of the viscosity of the electrolyte solution.[5] In Fig. 3, the half-wave potentials are plotted against the logarithm of the various concentrations of the ligand. The resultant curves are straight, so only one ionic species is predominant in this concentration range.[12] The slope of $E_{1/2}$ *vs.* log C for en was 0.056 V, for 1,2-pn 0.057 V, for 1,3-pn 0.055 V and for den 0.056 V, indicating that two molecules of en, 1,2-pn, 1,3-pn or den were attached to lead(II) ion,[12] while for trien

Table 1. Polarography of lead(II)-polyamine complexes

Concen (M)	$-E_{1/2}$ (V *vs.* SCE)	i_d (μA)	Reciprocal slope of log plot (mV)	$-\log k_d$
		en		
0.194	0.600	3.45	29	8.47
0.388	0.617	3.38	30	8.44
0.575	0.627	3.32	29	8.41
0.766	0.632	3.17	29	8.31
0.957	0.645	3.06	29	8.56
			average	8.44
		1,2-pn		
0.053	0.576	3.37	30	8.78
0.071	0.584	3.27	29	8.78
0.089	0.590	3.25	28	8.78
0.178	0.599	3.18	28	8.49
0.356	0.617	3.33	28	8.48
0.534	0.629	3.10	29	8.54
0.713	0.638	2.98	29	8.58
0.891	0.641	2.98	29	8.51
			average	8.62
		1,3-pn[a]		
0.100	0.577	2.00	30	8.21
0.200	0.596	1.84	29	8.21
0.400	0.614	1.77	28	8.21
0.600	0.623	1.73	29	8.17
1.00	0.631	1.57	29	8.00
			average	8.16
		den		
0.053	0.627	3.25	31	10.50
0.088	0.640	3.25	31	10.47
0.176	0.657	3.03	29	10.47
0.355	0.672	3.01	29	10.30
0.533	0.679	2.75	29	10.27
0.710	0.688	2.80	29	10.30
0.888	0.697	2.80	29	10.40
			average	10.39
		trien		
0.043	0.654	3.03	29	10.21
0.089	0.666	3.11	29	10.32
0.107	0.671	2.93	29	10.37
0.215	0.679	2.88	29	10.37
0.431	0.693	2.55	29	10.50
0.646	0.702	2.23	29	10.63
0.863	0.705	2.05	29	10.64
			average	10.43

a) [Pb(II)]: 0.22 mM

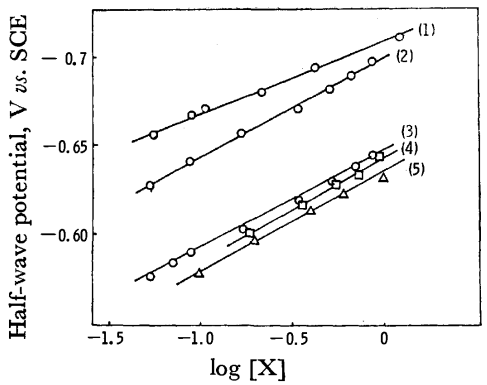

Fig. 3. Relation between $E_{1/2}$ of lead (II) complexes and log [X].
(1) trien; (2) den; (3) 1,2-pn; (4) en; (5) 1,3-pn

the slope was 0.034 V, indicating that one molecule of trien was attached. Because white precipitates were observed when 0.44 mM of Pb(II) was used in the case of the Pb(II)-1,3-pn system, 0.22 mM of Pb(II) was used. The limiting current of the Pb(II)-1,3-pn complex was linearly proportional to the concentration from 0 to 0.33 mM Pb(II) ion. The den complex is of interest because its maximum coordination number is three. The 1:2 complex for the den complex was observed in the case of copper-(II),[2] cadmium(II),[3] mercury(II),[13] and zinc(II)[14] complexes. The dissociation constants (k_d), which were calculated from Lingane's equation,[12] are given in Table 1. The stability constant of the trien complex was in good agreement with that obtained potentiometrically by Reiley and Schmid,[15] but slightly higher than that obtained by Lai and Chen,[6] probably because of the hydrolysis of the lead(II) ion. The stability constants increased in the order of: 1,3-pn complex<en complex<1,2-pn complex<den complex<trien complex; this tendency was identical with that of the copper(II)[2] and cadmium(II)[3] complexes. The stability constant of the complexes with a tri- or tetradentate ligand was larger than that of those with a bidentate ligand. Among these diamine complexes, the stability constant of the 1,2-pn complex was largest, probably because of its five-membered ring and one methyl group.

Polarography of Zinc(II) Complexes. The polarography of zinc(II)-1,2-pn, 1,3-pn, den, and trien complexes was studied in this work. A typical DC polarogram of Zn(II)-polyamine complex is given in Fig. 2(b). All the zinc(II)-polyamine complexes gave one-step waves. The currents varied with the mercury column height and the $i_l/\sqrt{H_{corr}}$ value was constant, indicating that the electrode reactions were entirely diffusion-controlled. The reciprocal slope of the log plot was 0.044 V for 1,2-pn, 0.049 V for 1,3-pn, 0.045 V for den and 0.050 V in trien concentration range from 0.006 to 0.030 M and 0.045 V in trien concentration range from 0.059 to 0.295 M for trien complex. These values demonstrated that these electrode reactions were irreversible reduction processes. When only the MX_N^{m+} complex, which is predominant in the bulk of the solution, dissociates very rapidly into the MX_p^{m+} complex in the vicinity of the electrode surface, when the MX_p^{m+} complex is reduced irreversibly at DME, and when its electrode reaction is diffusion-controlled, then Matsuda-Ayabe's equation for the irreversible half-wave potential of the complex ion[16] is expressed as:

$$(E_{1/2})_{irr} = 2.3\frac{RT}{\alpha nF}\left\{\log\frac{(k_f^\circ)_B}{\sqrt{D_N}} - (N-p)\log[X] + \frac{1}{2}\log\tau - 0.053\right\} \quad (1)$$

where [X] is the concentration of the polyamine, α is the transfer coefficient, τ is the dropping time of DME, $(k_f^\circ)_B$ is the forward (reduction) rate constant of the electron transfer process at the potential of the normal hydrogen electrode, and D_N is the diffusion coefficient of the complex ion MX_N^{m+} (all activities are assumed to be unity in above equation). The $(N-p)$ value can be obtained from the slope of the $(E_{1/2})_{irr}$ *vs.* log [X.] plot and the value of the reciprocal slope of log plot. The relation between $(E_{1/2})_{irr}$ and log [X] is given in Fig. 4. The slope obtained for 1,2-pn was 0.045 V, for 1,3-pn 0.054 V, for den 0.045 and for trien 0.050 V and 0.005 V. The calculated $(N-p)$ values for the zinc-(II)-polyamine complexes are given in Table 2(i). If

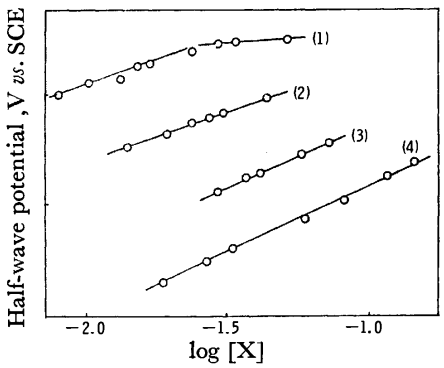

Fig. 4. Relation between $E_{1/2}$ of zinc(II) complexes and log[X].
(1) trien; (2) den; (3) 1,2-pn; (3) 1,2-pn; (4) 1,3-pn

TABLE 2. THE CALCULATED VALUE OF $(N-p)$ OF Zn(II) AND Ni(II)-POLYAMINE COMPLEXES

i) Zn(II)-polyamine complexes	1, 2-pn	1, 3-pn	den	trien	
$(N-p)$	1.1	1.2	1.0	1.0[a]	0.01[b]

ii) Ni(II)-polyamine complexes	1, 3-pn	den		trien	
$(N-p)$	1.8	1.0[c]	0.0[d]	0.96[e]	0.0[f]

a) 0.006 M≦trien≦0.030 M. b) 0.059 M≦trien≦0.295 M. c) 0.003 M≦den≦0.035 M. d) 0.071 M≦den≦0.284 M. e) 0.003 M≦trien≦0.028 M. f) 0.042 M≦trien≦0.056 M.

the value of N is known, p may be assumed. The zinc(II)-polyamine complexes have been studied potentiometrically and the ionic species in the bulk of solution were known except for the zinc(II)-1,3-pn system.[17] $Zn(1,2\text{-pn})_3^{2+}$, $Zn(den)_2^{2+}$, and $Zn(trien)^{2+}$ were predominant in the aqueous solution of each polyamine. From the values of $(N-p)$ and the complexes in the bulk

of the solution, the following rapid dissociation-association reactions were assumed for the electrode reactions of the zinc(II)-polyamine complexes:
for the 1,2-pn complex:

$$Zn(1,2\text{-pn})_3^{2+} \rightleftarrows Zn(1,2\text{-pn})_2^{2+} + 1,2\text{-pn}$$

for the 1,3-pn complex:

$$Zn(1,3\text{-pn})_N^{2+} \rightleftarrows Zn(1,3\text{-pn})_{N-1}^{2+} + 1,3\text{-pn}$$

for the den complex:

$$Zn(den)_2^{2+} \rightleftarrows Zn(den)^{2+} + den$$

for the trien complex:

$$Zn(trien)^{2+} \rightleftarrows Zn^{2+} + trien$$
$$(0.006M \leqq trien \leqq 0.030M).$$

Above 0.059 M trien, $Zn(trien)^{2+}$ would participate in the electrode reaction.

Polarography of Nickel(II) Complexes. The polarography of nickel(II)-1,3-pn, den, and trien complexes were investigated in this work. The polarography of the nickel(II)-1,2-pn complex had been reported elsewhere.[8] A typical DC polarogram of the nickel(II)-polyamine complex is given in Fig. 2(c). All the nickel(II)-polyamine complexes investigated in this work gave a one-step wave. The $i_l/\sqrt{H_{corr}}$ value was also constant, indicating that the electrode reaction was entirely diffusion-controlled. Polarograms were recorded in the ranges of concentration of 1,3-pn from 0.018 to 1.03 M, of den from 0.003 to 0.284 M and of trien from 0.003 to 0.056 M. The half-wave potentials were shifted to more negative value with an increase in the concentration of polyamine as is shown in Fig. 5. However, the half-wave potentials of the den or

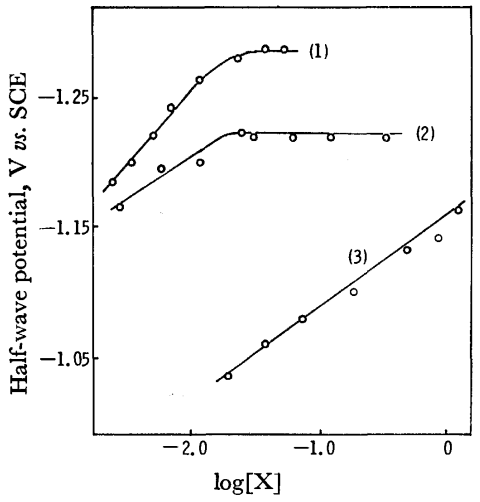

Fig. 5. Relation between $E_{1/2}$ of nickel(II) complexes and log[X].
(1) trien; (2) den; (3) 1,3-pn

trien complex were constant from 0.071 to 0.284 M den or from 0.042 to 0.056 M trien respectively. The reciprocal slope of the log plot was 0.038 V for the 1,3-pn complex, 0.056 V for the den complex in the concentration from 0.003 to 0.284 M den and 0.120 V for the trien complex in the concentration range of 0.003 to 0.056 M trien. These values demonstrated that these electrode reactions were irreversible electrode process and that Eq. (1) can be used to interpret the waves. The slope of $(E_{1/2})_{irr}$ *vs.* log [X] plot was 0.075 V for the 1,3-pn complex, 0.055 V in the ranae of 0.003—0.035 M of den and 0.00 V in the range of 0.071—0.288 M of den and 0.115 V in the range of 0.003—0.028 M trien, and 0.00 V in the range of 0.042—0.056 M trien. The ionic species of Ni(II)-polyamine complexes in thebulk ofsolution had been studied potentiometrically,[17] and $Ni(1,3\text{-pn})_3^{2+}$, $Ni(den)_3^{2+}$ and $Ni(trien)_2^{2+}$ were observed. The calculated $(N-p)$ values of Ni(II)-polyamine complexes are given in Table 2(ii). Thus, the following dissociation-association reactions were assum ed for the electrode reaction of Ni(II)-polyamine complexes:
for the 1,3-pn complex:

$$Ni(1,3\text{-pn})_3^{2+} \rightleftarrows Ni(1,3\text{-pn})^{2+} + 2(1,3\text{-pn})$$

for the den complex:

$$Ni(den)_2^{2+} \rightleftarrows Ni(den)^{2+} + den$$
$$(0.003M \leqq den \leqq 0.035M)$$

for the trien complex:

$$Ni(trien)_2^{2+} \rightleftarrows Ni(trien)^{2+} + trien$$
$$(0.003M \leqq trien \leqq 0.028M).$$

It is shown that the ionic states of these complexes which participate in the electrode reaction must form a 1: 1 complex at lower concentrations of these polyamines. Above 0.071 M den and 0.042 M trien, $Ni(den)_2^{2+}$ and $Ni(trien)_2^{2+}$ must directly participate in the electrode reaction.

Anodic Stripping Polarography. The present work and past works demonstrated that Cu(II), Pb(II), Cd(II), and Zn(II) formed stable complexes with en, 1,2-pn, 1,3-pn, den, and trien. As an application of these polyamine complexes to trace analysis, anodic stripping polarographic studies of these four metal ions were carried out in aqueous solutions of these polyamines. The peak potentials were measured in an aqueous solution of 0.05 M of each polyamine, they are shown in Fig. 6. 1,3-pn was found to be the best reagent among these polyamines, because it gave the best separation of the peaks of these metal ions. Typical anodic stripping polarograms of Zn(II), Cd(II), Pb-

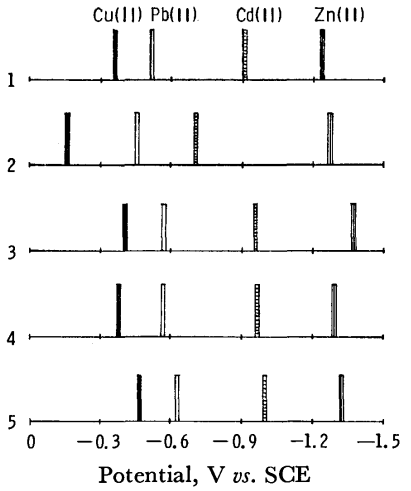

Fig. 6. Peak potentials of 0.1 ppm of Zn(II), Cd(II), Pb(II) and Cu(II) in 0.05 M polyamine and 0.2 M KCl.
(1) en; (2) 1,3-pn; (3) 1,2-pn; (4) den; (5) trien

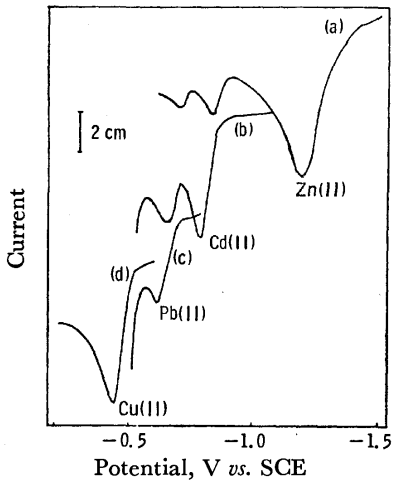

Fig. 7. Anodic stripping polarograms of 0.1 ppm of Zn(II), Cd(II), Pb(II), and Cu(II) in 0.4 M 1,3-pn and 0.2 M KCl.
Pre-electrolysis potential (V *vs.* SCE): (a), −1.50 V; (b), −1.10 V; (c), −0.80 V; (d), −0.60 V
Pre-electrolysis time (min): (a), 1; (b), 1; (c), 2; (d), 1
Record. sens., 0.04 μA/cm

(II), and Cu(II) in 0.4 M 1,3-pn are given in Fig. 7. The pre-electrolysis potential was −1.50 V *vs.* SCE for Zn(II), −1.10 V *vs.* SCE for Cd(II), −0.80 V *vs.* SCE for Pb(II) and −0.60 V *vs.* SCE for Cu(II). With choices of these pre-electrolysis potentials, interference by more cathodic waves could be omitted. Because the electrode reaction of Cu(II)-polyamine complex is a two-electron transfer process, its anodic stripping peak current could be sharper than that of Cu(II) in thiocyanate, NH_3, chloride or pyridine, in which a two-step wave of Cu(II) appears.[12] The calibration curves are given in Figs. 8 and 9. The wave height of these ions were linearly proportional to the concentration of the metal ions. The effects of acid and base on these anodic stripping polarograms

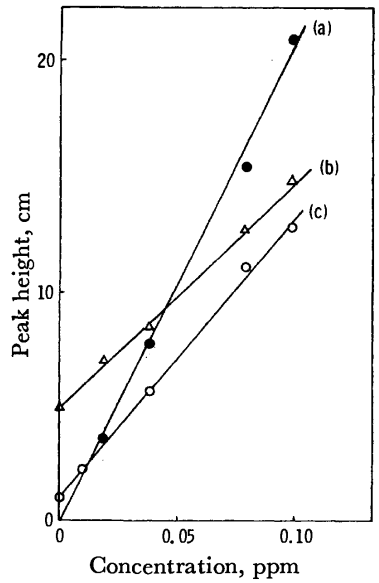

Fig. 8. Calibration curves of Cu(II), Pb(II), and Zn(II).
Pre-electrolysis time for (a) Zn(II) and (b) Cu(II): 2 min; and for (c) Pb(II): 5 min.
Other conditions: the same as those in Fig. 7.

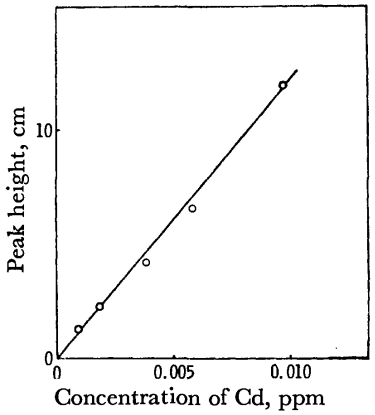

Fig. 9. Calibration curve of Cd(II)
Pre-electrolysis time: 5 min; Record. sens., 0.016 μA/cm
Other conditions: the same as those in Fig. 7.

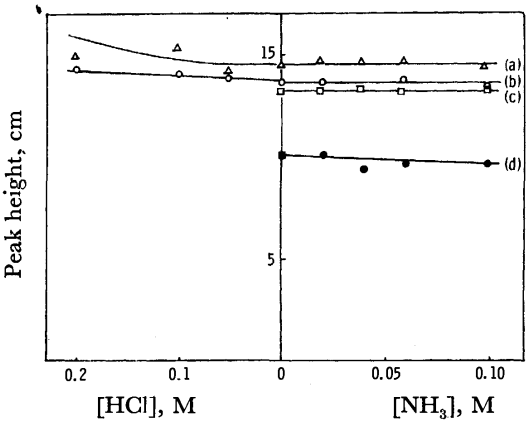

Fig. 10. Effects of hydrochloric acid and NH_3 on the peak heights of Zn(II), Cd(II), Pb(II), and Cu(II).
(a) [Zn(II)]: 0.150 ppm; (b) [Cd(II)]: 0.10 ppm; (c) [Pb(II)]: 0.080 ppm; (d) [Cu(II)]: 0.070 ppm
Pre-electrolysis time for Zn(II), Cu(II) and for Pb(II): the same as those in Fig. 8; and for Cd(II): 2 min.
Other conditions: the same as those in Fig. 7.

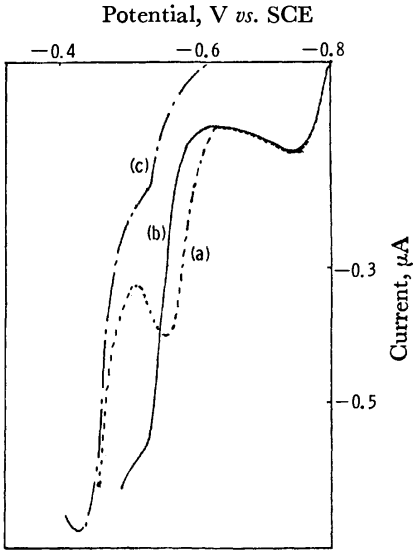

Fig. 11. Effect of hydrochloric acid on the anodic stripping polarograms of Cd(II), Pb(II), and Cu(II)
HCl: (a), 0.1 M; (b), 0.2 M; (c), 0.2 M
Pre-electrolysis potential: (a) and (b), −0.80 V *vs.* SCE, and (c), −0.60 V *vs.* SCE
Other conditions: the same as those in Fig. 10.

were also studied. 0.01—0.10 M NH_3 or 0.1—0.2 M hydrochloric acid was added to a mixture of Zn(II), Cd(II), Pb(II), and Cu(II), 0.4 M 1,3-pn and 0.2 M KCl, and then anodic stripping polarograms were recorded. The results are shown in Figs. 10 and 11. The wave heights of Cu(II), Pb(II), Cd(II), and Zn(II) were almost constant when NH_3 was added, but a slight increase in the wave heights of Zn(II) and Cd-(II) was observed with an increase of the concentration of hydrochloric acid. And also, by the addition of hydrochloric acid the peak potentials of Cu(II) and Pb(II) were shifted to so positive a potential that the peak height of Pb(II) and Cu(II) could not be exactly measured (Fig. 11). Accordingly, it is necessary to neutralize the acidic test solution by NH_3 prior to the determination.

The author is grateful to Professor S. Misumi of Kyushu University for his kind discussions and also to Dr. H. Kakiyama of the National Industrial Research Institute, Kyushu, for his continual encouragement.

References

1) A. E. Martell and M. Calvin, "Chemistry of the Metal Chelate Compounds," 5th Ed., Prentice-Hall, New York (1962).
2) H. A. Laitinen, J. C. Bailar, Jr., and S. Swann, Jr., *J. Amer. Chem. Soc.*, **71**, 1550 (1949).
3) B. E. Douglas, H. A. Laitinen, and J. C. Bailar, Jr., *ibid.*, **72**, 2486 (1950).
4) H. Irving, R. J. P. Williams, D. J. Ferret, and A. E. Williams, *J. Chem. Soc.*, **1954**, 792.
5) K. Morinaga, This Bulletin, **20**, 413 (1956).
6) T.-T. Lai and J.-Y. Chen, *J. Electroanal. Chem.*, **16**, 413 (1968).
7) M. Komatsu, *Nippon Kagaku Kaishi*, **1973**, 1701.
8) E. Barendrecht, "Electroanalytical Chemistry," Vol. 2, ed. by A. J. Bard, M. Dekker, New York (1967), p. 53.
9) M. Komatsu, *Bunseki Kagaku*, **22**, 975 (1973).
10) Y. Yamazaki, *Rev. Polarogr.* (Kyoto), **13**, 26 (1965).
11) M. Komatsu, *Bunseki Kagaku*, **21**, 1516 (1972).
12) I. M. Kolthoff and J. J. Lingane, "Polarography," Vol. 1, Interscience Publishers, New York, London (1952), p. 97.
13) C. J. Nyman, D. K. Roe, and D. B. Mason, *J. Amer. Chem. Soc.*, **77**, 4191 (1955).
14) J. E. Prue and G. Schwarzenbach, *Helv. Chim. Acta*, **33**, 985 (1950).
15) C. N. Reilley and R. W. Schmid, *J. Elisha Mitchell Sci. Soc.*, **73**, 273 (1957).
16) H. Matsuda and Y. Ayabe, *Z. Electrochem.*, **63**, 1164 (1959).
17) L. G. Sillen and A. E. Martell, "Stability Constants," The Chemical Society, London (1964). A. Ringbom, "Complexation in Analytical Chemistry," John Wiley and Sons, New York (1963).

The Solvent Extraction of the Copper-Pyrocatechol Violet Chelate with Tridodecylethylammonium Bromide

Yoshio SHIJO

Department of Industrial Chemistry, Faculty of Engineering, Univereity of Utsunomiya, Ishii-machi, Utsunomiya 321-31

(Received September 20, 1973)

The solvent extraction of the copper–Pyrocatechol Violet chelate with tridodecylethylammonium bromide (abbreviated TDEA) in benzene as an ion-association system has been investigated by the spectrophotometric method. The copper–PV–TDEA complex can be extracted into such aromatic hydrocarbons as benzene, toluene, and xylene, but not into such polar solvents as *n*-butanol, ethyl acetate, methylisobutylketone, and nitrobenzene. When a sample solution containing copper and PV, the pH of which has been adjusted to 7.5—8.5, is shaken with TDEA in benzene for 10 s, the maximum extraction of the ternary complex is obtained. The extractability of the complex from 50 ml of an aqueous solution into 10 ml of benzene is 98.3% under the optimum conditions. The absorbance and stability of the complex increase upon the addition of a small amount of ethanol to the extracted layer. Beer's law is obeyed up to 6.5 μg copper per 10 ml of benzene, and the molar absorptivity of the complex is 7.9×10^4 $cm^{-1}\cdot mol^{-1}\cdot l$ at 663 nm. The composition of the complex is confirmed to be Cu: PV: TDEA = 1: 2: 2 by the continuous variation method. A structure for the complex is proposed.

Pyrocatechol Violet (abbreviated as PV) forms water-soluble chelates with many metal ions and has been used as a metallochromic indicator or as a colorimetric reagent for several metal ions. The PV metal chelate anions react with quaternary ammonium salts as cetylpyridinium to form a water-soluble or a water-insoluble ion-association complex. The solvent extraction of the ion pair formed by the interaction of PV metal chelate anions with cations of 1,3-diphenylguanidinium, cetylpyridinium, *etc.* has been applied to the spectrophotometric determination of molybdenum(VI),[1] indium,[2] gallium,[3] and iron(III).[4] Recently, Přibil and Vesely[5] used a chloroform solution of Aliquat 336-S (methyltricaprylammonium chloride) in the solvent extraction of the Xylenol Orange metal cheletes. Because of its superior extraction efficiency, the oleophilic quaternary ammonium salt as Aliquat 336-S has been used for the extraction of many inorganic or organic anions[6-10] and also used as an ion exchanger for a liquid-membrane ion-selective electrode.[11,12] In this paper, the fundamental conditions for the solvent extraction of the copper–PV chelate anion with a benzene solution of tridodecylethylammonium bromide which has been synthesized in our laboratory and the composition of the ternary complex extracted into benzene are discussed in terms of the spectrophotometric method.

Experimental

Reagent. About a 2.5×10^{-3} M copper solution was prepared by dissolving a definite amount of cupric chloride in 1 M hydrochloric acid and by subsequent dilutions with deionized water. The resulting solution was standardized by EDTA titration. A working standard solution was prepared as needed by the dilution of the 2.5×10^{-3} M solution with deionized water to the desired concentration. A 5.0×10^{-4} M PV solution was prepared by dissolving the Dotite PV in deionized water without any further purification. The TDEA was prepared by the reaction[13] of tridodecylamine with ethylbromide in an alcoholic solution. The salt was recrystallized from petroleum benzine. A 6.0×10^{-4} M TDEA solution was prepared by dissolving the above TDEA in benzene.

All the other chemicals used were of a guaranteed reagent quality.

Apparatus. All the absorption spectra were obtained on a JASCO automatic recording spectrophotometer, model ORD-UV5. On the other hand, at a fixed wavelength measurements were made on a Hitachi manual spectrophotometer, model 101. Matched 1 cm absorption cells were used in all instances. The pH measurements were made with a Hitachi-Horiba model M-5 glass electrode pH meter.

Standard Procedure. Place up to 6.5 μg of copper in a 100 ml separatory funnel and add a definite amount of 0.2 M hydrochloric acid. Adjust the pH to 7.6 with a sodium acetate-sodium phosphate buffer solution. Add 4.0 ml of a 5.0×10^{-4} M PV solution and dilute to 50 ml with deionized water. Add 10 ml of 6.0×10^{-4} M TDEA in benzene and extract for 10 s with vigorous shaking. After the phases have separated, draw off the aqueous layer and centrifuge the extract for 5 min at 6000 rpm. Transfer 3.0 ml of the extract into a absorption cell and add 0.2 ml of ethanol. Measure the absorbance at 663 nm against the reagent blank obtained in the same way.

Results and Discussion

Absorption Spectra. The absorption spectra of the ternary complex extracted into benzene and the copper–PV chelate in an aqueous solution are given in Fig. 1, along with that of the reagent blank. The absorption curves of the ternary complex and the copper–PV chelate all have their maximum at 663 and 632 nm respectively. In the former, however, the absorbance is about three times greater than that of the latter. The bathochromic effect and the increase in the absorbance in the former are probably due to the combination with TDEA. By the addition of 0.2 ml of ethanol to 3.0 ml of the extract, the absorbance and stability of the ternary complex increase, but the absorbance of the reagent blank decreases. By the addition of ethanol into the initial organic phase, however, the extraction of the ternary complex is decreased extremely. PV is extracted into the organic layer under the conditions used in the standard procedure.

Effect of pH. The effect of the pH of the aqueous phase on the extraction was examined. The results are shown in Fig. 2. The maximum extraction of the

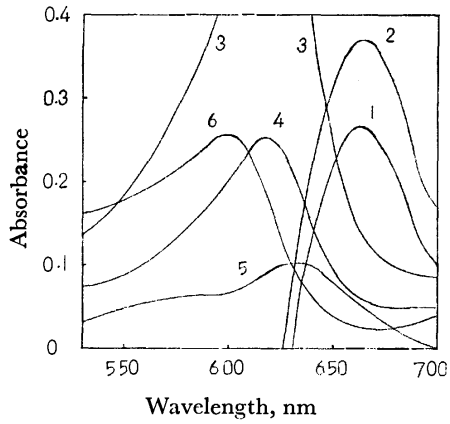

Fig. 1. Absorption spectra of the Cu-PV-TDEA complex in benzene and the Cu-PV chelate in aqueous solution.
pH: 7.6, Volume of aq. layer $V_w=50$ ml, $[acetate]_w=0.16$ M; Volume of org. layer $V_O=10$ ml, [secondary phosphate]$_w=0.08$ M
(1): Cu-PV-TDEA in benzene $[Cu]_O=5.0\times10^{-6}$ M,
(2): (1)+ethanol 6 vol% $[Cu]_O=4.7\times10^{-6}$ M,
(3): PV-TDEA in benzene $[PV]_w=4.0\times10^{-6}$ M,
(4): (3)+ethanol 6 vol% $[PV]_w=4.0\times10^{-6}$ M,
(5): Cu-PV in aq. solution $[Cu]_w=5.0\times10^{-6}$ M,
(6): PV in aq. solution $[PV]_w=2.0\times10^{-5}$ M.

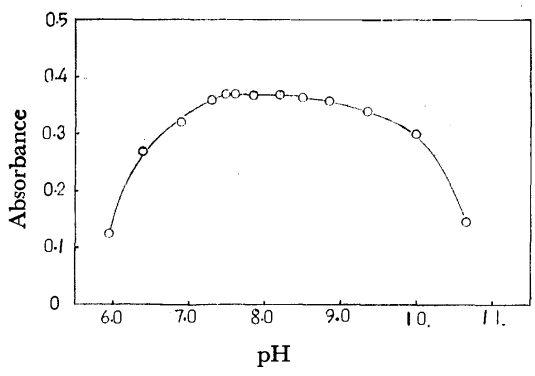

Fig. 2. Effect of pH on the extraction of the Cu-PV-TDEA complex.
pH: 7.6 $V_w=50$ ml, $V_O=10$ ml; Cu: 3.2 μg, $[PV]_w=4.0\times10^{-5}$ M, $[TDEA]_O=6.0\times10^{-4}$ M, $[ethanol]_O=6$ vol%, $[acetate]_w=0.16$ M, [secondary phosphate]$_w=$ 00.8 M.

ternary complex is reached at pH values from 7.5 to 8.5. This pH range is extended to lower pH values by increasing the concentration of TDEA in benzene. The absorbance of the reagent blank in the organic layer increases extremely with an increase in the pH value.

Organic Solvents. Several kinds of organic solvents were tested in order to achieve a quantitative extraction of copper. The ternary complex can be extracted into such aromatic hydrocarbons as benzene, toluene, and xylene, but not into such polar solvents as *n*-butanol, ethyl acetate, methylisobutylketone, and nitrobenzene. Benzene was chosen as the solvent which gave the highest absorbance.

The Effect of the PV Concentration. The effect of the PV concentration in the aqueous phase on the

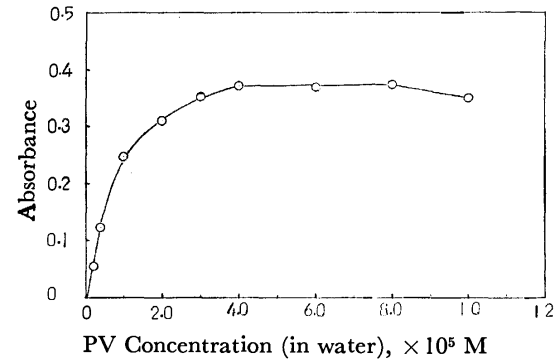

Fig. 3. Effect of the Pyrocatechol Violet concentration in aqueous phase on the extraction of the Cu-PV-TDEA complex.
pH: 7.6, $V_w=50$ ml, $V_O=10$ ml; Cu: 3μg, .2 $[TDEA]_O=6.0\times10^{-4}$ M, $[ethanol]_O=6$ vol%, $[acetate]_w=0.16$ M, [secondary phosphate]$_w=0.08$ M

extraction of the ternary complex was examined by varying the PV concentration, while other variables were held constant. The absorbance of the extract was constant when the PV in the initial aqueous phase was in the concentration range from 4.0×10^{-5} M to 8.0×10^{-5} M, as is shown in Fig. 3. The absorbance of the extract gradually decreased upon the further addition of PV. The absorbance of the reagent blank in the organic layer increased extremely with the increase in the PV concentration because the bulk of the PV was extracted into the organic layer. Therefore, the PV concentration was kept at 4.0×10^{-5} M.

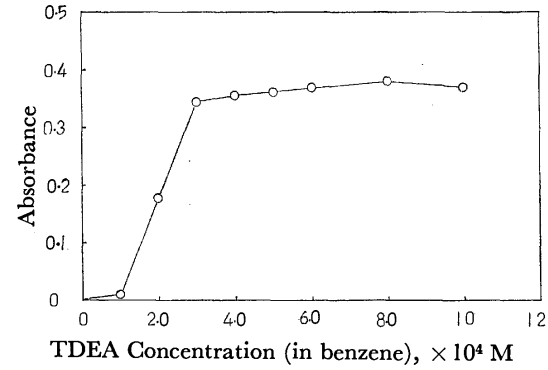

Fig. 4. Effect of tridodecylethylammonium bromide concentration in benzene on the extraction of the Cu-PV-TDEA complex.
pH: 7.6, $V_w=50$ ml, $V_O=10$ ml; Cu: 3.2 μg, $[PV]_w=4.0\times10^{-5}$ M, $[ethanol]_O=6$ vol%, $[acetate]_w=0.16$ M, [secondary phosphate]$_w=0.08$ M

The Effect of the TDEA Concentration. The effect of the concentration of TDEA in benzene on the extraction of the ternary complex was examined. The absorbance of the extract increased gently when the TDEA in benzene was in the concentration range from 3.0×10^{-4} M to 8.0×10^{-4} M, as is shown in Fig. 4. The absorbance of the reagent blank increased with the increase in the TDEA concentration in benzene. Therefore, the TDEA concentration was kept at 6.0×10^{-4} M.

The Effect of the Shaking Time. The shaking time

was varied from 5 s to 10 min. The absorbance of the extract was constant for the shaking times from 5 s to 30 s, but upon further shaking it gradually decreased. A shaking time of 10 s was, therefore, selected.

The Effect of the Ethanol. The effect of the addition of ethanol to the extract on the absorbance of the ternary complex was examined. The absorbance became highest when the ethanol concentration in the extract was about 6 vol%. The absorbance of the extract decreased upon the further addition of ethanol. The stability of the ternary complex and the reproducibility of the absorbance increased upon the addition of ethanol to the extract. The absorbance of the reagent blank, however, decreased upon the addition of ethanol.

Extractability, Distribution Ratio, and Molar Absorptivity. The extractability of the ternary complex under the optimum conditions was determined by a repetition of the extraction procedure on the same aqueous layer. When a 50 ml portion of the aqueous layer containing 6.4 μg of copper was shaken with 10 ml of benzene, 98.3% of copper was extracted by one extraction and almost completely by two. The distribution ratio and the molar absorptivity calculated by using the percentage extraction and the absorbance were 3.78×10^2 and 7.9×10^4 $cm^{-1}\cdot mol^{-1}\cdot l$ respectively.

Calibration Curve. A calibration curve for the determination of copper was made under the optimum conditions. A good linear relationship was obtained over the concentration range from 0 to 6.5 μg of copper per 10 ml of benzene.

The Effect of Diverse Ions. The effect of foreign ions on the determination of copper according to the standard procedure was also examined. Thorium, iron(III), cobalt, and nickel interfered at all the concentrations investigated. Up to about 10 μg of vanadium(V), aluminum, beryllium, manganese, zirconium, and uranium(VI) did not interfere with the determination of copper. Of the anions examined, chloride, sulfate, nitrate, and citrate did not interfere. However, thiosulfate and EDTA interfered seriously, giving negative errors.

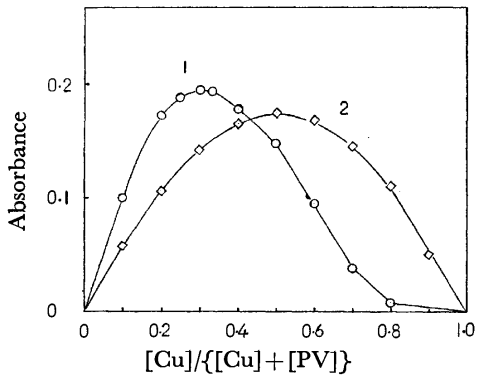

Fig. 5. Continuous variation method applied to the Cu–PV–TDEA complex and the Cu–PV chelate.
pH: 7.6, $V_w=10$ ml, $V_O=10$ ml; [acetate]$_w$=0.16 M, [secondary phosphate]$_w$=0.08 M
1 Cu–PV–TDEA complex, $[Cu]_w+[PV]_w=2.5\times10^{-5}$ M, $[TDEA]_O=6.0\times10^{-4}$ M, $[ethanol]_O$=6 vol%
2 Cu–PV chelate, $[Cu]_w+[PV]_w=4.0\times10^{-5}$ M

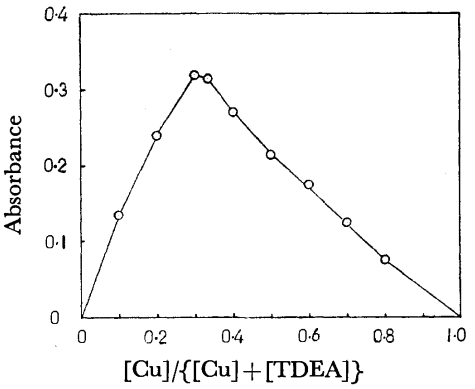

Fig. 6. Continuous variation method applied to the Cu–PV–TDEA complex.
pH: 7.6, $V_w=10$ ml, $V_O=10$ ml; $[Cu]_w+[TDEA]_O=5.0\times10^{-5}$ M, $[PV]_w=2.0\times10^{-4}$ M, $[ethanol]_O$=6 vol %, [asetate]$_w$=0.16 M, [secondary phosphate]$_w$=0.08M

The Composition and Structure of the Ternary Complex. Using the continuous variation method, the molar ratio of copper to PV was found to be 1:2, as is shown in Fig. 5. The molar ratio of copper to TDEA was also found to be 1:2, as is shown in Fig. 6. Thus, the composition of the ternary complex was estimated to be $Cu(PV)_2(TDEA)_2$. Recently, the structures of the ternary complexes of Sn–PV–cetyltrimethylammonium, Al–PV–cetyltrimethylammonium, and Mo–PV–diaklylmonomethylbenzylammonium were proposed by Bailey *et al.*,[14] Chester *et al.*,[15] and Kohara *et al.*[1] respectively. A similar structure, such as is shown in Fig. 7, may be possible for the ternary complex $Cu(PV)_2$-$(TDEA)_2$.

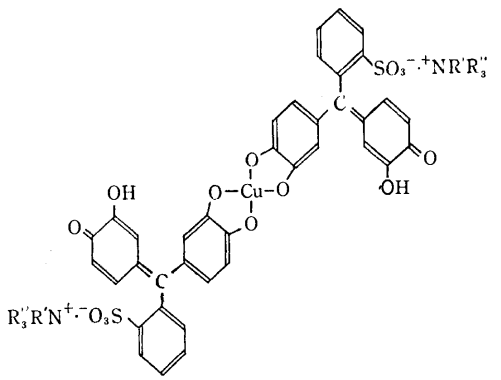

Fig. 7. Structure of the Cu–PV–TDEA complex.
$R'=C_2H_5$, $R''=C_{12}H_{15}$

The author wishes to thank Miss Hiroko Otsuka for her laboratory work.

References

1) H. Kohara, N. Ishibashi, and K. Abe, *Bunseki Kagaku*, **19**, 48 (1970).
2) T. Ishito and K. Tonosaki, *ibid.*, **20**, 689 (1971).
3) M. K. Akhmedli, E. L. Glushchenko, and Z. L. Gasanova, *Zh. Anal. Khim.*, **26**, 1947 (1971).
4) R. U. Yuryavichus and C. A. Valyukyavichyus, *ibid.*, **27**, 1125 (1972).
5) R. Přibil and V. Vesely, *Talanta*, **17**, 801 (1970).

6) G. B. S. Salaria and C. L. Rulfs, *Anal. Chem.*, **35**, 983 (1963).
7) A. M. Wilson and O. K. McFarland, *ibid.*, **36**, 2488 (1964).
8) F. L. Moore, *ibid.*, **38**, 510 (1966).
9) M. H. Campbell, *ibid.*, **40**, 6 (1968).
10) F. L. Moore, *ibid.*, **41**, 1658 (1969).
11) C. J. Coetzee and H. Freiser, *ibid.*, **41**, 1128 (1969).
12) H. James, G. Carmack, and H. Freiser, *ibid.*, **44**, 856 (1972).
13) A. B. Scott and H. V. Tartar, *J. Amer. Chem. Soc.*, **65**, 692 (1943).
14) B. W. Bailey, J. E. Chester, R. M. Dagnall, and T. S. West, *Talanta*, **15**, 1359 (1968).
15) J. E. Chester, R. M. Dagnall, and T. S. West, *ibid.*, **17**, 13 (1970).

Conditions for the Formation of Fe_3O_4 by the Air Oxidation of $Fe(OH)_2$ Suspensions.

Masao KIYAMA

Institute for Chemical Research, Kyoto University, Uji, Kyoto 611

(Received September 25, 1973)

The optimum conditions were studied for the formation of Fe_3O_4 by the air oxidation of $Fe(OH)_2$. The suspensions obtained by mixing NaOH and $FeSO_4$ solutions in various values of $R(=2NaOH/FeSO_4)$ were subjected to oxidation with air at various temperatures. The oxidation products were then examined by X-ray powder diffraction, chemical analysis, electron microscopic observation, and BET surface-area determination. Fe_3O_4 is formed at higher temperatures than is FeOOH. The temperature of formation becomes low as R approaches 1.0. In neutral suspensions ($R<1$), Fe_3O_4 is formed *via* green rust II or a mixture of green rust II and $Fe(OH)_2$. By further oxidation, the Fe_3O_4 formed gradually changes to γ-Fe_2O_3. A mixture of α-FeOOH and either $NaFe_3(OH)_6(SO_4)_2$ or α-Fe_2O_3 is formed as the final oxidation product. In alkaline suspensions ($R>1$), Fe_3O_4 is formed directly. The morphology and ferrous-ion content of Fe_3O_4 powder change considerably with the presence of green rust II before the formation of Fe_3O_4. It is suggested that Fe_3O_4 is formed near the surface of the particles of $Fe(OH)_2$ and green rust II by the coprecipitation of ferrous ions with ferric hydroxo-complexes.

The formation of iron oxides and oxyhydroxides, such as α-Fe_2O_3, γ-Fe_2O_3, Fe_3O_4, α-FeOOH, β-FeOOH, γ-FeOOH, and δ-FeOOH, has thus far been achieved by means of wet methods, such as the hydrolysis and oxidation of iron salt solutions. α-FeOOH, β-FeOOH, and α-Fe_2O_3 have been obtained by the hydrolysis of ferric salts.[1-7] A mechanism of hydrolysis was suggested on the basis of the spectrophotometric and magnetic properties of the ferric complexes present in the solution prior to the formation of precipitates.[8]

δ-FeOOH is formed when $Fe(OH)_2$ is oxidized rapidly in an alkaline solution by the addition of hydrogen peroxide.[9,10] If oxidation is carried out slowly by passing air into a suspension obtained by mixing ferrous salt and alkaline solutions, α-FeOOH, γ-FeOOH or Fe_3O_4, or a mixture of them is obtained according to the pH, the temperature, and the kind of anion present.[11-15] Feitknecht proposed the following mechanism:[16] (1) γ-FeOOH, δ-FeOOH, and γ-Fe_2O_3 are formed by the surface oxidation of green rust, $Fe(OH)_2$, and Fe_3O_4 particles respectively. (2) The formation of α-FeOOH proceeds in a liquid phase of suspension. (3) The formation of Fe_3O_4 takes place by the surface oxidation of the green rust particles in a neutral suspension medium. The formation can also take place in a liquid phase of alkaline suspension. From crystallochemical considerations, Bernal *et al.* suggested that the reaction of solid phase proceeds topotaxially in the particles of intermediate oxidation products.[17]

These theories hold except for the formation of γ-FeOOH and Fe_3O_4. The presence of green rust is not indispensable for the formation of γ-FeOOH.[18-20] In this paper, the conditions and the mechanism of the formation of Fe_3O_4 will be given.

Experimental

Material. Chemical reagents of an analytical grade were used. The air for stirring and oxidation was bubbled through washing vessels containing a KOH solution to remove carbon oxides and dust. Distilled water into which nitrogen had been bubbled at the boiling point for 2 hr to remove any dissolved oxygen was used.

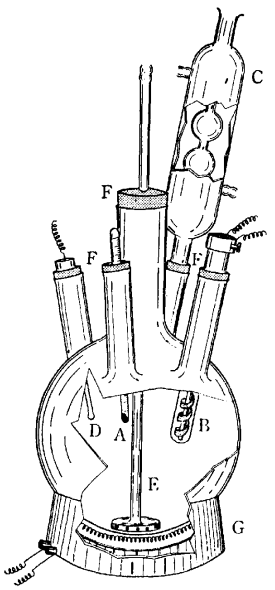

Fig. 1. The reaction vessel.
A: Thermometer, B: Temperature regulator, C: Reflux condenser, D: Electrode for self-recording pH meter, E: Glass tube, F: Rubber stopper, G: Electrical heater.

Apparatus. Figure 1 shows the reaction vessel specially constructed for the air-oxidation experiments. A spherical flask with a capacity of about 4 l is fitted with five inlet necks. A glass tube (E) with a flat end having eight holes (0.1 cm in diameter) at equal intervals is kept in contact with the bottom of the flask. The temperature regulator (B) consists of a spiral bimetal strip dipped in oil in a glass tube. Since the $Fe(OH)_2$ suspension in the flask is thoroughly stirred with air, a small portion (50—100 ml) taken out of the suspension can be considered to be an appropriate sample.

Procedure. The suspensions of $Fe(OH)_2$ were prepared by adding various amounts of a NaOH solution to 1 l of 0.72 M-$FeSO_4$ in each flask, the total volume of each suspension then being made 3 l with water. The suspensions in the flasks were quickly heated to the desired temperatures. Nitrogen was passed through the suspension from the eight holes at a rate of 1 l/min to prevent bumping and oxidation. When the suspension reached the desired temperature, compressed air was passed through in place of nitrogen. The

temperature was kept constant during the course of oxidation.

The oxidation conditions were confined as follows: a) The $R(=2NaOH/FeSO_4)$ molar ratio was kept at 0.1—4.0. b) Air was passed through at a rate of 200 l/hr. c) Oxidation was carried out at temperatures between 5 and 85 °C. The oxidation product was collected on filter paper, washed with water, and then dried at about 50 °C under reduced pressure.

Analysis of the Oxidation Product. The amounts of ferrous and ferric ions were determined by chemical analysis. The ferrous-ion content was determined by means of $KMnO_4$ titration after the sample had been dissolved in dilute H_2SO_4 by heating under a nitrogen atmosphere. The total iron content was determined by the gravimetry of the precipitate obtained from the solution prepared by the dissolution of the sample in a mixture of dilute HNO_3 and HCl solutions by heating.

The samples were examined by means of X-ray diffraction using FeKα radiation. By means of electron microscopic examination, it was found that FeOOH particles are needle-like, while Fe_3O_4 particles are spherical, cubic, and octahedral. The presence of a small amount of FeOOH was detected by electron-microscopic examination. For the sake of confirmation, the samples found by X-ray analysis to consist only of Fe_3O_4 were subjected to electron-microscopic examination. When $Fe(OH)_2$ and green rust remained in the suspension, the wet precipitate obtained by filtration was also subjected to those examinations. In order to prevent oxidation during X-ray analysis, the wet precipitate was sealed with cellophane tape.

The mean particle size of the samples was estimated from their surface area as measured by the BET method using nitrogen gas.

Results and Discussion

Formation of Fe_3O_4. Precipitates were formed when NaOH and $FeSO_4$ solutions were mixed: (a) When the amount of NaOH was insufficient ($R<1$), the resulting whitish suspension was neutral (pH 7—9). The precipitate was usually amorphous, but the precipitate in the suspension with $R<0.6$ changed to a crystalline precipitate of ferrous basic sulfate when subjected to aging in an inert gas.[21] (b) When excess NaOH ($R>1$) was added, the suspension became alkaline (pH>10) enough to give a white precipitate. The precipitate in (b) consisted of fine crystal particles of $Fe(OH)_2$, the size of which increased with the NaOH concentration.

The black ferromagnetic precipitate (Fe_3O_4) was formed by the oxidation of the suspension at higher temperatures than was the yellowish brown and non-ferromagnetic precipitate (FeOOH). The process of the Fe_3O_4 formation in (a) differs from that in (b). Electron-micrographs of the precipitates formed at 70 °C in the course of oxidation, corresponding to the R values of 0.5 and 2.0, are shown in Figs. 2(a) and (b) respectively. After 90 min, a whitish precipitate (Fig. 2(a(0)) was oxidized; thereafter it turned dark green. It consists of hexagonal particles (a(1.5)), the pH of the suspension being reduced from 7.2 to 6.5.* About 40% of the total iron ions were ferric ions in the

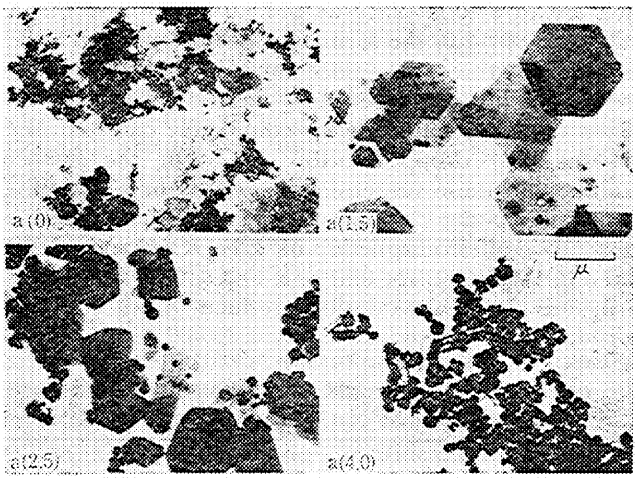

(a)

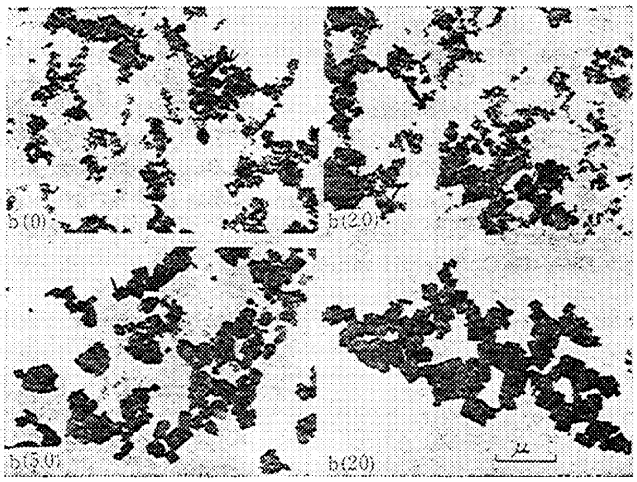

(b)

Fig. 2. Electron micrographs of the precipitates during the course of oxidation at 70 °C. (a) $R=0.5$; (0) amorphous, (1.5) green rust II, (2.5) green rust II> Fe_3O_4, (4.0) $Fe_3O_4 \gg \alpha$-FeOOH. (b) $R=2.0$; (0) $Fe(OH)_2$, (2.0) and (5.0) mixtures of $Fe(OH)_2$ and Fe_3O_4, (20) Fe_3O_4.
Number in parentheses indicates the time of oxidation in hr.

precipitate, and its X-ray diffraction data agreed with those of green rust II (hexagonal crystal unit cell, a 3.17 and c 10.7 Å).[17] The precipitate of Fe_3O_4 began to be formed at pH 6.5. After 4 hr, green rust II was transformed into Fe_3O_4 and a small amount of α-FeOOH, the former being spherical and the latter needle-like (Fig. 2(a(4.0)), the pH being suddenly reduced from 6 to 3.7. On the other hand, distinct octahedral and cubic particles of Fe_3O_4 were obtained directly from the alkaline suspension of $Fe(OH)_2$(b (0), (2), (5), and (20), Fig. 2). The appreciable difference in particle shape between the precipitates of $Fe(OH)_2$ and green rust II, and the precipitate of Fe_3O_4 indicates that the formation of Fe_3O_4 does not take place by the surface oxidation of the particles of $Fe(OH)_2$ and green rust II.

In the case where $R<0.6$, all the whitish precipitate turned to green rust II, irrespective of the oxidation temperature. The formation of Fe_3O_4 or FeOOH, or

* When the suspension was not stirred, its pH decreased to about 5.

their mixture took place at pH 6.0 ± 0.5. For the R values of 0.6—1.0, the formation of Fe_3O_4 or FeOOH, or their mixture took place at pH 7—9 due to the presence of colloidal $Fe(OH)_2$ besides green rust II. When these precipitates were completely oxidized, the pH suddenly dropped below 4.5. On the further oxidation of these suspensions at 70 °C or above, the Fe_3O_4 precipitate disappeared very gradually, and a mixture (nonferromagnetic) of α-FeOOH and either $NaFe_3(OH)_6(SO_4)_2$($R<0.6$) or α-Fe_2O_3($0.6<R<1$) was formed as the final oxidation product.

TABLE 1. PRECIPITATES FORMED DURING THE COURSE OF OXIDATION OF THE SUSPENSION CONTAINING 0.24 M-$FeSO_4$ AND 0.48 M-NaOH AT 40, 70, AND 85 °C

Oxidation time (hr)	40 °C		70 °C		85 °C	
5	A>B	(8.5)	A≈B	(6.4)	B	(4.1)
8	A≈B>C	(8.4)	B	(3.6)	B	
25	B>C	(4.1)	B	(3.3)	B	(3.1)
150	B>C	(3.7)	B≫C	(2.9)	B≫D	(2.6)
300	B>C	(3.6)	B≫C>D	(2.9)	B≈D≫C	
750	B>C	(3.5)	B≈D>C	(2.8)	D≫C	(2.6)

A=$Fe(OH)_2$ B=Fe_3O_4 or γ-Fe_2O_3 C=α-FeOOH
D=α-Fe_2O_3 The pH values are in brackets.

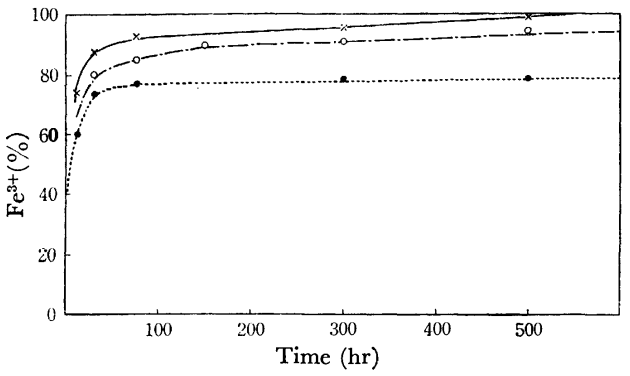

Fig. 3. Change in the ferric ion content of the suspension given in Table 1 with time. Temperature of oxidation: 40 ···●···, 70 ○---○ and 85 °C ×—×.

In order to study the formation and the decomposition of Fe_3O_4, the suspension with $R=1.0$ was oxidized at 40, 70, and 85 °C for a very long time. Table 1 shows the precipitates present in the suspension, together with the pH values at different times. The ferric-ion contents of the suspension are plotted against the time in Fig. 3. When the pH remained in the 7—9 range, the rate of oxidation was great because of the presence of $Fe(OH)_2$. When the precipitate of $Fe(OH)_2$ was completely oxidized to Fe_3O_4 or a mixture of Fe_3O_4 and α-FeOOH, the pH dropped below 4.5 and the changes in pH and ferric-ion content became very slow. By oxidation at 40 °C, a small amount of α-FeOOH is formed in addition to Fe_3O_4, the composition of the precipitate being nearly independent of the oxidation time. Fe_3O_4 is gradually oxidized to γ-Fe_2O_3 at 70 and 85 °C, since the surface oxidation of the Fe_3O_4 particles takes place topotaxially. The

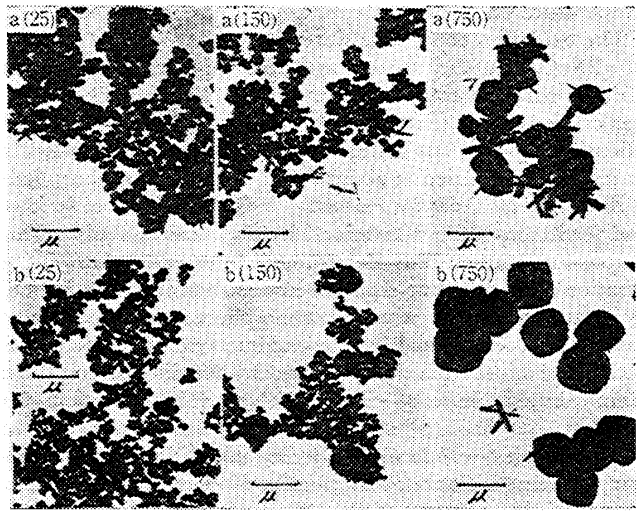

Fig. 4. Electron micrographs of the precipitates during the course of oxidation at 70 (a) and 85 °C (b). Number in parentheses indicates the time of oxidation in hr.

black color remained unchanged until the ferrous-ion content decreased to about 10% of the total iron ions. Electron-micrographs of the precipitates during the course of oxidation at 70 and 85 °C are given in Fig. 4. Electron microdiffraction showed that the X-, Y-, and I-shaped particles were all α-FeOOH. The spherical particles below 0.2 μm in size were of the spinel type (a solid solution of γ-Fe_2O_3 and Fe_3O_4), and the bigger ones, α-Fe_2O_3. This indicates that α-FeOOH and α-Fe_2O_3 are formed on the further oxidation of the particles (the solid solution) in an acidic solution. This might result from the hydrolysis of the ferric hydroxo-complexes formed by the dissolution of the precipitate of γ-Fe_2O_3, which is unstable in an acidic solution.

A kinetic study of the aerial oxidation of mixtures of $FeSO_4$ and NaOH solutions was made by Miyamoto.[22] He found that the oxidation of the suspensions proceeds in proportion to the time, irrespective of the R values. This could be explained by considering the fact that oxidation takes place in the liquid phase and not in the solid phase. In the present experiments, the ferric-ion content in the suspension increased in proportion to the oxidation time until 70% or more of the total precipitates of $Fe(OH)_2$ or green rust II had been transformed into Fe_3O_4 (or FeOOH). At a given temperature, the smaller the concentration of excess NaOH, the greater the acceleration of oxidation, in line with Miyamoto's result. The concentration of $FeSO_4$ in the neutral suspensions with $R<0.8$ slightly influenced the oxidation rate, which increased as R approached 1.0.

If the solid-phase reaction is predominant, the increase in the ferric-ion content in the suspension must be apporoximately represented by the parabolic law because the oxidation rate decreases with the increase in the thickness of the Fe_3O_4 layer on the particles of Fe $(OH)_2$ and green rust II. The fact that the oxidation of the suspension proceeds in proportion to the time indicates that the formation of Fe_3O_4 takes place in

liquid phases of alkaline and neutral suspensions. The suspension medium is saturated with respect to $Fe(OH)_2$ or green rust II. When air was bubbled into the suspension, the ferrous ions in the suspension medium react with the dissolved oxygen, thus giving rise to the formation of a ferric hydroxo-complex (polynuclear complex). When the suspension is well stirred by bubbling air, the ferrous ion consumed by oxidation is incessantly supplied by the dissolution of the precipitates of $Fe(OH)_2$ and green rust II in the suspension medium. If bubbling is carried out at a constant rate, the oxidation might proceed in proportion to the time since the rate of the dissolution of oxygen is constant. The rate of oxidation is determined by the rate of the dissolution of oxygen or the precipitates of $Fe(OH)_2$ and green rust II into the suspension medium.

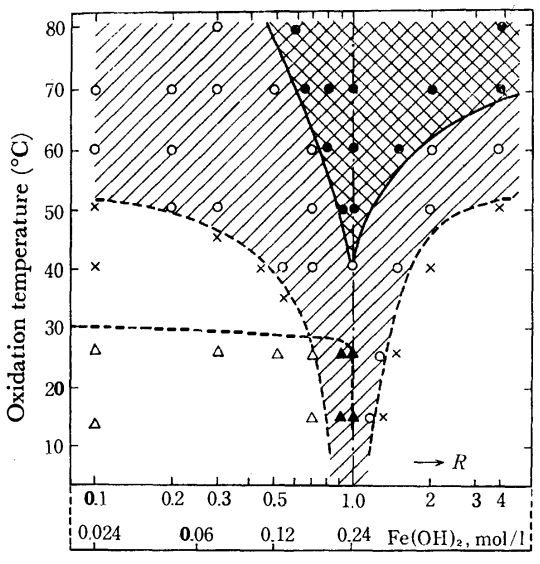

Fig. 5. Oxidation conditions for the formation of Fe_3O_4. ●: Fe_3O_4, ×: α-FeOOH, ○: A mixture of Fe_3O_4 and α-FeOOH, ▲: A mixture of Fe_3O_4, α-FeOOH and γ-FeOOH, △: A mixture of α-FeOOH and γ-FeOOH.

Conditions for the Formation of Fe_3O_4. Oxidation in the alkaline suspensions ($R>1$) was continued until the precipitate of $Fe(OH)_2$ completely disappeared, whereas oxidation in the neutral suspensions ($R<1$) was stopped as soon as the pH dropped below 4.5. The formation of precipitates is shown in Fig. 5 in terms of the temperature (ordinate) and the R value (abscissa). For the R values up to 1.0, the amount of ferrous precipitates such as $Fe(OH)_2$, formed by the addition of the NaOH solution to the $FeSO_4$ solution increases with the increase in R. The amount of ferrous precipitate in the starting suspension as calculated from the R value, is also indicated in terms of $Fe(OH)_2$ on the other abscissa. We see that the temperature at which Fe_3O_4 is formed is lowered as R approaches 1.0. Only Fe_3O_4 is formed in the upper triangular region, but FeOOH is also formed in the lower region. The influence of R on the Fe_3O_4 formation is almost symmetrical with respect to the line with $R=1.0$.

Either Fe_3O_4 or FeOOH, or their mixture, is formed in the suspension of the same value of R, depending on the oxidation temperature. Such a variety in the product formation may be due to the difference in the pH in the suspension. From the measurements of the hydrolysis constants of ferrous ions, it is generally considered that the $FeOH^-$ ion** is in equilibrium with the Fe^{2+} ion** in a neutral suspension medium or with $HFeO_2^-$ ion** in an alkaline suspension medium[23,24] and that the saturated solution of only $Fe(OH)_2$, in which most ferrous ions are present as $FeOH^+$ ions, has a pH value of 9.3 or 9.4.[25] Each particle of $Fe(OH)_2$ or green rust II in the suspension might be surrounded by a thick and dense layer of $FeOH^+$ ions. The R value most favorable for the formation of Fe_3O_4 was 1.0. The starting suspensions with the R of 1.0 had a pH of 9—10. The pH value in the layer of $FeOH^+$ ion can also be taken as 9—10.

The Fe_3O_4 particles are considered to be formed and to grow on (or in) the layer with pH 9—10 by the slow coprecipitation of $FeOH^+$ with ferric hydroxo-complexes formed by oxidation. Some of the particles of Fe_3O_4 might migrate outside the layer with pH 9—10 and be gradually oxidized to γ-Fe_2O_3. On the other hand, FeOOH may be formed outside the layer by the hydrolysis of the ferric hydroxo-complexes. Favorable conditions for the formation of Fe_3O_4 include an increase in the surface area and volume of the layer (roughly given by the product of the thickness and the total surface area of the particles of green rust II and $Fe(OH)_2$ in the suspension). The thickness of the layer might increase with the temperature, so that a temperature rise is favorable for the formation of Fe_3O_4.

Morphology and Ferrous-ion Content of the Fe_3O_4 Powders. Electron-micrographs of the Fe_3O_4 powders are given in Fig. 6. The particles of the Fe_3O_4 powders obtained in the neutral suspensions (A–D) are spherical and cubic (the needle-like particles are α-FeOOH); those in the alkaline suspensions (E and F) are cubic, octahedral, and orthorhombic. The mean particle size of the Fe_3O_4 powders obtained in the neutral suspensions,

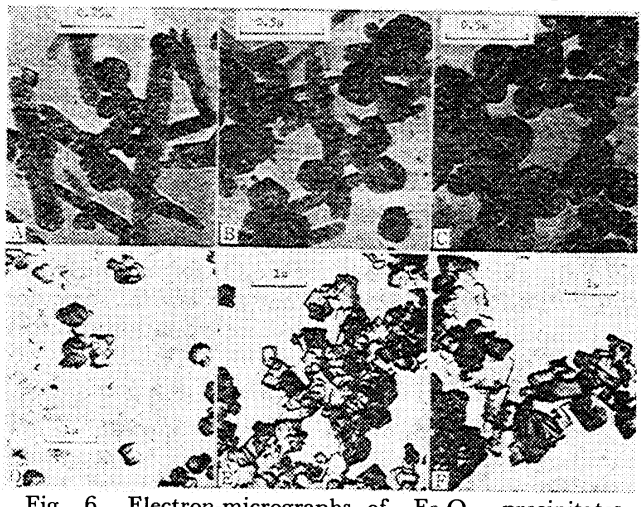

Fig. 6. Electron-micrographs of Fe_3O_4 precipitates formed by the oxidation of the suspensions at 70 °C with R values 0.1 (A), 0.3(B), 0.8(C), 1.0(D), 2.0(E) and 4.0(F). D, E and F were observed by the carbon replica method.

** H_2O ligands are omitted.

under the conditions where only Fe_3O_4 is formed, was found to be below 0.1 μm. The ferrous-ion content of the powders was less than 25% of the total iron ions, decreasing with the rise in the temperature and with the decrease in *R*. On the other hand, the mean particle size of the Fe_3O_4 powders in the alkaline suspensions was found to increase remarkably with the rise in the temperature and the *R* value, their ferrous-ion contents being about 30%. The absence of green rust II before the formation of Fe_3O_4 does not hinder the growth of Fe_3O_4 particles.

It is known that the rate of oxidation of Fe_3O_4 particles in an aqueous solution changes with the pH, the temperature, the particle size, *etc.* Oxidation may take place upon the dissolution of the ferrous ions in Fe_3O_4 particles into the aqueous solution or upon the adsorption of the oxygen atom on the Fe_3O_4 particles. In either case, the iron ions should diffuse toward the surface of Fe_3O_4 particles, thus causing oxidation. Since the oxidation of Fe_3O_4 particles takes place topotaxially, and since its rate depends on the surface area, the ferrous-ion content in each particle of Fe_3O_4 in the suspension is determined by its size. The fact that non-stoichiometric Fe_3O_4 (ferrous ion content$<$ 33.3%) was obtained in the present work might be a result of the particle-size distribution in the powder.

Additional Remarks on the Conditions for Fe_3O_4 Formation.

a): An air-flow rate greater or less than 100—400 l/hr was unfavorable for Fe_3O_4 formation. This indicates that the rate of movement of the particles of green rust II and $Fe(OH)_2$ in suspension affects the total surface area of the $FeOH^+$ layer with pH 9—10. When the flow rate is too small, the surface area of the layer with pH 9—10 diminishes as a result of a coagulation of the particles of $Fe(OH)_2$ and green rust II. When it is too great, the surface area of the layer with pH 9—10 diminishes as a result of the reduction of the thickness of the layer.

b): An increase in the concentrations of all ferrous ions in the starting suspension was favorable for Fe_3O_4 formation.

c): The use of $FeCl_2$, $FeBr_2$, or FeI_2 instead of $FeSO_4$ facilitated the formation of Fe_3O_4 or γ-FeOOH in the neutral suspension. The precipitate of Fe_3O_4 was formed *via* green rust I (not green rust II). The temperature for Fe_3O_4 formation could be lowered as compared with the case of $R<1$ in Fig. 5. For example, when suspensions with $R=0.5$ contained $FeCl_2$, $FeBr_2$, and FeI_2, the temperature for Fe_3O_4 formation fell to 25 °C. This might indicate that the crystal structure and composition of the intermediate oxidation product affect the thickness of the layer with pH 9—10.

d): When LiOH or KOH was used as a precipitant, the temperature for Fe_3O_4 formation ($R>1$, Fig. 5) became lower in the former and rose in the latter.

When a small amount of divalent metal ions (M^{2+}), such as Mg^{2+}, Mn^{2+}, and Co^{2+} ions, existed in the starting suspension, a ferromagnetic precipitate of $M_xFe_{3-x}O_4$ was obtained on slow oxidation. The conditions for $M_xFe_{3-x}O_4$ formation were similar to those for Fe_3O_4 formation, the amount of divalent metal ion in the precipitate depending on the pH.

The author is indebted to Professor Toshio Takada for drawing his attention to this problem and to Mr. Hisato Ihara and Mr. Toshikazu Akita for their assistance in the experiments.

References

1) K. Wefers, *Ber.*, **43**, 677 (1966).
2) U. Schwertmann, *Z. Anorg. Allg. Chem.*, **298**, 23 (1959).
3) R. J. Atkinson, A. M. Posner, and J. P. Quirk, *J. Inorg. Nucl. Chem.*, **30**, 3271 (1968).
4) I. Kataoka, *Nihon Dojo Hiryo Gakkai Shi*, **29**, 9 (1959).
5) W. O. Milligan and H. B. Weiser, *J. Amer. Chem. Soc.*, **57**, 238 (1935).
6) A. L. Mackay, *Mineral. Mag.*, **32**, 545 (1960).
7) R. H. H. Wolf, M. Wrisscher, and J.Siparo-Zulijevic, *Kolloid-Z. Z. Polym.*, **215**, 57 (1967).
8) M. Kiyama and T. Takada, This Bulletin, **46**, 1680 (1973).
9) M. H. Francombe and H. P. Rooksby, *Clay Min. Bull.*, **4**, 1 (1959).
10) S. Okamoto, *J. Amer. Ceram. Soc.*, **51**, 594 (1968).
11) W. H. Albrecht, *Ber.*, **62**, 1473 (1929).
12) G. Schikorr, *Z. Anorg. Allg. Chem.*, **191**, 322 (1930).
13) U. Schwertmann, *ibid.*, **298**, 337 (1959).
14) A. Krause and A. Borkowska, *Rocz. Chem.*, **29**, 999 (1955).
15) T. Misawa, T. Kyuno, W. Suetaka, and S. Shimodaira, *Corros. Sci.*, **11**, 35 (1971).
16) W. Feitknecht, *Z. Elektrochem.*, **63**, 34 (1959).
17) J. D. Bernal, E. R. Dasgupta, and A. L. Mackay, *Clay Min. Bull.*, **4**, 15 (1959).
18) M. Kiyama and T. Takada, This Bulletin, **45**, 1923 (1972).
19) M. Kiyama, T. Akita, S. Shimizu, Y. Okuda, and T. Takada, *ibid.*, **45**, 3422 (1972).
20) M. Kiyama, Y. Jikuhara, and T. Takada, *ibid.*, **46**, 323 (1973).
21) T. Takada, T. Akiyama, N. Yamamoto, and M. Kiyama, *Bull. Inst. Chem. Res., Kyoto Univ.*, **46**, 295 (1968).
22) S. Miyamoto, This Bulletin, **2**, 40 (1927); **3**, 137 (1928).
23) M. Ehrenfreund and J. Leibenguth, *Bull. Soc. Chim. Fr.*, 2498 (1970).
24) K. H. Gayer and L. Woontner, *J. Phys. Chem.*, **60**, 1569 (1956).
25) D. L. Leussing and I. M. Kolthoff, *J. Amer. Chem. Soc.*, **75**, 2476 (1953).

The Reduction of [Ru(Hedta)(H_2O)] at the Mercury Electrode and Subsequent Reactions*

Kunio SHIMIZU, Tadashi MATSUBARA, and Gen P. SATÔ

Department of Chemistry, Faculty of Science and Technology, Sophia University, Chiyoda-ku, Tokyo 102

(Received November 9, 1973)

The reduction of [Ru(Hedta)(H_2O)] at the mercury electrode and the subsequent chemical reactions in buffer solutions were investigated by AC and DC polarography and by large-scale electrolysis. Two polarographic steps were observed; the more positive step is discussed in this paper. The step was a diffusion-controlled, one-electron reduction of ruthenium(III) to ruthenium(II). For $[H^+]=(10^{-3}—10^{-5})$ mol dm^{-3} the reduction was reversible, and it became less reversible if $[H^+]<10^{-5}$ mol dm^{-3}. Large-scale electrolysis in formate buffer solutions at the potential of the polarographic diffusion current plateau confirmed that the reduction is a one-electron process. In formate buffer, the reduced form of the complex is deactivated. Furthermore, in the presence of perchlorate ions the reduced form is reoxidized to the original form. The rate constant for the reoxidation reaction at 25.0 °C was $k_2=(1.38\pm0.26)\times10^{-3}$ mol^{-1} dm^3 s^{-1}. The activation parameters for the reoxidation reaction were $\Delta H^*=(94.1\pm17.6)\times10^3$ J mol^{-1} and $\Delta S^*=(19.0\pm6.3)$ J K^{-1} mol^{-1}.

Although electrochemical studies of ruthenium have been reported by several authors,[1-7] most of the work dealt with aqua or chloro complexes in aqueous solutions. In fact, the electrode processes of ruthenium complexes are not well understood.

All the known complexes of ruthenium(II) and ruthenium(III) take the low-spin d^6 and d^5 configurations respectively, which are considerably substitution-inert. Taube and co-workers[8-11] first studied redox reactions of ammine complexes of ruthenium(II) and ruthenium(III) in aqueous solutions and proposed that the electron transfer process between them proceeds *via* an outer-sphere mechanism. They reported also that ruthenium(II) complexes can be oxidixed by perchlorate ions, which are known to be relatively weak oxidizing agents. Recently the oxidation of ruthenium(II) aqua complexes by perchlorate ions[12] and substitution reactions on ruthenium(II) complexes[13-16] have been reported, and these data are in agreement with those reported by Taube. Recent progress in the study of redox reactions of ruthenium complexes has been reviewed by Ford[17] and Taube.[18]

In the present work, (hydrogenethylenediaminetetraacetato)aquaruthenium(III), which has been proved to take the low-spin d^5 configuration,[19] was investigated by means of polarography, and the effect of perchlorate ions on the reduced form of the complex was investigated by using a large-scale electrolytic method.

Experimental

Materials. (Hydrogenethylenediaminetetraacetato)-aquaruthenium(III)-3-water, [Ru(Hedta)(H_2O)]·3H_2O was prepared according to the procedure described by Mukaida.[19] The product was a dull-yellow powder and readily soluble in water (Found: C, 25.73; H, 3.29; N, 6.18%. Calcd: C, 25.97; H, 4.59; N, 6.06%). The IR spectrum of the product obtained agreed with that reported by Mukaida. Its purity as determined by alkalimetric titration was 99.96%. The alkalimetric titration curve showed two pH-jumps indicating the existence of two dissociable protons. The pK values** calculated from the pH-titration curve were 2.37 and 7.63. This pK_1 value was very similar to that of [Rh(Hedta)(H_2O)] (pK_1=2.32, pK_2=9.12),[20] but the aqua group was more acidic than in the rhodium complex. The corresponding equilibria are represented by;

$$[Ru(Hedta)(H_2O)] \overset{K_1}{\rightleftharpoons} [Ru(edta)(H_2O)]^- + H^+$$

$$[Ru(edta)(H_2O)^-] \overset{K_2}{\rightleftharpoons} [Ru(edta)(OH)]^{2-} + H^+$$

The near ultraviolet-visible absorption spectrum of the complex in 0.2 mol dm^{-3} formic acid–sodium formate solution (pH=2.80) showed one absorption band at 283 nm ($\varepsilon=2.75\times10^2$ m^2 mol^{-1}). The spectrum remained identical in 0.01 mol dm^{-3} (pH=1.88) and 1.0 mol dm^{-3} (pH=0.88) perchloric acid solutions as well.

Sodium perchlorate-1-water was prepared from perchloric acid and sodium carbonate, according to the procedure reported earlier.[21]

All the other reagents were of Guaranteed Reagent grade and used without further purification. Twice distilled water was used except for the synthesis of the complex.

Polarography. All the polarograms were recorded with a potentiostat type AC-DC polarograph constructed locally. For AC polarography, alternating voltage of 10 mV (rms) was superimposed, the frequency was 35 Hz unless otherwise stated. The characteristics of the dropping mercury electrode (DME) were as follows: $m=1.685$ mg s^{-1}, $t_d=4.89$ s under a mercury head of 60 cm (−0.4 V *vs.* SCE, acetate buffer, ionic strength=0.5 mol dm^{-3}, 25.0 °C).

A conventional beaker type cell was used for polarographic measurements. A spiral of platinum wire served as the counter electrode. A reference saturated calomel electrode (SCE) was connected to the cell solution through a series of two H-type salt bridges (saturated sodium nitrate) with filter paper plugs. Dissolved oxygen was expelled by passing nitrogen which had been passed through vanadium(II) sulfate solution and water.

The following supporting electrolytes were used for the polarographic measurements: sodium acetate – acetic acid buffer (pH$_c$***>3.5), sodium formate – formic acid buffer (2>pH$_c$>3.5), 0.02 mol dm^{-3} sodium perchlorate – 0.18 mol dm^{-3} perchloric acid (pH$_c$=0.72). The ionic strength of all the buffer solutions was adjusted to 0.2 mol dm^{-3} with sodium perchlorate. Each solution contained 0.002% gelatin as maximum suppressor.

* Partly presented at the 18th Meeting of the Polarographic Society of Japan, Tokyo, October, 1972.

** pK represents $-\log(K/\text{mol dm}^{-3})$.

*** pH$_c$ represents $-\log([H^+]/\text{mol dm}^{-3})$.

All the potentials reported in this paper refer to SCE. All measurements were performed at (25.0±0.1)°C unless otherwise stated.

Controlled-Potential Electrolysis. The electrolytic measurement was performed with a potentiostat type electrolyzer constructed locally. About 20 μmol of the complex dissolved in 10 cm^3 of supporting electrolyte solution was electrolyzed at −0.40 V under a nitrogen atmosphere in a glass cell having two side compartments. The side compartments were separated from the cell by agar plugs. The working electrode was a mercury pool at the bottom of the cell (surface area, about 7.1 cm^2). Another mercury pool in one of the side compartments served as the counter electrode, and an SCE was connected to the solution in the other side compartment. The solution was stirred during electrolysis with a stirrer made of polyformaldehyde resin rotating at 700 revolutions per minutes. The cell was equipped with a DME for recording polarograms in the course of electrolysis. The quantity of electricity was determined by integrating the recorded electrolytic current-time curve graphically. The electrolytic current was corrected for the residual current.

For all electrolytic measurements, a mixture of sodium formate – formic acid was used as buffer, sodium perchlorate being added when perchlorate ion effect was studied. The ionic strength of the solutions was adjusted to 0.5 mol dm^{-3} by adding sodium chloride.

Others. Alkalimetric titration of the complex was performed with an automatic titrator (Radiometer; Type ASU1a Auto Burette, TTC1c Titrator, SBR2c Titrigraph). An appropriate amount of the complex was titrated with a carbon-dioxide free sodium hydroxide solution standardized against potassium hydrogenphthalate.

All the pH_c values of the solutions were determined with a Radiometer pH Meter 25E, whose meter readings were calibrated against standard hydrochloric acid solutions, and the hydrogen ion concentrations of the solutions were directly calculated from their pH_c values.

Results

Polarography. Typical AC and DC polarograms of [Ru(Hedta)(H_2O)] are shown in Fig. 1. Two DC steps appeared at −0.2 and −1.0 V. A symmetrical AC wave appeared at the potential of the more positive (first) step; but no AC wave corresponding to the more negative (second) step was observed. The heights of both DC steps were nearly equal, but the second step appeared to be less steep than the first and was accompanied by a maximum, which could not be suppressed even in the presence of 0.02% gelatin. The maximum became larger at higher hydrogen ion concentration, and no distinct second step was observed in formic acid – sodium formate buffer solutions. It was impossible to infer the nature of the first reduction product from the analysis of the second step.

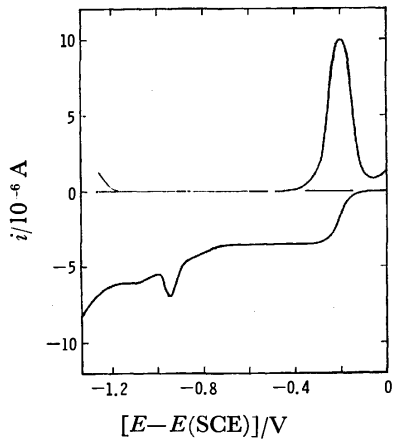

Fig. 1. AC (upper) and DC (lower) Polarograms of [Ru(Hedta)(H_2O)]. 1 mmol dm^{-3} [Ru(Hedta)-(H_2O)]; acetate buffer; 0.002% gelatin; pH_c=3.68; ionic strength=0.2 mol dm^{-3}.

The limiting current of the first step was directly proportional to both the concentration of the complex and the square root of the corrected head of mercury. No kinetic contribution was detected even at 40.0 °C. The half-wave potential was affected neither by the concentration of the complex nor the drop time.

The plot of $\log[i/(i_d-i)]$ against E, where i_d and i are the diffusion current and the current at potential E, respectively resulted in a straight line whose reciprocal slope was −62——63 mV at $pH_c<5$. At pH_c higher than 5, the reciprocal slope was larger and increased gradually over a long period of time (a few hours at 25.0 °C), presumably owing to slow hydrolysis of the complex. The half-wave potential became more negative at higher pH_c, and tended to reach a constant value at pH_c higher than 5 (Fig. 2). It was independent of free edta added to the solution up to 100 mmol dm^{-3} at pH_c=3.68.

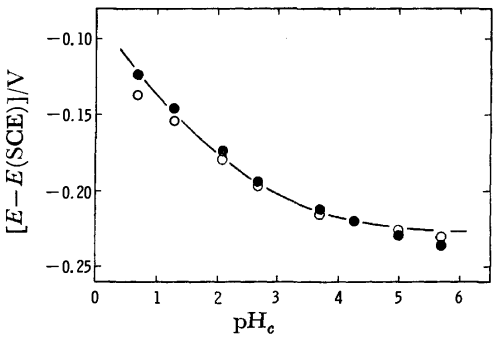

Fig. 2. pH_c-Dependence of half-wave potential and summit potential. 1 mmol dm^{-3} [Ru(Hedta)(H_2O)]; buffer solution; ionic strength=0.2 mol dm^{-3}; ●: $E_{1/2}$, ○: E_s, ——Calculation from Eq. (1b) using the best-fit set of K_O, K_R, and K'_R.

The polarographic diffusion coefficient of the complex (pH_c=3.68) calculated by using the Ilkovic equation modified by Koutecký[22] was 6.00×10^{-10} m^2 s^{-1}. This value is quite reasonable when compared with those of similar depolarizers obtained by the same method: (Cu(II)edta,[23] 5.47×10^{-10} m^2 s^{-1}; Tl(III)-edta,[24] 5.8×10^{-10} m^2 s^{-1}; H_4edta,[25] 5.01×10^{-10} m^2 s^{-1}).

The summit potential, E_s, of the corresponding AC wave coincided with $E_{1/2}$ within ±2 mV when the pH_c of the solution was higher than about 2. At a lower pH_c, E_s became more negative than $E_{1/2}$ (Fig. 2).

When $\log[(i_s/i)^{1/2}-(i_s-i)/i^{1/2}]$ (where i_s and i are the alternating currents at E_s and at E, respectively) was plotted against E, a pair of straight lines with reciprocal slopes of +125 and −106 mV was obtained (pH_c=3.68). The summit current was maximum at

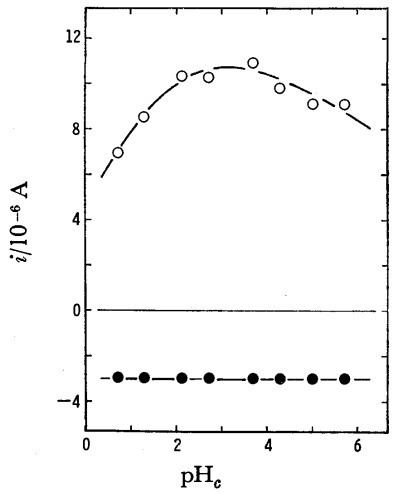

Fig. 3. pH_c-Dependence of i_d and i_s. 1 mmol dm^{-3} [Ru(Hedta)(H_2O)]; buffer solution; ionic strength= 0.2 mol dm^{-3}; ●: i_d; ○: i_s, ΔV=10 mV, f=35 Hz.

pH_c values between 3 and 4, decreasing at higher and lower pH_c (Fig. 3). The dependence of i_s on the frequency of the superimposed alternating voltage was examined at pH_c=0.72, 3.68, and 5.78 in the frequency range of 35—190 Hz, and i_s was found to be proportional to the square root of the frequency at pH_c= 3.68; in the other cases, the relation between i_s and the frequency was not linear.

Controlled-Potential Electrolysis. When the complex was partially reduced at the potential of the diffusion current plateau of the first step (−0.40 V), a redox polarographic step appeared at about −0.2 V. It was also noted that the reduced form of the complex was oxidized to the original form of the complex by passing air into the solution. The solution became slightly greenish when the electrolysis roceeded.

In the absence of perchlorate ions, the polarographic oxidation and reduction diffusion currents, i_d^a and i_d^c, recorded by suspending the electrolysis were plotted against the quantity of electricity consumed (Q) (Fig.

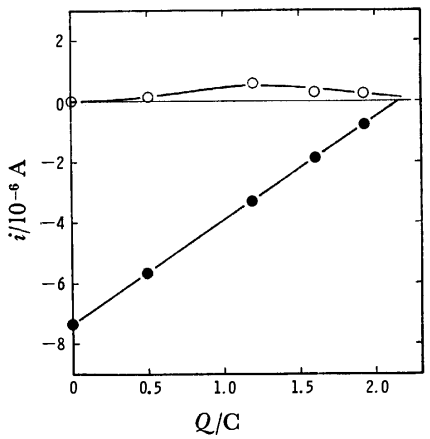

Fig. 4. Polarographic diffusion current against quantity of electricity consumed. Solution volume, 10 cm^3; 2.26 mmol dm^{-3} [Ru(Hedta)(H_2O)]; formate buffer; pH_c=4.34; ionic strength=0.5 mol dm^{-3}; 25 °C; ○: i_d^a, ●: i_d^c.

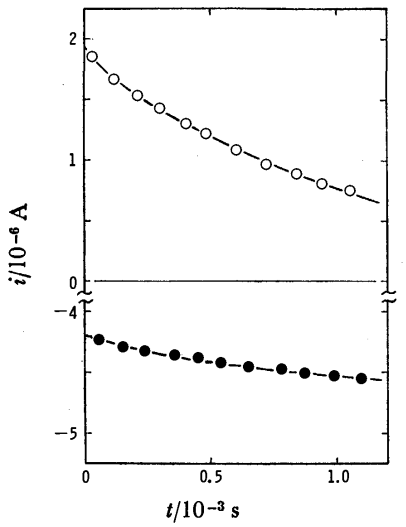

Fig. 5. Time-dependence of i_d^a and i_d^c. Formate buffer; 0.15 mol dm^{-3} $NaClO_4$; pH_c=4.35; ionic strength= 0.5 mol dm^{-3}; 25 °C; ○: i_d^a, ●: i_d^c.

4). The reduction diffusion current decreased in proportion to the advancement of the electrolysis. The slope obtained from the decrease in $|i_d^c|$ indicated that the reduction is a one-electron process. On the contraty, i_d^a remained small during the electrolysis instead of increasing proportionally. When the partially electrolyzed solution was allowed to stand, i_d^a decreased with a half-decay time of about 30 min while i_d^c remained constant.

In the solution containing perchlorate ions, the dependence of i_d^c on Q was not linear. When the electrolysis was suspended, i_d^a decreased faster than in the absence of perchlorate ions while $|i_d^c|$ increased (Fig. 5).

Discussion

Electrode Processes and Equilibria. In acid buffer solutions the first reduction step is DC-polarographically reversible, and its $E_{1/2}$ is independent of the concentration of $edta^{4-}$ in the solution. On the basis of these observations the pH-dependence of $E_{1/2}$ can be explained in terms of a set of acid-base equilibria (Fig. 6).

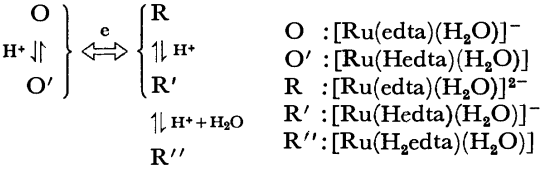

Fig. 6. Electrode process and acid-base equilibria.

Here $[Ru(edta)(OH)]^{2-}$ is ignored, because its concentration is negligible in acid solutions. Furthermore, any protonated species of the Ru(III) complex can be excluded by the fact that the electronic spectra of the complex in acid solutions were unchanged up to pH_c= 1. If each reaction is virtually in equilibrium in the course of the DC-polarographic reduction, the current-potential curve should follow Eqs. (1a) and (1b).

$$E = E_{1/2} - \frac{RT}{F} \ln \frac{i}{i_d - i} \quad (1a)$$

with

$$E_{1/2} = E_c + \frac{RT}{F} \ln \frac{([H^+]/c^\ominus)^2 + K_R[H^+]/c^\ominus + K_R K_R'}{([H^+]/c^\ominus) + K_O} \quad (1b)$$

where

$$K_O = [O][H^+]/[O']c^\ominus$$

$$K_R = [R][H^+]/[R']c^\ominus$$

$K_R' = [R'][H^+]/[R'']c^\ominus$ with $c^\ominus = 1$ mol dm^{-3}.

Among these constants $K_O = 4.29 \times 10^{-3}$ was determined by the titration of [Ru(Hedta)(H_2O)]. The others were calculated by applying the method of least squares to Eq. (1b). The best fit was obtained by the following set: $E_c = -0.078$ V, $K_R = 6.20 \times 10^{-4}$, and $K_R' = 2.53 \times 10^{-2}$. The agreement between the 'best' curve and the experimental data is excellent (Fig. 2).

The points in Fig. 2 lying along a single curve were obtained by using different buffer solutions. It follows that no anion is involved in the proton uptake of the reduced form. Although no direct evidence has yet been obtained for the protonated reduced form, the value of K_R' seems reasonable.

Polarographic Reversibility. The result of coulometry shows that the charge number of the reduction step is one. The log-plot of the DC step and the single redox step observed in the partially electrolyzed solutions show that the first step is reversible at $pH_c < 5$.

The AC reversibility was tested by analyzing the shape and height of the AC wave and the frequency dependence. The AC log-plot resulted in a pair of straight lines whose reciprocal slopes were in fair agreement with the reversible value of ± 118 mV.[26] For an AC-reversible wave the ratio of the summit AC current (i_s) to the diffusion current (i_d) is given by Eq. (2).

$$\frac{i_s}{i_d} = \frac{nF\Delta V(2\pi f)^{1/2}}{4RT(7/3\pi)^{1/2} t_d^{-1/2}(1+x)} \quad (2)$$

with

$$x = bD^{1/2}m^{1/3}t_d^{1/6}$$

Where ΔV and f are the amplitude and frequency of the superimposed AC voltage and t_d is the mean drop time in the potential region where i_s and i_d are measured; the constant b is 39.7 m^{-1} kg$^{1/3}$ given by Koutecký.[22] Inserting the necessary values into Eq. (2) one obtains $i_s/i_d = 3.34$. The corresponding experimental value at $pH_c = 3.68$ was 3.11; the agreement is reasonable. The summit current was proportional to $f^{1/2}$ up to $f = 190$ Hz as expected for a reversible case. All these data demonstrate that at $pH_c = 3$—5 the reduction process is reversible in both AC- and DC-polarographic senses.

However, at $pH_c > 5$ both AC and DC polarograms became more or less irreversible. This seems to suggest that the reduction of $[Ru(edta)(OH)]^{2-}$ is less reversible. At $pH_c < 2$, on the other hand, the DC step remained reversible, but the AC wave broadened and its height decreased. A study on the AC wave using a phase-selective AC polarograph indicated a reversible electron-transfer followed by a relatively slow chemical reaction.[27] The less reversible behavior of the AC wave may be explained by assuming that the proton dissociation of the reduced form, which involves the substitution of one of the ligating water molecules by the carboxyl group, is sluggish compared with the frequency of the superimposed AC voltage.

Chemical Reactions Subsequent to Electrode Reaction. As mentioned earlier, the reduction of the complex proceeds through a one-electron process. But the polarograms recorded in the course of the electrolysis showed an unusual behavior of the reduced form of the complex. The gradual decrease in i_d^a observed in the absence of perchlorate ions, when the partially electrolyzed solution was allowed to stand, shows the existence of at least one following chemical reaction by which the reduced form is consumed. We call this chemical reaction the deactivation reaction since the product is polarographically inactive as demonstrated by the fact that no polarographic step was observed when the solution was left to stand for a sufficient time after the completion of the electrolysis.

In the presence of perchlorate ions not only did i_d^a decrease but $|i_d^c|$ increased (Fig. 5). The faster decrease in i_d^a than that observed in the absence of perchlorate ions indicates the contribution of another chemical reaction in which the reduced form and perchlorate ions react. The increase in $|i_d^c|$ indicates the regeneration of the original form of the complex. These facts suggest that perchlorate ions reoxidize the reduced form to the original oxidized form. We call this reaction the reoxidation reaction. In the presence of perchlorate ions, the deactivation and reoxidation reactions occur simultaneously.

Kinetic Study of Chemical Reactions. The rate constants of both reactions can be determined by analyzing the time-dependence of i_d^a and i_d^c when the electrolysis is suspended.

The following reaction scheme is proposed:

$$\mathrm{Ox} \overset{e}{(\rightleftharpoons)} \mathrm{Red} \xrightarrow{k_3'[\mathrm{Red}]} \mathrm{Z}$$

$$\uparrow \quad\quad\quad\quad\quad\quad\quad\quad \downarrow$$

$$\underset{k_2'[\mathrm{Red}]}{\longleftarrow}$$

where Ox, Red, and Z represent the oxidized (equilibrium mixture of O and O'), reduced (equilibrium mixture of R, R', and R''), and deactivated forms of the complex, respectively, and [Red] is the concentration of Red. If the rate of decrease of [Red] is assumed to be first-order with respect to [Red], the time differentiation of [Red], when the electrolysis is suspended, is given by:

$$-\frac{d[\mathrm{Red}]}{dt} = (k_2' + k_3')[\mathrm{Red}] \quad (3)$$

where k_2' and k_3' are the apparent first-order rate constants for the respective reactions. Integrating Eq. (3) with the boundary condition, $[\mathrm{Red}] = [\mathrm{Red}]_0$ at $t = 0$, one obtains:

$$[\mathrm{Red}] = [\mathrm{Red}]_0 \exp\{-(k_2' + k_3')t\}. \quad (4)$$

Similarly, the time differentiation of the concentration of Ox under the same conditions is

$$\frac{d[\mathrm{Ox}]}{dt} = k_2'[\mathrm{Red}]. \quad (5)$$

The equation obtained by inserting Eq. (4) into Eq. (5) is integrated with the boundary condition, $[Ox]=[Ox]_0$ at $t=0$. Rearranging the resulting expression, we have

$$\frac{k_3}{k_2'+k_3'} = \frac{[Ox]-[Ox]_0}{[Red]-[Red]_0}. \quad (6)$$

By assuming equal diffusion coefficients for both Red and Ox, Eqs. (4) and (6) are expressed as follows:

$$\ln (i_d^a/i_{d,0}^a) = -(k_2'+k_3')t \quad (7)$$

$$\frac{i_d^c - i_{d,0}^c}{i_{d,0}^a - i_d^a} = \frac{k_2'}{k_2'+k_3'} \quad (8)$$

where $i_{b,0}^a$ and $i_{b,0}^a$ are the respective diffusion currents at $t=0$.

Table 1. Kinetic data for reoxidation and deactivation rates

No.	$[H^+]$ / 10^{-4} M	$[ClO_4^-]$ / M	[NaCl] / M	k_2' / 10^{-4} s^{-1}	k_3' / 10^{-4} s^{-1}
1	3.39	0	0.30		19.1
2	2.19	0	0.25		15.6
3	0.457	0	0.15		7.00
4	1.17	0	0.195		11.1
5	0.457	0.15	0	2.66	6.28
6	0.437	0.15	0	2.71	6.25
7	3.24	0.15	0.05	1.79	19.0
8	0.457	0.10	0.05	1.54	6.06
9	0.457	0	0.15		6.24
10	0.457	0.15	0	2.37	5.97
11	0.457	0.04	0.11	0.50	6.57
12	0.457	0.05	0.10	0.57	6.52
13	1.41	0.15	0.045	2.23	10.9
14	3.16	0.15	0.10	2.75	17.3
15	2.75	0.15	0.10	2.97	15.8
16	0.59	0	0.15		6.33[a]
17	3.63	0	0.30		18.7
18	3.63	0	0.30		18.3[a]
19	1.05	0	0.195		11.7
20	1.05	0	0.195		11.8
21	1.05	0.15	0.045	2.54	12.0
22	1.05	0	0.195		19.7 (30.0 °C)
23	1.05	0.15	0.045	5.25	20.7 (30.0 °C)
24	1.05	0	0.195		4.15(10.0 °C)
25	1.05	0.15	0.045	0.36	4.54(10.0 °C)
26	1.05	0	0.195		5.39(15.0 °C)
27	1.05	0.15	0.045	0.645	5.06(15.0 °C)
28	1.05	0	0.195		7.60(20.0 °C)
29	1.05	0.15	0.045	1.27	8.35(20.0 °C)

M represents mol cm^{-3}. a) The solution contains 0.1 mol dm^{-3} H_4edta.

Equations (7) and (8) were experimentally satisfied, and by solving them k_2' and k_3' were obtained as shown in Table 1. k_3' was found to be independent of perchlorate ion concentration. It seems that the deactivation process involves a reaction between Ru(II)edta species and formic acid similar to that reported in the case of the tetrachlororuthenate(II)–formic acid system.[28] Details on the kinetics of this reaction and identification of the reaction product will be reported separately.

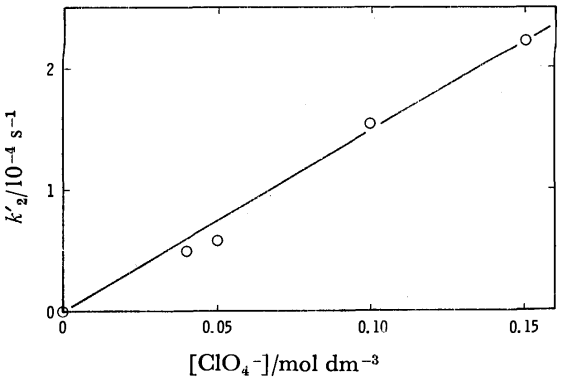

Fig. 7. Effect of perchlorate ion concentration on reoxidation rate. Formate buffer; ionic strength= 0.5 mol dm^{-3}; 25 °C.

The apparent rate constant of the reoxidation, k_2', was independent of the hydrogen ion concentration and formic acid concentration. When k_2' was plotted against perchlorate ion concentration a straight line was obtained (Fig. 7), from which the rate constant for the reoxidation, k_2 at 25.0 °C is estimated at the 90% confidence limit as follows:

$$k_2 = \frac{k_2'}{[ClO_4^-]} = (1.38\pm0.26)\times10^{-3}\ \text{mol}^{-1}\ \text{dm}^3\ \text{s}^{-1}$$

Linear Arrhenius plots are obtained for k_2. The activation parameters for the reoxidation process are calculated at the 90% confidence limit by applying the rate theory of Eyring with the assumption tnat the transmission coefficient and quotient of activity coefficients are unity. At 25.0 °C, ΔH^* and ΔS^* obtained are as follows:

$$\Delta H^* = (9.41\pm17.6)\times10^3\ \text{J mol}^{-1},$$

$$\Delta S^* = (19.0\pm6.3)\ \text{J K}^{-1}\ \text{mol}^{-1}.$$

The value of ΔH^*, which is very similar to those for other ruthenium(II) substitution reactions[13-15] but much larger than those for ruthenium(II)—ruthenium(III) electron transfer reactions,[11] seems to indicate that the rate determining step of the reoxidation reaction is the substitution of perchlorate ion on the reduced form of the complex. The most probable mechanism for the attack of perchlorate ion on the reduced form is similar to that proposed by Taube[9] in the case of hexaammineruthenium(II) ions.

The authors wish to thank to Dr. M. Mukaida of Sophia University, for his kind help in the synthesis of the complex. Thanks are due to Mr. T. Kimura of St. Paul University, for permission to use his computer program for the calculation of acid-base equilibrium constants. The authors also thank Sr. Jean Michalec for correcting the manuscript.

References

1) L. W. Niedrach and A. D. Tevebaugh, *J. Amer. Chem. Soc.*, **73**, 2835 (1951).

2) D. T. Sawyer, R. J. Kula, and A. I. Budd, *J. Electroanal. Chem.*, **4**, 242 (1962).

3) D. K. Atwood and T. De Vries, *J. Amer. Chem. Soc.*, **84**, 2659 (1962).
4) E. E. Mercer and R. R. Backley, *Inorg. Chem.*, **4**, 1692 (1965).
5) R. R. Backley and E. E. Mercer, *J. Phys. Chem.*, **70**, 3103 (1966).
6) R. M. Wallsce and R. C. Propst, *J. Amer. Chem. Soc.*, **91**, 3779 (1969).
7) H. S. Lim, D. J. Barclay, and F. C. Anson, *Inorg. Chem.*, **11**, 1460 (1972).
8) J. F. Endicott and H. Taube, *J. Amer. Chem. Soc.*, **86**, 1686 (1964).
9) J. F. Endicott and H. Taube, *ibid.*, **84**, 4984 (1962).
10) J. F. Endicott and H. Taube, *Inorg. Chem.*, **4**, 437 (1965).
11) T. J. Meyer and H. Taube, *ibid.*, **7**, 2369 (1968).
12) T. W. Kallen and J. E. Earley, *ibid.*, **10**, 1152 (1971).
13) B. Bosich and F. P. Dwyer, *Aust. J. Chem.*, **19**, 2235 (1966).
14) N. R. Daves and T. L. Mullins, *ibid.*, **21**, 915 (1968).
15) T. W. Kallen and J. E. Earley, *Inorg. Chem.*, **10**, 1149 (1971).
16) R. J. Allen and P. C. Ford, *ibid.*, **11**, 679 (1972).
17) P. C. Ford, *Coordin. Chem. Rev.*, **5**, 75 (1970).
18) H. Taube, "Electron Transfer Reactions of Complex Ions in Solutions," Academic Press, New York, (1970), p. 76.
19) M. Mukaida, H. Okuno, and T. Ishimori, *Nippon Kagaku Zasshi*, **86**, 598 (1965).
20) F. P. Dwyer and F. L. Garvan, *J. Chem. Soc., A*, **1966**, 4823.
21) K. Higaki and G. P. Satô, *Rev. Polarog.* (Kyoto), **17**, 109 (1971).
22) J. Koutecký, *Czech. J. Phys.*, **2**, 50 (1953).
23) R. L. Pecsok, *Anal. Chem.*, **25**, 561 (1953).
24) T. Kitagawa and Y. Maruyama, *Bunseki Kagaku*, **19**, 362 (1970).
25) K. Niki, K. Suzuki, G. P. Satô, and N. Mori, *J. Electroanal. Chem.*, **49**, 27 (1974).
26) A. J. Bard, "Electroanalytical Chemistry," vol. 1, Marcel Dekker Inc., New York, (1966), p. 23.
27) M. Kobayashi, M. Sc. Thesis, Sophia Univ., Tokyo, Japan, (1973).
28) J. Halpern and A. L. W. Kemp, *J. Amer. Chem. Soc.*, **88**, 5147 (1966).

The Complexing of the Sodium Ion in Acetonitrile with Other Solvents. Investigation by the Use of a Cation-sensitive Glass Electrode

Kosuke Izutsu, Toshiaki Nomura, Toshio Nakamura,
Hidetoshi Kazama, and Shigeo Nakajima
Chemistry Department, Faculty of Science, Shinshu University, Asahi, Matsumoto 390
(Received November 16, 1973)

The complexing of the sodium ion in acetonitrile (AN) with such solvents as methanol, water, DMF, DMA, DMSO, HMPA, and pyridine has been studied potentiometrically by using a monovalent cation-sensitive glass electrode. The reference electrode of Ag-0.005 M $AgNO_3$(AN) and the salt bridge of 0.1 M Et_4NPi(AN) were used. Mono- and di-solvated ions were formed for methanol, water, and pyridine. For DMF, DMA, DMSO, and HMPA, tri-solvated species were also formed. The formation constants for the mono-solvated sodium ion were 0.7 for pyridine, 1 for methanol, 1.8 for water, 2.5 for DMF, 5 for DMA, 6 for DMSO, and 30 for HMPA.

The hydration constants of alkali metal ions and several monovalent anions in acetonitrile(AN) have been determined by Chantooni and Kolthoff.[1] This was done by measuring conductometrically the ionic solubility of a slightly soluble salt in AN in the presence of a known concentration of water.

In the present paper, we investigated the complexing of the sodium ion in AN with such solvents as methanol, water, dimethylformamide(DMF), dimethylacetoamide (DMA), dimethylsulfoxide(DMSO), hexamethylphosphoramide(HMPA), and pyridine by using a monovalent cation-sensitive glass electrode. The emf of the following cell was measured:

$$\underset{(A)}{Ag|0.005\ M\ AgNO_3(AN)}\|\underset{(B)}{0.1\ M\ Et_4NPi(AN)}\|\underset{(C)}{10^{-3}\ M\ NaClO_4+0.01\ M\ Et_4NClO_4(AN+D)}|Glass\ electrode$$

Cell I

where D denotes a solvent added to the AN solution in the compartment (C). The liquid junction potential between the salt bridge (B) and the solution in the compartment (C) was assumed to change only negligibly upon the addition of a solvent (D). The salt bridge of the 0.1 M tetraethylammonium picrate (Et_4NPi) in AN was used because Parker *et al.*[2,3] reported that the junction potential between this salt bridge and a 0.01 M $AgClO_4$ solution in other dipolar solvents is usually relatively small. The Nernstian response of the cation-sensitive glass electrode towards alkali-metal ions has been verified in several nonaqueous solvents.[4,5] We found, in the present study, that the glass electrode can also be used to measure the difference in the activity of the sodium ion in various solvents, provided that a suitable reference electrode system is employed.

In the mixture of AN and D, the following equilibrium is attained between sodium ions solvated only by AN (denoted by Na_s^+) and those which are solvated also by D (denoted by Na_{xD}^+, where x is the number of solvating D molecule(s)):

$$Na_s^+ + xD = Na_{xD}^+ \quad (1)$$

$$K_x = \frac{[Na_{xD}^+]}{[Na_s^+][D]^x} \quad (2)$$

where K_x is the corresponding formation constant. If we denote the activity of Na_s^+ in pure AN by $[Na_s^+]_{AN}$, and that in the mixture of AN and D by $[Na_s^+]_{AN-D}$, the following relations hold:

$$R \equiv \left\{\frac{[Na_s^+]_{AN}}{[Na_s^+]_{AN-D}} - 1\right\}/[D] = K_1 + K_2[D] + K_3[D]^2 + \cdots \quad (3)$$

and

$$(R-K_1)/[D] = K_2 + K_3[D] + \cdots \quad (4)$$

Here, the values of $[Na_s^+]_{AN}/[Na_s^+]_{AN-D}$ can be obtained from the potentials of the glass electrode in pure AN and an AN–D mixture as follows:

$$[Na_s^+]_{AN}/[Na_s^+]_{AN-D} = 10^{(E_{AN}-E_{AN-D})/59} \quad (5)$$

where E_{AN} and E_{AN-D} are in mV. By plotting the relations between R and [D] and between $(R-K_1)/[D]$ and [D], we can obtain the values of the formation constants of Reaction (1).

In the determination of formation constants, the following assumptions are made: (i) the solvent (D) in AN–D mixtures is monomeric, and the activity of D is equal to the analytical concentration; (ii) the activity of AN does not change upon the addition of D and is equal to unity; and (iii) the salt-effect activity coefficient of the sodium ion, calculated by the Debye-Hückel equation, is equal in pure AN and in AN–D mixtures. We also assume that the amount of the solvent(D) consumed by the solvation of the ions of an indifferent electrolyte is negligible. The last assumption seems to be justified when the indifferent electrolyte is 0.01 M Et_4NClO_4 if we consider that the hydration constant of perchlorate ion in AN has been reported to be 0.7.[1]

Apparatus and Reagents

Apparatus. The assembly of Cell I is shown in Fig. 1. In each experiment, the solution in the compartment (C) was initially composed of 50 ml of the AN solution which was 10^{-3} M in $NaClO_4$ and 0.01 M in Et_4NClO_4; from the solvent inlet, the solvent (D) was titrated with a microsyringe. The maximum volume of D added to the cell was 0.85 ml for water, 1.25 ml for methanol, 1.8 ml for HMPA, and 2.5 ml for DMF, DMA, DMSO, and pyridine. After each addition of solvent, the solution was stirred with a magnetic stirrer. The emf was measured with the expanded scale of a Hitachi-Horiba pH meter, model F-7ss, to ± 0.1 mV. The mono-

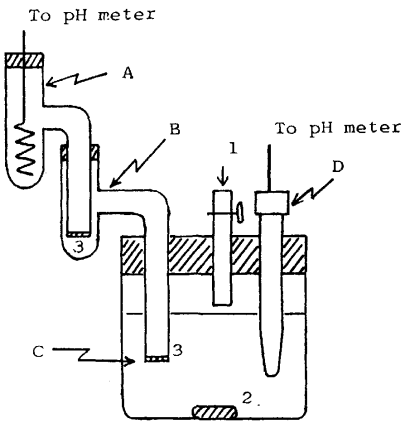

Fig. 1. Diagram of cell assembly.
A: reference electrode, B: salt bridge, C: cell for test solution, D: cation-sensitive glass electrode, 1: solvent inlet, 2: magnetic stirrer, and 3: fine porosity sintered glass. The cell is kept in a bath at 25±0.1 °C.

valent cation-sensitive glass electrode was a Beckman 39047. The reference electrode of Ag-0.005 M $AgNO_3$ in AN was connected to the solution in (C) through a salt bridge of 0.1 M Et_4NPi in AN. The reference electrode and the salt bridge were prepared every day before measurement in order to avoid mixing of solutions between compartments. When the reference electrode and the salt bridge were too fresh, however, the emf of the cell changed with the time. Therefore, the titration was carried out after the shift of emf had become less than 0.5 mV/hr. The emf of the cell of the initial AN solution was reproducible; it was 75±1 mV. Polarograms were measured with a three-electrode polarograph, Yanagimoto P8-PS. All the experiments were carried out at 25±0.1 °C.

Reagents. Unhydrated sodium perchlorate was dried before use at 130 °C under a vacuum. The tetraethylammonium picrate was prepared by the method of Coetzee and Padmanabhan.[6] The tetraethylammonium perchlorate was prepared and dried by the conventional method. Acetonitrile was purified by distilling it three times using an adiabatic vacuum fractional distillation column, first from P_2O_5, next from CaH_2, and finally without any addition.[7] The purified AN was used within a day after distillation. The pyridine was used after the purification of the spectrophotometric product by fractional crystallization. The other solvents were of an analytical reagent grade and were used without further purification.

Results

Response of the Glass Electrode to the Activity of Sodium Ion in Different Solvents. The slope of the response of the glass electrode to the concentration of the sodium ion in AN has been reported to be 56 mV in the presense of 0.1 M Bu_4NClO_4.[4] The glass electrode used in the present study showed a slope of 58 mV to the sodium ion between 10^{-4} and 10^{-2} M in AN–0.01 M Et_4NClO_4. If corrected for the change in the salt-effect activity coefficient, the response towards pa_{Na^+} is very near to the Nernstian slope of 59 mV.

For the present study, it is also necessary for the electrode to respond to the difference in the activity of the sodium ion between solvents of different species or compositions. This was verified by comparing the emfs of the following cell with the polarographic half-wave potentials of the sodium ion, which are considered to make a Nernstian response to the solvent effect on the activity of the sodium ion:

Ag|0.005 M $AgNO_3$(AN)‖0.1 M Et_4NPi(AN)‖
10^{-3} M $NaClO_4$ + 0.01 M Et_4NClO_4(D)|Glass electrode
(D denotes AN, MeOH, H_2O, DMF, and DMSO)
Cell II

The half-wave potentials were measured in a solution of 10^{-3} M $NaClO_4$+0.01 M Et_4NClO_4 by using a reference electrode and salt bridge similar to those in Cell II.

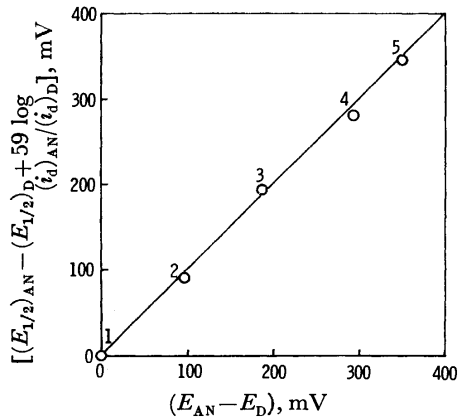

Fig. 2. Relations between the emf of Cell II and the half-wave potential of sodium ion in various solvents. Referred to the values in AN. Circle 1 is in AN, 2 in MeOH, 3 in H_2O, 4 in DMF, and 5 in DMSO.

The results in Fig. 2 show that the emf and the half-wave potential (corrected for the change in diffusion current) in each solvent, both referred to the values in AN, agree quite well, suggesting that the glass electrode can respond to the activity of the sodium ion in different solvents.

Complexing of the Sodium Ion in AN with Other Solvents. From the emf measurement of Cell I, the values of the formation constants of Reaction (1) were calculated by using the relations of Eqs. (3) to (5). The results are summarized in Table 1. Figures 3 to 6 show some

Table 1. Complex formation constants of sodium ion in AN with other solvents

Solvent	K_1	K_2	K_3
H_2O	1.8	1.8	
	1.8	1.8	
	1.8	1.9	
MeOH	$1._0$	0.4	
	$1._2$	0.4	
DMF	2.4	$2._1$	$1._1$
	2.5	$2._0$	$1._2$
DMA	5.3	10	$7._6$
	5.2	12	$5._2$
DMSO	5.8	10	$1._3\times10$
	6.2	12	$1._5\times10$
HMPA	28	$3._2\times10^2$	$1._4\times10^3$
	30	$3._1\times10^2$	$1._2\times10^3$

examples of R-[D] and $(R-K_1)/[D]$-[D] relations.

By the addition of water, mono- and di-hydrated sodium ions are formed, with K_1 and K_2 equal to 1.8 and 1.8 respectively. These values are in fairly good agreement with those of 2 and 3 respectively obtained by Chantooni and Kolthoff from the conductometric measurement of the solubility.[1] The solvation of methanol is weaker than hydration, and K_1 and K_2 are 1 and 0.4 respectively. The solvation becomes easier with the increase in the solvent basicity in the order: MeOH<H_2O<DMF<DMA~DMSO<HMPA. For DMF, DMA, DMSO, and HMPA, a complexing up to three solvent molecules is observed. It is interesting, however, that pyridine, which is strongly basic, solvates only weakly with a K_1 of approximately 0.7. The weak solvation of pyridine to the sodium ion is consistent with the results of the calorimetric investigation in acetone.[8]

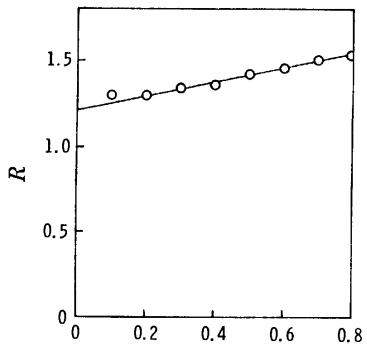

Fig. 3. R-[MeOH] relation.

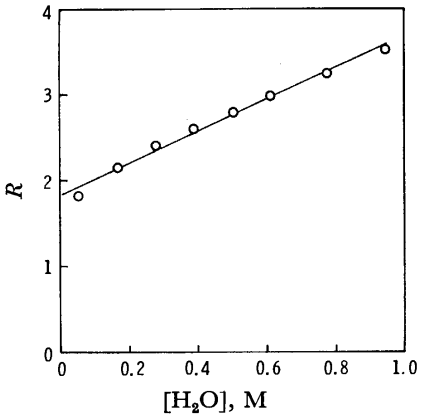

Fig. 4. R-[H_2O] relation.

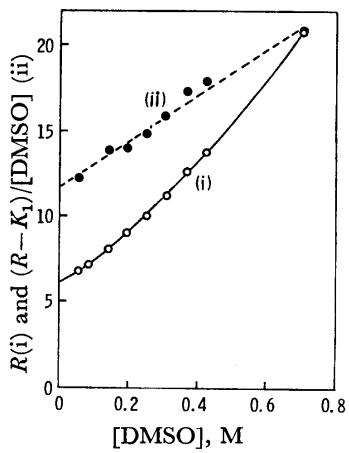

Fig. 5. R-[DMSO] (Curve i) and $(R-K_1)/[DMSO]$ -[DMSO] (Curve ii) relations.

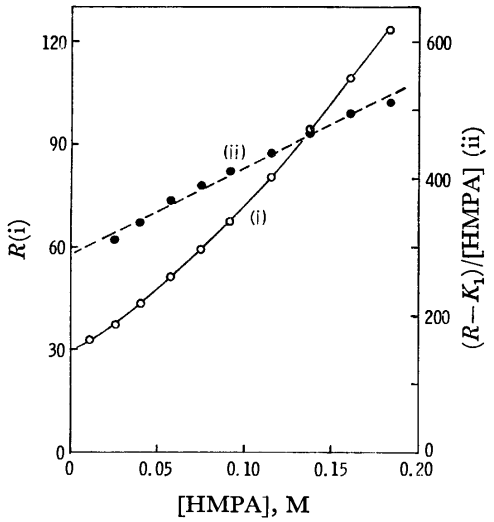

Fig. 6. R-[HMPA] (Curve i) and $(R-K_1)/[HMPA]$-[HMPA] (Curve ii) relations.

Discussion

From the results in Fig. 2, the glass electrode may be considered to respond with a Nernstian slope to the solvent effect on the activity of the sodium ion.

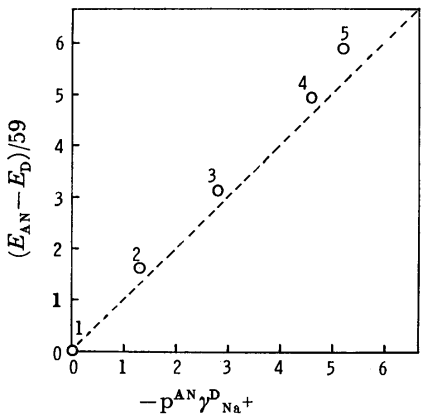

Fig. 7. Relations between the emf of Cell II and the solvent activity coefficient of sodium ion in various solvents. Referred to the values in AN. Circle 1 is in AN, 2 in MeOH, 3 in H_2O, 4 in DMF, and 5 in DMSO. E_{AN} and E_D are in mV.

Figure 7 shows the relation between the emfs of Cell II and the solvent activity coefficients of the sodium ion in several solvents, all referred to the values in AN. As the solvent activity coefficients, the values reported by Kolthoff and Chantooni ($p^{H_2O}\gamma^{MeOH}=1.5$, $p^{H_2O}\gamma^{AN}=2.8$, $p^{H_2O}\gamma^{DMF}=-1.8$, and $p^{H_2O}\gamma^{DMSO}=-2.4$)[9] were used. As is apparent from this figure, the values of $(E_{AN}-E_D)/59$ and $p^{AN}\gamma^{D}_{Na^+}$ for each solvent are in fairly good agreement. This may support the con-

sideration that the solvent activity coefficients quoted here are reasonable values and allow us to speculate that the junction potentials between the salt bridge and the solutions in these different solvents are relatively small, as has been reported by Cox *et al.*[3]

In the determination of formation constants, the junction potential between the salt bridge and the solution in (C) of Cell I was assumed to change only negligibly upon the addition of the solvent (D). According to Cox *et al.*,[3] the junction potential between the salt bridge of 0.1 M Et_4NPi(AN) and an aqueous 0.01 M $AgClO_4$ solution is approximately 10 mV (Fig. 1, Ref. (3)). If this is correct, the change in the junction potential in the present study, in which water up to *ca.* 1 M (1.7 v/v%) is added to the AN solution, is expected to be small (probably less than 1 mV) and it will tend to decrease the apparent value of $(E_{AN}-E_{AN-D})$. On the contrary, if a salt bridge of 0.1 M Et_4NPi in acetone is used instead of 0.1 M Et_4NPi in AN, the junction potential may be expected, according also to Cox *et al.*, to change to the opposite direction and to increase the apparent value of $(E_{AN}-E_{AN-D})$ (Fig. 1, Ref. (3)). The values of K_1 and K_2 for the hydration of the sodium ion, obtained by using a salt bridge of 0.1 M Et_4NPi in acetone, are 1.8 and 1.9

Table 2. Effect of salt bridge on hydration constants of sodium ion in AN

Salt bridge	K_1	K_2
0.1 M Et_4NPi in AN	1.8	1.8
	1.8	1.8
	1.8	1.9
0.1 M Et_4NPi in Acetone	1.7	2.0
	1.8	1.9
	1.8	1.9

(Table 2) respectively, in good agreement with the values of 1.8 and 1.8 respectively obtained with Cell I. This seems to support the assumption that the change in the junction potential by the addition of water is negligibly small. For the addition of methanol, however, the change in the junction potential may be somewhat larger than for water (Fig. 1, Ref. (3)). For other aprotic solvents, the change in the junction potential seems to be smaller than in the case of water.[3]

In the present study, the solution of the sodium ion usually contained 0.01 M Et_4NClO_4 as an indifferent electrolyte. According to the conductance measurement,[10] sodium ions in AN associate with perchlorate ions with an association constant of *ca.* 11. The hydration constants of the sodium ion in Table 3, determined in the presence of the indifferent electrolyte of 0, 0.01 and 0.1 M Et_4NClO_4 are, however, in good agreement with each other, suggesting that the effect of ion association is small in this case.

Table 3. Effect of concentration of indifferent electrolyte on hydration constants of sodium ion in AN

Concn. of Et_4NClO_4(M)	K_1	K_2
0	1.7	1.7
	1.8	1.8
	1.7	1.9
0.01	1.8	1.8
	1.8	1.8
	1.8	1.9
0.1	1.8	1.7
	1.8	1.8
	2.0	1.7

In addition to the factors considered above, the values of formation constants may also be affected by such factors as follows: (i) Some part of the solvent added may be self-associated, and the activity of the solvent may be less than the concentration. (ii) Both the activity of AN and the medium character may change upon the addition of other solvent. Because the effect of these factors increases with the increase in the amount of solvent added, the deviation of the values of K_2 and K_3 from the true values may be larger than the deviation of K_1. The values of K_1 in Table 1 seem to be reliable within $\pm 10\%$, except for the case of methanol, in which the reliability is somewhat less.

Due to the importance of solvation phenomena in the mechanism of various chemical reactions, the solvation of the sodium ion has recently been studied extensively by a variety of experimental techniques, among which infrared[11] and NMR[12] spectroscopies, conductometry[1] and calorimetry[8] are most significant. The present potentiometric method, however, seems to be superior to these techniques in the point that the activity of the sodium ion is directly measured.

The complexing of the lithium ion in AN with other solvents is now under investigation by using a similar method.

This work partly supported by a grant from the Ministry of Education of Japan.

References

1) M. K. Chantooni, Jr. and I. M. Kolthoff, *J. Amer. Chem. Soc.*, **89**, 1582 (1967).
2) R. Alexander, A. J. Parker, J. H. Sharp, and W. E. Waghorne, *ibid.*, **94**, 1148 (1972).
3) B. G. Cox, A. J. Parker, and W. E. Waghorne, *ibid.*, **95**, 1010 (1973).
4) J. E. McClure and T. B. Reddy, *Anal. Chem.*, **40**, 2064 (1968).
5) M. K. Chantooni, Jr. and I. M. Kolthoff, *J. Phys. Chem.*, **77**, 1 (1973).
6) J. F. Coetzee and G. R. Padmanabhan, *ibid.*, **66**, 1708 (1962).
7) J. F. Coetzee, *Pure Appl. Chem.*, **13**, 429 (1966).
8) E. M. Arnett, H. C. Ko, and C. C. Chao, *J. Amer. Chem. Soc.*, **94**, 4776 (1972).
9) I. M. Kolthoff and M. K. Chantooni, Jr., *J. Phys. Chem.*, **76**, 2024 (1972).
10) R. L. Kay, B. J. Hales, and G. P. Cunningham, *ibid.*, **71**, 3925 (1967).
11) B. W. Maxey and A. I. Popov, *J. Amer. Chem. Soc.*, **91**, 20 (1969); W. J. McKinney and A. I. Popov, *J. Phys. Chem.*, **74**, 535 (1970).
12) E. Schaschel and M. C. Day, *J. Amer. Chem. Soc.*, **90**, 503 (1968); B. W. Maxey and A. I. Popov, *ibid.*, **90**, 4470 (1968).

Effect of Ethanol on the Outer-sphere Association of Λ- or Δ-Tris(ethylenediamine)cobalt(III) with *d*-Tartrate Ions in Aqueous Solutions

Hayami YONEDA, Katsuhiko MIYOSHI, Shingo SUZUKI, and Toshiaki TAURA

Department of Chemistry, Faculty of Science, Hiroshima University, Hiroshima 730

(Received December 24, 1973)

The effect of ethanol on the outer-sphere association of Λ- or Δ-$[Coen_3]^{3+}$ ion (en=ethylenediamine) with *d*-tartrate ion was investigated in aqueous solutions containing 0, 1, 3, and 5 wt% of ethanol at 25 °C by measuring the change in optical density of the charge-transfer spectra at 265 nm. It was found that the association constant of Λ-$[Coen_3]^{3+}$ ion with *d*-tartrate ion $K_{A(\Lambda)}$ was a little larger than that of Δ-$[Coen_3]^{3+}$ ion $K_{A(\Delta)}$, and that the addition of ethanol increased both $K_{A(\Lambda)}$ and $K_{A(\Delta)}$ but decreased the ratio $K_{A(\Lambda)}/K_{A(\Delta)}$. The diminished discrimination between Λ- and Δ-$[Coen_3]^{3+}$ ions by *d*-tartrate ion was discussed in terms of the solubility of these diastereoisomers in aqueous ethanol and was attributed to the increased electrostatic interaction between the complex and *d*-tartrate ions arising from the decrease in the dielectric constant of the medium.

It is well-known that the racemic $[Coen_3]^{3+}$ ion is resolved from the fact that the Λ-form precipitates as Λ-$[Coen_3]X$*d*-tart (X=halide anion and *d*-tart=*d*-tartrate dianion), while the corresponding Δ-form remains gelatinous when evaporated in aqueous solution. The discrimination of Λ- from Δ-forms by *d*-tart ion is expected to take place also in solution, *viz.*, the differential outer-sphere association with *d*-tart ion is anticipated for Λ- and Δ-$[Coen_3]^{3+}$ ions. Addition of alcohol decreases solubility of many inorganic salts. This is the case with this system. Thus, it seems of interest to examine the effect of alcohol on the outer-sphere association of Λ- or Δ-$[Coen_3]^{3+}$ ion with *d*-tart ion in aqueous solution. The purpose of this investigation is to find optimum conditions for the discrimination between Λ- and Δ-forms. As the first step, the association constants were determined by spectrophotometry in aqueous ethanol.

Ogino and Saito[1] and Nordén[2] reported from the measurements of charge-transfer (CT) and the corresponding circular dichroism (CD) spectra that *d*-tart ion associates to a greater extent with Λ-$[Coen_3]^{3+}$ than with Δ-$[Coen_3]^{3+}$ ion in aqueous solution. They neglected the association of $[Coen_3]^{3+}$ ion with perchlorate ion added to adjust ionic strength constant, on the ground that the spectra are not altered by its addition. However, it is not plausible from both electrostatic[3] and experimental[4] viewpoints that $[Coen_3]^{3+}$ ion does not associate at all with ClO_4^- ion even in aqueous solution. Addition of alcohol is expected to promote ionic association of the complex cation not only with *d*-tart ion but also with ClO_4^- ion owing to the accompanying decrease in the dielectric constant of the medium. Therefore, measurements should be carried out on a system which contains no anions other than *d*-tart ion.[5]

Experimental

Materials. Λ-$[Coen_3](d\text{-tart})_{3/2}\cdot 6H_2O$(or $5.5H_2O$) was prepared by the double decomposition of Λ-$[Coen_3]Brd$-tart$\cdot 5H_2O$ with an equivalent amount of Ag_2*d*-tart. Found: C, 25.32; H, 6.99; N, 15.15%. Calcd for $C_{12}H_{42}N_6O_{15}Co$(or $C_{12}H_{41}N_6O_{14.5}Co$): C, 25.31(25.72); H, 7.43(7.37); N, 14.76 (15.00)%. Similar procedures gave Δ-$[Coen_3](d\text{-tart})_{3/2}\cdot 6H_2O$(or $6.5H_2O$) when Δ-$[Coen_3]Br_3\cdot 2H_2O$ was used in place of Λ-$[Coen_3]Brd$-tart$\cdot 5H_2O$. Found: C, 24.73; H, 7.18; N, 14.46%. Calcd for $C_{12}H_{42}N_6O_{15}Co$(or $C_{12}H_{43}N_6O_{15.5}Co$): C, 25.31(24.92); H, 7.43(7.49); N, 14.76(14.53)%. Since the number of molecules of the water of crystallization in these complex salts was not definite, the concentration of the stock solutions was determined spectrophotometrically by using the absorption band at 465 nm, the magnitude and the shape of which do not change on the addition of *d*-tart ion. Its molar extinction coefficients are listed in Table 1. Molar rotation at 589 nm was +620 and −380° for Λ- and Δ-form, respectively.[6] Their optical purity is thus satisfactory, taking the contribution from 3/2 *d*-tart ion (+126°) into consideration.

The starting materials Λ-$[Coen_3]Brd$-tart$\cdot 5H_2O$ and Δ-$[Coen_3]Br_3\cdot 2H_2O$ were prepared by the usual method,[7] their specific rotations being in good agreement with those given in the literature.[7] $[Coen_3](ClO_4)_3$ was prepared by the usual method[7] starting with $CoSO_4\cdot 7H_2O$ and $HClO_4$ in place of $CoCl_2\cdot 6H_2O$ and HCl, respectively. Found: C, 13.41; H, 4.53; N, 15.86%. Calcd for $C_6H_{24}O_{12}Cl_3Co$: C, 13.41; H, 4.50; N, 15.63%.

Ion-exchanged water was purified by distillation. Ethanol was refluxed over calcium oxide and then over magnesium ethoxide, and then fractionated. Mixed solvents were prepared by weight. KNa*d*-tartrate$\cdot 4H_2O$ of reagent grade was used without further purification.

Apparatus. A Shimadzu double beam spectrophotometer UV-200 with 1 cm quartz cells was used for the measurement of CT absorption spectra. Its cell compartment was kept at 25±0.2 °C with a Komatsu-Yamato Coolnics CTR-120.

Procedure. Sample solutions used for measurements were prepared with appropriate amounts of stock solutions of Λ- and Δ-$[Coen_3](d\text{-tart})_{3/2}$ (0.01 mol/l) and of KNa*d*-tart (0.05 mol/l). Reference solutions prepared from the stock solutions of $[Coen_3](ClO_4)_3$ (0.01 mol/l) had strictly the same total concentration of $[Coen_3]^{3+}$ ion as in the corresponding sample solutions so that the spectrophotometer could allow us to measure directly the absorption at 265 nm due to the ion-pair formation between Λ- or Δ-$[Coen_3]^{3+}$ and *d*-tart ions. The concentration of $[Coen_3]^{3+}$ ion was $(1.0—6.0)\times 10^{-3}$ mol/l and that of *d*-tart ion was $(1.0—1.2)\times 10^{-2}$ mol/l, giving the final ionic strength 0.033 taking the decrease by ion-pair formation into consideration. Since pH of the sample solutions was around 7, the formation of H*d*-tart$^-$ ion or H_2*d*-tart was negligible.

Solubility was measured at 25 °C by a conventional method in the mixed solvents with ethanol, the concentration of the saturated solutions being determined by spectrophotometry.

Results and Discussion

Let M^{3+} and A^{2-} denote $[Coen_3]^{3+}$ and *d*-$tart^{2-}$ ions, respectively. Then the outer-sphere association equilibrium is

$$M^{3+} + A^{2-} \rightleftarrows MA^{+}$$

if only the first step association is assumed. The outer-sphere association constant K_A is given by

$$K_A = [MA^+]/[M^{3+}][A^{2-}] = x/(C_M - x)(C_A - x) \quad (1)$$

where C_M and C_A refer to the total concentration of M^{3+} and A^{2-}, respectively, and x refers to the concentration of MA^+ at equilibrium. Since no other species than M^{3+} and M^+ present in solution contributes to the absorbance at the wavelength employed for the measurement (265 nm), the difference of the absorbance ΔD between a sample solution and its reference solution can be given by

$$\Delta D = x(\varepsilon_{MA} - \varepsilon_M) \quad (2)$$

if both sample and reference solutions have the same total concentration of M^{3+} and the cell length is 1 cm. ε denotes the molar extinction coefficient of the species indicated by the subscript. Combining Eqs. (1) and (2) we have

$$C_M(C_A - x)/\Delta D = (C_A - x)/(\varepsilon_{MA} - \varepsilon_M) + 1/K_A(\varepsilon_{MA} - \varepsilon_M) \quad (3)$$

which is valid at a constant ionic strength and constant temperature.

Firstly an appropriate value of K_A is assumed and x's obtained from Eq. (1) are substituted into Eq. (3). The plot of the quantity on the left-hand side of Eq. (3) *vs.* $(C_A - x)$ gives a refined association constant as (slope)/(intercept), which is again substituted into Eq. (1). The same procedures are continued until a constant K_A is attained. Calculation should be carried out with the data having the same final ionic strength I, which is given by

$$I = 3C_M + 3C_A - 6x.$$

Details of analysis have been given by Tanaka *et al.*[5]

Typical examples of the plot of ΔD *vs.* C_M are shown in Fig. 1, where for any value of C_M, the amount of A added to Λ-solution is equal to that to Δ-solution. Thus we see in Fig. 1 that ΔD of Λ-solution is larger than that of Δ-solution and that the addition of ethanol increases ΔD of both solutions but decreases the difference in ΔD between them. Figure 2 shows some of the final plots of Eq. (3) obtained along the line described above. The linearity in Fig. 2 supports the assumption that only the first step association occurs under these experimental conditions.

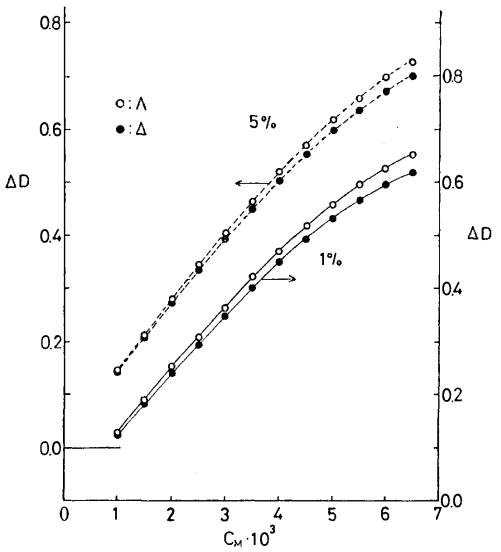

Fig. 1. Plot of ΔD *vs.* C_M.
5% (----) and 1% (——) solutions correspond to the left- and right-hand scales, respectively. Open and closed circles for Λ- and Δ-solutions, respectively.

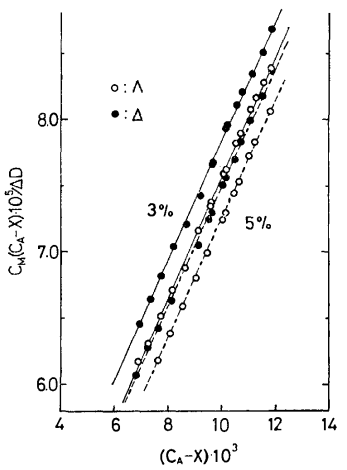

Fig. 2. Some final plots of Eq. (3).
3% (——), 5% (----). Open and closed circles for Λ- and Δ-solutions, respectively.

Derived parameters along with the values of ε_M (at 265 nm) are summarized in Table 1, where $K_{A(\Lambda)}$ and $K_{A(\Delta)}$ refer to the association constant of *d*-tart ion with Λ- and Δ-$[Coen_3]^{3+}$ ions, respectively, the final ionic strength being 0.033 in all cases. These para-

Table 1. Association constant at 25 °C (I=0.033)

	0 %	1 %	3 %	5 %	0 %
K_A (Λ)	131.7±3.2	139.8±3.6	156.9±3.1	170.9±3.5	
K_A (Δ)	118.9±4.3	125.6±4.4	143.7±2.6	159.3±3.7	
ε_{MA}-ε_M (Λ)	210.5±3.2	213.5±3.3	216.4±2.3	219.3±2.2	366[a], 350[b]
ε_{MA}-ε_M (Δ)	211.3±5.4	212.5±4.9	216.2±2.3	217.6±2.7	415[a], 390[b]
$K_{A(\Lambda)}/K_{A(\Delta)}$	1.11	1.11	1.09	1.07	1.30[c], 1.18[b]
ε_M (at 465 nm)	88.9	89.0	89.2	89.3	
ε_M (at 265 nm)	165	167	170	172	158[a], 165[b]

a) Ref. 1. b) Ref. 2. c) recalculated value. 1.24 is reported in Ref. 1.

Table 2. Association constant extrapolated to $I=0.1$ in water at 25 °C

a[a)]	$K_{A(\Lambda)}$		$K_{A(\Delta)}$		Theoretical	
	This work	Literature	This work	Literature	Fuoss	Bjerrum
5 Å	50.7±1.2	23.4±1.0[b)]	45.7±1.7	18.0±0.7[b)]	89	77
6 Å	55.8±1.4	26±2[c)]	50.4±1.8	22±2[c)]	44	56

a) $\log f_z=-AZ^2I^{1/2}/(1+BaI)$. b) Recalculated in Ref. 1. c) Ref. 2.

meters indicate that $K_{A(\Lambda)}$ is a little larger than $K_{A(\Delta)}$ and that the addition of a small amount of ethanol promotes ionic association. The promotion might be interpreted in terms of the decrease in the dielectric constant of the medium. It should be noted that $(\varepsilon_{MA}-\varepsilon_M)$ as well as ε_M increases with the increase of ethanol content, but the values for Λ-form are equal to those for Δ-form in every case investigated within experimental error. On the other hand, Ogino and Saito[1] obtained 366±15, 415±16, and 365±13[3] as the value of $(\varepsilon_{MA}-\varepsilon_M)$ for Λ-, Δ-, and racemic forms, respectively, in aqueous solutions at $I=0.1$ ($NaClO_4$).[2] ε_M (at 265 nm) we obtained in water differs somewhat from the value 158 reported by Ogino and Saito but agrees well with that by Nordén. Though the origins of the differences are not known, it is certain that the value of $(\varepsilon_{MA}-\varepsilon_M)$ for the racemate should lie between the corresponding values for Λ- and Δ-forms if they are different.

The ratio $K_{A(\Lambda)}/K_{A(\Delta)}$, a measure of the discrimination between Λ- and Δ-forms by *d*-tart ion in solution and defined to be a *discrimination factor*, is diminished on the addition of ethanol. Ogino and Saito,[1] and Nordén[2] reported 1.30 and 1.18, respectively, for the value of the factor in water, both of which are considerably larger than the value 1.11 we obtained. In order to compare our results with theirs in detail, our association constants in water were extrapolated to $I=0.1$ with the aid of the extended Debye-Hückel equation for activity coefficients with $a=5$ and 6 Å. The results are listed in Table 2 together with the values estimated by means of Fuoss[9] and Bjerrum[3] equations derived on the basis of pure electrostatics. We see that our association constant is about twice as large as theirs and that 6 Å[10] substituted as a into the theoretical equations reproduces our association constants satisfactorily. The interionic distance seems reasonable from molecular models though *d*-$tart^{2-}$ ion is not an ideal rigid-sphere with its charge uniformly distributed. Thus it may be concluded that the neglect of the association of $[Coen_3]^{3+}$ ion with ClO_4^- ion is responsible for the smaller K_A values obtained by Ogino and Saito, and Nordén and that outer-sphere association of *d*-tart ion with Λ- or Δ-$[Coen_3]^{3+}$ ion is described almost completely by pure electrostatic theories; the contribution from non-electrostatic interaction which is thought to discriminate Λ- from Δ-forms, is much smaller than that from the electrostatic one.

In order to explain the large discrimination factors obtained by Ogino and Saito, and Nordén, it is assumed that the electrostatic field of $[Coen_3]^{3+}$ ion is reduced by the ion-pair formation with ClO_4^- ion, and the electrostatic interaction between the complex ion and *d*-tart ion is weakened, *viz.*, non-electrostatic interaction is enhanced as compared with an electrostatic one when a large amount of $NaClO_4$ is added. Thus it follows that presence of some univalent anions such as ClO_4^- or Br^- ion in solution seems more effective in the discrimination between Λ- and Δ-forms by *d*-tart ion than the addition of alcohol which causes increase in the electrostatic interaction between Λ- or Δ-$[Coen_3]^{3+}$ and *d*-tart ions. In fact Br^- ion in crystalline Λ-$[Coen_3]$-Br*d*-tart·$5H_2O$ is attached closely to $[Coen_3]^{3+}$ ion from the direction of its three-fold axis and is considered to play an important role in the crystal formation.[11]

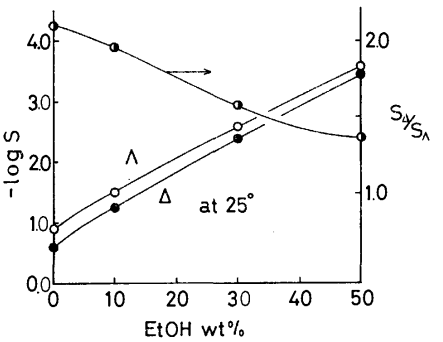

Fig. 3. Variation of solubilities of Λ- and Δ-$[Coen_3]$ (d-tart)$_{3/2}$ with the content of ethanol at 25 °C. Solubility ratio S_Δ/S_Λ (◑) corresponds to the right-hand scale. Open and closed circles for Λ- and Δ-forms, respectively.

The discrimination factor is very close to unity in solution and is therefore regarded at most as a part of the causes that precipitate only Λ-form as Λ-$[Coen_3]$-Br*d*-tart·$5H_2O$. In this connection, the effect of ethanol on the solubility of Λ- and Δ-$[Coen_3](d\text{-tart})_{3/2}$ was examined at 25 °C. The results are given in Fig. 3, where S denotes the concentration of the saturated solution in mol/l. The solubility difference between Λ- and Δ-forms decreases with the increase in ethanol content just like the discrimination factor in solution, but the solubility ratio S_Δ/S_Λ is considerably larger than the factor. Thus it might be concluded that the addition of alcohol is unfavourable to the discrimination of Λ- from Δ-forms by *d*-tart ion, since it only leads to increased electrostatic interaction between the complex and *d*-tart ions.

Reference and Notes

1) K. Ogino and U. Saito, This Bulletin, **40**, 826 (1967).
2) B. Nordén, *Acta Chem. Scand.*, **26**, 111 (1972).
3) R. A. Robinson and R. H. Stokes, "Electrolyte Solu-

tions", Butterworths, London (1959), p. 392. Bjerrum's critical distance amounts to 10.7 Å for 3–1 electrolytes in water at 25 °C.

4) S. Katayama and R. Tamamushi, This Bulletin, **41**, 606 (1968); H. Kaneko, N. Wada, and Y. Saito, Presented at the 28th Annual Meeting of the Chemical Society of Japan, Tokyo, 1973.

5) N. Tanaka, H. Kaneko, and T. Shirakashi, *Nippon Kagaku Zasshi*, **92**, 957 (1971).

6) These values are at $C=4\times10^{-3}$ mol/l. In more concentrated solutions, somewhat large deviation from additivity is observed. See also Ref. 2.

7) J. B. Work, "Inorganic Syntheses", Vol. II, McGraw-Hill, New York (1946), p. 221; J. A. Broomhead, F. P. Dwyer, and F. W. Hogarth, *ibid.*, Vol. VI (1960), p. 183.

8) These are recalculated values; in the original paper, 358 and 397 are listed as $(\varepsilon_{MA}-\varepsilon_{M})$ for Λ- and Δ-forms, respectively.

9) R. M. Fuoss, *J. Amer. Chem. Soc.*, **80**, 5059 (1958).

10) 5.8 Å is obtained from $K_{A(\Delta)}$ in water by using a more elaborate equation derived by H. Yokoyama, and H. Yamatera, *Chem. Lett.*, **1973**, 337.

11) H. Yoneda *et al.*, Proc. of the 29th Annual Meeting of the Chemical Society of Japan, Hiroshima, 1973, p. 1076.

Potentiometric and Spectrophotometric Studies of Fluoride Complexes of Uranium(IV)

Hidetake KAKIHANA and Shin-ichi ISHIGURO

Research Laboratory for Nuclear Reactors, Tokyo Institute of Technology, O-okayama, Meguro-ku, Tokyo 152

(Received December 25, 1973)

The stability constants and the molar extinction coefficients of uranium(IV) fluoride complexes were determined in aqueous solutions containing 1 M $(Na^+ + H^+)Cl^-$ as a constant ionic medium at 25 °C. The emf data obtained by the use of a fluoride-ion-selective electrode were explained in terms of the formation of a series of mononuclear complexes, UF^{3+}, UF_2^{2+}, UF_3^+, and UF_4, with stability constants $\beta_1=(2.2\pm0.13)\times10^7$, $\beta_2=(1.33\pm0.05)\times10^{13}$, $\beta_3=(2.9\pm0.5)\times10^{17}$, and $\beta_4=(6\pm1)\times10^{21}$ respectively. Using these values for β's the spectra observed in the 350—700 nm region were analyzed by means of a computer in order to estimate the molar extinction coefficients of each uranium(IV) fluoride complex species.

The visible and ultraviolet spectra of uranium(IV) have thus far been investigated in crystal, gases, and aqueous solutions. Conway[1] measured the absorption spectra of UF, dissolved in a matrix of CaF_2 and assigned all the absorption peaks to the transition caused by two 5f electrons. Pappalardo and Jørgensen[2] studied the absorption spectra of uranium(IV) in the octahedral coordination. Satten *et al.*[3] calculated the energy parameters of $5f^2$ electrons in crystals.

The absorption spectra of aquated uranium(IV) ions in $HClO_4$[4] and $DClO_4$[5] solutions were reported. Spectrophotometric studies of uranium(IV) fluoride complexes were carried out by Stein *et al.*[6] in 1 M $HClO_4$ and 1 M H_2SO_4 solutions over the range of 300—1300 nm. They prepared complex salts $UFSO_4$-$(HSO_4)\cdot2H_2O$, $UF_2SO_4\cdot2H_2O$, and $(UF_3)_2SO_4\cdot4H_2O$ and discussed the infrared spectra and X-ray powder patterns. Baran and Tympl[7] measured the absorption spectra of the hydroxo and carbonato complexes of uranium(IV).

In solutions, the absorption spectra usually change in band shape and in position with the change in ligand concentration, because several species can coexist in a solution and because the mole fraction of each species varies with the ligand concentration.

A potentiometric titration is one of the most accurate methods for studying chemical equilibria in solution. Recently-developed fluoride-ion-selective electrodes are very useful for studying fluoride complexes in solution. Uranium(IV) fluoride complexes were studied by means of the fluoride-ion-selective electrodes by Norén[8] in a 4 M $HClO_4$ solution and by Grenthe and Varfeldt[9] in a mixture of 3.4 M $NaClO_4$ and 0.6 M $HClO_4$ and the formations of UF^{3+}, UF_2^{2+}, and UF_3^+ complexes have been reported. The electronic spectra of these species, however, have not yet been measured.

In the present study, the stability constants of uranium(IV) fluoride complexes were determined in a 1 M $(Na^+ + H^+)Cl^-$ solution by potentiometry with a fluoride-ion-selective electrode, and on the basis of these constants the spectrophotometric data were analyzed by means of a computer in order to estimate the molar extinction coefficients of each uranium(IV) fluoride complex species.

Experimental

Reagents. The uranium(IV) chloride used was prepared by the following method. The uranium metal was dissolved in dilute hydrochloric acid and then treated with nitric acid. The uranyl nitrate thus prepared was recrystallized twice from water and then converted to ammonium diuranate by the addition of ammonia. The ammonium diuranate precipitates were washed with water, dried under an infrared lamp, and decomposed to triuranium octoxide, U_3O_8, by heating at 900 °C for about 6 hr. The test solutions were prepared by the electrolytic reduction of UO_2Cl_2 solutions which had been prepared by dissolving U_3O_8 in hydrochloric acid.

The other chemicals used were of a reagent grade. Sodium fluoride was once recrystallized from water and dried in an electric furnace at 120 °C for 16 hr.

Apparatus. The test solutions containing fluoride ions were stored in polyethylene bottles. A fluoride-ion-selective electrode (Orion 94-09) was used for the determination of the free-fluoride-ion concentration. A specific-ion meter (Orion model 404) was employed to measure the potential of the fluoride-ion-selective electrode against a saturated calomel electrode used as reference.

The visible spectra were measured by means of an MPS 50L (Shimadzu Seisakusho Co. Ltd.) double-beam spectrophotometer, using a quartz cell 1.00 cm thick.

Measurements. In the solution used, the electrode exhibited Nernst behavior throughout the region of the free-fluoride-ion concentration of $10^{-4}\geq[F^-]\geq10^{-6}$ M. The constant ionic medium was kept at 1 M with sodium chloride. A back-titration technique starting at a high fluoride-ion concentration was employed in the present experiment in order to avoid the formation of precipitates during the titration and the corrosion of burets. A solution containing C_U M uranium(IV) and C_F M fluoride ions was titrated with a solution containing C_U M uranium(IV) ions to keep the total concentration of uranium(IV) constant (C_U) throughout the titration. The concentration of uranium(IV) was gravimetrically determined in the form of U_3O_8. Uranium-(IV) was gradually oxidized to uranium(VI) even in a solution under an atmosphere of nitrogen. To avoid errors caused by oxidation, the test solution was prepared immediately before each titration.

The test solutions for spectrophotometric measurements were prepared under the same ionic medium conditions as in the emf measurements.

Results and Discussion

Potentiometric Measurements. Formation curves at different total concentrations of uranium(IV) are shown in Fig. 1. The experimental results are discribed in terms of n_{exp}, the average number of fluoride ions

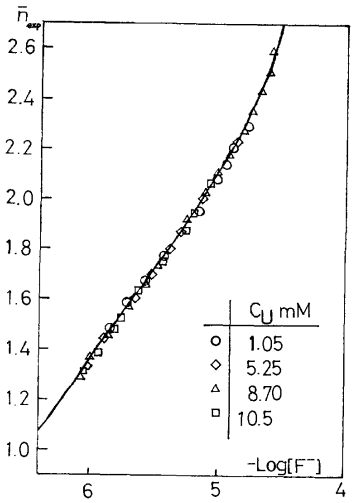

Fig. 1. Average number, $\bar{n}_{exp}$, of F⁻ bound per uranium(IV), as a function of $-\log [F^-]$. The curve was calculated using the constants obtained.

bound to the uranium(IV) ion, as a function of $-\log[F^-]$. Potentiometric measurements were carried out in the region where the fluoride-ion concentration was larger than 10^{-6} M, where the fluoride-ion-selective electrode exhibited Nernst behavior and a quick response to the change in the fluoride-ion concentration. Since the hydrogen fluoride complexes, HF and HF_2^-, are formed in an acidic solution ($[H^+] \gtrsim 0.1$ M),[10,11] $\bar{n}_{exp}$ was calculated by means of the equation:

$$\bar{n}_{exp} = (C_F - [F^-] - [HF] - 2[HF_2^-])/C_U = (C_F - f - K_{11}hf - 2K_{11}K_{12}hf^2)/C_U \quad (1)$$

where C_F, C_U, f, and h stands for the total fluoride, total uranium(IV), free-fluoride-ion, and free-hydrogen-ion concentrations respectively, and where K_{11} and K_{12} denote the step-by-step stability constants of these reactions:

$$H^+ + F^- = HF;\ K_{11} = [HF]/[H^+][F^-] \quad (2)$$

$$HF + F^- = HF_2^-;\ K_{12} = [HF_2^-]/[HF][F^-] \quad (2')$$

The values of K_{11} and K_{12} are given as 6.93×10^2 and 3.2 respectively.[10]

As is shown in Fig. 1, the formation curves are independent of the uranium(IV) concentration. This fact indicates the formation of a series of mononuclear complexes. The approximate values of the stability constants of the complexes were estimated by the graphical method as has been described by Rossotti and Rossotti.[12] The formation function:

$$\bar{n}_{exp} = \sum n\beta_n f^n / (1 + \sum \beta_n f^n) \quad (3)$$

can be rearranged as follows:

$$\sum_{i=0}^{n-1} \left(\frac{\bar{n} - i}{n - \bar{n}} \right) \beta_i f^{i-n} = \beta_n + \sum_{i=n+1}^{N} \left(\frac{i - \bar{n}}{n - \bar{n}} \right) \beta_i f^{i-n} \quad (4)$$

where β_n denotes the cumulative stability constant of this reaction:

$$U^{4+} + nF^- = UF_n^{4-n};\ \beta_n = [UF_n^{4-n}]/[U^{4+}][F^-]^n \quad (5)$$

The initial part of the plot of $\sum_{i=0}^{n-1} (\bar{n} - i)\beta_i f^{i-n}/(n - \bar{n})$ against $(i - \bar{n})f/(n + 1 - \bar{n})$ gives a straight line with an intercept of β_n and a slope of β_{n+1}. The procedure is continued until the plot of $\sum_{i=0}^{n-1} (\bar{n} - i)\beta_i f^{i-n}/(n - \bar{n})$ against $(i - \bar{n})f/(n + 1 - \bar{n})$ becomes horizontal. In our case, the procedure could be carried out until $n=4$, the plot was so spread that the formation of UF_5^- was not conclusive.

If we assume the formation of four complexes, UF^{3+}, UF_2^{2+}, UF_3^+, and UF_4, the mole balances for uranium(IV), fluoride, and hydrogen ions can be expressed by the following equations:

$$C_U = [U^{4+}] + [UF^{3+}] + [UF_2^{2+}] + [UF_3^+] + [UF_4] = u(1 + \sum_{n=1}^{4} \beta_n f^n) \quad (6)$$

$$C_F = [F^-] + [HF] + 2[HF_2^-] + [UF^{3+}] + 2[UF_2^{3+}] + 3[UF_3^+] + 4[UF_4] = f + K_{11}hf + 2K_{11}K_{12}hf^2 + u\sum_{n=1}^{4} n\beta_n f^n \quad (7)$$

$$C_H = [H^+] + [HF] + [HF_2^-] = h + K_{11}hf + K_{11}K_{12}hf^2 \quad (8)$$

where u represents the free-uranium(IV)-ion concentration. n_{calcd} is given by the following equation:

$$\bar{n}_{calcd} = \sum_{n=1}^{4} n\beta_n f^n / (1 + \sum_{n=1}^{4} \beta_n f^n) \quad (9)$$

Finally, the error-square sum, $U = \sum (1 - \bar{n}_{exp}/\bar{n}_{calcd})^2$ was minimized in order to obtain a set of the best-fit values of the stability constants by the least-squares method with the help of an electronic computer (HITAC 8500 and 8700). The formation curve was calculated using the four stability constants thus obtained. The calculated formation curve well explains the experimental points, as Fig. 1 shows. If only three complexes, UF^{3+}, UF_2^{2+}, and UF_3^+, were taken into consideration, the formation curve deviated from the experimental points at high $\bar{n}$ values ($\bar{n} \geq 2.2$). Since the calculation on the assumption of the formation of the UF_5^- complex in addition to the other four did not reduce the error-square sum remarkably, it may be concluded that there is very little mole fraction of the UF_5^- complex, if any, in this system. The final values of the stability constants obtained for the four uranium(IV) fluoride complexes, UF^{3+}, UF_2^{2+}, UF_3^+, and UF_4, are $\beta_1 = (2.2 \pm 0.13) \times 10^7$, $\beta_2 = (1.33 \pm 0.05) \times 10^{13}$, $\beta_3 = (2.9 \pm 0.5) \times 10^{17}$, and $\beta_4 = (6 \pm 1) \times 10^{21}$ respectively. They are listed in Table 1, together with the values reported in Ref. 8 and 9 and those obtained by solubility measurements by Savage and Browne.[13] As for β_2 and β_3, our results agreed well with Ref. 8, while for β_4 they agreed fairly well with Ref. 13. In Fig. 2, we show the distribution of the species of uranium(IV) fluoride complexes.

Mesmer and Baes[14] have studied a general correlation for the step-by-step stability constants of the fluoride complexes of a large number of metal ions and reported that the $\Delta \log K_n$ values can be well represented by:

$$\Delta \log K_n = -\alpha \Delta n \quad (10)$$

where K_n is the step-by-step stability constant ($=\beta_n/\beta_{n-1}$) and where n is the number of fluoride ions in the complex formed. They have concluded that the best-fitting value for α is 1.1. The $\Delta \log K_n$ values for uranium(IV) are plotted against n, together with those for other metals such as uranium(VI),[10] thorium(IV),[8,16,17] hafnium(IV),[18] and beryllium(II).[14] The

TABLE 1. THE STABILITY CONSTANTS OF URANIUM(IV) FLUORIDE COMPLEXES

Reference	Medium	Temp.	β_1^*	β_2^*	β_3^*	β_4^*
This work	1 M $(Na^+ + H^+)Cl^-$	25 °C	$(3.1\pm0.3)\times10^4$	$(2.8\pm0.1)\times10^7$	$(9\pm1)\times10^8$	$(1.3\pm0.5)\times10^{10}$
Ref. 8	4 M $HClO_4$	20 °C	$(8.8\pm0.2)\times10^4$	$(3.3\pm0.2)\times10^7$	$(8\pm1)\times10^8$	—
Ref. 9	3.4 M $NaClO_4$ + 0.6 M $HClO_4$	25 °C	$(2.34\pm0.06)\times10^5$	$(1.94\pm0.04)\times10^8$	$(2.8\pm0.2)\times10^9$	—
Ref. 13	0.12 M $HClO_4$	25 °C	—	—	2.5×10^{10}	2.8×10^{10}

Uncertainties of the stability constants were estimated as 3σ where σ denotes the standared deviation. The results are described in terms of β_p^*, $\beta_p^*=\beta_p/K_{11}^p$, for comparison with other data. β_p^* is the over-all stability constants of the following reaction,

$$U^{4+}+pHF=UF_p^{4-p}+pH^+;\ \beta_p^*=[UF_p^{4-p}][H^+]^p/[U^{4+}][HF]^p$$

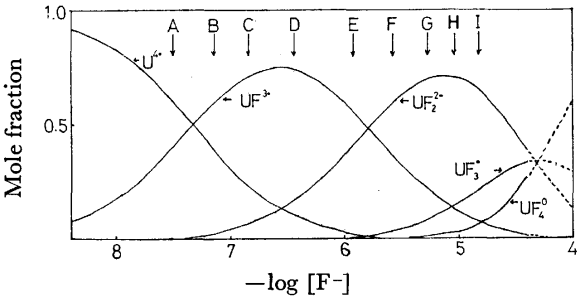

Fig. 2. The distribution of species of uranium(IV) fluoride complexes calculated using the stability constants obtained. Arrows (A-I) indicate compositions of species and free fluoride ion concentrations used for spectrophotometric measurements.

same α value of 1.1 is obtained for uranium(VI) and beryllium(II) fluoride complexes. A little larger value of 1.5 is found for the uranium(IV) and thorium(IV) fluoride complexes, with the exception of UF_4, the step-by-step stability constant of UF_4 being larger than would be expected from Eq. (10) on the assumption that $\alpha=1.5$. The plots for thorium(IV) fluoride complexes in different ionic media give the same slope.

Spectrophotometric Measurements. Without the fluoride ion, the spectra of the aquated uranium(IV) ion

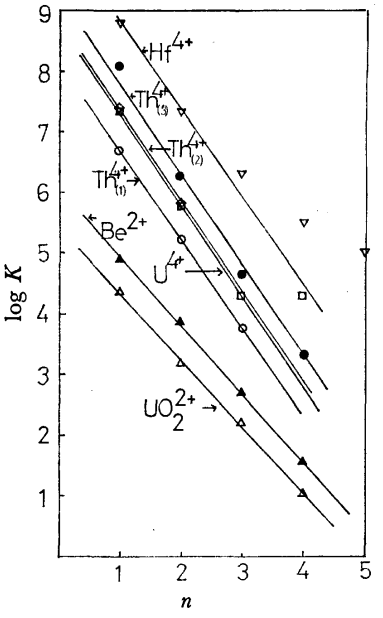

Fig. 3. The correlation of stepwise formation constants with n, the number of fluoride ion in the complex.

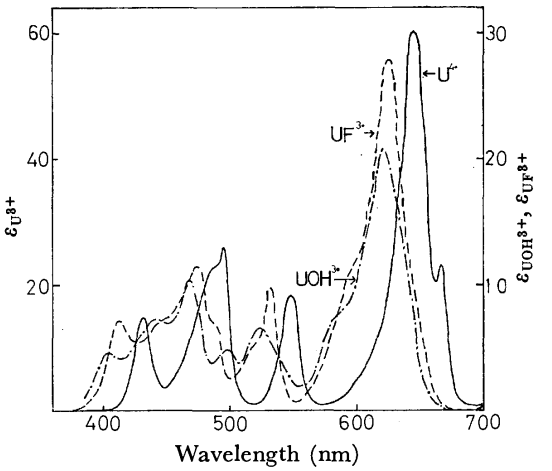

Fig. 4. The spectra of the aquated U^{4+} and UOH^{3+} ions and the calculated spectrum of UF^{3+}.

were measured in a 1 M HCl solution with various uranium(IV) concentrations in the 350—700 nm region, where the formation of chloro complexes of uranium(IV) is negligible.[15] The molar extinction coefficients of the aquated uranium(IV) ion in this region are shown in Fig. 4, together with those of UOH^{3+} as measured by Baran and Tympl.[7] The spectra of the uranium(IV) fluoride complexes were measured in the same ionic media as those used for the potentiometric titrations. The 9 fluoride-ion concentrations at which the spectra have been measured are marked with arrows (A-I) in Fig. 2.

Since four mononuclear complexes of uranium(IV) fluoride were found by the potentiometric measurements, the total absorbance, A, in solution can be expressed as follows:

$$\begin{aligned} A &= \varepsilon_0[U^{4+}] + \varepsilon_1[UF^{3+}] + \varepsilon_2[UF_2^{2+}] \\ &\quad + \varepsilon_3[UF_3^{+}] + \varepsilon_4[UF_4] \\ &= u\sum_{n=0}^{4}\varepsilon_n\beta_n f^n \end{aligned} \qquad (11)$$

where ε_n denotes the molar extinction coefficient of the relevant species and where β_0 is unity. Nine sets of data obtained by spectrophotometric measurements were used for the estimation of the molar extinction coefficients of the uranium(IV) fluoride complexes. The value of ε_0 at a given wavelength was adopted from the results in Fig. 4 (the spectrum of U^{4+}). In order to avoid errors in the calculation at a given uranium(IV) concentration, the total absorbance of the solution at the absorption maximum (600—650 nm)

was kept approximately constant (about 0.8) by varying the uranium(IV) concentration from 0.023 to 0.047 M. The values of ε's of the complexes can be calculated by solving Eqs. (6), (7), (8), and (11) at any point in the 350—700 nm region. The most suitable values of ε's were obtained by minimizing the error-square sum, $U=\Sigma(A_{calcd}-A_{exp})^2$, at given wavelength. The calculated molar extinction coefficients of the UF^{3+} complex are graphically shown in Fig. 4, while those of UF_2^{2+} and UF_3^+ are shown in Fig. 5. Using these values for ε_n, the total absorbance was calculated and compared with the observed absorbance. Some typical results of the comparison are shown in Fig. 6. This good agreement between the observed and calculated spectra may support the above-mentioned analysis and may make it possible to discuss ε_n a little further.

The spectrum of UOH^{3+}, as measured by differential spectroscopy by Baran and Tympl,[7] is depicted for comparison in Fig. 4. It may be seen from Fig. 4

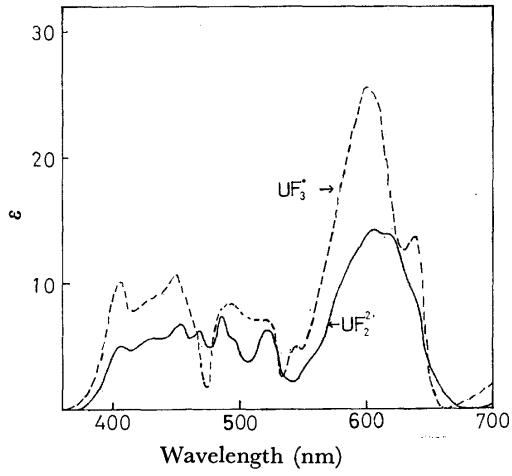

Fig. 5. The calculated spectra of UF_2^{2+} and UF_3^+.

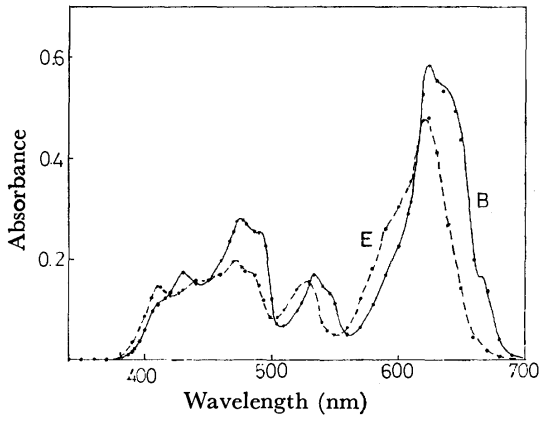

Fig. 6. Typical absorption spectra of uranium(IV) fluoride complexes. The calculated total absorbances are represented by dots. Solid and broken lines show measured absorption spectra of solutions with the following compositions of species.
(B) U^{4+}: 38.7%, UF^{3+}: 58.8%, UF_2^{3+}: 2.5% (indicated by arrow B in Fig. 2)
(E) U_4^+: 2%. UF^{3+}: 54.8%, UF_2^{2+}: 42%, UF_3^+: 1.2% (arrow E)

that, as a rule, the absorption peaks of the aquated U^{4+} ion shift to a wavelength shorter by 20—25 nm when a water molecule in the aquated U^{4+} ion is replaced with F^- or OH^- ions. Furthermore, the spectrum of UOH^{3+} has small absorption peaks at about 430 and 500 nm and a shoulder at 580 nm, while the spectrum of UF^{3+} has shoulders at about 430, 490, 520, and 595 nm. These small absorption peaks and shoulders of UOH^{3+} and UF^{3+} do not correspond to any peaks of the aquated U^{4+}. They may be supposed to be caused by changes in the ligand-field symmetry of UOH^{3+} and UF^{3+}. The hydroxyl ion may have a larger effect on the splitting of the degenerated states of $5f^2$ electrons in uranium(IV) than does the fluoride ion.

As for the spectrum of UF_2^{2+}, the peaks shift by about 10 nm to a wavelength shorter than those of UF^{3+}, and several additional peaks appear in the 400—500 nm region. The large absorption band at about 610 nm becomes weaker in intensity (about half of that of UF^{3+}) and broader in width.

Since the mole fraction of UF_3^+ is, at most, 35%, much less than those of UF^{3+} (75%) and UF_2^{2+} (70%), the calculated spectrum of UF_3^+ is uncertain compared with those of UF^{3+} and UF_2^{2+}. The absorption peaks of UF_3^+ also seem to shift to a shorter wavelength, but become stronger in intensity than those of UF_2^{2+}, even if uncertainities in calculation are considered.

The authors wish to thank Professor Hitoshi Ohtaki for his helpful advice and also Dr. Isao Okada for his discussions of the manuscript.

References

1) J. G. Conway, *J. Chem. Phys.*, **31**, 1002 (1959).
2) R. Pappalardo and K. Jørgensen, *Helv. Phys. Acta*, **37**, 79 (1964).
3) R. A. Satten, C. L. Schreiber, and E. Y. Wong, *J. Chem. Phys.*, **42**, 162 (1965).
4) D. Brown and R. G. Wilkins, *J. Chem. Soc.*, **1961**, 3804.
5) D. Cohen and W. T. Carnall, *J. Phys. Chem.*, **64**, 1933 (1960).
6) L. Stein, C. W. Williams, I. M. Fox, and E. Gebert, *Inorg. Chem.*, **5**, 662 (1963).
7) V. Baran and M. Tympl, *Collect. Czech. Chem. Comm.*, **34**, 756 (1969).
8) B. Norén, *Acta Chem. Scand.*, **23**, 931 (1969).
9) I. Grenthe and J. Varfeldt, *ibid.*, **23**, 988 (1969).
10) H. Kakihana, C-F. Kao, and S. Ishiguro, to be published.
11) L. Ciavatta, *Aekiv För Kemi.*, **21**, 129 (1963).
12) F. J. C. Rossotti and H. Rossotti, *Acta Chem. Scand.*, **9**, 1166 (1956).
13) A. W. Savage and J. C. Browne, *J. Amer. Chem. Soc.*, **82**, 4817 (1960).
14) K. A. Kraus and F. J. Nelson, *ibid.*, **72**, 3901 (1950).
15) R. E. Mesmer and C. F. Baes, *Inorg. Chem.*, **8**, 618 (1969).
16) E. W. Baumann, *J. Inorg. Nucl. Chem.*, **32**, 3823 (1970).
17) P. Klots, A. Mukherji, S. Feldberg, and L. Newman, *Inorg. Chem.*, **10**, 740 (1971).
18) B. Norén, *Acta Chem. Scand.*, **21**, 2457 (1967).

Binuclear Metal Complexes. IX.[1] Syntheses and Magnetic Properties of Copper(II) and Nickel(II) Complexes of Schiff Bases Derived from 3-Formylsalicylic Acid and Alkyl Amines

Mitsunori TANAKA, Hisashi OKAWA,* Tomoko TAMURA, and Sigeo KIDA*

Faculty of Education, Kagawa University, Takamatsu, Kagawa 760

**Department of Chemistry, Faculty of Science, Kyushu University, Hakozaki, Higashi-ku, Fukuoka 812*

(Received April 1, 1974)

Copper(II) and nickel(II) complexes of H_2fsac-R have been synthesized, where H_2fsac-R denotes the Schiff bases prepared from 3-formylsalicylic acid and alkylamines (alkyl(R)=methyl, ethyl, hydroxyethyl, *n*-propyl, *n*-butyl, isobutyl, and *sec*-butyl). On the bases of elemental analyses, IR spectra, visible spectra and cryomagnetic measurements, it was found that the complexes have a binuclear structure connected by two phenolic oxygens; the complexes are abbreviated to M_2(fsac-R)$_2$. The nickel(II) complexes contain two, three or four molecules of coordinated water. The cryomagnetic data for Cu_2(fsac-R)$_2$ are interpreted in terms of the Bleaney-Bowers equation with large $-2J$ values (>700 cm^{-1}), indicating the presence of strong intramolecular antiferromagnetic spin-exchange interactions. The Ni_2(fsac-R)$_2\cdot nH_2O$ obey the Curie-Weiss law, the Weiss constants being estimated to -35——41 K.

In the previous paper of this series,[2] it was shown that 3-formylsalicylic acid forms binuclear copper(II) and nickel(II) complexes bridged by the phenolic oxygens. This report relates to the syntheses and characterization of the copper(II) and nickel(II) complexes of the Schiff bases derived from 3-formylsalicylic acid and alkylamines (R–NH_2). The Schiff bases are abbreviated to H_2fsac-R, in which R is methyl, ethyl, hydroxyethyl, *n*-propyl, *n*-butyl, isobutyl, or *sec*-butyl. Based on elemental analyses, IR spectra, visible spectra, and cryomagnetic data, the complexes seem to possess the binuclear structure shown in Fig. 1. The complexes are denoted by M_2(fsac-R)$_2$.

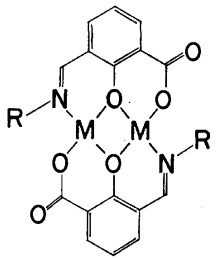

R=alkyl
M=Cu(II), Ni(II)

Fig. 1.

The copper(II) complexes are similar in structure to dihalogenobis(N-alkylsalicylaldimino)dicopper(II) complexes,[3-7] whose magnetic properties have been well elucidated. The exchange integrals of Cu_2(fsac-R)$_2$ were discussed in comparison with those of the above complexes.

Experimental

Syntheses. 3-Formylsalicylic acid was prepared after the method of Duff and Bills.[8] The synthetic methods of the complexes are nearly the same. A typical procedure is as follows. To an aqueous solution (30 ml) of sodium carbonate (106 mg) containing 3-formylsalicylic acid (154 mg) and ethylamine (70% aqueous solution, 75 mg), was added an aqueous solution (30 ml) of copper(II) acetate monohydrate (200 mg). The mixture was heated at 60 °C on a water-bath for a while to give blue prisms, which were collected and thoroughly washed with hot water. The nickel(II) complexes were obtained as yellowish green prisms using nickel(II) acetate tetrahydrate as a metal source. The analytical data are given in Table 1.

Table 1. Elemental analyses of complexes

	Found (%)			Calcd (%)		
	C	H	N	C	H	N
Cu_2(fsac-Me)$_2$	44.56	2.93	5.45	44.91	2.93	5.82
Cu_2(fsac-Et)$_2\cdot 1/2H_2O$	46.23	3.38	4.93	46.33	3.69	5.40
Cu_2(fsac-enOH)$_2$	44.03	3.34	5.04	44.37	3.35	5.17
Cu_2(fsac-Pr)$_2\cdot H_2O$	47.96	4.02	4.56	47.57	4.35	5.04
Cu_2(fsac-*n*-Bt)$_2\cdot 1/2H_2O$	49.82	4.70	4.71	50.17	4.74	4.88
Cu_2(fsac-*i*-Bt)$_2\cdot 1/2H_2O$	49.85	4.48	4.51	50.17	4.74	4.88
Cu_2(fsac-*s*-Bt)$_2\cdot 1/2H_2O$	50.26	4.58	4.77	50.17	4.74	4.88
Ni_2(fasc-Me)$_2\cdot 2H_2O$	41.25	3.59	4.80	41.12	3.83	5.33
Ni_2(fsac-Et)$_2\cdot 3H_2O$	43.03	4.12	4.55	43.37	4.37	5.06
Ni_2(fsac-enOH)$_2\cdot 2H_2O$	41.44	3.78	4.54	41.65	3.84	4.86
Ni_2(fsac-*n*-Bt)$_2\cdot 4H_2O$	46.28	5.10	4.15	45.91	5.45	4.46

Measurements. Magnetic susceptibilities of the complexes were measured by the Faraday method from liquid nitrogen temperature to room temperature. The Pascal constants[9] were used for diamagnetic correction. The effective magnetic moments were determined by the equation, $\mu_{eff}=2.828\sqrt{(\chi_A-N\alpha)T}$, where the temperature-independent paramagnetism for nickel(II) ion is estimated at 193×10^{-6} e.s.u./mol.[10] The infrared spectra were measured with a Hitachi 215 grating infrared spectrophotometer in the region 4000—650 cm^{-1}. In some cases the hexachlorobutadiene-mull method was applied for the measurements in the region 4000—2000 cm^{-1}. Electronic spectra on solids and in pyridine solutions were obtained with a Hitachi EPS-3T spectrophotometer.

Results and Discussion

Copper(II) Complexes. Some IR bands, ligand field bands (powder and pyridine solution) and effective magnetic moments at room temperature are given in Table 2. The IR bands near 1640 and 1545 cm^{-1} were tentatively assigned to the azomethine and the

Table 2. Properties of $Cu_2(fsac\text{-}R)_2$ complexes

	IR (cm^{-1})		d-d (kK)		μ_{eff} (K) (B.M.)
	C=N	COO^-	solid	py (ε)	
$Cu_2(fsac\text{-}Me)_2$	1645	1550	15.3	15.1 (124)	0.68 (297.7)
$Cu_2(fsac\text{-}Et)_2$	1640	1545	14.9	14.8 (118)	0.66 (291.6)
$Cu_2(fsac\text{-}enOH)_2$	1635	1540	15.4	15.1 (128)	0.54 (297.7)
$Cu_2(fsac\text{-}Pr)_2$	1635	1540	14.7	14.4 (114)	0.66 (294.2)
$Cu_2(fsac\text{-}n\text{-}Bt)_2$	1635	1545	14.8	14.6 (101)	0.71 (296.6)
$Cu_2(fsac\text{-}i\text{-}Bt)_2$	1630	1550	14.8	14.6 (119)	0.63 (294.1)
$Cu_2(fsac\text{-}s\text{-}Bt)_2$	1635	1545	14.7	14.4 (101)	0.63 (295.4)

carboxylate groups respectively. The skeletal vibration near 1550 cm^{-1} is useful to distinguish the binuclear structure bridged by phenolic oxygen.[3,11] In the present complexes, however, this band could not be well recognized owing to the strong absorption of the carboxylate group. The reflectance spectra of the complexes show a d-d band in the region 15.4—14.9 kK, that is higher in energy than that (14.1 kK) for bis(3-formylsalicylato)dicopper(II)[2] (which is a $[CuO_4]$-chromophore). The spectral data are consistent with the binuclear structure of the $[CuO_3N]$-chromophore (Fig. 1), since most $[CuO_2N_2]$-chromophores containing bridging oxygen atoms exhibit a ligand field band in the region 15.4—18.5 kK.[12-15] The effective magnetic moments at room temperature are much lower than the spin-only value. From all of these facts, it is concluded that the complexes possess a binuclear structure given in Fig. 1. The oxygen of the hydroxyethyl substituent in $Cu_2(fsac\text{-}enOH)_2$ does not seem to coordinate to the copper(II) ion, since the O–H stretching vibration is found around 3400 cm^{-1}. This fact is in line with Tokii *et al.*'s finding[7] that dichlorobis(*N*-hydroxyethylsalicylaldimino)dicopper(II) has a binuclear structure as shown in Fig. 2 and the hydroxy group in the *N*-substituent is not concerned with coordination.

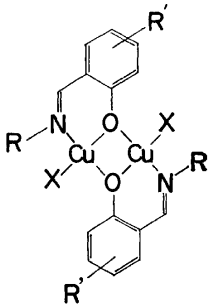

R=alkyl, aryl
R'=alkyl
X=Cl, Br

Fig. 2.

The ligand field band determined from pyridine solution spectrum of each complex is located to lower energy region than that from the corresponding powder spectrum. Since the shifts, however, are small (0.1—0.3 kK) and no splitting is found in each spectrum, the complexes seem to keep binuclear structure in pyridine, in which no coordination of pyridine to the metal is supposed. When the pyridine solution was concentrated, the pyridine-free complexes were recovered.

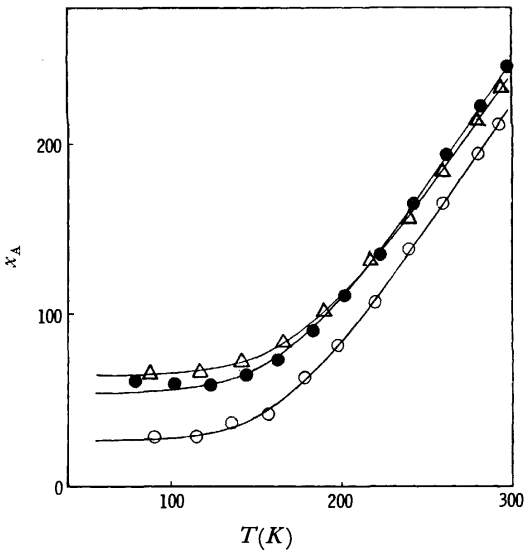

Fig. 3. Variation of molar susceptibility of $Cu_2(fsac\text{—}R)_2$ complexes; (●) R=Me, (○) R=Et, and (△) R=Pr.

The magnetic susceptibilities of the complexes were measured at various temperatures. The results were well interpreted on the basis of the Bleaney-Bowers equation,[16]

$$\chi_A = \frac{Ng^2\beta^2}{3kT}\left[1+\frac{1}{3}\exp(-2J/kT)\right]^{-1} + N\alpha,$$

where J is the exchange integral, k the Boltzmann constant, N the Avogadro number, β the Bohr magneton and g the Lange g-factor. The typical examples are shown in Fig. 3. The magnetic parameters, $-2J$, g and $N\alpha$, determined from the best fit of the data to the Bleaney-Bowers equation are given in Table 3. Judging from the $-2J$ values (which are energy separation between the singlet and triplet states) of the complexes presented here, it does not seem that the substituents attached to the imino-nitrogen exert any appreciable effect upon the spin-exchange interaction.

Table 3. Magnetic parameters of $Cu_2(fsac\text{-}R)_2$ complexes

	$-2J$ (cm^{-1})	g	$N\alpha\times10^6$ (e.s.u./mol)
$Cu_2(fsac\text{-}Me)_2$	720	2.20	55
$Cu_2(fsac\text{-}Et)_2$	715	2.20	27
$Cu_2(fsac\text{-}enOH)_2$	820	2.20	37
$Cu_2(fsac\text{-}Pr)_2$	725	2.20	55
$Cu_2(fsac\text{-}n\text{-}Bt)_2$	705	2.20	35
$Cu_2(fsac\text{-}i\text{-}Bt)_2$	735	2.17	65
$Cu_2(fsac\text{-}s\text{-}Bt)_2$	750	2.20	50

The magnetic properties of dihalogenobis(*N*-alkylsalicylaldimino(dicopper(II) complexes, which are similar to the present complexes, were explored by Kato *et al.*[6,7] and Harris *et al.*[3-5] The $-2J$ values of these complexes are in the range 194—580 cm^{-1}, depending upon the substituents attached to the aromatic ring and the

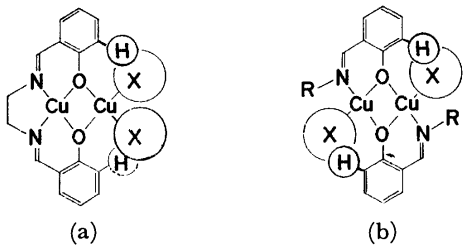

(a) (b)

Fig. 4.

imino-nitrogen. Therefore, it is evident that our complexes exhibit a very strong antiferromagnetic spin-exchange interaction compared to the dihalogenobis-(*N*-alkylsalicylaldimino)dicopper(II) complexes.

The difference in magnetic properties between the present complexes and dihalogenobis(*N*-alkylsalicylaldimino)dicopper(II) complexes can be explained in terms of the geometries of the complexes. It was demonstrated from X-ray investigation[17] that the coplanarity of two tetragonal planes of the copper(II) ion in dichloro [*N*, *N'*-ethylenebis (salicylaldimino) copper (II)]-copper(II) is considerably distorted owing to the steric repulsions between the chloro group and the hydrogen attached to the 3-position of the salicylaldehyde moiety (Fig. 4a). From the same steric requirement (Fig. 4b), it is also expected that the $\overset{X}{N}\!>\!Cu\!<\!\overset{O}{O}\!>\!Cu\!<\!\overset{N}{X}$ plane in dihalogenobis(*N*-alkylsalicylaldimino)dicopper(II) complexes is distorted. In fact Sinn *et al.*[18] have recently studied the structures of dichlorobis(*N*-methylsalicylaldimino) dicopper (II), dichlorobis (*N*-ethylsalicylaldimino)dicopper(II) and dibromobis(*N*-ethylsalicylaldimino)dicopper(II) and found that the dihedral angles between the planes formed by Cu_2O_2 and $Cu_2N_2Cl_2$ are appreciably large (39.3° for R=methyl and X=chloro, 33.1° for R=ethyl and X=chloro, and 35.7° for R=ethyl and X=bromo). On the other hand, such a steric hindrance is not anticipated for the present complexes, since the carboxyl group attached to 3-position is involved in coordination to the copper(II) ion. Accordingly our complexes seem to have a nearly coplanar structure in regard to the $\overset{N}{O}\!>\!Cu\!<\!\overset{O}{O}\!>\!Cu\!<\!\overset{O}{N}$ plane. In this case the overlapping of $d_\pi(Cu)$-$p_\pi(O)$-$d_\pi(Cu)$ orbitals is sufficiently large, thereby strengthening the spin-exchange interaction. An importance of π-superexchange pathway in spin-exchange interaction for binuclear copper(II) complexes has been reported.[13,19] The present result is in line with the previous findings[20-22] that the more coplanar the tetragonal planes of the copper(II) ions is, the larger the magnetic exchange interaction between the copper-(II) ions becomes.

Nickel(II) Complexes. The nickel(II) complexes forms yellowish green prisms containing two, three or four water molecules. Some IR bands, d-d bands (powder and pyridine solution) and effective magnetic moments at room temperature and near liquid nitrogen temperature are given in Table 4. The IR bands near 1635 and 1565 cm^{-1} may be attributed to the azomethine and the carboxylate groups respectively. The broad band around 3300 cm^{-1} is assigned to the O–H vibration of coordinated water. The reflectance spectra of the complexes show two bands in visible region: 8.7—8.9 and 15.4—15.7 kK. This fact clearly indicates that the nickel(II) ion has a nearly octahedral geometry, although the complexes have only two or three molecules of water except Ni_2(fsac-*n*-Bt)$_2$·$4H_2O$. The solution spectrum of each complex in pyridine shows the first d-d band (which corresponds to 10 Dq) in the region 9.5—9.6 kK, which is higher by 0.7—0.9 kK than that from the corresponding powder spectrum. This fact implies that in pyridine solution the complexes are coordinated with solvents in apical positions.

The magnetic moments at room temperature are comparable to the values for common octahedral nickel-(II) complexes. On the other hand, the values near liquid nitrogen temperature are lower than the spin-only value, 2.83 B.M. These facts imply an antiferromagnetic spin-exchange interaction between nickel-

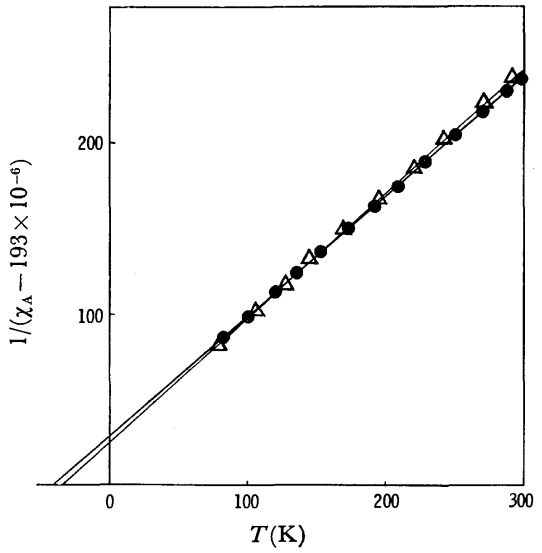

Fig. 5. Plots of inverse susceptibilities of (●) Ni_2(fsac—Et)$_2$·$3H_2O$ and (△) Ni_2(fsac–enOH)$_2$·$2H_2O$ per a nickel atom as a function of temperature.

Table 4. Properties of Ni_2(fsac-R)$_2$·nH_2O complexes

	IR (cm^{-1})			d-d (kK)				μ_{eff} (K) (B.M.)	
				powder		py (ε)			
	O–H	C=N	COO^-						
Ni_2(fsac-Me)$_2$·$2H_2O$	3300	1640	1560	8.8	15.4	9.6(42)	15.9(38)	3.14(197.8)	2.76(87.0)
Ni_2(fsac-Et)$_2$·$3H_2O$	3300	1640	1560	8.7	15.7	9.5(35)	15.7(33)	3.10(293.0)	2.64(77.5)
Ni_2(fsac-enOH)$_2$·$2H_2O$	3300	1630	1570	8.7	15.6	9.6(37)	16.0(35)	3.06(291.7)	2.74(83.5)
Ni_2(fsac-*n*-Bt)$_2$·$4H_2O$	3300	1635	1570	8.9	15.5	9.6(42)	16.1(40)	3.17(296.6)	2.72(87.1)

(II) ions. To elucidate the magnetic behaviors of the complexes, the magnetic susceptibilities were measured as a function of temperature. The results were well interpreted on the basis of the Curie-Weiss law, $\chi_A = C/(T-\theta)$. The representatives of the $1/(\chi_A - 193 \times 10^{-6})$ *versus* T plots are shown in Fig. 5. The Weiss constants obtained are −35 K for R=methyl, −41 K for R=ethyl, −35 K for R=hydroxyethyl, and −40 K for R=*n*-butyl.

There are a few binuclear nickel(II) complexes, in which two nickel(II) ions are connected by the phenolic oxygens.[2,23,24] These complexes show demagnetization by the spin-coupling *via* the phenolic oxygen bridges; the Weiss constants are estimated at −50—−125 °C. In general, the Weiss constants of the mononuclear nickel(II) complexes are small, say a few degrees at best. Therefore, judging from the magnitude of the Weiss constants it may be concluded that the demagnetization in $Ni_2(fsac\text{-}R)_2 \cdot nH_2O$ is caused by the intramolecular spin-exchange interaction through the oxygen bridges.

The authors are grateful to the Ministry of Education for a Scientific Research Grant-in-aid.

References

1) Part VIII: Ref. 2.
2) M. Tanaka, H. Okawa, I. Hanaoka, and S. Kida, *Chem. Lett.*, **1974**, 71.
3) C. M. Harris and E. Sinn, *J. Inorg. Nucl. Chem.*, **30**, 2723 (1968).
4) C. M. Harris, J. M. James, P. J. Milham, and E. Sinn, *Inorg. Chim. Acta*, **3**, 81 (1969).
5) R. B. Coles, C. M. Harris, and E. Sinn, *Inorg. Chem.*, **8**, 2607 (1969).
6) M. Kato, K. Imai, Y. Muto, and T. Tokii, *J. Inorg. Nucl. Chem.*, **35**, 109 (1973).
7) T. Tokii, Y. Muto, M. Kato, K. Imai, and H. B. Jonassen, *ibid.*, **34**, 3377 (1972).
8) J. C. Duff and E. J. Bills, *J. Chem. Soc.*, **1932**, 1987.
9) P. W. Selwood, "Magnetochemistry," pp. 78, 91, Interscience, New York (1956).
10) C. J. Ballhausen, "Introduction to Ligand Field Theory" McGraw-Hill, Inc. (1962), p. 142.
11) S. J. Gruber, C. M. Harris, and E. Sinn, *J. Inorg. Nucl. Chem.*, **30**, 1805 (1968).
12) H. Okawa, T. Tokii, Y. Nonaka, Y. Muto, and S. Kida, This Bulletin, **46**, 1462 (1973).
13) Y. Ishimura, Y. Nonaka, Y. Nishida, and S. Kida, *ibid.*, **46**, 3728 (1973).
14) W. E. Hatfield, T. S. Piper, and U. Klabunde, *Inorg. Chem.*, **2**, 629 (1963).
15) C. M. Harris, E. Sinn, W. R. Walker, and P. R. Woolliams, *Aust. J. Chem.*, **21**, 631 (1968).
16) B. Bleaney and K. D. Bowers, *Proc. Roy. Soc. Lond.*, **A214**, 451 (1952).
17) C. A. Bear, J. M. Waters, and T. N. Waters, *Chem. Commn.*, **1971**, 703.
18) R. M. Countryman, W. T. Robinson, and E. Sinn, private communication.
19) S. Kida, Y. Nishida, and M. Sakamoto, This Bulletin, **46**, 2428 (1973).
20) Y. Muto, M. Kato, H. B. Jonassen, and L. C. Cusachs, *ibid.*, **40**, 1732 (1967).
21) M. Kato, Y. Muto, and H. B. Jonassen, *ibid.*, **40**, 1738 (1967).
22) K. T. McGregor, N. T. Watkins, D. L. Lewis, R. F. Drake, D. J. Hodgeson, and W. E. Hatfield, *Inorg. Nucl. Chem. Lett.*, **9**, 423 (1973).
23) H. Okawa, T. Tokii, Y. Muto, and S. Kida, This Bulletin, **46**, 2464 (1973).
24) N. F. Pilkington and R. Robson, *Aust. J. Chem.*, **23**, 2225 (1970).

Diels-Alder Reactions of 5,5,5-Trichloro-3-penten-2-one and Related Compounds[1]

Sadao Tsuboi, Yasuhiro Ishiguro, and Akira Takeda

Department of Synthetics Chemistry, School of Engineering, Okayama University, Tsushima, Okayama 700

(Received August 8, 1973)

The Diels-Alder reaction of 5,5,5-trichloro-3-penten-2-one (**1a**) with cyclopentadiene afforded *exo*-2-acetyl-*endo*-3-trichloromethylbicyclo[2.2.1]hept-5-ene (**2a**) stereoselectively. The stereochemistry of the reactions of cyclopentadiene with several γ-chlorinated α,β-unsaturated ketones was examined. The *endo*-directive abilities decreased in the following order: $CCl_3 > CCl_2CH_3$, $CHCl_2$, $CCl(CH_3)_2 > CH(CH_3)_2 > CH_3$. Compound **1a** reacted with butadiene and furan to give 4-acetyl-5-trichloromethylcyclohexene (**3**) and 4-(2-furyl)-5,5,5-trichloropentan-2-one (**7**) respectively.

We have recently published several works on the allylic rearrangement of 5,5,5-trichloro-3-penten-2-one (**1a**)[2,3] and on the reaction of **1a** with nucleophiles.[4] To expand the knowledge of its chemical properties, especially its dienophilic reactivity, we have now carried out the reaction of the compound **1a** and related compounds with such dienes as cyclopentadiene, butadiene, and furan.

A great number of examples have manifested a wide applicability of the well-known rule[5] of *endo* addition in the Diels-Alder reaction. However, many examples have also disclosed deviations from the *endo* rule.[6-8] Williamson and Hsu have reported that pentachlorocyclopentadiene with many dienophiles gives bicycloheptene Diels-Alder adducts in which the predominant isomer has the chlorine atom on the bridge *anti* to the double bond.[9] Recently, McBee *et al.* have reported that fluorine substituents dominate the stereochemical course of the Diels-Alder reactions.[10]

Results and Discussion

A list of dienophiles prepared for this study is given in Table 1. The methyl ketone **1d** was prepared by the reaction of triethylphosphonoacetone with 2-chloro-2-methylpropanal in the presence of sodium hydride. Compound **1i** was prepared by the condensation of chloral with 4-methyl-2-pentanone. Other α,β-unsaturated ketones were prepared by the methods described in the literature. All the dienophiles listed here were assigned to the *trans* configuration on the basis of the large coupling constants (J=14—17 Hz) observed of olefin protons and the infrared absorption at *ca.* 970 cm^{-1}.

Table 1. Preparation and properties of dienophiles (**1**)

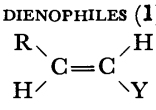

Compd.	R	Y	Yield %	Bp, °C/mmHg (Mp, °C)	Ref.
1a	CCl_3	$COCH_3$	80	95—100/20	a
1b	$CHCl_2$	$COCH_3$	65	91—92/17	b
1c	CCl_2CH_3	$COCH_3$	52	77—80/6	b
1d	$CCl(CH_3)_2$	$COCH_3$	55	53—55/4	g
1e	$CH(CH_3)_2$	$COCH_3$	13	59—61/25	c
1f	CH_3	$COCH_3$	41	119—125	d
1g	CCl_3	COC_6H_5	86	(97—99)	e
1h	CH_3	COC_6H_5	12	140—145/30	f
1i	CCl_3	$COCH_2CH(CH_3)_2$	83	96—97/6	g

a) Ref. 2. b) Ref. 3. c) E. N. Eccot and R. P. Linstead, *J. Chem. Soc.*, **1930**, 905. d) Ref. 17. e) W. Koenigs, *Chem. Ber.*, **25**, 795 (1892). f) Ref. 18. g) New compound.

When the trichloromethyl compound **1a** (*trans*) was allowed to react with cyclopentadiene at 90—100 °C for 40 hr, a cycloaddition product (**2a**) was formed in a high yield. The yield was quantitative when the reaction was conducted for 3 day, even at room temperature. The elemental analysis and mass spectral data clearly indicated the formation of the 1 : 1 adduct of **1a** and cyclopentadiene (see Table 3). The infrared spectrum of **2a** showed a strong band at 1724 cm^{-1} due to an isolated carbonyl group and a weak band at 1583 cm^{-1} due to a norbornene ring double bond. In the NMR spectrum of **2a**, which is shown in Fig. 1, the signals at 2.32 ppm (clean singlet, 3H) and at 4.01 ppm (q, 1H, J=3.4 and 5.5 Hz) are attributable to acetyl protons and a C_3-methine proton[11] respectively. The signals of two olefin protons appeared at 6.28 ppm (t, 2H, J=1.3 Hz). It is reasonable to conclude that the adduct **2a** has an *exo*-2-acetyl-*endo*-3-trichloromethyl structure, because signals of olefin protons in *endo*-2-acetylbicyclo[2.2.1]hept-5-ene tend to appear as two multiplets, with the result that the resonance due to the C_6-olefin proton is shifted to a higher field than that of the *exo*-acetyl isomer.[12] The

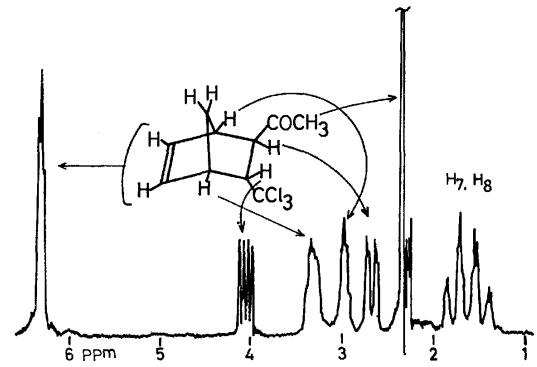

Fig. 1. NMR spectrum of *exo*-2-acetyl-*endo*-3-trichloromethylbicyclo[2.2.1]hept-5-ene (**2a**) in $CDCl_3$.

endo structure of **2a** was further substantiated by the fact that it was reduced with zinc in acetic acid, giving *exo*-2-acetyl-*endo*-3-methylbicyclo[2.2.1]hept-5-ene (*endo* **2f**), one of the two isomers derived from the reaction of 3-penten-2-one (**1f**) with cyclopentadiene, whose structure has been unambiguously established. The NMR spectrum ($COCH_3$, 2.20 ppm; CH_3, 0.93 ppm) of the compound **2f** which we obtained was identical with that of the authentic sample of the *endo* **2f** prepared independently by Kobuke's procedure.[8]

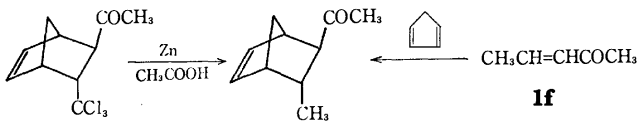

2a *endo*-**2f** **1f**

The yields, *endo* percentages, and physical properties of the adducts of cyclopentadiene with ketones listed in Table 1 are summarized in Table 2. Their elemental analyses and the spectral data are tabulated in Table 3. The configurational determination of the Diels-Alder adducts was accomplished by analyzing the NMR spectrum. The NMR spectra of trichloromethyl compounds, **2a**, **2g**, and **2i**, which were free from an *exo* component, showed clear patterns of chemical shifts and coupling constants. Those of other compounds containing both *endo* and *exo* components showed more complicated patterns. The C_3-protons of compounds **2a**, **2c**, **2g**, and **2i** showed a sharp quartet with a small width of the peak at half-height (*ca.* 0.75 Hz),[13] indicating that these protons are in the *exo* configuration. If they were in the *endo* configuration, a long-range coupling between the C_3-proton and the bridge proton would be expected to work over the coplanar W in the order of 1—2 Hz.[9] The signals of the C_2-protons of the adducts **2** usually appeared at 2.5—3 ppm. The methyl protons of the *exo*-acetyl isomers appeared as a singlet at a lower field than those of the *endo*-acetyl isomers.[14] The configurations of compounds **2b**, **2d**, **2e**, and **2f** were determined on the basis of the signals due to acetyl and olefin protons, while that of **2h** was determined by comparing its NMR spectrum with that of **2f**, especially on the basis of the signals due to olefin and methyl protons.

From the data given in Table 2, it is apparent that chlorine substituents exert the principal influence on the stereochemical course of the Diels-Alder reaction.[15] It should be noted as remarkable that the dienophiles **1a**, **1g**, and **1i**, each possessing a trichloromethyl group, afforded *endo* products exclusively. When we compare the *endo* percentages of **2a**, **2g**, and **2i** with each other, and also those of **2f** and **2h** with each other, it is understandable that the group Y is of minor importance in predicting the stereochemical course of the reaction of the dienophiles **1** with cyclopentadiene. Thus, the *endo*-directive abilities of substituents in the Diels-Alder reactions of a series of γ-chlorinated α,β-unsaturated ketones with cyclopentadiene may be regarded as decreasing in this order: $CCl_3 > CCl_2CH_3$, $CHCl_2$,

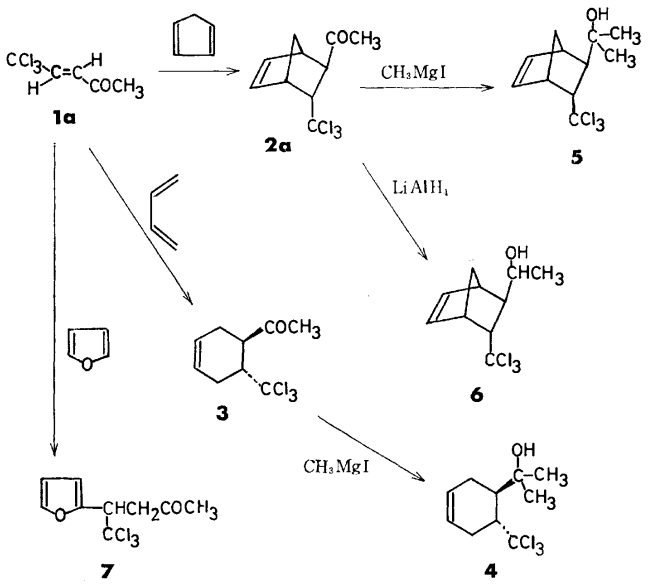

Scheme 1.

Table 2. The *endo* percentage and properties of Diels-Alder adducts (**2**)

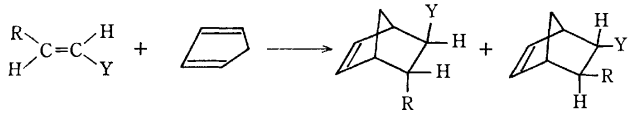

endo R *exo* R

Compd.	R	Y	Yield %	*endo* R, %	Bp, °C/mmHg[a] (Mp, °C)
2a	CCl_3	$COCH_3$	83—96	100[c]	131—132/7 (49.0—50.5)[d]
2b	$CHCl_2$	$COCH_3$	65	72	102—112/5 (66.0—67.5)[d]
2c	CCl_2CH_3	$COCH_3$	72	76	117—118/0.6
2d	$CCl(CH_3)_2$	$COCH_3$	9	70	94—95/4
2e	$CH(CH_3)_2$	$COCH_3$	11	60	70—81/4
2f	CH_3	$COCH_3$	62	35[b]	
2g	CCl_3	COC_6H_5	59	100	(65.0—67.5)[d]
2h	CH_3	COC_6H_5	68	31	119—121/0.5
2i	CCl_3	$COCH_2CH(CH_3)_2$	62	100	108/0.42

a) Data of the *exo*:*endo* mixture. b) The *endo* percentage was determined by glpc analysis, and it was nearly identical with that of Kobuke's experiment.[8] c) The configuration of the adduct obtained from the reaction at room temperature for 3 day was the same one. d) Recrystallized from petroleum ether (bp 45—51°C).

TABLE 3. ANALYSES AND PROPERTIES OF DIELS-ALDER ADDUCTS (**2**)

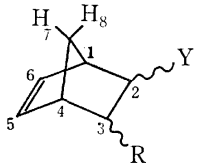

Compd.[a]	Anal (Calcd), % C	Anal (Calcd), % H	IR[b] and MS *m/e* (rel. intensity)	NMR[c] δ ppm
2a	47.17 (47.37	4.77 4.37)	IR 1724, 1583, 795 cm^{-1} MS 252 (0.2, M^+), 217 (5, M^+–Cl), 173 (10), 139 (22), 135 (100)	1.42 (dq, H_8), 1.73 (dt, H_7), 2.32 (s, *exo* $COCH_3$), 2.65 (dd, H_2), 2.98 (dt, H_1), 3.27 (m, H_4), 4.01 (dd, H_3), 6.28 (t, H_5 and H_6), J_{34}=3.4 Hz, J_{23}=5.5 Hz, J_{56}=1.3 Hz, J_{78}=8.8 Hz
2b	54.60 (54.81	5.58 5.52)	IR 1715, 1577, 742 cm^{-1}	1.30—1.90 (m, H_7 and H_8), 2.15 (s, 0.9 H, *endo* $COCH_3$), 2.24 (s, 2.1 H, *exo* $COCH_3$), 2.30—3.20 (m, H_1, H_2, and H_4), 3.20—3.60 (m, H_3), 5.01 (d, 0.72H, J=11 Hz, *endo* $CHCl_2$), 5.59 (d, 0.28 H, J=9 Hz, *exo* $CHCl_2$), 5.80—6.60 (m, H_5 and H_6)
2c	56.97 (56.69	6.10 6.05)	IR 1720, 1580, 700 cm^{-1}	1.22—1.93 (m, H_7 and H_8), 2.05 (s, 2.28 H, *endo* CCl_2CH_3), 2.12 (s, 0.72H, *exo* CCl_2CH_3), 2.21 (s, 0.72H, *endo* $COCH_3$), 2.29 (s, 2.28H, *exo* $COCH_3$), 3.54 (q, 0.76H, *exo* H_3), 5.83—6.56 (m, H_5 and H_6)
2d	67.68 (67.76	8.20 8.06)	IR 1710, 1575 cm^{-1}	1.21—1.87 (m, H_7 and H_8), 1.48 (d, 4.2H, J=2 Hz, *endo* $CCl(CH_3)_2$), 1.69 (d, 1.8H, J=7 Hz, *exo* $CCl(CH_3)_2$), 2.22 (s, 0.9H, *endo* $COCH_3$), 2.31 (s, 2.1H, *exo* $COCH_3$), 2.42—2.63 (m, H_2), 2.69—3.32 (m, H_1, H_4 and H_3), 5.77—6.55 (m, H_5 and H_6)
2e[d]			IR 1710, 1575 cm^{-1}	0.89 (d, 3.6H, J=8 Hz, *endo* $CH(C\underline{H}_3)_2$), 0.98 (d, 2.4H, J=7 Hz, *exo* $CH(C\underline{H}_3)_2$), 1.10—1.30 (m, $C\underline{H}(CH_3)_2$), 1.30—1.60 (m, H_7 and H_8), 2.12 (s, 1.2H, *endo* $COCH_3$), 2.23 (s, 1.8H, *exo* $COCH_3$), 2.50—3.00 (m, H_1 and H_4), 1.90—3.30 (m, H_2 and H_3), 5.70—6.53 (m, H_5 and H_6)
2g	56.80 (57.08	4.10 4.15)	IR 1680, 1604, 1585 cm^{-1} MS 314 (0.5, M^+), 279 (7, M^+–Cl), 278 (8, M^+–HCl), 196 (100)	1.33—2.21 (m, H_7 and H_8), 3.00 (m, H_2), 3.31—3.61 (m, H_1 and H_4), 4.30 (dd, H_3), 6.36 (t, H_5 and H_6), 7.43—8.20 (m, COC_6H_5); J_{34}=3 Hz, J_{23}=6 Hz, J_{16}=J_{45}=J_{56}=2 Hz
2h	84.52 (84.87	7.96 7.60)	IR 1680, 1601, 1582 cm^{-1}	0.89 (d, 0.9H, J=8 Hz, CH_3), 1.17 (d, 2.1H, J=8 Hz, CH_5), 1.30—1.95 (m, H_7 and H_8), 5.60—6.45(m, H_5 and H_6), 7.19—8.24 (m, COC_6H_5)
2i	58.90 (58.82	5.73 5.80)	IR 1715, 1578 cm^{-1}	0.94 (d, J=7 Hz, $CH(C\underline{H}_3)_2$), 1.26—1.90 (m, H_7 and H_8), 1.90—2.30 (m, $C\underline{H}(CH_3)_2$), 2.48 (d, J=5 Hz, $COCH_2$–), 2.60 (dd, H_2), 2.90 (m, H_1), 3.30 (m, H_4), 4.39 (dd, H_3), 6.24 (t, H_5 and H_6); J_{12}=2 Hz, J_{23}=6 Hz, J_{34}=3 Hz, J_{16}=J_{56}=J_{45}=2 Hz

a) *Endo* and *exo* materials from **2f** were separated by glpc and each component was analyzed. NMR spectra were identical with those of authentic samples.[8] b) Compound **2g** was measured by a Nujol method. All the others were measured in neat. c) Measured in $CDCl_3$. d) This compound was too volatile to be analyzed.

$CCl(CH_3)_2$>$CH(CH_3)_2$>CH_3.

Compound **1a** further gave the Diels-Alder adduct **3** with butadiene, as is shown in Scheme 1. The adduct **3** was converted to 4-(1-hydroxy-1-methylethyl)-5-trichloromethylcyclohexene (**4**) in a 50% yield by the action of methylmagnesium iodide. On the other hand, the Grignard reaction of the adduct **2a** afforded 2-(1-hydroxy-1-methylethyl)-3-trichloromethylbicyclo[2.2.1]hept-5-ene (**5**) in only a 5% yield, probably because of the steric restriction of the norbornene skeleton. The reduction of **2a** with lithium aluminum hydride gave the corresponding carbinol **6** in a 38% yield. When the dienophile **1a** was allowed to react with furan, a substitution-addition product **7** was obtained in a low yield.[16] The structural assignments of these compounds were accomplished by the aid of the IR, NMR, and Mass spectra and by elemental analyses (see Experimental).

Experimental

The melting points and boiling points are uncorrected. The elemental analyses were carried out by Mr. Eiichiro Amano. The analytical determinations by glpc were performed on a Hitachi K-53 model gas chromatograph fitted with 10% Apiezon Grease L on Chromosorb W (3 mm o.d.×1 m). The preparative isolations by glpc were performed on 10% Apiezon Grease L on Chromosorb W (3 mm o.d.×2.25 m). The mass spectra were measured on a Hitachi RMS-4 model mass spectrometer with an ionization energy of 70 eV. We are indebted to Mr. Heizan Kawamoto and Miss Hiromi Ootani for the NMR (60 MHz) measurement.

Compounds **1a**, **1b**, and **1g** were prepared by the procedures described in the literature. Compound **1f** was prepared by the method of Claisen[17] by dehydrating 4-hydroxypentan-2-one: bp 119—125 °C; IR (cm^{-1}, liquid) 1675 (C=O) and 1635 (C=C). Ethylideneacetophenone (**1h**) was prepared by the method of Kohler from crotonyl chloride and benzene[18]: bp 140—145 °C/30 mmHg; IR (cm^{-1}, liquid) 1670 (C=O), 1628 (C=C), 1603, 1585 (benzene C=C). Cyclopentadiene was generated from its dimer by a standard procedure[19] just prior to use.

*5-Chloro-5-methyl-3-hexen-2-one (**1d**).* To a mixed solution of 1.9 g (0.04 mol) of sodium hydride (52% in mineral oil) in 40 ml of dry tetrahydrofuran (THF) was added 7.8 g (0.04 mol) of diethylphosphonoacetone at 30—35 °C with stirring. Freshly-distilled 2-chloro-2-methylpropanal (4.3g, 0.04 mol) was then added at 20—25 °C, and the mixture was stirred for 15 min at 45 °C. After 50 ml of water had then been added, the organic layer was extracted with ether. The ethereal layer was washed with water and dried over $MgSO_4$. After the removal of the solvent, the residue was distilled to give 3.1 g (55%) of **1d**: bp 53—55 °C/4 mmHg; IR (cm^{-1}, liquid) 1695 (cisoid C=O), 1670 (transoid C=O), 1625 (C=C); NMR ($CDCl_3$) δ 1.73 (s, 6H, $CCl(CH_3)_2$), 2.28 (s, 3H, $COCH_3$), 6.21 and 6.92 (2d, 2H, J=17 Hz, -CH=CH-).

Found: C, 57.10; H, 7.70. Calcd for $C_7H_{11}ClO$: C, 57.34; H, 7.56.

*6-Methyl-1,1,1-trichloro-2-hepten-4-one (**1i**).* A mixture of chloral hydrate (82 g, 0.5 mol), 4-methyl-2-pentanone (60 g, 0.6 mol), acetic anhydride (50 g, 0.5 mol), glacial acetic acid (30 g, 0.5 mol), and sodium acetate (2.0 g, 0.024 mol) was refluxed for 24 hr. After the removal of the solvent, the residue was dissolved in ether and the ether solution was treated with charcoal. After most of the ether had been removed, the precipitate was collected and recrystallized from ether to give 51.4 g (42%) of 2-hydroxy-6-methyl-1,1,1-trichloroheptan-4-one:[20] mp 86—87 °C; IR (cm^{-1}, nujol) 3400 (OH), 1710 (C=O), 820, 793; NMR ($CDCl_3$) δ 0.97 (d, 6H, J=6 Hz, $-CH(C\underline{H}_3)_2$), 2.23 (m, 1H, $-C\underline{H}(CH_3)_2$), 2.27 (d, 2H, J=12 Hz, $C\underline{H}_2CH(CH_3)_2$), 3.00 (m, 2H, $-CH(OH)C\underline{H}_2-$), 3.60 (broad s, 1H, OH), and 4.69 (dd, 1H, J=4 and 7 Hz, $>C\underline{H}(OH)$).

Found: C, 38.75; H, 5.30. Calcd for $C_8H_{13}Cl_3O_2$: C, 38.82; H, 5.29.

To 320 ml of conc. H_2SO_4 was added 51 g (0.21 mol) of 2-hydroxy-6-methyl-1,1,1-trichloroheptan-4-one at −5—0 °C with stirring. After the mixture had been stirred for 4 hr at room temperature, it was poured onto crashed ice. The organic layer was extracted with ether, and the ethereal layer was washed with water and then dried over $MgSO_4$. After the evaporation of the solvent, the residue was distilled to yield 40.4 g (83%) of **1i**: bp 96—97 °C/6 mmHg; IR (cm^{-1}, liquid) 1705 (cisoid C=O), 1678 (transoid C=O), 1632 (C=C); NMR ($CDCl_3$) δ 0.98 (d, 6H, J=6 Hz, $2CH_3$), 1.80—2.70 (m, 1H, $-C\underline{H}(CH_3)_2$), 2.50 (d, 2H, J=5 Hz, $-C\underline{H}_2CH(CH_3)_2$), 6.51 (d, 1H, J=17 Hz, $-CH=C\underline{H}CO$), 7.01 (d, 1H, J=17 Hz, $CCl_3C\underline{H}=CH-$).

Found: C, 41.85; H, 4.78. Calcd for $C_8H_{11}Cl_3O$: C, 41.87; H, 4.83.

Diels-Alder Additions. Most of the reactions were conducted in autoclaves or ampoules. A solution of two mols of diene and one mol of dienophile in benzene ([c]=*ca.* 10 mol/l) was heated at 90—100 °C for 40 hr,[21] under an atmosphere of nitrogen. After the solvent had then been evaporated, the residue was distilled to give nearly pure Diels-Alder adducts. The crystallized materials were collected and purified by recrystallization from petroleum ether (bp 45—50 °C). If necessary, the microanalyses and spectral measurements were performed on samples collected by glpc or tlc.

exo-*2-Acetyl*-endo-*3-methylbicyclo[2.2.1]hept-5-ene (endo **2f**).* To a solution of 5.1 g (0.02 mol) of **2a** in 10 ml of acetic acid was added, in several portions, 5.2 g (0.08 mol) of zinc powder at 0—5 °C. The mixture was then stirred at 5 °C for 30 min. Zinc chloride and the resinous material were filtered off, and the filtrate was extracted with ether. The ethereal layer was washed with water and dried over $MgSO_4$. The removal of the solvent left 1.9 g of a brown oil which, on distillation, gave 0.7 g of a clean oil: bp 67—69 °C/7 mmHg. The glpc analysis (column temp., 110 °C; carrier gas, N_2, 0.5 kg/cm^2, 40 ml/min) of this oil showed two peaks. The peaks, retention times (min), and peak areas were as follows: 1, 7.3, 57%; 2, 8.0, 43%.

The component 1 collected by preparative glpc was identified as the *endo* **2f** by comparison of the NMR spectrum and retention time with that of the *endo* isomer isolated from the Diels-Alder adducts (see Table 2) of 3-penten-2-one (**1f**) with cyclopentadiene: yield, 13%: IR (cm^{-1}, liquid) 1700 (C=O), 1570 (C=C); NMR ($CDCl_3$)[8] δ 0.93 (d, 3H, J=7 Hz, *endo*-CH_3), 2.20 (s, 3H, *exo*-$COCH_3$), 6.02—6.35 (m, 2H, olefin protons); Mass *m/e* (rel. intensity) 150 (M^+, 20), 135 (M^+-CH_3, 31), 126 (66), 117 (M^+-COCH_3, 26), 107 (71), 105 (56), 92 (56), 91 (79), 85 (100), 79 (75).

The structure of the component 2 collected by preparative glpc was not resolved: IR (cm^{-1}, liquid) 1710, 1635, 1360, 1160, 910, 740; NMR ($CDCl_3$) δ 0.80—1.35 (m, 1H), 2.15 (s, 3H, $COCH_3$), 2.0—3.6 (m, 5H), 4.85—5.22 (m, 2H), 5.68 (s, 2H), 5.52—6.15 (m, 1H); Mass *m/e* (rel. intensity) 150 (2), 135 (10), 117 (38), 93 (56), 92 (100), 91 (86), 79 (58), 77 (60), 66 (58).

4-Acetyl-5-trichloromethylcyclohexene (*3*) was prepared by the Diels-Alder reaction of **1a** with butadiene: yield, 77%; bp 114—117 °C/3 mmHg; IR (cm^{-1}, liquid) 1718 (C=O), 1670 (C=C); NMR ($CDCl_3$) δ 1.88—3.96 (m, 4H, H_3 and H_6), 2.30 (s, 3H, $COCH_3$), 3.17 (q, 1H, $>C\underline{H}COCH_3$), 3.41 (q, 1H, $CHCCl_3$), 5.79 (t, 2H, -CH=CH-); Mass *m/e* (rel. intensity) 240 (0.6, M^+), 204 (4, M^+-HCl), 169 (39), 162 (39), 127 (100), 123 (58), 105 (44), 91 (87), 79 (90).

Found: C, 44.42; H, 4.23. Calcd for $C_9H_{11}Cl_3O$: C, 44.75; H, 4.59.

*4-(1-Hydroxy-1-methylethyl)-5-trichloromethylcyclohexene (**4**).* The ethereal solution of methyl magnesium iodide was prepared from magnesium (0.61 g, 0.025 mol), methyl iodide (4.3 g, 0.030 mol), and ether (20 ml) in the usual manner. To this solution was added a solution of 3.0 g (0.015 mol) of **3** in 20 ml of dry ether at −10—−5 °C. After the complete addition, the mixture was stirred for 30 min at room temperature. It was then acidified with 10% HCl at −5 °C, and the organic layer was extracted with ether. The extract was washed with saturated sodium chloride solution and dried

over $MgSO_4$. The subsequent removal of the solvent gave 2.8 g of a brown oil. The tlc analysis[22] of this oil showed two spots at R_f values of 0.42 and 0.52 in the ratio of 3: 1. The spot of **3** appeared at R_f 0.52. The component with the R_f value of 0.42 separated by preparative tlc was identified as **4**: yield, 50%; IR (cm^{-1}, liquid) 3500 (OH), 1677 (C=C); NMR ($CDCl_3$) δ 1.26 (s, 3H, CH_3), 1.34 (s, 3H, CH_3), 1.68 (s, 1H, OH), 2.20—2.80 (m, 5H, H_3, H_4 and H_6), 3.14—3.40 (m, 1H, >CHCCl$_3$), 5.78 (broad s, 2H, -CH=CH-).

Found: C, 46.43; H, 5.82. Calcd for $C_{10}H_{15}Cl_3O$: C, 46.63; H, 5.87.

2-(1-Hydroxy-1-methylethyl)-3-trichloromethylbicyclo[2, 2, 1]hept-5-ene (5). The adduct **2a** (2.5 g, 0.01 mol) was allowed to react with methyl magnesium iodide (methyl iodide, 0.018 mol; magnesium, 0.015 mol) in ether. When the mixture was treated as usual, 1.98 g of a clean oil was obtained. The tlc analysis[22] of this oil showed two spots at R_f values of 0.37 and 0.51 in the ratio of 1: 4. The spot of **2a** appeared at R_f 0.51. The component with the R_f value of 0.37 was separated by preparative tlc and was identified as **5**: yield 5%; IR (cm^{-1}, liquid) 3530 (OH), 1571 (C=C); NMR ($CDCl_3$) δ 1.12—1.77 (m, 2H, $2H_7$), 1.33 and 1.42 (2s, 6, -C(C$\underline{H}_3$)$_2$), 1.77—2.10 (m, 1H, H_2), 1.87 (s, 1H, OH), 2.90 (m, 1H, H_1), 3.40 (m, 2H, H_3 and H_4), 6.20 (m, 2H, -CH=CH-).

OH

Found: C, 49.28; H, 5.57. Calcd for $C_{11}H_{15}Cl_3O$: C, 49.01; H, 5.56.

2-(1-Hydroxyethyl)-3-trichloromethylbicyclo[2.2.1]hept-5-ene (6). To a mixture of 30 ml of dry ether and 0.75 g (0.02 mol) of lithium aluminum hydride was added dropwise a solution of 10.1 g (0.04 mol) of **2a** in 30 ml of dry ether at reflux temperature. After the complete addition, the mixture was refluxed for a further 30 min. To the mixture was added 10 ml of ice–water, and it was acidified with 10% H_2SO_4. The organic layer was extracted with ether. The extract was washed with water and dried over $MgSO_4$. The subsequent removal of the solvent left a residue which, on distillation, gave 3.8 g (38%) of **6**: bp 124 °C/0.25 mmHg; IR (cm^{-1}, liquid) 3375 (OH), 1572 (C=C); NMR ($CDCl_3$) δ 1.28 and 1.34 (2d, 3H, J=7 Hz, -CH(OH)C$\underline{H}_3$), 1.40—1.60 (m, 2H, $2H_7$), 1.79—1.95 (m, 1H, H_2), 2.01 (s, 1H, OH), 2.82—3.55 (m, 3H, H_1, H_3, and H_4), 3.91—4.73 (m, 1H, >C$\underline{H}$(OH)), 6.23 (m, 2H, -CH=CH-).

Found: C, 47.26; H, 5.26. Calcd for $C_{10}H_{13}Cl_3O$: C, 47.00; H, 5.13.

4-(2-Furyl)-5,5,5-trichloropentan-2-one (7). A mixed solution of **1a** (5.6 g, 0.3 mol) and furan (4.1 g, 0.06 mol) in benzene (20 ml) was heated for 40 hr at 80 °C under an atmosphere of nitrogen. The solvent and excess furan were then removed *in vacuo*; the residue, on distillation, gave 0.9 g (11%) of **7**: bp 111 °C/4 mmHg; IR (cm^{-1}, liquid) 1730 (C=O), 1506 (furan C=C); NMR ($CDCl_4$) δ 2.14 (s, 3H, $COCH_3$), 3.34 (d, 2H, J=7 Hz, $-CH_2-$), 4.49 (t, 1H, J= 7 Hz, >CH), 6.37 (m, 2H, furan H_3 and H_4), 7.37 (m, 1H, furan H_5); MS *m/e* (rel. intensity) 218 (49, M^+-HCl), 183 (40), 162 (10), 149 (37), 141 (27), 137 (11), 81 (10), 43 (100).

Found: C, 42.43; H, 4.02. Calcd for $C_9H_9Cl_3O_2$: C, 42.30; H, 3.55.

References

1) Presented in part at 26th Annual Meeting of the Chemical Society of Japan, Hiratsuka, April 2, 1972.

2) A. Takeda and S. Tsuboi, *J. Org. Chem.*, **35**, 2690 (1970).

3) A. Takeda and S. Tsuboi, *ibid.*, **38**, 1709 (1973).

4) A. Takeda, S. Tsuboi, T. Moriwake, and E. Hirata, This Bulletin, **45**, 3685 (1972).

5) See, for instance, A. Wasserman, "Diels-Alder Reactions," Elsevier, Amsterdam, 1965; J. Sauer, *Angew. Chem.*, **79**, 76 (1967).

6) See, for instance, J. G. Martin and R. K. Hill, *Chem. Rev.*, **61**, 537 (1961).

7) J. A. Berson, Z. Hamlet, and W. A. Muller, *J. Amer, Chem. Soc.*, **84**, 297 (1962).

8) Y. Kobuke, T. Fueno, and J. Furukawa, *ibid.*, **92**, 6548 (1970).

9) (a) K. L. Williamson and Y-F. Li Hsu, *J. Amer. Chem, Soc.*, **92**, 7385 (1970); (b) K. L. Williamson, Y-F. Li Hsu, R. Lacko, and C. He Youn, *ibid.*, **91**, 6129 (1969).

10) E. T. McBee, M. J. Keogh, R. P. Levek, and E. P. Wesseler, *J. Org. Chem.*, **38**, 632 (1973).

11) Trichloromethyl-substituted methine protons show signals at *ca.* 3.5—5 ppm (see Reference (4)).

12) J. G. Dinwiddle, Jr. and S. P. McManus, *J. Org. Chem.*, **30**, 766 (1965).

13) Compound **2c** contains both components.

14) The electrochemical reduction of **2a** afforded the *endo* **2b**, whose *exo*-acetyl protons in NMR sppeared as a singlet at a lower field (2.24 ppm) than did the *endo*-acetyl protons (2.15 ppm) of the *exo* **2b**, the minor component of the two isomers derived from the reaction of **1b** with cyclopentadiene. The details of the electrochemical reduction of **2a** and related compounds will be published elsewhere.

15) It is also known that, with cyclopentadiene, ethyl 4-chlorocrotonate and ethyl 4-bromocrotonate gave 78 and 73.5% *endo* (CH_2X) products respectively; H. Christol, A. Donche, and F. Plenat, *Bull. Soc. Chim. Fr.*, **1966**, 1315.

16) The so-called "substitution-addition reaction" is exemplified by the formation of β-(2-furyl)propionaldehyde from furan and acrolein: S. M. Sherlin, A. Ya. Berlin, T. A. Serebrennikova, and F. E. Rabinovich, *J. Gen. Chem. (U.S.S.R.)*, **8**, 7 (1938) *(Chem. Abstr.*, **32**, 5397 (1938)); K. Alder and C. H. Schmidt, *Chem. Ber.*, **76**, 183 (1943).

17) L. Claisen, *Ann.*, **306**, 324 (1899).

18) E. P. Kohler, *Amer. Chem. J.*, **42**, 395.

19) R. B. Moffett, "Organic Syntheses," Collect. Vol. IV, N. Rabjohn, ed., Wiley, New York, N. Y. (1963), p. 238.

20) Champs (François de Champs, Doctoral Dissertation, Univ. of Paris., October 31, 1970) has synthesized this compound by the reaction of chloral hydrate with 4-methyl-2-pentanone in the presence of $TiCl_4$.

21) The reaction of **1f** was discontinued after heating for 20 hr.

22) Conditions of tlc: support, Silica gel GF_{254} (E. Merck AG, Darmstadt), 0.2 mm; developer, *n*-hexane–acetone (5:1 v/v).

The Synthesis of 1,3-Thiazines by the Reaction of Non-isolable β-Imino(dithiocarboxylic) Acids with Aldehydes

Tetsuko MIYAUCHI, Yutaka KADOKURA, Naoaki FUKADA, and Tatsuo TAKESHIMA

Department of Chemistry, Faculty of Science, Chiba University, Yayoi-cho, Chiba-shi 280

(Received November 5, 1973)

1,3-Thiazines, (**1**)—(**6**), were synthesized, in yields ranging from 2.9 to 43%, by the reaction of aldehyde with the intermediate β-iminodithiocarboxylic acids which are formed by the reaction of ketones with carbon disulfide in the presence of ammonia.

We have previously reported that a series of 1,3-thiazines were synthesized by means of the reaction of 2-iminocyclopentanedithiocarboxylic acid with carbonyl compounds.[1] This method, however, requires an isolated β-iminodithiocarboxylic acid as the starting material, and the preparation of the free acid is possible in only a few limited cases; thus, the scope of this method is restricted. Though there are many *N*-substituted β-iminodithiocarboxylic acids, they do not undergo the present reaction.

Only a few specific ketones, such as cyclopentanones and 4,5-dihydro-3-methyl-1-phenyl-1*H*-pyrazol-5-one, afforded the corresponding β-iminodithiocarboxylic acid when reacted with carbon disulfide in the presence of ammonia.[2-4] Other ketones, such as methyl ethyl ketone, cyclohexanone, cycloheptanone, and cyclooctanone, immediately give 1,3-thiazines, which are considered to be formed from the intermediate β-iminodithiocarboxylic acids by a reaction with the material ketones present.[5] All attempts to isolate the intermediate acids from the reaction products were unsuccessful. An attempt at the synthesis of the iminodithiocarboxylic acids from the corresponding β-ketodithiocarboxylic acids also failed.

The present investigation was undertaken in order to extend the method of preparing the 1,3-thiazines by making use of the supposed intermediate iminodithiocarboxylic acids mentioned above. Thus, a mixture of two kinds of carbonyl compounds, and carbon disulfide were allowed to react in the presence of ammonia to give the cross-reaction products. Cyclohexanone, 4-methylcyclohexanone, cycloheptanone, and cyclooctanone were chosen as the sources of the intermediate. Vanillin and salicylaldehyde were used as the other parts of the reactant because they gave easily crystallizable products. The yields of the present reaction ranged from 2.9 to 43%.

The limitation of the present reaction is that the use of two kinds of carbonyl compounds, both which have α-hydrogen atom, is unfavorable, because four kinds of 1,3-thiazines may be formed including the cross-reaction products.

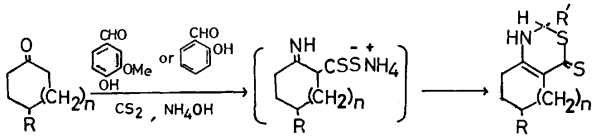

(1) $n=1$, R=H, R′=*p*-hydroxy-*m*-methoxyphenyl
(2) $n=1$, R=H, R′=*o*-hydroxyphenyl
(3) $n=1$, R=Me, R′=*p*-hydroxy-*m*-methoxyphenyl
(4) $n=1$, R=Me, R′=*o*-hydroxyphenyl
(5) $n=2$, R=H, R′=*p*-hydroxy-*m*-methoxyphenyl
(6) $n=3$, R=H, R′=*p*-hydroxy-*m*-methoxyphenyl

Scheme

The products which were obtained here were identified on the basis of IR and UV spectra, and elemental analyses (see Experimental section). The spectra were similar to that of 4(1*H*)-thiono-5,6,7,8-tetrahydro-4*H*-3,1-cyclohexathiazine-2-spirocyclohexane.[5]

Experimental

2-(p-Hydroxy-m-methoxyphenyl)-4(1H)-thiono-5,6,7,8-tetrahydro-4H-3,1-cyclohexathiazine (1). A mixture of carbon disulfide (15.2 g, 0.20 mol) and cyclohexanone (1.5 g, 0.015 mol) was added to a solution of vanillin (3 g, 0.02 mol) in 28% aqueous ammonia (140 ml), and then the mixture was shaken at room temperature for 4 hr. The solid product was collected, washed with water, ether and ethanol, and dried (yield, *ca.* 2 g; 43%). Recrystallization from pyridine–ethanol gave yellow crystals; mp 222—224 °C (slow heating) and 240—242 °C (rapid heating). IR (KBr): 3290 (m, s NH), 3080 (m, br OH and aromatic CH), 1600 (m, aromatic C=C), and 1515 (s, br conj. C=C) cm^{-1}. UV: λ_{max}^{EtOH} 234 (log ε 4.19), 280 (3.37), 341 (3.79), 406 (4.26) nm.

Found: C, 58.73; H, 5.55; N, 4.71; S, 20.60%; mol wt (Mass), 307. Calcd for $C_{15}H_{17}NO_2S_2$: C, 58.63; H, 5.58; N, 4.56; S, 20.82%; mol wt, 307.3.

2-(o-Hydroxyphenyl)-4(1H)-thiono-5,6,7,8-tetrahydro-4H-3,1-cyclohexathiazine (2). A mixture of carbon disulfide (5 g, 0.066 mol) and cyclohexanone (3 g, 0.031 mol) was added to a solution of salicylaldehyde (5 g, 0.041 mol) in 28% aqueous ammonia (50 ml), and then the mixture was worked up as has been described for **1**. The crude product was washed with water and acetic acid, and dried (yield, *ca.* 3 g; 35%). Recrystallization from methanol gave orange crystals; mp 222—224 °C (slow heating) and 240—242 °C (rapid heating). IR (KBr): 3290 (s, NH), 3140 (s, br OH and aromatic CH), 1610 (w, NH), 1600 (s, aromatic C=C), 1500 (*vs.* conj. C=C) cm^{-1}. UV: λ_{max}^{EtOH} 275 (log ε 3.42), 343 (3.74), 406 (4.24) nm.

Found: C, 60.63; H, 5.43; N, 5.03; S, 22.99%; mol wt (Mass), 277. Calcd for $C_{14}H_{15}NOS_2$: C, 60.64; H, 5.45; N, 5.05; S, 23.08%; mol wt, 277.3.

2-(p-Hydroxy-m-methoxyphenyl)-6-methyl-4(1H)-thiono-5,6,7,8-tetrahydro-4H-3,1-cyclohexathiazine (3). A mixture of 4-methylcyclohexanone (1 g, 0.009 mol), carbon disulfide (2 g, 0.026 mol), vanillin (1.5 g, 0.01 mol), and 28% aqueous ammonia (15 ml) was shaken at room temperature for 5 hr and then kept overnight in an ice box. The solid product was collected, washed with ethanol, and dried (yield, 0.48 g; 17%). Recrystallization from pyridine–water gave yellow crystals; mp 247—248 °C (in a sealed tube, slow heating) and

263—265 °C (decomp.) (in a sealed tube, rapid heating). IR (KBr): 3270 (s, br NH), 3200 (br, sh OH), 3040 (sh aromatic CH), 1615 (w, NH), 1605 (m, aromatic C=C), 1520 (s, br conj. C=C) cm^{-1}. UV: λ_{max}^{EtOH} 235 (log ε 4.15), 285 (3.29), 338 (3.74), 350 (3.79), 406 (4.26) nm.

Found: C, 59.99; H, 5.98; N, 4.49; S, 19.74%; mol wt (Mass), 321. Calcd for $C_{16}H_{19}NO_2S_2$: C, 59.80; H, 5.96; N, 4.36; S, 19.92%; mol wt, 321.3.

2-(o-Hydroxyphenyl)-6-methyl-4(1H)-thiono-5,6,7,8-tetrahydro-4H-3,1-cyclohexathiazine (4). A mixture of 4-methylcyclohexanone (10 g, 0.089 mol), carbon disulfide (20 g, 0.26 mol), salicylaldehyde (15 g, 0.12 mol), and 28% aqueous ammonia (100 ml) was worked up as has been described for **1.** The reaction mixture was then shaken with some ether and filtered. The filtrate was evaporated under reduced pressure, and to this chloroform was added. The solid product was collected and recrystallized from ethanol to give yellow crystals (yield, 0.75 g; 2.9%); mp 222—223 °C (decomp.) (slow heating) and 238—240 °C (decomp.) (rapid heating). IR (KBr): 3270 (s, NH), 3100 (s, br OH and aromatic CH), 1605 (w, NH), 1595 (s aromatic C=C), 1500 (*vs.* conj. C=C) cm^{-1}. UV: λ_{max}^{EtOH} 343 (log ε 3.78), 405 (4.24) nm.

Found: C, 61.71; H, 5.67; N, 4.94; S, 21.93%; mol wt (Mass), 291. Calcd for $C_{15}H_{17}NOS_2$: C, 61.85; H, 5.88; N, 4.81; S, 21.97%; mol wt, 291.3.

2-(p-Hydroxy-m-methoxyphenyl)-4(1H)-thiono-5,6,7,8-tetrahydro-4H-3,1-cycloheptathiazine (5). A mixture of cycloheptanone (1 g, 0.009 mol), carbon disulfide (2 g, 0.026 mol), vanillin (1.5 g, 0.01 mol), and 28% aqueous ammonia (20 ml) was worked up as has been described for **1.** Recrystallization from pyridine–methanol gave yellow crystals (yield, 0.57 g; 19%); mp 225—226 °C (decomp.) (slow heating) and 241—243 °C (rapid heating). IR (KBr): 3240 (s, NH), 3090 (m, br OH and aromatic CH), 1610 (w, NH), 1595 (s, aromatic C=C), 1510 (s, br conj. C=C) cm^{-1}. UV: λ_{max}^{EtOH} 233 (log ε 4.22), 282 (3.62), 336 (3.77), 404 (4.22) nm.

Found: C, 59.82; H, 5.84; N, 4.67; S, 19.63%; mol wt (Mass), 321. Calcd for $C_{16}H_{19}NO_2S_2$: C, 59.80; H, 5.96; N, 4.36; S, 19.92%; mol wt, 321.3.

2-(p-Hydroxy-m-methoxyphenyl)-4(1H)-thiono-5,6,7,8,9,10-hexahydro-4H-3,1-cyclooctathiazine (6). A mixture of cyclooctanone (1 g, 0.008 mol), carbon disulfide (2.5 g, 0.33 mol), vanillin (1.5 g, 0.01 mol), and 28% aqueous ammonia (20 ml) was worked up as has been described for **1.** The solid product was collected and recrystallized from ethanol–ether (yield, 0.65 g; 26%) and then from acetone–ethanol to give yellow crystals; mp *ca.* 135 °C. IR (KBr): 3270 (s, NH), 3140 (m, sh OH), 3040 (w, aromatic CH), 1600 (m, aromatic C=C), 1510 (*vs.* conj. C=C) cm^{-1}. UV: λ_{max}^{EtOH} 235 (sh) (log ε 4.15), 290 (3.53), 340 (3.77), 412 (4.23) nm.

Found: C, 60.80; H, 6.51; N, 3.90; S, 18.92%; mol wt (Mass), 335. Calcd for $C_{17}H_{21}NO_2S_2$: C, 60.88; H, 6.31; N, 4.18; S, 19.09%; mol wt, 335.4.

References

1) M. Muraoka, M. Yokoyama, K. Yamamoto, and T. Takeshima, This Bulletin, **43**, 2134 (1970).

2) T. Takeshima, M. Yokoyama, T. Imamoto, M. Akano, and H. Asaba, *J. Org. Chem.*, **34**, 730 (1969).

3) G. Matolcsy, P. Sohár, and B. Bordás, *Chem. Ber.*, **104**, 1155 (1971).

4) T. Takeshima, T. Miyauchi, N. Fukada, S. Koshizawa, and M. Muraoka, *J. Chem. Soc., Perkin Trans. I*, **1973**, 1009.

5) T. Takeshima, T. Hayashi, M. Muraoka, and T. Matsuoka, *J. Org. Chem.*, **32**, 980 (1967); T. Takeshima, T. Imamoto, M. Yokoyama, K. Yamamoto, and M. Akano, *ibid.*, **33**, 2877 (1968).

The Iodination of Benzene with Iodine in the Thallium(III) Trifluoroacetate-Trifluoroacetic Acid System

Nobuo ISHIKAWA and Akira SEKIYA

Department of Chemical Engineering, Tokyo Institute of Technology, Ookayama, Meguro-ku, Tokyo 152

(Received November 20, 1973)

Molecular iodine in the system of thallium(III) trifluoroacetate-trifluoroacetic acid has been found to possess a high potency for aromatic iodination. Under controlled conditions, benzene and also mesitylene were step-by-step mono-, di-, and triiodinated, whereupon whole iodine was consumed for the iodination by the oxidation process of the thallium(III) salt. In the course of the iodination of benzene, an intermediate has been revealed to consist of thalliated benzenes, which were transformed into iodinated benzenes by the electrophilic attack of iodine.

Recently, Taylor *et al.*[1,2] reported a new aromatic iodination process, one which involves thalliation with thallium(III) trifluoroacetate to aryl thallium(III) ditrifluoroacetate, followed by iodination with potassium iodide to aryl iodide. On the other hand, the iodination with molecular iodine in the presence of thallium(III) trifluoroacetate in carbon tetrachloride was additionally described in their experimental section,[2] which attracted our attention for practical purposes. This iodination, however, was not investigated in the mechanistic aspect.

In this paper we will describe our finding that molecular iodine in the system consisting of thallium(III) trifluoroacetate and trifluoroacetic acid possesses a high potency for direct aromatic iodination.

Results and Discussion

A preliminary test for the aromatic iodination with molecular iodine was carried out in order to examine the effect of metal trifluoroacetate on the iodination of benzene. Several metal trifluoroacetates, such as Fe(III),[3] Cu(II),[3] Ag(I), Hg(II), and Tl(III) salts, were prepared, and the iodination was carried out in the presence of these metal salts in a large excess of benzene at its refluxing temperature. The results are summarized in Table 1. As can be seen, Tl(III), Ag(I), and Hg(II) salts showed a considerable effect in the reaction, while the other salts were almost inert. Among these three salts, particularly thallium(III) trifluoroacetate exhibited a noticeable result. The yield in this case was 83% for a two-molar-equivalent formation from a one-molar equivalent of iodine,

Table 1. Effect of metal trifluoroacetates on the iodination of benzene

$$C_6H_6 \xrightarrow[M(CF_3CO_2)_n\text{-}C_6H_6]{I_2^{a)}} C_6H_5I$$

M(n)	Fe(III)	Cu(II)	Ag(I)	Hg(II)	Tl(III)
Yield[b] (%)	trace	trace	48	48	83
Solubility[c] of $M(CF_3CO_2)_n$	p.s.	p.s.	s.	s.	p.s.

a) A mixture of I_2 (2.5 mmol), $M(CF_3CO_2)_n$ (3.75 m mol) and benzene (10 ml) was refluxed for 2.5 hr. b) Yield is based on the formation of 2 mol of iodobenzene from 1 mol of iodine, and determined by glc using nitrobenzene as an internal standard. c) s., soluble; p.s., partly soluble.

Table 2. Solvent effect on the iodination of benzene[a)]

Solvent	Reaction temp. (°C)	Yield[b] (%) of iodobenzene
MeCN	80	13
$CHCl_3$	63	34
CCl_4	76	87
DMF	85	0
Dioxane	85	0
MeOH	65	3
CF_3CO_2H	68	100

a) A mixture of C_6H_6 (5.5 mmol), I_2 (2.5 mmol), and $Tl(CF_3CO_2)_3$ (2.75 mmol) in solvent (8 ml) was heated for 2.5 hr. b) Similar to the b) of Table 1.

suggesting that an oxidation-reduction process is involved.

On the basis of these results, further study was centered on the behavior of thallium(III) trifluoroacetate toward the iodination. Experiments with this thallium salt in various solvents were carried out, generally at the refluxing temperature of the solvents used. The results are summarized in Table 2. As can be seen, trifluoroacetic acid, carbon tetrachloride and benzene showed marked effects on the iodination. The effect of trifluoroacetic acid was most remarkable, affording an almost quantitative yield of iodobenzene even at room temperature (30 °C) in a 15 min reaction period. The formation of thallium(I) salt equivalent to the reacted thallium(III) trifluoroacetate was confirmed as thallium(I) chromate by the quantitative analysis of the reaction mixture. Therefore, the reaction can be represented by the following overall equation:

$$Tl(CF_3CO_2)_3 + I_2 + 2C_6H_6 \longrightarrow Tl(CF_3CO_2) + 2C_6H_5I + 2CF_3CO_2H \quad (1)$$

The effectiveness of the iodination in trifluoroacetic acid in the presence of thallium(III) trifluoroacetate was further realized for the polyiodination of benzene. The di-, tri-, and tetraiodinations of benzene were performed step-by-step with appropriate amounts of iodine and thallium(III) trifluoroacetate, as is shown in Table 3. 1,4-Diiodobenzene, 1,2,4-triiodobenzene, and 1,2,4,5-tetraiodobenzene were obtained in fair yields by this method. Despite the high efficiency of this method for iodination, though, the insolubility of the polyiodobenzenes in the reaction medium appears

Table 3. Iodination of benzene and mesitylene[a)]

Substrate	Molar ratio Sub : I_2 : $Tl(TFA)_3$	Solv.	Temp. (°C)	Time (hr)	Product	Yield (%)
C_6H_6	1.1 : 0.5 : 0.55	TFA	30	0.25	C_6H_5I	94[b)]
C_6H_6	1.1 : 0.5 : 0.55	TFA	68	2.5	C_6H_5I	100[b)]
C_6H_6	1.1 : 0.5 : 0.55	CCl_4	76	2.5	C_6H_5I	87[b)]
C_6H_6	1.0 : 1.0 : 1.1	TFA	68	2.5	p-$C_6H_4I_2$	86[b)]
C_6H_6	1.0 : 1.0 : 1.1	CCl_4	76	2.5	C_6H_5I p-$C_6H_4I_2$	89[b)] 2[c)]
C_6H_6	1.0 : 1.5 : 1.7	TFA	68	12.5	1,2,4-$C_6H_3I_3$ 1,2,4,5-$C_6H_2I_4$	70[c)] 13[c)]
C_6H_6	1.0 : 2.0 : 2.2	TFA	68	20	1,2,4-$C_6H_3I_3$ 1,2,4,5-$C_6H_2I_4$	38[c)] 41[c)]
1,3,5-$C_6H_3Me_3$	1.0 : 0.5 : 0.55	TFA	68	0.5	$C_6H_2IMe_3$ $C_6HI_2Me_3$	60[c)] 11[c)]
1,3,5-$C_6H_3Me_3$	1.0 : 1.0 : 1.1	TFA	68	0.75	$C_6HI_2Me_3$	92[c)]
1,3,5-$C_6H_3Me_3$	1.0 : 1.5 : 1.7	TFA	68	1.5	$C_6I_3Me_3$	82[c)]

a) A mixture of benzene or mesitylene (3 mmol), I_2 and $Tl(CF_3CO_2)_3$ in solvent (8 ml) was allowed to react. b) Yield is determined by glc using nitrobenzene as an internal standard. c) Yield is based on the product actually isolated.

to resist further penta- or hexa-iodination. The use of carbon tetrachloride instead of trifluoroacetic acid as a solvent failed in the diiodination of benzene. By the same procedure as has been described for benzene, mesitylene was iodinated step-by-step to give mono-, di-, and triiodomesitylene in good yields (Table 3).

In view of the above iodination results, iodine in the system of thallium(III) trifluoroacetate-trifluoroacetic acid has been revealed to be a powerful iodinating agent. The effect of trifluoroacetic acid was recognized from the fact that iodine in thallium(III) acetate-acetic acid did not work even for the monoiodination of benzene.

It is obvious that the overall reaction (1) for the iodination of benzene involves successive iodination with iodine formed through the oxidation of I^- with Tl^{3+} [Eq. (3)] after the initial iodination [Eq. (2)]. The iodine formed in Eq. (3) retraces the same path over again:

$$C_6H_6 + I_2 \xrightarrow{Tl(CF_3CO_2)_3} C_6H_5I + HI \quad (2)$$

$$2HI + Tl(CF_3CO_2)_3 \longrightarrow Tl(CF_3CO_2) + I_2 + 2CF_3CO_2H \quad (3)$$

The formation of less than a half molar equivalent of iodobenzene in the use of silver(I) and mercury(II) trifluoroacetates seems to be due to the inertness of these salts for the oxidation of I^- to iodine.

A problem is how Reaction (2) proceeds mechanistically under these conditions. The aromatic thallation has been reported by Taylor *et al.*[4)] to proceed smoothly in trifluoroacetic acid by the use of thallium(III) trifluoroacetate.

$$C_6H_6 + Tl(CF_3CO_2)_3 \longrightarrow C_6H_5Tl(CF_3CO_2)_2 + CF_3CO_2H \quad (4)$$

The rapidity of this reaction is enough to consider phenyl thallium bis-trifluoroacetate as an intermediate for the iodination. In order to confirm this consideration, phenyl thallium bis-trifluoroacetate was allowed to react with one half and with one molar equivalent of iodine in trifluoroacetic acid under the conditions used for the above-mentioned iodination. The reaction proceeded with sufficient rapidity to give mainly iodobenzene in the former case and mainly 1,4-diiodobenzene in the latter, in yields of 78 and 86% respectively. These reactions can be written as follows:

$$C_6H_5Tl(CF_3CO_2)_2 + \frac{1}{2}I_2 \longrightarrow C_6H_5I + \frac{1}{2}Tl(CF_3CO_2) + \frac{1}{2}Tl(CF_3CO_2)_3 \quad (5)$$

$$C_6H_5Tl(CF_3CO_2)_2 + I_2 \longrightarrow C_6H_4I_2(p\text{-}) + Tl(CF_3CO_2) + CF_3CO_2H \quad (6)$$

A possible pathway of Reaction (5) can be represented by the following equations:

$$C_6H_5Tl(CF_3CO_2)_2 + I_2 \longrightarrow C_6H_5I + TlI(CF_3CO_2)_2 \quad (7)$$

$$TlI(CF_3CO_2)_2 + CF_3CO_2H \longrightarrow Tl(CF_3CO_2)_3 + HI \quad (8)$$

$$HI + \frac{1}{2}Tl(CF_3CO_2)_3 \longrightarrow \frac{1}{2}Tl(CF_3CO_2) + \frac{1}{2}I_2 + CF_3CO_2H \quad (9)$$

The reaction is presumed to be initiated by Eq. (7), which is regarded as an electrophilic substitution attacked by iodine, thus affording iodobenzene. The succeeding stages, (8) and (9), involve oxidation of I^- to iodine by the action of Tl^{3+}. By the summation of Eqs. (7), (8), and (9), an overall Eq. (5) is given. In Reaction (5) it is supposed that the iodobenzene and thallium(III) trifluoroacetate formed react further in an equimolar ratio to form thalliated iodobenzene ($C_6H_5I + Tl(CF_3CO_2)_3 \rightarrow IC_6H_4Tl(CF_3CO_2)_2 + CF_3CO_2H$). Actually, when iodobenzene was refluxed with an equimolar amount of thallium(III) trifluoroacetate in trifluoroacetic acid for 2.5 hr, a loss of about two-thirds the iodobenzene was observed by glc.

This is consistent with the above finding that Reaction (5) gave only a moderate yield of iodobenzene. Also,

Reaction (6) must have proceeded through the *para*-thalliated iodobenzene.

It may be concluded that the iodination of benzene [Eq. (1)] in the system of thallium(III) trifluoroacetate–trifluoroacetic acid proceeds by the pathway of (4), (7), (8), and (9), which are summed up by Eq. (1). It should be emphasized that the iodination reaction described here involves two important stages; one is the electrophilic substitution of phenyl thallium di-trifluoroacetate with iodine, and the other is the oxidation of the resultant iodide anion to iodine with thallium(III) salt. This mechanism is quite different from that of the iodination of aryl thallium di-trifluoroacetate with potassium iodide reported by Taylor *et al.*[2] They speculated that the reaction proceeds *via* aryl thallium diiodide:

$$ArTl(CF_3CO_2)_2 + 2KI \longrightarrow [ArTlI_2] \longrightarrow ArI + 2CF_3CO_2K + TlI.$$

Experimental

Metal Trifluoroacetates. The Tl(III),[2,4] Hg(II),[5] and Ag(I) trifluoroacetates[6] were prepared according to the methods of the literature. The Fe(III) and Cu(II) trifluoroacetates were prepared as follows.

Into a solution of $Fe(CF_3CO_2)_2$, which had been prepared by the addition of iron powder to an aqueous trifluoroacetic acid solution (more than 3 molar equivalents), 30% H_2O_2 was added; the resulting solution of the Fe(III) salt was then concentrated to dryness.

Copper(I) oxide freshly prepared from $CuSO_4 \cdot 5H_2O$ and NaOH was dissolved in aqueous trifluoroacetic acid, and the resulting solution was concentrated to dryness to give $Cu(CF_3CO_2)_2$.

These metal trifluoroacetates were used after having been thoroughly dried over P_2O_5 *in vacuo*.

Iodination Procedure. The iodinations shown in Table 1, Table 2, and Table 3 were carried out as follows.

To the solvent (in Table 1 benzene itself was used) placed in a flask, metal trifluoroacetate and iodine were added. The mixture was immediately refluxed or warmed at the fixed temperature. Ag(I) and Hg(II) trifluoroacetates were easily soluble in benzene, but the other Fe(III), Cu(II) and Tl(III) salts were only partly soluble. In the run with Ag(I) trifluoroacetate, AgI was precipitated as the reaction proceeded (Table 1). In the iodinations in several solvents (Table 2), acetonitrile, DMF, methanol, and trifluoroacetic acid gave a homogeneous reaction solution, but chloroform and carbon tetrachloride were able to dissolve Tl(III) trifluoroacetate to only a limited extent. When 1,4-di-, 1,2,4-tri- or 1,2,4,5-tetraiodobenzene, and mono-, di- or triiodomesitylene were formed (Table 3), these products were deposited during the reaction because of their low solubility. In the polyiodination of benzene in trifluoroacetic acid, a mixture of tri- and tetraiodobenzene made a mass such as was formed in the reaction mixture. Therefore, in these cases the reaction required a longer period. In general, monoiodobenzene was quantitatively analyzed from the reaction mixture by glc, using a column of silicone DC 550 and with nitrobenzene as the internal standard.

All the iodinated benzenes except iodobenzene were isolated by the following procedure. After the evaporation of trifluoroacetic acid from the reaction mixture, the residue (in the case of tri- and tetraiodobenzene) or its benzene solution (in the case of 1,4-diiodobenzene) was washed with 10% nitric acid and then with aqueous sodium bisulfite to remove the metal trifluoroacetate and unreacted iodine. The crystals obtained as 1,4-diiodobenzene by the evaporation of benzene were almost pure, colorless crystals: mp 128 °C (lit,[7] mp 128—129 °C). Its IR spectrum was consistent with that of an authentic specimen. The 1,2,4-tri and 1,2,4,5-tetraiodobenzene were obtained as a mixture, which was separated by alumina-column chromatography. The 1,2,4-triiodobenzene was obtained by elution with *n*-hexane, and then 1,2,4,5-tetraiodobenzene was eluted with benzene. 1,2,4-Triiodobenzene: colorless crystals, mp 91 °C (lit,[7] mp 90—91 °C). 1,2,4,5-Tetraiodobenzene: colorless crystals, mp 250—251 °C (lit,[7] mp 252—253 °C). Their IR spectra were consistent with those of authentic specimens.

The monoiodomesitylene was obtained in the same manner as has been described for 1,4-diiodobenzene. Monoiodomesitylene: colorless crystals, mp 31—32 °C (lit,[8] mp 32—34 °C). Most of the di- and tri-iodomesitylenes were deposited from the reaction mixture; filtration gave almost pure crystals. Diiodomesitylene: colorless crystals mp 80—81 °C (lit,[8] mp 81—82 °C). Triiodomesitylene: colorless crystals, mp 206 °C (lit,[8] mp 206—208 °C).

Reaction of Phenyl Thallium bis-Trifluoroacetate with Iodine in Trifluoroacetic Acid. To a solution of 1.27 g (0.0025 mol) of phenyl thallium bis-trifluoroacetate in 8 ml of trifluoroacetic acid, 0.32 g (0.0012 mol) of iodine was added, after which the mixture was refluxed for 1 hr. The brown color of the iodine disappeared about 10 min after the beginning of refluxing. When the reaction mixture was cooled, crystals came out; these were collected (0.04 g) and identified with 1,4-diiodobenzene. The reaction mixture was carefully concentrated, and after the resulting residue has been washed with 10% nitric acid it was dissolved in benzene. The benzene solution was subjected to glc, using nitrobenzene as the internal standard. The yield of iodobenzene was 78%. Using 0.64 g (0.0025 mol) of iodine, the reaction was carried out in the way described above; 1,4-diiodobenzene was thus obtained in an 86% yield, while the formation of only a trace of monoiodobenzene was detected by glc.

References

1) A. McKillop, J. S. Fowler, M. J. Zelesko, J. D. Hunt, E. C. Taylor, and G. McGillivray, *Tetrahedron Lett.*, **1969**, 2427.

2) A. McKillop, J. D. Hunt, M. J. Zelesko, J. S. Fowler, E. C. Taylor, G. McGillivray, and F. Kienzle, *J. Amer. Chem. Soc.*, **93**, 4841 (1971).

3) The trifluoroacetates of Fe(III) and Cu(II) in trifluoroacetic acid were also inert for the iodination of benzene under refluxing conditions.

4) A. McKillop, J. S. Fowler, M. J. Zelesko, J. D. Hunt, E. C. Taylor, and G. McGillivray, *Tetrahedron Lett.*, **1969**, 2423.

5) P. E. Aldrich, U. S. 3043859 (1962).

6) R. N. Haszeldine, *J. Chem. Soc.*, **1951**, 584.

7) R. Goto and H. Suzuki, *Nippon Kagaku Zasshi*, **84**, 167 (1963).

8) H. Suzuki and R. Goto, *ibid.*, **84**, 284 (1963).

The Oxyphenylation of Cyclic Olefins Conjugated to the Benzene Ring by Means of Palladium Chloride[1]

Hiroshi HORINO, Mannosuke ARAI, and Naoto INOUE
College of General Education, Tohoku University, Kawauchi, Sendai 980

(Received November 28, 1973)

The reaction of 1,2-dihydronaphthalene, indene, and acenaphthylene with phenylpalladium chloride prepared *in situ* from phenylmercuric chloride and lithium chloropalladate in aqueous acetone afforded 2-phenyltetrarol, 2-phenylindanol, and 2-phenylacenaphthenol respectively, accompanying by the corresponding phenylated olefins. Acetoxyphenylation products were also obtained in the reactions in acetic acid. The configurations of these oxyphenylated compounds were determined to be *trans*.

Recently, extensive studies of the arylation of olefins using palladium complexes have been reported.[2-5] Heck reported that the reaction of olefins with the reactive organopalladium compounds prepared *in situ* from organomercurials and palladium salts gave the substituted olefins.[3] The Heck reaction is a representative example of the addition of a reactive carbon-palladium-σ-complex to olefins. In addition, the reaction has the valuable characteristic that the arylation takes place at the carbon atom bonded to the mercury of the organomercurials. When this reaction was applied to the cyclic olefin conjugated to the benzene ring in a protic solvent, a new reaction was found in which an aryl group and an anion part of the solvents were added simultaneously to the olefins.[1]

In spite of many studies of the Heck reaction,[3,4] no report describing such a kind of product has appeared. In this paper, we will report the oxyphenylation of 1,2-dihydronaphthalene, indene, and acenaphthylene in various protic solvents.

Results and Discussion

The reaction of 1,2-dihydronaphthalene (I) with phenylmercuric chloride and lithium chloropalladate in aqueous acetone (1: 1) at room temperature gave an unexpected oxygenated compound, $C_{16}H_{16}O$ (IIIa) (mp 76—77 °C), in a 60% yield, accompanied by 2-phenyl-3,4-dihydronaphthalene (II).[6] The IR spectrum of IIIa showed an absorption band at 3300 cm^{-1} (OH) and 1020 cm^{-1} (C–O), with a characteristic signal of a doublet (1H, J=9 Hz) at 4.65 ppm in its NMR spectrum. The structure of IIIa was confirmed to be *trans*-2-phenyltetrarol by a mixed-melting-point test with an authentic sample.[7] The experiment in a mixture of dioxane and water (1: 1) gave also IIIa in a 52% yield.

In the reaction of I with phenylpalladium chloride in methanol or ethanol, methyl (IIIb) or ethyl ether (IIIc) of 2-phenyltetrarol was obtained in a 45 to 50% yield. However, the yield of isopropyl ether

TABLE 1. RESULTS OF OXYPHENYLATION IN VARIOUS SOLVENTS

Olefin	Organomercurial	Solvent	Product (% to Pd)
I	PhHgCl	Acetone–H_2O (1:1)	II (13) IIIa (60)
I	PhHgCl	Dioxane–H_2O (1:1)	II (14) IIIa (52)
I	PhHgCl	Methanol	II (12) IIIa (45)
I	PhHgCl	Ethanol	II (10) IIIc (49)
I	PhHgCl	Isopropanol	II (23) IIId (27)
I	PhHgCl	*t*-Butanol	II (57)
I	PhHgCl	Acetic acid	II (40) IIIe (14)
I	PhHgCl	Acetic acid (sodium acetate 4 mol. eq.)	II (28) IIIe (47)
I	PhHgCl	Acetone (Phenol 10 mol. eq.)	II (67)
I	*p*-Cumylmercuric chloride	Acetone–H_2O (1: 1)	IV (9) V (43)
I	β-Naphthylmercuric chloride	Acetone–H_2O (1: 1)	VI (21) VII (53)
VIII	PhHgCl	Acetone–H_2O (1: 1)	IX (16) Xa (53)
VIII	PhHgCl	Dioxane–H_2O (1: 1)	IX (26) Xa (50)
VIII	PhHgCl	Acetic acid–H_2O (1: 1)	IX (19) Xa (36) Xb (17)
VIII	PhHgCl	Acetic acid	IX (72) Xb (4)
VIII	PhHgCl	Acetic acid (Sodium acetate 4 mol.eq.)	IX (25) Xb (35)
VIII	PhHgCl	Acetone–H_2O (1: 1) (Sodium acetate 4 mol.eq.)	IX (17) Xa (62)
XI	PhHgCl	Acetone–H_2O (1: 1)	XII (—) XIIIa (48)
XI	PhHgCl	Acetic acid (Sodium acetate 4 mol.eq.)	XII (28) XIIIb (13)

(IIId) was relatively low and no alkoxy derivative was found in the reaction in *t*-butanol, while the yeild of the substitution product, II, increased with the size of the alkoxy group. The major product of the reaction in acetic acid was II, and the oxyphenylation product, IIIe, was obtained in only a 14% yield.

When the reaction was carried out in the presence of 4 molar equivalents of sodium acetate to palladium chloride, the formation of IIIe was the main reaction.

The structures of these oxyphenylated products were determined by their elemental analyses and by means of their IR and NMR spectra.

These results are shown in Table 1.

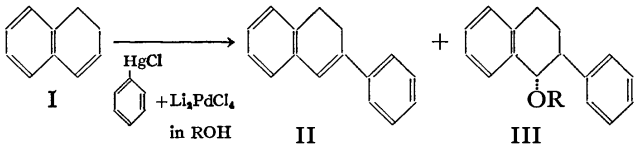

a; R=H
b; R=CH_3
c; R=CH_2CH_3
d; R=$CH(CH_3)_2$
e; R=$COCH_3$

trans-2-Phenyltetrarol and its acetate, synthesized according to the method of Hanaya,[7] were identical with the oxyphenylation products, IIIa and IIIe respectively. The treatment of IIIa with sodium hydride and subsequently with methyl iodide afforded IIIb.

The NMR data of the oxyphenylated products are shown in Table 2.

The coupling constants of hydrogen attached to carbinol carbon in the NMR spectra are found in the range of 7 to 9 Hz: this shows that the *trans* configuration is between the phenyl group and the hydroxy one.

In the reaction of I with *p*-cumyl- and *β*-naphthylmercuric chloride in aqueous acetone, the respective corresponding alcohols (V) and (VII) were obtained, accompanied by the arylated olefins, (IV) and (VI).

Table 2. IR and NMR data of oxyphenylation products

Compound No	IR (cm^{-1})			NMR	
	ν(OH)	ν(C=O)	ν(C–O)	H_1 (ppm)[a]	$J_{1,2}$ (Hz)[b]
IIIa	3300		1020	4.65	9
IIIb[c]			1040	4.58	8
IIIc[c]			1070	4.50	8
IIId[c]			1025	4.48	7
IIIe		1735	1235, 1030	6.20	8
V	3260		1030	4.72	8
VII	3390		1030	4.70	9
Xa	3200		1055	5.00	6
Xb[c]		1735	1230, 1020	6.25	5
XIIIa	3400		1030	5.24	3
XIIIb[c]		1745	1230, 1030	6.52	3

a) The chemical shift of H_1.
b) The coupling constant between H_1 and H_2. $-\overset{H_1}{\underset{OR}{C}}-\overset{H_2}{\underset{Ar}{C}}-$
c) neat.

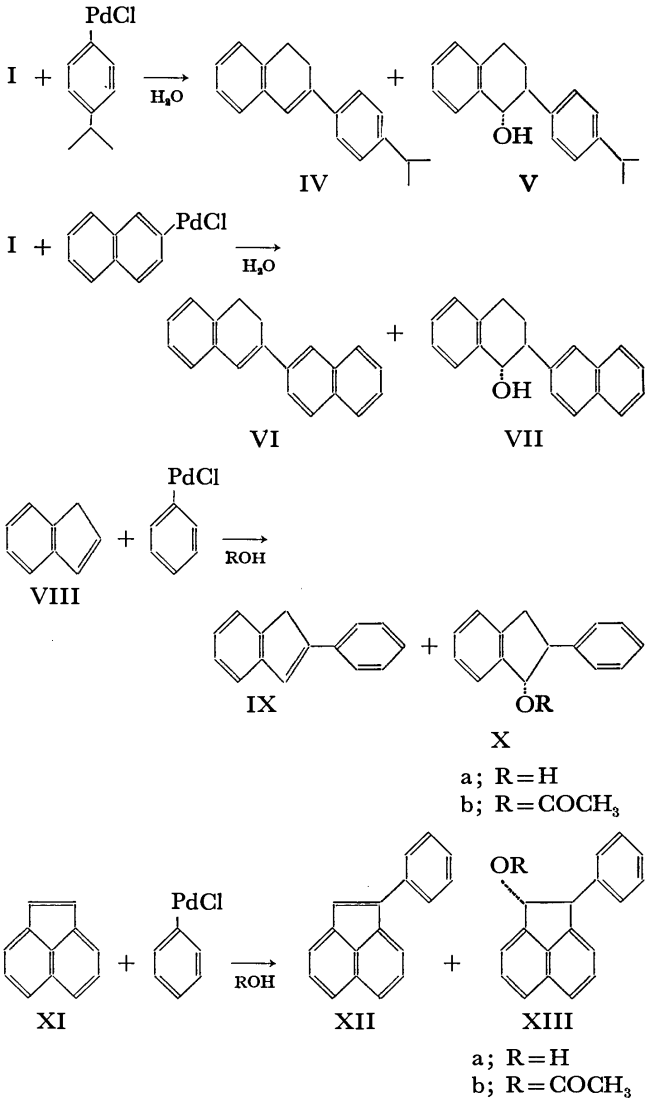

a; R=H
b; R=$COCH_3$

These structures were proved by their elemental analyses and by the spectral data shown in Table 2.

trans-2-Phenylindanol (Xa) and *trans*-2-phenylacenaphthenol (XIIIa) were obtained by the reaction of indene (VIII) and acenaphthylene (XI) respectively, with phenylpalladium chloride in aqueous acetone. The oxyphenylation products of VIII or XI in an acetic acid solution of sodium acetate were found to be *trans*-2-phenylindanol acetate (Xb) and *trans*-2-phenylacenaphthenol acetate (XIIIb). These structures were confirmed by the following experiments.

The application of hydroboration to 2-phenylindene (IX)[8] and 1-phenylacenaphthylene (XII)[9] gave the corresponding *trans* alcohols, which were identical with the oxyphenylation products, Xa and XIIIa.

These substances were then acetylated to Xb and XIIIb with acetic anhydride and pyridine.

According to the reaction mechanism proposed by Heck,[3] hydrochloric acid and mercuric chloride are produced in the reaction of olefins with phenylmercuric chloride and lithium chloropalladate.

Thus, the catalytic action of these acids might bring about an addition reaction of water to the arylated olefins.

The treatment of II (or IX) with hydrochloric acid

(two molar equivalents of II) or mercuric chloride (equimolecular) in an aqueous acetone mixture (1: 1) resulted in the recovery of II (or IX).

The same results were observed in the case of methanol.

The presence of sodium acetate in the reaction mixture of I or VIII with phenylpalladium chloride caused an increase in the acetoxy- and hydroxyphenylation products at the expense of the arylated olefin, as is shown in Table 1. Therefore, it is clear that the oxyphenylation products were not derived from the arylated olefins.

The function of sodium acetate is probably not only to neutralize hydrochloric acid, but also to raise the nucleophilic attack of acetic acid on the reactive intermediate. Taking into account the fact mentioned above, the same reaction intermediate as that of the Heck reaction may be assumed to give the oxyphenylation product as well as the arylated olefin:

$$ArHgCl + PdCl_2 \longrightarrow ArPdCl + HgCl_2$$

$$ArPdCl + \underset{}{\overset{H}{\diagdown}}C{=}C\underset{}{\overset{}{\diagup}} \longrightarrow$$

$$\longrightarrow \underset{}{\overset{Ar}{\diagdown}}C{=}C\underset{}{\overset{}{\diagup}} + HPdCl \quad \text{(Heck reaction)}$$

$$Ar\text{-}\overset{H}{\overset{|}{C}}\text{-}\overset{|}{C}\text{-}PdCl \xrightarrow{ROH} Ar\text{-}\overset{H}{\overset{|}{C}}\text{-}\overset{|}{C}\text{-}OR + HPdCl \quad \text{(Oxyphenylation)}$$

Heck suggested a step-by-step and stereospecific reaction mechanism including a *cis*-elimination of the hydridopalladium species.[3]

When this reaction mechanism is applied to the cyclic olefins, I, VIII, and XI, the organopalladium intermediates may be represented by the following formulae, (XIVa), (XIVb), and (XIVc) respectively.

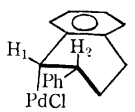

XIVa

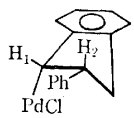

XIVb

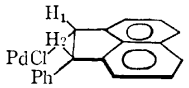

XIVc

The *trans*-configurations of benzylic hydrogen, H_2, and the palladium atom in XIVa, XIVb, and XIVc make the *cis*-elimination of hydridopalladium chloride difficult. Thus, the reaction intermediates with long lives are subjected to nucleophilic replacement by protic solvents. The *trans*-configuration between the phenyl group and the acetoxy, alkoxy, or hydroxy group means that the solvent anion attacks the carbon atom bearing a palladium atom from the back side of the metal. The reaction mechanism proposed above is consistent with the results of the acetoxypalladation studies of cyclohexene by Henry,[10] in which the nucleophilic attack of the acetate ion on palladium occurred from outside the co-ordination sphere in an S_N2 fashion.

In conclusion, the oxyphenylation has presented an useful method for synthesizing *trans*-2-phenylcycloalkanols from benzocycloalkenes. The extension of the reaction to acyclic olefins, *e.g.*, methylstyrenes, is now under investigation.

Experimental

All the melting points are uncorrected. The IR and NMR spectra were measured with a Hitachi 215 grating infrared spectrometer by the KBr disk method, and with Varian A-60D (60 MHz) in carbon tetrachloride, using TMS as the internal standard.

Materials. The following compounds were synthesized by the method described in the literature: phenylmercuric chloride,[11] *p*-cumylmercuric chloride,[3] *β*-naphthylmercuric chloride,[12] and 1,2-dihydronaphthalene.[13] Indene and acenaphthylene of a commercial grade were used.

Reaction of I with Phenylmercuric Chloride and Lithium Chloropalladate in a Mixture of Acetone and Water (1: 1). To a solution of palladium chloride (356 mg, 2 mmol) and lithium chloride (168 mg, 4 mmol) in a mixture of acetone and water (1: 1) (20 ml), I (290 mg, 2.2 mmol) and then phenylmercuric chloride (626 mg, 2 mmol) were added, after which the mixture was stirred for 6 hr at room temperature. The mixture was then added to 100 ml of a saturated solution of sodium chloride, and the resulting oil was extracted with benzene.

The benzene layer was dried over anhydrous sodium sulfate and evaporated under reduced pressure to give a yellow oily residue (430 mg). The residue was chromatographed on silica gel. Elution with *n*-hexane and a mixture of benzene and *n*-hexane (1: 1) gave colorless crystals (II) (51 mg, 13%, mp 58—60 °C) and a yellow oil (IIIa) (269 mg, 60%) respectively. The latter was crystallized from *n*-hexane; mp 76—77 °C. Neither showed any depression in a mixed-melting-point test with 2-phenyl-3,4-dihydronaphthalene[6] and *trans*-2-phenyltetrarol.[7]

In a similar way, the following experiments in various solvents were carried out. The yields and spectrographic data of the oxyphenylation products are shown in Table 1 and Table 2.

In Methanol; *trans*-2-Phenyltetrarol methyl ether IIIb; colorless oil; bp 133—136 °C/1 mmHg.

Found: C, 85.86; H, 7.50%. Calcd for $C_{17}H_{18}O$: C, 85.67; H, 7.61%.

In Ethanol; *trans*-2-Phenyltetrarol ethyl ether IIIc; colorless oil; bp 142—144 °C/3 mmHg.

Found: C, 85.16; H, 8.38%. Calcd for $C_{18}H_{20}O$: C, 85.67; H, 7.99%.

In 2-Propanol; *trans*-2-Phenyltetrarol isopropyl ether IIId; colorless crystals; mp 59—60 °C; recrystallized from *n*-hexane.

Found: C, 84.94; H, 8.46%. Calcd for $C_{19}H_{22}O$: C, 85.67; H, 7.99%.

In an Acetic Acid Solution of Sodium Acetate; To an acetic acid solution of palladium chloride (356 mg, 2 mmol) and lithium chloride (168 mg, 4 mmol), I (290 mg, 2.2 mmol), sodium acetate (656 mg, 8 mmol), and phenylmercuric chloride (626 mg, 2 mmol) were added successively. The mixture was then stirred for 7 hr at room temperature, and the reaction mixture was treated as has been described above.

trans-2-Phenyltetrarol acetate IIIe: colorless crystals; recrystallized from ethanol; mp 113—114 °C.

Found: C, 81.15; H, 6.83%. Calcd for $C_{18}H_{18}O_2$: C, 81.17; H, 6.81%.

This substance showed no depression in a mixed-melting-point with an authentic sample.[7]

The following procedure was carried out in the same way as in the reaction of I with phenylmercuric chloride and lithium

chloropalladate except for the use of *p*-cumylmercuric chloride and *β*-naphthylmercuric chloride instead of phenylmercuric chloride.

Reaction of I with p-*Cumylmercuric Chloride and Lithium Chloropalladate in a Mixture of Acetone and Water (1: 1).* 2-Isopropylphenyl-3,4-dihydronaphthalene IV; mp 68 °C.

Found: C, 92.26; H, 7.74%. Calcd for $C_{19}H_{20}$: C, 91.88; H, 8.12%.

trans-2-Isopropylphenyltetrarol V; mp 116 °C.

Found: C, 85.70; H, 8.64%. Calcd for $C_{19}H_{22}O$: C, 85.67; H, 8.33%.

Reaction of I with β-Naphthylmercuric Chloride and Lithium Chloropalladate in a Mixture of Dioxane and Water (1: 1). 2-*β*-Naphthyl-3,4-dihydronaphthalene VI; mp 150—151 °C; recrystallized from ethanol.

Found: C, 93.71; H, 6.29%. Calcd for $C_{20}H_{16}$: C, 93.67; H, 6.34%.

trans-2-*β*-Naphthyltetrarol VII; mp 118—119 °C: recrystallized from *n*-hexane.

Found: C, 87.46; H, 6.73%. Calcd for $C_{20}H_{18}O$: C, 87.56; H, 6.61%.

Analogous procedures were undertaken in the reaction of indene VIII with phenylmercuric chloride and lithium chloropalladate in a mixture of acetone and water (1: 1) and also in an acetic acid solution of sodium acetate.

2-Phenylindene IX;[9] mp 164—165 °C; recrystallized from benzene.

Found: C, 94.01; H, 6.44%. Calcd for $C_{15}H_{12}$: C, 93.71; H, 6.29%.

trans-2-Phenylindanol Xa; mp 82—83 °C; recrystallized from *n*-hexane.

Found: C, 85.49; H, 6.55%. Calcd for $C_{15}H_{14}O$: C, 85.68, H, 6.71%.

trans-2-Phenylindanol acetate Xb; bp 163—165 °C/1 mmHg;

Found: C, 80.00; H, 6.31%. Calcd for $C_{17}H_{16}O_2$: C, 80.92; H, 6.83%.

Reaction of Acenaphthylene (XI) with Phenylmercuric Chloride and Lithium Chloropalladate in a Mixture of Acetone and Water (1: 1). In a similar manner, the reaction of XI (457 mg 3.3 mmol) with phenylmercuric chloride (940 mg, 3 mmol) in a solution of lithium chloropalladate (130 mg, 3 mmol) was carried out to give yellow crystals (XIIIa) (354 mg, mp 97—98 °C) which were later recrystallized from a mixture of benzene and *n*-hexane. The crystals were found to be identical with the *trans*-2-phenylacenaphthenol synthesized as will be described below by a comparison of their IR spectra and by a mixed-melting-point test.

Synthesis of trans-*2-Phenylacenaphthenol from 1-Phenylacenaphthylene.* 1-Phenylacenaphthylene (684 mg) was dissolved in a solution of sodium borohydride (324 mg) in dried tetrahydrofuran (30 ml).

To the solution boron trifluoride etherate (1.2 ml) was added, drop by drop, at 23 °C for 20 min. After the reaction mixture had then been stirred for 1 hr, water (1 ml) was added to decompose the excess diborane. To the solution was added 3 M sodium hydroxide (1.5 ml) and then 30% hydrogen peroxide (1.5 ml), drop by drop, at 40 °C. After the solution had been stirred for 1 hr, it was poured into water and extracted with ether. The ether extract was concentrated, and the residual paste (820 mg) was chromatographed on a silica gel column. Elution with benzene gave *trans*-2-phenylacenaphthenol as colorless crystals (298 mg); mp 99—100 °C; recrystallized from a mixture of benzene and *n*-hexane.

Found: C, 87.43; H, 5.74%. Calcd for $C_{18}H_{14}O$; C, 87.77; H, 5.73%.

Besides, elution with a mixture of benzene and *n*-hexane (1: 10) gave a recovery of 1-phenylacenaphthylene (XII) (338 mg).

The authors wish to express their thanks to the Kawaken Fine Chemical Co., Ltd., for its gift of palladium chloride.

References

1) A part of this paper has been reported in a preliminary communication; H, Horino and N. Inoue, This Bulletin, **44**, 3210 (1971).

2) Y. Fujiwara, I. Moritani, R. Asano, and S. Teranishi, *J. Amer. Chem. Soc.*, **91**, 1766 (1969).

3) R. F. Heck, *ibid.*, **90**, 5518 (1968). R. F. Heck, *ibid.*, **91**, 6707 (1969).

4) A. Kasahara, T. Izumi, G. Saito, M. Yodono, K. Saito, and Y. Goto, This Bulletin, **45**, 895 (1972).

5) T. Mizoroki, K. Mori, and A. Ozaki, *ibid.*, **44**, 581 (1971).

6) N. C. Campbell and D. Kidd, *J. Chem. Soc.*, **1954**, 2154.

7) K. Hanaya, *Nippon Kagaku Zasshi*, **87**, 745 (1966).

8) J. von Braun and G. Manz, *Ber.*, **62**, 1062 (1929).

9) W. A. Bonner and C. J. Callin, *J. Amer. Chem. Soc.*, **75**, 3831 (1957).

10) P. M. Henry, *ibid.*, **93**, 1494 (1971).

11) H. C. Brown and C. W. McGray, *ibid.*, **77**, 2300 (1955).

12) A. N. Nesmejanow, "Organic Syntheses," Coll. Vol. II, p. 432 (1943).

13) H. Hock and F. Depke, *Chem. Ber.*, **83**, 317 (1950)

Pyridoxal Model Compounds. I. The Regioselective Formylation of Methoxy-substituted Aromatic Compounds[1]

Masaaki IWATA and Sakae EMOTO

The Institute of Physical and Chemical Research, Wako-shi, Saitama 351

(Received December 8, 1973)

9-Substituted 2-methoxyanthracenes (IVa—d) and -triptycenes (Va, b), and 3-substituted anisoles (VIa, b) were formylated by the use of the Vilsmeier-Haack method (Method A) and the metallation method using *n*-butyllithium (Method B). By the Method A, IVa—c, Vs', and VIs' were regioselectively formylated at C-1, C-3, and C-6 respectively, without exception, while by the Method B IVa—c, Va, VIa, and VIb were regioselectively formylated at C-3, C-3, C-2, and C-6 respectively, and Vb gave C-1 and C-3 formylated derivatives in the ratio of 10 to 1 respectively. Possible transition states concerning the occurrence of the regioselectivity were proposed and discussed.

Pyridoxal catalyzes many reactions of amino acids,[2] and the study of the reaction mechanism has shown that the *ortho*-positioning of the formyl and the hydroxy groups on the pyridine ring is essential to the activity.[3] In practice, it has been demonstrated that salicylaldehyde derivatives with a similar interrelation of these two functional groups to pyridoxal indicate a pyridoxal-like activity for amino acids.[4] On the basis of this advanced knowledge, we designed synthetic schemes to obtain new model compounds of pyridoxal functioning, as expected, as an "asymmetric inversion catalyst".[5] In the present paper we wish to report the first example of the regioselective formylation at *ortho*-positions of these methoxy-substituted aromatic compounds: 9-substituted 2-methoxyanthracenes (IVa—c), 9-substituted 2-methoxytriptycenes (Va, b), and 3-substituted anisoles (VIa, b).

Since, to our knowledge, there is a dearth of systematical investigations concerning the regioselective introduction of a formyl group into methoxy-substituted aromatic compounds, our interest was focused on the elucidation of the reactivity of these compounds for Vilsmeier-Haack reagents and *n*-butyllithium.

Results and Discussion

Synthesis of Starting Materials. The 2-methoxyanthracenes (IVa—d) were prepared in four steps from the reaction of phthalic anhydride with anisole. The reduction of *o*-(*p*-methoxybenzoyl)benzoic acid (I) with zinc–ammonia gave *o*-(*p*-methoxybenzyl)benzoic acid (II) quantitatively. In this step, the Clemmensen reduction (zinc–hydrochloric acid) of (I) yielded II and 3-(*p*-methoxyphenyl)phthalide (IIa) in a ratio of about 2 to 1 respectively.[6] The Wolff-Kishner reduction (hydrazine–*n*-butanol–potassium hydroxide) of (I) afforded only 3-(*p*-methoxyphenyl)-6-oxo-1H-phthalazine (IIb). The dehydrative cyclization of II with concd. sulfuric acid gave 2-methoxy-9-anthrone (III) in a good yield; it was then treated with the corresponding Grignard reagents to give IVa—c. To exemplify and compare the results with those of the literature,[7] 2-methoxyanthracene (IVd) was prepared by the reduction of III with sodium borohydride. 2-Methoxytriptycenes (Va, b) were synthesized by the addition of IVa and IVd respectively to benzyne.

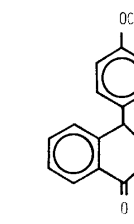

IIa

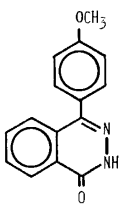

IIb

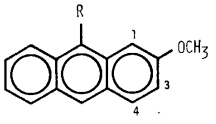

IVa R=2-*p*-cymenyl
IVb R=$-C_6H_5$
IVc R=$-CH_3$
IVd R=–H

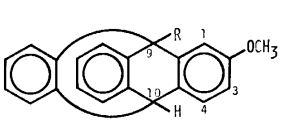

Va R=2-*p*-cymenyl
Vb R=–H

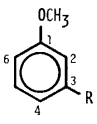

VIa R=$-OCH_3$
VIb R=*tert*-C_4H_9

Regioselective Formylation. Formylation was carried out by the use of two methods: the Vilsmeier-Haack method (Method A)[8] and the metallation method using *n*-butyllithium–*N*-methylformanilide (Method B).[9] The results obtained are shown in Table 1.

Table 1. The regioselective formylation of methoxy-substituted aromatic compounds. Yields and the formylated positions

Compound	Method A		Method B	
	Formylated position	Yield(%)	Formylated position	Yield(%)
IVa	1	98	3	71
IVb	1	50	3	64
IVc	1	48	3	63
IVd[a]	1, 3	40, 23[b]	—	—
Va	3	79	3	58
Vb	3	82	1, 3	41, 4[c]
VIa	6[d]	62[d]	2[e]	75[e]
VIb	6	95	6	17

a) In the lit.[7] 1 and 3 formylated products have been obtained in almost equal amounts in about 70% total yield. b) 40% for 1 and 23% for 3. c) 41% for 1 and 4% for 3. d) By use of dimethylformamide and phosphorus oxychloride,[10] the same C-6 formylated product has been regioselectively obtained in 85% yield. e) By metallation with phenyllithium and subsequent formylation with *N*-methylformanilide in abs. ether at r.t.,[11] the same C-2 formylated product has been regioselectively obtained in 55% yield.

The data listed in Table 1 indicate (a) that the formylation according to Method A is strictly regioselective for all types of compounds and that the formylated position is independent of the substituent group in each case and (b) that the formylation according to Method B is less selective and that the regioselectivity is dependent on the substituent group except for the case of anthracenes.

The Determination of the Structures of Formylated Compounds. The structures of the formylated compounds were determined by the use of IR, UV, NMR, and elemental analyses. The lanthanide-induced NMR spectra were especially effective for the determination of the introduced position of the formyl group.

The NMR Spectral Data. The lanthanide-induced spectra with the aid of tris(dipivalomethanato)europium(III), $Eu(DPM)_3$, were measured for all the formylated anthracenes and triptycenes. From the spectra, the following findings were obtained: (a) the metal ion of the shift reagent associated more tightly with the aldehyde oxygen atom than with the methoxy group: (b) the formyl proton of the C-3 position experiences greater shift than that of the C-1 position by about 10 factors, and (c) the effect of the interaction between the shift reagent and the neighboring protons of the formyl group is transferred more effectively through the bond than the space. Detailed analyses of the induced spectra are in progress; the results will be published in the forthcoming paper.

On the basis of these findings the chemical shifts and the coupling constants of the main protons of the formylated compounds in the original NMR spectra were assigned as is shown in Tables 2 and 3. In the C-1 formylated 9-arylanthracenes, the aldehydic protons appears in a higher field than that of the other aldehydic protons by *ca.* 1.3 ppm (Table 2). The shift may be due to the anisotropic effect of the ring current of the peri-aryl substituent and to the steric effect of the peri-substituent affecting the non-coplanarity of the formyl group and the aromatic ring. The C-1 aromatic proton of the C-3 formylated anthracenes may experience a similar ring current anisotropy of the 9-aryl group and reveals a chemical shift at a higher field. In the NMR data of triptycenes (Table 3), the formyl protons showed the normal chemical shifts. However, in the C-1 formylated triptycene the C-9 methine proton was deshielded by the anisotropic effect of the adjacent formyl group and showed a chemical shift at a field lower by 1.97 ppm than that of the C-3 formylated triptycene. In Table 4, the chemical shifts and the coupling constants of the formylated anisoles are collected. One of the aromatic protons at the *meta*-position of the formyl group showed spin-spin coupling with the formyl proton when one of the *ortho*-positions of the formyl group was not substituted.[12]

The UV Spectral Data. The structural features of the formylated compounds were well reflected on the UV spectra. The UV spectral data of some of the anthracene derivatives are summarized in Table 5. In the table the original ^1B_b band, the longitudinally-polarized transition, at 255—259 nm splits into two electronic transitions of nearly equal intensities when the C-3 position is formylated. One appears on the shorter-wavelength side, and the other, on the side longer than the original band. The spacings of these bands are almost constant; in the C-3 formylated compound of IVd, 266.5—244.2=22.3 nm, and in that of IVa, 277—256=21 nm. Therefore, it is apparent that these two ^1B_b bands are due to the longitudinal polarization in the directions of both the methoxy and the formyl groups. The vibrational structures of the transversely-polarized ^1L_a bands on the side with wave-

TABLE 2. NMR DATA OF FORMYLATED COMPOUNDS OF 2-METHOXYANTHRACENES

δ ppm (J in Hz)

Compounds		Solv.	C_1–H	C_3–H	C_4–H	C_{10}–H	$-OCH_3$	–CHO
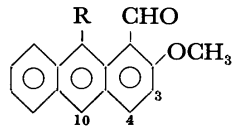	R=2-*p*-cymenyl	CCl_4	—		8.01 J=9.5	8.33	3.82	9.41
	R=–C_6H_5	CCl_4	—	7.03 J=9.2	7.71 J=9.2	8.14	3.76	9.41
	R=–CH_3	$CDCl_3$	—	7.23 J=9.5	8.06 J=9.5	8.21	4.03	10.85
	R=–H	$CDCl_3$	—	7.45 J=9.0	8.07 J=9.0	8.31	4.06	10.94
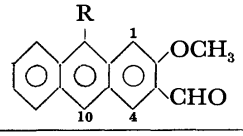	R=2-*p*-cymenyl	$CDCl_3$	6.76	—	8.54	8.60	3.74	10.56
	R=–C_6H_5	CCl_4	6.76	—	8.46	8.46	3.73	10.47
	R=–CH_3	$CDCl_3$	7.34	—	8.35	8.47	4.07	10.52
	R=–H	$CDCl_3$	7.23	—	8.46	8.46	3.97	11.36

TABLE 3. NMR DATA OF FORMYLATED COMPOUNDS OF 2-METHOXYTRIPTYCENES

δ ppm (J in Hz)

Compounds		Solv.	C_1–H	C_3–H	C_4–H	C_9–H	C_{10}–H	$-OCH_3$	–CHO
1-Formyl-2-methoxytriptycene		$CDCl_3$	—	6.44 J=8.0	7.37 J=8.0	7.33	5.29	3.74	10.55
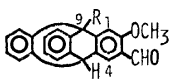	R=2-*p*-cymenyl	$CDCl_3$	6.92	—	7.75	—	5.34	3.76	10.24
	R=–H	CCl_4	7.02	—	7.76	5.36	5.36	3.85	10.25

Table 4. NMR data of formylated compounds of anisoles

Compounds	Solv.	C_2–OCH_3	C_4–OCH_3	C_6–OCH_3	C_3–H	C_4–H	C_5–H	C_6–H	–CHO
					δ ppm (J in Hz)				
2,6-Dimethoxybenzaldehyde	CCl_4	3.86	—	3.86	6.51 J=8.5	7.35 J=8.5	6.51 J=8.5	—	10.39
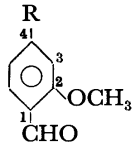 R=–OCH_3	CCl_4	3.88	3.84	—	6.34 J=2.2	—	6.47 J=8.5 2.2 0.75	7.71 J=8.5	10.20 J=0.75
R=*tert*-C_4H_9	CCl_4	3.93	—	—	6.92 J=1.8	—	6.98 J=8.0 1.8 0.8	7.68 J=8.0	10.33 J=0.8

Table 5. The UV spectral data of the anthracene derivatives (in Ethanol)

IVa		λ_{max}	259	318	333.5	351	376	396.5	
		log ε	5.07	3.41	3.69	3.79	3.79	3.79	
IVd		λ_{max}	255	314	329	346.5	368.5	388.5	
		log ε	5.15	3.38	3.61	3.67	3.60	3.59	
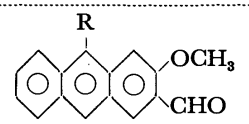	R=–H	λ_{max}	244.2	266.5	354^s	371	419		
		log ε	4.68	4.76	3.64	3.91	3.80		
	R=2-*p*-cymenyl	λ_{max}	256	277	330	347	365	399	432 451^s
		log ε	4.67	4.70	3.70	3.83	3.72	3.35	3.39 3.33
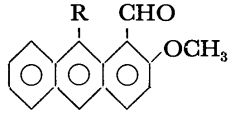	R=–H	λ_{max}	251	263.5^s	281^s	295^s	314^s	346	364 416.5
		log ε	4.84	4.50	4.25	4.01	3.63	3.64	3.83 3.65
	R=2-*p*-cymenyl	λ_{max}	261	324.5	343	361	394	415.5^s	
		log ε	4.94	3.50	3.62	3.74	3.80	3.72	

s: shoulder band

lengths longer than 314 nm disappeared when the C-1 or C-3 positions of IVd and the C-3 position of IVa were formylated. However, in the C-1 formylated derivative of IVa the vibrational characteristics remained considerably clear, although the bands showed slightly bathochromic shifts. This may be assumed to be due to the non-coplanarity of the formyl group and the anthracene ring affected by the steric overlap of the formyl group with the aryl group at the peri-position and the methoxy group at C-2; this reliable assumption coincides with the results of the analysis of the NMR spectral data.

Possible Transition States of Formylation. By many authors[13] since Vilsmeier,[8] several reaction mechanisms have been proposed for the Vilsmeier-Haack reaction. Of these proposals, it seems most reasonable to adopt the mechanism suggested by Bosshard and Zollinger,[14] where the following reactive intermediate (VII) of the formylating reagents attacks the most electron-rich

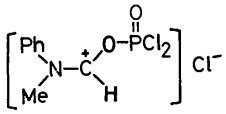

VII

position of the substrate molecule. However, it should be noted that VII is bulky around the positive charge and that, thus, VII would select the reaction point of the substrate with respect not only to the electronic density but also to the steric environment if there is not much difference in electronic density. Practically, from the results shown in Table 1, it seems clear that, in methoxyanthracenes (IVa—d), the regioselectivity of formylation by Method A is due only to the difference in electronic density,[15] and that in methoxytriptycenes (Va, b) and methoxybenzenes (VIa, b) the steric factors govern the reaction predominantly. Typically, for example, in methoxytriptycenes involving a C_s point group the transition state of formylation attacking the C-1 position could be shown by a tetrahedral intermediate like VIII. In this model it is apparent that the attack of the formylating active species (VII) on the C-1 position may be prevented because of the steric interaction of VII with the bridged benzene rings and the C-9 substituent. Therefore, the C-3 position will be regioselectively formylated in methoxytriptycenes. In a similar manner, it may be

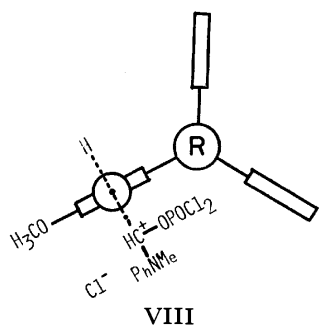

VIII

Fig. 1. A transition state model of formylation of methoxytriptycenes. VIII is projected from the front side of the R-axis and C-9 carbon is on the plane. The rectangle shows the hydrogen-abbreviated benzene ring.

suggested that the results of formylation in anisoles can be explained by the steric interaction of VII and the substituent, and that the C-6 position is regioselectively formylated.

In formylation by the metallation method (Method B), it was empirically observed that no types of aromatic compounds were formylated by the addition of *N*-methylformanilide without the formation of the dark green or blue colored complex of the substrate with *n*-butyllithium. Thus, the driving force of formylation by Method B seems to be the formation of the lithium complex, doubtless a radical anion. Although, unfortunately, the reactivity of the radical anions is not yet known in detail,[16] the results found by Method B may be explained on the basis of the following assumptions: (a) the electronic distribution of the substrate is quite different from that of the substrate-lithium complex, and (b) the unstable lithium complex and the transition state of formylation have nearly the same energy content, and thus their interconversion will involve only a small reorganization of the molecular structure, in agreement with the Hammond's postulation.[17] In methoxyanthracenes the fact that the C-3 position is regioselectively formylated without exception may be understood on the basis of the (a) assumption; that is, the C-3 position may be nucleophilically more active than the C-1 position in the complex state. The experimental results that the dependency of formylation on the substituents was shown in triptycenes and anisoles seem to give evidence of the least gap of the energy content being between two reactive positions in the complex, as is indicated in the cases of Vb and VIa. Also, the results in Va and VIb seem alternatively to demonstrate that the substituent effects on formylation may be due to mainly the steric effect. Therefore, it could be concluded that, in the case of Method A, the reaction selectivity may be determined by the steric interaction of the formylating reagents with the substrate in the transition state and the electronic density, while in Method B the perturbation of the electronic distribution of the substrate in the complex state may cause the regioselectivity of the formylated positions.

Experimental

The instruments for spectral measurements were a Shimadzu IR-27 (IR) apparatus, a Hitachi 124 spectrophotometer (UV), and a Varian HA-100D (NMR) apparatus. Merck Art. 7734 was used for the preparative separation of products on a silica gel column by elution chromatography, and Wakogel B-5 UA, for thin-layer chromatography. The *m*-methoxyanisole (VIa) was commercially available, and the *m-tert*-butylanisole (VIb) was obtained by the methylation of the corresponding phenol (commercially available) with dimethyl sulfate in a good yield. The melting points are uncorrected.

o-(p-Methoxybenzoyl)benzoic Acid (I). To a mixture of phthalic anhydride (148 g, 1 mol) and anisole (250 ml) in 250 ml of carbon disulfide we added 140 g of aluminium chloride under vigorous stirring at room temperature. After all the anhydride disappeared to form a viscous dark red solution, the solution was hydrolyzed with ice water, and the solvents were removed by steam distillation. From the cooled residual solution, a grey solid was precipitated. After most of the supernatant solution had been decanted, *ca.* 1000 ml of chloroform was poured into the flask to dissolve the solid and the organic layer was separated. The solvent was then evaporated to give almost pure (I) (204—250 g; 80—97%). For analytical use, a part of the solid was recrystallized from acetic acid; colorless plates; mp 122—123.5 °C. Found: C, 70.30; H, 4.65%. Calcd for $C_{15}H_{12}O_4$: C, 70.30; H, 4.72%. IR (KBr disk): ν_{max} 1664 (–CO–) and 1689 (–COOH) cm^{-1}.

o-(p-Methoxybenzyl)benzoic Acid (II). In a three-necked flask, 64 g (0.25 mol) of (I), 600 ml of 20% ammonia, and 60 ml of 20% ammonia containing 5 g of cupric sulfate were successively added, after which the mixture was heated until gentle reflux. Then 150 g of zinc powder was added in limited amounts. After having been stirred at 95—100 °C for 24 hr, the mixture was cooled and filtered to give a transparent solution which was acidified by the addition of *ca.* 1500 ml of 10% hydrochloric acid. The white precipitate was collected and dried to give II (50.6—57.6 g; 84—95%). For analytical use, a part of the solid was recrystallized from 50% aqueous ethanol; colorless fine crystals; mp 117—118 °C. Found: C, 74.29; H, 5.75%. Calcd for $C_{15}H_{14}O_3$: C, 74.36; H, 5.83%. IR (KBr disk): ν_{max} 1680 (–COOH) and 1250 (=C–O–C) cm^{-1}.

2-Methoxy-9-anthrone (III). Fine powdered II (57.6 g, 0.238 mol) was dissolved in 250 ml of ice-cold concd. sulfuric acid, after which the mixture was stirred at 0—5 °C for 2 hr. Then the solution was poured into *ca.* 2000 ml of ice water to give III (35.8 g; 67%) as a yellow solid. The solid was purified by elution chromatography with THF; fine yellow needles; mp 96—97.5 °C. IR (KBr disk): ν_{max} 1648 (–CO–) and 1296 (=C–O–C) cm^{-1}. The purified III was used for the subsequent reactions.

Synthesis of 9-Substituted 2-Methoxyanthracenes by the Grignard Reaction. General Procedure. The compounds from IVa—IVc were synthesized by the following procedure. Into 0.02 mol of turnings-magnesium in 30 ml of dry THF, 0.02 mol of the corresponding aryl or alkyl bromide was vigorously stirred under a nitrogen atmosphere at room temperature. To the resulting Grignard reagent 0.01 mol of III in 20 ml of THF was added drop by drop at the temperature of ice water. After the completion of the reaction, followed by tlc, the reaction mixture was hydrolyzed with ice water containing ammonium chloride, acidified with *ca.* 6M HCl, and stirred until all the corresponding 9-substituted 2-methoxy-9-anthranol had been dehydrated to the corresponding 9-substituted 2-methoxyanthracene. The mixture was extracted with ethyl acetate, and the organic layer was separated and dried with anhydrous Na_2SO_4. After the removal of the solvents under reduced pressure, the residue was chromatographed on a silica gel column with benzene to give the corresponding pure 9-substituted 2-methoxyanthracenes.

9-(2-p-Cymenyl)-2-methoxyanthracene (IVa). Obtained in a 76% yield; a yellow green viscous liquid. Found: C, 88.09; H, 7.10%. Calcd for $C_{25}H_{24}O$: C, 88.19; H, 7.11%. NMR (CCl_4): δ 1.27 (6H, d, J=7.0 Hz, $-CH(C\underline{H}_3)_2$), 1.83 (3H, s, $Ar-C\underline{H}_3$), 3.86 (1H, qui, J=7.0 Hz, $-C\underline{H}(CH_3)_2$), 7.03 (1H, quar, J=2.7, 9.0 Hz, C_3–H), and 7.82 (1H, d, J=9.0 Hz, C_4–H) ppm. IR (neat): ν_{max} 1632, 1468, 1268, 1230, and 1210 cm^{-1}. UV data are shown in Table 5.

9-Phenyl-2-methoxyanthracene (IVb). Yield, 96%; pale yellow plates; mp 100—102 °C. Found: C, 88.71; H, 5.62%. Calcd for $C_{21}H_{16}O$: C, 88.70; H, 5.67%. NMR (CCl_4): δ 3.63 (3H, s, $-OCH_3$), 6.71 (1H, d, J=2.7 Hz, C_1–H), 7.04 (1H, quar, J=2.7, 9.0 Hz, C_3–H), 7.80 (1H, d, J=9.0 Hz, C_4–H), and 8.27 (1H, s, C_{10}–H) ppm. UV (ethanol): λ_{max} (log ε) 258.2 (5.10), 318 (3.41), 333.8 (3.67), 351.5 (3.78), 376.5 (3.76), and 396 (3.76) nm. IR (KBr disk): ν_{max} 1628 and 1225 cm^{-1}.

9-Methyl-2-methoxyanthracene (IVc). Yield, in 64%; light yellow needles; mp 147—149 °C. Found: C, 86.25; H, 6.18%. Calcd for $C_{16}H_{14}O$: C, 86.45; H, 6.35%. NMR (CCl_4): δ 2.97 (3H, s, Ar–CH_3), 3.95 (3H, s, –OCH_3), 7.70 (1H, quar, J=2.7, 9.0 Hz, C_3–H), 7.79 (1H, d, J=9.0 Hz, C_4–H), 7.26 (1H, d, J=2.7 Hz, C_1–H), and 8.13 (1H, s, C_{10}–H) ppm. UV (ethanol): λ_{max} (log ε) 259 (5.16), 319 (3.36), 334 (3.61), 352 (3.71), 377 (3.72), and 397 (3.71) nm. IR (KBr disk): ν_{max} 1630, 1469, 1213, and 735 cm^{-1}.

2-Methoxyanthracene (IVd). III (1.5 g, 0.067 mol) was reduced with 0.265 g (0.07 mol) of sodium borohydride in ethanol and hydrolyzed with ice water containing methanol and *ca.* 6 M HCl. The precipitate was collected by filtration, and the solid was dehydrated in benzene by then addition of concd. sulfuric acid with vigorous stirring overnight. The supernatant solution was then separated, and the solvent was removed under reduced pressure. The residue was chromatographed on a silica gel column with benzene to give IVd (1.20 g, 86%) as a pale yellow solid; mp 163—165 °C. Found: C, 86.66; H, 5.85%. Calcd for $C_{15}H_{12}O$: C, 86.51; H, 5.81%. NMR ($CDCl_3$): δ 3.76 (3H, s, –OCH_3), 7.04 (1H, quar, J=2.4, 9.0 Hz, C_3–H), 7.85 (1H, d, J=9.0 Hz, C_4–H), 8.21 (1H, s, C_9–H), and 8.29 (1H, s, C_{10}–H) ppm. IR (KBr disk): ν_{max} 1640, 1465, 1214 (=C–O–C), and 875 $cm.^{-1}$ The UV data are shown in Table 5.

Synthesis of 9-(2-p-Cymenyl)-2-methoxytriptycene (Va) and 2-Methoxytriptycene (Vb). The preparation of benzyne and its addition to anthracenes were carried out by the same method as has been described previously.[18] Then the products were isolated by elution-column chromatography with cyclohexane–benzene (1 : 9 v/v). Va was obtained in a 27% yield as a yellow viscous liquid. Found: C, 89.39; H, 7.04%. Calcd for $C_{31}H_{28}O$: C, 89.38; H, 6.78%. UV (cyclohexane): λ_{max} (log ε): 226 (4.42), 244 (s) (4.01), 255 (s) (3.74), 261 (3.60), 269.5 (3.57), 277 (3.60) and 289.5 (3.49) nm. IR (neat): ν_{max} 1460, 1280, and 1230 $cm.^{-1}$ NMR (CCl_4): δ 1.39 (6H, d, J=7.5 Hz, –$CH(CH_3)_2$), 1.77 (3H, s, Ar–CH_3), 3.59 (3H, s, –OCH_3), 5.19 (1H, s, C_{10}–H), 6.36 (1H, quar, J=2.5, 8.0 Hz, C_3–H), and 7.17 (1H, d, J=8.0 Hz, C_4–H) ppm. Vb was obtained in a 33% yield as pale yellow crystals from petroleum ether; mp 173—174 °C. Found: C, 88.75; H, 5.50%. Calcd for $C_{21}H_{16}O$: C, 88.70; H, 5.67%. UV (cyclohexane): λ_{max} (log ε) 224.5 (4.19), 273 (3.62), 280 (3.75), and 291 (3.62) nm. NMR (CCl_4): δ 3.65 (3H, s, –OCH_3), 5.23 (2H, s, C_9–H and C_{10}–H), 7.12 (1H, d, J=2.0 Hz, C_1–H), 6.37 (1H, quar, J=2.0, 8.0 Hz, C_3–H) ppm.

General Procedure of Formylation. The formylation of the compounds from IV to VI was carried out by two kinds of procedure. One was the Vilsmeier-Haack method using *N*-methylformanilide (MFA) and phosphorus oxychloride (Method A); the other was the metallation method using *n*-butyllithium and MFA (Method B).

Method. A. To a solution of a methoxyaromatic compound (1 mmol) in MFA (2.6 mmol), we added phosphorus oxychloride (3.7 mmol) drop by drop after which the mixture was heated at 70—80 °C for 2 hr. After the mixture had been treated with sodium acetate–ice water, it was extracted with benzene or chloroform. After the removal of the solvents, the residue was chromatographed on a silica gel column with benzene–ethyl acetate to give the products.

Method B. A solution of a methoxyaromatic compound (1 mmol) in THF was added to a solution of *n*-butyllithium (1.5—2.5 mmol) in hexane (*ca.* 20%) under a nitrogen atmosphere, and then MFA (1.5—2.5 mmol) was added. The mixture was stirred at room temperature or in an ice-bath for 1.5—2 hr. After the usual work-up, the products were isolated by silica-gel column chromatography with benzene or chloroform.

Formylation of IVa by Method A. Yield of 9-(2-*p*-cymenyl)-1-formyl-2-methoxyanthracene, 98%; dark brown shell ligaments; mp 110—112 °C. Found: C, 84.73; H, 6.61%. Calcd for $C_{26}H_{24}O_2$: C, 84.75; H, 6.57%. The NMR and UV data are shown in Tables 2 and 5 respectively. IR (KBr disk): ν_{max} 1690 (–CO–) and 1250 (=C–O–C) cm^{-1}.

Formylation of IVb by Method A. Yield of 1-formyl-2-methoxy-9-phenylanthracene, 50%; mp 131.5—132.5 °C. The NMR data are shown in Table 2.

Formylation of IVc by Method A. Yield of 1-formyl-2-methoxy-9-methylanthracene, 48%; yellow crystals; mp 177.5—179 °C. Found: C, 81.55; H, 5.58%. Calcd for $C_{17}H_{14}O_2$: C, 81.58; H, 5.64%. UV (cyclohexane): λ_{max} (log ε) 256 (4.67), 319 (s) (3.56), 350 (3.45), 368 (3.59), and 421 (3.52) nm. IR (KBr disk): ν_{max} 1650 (–CO–) and 1250 (=C–O–C) cm^{-1}.

Formylation of IVd by Method A. Yield of 1-formyl- and 3-formyl-2-methoxyanthracenes, 40 and 23% respectively.

The 1-formyl derivative; pale yellow needles; mp 185—186 °C (lit.[7] 192—194.5 °C). Found: C, 81.62; H, 5.18%. Calcd for $C_{16}H_{12}O_2$: C, 81.34; H, 5.12%. IR (KBr disk); ν_{max} 1650 (–CO–) and 1250 (=C–O–C) cm^{-1}. The NMR and UV data are shown in Tables 2 and 5 respectively.

The 3-formyl derivative; pale yellow needles; mp 113—114 °C (lit.[7] 116—117 °C). Found: C, 81.41; H, 5.00%. IR (KBr disk): ν_{max} 1668 (–CO–), 1265, and 1215 (=C–O–C) cm^{-1}. The NMR and UV data are shown in Tables 2 and 5 respectively.

Formylation of Va by Method A. Yield of 9-(2-*p*-cymenyl)-3-formyl-2-methoxytriptycene, 79%; yellow red crystals; mp 93.2—94.5 °C. Found: C, 86.65; H, 6.39%. Calcd for $C_{32}H_{28}O_2$: C, 86.45; H, 6.35%. UV (cyclohexane): λ_{max} (log ε) 226 (4.51), 248.5 (s) (4.20), 254 (4.05), 261 (4.00), 266 (3.78), 278 (3.96), 278 (s) (3.94), and 333 (3.81) nm. IR (KBr disk): ν_{max} 1680 (–CO–), 1260, and 1230 (=C–O–C) cm^{-1}. The NMR data are shown in Table 3.

Formylation of Vb by Method A. Yield of 3-formyl-2-methoxytriptycene, 82%; pale yellow crystals from cyclohexane-ethanol; mp 242.5—243 °C. Found: C, 84.58; H, 4.87%. Calcd for $C_{22}H_{16}O_2$: C, 84.59; H, 5.16%. UV (cyclohexane): λ_{max} (log ε) 234 (4.60), 256 (3.91), 263.5 (3.97), 272.5 (4.02), 275 (s) (4.00), 323 (3.85), and 331 (3.85) nm. IR (KBr disk): ν_{max} 1670 (–CO–) and 1250 (=C–O–C) cm^{-1}. The NMR data are shown in Table 3.

Formylation of VIa by Method A. Yield of 4-methoxy-*o*-anisaldehyde, 62%; pale yellow crystals; mp 70.5—71.5 °C. Found: C, 65.27; H, 5.77%. Calcd for $C_9H_{10}O_3$: C, 65.05; H, 6.07%. IR (KBr disk): ν_{max} 1674 (–CO–), 1265, and 1220 (=C–O–C) cm^{-1}. The NMR data are shown in Table 4.

Formylation of VIb by Method A. Yield of 4-*tert*-butyl-*o*-anisaldehyde, 95%; colorless liquid. Found: C, 74.83; H, 8.38%. Calcd for $C_{12}H_{16}O_2$: C, 74.97; H, 8.39%. IR (neat): ν_{max} 1684 (–CO–) and 1230 (=C–O–C) cm^{-1}. The NMR data are shown in Table 4.

Formylation of IVa by Method B. Yield of 9-(2-*p*-cymenyl)-3-formyl-2-methoxyanthracene, 71%; brown red needles; mp 118—119 °C. Found: C, 84.64; H, 6.26%. Calcd for $C_{26}H_{22}O_2$: C, 84.75; H, 6.57%, IR (KBr disk): ν_{max} 1695 (–CO–), 1231, and 1210 (=C–O–C) cm^{-1}. The NMR and UV data are shown in Tables 2 and 5 respectively.

Formylation of IVb by Method B. Yield of 3-formyl-2-methoxy-9-phenylanthracene, 64%; yellow needles; mp 160.4—162.6 °C. IR (KBr disk): ν_{max} 1680 (–CO–), 1225, and 1215 (=C–O–C) cm^{-1}. The NMR data are shown in Table 2.

Formylation of IVc by Method B. Yield of 3-formyl-2-methoxy-9-methylanthracene, 63%; yellow needles; mp 150.4

—152.4 °C. The NMR data are shown in Table 2.

Formylation of IVd by Method B. A trace of 1-formyl-2-methoxyanthracene was detected on tlc. However, its isolation was not attempted.

Formylation of Va by Method B. This yielded the same product as was detected by Method A in a 58% yield. Its behavior on tlc, EA, NMR, UV, and IR data were consistent with 9-(2-*p*-cymenyl)-3-formyl-2-methoxytriptycene.

Formylation of Vb by Method B. Yields of 1-formyl and 3-formyl-2-methoxytriptycenes, 41 and 4% respectively.

The 1-formyl isomer; fine crystals from cyclohexane; mp 210.5—212 °C. Found: C, 84.68; H, 5.07%. Calcd for $C_{22}H_{16}O_2$: C, 84.59; H, 5.16%. UV (cyclohexane): λ_{max} (log ε) 223 (4.24), 236.7 (4.16), 257 (s) (3.97), 269.7 (3.82), 277.5 (3.86), and 333.5 (3.68) nm. IR (KBr disk): ν_{max} 1675 (–CO–), 1266, and 1237 (=C–O–C) cm^{-1}. The NMR data are shown in Table 3.

Formylation of VIa by Method B. Yield of 6-methoxy-*o*-anisaldehyde, 75%; needles; mp 98—99 °C (lit.[11] mp 98—99 °C). Found: C, 65.04; H, 5.99%. Calcd for $C_9H_{10}O_3$: C, 65.05; H, 6.07%. IR (KBr disk): ν_{max} 1675 (–CO–) and 1250 (=C–O–C) cm^{-1}. The NMR data are shown in Table 4.

Formylation of VIb by Method B. This yielded the same product as was isolated by formylation with Method A in a 17% yield. Its behavior on tlc, IR, and NMR were coincident with 4-*tert*-butyl-*o*-anisaldehyde.

This study was supported in part by a Grant for Life Science from this Institute.

The authors wish to thank the following: Mr. Jun Uzawa and Mrs. Tamiko Chijimatsu for their NMR spectral measurements; the staff of the Organic Microanalytical Laboratory in this Institute for their elemental analyses, and Assistant Professor Kazutoshi Yamada, Chiba University, for his computer calculations and helpful discussions.

References and Notes

1) (a) A portion of this work has been published as a communication: M. Iwata and S. Emoto, *Chem. Lett.*, **1973**, 477. (b) Presented in part at the 29th Autumn Annual Meeting of the Japan Chemical Society, Hiroshima University, Oct. 10, 1973, Abstract No. 1R08.

2) E. E. Snell and S. J. Di Mari, "The Enzymes," Vol. 2, 3rd Ed., ed. by P. D. Boyer, Academic Press, New York (1970), p. 335.

3) D. E. Metzler, M. Ikawa, and E. E. Snell, *J. Amer. Chem. Soc.*, **76**, 648 (1954).

4) (a) M. Ikawa and E. E. Snell, *ibid.*, **76**, 653 (1954). (b) M. Ando and S. Emoto, This Bulletin, **42**, 2624 (1969).

5) The term "asymmetric inversion catalyst" is tentatively used to denote the catalyst which can catalyze the stereoisomerization of an optically-active compound to its enantiomer, in contrast to the racemization catalyst, which catalyzes the conversion of an optically-active compound to its racemic mixture. In other words, it can generally be said that an asymmetric inversion catalyst is an enantioselective catalyst: Y. Izumi, *Angew. Chem. Int. Ed. Engl.*, **10**, 871 (1971).

6) Similar results have been reported in the literature; D. P. Weeks and J. Celia, *J. Org. Chem.*, **34**, 3713 (1969). Moreover, a reasonable reaction mechanism was elucidated in the report; G. E. Risinger and J. A. Thompson, *Rec. Trav. Chim. Pays-Bas*, **82**, 801 (1963).

7) (a) J. L. Ferrari and I. M. Hunsberger, *J. Org. Chem.*, **25**, 485 (1960). (b) J. L. Ferrari, I. M. Hunsberger, and H. S. Gutowsky, *J. Amer. Chem. Soc.*, **87**, 1247 (1965).

8) Originally: A. Vilsmeier and A. Haack, *Ber.*, **60**,119 (1927). Practically the modified method was used according to: V. P. Bronovitskaya, A. A. Kizil'shtein, and A. Ya. Berlin, *Zh. Org. Khim.*, **4**, 340 (1968); *Chem. Abstr.*, **68**, 114284e.

9) Originally: H. Gilman and J. W. Morton Jr., "Organic Reactions," Vol. 8, ed. by R. Adams, John Wiley & Sons, New York (1954), p. 258. Practically the modified method was used, see Experimental Part.

10) A. H. Sommers, R. J. Michaels Jr., and A. W. Weston, *J. Amer. Chem. Soc.*, **74**, 5546 (1952).

11) G. Wittig, "Newer Methods of Preparative Organic Chemistry," Vol. 1, ed. by W. Forest, Interscience Publishers, New York, N. Y. (1948), p. 579.

12) The observed splitting is due to a coupling with a ring proton situated five bonds away. For detail discussion see: D. G. de Kowalewski and V. J. Kowalewski, *J. Chem. Phys.*, **37**, 1009 (1962).

13) See, for example, the review: M.–P. de Maheas, *Bull. Soc. Chim. France*, **1962**, 1989.

14) H. H. Bosshard and H. Zollinger, *Helv. Chim. Acta*, **42**, 1659 (1959).

15) The simple Hückel MO calculation of 9-aryl-2-methoxyanthracenes demonstrated the following decreasing order of electronic density; 1>3>6>8>7>5>4>10.

16) M. T. Jones, "Radical Ions," ed. by E. T. Kaiser and L. Kevan, Interscience Publishers, New York, N. Y. (1968), p. 245.

17) G. S. Hammond, *J. Amer. Chem. Soc.*, **77**, 324 (1955).

18) L. F. Fieser, "Organic Experiments," D. C. Heath and Company, Boston, Massachussets, (1964), p. 315.

The Reaction of Alcohols with Hexamethylphosphoric Triamide[1]

Seiji ARIMATSU, Ryohei YAMAGUCHI, and Mituyosi KAWANISI*)

Department of Industrial Chemistry, Faculty of Engineering, Kyoto University, Yoshida, Sakyo-ku, Kyoto 606

(Received December 17, 1973)

The thermal treatment of 4-homoadamantanol and bicyclo[3.3.1]nonanols with hexamethylphosphoric triamide (HMPT) gave the corresponding olefins in moderate yields. The application of this dehydration method to a system in which olefin formation was regarded as difficult or impossible stereochemically led to various types of reactions, *i.e.*, reduction, substitution, and phosphorodiamidation. Upon being heated in HMPT, 2-adamantanol afforded 2-adamantyl tetramethylphosphorodiamidate, whereas 1-adamantanol was transformed into adamantane *via* 1-adamantyl tetramethylphosphorodiamidate. In the case of allylic or benzylic alcohols, dimethylamino-substituted compounds were obtained. The reduction of the amount of HMPT promoted the formation of an ether, while dibenzhydryl ether was produced exclusively from benzhydrol. The mechanism of these reaction is discussed.

Recently Hexamethylphosphoric triamide (HMPT) has been widely used as a reaction medium because of its excellent properties as a dipolar aprotic solvent.[2] More recently it was found that HMPT behaved as a reagent for dehydrohalogenation,[3a] dehydration,[3b-d] and various types of reactions in organic synthesis.[3e-m]

In line with the interest in the behavior of HMPT as a reagent, we attempted to apply Monson's method[3b-d] for the dehydration of alcohols to bicyclo[3.3.1]-nonane and homoadamantane systems; the corresponding olefins were thus obtained in a moderate yield. However, when this method was extended to a system in which the olefin formation was regarded as difficult judging from the Bredt rule,[4] divergent types of reactions were observed. Among these reactions, in view of the fact that dimethylamino-substituted compounds were obtained from allylic or benzylic alcohols, we investigated the reaction of benzylic alcohols with HMPT in more detail.

This paper will describe the results obtained in the reaction of HMPT (a) with some alicyclic alcohols, and (b) with benzyl alcohols, including (b-1) the effect of the reaction temperature, (b-2) the formation of an ether, and (b-3) the detection of benzylpentamethylphosphoric triamide.

Finally, (c) some mechanistic aspects will be considered particularly, with particular attention being paid to the reaction of benzyl alcohols.

Results and Discussion

The Reaction of Alicyclic Alcohols with HMPT. As shown in Table 1, the dehydration of alcohols took place readily and gave the corresponding olefins in moderate yields. Among these, it should be noted that 4-homoadamantanol is converted to 4-homoadamantene in an excellent yield; this provides the most convenient method yet for the preparation of this cage olefin.[5]

When 2-adamantanol (**1**) was treated with HMPT, 2-adamantyl tetramethylphosphorodiamidate (**2**) could be isolated in a 15% yield, as is shown in Scheme 1.[6] On the other hand, 1-adamantanol (**3**) afforded only the reduction product, adamantane (**4**). When the reaction of **3** with HMPT was followed by glc, combined with MS, however, it was found that 1-adamantyl tetramethylphosphorodiamidate (**5**) was an intermediate leading to the final product, **4**. Compared with the MS spectrum of **2**, that of **5** indicates the base peak at *m/e* 135, corresponding to the adamantyl cation, whereas that of **2** indicates the base peak at *m/e* 151, corresponding to the adamantyloxy cation. This may reflect the more facile formation of adamantane (**4**) from **5** than from **2**.

Table 1. DEHYDRATION OF ALCOHOLS IN HMPT

Alcohol	Olefin	Yied (%)
4-Homoadamantanol	4-Homoadamantene	91
exo-Bicyclo[3.3.1]nonan-2-ol	Bicyclo[3.3.1]non-2-ene	43
endo-Bicyclo[3.3.1]nonan-2-ol	Bicyclo[3.3.1]non-2-ene	28
Bicyclo[3.3.1]nonane-2,6-diol[a]	Bicyclo[3.3.1]nona-2,6-diene	35

a) Epimeric mixture; *endo, endo*-, and *endo, exo*-diols.

A similar reaction of *exo*-bicyclo[3.3.1]non-3-en-2-ol (**6**) gave 2-*exo*-dimethylaminobicyclo[3.3.1]non-3-ene (**7**), together with a reduction product, bicyclo[3.3.1]-non-2-ene (**8**). The *exo*-configuration of the dimethylamino group at the 2 position of **7** was established by NMR, which indicated a narrow half-band width of 5.0 Hz assignable to the methine proton at the 2 position.[7] Furthermore, 2-phenyl-2-adamantanol (**9**) gave 2-phenyl-2-dimethylaminoadamantane (**10**) in an 80% yield.

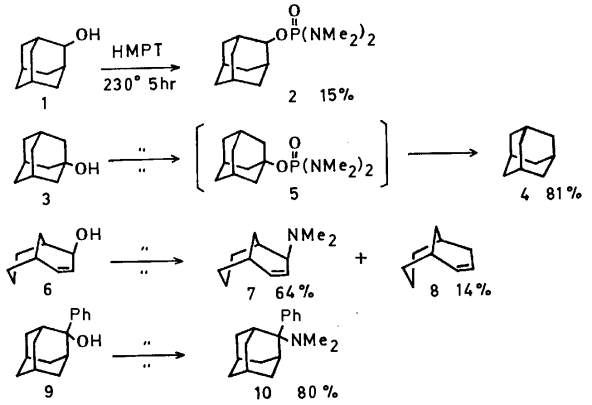

Scheme 1.

* To whom all correspondence should be addressed.

The Reaction of Benzyl Alcohols with HMPT. The fact that dimethylamino-substituted compounds were obtained from allylic or benzylic alcohols such as **6** and **9** prompted us to investigate the reaction of benzyl alcohols with HMPT. The results obtained are listed in Table 2.

Table 2. Reaction of benzyl alcohols with HMPT

Alcohol	Product	Yield (%)
Benzyl alcohol	Benzyldimethylamine	10
	Dibenzylmethylamine	40
Benzhydrol	Diphenylmethane	8
	Benzhydryldimethylamine	56
Triphenylmethanol	Triphenylmethane	44

Monson and Priest have already reported that benzyl alcohols were converted to the corresponding dimethylamino derivatives.[3f] However, we could obtain some additional results—that is, the formation of dibenzylmethylamine and two reduction products, diphenylmethane and triphenylmethane.

The Effect of the Reaction Temperature: The reaction of benzyl alcohols with HMPT seems to be highly sensitive to the reaction temperature employed. As is shown in Table 3, dibenzylmethylamine was produced over 215 °C, whereas benzyldimethylamine was a sole product at 200 °C. In the case of benzhydrol, a temperature dependency could be also observed, as is shown Table 4, but it was extremely small as compared with the result in the case of benzyl alcohol. Triphenylmethanol gave only triphenylmethane in the temperature range of 200—230 °C. The formation of reduction products seems to be dependent upon the steric effects; that is, although toluene escaped from detection in the case of benzyl alcohol, the yield of the reduction products increased as the number of phenyl group increased.

Table 3. Reaction of benzyl alcohol with HMPT

Reaction time hr	Reaction temp. °C	Product distribution (%)[a]	
		$PhCH_2NMe_2$	$(PhCH_2)_2NMe$
1	200	100	—
1	215	85	15
1	230	59	41
5	230	25	75

a) Determined by glc analysis. The yield was almost quantitative except in the case of last run, which is shown in Table 2.

Table 4. Reaction of benzhydrol with HMPT

Reaction time hr	Reaction temp. °C	Product distribution (%)[a]	
		Ph_2CH_2	Ph_2CHNMe_2
1	200	6	94
1	215	7	93
1	230	9	91
5	230	11	89

a) Determined by glc analysis. The yield was almost quantitative except in the case of last run, which is shown in Table 2.

The Formation of an Ether: When a series of experiments was performed on the reaction of benzyl alcohol with varying amounts of HMPT, a novel type of reaction was discovered—namely, the formation of an ether.[8] These data, summarized in Table 5, show that, in the presence of smaller amounts of HMPT, the production of the ether is favored. HMPT was fully consumed when 3 mol of benzyl alcohol was treated with 1 mol of HMPT at 230—240 °C. Since the ratio of benzyldimethylamine (**11**) and dibenzylmethylamine (**12**) was almost unchanged in varying amounts of HMPT, HMPT might be indifferent to the formation of **11** and **12** from the presumed intermediate, benzyl tetramethylphosphorodiamidate (**13**).[3f]

Table 5. Reaction of benzyl alcohol with varying amounts of HMPT

Molar ratio of benzyl alcohol and HMPT	Product distribution (%)[a]		
	$PhCH_2NMe_2$	$(PhCH_2)_2NMe$	$(PhCH_2)_2O$
1 : 1	56	39	5
1 : 2/3	55	38	7
1 : 1/3	50	35	15

a) Determined by glc analysis. The yield was almost quantitative.

When 3 mol of benzhydrol was treated with 1 mol of HMPT, dibenzhydryl ether (**14**) was obtained as the sole product in a 71% yield after recrystallization from ethanol.

These results further prompted us to investigate the reaction of phthalyl alcohol (**15**) with HMPT, which was supposed to give rise to intramolecular ether-formation affording phthalan (**16**) (Eq. (1)). Actually, although the yield was far from satisfactory, **16** was obtained in an 8% yield from a mixture of equimolar amounts of **15** and HMPT.

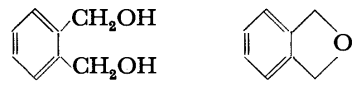

15 **16** (1)

Detection of Benzylpentamethylphosphoric Triamide: When a solution of benzyl alcohol and HMPT was refluxed for 5 hr, a small amount of a new product was detected; this product identified as benzylpentamethylphosphoric triamide (**17**) from the spectroscopic data (see Experimental section). It is highly probable that this compound was formed by the amine-exchange reaction of the benzyldimethylamine produced with HMPT.

Mechanistic Investigations. Intermediacy of Alkyl Tetramethylphosphorodiamidate in the Reaction of Alcohols with HMPT: Concerning the mechanism of the reaction of alcohols with HMPT, Monson and Priest suggested, without rigorous proof, that the initial step of the reaction was the formation of alkyl tetramethylphosphorodiamidate (**18**) (Eq. (2)).[3d]

$$ROH + (Me_2N)_3P{=}O \longrightarrow ROP(NMe_2)_2 + HNMe_2\uparrow \quad (2)$$

18

As is shown in Scheme 1, this presumed intermediate was actually isolated by using an adamantanol.

Also, with regard to the mechanism of the reaction of benzyl alcohols with HMPT, Monson and Priest suggested that the benzyl tetramethylphosphorodiamidates initially produced rearranged to benzyldimethylamine (**11**).[3f] In order to establish this mechanism, we prepared benzyl tetramethylphosphorodiamidate (**13**) from sodium benzylate and tetramethylphosphorodiamidic chloride in ether, and thermally treated **13** *without* solvents. The treatment of **13** at 230—240 °C for 1 hr gave **11** and dibenzylmethylamine (**12**) in the same ratio as in the reaction of benzyl alcohol with HMPT. This implies that **13** is actually an intermediateto the two final products, **11** and **12**. According to the Monson mechanism, it is understandable that **11** was produced by the rearrangement of the **13** intermediate. However, it is still not clear how **12** was obtained from **13**. Since Monson did not obtain **12**, we are left with the intriguing question of how **12** was formed from **13**.

The Formation of Dibenzylmethylamine by the Reaction of Benzyl Tetramethylphosphorodiamidate and Benzyldimethylamine: One explanation of the formation of **12** is that the benzyldimethylamine produced (**11**) attacks the benzylic carbon atom of the still-surviving benzyl tetramethylphosphorodiamidate (**13**), which is an intermolecular analogy of the rearrangement of the **13** intermediate (Scheme 2).

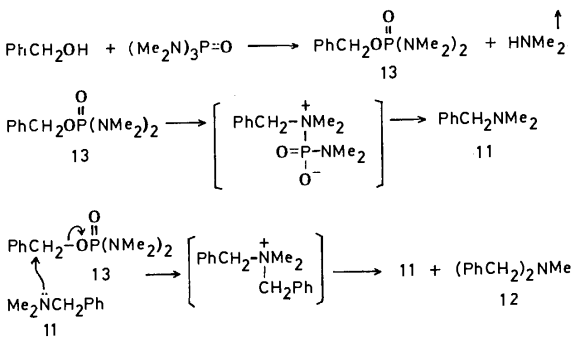

Scheme 2.

In order to test this hypothesis, we investigated the crossed reactions between benzyl tetramethylphosphorodiamidate (**13**) and benzyldiethylamine (**19**)[9] as well as those between benzyl tetraethylphosphorodiamidate (**20**) and benzyl dimethylamine (**11**).[10] It was preliminarily observed that **20** was also thermally converted to benzyldiethylamine (**19**) and dibenzylethylamine (**21**), but the ratio of **21**/**19** was smaller than that of **12**/**11**. In the former case, no crossed reaction was observed, but in the latter case, the crossed reaction did take place and dibenzylmethylamine (**12**) was obtained (Scheme 3).

These observations imply that the rate of the attack of **19** must be slower than that of **11** for steric reasons and also well explain the fact that dibenzhydrylmethylamine is not obtained in the case of benzhydrol.

From these results we concluded that **12** was derived from the nucleophilic substitution reaction of **13** by **11** as is shown in Scheme 2.

Additionally, when an equimolar mixture of **20** and

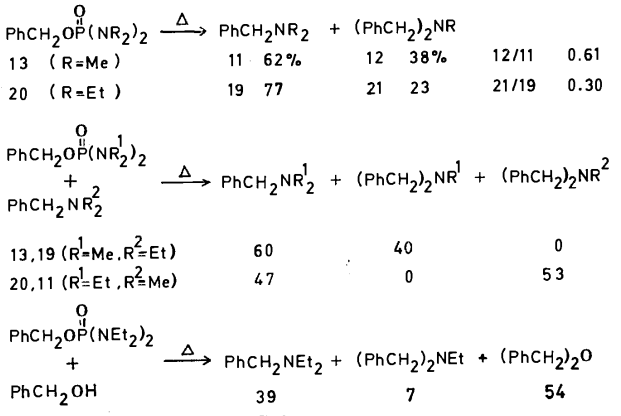

Scheme 3.

benzyl alcohol was treated at 230—240 °C for 1 hr, dibenzyl ether was obtained at the expense of **20**, together with **19** and **21**. (Scheme 3) Therefore, it is highly probable that the ether-formation proceeds by the nucleophilic substitution reaction of **18** by the still-remaining alcohol.

Mechanism Concerning the Formation of the Reduction Products: As for the formation of the reduction products, such as diphenylmethane and triphenylmethane, we tentatively propose the mechanism depicted in Scheme 4.

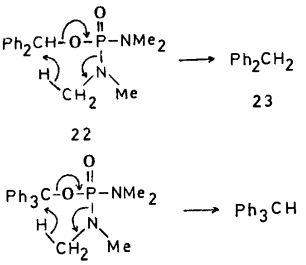

Scheme 4.

When the intramolecular rearrangement occurs, hydrogen from the methyl group attached to nitrogen transfers to the benzylic carbon atom. An attempt to prepare benzhydryl tetramethylphosphorodiamidate (**22**) did not succeed, but instead of **22**, we directly obtained diphenylmethane (**23**) and benzhydryldimethylamine (**24**) in refluxing ether, though the ratio of **23** and **24** was *ca.* 1 : 1, different from the results of the reaction of benzhydrol with HMPT. This explanation can also be extended to the formation of adamantane and bicyclo[3.3.1]non-2-ene from their precurcors. However, these observations can not be explicitly explained at present, and an intermolecular pathway cannot be ruled out.

Experimental

All the temperature are uncorrected. The IR spectra were obtained on a Shimadzu IR-27 spectrophotometer. The mass spectra were taken by using a Hitachi RMS-4 mass spectrometer. The NMR spectra were obtained on a EM-360 spectrometer, TMS being chosen as the internal standard. The microanalyses were performed by Mrs. Kiyoko Fujimoto.

Hexamethylphosphoric Triamide (HMPT). Commercially-available HMPT was refluxed for 5 hr under N_2 with calcium

hydride and then distilled; bp 110—115 °C/15 mmHg.

Starting Materials. The following compounds were prepared according to the reported methods: 4-homoadamantanol,[5] *exo*-bicyclo[3.3.1]nonan-2-ol,[11] *endo*-bicyclo[3.3.1]-nonan-2-ol,[11] bicyclo[3.3.1]nonane-2,6-diol,[12] 1-adamantanol,[13] 2-adamantanol,[14] *exo*-bicyclo[3.3.1]non-3-en-2-ol,[11] benzhydrol,[15] triphenylmethanol,[16] and phthalyl alcohol.[17]

Preparation of 2-Phenyl-2-adamantanol. The Grignard reagent prepared from bromobenzene (9.7 g; 0.062 mol) and magnesium (1.5 g; 0.062 atom) in ether (35 ml) was treated with adamantanone (4.5 g; 0.03 mol) in ether (55 ml) and then hydrolyzed with 20% H_2SO_4. The ether layer was separated, combined with an ether extract of the aqueous layer, and dried over Na_2SO_4. The subsequent evaporation of the solvent yielded 4.2 g (63%) of 2-phenyl-2-adamantanol: mp 89.5—90.5 °C, mass spectrum: *m/e* 228 (M^+), NMR ($CDCl_3$): δ 7.1—7.45 (m, 5H), IR (Nujol mull): 3220, 1601, 1008, 697 cm^{-1}. Found: C, 84.38; H, 8.53%. Calcd for $C_{16}H_{20}O$: C, 84.16; H, 8.83%.

General Procedure for Dehydration of Alcohols by HMPT. The substrate (0.01 mol) was dissolved in HMPT (10 ml) and heated at 230—240 °C under N_2 for 5 hr. The reaction mixture was then poured onto water and extracted five times with petroleum ether (bp 40—50 °C). The extract was washed two times with brine and dried over Na_2SO_4. The subsequent evaporation of the solvent gave crude materials. Since 4-homoadamantene[5] and bicyclo[3.3.1]non-2-ene[11] sublimed during the reaction, they could be obtained in pure form from the sublimates. Bicyclo[3.3.1]nona-2,6-diene was purified by distillation; bp 60—65 °C/20 mmHg (lit,[18] 51—51.5 °C/15 mmHg).

Thermal Reaction of Alcohols with HMPT. The treatment was essentially the same as was been described above. The reaction mixture was poured onto water and extracted five times with benzene. The extract was washed two times with brine and dried (Na_2SO_4). After the evaporation of the solvent, a crude material was obtained; this material was purified by a combination of column chromatography and preparative glc.

2-Adamantyl Tetramethylphosphorodiamidata (2): Mp 51.5—53 °C (from *n*-hexane), mass spectrum: *m/e* 286 (M^+), 151 (100%), 135, NMR (CCl_4): δ 2.59 (d, J_{PH} 9.0 Hz, 12H), 4.19—4.60 (b, 1H), IR (Nujol mull): 1290, 1195, 999, 988, 750 cm^{-1}. Found: C, 58.70; H, 9.62; N, 9.59%. Calcd for $C_{14}H_{27}N_2O_2P$: C, 58,72; H, 9.50; N, 9.78%.

2-exo-Dimethylaminobicyclo[3.3.1]non-3-ene (7): Mass spectrum: *m/e* 165 (M^+), NMR (CCl_4): δ 2.20 (s, 6H), 2.68 (m, 1H, $W_{1/2}$ 5.0 Hz), 5.87 (m, 2H), IR (liquid film): 1180, 1040, 1000, 720 cm^{-1}. Found: C, 80.21; H, 11.46; N, 8.73%. Calcd for $C_{11}H_{19}N$: C, 79.94; H, 11.59; N, 8.48%.

2-Phenyl-2-dimethylaminoadamantane (10): Mp 109.5—111 °C, mass spectrum: *m/e* 255 (M^+), NMR ($CDCl_3$): δ 1.36—1.79 (m, 10H), 1.82 (s, 6H), 2.17—2.42 (b, 1H), 2.40—2.78 (b, 3H), 7.02—7.26 (m, 5H), IR (Nujol mull): 1491, 755, 703 cm^{-1}. Found: C, 84.65; H, 10.11; N, 5.55%. Calcd for $C_{12}H_{25}N$: C, 84.65; H, 9.87; N, 5.48%.

Reaction of Benzyl Alcohols with HMPT. The procedure was the same as that described above. The products were identified by comparison with the reported spectral data (Sadtler Standard Spectra, The Aldrich Library of IR Spectra).

Formation of Dibenzhydryl Ether (14) by the Reaction of Benzhydrol with HMPT: A mixture of 1.84 g (0.01 mol) of benzhydrol and 0.6 g (0.003 mol) of HMPT was heated at 230—240 °C for 1 hr under N_2. The usual work-up and recrystallization from ethanol gave 1.25 g (71%) of dibenzhydryl ether (**14**): mp 107—108 °C (lit,[19] 109 °C), mass spectrum: no parent, *m/e* 167 (100%), NMR (CCl_4): δ 5.33 (s, 2H), 7.30 (m, 20H), IR (Nujol mull): 1050 cm^{-1}.

Formation of Phthalan (16) by the Reaction of Phthalyl Alcohol (15) with HMPT: A mixture of 1.38 g (0.01 mol) of phthalyl alcohol and 1.79 g (0.01 mol) of HMPT was heated for 1 hr according to the procedure described above. Column Chromatography (Al_2O_3, *n*-hexane: benzene=4: 1) of the crude material afforded 0.1 g (8%) of phthalan (**16**):[20] mass spectrum: *m/e* 120 (M^+), 91 (100%), NMR (CCl_4): δ 5.0 (s, 4H), 7.13 (s, 4H), IR (liquid film): 3030, 1040, 900, 740 cm^{-1}.

Isolation of Benzylpentamethylphosphoric Triamide (17) in the Reaction of Benzyl Alcohol with HMPT: The procedure was as has been described above except that the reaction time was 5 hr. The benzene extract was evaporated; subsequent column chromatography of the residue afforded 3% of benzylpentamethylphosphoric triamide, together with benzyldimethylamine and dibenzylmethylamine. **17**: mass spectrum: *m/e* 255 (M^+), 211, 120 (100%), NMR (CCl_4): δ 2.47 (d, J_{PH} 7.8 Hz, 3H), 2.62 (d, J_{PH} 10.2 Hz, 12H), 4.15 (d, J_{PH} 9.0 Hz, 2H), 7.2—7.4 (m, 5H), IR (liquid film): 1600, 1500, 1300, 1200, 980, 775, 740, 700 cm^{-1}.

Preparation of Benzyl Tetramethylphosphorodiamidate (13). To 2.16 g (0.02 mol) of benzyl alcohol dissolved in 40 ml of anhydrous ether, we added 0.48 g (0.02 mol) of sodium hydride. The mixture was stirred and refluxed for 2 hr. To the suspention of sodium benzylate in ether we then slowly added tetramethylphosphorodiamidic chloride.[21] The mixture was stirred and refluxed overnight. The precipitates were removed by filtration, and the organic layer was washed two times with brine and dried (Na_2SO_4). The subsequent evaporation of the solvent, followed by distillation at 140—145 °C/5 mmHg, yielded 3.8 g (79%) of benzyl tetramethylphosphorodiamidate (**13**)[22]: mass spectrum: *m/e* 242 (M^+), 151 (40%), 91 (100%), NMR (CCl_4): δ 2.53 (d, J_{PH} 9.6 Hz, 12H), 4.85 (d, J_{PH} 9.6 Hz, 2H), 7.30 (s, 5H), IR (liquid film): 1305, 1200, 990, 750, 700 cm^{-1}.

Preparation of Benzyl Tetraethylphosphorodiamidate (20). The procedure described above was followed, but we used tetraethylphosphorodiamidic chloride[23] instead of tetramethylphosphorodiamidic chloride. Thus, 2.8 g (94%) of the pure material was obtained after decolorizing with active carbon. **20**: mass spectrum: *m/e* 298 (M^+, feeble), 91 (100%), NMR (CCl_4): δ 1.06 (t, 12H), 3.02 (d of quartet, J_{PH} 12.6 Hz, 8H), 4.87 (d, J_{PH} 7.8 Hz, 2H), 7.30 (s, 5H), IR (liquid film): 1235, 1010 cm^{-1}. Found: C, 60.54; H, 9.38; N, 9.38%. Calcd for $C_{15}H_{27}N_2O_2P$: C, 60.37; H, 9.12; N, 9.38%.

Thermolysis of 13 and 20. The substrate (0.002 mol) was heated for 1 hr at 230—240 °C under N_2. During the period of the reaction, an insoluble oily layer appeared; upon cooling, it solidified to a gummy, crystalline mass. This phenomenon was also observed upon the reaction of benzyl alcohol with HMPT. This compound was identical with bisdimethylammonium dihydrogen pyrophosphate, $(Me_2NH_2)_2H_2P_2O_7$, which Monson and Priest have reported on.[3f] The upper layer was immediately subjected to glc analysis; the products shown in Scheme 3 were observed in the specified ratio.

Thermal Reaction between 13 and 19, as well as between 20 and 11. Benzyldimethylamine (**11**)[10] and benzyldiethylamine (**19**)[9] were prepared according to the reported methods. Each equimolar mixture of the substrates was treated by the procedure described above. The reaction mixture was immediately subjected to glc analysis. The relative ratios are shown in Scheme 3.

The authors wish to thank Professor Hitosi Nozaki

for his valuable advice and continuous encouragement, and also Mr. Koichi Kimoto for his skillful technical assistance and discussions.

References

1) Partly presented at the 26th and 27th Annual Meetings of the Chemical Society of Japan, Hiratsuka and Nagoya, 1972.

2) H. Normant, *Angew. Chem. Int. Ed. Eng.*, **6**, 1046 (1967).

3) a) R. S. Monson, *Chem. Commun.*, **1971**, 113; b) R. S. Monson, *Tetrahedron Lett.*, **1971**, 567; c) J. S. Lomas, D. S. Sagatys, and J.-E. Dubois, *ibid.*, **1972**, 165; d) R. S. Monson and D. N. Priest, *J. Org. Chem.*, **36**, 3826 (1971); e) J. Kopecký and J. Šmejkal, *Chem. Ind.* (London), **1966**, 1529; f) R. S. Monson and D. N. Priest, *Chem. Commun.*, **1971**, 1018; g) R. S. Monson, D. N. Priest, and J. C. Ullrey, *Tetrahedron Lett.*, **1972**, 929; h) M. Kawanisi, S. Arimatsu, R. Yamaguchi, and K. Kimoto, *Chem. Lett.*, **1972**, 881; i) R. S. Monson and D. N. Priest, *Can. J. Chem.*, **49**, 2897 (1971); j) E. B. Pedersen, N. O. Vesterager, and S.-O. Lawesson, *Synthesis*, **1972**, 547; k) N. O. Vesterager, R. Dynesli, E. B. Pedersen, and S.-O. Lawesson, *ibid.*, 548 (1972); l) M. Kawanisi, S. Arimatsu, and R. Yamaguchi, *Chem. Lett.*, **1972**, 1031; m) R. S. Monson and B. M. Broline, *Can. J. Chem.*, **51**, 942 (1973).

4) G. Köblich, *Angew. Chem.*, **85**, 494 (1973).

5) a) J. E. Nordlander, F. Y.-H. Wu, S. P. Jindal, and J. B. Hamilton, *J. Amer. Chem. Soc.*, **91**, 3962 (1969); b) P. v. R. Schleyer, E. Funke, and S. H. Liggero, *ibid.*, **91**, 3965 (1969); c) R. M. Black and G. B. Gill, *J. Chem. Soc., C*, **1970**, 671; d) S. Arimatsu, *Yuki Gosei Kagaku*, **31**, 339 (1973).

6) A high-molecular-weight product was also obtained (272 mg from 800 mg of 2-adamantanol); it was considered to be di(2-adamantyl) dimethylphsophorodiamidate judging from its NMR and IR data. Moreover, its precise structure was not confirmed. An intractable tarry matter was also formed.

7) This deduction is in accordance with the report by Garbisch that, for 6-substituted 1-phenylcyclohexene, the C-6 substituent may be considered to have preference for the equatorial position for the $W_{1/2}$ of C-6 proton bands$>$15 Hz, and to have preference for the axial position for the $W_{1/2}$ of C-6 proton bands$<$13 Hz; see E. W. Garbisch, Jr., *J. Org. Chem.*, **27**, 4249 (1962).

8) This ether formation has also been observed in the thermal reaction of alcohol with dimethyl sulfoxide (DMSO). *cf.* V. J. Traynelis, W. L. Hergenrother, H. T. Hanson, and J. A. Valicenti, *J. Org. Chem.*, **29**, 123 (1964).

9) V. Meyer, *Ber.*, **10**, 310 (1877).

10) M. L. Moore, "Organic Reactions," Vol. 5, ed. by R. Adams, John Wiley & Sons, New York (1949), p. 323.

11) J. P. Schaefer, J. C. Lark, C. A. Flegal, and L. M. Honig, *J. Org. Chem.*, **32**, 1372 (1967).

12) J. P. Schaefer and L. M. Honig, *ibid.*, **33**, 2655 (1968).

13) H. W. Geluk and J. L. M. A. Schlatmann, *Tetrahedron*, **24**, 5361 (1968).

14) P. v. R. Schleyer and R. D. Nicholas, *J. Amer. Chem. Soc.*, **83**, 182 (1961).

15) F. Y. Wiselogle and H. Sonneborn, II, "Organic Syntheses," Coll. Vol. I, p. 90 (1941).

16) L. F. Fieser, "Experiments in Organic Chemistry," 3rd ed., Heath & Co., Boston (1955), p. 77.

17) R. F. Nystrom and W. G. Brown, *J. Amer. Chem. Soc.*, **69**, 1197 (1947).

18) a) H. Musso and U. Biethan, *Chem. Ber.*, **100**, 119 (1967); b) H. Stetter and E. F. Schwartz, *ibid.*, **101**, 2464 (1968).

19) A. Sagaumenny, *Ann.*, **184**, 174 (1877).

20) A. Ludwig, *Ber.*, **40**, 3060 (1907).

21) P. Lester, U.S. 2678335 (1954) through *Chem. Abstr.*, **49**, 6300g (1954).

22) P. C. Hamm, U.S. 3397270 (1968); *Chem. Abstr.*, **69**, P 105339v (1968).

23) B. Loev and J. T. Massengale, *J. Org. Chem.*, **22**, 1186 (1957).

Asymmetric Hydroformylation of Styrene. The Effects of the Reaction Conditions on the Stereoselectivity

Masato TANAKA, Yoshihisa WATANABE, Take-aki MITSUDO, and Yoshinobu TAKEGAMI

Department of Hydrocarbon Chemistry, Faculty of Engineering, Kyoto University, Sakyo-ku, Kyoto 606

(Received December 26, 1973)

The effects of the reaction conditions on the asymmetric hydroformylation of styrene with rhodium catalysts have been studied. The $[\alpha]_D$ value and the configuration of the product, hydratropaaldehyde, were much affected by the phosphine/rhodium ratios, the reaction temperatures (20—110 °C), and the partial pressures of carbon monoxide and hydrogen (10—100 atm). The results were mainly explained in terms of the structures of the catalysts and the skeletal isomerization of acyl complexes. The predominant species of the catalysts and the participation of a π-benzyl-type intermediate were also discussed.

Recently, catalytic asymmetric syntheses with chiral phosphine transition-metal complexes have attracted much interest, and several papers on the asymmetric hydroformylation of olefins with chiral phosphine rhodium complexes have been published.[1-4] However, there has been no example of an investigation of the effects of the reaction conditions on the asymmetric hydroformylation. The hydroformylation reaction is believed to proceed *via* the π-olefin, alkyl, and acyl complexes:

$$\rangle{=}\langle + \text{H-M(CO)}_{3-n}\text{L}_n \longrightarrow \rangle\underset{|}{\text{C}}\text{-M(CO)}_{3-n}\text{L}_n \quad (1)$$

$$\rangle\underset{|}{\text{C}}\text{-M(CO)}_{3-n}\text{L}_n \longrightarrow \text{R-M(CO)}_{3-n}\text{L}_n \quad (2)$$

$$\text{R-M(CO)}_{3-n}\text{L}_n + \text{CO} \longrightarrow \text{R-}\underset{\underset{\text{O}}{\|}}{\text{C}}\text{-M(CO)}_{3-n}\text{L}_n \quad (3)$$

$$\text{R-}\underset{\underset{\text{O}}{\|}}{\text{C}}\text{-M(CO)}_{3-n}\text{L}_n + \text{H}_2 \longrightarrow \text{RCHO} + \text{H-M(CO)}_{3-n}\text{L}_n \quad (4)$$

where L is carbon monoxide or a phosphorus ligand and M is cobalt or rhodium. Great effects on the reaction rate and the distribution of the products (the straight/branched ratio) are brought about by changing the reaction conditions, the structure of the active species and the reaction mechanisms have been discussed on the basis of these results.[5]

In this paper, the authors will describe the effects of the reaction conditions (the reaction temperatures, the phosphine/rhodium ratios, and the partial pressures of carbon monoxide and hydrogen) on the asymmetric hydroformylation of styrene with chiral phosphine rhodium complexes.

Experimental

Benzene was refluxed over lithium aluminum hydride, distilled under argon, and stored over calcium hydride. Styrene was distilled at a reduced pressure of argon and was stored with *p-tert*-butylcatechol as a radical inhibitor in a refrigerator. Neomenthyldiphenylphosphine[6] and (*R*)-benzylmethylphenylphosphine[7] were prepared according to the methods of the literature.

The glpc analysis was carried out on a Shimadzu model GC-3B apparatus equipped with a stainless steel column (3 mm$^{\phi}$ × 3 m) packed with diethylene glycol adipate polyester on chromosorb. The optical rotations were measured neat on a JASCO model DIP-180 automatic polarimeter.

Reaction Procedure. An autoclave (100 ml) made of stainless steel (SUS-32) and equipped with a magnetic stirrer was used. Ten ml of benzene, 10 ml of styrene, 3.1 mg of μ,μ'-dichlorotetracarbonyldirhodium, and a desired amount of a chiral phosphine were placed into the autoclave under a slow stream of argon. After the autoclave has been purged with 20 atm of hydrogen several times, hydrogen and carbon monoxide were introduced at certain pressures, after which the mixture was heated up to the desired temperature. The reaction temperature was regulated automatically within a variation of ±1 °C. After having been agitated for a certain time, the autoclave was discharged and an aliquot of the reaction mixture was analyzed by gas chromatography. The optically-active hydratropaaldehyde produced was isolated by the distillation of the reaction mixture, and then the optical rotation was measured.

Reduction of Hydratropaaldehyde. The configuration and the maximum rotation of hydratropaaldehyde are unknown. Therefore, the aldehyde was transformed into 2-phenyl-1-propanol, whose configuration and maximum rotation are known. To a suspension of lithium aluminum hydride (2.19 g) in ether (120 ml), an ether solution (20 ml) of hydratropaaldehyde (5.4 g, $[\alpha]_D$ +1.28°) was added, drop by drop, at 0 °C, and then the mixture was refluxed for 2 hr. The resultant solution was hydrolyzed with 3 M H_2SO_4 (60 ml), and the aqueous layer was extracted three times with 30 ml portions of ether. The combined organic layer was washed with water, dried over magnesium sulfate, and distilled to give 4.7 g of 2-phenyl-1-propanol; bp 63.0—64.2 °C/0.6 mmHg, $[\alpha]_D$ −0.120° (neat). As the maximum rotation of (*S*)-2-phenyl-1-propanol is $[\alpha]_D$ −15.16° (neat),[8] that of (*S*)-hydratropaaldehyde is estimated to be $[\alpha]_D$ +160° (neat) if the reduction of the aldehyde proceeds without racemization. However, since such a racemization has been noted,[2] the authors will use not the "optical yield" but the $[\alpha]_D$ value in this text.

Results and Discussion

The effects of the reaction conditions (the reaction temperatures, the partial pressures of hydrogen and carbon monoxide, and the phosphine/rhodium ratios) on the $[\alpha]_D$ value of the product were examined; some typical results are summarized in Tables 1 and 2. Under the conditions used, styrene was converted into hydratropaaldehyde and hydrocinnamaldehyde. The former was always the main product, and no other by-products were detected by gas chromatography.

The Effects of the Phosphine/Rhodium Ratio. The

Table 1. Asymmetric hydroformylation of styrene catalyzed by (*R*)-benzylmethylphenylphosphine–rhodium complexes[a]

Exp. No.	Reaction conditions: Temp. (°C)	Partial pressure,[b] (atm) CO	H_2	P/Rh[c]	Time (hr)	Yield[d] (%)	Iso-%[e]	$[\alpha]_D$ (neat)
1	75	70	70	1	8	41.8	89.7	+0.07
2	75	70	70	8	21	36.0	94.9	+60.2
3	110	70	70	4	6	15.8	78.5	+41.6
4	90	70	70	4	8	26.7	89.2	+46.0
5	60	70	70	4	72	18.5	98.0	+67.4
6	110	10	50	2	2	29.6	68.6	+11.0
7	110	70	50	2	2	96.5	88.6	+27.0
8	110	100	50	2	2	90.5	85.1	+18.7
9	90	30	70	4	8	22.9	89.9	+45.6
10	110	15	50	3	6	37.5	85.3	+29.2
11	110	70	50	3	5	53.0	90.4	+38.3
12	110	100	50	3	2	~100	86.9	+21.8
13	110	50	10	2	3	22.0	65.4	+9.6
14	110	50	95	2	1.5	96.1	89.5	+29.3
15	110	50	10	3	7	22.6	87.6	+26.4
16	110	50	100	3	2	86.8	91.3	+37.6
17	90	70	30	4	23	38.6	89.2	+43.6

a) Styrene: 10 ml, benzene (solvent): 10 ml, $[Rh(CO)_2Cl]_2$: 3.1 mg. b) Initial pressure. c) Phosphine/rhodium ratio. d) Total yield of hydratropaaldehyde and hydrocinnamaldehyde based on the amount of styrene used. e) 100×Hydratropaaldehyde/(hydratropaaldehyde+hydrocinnamaldehyde).

Table 2. Asymmetric hydroformylation of styrene catalyzed by neomenthyldiphenylphosphine–rhodium complexes[a]

Exp. No.	Reaction conditions: Temp. (°C)	P/Rh[b]	Time (hr)	Yield[c] (%)	Iso-%[d]	$[\alpha]_D$ (neat)
18	75	2	12	67.5	89.3	+1.28
19	75	50	6.5	68.1	93.1	−1.61
20	100	2	2	96.1	70.8	+0.67
21	20	2	216	42.1	96.7	−4.61

a) Styrene: 10 ml, benzene (solvent): 10 ml, $[Rh(CO)_2Cl]_2$: 3.1 mg, initial partial pressure of carbon monoxide and hydrogen: 70 atm, respectively. b) Phosphine/rhodium ratio. c) Total yield of hydratropaaldehyde and hydrocinnamaldehyde based on the amount of styrene used. d) 100×Hydratropaaldehyde/(hydratropaaldehyde+hydrocinnamaldehyde).

effects of the phosphine/rhodium ratio on the $[\alpha]_D$ value and the percentage of hydratropaaldehyde were examined under the conditions, initial partial pressure of hydrogen and carbon monoxide of 70 atm and at 75 °C. Two kinds of chiral phosphines were used: (*R*)-benzylmethylphenylphosphine and neomenthyldiphenylphosphine (nmdpp). The former has an asymmetric center on phosphorus, while the latter has three asymmetric centers on the alkyl group. The results are illustrated in Figs. 1 and 2.

In the case of (*R*)-benzylmethylphenylphosphine, when the phosphine/rhodium ratio was 1 the stereochemical control was not so effective, so the $[\alpha]_D$ value was nearly zero. However, an increase in the ratio resulted in a larger stereoselectivity, and the $[\alpha]_D$ value amounted to +50.8° at the 2: 1 ratio. Then it approached asymptotically to a limit with an increase in the ratio (4: 1 and 8: 1). These results suggest an equilibrium among active species which is affected by both the phosphine/rhodium ratio and the partial pressure of carbon monoxide, which will be discussed later:

$$HRh(CO)_3 \underset{CO,\,-P^*}{\overset{P^*,\,-CO}{\rightleftarrows}} HRh(CO)_2P^* \underset{CO,\,-P^*}{\overset{P^*,\,-CO}{\rightleftarrows}} HRh(CO)P_2^* \quad (5)$$

where P* is a chiral phosphine. $HRh(CO)_3$ may be predominant at the 1: 1 ratio, and in principle, the

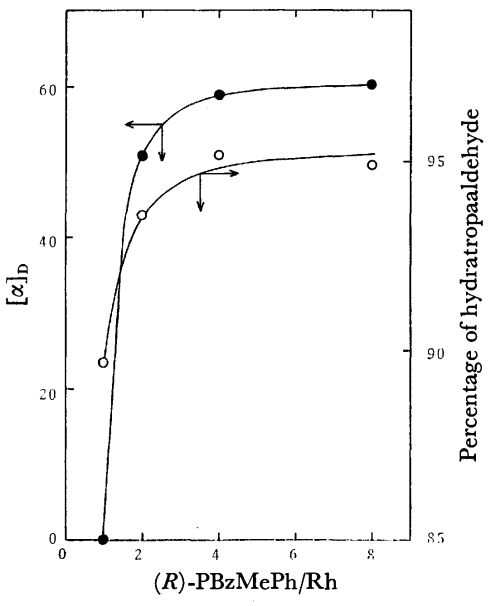

Fig. 1. Effects of (*R*)-benzylmethylphenylphosphine/rhodium ratios on the $[\alpha]_D$ value and the percentage of hydratropaaldehyde. ($P_{CO}=P_{H_2}=70$ atm, 75 °C)

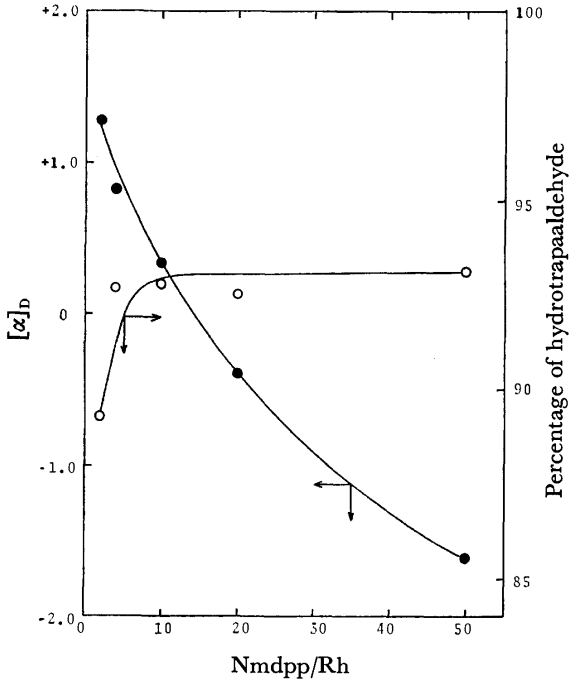

Fig. 2. Effects of neomenthyldiphenylphosphine/rhodium ratios on the $[\alpha]_D$ value and the percentage of hydratropaaldehyde. ($P_{CO}=P_{H_2}=70$ atm, 75 °C)

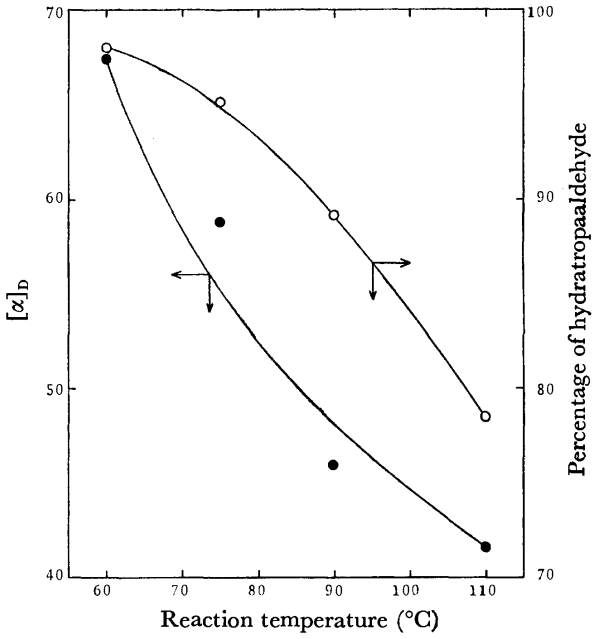

Fig. 3. Effects of reaction temperatures on the $[\alpha]_D$ value and the percentage of hydratropaaldehyde. ($P_{CO}=P_{H_2}=70$ atm, (*R*)-benzylmethylphenylphosphine /rhodium=4)

hydroformylation proceeds without any asymmetric induction. Therefore $HRh(CO)_2P^*$ may be the dominant species at larger ratios, and it may be alternated with $HRh(CO)P_2^*$ when the ratio becomes much larger. With catalytic activities, there may be no drastic differences among the species, judging from the results shown in Table 1. Therefore, it can be concluded that Equilibrium (5) is responsible for the relationship between the phosphine/rhodium ratio and the $[\alpha]_D$ value.[9]

As Fig. 2 shows, when nmdpp was used the effect on the $[\alpha]_D$ value was very different from that in the case of (*R*)-benzylmethylphenylphosphine. Thus, the $[\alpha]_D$ value decreased monotonously from $+1.28°$ to $-1.61°$ when the phosphine/rhodium ratio increased gradually from 2: 1 to 50: 1. The configuration of hydratropaaldehyde was reversed from *S* to *R* at a ratio around 14: 1. These results clearly suggest the participation of the equilibrium mentioned above. It seems reasonable that, when the phosphine/rhodium ratio is smaller, $HRh(CO)_2P^*$, which may be responsible for the formation of *S*-aldehyde, is predominant, and that $HRh(CO)P_2^*$, responsible for the formation of *R*-aldehyde, may take the place of $HRh(CO)_2P^*$ at larger ratios.

The difference in the behavior of the $[\alpha]_D$ value between these two phosphines may be attributed to the differences in their structures and coordination abilities.

On the other hand, the percentage of hydratropaaldehyde was slightly increased with an increase in the ratio both in the case of (*R*)-benzylmethylphenylphosphine and in that of nmdpp.

The Effect of the Reaction Temperature. The relationships between the reaction temperature and the $[\alpha]_D$ value, and the percentage of hydratropaaldehyde

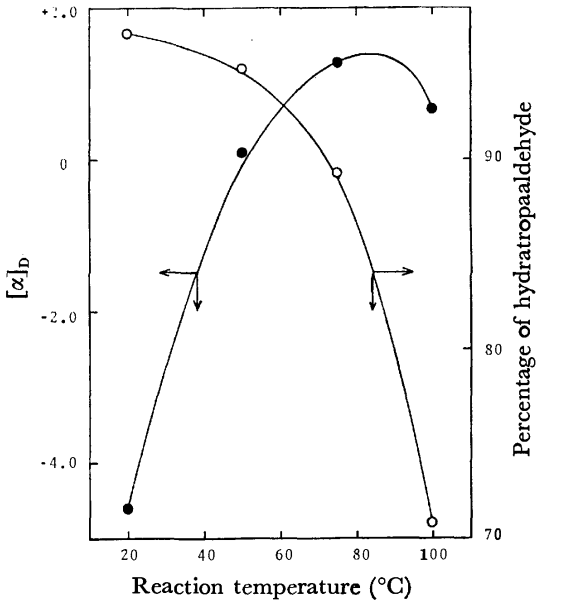

Fig. 4. Effects of reaction temperatures on the $[\alpha]_D$ value and the percentage of hydratropaaldehyde. ($P_{CO}=P_{H_2}=70$ atm, neomenthyldiphenylphosphine/ rhodium=2)

respectively, were examined under the conditions of a phosphine/rhodium ratio of 4: 1 for (*R*)-benzylmethylphenylphosphine, or one of 2: 1 for nmdpp, and with initial partial pressures of carbon monoxide and hydrogen of 70 atm. The results are illustrated in Figs. 3 and 4.

As Fig. 3 shows, when (*R*)-benzylmethylphenylphosphine was used as a chiral ligand, the $[\alpha]_D$ value of hydratropaaldehyde increased almost proportionally with a decrease in the reaction temperature. The $[\alpha]_D$

value reached +67° at 60 °C.* In considering the effect of the reaction temperature on the $[\alpha]_D$ value, two factors may be mainly taken into account: the reaction rate and the stability of the conformations of the reaction intermediates. Lowering the reaction temperature made the overall reaction slow down (see Tables 1 and 2). Though the real mechanism of the asymmetric induction is not clear, the reactions involving the diastereomeric key intermediate, which decides the configuration of the product, may also become slower, and so the stereoselection may be effective. About the second factor, the conformation and configuration of catalytically-active species and reaction intermediates may be more stable at lower temperatures. This means that the chiral environment at the reaction site is fixed and that the epimerization of the intermediates (the racemization of the alkyl or acyl group of the intermediates) does not occur easily. This factor, therefore, may result in a high $[\alpha]_D$ value.

In the case of nmdpp, a different type of relationship was observed. When the reaction temperature was lowered from 100 to 75 °C, the $[\alpha]_D$ value increased by a factor of about 2. This dependency is analogous to that in the case of (*R*)-benzylmethylphenylphosphine. However, the $[\alpha]_D$ value decreased when the temperature lowered further (50 and 20 °C). Thus, it was +1.28° at 75 °C, nearly zero at 50 °C, and −4.61° at 20 °C with a change in the configuration of hydratropaaldehyde from *S* to *R*. These facts clearly imply that the mode of the stereochemical control is delicately altered by changing the reaction temperature. The phosphine coordinated to rhodium can rotate around the coordination bond axis, and several metastable conformations of the catalytically-active species are possible. Therefore, the unexpected phenomenon may be attributed to this type of conformational alternation in the catalyst molecule. This conformational factor may be rather important with nmdpp, for neomenthyl group has three asymmetric carbons. On the other hand, as has been described above, the phosphine/rhodium ratio affects the $[\alpha]_D$ value and the configuration; these results have been discussed from the standpoint of the number of the phosphine coordinated to rhodium. The effect of the reaction temperature can be partly explained on the basis of this consideration. Lowering the reaction temperature has the same effect on the $[\alpha]_D$ value as the increase in the phosphine/rhodium ratio. Therefore, it is likely that the number of the phosphine on the rhodium is larger at lower temperatures. The unexpected phenomenon of the effect of the reaction temperature may also be attributed to this factor.

As is shown in both Figs. 3 and 4, the percentage of hydratropaaldehyde gradually decreases as the reaction temperature becomes higher. Previous work[10] in this laboratory has demonstrated that α-phenylpropionyltetracarbonylcobalt, which is formed by the reaction of hydridotetracarbonylcobalt with styrene under a carbon monoxide atmosphere, easily undergoes a skeletal isomerization to give the β-isomer, and that this type of isomerization is accelerated by elevating the reaction temperature. Under the conditions of the asymmetric hydroformylation;

$$PhCH(CH_3)CORh(CO)_{3-n}P_n^* \longrightarrow PhCH_2CH_2CORh(CO)_{3-n}P_n^* \quad (6)$$

an analogous isomerization seems to occur; therefore the percentage of hydratropaaldehyde decreases with an increase in the reaction temperature.

The Effect of the Partial Pressure of Carbon Monoxide. The effects of the partial pressures of carbon monoxide on the $[\alpha]_D$ value and the percentage of hydratropaaldehyde were examined by the use of (*R*)-benzylmethylphenylphosphine under the following

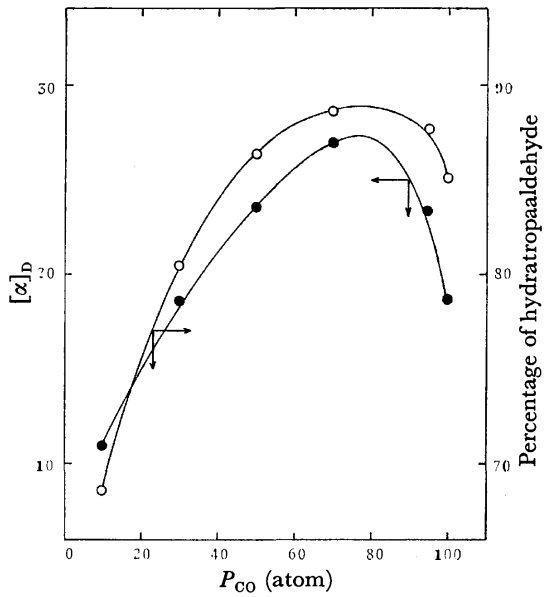

Fig. 5. Effects of partial pressures of carbon monoxide on the $[\alpha]_D$ value and the percentage of hydratropaaldehyde. (P_{H_2}=50 atm, 110 °C, (*R*)-benzylmethylphenylphosphine/rhodium=2)

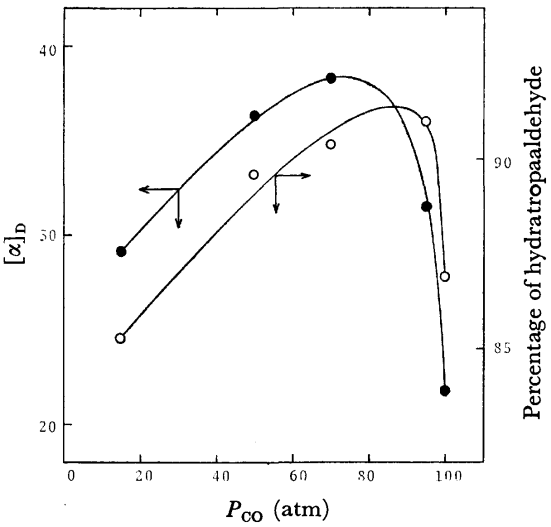

Fig. 6. Effects of partial pressures of carbon monoxide on the $[\alpha]_D$ value and the percentage of hydratropaaldehyde. (P_{H_2}=50 atm, 110 °C, (*R*)-benzylmethylphenylphosphine/rhodium=3)

* Taking the optical purity of the phosphine (76.6%) into consideration, this optical rotation indicates a 52% optical yield.

conditions; 110 °C, an initial partial pressure of hydrogen of 50 atm, and a phosphine/rhodium ratio of 2: 1 or 3: 1. The results are illustrated in Figs. 5 and 6.

As Figs. 5 and 6 show, the $[\alpha]_D$ value and the percentage of hydratropaaldehyde at first increased monotonously to a maximum, and then decreased with an increase in the partial pressure of carbon monoxide, when the other reaction conditions were fixed. These relations may be partly explained by the equilibrium of the active species. As the partial pressure of carbon monoxide increases, the Equilibrium (5) is shifted to the left; this shift brings about a decrease in the $[\alpha]_D$ value and the percentage of hydratropaaldehyde, as has been described in connection with the effect of the phosphine/rhodium ratio. The tendency of the right-hand half of the curves in Figs. 5 and 6 to decrease may be attributed to this factor. However, the left-hand half can not be explained clearly.

In contrast with the results shown in Figs. 5 and 6, the change in the partial pressure of carbon monoxide did not result in any appreciable effect at the phosphine/rhodium ratio 4: 1 (see Exps. No. 4 and 9 in Table 1). The (5) equilibrium seems to lie very far to the right at larger ratios; therefore, the equilibrium is not profoundly affected by changing the partial pressure of carbon monoxide in the range examined.

The Effect of the Partial Pressure of Hydrogen. The effects of the initial partial pressure of hydrogen were also examined; the results are shown in Figs. 7 and 8. As Figs. 7 and 8 show, the $[\alpha]_D$ value and the percentage of hydratropaaldehyde increased monotonously as the partial pressure increased, when the phosphine/rhodium ratio, the partial pressure of carbon monoxide, and the temperature were fixed at 2: 1 or 3: 1, 50 atm, and 110 °C respectively.

As has been described above, the effect of the partial pressure of carbon monoxide was much larger at a phosphine/rhodium ratio of 3: 1 or 2: 1 than that at

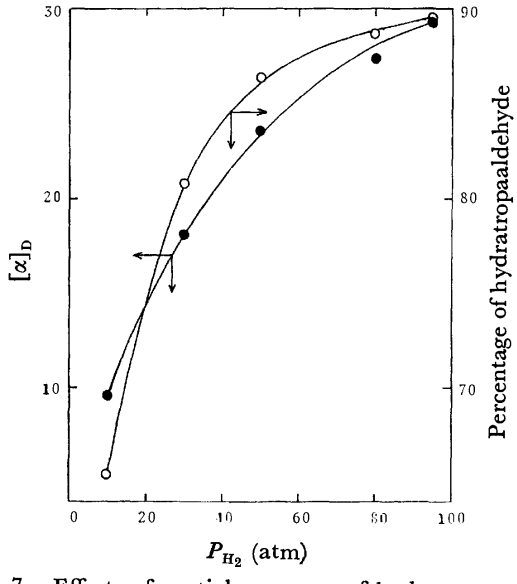

Fig. 7. Effects of partial pressures of hydrogen on the $[\alpha]_D$ value and the percentage of hydratropaaldehyde. (P_{CO}=50 atm, 110 °C, (*R*)-benzylmethylphenylphosphine/rhodium=2)

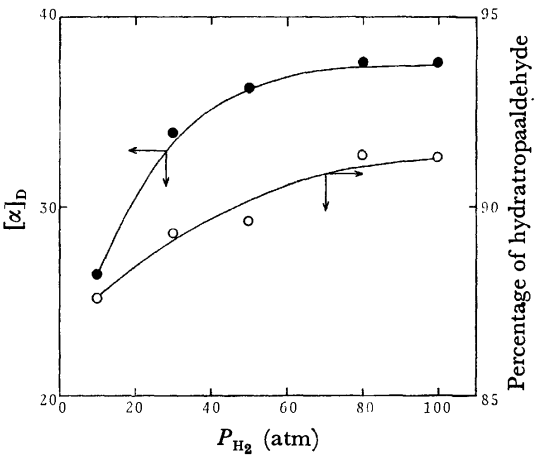

Fig. 8. Effects of partial pressures of hydrogen on the $[\alpha]_D$ value and the percentage of hydratropaaldehyde. (P_{CO}=50 atm, 110 °C, (*R*)-benzylmethylphenylphosphine/rhodium=3)

the 4: 1 ratio. This observation is also applicable to the present case. At the 4: 1 ratio, no significant effect of the partial pressure of hydrogen was observed (see Exps. No. 4 and 17 in Table 1).

General Discussion. As has been mentioned above, the $[\alpha]_D$ value and the percentage of hydratropaaldehyde show a fairly good parallelism in Figs. 5—8. This parallelism seems to indicate that the $[\alpha]_D$ value is also dependent on the route through which the hydratropaaldehyde is formed. According to the generally-accepted mechanism of hydroformylation, hydratropaaldehyde is thought to be formed *via* a styrene–rhodium π-complex (**1**), an α-phenethyl–rhodium complex (**2**), and an α-phenylpropionyl–rhodium complex (**3**) as intermediates. However, styrene shows behavior different from that of simple olefins in hydroformylation. With simple 1-olefins, the formylation mainly occurs on a terminal carbon to give a straight-chain aldehyde as a major product.[5] On the other hand, with styrene the inner carbon is predominantly formylated to give hydratropaaldehyde, a branched-chain aldehyde. Furthermore, with simple olefins an incremental addition of phosphine causes an increase in the percentage of the straight-chain aldehyde and a decrease in that of the branched-chain one, while with styrene an increase in the phosphine/rhodium ratio brings about an increase in the percentage of hydra-

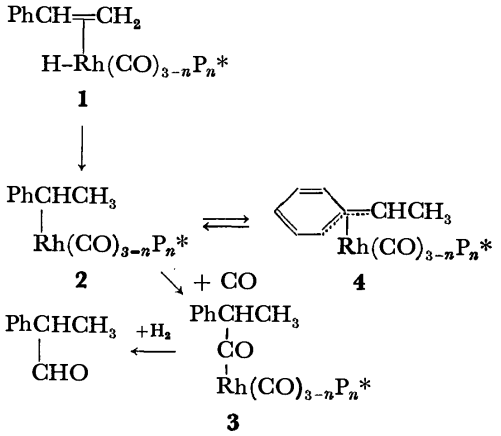

tropaaldehyde. These facts show that styrene has a marked tendency to be formylated on the inner carbon. From these considerations, an alternative route which contains a π-benzyl-type complex (**4**) as an intermediate may reasonably be suggested. This is supported by the fact that a π-benzyl-rhodium complex is formed in the reaction of benzyl chloride and Rh(I) complexes ($RhClL(PPh_3)_2$, L; CO or PPh_3).[11] This hypothesis of a participation of the π-benzyl-type complex is not only consistent with the fact that styrene is mainly formylated on the inner carbon, but is also reasonable in view of the stereoselectivity. Thus, in the asymmetric hydroformylation of olefins such as styrene derivatives, simple olefins, and unsaturated ethers, the stereoselectivity is highest in styrene, while that of the other olefins is far lower.[12] The π-benzyl-type complex of styrene will construct a rigid conformation of the diastereomeric intermediate to make the asymmetric induction more effective. This is probably the reason why styrene shows a larger stereoselectivity than the other olefins examined in the asymmetric hydroformylation.

References

1) M. Tanaka, Y. Watanabe, T. Mitsudo, K. Yamamoto, and Y. Takegami, *Chem. Lett.*, **1972**, 483.
2) I. Ogata and Y. Ikeda, *ibid.*, **1972**, 487.
3) G. Consiglio, C. Botteghi, C. Salomon, and P. Pino, *Angew. Chem.*, **85**, 663 (1973), and the preceeding papers.
4) R. Stern, A. Girschauer, and L. Sajus, *Tetrahedron Lett.*, 3247 (1973).
5) F. E. Paulik, *Catal. Rev.*, **6**, 49 (1972).
6) J. D. Morrison, R. E. Burnett, A. M. Aguiar, C. J. Morrow, and C. Phillip, *J. Amer. Chem. Soc.*, **93**, 1301 (1971).
7) Naumann, G. Zon, and K. Mislow, *ibid.*, **91**, 7012 (1969).
8) C. B. Cohen, J. Marshall, and H. E. Woodman, *J. Chem. Soc.*, **107**, 887 (1915).
9) A similar relationship between the $[\alpha]_D$ value and the phosphine/rhodium ratio has been reported.[2]
10) Y. Takegami, C. Yokokawa, Y. Watanabe, H. Masada, and Y. Okuda, This Bulletin, **37**, 1190 (1964).
11) C. O'Connor, *J. Inorg. Nucle. Chem.*, **32**, 2299 (1970).
12) M. Tanaka, Y. Watanabe, T. Mitsudo, and Y. Takegami, unpublished results which were presented at the 27th annual meeting of the chemical society of Japan, Nagoya, October 13, 1972.

The Novel Synthesis of L-Hydroxyproline from D-Glutamic Acid

Chikahiko EGUCHI and Akio KAKUTA

Central Research Laboratories, Ajinomoto Co., Inc., Suzuki-cho, Kawasaki-ku, Kawasaki 210

(Received December 27, 1973)

L-Hydroxyproline (**1**) and D-*allo*-hydroxyproline (**2**) were synthesized from D-glutamic acid (**3**) using the asymmetric center of **3** as that at C_4 of 4-hydroxyproline. When the aqueous solution of **1** or **2** was heated at 200 °C for 2 hr, a solution in the equilibrium state, containing 55% of **1** and 45% of **2**, was obtained. From this mixture, **1** was obtained by fractional crystallization.

Since 4-hydroxyproline was first synthesized in 1905 by Leuchs,[1] several synthetic routes have been studied by many researchers.[2-7] In these routes, comparable amounts of racemic diastereomers, *i.e.*, DL-hydroxyproline (DL-Hyp) and DL-*allo*-hydroxyproline (DL-*a*Hyp), have been formed. Therefore, difficult procedures, that is, the fractionation of DL-Hyp and DL-*a*Hyp and the optical resolution of DL-Hyp, were unavoidable, if one was to obtain L-hydroxyproline (**1**) from these racemic diastereomers.[8-9]

This paper will deal with a new synthesis of (4*R*)-4-hydroxyproline, *i.e.*, **1** and D-*allo*-hydroxyproline (**2**), from D-glutamic acid (**3**) using the asymmetric center of **3** as that at C_4 of 4-hydroxyproline, and with a new method of the interconversion between **1** and **2**. By these methods, **1** can be easily obtained without optical resolution, as will be described below.

Results and Discussion

Synthesis of L-*Hydroxyproline and* D-allo-*Hydroxyproline.*

(*R*)-γ-Butyrolactone-γ-carboxylic acid (**4**) was prepared from **3** in an 85% yield by a reaction with nitrous acid in an aqueous solution. This reaction is known to proceed with a full retention of the configuration due to the participation of the neighboring carboxylate group.[10,11] The treatment of **4** with thionyl chloride afforded (*R*)-γ-butyrolactone-γ-carboxylic acid chloride (**5**) in a 96% yield. This reaction is considered to proceed with a full retention of its configuration by analogy with the conversion of *N*-trifluoroacetyl-L-proline to *N*-trifluoroacetyl-L-prolyl chloride.[12]

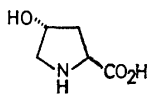

1

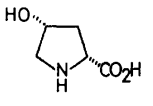

2

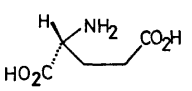

3

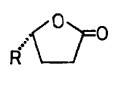

4 R=CO_2H **5** R=COCl
6 R=CH_2OH **7** R=CH_2Cl

Formulae.

(*R*)-γ-Hydroxymethyl-γ-butyrolactone (**6**) was prepared from **5** in a 77% yield by reduction with sodium borohydride in dry diglyme. A small amount of 1,2,5-trihydroxypentane was also formed in this reduction. However, it was easily removed by silica gel chromatography.

In the case of sodium borohydride reduction, it is occasionally troublesome to decompose the reaction products and to remove the resulting boric acid.[13] However, in the present case, when methanol was poured into the reaction mixture we could easily decompose the reaction products and convert the boric acid into volatile trimethyl borate. The reduction mechanism of acid chloride with sodium borohydride has not been exactly reported, however, the reaction-equation seems to be as follows, by analogy with the reduction with lithium borohydride:[14]

$$4\,RCOCl + 2\,NaBH_4 \longrightarrow NaCl + BCl_3 + NaB(OCH_2R)_4 \quad (1)$$

$$BCl_3 + CH_3OH \longrightarrow B(OCH_3)_3 + 3\,HCl \quad (2)$$

$$NaB(OCH_2R)_4 + 3\,CH_3OH + HCl \longrightarrow NaCl + B(OCH_3)_3 + 4\,RCH_2OH \quad (3)$$

Fickett, Govner, and Leres reported that the optically-active alcohol, 2-chloropropanol, was obtained, with a retention of its configuration, from the optically-active acid chloride, 2-chloropropionyl chloride, by reduction with litium aluminium hydride.[15] By analogy with this reaction and by a comparision between the specific rotation of **6** and that of its (*S*)-isomer, which was synthesized by Koga, Taniguchi, and Yamada from (*S*)-γ-butyrolactone-γ-carboxylic acid methyl ester,[16] this reduction step may be considered to proceed with a full retention of configuration.

(*R*)-γ-Chloromethyl-γ-butyrolactone (**7**) was prepared from **6** in a 93% yield by reaction with thionyl chloride in the presence of pyridine. In this reaction, the configuration is considered to be retained.

At the next step, the halogenation of the α-position of **7** was examined. The α-position of the lactone or the ester is known to be hardly halogenated without the cleavage of the ester group.[17,18] However, in the present case the halogenation must be carried out without opening the lactone ring if we are to retain the configuration of the γ-position. A mixture of **7** and sulfuryl chloride was heated in a sealed glass tube. α-Monochloro-compounds (**8**), α,α-dichloro-compound (**9**), α,β-dichloro-compound (**10**) and polychloro-substituted protoanemonins (**11**) were formed. The gas-liquid chromatographic analyses (glc) showed two α-monochloro-compounds, *i.e.*, one with a shorter retention time (**8a**) and the other with a longer retention time (**8b**); their stereochemistries were deduced from the products of their amination, as will be discussed later. **11** was a mixture of tetra-, tri-, and dichloro-substituted protoanemonins. The component ratios of these products were determined by means of the ratios of their peak-areas in glc. A part of the results are shown in

Table 1. Chlorination of (*R*)-γ-chloromethyl-γ-butyrolactone (**7**) with sulfuryl chloride or gaseous chlorine

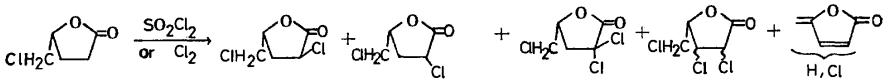

7 **8a** **8b** **9** **10** **11**

Expt. No.	$[SO_2Cl_2]$ / [7] [a]	Temp., C°	Time, hr	Products, % Unchanged 7	8a	8b	9	10	11
1	10.0	reflux	12	95	+[b]	+	+	—[c]	+
2	5.5	100	13	70	14	5	+	—	11
3	1.8	110	20	22	28	13	25	+	12
4	3.0	112	25	18	24	10	38	+	10
5	4.9	115	23	17	29	14	35	+	5
6	4.2	120	15	10	37	12	28	+	13
7	1.0	120	15	70	16	9	+	—	9
8	4.0	130	15	7	11	6	20	4	52
9	10.8	160	4.5	21	3	—	14	9	53
10[d]		134	7.5	12	17	9	27	3	34

a) Molar ratio. b) Trace amount. c) Undetectable. d) Gaseous chlorine was bubbled into **7**.

Table 1. Hardly any reaction took place under 100 °C, and above 130 °C the amount of **11** rapidly increased. The amount of sulfuryl chloride required was more than twice the molar equivalent of **7**.

When **7** was chlorinated by gaseous chlorine, the same products (**8**—**11**) were formed, as is shown in Table 1. However, in this case **11** was more easily formed than in the case of the chlorination with sulfuryl chloride.

When **7** was heated for 15—25 hr with three—five times molar sulfulyl chloride at 110—120 °C, the total amount of α-chloro-compounds (**8a**, **8b**, and **9**) was the largest, as is shown in Table 1. However it was impossible to prepare only α-monochloro-compounds. Therefore, the selective conversion of **9** to **8** was examined. The chlorination products were hydrogenated in acetic acid under atmospheric pressure in the presence of sodium acetate and 5% Pd–C. The rate of the dehalogenation of **9** to **8a** and **8b** was much faster than that of **8** to **7**. Therefore, the reaction rate was followed by glc, and then the hydrogenation was stopped at the time when **9** was almost completely converted to **8** without the dehalogenation of **8**. The hydrogenated mixture generally contained 40—45% of **8a**, 30—40% of **8b**, and 2—3% of **9**.

These mixtures were aminated with conc. ammonium hydroxide and hydrolyzed with 3 M hydrochloric acid or 1 M sodium hydroxide. The Hyp and *a*Hyp thus produced were treated by means of an ion-exchange column (acid form) and decolorizing resin and were estimated by means of an automatic amino-acid analyzer. The results are shown in Table 2. The chlorination of **7** with sulfuryl chloride, followed by hydrogenation, amination, and hydrolysis, gave Hyp and *a*Hyp in a 46% overall yield.

The optical purities of these amino acids were determined by Manning and Moore's method,[19] with some modifications. Thus, four dipeptides, *i.e.*, L-leucyl-L-hydroxyproline, L-leucyl-D-hydroxyproline, L-leucyl-L-*allo*-hydroxyproline and L-leucyl-D-*allo*-hydroxyproline, were prepared from the amino acid mixture by reaction with *N*-carboxy-L-leucine anhydride. Then, the optical purity of Hyp was determined from the amounts of L-leucyl-L-hydroxyproline and L-leucyl-D-hydroxyproline. On the other hand, for the determination of the optical purity of *a*Hyp, the amino acid mixture was

Table 2. Amination of (γ*R*)-α-chloro-γ-chloromethyl-γ-butyrolactone (**8a** and **8b**)

Expt. No.	[8b]/[8a] [a]	Reaction conditions[b] Amination	Hydrolysis	4-Hydroxyprolines Yield[c] (%)	[1]/[2] [d]	Content of enantiomer, % D-Hyp[e]	L-*a*Hyp[f]
1	39/61	A	C	38	41/59	4.7	3.1
2	46/54	A	C	46	46/54	4.1	2.9
3	45/55	A	C	46	44/56	4.2	2.5
4	45/55	B	C	45	55/45	4.6	3.6
5	41/59	A	C	12	39/61		
6	41/59	A	D	10	40/60		

a) Molar ratio of **8b** to **8a** in the starting material of amination. b) A; at room temperature for 2 day in conc. ammonium hydroxide. B: at 100—110°C for 7.5 hr in conc. ammonium hydroxide. C; reflux for 2 hr in 3 M hydrochloric acid. D; reflux for 0.5 hr in 1 M sodium hydroxide. c) The yield is based on **7** by chlorination with sulfuryl chloride followed by hydrogenation, amination and hydrolysis in Expt. No. 1—4. In Expt. No. 5 and 6, that is based on **7** by chlorination with gaseous chlorine, amination, and hydrolysis. d) Molar ratio of **1** to **2** in the formed 4-hydroxyproline. e) [D-Hyp]/([D-Hyp]+[L-Hyp]). f) [L-*a*Hyp]/([L-*a*Hyp]+[D-*a*Hyp]).

reacted with *N*-carboxy-L-valine anhydride instead of *N*-carboxy-L-leucine anhydride, and the L-valyl-L-*allo*-hydroxyproline and L-valyl-D-*allo*-hydroxyproline thus formed were estimated by means of the automatic amino-acid analyzer. The Hyp was composed of about 4% of the D-isomer and about 96% of the L-isomer, while the *a*Hyp was composed of about 3% of the L-isomer and about 97% of the D-isomer, as is shown in Table 2.

By recrystallization from water–ethanol, **1** and **2** were obtained in a 40% yield based on **7** (*i.e.*, in a 23% yield based on **3**). In this mixture, D-hydroxyproline and L-*allo*-hydroxyproline were not found by the above-mentioned method used to determine the optical purity.

When the amination was carried out at room temperature, as is shown in Table 2, the molar ratio of **1** to **2** was in fair agreement with that of **8b** to **8a**. On the other hand, α-amino acid is known to be formed at room temperature from α-chlorocarboxylic acid with a full inversion of the configuration.[20] Therefore, it could unambiguously be deduced that **1** and **2** were formed from **8b** and **8a** respectively. Thus, **8a** must be (α*S*,γ*R*)-α-chloro-γ-chloromethyl-γ-butyrolactone and **8b** must be (α*R*,γ*R*)-α-chloro-γ-chloromethyl-γ-butyrolactone.

Interconversion between L-*Hydroxyproline and* D-allo-*Hydroxyproline and Isolation of* L-*Hydroxyproline.* To obtain **1** from the mixture of **1** and **2**, novel methods of interconversion and fractination were examined. Until now, the interconversion between **1** and **2** has been made by two methods: (A) by heating an aqueous solution of the amino acid in the presence of excess barium hydroxide at 200 °C for several hours[21] and (B) by treating the amino acid with an excess of acetic anhydride in refluxing glacial acetic acid.[22] The reaction mixtures at the equilibrium state contained about 50% of **1** in Method (A) and about 25% of **1** in Method (B).

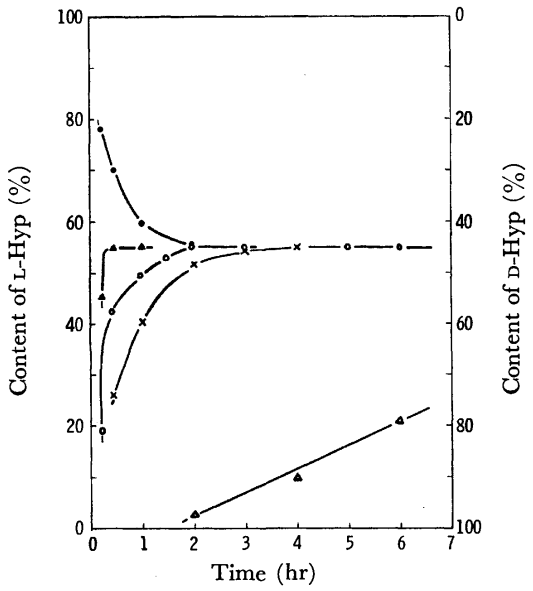

Fig. 1. Interconversion between L-hydroxyproline (**1**) and D-*allo*-hydroxyproline (**2**) in an aqueous solution: (△), **2** (starting material), 150 °C (reaction temperature); (×), **2**, 180 °C; (○), **2**, 200 °C; (▲), **2**, 220 °C; (●), **1**, 200 °C.

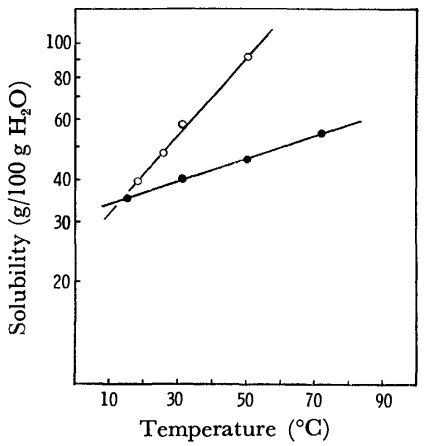

Fig. 2. Solubilities of L-hydroxyproline (●) and D-*allo*-hydroxyproline (○).

An aqueous solution of **1** or **2** was heated at 150, 180, 200, and 220 °C, and the contents of **1** and **2** in the solution were estimated using the optical rotation or an automatic amino-acid analyzer. The results are shown in Fig. 1. When the aqueous solution of **1** or **2** was heated at 200 °C for 2 hr, a solution at the equilibrium state, which contained 55% of **1** and 45% of **2**, was easily obtained.

The solubilities of **1** and **2** in water were also examined. The results are shown in Fig. 2. The temperature dependence of the solubility is apparently different between **1** and **2**. The solubility of **1** in water was constant regardless of the presence of **2**. Therefore, 9.00 g of a mixture of 55% of **1** and 45% of **2** gave 0.85 g of optically-pure **1** by fractional crystallization from 10 ml of water at 30 °C. Thus, the conversion of the mixture of **1** and **2** to **1** was carried out by a combination of interconversion and fractional crystallization in water. Also, by a method previously reported by the present authors, *i.e.*, the method through cyclic dipeptides, these mixtures could be easily converted to **1**.[23]

Experimental

The melting points are uncorrected. The IR spectra were recorded on a JASCO IR-S spectrometer. The NMR spectra were measured with a Varian T-60 or XL-100 spectrometer, using TMS as the internal standard. The mass spectra were obtained using a Hitachi RMU-6E spectrometer. The optical rotations were measured with a JASCO DIP-SL automatic polarimeter. The 4-hydroxyprolines were analyzed using a Hitachi KLA-3B automatic amino-acid analyzer (column size, 50×0.9 cm; resin, Hitachi Type 2612; column flow rate, 60 ml/hr; buffer, citrate (0.2 M) pH 3.25; temperature, 55 °C).

*Identification of the Chlorination Products of (*R*)-γ-Chloromethyl-γ-butyrolactone (***7***).* The reaction mixture was fractionated using a Shimadzu Gas Chromatograph GC-4A equipped with TCD and a glass column (5 ft×1/4 in. with 10% PEG-6000 on Chromosorb W (HMDS), 60—80 mesh; column temperature, 145 °C; flow rate of helium gas, 35 ml/min). The component ratios were determined by using a Hewlet Packard 402 High Efficiency Gas Chromatogram equipped with FID

and a glass column (4 ft×1/4 in. with 20% PEG-4000 on Chromosorb W (HMDS), 80—100 mesh; column temperature, 160 °C; flow rate of helium gas, 30 ml/min); the retention times (r.t.) will be shown below.

*(αS, γR)-α-Chloro-γ-chloromethyl-γ-butyrolactone (**8a**)*: r.t., 11.6 min; Mass spectrum *m/e* 119 (M–CH_2Cl, $C_4H_4O_2Cl$), 88, 83, 75 (C_3H_4Cl), 63 (C_2H_4Cl), 62 (C_2H_3Cl), 49 (CH_2Cl); IR (liquid film) 1960, 1795 (C=O), 1175, 1035 and 924 cm^{-1}.

*(αR, γR)-α-Chloro-γ-chloromethyl-γ-butyrolactone (**8b**)*: r.t., 15.6 min. The mass spectrum was identical with that of **8a**.

*(R)-α,α-Dichloro-γ-chloromethyl-γ-butyrolactone (**9**)*: r.t., 8.4 min; Mass spectrum *m/e* 153 (M–CH_2Cl, $C_4H_3O_2Cl_2$), 125, 109 (C_3H_3Cl), 96 ($C_2H_2Cl_2$), 61 (C_2H_2Cl), 49 (CH_2Cl); IR (liquid film) 2970, 1810 (C=O), 1179, 1034 and 963 cm^{-1}; NMR (in $CDCl_3$) $ClCH_dH_e$–$C_\gamma H_c$–$C_\beta H_bH_a$– δ_a 3.26, δ_b 2.97, 4.95, δ_d 3.79, δ_d 3.86, J_{ab}=14.6 Hz, J_{ac}=5.5 Hz, J_{bc}=9.3 Hz, J_{de}=12.3 Hz, J_{dc}=4.9 Hz, J_{ec}=4.6 Hz. The assignment of this five-spin system was confirmed by computor simulation.

*(γR)-α,β-Dichloro-γ-chloromethyl-γ-butyrolactone (**10**)*: r.t., 9.8 min. The mass spectrum was almost identical with that of **9**; however, they differed in the relative strengths of their peaks.

*Polychloro-substituted Protoanemonins (**11**)*: r.t., 1.8—2.8 min; Mass spectrum *m/e* 268 ($C_5HO_2Cl_5$), 233 ($C_5HO_2Cl_4$), 222 ($C_5O_2Cl_4$), 198 ($C_5HO_2Cl_3$), 185 ($C_4O_2Cl_3$), 151 ($C_4HO_2Cl_2$), 123. In NMR spectrum, the signals appeared between δ 6.13 and 7.70.

Determination of the Optical Purity of 4-Hydroxyproline by Ion-exchange Chromatography. allo-*Hydroxyproline*: The borate buffer (0.45 M, 500 ml) was prepared by dissolving boric acid (13.9 g) in 497 ml of boiled, distilled water and then by adding 50% sodium hydroxide to bring the solution to pH 10.2 at 25 °C. In 15 ml of this borate buffer, 20 mg (0.152 mmol) of an amino acid mixture of hydroxyproline and *allo*-hydroxyproline was dissolved, and then a small amount of silicone grease was added to minimize foaming. To the vigorously-stirred solution we then rapidly added, at 0—2 °C, a solution of *N*-carboxy-L-valine anhydride (26 mg, 0.18 mmol) in dioxane (1.0 ml). After this mixture has been vigorously stirred for 3 min, 3 ml of 2 M hydrochloric acid was added rapidly to stop the reaction. The solution was filled up to 25 ml with a citrate buffer (0.2 M, pH 2.2), and the contents of L-valyl-L-*allo*-hydroxyproline and L-valyl-D-*allo*-hydroxyproline in the solution were estimated by comparison with authentic mixtures using a Hitachi KLA-5 automatic amino-acid analyzer (column size, 50×0.9 cm; resin, Hitachi Type 2613; column flow rate, 60 ml/hr; buffer, citrate (0.2 M), pH 3.25; temperature, 55 °C).

The elution times were 142 min for L-valyl-D-hydroxyproline and L-valine, 170 min for L-valyl-D-*allo*-hydroxyproline, 190 min for L-valyl-L-hydroxyproline, and 207 min for L-valyl-L-*allo*-hydroxyproline. The detectable amount of L-*allo*-hydroxyproline in the amino acid mixture was checked by using an authentic mixture. A 0.5% amount of L-*allo*-hydroxyproline in *allo*-hydroxyproline was detectable; however, any amount less than 0.5% of L-isomer was not detectable.

Hydroxyproline: Using *N*-carboxy-L-leucine anhydride (29 mg, 0.18 mmol), the contents of L- and D-hydroxyprolines in a mixture of hydroxyproline and *allo*-hydroxyproline were estimated in a manner similar to that described in the part of *allo*-hydroxyproline. The elution times were 155 min for L-leucyl-D-hydroxyproline, 220 min for L-leucyl-L-hydroxyproline, and 254 min for L-leucyl-L-*allo*-hydroxyproline, L-leucyl-D-*allo*-hydroxyproline, and L-leucine. Any amount less than 0.5% of D-hydroxyproline was not detectable.

*(R)-γ-Butyrolactone-γ-carboxylic Acid (**4**)*. From D-glutamic acid ($[\alpha]_D^{27}$ −31.6° (*c* 10.2, 2 M HCl)), **4** was obtained in an 85% yield by the method of Austin and Howard:[24] bp 165.5—167.5 °C/0.30 mmHg; mp 73.5—74.0 °C (recrystallization from ethyl acetate–benzene–petroleum ether); $[\alpha]_D^{20}$ −15.9° (*c* 1.10, ethanol), +7.29° (*c* 1.03, water), −14.3° (*c* 1.19, methanol). Lit,[11] bp 150—155 °C/0.2 mmHg, mp 71—72 °C, $[\alpha]_D^{20}$ −2.8° (*c* 5.8, water), +10.6° (*c* 5.0, methanol) for (*S*)-isomer.

*(R)-γ-Butyrolactone-γ-carboxylic Acid Chloride (**5**)*. A mixture of **4** (55.7 g, 0.429 mol) and thionyl chloride (102.0 g, 0.857 mol) was refluxed for 2 hr and then allowed to stand at room temperature overnight. After the removal of the excess thionyl chloride, the residue was distilled under reduced pressure to give 61.1 g (0.413 mol) of **5** in a 96% yield: bp 117.1 °C/4.5 mmHg; $[\alpha]_D^{30}$ +0.196° (*c* 4.34, dioxane), −44.5° (*c* 3.70, benzene); IR (liquid film) 2970, 1805—1780, 1458, 1490, 1355, 1138, 1060, and 910 cm^{-1}; NMR (in $CDCl_3$) δ 2.7 (4H, m, $-CH_2-CH_2-$) and 5.3 (1H, m, C_γ–H); Mass spectrum *m/e* 85 (M–COCl, $C_4H_5O_2$), 57, 36, 29. Found: C, 40.65; H, 3.49; Cl, 23.59%. Calcd for $C_5H_5O_3Cl$: C, 40.42; H, 3.39; Cl, 23.87%. Lit,[25] bp 136—137 °C/12 mmHg for the racemic form.

*(R)-γ-Hydroxymethyl-γ-butyrolactone (**6**)*. A solution of **5** (24.8 g, 0.168 mol) in dry diglyme (50 ml) was added at 0—5 °C to a solution of sodium borohydride (4.12 g, 0.109 mol) in dry diglyme (175 ml). The mixture was then stirred for 30 min at room temperature. To the mixture, methanol (70 ml) was added. After the filtration of sodium chloride, the filtrate was concentrated under reduced pressure. The resulting syrup was placed on a silica gel column containing 100 ml of WAKO GEL C-200 and eluted with 2.5% ethanol in chloroform. **6** was eluted faster than 1,2,5-trihydroxypentane, so the two products were easily separated. After the removal of the solvent from the elute containing **6**, the residue was distilled under reduced pressure to give 14.7 g (0.127 mol) of **6** in a 76% yield: bp 101.0—102.0 °C/0.048 mmHg; $[\alpha]_D^{30}$ −53.5° (*c* 3.17 chloroform), −33.5° (*c* 3.12, ethanol); IR (liquid film) 3400, 1765, 1350, 1185, 1060, 935, and 803 cm^{-1}; NMR (in $CDCl_3$) δ 1.95—2.75 (4H, $-CH_2-CH_2-$), 3.80 (2H, $-CH_2OH$) and 4.63 (1H, C_γ–H); Mass spectrum *m/e* 116 (M^+), 85 (M–CH_2OH), 57, 31 (CH_2OH). Found: C, 51.90; H, 6.67%. Calcd for $C_5H_8O_3$: C, 51.72; H, 6.94%. Lit,[16] $[\alpha]_D^{28}$ +31.1° (ethanol) for the (*S*)-isomer.

*(R)-γ-Chloromethyl-γ-butyrolactone (**7**)*. Thionyl chloride (26.9 g, 0.226 mol) was added to a mixture of **6** (23.2 g, 0.200 mol) and dry pyridine (17.6 g, 0.222 mol) at 40—50 °C. The mixture was stirred for 1 hr at 60 °C. To the mixture, chloroform (200 ml) was then added. The resulting chloroform solution was washed with water (50 ml) (three times), saturated sodium bicarbonate (20 ml), and water (50 ml), dried with anhydrous sodium sulfate, and decolorized with active charcoal. After the removal of the chloroform, the residue was distilled under reduced pressure to give 25.0 g (0.187 mol) of **7** in a 94% yield; bp 94.0—94.2 °C/2.0 mmHg; $[\alpha]_D^{27}$ −12.9° (*c* 3.03, chloroform), −33.2° (*c* 3.51, ethanol); IR (liquid film) 2965, 1775, 1169, 1040, 915, and 738 cm^{-1}; NMR (in $CDCl_3$) δ 1.95—2.77 (4H, $-CH_2-CH_2-$), 3.70 (2H, CH_2Cl), 4.76 (1H, C_γ–H); Mass spectrum *m/e* 134 (M^+, 2%), 85 (M–CH_2Cl, 100%), 57, 55, 29. Found: C, 44.85; H, 5.17; Cl, 26.65%. Calcd for $C_5H_7O_2Cl$: C, 44.63; H, 5.24; Cl, 26.35%.

L-*Hydroxyproline (**1**) and* D-allo-*Hydroxyproline (**2**)*. A mixture of **7** (1.98 g, 14.8 mmol) and sulfuryl chloride (6.04 g, 44.7 mmol) was heated at 112 °C for 25 hr in a glass tube.

After the removal of the excess sulfuryl chloride from the mixture under reduced pressure, chloroform (50 ml) was added to the residue. The resulting chloroform solution was washed with water (10 ml), saturated sodium bicarbonate (10 ml), and water (10 ml), and dried with anhydrous sodium sulfate. The removal of the chloroform gave 3.39 g of a syrup. The results of glc analysis showed that the sryup contained 24% of **8a**, 10% of **8b**, 38% of **9**, a trace amount of **10**, 10% of **11**, and 18% of unchanged **7**.

This syrup was dissolved in 30 ml of acetic acid and hydrogenated in the presence of sodium acetate (1.0 g) and 5% Pd–C (250 mg) at atmospheric pressure. The conversion of **9** to **8a** and **8b** was followed by glc. When 230 ml of hydrogen gas had been absorbed, the reaction was stopped. After the filtration of the catalyst and the sodium acetate, the filtrate was concentrated under reduced pressure. Toluene (10 ml) was added to the residue. The toluene solution was evaporated to remove acetic acid under reduced pressure. The syrup (2.88 g) thus obtained was found by glc to contain 43% of **8a**, 37% of **8b**, 2% of **9**, 4% of **10**, 9% of **11**, and 5% of **7**.

This syrup was dissolved in 30 ml of conc. ammonium hydroxide, and the solution was stirred for 2 days at room temperature. The excess of ammonium hydroxide was evaporated under reduced pressure, 90 ml of 3 M hydrochloric acid was added, and the solution was refluxed for 2 hr. The solution was then evaporated under reduced pressure. The residue was dissolved in water (30 ml), and the aqueous solution was placed in an ion-exchange column containing 100 ml of IR-120 resin (acid form). The resin was washed with water, and the absorbed amino acids were eluted with 0.2 M ammonium hydroxide. The elute was concentrated under reduced pressure and decolorized by the use of decolorizing resin (Hokuetsu Tanso Co.'s HS decolorizing resin). By analysis using the automatic amino-acid analyzer, the solution was found to contain 0.409 g (31.2 mmol) of hydroxyproline, 0.478 g (36.5 mmol) of *allo*-hydroxyproline, and trace amounts of unidentified ninhydrin positive substances. The optical purity of the 4-hydroxyproline thus obtained was determined by the above-mentioned method. The hydroxyproline was composed of 95.9% of the L-isomer and 4.1% of the D-isomer, while the *allo*-hydroxyproline was composed of 97.1% of the D-isomer and 2.9% of the L-isomer.

The solution was evaporated to dryness under reduced pressure. The residue was recrystallized from water–ethanol to give 0.784 g (5.98 mmol) of a mixture composed of 44.8% of **1** and 55.2% of **2** in a 40% yield based on **7**: mp 239 °C (decomp.); $[\alpha]_D^{31}$ $-1.72\pm0.25°$ (*c* 2.03, water). Found: C, 45.71; H, 7.02; N, 10.89%. Calcd for $C_5H_9O_3N$: C, 45.79; H, 6.91; N, 10.68%. In the mixture thus obtained, D-hydroxyproline and L-*allo*-hydroxyproline were not found by the above-mentioned method used to determine the optical purity.

Interconversion between L-*Hydroxyproline (1) and* D-allo-*Hydroxyproline (2).* A solution of **2** (0.500 g, 3.82 mmol) in water (5 ml) was sealed in a glass tube and heated for 2 hr at 200 °C. The tube was then cooled and opened, and the solution was filled up to 50 ml. The specific rotations, $[\alpha]_D^{30}$ (*c* 1.00, water), of the solution and authentic **1** and **2** were -16.0, -76.0, and $+58.6°$ respectively. Therefore, the solution contained 55.4% of **1** and 44.6% of **2**. The analytical results obtained by means of the automatic amino-acid analyzer showed that the solution was composed of 56.2% of **1** and 43.8% of **2**. The experiments were similarly carried out while varying the heating time. The following results were obtained: 19.1% of **1** at 15 min, 42.4% of **1** at 30 min, 49.5% of **1** at 1 hr, 52.1% of **1** at 1.5 hr, 55.4% of **1** at 2 hr, 55.8% of **1** at 3 hr, 54.9% of **1** at 5 hr, and 55.5% of **1** at 6 hr. The experiments were similarly done at 150, 180, 200, and 220 °C by using **1** or **2** as the starting material.

Solubility of L-*Hydroxyproline (1) or* D-allo-*Hydroxyproline (2) in Water.* A suspension of **2** (10 g) in water (10 ml) was stirred at 32.0 ± 0.1 °C overnight. The supernatant solution (1.585 g) was then taken up and dried at 80 °C until the weight became constant. The rsidue weighed 0.580 g. Therefore, the solubility of **2** in water at 32 °C was determined to be 57.7 g/100 g-water. The solubilities of **1** or **2** in water were similarly determined at different temperatures.

The authors wish to express their thanks to Professor Naoki Inamoto of the University of Tokyo for his valuable suggestions and to Dr. Takehiko Ichikawa for his many helpful discussions.

References

1) H. Leuchs, *Ber.*, **38**, 1937 (1905).
2) R. Gaudry and C. Godin, *J. Amer. Chem. Soc.*, **76**, 139 (1954).
3) R. Kuhn and G. Osswald, *Chem. Ber.*, **89**, 1423 (1956).
4) W. Traube, R. Johow, and W. Tepohl, *Ber.*, **56**, 1861 (1923).
5) H. McIlwain and G. M. Richardson, *Biochem. J.*, **33**, 44 (1939).
6) N. Izumiya and B. Witkop, *J. Amer. Chem. Soc.*, **85**, 1835 (1963).
7) Y. K. Lee and T. Kaneko, This Bulletin, **46**, 2924 (1973).
8) H. Leuchs and J. F. Brewster, *Ber.*, **46**, 986 (1913).
9) H. Leuchs and K. Barmann, *ibid.*, **52**, 2086 (1919).
10) P. Brewster, F. Hiron, E. D. Hughes, C. K. Ingold, and P. A. D. S. Rao, *Nature*, **166**, 179 (1950).
11) O. Červinka and L. Hub, *Collect. Czech. Chem. Commun.*, **33**, 2927 (1968).
12) W. A. Bonner, *J. Chromatogr. Sci.*, **10**, 159 (1972).
13) S. W. Chaikin and W. G. Brown, *J. Amer. Chem. Soc.*, **71**, 122 (1949).
14) N. G. Gaylord, "Reduction with Complex Metal Hydrides," Interscience Publisher Inc., New York, N. Y., (1956), p. 379.
15) W. W. Fickett, K. Govner, and H. Leres, *J. Amer. Chem. Soc.*, **73**, 5063 (1951).
16) K. Koga, M. Taniguchi, and S. Yamada, *Tetrahedron Lett.*, **1971**, 263.
17) C. A. Buehler and D. E. Pearson, "Survey of Organic Syntheses," John Wiley & Sons Inc., New York, N. Y., (1970), p. 386.
18) H. Plieninger, *Chem. Ber.*, **83**, 265 (1950).
19) J. M. Manning and S. Moore, *J. Biol. Chem.*, **243**, 5591 (1968).
20) L. Fowden, *Biochem. J.*, **64**, 323 (1956).
21) H. Leuchs and H. Felser, *Ber.*, **41**, 726 (1908).
22) D. S. Robinson and J. P. Greenstein, *J. Biol. Chem.*, **195**, 383 (1952).
23) C. Eguchi and A. Kakuta, *J. Amer. Chem. Soc.*, submitted for publication.
24) A. T. Austin and J. Howard, *J. Chem. Soc.*, 3593 (1961).
25) H. Blieniger, G. Ege, R. Fisher, and W. Hoffmann, *Chem. Ber.*, **94**, 2106 (1961).

The One-electron Reduction of Carbonium Ions. VI. The Trapping of the Cycloheptatrienyl Radical with 2-Methyl-2-nitrosopropane in the Course of the Zinc Reduction of the Tropylium Ion*

Kunio OKAMOTO and Koichi KOMATSU

Department of Hydrocarbon Chemistry, Faculty of Engineering, Kyoto University, Sakyo-ku, Kyoto 606

(Received January 5, 1974)

The zinc reduction of the tropylium ion was carried out in the presence of 2-methyl-2-nitrosopropane (a radical scavenger) in H_2O–THF (7: 3 by volume) at room temperature. In the reaction mixture with a short reaction time (5 min), *t*-butyl tropyl nitroxide (II) (a radical-trapping product) was identified by the ESR analysis. α-Phenyl-*N*-*t*-butylnitrone (I), which was isolated from the reaction mixture during a prolonged reaction time (30 min), was proved to be derived from the nitroxide II through the hydrogen abstraction by *t*-butyl nitroxide, which was itself formed from 2-methyl-2-nitrosopropane *in situ* in the acidic reaction mixture in the presence of zinc powder. The hydrogenation (on Pd/C) of the product mixture for a short reaction time (1 min) gave *N*-*t*-butyl-*N*-cycloheptylhydroxylamine and bicycloheptyl. On the basis of these observations, it is concluded that the primary product of the zinc reduction of the tropylium ion must be the tropyl radical.

The formation of bitropyl by the zinc reduction of the tropylium ion was first found by Doering and Knox.[1] They suggested an initial "one-electron" reduction, resulting in the formation of the tropyl (cycloheptatrienyl) radical, and a subsequent radical coupling. Since this mechanism seems certainly to be the most probable one, we have been considering the same mechanism in our series of studies of the reduction of substituted tropylium ions.[2] However, there has been no clear and direct evidence for the intervention of the tropyl radical in the course of the bitropyl formation. Thus, in order to confirm the validity of this mechanism, we have applied the "spin-trapping" technique[3] using *t*-nitrosobutane (2-methyl-2-nitrosopropane) to the zinc reduction of the tropylium ion.

Results and Discussion

The tropylium ion was allowed to react with an excess of zinc powder in the presence of 8 molar equivalents of *t*-nitrosobutane in H_2O–THF (7: 3 by volume) at room temperature for 30 min. The reaction products were then separated by elution chromatography to give bitropyl, α-phenyl-*N*-*t*-butylnitrone (I), and a comparable amount of *N*-*t*-butylhydroxylamine. The product distributions for the shorter reaction times were also examined to give the results summarized in Table 1.

The yields of bitropyl are almost invariable (50± 5%), whereas those of the nitrone I and *N*-*t*-butylhydroxylamine definitely increase with a prolonged reaction time. On the other hand, an analysis of the aqueous layer by means of ultraviolet spectroscopy revealed that the tropylium ion was completely consumed within one minute.

These results seem to indicate that the zinc reduction, which initially gives a primary product (presumably the tropyl radical), is rapidly completed and that about a half of the primary product so formed is trapped by *t*-nitrosobutane to give a transient product (II), which subsequently rearranges to the nitrone I[4] (see Scheme 1).

Table 1. The product distribution for the zinc reduction of the tropylium ion in the presence of *t*-nitrosobutane[a]

Reaction time, min	Temp. °C	Yield, %		
		Bitropyl	Nitrone I	Hydroxylamine[b]
1	24.0	50.4	4.4	~0
2	31.0	54.3	8.6	~0
15	31.0	45.5	32.0	~10.7
30	31.0	47.1	42.6	~21.0

a) [Tropylium fluoroborate] = 1.91×10^{-2} M; [Zn] = 5.0 atom equivalent with respect to the tropylium ion; [*t*-BuNO] = 0.153 M; Solvent = H_2O–THF (7: 3 by volume).
b) *N*-*t*-Butylhydroxylamine; the yield is calculated with reference to the tropylium ion. The real yield of this compound is supposed to be greater; see Ref. 15 in the Experimental.

The attempt to isolate this transient product was unsuccessful because of its instability and volatility. However, the reaction mixture with a short reaction time (5 min), after the usual work-up and vacuum distillation, gave a red oil which, after an immediate dissolution in benzene, exhibited an ESR spectrum composed of an equivalent triplet of the doublet; this radical was assigned to be *t*-butyl tropyl nitroxide (II) (a_N = 14.6 G, a_H = 2.2 G), the trapping product. The identical ESR spectrum was observed in the reaction of *t*-nitrosobutane with the tropyl radical, which was itself produced by the thermal dissociation of bitropyl[5] in *m*-xylene at 60 °C (see Experimental). Furthermore, when the product mixture with a short reaction time (1 min) was catalytically hydrogenated on palladium-carbon, *N*-*t*-butyl-*N*-cycloheptylhydroxylamine (III), which was supposedly derived from the trapping product (the nitroxide II), was isolated (9% yield), along with bicycloheptyl, which was produced by the hydrogenation of bitropyl. These results are illustrated in Scheme 1.

The control experiments to examine the course of the

* Presented at the 24th Annual Meeting of the Chemical Society of Japan, Osaka, April, 1971.

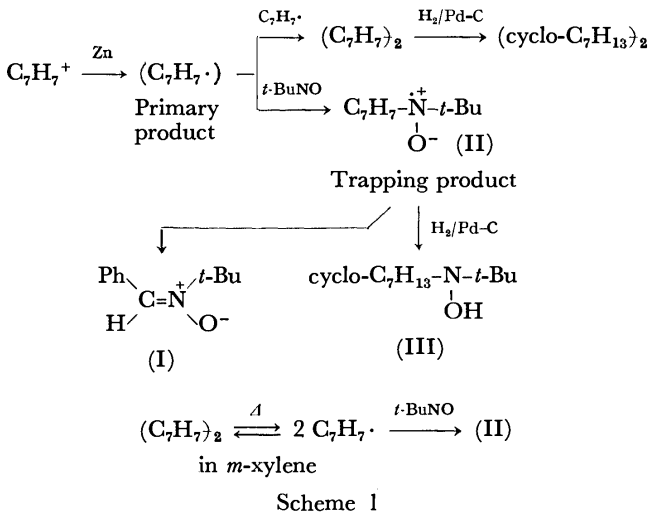

Scheme 1

formation of I indicated that the coexistence of three components, *i.e.*, *t*-nitrosobutane, zinc, and proton,[6] is a necessary condition in order to transform II into I. That is, the three reactions were continued for 30 min each after the immediate removal of the *t*-nitrosobutane (by bubbling off with air), zinc powder (by filtration), and proton[6] (by neutralization with NaOH) from the reaction mixtures with a short reaction time (1 min); no more than a trace amount of the nitrone I was detected in any of the reaction mixtures, whereas bitropyl was always found as the major product.

In another control experiment, the interaction of *t*-nitrosobutane with zinc in an aqueous tetrahydrofuran solution, acidified by the addition of acetic acid,[6] was found to give *t*-butyl nitroxide (IV), which was identified by means of its ESR spectrum (an equivalent triplet of doublet; $a_N = 13.9$ G, $a_H = 12.9$ G[7]). In addition, a nitroxide radical is known to be able to abstract a hydrogen atom.[8]

Consequently, it is most probable that, in the mixture with a prolonged reaction time, the nitroxide IV is produced *in situ* and that it immediately abstracts a hydrogen atom from the nitroxide II or its valence tautomer, II', to give *N*-*t*-butylhydroxylamine. This is illustrated in Scheme 2.

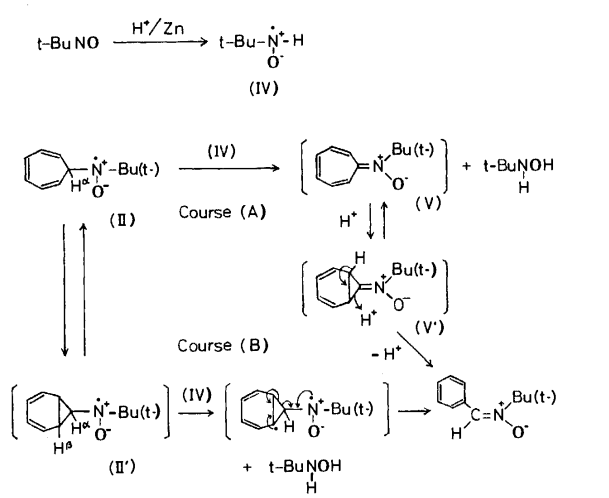

Scheme 2.

In Course (A), the nitrone V would be produced by the abstraction of α-hydrogen of the nitroxide II, and would subsequently be converted into the nitrone I through a norcaradiene-type intermediate, V', under acidic conditions in the reaction mixture or in the course of isolation, *e.g.*, during elution chromatography on silica gel.

As for Course (B), it is supposed that the cycloheptatriene-norcaradiene equilibrium lies to the norcaradiene side (II') when the electron-withdrawing nature of the partially polarized N–O bond in the nitroxide II is taken into consideration.[9] The subsequent β-hydrogen abstraction from the norcaradienyl system (II') to give the benzal system (I) seems plausible by analogy with the ionic rearrangements of a similar type found in the literature.[1,10] Thus, the preferred course (A or B) of the formation of the nitrone I from the nitroxide II has not yet been completely clarified.

However, on the basis of the ESR spectrum of the nitroxide II and of the isolation of the nitrone I and also the hydroxylamine III from the reaction mixture, it may be concluded that the primary product of the zinc reduction of the tropylium ion must be the tropyl radical.

Experimental[11]

Materials. Tropylium fluoroborate and *t*-nitrosobutane were prepared according to the methods of Conrow[12] and of Emmons[13] respectively. The zinc powder was of a reagent-grade quality. THF was distilled over 2,6-di-*t*-butyl-*p*-cresol; bp 66.0—66.2 °C.

Zinc Reduction of the Tropylium Ion in the Presence of t-*Nitrosobutane.* The Procedures for a representative run with the reaction time of 30 min will now be described. To a stirred solution of 0.750 g (4.20 mmol) of tropylium fluoroborate and 2.95 g (33.9 mmol) of *t*-nitrosobutane in 220 ml of H_2O–THF (7: 3 by volume), we added 1.38 g (21.0 mg-atom) of zinc powder under an atmosphere of nitrogen. After a 30 min reaction at 31 °C in the dark, the excessive zinc powder was filtered off. The filtrate was then worked up in the usual way to give 0.667 g of a partially-solidified red oil, which was then chromatographed over 25 g of silica gel (Nakarai, No. II-A, 100—200 mesh). Elution with *n*-hexane–benzene (4: 1 by volume) afforded 0.180 g (0.989 mmol) of bitropyl as white crystals, with an infrared spectrum identical with that of the authentic sample; 47.1% yield. The fractions eluted with benzene–ether (3: 2 by volume) gave 0.317 g (1.79 mmol) of the nitrone I as white crystals; its identity was established by means of the infrared and ultraviolet spectra and by a mixed mp; 42.6% yield; mp 73.0—74.5 °C (lit,[14] mp 75—76 °C). On the other hand, fractions eluted with ethanol and the ethereal extracts of the aqueous layer, which had been made alkaline, gave 0.0870 g[15] (0.978 mmol) of *N*-*t*-butylhydroxylamine as pale yellow crystals, which exhibited an infrared spectrum identical with that of the authentic sample; 2.9% yield based on *t*-nitrosobutane; 23.3% of the tropylium ion used.

In another run on half the scale of the above-mentioned reaction, after a reaction time of 5 min and the usual work-up, the reaction mixture was distilled under a vacuum to give 0.0184 g of a brownish-red oil; bp 70—85 °C (bath temperature)/0.4 mmHg. The distillate was immediately dissolved in benzene and sealed in a Pyrex tube (outer diameter, 4 mm) under a vacuum. An ESR spectrum was taken on

the sample to give the results described in the text.

Hydrogenation of the Crude Product Mixture. In the same way as has been described above, 1.00 g (5.60 mmol) of tropylium fluoroborate was reduced with 1.83 g (28.0 mg-atom) of zinc powder in the presence of 3.90 g (44.8 mmol) of *t*-nitrosobutane in 292 ml of H_2O–THF (7: 3 by volume) at room temperature. After 1 min, the reaction mixture was worked up and concentrated *in vacuo* to *ca.* 10 ml, which was subsequently hydrogenated over 0.8 g of palladium carbon (Nakarai, 5%) in dry THF to give 0.519 g of a yellowish oil. From this oil we isolated 0.315 g (1.62 mmol) of bicycloheptyl (58% yield; NMR, τ_{CCl_4} 7.9 (br, m, 2H, methine), 8.5 (br, s, 24H, methylene); $\nu_{max}^{CCl_4}$ 1450 (sh), 1460, 2870, 2940 cm^{-1}) and 0.088 g (0.51 mmol) of *N*-*t*-butyl-*N*-cycloheptylhydroxylamine (9.2% yield; NMR, τ_{CCl_4} 6.3 (br, s, 1H, methine), 7.1 (br, s, 1H, OH), 8.5 (br, s, 21H, methylene, methyl); $\nu_{max}^{CCl_4}$ 1025, 1120, 1215, 1350, 1380, 1450 (sh), 1460, 2870, 2930, 3420, 3630 cm^{-1}), by the use of preparative thin-layer chromatography over silica gel (Merck, Kieselgel PF_{254}), with benzene–ether (2: 1) as the eluent.

Found: C, 71.53; H, 12.30%. Calcd for $C_{11}H_{23}NO$: C, 71.30; H, 12.51%.

Reaction of t-*Nitrosobutane with Zinc in an Acidic Solution. ESR Measurements.* Into a Pyrex tube (outer diameter, 10 mm) with a capillary side tube (outer diameter, 1 mm) for ESR measurement, we charged 0.020 g (0.23 mmol) of *t*-nitrosobutane and 0.10 g (1.5 mg-atom) of zinc powder. The tube was then connected to a vacuum line, and 1.6 ml of a solution of acetic acid (0.04 M) in H_2O–THF (1: 1 by volume) was transferred into the tube with vacuum distillation. After sealing off the tube under a vacuum, the mixture was shaken at room temperature in the dark and an ESR spectrum of the supernatant solution was immediately recorded to give the results described in the text.

Thermal Dissociation of Bitropyl in the Presence of t-*Nitrosobutane. ESR Measurements.* Into a Pyrex tube (outer diameter, 5 mm) for ESR measurement, we charged 0.015 g (0.17 mmol) of *t*-nitrosubutane and 0.090 g (0.50 mmol) of bitropyl, which had been purified by sublimation (50 °C/1 mmHg). The tube was then connected to a vacuum line, and 0.5 ml of dry *m*-xylene was added by vacuum distillation. After being sealed off under a vacuum, the tube was shaken well in the dark and introduced into the ESR cavity, which had been kept at 60 °C with JEOL variable-temperature equipment, JES-UCT-2X. After 10 min, signals composed of an equivalent triplet of a doublet (a_N=14.5 G, a_H=2.2 G) began to appear in the ESR spectrum and kept increasing in intensity.

References

1) W. von E. Doering and L. H. Knox, *J. Amer. Chem. Soc.*, **79**, 352 (1957).

2) a) K. Okamoto, K. Komatsu, and H. Shingu, This Bulletin, **42**, 3249 (1969); b) K. Okamoto, K. Komatsu, O. Murai, and O. Sakaguchi, *Tetrahedron Lett.*, **1972**, 4989; c) K. Okamoto, K. Komatsu, S. Tsukada, and O. Murai, This Bullein, **46**, 1780 (1973); d) K. Okamoto, K. Komatsu, O. Murai, O. Sakaguchi, and Y. Matsui, *ibid.*, **46**, 1785 (1973).

3) *cf.* E. G. Janzen, *Accounts Chem. Res.*, **4**, 31 (1971).

4) A control experiment indicated that the tropylium ion itself reacts slowly with *t*-nitrosubutane to yield a small amount (1.6%) of the nitrone I after 30 min at room temperature. However, 68.5% of the tropylium ion was recovered unchanged in this case. An ionic mechanism may be supposed to be operating.

5) Bitropyl is reported to yield the tropyl radical by homolytic thermal dissociation (G. Vincow, H. J. Dauben, Jr., F. R. Hunter, and W. V. Volland, *J. Amer. Chem. Soc.*, **91**, 2823 (1969)). Thus, it is most probable that the tropyl radical is trapped by *t*-nitrosobutane to give *t*-butyl tropyl nitroxide (II).

6) The acidity of an aqueous solution of the tropylium ion is reported to be almost equal to that of an aqueous solution of acetic acid (W. von E. Doering and L. H. Knox, *J. Amer. Chem. Soc.*, **76**, 3203 (1954)).

7) The lit. ESR: a_N=13.4 G, a_H=12.5 G (in methanol), a_N=13.8 G, a_H=13.8 G (in water); the ratio of a_N to a_H is strongly dependent on the solvent polarity (Th. A. J. W. Wajer, A. Mackor, and Th. J. de Boer, *Tetrahedron*, **25**, 175 (1969)).

8) For examples of such a hydrogen abstraction by the nitroxide radical, see a) R. Dupeyre and A. Rassat, *J. Amer. Chem. Soc.*, **88**, 3180 (1966); b) M. Iwamura and N. Inamoto, This Bulletin, **40**, 703 (1967); c) K. Murayama and T. Yoshioka, *ibid.*, **42**, 2307 (1969).

9) R. Hoffmann, *Tetrahedron Lett.*, **1970**, 2907; and the references cited therein.

10) a) D. Bryce-Smith and W. A. Perkins, *J. Chem. Soc.*, **1962**, 5295; b) A. G. Anderson, Jr., and L. L. Repologle, *J. Org. Chem.*, **28**, 262 (1963); c) P. Beresford, A. Ledwith, and H. J. Woods, *J. Chem. Soc., B*, **1970**, 257.

11) The melting point and boiling point are uncorrected. The infrared and ultraviolet spectra were recorded with Shimadzu spectrometers, model IR-27 and model UV-50M, respectively. The ESR spectra were taken on a JEOL X-band spectrometer, model JES-3BS-X, equipped with a 100 kHz field modulation unit. The NMR spectra were taken on a Hitachi model R-24 spectrometer.

12) K. Conrow, "Organic Syntheses," Vol. 43, p. 101 (1963).

13) W. D. Emmons, *J. Amer. Chem. Soc.*, **79**, 6552 (1957).

14) W. D. Emmons, *ibid.*, **79**, 5739 (1957).

15) The observed yield of *N*-*t*-butylhydroxylamine may be somewhat lower than the real value because of the experimental loss caused by the high volatility of this compound.

Oxidation by Iron(III) Complexes. VIII. The Reactions of Iron(III) Chloride with Toluene and Substituted Toluenes[1]

Hiroo Inoue, Megumu Izumi, and Eiji Imoto
Department of Applied Chemistry, College of Engineering, University of Osaka Prefecture, Sakai-shi, Osaka 591

(Received January 21, 1974)

The thermal and photochemical reactions of toluene with anhydrous iron(III) chloride in the solid state result in nuclear chlorination. In a homogeneous system, a side-chain reaction occurs under irradiation with light, although no product is obtained in the thermal reaction. The addition of water to the iron(III) chloride–toluene system in the range of the molar ratio of 1—5 changes the course of the photochemical reaction; in the water/iron(III) chloride molar ratios of 1—1.7, 3, and 4—5, the main products are the diphenylmethane-type compound, *o*- or *p*-chlorotoluene (*o*>*p*), and benzyl chloride respectively. Pyridine as a ligand acts to give benzyl chloride selectively. The Mössbauer data of the $FeCl_3/nH_2O$ solid show that the arrangement of the Cl^- ion around the Fe(III) ion changes upon the addition of water. The thermal and photochemical reactions of *p*-methoxytoluene with anhydrous iron(III) chloride give 2,2′-dimethoxy-4,4′-dimethylbiphenyl by oxidative aryl coupling. Water inhibits the aryl coupling reaction.

Previously we investigated the photo-oxidative cleavage of the carbon-carbon bond of 1,2-glycols[2] and the carbon-carbon coupling of the active methylene group of alkyl aryl ketones in the presence of iron(III) chloride.[3] As part of a series of studies of oxidation by iron(III) salts, we will here investigate the oxidation of toluenes by iron(III) chloride.

Anhydrous iron(III) chloride reacts with alkylbenzenes to bring about nuclear chlorination, the formation of diphenylmethane-type hydrocarbons, and polymerization.[4,5] Furthermore, the reaction of toluene and iron(III) chloride-lithium chloride in acetic acid under ultraviolet irradiation gives benzyl chloride and iron(II) chloride.[6] In this paper, we will describe the role of a ligand environment around the Fe(III) ion in controlling various competing reactions and the effect of the substituent at the *p*-position of toluene upon the reaction pathway. Some of the results of this investigation have been reported in a previous communication.[7]

Results and Discussion

Reaction of Toluene with Iron(III) Chloride. Thermal Reaction: When a homogeneous solution of iron(III) chloride in toluene was heated at 70 °C, no product was detected by glc. In a heterogeneous system, however, the isomeric chlorotoluenes (I) (*o*: (*m*+*p*)=13: 87) were produced in a satisfactory yield, along with iron(II) chloride (Table 1). The isomer distribution reflects the electrophilic property of the chlorination species.

$$C_6H_5CH_3 \xrightarrow[\Delta]{(FeCl_3)_m} ClC_6H_4CH_3$$
I

Photo-reaction: The irradiation of a homogeneous solution of iron(III) chloride in toluene yielded 98% phenyltolylmethanes (II) with an isomer ratio of *o*: *p*= 46: 54, plus a small amount of bibenzyl. When the iron(III) chloride was dispersed in toluene, I was produced along with II. The isomer distribution coincided with that in the thermal reaction. Although the amount of I produced under irradiation with light increased with the increase in the amount of iron(III) chloride dispersed, the amount of II came to be nearly constant independently of the dispersion amount; it depended on that of the iron(III) chloride dissolved in the toluene, as is shown in Fig. 1. Thus, anhydrous iron(III) chloride in the solid state undergoes nuclear chlorination. Iron(III) chloride has been reported to exist as a dimer (III) in non-polar solvents.[8] On the other hand, the iron(III) chloride in the solid state has a $FeCl_6$ octahedral structure (IV) as a structural unit, as will be described later. Thus, the structure of the iron(III) chloride in the reaction system affects the reaction course of either the nuclear chlorination or the side-chain reaction.

$$C_6H_5CH_3 \xrightarrow[h\nu]{FeCl_3} C_6H_5CH_2C_6H_4CH_3$$
II

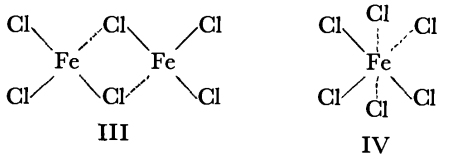

III

IV

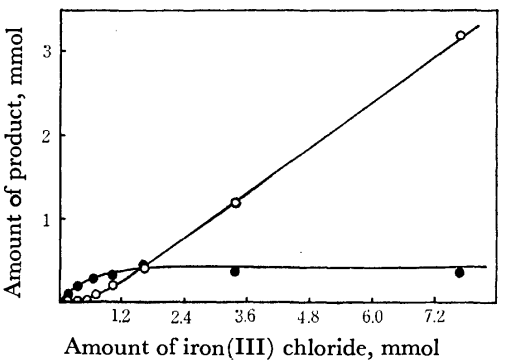

Fig. 1. The relationship between the amount of I (—○—) or II (—●—) produced and that of iron(III) chloride added in toluene (10 ml). (under irradiation with light).

Effect of Water. Water was added to an anhydrous iron(III) chloride–toluene system consisting of 1.4 mmol of iron(III) chloride in 10 ml of toluene (Table 1).

At the water/iron(III) chloride molar ratio (n) of 1.7, the thermal reaction gave I and II in low yields of 6 and 10% respectively (70 hr). At molar ratios higher than 3, no product was detected by glc. In the photoreaction, however, I, II, and benzyl chloride (V) were obtained in higher yields. Furthermore, the yields changed depending on the value of n (Table 1). At n=1—1.7, the reaction yielded II along with the small amount of I. This phenomenon was similar to the results of the thermal toluene–copper(II) bromide reaction.[9] However, the course of the reaction again altered in the direction of nuclear chlorination with the predominance of the o-position (o: (p+m)=67: 33) upon the further addition of water. In addition, V was obtained. The maximum selectivity for nuclear chlorination was observed at n=3. When n became larger than 3, the yields of I and II decreased and that of V increased. The maximum yield of V was observed at n=4—5. Thus, water significantly changes the course of the photochemical reaction of toluene with iron(III) chloride.

$$C_6H_5CH_3 \xrightarrow[h\nu]{FeCl_3/(4-5)H_2O} C_6H_5CH_2Cl$$
V

Table 1. The reaction of toluene with iron(III) chloride[a]

Additive	Molar ratio Additive/$FeCl_3$	Therm. or $h\nu$	Yield of product, %[b] I(o/p+m)	II(o/p)[e]	V
None[c]	0	70 °C	60(13/87)	0	0
None[d]	0	$h\nu$	44(13/87)	51(46/54)	0
H_2O	1.7	70 °C	6	10	0
H_2O	1.7	$h\nu$	12(65/35)	52(46/54)	0
H_2O	3	70 °C	0	0	0
H_2O	3	$h\nu$	54(67/33)	10(48/52)	28
H_2O	4—5	$h\nu$	0	8	91
C_5H_5N	5	$h\nu$	0	0	100

a) Reaction time: 70 hr. Amount of $FeCl_3$: 1.4—1.6 mmol in 10 ml of toluene. b) The yields of I, II, and V were calculated from 2 × (number of moles of the products/that of $FeCl_3$) × 100. c) Yield of $FeCl_2$: 77%. d) Yield of $FeCl_2$: 96%. e) The isomer distribution of phenyltolylmethanes which were prepared by the reaction of toluene with benzyl chloride in the presence of iron(III) chloride was o/p=43/57.

Effect of Pyridine. When the pyridine/iron(III) chloride molar ratio was higher than 1, the thermal reaction (70 °C, 70 hr) yielded I in a yield lower than 10% and the photochemical reaction gave (V) selectively; thus, the yield of V was 100% in the molar ratio of 5 (Table 1). II was not obtained at all in the thermal and photochemical reactions. This finding was similar to that in the case of water.

Mössbauer Data. The Mössbauer spectra were measured at room temperature for the iron(III) chloride solid containing water at n=1.7, 3, and 6. The results are compared in Table 2. All the samples are characterized by approximately the same isomer shift (0.38—0.44 mm/s). Thus, the electron density at the Fe nucleus appears to be about the same. However, the quadrupole splitting (Q.S.) changes with the amount of water. Anhydrous iron(III) chloride exhibits a single narrow resonance line, Q.S.=0. This means that the anhydrous salt has a $FeCl_6$ octahedra (IV) as a structural unit.[10] In $FeCl_3/6H_2O$, we found Q.S.= 0.83 mm/s, which was the same as was found by Nozik and Kaplan.[10] An X-ray diffraction study[11] shows that the structural unit in the crystal is the octahedral complex $Fe(H_2O)_4Cl_2$, with the Cl^- ions being coaxial (VI). On the other hand, in $FeCl_3/3H_2O$ we found Q.S.=0.36 mm/s. This indicates that the arrangement of the Cl^- ion and H_2O surrounding the central Fe(III) ion differs from the case of $FeCl_3/6H_2O$. The $FeCl_3/1.7H_2O$ solid exhibits a broad resonance line, thus indicating that the arrangement of the Cl^- ions is disturbed by water.

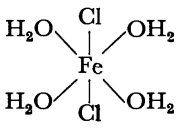

VI

Table 2. Mössbauer data of the $FeCl_3/nH_2O$ solid

$FeCl_3/nH_2O$	Isomer shift mm/s	Q.S. mm/s
$FeCl_3$	0.44	0
$FeCl_3/1.7H_2O$	0.44	—
$FeCl_3/3H_2O$	0.38	0.36
$FeCl_3/6H_2O$	0.45	0.83

Reaction Pathway. When the $FeCl_3/nH_2O$ solid is irradiated with light, the Cl· ion is oxidized by the excited Fe(III) ion, thus leading to the formation of Cl·(VII). The reactivity of the Cl· thus formed is

$$(FeCl_3\text{-}nH_2O)_m \xrightarrow{h\nu} (Cl\cdot FeCl_2\text{-}nH_2O)(FeCl_3\text{-}nH_2O)_{m-1}$$
VII

affected by the ligand environment around the Fe(III) ion and affords either nuclear chlorination or hydrogen abstraction from the methyl group leading to the benzyl radical. That is, the iron(III) chloride solid (n=0) with the structure of Fe–Cl···Fe undergoes nuclear chlorination. When the iron(III) chloride solid contains water, the reaction proceeds *via* the formation of the benzyl radical, followed by the Friedel-Crafts reaction giving II in the case of n=1—1.7, or by ligand-transfer oxidation[12] giving V in the case of n=4—5. In the case of n=3, however, the reaction pathway is uncertain. The formation of I (o>p) may mean that the ligand-transfer oxidation of the benzyl radical occurs at the o- or p-position. However, the reason why the reaction pathway changes with the arrangement of the Cl^- ion and water around the Fe(III) ion is not yet clear.

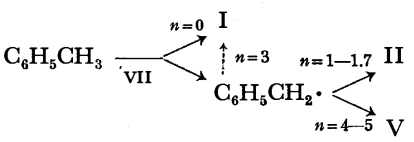

Table 3. The reactions of the substituted toluenes with iron(III) chloride[a]

p-Substituent	Additive	*n*	Therm. or *hν*	Yield of product,[b] %					Polymer mg
				N–Cl	S–Cl	$-CH_2-$	N–N	$FeCl_2$	
Cl	None	0	70 °C	23	0	6	0	52	7
Cl[c]	None	0	*hν*	7	0	28	0	70	71
Cl	H_2O	3	*hν*	18	11	7	0	—	—
CH_3O	None	0	70 °C	—	—	13	19	88	110
CH_3O	None	0	*hν*	—	—	21	41	64	81
CH_3O	H_2O	3	*hν*	—	—	35	0	53	40

a) Amount of $FeCl_3$: 1.4—1.7 mmol in 10 ml of toluene. Reaction time: 40 hr for *p*-chlorotoluene and 20 hr for *p*-methoxytoluene. b) N–Cl, S–Cl, $-CH_2-$, and N–N: nuclear chlorination, side-chain chlorination, formation of diphenylmethanes, and aryl coupling, respectively. c) This run was made at ten times scale (86 hr).

Reactions of the p-*Substituted Toluenes with Iron(III) Chloride. Chloro Group*: The thermal and photochemical reactions of *p*-chlorotoluene with dispersed iron(III) chloride resulted in nuclear chlorination and a side-chain reaction, although the total yields of the products became lower than that of iron(II) chloride, as Table 3 shows. The other products could not be detected by means of glc. In the thermal reaction, the yield of the nuclear chlorination product, 2,4-dichlorotoluene (VIII), became lower than that in the case of toluene, but the mixture (IX) of 2,4′-dichloro-5-methyldiphenylmethane and 3,4′-dichloro-6-methyldiphenylmethane was produced in addition to the (VIII). In the photo-reaction, the yield of (IX) became higher than that of (VIII). When the $FeCl_3/3H_2O$ solid was used, *p*-chlorobenzyl chloride (X) was produced in addition to (VIII) and (IX). Among these products, the yield of (VIII) became higher in spite of deactivation by the chloro group at the *p*-position. These results were similar to those in the case of toluene.

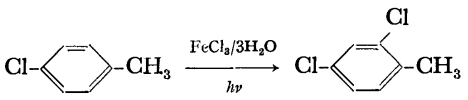

VIII

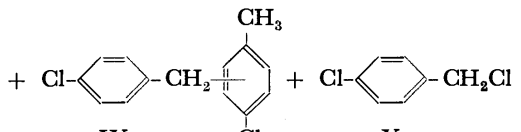

IX Cl X

Methoxy Group: A solution of iron(III) chloride in *p*-methoxytoluene, containing partially-insoluble iron(III) chloride, was heated at 70 °C for 20 hr. As Table 3 shows, 2,2′-dimethoxy-4,4′-dimethyldiphenyl (XI) was thus produced in a 19% yield by the coupling of two benzene nuclei, accompanied by the formation of 2,4′-dimethoxy-5-methyldiphenylmethane (XII) in a 13% yield. The other aryl coupling products were not obtained. In the reaction, iron(III) chloride was converted to iron(II) chloride. As another product, *p*-cresol was detected by means of glc, although the amount produced was very small. The total yields of the products became lower than that of iron(II) chloride because of the formation of a polymeric material. The yield of (XI) increased under irradiation with light; (XI) and (XII) were obtained in 41 and 21% yields respectively, while in the dark the yields of (XI) and (XII) were 5—6 and 2% respectively. The formation of (XI) and *p*-cresol indicates that the reaction proceeded *via* the cation radical (XIII) of *p*-methoxytoluene, which is formed by the oxidation of *p*-methoxytoluene by iron(III) chloride, followed by the reaction of (XIII) with *p*-methoxytoluene. The formation of the cation radical as an intermediate has been considered to occur in the oxidative coupling of methyl-substituted benzenoid compounds by lead tetra-acetate,[13] the radical-initiated oxidation of anisol,[14] the metal-catalyzed cyclodimerisation of aromatic enamines,[15] and the reaction of methylated benzil and bibenzyl derivatives with tris-(*p*-bromophenyl)ammonium hexachloroantimonate.[16]

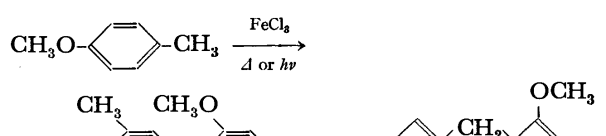

XI XII

On the other hand, the facts that the diphenylmethane-type compound is produced in the homogeneous, thermal reaction and that the reaction occurs at the *o*-position of the methoxy group of *p*-methoxytoluene suggest that the *p*-methoxybenzyl cation (XIV) is formed from XIII and then reacts with *p*-methoxytoluene to give XII. When water was added to the iron(III) chloride-*p*-methoxytoluene system at $n=3$ and the solution was irradiated with light, XII was pro-

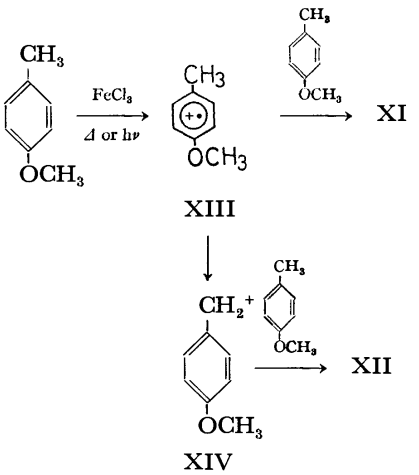

duced selectively in a 35% yield, along with a small amount of *p*-cresol. Thus, the aryl coupling was inhibited by water. The amount of the polymeric material produced became smaller.

Experimental

Materials. Anhydrous iron(III) chloride was prepared by the sublimation of commercial iron(III) chloride under the reduced pressure of 1 mmHg at 300 °C. The purity of the iron(III) chloride used was 99—99.8%; it was measured by the methods described in a previous paper.[3]

Toluene and Iron(III) Chloride, General Procedure. Thermal Reaction: The homogeneous solution was prepared by dissolving 0.3 mmol of iron(III) chloride in 10 ml of toluene. In the heterogeneous system, 1.4—1.6 mmol of iron(III) chloride was dispersed under stirring in 10 ml of toluene. The solution was placed in a tube (2 cm × 15 cm) and heated at 70 °C under a nitrogen atmosphere for a desired time. After the resulting reaction mixture had been filtered off to separate the iron(II) chloride, the filtrate was submitted to glc analysis. The products, *o*-, *m*-, and *p*-(I), which were obtained in the heterogeneous system were identified by a comparison of their retention times in glc with those of authentic specimens, and their amounts were determined by means of glc. The grey precipitate was repeatedly washed with benzene, dried, and submitted to the quantitative analysis of the Fe(II) ion.

Photo-reaction: The homogeneous or heterogeneous solution which was prepared above was placed in a Pyrex tube and irradiated with a Pyrex-covered 100 W high-pressure mercury lamp at a distance of 6 cm under a nitrogen atmosphere at room temperature for a desired time. During the reaction, the solution was stirred vigorously. After the reaction mixture had then been filtered off to separate the iron(II) chloride, the amount of I was determined by the glc analysis of the filtrate. II was isolated by glc as a mixture of the *o*- and *p*-isomers and bibenzyl. The NMR spectrum (CCl_4) of II showed signals at δ 2.15 (s, 3H, CH_3), 3.85 (s, 2H, CH_2), and 6.9—7.3 (m, 9H, aromatic protons) for the *o*-isomer, at δ 2.22 (s, 3H, CH_3), 3.90 (s, 2H, CH_2), and 6.9—7.3 (m, 9H, aromatic protons) for the *p*-isomer, and at δ 2.83 (s, 4H, CH_2) and 7.06 (s, 10H, aromatic protons) for bibenzyl. The isomer distribution was calculated from the relative heights of the integrated spectrum. The grey precipitate was iron(II) chloride and did not contain any polymeric material at all. Similar procedures were used for the experiments investigating the effect of the amount of the dispersed iron(III) chloride on the reaction.

Iron(III) Chloride–Water or Pyridine System. Various amounts of water or pyridine were added to 10 ml of toluene containing 1.4 mmol of iron(III) chloride. The solution was then heated or irradiated under conditions similar to those in the case of anhydrous iron(III) chloride. The amounts of I, II, and V thus produced were determined by means of glc.

p-*Chlorotoluene and Iron(III) Chloride.* *(a)*: Anhydrous iron(III) chloride (14.5 mmol) was dispersed in 100 ml of *p*-chlorotoluene, and the solution was irradiated with light for 86 hr under conditions similar to those in the case of toluene. The grey solid (1.71 g) then filtered out had 10.2 mmol of iron(II) chloride. A part of the filtrate was submitted to glc analysis. The products, VIII and IX, were identified by a comparison of their retention times in glc with those of authentic specimens, and their amounts were determined by means of glc. The authentic specimen of IX was prepared by the reaction of X and *p*-chlorotoluene in the presence of iron(III) chloride. Furthermore, IX was isolated by glc as a mixture of 2,4′-dichloro-5-methyldiphenylmethane and 3,4′-dichloro-6-methyldiphenylmethane. The NMR (CCl_4) of (IX) showed signals at δ 2.22 and 2.11 (s, 3H, CH_3), 3.95 and 3.81 (s, 2H, CH_2), and 6.8—7.4 (m, 7H, aromatic protons). The other part of the filtrate was submitted to chromatography on alumina (elution with carbon tetrachloride and then methanol). The elution with methanol gave a brown polymeric material (71 mg).

(b): Anhydrous iron(III) chloride (1.4 mmol) was dispersed in 10 ml of *p*-chlorotoluene, and the solution was heated at 70 °C under a nitrogen atmosphere for 40 hr. The grey solid (198 mg) filtered out had 0.73 mmol of iron(II) chloride. The amounts of VIII, IX, and the polymeric material were determined by a method similar to that used in the case of the photo-reaction (a).

(c): A mixture of anhydrous iron(III) chloride (1.4 mmol) and water (4.3 mmol) was allowed to react with 10 ml of *p*-chlorotoluene under irradiation with light for 40 hr. The identification and the determination of VIII, IX, and X were carried out by methods similar to those used in the cases of (a) and (b).

p-*Methoxytoluene and Iron(III) Chloride.* *(a)*: Anhydrous iron(III) chloride (1.4 mmol) was added to 10 ml of *p*-methoxytoluene, and the solution was irradiated with light for 20 hr under conditions similar to those used in the case of toluene. A red-brown solid (154 mg) was then filtered off, washed twice times with 3-ml portions of benzene, and dried. The solid contained 0.9 mmol of iron(II) chloride. The mixture of the filtrate and the benzene solution was freed off the solvent at 74 °C/25 mmHg. The residue was submitted to chromatography on alumina. Elution with benzene, carbon tetrachloride, and then methanol gave XI, XII, and a brown, oily material containing *p*-cresol respectively. The amounts of XI and XII were determined by means of glc (Table 3). XI, mp 59.5—60 °C (lit,[17] mp 61 °C), exhibited NMR (CCl_4) signals at δ 2.26 (s, 6H, CH_3), 3.62 (s, 6H, OCH_3), and 6.5—7.1 (m, 6H, aromatic protons). Mass spectrum *m/e*; 242 (parent peak).

Found: C, 79.30; H, 7.35%. Calcd for $C_{16}H_{18}O_2$: C, 79.31; H, 7.49%.

XII, mp 72—73.5 °C (lit,[17] 74 °C), exhibited NMR (CCl_4) signals at δ 2.18 (s, 3H, CH_3), 3.65 and 3.68 (s, 6H, OCH_3), 3.76 (s, 2H, CH_2), and 6.4—7.1 (m, 7H, aromatic protons). Mass spectrum *m/e*; 242 (parent peak).

Found: C, 79.20; H, 7.30%. Calcd for $C_{16}H_{18}O_2$: C, 79.31; H, 7.49%.

A similar procedure was used for the photo-reaction in the iron(III) chloride–water system.

(b): Anhydrous iron(III) chloride (1.44 mmol) was allowed to react with *p*-methoxytoluene (10 ml) under a nitrogen atmosphere at 70 °C for 20 hr. The products, XI, XII, *p*-cresol, a red-brown oily material, and iron(II) chloride, were isolated or detected by methods similar to those used in the case of (a).

Mössbauer Spectra. Anhydrous iron(III) chloride was evaporated on aluminium foil supports with spacing of less than 1 mm. The cell was covered by a polyethylene film to prevent the salt from absorbing atmospheric water. An appropriate amount of water was then dropped on the iron(III) chloride film. Gamma rays emitted by the ^{57}Co-in-copper source impinged upon the absorber sample at room temperature. Velocity calibrations were made using the well-known spectrum of natural iron metal as the standard.

Analyses. The quantitative analyses of iron(III) chloride and iron(II) chloride were carried out by the methods

described in the literature.[18] The amounts of the products were determined by means of glc using a 3 mm × 1 m column of 30% high-vacuum silicone grease or 3% Apieson grease L on Celite 545.

The authors are grateful to Dr. Akihiro Tomita, University of Osaka Prefecture, for measuring the Mössbauer spectra.

References

1) Part VII of this series: H. Inoue, Y. Kimura, and E. Imoto, This Bulletin, **46**, 3303 (1973). Part I, II, III, IV, V, and VI: H. Inoue, K. Tamaki, N. Komakine, and E. Imoto, *ibid.*, **39**, 1577 (1966); *ibid.*, **40**, 875 (1967); H. Inoue, N. Komakine, and E. Imoto, *ibid.*, **41**, 2726 (1968); H. Inoue, M. Sakata, and E. Imoto, *ibid.*, **44**, 3490 (1971); H. Inoue, M. Izumi, and E. Imoto, *Chem. Lett.*, **1973**, 571; H. Inoue, M. Sakata, and E. Imoto, This Bulletin, **46**, 2211 (1973).
2) Part III of this series, Ref. 1.
3) Part VI of this series, Ref. 1.
4) P. Kovacic, C. Wu, and R. W. Stewart, *J. Amer. Chem. Soc.*, **82**, 1917 (1960).
5) P. Kovacic and C. Wu, *J. Org. Chem.*, **26**, 759, 762 (1961).
6) A. I. Kryukov and S. A. Ivanitskaya, *Ukr. Khim. Zh.*, **34**, 3 (1968); *Chem. Abstr.*, **69**, 35599 (1968).
7) Part V of this series, Ref. 1.
8) A. F. Wells, "Structural Inorganic Chemistry", Oxford University Press, London (1950), p. 110.
9) P. Kovacic and K. E. Davis, *J. Amer. Chem. Soc.*, **86**, 427 (1964).
10) A. J. Nozik and M. Kaplan, *J. Chem. Phys.*, **49**, 4141 (1968).
11) M. D. Lind, *ibid.*, **46**, 2010 (1967).
12) C. L. Jenkins and J. K. Kochi, *J. Org. Chem.*, **36**, 3095, 3103 (1971).
13) R. O. C. Norman, C. B. Thomas, and J. S. Willson, *J. Chem. Soc., Parkin I*, **1973**, 325.
14) R. A. McClelland, R. O. C. Norman, and C. B. Thomas, *ibid., I*, **1972**, 562.
15) F. A. Bell, R. A. Crellin, H. Fujii, and A. Ledwith, *Chem. Commun.*, **1969**, 251.
16) L. J. Kricka and A. Ledwith, *J. Chem. Soc., Parkin I*, **1973**, 294.
17) R. Pummerer, H. Puttfarcken, and P. Schopflocher, *Chem. Ber.*, **58**, 1808 (1925).
18) Part II of this series, Ref. 1.

Carbonylation of Alcohols, Olefins, and Saturated Hydrocarbons by CO in the Ag(I)-H_2SO_4 System

Yoshie SOUMA and Hiroshi SANO

Government Industrial Research Institute, Osaka, Midorigaoka, Ikeda, Osaka 563

(Received July 26, 1973)

In the presence of an Ag carbonyl-ion catalyst, prepared *in situ* from the Ag compound and carbon monoxide in H_2SO_4, olefins or alcohols reacted with carbon monoxide at room temperature and atmospheric pressure to produce exclusively tertiary carboxylic acids in high yields. The amount of Ag compound sufficient for carrying out the reaction is *ca.* 0.2 mol/l. The optimum reaction temperature is 0—40 °C. The reaction proceeds practically at above a 90% H_2SO_4 concentration. Saturated hydrocarbons, containing a tertiary hydrogen, also reacted with carbon monoxide in the presence of alcohols or olefins as carbonium ion precursors, thus producing tertiary carboxylic acids.

In our previous papers, we have reported the carbonylation reactions of olefins,[1] alcohols,[2] and saturated hydrocarbons[3] by the catalysis of the Cu(I) carbonyl ion[4] to produce tertiary carboxylic acids in high yields at room temperature and atmospheric pressure. The present investigation will deal with the use of the Ag compound as a catalyst for the same reaction.

Results

Olefins or alcohols react with carbon monoxide in the presence of the Ag carbonyl ion catalyst in a concd H_2SO_4 solution at room temperature and atmospheric pressure to produce tertiary carboxylic acids exclusively, because olefins or alcohols are protonated and rearrange to the most stable tertiary carbonium ion prior to the carbonylation. The results are shown in Table 1.

Table 1. Carbonylation of olefin or alcohol[a]

Substrates	Temp. (°C)	Time (min)	Products R_1	R_2	Yield (%)
1-Hexene	30	40	*n*-C_3H_7	CH_3	80
			C_2H_5	C_2H_5	16
1-Octene	30	40	*n*-C_5H_{11}	CH_3	61
			n-C_4H_9	C_2H_5	24
			n-C_3H_7	*n*-C_3H_7	12
1-Decene	30	60	*n*-C_7H_{15}	CH_3	60
			n-C_6H_{13}	C_2H_5	24
			n-C_5H_{11}	*n*-C_3H_7	10
Cyclohexene	10—12	55			84
1-Butanol	30	3 hr	CH_3	CH_3	29
			C_2H_5	H	17
1-Hexanol	30	2 hr	*n*-C_3H_7	CH_3	79
			C_2H_5	C_2H_5	19
Cyclohexanol	30	1 hr			81
2,5-Dimethyl-cyclohexanol	30	1 hr	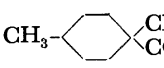		*cis* 33
					trans 33

a) In all cases, 8 mmol of Ag_2O, 40 ml of 98% H_2SO_4, and 20 mmol of olefins or alcohols were used. The pressure of carbon monoxide was 1 atm.

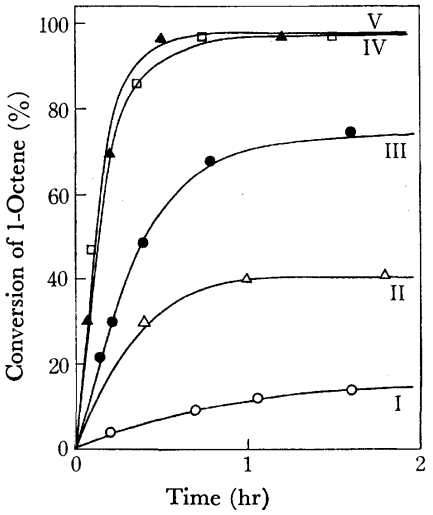

Fig. 1. The catalytic effect of Ag_2O.
1-Octene 5 mmol and 98% H_2SO_4 10 ml were used at 30 °C.
I: Ag_2O 0 mmol, II: Ag_2O 0.1 mmol, III: Ag_2O 1 mmol, IV: Ag_2O 2 mmol, V: Ag_2O 4 mmol.

The effect of the amount of Ag compound is illustrated in Fig. 1. Without Ag_2O, the rate of reaction is very slow and the yield of carboxylic acid is less than 15%. When Ag_2O is added in concd H_2SO_4, the rate of reaction and the yield increase considerably. The amount of Ag_2O sufficient for carrying out carbonylation is *ca.* 0.2 mol/l. In concd. H_2SO_4, the polymerization reaction proceeds in competition with the carbonylation reaction of olefin. When the amount of Ag_2O is not enough, the CO concentration enriched by Ag^+ in the solution is not sufficient for its reaction with the carbonium ion. Therefore, polymerization predominates over carbonylation.

Saturated hydrocarbons bearing tertiary hydrogen also react with carbon monoxide in the presence of olefins or alcohols, which form carbonium ions and which can abstract hydride from branched hydrocarbons. The results are shown in Table 2. The added olefins or alcohols in the reaction mixture also yield tertiary carboxylic acid.

As shown in Table 3, the effect of the H_2SO_4 concentration upon the carbonylation is parallel to its

Table 2. The carbonylation of saturated hydrocarbon in the presence of olefin or alcohol[a)]

Substrates	Olefin or alcohol	Reaction time (min)	Products	Yield (%)
Methylcyclohexane	1-Hexene	40	Methylcyclohexanecarboxylic acid	45
			tert-C_7 acids	33
Methylcyclohexane	1-Hexanol	90	Methylcyclohexanecarboxylic acid	42
			tert-C_7 acids	31
Methylcyclohexane	1-Octene	60	Methylcyclohexanecarboxylic acid	72
			tert-C_9 acids	23
1,4-Dimethylcyclohexane	1-Octene	60	1,4-Dimethylcyclohexanecarboxylic acid (*cis*: *trans*=1: 1)	60
			tert-C_9 acids	30
Methylcyclopentane	1-Octanol	120	Methylcyclopentanecarboxylic acid	60
			tert-C_9 acids	27
n-Octane	1-Hexanol	90	*tert*-C_9 acids	0
			tert-C_7 acids	75

a) In all cases, 1.856 g of Ag_2O, 40 ml of 98% H_2SO_4, 20 mmol of saturated hydrocarbons, and 20 mmol of olefins (or alcohols) were used. The reaction temperature was approximately 30 °C. The CO pressure was 1 atm. The components of *tert*-C_7 acids and *tert*-C_9 acids were the same as in Table 1.

effect upon the formation of the unstable Ag carbonyl ion, $Ag(CO)_n^+$, in the H_2SO_4 solution. As was shown in our previous paper, Ag^+ does not absorb carbon monoxide in H_2SO_4 of less than an 80% concentration.

Table 3. The effect of the H_2SO_4 concentration upon the carbonylation[a)]

Concn of H_2SO_4 (wt%)	$Ag(CO)^+/Ag^+$ mol ratio	Conversion of 1-octene, %	Reaction time (min)
100	0.14	97	20[b)]
95	0.07	90	25[b)]
90	0.04	80	90[c)]
85	0.01	17	150[c)]
80	0	0	—

a) 0.928 g of Ag_2O, 1.57 ml of 1-octene, and 20 ml of H_2SO_4 were used at 30°C. The 1-octene was added drop by drop in order to prevent polymerization. b) In concd H_2SO_4, 1-octene reacted with CO immediately after the addition of 1-octene. c) The reaction rate became slower when the concentration of H_2SO_4 was less than 90%.

It seems that Ag compounds form the unstable Ag carbonyl ion by absorbing carbon monoxide in concd H_2SO_4, as in the case of the Cu(I) carbonyl ion:[5)]

$$Ag^+ + nCO \overset{H_2SO_4}{\rightleftharpoons} Ag(CO)_n^+ \quad n=1\sim2$$

The $Ag(CO)_n^+$ is very unstable, and in the presence of such CO acceptors as carbonium ions, CO is liberated from $Ag(CO)_n^+$ and combines with the carbonium ion immediately. That Ag^+ seems to act as a CO carrier to keep a high CO concentration in solution.

Among the compounds, Ag_2O, Ag_2SO_4, and $AgClO_4$ are effective in this reaction. On the other hand, AgCl, AgBr, AgI, and AgCN do not show any catalytic activity. The presence of the halogen atom and CN^- may be supposed to prevent the formation of silver carbonyl ions.

The influence of the reaction temperature was also studied. The results are shown in Table 4.

1-Hexanol reacts with carbon monoxide at 0—30 °C and gives tertiary C_7 carboxylic acids in high yields. The rate of reaction becomes rapid with an increase in the temperature. A linear relationship between $\log k$ and $1/T$ was observed. However, the total yield of carboxylic acids and the proportion of tertiary C_7 carboxylic acid decrease with the increase in the temperature. The explanation of this is that the formation of unstable silver carbonyl ion decreases and the polymerization predominates over carbonylation. In addition, the β scission of carbonium ions begins to proceed with the increase in the temperature. In the reaction of 1-hexene or cyclohexene, the influence of the temperature is almost the same as that in the case of 1-hexanol. However, the rate of reaction is very rapid

Table 4. The influence of the temperature on the reaction of 1-hexanol[a)]

Reaction temp., °C	The total yield of carboxylic acids, %	The component of carboxylic acids				Rate constant $k\times10_5\,s^{-1}$ [b)]	$\frac{Ag(CO)^+}{Ag}$
		t-C_5	*t*-C_6	*t*-C_7	higher acids		
0	99	0	0	100	0	2.78	0.37
10	99	0	0	100	0	4.63	0.30
30	99	0	1	99	0	18.50	0.14
40	83	7	10	77	6	56.0	0.08
55	32	57	25	15	3	—[c)]	0.02

a) 1-Hexanol (10 mmol), Ag_2O (4 mmol), and 98% H_2SO_4 (20 ml) were used. b) The first-order rate constant was calculated from $-d[ROH]/dt=k[ROH]$. c) The rate constant could not be measured because the rate of reaction was too rapid and because the reaction proceeded immediately after the addition of 1-hexanol.

and depends on the rate of the addition of the reactant. The reactant must be added drop by drop to prevent polymerization.

Experimental

Preparation of the Ag Carbonyl Catalyst Solution. In a 300 ml three-necked flask, equipped with a thermometer and a CO gas buret, we placed 1.856 g of Ag_2O and 40 ml of 98% H_2SO_4. The apparatus was evacuated by means of a vacuum pump to remove the air, and then carbon monoxide was introduced from the gas buret. When the mixture was stirred, CO was absorbed by the Ag^+ solution in 10 min.

Carbonylation of Olefins, Alcohols, and Saturated Hydrocarbons. From a syringe, 20 mmol portion of olefins (or alcohols or equimolar mixtures of saturated hydrocarbons and alkylcation sources) was added, drop by drop, to the Ag carbonyl catalyst solution. The carbon monoxide was soon absorbed. After the reaction, the reaction mixture was poured over ice water, and the products were extracted by benzene. The yield of tertiary carboxylic acid was determined by the titration of the benzene extract with a 1/10 M NaOH ethanol solution, and also by gas chromatography by adding a known amount of the internal standard. Glpc analysis was performed using a 3 m FFAP column (10% on Chromosorb WAW).

All the identifications were carried out using authentic samples which had been obtained and characterized by the carbonylation of olefins, alcohols, or saturated hydrocarbons using a Cu(I) carbonyl catalyst.[1-3] The ratios of each isomer of *tert*-C_9 acids and *tert*-C_{11} acids were determined by ^{13}C NMR according to the method described in a previous paper.[2]

The author would like to thank Mr. Nobuyoshi Ookura for his valuable assistance.

References

1) Y. Souma and H. Sano, *J. Org. Chem.*, **38**, 2016 (1973).
2) Y. Souma and H. Sano, This Bulletin, **46**, 3237 (1973).
3) Y. Souma and H. Sano, *J. Org. Chem.*, **38**, 3633 (1973).
4) Y. Souma and H. Sano, *Nippon Kagaku Zasshi*, **91**, 625 (1970).
5) Y. Souma and H. Sano, *Chem. Lett.*, **1973**, 1059.

Reaction of 2-Benzoylamino-2-methylpropionamidine and 2-Benzoylaminoacetamidine with Bifunctional Compounds

Hiroaki UCHIDA, Akiko CHINONE, and Masaki OHTA

Department of Chemistry, Faculty of Science, Tokyo Institute of Technology, Ookayama, Meguro-ku, Tokyo 152

(Received November 29, 1973)

The reaction of 2-benzoylamino-2-methylpropionamidine (III) with 1,3-bifunctional compounds was investigated in connection with studies on 2-benzoylaminoacetamidine (I). In case of the reaction of III an appreciable amount of 5,5-dimethyl-2-phenylimidazolin-4-imide (VIII) was formed, the yield of 2-(1-benzoylamino-1-methylethyl)-4,6-dimethylpyrimidine (VI) being low. On the other hand, III reacted with ethyl acetoacetate to give 2-(1-benzoylamino-1-methylethyl)-4-hydroxy-6-methylpyrimidine (IX) in about 50% yield besides VIII. Both III and I were made to react with ethoxymethyleneacetylacetone to yield 5-acetyl-2-(1-benzoylamino-1-methylethyl)-4-methylpyrimidine (X) and 5-acetyl-2-(*N*-benzoylaminomethyl)-4-methylpyrimidine (XI), respectively. Reaction of I with ethoxymethylenemalononitrile gave 4-amino-2-(*N*-benzoylaminomethyl)-5-cyanopyrimidine (XII), but did not proceed with benzoin, malondialdehyde, tetraethoxypropane or phenacyl bromide.

In a previous paper[1] the reactions of 2-benzoylaminoacetamidine (I)[2] and 2-benzyloxycarbonylaminoacetamidine (II)[2] with various 1,3-bifunctional compounds were described. It was pointed out that both I and II react with acetylacetone to produce 2-amino-3-benzoylamino- and 2-amino-3-benzyloxycarbonylamino-4,6-dimethylpyridine, respectively, erroneously reported by Goldberg and Kelly[3] to be pyrimidine derivatives. Reaction of I with ethyl acetoacetate gave 2-(*N*-benzoylaminomethyl)-4-hydroxy-6-methylpyrimidine. However, in every case, concurrent formation of a considerable amount of acylaminoacetamide was observed. The formation of pyridine derivatives is ascribed to the reactive α-methylene group of amidines and depends on the function of 1,3-bifunctional compounds. An amidine which has no α-hydrogen might therefore produce a pyrimidine derivative exclusively. We have investigated the reaction of 2-benzoylamino-2-methylpropionamidine (III) with acetylacetone and ethyl acetoacetate in the presence of alkali.

Amidine (I and III) hydrochlorides were prepared from the nitriles *via* the imidate hydrochlorides following the usual procedure. Shirai and Kurashige[4] reported that the reaction of 2-(*N*-acetyl-*N*-methylamino)-2-methylpropionitrile (IV) with hydrogen chloride and ethanol afforded the corresponding imidate hydrochloride and imidazolone hydrochloride, and ammonolysis of the imidate hydrochloride afforded imidazolinimide hydrochloride instead of the corresponding amidine hydrochloride.

As regards the imidate hydrochloride or amidine hydrochloride we prepared, contaminants in III hydrochloride were trace amounts of ammonium chloride and 2-benzoylamino-2-methylpropionamide (V), formation of imidazolone or imidazolinimide[4] not being observed. Purification of crude III hydrochloride was effected by fractional precipitation by adding ether to the alcoholic solution of the crude product.

Reaction of III with acetylacetone was carried out under various conditions, as shown in Table 1. It can be seen that attempts to improve the yield of 2-(1-benzoylamino-1-methylethyl)-4,6-dimethylpyrimidine (VI) were unsuccessful under all the conditions. The empirical formula of the main product was $C_{11}H_{13}N_3$ which did not change on heating in water. The compound did not seem to change under alkaline conditions where III and acetylacetone undergo reaction, but turned to 5,5-dimethyl-2-phenyl-4-imidazolone (VII) quantitatively on being left to stand with 10% hydrochloric acid at room temperature. Compound $C_{11}H_{13}N_3$ was warmed with acetic anhydride to give a monoacetylated compound. These results and the spectral data identified the product as 5,5-dimethyl-2-phenylimidazolin-4-imide (VIII).

Reaction of III and acetylacetone in ethanol formed VI in relatively high yield in the presence of weak alkali, and in water moderate temperature seemed to be required. Compound V was obtained in trace amount in Expt. 1—3, in several percent yield in Expt. 4—6, and in 17% yield in Expt. 7. Compound VII was obtained in 7% yield in Expt. 7. This might be caused by hydrolysis of VIII, or by cyclization of V

TABLE 1. REACTION OF III[a] WITH ACETYLACETONE

Expt. No.	Solvent	Reaction		Alkali	Molar ratio of III·HCl: alkali	Yield of	
		temp. (°C)	time			VI(%)	VIII(%)
1	C_2H_5OH	reflux	7.5 hr	K_2CO_3	1:1	17	72
2	C_2H_5OH	reflux	7.5 hr	C_2H_5ONa	1:0.2[b]	2	75
3	C_2H_5OH	r.t.	3 day	C_2H_5ONa	1:0.3[b]	5	90
4	H_2O	r.t.	5 day	K_2CO_3	1:1.1	5	26
5	H_2O	r.t.	5 day	NaOH	1:2.2	—	55
6	H_2O	55—60	2 hr	K_2CO_3	1:1.1	17	43
7	H_2O	reflux	1 hr	K_2CO_3	1:1.1	—	56

a) Used in the form of hydrochloride with exception of Reactions 2 and 3. b) Ratio of free III: alkali.

in the presence of alkali as reported by Mohr.[5]

Conversion of III hydrochloride itself was examined under nearly the same conditions as in the reaction with acetylacetone. Under reflux for 5.5 hr in ethanol with an equimolecular amount of potassium carbonate, 82% of III hydrochloride was recovered unchanged and a small quantity of amide V was obtained. Refluxing for 4.5 hr with two molar quantities of sodium ethoxide in ethanol gave VIII quantitatively.

Reaction of III and ethyl acetoacetate gave 2-(1-benzoylamino-1-methylethyl)-4-hydroxy-6-methylpyrimidine (IX), which showed a ring carbonyl band at 1682 cm^{-1} and no hydroxyl group absorption, suggesting it to have the keto form in solid state.

The above results show that competitive reactions occurred between intramolecular cyclization of III to VIII and pyrimidine ring formation from III with acetylacetone or ethyl acetoacetate. An attempt to react III with ethoxymethyleneacetylacetone, which is considered to be highly reactive and favorable for pyrimidine ring formation, gave 5-acetyl-2-(1-benzoylamino-1-methylethyl)-4-methylpyrimidine (X) in a satisfactory yield. The reaction with ethoxymethyleneacetylacetone I was also tried, and 5-acetyl-2-(*N*-benzoylaminomethyl)-4-methylpyrimidine (XI) was obtained. In this case α-methylene group of I did not participate in the reaction and no pyridine compound was formed. The reaction of I with ethoxymethylenemalononitrile resulted in the formation of 4-amino-2-(*N*-benzoylaminomethyl)-5-cyanopyrimidine (XII) which was identified by an alternative synthesis from ethyl 2-benzoylaminoacetimidate and aminomethylenemalononitrile. However, reactions of I with benzoin, malondialdehyde, tetraethoxypropane, and phenacyl bromide resulted in the formation of 2-benzoylaminoacetamide.

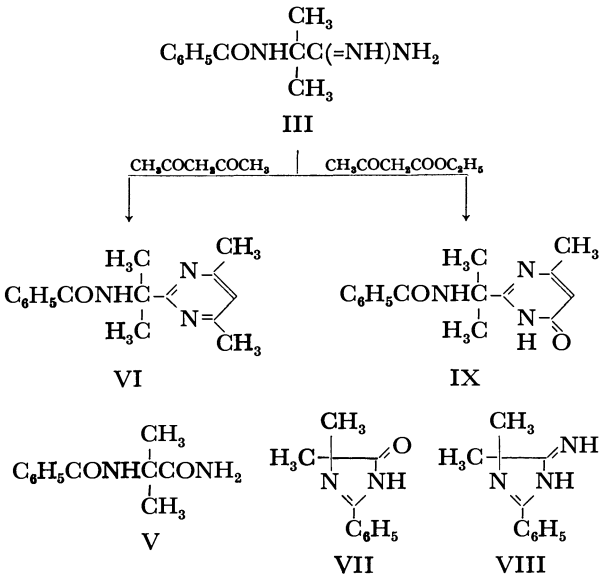

Chart 1

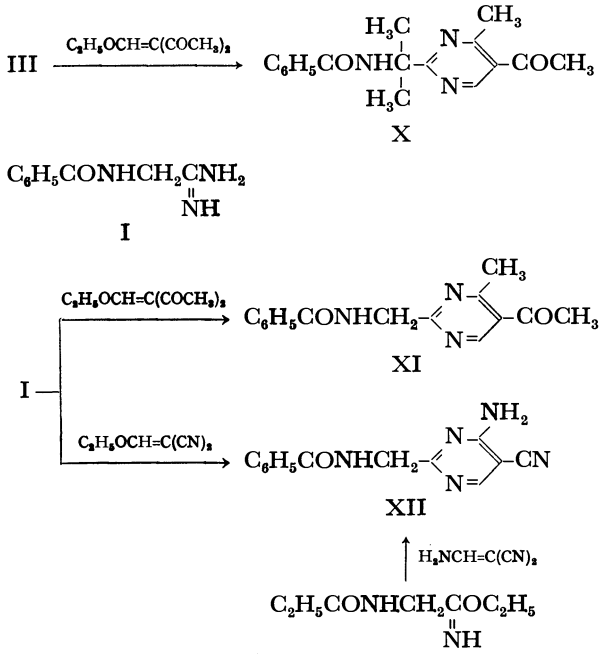

Chart 2

Experimental

All melting points were uncorrected. The NMR spectra were recorded at 60 MHz using tetramethylsilane as an internal standard.

2-Benzoylamino-2-methylpropionamidine(III) Hydrochloride. Hydrogen chloride was introduced to a suspension of 9.4 g (50 mmol) of 2-(*N*-benzoylamino)-2-methylpropionitrile[6] in a mixed solvent of chloroform (55 ml) and benzene (90 ml) containing 2.5 g of ethanol under cooling with ice-salt with occasional shaking, until the nitrile dissolved completely. On being left to stand in a refrigerator a viscous oily product separated which, after removal of the solvent by decantation, was crystallized by the addition of dry ether (150 ml). The resulting crystals were 12.4 g of crude ethyl 2-benzoylamino-2-methylpropionimidate hydrochloride, very hygroscopic, mp 200—202 °C. Found: N, 11.80%. Calcd for $C_{13}H_{19}O_2N_2Cl$: N, 10.35%.

To a solution of ammonia in ethanol (60 ml, 15% by wt) was added the imidate hydrochloride obtained above and the mixture was stirred for 1 hr under cooling with ice. The resulting solution, after being allowed to stand at room temperature for 1 day, was concentrated until crystals began to separate out. Dry petroleum ether (150 ml) was added to the residue, and 10.6 g of crude III hydrochloride was obtained, mp 212—214 °C. Recrystallization from acetonitrile gave colorless needles of III hydrochloride, mp 222—223.5 °C. Found: C, 54.50; H, 6.62; N, 17.68%. Calcd for $C_{11}H_{16}ON_3Cl$: C, 54.66; H, 6.67; N, 17.38%. IR (KBr) cm^{-1}: 3600—2800, 1645, 1536. NMR (DMSO-d_6) τ: 1.09 (s, 4H), 1.31 (s, 1H), 1.83—2.83 (m, 5H), 8.36 (s, 6H).

Crude III hydrochloride (5 g) was dissolved in 70 ml of ethanol, and a small amount of ammonium chloride was precipitated by the addition of 20 ml of dry ether. Additional 125 ml of dry ether gave 4.3 g of colorless needles of III hydrochloride, mp 221—223 °C. The filtrate was concentrated after III hydrochloride had been collected by filtration, and the residue was recrystallized from ethyl acetate to give 0.4 g of colorless needles of V, mp 205—206 °C. Found: C, 63.82; H, 6.89; N, 13.29%. Calcd for $C_{11}H_{14}O_2N_2$: C, 64.06; H, 6.84; N, 13.58%. IR (KBr) cm^{-1}: 3410, 3310, 3225, 3180, 1660, 1640, 1610, 1535. NMR (DMSO-d_6) τ: 1.83 (s, 1H), 1.97—2.69 (m, 5H), 2.97 (bs, 2H), 8.49 (s, 6H).

2-(1-Benzoylamino-1-methylethyl)-4,6-dimethylpyrimidine (VI).

a) Reaction of III with Acetylacetone in Ethanol (Expt. 1, Table 1): To a solution of 1.3 g (13 mmol) of acetylacetone in 30 ml of ethanol was added 2.4 g (10 mmol) of III hydrochloride and 1.5 g (11 mmol) of potassium carbonate, and the mixture was refluxed for 7.5 hr with stirring. The reaction mixture was filtered and the filtrate was concentrated to give crystalline residue. Recrystallization from methanol gave colorless prisms of VIII, mp 246 °C, 0.89 g. Found: C, 70.33; H, 6.88; N, 22.39%. Calcd for $C_{11}H_{13}N_3$: C, 70.56; H, 7.00; N, 22.44%. IR (KBr) cm^{-1}: 3325, 1675, 1603, 1550, 1320, 1290, 703. NMR (DMSO-d_6) τ: 1.65—2.83 (m, 5H), 2.28 (bs, 2H), 8.70 (s, 6H).

The filtrate, after VIII had been collected, was concentrated and the residue was subjected to column chromatography on silica gel. Crystals eluted with methylene chloride were recrystallized from acetonitrile to give colorless prisms of VI, mp 170—171 °C, 0.46 g (17%). Found: C, 71.63; H, 7.10; N, 15.78%. Calcd for $C_{16}H_{19}ON_3$: C, 71.34; H, 7.11; N, 15.60%. IR (KBr) cm^{-1}: 3350, 1664, 1600, 1530, 710. NMR (DMSO-d_6) τ: 1.32 (s, 1H), 2.02—2.63 (m, 5H), 2.86 (s, 1H), 7.58 (s, 6H), 8.27 (s, 6H).

With methylene chloride and ethyl acetate, 0.46 g of VIII was eluted, the total yield being 1.35 g (72%).

b) Reaction of III with Acetylacetone in Water (Expt. 6, Table 1): A solution of 1.5 g (15 mmol) of acetylacetone, 2.4 g (10 mmol) of III hydrochloride, and 1.5 g (11 mmol) of potassium carbonate in 20 ml of water was warmed to 55—60 °C for 2 hr. Crystals, a part of which began to separate out on being warmed for 30 min, were collected by filtration and recrystallized from acetonitrile to give colorless prisms of VI, mp 170—171 °C, 0.45 g (17%). Spectral data were identical with those obtained in the preceding experiment.

The filtrate of the reaction mixture was concentrated, and the residue was subjected to column chromatography on silica gel. Crystals eluted with methylene chloride were recrystallized from ethyl acetate to give colorless prisms of VII, mp 202—204 °C (lit,[7] mp 202 °C), 0.04 g (2%). Found: C, 70.04; H, 6.52; N, 14.94%. Calcd for $C_{11}H_{12}ON_2$: C, 70.18; H, 6.43; N, 14.88%. IR (KBr) cm^{-1}: 3425, 1740, 1713, 1620, 1606, 1550, 702. NMR (DMSO-d_6) τ: 1.46 (s, 1H), 1.69—2.72 (m, 5H), 8.70 (s, 6H).

Continued elution with methylene chloride gave 0.08 g (4%) of V, mp 205—206 °C (ethyl acetate).

With methylene chloride and ethyl acetate, 0.80 g (43%) of VIII was eluted, mp 248—249 °C (ethyl acetate).

2-(1-Benzoylamino-1-methylethyl)-4-hydroxy-6-methylpyrimidine (IX). *a) Reaction of III with Ethyl Acetoacetate in the Presence of Sodium Ethoxide*: An ethanol solution of sodium ethoxide prepared from 0.46 g (20 mmol) of sodium and 20 ml of ethanol was added to a solution of 2.4 g (10 mmol) of III hydrochloride in 30 ml of ethanol under ice cooling, and the precipitated sodium chloride was removed by filtration. To the filtrate was added 1.3 g (10 mmol) of ethyl acetoacetate. The mixture was warmed at 60 °C for 5 hr, and then concentrated. The residue was dissolved in 30 ml of water and neutralized with acetic acid to give a white precipitate. Recrystallization from *n*-butanol gave white powder of IX, mp 276—278 °C, 1.25 g (46%). Found: C, 66.29; H, 6.33; N, 15.22%. Calcd for $C_{15}H_{17}O_2N_5$: C, 66.49; H, 6.32; N, 15.49%. IR (KBr) cm^{-1}: 3230, 1682, 1633, 1600, 1550. NMR (DMSO-d_6) τ: 1.57 (s, 1H), 1.92—2.58 (m, 5H), 3.95 (s, 1H), 7.23 (s, 1H), 7.77 (s, 3H), 8.37 (s, 6H).

The aqueous filtrate, after IX had been separated, was concentrated and the residue was subjected to column chromatography on silica gel. Elution with ethyl acetate gave 0.04 g (2%) of V, mp 207—208 °C (ethyl acetate), and 0.62 g (33%) of VIII, mp 246—248 °C (ethyl acetate).

b) Reaction of III with Ethyl Acetoacetate in the Presence of Sodium Hydroxide: To a solution of III in 40 ml of ethanol, prepared from 2.4 g (10 mmol) of III hydrochloride and 0.23 g (10 mmol) of sodium by the same procedure as in the preceding experiment, was added 1.3 g (10 mmol) of ethyl acetoacetate. The reaction mixture was transferred to an evaporating dish and evaporated to dryness in a desiccator over sulfuric acid. The residue was added to a mixture of 5 ml of 20% aqueous sodium hydroxide and 25 ml of ethanol, and then stirred at room temperature for 1 day. The mixture was concentrated, and the work up as described in the preceding experiment gave white powder of IX, mp 277—278 °C (*n*-butanol), 1.4 g (52%). Spectral data were identical with those of IX obtained in *a*).

The aqueous filtrate after separating IX was concentrated and then subjected to column chromatography on silica gel. The elution with ethyl acetate gave 0.15 g (8%) of VII, mp 201—202 °C (ligroin), and 0.49 g (26%) of VIII, mp 247—248 °C (ethyl acetate).

5,5-Dimethyl-2-phenylimidazoline-4-acetimide. In 10 ml of acetic anhydride, 0.94 g (5 mmol) of VIII was heated at 80 °C for 30 min. The reaction mixture was concentrated and the residue was recrystallized from ethyl acetate to give colorless prisms of 5,5-dimethyl-2-phenylimidazoline-4-acetimide, mp 159 °C, 0.92 g (80%). Found: C, 68.40; H, 6.71; N, 18.45%. Calcd for $C_{13}H_{15}ON_3$: C, 68.10; H, 6.59; N, 18.33%. IR (KBr) cm^{-1}: 3235, 3160, 1690, 1530, 1280. NMR (DMSO-d_6) τ: −0.93 (s, 1H), 1.67—2.73 (s, 5H), 7.50 (s, 3H), 8.54 (s, 6H).

5-Acetyl-2-(1-benzoylamino-1-methylethyl)-4-methylpyrimidine (X). To an ethanol solution of III, prepared from 0.10 g (4.4 mmol) of sodium in 10 ml of ethanol and 1.10 g (4.6 mmol) of III hydrochloride in 15 ml of ethanol, was added 0.78 g (5 mmol) of ethoxymethyleneacetylacetone.[7] The mixture was allowed to stand at room temperature for 13 hr, heated to 80 °C for 1 hr and then concentrated. The residual crystals were recrystallized from ethyl acetate to give colorless needles of X, mp 155—156 °C, 0.83 g (64%). Found: C, 68.92; H, 6.48; N, 14.26%. Calcd for $C_{17}H_{19}O_2N_3$: C, 68.66; H, 6.44; N, 14.13%. IR (KBr) cm^{-1}: 3300, 1688, 1633, 1602, 1532. NMR (DMSO-d_6) τ: 0.63 (s, 1H), 1.10 (s, 1H), 1.73—2.50 (m, 5H), 7.16 (s, 6H), 8.06 (s, 6H).

Crystals insoluble in hot ethyl acetate were recrystallized from ethanol to give colorless needles of unchanged III hydrochloride, mp 225—227 °C, 0.3 g (12%). Spectral data were identical with those of authentic III hydrochloride.

5-Acetyl-2-(N-benzoylaminomethyl)-4-methylpyrimidine (XI). To an ethanol solution of I, prepared from 0.35 g (15 mmol) of sodium in 20 ml of ethanol and 3.2 g (15 mmol) of I hydrochloride in 20 ml of ethanol, was added 2.4 g (15.4 mmol) of ethoxymethyleneacetylacetone. Crystals, once precipitated in large quantities after 5 min stirring, were dissolved completely after 1 hr at room temperature. The mixture, after being allowed to stand at room temperature for 18 hr, was heated at 80 °C for 1 hr and then concentrated. Recrystallization of the residue from benzene gave colorless prisms of XI, mp 110—111 °C, 3.1 g (77%). Found: C, 66.99; H, 5.68; N, 15.72%. Calcd for $C_{15}H_{15}O_2N_3$: C, 66.90; H, 5.61; N, 15.61%. IR (KBr) cm^{-1}: 3410, 1688, 1650, 1600, 1536. NMR (DMSO-d_6) τ: 0.80 (s, 1H), 0.90 (s, 1H), 1.87—2.63 (m, 5H), 5.28 (d, 2H), 7.36 (s, 6H).

4-Amino-2-(N-benzoylaminomethyl)-5-cyanopyrimidine (XII). *a) Reaction of I with Ethoxymethylenemalononitrile*: To an ethanol solution of I, prepared from 0.15 g (6.5 mmol) of sodium in 20 ml of ethanol and 1.1 g (5 mmol) of I hydro-

chloride, was added 0.6 g (5 mmol) of ethoxymethylenemalononitrile[8] at 0 °C. The mixture was stirred at 0 °C for 1 hr and at 30 °C for an additional 1 hr. Crystals separated out were collected and recrystallized from ethanol to give colorless needles of XII, mp 208—209 °C, 0.7 g (56%). Found: C, 61.56; H, 4.43; N, 27.58%. Calcd for $C_{13}H_{11}ON_5$: C, 61.65; H, 4.38; N, 27.66%. IR (KBr) cm^{-1}: 3375, 3325, 3200, 2220, 1670, 1650. NMR (DMSO-d_6) τ: 1.13 (s, 1H), 1.14 (s, 2H), 1.88—2.62 (m, 6H), 5.53 (d, 2H).

b) Reaction of Ethyl Benzoylaminoacetimidate with Aminomethylenemalononitrile: An ethanol solution of sodium ethoxide, prepared from 0.23 g (10 mmol) of sodium and 20 ml of ethanol, was added to a solution of 2.4 g (10 mmol) of ethyl benzoylaminoacetimidate hydrochloride[3] in 30 ml of ethanol under ice cooling and the precipitated sodium chloride was removed by filtration. To the filtrate was added 0.9 g (10 mmol) of aminomethylenemalononitrile.[9] The mixture was warmed at 50 °C for 3 hr, and then concentrated. The oily residue was subjected to column chromatography on alumina. Crystals eluted with ethanol were recrystallized from ethanol to give XII, mp 208—209 °C, 0.25 g (10%). Spectral data were identical with those of XII obtained in the preceding experiment.

References

1) H. Uchida, H. Iwasawa, and M. Ohta, This Bulletin, **46**, 3277 (1973).
2) Nomenclature of this compound in Ref. 1 is corrected.
3) A. A. Goldberg and W. Kelly, *J. Chem. Soc.*, **1947**, 1372.
4) T. Shirai and S. Kurashige, *Yuki Gosei Kagaku*, **31**, 88 (1973).
5) E. Mohr, *J. Prakt. Chem.* [2] **81**, 49 (1910).
6) W. Gulewitsch and T. Wasmus, *Ber.*, **39**, 1181 (1906).
7) J. D. Kendall and G. F. Duffin, Brit. 749191 (1956); *Chem. Abstr.*, **51**, 1289d (1957).
8) L. Claisen, *Ann.*, **297**, 1 (1897).
9) O. Diels, H. Gurther, and R. Kaack, *Ber.*, **55B**, 3439 (1922).

Photoinduced Reactions. LXXVII. On the Applicability of Excited Acetone to Induce Photoaromatization of Dihydroheteroaromatics[1]

Teruo MATSUURA and Yoshikatsu ITO

Department of Synthetic Chemistry, Faculty of Engineering, Kyoto University, Yoshida, Sakyo-ku, Kyoto 606

(Received February 4, 1974)

Photoaromatization of various dihydroheteroaromatics and some carbocyclic dihydroaromatics with excited acetone was examined. Among the tested compounds, indoline, 2,3-dihydro-2-methylbenzofuran, and 9,10-dihydroanthracene were found to be photoaromatized. 2-Thiazolines, 2-oxazolines, 2-isoxazolines, 9,10-dihydrophenanthrene, 2,3-dihydro-5,6-dimethylpyrazine, 3,4-dihydro-1-methylisoquinoline, and 6-methyl-3(2*H*)-pyridazinone did not undergo photoaromatization, but recovered unchanged or underwent their own photochemical reactions.

In a previous paper,[2] we have reported that excited states of acetone could be used to dehydrogenate imidazolines to imidazoles. Our attention, then, was focused to see whether this photoaromatization could be extended to other dihydroaromatics. The present paper shows that it is not always the case but various types of reactions take place, although the photoaromatization occurs in some cases. Interpretation of the results with the Hückel molecular orbital (HMO) energy was attempted with some success.

An acetone solution of various dihydroheteroaromatics (AH_2), including a few carbocyclic dihydroaromatics, was irradiated with light mainly at 2537 Å and the products were separated by chromatographic methods. The results are summarized in Table 1, which also includes the results obtained with 2-imidazolines (No. 3—5)[2] for comparison. Various types of reactions occurred and they can be classified into the following six categories. A hydroaromatic radical (·AH), which is produced by hydrogen abstraction with excited acetone from AH_2, may undergo four types of processes; (i) dehydrogenation to an aromatic compound (A), (ii) coupling with the acetone ketyl radical (iii) dimerization, and (iv) regeneration of AH_2 by hydrogen transfer from the acetone ketyl radical. Process (iv) has been proved to occur in part in the case of imidazolines.[2] Other processes will involve the excited states (AH_2*) of the substrate itself; namely, (v) deactivation to AH_2 and (vi) its own photochemical reaction leading to products.

$$AH_2 + Me_2CO^* \longrightarrow \cdot AH + Me_2\dot{C}OH$$

$$A \xleftarrow{\text{(i) } -H\cdot} \cdot AH \xrightarrow{\text{(ii) } Me_2\dot{C}OH} Me_2C(OH)\text{-}AH$$

$$\cdot AH \xrightarrow{\text{(iii) } \cdot AH} (AH)_2 \qquad \cdot AH \xrightarrow{\text{(iv) } Me_2\dot{C}OH} AH_2 + Me_2CO$$

$$AH_2 \underset{\text{(v)}}{\overset{h\nu \text{ or } Me_2CO^*}{\rightleftharpoons}} AH_2^* \xrightarrow{\text{(vi)}} \text{Products}$$

Only indoline (No. 1), 2,3-dihydro-2-methylbenzofuran (No.2), and 9,10-dihydroanthracene (No.11) gave the corresponding aromatized product or its further photolysis product, *e.g.* dianthracene from dihydroanthracene.[11] The intermediary formation of radical ·AH is demonstrated in the latter two cases giving a cross-coupling product and a dimer, respectively. While 2-methyl-2-thiazoline (No. 6) and 3,5-diphenyl-2-isoxazoline (No. 10) gave *N*-vinylthioacetamide[5] and 4,5-diphenyl-3-oxazoline,[7] respectively, other compounds (No. 7, 9, 12, 14, and 15) were unreactive under the conditions except 2-methyl-2-oxazoline (No. 8) which gave a complex mixture of products. The photochemical isomerization of 2,3-dihydro-5,6-dimethylpyrazine (No. 13) to 1,4,5-trimethylimidazole has already been reported.[12] Since the transformation of this imidazole to the imidazole-acetone adduct, 1-(2-hydroxy-2-methylpropyl)-4,5-dimethylimidazole, did not occur under the similar photolytic conditions, it is assumed that the adduct is formed by a similar photoisomerization of the dihydropyrazine-acetone adduct [t pe (ii) product] as depicted below.

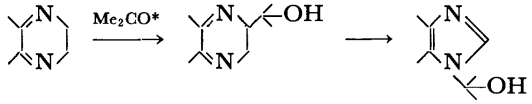

Although the present data are insufficient to make a proper prediction about the reaction courses which dihydroaromatic compounds will follow, we have attempted to interpret the results, particularly on photoaromatization, in terms of HMO π-electron energy (Table 1). We previously showed[2] that $\Delta E_{\pi 2}$ value, which implies the stabilization energy of π-electron for the aromatization step (·AH→A), has a more important meaning to the photodehydrogenation of imidazolines to imidazoles than $\Delta E_{\pi 1}$ value which might contribute to lowering the activation energy of the hydrogen abstraction step (AH_2→·AH). This argument may be valid in the case of the five-membered dihydroheteroaromatics. Thus, indoline (No. 1) having a higher $\Delta E_{\pi 2}$ value than those of imidazolines is easily photoaromatized and 2,3-dihydro-2-methylbenzofuran (No. 2) having a somewhat low $\Delta E_{\pi 2}$ value undergoes slow photoaromatization. 2-Methyl-2-thiazoline (No. 6), and 2-phenyl-2-oxazoline (No. 9) having a low $\Delta E_{\pi 2}$ value suffered no photoaromatization. These results are not interpreted in terms of the $\Delta E_{\pi 1}$ value. Attempts to interpret the data for the six-membered hydroaromatics in terms of either $\Delta E_{\pi 1}$ or $\Delta E_{\pi 2}$ value proved unsuccessful.

Experimental

All the melting points are uncorrected. NMR spectra were taken on an NEVA T-60 spectrometer with tetramethylsilane

TABLE 1. PHOTOCHEMICAL REACTIONS OF DIHYDROAROMATICS (AH_2) IN ACETONE AT 2537Å

No.	AH_2	Concn. g/220 ml	Irrad. time (hr)	Recovered (%) (iv or v)	Products (% yield)[a] [Type of product][b]	HMO calculation[c] $\Delta E_{\pi 1}(\beta)$	HMO calculation[c] $\Delta E_{\pi 2}(\beta)$
1	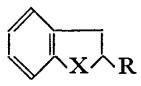 R=H, X=NH[3]	0.70	21	0	Indole (46) [i]	0.61668[d]	2.71792
2	R=Me,[4] X=O	2.19	186	31	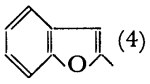 (4) [i] 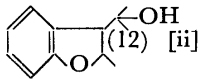 (12) [ii]	0.72735[d]	2.41491
3	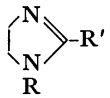 R=H, R'=Me[2]	2.09	26	0	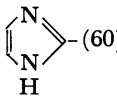 (60) [i] 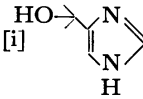 (9) [ii]	0.67520	2.58100
4	R=Me, R'=Me[2]	1.85	24	0	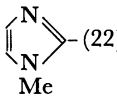 (22) [i] 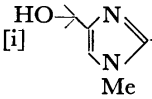 (6) [ii] 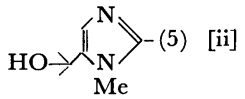 (5) [ii]	0.69020	2.55070
5	R=H, R'=Ph[2]	2.60	75	36	2-Phenylimidazole (36) [i]	0.73246	2.52744
6	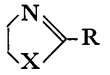 R=Me, X=S[5]	2.26	113	e)	*N*-Vinylthioacetamide (15)[5] [vi]	0.75309[d]	2.39559
7	R=Ph, X=S[5]	2.39	48	f)	—	—	—
8	R=Me, X=O[6]	2.80	119	g)	—	—	—
9	R=Ph, X=O[6]	2.20	45	f)	—	0.68715[d]	2.28541
10	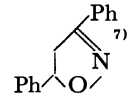 [7]	2.26	52	29	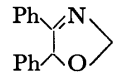 *etc.* (7)[7] [vi]	—	—
11	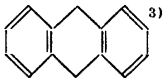 [3]	3.10	88	19	Dianthracene (15) [i] 9,10,9',10'-Tetrahydrodianthranyl (15) (iii)	1.09174	2.22194
12	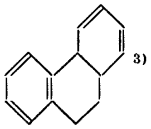 [3]	2.04	24	f)	—	0.63098	2.50456
13	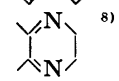 [8]	2.17	22	e)	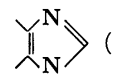 (19) [ii] (40) [vi]	0.73885	2.94457
14	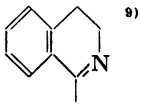 [9]	2·24	142	f)	—	0.68485[d]	2.67979
15	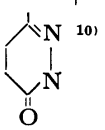 [10]	1.86	48	f)	—	0.74023[d]	2.60967

a) Based on the initial amount of the starting material. b) A[i], HA-C(OH)Me_2[ii], $(HA)_2$[iii], and others[vi]. c) See ref. 2) for the method of calculation. E_π: total π-electron energy of the aromatic system ($E_{\pi A}$), ·AH ($E_{\pi\cdot AH}$), or AH_2 ($E_{\pi AH_2}$). $\Delta E_{\pi 1}=E_{\pi\cdot AH}-E_{\pi AH_2}$. $\Delta E_{\pi 2}=E_{\pi A}-E_{\pi\cdot AH}$. d) Intermediates having the radical center at 3 position for indoline, 2 for 2,3-dihydro-2-methylbenzofuran, 4 for 2-methyl-2-thiazoline, 4 for 2-phenyl-2-phenyl-2-oxazoline, 3 for 3,4-dihydro-1-methylisoquinoline, and 5 for 4,5-dihydro-6-methyl-3(2*H*)-pyridazinone were assumed as ·AH on the basis of their larger π-delocalization energy than those having the radical center at another position. e) The starting material decomposed during column chromatography on silica gel. f) Essentially no reaction occurred judging from NMR, IR, and tlc analyses of the photolysate. g) It gave a complex mixture which contained no 2-methyl-2-oxazole.

as the internal standard. IR spectra were measured on a JASCO IRS spectrophotometer. Mass spectra were determined on a HITACHI RMS-4 spectrometer. Vapor phase chromatography (vpc) was carried out with a Shimadzu GC-2C. Unless otherwise specified, column chromatography (cc) was carried out with Mallinckrodt silica gel (100 mesh) and thin layer chromatography (tlc) with Merck Kieselgel GF_{254}.

Materials. The starting materials were commercially available or prepared according to the methods of literatures cited in Table 1.

Irradiation. A given amount (Table 1) of the substrate was dissolved in 220 ml of acetone and the solution was irradiated internally with a 10-W low-pressure mercury lamp (Vycor housing) under bubbling nitrogen with external cooling with tap water. After evaporation of the solvent under reduced pressure, the residue was submitted to separation in the following way.

Isolation and Characterization of Photoproducts. Indole was isolated by vpc (Silicone DC 550, 40—60 mesh; helium, 1.1 kg/cm² gauge; 140 °C), mp 48.5—51 °C (lit,[13] mp 52 °C), which was identical with an authentic sample (IR). Yield of indole was determined by vpc using diphenyl as the internal standard.

The crude photolysate obtained from 2,3-dihydro-2-methylbenzofuran was chromatographed on 70 g of silica gel. Elution with 300 ml of petroleum ether gave 90 mg of 2-methylbenzofuran. The IR spectrum was identical with the Sadlter Standard Spectrum of this compound. Further elution with 1.3 l of petroleum ether afforded 680 mg of the starting material (tlc and IR). After elution of 440 mg of unidentified products, 380 mg of 2,3-dihydro-3-(α-hydroxyisopropyl)-2-methylbenzofuran was eluted with 1.1 l of benzene–chloroform (1 : 1) which was further purified by preparative tlc (benzene–chloroform, 5 : 1), and distilled to give a colorless oil; bp 75—80 °C (bath temp.)/2 mmHg; ν_{max}^{neat} 3470, 1595, 1240, 1135, 750 cm^{-1}; λ_{max}^{EtOH} 289 nm (ε 3600), 283 nm (4300); τ^{CDCl_3} 2.60—3.34 (4H, m, aromatic H), 5.18 (1H, d-q, J=3 Hz, J'=7 Hz, –CH–O), 7.02 (1H, slightly diffused d, J=3 Hz, –CH–CH–O), 7.83 (1H, broad s, disappeared on deuteration, OH), 8.63 (3H, d, J=7 Hz, CH_3–CH–), 8.78 (6H, d, J=1.5 Hz, $(CH_3)_2$–C–); *m/e* (rel. int.) 192 (M^+, 11), 134 ($M^+-(CH_3)_2CO$, 100), 133 ($M^+-(CH_3)_2COH$, 83), 119 (134—CH_3, 79), 105 (73), 91 (58), 59 (70).

Found: C, 74.77; H, 8.42%. Calcd for $C_{12}H_{16}O_2$: C, C, 74.97; H, 8.39%. Further elution with more polar solvents (chloroform and acetone) gave 1.20 g of a mixture of unidentified products.

During the photolysis of 9,10-dihydroanthracene, dianthracene (450 mg) precipitated as colorless crystals which were identical with an authentic sample[11] (IR). After removal of dianthracene and the solvent, the residue was chromatographed on 90 g of silica gel. Elution with 1.1 l of petroleum ether yielded 590 mg of the recovered starting material (tlc and IR). Further elution with 2.4 l of the same solvent gave 470 mg of 9,10,9′,10′-tetrahydrodianthranyl, mp273—274°C (lit,[14] mp 256—257 °C), which was identical with an authentic sample[14] (IR, NMR). Further elution with more polar solvents (benzene and chloroform) gave 1.57 g of a mixture of unidentified products.

The photolysate from 2,3-dihydro-5,6-dimethylpyrazine was found by NMR analysis to consist of mainly three components, the starting material, 1,4,5-trimethylimidazole, and 1-(2-methylpropyl)-4,5-dimethylimidazole, in the ratio of 0.8 : 2.6 : 1.6. The product mixture was chromatographed on 80 g of neutral alumina (Merck). Elution with 1 l of benzene–chloroform (2 : 1) gave 90 mg of a mixture of unidentified products. Further elution with 2.2 l of the same solvent afforded 870 mg of crude 1,4,5-trimethylimidazole, which was purified by preparative tlc (Aluminiumoxid GF_{254} Type E, Merck; chloroform–acetone, 2 : 1). Picrate, mp 216—217.5 °C (lit,[12] mp 219—220 °C). The NMR and IR spectra were consistent with those reported.[12] Further elution with 1.8 l of benzene–chloroform (1 : 2) and 1 l of chloroform yielded 610 mg of 1-(2-hydroxy-2-methylpropyl)-4,5-dimethylimidazole, which was purified by preparative tlc as mentioned above. A colorless viscous oil crystallized on standing; mp 90.5—92.5 °C; ν_{max}^{neat} 3150, 1500, 1220, 1180, 915, 725 cm^{-1}; λ_{max}^{EtOH} 226 nm (ε 5600); *m/e* (rel. int.) 168 (M^+, 100), 110 ($M^+-(CH_3)_2CO$, 93), 109 ($M^+-(CH_3)_2CHO$, 89), 95 (110—CH_3, 76), 59 (67); τ^{CDCl_3} 2.64 (1H, s, –CH=), 4.86 (1H, s, disappeared on deuteration, OH), 6.28 (2H, s, $-CH_2-$), 7.90 (6H, s, =C–CH_3), 8.80 (6H, s, $(CH_3)_2$–C–).

Found: C, 64.00; H, 9.66; N, 16.77%. Calcd for $C_9H_{16}N_2O$: C, 64.25; H, 9.59; N, 16.65%.

Further elution with more polar solvents (ethanol) gave 370 mg of a mixture of unidentified products. The starting dihydropyrazine decomposed during chromatography and could not be recovered.

References

1) Part LXXVI: I. Saito, M. Takami, and T. Matsuura, submitted for publication.

2) T. Matsuura, Y. Ito, and I. Saito, This Bulletin, **48**, 3805 (1973).

3) Commercially available.

4) J. Entel, C. M. Ruof, and M. C. Howard, *J. Amer. Chem. Soc.*, **73**, 2365 (1951).

5) T. Matsuura and Y. Ito, *Chem. Commun.*, **1972**, 897.

6) H. Wenker, *J. Amer. Chem. Soc.*, **57**, 1079 (1935).

7) T. Matsuura and Y. Ito, *Tetrahedron Lett.*, **1973**, 2283.

8) T. Ishigura and M. Matsumura, *Yakugaku Zasshi*, **78**, 229 (1958).

9) E. Späth, F. Berger, and W. Kuntara, *Ber.*, **63**, 134 (1930).

10) M. Kumagai, *Nippon Kagaku Zasshi*, **81**, 139 (1960).

11) A. Schönberg, G. O. Schenck, and O. -A. Neumüller, "Preparative Organic Photochemistry," Springer-Verlag New York Inc., New York (1968), p. 99.

12) P. Beak and J. L. Miesch, *J. Amer. Chem. Soc.*, **89**, 2375 (1967).

13) The Merck Index, 18th Ed., Merck & Co. (1968), p. 565.

14) J. W. Cook, *J. Chem. Soc.*, **1926**, 1683.

Règles Concernant la Stéréochimie de L' Hydrogénation Catalytique

Eric BROWN et Michel RAGAULT

Laboratoire de Synthèse Organique, Faculté des Sciences, Centre Universitaire, Route de Laval, 72000, Le Mans, France

(Reçu, 4, Mai 1973)

The rule of maximum compactness is put forward as a guide for establishing the stereochemistry of catalytic hydrogenation in many cases. This rule complements the well-known Auwers-Skita rule.

La réaction globale d'hydrogénation catalytique:

$$R + H_2 \xrightarrow{Cat} P$$

est généralement la résultante des processus élémentaires I à V ci-après:[1-3]

$Cat + H_2 \rightleftharpoons Cat\cdot HH$	(I)	Adsorption de H_2
$Cat\cdot HH + R \rightleftharpoons Cat\cdot HHR$	(II)	Adsorption de R
$Cat\cdot HHR \rightleftharpoons Cat\cdot H\cdot(HR)$	(III)	Hydrogénation de R
$Cat\cdot H\cdot(HR) \rightleftharpoons Cat\cdot P$	(IV)	Hydrogénation de R
$Cat\cdot P \rightleftharpoons Cat + P$	(V)	Désorption de P

Bien que l'on puisse souvent prévoir plusieurs composés hydrogénés P stéréoisomères (4 au maximum), l'expérience montre que l'hydrogénation catalytique est une réaction d'une grande stéréospécificité et que l'on obtient dans de nombreux cas un produit P unique résultant d'une addition *cis* d'hydrogène. Cette observation a conduit à admettre que le réactif R s'adsorbe sur le catalyseur par la face la plus dégagée et que, dans l'étape suivante, deux atomes d'hydrogène adsorbés viennent attaquer la molécule R par cette même face, conduisant ainsi à un composé *cis* dihydrogéné. Cette règle de l'encombrement catalytique d'Auwers-Skita,[4-8] si elle a le mérite de la simplicité, souffre malheureusement dans la pratique de nombreuses limitations, ainsi que nous l'illustrerons par la suite.

Pour interpréter et expliquer la stéréochimie des produits P obtenus par hydrogénation catalytique, les théories d'Auwers, Skita[4-6] et de leurs successeurs[1-3,7,8] considèrent uniquement les étapes d'adsorption (I) et (II) et de réduction (III) et (IV), sans se préoccuper des facteurs qui influent sur l'étape (V) de désorption du produit final P. Un tel point de vue est sans doute trop restrictif, ainsi que nous allons tenter de le montrer maintenant.

Nous pouvons admettre, avec Langmuir,[9] que dans Cat·HHR, le solvant utilisé, l'hydrogène et le réactif R sont fixés par physisorption (liaisons de van der Waals) et chimisorption, en formant une couche monomoléculaire à la surface du catalyseur. Les processus de sorption II et de désorption V sont certainement lents et imposent leur vitesse à la réaction globale d'hydrogénation. La désorption du produit P sera facilitée si ce dernier occupe sur le catalyseur une surface plus réduite que l'ensemble initial (R+2H), car ainsi les interactions de van der Waals avec les autres molécules adsorbées seront plus faibles qu'au départ. De plus, P aura d'autant moins d'affinité pour le catalyseur qu'il sera moins plan et que ses groupements fonctionnels polaires ou insaturés seront moins accessibles, par suite de la diminution corrélative du nombre des liaisons (de van der Waals, essentiellement) entre P, le catalyseur et les autres molécules adsorbées. Ainsi donc, plus P sera "recroquevillé" sur lui-même et plus ses groupements fonctionnels seront "masqués", plus le processus V de désorption, et par conséquent la réaction globale d'hydrogénation seront rapides. Ces arguments conduisent à énoncer la règle suivante qui modère la règle d'Auwers-Skita trop souvent mise en défaut: "Lorsque l'hydrogénation catalytique (effectuée en milieu neutre) d'un composé polycyclique insaturé est susceptible de conduire à plusieurs isomères saturés, il se forme de préférence l'isomère dans lequel les groupements fonctionnels polaires ou riches en électrons (π) sont le plus masqués et par conséquent le moins aptes à former des complexes avec le catalyseur et les molécules adsorbées sur ce dernier". Dans la plupart des cas habituels, cette règle pourra s'énoncer plus simplement de la façon suivante ("Règle de la compacité maximum"): "L'hydrogénation catalytique en milieu neutre d'un composé polycyclique insaturé conduit de préférence à l'isomère saturé le plus compact et le plus *gauche* compatible avec les exigences thermodynamiques". Exprimée sous cette forme, la règle précédente permet de comprendre pourquoi l'hydrogénation catalytique des doubles liaisons carbone-carbone conduit presque toujours aux composés hydrogénés *cis*, que la double liaison initiale soit en position intra- ou juxtanucléaire. Cependant, si la molécule R de départ est très volumineuse, l'hydrogénation ne modifiera que peu la compacité et on doit s'attendre à obtenir l'isomère d'hydrogénation le plus stable.

Les quelques exemples suivants nous paraissent significatifs et de nature à illustrer ce qui précède. La règle d'Auwers-Skita prévoit la formation de la cétone thermodynamique *trans* 2, par hydrogénation catalytique

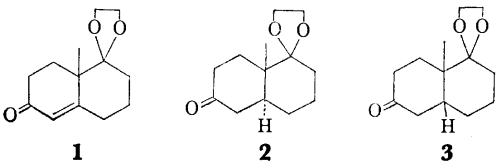

1 **2** **3**

de la cétone éthylénique 1, du fait d'une arrivée *trans* (supposée) de l'hydrogène par rapport au méthyle angulaire. En réalité, nous avons obtenu presque exclusivement la cétone saturée *cis* **3**, laquelle est nettement plus compacte que son isomère *trans* **2**.[10]

De même, l'hydrogénation catalytique de la méthyl octalone-2 **4** devrait conduire à la cétone saturée *trans* **5**, toujours selon la règle d'Auwers-Skita. En fait, là encore, on obtient essentiellement la cétone *cis* **6**, qui est plus compacte.[11]

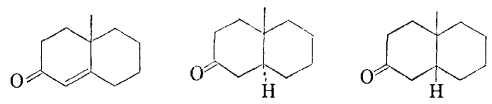

4 **5** **6**

L'hydrogénation catalytique suit un autre cours si le méthyle angulaire de l'octalone **4** est remplacé par un groupement fonctionnel polaire. Ainsi, l'ester **7** fournit par hydrogénation le composé *trans* **8**,[12] dans lequel la fonction ester est plus masquée que dans l'isomère *cis* **9** correspondant.

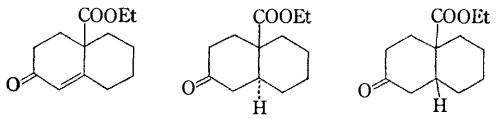

7 **8** **9**

Dans les exemples suivants, nous constatons que l'hydrogénation catalytique de l'indénone **10**,[13] de la phénanthrone **11**[14] et de l'hexahydrophénanthrène **13**[15] suivent bien la règle de la compacité maximum. Ainsi, l'hydrogénation du composé **11** conduit à une phénanthrone **12** à jonction *cis* alors que la règle d'Auwers-Skita laisserait prévoir un composé à jonction *trans*.

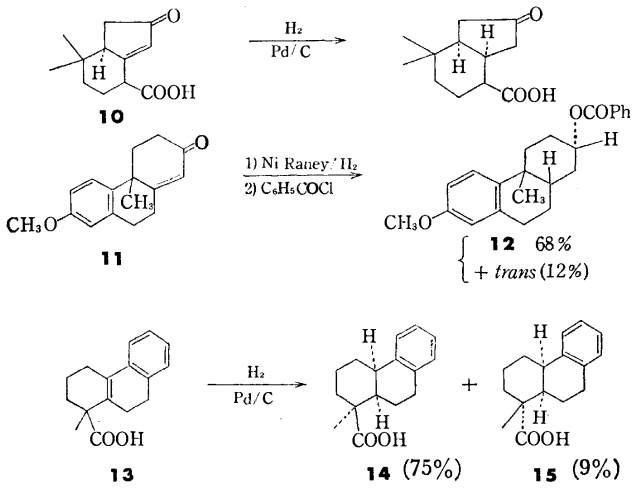

Le composé **13**, quant à lui, est susceptible de fournir par hydrogénation catalytique deux composés à jonction *cis* **14** et **15**. En fait, Ghatak et ses collaborateurs ont obtenu essentiellement l'isomère **14** dans lequel le groupement CO_2H occupe la position *endo*. L'examen des modèles moléculaires nous a montré que dans le composé **14**, le groupement CO_2H peut former des liaisons hydrogène avec le cycle aromatique, ce qui a pour effet de rendre ce composé plus compact que ses trois autres isomères possibles, et en particulier que son isomère **15**.

Pour en terminer avec cet exposé, nous allons donner un exemple qui a été souvent cité avant nous dans divers ouvrages[16-18] pour illustrer la règle d'Auwers-Skita:

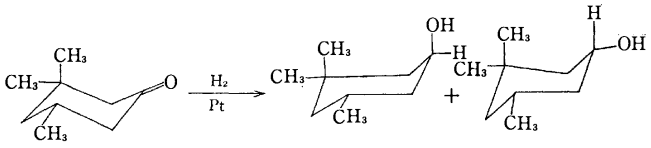

L'hydrogénation sur platine de la cyclohexanone **16** fournit principalement l'alcool axial **17**. Si la formation de **17** suit bien la règle d'Auwers-Skita, il est manifeste qu'elle suit également la règle de la compacité maximum car **17** est plus compact que son isomère équatorial **18**.

Nous tenons à remercier les professeurs D. H. R. Barton, P. F. Casals et J. M. Conia pour les conseils qu'ils nous ont donnés à l'occasion de ce travail.

Bibliographie

1) I. Horiuti et M. Polanyi, *Trans. Faraday Soc.*, **30**, 1164 (1934).
2) F. G. Gault, J. J. Rooney et C. Kemball, *J. Catal.*, **1**, 255 (1962).
3) W. R. Moore, *J. Amer. Chem. Soc.*, **84**, 3788 (1962).
4) D. von Auwers, *Ann.*, **420**, 91 (1920).
5) A. Skita, *Chem. Ber.*, **53**, 1792 (1920).
6) A. Skita et W. Faust, *Chem. Ber.*, **64**, 2878 (1931).
7) R. P. Linstead, W. E. Doering, S. B. Davis, P. Levine et R. R. Whetstone, *J. Amer. Chem. Soc.*, **64**, 1985 (1942) (et publications suivantes).
8) J. H. Brewster, *J. Amer. Chem. Soc.*, **76**, 6361 (1954).
9) G. Arditti, "Technologie chimique industrielle," Eyrolles, Paris (1968), Tome 2, p. 171.
10) E. Brown et M. Ragault, *Tetrahedron Lett.*, **1973**, 1927.
11) W. G. Dauben, J. B. Rogan et E. J. Blanz, *J. Amer. Chem. Soc.*, **76**, 6384 (1954).
12) W. G. Dauben, R. C. Tweit et R. L. MacLean, *ibid.*, **77**, 48 (1955).
13) M. Miyano et C. R. Dorn, *J. Org. Chem.*, **37**, 268 (1972).
14) R. E. Ireland et L. N. Mander, *J. Org. Chem.*, **34**, 142 (1969).
15) U. R. Ghatak, N. R. Chatterjee, A. K. Banerjee, J. Chakravarty et R. E. Moore, *J. Org. Chem.*, **34**, 3739 (1969).
16) H. O. House, "Modern Synthetic Reactions," W. A. Benjamin, New York (1965), p. 17.
17) W. Carruthers, "Some Modern Methods of Organic Synthesis," Cambridge University Press, London (1971), p. 315.
18) J. Mathieu et R. Panico, "Mécanismes Réactionnels en Chimie Organique," Hermann, Paris (1972), p. 686.

Stéréochimie des Perhydrobenz(*e*) Indénones-2

Eric BROWN et Michel RAGAULT

Laboratoire de Synthèse Organique, Faculté des Sciences, Centre Universitaire, Route de Laval, 72000, Le Mans, France

(Reçu, 4, Mai 1973)

The stereochemistry is given of various perhydrobenz(e) inden-2-ones, which have been synthesized as potential intermediates for C-nor-D-homo-steroids.

Nous avons décrit récemment[1] les synthèses des perhydrobenz(e)indénones-2 **4**, **5** et **6** en deux étapes à partir de la γ-dicétone **1**. La *trans-anti-trans* perhydrobenz(e) indénone-2 **6** devrait, selon nous, se révéler un intermédiaire utile dans la synthèse totale des C-nor D-homostéroïdes.

Nous allons exposer ci-après les arguments qui militent en faveur des structures **2**, **3**, **4**, **5** et **6** proposées pour les cinq benz(e) indénones-2 que nous avons préparées (schéma 1).

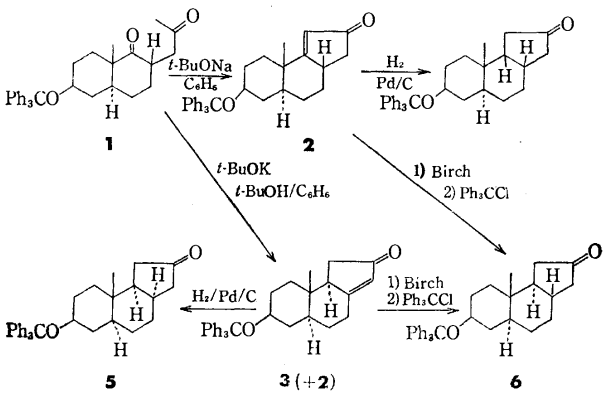

Schéma 1.

La cétone normale **2** est obtenue par crotonisation intramoléculaire de **1** par le *t*-butylate de sodium dans le benzène. Dans ce milieu alcalin et aprotique, la cétone déconjuguée **7** a peu de chances de se former et par conséquent, il n'y a aucune raison pour que la double liaison initialement en position 1,3b migre en position 3,3a.[2]

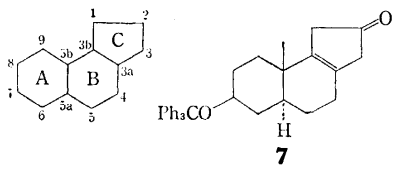

L'examen de modèles moléculaires montre que le cycle B a la forme chaise dans la structure **2** (qui possède un hydrogène 3a-β), tandis que dans l'isomère 3a-α correspondant, le cycle B adopterait la forme bateau moins stable. Dans les conditions de la crotonisation de **1**, l'hydrogène en 3a du composé **2** est épimérisable pour des raisons de vinylogie, et on doit donc obtenir finalement le produit thermodynamique, c'est-à-dire le composé **2** lui-même, à l'exclusion de son isomère 3a-α.

La crotonisation intramoléculaire de **1**, réalisée en milieu alcalin protique (*t*-butylate de potassium dans le mélange *t*-butanol/benzène), a fourni un mélange de cétones conjuguées **2** et **3** (d'après l'I.R. et la R.M.N.).

La formation de **3** passe nécessairement par l'intermédiaire de la cétone éthylénique déconjuguée **7**, laquelle résulte du mécanisme représenté sur le schéma 2.

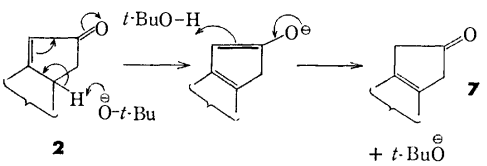

Schéma 2.

Après examen de modèles moléculaires, et en se livrant aux mêmes considérations que pour la cétone **2**, on doit conclure que l'hydrogène en 3b de la cétone **3** occupe la position α, ainsi que nous l'avons d'ailleurs représenté.

On peut prévoir que le méthyle angulaire en position 5b des benz(e)indénones-2 précédentes subira de la part du système cyclopenténone un effet de blindage d'autant plus prononcé que l'axe de la liaison $C_{(9b)}$-CH_3 fera un angle plus faible avec le plan du cycle considéré.[3-5] Dans ces conditions, les structures **2** et **3** proposées sont en accord avec les spectres de R.M.N. des composés correspondants. En ce qui concerne le composé **2**, où la cyclopenténone est relativement éloignée du méthyle angulaire, ce dernier résonne à δ 1.04 ppm (R.M.N. 100 MHz, avec $CDCl_3$ comme solvant). Par contre, dans l'isomère **3**, le cyclopentane est très proche du méthyle et exerce sur ce dernier un effet de blindage anormalement marqué, puisqu'on observe dans ce cas un $\delta(CH_3)\approx 0.56$ ppm (Fig. 1).

La stéréochimie des cétones saturées **4**, **5** et **6** pose des problèmes plus délicats. A priori, on aurait pu croire, en se fiant à la règle de l'encombrement catalytique d'Auwers-Skita que la molécule **2** s'adsorberait

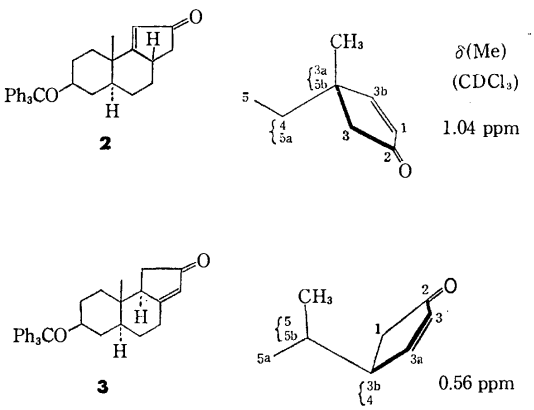

Fig. 1.

sur le catalyseur par la face dégagée, opposée au méthyle angulaire, et que, par conséquent, les deux atomes d'hydrogène viendraient s'additionner sur la double liaison en *trans* par rapport au groupement méthyle. S'il en était ainsi, on aurait normalement dû obtenir la cétone *trans-anti-trans* **6**, laquelle, étant la plus plane des quatre isomères possibles d'après l'examen des modèles, doit être également la cétone réduite la plus stable (car il y a espacement maximum des substituants et des hydrogènes des cycles). Nous aurions donc dû obtenir la même cétone **6**, à la fois par hydrogénation catalytique et par réduction de BIRCH du composé **2**, étant donné que les réductions chimiques conduisent généralement au produit thermodynamique. En fait, par réduction de BIRCH, nous avons obtenu une cétone saturée différente de celle résultant de l'hydrogénation catalytique de **2**, et par conséquent la structure 3a, 3b *cis* **4** a été attribuée au composé d'hydrogénation de **2**. De même, nous attribuons la structure compacte *trans-anti-cis* **5** au composé résultant de l'hydrogénation catalytique de la cétone éthylénique **3** isomère de **2**.

Par réduction de BIRCH (Li/NH_3 liquide), les cétones insaturées isomères **2** et **3** conduisent toutes les deux à un même composé (mêmes points de fusion, spectres I.R. superposables), auquel nous avons attribué la structure *trans-anti-trans* **6**. La structure *trans-anti-trans* de **6** est démontrée par le fait que ce composé est le seul qui puisse être obtenu par réduction à la fois de **2** et de **3**.[6] Nour pouvons également affirmer sans grand risque que le produit obtenu est le plus stable des benz(e)indénones-2 possibles, car il est obtenu par réduction chimique de deux cyclopenténones isomères. Ainsi que nous l'avons déjà dit précédemment, l'examen des modèles montre que la cétone *trans-anti-trans* **6** est la plus plane des quatre perhydrobenz(e)indénones-2 possibles et pour cette raison, ce doit être la plus stable thermodynamiquement. Le quatrième isomère, la cétone *trans-syn-trans* **8**, paraît peu probable car elle implique que le cycle B adopte la forme bateau peu stable.

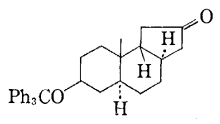

8

Les structures **4**, **5** et **6** avancées pour les cétones saturées sont confirmées par leurs spectres de R.M.N. Sur la Fig. 2, nous avons représenté en perspective les cycles B et C des structures **4**, **5** et **6**, ainsi que les déplacements chimiques δ (ppm) des signaux observés pour les méthyles angulaires correspondants. Si on admet comme exactes les structures précédentes, on constate que la cyclopentanone exerce sur le méthyle angulaire un effet de blindage en R.M.N. d'autant plus marqué que le plan du cycle fait un angle plus faible avec l'axe de la liaison C_{5b}–CH_3, ce qui est conforme aux résultats indiqués dans la littérature[3-5] (Fig. 2).

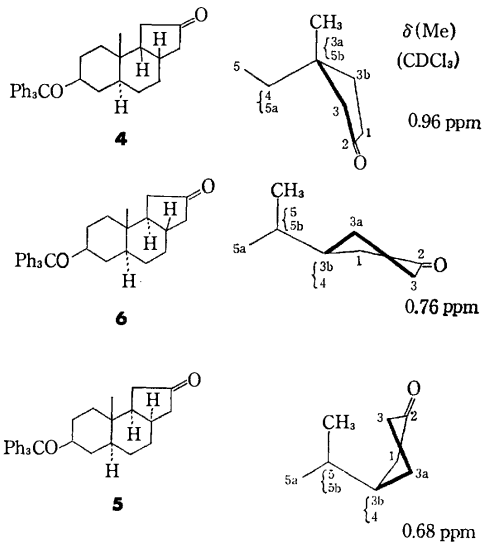

Fig. 2.

Il convient de noter que la cétone **6** est pour nous la plus digne d'intérêt, car elle présente la structure *trans-anti-trans* du système tricyclique A, B, C des C-nor D-homostéroïdes d'origine naturelle.[1] Etant donné qu'une telle molécule est pratiquement plane, elle constitue l'analogue d'un stéroïde, et par conséquent son méthyle angulaire doit avoir un déplacement chimique voisin de ceux des méthyles angulaires situés à la jonction des cycles A, B des stéroïdes normaux. En effect, l'examen des tables[7] montre que le méthyle angulaire à la jonction des cycles A, B des stéroïdes résonne à δ 0.8 ppm, valeur qui est par conséquent très voisine de la valeur δ=0.76 ppm observée pour le déplacement chimique du méthyle angulaire de la *trans-anti-trans* benz(e)indénone-2 **6**.

Nous tenons à remercier les professeurs D. H. R. Barton, P. F. Casals et J. M. Conia pour les conseils qu'ils nous ont donnés à l'occasion de ce travail.

Bibliographie

1) E. Brown et M. Ragault, *Tetrahedron Lett.*, **1973**, 1927.
2) P. Caubère, Communication personnelle.
3) M. Rey, S. Roberts, A. Diffenbacher et A. S. Dreiding, *Helv. Chim. Acta*, **53**, 417 (1970).
4) P. F. Casals, Communication personnelle.
5) J. M. Conia, Communication personnelle.
6) D. H. R. Barton, Communication personnelle.
7) N. S. Bhacca, L. S. Johnson et J. N. Shoolery, "High Resolution of NMR Spectra Catalogue," Vol. 1, Varian Analytical Instruments Division (1962).

Inositol Derivatives. 7. Azidolysis of Disulfonates of *myo*-Inositol and 1,2-*O*-Cyclohexylidene Derivative[1]

Tetsuo SUAMI, Seiichiro OGAWA, Shuichi OKI, and Haruo SATO

Department of Applied Chemistry, Faculty of Engineering, Keio University, Hiyoshi, Yokohama 223

(Received November 30, 1973)

Reactions of azide ion with three disulfonates (1,4-, 1,5-, and 1,6-) of *myo*-inositol and its 1,2-*O*-cyclohexylidene derivative were studied. The structures of the new azido compounds thus obtained were established by PMR spectroscopy and reaction sequences. The reaction mechanisms of the neighboring-group participation reactions were discussed. Hydrogenation of the azido compounds followed by acetylation afforded the corresponding six inosadiamines as their hexaacetates: three known (*allo*-1,5, *muco*-1,3, and *myo*-4,5) and three hitherto unknown inosadiamines (*allo*-1,4, *muco*-1,2, and *chiro*-2,4).

Azido-deoxy- and diazido-dideoxy-inositols are useful intermediates for the synthesis of inosamines and inosadiamines or certain kinds of nucleoside analogs having pseudo sugar moieties. Investigations have been carried out on nucleophilic displacement reactions by azide ion with readily accessible sulfonate derivatives of inositols.[2] In the present paper, we wish to report on the azidolysis of three ditosylates of *myo*-inositol and its 1,2-*O*-cyclohexylidene derivative. The structures of the new azido compounds were established by PMR spectroscopy of their acetyl derivatives, and also by their transformation into known aminocyclitols. The reaction mechanisms in azidolysis were discussed.

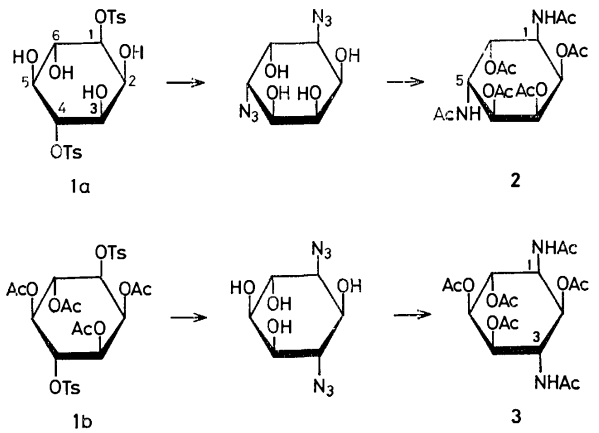

Scheme 1

1,4-Ditosylates. Treatment of 1,4-di-*O*-tosyl-*myo*-inositol (**1a**)[3] with an excess amount of sodium azide in refluxing aqueous 2-methoxyethanol for 20 hr, followed by conventional acetylation, afforded an azido derivative as a syrup. The crude azido compound was catalytically hydrogenated and subsequently acetylated to give hexaacetyl *allo*-inosadiamine-1,5 (**2**)[4] in 58% yield. On the other hand, when 1,4-di-*O*-tosyl-*myo*-inositol tetraacetate (**1b**)[3] was treated with sodium azide under the same conditions, hexaacetyl *muco*-inosadiamine-1,3 (**3**)[4] was obtained exclusively in 44% yield. In the former reaction (**1a**→**2**), displacement of the sulfonyloxy group at C-4 takes place initially by participation of the hydroxyl group at C-5 forming an intermediary 4,5-epoxide. The epoxide ring is opened by azide ion preferentially in a *trans*-diaxial manner. Another sulfonyloxy group at C-1 is replaced by the participation of the hydroxyl group at C-6 to give a 1,6-epoxide, which is attacked by the nucleophile in the manner described above. In the latter reaction (**1b**→**3**), the initial formation of a 1,6- or 3,4-acetoxonium ion, and its *trans*-diaxial opening by the azide ion results in the formation of compound **3**.

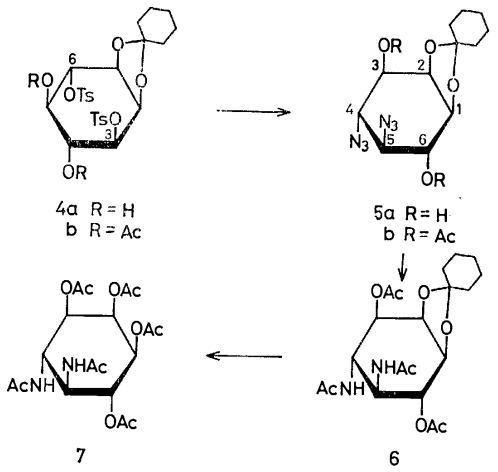

Scheme 2

In order to remove participation of the acetoxy group at C-3 in the replacement reaction of the sulfonyloxy group at C-4 in **1b**, two hydroxyl groups of **1a** at C-2 and C-3 were blocked by a nonparticipating cyclohexylidene group to give 1,2-*O*-cyclohexylidene-3,6-di-*O*-tosyl-*myo*-inositol (**4a**).[3] Compound **4a** and its diacetate (**4b**)[3] were subjected to azidolysis under the same conditions to give an azido compound (**5a**) as the sole crystalline product in fairly good yield. Acetylation of **5a** gave the diacetate (**5b**). Catalytic reduction of **5a**, followed by acetylation, afforded tetraacetyl *O*-cyclohexylidene-inosadiamine (**6**). Mild hydrolysis of **6** in aqueous acetic acid followed by acetylation gave hexaacetyl *myo*-inosadiamine-4,5 (**7**).[4] Compound **6** was thus assigned to 4,5-diacetamido-3,6-di-*O*-acetyl-1,2-*O*-cyclohexylidene-4,5-dideoxy-*myo*-inositol and **5a** to 4,5-diazido-1,2-*O*-cyclohexylidene-4,5-dideoxy-*myo*-inositol. The structure of **5b** was further confirmed by its PMR spectrum which allowed an interpretation by a first-order method with nicely resolved signals. The narrow doublets at τ 5.87 and 5.50 were respectively assigned to the protons at C-1

TABLE 1. CHEMICAL SHIFTS OF ACETYL METHYL PROTONS OF HEXAACETYL INOSADIAMINES[a)]

Compound	Configuration	Solvent	Chemical shifts
2	*allo*-1,5	C	8.06 (3)
			7.98 (9)
			7.89 (3)
			7.85 (3)
3	*muco*-1,3	C	8.02 (3)
			7.97 (3)
			7.92 (9)
			7.89 (3)
7	*myo*-4,5	C	8.07 (6)
			8.02 (3)
			7.99 (3)
			7.87 (3)
			7.80 (3)
10	*allo*-1,4	D	8.10 (6)
			7.96 (6)
			7.93 (6)
13	*muco*-1,2	C	7.99 (6)
			7.90 (6)
			7.87 (6)
20	*chiro*-2,4	D	8.23 (3)
			8.20 (3)
			8.07 (6)
			7.82 (6)

a) Measured at 60 MHz. Chemical shifts are expressed in terms of τ-values. Values in parentheses show number of protons. Abbreviations: C, $CDCl_3$; D, DMSO-d_6. The chemical shifts and pattern of the signals of known compounds (**2**, **3**, and **7**) are in good agreement with those reported by Nakajima *et al.*[4)]

and C-2 carrying the blocking group. The protons were shown to be coupled neither with H-4 (τ 6.72) nor with H-5 (τ 6.10).[5)]

In both reactions with **4a** and **4b**, the azidolysis involves the formation of an intermediary epoxide and acetoxonium ion, respectively, by participation of the neighboring group and its opening by an azide ion which is appreciably affected by the adjacent cyclohexylidene group in terms of steric and polar effects. Thus it is deduced that the opening of the 5,6-epoxide initially formed occurs in a *trans*-diaxial manner and the 3,4-epoxide is subsequently opened in a *trans*-diequatorial manner.

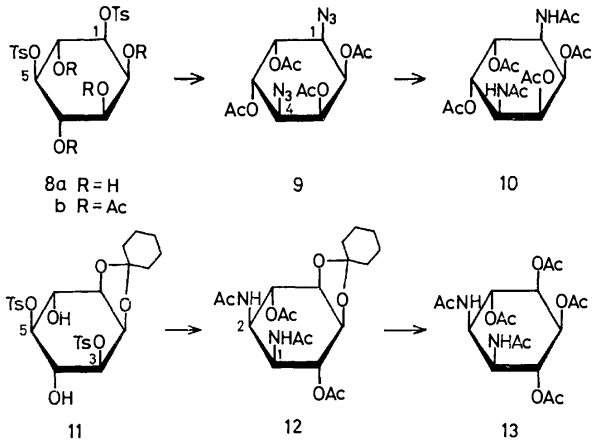

Scheme 3

1,5-Ditosylates. Treatment of 1,5-di-*O*-tosyl-*myo*-inositol (**8a**)[3)] and its acetyl derivative (**8b**)[3)] with sodium azide under similar conditions, followed by acetylation, gave diazidodideoxyinositol tetraacetate (**9**) as the sole crystalline product in 13 and 39% yields, respectively. Besides product **9**, two other unidentified minor products were detectable on tlc. Catalytic reduction of **9**, followed by acetylation, afforded hitherto unknown hexaacetyl inosadiamine (**10**). The PMR spectrum of **10** revealed three singlets of equal intensity in the vicinity of τ 8, ascribed to two acetamido, two acetoxy, and two acetoxy groups.[6)] From the pattern of the signals and their chemical shifts, it was deduced to be the time-averaged spectrum derived from a rapid interconversion between two equivalent conformations. The PMR spectrum of **9**, however, showed a wide double doublet (J=3 and 11 Hz) and a narrow triplet (J=3 Hz) at τ 6.00 and 5.56, respectively, which do not couple with each other and are ascribable to the protons on the carbon atoms carrying the azido groups.[5)]

TABLE 2. PMR SPECTRAL DATA IN $CDCl_3$ AT 60 MHz[a)]

Compound	H_1 ($J_{1,2}$)	H_2 ($J_{2,3}$)	H_3 ($J_{3,4}$)	H_4 ($J_{4,5}$)	H_5 ($J_{5,6}$)	H_6 ($J_{1,6}$)	OAc	OTs
5b	5.87 dd	5.50 dd	4.96 dd	6.72 t	6.10 t	4.82 dd	7.84 (3)[b)]	
	(5)	(4)	(10)	(10)	(10)	(7.5)	7.79 (3)	
9	5.56 t	—	4.34 t	6.00 dd	—	4.34 t	7.99 (3)	
	(3)		(3)	(11)		(3)	7.87 (3)	
							7.83 (3)	
							7.79 (3)	
18	—	6.22 dd	4.68 dd	6.13 t	4.90 dd	—	7.94 (3)	
	(3)	(10)	(10)	(10)	(3)		7.82 (6)	
							7.79 (3)	
19	5.43 dd	4.32 t	4.99 dd	4.58 dd	5.00 t	6.05 t	8.03 (3)	7.52 (3)
	(3)	(3)	(10.5)	(10)	(10)	(10.5)	8.01 (3)	
							7.91 (3)	
							7.84 (3)	

a) Chemical shifts are given in terms of τ-values. Values given for coupling constants (Hz) are of first-order. Abbreviations: t (triplet); dd (double doublet). b) Values in parentheses show number of protons.

A narrow triplet (τ 4.34) should be due to an equatorial proton on the carbon atom attached by the acetoxy group. Besides the expectation from analogous reaction mechanism, the results indicate that **9** should possess either *allo*-1,4- or *neo*-1,5-configuration. Since the former configuration satisfied the behavior of **10** in PMR spectroscopy, **9** was assigned to 1,4-diazido-1,4-dideoxy-*allo*-inositol tetraacetate and **10** to hexaacetyl *allo*-inosadiamine-1,4. Mechanistically, participation of the hydroxyl or the acetoxy group on C-4 to C-5 occurs initially to give rise to a 4,5-cyclic intermediate.

On the other hand, two hydroxyl groups at C-2 and C-3 of **8a** were blocked by a cyclohexylidene group to give compound **11**.[3] Azidolysis of **11** under similar conditions and subsequent acylation afforded tetraacetyl *O*-cyclohexylidene-inosadiamine (**12**) in 34% yield, which was converted into hitherto unknown inosadiamine (**13**). The PMR spectrum of **12** revealed four acetyl methyl protons as two singlets of equal intensities at τ 8.00 and 7.86, which were ascribed to two equivalent acetamido and acetoxy groups, respectively. The configuration of **12** is thus limited to *muco*-1,2 and *allo*-1,4. The PMR spectrum of **13** showed three singlets (1 : 1 : 1) due to six acetyl methyl protons, also supporting the above assignments.

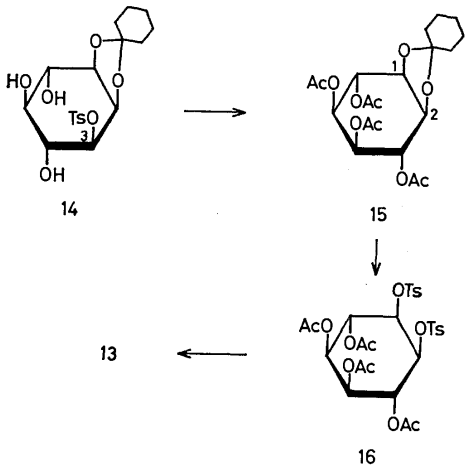

Scheme 4

For the sake of confirmation, an alternative synthesis of **13** was successfully attempted as follows. 1,2-*O*-Cyclohexylidene-3-*O*-tosyl-*myo*-inositol (**14**)[3] was heated in aqueous 2-methoxyethanol with sodium carbonate and subsequently acetylated to give 1,2-*O*-cyclohexylidene-*muco*-inositol tetraacetate (**15**) in 65% yield. By removing the cyclohexylidene group in aqueous acetic acid, **15** was converted into *muco*-inositol tetraacetate, which was treated with tosyl chloride in pyridine to give 1,2-di-*O*-tosyl-*muco*-inositol tetraacetate (**16**). Azidolysis of **16** in the usual way followed by reduction and acetylation afforded **13** in 30% yield.

Consequently, the structure of **13** was established as hexaacetyl *muco*-inosadiamine-1,2. In the case of **11**, the nucleophilic substitution of the intermediate epoxides is also affected by the cyclohexylidene group located in *trans* orientation to them resulting in the initial *trans*-diequatorial opening of the 5,6-epoxide[7] followed by subsequent *trans*-diaxial opening of the 3,4-epoxide.

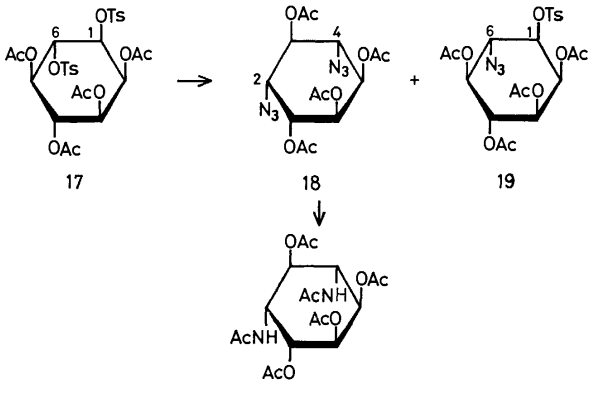

Scheme 5

1,6-Ditosylates. Treatment of 1,6-di-*O*-tosyl-*myo*-inositol tetraacetate (**17**)[3] with sodium azide by the usual method gave two major products, which were separated by fractional crystallization from ethanol into diazido compound (**18**) and monoazido compound (**19**) in 44 and 18% yields, respectively. Catalytic reduction of **18** and subsequent acetylation afforded a new hexaacetyl inosadiamine (**20**) in 42% yield. By analogy with the preceding results, the reaction involves the initial formation of the 5,6-acetoxonium ion, followed by its preferential diaxial opening with azide ion. However, in a favorable conformation of the intermediate, an attack of azide ion at C-5 would be somewhat interrupted by the adjacent *trans*-acetoxy group in pseudo equatorial orientation, which is probably reflected to a formation of **18** and **19** with a ratio of 2.4: 1. Another tosyloxy group at C-1 in **18** is replaced by the nucleophile in a direct S_N2 manner. **18** is therefore tentatively assigned to 2,4-diazido-2,4-dideoxy-*chiro*-inositol tetraacetate and **19** to 6-azido-6-deoxy-1-*O*-tosyl-*myo*-inositol tetraacetate.

The PMR spectrum of **18** (Table 1) shows a triplet (τ 6.13) and a double doublet (τ 6.22) which do not couple with each other, indicating the presence of the azido groups at C-2 and C-4. The chemical shifts of acetyl methyl protons of **20** also support its *chiro*-2,4 configuration. In the PMR spectrum of **19** (Table 1), the triplet (τ 6.05) due to a proton on the carbon atom bearing the azido group is coupled with H-1 double doublet (τ 5.43), supporting the above assignment.

In the case of **19**, the displacement of tosyloxy group at C-1 is significantly retarded by the existence of the neighboring azido group in *trans* orientation.

For the sake of comparison, 2,3-*O*-cyclohexylidene derivatives of the 1,6-ditosylates (**21a** and **21b**)[3] were subjected to azidolysis. Azidolysis of **21a** and **21b** proceeded in a quite different way to give 1,4-anhydro-5,6-*O*-cyclohexylidene-3-*O*-tosyl-*chiro*-inositol (**22**)[7] in 73 and 65% yields, respectively. This shows that the attack of the hydroxyl group (at C-6) on C-3 is preferential, the conformation being brought closer to that of boat form.[8]

Experimental

Unless otherwise stated, melting points were determined on a Mitamura Riken micro hot stage and are uncorrected. The melting points marked with asteriks were determined in a liquid bath and are uncorrected. IR spectra were measured on a JASCO IR-E spectrophotometer in KBr disks. PMR spectra were obtained on a Varian Associates A-60D (60 MHz) spectrometer at a concentration *ca.* 10% in deuteriochloroform ($CDCl_3$) or dimethylsulfoxide-d_6 (DMSO-d_6), with tetramethylsilane as an internal standard. Chemical shifts are given in terms of τ-values, signals being denoted by s (singlet), d (doublet), t (triplet), dd (double doublet), or m (complex multiplet). Values given for coupling constants are of first-order. All the solutions were concentrated by a rotary evaporator at 40—50 °C under reduced pressure, and a trace of residual pyridine was removed by coevaporation with toluene. Catalytic hydrogenation was carried out with a Parr shaker apparatus in the presence of Raney nickel T-4[9] catalyst in the initial hydrogen pressure of 3.5 kg/cm² at room temperature. Tlc was performed on silica gel (Wakogel B-10, Wako Pure Chemical Industries, Ltd.) using a mixture of 2-butanone and toluene. The spots were indicated by heating above 150 °C after spraying with 30% sulfuric acid.

Hexaacetyl allo-*Inosadiamine-1,5 (2).* A mixture of 1,4-di-*O*-tosyl-*myo*-inositol (**1a**)[3] (3.0 g), sodium azide (3.0 g), and 90% aqueous 2-methoxyethanol (100 ml) was refluxed for 20 hr. The mixture was then evaporated to dryness and the residue was treated with acetic anhydride (10 ml) and pyridine (10 ml) overnight at room temperature. The insoluble material was removed by filtration and the filtrate was evaporated to dryness. The residue was extracted with hot ethyl acetate (50 ml) and the extract was purified by passing through a short alumina column. The solution was evaporated to give a syrup, which was, without further purification, hydrogenated in an ethanol solution (20 ml) for 15 hr. The catalyst was filtered off and the filtrate was concentrated to give an oily product, which was acetylated in the usual way to give crystals (1.56 g, 58%) of **2**, mp 202—204 °C. Recrystallization from ethanol–ether afforded an analytically pure sample, mp 204.5—205.5 °C (lit,[4] 203—204 °C). Found: C, 50.21; H, 6.08; N, 6.43%.

Hexaacetyl muco-*Inosadiamine-1,3 (3).* A mixture of 1,4-di-*O*-tosyl-*myo*-inositol tetraacetate (**1b**)[3] (2.5 g), sodium azide (2.5 g), and 90% aqueous 2-methoxyethanol (100 ml) was refluxed for 16 hr. The reaction mixture was then treated as in the preparation of **2**. The crude crystals were recrystallized from ethyl acetate to afford pure crystals (0.72 g, 44%) of **3**, mp 229—231 °C (lit,[4] 227—228 °C). Found: C, 49.81; H, 6.01; N, 6.35%.

*4,5-Diazido-1,2-*O*-cyclohexylidene-4,5-dideoxy-*myo*-inositol (5a).*

a): A mixture of 1,2-*O*-cyclohexylidene-3,6-di-*O*-tosyl-*myo*-inositol (**4a**)[3] (1.4 g), sodium azide (1.4 g), and 90% aqueous 2-methoxyethanol (30 ml) was refluxed for 20 hr. The reaction mixture was evaporated to dryness and the residue was extracted with hot ethyl acetate (60 ml). The extract was passed through a short alumina column and was then concentrated to give a syrup, which was crystallized from ethanol to afford colorless plates (0.46 g, 60%) of **5a**, mp 70—90 °C. Recrystallization twice from ethanol gave an analytical sample, mp 102—105 °C (after melting and resolidifying at 68—83 °C).

Found: C, 47.35; H, 6.86; N, 23.49%. Calcd for $C_{12}H_{18}N_6O_4$: C, 46.44; H, 5.85; N, 27.08%. Calcd for $C_{12}H_{18}N_6O_4 \cdot C_2H_5OH$: C, 47.18; H, 6.79; N, 23.58%.

The crystals lose ethanol by drying *in vacuo* over phosphorus pentoxide at 80—90 °C overnight.

Found: C, 46.49; H, 5.78; N, 26.91%.

b): 1,2-*O*-Cyclohexylidene-3,6-di-*O*-tosyl-*myo*-inositol diacetate (**4b**)[3] (2.0 g) was allowed to react with sodium azide (2.0 g) in refluxing 90% aqueous 2-methoxyethanol (60 ml) for 19 hr followed by a similar treatment to that described above to yield crystals (0.42 g, 43%) of **5a**, mp 70—90 °C.

Compound **5a** (69 mg) was treated with acetic anhydride (0.5 ml) in pyridine (0.5 ml) for 30 min at 80 °C. The mixture was then poured into ice and water giving crystals (69 mg, 78%) of the diacetate (**5b**), mp 149—150.5 °C. Recrystallization from ethanol afforded a pure sample. needles, mp 150—151 °C.

Found: C, 49.03; H, 5.76; N, 20.90%. Calcd for $C_{16}H_{22}N_6O_6$: C, 48.72; H, 5.62; N, 21.31%.

*4,5-Diacetamido-3,6-di-*O*-acetyl-1,2-*O*-cyclohexylidene-4,5-dideoxy-*myo*-inositol (6).* The crude crystals of **5a** derived from **4a** (1.5 g) was hydrogenated in an ethanol solution (10 ml) overnight. The product was treated with acetic anhydride (2 ml) and pyridine (3 ml) overnight at room temperature to give a crystalline product, which was crystallized from ethanol affording crystals (0.45 g, 43%) of **6**, mp* 249—250.5 °C. An analytical sample was obtained by recrystallization from chloroform–ethanol, needles, mp* 249—250 °C. PMR ($CDCl_3$): τ 8.08, 8.06, 7.91, 7.86 (3-proton s, OAc), 4.78 (dd, $J_{1,6}=7.5$ Hz, $J_{5,6}=11$ Hz, H-6), 4.70 (dd, $J_{2,3}=4$ Hz, $J_{3,4}=10$ Hz, H-3).

Found: C, 56.39; H, 6.93; N, 6.51%. Calcd for $C_{20}H_{30}N_2O_8$: C, 56.32; H, 7.09; N, 6.57%.

Hexaacetyl myo-*Inosadiamine-4,5 (7).* Compound **6** (0.20 g) was refluxed with 80% aqueous acetic acid (10 ml) for 2 hr and the mixture was evaporated to dryness. The residue was treated with acetic anhydride (0.5 ml) and pyridine (1 ml) overnight at room temperature. The product was crystallized from chloroform–ethanol to afford pure needles (0.18 g, 84%) of **7**, mp* 303—303.5 °C (lit[4], 294—295 °C). Found: C, 50.04; H, 6.03; N, 6.37%. In the PMR spectrum of **7** in $CDCl_3$, the chemical shifts of signals due to the acetyl groups (Table 1) were in good agreement with those of an authentic sample.[4]

*1,4-Diazido-1,4-dideoxy-*allo-*inositol Tetraacetate (9).*

a): A mixture of 1,5-di-*O*-tosyl-*myo*-inositol (**8a**)[3] (2.0 g), sodium azide (2.0 g), and 90% aqueous 2-methoxyethanol (80 ml) was refluxed for 14 hr. The reaction mixture was treated as in the preparation of **5a** to yield a syrupy compound. Tlc (1:5 2-butanone–toluene) indicated the formation of three components having close R_f values. The syrup was dissolved in ethanol–ligroin and the solution was allowed to stand in a refrigerator for a week giving crystals (0.22 g, 13%) of **9**, mp 145—150 °C. Recrystallization from ethanol gave an analytical sample, mp 151—152 °C.

Found: C, 42.32; H, 4.54; N, 20.94%. Calcd for $C_{14}H_{18}N_6O_8$: C, 42.21; H, 4.55; N, 21.10%.

The mother liquor of **9** was concentrated to give a syrup. which was hydrogenated in an ethanol solution (20 ml) overnight. The product was acetylated in the usual way to afford a syrupy product, which was without further purification de-*O*-acetylated by treatment with a catalytic amount of sodium methoxide in a methanol solution. The product was crystallized from ethanol to give white powder (0.13 g) of di-*N*-acetyl inosadiamine. A 52 mg portion of this compound was acetylated in the usual way to give crystals of hexaacetyl *allo*-inosadiamine-1,4 (**10**), mp* 247.5—248 °C. The yield of **10** was 10% based on **8a**.

Found: C, 50.15; H, 6.05; N, 6.30%. Calcd for $C_{18}H_{26}N_2O_{10}$: C, 50.23; H, 6.09; N, 6.51%.

b): A mixture of 1,5-di-*O*-tosyl-*myo*-inositol tetraacetate (**8b**)[3] (1.0 g), sodium azide (1.0 g) and 90% aqueous 2-methoxyethanol (40 ml) was refluxed for 17 hr. The reaction mixture was then treated as in the preparation of *a)* to give crystals (0.24 g, 39%) of **9**, mp 147—150 °C. The product was identified with the compound obtained before by comparison of IR spectra.

Hexaacetyl allo-*Inosadiamins-1,4 (10).* Compound **9** (154 mg) was hydrogenated in an ethanol solution (15 ml) overnight. The product was acetylated in the usual way to give crystals after crystallization from ethanol–ether: yield 52 mg (31%), mp* 247.5—248 °C. It was shown to be identical with the compound obtained before by comparison of IR spectra.

1,2-Diacetamido-3,6-di-O-*acetyl-4,5*-O-*cyclohexylidene-1,2-dideoxy*-muco-*inositol (12).* A mixture of 1,2-*O*-cyclohexylidene-3,5-di-*O*-tosyl-*myo*-inositol (**11**)[3] (1.0 g), sodium azide (1.0 g), and 90% aqueous 2-methoxyethanol (20 ml) was refluxed for 17 hr. The reaction mixture was then treated as in the preparation of **5a** to give an oily azido compound. Tlc (1: 5 2-butanone-toluene) showed the formation of one major component along with a trace of one minor component. The crude compound was directly hydrogenated and then acetylated in the usual manner to give crystals, which were recrystallized from ethanol to afford thin needles (0.25 g, 34%) of **12**, mp* 182—185 °C. An analytical sample was obtained by recrystallization from ethanol; mp* 186—187 °C. PMR ($CDCl_3$): τ 8.00 (3-proton s, NHAc), 7.87 (6-proton s, OAc), 5.64 (2-proton broad d, J=4 Hz, H-4 and H-5), 5.45 (2-proton broad d, H-1 and H-2), 4.73 (2-proton m, H-3 and H-6), 3.50 (2-proton d, J=8 Hz, NHAc).

Found: C, 55.94; H, 6.97; N, 6.35%. Calcd for $C_{20}H_{30}N_2O_8$: C, 56.32; H, 7.09; N, 6.57%.

Hexaacetyl muco-*Inosadiamine-1,2 (13).* Compound **12** (0.10 g) was refluxed with 80% aqueous acetic acid (5 ml) for 1 hr, and then acetylated in the usual way to give crystals (62 mg, 57%) of **13**, mp 90—120 °C. Recrystallization from ethanol–ether afforded an analytical sample, needles, which melted* at 220—221.5 °C sharply after melting at 90—120 °C and then resolidifying at 150—155 °C.

Found: C, 50.18; H, 6.36; N, 6.37%. Calcd for $C_{18}H_{26}N_2O_{10}$: C, 50.23; H, 6.09; N, 6.51%.

1,2-O-Cyclohexylidene-muco-*inositol Tetraacetate (15).* A mixture of 1,2-*O*-cyclohexylidene-3-*O*-tosyl-*myo*-inositol (**14**)[3] (0.50 g), potassium carbonate (0.50 g), and 80% aqueous 2-methoxyethanol was refluxed for 4.5 hr. The reaction mixture was evaporated to dryness and the residue was treated with acetic anhydride (10 ml) and pyridine (10 ml) overnight at room temperature. The insoluble material was filtered off and the filtrate was evaporated to give a syrup, which was crystallized from ethanol to afford plates (0.34 g, 65%) of **15**, mp 130—131 °C. Recrystallization from ethanol–petroleum ether afforded an analytical sample, mp 134—134.5 °C PMR ($CDCl_3$): τ 7.93, 7.89 (6-proton s, OAc), 5.75 (2-proton m, H-1 and H-2), 4.77 (2-proton m, H-4 and H-5). The two multiplets are consistent with the A_2 portion of the A_2X_2 system.

Found: C, 56.42; H, 6.54%. Calcd for $C_{20}H_{28}O_{10}$: C, 56.07; H, 6.59%.

1,2-Di-O-*tosyl*-muco-*inositol Tetraacetate (16).* A mixture of **15** (1.5 g) and 30% aqueous acetic acid (20 ml) was heated for 3 hr at 75 °C. The reaction mixture was then evaporated to give a partly crystalline compound, from which **15** (0.12 g) was recovered. The resulting syrup was concentrated to dryness and treated with tosyl chloride (3.5 g) in pyridine (20 ml) overnight at room temperature. The mixture was poured into ice water and the resulting crystals were collected by filtration. Recrystallization from ethanol afforded pure crystals (1.15 g, 56%) of **16**, mp 160 °C. PMR ($CDCl_3$): τ 7.99, 7.97 (6-proton s, OAc), 7.53 (6-proton s, OTs), 5.16 (2-proton m, H-1 and H-2), 4.73 (2-proton m, H-4 and H-5). The two multiplets are consistent with the A_2 portion of the A_2X_2 system.

Found: C, 51.38; H, 5.16; S, 9.64%. Calcd for $C_{28}H_{32}O_{14}S_2$: C, 51.21; H, 4.91; S, 9.76%.

Preparation of 13 from 16. A mixture of **16** (0.51 g), sodium azide (0.55 g), and 90% aqueous 2-methoxyethanol (30 ml) was refluxed for 20 hr. The reaction mixture was evaporated to dryness and the residue was dried by coevaporation with toluene. The solid residue was treated with acetic anhydride (10 ml) and pyridine (10 ml) overnight at room temperature. The insoluble material was removed by filtration and the filtrate was evaporated. The syrupy residue was purified with a short alumina column with chloroform as an eluent. The product was then hydrogenated and subsequently acetylated in the usual manner to give crystals, which were recrystallized from ethanol–ether to afford needles (97 mg, 30%) of **13**, mp* 213—216 °C. It was identified with the compound obtained before by comparison of IR spectra.

2,4-Diazido-2,4-dideoxy-chiro-*inositol Tetraacetate (18) and 6-Azido-6-deoxy-1*-O-*tosyl*-myo-*inositol Tetraacetate (19).* A mixture of 1,6-di-*O*-tosyl-*myo*-inositol tetraacetate (**17**)[3] (4.0 g), sodium azide (4.0 g), and 90% aqueous 2-methoxyethanol (150 ml) was refluxed for 12 hr. The reaction mixture was then treated as in the preparation of **9** to yield an oily azido compound which was found to consist of two major components. They were fractionally crystallized from ethanol to afford almost pure crystals (1.25 g, 47.8%) of **18** and pure prisms (0.695 g, 22.7%) of **19**. Recrystallization from ethanol gave needles (1.16 g, 44.4%) of **18**, mp 147—148 °C.

Found: C, 42.15; H, 4.57; N, 21.32%. Calcd for $C_{14}H_{18}N_6O_8$: C, 42.21; H, 4.55; N, 21.10%.

Recrystallization from chloroform-ethanol gave prisms (0.633 g, 18.3%) of **19**, mp 163.5—164.5 °C.

Found: C, 47.99; H, 4.83; N, 7.81; S, 6.31%. Calcd for $C_{21}H_{25}N_3O_{11}S$: C, 47.82; H, 4.78; N, 7.97; S, 6.08%.

Hexaacetyl chiro-*Inosadiamine-2,4 (20).* Compound **18** (0.22 g) was hydrogenated in an ethanol solution (20 ml) overnight. The product was acetylated in the usual way and the product was crystallized from ethanol–ether to afford prisms (0.10 g, 42%) of **20**, mp 253—256 °C. Recrystallization from ethanol–ether gave large prisms after long storage in a refrigerator; mp 160—170 °C.

Found: C, 48.31; H, 6.34; N, 6.33%. Calcd for $C_{18}H_{26}N_2O_{10}\cdot H_2O$: C, 48.21; H, 6.29; N, 6.25%.

1,4-Anhydro-5,6-O-cyclohexylidene-2-O-*tosyl*-chiro-*inositol (22).* A mixture of 5,6-di-*O*-acetyl-1,2-*O*-cyclohexylidene-3,4-di-*O*-tosyl-*myo*-inositol (**21b**)[3] (1.1 g), sodium azide (1.1 g), and 90% aqueous 2-methoxyethanol (20 ml) was refluxed for 15 hr. The reaction mixture was evaporated to dryness and the residue was extracted with hot ethyl acetate. The extracts were evaporated to give crystals which were recrystallized from ethanol to afford crystals (0.47 g, 65%) of **22**, mp 114.5—116 °C. The product was identified with an authentic IR spectrum.

The authors wish to thank Prof. Sumio Umezawa for his kind advice. They are grateful to Mr. Saburo Nakada for elementary analyses and to Mr. Hayashi Uchino for the preparation of compound **13** from **14**. The work was carried out with financial support from the Ministry of Education.

References

1) Part of the work was presented at the Annual Meeting of the Chemical Society of Japan, Osaka, April 1, 1971 (Abstracts of Papers of the Meeting, Vol. III, p. 1529). In this paper, all the compounds except meso compounds are racemic. All the formulas depict only one enantiomer of the respective racemate.

2) a) T. Suami, S. Ogawa, K. Yabe, and M. Uchida, This Bulletin, **44**, 2804 (1971); b) L. Goodman, *Advan. Carbohyd. Chem.*, **22**, 109 (1968); c) J. G. Buchanan and H. Z. Sable, "Selective Organic Transformations," Vol. 2, ed. by B. S. Thyagarajan, Interscience Publishers, New York, N. Y. (1972), p. 11.

3) T. Suami, S. Ogawa, T. Tanaka, and T. Otake, This Bulletin, **44**, 835 (1971).

4) M. Nakajima, A. Hasegawa, and F. W. Lichtenthaler, *Ann. Chem.*, **669**, 75 (1963).

5) T. Suami, S. Ogawa, and M. Uchida, This Bulletin, **43**, 3577 (1970).

6) F. W. Lichtenthaler and P. Emig, *Carbohyd. Res.*, **7**, 121 (1968); F. W. Lichtenthaler, G. Bambach, and P. Emig, *Chem. Ber.*, **102**, 994 (1969).

7) T. Suami, S. Ogawa, S. Oki, and K. Ohashi, This Bulletin, **45**, 2597 (1972).

8) S. J. Angyal and R. M. Hoskinson, *J. Chem. Soc.*, **1963**, 2043.

9) S. Nishimura, This Bulletin, **32**, 61 (1959).

Inositol Derivatives. 8. Azidolysis of Tri- and Tetra-sulfonates of *myo*-Inositol[1]

Tetsuo SUAMI, Seiichiro OGAWA, Shuichi OKI, and Hideo KUNITOMO
Department of Applied Chemistry, Faculty of Engineering, Keio University, Hiyoshi, Yokohama 223
(Received November 30, 1973)

Reactions of the azide ion with four trisulfonates (1,4,5-, 1,4,6-, 1,5,6-, and 4,5,6-) and one tetrasulfonate (1,4,5,6-) of *myo*-inositol were studied. The structures of the new azido compounds were established by PMR spectroscopy and reaction sequences. The mechanism of neighboring-group participation reactions were discussed.

In continuation of the preceding work,[2] studies have been made on the azidolysis of four tritosylates (1,4,5,-1,4,6-, 1,5,6-, and 4,5,6-) of *myo*-inositol and some of their 2,3-*O*-cyclohexylidene derivatives, together with 1,4,5,6-tetra-*O*-tosyl-*myo*-inositol.

1,4,5-Tritosylate. Refluxing of 1,4,5-tri-*O*-tosyl-*myo*-inositol (**1**)[3] with sodium azide in 90% aqueous 2-methoxyethanol for 22 hr, followed by acetylation, exclusively gave crystalline triazidotrideoxyinositol triacetate (**2**) in 42% yield. Hydrogenation of **2** and subsequent acetylation gave the corresponding hexaacetyl inosatriamine (**3**) in 54% yield. Compound **2** was assigned to 1,3,5-triazido-1,3,5-trideoxy-*muco*-inositol triacetate on the basis of elemental analysis and IR and well-defined PMR spectra. In the PMR spectrum in deuteriochloroform ($CDCl_3$) (Table 1), the H-3 wide triplet (τ 5.80) shifted downfield remarkably as compared with two-proton double doublet (τ 6.02) due to two equivalent equatorial protons on C-1 and C-5, attributable to the deshielding effect of two *syn*-axial azido groups on C-1 and C-5.[4] The PMR spectrum of **3** in dimethylsulfoxide-d_6 (DMSO-d_6) also supported its *muco*-1,3,5 configuration. Thus, the acetyl methyl protons appearing as four singlets (2:1:1:2) at τ 8.18, 8.07, 8.04, and 7.87, could be ascribed to two equatorial and one axial acetamido, and one equatorial and two axial acetoxy groups, respectively.[5] The H-6 wide triplet (J=10 Hz) appeared in a lower field (τ 4.75) due to deshielding effect of two *syn*-axial acetoxy groups on C-2 and C-4.[4] It is interesting to note that, in the favored conformation of **2**, the two substituents located in *syn*-axial orientation appear to be not the acetoxy but the azido groups, in contrast with that of **3**, whose substituents on the same carbons were of *syn*-equatorial orientation.

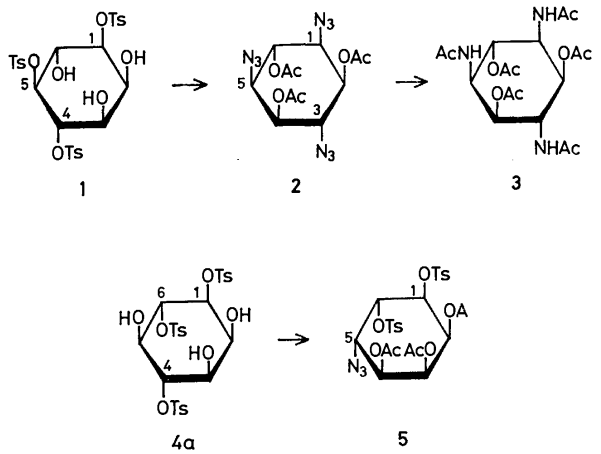

Scheme 1

It is reasonable to deduce that the azidolysis proceeds *via* neighboring-group participation reaction initiated by the intramolecular attack of the 3-hydroxyl group to C-4 leading to the intermediate 3,4-epoxide. From the structure of **2**, it is feasible that the intermediate epoxides formed successively are opened by azide ion in *trans*-diaxial manner.

1,4,6-Tritosylates. On treatment with sodium azide under similar conditions to those for **1**, 1,4,6-tri-*O*-tosyl-*myo*-inositol (**4a**)[3] yielded, after subsequent acetylation, the monoazido compound (**5**) as the sole crystalline product in 6% yield. The structure of **5** was deduced to be 5-azido-5-deoxy-1,6-di-*O*-tosyl-*allo*-inositol triacetate on the basis of its PMR spectrum, which exhibited the H-5 signal as a double doublet (J=3 and 10 Hz) at τ 5.86.[6] Mechanistically, the 5-hydroxyl group is likely to form the 4,5-epoxide which is opened diaxially by azide ion.

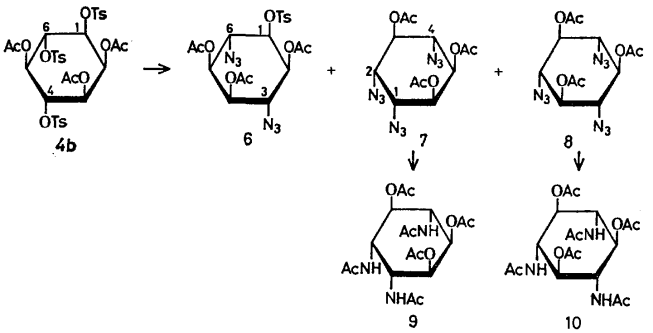

Scheme 2

On the other hand, when the triacetate (**4b**)[3] was treated with sodium azide under identical conditions, three azido compounds were formed, which were successively separated by fractional crystallization from ethanol and methanol to give one diazido compound (**6**) (34%), and two triazido compounds (**7** (9%) and **8** (2%)). Syrupy **8**, which was later obtained in a crystalline form, was further characterized by converting it into known hexaacetyl *scyllo*-inosatriamine-1,3,5 (**10**).[7] The structure of **8** was then established to be 1,3,5-triazido-1,3,5-trideoxy-*scyllo*-inositol triacetate.[8] From the data of analysis and IR and PMR spectra **6** and **7** were assigned to 3,6-diazido-3,6-dideoxy-1-*O*-tosyl-*muco*-inositol triacetate and 1,2,4-triazido-1,2,4-trideoxy-*chiro*-inositol triacetate,[9] respec-

TABLE 1. PMR SPECTRAL DATA IN $CDCl_3$ AT 60 MHz[a)]

Compound	H_1 ($J_{1,2}$)	H_2 ($J_{2,3}$)	H_3 ($J_{3,4}$)	H_4 ($J_{4,5}$)	H_5 ($J_{5,6}$)	H_6 ($J_{1,6}$)	OAc	Others
2	6.02 dd (4)	4.82 dd (8)	5.80 t (8)	4.82 dd (4)	6.02 dd (6)	4.60 t (6)	7.82 (9) [b)]	
6		(4.5)	5.88 t (4.5)		(9)	5.85 t (9)	8.08 (3) 7.92 (3) 7.89 (3)	7.50 (3) OTs
7	6.0 m (10)	6.0 m (10)	4.66 t (10)	6.20 t (10)	4.91 dd (3.5)	4.57 t (3.5)	7.93 (3) 7.82 (3) 7.73 (3)	
8	6.36 t (10)	4.92 t (10)	6.36 t (10)	4.92 t (10)	6.36 t (10)	4.92 t (10)	7.82 (9)	
21	5.08 dd (4)	(8)	5.78 t (8)		(6)	5.66 t (6)	7.86 (3) 7.84 (3) 7.80 (3)	6.87 (3) OMs
23a	4.78 t (3.5)	6.00 dd (8)	4.86 dd (10)	6.39 dd	6.0 m	6.0 m (3.5)	7.80 (3)	6.79 (3) OMs
27b	4.97 dd (3.5)	6.03 dd (11)	4.64 t (11)	6.05 t (11)	4.72 dd (3)	4.35 dd (4)	7.88 (3) 7.77 (3) 7.74 (3)	6.73 (3) OMs

a) Chemical shifts are given in terms of τ-values. Values given for coupling constants (Hz) are of firts order. Abbreviations: s (singlet); d (doublet); t (triplet); dd (double doublet); m (complex multiplet). b) Values in parenthesis show number of protons.

tively. The PMR spectrum of **6** exhibited the H-3 signal as a narrow triplet and H-6 signal as a wide triplet at τ 5.88 and 5.85, respectively. The downfield shift of H-6 axial proton as compared with H-3 equatorial proton might be attributed to the deshielding effect of two *syn*-axial acetoxy groups on C-2 and C-4.[4)] The structure of **6** was finally confirmed by transforming it into known hexaacetyl *chiro*-inosadiamine-1,4 (**12**)[10)] in the following way. On reduction and

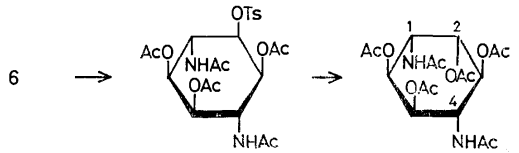

Scheme 3

subsequent acetylation, **6** gave 3,6-diacetamido-3,6-dideoxy-1-*O*-tosyl-*muco*-inositol triacetate (**11**). Without further purification, this was refluxed with sodium acetate in 90% aqueous 2-methoxyethanol followed by acetylation to afford **12** in 61% yield with an inversion of the configuration at C-1. The PMR spectral data of **7** established the axial orientation for H-3, H-4, and H-5, and the equatorial orientation for H-6. The PMR spectrum of hexaacetyl inosatriamine (**9**) derived from **7** showed the acetyl methyl protons as four singlet (2:1:2:1) at τ 8.21, 8.10, 8.06, and 7.85, which were assigned to two equatorial and one axial acetamido, and two equatorial and one axial acetoxy groups, respectively.[5)] These chemical shifts were found to be very similar to those of **12**. Consequently, the configuration of **7** was proved to be *chiro*-1,3,4. From these results, the azidolysis reactions of **4a** and **4b** should involve quite different mechanisms. In the case of **4b**, the initial formation of the intermediate 3,4- or/and 5,6-cyclic acetoxonium ion might be proposed.

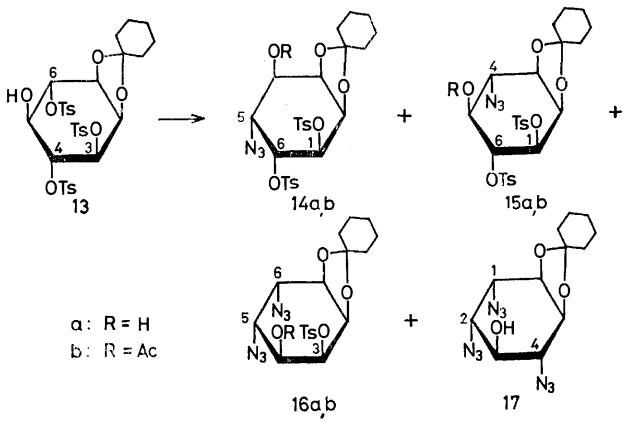

Scheme 4

1,2-*O*-Cyclohexylidene-3,4,6-tri-*O*-tosyl-*myo*-inositol (**13**)[3)] was subjected to a similar azidolysis. In compound **13**, the neighboring-group participation of the 3-hydroxyl group to C-4 as would be expected in the azidolysis of **5** was not possible, since the two hydroxyl groups at C-2 and C-3 were blocked by *O*-cyclohexylidene group. The reaction was monitored by tlc. After 3 hr, **13** disappeared completely and the formation of two major components (**14a** and **15a**) was detected. **15a**, a slightly faster-moving component, was then disappeared slowly and the third component **16a** was formed. By a prolonged treatment, **16a** was converted almost completely into the more faster-moving component (**17**), while **14a** remained unchanged during the course of the reaction. Thus, when **13** was allowed to react with sodium azide on being refluxed in 90% aqueous 2-methoxyethanol for 3 hr, monoazido compounds (**14a** and **15a**) and a diazido compound (**16a**) were obtained in 26, 28, and 7% yields, respectively, after separation by fractional crystallization from ethanol or ethyl acetate. When the reaction time

was extended to 22 hr, compound **14a**, **16a**, and a triazido compound (**17**) were isolated in 26, 1.4, and 13% yields, respectively, after fractionation by a silica gel chromatography. Since **13** yielded the 4,5-epoxide selectively on treatment with sodium methoxide,[11] the intermediary-formation of the same epoxide might be postulated as in the azidolysis of **13**. The monoazido compounds are therefore formed through nucleophilic cleavage of the 4,5-epoxide by azide ion. The 5-azido compound seems to be less reactive for further substitution as compared with the 4-azido compound, because of lack of the participating group. Compounds **14a** and **15a** were thus reasonably assigned to 5-azido-2,3-*O*-cyclohexylidene-5-deoxy-1,6-di-*O*-tosyl-*allo*-inositol and 4-azido-2,3-*O*-cyclohexylidene-4-deoxy-1,6-di-*O*-tosyl-*myo*-inositol, respectively. Compound **15a** would readily undergo nucleophilic substitution *via* the intermediate 5,6-epoxide to give 5,6-diazido-1,2-*O*-cyclohexylidene-5,6-dideoxy-3-*O*-tosyl-*allo*-inositol (**16a**) as a predominant product, which was further transformed into a triazido compound (**17**), 1,2,4-triazido-5,6-*O*-cyclohexylidene-1,2,4-trideoxy-*chiro*-inositol. The structure of **17** was confirmed by its conversion into **7** by hydrolysis with 80% aqueous acetic acid followed by acetylation.

The tentatively assigned structures of **14a**, **15a**, and **16a** were supported by the PMR spectra of their corresponding acetyl derivatives (**14b**, **15b**, and **16b**). The PMR spectrum of **14b** showed a double doublet (J=3.5 and 9.5 Hz) at τ 5.78, which was ascribed to the proton attached to the carbon atom carrying the azido group. In the spectrum of **15b**, H-4 signal appeared as a multiplet, which was coupled with the adjacent signal due to H-3 proton. The PMR spectrum of **16b** exhibited three narrow multiplets at τ 6.00, 4.98, and 4.68 in the ratio 1 : 1 : 1, ascribable to three pairs of protons being vicinally located: H-5 and H-6, H-1 and H-2, and H-3 and H-4, respectively.

Hydrolysis of **14a** followed by acetylation gave **5** in 55% yield, supporting the proposed structure of **5**.

1,5,6-Tritosylate. Treatment of 1,5,6-tri-*O*-tosyl-*myo*-inositol triacetate (**18**)[3] with sodium azide under the usual conditions, followed by acetylation, gave predominantly the monoazido compound (**19**) in 26% yield. Tlc showed the formation of a trace of the more faster-moving component, probably the diazido compound, in addition to **19**. The structure of **19** was assigned to 1-azido-1-deoxy-4,5-di-*O*-tosyl-*allo*-inositol triacetate on the basis of its PMR spectrum. The two double doublets (τ 5.90 and 4.34) showed splittings of 3.5 and 10.5 Hz, coupled with each other. Thus they were ascribed to H-1 and H-6 protons, respectively. Compound **19** should be formed by diaxial scission of the intermediate 4,5-epoxide with azide ion.

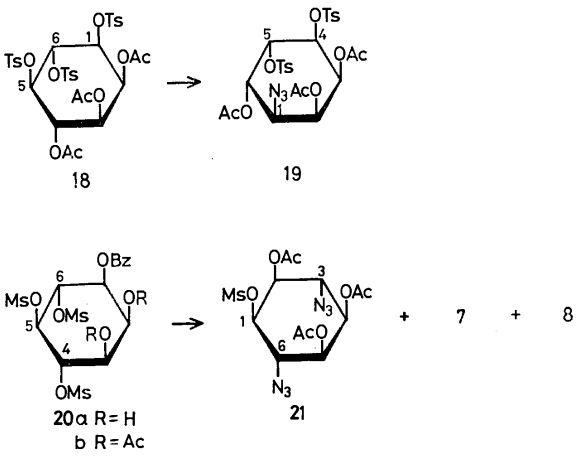

Scheme 5

4,5,6-Trisulfonates. 1-*O*-Benzoyl-4,5,6-tri-*O*-mesyl-*myo*-inositol (**20**)[12] was subjected to azidation. The products were fractionated by silica gel column chromatography to afford the monoazido compound (**21**), **7** and **8** in 31, 14, and 9.5% yields, respectively. The PMR spectrum of **21** (Table 1) was very close to that of **6**. Thus its structure was assigned to the corresponding 3,6-diazido-3,6-dideoxy-1-*O*-mesyl-*muco*-inositol. If the reaction is initiated by the participation of 1-benzoyloxy or 3-hydroxyl group to C-6 or C-4, the diaxial opening of the cyclic intermediates with azide ion should proceed preferentially to yield **21** as the predominant product along with the minor **8**. Compound **7** should have arisen from **21** by further direct S_N2 substitution of 1-mesyloxy group with azide ion. For the sake of confirmation, **21** was treated with sodium azide under the same conditions, but **7** was found to be only slightly formed by tlc. It was thus necessary to deduce an alternative reaction mechanism. We reported that the direct S_N2 displacement reaction of 5-tosyloxy function with chloride ion occurred readily in the tosylation of 1,2-*O*-cyclohexylidene-*myo*-inositol and its related compound.[12] By analogy with this, the initial substitution of the 5-mesyloxy group might be also feasible, and would account for the formation of **7** as well as **8** in relatively good yields.

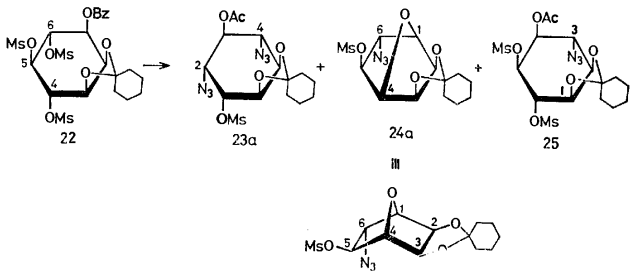

Scheme 6

The azidolysis of the 2,3-*O*-cyclohexylidene derivative (**22**)[12] was carried out. Following the reaction by tlc, the formation of two major components was shown, together with two minor components which gradually disappeared with prolonged treatment. After 45 hr, the products were fractionated with a silica gel column to afford the diazido compound (**23a**) (8%), and monoazido compounds (**24a** (9%) and **25** (1.5%)). Since the reaction might proceed *via* the cyclic intermediate, 1,6-benzoxonium ion, azidolysis of an epoxide with a similar configuration was studied. Epoxides, 2,3-anhydro-4,5-*O*-cyclohexylidene-1,6-di-*O*-mesyl-*epi*-inositol (**26a**)[12] and -1,6-di-*O*-tosyl-*epi*-inositol (**26b**)[11] were subjected to azidolysis. Compounds **23a**,**b** and **24a**,**b** were obtained as expected from **26a**,**b** in comparatively good yields.

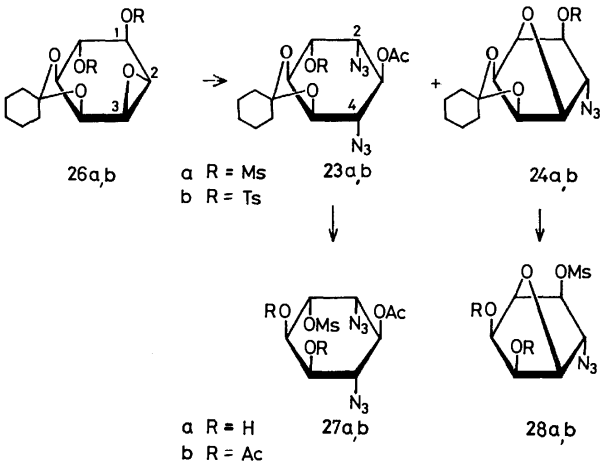

Scheme 7

Removal of the cyclohexylidene group of **23a** led to dihydroxyl compound (**27a**) which gave triacetate (**27b**). Similarly, **24a** was converted into dihydroxyl compound (**28a**) and diacetate (**28b**). On the basis of elemental analysis and IR and PMR spectra, **23a** and **24a** were assigned to 3-*O*-acetyl-2,4-diazido-5,6-*O*-cyclohexylidene-2,4-dideoxy-1-*O*-mesyl-*chiro*-inositol and 1,4-anhydro-6-azido-2,3-*O*-cyclohexylidene-6-deoxy-5-*O*-mesyl-*epi*-inositol, respectively. In the PMR spectrum of **27b**, a pattern of the signals due to the ring protons was shown to be essentially similar to that of 2,4-diazido-2,4-dideoxy-*chiro*-inositol tetraacetate,[2] supporting the proposed structure.

In the first step of the azidolysis, it is mechanistically reasonable to conclude that the 2,3-epoxide ring is opened by azide ion to give rise to 2- and 3-azido compounds, both of which are lacking in the participating groups for nucleophilic substitution of the sulfonyloxy group in a vicinal position. Thus in the case of the latter, substitution of the sulfonyloxy group at C-1 would proceed in direct S_N2 fashion to give **23a**. In the case of the former, a direct S_N2 attack on C-1 is considerably interrupted by steric and electronic effects due to the adjacent azido group, but the hydroxyl group at C-3 can attack the rear-side of C-6 intramolecularly in a boat-like conformation, resulting in the transannular epoxide (**24a**).[2,13]

The PMR spectral data of **24a** and its derivatives (Table 2) were consistent with the assigned structures. The C-2 and C-3 protons appeared at τ 5.31 and 5.67, respectively, as the AB quartet. The downfield shift of the former might be accounted for by assuming the proximity effect[14] and/or a strong magnetic field, excerted by the 6-*endo* azido group. No detectable coupling could be observed between the bridge head proton H-1 or H-4 and H-2 *endo* or H-3 *endo* protons, supporting the bicyclic structure. The coupling constants measured from **24a**, **24b**, and **28** were in good accord with those of bicyclo[2.2.1]heptane system.[15]

Table 2. PMR data of derivatives of 1,4-anhydro-*epi*-inositol in $CDCl_3$ at 60 MHz[a]

	24a	**24b**	**28b**
H_1	5.55 d	5.72 d	5.17 d
H_2	5.31 d	5.31 d	4.62 d
H_3	5.67 d	5.74 d	4.87 d
H_4	5.45—5.55 m	5.53 s	5.38 s
H_5	5.45—5.55 m	5.47 dd	5.60—5.80 m
H_6	5.88 dd	5.94 dd	5.25 m
OAc			7.87[b]
OMs	6.86		6.78
OTs		7.50	
$J_{1,2}$	0	0	0
$J_{2,4}$	5.5	6.0	6.7
$J_{3,4}$	0	0	0
$J_{4,5}$	—	1.0	—
$J_{5,6}$	6.0	5.5	—
$J_{1,6}$	2.0	2.3	—

a) see Table 1. b) Singlet due to two acetoxy groups.

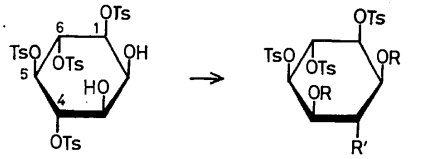

Scheme 8

1,4,5,6-Tetratosylate. Reaction of 1,4,5,6-tetra-*O*-tosyl-*myo*-inositol (**29**)[3] with sodium azide in the usual way gave the monoazido compound (**30a**) selectively in 62% yield, which was converted into the diacetate (**30b**). By a similar reaction with sodium acetate followed by acetylation, **29** yielded the triacetyl compound (**30c**) in 63% yield. The reactions seem to proceed *via* the intermediate 3,4-epoxide, followed by nucleophilic attack in diaxial manner. Exclusive products would possess *muco*-configuration. The PMR spectra of **30b** and **30c** supported the assigned structures. In **30b**, the acetyl methyl protons appeared as a single peak at τ 8.09, indicating a symmetrical structure. In **30c**, three acetoxy groups occurred as two singlets (2: 1) at τ 8.18 and 8.02, satisfying *muco*-configuration. The structures of **30a** and **30c** could thus be established as 3-azido-3-deoxy-1,5,6-tri-*O*-tosyl-*muco*-inositol and 2,3,4-tri-*O*-tosyl-*muco*-inositol triacetate, respectively.

Experimental

Unless otherwise noted, melting points were determined on a Mitamura Riken micro hot stage and are uncorrected. IR spectra were measured on a JASCO IR-E spectrophotometer in KBr disks. PMR spectra were obtained on a Varian Associates A-60D (60 MHz) spectrometer at a concentration of approximately 10% $CDCl_3$ or DMSO-d_6, with tetramethylsilane as an internal standard. Chemical shifts are given in terms of τ-values, signals being denoted by s (singlet), d (doublet), dd (double doublet), t (triplet), or m (complex multiplet). Values given for coupling constants are of first-order. All the solutions were concentrated with a rotary evaporator at 40—50 °C under reduced pressure, a trace of residual pyridine being removed by coevaporation with toluene. Catalytic hydrogenations were carried out with a Parr shaker apparatus in the presence of Raney nickel T-4[16] catalyst in the initial hydrogen pressure of 3.5 kg/cm^2 at room temperature. Tlc was performed on silica gel

(Wakogel B-10, Wako Pure Chemica lIndustries, Ltd.) using a mixture of 2-butanone and toluene. The spots were indicated by heating above 150 °C after spraying with 30% sufuric acid.

1,3,5-Triazido-1,3,5-trideoxy-muco-*inositol Triacetate (2).* A mixture of 1,4,5-tri-*O*-tosyl-*myo*-inositol (**1**)[3] (1.50 g), sodium azide (1.50 g), and 90% aqueous 2-methoxyethanol (75 ml) was refluxed for 22 hr. The reaction mixture was then evaporated to dryness and the residue was treated with acetic anhydride (10 ml) and pyridine (10 ml) overnight at room temperature. An insoluble material was removed by filtration and the filtrate was evaporated to yield an oil which was purified by passing through a short alumina column with chloroform as an eluent. The solution was concentrated and the product was crystallized from ether to afford crystals (0.37 g, 42%) of **2**. Recrystallization from ethanol–ether afforded an analytical sample (0.33 g, 37%), mp 92—93 °C.

Found: C, 37.81; H, 3.95; N, 33.19%. Calcd for $C_{12}H_{15}N_9O_6$: C, 37.79; H, 3.97; N, 33.07%.

Hexaacetyl muco-*Inosatriamine-1,3,5 (3).* A solution of **2** (100 mg) in ethanol (10 ml) was hydrogenated for 6 hr. The catalyst was filtered off and the filtrate was evaporated to dryness. The residue was treated with acetic anhydride (1.5 ml) and pyridine (2 ml) overnight at room temperature. The reaction mixture was evaporated to give a crystalline residue which was recrystallized from ethanol–ether to give tiny needles (60 mg, 54%) of **3**, mp 259—260 °C (decomp.).

Found: C, 50.49; H, 6.42; N, 9.99%. Calcd for $C_{18}H_{27}N_3O_9$: C, 50.34; H, 6.34; N, 9.79%.

*5-Azido-5-deoxy-1,6-di-*O*-tosyl*-allo-*inositol Triacetate (5).* A mixture of 1,4,6-tri-*O*-tosyl-*myo*-inositol (**4a**)[3] (2.0 g), sodium azide (2.0 g), and 90% aqueous 2-methoxyethanol (50 ml) was refluxed for 22 hr. The mixture was evaporated to dryness and the residue was acetylated in the usual manner. Tlc showed the formation of one major component and two minor components. The products were extracted with chloroform and the extracts were evaporated to give an oil which was crystallized from ethanol to give needles (0.14 g, 6.3%) of **5**, mp 157—158 °C. Recrystallization from ethanol afforded a pure sample, mp 158—160 °C. PMR ($CDCl_3$): τ 8.13, 7.92, 7.90 (3-proton s, OAc), 7.50 (3-proton s, $OSO_2C_6H_4C\underline{H}_3$).

Found: C, 48.97; H, 4.70; N, 6.31; S, 9.98%. Calcd for $C_{26}H_{29}N_3O_{12}S_2$: C, 48.82; H, 4.57; N, 6.57; S, 10.02%.

*Azidolysis of 1,4,6-tri-*O*-tosyl*-myo-*inositol Triacetate (4b).*[3] A mixture of **4b** (3.25 g), sodium azide (3.85 g), and 90% aqueous 2-methoxyethanol (100 ml) was refluxed for 16 hr. The reaction mixture was then treated in a similar way to that for **1** to give a crystalline mixture (1.04 g), mp 121—134 °C. Tlc (1: 4 2-butanone–toluene) indicated the formation of two major components. Fractional crystallization from ethanol gave two crystals: 3,6-diazido-3,6-dideoxy-1-*O*-tosyl-*muco*-inositol triacetate (**6**), yield 0.73 g (33.8%), mp 134—135 °C, and 1,2,4-triazido-1,2,4-trideoxy-*chiro*-inositol triacetate (**7**), yield 0.122 g (8.7%), mp 112—113 °C. Analytical samples of **6** and **7** were obtained by recrystallization from ethanol and dried *in vacuo* over phosphorus pentoxide overnight at room temperature.

6: Found: C, 45.09; H, 4.51; N, 16.35; S, 6.00%. Calcd for $C_{19}H_{22}N_6O_9S$: C, 44.70; H, 4.34; N, 16.46; S, 6.28%.

7: Found: C, 38.05; H, 3.96; N, 33.30%. Calcd for $C_{12}H_{15}N_9O_6$: C, 37.80; H, 3.97; N, 33.06%.

Evaporation of the mother liquor gave a syrup which was shown by tlc to consist of a faster-moving major component together with traces of **6** and **7**. The syrupy crude 1,3,5-triazido-1,3,5-trideoxy-*scyllo*-inositol triacetate (**8**) was, without further purification, hydrogenated in an ethanol solution (10 ml) for 5.5 hr. The product was treated with acetic anhydride (5 ml) and pyridine (5 ml) overnight at room temperature, and the mixture was then evaporated to give an oil, which crystallized upon addition of methanol to give plates (40 mg, 2.2%) of hexaacetyl *scyllo*-inosatriamine-1,3,5 (**10**), which did not melt below 330 °C, but sublimed at 305 °C turning brown at 310 °C (lit,[7] mp 310—315 °C). The compound was identified with an authentic sample[7] by comparison of IR spectra.

Hexaacetyl chiro-*Inosatriamine-1,2,4 (9).* A solution of **7** (0.20 g) in ethanol (30 ml) was hydrogenated for 20 hr. After the catalys had been removed by filtration, the solution was evaporated and the residue was acetylated in the usual way to give crystalline product. Recrystallization from ethanol afforded crystals (136 mg, 60.4%) of **9**, mp 167—168 °C. Recrystallization from ethanol gave an analytical sample as needles, mp 166—169 °C.

Found: C, 48.51; H, 6.25; N, 9.33%. Calcd for $C_{18}H_{27}N_3O_9\cdot H_2O$: C, 48.31; H, 6.51; N, 9.39%.

Preparation of Hexaacetyl chiro-*Inosadiamine-1,4 (12) from 6.* Compound **6** (0.91 g) was hydrogenated in an ethanol solution (150 ml) for 16 hr. The product was acetylated in the usual manner to give syrupy 1-*O*-tosyl-*muco*-inosadiamine-3,6 triacetate (**11**). Without further purification, **11** was treated with anhydrous sodium acetate (0.80 g) in refluxing 90% aqueous 2-methoxyethanol (45 ml) for 45 hr, and the reaction mixture was then evaporated to dryness and subsequently acetylated to give a crystalline compound, which was crystallized from chloroform to afford crystals (0.47 g, 61%) of **12**, mp 126—131 °C (lit,[10] 127—129 °C). This compound was identified with an authentic sample by comparison of their IR and PMR (DMSO-d_6) spectra.

*Azidolysis of 1,2-*O*-Cyclohexylidene-3,4,6-tri-*O*-tosyl*-myo-*inositol (13).*[3] *a)*: A mixture of **13** (6.0 g), sodium azide (6.0 g), and 90% aqueous 2-methoxyethanol (90 ml) was refluxed, and the progress of the reaction was followed by tlc (1: 4 2-butanone–toluene). After 3 hr, **13** disappeared completely in the reaction mixture. It was then evaporated to dryness and the residue was extracted with hot ethyl acetate (3×50 ml). The extract was concentrated to give a crystalline mixture, whose tlc showed the formation of major three components along with a trace of a faster-moving component. Crystallization from ethyl acetate gave crystals (1.29 g, 26%) of 5-azido-5-deoxy-2,3-*O*-cyclohexylidene-1,6-di-*O*-tosyl-*allo*-inositol (**14a**), mp 165—169 °C. The crystals were shown by IR spectrum to contain ethyl acetate. Recrystallization twice from ethanol gave an analytical sample, mp 163.5—164 °C.

Found: C, 52.77; H, 5.52; N, 7.08; S, 10.37%. Calcd for $C_{26}H_{31}N_3O_9S_2$: C, 52.60; H, 5.26; N, 7.08; S, 10.80%.

Compound **14a** (0.33 g) was treated with acetic anhydride (2 ml) and pyridine (3 ml) overnight at room temperature. The reaction mixture was evaporated with toluene to give a syrup which was crystallized from ethanol–ether to afford crystals (0.33 g, 94%) of the acetate (**14b**), mp 163.5—165.5 °C. Recrystallization from ethanol–chloroform gave an analytical sample, mp 150—151 °C. PMR ($CDCl_3$): τ 7.86 (3-proton s, OAc), 7.52 (6-proton s, $OSO_2C_6H_4C\underline{H}_3$).

Found: C, 52.70; H, 5.22; N, 6.47; S, 10.08%. Calcd for $C_{28}H_{33}N_3O_{10}S_2$: C, 52.90; H, 5.23; N, 6.61; S, 10.09%.

The mother liquor of **14a** was concentrated to a small volume and allowed to stand at room temperature yielding thin needles, which were recrystallized from ethanol to afford tiny needles (1.37 g, 27.8%) of 4-azido-4-deoxy-2,3-*O*-cyclohexylidene-1,6-di-*O*-tosyl-*myo*-inositol (**15a**), mp 173—175 °C, after melting and resolidifying at 165—167 °C.

Found: C, 52.90; H, 5.17; N, 7.05; S, 11.10%. Calcd

for $C_{26}H_{31}N_3O_9S_2$: C, 52.60; H, 5.26; N, 7.08; S, 10.80%.

Compound **15a** (0.36 g) was acetylated as described above to give crystals, which were recrystallized from chloroform–ethanol to afford crystals (0.37 g, 95%) of the acetate (**15b**), mp 156.5—158.5 °C. PMR ($CDCl_3$): τ 7.94 (3-proton s, OAc), 7.55 (6-proton s, $OSO_2C_6H_4C\underline{H}_3$), 5.71 (dd, $J_{1,2}$= 3.5 Hz, $J_{2,3}$=5 Hz, H-2).

Found: C, 53.14; H, 5.44; N, 6.43; S, 10.14%. Calcd for $C_{2,}H_{33}N_3O_{10}S_2$: C, 52.90; H, 5.23; N, 6.61; S, 10.09%.

The mother liquor of **15a**, kept at room temperature for a long time, yielded crystals which were recrystallized from ethanol to afford pure crystals (0.26 g, 6.9%) of 5,6-diazido-1,2-*O*-cyclohexylidene-5,6-dideoxy-3-*O*-tosyl-*allo*-inositol(**16a**), mp 142—143.5 °C.

Found: C, 49.18; H, 5.20; N, 17.97; S, 7.15%. Calcd for $C_{19}H_{24}N_6O_6S$: C, 49.12; H, 5.21; N, 18.10; S, 6.90%.

Acetylation of **16a** gave a homogeneous syrupy acetate (**16b**), which did not crystallize in spite of several attempts.

b): A mixture of **13** (10.0 g), sodium azide (10.0 g), and 90% aqueous 2-methoxyethanol (200 ml) was refluxed for 22 hr, when, tlc showed the formation of a faster-moving component, together with **14a** and **16a**. The reaction mixture was evaporated to dryness and the residue was extracted with ethyl acetate (3×100 ml). The extracts were purified by passing through a short alumina column and then concentrated to a syrup, which was crystallized from ethyl acetate to give crystals (1.76 g, 21.4%) of **14a**, mp 145—148 °C. The mother liquor was evaporated to give a syrup which was chromatographed on a silica gel column (90 g) with 1:6 2-butanone–toluene as an eluent. The three fractions were separated in accord with the results of tlc.

Fraction 1 gave a syrup which slowly crystallized upon trituration with ligroin, affording needles (0.61 g, 13.2%) of 1,2,4-triazido-5,6-*O*-cyclohexylidene-1,2,4-trideoxy-*chiro*-inositol (**17a**), mp 95—97 °C.

Found: C, 42.55; H, 5.01; N, 37.53%. Calcd for $C_{12}H_{17}N_9O_3$: C, 42.98; H, 5.11; N, 37.60%.

Fraction 2 gave crystals (0.089 g, 1.4%) of **16a**, mp 140—142 °C, after crystallization from ethanol.

Fraction 3 gave crystals (0.372 g) of **14a**, mp 142—145 °C, after crystallization from ethanol. The total yield of **14a** was then 26%.

Acetylation of **17a** gave a homogeneous syrupy acetate (**17b**) which did not crystallize in spite of several attempts.

Treatment of **17a** (0.30 g) with refluxing 80% aqueous acetic acid (10 ml) for 1.5 hr, followed by acetylation, gave crystals (0.26 g, 65%) of **7**, mp 111.5—112.5 °C. The compound was identified with a sample obtained from **4b**.

Compound **14a** (0.28 g) was successively hydrolyzed and acetylated as described above to give crystals (0.17 g, 55%) of **5**, mp 157—159 °C, after recrystallization from chloroform–ethanol. The compound was identified with a sample obtained from **4a**.

*1-Azido-1-deoxy-4,5-di-*O*-tosyl-*allo*-inositol Triacetate (19).* A mixture of 1,5,6-tri-*O*-tosyl-*myo*-inositol triacetate (**18**)[3] (0.50 g), sodium azide (0.50 g), and 90% aqueous 2-methoxyethanol (15 ml) was refluxed for 6 hr. The reaction mixture was then treated in a similar way to that for **4b** to give crystals (0.11 g, 26.4%) of **19**, mp 179.5—180.5 °C. Recrystallization from chloroform–ethanol, mp 182—183 °C.

Found: C, 49.22; H, 4.76; N, 6.34; S, 10.11%. Calcd for $C_{26}H_{29}N_3O_{12}S_2$: C, 48.82; H, 4.57; N, 6.57; S, 10.03%.

*1-*O*-Benzoyl-4,5,6-tri-*O*-mesyl-*myo*-inositol (20a).* 1-*O*-Benzoyl-2,3-*O*-cyclohexylidene-4,5,6-tri-*O*-mesyl-*myo*-inositol (**22**)[12] (3.0 g) was treated with refluxing 80% aqueous acetic acid (60 ml) for 3 hr. On being cooled to room temperature, the resulting crystals were collected by filtration: yield 1.98 g (77%), mp 215—221 °C. An additional crop (0.31 g, total yield 89%) was obtained by evaporation of the water layer. An analytical sample melted at 228—230 °C.

Found: C, 36.99; H, 4.46; S, 18.51%. Calcd for $C_{16}H_{23}O_{13}S_3$: C, 37.10; H, 4.27; S, 18.21%.

Acetylation of **20a** (1.5 g) in the usual manner gave the diacetate (**20b**): yield 1.74 g (99%), mp 209—212 °C. Recrystallization from chloroform–ethanol afforded an analytical sample, mp 214—216 °C.

Found: C, 39.80; H, 4.51; S, 15.94%. Calcd for $C_{20}H_{27}O_{15}S_3$: C, 39.74; H, 4.31; S, 16.21%.

Azidolysis of 20a. A mixture of **20a** (2.0 g), sodium azide (1.25 g), and 90% aqueous 2-methoxyethanol (75 ml) was refluxed for 28 hr. The reaction mixture was then treated in a similar way to that for **4b** to give a syrupy mixture of azido acetates. Tlc showed the formation of three major components. The mixture was chromatographed on a silica gel column (80 g) with 1:6 2-butanone–toluene as an eluent. The three fractions were separated in accord with the results of tlc.

Fraction 1 gave needles (0.14 g, 9.5%) of **8**, mp 127—132 °C, after crystallization from methanol.

Found: C, 37.80; H, 3.97; N, 33.06%. Calcd for $C_{12}H_{15}N_9O_6$: C, 37.69; H, 3.93; N, 32.85%.

Fraction 2 gave needles (0.20 g, 13.6%) of **7**, mp 109—111 °C, after crystallization from ethanol.

Fraction 3 gave crystals (0.51 g, 30.5%) of 3,6-diazido-3,6-dideoxy-1-*O*-mesyl-*muco*-inositol triacetate (**21**), mp 111—113 °C, after crystallization from chloroform–methanol.

Found: C, 35.95; H, 4.18; N, 19.35; S, 7.38%. Calcd for $C_{13}H_{18}N_6O_9S$: C, 36.14; H, 4.15; N, 19.32; S, 7.11%.

*Azidolysis of 1-*O*-Benzoyl-2,3-*O*-cyclohexylidene-4,5,6-tri-*O*-mesyl-*myo*-inositol (22).* A mixture of **22** (2.0 g), sodium azide (0.90 g), and 90% aqueous 2-methoxyethanol (70 ml) was refluxed for 45 hr. The reaction mixture was then treated in a similar way to that for **13**, and the resulting product was acetylated in the usual way to give a syrup which was purified by being passed through a short alumina column with chloroform. The solution was concentrated to afford a small amount of crystals (92 mg) of 3-*O*-acetyl-2,4-diazido-5,6-*O*-cyclohexylidene-2,4-dideoxy-1-*O*-mesyl-*chiro*-inositol (**23a**), mp 127—129 °C. The mother liquor was evaporated to give a syrup which was chromatographed on a silica gel column (100 g) with 1:9 2-butanone–toluene as an eluent. The three fractions were separated in accord with the results of tlc.

Fraction 1 gave crystals (35 mg, total yield 7.7%) of **23a**, mp 128—129 °C, after crystallization from ethanol–ether.

Found: C, 42.00; H, 5.18; N, 19.72; S, 7.36%. Calcd for $C_{15}H_{22}N_6O_7S$: C, 41.86; H, 5.15; N, 19.52; S, 7.45%.

Fraction 2 gave crystals (116 mg, 8.7%) of 1,4-anhydro-6-azido-2,3-*O*-cyclohexylidene-6-deoxy-5-*O*-mesyl-*epi*-inositol (**24a**), mp 127—128.5 °C, after crystallization from ethanol–ether. An analytical sample melted at 130—132 °C.

Found: C, 45.56; H, 5.50; N, 12.24; S, 9.06%. Calcd for $C_{13}H_{19}N_3O_6S$: C, 45.21; H, 5.55; N, 12.17; S, 9.28%.

Fraction 3 gave crystals (27 mg, 1.5%), mp 190—191 °C. The structure was deduced to be 2-*O*-acetyl-3-azido-4,5-*O*-cyclohexylidene-3-deoxy-1,6-di-*O*-mesyl-*muco*-inositol (**25**). PMR (DMSO-d_6): τ 7.80 (3-proton s, OAc), 6.83, 6.74 (3-proton s, OMs).

Found: C, 39.92; H, 5.01; N, 8.40; S, 13.13%. Calcd or $C_{12}H_{25}N_3O_{10}S_2$: C, 39.75; H, 5.21; N, 8.69; S, 13.26%.

*Azidolysis of 2,3-Anhydro-4,5-*O*-cyclohexylidene-1,6-di-*O*-mesyl-epi-inositol (26a).*[12] *a)*: A mixture of **26a** (1.0 g), sodium azide (0.66 g), ammonium chloride (0.27 g), and 90% aqueous 2-methoxyethanol (50 ml) was refluxed for

24 hr. The reaction mixture was then treated in a similar way to that for **13**. The syrupy azido compounds thus obtained were crystallized from ethanol–ether to give crystals (246 mg, 28.3%) of **24a**, mp 127—128.5 °C. The mother liquor was evaporated to dryness and the residue was acetylated in the usual way to give a syrup which was crystallized from ethanol–ether to afford crystals (360 mg, 33.3%) of **23a**, mp 128—129 °C.

b): Under the same conditions except for the absence of ammonium chloride, **26a** (1.0 g) afforded **23a** (230 mg, 21.3%), mp 128—129 °C, and **24a** (303 mg, 34.9%), mp 127—128.5 °C.

Azidolysis of 2,3-Anhydro-4,5-O-cyclohexylidenle-1,6-di-O-tosyl-epi-inositol (26b).[11] Compound **26b** (1.0 g) was refluxed with sodium azide (0.59 g) and ammonium chloride (0.24 g) in 2-methoxyethanol (30 ml) for 22 hr. The reaction mixture was treated in a similar way to that for **13** to give crystals (373 mg, 39.7%) of 1,4-anhydro-6-azido-2,3-*O*-cyclohexylidene-6-deoxy-5-*O*-tosyl-*epi*-inositol (**24b**), mp 115—123 °C. Recrystallization from ethanol gave an analytical sample, mp 126—127 °C.

Found: C, 54.24; H, 5.44; N, 9.62; S, 7.87%. Calcd for $C_{19}H_{23}N_3O_6S$: C, 54.15; H, 5.50; N, 9.97; S, 7.61%.

The mother liquor was concentrated and acetylated in the usual way to give a syrup. Tlc indicated the formation of one major component in addition to **24b**, which was probably diazido compound (**23b**) corresponding to **23a**. The syrup did not crystallize.

*3-O-Acetyl-2,4-diazido-2,4-dideoxy-1-O-mesyl-*chiro*-inositol (27a).* Compound **23a** (854 mg) was treated with refluxing 80% aqueous acetic acid (20 ml) for 1.5 hr, and then the reaction mixture was evaporated to dryness. The residual syrup crystallized spontaneously to give crystals (538 mg, 77.4%) of **27a**, mp 101—104 °C. Recrystallization from ethanol gave an analytical sample, mp 102—104 °C.

Found: C, 31.10; H, 4.12; N, 24.01; S, 8.86%. Calcd for $C_9H_{14}N_6O_7S$: C, 30.86; H, 4.03; N, 23.99; S, 9.15%.

Compound **27a** (100 mg) was acetylated in the usual way to give crystals (92 mg, 74%) of 2,4-diazido-2,4-dideoxy-1-*O*-mesyl-*chiro*-inositol triacetate (**27b**), mp 114—116 °C. Recrystallization from chloroform–ethanol gave an analytical sample, mp 115.5—117 °C.

Found: C, 35.90; H, 4.17; N, 19.48; S, 7.27%. Calcd for $C_{13}H_{18}N_6O_9S$: C, 35.95; H, 4.18; N, 19.35; S, 7.38%.

*1,4-Anhydro-6-azido-6-deoxy-5-O-mesyl-*epi*-inositol (28a).* Compound **24a** (0.50 g) was refluxed with 80% aqueous acetic acid (15 ml) for 1.5 hr. After cooling, the resulting crystals were collected by filtration: yield 162 mg (42%), mp 177.5—178 °C. Another crop of crystals was obtained by evaporation of the filtrate: yield 103 mg. The total yield of **28a** was 69%. An analytical sample was obtained by recrystallization from ethanol, mp 177—178 °C.

Found: C, 31.71; H, 4.13; N, 15.92; S, 12.11%. Calcd for $C_7H_{11}N_3O_6S$: C, 31.70; H, 4.18; N, 15.84; S, 12.09%.

Compound **28a** (67 mg) was acetylated in the usual way to give crystals (83 mg, 95%) of the diacetate (**28b**), mp 141—142 °C, after crystallization from ethanol. An analytical sample was obtained by recrystallization from chloroform–ethanol, mp 158.5—159 °C.

Found: C, 37.67; H, 4.27; N, 12.02; S, 8.93%. Calcd for $C_{11}H_{15}N_3O_8S$: C, 37.82; H, 4.33; N, 12.03; S, 9.18%.

*3-Azido-3-deoxy-1,5,6-tri-O-tosyl-*muco*-inositol (30a).* A mixture of 1,4,5,6-tetra-*O*-tosyl-*myo*-inositol (**29**)[3] (2.0 g), sodium azide (2.0 g), and 90% aqueous 2-methoxyethanol (50 ml) was refluxed for 15 hr. The reaction mixture was evaporated and the residue was extracted with 2-butanone (2×20 ml). The extract was passed through an alumina column and then evaporated to give crystals (0.98 g, 62%) of **30a**, mp 162—163.5 °C. Recrystallization from ethanol afforded an analytical sample, mp 168.5—169.5 °C.

Found: C, 49.02; H, 4.61; N, 6.16; S, 14.50%. Calcd for $C_{27}H_{29}N_3O_{11}S_3$: C, 48.57; H, 4.38; N, 6.29; S, 14.41%.

Compound **30a** (0.33 g) was acetylated in the usual way to give crystals which were recrystallized from chloroform–ethanol to afford plates (0.32 g, 84%) of the diacetate (**30b**), mp 172.5—173 °C.

Found: C, 49.89; H, 4.67; N, 5.48; S, 12.50%. Calcd for $C_{31}H_{33}N_3O_{13}S_3$: C, 49.52; H, 4.42; N, 5.59; S, 12.80%.

*2,3,4-Tri-O-tosyl-*muco*-inositol Triacetate (30c).* A mixture of **29** (2.0 g), anhydrous sodium acetate (2.0 g), and 90% aqueous 2-methoxyethanol (50 ml) was refluxed for 19 hr. The reaction mixture was treated in a similar way to that for **4b**, and the product was crystallized from ethyl acetate–ether to give crystals (1.2 g, 63%) of **30c**, mp 162.5—163.5 °C.

Found: C, 51.81; H, 4.87; S, 12.29%. Calcd for $C_{33}H_{36}O_{15}S_3$: C, 51.55; H, 4.72; S, 12.51%.

The authors wish to thank Prof. Sumio Umezawa for his kind advice. They are grateful to Mr. Saburo Nakada for elementary analyses and to Mr. Takatoshi Tanaka for assistance in the preparative experiments. The work was carried out with financial support from the Ministry of Education.

References

1) Presented in part at the Annual Meeting of the Chemical Society of Japan, Tokyo, April 6, 1970 (Abstracts of Papers of the Meeting, Vol. III, p. 1903). In this paper, all the compounds except for meso compounds are racemic. All the formulas depict only one enantiomer of the respective racemate.

2) T. Suami, S. Ogawa, S. Oki, and H. Sato, This Bulletin, **47**, 1731 (1974).

3) T. Suami, S. Ogawa, T. Tanaka, and T. Otake, *ibid.*, **44**, 835 (1971).

4) N. S. Bhacca and D. H. Williams, "Applications of NMR Spectroscopy in Organic Chemistry," Holden-Day, Inc., San Francisco, Calif., (1964), p. 183.

5) F. W. Lichtenthaler and P. Emig, *Carbohyd. Res.*, **7**, 121 (1968); F. W. Lichtenthaler, G. Bambach, and P. Emig, *Chem. Ber.*, **102**, 994 (1969).

6) T. Suami, S. Ogawa, and M. Uchida, This Bulletin, **43**, 3577 (1970).

7) S. Ogawa, T. Abe, H. Sano, K. Kotera, and T. Suami, *ibid.*, **40**, 2405 (1967).

8) This compound had also been obtained in syrupy form,[7] and characterized by conversion into **10**.

9) R. Schwesenger and H. Prinzbach prepared 1,2,4-triazido-1,2,4-trideoxy-*chiro*-inositol as an intermediate compound for their synthesis of "*cis*-benzene-triimine." The data will appear in *Angew. Chem. (Nachr. Chem. Techn.*, **21**, 305 (1973)).

10) T. Suami, S. Ogawa, H. Uchino, and M. Uchida, This Bulletin, **46**, 3840 (1973).

11) T. Suami, S. Ogawa, S. Oki, and K. Ohashi, *ibid.*, **45**, 2597 (1972).

12) T. Suami, S. Ogawa, K. Ohashi, and S. Oki, *ibid.*, **45**, 3660 (1972).

13) S. J. Angyal and R. M. Hoskinson, *J. Chem. Soc.*, **1963**, 2043; J. S. Brimacombe, F. Hunedy, and A. K. Al-Radhi, *Carbohyd. Res.*, **11**, 331 (1969).

14) B. E. Smart, *J. Org. Chem.*, **38**, 2027, 2366 (1973).

15) L. M. Jackman and S. Sternhell, "Applications of Nuclear Magnetic Resonance Spectroscopy in Organic Chemistry," Pergamon Press, Oxford (1969), p. 228.

16) S. Nishimura, This Bulletin, **32**, 61 (1959).

Note added in proof: The data[9] appeared in *Angew. Chem.*, **85**, 1107 (1973).

Chemiluminescence of Succinylfluorescein and Related Compounds. I. Emitting Species Produced by the Reaction of Succinylfluorescein with Oxygen in Aprotic Solvents

Isao KAMIYA and Keizo AOKI

Department of General Education, Nagoya University, Chikusa-ku, Nagoya 464

(Received December 24, 1973)

In the course of our studies of the chemiluminescence of xanthene dyes, we found the violet chemiluminescence emission (CL-emission) resulting from the reaction of succinylfluorescein with oxygen in an aerated alkaline aqueous system of a high concentration of an aprotic solvent (DMSO or DMF), an especially intense emission occurring in aerated dry DMSO or DMF with *tert*-BuOK as base. The CL-emission comprised two emission components: an intense violet emission (a peak, at 410 nm) whose spectral distribution was similar to that of the fluorescence band which appeared during the course of the reaction, and a weak greenish-yellow emission similar to the fluorescence of the dye. By isolating and identifying the violet-fluorescent reaction product with an authentic sample, and by comparing the CL-emission with the fluorescence emission of the isolated product, it was concluded that the violet CL-emission may be attributed to the formation of an excited dianion of 3,6-dihydroxyxanthone. The reaction path leading to the dioxetane intermediate which will be produced by the elimination of a proton from the C atom at the β-position of the dye, followed by the oxygenation *via* the caged radical pair, was discussed as a likely mechanism for the formation of the excited dianion.

In the previous paper,[1] the blue spectral component of the chemiluminescence (with a peak at 480 nm) observed in the reaction of such an xanthene dye as eosin Y with hydrogen peroxide in an alkaline solution was found to correspond to the fluorescence emission (FL-emission) of a blue-fluorescent product isolated from the reaction mixture; we concluded that the blue-fluorescent species is the primary excited product in the chemiluminescent reaction. Further study by means of a kinetic analysis of the blue-fluorescent product provided additional support for that conclusion.[2] However, the quantity of the isolated product was too small for it to be weighed or identified, so a question as to the identification of the product remained unanswered.

From the findings that several xanthene dyes other than eosin Y, uranin, eosin R, erythrosin B, 2',7'-dichlorofluorescein, rhodamine B, and even rhodamine S, which is not phthalyl, exhibited a similar blue emission with a production of an analogous blue-fluorescent species, we presupposed that the excited product might be a xanthone compound since excited species generated in many chemiluminescent systems have been reported to be carbonyl compounds,[3] thus we expected that a similar blue emission would arise from the oxidation of succinylfluorescein (**1**).

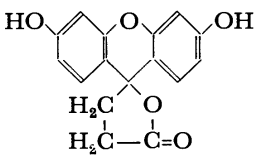

(**1**)

When succinylfluorescein was oxidized with hydrogen peroxide in an alkaline solution, however, a violet emission appeared with a peak at 410 nm in addition to a (weak) greenish-yellow emission. The violet emission was also found to appear from the oxidation of the dye with oxygen in an aerated alkaline aqueous system of a high concentration of such aprotic solvents as dimethylsulfoxide (DMSO) and *N'*,*N'*-dimethylformamide (DMF). Especially, an intense emission appeared in aerated dry DMSO (or DMF), with potassium *tert*-buthoxide (*tert*-BuOK) as the base. This paper will describe the chemiluminescent reaction of succinylfluorescein with oxygen in detail.

Experimental

Preparation of Succinylfluorescein (SF).[4] A 20 g portion of zinc chloride powder was added to a mixture of 11.01 g of resorcinol and 5.00 g of succinic anhydride, and then the mixture was heated to 180 °C for 4 hr. The reaction product was extracted with 4% hot hydrochloric acid, and the hot extract was filtered as quickly as possible. The product which precipitated on cooling was purified by repeated recrystallizations from 4% hydrochloric acid. Thin-layer chromatography showed only one spot, indicating the purity of the SF thus prepared.

Preparation of an Authentic Sample of 3,6-Dihydroxyxanthone.[5] After fluorescein had been chlorinated with phosphorous pentachloride, the produced fluorescein chloride was hydrolyzed by heating it in a concentrated aqueous sodium hydroxide solution to give 2,4,2',4'-tetrahydroxybenzophenone. With the dehydration of the benzophenone on heating, 3,6-dihydroxyxanthone was obtained. The purity of the prepared sample was confirmed by the thin-layer chromatographic method.

The Chemiluminescent Systems. Two systems were employed to investigate the chemiluminescence emission (CL-emission) of SF with oxygen.

DMSO (or DMF)–$NaOH_{aq}$ System: After 10—20 mg of the prepared SF had been dissolved in 10 ml of a mixture of DMSO (or DMF) and $NaOH_{aq}$, a portion of the reaction mixture (about 3 ml) was quickly transferred into a quartz cell ($10\times10\times45$ mm) which had been placed in a thermostat with circulating water at a constant temperature (40 °C). The volume ratio of DMSO to $NaOH_{aq}$ and the concentration of $NaOH_{aq}$ for the system employed are noted in the experimental results.

DMSO (or DMF)–tert-*BuOK System*: 6 mg of SF and 60 mg of *tert*-BuOK were dissolved in 10 ml of DMSO (or DMF) and 10 ml of *tert*-buthanol (*tert*-BuOH) respectively (the concentrations of SF and *tert*-BuOK were about $2.1\times$

10^{-3} and 5.3×10^{-2} M respectively), and when necessary, the two solutions were diluted with these solvents. The luminescent reaction was initiated by vigorously stirring 0.5 ml of the *tert*-BuOK solution (in *tert*-BuOH) into 2 ml of an aerated SF solution in DMSO (or DMF) in a quartz cell ($10\times10\times45$ mm) which had been placed in a thermostat.

The measurements of the intensity *versus* the reaction time and the spectrum of the CL-emission, and the absorption spectra of reaction mixture and the isolated product were carried out by a method essentially identical with those described in the previous paper.[1]

Results

The CL-Emission Spectrum of SF in Aerated-$NaOH_{aq}$ System. The CL-emission spectra of SF with oxygen in the system of DMSO–2 M $NaOH_{aq}$ (3: 1 v/v), measured at different reaction times, are shown in Fig. 1,

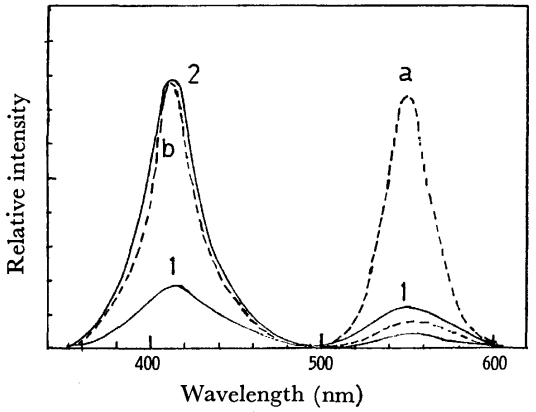

Fig. 1. CL-emission spectra of SF with oxygen measured at different reaction times; 1: after 1 min, 2: after 10 min, and FL-emission spectra of the reaction system measured at initial stage (a), and final stage (b) (DMSO–2 M $NaOH_{aq}$ system).

together with the fluorescence spectra (FL-emission) measured at the initial and final stages of the reaction. The results indicate that the CL-emission comprises two emission components: a weak greenish-yellow emission whose spectral distribution is similar to that of the fluorescence of SF (a peak at 555 nm), and an intense violet emission similar to the fluorescence band which appears during the course of the reaction (a peak at 410 nm). The intensity of the greenish-yellow emission at 555 nm showed a rapid decay, whereas that of the violet emission at 410 nm initially rose to a maximum and then showed a slight decay, followed by a long-lived steady glow, as is illustrated in Fig. 2.

The following two findings are noticeable. When nitrogen was bubbled into the luminescing system to remove the oxygen, the emission disappeared. Such xanthene dyes as uranin, eosin Y, erythrosin B, 2′,7′-dichlorofluorescein, rhodamine B and rhodamine S, which chemiluminesce as a blue emission upon oxidation with hydrogen peroxide, neither decomposed nor chemiluminesced with oxygen under comparable conditions.

The Effect of Solvent on the Chemiluminescence Emission. In DMSO–$NaOH_{aq}$ systems (0.25 M NaOH), the CL-emission appears only when the solution contains more

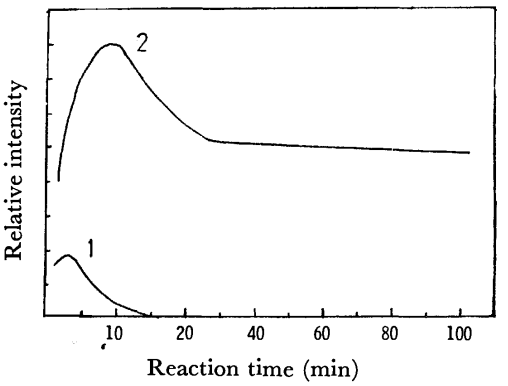

Fig. 2. Changes in the intensities of two components of CL-emission of SF in DMSO–2 M $NaOH_{aq}$ system, 1: violet emission component, 2: greenish-yellow component.

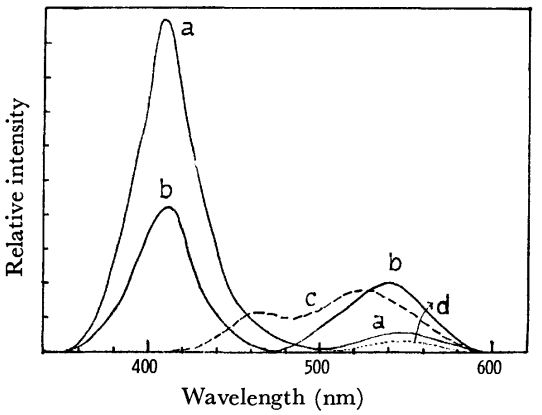

Fig. 3. CL-emission spectra of SF measured in DMSO– (a), DMF– (b), dioxane– (c), ethanol– (d), and methanol–2 M $NaOH_{aq}$ (3: 1 v/v) system (d).

than 50% DMSO in volume, and the higher the concentration of DMSO, the more intense the light which appears. Figure 3 shows the CL-emission spectra in DMSO–, DMF–, dioxane–, methanol–, and ethanol–2M $NaOH_{aq}$ (3: 1 v/v) systems. The spectrum in DMF is similar, but that in dioxane is dissimilar to the CL-emission spectrum in DMSO, and only a greenish-yellow emission appears in such protic solvents as methanol and ethanol. No emission could be observed in the acetone–, *tert*-BuOH–, and acetonitrile–2M $NaOH_{aq}$ (3: 1 v/v) systems, probably because the high concentration of these solvents prevents the dissolution of sodium hydroxide.

The Requisite Molar-ratio of Sodium Hydroxide to Succinylfluorescein for the Generation of the CL-Emission. Table 1 shows the relative intensities of CL-emissions measured when 10 and 20 mg of SF were dissolved in 10 ml of mixtures of DMSO and $NaOH_{aq}$ of different concentrations (3: 1 v/v). The results indicate that no appreciable emission appears when the molar-ratio of NaOH to SF is less than 3. The same requisite molar-ratio of NaOH to SF was found in DMF–$NaOH_{aq}$ systems.

The Effect of Adding Oxidizing Agent on the CL-Emission. When 0.5 ml of a 0.05 M aqueous solution of potassium ferricyanate was added to the luminescing DMSO–2M

TABLE 1. RELATIVE INTENSITIES OF CL-EMISSION IN DMSO–$NaOH_{aq}$–SF SYSTEMS OF DIFFERENT CONCENTRATIONS OF NaOH AND SF

[SF]=6.8×10^{-3}M		[SF]=3.4×10^{-3}M	
[NaOH] (M)	Relative intensity	[NaOH] (M)	Relative intensity
1/2	190	3/160	41
1/4	140	9/800	6
1/8	16	7/800	0
1/16	10		
1/40	8		
9/400	8		
3/160	0		
1/80	0		

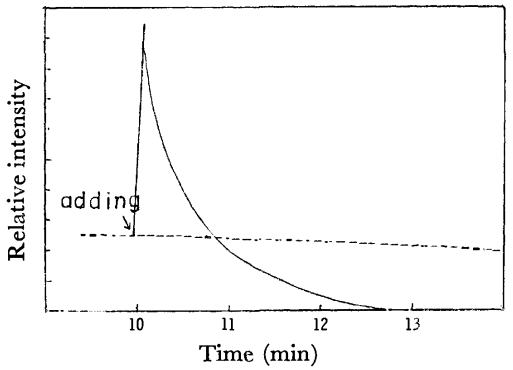

Fig. 4. Effect of adding $K_3Fe(CN)_{6aq}$ on the CL-emission intensity *versus* time; broken line shows intensity *versus* time when oxidizing agent was absent, and full line shows that after adding the agent (40 °C).

$NaOH_{aq}$ (3: 1 v/v) system, the intensity of the emission rapidly increased, then it vanished with a fast decay. A typical example of the effect of adding an oxidizing agent is illustrated in Fig. 4, where the dotted line shows an intensity *versus* reaction time curve measured when the oxidizing agent was absent, while the solid line shows the curve obtained after the agent was added. A similar effect was observed by adding aqueous solutions of bromine and potassium permanganate to the system. No emission, however, appeared when these agents were added to a deaerated system or to a system where the molar-ratio of NaOH to SF was less than three.

The Isolation and Identification of the Violet-fluorescent Product. During the course of the luminescent reaction in a DMSO–2M $NaOH_{aq}$ (3: 1 v/v) system, the absorption peak at 510 nm decreased; simultaneously a new absorption peak appeared at 370 nm, as is shown as the solid line curve in Fig. 5. The change in the absorption spectrum seems to be attributable to the decomposition of SF and the formation of a species. In an aerated aqueous solution of sodium hydroxide (containing no aprotic solvent), the absorption spectrum also changed, as is shown by the dotted line in Fig. 5. From the results, we can expect that the same reaction product may be formed in the two systems since the new absorption peak appeared at the same wavelength (370 nm). This was confirmed by the findings that

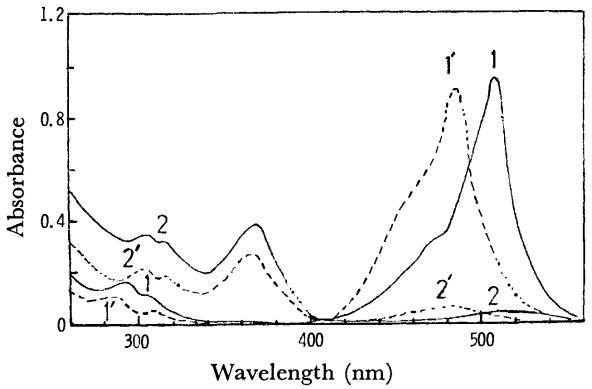

Fig. 5. Absorption spectra of reaction mixture in DMSO–2 M $NaOH_{aq}$ system (1: initial stage, 2: final stage) and those in 1/4 M $NaOH_{aq}$ system (1′: initial stage, 2′: final stage).

thin-layer chromatography (Silica gel G, $CHCl_3$–CH_3COOH, 1: 1) showed the same spot at R_f 0.14 (ascending method) and that paper chromatography (Toyo Filter Paper No. 50, 20% aqueous ethanol–5% aqueous ammonia, 1: 1) showed the same spot at R_f 0.30 (the descending method) for the products in the two systems. A large amount of the (violet-fluorescent) product could be prepared by the following method. Four grams of SF and 10 g of sodium hydroxide were dissolved in 300 ml of aerated water, and then the reaction mixture was kept at 40 °C with stirring in an open flask for three days. The residual reaction mixture was acidified with hydrochloric acid, and the precipitated crude brownish product was filtered off and adsorbed on a column of Mallinckrodt Silicic Acid (100 mesh). The column was eluted with ether; then, after the removal of the solvent, white needles were obtained. Recrystallization from 20% aqueous ethanol gave 50 mg of a pure product, which did not melt below 300 °C. The analytical data of the product are listed in Table 2. These data support the idea that the product is 3,6-dihydroxyxanthone. The product was further identified by its position on thin-layer chromatography (R_f 0.14,

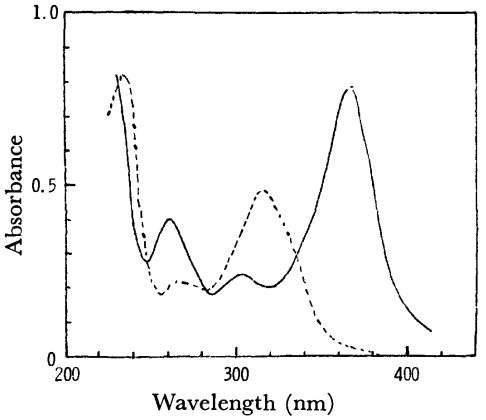

Fig. 6. Absorption spectra of reaction product; ——: dianion in KOH–H_2O system,----: neutral molecule in H_2O (in KOH_{aq}: λ_{max}=368 nm, $\epsilon=3.99\times10^4$; 304 nm, 1.05×10^4; 263 nm, 1.93×10^4; 225 nm, 4.49×10^4, in H_2O: λ_{max}=315 nm, $\epsilon=2.40\times10^4$; 267 nm, 1.02×10^4; 237 nm, 4.00×10^4).

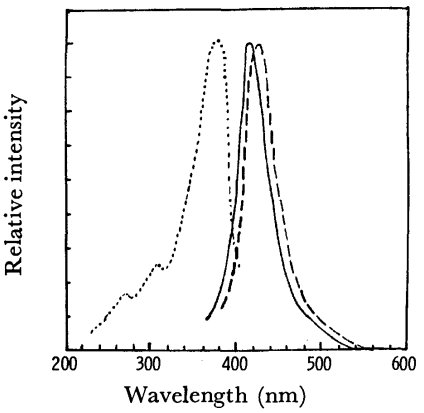

Fig. 7. FL-emission spectra of reaction product; ——: in DMSO–*tert*-BuOK system, ----: in H_2O–KOH system (exciting at 480 nm), and excitation spectrum for the FL-emission peak at 410 nm in DMSO–*tert*-BuOK system (·····).

TABLE 2. ANALYTICAL DATA FOR THE REACTION PRODUCT

Elemental analysis				
	Found (%)	Calcd for $C_{13}H_8O$(%)	Mass (M^+)	NMR (δ, ppm)
C	68.29	68.42	228	8.07 (d, J=9.0 Hz)
H	3.74	3.53		6.94 (dd, J=1.5, 9.0 Hz)
				6.88 (s)

(The NMR spectrum was taken in DMSO-d_6 with a JEOL MH-100 type spectrometer at 100 MHz using TMS as an internal standard.)

the ascending method) as well as by its position on paper chromatography (R_f 0.30, the descending method) compared with those of an authentic sample. The absorption and fluorescence spectra of the product in different media are illustrated in Figs. 6 and 7 respectively. These spectra also match those of the authentic sample.

Emission Characteristic in the DMSO (or DMF)–tert-BuOK System. The intensity of the CL-emission of SF in an aerated dry DMSO (or DMF)–*tert*-BuOK system was about 150 times greater than that in a DMSO–2M $NaOH_{aq}$ (3: 1 v/v) system. The spectra of the CL-emissions measured in the DMSO–, DMF–, and acetonitrile–*tert*-BuOK systems are illustrated in Fig. 8. The observed intense peak at 410 nm indicates that the CL-emission in the systems can be attributed to the formation of the excited dianion of 3,6-dihydroxyxanthone.

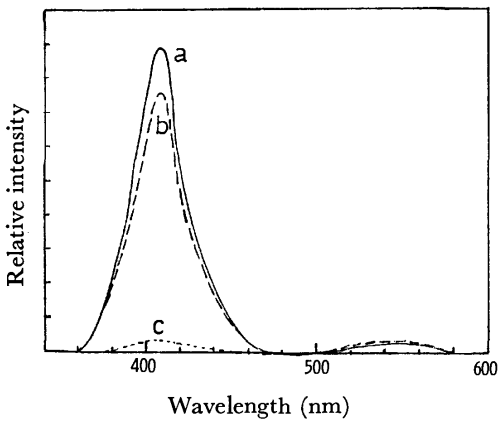

Fig. 8. CL-emission spectra of SF in DMSO– (a), DMF– (b), acetonitrile–*tert*-BuOK system (c)

The dependence of the molar-ratio of *tert*-BuOK to SF on the generation of the CL-emission in a DMSO–*tert*-BuOK system was investigated. The results, which are summarized in Table 3, indicate that no appreciable emission is generated when the molar-ratio of *tert*-BuOK to SF is less than 3.

TABLE 3. DEPENDENCE OF MOLAR-RATIO OF *tert*-BuOK TO SF (ρ) ON THE GENERATION OF CL-EMISSION IN AERATED DRY DMSO-*tert*-BuOK SYSTEM

[SF] (M)	[*tert*-BuOK] (M)							
	1.6×10^{-2}		2.6×10^{-3}		1.2×10^{-3}		6×10^{-4}	
	ρ	emission	ρ	emission	ρ	emission	ρ	emission
1.68×10^{-3}	6.8	G	1.57	N	—	—	—	—
8.4	12.6	G	3.15	G	1.43	N	—	—
5.6	18.9	G	4.7	G	2.14	N	—	—
4.2	25.2	G	6.3	G	2.86	N	1.43	N
2.1	50.4	G	12.6	G	5.7	G	2.86	N
1.05	100	G	25.2	G	11.4	G	5.7	U
5.25	—	—	50.4	G	22.8	G	11.4	G

(G: generated, N: did not generate, U: undefined)

The absorption spectrum of SF in an aerated DMSO solution showed no appreciable peak in the visible region. By adding a *tert*-BuOK solution (in *tert*-BuOH), a strong absorption at about 525 nm appeared, probably because of the structural change in the dye. (In a deaerated system, the absorption at 525 nm was found to be not so strong that oxygen would participate in the reaction which leads to the structural change.) During the course of the reaction, the spectrum changed as is shown in Fig. 9. It is of interest to find that a new absorption peak at 370 nm increases gradually and that the isobestic point appears at 364 nm. It seems reasonable to speculate that the main product is 3,6-dihydroxyxanthone, so the intense emission can be observed in a DMSO–*tert*-BuOK system. Figure 10 shows the intensity of the CL-emission and the change in the absorbance at 525 nm *versus* the reaction

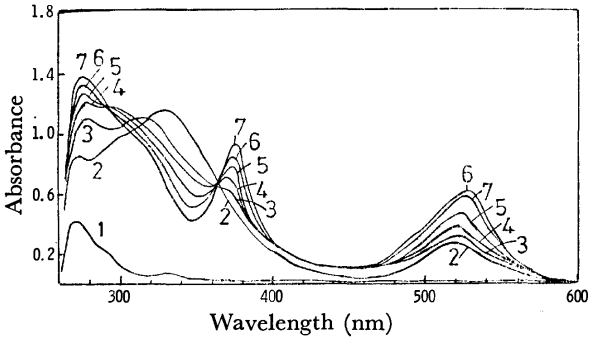

Fig. 9. Change of absorption spectrum of reaction mixture in DMSO–*tert*-BuOK–SF system ([*tert*-BuOK] $=2.6\times10^{-3}$ M, [SF]$=5.25\times10^{-5}$ M); 1: before adding *tert*-BuOK, 2→7: after adding *tert*-BuOK.

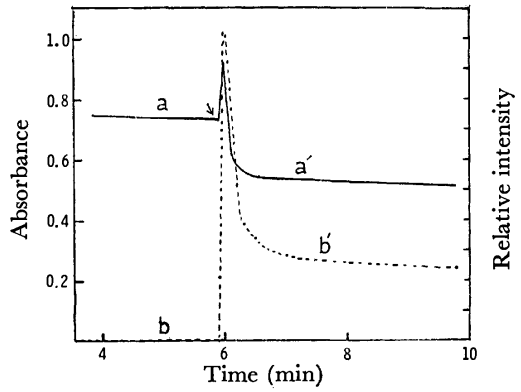

Fig. 10. Changes in the absorbance of reaction system at 525 nm (——a) and CL-emission intensity at 410 nm (----b) when adding 0.05 ml of a 6.6×10^{-3} M solution of *tert*-BuOK in *tert*-BuOH in 2 ml of a 6.8×10^{-5} M solution of SF in DMSO ($\rho=2.3$; *tert*-BuOK deficient system), and those (——a' and ----b') after adding 0.5 ml of the *tert*-BuOK solution ($\rho=23$; *tert*-BuOK sufficient system).

time measured when 0.05 ml of a 6.6×10^{-3} M solution of *tert*-BuOK was added to 2 ml of a 6.8×10^{-5} M solution of SF (the molar-ratio of *tert*-BuOK to SF is 2.3; it is a *tert*-BuOK deficient system) and also those measured when 0.5 ml of a *tert*-BuOK solution was added again to the system to make a *tert*-BuOK sufficient system (the molar-ratio is 23). The absorbance at 525 nm was found to increase to a maximum without any emission in the *tert*-BuOK deficient system (the peak at 370 nm did not appear in the system), whereas the absorbance decreased with emission in the *tert*-BuOK sufficient system.

The characteristics of the emission intensity *versus* the reaction time, which is strongly dependent upon the molar-ratio of *tert*-BuOK to SF, are so complicated that no kinetic analysis of the emission intensity could be made in the present study.

When such protic solvents as water, methanol, and ethanol were added drop by drop (each drop was about 0.02 ml) to the luminescing system (2.5 ml), a decrease in the intensity was found upon each addition. On the other hand, when a 0.05 M solution of benzoyl peroxide in DMSO was added, drop by drop, to the system, a bright flash appeared, with a lowering of the

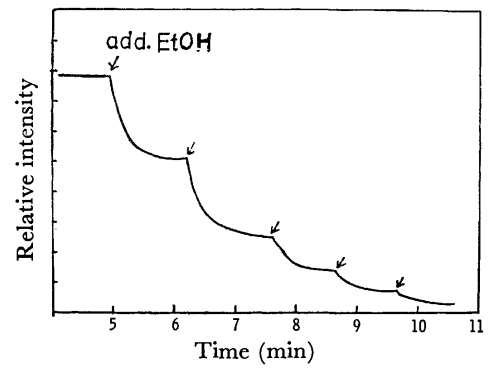

Fig. 11. Effect of adding H_2O or EtOH on the CL-emission intensity versus time in DMSO–*tert*-BuOK–SF system.

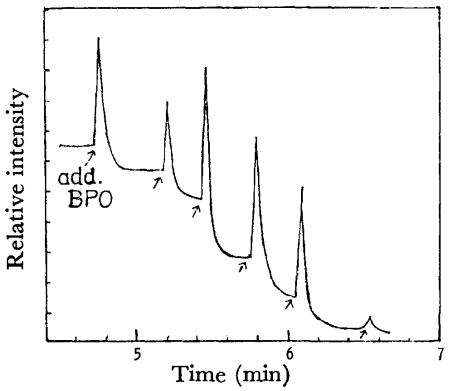

Fig. 12. Effect of adding benzoyl peroxide on the CL-emission intensity *versus* time in DMSO-*tert*-BuOK-SF system.

intensity of the steady glow, at each addition. Typical examples of the effects of adding a protic solvent and oxidizing agent are illustrated in Figs. 11 and 12 respectively. Neither an appreciable lowering of the intensity nor a flash was observed when a drop of DMSO was added to the luminescent system.

Discussion

The appearance of a strong absorption peak at 525 nm upon the addition of NaOH or *tert*-BuOK to an aerated solution of SF may be attributed to the following structural change in SF:

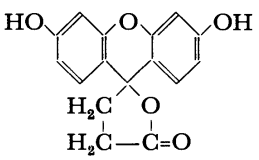

(1)

Lactone form of a neutral molecule of SF in DMSO

↓ 2 *tert*-BuOK or 2 NaOH and O_2

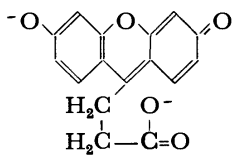

(2)

Quinoid form anion of SF in an aerated alkaline solution

A further reaction of SF with *tert*-BuOK will be necessary to initiate the luminescent reaction, because no appreciable emission appeared when the molar-ratio of *tert*-BuOK to SF was less than 3.

It has been reported that *tert*-BuOK prevents the reaction of DMSO with *tert*-BuOK under the experimental conditions employed here.[6]

A reasonable step may be the following elimination of a proton from the C atom at the β-position:

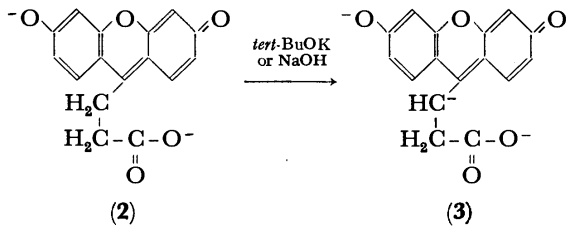

(2) (3)

Therefore, one possible mechanism for the reaction of **3** with oxygen may be the following oxygenation *via* a caged radical pair, **4**:[7]

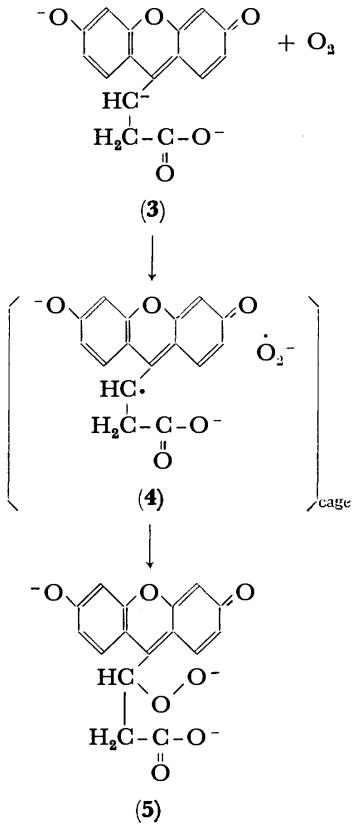

(3) (4) (5)

The experimental finding that the CL-emission rapidly increased upon the addition of an oxidizing agent will support this scheme.

The experimental results also indicate that the CL-emission is attributable to the formation of the excited dianion of 3,6-dihydroxyxanthone (**7**); thus, the reaction path leading to the dioxetane intermediate, **6**, may be the most probable mechanism for the formation of **7**, as has been proposed by many investigators.[8]

A finding similar to our finding that no appreciable emission arises in a protic solvent system has also been reported in the chemiluminescent reaction of photinus-ruciferin with oxygen;[9] also, a sharp rize in the intensity at the initial stage followed by a slight decay and then

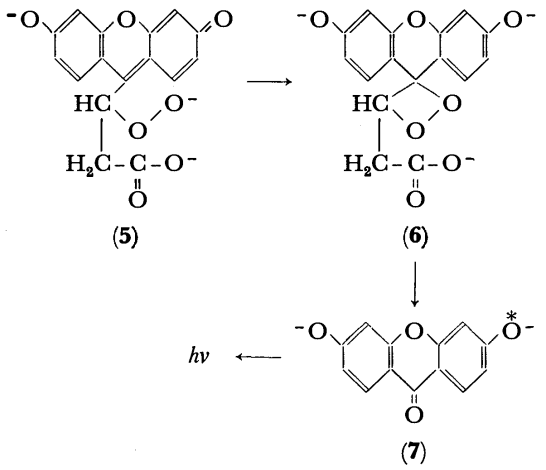

(5) (6) (7)

a long-lived steady glow, has been demonstrated for the CL-emission of 3,3′-tetrahydro-1,1′-biisoquinolinium iodide with oxygen.[10]

The authors wish to express their thanks to Professor Teruo Matsuura of the Faculty of Engineering, Kyoto University, for his useful discussion, to Mr. Tatsuyuki Yamakawa for his measurements of the intensity and the spectrum of the reaction system, to Miss Kyoko Toya for the elemental analysis, and to Mr. Kozo Matsumoto of Nagoya University and Dr. Nobutaka Suzuki of Mie University for their measurements of the MS and NMR spectra and for their helpful discussions.

This work was supported in part by a Scientific Research Grant of the Ministry of Education.

References

1) I. Kamiya and S. Kato, This Bulletin, **43**, 1284 (1970).
2) I. Kamiya and K. Aoki, This Bulletin, **47**, in press.
3) For example, M. J. Cormier, D. M. Hercules, and J. Lee, eds., "Chemiluminescence and Bioluminescence," Plenum Press, New York (1973).
4) The preparation was carried out by a modification of the preparation of fluorescein ("Beilstein's Handbuch d. org. chem.," Vol. 19, Hw p. 222).
5) R. Meyer and A. Conzetti, *Chem. Ber.*, **30**, 969 (1897); R. Meyer and A. Conzetti, *ibid.*, **32**, 2103 (1899).
6) G. A. Russell, E. G. Janzen, H. D. Becker, and F. J. Smentowski, *J. Amer. Chem. Soc.*, **84**, 2652 (1962).
7) J. W. Haap, E. G. Janzen, and B. C. Rudy, *J. Org. Chem.*, **35**, 3382 (1970).
8) For example, F. McCapra, *Quart. Rev.*, **20**, 485 (1965); K. R. Koppecky, J. H. van de Sande, and C. Mumford, *Can. J. Chem.*, **46**, 25 (1968); M. Mathew and G. J. Palenik, *ibid.*, **47**, 705 (1969); M. M. Rauhut, *Accounts Chem. Res.*, **2**, 80 (1969); E. H. White and C. C. Wei, *Biochem. Biophys. Res. Commun.*, **39**, 1219 (1970).
9) H. H. Seliger and W. D. McElroy, *Science*, **138**, 683 (1962).
10) R. A. Henry and C. A. Heller, *J. Lumines.*, **4**, 105 (1971).

The Reaction of 3-(ω-Ethoxycarbonylacetyl)-2*H*-cyclohepta[*b*]-furan-2-one with Active Methylene Compounds

Tetsuo NOZOE,* Kahei TAKASE,** Tomoo NAKAZAWA,*** Satoko SUGITA,**** and Motoyasu SAITO

Department of Chemistry, Faculty of Science, Tohoku University, Aramaki-aza-Aoba, Sendai 980

(Received December 27, 1973)

The reaction of 3-(ω-ethoxycarbonylacetyl)-2*H*-cyclohepta[*b*]furan-2-one (**4**) with malononitrile and with cyanoacetamide, in the presence of sodium ethoxide, gave 4-hydroxyazuleno[2,1-*b*]pyrid-2(1*H*)-one derivatives, (**5**) and (**9**) respectively, in good yields. On the other hand, the reaction of **4** with ethyl cyanoacetate gave 3-cyano-2-ethoxycarbonylmethylazulene-1-carboxylic acid (**12**). The structures of these products were determined on the basis of the spectral data and some chemical evidences.

It is known[1] that the reaction of 2-chloro- or 2-methoxytropones with active methylene compounds, such as malononitrile, ethyl cyanoacetate, and diethyl malonate, is a useful method for synthesizing azulene derivatives, especially those with various functional groups at the 1-, 2-, and 3-positions. In addition, it has been found[2] that 2*H*-cyclohepta[*b*]furan-2-one derivatives were the reaction intermediates in this azulene-formation reaction and that their reactions with active methylene compounds also gave azulene derivatives. Of these, the reaction of 3-acetyl-2*H*-cyclohepta-[*b*]furan-2-one (**1**) with malononitrile or cyanoacetamide gave a 1-acetyl-2-aminoazulene derivative (**2a**) or (**2b**), whereas that with ethyl cyanoacetate gave a 2-methylazulene derivative (**3**) as the major product, together with a minor amount of an 1-acetyl-2-aminoazulene derivative (**2c**).[2b] On the application of such types of reactions to 3-(ω-ethoxycarbonylacetyl)-2*H*-cyclohepta[*b*]furan-2-one (**4**),[3] we have now found that azuleno[2,1-*b*]pyridine derivatives were easily synthesized; the results will be reported in this paper.

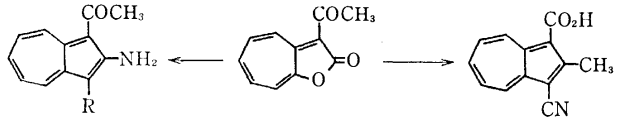

2a: R=CN
2b: R=$CONH_2$
2c: R=$CO_2C_2H_5$

1

3

Results and Discussion

The reaction of **4** with malononitrile took place easily, in the presence of sodium ethoxide, at room temperature; an azulenic compound (**5**), $C_{14}H_8O_2N_2$, was formed in a good yield. Compound **5** is only slightly soluble in organic solvents, but it is easily soluble in aqueous alkali. The infrared spectrum of **5** in KBr exhibits absorptions at 3300—2500 (associated enolic OH), 2203 (C≡N), and 1634 and 1626 cm^{-1} (C=O). The ultraviolet absorption curve is similar to that of ethyl 2(1*H*)-oxoazuleno[2,1-*b*]pyridine-3-carboxylate,[4] as is shown in Fig. 1. The mass spectrum reveals a molecular ion peak at *m/e* 236. On the basis of these spectral data and some chemical evidence to be described below, as well as a consideration of the reaction mechanism to be described later, the structure of **5** is assumed to be 10-cyano-4-hydroxyazuleno-[2,1-*b*]pyrid-2(1*H*)-one (**5a**). As is confirmed apparently by its spectral data, **5** exists in the 2(1*H*)-pyridone form, **5a**, but not in the 2-hydroxypyridine form, **5b**. However, **5** gave both types of diacetyl derivatives, that is, *O,N*- (**6a**) and *O,O'*-diacetyl derivatives (**6b**), derived from **5a** and **5b** respectively. Thus, when heated with acetic anhydride at 130 °C, **5** gave **6a**. Its infrared spectrum exhibits absorptions at 1637 (*N*-acetyl) and 1783 cm^{-1} (*O*-acetyl), and its ultraviolet absorption curve is similar to that of **5** (Fig. 1). On the other hand, the acetylation of **5** with acetic anhydride in pyridine gave **6b**. Its infrared spectrum exhibits an absorption at 1773 cm^{-1} (*O*-acetyl), and its ultraviolet absorption curve is similar to that of ethyl 2-methoxyazuleno[2,1-*b*]pyridine-3-carboxylate[4] (Fig. 2). On methylation with diazomethane or with dimethyl sulfate, **5** gave only an azuleno[2,1-*b*]pyridone-type *O,N*-

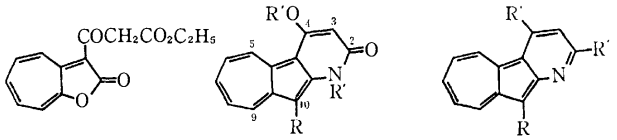

4

5a: R=CN; R'=H
6a: R=CN; R'=$COCH_3$
7: R=CN; R'=CH_3
9: R=$CONH_2$; R'=H
10: R=R'=H

5b: R=CN; R'=OH
6b: R=CN; R'=$OCOCH_3$
8: R=CN; R'=Cl
11: R=H; R'=Cl

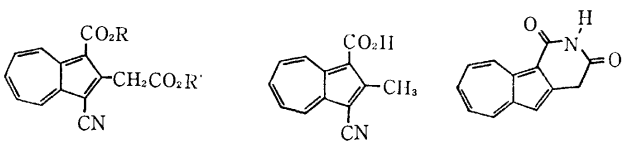

12: R=H; R'=C_2H_5
13: R=CH_3; R'=C_2H_5
14: R=R'=H
15: R=R'=CH_3

16

17

* Present address: No. 811, 2-5-1, Kamiyoga, Setagaya-ku, Tokyo 158.

** To whom correspondence should be addressed.

*** Present address: Department of Chemistry, Faculty of Science, Osaka University, Toyonaka, Osaka 560.

**** Nee Satoko Fukuda.

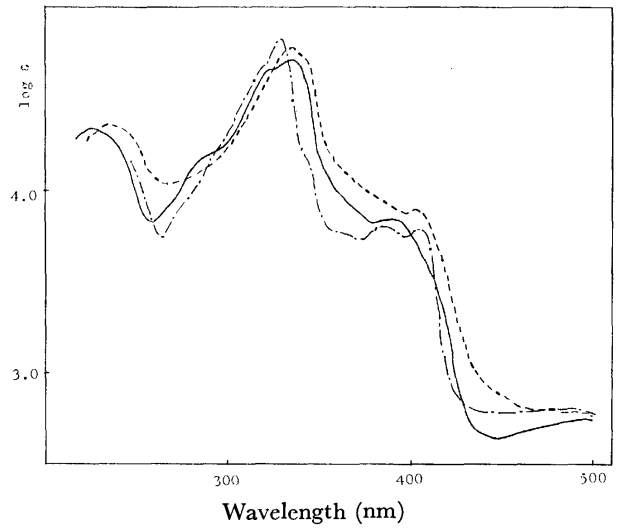

Fig. 1. The UV spectra of **5** (——), **6a** (----) and **10** (-·-·-) in methanol

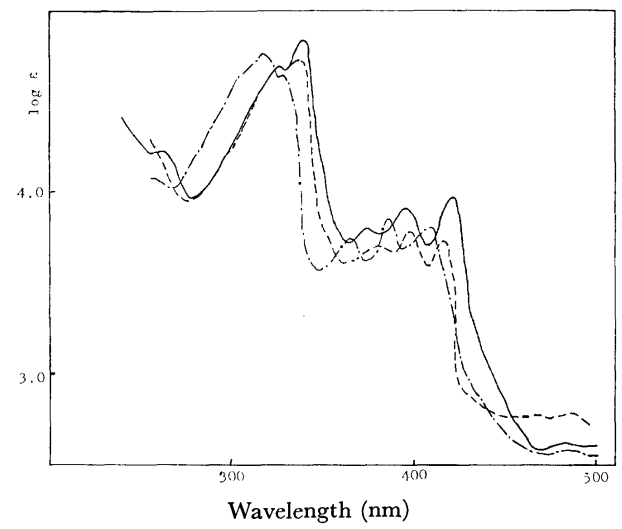

Fig. 2. The UV spectra of **6b** (——), **8** (----) and **11** (-·-·-) in methanol.

dimethyl derivative (**7**), derived from **5a**. The infrared spectrum of **7** exhibits absorptions at 2208 (C≡N) and 1656 cm^{-1} (C=O). The ultraviolet absorption curve of **7** is similar to that of **5**. On the other hand, the treatment of **5** with phosphorus oxychloride afforded an azuleno[2,1-*b*]pyridine-type dichloro compound (**8**). Its ultraviolet absorption curve is similar to that of **6b** (Fig. 2).

The reaction of **4** with cyanoacetamide, in the presence of sodium ethoxide, gave an azulenic compound (**9**) in a good yield. The same compound was also obtained from **5** when the latter was heated in 100% phosphoric acid at 100 °C. The infrared spectrum of **9** exhibits absorptions at 3300—2500 (associated enolic OH), and 1658, 1631, and 1621 cm^{-1} (C=O), but no absorption corresponding to the cyano group. The ultraviolet absorption curve is similar to that of **5**. The mass spectrum reveals a molecular ion peak at *m/e* 254. From these findings, **9** is assigned the structure of 10-carbamoyl-4-hydroxyazuleno[2,1-*b*]pyrid-2-(1*H*)-one. When **9** was heated in 100% phosphoric acid at 130 °C, decarbamoylation took place, with the formation of 4-hydroxyazuleno[2,1-*b*]pyrid-2(1*H*)-one (**10**). The same compound, **10**, was also obtained from **5** upon heating with 100% phosphoric acid at 130 °C. The infrared spectrum of **10** exhibits absorptions at 3300—2500 (associated enolic OH) and 1618 cm^{-1} (C=O). The ultraviolet absorption curve is similar to that of **5** (Fig. 1). These spectral data have substantiated the structure of **10**. Compound **10** gave an *N*-acetyl derivative on acetylation with acetic anhydride–pyridine. Further, the treatment of **10** with phosphorus oxychloride gave 2,4-dichloroazuleno[2,1-*b*]pyridine (**11**). Its ultraviolet absorption curve is similar to that of **8** (Fig. 2).

In the reaction of **4** with ethyl cyanoacetate, an azulenic compound (**12**) was obtained in a good yield. The infrared spectrum exhibits absorptions at 3300—2500, 1656 and 920 (COOH), 2212 (C≡N), and 1742 cm^{-1} (ester C=O). The methylation of **12** with diazomethane afforded an ester (**13**), while the alkaline hydrolysis of **12**, followed by the methylation of the resulting dicarboxylic acid (**14**) with diazomethane, yielded a dimethyl ester (**15**). Further, on heating in pyridine **14** gave 3-cyano-2-methylazulene-1-carboxylic acid (**16**).[2b] On the basis of these spectral data and chemical evidence, **12** was assigned the structure of 3-cyano-2-ethoxycarbonylmethylazulene-1-carboxylic acid.

When **12** or **14** was heated with acids, such as 75% sulfuric, 85% phosphoric, or concentrated hydrobromic acid, at about 100 °C, cyclization took place, with the formation of an imide (**17**). Its infrared spectrum exhibits absorptions at 3215 (NH), 1686 and 1678 cm^{-1} (C=O), but no absorption corresponding to the cyano group. Its NMR spectrum reveals a two-proton singlet at 4.31 ppm associated with the methylene protons. The mass spectrum reveals a molecular ion peak at *m/e* 211. These spectral data have substantiated the structure of **17**. The acetylation of **17** with acetic anhydride in pyridine gave an *N*-acetyl derivative, whereas that with acetic anhydride in the presence of concentrated sulfuric acid gave an *O*-acetyl derivative.

As has been described above, it has been found that the reaction of **4** with malononitrile or cyanoacetamide yielded directly the azuleno[2,1-*b*]pyrid-2(1*H*)-one derivative, **5** or **9** respectively. On the other hand, it has been found that the reaction of **4** with ethyl cyanoacetate yielded the azulene derivative, **12**, but no azuleno[2,1-*b*]pyrid-2(1*H*)-one derivative. The forma-

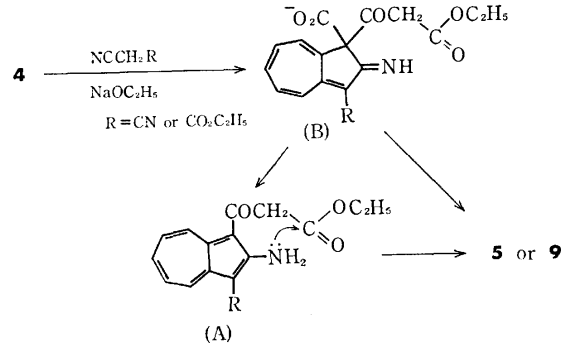

tion of **5** or **9** is presumed to be as follows. It had been found that, in the reaction of 3-acetyl-2*H*-cyclohepta[*b*]furan-2-one, **1**, with malononitrile or cyanoacetamide, the 1-acetyl-2-aminoazulene derivative, **2a** or **2b**, was formed *via* a dihydroazulene-type intermediate.[2b] Similarly, in the reaction of **4** with malononitrile or cyanoacetamide, an 2-amino-1-(ω-ethoxycarbonylacetyl)azulene derivative (A) should be formed at first *via* a dihydroazulene-type intermediate (B). In this case, however, cyclization between the amino and ester groups, which are present in a position favorable to lactam-formation, should occur subsequently to yield the azuleno[2,1-*b*]pyrid-2(1*H*)-one derivative, **5** or **9**. A similar cyclization should also be possible between the imino and ester groups in the intermediate (B), accompanying decarboxylation, to yield **5** or **9**. In the reaction of **4** with ethyl cyanoacetate, the azulene, **12**, is presumed to be formed through the same reaction mechanism as in the formation of 2-methylazulene derivative, **3**, in the reaction of **1** with ethyl cyanoacetate.[2b]

Experimental

All the melting points are uncorrected. The infrared spectra were taken on a Shimadzu IR-27 infracord. The ultraviolet spectra were run on a Hitachi EPS-3 spectrophotometer. The NMR spectra were determined with a Varian A-60 spectrometer. The mass spectral analyses were done on a Hitachi RMU-60 mass spectrometer.

10-Cyano-4-hydroxyazuleno[2,1-b]pyrid-2(1H)-one (5). To a solution of 1.30 g of **4** and 460 mg of malononitrile in 25 ml of anhydrous ethanol, 7.5 ml of a 1M sodium ethoxide solution was added, after which the mixture was stirred for 8 hr at room temperature. The reaction mixture was then diluted with water and acidified with 6M hydrochloric acid. The crystals thereby formed were recrystallized from dimethylformamide to give 1.23 g of **5** as reddish-violet needles; mp 354—360 °C (decomp.); UV (MeOH): λ_{max} 228 nm (log ε 4.35), 325 (4.68), 337 (4.69), 392 (3.86), and 500 (2.75).

Found: C, 71.38; H, 3.70; N, 12.04%. Calcd for $C_{14}H_8O_2N_2$: C, 71.18; H, 3.41; N, 11.86%.

1-Acetyl-4-acetoxy-10-cyanoazuleno[2,1-b]pyrid-2(1H)-one (6a). A mixture of 100 mg of **5** and 1 ml of pyridine was heated at 130 °C for 2 hr. After cooling, the addition of water to the reaction mixture yielded 90 mg of crystals. Recrystallization from dimethylformamide afforded **6a** as violet microcrystals; mp over 300 °C; IR (KBr): 2212 (C≡N), 1783, and 1637 cm^{-1} (C=O); UV (dioxane): λ_{max} 329 nm (log ε 4.75), 343 (4.85), 405 (3.94), 510 (2.16), and 554 (2.23); mass spectrum *m/e* 320 (M^+).

Found: C, 67.46; H, 3.84; N, 8.61%. Calcd for $C_{18}H_{12}O_4N_2$: C, 67.50; H, 3.78; N, 8.75%.

2,4-Diacetoxy-10-cyanoazuleno[2,1-b]pyridine (6b). A mixture of 100 mg of **5**, 0.5 ml of pyridine, and 0.5 ml of acetic anhydride was warmed in a water-bath for 1 hr. After cooling, the addition of water yielded 110 mg of crystals. Recrystallization from dimethylformamide afforded **6b** as violet micro-crystals; mp 234 °C (decomp.); IR (KBr): 2208 (C≡N) and 1773 cm^{-1} (C=O); UV (dioxane): λ_{max} 315 nm (log ε 4.66), 328 (4.74), 370 (3.71), 391 (3.82), 415 (3.84), 510 (2.45), and 543 (2.41).

Found: C, 67.66; H, 3.96; N, 8.85%. Calcd for $C_{18}H_{12}O_4N_2$: C, 67.50; H, 3.78; N, 8.75%.

10-Cyano-4-methoxy-1-methylazuleno[2,1-b]pyrid-2(1H)-one (7). a) To a solution of 100 mg of **5** in a mixture of 5 ml of ether and 1 ml of methanol, 3 ml of an ethereal solution of diazomethane was added, after which the mixture was stirred for 2 hr under ice-cooling and then allowed to stand overnight in a refrigerator. The crystals thereby formed were recrystallized from dimethylformamide, thus affording 80 mg of **7** as brownish-violet micro-crystals; mp 280—281 °C; IR (KBr): 2208 (C≡N) and 1656 cm^{-1} (C=O); UV (dioxane): λ_{max} 297 nm (log ε 4.09), 330 (4.71), 345 (4.78), and 525 (2.79); mass spectrum *m/e* 264 (M^+).

Found: C, 72.55; H, 4.76; N, 10.45%. Calcd for $C_{16}H_{12}O_2N_2$: C, 72.71; H, 4.58; N, 10.60%.

b) To a solution of 100 mg of **5** dissolved in a mixture of 2 ml of 6M potassium hydroxide solution and 15 ml of water, 1 ml of dimethyl sulfate and 2 ml of 6 M potassium hydroxide solution were added, after which the mixture was stirred for 9 hr at room temperature and then allowed to stand overnight. The reaction mixture was acidified with 6 M hydrochloric acid, and the crystals thereby formed were recrystallized from dimethylformamide to afford 90 mg of **7** as brownish-violet micro-crystals; mp 280—281 °C.

2,4-Dichloro-10-cyanoazuleno[2,1-b]pyrid-2(1H)-one (8). A mixture of 150 mg of **5** and 3 ml of phosphorus oxychloride was heated under reflux. The reaction mixture was poured into ice water, and the crystals thereby formed were recrystallized from dimethylformamide, thus giving 120 mg of **8** as violet plates; mp 295 °C; IR (KBr): 2217 cm^{-1} (C≡N); UV (dioxane): λ_{max} 320 nm (log ε 4.70), 332 (4.85), 355 (4.22), 368 (3.81), 380 (3.81), 390 (4.16), 414 (4.00), 476 (2.62), 496 (2.63), 510 (2.66), 528 (2.67), and 546 (2.65); mass spectrum *m/e* 272 (100%, M^+), 274 (65%, M^++2), and 276 (10.5%, M^++4).

Found: C, 61.03; H, 2.18; N, 10.01%. Calcd for $C_{14}H_6N_2Cl_2$: C, 61.56; H, 2.22; N, 10.26%.

10-Carbamoyl-4-hydroxyazuleno[2,1-b]pyrid-2(1H)-one (9). a) To a solution of 160 mg of **4** and 65 mg of cyanoacetamide in 10 ml of anhydrous ethanol, a 2 ml portion of a 1 M sodium ethoxide solution was added, after which the mixture was stirred for 10 hr at room temperature. The reaction mixture was then diluted with water and acidified with 6 M hydrochloric acid. The crystals thereby formed were recrystallized from dimethyl sulfoxide, thus giving 120 mg of **9** as brownish-violet prisms; mp 322—324 °C (decomp.); UV (DMF): λ_{max} 325 nm (log ε 4.51), 340 (4.46), 410 (2.79), and 520 (2.74).

Found: C, 65.81; H, 4.21; N, 11.31%. Calcd for $C_{14}H_{10}O_3N_2$: C, 66.13; H, 3.96; N, 11.02%.

b) A mixture of 100 mg of **5** and 2 ml of 100% phosphoric acid was heated at 230 °C for 1 hr. Then, a similar treatment gave 90 mg of **9** as brownish-violet prisms; mp 322—324 °C (decomp.). The treatment of **5** with conc. sulfuric acid in a similar manner gave the same product.

4-Hydroxyazuleno[2,1-b]pyrid-2(1H)-one (10). A mixture of 100 mg of **5** and 2 ml of 100% phosphoric acid was heated at 130 °C for 3 hr. The reaction mixture was then cooled to room temperature and diluted with water. The crystals thereby formed were recrystallized from dimethylformamide, thus giving 80 mg of **10** as violet microcrystals; mp over 290 °C; UV (dioxane): λ_{max} 322 nm (log ε 4.75), 336 (4.76), 358 (4.08), 400 (3.78), 500 (2.60), and 540 (2.60); mass spectrum *m/e* 211 (M^+).

Found: C, 74.10; H, 4.50; N, 6.39%. Calcd for $C_{13}H_9O_2N$: C, 73.92; H, 4.30; N, 6.63%.

The treatment of 100 mg of **9** in a manner similar to that described above also gave 84 mg of **10**; mp over 290 °C.

N-Acetyl Derivative: Violet crystals from dimethylformamide; mp over 290 °C; IR (KBr): 1647 and 1613 cm^{-1};

UV (MeOH): λ_{max} 218 nm (log ε 4.32), 282 (4.21), 344 (4.81), 330 sh (4.70), 316 sh (4.35), and 410 (3.94).

Found: C, 69.08; H, 4.91; N, 5.52%. Calcd for $C_{15}H_{11}O_3N \cdot 1/2H_2O$: C, 68.69; H, 4.61; N, 5.34%.

2,4-Dichloroazuleno[2,1-b]pyridine (11). A mixture of 150 mg of **10** and 3 ml of phosphorus oxychloride was heated under reflux for 2 hr and then poured into ice water. The crystals thereby formed were dissolved in chloroform and chromatographed on a silica gel column. The evaporation of the solvent from the effluent left green crystals. Recrystallization from benzene afforded 60 mg of **11** as green needles; mp 163—164 °C; UV (dioxane): λ_{max} 307 nm (log ε 4.68), 317 (4.75), 327 (4.64), 364 (4.75), 384 (3.86), 410 (3.57), 480 (2.23), 427 (2.46), 466 (2.54), and 616 (2.42); NMR (DMSO-d_6): δ ppm 7.2—7.8 (5H, m), 8.5 (1H, s), and 9.5 (1H, s); mass spectrum *m/e* 247 (100%, M+), 249 (64.7%, M+2), and 251 (10.6%, M+4).

Found: C, 62.65; H, 2.85; N, 5.35%. Calcd for $C_{13}H_7NCl_2$: C, 62.93; H, 2.84; N, 5.65%.

3-Cyano-2-ethoxycarbonylmethylazulene-1-carboxylic Acid (12). To a solution of 520 mg of **4** and 280 mg of ethyl cyanoacetate in 30 ml of anhydrous ethanol, a 4 ml portion of a 1 M sodium ethoxide solution was added, after which the mixture was stirred for 10 hr at room temperature. After standing overnight, the mixture was diluted with water and acidified with 6 M hydrochloric acid. The crystals thereby formed were recrystallized from dioxane, thus affording 480 mg of **12** as red prisms; mp 187—188 °C; UV (MeOH): λ_{max} 233 nm (log ε 4.61), 254 sh (4.22), 262 (4.27), 292 (4.64), 303 (4.75), 340 (3.84), 370 (3.83), and 503 (2.76).

Found: C, 67.37; H, 4.68; N, 4.66%. Calcd for $C_{16}H_{13}O_4N$: C, 67.84; H, 4.63; N, 4.95%.

Methyl 4-Cyano-2-ethoxycarbonylmethylazulene-1-carboxylate (13). To a suspension of 100 mg of **12** in a mixture of 10 ml of ether and 2 ml of methanol, 2 ml of an ethereal solution of diazomethane was added, after which the mixture was stirred for 2 hr under ice-cooling. The solvent was then evaporated, and the residue was dissolved in benzene and passed through an alumina column. The evaporation of the solvent gave 100 mg of **13** as red prisms; mp 128—129 °C; IR (KBr): 2217 (C≡N), 1742, and 1692 cm^{-1} (C=O); UV (MeOH): λ_{max} 234 nm (log ε 4.54), 265 (4.33), 293 (4.61), 304 (4.71), 340 (3.79), 370 (3.81), and 503 (2.73); NMR ($CDCl_3$): δ ppm 1.8 (3H, t, J=7.5 Hz), 4.0 (3H, s), 4.25 (2H, q, J=7.5 Hz), 4.41 (2H, s), 7.6—8.1 (3H, m), 7.75 (1H, m), and 9.73 (1H, m).

Found: C, 68.43; H, 5.01; N, 4.63%. Calcd for $C_{17}H_{15}O_4N$: C, 68.67; H, 5.08; N, 4.71%.

4-Cyano-2-carboxymethylazulene-1-carboxylic Acid (14). A solution of 220 mg of **12** dissolved in a mixture of 3 ml of ethanol and 3 ml of 1 M potassium hydroxide solution was heated under reflux for 2 hr. The reaction mixture was then diluted with water and acidified with 6 M hydrochloric acid, thus affording 185 mg of crude **14**. Recrystallization from ethanol afforded red prisms; mp 208—209 °C; IR (KBr): 3300—2500, 1701, 1653 (COOH), and 2217 cm^{-1} (C≡N); UV (MeOH): λ_{max} 234 nm (log ε 4.54), 264 (4.25), 294 (4.58), 305 (4.04), 341 (3.77), 370 (3.78), and 508 (2.74).

Found: C, 65.90; H, 3.76; N, 5.32%. Calcd for $C_{14}H_9O_4N$: C, 65.88; H, 3.55; N, 5.49%.

Methyl 4-Cyano-2-methoxycarbonylmethylazulene-1-carboxylate (15). To a suspension of 130 mg of **14** in a mixture of 3 ml of ether and 3 ml of methanol, 10 ml of an ethereal solution of diazomethane was added, after which the mixture was stirred for 2 hr under ice-cooling. The subsequent evaporation of the solvent left a crystalline material, which was dissolved in benzene and passed through a short column of alumina. The evaporation of the solvent from the effluent gave 110 mg of **15** as red needles; mp 138—139 °C; IR (KBr): 2212 (C≡N), 1736, and 1686 cm^{-1} (C=O); UV (MeOH): λ_{max} 234 nm (log ε 4.57), 264 (4.35), 293 sh (4.60), 304 (4.72), 340 (3.86), 369 (3.87), and 503 (2.92); NMR ($CDCl_3$): δ ppm 3.75 (3H, s), 3.98 (3H, s), 4.41 (2H, s), 7.6—8.1 (3H, m), 8.75 (1H, m), and 9.73 (1H, m).

Found: C, 67.84; H, 4.97; N, 4.73%. Calcd for $C_{16}H_{13}O_4N$: C, 67.84; H, 4.63; N, 4.95%.

3-Cyano-2-methylazulene-1-carboxylic Acid (16). A mixture of 100 mg of **14** and 1.5 ml of pyridine was heated at 130 °C for 2 hr. The reaction mixture was then diluted with water and acidified with 6 M hydrochloric acid, thus affording 76 mg of crude **16**; mp 272—273 °C. Recrystallization from dimethylformamide gave orange red needles; mp 273 °C. This was identified with an authentic sample[2b] by a mixed-melting-point determination and by an infrared spectral comparison.

1,2,3,4-Tetrahydroazuleno[1,2-c]pyridine-2,4-dione (17). A mixture of 100 mg of **12** and 2 ml of conc. sulfuric acid was heated at 100 °C for 30 min. The reaction mixture was then allowed to cool and poured into ice water, thus giving 65 mg of **17** as violet crystals; mp 226—230 °C. Recrystallization from dimethylformamide afforded violet columns; 232 °C (decomp.); UV (dioxane): λ_{max} 296 nm (log ε 4.71), 308 (4.82), 359 (3.79), 367 (3.77), 377 (4.02), 490 sh (2.57), 520 (2.68), 550 (2.60), and 600 (2.13); NMR (DMSO-d_6): δ ppm 4.31 (2H, s), 6.98 (1H, S s), 7.4—8.1 (3H, m), 8.67 (1H, m), 9.58 (1H, m), and 10.8 (1H, bs).

Found: C, 73.73; H, 4.57; N, 6.56%. Calcd for $C_{13}H_9O_2N$: C, 73.92; H, 4.30; N, 6.63%.

The treatment of 100 mg of **12** with conc. hydrobromic (3 ml) or 85% phosphoric acid (2 ml) in a manner similar to that described above also gave **17** (mp 232 °C) in yields of 65 mg and 65 mg respectively.

N-*Acetyl Derivative*: Violet columns (from dimethylformamide); mp 275 °C (decomp.); IR (KBr): 1634 cm^{-1} (C=O); UV (dioxane): λ_{max} 310 nm (log ε 4.65), 338 (4.90), 360 (4.59), 400 (4.46), 528 (2.76), 548 (2.82), and 594 (2.44); mass spectrum *m/e* 253 (M+).

Found: C, 71.40; H, 4.73; N, 5.74%. Calcd for $C_{15}H_{11}O_3N$: C, 71.14; H, 4.37; N, 5.53%.

O-*Acetyl Derivative*: Violet needles (from ethanol); mp 168—170 °C; IR (KBr): 1786 and 1626 cm^{-1} (C=O); UV (dioxane): λ_{max} 296 nm (log ε 4.62), 307 (4.73), 329 (4.15), 360 (4.01), 378 (4.01), 522 (2.97), 556 (2.90), and 604 (2.61); mass spectrum *m/e* 253 (1.5%, M+) and 211 (100%).

Found: C, 71.38; H, 4.62; N, 5.80%. Calcd for $C_{15}H_{11}O_3N$: C, 71.14; H, 4.37; N, 5.53%.

This work was financially supported by grants from the Ministry of Education of Japan and the Sankyo Co., Ltd., to which the authors' thanks are due.

References

1) For reviews, see: a) T. Nozoe, *Croat. Chim. Acta*, **29**, 207 (1957); b) T. Nozoe and S. Ito, *Fortschr. Chem. Org. Naturstoffe*, **19**, 32 (1961); c) T. Nozoe and T. Asao, "Dai-Yuki-Kagaku," **13**, Asakura Shoten, Tokyo (1960), pp. 439—534.

2) a) T. Nozoe, S. Seto, K. Takase, S. Matsumura, and T. Nakazawa, *Nippon Kagaku Zasshi*, **86**, 346 (1965); b) T. Nozoe, K. Takase, T. Nakazawa, and S. Fukuda, *Tetrahedron*, **27**, 3357 (1971).

3) J. W. Cook, J. D. Loudon, and R. K. Razdan, *J. Chem. Soc.*, **1954**, 4041.

4) T. Nozoe and K. Kikuchi, This Bulletin, **36**, 633 (1963).

A Base-induced Elimination Reaction of Phenylsulfonylacetates. I. General Aspect and Stereochemistry

Akira SERA, Hiroshi MANO, and Kazuhiro MARUYAMA
Department of Chemistry, Faculty of Science, Kyoto University, Sakyo-ku, Kyoto 606
(Received December 27, 1973)

Esters of phenylsulfonylacetic acid were found to undergo a base-induced β-elimination reaction with *t*-butoxide in *t*-butyl alcohol. The intervention of a carbanion as an intermediate of the elimination was proposed. The stereochemistry of the elimination was examined by the use of *erythro*- and *threo*-2-deuterio-1,2-diphenylethyl phenylsulfonylacetates. From the deuterium content in a product, *i.e.*, *trans*-stilbene, the elimination was found to occur predominantly in a *syn* fashion.

The pyrolytic elimination reaction of acetates has been investigated extensively, and it is well known that almost all of the reactions proceed through a cyclic six-membered transition state.[1] However, little is known about the base-induced β-elimination reaction of the acetates in solution.[2,3] Curtin and Kellom[3] observed that 1,2-diphenylethyl acetate predominantly undergoes a *syn* elimination with potassium amide in liquid ammonia to give stilbene. With *t*-butoxide in *t*-butyl alcohol, however, no elimination was observed. In a previous paper,[4] we reported that 1,2-diphenylethyl phenylsulfonylacetate produces *trans*-stilbene and methyl phenyl sulfone upon treatment with *t*-butoxide in *t*-butyl alcohol.[5] Experiments with a deuterium-labeled diastereoisomeric pair of the ester suggested that the stereochemistry of the reaction was a *syn* elimination. The present paper will be concerned with a more detailed investigation of the mechanism of this and related base-induced *syn* elimination reactions.

Results and Discussion

In order to shed light on the mechanism of elimination reactions of phenylsulfonylacetates, we first employed 2-phenylethyl phenylsulfonylacetate (**1a**). This ester did not react when heated in diphenyl ether (259 °C). Thus, we anticipated that no thermal elimination operated below this temperature. On the other hand, it was found that the ester gives methyl phenyl sulfone on treatment with potassium *t*-butoxide in *t*-butyl alcohol (reflux) or on treatment with sodium methoxide in diphenyl ether (reflux). Because the presence of a styrene-forming elimination reaction with bases had been suggested, kinetic studies of the base-induced elimination reactions were performed for *para*-substituted 2-phenylethyl phenylsulfonylacetates (**1a**—**d**) using potassium *t*-butoxide in absolute *t*-butyl alcohol. The rates of the olefin-forming elimination reactions from **1** were followed spectrophotometrically by means of the characteristic absorption of the styrenes produced. An excess of the base was required to bring

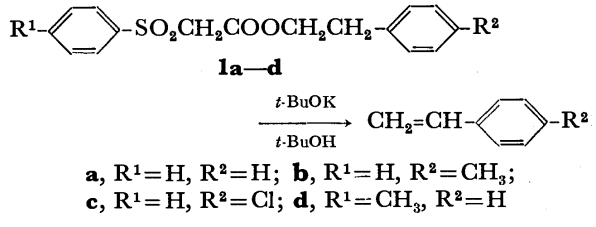

1a—d

a, $R^1=H$, $R^2=H$; **b**, $R^1=H$, $R^2=CH_3$;
c, $R^1=H$, $R^2=Cl$; **d**, $R^1=CH_3$, $R^2=H$

Table 1. Pseudo-first-order rate constants and activation parameters for eliminations from arylsulfonylacetates (**1a—d**) and 2-methyl-2-(phenylsulfonyl)propanoate (**2**) with *t*-butoxide in *t*-butyl alcohol

Substrate	Temp.[a] (°C)	$k\times10^6$ (s^{-1})[b,c]	$\Delta H^{\ddagger}$[d] (kcal·mol^{-1})	$\Delta S^{\ddagger}$[d] (e.u.)
1b	40.0	0.899±0.038		
1b	50.0	2.25 ±0.01	19.8	−23.2
1b	60.0	6.49 ±0.03		
1a	40.0	2.15 ±0.02		
1a	50.0	6.39 ±0.03	21.4	−16.1
1a	60.0	18.0 ±0.4		
1c	40.0	7.62 ±0.08		
1c	50.0	20.9 ±0.2	20.9	−15.5
1c	60.0	60.8 ±0.6		
1d	40.0	1.98 ±0.01		
1d	50.0	6.00 ±0.05	21.5	−16.1
1d	60.0	16.8 ±0.2		
2	40.0	0.679±0.026		
2	50.0	1.28 ±0.04	11.6	−49.7
2	60.0	2.24 ±0.26		

a) Bath temperature was kept within ±0.05 °C. b) Initial concentrations; [substrate]=5.00×10^{-3}M, and [base]=1.00 M. c) Deviations listed are standard deviations. d) At 50.0 °C.

about the elimination reaction of **1** effectively. The pseudo-first-order rate constants and the other thermodynamic data for the eliminations from **1a—d** are given in Table 1. In the reaction of **1a** with an excess amount of potassium *t*-butoxide in *t*-butyl alcohol, the reaction mixture was quenched by hydrochloric acid-*d* at an appropriate stage of the reaction, and the recovered starting material was submitted to NMR examination. The NMR spectra of the recovered **1a** showed that the methylene hydrogen atoms positioned α to the sulfonyl group were considerably displaced by deuterium atoms.[4] This observation suggests that a large portion of **1** must be converted into its conjugate base (carbanion) under the above conditions. Numerous examples illustrating the base-induced hydrogen exchange of methylene hydrogens positioned α to a sulfonyl group have been reported, and they have been explained on the basis of the formation of a carbanion stabilized by a strongly electron-withdrawing inductive effect of the sulfonyl group and a 3d-orbital resonance

with the adjacent sulfur atom.[6]

Since 2-phenylethyl 2-methyl-2-(phenylsulfonyl)propanoate (**2**) has no methylene hydrogens positioned α to the sulfonyl group, it is unlikely to anticipate **2** to

$$PhSO_2-\overset{\overset{CH_3}{|}}{\underset{\underset{CH_3}{|}}{C}}-COOCH_2CH_2Ph$$

2

give a carbanion similar to that of **1**. Accordingly, the reaction of **2** with potassium *t*-butoxide in absolute *t*-butyl alcohol was examined. The rate data and the activation parameters for the elimination reaction from **2** are also given in Table 1. As is shown in Table 1, the rate constant for the elimination from **2** is smaller than that for the elimination from **1a**. The values of the activation enthalpy and entropy for the elimination from **2** are quite different from those for the eliminations from **1a—d**. These results imply that the reaction mechanism of the elimination from **2** differs from that of **1**. It should be emphasized that a rapid formation of the carbanion occurs in the reaction of **1**, but not in the reaction of **2**. Judging from the facts described above, it is likely that the carbanion plays an important role in the olefin-forming elimination reaction of **1**. The carbanionic center thus formed in **1** should considerably lower the leaving ability of the leaving group ($ArSO_2CH_2COO^-$), thus decreases the rate of the E2 reaction of **1**. However, this is not the case. An alternative possibility is that the carbanionic center acts intramolecularly as an attacking base against β-hydrogen to promote the elimination; that is, an intramolecular carbanionic elimination takes place in the present case. A carbanionic mechanism has frequently been supposed to account for the *syn* eliminations in the systems where the favored *anti* co-planarity can not be readily attained.[7] However, the role of the carbanionic center in the present reaction is apparently distinct from those described in the literature.[7] It seems to act as a base to abstract β-hydrogen through a six-membered cyclic transition state. If so, the elimination should proceed in a *syn* fashion. Consequently, the stereochemistry of the elimination reaction was examined. The substrates used were two deuterium-labeled diastereoisomers of 1,2-diphenylethyl phenylsulfonylacetate (**3**)—that is, *dl-erythro-* and *dl-threo-*2-deuterio-1,2-diphenylethyl phenylsulfonylacetates (**4e** and **4t**).

$PhSO_2CH_2COOCHPhCH_2Ph$

3

$PhSO_2CH_2COOCHPhCHDPh$

4e, t

e, *erythro-*; **t**, *threo-*

The products resulting from the reaction of **3** or **4** with potassium *t*-butoxide in absolute *t*-butyl alcohol were found by gas chromatography to be *trans*-stilbene, 1,2-diphenylethanol, and methyl phenyl sulfone. No *cis*-stilbene was detected; that is, this elimination is stereoselective. Under the conditions employed, no isomerization from **4e** to **4t** or the reverse occurred, as checked by NMR. Both *trans*-stilbene and 1,2-diphenylethanol were quite stable under the conditions employed, as checked by gas chromatography. Furthermore, **4e** or **4t** recovered from the reaction mixture was found to retain its deuterium atom, as checked by NMR and mass spectrometries; that is, no D–H exchange was present. Also, no hydrogen exchange of *trans*-stilbene was observed with potassium *t*-butoxide in *t*-butyl alcohol-*O-d*. These observations clearly show that the stereochemistry of the elimination can be elucidated by examining the deuterium content of *trans*-stilbene obtained from **4e** and **4t**.

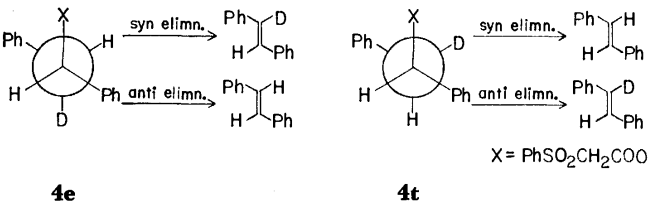

4e **4t**

Scheme 1.

From a consideration of a stereo-model of **4**, the most favorable conformations are those depicted in Scheme 1. If the elimination occurred in a *syn* fashion, **4e** should give *trans*-stilbene-α-*d*, while if it occurred in an *anti* fashion, **4e** should give *trans*-stilbene with no deuterium. On the other hand, **4t** should give *trans*-stilbene with no deuterium in a *syn* elimination, while in an *anti* elimination **4t** should give *trans*-stilbene-α-*d*. The deuterium contents of *trans*-stilbene obtained from the reactions of **4e** and **4t** with potassium *t*-butoxide in *t*-butyl alcohol were determined by mass spectrometry. The results are shown in Table 2. It is quite clear

Table 2. Deuterium contents of *trans*-stilbene obtained from *erythro-* and *threo*-2-deuterio-1,2-diphenylethyl phenylsulfonylacetates (**4e** and **4t**) with *t*-butoxide in *t*-butyl alcohol[a]

[*t*-BuOK] (M)	Deuterium content of *trans*-stilbene[c]	
	from **4e**[b] (%)	from **4t**[b] (%)
0.10	84.2±1.9	29.5±2.5
0.30	82.6±2.0	50.1±2.3
0.50	82.0±2.0	50.8±1.7
0.70	81.8±0.7	53.0±1.2
1.00	82.6±2.4	53.9±1.1
1.30	82.4±0.8	53.1±2.5

a) Reaction temperature was 90.0 °C. b) Initial concentration was [substrate] = 5.00×10^{-3}M. c) Deviations listed are standard deviations.

that the stereochemically-favored course of the elimination from **4** is *syn*, but the predominance of *syn* elimination is not overwhelming. It seems that a dual mechanism is operating in these eliminations—a predominant *syn* elimination accompanied by a concomitant *anti* elimination. The deuterium content of *trans*-stilbene obtained from the elimination of **4e** is almost independent of the concentration of the base, while that obtained from **4t** increases with an increase in the concentration of the base.

From these results, it can be concluded that the carbanion, the conjugate base of the substrate, is

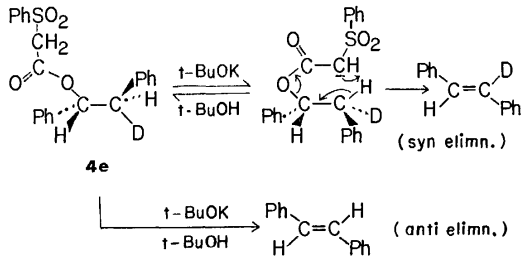

Scheme 2.

rapidly formed as an intermediate which successively undergoes the *syn* unimolecular elimination reaction through a six-membered cyclic transition state (Ei), as is depicted in Scheme 2. An *anti* elimination also occurs concomitantly with a *syn* elimination. A possible alternative may be a *syn* E2 mechanism. However, it is unlikely that a *syn* concerted bimolecular elimination occurs predominantly in the present case.[8]

Previously, Curtin and Kellom[3] treated *erythro*- and *threo*-2-deuterio-1,2-diphenylethyl acetates with potassium amide in liquid ammonia and explained their results in terms of the *syn* elimination mechanism. They proposed the cyclic mechanism, which had been rejected by Hauser, Shivers, and Skell[2] because an excess amide ion was required to convert 2-phenylethyl acetate into styrene. Our observations are compatible with Curtin's cyclic intramolecular mechanism for the *syn* elimination.[3] That the presence of the excess base is necessary to bring about the reaction effectively indicates that the excess base is required to displace the equilibrium toward carbanion formation.[4] As is shown in Scheme 2, in the *syn* elimination from **4e** to give *trans*-stilbene-α-*d* the β-proton should be abstracted by a base, the carbanionic center in **4e**. On the other hand, in the corresponding *anti* elimination from **4e** the β-deuteron should be abstracted by an external base, *t*-butoxide. The reverse operates in the elimination reaction from **4t**. Thus, the kinetic isotope effect may be thought to be responsible for the apparently higher *syn* path: *anti* path ratio for **4e** than for **4t** (Table 2). An increase in the fraction of a bimolecular elimination, which results from an increase in the base concentration, should be more significant in the reaction of **4t** than in that of **4e**, because the value of the primary kinetic isotope effect (k_H/k_D) for the *anti* elimination reaction of **4** must be appreciably higher than unity. Table 2 indicates that this is the case. Especially, a change in the base concentration from 0.1 to 0.3 M gives rise to a considerable increase in the fraction of *anti* elimination from **4t**; whereas the corresponding increase is not so significant in the case of **4e**. However, a leveling effect upon the change in deuterium content is observed with a further increase in the base concentration. This effect suggests a possibility of the contribution of ion pairs. A study of the effect of ion pairs will be presented elsewhere.

The *syn* elimination mechanism described above resembles the so-called α',β-elimination mechanism. Both reactions include the preliminary abstraction of hydrogen in the leaving groups, and both proceed through cyclic transition states. However, the α',β-elimination is mainly a reaction of an 'onium salt with an organometallic compound[9] and necessarily includes an ylide intermediate, which leads inevitably to a five-membered transition state; this is in contrast with the elimination from phenylsulfonylacetates with alkoxides described in the present paper.

Experimental

All the melting points are uncorrected. The NMR spectra were taken on a JEOL JNM-PS-100 spectrometer, using tetramethylsilane as the internal standard, and the UV spectra on a Shimadzu UV-200 double-beam spectrophotometer. The gas chromatographic analyses were performed by means of a JEOL JGC-20K (f.i.d.) gas chromatograph. The mass spectra were recorded on a Hitachi RMS-4 mass spectrometer connected with a Hitachi K-53 gas chromatograph.

Materials. All the carboxylic esters were prepared in the usual way from the corresponding acid chlorides and the alcohols. These alcohols and carboxylic acids were prepared using methods reported in the literature.

*2-Phenylethyl Phenylsulfonylacetate (**1a**).* Recrystallized from ethanol; mp 81.0—81.5 °C; NMR ($CDCl_3$) δ 2.78 (t, 2H), 4.06 (s, 2H), 4.21 (t, 2H), and 7.01—7.90 (m, 10H). Found: C, 62.99; H, 5.34%. Calcd for $C_{16}H_{16}O_4S$: C, 63.14; H, 5.30%.

*2-(p-Tolyl)ethyl Phenylsulfonylacetate (**1b**).* Recrystallized from ethanol; mp 76.0—76.5 °C; NMR ($CDCl_3$) δ 2.25 (s, 3H), 2.73 (t, 2H), 4.05 (s, 2H), 4.18 (t, 2H), 7.01 (s, 4H), and 6.91—7.91 (m, 5H). Found: C, 64.20; H, 5.69%. Calcd for $C_{17}H_{18}O_4S$: C, 64.13; H, 5.70%.

*2-(p-Chlorophenyl)ethyl Phenylsulfonylacetate (**1c**).* Recrystallized from ethanol; mp 56 °C; NMR ($CDCl_3$) δ 2.76 (t, 2H), 4.08 (s, 2H), 4.20 (t, 2H), 7.03 (d, 2H), 7.16 (d, 2H), and 7.36—7.89 (m, 5H). Found: C, 56.77; H, 4.45%. Calcd for $C_{16}H_{15}ClO_4S$: C, 56.72; H, 4.46%.

*2-Phenylethyl p-Tolylsulfonylacetate (**1d**).* Recrystallized from ethanol; mp 63.5—64.0 °C; NMR ($CDCl_3$) δ 2.39 (s, 3H), 2.80 (t, 2H), 4.04 (s, 2H), 4.22 (t, 2H), 7.03—7.32 (m, 7H), and 7.74 (d, 2H). Found: C, 64.37; H, 5.66; S, 10.19%. Calcd for $C_{17}H_{18}O_4S$: C, 64.13; H, 5.70; S, 10.07%.

*2-Phenylethyl 2-Methyl-2-(phenylsulfonyl)propanoate (**2**).* Purified by column chromatography on silica gel, with chloroform as the eluent. Viscous sirup; n_D^{25} 1.5510; NMR (CCl_4) δ 1.48 (s, 6H), 2.75 (t, 2H), 4.14 (t, 2H), and 6.97—7.76 (m, 10H). Found: C, 64.92; H, 6.07%. Calcd for $C_{18}H_{20}O_4S$: C, 65.04; H, 6.06%.

*1,2-Diphenylethyl Phenylsulfonylacetate (**3**).* Recrystallized from ethanol; mp 97.0—97.5 °C; NMR ($CDCl_3$) δ 3.10 (seven lines, 2H), 4.05 (s, 2H), 5.90 (t, 1H), and 6.99—7.79 (m, 15H). Found: C, 69.28; H, 5.32%. Calcd for $C_{22}H_{20}O_4S$: C, 69.45; H, 5.30%.

dl-erythro-*2-Deuterio-1,2-diphenylethanol.* This alcohol was prepared from *trans*-stilbene oxide by treatment with lithium aluminum deuteride, and was then recrystallized from hexane; mp 66—67 °C (lit,[3] 64.4—65.4 °C); NMR ($CDCl_3$) δ 2.43 (s, 1H), 2.77 (d, J=8 Hz, 1H), 4.51 (d, J=8 Hz, 1H), and 6.80—7.04 (m, 10H).

dl-threo-*2-Deuterio-1,2-diphenylethanol.* This alcohol was prepared from *cis*-stilbene oxide by treatment with lithium aluminum deuteride, and was then recrystallized from hexane; mp 66—67 °C (lit,[3] 64.4—65.4 °C); NMR ($CDCl_3$) δ 2.53 (s, 1H), 2.85 (d, J=5 Hz, 1H), 4.68 (d, J=5 Hz, 1H), and 7.00—7.28 (m, 10H).

dl-erythro-*2-Deuterio-1,2-diphenylethyl Phenylsulfonylacetate (**4e**).* Recrystallized from ethanol; mp 97.0—97.5 °C;

NMR ($CDCl_3$) δ 3.13 (d, J=8 Hz, 1H), 4.03 (s, 2H), 5.83. (d, J=8 Hz, 1H), and 6.94—7.74 (m, 15H).

dl-threo-*2-Deuterio-1,2-diphenylethyl Phenylsulfonylacetate (4t)* Recrystallized from ethanol; mp 97.0—97.5 °C; NMR ($CDCl_3$) δ 2.98 (d, J=6.5 Hz, 1H), 4.03 (s, 2H), 5.87 (d, J=6.5 Hz, 1H), and 6.97—7.80 (m, 15H).

Solvent and Base. *t*-Butyl alcohol was distilled twice from clean metallic sodium under anhydrous conditions. Potassium metal was cut clean of all oxides and rinsed in purified *t*-butyl alcohol. The metal was immediately transferred into an appropriate amount of anhydrous *t*-butyl alcohol and allowed to dissolve under anhydrous conditions.

Kinetic Measurements. The reactions of **1a—d** and **2** with potassium *t*-butoxide in *t*-butyl alcohol were carried out in a 20 ml flask. The initial concentration of the substrate was 5.00×10^{-3} M, while that of the base was 1.00 M. Runs were carried out in a thermostatted bath. The temperature was controlled within $\pm$0.05 °C. At appropriate intervals of time, 2 ml aliquots were withdrawn from the flask and quenched in ethanol—water (1: 1 by volume) in a 25 ml volumetric flask. The volumetric flask was filled to the mark with the ethanol—water mixture and shaken. The concentration of olefin in this solution was measured spectrophotometrically. The pseudo-first-order rate constants were obtained from the measured absorbances at the absorption maximum of styrene or substituted styrenes. Each rate constant was calculated by following the reaction till 10—15% completion; after that time a concomitant alcohol-forming reaction caused it to give complex kinetics. The molar extinction coefficients in ethanol—water (1: 1 by volume) are as follows: styrene, λ_{max} 248 nm (ε, 1.42×10^4); *p*-methylstyrene, λ_{max} 252 nm (ε, 1.66×10^4); and *p*-chlorostyrene, λ_{max} 253 nm (ε, 1.84×10^4).

Product Analysis. To a 20ml solution of potassium *t*-butoxide in absolute *t*-butyl alcohol, we added 0.100 mmol of the substrate. After having been maintained at 90.0 °C for 1 hr, the mixture was poured into water and extracted with ether. The ethereal solution was washed with water, dried, and analyzed by gas chromatography using a 2 m column of 2% PEG 20 M on Celite 545 (60—80 mesh) at 200 °C. The reaction products detected were *trans*-stilbene and 1,2-diphenylethanol.

Deuterium Analysis. To a 20 ml solution of potassium *t*-butoxide in absolute *t*-butyl alcohol, we added 0.100 mmol of the substrate (**4e** or **4t**). The mixture in a sealed ampoule was maintained at 90.0 °C for 1 hr and then treated in a manner similar to that above. The deuterium content of *trans*-stilbene was determined by mass spectrometry using a mass spectrometer connected with a gas chromatograph. The ionizing energy used for the analyses was 70 eV. The deuterium content was evaluated from the intensities of the corresponding mass peaks, corrected for the natural abundances of isotopes. The calculation method was based on the assumptions that hydrogen randomization precedes the formation of M^+–H· species from the stilbene molecular ion and that the value of the deuterium isotope effect (k_H/k_D) on fragmentation is unity.[10]

Control Experiments. When *cis*-stilbene was treated with potassium *t*-butoxide in *t*-butyl alcohol at 90.0 °C for 1.5 hr, it showed no detectable isomerization to *trans*-stilbene as checked by gas chromatography.

trans-Stilbene and 1,2-diphenylethanol were treated with potassium *t*-butoxide as has been described above. No detectable change was observed, as checked by gas chromatography.

The NMR spectrum of *trans*-stilbene treated with potassium *t*-butoxide in *t*-butyl alcohol-*O*-*d* as described above showed no H–D exchange. *t*-Butyl alcohol-*O*-*d* was prepared from potassium *t*-butoxide and deuterium oxide using a modification of a method described in the literature.[11] The isotopic purity of this alcohol was checked by NMR before use.

The starting ester (**4e** or **4t**) recovered from the reaction mixture showed neither interconversion into the corresponding epimer nor H–D exchange, as checked by NMR and mass spectrometries.

We wish to express our appreciation to Dr. Tamio Ueno, Kyoto University, and the staff of Hitachi, Ltd., for their valuable comments and co-operation in the mass spectrometry.

References

1) W. H. Saunders, Jr. and A. F. Cockerill, "Mechanisms of Elimination Reactions," John Wiley & Sons, New York, N. Y. (1973), p. 377.

2) C. R. Hauser, J. C. Shivers, and P. S. Skell, *J. Amer. Chem. Soc.*, **67**, 409 (1945).

3) D. Y. Curtin and D. B. Kellom, *ibid.*, **75**, 6011 (1953).

4) H. Mano and A. Sera, *Chem. Lett.*, **1972**, 495.

5) Similar base-induced eliminations were also observed for esters with active hydrogen atoms positioned α to the carboxyl group (for example, bis(1,2-diphenylethyl) malonate). Unpublished results.

6) D. J. Cram, "Fundamentals of Carbanion Chemistry," Academic Press, New York, N. Y. (1965), p. 105.

7) S. J. Cristol and his co-workers, *J. Amer. Chem. Soc.*, **69**, 338 (1947); **73**, 674 (1951); **79**, 3438, 3441 (1957).

8) W. F. Bayne and E. I. Snyder, *Tetrahedron Lett.*, **1971**, 571, and the references cited therein.

9) Recently, it was reported that 3-pentyldimethylsulfonium compounds are able to react *via* α',β-mechanism upon treatment with potassium *t*-butoxide in *t*-butyl alcohol; J. K. Borchardt, R. Hargreaves, and W. H. Saunders, Jr., *Tetrahedron Lett.*, **1972**, 2307.

10) P. F. Donaghue, P. Y. White, J. H. Bowie, B. D. Roney, and H. J. Rodda, *Org. Mass Spectrom.*, **2**, 1061 (1969).

11) A. Murray, III, and D. L. Williams, "Organic Syntheses with Isotopes," Interscience Publishers, New York, N. Y. (1958), p. 1341.

A Base-induced Elimination Reaction of Phenylsulfonylacetates. II. Effects of the Base and the Solvent on the Stereochemistry of Elimination

Hiroshi MANO, Akira SERA, and Kazuhiro MARUYAMA

Department of Chemistry, Faculty of Science, Kyoto University, Sakyo-ku, Kyoto 606

(Received December 27, 1973)

The base-induced elimination reaction[1] of 1,2-diphenylethyl phenylsulfonylacetate was investigated in a variety of base–solvent systems. A stronger base was found to facilitate *syn* elimination. The addition of crown ether caused a remarkable change in the stereochemistry of elimination from *syn* to *anti*. In aprotic solvents, an overwhelming *syn* elimination was observed.

In the preceding paper we reported that 1,2-diphenylethyl phenylsulfonylacetate (**1**) undergoes β-elimination with potassium *t*-butoxide in *t*-butyl alcohol, predominantly through a *syn* pathway.[1] An intervention of a carbanion intermediate was described, and a cyclic transition state for the *syn* elimination was proposed. It was also suggested that an ion pair or an ion aggregate more or less controlled the stereochemistry of elimination.

Pedersen[2] has shown that cyclic polyethers containing from five to ten oxygen atoms can form stable complexes with a potassium ion as well as with other cations. Recently, the cyclic polyethers have been used in studies of bimolecular elimination reactions exhibiting *syn–anti* dichotomy, and a pronounced effect of base ion-pairing and association on the stereochemistry of β-eliminations has been observed.[3-5] The present paper will deal with the effect of base association on the stereochemistry of the base-induced carbanionic elimination from 1,2-diphenylethyl phenylsulfonylacetate. Dicyclohexyl-18-crown-6 ether (**3**) was employed as a mechanistic probe.

Results and Discussion

The stereochemistry of elimination from 1,2-diphenylethyl phenylsulfonylacetate ($PhSO_2CH_2COOCHPh\text{-}CH_2Ph$, **1**) was examined under a variety of conditions. Four base–solvent systems, KOH–aq.EtOH, MeOK–MeOH, EtOK–EtOH, and *t*-BuOK–*t*-BuOH, were employed, as well as systems of *t*-BuOK in THF and DMF. The substrates examined in the present investigation were *dl-erythro-* and *dl-threo*-2-deuterio-1,2-diphenylethyl phenylsulfonylacetates (**2e** and **2t**). The reaction products from **1** and **2** were *trans*-stilbene, 1,2-diphenylethanol, and methyl phenyl sulfone. The deuterium content of *trans*-stilbene was examined in order to find out the stereochemical course of elimination. If the elimination were to occur in a *syn* fashion, **2e** should give *trans*-stilbene-α-*d* and **2t** should give *trans*-stilbene with no deuterium, while if it were to occur in an *anti* fashion, **2e** should give *trans*-stilbene with no deuterium and **2t** should give *trans*-stilbene-α-*d*.[1] Table 1 shows the results. The yield of *trans*-stilbene is also shown.

In protic solvents (water, methanol, ethanol, and *t*-butyl alcohol), the deuterium content of *trans*-stilbene produced from **2e** increases with the following order of base–solvent systems. KOH–aq.EtOH, MeOK–MeOH, EtOK–EtOH, *t*-BuOK–*t*-BuOH, while that produced from **2t** decreases with the same order; that is, the stereochemical course of the elimination reaction from **2** with potassium *t*-butoxide in *t*-butyl alcohol is more *syn*-favored. Since *t*-butoxide is stronger as a base, it seems to be more effective to form a carbanion positioned α to the sulfonyl group of the substrate. The fact that the *syn* elimination reaction is caused by this carbanion was pointed out in the preceding paper.[1] These observations imply that the *syn* elimination from **2** is facilitated by the use of a stronger base, *t*-butoxide, in a solvent of a low dielectric constant, *t*-butyl alcohol. In addition, an ion pairing or ion aggregation of the base must be operating in the present base–solvent system, because it was necessary to employ a rather high base concentration in order to bring about the reaction effectively. It was suggested by Závada and Svoboda[6] that both the dissociated and ion-paired bases take part in the elimination reactions of cycloalkyl tosylates simultaneously; the former prefers an *anti* elimination, and the latter, a *syn*. Very recently, evidence has been presented to indicate that the base association is one of the essential requisites for *syn* elimination by using a macrocyclic polyether.[3-5] Macrocyclic polyethers (crown ethers) are known to co-ordinate with alkali metal cations; hence, they convert contact ion pairs into separated ions.[7,8] Accordingly, the effect of dicyclohexyl-18-crown-6 ether (**3**) was investigated.

The results shown in Table 1 clearly indicate that the

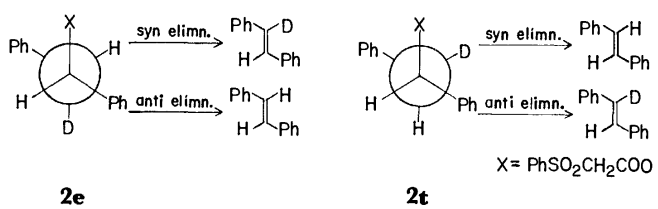

2e **2t**

Scheme 1.

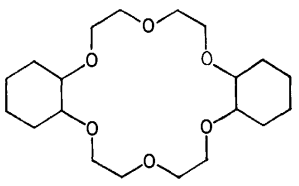

3

Table 1. Deuterium contents and yields of *trans*-stilbene obtained from *erythro*- and *threo*-2-deuterio-1,2-diphenylethyl phenylsulfonylacetates (**2e** and **2t**) with bases[a]

Base	Solvent	From **2e**[b]		From **2t**[b]	
		D-content[c] (%)	(Yield)[d] (%)	D-content[c] (%)	(Yield)[d] (%)
0.50 M KOH	EtOH–H_2O[e]	70.9±1.4	(7)	56.3±0.9	(7)
0.50 M MeOK	MeOH	71.0±3.7	(9)	52.3±2.8	(10)
0.50 M EtOK	EtOH	72.6±1.4	(14)	51.6±2.6	(12)
0.50 M *t*-BuOK	*t*-BuOH	82.0±2.0[f]	(4)	50.8±1.7[f]	(3)
1.00 M *t*-BuOK	*t*-BuOH	82.6±2.4[f]	(12)	53.9±1.1[f]	(11)
0.50 M *t*-BuOK	*t*-BuOH+**3**[g]	28.5±0.8	(—)	91.2±1.3	(—)
1.00 M *t*-BuOK	*t*-BuOH+**3**[h]	24.7±1.1	(—)	91.7±3.0	(—)
0.50 M *t*-BuOK	THF	93.8±1.8	(100)	21.4±1.6	(100)
1.00 M *t*-BuOK	THF	102.5±6.3	(100)	23.8±1.7	(100)
0.50 M *t*-BuOK	DMF	97.2±5.7	(100)	41.6±2.4	(100)
1.00 M *t*-BuOK	DMF	98.2±6.8	(100)	37.9±0.9	(100)

a) Reaction temperature was 90.0 °C (1 hr). b) Initial concentration was [substrate]$=5.00\times10^{-3}$M. c) Deviations listed are standard deviations. d) Overall yield of *trans*-stilbene. e) EtOH–H_2O; 80:20 by volume. f) Taken from Ref. 1. g) Concentration of crown ether **3** was 0.50 M. h) Concentration of crown ether **3** was 1.00 M.

addition of an equimolar amount of the crown ether, **3**, to the reaction mixture effected a remarkable change in the stereochemical course of the elimination. The deuterium contents of *trans*-stilbene produced show that the elimination reaction proceeds, for the most part, in an *anti* fashion in the presence of **3**. Roitman and Cram[8] studied the effect of crown ether on the rates and the stereochemical course of a potassium *t*-butoxide-catalyzed carbanion-generating reaction in *t*-butyl alcohol. They showed that the presence of crown ether dramatically increased the rates of both isotopic exchange and racemization. The occupation of the co-ordination sites of the potassium ion by crown ether was thought to be responsible for the restricted availability of these sites to both the leaving and entering groups in the reaction. Thus, the possibility of the association of a carbanion with the potassium ion complexed with crown ether was suggested.

A similar concept can account well for the present preferential *anti* elimination observed in the presence of **3** (Table 1). In *t*-butyl alcohol, the potassium ion was thought to associate with the carbanionic center of the substrate. In the presence of crown ether, the added ether must occupy a part of the co-ordination sites of the potassium ion. In the present case, however, the complexed potassium ion is supposed to be still held in the neighborhood of the carbanionic center of the substrate; hence, the carbanion may be prevented from taking the favored position for the intramolecular abstraction of the β-proton at the front face. Undoubtedly, the low dielectric nature of *t*-butyl alcohol plays an important role in the ion pairing between the carbanion and the complexed potassium ion.[9] Furthermore, it is known that a phenylsulfonyl group is one of the functional groups that induce carbanion asymmetry.[10] Consequently, the carbanion positioned α to the sulfonyl group is unable to react at the backside. On the other hand, since ion-paired potassium *t*-butoxide is forced to dissociate more or less by the added crown ether,[7] and since the thus-dissociated *t*-butoxide possesses a much greater kinetic basicity than ion-paired *t*-butoxide,[8] a bimolecular reaction with *t*-butoxide may be accelerated. Therefore, the addition of the crown ether could depress the *syn* elimination reaction and increase the *anti* elimination.

In aprotic solvents (THF and DMF), the deuterium contents of *trans*-stilbene produced indicate that the stereochemical course of the elimination reaction is more *syn*-favored than in *t*-butyl alcohol. Recently, it was reported that, in a bimolecular elimination with potassium *t*-butoxide, both the addition of the crown ether and the change in solvent from *t*-butyl alcohol to DMF operate to increase the *anti* pathway.[3] However, in the present case, the change in solvent from *t*-butyl alcohol to aprotic solvents operates to increase the *syn* pathway. This result can also be explained on the basis of the *syn* elimination mechanism described in the preceding paper.[1] It was shown there that the *syn* elimination requires the carbanion positioned α to the sulfonyl group of the substrate as an effective base. In THF and DMF, the potassium cation must be solvated nucleophilically; hence, the reactivity of the carbanion is increased. Consequently, the *syn* elimination may be highly favored.[11]

No interconversion between **2e** and **2t** was observed with *t*-butoxide in *t*-butyl alcohol.[1] However, in THF and DMF the base-induced interconversion was observed. Preliminary experiments showed that, in the reaction of **2e** with potassium *t*-butoxide in THF or DMF, the recovered ester[12] consisted of **2e** and **2t** (approximately 1 : 1), while in the reaction of **2t** under the same conditions the recovered ester[12] consisted of **2t** only. These results may reasonably be understood in terms of the existence of carbanion intermediates which are responsible for the interconversion of the ester. The kinetic isotope effect will make the rate of *syn* elimination from **2e** faster than that from **2t**. Therefore, the **2e** produced by the isomerization of **2t** is assumed to be exhausted, resulting in the absence of **2e** in the reaction mixture. If this is the case, the *syn*

selectivities for **2e** and **2t** must be larger than the values presented in Table 1.[13]

The reactions of **1** and **2** with potassium *t*-butoxide in DMSO were also examined. However, in DMSO, *trans*-stilbene produced reacted further with the solvent to give secondary products. The details will be reported elsewhere.

Experimental

Materials. Compounds **1**, **2e**, and **2t** have been described previously.[1] Crown ether **3** (2,5,8,15,18,21-hexaoxatricyclo[20.4.0.0^{9,14}]hexacosane) was prepared as has been described in the literature.[2]

Solvents and Bases. *t*-Butyl alcohol was purified as previously reported.[1] Ethanol and methanol were treated with magnesium and distilled twice under anhydrous conditions. Tetrahydrofuran was dried over sodium and distilled from lithium aluminum hydride under anhydrous conditions. *N,N*-dimethylformamide and dimethyl sulfoxide were treated with calcium hydride and distilled under reduced pressure. The alkoxide solutions were prepared from freshly-cut potassium metal and the appropriate alcohol under anhydrous conditions.

Product Analysis. The procedures employed were similar to those described in the preceding paper.[1] The reactions were performed by the sealed-ampoule technique, and the quantitative analyses of the reaction products were carried out by means of gas chromatography. The deuterium content of *trans*-stilbene was determined by mass spectrometry. The mass spectra were recorded on a Hitachi RM-50GC g.c. mass spectrometer at 70 eV.

We wish to express our appreciation to Professor Rikisaku Suemitsu for his help with the mass spectrometry.

References

1) A. Sera, H. Mano, and K. Maruyama, This Bulletin, **47**, 1754 (1974).
2) C. J. Pedersen, *J. Amer. Chem. Soc.*, **89**, 7017 (1967).
3) M. Svoboda, J. Hapala, and J. Závada, *Tetrahedron Lett.*, **1972**, 265.
4) J. Závada, M. Svoboda, and M. Pánková, *ibid.*, **1972**, 711.
5) R. A. Bartsch and K. E. Wiegers, *ibid.*, **1972**, 3819.
6) J. Závada and M. Svoboda, *ibid.*, **1972**, 23.
7) K. H. Wong, G. Konizer, and J. Smid, *J. Amer. Chem. Soc.*, **92**, 666 (1970).
8) J. N. Roitman and D. J. Cram, *ibid.*, **93**, 2231 (1971).
9) J. Závada, M. Pánková, and J. Sicher, *Chem. Commun.*, **1968**, 1145.
10) D. J. Cram, "Fundamentals of Carbanion Chemistry," Academic Press, New York, N. Y. (1965), p. 105.
11) One can also anticipate that potassium *t*-butoxide must dissociate more or less in DMF, and that the dissociated *t*-butoxide must operate as a strong base in the *anti* elimination, just as has been observed for usual E2 reactions. However, this is not the case. The reason for those conflicting observations remains to be determined.
12) Unpublished results. Recovered at an about 50% completion of the reaction at 25 °C. Analysis was performed by NMR.
13) Investigations of this problem are now in progress.

Optically Active Triptycenes. VII.[1] Synthesis, Optical Resolution and Absolute Configuration of 3-Chloro and 4-Chloro-7-substituted Triptycenes.

Michiaki HASHIMOTO, Yasumi SHIMIZU, Fumio OGURA, and Masazumi NAKAGAWA

Department of Chemistry, Faculty of Science, Osaka University, Toyonaka, Osaka 560

(Received February 2, 1974)

Isomeric 3- or 4-chlorotriptycene-7-carboxylic acid was synthesized from sodium anthraquinone-β-sulfonate and resolved with quinidine methohydroxide. The absolute configurations of (−)-3-chloro- and (−)-4-chlorotriptycene-7-carboxylic acids could be determined to be 1*S*,6*S* and 1*S*,6*R*, respectively, by the chemical correlation with (+)-2,5-dimethoxy-8-chlorotriptycene whose absolute configuration was proved to be 1*R*,6*S* by X-ray and chemical means.

The synthesis, optical resolution and absolute configuration of 2,5,7-[2] and 2,5,8-trisubstituted triptycenes[3] and 2,5- and 2,7-disubstituted triptycenes[4,5] as well as the analysis of CD spectra of these and related compounds[6] have been reported. The present paper deals with the synthesis, optical resolution of 3- or 4-chloro-7-substituted triptycenes and the determination of their absolute configuration by chemical correlation which were performed with the purpose of clarifying the effect of difference in the mode of coupling on chiroptical properties.

Synthesis and Optical Resolution. The route of synthesis is outlined in Scheme 1. Chloronitroanthraquinone (IIIa or IIIb) was prepared starting from sodium anthraquinone-β-sulfonate (I) *via* sodium nitroanthraquinonesulfonate (IIa or IIb) according to a modified method of Fierz-David.[7] Aminochloroanthraquinone (IVa or IVb) obtained by reduction of the nitro compound (IIIa or IIIb) with sodium sulfide was converted into nitrile (Va or Vb) by the Sandmeyer reaction. Acid hydrolysis of the nitrile (Va or Vb) afforded carboxychloroanthraquinone (VIa or VIb), which was reduced with zinc dust and aqueous ammonia to give 6- or 7-chloroanthracene-1-carboxylic acid (VIIa or VIIb). The acid (VIIa or VIIb) was converted into methyl or ethyl ester (VIIIa or VIIIb) by the usual method.

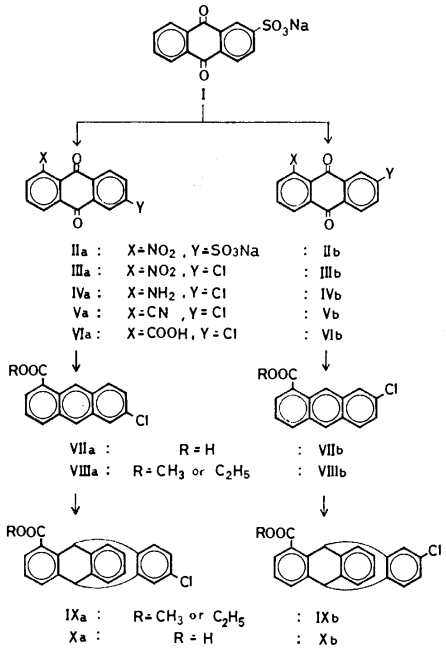

Scheme 1. Synthesis of 3,7- and 4,7-disubstituted triptycenes.

Reaction of benzyne generated by the decomposition of benzenediazonium carboxylate[8] with the ester (VIIIa or VIIIb) gave 3- or 4-chloro-7-methoxy(or ethoxy)carbonyltriptycene (IXa or IXb). Ethyl esters gave a less satisfactory result with respect to the yield and crystallinity. No significant increase in the yield of IX could be attained by varying the solvent from dichloromethane to 1,2-dimethoxyethane.[9]

The IR spectrum of IXa is almost superimposable with that of IXb, the difference in their NMR spectra being distinct in the region of aromatic protons. Racemate of 3- or 4-chlorotriptycene-7-carboxylic acid (Xa or Xb) was obtained hydrolyzing the ester (IXa or IXb) by the usual method. After several unsuccessful trials, optical resolution of Xa or Xb was accomplished with equimolar quinidine methohydroxide.[10] (−)-3-Chloro-7-carboxytriptycene (Xa) and (−)-4-chloro-7-carboxytriptycene (Xb) were isolated from the optically pure salts by decomposition with hydrochloric acid.

Absolute Configuration. Relative and absolute configurations of (−)-Xa and (−)-Xb were determined by chemical means as shown in Scheme 2. (−)-Xa

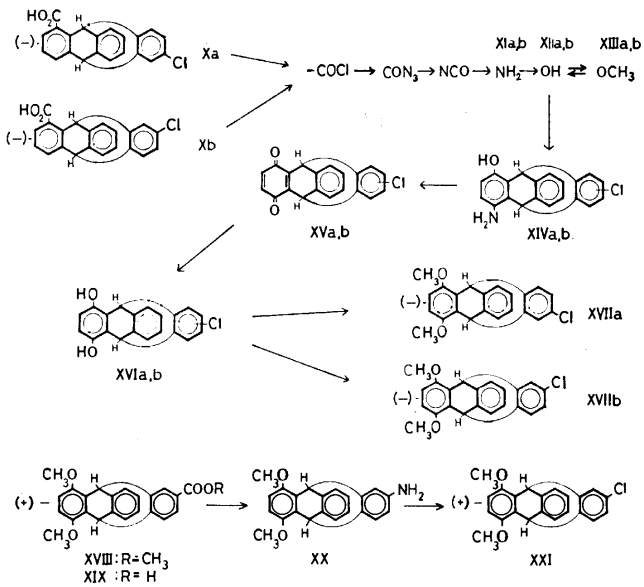

Scheme 2. Chemical correlation.

and (−)-Xb were converted into amine (XIa) and (XIb), respectively, by the Curtius reaction *via* acid chloride, acid azide, and isocyanate. In the case of XIb, a certain amount of urea derivative possibly resulting from the reaction of isocyanate with XIb was isolated. Phenols (XIIa and XIIb) were obtained by hydrolysis of diazonium salts of the amines (XIa and XIb) and purified as methyl ethers (XIIIa and XIIIb). Coupling of diazotized sulfanilic acid with the pure phenol (XIIa or XIIb) followed by reduction afforded *p*-aminophenol derivative (XIVa or XIVb) which was oxidized with ferric sulfate to yield *p*-benzoquinone derivative (XVa or XVb). Attempts to obtain the *p*-benzoquinone derivative (XVa or XVb) directly from the amine (XIa or XIb) by oxidation with sodium dichromate or chromium trioxide were unsuccessful, the only product isolated being 2-chloroanthraquinone. Oxidation of the phenol (XIIa or XIIb) with potassium nitrosodisulfonate or chromium trioxide gave the quinone (XVa or XVb) in a very poor yield, 2-chloroanthraquinone being isolated also in the case of chromium trioxide. Hydroquinone derivative (XVIa or XVIb) obtained from the quinone (XVa or XVb) by reduction with sodium hydrosulfite was converted into dimethyl ether (XVIIa or XVIIb) with dimethyl sulfate. The dimethyl ether derivatives thus prepared were found to be the same, including their chiroptical properties.

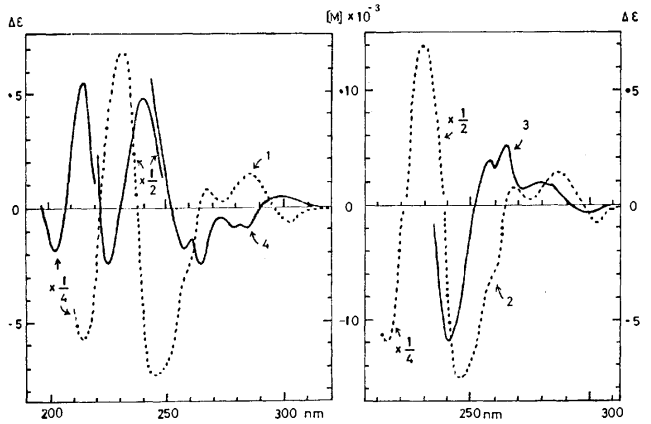

Fig. 1. CD (——) and ORD (----) spectra of (−)- and (+)-2,5-dimethoxy-8-chlorotriptycenes.
1: (−)-XVIIa, 2,3: (−)-XVIIb, 4: (+)-XXI

On the other hand, (+)-1*R*,6*S*-2,5-dimethoxy-8-methoxycarbonyltriptycene (XVIII)[3] was hydrolyzed to carboxylic acid (XIX) and then converted into amine (XX) by the Curtius reaction. (+)-2,5-Dimethoxy-8-chlorotriptycene (XXI) prepared from the amine (XX) by the Sandmeyer reaction was found to be the same as the above-mentioned chlorides (XVIIa and XVIIb) in melting point, IR, UV, and NMR spectra, but their chiroptical properties were antipodal (Fig. 1). The absolute configuration of (−)-2,5-dimethoxy-8-chlorotriptycene (XVII) was thus determined to be 1*S*,6*R*. Consequently the absolute configuration of (−)-3-chlorotriptycene-7-carboxylic acid (Xa) and (−)-4-chlorotriptycene-7-carboxylic acid (Xb) could be assigned to be 1*S*,6*S* and 1*S*,6*R*, respectively, on the combined evidence of X-ray[11] and chemical correlation.[3] Recently the X-ray crystal structure analysis was carried out on a single crystal of (+)-XXI. The absolute configuration was shown to be 1*R*,6*S* by the Bijvoet method[12] which is consistent with the results of chemical correlation.

Experimental

The melting points were measured on a Mettler FP2 apparatus and a Shimazu Kohfler micro hot stage, and are uncorrected. Purified and anhydrous solvents were used throughout the whole experiments, unless otherwise stated. The IR spectra were obtained on a Hitachi EPI-2 or a JASCO DS-301 spectrometer, electronic spectra on Hitachi EPS-3T and Zeiss PMQII4QIIId sopectrometers, NMR spectra in deuteriochloroform on a Varian A-60 spectrometer using TMS as an internal standard and given in τ-units. The optical rotations and CD spectra were obtained on Rudolf 200S-80, Yanagimoto ORD-185 spectropolarimeter, Roussel Jouan Dichrograph B, II-CD-185 and JASCO J-20 spectrometers, respectively. Shoulders and inflections are denoted by an asterisk.

6-Chloro-1-nitroanthraquinone (IIIa) and 7-Chloro-1-nitroanthraquinone (IIIb). The synthesis was performed by the reported method[7] with some modification. Sodium anthraquinone-β-sulfonate (310 g, 1 mol), dried thoroughly at 150 °C *in vacuo*, was added to 100% sulfuric acid (620 g) in small portions under stirring. To the dark brown solution was added dropwise at 90—95 °C a mixture of fuming nitric acid (d=1.52, 82 g) and 100% sulfuric acid (82 g). The reaction mixture containing yellow precipitates was heated to 100 °C for 30 min. The cooled reaction mixture was added to cold water (1.5 l). To the clear solution obtained on heating the mixture was added sodium chloride (82 g) to precipitate yellow crystals which were recrystallized from boiling water (1 l) to give sodium 1-nitroanthraquinone-6-sulfonate (IIa). 1-Nitro-7-sulfonate (IIb) in the mother liquor was not isolated as solid and subjected directly to further reaction.

1-Nitro-6-sulfonate (IIa) was dissolved in water (2.5 l) and mixed with concd. hydrochloric acid (460 g). To this solution was added at 100 °C dropwise an aqueous sodium chlorate (80 g in 800 ml) for 3 hr under stirring. After the mixture had been stirred for further 24 hr at 100 °C, light yellow precipitates were collected by filtration from the hot solution and recrystallized from benzene to give 6-chloro-1-nitroanthraquinone (IIIa 190 g, 22% based on I). 1-Nitro-7-chloro-isomer (IIIb) was prepared from 1-nitro-7-sulfonate (IIb) by essentially the same procedure and purified by recrystallization from benzene (180 g, 21% based on I).

1,6-Isomer: Mp 274—275 °C, light yellow rods (sublimed from *ca.* 220 °C), IR (KBr-disk): $\nu_{C=O}$ 1680 cm^{-1}.

Found: C, 58.34; H, 2.18%. Calcd for $C_{14}H_6O_4NCl$: C, 58.45; H, 2.11%.

1,7-Isomer: Mp 256—257 °C, yellow needles (sublimed from *ca.* 230 °C), IR (KBr-disk): $\nu_{C=O}$ 1682, 1670 cm^{-1} (doublet).

Found: C, 58.63; H, 2.22%. Calcd for $C_{14}H_6O_4NCl$: C, 58.45; H, 2.11%.

1-Amino-6-chloroanthraquinone (IVa) and 1-Amino-7-chloroanthraquinone (IVb). A stirred suspension of IIIa (50 g) in water (1.4 l) containing sodium sulfide (130 g) was refluxed for 4.5 hr. After cooling, red precipitates were collected by filtration and crystallized from benzene to yield IVa as dark red needles (34 g, 79.1%), mp 214—216 °C (sublimed from *ca.* 150 °C), IR (KBr-disk): ν_{NH} 3440, 3320, $\nu_{C=O}$ 1665, 1645 cm^{-1}.

Found: C, 65.16; H, 2.96%. Calcd for $C_{14}H_8O_2NCl$: C, 65.26; H, 3.13%.

The product obtained on treatment of IIIb by essentially the same procedure was recrystallized from benzene to afford IVb (83.9%) as bright brick red needles, mp 234—235 °C, IR (KBr-disk): ν_{NH} 3445, 3340, $\nu_{C=O}$ 1670, 1635 cm^{-1}.

Found: C, 65.40; H, 3.20%. Calcd for $C_{14}H_8O_2NCl$: C, 65.26; H, 3.13%.

6-Chloro-1-cyanoanthraquinone (Va) and 7-Chloro-1-cyanoanthraquinone (Vb). To a vigorously stirred solution of IVa (35 g, 0.13 mol) in concd. sulfuric acid (175 ml) was added powdered sodium nitrite (12.2 g, 0.18 mol) in small portions over a 40 min-period. Cracked ice (115 g) was added to the dark brown mixture maintaining the temperature at 50—60 °C. After stirring for further 1 hr, the mixture was poured onto ice (530 g) to precipitate diazonium salt. A suspension of the diazonium salt in water (900 ml) was added dropwise to an aqueous solution (350 ml) of copper sulfate (63 g) and potassium cyanide (70 g) maintained at 70 °C. After the mixture was stirred for 40 min at 100 °C, precipitate was collected by filtration and digested with 3 M nitric acid to yield brown crystals. Recrystallization of the crystals from toluene afforded pure Va as brown needles (28.0 g, 79.4%), mp 299.5—300.5 °C (decomp.) in a sealed tube, IR (KBr-disk): ν_{CN} 2220, $\nu_{C=O}$ 1680 cm^{-1}.

Found: C, 67.31; H, 2.29%. Calcd for $C_{15}H_6O_2NCl$: C, 67.31; H, 2.26%.

Application of a similar procedure to 1-amino-6-chloro-isomer (IVb) afforded Vb (crude yield 90%). Prolonged reaction time of diazotization resulted in a better yield of Vb. Recrystallization of crude product from benzene gave pure Vb as yellowish green needles, mp 299—300 °C (decomp.), IR (KBr-disk): ν_{CN} 2235, $\nu_{C=O}$ 1680 cm^{-1}.

Found: C, 67.31; H, 2.21%. Calcd for $C_{15}H_6O_2NCl$: C, 67.31; H, 2.26%.

6-Chloroanthracene-1-carboxylic Acid (VIIa) and 7-Chloroanthracene-1-carboxylic Acid (VIIb). Water (223 ml) was added dropwise under stirring to an ice-cooled solution of Va (55.7 g, 0.20 mol) in concd. sulfuric acid (668 ml). The mixture was heated to 160—170 °C for 4 hr and then poured into cold water (1 l) to give a black purple precipitate of VIa. To a stirred purple red solution of crude VIa in 15% aqueous ammonia was added zinc dust at 80—90 °C. Occasional addition of aqueous ammonia and zinc dust gave a greyish green suspension in *ca.* 7 hr. Brown filtrate, after treatment with active charcoal, was acidified with concd. hydrochloric acid to precipitate yellowish green VIIa (52.0 g, 97.1%). The precipitate could be used for esterification without further purification. Pure VIIa was obtained by recrystallization from toluene as greenish yellow needles, mp 258—266 °C (decomp.), IR (Nujol mull): $\nu_{C=O}$ 1685 cm^{-1}.

A similar reaction applied to Vb afforded VIIb (95.6%), which could be used directly for further reactions. Pure VIIb was obtained by recrystallization from benzene as yellow needles, mp 262—264 °C (decomp.), IR (Nujol mull): $\nu_{C=O}$ 1680 cm^{-1}.

6-Chloro-1-ethoxy(or methoxy)carbonylanthracene (VIIIa) and 7-Chloro-1-ethoxy(or methoxy)carbonylanthracene (VIIIb).

VIIIa (ethyl ester): To a solution of VIIa (17.8 g, 0.0690 mol) in ethanol (1500 ml) was added dropwise concd. sulfuric acid (150 nil) and the mixture was refluxed for 13 hr. After removal of a major portion of ethanol under reduced pressure, the reaction mixture was poured into water (1 l) and extracted with benzene. The extract, after being washed and dried, was concentrated under reduced pressure to yield brown crystals, which were dissolved in benzene and passed through a short column of alumina. Yellow crystals obtained by drying up benzene eluate under reduced pressure were recrystallized from ligroin to give pure VIIIa as yellow needles (14.1 g, 71.4%), mp 113—114 °C, IR (KBr-disk): $\nu_{C=O}$ 1718 cm^{-1}.

Found: C, 71.69; H, 4.58%. Calcd for $C_{17}H_{13}O_2Cl$: C, 71.71; H, 4.60%.

VIIIa (methyl ester): A mixture of VIIa (35 g), methanol (3 l) and concd. sulfuric acid (300 ml) was refluxed for 15 hr. Yellowish brown crystals deposited on cooling the mixture were collected by filtration. The filtrate neutralized by sodium hydrogen carbonate and concentrated under reduced pressure was poured into water and extracted with benzene. The extract was worked up in the usual way to give an additional amount of VIIIa (6 g). Benzene solutions of both crops of crystals were passed through short columns of alumina and the crystals obtained from the filtrates were recrystallized from benzene to afford pure material, yellow needles (total 28.1 g, 76.8%), mp 130—131 °C, IR (KBr-disk): $\nu_{C=O}$ 1710 cm^{-1}.

Found: C, 71.12; H, 4.10%. Calcd for $C_{16}H_{11}O_2Cl$: C, 70.98; H, 4.10%.

VIIIb (ethyl ester): By a similar procedure to that used for VIIIa, VIIb was converted into ethyl ester which was recrystallized from ligroin to give pure substance, yellow needles, mp 91—92 °C, IR (KBr-disk): $\nu_{C=O}$ 1718 cm^{-1}.

Found: C, 71.75; H, 4.61%. Calcd for $C_{17}H_{13}O_2Cl$: C, 71.71; H, 4.60%.

VIIIb (methyl ester): Treatment of VIIb by a similar procedure to that used for VIIIa afforded methyl ester, yellow needles, mp 128—129 °C (from methanol), IR (KBr-disk): $\nu_{C=O}$ 1710 cm^{-1}.

Found: C, 70.71; H, 4.13%. Calcd for $C_{16}H_{11}O_2Cl$: C, 70.98; H, 4.10%.

3-Chloro-7-ethoxy(or methoxy)carbonyltriptycene (IXa) and 4-Chloro-7-ethoxy(or methoxy)carbonyltriptycene (IXb). IXa (ethyl ester): To a gently refluxing mixture of VIIIa (ethyl ester, 12.3 g, 0.0432 mol), isoamyl nitrite (7.2 g, 0.0615 mol) and dichloromethane (200 ml) was added dropwise a solution of anthranilic acid (7.8 g, 0.0569 mol) in acetone (40 ml) under stirring over a period of 9.25 hr. After removal of volatile components under reduced pressure, xylene (123 ml) and maleic anhydride (6 g, 0.06 mol) were added. The mixture was refluxed for 1 hr and poured into cold water (360 ml). This was extracted with dichloromethane and the extract was worked up in the usual way to give a red brown oil. A benzene solution of the crude material was chromatographed on alumina to remove unreacted anthracene ester (VIIIa). The desired product (IXa) was obtained as colorless liquid (10.0 g, 63.5%), which was identified by NMR spectroscopy [NMR (CCl_4): 8.65 (t, CH_3), 5.65 (q, CH_2), 4.72 (s, bridgehead C^6), 2.29—3.34 (m, aromatic and bridgehead C^1)]. The reaction carried out in 1,2-dimethoxyethane reduced the yield of adduct to 52.5%. The compound showed an almost identical IR spectrum (Nujol mull) with that of IXb (ethyl ester).

IXa (methyl ester): By essentially the same procedure, VIIIa (methyl ester) could be converted into IXa (methyl ester), colorless rods, mp 153—155 °C (from methanol), IR (KBr-disk): $\nu_{C=O}$ 1718 cm^{-1}.

Found: C, 75.76; H, 4.34; Cl, 10.64%. Calcd for $C_{22}H_{15}O_2Cl$: C, 76.19; H, 4.36; Cl, 10.22%.

IXb (ethyl ester): This was prepared according to the method used for IXa (ethyl ester) in yields of 58.9% (in dichloromethane) and 38.1% (in dimethoxyethane), colorless needles, mp 178—180 °C (from methanol), NMR (CCl_4): 8.65 (t, CH_3), 5.66 (q, CH_2), 4.76 (s, bridgehead C^6), 2.29—3.34 (m, aromatic and bridgehead C^1).

Found: C, 76.48; H, 4.70%. Calcd for $C_{23}H_{17}O_2Cl$: C, 76.55; H, 4.75%.

IXb (methyl ester): The ester was prepared from VIIIb (methyl ester) by essentially the same procedure in 63% yield, colorless leaflets, mp 192.5—193.5 °C (from methanol), IR (KBr-disk): $\nu_{C=O}$ 1720 cm^{-1}.

Found: C, 75.81; H, 4.43; Cl, 10.02%. Calcd for $C_{22}H_{15}O_2Cl$: C, 76.19; H, 4.36; Cl, 10.22%.

3-Chlorotriptycene-7-carboxylic Acid (Xa). From Ethyl Ester (IXa): IXa (ethyl ester, 10.0 g, 0.0277 mol) dissolved in 99% ethanol (1400 ml) was mixed with powdered potassium hydroxide (7.8 g) and water (800 ml). The mixture was refluxed for 24 hr and then concentrated *in vacuo* to remove the solvent. A small amount of water was added to the hot residue until a faint turbidity was produced and the mixture was allowed to stand to precipitate colorless leaflets. The potassium salt collected by filtration was washed with ether and dissolved in a small amount of 99% ethanol. The ethanol solution was mixed with concd. hydrochloric acid and extracted with ether. The extract was worked up in the usual way to give Xa (5.0 g). An additional amount of Xa was obtained from the filtrate of the potassium salt (total yield 6.7 g, 72.7%). Combined crystals were recrystallized from ligroin to give pure Xa, colorless needles, mp 227—228 °C (sublimed from *ca.* 195 °C), IR (KBr-disk): $\nu_{C=O}$ 1685 cm^{-1} (the IR spectrum was found to be similar to that of Xb over the entire region), UV: $\lambda_{max}^{95\%EtOH}$ (ε) 292.5 (4190), 279.5 (4000), 270* (2240), 240* (12700), 217.5 (50400), 207.5 (61700) nm.

Xa could be obtained also by hydrolysis in acetic acid with 3 M sulfuric acid in 81% yield, but above-stated alkaline hydrolysis was superior as regards the purity of product.

Found: C, 75.92; H, 4.09%. Calcd for $C_{21}H_{13}O_2Cl$: C, 75.79; H, 3.94%.

From Methyl Fster (IXa): An alkaline hydrolysis of IXa (methyl ester) under the above-mentioned conditions afforded Xa in 96.3% yield.

4-Chlorotriptycene-7-carboxylic Acid (Xb). Hydrolysis of IXb (ethyl or methyl ester) according to the method used in the preparation of Xa gave Xb in 90 or 99% yield, respectively, mp 243—245 °C (from ligroin), IR (KBr-disk): $\nu_{C=O}$ 1685 cm^{-1}, UV: $\lambda_{max}^{99\%EtOH}$ (ε) 293 (4170), 278.5 (4070), 270* (2320), 240* (12200), 216.5* (53500), 209 (60800), 203* (53000) nm.

Found: C, 75.81; H, 3.83%. Calcd for $C_{21}H_{13}O_2Cl$: C, 75.79; H, 3.94%.

Optical Resolution of (±)-3-Chlorotriptycene-7-carboxylic Acid (Xa). Xa (2.157 g, 0.00648 mol) dissolved in 99% ethanol (40 ml) was mixed with aqueous quinidine methohydroxide (0.592 M, 10.9 ml, 0.0065 mol). After being left to stand overnight, the solvent was removed under reduced pressure and partly crystalline residue was recrystallized from dioxane. Repeated fractional recrystallization (7 times) afforded colorless crystals of optically pure salt, 0.389 g, mp 177—179 °C, $[\alpha]_{600}^{17.5}$ +95.10°, $[\alpha]_{589}^{17.5}$ +97.96°, $[\alpha]_{500}^{17.5}$ +154.7°, $[\alpha]_{400}^{17.5}$ +326.1° (*c* 0.490, EtOH). The crystals contained two molecules of dioxane as a solvent of crystallization and were slightly hygroscopic.

Found: C, 70.66; H, 6.47; N, 3.53%. Calcd for $C_{42}H_{39}N_2O_4 \cdot 2C_4H_8O_2$: C, 70.86; H, 6.54; N, 3.31%.

An effective resolution could not be attained by the use of ethanol or ethanol–ether.

The optically pure salt was decomposed by 5% aqueous hydrochloric acid to obtain (−)-Xa (0.13 g), which was recrystallized from ligroin, mp 236—238 °C, IR (KBr-disk): $\nu_{C=O}$ 1685 cm^{-1} (almost identical over entire region with (−)-Xb, (±)-Xa, and (±)-Xb), $[\alpha]_{600}^{16}$ −15.2°, $[\alpha]_{589}^{16}$ −16.3°, $[\alpha]_{500}^{16}$ −27.7°, $[\alpha]_{400}^{16}$ −70.8°, $[\alpha]_{350}^{16}$ −168° (*c* 0.516, 99% EtOH), CD: $\lambda_{max}^{99\%EtOH}$ ($\Delta\varepsilon$) 292 (−2.1), 278* (−0.89), 260* (+1.2), 254 (+2.1), 247 (−0.816), 240 (−1.14), 232 (−0.245), 220 (+11.4), 210 (−18.9) nm.

Found: C, 75.77; H, 4.18%. Calcd for $C_{21}H_{13}O_2Cl$: C, 75.79; H, 3.94%.

Optical Resolution of 4-Chlorotriptycene-7-carboxylic Acid (Xb). A solution of Xb (2.27 g, 0.00683 mol) in 99% ethanol (80 ml) was mixed with aqueous quinidine methohydroxide (0.614 M, 11.1 ml, 0.0068 mol) and left to stand overnight. The solid obtained by evaporating the solvent under reduced pressure was recrystallized from ethanol–ether. Repeated fractional recrystallization (16 times) from ethanol–ether or ethanol afforded colorless crystals of optically pure salt containing one molecule of ethanol as a solvent of crystallization, 1.134 g, mp 175—177 °C, $[\alpha]_{600}^{16}$ +133.9°, $[\alpha]_{589}^{16}$ +137.1°, $[\alpha]_{500}^{16}$ +213.4°, $[\alpha]_{400}^{16}$ +461.7° (*c* 0.440, EtOH).

Found: C, 73.76; H, 6.47; N, 3.91%. Calcd for $C_{42}H_{39}N_2O_4Cl \cdot C_2H_6O$: C, 73.67; H, 6.32; N, 3.91%.

The salt was decomposed with 5% aqueous hydrochloric acid to obtain (−)-Xb. Recrystallization of (−)-Xb from ligroin yielded colorless crystals of mp 90 °C containing some unidentified hydrocarbon as a solvent of crystallization. Upon heating *in vacuo* they gradually lost the solvent and showed a gradual rise in the melting point. After heating to 120 °C for 6 hr under reduced pressure, crystals free from the solvent were obtained, mp 204—205 °C, IR (KBr-disk): $\nu_{C=O}$ 1685 cm^{-1}, $[\alpha]_{436}^{21}$ −4.74°, $[\alpha]_{405}^{21}$ −9.95°, $[\alpha]_{365}^{21}$ −33.1° (*c* 0.980, 99% EtOH), CD: $\lambda_{max}^{99\%EtOH}$ ($\Delta\varepsilon$) 290 (−2.7), 274 (+2.0), 264* (+0.79), 250 (+2.0), 240 (−3.5), 225 (+33) nm.

Found: C, 75.86; H, 3.91; Cl, 10.42%. Calcd for $C_{21}H_{13}O_2Cl$: C, 75.79; H, 3.94; Cl, 10.66%.

7-Amino-3-chlorotriptycene (XIa). (−)-Xa (5.0 g, 0.015 mol) dissolved in ether (250 ml) was mixed with thionyl chloride (21.4 g) and refluxed for 7 hr. The mixture was concentrated under reduced pressure to yield colorless crystals of acid chloride, 5.3 g, mp 159—161 °C, IR (Nujol mull): $\nu_{C=O}$ 1755 cm^{-1}. To an ice-cooled solution of the chloride in acetone (200 ml), sodium azide (1.06 g) in water (10 ml) was added dropwise under stirring. The mixture was stirred for further 1.5 hr at the same temperature and then a major portion of the solvent was removed under reduced pressure. The residue was mixed with cold water (300 ml) and extracted with ether. The extract was worked up as usual, giving colorless crystals of acid azide, 5.45 g, mp 105—107 °C (decomposed with frothing), IR (Nujol mull): ν_{N_3} 2150, $\nu_{C=O}$ 1685 cm^{-1}. Thoroughly dried azide spread over the bottom of 1 l Erlenmeyer flask was heated gradually to 105 °C and kept at the temperature for 1 hr to yield light yellow crystals of isocyanate, mp 124—132 °C, IR (Nujol mull): $\nu_{N=C=O}$ 2250 cm^{-1}.

The isocyanate mixed with powdered potassium hydroxide (40 g) and 99% ethanol (500 ml) was refluxed for 6 hr and then a major portion of the solvent was removed *in vacuo*. The residue was mixed with water and extracted with ether. The extract was worked up in the usual way to yield light yellow crystals which gave, after sublimation *in vacuo* followed by recrystallization from ligroin, pure XIa, 3.542 g (77.6%), colorless needles, mp 201.2—203.2 °C, IR (KBr-disk): ν_{NH} 3470, 3380, δ_{NH} 1620 cm^{-1}, UV: $\lambda_{max}^{99\%EtOH}$ (ε) 295 (2140), 284.5 (4360), 278.8 (4120), 265.5 (4400), 255* (5910), 249* (8200), 245* (9890), 217 (50400), 207.5* (15900), 202 (11800) nm, $\lambda_{max}^{99\%EtOH\text{-}HCl}$ (ε) 283.4 (2710), 277.3 (3520), 270 (2740), 214 (64000), 203.5 (58200) nm, CD: $\lambda_{max}^{99\%EtOH}$ ($\Delta\varepsilon$) 302 (−0.65), 282 (−3.21), 278* (−2.38), 266 (+0.69), 250 (−4.0), 234 (+6.50), 226 (−7.58), 214 (−8.67), 206 (−3.03)

nm, $\lambda_{max}^{99\%EtOH\text{-}HCl}$ ($\Delta\varepsilon$) 282 (+0.78), 274* (−0.84), 270 (−1.31), 255 (+4.91), 236 (−13.7), 218 (+14.3) nm.

Found: C, 79.08; H, 4.58; N, 4.71; Cl, 11.75%. Calcd for $C_{20}H_{14}NCl$: C, 79.07; H, 4.64; N, 4.61; Cl, 11.67%.

By a similar sequence of reactions (±)-Xb afforded racemate, faintly brown crystals, 87.2%, mp 198—201 °C (from ligroin), IR (KBr-disk): ν_{NH} 3470, 3380 cm^{-1}. In the case of racemate, a small amount of urea derivative was obtained in the last stage of the reactions.

7-Amino-4-chlorotriptycene (XIb). The Curtius reaction of (−)-Xb under similar reaction conditions described above afforded optically active XIb (81.9%) which was recrystallized from ligroin to give pure XIb, mp 169—172 °C. IR (KBr-disk): ν_{NH} 3380, 3460 cm^{-1}, δ_{NH} 1620 cm^{-1}, UV: $\lambda_{max}^{99\%EtOH}$ (ε) 295 (2070), 284 (4290), 278.7 (3960), 266 (4040), 217 (50000), 202 (47100) nm, $\lambda_{max}^{99\%EtOH\text{-}HCl}$ (ε) 283.8 (2480), 277.5 (3260), 270.5 (2510), 214 (59600), 203 (53300) nm, CD: $\lambda_{max}^{99\%EtOH}$ ($\Delta\varepsilon$) 302 (+0.58), 283 (+4.93), 268 (+0.56), 248 (−6.91), 228 (+12.2), 216 (−23.3) nm, $\lambda_{max}^{99\%EtOH\text{-}HCl}$ ($\Delta\varepsilon$) 283 (−2.36), 274 (+0.49), 269 (+2.26), 254 (+5.45), 237 (−12.7), 220 (+16.6) nm.

Found: C, 78.61; H, 4.70; N, 4.64; Cl, 11.60%. Calcd for $C_{20}H_{14}NCl$: C, 79.07; H, 4.64; N, 4.61; Cl, 11.67%.

Racemate was prepared similarly from (±)-Xb, mp 181—184 °C (from ligroin), IR (KBr-disk): ν_{NH} 3480, 3380 cm^{-1}.

Formation of a small amount of urea derivative was observed in the reaction both of (±)- and (−)-Xb. In the case of optical isomer, the urea derivative was purified by recrystallization from ligroin, mp 301—302 °C, IR (KBr-disk): ν_{NH} 3320, δ_{NH} 1550, $\nu_{C=O}$ 1650 cm^{-1}, UV: $\lambda_{max}^{99\%EtOH}$ (ε) 284.5 (6910), 274* (12300), 261* (24700), 249* (28000), 214 (99500), 207.4 (77500), 203.5 (44400) nm, CD: $\lambda_{max}^{99\%EtOH}$ ($\Delta\varepsilon$) 290 (−0.71), 280* (+7.6), 276 (+8.5), 264 (+4.0), 256* (+2.8), 242 (−1.6), 238 (+2.4) nm

Found: C, 77.36; H, 4.05; N, 4.36; Cl, 11.04%. Calcd for $C_{41}H_{26}N_2OCl_2$: C, 77.72; H, 4.14; N, 4.42; Cl, 11.19%.

4-Chloro-7-hydroxytriptycene (XIIb). Optically active XIb (0.86 g, 2.8 mmol) dissolved in acetic acid (12 ml) was added over a period of 35 min to a stirred solution of nitrosyl sulfate at 10—15 °C prepared from sodium nitrite (0.220 g) and concd. sulfuric acid (2 ml). The mixture was stirred for further 55 min and mixed with water (3 ml) to give a reddish green solution. The cooled solution of diazonium salt was added dropwise to a refluxing 3 M sulfuric acid (60 ml) under stirring. After being refluxed for further 1 hr, the mixture was extracted with benzene. Red amorphous solid obtained by working up the extract by the usual way was difficult to purify. Pure phenol (XIIb) could be prepared *via* methyl ether (XIIIb, see below). Purified ether (XIIIb, 0.60 g) dissolved in a mixture of acetic acid (35 ml) and 47% hydrobromic acid (20 ml) was refluxed for 8 hr. The mixture was poured into water and extracted with ether. Light yellow crystals (0.551 g) obtained by working up the extract were recrystallized from ligroin to give pure optically active XIIb, colorless crystals, mp 242—246 °C, IR (KBr-disk): ν_{OH} 3520—3400 cm^{-1}, UV: $\lambda_{max}^{99\%EtOH}$ (ε) 284 (4370), 278 (4340), 265.4 (3470), 216 (58700), 195 (56600) nm, CD: $\lambda_{max}^{99\%EtOH}$ ($\Delta\varepsilon$) 278 (+3.27), 273 (+3.22), 266 (+3.09), 252 (−6.27), 240* (−3.13), 224 (+19.0), 215 (−28.2) nm.

Found: C, 78.90; H, 4.15; Cl, 11.76%. Calcd for $C_{20}H_{13}OCl$: C, 78.82; H, 4.30; Cl, 11.63%.

3-Chloro-7-hydroxytriptycene (XIIa). By the procedure used for the preparation of XIIb, optically active XIa was converted into optically active XIIa. Though analytically pure XIIa could not be obtained by the hydrolysis of pure XIIIa, it could be used for subsequent reaction.

3-Chloro-7-methoxytriptycene (XIIIa). A mixture of crude XIIa (1.036 g), potassium carbonate (6 g), dimethyl sulfate (1.1 g) and acetone (60 ml) was refluxed for 6 hr under stirring. The residue obtained by evaporating the solvent *in vacuo* was mixed with water and extracted with ether. Crude XIIIa obtained by working up the extract was dissolved in benzene and the solution was passed through a short column of alumina (30 g). Colorless crystals (0.885 g, 85.4%) obtained from the filtrate were recrystallized from ligroin to give pure XIIIa, mp 211—214 °C, IR (KBr-disk): $\nu_{CH(OCH_3)}$ 2850 cm^{-1}, UV: $\lambda_{max}^{99\%EtOH}$ (ε) 284.1 (3710), 277.5 (3870), 265 (3470), 261* (3000), 252* (3170), 215.8 (58500), 207 (25300), 202.5 (17800) nm, $\lambda_{max}^{isooctane}$ (ε) 284.5 (3740), 278 (3810), 265 (3460), 261.4 (3140), 254* (3100), 216.5 (63800), 199.3 (52900), 196 (47900), 194.5 (44000) nm, CD: $\lambda_{max}^{99\%EtOH}$ ($\Delta\varepsilon$) 284 (+1.8), 280* (+0.60), 270 (−1.4), 250 (−3.6), 232 (−5.2), 226 (−2.4) nm, $\lambda_{max}^{isooctane}$ ($\Delta\varepsilon$) 290 (+0.14), 284 (+1.9), 280* (+0.94), 272 (−0.85), 268* (−0.70), 252 (−3.7), 232 (−5.9), 228 (−1.9) nm.

Found: C, 79.31; H, 4.84; Cl, 10.99%. Calcd for $C_{21}H_{15}OCl$: C, 79.11; H, 4.74; Cl, 11.12%.

Racemate: Mp 196.5—198 °C (sublimed from *ca.* 150 °C), IR (KBr-disk): $\nu_{CH(OCH_3)}$ 2850 cm^{-1}.

4-Chloro-7-methoxytriptycene (XIIIb). Methylation of optically active XIIb by the above-mentioned procedure afforded XIIIb (79.7%) which was sublimed *in vacuo* and recrystallized from ligroin to give pure material, colorless crystals, mp 243—243.5 °C, IR (KBr-disk): $\nu_{CH(OCH_3)}$ 2850 cm^{-1}, UV: $\lambda_{max}^{99\%EtOH}$ (ε) 284.3 (3980), 277.6 (3900), 265.5 (3440), 215.5 (61000), 202 (51300) nm, $\lambda_{max}^{isooctane}$ (ε) 284.5 (3940), 278 (3820), 265.5 (3410), 262* (3000), 216.6 (64700), 199 (54800), 196.5* (50500), 194.5* (45100), 192* (27700) nm, CD: $\lambda_{max}^{99\%EtOH}$ ($\Delta\varepsilon$) 290 (+0.14), 270* (+2.7), 265 (+3.7), 250* (−5.4), 240 (−13), 226 (+20) nm, $\lambda_{max}^{isooctane}$ ($\Delta\varepsilon$) 290 (+0.10), 270* (+2.5), 264 (+3.6), 250 (−5.4), 240 (−12), 226 (+23) nm.

Found: C, 79.52; H, 4.80; Cl, 11.14%. Calcd for $C_{21}H_{15}OCl$: C, 79.11; H, 4.74; Cl, 11.12%.

Racemate: Mp 244—246 °C, IR (KBr-disk): $\nu_{CH(OCH_3)}$ 2850 cm^{-1}.

(−)-2,5-Dimethoxy-8-chlorotriptycene (XVIIa and XVIIb).

XVIIa from XIIa: To an ice-cooled and stirred solution of sulfanilic acid (0.150 g, 0.720 mmol) in aqueous sodium carbonate (0.032 g in 12 ml of water) was added a mixture of sodium nitrite (0.050 g, 0.720 mmol), ice (1 g) and concd. hydrochloric acid (0.12 ml). After 30 min, diazonium salt deposited as colorless crystals. To this mixture was added under stirring a solution of pure XIIa (0.210 g, 0.689 mmol) in methanol (3 ml) containing sodium hydroxide (0.56 g) and water (0.4 ml). After being left to stand overnight, the scarlet mixture was slightly warmed with sodium hydrosulfite (10 g) and concd. hydrochloric acid. The reaction mixture was poured into water and extracted with ethyl acetate. The extract was worked up in the usual way to give crude aminophenol (XIVa, 0.204 g, light yellow crystals). Ferric sulfate (4 g) was added to a solution of the crude XIVa in ethanol (25 ml), concd. sulfuric acid (4 ml) and water (50 ml) and the mixture was refluxed for 2 hr. The reaction mixture was concentrated under reduced pressure and extracted with ether. Evaporation of the extract, after washing and drying, afforded brown yellow crystals (0.198 g), which were dissolved in benzene and passed through a short column of alumina (7 g) to give pure quinone (XVa) as yellow crystals (0.105 g, 45.5% based on XIIa), IR (Nujol mull): $\nu_{C=O}$ 1655 cm^{-1} (racemate 1650 cm^{-1}). XIIa was recovered in a yield of 35%. Pure XVa (0.105 g, 0.33 mmol) dissolved in ether (8 ml) was mixed with aqueous

sodium hydrosulfite (0.2 g in 0.5 ml of water) and the mixture was stirred vigorously for 20 min. The colorless reaction mixture was poured into water and extracted with ether. Hydroquinone derivative (XVIa, 0.116 g, colorless crystals) obtained by working up the extract was methylated in the usual manner with potassium carbonate (1 g) and dimethyl sulfate (0.2 g) in acetone (10 ml). Crude XVIIa (light yellow crystals) was chromatographed on alumina and then recrystallized from methanol to give pure XVIIa, mp 209.0—210.5 °C, IR (KBr-disk): $\nu_{CH(OCH_3)}$ 2840 cm^{-1}, UV $\lambda_{max}^{99\%EtOH}$ (ε) 301* (3930), 295 (4090), 284.4 (5280), 278.8 (4270), 266 (2980), 256.8 (2500), 214.2 (58000), 202.3 (48200) nm, ORD: $[M]_{302}$ −1710°, $[M]_{286}$ +3230°, $[M]_{280}$* +1750°, $[M]_{266}$ +1770°, $[M]_{260}$* −5440°, $[M]_{246}$ −14600°, $[M]_{230}$ +26400°, $[M]_{215}$ −48100° (*c* 0.00898, EtOH).

Found: C, 75.40; H, 4.96; Cl, 9.87%. Calcd for $C_{22}H_{17}O_2Cl$: C, 75.75; H, 4.91; Cl, 10.17%.

Racemate: Mp 205.5—207 °C.

XVIIb from XIIb: According to an analogous sequence of reactions used for the preparation of XVIIa, pure XIIb was converted into(−)-2,5-dimethoxy-8-chlorotripycene (XVIIb), mp 209.0—210.5 °C. IR (KBr-disk): $\nu_{CH(OCH_3)}$ 2840 cm^{-1}, CD: $\lambda_{max}^{99\%EtOH}$ ($\Delta\varepsilon$) 298 (−0.22), 284 (+0.93), 280 (+1.0), 265 (+2.8), 258 (+2.0), 241 (−6.0) nm, ORD: $[M]_{302}$ −1720°, $[M]_{286}$ +3250°, $[M]_{280}$* +1580°, $[M]_{266}$ +1100°, $[M]_{260}$* −5420°, $[M]_{246}$ −15000°, $[M]_{230}$ +25600°, $[M]_{215}$ −48100° (*c* 0.00885, EtOH).

Found: C, 75.33; H, 4.83; Cl, 10.03%. Calcd for $C_{22}H_{17}O_2Cl$: C, 75.75; H, 4.91; Cl, 10.17%.

UV and IR spectra of XVIIb thus obtained were found to be completely superimposable with those of XVIIa.

Racemate: Mp 204.5—206.0 °C.

(+)-2,5-Dimethoxy-8-carboxytriptycene (XIX). To a refluxing solution of (+)-2,5-dimethoxy-8-methoxycarbonyltriptycene[3] (XVIII, 500 mg, 1.34 mmol) in acetic acid (25 ml) was added dropwise 3 M sulfuric acid (7 ml) and the mixture was refluxed for 12 hr. Colorless crystals deposited on cooling the reaction mixture were recrystallized from methanol to give pure (+)-XIX, mp 147.9—148.9 °C $[\alpha]_D$ +15° (*c* 0.2673, dioxane).

Found: C, 76.52; H, 5.04%. Calcd for $C_{23}H_{18}O_4$: C, 77.08; H, 5.06%.

(+)-2,5-Dimethoxy-8-aminotriptycene (XX). A mixture of (+)-XIX (533 mg, 1.34 mmol), thionyl chloride (1.5 ml) and tetrahydrofuran (11 ml) was refluxed for 3 hr to afford acid chloride [IR (Nujol mull): $\nu_{C=O}$ 1765 cm^{-1}] quantitatively. Sodium azide (252 mg) dissolved in water (3 ml) was added to a stirred and ice-cooled solution of the acid chloride in tetrahydrofuran (30 ml). After the mixture had been stirred for further 3 hr at the same temperature, water was added to precipitate acid azide [IR (Nujol mull): ν_{N_3} 2150, $\nu_{C=O}$ 1690 cm^{-1}]. Thoroughly dried acid azide (552 mg) dissolved in benzene (80 ml) was refluxed for 4 hr to yield isocyanate [553 mg, IR (Nujol mull): ν_{NCO} 2280 cm^{-1}]. A mixture of the isocyanate, 99% ethanol (50 ml), water (8 ml) and potassium hydroxide (5.0 g) was refluxed to afford (+)-XX (384 mg). Vacuum sublimation of the crude product (bath temp. 210—240 °C/800 Pa) afforded pure (+)-XX, colorless crystals, mp 287—289 °C (racemate, mp 243.5—245 °C), IR (KBr-disk): ν_{NH} 3420, 3350, δ_{NH} 1630 cm^{-1}, UV: $\lambda_{max}^{99\%EtOH}$ (ε) 300* (5900), 292.5 (6730), 269* (7260), 262 (7760), 220.5* (45300), 207.5* (56300), 203 (58300), 198 (58300) nm, CD: $\lambda_{max}^{99\%EtOH}$ ($\Delta\varepsilon$) 304.5 (+1.45), 274 (−13.6), 250* (+16.2), 242.5 (+16.9), 225.8 (−21.7), 218* (−4.77), 207.5 (−17.7) nm.

Found: C, 79.88; H, 5.96; N, 4.18%. Calcd for $C_{22}H_{19}O_2N$: C, 80.22; H, 5.81; N, 4.25%.

(+)-2,5-Dimethoxy-8-chlorotriptycene (XXI). To a stirred suspension of (+)-XX (60.6 mg, 0.184 mmol) in 6 M hydrochloric acid was added sodium nitrite (13.4 mg, 0.194 mmol) in water (3 ml) over a 15 min-period at 11—15 °C. The mixture, after being stirred for further 50 min, was added dropwise to a solution of cuprous chloride (36 mg) in 6 M hydrochloric acid (6 ml). Stirring was continued for 30 min at 20 °C and then for 1 hr at 100 °C. The reaction mixture was poured into water and extracted with ether. Crude product obtained by working up the extract was chromatographed on alumina and eluted with carbon tetrachloride. The crystals thus prepared were recrystallized from ligroin to give pure (+)-XXI, mp 209.6—210.4 °C (racemate, mp 206.1—207.1 °C), UV: $\lambda_{max}^{99\%EtOH}$ (ε) 301* (4020), 294.5 (4230), 284.5 (5510), 278.9 (4400), 266 (3320), 257 (2750), 240* (8290), 214.5* (61400), 212* (60600), 202* (57900), 198.5 (59600) nm, CD: $\lambda_{max}^{99\%EtOH}$ ($\Delta\varepsilon$) 300 (+0.52), 285 (−0.98), 278.5 (−0.88), 265.5 (−2.82), 258 (−1.98), 240 (+9.49), 225.5 (−5.08), 214 (+21.8), 202.5 (−17.9) nm, $[M]_{247}^{20}$ +14000° (*c* 1.417×10^{-4} mol/l, 99%EtOH).

Found: C, 75.61; H, 4.92; Cl, 10.15%. Calcd for $C_{22}H_{17}O_2Cl$: C, 75.75; H, 4.91; Cl, 10.16%.

References

1) For Part VI of this series, see, Ref. 3.

2) A. Sonoda, F. Ogura, and M. Nakagawa, This Bulletin, **35**, 853 (1962); F. Ogura, Y. Sakata, and M. Nakagawa, *ibid.*, **45**, 3646 (1972); F. Ogura and M. Nakagawa, *ibid.*, **46**, 651 (1973).

3) Y. Shimizu, T. Naito, F. Ogura, and M. Nakagawa, *ibid.*, **46**, 1520 (1973).

4) Y. Sakata, F. Ogura, and M. Nakagawa, *ibid.*, **46**, 611 (1973).

5) M. Kuritani, Y. Sakata, F. Ogura, and M. Nakagawa, *ibid.*, **46**, 605 (1973).

6) J. Tanaka, F. Ogura, M. Kuritani, and M. Nakagawa, *Chimia*, **26**, 471 (1972); J. Tanaka, K. Ozeki-Minakata, F. Ogura, and M. Nakagawa, *Nature Phys. Sci.*, **241**, 22 (1973); *idem.*, *Spectrochim. Acta*, **29A**, 877 (1973); J. Tanaka, C. Katayama, F. Ogura, H. Tatemitsu, and M. Nakagawa, *Chem. Commun.*, **1973**, 21.

7) H. E. Fierz-David, *Helv. Chim. Acta*, **10**, 206 (1927).

8) L. Friedman and F. M. Logullo, *J. Amer. Chem. Soc.*, **85**, 1549 (1963).

9) L. F. Fieser, "Organic Experiments," D. C. Heath and Co., Boston (1964), p. 315.

10) R. T. Major and J. Finkelstein, *J. Amer. Chem. Soc.*, **63**, 1318 (1941).

11) N. Sakabe, K. Sakabe, K. Ozeki-Minakata, and J. Tanaka, *Acta Cryst.*, **B28**, 3441 (1972).

12) T. Kaneda, N. Sakabe, and J. Tanaka, 28th Annual Meeting of the Chemical Society of Japan, Abstract, Part III, p. 1610, Tokyo, April (1973); *idem.*, This Bulletin, in press.

Synthetic Photochemistry. III.[1] The Addition Reaction of Methyl Acetopyruvate to Cycloheptatriene: An Ene Reaction and $(4+2)\pi$ and $(6+2)\pi$ Cycloadditions

Hitoshi TAKESHITA,* Akira MORI,* and Shô ITÔ**

*Research Institute of Industrial Science, Kyushu University, Hakozaki, Fukuoka 812

**Department of Chemistry, Tohoku University, Aramaki-Aoba, Sendai 980

(Received February 16, 1974)

The irradiation of methyl acetopyruvate with cycloheptatriene by means of a high-pressure mercury lamp has yielded $(6+2)\pi$ and $(4+2)\pi$ cycloadducts, together with tropylcarbinol derivatives formed by a formal abstraction of allylic hydrogen by the excited carbonyl group, this being the major process in this reaction.

As part of our series of studies of the photo-cycloaddition reactions of α,β-unsaturated carbonyl compounds with functional substituents to olefins,[2] we have now extended the investigation to that of methyl acetopyruvate (I) with cycloheptatriene (II), a cyclic conjugated triene, in order to determine the generality of the reaction. One of our primary interests in this reactant is to ascertain whether or not we can see a $(6+2)\pi$ cycloaddition.[3] At the same time, it will be valuable from the preparative point of view if we can see the hydrogen transfer process from a very reactive allylic methylene of II by an excited carbonyl group of I, since this should produce substituted tropylidenes, whose utilization might offer a novel entry to non-benzenoid aromatic systems. In fact, the experiments which will be described below have shown the occurrences of these two features.

Results and Discussion

The irradiation of a mixture of I and II by a 450 W high-pressure mercury lamp with a Pyrex glass filter has slowly given a mixture of products.[4] After the completion of the reaction, as monitored by a ferric chloride test, the solvent was removed *in vacuo*; the residual oil was then chromatographed through a silica gel column to give as photoproducts III (a pale yellow liquid, 50%), IV (a faint yellow liquid, 14%), V (a faint yellow liquid, 14%), and VI (a faint yellow liquid, 5.8%). Their structure elucidation is as follows:

The Structure of III. The NMR of III indicates that it is an isomeric mixture, and repeated chromatographic fractionation of III afforded a practically pure 7-tropyl isomer, IIIa [δ: 2.12 (3H, s), 2.94 (1H, d, J=16 Hz), 3.12 (1H, d, J=16 Hz), 3.71 (3H, s), and 5.0—6.7 (6H, m)]. The mixture of III was then reduced to a single hexahydro-derivative (VII), which gave a 2,4-dinitrophenylhydrazone (DNP), (λ_{max}^{MeOH}: 359 nm (ε: 19400)), confirming that they have the same carbon skeleton. When III was heated in a sealed tube for 190 °C, a dealdolized product, VIII, was obtained after the fractionation of the pyrolysate.[5] According to the NMR spectral analysis, VIII was again shown to be an isomeric mixture of VIIIa, VIIIb, and VIIIc, the components differing in the positions of the double bonds, and through an extensive fractionation by silica gel column chromatography, an enriched sample of the VIIIa isomer was obtained. The rest of the isomers, however, could not be separated. VIIIa revealed the presence of a glyoxaloyl group in the IR ($\nu_{C=O}$: 1723, 1670 cm^{-1}) and the NMR [δ: 2.70 (2H, d, J=6.8 Hz), 3.86 (3H, s), and 5.3—7.45 (5H, complex m)] spectra. Since the presence of a tropyl chromophore is evident from the UV (λ_{max}^{MeOH}: 287 (ε: 4000) and 301 nm (3900)) spectrum as well as from the above NMR evidence, VIIIa is deduced to be methyl 1-tropylglyoxalate. VIIIb and VIIIc are considered to be 2-tropyl- and 3-tropyl-derivatives on the basis of NMR spectral evidence.[6] A mixture of VIII was easily hydrogenated to a single octahydro-derivative (IX), which was then hydrolyzed to a crystalline carboxylic acid. IX was oxidized by potassium permanganate to give pimelic acid, whose identity with an authentic specimen was proved by direct comparisons (IR and NMR spectra and glc of its methyl ester). In addition, the presence of unconjugated keto-groups ($\nu_{C=O}$: 1720 cm^{-1}) and a simple cyclic triene chromophore (λ_{max}^{MeOH}: 254 nm (ε: 3700)) clarifies that III is a methyl 2-tropyl-2-hydroxylevulinate.

The Structures of IV and V. IV and V were shown to be *cycloadducts* by the observed substitution patterns of the seven-membered rings, which exhibit four olefinic protons in the NMR. Since IV and V possess a hydroxyketo-ester function, they cannot be $(2+2)\pi$ adducts. This was confirmed as follows: The independent hydrogenation of IV and V, using platinum oxide as the catalyst, resulted in the formation of the same tetrahydro-derivative (X), which gave a crystalline DNP (λ_{max}^{MeOH}: 362 nm (ε: 19500)). On the other hand, cycloheptene and I were irradiated in a similar manner to give the photo-adduct (XI) in a good yield together with a dimer of cycloheptene (a colorless liquid).[7] The non-identity of XI, which is a normal glyoxaloyl derivative, with X has been established by IR and NMR spectral comparisons. Therefore, IV and V should possess a bicyclo [3,2,2] nonadiene frame-work, derived by the $(4+2)\pi$ cycloaddition process; otherwise, the occurrence of a positional isomerism of the double bond is impossible. Interestingly, neither the dehydration nor the dealdolization of X has been successful so far; always unreacted X has been recovered quantitatively, while XI gives a normal α,β-unsaturated keto-ester (XII, a colorless liquid), whose *mono*-DNP, (λ_{xeau}^{MeOH}: 377.5 nm (ε: 24600)) shows reasonable physical properties.

The Structure of VI. VI has also retained the

aldolic moiety, as evidenced by its NMR [δ: 2.09 (3H, s), 3.60 (3H, s), and 5.85 (4H, br.s)] and IR (ν: 3500, 1723 (strong) cm^{-1}) spectra. The presence of cyclohepta-1,3-diene chromophore is confirmed by a measurement of the UV spectrum (λ_{max}^{MeOH}: 268 nm (ε: 3370)). On catalytic hydrogenation by platinum oxide, VI afforded a single tetrahydro-derivative (XIII, colorless liquid), which was further characterized by the formation of *mono*-DNP (yellow crystals, λ_{max}^{MeOH}: 360 nm (ε: 19200). XIII was not identical with either X or XI, judging from IR and NMR spectral comparisons. The remaining carbon skeleton for VI is, therefore, bicyclo [4,2,1] nonadiene, that of a (6+2)π adduct.

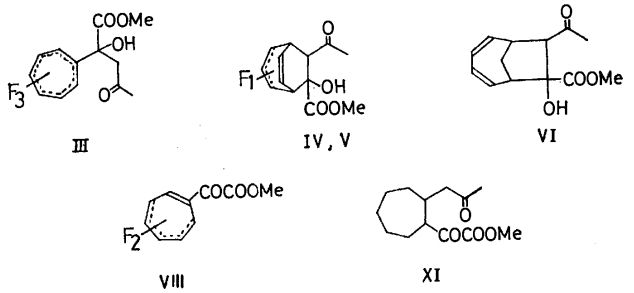

In connection with the above results, a few points should be noted. First, the main product, III, was formed by an ene-reaction which was not previously observed in the photochemical reaction of I, but the phenomenon is not surprising since electron deficient oxygen of the n,π^* excited carbonyl group of I can abstract a partially-negative allylic hydrogen of II, leaving a symmetrical tropyl radical. Secondly, the mode of the concerted formation of IV and V has to be photochemically disallowed, and yet the formation of IV and V was stereospecific despite being not regiospecific, while the (4+2)π photoaddition of the cyclopentadiene and α-acetoxyacrylonitrile has been reported to be non-stereospecific.[8] Third, the acquisition of VI constitutes, to the best of our knowledge, the first example of genuine (6+2)π photocycloaddition, although a thermal (6+2)π process has been reported in the reaction of acrylonitrile and II[9] and, in a formal sense, the intramolecular[3] and intermolecular photocycloadditions[10,11] of activated olefins and benzenes to give cyclobutanes are examples of the (6+2)π process, as has been mentioned.[3] Finally, an apparent absence of the genuine (2+2)π cycloadduct in the reaction mixture is in contrast with the photocycloadditions of ordinary olefins.

This complicated behavior itself makes the mechanistic analyses of the reaction difficult. However, at least one thing is clear; since the photoreaction is strongly concentration-dependent, *i.e.*, a slight dilution of II by an inert solvent diminishes the rate considerably, there is no involvement of a charge-transfer intermediate in this reaction. Other than this, since photoproducts are extremely unstable and sensitive to the air, and since addition of arylketones to the reaction system causes a consumption of the additives,[12] an intensive investigation will be needed to obtain a deeper understanding of the reaction.

Experimental

Reaction of Cycloheptatriene (II) and Methyl Acetopyruvate (I). a) I (7.24 g) was dissolved in II (200 ml) and was then internally irradiated by a 450 W high-pressure mercury lamp through a Pyrex glass filter under a nitrogen atmosphere for 54 hr. Then the reaction mixture was heated on an oil bath under reduced pressure to remove the II. The residual oil thus obtained was repeatedly fractionated by silica gel column chromatography, using hexane–benzene–ether system as eluant, to give as products III (a pale yellow oil; 5.9 g), IV (a pale yellow oil; 1700 mg), V (a faint yellow oil; 1700 mg), and VI (a faint yellow oil; 600 mg).

b) I (4.3 g) was dissolved in II (45 ml) and anhydrous ether (180 ml) and was then similarly irradiated. After 70 hr, the presence of I in the clean mixture was still recognized, but the crude mixture (*ca.* 2.1 g) obtained by the removal of the solvent and the unreacted I showed a similar product composition.

c) I (120 mg) was dissolved in II (3 ml) and externally irradiated by means of a high-pressure mercury lamp in the presence of various amount of benzophenone (10—100 mg). Every time, the formation of benzopinacol and a tropyl carbinol derivative exceeded that of the photoadducts.

Further Fractionation of III; Isolation of Methyl 2-(7-Tropyl)-2-hydroxylevulinate (IIIa). Above isomeric mixture of III (450 mg) was further chromatographed through a silica gel column; from the least polar fraction, a practically pure isomer, IIIa (a faint yellow oil; 30 mg), was obtained.

Hexahydro-derivative of III. III (98 mg) was dissolved in methanol and hydrogenated over platinum oxide to give a hexahydro-derivative (VII) as a colorless liquid in quantitative yield.

The DNP of VII was prepared in the usual manner as yellow needles; mp 168—168.5 °C (from ethanol-ethyl acetate) (Found: C, 53.81; H, 6.10; N, 13.46%. Calcd for $C_{19}H_{26}O_7N_4$: C, 54.02; H, 6.20; N, 13.26%).

Pyrolysis of III: Formation of Methyl Tropylglyoxalates (VIII). A degassed sample of III (305.7 mg) was heated in a sealed tube for 3 hr. The pyrolysate was then separated by silica gel column chromatography to yield, together with the recovered III (76 mg), 20 mg of a pale yellow liquid (VIII).

Fractionation of Isomeric Mixture of VIII; Enrichment of VIIIa. The above sample of VIII (120 mg) was further fractionated by silica gel column chromatography. The least polar fraction, eluted by hexane–benzene (1: 10), consisted of VIIa (70% pure) as a pale yellow liquid after distillation on a cold finger (Found: C, 67.23; H, 5.75%. Calcd for $C_{10}H_{10}O_3$: C, 67.40; H, 5.66%).

Catalytic Reduction of VIII: Formation of Methyl Cycloheptylglycolate (IX). VIII (105 mg) was reduced in methanol over platinum oxide to give an octahydro-derivative, IX (bp 110—112 °C/3 mmHg) as a colorless liquid after a cold-finger distillation; the homogeneity of distillate was proven by glc (Found: C, 64.23; H, 9.59%. Calcd for $C_{10}H_{18}O_3$: C, 64.49; H, 9.74%. ν: 3500, 1740 cm^{-1}, δ: ~1.5 (13H, br.), 3.86 (3H, s), 3.93 (1H, d, J=2 Hz)).

Alkaline Hydrolysis of IX to Cycloheptylglycolic Acid. IX (20 mg) was treated with aqueous sodium hydroxide solution to give colorless needles, mp 88—90 °C (from ethanol–ethyl acetate) (Found: C, 62.72; H, 9.39%. Calcd for $C_9H_{16}O_3$: C, 62.76; H, 9.36%).

Potassium Permanganate Oxidation of IX; Formation of Pimelic Acid. IX (98.2 mg) was mixed with water (3 ml), and into the mixture aqueous potassium permanganate (330 mg in 10 ml) was added, drop by drop, at 0 °C, and then

it was kept overnight. The mixture was subsequently acidified by hydrochloric acid and extracted with ether. An acidic material obtained by the re-extraction of the above was esterified by diazomethane to give dimethyl pimelate (40 mg (40%)) as a colorless liquid after cold-finger distillation. The sample showed essentially a single peak on a gas-liquid chromatogram and was identical with an authentic specimen (IR, NMR, and glc).

Catalytic Reduction of IV; *Formation of the Tetrahydro-derivative, X.* IV (155 mg) was dissolved in methanol and reduced with platinum oxide at room temperature. The product (X), a colorless liquid, was shown to be homogeneous; it consisted of a single peak on several gas-liquid chromatograms (ν: 3500, 1720, 1270, 1200 cm^{-1}. *m/e*: 240 (M^+), 95 (base peak)).

The DNP of X was obtained as yellow needles, mp 188—190 °C (Found: C, 54.04; H, 5.79; N, 13.37%. Calcd for $C_{19}H_{24}O_7N_4$: C, 54.28; H, 5.75; N, 13.33%).

Catalytic Reduction of V; *Formation of X.* V (255 mg) was similarly hydrogenated to give X, which was identical with those obtained from IV by a study of its IR and NMR spectra, glc, and a mixed-mp comparison with DNP.

Photochemical Reaction of I and Cycloheptene. I (115mg) was dissolved in cycloheptene (1 ml) and externally irradiated by a high-pressure mercury lamp through a Pyrex glass filter. After the evaporation of the excess olefin, the mixture was chromatographed through silica gel column to give a hydrocarbon and a 1: 1-cycloadduct (XI) (a colorless liquid (*m/e*: 240 (M^+), 95 (base peak), ν: 1730, 1270 cm^{-1})) which was not identical with either VII or X (IR, NMR, and glc).

Acid-Catalyzed Dehydration of XI; *Formation of the α,β-Unsaturated Keto-ester, XII.* XI (144 mg) was dissolved in benzene and heated with a small amount of *p*-toluenesulfonic acid to give XII (103 mg, 77.5%) as a colorless liquid (λ_{max}^{MeOH}: 245 nm (ε: 7100), ν: 1730, 1690, 1250 cm^{-1}).

The DNP of XII was obtained as orange-yellow needles; mp 180—181 °C (Found: C, 56.80; H, 5.53; N, 14.24%. Calcd for $C_{19}H_{22}O_6N_4$: C, 56.71; H, 5.51; N, 13.92%).

Catalytic Reduction of VI; *Formation of the Tetrahydro-Derivative XIII.* VI (83 mg) was dissolved in methanol and reduced over platinum oxide at room temperature. A single product (a colorless liquid), obtained after the usual work up, was characterized by the formation of crystalline DNP; yellow needles; mp 141—143 °C (Found: C, 54.33; H, 5.79; N, 13.29%. Calcd for $C_{19}H_{24}O_7N_4$: C, 54.28; H, 5.75; N, 13.33%).

H. T. and A. M. wish to thank The Ministry of Education for its financial support.

References and Notes

1) Part II: H. Takeshita, R. Kikuchi, and Y. Shoji, This Bulletin, **46**, 690 (1973).

2) H. Takeshita and S. Tanno, *ibid.*, **46**, 880 (1971).

3) A. S. Kushner, *Tetrahedron Lett.*, **1971**, 3275.

4) When the irradiation was also carried out in dioxane and in tetrahydrofuran solutions, a formation of polymeric material prevented the completion of the reaction, but the product distribution was similar to that of the present system.

5) The formation of azulenes has been observed. This will be the subject of another paper.

6) The NMR spectrum of VIII disclosed signals at δ: 3.87 (3H, s) and 2.47 (2H, t) for one isomer and at 3.89 (3H, s) and 2.40 (2H, t) for another isomer. However, the complexity of the overlapped vinyl proton signals prevented their distinguishment.

7) This showed no olefinic proton in the NMR, and no further study was carried out. However, it is interesting to note that its formation is attributable to the energy transfer of the triplet species of I to cycloheptene. This was not observed in the reaction of cyclohexene and I.

8) W. L. Dilling, and R. D. Kroening, *Tetrahedron Lett.*, **1968**, 5601. *cf.* T. S. Cantrell who also reported the formation of five photoadducts by the irradiation of cyclohexenone and cyclopentadiene; *Chem. Commun.*, **1970**, 1656.

9) D. Bellus, G. Helferich, and C. D. Weis, *Helv. Chim. Acta*, **54**, 463 (1971).

10) For example, a) H. J. F. Angus and D. Bryce-Smith, *Proc. Chem. Soc.*, **1959**, 326; b) D. Bryce-Smith, *Pure Appl. Chem.*, **16**, 47 (1968); c) H.-D. Scharf, and R. Klar, *Chem. Ber.*, **105**, 575 (1972).

11) H. E. Zimmerman, R. S. Givens, and R. M. Pagni, *J. Amer. Chem. Soc.*, **90**, 6096 (1968).

12) The results along this line will be reported in the future.

Stereochemical Studies on the Nuclear Alkylation of Phenols with 1-Phenylethyl Chloride and the Acidic Rearrangement of the 1-Phenylethyl Ethers of Phenols in the Phenolic Solvents

Kunio Okamoto, Tomomi Kinoshita, and Osamu Makino

Department of Hydrocarbon Chemistry, Faculty of Engineering, Kyoto University, Sakyo-ku, Kyoto 606

(Received March 22, 1974)

Phenolyses of optically active 1-phenylethyl chloride were carried out in phenol (50 °C), *p*-cresol (100 °C), *p*-chlorophenol (100 °C), and 2,6-xylenol (100 °C) in the presence of variable concentrations of the sodium salts of the respective phenols or triethylamine; the distributions (%) for the O- and C-alkylation products and the net steric courses (α%) for each product were examined. The distribution and the steric course which were graphically extrapolated to the zero base concentration indicated that, if the influence of the liberated hydrogen chloride was excluded, in the phenolyses without an added base the major products are the 1-phenylethyl ethers of the respective phenols with net *retained* configurations and the minor products are the *o*- and *p*-1-phenylethylated phenols with net *inverted* configurations. The hydrogen chloride rearrangement of the optically active 1-phenylethyl ethers of the respective phenols proceeded rapidly to give *o*-1-phenylethylated phenols with predominantly *retained* configurations (for phenol, *p*-cresol, and *p*-chlorophenol) and *p*-1-phenylethylated phenols with net *inverted* configurations (for phenol and 2,6-xylenol) in the respective phenol–benzene (1 : 1 by wt) solvents. The *p*-toluenesulfonic acid rearrangement of 1-phenylethyl phenyl ether-^{18}O proceeded to give *o*- and *p*-1-phenylethylphenols with partial loss of the oxygen-18 atom in the phenol–benzene (1 : 1 by wt) solvent, indicating the coexistence of the *intermolecular* course for the acidic rearrangement in the phenolic solvents. From these findings, it is concluded that the formation of the *ortho*-alkylates with retention of configuration, experimentally observed in the respective phenolyses without an added base, is attributed not to the direct retentive alkylation of the phenols, but to the rapid rearrangement of the 1-phenylethyl ethers with net retention of configuration, caused by the hydrogen chloride liberated in the S_N1-phenolysis of 1-phenylethyl chloride in the respective phenolic solvents.

When the S_N1 phenolysis of optically active 1-phenylethyl chloride was conducted in the presence of a base, partially (20—50%) retained 1-phenylethyl phenyl ether and partially (25—87%) inverted *o*- and *p*-1-phenylethylphenols were obtained in phenol, *p*-cresol, *p*-chlorophenol, and *p*-nitrophenol solvents.[1]

On the other hand, when the phenolysis was carried out without an added base, no phenolic ether was obtained. Instead, 1-phenylethylphenols alone were isolated; the *ortho* alkylated phenol possessed partially retained configuration, whereas the *para* isomer configuration was partially inverted.[2] These are illustrated in the following scheme.

In the presence of a base:

$$(R)\text{-RCl} + \text{PhOH} \longrightarrow (R)\text{-ROPh} + (S)\text{-}o\text{-RC}_6\text{H}_4\text{OH} + (S)\text{-}p\text{-RC}_6\text{H}_4\text{OH}$$

Without an added base:

$$(R)\text{-RCl} + \text{PhOH} \longrightarrow (R)\text{-}o\text{-RC}_6\text{H}_4\text{OH} + (S)\text{-}p\text{-RC}_6\text{H}_4\text{OH}$$

Prior to these investigations,[1,2] Hart and his collaborators[3] had already reported that *ortho*-alkylations of *p*-cresol and *p*-chlorophenol with optically active 1-phenylethyl chloride proceeded with retention of configuration, but the *para*-alkylation of 2,6-xylenol involved inversion; they suggested that the *ortho*-alkylation with retention of configuration would be a direct retentive C-alkylation with a cyclic transition state as follows.

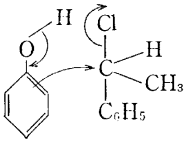

However, as we pointed out in the previous paper,[2] in view of the fact that in the phenol–acetonitrile solvent optically active 1-phenylethyl phenyl ether undergoes a rapid rearrangement to give the predominantly retained *o*-(1-phenylethyl)phenol in the presence of hydrogen chloride, it is probable that the product distribution and the steric course observed in the experiments[2,3] without an added base do not reflect the true reaction result between 1-phenylethyl chloride and phenol, but they are perturbed by the facile acidic rearrangement of 1-phenylethyl phenyl ether formed as a precursor of *o*- and *p*-alkylated phenols.

In order to confirm this anticipation, we intended to know the true product distribution and the true steric course avoided from the perturbation by the hydrogen chloride rearrangement. For this purpose we adopted an extrapolation method which we had applied to several phenolyses without an added base.[4] Namely, we carried out the phenolyses of optically active 1-phenylethyl chloride in phenol, *p*-cresol, *p*-chlorophenol, and 2,6-xylenol solvents, and examined the product distribution and the steric course for each product in the respective phenolyses with variable concentrations of sodium salts of the phenoxides or triethylamine; then extrapolated the results graphically to the zero base concentration. We considered the extrapolated values as the intrinsic results which are not affected by the liberated hydrogen chloride.

In this paper we will report that, contrary to the results of the experiments carried out without an added base,[2,3] the extrapolated results indicate that the direct *ortho*-alkylation with optically active 1-phenylethyl chloride proceeds with predominant *inversion* of configuration in phenol, *p*-cresol, and *p*-chlorophenol solvents, and that the *retained ortho*-1-phenylethylated phenols

which were obtained in the experiments without an added base are mostly produced by the retentive and rapid hydrogen chloride rearrangement of 1-phenylethyl phenyl ethers, initially-formed from the respective phenols and with net retained configurations, and consequently that a direct retentive C-alkylation[3] is not a major mechanism for the formation of the retained *ortho*-alkylates in the nuclear alkylations of phenol, *p*-cresol, and *p*-chlorophenol.

The S_N1 Phenolysis Rates and the Product Distributions in the Absence of a Base. In the presence of a base the phenolysis of 1-phenylethyl chloride obeys a good first-order kinetics, showing a good S_N1 characteristics, and gives the phenyl ethyl eher and *o*- and *p*-alkylated phenols.[1] However, as mentioned above, in the experiments without an added base the liberated hydrogen chloride seems to perturb the S_N1 phenolysis by the acidic rearrangement of the phenyl ether[2] and also by the cleavage reaction[5] of the phenyl ether with hydrogen chloride (*vide infra*).

In order to confirm such perturbation, we carried out the rate measurements without an added base. As anticipated, the first-order titrimetric rate constants of the phenolysis of 1-phenylethyl chloride tended to decrease after 19—26% completion in the mixtures of benzene and the respective phenols (1: 1 by weight). This is most probably ascribed to the occurrence of the cleavage reaction[5] of the respective phenyl ether by hydrogen chloride to give the starting 1-phenylethyl chloride. The initial first-order rate constants are summarized in Table 1.

Table 1. First-order rate constants for phenolyses of 1-phenylethyl chloride in phenol (ArOH)–benzene (1: 1 by wt) solvent in the absence of a base

Solvent ArOH–C_6H_6	Temp. °C	RCl M	k_1 s^{-1}	Conversion %
C_6H_5OH–C_6H_6	50	0.100	3.95×10^{-4}	25
p-MeC_6H_4OH–C_6H_6	50	0.103	3.85×10^{-4}	19
p-ClC_6H_4OH–C_6H_6	50	0.101	3.66×10^{-4}	20
2,6-Xylenol–C_6H_6	50	0.100	6.86×10^{-7} a)	26

a) Extrapolated value from data at 75 and 100 °C.

Hart and his collaborators[3] found that mixtures of various phenols and 1-phenylethyl chloride evolved hydrogen chloride to give 1-phenylethylated phenols, but they neither carried out the kinetic measurement, nor interpreted the reaction in terms of the typical S_N1 phenolysis.

In order to know the true product distribution which is not perturbed by the liberated hydrogen chloride, the distribution values in the phenolyses with variable concentrations of triethylamine or the sodium salt of the respective phenols were examined and extrapolated to the zero base concentration. The results obtained for the phenolyses in *p*-cresol (100 °C), *p*-chlorophenol (100 °C), 2,6-xylenol (100 °C), and phenol (50 °C) are summarized in Table 2, and illustrated in Figs. 1, 2, 3, and 4.

As it is shown in Figs. 1—4, the extrapolated values for the yield of the phenyl ether clearly indicate that, if the influence of hydrogen chloride is excluded from the reaction medium, the phenyl ether would be the major product for each phenolysis. The results, which were obtained by Hart and his collaborators[3] and confirmed in our duplicate runs, are clearly different from our extrapolated results (see Table 2).

The Steric Course of the S_N1 Phenolysis in the Absence of a Base. Hart and his collaborators[3] found that 1-phenylethyl chloride gives partially *retained ortho* 1-phenylethylated phenol in *p*-cresol and in *p*-chlorophenol. We confirmed their results under similar reaction conditions (see Table 2).

However, in the previous experiments[1b] carried out with added triethylamine in the mixtures of *p*-substituted phenols (phenol, *p*-cresol, and *p*-chlorophenol) and organic solvents (benzene and acetonitrile), we found that *ortho* 1-phenylethylated phenols exhibited partially *inverted* configurations.

In order to make the situation clearer, we examine

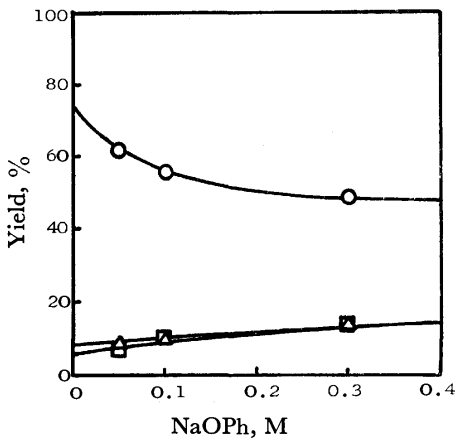

Fig. 1. The product composition for 1-phenylethyl chloride phenolysis in phenol in the presence of sodium phenoxide at 50 °C.

○: R-O- , △: *o*-RC_6H_4OH, □: *p*-RC_6H_4OH

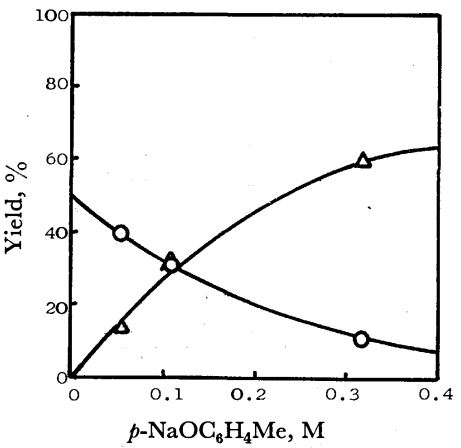

Fig. 2. The product composition for 1-phenylethyl chloride phenolysis in *p*-cresol in the presence of sodium *p*-cresoxide at 100 °C.

○: R-O- 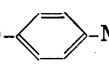 -Me, △: HO- 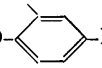 -Me

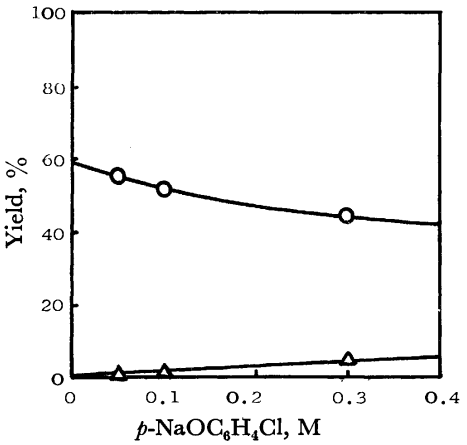

Fig. 3. The product composition for 1-phenylethyl chloride phenolysis in *p*-chlorophenol in the presence of sodium *p*-chlorophenoxide at 100 °C.

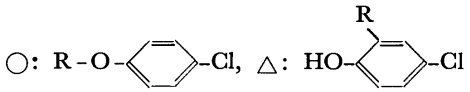

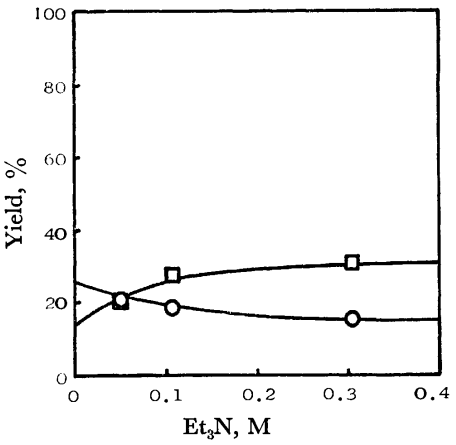

Fig. 4. The product composition for 1-phenylethyl chloride phenolysis in 2,6-xylenol in the presence of triethylamine at 100 °C.

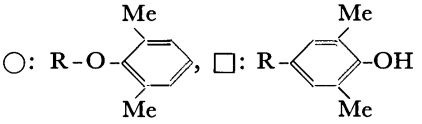

Table 2. Effect of added sodium phenoxides upon the product compositions and the steric courses for the phenolyses of 1-phenylethyl chloride in phenolic solvents

Solvent	Base[a] M	Product: Phenolic ether Yield %	Phenolic ether Net steric course, α%[b]	*o*-Alkylated phenol Yield %	*o*-Alkylated phenol Net steric course, α%[b]	*p*-Alkylated phenol Yield %	*p*-Alkylated phenol Net steric course, α%[b]
Phenol[c]	0.000	0.00	—	34.5	15.1 Ret.	63.8	35.1 Ret.
	0.051	61.8	30.3 Ret.	9.19	10.9 Inv.	6.78	29.7 Inv.
	0.109	56.3	29.7 Ret.	9.79	14.4 Inv.	10.3	31.2 Inv.
	0.309	49.3	33.5 Ret.	14.2	33.5 Inv.	14.4	32.3 Inv.
p-Cresol[d]	0.000	0.00[e]	—	60[e]	4.15 Ret.[e]		—
	0.000	2.25	8.66 Ret.	87.3	2.50 Ret.		—
	0.054	39.8	6.16 Ret.	13.9	7.34 Inv.		—
	0.124	31.6	4.93 Ret.	31.4	9.13 Inv.		—
	0.333	11.5	2.20 Ret.	60.0	19.1 Inv.		—
p-Chlorophenol[d]	0.000	0.00[e]	—	62[e]	2.26 Ret.[e]		—
	0.000	1.05	—	56.2	0.97 Ret.		—
	0.051	55.9	22.1 Ret.	0.976	24.7 Inv.		—
	0.101	53.0	20.7 Ret.	1.25	28.5 Inv.		—
	0.302	44.3	16.3 Ret.	4.56	54.0 Inv.		—
2,6-Xylenol[f]	0.000	0.00[e]	—		—	50[e]	5.46 Inv.[e]
	0.000	4.20	27.6 Ret.		—	41.5	7.06 Inv.
	0.051[g]	20.8	38.4 Ret.		—	20.1	18.8 Inv.
	0.115[g]	19.1	29.3 Ret.		—	27.2	30.0 Inv.
	0.310[g]	15.7	19.1 Ret.		—	32.1	77.9 Inv.

a) Sodium salts of the respective phenols. RCl=0.050 M. b) Calculated taking into account lack of optical purity of the starting substrate; the rotations of optically pure materials are taken to be 125° for *R*-(+)-1-phenylethyl chloride (H.M.R. Hoffmann and E.D. Hughes, *J. Chem. Soc.*, **1964**, 1244), 46.6° for *S*-(+)-1-phenylethyl phenyl ether (Ref. 1b), 20.4° for *S*-(+)-1-phenylethyl *p*-cresyl ether (Ref. 1b), −22.40° for *R*-(−)-1-phenylethyl *p*-chlorophenyl ether (Ref. 1b), −57.9° for *R*-(−)-1-phenylethyl 2,6-xylyl ether, 27.85° for *R*-(+)-*o*-(1-phenylethyl)phenol (Ref. 1b), 10.26° for *S*-(+)-*p*-(1-phenylethyl)phenol (Ref. 1b), 17.1° for *S*-(+)-*o*-(1-phenylethyl)*p*-cresol (Ref. 9), 44.7° for *S*-(+)-*o*-(1-phenylethyl)-*p*-chlorophenol (Ref. 9), and 8.6° for *S*-(+)-4-(1-phenylethyl)-2,6-xylenol (Ref. 9). Reported value for the 2,6-xylyl ether, −51° (Ref. 5a), was recalculated on the basis of the new value for the maximum rotation of the chloride (H. and H., *loc. cit.*). c) At 50 °C for 2 hr. d) At 100 °C for 5 hr. e) Hart *et al.* (Ref. 3). f) At 100 °C for 20 hr. g) Triethylamine.

TABLE 3. PRODUCT COMPOSITION AND STERIC COURSES FOR PHENOLYSES OF 1-PHENYLETHYL CHLORIDE IN VARIOUS PHENOLS.
Extrapolated values to the zero base concentration

Solvent	Temp. °C	Product					
		Phenolic ether		*o*-Alkylated phenol		*p*-Alkylated phenol	
		Yield %	Net steric course, α%	Yield %	Net steric course, α%	Yield %	Net steric course, α%
Phenol	100	75	29 Ret.	9.0	7.0 Inv.	7.0	29 Inv.
p-Cresol	100	49	8.7 Ret.	0—1	6.0 Inv.		—
p-Chlorophenol	100	59	59 Ret.	0—1	17 Inv.		—
2,6-Xylenol	100	25	50 Ret.		—	15	10 Inv.

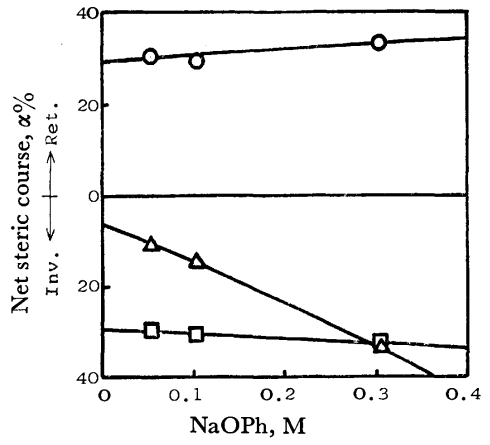

Fig. 5. The steric course for 1-phenylethyl chloride phenolysis in phenol in the presence of sodium phenoxide at 50 °C.

○: R-O-⟨⟩, △: *o*-RC_6H_4OH, □: *p*-RC_6H_4OH

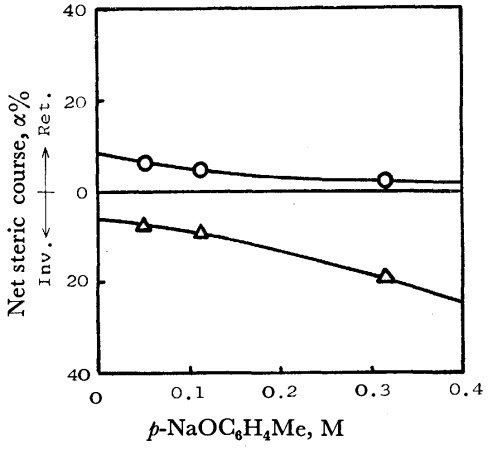

Fig. 6. The steric course for 1-phenylethyl chloride phenolysis in *p*-cresol in the presence of sodium *p*-cresoxide at 100 °C.

○: R-O-⟨⟩-Me, △: HO-⟨R⟩-Me

the effect of the base concentration on the steric course of the *ortho* 1-phenylethylated phenol formation by carrying out the phenolyses of optically active 1-phenylethyl chloride in the presence of variable concentrations of the sodium salts of phenol, *p*-cresol, and *p*-chlorophenol. The results are graphically extrapolated to the zero concentration of the respective phenoxides. These are illustrated in Table 3 and Figs. 5, 6, and 7 along

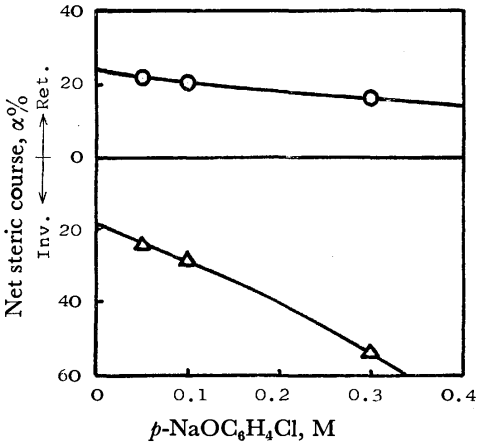

Fig. 7. The steric course for 1-phenylethyl chloride phenolysis in *p*-chlorophenol in the presence of sodium *p*-chlorophenoxide at 100 °C.

○: R-O-⟨⟩-Cl, △: HO-⟨R⟩-Cl

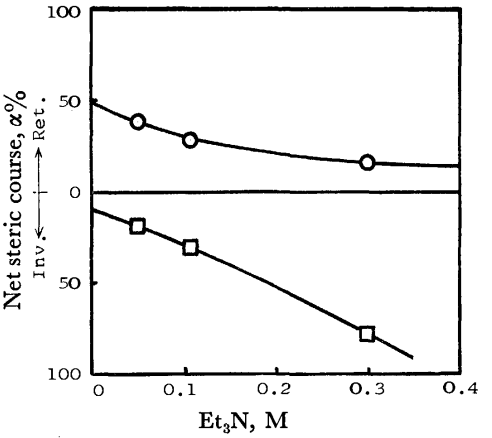

Fig. 8. The steric course for 1-phenylethyl chloride phenolysis in 2,6-xylenol in the presence of triethylamine at 100 °C.

○: R-O-⟨Me, Me⟩, □: R-⟨Me, Me⟩-OH

with the steric courses for the formation of 1-phenylethyl ether of the respective phenols. In Fig. 8 the steric course for the formation of *para* 1-phenylethylated 2,6-xylenol and 1-phenylethyl 2,6-xylyl ether in the xylenolyses with variable concentrations of triethylamine are illustrated.

It is evident that the extrapolated results show that even in the absence of the base the phenolyses give *ortho* 1-phenylethylated phenols with partially *inverted* configuration, if the perturbation of hydrogen chloride was excluded. From these results we can conclude that the intrinsic steric course for the *ortho* alkylation of phenol with 1-phenylethyl chloride is predominantly *inverted.*

The Steric Course of the Formation of 1-Phenylethylphenols from 1-Phenylethyl Ethers of Various Phenols in the Acidic Phenol Solvents. In order to confirm the rate and the steric course of the acidic rearrangement of 1-phenylethyl group under the phenolysis condition, the rearrangement of optically active 1-phenylethyl ethers of phenol, *p*-cresol, *p*-chlorophenol, and 2,6-xylenol were carried out in the presence of hydrogen chloride in the respective phenolic solvents. The respective 1-phenylethyl ethers rearranged rapidly to the corresponding 1-phenylethylphenols (92—97% yield) in the respective phenol–benzene (1: 1 by wt.) solvents at the same temperature as the phenolyses were conducted. A summary of the stereochemical results is given in Table 4.

It is shown for each rearrangement that the 1-phenylethyl group rearranges to the *ortho* position with partial retention of the configuration whereas the *para* rearrangement proceeds with predominant inversion of configuration.

Besides the acidic intramolecular rearrangement of 1-phenylethyl phenyl ether, the rearrangement products, *i.e.*, *ortho*- and *para*-alkylated phenols may partly stem from the S_N1 phenolysis of reproduced 1-phenylethyl chloride due to the hydrogen chloride cleavage[5] of the 1-phenylethyl phenyl ether. This is a sort of intermolecular course for the rearrangement of 1-phenylethyl phenyl ethers in the acidic phenol solvent, and illustrated in the following scheme, using ^{18}O-labelled phenyl ether.

$$R^{18}OPh + HCl \longrightarrow RCl + Ph^{18}OH$$

$$RCl + PhOH \longrightarrow ROPh + o\text{-}RC_6H_4OH + p\text{-}RC_6H_4OH$$

In fact, it is known that this ether is cleaved by hydrogen chloride to give partially retained 1-phenylethyl chloride in toluene,[5c] 3-pentanone,[5c] isobutyl alcohol,[5b] benzene,[5b] acetone,[5b] and phenol–dioxane.[5d]

Furthermore, it is also conceivable as another course for the intermolecular rearrangement in the phenolic solvent that the protonated 1-phenylethyl phenyl ether might be phenolyzed, and give intermolecularly the alkylated phenols, as is shown in the following scheme.

$$R^{18}OPh + H^+ (Cl^-) \longrightarrow R^{18}\overset{\overset{H}{|}}{O}\text{-}Ph$$

$$R^{18}\overset{\overset{H}{|}}{O}\text{-}Ph + PhOH \longrightarrow ROPh + o\text{-}RC_6H_4OH + p\text{-}RC_6H_4OH + Ph^{18}OH$$

In order to estimate the amounts of these intermolecular courses in the acidic rearrangement of 1-phenylethyl phenyl ether, ^{18}O-labelled 1-phenylethyl phenyl ether was subjected to the acidic rearrangement in the presence of *p*-toluenesulfonic acid in the phenol–benzene (1: 1 by wt) solvent at 25 °C. As illustrated in Table 5, it is evident that only 44.9% of *o*-1-phenylethylphenol and 25.7% of *p*-1-phenylethylphenol were intramolecularly produced from the labelled phenyl ether, but the rest of the alkylphenols was produced by the phenolysis of the oxonium ion of the phenyl ether or, less probably, by the phenolysis of 1-phenyl-

Table 4. The product compositions and the steric courses for the acidic rearrangements of 1-phenylethyl phenyl ethers (ROAr) in the presence of HCl in phenol(ArOH)–benzene (1: 1 by wt) solvents[a]

Ar–O–(1-Phenylethyl) Ar	α_D[c] M	HCl[b] M	Product: *o*-Alkylated phenol Yield %	*o*-Alkylated phenol $[\alpha]_D$[d] Net steric course, α%	*p*-Alkylated phenol Yield %	*p*-Alkylated phenol $[\alpha]_D$[d] Net steric course, α%
Phenyl[e]	+3.25° (±0.05°) 0.050	0.050	54.8	−0.925° (±0.025°) 47.9 Ret.	39.7	−0.520° (±0.026°) 73.0 Inv.
Phenyl[f]	−6.41° (±0.02°) 0.0968	0.0234	23.4	+2.85° (±0.32°) 74.5 Ret.	75.8	+1.21° (±0.09°) 85.8 Inv.
p-Cresyl[g]	+0.378° (±0.006°) 0.050	0.051	93.5	+0.036° (±0.003°) 10.1 Ret.		—
p-Chlorophenyl[g]	−4.56° (±0.05°) 0.050	0.051	92.2	−0.448° (±0.022°) 4.93 Ret.		—
2,6-Xylyl[h]	−2.86° (±0.01°) 0.050	0.052		—	96.5	−0.012° (±0.002°) 2.86 Inv.

a) The maximum rotations for the relevant optically active compounds in this table are shown in Table 2. b) Determined by titration. c) The rotations for a neat sample at 24—32°C in a 1 dm tube. d) The rotations for a benzene solution (*c* 4.8—73.6) at 22—30 °C. e) At 50 °C for 2 hr. f) At 40 °C for 5 hr (in PhOH–MeCN (1: 1 by wt)). g) At 100 °C for 5 hr. h) At 100 °C for 20 hr.

Table 5. ^{18}O content of alkylphenols produced by the rearrangement of 1-phenylethyl phenyl ether-^{18}O in a phenol–benzene (1:1 by wt) solvent in the presence of *p*-toluenesulfonic acid at 25 °C at 49% conversion[a)]

Material	Yield %	^{18}O atom% excess[a)]	Retention % of ^{18}O atom% excess
ROPh (0.100M)	—	0.863	—
o-RC_6H_4OH	31.3	0.387	44.9
p-RC_6H_4OH	17.7	0.222	25.7

a) $TsOH=3.96\times10^{-3}M$; $H_2O=7.8\times10^{-3}M$; oxygen-18 contents were determined by the method of Rittenberg and Ponticorvo (Ref. 8).

ethyl *p*-toluenesulfonate, produced by the acidic cleavage of the phenyl ether with *p*-toluenesulfonic acid.

In conclusion, in view of these findings mentioned above, the formation of the *ortho*-alkylates with *retained* configuration in the phenolysis without an added base is attributed not to the direct retentive alkylation of the phenols, but to the rapid rearrangement of the 1-phenylethyl ethers with net *retention* of configuration, caused by the hydrogen chloride liberated in the S_N1 phenolysis of 1-phenylethyl chloride in the respective phenolic solvents.

Experimental[6)]

Materials. *S*-(−)-1-Phenylethyl chloride was prepared by the reaction of *S*-(−)-1-phenylethanol with thionyl chloride in a manner previously described.[1)] Sodium *p*-substituted phenoxide was prepared by refluxing the toluene solution of *p*-substituted phenol with sodium metal. All the other reagents employed were of an analytical reagent grade and were fractionated just prior to use.

Synthesis of 1-Phenylethyl Phenyl Ether-^{18}O. According to the method of Stevens and Bentel,[7)] phenol-^{18}O (4.46 g; containing some ether) was prepared by a diazotization of aniline (2.8 g, 0.030 mol) with sodium nitrite (2.1 g, 0.030 mol) in $H_2{}^{18}O$ (^{18}O 3 atom% excess; 15 ml). 1-Phenylethyl phenyl ether-^{18}O (0.66 g; ^{18}O 0.863 atom% excess) was synthesized by refluxing an acetone solution (60 ml) of phenol-^{18}O (4.46 g; containing some ether), 1-phenylethyl chloride (3.3 g, 0.020 mol), and potassium carbonate (4.1 g, 0.030 mol) after the method described by Hart and Eleuterio.[9)] The ^{18}O content was determined by the method of Rittenberg and Ponticorvo.[8)]

Rate Measurement. The previous procedure[1)] was followed. Aliquots (1 ml) were removed at intervals from a reaction mixture (15 ml) placed in a constant-temperature bath. The increase of acid concentrations was followed by titration with standard sodium acetate in acetic acid, using crystal violet as an indicator. In each case, a first-order linear relationship was obtained to *ca.* 20% conversion. Infinity titers were calculated from the weight of the chloride used. These results are summarized in Table 1.

Product Isolation (General Procedure). The vessel, containing a reaction mixture, was placed in a constant-temperature bath; at the desired time the reaction was quenched by cooling and dilution with ether. The mixture was successively washed with 10% aq. NaOH and 10% aq. NaCl, dried with $MgSO_4$, and concentrated. The concentrate was subjected to preparative thin-layer chromatography on silica gel. The detailed procedures are described in representative cases which follow.

1-Phenylethyl Chloride Phenolysis in p-*Cresol in the Presence of Sodium* p-*Cresoxide.* A mixture of 1-phenylethyl chloride (1.500 ml, 0.01136 mol; $\alpha_D^{27.2}$ −34.50±0.05° (neat, 1 dm)) and *p*-cresol (220 ml) containing sodium *p*-cresoxide (0.0541 M: determined by titration) was kept at 100.0±0.1 °C for 5 hr. After the working-up mentioned above, 1-phenylethyl *p*-cresyl ether (0.9601 g, 39.8% yield; bp 160—165 °C/4 mmHg; $\alpha_D^{32.0}$ −0.201±0.013° (neat, 1 dm)) and *o*-(1-phenylethyl)-*p*-cresol (0.3350 g, 13.9% yield; bp 170—175 °C/4 mmHg; $[\alpha]_D^{34.0}$ +1.12±0.074° (*c* 2.016, benzene)) were obtained.

1-Phenylethyl Chloride Phenolysis in p-*Cresol in the Absence of an Added Base.* A mixture of 1-phenylethyl chloride (0.6410 g, 0.00456 mol; $\alpha_D^{27.2}$ −34.5° (neat, 1 dm)) and *p*-cresol (90 ml) was maintained at 100 °C for 5 hr and worked up as mentioned above: *o*-(1-phenylethyl)-*p*-cresol (0.8442 g, 87.3% yield; bp 170—175 °C/4 mmHg; $[\alpha]_D^{32.6}$ +0.118±0.010° (*c* 9.31, benzene)) and 1-phenylethyl *p*-cresyl ether (24.2 mg, 2.50% yield; bp 155—160 °C/4 mmHg; $[\alpha]_D^{34.0}$ +0.431±0.330° (*c* 0.232, benzene)) were obtained.

The Acidic Rearrangement of 1-Phenylethyl p-*Cresyl Ether in* p-*Cresol–Benzene (1:1 by wt).* A mixture of 1-phenylethyl *p*-cresyl ether (1.0651 g, 0.00502 mol; $\alpha_D^{32.0}$ +1.890± 0.030° (neat, 1 dm)) and *p*-cresol–benzene (1:1 by wt.; 100 ml) containing anhydrous hydrogen chloride (0.0505 M) was kept at 100 °C for 5 hr. After the working-up mentioned above, *o*-(1-phenylethyl)-*p*-cresol (0.9971 g, 93.5% yield; bp 170—177 °C/4 mmHg; $[\alpha]_D^{29.8}$ +0.182±0.051° (*c* 18.5, benzene)) was obtained.

The Acidic Rearrangement of 1-Phenylethyl Phenyl Ether-^{18}O in Phenol–Benzene (1:1 by wt). A mixture of 1-phenylethyl phenyl ether-^{18}O (0.2911 g; 0.00147 mol; ^{18}O 0.863 atom% excess) and phenol–benzene (1:1 by wt.; 14.5 ml) containing anhydrous *p*-toluenesulfonic acid (0.00396 M) was kept at 25 °C for 10 min (49% conversion by glc) and worked up in a manner mentioned above. *o*-(1-Phenylethyl)phenol (0.9115 g, 31.3% yield; ^{18}O 0.387 atom% excess) and *p*-(1-phenylethyl)phenol (0.0515 g, 17.7% yield; ^{18}O 0.222 atom% excess) were obtained.

We wish to thank Prof. Kameo Asada, Department of Nuclear Engineering, Kyoto University, for his kind technical guidance in the measurement of mass spectrograph and Prof. Jyun Oishi, Dept. N. E., Kyoto Univ., for his good offices with Prof. Asada.

References

1) a) K. Okamoto, K. Takeuchi, and H. Shingu, This Bulletin, **35**, 525 (1962); b) K. Okamoto, H. Yamada, I. Nitta, and H. Shingu, *ibid.*, **39**, 299 (1966).

2) K. Okamoto, T. Kinoshita, and H. Shingu, *ibid.*, **43**, 1545 (1970).

3) H. Hart, W. L. Spliethoff, and H. S. Eleuterio, *J. Amer. Chem. Soc.*, **76**, 4547 (1954).

4) a) K. Okamoto, K. Matsubara, and T. Kinoshita, This Bulletin, **45**, 1191 (1972); b) K. Okamoto and T. Kinoshita, *ibid.*, **45**, 2802 (1972); c) K. Okamoto, T. Kinoshita, and Y. Ito, *ibid.*, **46**, 2905 (1973).

5) a) H. Hart and H. S. Eleuterio, *J. Amer. Chem. Soc.*, **76**, 518 (1954); b) H. Hart and H. S. Eleuterio, *ibid.*, **76**, 1379 (1954); c) H. Hart and R. J. Elia, *ibid.*, **83**, 985 (1961); d) K. Okamoto, K. Takeuchi, and H. Shingu, This Bulletin, **37**, 276 (1964).

6) A Hitachi Model 023-6001 gas chromatographic instrument, with a thermocouple detector, a Hitachi Model 215 spectrophotometer, a Hitachi Model R-24 60 MHz NMR instrument, and an Atlas Model CH-4 mass spectrometer were used for analytical works. Optical rotations were measured with a JASCO Model DIP–SL polarimeter.

Each product was identified by the fact that the IR and NMR spectra and the retention time of glc (Apiezon Grease L on Neopak 1A 3 mm$^{\phi}$ × 2 m column, at 200°) were the same as those of an authentic sample.

7) J. R. Stevens and R. H. Bentel, *J. Amer. Chem. Soc.*, **63**, 311 (1941).

8) D. Rittenberg and L. Ponticorvo, *Int. J. Appl. Radiat. Isotopes*, **1**, 208 (1956).

9) H. Hart and H. S. Eleuterio, *J. Amer. Chem. Soc.*, **76**, 516 (1954).

A Convenient Method for the Preparation of Ketones by the Reaction of Grignard Reagents with Carboxylic Acid Derivatives

Masashi ARAKI, Shigeru SAKATA, Hisashi TAKEI, and Teruaki MUKAIYAMA

Laboratory of Organic Chemistry, Tokyo Institute of Technology, Ookayama, Meguro-ku, Tokyo 152

(Received March 20, 1974)

It was found that ketones were prepared in excellent yields by the reaction of Grignard reagents with *S*-(2-pyridyl) thioates and their analogues or with 2-pyridyl esters. The mechanism of this reaction was also discussed. This useful method for the preparation of ketones was successfully applied to the syntheses of *cis*-jasmone and dihydrojasmone.

Many works have been reported on the synthesis of ketones from carboxylic acid derivatives and organometallic compounds.[1] The reaction of Grignard reagents with acid chlorides, nitriles, acid amides, or acid anhydrides is frequently employed for this purpose; however, tertiary alcohols, undesirable by-products, are invariably accompanied with the formation of ketones except in the case of nitriles.

Staab and Jost[2] reported that the treatment of Grignard reagents with *N*-acylimidazoles affords ketones in fairly good yields. Recently, a convenient method for the synthesis of ketones from Grignard reagents and 8-acyloxyquinolines was reported by Sakan and Mori.[3] The reaction was suggested to proceed through an important intermediate of 8-acyloxyquinoline metal complex.

As part of our study on the carbon-carbon bond forming reaction by the use of 2-pyridyl sulfides,[4] it was found that various *S*-(2-pyridyl) thioates react very rapidly with Grignard reagents to give ketones in excellent yields by simple procedures. The preliminary report of this work was published elsewhere.[5]

This paper describes a scope and a limitation of this useful method for the preparation of ketones by the reaction of Grignard reagents with *S*-(2-pyridyl) thioates and their analogues or with 2-pyridyl esters, and the application of this method to the syntheses of *cis*-jasmone and dihydrojasmone.

S-(2-Pyridyl) thioates of various carboxylic acids were prepared according to the following two methods; (A) the reaction of 2-pyridinethiol with carboxylic acid halides in the presence of tertiary amine such as triethylamine, or (B) the reaction of carboxylic acids with triphenylphosphine and 2,2′-dipyridyl disulfide.[6] In general, the reaction of *S*-(2-pyridyl) thioates with Grignard reagents was carried out in dry tetrahydrofuran (THF) at 0 °C under argon atmosphere by the inverse addition. Usual work-up afforded various ketones in excellent yields as shown in Table 1.

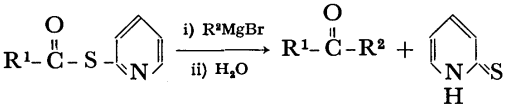

The effects of the solvents on this reaction clearly indicate that THF is the most suitable solvent (see Table 2). In THF, the reaction proceeded in homogeneous solution throughout the addition of Grignard reagents. While, in the cases of other solvents, white precipitates immediately appeared when Grignard reagents were added to the solution of *S*-(2-pyridyl) thioates.

Table 1. Reaction of *S*-(2-pyridyl) thioates with Grignard reagents in THF

R^1	R^2	R^1–CO–R^2 (%)[a]	Mp °C, (Bp °C/mmHg)
Ph	Ph	quant.	46.0—47.0
CH_3	Ph	91	oil
n-C_5H_{11}	Ph	86	oil
n-C_5H_{11}	Ph	83[b]	(134—137/17)
$(CH_2)_4$	Ph[c]	92[d]	107.0—107.5
$PhCH_2CH_2$	*n*-C_4H_9	97	oil
$PhCH_2CH_2$	*c*-C_6H_{11}	95	oil
$PhCH_2CH_2$	*sec*-C_4H_9	83	oil
$C_2H_5OCO(CH_2)_4$	Ph	85	27.0—28.0
$CH_3CO(CH_2)_4$	Ph	73	42.0—43.0

a) Isolated yields by preparative tlc (silica gel). b) Isolated yield by distillation. c) Two molar amounts of phenylmagnesium bromide were used. d) The yield of 1,4-dibenzoylbutane.

Table 2. Solvent effect

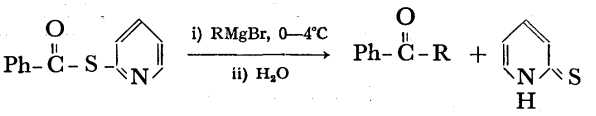

R	Solvent	Ph–CO–R(%)[a]	R_2(Ph)COH(%)
Ph	THF	quant.	—
Ph	Ether	54[b]	18
Ph	Benzene	80[b]	4
n-C_4H_9	Benzene	74	

a) Isolated yields by preparative tlc (silica gel). b) The mixture of benzophenone and triphenylmethanol was isolated and their ratio was determined by glpc.

In the early stage of this study, it was assumed that the preferential formation of ketones would be accomplished by the formation of a stable six-membered intermediate **I** which would react very sluggishly with

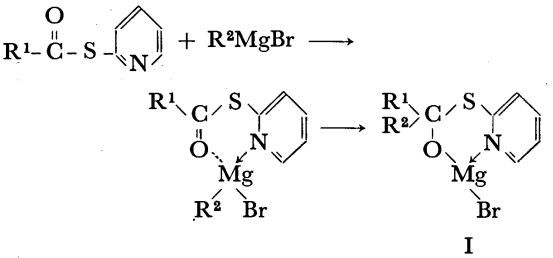

I

Grignard reagents as compared with *S*-(2-pyridyl) thioates. But, the IR spectra of the reaction mixture of *S*(2-pyridyl) isobutanethioate and cyclohexylmagnesium bromide in argon atmosphere showed the absorption at 1710 cm^{-1} which was assigned to the stretching vibration of the carbonyl group of the ketone. This result may indicates that the intermediate I is not kept stable under the reaction condition, but decomposes rapidly into ketones and magnesium thiolate. Thus, it can be concluded that the preferential formation of ketones by the present reaction depends only on the high reactivity of Grignard reagents toward *S*-(2-pyridyl) thioates as compared with ketones. This was confirmed by the following results; 1) benzophenone was obtained quantitatively by the reaction of *S*-(2-

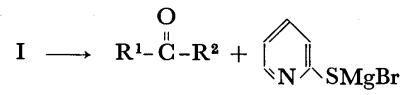

pyridyl) benzothioate with phenylmagnesium bromide in the presence of an equimolar amount of benzophenone without accompanying triphenylmethanol, and 2) the treatment of the *S*-(2-pyridyl) thioate of 6-oxoheptanoic acid or 5-carboethoxyvaleric acid with phenylmagnesium bromide without protection of the carbonyl group afforded the corresponding diketone or ketoester in high yields.

High reactivity of *S*-(2-pyridyl) thioates toward Grignard reagents would be attributed to the following three reasons; (1) Grignard reagents are activated by the formation of complex II with *S*-(2-pyridyl) thioates, (2) the addition reaction of Grignard reagents to the carbonyl group of *S*-(2-pyridyl) thioates proceeds through the favorable six-membered intermediate, (3) after the addition of Grignard reagents to the carbonyl group, magnesium thiolate IV is eliminated smoothly through electrocyclic mechanism as sketched in III.

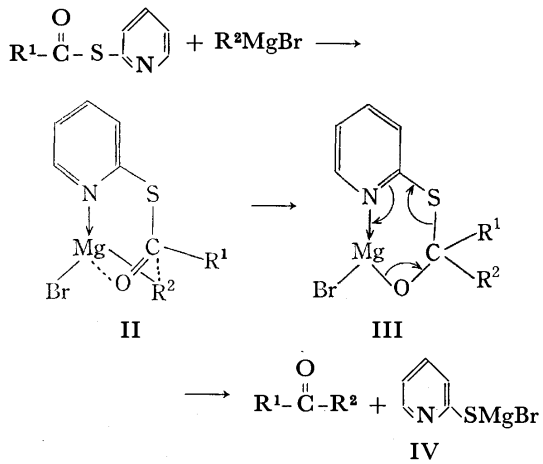

II III IV

The above-mentioned mechanism indicates that 2-pyridyl esters 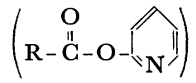 or the thioates having

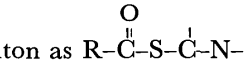

such a skelton as R–C–S–C–N– would similarly react with Grignard reagents to result in the exclusive formation of ketones. Expectedly, ketones were obtained in high yields by the addition of Grignard reagents to a

Table 3. Reaction of 2-pyridyl esters with Grignard reagents in THF

R^1	R^2	R^1COR^2(%)	Mp(°C)
Ph	Ph	93	46.0—47.0
Ph	*n*-C_4H_9	77	oil
Ph	*c*-C_6H_{11}	97	53.0—55.0
$PhCH_2CH_2$	Ph	88	67.0—68.0
$PhCH_2CH_2$	*n*-C_4H_9	87	oil
$PhCH_2CH_2$	*c*-C_6H_{11}	88	oil
$PhCH_2CH_2$	*t*-C_4H_9	<64	oil

a) Isolated yields by preparative tlc (silica gel).

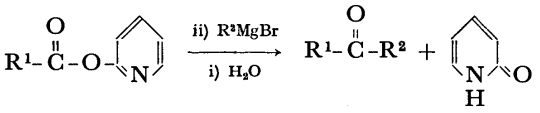

THF solution of 2-pyridyl esters at 0 °C as shown in Table 3.

The IR spectra of the reaction mixture of 2-pyridyl benzoate and phenylmagnesium bromide in argon atmosphere showed the absorption at 1663 cm^{-1} assigned to the carbonyl group of benzophenone formed by the reaction.

The thioates obtained from benzoyl chloride and 2-benzothiazolethiol or 2-(*N*-methylimidazole)thiol also reacted with Grignard reagents to give ketones as shown in Table 4.

Table 4. Reaction of thioates with Grignard reagents in THF

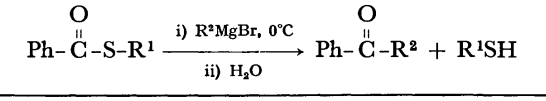

R^1	R^2	Ph–CO–R^2(%)	Mp (°C)
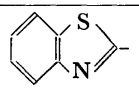	Ph	98	46.0—47.0
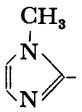	Ph	98	46.0—47.5
	n-C_4H_9	30[a]	oil
	n-C_4H_9	70[b]	oil

a) 1-Butyl-1-phenylpentanol was isolated in *ca.* 29% besides the ketone. b) Reaction at −78°C.

The present ketone synthesis by using *S*-(2-pyridyl) thioates was successfully applied to the preparation of *cis*-jasmone and dihydrojasmone through 1,4-diketones starting from levulinic acid as in Scheme 1.

In the above scheme, the protection of the carbonyl group by ethanedithiol seems to be unnecessary from the results shown in Table 1. But, *S*-(2-pyridyl) 6-oxopentanethioate (X), prepared by the reaction of levulinic acid with triphenylphosphine and 2,2′-dipyridyl disulfide, is not stable at room temperature and is readily converted to γ-pyridylthio-γ-valerolactone (XI).

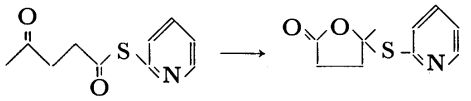

X XI

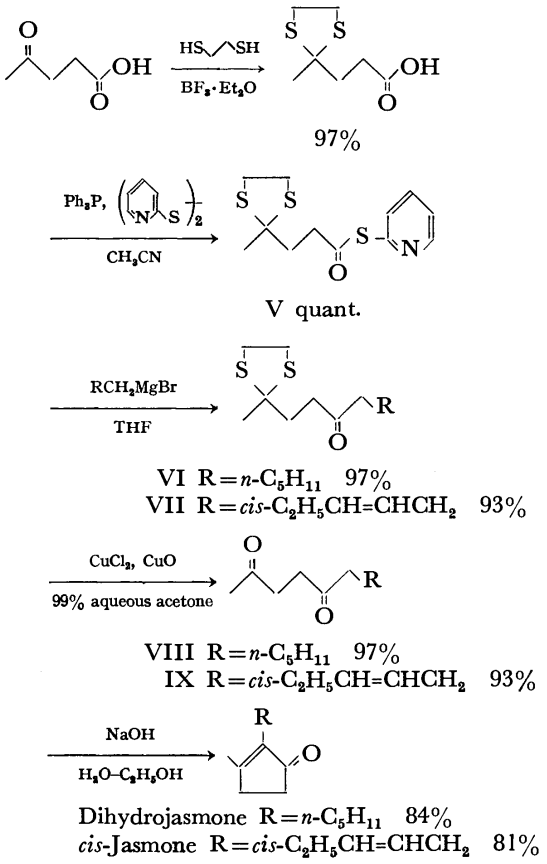

Scheme 1. Syntheses of *cis*-jasmone and dihydrojasmone

Therefore, the carbonyl group was led to ethylene dithioacetal in order to isolate the pure thioate V. The thioate V was isolated by silica gel column chromatography in 97% yield based on levulinic acid. The ketone VI was obtained in 97% yield by the reaction of V with *n*-hexylmagnesium bromide, and the hydrolysis of VI by our method[7] afforded 1,4-diketone (VIII) in 98% yield. Dihydrojasmone was obtained from VIII according to the method of Hunsdieker[8] in 84% yield. Analogously, olefinic 1,4-diketone IX was isolated in 82% yield by the reaction of V with 3-*cis*-hexenyl magnesium bromide, followed by the deprotection of the carbonyl group.[7] IX was converted to *cis*-jasmone in 81% yield by the ordinary procedure.[8]

In conclusion, it is noted that all the common ketones were easily prepared in high yields without accompanying tertiary alcohols by treating *S*-(2-pyridyl) thioates and 2-pyridyl esters with Grignard reagents. Further, this procedure was proved to be applicable to the syntheses of 1,6-diketone as 1-phenyl-1,6-dioxoheptane without the protection of carbonyl group or 1,4-diketones as 2,5-dioxo-*cis*-8-undecene and 1,5-dioxoundecane, precursors of *cis*-jasmone and dihydrojasmone.

Experimental

All the melting points and boiling points are uncorrected.

General Method for the Preparation of S-(2-Pyridyl) Thioates. *S*-(2-Pyridyl) thioates were prepared by the following two methods. (A) To a solution of 2-pyridinethiol[9] (2.22 g, 20 mmol) and triethylamine (2.02 g, 20 mmol) in dry THF (30 ml) was added 20 mmol of an acid halide at 0 °C with stirring. The reaction mixture was stirred for 4 hr at room temperature. After removal of triethylamine hydrochloride by filtration, the solvent was removed under reduced pressure and the residue was dissolved in ether. The ether layer was washed with saturated sodium chloride solution and dried over sodium sulfate. Removal of the solvent gave a crude *S*-(2-pyridyl) thioate quantitatively. The crude thioate was purified by distillation or recrystallization. (B) To a mixture of 2,2'-dipyridyl disulfide (2.20 g, 10 mmol), triphenylphosphine (2.62 g, 10 mmol), and a carboxylic acid (10 mmol) was added dry acetonitrile (30 ml) at once with stirring. The reaction mixture was stirred for 10 min and then the solvent was removed under reduced pressure. The residue was chromatographed over silica gel to give a *S*-(2-pyridyl) thioate.

S-(2-Pyridyl) thioates obtained by the method A or B were listed in Table 5.

Table 5. *S*-(2-Pyridyl)thioates $\left(R-\overset{O}{\overset{\|}{C}}-S-\text{(2-pyridyl)}\right)$

R	Method	Yield (%)	Mp °C (Bp °C/mmHg)
Ph	A	80	50.0—51.0[a]
CH_3	A	60	(98—99/4)
n-C_5H_{11}	A	84	(111—112/1)
$PhCH_2CH_2$	A	82	56.0—58.0[b]
$(CH_2)_4$	A	57	44.5—45.0[c]
$CH_3CO(CH_2)_4$	A	80[d]	oil
$C_2H_5OCO(CH_2)_4$	B	78[d]	oil

Recrystallized from a) benzene–hexane, b) cyclohexane, c) ether. d) Purified by silica gel column chromatography.

Other Thioates. *S*-[2-(*N*-Methylimidazolyl)] benzothioate and *S*-(2-benzothiazolyl) benzothioate were prepared similarly according to the method A mentioned above using 2-(*N*-methylimidazole)thiol of 2-benzothiazolethiol instead of 2-pyridinethiol (74% mp 104.5—105.0 °C (benzene–hexane), 75% mp 125.0—126.0 °C (cyclohexane)).

2-Pyridyl Esters. To a mixture of 2-hydroxypyridine (0.951 g, 10 mmol) and triethylamine (1.012 g, 10 mmol) in 50 ml of dry ether was added benzoyl chloride (1.406 g, 10 mmol) at 0 °C with stirring. After stirring for 4 hr at room temperature, precipitated triethylamine hydrochloride was removed by filtration. The filtrate was washed with saturated sodium chloride solution and dried over sodium sulfate. Removal of the ether gave a solid, which was recrystallized from cyclohexane–hexane to afford 2-pyridyl benzoate (1.05 g, 53% mp 41.0—42.0 °C).

In a similar manner, 2-pyridyl β-phenylpropionate was prepared using β-phenylpropionyl chloride instead of benzoyl chloride in benzene as a solvent. It is necessary that the benzene solution containing 2-pyridyl β-phenylpropionate is dried quickly over sodium sulfate, since this ester is readily hydrolyzed. (68% bp 128—130 °C/1.3×10^{-1} mmHg).

General Procedure for the Reaction of Thioates with Grignard Reagents under Argon. In a 50 ml two-necked flask equipped with dropping funnel and gas inlet tube were placed 20 ml of dry THF and 2 mmol of a thioate. The flask was cooled in ice-water bath and a THF solution of Grignard reagent (approximately 1 equivalent) was added from the dropping

funnel until the thioates were consumed (checked by tlc). The reaction mixture was quenched with 10% ammonium chloride and the resulting solution was extracted with ether. The organic layer was washed with 1 M sodium hydroxide to remove the thiol formed, with saturated sodium chloride and dried over sodium sulfate. After removal of the solvent the residue, almost pure ketone, was further purified by silica gel chromatography or distillation.

General Procedure for the Reaction of 2-Pyridyl Esters with Grignard Reagents under Argon. In 10 ml of THF a 2-pyridyl ester (1 mmol) was allowed to react with a Grignard reagent according to the above procedure. After quenching with 10% ammonium chloride, the resulting mixture was extracted with ether. The organic layer was washed with saturated sodium chloride and dried over sodium sulfate. After removal of the solvent the residue, whose IR spectra showed no absorption assigned to the stretching vibration of alcoholic O–H bond, was chromatographed over silica gel to give pure ketone.

Levulinic Acid Ethylene Dithioacetal. To a mixture of levulinic acid (0.231 g) and ethanedithiol (0.234 g) was added boron trifluoride etherate (0.2 ml) with stirring. An exothermic reaction occurred and after 2.5 hr, the resulting white solid was dissolved in ether. The ether layer was washed with water and dried over sodium sulfate. After removal of the ether, the obtained acid was purified by silica gel thin layer chromatography (0.370 g 97% mp 53.0—55.0 °C). In the case of larger scale experiment, recrystallization may be recommended instead of the chromatography.

References

1) a) D. A. Shirley, "Organic Reactions," Vol. 8, John Wiley & Sons, Inc., New York, N. Y. (1954), p. 28; b) M. S. Kharasch and O. Reinmuth, "Grignard Reactions of Nonmetallic Substances," Prentice-Hall, Englewood Cliffs, N. J., (1954); c) G. Posner and C. E. Witten, *Tetrahedron Lett.*, **1970**, 4647; d) A. Meyers and E. M. Smith, *J. Org. Chem.*, **37**, 4289 (1972); e) A. Meyers and N. Nazarenko, *ibid.*, **38**, 175 (1973); f) M. J. Jorgensen, "Organic Reactions," Vol. 18, John Wiley & Sons, Inc., New York, N. Y. (1970), p. 1; g) T. H. Chan, E. Chang, and E. Vinokur, *Tetrahedron Lett.*, **1970**, 1137; h) J. E. Dubois and M. Boussu, *ibid.*, **1970**, 2523.

2) H. A. Staab and E. Jost, *Ann. Chem.*, **655**, 90 (1962).

3) T. Sakan and Y. Mori, *Chem. Lett.*, **1972**, 793.

4) a) T. Mukaiyama, K. Narasaka, K. Maekawa, and M. Furusato, This Bulletin, **44**, 2285 (1971); b) T. Mukaiyama, S. Yamamoto, and M. Shiono, *ibid.*, **45**, 2244 (1972); c) K. Narasaka, M. Hayashi, and T. Mukaiyama, *Chem. Lett.*, **1972**, 259.

5) T. Mukaiyama, M. Araki, and H. Takei, *J. Amer. Chem. Soc.*, **95**, 4763 (1973).

6) *cf.* T. Endo, S. Ikenaga, and T. Mukaiyama, This Bulletin, **43**, 2632 (1970).

7) K. Narasaka, T. Sakashita, and T. Mukaiyama, *ibid.*, **45**, 3724 (1972).

8) H. Hunsdieker, *Chem. Ber.*, **75**, 460 (1942).

9) M. A. Phillips and H. Shapiro, *J. Chem. Soc.*, **1942**, 584.

The Configuration at C-21 of Hydroxyhopanone

Kazuo SEKIGUCHI, Hiroaki KANEMOTO, Yoji HIRAO, Takahiko TSUYUKI, and Takeyoshi TAKAHASHI

Department of Chemistry, Faculty of Science, The University of Tokyo, Bunkyo-ku, Tokyo 113

(Received March 29, 1974)

Hydroxyhopanone (**1**) was converted *via* two alternative routes (**1**→**9**→**11a**→**12**→**14**→**15**→**16** and **1**→**10**→**17**→**18**→**19**→**20**) to A-neohop-21-ene (**16**) and A-neohop-3-ene (**20**), respectively. These unsaturated hydrocarbons (**16** and **20**) were found to be identical; this provided evidence to confirm the 21β-H configuration for **1**.

Hydroxyhopanone is a pentacyclic triterpene isolated from dammar resin.[1] The structure had been determined as **1**[2] with a 21β-H configuration based on an isomerization of the norketone (**2**) to its isomeric norketone (**3**).[2a]

Later, this configuration at C-21 of **1** was questioned in connection with studies which led to a revision of the 21β-H (**4a** and **5a**) to the 21α-H structures (**4b** and **5b**) for zeorin and hopane, respectively.[3] However, this revision has recently been withdrawn by the same authors[4] on re-investigation of some derivatives of leucotylin (**6**). The 21β-H configuration was thus confirmed for hopane (**5a**) in accordance with the earlier observation[2a] as well as with the results obtained for adipedatol (**7**)[5] and adiantol B bromoacetate (**8**).[6]

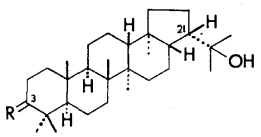

1 R=O
22 R=H_2

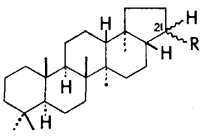

2 21β-H; R=-$COCH_3$(α)
3 21α-H; R=-$COCH_3$(β)
8 21β-H; R=-$CHOCOCH_2Br$(α)
CH_3

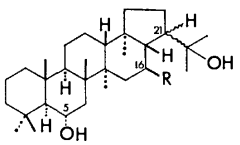

4a R=H; 21β-H
4b R=H; 21α-H
6 R=OH; 21β-H

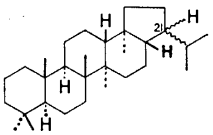

5a 21β-H
5b 21α-H

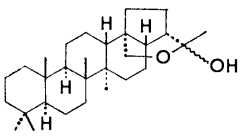

7

We wish to present another chemical evidence to confirm the 21β-H configuration for hydroxyhopanone (**1**).

Dehydration of **1** with phosphorus oxychloride in pyridine gave hop-21-en-3-one (hopenone-a) (**9**)[7] and hop-22(29)-en-3-one (hopenone-b) (**10**)[7] in a ratio of about 2: 1. The isopropylideneketone (**9**) was reduced with sodium borohydride to give hop-21-en-3β-ol (**11a**) and hop-21-en-3α-ol (**11b**) in a ratio of 4: 1. The former alcohol (**11a**) was converted to its mesylate (**12**). Solvolysis of **12** in a mixture of dioxane and water (1: 1) in the presence of calcium carbonate afforded A-neohopa-3,21-diene (**13**) (yield: 53%), A-neohop-21-en-4-ol (**14**) (y: 24%), and A-neohopa-4(23),21-diene (**15**) (y: 5%). Dehydration of **14** with phosphorus oxychloride in pyridine yielded **13** and **15** in a ratio of about 2: 1. The latter (**15**) in ethanol was hydrogenated over platinum catalyst to give A-neohop-21-ene (**16**).

On the other hand, hydrogenation of the isopropenylketone (**10**) in ethanol[4] over platinum catalyst yielded hopan-3-one (**17**) which was reduced with sodium borohydride to give hopan-3β-ol (**18**) as a main product. The alcohol (**18**) was converted to its mesylate (**19**) and then submitted to solvolysis to give A-neohop-3-ene (**20**) (y: 34%) and A-neohopan-4-ol (**21**) (y: 18%).

Two unsaturated hydrocarbons (**16** and **20**) thus obtained were found to be identical.

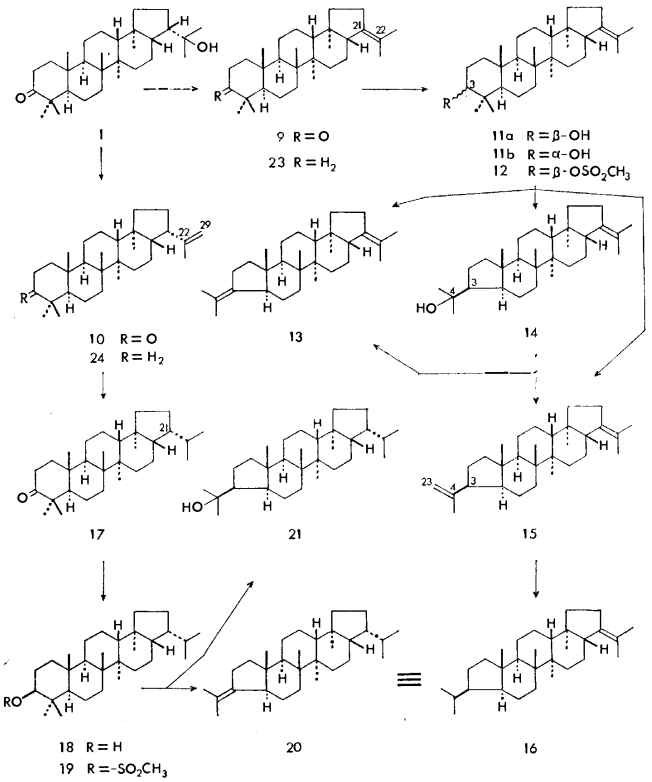

1
9 R=O
23 R=H_2
11a R=β-OH
11b R=α-OH
12 R=β-OSO_2CH_3
10 R=O
24 R=H_2
13
14
17
21
15
18 R=H
19 R=-SO_2CH_3
20
16

It has already been reported that dehydration of hydroxyhopane (**22**) with phosphorus oxychloride in

pyridine gave hop-21-ene (hopene-a) (**23**) and hop-22(29)-ene (hopene-b) (**24**),[7] and that reaction of methylmagnesium iodide with the norketone (**2**), obtained by oxidation of **24**, reproduced **22**.[2a] This showed that the configurations of the side chain at C-21 of **24** and **22** are the same. A parallel argument could lead to the same configuration at C-21 for the isopropenylketone (**10**) and hydroxyhopanone (**1**).

When treated with *p*-toluenesulfonic acid in chloroform, **10** isomerized completely to the isopropylideneketone (**9**). During hydrogenation of **10** in neutral conditions (ethanol, platinum catalyst) to give hopan-3-one (**17**), an isomerization of **10** *via* **9** to form an isomeric isopropenylketone (**25**) and successive hydrogenation leading to isohopan-3-one (**26**) are less probable. The isopropylideneketone (**9**) was found unchanged on hydrogenation in neutral conditions. The Wolff-Kishner reduction of **17** furnished hopane (**5a**)[8] whose configuration at C-21 has been shown to be the same as that of **1**.[8] Thus, no isomrization at C-21 has taken place during the hydrogenation of **10** to give **17**.

Based on a parallel argument, it could be concluded that the configurations at C-3 of **15** and **16** must be the same.

A β(equatorial) nature for the hydroxyl group at C-3 of **11a** and **18** was shown by the formation of A-neo derivatives from the tosylates (**13**, **14**, and **15** from **12**; **20** and **21** from **19**) in accordance with the stereochemistry required by the mechanism of ring contraction.[9] Thus, the side chains at C-3 of **14**, **15**, and **21** should be in a β-configuration.

These findings showed the structure with 3β-isopropyl side chain (**16**) for A-neohop-21-ene. The identity of **16** with **20** as shown above led to a 21α-configuration for the isopropyl group of A-neohop-3-ene (**20**) due to the C_2 symmetry of hexanor-A-neohopane (**27**). As stereochemistry at C-21 of **20** has been shown to be retained as that of **1**, the configuration at C-21 of hydroxyhopanone (**1**) should be 21β-H.

For a further confirmation of the result, A-neoisohop-3-ene (**28**) was prepared by the following transformation. Hydrogenation of **9** in acidic conditions (acetic acid, platinum catalyst)[4,10] gave isohopan-3-one (**26**) which was reduced with sodium borohydride to yield 3β-hydroxyisohopane (**29**) as a main product. The alcohol (**29**) was converted to the mesylate (**30**). Solvolysis of **30** gave **28** which was found to be not identical with **16** (=**20**).

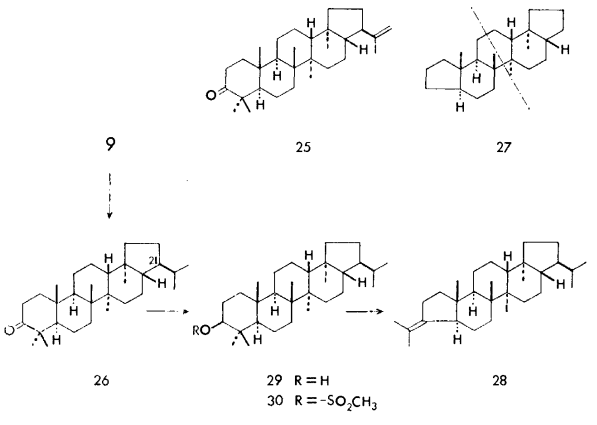

Thus, 21β-H configuration of hydroxyhopanone (**1**) was confirmed.

Experimental

IR spectra were measured using a Hitachi EPI-G2 spectrometer in Nujol mull, unless otherwise stated. NMR spectra were taken on a JEOL JNM-C-60 or a Hitachi R-24 spectrometer in deuteriochloroform solution containing tetramethylsilane as an internal standard. Mass spectra were measured using a Hitachi RMU-6-Tokugata mass spectrometer with a direct inlet system operating at 70 eV. Measurements of optical rotation were carried out using a JASCO polarimeter DIP-SL in chloroform solution. Gas chromatographic (glc) analyses were performed on a Shimadzu gas chromatograph model GC-4A. For column chromatography Wakogel C 200 (Wako Pure Chemical Industries) and Activated Alumina (Mesh 200—300, Showa Chemical Co.) were used. Thin layer chromatography (tlc) was carried out on Kieselgel PF_{254} (E. Merck, Darmstadt) in 0.25 mm thickness. All melting points were determined on a hot block and reported uncorrected.

Hydroxyhopanone (1): Hydroxyhopanone (**1**) was isolated from dammar resin by the procedure described by Dunstan *et al.*[7] Mp 249—250 °C; $[\alpha]_D^{19}$ +58° (*c* 0.76); IR 3450 (OH) and 1710 cm^{-1} (C=O); NMR δ 0.79, 0.95, 0.98, 1.09 (each 3H, s, *t*-CH_3), 1.03 (6H, s, 2×*t*-CH_3), and 1.23 (6H, s, -C(OH)($C\underline{H}_3$)$_2$); mass *m/e* 442 (M^+), 424, 205, and 189 (base peak); Found: C, 81.51; H, 11.62%. Calcd for $C_{30}H_{50}O_2$: C, 81.39; H, 11.38%; glc retention time 9.7 min (column: OV-1 (2%), 260 °C).

Dehydration of Hydroxyhopanone (1): To a solution of hydroxyhopanone (**1**; 0.6 g) in pyridine (55 ml), phosphorus oxychloride (6 ml) was added with stirring at 0 °C. The reaction mixture was allowed to stand overnight at room temperature, poured into ice-water, and extracted with ether. The ethereal extract was washed with diluted hydrochloric acid, sodium hydrogen carbonate solution and then water, and dried over sodium sulfate. After evaporation, the mixture was chromatographed on silica gel (50 g, impregnated with 25% silver nitrate; each fraction 200 ml). The fractions 34—41, eluted with petroleum ether–benzene (4: 1) were combined, and crystallized from acetone to afford hop-21-en-3-one (**9**; 0.35 g) as needles. Mp 209—210.5 °C; $[\alpha]_D^{19}$ +54° (*c* 1.10); IR 1700 cm^{-1} (C=O); NMR δ 0.61, 0.94, 0.98, 1.07 (each 3H, s, *t*-CH_3), 1.02 (6H, s, 2×*t*-CH_3), 1.58, and 1.73 (each 3H, s, C=C(CH_3)$_2$); mass *m/e* 424 (M^+), 205, and 189 (base peak); Found: C, 84.87; H, 11.34%. Calcd for $C_{30}H_{48}O$: C, 84.84; H, 11.39%; glc retention time 13.8 min (column: OV-1 (2%), 250 °C).

The fractions 43—51, eluted with petroleum ether–benzene (2: 1), gave 0.15 g of hop-22(29)-en-3-one (**10**) as needles after crystallization from acetone. Mp 219—220 °C; $[\alpha]_D^{19}$ +89° (*c* 0.57); IR 1700 (C=O), 1640, and 885 cm^{-1} (C=CH_2); NMR δ 0.75, 1.08 (each 3H, s, *t*-CH_3), 0.95, 1.03 (each 6H, s, 2×*t*-CH_3), 1.75 (3H, s, C=C-CH_3), and 4.78 (2H, br.s, C=CH_2); mass *m/e* 424 (M^+), 205, and 189; Found: C, 84.73; H, 11.58%. Calcd for $C_{30}H_{48}O$: C, 84.84; H, 11.39%; glc retention time 15.1 min (column: OV-1 (2%), 260 °C).

Isomerization of Hop-22(29)-en-3-one (10) to Hop-21-en-3-one (9): Hop-22(29)-en-3-one (**10**; 27 mg) in chloroform was treated with *p*-toluenesulfonic acid overnight at room temperature. After usual work-up, the solvent was removed to afford crude crystals (one spot on tlc), which was recrystallized from acetone. The isomerized product (20 mg) was

identical with hop-21-en-3-one (**9**) in respects of IR, NMR, mass spectra, and glc.

On the same treatment of hop-21-en-3-one (**9**; 22 mg), only the starting material (**9**; 19 mg) was recovered. No formation of the other product was observed.

Reduction of Hop-21-en-3-one (9): To a solution of hop-21-en-3-one (**9**; 2.92 g) in ethanol (1.4 l), sodium borohydride (1.6 g) was added and allowed to stand overnight at room temperature. After the reaction mixture was concentrated, acetone was added and left overnight at room temperature to destroy the excess sodium borohydride. Evaporation of the solvents gave crude products (2.54 g), which were subjected to silica gel column chromatographic separation: fractions 1—12, benzene (each fraction 200 ml); and fractions 13—20, benzene–ether (5: 1, each fraction 100 ml).

Fractions 8—11, on evaporation of the solvent, gave crude crystals, which were recrystallized from ethanol to give hop-21-en-3α-ol (**11b**; 0.56 g). Mp 161—162.5 °C; $[\alpha]_D^{13}$ +3° (*c* 0.31); IR 3470 cm^{-1} (OH); NMR δ 0.60, 0.96 (each 3H, s, *t*-CH_3), 0.85, 1.00 (each 6H, s, 2×*t*-CH_3), 1.57, 1.73 (each 3H, br.s, C=C(CH_3)$_2$), and 3.39 (1H, t, J=3 Hz, –CH_2–C<u>H</u>–OH).

Fractions 17 and 18 were combined, evaporated and crystallized from ethanol. Hop-21-en-3β-ol (**11a**; 1.91 g) was obtained. Mp 200—201.5 °C; $[\alpha]_D^{14}$ +40° (*c* 0.49); IR 3270 cm^{-1} (OH); NMR δ 0.60, 0.77, 0.83 (each 3H, s, *t*-CH_3), 0.97 (9H, s, 3×*t*-CH_3), 1.57, 1.72 (each 3H, br.s, C=C(CH_3)$_2$) and 3.20 (1H, dd, J=10 and 6 Hz, –CH_2–C<u>H</u>–OH); mass *m/e* 426 (M^+), 207, and 189 (base peak); Found: C, 84.60; H, 11.51%. Calcd for $C_{30}H_{50}O$: C, 84.44; H, 11.81%.

Mesylation of Hop-21-en-3β-ol (11a): Hop-21-en-3β-ol (**11a**; 1.32 g) was dissolved in dry pyridine (45 ml) and kept at 0 °C. To the solution, methanesulfonyl chloride (1 ml) in pyridine (5 ml) was added dropwise with agitation. The mixture was further stirred for 30 min and then left overnight at room temperature. The reaction mixture, after addition of ice-water in order to destroy the excess reagent, was extracted with ether and worked up as usual giving rise to 1.20 g of crude crystals. On recrystallization from acetone, hop-21-en-3β-yl mesylate (**12**; 0.70 g) was obtained as colorless needles. Mp 145—145.5 °C; $[\alpha]_D^{22}$ +26° (*c* 0.10); IR 1350 and 1180 cm^{-1}; NMR δ 0.59, 1.02 (each 3H, s, *t*-CH_3), 0.86, 0.97 (each 6H, s, 2×*t*-CH_3), 1.57, 1.73 (each 3H, s, C=C-(CH_3)$_2$), and 2.97 (3H, s, CH_3–SO_2–).

Solvolysis of Hop-21-en-3β-yl Mesylate (12): A mixture of hop-21-en-3β-yl mesylate (**12**; 0.44 g) and calcium carbonate (0.4 g) in dioxane–water (100 ml, 1: 1) was heated under reflux for several hours. Most of the solvents were removed under reduced pressure, acetic acid was added to dissolve calcium carbonate and the reaction product was extracted with chloroform. The extract was washed with sodium hydrogen carbonate solution, water and then saturated sodium chloride solution, and the solvents were removed. The crude crystal in benzene was passed through a column of alumina (15 g) and eluted with the following solvents: fractions 1—3, benzene (each fraction 30 ml); fractions 4—6, benzene–ether (1: 1, each fraction 20 ml); and fractions 7 and 8, ether (each fraction 30 ml).

On evaporation of the solvent, fraction 1 gave white crystals (0.31 g, mp 168—188 °C; IR 892 cm^{-1}) which were shown to be a mixture of olefins by NMR measurement. Signals due to olefinic protons were observed at δ 4.78 and 5.74, and each was a broad singlet with intensity less than one proton. The mixture was further chromatographed on silica gel impregnated with 10% silver nitrate and eluted with petroleum ether–benzene (9: 1, each fraction 40 ml). Evaporation of fraction 3 followed by recrystallization from dichloromethane–methanol gave A-neohopa-3,21-diene (**13**; 190 mg) as colorless plates. Mp 190—191 °C; $[\alpha]_D^{14}$ +45° (*c* 0.77); NMR δ 0.60, 0.98 (each 6H, s, 2×*t*-CH_3), 1.59, and 1.73 (each 6H, s, C=C(CH_3)$_2$); mass *m/e* 408 (M^+) and 189 (base peak); Found: C, 87.98; H, 11.76%. Calcd for $C_{30}H_{48}$: C, 88.16; H, 11.84%. Fractions 9—12 were combined and crystallized from chloroform–ethanol to afford A-neohopa-4(23),21-diene (**15**; 19 mg) as colorless needles. Mp 185—186 °C; IR 1640 and 894 cm^{-1} (C=CH_2); NMR δ 0.57, 0.72 (each 3H, s, *t*-CH_3), 0.95 (6H, s, 2×*t*-CH_3), 1.59 (3H, br.s, C=C–CH_3), 1.75 (6H, br.s, 2×C=C–CH_3), and 4.77 (2H, br.s, C=CH_2); mass *m/e* 408 (M^+) and 189 (base peak); Found: C, 88.04; H, 11.58%. Calcd for $C_{30}H_{48}$: C, 88.16; H, 11.84%.

Fraction 8 of the first chromatography afforded A-neohop-21-en-4-ol (**14**; 91 mg) as colorless needles by crystallization from chloroform–ethanol. Mp 193—194 °C; $[\alpha]_D^{20}$ +46° (*c* 0.17); IR 3400 cm^{-1} (OH); NMR δ 0.59, 0.78 (each 3H, s, *t*-CH_3), 0.98 (6H, s, 2×*t*-CH_3), 1.19, 1.22 (each 3H, s, –C(OH)(C<u>H</u>$_3$)$_2$), 1.59, and 1.73 (each 3H, s, C=C(CH_3)$_2$); mass *m/e* 426 (M^+), 408, and 189 (base peak).

Dehydration of A-Neohop-21-en-4-ol (14): To a solution of A-neohop-21-en-4-ol (**14**; 36 mg) in dry pyridine (10 ml), phosphorus oxychloride (1 ml) was added dropwise with stirring at 0 °C. The reaction mixture was allowed to stand overnight at room temperature, poured into ice-water and extracted with chloroform. The extract was washed with diluted hydrochloric acid, sodium hydrogen carbonate solution, water and then with saturated sodium chloride solution. After drying over sodium sulfate, evaporation of the solvent gave a residue (24 mg), which was chromatographed on silica gel impregnated with 10% silver nitrate and eluted with the following solvents (each fraction 20 ml): fractions 1—3, petroleum ether; fractions 4—7, petroleum ether–benzene (10: 1); fractions 8—10, petroleum ether–benzene (5: 1).

From fraction 4, on evaporation of the solvent, 15 mg of colorless crystal was obtained by crystallization from chloroform–ethanol. The mp and spectral data were identical with those of A-neohop-3,21-diene (**13**), obtained by solvolysis of hop-21-en-3β-yl mesylate (**12**).

Fractions 5—8, after crystallization from chloroform–ethanol, gave 7 mg of colorless needles, which was identical with A-neohopa-4(23),21-diene (**15**) in respects of IR, NMR, and tlc.

Hydrogenation of A-Neohopa-4(23),21-diene (15): A-neohopa-4(23),21-diene (**15**; 17 mg) in ethanol (30 ml) was catalytically hydrogenated in the presence of platinum oxide (about 5 mg) with stirring at 40 °C overnight. The solvent was removed under reduced pressure to afford crude crystals, which were recrystallized from chloroform–ethanol. A-neohop-21-ene (**16**) was obtained and weighed 8 mg. Mp 191.5—192.5 °C; $[\alpha]_D^{16}$ +49° (*c* 0.30); IR (KBr disk) 1380, 1360, 1165, and 1145 cm^{-1}; NMR δ 0.59, 0.72 (each 3H, s, *t*-CH_3), 0.97 (6H, s, 2×*t*-CH_3), 1.57, and 1.73 (each 3H, s, C=C(CH_3)$_2$), (signals due to protons of two secondary methyls could not be assignable); tlc R_f 0.4 (10% $AgNO_3$–SiO_2, petroleum ether); mass *m/e* 410 (M^+), 191 (base peak), and 189; Found: C, 87.39; H, 12.54%. Calcd for $C_{30}H_{50}$: C, 87.73; H, 12.27%; glc retention time 19.1 min (column: SE-30 (0.7%), 220°) and 20.2 min (column: OV-17 (2%), 250 °C).

Hydrogenation of Hop-22(29)-en-3-one (10): Hop-22(29)-en-3-one (**10**; 0.21 g) in ethanol (200 ml) was hydrogenated in the presence of platinum oxide (0.07 g) for 12 hr to the same procedure as above. Filtration of the catalyst followed by evaporation of the solvent gave a residue (0.21 g), which was recrystallized from acetone to afford hopan-3-one (**17**) as needles. Mp 230—232 °C; $[\alpha]_D^{19}$ +78° (*c* 0.75); IR 1700

0.97 (6H, s, 2×*t*-CH_3), 1.59, and 1.73 (each 3H, br.s, C=C-(each 3H, s, *t*-CH_3); mass *m/e* 426 (M^+), 205, and 191 (base peak); Found: C, 84.29; H, 11.91%. Calcd for $C_{30}H_{50}O$: C, 84.44; H, 11.81; glc retention time 14.6 min (column: OV-1 (2%), 260°) and 63.5 min (column: OV-17 (2%), 250 °C).

Hydrogenation of Hop-21-en-3-one (9): Hop-21-en-3-one (**9**; 62 mg) in ethanol (100 ml) was hydrogenated in the presence of platinum oxide (19 mg) overnight. Treatment as usual gave a substance (61 mg; one spot on tlc) which was found to be identical with the starting material (**9**). No formation of the other product was observed.

Reduction of Hopan-3-one (17): Hopan-3-one (**17**; 0.85 g) was dissolved in ethanol (650 ml), sodium borohydride (0.67 g) was added and left overnight at room temperature. After a small quantity of acetone was added, the solvents were removed. The residue, dissolved in chloroform, washed with water and evaporated, gave crude crystals (0.85 ; two spots on tlc), which were chromatographed on silica gel (100 g). The fractions 20—29 (one spot on tlc), eluted with benzene, were collected and recrystallized from ethanol to afford hopan-3β-ol (**18**; 0.46 g) as a main product. Mp 238—239 °C; IR 3300 cm^{-1} (OH); NMR δ 0.74, 0.78, 0.85, 0.99 (each 3H, s, *t*-CH_3), and 0.96 (6H, s, 2×*t*-CH_3); mass *m/e* 428 (M^+), 207, and 191 (base peak).

Mesylation of Hopan-3β-ol (18): To a solution of hopan-3β-ol (**18**; 0.4 g) in pyridine (20 ml), methanesulfonyl chloride (1 ml) in pyridine (9 ml) was added dropwise with agitation at 0 °C. The reaction mixture was allowed to stand overnight at room temperature and poured into ice-water. Extraction with ether and usual work-up gave a residue (0.39 g), which was recrystallized from ether to afford hopan-3β-yl mesylate (**19**; 0.12 g). Mp 119—120 °C; $[\alpha]_D^{21}$ +35° (*c* 0.49); IR 1170 cm^{-1} (SO_2); NMR δ 0.73, 1.02 (each 3H, s, *t*-CH_3), 0.87, 0.96 (each 6H, s, 2×*t*-CH_3), and 3.00 (3H, s, CH_3–SO_2–).

Solvolysis of Hopan-3β-yl Mesylate (19): A mixture of hopan-3β-yl mesylate (**19**; 0.32 g) and calcium carbonate (0.5 g) in dioxane (150 ml) and water (150 ml) was heated under reflux for 5 hr. The solvents were removed under reduced pressure and the residue was dissolved in ether. The ethereal solution was treated as usual manner and the residue was dissolved in petroleum ether–benzene, which was chromatographed on silica gel (10 g) and the following solvents (each fraction 40 ml) were eluted: fractions 1 and 2, petroleum ether–benzene (2: 1); fraction 3, petroleum ether–benzene (1: 1); and fraction 4, ether.

On evaporation of the solvents, fraction 1 gave a mixture (0.20 g) of olefins. IR 1640 and 894 cm^{-1}; NMR δ 1.58, 1.73 (each 3H, s, C=C(CH_3)$_2$), 4.8, and 5.4 (each less than 1H, olefinic proton); mass *m/e* 410 (M^+). The mixture gave four spots (R_f 0.9, 0.8, 0.5, and 0.2) on tlc (10% $AgNO_3$–SiO_2, petroleum ether). The olefin mixture was subjected to column chromatographic separation using silica gel impregnated with 10% silver nitrate, and eluted with petroleum ether (each fraction 30 ml). Fractions 8—15, after recrystallization from ethanol, gave A-neohop-3-ene (**20**; 88 mg) as colorless needles. Mp 193.5—193.7 °C; $[\alpha]_D^{16}$ +52° (*c* 0.28); IR (KBr disk) 1380, 1360, 1165, and 1145 cm^{-1}; NMR δ 0.60, 0.72 (each 3H, s, *t*-CH_3), 0.97 (6H, s, 2×*t*-CH_3), 1.58, and 1.73 (each 3H, s, C=C(CH_3)$_2$), (signals due to protons of two secondary methyls could not be assignable); tlc R_f 0.4 (10% $AgNO_3$–SiO_2, petroleum ether); mass *m/e* 410 (M^+), 191 (base peak), and 189; Found: C, 87.74; H, 12.42%. Calcd for $C_{30}H_{50}O$: C, 87.73; H, 12.27%; glc retention time 19.1 and 10.4 min (column: SE-30 (0.7%), 220 and 250 °C respectively) and 20.2 min (column: OV-17 (2%), 250 °C). This compound was shown to be identical (mp, mixed mp, IR, NMR, mass spectra, tlc, and glc) with **16**.

Fraction 4, eluted with ether, afforded A-neohopan-4-ol (**21**; 0.05 g). Mp 198.5—199 °C; $[\alpha]_D^{19}$ +64° (*c* 0.75); IR 3470 cm^{-1} (OH); NMR δ 0.70, 0.77 (each 3H, s, *t*-CH_3), 0.96 (6H, s, 2×*t*-CH_3), 1.18, and 1.21 (each 3H, s, –C(OH)-($C\underline{H}_3$)$_2$); mass *m/e* 428 (M^+), 410, 191, and 189 (base peak); Found: C, 84.03; H, 12.42%. Calcd for $C_{30}H_{52}O$: C, 84.04; H, 12.23%.

Reduction of Hopan-3-one (17): A mixture of hopan-3-one (**17**; 70 mg), potassium hydroxide (0.2 g), diethylene glycol (5 ml) and hydrazine hydrate (80%, 0.1 ml) was heated under reflux for 1 hr. After removal of water and hydrazine by distillation, the reaction mixture was further heated under reflux for 1 hr. Completion of the reaction was confirmed by tlc examination and then water was added to the reaction mixture. Extraction with ether, usual treatment and recrystallization from *n*-hexane–ethanol gave hopane (**5a**; 19 mg) as colorless needles. Mp 209.5—211 °C; $[\alpha]_D^{20}$ +50° (*c* 0.14); NMR δ 0.70, 0.79, 0.81, 0.84 (each 3H, s, *t*-CH_3) and 0.95 (6H, s, 2×*t*-CH_3), (signals due to protons of two secondary methyls could hardly be assignable); mass *m/e* 412 (M^+). These data coincide with those published for hopane (**5a**)[8] rather than for isohopane (**5b**) (moretane).[8]

Hydrogenation of Hop-21-en-3-one (9) in Acidic Condition: A solution of hop-21-en-3-one (**9**; 113 mg) in ethyl acetate (15 ml) and acetic acid (0.5 ml) was catalytically hydrogenated in the presence of platinum oxide at room temperature. After removal of the catalyst by filtration, evaporation under reduced pressure gave crude crystals, which were crystallized from chloroform–ethanol to give crude isohopan-3-one (**26**; 96 mg). IR 1700 cm^{-1} (C=O); NMR: signals due to vinyl methyls were not observed.

Reduction of Isohopan-3-one (26): Crude isohopan-3-one (**26**; 96 mg) without further purification, was dissolved in ethanol (50 ml) and treated with sodium borohydride and allowed to stand overnight. Addition of acetone followed by evaporation of the solvents under reduced pressure afforded a residue, which showed two spots on tlc. This was dissolved in benzene, passed through a column of silica gel (10 g) and eluted with the following solvents (each fraction 50 ml): fraction 1, benzene; fractions 2 and 3, benzene–ether (50: 1); and fractions 4—8, benzene–ether (10: 1).

A main component, isohopan-3β-ol (29), eluted in fractions 5 and 6, was obtained as crude crystals (78 mg), which gave one spot on tlc. IR 3350 cm^{-1} (OH).

Mesylation of Isohopan-3β-ol (29): Crude isohopan-3β-ol (**29**; 78 mg) obtained above, was dissolved in pyridine (6 ml) and kept at 0 °C. Methanesulfonyl chloride (about 0.5 ml) in pyridine was added and usual treatment gave crude isohopan-3β-yl mesylate (**30**; 90 mg) as pale yellow crystals, in which no starting material (**29**) was detected by tlc.

Solvolysis of Isohopan-3β-yl Mesylate (30): Calcium carbonate (0.1 g) and crude isohopan-3β-yl mesylate (**30**; 90 mg) without further purification, were suspended in dioxane (10 ml) and water (10 ml), and the mixture was heated under reflux for 13 hr. After the same treatment as in the case of solvolysis of hop-21-en-3β-yl mesylate (**12**), the residue was chromatographed on silica gel (5 g). Elution with benzene (30 ml) and evaporation of the solvent gave a mixture (52 mg) of olefins, which was subjected to column chromatographic separation on silica gel (3 g) impregnated with 10% silver nitrate using petroleum ether as eluent (each fraction 30 ml). Fractions 2—6, on crystallization from acetone, gave A-neoisohop-3-ene (**28**; 30 mg) as colorless needles. Mp 156—158 °C; IR (KBr disk) 1440, 1380, 1365, 1170, and 1140 cm^{-1}; NMR δ 0.62, 0.68 (each 3H, s, *t*-CH_3),

cm^{-1} (C=O); NMR δ 0.73, 0.94, 0.96, 1.00, 1.03, and 1.10 $(CH_3)_2$), (signals due to protons of two secondary methyls could not be assignable); mass *m/e* 410 (M^+); glc retention time 7.8 min (column: OV-1 (2%), 250 °C).

References

1) J. S. Mills and A. E. A. Werner, *J. Chem. Soc.*, **1955**, 3132.

2) a) G. V. Baddeley, T. G. Halsall, and E. R. H. Jones, *J. Chem. Soc.*, **1961**, 3891; b) K. Schaffner, L. Caglioti, D. Arigoni, O. Jeger, H. Fazakerley, T. G. Halsall, and E. R. H. Jones, *Proc. Chem. Soc.*, **1957**, 353; K. Schaffner, L. Caglioti, D. Arigoni, and O. Jeger, *Helv. Chim. Acta*, **41**, 152 (1958); H. Fazakerley, T. G. Halsall, and E. R. H. Jones, *J. Chem. Soc.*, **1959**, 1877; c) G. V. Baddeley, T. G. Halsall, and E. R. H. Jones, *ibid.*, **1960**, 1715.

3) I. Yosioka, T. Nakanishi, and I. Kitagawa, *Tetrahedron Lett.*, **1968**, 1485; I. Yosioka, T. Nakanishi, and I. Kitagawa, *Chem. Pharm. Bull.* (Tokyo), **17**, 279 (1969); I. Yosioka, T. Nakanishi, and I. Kitagawa, *ibid.*, **17**, 291 (1969). *cf.* T. Nakanishi, T. Fujiwara, and K. Tomita, *Tetrahedron Lett.*, **1968**, 1491.

4) I. Yosioka, T. Nakanishi, H. Yamauchi, and I. Kitagawa, *Tetrahedron Lett.*, **1971**, 1161; I. Yosioka, T. Nakanishi, H. Yamauchi, and I. Kitagawa, *Chem. Pharm. Bull.* (Tokyo), **20**, 147 (1972). *cf.* T. Nakanishi, H. Yamauchi, T. Fujiwara, and K. Tomita, *Tetrahedron Lett.*, **1971**, 1157.

5) H. Ageta and K. Shiojima, *Chem. Commun.*, **1968**, 1372.

6) H. Koyama and H. Nakai, *J. Chem. Soc.*, *B*, **1970**, 546.

7) W. J. Dunstan, H. Fazakerley, T. G. Halsall, and E. R. H. Jones, *Croat. Chem. Acta*, **29**, 173 (1957).

8) R. E. Corbett and R. A. J. Smith, *J. Chem. Soc.*, *C*, **1967**, 1622. *cf.* M. N. Galbraith, C. J. Miller, J. W. L. Rawson, E. Ritchie, J. S. Shannon, and W. C. Taylor, *Aust. J. Chem.*, **18**, 226 (1965).

9) J. F. Biellmann and G. Ourisson, *Bull. Soc. Chim. Fr.*, **1962**, 331.

10) R. E. Corbett and H. Young, *J. Chem. Soc.*, *C*, **1966**, 1556.

Studies on Benzoquinolines(f) and (h). Part II

Rameshwar P. TYAGI and Bhuwan C. JOSHI
Chemical Laboratories, University of Rajasthan, Jaipur 302004, India
(Received January 14, 1972)

3-Hydrazino-1-methyl, 1-hydrazino-3-methylbenzo(f) quinoline (IA, IIA) and 2-hydrazino-4-methyl, 4-hydrazino-2-methylbenzo(h) quinoline (IIIA, IVA) were reported[1] to give triazines and diazepines with nitrous and formic acids. It would be interesting to study the reactions of IA—IVA with acetylacetone and ethyl acetoacetate respectively.

Reactions of alcoholic solution of IA with acetylacetone yielded IB, $C_{19}H_{19}ON_3$. A characteristic absorption band at 1730 cm^{-1} in IR spectrum indicated the presence of a carbonyl group. NMR spectrum indicated the presence of six aromatic protons at δ 7.6—8.0 ppm, one aromatic proton as singlet at δ 7.10 ppm, nine protons as three singlets for methyl groups at δ 2.50, 2.25, and 2.10 ppm and the presence of two protons of a methylene group as singlet at δ 3.25 ppm. Therefore, IB had the structure as assigned, thereby indicating the formation of an intermediate hydrazone. IB on further refluxing in glycerol in the presence of fused sodium acetate, gave a mixture of products from which a compound, IC ($C_{19}H_{17}N_3$) was isolated. In IC, absence of an absorption band at 1730 cm^{-1} and the presence of an absorption band at 1602 cm^{-1} indicated the existence of a 1,2-diazepine system in it.[2] NMR spectrum indicated the presence of six aromatic protons at δ 7.60—8.00 ppm and nine protons of three methyl groups as singlets at δ 2.95,

TABLE 1.

Compound number	Molecular formula	Infrared in cm^{-1}	NMR chemical shifts (δ) expressed in ppm					
			=CH	-NH	Aromatic	$-\overset{O}{\overset{\|\|}{C}}-CH_2-$	$=\overset{\|}{C}-CH_3$	$-C-CH_3$
IB	$C_{19}H_{19}ON_3$	1730	—	—	7.60—8.00 (6)	3.25 (2)	2.50 (3)	
					7.10 (1)		2.25 (3)	—
							2.10 (3)	
IC	$C_{19}H_{17}N_3$	1602	6.10 (1)	9.20 (1)	7.60—8.00 (6)	—	2.95 (3)	
							2.80 (3)	—
							2.40 (3)	
IIB	$C_{19}H_{19}ON_3$	1728	—	—	—	—	—	—
IIC	$C_{19}H_{17}N_3$	1605	6.05 (1)	8.80 (1)	7.60—8.00 (6)	—	3.15 (3)	
							2.85 (3)	—
							2.40 (3)	
IIIB	$C_{19}H_{19}ON_3$	1730	—	—	—	—	—	—
IIIC	$C_{19}H_{17}N_3$	—	6.10 (1)	9.15 (1)	7.60—8.00 (6)	—	2.95 (3)	
							2.80 (3)	—
							2.40 (3)	
IVB	$C_{19}H_{19}ON_3$	1725	—	—	—	—	—	—
IVC	$C_{19}H_{17}N_3$	—	6.05 (1)	8.90 (1)	7.60—8.00 (6)	—	3.10 (3)	
							2.85 (3)	—
							2.40 (3)	

Compound number	Molecular formula	Infrared in cm^{-1}	NMR chemical shifts (δ) expressed in ppm						
			=CH	-NH	Aromatic	$-\overset{O}{\overset{\|\|}{C}}-CH_2$	$H-C\overset{H}{\diagup}$	$-O\diagdown C\overset{H}{\diagup}$	$=C-CH_3$
ID	$C_{20}H_{21}O_2N_3$	1735	—	—	—	—	—	—	—
IE	$C_{18}H_{15}ON_3$	1702 1602	—	8.8 (1)	7.60—8.00 (6)	3.10 (2)	—	—	2.60 (3) 2.50 (3)
IID	$C_{20}H_{21}O_2N_3$	1735	—	—	7.10—8.00 (7)	3.10 (2) 3.50 (2)	—	—	2.50 (6) 2.25 (3)
IIE	$C_{18}H_{15}ON_3$	1702 1590	—	8.80 (1)	7.60—8.00 (6)	3.00 (2)	—	—	2.50 (6)
IIID	$C_{20}H_{21}O_2N_3$	1735	—	—	—	—	—	—	—
IIIE	$C_{18}H_{15}ON_3$	1705 1600	—	8.90 (1)	7.60—8.00 (6)	3.10 (2)	—	—	2.55 (3) 2.40 (3)
IVD	$C_{20}H_{21}O_2N_3$	1735	—	—	—	—	—	—	—
IVE	$C_{18}H_{15}ON_3$	1705 1600	—	8.80 (1)	7.60—8.00 (6)	3.10 (2)	—	—	2.50 (3) 2.40 (3)

	Melting points	Analysis				Melting points	Analysis		
		C	H	N			C	H	N
IB	decomp.[a]	Calcd 74.75%	6.23%	13.77%	IC	114—115°C	Calcd 79.44%	5.92%	14.63%
		Found 74.54	6.08	13.52			Found 79.22	5.81	14.34
IIB	decomp.[a]	Calcd —	—	13.77	IIC	85—86	Calcd —	—	14.63
		Found —	—	13.49			Found —	—	14.28
IIIB	decomp.[a]	Calcd —	—	13.77	IIIC	103—104	Calcd —	—	14.63
		Found —	—	13.52			Found —	—	14.19
IVB	decomp.[a]	Calcd —	—	13.77	IVC	78—79	Calcd —	—	14.63
		Found —	—	13.43			Found —	—	14.29
ID	decomp.[a]	Calcd 71.64	6.26	12.53	IE	178—179	Calcd 74.74	5.19	14.53
		Found 71.34	5.97	12.37			Found 74.34	4.98	14.27
IID	decomp.[a]	Calcd —	—	12.53	IIE	122—123	Calcd —	—	14.53
		Found —	—	12.62			Found —	—	14.19
IIID	decomp.[a]	Calcd —	—	12.53	IIIE	156—157	Calcd —	—	14.53
		Found —	—	12.36			Found —	—	14.27
IVD	decomp.[a]	Calcd —	—	12.53	IVE	117—118	Calcd —	—	14.53
		Found —	—	12.73			Found —	—	14.30

a) No sharp melting point obtained.

2.80, and 2.40 ppm respectively. A signal at δ 9.20 ppm due to the –NH proton and a singlet at δ 6.10 ppm due to =CH- proton also indicated the presence of a 1,2-diazepine system.[2] The absence of a proton at position 2 of the benzoquinoline ring, the presence of an –NH proton and an absorption band at 1602 cm^{-1} would explain the fusion of a 1,2-diazepine ring with benzoquinoline system. Based on these observations, IC proved to be 10,12,13-trimethyl-8*H*-benzo(f)-[1,2]diazepino[3,4-*b*]quinoline.

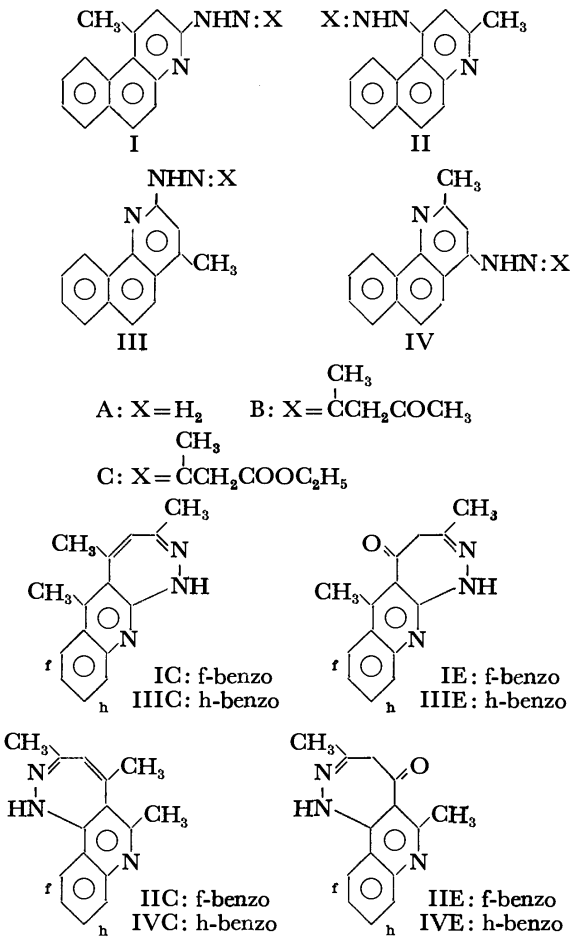

Fig. 1.

IA with ethyl acetoacetate yielded an intermediate hydrazone, ID ($C_{20}H_{21}O_2N_3$), the IR spectrum of which with an absorption band at 1735 cm^{-1} indicated the presence of an ester group. On further refluxing in glycerol in the presence of fused sodium acetate, IE ($C_{18}H_{15}ON_3$) was obtained. IR spectrum gave absorption bands at 1702 and 1602 cm^{-1} showing the presence of diazepinone moiety in it. NMR spectrum indicated the presence of six aromatic protons at δ 7.6—8.00 ppm, six protons as two singlets of methyl groups at δ 2.60 and 2.50 ppm, two protons of methylene group as singlet at δ 3.10 ppm, an –NH proton at δ 8.80 ppm and there was no proton at position 2 of the benzoquinoline ring. Thus, IE was assigned the structure to be 10,13-dimethyl-12-oxo-8*H*-11,12-dihydrobenzo(f)[1,2]diazepine[3,4-*b*]quinoline.

Similar observations were made when IIA—IVA were reacted with acetyl acetone and ethyl acetoacetate respectively (Fig. 1). The characteristic absorption bands and chemical shifts obtained in the NMR spectra of various products are compiled in Table 1. From these observations it can be concluded that cyclization of intermediates, hydrazones, occurred at position 2 in benzo(f) or at position 3 in benzo(h) quinolines to yield benzo(f) or benzo(h) quinolino-1,2-diazepine compounds.

Experimental

All the reported melting points are uncorrected. Microanalyses, IR and NMR spectra were from Central Drug Research Institute, Lucknow. IR spectra were recorded on Perkin-Elmer infrared in nujol and NMR spectra on a Varian A-60D model (using $CDCl_3$ or TFA as solvent and TMS as internal reference standard).

Acetylacetone-1-methyl-benzo(f)quinolyl-3-hydrazone(IB). To a well stirred solution of 3-hydrazino-1-methyl-benzo(f)-quinoline (IA) (8.92 g, 0.04 M) in absolute alcohol, acetylacetone (4.49 g, 0.045 M) was added dropwise and the reaction mixture was refluxed for 1 hr. It was cooled, poured

into ice-cold water and kept overnight at 0°C. The solid was washed well with water and dried. After repeated crystallization from ethanol IB, 9.8 g (80%) was obtained having no sharp melting point.

Similarly, IIB from IIA, IIIB from IIIA, and IVB from IVA were prepared. These hydrazones have no sharp melting points.

*10,12,13-Trimethyl-8*H-*benzo(f)* [*1,2*] *diazepino* [*3,4-*b] *quinoline (IC).* IB (7.6 g, 0.025 M) was refluxed in glycerol in the presence of fused sodium acetate for 4—5 hr with occasional shaking. It was poured into ice-cold water, kept overnight at 0 °C. The solid was washed well with water and repeatedly crystallized from ethanol to give pure IC, 3.58 g (50%), mp 114—115 °C.

Similarly, IIB yielded IIC, 8,9,11-trimethyl-13*H*-benzo(f)-[1,2]diazepino[3,4-*c*]quinoline. IIIB yielded IIIC, 10,12,13-trimethyl-8*H*-benzo(h)[1,2]diazepino[3,4-*b*]quinoline.

IVB yielded IVC, 8,9,11-trimethyl-13*H*-benzo(h)[1,2]-diazepino[3,4-*c*]quinoline.

Ethyl Acetoacetate-1-methyl-benzo(f) quinolinyl-3-hydrazone (ID). To a well stirred solution of IA (8.92 g, 0.04 M) in absolute alcohol, freshly distilled ethyl acetoacetate (5.72 g, 0.045 M) was added dropwise and the reaction mixture was refluxed for 1 hr. It was cooled and poured into ice-cold water. The solid obtained was washed well with water and repeatedly crystallized from ethanol to give pure ID, 9.38 g (70%).

Similarly, IID from IIA, IIID from IIIA and IVD from IVA were prepared.

*10,13-Dimethyl-12-oxo-8*H-*11,12-dihydro-benzo(f)* [*1,2*] *diazepino-* [*3,4-*b] *quinoline (IE).* ID (8 g) was refluxed in glycerol in the presence of fused sodium acetate for 6—7 hr, with occasional shaking. The reaction mixture was cooled, poured into ice-cold water and kept overnight at 0 °C. The crude product was crystallized from ethanol, when a pure compound, IE (3.45 g), was obtained.

Similarly, IID yielded IIE, 8,11-dimethyl-9-oxo-13*H*-9,10-dihydro-benzo(f)[1,2]diazepino[3,4-*c*]quinoline.

IIID yielded IIIE, 10,13-dimethyl-12-oxo-8*H*-11,12-dihydro-benzo(h)[1,2]diazepino[3,4-*b*]quinoline.

IVD yielded IVE, 8,11-dimethyl-9-oxo-13*H*-9,10-dihydro-benzo(h)[1,2]dizepino[3,4-*c*]quinoline.

Authors are thankful to the Head, Chemistry Department of this University for providing necessary facilities and University Grants Commission for financial assistance.

References

1) R. P. Tyagi and B. C. Joshi, This Bulletin, **45**, 2507 (1972).

2) O. Buchardt, C. L. Pedersen, U. Svanholm, A. M. Duffield, and A. T. Balaban, *Acta Chem. Scand.*, **23**, 3125 (1968).

Synthesis of Succin-as-eins*

R. GOPAL,** P. C. GUPTA, and S. P. GARG***
Department of Chemistry, University of Allahabad, India

(Received February 12, 1973)

A new series of compounds, succin-as-eins(SAE)—methyl phenol SAE, methyl resorcinol SAE, methyl catechol SAE, methyl quinol SAE, methyl phloroglucinol SAE, methyl pyrogallol SAE and methyl orcinol SAE have been prepared by condensing 2-acetyl propionic acid with appropriate phenols. The structure of methyl resorcinol SAE, based on chemical reactions and spectral data is discussed. The λ_{max} values for few of the dyes are comparable with their analogous succineins and phthaleins.

2-Acetyl propionic acid (I) has been shown to be a mixture of ring (II) and chain (I) tautomers by various workers.[2-4] The lactol (II), which yields well crystalline acetyl derivative (III),[5] on condensation with phenols gave a new series of compounds, succin-as-eins (IV). The condensation process proceeds through the equilibrium process of lactol (II) of acid (I) and with excess of phenol whole of the acid reacts as lactol.

Seven succin-as-eins (SAE)—methyl phenol SAE (IVa), methyl resorcinol SAE (IVb), methyl catechol SAE (IVc), methyl quinol SAE (IVd), methyl phloroglucinol SAE (IVe), methyl pyrogallol SAE (IVf) and methyl orcinol SAE (IVg) have been prepared by condensing acid (I) with respective phenols.

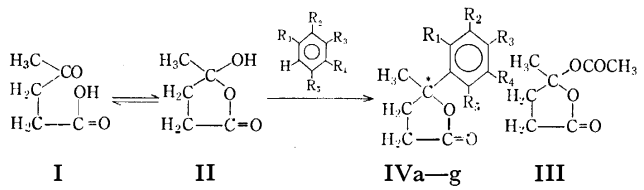

I II IVa—g III

(IVa) $R_1=R_2=R_4=R_5=H$; $R_3=OH$
(IVb) $R_2=R_4=R_5=H$; $R_1=R_3=OH$
(IVc) $R_3=R_4=R_5=H$; $R_1=R_2=OH$
(IVd) $R_2=R_3=R_5=H$; $R_1=R_4=OH$
(IVe) $R_2=R_4=H$; $R_1=R_3=R_5=OH$
(IVf) $R_4=R_5=H$; $R_1=R_2=R_3=OH$
(IVg) $R_2=R_4=H$; $R_5=CH_3$; $R_1=R_3=OH$
(V) $R_2=R_4=R_5=H$; $R_1=R_3=OCOCH_3$
(VI) $R_5=H$; $R_2=R_4=Br$; $R_1=R_3=OH$

The column chromatography, supplemented with thin-layer chromatography, was used for the purification of condensed products. Their IR (KBr) spectra show a strong band at 1760 cm^{-1} due to γ-lactone. The KOH treatment of IVb followed by acid hydrolysis yielded resorcinol and the acid (I). The dye (IVb; 1760 cm^{-1}) when refluxed with Zn-dust and acetic acid gave methyl resorcinol succin-as-in[6] (VII; IR (KBr) bands at 3600—3000 cm^{-1}, -OH in -COOH; 1700 cm^{-1}, >CO in -COOH). The acid (VII) on acetylation gave diacetyl compound (V). The diacetyl (V; IR (KBr) bands at 1760, 1200, and 1125 cm^{-1} due to γ-lactone and phenolic acetate) and dibromo (VI; 1760 cm^{-1}, γ-lactone) derivatives of IVb are also indicative of resorcinol molecule in it.

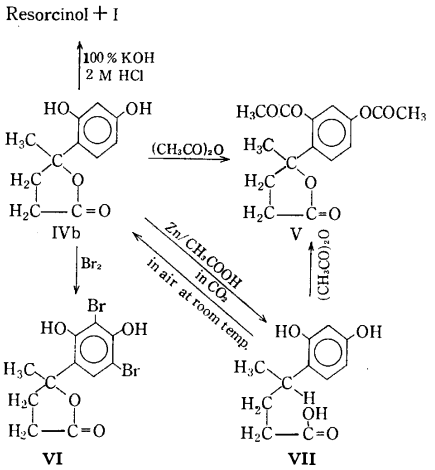

The absorption maxima (λ_{max}) of SAE (IV) given in Table 1 have been found comparable with their analogous succineins and phthaleins.

Experimental

All melting points are uncorrected. The λ_{max} (UV and visible) have been recorded on model DU-2 Beckmann Spectrophotometer and IR determined using a Perkin-Elmer Infracord.

The phenols have been taken in a little excess of molecular proportion than the acid (I). Conc H_2SO_4 (4—6 drops) was used as a condensing agent throughout.

Methyl Resorcinol SAE (IVb). An intimate mixture of acid (I) (5 g) and resorcinol (5 g) was heated at 120 °C for 2 hr. Conc H_2SO_4 (4—6 drops) was added cautiously and the heating was continued for additional 6 hr at 160 °C. The brittle product was extracted with 3% NaOH and precipitated with dil HCl. The precipitate was chromatographed over silica gel with chloroform–acetone mixture (80:20). The third fraction (200 ml) on crystallization gave a red crystalline dye (6.4 g), mp 300 °C, which dissolved with yellow-red colour in ethanol while in alkali (pH, 8) gave a bright pink-violet colour with light green fluorescence.

The preparation of the rest of compounds given in Table 1 was done in identical manner as described in IVb above taking acid (I) and appropriate phenols (yield, 60—65%).

* Owing to unsymmetric central carbon atom (C*) present in IV they may be named as succin-as-eins; -as representing unsymmetry and -ein the class of compound (Succin-ein[1]).

** Present address: Defence Laboratory, Jodhpur, India.
*** Present address: Department of Chemistry, University of Jodhpur, India.

TABLE 1. PREPARATION AND PROPERTIES OF METHYL SUCCIN-AS-EINS (IV)

Dyes	Condensation Temp (°C)	Condensation Time (hr)	Mp (°C)	Appearance	λ_{max}^{EtOH} (mμ); ε Neutral	λ_{max}^{EtOH} (mμ); ε at (pH)	Found % C	Found % H	Calcd % C	Calcd % H
IVa	110	12	225	Brown	—	411(9.0); 426	68.92	5.98	68.75	6.25
IVb	160	6	300	Red	480; 850	500(8.3); 1183	63.42	5.70	63.46	5.77
IVc	170	4	300	Dark brown	—	465(10.2); 619	63.74	5.54	63.46	5.77
IVd	170	4	300	Dark brown	—	a)	63.66	5.62	63.46	5.77
IVe	180	2.5	300	Dark red	—	470(8.4); 1142	58.82	5.54	58.92	5.36
IVf	160	5	300	Dark brown	—	485(8.6); 1366	58.86	5.44	58.92	5.36
IVg	140	1.5	300	Brown	—	500(10.0); 1966	65.10	6.12	64.86	6.30

a) The alkaline solution decomposed during the measurement of λ_{max} value.

Acetylation of IVb. The dye (IVb) (0.5 g), acetic anhydride (10 ml) and fused sodium acetate (1 g) were refluxed at 130—140 °C for 3 hr to give pale yellow crystalline diacetyl compound (V) (0.5 g), mp 190 °C (from 80% ethanol); $\lambda_{max}^{EtOH}(\varepsilon)$ 330 (3358).

Found: C, 61.82; H, 5.28; CH_3CO, 29.28%. Calcd for $C_{15}H_{16}O_6$: C, 61.64; H, 5.48; CH_3CO, 29.45%.

Bromination of IVb. The dye (0.5 g) was dissolved in ethanol (10 ml) and to this solution Br_2 (1 ml) was slowly added with stirring. It was refluxed for 45 min, on a water bath to give red crystalline dibromo compound (from 90% ethanol) (VI; 0.6 g), mp 300 °C; λ_{max}^{EtOH} (at neutral and at pH, 8.5) (ε) 530 (1390).

Found: Br, 43.96%. Calcd for $C_{11}H_{14}O_4Br_2$: Br, 43.7%.

Potassium-hydroxide Treatment of IVb. The dye (IVb) (2 g) and aqueous KOH (100%, 25 ml) were refluxed for 1 hr. The solution was diluted with 500 ml water and acidified with dil HCl, filtered and washed well with water. The solid residue was boiled with acidic water (50 ml, 1 ml 2 M HCl) to give the acid (I), mp 37 °C (lit,[4] mp 33—35 °C); bp 137—139 °C/10 mmHg (lit,[4] bp 137—139 °C/10 mmHg); amide, mp 106 °C (lit,[5] mp 107 °C); acetyl, mp 77 °C (lit,[5] mp 78 °C).

The light brown filtrate from solid residue was extracted with ether to give resorcinol (0.9 g), mixed mp 110 °C and identical IR with its authentic sample.

Zn-dust Reduction of IVb. The dye (IVb) (2 g) was refluxed in glacial acetic acid (100 ml) with Zn-dust (5 g) for 15 min, to yield a colourless crystalline acid (VII; 1.7 g), mp 245 °C, which does not give fluorescence in alkaline solution.

Found: C, 63.02; H, 6.48%. Calcd for $C_{11}H_{14}O_4$: C, 62.85; H, 6.66%.

The acid (VII) when left overnight changed to red compound IVb, with superimposible IR and the same λ_{max} values. The acetylation of the mixture of acid (VII) and red compound was carried out as in V above to give diacetyl (V), mixed mp and identical IR, λ_{max} values and elemental analysis.

The authors are grateful to Dr. J. D. Tewari for his useful suggestions. A grant and fellowship (to R. G.) from CSIR, New Delhi is acknowledged.

References

1) Biggs and Pope, *J. Chem. Soc.*, **123**, 2934 (1923); Dutt and Thorpe, *ibid.*, **125**, 2524 (1924).
2) K. Von Auwers and A. Heinze, *Ber.*, **52**, 584 (1919).
3) S. Racine, *Ann. Chem.*, **78**, 239 (1887).
4) I. Heilbron and H. M. Bunbury, "Dictionary of Organic Compounds", Vol. 3, Oxford Univ. Press, New York (1953), p. 178.
5) E. H. Rodd, "Chemistry of Carbon Compounds," Vol. IB, Elsevier, New York (1952), p. 881.
6) The nomenclature is according to "The Chemistry of Carbon Compounds" Vol. IIIB, ed. by E. H. Rodd, Elsevier, New York (1956), p. 1110.

NOTES

BULLETIN OF THE CHEMICAL SOCIETY OF JAPAN, VOL. 47(7), 1791—1792 (1974)

High-precision Flow Meter for Gas Chromatography

Yoshio HORI* and Riki KOBAYASHI

Department of Chemical Engineering, Rice University, Houston, Texas 77001, U.S.A.

(Received September 28, 1973)

Synopsis. A gas-chromatographic apparatus with an empty tubing in place of a packed column can be used as a flow meter. The detector signal, processed by a differentiator-timer system, gives a precision of 0.06% in the measurement of the flow rate.

Gas chromatography in physico-chemical application requires precise measurements of the retention volume. Sources of error in the measurements of retention time have been analyzed, and various improvements have been made.[1-2] On the other hand, a soap film flow meter has been conventionally used for the measurement of the carrier-gas flow rate. Because of the visual observation of the soap film motion, the experimental uncertainty in the retention volume is at least 0.2—0.5%. No flow-measuring device can give much more precise measurements.

During the gas-chromatographic studies of physical adsorption and gas-liquid equilibrium at elevated pressures, a new flow meter was developed in this laboratory to give more precise measurements.

Apparatus

High-pressure Gas-chromatographic Apparatus. The main features of the equipment are similar to those described previously.[3] Two high-pressure regulators made by the Matheson and Grove Valve & Regulator Co. were connected in series; they held such a constant pressure of the carrier gas that no change was detected in the Heise Gauge during any experimental run. The pressure was measured by means of Heise Gauges with certified accuracy of 0.1% of the full scale. Their ranges were 200, 1000, and 2000 psi. The pressure was kept constant at all experimental conditions (up to 120 atm) between the inlet and the expansion valve; the pressure drop across the packed column is negligible, as has been verified previously.[3] The pressure of the carrier gas is reduced to 1 atm at the expansion valve.

Flow-measuring Device. In a common gas chromatographic apparatus, a packed column can be replaced with an empty tubing of a known volume. Then one can obtain a definite retention time in accordance with the flow rate. This is the principle of the present flow meter.

A six-way linear gas-sampling valve manufactured by Varian Aerograph was used as the perturbation gas-injection valve. The volume of the sample loop of the valve was 0.18 ml. Two sets of copper tubing 1/4 inch in diameter were used as the empty tubing; one was 2 m long, and the other, 8.6 m long. Either of the two empty tubings was used according to the flow conditions. The pressures at both the inlet and the outlet of the empty tubings were measured by means of manometers filled with water. A Gow-Mac thermal conductivity cell (Model 10-460, Flo-thru type) was used. The flow-meter system was immersed in a thermostat, filled with silicone oil and maintained at 35.0± 0.03 °C.

The flow-meter system was connected to the outlet of the high-pressure gas-chromatographic apparatus. The flow-meter system is regulated at the constant temperature (35 °C), and the pressure in the empty tubing is measured (atmospheric pressure), so that the flow meter can work under any experimental conditions of the high-pressure equipment.

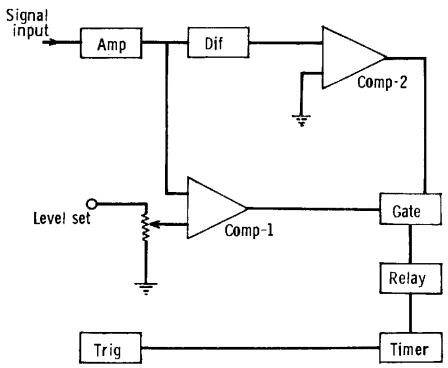

Fig. 1. Block diagram of the differentiator-timer system.

After the carrier-gas (methane) flow reaches a steady state, a dose of perturbation gas (argon) is injected by means of the sample injection valve, which triggers a microswitch at the same time. Then the timer starts. The perturbation gas, passing through the empty tubing, reaches the detector. The signal from the detector is differentiated by the differentiator and is compared with zero level by means of the comparator-2 (Fig. 1). When the elution peak reaches its maximum, the differentiated signal becomes zero, the relay system being driven to turn off the timer. The timer stops only when the input signal exceeds the preset threshold level (comparator-1) and the differentiated signal reaches zero. The timer, a Model S-6 Precision Timer manufactured by the Standard Electric Company, gives readings as precise as 1/1000 minute.

The present flow meter was calibrated against a soap-film flow meter, the volume of which had previously been calibrated. The retention time, t (min), is related to the carrier gas flow rate, f (cm³/min) (at 35.0 °C, atmospheric pressure), and the effective volume between the injection valve and the detector cell, v (cm³):

$$f \cdot t = v + f \cdot \Delta t \qquad (1)$$

where Δt (min) is a constant. Δt corresponds to the delay in the detector system and the variation in the flow pattern according to the flow rate. The linear relationship (1) was found to hold for flow rates less than 180 cm³/min, using an

* Present address: Research Department, Kikumoto Works, Sumitomo Chemical Co., Ltd., Niihama, Ehime 792.

appropriate one of the empty tubings (2 m and 8.6 m long). The *accuracy* of the present flow meter depends upon that of the soap-film flow meter. However, the *precision* is much improved, as is exemplified below.

Results of Measurements

A lot of flow measurements were made for each experimental run by means of the present flow meter. Some of them are tabulated in Table 1. The retention times in the third line were obtained during the time shown in the fourth line. The constancy of the measurements is excellent.

Table 1. Reproducibilty of the measurements of flow rate

Chromatographic pressure in the high pressure part[a] (atm)	3.0	10.5	15.5
Average flow rate at 35.0 °C, latm (cm^3/min)	12.539	36.754	62.385
Measured retention time by the flow meter (min)	3.3109	1.1329	0.6701
	3.3114	1.1331	0.6692
	3.3117	1.1331	0.6701
	3.3113	1.1332	0.6701
		1.1331	0.6698
		1.1330	0.6698
		1.1322	0.6701
Duration in which the measurements were made (min)	39	25	34

a) The flow meter is connected to the outlet of the high pressure gas chromatographic apparatus. The pressures before the expansion valve in high pressure apparatus are shown here.

According to the series perturbation technique,[3-6] the adsorption of methane on Porasil was precisely measured by means of a high-pressure gas chromatograph equipped with the present flow meter. The carrier gas was methane, and the retention volume of the methane was measured by the use of radioactive methane. The detailed experimental results will be reported elsewhere.[7] The retention volume of helium perturbation is a first-order approximation of the gas-phase volume of the column packed with Porasil. Figure 2 gives the helium perturbation obtained by means of the apparatus equipped with the present flow meter in comparison with those obtained with a soap-film flow meter. If the density of the adsorbed methane is constant at a fixed temperature, the gas-phase volume decreases linearly with the methane adsorption.[3] The present flow meter improved the measurement very much. As may be seen in Table 1, the scattering is approximately 0.06%, at least 4 times better than in careful measurements by means of a soap-film flow meter.

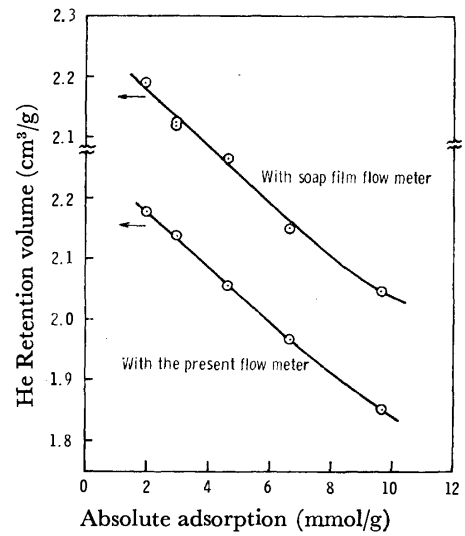

Fig. 2. Measurement of He retention volume by high pressure gas chromatographic apparatus equipped with and without differentiator.

Financial support was supplied by the U. S. National Science Foundation.

References

1) J. F. Oberholtzer and L. B. Rogers, *Anal. Chem.*, **41**, 1234 (1969).
2) M. Goedert and G. Guiochon, *ibid.*, **42**, 962 (1970).
3) Y. Hori and R. Kobayashi, *J. Chem. Phys.*, **54**, 1226 (1971).
4) H. B. Gilmer and R. Kobayashi, *A. I. Ch. E. J.*, **11**, 702 (1965).
5) J. J. Haydel and R. Kobayashi, *Ind. Eng. Chem., Fundametal*, **6**, 546 (1967).
6) S. Masukawa and R. Kobayashi, *J. Gas Chromatogr. Sci.*, **6**, 257 (1968).
7) Y. Hori and R. Kobayashi, This Bulletin, to be published.

BULLETIN OF THE CHEMICAL SOCIETY OF JAPAN, VOL. 47(7), 1793—1794 (1974)

Tritium Fractionation in the Crystallization of Aluminum Alums from Their Aqueous Solutions

Haruhiko TANAKA,* Hiroko ANDO, and Hisao NEGITA

*Shinonome Branch School, Faculty of Education, Hiroshima University, Shinonome, Hiroshima 734
Department of Chemistry, Faculty of Science, Hiroshima University, Higashisenda-machi, Hiroshima 730

(Received November 12, 1973)

Synopsis. The tritium fractionation in the crystallization of $NH_4Al(SO_4)_2 \cdot 12H_2O$ from a solution was found to be larger than those in $NaAl(SO_4)_2 \cdot 12H_2O$ and $KAl(SO_4)_2 \cdot 12H_2O$. This fact was discussed in terms of the proton exchange between NH_4^+ and H_2O.

In previous studies,[1] the fractionation of tritiated water (HTO) has been investigated in the crystallization of a number of hydrated crystals. It was found that HTO is generally diluted with crystallization water to a small percentage. It seems to be of some importance to examine the behavior of NH_4^+ in the tritium fractionation in $NH_4Al(SO_4)_2 \cdot 12H_2O$, with reference to the results in $NaAl(SO_4)_2 \cdot 12H_2O$ and $KAl(SO_4)_2 \cdot 12H_2O$.

Experimental

The aluminum alums of commercial origin were purified by recrystallization. The large single crystal of the salt was grown from a slightly supersaturated aqueous solution containing a trace of HTO at around 20 °C.

The water from the single crystals of sodium- and ammonium alums was recovered by heating them at *ca.* 300 °C in a stream of nitrogen gas and at *ca.* 50 °C *in vacuo* respectively. The water from the mother solution was recovered through distillation and subsequent dehydration. The tritium radioactivity was compared between the dehydrated water and the mother liquid as has been described in a previous paper.[1] Simultaneous TGA and DTA were carried out for the dehydration of the three kinds of alums with a thermal analyzer, M8002 TG-DTA, of the Rigaku Denki Co. Ltd., at the rate of 5 °C/min in an atmosphere of nitrogen.

Results and Discussion

The separation factor, S, of HTO for the crystallization of a hydrated salt from an aqueous solution can be given as $S=N_s/N_l$, where N_s and N_l are the net count rates for a 0.1 g portion of water recovered from the solid and liquid phases respectively.[1] Table 1 gives the separation factors, S, for the aluminum alums. We see that there is only a small percentage of dilution of HTO in the water of crystallization of sodium- and potassium aluminum alums,[2] as is the case with many inorganic hydrated crystals.[1]

TABLE 1. THE SEPARATION FACTOR, S, OF HTO FOR ALUMS

Crystal	Net count rate (cpm) of HTO[a]		$S(N_s/N_l)$
	N_s	N_l	
$NaAl(SO_4)_2 \cdot 12H_2O$	19419	20076	0.967 ± 0.006
$KAl(SO_4)_2 \cdot 12H_2O$	26426	27097	0.975 ± 0.004[b]
$NH_4Al(SO_4)_2 \cdot 12H_2O$	13121	14061	0.933 ± 0.006

a) Averaged from 5—6 independent experiments for 0.1 g of water with 35% efficiency.
b) From Ref. 2.

The fractionation in $NaAl(SO_4)_2 \cdot 12H_2O$ can be explained by a mechanism similar to that in $KAl(SO_4)_2 \cdot 12H_2O$. On the contrary, a remarkable dilution of HTO is found in $NH_4Al(SO_4)_2 \cdot 12H_2O$. It seems that hydrogen atoms in the NH_4^+ ion are responsible for the considerable dilution, because the dilution due to the crystallization water in sodium- and potassium aluminum alums is found to be small.

It can be assumed here that the dilution in the crystallization water of $NH_4Al(SO_4)_2 \cdot 12H_2O$ is equal to that in $KAl(SO_4)_2 \cdot 12H_2O$, This is supported by the facts that (1) the crystal-growth mechanism of these alums is identical,[3] (2) the K^+ and NH_4^+ ions have similar ionic radii and viscosity-B coefficients,[4] and (3) these alums give very similar DT–TGA curves for the dehydration, as is shown in Fig. 1.

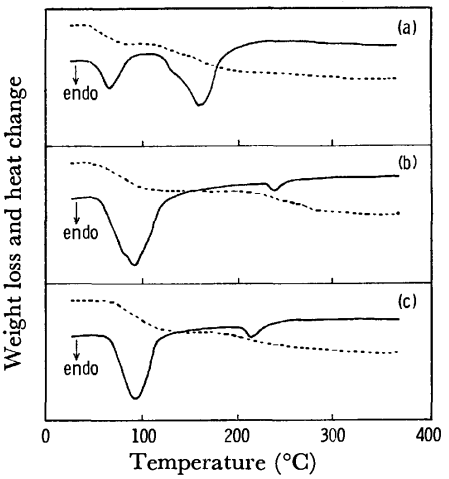

Fig. 1. DTA (——) and TGA (-----) diagrams for dehydration of alums.
(a): $NaAl(SO_4)_2 \cdot 12H_2O$, (b) :$KAl(SO_4)_2 \cdot 12H_2O$,
(c): $NH_4Al(SO_4)_2 \cdot 12H_2O$.

It is well-known that the proton-exchange reaction occurs readily in the aqueous solution of NH_4^+:[7]

$$HTO + NH_4^+ \rightleftharpoons H_2O + NH_3T^+ \quad (1)$$

In Eq. (1), tritium may be diluted in NH_4^+ according to the theory of isotope effect in an equilibrium reaction, because the proton in NH_4^+ is labile in comparison with that in H_2O.[8] It follows that tritium is diluted in the NH_4^+ of the crystal of $NH_4Al(SO_4)_2 \cdot 12H_2O$ grown from the aqueous solution.

Accordingly, a considerable dilution of tritium in the dehydrated water may become possible since a proton-exchange reaction is expected to occur between NH_4^+ in the amorphous $NH_4Al(SO_4)_2$ and dehydrated water during the vacuum dehydration, as has been suggested for the dehydration of $(COOH)_2 \cdot 2H_2O$ by Okazaki and Takemura.[9,10]

In conclusion, the too small S value for $NH_4Al(SO_4)_2 \cdot 12H_2O$ compared with those for the other alums can be explained qualitatively in terms of the proton-exchange reaction between NH_4^+ and H_2O in both the aqueous solution and the vacuum dehydration.

The authors wish to express their thanks to Dr. Osamu Yamamoto for his help in analysing the activity of tritium.

References

1) H. Tanaka and H. Negita, This Bulletin, **43**, 3079 (1970); H. Tanaka, M. Tanga, and H. Negita, *ibid.*, **46**, 1000 (1973).

2) H. Tanaka, *ibid.*, **45**, 339 (1972).

3) P. Bennema, Thesis, The Technical University of Delft (1965).

4) The B coefficient was originally given by Jones and Dole.[5] This value accounts for the interaction between an ion and water in the aqueous solution.[6]

5) G. Jones and M. Dole, *J. Amer. Chem. Soc.*, **51**, 2950 (1929).

6) R. W. Gurney, "Ionic Processes in Solution," McGraw-Hill Book Co. Inc., New York (1954), Chap. 9.

7) E. A. Evans, "Tritium and Its Compounds," Butterworths & Co. Ltd., London (1966), p. 350.

8) R. W. Gurney, "Ionic Processes in Solution," McGraw-Hill Book Co. Inc., New York (1954), Chap. 7.

9) N. Okazaki and E. Takemura, This Bulletin, **34**, 977 (1961).

10) H. Tanaka, T. Kado, and H. Negita, *ibid.*, **47**, 278 (1974).

BULLETIN OF THE CHEMICAL SOCIETY OF JAPAN, VOL. 47(7), 1795—1796 (1974)

Extrinsic Photoconductivity of *N*-Ethylcarbazole Single Crystals

Keishi KATO, Masaaki YOKOYAMA, and Hiroshi MIKAWA

Department of Applied Chemistry, Faculty of Engineering, Osaka University, Yamadakami, Suita, Osaka 565

(Received February 20, 1974)

Synopsis. An extrinsic photocurrent was observed in pure *N*-ethylcarbazole single crystal, contrary to the current view that it does not exist in *N*-isopropylcarbazole.[8] It was reduced to a great extent in anthracene-containing crystal due to the decrease in carrier quantum yield caused by the energy transfer from *N*-ethylcarbazole (host) to anthracene (guest) molecules.

Studies have been made on the photoconductivity of poly-*N*-vinylcarbazole (PVCz),[1-7] as regards application to electrophotography. For a better understanding of the photoconductive properties of this polymer, it is desirable to investigate the differences in photoconductive property of the polymer and the corresponding molecular crystals. *N*-Ethylcarbazole (EtCz) and *N*-isopropylcarbazole (IPCz) were chosen as suitable model compounds, each corresponding to the monomeric unit of PVCz.

The photoconductivity of IPCz was studied by Sharp who reported that the compound exhibits no extrinsic photoconduction in the lowest π-π^* absorption region in contrast to the presence of both extrinsic and intrinsic photoconduction in PVCz. In view of current aspects of the photoconductivity of anthracene, the absence of extrinsic photoconduction in IPCz seems unusual. It seems necessary to reinvestigate the photoconductive properties of molecular crystals of the model compounds.

The present paper gives the results concerning the photoconductivity of EtCz single crystal. EtCz exhibits extrinsic photoconduction in the lowest π-π^* absorption region which could be largely reduced by the presence of a small amount of anthracene.

Experimental

Commercial EtCz contains anthracene as an impurity which is very difficult to remove by the usual methods of purification.[9] EtCz of high purity could be obtained only when synthesized EtCz was used as a starting material.

In our present work we used two kinds of EtCz crystal, one obtained from commercial EtCz purified first by repeated recrystallization and finally by vacuum distillation followed by zone melting, and containing about 2×10^{-3} mol/mol anthracene, the other a zone-refined EtCz crystal prepared from synthetic carbazole, the purity of the crystal being confirmed by the fact that the fluorescence lifetimes remained constant (about 20 ns) over the whole spectral region. Single crystals were obtained in a Bridgman furnace. Pillar crystals (about 2 mm×2 mm×5 mm) cut from the ingot along the a-axis (crystallographical) were used for the DC steady-state measurements, the surfaces of both ends being painted with silver-paste (Du Pont). A 500 W-xenon light source was used together with a prism-monochromator. Monochromatic light was cast onto the crystal perpendicular to the applied electric field. The photocurrent was measured with a vibrating-reed electrometer (Takeda Riken TR-81).

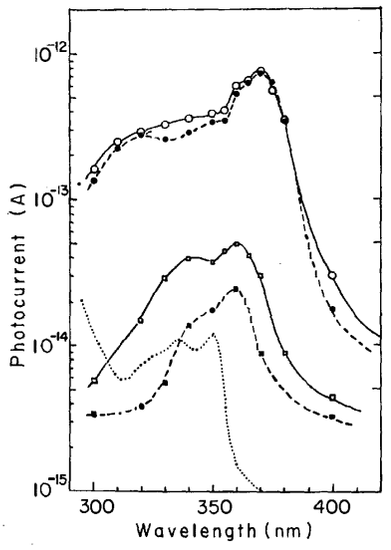

Fig. 1. The spectral dependence of the photocurrent for both pure and anthracene-containing EtCz crystals, applied field strength being 5000 V/cm.
(—○—); pure EtCz crystal in high vacuum, (--●--); pure EtCz crystal in air, (—□—); anthracene-containing EtCz crystal in high vaccum, (--■--); anthracene-containing EtCz crystal in air. The dashed line indicates the absorption spectrum of EtCz solid (KBr disk).

Results and Discussion

Figure 1 shows the spectral dependence of the photocurrent for both pure and anthracene-containing crystals of EtCz. The photocurrent was proportional to the light intensity irrespective of the exciting wavelength.

The pure EtCz crystal shows a relatively large photocurrent, nearly equal to that of PVCz. The photocurrent rises at the onset of the lowest singlet absorption, its peak being located at about 370 nm. This antibatic behaviour of the action spectrum of the photocurrent is similar to that of PVCz reported by Bauser and Klöpffer[1] and Okamoto *et al.*,[3] carriers are generated by extrinsic processes involving the interaction of singlet excitons with impurity or defects in the bulk of the crystal.

In anthracene-containing crystals, a considerable reduction of the photocurrent is observed over the whole spectral range by factor of about 10. This results is similar to the case of tetracene-doped and acridine-doped anthracene crystals.[10] The reduction of the photocurrent might be due to either the decrease of the quantum efficiency of the charge-carrier formation process or the decrease of the effective mobility of the carriers. The latter effect can be neglected for the following reasons. (1) Carrier mobility is independent of the wavelength of the incident light. In spite of

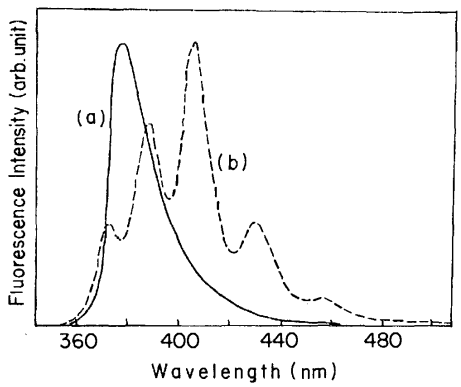

Fig. 2. The fluorescence spectra of pure and anthracene-containing crystals of EtCz at room temperature. (a); pure EtCz single crystal, (b); anthracene-containing crystal of EtCz (2×10^{-3} mol/mol).

this, the spectral dependence of the photocurrent changes in anthracene-containing crystals, the photocurrent peak showing a blue shift to 360 nm. (2) In anthracene-containing crystals, the fluorescence of EtCz is remarkably quenched and the intensive fluorescence of anthracene is observed as shown in Fig. 2. This is due to an efficient energy transfer from the lowest excited singlet state of EtCz (3.5 eV) to that of anthracene (3.3 eV). Thus it can be concluded that the reduction of the photocurrent in anthracene-containing crystals is mainly due to the decrease in the carrier-generation efficiency due to the energy transfer. The shift of the photocurrent peak to about 360 nm can be interpreted as follows. Since anthracene molecules are distributed uniformly in the crystal, anthracene molecules available as the dissipating center of the singlet-excitation energy decrease if the light is absorbed near the surface of the crystal, thus causing a blue-shift of the action spectrum of photoconductivity.

Preliminary experiments on the transient photoconductivity of EtCz single crystal with a pulsed light of the π-π^* absorption region showed that the hole photocurrent was remarkably larger than the electron photocurrent. Hence, the photocurrent measured with pillar crystals is mainly due to the hole photocurrent in the lowest π-π^* absorption region.

Thus the photoconductivity of EtCz crystal can be described as follows: The photocarrier (mainly holes) are generated by an extrinsic process involving the interaction of singlet excitons with impurity or defects in the bulk of the crystal. The small contribution of photocarrier generation on the surface of the crystal is explained by the experimental result in which the photocurrent was not affected, or only a little, by the atmosphere. If the crystal contains anthracene molecules, they act as traps of the singlet-excitation energy in EtCz crystal causing a decrease in carrier generation efficiency. Complete quenching of the photoconductivity may thus occur in the lowest π-π^* absorption region, if the crystal contains a considerable amount of impurity which quenches the excited energy of the host EtCz molecules. The result obtained by Sharp[8] showing no photoconduction in the lowest π-π^* absorption region, a sharp contrast to the present results of

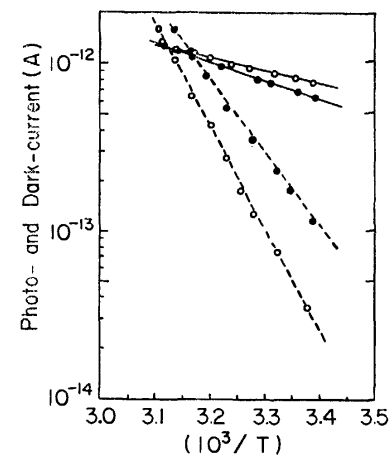

Fig. 3. The temperature dependence of the photo- and dark-currents of pure EtCz single crystal. (—○—); photocurrent in high vacuum, (—●—); photocurrent in air, (--○--); dark-current in high vacuum, (--●--); dark-current in air.

Table 1. The activation energies of EtCz crystal and PVCz film (eV)

Current	EtCz crystal		PVCz film[2]	
	photo-	dark-	photo-	dark-
In vacuum	0.06	0.5	0.1—0.3	1.0—1.3
In air	0.08	0.45	0.5—0.6	0.7—0.8

EtCz crystal, might be attributed to the presence of some impurity such as anthracene in the crystal.

Figure 3 shows the temperature dependence of the photo- and dark-currents in pure EtCz crystal. The relation $i \propto \exp(-E_a/kT)$ holds for dark- and photocurrents. The activation energies (E_a) are given in Table 1, compared with those of PVCz. The activation energies of both dark- and photo-current in EtCz crystal are smaller than those of PVCz. Since it is expected that carrier-generation process requires a very small activation energy, these differences in activation energy seem to reflect the differences of the behaviours in carrier transport between molecular crystals and polymers.

References

1) H. Bauser and W. Klöpffer, *Chem. Phys. Lett.*, **7**, 137 (1970).
2) K. Okamoto, S. Kusabayashi, and H. Mikawa, This Bulletin, **46**, 1948 (1973).
3) K. Okamoto, S. Kusabayashi, and H. Mikawa, *ibid.*, **46**, 2324 (1973).
4) K. Okamoto, K. Kato, K. Murao, S. Kusabayashi, and H. Mikawa, *ibid.*, **46**, 2883 (1973).
5) D. M. Pai, *J. Chem. Phys.*, **52**, 2285 (1970).
6) A. Szymanski and M. M. Labes, *ibid.*, **50**, 3568 (1969).
7) J. Mort, *Phys. Rev.*, **B5**, 3329 (1972).
8) J. H. Sharp, *J. Phys. Chem.*, **71**, 2587 (1967).
9) K. Kato, M. Yokoyama, K. Okamoto, S. Kusabayashi, H. Mikawa, K. Yoshihara, and S. Nagakura, *Mol. Cryst. and Liq. Cryst.*, in press.
10) R. F. Chaiken and D. R. Kearns, *J. Chem. Phys.*, **45**, 3966 (1966).

BULLETIN OF THE CHEMICAL SOCIETY OF JAPAN, VOL. 47(7), 1797—1798 (1974)

ENDOR Studies of 1,3,5-Triphenylverdazyl Radical and Its Methyl Derivatives. V.

Kazuo MUKAI, Takamitsu YAMAMOTO,* Masahiro KOHNO,*
Nagao AZUMA,† and Kazuhiko ISHIZU
Department of Chemistry, Faculty of Science, Ehime University, Matsuyama 790
**JEOL LTD., Akishima, Tokyo 196*

(Received March 4, 1974)

Synopsis. The ENDOR spectra of 1,3,5-triphenylverdazyl radical and its methyl derivatives were observed in toluene, and the effects of methyl substitution on the proton hyperfine coupling constants were investigated.

Verdazyls, a series of very stable neutral radicals containing four nitrogen nuclei, were previously studied by Kuhn, Neugebauer, and Trischmann.[1,2] Recent studies of the magnetic susceptibility of 1,3,5-triphenylverdazyl and its methoxy or methyl derivatives have clarified some interesting magnetic properties in these radicals,[3-5] as is explained by the one-dimensional Heisenberg model or the linear Ising model. The X-ray diffraction analyses[6,7] of the above verdazyls revealed the variety of molecular packing. The magnetic property is very sensitive to both the packing of the radical molecules in the crystal and the distribution of the unpaired electron on the radical. ESR is a frequently used method for determining the distribution of the unpaired electron on radical molecules. However, the ESR spectra of verdazyl radicals usually show only nine line splittings (a^N=6G[1]) due to the four nitrogen atoms in verdazyls.

Electron nuclear double resonance (ENDOR) spectroscopy is a valuable method for the determination of proton isotropic hyperfine couplings of organic radicals in solution, since the effective resolution is much higher than for ESR.[8] However, due to the quadrupole moment of the nitrogen atom, the observation of ENDOR spectra of the radicals which include nitrogen atoms is generally difficult compared to those of other radicals. Particularly, in the case of verdazyl radicals, four nitrogens are contained in the heterocyclic ring. Thus, we carefully selected adequate temperature, solvent, radical concentration, ESR and NMR powers, and ESR and NMR modulations.[9]

In the present paper, proton hyperfine splitting constants measured from the solution ENDOR spectra of the 1,3,5-triphenylverdazyl radical and its methyl derivatives in toluene are reported, in order to present fundamental data which are essential for a more detailed understanding of the magnetic properties of these radicals.

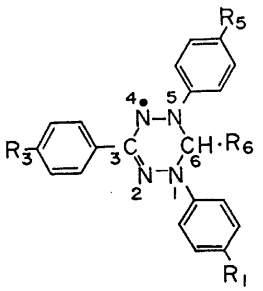

Fig. 1. The verdazyl radicals (I—V).

Radical	R_1,R_5	R_3	R_6
I	H	H	H
II	H	CH_3	H
III	CH_3	H	H
IV	CH_3	CH_3	H
V	H	H	CH_3

Experimental

Verdazyls (I—V) (see Fig. 1) were prepared by the method of Kuhn and Trischmann,[1] followed by recrystallization from an acetone–ethanol mixture. They were identified by their elementary analyses and melting points, and the values obtained were in good agreement with those presented in the literature.[1] The radical concentrations were determined by their magnetic susceptibilities in the temperature range from 77 to 300 K. The respective spin concentrations were 100% as $S=1/2$, within the limit of the experimental error.

The paramagnetic susceptibility measurements were carried out with a Shimadzu type MB-2 magnetic torsion balance, equipped with a low temperature cryostat. The ENDOR spectra were recorded by a JEOL type ES-EDX-1 spectrometer, operated with 80 Hz magnetic field modulation. About 150 watts of the continuous radio wave frequency modulated at 6.5 kHz were running inside of the cavity for NMR excitation.[10]

Results and Discussion

The ESR spectra of 1,3,5-triphenylverdazyl (I) and its methyl derivatives (II), (III), (IV), and (V) show only nine line splittings due to four nitrogens in the heterocyclic ring. We were unable to resolve splittings from the protons. The nitrogen hyperfine splittings, a^N, observed in 2-methyltetrahydrofuran (2-MeTHF)

TABLE 1. HYPERFINE SPLITTING CONSTANTS OF VERDAZYL RADICALS (in Gauss)

Radical	a^{N} a)	a_p^H	a_o^H	a_m^H, $a_{3\text{-}o}^H$	$a_{3\text{-}p}^{CH_3}$	$a_6^{CH_3}$
I	5.79	1.22_2	1.11_2	0.42_5	—	—
II	5.67	1.21_8	1.11_3	0.42_4	0.30_0	—
III	5.75	1.29_3	1.12_4	0.41_9	—	—
IV	5.62	1.29_0	1.12_4	0.41_3	0.30_2	—
V	5.60	1.26_5	1.15_4	0.42_2	—	0.97_6

a) The values in 2-MeTHF observed by ESR.

† Present address: Department of Chemistry, Faculty of Science, Kyoto University, Kyoto.

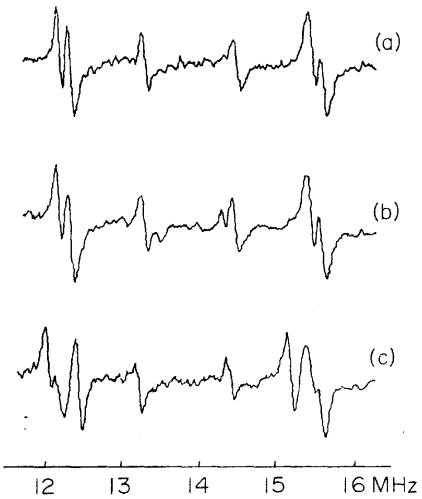

Fig. 2. ENDOR spectra of (a) verdazyl (I) at −78 °C, (b) verdazyl (II) at −74 °C, and (c) verdazyl (V) at −70 °C in toluene.

at room temperature are listed in the first column of Table 1.

Figure 2 shows three typical ENDOR spectra of the verdazyls in toluene at temperature −70∼−80 °C. Toluene, chloroform, 2-MeTHF and *n*-heptane were used as solvents, and it was found that toluene is the most suitable solvent for the verdazyls.

The ENDOR spectrum of 1,3,5-triphenylverdazyl radical (I) (see Fig. 2(a)) clearly exhibits three different proton hyperfine splittings (1.22_2, 1.11_2, and 0.42_5 G). The orbitals containing the unpaired electron of the 1,3,5-triphenylverdazyl have, at least in the Hückel approximation, a node in 3-phenyl ring, giving a zero spin density on the phenyl ring. In the McLachlan approximation, the orbitals are spin polarized so as to yield nonvanishing spin densities in the 3-phenyl ring of the radical.[11] However, these spin densities are not large enough to account for the above proton hyperfine splittings. In fact, aryl-substituted verdazyls with selectively introduced D-, Cl-, Br-, F- and ethoxycarbonyl groups give well resolved ESR spectra[12] at room temperature, and the observed proton hyperfine splittings are explained as splittings ($a_o^H = a_p^H = 1.06$—1.09 G, $a_m^H = 0.41$—0.49 G) in equivalent 1,5-phenyl rings. On the other hand, recent NMR study[13] of 1,3,5-triphenylverdazyl in $CDCl_3$ shows paramagnetic shift lines due to all protons contained in the verdazyl radical. The hyperfine splittings are assigned for 1,5-phenyl ring protons ($a_6^H = 1.195$, $a_o^H = 1.12$ and $a_m^H = 0.425$ G), for 3-phenyl ring protons ($a_p^H = 0.31$, $a_o^H = 0.425$, and $a_m^H = 0.16$ G), and for C-6-methylene protons in the verdazyl ring ($a_6^H = 0.027$ G[14]). A comparison of the hyperfine splittings obtained in the present ENDOR study with those of ESR and NMR studies indicates that the hyperfine splittings (1.22_2 and 1.11_2 G) arise from the *para* and *ortho* protons respectively in the 1,5-phenyl rings, and 0.42_5 G from both *meta* protons in the 1,5-phenyl rings and *ortho* protons in the 3-phenyl ring. The verdazyl (III) also shows three pairs of similar hyperfine splittings.

As shown in Fig. 2(b), in addition to the above three splittings of verdazyl (I), a pair of signals with weak intensity and smaller splitting (0.30_0 G) is clearly observed for verdazyl (II), in which the *para* proton in the 3-phenyl ring is substituted by methyl group. This signal is attributed to the methyl protons. Verdazyl (IV) also shows four pairs of similar hyperfine splittings. These values are listed in Table 1. Hyperfine splittings of *ortho* and *para* ring protons remain constant within experimental error, indicating that methyl substitution does not affect the distribution of the unpaired electron. The small increase in hyperfine splitting of the *para* proton observed for verdazyls (III) and (IV) is explained as a larger Q-value for the methyl proton than for the ring α-proton.

In addition to the hyperfine splittings of 1.26_5, 1.15_4, and 0.42_2 G due to 1,3,5-phenyl ring protons, an abnormally large hyperfine splitting (0.97_6 G) was observed for verdazyl (V), in which one of C-6-methylene protons is substituted by a methyl group. C-6-Methylene protons have small hyperfine splittings of about 0.03 G,[13,14] and thus this large hyperfine splitting should be attributed to the substituted methyl γ-protons. We usually cannot expect such a large splitting for a γ-proton. However, the Stuart model shows that the methyl protons locate just above the 1- and 5-nitrogen atoms having large spin densities and should couple more strongly, because of hindered rotation of C-6-methylene group. In fact, X-ray studies have revealed such a configuration, with the shortest distance of 2.72 Å between the 1-nitrogen and the methyl protons.[15] A small change in hyperfine splittings of *ortho* and *para* proton was also observed for verdazyl (V). This arises from the variation of the distortion angle of the 1,5-phenyl rings connected to the centeral verdazyl ring by substituted methyl group.

In conclusion, as was expected, the effect of the methyl substitution on the spin distribution is fairly small. Therefore, these radicals are useful for the study of how molecular packing affects the magnetic properties of the organic radical crystalline.

References

1) R. Kuhn and H. Trischmann, *Angew. Chem.*, **75**, 294 (1963); *Monatsh. Chem.*, **95**, 457 (1964).
2) R. Kuhn, F. A. Neugebauer, and H. Trischmann, *Angew. Chem.*, **76**, 691 (1964); *Monatsh. Chem.*, **97**, 525 (1966).
3) K. Mukai, N. Azuma, and K. Ishizu, This Bulletin, **43**, 3618 (1970).
4) N. Azuma, J. Yamauchi, K. Mukai, H. O. Nishiguchi, and Y. Deguchi, *ibid.*, **46**, 2728 (1973).
5) K. Mukai, K. Oishi, K. Ishizu, and N. Azuma, *Chem. Phys. Lett.*, **23**, 522 (1973).
6) D. E. Williams, *Acta Crystallogr.*, **B29**, 96 (1973).
7) N. Azuma *et al.*, to be published.
8) J. S. Hyde, *J. Chem. Phys.*, **43**, 1806 (1965).
9) J. H. Freed, D. S. Leniart, and J. S. Hyde, *ibid.*, **47**, 2762 (1967). Other references are therein.
10) T. Yamamoto, K. Sato, and T. Miyamae, *J. Appl. Phys.*, **11**, 1508 (1972).
11) P. H. H. Fischer, *Tetrahedron*, **23**, 1939 (1967).
12) F. A. Neugebauer, *Monatsh. Chem.*, **98**, 231 (1967).
13) P. Kopf, K. Morokuma, and R. Kreilick, *J. Chem. Phys.*, **54**, 105 (1971).
14) F. A. Neugebauer, H. Trischmann, and G. Taigel, *Monatsh. Chem.*, **98**, 713 (1967).
15) N. Azuma *et al.*, to be published.

BULLETIN OF THE CHEMICAL SOCIETY OF JAPAN, VOL. 47(7), 1799—1800 (1974)

The Back-extraction Behavior of Chelate Compounds. I. The Extraction and the Back-extraction of the Metal Oxinates

Takaharu HONJO, Kiyoshi AMENO, Masanobu HORIUCHI, and Toshiyasu KIBA
Department of Chemistry, Faculty of Science, Kanazawa University, Kanazawa, Ishikawa 920
(Received November 15, 1973)

Synopsis. The behavior of trace amounts of silver, bismuth, cadmium, cerium, cobalt, europium, iron, mercury, indium, manganese, lead, scandium, and zinc in back-extraction have been examined in order to ascertain the basic conditions for the mutual separation of metals as their oxinates by back-extraction.

In recent years a number of investigations concerning the liquid-liquid extraction of metal oxinates have been reported and reviewed, but only a few back-extraction techniques have been treated and applied to the separation of metals.[1,2] In this investigation, the behavior of trace amounts of silver(I), bismuth(III), cadmium(II), cerium(III), cobalt(II), europium(III), iron(III), mercury(II), indium(III), manganese(II), scandium(III), and zinc(II) in back-extraction have been examined in order to ascertain the basic conditions for the mutual separation of metals as their oxinates by back-extraction. The results have then been applied to the separation of cobalt from mixtures of iron radioisotopes by means of back-extraction.

Experimental

Extraction. Extraction was carried out for a buffered solution containing a radioactive tracer; the solution was made to have 0.1 M acetic acid (in the acidic region) or 0.1 M boric acid (in the basic region), and its pH was adjusted to an appropriate value. A solution of 0.01—0.1 M oxine in chloroform (5 ml) was shaken by means of a mechanical shaker with an equal volume of an aqueous solution containing each metal for 30 min at room temperature (20—25 °C). After centrifugation, a 3 ml portion of each phase was pipetted out into a test tube, and the radioactivity was counted with the NaI(Tl) scintillation counter. The pH of the aqueous phase was measured again after extraction by means of the pH meter.

Back-extraction. A 5 ml aliquot of an organic phase which had been prepared by the standard extraction procedure was shaken with a 5 ml portion of an aqueous solution adjusted to a desired pH for 30 min at room temperature. The distribution was determined as in the case of the extraction.

Theoretical

The percentage of extraction, % E, and the percentage of back-extraction, % E_{back}, can be calculated by means of the following equations:

$$\%E = D/(1+D)\cdot 100 \quad (1)$$

$$\%E_{back} = D^*/(1+D^*)\cdot 100 \quad (2)$$

where D and D^* are the net distribution ratios of a metal in the extraction and in the back-extraction respectively.

Results and Discussion

The extraction of trace amounts of 13 metals was carried out with 0.01—0.1 M oxine in chloroform for each, while the back-extraction of the metal oxinates was done with various acidic and basic aqueous solutions.

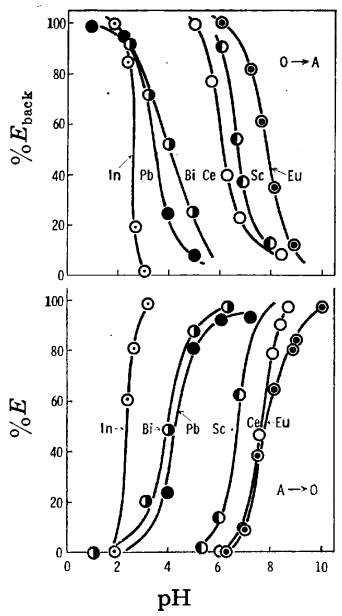

Fig. 1. The effect of pH or HCl(M) on the extraction and the back-extraction of trace amounts of Ag(I), Cd(II), Co(II), Fe(III), Hg(II), Mn(II), and Zn(II)-0.01—0.1 M oxine-chloroform system.

The results are shown in Figs. 1—2 as a function of the pH or HCl(M) of the aqueous phase. The symbols in the two figures, A→O and O→A, denote the extraction and the back-extraction of chemical species respectively.

The data on the $pH_{1/2}$ values of metal oxinates obtained in the present extraction system are summarized in Table 1. The difference in $pH_{1/2}$ gaves larger in the order of Fe(III), Sc(III), Zn(II)<Cd(II), Eu(III)<Bi(III)<In(III)<Hg(II)<Ce(III)<Ag(I)<Pb(II)<Mn(II)<Co(II). The disagreement of the $pH_{1/2}$ values appearing in the liquid-liquid extraction of the chelates indicates that the extraction equilibrium is not strictly reached under the present conditions. The fact that the extraction and the back-extraction curves of cobalt oxinate are quite different, *i.e.*, the nonequilibrium nature of the process, may be useful for the back-extraction separation of metals.

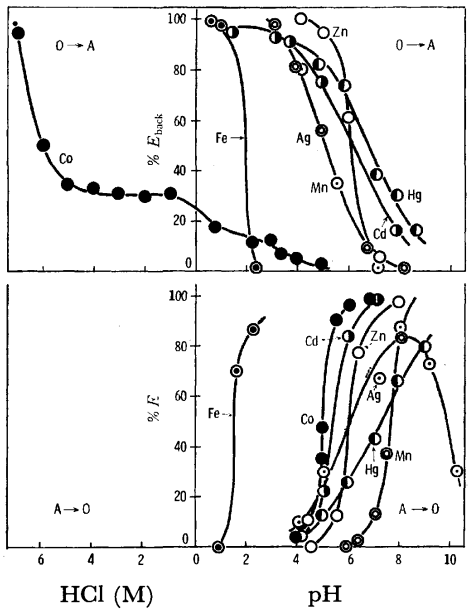

Fig. 2. The effect of pH on the extraction and the back-extraction of trace amounts of Bi(III), Ce(III), Eu-(III), In(III), Pb(II), and Sc(III)-0.01—0.1 M oxine–chloroform system.

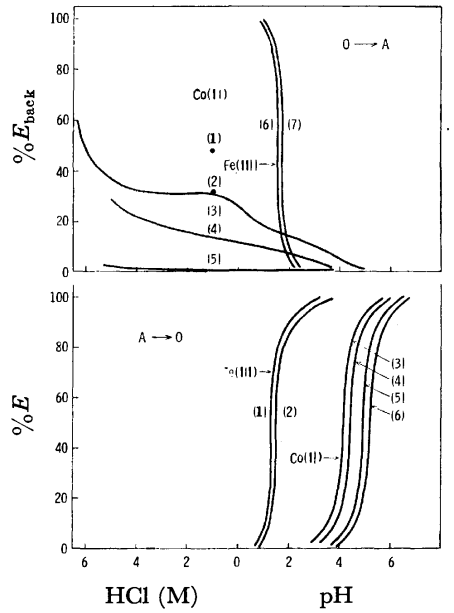

Fig. 3. The extraction and the back-extraction of Co(II) and Fe(III) with 0.01 M oxine in chloroform under various conditions.

Extraction: Co(II) (M)							
(1)	(2)	(2)	(3)	(4)	(5)	(5)	(6)
None	None	10^{-3}	Trace	Trace	Trace	10^{-3}	Trace
Fe(III) (M)							
(1)	(2)	(2)	(3)	(4)	(5)	(5)	(6)
10^{-3}	Trace	Trace	10^{-3}	10^{-4}	10^{-5}	None	None

Back-extraction:	(1)	(2)	(3)	(4)	(5)
Extraction pH	6.0	6.0	6.0	8.0	6.0
Shaking time (min)	30	5	30	30	90
Co(II) (M)	10^{-1}	Trace	Trace	Trace	Trace
Fe(III) (M)	None	None	None	None	None

	(5)	(6)	(6)	(8)
Extraction pH	6.0	3.5	3.5	3.5
Shaking time (min)	90	30	30	30
Co(II) (M)	Trace	None	10^{-3}	None
Fe(III) (M)	10^{-3}	Trace	Trace	10^{-3}

As can been seen in Fig. 3, the back-extractability of cobalt decreases as the shaking time becomes longer, and the pH values increase.

This abnormal behavior of cobalt oxinates seems to be caused by the transformation of $Co(Ox)_2$ into a certain inert complex such as $Co(Ox)_3$.[3]

The range of the extraction of cobalt shifts to a lower pH as the concentration of the coexisting iron increases; that is, the mutual separation of cobalt and iron with oxine in chloroform seems to be unattainable in the regular extraction. When a sample solution the pH of which had been adjusted to 6.0 was shaken with a 0.01 M oxine-chloroform solution for 90 min, the extraction of cobalt and iron proceeded quantitatively. Iron, however, could be stripped out of the organic phase by shaking it with an aqueous solution of a 1 M HCl solution for 30 min, while all cobalt remained in the organic phase. Thus, the data on metal oxinates in the extraction and the back-extraction may give valuable hints for finding the best conditions for the mutual separation of other metals as their oxinates by back-extraction, as has already been reported by the present authors for the Co(II)–Ni(II)–STTA–cyclohexane system.[4]

Table 1. $pH_{1/2}$ determined by the extraction and the back-extraction of metals with 0.01—0.1 M oxine in chloroform

Metal	HOx (M)	$pH_{1/2}$	
		Extraction	Back-extraction
Ag(I)	0.1	6.10	5.10
Bi(III)	0.01	4.20	4.05
Cd(II)	0.1	5.40	5.50
Ce(III)	0.01	7.68	6.70
Co(II)	0.01	5.10	5 M HCl
Eu(III)	0.01	7.85	7.75
Fe(III)	0.01	1.50	1.50
Hg(II)	0.01	7.80	7.50
In(III)	0.01	2.35	2.60
Mn(II)	0.01	7.70	5.35
Pb(II)	0.01	4.45	3.00
Sc(III)	0.01	6.67	6.67
Zn(II)	0.01	6.10	6.10

We would like to thank the Ministry of Education for its Scientific Research Grant to one of us (T.H.).

References

1) K. Motojima and H. Hashitani, *Bunseki Kagaku*, **9**, 151 (1960).
2) J. Stary, *Anal. Chim. Acta*, **28**, 132 (1963).
3) S. Oki, *ibid.*, **50**, 465 (1970).
4) T. Honjo, T. Unemoto, and T. Kiba, *Bunseki Kagaku*, **23**, 203 (1973).

BULLETIN OF THE CHEMICAL SOCIETY OF JAPAN, VOL. 47(7), 1801—1802 (1974)

The Standard Free Energy of the Formation of $LaFeO_3$ at 1204°C

Noboru KIMIZUKA and Takashi KATSURA*

National Institute for Researches in Inorganic Materials, Sakuramura, Niiharigun, Ibaragi 300-31

**Department of Chemistry, Tokyo Institute of Technology, Ookayama, Meguro-ku, Tokyo 152*

(Received November 20, 1973)

Synopsis. The standard free energy of the formation of $LaFeO_3$ was detemined to be -68700 ± 200 cal·mol^{-1} at 1204 °C by the following reaction: 1/2 $La_2O_3(s)+Fe(s)+3/4\ O_2(g)=LaFeO_3(s)$, based on precise phase equilibria in the Fe–Fe_2O_3–La_2O_3 system.

Moruzzi and Shafer[1] have investigated phase equilibria in the La_2O_3–iron oxide system at high temperatures up to 1900 °C in air. They found two compounds in this system; one is the orthorhombic perovskite-type $LaFeO_3$, while the other is a compound, $LaFe_{12}O_{19}$, with a magnetoplumbite structure. The latter is stable at temperatures between 1380 and 1421 °C. Cassedanne and Forestier[2] have also studied the Fe_2O_3–La_2O_3 system at temperatures from 900 to 1300 °C in air, and determined the cell constants of $LaFeO_3$.

One objective of the present study is to determine the standard free energy of the formation of $LaFeO_3$ on the basis of precise phase equilibria in the Fe–Fe_2O_3–La_2O_3 system at 1204 °C by changing the oxygen partial pressure from one to $10^{-15.75}$ atm under one atmospheric total pressure.

Experimental

Since the experimental methods and apparatus used in this study are the same as those described elsewhere,[3,4] a brief description will suffice for the general procedure.

A vertical quench furnace was used for every equilibrium run under a controlled oxygen partial pressure at 1204 °C. The atmospheres of the desired oxygen partial pressures were obtained by using CO_2–H_2 mixtures. Every value of P_{O_2} was measured by means of a solid electrolyte cell composed of $(ZrO_2)_{0.85}(CaO)_{0.15}$.[5] The calculated values of P_{O_2} based on the thermochemical data[6] and the measured ones showed a very good consistence within ±0.01 in terms of $\log P_{O_2}$. The funance temperature was measured by means of a Pt-87%Pt13%Rh thermocouple calibrated against the gold point; it was kept constant within ±1 °C.

A guaranteed reagent, Fe_2O_3, metallic iron powder (99.98%), and optical-grade La_2O_3 were used as the starting materials. The mixture of Fe_2O_3/La_2O_3 or Fe/La_2O_3 was primarily calcined at 1300 °C, then it was ground finely in an agate mortar and heated again at 1300 °C for 20 hr in air. The sintered material thus obtained was put into an alumina crucible, and the weight change was followed thermogravimetrically with an automatic balance at every controlled P_{O_2} value at 1204 °C. The equilibrated specimens were quenched rapidly, as has been described before,[3,4] and the phases present were identified by an X-ray powder method.

Results and Discussion

The phase equilibria obtained in the present study are illustrated in Fig. 1. No solubility of the lanthanum

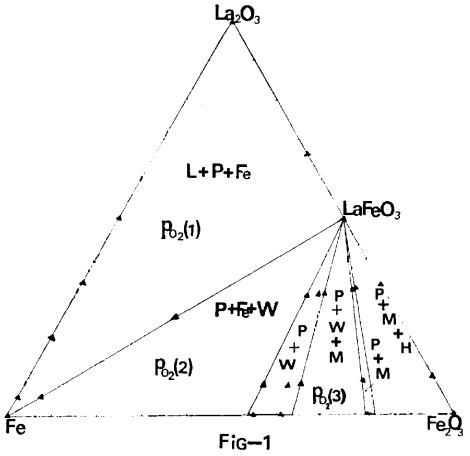

Fig-1

Fig. 1. Phase diagram of the Fe–Fe_2O_3–La_2O_3 system at 1204 °C.
L: La_2O_3, P: $LaFeO_3$, Fe: γ-iron, W: wüstite, M: magnetite, H: hematite.
$-\log P_{O_2}(1)=13.57$, $-\log P_{O_2}(2)=11.92$, $-\log P_{O_2}(3)=9.12$
where $P_{O_2}(1)$, $P_{O_2}(2)$, and $P_{O_2}(3)$ mean the equilibrium oxygen partial pressures over the three phases L+P+Fe, P+Fe+W, and P+W+M, respectively.

ion in the hematite, wüstite, and metallic iron phases was observed within present limits of experimental error. The La_2O_3 phase was stable in reducing atmospheres below $10^{-15.75}$ atm P_{O_2} without any deviation from the stoichiometry.

A perovskite-type compound, $LaFeO_3$, was stable in the range of oxygen partial pressures from one to $10^{-13.57}$ atm P_{O_2}, at which point $LaFeO_3$ was decomposed to form metallic iron and La_2O_3. The equilibrium state may be written as follows at an oxygen partial pressure of $10^{-13.57}$ atm:

$$1/2La_2O_3(s) + Fe(s) + 3/4O_2(g) = LaFeO_3(s) \qquad (1)$$

The existence of ferric iron in the $LaFeO_3$ structure under such an extremely low oxygen partial pressure may be attributed to the stable lattice energy of the perovskite-type structure, and also to the fact that the association of the oxygen ion with the La^{3+} ion in the structure has a profound influence upon the bonding between Fe^{3+} and oxygen ions.

The lattice constants of $LaFeO_3$ equilibrated with Fe_2O_3 and with La_2O_3 are almost identical within the limits of experimental errors (see Table 1). On the basis of these X-ray data, together with the thermogravimetric results, it may be safely said that the $LaFeO_3$ phase exists only as a stoichiometric compound under the present experimental conditions.

Since the La_2O_3, metallic iron, and $LaFeO_3$ phases

Table 1. Lattice constants of $LaFeO_3$
(Space group: D_{2h}^{16}–Pbnm, distorted Perovskite structure)

Lattice constant (A)	$LaFeO_3$ equilibrated with		$LaFeO_3$ pure phase	$LaFeO_3$[a]
	La_2O_3	Fe_2O_3		
a	5.566	5.558	5.553	5.556
b	5.557	5.557	5.560	5.565
c	7.846	7.856	7.865	7.862
$V(A^3)$	242.7	242.7	242.8	243.1

a) After Ref. 9.

are all stoichiometric at 1204 °C, the standard free energy of the formation of $LaFeO_3$ from La_2O_3, Fe, and oxygen may be directly calculated on the bais of Eq. (1) as follows:

$$\Delta G^\circ(1) = -3/4RT \ln P_{O_2}(1)$$
$$= -68700 \pm 200 \text{ cal} \cdot \text{mol}^{-1}$$

where R means the gas constant and T is the absolute temperature. The experimental error was estimated on the basis of the fluctuations of both temperature and oxygen partial pressure during the present study. In addition, as is shown in Fig. 1, the equilibrium oxygen partial pressures, $P_{O_2}(2)$ for metallic iron and wüstite, and $P_{O_2}(3)$ for wüstite and magnetite, were identical with those obtained by Darken and Gurry.[7,8]

The authors are grateful to Dr. Mitsuoki Nakahira and Mr. Jiichiro Yoshimoto, National Institute for Researches in Inorganic Materials, for their many useful discussions, and to Mr. Kenzo Kitayama, Tokyo Institute of Technology, who assisted in the present study.

References

1) V. L. Moruzzi and M. W. Shafer, *J. Amer. Ceram. Soc.*, **63**, 367 (1960).
2) J. Cassedane and H. Forestier, *C. R. Acad. Sci. Paris*, **250**, 2898 (1960).
3) T. Katsura and M. Hasegawa, This Bulletin, **40**, 561 (1960).
4) T. Katsura and A. Muan, *Trans. Met. Soc. AIME*, **230**, 77 (1964).
5) K. Hirota, This Bulletin, **42**, 1892 (1969).
6) "JANAF Thermochemical Tables," U.S. Department of Commerce, N.B.S. Institute for Applied Technology, Distributed by Clearinghouse. Aug. 1965.
7) L. S. Darken and R. W. Gurry, *J. Amer. Chem. Soc.*, **67**, 1398 (1945).
8) L. S. Darken and R. W. Gurry, *ibid.*, **68**, 798 (1946).
9) S. Geller and E. A. Wood, *Acta Crystallogr.*, **9**, 561 (1956).

BULLETIN OF THE CHEMICAL SOCIETY OF JAPAN, VOL. 47(7), 1803—1804 (1974)

The Synthesis of Methylthio- and Bis(methylthio)phenazine Derivatives

Masao TADA

The Research Institute for Tuberculosis, Leprosy and Cancer, Tohoku University, Hirosemachi, Sendai 980

(Received October 6, 1973)

Synopsis. A number of methylthio- and bis(methylthio)phenazine derivatives have been prepared by the reactions of various halogenophenazines and their *N*-oxides with sodium methyl sulfide.

Phenazine derivatives have received much attention because of their potential biological activities.[1] In previous paper,[2-4] the syntheses of piperidino-, morpholino-, and carboxymethylthiophenazines were reported. This note will describe the preparation of methylthiophenazines. Kidani *et al.*[5] reported that 1- and 2-methylthiophenazine were prepared from 1- and 2-phenazine isothiouronium chloride respectively. Recently 1-methylthiophenazine 5-oxide was derived from *N*-acyl-2'-methylthio-2-nitrodiphenylamine by a photochemical reaction.[6] In the present work, methylthio- and bis(methylthio)phenazines were prepared by nucleophilic displacement on the corresponding halogenophenazine derivatives.

The reactions of monohalogenophenazines, their *N*-oxides, and *N,N'*-dioxides with an equimolecular quantity of sodium methyl sulfide gave the corresponding methylthiophenazine derivatives in good yields. The reactions of dihalogenophenazines, their *N*-oxides, and *N,N'*-dioxides with a two-molar quantity of the sulfide gave the corresponding bis (methylthio)phenazine derivatives. In these reactions, the *N*-oxides, and *N,N'*-dioxides underwent a partial elimination of the oxide group to form the desired methylthiophenazines and their *N*-oxides respectively. In the presence of an excess of the reagent, the replacement reaction of the halogenophenazine *N*-oxide or *N,N'*-dioxide is accompanied by the removal of the oxide group to give the methylthio compound, as was found during substitution with sodium mercaptoacetate.[4,7] The results of the deoxygenation reactions observed during the nucleophilic displacement of halogen atoms of the monohalogenophenazine *N*-oxides are summarized in Table 1. By these replacement reactions, all the isomers of methylthio- and bis(methylthio)-phenazine could be prepared from the corresponding halogenophenazine derivatives.

The results of the series of reactions show that the halogen atoms of the mono- and dihalogenophenazines are easily displaced with the methyl sulfide, in

TABLE 1. REACTION OF HALOGENOPHENAZINE *N*-OXIDES WITH METHANETHIOL

Halogeno-phenazine 5-oxide	(Product Yield,[a] %) Methylthio-phenazine	Its oxide	Its dioxide
1-Cl	4	87	
	98		
2-Cl	18	79	
	98		
2-Br	8	90	
	99		
3-Cl	2	95	
	98		
3-Br	1	97	
	98		
2-Cl[b]	2	8	76
	81	1	
2-Br[b]	1	3	87
2-Cl, 7-OMe	16	74	
	63		

a) The numerical data in the upper column are the yield when the reactions are run in the equimolecular quantity of the thiol, and those in the lower column are the yield when the reactions are run in five molar quantity of the reagent.
b) This compound is 5,10-dioxide.

TABLE 2. SYNTHESES AND PROPERTIES OF METHYLTHIO- AND BIS(METHYLTHIO)PHENAZINE DERIVATIVES

Compound: Ring	Substituent	Mp (°C)	Synth. method	Reaction time (hr)	Yield (%)
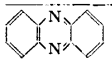	1-SMe	173—174[a]	A, F	10, 0.1	98, 86
	1-SMe, 6-OMe	227—228	A	10	79
	2-SMe	159—160[b]	A, B, F	5, 4, 0.1	98, 79, 96
	2-SMe, 7-OMe	211—212	A, F	6, 0.2	63, 85
	2-SMe, 9-OMe	132—133	A	10	81
	2-SMe, 9-Me	132—133	A	8	90
	1,2-Bis(SMe)	161—162	C, F	10, 0.2	92, 97
	1,3-Bis(SMe)	185—186	C, F	10, 0.2	85, 88
	1,4-Bis(SMe)	264—265	C	8	92
	1,6-Bis(SMe)	270—271	C	10	93
	1,7-Bis(SMe)	184—185	B	10	83
	1,8-Bis(SMe)	190—191	C, F	10, 0.2	92, 90
	1,9-Bis(SMe)	225—226	C	10	88
	2,3-Bis(SMe)	123—125	C	10	90
	2,7-Bis(SMe)	217—218	C	10	91
	2,8-Bis(SMe)	200—201	C	10	91
	1-SO_2Me	230—231	D, F	3, 0.2	85, 87
	2-SO_2Me	223—224	D, F	2.5, 0.3	85, 98
	2-SO_2Me, 7-OMe	220—222	D, F	2, 0.2	70, 83
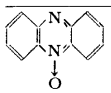	1-SMe	208—209(dec)[c]	B	7	87
	2-SMe	147—148	B	4	90
	3-SMe	171—172	B	4	97
	2-SMe, 7-OMe	187—188	B	6	74
	3-SMe, 8-OMe	195—196	B	4	3
	1,2-Bis(SMe)	181—182	B	8	57
	1,3-Bis(SMe)	223—224(dec)	B	7.5	71
	1,7-Bis(SMe)	234—235(dec)	B	10	15
	1,8-Bis(SMe)	200—201	B	8	66
	1,9-Bis(SMe)	242—243(dec)	B	8	50
	2,3-Bis(SMe)	209—210	B	8	37
	2,7-Bis(SMe)	210—211	B	8	37
	2,8-Bis(SMe)	213—214(dec)	B	8	51
	1-SO_2Me	241—242(dec)	E, D	18, 3	86, 68
	2-SO_2Me	207—208	D	3	91
	3-SO_2Me	187—188	D	3	90
	2-SO_2Me, 7-OMe	217—218(dec)	D	2	64
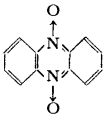	2-SMe	187—188(dec)	B	4	87
	2-SMe, 7-OMe	218—219(dec)	B	4	86
	2,3-Bis(SMe)	225—226(dec)	B	8	30
	2,7-Bis(SMe)	222—223(dec)	B	7	32
	2,8-Bis(SMe)	228—229(dec)	B	8	33
	2-SO_2Me	202—203(dec)	E, D	18, 5	84, 78
	2-SO_2Me, 7-OMe	205—206(dec)	E, D	18, 2	90, 83

a) Reported mp: 172—173°C.[5] b) Reported mp: 159.5—160°C.[5] c) Reported mp: 213°C.[6]

contrast to the cases of the alcoholysis[8] and the hydrolysis,[8,9] as can be expected in view of the high nucleophilicity of the sulfide.[10] These substitutions are especially useful for the identification of the halogenophenazine derivatives.

The methylthiophenazine *N*-oxides and *N,N'*-dioxides were deoxygenated more effectively by treatment with zinc powder in acetic acid to give the methylthiophenazines, from which the sulfones were then prepared by oxidation with a limited amount of hydrogen peroxide in acetic acid. The oxidation of these compounds with an excess of hydrogen peroxide afforded the methylsulfonylphenazine *N*-oxide or *N,N'*-dioxide, which was subsequently converted into the methylsulfonylphenazine by reduction with zinc powder in acetic acid.

The syntheses and properties of the methylthio- and bis(methylthio)phenazine derivatives thus obtained are listed in Table 2.

Experimental

All the melting points are uncorrected.

Starting Materials. The following compounds were prepared by the methods given in the literature: phenazine (1-chloro-,[8] 1-chloro-6-methoxy-,[11] 2-bromo-,[12] 2-chloro-,[8] 2-chloro-7-methoxy-,[13] 2-chloro-9-methoxy-,[11] 2-chloro-9-methyl-,[14] 1,2-dichloro-,[15] 1,3-dichloro-,[15] 1,4-dichloro-,[15] 1,6-dichloro-,[16] 1,8-dichloro-,[17] 1,9-dichloro-,[17] 2,3-dichloro-,[15] 2,7-dibromo-,[18] 2,7-dichloro-,[9] and 2,8-dichloro-[15]), phenazine 5-oxide (1-chloro-,[8] 2-bromo-,[12] 2-chloro-,[8] 2-chloro-7-methoxy,[8] 3-bromo-,[12] 3-chloro-,[8] 1,2-dichloro-,[15] 1,3-dichloro-,[15] 1,7-dichloro-,[17] 1,8-dichloro-,[17] 1,9-dichloro-,[17] 2,3-dichloro-,[17] 2,7-dibromo-,[18] 2,7-dichloro-,[8] and 2,8-dichloro-[15]), and phenazine 5,10-dioxide (2-bromo-,[19] 2-chloro-,[9] 2-chloro-7-methoxy-,[19] 2,3-dichloro-,[17] 2,7-dichloro-,[8,9] and 2,8-dichloro-[17]).

Syntheses of Methylthio- and Bis(methylthio)phenazine Derivatives. These compounds were prepared by the six general methods (A, B, C, D, E, and F). The mthods, the reaction times, the yields, and the melting points, for each compound are summarized in Table 2. All the products had satisfactory elemental analyses (C, H, and N).

Method A. To a hot solution of the halogenophenazine derivative (10 mmol) in ethanol (80—500 ml), a 20% aqueous solution of sodium methyl sulfide (50 mmol) was added. After refluxing, the hot mixture was diluted with water. The crystals thereby separated were chromatographed over alumina, using benzene as the solvent, and then recrystallized from an appropriate solvent.

Method B. This method is the same as Method A except that the theoretical quantity of the sulfide is used.

Method C. This method is the same as those above except that a ten molar quantity of the sulfide is used.

Method D. A solution of methylthiophenazine (5 mmol) in a 30% aqueous solution (2 ml) of hydrogen peroxide and acetic acid (50 ml) was warmed at 55 °C and then poured into water. To the aqueous solution, sodium bicarbonate (15 g) was added. The crystals thus separated were recrystallized from an appropriate solvent.

Method E. To a solution of methylthio- or methylsulfonylphenazine (5 mmol) in acetic acid (100—200 ml) and acetic anhydride (10 ml), a 30% aqueous solution (20 ml) of hydrogen peroxide was added. The mixture was warmed at 55 °C and then poured into water (1—1.5 l). The crystals thus separated were recrystallized from an appropriate solvent.

Method F. Into a solution of the pheanzine *N*-oxide (2 mmol) in acetic acid (20—50 ml), zinc powder (1—1.5 g) was stirred in small portions. The mixture was then heated on a water bath and filtered while hot. After the ordinary treatment, the recrystallization of the product from an appropriate solvent afforded the phenazine.

The author wishes to express his gratitude to Miss Mieko Sasaki for her assistance in these experiments.

References

1) For example, K. Katagiri, H. Endo, M. Tada, and Y. Niinomi, *Ann. Rept. Shionogi Res. Lab.*, **18**, 130 (1968); H. Endo, M. Tada, and K. Katagiri, *Sci. Rep. Res. Inst. Tohoku Univ., Ser. C*, **16**, 18 (1969).

2) H. Endo, M. Tada, and K. Katagiri, This Bulletin, **42**, 502 (1969).

3) H. Endo, M. Tada, and K. Katagiri, *ibid.*, **42**, 506 (1969).

4) H. Endo, M. Tada, and K. Katagiri, *ibid.*, **42**, 566 (1969).

5) Y. Kidani and K. Ukai, *Chem. Pharm. Bull.* (Tokyo), **14**, 293 (1966).

6) Y. Maki, T. Hosokami, and M. Suzuki, *Chem. Comm.*, **1972**, 693.

7) J. K. Landquist, *J. Chem. Soc.*, **1956**, 2550.

8) I. J. Pachter and M. C. Kloetzel, *J. Amer. Chem. Soc.*, **74**, 971 (1952).

9) D. L. Vivian, *ibid.*, **73**, 457 (1951).

10) N. B. Chapman, "Rodd's Chemistry of Carbon Compounds," 2nd ed., Vol. III. Part A, ed. by S. Coffey, Elsevier Publishing Co., Amsterdam (1971), p. 106.

11) I. Yoshioka and R. Ashikawa, *Yakugaku Zasshi*, **79**, 896 (1959).

12) V. P. Chernetskii and A. I. Kiprianov, *Zh. Obshch. Khim.*, **26**, 3032 (1956); through *Chem. Abstr.*, **51**, 8762 (1957).

13) D. L. Vivian, G. Y. Greenberg, and J. L. Hartwell, *J. Org. Chem.*, **16**, 1 (1951).

14) S. Maffei, S. Pietra, and A. M. Rivolta, *Ann. Chim.* (Rome), **43**, 611 (1953).

15) V. P. Chernetskii and A. I. Kiprianov, *Zh. Obshch. Khim.*, **23**, 1743 (1953); through *Chem. Abstr.*, **48**, 13695 (1954).

16) I. J. Pachter and M. C. Kloetzel, *J. Amer. Chem. Soc.*, **73**, 4958 (1951).

17) H. Otomasu, *Chem. Pharm. Bull.*, **3**, 365 (1955).

18) E. Banberger and W. Ham, *Ann. Chem.*, **382**, 82 (1911).

19) H. Endo, M. Tada, and K. Katagiri, *Sci. Rep. Res. Inst. Tohoku Univ., Ser. C*, **14**, 164 (1968).

BULLETIN OF THE CHEMICAL SOCIETY OF JAPAN, VOL. 47(7), 1805—1806 (1974)

The Reaction of Dicarboximides with Benzonitrile in Liquid Ammonia

Choji KASHIMA, Makoto YAMAMOTO,* Susumu KOBAYASHI, and Noboru SUGIYAMA
Department of Chemistry, Tokyo Kyoiku University, Otsuka, Tokyo 112

(Received November 10, 1973)

Synopsis. Acyclic dicarboximides were treated with benzonitrile in the presence of sodium amide to give 4-hydroxypyrimidines. However, the reaction of succinimide with benzonitrile gave 5-hydroxy-2-phenyl-2-pyrroline-3-carboxamide. Also, glutarimide gave a similar product.

In a previous paper[1] we reported that β-diketone condensed with benzonitrile (**1**) to give 4(1*H*)-pyridone directly. In this reaction it was assumed that an intermediately-formed imino-β-diketone was dehydrocyclized to 4(1*H*)-pyridone. A similar reaction has been shown in the reaction of **1** with ethyl acetoacetate.[2]

Diacetimide (**2**), *N*-acetylbenzamide (**3**), ethyl *N*-acetylcarbamate (**4**), succinimide (**5**) and glutarimide (**6**) all have the same $-CH_2CONHCO-$group. Since this group is expected to behave in liquid ammonia much like the $-CH_2COCH_2CO-$group, these compounds were subjected to a reaction with **1** in the presence of alkali amide in liquid ammonia.

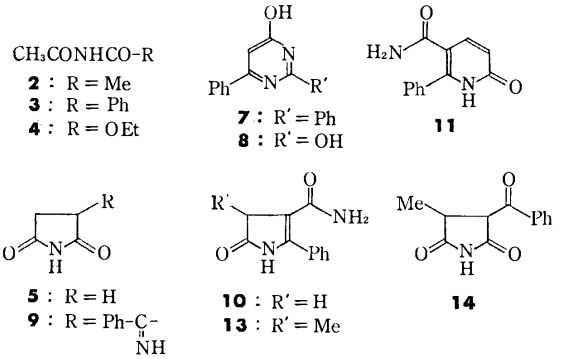

Fig. 1.

Compound **2** did not react with **1** in the presence of sodium amide in liquid ammonia. However, **3** reacted with an equimolar **1** in the presence of three molar equivalents of sodium amide to give 4-hydroxy-2,6-diphenylpyrimidine (**7**). The structure of **7** was verified by comparing the spectral data of **7** with those described in the literature.[3] Compound **7** was also identified with the product which was obtained by the reaction of ethyl benzoylacetate with benzamidine hydrochloride. Ethyl *N*-acetylcarbamate (**4**) also reacted with **1** in the presence of three molar equivalents of potassium amide in liquid ammonia to give 10.8% of 2,4-dihydroxy-6-phenylpyrimidine (**8**). The structure of **8** was identified by mean of a comparison with an authentic sample[4] and was also supported by the infrared spectrum.

Compound **5** was allowed to react with equimolar **1** in the presence of three molar equivalents of sodium amide in liquid ammonia. However, instead of the expected product, *i.e.*, 3-benzimidoylsuccinimide (**9**),[5] colorless needles were obtained in a 58.2% yield. The infrared spectrum of this compound showed three amide bands, at 3450, 3320, and 3300 cm^{-1}, and two carbonyl bands, at 1730 and 1675 cm^{-1}. The NMR spectrum was assignable for the signals at δ 3.33 and 7.40 ppm for the methylene and aromatic protons; moreover, the amino protons were observed at δ 8.13 and 11.98 ppm, but they disappeared with the use of deuterium oxide. From these spectral data and the elemental analysis, the structure of this compound was proved to be 5-oxo-2-phenyl-2-pyrroline-3-carboxamide (**10**). When glutarimide (**6**) and **1** were treated under conditions similar to those described above, 3,4-dihydroxy-6-phenyl-2(1*H*)-pyridone-5-carboxamide (**11**) was obtained in a 35% yield. The structure of **11** was proved by the spectral data and the elemental analysis. Although this type of synthesis is known in the literature,[6] our synthetic method is still simpler and more useful.

In order to investigate the change in the reactivity of succinimide with a substituent at the 2-position, the reaction of 2-methylsuccinimide (**12**) with **1** was carried out. However, instead of the expected pyrrolinecarboxamide (**13**), 3-benzoyl-2-methylsuccinimide (**14**) was obtained in a 22% yield.

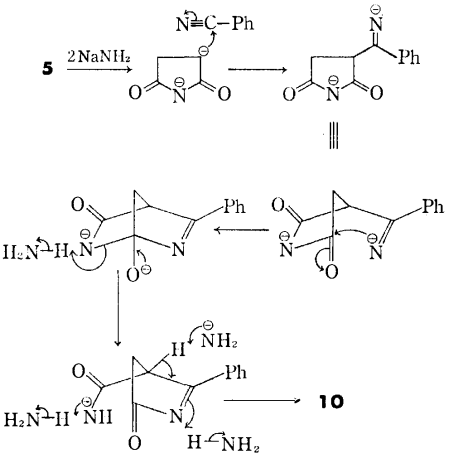

Scheme 1.

The formation mechanism of **10** from **5** and **1** was speculated as follows: Imide **5** reacted with **1** to give **9**, followed by recyclization to **10**, as is illustrated in Scheme 1. On the reaction of **12** and **1**, we supposed that the benzimidoyl intermediate was also formed first and was then hydrolyzed to **14**, because of some steric

* Present Address: Department of Chemistry, Saga University, Saga-shi 840.

hindrance and inductive effect of the methyl group at the cyclization stage.

Experimental

4-Hydroxy-2,6-diphenylpyrimidine (7). *Method A*: To a solution of 0.15 mol of sodium amide in about 300 ml of liquid ammonia in a three-necked flask, we added 0.05 mol (8.15 g) of **3**. After 1 hr's stirring, 0.05 mol (5.2 g) of **1** in 30 ml of anhydrous ether was added. The mixture was then stirred for an additional 3 hr at −33 °C and then neutralized with 8.1 g of solid ammonium chloride. The liquid ammonia was driven off rapidly, and 100 ml of dilute hydrochloric acid was added. The white precipitates thus obtained were collected, washed with ether, and recrystallized from hot pyridine to give 2.80 g (22.6%) of **7** as colorless needles; mp 284—286 °C (lit, 289—290 °C[5]).

Method B: Compound **7** was also prepared by the following method. To a solution of 0.2 mol of sodium amide in 300 ml of liquid ammonia, we added 0.05 mol (8.0 g) of benzamidine hydrochloride dihydrate.[7] After 1 hr's stirring, 0.05 mol (9.6 g) of ethyl benzoylacetate in 30 ml of anhydrous ether was added, drop by drop. The mixture was then stirred for an additional 3.5 hr at −33 °C and subsequently treated as above.

2,4-Dihydroxy-6-phenylpyrimidine (8). According to Method A, **8** was synthesized from 0.15 mol of potassium amide, 0.05 mol (6.6 g) of **4** and 0.05 mol (5.2 g) of **1**. Yield, 1.02 g (10.8%); yellowish white prisms (from hot water); mp 269—271 °C (lit, 270 °C[6]).

Reaction of **2** *with* **1**. According to Method A, 0.05 mol of **2**, 0.05 mol of **1**, and 0.15 mol of sodium amide were treated in liquid ammonia. No pyrimidine compound could be detected.

5-Oxo-2-phenyl-2-pyrroline-3-carboxamide (10). According to Method A, 0.15 mol of sodium amide, 0.05 mol (4.95 g) of **5**,[8] and 0.05 mol of **1** were treated in liquid ammonia. After neutralization with 8.1 g of solid ammonium chloride, the liquid ammonia was completely evaporated. Then 400 ml of ethanol was added to the residue, and the insoluble substance was dissolved in 100 ml of pyridine. The ethanol solution was then concentrated to about 50 ml under reduced pressure to yield 2.98 g of a white precipitate after standing overnight. The pyridine solution was evaporated to dryness under reduced pressure to give 2.90 g of a white substance. The combined precipitate (5.88 g, 58%) was again recrystallized from ethanol to give pure **10** as colorless needles; mp 197—197.5 °C. Found: C, 65.36; H, 5.16; N, 13.76%. Calcd for $C_{11}H_{10}N_2O_2$: C, 65.33; H, 4.98; N, 13.86%. UV: λ_{max}^{EtOH} 230 (ε 5100) and 314 nm (14700).

3,4-Dihydro-6-phenyl-2(1H)-pyridone-5-carboxamide (11). According to Method A, **11** was prepared from 0.15 mol of sodium amide, 0.05 mol of **1**, and 0.05 mol (5.65 g) of **6**.[9] After the evaporation of the liquid ammonia, we added 300 ml of hot pyridine to the residue; after filtration, the filtrate was concentrated to dryness, and to this residue we added a benzene–ethanol mixture. The resulting insoluble substance (2.75 g) was filtered, and the filtrate was concentrated. The residue was chromatographed on a silica gel (Merck 7734, 0.05—0.2 mm) column using a benzene–ethyl acetate (1: 1 v/v) mixture. The fraction which showed an R_f value of 0.56 on silica gel (Wakogel B-5) thin layer chromatography (tlc) with the benzene–ethyl acetate (1: 1 v/v) mixture was collected and concentrated to give a white solid (1.03 g), which was proved to be the same compound as the above insoluble substance by the results of tlc and by the spectral data. The combined product (3.78 g, 35.0%) was recrystallized from hot pyridine to give pure **11** as colorless crystals; mp 231—232 °C. Found: C, 66.42; H, 5.66; N, 13.19%. Calcd for $C_{12}H_{12}N_2O_2$: C, 66.65; H, 5.59; N, 12.96%. IR (KBr): 3410, 3220, 3130, 1700, 1650, 1635, 1615, and 695 cm^{-1}. UV: λ_{max}^{EtOH} 225 (ε 10600) and 281 nm (8030). NMR: $\delta^{pyridine-d_5}$ 2.80 (m, 4H), 7.05 (broad s, 2H), 7.40 (m, 5H), and 10.90 ppm (broad s, 1H).

3-Benzoyl-2-methylsuccinimide (14). According to Method A, **14** was obtained from 0.15 mol of sodium amide, 0.05 mol of **1**, and 0.05 mol of **12**. After the evaporation of the liquid ammonia, to the residue we added 200 ml of dilute hydrochloric acid and the resulting white precipitate (**14**) was collected. The filtrate was extracted with two 200 ml portions of ether. The ether extracts were combined and washed with water and dried over anhydrous sodium sulfate. After evaporating the solvent, we added an *n*-hexane–benzene (1: 1 v/v) mixture to the viscous product. The resulting precipitate was recrystallized from benzene to give 2.40 g (22.1%) of **14** as colorless leaflets; mp 147—149 °C. Found: C, 66.26; H, 5.08; N, 6.56%. Calcd for $C_{12}H_{11}NO_3$: C, 66.35; H, 5.10; N, 6.45%. IR (KBr): 3075, 3200, 1780, 1710, 1670, and 700 cm^{-1}. UV: λ_{max}^{EtOH} 250 (ε 13100) and 287 nm (2420). NMR: $\delta^{acetone-d_6}$ 1.77 (d, 3H), 3.22—3.68 (oct, 1H), 4.87 (d, 1H), 7.31—7.81 (m, 3H), 8.04—8.22 (m, 2H) and 10.15 ppm (broad s, 1H, disappeared by D_2O).

References

1) N. Sugiyama, M. Yamamoto, S. Kobayashi, and C. Kashima, This Bulletin, **42**, 2389 (1969).

2) N. Sugiyama, M. Yamamoto, S. Kobayashi, and C. Kashima, *ibid.*, **45**, 296 (1972).

3) G. Shaw and G. Sugowdz, *J. Chem. Soc.*, **1954**, 665.

4) T. B. Johnson and E. H. Hemingway, *J. Amer. Chem. Soc.*, **37**, 381 (1915).

5) D. R. Bryant and C. R. Hauser, *ibid.*, **83**, 3468 (1961).

6) Y. Hayashi and T. Sakan, *Nippon Kagaku Zasshi*, **81**, 1894 (1960).

7) A. W. Dox, "Organic Syntheses," Coll. Vol. I (1941), p. 5.

8) H. T. Clarke and L. D. Behr, "Organic Syntheses," Coll. Col. II (1942), p. 562.

9) G. Paris, L. Berlinguet, and R. Gaudry, "Organic Syntheses," Coll. Vol. IV (1962), p. 496.

BULLETIN OF THE CHEMICAL SOCIETY OF JAPAN, VOL. 47(7), 1807—1808 (1974)

A Platinum Complex Bound to Iodinated Polystyrene by a Platinum-Carbon σ-Bond

Noboru KAWATA, Tsutomu MIZOROKI, and Atsumu OZAKI

Research Laboratory of Resources Utilization, Tokyo Institute of Technology, Ohokayama, Meguro-ku, Tokyo 152

(Received December 28, 1973)

Synopsis. A platinum complex bound to iodinated polystyrene was prepared by the reaction of $Pt(P\phi_3)_4$ with iodinated polystyrene. The reaction of the synthesis was confirmed by means of direct oxidative addition of aryl iodide to $Pt(P\phi_3)_4$.

Recently much attention has been paid to the immobilizing of a soluble organotransition metal complex catalyst by fixing it on a polymer, not only from a practical point of view, but also for examining the effect of polymer ligand on the catalytic activity and selectivity. Polystyrene containing phosphorus, nitrogen or cyclopentadiene has been widely used to immobilize transition metal complexes such as $RhCl(CO)(P\phi_3)_2$ ($\phi=C_6H_5$)[1-3] and $TiCp_2Cl_2$ ($Cp=C_5H_5$)[4] through the coordination bond of metal-phosphine, metal-nitrogen or metal-cyclopentadiene.

In the preceding paper,[5] it was reported that treatment of a halogenated polystyrene with tetrakis(triphenylphosphine) nickel (0) or palladium(0) gave an insoluble nickel(II) or palladium(II) complex combined to polystyrene by metal-carbon σ-bond as follows:

$$\}\text{-}C_6H_4X + M(P\phi_3)_4 \longrightarrow \}\text{-}C_6H_4\text{-}\underset{\displaystyle P\phi_3}{\overset{\displaystyle P\phi_3}{M}}\text{-}X + 2P\phi_3$$

(M=Ni or Pd, X=Br or I)

This method of immobilizing metal complexes was extended to the reaction of tetrakis(triphenylphosphine)-platinum(0) (denoted by [I]) with iodinated polystyrene. An insoluble polystyrene containing platinum complex was obtained. The present paper reports on the oxidative addition of iodinated polystyrene to complex [I].

Platinum Complex Supported on Iodinated Polystyrene. To a benzene solution (150 ml) of iodinated polystyrene (3.0 g, average P.D. 1100, 96.4% iodination on *para*-position) prepared according to the method given in the literature[6] was added another benzene solution (100 ml) of [I] (5 g) under nitrogen atmosphere. The mixture was warmed up to 70—80 °C and kept for 5—6 hr with stirring, during which a precipitate was obtained. The precipitate was washed three times with benzene and twice with *n*-hexane, and then dried under vacuum. Pale yellow powder (3.6 g), insoluble in common solvents and stable in the air at ambient temperature, was obtained. The amount of platinum supported on iodinated polystyrene could be estimated to be about 4 atoms per ten phenyl rings by assuming that platinum was bound to the polymer as $\}\text{-}C_6H_4\text{-}Pt(P\phi_3)_2I$. ^{31}P-FT-NMR[7] of the platinum-polystyrene complex suspended in methylene dichloride showed a fairly sharp absorption (26.7 ppm, $J_{Pt-P}=3066$ Hz) in a low field in reference to free triphenylphosphine. This indicates that the platinum-polystyrene complex has *trans*-square planar structure, since only one absorption and one large coupling constant of J_{Pt-P} were observed. It is to be noted that the local magnetic field around the platinum atom is well averaged out in the solvent, since NMR absorptions of solid materials are usually too broad to be detected due to local magnetic fields.

In order to clarify the synthesis reaction and to characterize the platinum-polystyrene complex, a direct oxidative addition of aryl iodide to complex [I] was attempted. The known method of preparing *trans*-bis(triphenylphosphine)σ-phenyl(halo) platinum(II) complexes is to utilize the thermal desulfurylation of $C_6H_5SO_2Pt(P\phi_3)_2X$,[8] which can be prepared from the oxidative addition of $C_6H_5SO_2X$ to complex [I]. The direct oxidative addition of phenyl halide to [I] has not been reported. This seems to be a difficult reaction, although $Pt(PEt_3)_4$ ($Et=C_2H_5$), which is regarded to have a more nucleophilic nature, is subjected to the oxidative addition of phenyl halide.[9] It was found, however, that σ-aryl platinum(II) complexes are readily synthesized only by warming the mixture of [I] and aryl iodide in benzene.

Oxidative Addition of Aryl Iodide to Complex [I]. A commercial iodobenzene (36 mmol) was added to a

Table 1. Characterization of bis(triphenylphosphine) σ-aryl(iodo)platinum(II)

Complex	Color	Found (%)			Calcd (%)			P-NMR (ppm[a])	J_{Pt-P} (Hz)	Yield[b] (%)
		C	H	I	C	H	I			
$C_6H_5Pt(P\phi_3)_2I$	White	55.1	3.95	13.5	54.6	3.79	13.8	27.2	3097	65
p-$C_6H_4CH_3Pt(P\phi_3)_2I$	White	55.9	3.98	13.1	55.1	3.94	13.6	26.9	3104	53
p-$C_6H_4NO_2Pt(P\phi_3)_2I$	Pale yellow	53.2	3.58 N(%): 1.29	12.7	52.1	3.51 N(%): 1.44	13.1	25.7	2971	71
p-$C_6H_4BrPt(P\phi_3)_2I$	White	51.1	3.51	20.2	50.3	3.39	20.7	26.4	3137	63
Pt Complex bound to polymer	Pale yellow	52.8	3.82	22.2				26.7	3065	

a) From free $P\phi_3$ in CH_2Cl_2. b) Based on the $Pt(P\phi_3)_4$ (mol) used.

benzene solution of [I] (4.5 g, 3.6 mmol) under nitrogen atmosphere. The solution was kept at 50—60 °C for 2—3 hr with stirring, during which a white crystal was deposited. The solution was decanted. The crystal was dissolved in hot benzene (200 ml), recrystallized by adding *n*-hexane, well washed with *n*-hexane, and then dried under vacuum. The same method was applied to *p*-tolyl, *p*-nitrophenyl, and *p*-bromophenyl iodide. There was practically no difference in the reactivity of these aryl iodides. No complex was obtained by the treatment with aryl bromide even at a higher temperature (80 °C), most of [I] being decomposed to metallic platinum. The results are summarized in Table 1. ^{31}P-FT-NMR of the complexes also shows that they all have the same *trans*-square planar structure as the platinum-polymer complex.

The authors wish to thank Mr. Y. Nakamura for his help in the NMR measurement.

References

1) R. H. Grubbs and L. C. Kroll, *J. Amer. Chem. Soc.*, **93**, 3061 (1972).
2) M. Capka, P. Svoboda, M. Cerney, and J. Hetfleje, *Tetrahedron Lett.*, **1971**, 4789.
3) J. P. Collman, L. S. Hegedus, M. P. Cooke, J. R. Norton, G. Dolcetti, and D. N. Marquardt, *J. Amer. Chem. Soc.*, **94**, 1789 (1972).
4) R. H. Grubbs, G. Gibbons, L. C. Kroll, W. D. Bond Jr., and C. H. Brubaker, Jr., *ibid.*, **95**, 2373 (1973).
5) N. Kawata, T. Mizoroki, A. Ozaki, and M. Ohkawara, *Chem. Lett.*, **1973**, 1165.
6) M. Ohkawara and K. Mizuta, *Kogyo Kagaku Zasshi*, **64**, 232 (1961).
7) Fourier Transform NMR (JEOL-JNM-PFT-100).
8) C. D. Cook and G. S. Jauhal, *Can. J. Chem.*, **45**, 301 (1967).
9) D. H. Gerlach, A. R. Kane, G. W. Parshall, J. P. Jesson, and E. L. Muetterties, *J. Amer. Chem. Soc.*, **93**, 3543 (1971).

BULLETIN OF THE CHEMICAL SOCIETY OF JAPAN, VOL. 47(7), 1809—1810 (1974)

Dissociation Constants of 2-Aminotropones

Kimiaki IMAFUKU, Yasuyoshi TAKATA,* and Hisashi MATSUMURA
Department of Chemistry, Faculty of Science, Kumamoto University, Kurokami, Kumamoto 860
(Received January 10, 1974)

Synopsis. The dissociation constants of 2-aminotropones were measured in 50% aqueous methanol at 20 °C and shown to be correlated by the Hammett equation with $\rho=3.40$. The difference between 4- and 6-substituents is discussed.

The dissociation constants of tropolone derivatives with a seven-membered ring structure have been reported[1] to be linearly correlated with Hammett's substituent constants. Furthermore, we have ourselves discussed[2] the Hammett relationships in the tropolone derivatives on the basis of a simple HMO method.

On the other hand, no systematic study of the dissociation of 2-aminotropones has been reported, although a few dissociation constants are known.[3]

This communication will deal with the measurements of the dissociation constants of 2-aminotropone derivatives (Fig. 1) and with their analysis by means of the Hammett relationships.

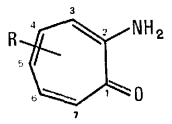

Fig. 1. 2-Aminotropones.

Results and Discussion

Dissociation Constants. The dissociation constants of 4-, 5-, and 6-substituted 2-aminotropones were determined spectrophotometrically in 50% aqueous methanol at 20 °C. The results expressed in terms of pK_a values are listed in Table 1, together with the Hammett substituent constants.[4]

TABLE 1. DISSOCIATION CONSTANTS OF 2-AMINOTROPONES

No.[a]	R	σ	pK_a
1	5-CH_3	−0.170	2.63
2	4-CH_3	−0.069	2.52
3	6-CH_3	−0.059[b]	2.36
4	6-CH=CH-Ph	−0.041[b]	2.30
5	H	0	2.16
6	4-CH=CH-Ph	0.025[c]	2.11
7	5-Cl	0.227	1.34

a) Numbering of substituents refers to that given in Fig. 2. b) Results in this work. c) Value in Ref. 8.

The 2-aminotropones show pK_a values between 2.63 (5-methyl) and 1.34 (5-chloro) and are less basic than the aniline derivatives. The pK_a values for the corresponding aniline derivatives are from 5.10 (*p*-methyl) to 3.98 (*p*-chloro).[5] This difference may be attributed to the electron-withdrawing effect of the carbonyl group adjacent to the amino group in the tropone ring.

The pK_a values for 2-amino-5-nitrotropone could not be measured, since the nitro group is a strong electron-attracting group ($\sigma_p=0.778$) and so reduced the basicity to $pK_a<1$.

Substituent Effects. When the pK_a values of 2-aminotropones are plotted against the substituent constants, the plot gives the straight line shown in Fig. 2. Here, the substituent constants, the σ_m and σ_p values, are respectively applied to the 4- and 5-positions in the tropone nucleus in the same manner as those of the tropolones.[1,2] The following equation was obtained by the least-squares method:

$$pK_a = 2.16-3.40\sigma \quad (r=0.982) \qquad (1)$$

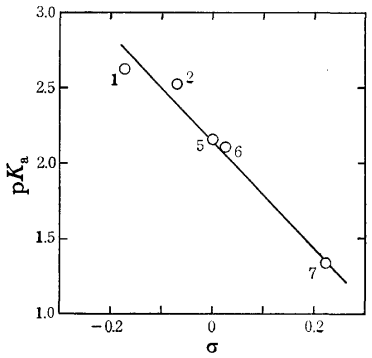

Fig. 2. The Hammett plot of pK_a.

It is of some interest to compare the ρ value obtained in the present work with those of tropolones, phenols, and anilines. The ρ value (3.40) for 2-aminotropones is comparable to that ($\rho=3.44$ in 30% ethanol at 25 °C) for anilines.[6] It has also been shown that the ρ value for tropolones ($\rho=2.68$ in water at 25 °C)[1] is comparable to that of phenols ($\rho=2.55$ in 48.9% ethanol at 20—22 °C).[7] The ratios of amino-substituted compounds to hydroxy-substituted compounds are 1.27 for troponoids and 1.35 for benzenoids. These ratios are almost equal.

4- and 6-Substituents. 4-Substituted tropolones show only one pK_a value, though they can exist in two non-equivalent tautomeric forms—as 4- and 6-substituted 2-hydroxytropones. On the other hand, 4- and 6-substituted 2-aminotropones were both obtained as pure materials, and the σ values for the 6-substituents could be estimated by using 6-substituted isomers.

The substituent constants for the 6-methyl and 6-styryl groups were estimated to be −0.059 and −0.041 respectively by using Eq. (1). The substituents in the 4- and 6-positions cannot conjugate with the

* Present address: Dainichi-seika Color & Chemicals Mfg. Co., Ltd., Iwata-shi, Shizuoka 438.

amino group; their effect is mainly due to the inductive effect.

As regards the methyl groups, the σ_6 value (−0.059) is larger than the $\sigma_4(\equiv\sigma_m)$ value (−0.069).[4] The electron-donating effect of the 6-methyl group decreases in comparison with that of the 4-methyl group. This may be attributed to the difference in distance between the methyl group and the amino group.

The 4-styryl group (σ_m=0.025)[8] decreased the basicity of 2-aminotropone by its inductive electron-attracting effect, while 6-styryl group enhanced the basicity to pK_a=2.30. The pK_a value gave σ_6=−0.041 for the 6-styryl group in the same manner as for the 6-methyl group. The resonance of the 6-styryl group with a carbonyl adjacent to the amino group enriches the electron density of the oxygen atom. Consequently, the hydrogen bonding of hydrogen in the amino group with the carbonyl oxygen atom is enhanced and the dissociation of the ammonium ion becomes difficult. This is consistent with the difference in $\nu_{C=O}$ values of the two series of 4- and 6-styryl-2-aminotropones.[9]

Experimental

Materials. The 2-aminotropones used for the measurements of the dissociation constants were prepared by the methods described in the references.

Their melting pointed are as follows: 2-Aminotropone, mp 107—108 °C (ref.[10,11] 106—107 °C); 4-methyl-2-aminotropone, mp 124.5—125.5 °C (ref.[12,13] 122—123 °C); 5-methyl-2-aminotropone, mp 109—111.5 °C (ref.[12] 105—107 °C); 6-methyl-2-aminotropone, mp 113.5—114.5 °C (ref.[12,14] 111—112 °C); 5-chloro-2-aminotropone, mp 160.5—161.5 °C (ref.[15] 157 °C); 4-styryl-2-aminotropone, mp 194—195 °C (ref.[16] 194.5—195 °C); 6-styryl-2-aminotropone, mp 137—138 °C (ref.[16,17] 137—138 °C).

Measurements of the Dissociation Constants. The dissociation constants of 2-aminotropones were measured spectrophotometrically in 50% aqueous methanol at 20 °C by the method of Albert and Serjeant.[18]

The absorption spectra were taken on a Hitachi EPS-3T spectrophotometer, while the pH values were measured by means of a Hitachi-Horiba pH meter.

The authors wish to thank Professor Tetsuo Nozoe and Sankyo Co. Ltd. for supply of tropolone.

References

1) N. Yui, *Sci. Repts. Tohoku Univ.*, I, **40**, 102, 114 (1956).
2) K. Imafuku and H. Matsumura, This Bulletin, **42**, 1772 (1969); **43**, 560 (1970).
3) S. Seto, T. Hiratsuka, and H. Toda, *Yakugaku Zasshi*, **89**, 1673 (1969).
4) H. H. Jaffe, *Chem. Rev.*, **53**, 191 (1953).
5) J. W. Smith, "The Chemistry of the Amino Group," ed. by S. Patai, Interscience, New York (1968), p. 182.
6) G. M. Bennett, G. L. Brooks, and S. Glastone, *J. Chem. Soc.*, **1934**, 1821.
7) S. Schwarzenbach and H. Egli, *Helv. Chim. Acta*, **17**, 1176, 1183 (1934); S. Schwarzehbach and E. Rudin, *ibid.*, **22**, 360 (1939).
8) J. K. Kochi and G. S. Hammond, *J. Amer. Chem. Soc.*, **75**, 3452 (1953).
9) K. Imafuku and H. Matsumura, This Bulletin, **46**, 199 (1973).
10) T. Nozoe, S. Seto, H. Takeda, S. Morosawa, and K. Matsumoto, *Proc. Japan Acad.*, **27**, 556 (1951); **28**, 192 (1952).
11) T. Nozoe, T. Mukai, and K. Takase, *Sci. Repts. Tohoku Univ.*, I, **39**, 164 (1956).
12) T. Sato, *Nippon Kagaku Zasshi*, **80**, 1167 (1959).
13) P. Akroyd, R. D. Haworth, and J. D. Hobson, *J. Chem. Soc.*, **1951**, 3427.
14) S. Seto, *Sci. Repts. Tohoku Univ.*, I, **37**, 367 (1953).
15) J. Kinumaki, Y. Ikegami, and K. Aida, *Bull. Chem. Research Inst. Non-Aq. Solns., Tohoku Univ.*, **6**, 49 (1956).
16) H. Matsumura, *Nippon Kagaku Zasshi*, **81**, 1763 (1960).
17) D. S. Tarbell, K. I. H. Williams, and E. J. Sehm, *J. Amer. Chem. Soc.*, **81**, 3443 (1959).
18) E. Albert and E. P. Serjeant, "Ionization Constants of Acids and Bases," Methuen & Co. Ltd., London (1962), Chap. 4.

BULLETIN OF THE CHEMICAL SOCIETY OF JAPAN, VOL. 47(7), 1811—1812 (1974)

Base Catalyzed Oxygenation of 3,5-Di-*t*-butylpyrocatechol and Its Related Compounds

Akira NISHINAGA, Toshio ITAHARA, and Teruo MATSUURA

Department of Synthetic Chemistry, Faculty of Engineering, Kyoto University, Kyoto 606

(Received Junuary 14, 1974)

Synopsis. The oxygenation of 3,5-di-*t*-butylcatechol (**1**) and its related compounds 3,5-di-*t*-butyl-*o*-benzoquinone (**2**), 4,6-di-*t*-butylpyrogallol (**3**), 2,4-di-*t*-butyl-5-oxo-2-hexenedioic acid (**4**), 2,4-di-*t*-butyl-4-(carboxyhydroxymethyl)-2-buten-4-olide (**5**), and 3,5-di-*t*-butyl-6-carboxy-2-pyrone (**6**) in DMF–Bu^{t}OK gave 2,4-di-*t*-butyl-4-hydroxy-2-buten-4-olide (**7b**). A possible mechanism and the relation between **4**, **5**, and **6**, the products in aqueous alkaline autoxidation of **1** and **3**, are discussed.

As a part of studies on model catalytic oxygenation for enzyme reactions, the base catalyzed oxygenation of 3,5-di-*t*-butylcatechol (**1**) and its related compounds has been investigated. The autoxidation of **1** in aqueous and methanolic NaOH solutions is known to give 2,4-di-*t*-butyl-5-oxo-2-hexenedioic acid (**4**) and 2,4-di-*t*-butyl-4-(carboxyhydroxymethyl)-2-buten-4-olide (**5**), respectively.[1,2] Compound **5** has also been obtained in the oxidation of 3,5-di-*t*-butyl-*o*-benzoqunone (**2**) with H_2O_2[2]. Campbell *et al.*[3] isolated **4** and 3,5-di-*t*-butyl-6-carboxy-2-pyrone (**6**) in the alkaline autoxidation of 4,6-di-*t*-butylpyrogallol (**3**). However, there has been no attempt to elucidate the relationship among these products sporadically obtained under different conditions.

We have found that the oxygenation of **1** in a DMF–Bu^{t}OK system newly gives 2,4-di-*t*-butyl-4-hydroxy-2-buten-4-olide (**7b**), and have made an attempt to correlate the products. When **1** was dissolved in DMF containing Bu^{t}OK under air, the solution assumed an intense blue color due to the formation of 3,5-di-*t*-butyl-*o*-benzosemiquinone (**8**) which was detected by ESR. The solution gradually turned brown with decay of the ESR signal. From the reaction mixture **7b**, the same product as that obtained in the photooxygenation of **3** in DMF–Bu^{t}OK showed the ESR spectrum of 4,6-di-*t*-butylpyrogallol anion radical (**9**), which rapidly disappeared by O_2 bubbling. The fact that **7b** was obtained in the oxygenation of **4**, **5**, and **6** in high yield suggests that they are correlated with each other to give an intermediary species in the oxygenation of **1**. Thus, the mechanistic pathway of the following scheme is suggested.

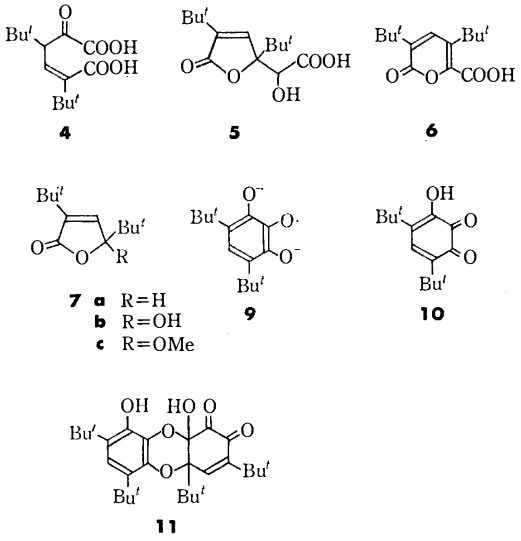

In aqueous alkaline oxygenation of **1** or **3**, one of **4**, **5**, or **6** is isolated depending on the conditions, while compounds **4**, **5**, and **6** are deprotonated to anion 2,4-di-*t*-butyl-5-oxo-2-hexen-4-idodioate (**13**) which would undergo further oxygenation to give **7b** in the DMF–Bu^{t}OK system. Hence, the poor yield of **7b** from **1** and **3** should be due to that of **13**.

As **5** is also obtained in high yield by the oxidation of 4,6-di-*t*-butylresorcinol[4] was isolated. The structure of **7b** was confirmed by the fact that its acid catalyzed methanolysis gave 2,4-di-*t*-butyl-4-methoxy-2-buten-4-olide (**7c**), and also by examination of its spectral data (Table 1) and elemental analyses. Compound **7b** was also obtained in the oxygenation of **1** in MeOH containing MeONa (yield, 41%), and in that of **2**, **3**, **4**, **5**, and **6** in DMF–Bu^{t}OK. The results are summarized in Table 2. The air saturated solu-

Table 1. The NMR and IR data of **7** and **5**

	NMR (τ_{CDCl_3}), ppm						IR (CO) cm^{-1}
	Bu^t		vinyl-H	–O–C–H	OH	OMe	
7a[a]	9.05	8.75	3.05	5.48			1740
7b	8.98	8.80	3.26		5.87		1740
7c	9.00	8.70	3.34			6.84	1760
5[b]	8.93	8.77	2.65	5.29			1755 1725

a) **7a** was prepared according to the method by Grinstead.[2] b) NMR; in CD_3OD.

Table 2. Formation of **7b** in the oxygenation of **1** and its related compounds in DMF–Bu^{t}OK

Substance	Bu^{t}OK/Subs. (mole ratio)	Reaction time (hr)	**7b** (%)
1	3	19	34
2	3	72	35
	3	40	36
3	3	12	16
	5	40	28
4	5	1	61
	5	17	76
5	6	24	82
6	6	3	47
	6	17	61

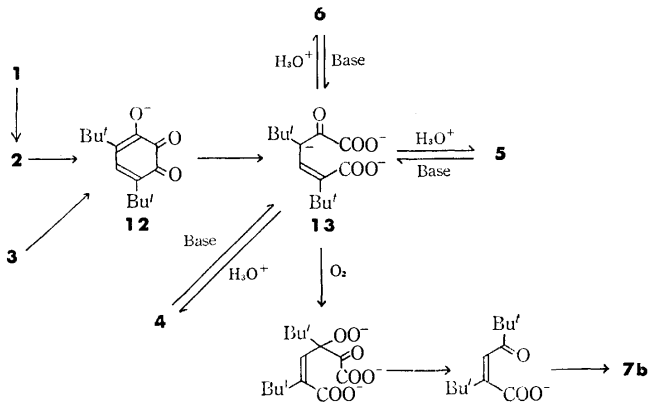

of **2** with H_2O_2[2], it is quite reasonable to assume the transient formation of 3,5-di-*t*-butyl-6-oxido-*o*-benzoquinone (**12**) just before **13** in the scheme, although 3,5-di-*t*-butyl-6-hydroxy-*o*-benzoquinone (**10**), protonated compound of **12**, has not been synthesized so far. The oxidation of **3** with *p*-benzoquinone,[5] Ag_2O,[6] and KIO_3[7] all gave a dimer, whose structure is believed to be **11**,[7] but not **10**. The dimer, upon dissolving in DMF–Bu^{t}OK, also gave **9**, and then **7b** by bubbling of O_2. It is obscure whether the formation of **13** is caused by the oxidation of quinones **2** and **12** with H_2O_2 formed during the course of reaction or by the coupling of semiquinones **8** and **9** with O_2 or O_2^- in the oxygenation.

Experimental

Oxygenation of 1 in DMF–Bu^{t}OK. A solution of **1** (0.54 g), prepared according to the method of Schulze and Flaig,[1] in DMF (15 ml) containing Bu^{t}OK (1 g) was bubbled with O_2 at room temperature for 19 hr. The resulting light brown reaction mixture was extracted with ether. The extract was washed with water, dried (Na_2SO_4), and evaporated. The silica gel tlc separation of the residue developed with a mixture of benzene–ether (3: 1 v/v) gave **7b**; colorless prisms; recrystallized from isooctane; mp 101.5—102 °C; yield, 0.18 g.

Found: C, 67.59; H, 9.45%. Calcd for $C_{12}H_{20}O_4$: C, 67.89; H, 9.50%.

Acid Catalyzed Methanolysis of 7b. A solution of **7b** (0.072 g) in MeOH (10 ml) containing a small amount of concd. H_2SO_4 was allowed to stand at room temperature for one week. The mixture was diluted with water and extracted with ether. The extract was washed (water), dried (Na_2SO_4), evaporated, and chromatographed on a silica gel column. The elution with a benzene–ether (5: 1 v/v) mixture gave **7c**; mp 60.5—61.5 °C; recrystallized from light petroleum; yield, 0.046 g (59%).

Found: C, 68.73; H, 9.75%. Calcd for $C_{13}H_{22}O_3$: C, 68.99; H, 9.80%.

Oxygenation of 2, 3, 4, 5, 6, and 11 in DMF–Bu^{t}OK. Compounds **3**, **4**, **5**, **6**, and **11** were prepared according to the method of Schulze and Flaig,[1] Grinstead,[2] Campbell,[4] and Critchlow *et al.*,[7] respectively. The compounds were oxygenated and worked up as described above to give **7b**. The results are summarised in Table 2.

References

1) V. H. Schulze and W. Flaig, *Ann.*, **573**, 231 (1952).
2) R. R. Grinstead, *Biochemistry*, **3**, 1308 (1964).
3) T. W. Campbell, *J. Amer. Chem. Soc.*, **73**, 4190 (1951); F. Stitt, G. F. Bailay, G. B. Coppinger, and T. W. Campbell, *ibid.*, **76**, 3642 (1954).
4) T. Matsuura, A. Nishinaga, N. Yoshimura, T. Arai, K. Omura, H. Matsushima, S. Kato, and I. Saito, *Tetrahedron Lett.*, **1969**, 1673.
5) W. Flaig, T. Ploez, and A. Biergans, *Ann.*, **597**, 196 (1955).
6) J. C. Salfeld, *Chem. Ber.*, **93**, 737 (1960).
7) A. Critchlow, E. Haslam, R. D. Haworth, P. B. Tinker, and N. M. Waldron, *Tetrahedron*, **23**, 2829 (1967).

BULLETIN OF THE CHEMICAL SOCIETY OF JAPAN, VOL. 47(7), 1813—1814 (1974)

Decomposition of 1,4-Dimethoxybenzene Radical Cations in CH_3NO_2–$AlCl_3$ System[1)]

Akira NISHINAGA, Hidetoshi HAYASHI, and Teruo MATSUURA

Department of Synthetic Chemistry, Faculty of Engneering, Kyoto University, Kyoto 606

(Received February 4, 1974)

Synopsis. The decomposition of 1,4-dimethoxybenzene cation (**2a**) and 1,4-dimethoxy-2,5-dimethylbenzene cation (**2b**) gave 2,2′,5,5′-tetramethoxydiphenyl and 2,5-dimethyl-*p*-benzoquinone indicating that the reaction pathway depends on substituent at nucleus of the radical cations **2**.

In a previous work,[1)] we reported that 1,4-dialkoxybenzenes are rapidly oxidized in various nitro compounds in the presence of $AlCl_3$ quantitatively to form fairly stable corresponding radical cations.[1,2)] In the CH_3NO_2–$AlCl_3$ system, however, they slowly decompose on being left to stand at room temperature. The initial step of oxidation of alkoxybenzenes has been considered to be radical cation formation,[3-5)] but the reaction of actual alkoxybenzene radical cations is little known. The chemical reactions of several stable radical cations, such as those from perylene,[6)] thianthrene,[7)] and aromatic amines[8)] have been reported. The present paper reports on the decomposition of 1,4-dimethoxybenzene radical cations in the CH_3NO_2–$AlCl_3$ system predominantly giving a dimerized product or quinoid compound depending on the substituent at nucleus of the radical cations.

When solutions of radical cations **2** quantitatively generated by dissolving **1** in CH_3NO_2–$AlCl_3$ sytsem were allowed to stand at room temperature, the radical cations slowly deteriorated with fading of the initial deep green color of **2**. **1a** (34%) and dimer **3** (39%) were isolated from decomposition products of **2a** and **1b** (45%), **4** (14%), and small amounts of **5** from those

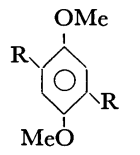

1a : R=H
b : R=Me

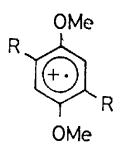

2a : R=H
b : R=Me

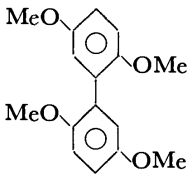

3

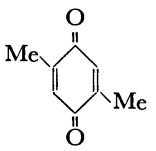

4

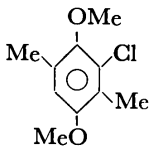

5

of **2b**. The products except for the starting materials (**1**) were not obtained from the solution of **1** in CH_3CN–$AlCl_3$, CH_2Cl_2–$AlCl_3$, or CH_3NO_2 alone where no **2** is formed, indicating that the products resulted from **2**.

The formation of **3** from **2a** provides a direct evidence for the proposed radical cation mechanism for the oxidation of methoxybenzenes to give such dimerized products (Scholl reactions).[5,9)]

In the case of **2b**, neither the dimer of type **3** nor one dimerized at the methyl carbon such as that formed in the reaction of 9,10-dimethylanthracene radical cation in which the highest spin density is at the methyl carbon[10)] was obtained, suggesting that the reaction path way is largely affected by the substitution of radical cations. It seems likely that coupling at the 3 and 6 positions in **2b** is hampered by the steric effects of the flanking groups, and coupling at the methyl group is put away by disproportionation to give the corresponding dication **7** which can be brought by the stabilizing effects of lone pairs in the 1,4-dimethoxy groups, and gives **4** either by leaving methyl cation or by reaction with water in working-up of the reaction mixture. Compound **5** is considered to form by chlo-

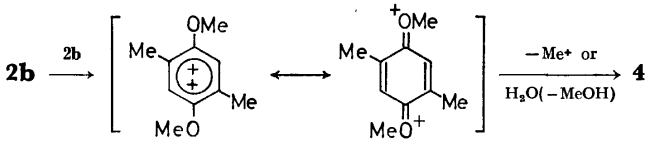

7

rination of **1b** reformed in a secondary reaction since the amount of **5** increases by longer standing of the reaction mixture with decrease in the yield of **1b**.

Experimental

Formation and Decomposition of **2**. To a solution of **1** (5 mmol) in CH_3NO_2 (50 ml) was added anhydrous $AlCl_3$ (1.33 g) under anhydrous atmosphere. The solution immediately assumed a green color due to the quantitative formation of **2** as determined by ESR. After the solution had been left to stand at room temperature for 1 hr, the mixture was poured into excess amount of ice-water and extracted with ether. The ether extract was washed (water), dried (Na_2SO_4), evaporated and chromatographed.

The separation of the products from **2a** by tlc (silica gel) developing with C_6H_6 gave **1a** (0.23 g) and **3**,[11)] mp 113—114 °C (0.265 g).

The products from **2b** were chromatographed on a silica gel (50 g) column. Elution with benzene gave **2a** (0.37 g), **5**, colorless plates, mp 135—137 °C (small amounts), and **4**, mp 121—122 °C (0.01 g) identified with authentic samples.

References

1) Aromatic Radical Cations IV. Part III: A. Nishinaga, H. Hayashi, and T. Matsuura, *Chem. Lett.*, **1973**, 141. Preceding papers: A. Nishinaga, P. Ziemek, and T. Matsuura, *Tetrahedron Lett.*, **1969**, 4905; *J. Chem. Soc.*, **1970**, 2613.

2) W. F. Forbes and P. D. Sullivan, *J. Amer. Chem. Soc.*, **88**, 2862 (1966).

3) A. Zweig, W. G. Hodgson, and W. H. Jura, *ibid*,. **86**, 4124 (1964).

4) P. J. Andrulis, Jr., M. J. S. Dewar, R. Dietz, and

R. L. Hunt, *J. Amer. Chem. Soc.*, **88**, 5473, 5483 (1966).
5) O. C. Musgrave, *Chem. Rev.*, **69**, 499 (1969).
6) C. V. Ristagno and H. J. Shine, *J. Amer. Chem. Soc.*, **93**, 1811 (1971); *J. Org. Chem.*, **36**, 4050 (1971).
7) H. J. Shine, C. F. Dais, and R. J. Small, *J. Org. Chem.*, **29**, 21 (1964); Y. Murata and H. J. Shine, *ibid.*, **34**, 3368 (1969); J. J. Silber and H. J. Shine, *ibid.*, **36**, 2923 (1971); H. J. Shine and Y. Murata, *J. Amer. Chem. Soc.*, **91**, 1872 (1969); V. D. Parker and L. Eberson, *ibid.*, **92**, 7488 (1970); H. J. Snine and J. J. Silber, *ibid.*, **94**, 1026 (1972); H. J. Shine and L. Piette, *ibid.*, **84**, 4798 (1962).
8) A. Ledwith, *Accounts Chem. Res.*, **5**, 133 (1972) and references cited therein; P. Bruni, M. Colonna, and L. Greci, *Tetrahedron*, **27**, 5893 (1971).
9) A. T. Balaban and C. D. Nenitzescu, "Friedel-Crafts and Related Reactions," Vol. II, Part 2, ed. by G. A. Olah, Interscience Publishers, New York, N. Y. (1964), p. 979.
10) V. D. Parker and L. Eberson, *Tetrahedron Lett.*, **1969**, 2839.
11) P. Kovacic and M. E. Kurz, *J. Org. Chem.*, **31**, 2011 (1966).

BULLETIN OF THE CHEMICAL SOCIETY OF JAPAN, VOL. 47(7), 1815—1816 (1974)

Carbon-13 Nuclear Magnetic Resonance Spectra of α-Ribonucleosides

Hiroshi SUGIYAMA, Naotaka YAMAOKA,* Bunji SHIMIZU,**
Yoshiharu ISHIDO,*** and Shuichi SETO

Chemical Research Institute of Non-Aqueous Solutions, Tohoku University, Sendai 980
**Faculty of Pharmaceutical Science, Kitazato University, Minato-ku, Tokyo 108*
***Central Research Laboratory, Sankyo Ltd., Shinagawa-ku, Tokyo 140*
****Department of Chemistry, Tokyo Institute of Technology, Meguro-ku, Tokyo 152*

(Received March 1, 1974)

Synopsis. The C-13 NMR spectra of four α- and two β-ribonucleosides have been measured and all carbon signals have been assigned.

Although a naturally occuring α-ribonucleoside is found only as a part of vitamine B_{12},[1] there is a great possibility to find α-ribonucleosides which are highly biologically active like vitamine B_{12}. Carbon-13 NMR spectroscopy is a useful tool for the investigation of biologically important substances because of large chemical shift differences and susceptibilities to conformational and configurational changes.[2] The present authors have shown its application to oligosaccharides and glucans.[3,4] At the present time, its application to α-ribonucleosides has been intended.

Carbon-13 NMR studies of β-ribonucleosides and nucleotides have been published by Dorman and Roberts[5] and Jones *et al.*[6] Recently, Mantsch and Smith have indicated the reverse assignment of C-13 signals due to C-2′ and C-3′.[7] Our assignment of C-13 signals in the spectra of α-ribonucleosides was based on a comparison with those studies. As shown in the Table, the signals due to carbons of the sugar moiety appear between δ 90 and 60 ppm and those of the base moiety do between δ 160 and 130 ppm except the methyl signals. The C-2′ and C-3′ signal assignments for the β-anomers by Dorman[5] and Jones[6] are reversed to those given in the Table. The present assignment is based on the sterical reason as follows. The anomeric change from α to β should afford a more marked effect on the C-2′ chemical shift than on the C-3′ chemical shift, and the C-2′ and C-3′ signals of the α-anomers appear at the same field strength. Therefore, the signal which shows a downfield shift should be assigned to C-2′ of the β-anomers. As a result, the signal at δ 74 ppm is attributed to C-2′, and the assignment by Mantsch and Smith seems more reasonable. The C-3′ and C-5′ signals of both anomers appear at the same field strength. The C-4′ signals of the α-anomers appear at a little lower field than those of the β-anomers except that of theophylline.

Carbons in the base moieties of the purine-α- and -β-ribosides show almost the same chemical shifts, but those of the pyrimidine-α- and -β-ribosides show little different chemical-shifts as seen from the Table. Jones *et al.* showed that the chemical shifts for a base moiety change according to the *syn* and the *anti* conformation of the C–N riboside bond.[8] Hence, the distribution of the rotamer of the purine ribosides on the riboside bond is the same in the both α- and β-anomers.[9] In the case of the pyrimidine ribosides, that is different between α- and β-anomers. Since *N*-acetylproline shows the higher Cα chemical shift in the *trans*-rotamer than in the *cis*-rotamer,[10] the signal at δ 27.6 ppm in the spectra of (IIα and β) can be assigned to N_1–Me and that at δ 29 ppm to N_3–Me. In the case of (IIβ), the C-3′, C-4′, and N_3–Me signals are shifted to higher fields than those of (IIa). This fact can be explained by the reason that N_3–Me of the *syn* rotamer comes over on C-3′ and C-4′ and interacts sterically with those atoms.

Experimental

Materials. The all α-ribosides[11] and theophylline[12] and thymine β-ribosides[13] were synthesized as reported before. Adenine and uracil β-ribosides were purchased from Seikagaku Kogyo.

Measurement of C-13 NMR Spectra. The spectra were measured with a JEOL PFT-100 spectrometer and an EC-6 computer at 25.15 MHz. Deuterium internal-lock on a solvent was used. Pulse width and repetition time were

TABLE 1. C-13 CHEMICAL SHIFTS OF α- AND β-RIBONUCLEOSIDES

		Me	C-2	C-4	C-5	C-6	C-8	C-1′	C-2′	C-3′	C-4′	C-5′
I	α		153.2	150.4	119.1	156.7	142.7	86.1	71.8	71.8	84.9	62.6
	β		153.4	149.9	120.3	157.1	141.1	89.0	74.6	71.7	86.9	62.7
II	α	27.6 29.6	151.0	148.0	105.9	154.5	142.3	66.7	71.2	70.6	85.1	61.3
	β	27.6 29.4	150.7	149.3	105.4	154.0	142.0	87.7	73.1	69.5	79.4	62.7
III	α		150.6	163.5	99.8	142.9		85.2	70.6	70.6	84.2	61.3
	β		152.4	164.7	103.1	142.2		89.1	74.9	71.1	86.0	62.2
IV	α	12.6	150.9	164.5	107.6	139.9		85.5	70.8	70.8	84.2	61.6
	β	12.1	150.9	164.4	109.7	137.7		87.3	73.8	70.2	85.0	61.5

δ_C (ppm downfield from TMS) which is converted using the factor of $\delta_C^{d_6\text{-DMSO}}$ 39.5 ppm.
I; adenine-riboside, II; theorphylline-ribosides, III: uracil-riboside, IV; thymine-riboside.

13 μs ($\pi/4$ pulse) and 2 s, respectively. All protons were decoupled by the noise modulation method with 30 W power. The material concentrations were 10—20 mg in 0.2 ml of d_6-dimethyl sulfoxide.

References

1) D. C. Hodgkin, J. Kamiper, J. Lindsey, M. MacKay, J. Pickworth, J. H. Robertson, C. B. Shoemaker, J. G. White, R. J. Prosen, and K. N. Trueblood, *Proc. Roy. Soc.*, **A242**, 228 (1957).

2) J. B. Stothers, "Carbon-13 NMR Spectroscopy," Academic Press, New York, N. Y. (1972).

3) T. Usui, M. Kobayashi, N. Yamaoka, K. Matsuda, K. Tuzimura, H. Sugiyama, and S. Seto, *Tetrahedron Lett.*, **1973**, 3397.

4) T. Usui, N. Yamaoka, K. Matsuda, K. Tuzimura, H. Sugiyama, and S. Seto, *J. Chem. Soc. Perkin I*, **1973**, 2425.

5) D. E. Dorman and J. D. Roberts, *Proc. Nat. Acad. Sci. U. S.*, **65**, 19 (1970).

6) A. J. Jones, D. M. Grant, M. W. Windley, and R. K. Robins, *J. Phys. Chem.*, **74**, 2684 (1970).

7) H. H. Mantsch and I. C. P. Smith, *Biochem. Biophys. Res. Commn.*, **46**, 808 (1972).

8) A. J. Jones, M. W. Winkley, and D. M. Grant, *Tetrahedron Lett.*, **1969**, 5197.

9) T. Imoto, K. Akasaka, and H. Hatano, *Chem. Lett.*, **1974**, 73.

10) W. A. Thomas and M. K. Williams, *Chem. Comm.*, **1972**, 994.

11) a) B. Shimizu, *Ann. Sankyo Res. Lab.*, **19**, 1 (1967); b) T. Nishimura, B. Shimizu, and I. Iwai, *Chem. Pharm. Bull.* (Tokyo), **12**, 1471 (1964).

12) T. Sato, T. Shimadate, and Y. Ishido, *Nippon Kagaku Zasshi*, **81**, 1440 (1960).

13) N. Yamaoka, H. Shiraishi, and K. Tuzimura, *Amino Acid Nucleic Acid*, No. 23, 127 (1971).

BULLETIN OF THE CHEMICAL SOCIETY OF JAPAN, VOL. 47(7), 1817—1817 (1974)

A Novel Rearrangement of Styryl Sulfoxide Induced by Phosphorus Pentachloride[1]

Norioki MIYAMOTO, Daisuke FUKUOKA, Kiitiro UTIMOTO, and Hitosi NOZAKI
Department of Industrial Chemistry, Kyoto University, Yosida, Sakyo-ku, Kyoto 606

(Received March 13, 1974)

Synopsis. The reaction of both isomers of methyl styryl sulfoxide (Ia) with the title chloride affords methyl phenacyl sulfide (IIa) and phenyl(α-methylthio)acetaldehyde (IIIa) besides β-chlorostyryl methyl sulfide (IVa). Phenyl styryl sulfoxide reacts similarly.

The reaction of sulfoxides with Lewis acids is well known to involve the Pummerer rearrangement.[2] We now wish to describe a novel rearrangement of methyl styryl sulfoxide (I) induced by phosphorus pentachloride in methylene chloride at room temperature. The isolated products were the β-keto sulfide II and the aldehyde III besides β-chlorostyryl sulfide (IV) (Scheme 1). A series of experiments gave results, which are given in the order of the starting sulfoxide and the

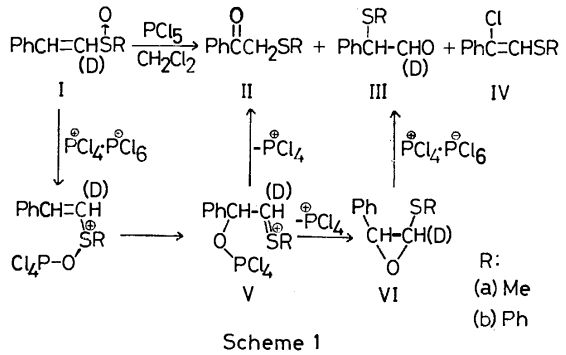

Scheme 1

products (% yield[3]): *cis* Ia,[4] IIa[5] (25), IIIa[6] (23), IVa[7] (42); *trans* Ia,[7] IIa[5] (30), IIIa[6] (10), IVa[7] (27); *cis* Ib,[4] IIb[5] (20), IIIb[8] (18), IVb (53). The aldehyde III was identified on the basis of the comparison of the spectra with those of the authentic specimen, which were independently synthesized by a novel procedure involving the reaction of the sulfur-stabilized anion with ethyl formate as follows:

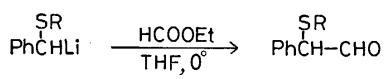

III

The formation of each product II, III, or IV is rationalized as shown in Scheme 1. The chlorination should proceed in the similar manner as suggested by Russell *et al.* in the reaction of the sulfoxide Ia with thionyl chloride.[7] The formation of II and III is explained by assuming V to be the common intermediate. The evidence supporting the proposed route to III is secured by the reaction of *trans* α-deuteriostyryl methyl sulfoxide[7] (Iad). Treatment of Iad with phosphorus pentachloride yielded the aldehyde IIIad having the deuterium at the formyl carbon. The structure of IIIad was determined on the basis of the NMR analysis. Since it is obvious from the above observations that the methylthio group shifts to the benzylic carbon, the formation of IIIa should involve the known, acid-catalyzed rearrangement[9] of the α,β-epoxy sulfide VI derived from the intermediary V. The formation of the β-keto sulfide III is explained by assuming V as the intermediate.

An additional proof for the proposed reaction scheme 1 is furnished by the observation that the methyl styryl sulfide[10] or phenyl styryl sulfide[10] reacts with thionyl chloride in carbon tetrachloride under reflux to yield the β-keto sulfide II (*a*, 42%[11]; *b*, 29) and III (*a*, 53; *b*, 38) besides the recovered vinylic sulfide. The formation of II and III can be rationalized in terms of the well-known [2,3]sigmatropic rearrangement[12] involving VII as the intermediate, whose structure is similar to that of V proposed in the reaction of the sulfoxide I with phosphorus pentachloride.

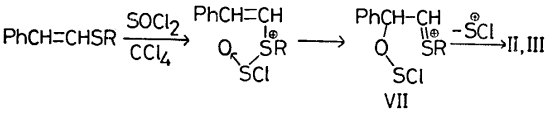

Experimental

The NMR spectra were obtained on a JEOL C-60H spectrometer in CCl_4. The chemical shifts are given in ppm from the TMS internal standard, and the abbreviations are used with their common meanings.

Reaction of Styryl Sulfoxide with Phosphorus Pentachloride. To the methylene chloride (20 ml) solution of the vinylic sulfoxide (I, 3.0 mmol) was added portionwise with stirring phosphorus pentachloride (630 mg, 3.0 mmol) at 0 °C. After the stirring at room temperature for 1 hr, the reaction mixture was poured into cold water in order to hydrolyze the remaining phosphorus pentachloride. Extraction with methylene chloride, drying (Na_2SO_4), and column chromatography (silica gel) gave the products II, III, and IV. IVa: bp 120—123 °C/3 mm, NMR δ 6.55 ppm (s, 1H, vinylic). Found: C, 68.3; H, 4.6%. Calcd for $C_{14}H_{11}ClS$: C, 68.1; H, 4.5%.

Independent Synthesis of the Aldehyde (III). The aldehyde III was prepared by the following new procedure in far better yield than the published ones.[6,8]

To the THF (10 ml) solution of benzyl methyl sulfide[13] (2.0 g, 15 mmol), was added *n*-butyl lithium (18 mmol) at 0 °C under nitrogen. The dark green solution was stirred for 30 min. Then the anion thus obtained was added with stirring to the THF (2.0 ml) solution of ethyl formate (30 mmol) at 0 °C. After the stirring at room temperature for 1 hr, the reaction mixture was poured into dilute hydrochloric acid. Extraction with ether, drying (Na_2SO_4), and distillation afforded the aldehyde (IIIa,[6] 2.1 g, 86%).

The aldehyde IIIb[8] was similarly prepared from benzyl phenyl sulfide[13] (84%).

Reaction of Styryl Sulfide with Thionyl Chloride. The

styryl sulfide (3.3 mmol) was allowed to react with thionyl chloride (1.0 g, 8.4 mmol) in carbon tetrachloride (20 ml) under reflux in a nitrogen atmosphere for 12 hr. Work-up with water, concentration *in vacuo*, and column chromatography (silica gel) gave II and III in addition to the recovered vinylic sulfide.

References and Notes

1) Parts of this work was presented in the 30th Annual Meeting of the Chemical Society of Japan, April, 1974, Osaka.

2) L. Horner and P. Kaiser, *Ann. Chem.*, **626**, 19 (1959).

3) The yields were based on the sulfoxide I initially added.

4) N. Miyamoto, D. Fukuoka, K. Utimoto, and H. Nozaki, This Bulletin, **47**, 502 (1974).

5) L. M. Long, *J. Amer. Chem. Soc.*, **68**, 2159 (1946).

6) P. Duhamel, L. Duhamel, and J. Chauvin, *C. R. Acad. Sci. Paris, C*, **277**, 1233 (1972).

7) G. A. Russell, E. Sabourin, and G. J. Mikol, *J. Org. Chem.*, **31**, 2854 (1966).

8) T. Kumamoto, S. Kobayashi, and T. Mukaiyama, This Bulletin, **45**, 866 (1972).

9) BF_3·EtO_2-catalyzed rearrangement of the α,β-epoxy sulfide to (α-arylthio)acetaldehyde was recently reported. See D. F. Tavares and R. E. Estep, *Tetrahedron Lett.*, **1973**, 1229. For the analogous rearrangement of the oxirane substituted by a hetero atom, see A. Kirrmann, P. Duhamel, and R. Nouri-Bimorghi, *Ann. Chem.*, **691**, 33 (1966); H. Newman and R. B. Angier, *Tetrahedron*, **26**, 825 (1970); P. F. Vogt and D. F. Tavares, *Can. J. Chem.*, **47**, 2875 (1969); D. F. Tavares, R. E. Estep, and M. Blezard, *Tetrahedron Lett.*, **1970**, 2373.

10) W. E. Truce and J. A. Simms, *J. Amer. Chem. Soc.*, **78**, 2756 (1956).

11) The yields were based on the vinylic sulfide initially added under consideration of recovered starting material (R=Me, 40%; R=Ph, 48).

12) U. Schöllkopf, *Angew. Chem.*, **82**, 795 (1970).

13) R. L. Shriner, H. C. Struck, and W. J. Jorison, *J. Amer. Chem. Soc.*, **52**, 2060 (1930).

BULLETIN OF THE CHEMICAL SOCIETY OF JAPAN, VOL. 47 (7), 1819—1820 (1974)

Syntheses of α-Hydroxyamino Acids from α-Keto Acids

Afzal AHMAD

Department of Chemistry, University of Islamabad, P.O. Box No. 1090, Islamabad, Pakistan

(Received May 7, 1973)

Synopsis. A new general method for the synthesis of α-hydroxyamino acids has been developed. Lithium cyanohydridoborate reduces α-keto acid oximes to the corresponding α-hydroxyamino acids and not to the corresponding α-amino acids.

During the course of investigations into the chemical and biological oxidation of α-amino acids it was considered essential to study the chemistry of analogous α-hydroxyamino acids. α-Hydroxyamino acids had been prepared earlier by several methods,[1-6] most of which gave contaminated products showing considerable discrepancies in their physical and chemical properties. One approach which appeared attractive entailed the synthesis of α-oximino acids from α-keto acids as the first step with a subsequent controlled reduction to obtain α-hydroxyamino acids as final products. All attempts, using methods to generate a stoichiometric amount of active hydrogen to convert α-oximino acid into the corresponding α-hydroxyamino acid resulted in complete failure. In every case a mixture of the corresponding α-amino acid and unchanged α-oximino acid was recovered.

Borch and Durst[7] have demonstrated a reaction of an aldehyde or ketone with ammonia in the presence of lithium cyanohydridoborate ($LiBH_3CN$) under neutral conditions in absolute methanol to give good yields of the corresponding amines. On application of this reaction, it was observed that when excess lithium cyanohydridoborate was stirred with α-oximino acids in aqueous medium at pH 5 for 48 hr at room temperature, α-hydroxyamino acids were also obtained in good yields. It was also found that in this reaction α-oximino acid could be replaced by the corresponding α-keto acid and hydroxylamine in equimolar quantities.

$$\begin{array}{l} R\text{-}\underset{\underset{O}{\|}}{C}\text{-}COOH + NH_2OH \text{ or } R\text{-}\underset{\underset{NOH}{\|}}{C}\text{-}COOH \\ \xrightarrow{LiBH_3CN} R\text{-}\underset{\underset{NHOH}{|}}{CH}\text{-}COOH \end{array}$$

α-Hydroxyamino acids prepared by this method are listed in Table 1. They are colorless crystalline compounds, having dipolar ion structure, and can be titrated with both acids and alkalies. pK_1 (2.05—2.45) and pK_2 (5.20—5.95) were measured in aqueous solutions and their isoelectric points calculated (pH 3.6—4.1). When they were titrated with sodium hydroxide in the presence of formaldehyde (Sørensen formal titration) a considerable decrease in the apparent values of pK_2 was observed. The dissociation constant pK_2 should therefore be associated with the hydroxyamino group ($R\text{-}NH_2^+OH \rightleftharpoons R\text{-}NHOH + H^+$), and constant pK_1 should thus be associated with the dissociation of carboxylic group ($R\text{-}COOH \rightleftharpoons R\text{-}COO^- + H^+$). An additional evidence in favor of the dipolar structure came from IR absorption studies. Like α-amino acids α-hydroxyamino acids show two characteristic bands for $-COO^-$ group, a prominent one occurring in the region 1580—1620 cm^{-1} and a weak one near 1410 cm^{-1}. Absorption band due to NH_2^+ deformation also appears near or coincident with the ionized carboxyl (1600 cm^{-1}) resulting in the broadening of the peak in this region. A complex series of medium scale continuous absorptions in the range 2400—2800 cm^{-1} were also observed in all cases.[8] Persistant absorption bands near 1300 cm^{-1} (NH_2 deformation) and 800 cm^{-1} (NH_2 rock) were displayed by all α-hydroxyamino acids.

Experimental

α-Keto Acids. Most of the α-keto acids were commercial products. Phenylglyoxylic acid[9] and phenylpyruvic acid[10] were prepared by known methods.

α-Oximino Acids. These were prepared by well-established methods, either from suitably substituted α-keto or malonic ester or malonic acids, by nitrosation with freshly prepared butyl nitrite,[11] or from α-keto acids and hydroxylamine.

α-Hydroxyamino Acids. A General Procedure: Either

Table 1.

α-Hydroxyamino acids $RCH(\overset{+}{N}H_2OH)COO^-$ R=	Yield[a] (%) from α-Keto acids	Yield[a] (%) from α-Oximino acids	Mp (°C) (decomp.)	Analysis (%) Found C	Found H	Found N	Calcd C	Calcd H	Calcd N
H–	53	71	135(139)[b]	26.43	5.49	15.40	26.38	5.53	15.38
CH_3–	38	55	146—147(194—195)[c]	34.32	6.79	13.28	34.29	6.71	13.34
CH_3CH_2–	45	68	173(193—194)[c]	40.48	7.51	11.81	40.35	7.62	11.76
$CH_3(CH_2)_2$–	49	70	167(194—195)[c]	45.31	8.39	10.75	45.11	8.27	10.53
$(CH_3)_2CH$–	43	57	193—194(192—193)[c]	45.32	8.41	10.35	45.11	8.27	10.53
$HOOC(CH_2)_2$–	41	48	138(138)[b]	36.73	5.71	8.48	36.81	5.56	8.59
C_6H_5–	47	59	135(133)[b]	57.51	5.38	8.29	57.48	5.43	8.38
$C_6H_5CH_2$–	41	54	159(159—160)[c]	59.77	6.21	7.83	59.69	6.12	7.73

a) Reaction time 48 hr in each case. b) Reported Mps.[9] c) Reported Mps.[5]

α-oximino acid (0.001 mol) or a mixture of the corresponding α-keto acid (0.001 mol) and $NH_2OH \cdot HCl$ (0.001 mol) is taken in water (10 ml). Enough alkali (NaOH) is added to raise the pH of the solution to approximately pH 5. A large excess of lithium cyanohydridoborate ($LiBH_3CN$) (0.002—0.003 mol) is added and the solution is stirred at room temperature for 48 hr. The reaction is interrupted by decomposing the unreacted $LiBH_3CN$ by adding concd HCl dropwise. The pH of the reaction mixture is adjusted to 1. The solution is filtered and the clear filtrate is evaporated to dryness under vacuum at room temperature. The residue so obtained is taken in water (10 ml) and evaporated again as before to remove free acid. The brown residue is then taken up in water (5 ml) and passed through a column (1 × 10 cm) of cation exchange resin (Bio-rad., Ag 50 W-x8, H^+ form). After thorough washing of the column with distilled water, α-hydroxyamino acid is taken off the column with aqueous ammonia (2%). The eluate is evaporated to dryness under vacuum at room temperature to give almost pure α-hydroxyamino acid. Further purification is achieved by crystallization from aqueous ethanol. Occasionally it was found necessary to purify α-hydroxyamino acids by passing through a column of anion exchange resin (Bio-Rad., Ag 1-x8, OH^- form) also. α-Hydroxyamino acids prepared by this method are recorded in Table 1. The IR spectrum of α-hydroxyaminopropionic acid is given (cm^{-1}) as a specimen: 655(s), 790(s), 895(s), 960(w), 1000(s), 1060(m), 1090(s), 1140(s), 1260(s), 1305(s), 1370—1620 (strong and broad), 2350(sh.) and 2400—2800 (a continuous medium absorption).

References

1) a) W. V. Miller and J. Plochl, *Ber.*, **26**, 1545 (1893). b) C. D. Hurd and J. M. Longfellow, *J. Org. Chem.*, **16**, 761 (1951).

2) L. Neelakantan and W. H. Hartung, *ibid.*, **23**, 964 (1958).

3) G. A. Snow, *J. Chem. Soc.*, **1954**, 2588.

4) a) T. Posner, *Ann.*, **389**, 120 (1912). b) N. Grossowicz and Y. Lichtenstein, *Nature*, **191**, 412 (1961). c) T. T. Emery, *Biochemistry*, **2**, 1041 (1963).

5) a) A. H. Cook and C. A. Slater, *J. Chem. Soc.*, **1956**, 4130. b) G. C. Lancini, A. Diena, and E. Lazzari, *Tetrahedron Lett.*, **1966**, 1769.

6) E. Buehler and G. B. Brown, *J. Org. Chem.*, **32**, 265 (1967).

7) R. F. Borch and H. D. Durst, *J. Amer. Chem. Soc.*, **91**, 3996 (1969).

8) R. A. Heacock and L. Marion, *Can. J. Chem.*, **34**, 1782 (1956).

9) T. S. Oakwood and C. A. Weisgerber, "Organic Syntheses," Coll. Vol. **3**, p. 114 (1955).

10) R. M. Herbst and D. Shemin, *ibid.*, Coll. Vol. 2, p. 519 (1943).

11) W. A. Noyes, *ibid.*, Vol. 2, p. 108 (1943).

BULLETIN OF THE CHEMICAL SOCIETY OF JAPAN, VOL. 47(7), 1821—1822 (1974)

Film Rupture of Polyvinyl Alcohol in the Presence of Surfactants

Waichi NAGASHIRO, Makoto TANAKA, Tadao OKABE, and Mitsuru OIKAWA
Central Research Laboratory, Hitachi Ltd. Kokubunji, Tokyo 185

(Received Junuary 26, 1974)

Synopsis. It was observed that polymer film coated over a mask hole broke down on drying. The phenomenon is related to the surface chemical properties of the coating solution.

Film rupture phenomenon of polyvinyl alcohol was studied in the presence of various surfactants. Polymer film coated over a mask hole breaks down little by little on drying. The rupture starts from the center of the hole. The coating solution consists of polyvinyl alcohol, graphite and surfactants. After the drying of the solution, hardened polymer consisting of graphite remains on the inner side of the hole, making the diameter of the hole reduced. The rupture is related to the surface chemical properties of the coating solution.

Experimental

Surface tension and foam stability were measured as regards surface chemical properties of the coating solution. Surface tension was determined with a Du Noüy tension meter. Various methods have been given[1-4] for the measurement of foam stability. The present work was carried out by measuring the relative foam height from the instant the foam formation ceased. Foam formation was carried out by stirring the coating solution uniformly. The relative foam stability was estimated by the foam height 90 min after foam formation was completed.

Results and Discussion

A schematic view of the reduction mechanism of the size of a mask hole is given in Fig. 1. The suspension of polyvinyl alcohol, graphite, and surfactants is coated over the mask hole (Fig. 1—1,2). Graphite particles at the center of the mask hole move toward the edge of the hole (Fig. 1—3), while the coating solution is dried at room temperature. We observed two types of drying processes resulting from the difference in additive surfactants; in one case the coated polymer film remained unbroken on being dried (Fig. 1—4,5), in the other the coated polymer film at the center of the hole gradually broke down on being dried (Fig. 1—4′,5′).

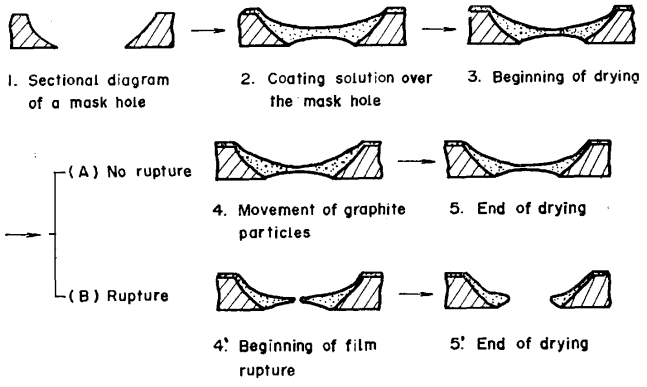

Fig. 1. Reduction mechanism of a mask hole coated with suspension solution

Table 1. Surface chemical properties of coating solutions with various surfactants

Commercial name	Structure	Maker[a]	Foam stability	Film rupture[b]	Surface tension[c] (dyne/cm)
(No surfactant)			92	×	54.0
Pluronic L31	Nonion	AD	92	×	47.2
Tween 60	Nonion	KA	91	×	51.2
Tween 40	Nonion	KA	90	×	50.0
OP-30	Nonion	NC	90	×	49.3
BC-30TX	Nonion	NC	90	×	48.8
Emal 20C	Anion	KA	90	×	49.6
Pluronic L64	Nonion	AD	88	×	45.0
Pluronic F38	Nonion	AD	88	×	53.2
Demol N	Anion	KA	88	×	55.0
Tween 80	Nonion	KA	86	×	50.9
Lipomin LH	Amphoteric	LO	85	×	51.2
Pluronic F108	Nonion	AD	82	×	44.6
Ameet 105	Cation	KA	82	○	47.5
R-2020	Nonion	NC	79	○	38.7
Tween 20	Nonion	KA	75	○	47.2
Emulgen A60	Nonion	KA	75	×	45.3
R-1020	Nonion	NC	73	○	40.3
Emulgen 911	Nonion	KA	71	○	39.2
Emulgen 120	Nonion	KA	65	○	39.9
MYL-10	Nonion	NC	64	○	37.7
Emulgen 810	Nonion	KA	63	○	36.3
Emanone 1112	Nonion	KA	17	○	39.9
Pluronic L92	Nonion	AD	12	○	38.3

a) KA (Kao Atlas Co. Ltd), NC (Nikko Chemical Co. Ltd), AD (Asahi Electro Chemical Co. Ltd), LO (Lion Fat and Oil Co. Ltd). b) ×; Rupture, ○; No rupture. c) Surface tension of the solution of 0.05% additive surfactants.

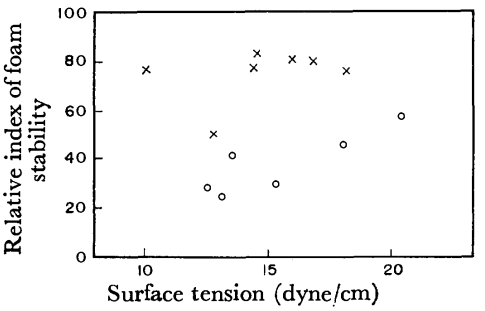

Fig. 2. Relation between foam stability and surface tension. (○; rupture, ×; no rupture)

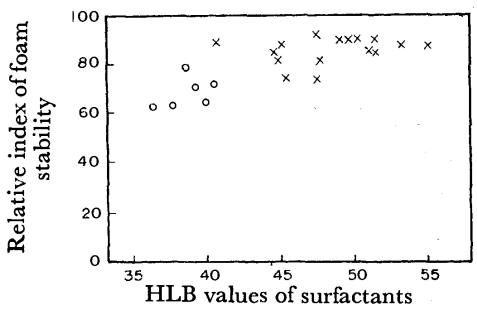

Fig. 3. Relation between foam stability and HLB value of additive surfactants. (○; rupture, × ; no rupture)

It is considered that this film rupture is related to the foam stability of the solution. The relation between film rupture and the surface chemical properties of the coating solution was studied. The results of the measurements of surface tension and foam stability of coating solutions containing various surfactants are summarized in Table 1, the film rupture being given in the order of foam stability.

The foam stability is plotted against the surface tension in Fig. 2. It is evident that film rupture occurs in a lower surface tension and lower foam stability region of a coating solution. A coating solution with a lower foam stability or a lower surface tension does not always rupture. The relation between foam stability and HLB value of surfactants is given in Fig. 3. The relation is not reliable. Film rupture does not seem to be related directly to any of the surface chemical properties of the coating solution. It occurs in the region of lower foam stability and lower surface tension.

References

1) C. Stiepel, *Seitfensieder-Ztg.*, **41**, 347 (1914).
2) L. E. Weeks, J. C. Harris, and E. L. Brown, *J. Amer. Oil Chem. Soc.*, **31**, 254 (1954).
3) J. Ross and G. D. Miles, *Oil Soap*, **18**, No. 5 (1941).
4) G. D. Miles and J. Ross, *J. Phys. Chem.*, **48**, 280 (1944).

Reductions of Cobalt(III) Complexes by Ferrous Chelates. II. The Reductions of Cobalt(III) Complex with Polymeric Ligands by Means of Some Ferrous Chelates

Yoshimi KURIMURA, Ikuko SEKINE, Eishun TSUCHIDA,* and Yukio KARINO*

Department of Chemistry, Ibaraki University, Mito, Ibaraki 310

**Department of Polymer Chemistry, Waseda University, Shinjuku-ku, Tokyo 160*

(Recieved May 28, 1973)

The effects of polymeric ligands on the electron-transfer reaction of the cobalt(III) complex have been studied for the reductions of the complex ions of *cis*-$Co(en)_2ACl^{2+}$ (A=poly-4-vinylpyridine, PVP, or pyridine, py) by the aquo ferrous ion and some Fe(II)-nitrilopolycarboxylate chelates. The specific rate of the Fe^{2+} reduction of the $Co(en)_2PVPCl^{2+}$ is smaller than that of the $Co(en)_2PyCl^{2+}$. The specific rate of the Fe(II)-chelate reduction increases considerable when the pyridine ligand in the $Co(en)_2$-$PyCl^{2+}$ is replaced by PVP. The effects of the chelating agents, the degree of coordination, the ionic strength, and the concentration of the reductant on the reduction rate of the $Co(en)_2ACl^{2+}$ by the Fe(II)-nitrilopolycarboxylate were also examined. The resulting reactivity patterns of the polymer complex ions could mainly explained by the effect of the higher electrostatic field caused by the positively-charged polymer structure.

Kinetic studies have been made of the $FeEDTA^{2-}$ reduction of $Co(NH_3)_5Y^{2+}$ (Y=halogen ions, NCS^-, NO_3^-, and N_3^-) and of $Fe^{II}Z^{m-}$ (Z=EDTA, CyDTA, EDTAOH, and EDTA)[1] reductions of $Co(NH_3)_5Cl^{2+}$: the results were reported in a previous paper.[2] The pattern of reactivities for the $FeEDTA^{2-}$ reductions of the $Co(NH_3)_5Y^{2+}$, in which the Y ligand is varied, indicates the inner-sphere natuer of the reactions: furthermore, the variation in the rate of reaction of the $Fe^{II}Z^{m-}$ with $Co(NH_3)_5Cl^{2+}$ were explained in terms of the steric, charge, and stabilization effects. For the reductions of the $Co(NH_3)_5Y^{2+}$ by the $Fe^{II}Z^{m-}$, it is suggested that the stabilization effect, the degree of which is expressed by the values of the logarithmic ratio of the stability constants ($\log K_{Fe^{III}Z}/K_{Fe^{II}Z}$), is the most important factor controlling the reaction rate.

A water-soluble polymer metal complex of *cis*-$[Co(en)_2PVPCl]Cl_2\cdot nH_2O$ (PVP=poly-4-vinylpyridine) was prepared,[3] and the specific rate and activation parameters for the ferrous-sulfate-ion reduction were determined in dilute sulfuric acid solution.[4] The rate of the reduction of the polymer complex ions is expected to be sensitive to the charge on the reductant species, since the polymer ion forms a "domain" with a greater charge density in the solution.

In the present study, the effects of the polymer ligand on the rate of the electron-transfer reactions were examined for the reduction of the polymer complex ion by ferrous chelate and aquo-ferrous ions.

Experimental

Materials. The *cis*-$[Co(en)_2Cl_2]Cl$[5] and *cis*-$[Co(en)_2pyCl]Cl_2$[6] were prepared by the procedures described in the references cited. Poly-4-vinylpyridines with degrees of polymerization (P_n) of 19 and 98 were prepared such as has been reported by Katchalsky *et al.*[7]

Preparations of cis-$[Co(en)_2PVPCl]Cl_2\cdot nH_2O$. $[Co(en)_2PVPCl]Cl_2\cdot nH_2O$ was prepared by means of substitution reaction between *cis*-$[Co(en)_2Cl_2]Cl$ and PVP in water-ethanol solution.[3] The identity and the purity of the *cis*-$[Co(en)_2PVPCl]Cl_2\cdot nH_2O$ were confirmed by the elementary analysis of C, H, and N, and the infrared and electronic spectra. The absorption peak at 1600 cm^{-1}, based on $\nu_{C=C,C=N}$ of the pyridine ring of the PVP, shifts to a wave number higher by about 20 cm^{-1} in the PVP complex. This indicates the coordination of the pendant pyridine to the Co(III). The absorption peaks due to the $\nu_{C=C}$, δ_{CH} (in plane) and the δ_{CH} (out of plane) also shift to a wave number higher by 2—10 cm^{-1} as a result of coordination. Some examples of the results of the elementary analysis are shown in Table 1. The degree of coordination (x) was determined from carbon content.[8] The absorption maximum and the molar extinction coefficient of the first absorption band of the $Co(en)_2$ $PVPCl^{2+}$ in the aqueous solution agree with those in the literature (λ_{max}=518 nm and $\varepsilon_{max}=72\pm2$).[3] The configuration of the *cis*-$[Co(en)_2$-$PVPCl]^{2+}$ is shown in Fig. 1. The *cis*-configuration of the $[Co(en)_2PVPCl]Cl_2\cdot nH_2O$ we prepared was ascertained from the sharp splitting of the $-CH_2$ rocking band (870—900

Table 1. Elementary analysis of $[Co(en)_2PVPCl]Cl_2\cdot nH_2O$

P_n[a]		C, %	H, %	N, %	x	n
98	Found	43.51	6.13	14.19		
	Calcd	43.5	6.74	14.6	0.36	2
98	Found	42.49	6.77	15.86		
	Calcd	42.5	6.45	15.7	0.45	2
98	Found	33.53	5.65	14.97		
	Calcd	33.5	5.96	15.0	0.68	4
19	Found	34.43	6.48	14.95		
	Calcd	34.4	6.75	14.9	0.64	4
19	Found	34.11	6.27	14.77		
	Calcd	34.1	5.97	14.9	0.65	4

a) Degree of polymerization of the PVP.

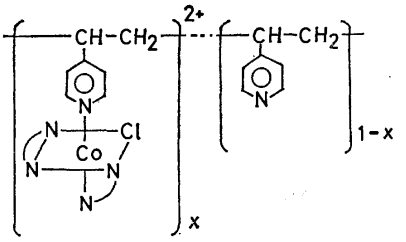

Fig. 1. Configuration of *cis*-$Co(en)_2PVPCl^{2+}$.

cm^{-1})[9] of the ethylenediamines in the complex.

Kinetic Measurements. The solution of the ferrous perchlorate was prepared by dissolving a known amount of analytical-grade iron wire, (Mallincroft Co.) in an excess of perchloric acid solution. The methods of determinations the ferrous, hydrogen and perchlorate ions in the ferrous perchlorate solution and the method of preparation for the ferrous chelate solutions were identical with those used in a previous work.[2]

The solution of the Co(III) complex was prepared by dissolving weighed amounts of the Co(III) complex into an acetate-buffered solution. The ionic strength of the reaction mixture was maintained at a constant value by the addition of sodium perchlorate. The reaction was followed spectrophotometrically at the wave-lengths in the vicinity of the first absorption maximum (—520 nm) of the Co(III) complex for higher concentrations of the complex and at the charge-transfer absorption maximum (~230 nm) of the Co(III) complex for lower Co(III) concentrations. The rate constants were calculated from the data which were obtained under pseudo-first-order conditions in which, in most cases, the concentration of the Fe(II) was in great excess over that of the Co(III). In some cases, the concentration of the Fe(II) was in not so great an excess over that of the Co(III): in such cases, then, the value of [Fe(II)] used for the calculation of the rate constant was an average value of the Fe(II) concentrations between the initial time and the half-life of the reaction. The values of k_{py} and k_{PVP} were obtained by means of this equation: $2.3\times m/[Fe(II)]$, where m is the slope of the straight line which was obtained from the slopes of the log (A_t-A_∞) *vs.* time plots, where A_t is the absorbance at time t, and A_∞, the absorbance after all the Co(III) has been reduced to Co(II).

Results

The rate equations for the reduction of $Co(en)_2pyCl^{2+}$ by Fe^{2+} and $Fe^{II}Z^{m-}$ and that of the $Co(en)_2PVPCl^{2+}$ by Fe^{2+} almost fit the second-order kinetics: $-d[Co(III)]/dt=k[Co(III)][Fe(II)]$ ($k=k_{py}$ or k_{PVP}), under the experimental conditions employed. The apparent second-order rate constant of k_{PVP} for the $Fe^{II}Z^{m-}$ reductions was calculated from the initial slopes of the log (A_t-A_∞) *vs.* time plots. In most cases, such plots give straight lines for about a half-life of the reaction.

Table 2 shows that the rate constant for the Fe^{2+} reduction of the polymer complex with $P_n=98$ is almost identical with that of the polymer complex with $P_n=19$ within the limits of experimental errors when the values of x are equal to each other ($x=0.68$ for $P_n=98$ and $x=0.65$ $P_n=19$). This indicates that the value of k_{PVP} for Fe^{2+} reduction is not so much affected by the chain length of the polymer ligand when the P_n value ranges between 19 and 98 under the experimental conditions given in Table 2. For the Fe^{2+} reduction, the reactivity of the polymer complex is lower than that of the monomeric one by about one-third.

TABLE 2. RATE CONSTANTS FOR THE Fe^{2+} REDUCTION OF $Co(en)_2ACl^{2+}$

A	P_n	x	k[a], $M^{-1}s^{-1}$
Py			1.1×10^{-3}
PVP	98	0.68	3.7×10^{-4}
PVP	19	0.65	3.7×10^{-4}

a) $[Co(III)]=4.0\times10^{-3}$ M, $[Fe(II)]=3.4\times10^{-2}$ M, $[Fe(II)]=3.4\times10^{-2}$ M, $[H^+]=2.0\times10^{-2}$ M, $\mu=0.12$, 40 °C.

Ferrous Chelate Reduction. All the reductions of the $Co(en)_2pyCl^{2+}$ and $Co(en)_2PVPCl^{2+}$ by $Fe^{II}Z^{m-}$ except for the Fe^{II}DTPA were followed in the solution of pH=5 in which the predominant species of Fe(II) are normal ferrous chelates. For the Fe^{II}DTPA reduction, the rate constants of Reactions (1) and (2) could be obtained separately from the pH dependence of the rate constant:

$$Co(en)_2ACl^{2+} + FeHDTPA^{2-} \rightarrow Co(II) + Fe(III) \quad (1)$$

$$Co(en)_2ACl^{2+} + FeDTPA^{3-} \rightarrow Co(II) + Fe(III) \quad (2)$$

where A=py or PVP. From Reactions (1) and (2), we obtaine:

$$k_a(1+K_{FeHZ}[H^+]) = k_1 + k_2K_{FeHZ}[H^+] \quad (3)$$

In this equation, k_1 and k_2 are the rate constants of Reactions (1) and (2) respectively, while K_{FeHZ} is the formation constant of the protonated chelate, $FeHDTPA^{2-}$, and k_a is k_{py} or k_{PVP}. The value of K_{FeHZ} was $10^{5.4}$ ($\mu=0.1$ and at 25 °C).[10] As is shown in Fig. 2, the plots of $k_a(1+K_{FeHZ}[H^+])$ *vs.* $[H^+]$ become linear in both cases. The slopes and intercepts of these lines give the values of k_2K_{FeHZ} and k_1 respectively.

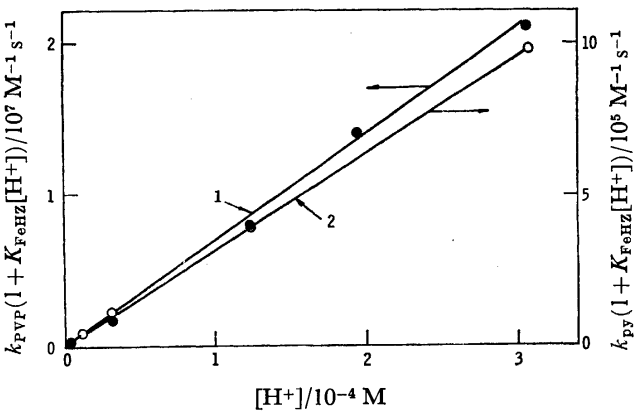

Fig. 2. Plots of $k_a(1+K_{FeHZ}[H^+])$ *vs.* $[H^+]$.
$[Co(III)]=1.0\times10^{-5}$ M, $[Fe^{II}DTPA]=5.1\times10^{-5}$ M, $\mu=0.02$, 25 °C,
1, $Co(en)_2PVPCl^{2+}$, 2, $Co(en)_2pyCl^{2+}$.

Unfortunately, the intercepts of such plots were too small for us to determine the values of k_1 for the $Co(en)_2pyCl^{2+}$ and the $Co(en)_2PVPCl^{2+}$. The values of k_1 were, however, estimated to be smaller than corresponding k_2 values by at least one-tenth in both cases. The rate constants for the reductions of $Co(en)_2pyCl^{2+}$ and $Co(en)_2PVPCl^{2+}$ by several ferrous chelates are summarized in Table 3.

The effects of the conentration of the ferrous chelate and the degree of the coordination and that of the polymerization on the rate of the reduction of the polymer complex are represented in Fig. 3 and Table 4 respectively. For the $Fe^{II}Z^{m-}$ reduction, The apparent rate constant is affected by the degree of coordination, x, in

Table 3. Rate constants for the reductions of $Co(en)_2pyCl^{2+}$ and $Co(en)_2PVPCl^{2+}$ by Fe(II)-chelates (μ=0.02, 25 °C)

Reductant	Rate constant, $M^{-1}s^{-1}$	
	k_{py}	k_{PVP}[a]
$FeEDTA^{2-}$	1.4×10^4	2.8×10^5
$FeCyDTA^{2-}$	1.2×10^4	1.9×10^5
$FeEDTAOH^-$	2.4×10^4	8.8×10^4
$FeHDTPA^{2-}$	1.3×10^4	2.8×10^5

a) Apparent rate constants for the $Co(en)_2PVPCl^{2+}$ with P_n=19 and x=0.64.
$[Co(III)]=1.0\times10^{-5}$ M, $[Fe(II)]=5.1\times10^{-4}$ M.

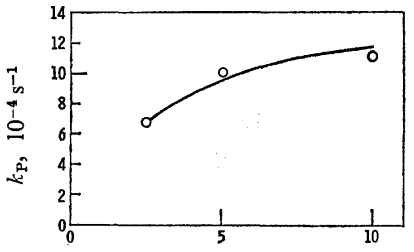

Fig. 3. Plots of the pseudo-first-order rate constant *vs.* $[FeEDTA^{2-}]/[Co(III)]$.
$[Co(en)_2PVPCl^{2+}]=1.0\times10^{-5}$ M (P_n=19, x=0.65), μ=0.02, pH=5.0, 25 °C.

Table 4. Effects of the degree of coordination and the degree of polymerization on the rate constant

P_n	x	$x/10^5$ $M^{-1}s^{-1}$
98	0.32	2.2
	0.36	3.6
	0.45	3.4
	0.69	4.5
19	0.65	2.8

$[Co(en)_2PVPCl^{2+}]=1.0\times10^{-5}$ M, $[FeEDTA^{2-}]=5.0\times10^{-5}$ M, pH=5.0, μ=0.02, 25 °C.

Table 5. Effect of ionic strength on the rate constants for the reductions of $Co(en)_2pyCl^{2+}$ and $Co(en)_2PVPCl^{2+}$ by $FeEDTA^{2-}$ [a]

	Rate constant/M^- s^{-1}	
	k_{py}	k_{PVP}[b]
0.02	1.4×10^4	2.8×10^5
0.10	7.3×10^3	2.3×10^4

a) $[Co(III)]=1.0\times10^{-5}$ M, $[FeEDTA^{2-}]=5.0\times10^{-5}$ M, pH=5.0, 25 °C. b) Apparent rate constants, P_n=19, x=0.65.

the polymer complex and by the degree of polymerization of the polymer ligand: the rate constant increases with an increase in the value of x and the rate constant in the complex of PVP with P_n=98 is greater than that for P_n=19 when the values of x are almost the same. A comparison the rate constants for the $Co(en)_2pyCl^{2+}$ and $Co(en)_2PVPCl^{2+}$ complexes at different ionic strengths is also shown in Table 5.

Discussion

It may be reasonable to assume that the reductions of the $Co(en)_2PVPCl^{2+}$ and $Co(en)_2pyCl^{2+}$ complexes by Fe^{2+}, $FeSO_4$,[11] and $Fe^{II}Z^{m-}$ proceed through a chloride-bridged mechanism, since it has been suggested that $Co(NH_3)_5Cl^{2+}$ reacts with Fe^{2+},[12] $FeEDTA^{2-}$,[12] and $FePDTA^{2-}$[13] *via* the chloride-bridged activated state.

The rate of reaction between two cationic species in an aqueous solution, for example, the reaction of $Co(NH_3)_5Cl^{2+}$ with Fe^{2+}, is markedly accelerated in the presence of small amounts of polyions, such as polyvinylsulfonate or polymethacryloxyethylsulfonate anions.[14-17] In dilute solution of a polyelectrolyte, the damains occupied by the polyions contain very high density of the ionized group, while the space between the domains has only a very low concentration of ionic species.[14] It was also demonstrated by means of several experimental techniques, such as electronic mobility,[18,19] osmotic pressure,[20] and potentiometric titration,[21,22] that appreciable amounts of the counter ions are fixed near the polyion structure in an aqueous solution of polyelectrolytes due to Coulombic attraction between the polyion and the counter ion. The polycation domain consisting of the $Co(en)_2PVPCl^{2+}$ also tends to concentrate the opposite-charged $Fe^{II}Z^{m-}$ species. This causes an increase in the local concentration of the $Fe^{II}Z^{m-}$ species, thus promotes the reduction rate. The results listed in Table 6 qualitatively support this electrostatic explanation: the results show that the acceleration factor depends essentially on the charges of the reductant. The reduction of the activity coefficient of the multiplycharged activated complex in the strong field of the polyion domain[23] is considered to be another factor controlling the rates of polyion catalyzed reactions. Among the reactions investigated, the latter factor, however, seems to be less important than the former, since the acceleration factor for the Fe^{2+} reduction of the $Co(en)_2PVPCl^{2+}$, in which the reaction takes place through the multiply positive-charged activated complex, is not so far from unity. The specific rate for the $FeEDTA^{2-}$ reduction of the $Co(en)_2PVPCl^{2+}$ complex increases as the degree of coordination increases (Table 5). This could also be explained in terms of the accumulation of the $FeEDTA^{2-}$ in the polycation doamin as the degree of

Table 6. Acceleration factors for the Fe(II) reduction of $Co(en)_2PVPCl^{2+}$

Reductant	Acceleration factor k_{PVP}/k_{py}
Fe^{2+}	0.33[a]
$FeSO_4$	0.59[b]
$FeEDTAOH^-$	3.7[c]
$FeEDTA^{2-}$	21[c]
$FeCyDTA^{2-}$	16[c]
$FeHDTPA^{2-}$	22[c]

a) μ=0.12, 40 °C, P_n=98, x=0.45, in 0.1 M $HClO_4$.
b) $\Sigma[SO_4^{2-}]=1.25$, $[H^+]=1.0$ M, P_n=98, x=0.45.[4]
c) μ=0.02, P_n=19, x=0.64.

coordination increases, since it is considered that the charge density of the polymer domain becomes larger with the degree of coordination. For a $FeEDTA^{2-}$ reduction, the pseudo-first order rate constant, k_p, increases with the concentration of the reductant, but the relationship between the rate constant and the $[FeEDTA^{2-}]/[Co(III)]$ is not linear as is shown in Fig. 3. This seems to suggest the existence of an equilibrium between the $FeEDTA^{2-}$ in the bulk and that in the domain in the polyion-$FeEDTA^{2-}$ system.

The greater influence of the ionic strength or the concentration of the nonparticipating salts on the specific rate of the $FeEDTA^{2-}$ reduction of the $Co(en)_2PVPCl^{2+}$ than the influence of the $Co(en)_2pyCl^{2+}$ (Table 5) also indicates greater effect of the Coulombic force between the polycations and the nonparticipating anions. As the amounts of the nonparticipating anions in the solution increase, their concentrations in the domain would increase also, this causing a partial neutralizing of the positive charges carring on the polyion domain. Therefore, the amounts of the $FeEDTA^{2-}$ will tend to be diluted in the polyion domains, resulting in a lower collision frequency.

References

1) The abbreviations of the chelating agents used here are: EDTA, ethylenediaminetetraacetic acid: CyDTA, cyclohexanediaminetetraacetic acid: EDTAOH, hydroxyethylethylenediaminetriacetic acid: DTPA, diethylenetriaminepentaacetic acid, and PDTA, propylenediaminetetraacetic acid.

2) Y. Kurimura, This Bulletin, **46**, 2093 (1973).

3) Y. Kurimura, E. Tsuchida, and M. Kaneko, *J. Polym. Sci.*, *A*-1, **9**, 3511 (1971).

4) Y. Kurimura, E. Tsuchida, and M. Kaneko, *ibid.*, *A*-1, **9**, 3521 (1971).

5) S. M. Jorgensen, *J. Prakt. Chem.*, **41**, 448 (1890).

6) J. C. Bailar, Jr. and L. B. Clapp, *J. Amer. Chem. Soc.*, **67**, 171 (1945).

7) A. Katchalsky, K. Rosenheck, and B. Altmann, *J. Polym. Sci.*, **23**, 955 (1955).

8) The degree of coordination, x, indicates the molar ratio of the Co(III) per monomer unit of PVP.

9) M. Baldwin, *J. Chem. Soc.*, 4369 (1960).

10) A. Ringbom, "Complexation in Analytical Chemistry," John Wiley & Sons., New York, 1963.

11) The experimental conditions for the Fe(II) reductions of $Co(en)_2PVPCl^{2+}$ and $Co(en)_2pyCl^{2+}$ in dilute sulfuric acid solutions were: $[Fe(II)]=2.0\times10^{-2}$ M, $[H^+]=1.0$ M, and $\sum[SO_4^{2-}]=1.25$ M.[4] Under such conditions, almost all of the Fe(II) species would be present as $FeSO_4$ since the logarithmic formation constant (log β) for the $FeSO_4$ has been estimated to be about 2, though this value has not yet been directly obtained. This estimation was derived from a comparison of the log β values for several $M^{II}SO_4$ species,[10] *e.g.*, Co^{2+} (2.5), Ni^{2+} (2.3), and Zn^{2+} (2.3).

12) H. Diebler and H. Taube, *Inorg. Chem.*, **4**, 1029 (1965).

13) B. Grossman and R. G. Wilkins, *J. Amer. Chem. Soc.*, **89**, 4230 (1967).

14) H. Morawetz and B. Vogel, *ibid.*, **91**, 563 (1963).

15) H. Morawetz and G. Gordimer, *ibid.*, **92**, 7532 (1970).

16) E. Gould, *ibid.*, **92**, 6797 (1970).

17) S. Bruckner, V. Crescenzi, and F. Quardrifoglio, *J. Chem. Soc.*, *A*, **1970**, 1168.

18) J. R. Huizenga, P. F. Grieger, and F. T. Wall, *J. Amer. Chem. Soc.*, **72**, 2636 (1950).

19) A. Katchalsky, *J. Chem. Soc.*, **1961**, 5198.

20) Z. Alexandrowitz, *J. Polym. Sci.*, **40**, 91 (1951).

21) M. Nagasawa and A. Holtzer, *J. Amer. Chem. Soc.*, **86**, 538 (1964).

22) M. Nagasawa, T. Murase, and K. Kondo, *J. Phys. Chem.*, **69**, 4005 (1965).

23) N. Ise and F. Matsui, *J. Amer. Chem. Soc.*, **90**. 4242 (1968).

The Thermal Decomposition and Reduction of Silver(I) Oxide

Issei NAKAMORI, Hidetsugu NAKAMURA, Toshiyuki HAYANO, and Shuichi KAGAWA*

Department of Chemical Engineering, Faculty of Engineering, Kyushu University, Hakozaki, Fukuoka 812

(Received October 5, 1973)

The thermal decomposition of silver(I) oxide and its reduction with reductive gases, such as ethylene, hydrogen, and carbon monoxide, have been studied by using a fixed-bed flow reactor. Under isothermal conditions, each reaction gave a sigmoidal shape to the fractional decomposition *vs.* time curves, and these curves were in good agreement with Avrami's equation. The temperature at which the reaction commenced corresponded well to the chemical affinity of the reaction, and a linear free-energy relationship holds between the apparent activation energy and the standard enthalpy change of the reaction. In the thermal decomposition, an enlargement in particle size resulting from the melting and sintering of the product silver was recognized, but in the reduction the particle size scarcely varied during the reaction. On the basis of these results, the mechanism of each reaction was discussed.

The thermal decomposition of silver(I) oxide has been investigated by various workers, but no reasonable explanation of the decomposition rate equation and the reaction mechanism were obtained. With regard to the fractional decomposition (α) *vs.* reaction time (t) curves, both sigmoidal and nonsigmoidal curves have been reported. Sigmoidal curves have been reported by Lewis[1] and by Hood and Murphy,[2] who proposed that the reaction proceeded autocatalytically obeying by Ostwald's equation: $d\alpha/dt=k\alpha(1-\alpha)$. Recently, Tobisawa[3] and Herley and Prout[4] have proposed a topochemical approach to these observed sigmoidal curves. Nonsigmoidal curves which have a maximum rate at the initial stage of the decomposition have been reported by Pavluchenko and Gurevich[5] and by Garner and Leaves.[6] Kato *et al.*[7] observed nonsigmoidal curves which showed that the reaction proceeded linearly with the time up to a great extent of the fractional decomposition. However, almost all the samples which have not shown sigmoidal curves have undergone grinding or preheating. These treatments may have an effect on the physical and chemical properties of the samples.

On the other hand, the reduction of silver oxide with ethylene has been studied in order to examine the role of silver as a catalyst in the direct oxidation of ethylene.[8-10] Kagawa *et al.*[9] found that, both in the thermal decomposition of silver oxide and in its reduction with ethylene, the reactions proceeded obeying Ostwald's equation and suggested that the two mechanisms of reactions were similar.

In this paper, on the basis of a comparison of the thermal decomposition with the reduction with several reductive gases, the reaction mechanisms will be discussed.

Experimental

Preparation of Silver(I) Oxide. The sample of silver oxide was prepared from silver nitrate and sodium hydroxide. In order to eliminate the silver carbonate formed at the surface of the silver oxide, the specimen was treated in a carbon dioxide-free nitrogen stream at 60—120 °C for 48—72 hr and stored *in vacuo* over silica gel under dark-room conditions. By a chemical analysis of the silver, the sample gave 100±0.2% as silver(I) oxide and was confirmed gas-chromatographically not to evolve oxygen gas below 250 °C, while the X ray diffraction patterns did not show any line of silver or of silver carbonate.

Apparatus and Procedure. The reaction was carried out in a fixed-bed flow reactor using a Pyrex tube 1 cm in inside diameter. A given amount of the silver oxide sample was packed in the reactor. In the case of the thermal decomposition, the nitrogen used as a carrier gas was passed through at a constant flow rate. The reactor was immersed in a fused-salts bath and heated; then the reaction commenced. The product oxygen in the effluent gas was analyzed by gas-chromatography. The reaction rate was determined from the flow rate of the carrier gas and from the oxygen concentration in the effluent gas. In the cases of the reductions with ethylene, hydrogen, and carbon monoxide, pure reactant gases and mixtures of them with nitrogen gas were passed through the reactor at a constant flow rate and the reaction product gases, such as ethylene oxide, carbon dioxide, and water vapour, were analyzed gas-chromatographically. In each reduction, no oxygen gas evolution as a result of the thermal decomposition was detected. One of the baths of the oil, the water or the water-methanol, was selected as a thermostat according to the reaction temperature.

Experiments were carried out both isothermally and dynamically. In the case of a dynamical operation, the heating rate was 2 °C/min. In the case of an isothermal operation, the required temperature could be obtained within 5 minutes and the temperature was controlled within ±0.5 °C during the course of the reaction. At slow flow rates up to 80 cm^3/min, the effect of the flow rate on the rates of the thermal decomposition and the reduction was observed. Therefore, experiments were carried out at flow rates above 80 cm^3/min. The sample weight did not effect the reaction rate. Considering the accuracy of analysis and the elimination of the heat of reaction, the sample weight was determined to be 0.5—1.5 g for the thermal decomposition and for the reduction with ethylene, and about 0.15 g for the reductions with hydrogen and carbon monoxide.

Results

Reaction under Dynamical Conditions. As is shown in Fig. 1, the thermal decomposition of silver oxide began at 330 °C, reached a maximum rate at about 440 °C, and was completed at 500 °C. On the other hand, the reduction with ethylene occurred over the range of temperature of 110—210 °C, that with hydrogen, at 10—130 °C, and that with carbon monoxide, at −40—30 °C. By balancing the oxygen atoms in

* Present address: Department of Industrial Chemistry, Faculty of Engineering, Nagasaki University, Nagasaki 852

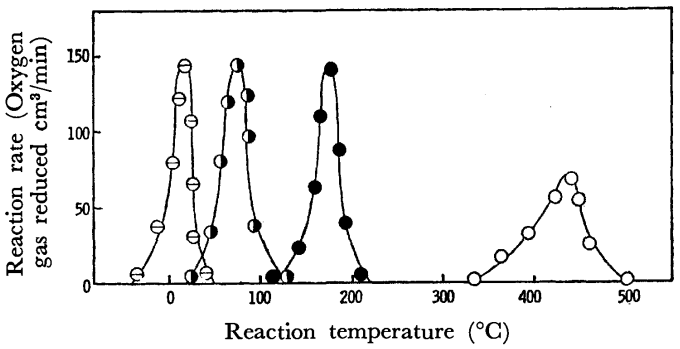

Fig. 1. Reaction under dynamical condition (heating rate 2 °C/min). ⊖ reduction with CO, ● reduction with C_2H_4, ◑ reduction with H_2, ○ thermal decomposition in N_2.

TABLE 1. OXYGEN BALANCE AND REACTION EQUATION

System	O in sample a (mg)	O in product b (mg)	O balance b/a	Reaction equation	ΔG°_{298} (kcal/mol)	T_c (°C)
Ag_2O-N_2	34.2	35.2	1.03	$Ag_2O \rightarrow 2Ag + \frac{1}{2}O_2$	2.6	330
Ag_2O-C_2H_4	33.6	34.9	1.04	$Ag_2O + C_2H_4 \rightarrow 2Ag + C_2H_4O$ $Ag_2O + \frac{1}{6}C_2H_4 \rightarrow 2Ag + \frac{1}{3}CO_2 + \frac{1}{3}H_2O$	−44.5	110
Ag_2O-H_2	33.8	34.9	0.97	$Ag_2O + H_2 \rightarrow 2Ag + H_2O$	−54.5	10
Ag_2O-CO	35.8	35.2	0.98	$Ag_2O + CO \rightarrow 2Ag + CO_2$	−58.7	−40

product gases with those in silver oxide used, the reaction equations were determined. The results are shown in the fifth column of Table 1. In the reduction of silver oxide with ethylene, two reactions occurred competitively and the selectivity of ethylene oxide based on the ethylene reacted was about 37%. In the sixth and seventh columns of Table 1 respectively, the temperature at which the reaction commenced (T_c) and the standard free energy change of the reaction (ΔG°_{298}) are described. Between T_c and ΔG°_{298} a fairly good correspondence is found; the smaller (the more negative) the ΔG°_{298}, the lower the T_c.

Reaction under Isothermal Conditions. The thermal decomposition under isothermal conditions was carried out between 410—430 °C. The fractional decomposition *vs.* time curves are shown in Fig. 2. These curves, which showed an accelerated period, gave a sigmoidal shape characteristic of a solid reaction. The reductions of silver oxide with ethylene, hydrogen, and carbon monoxide were carried out at the temperature ranges of 136—145 °C, 65—75 °C, and −8—10 °C respectively. The results[11] are shown in Figs. 3, 4 and 5. Although the reaction temperatures were different from each other, the shapes of the curves were sigmoidal, similar to those of the thermal decomposition in nitrogen.

In the case of the reduction with ethylene, the effect of the partial pressure of ethylene on the reduction rate is illustrated in Fig. 6.[12] The partial pressure of

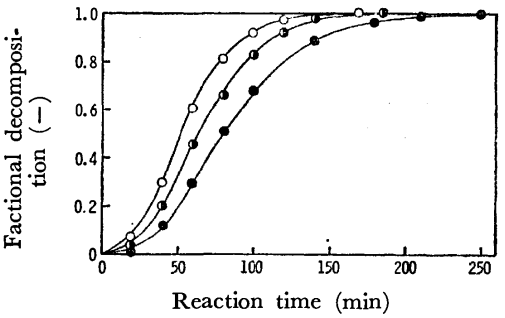

Fig. 3. Reduction with C_2H_4.
○ at 145 °C, ◑ at 140 °C, ● at 136 °C

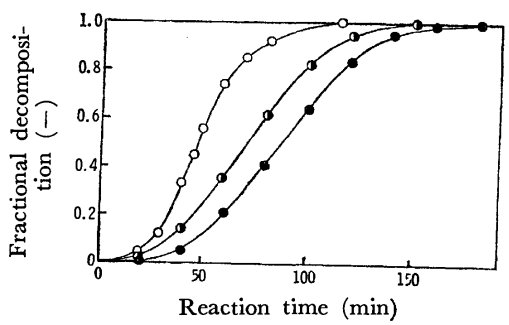

Fig. 2. Thermal decomposition in N_2.
○ at 430 °C, ◑ at 420 °C, ● at 410 °C

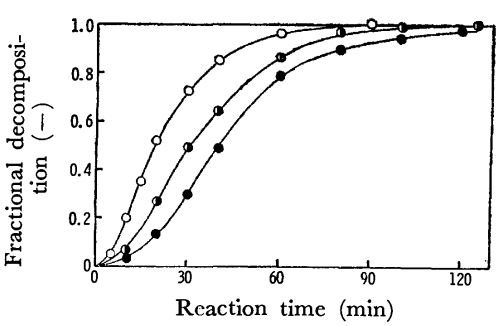

Fig. 4. Reduction with H_2.
○ at 75 °C, ◑ at 70 °C, ● at 65 °C

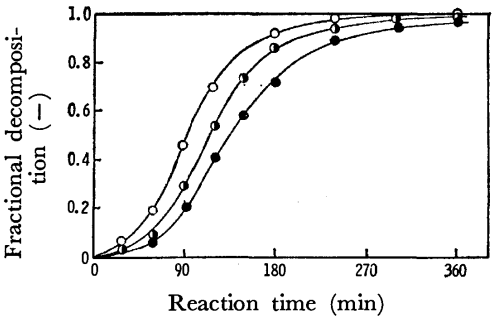

Fig. 5. Reduction with CO.
○ at 10 °C, ◑ at 0 °C, ● at −8 °C

ethylene below 0.4 atm had a considerable influence on the reaction rate constant, but above 0.4 atm the effect was negligible. For the other reductive gases, similar results were obtained.

Scanning-Electron-Microscope Observation. The sample of silver oxide consisted of opaque polycrystalline particles. From scanning electron micrographs it was observed that some dozens of primary particles about 0.1 μ in size aggregate to form a secondary particle several ten microns in size. Some examples of scanning electron micrographs are shown in Fig. 7. In the case of the thermal decomposition, the product silver somewhat melted in the course of the reaction. After the completion of the decomposition, the particle size of silver came to about several ten times larger than that of the sample of silver oxide.

On the other hand, in the case of the reduction, the primary particle decreased in size as the density changed from oxide to metallic silver, and no enlargement in size as a result of sintering was observed. From this result an enlargement in size resulting from the aggregation or sintering of primary particles does not seems to affect the fractional decomposition *vs.* time curves or, therefore, the reaction mechanism.

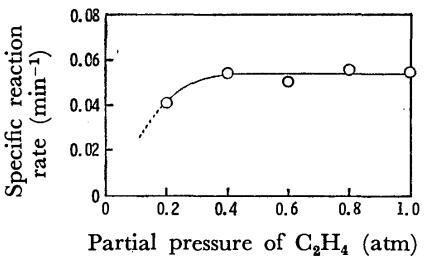

Fig. 6. Effect of partial pressure of C_2H_4 on reaction rate at 138 °C.

Discussion

The overall reaction of the thermal decomposition and reduction of silver(I) oxide can be written commonly by this equation:

$$Ag_2O(solid) + Reactant(gas) \rightarrow Ag(Solid) + Product(gas) \quad (1)$$

In the thermal decomposition, there is nothing corresponding to the reactant in Eq. (1), and the product is oxygen. The results in these experiments showed that, in a series of reactions, the thermal decomposition

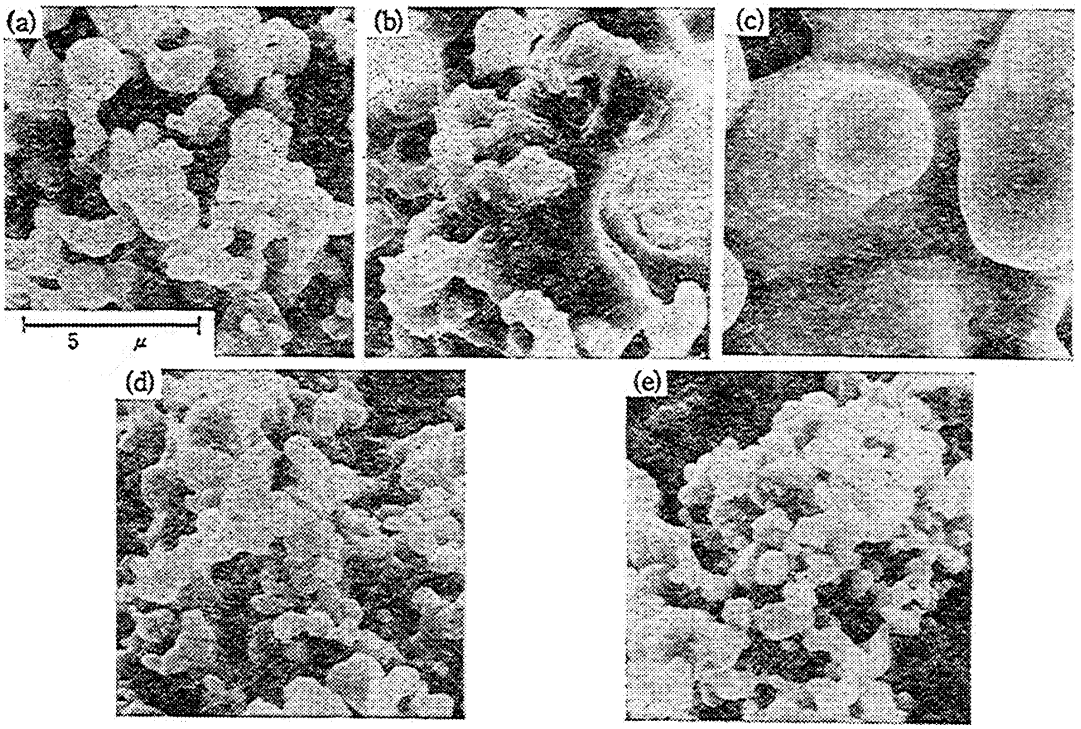

Fig. 7. Scanning electron micrographs of some selected samples.
a) Silver(I) oxide undecomposed. b) Sample at fractional decomposition of 0.5 in the thermal decomposition. c) Sample at complete decomposition in the thermal decomposition. d) Sample at fractional decomposition of 0.5 in the reduction with C_2H_4. e) Sample at complete decomposition in the reduction with C_2H_4.

occurred at the highest temperature (330 °C) and that the reduction with carbon monoxide occurred at the lowest temperature (−40 °C). The temperature at which the reaction commenced varied approximately linearly with ΔG°_{298}. It is interesting that each of these reactions gave the same sigmoidal shape to the fractional decomposition *vs.* time curves, although these reactions occurred at different temperatures, extending over a wide range.

Two kinds of theories to explain sigmoidal curves in a phase transformation and a thermal decomposition have been proposed. One kind is exemplified by those of Garner and of Prout and Tompkin, which explain the growth of nuclei in terms of the branching chain-reaction mechanism; the other kind is exemplified by Avrami, Mampel, Erofeev, and Cahn's theories, which take into account the overlapping of growing nuclei. Prout and Tompkin's rate equation is identical with Ostwald's equation, which was used by Lewis and by Hood and Murphy. However, it is unreasonable to apply this equation over the entire range of decomposition, because an equation of this form requires that all the solid product be in a position to catalyse all the particles of the solid reactant equally throughout the complete course of the reaction. In a solid decomposition where the mobility of the reacting constituents is low, such a situation is not feasible.[13] Besides, the results of this experiment did not fit in well with Prout-Tompkin's equation.

On the other hand, the latter contains complicated equations, none of which can be applied to any practical problem. However either of the following approximate equations can be utilized:

$$\alpha/(1-\alpha) = Bt^k \tag{2}$$

$$\alpha = 1 - \exp(-Bt^k) \tag{3}$$

where α is the fractional decomposition; t, the reaction time, and B and K, the constants characteristic of the reaction system.

As is shown in Figs. 8—11, the present experimental results fit in well with Eq. (3) except in the case of the

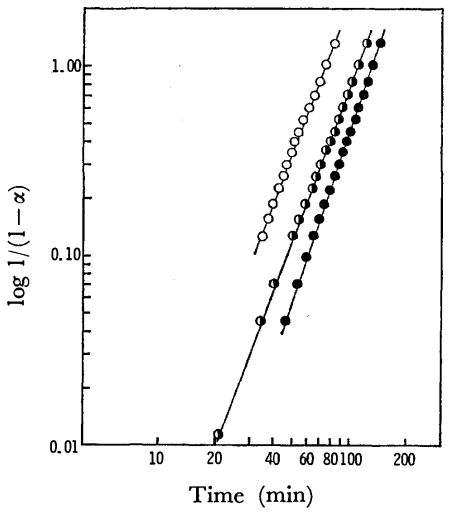

Fig. 8. Avrami plot in the case of thermal decomposition.
○ at 430 °C, ◑ at 420 °C, ● at 410 °C

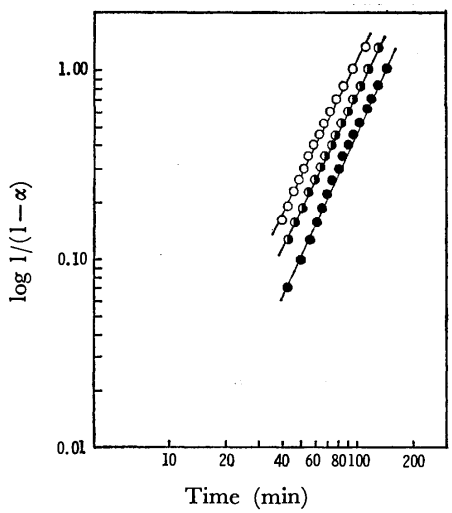

Fig. 9. Avrami plot in the case of reduction with C_2H_4.
○ at 145 °C, ◑ at 140 °C, ● at 136 °C

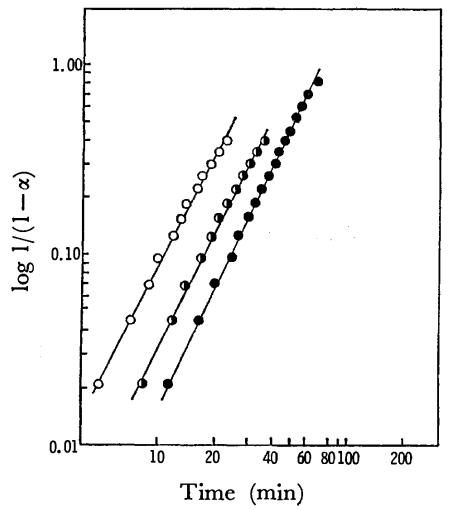

Fig. 10. Avrami plot in the case of reduction with H_2.
○ at 75 °C, ◑ at 70 °C, ● at 65 °C

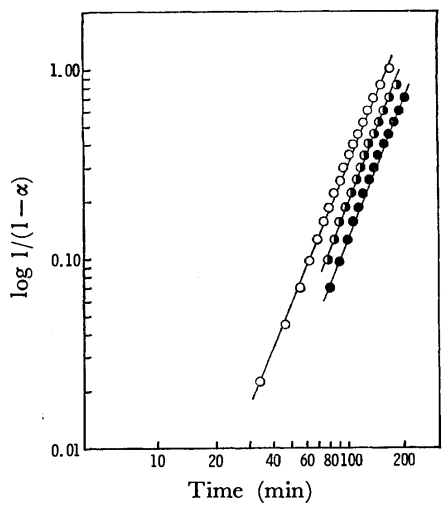

Fig. 11. Avrami plot in the case of reduction with CO.
○ at 10 °C, ◑ at 0 °C, ● at −8 °C

TABLE 2. EXAMINATION OF VALIDITY TO AVRAMI'S EQUATION AND APPARENT ACTIVATION ENERGY

System	Reaction temperature (°C)	k	B	Applicable range of Avrami's equation	E_a (kcal/mol)
Ag_2O-N_2	430	2.75	17.36×10^{-6}	$0.25<\alpha<0.95$	
(thermal decompn.)	420	2.61	8.67×10^{-6}	$0.03<\alpha<0.95$	96.5
	410	2.81	2.32×10^{-6}	$0.10<\alpha<0.95$	
Ag_2O-C_2H_4	145	2.04	2.15×10^{-4}	$0.30<\alpha<0.95$	
	140	2.08	1.22×10^{-4}	$0.25<\alpha<0.95$	38.5
	136	2.17	0.67×10^{-4}	$0.15<\alpha<0.95$	
Ag_2O-H_4	75	2.00	8.31×10^{-4}	$0.05<\alpha<0.60$	
	70	2.00	7.45×10^{-4}	$0.05<\alpha<0.60$	24.8
	65	2.10	2.90×10^{-4}	$0.05<\alpha<0.85$	
Ag_2O-CO	10	2.44	9.51×10^{-6}	$0.05<\alpha<0.90$	
	0	2.61	2.70×10^{-6}	$0.15<\alpha<0.95$	16.2
	−8	2.68	1.30×10^{-6}	$0.10<\alpha<0.80$	

reduction with hydrogen, where the range of applicability of Eq. (3) is somewhat small. From these figures, the values of k and B were determined. They are shown in Table 2. The values of k, being within 2.00—2.81, were approximately constant in all the reaction systems. From the finding that the thermal decomposition and the reduction occur obeying the same rate equation, it can be considered that the rate-determining step is similar. Plots of log B against $1/T$ (K^{-1}) gave straight lines, and from their slopes the apparent activation energies (E_a) were determined. The plot of this activation energy against the standard enthalpy change of the reaction at the average temperature investigated (ΔH°_T) gave a fairly good straight line (Fig. 12). Let us now discuss this free-energy relationship.

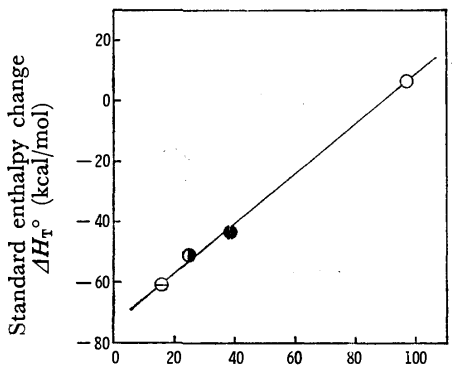

Fig. 12. Linear free energy relationship.
⊖ reduction with CO, ◑ reduction with H_2, ● reduction with C_2H_4. ○ thermal decomposition in N_2

Although the mechanism of Reaction (1) is not yet known in detail, generally the following steps may be considered: Silver oxide decomposes at the active point which exists in the interior of crystal or on the surface layer, thus producing silver and oxygen atoms. Then this oxygen atom diffuses to the outer surface to react with the reactant gas, and the silver atom diffuses to the interface between metallic silver and silver oxide to form a silver crystal.

Since the fractional decomposition *vs.* time curves gave a sigmoidal shape, the diffusion step may not be the rate-determining step. If the chemical reaction of an oxygen atom with a reactant gas occurs at the surface of silver oxide, the reaction rate depends upon the surface area of the silver oxide and on the partial pressure of the reactant gas. Since the surface area of silver oxide decreases as the reaction proceeds, the reaction rate must decrease monotonously and does not have an accelerated period. Even if this chemical reaction occurs over the whole surface of both silver oxide and silver, the sigmoidal curves cannot be explained, for the total surface area either remains constant (in the case of the reduction) or decreases gradually (in the case of the thermal decomposition), as may be seen in scanning electron micrographs. Moreover, the rate of the reaction is not first-order with respect to the partial pressure of reductive gas. Thus, the chemical reaction may not be the rate-determining step.

From Allen's[14] study it is reasonable to consider that silver-oxygen bond secession occurs at the initial stage of the reaction. However this step may not be the rate-determining step, for if it is so, the activation energies of each reaction must be constant in all the reaction systems, while in reality the apparent activation energy of each reaction, as calculated from the initial reaction rate, varied with the reaction system—the higher the reaction temperature, the larger this value.

Dubinin *et al.*[15] and Kato *et al.*[7] have reported that the thin layer silver coating on silver oxide and silver produced by the reduction with ethylene considerably increases the reaction rate. From these reports, and the finding that a series of these reactions occur obeying the same rate equation, similar to the equation of an ordinary phase transformation, it is more reasonable to consider that the step of the nucleation of silver and its development is the rate-determining step.

Though the results of this experiment can not reveal the detailed reaction mechanisms, from the above considerations we can estimate Eqs. (4) and (5) to be:

$$Ag_2O(solid) + Reactant(gas) \rightarrow Ag(interface) + Product(gas) \quad (4)$$

$$Ag(interface) \rightarrow Ag(solid) \quad (5)$$

From the previous discussion it can be considered that Reaction (4) steadily occurs in a preliminary equilibrium, and that Reaction (5) is rate-determining. Therefore:

$$\Delta G^\circ_{(1)} = \Delta G^\circ_{(4)} + \Delta G^\circ_{(5)} \quad (6)$$

$$\Delta G^\circ_{(4)} = -RT\ln(C_{Ag}\cdot C_{prod.}/C_{react.}) \quad (7)$$

The B is Avrami's rate equation is some function of the formation rate of the nuclei ($\dot{N}$) and the growth rate of the nuclei (G).[16] Though the form of this function depends upon the dimensionality of the development of the nuclei, in general it takes the form of const$\cdot G^a\cdot \dot{N}^b$.

The volume nucleation rate is approximately[16]:

$$\dot{N}_j = vn(\delta/D)^{3-j}\exp\{-(\Delta G_j^* + \Delta G_A^*)/RT\} \quad (8)$$

where j is the dimensionality of the nucleation site; v, a frequency factor; n, the number of atoms per unit volume; δ, an effective grain boundary thickness; D, the grain diameter; ΔG_j^*, the minimum free energy required to form a nucleus, and ΔG_A^*, the free energy of activation for a nucleus to continue to grow.

The linear growth rate would be:

$$G = v\delta(n/s)\exp(-\Delta G_A^*/RT) \quad (9)$$

where n/s is the density of atoms per unit area of the reactive molecules.

By rearranging Eqs. (1), (4) and (5), we get:

$$C_{Ag} = (C_{react.}/C_{prod.})\exp\{-(\Delta G^\circ_{(1)} - \Delta G^\circ_{(5)})/RT\} \quad (10)$$

where C_{Ag} is the concentration of silver atoms and is proportional to n.

Since the experiments in this study were carried out under similar conditions, the values of ($C_{react.}/C_{prod.}$) during the course of the reaction are equal in each reaction; thus, the apparent activation energy obtained from the Arrhenius plot of B becomes:

$$E_a = b\Delta H_j^* + (a+b)(\Delta H_A^* + \Delta H^\circ_{(1)} - \Delta H^\circ_{(5)}) \quad (11)$$

where ΔH° is an enthalpy change term corresponding to a free-energy change term. Since ΔH_j^*, ΔH_A^*, and $\Delta H^\circ_{(5)}$ are considered to be constant in all the reaction systems, we can understand that the plot of the apparent activation energy against $\Delta H^\circ_{(1)}$ should be a straight line.

From the above discussion, we may conclude that, since the chemical reaction process is very rapid, and since the process of the crystallization of new-phase silver is the rate-determining step, the thermal decomposition and reduction of silver oxide show the same kinetic behaviour as a phase transformation.

About the thermal decomposition of silver oxide, Allen[14] reported that the activation energy calculated from the reaction rate and the reaction temperature was 36 kcal/mol. A differentiation of Eq. (3) with t yields:

$$d\alpha/dt = kB^{1/k}f(\alpha) \quad (12)$$

Thus, the activation energy determined by Allen must be equal to $1/k$ times our apparent activation energy. Actually, the two give approximately equal values.

In this study, it is difficult to discuss the sites of nucleation and the dimensionality of the growth of the nuclei in detail considering the accuracy of our experiments. Moreover, whether or not the sites where the bond secession of silver oxide occurs are identical with the sites where the nuclei of a silver crystal generates is an interesting problem for future study.

References and Notes

1) G. N. Lewis, *Z. Phys. Chem.*, **52**, 310 (1905).
2) G. C. Hood Jr. and G. W. Murphy, *J. Chem. Educ.*, **26**, 169 (1949).
3) S. Tobisawa, This Bulletin, **32**, 1173 (1959).
4) P. J. Herley and E. G. Prout, *J. Amer. Chem. Soc.*, **82**, 1540 (1960).
5) M. M. Pavluchenko and E. Gurevich, *Zh. Obshch. Khim.*, **21**, 517 (1951).
6) W. E. Garner and L. W. Reaves, *Trans. Faraday Soc.*, **54**, 254 (1954).
7) A. Kato, Y. Anju, and T. Seiyama, *Nippon Kagaku Zasshi*, **91**, 56 (1970).
8) T. Yamashina and M. Seo, This Bulletin, **41**, 2547 (1968).
9) S. Kagawa, K. Kono, H. Futata, and T. Seiyama, *Kogyo Kagaku Zasshi*, **74**, 819 (1971).
10) H. T. Spath, H. G. Winkler, and K. Torker, "Proceedings of the Seventh Internetional Symposium on the Reactivity of Solid" Chapman & Hall, London (1972), p. 745.
11) In the reduction with ethylene a fractional decomposition of silver oxide was calculated from the amounts of products carbon dioxide and ethylene oxide.
12) Specific reaction rate was calculated by Eq. (12) described later.
13) D. A. Young, "The International Encyclopedia of Physical Chemistry and Chemical Physics. Topic 21, Solid and Surface Kinetics. Vol. 1, Decomposition of Solids" Pergamon Press, London (1966), p. 49.
14) J. A. Allen, *Aust. J. Chem.*, **13**, 431 (1960).
15) M. M. Dubinin, O. Kadlets, and V. Pouet, *Kinet. Katal.*, **8**, 292 (1967); *Chem. Abstr.*, **67**, 47594 (1967).
16) J. W. Cahn, *Acta Met.*, **4**, 449 (1956).

An Infrared Study of the Steric Effects of Alkyl Substituents on the N–H Stretching Absorptions of *sym*-Dialkylureas

Yoshiyuki MIDO

Department of Chemistry, Faculty of Science, Kobe University, Nada, Kobe 657

(Received October 6, 1973)

By examining their N–H stretching absorptions in the hydrogen-bonding system, the steric effects of the substituent on the C=O or N–H group have been studied for *sym*-disubstituted alkylureas of the *R*HNCONH*R'* type in carbon tetrachloride. By comparing the estimated percentage of the monomer, it is concluded that the steric effects are not large enough to convert the *trans* conformation into the *cis* conformation, though the branched alkyl groups may prevent another molecule from approaching more strongly than the normal alkyl groups. Correlations among some spectral parameters have been examined, such as the estimated percentage of the monomer, the frequency shift upon hydrogen-bond formation, the apparent integrated absorption intensity, and the half-intensity width of the associated band.

The peptide group in secondary amides has been shown to adopt possibly the *trans* and/or *cis* conformation under certain conditions:[1,2]

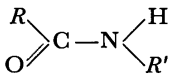

trans

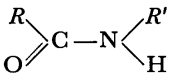

cis

The more favorable conformation and its percentage in solution are mainly decided by the steric factor between the substituents, *R* and *R'*, and the C=O group.[1-6] The steric factor can affect the intensity of the associated band; that is, the larger the size of the *R* and *R'* groups, the weaker the intensity.[5,6] The N–H stretching frequencies characteristic of their conformations have been established.[1-6]

As *sym*-dialkylureas have the –CO–NH– structure, such as in secondary amides, it seemed that it would be interesting to examine the relationships between the size of *N*-alkyl substituents and the intensity of the associated N–H stretching band in solution, and to estimate the limit of the size which can convert the dominant *trans* conformation into the *cis* conformation, if the steric hindrance of a bulky group such as *tert*-butyl can convert in that manner.

We have studied various alkylureas by infrared spectrometry and have shown that *sym*-dialkylureas are dominantly in the *trans-trans* conformation in the solid[7,8] and liquid states,[7] and in solutions.[9,10]

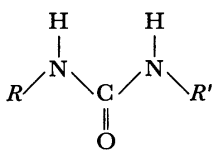

trans-trans

However, our conclusion regarding *sym*-di-*tert*-butylurea (*s*-D*t*BU) in solutions did not agree with that of Rao *et al.*,[11] suggesting that, of the two closely-spaced monomeric N–H stretching bands, the stronger band, at 3437 cm^{-1}, arises from the *cis* rotamer.[12] The other band, at 3469 cm^{-1} (indicated as a weak band by an arrow sign in Fig. 1) could be interpreted as being due to the *cis* conformation; we do not, however, have any conclusive evidence yet, though it is certain that the 3469 cm^{-1} band does not originate from the *trans* conformation.

The purposes of the present study are: (1) to examine whether or not the steric hindrance of a bulky group or groups such as *tert*-butyl is large enough to convert the *trans* conformation into the *cis* conformation, and (2) to establish possible correlations among the spectral parameters obtained from the N–H stretching absorptions for various *sym*-dialkylureas in a dilute carbon tetrachloride solution.

Experimental

All the dialkylureas used had already been identified in our previous studies.[7,8] Carbon tetrachloride for spectroscopy was used. The spectra (3600—3200 cm^{-1}) were recorded with solvent compensation at a slow speed and using a five-fold-scale expansion in frequency. The measurements were made at 27°±2 °C with a Hitachi EPI-G2 Infrared Grating Spectrophotometer.

The 0.0025 M solutions in carbon tetrachloride were examined using a 2.0-cm NaCl cell. Some typical spectra are shown in Fig. 1. The apparent molar extinction coefficient, ε, for the monomeric N–H stretching band of each sample was determined by measuring its apparent optical density, $O.D._{mono}$ of a 0.0005 M solution (using a 5.0-cm NaCl cell), in which the associated band no longer appears. The ε is defined as:

$$\varepsilon = \frac{1}{CL}\log_{10}\left(\frac{T_0}{T}\right)_{\nu_{max}}$$

where C is the concentration of the solute in moles per liter, L is the cell length in cm, and T_0 and T are the apparent intensities of the incident and transmitted radiation at the maximum wave number respectively.

In order to obtain reliable data, three or more samples were independently prepared for each of the dialkylureas, and their spectra were recorded. The spectral parameters were independently estimated from three or four of their reproducible spectra. The average value of the estimations is listed in Table 1. As the monomeric and associated bands significantly overlap one another, and as the latter band is much broader, as is shown in Fig. 1, the average values are considered to have some certainty. Therefore, the $O.D._{mono}$, the $O.D._{asso}$, and the frequency shift, $\Delta\nu$, were obtained from the band-contours before the graphical separation by Jones' method,[6] while the apparent integrated absorption intensity, B, and the half-intensity width, $\nu_{1/2}$, of the associated band were obtained from the band contours after the graphical separation. The estimated concentration percentage of the monomer, C_{mono}/C, was calculated from the $O.D._{mono}$ and

Table 1. IR data for N-H stretching bands of dialkylureas (0.0025 mol/lit. in CCl_4)

Compound No.[a]	R'		ε[b]	Monomer band O.D.	Monomer band C_{mono}/C (%)	Association band O.D.	Association band B[c] ($\times 10^{-3}$)	Association band $\nu_{1/2}$ (cm^{-1})	Association band $\Delta\nu$[d] (cm^{-1})
	$CH_3NHCONHR'$								
1	Methyl	*s*-DMU	127	0.475	75	0.176	10	123	88
2	Ethyl	MUE	107.5	0.424	79	0.191	9.5	113	90
3	Propyl	MUP	110	0.417	76	0.184	9	110	87
4	Isopropyl	MU*i*P	90 (49)[e]	0.382 (0.229)	85 (93.5)	0.165	7.5	109	79[f]
5	Butyl	MUB	112.5	0.439	78	0.163	8	110	90
6	*s*-Butyl	MU*s*B	90.5 (46)[e]	0.371 (0.205)	82 (89)	0.165	7	108	81[f]
7	*t*-Butyl	MU*t*B	91.5 (41)[e]	0.419 (0.204)	91.5 (99.5)	0.082	3.5	90	65[f]
	$C_2H_5NHCONHR'$								
8	Ethyl	*s*-DEU	98.5	0.399	81	0.189	9	113	84
9	Propyl	EUP	97.5	0.403	82.5	0.152	6.5	108	80
10	Isopropyl	EU*i*P	79	0.369	93.5	0.125	4.5	99	76
11	Butyl	EUB	93.5	0.404	86.5	0.147	6	104	81
12	*s*-Butyl	EU*s*B	83	0.369	89	0.139	5.5	102	81
13	*t*-Butyl	EU*t*B	80	0.379	95	0.084	2.5	77	71
	n-$C_3H_7NHCONHR'$								
14	Propyl	*s*-DPU	93	0.381	82	0.161	7	103	82
15	Isopropyl	PU*i*P	74	0.334	90.5	0.127	5	97	75
16	Butyl	PUB	87	0.367	84.5	0.177	8	106	83
17	Isobutyl	PU*i*B	86	0.365	85	0.190	8.5	106	86
18	*s*-Butyl	PU*s*B	76.5	0.336	88	0.143	5.5	93	78
19	*t*-Butyl	PU*t*B	75	0.342	91	0.079	2	77	73
	n-$C_4H_9NHCONHR'$								
20	Isopropyl	BU*i*P	76	0.342	90	0.114	4	89	70
21	Butyl	*s*-DBU	91.5	0.376	82	0.150	6.5	107	79
22	*s*-Butyl	BU*s*B	77.5	0.343	88.5	0.133	5	96	74
23	*t*-Butyl	BU*t*B	71.5	0.339	95	0.077	2.5	80	75
	The other $R'NHCONHR'$								
24	Isobutyl	*s*-D*i*BU	96	0.369	77	0.221	9	100	88
25	*s*-Butyl	*s*-D*s*BU	83	0.386	93	0.117	4	86	67
26	*t*-Butyl	*s*-D*t*BU	77.5	0.362	93.5	—	(0.5)	—	(60)
27	*t*-Amyl	*s*-D*t*AU	80.5	0.376	93.5	—	(0.5)	—	(60)

a) Point number in figures. b) Apparent molar extinction coefficient ($mol^{-1}\cdot l\cdot cm^{-1}$). c) $B=\int\frac{1}{CL}\log_e\left(\frac{T_0}{T}\right)d\nu$ ($mol^{-1}\cdot l\cdot cm^{-2}$). d) $\Delta\nu=\nu_{mono}-\nu_{asso}$, see Ref. 9 for ν_{mono}. e) Side band (monomer), see Experimental. f) The average value, see Experimental.

ε values. The B is defined as:

$$B=\frac{1}{CL}\int\log_e\left(\frac{T_0}{T}\right)d\nu$$

where $d\nu$ is the differential of the wave number.

In a special case with such a band-splitting as is seen in MU*i*P, MU*s*B and MU*t*B, when the values of parameters are as plotted in Figs. 2—7, the average value of two for the splitting in a spectral parameter was used except in C_{mono}/C and the corresponding ε in Figs. 2 and 4 respectively, since, generally, the N–H vibrations, which derive from two components due to two N–H groups on dialkylurea, appear as only one band. The exceptional C_{mono}/C in Fig. 2 for the special three was estimated for only the higher component in splitting because the intensity of the lower component is considerably affected by the neighboring associated band.

The uncertainties of C_{mono}/C, B, $\nu_{1/2}$, and $\Delta\nu$ may be estimated to be about 4%, 0.5×10^3 $mol^{-1}\cdot cm^{-2}$, 7 cm^{-1}, and 5 cm^{-1} respectively.

Results and Discussion

It is expected that the bulkier the effective size of alkyl substituents on dialkylureas is, the larger the steric hindrance between the C=O and the substituents will be, and the harder the intermolecular association through hydrogen bond will be, thus weakening the intensities of associated bands. Figure 1 shows the expected spectral behavior of the broader associated N–H band in dialkylureas; in their associated band-intensities, *s*-DMU, with the smallest methyl groups, is the strongest, while *s*-D*t*BU, with the largest *tert*-butyl groups, is the weakest, the other two being in the middle.

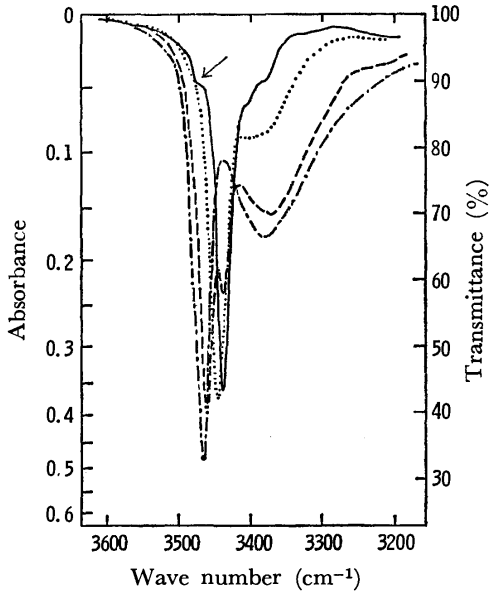

Fig. 1. Infrared spectra, N-H stretching region, of dialkylureas in CCl_4 (0.0025 M), ——————: *s*-DMU (1), ------: MU*i*P (4), ·····: EU*t*B (13), ——: *s*-D*t*BU (26). An arrow sign indicates the questionable band, which was assigned to the *trans* ν(N-H) vibration by Rao *et al.*[1]

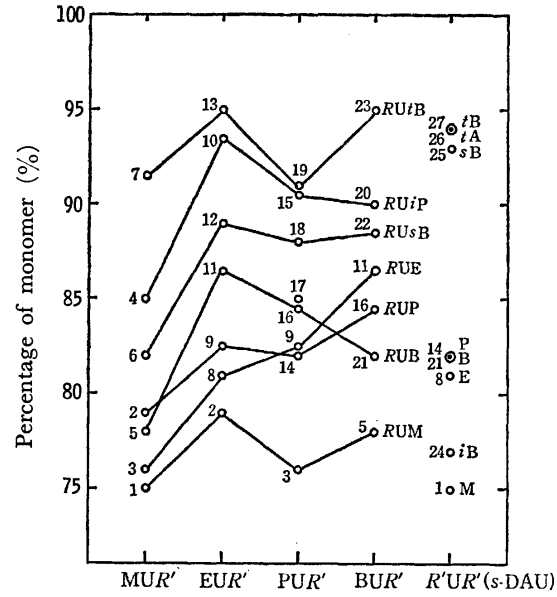

Fig. 2. The estimated percentage of monomer of dialkylureas in CCl_4 (0.0025 M). The points are numbered as in Table 1, column 1 (as in Figs. 3—7). The observed data for dialkylureas with the same *R*′ group are connected by a line.

The band-splitting of the monomeric absorption in MU*i*P (as well as in MU*s*B and MU*t*B) results from two different types of N-H groups, the higher component resulting from the methyl group, and the lower component, from the branched alkyl group, but not from rotational isomerism.[9,10] As the above monomeric band has been already assigned to the *trans* conformation except for the 3469 cm^{-1} band in *s*-D*t*BU,[9,10] it is also reasonable to similarly assign the associated band to the *trans* conformation.[13] Several spectral data obtained quantitatively are summarized in Table 1.

The estimated percentage of the monomer is plotted in Fig. 2 for four series of *R*HNCONH*R*′ (*RUR*′) according to the *R* group and a series with the same substituents (*s*-DAU). As may be seen in Fig. 2, the percentages are sensitive to the alkyl substituent and may be classified into three groups; the derivatives with a methyl group (*R*UM) have the lowest value, those with another primary alkyl group have a middle value, while those with such a branched alkyl group as isopropyl, *sec*- and *tert*-butyl have the highest value. The values for *s*-DAU are more sensitive to the alkyl substituents.

This suggests that the percentage roughly differentiates the alkyl substituent on dialkylurea. Also, the monomeric N-H stretching frequency of dialkylurea has been found to differentiate the alkyl substituent.[9,10] Therefore, we examined the correlation between the frequency and the percentage (Fig. 3). Figure 3 shows that the larger the percentage, the lower the frequency. It is interesting to note that the hydrogen-bonding formation ability of dialkylurea may, qualitatively but directly, be deduced from its monomeric N-H stretching frequency itself, though it can also, of course, be deduced from the well-established correlations of the frequency shift, $\Delta\nu$, with the physical properties.[14]

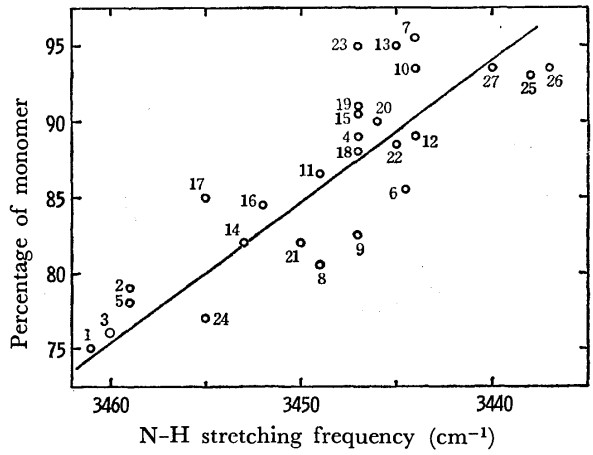

Fig. 3. The correlation between the monomeric N-H stretching frequency and the percentage of monomer.

Among the percentages of dialkylureas with a branched alkyl group or groups, there is no drastic difference, though there is a slightly increasing inclination in the percentage order: *RUs*B<*RUi*P<*RUt*B. This indicates that the steric hindrance between C=O and a *tert*-butyl group or groups is not large enough to drastically convert the *trans* conformation into the *cis* conformation. The indication adds support to our conclusions[9,10] that the dialkylureas examined exist dominantly in the *trans-trans* conformation in solution and that the stronger band at 3437 cm^{-1} of the two monomeric N-H stretching bands of *s*-D*t*BU arises from the *trans* conformation, contrary to the assignment by Rao *et al.*[11]

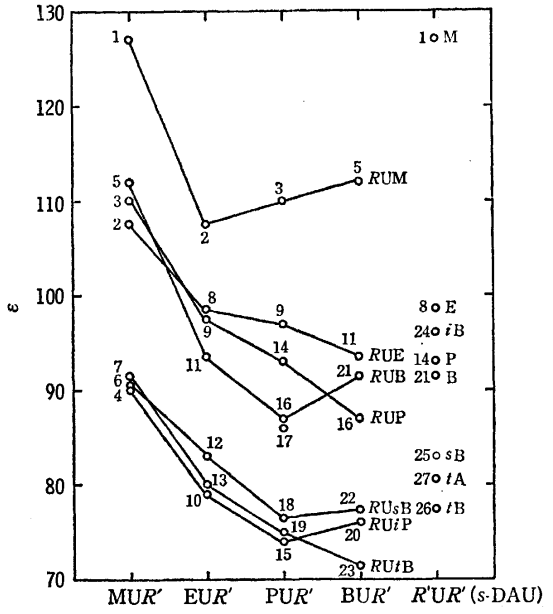

Fig. 4. The apparent molar extinction coefficient ε of dialkylureas in CCl_4 (0.0005 M, 5 cm).

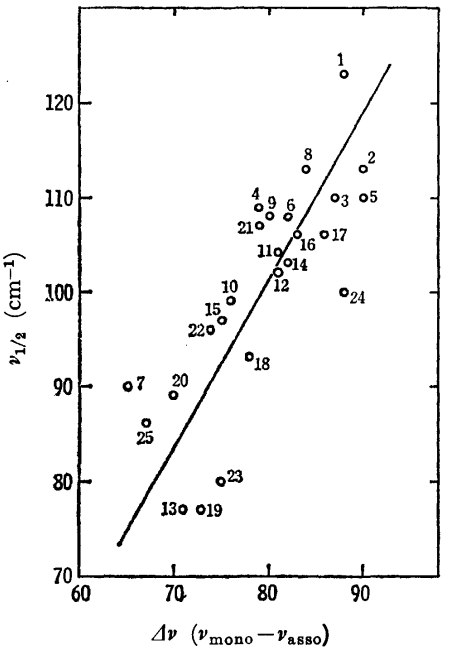

Fig. 5. The correlation between the frequency shift $\Delta\nu$ and the half-intensity width $\nu_{1/2}$.

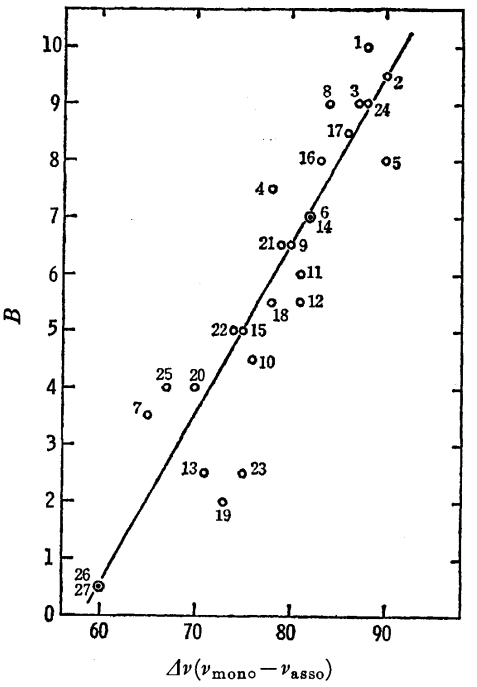

Fig. 6. The correlation between the frequency shift $\Delta\nu$ and the apparent integrated absorption intensity B.

The zig-zag-like line-plots in Fig. 2 seem to stem from the steric effect characteristic of the substituent on the hydrogen bond. The fact that no line-plots of the apparent molar extinction coefficients, ε, shown in Fig. 4 are zig-zag suggests that the steric effect affects the hydrogen-bonding formation and that the effect of the ethyl group is quite effective. Similar studies of *N*-alkylamides *R*CONH*R'* have shown that, of the *n*-alkyl groups, the ethyl group most greatly hinders the hydrogen-bonding formation, and that the effects of the longer-chain alkyl group are constant.[5,6]

The plots for ε may also be classified into three groups according to the *R'* group in *RUR'*. As there are large differences in ε among the three groups, it must be emphasized that when a hydrogen-bonding system is quantitatively studied, an examination should be made not only of the intensity of the associated band, but also of that of the monomeric band.

The amount of the X–H stretching frequency shift, $\Delta\nu$, upon a hydrogen-bonding system (X–H···Y) has generally been accepted as a measure of the strength of the hydrogen bond, and it has been directly related to the half-intensity width, $\nu_{1/2}$, and the intensity, B, of the associated band, the enthalpy of the hydrogen-bonding formation, and the X–H distance, but inversely related to the X···Y distance and the Hammett sigma function.[14,15]

In the present study, some correlations among spectral parameters have been examined for the hydrogen-bonding system of dialkylureas in a 0.0025 M carbon tetrachloride solution. It is quite evident from Table 1 and Fig. 1 that the bulkier the *R* and *R'* groups in *RUR'*, the smaller the $\Delta\nu$, $\nu_{1/2}$, or B value. The correlations between $\Delta\nu$ and $\nu_{1/2}$ or B were found to be linear (Figs. 5 and 6). A similar correlation was established between B and the estimated percentage of the associated species, C_{asso}/C (Fig. 7). The remarkable deviation of Points 26 (for *s*-D*t*BU) and 27 (*s*-D*t*AU) in Fig. 7 is considered to arise because their percentages of associated species were overestimated, since the questionable band at 3469 cm^{-1} in *s*-D*t*BU and the corresponding band in *s*-D*t*AU, which are also monomeric bands, as described, were not estimated to be added to their percentages of the monomer.

It is natural that the bulkier the alkyl substituents of dialkylureas are, the smaller the values of the $\Delta\nu$, $\nu_{1/2}$, B and C_{asso}/C become and, accordingly, the more closely the points approach to the original in Figs. 5—7.

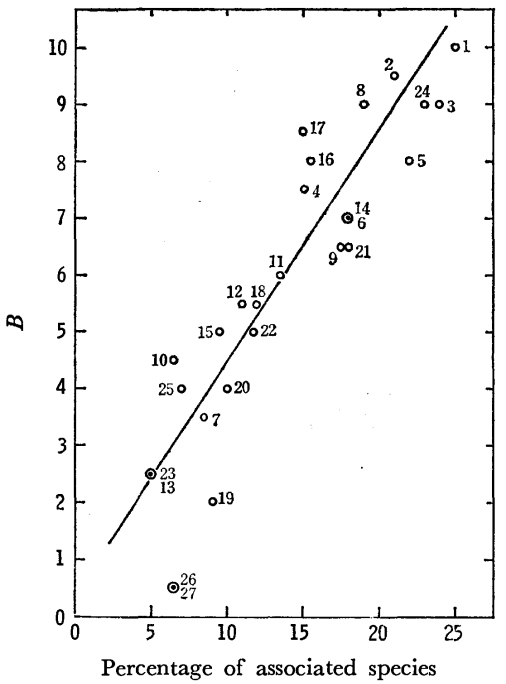

Fig. 7. The correlation between the estimated percentage of associated species C_{asso}/C and the apparent integrated absorption intensity B.

A comparison of the spectra of dialkylureas and *N*-alkylamides[6] shows clear differences in their spectral properties: (1) The $\Delta\nu$ values of the latter (*N*-alkylamides), when estimated from the spectra with N–H stretching band-intensities similar to those of the former, are approximately one and a half times as large as those of the former. (2) The former can form hydrogen bonds in a solution at a lower concentration than the latter. Probably, those spectral differences originate mainly from the differences in the electronic structure and the number of N–H groups per molecule. This consideration is supported by the facts that the C=O stretching frequencies of the former are generally higher than those of the latter, indicating the stronger tendency in the former to impart a double-bond character to the C=O bond, and that trialkylureas with only one N–H group give spectra with band-intensities similar to the latter at the same concentration.[16]

The author wishes to express his deep gratitude to Dr. Hiroatsu Matsuura of the Institute for Protein Research of Osaka University for his kind advice and to Prof. Hiromu Murata of Hiroshima University for his encouragement.

References

1) L. J. Bellamy, "The Infrared Spectra of Complex Molecules," 2nd ed., Methuen, London (1958), Chap. 12.
2) H. E. Hallam and C. M. Jones, *J. Mol. Struct.*, **5**, 1 (1970).
3) R. A. Russell and H. W. Thompson, *Spectrochim. Acta*, **8**, 138 (1956).
4) I. Suzuki, M. Tsuboi, T. Shimanouchi, and S. Mizushima, *ibid.*, **16**, 471 (1960).
5) R. L. Jones, *ibid.*, **23A**, 1745 (1967).
6) R. L. Jones, *ibid.*, **22**, 1555 (1966).
7) Y. Mido and H. Murata, This Bulletin, **42**, 3372 (1969).
8) Y. Mido, *Spectrochim. Acta*, **28A**, 1503 (1972).
9) Y. Mido, *ibid.*, **29A**, 1 (1973).
10) Y. Mido, *ibid.*, **29A**, 431 (1973).
11) C. N. R. Rao, G. C. Chaturvedi, and R. K. Gosavi, *J. Mol. Spectry*, **28**, 526 (1968).
12) For dialkylureas, Rao *et al.* did not define the term "*cis* rotamer" with regard to the two C–N rotational axes. Three forms could be considered: the *trans-trans*, the *trans-cis*, and the *cis-cis* forms, but the *cis-cis* form is unlikely on steric grounds.[9] It is possible that there is no difference in the N–H frequency for the *trans* conformation between the *trans-trans* and the *trans-cis* forms. We propose that the *cis* conformation represents only a *cis* relation between an N–H group and a C=O group about the C–N rotational axis.
13) If the associated band of the *cis* conformation is considered in relation to the case of secondary amides, it must appear 100—150 cm^{-1} lower than that of the *trans* conformation.[1,4,5]
14) G. C. Pimentel and A. L. McClellan, "The Hydrogen Bond", W. H. Freeman and company, San Fracisco and London (1960), Chap. 3.
15) Chap. 23 in Ref. 1.
16) Y. Mido, to be published.

The Molar Volume and Entropy of Adsorbed Methane on Porasil

Yoshio HORI* and Riki KOBAYASHI

Department of Chemical Engineering, Rice University, Houston, Texas 77001, U. S. A.

(Received October 25, 1973)

With the use of high-precision gas-chromatography, the multilayer adsorption of methane on fused silica beads was precisely measured between 145.0 K and 213.6 K. The molar volume and the partial molar entropy of the adsorbed methane were determined as a function of the temperature. The molar volume in the monolayer region depends much less on the temperature than that of the bulk liquid. However, the molar volume of multilayer adsorbed methane shows a dependence on the temperature similar to that of bulk liquid, which is at a lower temperature. The volume of the monolayer is practically constant under the present experimental conditions. The apparent thickness of the adsorbed monolayer was interpreted in terms of a simple collision model. The partial molar entropy of the adsorbed phase is much lower than that of the saturated bulk liquid. The lower dependence of the molar volume on the temperature and the lower entropy suggest that the freedom of motion of the adsorbed molecules is restricted as compared with those in bulk liquid.

The series perturbation technique,[1] a refined form of "Hypothetical perfect gas perturbation,"[2] was described in a previous paper and shown to be useful in the study of adsorption. The absolute adsorption and the molar volume of adsorbed methane can be measured by means of this technique. The molar volume of adsorbed methane was verified by the analysis of the dependence of Gibbs adsorption on the gas phase density, which was discussed previously.[1]

In order to measure the precise values of the molar volume of the adsorbed phase, a high-precision gas-chromatography was developed. The apparatus was equipped with a high-precision flow meter described elsewhere.[3] In addition to the molar volume of the adsorbed phase, the entropy of the adsorbed phase will be presented here.

Experimental

Apparatus. The high-pressure gas-chromatographic apparatus[1] was modified for the precise measurement of the retention volume. The apparatus consists of two sets of the ordinary gas-chromatographic apparatus. One has a column packed with an adsorbent for the measurement of the physical adsorption. The other is connected to the outlet of the former one and is used as a flow meter. A differentiator and a high-precision timer are combined with the latter chromatographic apparatus to give precise measurements of the flow rate of the carrier gas.[3] The general features of the apparatus are similar to the one described previously.[1] Therefore, only the modifications for precise measurement will be described here.

The pressure of the perturbation gases was kept equal to that of the carrier gas. The volume of the loop of the sample injection valve (a dose of perturbation gas) was about 50 μl. The carrier gas and all the perturbation gases were dried with magnesium perchlorate before entering the system. The column packed with the adsorbent was immersed in a thermostat filled with isohexane or isopentane. The thermostat was cooled by liquid nitrogen, and the temperature was maintained as constant as ±0.02° by means of a Thermotrol, Model 1053 A, manufactured by Hallikainen Instruments. The temperature distribution in the thermostat was uniform at any temperature in the present study in the range of ±4 inches from the column position. A flow-through thermal conductivity cell, Model 10-460 by Gow-Mac, was used. The gas volume of the thermal conductivity cell was 0.35 ml. The signal was recorded by means of a recorder, Speedomax W/L, made by Leeds & Northrup. The response time (full span) of the recorder was 0.5 s. The thermal conductivity cell and the expansion valves were immersed in the thermostat at 35.0 °C.

Materials. All the gases except radioactive methane and the adsorbent Porasil are the same as those used in the previous study.[1] The tritiated methane was purchased from New England Nuclear. The perturbation gases were diluted with the carrier gas (methane) in the following ratios: helium 1/32, neon 1/16, argon 1/32, and tritiated methane 0.5 curie in 560 ml of methane at 130 atm. The diluted perturbation gases were stored in 560 ml cylinders made of stainless steel.

Determination of Retention Time. The shape of an elution peak corresponds to the concentration distribution of a perturbation gas in the eluted carrier gas. The retention time is defined as the value averaged over this distribution curve:

$$t_r = \int_0^\infty y \cdot t dt \Big/ \int_0^\infty y dt$$

Here, y is the height of the elution peak at time t. When a perturbation gas is injected, a precision timer is triggered by a microswitch attached to the sample injection valve. The precision timer is turned off manually in the vicinity of the top of the elution peak, and this turn-off signal is marked on the recorder chart by an event marker. The precision timer is used to minimize the effect of any possible shrinkage or expansion of the chart paper.

The retention time, t (min), was calculated as below:

$$t_r = t_0 + \frac{l_c - l_m}{u}$$

t_0 (min) is the time elapsed between the turning on and off of the timer described above. l_m (cm) is the position of the turn-off mark on the recorder chart with reference to the outset of the elution peak. u (cm/min) is the chart speed of the recorder. u was taken at 10.16 cm/min during the course of this work. l_c is the center of gravity of the eluted peak:

$$l_c = \int_0^{l_2} y \cdot x dx \Big/ \int_0^{l_2} y dx = \sum_{i=0}^{s} x_i \cdot y_i \cdot \Delta x \Big/ \sum_{i=0}^{s} y_i \cdot \Delta x$$

where x (cm) is the position in the chart with reference to the outset of the peak and where l_2 is the position of the end of the peak. The other values follow the usual substitution

* Present address: Research Department, Kikumoto Works, Sumitomo Chemical Co., Ltd., Niihama, Ehime 792

of an integration with summation. The value of s was taken between 25 and 40 for an elution peak.

Source of Experimental Error. The retention times for He, Ne, Ar, and CH_3T were reproducible within 0.1% in any experimental run in this apparatus. The precision of the flow meter was 0.06% as has been discussed elsewhere.[3] Therefore, there must be other sources of experimental error. As a matter of fact, the flow rate was found to change when an eluted perturbation gas passed through the expansion valve. The carrier gas flows through the expansion valve in a viscous flow across a great difference of pressure. On the other hand, the composition of the part of the carrier gas including an eluted perturbation gas is a little different from pure carrier gas. This difference in composition gives rise to a change in the viscosity, resulting in the slight change in the flow rate mentioned above. Since the retention volume is calculated as the difference between the column value and the by-pass one (see Eq. (1) in Ref. 1), the viscosity effect will be cancelled out in the first order approximation. However, a delicate difference in flow pattern may bring about some scattering of the retention volumes. This viscosity effect will cause the sample-size effect, which was minimized in the present study by choosing the concentration of the perturbation gases stated above.

Results and Discussion

Adsorption Isotherm. The experimental data obtained by means of present apparatus were treated according to the series perturbation method previously reported.[1] The values of the absolute adsorption* of methane on Porasil between 145.0 K and 213.16 K are tabulated in Table 1. The isotherms show typical multilayer adsorption.

Molar Volume of the Adsorbed Methane. The free gas volume of the chromatographic column varies with the amount of adsorption. Figure 1 shows this relation in the present study after the correction of the thermal expansion of the stainless steel column and Porasil. In the interests of simplicity, the results at 193.16 K and 181.23 K are not shown in Fig. 1. The free gas volume decreases linearly up to 7 mmol/g,

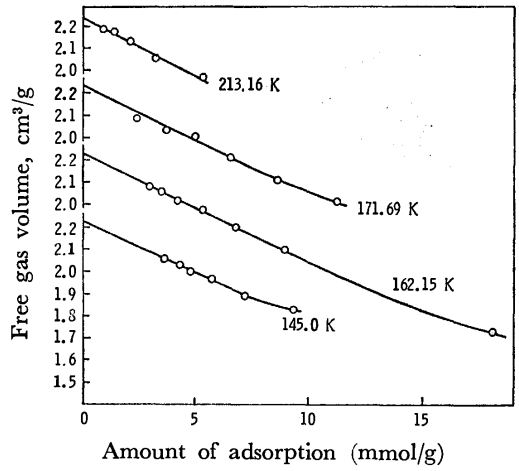

Fig. 1. Dependence of the free gas volume upon the amount of adsorption.

* The amount of adsorption discussed in this paper is the "absolute adsorption" described previously.[1]

Table 1. Absolute adsorption of methane on porasil

T K	P atm	Abs. ads. mmol/g
213.16	3.00	0.930
	5.00	1.381
	10.00	2.051
	20.00	3.191
	40.00	5.293
193.16	5.00	1.977
	10.00	2.968
	20.00	4.658
	30.00	6.689
	40.00	9.672
181.23	5.00	2.530
	10.00	3.793
	15.96	5.206
	20.07	6.332
	26.62	8.979
171.69	3.00	2.374
	6.64	3.693
	10.47	4.908
	14.79	6.529
	18.42	8.606
	20.89	11.239
162.15	3.00	2.981
	4.00	3.491
	5.50	4.170
	8.00	5.303
	10.50	6.755
	13.00	8.921
	15.50	18.073
145.00	1.80	3.641
	2.50	4.306
	3.00	4.790
	4.00	5.774
	5.00	7.178
	6.00	9.325

but the plots become curved near 10 mmol/g. The slopes of the straight lines were computed by the least-squares method between 0 and 7 mmol/g. The results, shown in Fig. 2, show the molar volume of the adsorbed phase between 0 and 7 mmol/g, V_a. The average molar volume, V_m, of the adsorbed phase near 10 mmol/g was estimated by means of:

$$V_m = \{V_g(0) - V_g(N_A)\}/N_A$$

where $V_g(0)$ and $V_g(N_A)$ are the free gas volume at the amount of adsorption 0 and N_A mmol/g. The value of $V_g(0)$ was estimated from the extrapolation linearly to zero adsorption in Fig. 1. The molar volume, V_m, is also plotted against the temperature in Fig. 2, with the molar volume of saturated liquid methane[4] shown for comparison. The data obtained from the previous paper are indicated by closed circles. The V_a is higher than that of liquid methane at lower temperatures and changes slowly with the temperature. On the other hand, V_m increases with the temperature in the linear extension of liquid methane at lower temperatures. These facts suggest that the adsorbed phase

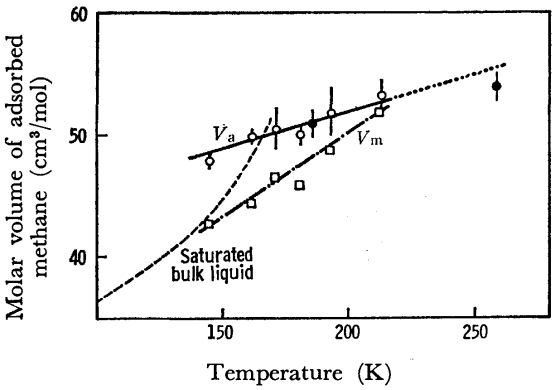

Fig. 2. Change of molar volumes of adsorbed methane with temperature. V_a is the molar volume near monolayer, and V_m is that averaged over 10 mmol/g of adsorption.

near the monolayer is quite different from the liquid phase, but that the multilayer adsorbed phase would be similar to the liquid phase at lower temperatures.

Temperature Dependence of the Monolayer Capacity. The adsorption data were processed according to a modified BET method which has three parameters:[5]

$$\Phi/N_A = 1/(N_0 \cdot C) + \Theta/N_0$$
$$\Phi \equiv x[(1-x^n)-nx^n(1-x)]/(1-x)^2$$
$$\Theta \equiv x(1-x^n)/(1-x)$$
$$x \equiv P/P_0$$

N_0 is the monolayer capacity (mmol/g). P and P_0 are the adsorption pressure and the saturation pressure of the bulk liquid at the same temperature. n is a parameter adjustable so as to give the best straight line in the Φ/N_A *vs.* Θ plot. Straight lines were obtained where x was less than 0.6. The values of n lie between 5.5 and 6. In Table 2 are tabulated the values of N_0 obtained by this procedure. It is remarkable that the monolayer capacity changes very slowly with the temperature. The volume of the monolayer, V_0, can be evaluated by means of:

$$V_0 = V_a \cdot N_0$$

with the V_a as shown in Fig. 2. The V_0 value appears in the third column of Table 2. The monolayer volumes are apparently independent of the temperature.

Apparent Thickness of the Monolayer. One can estimate the apparent thickness of the monolayer, h_0, from this relationship:

Table 2. The monolayer properties of adsorbed methane on porasil

T K	N_0 mmol/g	V_0 cm³/g	h_0 Å
213.16	3.04±0.02	0.161	3.34
193.16	3.13±0.01	0.162	3.36
181.23	3.17±0.01	0.159	3.30
171.69	3.18±0.02	0.161	3.34
162.15	3.23±0.01	0.161	3.34
145.00	3.28±0.02	0.157	3.26

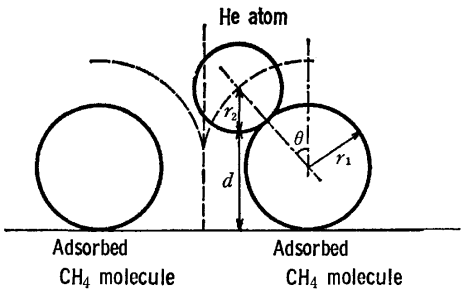

Fig. 3. A collision model of a perturbation gas atom and adsorbed methane molecules.

$$h_0 = V_0/A$$

where A is the surface area of the adsorbent, 482 m²/g according to conventional BET, using nitrogen with molecular cross-sectional area of 16.2 Å². The thickness of the monolayer, shown in the fourth column of Table 2, is virtually constant.

Since an adsorbed molecule will vibrate normal to the surface, the thickness of the monolayer must be larger than the collision diameter of the adsorbate molecule. Therefore, it seems to be contradictory that the apparent thickness of the monolayer is 3.31 Å, while the collision dimaeter of methane is 3.817 Å.[6] This will now be explained. Let us take an example of a helium atom moving normal toward the surface (Fig. 3). The helium atom will hit an adsorbed methane molecule and fly back to the gas phase again. The distance between the center of the helium atom and the surface is r_2+d when a helium atom is in contact with a methane molecule (Fig. 3), where r_1 and r_2 are 1/2 of the collision diameters of methane and helium respectively. The contribution of r_2 has already been corrected to the steric effect in the series-perturbation theory by adding $A \cdot r_2$ to the retention volume of helium,[1] where A is the surface area of the adsorbent. Thus, the thickness of the adsorbed layer may be observed to be d in that collision. The apparent thickness of the adsorbed layer can be estimated by averaging the d values over the surface of the adsorbed methane molecule. If adsorbed methane molecules are arranged in a hexagonal closed packing position, and if the monolayer capacity is assumed to be 3.20 mmol/g, the apparent thickness of the adsorbed layer can be estimated to be 3.0 Å by a simple calculation. In this estimation, the collision diameters of helium and methane are taken to be 2.56 Å and 3.82 Å respectively.[6] If the helium atom moves parallel to the surface, the apparent thickness will be observed to be equal to 3.82 Å. Therefore, the actual value of the apparent thickness must be a certain value between 3.0 Å and 3.82 Å. If one takes into account the vibrational motion of adsorbed methane normal to the surface, the observed apparent thickness (3.31 Å) is in good agreement with the value estimated above.

Entropy of the Adsorbed Methane. The experimental data were treated according to a procedure described previously.[7] Figure 4 shows the plots of $\log f$ *vs.* $1/T$ at fixed amounts of adsorption, where f

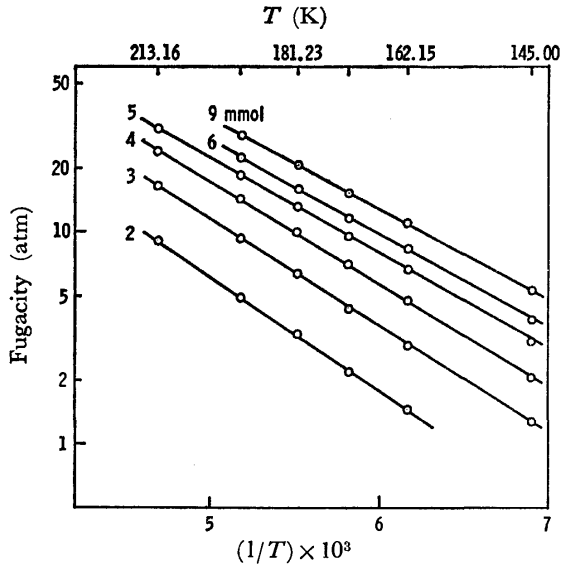

Fig. 4. Plots of $\log f$ *vs.* $1/T$ at fixed amounts of adsorption.

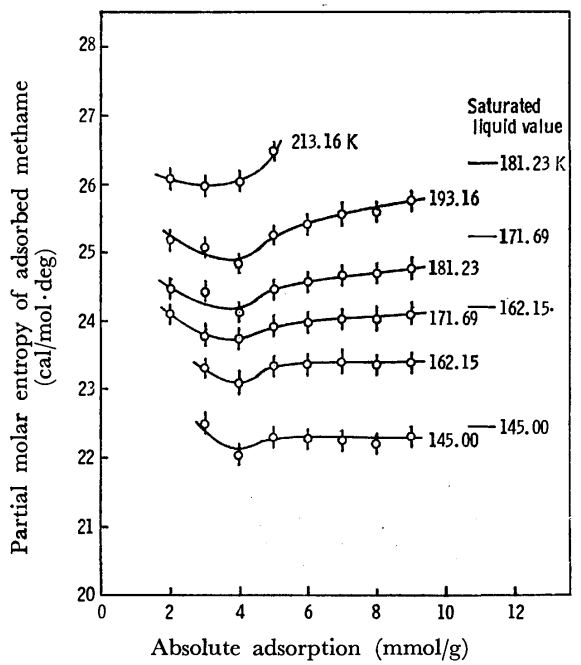

Fig. 5. Entropy of saturated liquid methane is indicated in the right-hand side.

is the equilibrium fugacity. The experimental points for 7 and 8 mmol/g are not shown for the sake of simplicity. Single straight lines can be drawn over all the range of temperatures. The slopes of the straight lines were determined by the least-squares method.

The partial molar entropy of the adsorbed methane was also calculated; it is shown in Fig. 5.** In Fig. 5 the molar entropy of saturated liquid methane is also shown at various temperatures. The partial molar entropy of the adsorbed phase at 145 K is nearly equal to the molar entropy of saturated liquid at the same temperature.*** However, above 145 K the partial molar entropy of the adsorbed methane is much lower than the molar entropy of the saturated liquid. As has been mentioned above, the temperature dependence of the molar volume of the adsorbed methane, V_m, is much lower than that of the bulk liquid (Fig. 2). V_m increases linearly with the temperature near the critical temperature (190.9 K[8]), like an extension of the molar volume of saturated liquid methane at lower temperatures. This may be explained as follows. The surface will attract adsorbate molecules and prevent the intermolecular distance from increasing steeply near the critical temperature. These facts suggest that the freedom of motion of the adsorbed molecules is restricted above 145 K as compared with that in bulk liquid.

Grant and Manes[9] stated that the liquidlike state may persist on the adsorbent at temperatures far above the critical temperature of the free liquid. Their assumption was previously verified by the present authors.[7]

Brunauer[10] suggested that multilayer adsorption probably occurs at temperatures where molecular clusters can exist in the gas phase, *i. e.*, for temperatures up to 10 to 15° above the critical. However, the present authors investigated the high-pressure adsorption of methane on Porasil, and found that multilayer adsorption takes place as much as 40° above the critical temperature. The −19.9 °C isotherm, 60° higher than the critical, reaches about 1.6 times the monolayer coverage.[1]

These findings indicate that the surface attracts adsorbate molecules very strongly, even over the monolayer coverage, and that multilayer adsorbed molecules possess less freedom of motion than those of bulk liquid at the same temperature.

Financial support was supplied by the U. S. National Science Foundation.

References

1) Y. Hori and R. Kobayashi, *J. Chem. Phys.* **54**, 1226 (1971).
2) S. Masukawa and R. Kobayashi, *J. Gas Chromatog.* **6**, 257 (1968).
3) Y. Hori and R. Kobayashi, This Bulletin, **47**, 1791 (1974).
4) H. E. Tester, "Thermodynamic Functions of Gases"

** The values of entropy above 4 mmol/g of adsorption at 213.16 K and 193.16 K differ somewhat from those reported in the previous paper.[7] This disagreement comes from the different temperature ranges of measurement in the two studies. It is impossible at present to tell whether or not the discrepancy is meaningful.

*** The measurement could not be made below 145.0 K for the following reason. In order to obtain precise values of the retention time, the flow rate must not be two low at the detectors. On the other hand the pressure drop across the column is to be low enough to be negligible. Therefore the pressure should be appreciably higher inside the column than at the detector. (*i.e.* 1 atm) However, the vapor pressure of methane becomes very low below 145.0 K (for example, 2.67 atm at 125 K). Consequently, it is impossible to measure an appropriate adsorption isotherm.

F. Din (Editor), Vol. 3, Butterworths, London (1961).
5) L. G. Joyner, E. B. Weinberger and C. W. Montgomery *J. Amer. Chem. Soc.*, **67**, 2182 (1945).
6) J. O. Hirschfelder, C. F. Curtiss and R. G. Bird, "Molecular Theory of Gases and Liquids," John Wiley and Sons, Inc., New York (1966).
7) Y. Hori and R. Kobayashi, *Ind. Eng. Chem. Fundamentals*, **12**, 26 (1973).
8) A. J. Vennix and R. Kobayashi, *A. I. Ch. E. J.* **15**, 926 (1969).
9) R. J. Grant and M. Manes, *Ind. Eng. Chem. Fundamentals* **3**, 211 (1964).
10) S. Brunauer, "The Adsorption of Gases and Vapors" Princeton U. P., Princeton, N. J. (1943).

The Electro-Initiated Polymerization of Acrylamide in an Aqueous Solution of Trifluoroacetic Acid and Potassium Trifluoroacetate*

Zenpachi OGUMI, Isao TARI,** Zenichiro TAKEHARA, and Shiro YOSHIZAWA

Department of Industrial Chemistry, Faculty of Engineering, Kyoto University, Yoshida, Sakyo-ku, Kyoto 606

(Received November 2, 1973)

The electro-initiated polymerization of acrylamide was investigated in an aqueous solution of trifluoroacetic acid and potassium trifluoroacetate. An oligomer with a molecular weight of 4000—6000 was thus obtained. The initiating ability of Kolbe's intermediate radicals was recognized by an analysis of the fluorine contained in the polymerized products as the end group. Kolbe's intermediate radicals, R·, react with monomers, M, to form RM·, which takes the paths of polymerization and other reactions. The rate of reaction to form RM· is so fast that no Kolbe's dimer, C_2F_6, is obtained. Gas analysis clarified the ratio of $CF_3COO\cdot$ to $CF_3\cdot$, which reacted with the monomer. The comparison of the molecular weights as measured by the two different methods suggests that the coupling reaction of radical ends terminates the propagation reaction. The rate of oligomer production was independent of the current density.

Over a period of years, much interest has been shown in electrolytic methods of initiating a polymerization, the so-called electro-initiated polymerization. A few papers have been reported concerning utilizing Kolbe's electrolysis as a source of free radicals for initiating polymerization. Yoshizawa *et al.*[1] obtained a polymerized acrylamide with a molecular weight of 700—1500 by the electro-initiated polymerization of acrylamide in an aqueous solution of acetic acid and potassium acetate. In this paper, the polymerization of acrylamide in an aqueous solution of trifluoroacetic acid and potassium trifluoroacetate was examined. The use of trifluoroacetate instead of acetate allows us to make sure whether Kolbe's radicals initiate the polymerization or produce the initiating species from an analysis of fluorine, which is considered to be present as the end group. From the results of the current efficiency of the production of oligomer and the relation between the rate of electrode reaction and that of polymerization, a path of the production of the oligomer may be suggested. Furthermore, information about Kolbe's intermediate radicals may be obtained.

Experimental

An H-shaped glass fitted with a fine fritted glass filter as a diaphragm was used as the electrolysis cell. Smooth platinum plates (3×3 cm^2) were used as electrodes. One of them was coated on one side with silicon resin for use as a working electrode, and this one was electrolyzed anodically and cathodically, alternately, and finally cathodically in 0.5 M H_2SO_4 at 20 mA/cm^2 as pretreatment. After that, it was washed with distilled water and electrolytes and then used immediately. Trifluoroacetic acid (commercial G.R. grade) was used.

The content of iron compound in it, which is known to affect the polymerization of acrylamide,[2] was less than 0.003 %, and this is low enough to have no effect on this experiment. Four mol of this reagent and 2 mol of potassium hydroxide (comercial G.R. grade) were dissolved in distilled water to 1 liter. This solution will be designated as TFA+TFK 4M from now on. The monomer of acrylamide was recrystallized from benzene and dried under air. The acrylamide thus refined, which will be designated as AAM, was stored in a dark and cold place and used within a week. The anolyte was prepared by dissolving a given amount of AAM in 100 ml of TFA+TFK 4M. TFA+TFK 4M was used as a catholyte without any addition of AAM. Electrolysis was carried out in an ice-water bath. Nitrogen was bubbled from 30 min before the beginning of the electrolysis to its end. The potential-current curve was potentiostatically obtained by the use of a rotating disk electrode (the surface area was 1 cm^2) in order to prevent the working electrode from being covered by the gas evolved. When the anolyte was poured into 1 liter of methanol after electrolysis, a white precipitate of an insoluble polymerized product came out. This was filtered through a #4 glass filter, dried at 60—80 °C under reduced pressure, and weighed. The viscosities were determined in an Ubellohde viscometer mounted in a thermostated bath held at 30.00±0.05 °C. The intrinsic viscosities were determined by means of the usual graphic plots. The weight-average molecular weight was calculated by means of the equation: $[\eta]=3.73\times10^{-4}\times M_w^{0.66}$.[3] To examine the possibility of the hydrolysis of the amide group to acid, the pH titration of the aqueous solution of the product was carried out. The results showed no hydrolysis occurring.

Results

Fluorine Content in Polymerized Products. The polymerized product obtained by the electrolysis of TFA+TFK 4M 100 ml+AAM 20 g at the anodic current of 400 mA/9 cm^2 was dissolved into the distilled water; this solution was poured into methanol in order to free the occluded fluorine from the product. The fluorine content in the product purified by repeating this process five times was examined by elemental analysis. Its content was between 2 and 3 percent. On the other hand, the polymerized product obtained by the electrolysis of a solution of acetic acid and its potassium salt was dissolved into TFA+TFK 4M, and then the fluorine content of this sample was examined. However, only a trace of fluorine was detected. These results clearly indicate that fluorine was included in the product *via* electrode processes.

Potential-current Relationship. The steady-state potential-current relationship was potentiostatically obtained. In this experiment, a rotating disk electrode

* Studies of the Electro-initiated Polymerization. Part 3.

** Present address: Department of Synthetic Chemistry, Faculty of Engineering, Okayama University, Tsushima, Okayama 700

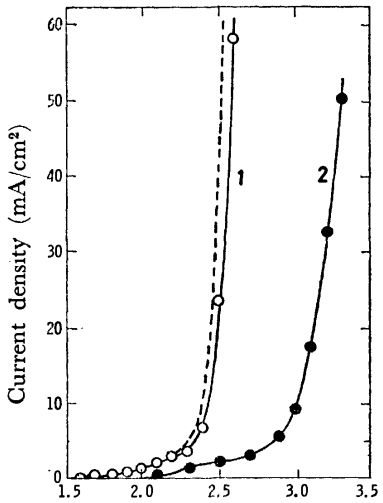

Fig. 1. Potentiostatic current-potential curves on the platinum rotating disk electrode in the solution of TFA+TFK 4M.
Rotating speed: 800 rpm.
-○-: without addition of AAM,
-●-: with addition of AAM 20 g
---: ohmic drop corrected

was used for the reason described above. The ohmic drop between the working and reference electrodes was not corrected in Fig. 1. This correction would cause Curve 2, measured in the solution containing AAM, to be almost the same as Curve 1, measured in the solution containing no AAM, as is shown by the dotted line. These curves show a current plateau which is characteristic of the Kolbe reaction.

Relationship between the Electrolysis Time and the Yield of an Oligomer. As is shown in Fig. 2, the yields of the oligomer increase linearly with the electrolysis time until four hours. This shows that the yield can be normalized independent of the electrolysis time, so that the induction period of oligomer production can be very short and the conditions can be kept constant during the electrolysis. Lying for eight hours under the same conditions except for a current passing through gave no polymerized product.

The Effect of the AAM Concentration on the Yields. The dependence of the yields on the concentration of AAM was examined at a current of 440 mA/9 cm².

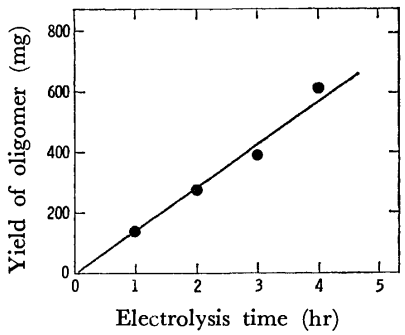

Fig. 2. Dependence of yields on electrolysis time in the solution of TFA+TFK 100 ml+AAM 20 g.
Current: 400 mA/9 cm²

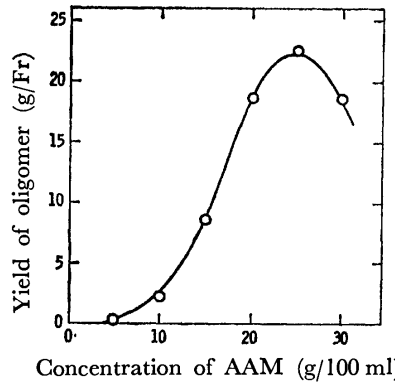

Fig. 3. Dependence of yields on the concentration of AAM in the solution of TFA+TFK 4M
Current: 400 mA/9 cm²

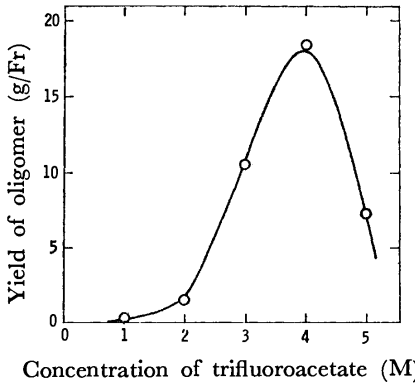

Fig. 4. Dependence of yields on the concentration of trifluoroacetate.
AAM 20 g per 100 ml of solution
Current: 400 mA/9 cm², $CF_3COOH:CF_3COOK=1:1$

The results are presented in Fig. 3.

The Effect of the Concentration of Trifluoroacetate on the Yields. The dependence of the yields on the concentration of trifluoroacetate was examined at the current of 400 mA/9 cm². In these experiments, the ratio of trifluoroacetic acid to potassium trifluoroacetate was kept constant at 1 : 1. The results shown in Fig. 4 show the maximum and the disagreement with the results obtained in the case of acetate, which shows a linear dependence.[1)]

The Effect of the Current Density on the Yield. In order to investigate the effect of the current density on the yield, electrolysis was carried out at different current densities under the conditions of TFA+TFK 4M 100 ml+AAM 20 g. The results are shown in Fig. 5.

Analysis of Evolved Gases. A gas chromatographic technique was utilized to determine the gaseous products which were formed during electrolysis. The oxygen, tetrafluoromethane, hexafluoroethane, and carbon dioxide were analyzed by using the stationary phase of silica gel, Porapak K, and molecular-sieve 5A. The retention time was used for the qualitative analysis. The relative sensitivities, $N_2 : O_2 : CO_2 : CF_4 : C_2F_6 = 1.00 : 1.05 : 0.872 : 0.541 : 0.485$, were used for the quantitative analysis. Table 1 shows that both carbon dioxide and hexafluoroehane were evolved at high current efficiencies when no AAM was added, while,

Table 1. Current efficiency of gaseous products
Solution: TFA+TFK 4 M, Platinum electrode

AAM (g/100 ml)		0			20		
C. D. (mA/cm²)		20	30	40	20	30	40
CE (%)	O_2	8.8	7.0	5.5	2.3	1.4	1.5
	CO_2	77.5	88.5	90.2	33.7	42.9	51.5
	C_2F_6	75.1	85.5	95.7	0	0	0

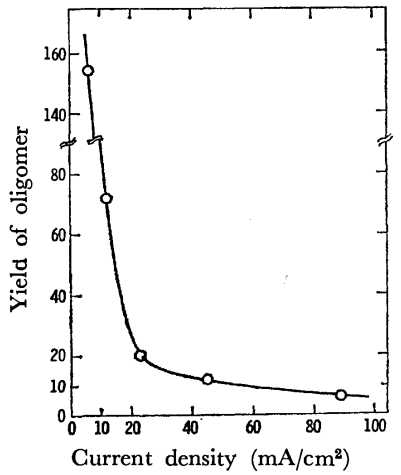

Fig. 5. Dependence of yields on current density in the solution TFA+TFK 4 M 100 ml+AAM 20 g.

on the other hand, the addition of AAM to anolyte caused a significant decrease in the current efficiency of the evolution of carbon dioxide and allowed the production of only a trace of hexafluoroethane. These results indicate that the intermediate radicals produced (R·) by electrolysis on the electrode do not further the normal coupling process of Kolbe's reaction, but react with the monomer (M) to form RM·. Whether CF_3COO· or CF_3· of the intermediate radicals reacts with the monomer was determined by a comparison of the current efficiencies of the evolution of gases between the cases without and with the addition of AAM. The results are shown in Table 2.

Table 2. The ratio of radicals which react with monomer
TFA+TFK 4 mol/l, AAM 20 g/100 ml

C.D. (mA/cm²)	Radical	
	CF_3COO%	CF_3%
20	44	33
30	45	43
40	37	52

Molecular Weight. The molecular weight was determined by means of two methods, one was based on viscosity measurements, and the other one, on a quantitative analysis of the end groups of the product by measuring the fluorine content. The results calculated by the two different measurements are listed in Table 3. The calculation in the latter method was carried out on the assumption that both ends of a product had a trifluoromethyl group. This table shows that the molecular weight does not depend on the current density.

Discussion

The facts that fluorine was detected in the polymerized products and that the molecular weights calculated from the fluorine contents were almost equal to those obtained by means of viscosity measurements indicate that Kolbe's electrochemical reaction produces the initiating species of polymerization and that termination is caused by a coupling reaction of radicals. It had previously been certified that the charge transfer of monomeric acrylamide on the anode does not take place under the experimental conditions adopted here. It has been reported that, in an experiment using acetic acid and potassium acetate, the oligomer with a molecular weight of about 1000 was produced.[1] On the other hand, in this experiment an oligomer with a molecular weight of 4000—6000 was obtained. This may be considered because of the difference in the possibilities of chain transfer to species in the electrolyte. The polymerized product was identified by means of IR spectroscopy as the oligomer of acrylamide. The electrochemical reaction of trifluoroacetate was extensively investigated in detail by Conway *et al.*[4] They proposed that trifluoroacetate furthers the process of Kolbe's reaction on the platiniumine electrode as follows, in the same way as in the case of acetate:

$$CF_3COO^- \longrightarrow CF_3COO\cdot + e \qquad (1)$$

Table 3. The effect of current density on the products
Solution: TFA+TFK 4 M, AAM: 20 g/100 ml

Current (mA/9 cm²)	800	400	200	100	50	means
Yield (g/Fr)	5.70	12.06	20.44	72.38	154.2	—
Viscosity[η]	0.1125	0.1198	0.1165	0.115	0.1222	0.1172
M. wt.[a]	5100	5700	5400	5300	5800	5460
F content	2.19	2.335	2.245	2.085	1.96	2.151
M. wt.[b]	5210	4880	5080	5470	5820	5290

a) Calculated by using [η]. b) Calculated by using F content.

$$CF_3COO\cdot \longrightarrow CF_3\cdot + CO_2 \quad (2)$$

$$CF_3\cdot \longrightarrow 1/2C_2F_6 \quad (3)$$

or

$$CF_3COO\cdot \longrightarrow 1/2C_2F_6 + CO_2 \quad (4)$$

Many workers have proposed different mechanisms for Kolbe's reaction. We consider that the free radical mechanism is most reasonable. In this work, however, gas analysis has clearly shown that the addition of AAM to the anolyte resulted in preventing the evolution of Kolbe's coupling product, C_2F_6. This indicates that the intermediate species, $CF_3COO\cdot$ and/or $CF_3\cdot$, produced by the charge transfer of trifluoroacetate on the anode react with the monomeric acrylamide existing near the anode much faster than they react in the path of Kolbe's coupling process which produces C_2F_6 and forms RM·. The radicals, RM·, produces in this way react among themselves or with R· and monomers. The current efficiencies of the production of oligomers can be calculated from the yields and molecular weights of oligomers. As is shown in Fig. 6, a straight-line relation on logarithmic coordinates was obtained. This means that the rate of the production of the oligomer is independent of the rate of the electrode process and becomes a very slow and almost constant value compared with the latter. All this indicates that most of the RM· produced disappeared without furthering the polymerization. This result can be explained by considering in the same way as in the "cage effect theory," which is extensively used on the discussion of polymer chemistry. The RM· produced exists on the electrode surface or in the vicinity of the electrode, where the concentration of radicals is so high that the coupling reaction occurs easily. This is why the initiating efficiency of R· becomes very low. Thus, the polymerization may proceed as follows.

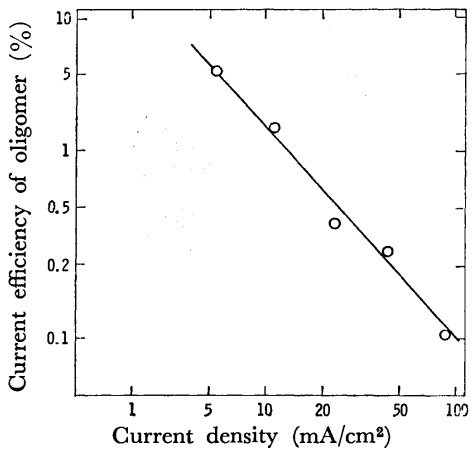

Fig. 6. Dependence of current efficiencies for polymerization on current density.

$$R\cdot + M \xrightarrow{\text{fast}} RM\cdot \quad (5)$$

$$2RM\cdot \longrightarrow RMMR \quad (6)$$

$$RM\cdot + R\cdot \longrightarrow RMR \quad (7)$$

$$RM\cdot + M \xrightarrow{\text{slow}} RMM\cdot \dashrightarrow \text{oligomer} \quad (8)$$

R· is $CF_3COO\cdot$ and/or $CF_3\cdot$, and the ratio of $CF_3COO\cdot$ to $CF_3\cdot$ can be calculated from the gas analysis, as is shown in Table 2. The production of the high polymer of acrylamide caused by the addition of iron compounds to the solution adopted here has already been reported.[2] With reference to this evidence, intermediate radicals, RM·, and Kolbe's radicals can not exist as literally "free" radicals, because, if so, they would react to the high polymer, instead, they interact with the electrode. The region where polymerization takes place will be discussed in detail in following papers.

References

1) S. Yoshizawa, I. Tari, and M. Suhara, *Denki Kagaku*, **40**, 650 (1972).

2) S. Yoshizawa, Z. Takehara, Z. Ogumi, and C. Nagai, *ibid.*, **40** 724 (1972).

3) "Polyacrylamide", American Cyanamid Co., New Products Bull. No. 34, (1955), p. 2.

4) B. E. Conway and M. Dzieciuch, *Can. J. Chem.*, **41** 38 (1963).

Force Field of Allene

Kazutoshi TANABE and Shinnosuke SAËKI

National Chemical Laboratory for Industry, Honmachi, Shibuyaku, Tokyo 151

(Received November 5, 1973)

The force constants based on the simple or modified Urey-Bradley, and the general force fields have been determined from the observed fundamental frequencies, Coriolis coupling constants and centrifugal distortion constants of allene C_3H_4, C_3D_4 and $C_3H_2D_2$ by the damped least-squares method. It is concluded that the simple or modified UBFF is not suitable for reproducing the observed data. In order to attain the best fit between the observed and calculated values, new bond-angle interaction constants q(CH, CCC) and q(CC, HCH) as well as the bond-bond and angle-angle interaction constants p and l should be added to the simple UBFF.

The intramolecular force field of an allene molecule is of interest in connection with the electronic structure of the adjacent double bond system in the molecule. Although there are many papers on the measurements and analysis of infrared or Raman spectra,[1-19] calculation of the force constants for the allene molecule has not yet been thoroughly accomplished.

Shuler and Fletcher[8] observed the infrared spectrum of allene-d_2 and calculated the force constants from the observed frequencies of allene-h_4 and -d_4 to support the assignment of the fundamental frequencies of allene-d_2. Sverdlov and Borisov[20,21] determined the force constants and calculated the normal frequencies allene-h_4, -d_1, -1,1-d_2, -1,3-d_2, -d_3 and -d_4 in order to to elucidate the peculiarity of the vibrational spectra of compounds with cumulated double bonds. Venkateswarlu and Pillai[22] determined the force constants from the observed Raman and infrared data, and compared these results with those of molecules having similar chemical bonds. Cyvin,[23] and Andersen *et al.*[24] determined the force constants in order to evaluate the mean amplitudes of vibration for allene-h_4, -d_1, -1,1-d_2, -1,3-d_2, -d_3, -d_4 and -t_4. Fletcher and Thompson[25] applied the Hybrid Orbital Force Fiele (HOFF) to the allene molecule, and determined the force constants from the vibrational frequencies and Coriolis coupling constants of allene-h_4, -d_4 and -1,1-d_2.

However, according to latest studies, some of the observed vibrational frequencies or Coriolis coupling constants used in these papers are proved to be based on erroneous assignment. Nemes *et al.*[26] determined the force constants from the observed data of the fundamental frequencies and the Coriolis zeta constants of allene-h_4, -d_4 and -d_2, but their analysis was made only on the E species vibrations of the allene molecule.

Very recently, the centrifugal distortion constants of allene-d_2 has been obtained from the analysis of microwave spectrum.[27] For allene-h_4 and -d_4, Maki and Toth[17] measured the vibration-rotation spectra with a high resolution, and obtained the values of D_J and D_{JK}. Inclusion of these centrifugal distortion constants into the calculation of the force constants will lead to a better determination of the force field of the allene molecule.

We have determined the force constants of the allene molecule in order to attain the best fit between the observed and calculated values of the thirty-seven fundamental frequencies, ten Coriolis coupling constants and five centrifugal distortion constants of allene-h_4, -d_4 and -1,1-d_2. From the values of the force constants based on the simple or modified Urey-Bradley, and the more general force field, the intramolecular force field of the allene molecule has been discussed in relation to the electronic structure of the adjacent double bond system in the molecule.

Calculation

The observed data of the fundamental frequencies, the Coriolis coupling constants and the centrifugal distortion constants of allene-h_4, -d_4, and -d_2 have been taken from the literature where the correct band assignment was made. Since the ν_7 and ν_{10} bands of allene-d_2 have not been observed in the spectra, their frequencies have roughly been estimated by the frequency product rule.[5,26] For the ν_{11} and ν_{15} bands of allene-d_2, the frequencies estimated from the combination bands have been adopted.[8]

In calculating the force constants from the observed data of the fundamental frequencies, the Coriolis coupling constants and the centrifugal distortion constants, the statistical weights for these data are of much significance in the least-squares determination. The final results are very sensitive to the allocation of the statistical weights for the observed data. We have taken the statistical weight of a given observed datum as the squared reciprocal of its experimental uncertainty, in accordance with Nemes *et al.*[26] and Aldous and Mills.[28]

For the experimental uncertainty of a fundamental frequency, 1% of the observed wave number has been taken, the vibrational anharmonicity or any resonance effect being taken into consideration. The value 0.02 has been taken for the uncertainty of a Coriolis coupling constant. The uncertainty of a centrifugal distortion constant has been taken from the experimental error given in the literature.[17,27] The uncertainty for the estimated vibrational frequencies of allene-d_2 (ν_7, ν_{10}, ν_{11} and ν_{15}) has been taken to be 15 cm^{-1} according to Nemes *et al.*[26] The observed data and their uncertainties used in the least squares calculation are summarized in Table 1.

The computation of normal frequencies by means of Wilson's GF matrix method and the refinement of force constants by the least squares method have been carried out using a FACOM Model 270-30 electronic computer system. The molecular structure parameters used in the computations are taken from the work of Maki and Toth[17] as follows: r(C–H)=1.087(A), R(C=C)=1.308, and $\angle$HCH=118°10′. The internal

TABLE 1(a). OBSERVED AND CALCULATED VALUES OF ALLENE-h_4

		Obsd	δ[a]	Ref.[b]	UBFF		MUBFF		GFF	
					Calcd	$\Delta\nu$[c]	Calcd	$\Delta\nu$[c]	Calcd	$\Delta\nu$[c]
A_1	ν_1	3015	30	R.G. (12)	3020	−5	3016	−1	3017	−2
	ν_2	1443	14	R.G. (12)	1461	−18	1468	−26	1453	−10
	ν_3	1073	11	R.G. (12)	1048	25	1060	12	1081	−9
B_1	ν_4	865	9	R.L. (1)	867	−2	867	−2	867	−2
B_2	ν_5	3407	30	I.G. (17)	3020	−13	3012	−5	3016	−9
	ν_6	1957	20	I.G. (3)	1984	−27	1973	−16	1957	0
	ν_7	1398	14	I.G. (3)	1410	−12	1405	−7	1398	−0
E	ν_8	3486	31	I.G. (16)	3107	−21	3145	−20	3121	−36
	ν_9	999	10	I.G. (16)	1037	−38	1037	−38	994	5
	ν_{10}	841	8	I.G. (16)	801	40	801	40	846	−5
	ν_{11}	355	4	I.G. (16)	347	9	347	8	351	4
	ζ_8	0.002	0.02	I.G. (16)	0.001	0.001	0.001	0.001	−0.007	0.009
	ζ_9	0.137	0.02	I.G. (16)	0.251	−0.114	0.250	−0.113	0.169	−0.032
	ζ_{10}	0.017	0.02	I.G. (16)	−0.159	0.176	−0.157	0.174	−0.008	0.025
	ζ_{11}	0.814	0.02	I.G. (16)	0.877	−0.063	0.877	−0.063	0.816	−0.002
	$\lvert\zeta_{9,10}\rvert$	0.563	0.02	I.G. (16)	0.530	0.033	0.524	0.039	0.562	0.001
	D_J[d]	0.116	0.02	I.G. (17)	0.090	0.026	0.088	0.028	0.084	0.032
	D_{JK}[d]	4.60	1.8	I.G. (17)	4.29	0.31	4.34	0.26	5.14	−0.54

a) Experimental uncertainty. b) R: Raman, I: infrared, G: gas, L: liquid. c) Error (=Obsd−Calcd). d) In units of 10^{-6} cm^{-1}.

TABLE 1(b). OBSERVED AND CALCULATED VALUES OF ALLENE-d_4

		Obsd	δ	Ref.	UBFF		MUBFF		GFF	
					Calcd	$\Delta\nu$	Calcd	$\Delta\nu$	Calcd	$\Delta\nu$
A_1	ν_1	2195	22	R.L. (1)	2199	−5	2205	−10	2205	−10
	ν_2	1228	12	R.L. (1)	1216	12	1231	−3	1227	1
	ν_3	874	9	R.L. (1)	865	9	865	9	877	−3
B_1	ν_4	615	6	R.L. (1)	613	2	613	2	613	2
B_2	ν_5	2229	22	I.G. (17)	2217	12	2232	−3	2218	11
	ν_6	1920	19	I.G. (17)	1944	−24	1915	5	1917	3
	ν_7	1034	10	I.G. (3)	1029	6	1025	9	1019	15
E	ν_8	2330	23	I.G. (16)	2308	22	2309	21	2296	34
	ν_9	825	8	I.G. (16)	845	−21	845	−20	822	2
	ν_{10}	666	7	I.G. (16)	643	23	643	23	662	4
	ν_{11}	307	3	I.G. (16)	299	7	299	7	309	−3
	ζ_8	0.013	0.02	I.G. (16)	0.002	0.011	0.002	0.011	−0.014	0.027
	ζ_9	0.354	0.02	I.G. (16)	0.434	−0.080	0.432	−0.078	0.350	0.003
	ζ_{10}	−0.122	0.02	I.G. (16)	−0.276	0.154	−0.274	0.152	−0.086	−0.036
	ζ_{11}	0.707	0.02	I.G. (16)	0.791	−0.084	0.791	−0.084	0.702	0.005
	$\lvert\zeta_{9,10}\rvert$	0.534	0.02	I.G. (16)	0.448	0.086	0.442	0.092	0.521	0.014
	D_J	0.041	0.02	I.G. (17)	0.055	−0.014	0.054	−0.013	0.052	−0.011
	D_{JK}	—	—		2.42	—	2.44	—	2.82	—

coordinates and the symmetry coordinates of the allene molecules are given in Tables 2 and 3, respectively.

The force constants have been adjusted by the damped least-squares method by the equation

$$\Delta K = (\tilde{J}WJ)^{-1}\tilde{J}W\Delta\nu,$$

where J and W are the Jacobian and weight matrices, respectively, and ΔK and $\Delta\nu$(obsd−calcd) are the column matrices. The standard deviations of the force constants have been evaluated by the equations

$$\sigma(K) = (\sigma_1^2+\sigma_2^2)^{1/2},$$

$$\sigma_1 = \left[\frac{N}{N-k}(\tilde{J}WJ)^{-1}\right]_{ii}^{1/2},$$

and

$$\sigma_2 = \left[\frac{N}{N-k}(\tilde{J}WJ)^{-1}(\tilde{J}W\Delta\nu)(\tilde{J}W\Delta\nu)(\tilde{J}WJ)^{-1}\right]_{ii}^{1/2},$$

where N, k denote the numbers of the available observed data and the adjusted force constants, respectively.[29]

Table 1(c). Observed and calculated values of allene-d_2

		Obsd	δ	Ref.	UBFF		MUBFF		GFF	
					Calcd	$\Delta\nu$	Calcd	$\Delta\nu$	Calcd	$\Delta\nu$
A_1	ν_1	3013	30	I.G. (10)	3020	−7	3002	11	3017	−4
	ν_2	2227	22	I.G. (10)	2209	18	2212	14	2212	15
	ν_3	1940	19	I.G. (10)	1964	−24	1964	−24	1937	3
	ν_4	1418	14	I.G. (8)	1438	−20	1420	−2	1428	−10
	ν_5	1176	12	I.G. (8)	1158	18	1149	27	1171	5
	ν_6	924	9	R.L. (5)	918	6	933	−9	928	−4
A_2	ν_7	750	15	Est. (5)[a]	751	−1	751	−1	751	−1
B_1	ν_8	2318	23	I.G. (10)	2308	10	2309	9	2296	22
	ν_9	841	8	I.G. (15)	862	−21	862	−21	846	−5
	ν_{10}	812	15	Est. (26)[a]	776	36	776	36	822	−10
	ν_{11}	336	15	Est. (8)[b]	318	18	319	17	317	19
B_2	ν_{12}	3084	31	I.G. (10)	3107	−22	3105	−21	3121	−37
	ν_{13}	996	10	I.G. (16)	1036	−40	1036	−40	994	2
	ν_{14}	667	7	I.G. (16)	656	11	656	11	663	4
	ν_{15}	327	15	Est. (8)[b]	325	2	325	2	343	−16
D_J		0.080	0.01	Mw. (27)[c]	0.070	0.010	0.068	0.012	0.066	0.014
D_{JK}		4.33	0.17	Mw. (27)[c]	3.40	0.93	3.49	0.84	4.05	0.28

a) Estimated from the frequency product rule. c) Estimated from the combination bands. c) Microwave spectrum.

Table 2. Internal coordinates of allene

Symbol	Description
r_1, r_2, r_3, r_4	CH stretching
R_1, R_2	CC stretching
α_1, α_2	HCH scissoring
β_1, β_2, β_3, β_4	HCC bending (in-plane)
γ_1, γ_2	CH_2 wagging (out-of-plane)
ϕ_1, ϕ_2	CCC bending
τ	Torsion

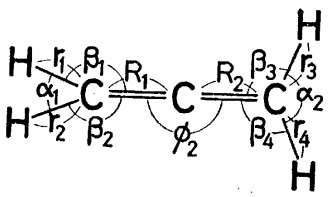

Results and Discussion

First, in order to confirm the validity of the simple Urey-Bradley force field (UBFF),

$$2V = \sum K_i(\Delta r_i)^2 + \sum H_{ij} r_i r_j (\Delta\phi_{ij})^2 + 2\sum F'_{ij} q^\circ_{ij} (\Delta q_{ij}) + \sum F_{ij}(\Delta q_{ij})^2 + \sum \pi(\Delta\gamma)^2 + Y(\Delta\tau)^2,$$

where K, H, F, π, Y are the stretching, bending, repulsive, out-of-plane bending, and torsional force constants, respectively, we determined these force constants by the least-squares method using the observed data. The converged values and their standard deviations of the UBFF force constants are given in Table 4. The calculated values of the normal frequencies, the Coriolis coupling constants and the centrifugal distortion constants of the allene molecules are given in Table 1 in comparison with the observed data.

Although the nine UBFF force constants were de-

Table 3. Symmetry coordinates of allene

h_4, d_4	A_1	$S_1 : (r_1+r_2+r_3+r_4)/2$	d_2	A_1	$S_1' : S_1$
		$S_2 : (2\alpha_1-\beta_1-\beta_2+2\alpha_2-\beta_3-\beta_4)/\sqrt{12}$			$S_2' : S_2$
		$S_3 : (R_1+R_2)/\sqrt{2}$			$S_3' : S_3$
	B_1	$S_4 : \tau$			$S_4' : S_5$
	B_2	$S_5 : (r_1+r_2-r_3-r_4)/2$			$S_5' : S_6$
		$S_6 : (R_1-R_2)/\sqrt{2}$			$S_6' : S_7$
		$S_7 : (2\alpha_1-\beta_1-\beta_2-2\alpha_2+\beta_3+\beta_4)/\sqrt{12}$		A_2	$S_7' : S_4$
	E	$S_8 : (r_1-r_2)/\sqrt{2}$		B_1	$S_8' : S_8$
		$S_9 : \gamma_2$			$S_9' : S_9$
		$S_{10} : (\beta_1-\beta_2)/\sqrt{2}$			$S_{10}' : S_{10}$
		$S_{11} : \phi_1$			$S_{11}' : S_{11}$
				B_2	$S_{12}' : (r_3-r_4)/\sqrt{2}$
					$S_{13}' : \gamma_1$
					$S_{14}' : (\beta_3-\beta_4)/\sqrt{2}$
					$S_{15}' : \phi_2$

Table 4. Converged values and standard deviations of the UBFF and MUBFF force constants

	UBFF	MUBFF	From GFF
K(CH)[a]	4.77 (0.09)	4.81 (0.04)	4.21 (1.09)
K(CC)[a]	8.62 (0.26)	8.86 (0.29)	7.84 (0.65)
H(HCH)[a]	0.33 (0.03)	0.33 (0.03)	0.26 (0.25)
H(HCC)[a]	0.19 (0.04)	0.22 (0.05)	−0.03 (0.13)
H(CCC)[a]	0.27 (0.01)	0.27 (0.01)	0.31 (0.03)
F(HH)[a]	0.01 (0.07)	−0.01 (0.08)	0.23 (0.74)
F(HC)[a]	0.57 (0.12)	0 49 (0.13)	1.22 (0.42)
π[b]	0.04 (0.00)	0.04 (0.00)	0.05 (0.00)
Y[b]	0.39 (0.01)	0.39 (0.01)	0.39 (0.01)
p(CH, CH)[a]		0.01 (0.07)	−0.25 (0.56)
p(CH, CC)[a]		−0.09 (0.07)	−0.53 (0.33)
p(CC, CC)[a]		0.24 (0.21)	0.45 (0.16)
l(HCC, CCC)[b]			−0.05 (0.02)
l(CCC, γ)[b]			0.05 (0.01)
q(CH, CCC)[c]			−0.22 (0.03)
q(CC, HCH)[c]			0.24 (0.17)

a) In units of mdyn/Å. b) In units of mdyn·Å. c) In units of mdyn.

termined (Table 4), the agreement between the observed and calculated values is not satisfactory as a whole. In particular, the disagreement in the normal frequencies ν_9 and ν_{10} of allene-h_4 and -d_4, ν_{13} and D_{JK} of allene-d_2, and the Coriolis coupling constants ζ_9, ζ_{10}, ζ_{11}, $|\zeta_{9,10}|$ is much larger than experimental uncertainty. The weighted sum of squared errors, a residual 389 in this case indicates the average difference between the observed and calculated values

$$\sqrt{389/52} = 2.7$$

is about three times larger than the experimental uncertainty. A disagreement to this extent cannot be ignored. Therefore, in order to reduce it, several other interaction force constants have been added to the above simple UBFF.

Shimanouchi[30] introduced several new interaction force constants for the purpose of revising the simple Urey-Bradley force field, and determined their values for various molecules:

$p : p(\Delta r_i)(\Delta r_j)$	bond-bond interaction (SiX_4)
$\rho : \rho(\Delta r_i)(\Delta r_j)$	resonance interaction (CO_3^{--})
$t : t(\Delta\phi_{ij})(\Delta\phi_{kl})$	trans interaction (CH_3CH_3)
$g : g(\Delta\phi_{ij})(\Delta\phi_{kl})$	gauche interaction (CH_3CH_3)
$l : l(\Delta\phi_{ij})(\Delta\phi_{ik})$	angle-angle interaction (CH_2X_2).

The bond-bond interaction force constants p(CH,CH), p(CH,CC), and, in particular, p(CC,CC) are considered to take important roles in the force field of the allene molecule. Thus we added the three force constants p to the UBFF, and determined the twelve MUBFF force constants by the least-squares method. Converged values are compared with those of the simple UBFF in Table 4, the calculated values of ν, ζ, D being given in Table 1.

Although the new interaction force constants p converged to have appreciable values (Table 4), the effect of introducing such force constants on the calculated values (Table 1) is not striking. The residual in this case is 376, and thus the average difference

$$\sqrt{376/52} = 2.7$$

is about three times larger than experimental uncertainty. This agreement is slightly better than in the case of the above simple UBFF. However, the disagreement cannot be overlooked, and the force field sould be improved.

For this purpose, we determined the force constants based on the more general force field (GFF), and transformed the converged values of the GFF force constants into the UBFF force constants. A modification of the Urey-Bradley force field was discussed.

The twenty-three force constants based on the general force field were adjusted by the least-squares method from the total fifty-two observed data. A refinement of all the GFF force constants led to large standard deviations for some force constants. Hence, in order to reduce them, and to determine individual force constants definitely, the number of adjusted force constants was reduced, on the assumption that interaction between non-adjacent bonds in the allene molecule can well be neglected.

Though the force constant $F(3,3)$ in the A_1 symmetry species of allene-h_4 or -d_4 still differs from $F(6,6)$ in B_2, the other five force constants in B_2 are equal to those in A_1, and the two force constants $F(8,9)$ and $F(9,10)$ in the E species are equal to zero. Thus the sixteen independent GFF force constants were adjusted by the least squares method from the observed ν, ζ, D data. The converged values and standard deviations of the GFF force constants are listed in Table 5.

The agreement between the observed and calculated values in this case is satisfactory as a whole. The residual is 34.1, hence the average difference between the observed and calculated values

$$\sqrt{34.1/52} = 0.81$$

is even smaller than experimental uncertainty. The disagreement between the observed and calculated

Table 5. Converged values and standard deviations of the GFF force constants

A_1	$F(1, 1)$[a]	5.13 (0.19)
	$F(2, 2)$[b]	0.44 (0.04)
	$F(3, 3)$[a]	10.20 (0.32)
	$F(1, 2)$[c]	−0.19 (0.37)
	$F(1, 3)$[a]	0.58 (0.42)
	$F(2, 3)$[c]	−0.24 (0.04)
B_1	$F(4, 4)$[a]	0.39 (0.01)
B_2	$F(5, 5)$[a]	5.13 (0.19)[d]
	$F(6, 6)$[a]	9.28 (0.19)
	$F(7, 7)$[b]	0.44 (0.04)[d]
	$F(5, 6)$[a]	0.58 (0.42)[d]
	$F(5, 7)$[c]	−0.19 (0.37)[d]
	$F(6, 7)$[c]	−0.24 (0.04)[d]
E	$F(8, 8)$[a]	5.28 (0.10)
	$F(9, 9)$[b]	0.05 (0.00)
	$F(10, 10)$[b]	0.51 (0.03)
	$F(11, 11)$[b]	0.41 (0.04)
	$F(8, 9)$[c]	0.00[d]
	$F(8, 10)$[c]	0.52 (0.20)
	$F(8, 11)$[c]	−0.31 (0.47)
	$F(9, 10)$[b]	0.00[d]
	$F(9, 11)$[b]	0.07 (0.01)
	$F(10, 11)$[b]	−0.06 (0.03)

a) In units of mdyn/Å. b) In units of mdyn·Å. c) In units of mdyn. d) See text.

values mentioned above in the case of UBFF and MUBFF is now well resolved in terms of the GFF force constants (Table 1). The agreement is satisfactory, and the GFF force constants (Table 5) are qualified as pertinent to the representation of the force field of the allene molecule.

They were thus converted into the UBFF force constants, and several interaction constants which should be added to the Urey-Bradley force field were determined. (See Table 4 for a comparison with force constants of UBFF and MUBFF). Some remarks are given concerning the results obtained for the MUBFF force constants derived from the GFF.

As new interaction force constants which should be added to the UBFF, in addition to the bond-bond interaction term p and the angle-angle interaction term l proposed by Shimanouchi, the necessity of introducing the bond-angle interaction term q should be stressed. The constant q(CC, HCH) is important for describing the normal frequencies of the A_1 and B_2 type vibrations.

The bond-angle interaction term q(CH,CCC) as well as the angle-angle interaction term l(HCC,CCC) and l(CCC,γ) are important for describing the normal frequencies and the Coriolis coupling constants of the E type vibrations. The necessity of introducing the term l was stressed by Shimanouchi for molecules such as methylene halides. The fact that the term l is also of significance in molecules containing double bonds such as allene is interesting in relation to the intramolecular force field.

The bond-bond interaction terms p(CH,CH), p(CH, CC) and p(CC,CC) suggest an electronic interaction between the bonds in the allene molecule. The strong electronic interaction between the adjacent double bonds in the allene molecule may give rise to the effectiveness of the value for p(CC,CC).

The authors thank Professor Eiji Hirota, Department of Chemistry, Kyushu University, and Dr. Chi Matsumura, National Chemical Laboratory for Industry, for their valuable discussions and suggestions.

References

1) R. C. Lord and J. Ocampo, *J. Chem. Phys.*, **19**, 260 (1951).
2) J. de Heer, *ibid.*, **20**, 637 (1952).
3) R. C. Lord and P. Venkateswarlu, *ibid.*, **20**, 1237 (1952)
4) K. N. Rao and E. D. Palik, *ibid.*, **23**, 2112 (1955).
5) J. C. Evans, J. K. Wilmshurst, and H. J. Bernstein, *Can. J. Chem.*, **34**, 1139 (1956).
6) J. Overend and H. W. Thompson, *Trans. Faraday Soc.*, **52**, 1295 (1956).
7) K. N. Rao and E. D. Palik, *J. Mol. Spectrosc.*, **1**, 24 (1957).
8) W. E. Shuler and W. H. Fletcher, *ibid.*, **1**, 95 (1957).
9) K. N. Rao, A. H. Nielsen, and W. H. Fletcher, *J. Chem. Phys.*, **26**, 1572 (1957).
10) D. R. Eaton and H. W. Thompson, *Proc. Roy. Soc., Ser. A*, **250**, 39 (1959).
11) J. Overend and B. Crawford Jr., *J. Chem. Phys.*, **29**, 1002 (1958).
12) S. Brodersen and E. H. Richardson, *J. Mol. Spectrosc.*, **4**, 439 (1960).
13) J. Blanc, C. Brecher, and R. S. Halford, *J. Chem. Phys.*, **36**, 2654 (1962).
14) I. M. Mills and J. L. Duncan, *J. Mol. Spectrosc.*, **9**, 244 (1962).
15) I. M. Mills, *Mol. Phys.*, **8**, 363 (1964).
16) I. M. Mills, W. L. Smith, and J. L. Duncan, *J. Mol. Spectrosc.*, **16**, 349 (1965).
17) A. G. Maki and R. A. Toth, *ibid.*, **17**, 136 (1965).
18) N. Van Thanh, *Ann. Phys. (Paris)*, **1967**, 241.
19) J. M. R. Stone, *J. Mol. Spectrosc.*, **38**, 503 (1971).
20) L. M. Sverdlov, *Opt. Spectrosc.*, **2**, 540 (1957).
21) L. M. Sverdlov and M. G. Borisov, *ibid.*, **9**, 227 (1961).
22) K. Venkateswarlu and M. G. K. Pillai, *Z. Phys. Chem.*, **18**, 396 (1958).
23) S. J. Cyvin, *J. Chem. Phys.*, **29**, 583 (1958).
24) B. Andersen, R. Sølevik, J. Brunvoll, S. J. Cyvin, and G. Hagen, *Acta Chem. Scand.*, **21**, 1759 (1967).
25) W. H. Fletcher and W. T. Thompson, *J. Mol. Spectrosc.*, **25**, 240 (1968).
26) L. Nemes, J. L. Duncan, and I. M. Mills, *Spectrochim. Acta*, **23A**, 1803 (1967).
27) E. Hirota and C. Matsumura, *J. Chem. Phys.*, **59**, 3038 (1973).
28) J. Aldous and I. M. Mills, *Spectrochim. Acta*, **18**, 1073 (1962).
29) T. Ogawa and T. Mayazawa, *ibid.*, **20**, 557 (1964).
30) T. Shimanouchi, *Pure Appl. Chem.*, **7**, 131 (1963).

The Kinetics and Mechanism of Hydrogen Adsorption and Hydrogen–Deuterium Equilibration on the Copper Surface

Makoto KIYOMIYA, Naohiro MOMMA, and Iwao YASUMORI

Department of Chemistry, Tokyo Institute of Technology, O-okayama, Meguro-ku, Tokyo 152

(Received November 13, 1973)

The mechanism of H_2–D_2 equilibration reaction over the copper surface was studied in the 40—90 °C range of temperature and in the pressure range of 4—45 Torr. From the studies of the hydrogen adsorption and the reaction between gaseous deuterium and preadsorbed hydrogen, the reaction was confirmed to proceed *via* combination between hydrogen and deuterium atoms on the surface. The rate constants for the adsorption and the desorption were optimized by a computer simulation of the reaction-time course and were found to be in satisfactory agreement with the observed results. A marked isotope effect was found in these rates; its influence on the partial pressure dependence of the reaction was discussed.

It has been known that copper, a typical "s-metal," is different from a "d-metal" in its catalytic activity for reactions such as the hydrogenation of olefins and the decomposition of alcohols or formic acid. Surface hydrogen is supposed to play an important role in these reactions. However, there have been few detailed reports on the adsorption and reaction of hydrogen on the copper surface.

Allen and Mitchell[1] have reported that hydrogen is not chemisorbed on the evaporated film of copper in the temperature range from 90 to 273 K. On the other hand, Prichard and Alexander[2] have found, from their measurements of the surface potential, that hydrogen is chemisorbed spontaneously on the evaporated film between 242 and 337 K. Though Shield and Russell[3] suggested that the adsorption of hydrogen is due to transition-metal impurities, Cadenhead and Wagner[4] have found that carefully reduced copper powder can adsorb approximately 0.4 of a monolayer of hydrogen at 77 K. Recently, Momma and Yasumori[5] have found, from a thermal desorption study, that there is only one dissociative state for the adsorbed hydrogen on copper powder.

In this work, we studied in detail the kinetics of the H_2-D_2 equilibration reaction in order to ascertain the behavior of adsorbed hydrogen on the copper surface.

Experimental

A circulating system of about 500 ml was used for the studies of adsorption and kinetics. This apparatus was incorporated with a reaction vessel, an inductance Bourdon gauge,[6] gas reservoirs, and a high-vacuum line. The temperature of the reaction vessel was controlled within ±0.5 °C. Isotopes of hydrogen were analyzed by the use of a gas chromatograph with a column of Mn^{2+} coated γ-alumina.[7]

The kinetics of the equilibration reaction was studied using an equimolar mixture of H_2 and D_2 in the temperature range of 40—90 °C at total pressures between 4 and 45 Torr. The dependences of the reaction rate on the partial pressures of H_2 and D_2 were also examined. Two series of experiments were carried out; in the first series, the initial pressure of H_2 (or D_2) was varied, while that of D_2 (or H_2) was kept constant, and in the second series, the fraction of hydrogen was varied under a constant total pressure.

During the course of the equilibration, the amounts of hydrogen and deuterium adsorbed on the surface were estimated from the introduced amounts and from the partial pressure of each isotopic molecule. The pressure change due to adsorption during the course of reaction was continuously followed by means of a Bourdon gauge. The rates of the adsorption and desorption of hydrogen and deuterium and the adsorption isotherms were determined using the same reaction vessel.

Copper powder, used as a catalyst, was prepared by the following procedure: cupric oxide was precipitated from an aqueous solution of copper nitrate by adding sodium hydroxide and was reduced with circulating hydrogen of 50—100 Torr at 180 °C. Guaranteed-reagent cupric nitrate was obtained from Wako-Pure Chemical Industries, Ltd. The reduction was continued for 50 hr until no decrease in the hydrogen or no trace of water could be found. The reduced copper powder was evacuated at the same temperature for several hours. The surface area of the catalyst was estimated as 4.4 m^2/g by means of the BET method using krypton at 77 K.

Transition-metal impurities in the cupric oxide were examined by emission spectroanalysis; the amounts of Fe and Ni were less than 5 ppm, and those of Co and Mn were less than 10 ppm. As for non-transition-metal impurities, the amounts of Al and Na were less than 2 and 0.5 ppm respectively, while those of Si and Mg slightly exceeded the limit of detection.

High-purity hydrogen, deuterium (HD less than 0.5%), and krypton purchased from the Takachiho Co., Ltd., were used without further purification.

In annealing, the copper powder was heated at definite temperatures up to 500 °C *in vacuo* below 10^{-5} Torr for an hour. Prior to each kinetic run, the annealed catalyst was evacuated again at room temperature for several hours.

The simulation and the numerical analysis of the reaction-time course were carried out by means of the Runge-Kutta-Gill method with the aid of a computer, HITAC 8700.

Results

The Adsorption of Hydrogen and Deuterium. The adsorption of hydrogen proceeded at a measurable speed at room temperature. Figures 1 and 2 show the time courses of the chemisorption of H_2 and D_2 respectively in the temperature range of 30—170 °C. It is evident that the chemisorption requires an activation energy. A marked isotope effect in the adsorption rate was found; the rate of hydrogen adsorption was about six times as fast as that of deuterium adsorption at room temperature. Figure 3 shows a linear relationship[8] between the rate of adsorption and the pressure, where the points on each line were obtained as those

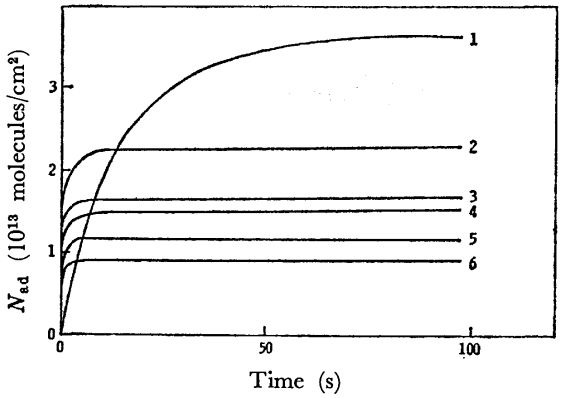

Fig. 1. Time course of hydrogen adsorption on copper at various temperatures.
1: 33.5, 2: 69, 3: 99, 4: 111, 5: 126, 6: 166 °C.

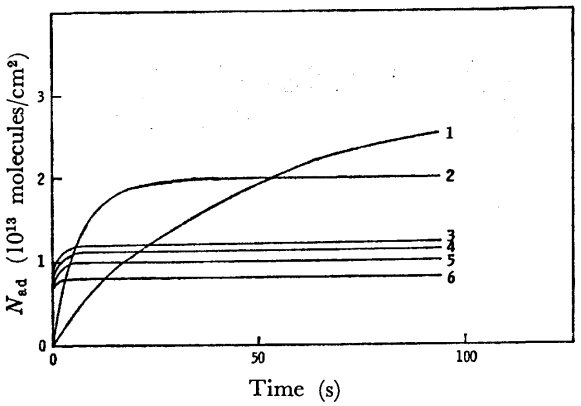

Fig. 2. Time course of deuterium adsorption on copper at various temperatures.
1: 36, 2: 62, 3: 99, 4: 111, 5: 126, 6: 166 °C.

for the same amount of adsorbed hydrogen from various time curves at 20 °C. The intercepts correspond to the desorption rates, which increase with the amount of adsorbed hydrogen. This result suggests that the adsorption is not controlled by any process such as diffusion in the gas phase or in surface migration, but by the simple collision of gaseous molecules with the surface.

The adsorption isotherms of hydrogen and deuterium were obtained in the temperature region from 0 to 60 °C and at pressures from 4 to 45 Torr. The adsorption of hydrogen was found to be reversible under these conditions. Plots of the reciprocal of $\sqrt{P_e}$ against the reciprocal of N^s_{ad} showed a linear relationship, where P_e is the equilibrium pressure and N^s_{ad} is the amount of adsorbed hydrogen. This result indicates that the adsorption isotherm obeys the Langmuir equation for dissociative adsorption. The monolayer capacity was evaluated as 2.8×10^{14} H atoms/cm^2. This value corresponds to approximately 20% of the surface copper atoms, 1.6×10^{15} atoms/cm^2, taken as the average of the (111) and (100) planes. The heats of adsorption of hydrogen and deuterium were determined to be 9.2±1.0 kcal/mol and 10.3±2.0 kcal/mol respectively.

The overall rate of adsorption may, therefore, reasonably be expressed as:

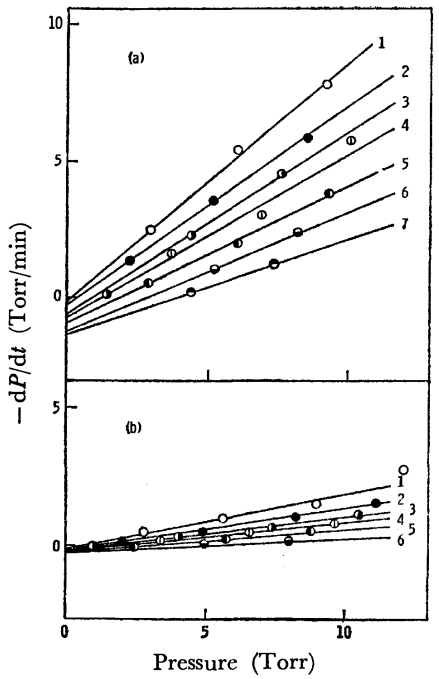

Fig. 3. Relationship between the net rate of adsorption and pressure at constant amount of adsorption at 20 °C.
a: H_2, b: D_2; 1: 0.306, 2: 0.612, 3: 0.918, 4: 1.22, 5: 1.53, 6: 1.84, 7: 2.14×10^{13} molecules/cm^2.

$$KV/\sigma_0^2 S\cdot dP/dt = -k_a P(1-\theta)^2 + k_d\theta^2 \qquad (1)$$

where K is the conversion factor (molecules/ml·Torr), V is the volume of the reaction system, σ_0 is the monolayer capacity, S is the surface area, and k_a and k_d are the rate constants for adsorption and desorption respectively.

Adsorption Measurements during H_2-D_2 *Equilibration.* The change in the adsorption during the H_2-D_2 equilibration was followed volumetrically; the results at 14 °C are shown in Fig. 4. The amount of adsorbed hydrogen or deuterium is conventionally expressed by the virtual pressure of H_2 or D_2 which would be

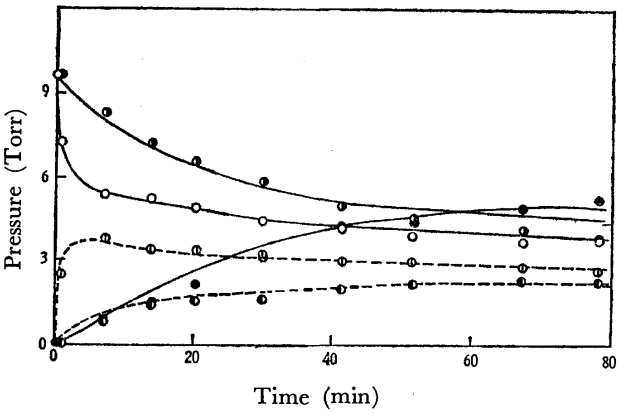

Fig. 4. Adsorption during the course of H_2-D_2 equilibration on copper at 14 °C. Lines indicate the best fitting curves obtained by computer simulation.
○: H_2(g), ◑: D_2(g), ●: HD(g), ⓘ: H_2(a), ◐: D_2(a).

expected if the adsorbed species were all present in the gas phase. When an equimolar mixture of H_2 and D_2 was introduced into the reaction system, the hydrogen in the gas phase decreased more rapidly than the deuterium. The adsorbed amount of hydrogen reached a maximum about ten minutes after the start of the reaction. As the reaction proceeded, the amount of adsorbed hydrogen decreased, whereas that of the adsorbed deuterium increased until it reached an amount similar to that of adsorbed hydrogen, their sum being almost kept constant after the maximum.

Exchange Reaction. In order to get information on the mechanism of the H_2-D_2 equilibration, the exchange reaction between the adsorbed hydrogen and gaseous deuterium was examined. Figure 5 shows the behavior of hydrogen species during the course of the exchange. In this case, H_2 was preadsorbed on the copper surface; then, the hydrogen in the circulating system was quickly replaced by deuterium except for the small amount of hydrogen in the catalyst vessel. An induction period for the HD formation and a maximum in the rate appeared, and the surface hydrogen was gradually displaced by deuterium.

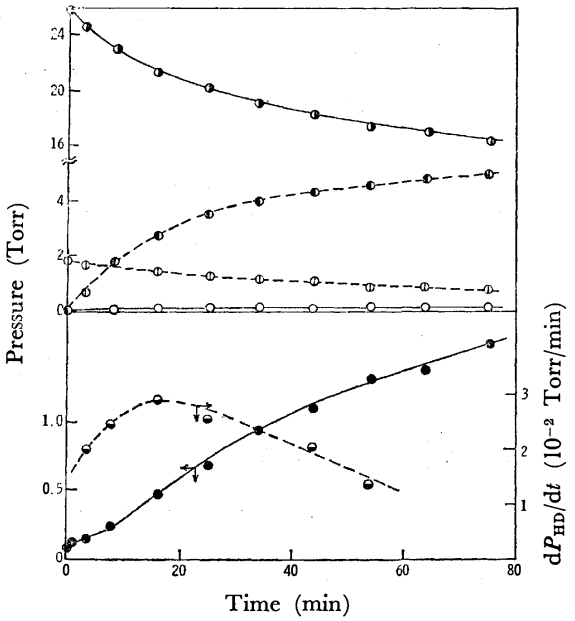

Fig. 5. Adsorption during the course of exchange reaction at 20 °C.
○: H_2(g), ◑: D_2(g), ●: HD(g), ◒: the rate of HD formation, ⓘ: H_2(a), ◐: D_2(a).

These results suggest that the equilibration takes place through the repetition of the dissociative adsorption of H_2 and D_2 and the desorption of HD. Hydrogen deuteride is formed from the recombination between the chemisorbed hydrogen and deuterium atoms; the rate of HD formation in this case should be proportional to the respective concentrations of adsorbed species. This view was further supported by a similar finding for the exchange between adsorbed D atoms and gaseous H_2 molecules.

If a reaction between adsorbed hydrogen atoms and gaseous deuterium molecules, $H(a)+D_2 \rightarrow HD+D(a)$,

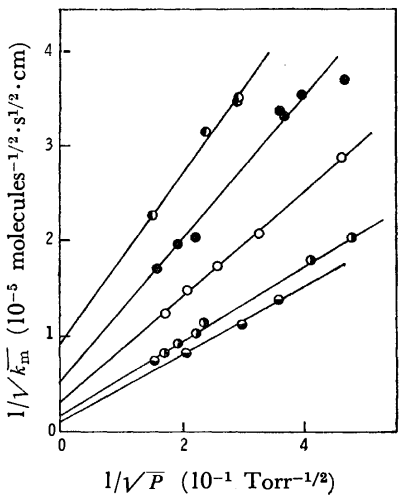

Fig. 6. Dependence of $1/\sqrt{k_m}$ on $1/\sqrt{P}$ at various temperatures.
◐: 43.5, ●: 51, ○: 64, ◑: 75.5, ◒: 85 °C,

occurs, a monotonous decrease in the rate may be observed, since the rate is expressed as $dP_{HD}/dt = k\theta_H P_{D_2}$.

Kinetics of H_2-D_2 Equilibration. The rate of the equilibration in an equimolar mixture of H_2 and D_2 obeyed the usual first-order equation:

$$k_e = 1/t \cdot \ln(x_0 - x_e)/(x_0 - x_t) \qquad (s^{-1}) \qquad (2)$$

where x_0, x_t, and x_e represent the fraction of hydrogen deuteride at the beginning, at time t, and at equilibrium respectively. The absolute rate, k_m, is derived from the constant, k_e, as:

$$k_m = nk_e/S \qquad (\text{molecules/cm}^2\cdot\text{s}) \qquad (3)$$

where n is the total number of hydrogen molecules in the reaction system and where S is the surface area of copper.

The dependences of the absolute rate on the pressure and the temperature were studied in the ranges from 4 to 45 Torr and from 40 to 90 °C. The apparent order of the reaction was 0.8 with respect to the total pressure of hydrogen. Since a linear relationship holds between the reciprocals of $\sqrt{k_m}$ and $\sqrt{P}$, as is shown in Fig. 6, the rate may be represented by the equation:

$$k_m = k_0(\sqrt{KP}/1 + \sqrt{KP})^2 \qquad (4)$$

where k_0 is the rate constant and is estimated as an extrapolated value of k_m when the pressure rises to infinity. The apparent activation energy and the heat of adsorption were evaluated as 17.9±1.5 kcal/mol and 9.7±1.5 kcal/mol respectively.

Dependence of the Rate on the Composition of the Reactant. In order to ascertain the dependence of the rate on the partial pressures of H_2 and D_2, two series of experiments were carried out. Figure 7 shows the initial rate of HD formation obtained at 79 °C, where the partial pressure of H_2 or D_2 was kept constant. A marked isotope effect was observed; when the partial pressure was lower than 3.2 Torr, the rate of reaction under a constant D_2 pressure was faster than that under a constant H_2 pressure. Plot of log P_{H_2} or log P_{D_2}

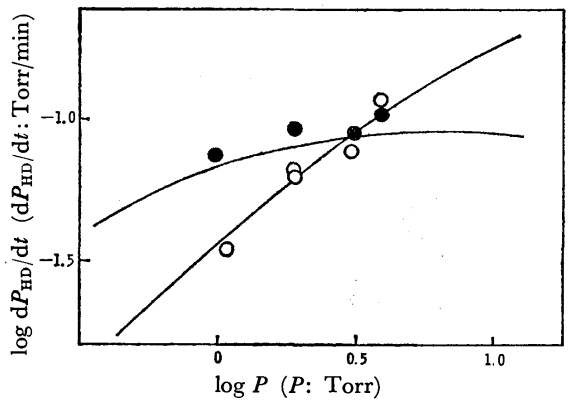

Fig. 7. Variation of initial rate of HD formation with hydrogen or deuterium pressure. Initial pressure was 3.2 Torr. Solid lines show theoretical curves. ○: initial P_{H_2}=3.2 Torr, ●: initial P_{D_2}=3.2 Torr.

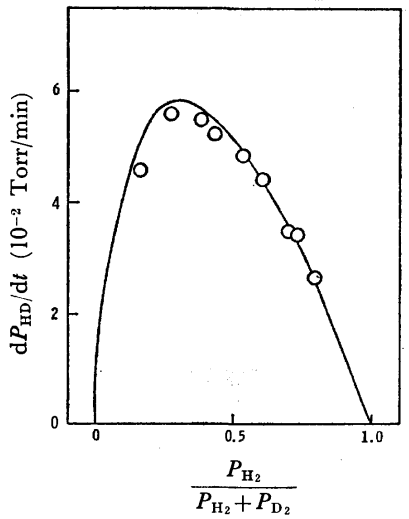

Fig. 8. Variation of initial rate of HD formation with the fraction of hydrogen. Total pressure was kept constant at 6.2 Torr. Solid line shows a theoretical curve.

against the logarithm of the initial rate of HD formation gives the apparent reaction order of 0.8±0.1 in deuterium and that of 0.2±0.1 in hydrogen within these pressure limits.

Figure 8 shows the correlation between the initial rate of HD formation and the fraction of hydrogen under a constant total pressure of 6.2 Torr at 84 °C. The maximum in the rate appears at a hydrogen fraction of 0.3—0.4; it deviates from the point of an equimolar composition. This result can be attributed to the kinetic isotope effect in the adsorption and desorption processes.

Effect of Annealing. The dependences of the reaction velocity and the apparent activation energy on the annealing temperature are shown in Table 1; the activity per unit of weight of copper decreased on annealing. However, it was found that the annealing also decreased the surface area of copper and that the reaction rate per unit of surface area remained almost unchanged.

Table 1. Effect of annealing on catalytic activity

Annealing temp. (°C)	Surface area (m^2/g)	Specific activity (molecules/s·g)	k_m (molecules/s·cm^2)	E_{ap} (kcal/mol)
180	4.4	2.48×10^{14}	5.6×10^{9}	12.6
280	4.1	2.15×10^{14}	5.2×10^{9}	12.6
380	3.4	1.72×10^{14}	5.1×10^{9}	12.2
480	2.2	0.69×10^{14}	4.4×10^{9}	11.9

Discussion

In the present study, it is revealed that hydrogen is dissociatively adsorbed on the copper surface and that an activation energy is needed for this process. The results obtained from the adsorption measurements during the course of the exchange reaction confirm that the equilibration reaction occurs *via* the dissociative adsorption of H_2 and D_2 and the desorption of HD as a result of a recombination of the chemisorbed hydrogen and deuterium atoms.[9] A recent study of the thermal desorption supports this mechanism; the desorption spectra showed only one dissociatively-adsorbed state for hydrogen on the reduced copper powder. The desorption was found, from the dependence of the peak shift on the amount of adsorption, to be second-order with respect to the surface concentration of hydrogen; further, the complete mixing of the hydrogen and deuterium atoms was observed.

There is no alternative mechanism for explaining the equilibration reaction. Since the Rideal-Eley mechanism[10] involves a surface reaction between the chemisorbed hydrogen atom and the physically-adsorbed molecule as the rate-controlling step, it does not accord with the present results on the exchange reaction. The Schwab-Killmann mechanism,[11] which presumes a molecular adsorption of H_2 and D_2 and a bimolecular rearrangement between them on the surface, also does not hold because the adsorbed hydrogen is in a dissociative state, as has been discussed above.

Subsequently, the results of the adsorption measurements during the H_2-D_2 equilibration can be analyzed according to the following scheme:

$$H_2 \underset{k_d^H}{\overset{k_a^H}{\rightleftharpoons}} 2H(a) \quad \text{(I)}$$

$$HD \underset{k_d^{HD}}{\overset{k_a^{HD}}{\rightleftharpoons}} H(a) + D(a) \quad \text{(II)}$$

$$D_2 \underset{k_d^D}{\overset{k_a^D}{\rightleftharpoons}} 2D(a) \quad \text{(III)}$$

where k_a and k_d are the rate constants for the adsorption and the desorption respectively, as defined above.

The rates are expressed in the same way as in Eq. (1):

$$KV/\sigma_0^2 S\cdot dP_H/dt = -k_a^H P_H(1-\theta_H-\theta_D)^2 + k_d^H\theta_H^2 \quad (5)$$

$$KV/\sigma_0^2 S\cdot dP_{HD}/dt = -k_a^{HD} P_{HD}(1-\theta_H-\theta_D)^2 + k_d^{HD}\theta_H\theta_D \quad (6)$$

$$KV/\sigma_0^2 S\cdot dP_D/dt = -k_a^D P_D(1-\theta_H-\theta_D)^2 + k_d^D\theta_D^2 \quad (7)$$

This set of simultaneous differential equations was solved numerically by applying the Runge-Kutta-Gill

TABLE 2. RATE CONSTANTS FOR DESORPTION AND ADSORPTION AT 14°C

	k_d (cm²/molecules·s)	k_a (cm²/molecules·Torr·s)
H_2	7.9×10^{-17}	5.4×10^{-18}
HD	7.0×10^{-17}	3.0×10^{-18}
D_2	1.7×10^{-17}	7.2×10^{-19}

method with the aid of a computer. The rate constants as parameters were chosen so as to obtain the best-fitting curves to the experimental time course by using the least-squares method. The rate constants thus determined are listed in Table 2; the coincidence of the theoretical curves with the experimental results is evident, as is shown in Fig. 4. The rate constants at 0 and 89 °C were also evaluated from the results of adsorption during the equilibration by means of the computer simulation procedure. The activation energies for the adsorption and desorption were determined from these constants at 0, 14, and 89 °C by combining the separate data of the adsorption rates of H_2 and D_2 at temperatures between 0 and 20 °C. These values are summarized in Table 3. The rate constants estimated from the adsorption and desorption rates of H_2 and D_2 at 20 °C are compared with those determined by the simulation in Table 4. The agreement between the calculated and the observed values offers an additional evidence for the validity of computer simulation. Therefore, it is confirmed that the reaction proceeds *via* the so-called Bonhoeffer-Farkas mechanism.

TABLE 3. ACTIVATION ENERGIES FOR DESORPTION AND ADSORPTION

	E_a (kcal/mol)	E_d (kcal/mol)
H_2	9±1	17±1
HD	9±1	17±2
D_2	10±1	18±2

TABLE 4. RATE CONSTANTS FOR DESORPTION AND ADSORPTION AT 20°C

	k_d (cm²/molecules·s)		k_a (cm²/molecules·Torr·s)	
	Obsd	Calcd	Obsd	Calcd
H_2	1.5×10^{-16}	1.5×10^{-16}	5.5×10^{-18}	7.4×10^{-18}
D_2	4.2×10^{-17}	3.6×10^{-17}	1.1×10^{-18}	1.0×10^{-18}

It may be seen that the rates are empirically represented by Eq. (4), which is derived on the basis of this mechanism by neglecting the isotope effect. The linear relationship shown in Fig. 6 is, however, rather accidental; Eq. (4) predicts that the reaction order of H_2 or D_2 must not exceed 0.5. The solid lines in Figs. 7 and 8 were obtained by the use of evaluated rate constants involving the isotope effect and were in good agreement with the experimental results.

Accordingly, the considerations given above indicate that the isotope effect can not be ignored in interpreting the pressure dependence of the reaction.

The equilibration reaction can now be precisely analyzed on the basis of the present results and the transition-state theory. It can easily be shown that the rate constants of adsorption, k_a, and desorption, k_d, are given by:

$$k_a = kT/h\cdot F^{\ddagger}/F_g F_{s_2}\cdot\exp(-E_a/RT)\cdot k'/T\cdot s/2L \quad (8)$$

$$k_d = kT/h\cdot F^{\ddagger}/F_{H(a)}{}^2\cdot\exp(-E_d/RT)\cdot s/2L \quad (9)$$

where L is the total number of sites per unit area of copper, s is the number of adjacent sites, and F_g, $F_{H(a)}$, F_{s_2}, and $F^{\ddagger}$ are the partition functions of gaseous hydrogen, the adsorbed hydrogen atom, the dual sites, and the activated complex respectively. The constant, k', in Eq. (8) is the conversion factor in unit of molecules·deg/Torr·ml. The transmission coefficient is assumed to be unity. The rates at 14 °C were evaluated by assuming F_{s_2}, $F^{\ddagger}$, and $F_{H(a)}$ to be unity, and s to be 6, and by assuming L as 2.8×10^{14} sites/cm². The results for hydrogen were:

$$k_a = 6.0\times10^{-18} \quad \text{(cm²/molecules·Torr·s)}$$

$$k_d = 7.9\times10^{-15} \quad \text{(cm²/molecules·s)}.$$

As is shown in Table 2, the calculated rate constant of adsorption is in satisfactory agreement with the experimental value. However, in the case of desorption, the theoretical value is larger than the experimental value by a factor of 10^2. This discrepancy is presumably a result of the low vibrational frequencies of the adsorbed hydrogen atom on the real surface.

By combining the difference between the zero-point energies of the molecular vibrations of H_2 and D_2, 1.8 kcal/mol with the values of the activation energies shown in Table 3, it is possible to estimate the difference between the zero-point energies of the Cu-H and Cu-D vibrations on the surface. The value, 0.9 kcal/mol, obtained for this difference seems reasonable in comparison with the value, 0.92 kcal/mol, of that between the dissociation energies of diatomic molecules, CuH and CuD.

It has been considered by several investigators that defect structures in metal surface may play an important role in heterogeneous catalysis. Uhara *et al.*[12] studied the effect of annealing on the catalytic activity of copper for the decomposition of benzene diazonium chloride and suggested that the fall in catalytic activity was attributable to a decrease in the concentration of dislocation which occurred around 400 °C. In the present study, the total activity per unit of weight decreased upon annealing in a way similar to that observed by them. However, the surface area also decreased upon annealing, and the reaction rate per unit of surface area was almost unvaried. Therefore, this reaction is not structurally sensitive, but belongs to a category of "facile" reaction[13] which depends only on the degree of exposure of metal atoms. Besides, it is known that the points or lines of the emergence of defects at silver films[14] and the lattice imperfection on silver crystals[15] are unimportant for the decomposition of formic acid. Woodward *et al.*[16] indicated that dislocations on silver do not act as active sites for the oxidation of ethylene. The present findings, together with these observations, lead us to conclude that the structural defects in s-metals do not play a dominant role in heterogeneous catalysis.

References

1) J. A. Allen and J. W. Mitchell, *Discuss. Faraday Soc.*, **8**, 361 (1950).
2) C. S. Alexander and J. Prichard, *J. Chem. Soc. Faraday I*, **68**, 202 (1972).
3) L. S. Shield and W. W. Russell, *J. Phys. Chem.*, **64**, 1592 (1960).
4) D. A. Cadenhead and N. J. Wagner, *J. Catal.*, **21**, 312 (1971).
5) To be published.
6) I. Yasumori, S. Ohno, and E. Miyazaki, This Bulletin, **40**, 769 (1967).
7) I. Yasumori and S. Ohno, *ibid.* **39**, 1302 (1966).
8) Y. Amenomiya, *J. Catal.*, **12**, 410 (1968).
9) K. F. Bonhoeffer and A. Farkas, *Z. Phys. Chem.*, **12B**, 231 (1931).
10) E. K. Rideal, *Proc. Cambridge Phil. Soc.*, **35**, 130 (1939).
11) G. M. Schwab and E. Killmann, *Z. Phys. Chem. (N. F.)*, **24**, 119 (1960).
12) I. Uhara, S. Yanagimoto, K. Tani, G. Adachi, and S. Teratani, *J. Phys. Chem.*, **66**, 2691 (1962).
13) M. Boudart, A. Aldag, J. E. Benson, N. A. Dougharty, and C. G. Harkins, *J. Catal.*, **6**, 92 (1966).
14) J. Bagg, H. Jaeger, and J. V. Sanders, *ibid.*, **2**, 449 (1963).
15) H. Jaeger, *ibid.*, **9**, 237 (1967).
16) J. W. Woodward, R. G. Lindgren, and W. H. Corcoran, *ibid.*, **25**, 292 (1972).

The Crystal Structure of (+)-2,5-Dimethoxy-8-Chlorotriptycene

Tsuguhiro KANEDA,* Noriyoshi SAKABE, and Jiro TANAKA

Department of Chemistry, Faculty of Science, Nagoya University, Chikusa, Nagoya 464

(Received November 16, 1973)

The crystal structure of (+)-2,5-dimethoxy-8-chlorotriptycene has been investigated by the X-ray method. The crystal system is monoclinic, and the space group is $P2_1$. The cell dimensions are $a=8.231$, $b=13.320$, $c=8.156$ Å, and $\beta=96.49°$. The structure was deduced from the Patterson map and from the calculation of the R-factor minimized by varying the rotational and translational parameters. The structure parameters were refined by the block-diagonal least-squares method by using 1227 independent reflections; the final R-value was 0.073. The absolute configuration was determined to be 1R6S from the Cu$K\alpha$ anomalous scattering of the chlorine atom.

Triptycene has a rigid molecular skeleton, with a three-fold symmetry axis. The crystal structures of several triptycene derivatives have been investigated,[1-5] and the high symmetry of the molecular structure has been characterized. A series of optically-active substituted triptycenes were synthesized by Ogura, Nakagawa, and their co-workers,[6-8] and the theoretical analysis of their circular dichroism spectra was carried out by the exciton method.[9-11] It was found that the absolute configuration of (+)-2,5-dimethoxy-7-dimethylaminotriptycene hydrobromide, as determined by the X-ray method, was not in agreement with that deduced by the analysis of the CD spectra.[5,9-11] The disagreement between the X-ray and CD analysis is serious problem for the foundation of stereochemistry; further investigation with other derivatives is earnestly desired.

The triptycene derivatives thus far studied have substitutents at the 2, 5, and 7-carbon atoms; however, other derivatives with substituents at different positions are also of much interest. The present investigation was undertaken in order to determine the absolute configuration of (+)-2,5-dimethoxy-8-chlorotriptycene in order to confirm the absolute configuration by the X-ray method.

Experimental

The (+)-2,5-dimethoxy-8-chlorotriptycene was synthesized and crystallized from the petroleum ether by Dr. Ogura.

The space group was determined from oscillation and Weissenberg photographs. The density was measured by the flotation method in a mixed solution of cyclohexane and carbon tetrachloride. The cell dimensions were determined by the least-squares method, using 12 reflections which had been carefully measured on a Hilger-Watts four-circule diffractometer with Ni-filtered Cu$K\alpha$ radiation ($\lambda=1.5418$ Å). The intensity data were also measured on the diffractometer in the ω-2θ scanning mode ($\theta\leq 72°$) with the same radiation, using a crystal whose size was $0.3\times0.3\times0.5$ mm^3.

1378 independent reflections were obtained, and no correction was made for absorption or extinction. The crystal data are shown in Table 1.

TABLE 1. CRYSTAL DATA

$M.\ F.$: $C_{22}H_{17}O_2Cl$
$M.\ W.=348.83$
Crystal system: monoclinic
Systematic absences: $0k0$ when k is odd.
Space group: $P2_1$
$a=8.231\pm0.002$, $b=13.320\pm0.002$,
$c=8.156\pm0.001$ Å; $\beta=96.49\pm0.01°$
$V=886.5$ Å^3, $Z=2$,
$D_m=1.280$, $D_c=1.284$ g·cm^{-3},
$F(000)=364$, $\mu=21.29$ cm^{-1} (for Cu$K\alpha$)

* Department of Chemistry, Faculty of Science, Hokkaido University, Kita, Sapporo 060

Structure Analysis

Since the molecule is rigid and since the bond lengths of related molecules are known,[5] the position of each atom may be easily estimated when the translational and rotational parameters of the molecule in the unit cell can be determined. The direction of the pseudo-three-fold axis could be easily found from the Patterson map, because the carbon-carbon vectors with lengths of ~1.4 Å and ~2.8 Å were superposed six and four times respectively along the axis. This implies that two of the rotational parameters, ω and χ, can be determined and that only the ϕ parameter remains to fix the rotational freedom (see Fig. 1).

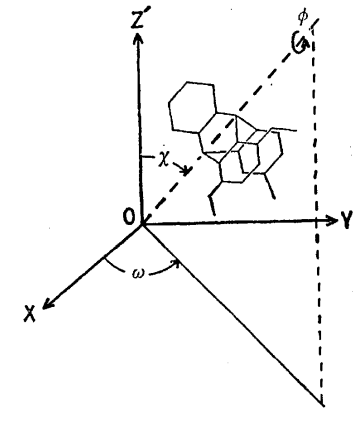

Fig. 1. Definition of rotational parameters with respect to the Cartesian coordinate axes.[12]

The translational and rotational searches were performed by the calculation of the R-values on the basis of the assumed model, which is rotated around the ϕ-axis and translated in the ac plane. Twenty-three $h0l$ reflections within $\theta<30°$ were selected for this calculation. The angle of the ϕ parameter was changed in the range from 0 to 2π with an interval of $\pi/90$ radian. At each setting of ϕ, the molecule was successively

translated in the *ac* plane by 1/50 for both Δx and Δz, and the *R*-value was calculated at each point. The position of the minimum *R*-value(0.30) was easily found on the *R*-map thus prepared. The calculation could be done within ten minutes machine time on the FACOM 230-60. Further refinement, using all the three-dimensional reflection data, confirmed that the position was actually adequate. The origin was adjusted so as to put all the *y*-parameters of atoms belonging to one molecule in the range from 0 to one.

The diagonal least-squares method was applied for the refinement of structure parameters by using 1227

Table 2. Atomic coordinates and their standard deviations

	x	*y*	*z*		*x*	*y*	*z*
C (1)	0.4281(12)	0.4415(8)	0.3635(12)	C (21)	0.7886(16)	0.3721(13)	0.0349(15)
C (2)	0.7310(11)	0.4379(8)	0.2961(12)	C (22)	1.0172(14)	0.5977(12)	0.8079(16)
C (3)	0.8900(12)	0.4587(8)	0.3461(13)	O (1)	0.6712(9)	0.3902(6)	0.1487(8)
C (4)	0.9373(12)	0.5042(8)	0.5005(13)	O (2)	0.8467(7)	0.5790(6)	0.7495(8)
C (5)	0.8153(11)	0.5312(8)	0.5988(11)	Cl	0.2712(5)	0.2452(4)	0.9903(4)
C (6)	0.5095(12)	0.5350(8)	0.6413(12)				
C (7)	0.3878(13)	0.3929(9)	0.8085(11)	Atomic coordinates of hydrogen atoms			
C (8)	0.3108(13)	0.3022(9)	0.8033(12)		*x*	*y*	*z*
C (9)	0.2677(12)	0.2499(10)	0.6602(12)	H(C 1)	0.370	0.401	0.254
C (10)	0.2993(13)	0.2939(8)	0.5129(12)	H(C 3)	0.987	0.447	0.265
C (11)	0.2424(12)	0.5876(9)	0.2469(13)	H(C 4)	1.076	0.515	0.541
C (12)	0.1775(13)	0.6829(9)	0.2753(14)	H(C 6)	0.555	0.571	0.760
C (13)	0.2189(14)	0.7324(9)	0.4226(14)	H(C 7)	0.416	0.419	0.915
C (14)	0.3270(12)	0.6882(8)	0.5457(13)	H(C 9)	0.212	0.174	0.648
C (15)	0.6089(11)	0.4610(7)	0.3958(11)	H(C 10)	0.278	0.260	0.427
C (16)	0.6560(11)	0.5108(7)	0.5488(12)	H(C 11)	0.222	0.545	0.147
C (17)	0.4241(11)	0.4361(7)	0.6624(11)	H(C 12)	0.065	0.725	0.200
C (18)	0.3788(11)	0.3845(8)	0.5124(11)	H(C 13)	0.175	0.793	0.445
C (19)	0.3477(11)	0.5459(8)	0.3704(12)	H(C 14)	0.349	0.719	0.631
C (20)	0.3899(10)	0.5958(8)	0.5209(11)				

Table 3. Anisotropic thermal factors* ($\times 10^4$) and their standard deviations

	B_{11}	B_{22}	B_{33}	B_{12}	B_{13}	B_{23}
C (1)	126(17)	41(7)	97(15)	−13(16)	42(25)	−13(16)
C (2)	149(18)	41(7)	111(16)	23(17)	110(28)	15(17)
C (3)	105(17)	55(8)	151(18)	7(18)	106(28)	−1(20)
C (4)	115(16)	50(7)	141(17)	−27(18)	71(28)	−40(19)
C (5)	95(15)	50(7)	98(16)	−19(16)	19(24)	14(17)
C (6)	126(17)	43(6)	106(16)	−27(17)	75(25)	−55(17)
C (7)	149(18)	58(8)	78(15)	−31(19)	34(25)	0(18)
C (8)	171(21)	66(9)	97(16)	−56(21)	87(30)	50(20)
C (9)	132(18)	66(8)	147(18)	−61(22)	94(29)	42(23)
C (10)	156(19)	62(8)	98(17)	−11(20)	14(29)	−34(19)
C (11)	105(16)	66(8)	134(18)	8(20)	24(27)	41(20)
C (12)	135(19)	46(7)	173(21)	14(19)	−12(31)	47(21)
C (13)	158(21)	50(8)	203(20)	−21(21)	64(33)	18(24)
C (14)	104(17)	36(6)	175(20)	31(17)	26(29)	−29(18)
C (15)	95(15)	42(6)	96(14)	12(15)	52(23)	−17(16)
C (16)	89(14)	36(6)	115(15)	21(15)	31(23)	−4(16)
C (17)	100(16)	41(6)	102(15)	−3(16)	28(24)	−19(16)
C (18)	101(15)	46(7)	105(15)	−30(17)	37(24)	5(17)
C (19)	92(15)	41(7)	116(16)	19(16)	12(24)	18(17)
C (20)	58(13)	60(7)	107(16)	12(16)	−3(22)	−19(18)
C (21)	214(27)	136(14)	149(22)	57(32)	176(38)	−89(30)
C (22)	127(20)	135(15)	191(24)	−66(30)	−36(43)	−133(32)
O (1)	180(14)	76(6)	93(11)	−9(16)	77(19)	−64(14)
O (2)	98(10)	62(5)	124(11)	1(13)	1(17)	−47(13)
Cl	335(8)	112(3)	147(5)	−175(9)	75(10)	54(7)

* The anisotropic thermal factors are of the form $\exp\{-(h^2B_{11}+k^2B_{22}+l^2B_{33}+hkB_{12}+hlB_{13}+klB_{23})\}$.

independent reflections with $|F^0|>6\sigma$, and the R-index was reduced to 0.130. Additional block-diagonal least-squares refinement was carried out with anisotropic thermal factors, and the R-index was converged to 0.097. The hydrogen atoms attached to the benzene rings and those attached to the bridge-head carbons were found on the difference Fourier map. Further refinement, including these hydrogen positions, resulted in the final R-value of 0.073, with an equal weight for each reflection. No other significant peaks were found in the final Fourier and difference Fourier maps.

The atomic scattering factors were taken from the International Tables for X-ray Crystallography.[13] The computation was carried out with the programs of UNICS coded by Dr. Ashida and those coded by ourselves on FACOM 230-60 at the Nagoya University Computation Center.

The atomic coordinates, with their standard deviations, and the anisotropic thermal factors, with their standard deviations, are listed in Table 2 and Table 3 respectively. The observed and calculated structure factors are listed in Table 4.[14]

Results and Discussion

(+)-2,5-Dimethoxy-8-chlorotriptycene is actually a rigid molecule with a pseudo-three-fold axis. The bond lengths and angles are shown in Table 5 and Table 6 respectively. The average bond length around the C(1) and C(6) of the bridge head carbons, 1.52 Å, is in good agreement with the expected value for an sp^2-sp^3 carbon bond.[15] The bonds which form the bicyclo-2,2,2-octatriene ring are longer than the normal value of the benzene ring by 0.02~0.04 Å. The tetrahedral angles around the bridge-head carbons are smaller by 2.4~4.6° than the normal tetrahedral angle. The external angles made by the bicyclo-2,2,2-octatriene ring and the benzenoid ring are about 127°, while the internal angles are about 113°. These results mean that a significant strain is exerted on the part of the

Table 5. Bond lengths and their standard deviations

C (2)-C (3)	1.352(15) Å	C (1)-C (15)	1.502(14) Å
C (2)-C (15)	1.395(14)	C (1)-C (18)	1.526(15)
C (3)-C (4)	1.413(16)	C (1)-C (19)	1.541(14)
C (4)-C (5)	1.400(15)	C (6)-C (16)	1.524(14)
C (5)-C (16)	1.354(14)	C (6)-C (17)	1.511(14)
C (15)-C (16)	1.428(14)	C (6)-C (20)	1.540(15)
average	1.390	average	1.524
C (7)-C (8)	1.362(17)	C (2)-O (1)	1.398(13)
C (7)-C (17)	1.387(15)	C (5)-O (2)	1.383(13)
C (8)-C (9)	1.370(17)	C (21)-O (1)	1.432(20)
C (9)-C (10)	1.387(17)	C (22)-O (2)	1.447(18)
C (10)-C (18)	1.372(16)	C (8)-Cl	1.767(13)
C (17)-C (18)	1.415(15)		
average	1.382		
C (11)-C (12)	1.407(17)		
C (11)-C (19)	1.370(16)		
C (12)-C (13)	1.378(17)		
C (13)-C (14)	1.392(17)		
C (14)-C (20)	1.358(15)		
C (19)-C (20)	1.404(15)		
average	1.385		

Table 6. Bond angles and their standard deviations

C (3)-C (2)-C (15)	120.8(10) °	C (15)-C (1)-C (18)	107.1(8) °
C (2)-C (3)-C (4)	121.1(10)	C (15)-C (1)-C (19)	104.9(8)
C (3)-C (4)-C (5)	118.5(10)	C (18)-C (1)-C (19)	105.4(8)
C (4)-C (5)-C (16)	120.5(10)	C (16)-C (6)-C (17)	106.0(8)
C (2)-C (15)-C (16)	118.1(9)	C (16)-C (6)-C (20)	106.1(8)
C (5)-C (16)-C (15)	120.8(9)	C (17)-C (6)-C (20)	105.1(8)
C (8)-C (7)-C (17)	118.9(11) °	C (6)-C (17)-C (18)	113.9(10) °
C (7)-C (8)-C (9)	123.6(11)	C (1)-C (15)-C (16)	113.4(8)
C (8)-C (9)-C (10)	117.8(11)	C (6)-C (16)-C (15)	112.4(8)
C (9)-C (10)-C (18)	120.7(11)	C (1)-C (18)-C (17)	112.2(9)
C (7)-C (17)-C (18)	118.8(10)	C (1)-C (19)-C (20)	113.3(9)
C (10)-C (18)-C (17)	120.2(10)	C (6)-C (20)-C (19)	112.6(9)
C (12)-C (11)-C (19)	117.7(11) °	C (1)-C (15)-C (2)	128.5(9) °
C (11)-C (12)-C (13)	120.9(11)	C (5)-C (16)-C (6)	126.8(9)
C (12)-C (13)-C (14)	120.1(11)	C (6)-C (17)-C (7)	127.3(9)
C (13)-C (14)-C (20)	119.8(10)	C (1)-C (18)-C (10)	127.6(10)
C (11)-C (19)-C (20)	121.5(10)	C (1)-C (19)-C (11)	125.2(10)
C (14)-C (20)-C (19)	119.9(10)	C (6)-C (20)-C (14)	127.5(10)
C (3)-C (2)-O (1)	125.9(10) °	Cl-C (8)-C (7)	118.9(9) °
C (15)-C (2)-O (1)	113.3(9)	Cl-C (8)-C (9)	117.4(9)
C (4)-C (5)-O (2)	123.6(9)		
C (16)-C (5)-O (2)	115.9(9)		
C (2)-O (1)-C (21)	115.9(10)		
C (5)-O (2)-C (22)	116.7(9)		

bicyclo-2,2,2-octatriene ring of the triptycene skeleton. A similar trend is found in the results of previous studies.[1-5]

The least-squares planes of three benzene rings are given by the following equations;

(1) Benzene ring:
$0.8201X+0.4291Y-0.3786Z'-4.0490=0$

(2) Chlorobenzene ring:
$0.8823X-0.4620Y+0.0906Z'-0.3395=0$

(3) Dimethoxybenzene ring:
$-0.0524X+0.8942Y-0.4446Z'-3.8398=0$

where X, Y, and Z' are coordinates in Å along the a, b, and c* axes respectively. The deviations of atoms from these planes are shown in Table 7. The planarity of the three benzene rings is remarkably good. The chlorine atom is nearly on the ring plane, and bridgehead carbons are on nearly three planes, but C(21) deviates from the dimethoxybenzene-ring plane by 0.13 Å.

Table 7. Deviations from the least-squares plane

(1)	Benzene-ring plane			
	C (11)	0.001 Å	C (1)[a]	−0.026 Å
	C (12)	−0.001	C (6)[a]	−0.005
	C (13)	−0.002		
	C (14)	0.004		
	C (19)	0.001		
	C (20)	−0.004		
(2)	Chlorobenzene-ring plane			
	C (7)	−0.005 Å	C (1)[a]	0.024 Å
	C (8)	−0.005	C (6)[a]	0.018
	C (9)	0.015	Cl[a]	0.043
	C (10)	−0.015		
	C (17)	0.005		
	C (18)	0.005		
(3)	Dimethoxybenzene-ring plane			
	C (2)	0.008 Å	C (1)[a]	−0.058 Å
	C (3)	0.010	C (6)[a]	0.033
	C (4)	−0.018	C (21)[a]	0.128
	C (5)	0.007	C (22)[a]	−0.031
	C (15)	−0.018	O (1)[a]	−0.010
	C (16)	0.011	O (2)[a]	0.027

a) Atoms not included in the least-squares plane calculation.

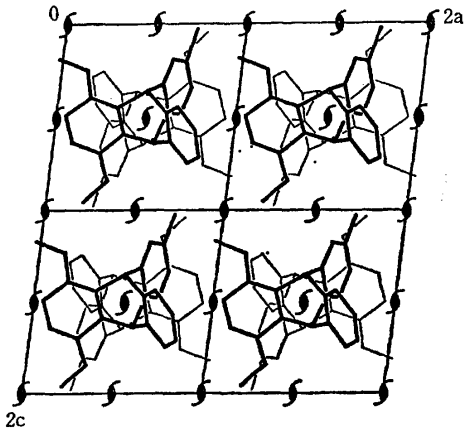

Fig. 2. Projection along the b axis.

The crystal structures as projected along the b axis and the c axis are shown in Figs. 2 and 3 respectively. The intermolecular distances within 3.6 Å are listed in Table 8. The closest distance occurs at 3.29 Å between the chlorine atom and the oxygen atom of the methoxyl group (O(2)).

The absolute configuration was determined by the Bijvoet method using the anomalous scattering of Cu$K\alpha$ radiation by the chlorine atom. The $\Delta f'$ and $\Delta f''$ values were taken from the International Tables for X-ray Crystallography.[13] The observed intensity differences and calculated ones between the Bijvoet pair for twenty reflections are listed in Table 9. The signs of the observed values are in good agreement with those calculated based on the positional parameters of Table 2 in the right-handed coordinate system. The absolute configuration thus determined is 1R6S, as is illustrated in Fig. 4. This result is in good agreement with the chemical correlation of (+)-2,5-dimethoxy-8-

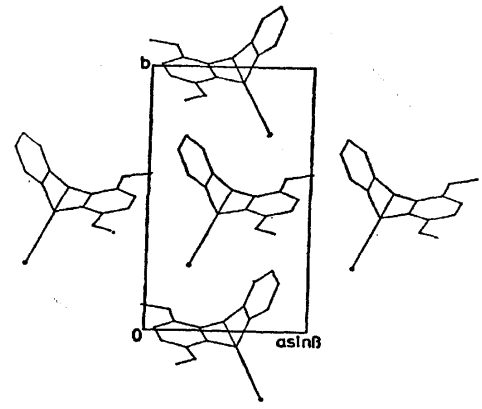

Fig. 3. Projection along the c axis.

Table 8. Intermolecular distances
≤ 3.6 Å

The Roman numerals represent the symmetry operators relevant to the atoms listed second.

Cl·····O (2[iv])	3.288(9) Å
O (1) ·····C (7[ii])	3.417(11)
C (2) ·····C (13[iii])	3.566(16)
C (3) ·····C (11[vii])	3.542(15)
C (7) ·····C (21[i])	3.604(16)
C (10)·····C (14[iii])	3.465(15)
C (11)·····C (4[vi])	3.604(15)
C (12)·····O (21[v])	3.604(19)

Symmetry code superscript	Symmetry operator		
i	x	y	$1+z$
ii	x	y	$-1+z$
iii	$-x$	$1/2+y$	$-z$
iv	$-x$	$1/2+y$	$1-z$
v	$-x$	$1/2+y$	$-1-z$
vi	$-1+x$	y	z
vii	$1+x$	y	z

TABLE 9. DETERMINATION OF ABSOLUTE CONFIGURATION

$100 \times \{I(hkl) - I(\bar{h}\bar{k}\bar{l})\}/I(hkl)$

h	k	l	Obsd	Calcd
1	1	−3	−5.1	−4.6
1	3	−4	9.1	6.0
1	5	1	2.3	3.4
1	9	1	−22.7	−25.2
2	1	−3	13.7	6.5
2	2	−4	14.7	7.9
2	2	5	−18.5	−5.8
2	6	−5	−15.0	−17.6
2	6	−1	27.8	17.2
2	6	2	−13.5	−9.2
3	1	−2	−9.9	−5.5
3	3	−1	−11.2	−4.3
3	3	2	−9.8	−5.7
3	5	2	9.6	7.0
3	7	1	24.2	21.9
4	2	4	30.3	23.2
4	3	−4	24.5	13.8
4	3	1	−19.4	−15.9
5	2	−3	−16.0	−14.1
5	4	−3	12.3	12.5

chlorotriptycene[16] with (+)-2,5-dimethoxy-7-dimethylaminotriptycene, since the absolute configuration of the latter molecule, as determined by the X-ray method,[5] is known to be 1R6S also.

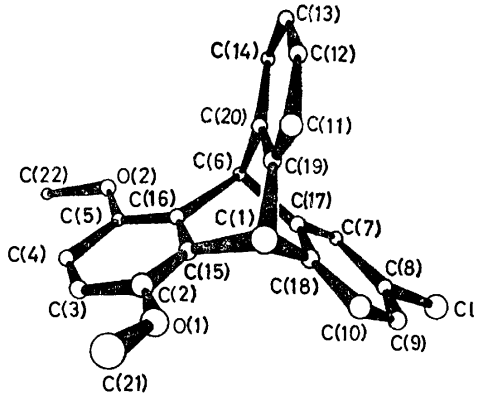

Fig. 4. Absolute configuration of (+)-2,5-dimethoxy-8-chlorotriptycene.

References

1) K. J. Palmer and D. H. Templeton, *Acta Crystallogr.*, B**24**, 1048 (1968).
2) I. L. Karle and J. A. Estlin, *Z. Kristallogr.*, **128**, 371 (1969).
3) K. Anzenhofer and J. J. de Boer, *ibid.*, **131**, 103 (1970).
4) M. A. Neuman, *Trans. Amer. Cryst. Assoc.*, **6**, 111 (1970).
5) N. Sakabe, K. Sakabe, K. Ozeki-Minakata, and J. Tanaka, *Acta Crystallogr.*, B**28**, 3441 (1972).
6) M. Kuritani, Y. Sakata, F. Ogura, and M. Nakagawa, This Bulletin, **46**, 605 (1973).
7) Y. Sakata, F. Ogura, and M. Nakagawa, *ibid.*, **46**, 611 (1973).
8) F. Ogura and M. Nakagawa, *ibid.*, **46**, 651 (1973).
9) J. Tanaka, K. Ozeki-Minakata, F. Ogura, and M. Nakagawa, *Nature, Phys. Sci.*, **241**, 22 (1973).
10) J. Tanaka, F. Ogura, M. Kuritani, and M. Nakagawa, *Chimia*, **26**, 471 (1972).
11) J. Tanaka, K. Ozeki-Minakata, F. Ogura, and M. Nakagawa, *Spectrochim. Acta*, **29**A, 897 (1973).
12) R. Huber, "Crystallographic Computing," ed. by F. R. Ahmed, Munksgaard, Copenhagen (1970), p. 96.
13) "International Tables for X-ray Crystallography," Vol. III, Birmingham: Kynoch Press (1968), p. 201.
14) Table 4 has been submitted to, and is kept by the office of the Chemical Society of Japan, 1-5, Kanda, Surugadai, Chiyodaku, Tokyo. (Doument No. 7416).
15) M. J. S. Dewar and H. N. Schmeising, *Tetrahedron*, **11**, 96 (1960).
16) M. Hashimoto, Y. Shimizu, F. Ogura, and M. Nakagawa, This Bulletin, **47**, 1761 (1974).

The Microwave Spectrum of 3,3,3-Trifluoropropene

Shuji SAITO and Fumio MAKINO
Sagami Chemical Research Center, Sagamihara, Kanagawa 229
(Received December 10, 1973)

The microwave spectra of normal, 2-^{13}C, and three monodeuterated isotopic species of 3,3,3-trifluoropropene have been studied. The combined structure of r_0 and r_s was obtained from the rotational constants observed. It has been necessary to take account of a tilt angle of the symmetry axis of the trifluoromethyl group. The following structural parameters have been determined: r(C–C)=1.489±0.002 Å, r(C=C)=1.312±0.010 Å, r(C–H$_1$)=1.085±0.011 Å, r(C–H$_2$)=1.092±0.009 Å, r(C–H$_3$)=1.109±0.003 Å, ∠F–C–F=106.8±0.3°, ∠C–C=C=124.8±0.4°, ∠C=C–H$_1$=120.6±1.0°, ∠C=C–H$_2$=122.8±1.0°, ∠C=C–H$_3$=121.2±1.0°, and θ_t=1.0±0.8° on the assumption that r(C–F)=1.345±0.003 Å, where θ_t denotes the tilt angle of the CF$_3$ top axis relative to the C–C bond away from the double bond of the vinyl group. The components of the electric dipole moment have been determined to be μ_a=2.331±0.014 D and μ_b=0.698±0.025 D; these values give a total dipole moment of 2.433±0.020 D at an angle of 7±1° with the symmetry axis of the trifluoromethyl group. The relative intensity between the rotational transitions in the ground state and in the first torsionally-excited state has been measured. The torsional frequency has been determined to be 88±25 cm^{-1}.

When a trifluoromethyl group, CF_3, is substituted in a molecule, a significant structural change can be expected because fluorine is the most electronegative element. There have been several studies of the structural determination of molecules containing the trifluoromethyl group by means of microwave spectroscopy or other methods. The results thus far have not, however, shown definitely the trend of the structural change upon trifluoromethyl substitution. Hilderbrandt *et al.*[1] studied hexafluoroacetone, hexafluoropropylimine, and hexafluoroisobutene by means of the electron-diffraction method and revealed that, upon fluorine substitution, the C-C bond length of the molecules studied increased, contrary to the trend previously observed in pairs of ethane[2] and 1,1,1-trifluoroethane,[3] ethylene[4] and 1,1-difluoroethylene,[5] and so on.

The real structural change upon fluorine substitution should be extractable from the accurately-determined structures of the fundamental and simplest molecules, in which such other effects as steric repulsion are not conspicuous. The pair of propene and 3,3,3-trifluoropropene is a good example for study. Recently, Tokue, Fukuyama and Kuchitsu[6] studied both the molecules by the electron-diffraction method. Making a joint analysis using the electron-diffraction intensities and the results of our microwave spectroscopic study which we will report in this paper, they determined the average structure of 3,3,3-trifluoropropene and found that the molecule follows the trend previously observed. The infrared spectrum of 3,3,3-trifluoropropene has been observed in the gas phase and assigned except for the torsional mode of the CF_3 top.[7] The dipole moment of this molecule in the gas phase was determined to be 2.45 D by the dielectric-constant method.[8]

In this paper we will report the microwave spectrum of 3,3,3-trifluoropropene, including one ^{13}C isotopic species and three monodeuterated species, and the determination of the molecular structural parameters, the dipole moment, the torsional frequency, and the barrier to internal rotation. While this work was in progress, Mukhtarov and Kuliev[9] reported the rotational constants of 3,3,3-trifluoropropene in the ground and torsionally-excited states, and its dipole moment.

Experimental

The spectra were observed with a conventional 110 KHz Stark-modulation spectrometer.[10] The measurements were carried out at the temperature of dry ice. The accuracy of the frequencies measured was estimated to be better than 0.1 MHz. Normal 3,3,3-trifluoropropene was obtained from the K & K Co. and was used without further purification. A mixture of three monodeuterated isotopic species was kindly provided by Y. Nakano. A deuterated sample was prepared by a hydrogen-exchange reaction of normal species with the deuterium gas on a powdered nickel catalyst. The product was purified by gas chromatography.

Microwave Spectrum

The spectra of the normal 3,3,3-trifluoropropene observed in the X to K bands consisted of a strong *a*-type *R*-branch and weak *b*-type *R*- and *Q*-branch transitions, characteristic of a nearly prolate symmetric top. Their assignment was made on the basis of the Stark effect on each transition. The weak *b*-type *R*-branch transitions were measured by means of a recorder. The frequencies of the observed transitions are listed in Table 1. The rotational constants of the normal species were determined by a least-squares fitting of the lowest fifteen transitions, as is shown in Table 4. The centrifugal distortion effect was discarded in the analysis, because only low-J transitions were measured.

The strong satellite lines in the vicinity of the ground-state transitions and showing similar Stark effect behavior were found at slightly higher frequencies with regularly varying intensities. These were assigned to the transitions in the first and second torsionally-excited states, since their intensities indicated that the states belong to the vibrations of very low frequencies which were not observed in the infrared spectrum.[7] The frequencies of the observed transitions are listed in Table 2. The rotational constants in the torsionally-excited states were obtained in the same way as those of the ground state. These results are also given in Table 4. The obtained B and C rotational constants in the ground and torsionally-excited states are nearly equal to those reported by Mukhtarov and Kuliev.[9]

Table 1. Rotational transitions of the normal 3,3,3-trifluoropropene in the ground state (MHz)

Transition	ν_{obsd}[a]	$\nu_{obsd}-\nu_{calcd}$[c]
a type		
$2_{12} \leftarrow 1_{11}$	11562.94	0.07
$2_{02} \leftarrow 1_{01}$	11631.77	0.04
$2_{11} \leftarrow 1_{10}$	11703.55	0.04
$3_{13} \leftarrow 2_{12}$	17343.50	0.10
$3_{03} \leftarrow 2_{02}$	17444.04	0.10
$3_{22} \leftarrow 2_{21}$	17449.58	−0.21
$3_{21} \leftarrow 2_{20}$	17455.55	−0.09
$3_{12} \leftarrow 2_{11}$	17554.30	−0.05
$4_{14} \leftarrow 3_{13}$	23122.87	−0.01
$4_{04} \leftarrow 3_{03}$	23251.87	0.08
$4_{23} \leftarrow 3_{22}$	23265.24	−0.01
$4_{32} \leftarrow 3_{31}$	23269.37[b]	0.11
$4_{31} \leftarrow 3_{30}$		0.00
$4_{22} \leftarrow 3_{21}$	23279.48	−0.36
$4_{13} \leftarrow 3_{12}$	23404.00	−0.05
b type[b]		
$1_{11} \leftarrow 0_{00}$	8315.90	0.09
$2_{02} \leftarrow 1_{01}$	9132.67	0.15
$2_{12} \leftarrow 1_{01}$	14062.10	0.02
$2_{20} \leftarrow 1_{11}$	19272.87	−0.06
$3_{13} \leftarrow 2_{02}$	19773.65	−0.11
$3_{21} \leftarrow 2_{12}$	25165.36	−0.33
$3_{31} \leftarrow 2_{20}$	30121.76	0.09
$3_{30} \leftarrow 2_{21}$	30122.54	−0.03

a) Accuracy better than ±0.1 MHz, unless otherwise indicated, b) ±0.2 MHz. c) Calculated frequencies were obtained using the rotational constants in Table 4.

Their values of the A rotational constants are quite different from ours. This difference is due to the fact that we have observed both the *a*- and *b*-type spectra in the ground and torsionally-excited states.

Though all three ^{13}C isotopically-substituted species were searched for in their natural abundances (1.1%), most of the lines were masked or disturbed by other strong lines. Only the *a*-type spectrum of the 2-^{13}C species was assigned and measured, as is shown in Table 3.

Table 2. Rotational transitions of the normal 3,3,3-trifluoropropene in the torsionally-excited states (MHz)

Transition	$v_t=1$		$v_t=2$	
	ν_{obsd}[a]	$\nu_{obsd}-\nu_{calcd}$[c]	ν_{obsd}[a]	$\nu_{obsd}-\nu_{calcd}$[c]
a type				
$2_{12} \leftarrow 1_{11}$			11610.53	0.17
$2_{02} \leftarrow 1_{01}$	11646.83	0.07	11661.91	0.12
$2_{11} \leftarrow 1_{01}$	11709.10	−0.20	11714.70	−0.15
$3_{13} \leftarrow 2_{12}$	17379.04	0.05	17414.83	−0.21
$3_{03} \leftarrow 2_{02}$	17467.44	0.10	17490.69	0.04
$3_{22} \leftarrow 2_{21}$	17471.72	−0.10	17493.83	−0.08
$3_{21} \leftarrow 2_{20}$	17476.25	−0.05	17497.01	−0.16
$3_{12} \leftarrow 2_{11}$	17563.22	−0.02	17571.72	−0.04
$4_{14} \leftarrow 3_{13}$	23170.83	0.12	23219.08	−0.04
$4_{04} \leftarrow 3_{03}$	23284.75	0.18	23317.22	0.13
$4_{23} \leftarrow 3_{22}$	23294.93	0.04	23324.55	−0.03
$4_{32} \leftarrow 3_{31}$	23297.58[b]	−0.38	23326.31[b]	−0.51
$4_{31} \leftarrow 3_{30}$		−0.46		−0.56
$4_{22} \leftarrow 3_{21}$	23305.77	−0.30	23332.57	−0.14
$4_{13} \leftarrow 3_{12}$	23416.29	−0.03	23428.01	−0.04
b type[b]				
$1_{11} \leftarrow 0_{00}$	8317.91	0.09	8319.97	0.19
$3_{03} \leftarrow 2_{12}$	15033.91	0.16	15053.86	0.25
$3_{13} \leftarrow 2_{02}$	19812.54	−0.03	19852.13	0.05
$3_{22} \leftarrow 2_{11}$	24953.36	−0.11	23959.34	0.00
$3_{21} \leftarrow 2_{12}$	25143.28	−0.06		
$3_{31} \leftarrow 2_{20}$	30094.48	0.12		
$3_{30} \leftarrow 2_{21}$	30095.50	0.00		

a) Accuracy better than ±0.1 MHz, unless otherwise indicated. b) ±0.2 MHz. c) Calculated frequencies were obtained using the rotational constants in Table 4.

There are three isotopic isomers of monodeuterated species. For the sake of simplicity, each isomer is designated by the number of the substituted atom, as given in Fig. 1. Also, only *a*-type *R*-branch transitions were observed for these species because of the low enrichment of the deuterium atom. The results are shown in Table 3. The rotational constants of the 2-^{13}C and monodeuterated species were determined

Table 3. Observed rotational transition of 2-^{13}C and monodeuterated 3,3,3-trifluropropene (MHz)[a,b,c]

Transition	2-^{13}C	D_1	D_2	D_3
$2_{12} \leftarrow 1_{11}$	11467.56(0.00)	11201.53(0.00)	10932.97(0.00)	11344.58(0.00)
$2_{02} \leftarrow 1_{01}$		11282.89(−0.09)		11457.62(−0.07)
$2_{11} \leftarrow 1_{10}$	11620.15(0.00)	11368.29(0.00)	11064.96(0.00)	11579.61(0.00)
$3_{13} \leftarrow 2_{12}$		16801.32(0.21)	16398.57(−0.15)	
$3_{03} \leftarrow 2_{02}$		16919.51(−0.14)	16493.70(0.00)	17175.54(0.00)
$3_{22} \leftarrow 2_{21}$		16927.42(0.05)		
$3_{21} \leftarrow 2_{20}$		16934.92(−0.17)		
$3_{12} \leftarrow 2_{11}$		17051.09(−0.13)	16596.99(0.30)	17366.99(0.33)
$4_{14} \leftarrow 3_{13}$	22931.53(0.31)			
$4_{32} \leftarrow 3_{31}$	23091.93 (0.41)			
$4_{31} \leftarrow 3_{30}$	(0.22)			

a) Accuracy better than ±0.2 MHz. b) Designation of isotopic species is given in Fig. 1. c) Differences between observed and calculated frequencies are shown in parentheses after observed values. Calculated values were obtained using the rotational constants listed in Table 4.

Table 4. Rotational constants (MHz) and moments of inertia (amu Å²)[a] for 3,3,3-trifluoropropene

	Normal	$v_t=1$	$v_t=2$	2-^{13}C
A	5442.67±0.10	5436.56±0.10	5430.25±0.10	5122 ±170
B	2943.47±0.03	2942.68±0.03	2941.77±0.03	2924.11±0.05
C	2873.14±0.03	2881.26±0.03	2889.53±0.03	2847.82±0.05
I_a	92.855±0.002	92.959±0.002	93.067±0.002	
I_b	171.695±0.002	171.740±0.002	171.793±0.002	172.831±0.003
I_c	175.897±0.002	175.401±0.002	174.899±0.002	177.461±0.003
ΔI[b]	88.653±0.005	89.298±0.005	89.961±0.005	

	D_1	D_2	D_3
A	5520 ±70	5500 ±140	5213 ±50
B	2862.92±0.05	2782.74±0.05	2924.28±0.05
C	2779.54±0.05	2716.74±0.05	2806.77±0.05
I_a			
I_b	176.525±0.003	181.611±0.003	172.821±0.003
I_c	181.820±0.003	186.023±0.003	180.056±0.003
ΔI[b]			

a) Conversion factor=505376 MHz amu Å². b) $\Delta I=I_a+I_b-I_c$.

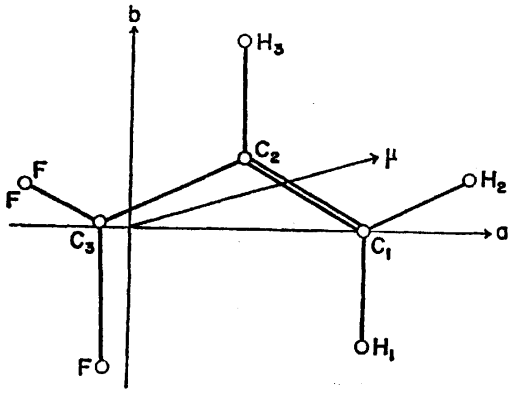

Fig. 1. Numbering of the hydrogen atoms in 3,3,3-trifluoropropene: the c principal axis is perpendicular to the paper.

from a few adequate transitions. The observed rotational constants and moments of intertia are given in Table 4. The large errors associated with the A rotational constants for the 2-^{13}C and monodeuterated species resulted from a lack of observation on b-type transitions.

Dipole Moment

The second-order Stark effect was measured for four transitions, as is shown in Table 5. The electrode spacing was calibrated using the $J=1\leftarrow0$ transition of OCS.[11] From the Stark coefficients, μ_a was determined to be 2.331±0.014 D, and μ_b, to be 0.698±0.025 D; these values gave a value of 2.433±0.020 D for the total dipole moment, where the error quoted was 2.5 times the standard deviation. The total dipole moment made an angle of 16°40′±40′ with the a principal axis. The orientation of the dipole moment relative to the molecular framework is not uniquely determined. It is reasonable to consider that the dipole moment

Table 5. Stark coefficients and dipole moment of 3,3,3-trifluoropropene

Transition	$\lvert M\rvert$	$\Delta\nu/E^2$[a] obsd	$\Delta\nu/E^2$[a] obsd−calcd
$2_{02}\leftarrow1_{01}$	0	-3.46_2	−0.015
	1	3.85_0	0.004
$2_{11}\leftarrow1_{10}$	0	2.98_1	0.009
$2_{12}\leftarrow1_{11}$	0	2.68_6	−0.023

$\mu_a=2.331\pm0.014$ D $\quad\mu_b=0.698\pm0.025$ D
$\mu_{total}=2.433\pm0.020$ D $\quad\angle\mu_{total}$ CF_3-axis$=7\pm1°$

a) Values in 10^{-5} MHz(V/cm)$^{-2}$

of 3,3,3-trifluoropropene is mainly made up of the group moment of the CF_3 top. The angle between the direction of μ_{total} and the symmetry axis of the CF_3 top was determined to be 7±1° on the basis of the structure determined in the following section. The dipole moment obtained in this study is in agreement with the value ($\mu=2.45$ D) obtained by the dielectric-constant measurement.[8] Mukhtarov and Kuliev[9] gave slightly different values for the components of the dipole moment: $\mu_a=2.17\pm0.05$ D and $\mu_b=0.42\pm0.05$ D.

Molecular Structure

When the symmetry axis of the trifluoromethyl group is assumed to be colinear with the C–C single bond, there are eleven independent parameters specifying the structure of 3,3,3-trifluoropropene. As 2-^{13}C and three monodeuterated species were observed, the r_s coordinates of the center carbon atom and three hydrogen atoms were calculated to be as listed in Table 6. Three moments of inertia for the normal species are not enough to determine the remaining six parameters. We assume that the C–F bond distance is 1.345±0.003 Å,

Table 6. The r_s coordinates of atoms in 3,3,3-trifluoropropene (Å)

Atom	a_s	b_s
2-C	1.0655±0.0023	0.6605±0.0039
H_1	2.2022±0.0011	−1.0868±0.0025
H_2	3.1732±0.0007	0.4899±0.0056
H_3	1.0499±0.0023	1.7699±0.0015

the value obtained by the electron-diffraction method[6] and the most precise among the observed parameters. Moreover, we made full use of two moments of intertia for the 2-^{13}C species. Assuming the proper values for the parameters concerning three hydrogen atoms, four skeletal parameters, r(C–C), r(C=C), ∠F–C–F, and ∠C–C=C, were calculated by using three moments of inertia for the normal species and the I_b and I_c of the 2-^{13}C species. The results thus obtained were unreasonable, however, even if the effect of the zero-point vibrations was assumed to be rather large. It was found that five moments of inertia were never reconciled to the parameters of the vinyl group within any reasonable range, because the structure of the CF_3 group was strictly conditioned by the assumed value of the r(C–F) bond and the following equation;

$$\Delta I = I_a + I_b - I_c = 4m_F r_{CF}^2 \sin^2 \theta_{FCF}/2 + \Delta_0 \qquad (1)$$

This means that it is necessary to consider a relative configuration between the trifluoromethyl group and the vinyl group. Therefore, we recalculated the structure by taking account of the tilt of the symmetry axis of the trifluoromethyl group relative to the C–C single bond. About a one-degree tilt of the symmetry axis from the C–C single bond outward from the C–C=C angle was enough to explain five moments of inertia. The results are shown in Table 7. The remaining six parameters concerning the three hydrogen atoms were fitted to give their r_s coordinate as is given in Table 6. The obtained structural parameters are also shown in Table 7. The a and b coordinates of the C_2 atom in the molecular structure determined were calculated to be 1.0667 Å and 0.6613 Å respectively; these values were in agreement with the r_s coordinates given in Table 6.

Table 7. Molecular structure of 3,3,3-trifluoropropene

r(C–C)	1.489±0.002 Å
r(C=C)	1.312±0.010 Å
r(C–H_1)	1.085±0.011 Å
r(C–H_2)	1.092±0·009 Å
r(C–H_3)	1.109±0.003 Å
∠F–C–F	106.8±0.3°
∠C–C=C	124.8±0.4°
∠C=C–H_1	120.6±1.0°
∠C=C–H_2	122.8±1.0°
∠C=C–H_3	121.2±1.0°
θ_t[a]	1.0±0.8°
Assumed[b]	
r(C–F)	1.345±0.003 Å

a) For the defininition, see the text. b) Ref. 6.

Internal Rotation

No splitting due to internal rotation was observed in any of the spectral lines in the torsionally-excited states up to $v=2$. The frequency of the torsional vibration was obtained from the relative intensities of the transitions in the ground state and in the first torsionally-excited state by the use of the method of Esbitt and Wilson.[12] Nine transitions of $J=2\leftarrow1$, $3\leftarrow2$, and $4\leftarrow3$ with $K_{-1}=0$ and 1 were investigated, but only three were suitable for measurement. The difficulties arose from the richness of the lines. The results for the three transitions which had the least interference are shown in Table 8. From the average relative intensity, the torsional frequency was found to be:

Table 8. Relative intensities of the transitions in the ground state and the $v_t=1$ torsional state of 3,3,3-trifluoropropene at 294 K

Transition	$I(v_t=1)/I(G.S.)$
$3_{03} \leftarrow 2_{02}$	0.66±0.01
$3_{12} \leftarrow 2_{11}$	0.72±0.03
$4_{04} \leftarrow 3_{03}$	0.57±0.03
Average	0.65±0.08

$$\nu_t = 88 \pm 25 \text{ cm}^{-1}.$$

This value is in good agreement with the frequency reported by Mukhtarov and Kuliev.[9] After the well-known method of the internal rotation analysis[13,14] and the molecular structure obtained, the three-fold barrier to the internal rotation of the trifluoromethyl top with respect to the vinyl group was calculated to be:

$$V_3 = 1640 \pm 800 \text{ cm}^{-1}.$$

The large uncertainty is due to the experimental error.

Discussion

The molecular structure of 3,3,3-trifluoropropene is conspicuous in a tilted trifluoromethyl group. Methyl group tilt has been found in several molecules from an analysis of the internal rotation or by structural analysis.[15] Tilted trifluoromethyl groups have not been reported since splittings due to the internal rotation are scarcely observed, and the detailed structures of the molecules containing a CF_3 top have rarely been determined. Though the magnitude of the tilt observed in this study is small, the heavy mass of the CF_3 top causes the effect to be noticeable, shifting the total moments of inertia. As has been described above, the moments of inertia including these shifts can never be explained within the plausible values of other skeletal parameters.

The tilt of the methyl group attached to an unsaturated carbon atom has not shown any definite direction,

such as is observed in propene,[16] acetone,[17] and methylketene.[18] It is not easy to find why the tilt of 3,3,3-trifluoropropene is away from the double bond of the vinyl group. In this connection, though, it should be noted that the distance between the H_1 atom and the fluorine atom in the plane of symmetry is 2.45 Å, slightly less than the sum of the atomic van der Waals radii, 2.55 Å.[19]

Tokue *et al.*[6] determined the average structure of 3,3,3-trifluoropropene by a joint analysis using the electron-diffraction intensities and our rotational constants. Their results agree with ours within the range of experimental error except for the C=C–H angle. The three C=C–H angles of 3,3,3-trifluoropropene have been determined separately in this study; their average is 121.5±1.0°. The corresponding value obtained by Tokue *et al.* is significantly small, 111.3±4.0°. Tokue *et al.* noticed that the C=C–H angle obtained in the joint analysis always became small if the weight of the rotational constants was increased relative to the diffraction intensities, while, inversely, if this angle was fixed to the r_α° parameter, 119.0°, some of the skeletal parameters were shifted appreciably. A similar situation was encountered in our structural analysis when the tilt of CF_3 top was not considered. It will be interesting to carry out the joint analysis with a tilted trifluoromethyl top.

When compared with the structures of related molecules, the partial structure of the CF_3 group of 3,3,3-trifluoropropene is very similar to those of analogous compounds.[3,20] The vinyl group of $CF_3CH{=}CH_2$ is slightly different from those of propene[21] and *cis*-3-fluoropropene.[22] The C–C single and C=C double bonds of 3,3,3-trifluoropropene are compared with those of related molecules in Table 9, which shows a systematic change in the bond distances upon trifluoromethyl substitution; a change in the C–C single bond connecting the methyl group and the rest of the molecule, which is brought about by the trifluoromethyl substitution, depends inversely on the electron-withdrawing force of the rest of the molecule. The molecules studied by Hilderbrandt *et al.*[1] may not act thus or may be influenced by other kinds of forces.

Table 9. Comparison of structures (Å)

Molecule	r(C–C)	r(C=C), r(C C) or r(C≡N)	Ref.
CH_3-CH_3	1.531_9±0.002		a)
CF_3-CH_3	1.492		b)
CH_3-CH=CH_2	1.501 ±0.004	1.336±0.004	c)
CF_3-CH=CH_2	1.489 ±0.002	1.312±0.010	This work
CH_3-C≡CH	1.4589	1.2062	d)
CF_3-C≡CH	1.46_4 ±0.002	1.201±0.002	e)
CH_3-C≡N	1.458_8	1.157_1	d)
CF_3-C≡N	1.46_1	1.15_3	b)

a) Ref. 2. b) Ref. 3. c) Ref. 21. d) C. C. Costain, *J. Chem. Phys.*, **29**, 864 (1958). e) Ref. 20.

References

1) R. L. Hilderbrandt, A. L. Andreassen, and S. H. Bauer, *J. Phys. Chem.*, **74**, 1586 (1970).
2) K. Kuchitsu, *J. Chem. Phys.*, **49**, 4456 (1968).
3) L. F. Thomas, J. S. Heeks, and J. Sheridan, *Z. Electrochem.*, **61**, 935 (1957).
4) L. S. Bartell and R. H. Bonham, *J. Chem. Phys.*, **27**, 1414 (1957).
5) V. W. Laurie and D. T. Pence, *ibid.*, **38**, 2693 (1963).
6) I. Tokue, T. Fukuyama, and K. Kuchitsu, *J. Mol. Structure*, **17**, 207 (1973).
7) G. A. Crowder and N. Smyrl, *J. Chem. Phys.*, **53**, 4102 (1970).
8) J. J. Conradi and N. C. Li, *J. Amer. Chem. Soc.*, **75**, 1785 (1953).
9) I. A. Mukhtarov and V. A. Kuliev, *Izv. Akad. Nauk Azerb. SSR.*, **1970**, 146.
10) S. Saito, *J. Mol. Spectrosc.*, **30**, 1 (1969).
11) J. S. Muenter, *J. Chem. Phys.*, **48**, 4544 (1968).
12) A. S. Esbitt and E. B. Wilson, Jr., *Rev. Sci Intsr.*, **34**, 901 (1963).
13) C. C. Lin and J. D. Swalen, *Rev. Mod. Phys.*, **31**, 841 (1959).
14) M. Hayashi and L. Pierce, Tables for the Internal Rotation Problem, University of Notre Dame, 1961.
15) L. Piece and M. Hayashi, *J. Chem. Phys.*, **35**, 479 (1961).
16) E. Hirota, *ibid.*, **45**, 1984 (1966).
17) R. Nelson and L. Pierce, *J. Mol. Spectrosc.*, **18**, 344 (1965).
18) B. Bak, J. J. Christiansen, K. Kunstmann, L. Nygaard, and J. Rastrup-Andersen, *J. Chem. Phys.*, **45**, 883 (1966).
19) L. Pauling, "The Nature of the Chemical Bond," Cornell University Press, Ithaca, New York (1960).
20) J. N. Shoolery, R. G. Shulman, W. F. Sheehan, Jr., V. Schomaker, and D. M. Yost, *J. Chem. Phys.*, **19**, 1364 (1951).
21) D. R. Lide, Jr., and D. Christensen, *ibid.*, **35**, 1374 (1961).
22) E. Hirota, *ibid.*, **42**, 2071 (1965).

The Reaction of β-Hydroxyalkylmercuric Perchlorate with Sodium Formate in an Aqueous Solution

Sumio SHINODA and Yasukazu SAITO

Department of Synthetic Chemistry, Faculty of Engineering, University of Tokyo, Hongo, Bunkyo-ku, Tokyo 113

(Received December 21, 1973)

The reaction of 2-hydroxy-1-propylmercuric perchlorate with sodium formate in an aqueous solution was found to be a redox-type reaction: $CH_3CH(OH)CH_2HgClO_4+HCOONa=CH_3CH=CH_2+Hg(0)+CO_2+H_2O+NaClO_4$. The concentration of the mercurial coordinated by the formate ion was determined *in situ* by analyzing the geminal ^{199}Hg–^1H spin-coupling constant. By changing the ratio of $[CH_3CH(OH)CH_2HgClO_4]/[HCOONa]$, the initial reaction rate was confirmed to be first-order with respect to the formato-mercurial: $v=k[CH_3CH(OH)CH_2HgOCOH]$. From the variation in k with the temperature, the values of $E_a=17.5$ kcal mol^{-1} and $A=4.0\times10^8$ s^{-1} were obtained. On the grounds of the kinetic isotope effect for DCOONa and the stereochemical study with *threo*- and *erythro*-$CH_3CH(OH)CHCH_3HgClO_4$, a mechanism is proposed in which the reaction proceeds solely through the unimolecular redox-decomposition of the formato-mercurial, involving an anti-elimination of olefin coupled with a two-electron transfer from the formate ligand to the mercurial.

A number of inorganic ions are known to oxidize formic acid in solution, and various mechanisms have been postulated for the redox processes.[1–5] In view of the ready redox-decomposition of β-hydroxyalkylmercurials,[6–9] it seemed of interest to investigate further the reactivity of the organomercurials through reactions with formate ions in aqueous media.

One of the unique features of the organomercurial is that it exhibits satellite peaks in the PMR spectra due to proton-mercury (^{199}Hg; $I=1/2$, natural abundance 16.84%) spin-spin interactions. In particular, the geminal proton-mercury coupling constants are useful in discriminating the dissociation or coordination of ligands, since they depend characteristically on the ligand species.[10–13] Accordingly, a quantitative analysis of formate-ion coordination during the reaction becomes possible. In the present work, we wish to report the application of geminal coupling constants of organomercurials to reaction kinetics, together with an elucidation of the reaction mechanism on the grounds of the rate expression, the isotope effect, and the stereochemistry of the reaction.

Experimental

Reagent. A mercuric solution was prepared by adding 28.703 g of 70% perchloric acid (0.20 mol) to 21.659 g of mercuric oxide (0.10 mol) suspended in 50 ml of water. Hydroxymercuration was effected by bubbling propene through the mercuric solution at 0 °C to obtain an aqueous 2-hydroxy-1-propylmercuric perchlorate solution quantitatively. Perchloric acid, formed stoichiometrically by the hydroxymercuration, was neutralized by an equivalent amount of sodium carbonate (5.299 g; 0.05 mol). The stock solution was prepared by diluting the solution to 100 ml with water (1.00 M; pH 0.75); the solution was then stored in a refrigerator. Aqueous *threo*- and *erythro*-3-hydroxy-2-butylmercuric perchlorate solutions were prepared in a similar manner using *cis*- and *trans*-2-butenes respectively. An aliquot of these solutions (2 to 10 ml) was used in each experiment. Sodium deuteroformate (DCOONa) of a minimum isotopic purity (atom % D) of 99% was obtained from Merck, Sharp, and Dohme of Canada, Ltd. The other chemicals were the G. R. grade, prepared by the Tokyo Kasei Co., Ltd. (Tokyo).

Experimental Procedure. A calculated amount of sodium formate (0.30 to 2.00 M) was added to 2 ml of the 2-hydroxy-1-propylmercuric perchlorate stock solution at 0 °C. A part of the solution maintained at 0 °C was quickly transferred to a PMR sample tube and put in the probe of the spectrometer kept at an adjusted temperature. The temperatures (45.2 to 63.2 °C) were calibrated by the relative chemical shifts of ethyleneglycol. The reaction was pursued by taking spectra in sequence with a JEOL PS-100 or a Hitachi R-20B PMR spectrometer.

In the determination of the amount of gas evolution, the solution of the reactants was introduced into a 100-ml flask connected to a vacuum line, and the amount was determined manometrically. A Hitachi RMU-6 mass spectrometer was used for the analysis of the gas-phase components. The amounts of *cis*- and *trans*-2-butenes were determined by gas chromatography using a column of 20% dimethylsulfolane on Celite.

Results and Discussion

Stoichiometry of the Reaction of $CH_3CH(OH)CH_2HgClO_4$ with Sodium Formate. The aqueous solution of 2-hydroxy-1-propylmercuric perchlorate (**1**) mixed with an equimolar amount of sodium formate was stable at 0 °C, but both the evolution of gas and the precipitation of elemental mercury were observed at *ca.* 50 °C. The reaction was pursued by taking the PMR spectra of a solution containing various concentrations (0.30 to 2.00 M) of sodium formate *in situ* after the temperature of the solution had been abruptly raised from 0 °C. The concentrations of the reactants were determined from the doublet peak (CH_3-; δ 1.21) for the mercurials and the singlet peak (HCO-; δ 9.12) for the formate ions respectively, in comparison with the peak intensity of the external tetramethylsilane reference. Some typical representative spectra are shown in Fig. 1, in which no other absorption peaks are obviously detected.

The time-course of the respective concentrations of the reactants is presented in Fig. 2, which evidently confirms the following equations:

$$[CH_3CH(OH)CH_2Hg^+]_0 - [CH_3CH(OH)CH_2Hg^+] = [HCOO^-]_0 - [HCOO^-] \quad (1)$$

$$d[CH_3CH(OH)CH_2Hg^+]/dt = d[HCOO^-]/dt \quad (2)$$

A mass-spectrometric analysis of the evolved gas showed that the gas-phase composition was an equi-

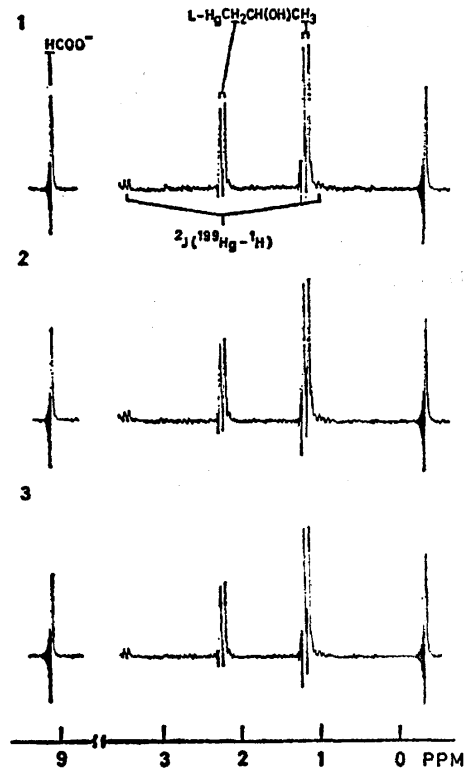

Fig. 1. The time-sequential PMR spectra obtained *in situ* for the reaction of 2-hydroxy-1-propylmercuric perchlorate with sodium formate in an aqueous solution at 51.0 °C. The unchanged singlet peak at −0.32 ppm is an absorption due to an external tetramethylsilane reference. Initial concentrations of the mercurial and sodium formate were 1.00 M and 0.70 M, respectively. These spectra were taken after (1) 14.0 min, (2) 37.0 min, (3) 136.3 min from the moment of raising the solution temperature.

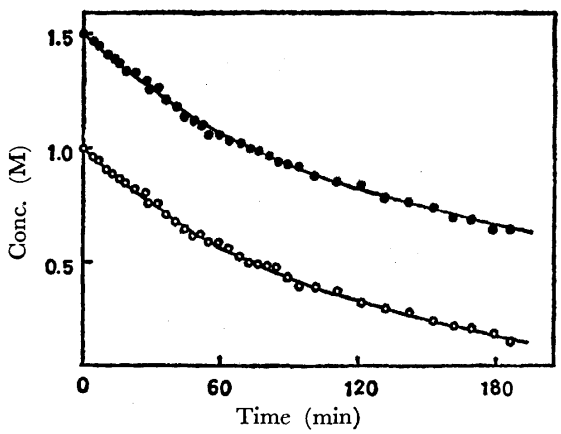

Fig. 2. The time-course of concentrations of the reactants for the reaction of 2-hydroxy-1-propylmercuric perchlorate with sodium formate in an aqueous solution at 63.2 °C. ○ and ● correspond to the mercurial and formate ions, respectively.

molar mixture of propene and carbon dioxide. No other gas, such as hydrogen or carbon monoxide, was detected by either mass-spectroscopic or gas-chromatographic analysis. It was also found by manometric measurement that the amounts of propene and carbon dioxide formed coincided (within 2%) with those of decomposed mercurials and formate ions. The stoichiometry of the reaction can, therefore, be expressed by Eq. (3), which obviously shows a redox-type reaction:

$$CH_3CH(OH)CH_2HgClO_4 + HCOONa = CH_3CH{=}CH_2 + Hg(0) + CO_2 + H_2O + NaClO_4 \quad (3)$$

Rate Equation for the Reaction of $CH_3CH(OH)CH_2HgClO_4$ with Sodium Formate. In the solution of the reactants, mercurials are present in the forms of both an aquo-complex, $CH_3CH(OH)CH_2HgOH_2^+$ (**2**),[14] and a formato-complex, $CH_3CH(OH)CH_2HgOCOH$ (**3**),[15] which are equilibrated as Eq. (4). Their ratio is reflected in the apparent value of the geminal ^{199}Hg-^1H spin-coupling constant, $^2J_{HgH}$, of the mercurial. Formate ions are found in the forms of ligands, free ions, and formic acid, which exchange with each other rapidly on the PMR time-scale. The peak intensities in Fig. 1 show the total amounts of the mercurials and formate ions respectively.

$$\underset{\mathbf{2}}{CH_3CH(OH)CH_2HgOH_2^+} + HCOO^- \rightleftharpoons \underset{\mathbf{3}}{CH_3CH(OH)CH_2HgOCOH} + H_2O \quad (4)$$

Since any observed value of $^2J_{HgH}$, J_{obs}, is expressed as a function of the molar fractions (Eq. (5)), the amounts of both **2** and **3** can be adequately evaluated through the use of Eq. (6) by monitoring the value of J_{obs} *in situ*, if the inherent values of $^2J_{HgH}$ for **2** and **3** (J_a and J_f, respectively) are properly determined:

$$J_{obs} = J_a x + J_f(1-x) \quad (5)$$

$$\left.\begin{aligned} x &= (J_{obs}-J_f)/(J_a-J_f) \\ 1-x &= (J_a-J_{obs})/(J_a-J_f) \end{aligned}\right\} \quad (6)$$

where x and $(1-x)$ are molar fractions of **2** and **3** respectively. As the complete dissociation of **1** had been confirmed,[14] it was possible to determine the value of J_a by simply measuring the $^2J_{HgH}$ for the aqueous solution of **1** (258.0 Hz). The increase in the added amount of sodium formate caused the decrease in the value of $^2J_{HgH}$ (Fig. 3). In the presence of a

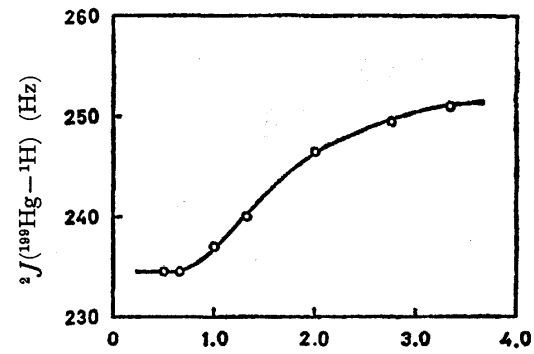

Fig. 3. Variation of geminal ^{199}Hg-^1H spin-coupling constant with the amount of added sodium formate. The concentration of $CH_3CH(OH)CH_2HgClO_4$ was commonly chosen as 1.00 M.

sufficient excess of sodium formate, the value became apparently constant. By extrapolating the plot to the intercept, the value of J_f was determined to be 234.5 Hz. The difference in value between J_a and J_f is large enough for us to determine x and $(1-x)$ with sufficient precision.

The reaction rates were determined for the solutions of the reactants with various ratios of [$CH_3CH(OH)CH_2HgClO_4$] to [HCOONa], where the initial concentrations of the mercurial were commonly chosen as 1.00 M. The increase in the amount of added sodium formate accelerated the reaction. Further, as is shown in Fig. 4, a plot of the initial rate against the concentration of **3**, as evaluated by Eq. (6), is linear. Each of the double circles represents three experimental values of the initial rates determined for solutions with different pH values, which were controlled by added amounts of both sodium formate and perchloric acid.

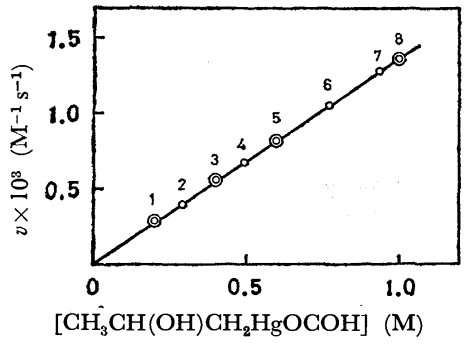

Fig. 4. Plot of initial rate *vs.* concentration of 2-hydroxy-1-propylmercuric formate at 63.2 °C.
Each point corresponds to the composition (HCOONa (M), $HClO_4$ (M)) of the solution: 1 (0.29, 0.10; pH 0.77. 0.58, 0.41; pH 0.52. 0.95, 0.82; pH 0.20), 2(0.30, 0.00; pH 1.60), 3(0.50, 0.10; pH 1.08. 0.79, 0.40; pH 0.85. 1.18, 0.80; pH 0.57), 4(0.50, 0.00; pH 1.80), 5(0.71, 0.10; pH 1.59. 1.02, 0.41; pH 1.34. 1.41, 0.81; pH 1.05), 6(0.80, 0.00; pH 2.27), 7(1.07, 0.00; pH 2.39), 8(1.50, 0.00; pH 3.41. 1.80, 0.00; pH 3.88. 2.00, 0.00; pH 4.20), where the concentration of $CH_3CH(OH)CH_2HgClO_4$ was commonly chosen as 1.00 M. Initial rates were calculated from the initial linear slopes of the plots of the conversion (below 5%) *vs.* time.

The observed absence of any appreciable variation in the rate with the pH evidently shows that the reaction is zero-order in proton activity in the pH range studied.

The rate equation for the reaction of **1** with sodium formate in an aqueous solution is, therefore, given by Eq. (7). This equation shows that the reaction proceeds only when the formate ligand is coordinated:

$$v = -d[CH_3CH(OH)CH_2Hg^+]/dt = -d[HCOO^-]/dt = k[CH_3CH(OH)CH_2HgOCOH] \quad (7)$$
$$(k = 1.35\times10^{-3}\ s^{-1} \text{ at } 63.2\ ^\circ C)$$

Kinetic Isotope Effect for the Reaction of $CH_3CH(OH)CH_2HgClO_4$ with Sodium Formate. Experiments with DCOONa indicated a kinetic isotope effect, k_H/k_D, of 2.1±0.1 (the mean of three experimental values), at 51.0 °C. This effect is similar in magnitude to those for the inorganic ions,[1,2] although considerably smaller than that for Hg^{2+} (3.4 at 46.5 °C).[2] The existence of the kinetic isotope effect confirms that the C–H bond of the formate ion is actually broken in the rate-determining step. Therefore, we can exclude a possible alternative path in which the slow deoxymercuration of the mercurial is succeeded by the fast oxidation of the formate ion by the free mercuric ion formed, even though this path is consistent with the data in Fig. 2. In fact, oxy-ligands are far less effective for the deoxymercuration than halo-ligands;[16] moreover, the reaction rate has been claimed to be first-order in proton activity in the case of deoxymercuration.[17,18]

Stereochemistry of the Reactions of $CH_3CH(OH)CHCH_3HgClO_4$ with Sodium Formate. *Threo-* and *erythro-*3-hydroxy-2-butylmercuric perchlorate, obtained by the hydroxymercuration of *cis-* and *trans-*2-butenes[19] respectively, were used to determine the stereochemical nature of the reaction. Both the evolution of gas and the precipitation of elemental mercury were also observed for the reactions of these mercurials with sodium formate. The gas-chromatographic analyses of the evolved 2-butenes showed that the stereo-isomerism was completely retained in comparison with the respective starting 2-butenes. This clearly indicates that the reaction involves the stereospecific anti-elimination of olefins.

Activation Parameters for the Decomposition of $CH_3CH(OH)CH_2HgOCOH$. From the variation in k in Eq. (7) with the temperature (45.2 to 63.2 °C), the values of E_a=17.5 (±0.5) kcal mol^{-1} and A=4.0 (±0.9)×10^8 s^{-1} were obtained as activation parameters for the unimolecular decomposition of **3**. The activation energy, E_a, is of a magnitude similar to those for the inorganic ions.[1,2] The value of the pre-exponential factor, A, reported for the unimolecular decomposition of the Tl^{3+}-formate ion adduct,[2] lies near to the normal magnitude of A ($\sim10^{13}$ s^{-1}) for simple unimolecular reactions in solutions.[20] Therefore, the comparatively large reduction of A for the unimolecular decomposition of **3** strongly suggests a restricted structure of the transition state.

Structural Consideration of the Activated Complex. Taking into consideration the results of the kinetic isotope effect and stereochemistry, the structure of the activated complex represented in Fig. 5 is proposed for the decomposition of the formato-mercurial, where the hydroxyl ion and the elemental mercury are eliminated in an anti-manner, coupled with two-electron transfer processes. The magnitude of A seems to be

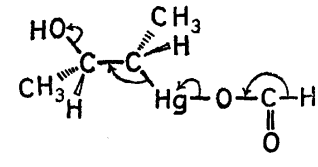

Fig. 5. Proposed structure of the activated complex for the redox decomposition of *threo*-3-hydroxy-2-butylmercuric formate.

compatible with this sterically-restricted structure. The observed stereospecificity of the reaction may be correlated with the predominant preference of antiperiplanar elimination in the *E*2 reactions.[21]

The authors wish to express their gratitude to Professor Yukio Yoneda for his helpful discussions and encouragement. They would also like to acknowledge the financial support received from the Kawakami Memorial Fund.

References

1) A. Aguilo, *J. Catal.*, **13**, 283 (1969).
2) J. Halpern and S. M. Taylor, *Discuss. Faraday Soc.*, **29**, 174 (1960).
3) H. N. Halvorson and J. Halpern, *J. Amer. Chem. Soc.*, **78**, 5562 (1956).
4) A. R. Tophan and A. G. White, *J. Chem. Soc.*, **1952**, 105.
5) C. E. H. Bawn and A. G. White, *ibid.*, **1951**, 339.
6) Y. Saito, "Some Theoretical Problems of Catalysis," ed. by T. Kwan, G. K. Boreskov, and K. Tamaru, University of Tokyo Press, Tokyo (1973), p. 241.
7) M. Matsuo and Y. Saito, *J. Org. Chem.*, **37**, 3350 (1972).
8) M. Matsuo and Y. Saito, This Bulletin, **44**, 2889 (1971).
9) Y. Saito and M. Matsuo, *J. Organometal. Chem.*, **10**, 524 (1967).
10) J. Relf, R. P. Cooney, and H. F. Henneike, *ibid.*, **39**, 75 (1972).
11) R. Scheffold, *Helv. Chim. Acta*, **52**, 56 (1969).
12) D. F. Evans, P. M. Ridout, and I. Wharf, *J. Chem. Soc.*, A, **1968**, 2127.
13) J. V. Hatton, W. G. Schneider, and W. Siebrand, *J. Chem. Phys.*, **39**, 1330 (1963).
14) It was concluded that methylmercuric perchlorate dissociated completely in water into perchlorate ions and the cations $[CH_3Hg\text{–}OH_2]^+$ on the basis of Raman spectroscopy ($\nu_{Hg-O}=463\ cm^{-1}$). This is also the case for **1** because the Raman spectrum showed in the far infrared region only one absorption band at 463 cm^{-1}, see P. L. Goggin and L. A. Woodward, *Trans. Faraday Soc.*, **58**, 1495 (1962).
15) The coordination number for the organomercurial is generally accepted as two, see reference (11).
16) W. Kitching, *Organometal. Chem. Rev.*, **3**, 61 (1968).
17) K. Ichikawa, K. Nishimura, and S. Takayama, *J. Org. Chem.*, **30**, 1593 (1965).
18) M. M. Kreevoy, *J. Amer. Chem. Soc.*, **81**, 1099 (1959).
19) M. M. Kreevoy, L. L. Schaleger, and J. C. Ware, *Trans. Faraday Soc.*, **58**, 2433 (1962).
20) E. A. Moelwyn-Hughes, "The Chemical Statics and Kinetics of Solutions," Academic Press Inc. (London) Ltd., London (1971), p. 88.
21) C. K. Ingold, "Structure and Mechanism in Organic Chemistry," 2nd Ed., Cornel University Press, Ithaca, New York (1969), Chap. 9.

The Crystal and Molecular Structure of β-Lactose

Ken HIROTSU and Akira SHIMADA†

Department of Chemistry, Faculty of Science, Osaka City University, Sugimoto-cho, Sumiyoshi-ku, Osaka 558

(Received December 24, 1973)

The crystal structure of β-lactose ($C_{12}H_{22}O_{11}$) was solved by direct phasing methods with integrated photographic intensity data. The structure was refined by the anisotropic least-squares method to give a final R value of 0.068 for the observed reflections. The space group is $P2_1$, with $Z=2$ and with unit cell dimensions of $a=10.839$ (6), $b=13.349$ (6), $c=4.954$ (5) Å, and $\beta=91.31$ (9)°. All the hydrogen atoms were located on different syntheses. The crystals are nearly isostructural with those of β-cellobiose except for the axial O(4) atom. The exocyclic C(5)–C(6) and C(5′)–C(6′) bonds are significantly shorter than the other C–C bonds. The lengths of the two ring C–O bonds are unequal in the galactose unit and equal in the glucose unit. The C(1)–O(1) and C(1′)–O(1′) bond lengths are shorter by 0.015 Å and 0.030 Å than the mean exocyclic C–O length of 1.417 Å. The structure contains an intramolecular hydrogen bond and exhibits an asymmetrical twist about the bridge bond. All the oxygen atoms, except the bridge oxygen atom, are involved in the hydrogen-bonding network, which comprises two terminating chains.

The crystal structure of β-lactose has been determined as a part of a series of X-ray diffraction studies of carbohydrates in this laboratory.[1] β-Lactose (*O*-β-D-galactopyranosyl-(1→4)-β-D-glucopyranoside) is a disaccharide which consists of glucose and galactose units, as is shown in (I):

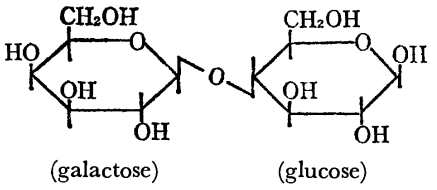

(galactose) (glucose)

(I)

The crystal structure of α-lactose monohydrate[2] was determined by Fries, Rao, and Sundaralingam. The main purpose of our investigation was to compare precisely the bond lengths and angles of β-lactose with those of α-lactose,[2] β-cellobiose,[3–5] and methyl β-cellobioside.[6] The conformation of the (β-1,4) glycosidic bond, which is present in a variety of natural polysaccharides, and the hydrogen-bond scheme in crystal was also of interest.

Experimental

Suitable crystals were prepared from a hot aqueous solution by the method reported by Tsuzuki and Mori.[7] The cell dimensions were measured from zero-layer Weissenberg photographs, which were calibrated with superimposed Al powder lines ($a=4.04934$ Å). The density was determined by the flotation technique using a mixture of cylohexane and carbon tetrachloride. The crystal data are summarized in Table 1. A crystal with the dimensions of $0.2\times0.2\times0.3$ mm was used for all the intensity measurements. The intensity data were recorded on multiple film, equi-inclination integrating Weissenberg photographs using Cu$K\alpha$ radiation. Layers from $h0l$ to $h2l$ and from $hk0$ to $hk5$ were obtained. The intensities were estimated visually by comparison with a calibrated intensity standard. No correction was applied for absorption and extinction. All the intensity data were corrected for spot shape and for Lorentz and polarization factors. The resulting data were correlated and reduced to the relative structure factor amplitudes using the method of Hamilton, Rollet, and Sparks.[8] A total of 1595 structure factors were evaluated; 129 were too weak to be measured. Finally, a Wilson plot was made estimating an approximate absolute scale and an overall temperature factor, in order to calculate normalized structure factor magnitudes, $|E|$.

† Deceased August 5, 1973.

TABLE 1. CRYSTAL DATA

$C_{12}H_{22}O_{11}$	F. W. 342.3
Monoclinic	Space group $P2_1$
$a=10.839(6)$ Å	$Z=2$
$b=13.349(6)$	$F(000)=364$
$c=4.954(5)$	$V=716.7$ Å^3
$\beta=91.31(9)°$	λ(Cu$K\alpha$)$=1.5418$ Å
$D_x=1.586$ g·cm^{-3}	$D_m=1.57$ g·cm^{-3} (by flotation)

Structure Determination and Refinement

The crystal structure of β-lactose was solved by the multisolution method described by Woolfson and Germain.[9] The starting set of phases is listed in Table 2. In order to apply the tangent formula,[10] numerical phases from 45° to 315° (=−45°) in steps of 90° were assigned to the A and B symbols. Tangent refinement was carried out for each of the 16 possible phase combinations, and the number of reflections included was gradually increased from 100 with $E>1.70$ to 350 with $E>1.22$. The values of R_{Karle}[11] ranged from 0.27 to 0.31, and those of Z[12], from 8842 to 10882. All sixteen E-maps were calculated in increasing order of R_{Karle} value. A cursory inspection revealed the site of the glucose unit in several of the E-maps, and so the unit was chosen as a trial partial structure.[13] How-

TABLE 2. THE STARTING SET OF PHASES

h	k	l	E	ϕ	
3	9	−2	2.85	0°	
4	0	3	2.14	0°	origin and enantiomorph
1	12	1	2.64	45°	(45° → 39.5°)
8	0	−2	3.36	0°	from Σ_1
4	10	−1	2.55	A	(45° → 41.8°)
7	7	−1	2.87	B	(90° → 115.7°)

ever, this partial structure could not be developed into a complete structure by means of tangent refinement. After completing the structure, it turned out that the unit was actually properly oriented, but not placed in the right position in the unit cell. After this initial failure, the following new sets of phases were assigned to the A and B symbols. Tangent refinement was again carried out for each of the additional 20 possible phase combinations: (A=±90°, B=±45°, ±135°), (B=±90°, A=±45°, ±135°), (A=±90°, B=±90°). A solution was finally obtained from an *E*-map calculated by means of the phases in the most consistent set (R_{Karle}=0.21 and Z=10470). The initial and refined phases in this set are shown in Table 2. The positions of all the non-hydrogen atoms were easily located and further confirmed by a least-squares refinement. Seven cycles of isotropic block-diagonal least-squares refinement resulted in an R ($=\Sigma||F_o|-|F_c||/\Sigma|F_o|$) value of 12.5%. Six more cycles of anisotropic block-diagonal least-squares and two difference-map calculations were necessary to locate the 22 hydrogen atoms. The isotropic thermal parameters of the hydrogen atoms were assumed to be equal to those of the parent atoms, which were obtained from the last stage of isotropic refinement (R=12.5%). These hydrogen atoms were included in the refinement, in which positional parameters were varied but thermal parameters were fixed. Additional cycles of refinement resulted in an R value of 7.4%. At this point, seven reflections with very large structure-factor amplitudes were removed from the data because they appeared to be affected by secondary extinction. Four final cycles of block-diagonal refinement gave an R of 6.8% for the observed reflections and one of 7.7% for all the reflections. Throughout the refinements,

Table 3. Fractional atomic coordinates and thermal parameters in β-lactose

Key to atomic numbering is given in Fig. 1. The temperature factor expression used was

$$\exp[-(h^2\beta_{11}+k^2\beta_{22}+l^2\beta_{33}+hk\beta_{12}+hl\beta_{13}++kl\beta_{23})].$$

Numbers in parentheses refer to standard deviations of the last place.

	x	y	z	β_{11}	β_{22}	β_{33}	β_{12}	β_{13}	β_{23}
C(1)	0.7544(3)	0.5881(3)	0.0177(8)	0.0036(3)	0.0026(2)	0.0184(12)	0.0000(4)	0.0036(9)	0.0007(9)
C(2)	0.7328(3)	0.6984(3)	−0.0391(8)	0.0038(3)	0.0025(2)	0.0149(10)	−0.0001(4)	0.0028(9)	0.0000(8)
C(3)	0.6660(4)	0.7460(3)	0.1955(8)	0.0046(3)	0.0019(2)	0.0174(12)	0.0001(4)	0.0049(10)	−0.0019(9)
C(4)	0.5466(4)	0.6880(3)	0.2375(9)	0.0044(3)	0.0022(2)	0.0206(13)	0.0004(4)	0.0027(10)	−0.0024(9)
C(5)	0.5744(4)	0.5768(3)	0.2829(8)	0.0041(3)	0.0023(2)	0.0167(11)	−0.0004(4)	0.0071(9)	−0.0017(8)
C(6)	0.4573(4)	0.5163(4)	0.3060(9)	0.0057(4)	0.0025(2)	0.0355(19)	−0.0014(5)	0.0098(13)	−0.0020(10)
C(1′)	0.9553(4)	0.2796(3)	−0.4780(9)	0.0043(3)	0.0024(2)	0.0237(14)	0.0011(4)	0.0039(11)	−0.0025(9)
C(2′)	0.8242(4)	0.2694(4)	−0.3760(9)	0.0047(3)	0.0026(2)	0.0295(16)	−0.0005(4)	0.0084(12)	−0.0034(10)
C(3′)	0.7684(4)	0.3742(4)	−0.3392(9)	0.0034(3)	0.0030(2)	0.0237(13)	−0.0008(4)	0.0073(10)	−0.0011(9)
C(4′)	0.8557(3)	0.4444(3)	−0.1800(8)	0.0036(2)	0.0016(2)	0.0227(13)	0.0006(4)	0.0045(10)	0.0023(8)
C(5′)	0.9857(4)	0.4431(3)	−0.2897(9)	0.0039(3)	0.0021(2)	0.0231(13)	0.0009(4)	0.0037(10)	0.0021(8)
C(6′)	1.0788(4)	0.5001(4)	−0.1179(9)	0.0037(3)	0.0032(2)	0.0341(17)	−0.0005(4)	0.0050(11)	−0.0012(11)
O(1)	0.8086(3)	0.5456(2)	−0.2101(6)	0.0046(2)	0.0020(1)	0.0182(8)	0.0011(3)	0.0052(7)	0.0013(6)
O(2)	0.8442(3)	0.7471(2)	−0.1082(7)	0.0061(3)	0.0030(2)	0.0244(9)	−0.0027(4)	0.0079(9)	−0.0041(7)
O(3)	0.6449(3)	0.8500(2)	0.1506(7)	0.0060(3)	0.0016(1)	0.0281(10)	0.0004(3)	0.0010(9)	−0.0022(6)
O(4)	0.4682(3)	0.6980(3)	0.0058(7)	0.0042(2)	0.0035(1)	0.0288(10)	0.0014(3)	−0.0027(9)	0.0007(8)
O(5)	0.6410(3)	0.5386(2)	0.0566(6)	0.0037(2)	0.0021(1)	0.0192(8)	−0.0005(3)	0.0075(7)	−0.0042(6)
O(6)	0.4802(4)	0.4118(3)	0.3041(7)	0.0079(3)	0.0021(2)	0.0339(12)	−0.0023(4)	0.0014(10)	0.0023(8)
O(1′)	1.0099(3)	0.1856(3)	−0.4838(8)	0.0048(2)	0.0027(2)	0.0322(11)	0.0014(3)	0.0062(9)	−0.0043(7)
O(2′)	0.7472(3)	0.2183(3)	−0.5615(9)	0.0054(3)	0.0042(2)	0.0614(21)	0.0018(4)	−0.0061(12)	−0.0173(11)
O(3′)	0.6516(3)	0.3647(3)	−0.2230(9)	0.0043(3)	0.0037(2)	0.0494(16)	−0.0016(4)	0.0137(10)	−0.0117(9)
O(5′)	1.0280(3)	0.3412(2)	−0.3000(6)	0.0034(2)	0.0021(1)	0.0293(10)	0.0015(3)	0.0020(8)	−0.0026(7)
O(6′)	1.1910(3)	0.5153(3)	−0.2549(9)	0.0043(3)	0.0031(2)	0.0579(19)	−0.0005(4)	0.0060(11)	0.0069(10)

	x	y	z		x	y	z
H(C1)	0.813(5)	0.585(5)	0.210(10)	H(C5′)	0.979(4)	0.473(4)	−0.480(9)
H(C2)	0.670(5)	0.703(5)	−0.190(10)	H(C6′-1)	1.099(4)	0.458(4)	0.080(9)
H(C3)	0.721(5)	0.737(5)	0.360(10)	H(C6′-2)	1.040(6)	0.566(6)	−0.054(12)
H(C4)	0.510(4)	0.718(4)	0.416(9)	H(O2)	0.882(6)	0.788(6)	0.013(12)
H(C5)	0.632(5)	0.571(4)	0.444(10)	H(O3)	0.575(6)	0.865(6)	0.050(12)
H(C6-1)	0.399(6)	0.533(6)	0.157(12)	H(O4)	0.361(6)	0.735(7)	−0.025(13)
H(C6-2)	0.418(6)	0.545(5)	0.495(11)	H(O6)	0.535(6)	0.400(6)	0.492(13)
H(C1′)	0.940(6)	0.309(5)	−0.676(10)	H(O1′)	1.077(5)	0.191(5)	−0.588(11)
H(C2′)	0.832(6)	0.233(6)	−0.215(12)	H(O2′)	0.794(6)	0.171(5)	−0.645(11)
H(C3′)	0.754(6)	0.410(6)	−0.543(13)	H(O3′)	0.652(6)	0.439(6)	−0.093(12)
H(C4′)	0.852(5)	0.422(5)	0.018(10)	H(O6′)	1.220(6)	0.455(6)	−0.246(12)

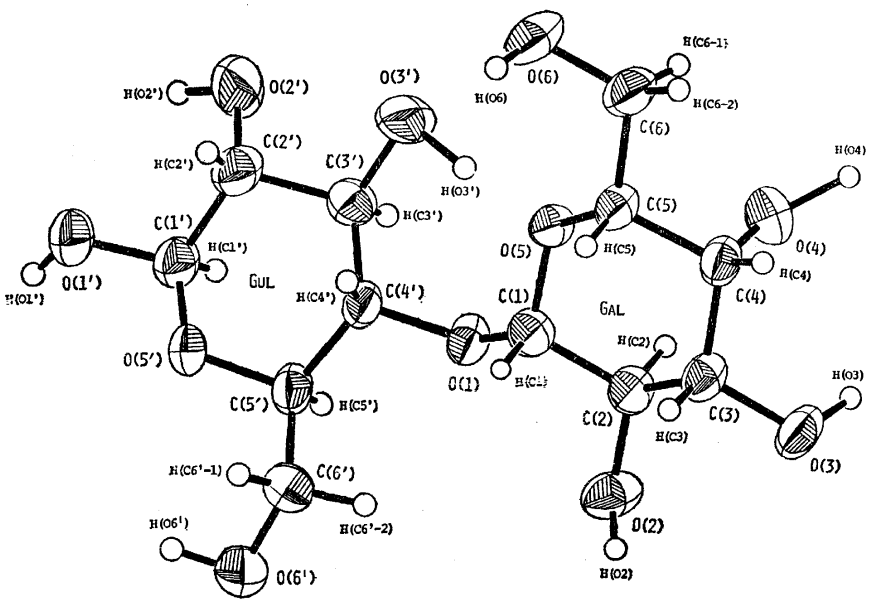

Fig. 1. Molecular conformation and atomic numbering in β-lactose.
The 74% probability thermal ellipsoids are shown for carbon and oxygen atoms.

the following weighting scheme was used:

$$w = 0.15 \text{ for } |F_o| < 1.4$$
$$w = (1.4/F_o)^2 \text{ for } |F_o| \geq 1.4.$$

The final atomic parameters are listed in Table 3. The atomic scattering factors used for the carbon and oxygen atoms were those of the International Tables for X-ray Crystallography,[14] and for the hydrogen atoms, those of Stewart, Davidson, and Simpson (1965).[15] The final structure factors are given in Table 4.*

After the completion of this work, this structure was found to be nearly isomorphous with β-cellobiose except for the atomic position of O(4).

Discussion

Figure 1 illustrates the conformation of the molecule of β-lactose, with the standard numbering for carbohydrates.

Bond Lengths and Angles. The bond lengths and angles involving carbon and oxygen atoms are shown in Fig. 2. The standard deviations are 0.005~0.006 Å for the carbon-carbon bonds and the carbon-oxygen bonds, and 0.3°~0.4° for the valence-bond angles. The bond lengths and angles in the β-galactosyl and β-glucosyl moieties agree well with the values previously reported by Berman, Chu, and Jeffrey.[16]

The carbon-carbon distances found in the unprimed ring (galactosyl moiety) range from 1.508 Å to 1.531 Å, with an average value of 1.524 Å, while those found in the primed ring (glucosyl moiety) range from 1.510 Å to 1.538 Å, with an average value of 1.530 Å. The average values of the corresponding ring C–C bonds in the four disaccharides listed in Table 5 range from 1.521 Å (C(1)–C(2)) to 1.533 Å (C(3')–C(4')) and are normal

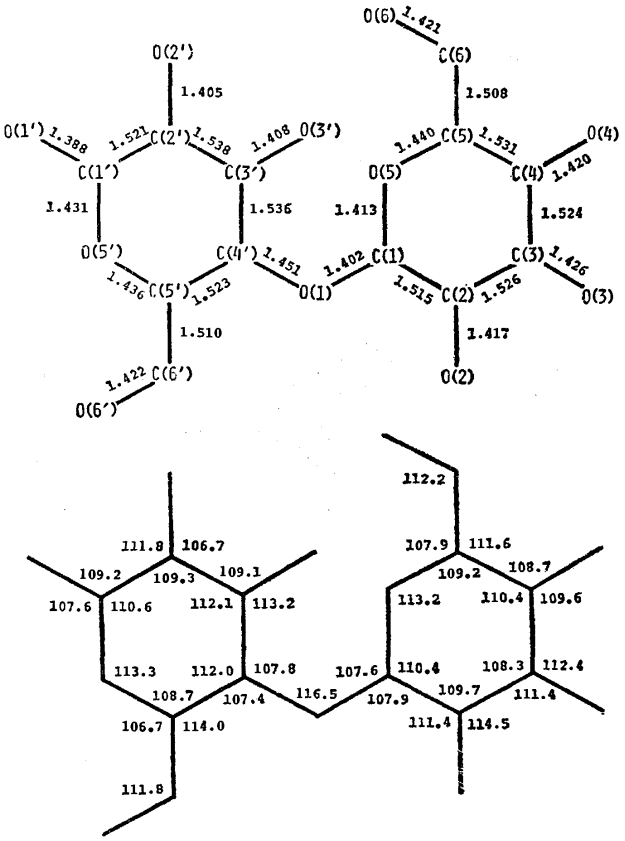

Fig. 2. Bond lengths(Å) and bond angles(°) in β-lactose.

values for carbohydrates, although C(1)–C(2) and C(1')–C(2') seem to be slightly short. The exocyclic C(5)–C(6) and C(5')–C(6') bonds are significantly shorter than the ring C–C bonds in all four disaccharides. The average value of the C(5)–C(6) bond is 1.514 Å, and that of C(5')–C(6') is 1.508 Å. This slight shortening with respect to the average ring C–C bonds has been

* Table 4 has been submitted to, and is kept by the office of the Chemical Society of Japan, 1-5 Kanda-Surugadai, Chiyoda-ku, Tokyo 113. (Document No. 7417).

pointed out by Ham and Williams.[6]

Two endocyclic C–O bonds [C(1)–O(5) and C(5)–O(5)] in the unprimed ring of β-lactose are found at 1.413 Å and 1.440 Å, the latter bond being about 5σ longer than the former. In the primed ring, the corresponding distances [C(1')–O(5') and C(5')–O(5')] are nearly equal: C(1')–O(5')=1.431 Å *versus* C(5')–O(5')=1.436 Å. The same trend was observed in β-cellobiose: C(1)–O(5)=1.425 Å *versus* C(5)–O(5)=1.436 Å and C(1')–O(5')=1.435 Å *versus* C(5')–O(5')=1.437 Å. However, the two endocyclic C–O bonds in methyl β-cellobioside[6] are nearly equal in the primed and the unprimed rings. In α-lactose,[2] the same pattern, C(1)–O(5)<C(5)–O(5), as in β-cellobiose and β-lactose was found in the unprimed ring, while the reverse trend, C(1')–O(5')<C(5')–O(5'), was found in the primed ring. These differences and the greater variation of C–O bond lengths may be significant and may be associated with the type of hydrogen bond involved, but no correlation is apparent.

The exocyclic C–O bonds in β-lactose range from 1.405 Å to 1.426 Å, with a mean value of 1.417 Å, excluding the anomeric and bridge C–O bonds. The corresponding average lengths of α-lactose, β-cellobiose, and methyl β-cellobioside are 1.427 Å with a spead of 0.018 Å, 1.419 Å with a spread of 0.017 Å, and 1.428 Å with a spread of 0.030 Å, respectively. There are no significant differences among these average values. The means value of the C(2)–O(2) bonds in the four compounds listed in Table 5 is 1.419 Å. The corresponding average values of C(3)–O(3), C(4)–O(4), C(6)–O(6), C(2')–O(2'), C(3')–O(3'), and C(6')–O(6') are shown in the 7th column of Table 5. There are no significant differences among these average values.

The C(1)–O(1) and C(1')–O(1') bond lengths in the anomeric positions of β-lactose are significantly shorter, by 0.015 Å and by 0.030 Å respectively, than the mean exocyclic C–O length of 1.417 Å. This shortening effect has been found in disaccharides in Table 5 and many other related compounds. The C(1)–O(1) bonds in the unprimed rings of α-lactose, β-cellobiose, and methyl β-cellobioside are all greater than the C(1')–O(1') bonds in the primed rings, as is shown in Table 5. The bridge C(4')–O(1) bond distance (1.451 Å) of β-lactose is in good agreement with the corresponding length (1.446 Å) in β-cellobiose. The average C(4')–O(1) bond length of four disaccharides in Table 5 is 1.443 Å, significantly longer than the normal C–O distance for carbohydrates.

The bond angles of four disaccharides with (β-1,4) linkage have been tabulated in Table 6. The average carbon valence-bond angle within the rings of β-lactose is 110.1° with a spread of 3.8°. The average deviations from the corresponding angles in β-cellobiose, α-lactose, and methyl β-cellobioside are 1.0°, 1.2°, and 2.2° respectively. The C–O–C ring angles are the largest among the ring angles in β-lactose, α-lactose, and β-cellobiose, but not in the primed ring of methyl

Table 5. Bond distances of four accurately determined disaccharides with (β-1,4) linkage

	β-Lactose	α-Lactose[2]	Cellobiose[5]	Methyl β-cellobioside[6]	Mean	Spread
C(1)-C(2)	1.515 Å	1.517 Å	1.525 Å	1.526 Å	1.521 Å	0.011 Å
C(2)-C(3)	1.526	1.523	1.520	1.535	1.526	0.015
C(3)-C(4)	1.524	1.533	1.543	1.528	1.532	0.019
C(4)-C(5)	1.531	1.536	1.532	1.530	1.532	0.006
C(5)-C(6)	1.508	1.514	1.519	1.515	1.514	0.011
C(1')-C(2')	1.521	1.531	1.514	1.513	1.520	0.018
C(2')-C(3')	1.538	1.516	1.519	1·529	1.526	0.022
C(3')-C(4')	1.536	1.533	1.530	1.533	1.533	0.006
C(4')-C(5')	1.523	1.525	1.527	1.526	1.525	0.004
C(5')-C(6')	1.510	1.514	1.501	1.505	1.508	0.013
C(1)-O(5)	1.413	1.427	1.425	1.432	1.424	0.019
C(5)-O(5)	1.440	1.448	1.436	1.430	1.439	0.018
C(1')-O(5')	1.431	1.443	1.435	1.434	1.436	0.012
C(5')-O(5')	1.436	1.425	1.437	1.432	1.433	0.012
C(2)-O(2)	1.417	1.425	1.416	1.416	1.419	0.009
C(3)-O(3)	1.426	1.433	1.427	1.431	1.429	0.007
C(4)-O(4)	1.420[a]	1.421[a]	1.420	1.410	1.415	0.011
C(6)-O(6)	1.421	1.419	1.416	1.434	1.423	0.018
C(2')-O(2')	1.405	1.429	1.423	1.439	1.424	0.034
C(3')-O(3')	1.408	1.434	1.410	1.429	1.420	0.026
C(6')-O(6')	1.422	1.430	1.423	1.440	1.429	0.018
C(1)-O(1)	1.402	1.389	1.397	1.390	1.396	0.013
C(1')-O(1')	1.388	1.387[a]	1.381	1.379	1.383	0.009
C(4')-O(1)	1.451	1.437	1.446	1.437	1.443	0.014
e.s.d.	0.005~0.006	0.003~0.005	0.004~0.005	0.005~0.006		

a) This value was not included in the calculation of the mean value, since the oxygen atom is in an axial position.

β-cellobioside.

In β-lactose, the exocyclic angles range widely from 106.7° to 114.5°, with an average value of 110.0°, excluding the valence-bond angle at the glycosidic oxygen atom. The average difference in the corresponding exocyclic bond angles between β-lactose and β-cellobiose is 0.8°, which is significantly small compared with the other two average differences (1.6° and 1.8°) between β-lactose and α-lactose, and between β-lactose and methyl β-cellobioside. This may be because β-lactose is nearly isostructural with β-cellobiose. The exocyclic bond angles are strongly affected by intermolecular forces, especially by the formation of hydrogen bonds. The larger differences in the average values found between β-lactose and α-lactose, and between β-lactose and methyl β-cellobioside, are caused by the different molecular packing, *i.e.*, the different hydrogen-bonding scheme.

The bond angle of 116.5° at the bridge oxygen atom of β-lactose agrees with the corresponding angles found in the crystal structures of β-cellobiose (116.1°), α-lactose (117.1°), methyl β-cellobioside (115.8°), lactose–calcium bromide heptahydrate (115.6°),[17] and lactose–calcium chloride heptahydrate (116.0°).[18]

Molecular Conformation. The conformational angles in the pyranose rings of β-lactose, α-lactose, β-cellobiose, and methyl β-cellobioside are listed in Table 7. The torsional angles in the galactose unit of β-lactose range only from 55.9° to 61.2°, with an average value of 58.2°. On the other hand, those of the glucose unit range more widely, from 48.9° to 65.0°, with a mean value of 55.7°. In the four disaccharides listed in Table 7, the torsional angles around the ring C–O bonds are generally the largest, while those around C(2)–C(3), C(3)–C(4), C(2′)–C(3′), and C(3′)–C(4′), which are at the position opposite to the ring C–O

TABLE 6. BOND ANGLES OF FOUR ACCURATELY DETERMINED DISACCHARIDES WITH (β-1,4) LINKAGE

	β-Lactose	α-Lactose[2]	Cellobiose[5]	Methyl β-cellobioside[6]	Mean	Spread
C(1)-C(2)-C(3)	109.7°	110.9°	108.3°	108.8°	109.4°	2.6°
C(2)-C(3)-C(4)	108.3	110.9	109.5	113.9	110.7	5.6
C(3)-C(4)-C(5)	110.4	108.9	111.0	108.5	109.7	2.5
C(4)-C(5)-O(5)	109.2	110.5	110.3	110.3	109.8	1.3
O(5)-C(1)-C(2)	110.4	111.2	108.3	107.4	109.3	3.8
C(1′)-C(2′)-C(3′)	109.3	110.9	110.0	113.6	111.0	4.3
C(2′)-C(3′)-C(4′)	112.1	110.3	111.8	111.8	111.5	1.8
C(3′)-C(4′)-C(5′)	112.0	111.1	112.3	109.1	111.1	3.2
C(4′)-C(5′)-O(5′)	108.7	107.9	109.2	108.3	108.5	1.3
O(5′)-C(1′)-C(2′)	110.6	109.7	109.3	108.7	109.6	1.9
C(5)-O(5)-C(1)	113.2	112.2	112.4	111.1	112.2	2.1
C(5′)-O(5′)-C(1′)	113.3	114.1	113.5	111.3	113.1	2.8
O(5)-C(1)-O(1)	107.6	107.0	107.4	107.6	107.4	0.6
C(2)-C(1)-O(1)	107.9	107.7	109.0	110.4	108.8	2.7
C(1)-C(2)-O(2)	111.4	108.8	110.0	111.0	110.3	2.6
C(3)-C(2)-O(2)	114.5	110.5	113.6	109.1	111.9	5.4
C(2)-C(3)-O(3)	111.4	108.1	112.0	110.3	110.5	3.9
C(4)-C(3)-O(3)	112.4	111.4	111.5	109.2	111.1	3.2
C(3)-C(4)-O(4)	109.6[a]	110.0[a]	108.1	110.2	109.2	2.1
C(5)-C(4)-O(4)	108.7[a]	108.4[a]	109.4	107.8	108.6	1.6
C(4)-C(5)-C(6)	111.6	112.0	111.0	112.0	111.7	1.0
O(5)-C(5)-C(6)	107.9	106.8	105.4	106.8	106.7	2.5
C(5)-C(6)-O(6)	112.2	110.3	112.2	111.0	111.4	1.9
O(5′)-C(1′)-O(1′)	107.6	111.5[a]	107.0	108.3	107.6	1.3
C(2′)-C(1′)-O(1′)	109.2	108.8[a]	110.2	107.0	108.8	3.2
C(1′)-C(2′)-O(2′)	111.8	111.1	110.6	107.2	110.2	4.6
C(3′)-C(2′)-O(2′)	106.7	112.7	106.5	110.3	109.1	6.2
C(2′)-C(3′)-O(3′)	109.1	107.0	107.1	105.0	107.1	4.1
C(4′)-C(3′)-O(3′)	113.2	111.6	112.5	112.5	112.5	1.6
C(3′)-C(4′)-O(1)	107.8	110.6	109.0	111.5	109.7	3.7
C(5′)-C(4′)-O(1)	107.4	107.0	106.4	106.7	106.9	1.0
C(4′)-C(5′)-C(6′)	114.0	113.7	113.6	114.9	114.1	1.3
O(5′)-C(5′)-C(6′)	106.7	107.2	106.4	108.3	107.2	1.9
C(5′)-C(6′)-O(6′)	111.8	111.2	111.2	110.6	111.2	1.2
C(1)-O(1)-C(4′)	116.5	117.1	116.1	115.8	116.4	1.3
e.s.d.	0.3∼0.4	∼0.2	0.2∼0.3	0.3∼0.4		

a) This value was not involved in the calculation of the mean value, since the oxygen atom is in an axial position.

Table 7. A comparison of the ring torsional angles in β-lactose, α-lactose, β-cellobiose and methyl β-cellobioside

	(I)	(II)	(III)	(IV)	Mean		(I)	(II)	(III)	(IV)	Mean
C(1)→C(2)	58.8°	53.7°	63.5°	58.7°	58.7°	C(1')→C(2')	55.8°	53.8°	57.8°	51.0°	54.6°
C(2)→C(3)	−56.7	−51.4	−57.3	−51.0	−54.1	C(2')→C(3')	−48.9	−51.2	−50.7	−45.0	−49.0
C(3)→C(4)	55.9	54.2	52.0	47.7	52.5	C(3')→C(4')	49.1	53.5	48.0	48.2	49.7
C(4)→C(5)	−56.8	−59.1	−51.9	−53.9	−55.4	C(4')→C(5')	−53.4	−57.5	−51.1	−59.9	−55.5
C(5)→O(5)	59.8	61.7	59.8	67.4	62.2	C(5')→O(5')	62.1	62.9	60.9	70.1	64.0
O(5)→C(1)	−61.2	−60.8	−65.7	−69.1	−64.2	O(5')→C(1')	−65.0	−61.6	−65.1	−64.3	−64.0

(I) β-Lactose (this work). (II) α-Lactose.[2] (III) β-Cellobiose.[5] (IV) Methyl β-cellobioside.[6]

Table 8. Exocyclic torsional angles

O(5)-[C(5)-C(6)]-O(6)	50.2°	O(5')-[C(5')-C(6')]-O(6')	71.9°
C(4)-[C(5)-C(6)]-O(6)	−170.8	C(4')-[C(5')-C(6')]-O(6')	−168.0
O(1)-[C(1)-C(2)]-O(2)	−56.4	O(1')-[C(1')-C(2')]-O(2')	−69.0
O(2)-[C(2)-C(3)]-O(3)	53.8	O(2')-[C(2')-C(3')]-O(3')	64.6
O(3)-[C(3)-C(4)]-O(4)	60.0	O(3')-[C(3')-C(4')]-O(1)	−69.4
O(4)-[C(4)-C(5)]-C(6)	−56.4	O(1)-[C(4')-C(5')]-C(6')	69.6

Table 9. Torsional angles[a] and pseudotorsional angles of the (β-1,4) linkage in the six determined disaccharides

Pseudotorsional angle is defined similarly to torsional angle, except that a line between C(1)---C(4') is used in place of a bond.

		(I)	(II)	(III)	(IV)	(V)	(VI)
Ψ_1	O(5)-C(1)-O(1)-C(4')	−76.3°	−70.7°	−92.6°	−91.1°	−77.0°	−76.0°
Ψ_1'	C(2)-C(1)-O(1)-C(4')	166.5	170.3	146.2	152.1	164.4	165.2
Ψ_2	C(1)-O(1)-C(4')-C(3')	106.4	180.0	94.6	80.3	106.5	108.3
Ψ_2'	C(1)-O(1)-C(4')-C(5')	−132.3	−131.3	−143.0	−160.7	−136.7	−134.9
	O(5)-C(1)---C(4')-C(3')	24.5	31.0	−0.2	−10.7	23.6	25.5
	O(5)-C(1)---C(4')-C(5')	171.1	176.9	144.5	125.9	166.9	169.8
	C(2)-C(1)---C(4')-C(3')	−106.4	−98.6	−144.7	−150.4	−109.9	−107.8
	C(2)-C(1)---C(4')-C(5')	40.2	47.3	2.6	13.8	33.4	36.5

(I) β-Cellobiose.[5] (II) β-Lactose (this paper). (III) α-Lactose.[2] (IV) Methyl β-cellobioside.[6] (V) Lactose-calcium bromide heptahydrate.[17] (VI) Lactose-calcium chloride heptahydrate.[18] a) Ψ_1, Ψ_1', Ψ_2 and Ψ_2' are defined according to Sundaralingam (1968).[20]

bonds, are the smallest, although there are some exceptions. This trend may be due to the smaller puckering around the C(2)-C(3) and C(3)-C(4) bonds and the larger puckering around the C(5)-O(5) and C(1)-O(5) bonds. The torsional angles involving exocyclic atoms in β-lactose are shown in Table 8. The exocyclic torsional angles around C(1')-C(2'), C(2')-C(3'), C(3')-C(4'), and C(4')-C(5') in the β-glucose residue of β-lactose are considerably larger than those in the galactose residue.

Both C(5)-C(6) and C(5')-C(6') bonds have the+ *synclinal* conformation.

The conformational twists about the C(1)-O(1) and C(4')-O(1) bonds are of interest in comparison with the models for cellulose. The torsional and pseudotorsional angles[19] of the (β-1,4) linkage in the five determined structures and the present one are given in Table 9. Because of the isomorphous structures, the torsional and pseudotorsional angles of β-lactose are approximately equal to those of β-cellobiose. These two molecules exhibit an asymmetrical twist about the bridge bond, $\Psi_1=-70.7°$ and $\Psi_2=108.0°$ in β-lactose, and $\Psi_1=-76.3°$ and $\Psi_2=106.4°$[20] in β-cellobiose. The two isostructural lactose complexes, lactose–calcium bromide heptahydrate and lactose–calcium chloride heptahydrate, also exhibit an asymmetrical twist. The conformations around the bridge bonds of these two complexes are very similar to those of β-lactose and β-cellobiose, as is shown in Table 9. In contrast to the above four structures, a symmetrical twist about the bridge bond is found in α-lactose: $\Psi_1=-92.6°$ and $\Psi_2=94.6°$. In methyl β-cellobioside, the conformation around the bridge bond is close to that of α-lactose, but it is not symmetrical. The conformations about the bridge bonds in disaccharides with (β-1,4) linkage are affected by the intermolecular forces in the crystal, especially hydrogen bonding, but, roughly speaking, the same conformation is maintained. This similarity in conformation about the bridge bond is caused by the fact that, in these molecules, the intramolecular hydrogen bond, O(3')···O(5), is always formed and plays an important role in determining the molecular conformation.

Hydrogen Bonding. The molecular packing and

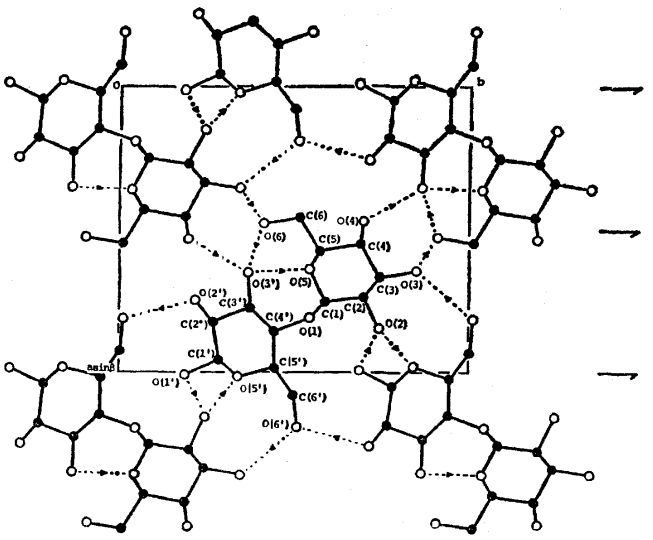

Fig. 3. Packing of the structure viewed down the *c* axis.

Table 10. Hydrogen bonding distances and angles

i	j	k	*d*(jk)	∠(ijk)
C(2)	O(2)	O(5, b)	2.731 Å	117.0°
C(3)	O(3)	O(6, c)	2.730	120.0
C(4)	O(4)	O(3′, c)	2.804	91.9
C(6)	O(6)	O(3′, d)	3.022	107.7
C(1′)	O(1′)	O(2, e)	2.722	90.3
C(2′)	O(2′)	O(6′, e)	2.941	120.3
C(3′)	O(3′)	O(5, a)	2.707	100.6
C(6′)	O(6′)	O(3, f)	2.873	110.3

Intermolecular non-bonded distances less than 3.3 Å between carbon and oxygen atoms

i	j	*d*(ij)
O(2)	C(1′, k)	3.052 Å
O(1′)	C(6′, e)	3.296
O(3′)	C(4, i)	3.191

Symmetry code

The letters refer to the symmetry operations to be applied to the coordinates listed in Table 3.

a	*x*,	*y*,	*z*
b	2−*x*,	1/2+*y*,	−*z*
c	1−*x*,	1/2+*y*,	−*z*
d	*x*,	*y*,	1+*z*
e	2−*x*,	−1/2+*y*,	−1−*z*
f	2−*x*,	−1/2+*y*,	−*z*
g	1−*x*,	1/2+*y*,	−1−*z*
h	−1+*x*,	*y*,	*z*
i	1−*x*,	−1/2+*y*,	−*z*
j	1−*x*,	−1/2+*y*,	1−*z*
k	2−*x*,	1/2+*y*,	−1−*z*

the hydrogen-bonding scheme are shown in Figs. 3 and 4. The hydrogen-bonding distances and angles are listed in Table 10. The crystal structure of β-lactose is nearly isomorphous with β-cellobiose. However, the hydrogen-bonding scheme around the axial O(4) atom is different from that of β-cellobiose. When the equatorial O(4) atom in the crystalline β-cellobiose is assumed to be replaced by the axial O(4) atom and the intermolecular distances are subsequently calculated, two hydrogen bonds, O(6)···O(4) and O(4)···O(2′), are missing and only one short contact, O(4)···O(3′), of 2.30 Å is found. This short contact can be lengthened to correspond to the hydrogen-bond length by slight changes in the atomic positions, and one more hydrogen bond can be formed between O(6) and O(3′), as is shown in Figs. 3 and 4. Therefore, crystalline β-lactose is isomorphous with β-cellobiose. β-Epicellobiose (*O*-β-D-glucopyranosyl-(1→4)-β-D-mannopyranoside) is different from β-cellobiose only in that the O(2′) atom is in an axial position. In a similar manner, the equatorial oxygen atom O(2′) in the crystalline β-cellobiose is assumed to be replaced by the axial O(2′). As a result, one short contact of 3.18 Å is found between O(2′) and O(6′). Although two hydrogen bonds, O(2′)–H···O(6′) and O(4)–H···O(2′), are missing, there appear to be two compensating hydrogen bonds, which are perhaps formed between axial O(2′) and O(6′) and between O(4) and O(3′) by slight changes

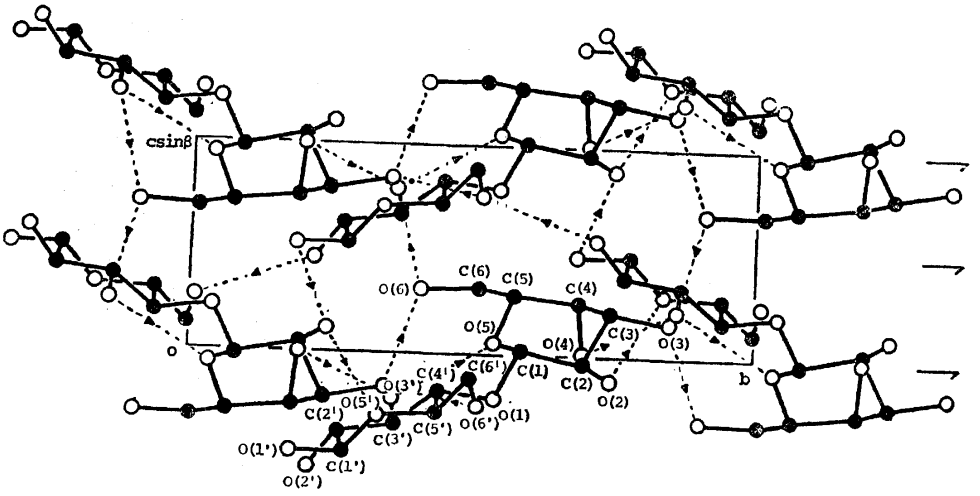

Fig. 4. Packing of the structure viewed down the *a* axis.

in atomic positions. Hence, crystalline anhydrous β-epi-cellobiose, as well as β-lactose, might be isomorphous with β-cellobiose.

Each of four hydroxyl groups, O(2)–H, O(3)–H, O(6)–H, and O(6′)–H, participates in hydrogen bonds as both one donor and one acceptor. O(4)–H, O(1′)–H, and O(2′)–H serve as donors only. O(3′)–H serves as one donor and two acceptors. Two ring oxygens, O(5) and O(5′), take part in hydrogen bonds as acceptors. The glycosidic linkage oxygen atom is not involved in hydrogen bonds, just as in all crystal structures of di- and tri-saccharides. The hydrogen-bond system comprises two terminated chains:

$$\begin{aligned} &O(2', g) \rightarrow O(6', h) \rightarrow O(3, i) \rightarrow \\ &\quad O(6, a) \rightarrow O(3', d) \rightarrow O(5, d) \\ &\qquad\qquad \uparrow \\ &\qquad\qquad O(4, j) \end{aligned}$$

$$O(1', d) \rightarrow O(2, f) \rightarrow O(5', a)$$

where → indicates the donor direction and where the small letter refers to the symmetry operations given in Table 10. The intramolecular hydrogen bond, O(3′)⋯O(5)=2.707 Å, is significantly short compared with that of 2.811 Å in α-lactose, that of 2.767 Å in cellobiose, that of 2.762 Å in methyl β-cellobioside, that of 2.76 Å in lactose–calcium bromide heptahydrate, and that of 2.75 Å in lactose–calcium chloride heptahydrate.

Computer Programs

All the calculations were performed on a FACOM 270/30 computer at the Computer Center of Osaka City University using the following programs: RSLC-3,[21] RSSFR-3,[21] HBLS-IV,[21] SCALE (film factor, Lp, and layer scaling),[22] DEAM,[23] PHASE-I, II, and III (direct method),[24] and BOND (bond length and angle, best plane, dihedral angle, and intermolecular distance).[25]

References

1) K. Hirotsu and A. Shimada, *Chem. Lett.*, **1973**, 83.
2) D. C. Fries, S. T. Rao, and M. Sundaralingam, *Acta Crystallogr.*, **B27**, 994 (1971).
3) R. A. Jacobson, J. A. Wunderlich, and W. N. Lipscomb, *ibid.*, **14**, 598 (1961).
4) C. J. Brown, *J. Chem. Soc., A*, **1966**, 927.
5) S. Chu and G. A. Jeffrey, *Acta Crystallogr.*, **B24**, 830 (1968).
6) J. T. Ham and D. G. Williams, *ibid.*, **B26**, 1373 (1970).
7) Y. Tsuzuki and N. Mori, *Nippon Kagaku Zasshi*, **77**, 994 (1956).
8) W. C. Hamilton, J. S. Rollet, and R. A. Sparks, *Acta Crystallogr.*, **18**, 129 (1965).
9) M. M. Woolfson and G. Germain, *ibid.*, **B24**, 91 (1968).
10) J. Karle and H. Hauptman, *ibid.*, **9**, 635 (1956).
11) J. Karle and I. L. Karle, *ibid.*, **21**, 849 (1966).
12) G. Germain, P. Main, and M. M. Woolfson, *ibid.*, **A27**, 368 (1971).
13) J. Karle, *ibid.*, **B24**, 182 (1968).
14) International Tables for X-ray Crystallography Vol. III. Birmingham: Kynoch Press (1962).
15) R. F. Stewart, E. R. Davidson, and W. T. Simpson, *J. Chem. Phys.*, **42**, 3175 (1965).
16) H. Berman, S. Chu, and G. A. Jeffrey, *Science*, **157**, 1576 (1967).
17) C. E. Bugg, *J. Amer. Chem. Soc.*, **95**, 908 (1973).
18) W. J. Cook and C. E. Bugg, *Acta Crystallogr.*, **B29**. 907 (1973).
19) D. C. Rohrer, *ibid.*, **B28**, 425 (1972).
20) M. Sundaralingam, *Biopolymers*, **6**, 189 (1968).
21) The Universal Crystallographic Computing System (I) ed. by T. Sakurai, The Crystallographic Society of Japan (1967).
22) H. Yoshioka, K. Hirotsu, and F. Takusagawa, unpublished work.
23) A. Takenaka, "Schematic Drawing of Crystal and Molecular Structure Containing Atomic Thermal Motions," (1972). Apply 270/23-503-001, Tokyo, Fujitsu Ltd.
24) K. Nakatsu and K. Hirotsu, unpublished work.
25) H. Yoshioka, unpublished work.

The Reaction of Hot Deuterium Atoms with *cis*-2-Butene

Shin SATO, Seishi NISHIDA, and Kiyoshi HOSOYA

Department of Applied Physics, Tokyo Institute of Technology, Ookayama, Meguro-ku, Tokyo 152

(Received December 25, 1973)

The photolysis of deuterium iodide at the wavelength of 2288 Å was carried out in the presence of *cis*-2-butene and iodine at 40 °C. Among the products, hydrogen (D_2 and HD), methane (CH_3D), propylene ($CH_3CH{=}CHD$), *n*-butane ($CH_3CHDCHDCH_3$), and 1-butene were measured as a function of the pressure of *cis*-2-butene. The formation of HD at higher pressures of *cis*-2-butene was attributed to the abstruction of H atoms from *cis*-2-butene-by hot D atoms. This reaction accounted for 8% of the total D atom-reaction. The formations of CH_3D, C_3H_5D, and $C_4H_8D_2$ were well explained by the successive reactions of hot butyl radicals, $C_4H_8D^*$.

In the reaction of recoil-tritium atoms with a saturated hydrocarbon,[1] the substitution reaction is well known to occur together with the abstraction reaction:

$$T^* + RH \begin{cases} \nearrow RT + H \\ \searrow HT + R \end{cases}$$

In a previous paper,[2] we reported that, when hot deuterium atoms were produced by the photolysis of DI at 2288 Å in the presence of ethylene, a large amount of HD was formed, and that the pressure dependence of this HD formation could be well explained in terms of the following reaction scheme:

$$D^* + C_2H_4 \rightarrow C_2H_4D^* \rightarrow \begin{cases} H + C_2H_3D \\ \xrightarrow{+DI} HD \end{cases}$$

The so-called "billiard-like" substitution reaction and also the abstraction reaction do not seem to occur with ethylene.[3] In the case of propylene, on the other hand, more than 10% of the reaction of hot deuterium atoms is attributable to the abstraction reaction producing HD.

In order to substantiate these findings, we have studied the reaction between hot deuterium atoms and *cis*-2-butene after a slight modification of the reaction system.

Experimental

The deuterium iodide and hydrogen iodide were prepared in a manner described previously.[2] The *cis*-2-butene was purchased from the Takachiho Shoji Co., which showed no impurity on gas chromatographic analysis. To keep the reaction system at 40 °C, a small air bath box was made. The temperature inside was kept within ±1 °C by using a modified Beckmann thermometer. The irradiation by a cadmium resonance lamp was performed through a quartz window attached to the box. In each experiment, the cell was saturated with iodine vapor before deuterium iodide and *cis*-2-butene were introduced.

The non-condensable products at 77 K were collected by means of Toepler pump equipped with a cuprous oxide furnace, which was used to combust hydrogen into water when the amount of methane produced was measured. Among the condensable products at 77 K, hydrocarbons were analyzed on the gas chromatograph of a 20-m-long dimethyl sulforane column. The D-content in the product was measured by mass spectrometry after each component had been separated by gas chromatography. Many kinds of alkyl iodides were found to be formed, but they were not analyzed quantitatively.

Results

The photolysis results are summarized in Fig. 1. All the data were obtained when the pressures of DI and I_2 were 10.3 and 1.1 Torr respectively, in a 120-ml reaction vessel; the irradiation time was 6 min. Experiments with HI in place of DI were also carried out. Those results are not shown here, because the curves for each product almost coincided with those for the corresponding products shown in Fig. 1. The plots for HD and D_2 were obtained after a correction was made for the initially-present impurity, HI, in the DI gas. The correction method has been previously described.[2]

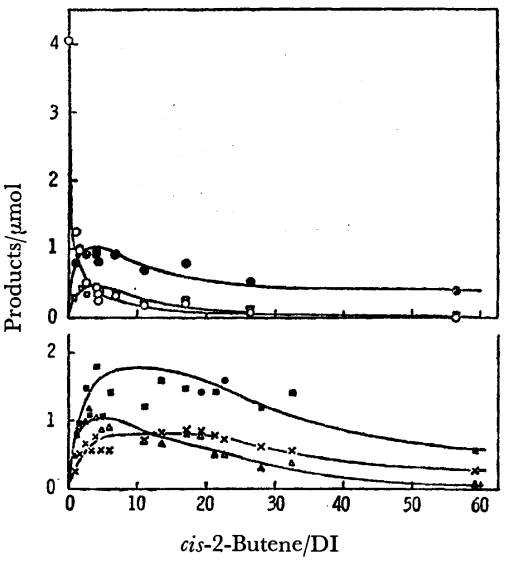

Fig. 1. The photolysis products as a function of the *cis*-2-butene/DI ratio. ○, D_2; ●, HD; □, CH_3D; ■, *n*-butane; △, propylene; ×, 1-butene.

Mass-spectrometric analysis showed that the methane formed in the present system consisted of CH_3D and CH_4. By estimating the contribution of the HI initially present in the DI gas, and that of the abstraction reaction of CH_3 from butene, to the formation of CH_4,[4] it was concluded that, if pure DI was used, all of the methane produced must be CH_3D. When a similar correction was applied to the mass spectra of propylene and *n*-butane, it was found that they were $CH_3CH{=}CHD$ and $CH_3CHDCHDCH_3$ respectively. In the case of 1-butene, however, no unique conclusion could be obtained.

According to Back and Cvetanović, iodine atoms initiate the *cis-trans* isomerization of 2-butene, and also the isomerization to 1-butene, although the latter process is very slow.[5] In the present system, obviously, these reactions are overlapped with the reactions initiated by the D atoms. Therefore, we will not discuss the formation of 1-butene in the present system, although it is itself of much interest.

Discussion

Abstraction Reaction of Hot D Atoms. As Fig. 1 shows, the amounts of HD, CH_3D, and $CH_3CH{=}CHD$ increase with the increase in the ratio of *cis*-2-butene/DI up to about 3, where the total pressure is 40 Torr. At the pressures higher than that, the three products gradually decrease with the increase in pressure. The curve for HD levels off at about 0.4 μmol, while those for CH_3D and $CH_3CH{=}CHD$ approach zero. The curve for HD is very similar to that obtained in the DI–C_3H_6 system.[2] These results may be interpreted in terms of the following reaction scheme:

$$DI + h\nu \longrightarrow D^* + I \quad (1)$$

$$D^* + DI \longrightarrow D_2 + I \quad (2)$$

$$D^* + I_2 \longrightarrow DI + I \quad (3)$$

$$D^* + C_4H_8 \longrightarrow \begin{cases} D + C_4H_8 & (4) \\ HD + C_4H_7 & (5) \\ C_4H_8D^* & (6) \end{cases}$$

$$C_4H_8D^* \longrightarrow \begin{cases} CH_3 + CH_3CH{=}CHD & (7) \\ H + C_4H_7D & (8) \\ D + C_4H_8 & (9) \end{cases}$$

$$C_4H_8D^* + M \longrightarrow C_4H_8D + M \quad (10)$$

$$C_4H_8D + DI \longrightarrow C_4H_8D_2 + I \quad (11)$$

$$C_4H_8D + I_2 \longrightarrow C_4H_8DI + I \quad (12)$$

$$CH_3 + DI \longrightarrow CH_3D + I \quad (13)$$

$$CH_3 + I_2 \longrightarrow CH_3I + I \quad (14)$$

$$CH_3 + C_4H_8 \longrightarrow C_5H_{11} \quad (15)$$

$$H(D) + DI \longrightarrow HD(D_2) + I \quad (16)$$

$$H(D) + I_2 \longrightarrow HI(DI) + I \quad (17)$$

$$H(D) + C_4H_8 \longrightarrow C_4H_9(C_4H_8D) \quad (18)$$

$$I + I + M \longrightarrow I_2 + M \quad (19)$$

In the presence of a large amount of *cis*-2-butene, all of the thermalized atoms and radicals are captured by *cis*-2-butene or I_2 and do not contribute to the formation of HD and CH_3D. Therefore, the HD formation observed at the higher pressures must be due to Reaction (5). In the absence of *cis*-2-butene, the amount of D_2 produced was 4.02 μmol. Using this value and assuming $k_1/k_2=3$,[6] the ratio of $k_5/(k_4+k_5+k_6)$ may be estimated to be as follows: $0.4/4.02(1+3\times1.1/10.3)=0.075$. This value, about 8%, is smaller than that previously obtained as the fraction of the abstraction reaction in the hot D atom reaction in the DI–C_3H_6 system (more than 10%). By comparing the curves of HD in both experiments, we feel that the figure of more than 10% previously obtained may be a little overestimated. However, the exact determination of these values is not feasible by the present technique.

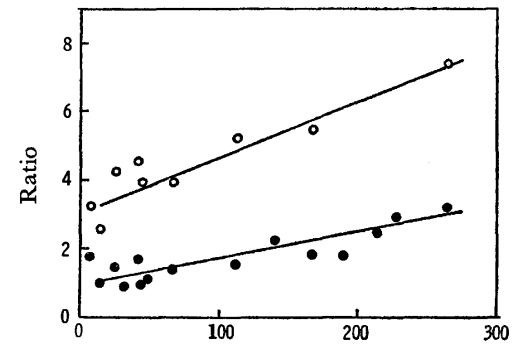

Fig. 2. The ratios of *n*-butane/methane (○) and *n*-butane/propylene (●) as a function of the *cis*-2-butene pressure.

Formation of CH_3D. Figure 2 shows the ratios of propylene/*n*-butane and methane/*n*-butane as a function of the pressure of *cis*-2-butene. On the appropriate assumption, the steady-state treatment of the reaction mechanism proposed above can predict these linear relationships.

In a previous paper, we concluded that the D* atoms produced in the photolysis of DI at 2288 Å did not give rise to the direct substitution reaction:

$$D^* + CH_2{=}CH_2 \longrightarrow CHD{=}CH_2 + H$$

The mechanism of the methane formation discussed above may be taken as one of the evidences supporting this conclusion.

Reaction (7) is a unimolecular reaction which competes with Reactions (8) and (9). If the hot radical has a lifetime long enough for the distribution of its excess energy to the vibrational freedom of the radical, Reaction (7) may predominate over Reactions (8) and (9), because the excess energy retained in the radical is only 50 kcal/mol. However, the pressure-dependent curve of HD in the range of the C_4H_8/DI ratios, 0∼10, is similar to that of CH_3D, as is shown in Fig. 1. There are two possible explanations for this similarity. One is that the lifetime of the hot radical is not long enough for the distribution of the excess energy, upon which Reaction (8) depends. The other is the participation of the substitution reaction of hot D atoms, such as

$$D^* + CH_3CH{=}CHCH_3 \longrightarrow CH_2DCH{=}CHCH_3 + H,$$

which may be possible, because the C–H bond, which is substituted, is aliphatic. Since we could not analyze the D content in *cis*-2-butene, though, no precise conclusion could be drawn.

General Discussion. The hot D atoms obtained in the present experiment are retained most at 2.4 eV.[2] According to the estimation of Wolfgang,[1] the characteristic hot atom reactions take place at more than 5 eV. The reactions reported here, therefore, are largely explainable by a small extension of the thermal reactions.

The decomposition of the *sec*-butyl radicals produced by the addition of hydrogen atoms to 2-butene has been extensively studied by Rabinovitch and his coworkers,[7]

and chemical activation is a well-known method of obtaining the hot radicals. For the production of hydrogen atoms, they used an electric discharge under a low pressure of hydrogen. Their data were mainly obtained at pressures lower than 1 Torr. Therefore, the results obtained here cannot be compared directly with theirs. According to their data on the D+*cis*-2-butene system,[8] k_a is about 2.0×10^7 s^{-1} at the pressure of 0.3 Torr. k_a is defined as follows:

$$k_a = \omega\frac{D}{S}$$

Here, ω is the collision frequency, while D and S are the fractions of the decomposition and of the stabilization of hot radicals. A rough estimation may be made in the present system as follows:

$$\frac{\text{methane}}{n\text{-butane}} \simeq \frac{D}{S} = k_a'/\omega$$

Using the data shown in Fig. 2, the value of k_a' could be calculated to be in the range of 10^8 s^{-1}, which is a little larger than the k_a value reported for the thermal D atom reaction. This difference may be attributed to the difference in the initial energy of the D atoms.

References

1) R. Wolfgang, "Progress in Reaction Kinetics," Vol. 3, edited by G. Porter, Pergamon Press, (1965) p. 97.

2) Y. Sano and S. Sato, This Bulletin, **44**, 3213 (1971).

3) In the recoil tritium reaction, both the abstraction reaction and the direct substitution reaction are assumed to occur. A. J. Johnston and D. S. Urch, *J. Chem. Soc. Faraday I*, **69**, 1173 (1973).

4) R. J. Cvetanović and R. S. Irwin, *J. Chem. Phys.*, **46**, 1694 (1967).

5) M. H. Back and R. J. Cvetanović, *Can. J. Chem.*, **41**, 1396, 1406 (1963).

6) R. A. Ogg and R. R. Williams, *J. Chem. Phys.*, **11**, 214 (1943); **13**, 586 (1945); **15**, 691 (1947).

7) B. S. Rabinovitch and D. W. Setser, "Advances in Photochemistry," Vol. 3, edited by W. A. Noyes, Jr., G. S. Hammond, and J. N. Pitts, Jr., Interscience Publishers, (1964) p. 1.

8) R. E. Harrington, B. S. Rabinovitch, and M. R. Hoare, *J. Chem. Phys.*, **33**, 744 (1960).

Calculation of the Widths for Isotropic Parts of Highly-polarized Raman Lines: Vibrational Relaxation of Infrared-inactive Levels

Masao KAKIMOTO and Tsunetake FUJIYAMA*

Department of Chemistry, Faculty of Science, The University of Tokyo, Hongo, Bunkyo-ku, Tokyo 113

**Department of Chemistry, Faculty of Science, Tokyo Metropolitan University, Fukazawa, Setagaya-ku, Tokyo 158*

(Received December 25, 1973)

A theoretical calculation is made to explain the widths of the isotropic parts of polarized Raman lines in liquids. The calculation is based on the model of the intermolecular resonance-type vibrational relaxation through the vibration-dependent term of the Lennard-Jones atom-atom interaction. The result is applied to the Raman lines of liquid nitrogen, oxygen, and carbon disulfide, and compared with the experimental data.

It is known that a polarized Raman line consists of two parts, the isotropic and anisotropic parts, and that the former originates from the trace, and the latter, from the anisotropy, of a scattering tensor.[1,2] Because the trace of a tensor is independent of any rotation of coordinates, the isotropic part does not reflect the rotational motion of molecules. The widths of the isotropic parts are very narrow in general and are considered to be related to the decay of the vibrationally-excited state or the vibrational relaxation. The anisotropic part, on the other hand, contains information not only about the vibrational relaxation, but about the molecular rotational motion (or the reorientational motion in the case of condensed phases). The line-shape of the anisotropic part is expressed as a convolution of two curves which give the line-shapes due to vibrational relaxation and rotational motion respectively. Many authors have tried, both from theoretical[2-6] and experimental[2,7-12] aspects, to extract information about the reorientational motion of molecules in liquids from the observed line-shape of a Raman line. However, very few but Valiev[13] have reported any theoretical evaluation of the widths of the isotropic part. The present work will be concerned with the calculation of the width of the isotropic part of a highly-polarized Raman line which is infrared-inactive, or with the calculation of the transition probability for vibrational relaxation of an infrared-inactive level.

Previously, the present authors[14] reported a theoretical evaluation of the vibrational-relaxation widths appearing in the infrared spectra. Those results were, however, confined to infrared-active vibrational levels, because dipole matrix elements are necessary to cause transitions. In the present case, a similar model is not applicable since a vibrational transition has no transition moment. Any attempt to seek an interaction which causes vibrational relaxation ends to failure so long as we confine ourselves to *molecule-to-molecule*-type interactions. Valiev[13] used an exchange interaction *between atoms* which participate in a molecular vibration and estimated only the order of magnitude for the vibrational-relaxation width. Our model is similar to that of Valiev, but differs in the following two points: first, the use of a more realistic potential function of the Lennard-Jones type for an interatomic interaction, and second, the use of a model of the resonance exchange of vibrational quanta between two molecules.

Theory

Consider a pair of two homonuclear diatomic molecules, the interaction geometry of which is shown in Fig. 1. The interaction potential between two atoms,

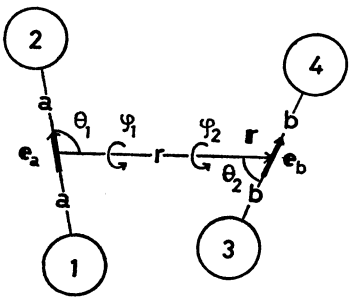

Fig. 1. A diagram showing a geometry of interacting two diatomic molecules.
1, 2, 3, and 4 indicate the atoms. $\mathbf{e}_a$ and $\mathbf{e}_b$ are unit vectors.

i and j, is written as $V(r_{ij})$, since the interaction, for which the Lennard-Jones potential is anticipated, is a function of the interatomic distance, r_{ij}, alone. Then the total intermolecular interaction, V, is:

$$V = \sum_{(i,j)} V(r_{ij}) \tag{1}$$

where (i, j) means all the pairs of interacting atoms, (1,3), (1,4), (2,3), and (2,4). The interatomic distances, r_{ij}'s, are the functions of r, θ_1, θ_2, φ_1, φ_2, a, and b (see Fig. 1):

$$r_{24} = r\left[1-\frac{2}{r}(a\cos\theta_1 - b\cos\theta_2) + \frac{1}{r^2}\{a^2+b^2 - 2ab(\sin\theta_1\cos\varphi_1\sin\theta_2\cos\varphi_2 + \sin\theta_1\sin\varphi_1\sin\theta_2\sin\varphi_2 + \cos\theta_1\cos\theta_2)\}\right]^{1/2} \tag{2}$$

and similar equations for the others.[15] As the molecules undergo vibrations, a and b, and hence r_{ij}'s also, change in magnitude. Therefore, we expand V in a series of the small changes of the bond distances, Δa and Δb, and retain only the term which is bilinear on Δa and Δb:

$$V' = \frac{\partial^2 V}{\partial a \partial b}\Delta a \Delta b \tag{3}$$

which, by virtue of Eq. (1), yields:

$$V' = \sum_{(i,j)} \left[\frac{\partial^2 V(r_{ij})}{\partial r_{ij}^2} \frac{\partial r_{ij}}{\partial a} \frac{\partial r_{ij}}{\partial b} + \frac{\partial V(r_{ij})}{\partial r_{ij}} \frac{\partial^2 r_{ij}}{\partial a \partial b} \right] \Delta a \Delta b \quad (4)$$

Note that $\frac{\partial^2 V(r_{ij})}{\partial r_{ij}^2}$ and $\frac{\partial V(r_{ij})}{\partial r_{ij}}$ are common for all the (i,j) pairs. Therefore, they are written simply as $\frac{d^2V}{dr^2}$ and $\frac{dV}{dr}$ respectively. On calculating the differentials in Eq. (4), we expand the square bracket in Eq. (2) in powers of $1/r$ and neglect the terms of orders higher than $(1/r)^2$. This approximation, and hence its validity, are similar to those of a dipole-dipole interaction.[15] Some manipulation leads to:

$$V' = \left[\frac{d^2V}{dr^2} \frac{4ab}{r^2} X + \frac{dV}{dr} \frac{4ab}{r^3} Y \right] \Delta a \Delta b \quad (5)$$

where:[16]

$$X = 1 + (\mathbf{e}_a \cdot \mathbf{e}_b)^2 + 8\left(\mathbf{e}_a \cdot \frac{\mathbf{r}}{r}\right)^2 \left(\mathbf{e}_b \cdot \frac{\mathbf{r}}{r}\right)^2 - 6(\mathbf{e}_a \cdot \mathbf{e}_b)\left(\mathbf{e}_a \cdot \frac{\mathbf{r}}{r}\right)\left(\mathbf{e}_b \cdot \frac{\mathbf{r}}{r}\right) - 2\left(\mathbf{e}_a \cdot \frac{\mathbf{r}}{r}\right)^2 - 2\left(\mathbf{e}_b \cdot \frac{\mathbf{r}}{r}\right)^2 \quad (5a)$$

and:

$$Y = -1 - 2(\mathbf{e}_a \cdot \mathbf{e}_b)^2 - 15\left(\mathbf{e}_a \cdot \frac{\mathbf{r}}{r}\right)^2 \left(\mathbf{e}_b \cdot \frac{\mathbf{r}}{r}\right)^2 + 12(\mathbf{e}_a \cdot \mathbf{e}_b)\left(\mathbf{e}_a \cdot \frac{\mathbf{r}}{r}\right)\left(\mathbf{e}_b \cdot \frac{\mathbf{r}}{r}\right) + 3\left(\mathbf{e}_a \cdot \frac{\mathbf{r}}{r}\right)^2 + 3\left(\mathbf{e}_b \cdot \frac{\mathbf{r}}{r}\right)^2 \quad (5b)$$

The vector products appearing in Eqs. (5a) and (5b), and hence X and Y, are written in terms of the spherical harmonics normalized to unity, $Y_l^m(\theta_a,\varphi_a)$, $Y_l^m(\theta_b,\varphi_b)$, and $Y_l^m(\theta_r,\varphi_r)$, where (θ_a,φ_a), (θ_b,φ_b), and (θ_r,φ_r) are the polar coordinates of $\mathbf{e}_a$, $\mathbf{e}_b$, and $\mathbf{r}$ respectively in a laboratory-fixed coordinate system. Though these expressions are too lenghty to be written here, the following relations will be necessary later:

$$\int X^2 d\tau' = \frac{2^{10}}{5^2}\pi^3$$
$$\int Y^2 d\tau' = \frac{2^{13}}{3 \times 5^2}\pi^3 \quad (6)$$
$$\int XY d\tau' = -\frac{2^{11} \times 7}{3^2 \times 5^2}\pi^3$$

where $d\tau' = \sin\theta_a \sin\theta_b \sin\theta_r d\theta_a d\varphi_a d\theta_b d\varphi_b d\theta_r d\varphi_r$, and where integrations are carried out over the entire configuration space.

Now, consider that the two molecules are initially on the vibrational states of $v_a=1$ and $v_b=0$ respectively, where v_a and v_b are the vibrational quantum numbers. Then, the transition probability for a coupled transition, $(v_a, v_b)=(1, 0)\rightarrow(0, 1)$, is given by:[17]

$$\frac{1}{\hbar^2}\int_{-\infty}^{\infty} \langle M(0)M(t)\rangle_{av} e^{-i(\omega_a-\omega_b)t} dt \quad (7)$$

where ω_a and ω_b are the vibrational angular-frequencies and where M means the matrix element of V':

$$M = \langle 01 | V' | 10 \rangle \quad (8)$$

The average, denoted by $\langle\ \rangle_{av}$ in Eq. (7), may be regarded either as a time-average or, if M is ergodic, as an ensemble average. The latter concept is used later in calculating the average. To obtain a probability, $P(1\rightarrow0)$ for ,one of the interacting molecules undergoing a transition, $1\rightarrow0$, one integrates Eq. (7) over ω_b and takes the square root:[18]

$$P(1\rightarrow0) = \frac{1}{\hbar}\left[\langle |M|^2\rangle_{av}\right]^{1/2} \quad (9)$$

We then insert Eq. (5) into Eq. (9), keeping in mind that $2\Delta a$ and $2\Delta b$ are the normal coordinates, Q_a and Q_b respectively, of vibrations. Further, when the interacting two molecules are of the same species, we can write:

$$a = b$$

and:

$$\langle 1|Q_a|0\rangle = \langle 1|Q_b|0\rangle = \sqrt{\frac{\hbar}{2m\omega}} \quad (10)$$

where m is the reduced mass and where $\omega=\omega_a=\omega_b$. Thus,

$$P(1\rightarrow0) = \frac{a^2}{2m\omega}\left[\left\langle\left(\frac{d^2V}{dr^2}\right)^2 \cdot \frac{1}{r^4}X^2\right\rangle_{av} + 2\left\langle \frac{d^2V}{dr^2}\frac{dV}{dr}\frac{1}{r^4}XY\right\rangle + \left\langle\left(\frac{dV}{dr}\right)^2 \cdot \frac{1}{r^6}Y^2\right\rangle_{av}\right]^{1/2} \quad (11)$$

To proceed further, an analytical expression for V is necessary. The best that is available, that has a simple form and whose parameters are determined well, may be the Lennard-Jones potential:

$$V(r) = 4\varepsilon\left[\left(\frac{r_0}{r}\right)^{12} - \left(\frac{r_0}{r}\right)^6\right] \quad (12)$$

The averages of Eq. (11) are calculated as:

$$\langle F\rangle_{av} = W\int F d\tau \quad (13)$$

where:

$$d\tau = r^2 dr d\tau'$$

and where W is a normalization constant which is determined, from the condition that n molecules are contained in 1 cm^3, to be:

$$W = \frac{n}{(4\pi)^2} \quad (14)$$

A lower limit, a_0, exists for the parameter, r, the physical meaning of which is that no two molecules can come closer than a_0. Remembering the relations of Eq. (6), we finally obtain:

$$P(1\rightarrow0) = \frac{8}{5}\frac{a^2}{m\omega}\sqrt{n\pi}\,4\varepsilon\left[A\frac{r_0^{24}}{a_0^{29}} - B\frac{r_0^{18}}{a_0^{23}} + C\frac{r_0^{12}}{a_0^{17}}\right]^{1/2} \quad (15)$$

where

$$A = \frac{4\times1909}{29},\quad B = \frac{4\times1123}{23},\quad \text{and}\quad C = \frac{661}{17}.$$

Comparison with the Experimental Data

To check the validity of our model as used in the present theory, the widths of the isotropic Raman lines of liquid N_2 and O_2 were calculated by means of Eq.

Table 1.

Molecule	$(cm^{-1})^{b)}$	FWHM[a] (cm^{-1})		Used parameters		
		Obsd[b]	Calcd	$2a$ (Å)[c]	ε/k (K)[d]	r_0 (Å)[d]
N_2	2331	0.067±0.004	0.037	1.0976	35.7	2.789
O_2	1555	0.117±0.008	0.067	1.2074	35.7	2.789
CS_2	656	0.50 ±0.02	0.72	3.108	124.0	3.418

a) Full-width at half-maximum, calculated from Eq. (15) through the relation; FWHM$=P(1\rightarrow0)/\pi c$, where c is the velocity of light. b) See Ref. 19. c) See Ref. 22. d) See Ref. 23.

(15) and compared with the observed ones.

The Raman lines of liquid N_2 and O_2 are extremely narrow; therefore, the widths cannot be measured precisely with a conventional grating spectrometer. Clements and Stoicheff[19] have reported the most reliable data to date; they made their observations by the use of a Fabry-Perot interferometer.

In the calculations of the theoretical widths, the values of n are estimated from the values of the molecular weight and density.[20] Since the Lennard-Jones parameters, ε and r_0, are not available for an N···N or O···O pair, they are transferred from those for an Ne pair. The estimation of a_0 is the most difficult problem, although the results are rather sensitive to it. We arbitrarily, mainly because of the ease of calculation, put a_0 equal to r_0.[21] The results are shown in Table 1.

The conclusion of Eq. (15) is also applicable to the estimation of the width for the totally-symmetric vibration of CS_2, although it is a triatomic molecule. In this case, Q_a is $\sqrt{2}\Delta a$ instead of $2\Delta a$; therefore Eq. (15) should be multiplied by a factor of two. The values of ε and r_0 are transferred from those of Ar. The result for CS_2 is also included in Table 1.

As may be seen from Table 1, the agreement between the calculated and the experimental values is fairly good. This agreement may confirm the validity of the model used in the present theory. There may be many causes for the broadening of the isotropic part of a Raman line, but it can be concluded that the resonance exchange of the vibrational quanta through the interatomic interaction is the most important.

The authors are indebted to all the members of the Shimanouchi Laboratory for their helpful correspondence about this work. They are particularly grateful to Professor Takehiko Shimanouchi of the University of Tokyo for giving them the opportunity of publishing this work.

References

1) G. Placzek, "The Rayleigh and Raman Scattering," U. S. At. Energy Comm. UCRL-TRANS-526(L), 1962 [translated from *Marx Handbuch der Radiologie*, 2nd ed., Vol. 6, Akademische Verlagsgesellschaft, Leipzig (1934), Pt. II, pp. 205—374].

2) F. J. Bartoli and T. A. Litovitz, *J. Chem. Phys.*, **56**, 404, 413 (1972).

3) K. A. Valiev and L. D. Eskin, *Opt. Spectrosc.*, **12**, 429 (1961); K. A. Valiev, *ibid.*, **13**, 282 (1962).

4) R. G. Gordon, *J. Chem. Phys.*, **42**, 3658 (1965).

5) S. Bratos and E. Marechal, *Phys. Rev.*, **A4**, 1078 (1971).

6) L. A. Nafie and W. L. Peticolas, *J. Chem. Phys.*, **57**, 3145 (1972).

7) M. F. Crawford, H. L. Welsh, and J. H. Harrold, *Can. J. Phys.*, **30**, 81 (1952).

8) A. V. Rakov, *Opt. Spectrosc.*, **7**, 128 (1959).

9) M. Scotto, *J. Chem. Phys.*, **49**, 5362 (1968).

10) J. P. Perchard, W. F. Murphy, and H. J. Bernstein, *Mol. Phys.*, **23**, 499 (1972).

11) J. H. R. Clarke and S. Miller, *Chem. Phys. Lett.*, **13**, 97 (1972).

12) K. T. Gillen and J. E. Griffiths, *ibid.*, **17**, 359 (1972).

13) K. A. Valiev, *Soviet Phys. JETP*, **13**, 1287 (1961).

14) M. Kakimoto and T. Fujiyama, This Bulletin, **45**, 2970 (1972).

15) See, for example, M. Bersohn, and J. C. Baird, "An Introduction to Electron Paramagnetic Resonance," Benjamin, New York (1966), Appendix B-1.

16) All the quantities subscripted with a or b in the text hereafter correspond to the left and the right molecules, respectively, in Fig. 1.

17) See, for example, R. Zwanzig, *J. Chem. Phys.*, **34**, 1931 (1961), Eqs. (3)—(9).

18) K. A. Valiev, *Opt. Spectrosc.*, **11**, 253 (1961), Eq. (24). The integration over ω_b must be carried out only within a certain limited range, $[\omega_a-\alpha, \omega_a+\alpha]$, because ω_b cannot spread over so widely. In obtaining Eq. (9) of the text, one is putting the integral

$$\int_{\omega_a-\alpha}^{\omega_a+\alpha}\int_{-\infty}^{\infty}\frac{\langle M(0)M(t)\rangle_{av}}{\langle|M|^2\rangle_{av}}e^{-t(\omega_a-\omega_b)t}dtd\omega_b$$

equal to 1. Although there is no theoretical reason to choose the value of 1, this simplification is permissible because we concern here only with the order of magnitude and because there is no way to estimate the correct value for α. In the limit of $\alpha\rightarrow\infty$, the final result (Eq. (11) or (15)) becomes about 2.5 (*i.e.* $\sqrt{2\pi}$) times larger.

19) W. R. L. Clements and B. P. Stoicheff, *Appl. Phys. Lett.*, **12**, 246 (1968): Though the spectra they measured contain not only isotropic but anisotropic parts, the widths reported may be regarded as those of isotropic parts, because of very low depolarization degrees.

20) "International Critical Tables," National Research Council, McGraw-Hill, New York (1928).

21) r_0 is the distance at which the potential has the value zero. If we choose, instead, a_0 to be the distance at which the potential has the value $(3/2)kT$ the results become about 3.3 times larger for N_2 and O_2, and about 3.6 times larger for CS_2. This may be an overestimation, since we do not take a radial distribution function into account. Anyhow, the present model gives the correct order of magnitude.

22) "Tables of Interatomic Distances and Configuration in Molecules and Ions," The Chemical Society, London (1958).

23) J. O. Hirschfelder, C. F. Curtiss, and R. B. Bird, "Molecular Theory of Gases and Liquids," Wiley, New York (1954).

Electrical Properties of Evaporated Thin Films of Copper Phthalocyanine

Yoshiro SAKAI, Yoshihiko SADAOKA, and Hirofumi YOKOUCHI

Department of Industrial Chemistry, Faculty of Engineering, Ehime University, Bunkyo-cho, Matsuyama, Ehime 790

(Received January 14, 1974)

The electrical properties of evaporated thin films of copper phthalocyanine(CuPc) were investigated by the ac method. The frequency dependence of conductivity and capacitance, and the activation energy for dc conductivity in α- and β-CuPc were determined. No significant variation in the electrical properties was observed with the difference in the phases of CuPc films *in vacuo*. The frequency dependence of conductivity and capacitance can be explained in terms of the simultaneous hopping and band conduction, *viz.*, $\sigma=\sigma_{dc}+A_1\cdot\omega^n$ and $C=C_\infty+A_2\cdot\omega^{1-n}$. The energy gap for α- and β-CuPc *in vacuo* is 1.80 eV and 1.89 eV, respectively. The adsorbed O_2 gas has a great effect on the dc conductivity but little on the ac conductivity of α-CuPc film. The adsorption of oxygen on α-phase CuPc might be the cause of high dc conductivity and low activation energy(0.5—0.7 eV) as compared with those *in vacuo*.

It is known that copper phthalocyanine(CuPc) can be obtained in two crystallographic modifications(α and β). Wihksne and Newkirk[1] found that the conductivity of form α is greater than that of form β by a factor of 10^5, the activation energies being 0.25 eV and 0.9 eV, respectively. On the other hand, Harrison and Ludewig[2] claimed that the difference in conductivity is due to the greater adsorptivity for oxygen on α-phase CuPc, and found that the conductivity of the α-phase film is similar to that of the β-phase one when the oxygen has been eliminated. Eley and Parfitt[3] studied the ac conductivity of aromatic compounds. They explained the frequency dependence of conductivity in a compressed powder disk in terms of contact resistance and contact capacitance(Maxwell-Wagner type dispersion). The frequency dependence of the conductivity in aromatic compounds can be explained in terms of the hopping conduction mechanism rather than the Maxwell-Wagner type dispersion.[4,5] We have studied the frequency and temperature dependence of conductivity as well as the capacitance of α- and β-phase CuPc films.

Experimental

Electrical measurements were carried out on evaporated thin α- and β-phase CuPc films, the surface of the film being expected to be in alignment with its *ab*-plane. An ac bridge TR 10C(Ando Electrics Co., Ltd.) was used to measure the conductivity and capacitance. The sample was held in O_2 or H_2 atmosphere or *in vacuo*(about 10^{-2} Torr). A sandwich type cell of thin film was prepared by evaporation on a microscope slide. The evaporation was carried out in a vacuum of the order of 10^{-6} Torr, the rate of deposition of CuPc being approximately 10^{-7} mm/s. The bottom electrode was an evaporated silver layer covered with an evaporated thin film of CuPc. The CuPc thickness was about 10^{-3} mm. The top electrode was also prepared by the evaporation of silver. The cell constant was determined to be about 2×10^3 cm. The β-phase CuPc was obtained by annealing the evaporated film at 320 °C for 30 min in N_2 atmosphere.[1,2] The transition from α to β-phase on annealing was confirmed by the IR spectrum of the CuPc film which was deposited on a KBr disk. This was also confirmed by the change of electrical conductivity, the result being similar to that obtained by Wihksne and Newkirk[1] as well as by Harrison and Ludewig.[2] Measurements of the conductivity and the capacitance were carried out at temperatures 13—130 °C (±2 °C). The frequency was varied from 30 Hz to 1 MHz. The amplitude of the alternating voltage amounted to 20 V.

Results and Discussion

Ebert and Gottlieb[6] studied the X-ray diffraction and IR spectra of α- and β-CuPc. Their results indicate that the IR spectrum of α-CuPc differs from that of β-CuPc at the wavelengths 7.6, 9.2, 11.4, 13 and 14 μm. The spectra of the deposited CuPc film on a KBr disk and the annealed one were found to be similar to those obtained by Ebert and Gottlieb, indicating that the evaporated film of CuPc on a slide glass is in the α-phase while the annealed one is in the β-phase.[2]

The frequency dependence of conductivity for the α- and β-CuPc films *in vacuo* at various temperatures is shown in Figs. 1 and 2. The temperature and the frequency dependences of the electrical properties for both α- and β-CuPc *in vacuo* were found to be similar, indicating that there is no significant difference between the two phases. In the high frequency region, it was found that the conductivity of both α- and β-CuPc is proportional to ω^n:

$$\sigma_{ac} = A_1\cdot\omega^n \qquad (1)$$

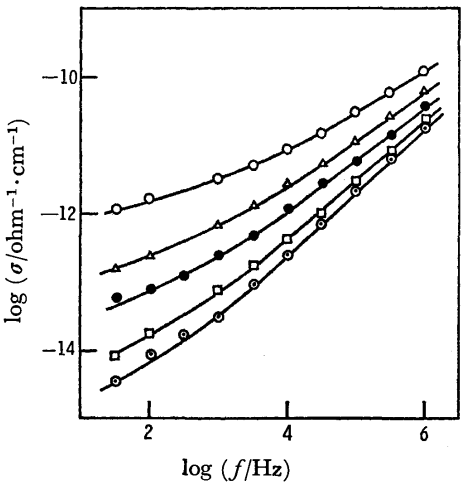

Fig. 1. Frequency dependence of conductivity of α-CuPc film *in vacuo*.
(○) 124 °C, (△) 98 °C, (●) 74 °C, (□) 47 °C, (⊙) 27 °C.

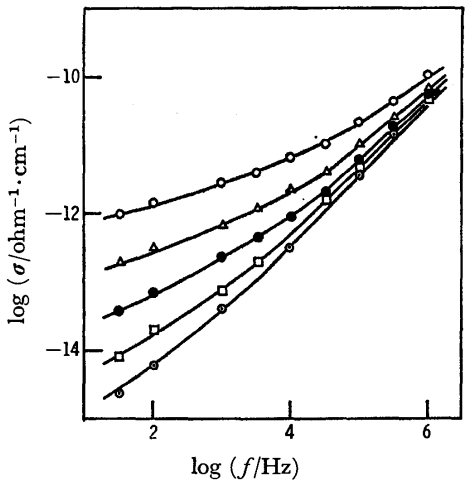

Fig. 2. Frequency dependence of conductivity of β-CuPc film *in vacuo*.
(○) 127 °C, (△) 99 °C, (●) 76 °C, (□) 45 °C, (⊙) 18 °C.

where ω is the angular frequency. The value of n decreases from 1.0 to 0.5 with an increase in temperature. σ_{ac} at low frequencies was calculated by extrapolation from the high frequency region on the assumption that σ_{ac} obeys Eq. (1) over the whole range of frequency. In the low frequency region the difference between σ_{ac} value thus obtained and the observed conductivity increases with an increase in temperature.

We have studied the frequency and temperature dependence of conductivity of aromatic compounds in both an evaporated thin film and a compressed powder disk and have found that the observed conductivity can be expressed as the sum of two terms, the band conduction and the hopping conduction.[4,5] The latter strongly depends on frequency, but not the former. Thus we have

$$\sigma = \sigma_{ac} + \sigma_{dc} = A\cdot\omega^n\cdot\exp[-E(T\cdot\omega)/kT] + \sigma_0\cdot\exp(-E/kT) \quad (2)$$

where σ_{ac} is the frequency dependent conductivity, σ_{dc} is the frequency independent conductivity, $E(T\cdot\omega)$, the apparent activation energy for hopping from one localized state to another, is a function of both temperature[7-9] and frequency, and E is the activation energy of the band conduction. When the conductivity is given by Eq. (2), the Kramers-Kronig relation[10] can be used to determine the frequency dependence of the capacitance:

$$C = C_\infty + A_2\cdot\omega^{1-n} \quad (3)$$

The values of n for conductivity and capacitance were obtained at various temperatures by use of Eqs. (2) and (3). It was assumed that C_∞ is roughly equal to the value of C at 1MHz. The values of n thus obtained are given in Table 1. The values of n in C are in fair agreement with those in σ_{ac}. The results indicate that the frequency dependence of conductivity and capacitance can be expressed by Eqs. (2) and (3) within experimental error. We see that σ_{ac} of α-CuPc and that of β-CuPc do not differ greatly (Fig. 3). The apparent activation energy of ac conductivity decreases with the increase in frequency and the decrease in temperature for both α- and β-CuPc *in vacuo*.

Table 1. Values of n for α-CuPc and β-CuPc films *in vacuo* and in H_2 atmosphere

Phase	Temp. °C	n in σ_{ac}	n in C
β *in vacuo*	127	0.4_9	0.5_2
	99	0.5_4	0.5_7
	76	0.6_8	0.6_4
	45	0.8_3	—
α *in vacuo*	124	0.5_0	0.5_7
	98	0.6_3	0.5_9
	74	0.6_9	0.7_5
	47	0.8_1	0.7_6
	27	0.8_3	0.7_6
α in H_2	122	0.5_0	0.5_0
	99	0.5_5	0.5_4
	73	0.6_5	0.5_9
	54	0.7_2	0.6_6
	31	0.8_4	—

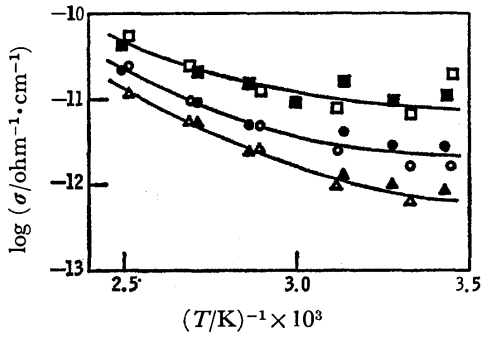

Fig. 3. Temperature dependence of conductivity in the high frequency region of α- and β-CuPc films *in vacuo*.
(□, ○, △) α-CuPc, (■, ●, ▲) β-CuPc, (□, ■) 300 kHz, (○, ●) 100 kHz, (△, ▲) 30 kHz.

The temperature dependence of σ_{dc} ($=\sigma - A_1\cdot\omega^n$) was obtained for both α- and β-CuPc (Fig. 4). The activation energy of σ_{dc} is 0.90 eV and 0.94 eV for the α-CuPc and the β-CuPc film *in vacuo*, respectively. These are in fair agreement with those obtained by Harrison and Ludewig.[2]

The effect of adsorbed O_2 gas on the electrical properties was investigated. The frequency dependence of conductivity for α-CuPc film in H_2 and O_2 is shown in Figs. 5 and 6. The frequency dependence of conductivity and capacitance in H_2 is similar to that *in vacuo* (Table 1) but the activation energy of dc conductivity is slightly larger than that *in vacuo*. In the low frequency range, the conductivity of α-CuPc in O_2 is larger than that *in vacuo* by a factor of 10^4 at room temperature. The magnitude of σ_{dc} was poorly reproducible, being strongly affected by the condition of O_2 gas adsorption. The activation energy was found to be 0.5—0.7 eV. When the contribution of σ_{dc} component is large, the frequency dependence of σ_{ac} can be obtained by subtracting σ_{dc} from σ on the assumption that the value of σ_{dc} is approximately equal to that of σ in the low

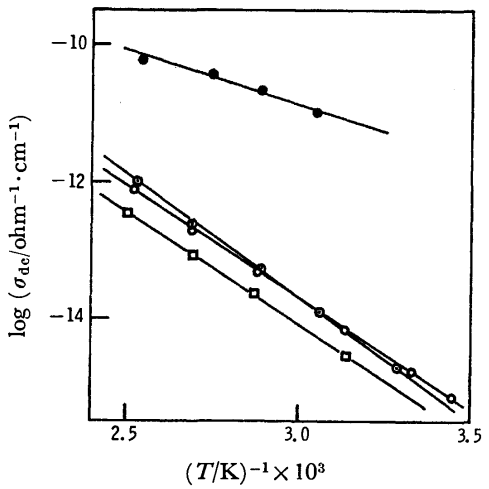

Fig. 4. Temperature dependence of dc conductivity of CuPc film in various conditions.
(□) β-CuPc film *in vacuo*, (○) α-CuPc film *in vacuo*, (⊙) α-CuPc film in H_2 atmosphere, (●) α-CuPc film in O_2 atmosphere.

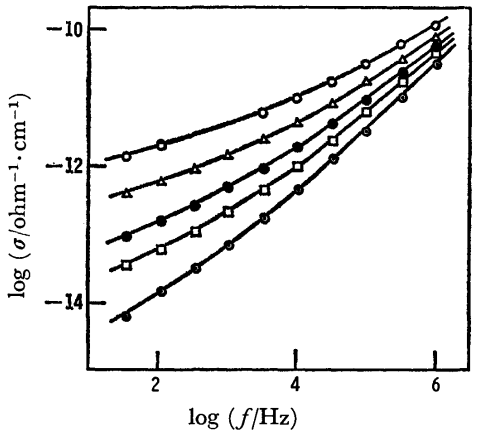

Fig. 5. Frequency dependence of conductivity of α-CuPc film in H_2 atmosphere.
(○) 122 °C, (△) 99 °C, (●) 73 °C, (□) 54 °C, (⊙) 31 °C.

frequency region. The frequency dependence of σ_{ac} is shown in Fig. 7. It can thus be said that the σ_{ac} is little affected by the adsorbed O_2.

The band conduction σ_{dc} becomes gradually predominant at low frequency range with temperature rise, so that in the high temperature region the conductivity depends little on the frequency. Such a remarkable tendency is observed in particular in α-CuPc under O_2 atmosphere. It seems that the hopping conduction σ_{ac} is mainly based on the localized state (and/or shallow traps) which might be produced by crystal

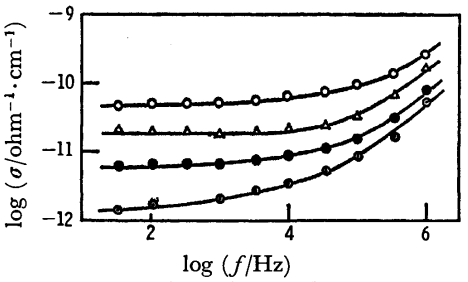

Fig. 6. Frequency dependence of conductivity of α-CuPc in O_2 atmosphere.
(○) 120 °C, (△) 74 °C, (●) 55 °C, (⊙) 34 °C.

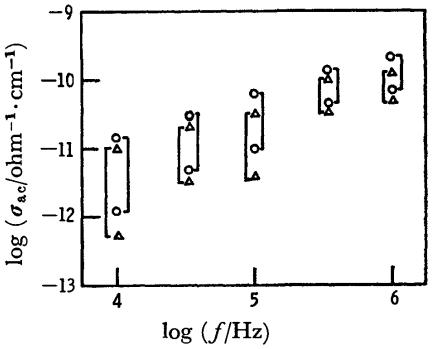

Fig. 7. Frequency dependence of σ_{ac} of α-CuPc films.
(○) in O_2 introduced after evacuation,
(△) in H_2 atmosphere.

defects but not adsorbed oxygen, and the band conduction σ_{dc} is due to electrons excited to the conduction band and/or holes to the valence band. Since the frequency at which traps produced by adsorbed oxygen are filled and emptied is greater than the applied field frequencies, the adsorbed oxygen has no effect on thermally and frequency assisted hopping conduction.

References

1) K. Wihksne and A. E. Newkirk, *J. Chem. Phys.*, **34**, 2184 (1961).
2) S. E. Harrison and K. H. Ludewig, *ibid.*, **45**, 343 (1966).
3) D. D. Eley and C. D. Parfitt, *Trans. Faraday Soc.*, **51**, 1529 (1955).
4) Y. Sakai and Y. Sadaoka, *Jap. J. Appl. Phys.*, **12**, 1463 (1973).
5) Y. Sakai and Y. Sadaoka, *ibid.*, **12**, 1952 (1973).
6) A. A. Ebert and H. B. Gottlieb, *J. Amer. Chem. Soc.*, **74**, 2806 (1952).
7) N. F. Mott, *J. Non-Crystalline Solids*, **1**, 1 (1969).
8) N. F. Mott, *ibid.*, **8**, 1 (1972).
9) S. K. Bahl and K. L. Chopra, *J. Appl. Phys.*, **41**, 2196 (1970).
10) H. K. Rockstad, *J. Non-Crystalline Solids*, **2**, 192 (1970).

The Radiolytic-chain Dechlorination of Polychlorinated Biphenyls in Alkaline 2-Propanol Solutions

Takeshi SAWAI, Toshinari SHIMOKAWA, and Yoshiharu SHINOZAKI

Tokyo Metropolitan Isotope Research Center, Fukazawa, Setagaya, Tokyo 158

(Received January 17, 1974)

The radiolysis of solutions of polychlorinated biphenyls(PCB's) and potassium hydroxide in simple aliphatic alcohols was studied. The major products in alkaline 2-propanol solutions were potassium chloride, acetone, lower chlorinated biphenyls, and biphenyl. Their yields increased and the concentration of the hydroxide ions decreased with the dose. Acetone and potassium chloride were formed in high yields, and their concentrations were almost equal to the diminution in the hydroxide ions. The dechlorination yield was determined as a function of the dose, the dose rate, and the concentrations of PCB's, potassium hydroxide, and organic solutes. The chain-dechlorination reaction proceeded in the alkaline 2-propanol solution, but not in alkaline methanol, ethanol, 1-propanol, and butanols. The 2-propoxide radical anion, which is formed by the electron transfer from the hydroxide ion to the 2-propanol radical, is the chain carrier for the dechlorination reaction of PCB's in alkaline 2-propanol solutions. The mechanism is discussed in detail.

In neutral or alkaline aliphatic alcohol solutions, carbon tetrachloride,[1] 1,1,1-trichloro-2,2-*bis*(*p*-chlorophenyl)ethane,[2] nitrous oxide, [3] and methyl halide[4] undergo radiolytic decomposition with high yields. For example, in alkaline alcoholic solutions of methyl halide, methane is produced in a high yield on exposure to ^{60}Co γ-rays, but the yields can be changed by varying the kinds of alcohol and solutes; *e.g.*, the dehalogenation yields of CH_3Cl, CH_3Br, and CH_3I in alkaline 2-propanol were 2.2, 130, and 179, respectively. Sherman has proposed the following reactions for the most important propagation steps in the chain decomposition in alkaline alcoholic solutions:[4]

$$R\cdot + \overset{|}{C}HOH \longrightarrow RH + -\overset{\cdot}{C}OH \ (I) \quad (1)$$

$$I + B^- \rightleftharpoons -\overset{|}{C}O^- \ (II) + BH \quad (2)$$

$$MX + II \longrightarrow M\cdot + X^- + -\overset{|}{C}O \quad (3)$$

$$N_2O + II \longrightarrow O^- + N_2 + -\overset{|}{C}O \quad (3')$$

$$M\cdot(\text{or } O^-) + \overset{|}{C}HOH \longrightarrow MH(\text{or } OH^-) + I \quad (4)$$

where R·, B^-, and MX are the radical, the base, and alkyl halide, respectively. Moreover, it has been suggested that the radical-induced chain decomposition of some compounds in the alkaline alcohol solution can be observed under the following conditions: 1. MX should have a sufficiently high electron affinity, so that electron transfer from the alcohol radical anion-(II) is an efficient process, and 2. the compound produced by the electron-transfer reaction (3) is able to abstract a carbinol hydrogen from alcohol, thus giving the alcohol radical (I).

In general, it is well known that organic halides have a very high reactivity toward hydrated electrons and form halide ions by dissociative electron attachment. The rate constants of hydrated electrons for monofluoro- or monochlorobenzene and polyfluorobenzenes are $5\times10^8\ M^{-1}s^{-1}$ and $10^9\sim10^{10}\ M^{-1}s^{-1}$.[5,6] Therefore, it may be expected that the reactivity for polychlorinated biphenyls (PCB's) is relatively high. The study of the dechlorination reactions of aromatic polychlorides in organic solutions, especially in alkaline alcoholic solutions, is very interesting. In a preliminary experiment,[7] it was found that the chain dechlorination of PCB's proceeded and yielded potassium or sodium chloride and biphenyl with high *G*-values in the alkaline 2-propanol solutions, but not in the neutral 2-propanol and the alkaline methanol. The authors suggested that the chain-propagation steps in the dechlorination of PCB's must be similar to that proposed by Sherman.[3,4] This radiolytic-chain dechlorination of PCB's in 2-propanol-alcoholate solutions has also been found independently by Arai *et al.*[8]

The present paper is concerned with a more detailed study of the chain-dechlorination reaction of PCB's.

Experimental

Sample. PCB's dissolved in alkaline alcohol solutions were placed in a Pyrex irradiation vessel 12 mm in o.d. The solutions were irradiated with 3K Ci ^{60}Co γ-rays at room temperature after having been purged with pure nitrogen gas for about 30 min or after having been degassed by freeze-pump-thaw cycles. The dose rate was determined by means of a ferrous sulfate solution, and the energy absorbed in the samples was corrected with the electron density of the solutions.

The PCB's (Kanechlor-300, 400, 500*), alcohols, and potassium hydroxide (special grade, from Wako Pure Chemical Co.) were used without further purification. As the PCB's used in our experiments consist of mixtures of various chlorinated biphenyls, the contents of chlorine were analyzed by means of elemental analysis with a Shimadzu UM-2 element analyzer.

Analysis. The potassium chloride produced by irradiation was dissolved in water and was determined by Mohr's method.[9] The hydroxide-ion concentration was measured by means of acid-base titration, with phenolphthalein as an indicator. The PCB's remaining in the solutions after irradiation were analysed with a Shimadzu 4B gas chromatograph with an electron-capture-type detector and using a 2 m glass column of SE-30 at 190—210 °C. The acetone and biphenyl were determined by means of a Shimadzu 4A gas chromatograph with a hydrogen flame detector at 60

* Kanechlor (identified as KC for short) is a commercial name of the PCB's manufactured by the Kanegafuchi Chemical Industrial Co., Ltd. The numeral indicates the average number of substituted chlorine; *e.g.*, 400 shows a PCB containing 4 chlorines as the average.

and 220 °C respectively; for these analyses, a 2 m stainless steel column of 20% polyethylene glycol 20 M on chromosorb was used. A gas chromatograph-mass spectrometer (Shimadzu LKB-9000) was also used for the confirmation of the PCB's, acetone, and biphenyl.

Results and Discussion

Yield of Chloride Ion, Acetone, and Biphenyl. As has been shown in the previous paper,[7] the chloride ion was effectively liberated from the PCB's in the alkaline 2-propanol solutions purged with nitrogen gas, and a complementary amount of the hydroxide ion was consumed on exposure to ^{60}Co γ-rays at room temperature; the dechlorination was completely suppressed when the OH^- was almost consumed. In the case of 2-propanol solution containing 0.05 M potassium hydroxide and 1% KC-400, the initial yield of the chloride ion ($G(Cl^-)$) was ~450; meanwhile, the decreasing yield of the hydroxide ion was equal to that of the dechlorination. These high yields suggest that the radiolytic-chain dechlorination reaction apparently occurred, because the radical yield in the radiolysis of 2-propanol was only ~7.[10] The chain dechlorination, on the other hand, did not occur in the presence of dissolved oxygen. In the presence of an excess of potassium hydroxide in relation to the PCB's, the formation of chloride ions and the decrease in the quantity of hydroxide ions with the dose are shown in Fig. 1. The formation and the consumption were almost equal in each dose, and these rates decreased with the dose. The acetone and biphenyl also increased with an increase in the dose in a 0.2 M alkaline 2-propanol solution of 0.5% KC-300, as is shown in Fig. 2. The yield of acetone was almost the same as that of the chloride ion, and the rate was also suppressed with the dose. The formation of biphenyl increased sharply at a dose between 6×10^{18} and 2×10^{19} eV/g. At a dose of 3.2×10^{19} eV/g, the dechlorination of PCB's

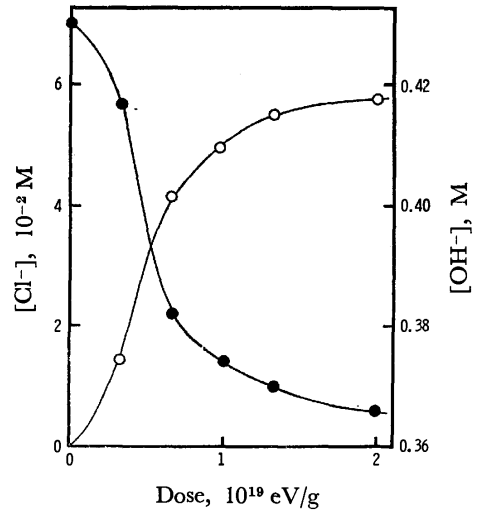

Fig. 1. Increase of chloride ion and decrease of hydroxide ion at various dose in 0.42 M KOH-2-propanol solutions of 0.3% KC-400.
○: chloride ion, ●: hydroxide ion
dose rate: 6.6×10^{18} eV/g hr

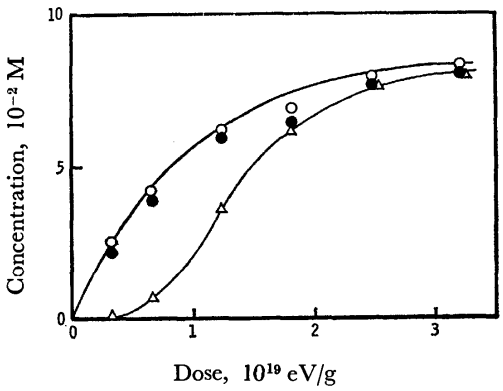

Fig. 2. Yields of products in 0.2 M KOH-2-propanol solutions of 0.5% KC-300.
○: chloride ion, ●: acetone, △: biphenyl
dose rate: 1.1×10^{19} eV/g hr

was found to reach about 100%, as calculated from the chlorine content. The amount of biphenyl multiplied by a factor of 3.2** was almost equal to the chloride-ion concentration at a dose of 3.2×10^{19} eV/g. This fact suggests that the dechlorination reaction of PCB's is predominant and that other reactions, such as C–C bond dissociation, the dimerization of PCB's, or the addition of radicals to a benzene ring, scarcely proceed. Pinacol was not detected.

The initial yields of the dechlorination and of the decrease in the quantity of hydroxide ions were affected by the alkaline concentration. These results are summarized in Table 1. As can be seen from Table 1, the yield obviously increased with the hydroxide-ion concentration; however, the effect of the PCB concentrations from 1% to 10% on the $G(Cl^-)$ value was small: we found no remarkable difference between KC-300, -400, and -500.

On irradiating 0.2 M alkaline 2-propanol solutions containing 0.5% KC-300 at a dose rate of $6.94\sim244\times10^{17}$ eV/g hr, the initial yields of Cl^- were found to be as given in Table 2. As is shown in Table 2, the yield

Table 1. Initial yields in alkaline 2-propanol solutions

PCB's	OH⁻/M	$G(Cl^-)$	$G(-OH^-)$	Dose rate eV/g hr
1% KC-400	1×10^{-2} a)	170	180	4.0×10^{18}
	5×10^{-2}	450	420	
	8×10^{-2}	670		
0.5% KC-400	0.25	600	600	2.4×10^{19}
1% KC-300	0.1	650		6.6×10^{18}
	0.25	680		
	0.5	730		
0.5% KC-300	0.2	630		2.4×10^{19}
0.3% KC-300	0.2	400		

a) NaOH was used.

** The average number of substituted chlorine in KC-300 was 3.2.

Table 2. Initial dechlorination yields in 0.2 M KOH-2-propanol solutions of 0.5% KC-300 at various dose rates

Dose rate (10^{17} eV/g hr)	$G(Cl^-)$
244	630
126	700
67.7	730
31.2	830
14.6	1200
6.94	1500

Table 3. Dechlorination of PCB's in 0.2 M KOH-2-propanol solutions as a function of concentration of additives

(1)	Biphenyl (M)	0	0.005	0.025	0.1
	Cl^- (M)	0.061	0.055	0.048	0.024
(2)	Acetone (M)	0	0.1	0.3	1.0
	Cl^- (M)	0.059	0.045	0.005	0.002
(3)	Nitrobenzene (M)	0	0.002		
	Cl^- (M)	0.060	0.001		
(4)	*n*-Hexane (M)	0	0.38	0.77	1.5
	Cl^- (M)	0.060	0.052	0.023	0.012

(1): 0.5% KC-300, dose rate 1.6×10^{19} eV/g hr, 1 hr
(2): 0.5% KC-400, dose rate 6.7×10^{18} eV/g hr, 1.5 hr
(3, 4): 0.5% KC-300, dose rate 8.4×10^{17} eV/g hr, 17 hr

increased with a decrease in the dose rate.

The dechlorination has to depend on additives such as electron acceptors or radical scavengers if the initiation step is Reaction (1) and if the chain-propagation steps are Reactions (3) and (4). Table 3 shows the effects of various additives on the chloride-ion concentration. The presence of a small amount of these electron acceptors inhibited the formation of chloride ions, this effect was especially notable in nitrobenzene. The addition of *n*-hexane had no particular effect, though. The reactivity of PCB's towards the solvated electrons has not been established, but it may be at least of the order of $10^9\sim10^{10}$ $M^{-1}s^{-1}$ in view of the facts that the rate constants of hydrated electrons for halogenated benzenes in aqueous solutions were 5×10^8 in monochlorobenzene,[5] $6\sim7\times10^7$ in monofluorobenzene,[5,6] $1\sim2\times10^9$ in difluorobenzene,[6] and $\sim2\times10^{10}$ $M^{-1}s^{-1}$ in tetra and hexafluorobenzene.[6] On the other hand, the rate constants were 5×10^9 for acetone or biphenyl and 3×10^{10} $M^{-1}s^{-1}$ for nitrobenzene.[5] The almost complete suppression of the dechlorination by the presence of these electron acceptors, in the case of nitrobenzene particularly, cannot be explained only by the competition reaction of electrons with the dissociative electron attachment for PCB's, because $G(e^-_{solv})$ was only 0.9~1.0, while $G(H)$, $G(H_2)$, and $G(CH_3)$ were 2.6, 1.27, and 1.06, respectively.[10-12] A simple explanation of the suppression of the dechlorination is to inhibit the charge-transfer reaction in the propagation steps. The inhibition may involve the competition for an intermediate in one of the propagation steps, as has been mentioned by Sherman:[3]

$$-\overset{|}{C}O^- + S \longrightarrow -\overset{|}{C}O + S^- \quad (9)$$

The effect of the irradiation temperature on the dechlorination was studied at ~20 °C, 60 °C, and 90 °C. The samples were irradiated in an oil bath with a regulator, and the temperature was monitored by means of a thermocouple on a recorder. The dechlorination yield at 60 °C showed an increase of ~30%, but there was a small decrease at 90 °C in comparison with the value at ~20 °C. Arai *et al.*[8] has shown that the yield decreased at higher temperatures in alcoholate solutions and that phenylcyclohexadiene instead of biphenyl was the main product at 200 °C. They presumed that a different reaction might occur at higher temperatures, *e.g.*, the decomposition of radicals or addition to a benzene ring.

Dechlorination of PCB's. In irradiating the PCB's in alkaline 2-propanol solutions, each peak height on the gas chromatogram varied with the dose. The gas chromatograms of the KC-300 solutions, irradiated and unirradiated, are shown in Fig. 3. From the analysis with the gas chromatograph-mass spectrometer, it was deduced that the peak numbers of 1, 2-3, 4-6, and 7 in Fig. 3 were identified with mono-, di-, tri-, and tetrachlorobiphenyl respectively. However, no special attention was paid to the concentration of each PCB and isomer. Figure 4 shows the effect of the dose on these peak heights. The yields of chloride ion are also plotted in Fig. 4. As the chloride ion was formed, the tetra- and trichlorobiphenyl decreased quickly, while the di- and monochlorobiphenyl decreased after having

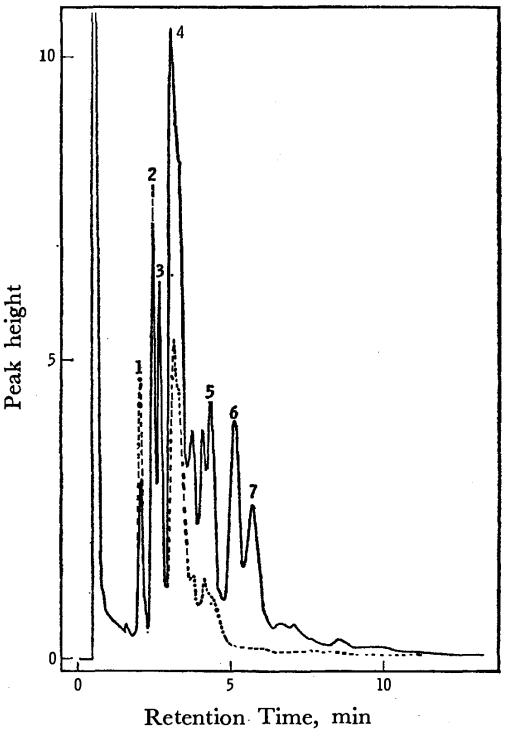

Fig. 3. Gas chromatogram of unirradiated and irradiated 0.2 M KOH-2-propanol solutions of 0.5% KC-300.
solid line: unirradiated solution
dashed line: irradiated solution

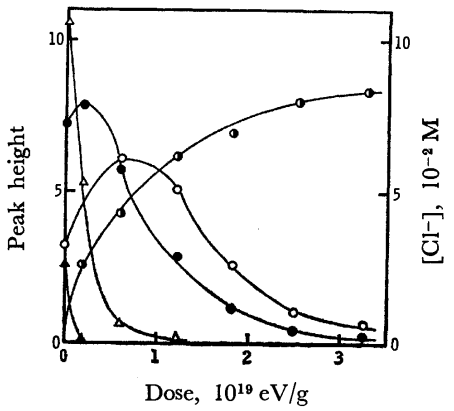

Fig. 4. Effect of irradiation dose on peak heights of chlorinated biphenyls in 0.2 M KOH-2-propanol solutions of 0.5% KC-300.
▲: tetrachlorobiphenyl, △: trichlorobiphenyl
●: dichlorobiphenyl, ○: monochlorobiphenyl
◑: chloride ion
dose rate: 1.1×10^{19} eV/g hr

increased temporarily. The facts indicate that the PCB's were dechlorinated by irradiation to form the less chlorinated biphenyls and were then finally converted to biphenyl *via* monochlorobiphenyl. It is well known that biphenyl is very stable to ionizing radiations. The variation in each peak height of the KC-400 and KC-500 solutions with the dose was similar to that of KC-300, but was a little more complicated.

Reaction of Chain Dechlorination. The radiolytic chain dechlorination of PCB's in the alkaline 2-propanol solution must be similar to the mechanism suggested by Sherman[3,4] for the decomposition of N_2O or of bromo- and iodobenzene in alkaline aliphatic alcohols.

In the dechlorination of PCB's: 1) Chain dechlorination did not occur in neutral alcohols but occurred in alkaline 2-propanol solutions and the $G(Cl^-)$ value depended on the concentration of the hydroxide ion. 2) The amounts of chloride ion and acetone formed, and the decrease in the hydroxide-ion concentration upon irradiation, were almost equal at each radiation dose. 3) The formation of the radical ion ($(CH_3)_2CO^-$) is known in alkaline aqueous solutions of 2-propanol,[13,14] and the rate of Reaction (2) was relatively fast and the pK-value was 12.2.[13] 4) The charge-transfer process was very important in the propagation steps of the chain-dechlorination reactions, because the dechlorination was effectively suppressed in the presence of a small amount of an electron acceptor such as nitrobenzene. 5) The dechlorination from highly chlorinated biphenyls was a predominant reaction in the first stage, and then the lowly chlorinated biphenyls were converted to biphenyl *via* monochlorobiphenyl.

On the basis of the above facts, the radiolytic-chain dechlorination of PCB's in deoxygenated alkaline 2-propanol solutions can be represented as follows:

$$(CH_3)_2CHOH \xrightarrow{\sim\sim} R\cdot,\ e^-_{solv},\ \text{other products} \quad (5)$$

$$C_{12}H_{10-n}Cl_n + e^-_{solv} \longrightarrow \cdot C_{12}H_{10-n}Cl_{n-1} + Cl^- \quad (6)$$

$$R\cdot + (CH_3)_2CHOH \longrightarrow (CH_3)_2\dot{C}OH + RH \quad (7)$$

$$\cdot C_{12}H_{10-n}Cl_{n-1} + (CH_3)_2CHOH \longrightarrow C_{12}H_{10-n+1}Cl_{n-1} + (CH_3)_2\dot{C}OH \quad (8)$$

$$(CH_3)_2\dot{C}OH + OH^- \rightleftharpoons (CH_3)_2CO^- + H_2O^{13)} \quad (9)$$

$$(CH_3)_2CO^- + C_{12}H_{10-n}Cl_n \longrightarrow (CH_3)_2CO + \cdot C_{12}H_{10-n}Cl_{n-1} + Cl^- \quad (10)$$

As Reactions (8), (9), and (10) proceed, n decreases to $n-1$, $n-2$, ···, and finally biphenyl is produced:

$$(CH_3)_2CO^- + C_{12}H_9Cl \longrightarrow (CH_3)_2CO + \cdot C_{12}H_9 + Cl^- \quad (11)$$

$$\cdot C_{12}H_9 + (CH_3)_2CHOH \longrightarrow C_{12}H_{10} + (CH_3)_2\dot{C}OH \quad (12)$$

The rate of the dechlorination, on the other hand, decreased with the dose, as is shown in Figs. 1, 2, and 4. This can be accounted for by the following reactions: 1. An electron acceptor such as biphenyl was formed. Indeed, the presence of a small amount of biphenyl decreased the $G(Cl^-)$. 2. The concentration of the hydroxide ion decreased with the dose. 3. Highly chlorinated PCB's changed into lowly chlorinated PCB's. The rate constant of Reaction (10) in the lowly chlorinated compounds may be lower than that in the highly chlorinated compounds, because the dechlorination yield of trichlorobenzene in the alkaline 2-propanol was higher than those of di- and monochlorobenzene.[15]

Assuming the initiation by Reactions (5)—(9), the propagation by (8)—(10), and a biomlecular termination by Reaction (13)[3];

$$2(CH_3)_2CO^- \xrightarrow[(CH_3)_2CHOH]{} (CH_3)_2CO + 2(CH_3)_2CHO\cdot \quad (13)$$

the initial yield of the dechlorination is given by Expression (I):

$$G(Cl^-) = G_e + k_{10}[\text{PCB's}]\{(G_e+G_R)/k_{13}\times D]\}^{1/2} \quad (I)$$

where G_e: yield of scavengable electrons by PCB's
G_R: yield of the radical R
D: dose rate

A straight line is obtained in a plot of $G(Cl^-)$ *vs.* $(1/D)^{1/2}$ as is shown in Fig. 5. The bimolecular reaction (13) should be very important in the chain dechlorination; however, the positive intercept at $(1/D)^{1/2}=0$ may

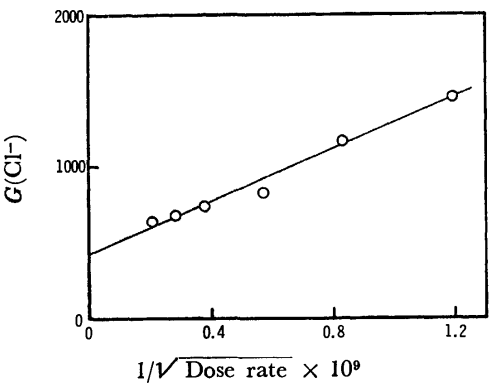

Fig. 5. Dechlorination yield as a function of dose rate.

Table 4. Dechlorination yields of PCB's in various alcohol solutions of 0.2 M KOH-0.5% KC-300

Solvent	$G(Cl^-)$	pK[13]
Methanol	4.2	10.7
Ethanol	4.9	11.6
1-Propanol	3.2	11.5
2-Propanol	700	12.2
n-Butanol	6.5	11.5
i-Butanol	9.0[a]	11.6
sec-Butyl alcohol	40	
t-Butyl alcohol	4.9	b)

Dose rate: 1.2×10^{19} eV/g hr. a) Dose rate 1.4×10^{18} eV/g hr. b) No observable dissociations up to pH 13.5.[14]

indicate an additional termination process.

Dechlorination of PCB's in Other Alcohols. It was found that the radiolytic dechlorination of PCB's in the alkaline 2-propanol solutions occurred efficiently. We studied whether a similar reaction proceeded in other simple aliphatic alcohols. The $G(Cl^-)$ values in various alcohols containing 0.5% KC-300 and 0.2 M KOH are shown in Table 4. The $G(Cl^-)$ in the solution of *sec*-butanol was relatively high, but it was only 4~9 in the other alcohols.

In alkaline alcohol solutions, the G(dechlorination) value of carbon tetrachloride were 270, 62, and 7.7 in 2-propanol, 1-propanol, and *tert*-butyl alcohol respectively.[1] The magnitude in 1-propanol was indicative of a chain reaction. Moreover, the $G(Cl^-)$ of DDT in neutral alcohols showed the same tendency.[2] The order of decreasing yield paralleled the order of increased C–H bond strength of the alcohols.

In our experiments, the chain-dechlorination reaction did not involve any alcohols other than 2-propanol and *sec*-butyl alcohol. It is known that in the pulsed radiolysis of alkaline aqueous solutions of aliphatic alcohol, the α-hydroxyl radicals dissociate to the transient RO^- and that the pK-value of the reversible reaction (9) in 2-propanol is 12.2, while the others are lower, as is shown in Table 4.[13,14] Therefore, the equilibrium in Reaction (9) apparently shifts to the right-hand side except for the case of *sec*- and *tert*-butyl alcohol. The fact that PCB's in alcoholic solutions other than 2-propanol did not undergo the radiolytic chain dechlorination may be attributed to either the fact that the electron-transfer process to PCB's from RO^- is inefficient or to the fact that the PCB radical cannot abstract the α-hydrogen of alcohols. We cannot decide which is the case. The 2-propoxide radical ion may release an electron more easily than the ions of other alcohols: also, the bond strength of α-hydrogen in 2-propanol is smaller than that of methanol, ethanol, 1-propanol, *n*-butanol, and isobutyl alcohol.

The authors are indebted to Mr. Nobuo Ito, Tokyo Metropolitan Research Institute for Environmental Protection, for his help in the analysis using a gas chromatograph-mass spectrometer.

References

1) C. Radlowski and W. V. Sherman, *J. Phys. Chem.*, **74**, 3043 (1970).
2) R. Evans, E. Nesyto, C. Radlowski, and W. V. Sherman, *ibid.*, **75**, 2762 (1971).
3) W. V. Sherman, *ibid.*, **71**, 1965 (1967).
4) W. V. Sherman, *ibid.*, **72**, 2287 (1968).
5) M. Anber and P. Neta, *Int. J. Appl. Radiat. Isotopes*, **18**, 493 (1967).
6) R. Koster and K. D. Asmus, *J. Phys. Chem.*, **77**, 749 (1973).
7) T. Sawai and Y. Shinozaki, *Chem. Lett.*, **1972**, 865.
8) S. Arai, M. Matsui, J. Moriguchi, and M. Imamura, *Reports Inst. Phys. Chem. Res.*, **48**, 185 (1972).
9) "Scott's Standard Methods of Chemical Analysis," ed. by N. H. Furman, D. Van Nostrand, New Jersey (1962), p. 332.
10) D. E. Adams, J. H. Baxendale, and R. D. Sedgwick, *J. Phys. Chem.*, **63**, 854 (1959).
11) M. C. Sauer, S. Arai, and L. M. Dorfman, *J. Chem. Phys.*, **43**, 708 (1965).
12) W. V. Sherman, *J. Phys. Chem.*, **70**, 667 (1966).
13) K. D. Asmus, A. Hengline, A. Wigger, and G. Beck, *Ber. Bunsenges. Phys. Chem.*, **70**, 756 (1966).
14) M. Simic, P. Neta, and E. Hayon, *J. Phys. Chem.*, **73**, 3794 (1969).
15) Unpublished result.

Vibrational Energy Transfer of Some X_2CO-type Molecules on Collision with Argon

Yoshiro YONEZAWA* and Takayuki FUENO

Department of Chemistry, Faculty of Engineering Science, Osaka University, Toyonaka, Osaka 560

(Received February 5, 1974)

Vibrational excitation of X_2CO-type polyatomic molecules (X=F, Cl, Br, and H) on collision with an argon atom at temperatures 1000—3000 K was treated by the SSH-Tanczos method with a more tractable formula of average vibrational factor. Bending modes are more easily excited than bond-stretching modes in carbonyl halides. Excitation of the carbonyl stretching mode, the most difficult to occur in T–V process, becomes realizable when coupled with other modes to satisfy the near-resonance conditions.

Energy transfer involved in molecular collision is of importance in chemical reactions. Theories have been developed considerably for diatomic molecules[1-6] but not much for polyatomic molecules. An approximation method was given by Schwartz, Slawsky, and Herzfeld (SSH[4,5]), and Tanczos.[6] Though it is based on the two-state distorted-wave approximation by the harmonic oscillator model, useful results can be deduced for the energy transfer process of vibrationally excited molecules.

We have applied this method to the vibrational excitation of X_2CO-type polyatomic molecules (X=F, Cl, Br, and H) on collision with an argon atom. From the results, the kinetic data of the thermal decomposition of carbonyl fluoride reported by Modica[7] are discussed.

Method of Calculation

According to the SSH theory,[4,5] the probability that a pair of molecules originally in vibrational states i_a and i_b will arrive at vibrational states f_a and f_b after a collision at temperature T K is given by

$$\langle P(a,b)\rangle = \tilde{p}\,p_0(a)p_0(b)V^2(a)V^2(b) \times 8\sqrt{\frac{\mu}{2kT}}\exp(\varepsilon_0/kT)\left(\frac{8\pi^3\mu\Delta E}{h^2}\right)^2 \times \int_0^\infty F(u)\mathrm{d}u \quad (1)$$

with

$$F(u) = \frac{u}{\alpha^4}(r_c/r_0)^2\exp\left(-\frac{\mu u^2}{2kT}\right)\frac{\exp(H-H')}{[1-\exp(H-H')]^2} \quad (2)$$

and

$$H = \frac{4\pi^2\mu u}{\alpha h}, \quad H' = \frac{4\pi^2\mu v}{\alpha h} \quad (3)$$

where μ is the reduced mass of the collision pair which approach each other with an effective relative velocity u and recede with a velocity v; ΔE is the net total change in translational energy involved during the collision, *i. e.*,

$$\Delta E = h\nu_a(i_a-f_a) + h\nu_b(i_b-f_b) = \mu(v^2-u^2)/2\ ; \quad (4)$$

ε_0 is the minimum value of the Lennard-Jones potential

$$\varepsilon(r) = 4\varepsilon_0[(r/r_0)^{12} - (r/r_0)^6]\ ; \quad (5)$$

α is an intermolecular force constant in reciprocal length units, for the repulsive exponential potential function

$$V(r) = V_0\exp(-\alpha r) - \varepsilon_0 \quad (6)$$

evaluated so as to best fit Eq. (5) at $r=r_0$ and $r=r_c$, where r_c is the distance between molecular centers at the classical turning point for each u; p_0 is the geometrical factor required for the orientation consideration, $p_0(i_a\to f_a)=2/3$ being assumed herewith, and $\tilde{p}$ is a cross-section factor which is approximated by

$$\tilde{p} = 1.364/(1+1.1\,\varepsilon_0/kT) \quad (7)$$

The average vibrational factor V^2 in Eq. (1) for polyatomic molecules has been given by Tanczos[6] as follows:

$$V^2(a) = V^2(i_a\to i_a\pm1) = \frac{h\left(i_a+\frac{1}{2}\pm\frac{1}{2}\right)}{8\pi^2\nu_a}\frac{(\alpha^*)^2}{N_s}\sum_s\frac{A_{sa}^2}{m_s} \quad (8)$$

where s denotes the atom to be taken into account in the breathing sphere model, N_s the number of atoms, $N_s=4$ being assumed herewith, m_s an atomic mass, and A_{sa} the Cartesian displacement coefficient of s in the normal vibration Γ_a whose vibrational frequency is ν_a. α^* is evaluated at $u=u^*$, the most favorable velocity for the vibrational transition involving a particular value of ΔE:

$$\alpha^* = \frac{1}{r_0-r_c}\ln\left(1+\frac{E_m}{\varepsilon_0}\right) \quad (9)$$

where

$$E_m = \mu(u^*)^2/2 = kT\left[\frac{2\pi^4\mu(\Delta E)^2}{(\alpha^*)^2h^2kT}\right]^{1/3} \quad (10)$$

Following the method of a normal coordinate analysis by Stretton,[8] we can express the summation in Eq. (8) in a compact form as follows:

$$\sum_s A_{sa}^2/m_s = (\tilde{L}_X L_X)_{a,a} \quad (11)$$

where L_X is a transformation matrix between the orthogonal coordinate X and normal coordinate Q, and the product $(\tilde{L}_X L_X)_{a,a}$ is to be taken over the matrix elements corresponding to Γ_a only. L_X can be determined by means of the GF matrix treatment of molecular vibrations.[9]

$$L_X = M^{-1}\tilde{B}L_G\Lambda_G^{-1/2}L_c \quad (12)$$

* Present Address: Department of Industrial Chemistry, Faculty of Engineering, Kyoto University, Yoshida, Kyoto 606.

where definitions of the matrices, M^{-1}, $\tilde{B}$, L_G, $\Lambda_G^{-1/2}$, and L_c are the same as in Ref. 9.

For the sake of convenience, we introduce the average amplitude factor $Y(X_s;\Gamma_a)$ for atom s in Γ_a:

$$Y(X_s;\Gamma_a) = (\tilde{L}_X)_{a,x_s}(L_X)_{x_s,a} + (\tilde{L}_X)_{a,y_s}(L_X)_{y_s,a} + (\tilde{L}_X)_{a,z_s}(L_X)_{z_s,a} \quad (13)$$

The right-hand side of Eq. (11) can thus be written as

$$(\tilde{L}_X L_X)_{a,a} = \sum_s Y(X_s;\ \Gamma_a) \quad (14)$$

We analyzed the in-plane vibrational motion of carbonyl halides and formaldehyde by using the potential function of Miyazawa.[10] We have omitted the mode Γ_6 (B_2 symmetry) throughout the calculation. Since it is the only mode corresponding to the out-of-plane motion, it cannot be mixed with the other five modes. Its omission does not affect our calculations. Molecular geometries were obtained from the literature.[11] Relevant Urey-Bradley force constants are summarized in Table 1.[12,13]

Vibrational transition probabilities of those molecules by translational-vibrational (T–V) or vibrational-vibrational (V–V) process on collision with an argon atom at T=1000—3000 K have been calculated by the above method. Relevant constants of the Lennard-Jones potentials for the collision pairs are given in Table 2. Calculations were carried out on a FACOM Computer at the Kyoto University Computation Center.

Table 1. Urey-Bradley force constants of X_2CO molecules in md/Å[a]

Molecule	Force constants					
	K_{CX}	K_{CO}	H_{XX}	H_{OX}	F_{OX}	F_{XX}
F_2CO	4.528	12.85	0.450	0.294	1.578	1.120
Cl_2CO	1.99	12.61	0.11	0.218	0.860	0.523
Br_2CO	1.565	12.83	0.060	0.189	0.631	0.528
H_2CO	3.842	11.044	0.349	0.338	0.88	0.0

a) The symbols K, H, and F denote the force constants for the bond-stretchings, bond-bendings, and nonbond interactions, respectively. The coefficients for the energy terms linear with respect to displacements were all assumed to be one-tenth the force constants.

Table 2. Lennard-Jones potential parameters[a] and reduced masses of the collision pairs

Collision pair	r_0 (Å)	ε_0/k (K)	μ (10^{-23} g)
F_2CO-Ar	5.331	117.8	4.166
Cl_2CO-Ar	5.562	210.4	4.763
Br_2CO-Ar	5.638	253.9	5.448
H_2CO-Ar	4.988	116.8	2.869
CO-Ar	3.504	116.8	2.756

a) Potential parameters of carbonyl halides-argon systems were approximated by

$r_0=[r_0(\text{CO-CO})+r_0(X_2-X_2)+r_0(\text{Ar}-\text{Ar})]/2$

$\varepsilon_0=\sqrt{\varepsilon_0(X_2-X_2)\varepsilon_0(\text{Ar}-\text{Ar})}$.

Parameter values of r_0(M−M) and ε_0(M−M) were taken from J. O. Hirschfelder, C. F. Curtiss, and R. B. Bird, "Molecular Theory of Gases and Liquids," John Wiley & Sons, New York, N. Y. (1954), Appendix.

Results and Discussion

Fundamental frequencies and average amplitude factors of all the molecules are summarized in Table 3.

Table 3. Fundamental frequencies[a] and average amplitude factors[b]

Molecule		$Y(X_s;\Gamma_a)$				
		Γ_1	Γ_2	Γ_3	Γ_4	Γ_5
F_2CO	$\bar{\nu}$	1925	968	580	1228	622
		(1928)	(965)	(584)	(1249)	(626)
	C	0.322	0.052	0.033	0.373	0.032
	O	0.129	0.111	0.043	0.003	0.156
	F	0.001	0.094	0.129	0.038	0.082
Cl_2CO	$\bar{\nu}$	1819	561	282	843	435
		(1827)	(567)	(285)	(849)	(440)
	C	0.297	0.107	0.033	0.429	0.000
	O	0.150	0.128	0.035	0.019	0.213
	Cl	0.000	0.037	0.071	0.007	0.036
Br_2CO	$\bar{\nu}$	1819	427	180	754	348
		(1828)	(425)	(181)	(757)	(350)
	C	0.295	0.150	0.021	0.438	0.018
	O	0.152	0.168	0.022	0.034	0.262
	Br	0.000	0.009	0.034	0.001	0.010
H_2CO	$\bar{\nu}$	1742	2805	1483	2865	1242
		(1744)	(2780)	(1503)	(2874)	(1280)
	C	0.262	0.027	0.009	0.044	0.108
	O	0.122	0.000	0.053	0.000	0.028
	H	0.437	2.802	2.488	2.700	2.097

a) Calculated and observed wavenumbers $\bar{\nu}$ in cm^{-1}. The experimental values for carbonyl halides (taken from Ref. 12) and formaldehyde (I. C. Hisatsune and D. F. Eggers, Jr., *J. Chem. Phys.*, **23**, 487 (1955)) are given in parentheses. b) $Y(X_s;\Gamma_a)$ given in units of 10^{23} g^{-1}.

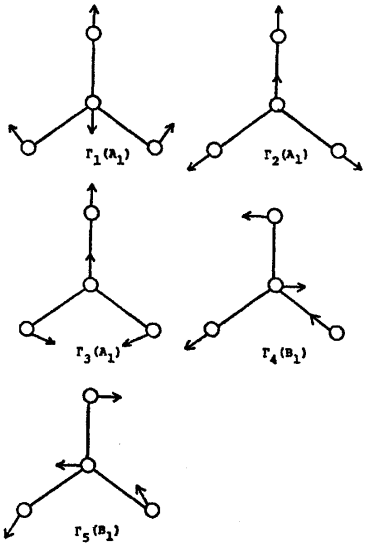

Fig. 1. The normal modes of F_2CO in Cartesian displacements.
The magnitude of the displacement vectors are arbitrary.

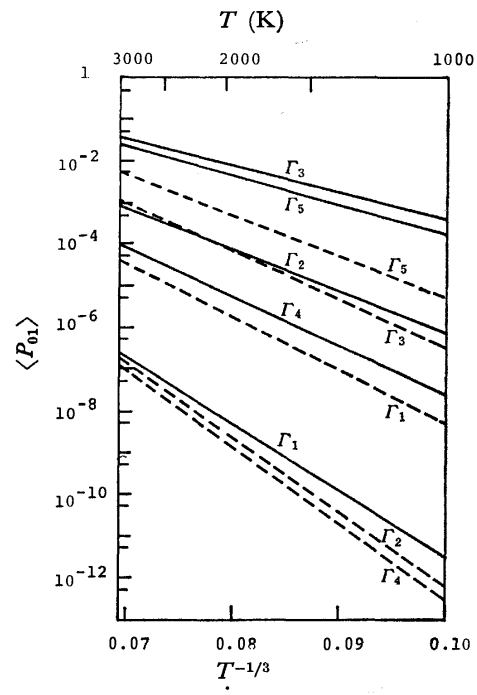

Fig. 2. Temperature dependences of the T-V vibrational transition probabilities, $\langle P_{01}\rangle$, of all the normal modes of F_2CO (solid line) and H_2CO (broken line).

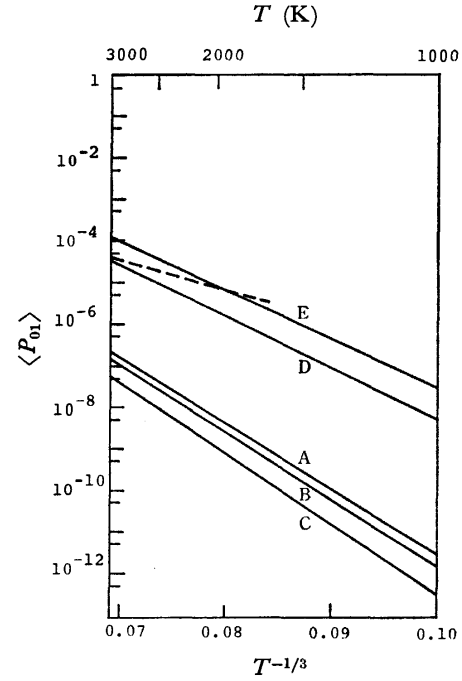

Fig. 3. Temperature dependences of the T-V vibrational transition probabilities, $\langle P_{01}\rangle$, of the carbonyl stretching mode (Γ_1) of X_2CO. The broken line represents the values calculated for CO from Eq. (15) with the aid of

$\langle P_{01}\rangle = \exp(h\nu/kT)/\{\tau Z_c[1-\exp(-h\nu/kT)]\}$

where Z_c denotes the average number of collisions which a CO molecule experiences per second under 1 atmospheric pressure.

A, F_2CO; B, Cl_2CO; C, Br_2CO; D, H_2CO; E, CO.

The normal modes of carbonyl fluoride in Cartesian displacements are represented in Fig. 1. There are three A_1 modes: carbonyl stretching Γ_1, symmetric CX stretching Γ_2, XCX bending Γ_3, and two B_1 modes: asymmetric CX stretching Γ_4, CO rocking Γ_5. It can be seen that vibrational wave numbers increase in the order $\bar{\nu}_3<\bar{\nu}_5<\bar{\nu}_2<\bar{\nu}_4<\bar{\nu}_1$ for carbonyl halides and in $\bar{\nu}_5<\bar{\nu}_3<\bar{\nu}_1<\bar{\nu}_2\leqq\bar{\nu}_4$ for formaldehyde.

Transition probabilities $\langle P_{01}\rangle$ for the 0—1 excitation of the various normal modes of carbonyl fluoride and formaldehyde by T-V process are plotted as functions of $T^{-1/3}$ in Fig. 2. As was the case with the vibrational excitation of diatomic molecules studied by Landau-Teller,[14] all the $\langle P_{01}\rangle$ are proportional to $\exp(-T^{-1/3})$. Transition probabilities of X_2CO molecules increase in the reverse order to that of the magnitude of vibrational wave numbers, *viz.*, $\langle P_{01}(\Gamma_1)\rangle<\langle P_{01}(\Gamma_4)\rangle<\langle P_{01}(\Gamma_2)\rangle<\langle P_{01}(\Gamma_5)\rangle<\langle P_{01}(\Gamma_3)\rangle$ for carbonyl halides, and $\langle P_{01}(\Gamma_4)\rangle\leqq\langle P_{01}(\Gamma_2)\rangle<\langle P_{01}(\Gamma_1)\rangle<\langle P_{01}(\Gamma_3)\rangle<\langle P_{01}(\Gamma_5)\rangle$ for formaldehyde. The results are due primarily to the decrease of ΔE in these orders.

Transition probabilities for the 0—1 excitation of carbonyl stretching modes (Γ_1) of carbonyl halides, formaldehyde, and carbon monoxide are shown in Fig. 3. As the vibrational wave number of carbon monoxide, we have assumed 2143 cm^{-1}.[13] Millikan *et al.* have observed that, in carbon monoxide–argon system, the vibrational relaxation time τ over 1700—3000 K is expressed by

$$\ln(p\tau) = \gamma T^{-1/3} + \delta \qquad (15)$$

with $\gamma=182$ and $\delta=-22.4$, where p is in atm, τ in second, and T in K.[15,16] $\langle P_{01}\rangle$ of carbon monoxide obtained from this equation is also given in Fig. 3. The two values agree with each other especially near 2000 K. The $\langle P_{01}\rangle$ value for carbon monoxide is larger than the values for carbonyl halides by a few order of magnitude, despite its larger value of ΔE.

The average vibrational factors $V^2(0\rightarrow1)$ of the Γ_1 mode are given in Table 4. The V^2 values for carbon monoxide and formaldehyde are several times greater than those for carbonyl halides. This is ascribable to the larger values of α^* and smaller reduced masses of this mode for these two molecules. The reduced mass of the carbonyl stretching mode is indicated by $[(\tilde{L}_X L_X)_{\Gamma_1,\Gamma_1}]^{-1}$ for carbonyl halides as well as formaldehyde and $[m_C m_O/(m_C+m_O)]$ for carbon monoxide, where m_C and m_O denote the mass of the carbon and oxygen atoms, respectively.

TABLE 4. AVERAGE VIBRATIONAL FACTORS $V^2(0\rightarrow1)$ OF THE CARBONYL STRETCHING MODE

Molecule	$V^2(0\rightarrow1)\times10^3$				
	T=1000	1500	2000	2500	3000 K
F_2CO	2.01	1.99	1.99	1.98	1.98
Cl_2CO	1.96	1.94	1.93	1.92	1.92
Br_2CO	1.92	1.90	1.88	1.88	1.87
H_2CO	7.08	7.02	6.99	6.97	6.96
CO	9.30	9.22	9.18	9.15	9.13

However, with V^2 alone we cannot account for the large $\langle P_{01} \rangle$ value for carbon monoxide. An even more important contribution to $\langle P_{01} \rangle$ is derived from the reduced mass μ involved in Eq. (2); the $F(u)$ becomes greater in magnitude as the reduced mass decreases. The relatively large $\langle P_{01} \rangle$ for formaldehyde can be interpreted in the same way. All the results emphasize the concurrent importance of small ΔE and μ as well as large V^2 in order that vibrational energy transfer proceeds more effectively. The intramolecular motion of halogen atom in carbonyl halides hardly affects the vibrational excitation of carbonyl stretching mode; the amplitude factors of the halogen atoms in Γ_1 are negligibly small as compared with those for the carbon and oxygen atoms (Table 3).

Transition probabilities were calculated for the 0—1 excitation of carbonyl stretching mode by V-V processes coupled with the 1—0 de-excitation of the other modes $\langle P_{01}^{10} \rangle$, with the 2—0 de-excitation of the Γ_2 mode $\langle P_{01}^{20} \rangle$, and with the 1—0 de-excitation of both the Γ_3 and Γ_5 modes $\langle P_{10}^{01,10} \rangle$. The results for carbonyl fluoride are plotted as functions of $T^{-1/3}$ in Fig. 4.

We see that the transition probabilities $\langle P_{01}^{10} \rangle$ increase in the reverse order to that of the magnitude of ΔE, *viz.*, $\langle P_{01}^{10}(\Gamma_1-\Gamma_3) \rangle < \langle P_{01}^{10}(\Gamma_1-\Gamma_5) \rangle < \langle P_{01}^{10}(\Gamma_1-\Gamma_2) \rangle < \langle P_{01}^{10}(\Gamma_1-\Gamma_4) \rangle$. A similar trend is also found in the case of formaldehyde: $\langle P_{01}^{10}(\Gamma_1-\Gamma_4) \rangle \leqq \langle P_{01}^{10}(\Gamma_1-\Gamma_2) \rangle < \langle P_{01}^{10}(\Gamma_1-\Gamma_5) \rangle < \langle P_{01}^{10}(\Gamma_1-\Gamma_3) \rangle$. Likewise, $\langle P_{01}^{20} \rangle$ is far larger than the corresponding $\langle P_{01} \rangle$ and $\langle P_{01}^{10} \rangle$ in the temperature range of our study. However, $\langle P_{01}^{10,10} \rangle$ is not so large as $\langle P_{01}^{20} \rangle$.

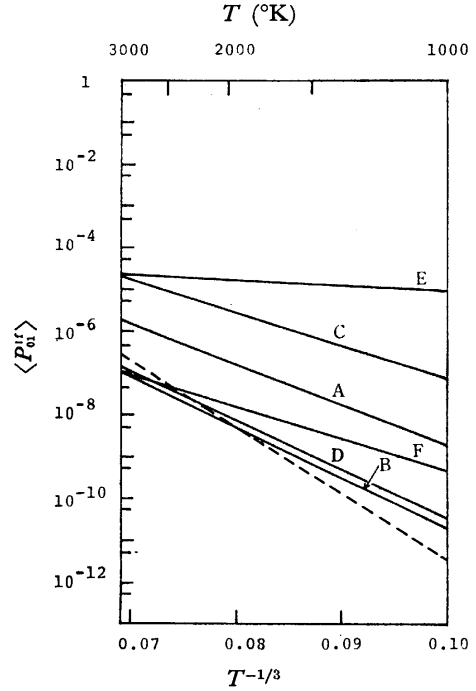

Fig. 4. Temperature dependences of the V-V vibrational transition probabilities, $\langle P_{01}^{10} \rangle$, $\langle P_{01}^{20} \rangle$, and $\langle P_{01}^{10,10} \rangle$ of F_2CO.
A, $\langle P_{01}^{10}(\Gamma_1-\Gamma_2) \rangle$; B, $\langle P_{01}^{10}(\Gamma_1-\Gamma_3) \rangle$; C, $\langle P_{01}^{10}(\Gamma_1-\Gamma_4) \rangle$; D, $\langle P_{01}^{10}(\Gamma_1-\Gamma_5) \rangle$; E, $\langle P_{01}^{20}(\Gamma_1-\Gamma_2) \rangle$; F, $\langle P_{01}^{10,10}(\Gamma_1-\Gamma_3,\ \Gamma_5) \rangle$.
The broken line indicates $\langle P_{01} \rangle$ for the T-V process.

In short, the transition probability for the 0—1 excitation of Γ_1 at lower temperature markedly increases on near-resonance coupling with another mode. Thus, it is probable that under the usual experimental conditions, vibrational excitation of a normal mode is caused mainly by a V-V process. At higher temperature ($T > 2000$ K), however, none of the V-V processes are more efficient than the T-V process.

Modica[7] has studied the kinetics of shock-tube decomposition of carbonyl fluoride in argon at 2200—3600 K:

$$F_2CO + Ar \longrightarrow FCO + F + Ar.$$

He concluded that in the transition state the bending modes (Γ_3, Γ_5, and Γ_6) are considerably deformed in constrast to the relatively insensitive bond-stretching modes (Γ_1, Γ_2, and Γ_4). Our present calculations show the relative ease of the vibrational excitation of Γ_3 and Γ_5. The Γ_6 mode should also be as easily excited as these two modes because of its small vibrational wave number (774 cm^{-1}).[12] The decomposition reaction might proceed through the V-V energy transfer from these bending modes to the C-F bond-stretching modes.

References

1) D. Rapp and T. Kassal, *Chem. Revs.*, **69**, 61 (1969).
2) Y. Yonezawa and T. Fueno, This Bulletin, **44**, 2976 (1971).
3) K. F. Herzfeld and T. A. Litovitz, "Absorption and Dispersion of Ultrasonic Waves", Academic Press, New York, N. Y. (1959).
4) R. N. Schwartz, Z. I. Slawsky, and K. F. Herzfeld, *J. Chem. Phys.*, **20**, 1591 (1952).
5) R. N. Schwartz and K. F. Herzfeld, *ibid.*, **22**, 767 (1954).
6) F. I. Tanczos, *ibid.*, **25**, 439 (1956).
7) A. P. Modica, *J. Phys. Chem.*, **74**, 1194 (1970).
8) J. L. Stretton, *Trans. Faraday Soc.*, **61**, 1053 (1965).
9) H. Takahashi, "Jikken Kagaku Koza," Supplement **10**, edited by T. Shimanouchi, The Chemical Society of Japan, Maruzen, Tokyo (1964), p. 465.
10) T. Miyazawa, *Nippon Kagaku Zasshi*, **74**, 915 (1953).
11) "Table of Interatomic Distances and Configuration in Molecules and Ions," ed. by A. D. Mitchell, The Chemical Society, London (1958).
12) J. Overend and J. R. Scherer, *J. Chem. Phys.*, **32**, 1296 (1960).
13) S. Mizushima and T. Shimanouchi, "Sekigaisen Kyushu to Raman Kouka," Kyoritsu Shuppan, Tokyo (1957), Appendix.
14) L. Landau and E. Teller, *Physik. Z. Sowjetunion*, **11**, 18 (1937).
15) W. J. Hooker and R. C. Millikan, *J. Chem. Phys.*, **38**, 214 (1963).
16) a) R. C. Millikan, *ibid.*, **38**, 2855 (1963). b) R. C, Millikan, *ibid.*, **40**, 2594 (1964).

Magnetic Properties of Nonbenzenoid Aromatic Hydrocarbons

Hiroyuki YAMAGUCHI* and Takeshi NAKAJIMA
Department of Chemistry, Tohoku University, Sendai 980
(Received March 18, 1974)

The magnetic susceptibilities for nonbenzenoid aromatic hydrocarbons have been examined by using the modified London-Hoarau method in the framework of the Wheland-Mann-type SCF MO approximation. By taking into account the double-bond fixation quite common in these molecules, we obtained a general agreement between the calculated results and the available experimental values.

The diamagnetic delocalization susceptibility of a ring π-electron system, attributable to induced ring currents in its π-electron network, is one of the important quantities indicative of π-electron delocalization. A quantum-mechanical theory for the diamagnetic delocalization susceptibility was first developed by London.[1] His method is based on the Hückel LCAO MO theory and has extensively been used for a variety of aromatic hydrocarbons.[2,3] The calculated diamagnetic anisotropies for benzenoid hydrocarbons are usually in quite good agreement with the experimental values. On the other hand, the direct application o London's technique to nonbenzenoid aromatic hydrocarbons[4,5] often brings about unsatisfactory results in view of the recently-reported experimental data.[15]

It is probable that such unsatisfactory results arise mainly from the employment of molecular orbitals obtained using the simple Hückel MO theory which does not take into account the double-bond fixation quite common in nonbenzenoid hydrocarbons and, hence, proves to be less reliable when applied to these molecules, and partly from the shortcomings inherent in London's original theory. Hoarau[6] has made improvements on the London theory by refining the calculation of the gauge factors.

It is the purpose of this paper to calculate the magnetic susceptibilities of several nonalternant hydrocarbons by using the modified London-Hoarau method in the framework of the Wheland-Mann-type SCF MO approximation.[7] This approximation allows us to obtain equilibrium geometrical structures with respect to the C–C bond lengths of these molecules.

Method of Calculation

London's theory is not necessarily related to the simple Hückel MO approximation. It can naturally be extended to the Wheland-Mann-type SCF LCAO MO method.[7] In this method, the Coulomb integral, α_μ, and the resonance integral, $\beta_{\mu\nu}$, are given by the following formulas, respectively:

$$\alpha_\mu = \alpha_0 + \omega(1-q_\mu)\beta_0 \quad (1)$$

where q_μ is the electron density and ω is taken to be unity, and:

$$\beta_{\mu\nu} = \beta_0 \exp[a(1.397-r_{\mu\nu})] \quad (2)$$

where $r_{\mu\nu}$ is the bond length and is correlated with the bond order, $p_{\mu\nu}$, by Eq. (3):[8]

$$r_{\mu\nu} = 1.520 - 0.186p_{\mu\nu} \quad (3)$$

The value of a in Eq. (2) is taken to be 4.4 Å^{-1}. This value was determined so as to reproduce the observed C–C bond lengths of butadiene[9] and naphthalene[10] and the dipole moments of pentafulvene[11] and heptafulvene.[12]

Improving the correlation between the experimental and calculated relative anisotropies of diamagnetic susceptibility, Hoarau proposed an expression for the molar susceptibility which includes a dependence on the delocalization energy, DE:[7]

$$\Delta K = \Delta K_L/3 + A\times 10^{-18}DE \quad (4)$$

where ΔK_L is the molar susceptibility according to London's theory.[1] The A parameter was fitted to ensure the best agreement with the experimental results; the value of 0.776 for the case of Hückel basis was found. Nakajima and Kohda[13] proposed a different value for A, 0.940. However, in both papers rather inaccurate experimental values of diamagnetic susceptibility were used. Reconsidering their procedure by the use of the more recent experimental values of the diamagnetic susceptibilities given in Ref. 14, we obtain a different least-squares fit:**

$$\Delta K = \Delta K_{SCF}/3 + 0.359\times 10^{-18}DE \quad (5)$$

where ΔK_{SCF} is the magnetic susceptibility calculated by using the Wheland-Mann-type SCF LCAO MO basis. Equation (5) can be used to calculate the magnetic susceptibilities of several nonbenzenoid aromatic hydrocarbons (Fig. 1).

Results and Discussion

In Table 1, the theoretical diamagnetic susceptibilities, ΔK, for nonalternant hydrocarbons are listed (in units of $\Delta K_{benzene}$) and compared with the experimental exaltations (in units of $\Lambda_{benzene}$).[15] The theoretical values are in good agreement with the experimental data, except for the case of aceheptylene (IX), whose experimental exaltation has been reported, unbelievably, to be zero. Recently, using the coupled perturbed Hartree-Fock method, Mikami *et al.*[16] have calculated the magnetic susceptibility of IX. The calculated value is almost the same as that obtained in this paper. It is, therefore, hoped that the experimental value of this molecule should be re-examined. In pentalene (I), heptalene (II), *s*-indacene (III), py-

* Present address: Department of Chemistry, Faculty of Science, Kumamoto University, Kurokami-machi, Kumamoto 860.

** We have re-examined the A value using the experimental values of benzene, naphthalene, anthracene, naphthacene, phenanthrene, chrysene, pyrene, perylene, triphenylene, and coronene, which do not exhibit any significant bond-length variation.

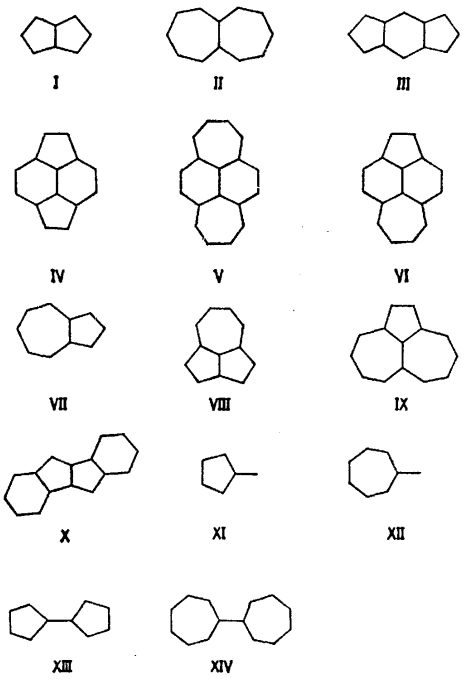

Fig. 1. Nonbenzenoid aromatic hydrocarbons.

TABLE 1. DIAMAGNETIC SUSCEPTIBILITIES OF NONALTERNANT HYDROCARBONS

Molecule	Theoretical $\Delta K/\Delta K_{benzene}$	Experimental $\Lambda/\Lambda_{benzene}$
Pentalene (I), D_{2h}	−1.35	
Pentalene (I), C_{2h}	−0.41	
Heptalene (II), D_{2h}	−4.41	
Heptalene (II), C_{2h}	−0.61	−0.45[a]
s-Indacene (III), D_{2h}	−0.88	
s-Indacene (III), C_{2h}	−0.38	
Pyracylene (IV)	−0.40	
Dipleiadiene (V)	−0.34	
Acepleiadylene (VI)	3.92	3.87[a]
Azulene (VII)	2.04	2.16[a]
Aceazulylene (VIII)	2.14	2.18[a,c]
Aceheptylene (IX)	1.72	0.0[a,d]
Dibenzopentalene (X)	1.10	1.00,[a,d] 0.87[b,d]
Fulvene (XI)	0.10	0.08[a]
Heptafulvene (XII)	0.16	
Fulvalene (XIII)	0.075	
Heptafulvalene (XIV)	0.18	0.15[a]

a) Ref. 15. b) Ref. 6. c) The value for a dimethylphenyl derivative. d) The value for a dimethyl derivative.

racylene (IV), and dipleiadiene (V), the last of which is yet unknown, the magnetic susceptibilities are predicted to be negative. Such an anomalously-reduced diamagnetism may be interpreted as an induced paramagnetism.[13,17–19]

Molecules I, II, and III are predicted to possess two equilibrium geometrical structures, one belonging to the molecular symmetry, D_{2h}, and the other to C_{2h}.[20] In the former, the C–C bond lengths are quite equalized, while in the latter there is a considerable double-bond fixation. The equilibrium structures with the reduced-molecular symmetry (C_{2h}) were obtained by taking a distorted C nuclear arrangement with the C_{2h} symmetry as the starting geometry for the iterative calculation. It has been shown that, as a result of the *pseudo*-Jahn-Teller effect, in such a case the structure with reduced symmetry is energetically more stable than the fully-symmetrical one. We calculated the magnetic susceptibilities for two molecular symmetries of these molecules. It can be seen that the double-bond fixation brings about a considerable decrease in the paramagnetic susceptibility. The good agreement with theory and experiment in heptalene (II) provides further support for the molecular-symmetry reduction occurring in this molecule and in Molecules I and III as well.

In Molecules IV, V, and VI, it is predicted that the calculated bond lengths of the naphthalene core are almost the same as those in the free naphthalene molecule and that there are marked double-bond fixations in the other region of the periphery.[21] The periphery of IV and V may give a paramagnetic ring current characteristic of the $4n$ perimeter.[18] On the other hand, naphthalene core in IV and V may exhibit a diamagnetic ring current to the same extent as that of a free naphthalene molecule. Therefore, it may be expected that the paramagnetic ring current and the diamagnetic ring current cancel each other out to give a small magnetic susceptibility in IV and V.

It may be concluded that the magnetically-induced ring currents decrease sensitively with the double-bond fixation, and that in I, II, III, IV, and V they are extremely impeded. Part of the evidence for these reduced magnetic susceptibilities is given by the NMR spectra of II,[22] III,[23] and IV,[24] which show the proton signals in the olefinic region.

References

1) F. London, *J. Phys. Radium*, **8**, 397 (1937).
2) B. Pullman and A. Pullman, "Les Théories Electroniques de la Chimie Organique," Masson, Paris (1952), p. 527.
3) R. McWeeny, *Proc. Phys. Soc.*, **A64**, 261, 921 (1951); *ibid.*, **A65**, 839 (1952); *ibid.*, **A66**, 714 (1953).
4) M. Mayot, G. Berthier, and B. Pullman, *J. Phys. Radium*, **12**, 652 (1951); *J. Chim. Phys.*, **50**, 176 (1953).
5) B. Pullman, A. Pullman, E. D. Bergmann, G. Bertheir, E. Fischer, Y. Hirshberg, and J. Pontis, *ibid.*, **49**, 24 (1952).
6) J. Hoarau, *Ann. Chim.*, **1**, 544 (1956).
7) G. W. Wheland and D. E. Mann, *J. Chem. Phys.*, **17**, 264 (1949).
8) T. Nakajima and S. Katagiri, *Mol. Phys.*, **7**, 149 (1964).
9) A. Almeningen, O. Bastiansen, and M. Treattberg, *Acta Chem. Scand.*, **12**, 1221 (1958).
10) D. W. J. Cruickshank and R. A. Sparks, *Proc. Roy. Soc.* (London), **A528**, 270 (1960); O. Bastainsen and P. N. Skanke, *Advan. Chem. Phys.*, **3**, 323 (1961).
11) J. Thiec and J. Wiemann, *Bull. Soc. Chim. Fr.*, **1956**, 177.
12) Y. Kurita, S. Seto, T. Nozoe, and M. Kubo, This Bulletin, **26**, 272 (1953).
13) T. Nakajima and S. Kohda, This Bulletin, **39**, 804 (1966).

14) J. Nowakowski, *Theor. Chim. Acta*, **10**, 79 (1968).
15) H. J. Dauben, Jr., J. D. Wilson, and J. L. Laity, *J. Amer. Chem. Soc.*, **91**, 1991 (1969).
16) Y. Mikami, S. Miyai, and T. Nakajima, This Bulletin, **46**, 787 (1973).
17) G. Wagnière and M. Couterman, *Mol. Phys.*, **5**, 621 (1962).
18) J. A. Pople and K. G. Untch, *J. Amer. Chem. Soc.*, **88**, 4811 (1966).
19) H. C. Longuet-Higgins, "Aromaticity," Spec. Publ. No. 21, The Chemical Society, London (1966), p. 109.
20) T. Nakajima, A. Toyota, and S. Fujii, This Bulletin, **45**, 1022 (1972); T. Nakajima, *Topics Current Chem.*, **32**, 1 (1972).
21) H. Yamaguchi and T. Nakajima, This Bulletin, **44**, 682 (1971).
22) H. J. Dauben and D. J. Bertelli, *J. Amer. Chem. Soc.*, **83**, 4659 (1961).
23) K. Hafner, K. H. Häfner, C. König, M. Kreuder, G. Ploss, G. Schulz, E. Sturm, and K. H. Vöpel, *Angew. Chem.*, **75**, 35 (1963); K. Hafner, *ibid.*, **75**, 1041 (1963).
24) B. M. Trost and G. M. Bright, *J. Amer. Chem. Soc.*, **89**, 4244 (1967).

Ligand-Ligand Interaction in the β-Diketonato Complexes of Be^{2+}, Al^{3+}, and Zn^{2+}

Takeshi OHNO and Shunji KATO

Institute of Chemistry, College of General Education, Osaka University, Toyonaka, Osaka 560

(Received September 13, 1973)

The fluorescence yield (Φ_F) and the phosphorescence yield (Φ_P) of acetylacetone, benzoylacetone, and dibenzoylmethane were enhanced by coordination of Zn^{2+}, Al^{3+}, and Be^{2+} in an increasing order. In the bis- and the tris-bidentate complexes, not only did the ratios of Φ_P to Φ_F increase, but also the lifetimes of the phosphorescences became a little longer than that of the corresponding mono-bidentate complex. This change originates from some kinds of interaction between the ligands in the excited and ground states. Such an inter-ligand interaction was supported by the measurement of the polarization. However, the interaction energy is smaller than the expected values in the analyses of the absorption spectra and the circular dichroism in the region of the ligand band. A difference in the absorption spectra between the mono- and the bis- or the tris-bidentate complexes was seen only in the Franck-Condon factors; this finding supports the extension of the excited state through the two or the three ligands due to the weak inter-ligand interaction.

It can be easily expected that an excited state of a ligand in a coordination compound has a different character from that of the free ligand because of the coordination bond and the other ligand(s) in close proximity. An enhancement of the ligand-triplet yield is caused by spin-orbit interaction due to a heavy metal ion,[1] and the excitation in the ligand is transferred to that in the metal ion,[2] with an excited state below that of the ligand. Further, the circular dichroism due to intra-ligand transition in some tris-bidentate complexes implies the presence of an inter-ligand effect through dipole-dipole interaction. However, effect of inter-ligand interaction on the excited state of ligand has been examined, through many types of inter-molecular interaction—redox reaction, dimer formation, luminescence quenching, and energy transfer—have been reported between molecules in the excited state and in the ground state. Because such a type of reaction has been known to depend on the extent of interaction between the molecules (see Table 1), one may ascertain the extent of the inter-ligand interaction by exploring the photochemistry of ligand. Consequently, each ligand in the bis- and tris-bidentate complexes suffers from ligand-ligand interaction and coordination effects; first, we examined the corresponding mono-bidentate complex, in which the coordination effect was revealed, and then the bis- and the tris-bidentate complexes were compared with it.

TABLE 1. PHENOMENA CAUSED BY INTERACTION BETWEEN MOLECULES IN THE EXCITED STATE AND THE GROUND STATE

Interaction	Phenomena
Strong	Excimer formation[3] Electron transfer[3]
Intermediate	Splitting of the vibronic band in the absorption spectrum[4]
Weak	Change of emission yield and lifetime[5] Energy transfer[6]

Three kinds of metal ions—beryllium(II), zinc(II), and aluminium(III)—were chosen as central metal ions, as they are practically inactive to electron-transfer reaction on photoexcitation and have no excited state below 45×10^3 cm^{-1}. Because these three metal ions arrange ligands in different conformations, the magnitudes and the characters of ligand-ligand interactions can be expected to be different. All the metal ions were easily chelated by various β-diketones, which showed strong luminescences at lower temperatures.[7] The acetylacetonato complexes emitted phosphorescence only, whereas the complexes of dibenzoylmethane and benzoylacetone emitted both fluorescence and phosphorescence. Therefore, some characteristics (yield, lifetime, and spectrum) of the emission in addition to the absorption spectrum were measured in order to ascertain the interaction between ligands in the excited state and the ground state.

Experimental

Materials. *Free Ligands*: The acetylacetone(AcAc), benzoylacetone(Ba), and dibenzoylmethane (Dbm) were purified in the following ways: vacuum distilation for AcAc, three recrystallizations from ethanol for Ba, and four recrystallizations from ethanol and benzene for Dbm.

Metal Complexes and Metal Salts: The metal complexes were prepared in the usual ways except of $Be(AcAc)_2$, which was obtained from Wako Pure Chemical Industries. The complexes of zinc prepared had the following molecular formula: $Zn(AcAc)_2(H_2O)$, $Zn(Ba)_2\cdot C_2H_5OH$, $Zn(Dbm)_2(H_2O)_2$. In aluminium and beryllium complexes, three β-diketones coordinate to Al^{3+}, and two, to Be^{2+}. The results of the elementary analyses agreed with the theoretical values within a deviation of 0.58% for carbon and that of 0.14% for hydrogen. The purifications of the metal salts, $BeSO_4$, $Zn(NO_3)_2$, $KAl(SO_4)_2\cdot12H_2O$, and H_3BO_3, were carried out through two recrystallizations from aqueous solutions.

Solvents: The ethanol was refluxed with silver nitrate and over calcium oxide, and then distilled. The methanol was purified in a similar way without drying. The water was distilled two times. The ether and isopentane were dried over calcium chloride and distilled over metalic sodium.

Procedure. All the solutions were buffered by 0.2 M borate at pH=8.0. The bis-bidentate and tris-bidentate complexes were examined soon after preparation, because, in solution, 10% of the complex was dissociated in a day. The spectrum of the mono-bidentate complex was measured for the solution containing β-diketone (10^{-5} M), together with a large excess of a metal ion ($10^{-4}\sim10^{-3}$ M), in which only the mono-β-diketonato complex was expected to exist.

This was supported by the set of successive formation constants,[8] by the changes in both the absorption and emission spectra and in the lifetime in the presence of excess metal ions. We used a mixture of water and methanol (1 : 4 by volume) as the solvent.

Measurements. The absorption spectra were measured by means of a Shimadzu MPS-50L spectrophotometer. For the measurements at the temperature of boiling nitrogen (77.4 K), a quartz Dewar vessel (diameter : 55 mm) filled with liquid nitrogen was set very near to the wide aperture of the head-on type photomultiplier in order to diminish the error due to light scattering.

For the luminescence studies, all the complexes and ligands were studied at 77 K at a concentration of about 10^{-5} M. The emission spectra were obtained by using MPF-2A Hitachi fluorescence spectrophotometer with a band-width of 2~8 nm; it had been calibrated by the method of Lippert[9] against the fluorescence of β-naphthol. The emission yields were determined relative to an EPA solution of benzophenone with a band-width of 6 nm.[10]

To measure the polarization of the emission, a Polacoat film (105 UV), put between two quartz plates, or a Gram-Thomson prism was used as the polarizer, and a Toshiba polarizing filter, as the analyzer. The emission monochromator, which had different transmittance with polarized lights perpendicular to each other, was corrected by means of unpolarized light scattered from a frosted glass.

Results and Discussion

Semi-empirical calculations have shown that the absorption band of AcAc in the near ultraviolet region is attributable to the π-π* transition[11] with a transition moment along the x-axis, as is shown in Fig. 1.

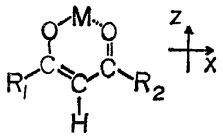

Fig 1. Structure of the ligand.
AcAc: $R_1=R_2=CH_3$
Ba: $R_1=CH_3$, $R_2=C_6H_5$
Dbm: $R_1=R_2=C_6H_5$

For Ba and Dbm, the intense band observed in a frequency region a little lower than AcAc can safely be assigned to the π-π* transition. Although the n-π* transitions are hidden by the strong π-π* transition, one of n-π* transitions may be shifted to a higher frequency because of the formation of an enol form†, this lifting one of the non-bonding orbitals. It is certain that, just as with the hydrogen bond, coordination to the metal ion makes a six-membered ring. However, because neither coordination nor protonation greatly changes the energy level of the other non-bonding orbital in the ring comformation, the non-bonding orbital may interact with the π-orbital of the neighboring ligand(s) in the complexes of aluminium, as will be discussed below.

† Burdett and Rogers reported, on the basis of PMR analysis, that 80% of the free AcAc, 100% of the Ba and 100% of the Dbm exists as the enol form in $CHCl_3$ or CCl_4.[12]

Effect of Coordination on the Excited States of β-Diketones. Absorption and Emission Spectra: A broad absorption band was observed at room temperature in the near-ultraviolet region for all the β-diketones examined, independent of the presence or absence of

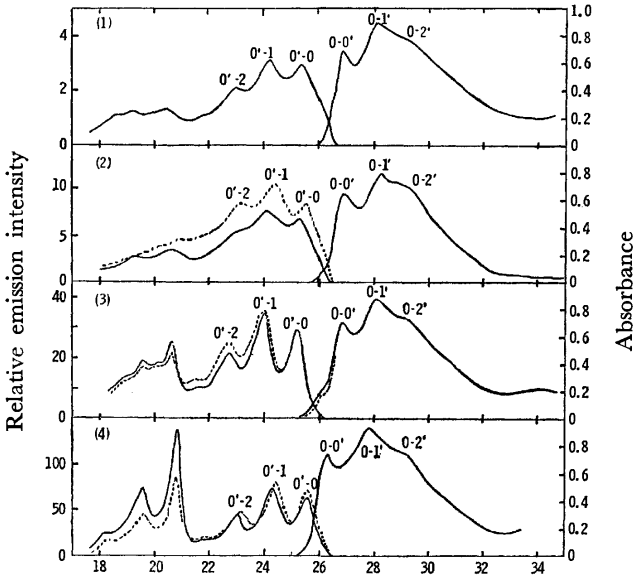

Wave number/10^3 cm^{-1}

Fig 2. Absorption and emission spectra of dibenzoylmethane and the dibenzoylmethanato complexes at 77 K in methanol and water (4 : 1 by volume).
(1) Dbm, (2) solid line : $Zn(Dbm)_2$, broken line : $Zn(Dbm)^+$, (3) solid line : $Al(Dbm)_2^+$, broken line : $Al(Dbm)^{2+}$, (4) solid line : $Be(Dbm)_2$, broken line : $Be(Dbm)^+$

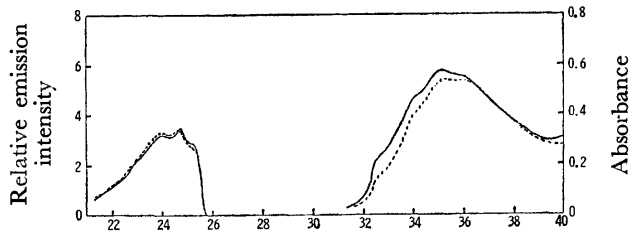

Wave number/10^3 cm^{-1}

Fig. 3. Absorption and emission spectra of $Al(AcAc)_3$ (solid line) and $Al(AcAc)^{2+}$ (dashed line) at 77 K in methanol and water (4 : 1 by volume)

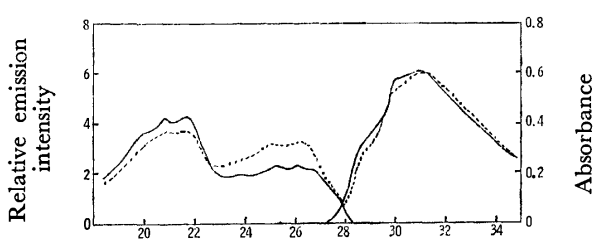

Wave number/10^3 cm^{-1}

Fig. 4. Absorption and emission spectra of $Al(Ba)_3$ (solid line) and $Al(Ba)^{2+}$ (broken line) at 77 K in methanol and water (4 : 1 by volume).

Table 2. Spectral data of absorption, fluorescence and phosphorescence in methanol and water at 77 K

Compound	Abs. 10^3 cm^{-1}	Fluo. 10^3 cm^{-1}	Phos. 10^3 cm^{-1} 0″—0
AcAc	(33.7),[a] (35.0), 36.23	—	—
$Be(AcAc)^+$	(32.5), (33.1), 34.25	—	25.45
$Be(AcAc)_2$	(32.5), (33.1), 34.25	—	25.45
$Al(AcAc)^{2+}$	(32.6), (33.8), 35.22	—	25.40
$Al(AcAc)_3$	(32·6), (33.8), 35.22	—	25.40
$Zn(AcAc)_2$	(32.6), (33.9), 35.21	—	25.45
Ba	(28.7), (30.0), 31.25	—	—
$Be(Ba)^+$	(28.4), (29.9), 30.08	27.76, 26.04, 25.25	22.08
$Be(Ba)_2$	(28.4), (29.9), 30.08	27.47, 26.04, 24.88	22.08
$Al(Ba)^+$	(28.7), (30.0), 31.10	27.2 25.87, 24.75	21.98
$Al(Ba)_3$	(28.7), (30.0), 31.10	27.14, 25.77, 24.47	21.88
$Zn(Ba)^+$	(28.7), (30.1), 31.2	27.4 26.2 25.00	—
$Zn(Ba)_2$	(28.9), (30.0), 31.3	27.2 25.8 24.7	21.83
Dbm	26.81, 28.01, (28.9)	26.04, 24.88, 23.7	20.70
$Be(Dbm)^+$	26.25, 27.55, (28.7)	25.57, 24.30, 23.04	20.88
$Be(Dbm)_2$	26.11, 27.40, (28.7)	25.45, 24.15, 22.94	20.88
$Al(Dbm)^{2+}$	(25.8), 26.74, 28.09, 29.15	25.31, 24.10, 22.78	20.75
$Al(Dbm)_2^+$	(25.8), 26.74, 28.09, 29.15	25.31, 24.10, 22.78	20.79
$Zn(Dbm)^+$	26.74, 28.17, (29.2)	25.55, 24.39, 23.26	—
$Zn(Dbm)_2$	26.74, 28.09, (29.1)	25.32, 24.2, 22.94	20.79

a) Parenthesis shows shoulder.

metal ions. Each of the mono-bidentate complexes had a broad absorption band, not greatly different from the free β-diketone. At 77 K, the fine structure of the absorption spectra emerged as is shown in Fig. 2—4; one may easily recognize that the peaks and shoulders of the coordinating β-diketones shift to a lower frequency than those of the free β-diketones (see Table 2). However, an exception is found in the case of $Al(Dbm)^{2+}$, in which a new band is weakly observed on the lower-frequency side of the 0—0′ band.

Coordination enhanced the emission intensity of β-diketones in all cases at 77 K, as is shown in Fig. 2. The fluorescence spectra of these mono-coordinated complexes have a well-resolved structure at 77 K and are practically independent of the metal ions (Fig. 2). The numerical data on the peaks and shoulders are shown in Table 2. As Fig. 2 shows, there are mirror-image relations between the absorption and the fluorescence spectra. Therefore, all of the peaks and the shoulders of the absorption may be regarded as 0—0′ bands or vibronic bands. However, $Al(Dbm)^{2+}$ is an exception; it is different from the others in its absorption spectrum, though similar in its fluorescence spectrum.

On the basis of rough analyses of the fine structures of the spectra, symmetric vibrations coupled with the π-π^* transition are assigned to C–C stretching in the six-membered ring and to C–R (R : CH_3 or C_6H_5) stretching (1300 cm^{-1}) (except for the case of $Be(AcAc)^+$) on the basis of Nakamoto's assignment of $Al(AcAc)_3$.[13]

Yields and Polarizations of Emission: All the free β-diketones showed a weak emission with quantum yields below 0.008 at 77 K. Fluorescence was observed only for Dbm. However, the coordination increased the emission very much, as has been mentioned above, and the fluorescence was easily observed even in the case of Ba. In view of all the emission yields listed in Table 3, it is noticeable that the emission yield was enhanced with the coordination in the following order: Be>Al>Zn. The simultaneous enhancement of the fluorescence and phosphorescence yields indicates that the strong metal-ligand bond restricts the internal rotation of the ligand in the singlet excited state and prevents it from making a radiationless transition. In fact, the fluorescence yields increase in an order of that of the ionic radii of metal ions (Be^{2+}: 0.34, Al^{3+}: 0.57, Zn^{2+}: 0.69 Å). Further, this presump-

Table 3. Emission yields observed at 77 K in methanol and water (4 : 1)

Compound	Φ_F	Φ_P	Φ_P/Φ_F	τ_P, s
$Be(AcAc)^+$	—	0.028	—	0.098
$Be(AcAc)_2$	—	0.031	—	0.098
$Al(AcAc)_3$	—	0.006	—	—
Zn(AcAc)	—	0.012	—	—
Ba	0.0001	0.001	—	—
$Be(Ba)^+$	0.023	0.065	2.8	0.32
$Be(Ba)_2$	0.020	0.10	5.0	0.35
$Al(Ba)^{2+}$	0.030	0.019	0.63	0.39
$Al(Ba)_3$	0.023	0.025	1.1	0.48
$Zn(Ba)_2$	0.0004	0.0015	3.8	—
Dbm	0.008	0.0003	0.33	—
$Be(Dbm)^+$	0.15	0.077	0.52	0.29
$Be(Dbm)_2$	0.11	0.13	1.1	0.40
$Al(Dbm)^{2+}$	0.088	0.032	0.37	0.60
$Zn(Dbm)^+$	0.028	0.007	0.24	0.45
$Zn(Dbm)_2$	0.019	0.007	0.31	0.45

tion is supported by the fact that an intense fluorescence is observed at low temperatures for all the complexes which have no emission at room temperature.

It is important that beryllium complexes do not have the smallest ratio of the phosphorescence yields to the fluorescence yield, contrary to the expectation that the ratio in the lightest metal complex would be the smallest on account of having the smallest spin-orbit interaction. This abnormality will be discussed later.

The polarization of emission is defined by Eq. (1) when excited with polarized light:

$$P = \frac{I_{\parallel} - I_{\perp}}{I_{\parallel} + I_{\perp}} \quad (1)$$

where $I_{\parallel}$ and $I_{\perp}$ are the emission intensities with electric vectors parallel and perpendicular to that of the exciting light respectively. When the emission moment at an angle(θ) with the absorption one, P is written as Eq. (2), assuming the random orientation of a solute in the solution:

$$P = \frac{3\cos^2\theta - 1}{\cos^2\theta + 1} \quad (2)$$

Moreover, the polarization is calculated to be 1/2 when the transition moment of the emission is the same in direction as that of absorption (θ=0°), and −1/3 when it is perpendicular (θ=90°). The fluorescence polarizations obtained have a small deviation from the ideal value (1/2) and are independent of the excitation light throughout the near-ultraviolet region for all the samples except Al(Dbm)$^{2+}$, as Table 4 shows. Phosphorescence polarizations have negative or small positive values, depending on the metal ions, for all the series of β-diketones; they are also independent of excitation wavelength except for the dibenzoylmethanato complex of aluminium. The independence of P for the mono-β-diketonato complex suggests that the broad absorption band in the near-ultraviolet region consists of one kind of transition except for the case of dibenzoylmethanato complexes, one of which has a new and weak absorption band in the lower frequency region, as has been mentioned above. The negative and small positive values of the phosphorescences indicate that the lowest triplet state is a π-π^* state in all cases, just as McGlynn *et al.* reported.[14] The assignment of the phosphorescence is supported by both the semi-empirical calculation of acetylacetone[13] and the relatively longer lives of the phosphorescences. The shortest lifetime, 0.1 s, which was found for Be(AcAc)$^+$, was longer than any other reported life-times of the n-π^* triplet state.

TABLE 4. POLARIZATION OF EMISSION ON EXCITATION TO THE FIRST EXCITED STATE IN METHANOL AND WATER (4 : 1) AT 77 K

Compound	P_{Fluo}	P_{Phos}
Be(AcAc)$_2$		0.10
Al(AcAc)$_3$		−0.018
Zn(AcAc)$_2$		−0.097
Be(Ba)$^+$	0.35	
Be(Ba)$_2$	0.14	
Al(Ba)$^{2+}$	0.28	
Al(Ba)$_3$	0.03	
Zn(Ba)$_2$	0.35	0.17
Be(Dbm)$^+$	0.33, 0.36[a]	0.01, 0.14[a]
Be(Dbm)$_2$	0.30, 0.12[a]	−0.13, 0.07[a]
Al(Dbm)$^{2+}$	0.25, 0.13[a]	0.020
Al(Dbm)$_2^+$	0.15, 0.11[a]	
Zn(Dbm)$^+$	0.40	
Zn(Dbm)$_2$	0.40	

a) The values were obtained on the excitation of the 0—1′ or 0—2′ band; they were different from the value on the excitation of the 0—0′.

It is interesting that the shortest lifetimes of the AcAc and Dbm complexes were found not for the zinc complexes but for the beryllium complexes, contrary to the expectation based on the spin-orbit coupling through the metal-ligand bond. Because the shortest lifetimes were accompanied by extraordinary enhancements of the yields in all the beryllium complexes, it is probable that the intersystem crossing rates ($S_1 \rightarrow T_0$, $T_0 \rightarrow S_0$) increase with the strength of the metal-ligand bond.

After all, the metal-ligand bond in a complex brings about: (i) a small radiationless transition rate in the singlet excited state, resulting in increasing yields of emission, and (ii) a large intersystem crossing rate, resulting in a larger yield and the shortest lifetime of the phosphorescence.

Ligand-ligand Interactions in Bis- and Tris-bidentate Complexes. Conformations of Ligands in Bis- and Tris-bidentate Complexes: The conformations of the coordinating β-diketones are different depending on the metal ions. In beryllium complexes, the six-membered rings of two ligands hold planes which are vertical with each other, so that the Coulomb exchange interaction of π-π electrons (inter-ligand π-π) between two ligands

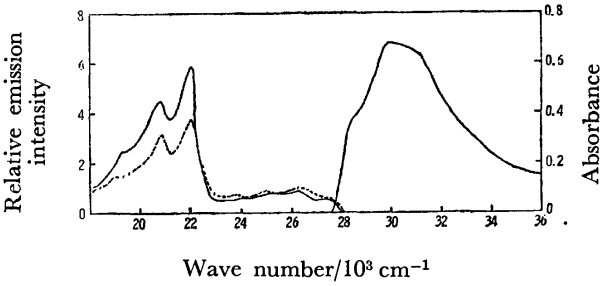

Fig. 5. Absorption and emission spectra of Be(Ba)$_2$ (solid line) and Be(Ba)$^+$ (broken line) at 77 K in methanol and water (4 : 1 by volume).

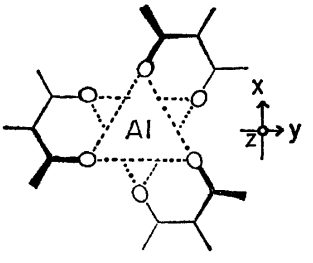

Fig. 6. Comformation of the tris-acetylacetonato complex of aluminium(III).

is impossible as the first approximation. However, weak interactions of two types cannot be ignored. One is the dipole-dipole interaction due to a weak component of the transition moment along the z-axis. The other is the interaction between non-bonding electrons localized on the oxygen atoms of one ligand and the π-electrons on the six-membered ring of the other ligand (inter-ligand n-π).

Aluminium complexes with the three same ligands have a conformation as in Fig. 6, belonging to the D_3 group. In these complexes, both Coulomb exchange interaction (inter-ligand π-π and n-π) and dipole-dipole interaction may be operative between the ligands. Especially, the circular dichroism of tris-(acetylacetonato)-silicon(IV) in the near-ultraviolet region has been understood on the basis of the dipole-dipole interaction,[15] which splitted the triply-degenerated state into two exciton-like state with A_2 and E symmetry with an allowed transition.

As for zinc complexes—$Zn(AcAc)_2 \cdot (H_2O)$[16] and $Zn(Ba)_2 \cdot C_2H_5OH$,[17] X-ray analysis has shown that two ligands of AcAc or Ba are approximately coplanar and that H_2O or C_2H_5OH is located at an apical position. It is probable that $Zn(Dbm)_2 \cdot (H_2O)_2$ has a similar structure, with two Dbm in the same plane and two H_2O at apical positions. Such a structure has also been reported in the case of Zn(8-hydroxyquinolinato)$_2(H_2O)_2$.[18] Two ligands in the same plane may interact with each other through both Coulomb-exchange (π-π and n-π) and dipole-dipole interactions; the latter produces a lower symmetric state with a forbidden transition and an antisymmetric higher one with an allowed transition.

Absorption Spectra and Emission Spectra: Each of the bis- and the tris-β-diketonato complexes has an absorption spectrum similar to that of the corresponding mono-β-diketonato complex, as is shown in Figs. 2—4. Although they are not finely resolved, some peaks and shoulders of the absorption spectra of the bis- and the tris-β-diketonato complexes can be assigned to a vibrational structure, just as those of the corresponding mono-β-diketonato complexes are (see Table 2). This assignment is supported by the fluorescence spectra in the case of the dibenzoylmethanato complexes (see Fig. 2). The fluorescence spectra of the bis-β-diketonato complexes, whose peaks and shoulders can be assigned to one kind of progression without ambiguity, have a good mirror image with the absorption spectra. After all, it is reasonable to say that there is not so strong an interaction between ligands in the bis- and tris-bidentate complexes as to produce a distinct new electronic transition.

This is contrary to the proposition which explains the absorption spectra and the circular dichroism of some tris-acetylacetonato complexes. Hanazaki *et al.*[11] have regarded the separation (1500 cm^{-1}) between the absorption maximum and the shoulder on the lower-frequency side observed at room temperature as the energy difference between the A_2 and E states for $Al(AcAc)_3$. For $Si(AcAc)_3^+$, 1500 cm^{-1} has been obtained in a similar way to that reported by Mason and Searle.[15] However, there remain some ambiguities in the assignments which are deduced without considering that the vibrational structure might appear as some sub-bands in the absorption spectra. Moreover, it must be recalled that the dipole-dipole interaction comes vibronically into play, according to Simpson,[19] when the vibrational interval (1300 cm^{-1}) is larger than the interaction energy (850 $cm^{-1} = 1/3 \times$ (the energy difference between E and A_2 states), which has been calculated by the method of P-P-P SCF-CI[11]). The splitting of the individual sub-band is calculated approximately to be one fourth of 2560 cm^{-1}, on the average, if the absorption spectrum is considered to consist of four sub-bands. Therefore, the absorption spectrum becomes more complex and broader, so that small splitting cannot be observe deasily. Moreover, if the dipole-dipole interaction in $Al(AcAc)_3$ is retained in the case of $Al(Dbm)_2^+$, which has a less broad absorption spectrum, a splitting of the individual sub-band should be observed.

In the case of α,α′-bipyridyl complexes of nickel(III) whose absorption spectra are well resolved into several sharp sub-bands, the splitting of the sharp individual sub-band may be expected to be visible since the total dipole-dipole interaction in $[Ni(\alpha,\alpha'\text{-bipyridyl})_3]^{2+}$ has been calculated to be 2680 cm^{-1}.[20] However, Bray *et al.* observed no difference between the well-resolved spectra of the mono- and the tris-α,α′-bipyridyl complexes at 77 K.[21] After all, then it is not improbable that the dipole-dipole interaction in the tris-β-diketonato complexes is smaller than the calculated values in the cases of $Al(AcAc)_3$ and $Si(AcAc)_3^+$.

However, in the relative intensities of the sub-bands of the absorption spectra, a distinct difference is observed between the bis- or the tris-bidentate complexes and the mono-bidentate complexes (Figs. 3 and 4). The intensities of the 0—0′ and 0—1′ bands are higher, and those of the 0—2′ and 0—3′ bands are a little lower, for $Al(AcAc)_3$ and $Al(Ba)_3$ than for the respective monobidentate complexes. As for the fluorescence, the intensity ratios of the vibronic bands to the 0—0′ band for the bis- and the tris-bidentate complexes in

Table 5. Relative intensities of the vibronic bands of emission normalized to the intensity of the 0′—0 or 0″—0 band

Compound	Fluorescence		Phosphorescence	
	0′—1	0′—2	0″—1	0″—2
$Be(AcAc)^+$	—		1.10	0.90
$Be(AcAc)_2$	—		1.07	0.87
$Al(AcAc)^{2+}$	—		0.92	
$Al(AcAc)_3$	—		0.88	
$Be(Ba)^+$	—		0.65	
$Be(Ba)_2$	—		0.62	
$Al(Ba)^{2+}$	1.88	1.95	0.96	
$Al(Ba)_3$	1.87	1.92	0.95	
$Be(Dbm)^+$	1.56	0.84	0.42	
$Be(Dbm)_2$	1.55	0.77	0.41	
$Al(Dbm)^{2+}$	1.30	0.72	0.74	0.68
$Al(Dbm)_2^+$	1.19	0.66	0.69	0.64
$Zn(Dbm)^+$	1.20	0.77	0.48	
$Zn(Dbm)_2$	1.15	0.65	0.42	

any case, are lower than those for the mono-bidentate complexes as is shown in Table 5; for instance, the ratio of the 0′—1 is 1.30 for $Al(Dbm)^{2+}$ while it is 1.19 for $Al(Dbm)_2^+$. A similar situation is also seen in the phosphorescence. The intensity ratios of the vibronic bands are lower for the bis- and the tris-bidentate complexes than for the mono-bidentate complexes except in the case of $Al(Ba)_3$.

These changes in the spectral pattern are reduced to the change in the Franck-Condon factors ($\langle 0|v'\rangle^2$, $\langle 0'|v\rangle^2$ and $\langle 0''|v\rangle^2$ where v and v' are zero or near to zero). The situation in which the Franck-Condon factors for the sub-bands of the bis- and the tris-bidentate complexes decrease compared to that of the mono-bidentate complexes may correspond to the reduction of the configurational deformation or displacement in the excited state with the bis- and the tris-bidentate complexes. Since a smaller deformation or displacement can be expected when a ligand-ligand interaction causes an extended excited state, the variation in the Franck-Condon factors can be understood in terms of ligand-ligand interaction. Further, it may be expected that the Franck-Condon factors of phosphorescence ($\langle 0''|v\rangle^2$, v: much higher) are smaller in the bis- and the tris-bidentate complexes. If this is the case, the phosphorescence may also be expected to have a larger yield and a longer lifetime, because smaller Franck-Condon factors with higher v-values reduce the rate of the radiationless transition for polyatomic molecules.[22]

Yields and Polarizations of Emissions: The sharing of excitation and emission by two or three ligands results in a depolarization of the emission. When the excited state of the bis-bidentate complexes of beryllium is a doubly degenerate state of E symmetry, with a transition moment of two components, the fluorescence polarization is calculated to be 0.14 (see Table 6). The polarizations measured for $Be(Ba)_2$ and $Be(Dbm)_2$ were nearly 0.14 as Table 4 shows*. Though these results do not enable us to decide what kind of inter-ligand interaction is operative, they support the idea that an interaction exists between ligands in the excited state and in the ground state. As for the tris-β-diketonato complexes belonging to the D_3 group, it can easily be seen that the transition moments of the three ligands couple to give a transition (z-polarized) with the A_2 symmetry and a transition (x- and y-polarized) with the E symmetry. Since the splitting of the two states is too small to be observed in the spectra, it is plausible that both of the states fluoresce at 77 K. In that case, the fluorescence polarization can be calculated to be 0.09 on excitation to both states. In fact, the measured polarization (0.03) of $Al(Ba)_3$ was near to the ideal value. Therefore, these results confirm the existence of the excited state extending through three ligands which has been proposed on the basis of the changes in the sub-band intensities.

* The polarization of $Be(Dbm)_2$ was different between the 0′—0 excitation and the 0—1′ or 0—2′ excitation. It is probable that ligand-ligand interaction produces such a splitting as was observed in the case of $Al(Dbm)_3^{2+}$ as has been described.

TABLE 6. IDEAL VALUES OF THE FLUORESCENCES OF BIS AND TRIS-BIDENTATE COMPLEXES[a]

Complex (symmetry group)	Absorption (moment)	Fluorescence (moment)	Polarization
Tris-bidentate (D_3)	$A_1 \rightarrow A_2$, E (x, y, z)	$A_2 \rightarrow A_1$ (z)	0.22
	$A_1 \rightarrow A_2$, E (x, y, z)	$E \rightarrow A_1$ (x, y)	−0.17
	$A_1 \rightarrow A_2$, E (x, y, z)	A_2, $E \rightarrow A_1$ (x, y, z)	0.09
Bis-bidentate (D_{2d})	$E \rightarrow E$ (x, y)	$E \rightarrow E$ (x, y)	0.14

a) The ideal values are calculated on the following conditions in the case of tris-β-diketonato complexes: (i) the ratio of the transition probability of $A_2 \leftrightarrow A_1$ to that of $E \leftrightarrow A_1$ is two, and (ii) the internal conversion rate between A_2 and E is very rapid.

No difference in fluorescence polarization between the mono- and bis-β-diketonato form was observed for zinc complexes. However, this does not imply that no delocalization of the excited state occurs through the two ligands of zinc complexes, because the two ligands have parallel transition moments.

As for the phosphorescence, the bis- and tris-β-diketonato complexes have longer lifetimes than the corresponding mono-β-diketonato complexes except for zinc complexes, as Table 3 shows. These changes may be caused by a decrease in the radiationless transition rate, because the rate is reduced with the decrease in Franck-Condon factors for higher v'-values which was expected from the change in the vibronic band intensities of the phosphorescences mentioned above.

There was a distinct change in the emission yields from the mono-β-diketonato complexes to the bis- and tris-β-diketonato ones (see Table 3). The fluorescence yields of the latter decreased, while the phosphorescence yields increased. The increase in the phosphorescence yields seems to arise from the same origin (a decrease in the radiationless transition rate of the triplet state) as the longer lifetime. However, because the increase in the yield was much larger than that in the lifetime, it may be assumed that it is mainly due to the increase in the intersystem crossing rate of the singlet-excited state and partially due to a decrease in the radiationless transition rate of the triplet state. This assumption is supported by the fact that the fluorescence yields decrease in the case of the bis- and tris-β-diketonato complexes. It is reasonable that the increase in the intersystem crossing rate is brought about by the spin-orbit coupling through the inter-ligand interaction as well as by inter-phenyl interaction in diphenylmethane and triphenylmethane.[5]

References

1) P. Yuster and S. I. Weissman, *J. Chem. Phys.*, **17**, 1182 (1949).

2) M. A. El-Sayed and M. L. Bhaumik, *ibid.*, **39**, 2391 (1963), Y. Ohashi, K. Yoshihara, and S. Nagakura, *J. Mol.*

Spectrosc., **38**, 43 (1971).
3) B. Stevens, "Advance in Photochemistry," Vol. 8, John Wiley & Sons, New York (1971), p. 161.
4) L. O. Edwards and W. T. Simpson, *J. Chem. Phys.*, **53**, 4237 (1970); M. E. Long, Y. H. Li, and E. Lim, *Chem. Phys. Lett.*, **16**, 445 (1972).
5) F. H. Watson and M. A. El-Bayoumi, *J. Chem. Phys.*, **55**, 5464 (1971).
6) Th. Förster, *Discuss. Faraday Soc.*, **27**, 7 (1959).
7) R. S. Becker and J. B. Allison, *J. Phys. Chem.*, **67**, 2669 (1963).
8) R. M. Izatt, W. C. Fernelius, B. P. Blck, and C. G. Hass, Jr., *ibid.*, **59**, 170 (1955).
9) E. Lippert, W. Nagele, I. Seibold-Blankenstein, U. Straiger, and W. Voss, *Z. Anal. Chem.*, **170**, 1 (1960).
10) E. H. Gilmore, G. E. Gibson, and D. S. McClure, *J. Chem. Phys.*, **20**, 829 (1952).
11) I. Hanazaki, F. Hanazaki, and S. Nagakura, *ibid.*, **50**, 265 (1969).
12) J. L. Burdett and M. T. Rogers, *J. Amer. Chem. Soc.*, **86**, 2105 (1964).
13) K. Nakamoto, Y. Morimoto, and A. E. Martell, *ibid.*, **66**, 346 (1962).
14) S. P. McGlynn, T. Azumi and M. Kinoshita, "Molecular Spectroscopy of The Triplet State," Prentice-Hall, New Jersey (1966), p. 246.
15) E. Larsen, S. F. Mason, and G. H. Searle, *Acta Chem. Scand.*, **20**, 191 (1966).
16) E. L. Lippert and M. R. Truter, *J. Chem. Soc.*, **1960**, 4996.
17) R. L. Belford, N. D. Chasteen, M. A. Hitchman, P. K. Hon, C. E. Pflungan, and I. C. Paul, *Inorg. Chem.*, **8**, 1312 (1969).
18) G. J. Palenik, *Acta Crystallogr.*, **17**, 696 (1964).
19) W. T. Simpson and D. L. Peterson, *J. Chem. Phys.*, **26**, 588 (1957).
20) S. F. Mason, *J. Chem. Soc., Ser. A*, **1969**, 1428.
21) R. G. Bray, J. Ferguson, and C. J. Hawkins, *Aust. J. Chem.*, **22**, 2091 (1969).
22) W. Siebrand, *J. Chem. Phys.*, **46**, 440 (1967).

Studies of the Chemiluminescence of Several Xanthene Dyes. VI. A Kinetic Analysis of a Blue-fluorescent Product in the Chemiluminescent Reaction of Eosin Y with Hydrogen Peroxide

Isao KAMIYA and Keizo AOKI

Department of General Education, Nagoya University, Chikusa-ku, Nagoya 464

(Received November 29, 1973)

In the present study, we found that the absorbance at 395 nm of the chemiluminescent reaction system of eosin Y with hydrogen peroxide initially increased to a maximum, and then gradually decreased. From the finding that the absorption spectrum of a chromatographically-isolated blue-fluorescent product (M_E) showed a peak at the same wavelength (395 nm), we could confirm that the increment of the absorbance at 395 nm (Δ_{395}) was mainly due to the generation of M_E; we then extended the investigation of the mechanism for the chemiluminescent reaction by a kinetic analysis of M_E. The observed value of Δ_{395} could be approximately calculated by the expression of $[M_E]$, which was derived from a kinetic scheme proposed in the previous paper.[1] The ratio of the generation rates of M_E in different media, which was calculated from the observed values of Δ_{395}, was in good agreement with that estimated from the curves of the chemiluminescence emission intensity *versus* the time measured in the media. These results gave additional evidence in support of the view that the blue-fluorescent species is the primary excited product in the reaction.

In the previous paper,[1] Kamiya and Kato showed that the chemiluminescence emission (CL-emission) in the reaction of such a xanthene dye as eosin Y with hydrogen peroxide in an alkaline solution was composed of two emission components: a greenish-yellow emission whose spectral distribution was similar to that of the fluorescence emission (FL-emission) of the dye, and a blue emission similar to the fluorescence band which appeared during the course of the reaction. The observed characteristics of the emission components indicated that the generation of an excited species which fluoresces blue light, and an energy-transfer process from the exicted product to an unoxidized dye were likely to be part of the mechanism for the chemiluminescent reaction.

In the present study, we found that the absorbance at 395 nm of the reaction system initially increased to a maximum, and then gradually decreased. From the finding that the absorption spectrum of a chromatographically-isolated blue-fluorescent product showed a peak at the same wavelength (395 nm), we could confirm that the increment of the absorbance at 395 nm (Δ_{395}) was mainly due to the generation of the blue-fluorescent product (M_E); we then extended the investigation of the mechanism for the chemiluminescent reaction by a kinetic analysis of M_E. The details of the experimental results and a discussion based on the results will be presented in this paper.

Experimental

The luminescent reaction was performed by adding 0.5 ml of a 20% aqueous solution of hydrogen peroxide to a mixture of 1 ml of a 0.3 M aqueous solution of sodium hydroxide and 3 ml of a 1.3×10^{-3} M eosin Y solution in 50% dimethylsulfoxide, in 50% ethanol, or in water, in a quartz cell ($10\times10\times45$ mm) at 40 °C.

The FL-emission spectra were measured on a Hitachi MPF-2A-type recording fluorescence spectrophotometer. With the exciting source turned off, the intensities of the CL-emission were measured on the same apparatus equipped with a thermostatic cell assembly. The absorption spectrum and the changes in the absorbances at 395 nm and 517 nm with the reaction time were measured on a Hitachi 124-type recording spectrophotometer. The temperature of the reaction system was maintained at 40 °C in a Komatsu SPR-D Coolnics cell holder.

The separation of the blue-fluorescent product from the reaction mixture could be performed by thin-layer chromatography (Silica Gel G on a glass plate; chloroform–acetic acid, 1 : 1, or acetone–benzene–acetic acid, 2 : 7 : 1, for development), as well as by paper chromatography (Toyo Filter Paper No. 50; 25% aqueous ethanol solution–5% aqueous ammonia solution, 1 : 1, for development). A part of the blue-fluorescent spot on the plate was scraped off, and the blue-fluorescent product was extracted with ethanol.

The spent reaction mixture was neutralized with dilute hydrochloric acid and evaporated to dryness; then the main product of the reaction was extracted with ethanol. The identification of the main product with an authentic sample of phthalic acid was performed on a Yanagimoto GCG-550-type gas chromatograph, in which nitrogen gas was used as carrier gas, and on a Hitachi EPI-G-type infrared spectrophotometer (KBr-disk method).

Results and Discussion

Figure 1 shows the change in the absorption spectrum of the chemiluminescent reaction system of eosin Y with hydrogen peroxide (50% dimethyl sulfoxide system) in the region of 330—470 nm.[2] This figure indicates that the absorbance at 395 nm initially increases to a maximum, and then gradually decreases. Figure 2 illustrates the curves of the absorbance at 395 nm *versus* the reaction time (Δ_{395}–t curves) for the reaction in three media: a 50% aqueous solution of dimethyl sulfoxide (50% DMSO), a 50% aqueous ethanol solution (50% EtOH), and water (H_2O). The results clearly demonstrate that the Δ_{395}–t curves are strongly characterized by the media; that is, Δ_{395} is remarkable in 50% DMSO, prolonged but not so remarkable in 50% EtOH, and slight in H_2O. It was found that the absorption spectrum of an ethanol solution of the isolated blue-fluorescent product showed a peak at 395 nm, as is illustrated in Fig. 3. This result strongly suggests that the change in the absorbance at

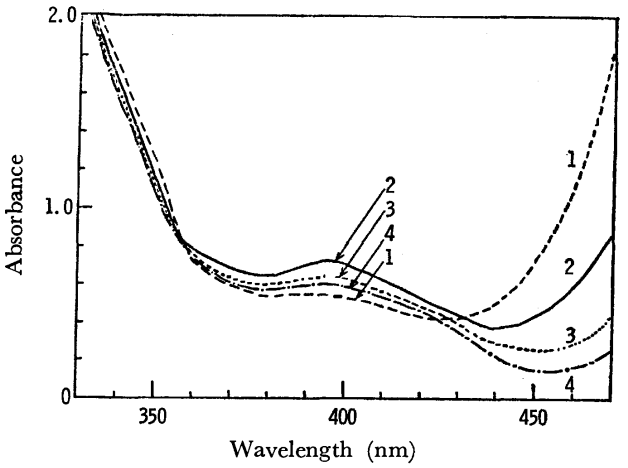

Fig. 1. The change of the absorption spectrum of the chemiluminescent reaction system of eosin Y with hydrogen peroxide (50% DMSO) in the region of 330—470 nm. 1: before adding H_2O_2, 2 → 4: after adding H_2O_2.

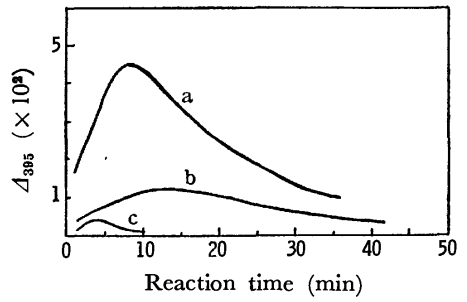

Fig. 2. Δ_{395}–t curves on the chemiluminescent reaction of eosin Y with hydrogen peroxide in three different media. a: in 50% DMSO, b: in 50% EtOH, c: in H_2O (40 °C).

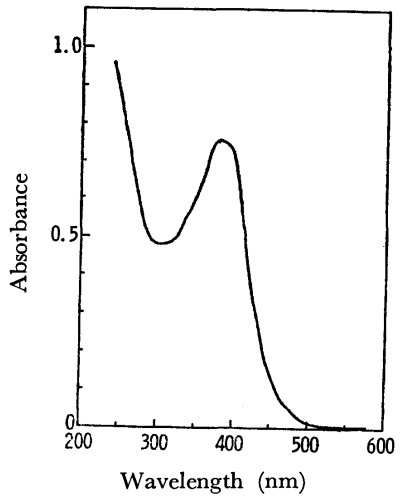

Fig. 3. Absorption spectrum of a ethanol solution of isolated blue-fluorescent product.

395 nm is mainly due to the generation of the blue-fluorescent product.

The overall reaction in the chemiluminescent system seems to be complicated, since several spots of minor unknown reaction products other than the main product (phthalic acid) and the blue-fluorescent product were separated by chromatography. However, without regard to the details, it has been found that the experimental results in the previous studies are consistent with the following kinetic scheme.[1,3]

Radical generation from the decomposition of hydrogen peroxide in an alkaline solution:

$$H_2O_2 \longrightarrow R^{\cdot}\ (O_2H^{\cdot} \text{ or } OH^{\cdot})$$

The generation of an excited (blue-fluorescent) species (M_E) by the decomposition of a short-lived energy-rich intermediate (M) which will be produced by the reaction of eosin Y (E) with R·:

$$E + R^{\cdot} \longrightarrow M \longrightarrow M_E^* \quad \text{(reaction rate } k_1') \quad \text{(i)}$$

An energy-transfer process:

$$M_E^* + E \longrightarrow M_E + E^* \quad (k_2) \quad \text{(ii)}$$

Blue FL-emission from M_E^*:

$$M_E^* \longrightarrow M_E + h\nu_1 \quad (k_3) \quad \text{(iii)}$$

Greenish-yellow FL-emission from E*:

$$E^* \longrightarrow E + h\nu_2 \quad (k_4) \quad \text{(iv)}$$

Radiationless deactivation of E*:

$$E^* \longrightarrow E + \text{heat} \quad (k_4') \quad \text{(iv')}$$

Self-quenching:

$$E^* + E \longrightarrow E + E \quad (k_5) \quad \text{(v)}$$

Since the Δ_{395}–t curve decreased in the course of the reaction,[4] the decomposition step of M_E may be taken into account:

$$M_E + R^{\cdot} \longrightarrow Q \quad (k_6) \quad \text{(vi)}$$

The quantity of blue-fluorescent species (M_E) produced must be small because of the low quantum yield of this chemiluminescent reaction.[5] Product Q, therefore, seems not to be the main reaction product (phthalic acid, P), since the yield of P (based on eosin Y consumed) was about 40%; therefore a further generation step of P which competes with reaction (i) must be present:

$$E + R^{\cdot} \rightarrow\rightarrow P \quad (k_7') \quad \text{(vii)}$$

According to the reaction scheme, the intensity of the greenish-yellow CL-emission ($h\nu_2$, I_E) is given by:

$$I_E = k_1'[R^{\cdot}]k_2k_4[E]^2/(k_2[E]+k_3)(k_4+k_4'+k_5[E]) \quad (1)$$

where [E] is the concentration of E at time t.

Since the intensity of blue CL-emission ($h\nu_1$), which is given by $k_1'[R^{\cdot}][E]k_3/(k_2[E]+k_3)$, and the fluorescence efficiency of eosin Y did not vary much with the change in [E] in the systems, assuming that $k_2[E] \gg k_3$ and $k_4+k_4' \gg k_5[E]$, and further assuming that the reactions of (i) and (vii) obey the pseudo-first order reaction in view of the previous result, that [R·] did not vary during the reaction provided [H_2O_2] was high (excess), we can write:

$$I_E = \{k_1k_4/(k_4+k_4')\}[E]_0 \exp\{-(k_1+k_7)t\} \quad (2)$$

where $k_1=k_1'[R^{\cdot}]$, $k_7=k_7'[R^{\cdot}]$, and where $[E]_0$ is the initial concentration of E.

The straight lines for the plots of log I_E(the lograithm of the CL-emission peak at 560 nm) *versus* the reaction time shown in Fig. 4 indicate that Eq. (2) is acceptable, and from the lines the values of k_1+k_7 in

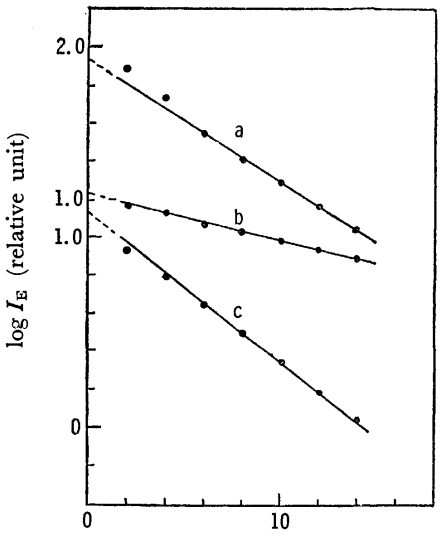

Fig. 4. Log plots of the relative intensities of emission peak (I_E) at 560 nm *versus* reaction time for the chemiluminescent reaction of eosin Y in 50% DMSO (a), 50% EtOH (b), and H_2O (c) at 40 °C.

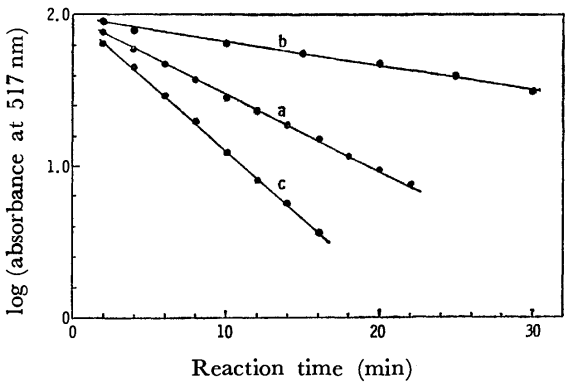

Fig. 5. Log plots of the absorbance at 517 nm of eosin Y (decomposed during the course of the chemiluminescent reaction) *versus* reaction time in 50% DMSO (a), 50% EtOH (b), and H_2O (c) at 40 °C.

50% DMSO, 50% EtOH, and H_2O are estimated to be 0.14, 0.05, and 0.19 min^{-1} respectively under the experimental conditions employed in the study. The same values of k_1+k_7 could be found from the lines for the log plots of the absorbance at 517 nm (the absorption peak of eosin Y) *versus* the reaction time (see Fig. 5).

The decomposition path of E being summarized by the following competitive and consecutive reaction diagram:

$$E + R^{\cdot} \begin{cases} \xrightarrow{k_1'} M_E^* \xrightarrow{\text{(fast)}} M_E \xrightarrow{k_6'} Q \\ \xrightarrow{k_7'} P \end{cases}$$

the concentration of the blue-fluorescent product ($[M_E]$) at time t can be given by:

$$[M_E] = \{k_1[E]_0/(k_1+k_7-k_6)\}[\exp(-k_6t) - \exp\{-(k_1+k_7)t\}] \quad (3)$$

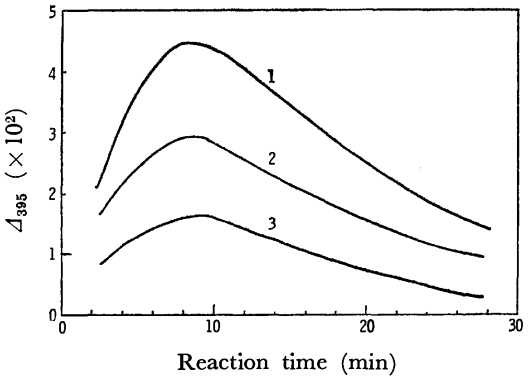

Fig. 6. Δ_{395}-t curves measured in 50% DMSO systems of different initial concentrations of eosin Y. 1: 8.7×10^{-4} M, 2: 5.8×10^{-4} M., 3: 4.3×10^{-4} M (40 °C).

where $k_6'[R\cdot]$ is put to k_6 by assuming that Reaction (vi) also obeys the pseudo-first order reaction.

Figure 6 shows Δ_{395}-t curves measured in 50% DMSO systems of different initial concentrations of eosin Y($[E]_0$). The results indicate that the value of Δ_{395} is strongly proportional to $[E]_0$, and so is proportional to $[M_E]$, if Eq. (3) is acceptable. From this argument, and recalling the results shown in Fig. 3, even though Δ_{395} may be changed a little by the decomposition of eosin Y and the generation of other minor, unknown reaction products, it seems reasonable to assume that:

$$\Delta_{395} \fallingdotseq \varepsilon_{395}[M_E] \quad (4)$$

where ε_{395} is the molar extinction coefficient of M_E at 395 nm. From Eq. (4), we can write:

$$\Delta_{395} = \{k_1\varepsilon_{395}[E]_0/(k_1+k_7-k_6)\}[\exp(-k_6t) - \exp\{-(k_1+k_7)t\}] \quad (5)$$

From Eqs. (3) and (4), putting t_m as the time required the reach to maximum of Δ_{395}, we can derive the following equation:

$$k_6\exp(-k_6t_m) = (k_1+k_7)\exp\{-(k_1+k_7)t_m\} \quad (6)$$

since $d[\Delta_{395}]/dt=0$; therefore $d[M_E]/dt=0$ at $t=t_m$. From the curves shown in Fig. 2, t_m being found to be 8, 12, and 2 min in 50% DMSO, 50% EtOH, and H_2O respectively, we can calculate the values of k_6 to be 0.10, 0.13, and 1.1 min^{-1} in 50% DMSO, 50% EtOH, and H_2O respectively, using the values of k_1+k_7 and t_m. From Eq. (6), the maximum value of $[M_E]$ at t_m ($[M_E]_m$) is given by:

$$[M_E]_m = (k_1/k_6)[E]_0\exp\{-(k_1+k_7)t_m\}$$

So that the maximum value of $\Delta_{395}(\Delta_m)$ is given by:

$$\Delta_m = \varepsilon_{395}(k_1/k_6)[E]_0\exp\{-(k_1+k_7)t_m\} \quad (7)$$

From Eqs. (5) and (7), we can finally write:

$$\Delta_{395} = \Delta_m[k_6/(k_1+k_7-k_6)\exp\{-(k_1+k_7)t_m] \times[\exp(-k_6t) - \exp\{-(k_1+k_7)t\}] \quad (8)$$

From the curves shown in Fig. 2, Δ_m being found to be 45×10^{-2}, 11×10^{-2}, and 4×10^{-2} in 50% DMSO, 50% EtOH, and H_2O respectively, the Δ_{395} values in these media can be calculated by the following numerical equations:

In 50% DMSO;

$$\Delta_{395} = \{0.10\times45\times10^{-2}/(0.14-0.10)\exp(-0.14\times8)\} \times\{\exp(-0.10t)-\exp(-0.14t)\}$$
$$= 3.45\{\exp(-0.10t)-\exp(-0.14t)\} \quad (9)$$

In 50% EtOH:

$$\Delta_{395} = \{0.13\times11\times10^{-2}/(0.05-0.13)\exp(-0.05\times12)\} \times\{\exp(-0.13t)-\exp(-0.05t)\}$$
$$= -0.325\{\exp(-0.13t)-\exp(-0.05t)\} \quad (10)$$

In H_2O:

$$\Delta_{395} = \{1.1\times4\times10^{-2}/(0.19-1.1)\exp(-0.19\times2)\} \times\{\exp(-1.1t)-\exp(-0.19t)\}$$
$$= -0.07\exp\{(-1.1t)-\exp(-0.19t)\} \quad (11)$$

In Table 1, the value of Δ_{395} in 50% DMSO, and 50% EtOH calculated using Eqs. (9) and (10) are tabulated, together with the observed values in the media. It can be seen from the table that the calculated Δ_{395} values are in fairly good agreement with the observed Δ_{395} values. The observed values of Δ_{395} in H_2O were, however, too small to make such a comparison.

Assuming that the value of ε_{395} does not appreciably vary in these media, we can calculate the ratio of k_1 (the generation rate of M_E) in the media from Eq. (7):

$$k_1(\text{DMSO}) : k_1(\text{EtOH}) : k_1(H_2O) = 0.10\times45\times10^{-2}/\exp(-0.14\times8) : 0.13\times11\times10^{-2}/\exp(-0.05\times12)$$
$$: 1.1\times4\times10^{-2}/\exp(-0.19\times2) = 5.3 : 1 : 2.47 \quad (12)$$

Table 1. Observed and calculated values of Δ_{395} in 50% DMSO and 50% EtOH

Reaction time (min)	50% DMSO		50% EtOH	
	Δ_{395} (obsd)	Δ_{395} (calcd)	Δ_{395} (obsd)	Δ_{395} (calcd)
2	10×10^{-2}	22.4×10^{-2}		
4	31	34.1		
5			8×10^{-2}	9×10^{-2}
6	41	40.3		
8	45	42.4		
10	44	41.7	10.5	10.8
12	41	39.7	11	11.2
14	37	36.6		
16	34	33.1		
18	30	29.3		
20	26	25.5	9	9.7
22	24	22.4		
24	21	19.3		
26	18	16.5		
28	16	14.1		
30	14	12.0	6	6.7
40			3.5	4.1
50			2	2.6

On the other hand, as Eq. (2) indicates that:

$$I_{E_0} = \{k_1k_4/(k_4+k_4')\}[E]_0$$

at $t=0$, the relative values of I_{E_0} in 50% DMSO, 50% EtOH, and H_2O can be estimated to be 87, 17, and 14 respectively by the extrapolation of the log plot of I_E (shown as relative intensities in Fig. 4) to zero-time. The ratio of the apparent efficiencies of the FL-emission ($k_4/(k_4+k_4')$) in the media was found to be 75 : 73 : 25, so we can also calculate the ratio of k_1 as follows:

$$k_1(\text{DMSO}) : k_1(\text{EtOH}) : k_1(H_2O) = 87/75 : 17/73 : 14/25 = 5.0 : 1 : 2.43 \quad (13)$$

The ratio in Eq. (13) is in good agreement with that in Eq. (12).

All of the results provide additional support for the view that the blue-fluorescent species is the primary excited product.

Unfortunately, the quantity of the isolated blue-fluorescent product was too small for it to be weighed or identified. 3,5-Dibromo-2,4-dihydroxybenzoate-2, which was produced when eosin Y was hydrolized in a 50% aqueous solution of sodium hydroxide for five hours at 140 °C,[6] showed no fluorescence at 480 nm. The fluorescence spectrum of 3,6-dihydroxyxanthone, which has been identified as the emitting species in the chemiluminescent reaction of succinylfluorescein, showed a peak at 410 nm.[7] The question as to the identification of the blue-fluorescent product, therefore, remains unanswered.

This work was supported in part by a Scientific Research Grant of the Ministry of Education.

References

1) I. Kamiya and S. Kato, This Bulletin, **43**, 1287 (1970).
2) The change of the spectrum in UV region (below 350 nm) could not be measured because the absorption of hydrogen peroxide retarded the measurement.
3) I. Kamiya and R. Iwaki, This Bulletin, **39**, 257, 264, 269, 277 (1966).
4) It was also found in the previous study,[1] that the FL-emission (a peak at 480 nm) which appeared during the course of the reaction decreased by successive oxidation.
5) The CL-emission intensity of xanthene dyes with hydrogen peroxide was about 100 times less than that of xanthene dyes with ozone whose quantum yield was reported to be $10^{-3}\sim10^{-4}$ einstein/mol (J. Nikokavouras and G. Vassilopoulos, *Z. Phys. Chem. (N.F.)*, **85**, 205 (1973).).
6) G. Heller, *Chem. Ber.*, **28**, 312 (1895); R. Meyer and H. Meyer, *ibid.*, **29**, 2623 (1896).
7) I. Kamiya and K. Aoki, This Bulletin, **47**, 1744 (1974).

The Electronic Spectra of Diphenylacetylene and 1,3-Butadiyne

Tetsuko TAKABE, Masashi TANAKA, and Jiro TANAKA
Department of Chemistry, Faculty of Science, Nagoya University, Chikusa-ku, Nagoya 464
(Received February 4, 1974)

The electronic absorption spectra of 2,4-hexadiyne-1,6-diol, diphenylacetylene, and diphenyldiacetylene were measured in a single crystalline state with a polarized light. The results of the polarization measurement and the theoretical calculations gave confirmative assignments of the electronic transitions of these molecules.

The electronic structures and electronic spectra of acetylene and poly-acetylenes have previously been investigated and have attracted considerable attention because of the simple molecular structures and the diveristy of electronic energy levels. Earlier extensive investigations of acetylene by Ingold *et al.*[1] and Innes[2] have revealed that the shape of the molecule in the excited state is not linear. The assignments of the electronic transitions of acetylene and poly-acetylenes have been discussed by many people.[3-9] The electronic spectra of diacetylene were studied by Woo and Chu[7] and by Price and Walsh,[8] and the bending of the excited state was suggested. Beer[9] investigated poly-acetylenes and classified the excited levels on the basis of the intensities of the electronic bands and the phosphorescence spectra. The polarization of band was measured on the crystal of dimethyldiacetylene, but the details of the analysis have not appeared. In this paper the polarization measurements in the near UV region of the derivatives of diacetylene, 2,4-hexadiyne-1,6-diol, diphenylacetylene and diphenyldiacetylene will be reported. The theoretical calculations of the energy levels of diacetylene and diphenylacetylene will also be presented in order to explain the observed spectra.

Experimental

2,4-Hexadiyne-1,6-diol was synthesized from propargyl alcohol.[10] The crystal for spectral measurements was obtained from a chloroform solution, and it was developed on the ac plane. The crystalline data will be reported in the Appendix. The projection of the molecules on the ac plane is shown in Fig. 1. The diphenylacetylene was obtained from the Tokyo Kasei Co. and was purified by recrystallization from methanol. The thin crystals for spectral measurement were obtained by sublimation; they were developed on the ab plane. The crystal structure was analyzed by Robertson and Woodward.[11] The diphenyldiacetylene was synthesized from phenylacetylene and was recrystallized from acetic acid. The crystal structure was analyzed by Wiebenga.[13] The crystalline absorption measurements were done with a microspectrophotometer.

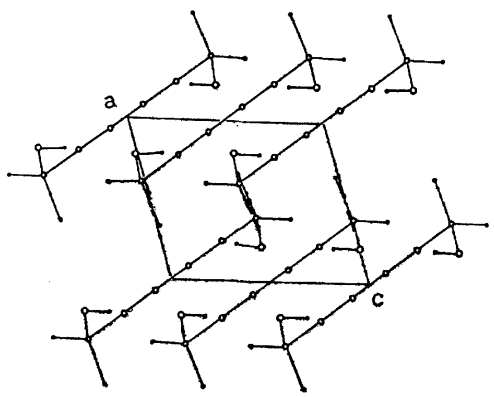

Fig. 1. Projection of 2,4-hexadiyne-1,6-diol crystal onto the ac plane.

Theoretical Calculations

The electronic energy levels of the diacetylene group and diphenylacetylene were calculated by a modification of the Pariser-Parr-Pople method, in which all the π and $\bar{\pi}$ electrons in the triple bonds are considered. The orthogonal MO sets, composed of $2p\pi$ and $2p\bar{\pi}$ atomic orbitals of carbon atoms, are calculated by the SCF method. The Hartree-Fock matrix elements are given as;

$$\begin{aligned}(\pi_\mu|\mathbf{F}|\pi_\mu) &= W_\mu + (\pi_\mu\pi_\mu|\pi_\mu\pi_\mu) - \sum_{\nu}^{m}(\pi_\nu\pi_\nu|\pi_\mu\pi_\mu) \\ &\quad - \sum_{\eta}^{n}(\bar{\pi}_\eta\bar{\pi}_\eta|\pi_\mu\pi_\mu) \\ &\quad + \sum_{\nu}^{m}\sum_{j}^{m}\{2C^*_{j\nu}C_{j\nu}(\pi_\nu\pi_\nu|\pi_\mu\pi_\mu) - C^*_{j\mu}C_{j\mu}(\pi_\mu\pi_\nu|\pi_\mu\pi_\nu)\} \\ &\quad + \sum_{\eta}^{n}\sum_{j}^{m}\{2C^*_{j\eta}C_{j\eta}(\bar{\pi}_\eta\bar{\pi}_\eta|\pi_\mu\pi_\mu) - C^*_{j\mu}C_{j\mu}(\bar{\pi}_\eta\pi_\mu|\bar{\pi}_\eta\pi_\mu)\} \\ (\pi_\mu|\mathbf{F}|\pi_\nu) &= \beta_{\mu\nu} - \sum_{j}^{m}C^*_{j\mu}C_{j\nu}(\pi_\mu\pi_\mu|\pi_\nu\pi_\nu) \\ (\pi_\mu|\mathbf{F}|\bar{\pi}_\eta) &= 0 \end{aligned} \quad (1)$$

where the subscript j denotes the filled MO, which varies from 1 to m, and where μ, ν, and η designate carbon atoms with orthogonal $2p\pi$ orbitals, π and $\bar{\pi}$. The one-electron Coulomb integrals are taken as:

$$(\pi_\mu\pi_\mu|\pi_\mu\pi_\mu) = (\bar{\pi}_\mu\bar{\pi}_\mu|\bar{\pi}_\mu\bar{\pi}_\mu) = 10.53 \text{ eV}$$

and

$$(\pi_\mu\pi_\mu|\bar{\pi}_\mu\bar{\pi}_\mu) = (\pi_\mu\pi_\mu|\pi_\mu\pi_\mu) - 1/2(\pi_\mu\bar{\pi}_\mu|\pi_\mu\bar{\pi}_\mu)$$

where

$$(\pi_\mu\bar{\pi}_\mu|\pi_\mu\bar{\pi}_\mu) = 0.91 \text{ eV}.$$

The valence-state ionization potential, W_p, is taken as -11.24 eV for the sp hybridized state and as -11.22 eV for the sp^2 hybridized state. The resonance integrals, β, were taken only for nearest neighbors; they were calculated by

$$\beta = -2.38\exp(2.375 - 1.7r) \text{ eV}.$$

All the calculations were based on the structure data determined by the X-ray crystal analysis. The configurational interaction of one-electron excited states were calculated with the SCF MO. The calculation for diphenylacetylene was performed similarly. The

Table 1. Transition energies of diacetylene

State	Calculated values			Experimental values		
	Transition energy (eV)	Oscillator strength f	Dichroic ratio $I_{//c}/I_{\perp c}$	Transition energy (eV)	Oscillator strength f	Dichroic ratio $I_{//c}/I_{\perp c}$
$^1A_{1u}$	4.41	forbidden		4.25	2×10^{-5}	1.1
$^1E_{2u}$	4.73	forbidden	1.63 (long-axis)	4.77	1×10^{-3}	1.5
$^1A_{2u}$	9.44	2.93		—	—	—
$^3A_{2u}$	3.42	forbidden		3.39[9]	—	—

Table 2. Molecular orbitals and state function of diacetylene

ε (eV)	j, j'	$c_{j\mu}=c_{j\mu'}$	
		$\mu=1$	2
−14.06	1	0.4236	0.5662
−11.32	2	0.5662	0.4236
−1.56	3	0.5662	−0.4236
1.18	4	0.4236	−0.5662

$^1A_{1u}$: $1/\sqrt{2}\{\psi_{2\to3'}-\psi_{2'\to3}\}$
$^1E_{2u}$: $1/2\{\psi_{2\to3'}+\psi_{2'\to3}+\psi_{2\to3}-\psi_{2'\to3'}\}$
$1/2\{\psi_{2\to3'}+\psi_{2'\to3}-\psi_{2\to3}+\psi_{2'\to3'}\}$
$^1A_{2u}$: $1/\sqrt{2}\{\psi_{2\to3}+\psi_{2'\to3'}\}$

Table 3. Transition energies of diphenylacetylene

State	Sym-metry	Calculated values		Experimental values	
		Transition energy (eV)	Oscillator strength f	Transition energy (eV)	Oscillator strength f
$^1B_{2u}$	y	4.20	1.50	4.21	0.66
$^1B_{3u}$	x	6.10	0.93	5.66	0.40
$^1B_{2u}$	y	6.40	0.82	6.30	—

results gave the transition energies and oscillator strengths shown in Tables 1 and 2. The observed spectral data are also shown there.

Results and Discussion

2,4-Hexadiyne-1,6-diol. The electronic absorption spectra in an ethanol solution are shown in Fig. 2. Two different series of absorption bands have been observed, one with a very weak intensity in the 30000—37000 cm^{-1} region and another with a medium intensity in the 37000—48000 cm^{-1} region. Both series are accompanied by vibrational progressions of 2200—2300 cm^{-1}, which can reasonably be correlated with the total symmetric vibration of the triple bonds. Because the intensities of these bands are rather weak, both series may be regarded as having a forbidden character.

The crystalline absorption spectra on the ac plane are presented in Fig. 3. Although the 0-0 band origin was not confirmed for this spectra, nevertheless the spectral pattern was clearly resolved, showing some vibrational progressions. The weakest and lowest transition starts at 30400 cm^{-1} and extends to 37000 cm^{-1}. The two band maxima at 33900 and 36100 cm^{-1} are separated by 2200 cm^{-1}, which is regarded as the total

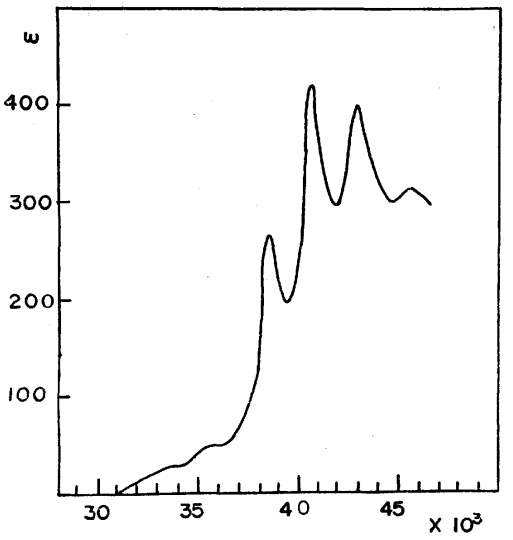

Fig. 2. Electronic absorption spectrum of 2,4-hexadiyne-1,6-diol in ethanol solution measured with Carl Zeiss spectrophotometer PMQ-II.

symmetric stretching vibration of the carbon-carbon triple bond. Taking the 0-0 band origin of the series as at 30400 cm^{-1}, one may suppose the presence of a coupled asymmetric mode which makes the forbidden transition active. For instance, the first vibronic allowed level may be assumed at 31700 cm^{-1}; therefore, a coupled frequency must be about 1300 cm^{-1} at its maximum.

The second, stronger series starts at 38500 cm^{-1}, followed by the vibrational progressions given by $38500+2200n$ cm^{-1} ($n=1,2,\cdots$). The dichroic intensity ratios for these two band series are estimated by taking the intensity ratio from the areas of these observed bands; they are tabulated in Table 1. The calculated value (1.63) is obtained from the crystal structure data by assuming that the electronic transitions are polarized parallel to the long axis of the molecule. With the second stronger transition, the observed value (1.5) is in good agreement with the predicted value of the long-axis polarization. For the first band, the polarization seems to be along the short-axis, because the observed intensity ratio (1.1) deviates from the value of the long-axis. As regards the transition polarized perpendicular to the long-axis, the direction could not be determined in $D_{\infty h}$ symmetry, but the dissimilar polarization ratio may be considered as proof of a different polarization character.

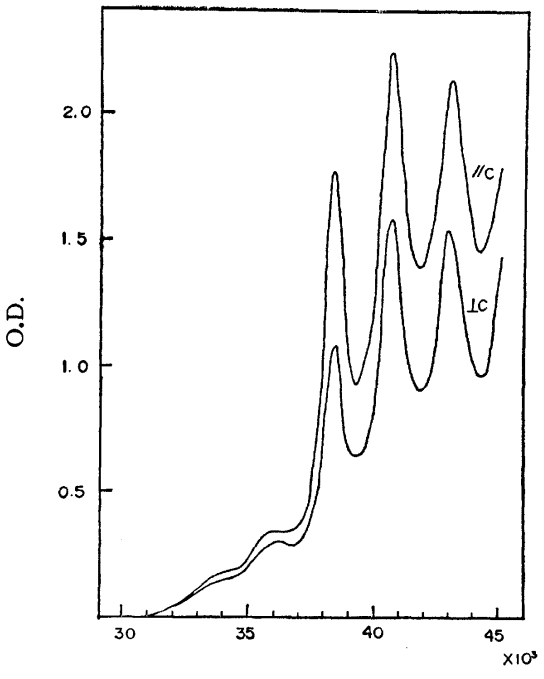

Fig. 3. Crystalline absorption spectra of 2,4-hexadiyne-1,6-diol for ac plane with the light polarized parallel and perpendicular to the c-axis.

Following the results of the theoretical calculations, the first forbidden band is assigned to the $^1A_{1u}$ state; it is shown that the transition is a $\pi \rightarrow \bar{\pi}^*$ type and is strictly forbidden. In the symmetry of the $D_{\infty h}$ of the linear system, the band is not active and it should appear when the excited state is deformed to the *trans*-form and/or when the molecule is coupled with the e_{1g}-type vibration. The vibronic analysis suggests that the observed vibronic excited state may be bent by a coupling with an asymmetric vibrational mode.

The second band is assigned to the transition to the $^1E_{2u}$ state, which is also forbidden but which has a mixed character of $\pi \rightarrow \pi^*$ and $\pi \rightarrow \bar{\pi}^*$-type transitions. The calculated energy values are in good agreement with the observed value. The $^1E_{2u}$ state of the linear system is changed to the ^1B_u state in the *trans*-form and to the $^1B_1$ state in the *cis*-form. The transition to these states will be allowed along the direction of the triple bond.[3-9] The presence of two band systems in the near UV region is in good agreement with the results of Woo and Chu,[7] who found a very weak system at 33700—37730 cm^{-1} and a diffuse and stronger band in the 38460 cm^{-1} region.

The results of polarization measurements on the crystalline spectra are in good agreement with the theoretical predictions of the transition directions. Thus, the assignments have been established for the first and second bands.

Diphenylacetylene. The UV spectrum in the ethanol solution is shown in Fig. 2. The first absorption band, starting at 33800 cm^{-1}, shows vibrational progressions of 2000 cm^{-1} and 950 cm^{-1}. The former is regarded as a totally symmetric vibration of the

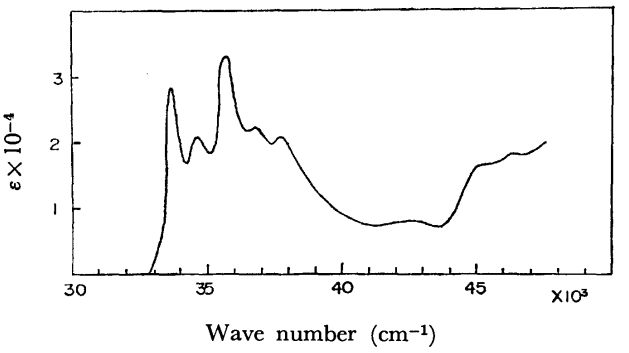

Fig. 4. Electronic absorption spectrum of diphenylacetylene in ethanol solution.

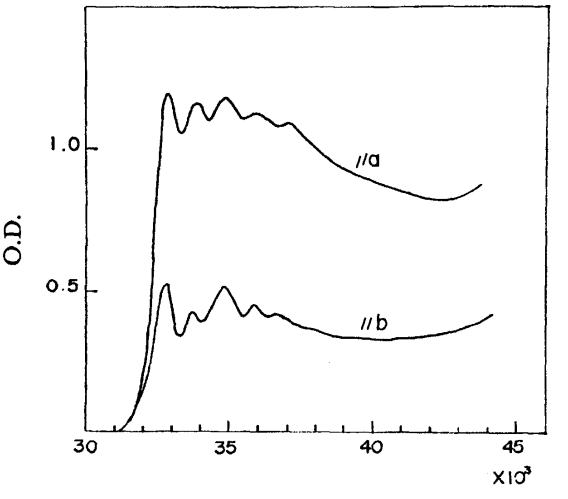

Fig. 5. Crystalline absorption spectra of diphenylacetylene for ab plane with the light polarized parallel to the a- and b-axes.

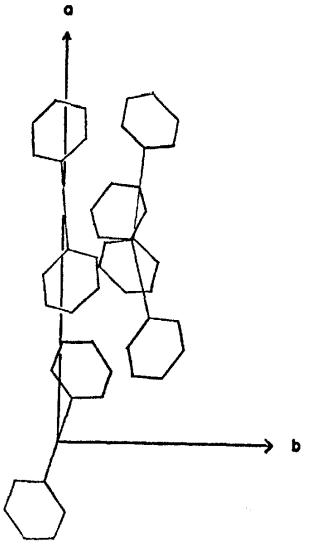

Fig. 6. Projection of diphenylacetylene in crystal onto the ab plane.

carbon-carbon triple bond, while the latter may be a vibration of the benzene ring. The results of the calculation show that the first band is the long-axis-polarized allowed transition. The crystalline absorption spectra are shown in Fig. 5. While the projection of molecules onto the developed ab plane is illustrated in Fig. 6. The intensity ratio observed on the crystalline spectra can reasonably be explained by the oriented gas model, and the first absorption band has been shown to be polarized parallel to the long-axis. These results support the earlier investigation by Mikailenko *et al.*[12] of the polarization study of the fluorescence.

Diphenyldiacetylene: The UV spectrum in the ethanol solution is shown in Fig. 7. The observed bands are very broad, and they seem to be composed of two or three band series starting at 30700 cm^{-1} and at 38500 cm^{-1}. The crystalline spectra are recorded with the ab plane, as is shown in Fig. 8. Following the crystalline structure data of Wiebenga,[13] the projection of molecules onto the ab plane is shown in Fig. 9. It will be easily found that the long-axis of the molecule is slightly more inclined to the a-axis than to the b-axis, and that the intensity ratio by the oriented gas model is $I_a/I_b=$ 1.4 : 1, while the observed value is 1.25 : 1 for both the first and second bands. Those results show that the polarization of the first and second bands are both along the long-axis.

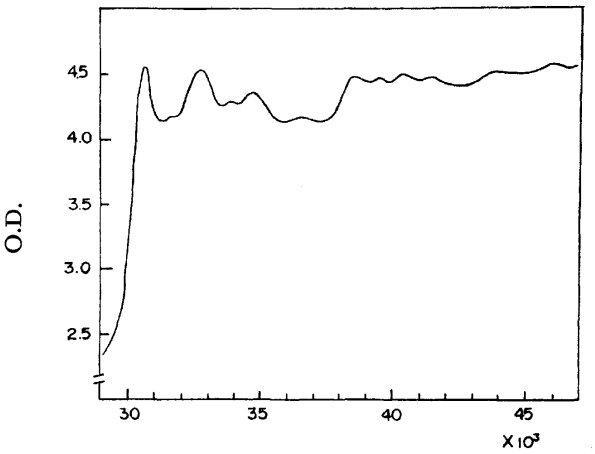

Fig. 7. Electronic absorption spectrum of diphenyldiacetylene in ethanol solution.

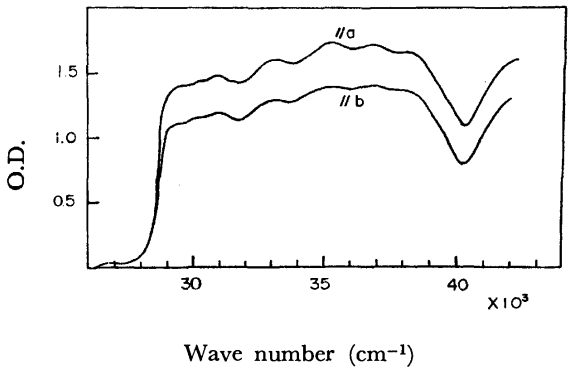

Fig. 8. Crystalline absorption spectra of diphenyldiacetylene for ab plane with the light polarized parallel to the a- and b-axes.

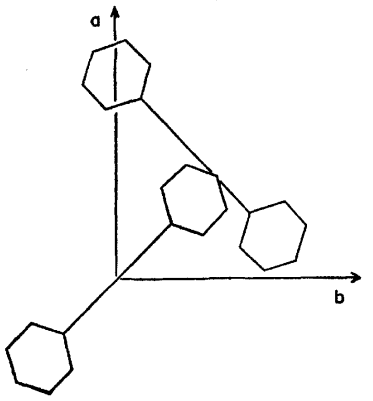

Fig. 9. Projection of diphenyldiacetylene molecules to the ab plane in the crystal.

Appendix

Crystalline Data of 2,4-Hexadiyne-1,6-diol. After the completion of our crystalline structure analysis, we found that an independent research has already been published.[14] However, the atomic coordinates were not given, and so we briefly describe our own results.

Crystal Data. From Weissenberg photographs and single-crystal diffractometry on a Hilger-Watt Four-circle diffractometer with Cu$K\alpha$, $\lambda=1.5418$ Å, $a=4.083(1)$, $b=16.000(1)$, $c=4.764(1)$ Å, $\beta=106.3°$, $Z=2$. $d_{obsd}=1.14$ g/cm³, and $d_{calcd}=1.19$ g/cm³. Space group $P2_1/c$. When the intensity data were collected on the diffractometer, 360 independent reflections were obtained. The data were corrected by the Lorentz and polarization factors. The absorption correction was not applied since the crystal size was so small as $0.1\times0.5\times$ 1 mm. The center of the molecule is coincident with the origin of the crystal for symmetry reasons. The molecule is linear, and the direction of the molecular axis can easily be found in the Patterson map. The refinement of the structure was performed by the block-diagonal least-squares method and by Fourier synthesis. A program of the UNICS written by Dr. Ashida was employed. The calculation was performed on the Hitac 5020 at Computer Centre, the University of Tokyo. The final R-index including hydrogen atoms was 0.107.

Atomic coordinates.

	x / a	y / b	z / c
C1	0.0814	0.0286	0.1083
C2	0.2235	0.0759	0.2883
C3	0.4094	0.1367	0.5144
O1	0.2133	0.2108	0.5057
H1	0.3970	0.1073	0.6755
H2	0.6669	0.1545	0.4664
H3	0.2178	0.2389	0.3716

We wish to thank Dr. Noriyoshi Sakabe of our Laboratory for his helpful advice on the X-ray crystal analysis.

References

1) C. K. Ingold and G. W. King, *J. Chem. Soc.*, **1933**, 2702.

2) K. K. Innes, *J. Chem. Phys.*, **22**, 863 (1954).
3) R. S. Mulliken, *Can. J. Chem.*, **36**, 10 (1958).
4) H. Howard and G. W. King, *ibid.*, **37**, 700 (1959).
5) L. Burnelle, *J. Chem. Phys.*, **35**, 311 (1961).
6) A. D. Walsh, *J. Chem. Soc.*, **1953**, 2290.
7) S. C. Woo and T. C. Chu, *J. Chem. Phys.*, **5**, 786 (1937).
8) W. C. Price and A. D. Walsh, *Trans. Faraday Soc.*, **41**, 381 (1945).
9) M. Beer, *J. Chem. Phys.*, **25**, 745 (1956).
10) K. Bowden, I. Heilbron, E. R. H. Jones, and K. H. Sargent, *J. Chem. Soc.*, **1947**, 1579.
11) J. M. Robertson and I. Woodward, *Proc. Roy. Soc., Ser. A*, **164**, 436 (1938).
12) V. I. Mikailenko, P. A. Tephyakov, V. V. Trusov, and V. M. Martynchenko, *Optics and Spectrosc.*, **20**, 29 (1966).
13) E. H. Wiebenga, *Z. Krist.*, **102**, 193 (1940).
14) E. Hädicke, K. Penzien, and H. W. Schnell, *Angew. Chem.*, **83**, 1024 (1972).

The Electronic Spectra of Paracyclophadiynes

Tetsuko TAKABE, Masashi TANAKA, and Jiro TANAKA

Department of Chemistry, Faculty of Science, Nagoya University, Chikusa-ku, Nagoya 464

(Received February 19, 1974)

The electronic absorption spectra of [3,3]-paracyclophadiyne and [4,4]-paracyclophadiyne have been investigated in solution and in the crystalline state. A *trans*-annular interaction between the diacetylene group and the benzene ring has been found, and a theoretical study has been made to confirm the assignment. The bathochromic shift and the CT band from the benzene ring to the diacetylene group are particularly noticeable for [3,3]-paracyclophadiyne, where the inter-group distance is significantly shorter than the normal van der Waals distance.

The *trans*-annular interaction between the different groups in composite molecules is a problem of great interest, because the mechanism of the electronic interaction between contact groups at close distances is not yet fully elucidated. A well-known case is that of [2,2]-paracyclophane, where a bathochromic shift of the UV absorption is observed. The CT bands of the complexes between TCNE and cyclophanes are also red-shifted by the *trans*-annular layer interaction.[1] The electronic structure and spectrum of [2,2]-paracyclophane were investigated by Vala *et al.*[2] and by Iwata *et al.*[3] and a significant change in spectrum from that of benzene was interpreted in terms of the presence of the CT transition between the benzene rings.

Recently a series of paracyclophadiynes were synthesized by Misumi and his collaborators;[4] a crystallographic study was carried out on one of these compounds in this laboratory. Each of the molecules consists of a diacetylene group and a benzene ring (Fig. 1), and the CT effect can be expected between the two groups. In this paper the electronic absorption spectra of 4,6-[10]-paracyclophadiyne ([3,3]-paracyclophadiyne) and 5,7-[12]-paracyclophadiyne ([4,4]-paracyclophadiyne) will be investigated in order to ascertain the *trans*-annular effect on the UV spectra. The inter-group CT transition is observed in [3,3]-paracyclophadiyne, while it is not found in [4,4]-paracyclophadiyne. A theoretical calculation for interpreting these spectra will be presented, and the assignment of the spectra will be presented in detail.

Experimental

The samples of [3,3]-paracyclophadiyne and [4,4]-paracyclophadiyne were gifts from Professor Misumi of Osaka University. The absorption spectra in solution were measured by means of a Carl Zeiss spectrophotometer, PMQ II. The crystalline absorption spectra of [3,3]-paracyclophadiyne were measured by means of thin crystals obtained by sublimation. A microspectrophotometer, composed of a Carl Zeiss monochromator and an Olympus microscope, was used for the crystalline spectral measurements. The crystal structure of [3,3]-paracyclophadiyne will be described in a separate paper. The crystalline data are as follows: monoclinic; space group $P2_1/a$; $a=14.509$; $b=8.539$, $c=10.623$ Å, and $\beta=112.37°$.[5] The crystal develops the ab plane by sublimation. The thin crystal of [4,4]-paracyclophadiyne were obtained from an acetone-water solution and were used for spectral measurements. The crystalline data were obtained by oscillation and Weissenberg photographs; $a=8.441\pm0.03$, $b=13.14\pm0.03$, $c=12.73\pm0.03$ Å, $\alpha=90.4\pm0.3°$, $\beta=90.4\pm0.3°$, and $\gamma=92.8\pm0.3°$. The crystal develops the ac plane.

Theoretical Calculations

The electronic energy levels of [3,3]-paracyclophadiyne are calculated by the molecular orbital method. The orthogonalized SCF MO for the diacetylene group, ϕ_{aj}, and the benzene ring, ϕ_{bi}, are calculated, and the ground configuration of the molecule is given as;

$$\Phi_0 = |\phi_{a1}(1)\cdots\bar{\phi}_{an}(2n)\phi_{b1}(2n+1)\cdots\bar{\phi}_{bm}(2n+2m)| \quad (1)$$

The excited configurations of each group will be denoted as $\Phi_{ai\to aj}$ and $\Phi_{bi\to bj}$. The singlet configuration of the charge transfer from the benzene ring to the diacetylene group may be described as;

$$\Phi_{bi\to aj} = \frac{1}{\sqrt{2}}\{|\cdots\phi_{bi}(2n+2i-1)\bar{\phi}_{aj}(2n+2i)\cdots| \pm|\cdots\phi_{aj}(2n+2i-1)\bar{\phi}_{bi}(2n+2i)\cdots|\} \quad (2)$$

The configurational energies and the matrix elements are calculated by using the Hamiltonian including the inter-group interaction:

$$\mathscr{H} = \sum_i\left\{-\frac{\hbar^2}{2\mu}\nabla_i^2 + V(\mathbf{r}_{ai}) + V(\mathbf{r}_{bi})\right\} + 1/2\sum_{i,j}e^2/r_{ij}. \quad (3)$$

The calculation of the excited energy levels is carried out by the composite molecule method. That is, the matrix elements between Φ_0, $\Phi_{ai\to aj}$ and $\Phi_{bi\to aj}$ are given in the zero-differential overlap approximation as follows:

$$\begin{aligned}
&(\Phi_{ai\to aj}|\mathscr{H}|\Phi_{ai\to aj}) = E_0 + \varepsilon_{aj} - \varepsilon_{ai} - (\phi_{ai}\phi_{ai}|\phi_{aj}\phi_{aj}) + 2(\phi_{ai}\phi_{aj}|\phi_{ai}\phi_{aj})\\
&(\Phi_{bi\to aj}|\mathscr{H}|\Phi_{bi\to aj}) = E_0 + \varepsilon_{aj} - \varepsilon_{bi} - (\phi_{bi}\phi_{bi}|\phi_{aj}\phi_{aj})\\
&(\Phi_{ai\to aj}|\mathscr{H}|\Phi_{ak\to al}) = 2(\phi_{ai}\phi_{aj}|\phi_{ak}\phi_{al}) - (\phi_{ai}\phi_{ak}|\phi_{aj}\phi_{al})\\
&(\Phi_{ai\to aj}|\mathscr{H}|\Phi_{bk\to bl}) = 2(\phi_{ai}\phi_{aj}|\phi_{bk}\phi_{bl})\\
&(\Phi_{ai\to bj}|\mathscr{H}|\Phi_{ak\to bl}) = -(\phi_{ai}\phi_{ak}|\phi_{bj}\phi_{bl})\\
&(\Phi_{bi\to aj}|\mathscr{H}|\Phi_0) = -\sqrt{2}\left(\phi_{bi}\left|-\frac{\hbar^2}{2\mu}\nabla^2\right|\phi_{aj}\right)\\
&(\Phi_{ai\to aj}|\mathscr{H}|\Phi_{ai\to bl}) = -\left(\phi_{aj}\left|-\frac{\hbar^2}{2\mu}\nabla^2\right|\phi_{bl}\right)\\
&(\Phi_{ai\to aj}|\mathscr{H}|\Phi_{bk\to aj}) = \left(\phi_{ai}\left|-\frac{\hbar^2}{2\mu}\nabla^2\right|\phi_{bk}\right)\\
&(\Phi_0|\mathscr{H}|\Phi_{ai\to aj}) = (\Phi_{ai\to aj}|\mathscr{H}|\Phi_{ak\to bl}) = (\Phi_{ai\to bj}|\mathscr{H}|\Phi_{bk\to al}) = 0
\end{aligned} \quad (4)$$

Here, the intermolecular kinetic and Coulomb integrals

are exactly calculated; the molecular orbitals, ϕ_{ai}, and the orbital energies, ε_{ai}, were given in a previous paper.[6] The results of the calculation are shown in Tables 1 and 2, where the polarization directions are described by the coordinates shown in Fig. 1.

It may be seen from Table 2 that the lower CT transitions are mostly of the $\phi_{bi}\rightarrow\phi_{aj}$ type, which implies that the donor property of the benzene ring exceeds that of the diacetylene group.

TABLE 1. OBSERVED AND CALCULATED TRANSITIONS OF [3,3]-PARACYCLOPHADIYNE

State (polarization)	Calculated		Observed	
	Transition energy(eV)	Oscillator strength f	Transition energy(eV)	Oscillator strength f
A_2	4.22	forbidden	4.10	—
$B_2(y)$	4.34	2×10^{-4}	4.20	3×10^{-3}
$B_1(x)$	4.49	1×10^{-4}		
$B_1(x)$	4.80	1×10^{-4}		
$B_2(y)$	4.88	1×10^{-3}		
$B_2(y)$	5.69	6×10^{-3}	5.27	3×10^{-2}
$B_1(x)$	5.75	2×10^{-2}		
$B_2(y)$	5.78	3×10^{-2}		
$A_1(z)$	5.97	1×10^{-3}		

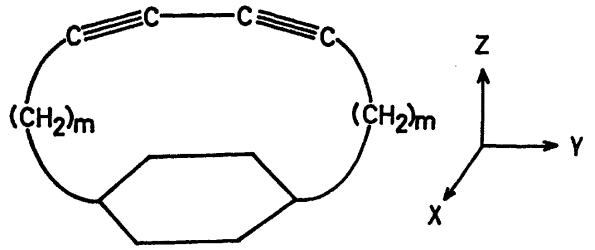

Fig. 1. The shape of [*m*,*m*]-paracyclophadiyne and the coordinate axes.

Results and Discussion

[4,4]-Paracyclophadiyne. The electronic absorption spectrum in solution is shown in Fig. 2, while that in a crystal is shown in Fig. 3. The spectra are considered to be superpositions of those of the two chromophores, the benzene and diacetylene groups, and a red shift of the $^1E_{1u}$-type band of benzene is observed. In the crystalline spectra, the weakest $^1A_{1u}$-type band of the diacetylene group is observed in the 33500—35500 cm^{-1} region, and the second transition, starting at 36700 cm^{-1}, may be reasonably correlated with the band at 38500 cm^{-1} of the diacetylene group, because it shows the vibrational progressions characteristic of the diacetylene group. Overlapping with this band series, the $^1B_{2u}$ parentage band of the benzene ring may exist in this region. Since the crystal structure is not known for this molecule, an extensive argument on the polarization and assignment can not be developed, but the band at 44500 cm^{-1} may be regarded as originating from the $^1E_{1u}$ level of the benzene group. The red shift of this band as compared to that of benzene may be caused by the CT-type interaction, which indicates that the level may be located in the higher energy region. The

TABLE 2. WAVE FUNCTIONS FOR THE SINGLET ELECTRONIC STATES OF [3,3]-PARACYCLOPHADIYNE

A_1 type state

Energy(eV)	Φ_0	$\Phi_{b3\rightarrow a\bar{3}}$	$\Phi_{a\bar{2}\rightarrow b4}$
0.00	0.9999	0.0053	−0.0141
5.01	−0.0052	0.9999	0.0009
5.97	−0.0141	0.0008	−0.0141

A_2 type state

Energy(eV)	$\Phi_{a2\rightarrow a\bar{3}}$	$\Phi_{a\bar{2}\rightarrow a3}$	$\Phi_{b2\rightarrow a\bar{3}}$	$\Phi_{a\bar{2}\rightarrow b5}$
4.22	0.7332	−0.6605	0.1611	0.0104
4.70	0.6188	0.7463	0.2445	0.0170
5.37	−0.2818	−0.0795	0.9562	0.0048
5.78	0.0042	0.0199	−0.0021	0.9998

B_1 type state

Energy(eV)	$\Phi_{b2\rightarrow b4}$	$\Phi_{b3\rightarrow b5}$	$\Phi_{b3\rightarrow a3}$	$\Phi_{a2\rightarrow b4}$
4.49	0.7069	0.6874	−0·0306	0.1639
4.80	0.0299	0.0101	0.9994	0.0150
5.75	−0.0062	0.2384	0.0123	−0.9711
6.48	0.7067	−0.6859	−0.0116	−0.1731

B_2 type state

Energy(eV)	$\Phi_{b2\rightarrow b5}$	$\Phi_{b3\rightarrow b4}$	$\Phi_{a2\rightarrow a3}$	$\Phi_{a\bar{2}\rightarrow a\bar{3}}$	$\Phi_{b2\rightarrow a3}$	$\Phi_{a2\rightarrow b5}$
4.34	0.0072	0.0003	−0.6957	0.6839	−0.2192	0.0152
4.88	0.0513	−0.0025	0.1229	−0.1878	−0.9729	0.0206
5.69	0.4789	−0.2983	−0.0162	−0.0249	0.0462	0.8238
5.78	−0.4779	0.6992	−0.0122	−0.0236	−0.0128	0.5308
6.44	0.7147	0.6309	−0.1625	−0.1555	0.0414	−0.1973
9.37	0.1696	0.1550	0.6885	0.6868	−0.0372	−0.0062

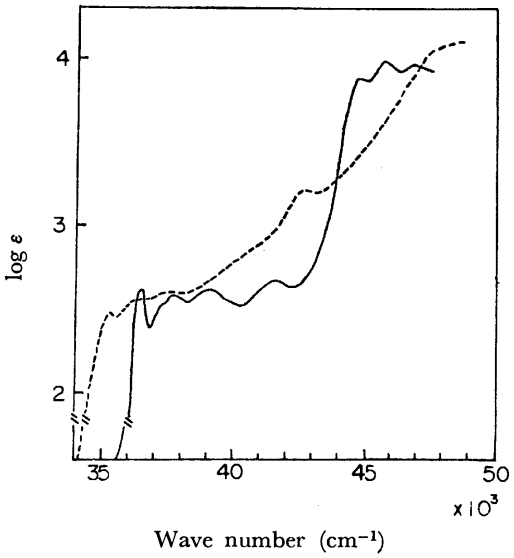

Fig. 2. The UV absorption spectra of
---- [3,3]-paracyclophadiyne and
—— [4,4]-paracyclophadiyne.

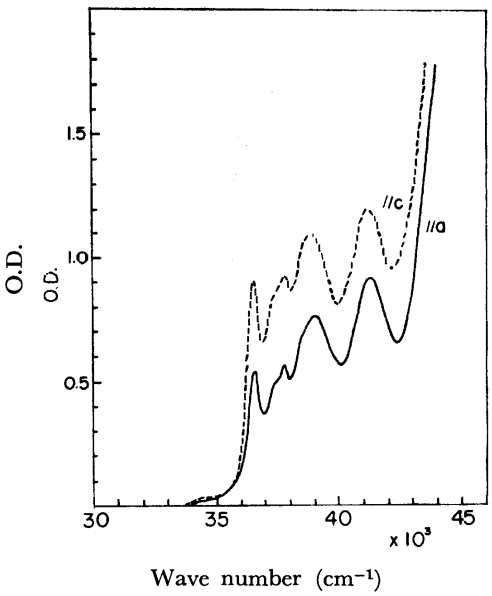

Fig. 3. The crystalline UV absorption spectra of [4,4]-paracyclophadiyne with (010) plane.

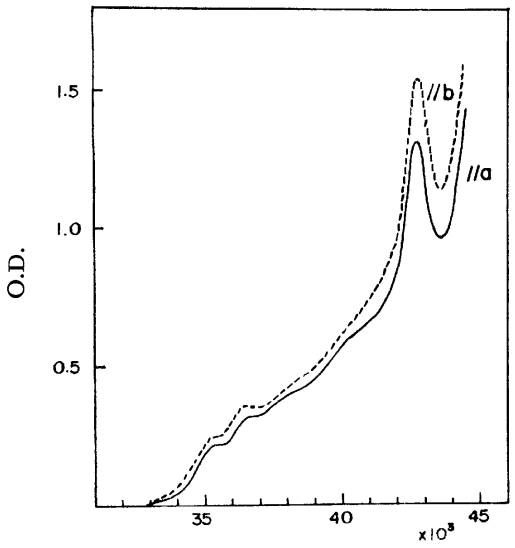

Fig. 4. The crystalline UV absorption spectra of [3,3]-paracyclophadiyne with (001) plane.

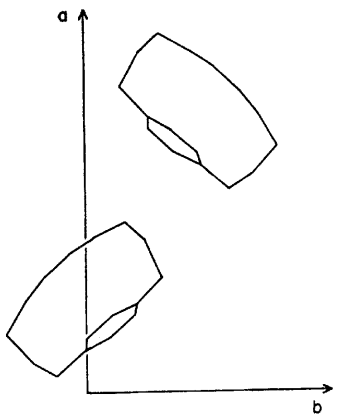

Fig. 5. The projection of [3,3]-paracyclophadiyne onto the (001) plane.

inter-group distance, separated by four methylene groups, will be larger than 3.3 Å, and the electronic overlap between the groups is not so effective that the CT transition may not appear at lower energies with a noticeable intensity.

[3,3]-Paracyclophadiyne. In the solution spectra of [3,3]-paracyclophadiyne (Fig. 2), a bathochromic shift of the UV absorption is apparent. The first absorption band in the 34500—37500 cm^{-1} region may be related to the diacetylene group,[6] but the transition to the $^1B_{2u}$ state of the benzene ring may overlap in this region. In the crystalline spectra (Fig. 4), a broad band with vibrational structures are observed in the 33500—37000 cm^{-1} region, and the band intensities along the a- and b-axes are nearly the same throughout this spectral region. These results seem consistent with the assignment of the $^1B_2(y)$-type transition, since the crystal structure analysis shows that the y-polarized band should give a nearly equal intensity along the a- and b-axes. If the $^1B_{2u}$-type transition of the benzene ring dominates in this region, the intensity should be predominant along the b-axis rather than distributed equally between the two axes; hence, the contribution of the $^1B_{2u}$-type band may not be so significant in the 38500—40000 cm^{-1} region.

Several CT transitions from the benzene ring to the diacetylene group are calculated to exist in this region, although they have weak intensities. In the shorter-wavelength region, a sharp prominent transition is observed at 42700 cm^{-1}; it is an extra band not belonging to either of the component chromophores. Following the theoretical calculation, a CT transition of the $^1B_2(y)$ type may be responsible for this transition, in which the charge transfer from the benzene ring to the diacetylene group is predominant. The polarization characteristic of this transition is that of the y-axis. However, the direction of the transition moment could

not unambiguously be determined by the observed polarization ratio (I_b/I_a), because the possibility of z polarization still remains to be solved.

According to the crystal-structure analysis, the inteatomic distances between the diacetylene group and the benzene-ring plane are in the range of 3.1—3.2 Å; a significant electronic interaction can be expected at such a short interatomic distance. Although the CT transition does not appear with strong intensities in the near UV region, the spectrum shows a bathochromic shift of the first band as large as 1300 cm^{-1}, in contrast to the case of [4,4]-paracyclophadiyne. The vibrational structure of the band is also blurred off. Moreover, the $^1E_{1u}$-type band of the benzene ring is blue-shifted in contrast to [4,4]-paracyclophadiyne because of the presence of the CT state at 42700 cm^{-1}, below the original position of the $^1E_{1u}$ level. The influence of the CT transition is thus shown to be important in determining the spectral properties of the system, with chromophores interacting through *trans*-annular interactions.

The authors are grateful to Professor Soichi Misumi and Drs. Yoshiteru Sakata and Takahiro Matsuoka of Osaka University for the gift of samples.

References

1) D. J. Cram and J. M. Cram, *Accounts Chem. Res.*, **4**, 204 (1971).
2) M. T. Vala, I. H. Hillier, S. A. Rice, and J. Jortner, *J. Chem. Phys.*, **44**, 23 (1966).
3) S. Iwata, K. Fuke, M. Sasaki, S. Nagakura, T. Otsubo, and S. Misumi., *J. Mol. Spectrosc.*, **46**, 1 (1973).
4) T. Matsuoka, T. Negi, T. Otsubo, Y. Sakata, S. Misumi, This Bulletin, **45**, 1825 (1972).
5) T. Aono, K. Sakabe, N. Sakabe, C. Katayama, and J. Tanaka, *Acta Crystallogr.*, **B**, to be submitted.
6) T. Takabe, M. Tanaka, and J. Tanaka, This Bulletin, **47**, 1912 (1974).

Estimation of Individual Ionic Activity Coefficients from Conductivity Data on Strong Electrolytes in Dilute Aqueous Solutions

Reita TAMAMUSHI

The Institute of Physical and Chemical Research, Hirosawa, Wako-shi, Saitama 351

(Received April 22, 1974)

The individual ionic activity coefficients of strong electrolytes in dilute aqueous solutions are derived from the ionic conductivity data, using the Debye-Hückel-Onsager theory of strong electrolyte solutions. The mean activity coefficients computed by the present method are in good agreement with the experimental values in most of the uni-univalent and some of the uni-multivalent electrolytes studied, which demonstrates the validity of the method in deriving the individual ionic activity coefficients. Comparisons are made of the values of individual activity coefficients of various ions in dilute aqueous solutions of strong electrolytes, as determined by different methods including measurements of potential differences across membranes at varying concentrations. The influence of the ion of opposite sign on the individual ionic activity coefficient has been observed.

The individual ionic activity coefficient is an important and useful quantity in the study of various phenomena in electrolyte solutions. Thermodynamics provides methods of determining mean activity coefficients of electrolytes, but it can offer no theoretical or experimental approach to the determination of individual ionic activity coefficients. Non-thermodynamic assumptions must be introduced in the calculation of individual ionic activity coefficients. Typical conventions used for computing ionic activities have been discussed in detail by Bates and Alfenaar.[1]

In solutions of low ionic strength ($I \leq 0.1$ M), individual ionic activity coefficients can be calculated with reasonable accuracy from the Debye-Hückel equation, if appropriate ion-size parameters are assumed. In his classical tabulation of ion-size parameters, Kielland[2] employed the so-called Stokes radius calculated from the ionic conductivity at infinite dilution. The application of conductivity data to the determination of ion-size parameters in the activity equation was suggested by Fuoss and Accascina.[3] Justice *et al.*[4] discussed the self-consistency of the Debye-Hückel theory of activity coefficients and the Fuoss-Onsager theory of electrolytic conductivity, and justified the use of conductivity data in the estimation of activity coefficients of electrolytes in dilute solutions ($I \leq 0.1$ M). Their study, however, was restricted to mean activity coefficients of electrolytes. The possibility of computing individual ionic activity coefficients from conductivity data has not been discussed.

In this paper, individual ionic activity coefficients are derived from ionic conductivity data, based upon the Debye-Hückel-Onsager theory of strong electrolyte solutions. The results are compared with the individual ionic activity coefficients calculated by various conventions[1] and with some experimental values obtained from membrane-potential measurements.

Theoretical

The Debye-Hückel-Onsager theory[5] of strong electrolyte solutions gives the following expressions for the individual ionic activity coefficient $\gamma_{+(-)}$ and ionic conductivity $\lambda_{+(-)}$, respectively, of the cation (anion) in a solution of a single electrolyte*:

$$\log \gamma_{+(-)} = -A^* z^2_{+(-)} \chi^{-1}_{+(-)} \tag{1}$$

$$\lambda_{+(-)} = \lambda^{\infty}_{+(-)} - (\alpha^* \lambda^{\infty}_{+(-)} + \beta^* |z_{+(-)}|) \chi^{-1}_{+(-)} \tag{2}$$

where $z_{+(-)}$ is the charge number, $\lambda^{\infty}_{+(-)}$ the ionic conductivity at infinite dilution, the coefficients A^*, α^*, and β^* are given in Table 1, and $\chi_{+(-)}$ is the distance parameter that determines the potential due to the environment of the given central ion. According to the Debye-Hückel theory, $\chi_{+(-)}$ is given by

$$\chi_{+(-)} = a_{+(-)} + \kappa^{-1} \tag{3}$$

where $a_{+(-)}$ is the distance of closest approach and κ^{-1} is often called the thickness of the ionic atmosphere. In the following treatment, however, it is not necessary to know the explicit expression for the quantity $\chi_{+(-)}$.

Eliminating $\chi_{+(-)}$ from Eqs. (1) and (2), we obtain

$$\log \gamma_{+(-)} = -\frac{A^* z^2_{+(-)}}{\alpha^* \lambda^{\infty}_{+(-)} + \beta^* |z_{+(-)}|} (\lambda^{\infty}_{+(-)} - \lambda_{+(-)}) \tag{4}$$

which relates the individual ionic activity coefficient to the ionic conductivity. Similarly, for the mean activity coefficient $\gamma_{\pm}$ of a completely dissociated electrolyte, we obtain

$$\log \gamma_{\pm} = -\frac{A^* |z_+ z_-|}{\alpha^* \Lambda^{\infty} + \beta^* (z_+ + |z_-|)} (\Lambda^{\infty} - \Lambda) \tag{5}$$

where Λ is the equivalent conductivity of the electrolyte.

Eq. (1) (the Debye-Hückel approach) and Eq. (2) (the Onsager-Robinson-Stokes approach) are less rigorous than more advanced theoretical expressions,[5] but do fit with reasonable accuracy the experimental data on mean activity coefficients and conductivities of completely dissociated electrolytes in aqueous solutions of ionic strengths below 0.1 M. The use of Eqs. (1) and (2) also has the following practical advantages for the present purpose:

(i) The equations can be combined in a straightforward way to give the expressions (4) and (5) for activity coefficients in terms of conductivity data.

(ii) The application of Eq. (2) is not restricted to solutions of symmetrical electrolytes, whereas some advanced conductivity equations (such as the Fuoss-Onsager equation) can be used only in solutions of

* The difference in activity coefficients due to the different concentration scales is ignored throughout the present paper.

TABLE 1. EXPRESSIONS FOR A^*, α^* AND β^* IN Eqs. (1) AND (2), AND THEIR NUMERICAL VALUES IN AQUEOUS SOLUTIONS OF 25 °C ($\varepsilon=78.30$, $\eta=0.008903$ poise)

	Theoretical expression[a]	Numerical value in aq. soln. of 25 °C
A^*	$\dfrac{e^2}{2\varepsilon kT(\ln 10)}$	1.554×10^{-8} cm
α^*	$\dfrac{\lvert z_+z_-\rvert e^2}{3\varepsilon kT}\dfrac{q}{1+\sqrt{q}}$	$2.3858\times10^{-8}\lvert z_+z_-\rvert\dfrac{q}{1+\sqrt{q}}$ cm
β^*	$\dfrac{F^2}{6\pi\eta N_A}$	$92.11\times10^{-8}\ \Omega^{-1}$cm^3 mol^{-1}
q	$\dfrac{\lvert z_+z_-\rvert}{z_+ + \lvert z_-\rvert}\dfrac{\lambda_+^\infty+\lambda_-^\infty}{z_+\lambda_-^\infty+\lvert z_-\rvert\lambda_+^\infty}$	

a) The symbols used have their usual meaning.

TABLE 2. COMPARISON OF THE CALCULATED AND EXPERIMENTAL MEAN ACTIVITY COEFFICIENTS OF STRONG ELECTROLYTES IN AQUEOUS SOLUTIONS AT 25 °C (calc.: calculated from the conductivity data by the present method)

A. Uni-univalent and uni-bivalent electrolytes.

Electrolyte		Equivalent concentration $c^*(=\nu zc)$[a]/mol dm^{-3} 0.01	0.02	0.05	0.1	Ref.	Electrolyte		Equivalent concentration $c^*(=\nu zc)$[a]/mol dm^{-3} 0.01	0.02	0.02	0.1	Ref.
HCl	calc.	0.894	0.862	0.810	0.763		KNO_3	calc.	0.892	0.855	0.792	0.735	
	exp.	0.905	0.876	0.830	0.796	5, 8		exp.	0.898	0.862	0.799	0.739	8
LiCl	calc.	0.901	0.869	0.817	0.772		$AgNO_3$	calc.	0.895	0.857	0.792	0.732	
	exp.	0.895	0.865	0.819	0.790	8		exp.	0.897	0.860	0.793	0.734	8
NaCl	calc.	0.901	0.869	0.817	0.772		$Na(CH_3COO)$	calc.	0.901	0.869	0.816	0.769	
	exp.	0.902	0.871	0.819	0.778	5, 8		exp.	—	—	—	0.791	8
KCl	calc.	0.899	0.867	0.815	0.772		$K(CH_3COO)$	calc.	0.919	0.888	0.836	0.780	
	exp.	0.902	0.869	0.816	0.770	8		exp.	—	—	—	0.796	5
NH_4Cl	calc.	0.900	0.866	0.809	0.761		Na_2SO_4	calc.	0.758	0.694	0.601	0.531	
	exp.	0.896	0.862	0.808	0.770	8		exp.	0.778	0.714	(0.615)[b]	0.536	8
KBr	calc.	0.901	0.872	0.822	0.777		K_2SO_4	calc.	0.745	0.675	0.582	0.513	
	exp.	0.906	0.876	0.824	0.778	8		exp.	0.777	0.711	(0.610)[b]	0.525	8
KI	calc.	0.901	0.870	0.821	0.782		$CaCl_2$	calc.	0.779	0.722	0.643	0.584	
	exp.	0.903	0.872	0.820	0.778	8		exp.	0.789	0.731	(0.645)[b]	0.583	8
HNO_3	calc.	0.887	0.858	0.807	0.758		$MgCl_2$	calc.	0.783	0.726	0.648	0.587	
	exp.	0.902	0.871	0.823	0.791	8		exp.	—	—	—	—	

B. Lanthanum salts.

Electrolyte		Molarity c/mol dm^{-3} 0.005	0.01	0.02	0.03	Ref.	Electrolyte		Molarity c/mol dm^{-3} 0.005	0.01	0.02	0.03
$LaCl_3$	calc.	0.611	0.543	0.479	0.444		$La(NO_3)_3$	calc.	0.606	0.531	0.465	0.429
	exp.	0.631	0.556	0.480	0.436	6		exp.	—	—	—	—
$LaBr_3$	calc.	0.628	0.563	0.502	0.470		$La(ClO_4)_3$	calc.	0.645	0.582	0.526	0.494
	exp.	0.638	0.567	0.490	0.449	6		exp.	—	—	—	—

a) Equivalent concentration c^* is defined by $c^*=\nu zc$, where c is the molarity and $\nu z=\nu_+z_+=\nu_-\lvert z_-\rvert$.
b) Interpolated values.

symmetrical electrolytes.

In this connection, it is important to remember that the formal expression for χ is not required in the derivation of Eqs. (4) and (5); these relations are satisfied if the effect of ionic interaction (considering only the Debye-Hückel type) on the activity and conductivity is expressed by the common parameter χ in Eqs. (1) and (2).

Results and Discussion

Equivalent Conductivities and Transport Numbers. Knowledge of equivalent conductivities and transport numbers is necessary in order to determine activity coefficients by using Eqs. (4) and (5). Ionic conductivities $\lambda_{+(-)}$ can be obtained from the equivalent conductivity Λ of the electrolyte and the transport numbers $t_{+(-)}$ of the ions according to the equation

$$\lambda_{+(-)} = t_{+(-)}\Lambda \qquad (6)$$

In the following calculations we used the conductivities and transport numbers reported by Spedding and Atkinson[6] (for the lanthanum salts) and those given in the Landolt-Börnstein Tables[7] (for the other electrolytes).

Mean Activity Coefficients of Strong Electrolytes. The validity of the present method of computing activity coefficients from conductivity data was examined by comparing the mean activity coefficients calculated by using Eq. (5) with the experimental data available in literature.[5,6,8] The results obtained with a variety of strong electrolytes are given in Table 2.

It is seen that the calculated activity coefficients o the majority of uni-univalent electrolytes are in good agreement with the experimental values at ionic strengths below 0.1 M. The agreement is also good for calcium chloride and for lanthanum chloride and bromide in solutions where $I \leq 0.1$ M. Some deviation of the calculated values from the experimental data is observed in solutions of hydrochloric and nitric acids. From the 62 sets of data in Table 2, the correlation between $\gamma_{\pm\text{calc}}$ and $\gamma_{\pm\text{exp}}$ is given by

$$\gamma_{\pm\text{calc}} = -0.00193 + 0.993\ \gamma_{\pm\text{exp}}$$

with

$$S = 0.0112,\ S_a = 0.00858,\ S_b = 0.0111$$

where S, S_a, and S_b are the standard deviations for $\gamma_\pm$, the intercept, and the slope, respectively.

Individual Activity Coefficients of Ions. Examination of the results given in Table 2 shows Eq. (4) to give reasonably good estimates of individual ionic activity coefficients in dilute solutions ($I \leq 0.1$ M). Table 3 presents the individual activity coefficients of various ions calculated by using Eq. (4) in aqueous electrolyte solutions of 25 °C.

It follows from the results in Table 3 that:

(i) In chloride solutions the individual activity coefficients of univalent cations increase in the order $H^+ < NH_4^+ < K^+ < Na^+ < Li^+$. This sequence of the alkali-metal cations is consistent with that obtained from potential measurements using a permselective membrane.[9] The activities of calcium and magnesium ions are almost the same in chloride solutions.

(ii) The values of $\gamma(H^+)$ are practically equal in chloride and nitrate solutions.

(iii) In solutions of a given ionic strength, $\gamma(K^+)$ varies with the nature of the anion, increasing in the order $SO_4^{2-} < NO_3^- < Cl^- < Br^- \lesssim CH_3COO^- < I^-$.

(iv) The values of $\gamma(La^{3+})$ increase in the following order: $NO_3^- \simeq Cl^- < Br^- < ClO_4^-$.

(v) The individual activity coefficient of chloride ion is almost the same in solutions of HCl, LiCl, NaCl, KCl, NH_4Cl, $CaCl_2$ and $MgCl_2$ of a given ionic strength ($I \leq 0.1$ M). In Fig. 1, $\log \gamma(Cl^-)$ is plotted as a function of $I^{1/2}$; the theoretical lines calculated from the Debye-Hückel limiting equation and from the Scatchard equation (*cf.* Eq. (8)) are also shown. Smaller values of $\gamma(Cl^-)$ observed in $LaCl_3$-solutions suggest the existence of some specific interaction between La^{3+} and Cl^-.

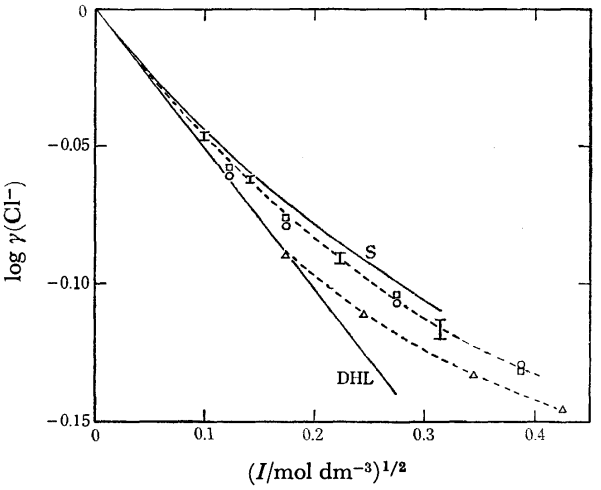

Fig. 1. Individual activity coefficients of chloride ion as a function of $I^{1/2}$ in aqueous solutions of uni-univalent and uni-multivalent electrolytes at 25 °C. I, uni-univalent electrolytes (HCl, LiCl, NaCl, KCl and NH_4Cl); O, $CaCl_2$; □, $MgCl_2$; △, $LaCl_3$. DHL, Debye-Hückel limiting slope; S, theoretical line by the Scatchard equation.

(vi) The values of $\gamma(NO_3^-)$ increase in the order $Ag^+ < K^+ < H^+$.

(vii) The activity of sulfate ion is almost the same in solutions of Na_2SO_4 and K_2SO_4 ($I \leq 0.15$ M).

Comparison of Individual Ionic Activity Coefficients Calculated by Different Methods. The following non-thermodynamic conventions have been commonly adopted in the estimation of individual ionic activities.[1]

The MacInnes Convention. MacInnes[10] assumes that

$$\gamma(K^+) = \gamma(Cl^-) = \gamma_\pm(KCl) \qquad (7)$$

in aqueous solutions of potassium chloride. It is also assumed that the activity of chloride ion in the presence of various univalent cations is independent of the nature of the cation at any concentration.

The pH Convention. In this convention[1,11] the individual activity coefficient of chloride ion in dilute aqueous solutions ($I \leq 0.1$ M) is assumed to be given by the Scatchard equation[12]

TABLE 3. INDIVIDUAL ACTIVITY COEFFICIENTS OF IONS IN AQUEOUS SOLUTIONS OF STRONG ELECTROLYTES AT 25 °C, AS COMPUTED FROM THE IONIC CONDUCTIVITY DATA

A. Individual activity coefficients of cations.

Ion	Electrolyte	Equivalent concentration $c^*(=vzc)$/mol dm^{-3}			
		0.01	0.02	0.05	0.1
H^+	HCl	0.893	0.861	0.809	0.761
	HNO_3	0.897	0.862	0.808	0.762
Li^+	LiCl	0.903	0.872	0.822	0.779
Na^+	NaCl	0.902	0.871	0.821	0.777
	$Na(CH_3COO)$	0.901	0.869	0.816	0.768
	Na_2SO_4	0.860	0.817	0.754	0.705
K^+	KCl	0.900	0.868	0.816	0.773
	KBr	0.899	0.869	0.820	0.778
	KI	0.901	0.870	0.822	0.784
	KNO_3	0.895	0.858	0.796	0.740
	$K(CH_3COO)$	0.924	0.891	0.839	0.780
	K_2SO_4	0.845	0.799	0.733	0.681
NH_4^+	NH_4Cl	0.901	0.868	0.811	0.763
Ag^+	$AgNO_3$	0.902	0.867	0.806	0.752
Ca^{2+}	$CaCl_2$	0.635	0.552	0.444	0.370
Mg^{2+}	$MgCl_2$	0.635	0.551	0.450	0.384
La^{3+}	$LaCl_3$	0.281	0.207	0.149	0.121
		(c^*=0.015)	(c^*=0.03)	(c^*=0.06)	(c^*=0.09)
	$LaBr_3$	0.295	0.222	0.163	0.135
		(c^*=0.015)	(c^*=0.03)	(c^*=0.06)	(c^*=0.09)
	$La(NO_3)_3$	0.281	0.204	0.147	0.120
		(c^*=0.015)	(c^*=0.03)	(c^*=0.06)	(c^*=0.09)
	$La(ClO_4)_3$	0.307	0.233	0.176	0.146
		(c^*=0.015)	(c^*=0.03)	(c^*=0.06)	(c^*=0.09)

B. Individual activity coefficients of anions.

Ion	Electrolyte	Equivalent concentration $c^*(=vzc)$/mol dm^{-3}			
		0.01	0.02	0.05	0.1
Cl^-	HCl	0.896	0.864	0.813	0.770
	LiCl	0.899	0.867	0.814	0.766
	NaCl	0.900	0.868	0.814	0.768
	KCl	0.899	0.867	0.815	0.771
	NH_4Cl	0.899	0.865	0.808	0.758
	$CaCl_2$	0.869	0.833	0.782	0.743
	$MgCl_2$	0.875	0.840	0.786	0.738
	$LaCl_3$	0.814	0.774	0.737	0.716
		(c^*=0.015)	(c^*=0.03)	(c^*=0.06)	(c^*=0.09)
Br^-	KBr	0.904	0.874	0.823	0.777
	$LaBr_3$	0.823	0.787	0.752	0.735
		(c^*=0.015)	(c^*=0.03)	(c^*=0.06)	(c^*=0.09)
NO_3^-	HNO_3	0.864	0.848	0.804	0.748
	KNO_3	0.889	0.851	0.788	0.730
	$AgNO_3$	0.889	0.848	0.778	0.713
	$La(NO_3)_3$	0.799	0.753	0.710	0.685
		(c^*=0.015)	(c^*=0.03)	(c^*=0.06)	(c^*=0.09)
ClO_4^-	$La(ClO_4)_3$	0.838	0.804	0.774	0.757
		(c^*=0.015)	(c^*=0.03)	(c^*=0.06)	(c^*=0.09)
CH_3COO^-	$Na(CH_3COO)$	0.901	0.869	0.816	0.770
	$K(CH_3COO)$	0.915	0.883	0.833	0.782
SO_4^{2-}	Na_2SO_4	0.591	0.503	0.383	0.303
	K_2SO_4	0.586	0.490	0.376	0.300

$$\log \gamma(Cl^-) = -\frac{A\sqrt{I}}{1+1.5\sqrt{I}} \quad (8)$$

where A is the Debye-Hückel limiting slope.

The Valance-relationship Convention. According to this convention,[1] the activity coefficients of ions are related as in the Debye-Hückel limiting law. In the case of an unsymmetrical electrolyte MA_2, for example, the relationship between $\gamma(M^{2+})$, $\gamma(A^-)$ and $\gamma_\pm(MA_2)$ is given by

$$\gamma(M^{2+}) = \gamma(A^-)^4 = \gamma_\pm(MA_2)^2 \quad (9)$$

For uni-univalent electrolytes the relationship is simply

$$\gamma_+ = \gamma_- = \gamma_\pm \quad (10)$$

which is equivalent to the assumption proposed by Guggenheim.[13]

If the individual activity coefficients of chloride ion at varying ionic strengths are defined either by the MacInnes convention or by the pH convention, the individual activity coefficients of other ions can be calculated in the following way:[1] *e.g.*, for the univalent cation M^+ and anion A^- of the electrolyte MA

$$\log \gamma(M^+) = 2 \log \gamma_\pm(MCl) - \log \gamma(Cl^-)$$

$$\log \gamma(A^-) = \log \gamma(Cl^-) + 2 \log \frac{\gamma_\pm(MA)}{\gamma_\pm(MCl)}$$

and for the univalent anion A^- of the salt MA_2

Table 4. Comparison of individual activity coefficients of various ions in aqueous solutions of strong electrolytes at ionic strength of 0.1 M and at 25 °C, as computed by different methods

Electrolyte	Ion	MacInnes-convention	pH-convention	Valence-convention	Present method	Exp.[9]
HCl	H^+	0.823	0.816	0.796	0.761	—
	Cl^-	0.770	0.777	0.796	0.770	—
HNO_3	H^+	0.823	0.816	0.791	0.762	—
	NO_3^-	0.760	0.767	0.791	0.748	—
LiCl	Li^+	0.811	0.804	0.790	0.779	0.76
	Cl^-	0.770	0.777	0.790	0.766	0.82
NaCl	Na^+	0.786	0.779	0.778	0.777	0.76
	Cl^-	0.770	0.777	0.778	0.768	0.80
$Na(CH_3COO)$	Na^+	0.786	0.779	0.791	0.768	—
	CH_3COO^-	0.796	0.803	0.791	0.770	—
KCl	K^+	0.770	0.763	0.770	0.773	0.75
	Cl^-	0.770	0.777	0.770	0.771	0.79
KBr	K^+	0.770	0.763	0.772	0.778	—
	Br^-	0.774	0.781	0.772	0.777	—
KI	K^+	0.770	0.763	0.778	0.784	—
	I^+	0.786	0.793	0.778	0.781	—
KNO_3	K^+	0.770	0.763	0.739	0.740	—
	NO_3^-	0.709	0.716	0.739	0.730	—
$K(CH_3COO)$	K^+	0.770	0.763	0.796	0.780	—
	CH_3COO^-	0.823	0.830	0.796	0.782	—
NH_4Cl	NH_4^+	0.770	0.763	0.770	0.763	—
	Cl^-	0.770	0.777	0.770	0.758	—
$AgNO_3$	Ag^+	—	—	0.734	0.752	—
	NO_3^-	—	—	0.734	0.713	—
Na_2SO_4	Na^+	0.786	0.779	0.763	0.733	0.75
	SO_4^{2-}	0.319	0.325	0.339	0.350	0.35
K_2SO_4	K^+	0.770	0.763	0.757	0.710	0.73
	SO_4^{2-}	0.317	0.323	0.328	0.340	0.35
$CaCl_2$	Ca^{2+}	0.401	0.394	0.384	0.415	0.42[a]
	Cl^-	0.770	0.777	0.787	0.765	0.75[a]
$MgCl_2$	Mg^{2+}	—	—	—	0.423	—
	Cl^-	0.770	0.777	—	0.765	—
$LaCl_3$	La^{3+}	0.137	0.133	0.125	0.162	—
	Cl^-	0.770	0.777	0.794	0.745	—
$LaBr_3$	La^{3+}	—	—	0.134	0.180	—
	Br^-	—	—	0.800	0.762	—
$La(NO_3)_3$	La^{3+}	—	—	—	0.162	—
	NO_3^-	—	—	—	0.720	—
$La(ClO_4)_3$	La^{3+}	—	—	—	0.190	—
	ClO_4^-	—	—	—	0.783	—

a) Estimated from the figure given in Ref. 1.

$$\log \gamma(A^-) = \log \gamma(Cl^-) + \frac{3}{2} \log \frac{\gamma_\pm(MA_2)}{\gamma_\pm(MCl_2)}$$

In this derivation of individual ionic activity coefficients, it is assumed that $\gamma(Cl^-)$ and $\gamma(M^+$ or $M^{2+})$ are independent of the nature of the ions of opposite sign present in the solution.

Application of all the conventions mentioned above more or less ignores the nature of the ions. On the other hand, the present method takes into account the nature of the ions as revealed by their characteristic ionic conductivities, and should give more reasonable estimates of individual ionic activity coefficients.

Table 4 compares the activity coefficients of various ions in aqueous solutions at ionic strength of 0.1 M, as determined by the different methods discussed earlier. The experimental values for cations in Table 4 were derived from potential measurements with a perm-selective membrane[9]; the experimental data were standardized at an ionic strength of 0.01 M or 0.015 M (in case of Na_2SO_4 and K_2SO_4). The experimental values for anions were calculated from those for the cations and those for the mean activity coefficients of the corresponding electrolytes. The membrane-potential measurements involve some error due to the difficulty of eliminating liquid-junction potentials; the uncertainty in the present experimental values is estimated to be between 1 and 5% most in cases.

Further experimental data will be required before it can be decided whether the present method gives more reliable estimates of individual ionic activity coefficients than the other conventions. From Table 4, however, it is already seen that the present method gives the best fit to the experimental values in the cases of calcium chloride and of sodium and potassium sulfates, where the other conventions result in appreciably different values.

References

1) R. G. Bates and M. Alfenaar, "Ion-selective Electrodes" ed. by R. A. Durst, National Bureau of Standards Special Publication 314 (1969), Chap. 6.

2) J. Kielland, *J. Amer. Chem. Soc.*, **59**, 1675 (1937).

3) R. M. Fuoss and F. Accascina, "Electrolytic Conductance," Interscience Publishers, New York-London (1959), p. 170.

4) J. -C. Justice, *J. Chim. Phys.*, **65**, 353 (1968); R. Bury, M. -C, Justice, and J. -C. Justice, *C. R. Acad. Sci. Paris*, **268**, 670 (1969); M. -C. Justice, R. Bury, and J. -C. Justice, *Electrochim. Acta*, **16**, 687 (1971).

5) R. A. Robinson and R. H. Stokes, "Electrolyte Solutions," Butterworths, London (1965), Chap. 7 and 9.

6) F. H. Spedding and G. Atkinson, "The Structure of Electrolytic Solutions," ed. by W. J. Hamer, John Wiley & Sons, Inc., New York (1959), pp. 319—339.

7) Landolt-Börnstein, "Zahlenwerte und Funktionen aus Physik, Chemie, Astronomie, Goephysik und Technik," II-Band, 7 Teil, Elektrische Eigenschaften II (1960).

8) R. Parsons, "Handbook of Electrochemical Constants," Butterworths Scientific Publications, London (1959), Tables 19 and 20.

9) R. Tamamushi and S. Goto, This Bulletin, **43**, 3420 (1970).

10) D. A. MacInnes, *J. Amer. Chem. Soc.*, **41**, 1086 (1919).

11) R. G. Bates, E. A. Guggenheim, Pure Appl. Chem., **1**, 163 (1960).

12) G. Scatchard, "The Structure of Electrolytic Solutions," John Wiley & Sons, Inc., New York (1959); ed. by W. J. Hamer, p. 9, *Chem. Rev.*, **19**, 309 (1936); W. J. Hamer, "Theoretical Mean Activity Coefficients of Strong Electrolytes in Aqueous Solutions from 0 to 100 °C," National Standard Reference Data Series - National Bureau of Standards 24, 1968.

13) E. A. Guggenheim, *Phil. Mag.*, **19**, 588 (1935).

The Catalytic Activity of Some Mixed Oxides for Depolymerization of Paraldehyde

S. P. WALVEKAR* and A. B. HALGERI

Department of Chemistry, Central College, Bangalore University, Bangalore-560001, India

(Received August 28, 1972)

Depolymerization of paraldehyde in benzene catalyzed by SiO_2–ZrO_2, SiO_2–TiO_2, Al_2O_3–ZrO_2, TiO_2–ZrO_2, Al_2O_3–TiO_2 (calcined at various temperatures) has been studied. It is observed that in all the cases the catalytic activity (first order rate constant, k) exhibited a maximum against the temperature of heat treatment of the catalyst. The acid sites at $pK_a \leqq -3.0$ correlate best with catalytic activity for depolymerization of paraldehyde.

It has been observed previously that mixed oxides show fairly strong acidic property on their surface and that the acidity changes remarkably on subjecting the samples to heat treatment.[1] In the present work an attempt has been made to study the depolymerization of paraldehyde in presence of some of these solid acids.

Depolymerization of paraldehyde proceeds in presence of mineral acids and carboxylic acids in non-aqueous media and can be followed by an accurate and easy method of analysis.[2,3] Depolymerization of paraldehyde in presence of solid acids like metal sulphates has been reported by Tanabe *et al.*[4,5] It was considered of interest to study this reaction in presence of mixed oxide catalysts for which no data exists. The rate constants have been correlated with the acidity of the catalysts.

Experimental

Materials. Paraldehyde and pure quality benzene were dried over sodium, distilled and used in this work. All other chemicals were extra pure grade reagents and were used as received.

Preparation of Catalysts. Silica gel was prepared by hydrolysis of dilute sodium silicate solution with 10% HCl.[6] Alumina was prepared from $Al(NO_3)_3 \cdot 9H_2O$ by precipitating $Al(OH)_3$ using ammonia water.[7] The precipitates obtained in the above two cases were heated for an hour and then filtered off and washed with distilled water till it was free from chloride and nitrate ions respectively. Finally the precipitates were dried at 100 °C for 20 hr and preserved. The binary oxides were prepared as follows.

1) Silica–titania: 85 g of SiO_2 gel prepared as above was suspended in 500 ml of distilled water and 18 ml of $TiCl_4$ was added. The mixture was boiled on a water bath for 1 hr and 50 ml of 28% ammonia water was added drop by drop to form the precipitate of titanic acid (H_4TiO_4). The final pH of the solution was near about 7.5. The mixture was heated for about an hour with continuous stirring and then the precipitate was filtered off and washed thoroughly with distilled water till it was free from chloride ions. The precipitate was dried at 100 °C for 20 hr and preserved. The weight % of TiO_2 in the mixture was calculated to be 15.

2) Silica–zirconia: 89 g of silica was suspended in 250 ml of distilled water and a solution of 26.9 g of $Zr(SO_4)_2 \cdot H_2O$ in 500 ml of water was added and to this mixture 46 ml of 28% ammonia was added dropwise with vigorous stirring. The mixture was heated for 2 hr. The final pH of the solution was 7.6. The precipitate was filtered off, washed with water until no sulfate ions were detected in the washings. The precipitate was dried as in 1). The weight % of ZrO_2 in the mixture was calculated to be 11.

3) Alumina–zirconia: This catalyst was prepared by the precipitation technique described above. 80 g of alumina prepared as above was suspended in 250 ml of distilled water and a solution of 48.9 g of $Zr(SO_4)_2 \cdot H_2O$ in 500 ml of water was added. The mixture was boiled on a water bath for 1 hr and 83 ml of 28% ammonia water was added dropwise until the pH of the solution was near about 7.2. The precipitate was washed and dried as in 1). The weight % of ZrO_2 in the mixture was calculated to be 20.

4) Titania–zirconia: The coprecipitated mixture of TiO_2–ZrO_2 was prepared as follows. 19.6 g of $Zr(SO_4)_2 \cdot H_2O$ was dissolved in 500 ml of distilled water and 20.5 ml of $TiCl_4$ was added to this solution. The solution was heated on a water bath for 2 hr and 322 ml of 28% ammonia water was added slowly with vigorous stirring to form a coprecipitate of the mixture. The final pH of the solution was near about 7.5. The precipitate was heated for 1 hr and was filtered off and washed thoroughly with distilled water until no chloride and sulfate ions were detected in the washings. The precipitate was dried at 120 °C for 20 hr. The weight % of ZrO_2 in the mixture was calculated to be 32.

5) Alumina–titania: 48.5 g of $AlCl_3 \cdot 6H_2O$ was dissolved in 360 ml of water and 7.8 ml of $TiCl_4$ was added. The solution was heated on a water bath for 1 hr and 290 ml of 28% ammonia water was added to the mixture in lots of 50 ml at a time. The last lot of ammonia water was added dropwise with continuous stirring until the pH of the solution was around 7.2. The mixture was boiled to complete the coprecipitation. The precipitate was washed and dried as in 4). The weight % of TiO_2 in the mixture was calculated to be 26.

The samples thus obtained in the above cases were powdered and only such samples collected between 100 and 150 mesh sieves were used. The powders were subjected to heat treatment in the temperature range of 120 to 1050 °C by heating for 6 hr in an electrical muffle furnace with temperature control arrangement. The samples after heat treatment were cooled in a desiccator and preserved in covered glass tubes, under vacuum.

Measurement of Surface Acidity and Acid Strength. The acidity (the number of acid sites) having an acid strength H_0 equal to or lower than the pK_a value of the indicator used were determined by using the amine titration method.[8,9]

Kinetic Studies. The procedure adopted was essentially the same as described by the earlier authors.[4,5] The reaction was studied at 25 °C by analyzing the acetaldehyde formed at various intervals of time by the bisulfite method.[10] Tests showed that none of the catalysts used, interfered with the determination of acetaldehyde by the above method.

Sufficient precautions were taken to study these reactions

* To whom all the correspondence has to be made.

in the absence of moisture, since even traces of moisture could greatly retard or even stop the reaction altogether, especially when very effective catalysts were being used in low concentrations. Since the reaction is heterogeneous and the rate depends upon the condition of the experiment, the experiments were carried out under similar conditions throughout this investigation.

Results and Discussion

It has been observed that the rate of depolymerization of paraldehyde catalyzed by metal sulphates[4] is of the first order and similarly with mixed oxides the rate was found to be of the first order with respect to paraldehyde concentration, as straight line graphs were obtained for the log $(a-x)$ against time 't' plots.

The results of the depolymerization of paraldehyde catalyzed by SiO_2–ZrO_2, SiO_2–TiO_2, Al_2O_3–ZrO_2, TiO_2–ZrO_2, and Al_2O_3–TiO_2 are presented in Tables 1 and 2. It is seen from these tables that the acidity at $pK_a \leqq -3.0$, increases with increasing temperature of heat treatment and attains a maximum and then decreases with further rise in temperature. A reference to the rate constant value, k, in these tables indicates that there exists a correlation between acidity and the catalytic activity. When the catalyst was poisoned by dicinnamal acetone ($pK_a = -3.0$), it could not depolymerize paraldehyde. Therefore acid sites having an acid strength of $pK_a \leqq -3.0$ correlate best with catalytic activity for depolymerization of paraldehyde. This conclusion is in agreement with the one obtained by us in case of some silica and alumina based binary oxide catalysts[11-13] and also with the one obtained by other workers with metal sulphates.[5] The dependence of catalytic activity on the temperature of heat treatment of catalyst is shown in Tables 1 and 2. It is observed that in all cases the catalytic activity (first order rate constant, k) exhibited a maximum against the temperature of heat treatment of the catalyst. The decrease in the catalytic activity of these mixed oxides after heat treatment at elevated temperatures is due to a decrease in the number of acid sites and acid strength rather than to a decrease in their surface area.[14]

It is interesting to note from the results presented in Tables 1 and 2 that acidity of 0.05 mmol/g or less at $pK_a \leqq -3.0$ is not effective for catalyzing this reaction. In case of Al_2O_3–ZrO_2 samples heat-treated at 260 and 800 °C have an acid value of 0.02 and 0.04 mmol/g respectively but these show no catalytic activity. Similarly in case of TiO_2–ZrO_2 and Al_2O_3–TiO_2 samples calcined at 120 and 220 °C have an acid value of 0.03 mmol/g but have no catalytic activity. It is further observed in case of SiO_2–TiO_2 that samples heat-treated at 120, 800, and 1000 °C have a number of acid sites having an acid strength of $pK_a \leqq +3.3$, but these samples show no catalytic activity. Similarly in case of Al_2O_3–TiO_2, TiO_2–ZrO_2 samples heat-treated at 120 and 800 °C have a number of acid sites having an acid strength of $pK_a \leqq +3.3$, but have no catalytic activity. A similar observation is made in case of Al_2O_3–ZrO_2 and Al_2O_3–TiO_2 for samples heat-treated at 260 and 220 °C respectively. Therefore even those relatively few acid sites at $pK_a \leqq -3.0$ (0.05 mmol/g or less) and those at $pK_a \leqq +3.3$ are catalytically inactive.

The reason for the ineffectiveness of acid sites with weaker acid strength than $pK_a = -3.0$ is probably to be found in the fact that no paraldehyde molecule will give a conjugated acid at any of these weaker sites, since the pK_a value of paraldehyde is about -3.3.[15] Similar correlations between activity and acid amount over limited ranges of acid strength were evident in both the hydration of propylene,[16] polymerization of isobutyl vinyl ether[17] catalyzed by various sulphates, and also hydrolysis of aliphatic esters catalyzed by

TABLE 1. ACIDIC PROPERTY OF MIXED OXIDE CATALYSTS AND DEPOLYMERIZATION OF PARALDEHYDE AT 25 °C

Catalyst and paraldehyde concentration	Calcination temperature °C	Acid amount, mmol/g $pK_a \leqq +3.3$	Acid amount, mmol/g $pK_a \leqq -3.0$	Rate constant ($k \times 10^3$ $min^{-1} \cdot g^{-1}$)
SiO_2–ZrO_2 Paraldehyde concn=0.073 M	110	0.18	0.08	4.02
	240	0.28	0.12	9.86
	320	0.39	0.16	18.48
	440	0.45	0.20	26.32
	500	0.52	0.30	42.50
	600	0.48	0.26	35.20
	710	0.40	0.24	32.50
	820	0.32	0.20	27.50
	1000	0.20	0.09	7.20
SiO_2–TiO_2 Paraldehyde concn=0.063 M	120	0.20	—	—
	260	0.31	0.12	8.45
	380	0.34	0.14	10.06
	440	0.37	0.16	12.34
	500	0.38	0.17	18.86
	550	0.42	0.20	26.52
	600	0.39	0.16	19.07
	700	0.37	0.08	8.42
	800	0.32	—	—
	1000	0.24	—	—

TABLE 2. ACIDIC PROPERTY OF MIXED OXIDE CATALYSTS AND DEPOLYMERIZATION OF PARALDEHYDE AT 25 °C

Catalyst and paraldehyde concentration	Calcination temperature °C	Acid amount, mmol/g $pK_a \leqq +3.3$	Acid amount, mmol/g $pK_a \leqq -3.0$	Rate constant ($k \times 10^3$ $min^{-1} \cdot g^{-1}$)
Al_2O_3–ZrO_2 Paraldehyde concn=0.093 M	120	0.12	—	—
	260	0.20	0.02	—
	380	0.33	0.08	8.26
	500	0.38	0.16	21.68
	610	0.31	0.12	17.92
	710	0.26	0.08	9.84
	800	0.14	0.04	—
	1000	0.04	—	—
TiO_2–ZrO_2 Paraldehyde concn=0.080 M	120	0.11	0.03	—
	220	0.18	0.09	6.45
	360	0.25	0.12	9.86
	440	0.30	0.15	18.82
	520	0.24	0.13	14.89
	600	0.18	0.09	10.08
	700	0.08	0.06	4.68
	800	—	—	—
Al_2O_3–TiO_2 Paraldehyde concn=0.096 M	120	0.18	—	—
	220	0.22	0.03	—
	320	0.26	0.06	4.60
	420	0.32	0.10	12.66
	500	0.30	0.07	7.34
	600	0.24	0.02	—
	700	0.18	0.01	—
	800	0.10	—	—

mixed oxides.[18] In these cases catalytic activities were found to be proportional to the activities at $-3.0 \leqq H_0 \leqq +1.5$, at $-5.6 \leqq H_0 \leqq -3.0$ and at $H_0 \leqq -3.0$ respectively.[16-18]

These observations show that every reaction requires acid sites of a particular acid strength for a particular reaction and hence it can be concluded that acidity and acid strength play an important role in every acid catalyzed reaction.

Authors wish to express their thanks to Professors M. Shadaksharaswamy and T. D. Bhaskar for providing research facilities and encouragement.

References

1) S. P. Walvekar and A. B. Halgeri, "58th Proc. Indian Sci. Congr. Abstracts," Part III (1971), p. 135.
2) R. P. Bell and B. G. Skinner, *J. Chem. Soc.*, **1952**, 2955.
3) R. P. Bell and A. H. Brown, *ibid.*, **1954**, 774.
4) K. Tanabe, *J. Res. Inst. Catal. Hokkaido Univ.*, **7**, 120 (1959).
5) K. Tanabe and A. Aramata, *ibid.*, **8**, 43 (1960).
6) P. W. Selwood and L. Lyon, *Discuss. Faraday Soc.*, **8**, 222 (1950).
7) I. V. Nikolesku and N. Chick, *Kinet. Katal.*, **10**, 910 (1969).
8) O. Johnson, *J. Phys. Chem.*, **59**, 827 (1955).
9) H. A. Benesi, *J. Amer. Chem. Soc.*, **61**, 970 (1957).
10) I. E. Friedmann, M. Cotonio, and G. A. Schaffer, *J. Biol. Chem.*, **73**, 342 (1972).
11) S. P. Walvekar and A. B. Halgeri, *J. Res. Inst. Catal. Hokkaido Univ.*, **20**, 219 (1972).
12) S. P. Walvekar and A. B. Halgeri, *J. Univ. Bombay*, **41**, 29 (1972).
13) S. P. Walvekar and A. B. Halgeri, *J. Indian Chem. Soc.*, **50**, 387 (1973).
14) S. P. Walvekar and A. B. Halgeri, *Indian J. Chem.*, **11**, 662 (1973).
15) K. Tanabe and T. Takeshita, *Advan. Catal.*, **17**, 135 (1967).
16) Y. Ogino, *Shokubai* (Tokyo), **10**, 242 (1968).
17) T. Kawakami and Y. Ogino, *ibid.*, **10**, 136 (1968).
18) S. P. Walvekar and A. B. Halgeri, *J. Indian Chem. Soc.*, **50**, 246 (1973).

The Telomerization of Methyl Acetate and Methyl Cyanoacetate with Ethylene

Tsutomu FUJIMOTO and Ichiro HIRAO

Laboratory of Organic Synthesis, Department of Chemical Engineering, Kyushu Institute of Technology, Tobata-ku, Kita-kyushu 804

(Received August 4, 1973)

The telomerization of methyl acetate and cyanoacetate with ethylene initiated by di-*tert*-butyl peroxide was investigated. Methyl esters of linear and α-branched alkanoic acids, and linear and α-branched alkyl acetates, as well as hydrocarbons, were identified in the system of methyl acetate. The methyl esters of linear and α-branched α-cyanoalkanoic acids were identified in the system of methyl cyanoacetate, but no alkyl cyanoacetates could be found. It was suggested that intramolecular 1,5-hydrogen transfer in telomer radicals with two ethylene units and a chain-transfer reaction to the telomers gave the branched telomers. The chain-transfer constants were estimated in the system of methyl cyanoacetate. The introduction of the cyano group to methyl acetate at the α-position gave a favorable system for chain-transfer reactions and facilitated intramolecular 1,5-hydrogen transfer in the telomer radicals. The relatively higher relative reactivity of the methoxy group to the acetyl group in methyl acetate in the telomerization with ethylene was discussed.

It is well known that a homolytic abstraction of an α-hydrogen atom from acetic and α-substituted acetic acids and their esters preferentially give the carboxymethyl radical and its homologous radicals.[1-3] The radicals react with olefins to give telomeric products.[4] The telomerization of ethylene with acetic acid and its derivatives is accompanied by 1,5-hydrogen transfer in telomer radicals, α-branched telomers being formed together with linear telomers.[5-7] Propagation, chain-transfer, and intramolecular hydrogen-transfer reactions of methoxycarbonylalkyl and cyanomethoxycarbonylalkyl radicals may be expected in the telomerization of methyl acetate and cyanoacetate with ethylene. An elucidation of the behavior of these radicals will give information of interest with regard to the reactivity of substituted alkyl radicals.

Some homologous series of telomers may be expected in the telomerization of methyl acetate with ethylene, but only linear aliphatic acids have been isolated from the telomerization products.[8] Free radical additions of ethyl cyanoacetate to unsaturated compounds have also been investigated,[9-14] but there has been no report on the telomerization of methyl cyanoacetate with ethylene. This paper will describe the telomerization products and the chain-transfer and intramolecular-rearrangement reactions of the telomer radicals in the telomerization of methyl acetate and cyanoacetate with ethylene.

Results and Discussion

Telomerization Products of Methyl Acetate with Ethylene. The telomerization was carried out in the presence of radical initiators in an autoclave. The product of the telomerization was fractionated into three fractions: I (insoluble in hot methyl acetate), II (soluble in hot methyl acetate, but insoluble at room temperature), and III (soluble in methyl acetate at room temperature). A product with a high molecular weight was obtained under an initial ethylene pressure of 40 kg/cm², but a product with a mean molecular weight of 235 was obtained using di-*tert*-butyl peroxide (DTBP) when ethylene was introduced to keep a pressure of 20 kg/cm² at 140 °C during the reaction. The product thus obtained was further fractionated to three fractions, III-1 (bp 60—150 °C/60 mmHg), III-2 (bp 150/60—170 °C/5 mmHg), and the residue (III-3). The compositions and molecular weights of the fractions are given in Table 1.

TABLE 1. COMPOSITION AND MOLECULAR WEIGHT OF THE FRACTIONS OF METHYL ACETATE TELOMER

Initiator	AIBN	DTBP	DTBP
Initial ethylene Press. (kg/cm²)	40	40	20[a]
Temp. (°C)	80	130	140
Time (hr)	7	7	8
Yield (g)	11.8	49.2	29.8
Composition (wt%) and M.wt.[b]			
I	73.3 (2400)	71.4 (1550)	—
II	16.1 (595)	22.3 (545)	—
III	10.6 (350)	6.3 (280)	100 (235)
III-1	—	—	37.5 (139)
III-2	—	—	39.7 (240)
III-3	—	—	22.8 (384)

a) Pressure of 20 kg/cm² was kept at 140 °C. b) Molecular weights are given in parentheses.

The gas chromatogram of lower boiling products is shown in Fig. 1. The identification of the products was carried out by gas chromatography (glc) and by a study of the IR, NMR, and mass spectra (see Experimental). The a_n peaks (n=1—7) were identified with methyl butanoate (LA_1), hexanoate (LA_2), octanoate (LA_3), decanoate (LA_4), dodecanoate (LA_5), tetradecanoate (LA_6), and hexadecanoate (LA_7) respectively. The b_n peaks (n=1—7) were identified with propyl (LM_1), pentyl (LM_2), heptyl (LM_3), nonyl (LM_4), undecyl (LM_5), tridecyl (LM_6), and pentadecyl (LM_7) acetates respectively. The c_n peaks (n=1—5) were identified with methyl 2-ethylbutanoate (BA_1), 2-ethylhexanoate (BA_2), 2-butylhexanoate (BA_3), 2-ethyloctanoate (BA_4), and 2-butyloctanoate (BA_5) respectively. The d_n peaks (n=1—3) were identified with

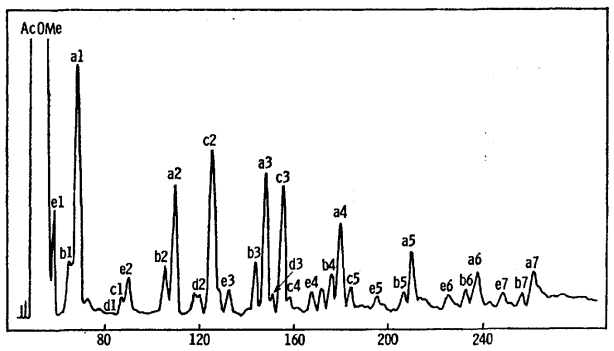

Fig. 1. Gas chromatogram of the telomerization product of methyl acetate with ethylene.

1-ethylpropyl (BM_1), 1-ethylpentyl (BM_2), and 1-butylpentyl(BM_3) acetates respectively. Although a peak which corresponds to 1-butylheptyl acetate in the retention time could not be detected because of the overlap of other peaks, the presence of the acetate was suggested by the formation of undecan-5-ol after the saponification of the telomerization product. The e_n peaks (n=1—7) were hydrocarbon homologues with an odd number of carbon atoms, from nonane to heneicosane respectively. The hydrocarbons were presumably formed by the addition of methyl radicals to ethylene. The result of silica-gel-column chromatography showed that hydrocarbons were included (at least 12% by weight) in the product obtained under a pressure of 20 kg/cm² at 140 °C. Chiang and Li have isolated and identified only linear acids from the same telomerization,[8] but the telomerization product was a complex mixture containing methyl esters of α-branched alkanoic acids (BA), linear alkyl (LM), and α-branched alkyl (BM) acetates and hydrocarbons in addition to methyl esters of linear alkanoic acids (LA).

The amounts of telomers relative to the amount of BA_2 were determined by glc because no suitable internal standard could be found. The results are given in Table 2. The content of the LA_1 telomer was 42% at 160 °C, while the contents of LA, BA, LM, and BM were 46—57, 24—29, 18—21, and 2—5% respectively in the telomers detectable by glc (Table 3).

Table 2. Relative amounts of methyl acetate telomers[a]

Temp. (°C)	140	140	140	140	140	130	150	160
Press. (kg/cm²)	20	20	20	30	40	20	20	20
Time (hr)	1	3	8	5	5	3	2	1
LA_1	1.91	1.92	1.91	1.72	1.53	0.99	2.45	2.68
LA_2	0.80	0.81	0.82	0.94	1.05	0.68	0.69	0.61
LA_3	0.63	0.62	0.61	0.94	1.20	0.82	0.41	0.23
LA_4	0.33	0.30	0.33	0.55	0.92	0.41	0.14	0.07
LA_5	0.18	0.13	0.16	0.36	0.68	0.28	0.06	—
LA_6	0.15	0.11	0.13	0.30	0.58	0.28	—	—
LM_1	0.42	0.44	0.44	0.37	0.30	0.20	0.49	0.52
LM_2	0.34	0.34	0.34	0.31	0.32	0.31	0.35	0.38
LM_3	0.25	0.26	0.24	0.26	0.30	0.25	0.21	0.15
LM_4	0.22	0.19	0.19	0.25	0.30	0.23	0.13	0.07
LM_5	0.14	0.11	0.13	0.21	0.28	0.19	0.06	—
LM_6	0.12	0.10	0.11	0.19	0.28	0.18	—	—
LM_7	0.09	0.09	0.09	0.17	0.24	0.20	—	—
BA_1	0.13	0.18	0.20	0.15	0.14	0.13	0.20	0.23
BA_2	1.00	1.00	1.00	1.00	1.00	1.00	1.00	1.00
BA_3	0.67	0.62	0.63	0.84	1.05	0.81	0.29	0.14
BA_4	0.07	0.11	0.11	0.13	0.12	0.07	0.08	0.06
BA_5	0.15	0.13	0.14	0.23	0.31	0.19	0.07	0.06
BM_1	0.03	0.04	0.05	0.05	0.04	0.01	0.02	0.02
BM_2	0.12	0.15	0.19	0.16	0.19	0.14	0.10	0.07
BM_3	0.11	0.13	0.13	0.13	0.16	0.12	0.07	0.05

a) Relative amounts of telomers are represented in mol/mol of methyl 2-ethylhexanoate (BA_2).

Table 3. Composition of series of methyl acetate telomers

Temp. (°C)	140	140	140	140	140	130	150	160
Press. (kg/cm²)	20	20	20	30	40	20	20	20
Time (hr)	1	3	8	5	5	3	2	1
LA_1 (%)	24	25	24	19	14	13	36	42
LA (%)	51	50	50	52	54	46	55	57
LM (%)	20	20	19	19	18	21	18	18
BA (%)	26	26	26	26	24	29	24	24
BM (%)	3	4	5	4	4	4	3	2

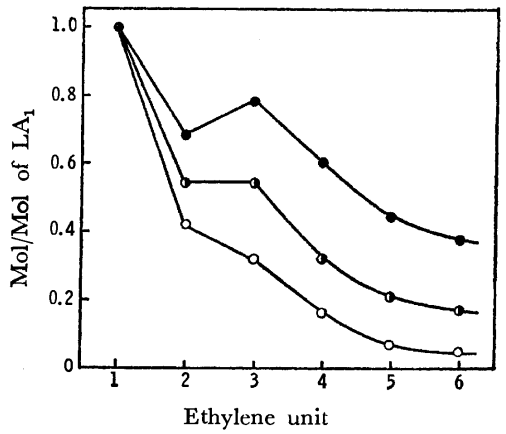

Fig. 2. Effect of ethylene pressure on the distribution of series LA at 140 °C.
Pressure
-○-: 20 kg/cm², -◑-: 30 kg/cm², -●-: 40 kg/cm².

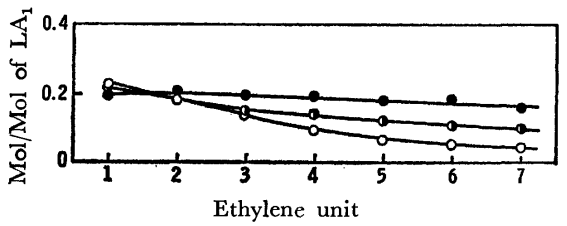

Fig. 3. Effect of ethylene pressure on the distribution of series LM at 140 °C.
Pressure
-○-: 20 kg/cm², -◑-: 30 kg/cm², -●-: 40 kg/cm².

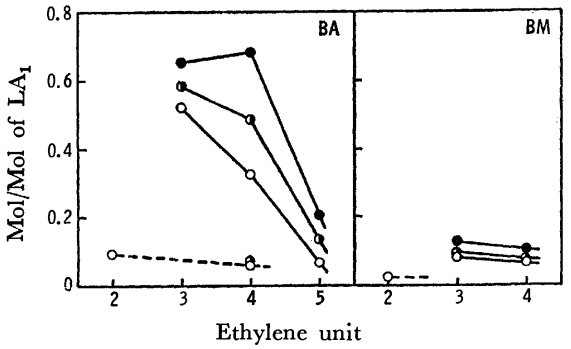

Fig. 4. Effect of ethylene pressure on the distribution of series BA and BM at 140 °C.
Pressure
-○-: 20 kg/cm², -◑-: 30 kg/cm², -●-: 40 kg/cm².
Full lines indicate butyl branched telomers.

The distributions of the telomers were almost unaffected by the reaction time. The effects of the pressure of ethylene on the distributions of LA, LM, BA, and BM are shown in Figs. 2, 3, and 4. In the distribution of LA, a remarkable minimum was found at two ethylene units, while a maximum at four ethylene units in the distribution of the methyl ester telomers with a branch of the butyl group under a high pressure of ethylene.

Telomerization Products of Methyl Cyanoacetate with Ethylene. The telomerization was carried out in the presence of DTBP at 140 °C in an autoclave. Ethylene was introduced into the autoclave to keep the prescribed pressure during the reaction. The gas chromatogram of the reaction mixture is shown in Fig. 5. The reaction products were identified by glc and by mass spectrometry (see Experimental). The 1, 4, and 6 peaks were identified with methyl 2-cyanobutanoate (N_1), 2-cyanohexanoate (N_2), and 2-cyanooctanoate (N_3) respectively. The 2, 5, 7, 8, and 9 peaks were identified with methyl 2-cyano-2-ethylbutanoate (B_1), 2-cyano-2-ethylhexanoate (B_2), 2-butyl-2-cyanohexanoate (B_3), 2-cyano-2-ethyloctanoate (B_4), and 2-butyl-2-cyanooctanoate (B_5) respectively. No propyl and pentyl cyanoacetates, which were expected to be formed *via* cyanoacetoxymethyl radicals, could be detected by glc. The component of the 3 peak was confirmed to be methyl 2-cyano-3-methyl-2-butenoate, which was a product of the thermal decomposition of DTBP in methyl cyanoacetate without ethylene, by a study of the IR, NMR, and mass spectra. A small amount of higher-boiling materials (bp> 110 °C/1 mmHg) was also obtained; however, the IR and NMR spectra showed the presence in the fraction of a few telomers with higher ethylene units.

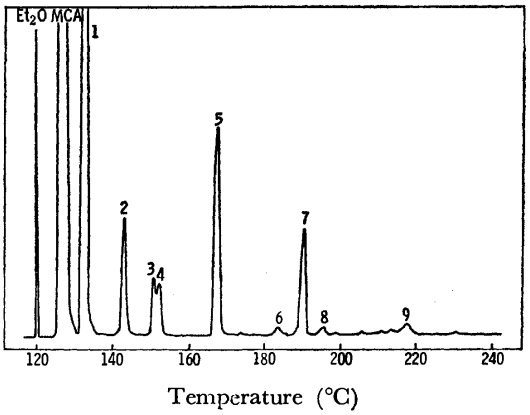

Fig. 5. Gas chromatogram of the telomerization product of methyl cyanoacetate with ethylene.

The analysis of the telomerization products was carried out by means of glc. The results are given in Table 4. The content of the N_1 telomer was over 50%, and a remarkable formation of the branched telomers, especially B_2, was observed in this system.

Chain-transfer Reactions in Telomerization of Methyl Cyanoacetate with Ethylene. In the telomerization, linear telomers, N_n, may be formed by the chain-transfer reaction of linear telomer radicals formed from cyanomethoxycarbonylmethyl radicals. The branched telomer, B_1, may be formed *via* the addition of ethylene to 1-cyano-1-methoxycarbonylpropyl radicals. The increase in the amount of B_1 with the reaction time suggests that the radicals were produced by the abstraction of a hydrogen atom at the α-position in the linear telomer N_1. The formation of the radicals by 1,3-hydrogen transfer in 3-cyano-3-methoxycarbonylpropyl radicals is presumed to be negligible because of the small possibility of 1,3-hydrogen transfer.[15] The formation of B_1, therefore, suggests that a part of the branched telomers may be formed by chain transfer to linear

Table 4. Composition of methyl cyanoacetate telomers[a]

Press. (kg/cm²)	20	30	30	30	40
Time (hr)	8	1	3	8	8
N_1	175 (63.6)	121 (62.3)	158 (56.5)	165 (54.5)	160 (49.4)
N_2	12.1 (4.4)	9.4 (4.8)	13.9 (5.0)	14.6 (4.8)	17.7 (5.5)
N_3	0.6 (0.2)	0.7 (0.4)	1.0 (0.4)	1.1 (0.4)	1.9 (0.6)
$HE_{\geq 4}CH$[b]	0.0 (0.0)	0.1 (0.0)	0.1 (0.0)	0.2 (0.1)	0.3 (0.1)
B_1	30.9 (11.2)	11.6 (6.0)	25.0 (8.9)	31.0 (10.2)	26.2 (8.1)
B_2	46.9 (17.0)	38.4 (19.8)	61.1 (21.8)	69.0 (22.8)	81.7 (25.2)
B_3	8.8 (3.2)	11.2 (5.8)	17.7 (6.3)	19.0 (6.3)	30.2 (9.3)
B_5	0.5 (0.2)	1.1 (0.6)	1.7 (0.6)	1.7 (0.6)	3.8 (1.2)
$HE_1CE_{\geq 3}H$[b]	0.5 (0.2)	0.5 (0.3)	1.1 (0.4)	1.3 (0.4)	2.0 (0.6)
$HE_2CE_{\geq 4}H$[b]	0.0 (0.0)	0.1 (0.0)	0.1 (0.0)	0.1 (0.0)	0.4 (0.1)
$[C_2H_4]/[MCA]$[c]	0.028	0.040	0.042	0.042	0.058
$[C_2H_4]$[d]	0.27	0.42	0.42	0.42	0.57

a) Yield and composition in parentheses are given in mmol and mol%, respectively. b) C and E in the telomer symbol represent $>C(CN)COOCH_3$ and ethylene unit, respectively. Yield was estimated. c) The average ratio of ethylene and methyl cyanoacetate concentrations during the reaction. d) The average concentration of ethylene during the reaction.

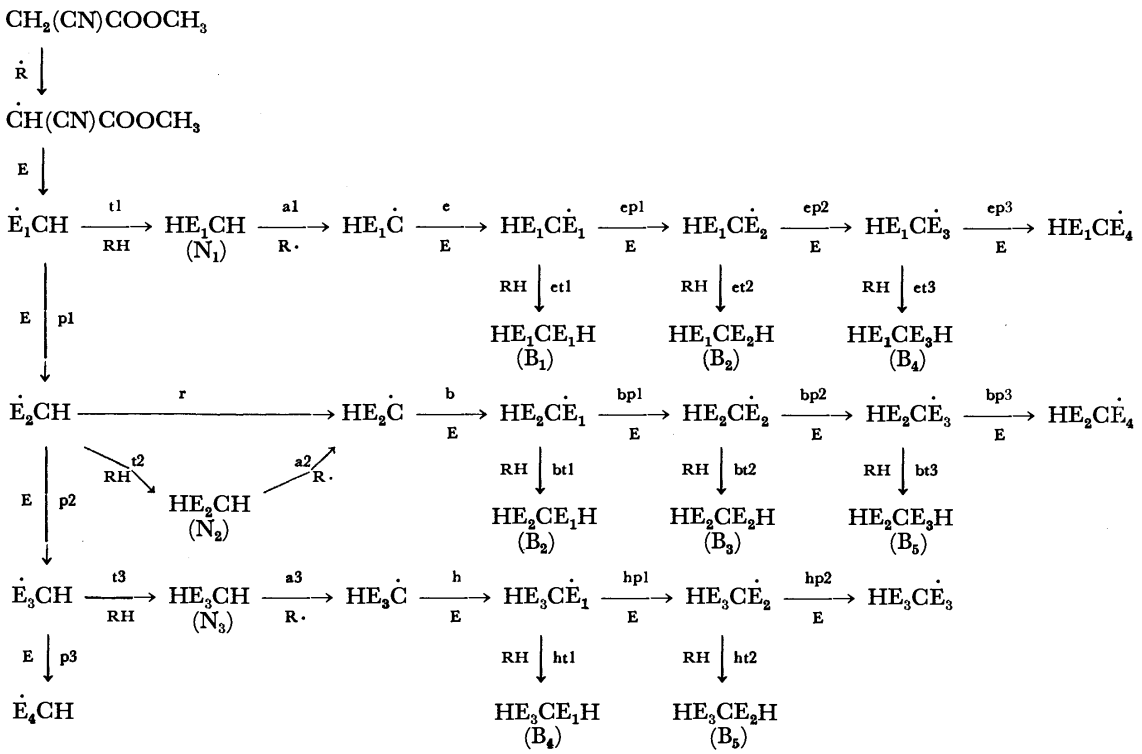

Chart 1. Reaction of methyl cyanoacetate with ethylene. C and E in the telomer symbol HE_nCE_mH represent $>C(CN)COOCH_3$ and ethylene unit, respectively. RH, E and R· represent chain transfer agent, ethylene and a free radical, respectively.

telomers.

The B_2 telomer may be formed by Reaction et2 from 5-cyano-5-methoxycarbonylheptyl radicals and by Reaction bt1 from 3-cyano-3-methoxycarbonylheptyl radicals (Chart 1). A part of the latter radicals may be formed through chain-transfer reaction to N_2 (a2); however, most of the radicals may be formed *via* intramolecular 1,5-hydrogen transfer in 5-cyano-5-methoxycarbonylpentyl radicals, which are telomer radicals with two ethylene units. The intramolecular 1,5-hydrogen transfer was suggested by the remarkable formation of the B_2 telomer, even at an initial stage of the reaction. Intramolecular 1,5-hydrogen transfer reaction is known in alkyl radicals in the gas phase[15] and has been suggested in the telomerization of ethylene with acetic acid and its derivatives.[5-7] Therefore, most of the telomers with a branch of the butyl group at the α-position may be formed from the radicals produced by the intramolecular hydrogen transfer. The possible formation pathways of the telomers identified in the system are summarized in Chart 1.

An estimation of the conversions (A_n and R) of the linear telomer N_n to branched telomers *via* chain-transfer to the telomer and of 5-cyano-5-methoxycarbonylpentyl radicals to branched telomers *via* intramolecular 1,5-hydrogen transfer in the radicals was attempted on the basis of the yields of telomers. For the estimation, it was necessary to determine the yields of branched telomers in each pathway. The yields were estimated from the following relations by assuming the same chain-transfer constant for the telomer radical, $RC(CN)(COOCH_3)\dot{E}_n$ (R=Et, Bu, and hexyl; E represents an ethylene unit), with the same n;

$$\frac{[B_2]_{et2}}{[B_1]_{et1}} = \frac{[B_3]_{bt2}}{[B_2]_{bt1}} = \frac{[B_5]_{ht2}}{[B_4]_{ht1}}$$

$$\frac{[B_4]_{et3}}{[B_2]_{et2}} = \frac{[B_5]_{bt3}}{[B_3]_{bt2}}$$

where $[B_n]_{etn}$, $[B_n]_{btn}$, and $[B_n]_{htn}$ represent the yields of branched telomers formed in the et$n$, bt$n$, and ht$n$ pathways respectively. There is no information on the chain-transfer constants of the branched telomer radicals; however, we may expect little change in the constants caused by the difference in alkyl groups, such as ethyl, butyl, and hexyl, in the telomer radical. A slight change may also be expected from the ratios (1.0—1.5)[6,7] of the chain-transfer constant of the branched telomer radical $BuC(X)(COOCH_3)\dot{E}_n$ to that of the linear telomer radical $CH(X)(COOCH_3)\dot{E}_n$ in the telomerizations of methyl propionate (X=CH_3) and methyl chloroacetate (X=Cl) with ethylene. The results, and the estimated conversions of linear telomer radicals with ethylene units of n by Reaction tn (T_n) and of branched telomer radicals $HE_2C(CN)(COOCH_3)\dot{E}_n$ by Reaction bt$n$ (T_{bn}), are given in Table 5. The mean value of A_1 and A_3 was used for A_2 in the estimation of the conversion, R. It was found that 5-cyano-5-methoxycarbonylpentyl radicals gave branched telomers in conversions of 75—79% under the present conditions.

TABLE 5. CONVERSION OF TELOMER RADICALS

Press. (kg/cm²)	20	30	30	30	40
Time (hr)	8	1	3	8	8
T_1[a]	77.4	70.4	68.7	68.3	61.1
T_2	23.7	19.0	21.4	21.4	19.3
R	75.1	79.2	76.7	76.6	78.1
T_{b1}	81.2	73.7	73.1	74.1	67.4
T_{b2}	94.9	90.6	91.3	92.1	88.6
A_1	17.9	11.5	17.8	20.2	19.5
A_3	18	17	34	37	34

a) Conversions are given in percentage.

The chain-transfer constants, C_n (k_{tn}/k_{pn}), for a linear telomer radical, $\dot{E}_nCH(CN)COOCH_3$, and C_{bn} (k_{btn}/k_{bpn}) for a branched telomer radical, $HE_2C(CN)(COOCH_3)\dot{E}_n$, were estimated by Mayo's equation[16] from the estimated yields of the telomers and from the average ratio of the ethylene and methyl cyanoacetate concentrations. The C_{rp} ratio of the rate constants, k_r (Reaction r) to k_{p2} (Reaction p2), was evaluated from the estimated yields of the branched telomers formed *via* Reaction r ($[B_n]_r$) and those of all of the linear and branched telomers formed *via* Reaction p2 ($[N_n+B_n]_{p2}$), and from the average concentration of ethylene;[7]

$$C_{rp} = \frac{k_r}{k_{p2}} = \frac{[B_n]_r[E]}{[N_n+B_n]_{p2}}$$

The estimated chain-transfer constants and C_{rp} values are given in Table 6. In the estimation, the formation of N_2 from 1-cyano-1-methoxycarbonylpentyl radicals by hydrogen abstraction was neglected.[6,7] Although the chain-transfer constant of the radical cannot be estimated, it should be much smaller than C_1 for the radicals stabilized by cyano and methoxycarbonyl groups. If the constant is not negligible, some higher value may be estimated for C_{rp} and some lower value for C_2. The estimated chain-transfer contants and C_{rp} values were larger than those in the telomerization

TABLE 6. CHAIN TRANSFER CONSTANTS

Press. (kg/cm²)	20	30	30	30	40	(Mean)
Time (hr)	8	1	3	8	8	
C_1	0.096	0.095	0.092	0.090	0.092	0.093
C_2	0.57	0.42	0.49	0.44	0.44	0.47
C_{b1}	0.12	0.11	0.11	0.12	0.12	0.12
C_{b2}	0.52	0.39	0.44	0.49	0.45	0.46
C_{rp}[a]	32	43	36	36	40	37

a) Represented in mol/l.

of methyl propionate and methyl chloroacetate with ethylene.[6,7]

Chain-transfer Reactions in the Telomerization of Methyl Acetate with Ethylene. In the telomerization product, telomers of methyl esters and acetates were found. The formation of these telomers suggests that hydrogen atoms of acetyl and methoxy groups in methyl acetate were abstracted to give methoxycarbonylmethyl and acetoxymethyl radicals. The formation of branched methyl ester telomers BA by chain transfer to linear telomers LA was also suggested by the formation of the BA_1 branched telomer. Intramolecular 1,5-hydrogen transfer in 5-methoxycarbonylpentyl radicals was also suggested by the minimum in the distribution of the LA telomer at two ethylene units (Fig. 2) and by the remarkable formations of BA_2 and of branched methyl ester telomers with a butyl group at the α-position. The formation of branched acetate telomers may be similar to that of methyl ester telomers, BA, as the formation of BM_1 and the amount of BM_2 suggest. These pathways of the formation of branched telomers are the same in manner as those in the system of methyl cyanoacetate.

The degree of chain transfer to linear telomers, LA, cannot be estimated because not all of the telomers could be analyzed by glc, but a convresion of more than 9% of the LA_1 formed during the reaction to the branched telomers was evaluated from the ratio of the amount of BA_1 to the sum of the amounts of LA_1 and BA_1 for 8 hr under a pressure of 20 kg/cm² at 140 °C. A considerable extent of the intramolecular hydrogen transfer in 5-methoxycarbonylpentyl radicals was also suggested by the ratio (1.6) of the sum of the amounts of BA_2, BA_3, and BA_5 to that of LA_3, LA_4, and LA_5, although it means only a rough measure.

A significant degree of the formation of branched telomers was also shown by the compositions of the series of telomers in the entire product (Table 7).

Table 7. Relative ratio of series of the telomers

Temp. (°C)	20	130	140	150	160
LA	—	1.00	1.00	1.00	1.00
LM	—	0.41	0.37	0.36	0.33
BA	—	0.74	0.61	0.47	0.32
BM	—	0.12	0.10	0.04	0.02
BA/LA	—	0.74	0.61	0.47	0.32
BM/LM	—	0.29	0.27	0.11	0.06
$(M/A)_t$	—	0.30	0.29	0.27	0.26
$(M/A)_d$	1.47	0.93	0.83	0.80	—
$(M/A)_0$	1.15	—	0.26	—	—

The compositions were obtained by means of NMR as follows:

$$LA = H_d - H_e/3$$
$$LM = H_f/2$$
$$BA = 2H_e/3 - H_d$$
$$BM = H_e/3 - H_f/2$$

where H_c, H_e, H_f, and H_d represent the relative intensities of the protons of CH_3COO–, –$COOCH_3$, –$COOCH_2$–, and of the sum of the protons of –CH_2COO– and >$CHCOO$– respectively. The high ratio of the branched telomer, BA, to the linear telomer, LA, was observed under a pressure of 20 kg/cm² at 130—140 °C, and the ratio decreased with a rise in the reaction temperature. In acetate telomers, the ratio (BM/LM) of branched to linear telomers also shows a tendency similar to that of methyl ester telomers. However, the lower ratio of BM/LM suggests that the α-hydrogen of the alkoxy moiety in the acetates is less reactive as a whole for homolytic hydrogen abstraction than that of the carboxylic moiety in the methyl esters.

The chain-transfer constants of the telomer radicals in this system could not be evaluated, but the broad distributions of the LA and LM telomers suggest quite small-chain-transfer constants of ω-methoxycarbonylalkyl and ω-acetoxyalkyl radicals (Figs. 2 and 3). A lower reactivity of ω-acetoxyalkyl radicals in the chain-transfer reaction than that of the ω-methoxycarbonylalkyl radicals was also suggested by the broader distribution in the acetate telomers, LM. The sharp distribution of the cyanoacetate telomers, N_n, compared with that of the methyl ester telomers, LA, shows that the introduction of the cyano group to methyl acetate at the α-position gave a favorable system for a chain-transfer reaction.

Relative Reactivity of the Methoxy Group to the Acetyl Group. In the telomerization of methyl acetate with ethylene, the abstraction of a hydrogen atom from methoxy and acetyl moieties in methyl acetate was indicated by the formation of acetate and methyl ester telomers. The relative reactivity of the methoxy group to the acetyl group in methyl acetate for hydrogen abstraction was estimated by means of the ratio ($(M/A)_t$) of the amounts of acetate telomers to that of methyl ester telomers in the telomerization. The ratio was 0.30 at 130 °C; it was slightly decreased with a rise in the reaction temperature (Table 7). The ratio suggests that the relative reactivity of the methoxy group is higher than that of the alkoxy moiety to the acetyl group in ethyl and isopropyl acetates.[17] Therefore, it was compared with the ratio ($(M/A)_d$) of the amount of the acetoxy group to that of the methoxycarbonyl group in the product of the decomposition of DTBP in methyl acetate, and with the formation ratio ($(M/A)_0$) of nonyl acetate to methyl decanoate in the addition of methyl acetate to 1-octene initiated by DTBP. The $(M/A)_d$ ratio was estimated from the ratio of the proton intensity of the acetyl group to that of the methoxy group in the product, which contained mainly methyl succinate, ethylene diacetate, and methyl 3-acetoxypropionate. The $(M/A)_0$ ratio was measured by means of glc. The ratios of $(M/A)_d$ and $(M/A)_0$ are given in Table 7.

The $(M/A)_d$ and $(M/A)_0$ ratios suggest that the methoxy group is more reactive for hydrogen abstraction than the acetyl group at 20 °C, and that the relative reactivity of the methoxy group decreases with a rise in the temperature. The value of $(M/A)_0$ was the same as that of $(M/A)_t$ at 140 °C; it was presumed to be higher than that in the addition of 1-octene with

methyl acetate initiated by di-isopropyl peroxydicarbonate.[18]. The $(M/A)_d$ ratio at the same temperature showed that the relative reactivity of the methoxy group was higher in the absence of ethylene or 1-octene. The difference in the relative reactivity of the methoxy group may be caused by a difference in the extent of contributions of the *tert*-butoxy, methyl, and telomer radicals to hydrogen abstraction from methyl acetate. In the decomposition of DTBP in methyl acetate, a hydrogen atom of methyl acetate may be abstracted by the methyl and *tert*-butoxy radicals formed by the decomposition of DTBP. Methyl radicals predominantly abstract a hydrogen atom from the acetyl group in methyl acetate,[19] whereas a hydrogen atom of the methoxy group in methyl acetate may be abstracted mainly by electrophilic *tert*-butoxy radicals.[20] Therefore, the high value of $(M/A)_d$ may be attributed to the large extent of the contribution of *tert*-butoxy radicals to the hydrogen abstraction. In the presence of olefins, the relative reactivity of the methoxy group may be apparently decreased by the contribution of additional hydrogen abstraction by telomer radicals, which are expected to be similar reactive with alkyl radicals in hydrogen abstraction. The relatively higher values of $(M/A)_t$ and $(M/A)_0$ may be caused by some contribution of *tert*-butoxy radicals to the hydrogen abstraction in the telomerizations with short kinetic chain lengths.

Experimental

Materials. Commercial methyl acetate was treated with acetic anhydride and with potassium carbonate in the usual way, then distilled. Commercial methyl cyanoacetate was dried over anhydrous magnesium sulfate, then distilled. Commercial 1-octene was distilled. The DTBP, ethylene, and methyl esters of linear alkanoic acids were obtained commercially. The methyl esters of α-branched alkanoic acids were prepared from the corresponding acids and methanol. The methyl 2-cyanoalkanoates and 2-alkyl-2-cyanoalkanoates were prepared from alkyl bromides and methyl cyanoacetate or the corresponding methyl 2-cyanoalkanoates.[21] Acetates and cyanoacetates were prepared from the corresponding alcohols and acetyl chloride or cyanoacetic acid. These reference samples were confirmed by elemental analyses and by a study of the IR and NMR spectra.

Telomerization. *Procedure A*: A mixture of methyl acetate (100 g) and an initiator (0.015 mol/mol) was placed in a 300 ml stainless-steel autoclave, air was displaced with ethylene, and ethylene was introduced until a pressure of 40 kg/cm² was reached at room temperature. The mixture was then heated at the prescribed temperature with stirring. *Procedure B*: A mixture of 150 g of methyl acetate and 7.5 g of DTBP was heated at the prescribed temperature in the autoclave. During the reaction, ethylene was introduced to keep the pressure prescribed for that temperature.

The telomerization of methyl cyanoacetate with ethylene was carried out by Procedure B, using 150 g of methyl cyanoacetate and 4.4 g of DTBP.

Hydrolysis of Telomers. A mixture of 7.6 g of the telomerization product of methyl acetate with ethylene, 5.0 g of potassium hydroxide, and 50 ml of ethanol was heated at 180 °C for 8 hr in an autoclave. The aicd (5.0 g) and the neutral fractions (1.9 g) were subsequently separated in the usual way.

Separation of Hydrocarbons. Hydrocarbons (0.127 g) were separated from the telomerization product (1.014 g) of methyl acetate with ethylene using a silica-gel-column with petroleum ether.

Identification of the Products. A gas chromatographic determination was made on 2.25 m and 4.0 m columns packed with PEG-20M (30% on Celite 545) for the telomerization products of methyl acetate with ethylene, and on a 2.25 m column packed with Apiezone Grease L (30% on Celite 545) for the telomerization products of methyl cyanoacetate with ethylene, with helium as the carrier gas. The IR and NMR spectra were measured on JASCO IR-A2 and JEOL JNM-C-60HL spectrometers respectively. The mass spectra were measured on a Hitachi RMU-6L mass spectrometer combined with a gas chromatograph. The reaction mixture was fractionated by the use of a spinning-band column.

Methyl Alkanoates LA_n: The retention times (min) of LA_1—LA_4, measured using a 4.0 m column at 140 °C and of LA_5—LA_7, measured using a 2.25 m column at 240 °C, agreed with those of authentic methyl esters as follows (LA_n, the retention time, reffered to methyl ester, and its retention time): LA_1, 1.75, butanoate, 1.72; LA_2, 4.45, hexanoate, 4.40; LA_3, 11.10, octanoate, 11.06; LA_4, 27.76, decanoate, 27.75; LA_5, 3.01, dodecanoate, 2.99; LA_6, 5.21, tetradecanoate, 5.22; LA_7, 9.02, hexadecanoate, 8.97. The IR and NMR spectra of LA_n (n=1—5), which were collected by preparative glc, and the mass spectra of LA_n(n=1—7) also supported the above identification. The signals in the NMR spectra were as follows (signal, τ value, and assignment): a, 9.07—9.15(t), CH_3–; b, 8.35—8.77 (m), $-CH_2-$; c, 7.82—7.84 (t), $-CH_2COO-$; d, 6.48—6.49 (s), $-COOCH_3$.

Alkyl Acetates LM_n: The retention times of LM_n (n=1—4), measured using a 4.0 m column at 140 °C, and of LM_n (n=5—7), measured using a 2.25 m column at 240 °C, agreed with those of authentic acetates as follows (LM_n, retention time, referred to acetate, and its retention time): LM_1, 1.66, propyl, 1.57; LM_2, 4.07, pentyl, 4.09; LM_3, 10.20, heptyl, 10.11; LM_4, 25.39, nonyl, 25.34; LM_5, 2.76, undecyl, 2.80; LM_6, 4.87, tridecyl, 4.90; LM_7, 8.44, pentadecyl, 8.50. The retention times of tridecyl and pentadecyl acetates were estimated using the relation between the retention times and the number of carbon atoms in the homologues. The mass spectra of LM_n (n=1—7) also supported the above identification.

Methyl α-Branched Alkanoates BA_n: The retention times of BA_n (n=1—5), measured using a 4.0 m column at 140 °C, agreed with those of authentic esters as follows (BA_n, retention time, referred methyl ester, and its retention time): BA_1, 2.86, 2-ethylbutanoate, 2.79; BA_2, 6.22, 2-ethylhexanoate, 6.17; BA_3, 13.16, 2-butylhexanoate, 13.10; BA_4, 14.70, 2-ethyloctanoate, 14.74; BA_5, 31.08, 2-butyloctanoate, 30.9. The retention time of methyl 2-butyloctanoate was estimated from those of the homologues. The IR and NMR spectra of BA_n (n=1—3), which were collected by preparative glc, and the mass spectra of BA_n (n=1—4) also supported the above identification. The signals in the NMR spectra were as follows (signal, τ value and assignment): a, 9.10—9.15 (t), CH_3–; b, 8.56—8.74 (m), $-CH_2-$; c, 7.82—7.87 (m), $>CHCOO-$; d, 6.38—6.47 (s), $-COOCH_3$.

α-Branched Alkyl Acetates BM_n: The retention times of BM_1, measured using a 2.25 m column at 80 °C, and of BM_2 and BM_3, measured using a 4.0 m column at 150 °C, agreed with those of authentic acetates as follows (BM_n, retention time, referred acetate, and its retention time): BM_1, 8.12, 1-ethylpropyl, 8.19; BM_2, 5.53, 1-ethylpentyl,

5.52; BM_3, 11.30, 1-butylpentyl, 11.31. BM_2 and BM_3 were also confirmed by mass spectrometry. The nonan-5-ol (with a retention time of 9.92 min at 150 °C using a 4.0 m column) in the neutral fraction was detected by glc, as were the alcohols corresponding to LM_n (n=1—7) and BM_n (n=1—3).

Hydrocarbons: The retention times of the e_1—e_4 peaks and of the e_5—e_7 peaks were measured at 140 °C with a 4.0 m column and at 240 °C with a 2.25 m column respectively. The retention times and the *m/e* of the parent ion peaks of the components of the e_n peaks (n=1—7) were as follows (e_n, retention time, *m/e* of parent ion peak, and n in CH_3-$(CH_2CH_2)_nH$): e_1, 1.13, 128, 4; e_2, 2.85, 156, 5; e_3, 7.02, 184, 6; e_4, 17.48, 212, 7; e_5, 2.17, 240, 8; e_6, 3.74, 268, 9; e_7, 6.50, —, 10.

Methyl α-Cyanoalkanoates N_n and B_n: The retention times of N_n (n=1—3) and B_n (n=1—5) at 190 °C agreed with those of authentic esters as follows (N_n or B_n, retention time, referred to methyl ester, and its retention time): N_1, 0.97, 2-cyanobutanoate, 0.96; N_2, 2.24, 2-cyanohexanoate, 2.24; N_3, 5.44, 2-cyanooctanoate, 5.45; B_1, 1.56, 2-cyano-2-ethylbutanoate, 1.57; B_2, 3.33, 2-cyano-2-ethylhexanoate, 3.32; B_3, 6.74, 2-butyl-2-cyanohexanoate, 6.72; B_4, 7.87, 2-cyano-2-ethyloctanoate, 7.85; B_5, 15.84, 2-butyl-2-cyano-octanoate, 15.83. The mass spectra of N_n (n=1—3) and B_n (n=1—5) also supported the above identification.

Propyl (1.18 min at 190 °C) and pentyl (2.97 min at 190 °C) cyanoacetates could not be detected by glc. Methyl 2-cyano-3-methyl-2-butenoate which had been collected by the use of a silica-gel-column with benzene was confirmed by elemental analysis, and by a study of its IR, NMR, and mass spectra.

Gas Chromatographic Analysis of Products. The gas chromatographic analysis of the telomerization products of methyl acetate with ethylene was made on a 2.25 m colum (PEG-20M, 30%). The column temperature was programed to rise at a rate of 4 °C/min from 80 °C to 240 °C. The amounts of the telomers relative to those of methyl 2-ethylhexanoate were determined by the use of calibration curves. The analysis of the telomerization products of methyl cyanoacetate with ethylene was made on a 2.25 m, column (Apiezone Grease L, 30%). The column temperature was programed to rise at a rate of 4 °C/min from 140 °C to 240 °C. Cyclododecane was used as the internal standard.

Determination of the Relative Ratios (M/A). Methyl acetate was removed from the reaction mixture of the telomerization of methyl acetate with ethylene by the use of a spinning-band column. The NMR spectra of the residues were measured in carbon tetrachloride.

The decomposition of DTBP (3.7 g) in methyl acetate (74 g) was carried out in an autoclave. The treatment of the reaction mixture was similar to that described above. The reaction of 1-octene (5.6 g) with methyl acetate (74 g) in the presence of DTBP was carried out much like the telomerization procedure. The ratio of the yield of nonyl acetate to that of methyl decanoate was determined by glc. In the experiments at 20 °C, the reaction mixture was irradiated with a high-pressure mercury lamp (UM-102).

The authors wish to thank Mr. Toshinori Shiraki, Mr. Keizo Fujiyama, Mr. Koichi Sonoda, Mr. Akira Morinaga, and Mr. Fumio Harada for their assistance in the experimental work.

References

1) M. S. Kharasch and M. T. Gladstone, *J. Amer. Chem. Soc.*, **65**, 15 (1943).
2) M. S. Kharasch, E. V. Jensen, and W. H. Urry, *J. Org. Chem.*, **10**, 386 (1945).
3) M. S. Kharasch, H. C. McBay, and W. H. Urry, *ibid.*, **10**, 394 (1945).
4) C. Walling, "Organic Reactions," Vol. 13, p. 91, John Wiley & Sons, Inc., New York, N. Y. (1963).
5) R. Kh. Freidlina, S. N. Aminov, and A. B. Terent'ev, *Dokl. Akad. Nauk SSSR*, **156**, 1133 (1964).
6) A. B. Terent'ev, N. S. Ikonnikov, and R. Kh. Freidlina, *ibid.*, **196**, 1373 (1971).
7) R. Kh. Freidlina, A. B. Terent'ev, and N. S. Ikonnikov, *ibid.*, **193**, 605 (1970).
8) M. Chiang and S. Li, *Hua Hsueh Hsueh Pao*, **28**, 379 (1962).
9) J. C. Allen, J. I. G. Cadogan, B. W. Harris, and D. H. Hey, *J. Chem. Soc.*, **1962**, 4468.
10) R. L. Huang, C. Ong, and S. H. Ong, *J. Chem. Soc., C*, **1968**, 2217.
11) M. Julia and J. C. Chottard, *C. R. Acad. Sci. Paris*, **259**, 2653 (1964).
12) M. Cazaux and R. Lalande, *Bull. Soc. Chim. Fr.*, **1966**, 3381.
13) E. Roe, D. A. Konen, and D. Swern, *J. Amer. Oil Chem. Soc.*, **42**, 457 (1965), *Chem. Abstr.*, **63**, 3179 (1965).
14) J. M. Surzur and P. Teissier, *Bull. Soc. Chim. Fr.*, **1970**, 653, 3060.
15) E. A. Hardwidge, C. W. Larson, and B. S. Rabinovitch, *J. Amer. Chem. Soc.*, **92**, 3278 (1970).
16) F. R. Mayo, *ibid.*, **70**, 3689 (1948).
17) S. Kato and F. Masuo, *Kogyo Kagaku Zasshi*, **60**. 1515 (1957).
18) J. C. Allen, J. I. G. Cadogan, and D. H. Hey, *J. Chem. Soc.*, **1965**, 1918.
19) K. C. Ferguson and J. T. Pearson, *Trans. Faraday Soc.*, **66**, 910 (1970).
20) C. Walling and M. J. Mintz, *J. Amer. Chem. Soc.*, **89**, 1515 (1967).
21) J. C. Hessler and R. M. Lamb, *ibid.*, **43**, 205, 672 (1921).

Studies of Tritylated Sucroses. III. NMR Studies of Tritylacetylsucroses

Toshiki Otake

Nippon Electric Varian, Ltd., Azabu Iigura-machi, Minato-ku, Tokyo 106

(Received October 22, 1973)

Seven tritylated derivatives have been synthesized by the tritylation of the primary hydroxyl group of sucrose. The ^{1}H NMR spectra of their peracetyl derivatives have been determined at 100 MHz and 220 MHz in order to assign the sugar-ring-proton signals with the aid of the double-resonance technique and NMR spin simulation. The relationship between the chemical shifts of their methine protons and the substituted position of the bonded trityl groups is discussed. Crystalline 1′-mono-*O*-tritylsucrose derived from 6,6′-di-*O*-palmitolysucrose is also described.

The preparations and the structures of two mono-*O*-tritylsucroses, 6′- (I) and 6-mono-*O*-tritylsucrose (II), and of 1′, 6-di-*O*-tritylsucrose (VI) were reported in previous papers.[1,2] The structures were mainly elucidated by ^{1}H NMR studies of the corresponding peracetyl derivatives and by gas-chromatographic studies of their partially-methylated derivatives. The structure of the tri-*O*-trityl derivative, 1′,6,6′-tri-*O*-tritylsucrose (VII), was established through complicated reaction routes without refering to the NMR spectra.[3-5]

In the NMR spectra of the tritylacetylsucroses, signals of protons on methylene carbons directly bearing an *O*-trityl group were observed in the region between δ 2 and 3.5. However, the author did not assign the

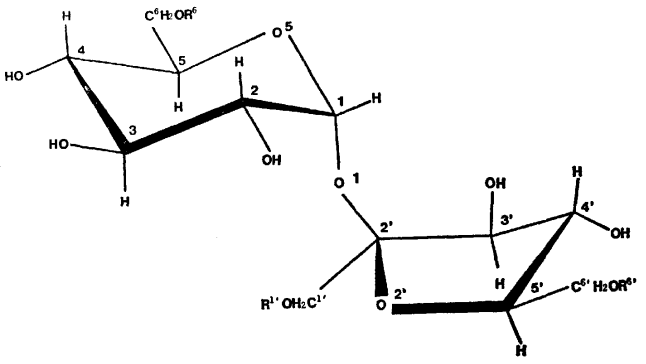

I $R^{6'}=Tr$ $R^{1'}=R^{6}=OH$
II $R^{6}=Tr$ $R^{1'}=R^{6'}=OH$
III $R^{1'}=Tr$ $R^{6}=R^{6'}=OH$
IV $R^{6}=R^{6'}=Tr$ $R^{1'}=OH$
V $R^{1'}=R^{6'}=Tr$ $R^{6}=OH$
VI $R^{1'}=R^{6}=Tr$ $R^{6'}=OH$
VII $R^{1'}=R^{6}=R^{6'}=Tr$

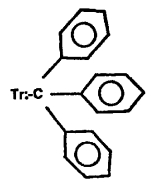

methine proton signals which appear in the region between δ 4.5 and 6.0; these signals show characteristic patterns according to the number and positions of trityl groups on a sucrose molecule. The chemical shifts and coupling constants for the methine and methylene protons of octa-*O*-acetylsucrose (VIII) had already been determined with the aid of the double-resonance technique and the multi solvent method.[6]

This paper will deal with the assignment of methine-proton signals in the tritylacetylsucroses and with the relationship between the methine chemical shifts and the anisotropic effects exerted by a trityl group. Further, it is suggested that the difference in the chemical shifts of methine or methylene protons between a tritylacetyl and a peracetyl derivative of an oligosaccharide provides valuable information about its stereostructure or conformation in solution.

Results and Discussion

As has been described in previous papers,[1,2] 1′-mono-*O*-tritylsucrose (III) was not found in the reaction product of sucrose with trityl chloride in pyridine, although di- and tri-*O*-tritylsucroses with a trityl group at the 1′-position were found in the product. The reaction of 6,6′-di-*O*-palmitoylsucrose[7] with trityl chloride in a 1 : 2 mole ratio in pyridine gave 1′-mono-*O*-trityl-di-*O*-palmitoylsucrose (IX) as the main product. In the reaction solution, the presence of unreacted trityl chloride and di-*O*-palmitoylsucrose, and a minor amount of poly-*O*-trityldi-*O*-palmitoylsucroses were also observed by thin-layer chromatography. Compound IX which had been isolated by column chromatography, was deacylated to give III. The procedure used to prepare the remaining six tritylacetylsucroses was described in the previous papers.[1,2] Recently, Buchanan[8] and Suami and Ikeda[9] have reported the synthesis of 6′-mono-*O*-tritylhepta-*O*-acetylsucrose (I′) and a peracetyl derivative of 1′,6′-di-*O*-tritylsucrose (V′) from 2,3,6,3′,4′-penta-*O*-acetylsucrose.

Figure 1 shows parts of the 220 MHz NMR spectrum of III′, which gives the expected seven signals of acetylmethyl-protons at δ 1.85 (3H), 1.97 (3H), 1.99(3H), 2.02(3H), 2.03(3H), 2.08(3H), and 2.10(3H), and also an AB-type quartet at δ 3.17 and 3.24 which arises from the isolated oxymethylene protons at the 1′-position. These signals together with the relative integrated intensity of the trityl group which corresponds to 14.83 protons (theory, 15 protons), and that of the acetyl groups, which corresponds to 20.96 protons (theory, 21 protons), account for the expected structure of III′.

In the NMR spectra of the tritylacetylsucroses with an acetyl group at the 6-position, such as 1′-mono- (III′), 6′-mono- (I′), and 1′,6′-di-*O*-tritylacetylsucrose (V′), all the methine-proton signals except those due to H-5 and H-5′ were readily assigned with the aid of the double-resonance technique, the results are shown in Figs. 1, 2, and 3. The analysis of the complicated signals between δ 5.2 and 5.6 in the spectrum of I′ was made by the spin-simulation method; these results are also shown in Fig. 2.

When a trityl group is situated at the 6-position, as in

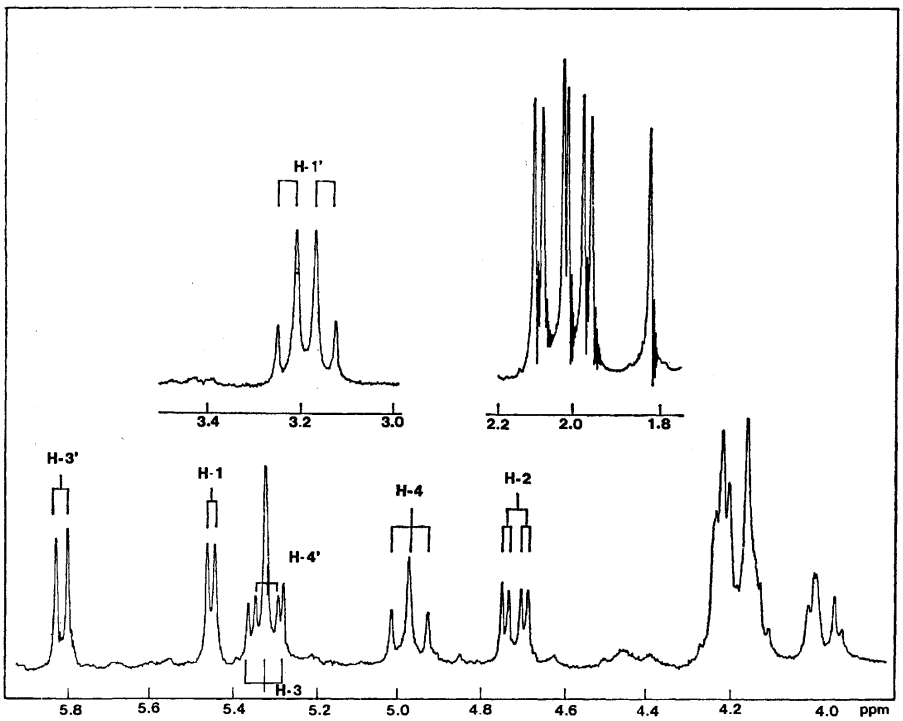

Fig. 1. Parts of the NMR spectrum at 220 MHz of III'.

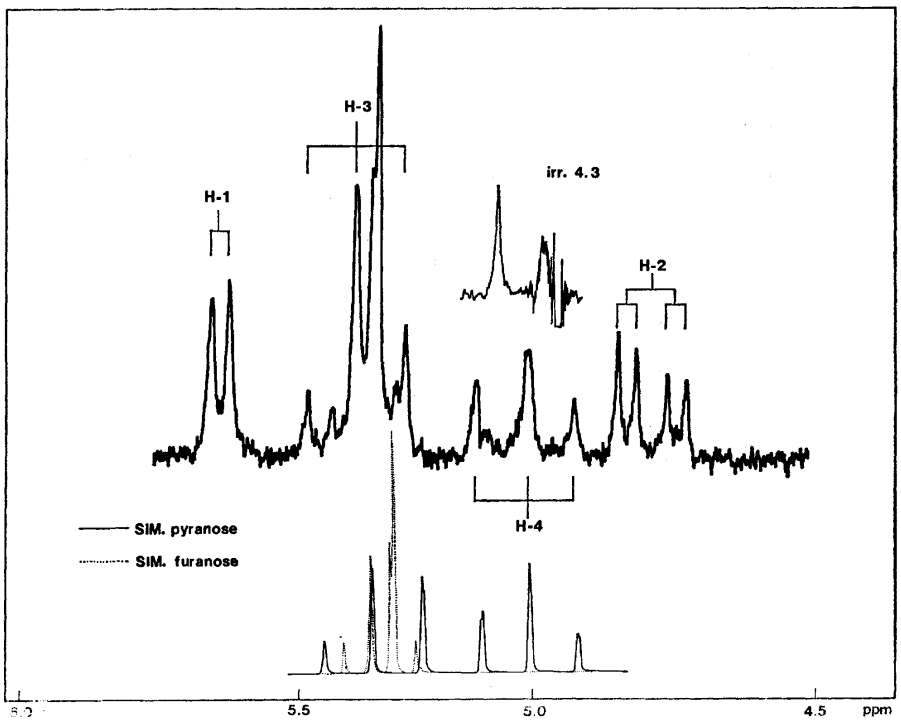

Fig. 2. A part of the NMR spectrum at 100 MHz of I'

the cases of 6-mono- (II'), 6,6'-di- (IV'), I',6-di- (VI'), and 1',6,6'-tri-*O*-tritylacetylsucrose (VII'), the access of the H-3 and H-4 signals and the overlapping of other signals make their assignments difficult, especially at 100 MHz. An approximate first-order analysis was applied to the methine-proton signals in the 220 MHz spectrum of II', which was confirmed by a spin simulation; the results are shown in Fig. 4. The signals due to H-3 and H-4 in IV' and VII' show symmetrical, but overlapping patterns near δ 5.2 in their 220 MHz spectra and correspond to the AB part of an ABXY system, where J_{AX} equal J_{BY}. They were simulated using appropriate parameters, as is shown in Figs. 5 and 6. In the 220 MHz spectrum of VI', the signals due to H-3 and H-4 lie between δ 5.20 and 5.35 (Fig. 7). By analogy with the cases of IV' and VII', the chemical shifts of H-3 and H-4 may have a value almost equal to that corresponding to

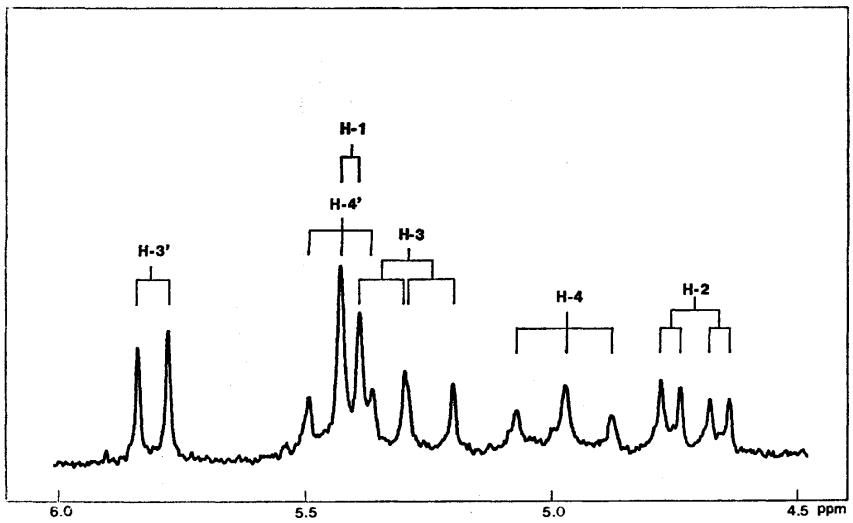

Fig. 3. A part of the NMR spectrum at 100 MHz of V'.

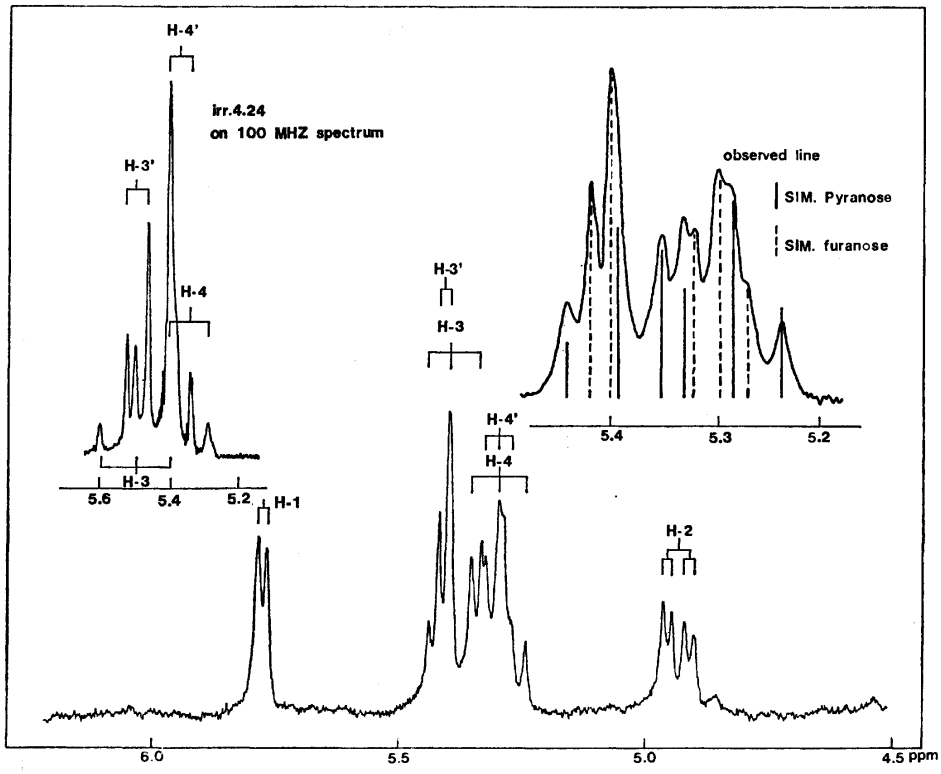

Fig. 4. Parts of the NMR spectrum at 220 MHz of II'.

the frequency of either of the two intense signals appearing in this region, that is, δ 5.31 or 5.27. The remaining methine-proton signals of this group of compounds, II', IV', VII', and VI' are well resolved and were readily assigned at 220 MHz.

The assignment of the signals of H-4 by irradiating H-5 signals was achieved only in the case of II'. For the other compounds of this group, the assignment of the H-4 signals was unsuccessful, because the chemical shifts of H-3 are too close to those of H-4.

The coupling constants applied to NMR spin simulation are listed in Table 1. The chemical shifts of all the methine protons except those of H-5 and H-5' in the tritylacetylsucroses examined are listed in Table 2.

Table 1. Coupling constants (Hz) applied to NMR spin simulation for tritylacetylsucroses

Compound	$J_{2,3}$	$J_{3,4}$	$J_{4,5}$	$J_{3',4'}$	$J_{4'5'}$
I'	9.5	10.0	10.0	5.3	5.5
II'	9.5	10.0	10.0	5.0	5.0
IV'	10.0	10.0	10.0	—	—
VII'	10.0	10.0	10.0	—	—

The differences in chemical shifts between a methine proton of octa-*O*-acetylsucrose (VIII) and the cor-

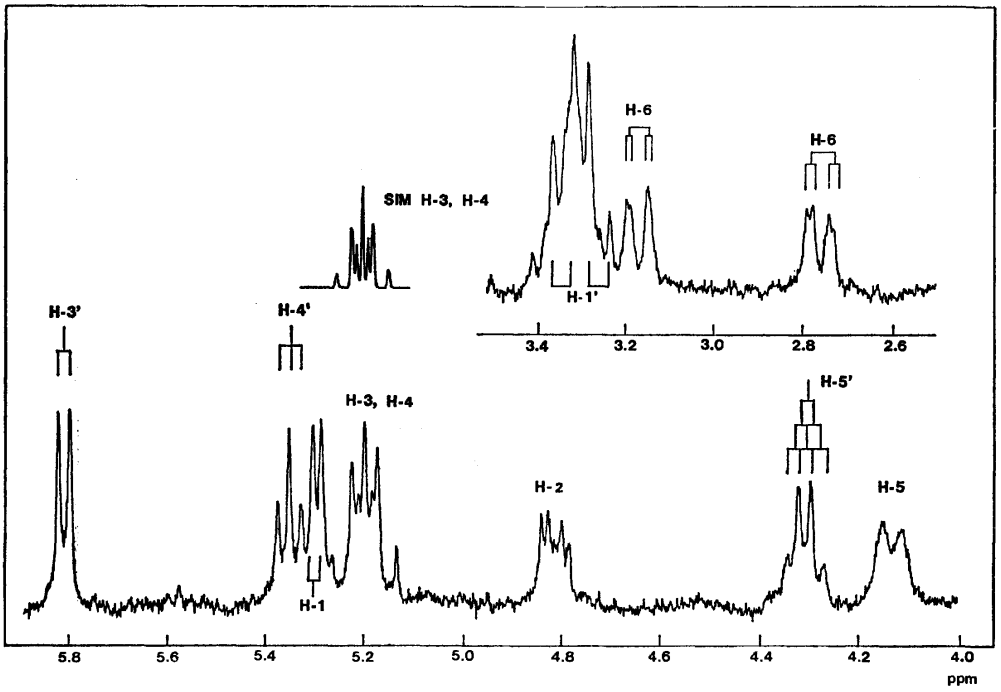

Fig. 5. Parts of the NMR spectrum at 220 MHz of VII'.

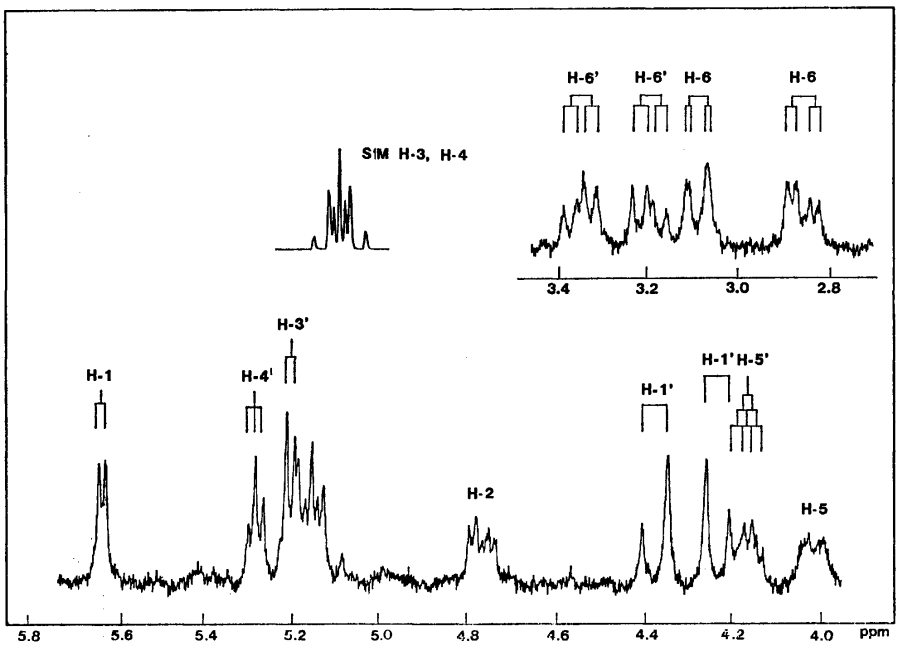

Fig. 6. Parts of the NMR spectrum at 220 MHz of V'.

responding proton of each tritylacetylsucrose (Δ) are listed in Table 3. A positive Δ value represents a downfield shift of a proton signal from VIII to a tritylacetylsucrose.

Each compound has its characteristic set of Δ values. The protons, H-3' in III', H-4 in II', and H-4' in I', resonate at lower fields than the corresponding protons in VIII. In spite of the similarity in the positional relationship between each proton and the trityl group, as will be shown below, the difference in the magnitude of the deshielding effects upon these protons should be considerable.

When a methine proton shares a hexose ring with a trityl group, it generally suffers a deshielding effect as in the cases of H-2 and H-3 in II', and that of H-4' in III', but not the case of H-3' in I'. In all the mono-*O*-tritylacetylsucroses, the methine protons bonded to the hexose ring with no trityl group resonate at a slightly higher field than the corresponding protons in VIII.

The anisotropic shielding effect, σ (expressed in ppm), that is, the ring-current effect of a benzene ring, is well known.[10] The surface where $\sigma=0$ is approximated by a double cone, the axis of which is shared

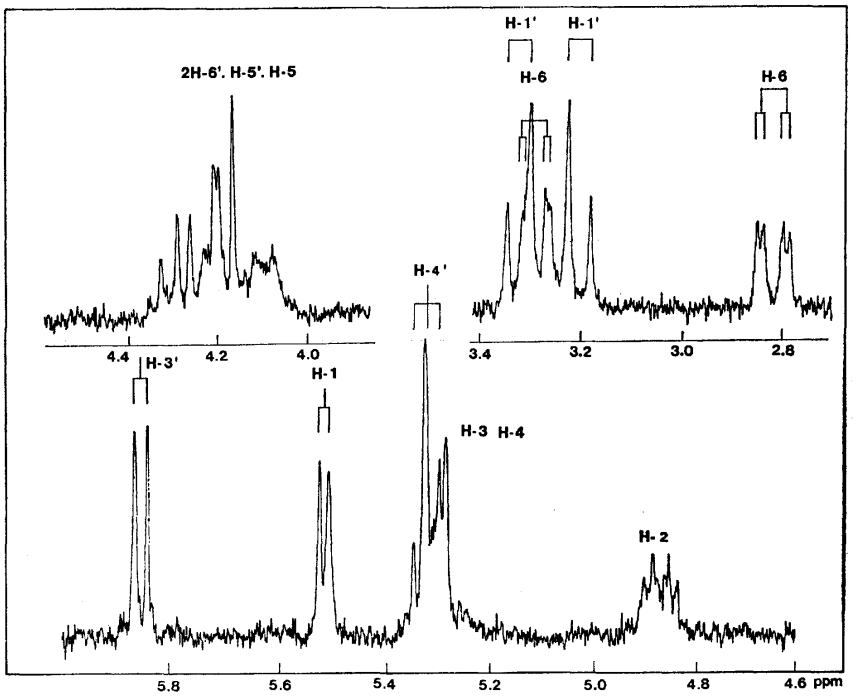

Fig. 7. Parts of the NMR spectrum at 220 MHz of VI'.

Table 2. Chemical shifts (δ) of methine protons in tritylacetylsucroses

Compound	H-1	H-2	H-3	H-4	H-3'	H-4'
I'	5.67	4.79	5.36	5.04	5.34	5.39
II'	5.79	4.96	5.42	5.32	5.43	5.32
III'	5.51	4.77	5.39	5.02	5.87	5.38
IV'	5.73	4.85	5.27 or 5.23	5.23 or 5.27	5.30	5.38
V'	5.52	4.86	5.32 or 5.28	5.28 or 5.32	5.87	5.32
VI'	5.40	4.70	5.29	4.96	5.81	5.42
VII'	5.30	4.79	5.22 or 5.17	5.17 or 5.22	5.82	5.35

Table 3. Chemical-shift differences between a proton of VIII and the corresponding proton of tritylacetylsucroses [$\Delta = \delta$(tritylacetylsucrose) $- \delta$(VIII)]

Compound	H-1	H-2	H-3	H-4	H-3'	H-4'
I'	−0.01	−0.06	−0.06	−0.02	−0.11	+0.03
II'	+0.11	+0.11	−0.03	+0.26	−0.02	−0.04
III'	−0.17	−0.08	−0.06	−0.04	+0.42	+0.02
IV'	+0.05	0.00	−0.18 or −0.22	+0.17 or +0.22	−0.15	+0.02
V'	−0.16	+0.01	−0.13 or −0.17	+0.22 or +0.26	+0.42	−0.04
VI'	−0.23	−0.15	−0.16	−0.10	+0.36	+0.06
VII'	−0.38	−0.06	−0.23 or −0.28	+0.11 or +0.16	+0.37	−0.01

with the hexad axis of the ring; the inside of the cone is the shielding region, and the outside, the deshielding region. The rotation of a phenyl of a trityl group about the bond to the methane carbon # (C_{TM}) is sterically hindered, while the trityl group as a whole can rotate around the C–O bond (TOB), thus dividing the space into several regions, as is shown in Fig. 8. A proton in the P region surrounding the TOB bond

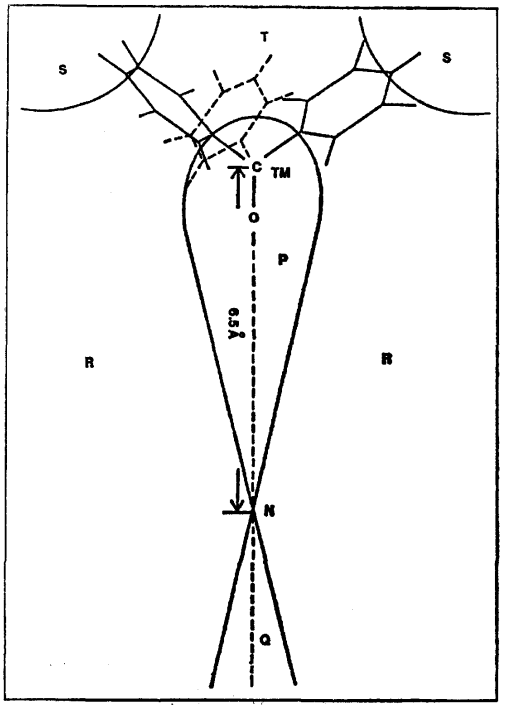

Fig. 8. A schematic representation of the anisotropic shielding effects exerted by a trityl group.

always suffers a deshielding effect, while that in the Q region suffers a shielding effect. The distance between C_{TM} and the node, N, of P and Q is estimated to be about 6.5 Å, with reference to the structure of triphenylmethane in the gas phase, as determined by the electron-diffraction method.[11] In the R region, the outside of the P and Q cores, the sign of the shielding effect, σ, is not clear. However, in view of the cancellation of a positive with a negative effect, the magnitude of σ in this region could not be very large. The methine protons in the tritylacetylsucroses should never be included in the S and T regions.

Thus, rotation about the bond which bears a trityl group causes a wide range of shielding or deshielding effects on a proton near this group. In all the tritylacetylsucroses, the rotation about the bond between the methylene carbon and the oxygen atom is appreciably restricted in such a conformation as (A). Any other conformations about the $C_{methylene}$–O bond make the distance between a phenyl group and various parts of the sucrose moiety too short. In III′, such a conformation as (B) is avoided, as by the Δ-2 effect in the case of glycopyranosides,[12] and the conformation illustrated as (C) is perferred. The trityl group is almost fixed; therefore, H-3′ may mostly be included in the P core, the deshielding region.

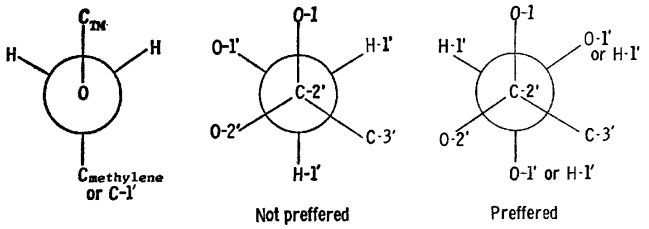

(A) (B) (C)

The C-5′ in I′ and C-5 in II′ are both attached with only one oxygen atom, and so the conformational restriction about C-5′–C-6′ or C-5–C-6 may be less than that about C-2′–C-1′. Then, H-4′ in I′ and H-4 in II′ may experience a shielding-deshielding averaging effect more than does H-3′ in III′. A proton on a ring with no trityl group may be included in the Q core, the shielding region which extends from the node, N.

The applicability of the additive rule for the Δ-value of di-*O*- and tri-*O*-tritylacetylsucroses has been examined. Each Δ value for a certain methine proton in a poly-*O*-tritylacetyl derivative agrees, in general, with the sum of the corresponding Δ values of mono-*O*-trityl derivatives, although there are some exceptions. This fact suggests that the disposition of a trityl group or the conformation of a sucrose moiety remains almost unchanged.

Experimental

General Methods. The NMR spectra were recorded on a Varian HA-100D (100 MHz) and an HR-220 (220 MHz) spectrometer, using chloroform-*d* solutions and with tetramethylsilane as the internal reference. The chemical shifts are expressed in δ. The NMR simulation was accomplished by means of a Varian Spectro System SS-100 equipped with a Varian 620/i computer. Thin-layer chromatography was carried out using Merck silica gel G as an adsorbent in a thickness of 0.25 mm. The developed plate was sprayed with 50% sulfuric acid and heated at 120 °C. Column chromatography was carried out using silica gel, 60—80 mesh (Kanto Chemical Co.).

1′-*Mono*-O-*tritylsucrose* (III). Crystalline 6,6′-di-*O*-palmitoylsucrose (1.278 g, mp 108—109 °C) which had been extracted from commercial sucrose palmitate, followed by crystallization, was reacted with recrystallized trityl chloride (0.834 g) which has twice the molarity of the ester, in dry pyridine (5 ml) at room temperature. Then the solution was allowed to stand for 96 hr. At the end of the reaction period, the solution was concentrated *in vacuo* at 40 °C until it became a hard syrup. Then the syrup was chromatographed on 10 g of silica gel. After the column had been washed with chloroform (200 ml) and 3% methanol–chloroform (70 ml), 6,6′-di-*O*-palmitoyl 1′-mono-*O*-tritylsucrose (IX) was eluted with 5% methanol–chloroform (200 ml). The evaporation of the last solution left 441 mg of IX as an amorphous solid. The thin-layer chromatogram developed by an admixture of methanol–tetrahydrofuran–water–methylene chloride 5 : 7 : 0.2 : 88 (vol/vol/vol/vol) showed the residue to be homogeneous, with an R_f value of 0.59. After the IX (400 mg) had then been dissolved by 5% ammoniac methanol (20 ml), the solution was allowed to stand for 24 hr at room temperature to remove the palmitoyl group. Then the solution was dried *in vacuo*, followed by the addition of methanol and reconcentration. The residue was chromatographed on a silica gel (10 g) column. After washing with 5% methanol–chloroform, III was eluted with 10% methanol–chloroform (200 ml). The residue of evaporation gave 201 mg of III.

Repeated crystallization from a 20% methanol–chloroform solution gave needles which melted at 193—196 °C and which had an $[\alpha]_D^{23}$ of +70.4° (*c* 1, methanol).

Found: C, 63.11; H, 6.40%. Calcd for $C_{31}H_{26}O_{11}$: C, 63.69; H, 6.21%.

1′-*Mono*-O-*tritylhepta*-O-*acetylsucrose(III′)*. 1′-Mono-*O*-tritylsucrose, III (100 mg), was dissolved in 2 ml of dry pyridine and then acetylated with acetic anhydride (0.3 ml) for 24 hr. The residue of evaporation *in vacuo* was chromatographed on silica gel (10 g) by washing the gel with 200 ml of toluene and 200 ml of 10% methyl ethyl ketone–toluene. The evaporation of the last washings gave 121 mg of III′, which had an $[\alpha]_D^{20}$ of +76.5° (*c* 1.59, $CHCl_3$).

Found: C, 61.67; H, 5.44%. Calcd for $C_{45}H_{50}O_{18}$: C, 61.50; H, 5.73%.

Other Materials. All the mono- and di-*O*-tritylacetylsucroses except III′ and V′ were prepared by the methods reported previously.[1,2] The tri-O-trityl derivative(VII′) was prepared by the method of Bredereck and his-co-workers. The authentic sample of V′ was synthesized by Suami and Ikeda through 2,3,6,3′,4′-penta-*O*-acetylsucrose; it melted at 100.0—102.0 °C and had an $[\alpha]_D^{20}$ of +58.4° (*c* 2.49, $CHCl_3$).

Found: C, 69.17; H, 5.70%. Calcd for $C_{62}H_{62}O_{17}$: C, 69.01; H, 5.79%.

The author wishes to thank Rrof. T. Suami, Keio University, for providing him with an authentic sample of 1′,6′-di-*O*-tritylhexa-*O*-acetylsucrose, Dr. T. Nishida for determining the 220 MHz NMR spectra, and Mr. K. Kushida for the 100 MHz NMR spectra.

References

1) T. Ōtake, This Bulletin, **43**, 3199 (1970).

2) T. Ōtake, *ibid.*, **45**, 2895 (1972).
3) G. G. McKeown, R. S. E. Serenius, and L. D. Hayward, *Can. J. Chem.*, **35**, 28 (1957).
4) G. G. McKeown and L. D. Hayward, *ibid.*, **35**, 992 (1957).
5) H. Bredereck, H. Zimmer, A. Wagner, G. Greiner, and W. Huber, *Chem. Ber.*, **91**, 2824 (1958).
6) W. W. Binkley, D. Horton, and N. S. Bhacca, *Carbohyd. Res.*, **10**, 245 (1969).
7) T. Ōtake and E. Tamate, *Kogyo Kagaku Zasshi*, **67**, 1586 (1964).
8) J. G. Buchanan, D. A. Cummerson and D. M. Turner, *Carbohyd. Res.*, **21**, 283 (1972).
9) T. Suami and Ikeda, Private Communication (1972).
10) For example, see C. E. Johnson, Jr., and F. A. Bovey, *J. Chem. Phys.*, **29**, 1012 (1958).
11) P. Andersen, *Acta Chem. Scand.*, **19**, 622 (1965).
12) R. E. Reeves, "*Advan. Carbohyd. Chem.*", 6th ed., Academic Press, New York (1951), p. 106.

Asymmetric Synthesis in the Oxymercuration Reaction Using Optically Active Mercuric Salts[1)]

Toshio SUGITA, Yasuo YAMASAKI, Osamu ITOH, and Katsuhiko ICHIKAWA

Department of Hydrocarbon Chemistry, Faculty of Engineering, Kyoto University, Sakyo-ku, Kyoto 606

(Received November 5, 1973)

The oxymercuration-demercuration of styrene with optically active mercuric tartrate, 2-phenylpropionate, mandelate, camphorate, menthoxyacetate, and monomethyl tartrate resulted in a partial asymmetric synthesis of 1-phenylethanol. When mercuric tartrate was used, exceptionally high optical yields (25—32%) were observed. The mechanisms for the asymmetric synthesis are discussed.

In many stereochemical investigations of the oxymercuration of olefins, asymmetric syntheses have recently been reported. Partial asymmetric syntheses were achieved in the methoxymercuration of the menthol and sugar esters of $\alpha\beta$-unsaturated acids.[2)] In these investigations, the chiral moiety resided in the olefinic part. As part of an investigation of asymmetric oxymercuration using optically active mercuric salt as a chiral center, Wright[3)] reported that two diastereomeric methoxymercurials were obtained in unequal amounts by the methoxymercuration of cyclohexene with mercuric (+)-lactate. After we had presented the results of asymmetric oxymercuration which would be included in the present paper, Carlson and Funk[4)] reported similar results using decene, octene, heptene, and allylbenzene as the olefinic substrates. However, the author did not refer to the stereochemical reaction mechanisms at all.

The present paper will deal with the results of the asymmetric synthesis of 1-phenylethanol (**3**) *via* the oxymercuration of styrene (**1**) with mercuric salts of chiral acids, utilizing the convenient and mild oxymercuration-demercuration procedure developed by Brown.[5)]

Styrene (**1**) was subjected to an oxymercuration reaction with an equivalent amount of mercuric salts in 50% aqueous tetrahydrofuran (THF) at 25 °C, and the resulting oxymercurials were submitted to demercuration *in situ* with alkaline sodium borohydride. The resulting **3** was purified by means of fractional distillation and, in some cases, by preparative vapor phase chromatography (vpc). The possibility of racemization of the reaction products during demercuration was safely excluded by the confirmation of the constant optical purity of chiral **3** in an alkaline medium. The results are summarized in Table 1.

$$\underset{(1)}{C_6H_5\text{-}CH{=}CH_2} \xrightarrow[H_2O\text{-}THF]{Hg(OCO\overset{*}{R})_2\ (2)} \xrightarrow{NaBH_4} \underset{OH}{C_6H_5\text{-}\overset{*}{C}H\text{-}CH_3}\quad (3)$$

As is shown in Table 1, an exceptionally high optical yield of **3** was observed when mercuric tartrate (**2a**) was used. On the contrary, the other chiral mercuric salts (**2b-g**) gave very low or no measurable optical yields.

It is well known in oxymercuration that the addition of perchloric acid or Lewis acids such as boron trifluoride effectively accelerates the reaction. Inouye[2a)] reported that the methoxymercurations of (−)-menthyl crotonate, cinnamate, and β-methylcinnamate were accelerated by boron trifluoride etherate, and that the optical yields of these reactions were comparable to those without the catalyst. In the present system, the addition of boron trifluoride accelerated the reaction; however, only a slight asymmetric induction was achieved and the predominant product was (−)-**3**, which was enantiomeric to that without the catalyst.

The role of the acid catalyst is looked upon as promoting the dissociation of mercuric salts leading to the highly active acyloxymercuric cation, which then added to the olefin to yield the mercurinium ion.

$$(RCOO)_2Hg \overset{H^+}{\rightleftharpoons} RCOOHg^+ + RCOOH$$

$$\text{>C=C<} + RCOOHg^+ \rightleftharpoons \text{>C(HgOCOR)C<}$$

The chiral environment which the mercury atom of the mercuric tartrate cation, HOOC·CHOH·CHOH·COOHg$^+$, experiences seems to be similar to that of mercuric methyl tartrate (**2g**). Therefore, it is conceivable, on the basis of assumptions described above, that low asymmetric induction was observed in either case.

On the other hand, the oxymercuration proceeds very smoothly in methanol solvent, under such neutral conditions, the dissociation of usual mercuric salts cannot be considered so favorable, and the reacting species seems not to be the acyloxymercuric cation but mercuric salt itself. In this case, a molecular adduct

$$\text{>C=C<} + Hg(OCOR)_2 \rightleftharpoons \text{>C(Hg(OCOR)}_2\text{)C<} \rightleftharpoons \text{>C(HgOCOR)C<}$$

or π-complex is formed at first, and the configuration of the product is determined at this stage if the product is formed by the attack of the solvent molecule in *trans* fashion on the π-complex or mercurinium ion formed subsequently, as is generally accepted. The oxymercuration with **2a** was very slow as compared with the reaction using the other salts such as **2h**. This fact also seems to indicate that the tartrate anion

TABLE 1. SYNTHESES OF OPTICALLY ACTIVE 1-PHENYLETHANOL (3) BY OXYMERCURATION-DEMERCURATION REACTION

Mercuric salt	Reaction condition[a] Time	3 Yield	3 α_D[b]	3 Opt. yield[c]
(+)-Tartrate (2a)	4 day[d]	4%	+5.64°	25.6%
(+)-Tartrate (2a)	7	5	+5.66	25.7
(+)-Tartrate (2a)	7.5	17	+6.66	30.3
(+)-Tartrate (2a)	14	20	+6.54	29.7
(+)-Tartrate (2a)	14[e]	15	+7.04	32.0
(+)-Tartrate (2a)	28	29	+5.69	25.9
(+)-Tartrate (2a)	1[f]	8	−0.02	0.1
(−)-2-Phenylpropionate (2b)	15 min	40	−0.10	0.5
(+)-Mandelate (2c)	15 hr	70	+0.05	0.2
(−)-Malate (2d)	3	64	±0.00	—
(+)-Camphorate (2e)	24	59	−0.54	2.5
(−)-Menthoxyacetate (2f)	15 min	40	−0.10	0.5
(+)-Monomethyl tartrate (2g)	10	61	+0.09	0.4
Acetate (2h)	15[g]	73	−0.06	0.3
Acetate (2h)	5[h]	62	−0.08	0.4

a) The reaction was carried on at 25 °C. b) The optical rotations were measured as pure liquid using 0.5 dm cell. c) Calculated from the value of α_D^{17} −11.0° (neat, l=0.25 dm): E. Downer and J. Kenyon, *J. Chem. Soc.*, **1939**, 1156. d) When the reaction was carried out for 1 day, no **3** was obtained. e) Under nitrogen atmosphere. f) BF_3-etherate (5 ml) was added. g) Equivalent amount of (+)-diethyl tartrate was added. h) Five equivalent amounts of (+)-diethyl tartrate were added.

strongly combines with mercury, and that the **2a** molecule adds to the olefinic double bond, making a molecular complex.

It is also interesting to note that the oxymercuration with mercuric acetate (**2h**) in a solvent containing (+)-diethyl tartrate produced asymmetric induction to some extent. Henbest[6] reported that, in the methoxymercurials obtained from 4-cyclohexenol and its derivatives, the mercury atom was oriented *cis* relative to the hydroxyl substituent, and he suggested that the coordination between the mercury atom and the substituent oxygen determined the stereochemical course of the addition. Although the complex-forming tendency of mercury toward oxygen is usually considered to be rather weak, it may be suggested that the glycol structure operates to endow a chiral environment to the mercury atom. Consequently, the mercury atom of **2a** becomes chiral by salt forming bonds as well as by coordinating bonds between mercury and hydroxyl oxygen, and it is likely that the complex-formation between **2a** and **1** is the stage of asymmetric synthesis.

When the mercury atom of **2a**, already coordinated by two carboxyl and two hydroxyl groups, makes a molecular complex with olefin, the mercury should have a coordination number more than four. Although the tetrahedral four-coordination is more common for mercury complexes, the six-coordinated mercury was suggested in an aqueous solution[7] and octahedral complexes of the type $(HgL_6)(ClO_4)_2$ were obtained when the donor atom was oxygen.[8] If octahedral six-coordination is assumed for mercuric (+)-(*R*,*R*)-tartrate (**2a**), the molecular complex of **2a** and **1** can be depicted as **4**, in which **1** favorably coordinates in the sterically less-hindered orientation. Mercuric (+)-tartrate (**2a**) in **4** has a C_2 chirality as a whole. Chiral complexes are usually more effective than simple chiral atoms in asymmetric inductions. It seems, therefore, to be a natural outcome that **2a** produces exceptionally high optical yields compared with **2b–g**, which is seemingly incapable of forming such a chiral complex. The S_N2-like attack of water on **4** or on the mercurinium ion derived from **4** gives (+)-(*R*)-**3**, which is the predominant isomer actually obtained. The results with **2a** reported by Carlson[4] are consistent with this mechanistic assumption.

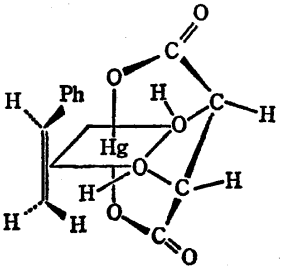

(4)

Experimental

All the boiling and melting points are uncorrected. The optical activity measurements were carried out on a Zeiss polarimeter and a Yanagimoto ORD-185 recording spectropolarimeter.

Materials. Commercially-available (+)-tartaric acid, (−)-malic acid (mp 105.5—106.5 °C; $[\alpha]_D^{28}$ −1.48°, c=8.29, H_2O), and (+)-camphoric acid (mp 189—193 °C; $[\alpha]_D^{20}$ +47.8°, EtOH) were used without further purification. (+)-Mandelic acid (mp 134—134.5 °C; $[\alpha]_D^{20}$ +155.3°, H_2O) and (−)-2-phenylpropionic acid[9] (bp 133—135 °C/6 mmHg; $[\alpha]_D^{21}$ +73.1°, $CHCl_3$) were obtained by the resolution of each racemic acid with cinchonine and (−)-1-phenylethylamine respectively. (−)-Menthoxyacetic acid[10] (bp 161—169 °C/7 mmHg; $[\alpha]_D^{20}$ −94.9°, MeOH), (+)-methyl hydrogen tartrate[11] (mp 54.5—55.5 °C (monohydrate); $[\alpha]_D^{18}$ +14.7°,

c=21, H_2O), and (+)-diethyl tartrate (bp 140—141 °C/7 mmHg; $[\alpha]_D^{20}$ +7.66°, neat) were prepared by the known procedures. Some of these acids were not completely optically pure; however, the optical purities of the resulting **3** are listed in Table 1 without corrections.

Styrene and THF were distilled before use in each experiment.

Preparations of Mercuric Salts. (+)-Tartaric acid (50.0 g, 0.33 mol) in 150 ml of water was added slowly to a stirred clear solution of mercuric acetate (95.7 g, 0.30 mol) in 400 ml of water. After the mixture was stirred for a while, the resulting white precipitates were washed with water until the filtrate became neutral. After drying under reduced pressure, 98.2 g (94%) of mercuric (+)-tartrate (**2a**) were obtained. Mp>200 °C, no clear mp indicated. Found: Hg, 57.7%. Calcd for $C_4H_4O_6Hg$: Hg, 57.5%.

Mercuric (−)-2-phenylpropionate (**2b**); mp 94—95 °C (recrystallized from EtOH); $[\alpha]_D^{24}$ −59.1° ($CHCl_3$); yield, 70.2%. Found: Hg, 39.0%. Calcd for $(C_9H_9O_2)_2Hg$: Hg, 40.2%. Mercuric (+)-mandelate (**2c**); mp 172—172.5 °C; yield, 95.3%. Found: Hg, 39.9%. Calcd for $(C_8H_7O_3)_2Hg$: Hg, 39.9%. Mercuric (−)-malate (**2d**); mp>200 °C, no clear mp indicated; yield, 86.5%. Found: Hg, 57.2%. Calcd for $C_4H_4O_5Hg$: Hg, 60.3%. Mercuric (+)-camphorate (**2e**); mp 266 °C (decomp.); yield, 95.6%. Found: Hg, 49.3%. Calcd for $C_{10}H_{14}O_4Hg$: Hg, 50.3%. Mercuric (−)-menthoxyacetate (**2f**); mp 64—66 °C (recrystallized from EtOH-H_2O), $[\alpha]_D^{20}$ −59.8° ($CHCl_3$); yield, 66.8%. Found: Hg, 30.8%. Calcd for $(C_{12}H_{21}O_3)_2Hg$: Hg, 32.0%. Methyl mercuric (+)-tartrate (**2g**); mp 171—172 °C (decomp.); $[\alpha]_D^{18}$ +27.4° (H_2O); quantitative yield. Found: Hg, 35.7%. Calcd for $(C_5H_7O_6)_2Hg$: Hg, 38.1 %; for $(C_5H_7O_6)_2Hg\cdot 2H_2O$: Hg, 35.6%.

Analysis of Mercury. Adams' procedure[12] was modified. To 0.2 g of the mercuric salt were added 10 ml of 7% fuming sulfuric acid and 5 ml of fuming nitric acid. The mixture was heated until reflux, and to it was added water sufficient to dissolve the mercuric salt. Refluxing was continued with the addition of water in small portions until the evolution of NO_2 gas ceased. To the cooled, colorless, clear solution was added 1 drop of 4% potassium permanganate solution, the color of which persisted for 5 min. The excess permanganate was removed by means of 5% ferrous sulfate solution. The mercury in the prepared sample was titrated with 0.05 N KSCN solution, using ferric alum as an indicator (Volhard method).[13]

General Method of Oxymercuration-demercuration. Mercuric (+)-tartrate (**2a**, 17.5 g, 50.2 mmol) was suspended in 50 ml of water, to which was added 50 ml of THF. Styrene (**1**, 5.23 g, 50.2 mmol) was then added dropwise to the suspension under well-stirring at 25 °C, and the reaction mixture was stirred in dark at that temperature for 7.5 day. To the mixture were added 50 ml of 3.0 M NaOH and then sodium borohydride (0.90 g, 23.8 mmol) in 50 ml of 3.0 M NaOH, and the mixture was stirred for 15 min. The resulting metallic mercury was filtered off and the filtrate was saturated with NaCl and extracted with ether. The ether extract was washed with water and dried over Na_2SO_4. Distillation under reduced pressure gave 1.03 g (16.8%) of crude **3** (bp 84—85 °C/8 mmHg, n_D^{20} 1.5292), which contained **1**, acetophenone, benzaldehyde, and benzyl alcohol up to a total of 5%. The crude product was purified by preparative vpc (PEG-20M 25% on C-22 fire-brick, 3 m column), and submitted to optical rotation measurements, α_D^{20} +6.66° (neat, l=0.50 dm). The product was identified by elemental analysis and by comparisons of the vpc retention time and the IR and NMR spectra with those of an authentic sample.

In the cases of **2b**, **2c**, **2e**, and **2f** the starting acids were recovered without racemization from the aqueous layer of ether extraction.

*Treatment of **3** in an Alkaline Medium.* (+)-1-Phenylethanol (**3**, α_D^{19} +6.41°, neat, l=0.50 dm; 0.61 g) was stirred with 20 ml of 3.0 M NaOH, 10 ml of water, and 10 ml of THF at 25 °C for 19 hr. After work-up and distillation, 0.40 g of **3** (α_D^{19} +6.40°, neat, l=0.50 dm) was recovered.

References

1) This work was presented in part at the 22nd Annual Meeting of the Chemical Society of Japan, April, 1969, Tokyo.

2) a) J. Oda, T. Nakagawa, and Y. Inouye, This Bulletin, **40**, 373 (1967). b) M. Kawana and E. Emoto, *ibid.*, **40**, 618 (1967).

3) J. Romeyn and G. F. Wright, *J. Amer. Chem. Soc.*, **69**, 697 (1947).

4) R. M. Carlson and A. H. Funk, *Tetrahedron Lett.*, **1971**, 3661.

5) H. C. Brown and M. -H, Rei, *J. Amre. Chem. Soc.*, **91**, 5646 (1969); H. C. Brown and P. J. Geoghegan, Jr., *J. Org. Chem.*, **35**, 1844 (1970).

6) H. B. Henbest and B. Nicholls, *J. Chem. Soc.*, **1959**, 227. On the stereochemical arguments of oxymercuration reaction, see also N. S. Zefirov, *Russ. Chem. Revs.*, **34**, **1959**, 527; W. Kitching, *Organometal. Chem. Rev.*, **3**, 61 (1968).

7) P. K. Gallagher and E. L. King, *J. Amer. Chem. Soc.*, **82**, 3510 (1960).

8) R. L. Carlin, J. Roitman, M. Dankleff, and J. O. Edwards, *Inorg. Chem.*, **1**, 182 (1962).

9) A. Campbell and J. Kenyon, *J. Chem. Soc.*, **1946**, 25.

10) M. T. Leffler and A. E. Calkins, "Organic Syntheses," Coll. Vol. III, p. 544 (1955).

11) W. Marckwald and L. Karczag, *Ber.*, **42**, 1518 (1909).

12) I. A. Koten and R. Adams, *J. Amer. Chem. Soc.*, **46**, 2746 (1924).

13) I. M. Kolthoff and E. B. Sandell, "Textbook of Quantitative Inorganic Analysis," 3rd ed., Macmillan Co., New York (1952), p. 547.

Catalytic Hydration of Pyridinecarbonitriles in the Presence of $[Cu(en)_2]Cl_2 \cdot 2H_2O$ and $CuCl_2 \cdot 2H_2O$

Ken-ichi WATANABE and Kiyoshi MURAYAMA

Department of Chemistry, Faculty of Science, Tokyo Metropolitan University, Setagaya-ku, Tokyo 158

(Received December 25, 1973)

Spectrophotometric studies on the catalytic hydration of 2-pyridinecarbonitrile derivatives in the presence of $[Cu(en)_2]Cl_2 \cdot 2H_2O$ and $CuCl_2 \cdot 2H_2O$ under nearly neutral conditions revealed that the products are their amides. In some cases, the yields were calculated from the weight of amides obtained. The hydration of the nitrile group was influenced by electronic and steric effects. Selective hydration of the nitrile group in α-position was observed in the case of dinitrile. The selectivity was applied to hydrolysis of nitriles to carboxylic acids.

It has been reported[1] that 2-pyridinecarbonitrile is easily hydrated to 2-pyridinecarboxamide in the presence of various complexes of Cu(II), Ni(II), and Co(II) in neutral solution at 60 °C. The nitrile group in α-position is presumed to interact with metal ions coordinated to the ring nitrogen and the activated nitrile group undergoes hydration to afford the free amide through ligand exchange. In order to elucidate the phenomenon, we studied the hydration of some 2-pyridinecarbonitrile derivatives (Table 1) in the presence of $[Cu(en)_2]Cl_2 \cdot 2H_2O$ and $CuCl_2 \cdot 2H_2O$. The results are given in this paper together with a discussion from theoretical and synthetic viewpoints.

Aqueous solutions of the nitriles containing the catalysts were kept at 60 °C (or 80 °C) for 5 hr in a sealed glass tube. The reactions were followed spectrophotometrically[1] and the yields of the reaction products were calculated.

Results and Discussion

The reaction conditions and main results are summarized in Tables 2 and 3. The UV analytical method could not be applied to compound III. No reaction occurred in IV and V at 60 °C even with a large amount of catalyst and an elongated reaction time of 20 hr. They were thus treated at 80 °C and the yields were calculated from the weight of free amides obtained (Table 3). I was a little more reactive than II as observed in the reactions with a large amount of the catalyst(Table 2). It was assumed that the higher basicity of I than II due to the methyl group made the pyridine ring easy to undergo coordination. On the other hand, II was more reactive than III presumably by electronic effect of the cyano group in 4-position(Table 3). The low reactivity of IV and V was attributed to steric hindrance in the coordination to the catalysts. In their Cu(II) ion catalyzed reactions, the amide complexes were not obtained, presumably for the same reason. In order to examine the reactivity of V, it was refluxed 5 hr with both catalysts and about 10% of the amide was obtained. We tried the addition of methanol to II and V in the presence of Cu(II) ion under reflux as follows:

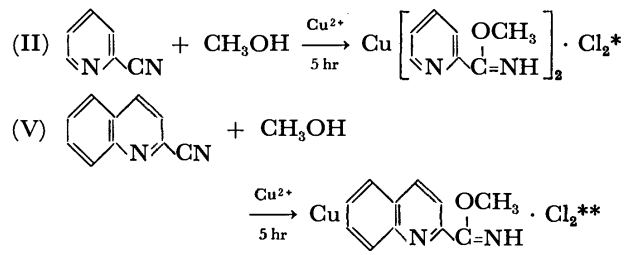

The reaction product from V was *O*-methyl-2-quinolinecarboximidate copper(II) chloride instead of bis-coordinated ligand complex. This also suggests a

TABLE 1. 2-PYRIDINECARBONITRILE DERIVATIVES AND THEIR HYDRATION PRODUCTS (AMIDES)

	I	II	III	IV	V
Samples	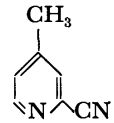	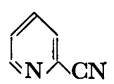	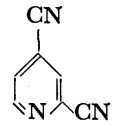	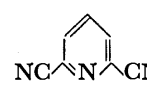	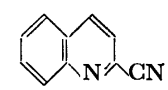
mp °C	88—89	28—29	91—92	126—127	93—94
Amides	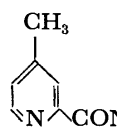	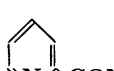	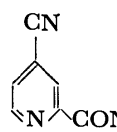	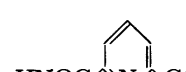	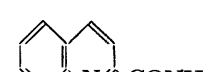
mp °C	125	105	255 (dec)	300 (dec)	129

* This complex was also prepared from bis(2-pyridinecarbonitrile)copper(II) chloride in methanol on addition of triethylamine: S. Suzuki, M. Nakahara, and K. Watanabe, This Bulletin, **47**, 645 (1974).

** New compound: Found: C, 41.33; H, 3.15; N, 8.70; Cl, 22.37% Calcd: C, 40.88; H, 3.12; N, 8.73; Cl, 22.15%.

Table 2. Catalytic hydration of nitriles. I
Reactivities of nitriles (%): spectrophotometry, sample: 5×10^{-3} mol/l, reaction temp.: 60 °C, reaction time: 5 hr

Catalyst	mol/sample	pH	I	II	IV	V
$[Cu(en)_2]\cdot Cl_2\cdot 2H_2O$	1/8	7.6	20	20	0	0
$[Cu(en)_2]\cdot Cl_2\cdot 2H_2O$	2	7.6	97	51	0	0
$CuCl_2\cdot 2H_2O$	3	4—5	100	95	0	0

Calculated from the remaining starting materials, separated by means of ion exchange resin and analyzed by UV method.

Table 3. Catalytic hydration of nitriles. II
(yields of free amides %)
sample: 1.6×10^{-3} mol/l, reaction temp.: 80 °C, reaction time: 5 hr

Catalyst	mol/sample	pH	II	III[a]	IV[b]	V
$[Cu(en)_2]Cl_2\cdot 2H_2O$	1/8	8	54	46	24	+
$CuCl_2\cdot 2H_2O$	1/8	4—5	49	32	2	+

a) Product: 4-cyano-2-pyridinecarboxamide. b) Product: 2,6-pyridinedicarboxamide.

steric hindrance in the coordination of the bulky ligand.

Thus, the electronic and steric effects of substituents were observed apparently in these catalytic hydration. The reactivity of compounds I–V was in the order: I>II>III>IV>V. This is attributed to their coordination ability caused by an electronic or steric factor which would also influence the mode of the reaction of IV.

In the reaction with $[Cu(en)_2]Cl_2\cdot 2H_2O$, all the reaction products, amides, were obtained in free form (Table 3). On the other hand, in the reaction with Cu(II) ion, I and II afforded stable copper(II) complexes of their amides. Thus, the net yield of amide from II should be estimated to be greater than 49% (free amide). However, III afforded scarcely any copper(II) complex of the amide, although free amide was obtained to some extent. The amide complexes obtained from I and II were found to have excellent catalytic ability. We examined the ligand exchange of the complex catalysts and found the formation of mixed amides in free form as follows:

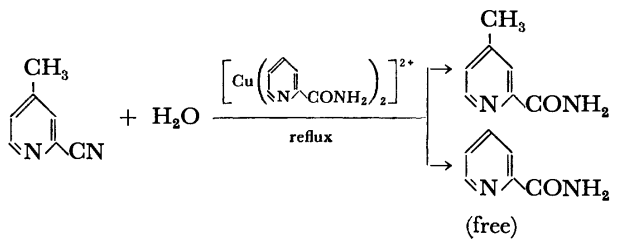

This suggested a catalytic function of labile metal complexes through ligand exchange.[1]

Remarkable selective hydration of the nitrile group in α-position was observed in dinitrile III to give 4-cyano-2-pyridinecarboxamide (Tables 1 and 3). In contrast, no selectivity was observed in the reaction with dinitrile IV. This indicates a particular interaction of metal ion with nitrile group in α-position.

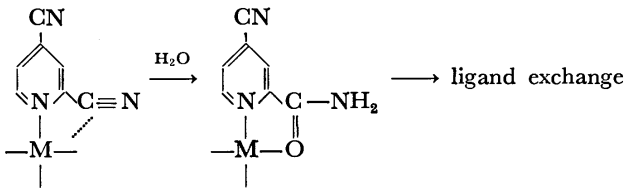

Such selectivity was not observed in the reaction in the presence of catalysts such as mineral acids, alkali, metals, or metal oxides.

For the synthetic application of this catalytic hydration, we tried selective hydrolysis of III with Cu(II) ion and nickel oxide catalysts under neutral conditions. For the sake of comparison, reactions of II and IV were also examined. It was found that selective hydrolysis of dinitrile III occurrs with Cu(II) ion, and simultaneous hydration occurrs in the presence of Ni-(or Cu) oxide catalyst. The results are summarized as follows:

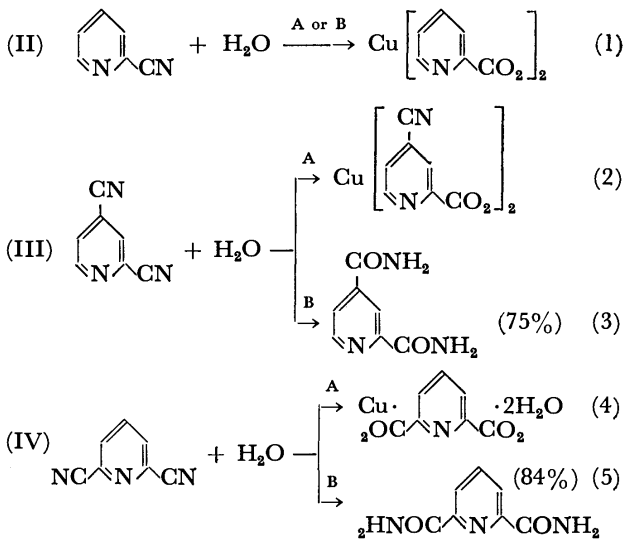

Method A: Cu(II) excess, pH *ca.* 4.5, reflux 15 hr
Method B: Ni-oxide(black), pyridine, reflux 2—5 hr

Use of an excess Cu(II) ion with a long reflux caused the hydrolysis of the nitrile group in α-position to afford copper(II) complexes of acids (Method A). In this case, III gave a 2 : 1 complex of 4-cyano-2-pyridinecarboxylic acid by selective hydrolysis(2), while IV gave 1 : 1 complex of diacid(4). The use of metal oxides[2] or metal[3] catalysts is excellent for the purpose of synthesizing amides from nitriles under neutral conditions, but the method lacks selectivity. Thus, III and IV gave free diamides in good yields(3 and 5, respectively) in contrast to the metal ion catalyzed reactions. II undergoes hydrolysis with metal oxide to afford copper(II) complex of 2-pyridinecarboxylic acid as in the case of Cu(II) ion catalyzed reactions(1). Although 4-carbamoyl-2-pyridinecarboxylic acid complex was expected, no selective hydrolysis of α-nitrile group in III was observed.

Exprimental

Materials. 4-Methyl-2-pyridinecarbonitrile was prepared[4] from 4-methylpyridine, recrystallized from ethanol

mp 88—89 °C. Commercial 2-pyridinecarbonitrile was recrystallized from ether, mp 28—29 °C. 2,4-Pyridinedicarbonitrile: 4-pyridinecarbonitrile-*N*-oxide was prepared[5] from 4-pyridinecarbonitrile and hydrogen peroxide solution, mp 206—215 °C. This was heated with dimethylsufonic acid and potassium cyanide to give 2,4-pyridinedicarbonitrile.[6] The crude dinitrile was purified by means of column chromatography(alumina) with benzene, mp 91—92 °C. 2,6-Pyridinedicarbonitrile was prepared[5,6] from 2-pyridinecarbonitrile by a similar method, mp 126—127 °C. 2-Quinolinecarbonitrile was prepared[7] from quinoline and recrystallized from methanol, mp 93—94 °C. $[Cu(en)_2]Cl_2 \cdot 2H_2O$ was prepared and recrystallized several times. Commercial extra-pure $CuCl_2 \cdot 2H_2O$ was used. Nickel oxide (black) was prepared by the decomposition of nickel carbonate at 250—300 °C.

Spectrophotometry (Table 2). In a sealed glass tube was placed 10 ml of a solution containing nitrile (5×10^{-3} mol/l) and catalyst, and the reaction mixture was kept at 60 °C for 5 hr. After the reaction, an aliquot quantity of the reaction mixture was poured into a column packed with ion exchange resin (Dowex 50, 2 × H-type) and developed with water (resin in column: diameter 1 cm, length 3 cm). The elute was a solution of unreacted pure nitrile which was separated completely from the reaction mixture. The decrease in the amount of starting material was followed spectrophotometrically (I: 274 nm, II: 265 nm, IV: 225 nm, V: 303 nm), and the yield of the reaction products, amides, was calculated. Yield(%) = 100 − unreacted nitrile. The separation was examined by the blank test. In the case of V, a water–ethanol mixture(2 : 1) was used for development.

Synthetic Method (Table 3). In a sealed flask was placed 50 ml of a solution containing nitrile (7.8×10^{-3} mol) and catalyst(9.7×10^{-4} mol) and the reaction mixture was kept at 80 °C for 5 hr. In the cases of III, IV, and V, deposition of white crystals was observed during the course of the reaction. After the reaction, the mixture was cooled and the precipitate was filtered off, dried and washed with benzene. The amide crystals thus obtained were recrystallized from acetic acid.

4-Cyano-2-pyridinecarboxamide. Mp 255—256 °C(dec), lit,[5] 256—258 °C. IR: νN-H 3410, νC≡N 2245, νC=O 1700 cm^{-1}, (KBr). Found: C, 56.87; H, 3.37; N, 28.38%. Calcd for $C_7H_5N_3O$: C, 57.14; H, 3.43; N, 28.56 %.

2,6-Pyridindiecarboxamide. Mp 298—302 °C(dec), lit,[6] 295—297 °C. IR: νN-H 3410, νC=O 1680 cm^{-1} (KBr). Found: C, 50.97; H, 4.32; N, 25.28%. Calcd for $C_7H_7N_3O_2$: C, 50.90; H, 4.28; N, 25.45%.

2-Quinolinecarboxamide(trace). Mp 129—131 °C, lit,[7] 132—133 °C. Determined by mixed melting point method and IR: νN-H 3440, νC=O 1680 cm^{-1}(KBr).

Hydration with Nickel Oxide Catalyst(black). Fifty ml of an aqueous solution containing nitrile(1g), II, III, or IV, and nickel oxide(0.1 g) was refluxed for 2—5 hr. In the reaction with IV, pyridine was added in order to dissolve the nitrile completely. After the reaction, the catalyst was filtered while hot and the filtrate was cooled. Amide crystals were precipitated, and were then filtered and recrystallized from water.

2,4-Dipyridinecarboxamide. Mp 256 °C, lit,[8] 258 °C. IR: νN-H 3450, 3310, νC=O 1715, 1695 cm^{-1} (KBr). Found: C, 50.97; H, 4.25; N, 25.33%. Calcd for $C_7H_7N_3O_2$: C, 50.90; H, 4.28; N, 25.45%.

Hydrolysis with Copper(II) Ion. A solution(100 ml) containing nitrile(1g), II, III, or IV, and $CuCl_2 \cdot 2H_2O$ (1.32 g) was refluxed for 15 hr(homogeneous, pH *ca.* 4.5). After the reaction, the reaction mixture was concentrated to a small quantity under reduced pressure, and then cooled. Crystals deposited were filtered, washed with ethanol, and recrystallized from water, dried *in vacuo*.

Copper (II) complex of 4-cyano-2-pyridinecarboxylic acid. IR: νC≡N 2240, νC=O 1650 cm^{-1}. Found: C, 46.76; H, 1.79; N, 16.17; Cl, 0%. Calcd for $C_{17}H_6O_4N_4Cu$: C, 46.99; H, 1.68; N, 15.67; Cl, 0%.

Copper(II) complex of 2,6-pyridinedicarboxylic acid. IR: νO-H 3440, νC=O 1160 cm^{-1}. Found: C, 31.80; H, 2.57; N, 5.38; Cl, 0%. Calcd for $C_7H_7NO_6Cu$: C, 31.76; H, 2.65; N, 5.29; Cl, 0%. When 2,6-pyridinedicarboxamide was treated similarly, the same complex was obtained.

The authors wish to express their hearty thanks to Dr. Shinnichiro Suzuki, Osaka University, for his valuable advice.

References

1) K. Watanabe, S. Komiya, and S. Suzuki, This Bulletin, **46**, 2792 (1973); **44**, 1440(1971).
2) K. Sakai, T. Ito, and K. Watanabe, *ibid.*, **40**, 1660 (1967).
3) K. Watanabe and K. Sakai, *ibid.*, **39**, 8(1966); K. Watanabe, *ibid.*, **37**, 1325 (1964).
4) F. H. Case and T. J. Kasper, *J. Amer. Chem. Soc.*, **78**, 5842 (1956).
5) H. Tani, *Yakugaku Zasshi*, **80**, 1418 (1960).
6) W. E. Feely and E. M. Beavers, *J. Amer. Chem. Soc.*, **81**, 4004 (1959).
7) M. Henze, *Ber.*, **69**, 1566 (1936).
8) N. Nishimoto and T. Nakashima, *Yakugaku Zasshi*, **81**, 1265 (1961).

Syntheses of Pyrrolotropone Derivatives from Benzocycloheptene-5,6-dione Monoarylhydrazones. II.[1,2] Syntheses of Benzo[5,6]cyclohept[1,2-*b*]-indole-6,11,12-triones

Kunihide FUJIMORI and Kameji YAMANE

Department of Chemistry, Faculty of Science, Shinshu University, Matsumoto 390

(Received January 16, 1974)

Benzo[5,6]cyclohept[1,2-*b*]indole-6,11,12-triones (benzoindolotropoquinones) (VIIIa—c) were prepared by the oxidation of 11,12-dihydrobenzo[5,6]cyclohept[1,2-*b*]indol-6-ones (Va—c) with sodium dichromate in acetic acid. Compound VIIIa was rearranged by means of a concd sodium hydroxide solution into a known benzocarbazole-1,4-quinone. The pyrrolotropolone derivative (VII) was also obtained through the ring closure of the 5-hydrazinotropolone derivative (VI).

Cyclohepta-3,6-diene-1,2,5-trione(*p*-tropoquinone) has been of interest as an *o*- and *p*-quinone-type compound with a seven-membered ring, but it was not successfuly synthesized until quite recently in spite of many attempts to do so.[3]

5-Nitrosotropolone and 5-arylazotropolone, however, have long been known to have the structures of monooxime and monoarylhydrazone respectively, and tropoquinone trioxime has been obtained from the former.[3]

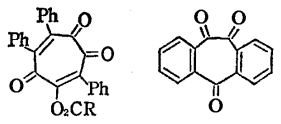

(I) (II)

Wittmann *et al.*[4] prepared the triphenylhydroxy derivative (I) and Ito *et al.*[5a] performed a successful synthesis of tropoquinone itself by the photosensitized oxidation of 2,5-substituted tropones. Improving its synthetic procedure, the latter[5b] later obtained tropoquinone quantitatively by the oxidation of 5-hydroxytropolone with DDQ in absolute methanol.

On the other hand, dibenzotropoquinone (II) had been obtained earlier.[6]

The present authors will describe the syntheses of benzoindolotropoquinones (VIII) by means of the oxidation of 11,12-dihydrobenzo[5,6]cyclohept[1,2-*b*]indol-6-ones (V) with dichromate.

Results and Discussion

Benzocycloheptene-5,6-dione monoarylhydrazones (IV) were obtained by treating a hydroxymethylene compound (III) of benzosuberone with a solution of aryldiazonium salts (Japp-Klingermann reaction). It was described in a previous paper[7] that those hydrazones (IV) could also be obtained by the reaction of benzocycloheptene-5,6-dione with arylhydrazines.

The resulting hydrazones (IVc and IVe), by analogy with IVa, *etc.*,[7] underwent Fischer indolization to form 11,12-dihydrobenzo[5,6]indol-6-ones (Vc and Ve).

The reaction of Compound III with diazonium salt from 5-aminotropolone led to the corresponding hydrazone (VI), which was then converted into the pyrrolotropolone derivative (VII) by ring closure with PPA.

The Oxidation of V with Sodium Dichromate. On treatment with NBS, Compounds Va—d were converted into benzo[5,6]cyclohept[1,2-*b*]indol-6-ones(ben-

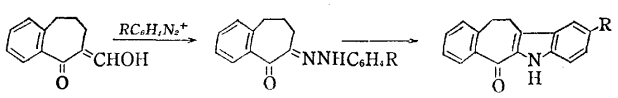

(III) (IV) (V)

a: R=H, b: R=Br, c: R=Cl, d: R=CH_3, e: R=NO_2

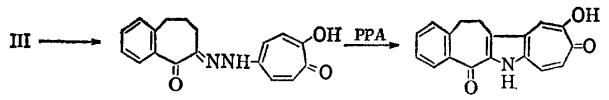

(VI) (VII)

zoindolotropones),[7] but the oxidation of V with selenium dioxide or chloranil resulted in the recovery of the unchanged starting materials. However, when Compound Va was treated with sodium dichromate in acetic acid, orange micro needles (mp 318—320 °C (dec)) were obtained.

The IR spectrum shows absorption bands at 3290 cm^{-1} (NH st.), and at 1680, 1641, and 1623 cm^{-1} (C–O st.). The elemental analysis revealed a composition with the formula of $C_{17}H_9NO_3$.

Further, the compound reacted with *o*-phenylenediamine to give the corresponding quinoxaline derivative. Therefore, the compound may be considered to have the structure of benzo[5,6]cyclohept[1,2-*b*]indole-6,11,12-trione(benzoindolotropoquinone) (VIIIa).

In the same way as with Compound VIIIa, VIIIb, and VIIIc were prepared by the dichromate oxidation of Vb and Vc; those compounds gave the corresponding quinoxaline derivatives, IXb and IXc respectively.

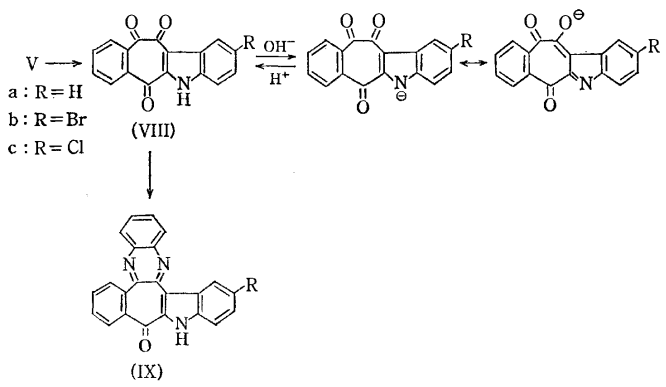

The UV spectra of VIIIa–c display the same absorption pattern in neutral and acidic media, but in an

alkaline medium they show more yellow color and the absorption maxima are shifted to longer wave lengths than in neutral and acidic media.

On changing to an acidic medium from an alkaline medium, the spectra returned to that in neutral and acidic media.

It was, therefore, supposed that VIIIa—c exsited in enolate ions in an alkaline medium.

The absorption spectra in an aprotic solvent such as chloroform or dimethyl sulfoxide are different from those in a protic solvent such as alcohol, so the formation of hemiketal can be taken into consideration in alcohol, by analogy with tropoquinone.[5]

TABLE 1. ULTRAVIOLET AND VISIBLE ABSORPTION MAXIMA

Compound	λ_{max}, nm(log ε)
VIII a	257(4.40), 265^{sh}(4.39), 295(3.85), 351(4.01)
VIII b	252(4.42), 257^{sh}(4.41), 269^{sh}(4.38), 356(4.05)
VIII c	252(4.42), 257^{sh}(4.42), 266^{sh}(4.39), 355(4.06)
	in CH_3OH or CH_3OH-0.1M HCl
VIII a	270(4.35), 285^{sh}(4.30), 375(3.89)
VIII b	276(4.37), 287^{sh}(4.36), 387(3.97)
VIII c	275(4.38), 286^{sh}(4.37), 387(3.97)
	in CH_3OH-0.1M NaOH

The NMR spectra were unable to measure since VIIIa—c were only slightly soluble in common organic solvents.

The Treatment of VIIIa with a Concd Sodium Hydroxide Solution. As has been mentioned above, VIIIa–c are considered to exist as enolate ions in slightly alkaline conditions. When VIIIa was heated in concd sodium hydroxide solution, the solution turned a greenish purple and gave orange micro needles (mp 280 °C). The results of the elemental analysis of the compound accord with the formula of $C_{16}H_9O_2N$, and the IR spectrum is identical with that for the known benzocarbazole-1,4-quinone (X).

The reaction process is supposed to cause a benzilic-acid rearrangement, followed by its decarboxylation and oxidation as well, thus producing stable benzocarbazole-1,4-quinone.

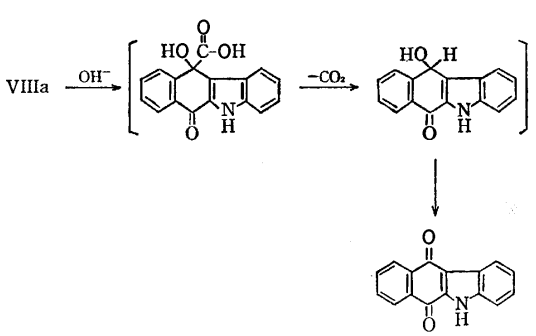

(X)

Experimental*

All the melting points are uncorrected.

General Procedure for the Preparation of Benzocycloheptene-5,6-dione Monoarylhydrazones(IV). Into a solution of aryldiazonium salt, prepared from arylamine and sodium nitrite in dilute sulfuric acid, the hydroxymethylene derivative (III) of benzocyclohepten-5-one was stirred, drop by drop, at 0 °C. When the stirring was continued, oily products solidified.

The resulting solid was collected and recrystallized from ethanol.

Benzocycloheptene-5,6-dione Monophenylhydrazone(IVa). Orange needles; yield, 44%; mp 111—112 °C. The mixed melting point with monophenylhydrazone, obtained by the reaction of benzocycloheptene-5,6-dione with phenylhydrazine, was not depressed.

Benzocycloheptene-5,6-dione Mono-p-tolylhydrazone(IVb). Orange needles; yield, 22%; mp 160—161 °C. The mixed melting point with mono-*p*-tolylhydrazone, obtained by the reaction of benzocycloheptene-5,6-dione with *p*-tolylhydrazine, was not depressed.

Benzocycloheptene-5,6-dione Mono-p-bromophenylhydrazone(IVc). Orange needles; yield, 36%; mp 160—161 °C. The mixed melting point with mono-*p*-bromophenylhydrazone, obtained by the reaction of benzocycloheptene-5,6-dione with *p*-bromophenylhydrazine, was not depressed.

Benzocycloheptene-5,6-dione Mono-p-chlorophenylhydrazone(IVd). Orange needles; yield, 69%; mp 165—166 °C. Found: C, 68.42; H, 5.16; N, 9.66%. Calcd for $C_{17}H_{15}ON_2Cl$: C, 68.34; H, 5.06; N, 9.38%.

Benzocycloheptene-5,6-dione Mono-p-nitrophenylhydrazone(IVe). Yellow needles; yield, 46%; mp 205—207 °C. Found: C 66.11; H, 4.87; N, 13.99%. Calcd for $C_{17}H_{15}N_3O_3$: C, 66.00; H, 4.89; N, 13.59%.

2-Chloro-11,12-dihydrobenzo[5,6]cyclohept[1,2-b]indol-6-one(Vc). A mixture of IVc (2.0 g) and concd hydrochloric acid (3 ml) in acetic acid (50 ml) was refluxed for 3 hr. After cooling, the reaction mixture was diluted with water and the resulting material was collected by filtration. Recrystallization from ethanol gave yellow micro needles (1.7 g, 90%); mp 232—233 °C. IR(KBr): ν_{NH} 3305, $\nu_{conjugated\ C=O}$ 1612 cm^{-1}. UV: $\lambda_{max}^{CH_3OH}$ 258(log ε=4.08) and 339(4.33) nm. Found: C, 72.69; H, 4.27; N, 5.13%. Calcd for $C_{17}H_{12}ONCl$: C, 72.47; H, 4.29; N, 4.97%.

2-Nitro-11,12-dihydrobenzo[5,6]cyclohept[1,2-b]indol-6-one(Ve). A mixture of IVe (0.19 g) and PPA (2 ml) was heated at 100 °C for 3 hr. After cooling, the reaction mixture was diluted with water. The resulting material was collected by filtration and dried. Recrystallization from acetic acid gave yellow needles (0.16 g, 89%); mp 280—282 °C. IR (KBr): ν_{NH} 3296, $\nu_{conjugated\ C=O}$ 1615 cm^{-1}. UV: $\lambda_{max}^{CH_3OH}$ 236(log ε=4.03), 260(3.96), and 313(4.49) nm. Found: C, 70.05; H, 4.18; N, 9.84%. Calcd for $C_{17}H_{12}N_2O_3$: C, 69.85; H, 4.14; N, 9.58%.

Benzocycloheptene-5,6-dione Mono-4,5-tropolonylhydrazone(VI). Into a solution of diazonium salt, prepared from 5-aminotropolone (1.0 g), III (1.4 g) was stirred, drop by drop, at 0 °C. The reaction mixture was then extracted with benzene, and the extract was dried over anhydrous sodium sulfate and condensed to leave a residue. Recrystallization from ethanol gave deep ruby red, scale-like crystals (0.28 g, 12%); mp 185—186 °C.

* The authors are grateful to the Sankyo Co., Ltd., for carrying out a part of the elemental analysis.

Found: C, 70.16; H, 5.28; N, 9.08%. Calcd for $C_{18}H_{16}N_2O_3$: C, 70.11; H, 5.23; N, 9.09%.

Pyrrolotropolone Derivative(VII). A mixture of the hydrazone (0.1 g) described above and PPA (2 ml) was heated at 120 °C for 3 hr. After cooling, the reaction mixture was diluted with water. The resulting material was collected by filtration and recrystallized to give yellowish-green micro crystals (0.05 g, 53%); mp>280 °C. UV: $\lambda_{max}^{CH_3OH}$ 240(log ε=4.19), 271(4.34), 299(4.37), 320(4.27), and 288 (4.27) nm. IR(KBr): ν_{OH} 3283, ν_{NH} 3258, $\nu_{conjugated\ C=O}$ 1611, 1591 cm^{-1}.

Found: C, 74.15; H, 4.70; N, 4.76%. Calcd for $C_{18}H_{13}O_3N$: C, 74.21; H, 4.50; N, 4.81%.

*Benzo[5,6]cyclohept[1,2-*b*]indole-6,11,12-trione(VIIIa).* A solution of Va (1.0 g) in acetic acid (30 ml) was heated at 100 °C, and then sodium dichromate (2.3 g) was added little by little. After the mixture has been refluxed for 30 min, the reaction mixture was stirred at room temperature for 2 hr. Water (5 ml) was then added, and the resulting material was collected by filtration. Recrystallization from acetic acid gave orange micro needles (0.24 g, 22%); mp 318—320 °C (dec).

Found: C, 74.15; H, 3.38; N, 4.56%. Calcd for $C_{17}H_9NO_3$: C, 74.18; H, 3.30; N, 5.09%.

Monophenylhydrazone: Reddish-brown needles; mp>280 °C IR(KBr): ν_{NH} 3283, 3238 cm^{-1}. Found: C, 75.69; H, 4.16; N, 11.30%. Calcd for $C_{23}H_{15}N_3O_2$: C, 75.60; H, 4.14; N, 11.50%.

Quinoxaline Derivative: Orange micro needles; mp>280 °C. UV: $\lambda_{max}^{CH_3OH}$ 242(log ε=4.49), 253(4.48), 277(4.58), and 427(4.09) nm. IR(KBr): ν_{NH} 3311, $\nu_{conjugated\ C=O\ or\ C=C}$ 1611, 1593 cm^{-1}. Found: C, 79.77; H, 3.85; N, 12.02%. Calcd for $C_{23}H_{13}N_3O$: C, 79.52; H, 3.77; N, 12.10%.

*2-Bromobenzo[5,6]cyclohept[1,2-*b*]indole-6,11,12-trione(VIIIb).* Compound was obtained from Vb (1.0 g) in acetic acid (60 ml) and sodium dichromate (1.89 g) by a method similar to that used for the preparation of VIIIa.

Recrystallization from acetic acid gave orange-yellow micro needles (0.26 g, 24%); mp>280 °C. UV: $\lambda_{max}^{CH_3OH}$ 242 (log ε=4.39), 253(4.40), 277(4.46), and 420(3.99) nm. IR(KBr): ν_{NH} 3305, $\nu_{conjugated\ C=O}$ 1680, 1638, and 1633 cm^{-1}.

Found: C, 57.67; H, 2.33; N, 4.15%. Calcd for $C_{17}H_8O_3NBr$: C, 57.65; H, 2.28; N, 3.96%.

Quinoxaline Derivative: Yellow micro needles; mp>280 °C. IR(KBr): ν_{NH} 3305, $\nu_{conjugated\ C=O\ or\ C=C}$ 1622 and 1590 cm^{-1}. Found: C, 64.88; H, 3.11; N, 9.68%. Calcd for $C_{23}H_{12}ON_3Br$: C, 64.80; H, 2.84; N, 9.86%.

*2-Chlorobenzo[5,6]cyclohept[1,2-*b*]indole-6,11,12-trione(VIIIc).* Compound was obtained from Vc (1.0 g) in acetic acid (50 ml) and sodium dichromate (2.6 g) by a method similar to that used for the preparation of VIIIa. Recrystallization from acetic acid gave yellow micro needles (0.26 g, 24%); mp>280 °C. UV: $\lambda_{max}^{CH_3OH}$ 242(log ε=4.41), 253(4.43), 277 (4.49), and 422(4.03) nm. IR(KBr): ν_{NH} 3236, $\nu_{C=O}$ 1683, 1643, and 1633 cm^{-1}. Found: C, 66.10; H, 2.64; N, 4.82%. Calcd for $C_{17}H_8O_3NCl$: C, 65.92; H, 2.60; N, 4.52%.

Quinoxaline Derivative: Yellow micro needles; mp>280 °C. Found: C, 72.42; H, 3.18; N, 10.96%. Calcd for $C_{23}H_{12}ON_3Cl$: C, 72.35; H, 3.17; N, 11.01%.

The Treatment of VIIIa with a Concd Sodium Hydroxide Solution. A suspension of VIIIa (1.0 g) in a 50% sodium hydroxide solution (50 ml) was heated on a water bath for 15 min. The reaction mixture turned a greenish purple and gave orange crystals. The resulting crystals were collected by filtration and recrystallized from ethanol to give orange prisms (0.05 g, 56%); mp 280 °C. The IR spectrum was identical with that of benzocarbazole-1,4-quinone which had been obtained by the oxidation of benzocarbazole with chromic anhydride. Found: C, 77.45; H, 3.65; N, 5.76%. Calcd for $C_{16}H_9O_2N$: C, 77.72; H, 3.67; N, 5.67%.

The authors wish to express their thanks to Professor Emeritus Tetsuo Nozoe of Tohoku University for his kind guidance. This research was supported by a grant from the Ministry of Education.

References

1) Part I of this series: Ref. 7.
2) Presented at the 28th Annual Meeting of the Chemical Society of Japan, Tokyo April, 1973.
3) T. Nozoe, K. Takase, and H. Matsumura, in "Dai-Yukikagaku (Comprehensive Organic Chemistry)," ed. M. Kotake, Asakura Shoten, Tokyo (1959), p. 274.
4) H. Wittman, V. Illi, H. Rathmayer, H. Sterk, and E. Zieglar, *Z. Naturforsch.*, **276**, 524—527 (1972).
5) a) Y. Shoji, N. Abe, H. Takeshita, and S. Ito, Preprints for the 5th Symposium on Non-benzenoid Aromatic Chemistry, Nagoya, October, 1972, p. 81. b) Y. Shoji and S. Ito, Preprints for the 6th Symposium on Non-benzenoid Aromatic Chemistry, Fukuoka, October, 1973, p. 132.
6) J. Rigaudy and L. Nédélec, *Bull. Soc. Chim. Fr.*, **1959**, 638.
7) K. Yamane and K. Fujimori, This Bulletin, **45**, 269 (1972).

Attempted Synthesis of Diphenylmethylenecyclobutanetrione and the Anomalous Behavior of Its Monoacetal, 4,4-Dimethoxy-2-diphenylmethylenecyclobutane-1,3-dione

Fumio Toda and Koji Yuwami

Department of Industrial Chemistry, Faculty of Engineering, Ehime University, Matsuyama 790

(Received January 21, 1974)

Neither the oxidation of 2-diphenylmethylenecyclobutane-1,3-dione (I) with SeO_2 nor the hydrolysis of 4,4-dibromo- (III) and 4,4-dimethoxy-2-diphenylmethylenecyclobutane-1,3-dione (IV) afforded the title cyclobutanetrione (II). The title acetal (IV) was dissolved in concd HCl-MeOH without hydrolysis, probably in the protonated form (X) on its carbonyl oxygen. The basification of a solution of IV in concd HCl-MeOH-d_4 recovered the IV undeuterated. On the other hand, IV was dissolved in KOH-MeOH in the form of the enolate anion (XII). The acidification of a solution of IV in KOH-MeOH-d_4 afforded the deuterated acetal (IV-d_6).

No derivative of methylenecyclobutanetrione has yet been reported, even though derivatives of 3,4-dimethylenecyclobutane-1,2-dione,[1] 2,4-dimethylenecyclobutane 1,3-dione,[2] and trimethylenecyclobutanone[3] have been prepared. All our attempts to prepare diphenylmethylenecyclobutanetrione (II) by the oxidation of 2-diphenylmethylenecyclobutane-1,3-dione (I) and by the hydrolysis of 4,4-dibromo- (III) and 4,4-dimethoxy-2-diphenylmethylenecyclobutane-1,3-dione (IV) failed. During the course of these attempts, however, we have found some anomalous behavior of IV in reaction to acid and base.

The treatment of I[2] with two molar amounts of Br_2 in $CHCl_3$ at room temperature afforded III in a 92% yield. The heating of III in MeOH under reflux for 2 hr afforded IV and 4-diphenylmethoxymethyl-3-methoxycyclobut-3-ene-1,2-dione (V) in 39 and 10% yields respectively. Because the reaction of III with MeOH in the presence of pyridine afforded IV in a 52% yield, but no any detectable amount of V, the HBr initially evolved by the methanolysis of III, thus leading to IV, is essential for the production of V. Therefore, a plausible pathway of the formation of V is as follows: a HBr-catalyzed addition of MeOH to the carbonyl of III gives VIII. The ketonization, accompanied by the attack of the methoxide ion on the diphenylmethyl carbon of the epoxide intermediate (IX) which is derived from VIII, affords V (Scheme 1).

The oxidation of I with SeO_2 in dioxane gave only a resinous material. The hydrolysis of III in boiling aqueous MeCN afforded benzophenone and an unidentified carboxylic acid ($C_{17}H_{11}O_3Br$) in 30 and 31% yields respectively. The formation of the benzophenone can be interpreted by assuming such an interme-

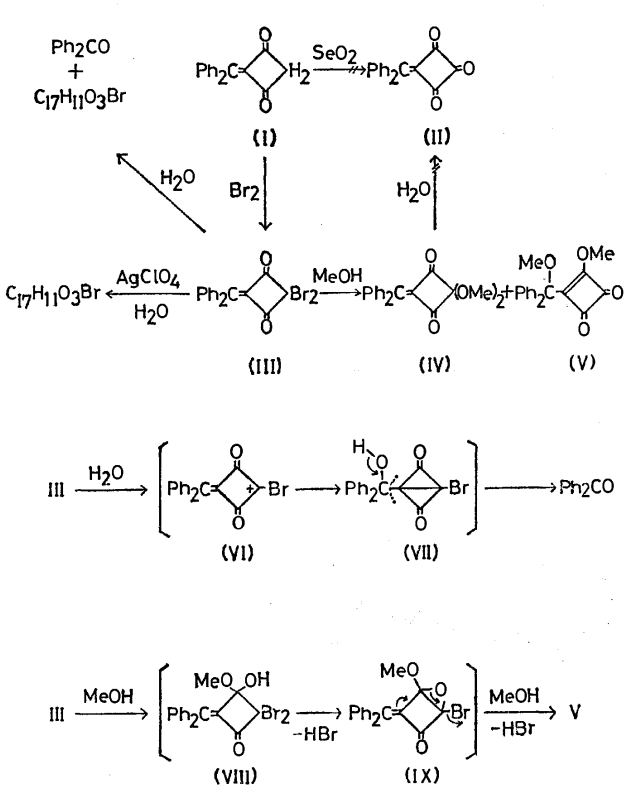

Scheme 1.

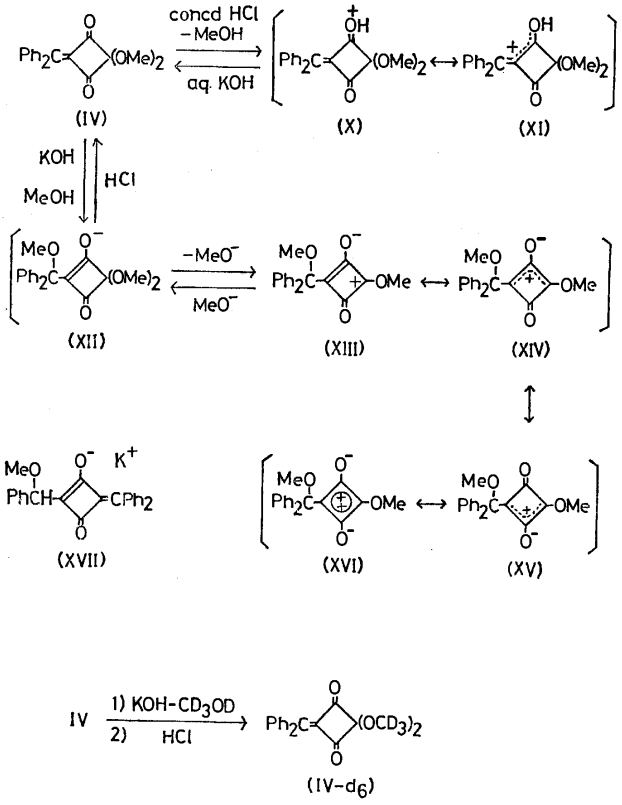

Scheme 2.

diate bearing diphenylhydroxymethyl moiety as VII. The formation of VII can be formulated by a homoallylic rearrangement across the four-membered ring (1,3-interaction), accompanied by the attack of the hydroxy ion on the diphenylmethyl carbon of VI initially produced from III (Scheme 1). The treatment of III with $AgClO_4$ in aqueous THF afforded the carboxylic acid in a 50% yield, but no II.

In contrast with usual acetals, IV was dissolved in concd HCl–MeOH without hydrolysis into the ketone (II), and the basification of the solution recovered the IV quantitatively. Because IV is almost insoluble in MeOH at room temperature, it is clear that HCl has a role in dissolving IV in MeOH. Because the basification of a solution of IV in concd HCl–MeOH-d_4 recovered the IV undeuterated, and because the UV spectral data of IV in concd HCl–MeOH are comparable to those of IV in MeOH (Table 1), the form of IV in the acidic media must be one derived by a protonation on its carbonyl oxygen (X). The contribution of XI to the resonance of X is considerable. However, it is not clear why the ε decreases as the concentration of concd HCl increases.

Table 1. The UV spectra of IV

Solvent	λ_{max} nm ($\varepsilon \times 10^{-2}$)		
MeOH	247 (94)	330 (69)	392 (128)
5% concd HCl–MeOH		331 (67)	393 (127)
20% concd HCl–MeOH		332 (39)	394 (83)
50% concd HCl–MeOH		332 (25)	400 (54)
5% KOH–MeOH	241 (107)		

In a similar manner, IV was dissolved in KOH–MeOH, and the acidification of the solution recovered the IV quantitatively. However, the UV spectrum of IV in 5% KOH–MeOH differs widely from that of IV in MeOH (Table 1). The IR spectrum of IV in 5% KOH–MeOH showed a very strong ν(C–O$^-$) band at such lower frequencies (1560 cm^{-1}) as does the carboxylate ion (1600—1540 cm^{-1}). The data are comparable to those of the potassium salt of the analogous enolate anion (XVII), which has been prepared by the reaction of 4-diphenylmethylene-2-benzylidenecyclobutane-1,3-dione with KOH–MeOH,[2] thus showing

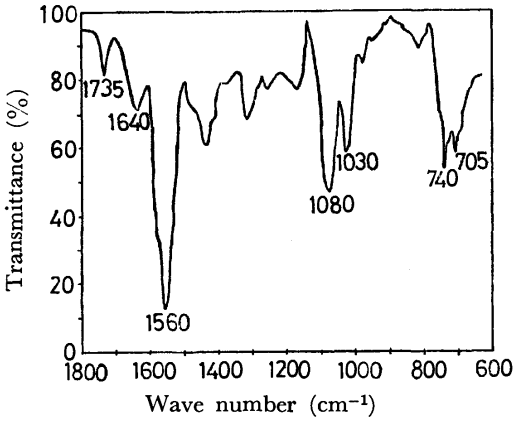

Fig. 1. The IR spectrum of IV in 5% KOH–MeOH (polyethylene-film window cell).

a very strong ν(C–O$^-$) band at 1580—1540 cm^{-1}. Therefore, it is reasonable to consider that the enolate anion (XII) is formed when the IV is dissolved in KOH–MeOH.

Nevertheless, the acidification of a solution of IV in KOH–MeOH-d_4 afforded the fully deuterated acetal (IV-d_6). The exchange of the two MeO with the CD_3O of the solvent can be interpreted by assuming an equilibrium between XII and XIII (Scheme 2). If the presence of XIII in the media is correct, the contribution of XIV and XV to its resonance is considerable. However, the contribution of the cyclobutadiene dication (XVI) to the resonance is doubtful, because even the tetraphenylcyclobutadiene dication is unstable and has been observed only at temperatures below —40 °C.[4]

Experimental

Reaction of I with Br_2. Into a solution of I (2.48 g) in $CHCl_3$ (100 ml), Br_2 (3.2 g) was stirred over a period of 10 min under cooling with an ice bath. The subsequent evaporation of the solvent left crude crystals. Recrystallization from acetone afforded III as red-prisms; 3.74 g (92%); mp 191 °C. IR (Nujol): 1790 (m), 1710 (vs), and 1505 cm^{-1} (vs); $\lambda_{max}^{CHCl_3}$: 246 sh (6300), 336 (9800), 407 (20700), and 425 sh nm (ε, 19600); NMR ($CDCl_3$): 2.45 τ (s, Ph).

Found: C, 50.54; H, 2.54%. Calcd for $C_{17}H_{10}O_2Br_2$: C, 50.29; H, 2.46%.

Reaction of III with MeOH. A solution of III (2.03 g) in MeOH (20 ml) was heated under reflux for 2 hr. The subsequent evaporation of the solvent left a mixture of purple rhombs and colorless needles, which were separated mechanically. The recrystallization of the purple rhombs from MeOH afforded IV; 0.6 g (39%); mp 129—130 °C. IR (Nujol): 1790 (m), 1700 (vs), 1085 (s), and 1040 cm^{-1} (vs); NMR ($CDCl_3$): 2.50 (s, Ph, 10H) and 6.36 τ (s, OMe, 6H).

Found: C, 73.88; H, 5.00%. Calcd for $C_{19}H_{16}O_4$: C, 74.01; H, 5.23%.

The recrystallization of the colorless needles from MeOH afforded V; 0.15 g (10%); mp 209—210 °C. IR (Nujol): 1790 (s), 1750 (m), 1585 (s), and 1360 cm^{-1} (s); λ_{max}^{MeOH}: 230 nm (ε, 23700); NMR ($CDCl_3$): 2.63 (s, Ph, 10H), 5.45 (s, OMe, 3H), and 6.87 τ (s, OMe, 3H).

Found: C, 73.87; H, 5.26%. Calcd for $C_{19}H_{16}O_4$: C, 74.01; H, 5.23%.

When the reaction of III (1.15 g) with MeOH (10 ml) was carried out in the presence of pyridine (0.1 g) by the same procedure as above, 0.4 g (52%) of IV was obtained.

Hydrolysis of III. A solution of III (0.406 g) in 5% aqueous MeCN (10 ml) was heated under reflux for 1 hr. After cooling, the reaction mixture was diluted with ether (100 ml). The ether solution was washed with dil KOH and water, and then dried over anhydrous Na_2SO_4. The evaporation of the solvent left benzophenone; 0.55 g (30%). The crude crystals obtained by the acidification of the alkaline extract were recrystallized from MeOH to afford an unidentified compound ($C_{17}H_{11}O_3Br$) as colorless needles; 0.106 g (31%); mp 189—190 °C. Mass spectrum *m/e*: 344 and 342 (M^+); IR (Nujol): 1690 (vs), 1625 (m), 1530 (m), and 1175 cm^{-1} (m); $\lambda_{max}^{CHCl_3}$: 330 nm (ε,←12100); NMR ($CDCl_3$): 2.5—2.9 τ (m, Ph).

Found: C, 59.56; H, 3.28%. Calcd for $C_{17}H_{11}O_3Br$: C, 59.50; H, 3.23%.

Reaction of III with $AgClO_4$. A mixture of III (0.406 g), $AgClO_4$ (0.45 g), and 10% aqueous THF (10 ml) was

kept at 0 °C for 5 min. Aqueous NaCl was then added to the reaction mixture. After the precipitates had been filtered off, the filtrate was diluted with ether (50 ml). The ether solution was washed with water and dried over anhydrous Na_2SO_4. The recrystallization from MeOH of the crude crystals left by the evaporation of the solvent afforded an unidentified compound ($C_{17}H_{11}O_3Br$): 0.17 g (50%).

The Formation of IV-d_6. The addition of dil HCl to a solution of IV (0.1 g) in 5% KOH-MeOH (10 ml) afforded IV-d_6; 0.1 g (100%). IR (Nujol): 2100 (w), 1790 (m), 1700 (vs), and 1525 cm^{-1} (vs); NMR ($CDCl_3$): 2.5 τ (s, Ph).

This work was supported by a grant from the Ministry of Education.

References

1) F. Toda, H. Ishihara, and K. Akagi, *Tetrahedron Lett.*, **1969**, 2531.
2) F. Toda, *Chem. Lett.*, **1972**, 621.
3) F. Toda and T. Kataoka, *ibid.*, **1972**, 173.
4) G. A. Olah and G. D. Masteescu, *J. Amer. Chem. Soc.*, **92**, 1430 (1970).

Dopaquinone and Related Compounds: Reactions with *o*-Phenylenediamine

Yoshimori OMOTE, Tokuo HIRAMA, and Toshihiko KOMATSU

Department of Chemistry, Tokyo Kyoiku University, Bunkyo-ku Otsuka, Tokyo 112

(Received January 22, 1974)

The oxidation of 4-substituted catechols including DOPA with *o*-chloranil or cerium(IV) sulfate to give the corresponding *o*-benzoquinones was examined. The trapping of *o*-benzoquinones with *o*-phenylenediamine immediately after oxidation was successfully used to isolate 2-substituted phenazines, the substituents being $-CH_3$, $-CH(CH_3)_2$, $-(CH_2)_2CO_2H$, $-(CH_2)_2CO_2CH_3$, $-CH{=}CHCO_2H$, $-CH{=}CHCO_2CH_3$, $-(CH_2)_2NHCOC_6H_5$, and $-CH_2CH(NHCOC_6H_5)CO_2CH_3$. Dopaquinone was identified in a protected form.

Raper[1] suggested the intermediacy of dopaquinone (I) in the melanogenesis of DOPA, and later Bu'Lock and Harley-Mason[2] reported the formation of dopachrome (II) based on the ultraviolet absorption spectrum. These intermediates are very unstable and have never been synthesized or trapped in spite of many reports on *o*-benzoquinones.[3-5]

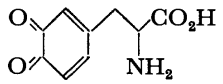

I

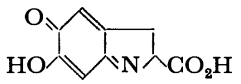

II

Recently Horspool *et al.* have shown that 4-substituted *o*-benzoquinones react with arylamines at the 4- and 5-positions.[6] Also, it is known that dopamine or 5-hydroxydopamine is easily cyclized into the corresponding indoline derivative by mild oxidation. Thus, it was of interest to synthesize and trap dopaquinone or dopachrome. This paper will be concerned with the synthesis of dopaquinone and related compounds in neutral or acidic media as well as with their reactions with *o*-phenylenediamine.

Results and Discussion

UV Spectral Studies. The oxidation of DOPA and related catechols were examined by means of the UV spectrum. Several oxidants are known to convert catechols to the corresponding *o*-benzoquinones: *e.g.*, *o*-chloranil,[3a] silver oxide,[7] cerium(IV) sulfate,[8] and potassium nitrosodisulfonate,[4a] among which *o*-chloranil is the best for the UV spectral studies. Equimolar solution of catechol and *o*-chloranil in ethanol were mixed, and the absorbance of the mixture was measured. The absorption maxima of the mixtures indicate that, in the case of catechols with no free amino group, the absorption of the corresponding quinone appears between 380—390 nm (Table 1). The absorbance of tetrachlorocatechol at 300 nm increased, while those of *o*-chloranil at 350 and 410 nm and catechol at 280 nm decreased. The isosbestic points were observed near 290 and 380 nm.

TABLE 1. THE ABSORPTION MAXIMA OF THE REACTION PRODUCTS OF 4-SUBSTITUTED CATECHOLS (IIIa—IIIh) WITH *o*-CHLORANIL

	λ_{max} (nm)		λ_{max} (nm)
IIIa	370	IIIe	385
IIIb	380	IIIf	384
IIIc	385	IIIg	—
IIId	386	IIIh	—

The final concentration of a substrate was 5×10^{-4} mol/l.

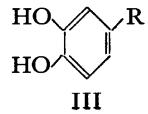

III

R

a : H
b : CH_3
c : $C(CH_3)_3$
d : $CH(CH_3)_2$
e : $(CH_2)_2CO_2H$
f : $(CH_2)_2NHCOC_6H_5$
g : $(CH_2)_2NH_2$
h : $CH_2CH(NH_2)CO_2H$

In the case of catechols with a free amino group, however, no absorption of *o*-benzoquinone appeared near 390 nm, while the absorptions at 350 and 410 nm of *o*-chloranil disappeared. These facts suggest that the oxidation by *o*-chloranil did not yield the corresponding *o*-benzoquinone. Dopamine (IIIg) did not show any absorption of *o*-benzoquinone after oxidation, but after 20 hr it showed an absorption at 470 nm which is similar to that of dopachrome.[9] DOPA (IIIh) itself did not show any absorption at 470—500 nm under similar oxidation conditions. Considering that dihydrocaffeic acid (IIIe), a desamino DOPA, gave a typical quinoid spectrum on oxidation, it could be concluded that a carboxyl group of DOPA has no relation to the instability of dopaquinone, but that an amino group contributes toward the cyclization of dopaquinone into an indoline derivative or an unidentified product.

Oxidation of 4-Substituted Catechols to o-Benzoquinone. 4-Isopropylcatechol (IIId), as a model compound of DOPA, was oxidized by *o*-chloranil according to the method which Horner *et al.*[3a] used in the oxidation of homocatechol, but 4-isopropyl-*o*-benzoquinone was an oily product and could not be obtained in a pure state. Therefore, cerium(IV) sulfate[8] was used as the oxidant. The acidic media are favorable for the stability of the quinone produced. The *o*-benzoquinone was obtained as a dark red oil which showed UV absorption band at 390 and 540 nm and an NMR spectrum characteristic of 4-substituted *o*-benzoquinone ring[10] (see Experimental), but an attempt at purification was unsuccessful. Therefore, it became necessary to trap such an unstable *o*-benzoquinone as a stable crystalline compound.

Reaction of o-Benzoquinones with o-Phenylenediamine. One of the most common methods of trapping *o*-benzoquinones is the reaction with *o*-phenylenediamine to give a phenazine derivative.[3a] On the other hand, Horspool *et al.*[6] have pointed out the possibility of substitution on the 4- or 5-position of *o*-benzoquinone upon treatment with arylamine. However, when the oily 4-isopropyl-*o*-benzoquinone was treated with *o*-phenylenediamine, 2-isopropylphenazine(Vb) was obtained in a 53% yield as yellow needles (Table 2).

TABLE 2. PHENAZINES (V) DERIVED FROM 4-SUBSTITUTED *o*-BENZOQUINONES (IV)

Phenazines	R	Yield%	mp °C
Va	CH_3	76	116—116.5
Vb	$CH(CH_3)_2$	53	90— 91
Vc	$(CH_2)_2CO_2H$	67	186—188 (dec)
Vd	$(CH_2)_2CO_2CH_3$	44	92— 93
Ve	$CH{=}CHCO_2H$	12	257—258 (dec)]
Vf	$CH{=}CHCO_2CH_3$	13	152—153
Vg	$(CH_2)_2NHCOC_6H_5$	37	171—172
Vh	$CH_2CHCO_2CH_3$ $\vert$ $NHCOC_6H_5$	31	211—212

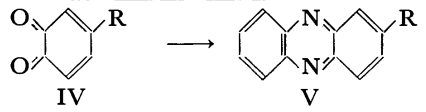

IV V

The quinones (IVc and IVd) from dihydrocaffeic acid and its methyl ester were also oily substances, but their corresponding phenazines (Vc and Vd) were crystals. The quinone from dihydrocaffeic acid is an isomer of a catechol (VII),[11] just as VI is a formal isomer of the unisolable dopamine quinone. However, the presence of these compounds could not be detected among the oxidation products. The quinone from caffeic acid was very unstable and could not be identified even by the NMR spectrum, but the trapping of this quinone to give the phenazine derivative (Vf) was successful. As is shown in Table 2, the method of trapping unstable *o*-benzoquinone by *o*-phenylenediamine is useful for the identification of dopaquinone related compound.

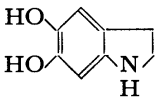

VI

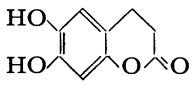

VII

Finally, DOPA was protected by methylation and benzoylation and then oxidized by cerium(IV) sulfate to give a dark red oil showing the UV and NMR spectra characteristic of 4-substituted *o*-benzoquinone, which was then converted into the crystalline phenazine derivative.

Experimental

Oxidation of 4-Isopropylcatechol (IIId). To a solution of IIId (137 mg) in chloroform (7 ml), we poured an ice-cooled solution of cerium(IV) sulfate (aq. 734 mg) in 20% sulfuric acid (13 ml), after which the mixture was stirred for 5 min. Then a solution of cerium(IV) sulfate (aq. 73.4 mg) in 20% sulfuric acid (2 ml) was added and the mixture was stirred for 1 min. The organic layer was washed three times with 0.01 M sulfuric acid, dried over anhydrous sodium sulfate, and then concentrated to give a red oil.

UV $\lambda_{max}^{CHCl_3}$: 390 and 580 nm; NMR ($CDCl_3$): δ 1.23 (d, J=7 Hz, 6H), 2.65 (septet, J=7 Hz, 1H), 6.2 (broad s, 1H), 6.4 (d, J=11 Hz, 1H), and 7.0 (dd, J=11 and 2 Hz, 1H); IR (film): 2940, 1735, 1680, 1665, 1280, 815, and 755 cm^{-1}.

Found: C, 71.40; H, 6.77%. Calcd for $C_9H_{10}O_2$: C, 71.98; H, 6.71%. R_f: 0.705(*n*-butyl acetate-heptane 1 : 1, DMF impregnated paper.[12]

Oxidation of N-Benzoyl DOPA Methyl Ester (IIIi). To a solution of IIIi (60 mg) in methanol-ethyl acetate (1 : 5) we added an ice-cooled solution of cerium(IV) sulfate (170 mg) in 20% sulfuric acid (4 ml) after which the mixture was vigorously stirred for 1 min. Then a solution of cerium(IV) sulfate (2 mg) in sulfuric acid was added to complete the reaction. The organic layer was washed three times with dilute sulfuric acid, dried over anhydrous sodium sulfate, and then concentrated to afford a dark red oil.

UV $\lambda_{max}^{CHCl_3}$: 386 and 580 nm; NMR ($CDCl_3$): δ 3.0 (broad d, J=7 Hz, 2H), 5.0 (broad t, J=7 Hz, 1H), 6.2 (broad s, 1H), 6.3 (d, J=10 Hz, 1H), and 7.0 (dd, J=10 and 2 Hz, 1H).

Phenazines. A typical example is shown below in the case of 2-methylphenazine.

2-Methylphenazine (IV).[13] A solution of 4-methylcatechol (IIIb) (170 mg) in chloroform was mixed with a solution of cerium(IV) sulfate in 20% sulfuric acid and stirred for 1 min. The organic layer was washed, dried and transferred into an ethereal solution of *o*-phenylenediamine with stirring at room temperature. After the mixture had stood for six days, the ether was distilled off and a mixture of acetic anhydride and pyridine (1 : 1, v/v) was added to the residue. After standing overnight, the reaction mixture was heated *in vacuo* to remove the acetic anhydride and pyridine. The residue was purified by column chromatography(benzene-ethyl acetate 5 : 1, silica gel) to give a yellow powder, which was recrystallized from ethanol to give yellow needles; 161 mg (76%), mp 116—116.5 °C (lit,[4] 117 °C).

2-Isopropylphenazine (Vb). 4-Isopropylcatechol (IIId) (150 mg) gave 115 mg (54%) of Vb; yellow needles, mp 90—91 °C; UV λ_{max}^{MeOH} (ε): 252 (124000) and 365 nm (13800); NMR ($CDCl_3$): δ 1.43 (d, J=7 Hz, 6H), 3.20 (septet, J=7 Hz, 1H), and 7.6—8.3 (m, 7H); IR (KBr): 1643, 1512, 1370, 835, and 758 cm^{-1}. Found: C, 81.22; H, 6.41; N, 12.55%. Calcd for $C_{15}H_{14}N_2$: C, 81.05; H, 6.35; N, 12.60%.

3-(2-Phenazinyl)propionic Acid (Vc). Dihydrocaffeic acid (IIIe) (364 mg) gave 338 mg (67%) of Vc; yellow prisms, mp 186—188 °C (dec): UV λ_{max}^{MeOH} (ε): 254 (124000) and 363 nm (15300); NMR (CF_3CO_2H): δ 3.16 (t, J=7 Hz, 2H), 3.50 (t, J=7 Hz, 2H), and 8.2—8.8 (m, 7H); IR (KBr): 1720, 1640, 825, and 775 cm^{-1}. Found: C, 71.19; H, 4.90; N, 11.08%. Calcd for $C_{15}H_{12}N_2O_2$: C, 71.41; G, 4.80; N, 11.11%.

Methyl 3-(1-Phenazinyl)propionate (Vd). The methyl ester of dihydrocaffeic acid (392 mg) gave 235 mg (44%) of Vd; yellow sticks, mp 92—93 °C; UV λ_{max}^{EtOH} (ε): 253 (143000) and 364 nm (20500); NMR ($CDCl_3$): δ 2.81 (t, J=7 Hz, 2H), 3.24 (t, J=7 Hz, 2H), 3.69 (s, 3H), and 7.5—8.3 (m, 7H): IR (KBr): 1740, 1640, 840, and 760 cm^{-1}. Found: C, 71.94; H, 5.23; N, 10.52%. Calcd for $C_{16}H_{14}N_2O_2$: C, 72.16; H, 5.30; N, 10.52%.

3-(2-Phenazinyl)-2-propenoic Acid (Ve). Caffeic acid (900 mg) gave 150 mg (12%) of Ve; dark yellow needles, mp 257—258 °C (dec); UV λ_{max}^{MeOH} (ε): 238 (21000), 282 (62000), 358 (7200), 380 (11000), and 395 nm (13000); NMR (CF_3CO_2H): δ 7.04 (d, J=15.6 Hz, 1H), 8.03 (d, J=15.6 Hz, 1H), and 8.3—8.8 (m, 7H); IR (KBr): 1690, 1620, 1290, 820, and 740 cm^{-1}. Found: C, 70.80; H, 4.06; N, 11.08%. Calcd for $C_{15}H_{10}N_2O_2$: C, 70.26; H, 4.03; N, 11.20%.

Methyl 3-(2-Phenazinyl)-2-propenoate (Vf). The methyl ester caffeic acid (388 mg) gave 68 mg (13%) of Vf; yellow needles, mp 152—154 °C; UV λ_{max}^{EtOH} (ε): 238 (19900) 285 (83500), 377 (16900), and 395 nm (15500); NMR

($CDCl_3$): δ 3.82 (s, 3H), 6.57 (d, J=16 Hz, 1H), and 7.6—8.3 (m, 8H); IR (KBr): 1725, 1630, 1312, 1290, 820, and 750 cm^{-1}. Found: C, 72.20; H, 4.60; N, 10.55%. Calcd for $C_{16}H_{12}N_2O_2$: C, 72.71; H, 4.58; N, 10.60%.

N-Benzoyl-3-(2-phenazinyl)ethylamine (Vg). *N*-Benzoyldopamine (IIIf) (376 mg) gave 178 mg (37%) of Vg; yellow needles, mp 171—172 °C; UV λ_{max}^{MeOH} (ε): 253 (107000) and 365 nm (13400); NMR ($CDCl_3$): δ 3.17 (t, J=7 Hz, 2H), 3.85 (q, J=7 Hz, 2H), 6.60 (broad s, 1H), and 7.2—83. (m, 12H); IR (KBr): 3320, 1640, 1550, 820, and 750 cm^{-1}. Found: C, 76.80; H, 5.25;N, 13.03%. Calcd for $C_{21}H_{17}N_3O$: C, 77.04; H, 5.23; N, 12.84%.

Methyl 3-(2-Phenazinyl)-2-benzoylaminopropionate (Vh). The methyl ester of N-benzoyldopa (IIIi) (100 mg) gave 38 mg (31%) of Vh; yellow needles, mp 211—212 °C; UV λ_{max}^{EtOH} (ε): 225 (25500), 254 (127000), and 363 nm (16800); IR(KBr): 3270, 1745, 1640, 815, and 760 cm^{-1}. Found: C, 71.83; H, 5.09; N, 11.16%. Calcd for $C_{23}H_{19}N_3O_3$: C, 71.67; H, 4.97; N, 10.90%.

References

1) H. S. Raper and A. Wormall, *Biochem. J.*, **19**, 84 (1925).

2) J. D. Bu'Lock and J. Harley-Mason, *J. Chem. Soc.*, **1951**, 2248.

3) a) L. Horner and W. Durckheimer, *Z. Naturforsch.*, **14b**, 741 (1959). b) L. Horner, K. H. Teichmann, K. H. Weber, and E. Geyer, *Chem. Ber.*, **98**, 1233 (1965).

4) H. J. Teuber and G. Staiger, *Chem. Ber.*, **88**, 802 (1955).

5) H. W. Wanzlick, "Newer Methods of Preparative Organic Chemistry," Vol. IV, Wilhelm Foerst, Academic Press (1968), p. 139.

6) a) W. M. Horspool, P. I. Smith, and J. M. Tedder, *J. Chem. Soc. C*, **1971**, 138. b) W. M. Horspool, P. I. Smith, and J. M. Tedder, *J. Chem. Soc. Perkin I*, **1972**, 1024.

7) R. Willstätter and F. Müller, *Ber.*, **44**, 2171 (1911).

8) R. Brockhaus, *Ann.*, **712**, 214 (1968).

9) a) H. S. Mason, *J. Biol. Chem.*, **172**, 83 (1948). b) S. Ducler, M. Wilchek, and D. Lavie, *Tetrahedron*, **27**, 607 (1971).

10) a) R. Hollenstein and W. von Philipsborn, *Helv. Chim. Acta*, **56**, 320 (1973). b) W. von Philipsborn, *Angew. Chem.*, **83**, 470 (1971).

11) A. Kaiser, W. Koch, M. Scheer, and U. Wölcke, *Helv. Chim. Acta*, **53**, 1708 (1970).

12) I. Buben and J. Pospíšil, *Collect. Czech. Chem. Commun.*, **34**, 1991 (1969).

13) Preparations of 2-substituted phenazines have been reported; Vb was synthesized by heating catechol with *o*-phenylenediamine in the presence of metallic oxides,[a] while Vc, Ve, and Vf were prepared from 2-phenazinecarboxaldehyde and malonic acid.[b] However, these methods are different from ours and the analytical details have not been described in these reports. a) Shell International Research Maatschappij N. V. Neth. appl. 6511395, March 4, 1965 [*Chem. Abstr.*, **66**, 2279e (1966)]. b) Yu. S. Rozum, *Ukrain. Khim. Zhur.*, **33**, 776 (1956) [*Chem. Abstr.*, **51**, 8762 (1957)].

The Photochemical Reaction of 1,4-Naphthoquinone Derivatives with Hydrogen Donors

Kazuhiro MARUYAMA and Seiichi ARAKAWA

Department of Chemistry, Faculty of Science, Kyoto University, Kyoto 606

(Received February 5, 1974)

The reaction products of the photochemical reactions of 1,4-naphthoquinone and its methyl- or halogeno-derivatives with xanthene were investigated. Methyl-substituted 1,4-naphthoquinones produce the corresponding 1,4-naphthohydroquinones, but naphthoquinone and its halogeno-derivatives react to give substituted or added products by the xanthyl group in addition to the hydroquinone derivatives. Stable free radicals, which remain unchanged under atmospheric pressure, are also obtained in the latter reactions. The courses of the photochemical reactions were investigated by means of the CIDNP technique, and the reaction mechanism was discussed.

The photochemical reaction of quinones has received extensive interests by many investigators.[1] According to Pfundt,[2] the irradiation of 9,10-phenanthraquinone with xanthene gave the "1,2-adduct", **1**, the reaction was reinvestigated by Maruyama and his co-workers.[3]

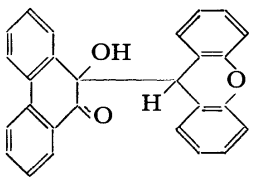

1

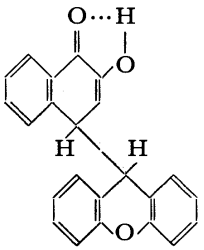

2

The irradiation of 1,2-naphthoquinone with xanthene, however, gave a different type of photo-adduct, **2**.[4] Recently the present authors have examined the photochemical reactions of *p*-quinones with xanthene by means of the CIDNP technique[5] and pointed out the formation of unstable intermediates in the course of reactions. Stable products such as hydroquinones and 9,9′-bixanthyl are also formed in the reactions.

In this work, the photochemical reactions of 1,4-naphthoquinone, 2-methyl-1,4-naphthoquinone, 2,3-dimethyl-1,4-naphthoquinone, 2,6-dimethyl-1,4-naphthoquinone, 2-chloro-1,4-naphthoquinone, 2,3-dichloro-1,4-naphthoquinone, 2-bromo-1,4-naphthoquinone, 2,3-dibromo-1,4-naphthoquinone with xanthene dissolved in benzene were mainly studied from the standpoint of stableproduct analyses. Examinations by means of the CIDNP technique were also extended to the above reactions in order to investigate the reaction mechanism.

Results and Discussion

In all of the photochemical reactions described below, a benzene solution of 1,4-naphthoquinone derivatives and xanthene sealed in a glass tube was irradiated by means of a 400W high-pressure mercury arc lamp from the outer side through a 5-cm-thick water layer under ice-water cooling or at room temperature.

Methyl-substituted 1,4-Naphthoquinones. The irradiation for about eight hours of the benzene solution of 2-methyl-1,4-naphthoquinone, **3a**, and xanthene gave 2-methyl-1,4-naphthohydroquinone, **4a**, and 9,9′-bixanthyl in a 70—80% yield. 2,3-Dimethyl-1,4-naphthoquinone, **3b**, and 2,6-dimethyl-1,4-naphthoquinone, **3c**, reacted as well as the **3a** with xanthene to give the corresponding 1,4-naphthohydroquinone derivatives and 9,9′-bixanthyl in good yields. The quantum yields of the naphthoquinone disappearance are tabulated in Table 1.

TABLE 1. QUANTUM YIELDS OF THE DISAPPEARANCE OF 1,4-NAPHTHOQUINONE DERIVATIVES

Quinones	Quantum yields[a]
1,4-Naphthoquinone	0.39
2-Methyl-1,4-naphthoquinone	0.29
2,3-Dimethyl-1,4-naphoquinone	0.12
2-Chloro-1,4-naphthoquinone	0.41

a) Non-degassed benzene solutions were used for the determination. Wavelength of light for excitation was longer than 400 nm.

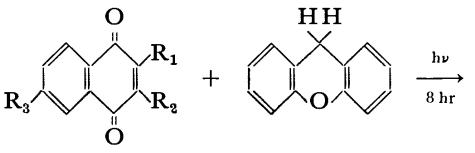

3

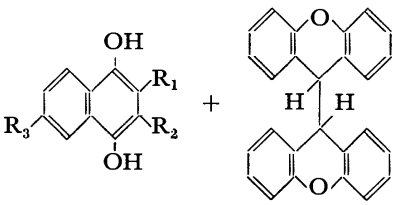

4

a; R_1=Me, R_2=R_3=H **b**; R_1=R_2=Me, R_3=H **c**; R_1=R_3=Me, R_2=H

1,4-Naphthoquinone and Its Halogeno-derivatives. In the photochemical reactions of 1,4-naphthoquinone and its halogeno-derivatives, other products of the **6** and **7** types, were obtained in addition to the corresponding hydroquinones and 9,9′-bixanthyl. Moreover, stable radicals could be isolated in the reaction of the halogeno-derivatives with xanthene. The relative yields of the respective compounds in the reaction products are profoundly dependent on the temperature, as is shown in Table 2. For example, under ice-water cooling compounds of the **8**, **9**, and **7** types were produced as the main products, but at room temperature

Table 2. Products in the photochemical reaction of 1,4-naphthoquinone derivatives with xanthene[a)]

Quinones	Reaction times (hr)	Products (%)				
		Hydroquinone or quinhydrone	9,9'-Bixanthyl	Adduct-1	Adduct-2	Radicals
5a	5[b)]	31	17	—	1.5	—
5b	4[b)]	48	23	0.5	4	—
5b	5[c)]	28	5	2.1	8.6	14
5c	11[c)]	trace	trace	24	—	17
5d	5[b)]	21	23	2.1	0.8	—
5d	5[c)]	3	4	5	trace	23
5e	10[c)]	trace	trace	11	—	5.3

a) Equivalent amounts of quinone and xanthene dissolved in benzene were irradiated. Yields were based on the amounts of quinones used. b) Under ice-water cooling. c) At room temperature.
Adduct-1: 2-[9'-Xanthyl]-1,4-naphthoquinone derivatives.
Adduct-2: 2,3-Di-[9'-xanthyl]-1,4-naphthoquinone derivatives.

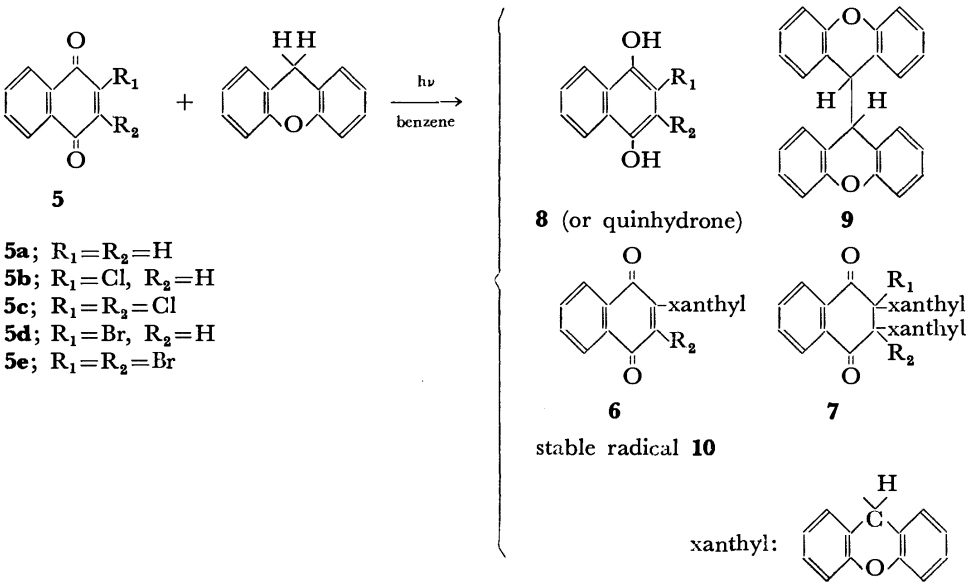

5

5a; $R_1=R_2=H$
5b; $R_1=Cl$, $R_2=H$
5c; $R_1=R_2=Cl$
5d; $R_1=Br$, $R_2=H$
5e; $R_1=R_2=Br$

8 (or quinhydrone) **9**

6 **7**

stable radical **10**

(*ca.* 25 °C) the principal products were of the **8**, **7**, and **10** types and the yield of **9** was considerably reduced. The reactions of **5d** and **5e** followed the same trend. The structures of the **6**—**9** products were determined by means of IR, PMR, mass, and elemental analyses.

Structure of Stable Radicals ***10***. In the photochemical reaction of halogeno-derivatives of 1,4-naphthoquinone with xanthene at room temperature, stable, greenish free radicals could be obtained in fairly high yields. The radicals show a well-resolved ESR hyperfine structure in a tetrahydrofuran solution. The typical ESR spectra of the radicals, which are obtained in the photochemical reaction of 2,3-dichloro- and 2,3-dibromo-1,4-naphthoquinone with xanthene, are shown in Fig. 1.

The analyses of the spectra are straightforward; five groups of lines split further to a quintet. This means that the radical center is at position 9' and almost all of the unpaired electrons delocalize on the xanthyl moiety. The physical properties of the stable radicals obtained are summarized in Table 3.

When the radicals were then submitted to chromic acid oxidation (or ferric chloride oxidation), they gave

Table 3. Physical properties of stable free radicals

Free radicals	**11a**[a)]	**11b**[a)]	**11c**[a)]
Color	green	dark green	black
Decomp. point (°C)	105—107	137	180—182
IR(KBr); (cm^{-1})	3200	3050	3050
ESR coupling constants (gauss) $a_{H_1',8'}$	3.23	3.00	3.30
ESR coupling constants (gauss) $a_{H_3',6'}$	3.90	3.60	3.81
ESR coupling constants (gauss) $a_{H_2',4',5',7'}$	0.79	0.74	0.76
g-Values	2.0029	2.0030	2.0034

a) The structures **11a**, **11b**, and **11c** correspond to the stable radicals **10b**, **10c**, and **10d** respectively.

9'-hydroxyderivatives, **12**. Reaction with zinc dust-hydrochloric acid, on the other hand, resulted in the corresponding 2-halogeno-3-[9'-xanthyl]-1,4-naphtho-hydroquinones, which were subsequently autoxidized in the air to the corresponding naphthoquinone derivatives, **6**. The radicals showed a broad IR absorption due to the hydroxy group in the region of ν_{OH}: 3000—3200 cm^{-1}. Therefore, the radicals were assigned to structure **10**.

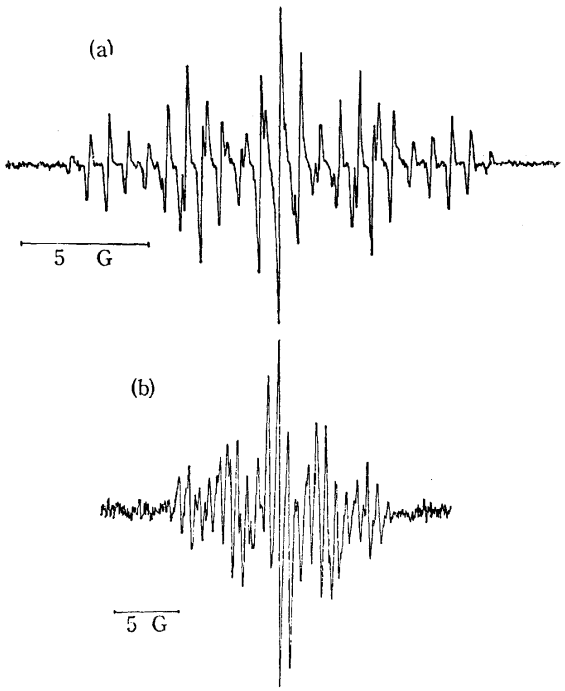

Fig. 1. ESR spectrum of stable radical (**10c**) obtained in the reaction of 2,3-dichloro-1,4-naphthoquinone with xanthene(a) and in the reaction of 2,3-dibromo-1,4-naphthoquinone with xanthene(b).

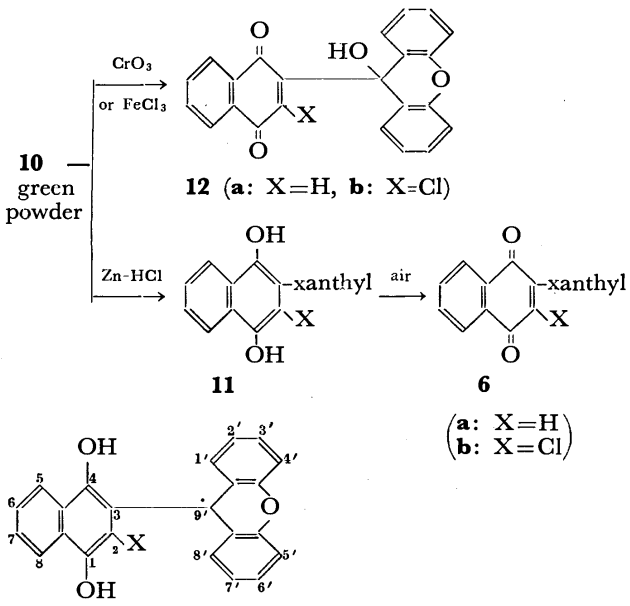

Thus, **5b** and **5d** convert to the same product, **10a**; **5c**, to **10b**, and **5e**, to **10c**. The radicals are stable in the solid state, but they gradually change to non-radical substances in a solution (*e.g.*, solvent THF). These radicals may be produced *via* photo-induced intramolecular hydrogen abstraction of the primary products, **6b—e**, accumulated in the reacting system, as is shown in the following equations;

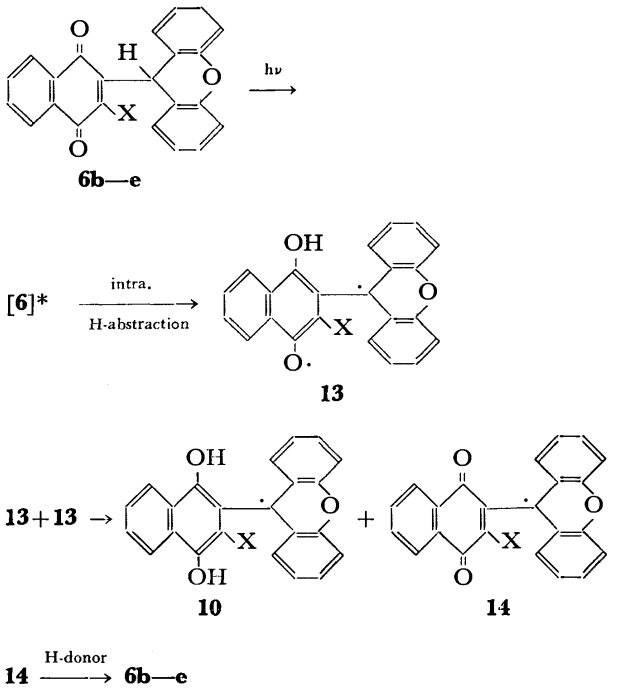

CIDNP Measurements and Reaction Mechanism. 1,4-Naphthoquinone derivatives examined in this work have n→π* absorption bands in the region of λ_{max}: 420—440 nm (ε: 20—60). The molecules of 1,4-naphthoquinone derivatives excited by the n→π* transition could be converted to the triplet state via inter-system crossing. The excited molecules in the triplet state can abstract hydrogen from xanthene to give the triplet radical pair, **18**—radical pair consisting of a semiquinone radical and a xanthyl radical—in the solvent cage. By means of the CIDNP technique we have previously investigated the photochemical reactions of 1,4-naphthoquinone derivatives with xanthene and pointed out the formation of the **15**, **16**, and **17** reaction intermediates.[5] These reaction intermediates decomposed thermally to give a solvent-separated semiquinone radical and xanthyl radical.

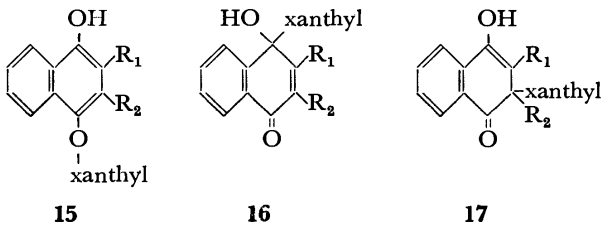

In addition to the strongly polarized PMR signals due to these intermediates, other polarized PMR signals corresponding to the isolated stable products could be observed. The PMR spectra observed during the course of the photochemical reactions of 1,4-naphthoquinone and its halogeno-derivatives with xanthene are shown in Figs. 2—4; Fig. 2 shows the PMR polarized signals observed in the reactions of 1,4-naphthoquinone with xanthene, Fig. 3, those of 2-chloro-1,4-naphthoquinone, and Fig. 4, those of 2,3-dichloro-1,4-naphthoquinone. The polarized PMR signals due to the stable products could be easily assigned to the

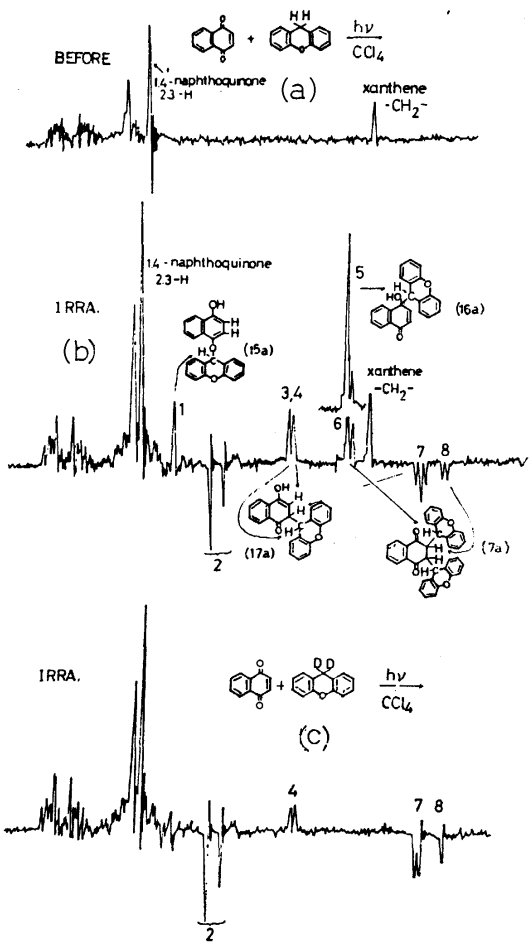

Fig. 2. PMR spectra observed in the photochemical reaction of 1,4-naphthoquinone with xanthene.
(a): before irradiation, (b): during irradiation; (c): during irradiation, when xanthene-9-d_2 was used.
Signals 2 in the Figure should be assigned to 2,3-protons of **16a**[15].

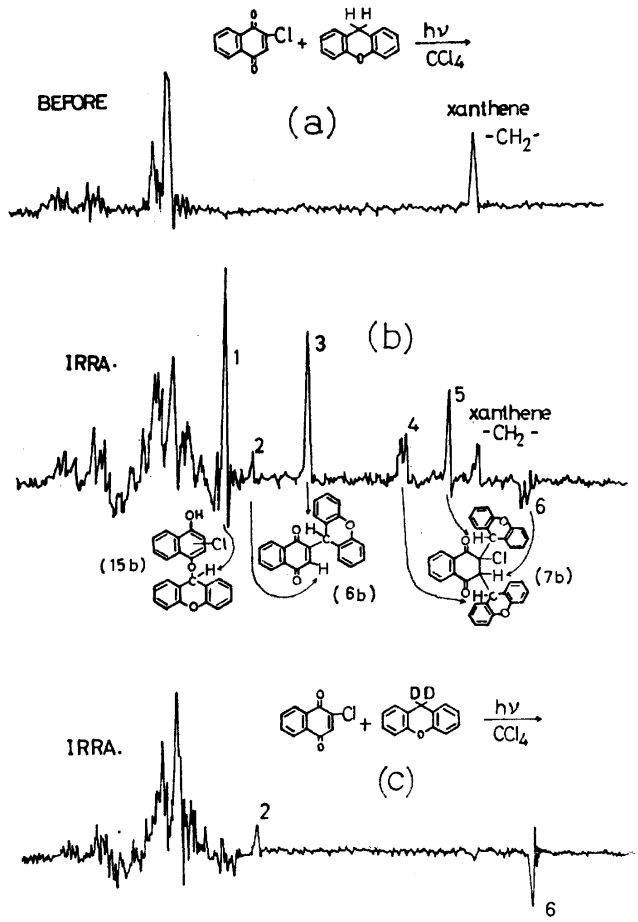

Fig. 3. PMR spectra observed in the photochemical reaction of 2-chloro-1,4-naphthoquinone with xanthene.
(a): before irradiation, (b): during irradiation, (c): during irradiation, when xanthene-9-d_2 was used.

respective compounds by comparison with the PMR spectra of the isolated products, but one can determine those due to reaction intermediates by comparison with the polarized PMR signals observed in the reaction of the corresponding quinones with xanthene-9-d_2 and their chemical shifts. The structures thus determined are indicated in Figs. 2—4. According to the CKO theory,[6] the polarized signals are developed by the reaction products formed through a radical process, regardless of their stabilities. Although these photochemical reactions obviously proceed through radical processes, fairly vigorous liberation of hydrogen halides could be observed in the course of the reactions of **5b**, **5c**, **5d**, and **5e**. This may be interpreted in terms of the decomposition of the thermally-unstable intermediates to give the substituted derivatives of 1,4-naphthoquinone by means of the xanthyl group. Since the structure of the reaction intermediates formed in the reacting system, as well as the stable products, could be determined by means of the CIDNP technique and by stable-product analyses, the following possible reaction scheme can be proposed. The disproportionation of the semiquinone radical (Step iv) was unambiguously confirmed by means of the CIDNP technique, the details were reported in a previous report.[5] The temperature dependence of the stable-product distributions described in Table 2 can be ingeniously interpreted by taking into consideration Steps v and vi; at higher temperatures the yield of 9,9′-bixanthyl is considerably reduced, and that of the stable radical is increased. The process of the stable free radical formation has already been considered in Section 3. In the photochemical reaction of 1,4-naphthoquinone with xanthene, Steps vii, viii, and ix might be unimportant.

The photochemical reactions of 1,4-naphthoquinone derivatives with thioxanthene proceeded quite smoothly, as those with xanthene, but the products were the corresponding hydroquinones, quinhydrones and 9,9′-bithioxanthyl, with the exceptions of **5b** and **5d**. In the phothochemical reactions of **5b** or **5d** with thioxanthene, a small amount of the adduct corresponding to **6b** was isolated in addition to the compounds described above.

Experimental

Materials. 1,4-Naphthoquinone (mp 125—126 °C) commercially available was further purified by sublimation.

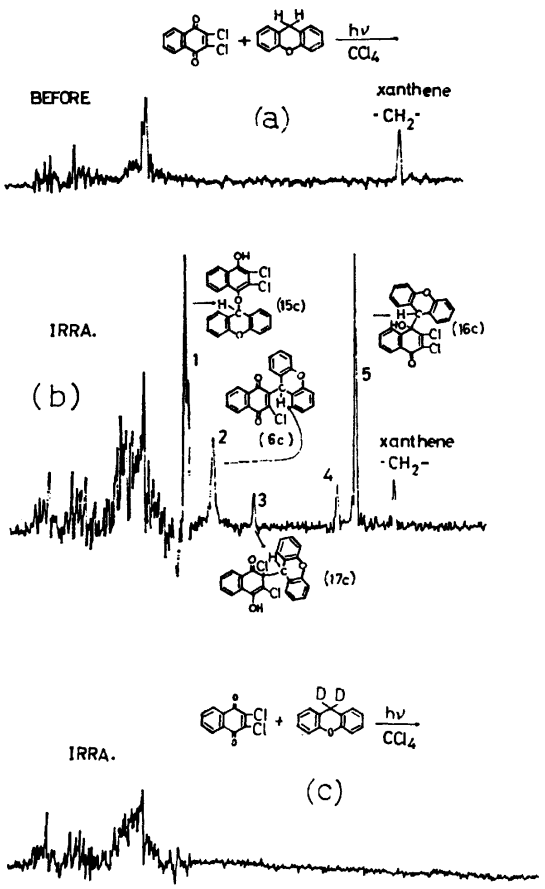

Fig. 4. PMR spectra observed in the photochemical reaction of 2,3-dichloro-1,4-naphthoquinone.
(a): before irradiation, (b): during irradiation, (c): during irradiation, when xanthene-9-d_2 was used.

2-Methyl-1,4-naphthoquinone (mp 104—105 °C),[7] 2,3-dimethyl-1,4-naphthoquinone (mp 126—127 °C),[8] and 2,6-dimethyl-1,4-naphthoquinone (mp 139 °C),[9] were prepared by the oxidation of the corresponding methylnaphthalenes with chromic acid. 2-Chloro-1,4-naphthoquinone (mp 116—117 °C) was prepared by the oxidation of 2,4-dichloronaphthol with chromic acid.[10] 2,3-Dichloro-1,4-naphthoquinone (mp 197—198 °C) commercially available was further purified by recrystallization. 2-Bromo-1,4-naphthoquinone (mp 135 °C) was prepared by the dibromination of 1,4-naphthoquinone, followed by dehydrobromination with sodium acetate.[11] 2,3-Dibromo-1,4-naphthoquinone (mp 220 °C) was prepared by the bromination of 2-bromo-1,4-naphthoquinone.[11] Xanthene commercially available was further purified by recrystallization. Thioxanthene (mp 130—131 °C) was prepared by the reduction of thioxanthone with lithium alminium hydride.[12] Thioxanthone was prepared by heating thiosalicyclic acid and benzene in conc. sulfuric acid.[13] Xanthene-9-d_2 was prepared with lithium aluminium deuteride.

Spectra. Infrared spectra were taken with a JASCO IR-G spectrophotometer, using a KBr disc. PMR spectra were observed with a JEOL PS-100 100 Hz spectrometer in suitable solvents using TMS as the internal standard. Ultraviolet spectra were recorded by means of a Shimadzu UV-200 spectrophotometer. ESR spectra were measured at room temperature using a JEOL X-band PE-3X spectrometer in THF.

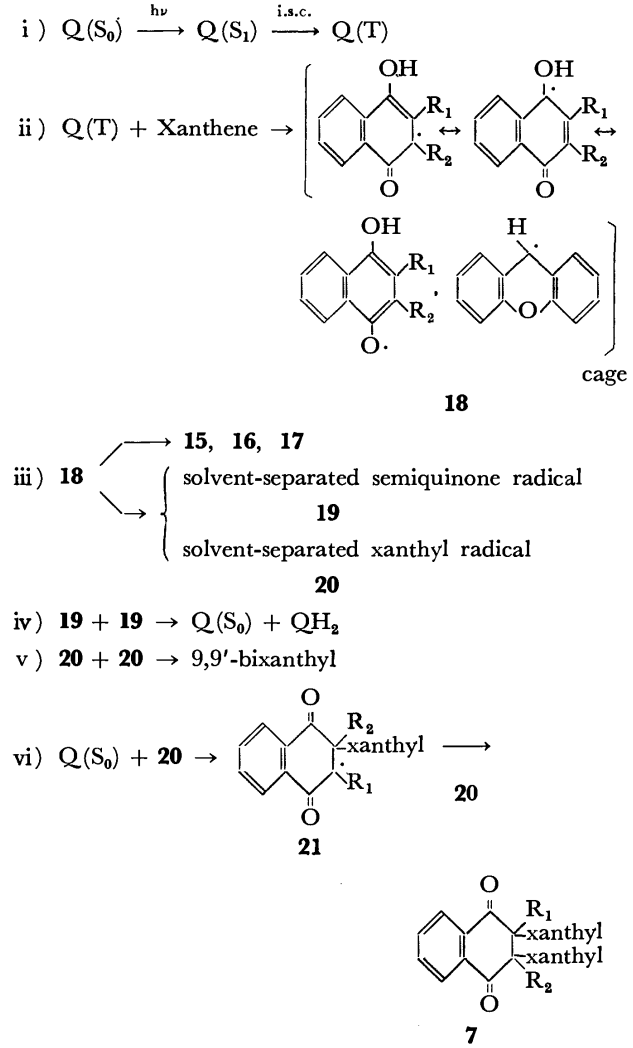

Reaction Scheme.

Photochemical Reactions. A typical photochemical reaction was performed as follows; 1,4-naphthoquinone derivatives (1—2 mmol) and one or two equivalents of xanthene were dissolved in 30 ml of benzene, and the solution was irradiated in an ordinary glass tube from outside by a 400W high-pressure mercury arc lamp through a water layer 5—10 cm thick under ice-water cooling or at room temperature.

i) Photochemical Reactions of Methyl-substituted 1,4-Naphthoquinone, 3, with Xanthene. A soluiton of 2-methyl-1,4-naphthoquinone, **3a** (300 mg, 1.7 mmol), and two equivalents of xanthene was irradiated for 8 hr. 2-Methyl-1,4-naphthohydroquinone, **4a**, thus deposited was filtered off, washed with benzene, and recrystallized from acetic acid. The filtrate was evaporated under reduced pressure and the residue was chromatographed on silica gel. Elution with light petroleum gave 9,9′-bixanthyl in 70—80% yield. 2,3-Dimethyl-1,4-

naphthoquinone, **3b**, and 2,6-dimethyl-1,4-naphthoquinone, **3c**, reacted with xanthene as smoothly as **3a** to give **4b**, **4c**, and 9,9′-bixanthyl. 2-Methyl-1,4-naphthohydroquinone, **4a**; white needles(readily turned violet in the air), mp 152 °C; ν_{OH} 3320 cm^{-1}. 2,3-Dimethyl-1,4-naphthohydroquinone, **4b**; white crystals (readily turned black), mp 141 °C; IR(KBr): ν_{OH} 3300 cm^{-1}, 2,6-Dimethyl-1,4-naphthohydroquinone, **4c**; white crystals tinged with violet; mp 175—176 °C; IR(KBr): ν_{OH} 3260 cm^{-1}. 9,9′-Bixanthyl; colorless needles; mp 211—211.5 °C.

*ii) Photochemical Reaction of 1,4-Naphthoquinone, **5a**, with Xanthene.* A solution of **5a** (632 mg, 4 mmol) and xanthene (4 mmol) in 30 ml of benzene was irradiated under ice-water cooling (at 0—5 °C) for hr 5. Dark violet needles of quinhydrone, **8a**, (195 mg, 31%) were deposited and then filtered off. The filtrate was evaporated under reduced pressure, and the residue was chromatographed on a column of florisil. Elution with light petroleum gave 9,9′-bixanthyl (120 mg, 17%). Elution with light petroleum–benzene (1 : 1 v/v) gave unreacted 1,4-naphthoquinone. Elution with benzene gave white crystals of 2,3-dixanthyl-2,3-dihydro-1,4-naphthoquinone, **7a** (31 mg, 1.5%). Quihydrone, **8a**; mp 165—166 °C, IR (KBr): ν_{OH} 3250 cm^{-1}. 2,3-Dixanthyl-2,3-dihydro-1,4-naphthoquinone, **7a**; mp 196 °C, IR(KBr): $\nu_{C=O}$ 1675 cm^{-1}, $\nu_{=C-O-}$ 1250 cm^{-1}. PMR($CDCl_3$) δ: 7.8—6.1(m, 20H), 4.30(d, 2H, methine protons of the xanthyl moleties), 3.12(d, 2H, 2,3-protons of the quinone moiety), J=4.0 Hz. Found: C, 83.20; H, 4.54%. Calcd for $C_{36}H_{24}O_4$: C, 83.06; H, 4.65%. Mass *m/e*: 520(M^+), 362, 338, 181.

*iii) Photochemical Reactions of 2-Chloro-1,4-naphthoquinone, **5b**, with Xanthene.* A solution of **5b** (964 mg, 5 mmol) and xanthene (5 mmol) in 60 ml of benzene was irradiated for 4 hr under ice-water cooling(at 0—5 °C). The violet leaflets quinhydrone, **8b**, (470 mg, 48%) thus deposited were filtered off, washed with petroleum-benzene, and recrystallized from petroleum–benzene(4 : 1 v/v). The filtrate was evaporated under reduced pressure to *ca.* 3 ml. Petroleum ether was added to the resulting solution, and crude solids were filtered off and recrystallized from peroleum–benzene to give colorless crystals of 2-chloro-2,3-dixanthyl-2,3-dihydro-1,4-naphthoquinone, **7b** (110 mg, 4%). The mother liquors from the filtration of **7a** were evaporated under reduced pressure, and the resulting residue was chromatographed on silica gel. Elution with petroleum gave 9,9′-bixanthyl (203 mg, 23%). Elution with petroleum–benzene(5 : 1 v/v) gave yellow needles of 2-xanthyl-1,4-naphthoquinone, **6b** (9 mg, 0.8%).

In the photochemical reaction of **5b** at room temperature, a solution of **5b** (385 mg, 2 mmol) and the equivalent mol of xanthene was irradiated for 5 hr. Greenish solids of **10b** (107 mg, 14%) were deposited, and filtered off, washed with petroleum-benzene. The greenish solids were proved to consist of free radicals by means of ESR spectroscopy. The filtrate was evaporated under reduced pressure to *ca.* 3 ml, and treated with petroleum; then the quinhydrone, **8b**, and **7b** deposited were collected and dissolved in petroleum-benzene (5 : 1 v/v) under heating. The quinhydrone was dissolved, and insoluble **7b** was separated out. The recrystallization of crude **7b** gave pure crystals (95 mg, 9%). When a hot solution containing quinhydrone was cooled, violet leaflets of quinhydrone, **8b** (94 mg, 24%), were obtained. The mother liquors left after the filtration of **8b** and **7b** were evaporated, and the resulting residue was chromatographed on silica gel. 17 mg of 9,9′-bixanthyl (5%) and 14 mg of **6b** (2.1%) were thus obtained.

Quinhydrone, **8b**; mp 141—142 °C, IR(KBr): ν_{OH}

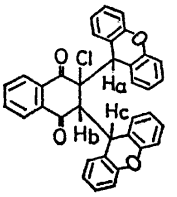

7b

3360 cm^{-1}. 2-Chloro-2,3-dixanthyl-2,3-dihydro-1,4-naphthoquinone, **7b**; mp 186 °C(decomp.), IR(KBr): $\nu_{C=O}$ 1700 cm^{-1} (due to carbonyl group bearing a chlorine atom at the equatorial position), 1675 cm^{-1}. PMR($CDCl_3$) δ: 8.08—6.36(m, 20H), 4.98(d, H_c), 4.43(s, H_a), 3.76(d, H_b), J_{bc}=4.0 Hz. In the PMR spectrum of the adduct corresponding to **7b** obtained from the photochemical reaction of **5b** with xanthene-9-d_2, the two signals at δ: 4.98 and 4.43 disappeared and the signal at δ: 3.76 changed to a singlet. Found: C, 78.11; H, 4.19; Cl, 6.12%. Calcd for $C_{36}H_{23}O_4Cl$: C, 77.90; H, 4.18; Cl, 6.39%. 2-Xanthyl-1,4-naphthoquinone **6b**; mp 196 °C, IR(KBr): $\nu_{C=O}$ 1650 cm^{-1}. PMR(CCl_4) δ: 7.0—8.3 (m, 12H), 6.31(s, 1H, proton at position 3 of the quinone moiety), 5.76(s, 1H, methine proton of the xanthene moiety). UV($CHCl_2$): λ_{max} (log ε), 430 nm(1.43), 340 nm(3.60), 286 nm(3.88), 254 nm(4.46). Found: C, 81.72; H, 4.06%. Calcd for $C_{23}H_{14}O_3$: C, 81.64; H, 4.17%. Stable radical, **10b**; greenish powder; mp 105—107 °C(decomp.), IR(KBr): ν_{OH} 3200 cm^{-1}.

*iv) Photochemical Reaction of 2-Bromo-1,4-naphthoquionne, **5d**, with Xanthene.* A solution of **5d** (1165 mg, 5 mmol) and xanthene (5 mmol) in 60 mg of benzene was irradiated for 5 hr under ice-water cooling (at 0—5 °C). Four products were isolated by the same treatment as in the case of **5b**. 250 mg (21%) of quinhydrone, **8d**, 210 mg(23%) of 9,9′-bixanthyl, 35 mg(2.1%) of **6b**, and 25 mg(0.8%) of 2-bromo-2,3-dixanthyl-2,3-dihydro-1,4-naphthoquinone **7d** were obtained. In the photochemical reaction of **5d** at room temperature, a solution of **5d** (354 mg, 1.5 mmol) and xanthene (1.5 mmol) was irradiated for 5 hr. The greenish solids, **10d**, deposited (117 mg, 23%) were filtered off, and washed with benzene–petroleum ether. The greenish solids were proved to be free radicals by means of ESR spectroscopy. The filtrate was evaporated under reduced pressure, and the resulting residue was chromatographed on silica gel. Small amounts 9,9′-bixanthyl and 25 mg(5%) of **6b** were thus obtained.

Quinydrone, **8d**; dark-violet leaflets; mp 113—115 °C, IR(KBr): ν_{OH} 3400 cm^{-1}. 2-Bromo-2,3-dixanthyl-2,3-dihydro-1,4-naphthoquinone, **7d**; white crystals; mp 151—152 °C, IR(KBr): $\nu_{C=O}$ 1700, 1780 cm^{-1}. PMR($CDCl_3$) δ: (m, 20H), 5.16(d, H), 4.56(s, H), 3.93(d, H), J_{bc}=4.0 Hz. Elemental and mass analyses could not be done, because **7d** was unstable and gradually decomposed. However, IR and PMR spectra showed the same patterns as those of **7b**. Stable radical, **10d**; greenish powder; mp *ca.* 110 °C (decomp.). **10d** and **10b** had almost the same decomposing points, and their chromic-acid oxidations gave the same

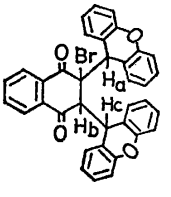

7d

product. Their ESR and IR spectra were, then, quite similar.

*v) Photochemical Reaction of 2,3-Dichloro-1,4-naphthoquinone, **5c**, with Xanthene.* A solution of **5c** (454 mg, 2 mmol) and xanthene (2 mmol) was irradiated for 11 hr. The dark-greenish solids thus deposited were filtered off, and washed with benzene. 130 mg(17%) of dark-greenish solids, **10c**, were thus obtained. The filtrate was evaporated under reduced pressure, and the resulting residue was chromatographed on silica gel. Elution with benzene gave red needles of 2-chloro-3-xanthylnaphthoquinone, **6c**, (178 mg, 24%). The dark-greenish solids were proved to be free radicals by means of ESR spectroscopy.

Stable radical, **10c**; dark-greenish powder; mp 135—140 °C(decomp.), IR(KBr): ν_{OH} 3050 cm^{-1}. 2-Chloro-3-xanthyl-1,4-naphthoquinone **6c**; PMR($CDCl_3$) δ: 7.5—8.2 (m, 4H), 6.7—7.3(m, 8H), 6.16(s, 1H), IR(KBr): $\nu_{C=O}$ 1660 cm^{-1}. UV($CHCl_3$): λ_{max} (log ε) 483 nm(1.80), 3.40 nm(3.75), 280 nm(4.18), 252 nm(4.30). Found: C, 73.98; H, 3.38; Cl, 9.77%. Calcd for $C_{23}H_{13}O_3Cl$: C, 74.11; H, 3.51; Cl, 9.51%. Mass *m/e*: 372(M$^+$), 337, 181.

*vi) Photochemical Reaction of 2,3-Dibromo-1,4-naphthoquinone, **5e**, with Xanthene.* A solution of **5e** (632 mg, 2 mmol) and xanthene (2 mmol) in 60 ml of benzene was irradiated for 10 hr. The black solids deposited were filtered off, and washed with benzene. 53 mg(5.3%) of black solids, **10d**, were thus obtained. The solids were proved to consist of free radicals by means of ESR spectroscopy. The filtrate was evaporated, and the resulting residue was chromatographed on silica gel. Elution with benzene gave red needles, which proved to be 2-bromo-3-xanthyl-1,4-naphthoquinone **6e** (107 mg, 11%).

Stable radical, **10e**; black powder; mp 181—182 °C(decomp.), IR(KBr): ν_{OH} 3050 cm^{-1}. 2-Bromo-3-xanthyl-1,4-naphthoquinone, **6e**; mp 210 °C(decomp.), IR(KBr): $\nu_{C=O}$ 1667 cm^{-1}. UV($CHCl_3$): λ_{max} (log ε) 490 nm(1.85), 340 nm (3.54), 290 nm(4.23), 254 nm(4.29). PMR($CDCl_3$) δ: 7.0—8.4(m, 12H), 6.36(s, 1H): Found: C, 66.49; H, 3.08; Br, 19.02%. Calcd for $C_{23}H_{13}O_3Br$: C, 66.20; H, 3.14; Br, 19.14%.

vii) Photochemical Reactions of 1,4-Naphthoquinone Derivatives with Thioxanthene. A solution of 1,4-naphthoquinone derivatives, **3a** and **5a**—**e** (2 mmol), and thioxanthene(4 mmol) in 30 ml of benzene was irradiated for 6—8 hr. Naphthohydroquinones, quinhydrones, and 9,9'-bithioxanthyl were thus obtained in nearly quantitative yields. In the photochemical reaction of **5b** or **5d** with thioxanthene, small amounts of the adduct corresponding to **6b** were isolated. 9,9'-Bithioxanthyl; white needles; mp>300 °C. 2-Thioxanthyl-1,4-naphthoquinone; orange needles; mp 236—237 °C, IR(KBr): $\nu_{C=O}$ 1650 cm^{-1}. PMR($CDCl_3$) δ: 7.04—8.0(m, 12H), 6.36(s, 1H), 5.74(s, 1H). Mass *m/e*: 354(M$^+$), 337, 197.

*Oxidation of Stable Free Radicals, **10b—d**.* A dilute aqueous chromic acid solution was added to a solution of stable free radicals, **10b, 10c,** or **10d** (100 mg), in acetic acid(30 ml) until the green solution turned reddish yellow. A 100-ml portion of water was then added to the solution, and it was extracted with ether. The dried extract was evaporated, and resulting residue was separated on thin-layer chromatography. 2-[9'-Hydroxyxanthyl]-1,4-naphthoquinone, **12a**, from **10b** and **10d**, and 2-chloro-3-[9'-hydroxyxanthyl]-1,4-naphthoquinone, **12b**, from **10c**, in about 30% yield.

2-[9'-Hydroxyxanthyl]-1,4-naphthoquinone, **12a**; red needles; mp 226—227 °C, IR(KBr): ν_{OH} 3490 cm^{-1}, $\nu_{C=O}$ 1660 cm^{-1}. PMR($CDCl_3$) δ: 6.92—8.10(m, 13H), 3.20 (s, 1H, –OH). Found: C, 78.25; H, 4.05%. Calcd for $C_{23}H_{14}O_4$: C, 77.96; H, 3.98%. Mass *m/e*: 354(M$^+$), 337, 197. 2-Chloro-3-[9'-hydroxyxanthyl]-1,4-naphthoquinone, **12b**; orange yellow needles; mp 165 °C (decomp.), IR(KBr): ν_{OH} 3370 cm^{-1}. $\nu_{C=O}$ 1680, 1640 cm^{-1} (the two IR absorptions due to carbonyl groups indicate the existence of chelated and non-chelated carbonyl groups, coinciding with the existence of an intramolecularly-hydrogen-bonded hydroxyl group). PMR($CDCl_3$) δ: 8.22—6.88(m, 12H), 6.84(s, 1H, –OH). Found: C, 71.38; H, 3.40; Cl, 9.35%. Calcd for $C_{23}H_{13}O_4Cl$: C, 71.04; H, 3.38; Cl, 9.12%. Mass *m/e*: 388(M$^+$), 371, 352, 336, 279, 197.

ESR Spectroscopy. ESR spectra of **10b—e** were observed at room temperature by the use of a JEOL X-band PE-3X spectrometer. THF used as a solvent was dried with metallic sodium and purified by distillation. Samples dissolved in THF were thoroughly degassed by four freeze-pump-thaw cycles and sealed. The ESR coupling constants and *g*-values of **10b—e** were measured by using Fremy's salt (a_N: 13.0 gauss, *g*: 2.0055) as a standard.

CIDNP Examinations. An investigation of these photochemical reactions by the CIDNP technique was performed using a JEOL C-60 HL spectrometer, equipped with a modified NMR probe for the photo-irradiation. The details of the method used were previously described in this Bulletin by Maruyama and his co-workers.[3]

Determination of Quantum Yields. A solution of 1,4-naphthoquinone derivatives(0.1 M) and xanthene(0.2 M) was irradiated with a 400W high-pressure mercury arc lamp through a uv-cut filter (Toshiba VY-42). The intensity was determined by means of a potassium ferrioxalate actinometer.[14] The rate of quinone disappearance was determined spectroscopically.

References

1) For example, see A. Schönberg, "Preparative Organic Photochemistry," Springer (1968).
2) G. Pfundt, Diss. Göttingen. c.f. A. Schönberg, "Preparative Organic Photochemistry," Springer (1968), p. 184.
3) K. Maruyama, T. Otsuki, H. Shindo, and T. Maruyama, This Bulletin, **44**, 2756, 2000, 2789, 2885 (1971).
4) K. Maruyama and A. Takuwa, *ibid.*, **46**. 1529 (1973).
5) K. Maruyama, T. Otsuki, A. Takuwa, and S. Arakawa, *ibid.*, **46**, 2470 (1973).
6) G. L. Closs, *J. Amer. Chem. Soc.*, **91**, 4552 (1969); G. L. Closs and A. D. Trifunac, *ibid.*, **91**, 4554 (1969); **92**, 2183, 2186 (1970); R. Kaptein and L. J. Oosterhoff, *Chem. Phys. Lett.*, **4**, 195, 214 (1969); R. Kaptein and J. A. den Hollander, *J. Amer. Chem. Soc.*, **94**, 6269 (1972).
7) L. F. Fieser, *J. Bio. Chem.*, **133**, 391 (1940).
8) L. I. Smith and I. M. Webster, *J. Amer. Chem. Soc.*, **59**, 664 (1937).
9) R. Wissgerber and O. Kruber, *Chem. Ber.*, **52**, 356 (1919).
10) P. T. Cieue, *ibid.*, **21**, 892 (1888).
11) Th. Zinke and M. Schmidt, *ibid.*, **27**, 2757 (1894).
12) A. Mustafa and M. K. Hilmy, *J. Chem. Soc.*, **1952**, 1343.
13) M. Gomberg and E. C. Britton, *J. Amer. Chem. Soc.*, **43**, 1921 (1945).
14) C. H. Hartchard and C. A. Parker, *Proc. Roy. Soc., Ser. A*, **235**, 518 (1956).
15) Signal 2 was erroneously assigned to 2,3-protons of quinone moiety in structure **15** in the previous report,[5] but this should be corrected to be assigned to 2,3-protons of quinone moiety in structure **16**.

The Addition of Arylpalladium Chloride to 1,5-Cyclooctadiene and *endo*-Dicyclopentadiene

Akira KASAHARA, Taeko IZUMI, Kazuyoshi ENDO, Toru TAKEDA, and Motomu OOKITA*

Department of Applied Chemistry, Faculty of Engineering, Yamagata University, Yonezawa, Yamagata 992

**Research Laboratory of Resources Utilization, Tokyo Institute of Technology, Ookayama, Meguro-ku, Tokyo 152*

(Received February 8, 1974)

1,5-Cyclooctdiene reacted with phenylpalladium chloride to give di-μ-chloro-bis-(1-phenylcyclooct-4-ene-8σ,4π)-dipalladium(II). Similarly, the reaction of *endo*-dicyclo-pentadiene with phenylpalladium chloride led to di-μ-chloro-bis-[*endo*-6-phenyl-3a,4,5,6,7,7a-hexahydro-*endo*-4,7-methanoindene-*endo*-5σ,(2—3)π]-dipalladium (II). The σ-bonded structures of these complexes have been confirmed by studies of the IR and NMR spectra.

Heck[1] has previously reported that the reaction of 1,3-diolefins with arylpalladium chloride gave 1-arylmethyl-π-allylpalladium chloride dimers in moderate yields. In this paper, we wish to report that 1,5-cyclooctadiene (**1**) and *endo*-dicyclopentadiene (**2**) react with arylpalladium chloride to form complexes containing a carbon–palladium σ bond.

Experimental

Materials. All the melting points are uncorrected. The arylmercuric chlorides were prepared by the methods described in the literature: *p*-tolylmercuric chloride,[2] mp 232—233 °C; *p*-anisylmercuric chloride,[3] mp 173—174 °C. The phenylmercuric chloride, 1,5-cyclooctadiene (**1**), and *endo*-dicyclopentadiene (**2**) were of a commercial grade and were used after purification.

*The General Procedure for The Preparation of Di-μ-chloro-bis-(1-arylcyclooct-4-ene-8σ,4π)-dipalladium(II) (**3a—c**) and Di-μ-chloro-bis-*[endo-*6-aryl-3a,4,5,6,7,7a-hexahydro-*endo-*4,7-methano-indene-*endo-*5σ,(2—3)π]-dipalladium(II) (**3d—f**).* A lithium chloropalladite solution was prepared by stirring 0.42 g (10 mmol) of anhydrous lithium chloride and 1.77 g (10 mmol) of anhydrous palladium chloride overnight at room temperature in 100 ml of acetonitrile. Into the lithium chloropalladite solution, arylmercuric chloride(10 mmol) was then added with stirring at room temperature for ten min, after which 12 mmol of **1** or **2** was added in one portion. After the mixture had been stirred at room temperature for 6 hr, the solution was filtered and evaporated to dryness. The residue was dissolved in chloroform and chromatographed on neutral alumina. The first elution with chloroform and recrystallization from methanol afforded colorless crystals, which were identified as biphenyls (**4a—c**). Further elution with chloroform and recrystallization from chloroform–cyclohexane afforded yellow products (**3a—f**). The results are summarized in Table 1.

*The Preparation of Chloro-(1-arylcyclooct-4-ene-8σ,4π)-pyridine-palladium Complexes (**5a—c**)* and *Chloro-*[endo-*6-aryl*]-*3a,4,5,6,7,7a-hexahydro-*endo-*4,7-methano-indene-*endo-*5σ,(2—3)π]-pyridine-palladium Complexes (**5d—f**).* A solution of the palladium complex (**3a—f**) (0.10 g) in methylene chloride was treated with a solution of pyridine (5% excess) in ether. After 30 min, the solvent was removed under reduced pressure; the residue was then recrystallized from benzene-cyclohexane to give yellow crystals. The results are summarized in Table 2.

*Sodium Borohydride or Deuteride Reductions of Arylated σ-Complexes (**3a—f**).* Into a suspension of sodium borohydride or deuteride in 50—70 ml of dry monoglyme **3a—f** was added with stirring over a period of 30 min (molar ratio of 2 : 1, hydride to complex). After the solution has been stirred at room temperature for 1 hr, an exual volume of water was added and the solution was heated on a steam bath for 1 hr. The reaction was heated on a steam bath for 1 hr. The reaction mixture was then cooled, and the palladium precipitate which had formed was collected on a filter. The filtrate was extracted with three 75-ml portions of *n*-hexane. The combined extracts were dried over anhydrous magnesium sulfate and then fractionally distilled to afford to product, **6a—f** or **7a—c** (see Table 3). The products were identified by comparison with authentic samples and by the observation of the NMR spectra.

Results and Discussion

At room temperature, **1** reacted with phenylpalladium chloride to give yellow di-μ-chloro-bis-(1-phenylcyclooct-4-ene-8σ,4π)-dipalladium(II) (**3a**) in a 28% yield, accompanied by a small amount of biphenyl (**4a**). *p*-Tolyl- and *p*-anisylpalladium chloride also reacted to afford yellow σ-complexes (**3b—c**).

The reduction of **3a** with sodium borohydride in monoglyme to afford phenylcyclooctane (**6a**) showed that the addition of the phenyl group occurred at an olefinic bond by means of the formation of a new carbon-carbon bond and that the reaction occurred without any rearrangement of the carbon skeleton. The σ-bonded structure of the complex (**3a**) was supported by the molecular-weight measurements and by the bridged splitting reaction with pyridine to give a readily soluble monomeric derivative (**5a**). Moreover, the far-infrared spectrum of **3a** showed a bridged Pd–Cl stretching absorption at about 278 and 227 cm^{-1}. The NMR spectrum of **3a** was consistent with the four resonances at 1.18—2.75 (the protons of methylene and methine groups), 6.09 (the olefinic proton), 6.46 (the olefinic proton), and 7.25 ppm (the phenyl protons), and was in agreement with the proposed structure. Similarly, in the NMR spectra of **3b—c**, all the resonances can be satisfactorily accounted for by the presence of the σ-bond.

In the presence of lithium chloropalladite, the reaction of **2** with arylmercuric chloride in acetonitrile also gave the yellow chloro-bridged complex, di-μ-chloro-bis[*endo*-6-aryl-3a,4,5,6,7,7a-hexahydro-*endo*-4,7-methanoindene-*endo*-5σ,(2—3)π]-dipalladium(II) (**3d—f**), accompanied by a small amount of **4a—c**. The molecular-weight measurements, the observation of far-infrared spectra, and the bridge-splitting reaction with pyridine supported the chloro-bridged binuclear structures for **3d—f**. Furthermore, the NMR spectra of **3d—f** were in agreement with the proposed structures.

TABLE 1. THE REACTION OF ARYLPALLADIUM CHLORIDE WITH 1,5-CYCLOOCTADIENE (**1**) AND *endo*-DICYCLOPENTADIENE (**2**)

Arylating Agent ArHgCl	Product	Yield (%)[a]	Mp °C (lit.)	Found % (Calcd) and mol wt[b]	IR (cm^{-1}) and NMR (δ, ppm) spectra.
a) Reaction with 1,5-cyclooctadiene (**1**).					
Ar=Ph	Biphenyl (**4a**)	8	68—69 (69—70[c])		
	3a (Ar=Ph)	28	176—178 (dec.)	C, 51.28 (51.40) H, 5.17 (5.23) Mol wt 645 (654)	IR 745, 690, 278 and 227. NMR 1.18—2.75 (m, 10H), 6.09 (m, 1H), 6.46 (m, 1H), and 7.25 (m, 5H).
Ar=*p*-Tolyl	Bi-*p*-tolyl (**4b**)	10	119—120 (120[c])		
	3b (Ar=*p*-Tolyl)	32	154—155 (dec.)	C, 52.77 (52.80) H, 5.57 (5.61) Mol wt 675 (682)	IR 800, 280, and 228. NMR 1.15—2.84 (m, 10H, methylene and methine protons), 2.28 (s, 3H, methyl protons), 6.11 (m, 1H, olefinic proton), 6.45 (m, 1H, olefinic proton), and 7.08—7.34 (m, 4H, *p*-tolyl protons).
Ar=*p*-Anisyl	Bi-*p*-anisyl **4c**)	11	170—171 (170—172[c])		
	3c (Ar=*p*-anisyl)	33	182—184 (dec.)	C, 50.35 (50.44) H, 5.30 (5.36) Mol wt 708 (714)	IR 805, 280, and 230. NMR 1.16—2.78 (m, 10H, methylene and methine protons), 3.65 (s, 3H, methoxy protons), 6.06 (m, 1H, olefinic proton), 6.43 (m, 1H, olefinic proton), and 7.01—7.43 (m, 4H, *p*-anisyl protons).
b) Reaction with *endo*-dicyclopentadiene (**2**).					
Ar=Ph	**4a**	10	68—69 (19—70[c])		
	3a (Ar=Ph)	40	108—110 (dec.)	C, 54.61 (54.72) H, 4.76 (4.87) Mol wt 693 (702)	IR 750, 690, 294, and 216. NMR 1.08—2.43 (m, 8H, methylene and methine protons), 2.80 (q, 1H, H_A, $J_{A,X}$= 9.5 and $J_{A,4}$=3.5 Hz), 6.86 (m, 2H, olefinic protons), and 7.23 (m, 5H, phenyl protons).
Ar=*p*-Tolyl	**4b**	12	119—120 (120[c])		
	3e (Ar=*p*-tolyl)	48	147—149 (dec.)	C, 55.83 (55.91) H, 5.17 (5.24) Mol wt 719 (730)	IR 800, 294, and 215. NMR 1.01—2.05 (m, 8H), 2.28 (s, 3H), 2.85 (q, 1H), 3.23 (q, 1H), 6.50 (m, 2H), and 7.23 (m, 4H).
Ar=*p*-Anisyl	**4c**	8	170—171 (170—172[c])		
	3f (Ar=*p*-anisyl)	42	118—120 (dec.)	C, 53.38 (53.52) H, 4.87 (5.01) Mol wt 758 (762)	IR 800, 297, and 215. NMR 1.10—2.55 (m, 8H, methylene and methine protons), 2.78 (q, 1H, H_X), 3.19 (q, 1H, H_A, $J_{A,X}$=9.5 and $J_{A,4}$=3.5 Hz), 3.65 (s, 3H, methoxy protons), 6.58 (m, 2H, olefinic protons), and 7.34 (m, 4H, anisyl protons).

a) Yields are based upon the arylmercuric chloride. b) IR spectra were measured on KBr disks (4000—650 cm^{-1}) or in Nujol mulls mounted on thin polythene windows (700—200 cm^{-1}). NMR spectra were observed in $CDCl_3$ by means of a Hitachi R-22 NMR spectrometer at 90 MHz, using TMS as an internal standard. The chemical shifts were followed by the splitting pattern (s, singlet; q, quartet; m, multiplet) and the relative strengths. Molecular weight was determined in $CHCl_3$, using a Hitachi 115 vapor-pressure osmometer. c) E. Müller and T. Topel, *Ber.*, **72**, 273 (1939).

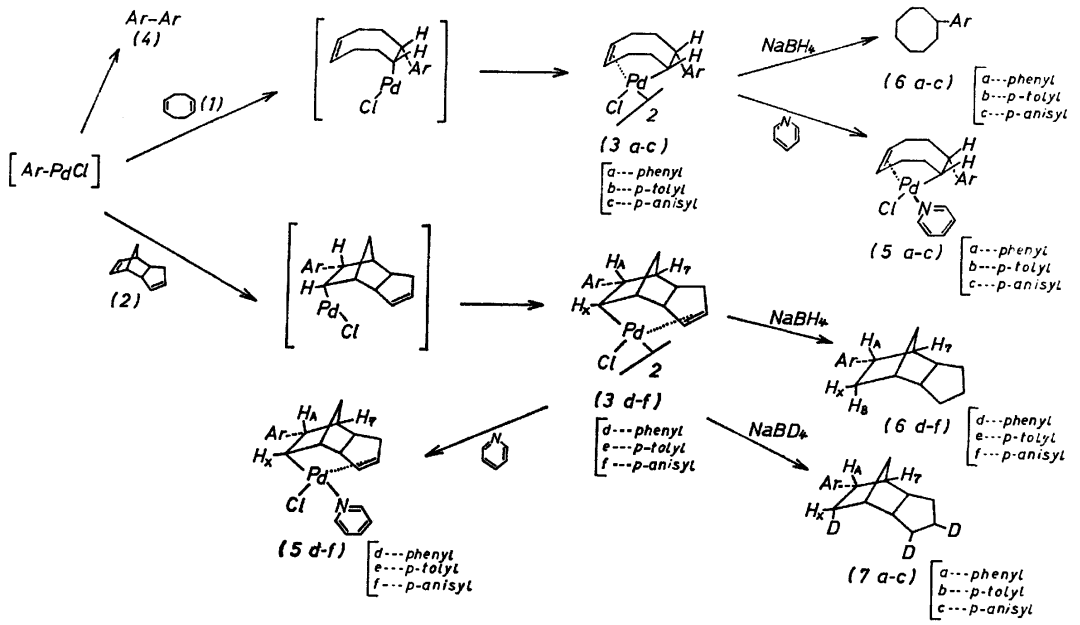

Fig. 1.

Table 2. The properties of pyridine derivatives (**5a—f**) of complexes (**3a—f**)

Complex	Mp °C (dec)	Found (Calcd) % and mol wt	IR (cm^{-1}) and NMR (δ, ppm) spectra
5a (Ar=Ph)	138—140	C, 55.95(56.10) H, 5.27 (5.45) N, 3.32 (3.44) Mol wt 394 (406)	IR 750, 740, 690, 284 (terminal Pd-Cl) and 235 (Pd-Py). NMR 1.14—2.78 (m, 10H, $-CH_2-+-CH-$), 6.12 (m, 1H, -C**H**=CH-), 6.51 (m, 1H, -CH=C**H**-), and 7.02—8.58 (m, 10H, phenyl+pyridine protons).
5b (Ar=*p*-tolyl)	157—160	C, 57.01(57.15) H, 5.58 (5.75) N, 3.25 (3.44) Mol wt 413 (420)	IR 800, 750, 287 (terminal Pd-Cl) and 238 (Pd-Py). NMR 1.10—2.83 (m, 10H, $-CH_2-+-CH-$), 2.29 (s, 3H, CH_3-), 6.14 (m, 1H, -C**H**=CH-), 6.48 (m, 1H, -CH=C**H**-), and 7.00—8.68 (m, 9H, tolyl+pyridine protons).
5c (Ar=*p*-anisyl)	156—157	C, 54.87(55.05) H, 5.39 (5.54) N, 3.14 (3.21) Mol wt 430 (436)	IR 800, 750, 283 (terminal Pd-Cl) and 235 (Pd-Py). NMR 1.15—2.74 (m, 10H, $-CH_2-+-CH-$), 3.68 (s, 3H, CH_3O-), 6.11 (m, 1H, -C**H**=CH-), 6.48 (m, 1H, -CH=C**H**-), and 6.98—8.64 (m, 9H, anisyl+pyridine protons).
5d (Ar=Ph)	129—131	C, 59.88(60.02) H, 5.14 (5.27) N, 3.26 (3.33) Mol wt 408 (420)	IR 740, 690, 293 (terminal Pd-Cl) and 233 (Pd-Py). NMR 1.10—2.51 (m, 8H, $-CH_3-+-CH-$), 2.84 (q, 1H, H_X), 3.22 (q, 1H, H_A, $J_{A,X}=9.0$ and $J_{A,4}=3.0$ Hz), 6.82 (m, 2H, olefinic protons), and 7.04—8.55 (m, 10H, phenyl+pyridine protons).
5e (Ar=*p*-tolyl)	155—157	C, 58.87(59.04) H, 5.41 (5.44) N, 3.06 (3.15) Mol wt 439 (444)	IR 800, 750, 291 (terminal Pd-Cl), and 235 (Pd-Py). NMR 1.06—2.14 (m, 8H, $-CH_2-+-CH-$), 2.27 (s, 3H, CH_3-), 2.91 (q. 1H, H_X), 3.28 (q, 1H, $J_{A,X}=9.5$ and $J_{A,4}=4$ Hz), 6.68 (m, 2H, olefinic protons), and 7.01—8.80 (m, 9H, tolyl+pyridine protons).
5f (Ar=*p*-anisyl)	144—146	C, 57.35(57.40) H, 5.07 (5.25) N, 2.96 (3.04) Mol wt 451 (460)	IR 804, 750, 294 (terminal Pd-Cl), and 235 (Pd-Py). NMR 1.08—2.58 (m, 8H, $-CH_2-+-CH-$), 2.81 (q, 1H, H_X), 3.25 (q, 1H, H_A, $J_{A,X}=9.5$ and $J_{A,4}=3.0$ Hz), 3.62 (s, 3H, CH_3O-), 6.65 (m, 2H, olefinic protons), and 7.01—8.84 (m, 9H, anisyl+pyridine protons).

TABLE 3. REDUCTION OF ARYLATED σ-COMPLEXES (**3a—f**) WITH $NaBH_4$ OR $NaBD_4$

Product[a]	Yield %	Bp °C/mmHg (lit.)	NMR spectra (δ, ppm).
6a (Ar=Ph)	68	110—115/1 (100—102/0.55—0.6[b])	
6b (Ar=*p*-tolyl)	70	123—125/1	1.38—1.81 (m, 14H, -CH_2-), 2.28 (s, 3H, CH_3), 2.80 (m, 1H, -CH-), and 7.22 (q, 4H, tolyl protons).
6c (Ar=*p*-anisyl)	71	118—121/1	1.40—1.79 (m, 14H, -CH_2-), 2.83 (m, 1H, -CH-Ar), 3.71 (s, 3H, CH_3O-), and 7.18 (q, 4H, anisyl protons).
6d (Ar=Ph)	75	134—136/2	1.36—1.90 (m, 14H, -CH_2-+-CH-), 3.03 (d-q, 1H, H_A, $J_{A,X}$=8.5 Hz, $J_{A,B}$=2.0 Hz, $J_{A,7}$=3.5 Hz), and 7.23 (m, 5H, phenyl protons).
7a (Ar=Ph)	70	132—135/2	1.35—1.90 (m, 11H, -CH_2-+-CH- -CHD-), 3.04 (q, 1H, H_A, $J_{A,X}$ =8.5 Hz, $J_{A,7}$=3.6 Hz), and 7.23 (m, 5H, phenyl protons).
6e (Ar=*p*-tolyl)	68	144—147/2	1.30—1.96 (m, 14H, -CH_2-+-CH-), 2.30 (s, 3H, CH_3-), 2.97 (d-q, 1H, H_A, $J_{A,X}$=8.4 Hz, $J_{A,B}$=2.1 Hz, $J_{A,7}$=3.6 Hz), and 7.11 (m, 4H, tolyl protons).
7b (Ar=*p*-tolyl)	65	144—148/2	1.34—1.93 (m, 11H, -CH_2-+-CH-+-CHD-), 2.29 (q, 1H, H_A, $J_{A,X}$ =8.6 Hz, $J_{A,7}$=3.6 Hz), and 7.13 (m, 4H, tolyl protons).
6f (Ar=*p*-anisyl)	65	150—151/3	1.30—1.98 (m, 14H, -CH_2-+-CH-), 2.96 (d-q, 1H, H_A, $J_{A,X}$=8.0 Hz, $J_{A,B}$=2.0 Hz, $J_{A,7}$=3.5 Hz), 3.74 (s, 3H, CH_3O-), and 7.25 (m, 4H, anisyl protons).
7c (Ar=*p*-anisyl)	68	148—150/3	1.28—1.98 (m, 11H, -CH_2-+-CH-+-CHD-), 2.94 (q, 1H, H_A, $J_{A,X}$ =8.2 Hz, $J_{A,7}$=3.5 Hz), 3.74 (s, 3H, CH_3O-), and 7.28 (q, 4H, anisyl protons).

a) The elemental analyses were consistent with the assigned structures and the deuterium-content of the products was calculated from the mass-spectral results. b) A. C. Cope and E. C. Hermann, *J. Amer. Chem. Soc.*, **72**, 3405 (1950).

For example, the NMR spectrum of **3e** consists of six groups of bands centered at δ 1.01—2.05 (the methylene and methine protons), 2.28 (the methyl protons), 2.85 (H_X proton), 3.23 (H_A proton), 6.50 (the olefinic protons), and 7.32 ppm (the tolyl protons), with relative intensities of 8 : 3 : 1 : 1 : 2 : 4. The quartet peak (J=10 and 4 Hz) at δ 3.23 ppm is assigned to the proton (H_A) on the aryl-bearing carbon, and the coupling of 10 Hz between the (CH-*p*-tolyl) and (CH-Pd) protons is a result of a coupling to a vicinal proton with a 0° dihedral angle ($J\simeq$7—9 Hz).[4] The palladium-carbon bond must be *endo* so that palladium can remain coordinated to the double bond; the *p*-tolyl moiety is, therefore, *endo*. In addition, the reduction of **3e** with sodium borohydride or deuteride gave a saturated hydrocarbon, $C_{17}H_{22}$ (**6e**) or $C_{17}H_{19}D_3$ (**7b**). The NMR spectrum of **6e** shows a very characteristic pair of quartets ($J_{A,X}$=8.4 Hz, $J_{A,B}$=2.1 Hz, $J_{A,7}$= 3.6 Hz) for the H_A proton at 2.97 ppm. The coupling constant of $J_{A,X}$ correlates with the calculated value ($J\simeq$7—9 Hz) between H_A and a proton at a 0° angle, and the coupling constant of $J_{A,B}$ is that expected for a 120° dihedral angle ($J\simeq$2 Hz). Furthermore, the NMR spectrum of deuterated hydrocarbon (**7b**) was very similar to that of **6e**, and the *endo*-configuration of the deuterium was established by the H_A quartet ($J_{A,X}$=8.6 Hz, $J_{A,7}$=3.6 Hz). These results support the proposed structure for **3e**. Similarly, in the NMR spectra for **3d** and **3f** and monomeric pyridine derivatives (**5d—f**), all the resonances can be satisfactorily accounted for by the proposed structures.

Recently, Maitlis[5] has reported that the reaction of diphenylmercury with dichloronorbornadiene palladium gave di-μ-chloro-bis-(*endo*-3-phenylnorbornen-2-yl-*endo*-palladium) and that the reaction proceeds *via* an *endo*-attack on co-ordinated norbornadiene. In the reaction of **1** or **2** with arylpalladium chloride, the reaction undoubtedly proceeds by means of *cis* arylpalladation at the double bond.

References

1) R. F. Heck, *J. Amer. Chem. Soc.*, **90**, 5542 (1968).
2) F. C. Whitemore, F. H. Hamilton, and N. Thurman, "Organic Syntheses," Coll. Vol. I, p. 519 (1941).
3) O. Dimroth, *Ber.*, **35**, 2867 (1902).
4) M. Karplus, *J. Amer. Chem. Soc.*, **85**, 2870 (1963).
5) A. Segnitz, P. M. Bailey, and P. M. Maitlis, *J. Chem. Soc. Chem. Comm.*, **1973**, 698.

The Stereochemistry of the Addition of Trimethylaluminum to Decalones and Methyl-substituted Cyclohexanones

Toshimitsu SUZUKI, Toshiaki KOBAYASHI, Yoshinobu TAKEGAMI, and Yuzo KAWASAKI*

Department of Hydrocarbon Chemistry, Faculty of Engineering, Kyoto University, Kyoto 606

(Received March 11, 1974)

The addition to the methyl-substituted 4-*t*-butylcyclohexanone was studied, providing that the β-axial methyl and α-axial methyl groups hindered the axial and equatorial attacks respectively. The results obtained with fused-ring system ketones (four decalones) were explained by considering the similar stereochemical influence of 2- and 3-methylene substituents as corresponding methyl substituents. A rapid conformation equilibrium was also considered for *cis*-decalones. In addition, the axial attack, especially at a molar ratio of two or more, was found to be hindered by the α-equatorial methyl group. This hindrance was explained by assuming the half-chair form of the cyclohexanone ring in the transition state.

The stereochemical factors of nucleophilic addition to cyclohexanone derivatives were reported for the first time by Dauben *et al.*[1] for the reduction by hydride, and two concepts, *i.e.*, "Steric Approach Control" and "Product Development Control", were proposed to explain the observed results.

Richer[2] excluded the concept of "Product Development Control" from his results on the addition reaction of small or rod-like reagents (*e.g.*, H^-, CN^-, $HC{\equiv}C^-$) to 4-*t*-butylcyclohexanone, and proposed that the steric course was determined by the relative seriousness of interactions between the entering group and 3,5-axial hydrogens. This concept was clarified by Marshall and Carroll,[3] considering the geometry of transition states.

On the other hand, Chérest and Felkin[4] considered "Steric strain" in the transition state of axial attack and "Torsional strain" in the transition state of equatorial attack, and proposed that the steric course of the reaction was controlled by the relative amounts of these strains.

Recently, the stereochemistry of the addition reaction of trialkylaluminum to substituted cyclohexanones was investigated by Ashby[5a] and our group. In these reactions, the steric course of the addition reaction was greatly dependent on the molar ratio of ketone to alkylaluminum. That is, in the reactions with the hydrocarbon solvent, it was found that the stereoselectivity changed with the reactant molar ratio. For example, in the cases of 4-*t*-butylcyclohexanone and trimethylaluminum in the benzene solvent, it was found that the amount of axial alcohol was about 75% of alcoholic products when the reactant molar ratio (Al/K) was one or less, and that the amount of equatorial alcohol was about 90% when the molar ratio was two or more.

Fig. 1.

The reaction of benzophenone with trimethylaluminum in benzene was investigated kinetically by Ashby *et al.*[6] They concluded that the reaction mechanism depended on the reactant molar ratio. When the molar ratio (Al/K) was unity, a slow unimolecular reaction proceeded through an intramolecular rearrangement of the ketone-Al complex, and when the molar ratio was two or more, a rapid bimolecular reaction took place between a second trimethylaluminum and a ketone-Al complex. 4-Centered and 6-centered transition states were proposed respectively. The relationship between the change in stereoselectivity in the cyclohexanone derivatives and the difference in mechanisms indicated by Ashby *et al.* is very interesting; it may be assumed that the equatorial attack corresponds to the unimolecular reaction, and the axial attack, to the bimolecular reaction.

In this paper, the reactions of fused-ring-system ketones (four decalones) with trimethylaluminum in a hydrocarbon solvent were investigated in order to clarify the stereochemistry of the addition reaction of trialkylaluminum to cyclohexanone derivatives. The reactions of several 2-alkylcyclohexanones with trimethylaluminum were also investigated in order to learn more details of the stereochemistry of this reaction.

Experimental

Materials. trans-*2-Decalone*:[7] $\Delta^{1(9)}$-Octalone-2 was synthesized by the method described in the literature. The reduction of $\Delta^{1(9)}$-octalone-2 (10 g) by liq. NH_3 and Li (2.5 g) gave *trans*-2-decalone. Quantitative analysis was carried out by GC. (Hitachi F6D model. Golay R45 column). Purity, 97%.

cis-*2-Decalone*: $\Delta^{1(9)}$-Octalone-2 (24.5 g) was hydrogenated in slightly acidic (HCl) aqueous ethanol on 2.5 g of a palladium-carbon (5%) catalyst.[8] The hydrogenation product was vacuum-distilled to give 19.7 g of a mixture of 90% *cis*-2-decalone and 10% *trans*-2-decalone (22 mmHg 126~127 °C). The mixture was purified by the recrystallization from *n*-pentane at about −100 °C. Purity, 99.2%.

cis-*1-Decalone*:[9] α-Naphthol, purified by vacuum distillation, was hydrogenated in acetic acid on platinum dioxide. *Cis-cis*-1-decalol (white solid, mp 89—90 °C. lit 88—89 °C) was obtained by the recrystallization of the hydrogenation product from *n*-hexane. A solution of 18.5 g of *cis-cis*-1-decalol in acetic acid (75 ml) was oxidized by a solution of 9 g of chromic acid in water. The subsequent vacuum distillation of the oxidation product afforded 88% *cis*-1-decalone. Purity, 88%. The only impurity was *trans*-1-decalone.

* Present address: Tokuyama Soda Co. Ltd., Tokuyama 745.

trans-*1-Decalone*: The mother solution of the above-mentioned recrystallization (containing decalin, decalones, and decalols) was oxidized in acetone by a solution of chromic acid and sulfuric acid. The oxidation product, which contained decalin, *trans*-1-decalone, and *cis*-1-decalone (*trans* : *cis*~1 : 1), was chromatographed on activated alumina to afford sufficiently pure *trans*-1-decalone (*cis*-1-decalone isomerizes to *trans*-1-decalone on activated alumina). Purity, 92%.

cis-*2,6-Dimethylcyclohexanone*: A solution of 29 g of 2,6-xylenol (purified by recrystallization from *n*-hexane) in 75 ml of acetic acid was hydrogenated on 0.67 g of platinum dioxide. The hydrogenation product was oxidized in acetone by the use of chromic acid and sulfuric acid. Vacuum distillation afforded 87% *cis*-2,6-dimethylcyclohexanone (69.5—70 °C/23 mmHg). The only impurity was the *trans* isomer. The structure of the product was checked by 220 MHz NMR. Purity, 87%.

cis-*2-Methyl-4-t-butylcyclohexanone*: Essentially pure *cis*-2-methyl-*4-t*-butylcyclohexanone was obtained from 2-methyl-4-*t*-butylphenol by the procedure described above. Purity, 96%.

trans-2-*Methyl-4-t-butylcyclohexanone*: *Trans*-2-methyl-4-*t*-butylcyclohexanone was obtained by the isomerization of *cis*-2-methyl-4-*t*-butylcyclohexanone following the procedure described by Huff *et al.*[10] The product thus obtained contained about 70% *trans* isomer and 30% *cis* isomer.

4-t-Butylcyclohexanone: 4-*t*-butylcyclohexanone was synthesized by the oxidation of 4-*t*-butylcyclohexanol with chromic acid and sulfuric acid. Purity, nearly 100%.

2-Methylcyclohexanone, 2,2,6-trimethylcyclohexanone, 3,3,5-trimethylcyclohexanone: Commercially-available reagents were used without further purification.

The toluene was purified by distillation after reflux on lithium aluminum hydride under an argon atmosphere for one day.

The trimethylaluminum was obtained from the Ethyl Corporation and was used without further purification. The concentration of the trimethylaluminum solution (in toluene) was determined by the volume of methane evolved on treating an aliquot of the solution with water.

All the ketones were used as 1 mol/l solutions prepared by weighing out the calculated amount of ketone in a volumetric flask and by subsequently diluting with toluene.

Procedure: A three-necked flask equipped with a magnetic stirrer, a gas inlet, a self-sealing rubber cap, and a gas outlet connected to a bubbler was flushed with argon. Toluene (about 9 ml) and 1 ml of a ketone solution was flushed with argon. Toluene (about 9 ml) and 1 ml of a ketone solution were introduced into the flask at the reaction temperature, and then a calculated amount of trimethylaluminum solution was stirred in. After a four-hour reaction, the solution was hydrolyzed with a small piece of ice and then 1 ml of an ammonium chloride solution (1M). The solution was washed with water to remove the aluminum hydroxide and then dried over calcium sulfate. A Hitachi model F6D gas liquid chromatograph with a Golay R45 column was employed for the qualitative and quantitative analyses. 220 MHz NMR was also employed to determine the configurations of the products.

Results and Discussion

Reactions of Three Cyclohexanones with Trimethylaluminum. The results are summarized in Table 1. In the case of 4-*t*-butylcyclohexanone, which has no substituent on the 3,5- or 2,6-position, the stereoselectivity is reversed, depending on the reactant molar ratio of ketone to trimethylaluminum (Al/K), indicating that the equatorial attack is the main course when the molar ratio is one or less, while the axial attack is the main course when the molar ratio is two or more. On the other hand, the results obtained from the reaction of trimethylaluminum with *trans*-2-methyl-4-*t*-butylcyclohexanone show a different steric course from that of 4-*t*-butylcyclohexanone. In this ketone, the 2-methyl group occupies the axial position, so the attack of trimethylaluminum from the equatorial side is blocked, resulting in the higher yield of equatorial alcohol. As has been shown in a previous paper, in the reaction of 3,5,5-trimethylcyclohexanone, the 3-axial methyl group hinders the trimethylaluminum attacking from the axial side. Therefore, these two cyclohexanones show steric courses different from that of 4-*t*-butylcyclohexanone.

The Reactions of Decalones. The results are summarized in Table 2.

trans-2-Decalone: The steric requirement of the carbonyl group in this ketone is the same as that of 4-*t*-butylcyclohexanone, so the results are almost the same as those of 4-*t*-butylcyclohexanone.

trans-1-Decalone: Although a reversal of the stereoselectivity depending on the ketone to aluminum molar ratio is observed, axial alcohol is formed in an amount of more than 40% even when the ratio (Al/K) is two, indicating that the axial attack is depressed to some extent. This might be explained by the presence of three axial

TABLE 1. REACTION OF KETONES WITH TRIMETHYLALUMINUM

Run	Ketone	$AlMe_3/K$	[K]	Conv. (%)	Product	
					-OHax. (%)	-OHeq. (%)
1	4-*t*-Butyl-CH	0.5[a]	0.28	—	80	20
2		1.0	0.093	45.2	81.0	19.0
3		2.0	0.095	95.0	14.2	85.8
4		3.0[a]	0.48	—	12	88
5	3,3,5-Trimethyl-CH	1.0	0.095	40.0	100	0
6		2.0	0.090	98.0	73.6	26.4
7	*trans*-2-Methyl-4-*t*-butyl-CH[b]	1.0	0.094	18.3	19.3	80.7
8		2.0	0.088	83.1	12.7	87.3

a) By E. C. Ashby *et al.*, b) *trans*:*cis*~70 : 30 mixture, temp. 0 °C, time 4 hr, K; ketone, CH; cyclohexanone.

TABLE 2. REACTION OF FOUR DECALONES WITH TRIMETHYLALUMINUM AND METHYLMAGNESIUM IODIDE

Run	Ketone	$AlMe_3$/K	[K]	Temp. (°C)	Conv.(%)	Product (%)	
						-OHax.	-OHeq.
9	*trans*-1	1.0	0.1	30	61.2	93.1	6.9
10		2.0	0.1	0	99.8	41.1	58.9
11		5.0	0.083	0	100	42.3	57.7
12	*trans*-2	1.0	0.075	30	75.1	73.3	26.7
13		5.0	0.063	0	100	18.0	82.0
						cis-cis	*cis-trans*
14	*cis*-1	1.0	0.1	30	74.4	9.3	90.7
15		5.0	0.083	0	100	4.0	96.0
16	*cis*-2	0.8	0.124	30	71.2	59.2	40.8
17		1.0	0.10	30	64.8	59.3	40.7
18		5.0	0.083	0	100	8.3	91.7
		MeMgI/K				-OHax.	-OHeq.
19	*trans*-1	2.0	0.1	0	100	94.9	5.1
20	*trans*-2	2.0	0.074	0	100	81.4	18.6
						cis-cis	*cis-trans*
21	*cis*-1	2.0	0.10	0	100	20.0	80.0
22	*cis*-2	2.0	0.10	0	100	56.3	43.7

Time 4 hr

Fig. 2. *trans*-2-decalone

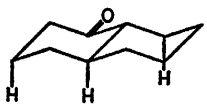

Fig. 3. *trans*-1-decalone

hydrogens (3, 8, and 10 positions) corresponding to the 3,5-axial hydrogens in cyclohexanone, which are believed to hinder the axial attack at a molar ratio of two or more. However, this ketone can be considered to be 2,3-di-equatorial-substituted cyclohexanone. It is known that the 3-equatorial substituent does not play any role in determining the stereoselectivity, so we should consider some effect of the 2-equatorial substituent. The effect of the 2-equatorial methyl substituent will be discussed below.

cis-Decalones:

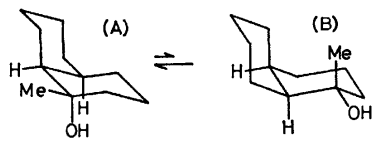

Fig. 4. Two conformations of *cis-cis*-alcohol produced by the reaction of *cis*-1-decalone and trimethylaluminum.

In the *cis*-decalone system, there exist two conformations, (A) and (B), which are believed to reach a very fast equilibrium, as is depicted in Figs. 5 and 6. The notations of the produced alcohols are as follows: in *cis-cis*-alcohol the hydroxyl group and bridge hydrogens are on the same side with the carbonyl-containing ring. On the other hand, in the *cis-trans*-alcohol they are on the opposite side. Therefore, in the case of *cis*-1-decalone, for example, as is depicted in Fig. 4, *cis-cis*-alcohol has an axial hydroxyl group in (A) and an equatorial hydroxyl group in (B) respectively.

cis-1-decalone: As is shown in Table 2, *cis-trans*-

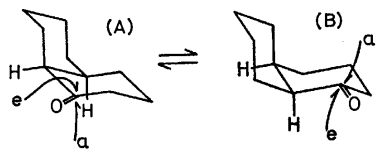

Fig. 5. *cis*-1-decalone, a; axial attack, e; equatorial attack.

alcohol is the predominant product at any molar ratio, and the steric course of the reaction apparently does not depend on the molar ratio. However, these results can be explained by the rapid conformation equilibrium between (A) and (B), considering the same steric course as in the case of 4-*t*-butylcyclohexanone.

At molar ratios of one or less, judging from the results of the reaction of trimethylaluminum with 4-*t*-butylcyclohexanone, the equatorial attack is predominant. The equatorial attack of trimethylaluminum on the (B) conformer gives *cis-trans*-alcohol. However, the equatorial attack on the (A) conformer is sterically hindered by the axial substituent (ring component). Thus, at molar ratios of one or less, the predominant reaction can be considered to be the equatorial attack of trimethylaluminum on the (B) conformer giving mainly *cis-trans*-alcohol.

At molar ratios of two or more, the prevailing attack on the cyclohexanone ring is an axial one. Accordingly, the (A) conformer gives *cis-trans*-alcohol by

the axial attack of trimethylaluminum; on the other hand, the axial attack on the (B) conformer is difficult by the presence of the 3-axial ring component.

The results can also be explained as follows: At any reactant molar ratio, trimethylaluminum attacks *cis*-1-decalone from the less hindered side (*i.e.*, the axial side in the (A) conformer and the equatorial side in the (B) conformer), so the product distribution is not affected by the reactant molar ratio. However, the axial attack at the molar ratio of unity is shown to be slow or difficult by the results obtained with *trans*-2-methyl-4-*t*-butylcyclohexanone. As is shown in Table 1, the reactivity of this ketone at the molar ratio of unity is very low (18.3%), even though the axial attack is the predominant steric course because of the fixed 2-axial methyl substituent. In addition, the equatorial attack at a molar ratio of two or more is the minor reaction path in most cases; it can become the major one only if the cyclohexanone ring contains a substituent which hinders the axial attack greatly, such as 3-axial methyl group in 3,3,5-trimethylcyclohexanone. Therefore, the latter explanation is not adequate.

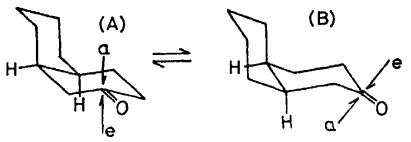

Fig. 6. *cis*-2-decalone, a; axial attack, e; equatorial attack.

cis-2-Decalone: When the molar ratio of ketone to aluminum is one or less, *cis-cis*-alcohol and *cis-trans*-alcohol are formed in nearly equal amounts; however, with an increase in the molar ratio, the *cis-trans*-alcohol increases to a large extent.

At a molar ratio of one or less, the equatorial attacks on the (A) and (B) conformers are equally favored, so *cis-trans*-alcohol and *cis-cis*-alcohol are produced from (A) and (B) respectively by the equatorial attack. Therefore, the two epimers are produced in almost equal amounts.

At a molar ratio of two or more, an axial attack on the (A) conformer is hindered by the presence of a 3-axial ring component. On the (B) conformer, however, an axial attack normally takes place and produces *cis-trans*-alcohol.

The results with four decalone isomers can be explained using the same concepts which were used in discussing the ketones listed in Table 1, considering the rapid conformation equilibrium of each isomer. Therefore, it may be concluded that, in these fused-ring-system ketones, the reactions proceed by means of the same steric course as in the monocyclic ketones.

From the results obtained by the reaction with *trans*-1-decalone, however, further study about cyclohexanones having 2-equatorial substituent is considered to be important.

Reactions of Cyclohexanones with an α-Equatorial Methyl Substituent. The results are summarized in Table 3. When the molar ratio (Al/K) is one, axial alcohols are produced in quantities of more than 96% in all the ketones investigated except 2,2,6-trimethylcyclohexanone, indicating that the stereoselectivity is greatly enhanced compared with the case of 4-*t*-butylcyclohexanone. The results for 2,2,6-trimethylcyclohexanone are anomolous. This ketone has a 2-axial methyl substituent, so the equatorial attack should be hindered. However, axial alcohol is still the main product, even though its percentage is about 10% smaller than those with other ketones.

At the reactant molar ratio of two, the extent of axial attack decreases in the order of 4-*t*-butylcyclohexanone, 2-methylcyclohexanone, and *cis*-2,6-dimethylcyclohexanone, as is shown in Table 3. It is known, therefore, that the axial attack decreases with the successive replacement of 2,6-equatorial hydrogens by methyl groups. In addition, a similar decrease in the axial attack is seen with a decrease in the flexibility of the ring system in the order of 2-methylcyclohexanone, *cis*-2-methyl-4-*t*-butylcyclohexanone, and *trans*-1-decalone. The results for *cis*-2,6-dimethylcyclohexanone and 2,2,6-trimethylcyclohexanone show that the 2-axial-methyl group plays a minor role in stereoselectivity at molar ratios of two or more. This may also be seen in the results for 4-*t*-butylcyclohexanone and *trans*-2-methyl-4-*t*-butylcyclohexanone (cf. Run 3 and Run 8 in Table 1).

Until now, the effect of the 2,6-equatorial substituent

TABLE 3. REACTION OF KETONES HAVING α-EQUATORIAL METHYL GROUP WITH TRIMETHYLALUMINUM

Run	Ketone	$AlMe_3$/K	[K]	Conv. (%)	Product	
					-OHax. (%)	-OHeq. (%)
23	2-Methyl-CH	1.0	0.094	52.8	96.0	4.0
24		2.0	0.090	100	27.8	72.2
25	*cis*-2-Methyl-4-*t*-butyl-CH	1.0	0.094	50.7	96.1	3.9
26		2.0	0.090	100	33.4	66.6
27	*trans*-1-decalone	1.0	0.10	40.2	97.8	2.2
28		2.0	0.10	100	41.1	58.9
29	*cis*-2,6-Dimethyl-CH	1.0	0.093	66.0	98.0	2.0
30		2.0	0.086	99.0	43.2	56.8
31	2,2,6-Trimethyl-CH	1.0	0.095	22.7	88.0	12.0
32		2.0	0.090	74.8	46·2	53.8

Temp. 0°C Time 4 hr, in toluene

on the stereoselectivity of the nucleophilic addition of an organometallic compound has not received any attention. However, as has been shown in the results obtained here, the 2,6-equatorial methyl groups causes a steric hindrance of the axial attack of trialkylaluminum at molar ratios of two or more.

Recently, Ashby *et al.*[5b] proposed the "Compression effect" to explain the reversal of stereoselectivity depending on the reactant molar ratio. Although the effect will be valid for the reversal of selectivity, it may be insufficient to explain the results for 2-alkylsubstituted cyclohexanones. If the "Compression effect" is enhanced through the replacement of 2,6-equatorial hydrogens by methyl groups, the axial attack should be more favored. On the contrary, the axial attack was decreased greatly by the 2,6-equatorial methyl substituent. Therefore, in working out a mechanism to explain the stereochemical effect of the 2,6-equatorial methyl group on the axial attack, one must consider the flexibility of the cyclohexanone ring.

At molar ratios of two or more, the trialkylaluminum complexed with ketone further complexed with a second trialkylaluminum moiety. The exact structure of this ketone : Al=1 : 2 complex cannot be depicted. However, as is to be expected from the amine trialkylaluminum complex, the distance between oxygen and trialkylaluminum is about 2 Å.[11] As has already been clarified, the distance between carbon and aluminum is about 2 Å. Such a structure as is shown in Fig. 7 may be considered. In this complex, the alkyl group of the first aluminum complexed to ketone has a very low activity toward carbonyl addition. Therefore the alkyl group of the second aluminum may attack the carbonyl group. In the transition state, the carbonyl plane will be distorted from the chair form to the half-chair form; consequently, the 2,6-equatorial substituent will come up to the carbonyl plane. This causes a large steric hindrance of the axial attack of

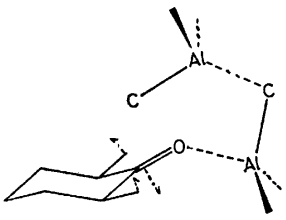

Fig. 7. ketone : $AlMe_3$=1 : 2 complex.

Table 4. Summary of the effect of hydrogen and methyl group at each position of cyclohexanone ring

$AlMe_3$/K molar ratio	1 or less		2 or greater	
Mode of attack	eq. attack	ax. attack	eq. attack	ax. attack
2,6 H(e)	−	−	−	−
2,6 H(a)	+	−	+	−
3,5 H(a)	−	+	−	+
2,6 Me(e)	−	+	−	++
2,6 Me(a)	++	−	++	−
3,5 Me(a)	−	++	−	++

+: having hindrance on the attack, —: little or no effect on the attack,

trialkylaluminum at molar ratios of two or more. In connection with this, the fact that *trans*-1-decalone gave a smaller amount of the axial attack product than did 2-methyl- or *cis*-2-methyl-4-*t*-butylcyclohexanone can be explained by the fact that the flexibility of carbonyl plane is depressed by the fused-ring system. This mechanism, which assumes the importance of the flexibility of the carbonyl group, explains the low reactivity of trimethylaluminum toward adamantanone. The reaction of trimethylaluminum with adamantanone at a molar ratio of two was carried out. It was found that the reactivity of this ketone was very low. Only a 20% conversion was observed in the reaction with trimethylaluminum at 0 °C for 4 hr. Adamantanone has so very rigid a cyclic system that it is difficult for the carbonyl plane to be distorted to the half-chair form. Table 4 summarizes the effects of hydrogens or methyl groups, which affect the direction of the attack of trimethylaluminum on cyclohexanone derivatives.

Temperature Dependence of the Product Distribution. In the case of 4-*t*-butylcyclohexanone, the product ratio (axial alcohol to equatorial alcohol) is not altered with the reaction temperature. However, it is affected by the reaction temperature in the cases of ketones containing 2-equatorial methyl substituents (listed in Table 3) or 3,3,5-trimethylcyclohexanone. Table 5 illustrates the results for 2,2,6-trimethylcyclohexanone, which showed the largest temperature dependence of the product distribution of all the ketones investigated.

A linear relationship is observed between the plot of log (-OHax./-OHeq.) *vs.* $1/T$ at Al/K=2. The dif-

Table 5. Reaction of 2,2,6-trimethylcyclohexanone with trimethylaluminum

Run	$AlMe_3$/K	[K]	Temp. (°C)	Conv. (%)	Product	
					-OHax. (%)	-OHeq. (%)
31	1.0	0.095	0	22.7	88.0	12.0
33	1.0	0.093	30	64.5	86.2	13.8
34	2.0	0.09	−30	~1	33.2	66.8
32	2.0	0.09	0	74.8	46.2	53.8
35	2.0	0.09	30	99.0	70.4	29.6
36	2.0	0.09	50	100	75.4	24.6
37	5.0	0.079	0	73.0	36.5	63.5
38	5.0	0.079	30	100	52.8	47.2

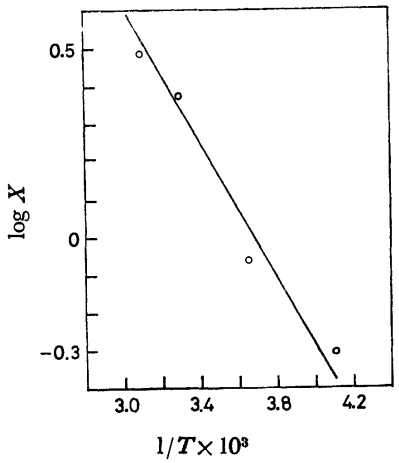

Fig. 8. log (−OHax./−OHeq.) *vs.* $1/T$ plot, Al/K=2.0.
Difference of activation energies; $E_{eq.}-E_{ax.}=4.06$ kcal/mol

ference between the activation energies was calculated to be about 4 kcal/mol. The difference in activation energy suggests a difference in mechanisms between axial and equatorial attacks. In addition, it should be noted that the results in $AlMe_3/K=2$ approach the results obtained at a molar ratio of one when the reaction temperature is elevated. From these two facts, it was considered that, in these ketones, the unimolecular reaction from the equatorial side contributed greatly even when the reactant ratio was two.

In these ketones, because of the large steric requirement, the rate of bimolecular axial attack decreased so as to be comparable with the rate of equatorial attack by the unimolecular process; therefore, the temperature dependence of the product distribution is observed.

On the other hand, in the case of 4-*t*-butylcyclohexanone, the rate of axial attack is sufficiently large and the temperature dependence is not observed.

References

1) W. G. Dauben, G. J. Fonken, and D. S. Noyce, *J. Amer. Chem. Soc.*, **78**, 2579 (1956).
2) J. C. Richer, *J. Org. Chem.*, **30**, 324 (1965).
3) J. A. Marshall and R. D. Carroll, *ibid.*, **30**, 2748 (1965).
4) M. Chérest and H. Felkin, *Tetrahedron Lett.*, **1968**, 2205.
5) a) E. C. Ashby, S. H. Yu, and P. V. Roling, *J. Org. Chem.*, **37**, 1918 (1972). b) J. Laemmle, E. C. Ashby, and P. V. Roling, *ibid.*, **38**, 2526 (1973).
6) E. C. Ashby, J. Laemmle, and H. M. Newmann, *J. Amer. Chem. Soc.*, **90**, 5179 (1968).
7) Richard S. Monson, "Advanced Organic Syntheses, Methods and Techniques," Academic Press, New York and London, (1971), pp. 27, 81.
8) R. L. Augustin, *J. Org. Chem.*, **23**, 1853 (1958).
9) H. E. Zimmerman and A. Mais, *J. Amer. Chem. Soc.*, **81**, 3644 (1959).
10) B. J. L. Huff, F. N. Tuller, and D. Caine, *J. Org. Chem.*, **34**, 3070 (1969).
11) C. D. Whitt, L. M. Parker, and J. L. Atwood, *J. Organometal. Chem.*, **32**, 291 (1971).

Reaction of Biguanides and Related Compounds. X.[1] The Cyclization of Arylbiguanides with Acyl Isothiocyanates

Mitsuru FURUKAWA, Motoo GOTO, and Seigoro HAYASHI

Faculty of Pharmaceutical Sciences, Kumamoto University, Oe-hon Machi, Kumamoto 862

(Received March 12, 1974)

The reactions of arylbiguanides with benzoyl and ethoxycarbonyl isothiocyanates gave 4(or 2)-arylguanidino-2(or 4)-phenyl-6-thioxo-1,6-dihydro-*s*-triazines and 4-arylguanidino-2-oxo-6-thioxo-1,4,5,6(or 1,2,3,6)-tetrahydro-*s*-triazines respectively, both of which were then converted into the corresponding oxo compounds, in which the thioxo group was converted into the oxo group, by oxidation with hydrogen peroxide. The condensation of 3-amidino-1-aryl-2-thioureas with aryl isothiocyanates afforded 1-aryl-2-arylimino-4-imino-6-thioxo-1,4,5,6-tetrahydro-*s*-triazines, which were also formed by the pyrolysis of 3-amidino-1-aryl-2-thioureas.

It has been reported by Somogyi[2] that the reaction of phenylbiguanide with an equimolar quantity of phenyl isothiocyanate gave 4,6-diimino-1-phenyl-2-phenyliminohexahydro-*s*-triazine, 6-amino-2,4-dianilino-*s*-triazine, and 4-imino-1-phenyl-2-phenylimino-6-thioxohexahydro-*s*-triazine in 29, 14—16, and 19% yields respectively, all *via* the same intermediate addition product. The interaction of biguanide and phenyl isothiocyanate has also been reported by Kurzer[3] to afford an excellent yield of 4,6-diimino-1-phenyl-2-thioxohexahydro-*s*-triazine, though no unequivocal evidence for its structure was provided. As an extension of our work on the reaction of biguanides with carbonyl compounds, we investigated the reaction of arylbiguanides with benzoyl and ethoxycarbonyl isothiocyanates, in both of which a carbonyl group is involved in the position adjacent to the isothiocyanate group.

Reaction of Arylbiguanides with Benzoyl Isothiocyanate. By analogy with the reaction of phenylbiguanide with phenyl isothiocyanate, several cyclization products are possible in the reaction between arylbiguanides (**1**) and benzoyl isothiocyanate (**2**). In addition, the participation of the carbonyl group in the cyclization is also possible.

When equimolar quantities of **1** and **2** were heated in ethanol for 4 hr, one product was obtained in a low yield. The product was positive in a lead acetate test for the sulfur atom. The infrared (IR) absorption spectra of the product exhibited the characteristic absorptions assignable to amino and imino groups near 3340 and 3140 cm^{-1} and that due to the thiocarbonyl group near 1250 cm^{-1}, but no absorption assignable to the carbonyl group was observed. Although the absorption assigned to the thiocarbonyl group was at a higher frequency than the normal absorption band of a thiocarbonyl group, its identity was confirmed by the fact that the absorption disappeared upon conversion to the carbonyl group by oxidation. The ultraviolet (UV) absorption spectra showed the maximum absorption at 265 nm. On the basis of these results and the analytical data, the product is presumed to be 4(or 2)-arylguanidino-2(or 4)-phenyl-6-thioxo-1,6-dihydro-*s*-triazines (**3**). A similar cyclization reaction has been known in the condensations of *N*-unsubstituted amidino compounds with aroyl isothiocyanates[4] and with substituted imidoyl isothiocyanates.[5] Support for the assigned structure **3** was provided by the mass spectra, in which the molecular ion and the fragment ion peaks

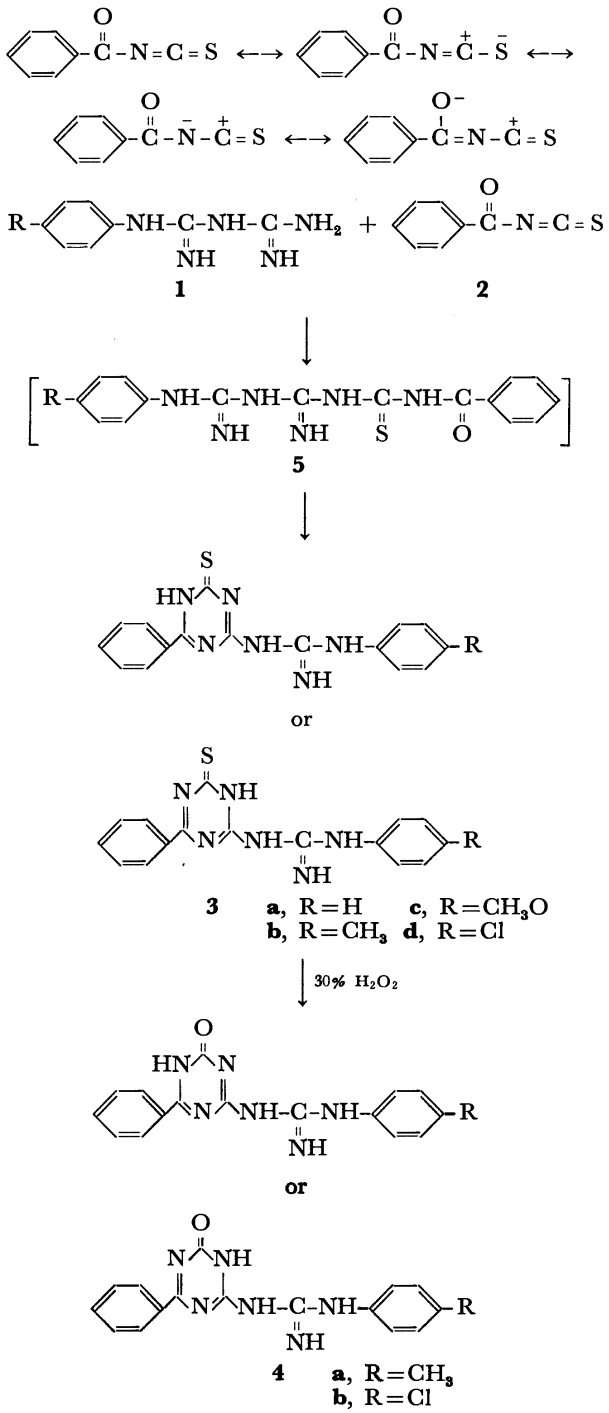

Scheme 1.

Table 1. 4(or 2)-Arylguanidino-2(or 4)-phenyl-6-thioxo-1,6-dihydro-*s*-triazine

Compd.	Mp (°C)	Yield (%)	Recryst. solvent	Formula	Analysis % Found (Calcd) C	H	N	IR cm^{-1} (KBr) $\nu_{C=S}$	UV λ_{max}^{EtOH} nm (log ε)
3a	269—270	20	EtOH	$C_{16}H_{14}N_6S$	59.65 (59.62)	4.37 (4.38)	26.22 (26.07)	1250	264 (4.56)
3b	251—252	10	EtOH+H_2O	$C_{17}H_{16}N_6S$	60.85 (60.70)	4.85 (4.80)	24.80 (24.99)	1260	265 (4.57)
3c	281—282	16	DMF+H_2O	$C_{17}H_{16}ON_6S$	58.05 (57.95)	4.54 (4.58)	23.64 (23.85)	1260	265 (4.51)
3d	271—272	19	DMF+H_2O	$C_{16}H_{13}N_6SCl$	53.67 (53.85)	3.73 (3.67)	23.20 (23.55)	1260	265 (4.51)

due to arylamidyl and arylamino ions were observed as an abundant peak.

In order to further elucidate the assigned structure, the product was converted into 4(or 2)-arylguanidino-2 (or 4)-phenyl-6-oxo-1,6-dihydro-*s*-triazines (**4**). The conversion was successfully carried out by heating with a 30% aqueous hydrogen peroxide solution in acetic acid at 80 °C for 30 min. The structure of **4** was established by the good agreement of the elemental analyses and by the IR spectra, in which the absorption of the thiocarbonyl group disappeared and the absorption assignable to the carbonyl group was observed near 1680 cm^{-1}. The absorption pattern was quite similar to that of **3**.

Somogyi[2] has reported that the cyclization reaction of phenylbiguanide with phenyl isothiocyanate proceeds through the intermediate addition product which is formed by the addition of the terminal amino group of phenylbiguanide to the isothiocyanate group. In view of the resonance formula of **2**, it seems that the initial addition of **1** to **2** would analogously occur at the positive carbon atom of the isothiocyanate group, but not at the adjacent carbonyl carbon atom, to form a similar intermediate (**5**), followed by cyclization to **3** by dehydration, though all efforts to isolate the intermediate under milder reaction conditions failed. The results are summarized in Table 1.

Reaction of Arylbiguanides with Ethoxycarbonyl Isothiocyanate. Recently Goerdeler and Neuffer[6] have reported that the amidino compounds, such as isoureas, isothioureas[7] and guanidines, reacted with ethoxycarbonyl isothiocyanate, with the elimination of ethanol, to give oxothioxotetrahydro-*s*-triazines. Compound **1** is also presumed to behave similarly toward ethoxycarbonyl isothiocyanate, because an amidino moiety is involved in the molecule.

When equimolecular quantities of **1** and ethoxycarbonyl isothiocyanate (**6**) were treated in ethanol at room temperature, 4-arylguanidino-2-oxo-6-thioxo-1,4, 5,6(or 1,2,3,6)-tetrahydro-*s*-triazines (**7**) were obtained in comparatively good yields, as had been expected.

The structure of **7** was assigned on the basis of the results of elemental analyses and the spectral data. The IR spectra exhibited characteristic absorptions assignable to amino and imino groups near 3450 and 3300 cm^{-1} and that due to the thiocarbonyl group near 1235 cm^{-1}. The mass spectra showed the molecular ion peak as an abundant peak. Fragment ion

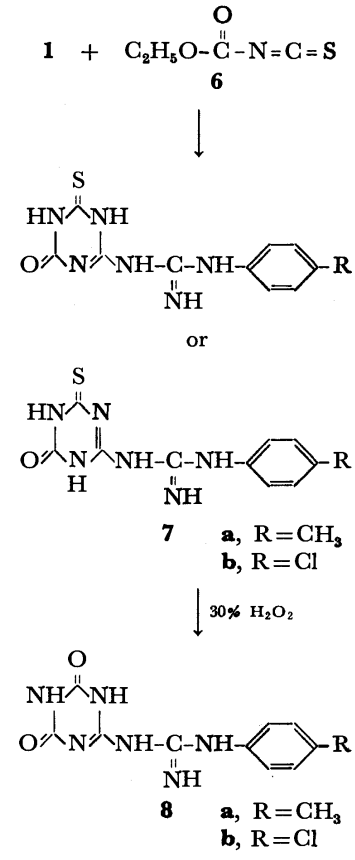

Scheme 2.

peaks presumably corresponding to the arylamidyl ion, the arylamino ion, and arylcyanamide were also observed. The UV spectra indicated the maximum absorption bands at 270 nm in a 0.01 M hydrochloric acid solution and at 275 and 250 nm in a 0.01 M sodium hydroxide solution; they must be due to the keto and enol forms respectively. Evidence for the structure was achieved by conversion with hydrogen peroxide into 4-arylguanidino-2,6-dioxo-1,2,5,6-tetrahydro-*s*-triazines (**8**), whose structures were established on the basis of the results of elemental analyses and the spectral data.

Reaction of 3-Amidino-1-aryl-2-thioureas with Phenyl Isothiocyanate. Because of the structural similarity, 3-aminido-1-aryl-2-thioureas (**9**) may be expected to behave much like **1** toward isothiocyanates. Crowther *et al.*[8] have reported that, in the preparation of 3-alkyl-

amidino-1-*p*-chlorophenyl-2-thioureas from alkylguanidines and *p*-chlorophenyl isothiocyanate, 4-alkylamino-2-*p*-chloroanilino-1-*p*-chlorophenyl-6-thioxo-1,6-dihydro-*s*-triazines were formed as by-products. This cyclization is presumed to proceed through the intermediate addition product which is formed by addition of 3-alkylamidino-1-*p*-chlorophenyl-2-thiourea, alone with further *p*-chlorophenyl isothiocyanate. Thus the condensation of **9** with several aryl isothiocyanates (**10**) was examined.

When equimolecular quantities of **9** and **10** were heated in dimethylformamide (DMF) at 110 °C, 1-aryl-2-arylamino-4-imino-6-thioxo-1,4,5,6-tetrahydro-*s*-triazines (**11**) were obtained in moderate yields.

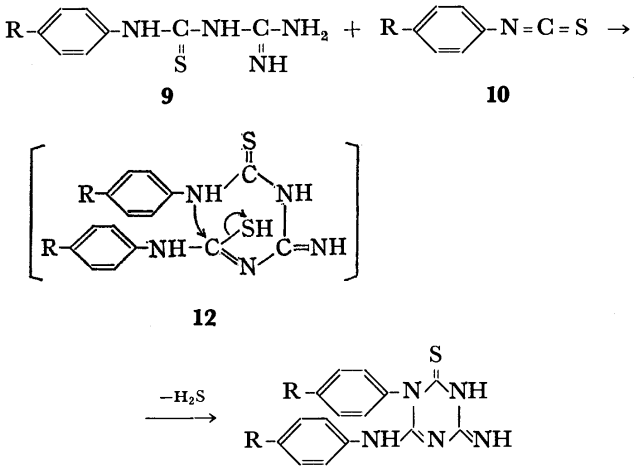

a, R=H **c**, R=C_2H_5O
b, R=CH_3 **d**, R=Cl

Scheme 3.

The structure of **11** was assigned on the basis of the results of elemental analyses and the spectral data. The IR spectrum exhibited absorptions assignable to amino and imino groups near 3430, 3370, and 3280 cm^{-1} and that due to the thiocarbonyl group near 1150 cm^{-1}. In the mass spectrum, the corresponding molecular ion was observed as the most abundant peak. Fragment ion peaks corresponding to the elimination of NCS group from the molecular ion and to arylamine were also observed. The reaction probably proceeds through the intermediate addition product (**12**), followed by the elimination of hydrogen sulfide, though attempts to isolate the intermediate were unsuccessful. The liberation of hydrogen sulfide was actually confirmed by the positive lead acetate test. Compound **11** was also obtained in a lower yield by the pyrolysis of **9** in DMF at 110 °C. It is probably formed by condensation of **9** with the **10** formed by the decomposition of **9**. The formation of **10** from **9** is detected in the mass spectrum of **9**.[9] The results are summarized in Table 2.

Contrary to expectations, however, the reactions of **9** with **2** and **6** resulted in failure, a small amount of the **9** being recovered unchanged and no anticipated product being isolated.

Experimental

*4(or 2)-Arylguanidino-2(or 4)-phenyl-6-thioxo-1,6-dihydro-s-triazine (**3**).* General Procedure: A solution of arylbiguanide (10 mmol) and benzoyl isothiocyanate (10 mmol) in ethanol (20 ml) was heated for 4 hr under reflux. The precipitates deposited during heating were collected by filtration. The filtrate was concentrated under reduced pressure, and the precipitates deposited on cooling were collected by filtration. The combined precipitates were recrystallized from a suitable solvent. The detailed data are summarized in Table 1. These compounds exhibited the corresponding molecular ion as an abundant peak in the mass spectra.

*2(or 4)-Phenyl-4(or 2)-p-tolylguanidino-6-oxo-1,6-dihydro-s-triazine (**4a**).* Into a suspension of 2(or 4)-phenyl-4(or 2)-*p*-tolylguanidino-6-thioxo-1,6-dihydro-*s*-triazine (0.6 g, 1.8 mmol) in acetic acid (7 ml), we stirred, drop by drop, a 30% aqueous hydrogen peroxide solution (0.3 ml) at 80 °C over a 5-min period. Stirring was continued for an additional 30 min, keeping the temperature at 80 °C, and then the insoluble parts were filtered off. The filtrate was basified with concentrated aqueous ammonia. The precipitates deposited upon cooling were collected by filtration, washed with water, and recrystallized from DMF-water to give colorless prisms (0.15 g, 26.3%) melting at 304—305 °C. IR(KBr): 1680 cm^{-1} (C=O). MS: 320 (M^+). Found: C, 63.34; H, 5.24; H, 25.84%. Calcd for $C_{17}H_{16}ON_6$: C, 63.73; H, 5.04; N, 25.84%.

*4(or 2)-p-Chlorophenylguanidino-2(or 4)-phenyl-6-oxo-1,6-dihydro-s-triazine (**4b**).* Into a suspension of 4(or 2)-*p*-chlorophenylguanidino-2(or 4)-phenyl-6-thioxo-1,6-dihydro-*s*-triazine (0.8 g, 2.24 mmol) in acetic acid (8.2 ml), we stirred, drop by drop, a 30% aqueous hydrogen peroxide solution (0.7 ml) at 80 °C over a 5-min period. The reaction mixture was then treated by the same procedure as that described above. The resulting product was recrystallized from DMF

Table 2. 1-Aryl-2-arylamino-4-imino-6-thioxo-1,4,5,6-tetrahydro-*s*-triazine

Compd.	Mp (°C)	Yield (%) Method a	Yield (%) Method b	Appearance	Formula	Analysis % Found(Calcd) C	H	N	IR cm^{-1} (KBr) $\nu_{C=S}$
11a	252	68	3	prism	$C_{15}H_{13}N_5S$	61.01 (61.01)	4.50 (4.44)	23.42 (23.72)	1155
11b	244	80	17	needle	$C_{17}H_{17}N_5S$	62.77 (63.14)	5.29 (5.30)	21.37 (21.66)	1155
11c	268	52	18	plate	$C_{19}H_{21}O_2N_5S$	59.49 (59.52)	5.54 (5.52)	18.18 (18.27)	1158
11d	290	31	23	needle	$C_{15}H_{11}N_5SCl_2$	50.30 (50.85)	3.00 (3.13)	19.55 (19.77)	1148

to give colorless prisms (0.2 g, 26.3%) melting at 314—315 °C. IR(KBr): 1660 cm^{-1} (C=O). MS: 341 (M^+). Found: C, 56.13; H, 3.96; N, 24.81%. Calcd for $C_{16}H_{13}ON_6Cl$: C, 56.39; H, 3.85; N, 24.66%.

*4-p-Tolylguanidino-2-oxo-6-thioxo-1,4,5,6(or 1,2,3,6)-tetrahydro-s-triazine (**7a**).* Into a solution of *p*-tolylbiguanide (1.9 g, 10 mmol) in ethanol (20 ml), we stirred, drop by drop, ethoxycarbonyl isothiocyanate (1.3 g, 10 mmol) at 0 °C under a stream of nitrogen gas. Stirring was continued for an additional 24 hr at room temperature under a nitrogen stream. The precipitates which were gradually deposited in the course of the reaction were collected by filtration, washed with water, dried, and recrystallized from DMF to give colorless prisms (1.86 g, 67.5%); mp>360 °C. IR (KBr): 1680 (C=O) and 1235 (C=S) cm^{-1}. UV $\lambda_{max}^{0.01M\ HCl}$ nm (log ε): 271 (4.42). UV $\lambda_{max}^{0.01M\ NaOH}$ nm (log ε): 248 (4.44) and 275 (4.44). Found: C, 47.99; H, 4.23; N, 29.95 %. Calcd for $C_{11}H_{12}ON_6S$: C, 47.82; H, 4.38; N, 30.42%.

*4-p-Chlorophenylguanidino-2-oxo-6-thioxo-1,4,5,6(or 1,2,3,6)-tetrahydro-s-triazine (**7b**).* Into a solution of *p*-chlorophenylbiguanide (2.12 g, 10 mmol) in ethanol (20 ml), we stirred, drop by drop, ethoxycarbonyl isothiocyanate (1.31 g, 10 mmol) at 0 °C under a stream of nitrogen gas. The reaction mixture was then treated by the same procedure as that described above to give colorless prisms (1.84 g, 62.0%); mp>360 °C. IR (KBr): 1680 (C=O) and 1235 (C=S) cm^{-1}. UV $\lambda_{max}^{0.01M\ HCl}$ nm (log ε): 270 (4.47). UV $\lambda_{max}^{0.01M\ NaOH}$ nm (log ε): 250 (4.37) and 275 (4.41). Found: C, 40.94; H, 3.08; N, 28.01%. Calcd for $C_{10}H_9ON_6SCl$: C, 40.47; H, 3.06; N, 28.32%.

*4-p-Tolylguanidino-2,6-dioxo-1,2,5,6-tetrahydro-s-triazine (**8a**).* Into a solution of 4-*p*-tolylguanidino-2-oxo-6-thioxo-1,4,5,6(or 1,2,3,6)-tetrahydro-*s*-triazine (0.5 g, 1.8 mmol) in an aqueous 1 M sodium hydroxide solution (16 ml), we stirred, drop by drop, an aqueous 30% hydrogen peroxide solution (4 ml) at 0 °C over a 20-min period. Stirring was continued for an additional 2 hr at room temperature. The precipitates which had been deposited were then collected by filtration. The filtrate was acidified with a 2 M sulfuric acid solution, and the precipitates thus deposited were collected by filtration. The combined precipitates were then washed with water, dried, and recrystallized from DMF to give colorless prisms (0.30 g, 64.1%); mp>360 °C. IR(KBr): 1720 and 1660 cm^{-1} (C=O). Found: C, 50.74; H, 4.72; N, 32.01%. Calcd for $C_{11}H_{12}O_2N_6$: C, 50.76; H, 4.65; N, 32.30%.

*4-p-Chlorophenylguanidino-2,6-dioxo-1,2,5,6-tetrahydro-s-triazine (**8b**).* Into a suspension of 4-*p*-chlorophenylguanidino-2-oxo-6-thioxo-1,4,5,6(or 1,2,3,6)-tetrahydro-*s*-triazine (0.8 g, 2.7 mmol) in an aqueous 1 M sodium hydroxide solution (20 ml), we added, drop by drop, an aqueous 30% hydrogen proxide solution (5.4 ml) at 0 °C over a 10-min period. Stirring was continued for an additional 1 hr at room tempreature, and then the insoluble part was filtered off and the filtrate was acidified with an aqueous 2 M sulfuric acid solution. The resulting precipitates were collected by filtration, washed with water, dried, and recrystallized from DMF to give colorless prisms (0.50 g, 65.8%) melting at 358—360 °C. IR(KBr): 1720 and 1660 cm^{-1} (C=O). Found: C, 42.92; H, 3.34; N, 29.73%. Calcd for $C_{10}H_9O_2N_6Cl$: C, 42.79; H, 3.23; N, 29.94%.

*1-Aryl-2-arylamino-4-imino-6-thioxo-1,4,5,6-tetrahydro-s-triazine (**11**).* General Procedure: a) A mixture of 3-amidino-1-aryl-2-thiourea (10 mmol), aryl isothiocyanate (10 mmol), and DMF (5 ml) was heated at 110 °C for 5 hr. After cooling, the mixture was poured into cold water and the precipitates thus deposited were collected by filtration, washed with water, and recrystallized from ethanol. The detailed data are summarized in Table 2. These compounds exhibited the corresponding molecular ions as the most abundant peak in the mass spectra. b) A solution of 3-amidino-1-aryl-2-thiourea (10 mmol) in DMF (5 ml) was heated at 110 °C for 10 hr. After cooling, the solution was poured into cold water and the resulting precipitates were collected by filtration, washed with water, and recrystallized from ethanol. The yield of the product is illustrated in Table 2. These compounds were identified with authentic samples obtained by the method described above by a mixed-melting-point determination and by an IR comparison.

References

1) Part IX: M. Furukawa, K. Matsuoka, T. Yoshida, Y. Kojima, and S. Hayashi, *Chem. Pharm. Bull.* (Tokyo), **22**, 1 (1974).

2) L. Somogyi, Z. Györgydeák, and R. Bognar, *Tetrahedron Lett.*, **1966**, 871; *Chem. Ber.*, **100**, 1975 (1967).

3) F. Kurzer and E. D. Pitchfork, *J. Chem. Soc.*, **1964**, 3459.

4) J. Goerdeler and J. Neuffer, *Chem. Ber.*, **104**, 1580 (1971).

5) J. Neuffer and H. Goerdeler, *ibid.*, **104**, 3498 (1971).

6) J. Goerdeler and J. Neuffer, *ibid.*, **104**, 1606 (1971).

7) J. Goerdeler and J. Neuffer, *Tetrahedron Lett.*, **1967**, 2791.

8) A. F. Crowther, F. H. S. Curd, D. N. Richardson, and F. L. Rose, *J. Chem. Soc.*, **1948**, 1636.

9) T. Ueda, A. Takada, K. Takahashi, and F. Ueda, *Chem. Pharm. Bull.* (Tokyo), **19**, 1990 (1971).

Preparation and Thermal Decomposition of Acyl Carbamoyl Peroxides

Renji OKAZAKI and Osamu SIMAMURA

Department of Chemistry, Faculty of Science, The University of Tokyo, Hongo, Tokyo 113

(Received January 29, 1974)

Thirteen acyl carbamoyl peroxides, a new class of peroxides, were prepared by addition of peroxy-acids to organic isocyanates and their properties were examined. The thermal decompositions, especially of benzoyl *N*-(*p*-nitrophenyl)carbamoyl peroxide and benzoyl *N*-benzoylcarbamoyl peroxide, were studied in crystalline state and in solution, and it was shown that they decompose via three different mechanisms, involving either an amino-radical, a nitrene or a protonated nitrene, depending on reaction conditions.

Peroxides having active hydrogens, such as hydrogen peroxide and alkyl hydroperoxides are known to undergo addition reaction with isocyanates; hydrogen peroxide produces azo-compounds *via* dicarbamoyl peroxides which are too unstable to be isolated,[1] whereas hydroperoxides form considerably stable peroxycarbamates.[2,3] We have preliminarily communicated elsewhere[4] that peroxy-acids also react with isocyanates to give acyl carbamoyl peroxides, a new class of peroxides:

$$RN{=}C{=}O + R'C(=O)OOH \rightarrow RNHC(=O)OOC(=O)R'$$

The present paper presents detailed accounts of the preparation and thermal decomposition of these peroxides.

Results and Discussion

Acyl carbamoyl peroxides were prepared at $-10\sim-15$ °C by adding a peroxy-acid in ether to an ethereal solution of an isocyanate containing a trace of pyridine as catalyst. The peroxides thus obtained and their characteristic infrared absorption bands are listed in Tables 1 and 2, respectively.

Reaction between *N*-methyl-*N*-(*p*-nitrophenyl)carbamoyl chloride and peroxybenzoic acid with 30% potassium hydroxide as a base gave benzoyl *N*-methyl-*N*-(*p*-nitrophenyl)carbamoyl peroxide, which was found so unstable as to decompose readily at room temperature yielding carbon dioxide. In Table 3 are summarized attempted syntheses which did not give the peroxides expected.

Tables 1 and 3 show that in order for acyl carbamoyl peroxides to be prepared isocyanates must carry an electronegative substituent. With *p*-nitrophenyl isocyanate, all the peroxy-acids examined gave the corresponding peroxides irrespective of the nature of their substituents and the substituent in isocyanates appears to have to be more electronegative than, say, a *m*-chloro substituent. This trend is similar to that observed in the preparation of substituted *N*-phenylperoxycarbamates, of which the *p*-methyl and *p*-methoxy derivatives were not prepared.[3] The aliphatic isocyanate does not seem to give peroxides with peroxy-acids, although the aliphatic peroxy-acid reacts with appropriate aromatic isocyanates to yield peroxides. Replacement of a hydrogen on the nitrogen of the carbamoyl group by a methyl group makes the peroxide remarkably unstable.

The effect of an electron-withdrawing substituent in the isocyanate is explained because it increases the reactivity of an isocyanate towards addition[5] and at the same time seems to make it less vulnerable to oxidative attack by peroxy-acids. Further, an electro-

TABLE 1. PREPARATION AND PROPERTIES OF ACYL CARBAMOYL PEROXIDES RNHC(=O)OOC(=O)R'

Compd.	R	R'	Yield (%)	Solvent[a]	Dp (°C)[b]	Purity[c] (%)	Analyses Found C	Found H	Found N	Calcd C	Calcd H	Calcd N
I	*p*-$O_2NC_6H_4$	C_6H_5	55	A	63	98	55.77	3.46	9.57	55.62	3.34	9.27
II	*p*-NCC_6H_4	C_6H_5	57	A	51	93	61.60	4.60	4.66	62.00	4.59	4.25
III	*p*-$EtO_2CC_6H_4$	C_6H_5	56	A	55	96	63.15	4.16	9.39	63.84	3.57	9.93
IV	*m*-ClC_6H_4	C_6H_5	55	B		d)						
V	*o*-$O_2NC_6H_4$	C_6H_5	69	A	64	94	55.34	3.60	9.09	55.62	3.34	9.27
VI	*p*-$O_2NC_6H_4$	*p*-$CH_3OC_6H_4$	68	A	68	100	53.78	3.93	8.27	54.22	3.64	8.43
VII	*p*-$O_2NC_6H_4$	*p*-$CH_3C_6H_4$	86	A	64	94	57.12	4.22	9.02	56.96	3.82	8.86
VIII	*p*-$O_2NC_6H_4$	*m*-ClC_6H_4	40	C	60	97	49.42	2.85	8.66	49.94	2.69	8.32
IX	*p*-$O_2NC_6H_4$	*p*-$O_2NC_6H_4$	19	D	55	84	47.91	3.19	12.02	48.42	2.61	12.10
X	*p*-$O_2NC_6H_4$	*n*-$C_{11}H_{23}$	47	D	49	95	59.82	7.62	7.30	59.98	7.42	7.36
XI	C_6H_5CO	C_6H_5	75	D	60	97	62.59	3.92	4.97	63.19	3.89	4.91
XII	$C_6H_5SO_2$	C_6H_5	74	D	80	82	51.97	3.63	4.76	52.33	3.45	4.36

a) Solvent for recrystallization: A, dichloromethane; B, ether-petroleum ether; C, dichloromethane-petroleum ether; D, ether. b) Decomposition point; all peroxides decompose explosively at these temperatures except compound XII. c) Active oxygen estimated by iodometry in acetic acid (A.T. Blomquist and A.F. Ferris, *J. Amer. Chem. Soc.*, **73**, 3408 (1951)). d) Too unstable to be analyzed correctly (see Experimental).

Table 2. Infrared spectra of acyl carbamoyl peroxides[a]

Compound	ν_{N-H} (cm^{-1})	$\nu_{C=O}$ (cm^{-1})		
I	3412[b]	1807	1777	
II	3410	1803	1780	
III	3415	1806	1783	1770
V	3321	1810	1780	
VI	3414	1806	1773	
VII	3412	1810	1787	
X	3417	1814	1789	
XI	3413	1835	1781	1728
XII	3385	1811	1781	

a) In chloroform in concentration of about 0.01 mol/l.
b) In carbon tetrachloride, 3420 cm^{-1}.

negative substituent seems to stabilize acyl carbamoyl peroxides as is observed with various types of peroxides, such as substituted benzoyl peroxides,[6] *t*-butyl *N*-phenylperoxycarbamates,[3] *t*-butyl peroxybenzoates[7] and *t*-butyl peroxyphenylacetates.[8] The destabilizing effect of a methyl group mentioned above seems to be due to its electron-releasing effect. Aliphatic isocyanates, which have low reactivity compared with aromatic ones,[5] do not yield acyl carbamoyl peroxides; on the other hand, benzoyl[9] and benzenesulfonyl[10] isocyanates, which are known for high reactivity, gave the corresponding peroxides in high yields.

The results of the thermal decompositions of benzoyl *N*-(*p*-nitrophenyl)carbamoyl peroxide in solutions as well as in crystalline state are summarized in Table 4. The yield of carbon dioxide exceeded 100 mol% by about 20% or more in benzene, chloroform and acetic acid, but it was about 100 mol% in the decomposition in crystalline state and in ethanol. Benzoic acid was produced in a relatively large amount in each case, but there was a definite difference in its yield between the decomposition in benzene, chloroform or acetic acid (about 50 mol%) on the one hand and that in crystalline state or in ethanol (70—80 mol%) on the other. Some products which appear to have been derived from phenyl radicals, such as biphenyl and benzene were formed in benzene, chloroform and acetic acid. The following nitrogen containing products were identified: *p,p'*-dinitroazobenzene in the decomposition in crystalline state; *p,p'*-dinitroazobenzene and *p*-nitroaniline in benzene and chloroform; *p*-nitroacetanilide in acetic acid; and 5-nitro-2-aminophenetole and 5-nitro-2-benzamidophenol in ethanol. Some of these findings strongly suggest a homolytic nature of the decomposition, but the concurrence of an ionic mechanism is very likely in view of the production of 5-nitro-2-aminophenetole and 5-nitro-2-benzamidophenol in ethanol.

The homolytic fission of the peroxidic linkage of benzoyl *N*-(*p*-nitrophenyl)carbamoyl peroxide would primarily produce an *N*-(*p*-nitrophenyl)-carbamoyloxy *p*-$O_2NC_6H_4NHCOO\cdot$ and a benzoyloxy $C_6H_5COO\cdot$ radicals. In order to know the behavior, under the prevailing conditions, of these radicals, *t*-butyl *N*-(*p*-nitrophenyl)peroxycarbamate[2,3] and benzoyl peroxide,[11] which are known to generate these radicals respectively, were separately decomposed in benzene and in ethanol and the products were examined. The results are summarized in Table 5. They show that the

Table 3. Attempted reactions[a] which gave no peroxides

Isocyanates	Peroxy-acids	Products isolated
p-ClC_6H_4NCO	$C_6H_5CO_3H$	*p,p'*-Dichloroazobenzene(10%) *p,p'*-Dichloroazoxybenzene(2%)
C_6H_5NCO	$C_6H_5CO_3H$	Nitrobenzene(1%), azobenzene(trace)
p-$O_2NC_6H_4NCO$	*o*-$HOOCC_6H_4CO_3H$	No reaction
$C_{11}H_{23}NCO$	$C_6H_5CO_3H$	No reaction
$C_{11}H_{23}NCO$	$C_{11}H_{23}CO_3H$	No reaction
p-$O_2NC_6H_4NCO$	H_2O_2	*p,p'*-Dinitroazobenzene(30%)
p-$OCNC_6H_4NCO$	$C_6H_5CO_3H$	Tarry material

a) Reactions were carried out by essentially the same procedure as described for the preparation of benzoyl *N*-(*p*-nitrophenyl)carbamoyl peroxide.

Table 4. Products of decomposition of benzoyl *N*-(*p*-nitrophenyl)carbamoyl peroxide

Reaction conditions		Products (yield in mol% of peroxide)[a]								
Solvent	Temp. °C	Carbon dioxide	Benzoic acid	Benzene	Biphenyl	*p*-Nitro-aniline	*p,p'*-Di-nitroazo-benzene	*p*-Nitro-acet-anilide	5-Nitro-2-benz-amido-phenol	5-Nitro-2-amino-phenetole
None	20	98	80			trace	15			
Benzene	80	117	48		20	15	12			
Chloroform	61	127	45	33		17	14			
Acetic acid	50	118	47	9				59		
Ethanol	78	96	68						10	63

a) The decomposition of benzoyl *N*-(*p*-nitrophenyl)carbamoyl peroxide usually gave a dark brown polymeric substance besides the compounds listed in this table.

TABLE 5. PRODUCTS OF DECOMPOSITION OF *t*-BUTYL *N*-(*p*-NITROPHENYL)PEROXYCARBAMATE AND BENZOYL PEROXIDE

Peroxide	Reaction conditions		Products (yield in mol% of peroxide)				
	Solvent	Temp. °C	Carbon dioxide	Benzoic acid	Biphenyl	*p,p'*-Dinitro-azobenzene	*p*-Nitro-aniline
Peroxycarbamate	Benzene	80	96		4	8	77
Peroxycarbamate	Ethanol	78	98			1	90
Benzoyl peroxide	Benzene	80	178	7	126[a]		

a) Biphenyl 90% and dihydrobiphenyl 36%.

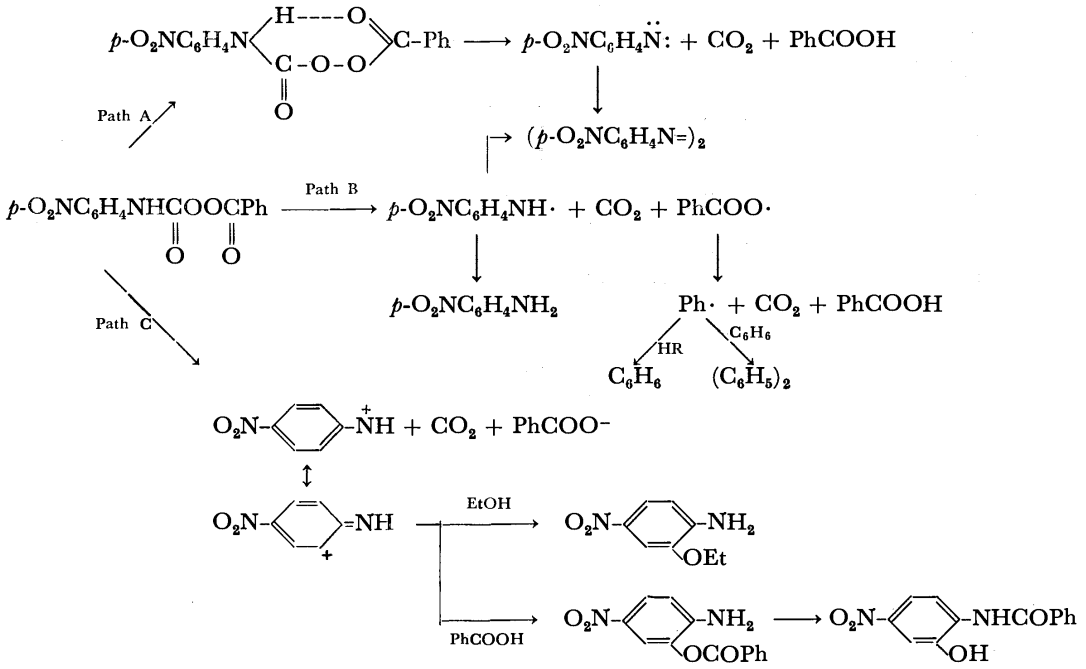

Scheme 1.

carbamoyloxy radical, when generated in benzene or in ethanol, gives mainly carbon dioxide (96—98%) and *p*-nitroaniline (77—90%) with *p,p'*-dinitroazobenzene as a minor product, and that 89% of the benzoyloxy radical generated in benzene loses carbon dioxide before it engages in other reactions, finally to form 63% of biphenyl, and only 3.5% of benzoic acid was obtained. No trace of 5-nitro-2-aminophenetole was detected in the decomposition in ethanol.

On the basis of the results presented above, three pathways are proposed as shown in Scheme 1 for the thermal decomposition of benzoyl *N*-(*p*-nitrophenyl) carbamoyl peroxide. Path A is a concerted mechanism via a seven-membered cyclic transition state giving rise to *p*-nitrophenylnitrene; path B is a radical mechanism beginning with the homolysis of the oxygen-oxygen bond usually observed in the thermal decomposition of peroxides; and path C is an ionic mechanism. The extent to which each of these mechanisms is operative depends on the experimental conditions under which the peroxide is decomposed.

Path A is straightforward and best explains the decomposition in crystalline state, since carbon dioxide and benzoic acid were obtained in nearly 100% yield and the fact that 30% of the *p*-nitrophenylcarbamoyloxy moiety was accounted for as *p,p'*-dinitroazobenzene strongly suggests the intermediacy of *p*-nitrophenylnitrene.[12]

Since the *p*-nitrophenylcarbamoyloxy moiety will liberate 100% of carbon dioxide in any of the postulated pathways, the fact that the carbon dioxide was evolved in excess of 100% in the decomposition in benzene, chloroform or acetic acid indicates the involvement of path B, in which the benzoyloxy radical generated decomposes also to give carbon dioxide at the expense of benzoic acid. However, if path B were the only mechanism operative in these solvents, the yield of benzoic acid would have been much less than actually found and as much as 180% or more of carbon dioxide would have been obtained, since benzoyloxy radicals extensively decompose to give phenyl radicals and carbon dioxide (cf. Table 5). Thus, the results of product analyses indicate that the decomposition in benzene proceeds via both paths A and B to the exclusion of path C, *viz.*, about 25%[13] through path B and consequently about 75% through path A.

The mode of decomposition in chloroform appears to be similar to that in benzene, but benzene was formed instead of biphenyl, the intermediate phenyl radical abstracting a hydrogen atom from chloroform.

Some of the *p*-nitrophenylamino radical produced in path B may undergo dimerization followed by dehydrogenation under the prevailing oxidizing conditions finally to give *p,p'*-dinitroazobenzene; but obviously its chief reaction is abstraction of a hydrogen atom from an appropriate hydrogen-donating species to give *p*-nitroaniline (cf. Table 5 and Ref. 2). It can also arise, however, from *p*-nitrophenylnitrene,[14] although this mode of formation seems to be a remote possibility in benzene.

As regards the decomposition in ethanol, product analysis suggests that it proceeds chiefly by path C, in which a protonated *p*-nitrophenylnitrene or a *p*-nitrophenylnitrenium ion[15] is postulated; a polar protic solvent such as ethanol is likely to favor such an ionic process. The production of 5-nitro-2-aminophenetole in a yield of as high as 63% supports this view and is best explained by nucleophilic attack on a mesomeric form of the nitrenium ion $p\text{-}O_2NC_6H_4NH^+$ by a molecule of ethanol as shown in Scheme 1. The formation of 5-nitro-2-benzamidophenol is similarly explained in terms of nucleophilic attack on the ring by benzoic acid or benzoate ion followed by migration of the benzoyl group to the nitrogen.[16] If path B were also operative to any perceptible extent, benzene and *p*-nitroaniline would have been detected. The intermediacy of *p*-nitrophenylnitrene is excluded because neither nitrogen-containing products expected from it nor products of dehydrogenation of ethanol such as acetaldehyde[17] were found.

The decomposition pattern in acetic acid is different from that in ethanol, especially in that such a product as 5-nitro-2-acetamidophenol, which would have readily arisen by way of path C was not detected; the intermediacy of protonated nitrene (path C) is thus ruled out. It is similar to that in benzene or chloroform as far as the yields of carbon dioxide and benzoic acid concerned; accordingly, path B is undoubtedly operating in some measure, and path A must be the major one, although *p,p'*-dinitroazobenzene and *p*-nitroaniline were absent from the reaction mixture. It is worth noting that 59% of *p*-nitroacetanilide was obtained as the sole product which accounts for the *p*-nitrophenylcarbamoyl group. A small part of the anilide may have been produced by prolonged contact of the *p*-nitroaniline initially formed with hot acetic acid solvent during the period of the reaction and the subsequent work-up, as was shown to be the case by separate experiments. The mechanism by which most of the *p*-nitroacetanilide was formed from *p*-nitrophenylnitrene or *p*-nitrophenylamino radical with acetic acid remains unexplained.

The thermal decomposition of benzoyl *N*-benzoylcarbamoyl peroxide in crystalline state was examined by measuring its infrared spectrum in Nujol mull, in which the peroxide was hardly soluble. A freshly prepared mull showed a ν_{N-H} band at 3420 cm^{-1} and $\nu_{C=O}$ bands at 1765 and 1685 cm^{-1}. When the same sample was measured after being kept 30 minutes at room temperature, the ν_{N-H} band had almost disappeared and new bands had appeared at 2350 and 2260 cm^{-1}, which are attributable to carbon dioxide and phenyl isocyanate, respectively. The $\nu_{C=O}$ band at 1765 cm^{-1} had considerably decreased in intensity, whereas the $\nu_{C=O}$ band at 1685 cm^{-1} was almost unchanged, although its band width had slightly increased. These facts would suggest that this peroxide decomposes in crystalline state giving carbon dioxide, benzoic acid and transitory benzoylnitrene, which seems to rearrange immediately to phenyl isocyanate.

The results of decompositions of benzoyl *N*-benzoylcarbamoyl peroxide in solutions are summarized in Table 6. The yield of carbon dioxide was higher than 100% in benzene, but lower in ethanol. Benzoic acid was formed nearly quantitatively in ethanol. Biphenyl, which was found in benzene, is a product indicative of the operation of a radical mechanism but in ethanol no such products were detected; for example, benzene, which would have readily resulted from phenyl radicals by abstraction of a hydrogen atom from ethanol, was absent from the reaction mixture. Products containing nitrogen were: in benzene solution, benzamide, phenyl isocyanate, carbanilide and γ-triphenylbiuret, the last two being produced from the reaction of phenyl isocyanate with benzoic acid;[18] and in ethanol solution, ethyl benzhydroxamate.

These findings may be accommodated in the reaction sequences shown in Scheme 2, which are formulated by the analogy with Scheme 1.

In path A', the intermediate formation of benzoylnitrene is postulated, which immediately rearranges to phenyl isocyanate,[19] and this in turn reacts with benzoic acid to give further products. Path B' represents a homolytic mechanism; the benzoyloxy radical will undergo a series of the usual reactions in benzene and the benzamido radical will abstract a hydrogen atom[20] from intermediate phenylcyclohexadienyl $C_6H_5C_6H_6\cdot$ radicals to give benzamide and biphenyl. Paths A' and B' are both operative in the decomposition in benzene; the former explains the formation of phenyl isocyanate and its subsequent reaction products with benzoic acid (carbanilide and γ-triphenylbiuret) and the latter that of biphenyl, benzamide, and more than 100 mol% of carbon dioxide.

Path C' postulated as a counterpart of path C in

Table 6. Products of decomposition of benzoyl *N*-benzoylcarbamoyl peroxide

Reaction conditions		Products (yield in mol% of peroxide)					
Solvent	Temp. (°C)	Carbon dioxide	Benzoic acid	Biphenyl	Benzamide	Phenyl isocyanate	Ethyl benzhydroxamate
Benzene[a]	80	124	28	34	34	2	
Ethanol	78	72	94				38

a) In addition to the products in this table carbanilide and γ-triphenylbiuret were isolated.

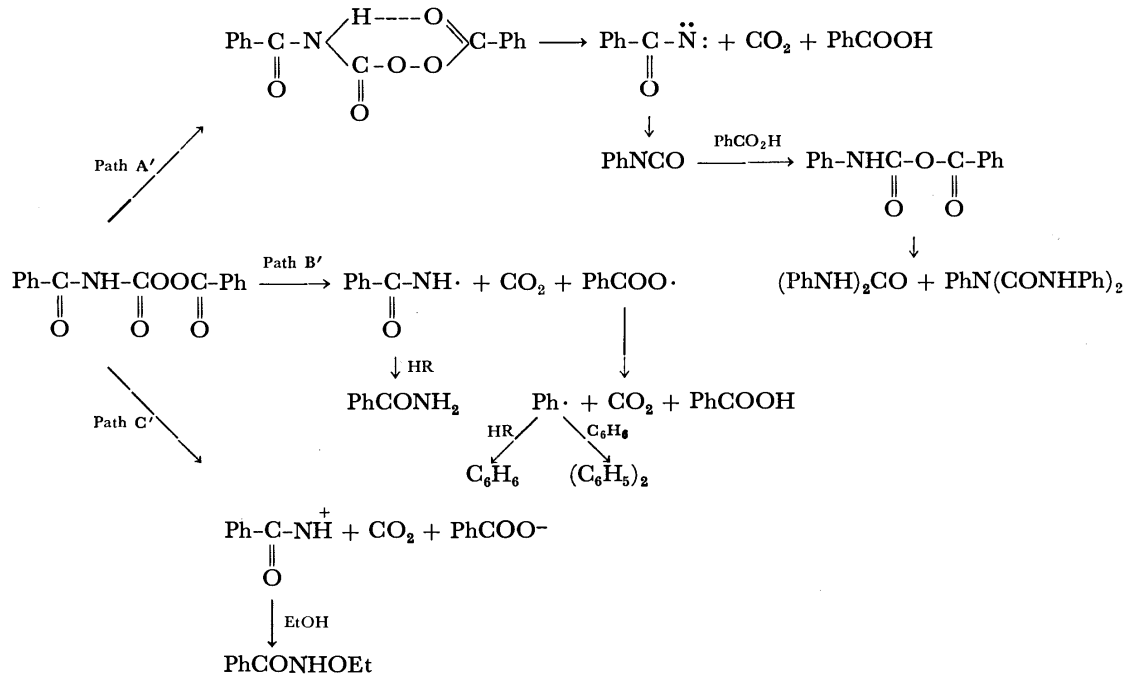

Scheme 2.

Scheme 1 involves protonated benzoylnitrene, which undergoes nucleophilic attack by ethanol, and best explains the formation of ethyl benzhydroxamate as the only isolable nitrogen containing compound in ethanol. It would seem possible that ethyl benzhydroxamate might have been formed by the action of solvent ethanol on benzoylnitrene produced by path A', thus,

$$C_6H_5CON: + EtOH \rightarrow C_6H_5CONHOEt.$$

Such a reaction is in fact reported by Horner, Bauer and Dorges,[21] but benzoylnitrene does not seem to be a proper intermediate in the present case, since no ethyl *N*-phenylcarbamate was detected, which ought to have been formed from ethanol and phenyl isocyanate, if benzoylnitrene had been involved, and which actually was obtained together with the benzhydroxamate.[21]

Experimental

Isocyanates and peroxy-acids were prepared by reported methods. *t*-Butyl *N*-(*p*-nitrophenyl)peroxycarbamate was prepared according to the directions given by O'Brien and his co-workers.[3]

Preparation of Acyl Carbamoyl Peroxides. A typical procedure is given below for the preparation of benzoyl *N*-(*p*-nitrophenyl)carbamoyl peroxide. Other peroxides were prepared similarly (see Table 1).

Benzoyl N-*(*p-*Nitrophenyl)carbamoyl Preoxide.* *p*-Nitrophenyl isocyanate (8.9 g, 0.055 mol) and two drops of pyridine were dissolved in 150 ml of absolute ether and to this solution, cooled to −15—−20 °C, was added slowly an ethereal solution (50 ml) of peroxybenzoic acid (purity 95%, 0.055 mol) with stirring while maintaining the temperature below −10 °C. The temperature was gradually raised to 0 °C after completion of the addition of the peroxy-acid. The precipitation of the peroxide set in after about 30 min. The mixture was stirred for a further 3 hr. The peroxide was filtered off and washed with cold ether three times (yield, 55%). The peroxide, at this stage, was almost pure and free from contamination with *p,p'*-dinitrodiphenylurea when pure starting materials were used. Recrystallization of 7.0 g of the peroxide from methylene chloride between 10 and −78 °C gave 4.0 g of almost white crystals, which explosively decomposed at 63 °C when heated at a rate of 4—5 °C per minute.

Benzoyl N-*(*m-Chlorophenyl)carbamoyl Peroxide.* Peroxybenzoic acid (3.2 g, 0.022 mol) in 20 ml of ether was added to 20 ml of an ethereal solution of *m*-chlorophenyl isocyanate according to the procedure described above for the *p*-nitro-derivative. After being stirred for 4 hr, the reaction mixture was added to 750 ml of petroleum ether (bp 35—40 °C) in order to precipitate the peroxide. Cooling the solution at −78 °C gave 3.3 g (55%) of a white solid material tinged with violet. This solid was certainly the desired peroxide, because it liberated iodine from an acetic acid solution of sodium iodide and violently detonated when allowed to stand for a few minutes at room temperature or heated on a spatula over a flame; it was too unstable to be submitted to elemental analysis and determination of active oxygen.

Benzoyl N-*Methyl*-N-*(*p-nitrophenyl)carbamoyl Peroxide.* An aqueous solution (30%) of potassium hydroxide (0.011 mol) was added dropwise with stirring to 170 ml of an ethereal solution of peroxybenzoic acid (1.7 g, 0.011 mole) and *N*-methyl-*N*-(*p*-nitrophenyl)carbamoyl chloride (2.2 g, 0.01 mole). After being stirred for 3 hr at −5 °C, the solution was kept at −78 °C for one day. Precipitated potassium chloride was filtered off and the filtrate was concentrated to 10 ml by evaporating the ether at −10 °C. Addition of cold petroleum ether to the concentrate gave a yellowish orange paste, which liberated iodine from an aqueous acetic acid solution of sodium iodide and decomposed even at 0 °C evolving carbon dioxide. The decomposition products of the peroxide at room temperature were *N*-methyl-*p*-nitroaniline (72%), mp and mixed mp 151 °C (lit,[22] 152 °C), benzoic acid (20%), and a trace of *N,N'*-bis-(p-nitrophenyl)ethylenediamine, mp 218—219°C (lit,[23] 220—221 °C), each of them being isolated by chromatography on alumina.

Thermal Decomposition of Peroxide. The decompositions

in solution were all performed under nitrogen or argon. Carbon dioxide evolved was measured by absorption in an Ascarite tube. Gas chromatographic analyses were carried out with a Perkin-Elmer Vapour Fractometer Model 154.

Decomposition of Benzoyl N-(p-Nitrophenyl)carbamoyl Peroxide in Crystalline State. The peroxide (1.839 g) was allowed to stand at room temperature (about 20 °C) for a week. The gas (0.261 g) evolved during the decomposition was shown to contain only carbon dioxide by mass spectrometric analysis. The residue was extracted with 400 ml of benzene for 13 hr in a Soxhlet extractor. From the benzene solution, benzoic acid (0.599 g) was recovered by using 5% sodium bicarbonate. The residual benzene solution was dried with anhydrous sodium sulfate, concentrated to 50 ml, and chromatographed on alumina to give *p,p'*-dinitroazobenzene (0.23 g), mp and mixed mp 218—219 °C (lit,[22] 220 °C), and a trace of *p*-nitroaniline, mp and mixed mp 147—148 °C (lit,[22] 148 °C).

Decomposition of Benzoyl N-(p-Nitrophenyl)carbamoyl Peroxide in Benzene. Benzene (900 ml) in a two-necked round-bottomed flask fitted with a gas inlet tube and a reflux condenser was flushed with a stream of nitrogen for an hour, and the peroxide (1.522 g, 5.03 mmol) was added quickly and dissolved by stirring. The solution was heated under reflux for 19 hr, nitrogen being slowly bubbled. Carbon dioxide (260 mg, 5.92 mmol) evolved. Removal of benzene by distillation gave 50 ml of a deep-red benzene solution. After the solution was shaken with 5% sodium bicarbonate to remove benzoic acid (297 mg, 2.43 mmol), it was dried with anhydrous sodium sulfate and analyzed; gas chromatography with an Apiezon grease column at 220 °C showed the presence of biphenyl only and chromatography on alumina and elution with benzene gave, in succession, biphenyl (152 mg, 0.99 mmol), *p,p'*-dinitroazobenzene (165 mg, 0.61 mmol), and unidentified brownish orange crystals (34 mg, mp 189—190 °C, from ethanol), and then elution with ether yielded *p*-nitroaniline (103 mg, 0.75 mmol).

Decomposition of Benzoyl N-(p-Nitrophenyl)carbamoyl Peroxide in Chloroform. The peroxide (2.673 g, 8.84 mmol) in 700 ml of chloroform was heated under reflux for 6 hr. The procedure was virtually the same as described above for the decomposition in benzene. The amount of carbon dioxide evolved was 494 mg (11.2 mmol). Chloroform was distilled from the reaction mixture through a concentric column of 80 cm in height to give 50 ml of a concentrated solution, a small portion of which was submitted to gas chromatographic analysis using an Apiezon grease column at 80 °C; it contained 227 mg (2.91 mmol) of benzene and no chlorobenzene. Isolation and identification of other products were carried out by chromatography on alumina as described above.

Decomposition of Benzoyl N-(p-Nitrophenyl)carbamoyl Peroxide in Acetic Acid. The peroxide (2.696 g, 8.94 mmol) in 665 ml of anhydrous acetic acid was decomposed at 50 °C for 12 hr. Acetic acid was carefully distilled through a 40 cm Vigreux column, an initial fraction (80 ml) boiling at 40—42 °C/35—38 mmHg being collected. This was fractionated through a concentric column of 80 cm in height under atmospheric pressure, an initial fraction (5 ml) being subjected to gas chromatographic analysis using a polyethylene glycol column at 100 °C to determine the quantity of benzene formed. The residual acetic acid solution in the first distillation was further concentrated almost to dryness at the same temperature and pressure as described above to give a brown solid, which was washed with 5% sodium bicarbonate to remove acidic compounds and then dissolved in a large amount of methylene chloride. The acid part extracted consisted of only benzoic acid (5.11 mg, 4.18 mmol), because methylation of the extract with diazomethane followed by gas chromatography showed the presence of methyl benzoate without any trace of other methyl esters such as methyl succinate which would have been formed from acetic acid solvent. Evaporation of the methylene dichloride solution gave only *p*-nitroacetanilide (952 mg, 5.29 mmol), which was identified by mixed melting point determination (213—215 °C, lit,[22] 215—216 °C) and comparison of the infrared spectrum.

Decomposition of Benzoyl N-(p-Nitrophenyl)carbamoyl Peroxide in Absolute Ethanol. The peroxide (1.409 g, 4.67 mmol) dissolved in 850 ml of absolute ethanol was heated under reflux for 24 hr. Carbon dioxide evolved weighed 196 mg (4.48 mmol). Removal of the solvent from the reaction mixture, an initial 100 ml of the distillate being retained for later examination, gave 70 ml of a deep-red solution, which was mixed with benzene and subjected to azeotropic distillation for complete removal of ethanol. The remaining benzene solution was filtered from insoluble dark brown precipitate, shaken with 5% sodium bicarbonate to extract benzoic acid (388 mg, 3.17 mmol), dried with anhydrous sodium sulfate and chromatographed on alumina, to give 5-nitro-2-aminophenetole (535 mg, 2.94 mmol) mp 90—91 °C (lit,[22] 91 °C). Found: C, 52.65; H, 5.72; N, 15.62%. Calcd for $C_8H_{10}N_2O_3$: C, 52.74; H, 5.53; N, 15.38%. Subsequent elution with benzene–ether mixture (1 : 9) gave two unidentified compounds in small amounts (20 mg and 30 mg). The dark brown precipitate insoluble in benzene mentioned above was recrystallized from ethanol and identified as 5-nitro-2-benzamidophenol (121 mg, 0.47 mmol), mp 266—267 °C. Found: C, 60.46; H, 4.07; N, 10.99%. Calcd for $C_{13}H_{10}N_2O_4$: C, 60.46; H, 3.90; N, 10.85%. The infrared spectrum in Nujol mull showed characteristic bands at 3340 (ν_{N-H}), 3110 (ν_{O-H}), and 1630 ($\nu_{C=O}$) cm^{-1}.

The initial fraction from the first distillation was submitted to gas chromatographic analysis for benzene using a polypropylene glycol column at 70 °C; but none was detected other than etanol.

Decomposition of Benzoyl N-benzoylcarbamoyl Peroxide in Benzene. The peroxide (2.846 g, 10.0 mmoles) was decomposed in 480 ml of benzene by heating under reflux for 49 hr. Carbon dioxide evolved weighed (544 mg 12.4 mmol). On cooling the solution, 0.0215 g of a light brown solid precipitated. It was filtered off and identified as a mixture of carbanilide (*sym*-diphenylurea) and γ-triphenylbiuret by comparing its infrared spectrum with those of authentic samples. The above filtrate, after being concentrated to 23 ml, was shown by gas chromatography (Apiezon grease L, at 150 °C) to contain biphenyl and phenyl isocyanate. The concentrate was shaken with 5% sodium bicarbonate, dried with anhydrous sodium sulphate and chromatographed on alumina to give biphenyl (402 mg), traces of carbanilide and γ-triphenylbiuret. The aqueous extract was dissolved in ether, methylated by diazomethane and submitted to gas chromatography using an Apiezon grease column at 161 °C; methyl benzoate (385 mg, 2.83 mmol) was detected. Evaporation of the ethereal solution and extraction of methyl benzoate from the residue with petroleum ether left benzamide (413 mg, 3.41 mmol), which was identified by the mixed mp (131—133 °C, lit,[22] 132.5—133.5 °C) and the infrared spectrum.

Decomposition of Benzoyl N-Benzoylcarbamoyl Peroxide in Absolute Ethanol. The peroxide (2.818 g, 9.89 mmol) was heated in ethanol (500 ml) under reflux for 20 hr, during which period 314 mg (7.13 mmol) of carbon dioxide evolved. The reaction mixture was concentrated to about 5 ml and

allowed to stand overnight in a refrigerator. After filtration of precipitated benzoic acid (266 mg), removal of the ethanol and addition of benzene, the solution was shaken with 5% sodium bicarbonate, dried with calcium chloride and evaporated to give 0.580 g of a light brown liquid residue. The acid portion extracted (1.937 g) with bicarbonate was methylated with diazomethane in ether and found to contain 0.861 g of benzoic acid by gas chromatographic determination of the methyl benzoate formed, and the remainder (1.112 g) of the aqueous extract, which was obtained of the extraction of the methyl benzoate with petroleum ether, was shown to be essentially identical with the above light brown liquid by comparison of the infrared spectra. A portion (0.417 g) of this liquid was dissolved in 3 ml of tetrahydrofuran and heated under reflux for 10 hr with 10 ml of 10% aqueous potassium hydroxide giving 0.152 g of benzoic acid and 0.151 g of ethyl benzhydroxamate, mp and mixed mp 63—64 °C (lit,[24] 64—65 °C), which is known to remain intact by treatment with alkali.[24] The light brown liquid was, therefore, considered to consist of ethyl benzhydroxamate (612 mg) and a compound which gave benzoic acid by alkaline hydrolysis.

Decomposition of t-*Butyl* N-*(*p-*Nitrophenyl)peroxycarbamate in Benzene.* Heating this peroxy-ester (1.282 g, 5.04 mmol) in benzene under reflux for 78 hr gave 213 mg (4.84 mmol) of carbon dioxide. The reaction mixture was concentrated to 29 ml and chromatographed on alumina to give biphenyl (29 mg 0.19 mmol), *p,p'*-dinitroazobenzene (103 mg, 0.38 mmol) and *p*-nitroaniline (536 mg, 3.88 mmol).

Decomposition of t-*Butyl* N-*(*p-*Nitrophenyl)peroxycarbamate in Ethanol.* The peroxy-ester (3.995 g, 15.7 mmol) was heated in ethanol (900 ml) under reflux for 22 hr to yield 681 mg (15.5 mmol) of carbon dioxide. Concentration of the reaction mixture to 70 ml and azeotropic distillation after addition of 150 ml of benzene gave 70 ml of a benzene solution and a precipitate (*p*-nitroaniline, 783 mg). The filtered benzene solution was chromatographed on alumina to give *p,p'*-dinitroazobenzene (35 mg, 0.13 mmol) and *p*-nitroaniline (1.145 g).

Decomposition of Benzoyl Peroxide in Benzene. Benzoyl peroxide (1.250 g, 5.17 mmol) was decomposed in boiling benzene for 46 hr to evolve 403 mg (9.18 mmol) of carbon dioxide. After the solution was concentrated to 26 ml, benzoic acid (46 mg, 0.38 mmol) was extracted with 5% sodium bicarbonate and the organic layer was submitted to gas chromatographic analysis for determination of biphenyl (716 mg) and dihydrobiphenyl (284 mg).

References

1) H. Esser, K. Rastadter and G. Reuter, *Chem. Ber.*, **89**, 685 (1956).
2) C. J. Pedersen, *J. Org. Chem.*, **23**, 252, 255 (1958).
3) E. L. O'Brien, F. M. Beringer and R. B. Mesrobian, *J. Amer. Chem. Soc.*, **79**, 6238 (1957); **81**, 1506 (1959).
4) R. Okazaki and O. Simamura, *Chem. Commun.*, **1969**, 1308.
5) R. G. Arnold, J. A. Nelson, and J. J. Verbanc, *Chem. Rev.*, **57**, 49 (1957).
6) C. G. Swain, W. H. Stockmayer, and J. T. Clarke, *J. Amer. Chem. Soc.*, **72**, 5426 (1950).
7) A. T. Blomquist and I. A. Berstein, *ibid.*, **73**, 5546 (1951).
8) P. D. Bartlett and C. Rüchardt, *ibid.*, **82**, 1756 (1960).
9) C. L. Arcus and B. S. Prydal, *J. Chem. Soc.*, **1954**, 4018.
10) O. C. Billeter, *Ber.*, **37**, 690 (1904).
11) G. S. Hammond and L. M. Soffer, *J. Amer. Chem. Soc.*, **72**, 4711 (1950).
12) P. A. S. Smith in "Nitrenes," W. Lwowski, Interscience Publishers, New York (1970), Chapter 4, reviews the chemistry of arylnitrenes.
13) Estimated from the yields of carbon dioxide and biphenyl given in Tables 4 and 5. From carbon dioxide: (117—98)/(178/2)=0.22; and from biphenyl: (20—4)/(126/2)=0.25.
14) The formation of arylamines from arylnitrenes by abstraction of hydrogen atoms is a recognized reaction,[12] but it was reported that thermolysis of *p*-nitrophenyl azide gave only a small amount of *p*-nitroaniline in decalin at 141° (P. A. S. Smith and J. H. Hall, *J. Amer. Chem. Soc.*, **84**, 480 (1962)) and none of it in boiling acetic anhydride (R. K. Smalley and H. Suschitzky, *J. Chem. Soc.*, **1963**, 5571).
15) The concept of protonated nitrene is not new; its intermediacy has often been invoked, for example in the reactions of aryl azides in acid solution and the rearrangement of phenylhydroxylamines. See, *e.g.*, R. A. Abramovitch and B. A. Davis, *Chem. Rev.*, **64**, 177 (1964) and H. J. Shine, "Aromatic Rearrangements," Elsevier Publishing Co., Amsterdam (1967) P. 188.
16) A. Einhorn and B. Pfyl, *Ann.*, **311**, 34 (1900); M. Bergmann, R. Ulpts, and F. Camacho, *Ber.*, **55**, 2801 (1922).
17) P. Walker and W. A. Waters (*J. Chem. Soc.*, **1962**, 1632) observed the formation of benzaldehyde in thermolysis of *p*-methoxyphenylazide in benzyl alcohol at 132 °C.
18) C. Walling and A. N. Naglieri, *J. Amer. Chem. Soc.*, **82**, 1820 (1960) and earlier references cited therein.
19) L. Horner and A. Christmann, *Chem. Ber.*, **96**, 388 (1963).
20) L. Horner and G. Bauer, *Tetrahedron Lett.*, **1966**, 3573.
21) L. Horner, G. Bauer, and J. Dorges, *Chem. Ber.*, **98**, 2631 (1965).
22) "Dictionary of Organic Compounds," ed. by J. R. A. Pollock and R. Stevens, Maruzen Company, Ltd., Tokyo, Japan (1965).
23) W. Borsche and J. C. Titsingh, *Ber.*, **40**, 5014 (1907).
24) M. E. Waldstein, *Ann. Chem.*, **181**, 386 (1876).

Crystal and Molecular Structure of ω-Amino Acids, ω-Amino-Sulfonic Acids and Their Derivatives. VII. The Crystal and Molecular Structure of DL-Carnitine Hydrochloride

Ken-ichi TOMITA, Keiko URABE, Yang Bae KIM,* and Takaji FUJIWARA

Faculty of Pharmaceutical Sciences, Osaka University, Toneyama, Toyonaka, Osaka 560

(Received April 24, 1974)

The crystal structure of DL-carnitine hydrochloride, $C_7H_{15}NO_3 \cdot HCl$, was determined by the heavy atom method using X-ray diffraction data on a Weissenberg photograph, and refined by the least-squares method to an *R*-factor of 0.13 for 1969 independent reflections. The crystals are monoclinic space group $P2_1/c$, $Z=4$, with $a=6.77(1)$, $b=11.41(2)$, $c=15.10(3)$ Å and $\beta=120.1(1)°$. By protonation at carboxyl oxygen atom, carnitine molecule has the cationic form, $N^+(CH_3)_3CH_2CH(OH)CH_2COOH$, with *trans-zigzag* skeletal configuration as similar as γ-amino-β-hydroxybutyric acid. The Cl^- ion mediates between adjacent carnitine cations by two O–H···Cl^- hydrogen bonds to form infinite chain elongated along the *c*-axis. The correlation between molecular structure and biological activity was also discussed.

Carnitine is a constituent of striated muscle and liver, being isolated from meat extract.[1] Its chemical structure was identified by M. Tomita et al. as L-γ-trimethylamino-β-hydroxybutyrobetaine by synthesis from L-γ-amino-β-hydroxybutyric acid.[2] Carnitine is well known as a vitamin B_T, a growth factor of certain insects, and medically used as a stimulant of gastric juice secretion. Furthermore, carnitine and its acetyl-derivatives have the muscarinic action in nervous system.[3] As its chemical structure is very similar to that of acetylchlorine and γ-amino-β-hydroxybutyric acid (GABOB), both chemical transmitters, we have carried out a single crystal X-ray analysis of DL-carnitine hydrochloride as a part of a series on the structural studies of ω-amino acids, and we also discuss very interesting correlation between structural specificity and biological activity.

Experimental

Using the commercial DL-carnitine hydrochloride, a colorless plate crystal was obtained from aqueous methanol solution by slow evaporation at room tempreature. The space group and cell constants were determined from precession photograph: the systematic absences of $0k0$ reflections with k odd and $h0l$ with l odd indicate that the space group is $P2_1/c$. The density was measured by flotation method using carbon tetrachloride-benzene mixture. The obtained crystallographic data are shown in Table 1. The intensities of 1969 independent reflections were collected from equi-inclination Weissenberg photographs around the *a*- and *b*-axes ($h=0$—5, $k=0$—3) with nickel-filtered Cu$K\alpha$ radiation and estimated by visual comparison with a calibrated scale. The usual corrections for Lorentz and polarization factors were made but none for absorption or extinction.

TABLE 1. CRYSTAL DATA

DL-Carnitine hydrochloride, $C_7H_{15}NO_3 \cdot HCl$	
Colorless transparent plates, Monoclinic system	
$a=6.77\pm0.01$ Å	$b=11.41\pm0.02$ Å
$c=15.10\pm0.03$ Å	$\beta=120.1\pm0.1°$
Volume of unit cell	1008.9 Å^3
Density (by flotation)	1.290 g/cm^3
Density (calculated)	1.301 g/cm^3
$Z=4$	$F(000)=428$
Space group: $P2_1/c$	

Structure Determination and Refinement

The structure was solved by heavy atom method. The position of the chlorine atom was easily determined from the inspection of sharpened Patterson map and all the non-hydrogen atoms were located by successive Fourier syntheses with phases based on the chlorine atom. By block-diagonal least-squares refinement with unit weight for the non-zero reflections and isotropic temperature factor, the initial *R*-factor, 0.26, was reduced to 0.19. Several cycles of refinement with anisotropic temperature factor for all non-hydrogen atoms were carried out to reduce *R*-factor to 0.17. The used anisotropic temperature factors are of the form: $\exp\{-(B_{11}h^2+B_{22}k^2+B_{33}l^2+B_{12}hk+B_{13}hl+B_{23}kl)\}$.

A three-dimensional difference Fourier synthesis was then calculated and the positions of seven hydrogen atoms except those of methyl groups, were properly found. Each one hydrogen atom peak of three methyl groups having reasonable bond length and angle in the difference Fourier map was fixed and the remaining two hydrogen atom positions in each methyl group were calculated. The final cycles of refinement including the hydrogen atoms with isotropic temperature factors reduced *R*-factor to 0.13 (0.14 including $|F_0|=0$).

Observed and calculated structure factors for each reflection are listed in Table 2. The atomic scattering factors used in all calculations were taken from International Tables for X-ray Crystallography (1692).[4] The final positional and thermal parameters together with their estimated standard deviations are gived in Tables 3(a) and 3(b).

All the computations were carried out on an NEAC 2200—700 Computer at this University using the programs of UNICS system.

Results and Discussion

Molecular Dimensions. The bond lengths and angles are shown in Table 4 with their estimated stand-

* Present address: College of Pharmacy, Seoul National University, Seoul, Korea

TABLE 2. OBSERVED AND CALCULATED STRUCTURE FACTORS

TABLE 3(a) FINAL POSITIONAL AND THERMAL PARAMETERS WITH THEIR STANDARD DEVIATIONS IN PARENTHESIS ($\times 10^4$)

Atom	x/a	y/b	z/c	B_{11}	B_{22}	B_{33}	B_{12}	B_{13}	B_{23}
Cl	870(3)	2888(2)	4220(1)	44(4)	35(1)	16(1)	49(5)	24(3)	21(2)
C(1)	5589(17)	6422(9)	2880(7)	182(30)	34(7)	32(6)	−140(24)	61(21)	−6(10)
C(2)	5876(15)	4453(8)	3526(6)	101(24)	22(6)	20(5)	74(21)	−51(16)	4(9)
C(3)	3330(15)	5856(8)	3639(6)	128(24)	35(6)	16(4)	−35(21)	57(17)	−31(9)
C(4)	2418(12)	5091(7)	1933(5)	29(18)	16(5)	1(4)	−10(16)	−3(11)	3(7)
C(5)	455(12)	4365(6)	1855(5)	55(19)	3(4)	1(4)	6(15)	15(11)	9(6)
C(6)	−1282(11)	4224(7)	717(5)	13(18)	27(5)	2(3)	−21(17)	−14(13)	6(7)
C(7)	−3536(11)	3776(7)	553(5)	20(18)	7(4)	7(4)	−8(15)	−1(13)	−2(7)
N	4271(10)	5439(5)	2999(4)	58(17)	3(4)	4(3)	−4(13)	11(11)	3(5)
O(1)	1204(10)	3256(5)	2291(4)	163(18)	6(3)	15(3)	28(14)	56(12)	29(5)
O(2)	−4190(10)	3869(5)	1159(5)	118(18)	56(5)	29(4)	−68(17)	112(14)	−40(7)
O(3)	−4729(10)	3249(5)	−343(4)	94(16)	55(5)	10(3)	−96(16)	19(11)	−25(7)

TABLE 3(b). POSITIONAL AND THERMAL PARAMETERS OF HYDROGEN ATOMS

Atom	Bound to	x/a(×10³)	y/b(×10³)	z/c(×10³)
H(1)	O(3)	−634	271	−45
H(2)	C(6)	−73	346	41
H(3)	C(6)	−97	504	51
H(4)	C(5)	−54	485	214
H(5)	O(1)	35	296	264
H(6)	C(4)	187	591	158
H(7)	C(4)	318	459	154
H(8)	C(2)	632	408	301
H(9)	C(2)	736	468	412
H(10)	C(2)	480	379	366
H(11)	C(3)	459	618	416
H(12)	C(3)	308	508	391
H(13)	C(3)	155	624	325
H(14)	C(1)	709	660	364
H(15)	C(1)	605	619	227
H(16)	C(1)	447	719	269

Over-all isotropic temperature factor is 1.244 Å²

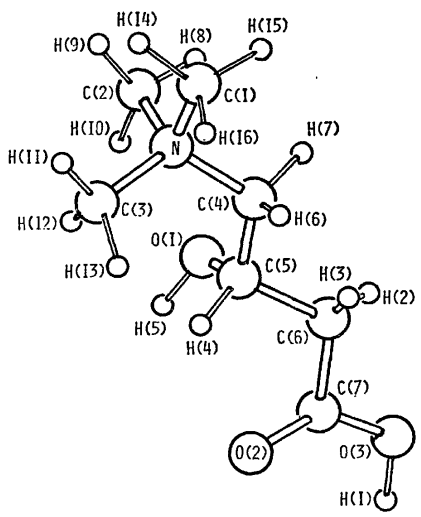

Fig. 1. The perspective drawing of the molecule of carnitine.

ard deviations in parentheses, in which the atomic numbering corresponds to that in Fig. 1, the perspective drawing of the molecule of carnitine as observed in crystals of the hydrochloride. They are in good agreement with those reported in the literatures. It is evident, from the difference in bond length between C_7–O_2 and C_7–O_3, that the protonation occurs at O_3 atom, being confirmed by difference Fourier synthesis.

The carnitine molecule has two planes, one is defined by the skeletal carbon, C_4, C_5, and C_6, and nitrogen N (plane 1), and another one by C_6, C_7, O_2 and O_3 (plane 2). The equations of least squares planes and deviations of the individual atoms from each plane are listed in Table 5. The experimental value of the dihedral angle between these two planes is 29.2°, indicating that all the non-hydrogen atoms in main carnitine molecule compose roughly a *trans-zigzag* configuration except two methyl carbon and hydroxyl oxygen atoms. The torsion angles around relevant bonds are shown in Fig. 2, with which it will be discussed later.

The hydrogen atoms of the trimethylammonium group have been observed to be in a staggered conformation and the C_4–N–C_1–H_{14}, C_4–N–C_2–H_9 and C_4–N–C_3–H_{11} torsion angles are all nearly 180°. This staggered conformation is also observed in the crystal

TABLE 4. BOND LENGTHS(Å) AND ANGLES(°) OF CARNITINE

Estimated standard deviations are listed in parentheses except the bonds including hydrogen atoms.

	Bond length		Bond angle		Bond angle
N-C(1)	1.499(13)	C(1)-N-C(2)	108.1(7)	H(6)-C(4)-N	101
N-C(2)	1.487(12)	C(1)-N-C(3)	108.4(7)	H(7)-C(4)-C(5)	108
N-C(3)	1.475(12)	C(1)-N-C(4)	107.1(7)	H(7)-C(4)-N	110
N-C(4)	1.518(10)	C(2)-N-C(3)	109.5(7)	H(8)-C(2)-H(9)	104
C(4)-C(5)	1.519(11)	C(2)-N-C(4)	111.4(7)	H(8)-C(2)-H(10)	108
C(5)-C(6)	1.529(11)	C(3)-N-C(4)	112.3(7)	H(8)-C(2)-N	108
C(5)-O(1)	1.419(10)	N-C(4)-C(5)	116.8(7)	H(9)-C(2)-H(10)	118
C(6)-C(7)	1.507(11)	C(4)-C(5)-O(1)	111.3(7)	H(9)-C(2)-N	115
C(7)-O(2)	1.203(10)	C(4)-C(5)-C(6)	107.2(6)	H(10)-C(2)-N	104
C(7)-O(3)	1.324(10)	C(5)-C(6)-C(7)	111.5(6)	H(11)-C(3)-H(12)	106
		C(6)-C(7)-O(2)	124.9(7)	H(11)-C(3)-H(13)	126
O(3)-H(1)	1.19	C(6)-C(7)-O(3)	111.8(7)	H(11)-C(3)-N	100
C(6)-H(2)	1.14	C(6)-C(5)-O(1)	108.7(7)	H(12)-C(3)-H(13)	101
C(6)-H(3)	1.03	O(2)-C(7)-O(3)	123.3(8)	H(12)-C(3)-N	101
C(5)-H(4)	1.11			H(13)-C(3)-N	119
O(1)-H(5)	1.01	H(1)-O(3)-C(7)	115	H(14)-C(1)-H(15)	114
C(4)-H(6)	1.05	H(2)-C(6)-H(3)	115	H(14)-C(1)-H(16)	106
C(4)-H(7)	1.12	H(2)-C(6)-C(7)	101	H(14)-C(1)-N	107
C(2)-H(8)	1.05	H(2)-C(6)-C(5)	108	H(15)-C(1)-H(16)	113
C(2)-H(9)	0.99	H(3)-C(6)-C(5)	95	H(15)-C(1)-N	110
C(2)-H(10)	1.14	H(3)-C(6)-C(7)	127	H(16)-C(1)-N	105
C(3)-H(11)	0.91	H(4)-C(5)-C(4)	112		
C(3)-H(12)	1.02	H(4)-C(5)-C(6)	102		
C(3)-H(13)	1.13	H(4)-C(5)-O(1)	115		
C(1)-H(14)	1.11	H(5)-O(1)-C(5)	111		
C(1)-H(15)	1.15	H(6)-C(4)-H(7)	109		
C(1)-H(16)	1.10	H(6)-C(4)-C(5)	112		

TABLE 5. EQUATIONS OF LEAST-SQUARES PLANES AND DEVIATIONS OF INDIVIDUAL ATOMS FROM THESE PLANES

Equation[a]	Deviations of atoms in Å		
0.55309X−0.83308Y+0.00833Z+4.7564=0 (plane 1)	C_4: −0.0291	C_5: 0.0247	C_6: 0.0378
	N: −0.0327		
0.25745X−0.87242Y+0.41545Z+4.17759=0 (plane 2)	C_6: 0.0009	C_7: −0.0012	O_2: 0.0012
	O_3: 0.0010		

a) X, Y, and Z are orthogonal coordinates in Å parallel to a, b, and c*.

structure of acetylcholine and its derivatives[5].

Molecular Enrivonment. Figure 3 shows the arrangement of the molecules in crystals as viewed along the *a*-axis. The chlorine ion mediates between adjacent carnitine cations by two O–H···Cl^- hydrogen bonds, $O_3H_1\cdots Cl^-$ (3.00 Å) and O_1–$H_5\cdots Cl^-$ (3.06 Å).

The contacts of the trimethylammonium group with the same group of neighboring molecules related by either a center of symmetry or two-fold screw axis have the normal van der Waals distances. There are no unusual short contacts in this crystal.

The Correlation between Molecular Structure and Biological Activity. As already mentioned in the introductory section, carnitine and its acetyl-derivatives have the muscarinic action in nervous system, and R. W. Baker *et al.* showed a strong correlation between structure and activity of muscarinic stimulants.[5] They pointed out that the torsion angles around relevant bonds and intramolecular distances between the nitrogen atom of trimethylammonium group and acetyl oxygen atom and so on in acetylcholine or its derivatives are of very important significance in performance of their activities. The torsion angle (τ) of the bonded group X–A–B–Y is defined as the angle between the plane X–A–B and the plane A–B–Y, and it is positive if clockwise and negative if anticlockwise from the near atom X to the further atom Y. As shown in Fig. 2, τ_1 of carnitine is +197.0°, τ_2 +174.8°, τ_3 +193.8° and τ_4 +203.3°, which correspond to all the anti-planar region of torsion angles defined by Klyne *et al.*[6] For comparison certain, torsion angles and interatomic distances observed in crystals of muscarinic stimulants are shown in Table 6(a) and (b), with that of carnitine hydrochloride and γ-amino-β-hydroxybutyric acid (GABOB). In this table, *ap*, *sc* or *ac* are the abbreviations of antiperiplanar, syn-clinal or anti-clinal, respectively. R. W. Baker *et al.* concluded that for potent muscarinic activity, τ_1 should be 180°, τ_2 in the range +73° to +137°,

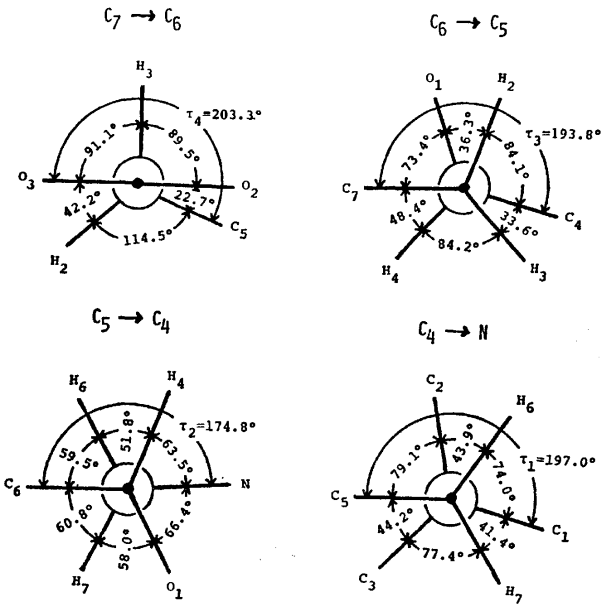

Fig. 2. The torsion angles around relevant bonds.

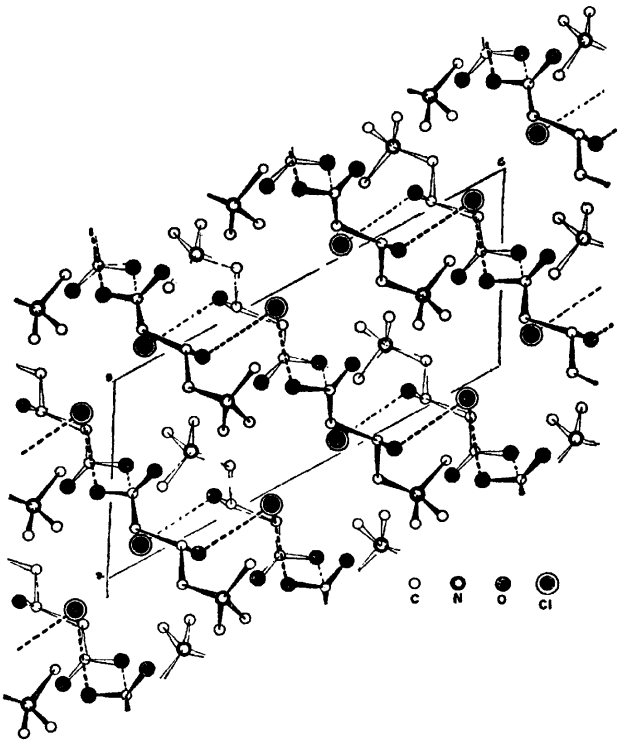

Fig. 3. The arrangement of the molecule in crystals as viewed along the *a*-axis.

τ_3 180±35° and τ_4 either 180° or −137°. The interatomic distances are: N^+–O (ester oxygen)=3.20 Å, N^+–C(carbonyl carbon)=4.50 Å and N^+–C(methyl carbon)=5.40 Å. Furthermore, the conformation of carbamoylcholine in crystals of its bromide is the only exceptional example of a potent muscarinic agonist with anti-periplanar conformation at τ_2(178°), and therefore, the relevant interatomic distances are significantly longer than those of the first three compounds in Table 6(b). On the other hand, the torsion angles and interatomic distances in crystals of carnitine hydrochloride and CABOB are very similar to those of carbamoylcholine because of having the *trans-zigzag* main chain configuration. It may be considered that there are two structurally different stimulants for muscarinic activity even if their conformations on interaction with the receptor molecule were modified from those observed in crystals. In other words, it may strongly suggest that the existence of two different receptor sites for muscarinic stimulants.

TABLE 6(a). CERTAIN TORSION ANGLES

Compound	τ_1	τ_2	τ_3	τ_4
Acetylcholine chloride[7]	*ap*	+*sc*	*ap*	*ap*
L(+)-Muscarine iodide[8]	*ap*	+*sc*	+*ac*	−*ac*
L(+)-*S*-Acetyl-β-methylcholine iodide[9]	*ap*	+*sc*	−*ac*	*ap*
Carbamoylcholine bromide[10]	*ap*	*ap*	*ap*	*ap*
Carnitine chloride (this work)	*ap*	*ap*	*ap*	*ap*
γ-Amino-β-hydroxybutyric acid[11]	*ap*	*ap*	*ap*	*ap*

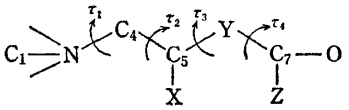

TABLE 6(b). CERTAIN INTERATOMIC DISTANCES

Compound	N-Y	N-C_7	N-Z
Acetylcholine	3.26 Å	4.40 Å	5.38 Å
L(+)-Muscarine iodide	3.07	4.49	5.40
L(+)-*S*-Acetyl-β-methylcholine iodide	3.21	4.25	5.16
Carbamoylcholine bromide	3.69	4.82	5.96
Carnitine chloride (this work)	3.87	5.08	6.18
γ-Amino-β-hydroxybutyric acid	3.79	4.94	6.05

The authors wish to thank the late Professor Masaji Tomita, Kobe Women's College of Pharmacy, for his valuable advice and continuous encouragement during the course of this work. This investigation was partly supported by the research grant from the Ministry of Education.

References

1) W. Gulewitsch and R. Krimberg, *Z. Physiol. Chem.*, **45**, 326 (1905); G. Fraenkel, *Biol. Bull.*, **104**, 359 (1953).
2) M. Tomita and Y. Sendju, *Z. Physiol. Chem.*, **169**, 263 (1927).
3) E. A. Hosein and P. Proulx, *Arch. Biochem. Biophys.*, **106**, 267 (1964); P. Weger, *Biochem. Z.*, **287**, 424 (1936).
4) "International Tables for X-Ray Crystallography," Vol. 3, Kynoch Press, England (1962).
5) R. W. Baker, C. H. Chothia, P. Pauling, and T. J. Petcher, *Nature*, **230**, 439 (1971).
6) W. Klyne and V. Perlog, *Experientia*, **16**, 521 (1960).
7) J. K. Herdklotz and R. L. Sass, *Biochem. Biophys. Res. Commun.*, **40**, 583 (1970).
8) F. Jellinek, *Acta Crystallogr.*, **10**, 277 (1957).
9) C. H. Chothia and P. J. Pauling, *Chem. Commun.*, **1969**, 626.
10) Y. Barrans and J. Clastre, *C. R. Acad. Sci., Paris, Ser. C*, **270**, 306 (1970).
11) K. Tomita, M. Harada, and T. Fujiwara, This Bulletin, **46**, 2854 (1973).

New Benzofuranosesquiterpenes from *Farfugium japonicum*. Farfugin A and Farfugin B[1]

Hajime NAGANO, Yoshihiko MORIYAMA, Yoshiaki TANAHASHI, and Takeyoshi TAKAHASHI
Department of Chemistry, Faculty of Science, The University of Tokyo, Bunkyo-ku, Tokyo 113
(Received April 27, 1974)

Two new benzofuranosesquiterpenes, farfugin A and farfugin B, have been isolated from *Farfugium japonicum* (L.) Kitamura, and their structures have been determined as **1** and **2**, respectively.

During chemical investigations on plants of the genus *Ligularia* (Compositae) and related plants,[2] two new sesquiterpenes, which we have named farfugin A and farfugin B, have been isolated from *Farfugium japonicum* (L.) Kitamura (=*Ligularia tussilaginea* Makino). We wish to report the structure determination leading to **1** and **2** for farfugin A and farfugin B, respectively.

A benzene extract of the rhizome of the plant was subjected to vacuum distillation and subsequent separation by column chromatography on silica gel to give farfugin A and farfugin B. Farfugin A (**1**) crystallized from methanol as colorless needles, mp 80.5—82.5 °C, $[\alpha]_D$+39°. The molecular formula of **1**, $C_{15}H_{18}O$, was determined by elemental analysis and the appearance of the molecular ion peak at *m/e* 214. Neither carbonyl nor hydroxyl absorption was observed in the IR spectrum. The UV and PMR spectra showed the presence of a β-methyl substituted benzofuran moiety with an α-proton,[3] an aromatic proton, an aromatic methyl, a secondary methyl spin coupled with a benzylic proton, two other benzylic protons, and four aliphatic protons (*Cf.* Experimental).

Hydrogenation of **1** over palladium–charcoal in methanol gave dihydrofurfugin A (**3**), whose PMR spectrum showed signals due to a part [$-OCH_2CH(CH_3)-$] of dihydrofuran moiety. An α-proton on the furan ring of **1** could be replaced by a bromine atom when **1** was treated with bromine in chloroform to afford bromofarfugin A (**4**).

Farfugin A (**1**) was dehydrogenated with palladium–charcoal to give a naphthofuran derivative (**5**) and a mixture of two naphthalene derivatives (**6** and **7**). Although a separation of the mixture failed due to paucity of the material, its UV, IR, and PMR spectra were closely related (*Cf.* Experimental) to those of 1,5-dimethyl-3-isopropylnaphthalene (**6**)[4] prepared from fukinone (**8**).[5] The sole difference between the two PMR spectra was that a *triplet* (J=7.5 Hz, $-CH_2\underline{CH}_3$) at δ 1.35 appeared in the spectrum of the mixture (**6** and **7**), while did not in that of **6** obtained from **8**. Combined glc-mass spectrometry of the mixture (**6** and **7**) revealed that it consisted of **6** [M^+ at *m/e* 198 ($C_{15}H_{18}$)] and **7**[M^+ at *m/e* 184 ($C_{14}H_{16}$)] in a ratio of 1 : 3. These observations showed that the mixture was composed of **6** and 1,5-dimethyl-3-ethylnaphthalene (**7**). The structure of the naphthofuran derivative (**5**) could be derived after completion of the structure determination of **1**.

The reference compound (**6**) was prepared as follows. Methylation of fukinone (**8**) with methyl iodide in a mixture of potassium *t*-butoxide and *t*-butyl alcohol gave 9-methylfukinone (**9**), which was hydrogenated over palladium–charcoal in ethanol to afford 9-methyldihydrofukinone (**10**). The ketone (**10**) was then reduced with lithium aluminium hydride to yield an alcohol (**11**). Treatment of **11** with phosphorus oxychloride in pyridine gave, besides a chloride (**12**), a mixture of hydrocarbons (**13**), which was subjected to dehydrogenation with palladium–charcoal to afford **6**[4] (Scheme 1).

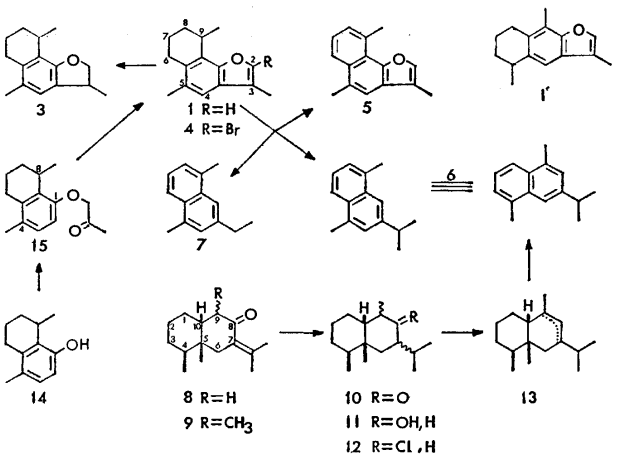

Scheme 1.

The result of dehydrogenation experiments along with spectral data of farfugin A described as above led to two alternative structures (**1** and **1'**) for farfugin A. The presence of intramolecular nuclear Overhauser effects (NOE)[6] between the aromatic proton (at C-4) and the aromatic methyl (at C-5), and between the same aromatic proton (at C-4) and the methyl (at C-3), observed for bromofarfugin A (**4**), showed that the structure of farfugin A must be represented by **1** rather than by **1'** (Table 1). This was confirmed by the following synthesis.

Treatment of 4,8-dimethyl-1-hydroxy-5,6,7,8-tetrahydronaphthalene (**14**)[7] with chloroacetone, potassium iodide, and potassium carbonate in dry acetone under reflux gave 1-acetonyloxy-4,8-dimethyl-5,6,7,8-tetrahydronaphthalene (**15**). The ether (**15**) was then heated with polyphosphoric acid to afford (±)-**1**, mp 73—73.5 °C, identical with natural (+)-**1** in all respects [IR in Nujol (**1** was soluble in Nujol), UV, PMR, MS, and tlc] except mp and $[\alpha]_D$ data (Scheme 1).

Farfugin B (**2**) was isolated as a colorless oil. A molecular ion peak at *m/e* 214 ($C_{15}H_{18}O$) was observed in the mass spectrum. The presence of an α-proton and a β-methyl on the benzofuran moiety, two aromatic protons, an aromatic methyl, an olefinic methyl, and

Table 1. Nuclear Overhauser effects[a]

Compounds	Observed protons	Saturated protons	NOE
4	4-H (7.00 s)	3-Me (2.12 s)	7
	4-H	5-Me (2.27 s)	15
	4-H	9-Me (1.38 d J=7 Hz)	nil
16	4-H (6.88 s)	5-Me (2.23 s)	14
	7-H (6.58 s)	5-Me	nil
	4-H	3-H (3.45m)	3
	7-H	3-H	nil
	1'-H (2.52m)	4-H (6.88 s)	nil
	3-Me (1.29 d J=7 Hz)	7-H (6.58 s)	nil
	1'-H	7-H	9
	4-H	1'-H (2.52m)	nil
	7-H	1'-H	19

a) The NOE's are expressed as increases in integrated signal intensities in %. The other indications are given in Experimental.

two olefinic protons was shown from its UV and PMR spectral data (*Cf.* Experimental).

Hydrogenation of **2** over palladium-charcoal in ethanol gave tetrahydrofarfugin B (**16**), whose PMR spectrum showed a multiplet as AM part of an AMX system due to a methylene of dihydrofuran moiety, and two *singlets* at δ 6.58 and 6.88 due to two aromatic protons (*Cf.* Experimental).

These observations led to a 3-methylbenzofuran structure with an additional methyl and a C_5H_9 substituent on C-5 and C-6 (that is, either 2 or 2'; each with the side chain replaced by C_5H_9) for farfugin B.

A nature of the C_5H_9 group was shown to be *trans-n*-3-pentenyl from the following evidences. Bromination of **2** yielded bromofarfugin B (**17**) and tribromofarfugin **B** (**18**). A doublet (J=7.5 Hz, $C\underline{H}_3CHBr$-) appeared at δ 1.86 in the PMR spectrum of **18**, in place of the olefinic methyl signal at δ 1.65 in that of **2**. The PMR spectrum of dihydrofarfugin B (**19**), obtained by hydrogenation of **2** over platinum catalyst in methanol, showed signals at δ 0.91 due to a primary methyl. An IR absorption band at 965 cm^{-1} due to *trans*-olefinic linkage was absent in the IR spectra of **16**, **18**, and **19** (Scheme 2).

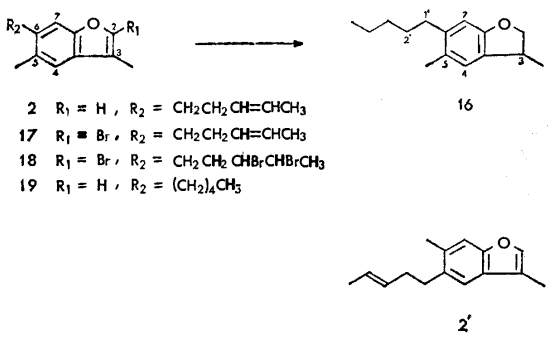

Scheme 2.

Two alternative structures of **2** and **2'** could thus be shown for farfugin B. The presence of NOE's between the aromatic proton (at C-4) and the aromatic methyl (at C-5), and between the other aromatic proton (at C-7) and the benzylic protons (at C-1'), observed for tetrahydrofarfugin B (**16**), favored the structure **2** over **2'** for farfugin B (Table 1). The structure of farfugin B should therefore be represented by 3,5-dimethyl-6-(*trans-n*-3-pentenyl)benzofuran (**2**). This received support from a recent synthesis of dihydrofarfugin B (**19**) from 1-methyl-2-bromo-4-methoxybenzene described elsewhere.[8]

Experimental

IR, UV, and mass spectra were measured using a Hitachi EPI-G2, a Hitachi EPS-3, and a Hitachi RMU-6-Tokugata spectrometers, respectively. A gas chromatograph, Hitachi K53, was equipped with this mass spectrometer for measurements by combined glc-mass spectrometry. Optical rotations, $[\alpha]_D$, were measured with a YANACO OR-50 spectrometer. PMR spectra were taken on a JEOL 4H-100 (100 MHz), a JEOL PS-100 (100 MHz), and a Hitachi R-20 (60 MHz) spectrometers. For the measurement of NOE's, the PMR spectra were taken with a Varian HA-100 spectrometer operating at 100 MHz in the frequency-swept and internal TMS-locked mode, for *ca.* 5% (w/v) degassed solution in $CDCl_3$. NOE experiments were performed with sweep rates of 0.4 Hz per sec for integration and 0.2 Hz per sec for signals on the spectrometer with a Hewlett-Packard HP-200ABR audio-oscillator and an HP-5212A electronic counter. Accuracies for NOE values are about ±2%. Chemical shifts are expressed in δ (TMS as internal standard), and coupling constants in Hz. All melting points were determined on a hot block and reported uncorrected. Merck Kieselgel G and Kieselgel 60 PF_{254} were used for analytical and preparative tlc, respectively. For column chromatography silica gel (Wakogel C-200) and neutral alumina (Showa Chemical Co.) were used.

Isolation of Farfugin A (1) and Farfugin B (2). The rhizomes of *Farfugium japonicum* (L.) Kitamura were extracted with hot benzene. The residue obtained (24 g) after evaporation of the solvent was subjected to distillation at 150 °C under 0.3 mmHg to give a brown oil (4 g), which, by repeated distillation, afforded a yellow oil(2.7 g). The oil was chromatographed on silica gel (150 g) using light petroleum as eluent (each 150 ml). The eluted fractions were collected and examined by tlc.

Fractions 6—8 were combined and the solvent was removed to give crude **1** (153 mg), which was further chromatographed on silica gel. Fractions eluted with light petroleum, on evaporation of the solvent, gave a residue, which afforded after crystallization from ethanol *farfugin A* (**1**; 102 mg), mp 80.5—82.5 °C, $[\alpha]_D^{20}$ +39° (c 0.34, in EtOH); UV (cyclohexane): λ_{max} 252.5 nm (ε 14500), 281 (2800), and 291 (3200); IR (Nujol): 1590 and 1540 cm^{-1}; PMR ($CDCl_3$): δ 1.37 (3H, d, J=7.5 Hz, $C_{(9)}$-CH_3), 2.16 (3H, d, J=1.2 Hz; $C_{(3)}$-CH_3), 2.27 (3H, s; $C_{(5)}$—CH_3), 2.63 (2H, m; $C_{(6)}$-H), 3.35 (1H, m; $C_{(9)}$-H), 7.05(1H, s; $C_{(4)}$-H), 7.20 (1H, m; $C_{(2)}$-H), and 1.5—2.0 (4H; $C_{(7)}$-H and $C_{(8)}$-H); MS: *m/e* 214 (relative intensity 79%, $M^+(C_{15}H_{18}O)$) and 199 (100%, $[M-CH_3]^+$). Found: C, 83.67; H, 8.24%. Calcd for $C_{15}H_{18}O$: C, 84.07; H, 8.47%.

Fractions 11—14 gave a residue (57 mg), which was chromatographed on silica gel. Fractions eluted with light petroleum were collected. Evaporation of the solvent gave

farfugin B (**2**; 49 mg), colorless liquid; UV (EtOH): λ_{max} 251.5 nm (ε 10500), 281.5 (3500), and 291.5 (3900); IR (liquid): 3020, 1575, and 965 cm^{-1}; PMR ($CDCl_3$): δ 1.65(3H, *m*; $-CH=CHC\underline{H}_3$), 2.19(3H, d, J=1.2 Hz; $C_{(3)}-C\underline{H}_3$), 2.37 (3H, s; $C_{(5)}-C\underline{H}_3$), 5.45 (2H, m; $-C\underline{H}=C\underline{H}-$), and 7.20 (3H, m; $C_{(2)}$-H, $C_{(4)}$-H, and $C_{(7)}$-H), and 2.5—3.0 (4H; $C_{(1')}$-H and $C_{(2')}$-H); MS: *m/e* 214 (37%, M^+ ($C_{15}H_{18}O$)) and 159 (100%).

*Hydrogenation of Farfugin A (**1**) over Palladium-Charcoal.* A solution of **1** (39 mg) in methanol (10 ml) was stirred with 10% palladium-charcoal (30 mg) in an atmosphere of hydrogen for 6 hr. Filtration of the catalyst and evaporation of the solvent under reduced pressure gave a crystalline product (32 mg), which was recrystallized from ethanol to give *dihydrofarfugin A* (**3**), mp 51—52 °C, UV (cyclohexane): λ_{max} 285 nm (ε 3200) and 292.5 (3500); IR (Nujol): 1610 and 1590 cm^{-1}; PMR ($CDCl_3$): δ 1.24 (3H, d, J=7 Hz; $C_{(9)}-CH_3$), 1.2 7(3H, d, J=6.5 Hz, $C_{(3)}-CH_3$), 2.15 (1H, s; $C_{(5)}-CH_3$), 2.55(2H, m; $C_{(6)}$-H), 3.00 (1H, m; $C_{(9)}$-H), 3.45 (1H, m; $C_{(3)}$-H), 4.03 (1H, dd, J=8 Hz and 7 Hz; $C_{(2)}$-H), 4.63 (1H, t, J=8 Hz; the other $C_{(2)}$-H), and 6.80 (1H, s; $C_{(4)}$-H); MS: *m/e* 216 (55%, M^+ ($C_{15}H_{20}O$)) and 201 (100%, $[M-CH_3]^+$).

*Bromination of Farfugin A (**1**).* A solution of bromine (23 mg) in chloroform (2 ml) was added dropwise to a solution of **1** (30 mg) in chloroform (5 ml) with stirring. The color of the solution disappeared immediately. Evaporation of the solvent gave a crystalline residue (40 mg), which was passed through a column of silica gel using light peroleum as eluent to afford *bromofarfugin A* (**4**; 38 mg), mp 99.5—100 °C (recrystallized from EtOH); IR (Nujol): 1590 cm^{-1}; PMR ($CDCl_3$): δ 1.38 (3H, d, J=7 Hz; $C_{(9)}-CH_3$), 2.12 (3H, s; $C_{(3)}-CH_3$), 2.27 (3H, s; $C_{(5)}-CH_3$), 2.63 (2H, m; $C_{(6)}$-H), 3.37 (1H, m; $C_{(9)}$-H), and 7.00 (1H, s; $C_{(4)}$-H); MS: *m/e* 294 (100%, M^+ ($C_{15}H_{17}OBr$)), 292 (100%, M^+), 279 (89%, $[M-CH_3]^+$), and 277 (90%, $[M-CH_3]^+$). Found: C, 61.66; H, 5.83%. Calcd for $C_{15}H_{17}OBr$: C, 61.44; H, 5.84%.

*Dehydrogenation of Farfugin A (**1**) over Palladium-Charcoal.* A mixture of **1** (51 mg) and 10% palladium-charcoal (53 mg) in a sealed tube under a nitrogen atmosphere was heated at 300 °C for 5 min. The reaction mixture was extracted with ether and evaporation of the solvent gave an oil (30 mg), which was submitted to separation by preparative tlc (silica gel impregnated with 1,3,5-trinitrobenzene, 10%; solvent: light petroleum). A silica gel layer (R_f 0.2) containing naphthofuran-trinitrobenzene adduct and that (R_f 0.4) containing naphthalene-trinitrobenzene adduct were collected respectively, and each of them was placed on the top of a column of alumina. Elution with benzene gave 3,5,9-trimethyl-naphtho[1,2-*b*]-furan (**5**; 7 mg), and a mixture (7 mg) of 1,5-dimethyl-3-isopropylnaphthalene (**6**) and 1,5-dimethyl-3-ethylnaphthalene (**7**), respectively. *3,5,9-trimethylnaphtho[1,2-b]furan* (**5**): mp 64.5—65.5 °C (recrystallized from EtOH); UV (MeOH): λ_{max} 248.5 nm (ε 49000), 253 (48000), 282.5 (5300, shoulder), 291 (5800), 302 (4300, shoulder), 324 (1800), and 339 (1500); IR (Nujol): 1570 cm^{-1}; MS: *m/e* 210 (100%, M^+($C_{15}H_{14}O$)), 209 (38%, $[M-H]^+$), and 195 (38%, $[M-CH_3]^+$).

Spectral data of the mixture of *naphthalene derivatives* (mixture of **6** and **7**) was as follows; UV (MeOH): λ_{max} 226 nm (ε 51700), 231 (72000), 278 (5100), 287 (5700), 293 (4800), and 324 (100) (ε was calculated based on assumption of molecular weight 198); IR (liquid): 1620, 1598, 865, 795, and 745 cm^{-1}; PMR ($CDCl_3$): δ 1.35 (t, J=7.5 Hz; $-CH_2C\underline{H}_3$), 1.37 (d, J=7.5 Hz; $-CH(C\underline{H}_3)_2$, 2.68 (s; aromatic $C\underline{H}_3$), and 7.2—8.0 (m, aromatic protons); glc (retention time): (i) 8.3 and 6.8 min (Diasolid H523 (2%), 1.5 m column, 160 °C, N_2 gas flow 80 ml/min); (ii) 17.0 min (Polydiethylene glycosuccinate on Chromosorb W (20%), 2 m column, 180 °C, N_2 gas flow 60 ml/min).

*Methylation of Fukinone (**8**).* To a solution of potassium *t*-butoxide in *t*-butanol, prepared from potassium (600 mg) and *t*-butanol (40 ml), a solution of fukinone[5] (**8**; 995 mg) in *t*-butanol (10 ml) and methyl iodide (6 g) were added dropwise under a nitrogen atmosphere. The reaction mixture was set aside for 5 hr at 25 °C. After neutralization with aqueous acetic acid (AcOH, 5 ml, and H_2O, 20 ml), the mixture was condensed under reduced pressure and extracted with ether. The extract was treated as usual and the resulting residue (1.97 g) was chromatographed on silica gel (150 g). Elution with light petroleum-ether (200 : 3; each fraction, 150 ml) gave an oil, 9-methylfukinone (**9**; 559 mg; from frs 15—19) and **8** (248 mg; from frs 22—25). *9-Methylfukinone* (**9**); UV (EtOH): λ_{max} 250 nm (ε 6500); IR (liquid): 1690 and 1630 cm^{-1}; PMR ($CDCl_3$): δ 0.81 (3H, d, J=7 Hz; $C_{(4)}-CH_3$), 0.94 (3H, s; $C_{(5)}-CH_3$). 1.07 (3H, d, J=7 Hz; $C_{(9)}-CH_3$), 1.80 (3H, s; $C=CCH_3$), and 1.91 (3H, s; $C=CCH_3$); MS: *m/e* 234 (30%, M^+ ($C_{16}H_{26}O$)), 219 (3%, $[M-CH_3]^+$), 187 (42%), 163 (39%), and 109 (100%).

*Hydrogenation of 9-Methylfukinone (**9**) over Palladium-Charcoal.* The methylated product (**9**; 559 mg) was hydrogenated with 10% palladium-charcoal (65 mg) in ethanol at room temperature. Filtration of the catalyst and evaporation of the solvent gave a residue (506 mg), which was passed through a column of silica gel (100 g) using light petroleum-ether (200 : 3) as eluent. The eluate was evaporated under reduced pressure to give oily *9-methyldihydrofukinone* (**10**; 402 mg), IR(liquid): 1710 cm^{-1}; MS: *m/e* 236 (31%, M^+ ($C_{16}H_{28}O$)), 221 (14%, $[M-CH_3]^+$), 194 (40%), 97 (52%), 84 (74%), 81 (51%). 69 (73%), 67 (55%), and 55 (100%).

*Reduction of **10** with Lithium Aluminium Hydride.* To a suspension of lithium aluminium hydride (464 mg) in dry ether (30 ml), a solution of **10** (403 mg) in dry ether was added and stirred for 4 hr at room tmeperature. The excess reagent was decomposed with water and the reaction mixture was extracted with ether. The extract was treated as usual to give an oily *9-methyldihydrofukinol* (**11**; 408mg), IR (liquid): 3450 cm^{-1}; MS: *m/e* 220 (6%, $[M-H_2O]^+$), 205 (24%, $[M-H_2O-CH_3]^+$) 177 (59%), 136 (75%), 109 (79%), 107 (66%), 95 (65%), 81 (56%), 67 (69%) and 55 (100%). A molecular ion peak at *m/e* 238 ($C_{16}H_{30}O$) was not observed.

*Dehydration of **11** with Phosphorus Oxychloride.* A solution of **11** (408 mg) and phosphorus oxychloride (2 ml) in pyridine (20 ml) was allowed to stand overnight at room temperature. The reaction mixture was poured into ice-water and extracted with ether. The extract was treated as usual to give a residue (341 mg), which was chromatographed on silica gel (100 g) using light petroleum as eluent (each fraction 20 ml). Fractions 10—12 gave a mixture of dehydrated products (**13**; 171 mg). Fractions 13—14 gave a residue, which was subjected to repeated chromatography on silica gel using light petroleum as eluent to afford the mixture of dehydrated products (**13**; 15 mg) and a chloride (**12**; 82 mg). The mixture of *9-methyleremophilenes* (**13**): colorless liquid, IR (liquid): 1650 cm^{-1}; PMR ($CDCl_3$): δ 5.16 (m, olefinic protons); MS: *m/e* 220 (5%, M^+ ($C_{16}H_{28}$)), 205 (4%, $[M-CH_3]^+$), 177 (70%), 109 (43%), 107 (44%), 97 (49%), 95 (100%), and 81 (71%). *Chloride* (**12**): colorless liquid, PMR ($CDCl_3$): δ 4.25 (m, $-CHCl-$); MS: *m/e* 258 (1.5%, M^+ ($C_{16}H_{29}OCl$)), 256 (2.5%, M^+), 221 (28%, $[M-Cl^+]$), 177 (57%), 109 (65%), 107 (96%), 81 (73%), 69 (65%), 67

(65%), and 55 (100%).

Dehydrogenation of ***13*** *over Palladium-Charcoal.* Dehydrated product (**13**; 60 mg) was heated with 10% palladium-charcoal (70 mg) at 300 °C for 5 min in a sealed tube under a nitrogen atmosphere. Another 60 mg of **13** was dehydrogenated described as above. The reaction mixtures were combined and extracted with ether. Evaporation of the solvent gave a residue (89 mg), which was submitted to preparative tlc. A diluted solution of 1,3,5-trinitrobenzene in methanol was sprayed on the plate. A zone developing a yellow color was collected and placed on the top of a column of alumina. The column was eluted with benzene to give oil 1,5-dimethyl-3-isopropylnaphthalene[4] (**6**; 24 mg). Picrate, orange needles, mp 110—113 °C (recrystallized from EtOH); trinitrobenzene-adduct, yellow needles, mp 139—141 °C (recrystallized from EtOH).

Spectral data of *1,5-dimethyl-3-isopropylnaphthalene* (**6**) were as follows; UV (EtOH): λ_{max} 225.5 nm (ε 49000), 231 (81000), 277.5 (4800), 287 (5700), 292.5 (4700), 318 (100), and 323 (100); IR (liquid): 1620, 1600, 865, 795, and 745 cm^{-1}; PMR ($CDCl_3$): δ 1.35 (6H, d, J=7.5 Hz; $-CH(C\underline{H}_3)_2$), 2.69 (6H, s, aromatic CH_3), and 7.2—8.0 (5H, m; aromatic protons); glc (retention time): (i) 8.3 min (Diasolid H523 (2%), 1.5 m column, 160 °C, N_2 gas flow 80 ml/min); (ii) 16.8 min (Polydiethylene glycosuccinate on Chromosorb W (20%), 2 m column, 180 °C, N_2 gas flow 60 ml/min).

*1-Acetonyloxy-4,8-dimethyl-5,6,7,8-tetrahydronaphthalene (****15****).* A solution of 1-hydroxy-4,8-dimethyl-5,6,7,8-tetrahydronaphtharene[7] (**14**; 896 mg) in dry acetone was refluxed with chloroacetone (964 mg), potassium iodide (314 mg), and potassium carbonate (2.50 g) for 6 hr. After the solvent was distilled off the residue was extracted with ether. The extract was washed, dried, and evaporated to afford a viscous oil (1.48 g), which was chromatographed on silica gel (75 g). Fraction eluted with benzene-light petroleum (2 : 1) gave *1-acetonyloxy-4,8-dimethyl-5,6,7,8-tetrahydronaphthalene* (**15**; 1.01 g), mp 50—51 °C (recrystallized from light petroleum); IR (Nujol): 1728, 1600, 1583, and 795 cm^{-1}; PMR ($CDCl_3$): δ 1.25 (3H, d, J=7 Hz; $C_{(8)}$–CH_3), 2.11 (3H, s; $C_{(4)}$–CH_3), 2.23 (3H, s; $-COCH_3$), 4.32 (2H, s; $-OCH_2CO-$), 6.32 (1H, d, J=9 Hz; $C_{(2)}$–H or $C_{(3)}$–H), and 6.78 (1H, d, J=9 Hz; $C_{(3)}$–H or $C_{(2)}$–H); MS: *m/e* 232 (20%, $M^+(C_{15}H_{20}O_2)$), 217 (10%, $[M-CH_3]^+$), 189 (20%, $[M-CH_3CO]^+$), 174 (100%), and 159 (88%). Found: C, 77.55; H, 8.64%. Calcd for $C_{15}H_{20}O_2$: C, 77.77; H, 8.77%.

*Cyclization of the Ether (****15****).* The ether (**15**; 971 mg) was heated with polyphosphoric acid (10 g) at 100 °C for 35 min under a nitrogen atmosphere. Ice-water was added and the reaction mixture was extracted with ether. The extract was washed with aqueous solution of sodium bicarbonate and then with water. After the solution was dried over anhydrous sodium sulfate, the solvent was removed to give a residue (860 mg), which was chromatographed on silica gel. Fractions eluted with light petroleum afforded a crystalline product, (±)-*farfugin A* (±**1**; 344 mg), mp 73—73.5 °C (recrystallized from EtOH); UV (cyclohexane): λ_{max} 253 nm (ε 13500), 281 (2800), and 290.5 (3000); IR (Nujol): 1590 and 1540 cm^{-1}; PMR ($CDCl_3$): δ 1.40 (3H, d, J=7 Hz; $C_{(9)}$–CH_3), 2.19 (3H, d, J=1 Hz; $C_{(3)}$–CH_3), 2.30 (3H, s; $C_{(5)}$–CH_3), 2.65 (2H, m; $C_{(6)}$–H), 3.37 (1H, m; $C_{(9)}$–H), 7.13 (1H, s; $C_{(4)}$–H), and 7.29 (1H, m; $C_{(2)}$–H); MS: *m/e* 214 (47%, $M^+(C_{15}H_{18}O)$), and 199 (100%, $[M-CH_3]^+$). Found: C, 84.02; H, 8.42%. Calcd for $C_{15}H_{18}O$: C, 84.07; H, 8.47%.

*Hydrogenation of Farfugin B (****2****) over Palladium-Charcoal.* A solution of **2** (29 mg) in ethanol was stirred with 10% palladium-charcoal (28 mg) for 5.5 hr under an atmosphere of hydrogen. Filtration of the catalyst and evaporation of the solvent gave a residue (22 mg), which was passed through a column of silica gel using light petroleum as eluent to afford oily *tetrahydrofarfugin B* (**16**; 19 mg); IR (liquid): 3020, 1618, and 1580 cm^{-1}; PMR ($CDCl_3$): δ 0.89 (3H, m; terminal CH_3 on the side chain), 1.29 (3H, d; J=7 Hz; $C_{(3)}$–CH_3), 2.23 (3H, s; $C_{(5)}$–CH_3), 2.52 (2H, m; benzyl) protons), 3.45 (1H, m; $C_{(3)}$–H), 4.01 (1H, dd, J=8 Hz and 7 Hz; $C_{(2)}$–H, 4.63 (1H, t, J=8 Hz; the other $C_{(2)}$–H), 6.58 (1H, s; $C_{(7)}$–H), and 6.88 (1H, s; $C_{(4)}$–H); MS: *m/e* 218 (100%, M^+ ($C_{15}H_{22}O$)), 203 (49%, $[M-CH_3]^+$), 162 (59%), and 161 (64%).

*Bromination of Farfugin B (****2****).* To a solution of **2** (36 mg) in carbon tetrachloride (5 ml), a solution of bromine (40 mg) in carbon tetrachloride (2 ml) was added dropwise with stirring and the resulting solution was allowed to stand at room temperature for 30 min. The products were examined by tlc. Evaporation of the solvent gave a residue (60 mg), which was chromatographed on silica gel using light petroleum as eluent to afford bromofarfugin B (**17**; 18 mg) and tribromofarfugin B (**18**; 36 mg). *Bromofarfugin B* (**17**): mp 36—37 °C (recrystallized from EtOH); IR (liquid): 3070, 3020, 1635, 1595, 1575, and 965 cm^{-1}; PMR ($CDCl_3$): δ 1.65 (3H, m; terminal CH_3), 2.12 (3H, s; $C_{(3)}$–CH_3), 2.34 (3H, s; $C_{(5)}$–CH_3), 5.45 (2H, m; $-C\underline{H}=C\underline{H}-$), and 7.13 (2H, s; $C_{(4)}$–H and $C_{(7)}$–H); MS: *m/e* 294 (71%, M^+ ($C_{15}H_{17}OBr$)), 292 (71%, M^+), 239 (100%), and 237 (100%). *Tribromofarfugin B* (**18**): mp 74—74.5 °C (recrystallized from EtOH); IR (Nujol): 1590, 1575, and 870 cm^{-1}; PMR ($CDCl_3$): δ 1.86 (3H, d, J=7.5 Hz; $-CHBr-C\underline{H}_3$), 2.13 (3H, s; $C_{(3)}$–CH_3), 2.40 (3H, s; $C_{(5)}$–CH_3), 4.20 (2H, m; $-C\underline{H}Br-C\underline{H}Br-$), 7.17 (1H, s; $C_{(4)}$–H or $C_{(7)}$–H), and 7.19 (1H, s; $C_{(7)}$–H or $C_{(4)}$–H); MS: *m/e* 456 (15%, $M^+(C_{15}H_{17}OBr_3)$), 454 (44%, M^+), 452 (44%, M^+), 450 (16%, M^+), 239 (100%), and 237 (100%). Found: C, 39.93; H, 3.77%. Calcd for $C_{15}H_{17}OBr_3$: C, 39.77; H, 3.78%.

*Hydrogenation of Farfugin B (****2****) over Paltinum Oxide.* Hydrogenation of **2** (8 mg) was effected over platinum oxide (8 mg) in methanol (2 ml) with stirring for 14 hr at 30 °C. Filtration of the catalyst and evaporation of the solvent gave oily *dihydrofarfugin B* (**19**; 8 mg), IR (liquid): 1575, 860, and 775 cm^{-1}; PMR ($CDCl_3$): δ 0.91 (3H, m; terminal CH_3), 2.23 (3H, d, J=1 Hz; $C_{(3)}$–CH_3), 2.42 (3H, s; $C_{(5)}$–CH_3), and 7.30 (3H, m; $C_{(2)}$–H, $C_{(4)}$–H, and $C_{(7)}$–H); MS: *m/e* 216 (19%, M^+ ($C_{15}H_{20}O$)) and 159 (100%).

The authors wish to thank Dr. M. Fukuyama and Mr. K. Sato, Sagami Chemical Research Center, Sagamihara-shi, for the measurements of NOE's.

References

1) A preliminary account of this paper: H. Nagano, Y. Moriyama, Y. Tanahashi, T. Takahashi, M. Fukuyama, and K. Sato, *Chem. Lett.*, **1972**, 13.

2) F. Patil, G. Ourisson, Y. Tanahashi, M. Wada, and T. Takahashi, *Bull. Soc. Chim. Fr.*, **1968**, 1047; T. Murae, Y. Tanahashi, and T. Takahashi, *Tetrahedron*, **24**, 2177 (1968); Y. Ishizaki, Y. Tanahashi, T. Takahashi, and K. Tori, *Chem. Commun.*, **1969**, 551; Y. Tanahashi, T. Takahashi, and H. Koyama, *Bull. Nat. Sci. Mus. Tokyo*, **12**, 633 (1969); Y. Ishizaki, Y. Tanahashi, T. Takahashi, and K. Tori, *Tetrahedron*, **26**, 5387 (1970); M. Tada, Y. Moriyama, Y. Tanahashi, T. Takahashi, M. Fukuyama, and K. Sato, *Tetrahedron Lett.*, **1971**, 4007; Y. Moriyama, T. Sato, H. Nagano, Y. Tanahashi, and T. Takahashi, *Chem. Lett.*, **1972**, 637; H. Nagano and T.

Takahashi, This Bulletin, **45**, 1935 (1972); H. Nagano, Y. Tanahashi, Y. Moriyama, and T. Takahashi, *ibid.*, **46**, 2840 (1973).

3) J. Romo and P. Joseph-Nathan, *Tetrahedron*, **20**, 2331 (1964); H. Hikino, K. Agatsuma, C. Konno, and T. Takemoto, *Tetrahedron Lett.*, **1968**, 4417.

4) L. Ruzicka, P. Pieth, T. Reichstein, and L. Ehmann, *Helv. Chim. Acta*, **16**, 268 (1933); A. S. Pfau and P. Plattner, *ibid.*, **19**, 858 (1936); B. Lacoume and L. H. Zalkow, *Tetrahedron Lett.*, **1966**, 5881.

5) K. Naya, I. Takagi, Y. Kawaguchi, Y. Asada, Y. Hirose, and N. Shinoda, *Tetrahedron*, **24**, 5871 (1968).

6) F. A. L. Anet and A. J. R. Bourn, *J. Amer. Chem. Soc.*, **87**, 5250 (1965).

7) O. P. Vig, S. S. Sanghu, and S. M. Mukherji, *J. Indian Chem. Soc.*, **34**, 81 (1957); S. M. Bloom, *J. Amer. Chem. Soc.*, **80**, 6280 (1958).

8) H. Shirasaki, H. Komatsu, H. Nagano, Y. Moriyama, Y. Tanahashi, and T. Takahashi, This Bulletin, **46**, 2918 (1973).

Furanoeremophilane-6β,10β-diol and Its Derivatives. New Furanosesquiterpenes from *Ligularia japonica* LESS[1]

Masahiro TADA, Yoshihiko MORIYAMA, Yoshiaki TANAHASHI, and Takeyoshi TAKAHASHI

Department of Chemistry, Faculty of Science, The University of Tokyo, Bunkyo-ku, Tokyo 113

(Received May 2, 1974)

Three new furanosesquiterpenes have been isolated from *Ligularia japonica* LESS., and their structures including absolute configurations have been determined as furanoeremophilane-6β,10β-diol (**1**), 10β-hydroxyfuranoeremophilan-6β-yl 2'ξ-methylbutanoate (**2**), and 10β-hydroxy-6β-methoxyfuranoeremophilane (**3**).

In connection with structural studies on constituents of the genus *Ligularia* (Compositae),[2] three new furanoereomophilane derivatives have been isolated from *Ligularia japonica* LESS. We wish to describe the structure determination leading to furanoeremophilane-6β,10β-diol (**1**), 10β-hydroxyfuranoeremophilan-6β-yl 2'ξ-methylbutanoate (**2**), and 10β-hydroxy-6β-methoxyfuranoeremophilane (**3**) for these sesquiterpenes.

A benzene extract of the roots of the plant was subjected to separation by column chromatography on silica gel to give **1** and **2**. Compound **1**, mp 120—122 °C, $[\alpha]_D$+33° (EtOH),* was positive to the Ehrlich test. The molecular formula of **1**, $C_{15}H_{22}O_3$, was determined by elemental analysis and the appearance of the molecular ion peak at *m/e* 250. The IR, UV, and PMR spectra showed the presence of a secondary methyl, a tertiary methyl, a β-methyl-substituted furan moiety with an α-proton,[2] an allylic methylene linked to carbon with no proton, and of hydroxyl group(s) (cf. Experimental). A monoacetate (**4**), obtained by acetylation of **1** with acetic anhydride in pyridine exhibited an absorption due to an additional hydroxyl group in its IR spectrum. In the PMR spectrum of **1** in benzene, on addition of deuterium oxide, a doublet at δ 4.41 (J=7.5 Hz) due to a proton on a hydroxyl-bearing carbon changed into a singlet, while both of a doublet at δ 2.72 (J=7.5 Hz) due to a secondary hydroxyl proton and a singlet at δ 2.93 due to a tertiary hydroxyl proton disappeared. The presence in **1** of a secondary and a tertiary hydroxyl group could thus be shown.

The presence of intramolecular nuclear Overhauser effects (NOE)[3] between a β-methyl (at C-11) on the furan ring and a proton (at C-6) on an acetoxyl-bearing carbon, as well as between the same methyl (at C-11) and an α-proton (at C-12) on the furan ring (Table 1), observed for **4**, showed that a secondary hydroxyl-bearing carbon (C-6) of **1** must be located on a β'-position (that is C-7) on the furan ring. This received support from an upfield shift[4,5] by 0.12 ppm of a doublet at δ 2.03 (in deuteriochloroform; J=1.5 Hz) due to a β-methyl on the furan ring, when **1** was acetylated. As a nature of three (at α, β, and β') of the four substituents on the furan ring was already clarified, the allylic methylene must be placed on an α'-position of the furan moiety for **1**. These observations led to a partial structure **A** (R=H), which could be extended, by means of biogenetic considerations, to two alternative structures, **B**(R=H) and **B'**(R=H), for **1**.

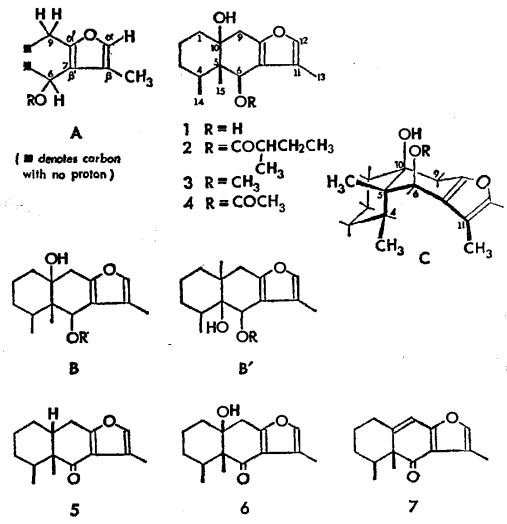

Table 1. Nuclear Overhauser effects

Compounds	Solvents	Observed protons	Saturated protons	NOE[a]
1	C_6D_6	9α-H	5-CH_3	nil
		9β-H	5-CH_3	nil
		12-H	11-CH_3	32
3	CCl_4	6-H	5-CH_3	13
4	C_6D_6	6-H	4-CH_3	21
		9α-H	5-CH_3	nil
		9β-H	5-CH_3	nil
		6-H	11-CH_3	4
		12-H	11-CH_3	20

a) The NOE's are expressed as increases in integrated signal intensities in %. The other indications are given in Experimental.

The IR spectrum of **2**, mp *ca.* 40 °C, showed a carbonyl absorption (ν_{max} 1725 cm^{-1}) due to an ester group. A molecular ion peak at *m/e* 334 ($C_{20}H_{30}O_4$) was observed in the mass spectrum of **2**, which was reduced with lithium aluminium hydride to give **1**. An acyl residue was therefore shown to be C_4H_9CO–. In the PMR spectrum of **2** in deuteriochloroform, a triplet at δ 0.88 (J=5.5 Hz) due to a primary methyl, a doublet at δ 1.14 (J=7 Hz) due to a secondary methyl, and a multiplet at δ 2.34 due to a methine proton of a –OCOCH(CH$_3$)– grouping appeared, besides signals due to protons of the structure moiety of

* Previously this value has been reported as +58° (EtOH).[1] The authors correct it to +33° for the same compound based on recent measurement data.

1. Thus, **2** must be an ester comprising from **1** and 2ξ-methylbutanoic acid.

Successive extraction of the roots with methanol and subsequent separation by column chromatography on silica gel gave a compound **3**, mp 82—84 °C, $[\alpha]_D$+ 5° (EtOH), whose molecular formula $C_{16}H_{24}O_3$ was given by elemental analysis and mass spectrometry (M^+ at *m/e* 264). The treatment of **1** with methanol in the presence of acetic acid, or with a mixture of methyl iodide, silver oxide, and dimethylformamide, afforded **3**. A secondary hydroxyl of **1** was thus methylated to give **3**. As the absence of **3** in the benzene extract was shown by thin layer chromatography, it was suggested that **3** might be an artifact produced by extraction with methanol.

A preference of the structure **B** (R=H) over **B'** (R=H) for **1** was shown as follows. The treatment of **1** with potassium periodate resulted in no consumption of the reagent. This showed the absence in **1** of an α-glycol (especially, of an α-*cis*-glycol) system. An NOE observed between a tertiary methyl (at C-5) and a proton (at C-6) on a methoxyl-bearing carbon for **3**, and the absence of NOE between a tertiary methyl (at C-5) and each of two allylic protons (at C-9) observed for **1** and **4**, suggested that the tertiary methyl was located on C-5 (Table 1). Finally, **1** was transformed to known ligularone (**5**).[4] Oxidation of **1** with chromium trioxide gave 10β-hydroxy-6-oxofuranoeremophilane (**6**), which was dehydrated with phosphorus oxychloride in pyridine to afford 6-oxofuranoeremophil-9-ene (**7**). Hydrogenation of **7** in the presence of palladium-charcoal in ethyl acetate proceeded stereoselectively to afford a ketone (yield: *ca.* 80%) as a main product, which was found to be identical with **5** in all respects. The structure **B** was thus derived for **1**.

The IR spectrum of **1** in carbon tetrachloride (0.005 M solution) showed the presence of an intramolecular hydrogen bond between the two hydroxyls. A tertiary hydroxyl at C-10 and a secondary hydroxyl at C-6 must therefore be in a 1,3-diaxial (that is, in *cis*) relationship to each other; this led to an equatorial conformation for a proton on C-6. These data along with the absence of NOE between the tertiary methyl at C-5 and each of methylene protons at C-9 (especially, an axial proton at C-9α) as described above, suggested an equatorial nature of this methyl (at C-5). This received support from a downfield shift by 0.23 ppm observed for a signal due to the tertiary methyl at C-5 of **1**, when the solvent was replaced from deuteriochloroform to pyridine-d_5.[6] In the PMR spectra of **3**, the corresponding downfield shift was relatively small (0.08 ppm) due to a strong intramolecular hydrogen bond (ν_{OH} 3488 cm^{-1}; in 0.005 M solution of carbon tetrachloride) which could inhibit competitively the solute-solvent association. The two hydroxyls and the tertiary methyl at C-5 are therefore in *cis* relationships to one another. The two methyls at C-4 and C-5 of **1** have been shown to be *cis* according to the conversion of **1** to **5** as mentioned above. The presence of NOE between a secondary methyl at C-4 and a proton at C-6 on an acetoxyl-bearing carbon was observed

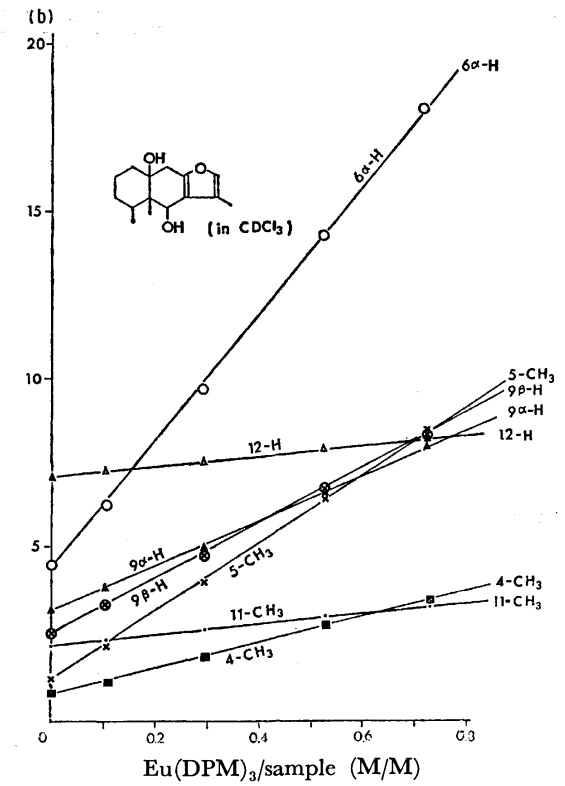

Fig. 1. Induced paramagnetic shifts for the diol(**1**)
[$Eu(DPM)_3$ was added to a 5% (w/v) soln of **1** in $CDCl_3$.]

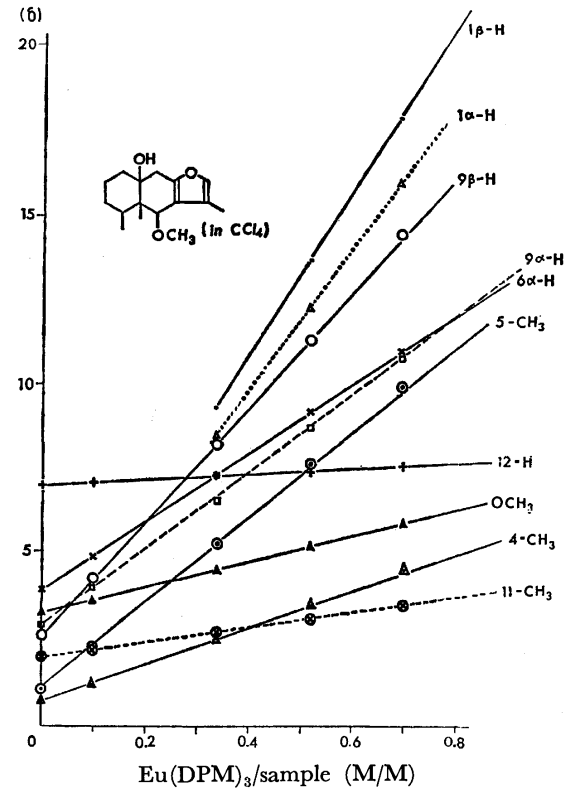

Fig. 2. Induced paramagnetic shifts for the monomethyl ether(**3**)
[$Eu(DPM)_3$ was added to a 5% (w/v) soln of **3** in CCl_4.]

for **4** (Table 1). These observations could only be explained based on a steroidal conformation of *cis*-decalin type depicted as in **C**.

The results of induced paramagnetic shift experiments[7] on the diol and the monomethyl ether were compatible with the structures **1** and **3**, respectively (Figs. 1 and 2). In the measurements for both of **1** and **3**, a large shift was observed for a signal due to a methyl at C-5. The signals due to a proton at C-9β and two protons at C-1 of **3**, as well as that due to a proton at C-6 of **1**, shifted very largely, while a smaller shift was observed for the corresponding signal due to a proton at C-6 of **3**. This could be interpreted by a preferencial association of the shift reagent, Eu(DPM)$_3$, with a hydroxyl rather than an ether group.[8]

As an absolute stereochemistry of **5** had been determined as in **5**,[4] the structure of the diol including absolute configuration should be represented by **1** with a conformation as shown in **C** (R=H). The structures **2**, **3**, and **4** followed for the ester, the monomethyl ether, and the monoacetate, respectively.

Experimental

IR spectra were measured using a Hitachi EPI-G2 spectrometer in Nujol mull, unless otherwise stated. UV spectra were determined on a Hitachi EPS-3 spectrophotometer. Measurements of optical rotation were carried out using a JASCO DIP-SL polarimeter. Mass spectra were taken on a Hitachi RMU-6-Tokugata mass spectrometer with a direct inlet system operating at 70 eV. PMR spectra were measured using a JEOL PS-100 (100 MHz) or a Hitachi R-20 (60 MHz) spectrometer. Chemical shifts were expressed in δ downfield from TMS as an internal standard, and coupling constants in Hz. For a measurement of NOE, PMR spectra were taken on a Varian HA-100 spectrometer operating at 100 MHz in the frequency-swept and internal TMS-locked mode, for *ca.* 5% (w/v) degassed solutions. NOE experiments were performed with sweep rates of 1 Hz per second for integrations and 0.2 Hz per second for signals on the spectrometer with a Hewlett-Packard HP-200ABR audio-oscillator and HP-5212A electronic counter. Accuracies are ±0.01 ppm for chemical shifts, ±0.2 Hz for coupling constants, and about ±2% for NOE values, for NOE experiments. Thin layer chromatography (tlc) was carried out on Kieselgel PF_{254} (E. Merck, Darmstadt). For column chromatography Wakogel C 200 (Wako Pure Chemical Co.) was used. All mps were determined on a hot block and reported uncorrected.

Isolation. Dried roots (1.6 kg) of *Ligularia japonica* LESS. were extracted with hot benzene (total 12 l). Evaporation of the solvent gave a residue (15 g) which was chromatographed on a column of silica gel (500 g). The eluted fractions were examined by tlc (silica gel). Fractions eluted with light petroleum–ether (10 : 1) gave, on evaporation of the solvents, a residue, which was crystallized from light petroleum to afford 10β-hydroxyfuranoeremophilan-6β-yl 2′ξ-methylbutanoate (**2**; 200 mg), mp *ca.* 40 °C; UV (EtOH) λ_{max} 218 nm (ε 9100); IR (CCl_4) 3570, 3500, 1725, 1640, 1565, 1245 cm^{-1}; PMR ($CDCl_3$) δ 0.83 (3H, d, J=7.5 Hz; methyl at C-4), 0.88 (3H, t, J=5.5 Hz; primary methyl in an acyl moiety), 1.14 (3H, d, J=7 Hz; secondary methyl in the acyl group), 1.25 (3H, s; methyl at C-5), 1.90 (3H, d, J=1.5 Hz; methyl at C-11), 2.34 (1H, m; –OCOCH(CH$_3$)– in the acyl residue), 2.65 and 3.20 (each, 1H, d, J=17.5 Hz; protons at C-9), 6.19 (1H, s; proton at C-6), 7.07 (1H, m; proton at C-12), ca. 3.3 (1H, broad signal; OH); mass spectrum *m/e* 334 (M$^+$; $C_{20}H_{30}O_4$), *m/e* 159 (base peak). Fractions eluted with light petroleum–ether (3 : 1) gave, on removal of the solvents, a solid, which was chromatographed on a column of silica gel (50 g). Elution with light petroleum–ether (3 : 1) and evaporation of the solvents gave a crude crystal, which was crystallized from a mixture of light petroleum and ether to afford furanoeremophilane-6β,10β-diol (**1**; 380 mg), mp 120—122 °C, $[\alpha]_D$ +33° (*c* 1.7, EtOH); UV(EtOH) λ_{max} 217 nm (ε 8000); IR (0.005 M solution of CCl_4) 3608, 3544, 3504, 1645, 1565, 1030 cm^{-1}; PMR (C_6D_6) δ 0.55 (3H, $\underline{A}_3B$, J=5.5 Hz; methyl at C-4), 1.11 (3H, s; methyl at C-5), 1.95 (3H, d, J=1.5 Hz; methyl at C-11), 2.42 (1H, d, J=17.8 Hz; proton at C-9β), 2.94 (1H, d, J=17.8 Hz; proton at C-9α), 7.00 (1H, m; proton at C-12); PMR (C_6H_6) (signals other than those described for C_6D_6) δ 2.72 (1H, d, J=7.5 Hz; OH at C-6), 2.93 (1H, s; OH at C-10), 4.41 (1H, d, J=7.5 Hz; proton at C-6); PMR ($CDCl_3$) δ 0.78 (3H, d, J=5.5 Hz; methyl at C-4), 1.22 (3H, s; methyl at C-5), 2.03 (3H, d, J=1.5 Hz; methyl at C-11), 2.53 (1H, d, J=17.8 Hz; proton at C-9β), 3.21 (1H, d, J=17.8 Hz; proton at C-9α), 4.52 (1H, s; proton at C-6), 7.08 (1H, m; proton at C-12); PMR (C_5D_5N) δ 0.75 (3H, d, J=5.5 Hz; methyl at C-4), 1.45 (3H, s; methyl at C-5), 2.11 (3H, d, J=1.5 Hz; methyl at C-11), 2.83 and 3.25 (each 1H, d, J=17.8 Hz; protons at C-9); mass spectrum *m/e* 250 (M$^+$), *m/e* 124 (base peak). Found: C, 72.23; H, 8.65%. Calcd for $C_{15}H_{22}O_3$: C, 71.97; H, 8.86%; mol wt 250.3.

Subsequent extraction of the roots with methanol and evaporation of the solvents gave a residue, which was passed through a column of silica gel (200 g). Fractions eluted with light petroleum–ether (5 : 1) gave, on removal of the solvents, a solid, which was sublimed at 60 °C (oil bath temperature) under 0.1 mmHg to afford 10β-hydroxy-6β-methoxyfuranoeremophilane (**3**: 60 mg), mp 82—84 °C; $[\alpha]_D$ +5° (*c* 2.0, EtOH); UV (EtOH) λ_{max} 220 nm (ε 9300); IR (0.005 M solution of CCl_4) 3488, 1634, 1560, 1084 cm^{-1}; PMR (CCl_4) δ 0.70 (3H, d, J=5.5 Hz; methyl at C-4), 1.12 (3H, s; methyl at C-5), 1.99 (3H, d, J=1.5 Hz; methyl at C-11), 2.59 (1H, d, J=17.8 Hz; proton at C-9β), 3.01 (1H, d, J=17.8 Hz; proton at C-9α), 3.28 (3H, s; methoxyl at C-6), 4.05 (1H, s; proton at C-6), 4.30 (1H, s; OH at C-10), 7.02 (1H, m; proton at C-12); PMR ($CDCl_3$) δ 0.73 (3H, d, J=5.5 Hz; methyl at C-4), 1.22 (3H, s; methyl at C-5), 2.07 (3H, d, J=1.5 Hz; methyl at C-11), 2.73 and 3.18, (each, 1H, d, J=17.8 Hz; protons at C-9), 3.39 (3H, s; methoxyl at C-6), 4.19 (1H, s; proton at C-6), 4.99 (1H, s; disappeared on addition of deuterium oxide; OH at C-10), 7.22 (1H, m; proton at C-12); PMR (C_5D_5N) δ 0.66 (3H, d, J=5.5 Hz; methyl at C-4), 1.30 (3H, s; methyl at C-5), 2.06 (3H, d, J=1.5 Hz; methyl at C-11), 2.87 and 3.20 (each, 1H, d, J=17.8 Hz; protons at C-9), 3.27 (3H, s; methoxyl at C-6), 4.25 (1H, s; proton at C-6); mass spectrum *m/e* 264 (M$^+$), *m/e* 138 (base peak). Found: C, 72.57; H, 9.27%. Calcd for $C_{16}H_{24}O_3$: C, 72.69; H, 9.15%; mol wt 264.4.

Acetylation of the Diol (1). A mixture of **1** (33 mg), acetic anhydride (1 ml), and pyridine (1 ml) was allowed to stand overnight at room temperature. After addition of methanol, the solvents were removed to give a residue, which was extracted with ether. The extract was treated as usual and the resulting residue was chromatographed on a column of silica gel (10 g). Elution with light petroleum–ether (10 : 1) gave, on removal of the solvents, 6β-acetoxy-10β-hydroxyfuranoeremophilane (**4**; 35 mg), an oil; IR (CCl_4) 3550, 1736, 1648, 1565, 1370, 1220, 1084, 1030 cm^{-1}; PMR (C_6D_6) δ 0.72 (3H, $\underline{A}_3B$, J=5.5 Hz; methyl at C-4), 1.04 (3H, s; methyl at C-5), 1.50 (3H, s; acetoxyl at C-6), 1.89 (3H, d, J=1.5 Hz;

methyl at C-11), 2.69 (1H, d, J=17.8 Hz; proton at C-9β), 2.99 (1H, d, J=17.8 Hz; proton at C-9α), 3.22 (1H, broad signal; OH at C-10), 6.34 (1H, s; proton at C-6), 6.94 (1H, m; proton at C-12); PMR ($CDCl_3$) δ 0.88 (3H, d, J=5.5 Hz; methyl at C-4), 1.05 (3H, s; methyl at C-5), 1.91 (3H, d, J=1.5 Hz; methyl at C-11), 2.05 (3H, s; acetoxyl at C-6), 2.65 and 3.20 (each, 1H, d, J=17.8 Hz; protons at C-9), 3.21 (1H, s; disappeared on addition of deuterium oxide; OH at C-10), 6.17 (1H, s; proton at C-6), 7.08 (1H, m; proton at C-12); PMR (C_5D_5N) δ 0.95 (3H, broad signal; methyl at C-4), 1.20 (3H, s; methyl at C-5), 1.96 (3H, d, J=1.5 Hz; methyl at C-11), 1.99 (3H, s; acetoxyl at C-6), 2.83 and 3.13 (each, 1H, d, J=17.8 Hz; protons at C-9), 6.46 (1H, proton at C-6); mass spectrum *m/e* 292 (M^+; $C_{17}H_{24}O_4$), *m/e* 124 (base peak).

*Methylation of the Diol (**1**).* (a) To a solution of **1** (30 mg) in methanol (4 ml) a drop of acetic acid was added and the resulting solution was allowed to stand at room temperature for 40 hr. After addition of water, the reaction mixture was extracted with ether. Usual work-up gave a residue which was chromatographed on a column of silica gel (10 g). Fractions eluted with light petroleum-ether (8 : 1) were collected and sublimed at 60 °C under 0.1 mmHg to afford the monomethyl ether (**3**; 20 mg), which was found to be identical (mp, mixed mp, IR, PMR, and $[\alpha]_D$) with an authentic sample of **3**. (b) A mixture of **1** (5 mg), methyl iodide (1 ml), silver oxide (20 mg), and dimethylformamide (2 drops) was heated under reflux for 6 hr. Extraction with ether and removal of the solvents gave a residue, which was purified as described above. A methylated product (2 mg) was found to be identical with the authentic specimen of **3**.

*Oxidation of the Diol (**1**).* To a solution of **1** (100 mg) in pyridine (1 ml), a solution of chromium trioxide (100 mg) in pyridine (5 ml) and water (2 drops) was added and stirred at room temperature for 40 hr. Extraction with ether and subsequent work-up as usual gave a crystal, which was crystallized from a mixture of light petroleum-ether to afford 10β-hydroxy-6-oxofuranoeremophilane (**6**; 50 mg), mp 147.5—148 °C, $[\alpha]_D$ +31° (*c* 1.3, EtOH); UV (EtOH) λ_{max} 268 nm (ε 3700); IR 3500, 1650, 1575, 1065 cm^{-1}; PMR ($CDCl_3$) δ 0.79 (3H, d, J=6 Hz; methyl at C-4), 1.18 (3H, s; methyl at C-5), 2.19 (3H, d, J=1.5 Hz; methyl at C-11), 2.72 and 3.50 (each, 1H, d, J=18 Hz; protons at C-9), 7.10 (1H, m; proton at C-12); mass spectrum *m/e* 248 (M^+; $C_{15}H_{20}O_3$), *m/e* 122 (base peak).

*Dehydration of the Hydroxyketone (**6**).* To a solution of **6** (50 mg) in pyridine (1 ml), phosphorus oxychloride (0.1 ml) was added dropwise with stirring. The reaction mixture was heated at 140 °C (oil bath temperature) for 35 min under an atmosphere of nitrogen. Extraction with ether and subsequent work-up as usual gave a residue, which was subjected to purification by preparative tlc to afford 6-oxofuranoeremophil-9-ene (**7**; 35 mg), mp 109—109.5 °C, $[\alpha]_D$ −410° (*c* 0.3, EtOH); UV (EtOH) λ_{max} 215 nm (ε 18000), 248 (7000), 334 (6700) (with shoulders at 242, 255, and 265 nm); IR 1640, 1610, 1595, 1550, 1080, 780 cm^{-1}; PMR ($CDCl_3$) δ 1.04 (3H, d, J=6 Hz; methyl at C-4), 1.22 (3H, s; methyl at C-5), 2.20 (3H, d, J=1.5 Hz; methyl at C-11), 6.37 (1H, broad s; proton at C-9), 7.01 (1H, m; proton at C-12); mass spectrum *m/e* 230 (M^+; $C_{15}H_{18}O_2$), *m/e* 175 (base peak).

*Hydrogenation of the Ketone (**7**).* The ketone (**7**; 13 mg) in ethyl acetate (5 ml) was hydrogenated in the presence of 10% palladium-charcoal (12 mg) with stirring for 1 hr. After filtration of the catalyst, the solvent was removed to give a residue (two spots on tlc). Separation by preparative tlc afforded ligularone (**5**) as a main product yield *ca.* 80%), mp 63 °C, $[\alpha]_D$ −58° (*c* 0.6, $CHCl_3$); UV (EtOH) λ_{max} 268 nm (ε 3300); IR 1670, 1610, 1565, 1070 cm^{-1}; PMR ($CDCl_3$) δ 0.86 (3H, d, J=7.5 Hz; methyl at C-4), 1.10 (3H, s; methyl at C-5), 2.17 (3H, d, J=1.5 Hz; methyl at C-11), 2.71 (1H, dd, J=17 and 6 Hz; proton at C-9), 2.89 (1H, dd, J=17 and 5.5 Hz; proton at C-9), 7.03 (1H, m; proton at C-12); mass spectrum *m/e* 232 (M^+; $C_{15}H_{20}O_2$), *m/e* 122 (base peak), which was found to be identical with an authentic sample of **5** in all respects. Compound corresponding to a minor spot on tlc was not further examined.

The authors wish to thank Dr. M. Fukuyama and Mr. K. Sato, Sagami Chemical Research Center, Sagamihara-shi, for the measurements of NOE's.

References

1) A preliminary account of this paper: M. Tada, Y. Moriyama, Y. Tanahashi, T. Takahashi, M. Fukuyama, and K. Sato, *Tetrahedron Lett.*, **1971**, 4007.

2) F. Patil, G. Ourisson, Y. Tanahashi, M. Wada, and T. Takahashi, *Bull. Soc. Chim. Fr.*, **1968**, 1047; T. Murae, Y. Tanahashi, and T. Takahashi, *Tetrahedron*, **24**, 2177 (1968); Y. Ishizaki, Y. Tanahashi, T. Takahashi, and K. Tori, *Chem. Commun.*, **1969**, 551; Y. Tanahashi, T. Takahashi, and H. Koyama, *Bull. Nat. Sci. Mus. Tokyo*, **12**, 633 (1969): Y. Ishizaki, Y. Tanahashi, T. Takahashi, and K. Tori, *Tetrahedron*, **26**, 5387 (1970); H. Nagano, Y. Moriyama, Y. Tanahashi, T. Takahashi, M. Fukuyama, and K. Sato, *Chem. Lett.*, **1972**, 13; Y. Moriyama, T. Sato, H. Nagano, Y. Tanahashi, and T. Takahashi, *ibid.*, **1972**, 637; H. Nagano and T. Takahashi, This Bulletin, **45**, 1935 (1972); H. Nagano, Y. Tanahashi, Y. Moriyama, and T. Takahashi, *ibid.*, **46**, 2840 (1973); Y. Moriyama, T. Tsuyuki, T. Takahashi, and H. Koyama, *Phytochemistry*, **13**, 288 (1974).

3) F. A. L. Anet and A. J. R. Bourn, *J. Amer. Chem. Soc.*, **87**, 5250 (1956).

4) H. Ishii, T. Tozyo, and H. Minato, *Tetrahedron*, **21**, 2605 (1965).

5) L. Rodríguez-Hahn, A. Guzmán, and J. Romo, *ibid.*, **24**, 477 (1968).

6) P. V. Demarco, E. Farkas, D. Doddrell, B. L. Mylari, and E. Wenkert, *J. Amer. Chem. Soc.*, **90**, 5480 (1968).

7) C. C. Hinckley, *ibid.*, **91**, 5160 (1969).

8) J. K. M. Sanders and D. H. Williams, *ibid.*, **93**, 641 (1971).

Codimerization of Butadiene and Ethylene Catalyzed by σ-Arylnickel(II) Compound in the Presence of Boron Trifluoride Etherate

Noboru KAWATA, Ken-ichi MARUYA, Tsutomu MIZOROKI, and Atsumu OZAKI

Research Laboratory of Resources Utilization, Tokyo Institute of Technology, Ohokayama, Meguro-ku, Tokyo 152

(Received December 10, 1973)

The codimerization of butadiene with ethylene was studied with use of the catalyst system consisting of bis(triphenylphosphine)σ-arylnickel(II) halide and boron trifluoride etherate in methylene dichloride. The codimerization took place readily at 15 °C under 20 kg/cm² to give *trans*- and *cis*-1,4-hexadiene and 3-methyl-1,4-pentadiene. A catalytic amount of water significantly enhanced the catalytic activity. The reaction path to form the codimers is discussed in terms of the variation in product distribution with time and the reaction kinetics.

During the course of studies on the dimerization of ethylene catalyzed by nickel(II) compound, it was found that the bis(triphenylphosphine)σ-arylnickel(II) halide-boron trifluoride etherate system significantly enhances the rate of dimerization to give butene selectively.[1] This catalyst system was found to be less efficient for the dimerization of propylene or its codimerization with ethylene,[2] but highly active for the dimerization of styrene with ethylene.[3] This suggests that it is particularly efficient for the codimerization of ethylene with conjugated olefins. For confirmation the codimerization of ethylene with butadiene was examined, the reaction conditions to give a selective formation of the codimers with high yield being investigated.

A number of homogenous catalyst systems have been reported for the codimerization of butadiene with ethylene. They frequently consist of a transition metal compound and an alkylaluminium compound as a reducing agent.[4~7] The present catalyst system is characterized by the absence of such reducing agent, exhibiting a considerably high activity in the presence of boron trifluoride etherate. Hata and Miyake employed boron trifluoride etherate for the codimerization catalyzed by a zerovalent iron complex $Fe(\phi_2PCH_2CH_2P\phi_2)_2\cdot C_2H_4$,[7] although the catalytic activity was not very high.

Experimental

Materials. Bis(triphenylphosphine)σ-arylnickel(II) halide was prepared according to the methods in the literature.[8,9] The results of elemental analysis of the nickel complex were as follows:

Complex		Calcd.		Found		Ref.
		C(%)	H(%)	C(%)	H(%)	
1-naphthyl-Ni($P\phi_3$)$_2$Br	(A)	69.9	4.7	69.9	4.5	8
phenyl-Ni($P\phi_3$)$_2$Br	(B)	68.2	4.7	68.4	4.6	9
o-tolyl-Ni($P\phi_3$)$_2$Br	(C)	68.5	4.9	67.1	4.6	9
mesityl-Ni($P\phi_3$)$_2$Br	(D)	69.1	5.3	69.1	4.7	8
o-tolyl-Ni($P\phi_3$)$_2$Cl	(E)	72.8	5.2	73.5	5.4	9
o-tolyl-Ni($P\phi_3$)$_2$I	(F)	64.5	4.6	65.7	4.7	9
o-tolyl-Ni[$P\phi(C_2H_5)_2$]$_2$Br ($\phi=C_6H_5$)	(G)	57.7	8.3	57.6	8.1	9

Butadiene was dried by passing through a molecular sieve column at room temperature. 1,4-Hexadiene was dried with anhydrous potassium carbonate and distilled under nitrogen. Cylinder ethylene was used without purification. Methylene dichloride was dried with a molecular sieve and distilled under nitrogen. Boron trifluoride etherate was also purified by distillation under nitrogen.

Procedure. All the operations were carried out under nitrogen atmosphere. Codimerization was performed in a Hasteloi autoclave(100 ml) equipped with a magnetic stirrer. The autoclave was first evacuated and flashed with ethylene, then cooled to −20 °C, at which temperature a methylene dichloride solution of a nickel complex and butadiene, separately prepared and kept at dry ice temperature, was introduced into the autoclave, followed by the addition of boron trifluoride etherate with or without water through a syringe. The autoclave was then warmed up to 15 °C, and ethylene was introduced to initiate codimerization. The pressure was kept constant during the course of reaction by supplying ethylene. Saturated aqueous solution of sodium hydroxide (*ca.* 15 ml) was added to terminate the reaction.

Analysis. The liquid product was separated by distillation at 110 °C into two parts, volatile(below C_8) and non-volatile (above C_{10}). The volatile part was analyzed by gas chromatography(PEG-6000 column), using benzene as an internal standard. The non-volatile part was well extracted with diethyl ether and the weight of extracted material was measured.

Identification. Most products were isolated by fractional distillation and identified by NMR, IR and/or Mass spectroscopy. 1,4-Hexadiene fraction(bp 65—67 °C) consisted of two components whose gas chromatographic retention times corresponded to those of authentic samples of *trans*- and *cis*-1,4-hexadiene. They were further confirmed by IR absorption (1653(C=C), 995 and 913 (vinyl), 967 (*trans* –CH=CH–), and 707 (*cis*–CH=CH–) cm^{-1}), and by NMR (an array of peaks from 6.10 to 4.80 ppm (CH_2=CH– and –CH=CH– 5H), and complex multiplets centered at 2.27 ppm (–CH_2– 2H) and 1.68 ppm (CH_3– 3H). 3-Methyl-1,4-pentadiene was estimated by means of the gas chromatographic retention time and mass spectroscopy, since its amount was too small to be isolated. 2,4-Hexadiene fraction (bp 81.5—82.5 °C) consisted of two components whose gas chromatographic retention times corresponded to those of authentic samples of *trans-trans* and *cis-trans* isomers. NMR spectra of the mixture showed an array of peaks from 6.50 to 4.8 ppm (–CH=CH–CH=CH– 4H) and a doublet centered at 1.65 ppm ($2CH_3$– 6H). IR absorption bands were observed at 1666(w), 1653(w), 987(s), 948(m), 926(m), 820(m), 735 (w), 707(m), and 675(m) cm^{-1}. The C_8-diene fraction (bp 108.6—110 °C) consisted of two major components, although they could not be isolated. Both components had the same molecular weight(110), which was determined by mass spectroscopy connected with gas chromatography. IR absorption bands of the fraction were observed at 1653, 991, and 917 cm^{-1} characterized by 1,4-diene. The NMR showed

that the peak area ratio of aliphatic to olefinic protons was 9/5, which was also in conformity with 1,4-C_8-dienes.

Results

Effect of Water. The codimerization of butadiene and ethylene takes place fairly rapidly at room temperature, but the reproducibility of yield and the selectivity of codimerization is poor. The purer the materials used in the reaction, the greater the decrease in yield. It was found that a catalytic amount of water present in the solution promotes catalytic activity. Such an effect was also found for the codimerization of styrene with ethylene by σ-phenylpalladium(II) complex catalyst.[10]

The effect of water added, when *o*-tolyl-bromo-nickel was used, is shown in Fig. 1. The products obtained were 1,4-hexadiene in *trans*/*cis* ratio 2.0—2.5 and 3-methyl-1,4-pentadiene in a 1/10—1/20 ratio to 1,4-hexadiene. The C_6+C_8 diene yield increases with the amount of water added and reaches a maximum at around 0.83 mmol (molar ratio, H_2O/BF_3OEt_2= 0.1), the higher oligomers monotonically increasing with the amount of water added. Although the C_6+C_8 diene yield depends on the amount of water, the selectivity of C_6-diene to C_6+C_8 dienes and that of 1,4-hexadiene to C_6-dienes is constant (Fig. 1-b). The effect of methanol and phenol instead of water were similarly tested. They also showed a promoting effect but less efficient than water. The effect of water was examined for ethylene dimerization and its codimerization with styrene, using the phenyl-bromo-nickel complex(B) at 0 °C under 1 atm. The results are summarized in Table 1. In both dimerization (Nos. 1 and 2) and codimerization (Nos. 3 and 4), the yield of butene or 3-phenyl-1-butene per min increases about 3 times with the addition of water (H_2O/BF_3OEt_2= 0.4). Formation of small amounts of styrene, phenylbutenes, and 3-methyl-3-phenyl-1-pentene was observed in the dimerization of ethylene, indicating that the ligand in the complex reacted with ethylene.

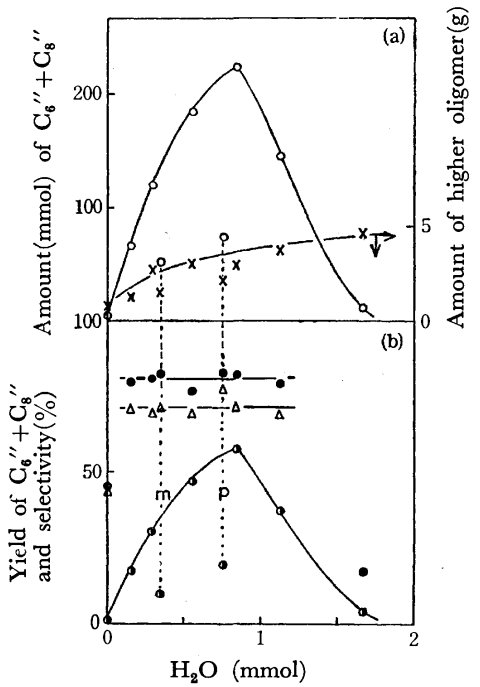

Fig. 1. Effect of added water.
Ni-complex(C), 0.5 mmol; BF_3OEt_2, 8 mmol; Butadiene, 0.39 mol; CH_2Cl_2, 20 ml; C_2H_4, 40 kg/cm²; 15 °C; 1 hr.
○, $C_6''+C_8''$; ×, higher oligomer; ●, $C_6''/(C_6''+C_8'')$; △, 1,4-hexadiene/C_6''; ◑, yield of $C_6''+C_8''$ in butadiene basis.
Methanol(m) and phenol(p) were added in place of water.

Effect of Ethylene Pressure. The effect of ethylene pressure under fixed conditions using the *o*-tolyl-bromo-

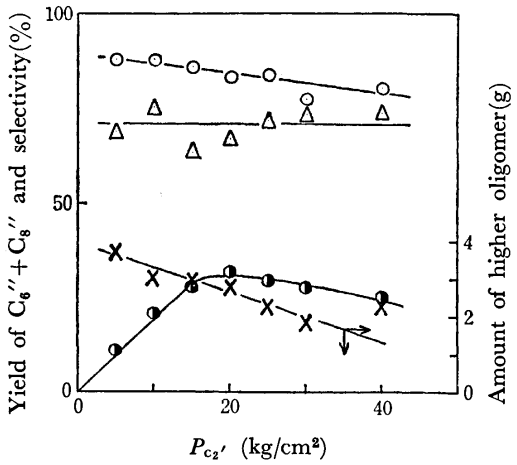

Fig. 2. Effect of ethylene pressure.
Ni-complex(C), 0.5 mmol; BF_3OEt_2, 8 mmol; H_2O, 0.83 mmol; Butadiene, 0.39 mol; CH_2Cl_2, 20 ml; 15 °C; 30 min.
◑, yield of $C_6''+C_8''$; ×, higher oligomer; ○, $C_6''/(C_6''+C_8'')$; △, 1,4-hexadiene/C_6''.

TABLE 1. DIMERIZATION OF ETHYLENE AND ITS CODIMERIZATION WITH STYRENE

No.	H_2O/BF_3OEt_2	Time (min)	Amounts (mmol) in product				
			Sty.[1]	3-p-1-b[2]	2-p-2-b[3]	3-m-3-p-1-p[4]	C_4'[5]
1	0	30	tr.	0.17	tr.	0.01	1.0
2	0.4	10	tr.	0.14	tr.	0.02	1.0
3	0	30	10.0	2.0	tr.	tr.	tr.
4	0.4	20	5.6	5.1	0.07	0.33	tr.

Phenyl-Ni($P\phi_3$)$_2$Br, 0.5 mmol; BF_3OEt_2, 0.5 mmol; Styrene (No. 3, 4), 17.4 mmol; CH_2Cl_2, 30 ml; 0 °C, 1 atm. 1) styrene, 2) 3-phenyl-1-butene, 3) 2-phenyl-2-butene, 4) 3-methyl-3-phenyl-1-pentene, and 5) butenes.

nickel complex(C) is illustrated in Fig. 2. The yield of C_6+C_8 diene increases linearly with ethylene pressure and reaches a maximum at around 20 kg/cm². The amount of butenes formed also increases, whereas the higher oligomers decrease with ethylene pressure. The higher oligomers obtained at 5 kg/cm² and above 10 kg/cm² were separately hydrogenated with Raney nickel catalyst. The amounts of absorbed hydrogen were 19.2 and 13.0 mmol/g respectively, suggesting that the oligomers formed under low pressure were more unsaturated and involved more butadiene than those under high pressure. The results are reasonable since the increase in ethylene concentration should be more favorable for cooligomerization than homooligomerization of butadiene.

Variation in Product Distribution with Time. In order to study the reaction path, variation in product distribution with time was examined using *o*-tolyl-bromo-nickel complex(C) as a catalyst component. The results are given in Fig. 3, where the amount of butadiene consumed for higher oligomers was estimated to be 40% at 100% conversion of butadiene. The rate of reaction, as given by the rate of increase in the amount of C_6+C_8 diene or 1,4-hexadiene, is rather insensitive to the decrease in butadiene concentration, suggesting a zero order reaction with respect to butadiene while 1,4-hexadiene rapidly disappears after butadiene is mostly consumed, being accompanied by an increase in C_8-dienes, higher oligomer and 2,4-hexadiene. Probably 1,4-hexadiene is first isomerized into its conjugated form 2,4-hexadiene, which, like butadiene, reacts readily with ethylene. The increase in higher oligomers in the later stage would be due to both homodimerization of hexadiene and codimerization of C_8-dienes with ethylene.

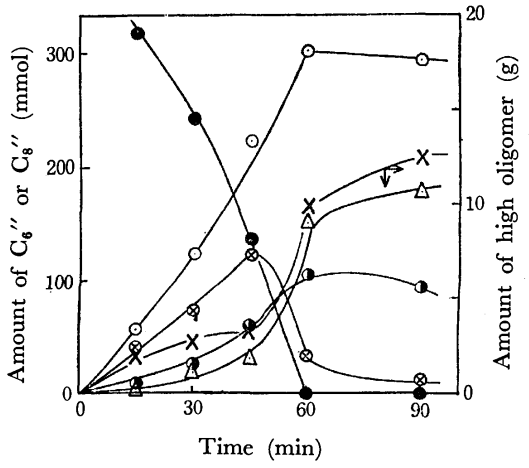

Fig. 3. Products distribution during the codimerization.
Ni-complex(C), 0.5 mmol; BF_3OEt_2, 8 mmol; H_2O, 0.83 mmol; Butadiene, 0.39 mol; C_2H_4, 20 kg/cm²; CH_2Cl_2, 20 ml; 15 °C.
○, $C_6''+C_8''$; ⊗, 1,4-hexadiene; ◑, 2,4-hexadiene; △, C_8''; ●, butadiene(calculated); ×, higher oligomer.

In order to confirm the above interpretation, the codimerization of 1,4-hexadiene with ethylene was examined using the same catalyst. The results are given in Fig. 4. 1,4-Hexadiene is rapidly isomerized

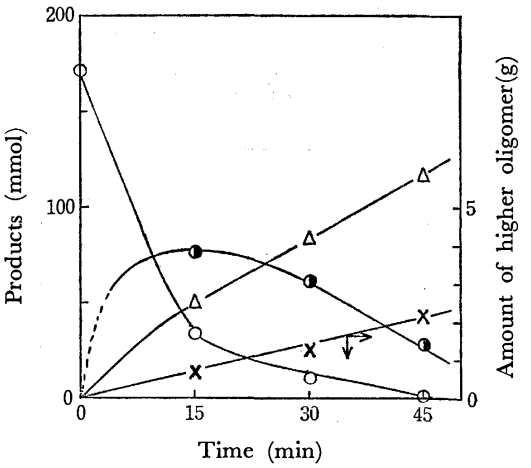

Fig. 4. Products distribution during the codimerization of ethylene with 1,4-hexadiene.
Ni-complex(C), 0.25 mmol; BF_3OEt_2, 4 mmol; H_2O, 0.41 mmol; 1,4-hexadiene(*trans*/*cis*=10), 0.172 mol; C_2H_4, 20 kg/cm²; 15 °C.
○, 1,4-hexadiene; ◑, 2,4-hexadiene; △, C_8''; ×, higher oligomer.

to 2,4-hexadiene, followed by the reaction with ethylene to give 1,4-C_8-dienes. Thus the reaction path might be deduced to be as follows:

$$C_4H_6 + C_2H_4 \longrightarrow CH_2{=}CH{-}CH_2{-}CH{=}CH{-}CH_3 \longrightarrow$$

$$CH_3{-}CH{=}CH{-}CH{=}CH{-}CH_3 \xrightarrow{C_2H_4}$$

$$CH_2{=}CH{-}\underset{\displaystyle CH_3}{\underset{|}{C}}H{-}CH{=}CH{-}CH_2{-}CH_3 \text{ and}$$

$$CH_2{=}CH{-}\underset{\displaystyle CH_2{-}CH_3}{\underset{|}{C}}H{-}CH{=}CH{-}CH_3$$

Effect of BF_3OEt_2 Concentration. The codimerization was carried out by varying the amount of BF_3OEt_2 using *o*-tolyl-bromo-nickel complex(C), the amount of the complex(0.5 mmol) and the molar ratio H_2O/BF_3OEt_2 being fixed. The rate of reaction can

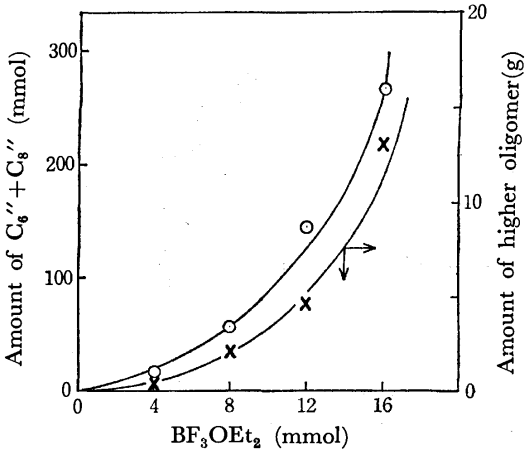

Fig. 5. Effect of amount of BF_3OEt_2.
Ni-complex(C), 0.5 mmol; $BF_3OEt_2/H_2O=10$; butadiene, 0.39 mol; C_2H_4, 20 kg/cm²; CH_2Cl_2, 20 ml; 15 °C; 15 min.
○, $C_6''+C_8''$; ×, higher oligomer.

TABLE 2. EFFECT OF LIGANDS

No.	Ni-Complex	Product					Yield and Selectivity		
		3-m-1,4-PD[a] (mmol)	1,4-HD[b] (mmol)	2,4-HD[c] (mmol)	C_8'' (mmol)	Olig[e] (g)	$C_6''+C_8''$ (%)	$(C_6''/C_6''+C_8'')$ (%)	$(1,4\text{-HD}/C_6'')$ (%)
1	D	7.3	83.3	32.0	27.2	4.0	38.4	81.9	67.9
2	C	5.6	70.8	28.0	20.4	2.9	32.0	83.6	67.8
3	B	6.0	72.9	21.6	15.9	2.6	29.8	86.3	72.5
4	A	2.7	39.5	9.5	6.9	1.7	15.0	88.2	76.4
5	E	6.8	81.2	23.0	14.0	2.4	32.1	88.8	73.1
6	F	5.0	66.6	18.8	15.3	2.9	27.1	85.5	73.7
7	G	4.7	56.5	24.7	14.1	3.4	25.6	85.9	65.8

Ni-Complex, 0.5 mmol; BF_3OEt_2, 8 mmol; H_2O, 0.83 mmol; butadiene, 0.39 mol; CH_2Cl_2, 20 ml; C_2H_4, 20 kg/cm^2; 15 °C; 30 min. a) 3-methyl-1,4-pentadiene, b) 1,4-hexadiene, c) 2,4-hexadiene, d) C_8-diene, and e) higher oligomers.

be estimated from the amount of C_6+C_8 dienes or higher oligomers formed in 15 min. (Fig. 5). It appears that the reaction rate obeys approximately the second order kinetics with respect to BF_3OEt_2, as in the codimerization of styrene with ethylene by the same catalyst system.

Effect of Ligands. Seven complexes with different ligands were prepared and tested for the effect of ligand on the selectivity and activity in codimerization. The results are summarized in Table 2. The difference in the selectivity of C_6-dienes or 1,4-hexadiene seems too small to estimate a ligand effect. The catalytic activity, as given by the yield of C_6-dienes or C_6+C_8 dienes, is affected by the σ-aryl ligand (Nos. 1—4), but to a smaller extent by the halide or phosphine ligand (Nos. 2, 5, 6, and 7), *viz.* the activity decreases in the order, mesityl>*o*-tolyl>phenyl>naphthyl.

Discussion

Reaction Path for Butadiene and Ethylene Codimerization. It was postulated that the active species of the present catalyst system is a nickel hydride complex formed from dissociative addition of olefin to σ-arylnickel(II) compound, with the σ-aryl ligand remaining on the nickel atom during the course of catalytic reaction.[2] The formation of 1,4-hexadiene can also be understood in terms of the nickel hydride intermediate as follows. Butadiene reacts with the nickel hydride(I) to give 1-methyl-π-allyl nickel(II), followed by an insertion of ethylene to form 4-hexenyl nickel(III) and elimination of β-hydrogen to give 1,4-hexadiene.

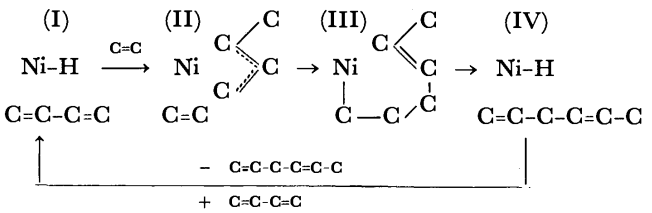

In this scheme, 1,4-hexadiene should be readily replaced by butadiene, since the codimerization rate is of nearly zero order in butadiene concentration. This would be reasonable if the conjugated diene preferentially occupies the coordination site of the nickel. An abrupt change in the distribution of 1,4-hexadiene and C_8-dienes was observed when butadiene is mostly consumed (Fig. 3). Although the isomerization of 1,4-hexadiene to 2,4-hexadiene is very fast in the absence of butadiene (Fig. 4), the formation of 2,4-hexadiene during the butadiene and ethylene codimerization was not so high in spite of very high concentration of 1,4-hexadiene. This suggests that the isomerization of 1,4-hexadiene is greatly retarded by the presence of butadiene. The nickel hydride is likely to be utilized for the isomerization. Thus after the consumption of butadiene, the nickel hydride becomes available for isomerization, resulting in the rapid decrease in 1,4-hexadiene. Since 2,4-hexadiene thus formed is conjugated, it is readily attacked by ethylene to give the C_8-dienes, resulting in the rapid increase in their amounts. In this way the variation in product distribution with time is explained in terms of preferential occupation of coordination site by conjugated dienes.

References

1) K. Maruya, T. Mizoroki, and A. Ozaki, This Bulletin, **45**, 2255 (1972).
2) K. Maruya, T. Mizoroki, and A. Ozaki, *ibid.*, **46**, 997 (1973).
3) N. Kawata, K. Maruya, T. Mizoroki, and A. Ozaki, *ibid.*, **47**, 413 (1974).
4) M. Iwamoto and S. Yuguchi, *ibid.*, **41**, 150 (1968).
5) M. Iwamoto and S. Yuguchi, *J. Org. Chem.*, **31**, 4290 (1966).
7) R. G. Miller, T. J. Kealy, and A. L. Barney, *J. Amer. Chem. Soc.*, **89**, 3756 (1967).
7) G. Hata and A. Miyake, This Bulletin, **41**, 2762 (1968).
8) J. Chatt and B. L. Show, *J. Chem. Soc.*, **1960**, 1718.
9) M. Hidai, T. Kashiwagi, T. Ikeuchi, and Y. Uchida, *J. Organometal. Chem.*, **30**, 279 (1971).
10) H. Nozima, N. Kawata, Y. Nakamura, K. Maruya, T. Mizoroki, and A. Ozaki, *Chem. Lett.*, **1973**, 1165.

Telomerization of Ethylene with Chloroform Initiated by *N*-Chloroalkylamines

Teruzo ASAHARA, Manabu SENŌ, and Noritaka OHTANI

Institute of Industrial Science, The University of Tokyo, Roppongi, Minato-ku, Tokyo 106

(Received February 15, 1974)

N-Chloroalkylamines initiate the telomerization of ethylene with chloroform to give α,α,α-trichloroalkanes $CCl_3(C_2H_4)_nH$(I), which are the same products as those obtained by peroxide-initiated reactions. The *N*-chloroalkylamine-iron and *N*-chloroalkylamine-ferrous chloride systems also initiate the reaction of ethylene with chloroform to afford α,α,ω-trichloroalkanes $CHCl_2(C_2H_4)_nCl$ (II) as the main product, and a small amount of I along with other telomers. The rate of the reaction and the composition of the products vary widely with the kind of *N*-chloroalkylamine. The reaction mechanism was discussed, a "caged radical" mechanism being proposed for the *N*-chloroalkylamine-ferrous chloride system.

A number of reports have appeared on the radical telomerization of olefins with polyhaloalkanes. Various initiators have been examined in these reactions. Some redox systems such as copper chloride–amine[1] or iron chloride–triethyl phosphite[2] gave the 1 : 1 adduct as the main product. It was found that *N*-chloroalkylamine and *N*-chloroalkylamine–metallic salt also initiate the reactions of ethylene with carbon tetrachloride to afford the 1 : 1 adduct and telomers with low molecular weights. A coordinated radical or a caged radical reaction process was suggested in addition to the free radical reaction process.[3]

A "free" radical is considered to abstract the hydrogen atom of chloroform.[4] The reactions of ethylene with chloroform initiated by peroxides give α,α,α-trichloroalkanes instead of α,α,ω-trichloroalkanes. The results prompted us to examine the reaction of ethylene with chloroform using *N*-chloroalkylamines as initiators in order to clarify the reaction mechanism.

Experimental

Materials. Ethylene (purity 99.8%) was used without further purification. Commercial chloroform was purified through an activated alumina column, the purity being examined by gas chromatography. *N*-Chloroalkylamines were prepared and purified as described previously.[3]

Reactions of Ethylene with Chloroform. The reaction was carried out in a 200 ml stainless steel autoclave with a magnetic stirrer. Chloroform and initiators were placed in the autoclave and air was replaced several times by ethylene. After ethylene was charged to a definite pressure, the autoclave was heated up to a prescribed temperature. After the reaction, the autoclave was cooled to room temperature and the reaction mixture was washed by an aqueous potassium iodide solution and then an aqueous sodium thiosulfate solution.

Analyses of the Products. The reaction products were analysed by a temperature programmed gas chromatograph using a 2 m column of Silicone DC 550 at 40—200 °C. *n*-Hexane was used as an internal standard. The authentic samples were prepared by the following methods. α,α,α-Trichloroalkanes, $CCl_3(C_2H_4)_nH$ (I) (n=1,2,3), α,α,ω-trichloroalkanes, $CHCl_2(C_2H_4)_nCl$ (II) (n=1,2) and α,α,α,ω-tetrachloroalkanes, $CCl_3(C_2H_4)_nCl$ (IV) (n=1,2) were prepared by the telomerization of ethylene with chloroform initiated by di-*t*-butylperoxide (DTBP), by that of ethylene with chloroform initiated by the iron chloride–hexamethylphosphoric triamide (HMPA) system[5] and by that of ethylene with carbon tetrachloride initiated by DTBP, respectively. The products were fractionally distilled several times and the purity was confirmed by glc. α,α-Dichloroalkanes, $CHCl_2(C_2H_4)_nH$ (III) (n=1,2) and γ,γ-dichloroalkanes, $HC_2H_4CCl_2(C_2H_4)_nH$ (VII) (n=1,2) were prepared by the reaction of the corresponding aldehydes or ketones with phosphorus pentachloride and purified by distillation. For quantitative analyses of α,γ,γ-trichloroalkanes $ClC_2H_4CCl_2(C_2H_4)_nH$ (V) (n=1,2) and α,γ,γ,ω-tetrachloroalkanes $ClC_2H_4CCl_2(C_2H_4)_nCl$ (VI) (n=1), type I and IV telomers with the same molecular weight as that of V and VI, respectively, were used.

Results and Discussion

The reaction products can be classified according to their structures into the following seven telomers; $CCl_3(C_2H_4)_nH$ (I), $CHCl_2(C_2H_4)_nCl$ (II), $CHCl_2(C_2H_4)_nH$ (III), $CCl_3(C_2H_4)_nCl$ (IV), $ClC_2H_4CCl_2(C_2H_4)_nH$ (V), $ClC_2H_4CCl_2(C_2H_4)_nCl$ (VI), and $H(C_2H_4)_mCCl_2(C_2H_4)_nH$ (VII). Telomers I and IV, having a trichloromethyl group, can act again as a telogen, giving telomers V, VI, and VII.

In the telomerization of ethylene with chloroform, *N*-chloroalkylamines possibly play three roles:

(i) *N*-chloroalkylamines act as initiators, *viz.*, they decompose thermally[6] or under the action of metal[7] to yield amino radicals:

$$RNXCl \xrightarrow{\Delta} R\dot{N}X + Cl\cdot \quad (1)$$

$$2RNXCl + Fe \longrightarrow 2R\dot{N}X + FeCl_2 \quad (2)$$

X=H, Cl, or alkyl; R=alkyl

(ii) *N*-chloroalkylamines have a large chain transfer constant and can act as chain transfer reagents.

$$R\cdot + RNXCl \longrightarrow RCl + R\dot{N}X \quad (3)$$

(iii) Though the basicity of *N*-chloroalkylamines is not so large as that of amines, they can coordinate metal ions at nitrogen and/or chlorine atoms and affect the reactivity of metal ions with chloroform.

$$Fe^{2+} + kRNXCl \rightleftharpoons Fe(RNXCl)_k^{2+} \quad (4)$$

Iron–*N*-chloroalkylamine complex is likely a mixture of complexes with a different value of k, the value of k increasing with the concentration of *N*-chloroalkylamine.

In the absence of metal or metallic salt, the main products were telomers I (Table I), irrespective of the kind of *N*-chloroalkylamines. This suggests that *N*-chloroamine yields the free radical which initiates the reaction. The initiating radical is probably amino

radical in Eq. 1 and/or aminium radical in the following reaction.[3]

$$RNXCl \longrightarrow R'CH{=}NX + HCl \quad (5)$$

$$RNXCl + HCl \longrightarrow R\overset{+}{N}HXCl\ Cl^- \longrightarrow R\overset{+\cdot}{N}HX\ Cl^- + Cl\cdot \quad (6)$$

The order of reactivity of *N*-chloroalkylamines is the same as that in the reaction with carbon tetrachloride;[3] *N*-chlorodibutylamine (CDBA)> *N*-chloromonobutylamine (CMBA)> *N*,*N*-dichlorobutylamine (DCBA). Among the products, a small amount of IV and a smaller amount of III were found. It is likely that α,α,α-trichloroalkyl radical abstracts chlorine atom not from chloroform but from *N*-chloroamine (Eq. 3), since the amount of IV is larger than that of III. The products of the reactions initiated by DTBP under the same conditions contain scarcely any IV and only 1% of III. Two explanations can be given for the formation of III. The amino radical abstracts chlorine atom from chloroform at 130 °C; *N*-chloroamine dissolves iron out of the surface of the autoclave and the stainless steel stirrer, especially in the case of DCBA leading to the formation of metallic salts which take part in the reaction.

In the presence of ferrous chloride (Table 1), the yield and composition of the products varied widely depending on the amount of ferrous chloride and the kind of *N*-chloroalkylamine. Addition of ferrous chloride to CDBA lowered the yield of telomers when the relative concentration of $FeCl_2$ to CDBA was below 25%. Above 25%, however, the reactivity of this initiating system increases remarkably. A similar tendency was observed in the case of DCBA. This indicates that the decomposition of *N*-chloroalkylamines into free radicals (Eqs. 1 and 6) is suppressed by the addition of ferrous chloride and that another radical formation process exists. The suppression of free radical formation can be attributed to the consumption of the *N*-chloroamine to form the iron–*N*-chloroalkylamine complex (Eq. 4). The formation of the complex is confirmed by the following investigation. An equimolar mixture of CDBA and ferrous chloride in methanol has a new broad absorption band at 320 nm at room temperature. This band is different from that of CDBA (275 nm) and ferric chloride (360 nm) and resembles that of ferrous chloride–dibutylamine complex (about 315 nm). The intensity of absorption increases with an increase in the relative concentration of CDBA and decreases gradually with an increase in the absorption of ferric chloride. The complex reacts probably with chloroform to generate dichloromethyl radicals like the copper chloride–amine complexes.[1] If the dichloromethyl radicals thus formed are free radicals, the reaction products would not be II but I, as revealed in the system of ferrous chloride alone. Thus we might suppose that *N*-chloroalkylamine coordinates iron ion to form a cage around the ion and the dichloromethyl radical formed is trapped within the cage (Eq. 7). When dichloromethyl radicals leave the cage, they react with ethylene and then chloroform to yield III and free trichloromethyl radicals (Eq. 10), which afford I by a chain reaction (Eqs. 12 and 13). When dichloromethyl radicals react with ethylene in the cage, the chain transfer reaction with ferric chloride immediately occurs to afford $n=1$ telomers of II (Eq. 8).

$$\underset{X_0}{Fe(RNXCl)_k^{2+}} + CHCl_3 \rightleftharpoons \underset{X}{[Fe(RNXCl)_kCl^{2+}\cdot CHCl_2]_{cage}} \quad (7)$$

Table 1. Telomerization of ethylene with chloroform using ferrous chloride–*N*-chloroalkylamine system[a]

Chloroamine ×10⁻² mol		$FeCl_2\cdot 4H_2O$ ×10⁻² mol	Time min	ΔP of Ethylene kg/cm²	Conv. of Chloroform %	Yield of Telomer g	Product mol%[b] I	II	III	IV	V	VI	VII
—		2.0	180	17	12	20	97	—	2	tr	—	—	1
(*n*-Bu)₂NCl	1.0	—	90	12	9	15	84	—	5	10	—	—	1
	2.0	0.5		1	1	2	8	59	15	18	—	—	—
		1.0		22	18	27	2	74	11	3	3	7	—
		1.5		25	18	27	5	60	16	5	6	8	tr
		2.0		22	16	24	4	61	16	5	5	9	tr
n-BuNHCl	1.0	—	120	12	6	10	74	1	9	14	—	—	2
	2.0	0.5	150	6	4	8	64	9	12	15	—	—	—
		1.0		6	5	10	37	19	19	20	5	—	—
		1.5		5	5	8	40	18	20	19	3	—	—
		2.0		1	1	2	38	20	22	18	—	—	2
n-$BuNCl_2$	1.0	—	120	1	3	4	34	19	18	26	3	—	—
		0.25		tr	2	3	31	23	21	25	tr	—	—
		0.5		2	3	4	45	13	19	22	1	—	1
		1.0		5	6	9	53	10	15	17	2	—	2
		2.0		6	6	9	65	9	10	12	1	—	1

a) Telomerization conditions: initial ethylene pressure, 20 Kg/cm² at 30 °C; chloroform, 1 mol; reaction temperature, 130 °C. b) The telomers except for those contained in Experimental were ignored since their amounts were very small in all runs.

$$[X+C_2H_4]_{cage} \longrightarrow X_0 + CHCl_2C_2H_4Cl \quad (8)$$

$$X \longrightarrow \underset{X_1}{Fe(RNXCl)_kCl^{2+}} + \cdot CHCl_2 \quad (9)$$

$$\cdot CHCl_2 \xrightarrow[CHCl_3]{nC_2H_4} III + \cdot CCl_3 \quad (10)$$

$$\cdot CCl_3 \xrightarrow[CHCl_3]{nC_2H_4} I + \cdot CCl_3 \quad (11)$$

$$CCl_3(C_2H_4)_n\cdot + X_1 \longrightarrow IV + X_0 \quad (12)$$

$$CCl_3(C_2H_4)_n\cdot + RNXCl \longrightarrow IV + R\dot{N}X \quad (13)$$

Figure 1 shows the telomer distribution of I and II. Although a considerable amount of $n \geq 2$ telomers was formed for type I, the $n=1$ telomer was selectively formed for type II. This indicates that the formation of II proceeds by a different mechanism from the free radical mechanism (Eqs. 14—16) and supports the above consideration.[8] The kind of *N*-chloroalkylamines would have some effect on the activation of ferrous ion in Eq. 7, on the stability of the cage (Eqs. 8 and 9), and on the reactivity of X_1 in Eq. 12.

$$FeL_k^{2+} + CHCl_3 \longrightarrow FeL_kCl^{2+} + \cdot CHCl_2 \quad (14)$$

$$\cdot CHCl_2 + nC_2H_4 \longrightarrow CHCl_2(C_2H_4)_n\cdot \quad (15)$$

$$CHCl_2(C_2H_4)_n\cdot + FeL_kCl^{2+} \longrightarrow CHCl_2(C_2H_4)_nCl + FeL_k^{2+} \quad (16)$$

L = ligand

Figures 2 and 3 show the dependence of the telomer composition on the concentration of CDBA, when the molar ratio of [CDBA]/[$FeCl_2 \cdot 4H_2O$] is 1 and 2, respectively. In both cases, the telomer composition hardly changes at low concentrations but the ratio of II becomes high at high concentrations. The increase of II at higher concentrations seems to be due to the low solubility of the ferrous chloride–CDBA complex in chloroform. The reaction of Eq. 8 becomes dominant over the reaction of Eq. 9, since it appears on the solid complex.

The results of telomerization using the *N*-chloroalkylamine–iron system are given in Table 2. As the amounts of iron increase, the rate of telomerization reaction and the product ratio of II increase, irrespective of *N*-chloroalkylamines used. In these systems, it is expected that the reaction of *N*-chloroamine with iron takes place first (Eq. 2). The amino radical then initiates the telomerization according to Eqs. 17 and 11. The ferrous chloride produced by Eq. 2 forms the complex (X_0) with *N*-chloroamine and also induces the telomerization (Eqs. 7—13). In the case of CDBA, the ratio of II

$$R\dot{N}X \xrightarrow[CHCl_3]{nC_2H_4} RNX(C_2H_4)_nH + \cdot CCl_3 \quad (17)$$

was not so large as that in the binary system of CDBA and ferrous chloride. This suggests that the free radical processes are not so feasible and supports the above explanation. However, in the cases of CMBA and CDBA, the ratio of II was larger than that in the binary system of *N*-chloroamine and ferrous chloride. The results can not be explained on the assumption that amino radicals abstract chlorine atom from chloroform. Since these reaction systems are heterogeneous,

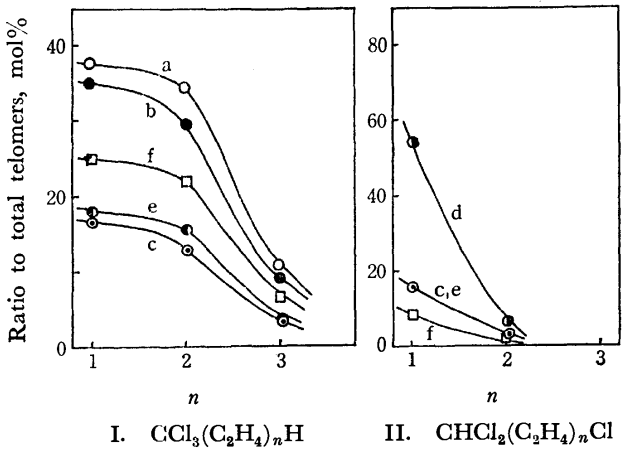

I. $CCl_3(C_2H_4)_nH$ II. $CHCl_2(C_2H_4)_nCl$

Fig. 1. Molecular weight distribution of homologous telomers.
a; $(n\text{-Bu})_2NCl$; b; *n*-BuNHCl; c; $n\text{-BuNCl}_2$; d; $(n\text{-Bu})_2NCl/FeCl_2 \cdot 4H_2O$; e; $n\text{-BuNHCl}/FeCl_2 \cdot 4H_2O$; f; $n\text{-BuNCl}_2/FeCl_2 \cdot 4H_2O$.

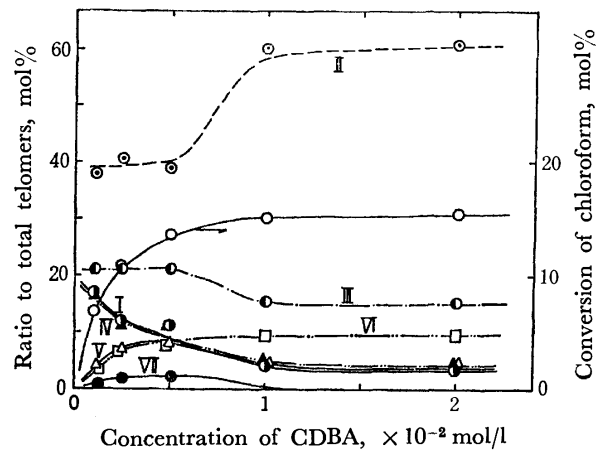

Concentration of CDBA, $\times 10^{-2}$ mol/l

Fig. 2. Effect of the concentration of CDBA–$FeCl_2$ complex.
[CDBA]$_0$/[$EeCl_2 \cdot 4H_2O$]$_0$ = 1; Chloroform, 1 mol; Reaction temperature, 130 °C; Reaction time, 90 min.

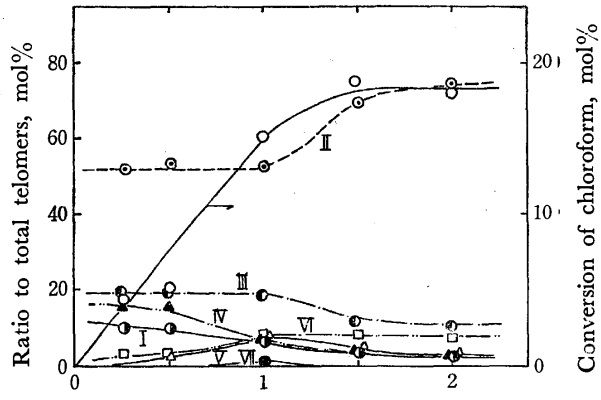

Concentration of CDBA, $\times 10^{-2}$ mol/l

Fig. 3. Effect of the concentration of CDBA–$FeCl_2$ complex.
[CDBA]$_0$/[$FeCl_2 \cdot 4H_2O$]$_0$ = 2; Chloroform, 1 mol; Reaction temperature, 130 °C; Reaction time, 90 min.

TABLE 2. TELOMERIZATION OF ETHYLENE WITH CHLOROFORM USING IRON-*N*-CHLOROALKYLAMINE SYSTEM[a]

Chloroamine ×10⁻² mol		Fe ×10⁻² mol	Time min	*ΔP* of Ethylene kg/cm²	Conv. of Chloroform %	Yield of Telomer g	Product mol%[b] I	II	III	IV	V	VI	VII
		2.0	120	7	5	8	98	—	2	—	—	—	—
(*n*-Bu)₂NCl	1.0	—	90	12	9	15	84	—	5	10	—	—	1
		0.25		13	11	18	72	3	7	13	3	—	3
		0.5		17	11	17	47	15	10	13	8	2	5
		1.0		27	21	34	24	35	11	8	12	7	3
		1.5		24	18	29	23	39	12	7	12	6	1
		2.0		25	20	32	23	40	12	6	11	7	1
n-BuNHCl	1.0	—	120	12	6	10	75	1	9	13	—	—	2
		0.25		13	9	15	57	8	11	14	5	—	5
		0.5		11	7	11	46	13	15	15	6	—	5
		1.0		10	9	14	23	32	18	13	7	4	3
		1.5		16	9	13	17	38	18	12	7	5	3
		2.0		12	10	14	16	39	17	12	7	6	3
n-BuNCl₂	1.0	—	120	1	3	4	34	19	18	26	3	—	—
		0.25		4	5	9	20	34	19	20	3	3	tr
		0.5		8	9	14	9	48	18	13	5	6	1
		0.75		11	12	18	7	51	17	11	5	8	tr
		1.0		13	13	21	6	54	17	10	5	8	tr
		1.5		14	14	22	5	56	16	9	5	9	tr
		2.0		11	12	19	6	55	16	10	4	8	tr

a) Telomerization conditions: initial ethylene pressure, 20 kg/cm² at 30 °C; chloroform, 1 mol; reaction temperature, 130 °C. b) The telomers except for those contained in Experimental were ignored since their amounts were very small in all runs.

we can presume that the reaction proceeds mainly on the surface of solid complexes or the iron particles making the chlorine abstraction by generated radicals easier. The surface of iron particles activated by *N*-chloroamines reacts presumably with chloroform to generate dichloromethyl radicals.[9]

The authors express their appreciation to Mr. T. Suzuki and Mr. H. Nojiri for assistance in the experiments.

References

1) D. J. Burton and L. J. Kehoe, *J. Org. Chem.*, **35**, 1339 (1970); T. Asahara, M. Senō, and C. C. Wu, This Bulletin, **43**, 1127 (1970); T. Asahara, M. Seno, and C. C. Wu, *Kogyo Kagaku Zasshi*, **72**, 1822 (1969).
2) T. Asahara and T. Sato, *ibid.*, **74**, 703 (1971): T. Asahara, A. Kurita, and T. Sato, *ibid.*, **74**, 1847 (1971).
3) T. Asahara, M. Seno, and N. Ohtani, This Bulletin, **46**, 3193 (1973).
4) D. F. Detar and D. V. Wells, *J. Amer. Chem. Soc.*, **82**, 5839 (1960).
5) T. Asahara and T. Sato, *Seisan Kenkyu* **23**, 138 (1971).
6) H. Okamoto, S. Hagiwara, and T. Kagiya, *Kogyo Kagaku Zasshi*, **74**, 1466 (1971).
7) T. Otsu, S. Aoki, M. Nishimura, M. Yamaguchi, and Y. Kusuki, *Polymer Lett.*, **5**, 835 (1967).
8) M. Assher and D. Vofsi, *J. Chem. Soc.*, **1963**, 3921.
9) F. Minisci and R. Galli, *Tetrahedron Lett.*, **1962**, 533.

A Polarographic Study of the Rates of the Dissociation Reactions of Aminopolycarboxylato-zinc(II), -lead(II), and -cadmium(II) Complexes

Mutsuo KODAMA[1], Kyoko NAMEKAWA,* and Takashi HORIUCHI*

Department of Chemistry, College of General Education, Hirosaki University, Bunkyo, Hirosaki 036

**Department of Chemistry, Ibaraki University, Bunkyo, Mito 310*

(Received March 22, 1973)

The rates and the mechanisms of the dissociation reactions of aminopolycarboxylato zinc(II), lead(II), and cadmium(II) complexes were studied by analyzing their kinetic waves by conventional DC polarography. The dissociations of the zinc(II)–HIDA and –NTA complexes and the cadmium(II)– and lead(II)–HIDA complexes in an acetate buffer solution, and those of protonated lead(II)–EDTA and –EDTA–OH complexes were found to proceed through the following direct dissociation mechanisms:

i) HIDA and NTA systems

$MX_2^{2-2m} \rightleftharpoons MX^{2-m} + X^{m-}$ in a rapid equil.

$MX^{2-m} \rightleftharpoons M^{2+} + X^{m-}$ r.d.s.

ii) EDTA and EDTA-OH systems

$MHY^{3-n} \rightleftharpoons M^{2+} + HY^{1-n}$ r.d.s.

On the other hand, the dissociation of the zinc(II)–EDTA-OH and its protonated DTPA complexes gave this rate law: $-d[MH_iY^{2+i-m}]/dt$ $(i=0$ or $1)=k_d^H\cdot[H^+]\cdot[MH_iY^{2+i-m}]$. From a comparison of the observed rate constants, the zinc(II)–HIDA and –NTA, lead(II)– and cadmium(II)–HIDA and protonated lead(II)–EDTA and –EDTA-OH complexes are concluded to dissociate through a simple glycinate reaction intermediate, and the zinc(II)–EDTA-OH and its protonated DTPA complexes, through a glycinate reaction intermediate which includes polyfurcated hydrogen bonds.

The dissociation reactions of metal complexes have been studied by analyzing the kinetic waves by conventional polarography.[2~7] Previously,[8~10] we also studied the dissociation reactions of aminopolycarboxylato nickel(II) and cobalt(II) complexes in alkaline solutions by DC polarography. In this paper, the dissociation reactions of aminopolycarboxylato zinc(II), cadmium(II), and lead(II) complexes will be studied by DC polarography. The structure of the reaction intermediate and the reaction mechanism will be discussed in detail on the basis of a comparison of the observed rate constant with that calculated from the reaction intermediate proposed.

Experimental

Reagents. Our previous paper[11] explained the preparation of standard zinc(II) and cadmium(II) solutions. The standard lead(II) solution was prepared by dissolving a known amount of pure lead(II) nitrate in redistilled water. EDTA, NTA, *N*-(2-hydroxyethyl)ethylenediamine-*N*,*N*′,*N*′-triacetic acid (EDTA-OH), 2,2′-ethylenedioxydi(ethylamine)-*N*,*N*,*N*′,*N*′-tetraacetic acid (GEDTA), and diethylenetriaminepentaacetic acid (DTPA) were recrystallized from their aqueous solutions. *N*-(2-hydroxyethyl)iminodiacetic acid (HIDA) was synthesized from ethanolamine and monochloroacetic acid and recrystallized from its aqueous solution three times by adding pure hydrochloric acid, ethanol, and acetone. All the other chemicals were of analytical-reagent grades and were used without further purification.

Apparatus and Experimental Procedures. All the DC current-voltage curves were measured with a manual polarograph similar to Kolthoff and Lingane's or with a Yanagimoto pen-recording polarograph PA-102. The characteristic features of the DME used were described in a previous paper.[8] All the other apparatuses and the experimental procedures were the same as those in that previous paper. In the HIDA, NTA, and GEDTA systems, an acetate buffer was used. For the EDTA, DTPA, and EDTA-OH systems, no buffer reagent was used, because the sample solutions contained a large excess of uncomplexed EDTA, EDTA-OH, or DTPA and had a sufficient buffer capacity in their pH ranges ($2.50<$ pH <3.50 in the EDTA-OH system, $2.00<$pH<3.00 in the EDTA system, and $2.40<$pH<3.00 in the DTPA system).

Results and Discussion

Reaction Rates and Mechanism. In an acetate buffer solution, zinc(II)–, cadmium(II)–, and lead(II)–HIDA complexes gave two step waves. The first waves were found to be kinetic waves due to the reduction of the aquo metal(II) ion and acetate complexes formed upon the slow dissociation of the metal(II) complexes, whereas the second waves, diffusion waves, were found to be the direct reduction of the metal(II) complexes. The zinc–(II)NTA complex also gave a kinetic wave due to its dissociation at the electrode surface. As was discussed in connection with the polarography of the aminopolycarboxylato cobalt (II) complexes,[10] the reaction mechanism and dissociation rates were determined from the i_k and i_d values using the treatment employed by Koryta.[4] Under the present experimental conditions, the Koryta equation for the kinetic waves of HIDA and NTA complexes could be formulated as:

$$\frac{i_k}{i_d-i_k}=0.886\cdot\sqrt{\frac{k_d\cdot t\cdot(\alpha_H)_X\cdot\beta_{Ac}}{K_{MX}\cdot[X]_f}}\,\frac{1}{1+\dfrac{K_2\cdot[X]_f}{(\alpha_H)_X}} \qquad (2)$$

corresponding to the (I) reaction mechanism:

(I)
- $MX_2^{2-2m} \rightleftharpoons MX^{2-m} + X^{m-}$ in a rapid equil.
- $MX^{2-m} \overset{k_d}{\rightleftharpoons} M^{2+} + X^{m-}$ (direct dissociation) (I_b) r.d.s.
- $M^{2+} + iAc^- \rightleftharpoons MAc_i^{2-i}$ (I_c) in a rapid equil.

$\underbrace{\qquad\qquad}_{Hg\downarrow 2e}$

M(Hg)

The β_{Ac} in Equation (1) is defined as $\beta_{Ac}=1+K_1^{Ac}\cdot[Ac^-]+K_1^{Ac}\cdot K_2^{Ac}\cdot[Ac^-]^2+\cdots$, and $(\alpha_H)_X$, $[X]_f$, $[Ac^-]$, K_{MX}, K_2, and K_1^{Ac} are, respectively, the (α_H) value of HIDA or NTA, the concentration of uncomplexed HIDA or NTA, the concentration of the free acetate ion, the second successive formation constant of the HIDA or NTA complex, and the i-th successive formation constant of the metal(II)-acetate complex.

From the slope of the linear relation between $i_k/(i_d-i_k)$ and $(\alpha_H)_X^{1/2}/(1+K_2'\cdot[X]_f)$ or $1/[X]_f^{1/2}\cdot(1+K_2'\cdot[X]_f)$, the k_d values were determined; they are listed in Tables 1, 2, and 3. The typical linear relations obtained are shown in Fig. 1. The lead(II)-EDTA-OH and -EDTA complexes in the pH range from 2.00 to 3.50 and the lead(II)-GEDTA complex in the pH range from 4.50 to 5.60 also gave kinetic waves due to their dissociations at the electrode surface. In the case of the EDTA-OH complex, we obtained a linear relation

TABLE 1. DISSOCIATION AND FORMATION RATE CONSTANTS OF THE ZINC(II)-AMINOPOLYCARBOXYLATE COMPLEXES
25 °C, $\mu=0.30$

System		NTA	HIDA
$\log K_{MX}$ [18]		10.0	8.06
$\log K_{st}$		0.48	0.30
$\log K_{elec}$		1.00	0.50
$\Delta \log k_d$	calcd	0	0.86
	obsd	0	0.86
k_d, s^{-1}		0.21	1.5
k_f, $M^{-1}s^{-1}$		2.1×10^9	2.7×10^8

TABLE 2. DISSOCIATION AND FORMATION RATE CONSTANTS OF THE CADMIUM(II)-AMINOPOLYCARBOXYLATE COMPLEXES
25 °C, $\mu=0.30$

System		NTA	EDTA (protonated)	HIDA
Reporter		13)	2)	present authors
$\log K_{MX}$		9.80	8.55	7.21
$\log K_{st}$		0.48	0.30	0.30
$\log K_{elec}$		1.00	0.50	0.50
$\Delta \log k_d$	calcd	0	0.90	1.91
	obsd	0	1.23	1.90
k_d, s^{-1}		~0.60	10.8	50
k_f, $M^{-1}s^{-1}$		$\sim4.0\times10^9$	6.0×10^9	8.1×10^8

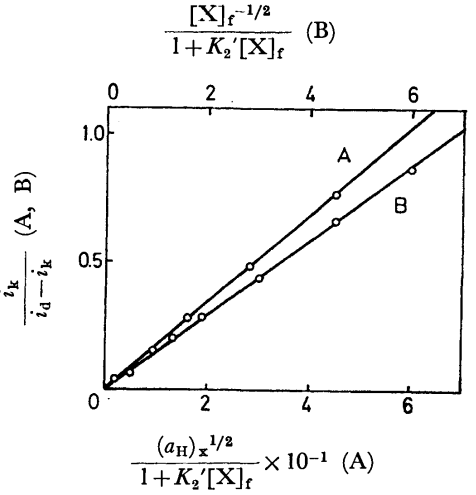

Fig. 1. The plot of $i_k/(i_d-i_k)$ against $(\alpha_H)_X^{1/2}/(1+K_2'[X]_f)$ or $(\alpha_H)_X^{1/2}/(1+K_2'\cdot[X]_f)\cdot[X]_f^{1/2}$
Cd(II)-HIDA system
25 °C, $\mu=0.30$
the concentration of cadmium(II) ion=0.60 mM
the concentration of acetate ion=0.06 M
A) The $i_k/(i_d-i_k)$ *vs.* $(\alpha_H)_X^{1/2}/(1+K_2'\cdot[X]_f)$ plot
the concentration of HIDA=30.0 mM
pH ranged from 4.80 to 5.82
B) The $i_k/(i_d-i_k)$ *vs.* $(\alpha_H)_X^{1/2}/(1+K_2'\cdot[X]_f)\cdot[X]_f^{1/2}$ plot
the concentration of HIDA ranged from 10.0 mM to 50.0 mM
pH=5.20

with an intercept of a finite value by plotting $((i_d-i_k)/i_k)\cdot(\alpha_H)_Y^{1/2}/[H^+]^{1/2}$ against the reciprocal of the hydrogen-ion concentration, $[H^+]^{-1}$ (at a given uncomplexed EDTA-OH concentration) (Fig. 2). This means that, under the present experimental conditions, the Koryta equation for the kinetic wave of the lead(II)-EDTA-OH complex may be expressed as:

$$\frac{i_k}{i_d-i_k}=0.886\cdot\sqrt{\frac{k_d\cdot t\cdot(\alpha_H)_Y}{K_{PbY}\cdot K^H\cdot[H^+]\cdot[Y]_f}}\,\frac{K^H\cdot[H^+]}{1+K^H\cdot[H^+]} \quad (2)$$

corresponding to the (II) reaction mechanism:

$$(II)\begin{cases} PbY^{2-m}+H^+ \rightleftharpoons PbHY^{3-m} & (II_a)\ \text{in rapid equil.} \\ PbHY^{3-m} \overset{k_d}{\rightleftharpoons} Pb^+ + HY^{1-m} & \text{(direct dissociation)} \\ & (II_b)\ \text{r.d.s.} \\ Pb^{2+}+2e^-+Hg \rightleftharpoons Pb(Hg) & (II_c) \end{cases}$$

TABLE 3. DISSOCIATION AND FORMATION RATE CONSTANT OF THE LEAD(II)-AMINOPOLYCARBOXYLATE COMPLEXES
25 °C, $\mu=0.30$

System		NTA	HIDA	EDTA-OH	EDTA	GEDTA
				protonated		
Reporter		13)	present authors			
$\log K_{MX}$		11.39	9.10	8.79	10.1	8.55
$\log K_{st}$		0.48	0.30	0.30	0.60	0.60
$\log K_{elec}$		1.00	0.50	0.50	0.50	0.50
$\Delta \log k_d$	calcd	0	1.61	2.74	1.74	2.98
	obsd	0	1.41	2.82	1.92	2.27
k_d, s^{-1}		~0.6	15.5	4.0×10^2	50	$1.0_5\times10^2$
k_f, $M^{-1}s^{-1}$		$\sim1.5\times10^{11}$	2.0×10^{10}	2.4×10^{11}	6.1×10^{11}	7.5×10^{10}

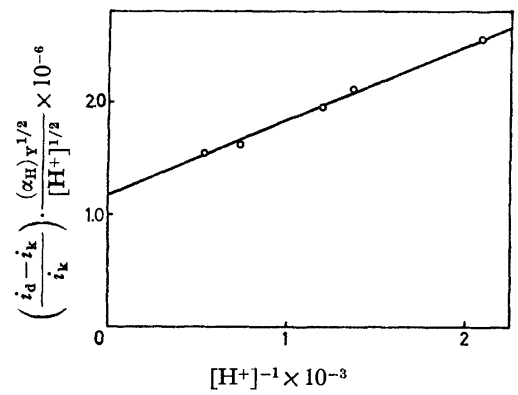

Fig. 2. The plot of $(i_d-i_k)\cdot(\alpha_H)_Y^{1/2}/i_k\cdot[H^+]^{1/2}$ against $[H^+]^{-1}$
Lead(II)-EDTA-OH system
25 °C, $\mu=0.30$
the concentration of lead(II) ion = 1.0 mM
the concentration of EDTA-OH = 14.0 mM
pH ranged from 2.60 to 3.50

Therefore, the ratio between the intercept and the slope of the above linear relation should correspond to the protonation constant of the lead(II)-EDTA-OH complex, K^H. From the above linear relation, the K^H value was determined to be 1.8×10^3. Although the formation of the protonated lead(II)-EDTA-OH complex has not yet been reported, if the pH dependence of the i_k value can be interpreted as due to the dissociation of the protonated lead(II)-EDTA-OH complex, the plot of the $i_k/(i_d-i_k)$ value against the $K^H\cdot[Y]_f^{-1/2}$ value (at a given $[Y]_f$) or the $[Y]_f^{-1/2}$ (at a given pH) should yield a straight line passing through the point of origin. These relations were examined successfully by using some typical experimental data (Fig. 3). The k_d value obtained from the slope of the above straight line is also listed in Table 3. In the GEDTA system, the straight line passing through the point of origin could be obtained by plotting $i_k/(i_d-i_k)$ against $K^H\cdot[H^+]\cdot(\alpha_H)_Y^{1/2}/(1+K^H\cdot[H^+])\cdot[H^+]^{1/2}$, $[Y]_f^{-1/2}$ or $\beta_{Ae}^{1/2}$, suggesting a reaction mechanism in which (II_b) is the slowest step. Therefore, the k_d value for the dissociation of the protonated lead(II)-GEDTA complex was determined from the slope of the above linear relation; it is listed in Table 3. In the case of the EDTA system, the plot of the $i_k^2\cdot[H^+]\cdot[(1+K^H\cdot[H^+])^2/(i_d-i_k)^2\cdot(\alpha_H)_Y\cdot(K^H\cdot[H^+])^2$ against $[H^+]$ gave a straight line with an intercept of a finite value. Furthermore, at a given pH, the plot of the $(i_k-(i_d-i_k))^2$ value against the $[Y]_f^{-1}$ value yielded a straight line passing through the point of origin. These facts evidently imply that the $i_k/(i_d-i_k)$ ratio is given by Eq. (3); hence, the dissociation of the protonated lead(II)-EDTA complex proceeds through (III_b) and (II_b):

$$\frac{i_k}{i_d-i_k}=0.886\cdot\sqrt{\frac{(k_d+k_d^H[H^+])\cdot t\cdot(\alpha_H)_Y}{K_{PbY}\cdot K^H\cdot[Y]_f\cdot[H^+]}}\;\frac{K^H\cdot[H^+]}{1+K^H\cdot[H^+]} \quad (3)$$

$$PbHY^{3-m}+H^+\overset{k_d^H}{\rightleftharpoons}Pb^{2+}+H_2Y^{2-m}$$ (proton-assisted dissociation) (III_b) r.d.s.

The k_d and k_d^H values were determined from the intercept and the slope of the linear relation between $i_k^2\cdot(1+K^H\cdot[H^+])^2/(i_d-i_k)^2\cdot(\alpha_H)_Y\cdot K^{H^2}\cdot[H^+]$ and $[H^+]$ (Table 3). Although the results are not shown here, the effects of the solution pH and the uncomplexed ligand concentration on the half-wave potential of kinetic waves of the lead(II) and cadmium(II) complexes were also examined. The shifts of the half-wave potential, as calculated on the basis of the proposed reaction mechanism, agreed well with those observed.

The zinc(II)-EDTA-OH and -DTPA complexes in an acid solution also produced kinetic waves due to their dissociations at the electrode surface. From the systematic examination of the nature of the kinetic waves, the $i_k/(i_d-i_k)$ ratios for the EDTA-OH and DTPA systems were found to be 0.886 $(k_d^H\cdot t\cdot[H^+]\cdot(\alpha_H)_Y/K_{ZnY}\cdot[Y]_f]^{1/2}$ and 0.886 $[k_d^H\cdot t\cdot(\alpha_H)_Y/K_{ZnY}\cdot[Y]_f]^{1/2}$ respectively. In considering the fact that all the zinc(II)-DTPA complex exists in the form of $ZnHY^{2-}$ under the present experimental conditions, the above fact suggests that the dissociation reactions of the zinc(II)-EDTA-OH and -DTPA complexes are given by (IVa) and (IVb) respectively:

$$ZnY^-+H^+\overset{k_d^H}{\rightleftharpoons}Zn^{2+}+HY^{2-}$$ (proton-assisted dissociation) (IV_a)

$$ZnHY^{2-}+H^+\overset{k_d^H}{\rightleftharpoons}Zn^{2+}+H_2Y^{3-}$$ (proton-assisted dissociation) (IV_b)

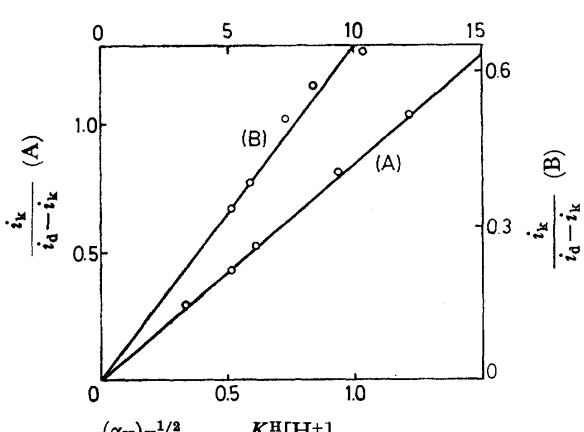

Fig. 3. The plot of $i_k/(i_d-i_k)$ against $(\alpha_H)_Y^{1/2}\cdot K^H\cdot[H^+]/[H^+]^{1/2}\cdot(1+K^H\cdot[H^+])$ or $[Y]_f^{-1/2}$
Lead(II)-EDTA-OH system
25.0 °C, $\mu=0.30$
the concentration of lead(II) ion = 1.0 mM
A) the $i_k/(i_d-i_k)$ *vs.* $(\alpha_H)_Y^{1/2}\cdot K^H\cdot[H^+]/[H^+]^{1/2}(1+K^H\cdot[H^+])$ plot. The concentration of EDTA-OH = 14.0 mM
pH ranged from 2.60 to 3.50
B) the $i_k/(i_d-i_k)$ *vs.* $[Y]_f^{-1/2}$ plot
the concentration of EDTA-OH ranged from 9.0 mM to 39.0 mM
pH = 3.09

TABLE 4. PROTON-ASSISTED DISSOCIATION AND FORMATION RATE CONSTANT OF THE ZINC(II)-AMINOPOLYCARBOXYLATE COMPLEXES
25 °C, μ=0.30

System	NTA	EDTA-OH	EDTA	DTPA (protonated)
Reporter	13)	present authors	12)	present authors
$\log K_{MX}$	10.0	14.0_5	15.9_1	13.2_0
$\log K_{st}$	0.30	0.30	0.60	0
$\log K_{elec}$	0.50	0.50	0.50	0
pK_a	1.86	5.26	5.97	4.10
$\log k_d^H$ calcd	1.50	0.85	0	−0.26
$\log k_d^H$ obsd	2.15	0.85	0	−0.26
k_d^H, $M^{-1}\cdot s^{-1}$	1×10^5	5×10^3	7×10^2	3.9×10^2
k_f, $M^{-1}\cdot s^{-1}$	—	1.7×10^8	5.7×10^8	1.1×10^8

The k_d^H values for the zinc(II)-EDTA-OH and -DTPA systems were determined from the slope of the linear relation between $i_k/(i_d-i_k)$ and $[Y]_f^{-1/2}$ or that between $i_k/(i_d-i_k)$ and $(\alpha_H)_Y^{1/2}\cdot[H^+]^{1/2}$ (EDTA-OH system) or $(\alpha_H)_Y^{1/2}$ (DTPA system). They are listed in Table 4, together with the reported rate constants and EDTA and NTA systems.[12,13]

Direct Dissociation. As has been stated above, metal(II)-HIDA and -NTA and protonated lead(II)-EDTA, -EDTA-OH, and -GEDTA complexes dissociate through the direct dissociation mechanism. As was discussed in connection with the dissociation reactions of nickel(II)-glutamate and -IDA complexes,[8] it is hard to believe that, in the dissociation of the cadmium(II)-aminopolycarboxylate complexes, all the bond breakages are involved in the rate-determining step. Day and Reilley, in their NMR study of metal-aminopolycarboxylate complexes,[14] mentioned that the breakage process of the cadmium(II)-nitrogen bond is much more sluggish than that of the cadmium(II) to the oxygen bond. Therefore, the dissociations of the cadmium(II)-HIDA and -NTA[4] complexes should proceed through a reaction intermediate in which the leaving HIDA or NTA anion is bonded to the cadmium(II) ion through the glycinate or iminodiacetate chelate ring (glycinate or IDA mechanism). If both complexes dissociate through the glycinate reaction intermediate (Fig. 4), the rate constant ratio between HIDA and NTA systems, $(k_d)_{HIDA}/(k_d)_{NTA}$, must be given by $(K_{CdX})_{NTA}\times2\times3.16/(K_{CdX})_{HIDA}\times3\times10=10$,[1.96] because the dissociation rate constant, k_d, is given by the well-known relation: $k_d=k_{rds}\cdot k_{inter}\cdot K_{st}\cdot K_{elec}/K_{MX}$.[8] Here, the symbols used have their usual meanings, while $(K_{CdX})_{NTA}$ and $(K_{CdX})_{HIDA}$ are the formation constants of 1 : 1 ratio cadmium(II)-NTA and -HIDA complexes. On the other hand, if the IDA mechanism is operative here, the rate-constant ratio between the two systems should be 10.[2,11] The observed ratio of $10^{1.90}$ evidently excludes the IDA mechanism. The rate-constant ratio calculated on the basis of the other reaction intermediates showed no satisfactory agreement with the observed one. As is clear from the dissociation rate constants for the zinc(II)-acetate[15] and -ammine complexes,[16] the zinc(II)-nitrogen bond has a life span longer than that of the zinc(II)-oxygen bond. Therefore, the zinc(II)-aminopolycarboxylate complex seems to dissociate through a glycinate or IDA reaction intermediate produced by the partial dissociation of the original complex. Ogino[17] suggested a water-loss mechanism for the formation of the zinc(II)-aminopolycarboxylate complex from the aquo zinc(II) ion and the aminopolycarboxylate anion. If the formation reaction of the zinc(II)-glycinate complex also has a water-loss mechanism, the dissociation rate constant of the zinc(II)-glycinate complex with a 1 : 1 ratio can be calculated by using the formation rate constant: $k_f=k_{Zn}^{H_2O}\cdot K_{os}$ and the K_{ZnX} value for the zinc(II)-glycinate complex. By using the $k_{Zn}^{H_2O}$ value of 5×10^7,[13] the K_{os} value of 5, and the K_{ZnX} value of 7×10^4,[18] the k_d value for the zinc(II)-glycinate complex was calculated to be 3.6×10^3 s^{-1}. Here, the zinc(II)-*N*-methyl-glycinate complex was employed as a model. By using the k_d value thus estimated as k_{rds}, the dissociation rate constant of the zinc(II)-NTA complex was calculated to be 0.1 on the basis of the glycinate dissociation mechanism. This value showed a satisfactory agreement with the observed k_d value (Table 1). None of the rate constants calculated on the basis of other reaction intermediates showed a satisfactory agreement with the observed one. The relative rate constant of the zinc(II)-HIDA system, calculated on the basis of the glycinate mechanism, is listed in Table 1 and compared with the observed one. The agreement between the observed and calculated rate constants can be regarded as satisfactory, lending strong support to the glycinate-mechanism explanation.

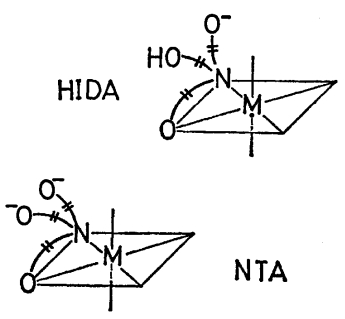

Fig. 4. Reaction intermediates for the direct dissociations of metal(II)-HIDA and -NTA complexes.

Rabenstein,[13] in his NMR study of the reaction of the lead(II)-NTA complex, reported several features

which support the conclusion that the lead(II)–NTA reaction also has a mechanism similar to those of the cadmium(II)- and zinc(II)–NTA reactions. Therefore it is natural to assume the glycinate mechanism for the dissociation of the lead(II)–aminopolycarboxylate complexes. As is shown by the data in Table 3, the relative dissociation rate constants evaluated on the basis of the glycinate mechanism agreed well with those observed. The dissociation rate constants of the protonated lead(II)–EDTA, –EDTA-OH, and –GEDTA complexes can also be understood in terms of the glycinate mechanism (Table 3). As is shown by the data in Table 3, the formation constant of the protonated complex evaluated from the K_{MY}, K^H, and pK_a values is always smaller than that of the corresponding normal complex, K_{MY}. This may mean that the formation of the protonated complex is always accompanied by the partial dissociation of the metal(II) ligand bonds in the original complex.[19] This would explain the dissociation of the protonated complex being more rapid than that of the normal complex. In exactly the same manner, the rapid dissociation of the protonated cadmium(II)–EDTA complex[2] can also be understood in terms of the glycinate mechanism.

Proton-Assisted Dissociation. As has been reported by several authors,[4,13] the proton-assisted dissociation of the metal(II)–aminopolycarboxylate complex proceeds much more rapidly than the corresponding direct dissociation. From a thermodynamic point of view, it can be said that when the metal complex of the polydentate ligand forms a binuclear complex with another metal ion through the free donor atom, its stability will increase appreciably. Therefore, it is reasonable to believe that, in the proton-assisted dissociation of the metal(II)–aminopolycarboxylate complex, the bond breakage in the course of the reaction intermediate formation always accompanied by the subsequent protonation at the freed donor atom, thus yielding a stable reaction intermediate. If the proton-assisted dissociations of zinc(II)–EDTA, –EDTA-OH, and –DTPA complexes proceed through the glycinate reaction intermediate, with the protonation occurring at the most basic free donor atom, one can estimate the relative rate constant by using the relation employed above. Here, the stability of the reaction intermediate, K_{inter}, should be the product of the stability constant of the zinc(II)-glycinate complex and the protonation constant of a free amino group, $K_h=1/K_a$. The relative rate constants calculated are listed in Table 4, together with the numerical values used in the calculation. The agreement between the calculated and observed values can be regarded as satisfactory. The rate constants for the proton-assisted dissociations of the lead(II)- and cadmium(II)–EDTA-OH, –EDTA, and –DTPA complexes also can be understood in terms of the glycinate reaction intermediate (Table 5). As is shown in Table 4 and 5, the rate constants for the proton-assisted dissociations of the zinc(II)–, lead(II)–, and cadmium(II)–NTA complex can also be understood by assuming a glycinate reaction intermediate where the carboxylate group is protonated (I in Fig. 5). If the reaction intermediates for the direct and proton-assisted dissociations of metal(II)–NTA complexes are given by the reaction intermediate in Fig. 4 and I in Fig. 5 respectively, the rate constant ratio between the two dissociation mechanisms should be 1 : 23.5. However, the observed ratios for the zinc(II)–,[13] lead(II)–,[13] and cadmium(II)–NTA[4,13,20] systems are $1:4\times10^4$, $1:5._5\times10^3$, and $1:1._3\times10^4$ respectively. As far as the $k_d=k_{rds}\cdot K_{inter}\cdot K_{st}\cdot K_{elec}/K_{MX}$ relation can be applied safely to the estimation of the relative dissociation rate constant, the above discrepancy would indicate that the protonation of the reaction intermediate results in not only an increase in the stability of the reaction intermediate, but also in an increase in the rate of the dissociation of the leaving ligand anion from the metal(II) ion. In order to describe the above effect, we propose an reaction intermediate with polyfurcated hydrogen bonds, shown by II in Fig. 5, in place of the simple binuclear complex, I. This structure can also explain why the zinc(II) system has a rate constant ratio different from those of the lead(II) and cadmium(II) systems. The rate constant for the proton-assisted dissociation of the nickel(II)–NTA complex[21] can also be understood by assuming the II reaction intermediate in Fig. 5. As is clear from the above discussion, it is not unreasonable to propose the III reaction intermediate in Fig. 5 for the proton-assisted dissociations of the metal(II) complexes of EDTA and its derivatives (Tables 4 and 5). The

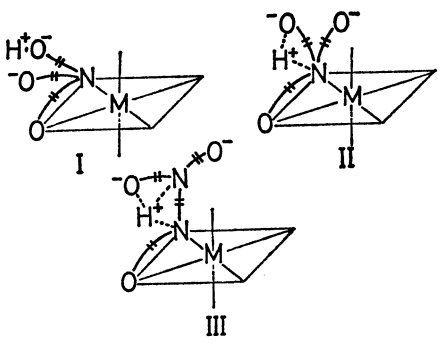

Fig. 5. Reaction intermediates for the proton-assisted dissociations of metal(II)-aminopolycarboxylate complexes.

TABLE 5. PROTON-ASSISTED DISSOCIATION RATE CONSTANTS OF CADMIUM(II)- AND LEAD(II)–AMINOPOLYCARBOXYLATE COMPLEXES

25 °C, $\mu=0.30$

A) Cadmium(II) system				
System Ref.	NTA 4)	EDTA 12)	EDTA-OH 12)	DTPA 12)
$\log k_d^H$	5.40	3.05	5.60	1.60
$\Delta \log k_d^H$ calcd	0	−2.20	−0.05	−3.90
$\Delta \log k_d^H$ obsd	0	−2.35	0.20	−4.00

B) Lead(II) system			
System Ref.	NTA 3, 13)	EDTA-OH 12)	DTPA 12)
$\log k_d^H$	4.70	4.87	2.46
$\Delta \log k_d^H$ calcd	0	0.19	−1.53
$\Delta \log k_d^H$ obsd	0	0.27	−2.24

rate constants for the direct and proton-assisted dissociations of the cobalt(II)–EDTA complex[22] can also be understood on the basis of the glycinate intermediate. However, in order to describe the precise role of the hydrogen ion in the dissociation of metal(II)–aminopolycarboxylate complexes, a further systematic investigation should be conducted.

Formation Reactions. The rate constants, k_f's, for the formation of the cadmium(II) complexes calculated with the aid of the $k_f=k_d \cdot K_{MX}$ relation were found to be slightly larger than the characteristic water-exchange rate constant of the cadmium(II) aquo ion[23] (Table 2). Since the equilibrium constant for the outer-sphere association of the cadmium(II) aquo ion with the aminopolycarboxylate anion, approximated by using the Fuoss exuation,[24] is expected to be larger than unity, the above fact can be taken as evidence for the usual water-loss mechanism. As in the case of cadmium(II) complex, the rate constants for the formation reactions of lead(II)- and zinc(II)-aminopolycarboxylate complexes, as calculated using the k_d values and the stability constants, can also be understood by assuming the usual water-loss mechanism (Tables 1 and 3).

References

1) To whom correspondence should be addressed.
2) N. Tanaka, R. Tamamushi, and M. Kodama, *Z. Phys. Chem., N. F.* **14**, 141 (1958).
3) K. Morinaga and T. Nomura, *Nippon Kagaku Zasshi*, **79**, 200 (1958).
4) a) J. Koryta, *Collect. Czech. Chem. Commun.*, **24**, 2903 (1959). b) J. Koryta, *ibid.*, **24**, 3057 (1959).
5) S. Misumi and Y. Masuda, *J. Electroanal. Chem.*, **6**, 434 (1963).
6) Y. Koike and H. Hamaguchi, *J. Inorg. Nucl. Chem.*, **29**, 473 (1967).
7) T. J. Bydalek, T. M. Stokich, and D. M. Coleman, *Inorg. Chem.*, **9**, 29 (1970).
8) M. Kodama, H. Nunokawa, and N. Oyama, This Bulletin, **44**, 2387 (1971).
9) M. Kodama and N. Oyama, *ibid.*, **44**, 2849 (1971).
10) M. Kodama, *ibid.*, **46**, 3422 (1973).
11) M. Kodama and N. Oyama, *ibid.*, **45**, 2619 (1972).
12) a) T. Fujisawa and N. Tanaka, *Nippon Kagaku Zasshi*, **87**, 965 (1966). b) T. Fujisawa and N. Tanaka, *ibid.*, **88**, 734 (1967). c) T. Fujisawa and N. Tanaka, *ibid.*, **89**, 1206 (1968). d) T. Fujisawa and N. Tanaka, *ibid.*, **92**, 962 (1971).
13) a) D. L. Rabenstein and R. J. Kula, *J. Amer. Chem. Soc.*, **91**, 2492 (1969). b) D. L. Rabenstein, *ibid.*, **92**, 2869 (1970).
14) R. J. Day and C. N. Reilley, *Anal. Chem.*, **36**, 1073 (1964).
15) M. Eigen and R. G. Wilkins, "Mechanisms of Inorganic Reactions," Advance in Chemistry Series, No. 49, R. K. Murman, R. T. M. Fraser, and J. Bauman, Ed., American Chemical Society, Washington, D.C., 1965, pp 55~65.
16) D. B. Rorabacher, *Inorg. Chem.*, **5**, 1891 (1966).
17) H. Ogino, "Formation, Substitution, and Isomerisation Reactions of Metal Complexes," p. 58 of "Mechanisms of Inorganic Reactions", edited by N. Tanaka, K. Tamaru, and S. Kawaguchi, Kagakudozin, Kyoto (1967).
18) L. G. Sillen and A. E. Martell, "Stability Constants of Metal-Ion Complexes," 2nd Ed., The Chemical Society, London (1964).
19) G. S. Smith and J. L. Hoard, *J. Amer. Chem. Soc.*, **81**, 556 (1959).
20) N. Tanaka, K. Ebata, T. Takahari, and T. Kumagai, This Bulletin, **35**, 1836 (1962).
21) M. Kimura, *Nippon Kagaku Zasshi*, **89**, 1209 (1968).
22) a) N. Tanaka, H. Osawa, and M. Kamada, This Bulletin, **36**, 67 (1963). b) H. Ogino and N. Tanaka, *ibid.*, **40**, 857 (1967).
23) M. Eigen, *Pure Appl. Chem.*, **6**, 97 (1963).
24) M. Fuoss, *J. Amer. Chem. Soc.*, **80**, 5059 (1958).

Oxidation of Chromium(II) Complexes. I. Kinetics of the Oxidation of Tris(2,2′-bipyridine)- and of Tris(1,10-phenanthroline)chromium(II) Complexes with Hexaamminecobalt(III) Ion[1]

Yoshio NARUSAWA, Masao KIMURA, and Kunio NAKANO

Department of Chemistry, College of Science, Rikkyo (St. Paul's) University, Nishi-Ikebukuro, Toshima-ku, Tokyo 171

(Received April 11, 1973)

Kinetic studies have been carried out on the oxidation of $[Cr(bipy)_3]^{2+}$ and $[Cr(phen)_3]^{2+}$ with $[Co(NH_3)_6]^{3+}$ (bipy and phen denote 2,2′-bipyridine and 1,10-phenanthroline, respectively). The rate law is found to be $-d[Cr(II)]/dt=k_1[Co(III)][Cr(II)]+k_2[Cr(II)]$. Simulation procedures with an analogue computer were applied for the analysis of these reactions. The rate constant k_1 (direct oxidation) and k_2 (dissociation) for $[Cr(bipy)_3]^{2+}$ were 180 M^{-1} s^{-1} and 0.120 s^{-1} ($\mu=0.11$ with NaCl, at 25 °C) and those for $[Cr(phen)_3]^{2+}$ were 310 M^{-1} s^{-1} and 0.630 s^{-1} ($\mu=0.20$ with NaCl, at 25 °C), respectively. The larger value of k_1 for $[Cr(phen)_3]^{2+}$ as compared with that of k_1 for $[Cr(bipy)_3]^{2+}$ was interpreted as being due to the good electron conductivity of the phenanthroline as a ligand in the activated state. The activation parameters were obtained as follows: in the case of $[Cr(bipy)_3]^{2+}$, $\Delta H^{\neq}=7.5$ kcal/mol and $\Delta S^{\neq}=-23$ e.u. for the k_1 path, and $\Delta H^{\neq}=17.2$ kcal/mol and $\Delta S^{\neq}=-5$ e.u. for the k_2 path; and in the case of $[Cr(phen)_3]^{2+}$, $\Delta H^{\neq}=8.2$ kcal/mol and $\Delta S^{\neq}=-20$ e.u. for the k_1 path, and $\Delta H^{\neq}=21.2$ kcal/mol and $\Delta S^{\neq}=+12$ e.u. for the k_2 path.

Many investigators[2-7] have pointed out that the oxidation reaction of $[Cr(bipy)_3]^{2+}$ with $[Co(NH_3)_6]^{3+}$ proceeds *via* an outer-sphere mechanism. Zwickel and Taube[6] reported on the rate constants under various conditions, and deduced from the ion-exchange of the product that there is no possibility of the formation of ligand-deficient species ($[Cr(H_2O)_2(bipy)_2]^{3+}$ or $[Cr(OH)_2(bipy)_2]^{+}$) in the course of the reaction. Murray and Waind[8] and Baker and Mehta[9] demonstrated, by spectrophotometric means in the case of the former and by polarographic means in the case of the latter, that $[Cr(H_2O)_2(bipy)_2]^{3+}$ is produced in the oxidation of $[Cr(bipy)_3]^{2+}$ with $[Co(NH_3)_6]^{3+}$. Endicott and Taube,[5] although their argument is not in line with that of Zwickel and Taube,[6] suggested that $[Cr(bipy)_3]^{2+}$ is very substitution-labile and the possibility exists that one of the coordination positions is exposed by opening one of the chelate rings in the activated state. The formation of $[Cr(H_2O)_2(bipy)_2]^{3+}$ and of $[Cr(OH)_2(bipy)_2]^{+}$ is not explained by the aquation of $[Cr(bipy)_3]^{3+}$ produced by oxidation, because Cr(III) complex is substitution-inert. This must be elucidated by a dissociative mechanism for $[Cr(bipy)_3]^{2+}$ into $[Cr(H_2O)_2(bipy)_2]^{2+}$, $[Cr(OH)(H_2O)(bipy_2)]^{+}$, or $[Cr(OH)_2(bipy)_2]$.

The present investigation was carried out following the kinetic work of Zwickel and Taube[6] by means of a stopped-flow technique, the rate equations being analyzed by simulation procedures with an analogue computer. The investigation also aims at a comparison of the kinetic parameters of $[Cr(bipy)_3]^{2+}$ with those of $[Cr(phen)_3]^{2+}$, which is similar to $[Cr(bipy)_3]^{2+}$ in structure.

Experimental

Reagents. Hexaamminecobalt(III) chloride monohydrate prepared by the usual method was purified several times. Hydrochloric acid was purified by distillation. The purity of 2,2′-bipyridine and 1,10-phenanthroline was examined by measuring the infrared spectra by KBr disk method. All other chemicals were of guaranteed grade and were not purified further.

Preparation of the Reactant Solutions. Solutions of $[Co(NH_3)_6]^{3+}$ were prepared by dissolving a weighed sample of $[Co(NH_3)_6]Cl_3\cdot H_2O$ in NaCl solution containing a given amount of 2,2′-bipyridine. Solutions of $[Cr(bipy)_3]^{2+}$ were prepared as follows: Cr metal (99.99%, Johnson Matthey) was dissolved in HCl which had been deaerated with a vacuum apparatus. After the excess HCl had been removed by distilling under reduced pressure, the residue was dissolved in NaCl solution containing a given amount of 2,2′-bipyridine. Solutions of $[Cr(phen)_3]^{2+}$ were prepared by the same procedure except that 1,10-phenanthroline was used instead of 2,2′-bipyridine. All the solutions were deaerated three times with a vacuum apparatus.

Measurements of Changes in the Absorbance. The stopped-flow apparatus used for following the reactions was a Yanaco SPS-1 spectrophotometer connected with an Iwasaki MS-5019A synchroscope with a memory device. The spectrophotometer used for measuring the absorption curves was a

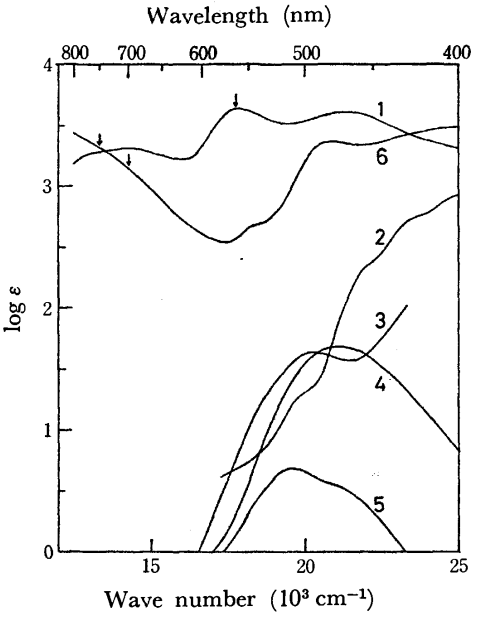

Fig. 1. Absorption spectra of various species.
1, $[Cr(bipy)_3]^{2+}$; 2, $[Cr(bipy)_3]^{3+}$; 3, $[Cr(H_2O)_2(bipy)_2]^{3+}$ [a]; 4, $[Co(NH_3)_6]^{3+}$; 5, Co^{2+}; 6, $[Cr(phen)_3]^{2+}$. a) From Ref. 11.

Hitachi 124 spectrophotometer. Introduction of the reactant solutions into the stopped-flow apparatus and the technique of the kinetic measurements followed the same procedures as the usual stopped-flow methods. Measurements of the absorption spectra of $[Cr(bipy)_3]^{2+}$ and $[Cr(phen)_3]^{2+}$ complexes were made by sealing the solution in a 10-mm quartz cell in the absence of air. The spectra are shown in Fig. 1 along with those of the other complexes concerned. The absorption spectra of $[Cr(bipy)_3]^{2+}$ and $[Cr(phen)_3]^{2+}$ complexes are in line with those reported,[10] except for slight differences in intensity.

Changes in the transmittance as a function of time were followed with the stopped-flow apparatus in an excess of $[Co(NH_3)_6]^{3+}$ at 562.5 nm ($\varepsilon=4340\,l\cdot mol^{-1}\,cm^{-1}$) for $[Cr(bipy)_3]^{2+}$ and at either 700 nm ($\varepsilon=1397$) or 750 nm ($\varepsilon=2046$) for $[Cr(phen)_3]^{2+}$. At each wavelength where the reaction was followed, the molar extinction coefficient of each reductant was *ca.* 500 times that of any other species present (Fig. 1). Oscilloscope trace of transmittance as a function of time is shown in Fig. 2. The gradual increase in transmittance with time (curve 2) corresponding to the disappearance of $[Cr(bipy)_3]^{2+}$ at a given wavelength was observed after the flow of the solution stopped (point A, curve 1). Curve 2 was converted into one showing the change in absorbance or concentration of Cr(II) complex *vs.* time using the molar extinction coefficient (ε), the value of % transmittance (T_∞) at 'infinite' time (curve 3), and the value of 5% calibration signal corresponding to $T_\infty\times0.05$ (curve 4). T_∞ was found to be 99.38% for the final solution in the kinetic run. The stopped-flow measurements were repeated several times for the same solution, and were repeated for $[Cr(phen)_3]^{2+}$ as well as for $[Cr(bipy)_3]^{2+}$ under various temperatures, oxidant concentrations and hydrogen ion concentrations.

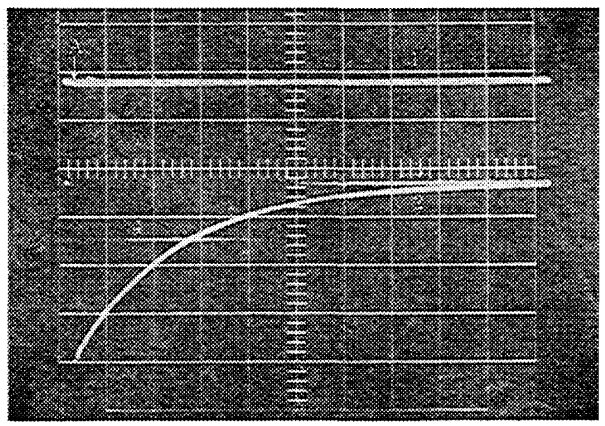

Fig. 2. Oscilloscope trace of transmittance (at 562.5 nm) of $[Cr(bipy)_3]^{2+}$ system as a function of time; $[Cr(bipy)_3^{2+}]=2.68\times10^{-4}$ M, $[Co(NH_3)_6^{3+}]=2.49\times10^{-3}$ M, $[bipy]=1.0\times10^{-2}$ M, pH=5.32, $\mu=0.10$ with NaCl, at 25.1 °C.
Curve 1, flow signal; 2, reaction signal; 3, transmittance (T_∞) at "infinite" time (99.38%); 4, 5% calibration signal. The abscissa scale is 1 sec per major division and the ordinate scale is in arbitrary unit of transmittance.

No attempt was made to identify the products of reaction or confirm directly the stoichiometry, which was assumed in each case to be $Cr(II)+Co(III)\rightarrow Cr(III)+Co(II)$ on the basis of the earlier observations of these and related reactions.

pH Measurements. The pH of the oxidant solution was measured with a pH meter. As it was impossible to measure directly the value of pH of the reductant solution, the value was estimated by measuring the pH of the solution in which Cr^{2+} ion was absent, because it was assumed that addition of Cr^{2+} ion to the solution does not affect the pH value under the experimental conditions of the present work, taking the acidity constants[12] of the bipyridinium and phenanthrolinium ions into consideration. The pH of the mixture of the reactant solutions was assumed to lie between the two pH's of the two reactant solutions, the values of which were within 0.1 pH unit of the average.

Analysis of Data

Analogue Computer Assembly. The analogue computer for analyzing the rate equations has circuits as shown in Figs. 3(a),[13] 3(b), and 4.

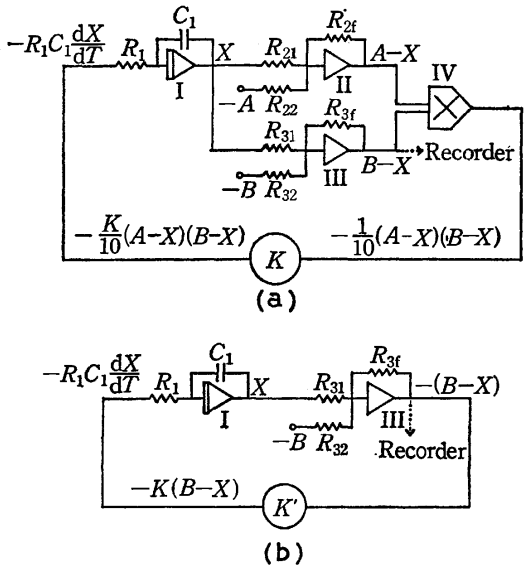

Fig. 3. Analogue computer circuit diagrams; (a) for the second-order reaction, and (b) for the first-order reaction, where inverter being omitted.
$C_1=10\,\mu F$; $R_1=100\,k\Omega$; $R_{21}=R_{22}=R_{2f}=R_{31}=R_{32}=10\,k\Omega$; $R_{3f}=10\,k\Omega$ or $100\,k\Omega$; $K=K'=1\,k\Omega$. I, SA-3a; II and III, SQ-10a; IV, Quarter-square multiplier, Model 4030/25.

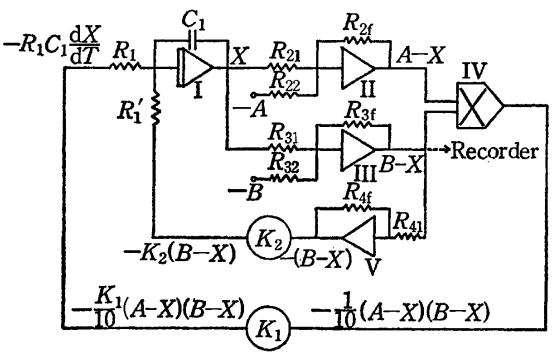

Fig. 4. Analogue computer circuit diagram for the composite first- and second-order reactions.
$C_1=10\,\mu F$; $R_1=R_1'=100\,k\Omega$; $R_{21}=R_{22}=R_{2f}=R_{31}=R_{32}=R_{41}=R_{4f}=10\,k\Omega$; $R_{3f}=10\,k\Omega$ or $100\,k\Omega$; $K_1=K_2=1\,k\Omega$.
I, SA-3a; II and III, SQ-10a; IV, Quarter-square multiplier, Model 4030/25; V, SA-3a.

Operational amplifiers and a function multiplier were supplied by Philbrick–Nexus and Burr-Brown, respectively. A voltage regulator Type VK 15012W, Volgen, was used as the D.C. power stabilizer. In the figures, I, II, III, and V are operational amplifiers; I integrator, II and III adder, and V inverter. Function multiplier IV was used for multiplying two variables, and attenuators K, K', K_1, and K_2 were used for multiplying a constant value. For the resistor R_{3f}, a value of either 10 kΩ or 100 kΩ was used, depending on the magnitude of the input signal of III. The analogue computer with the circuit shown in Fig. 4 was used for the first time for simulating the composite first- and second-order reactions. The voltage change corresponding to the change in the concentration of the chromium(II) complex was followed by the output signal of III as a function of time and was recorded with an EPR-2TC Toa Electronics recorder. The exact values of the individual components were determined prior to use and applied as corrections in the final evaluation of the rate constants measured by the analogue computer simulations.

Simulation Procedures for Measuring Rate Constants. For determining the rate constants graphically by using the change in a concentration as a function of time, the initial concentration of each of the reactants and the concentration at each instantaneous time after the reaction starts should be known. In the present investigation, however, it is supposed that Cr(II) complex was oxidized partially before the reactant solutions were mixed, owing to its sensitiveness to oxidation, that the reactant solutions were not mixed instantaneously because of the so-called dead-time resulting from the mechanical restriction of the stopped-flow apparatus, and that both reactants are consumed during the time in which reactants go from the mixing point to the cell through which a light beam for the observation passes. For these reasons, the rate constants cannot be determined exactly by a graphical method. Thus the simulation method with an analogue computer was attempted for analyzing the reaction. The simulation for the second-order reaction, assumed to be Cr(II)+Co(III)→Cr(III)+Co(II), was carried out according to Nakanishi's method,[13] *viz.*, with an analogue computer (Fig. 3(a)); the voltage, $-B$, corresponding to the effective initial concentration (calculated from the absorbance at the starting point of the curve of the absorbance change and the molar extinction coefficient) of Cr(II) complex was applied to the adder III as the input signal, and the circuit was closed at the machine time $T=0$. The output voltage of III was then followed as a function of time T, and the voltage change with time was recorded on the recorder. Thus, if the curve obtained by the simulation procedure was fitted to the curve of the change in concentration with time by adjusting the input voltage ($-A$) of adder II and the dial reading of the helipot K, $-A$ could be considered to correspond to the effective initial concentration of Co(III) complex and the reading of K to a value proportional to the rate constant. Thus, by comparing the assumed rate equation (1) or (1') with machine equation (2), equation (3) is obtained as follows:

$$-\frac{d[Cr(II)]}{dt} = k_{obs}[Co(III)][Cr(II)] \quad (1)$$

$$\frac{dx}{dt} = k_{obs}(a-x)(b-x) \quad (1')$$

$$\frac{dX}{dT} = -\frac{K}{10R_1C_1}(A-X)(B-X) \quad (2)$$

$$k_{obs} = \frac{\alpha\beta K}{10R_1C_1} \quad (3)$$

where k_{obs} is an apparent rate constant obtained by analyzing the rate equation as a second-order reaction; a and b are effective initial concentrations of Co(III) and Cr(II) complexes, respectively; x is the amount of reactant consumed at an effective time t after the reaction signal became observable; X is the voltage on C_1 at time T after the circuit is switched on and is proportional to x; α is a factor in $V\cdot l\cdot mol^{-1}$ to convert the voltage $(B-X)$ into the concentration $(b-x)$; β is a dimensionless factor to convert the machine time T into the reaction time t; and $1/R_1C_1$ is a correction factor whose reciprocal is a time constant of the integrator I. Examples of the simulation actually performed are shown (Fig. 5(a) and (b), curve 1).

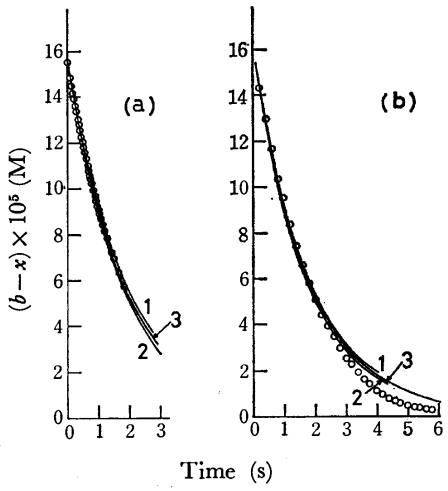

Fig. 5. Typical examples of analogue computer simulations for the oxidation of $[Cr(bipy)_3]^{2+}$ with $[Co(NH_3)_6]^{3+}$.
The open-circled points in (a) and (b) refer to No. 2—4 and No. 2—2 in Table 1, respectively. Solid curves 1, 2, and 3 are those obtained by the simulations for the second-order reaction (Eq. (1)) with the circuit of Fig. 3(a), the first-order reaction (Eq. (5)) with that of Fig. 3(b), and the composite first- and second-order reaction (Eq. (9)) with that of Fig. 4, respectively.

However, the values of k_{obs} thus obtained at the same temperature decrease as $[Co(NH_3)_6]^{3+}$ concentration increases (Tables 1 and 2). The results obtained by the graphical method are also shown.

It was assumed that k_{obs} is expressed by the sum of the term independent of [Co(III)] and the term reciprocally proportional to it:

$$k_{obs} = k_1 + \frac{k_2}{[Co(III)]} \quad (4)$$

TABLE 1. APPARENT SECOND-ORDER RATE CONSTANTS FOR $[Cr(bipy)_3]^{2+}$ SYSTEMS[a]

Run No.[b]	$[Cr(bipy)_3^{2+}]$ (mM)[c]	$[Co(NH_3)_6^{3+}]$ (mM)[c]	Temp (°C)	k_{obs} ($M^{-1}s^{-1}$) (graphical)	k_{obs} ($M^{-1}s^{-1}$) (simulation)
1— 3	0.252	0.275	25.4	1980	1890
1— 4	0.252	0.275	25.4	—[d]	1930
1— 5	0.252	0.275	25.4	2280	1910
2—21	0.249	2.52	39.9	524	547
2—25	0.249	2.52	39.9	543	561
2—30	0.249	2.52	34.8	450	414
2—31	0.249	2.52	34.8	436	413
2—16	0.249	2.52	29.9	295	311
2—17	0.249	2.52	29.9	301	314
2— 2	0.249	2.52	25.1	253	226
2— 4	0.249	2.52	25.1	247	225
2— 8	0·249	2.52	20.3	204	172
2—12	0.249	2.52	20.1	174	173
3— 1	0.268	2.49	34.6	511	410
3—12	0.268	2.49	25.1	219	233
3— 8	0.268	2.49	16.1	144	130

a) At 562.5 nm. b) No. 1-series; pH=6.32, μ=0.11(NaCl): 2-series; pH=6.30, μ=0.11(NaCl): 3-series; pH =5.32, μ=0.10(NaCl). c) Each reactant solution contains 0.010 M 2,2′-bipyridine. d) Graphical analysis not carried out.

TABLE 2. APPARENT SECOND-ORDER RATE CONSTANTS FOR $[Cr(phen)_3]^{2+}$ SYSTEMS[a]

Run No.	$[Cr(phen)_3^{2+}]$ (mM)[b]	$[Co(NH_3)_6^{3+}]$ (mM)[b]	Temp (°C)	k_{obs} ($M^{-1}s^{-1}$) (graphical)	k_{obs} ($M^{-1}s^{-1}$) (simulation)
28— 7	1.24	2.50	24.8	763	762
27—14[c]	1.27	4.98	25.1	522	520
27—15	1.27	4.98	25.1	512	514
29—33	1.12	9.99	39.8	1060	1010
29—28	1.12	9.99	35.1	813	786
29—17	1.12	9.99	30.0	540	530
29— 5	1.12	9.99	25.1	434	372
29— 8	1.12	9.99	25.1	371	373
29—11	1.12	9.99	20.0	326	263
29— 9	1.12	9.99	19.7	303	268

a) pH=6.05±0.10, μ=0.20(NaCl), λ=750 nm except No. 27—14. b) Each reactant solution contains 0.012 M 1,10-phenanthroline. c) λ=700 nm.

The rate constants k_1 and k_2 should be obtained from the intercept and the slope, respectively, by plotting k_{obs} against $[Co(III)]^{-1}$ (Fig. 6, lines 1 and 2). The results for $[Cr(bipy)_3]^{2+}$ and $[Cr(phen)_3]^{2+}$ complexes are given in Table 4.

The reaction was analyzed by assuming that it is of first-order:

$$-\frac{d[Cr(II)]}{dt} = k'_{obs}[Cr(II)] \tag{5}$$

For circuit diagram, see Fig. 3(b). The simulation procedure was almost the same as in the case of the second-order reaction. Examples are shown by curve 2 in Fig. 5(a) and (b). In this case, the machine equation is expressed as follows:

$$\frac{dX}{dT} = \frac{K'}{R_1C_1}(B-X) \tag{6}$$

If the dial of the helipot K' is properly adjusted, this turns out to correspond to Eq. (5), and we have

$$k'_{obs} = \frac{\beta K'}{R_1C_1} \tag{7}$$

The values of k'_{obs} thus obtained increase with the increase in concentration of $[Co(NH_3)_6]^{3+}$ at the same temperature (Table 3). Thus, it was assumed that k'_{obs} contains a term proportional to the concentration of Co(III):

$$k'_{obs} = k_1[Co(III)] + k_2 \tag{8}$$

The values of k_1 and k_2 obtained are given in Table 4.

Both equations obtained by substituting Eq. (4) into Eq. (1) and Eq. (8) into Eq. (5), respectively, become the same as the following equation:

$$-\frac{d[Cr(II)]}{dt} = k_1[Co(III)][Cr(II)] + k_2[Cr(II)] \tag{9}$$

However, the rate constants k_1 and k_2 obtained from

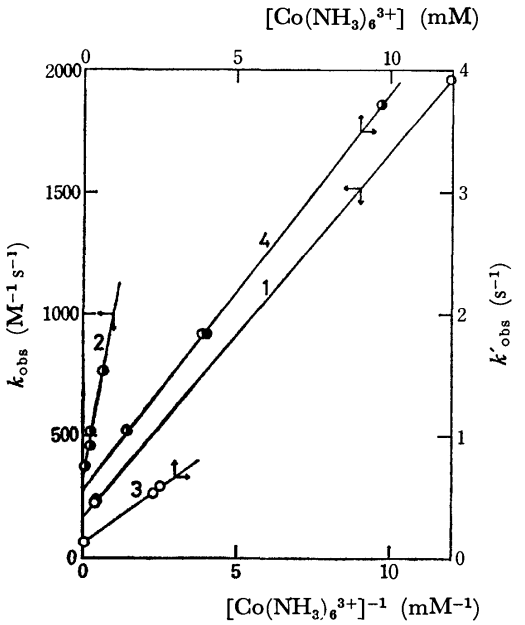

Fig. 6. Relationships of k_{obs} and k'_{obs} at 25 °C to $[Co(NH_3)_6^{3+}]^{-1}$ and $[Co(NH_3)_6^{3+}]$, respectively.[a] Data are taken from Tables 1, 2, and 3. ○, $[Cr(bipy)_3]^{2+}$; ◑, $[Cr(phen)_3]^{2+}$.
a) The concentration of $[Co(NH_3)_6]^{3+}$ ion was evaluated by using voltages $-A$ and $-B$ for $[Co(NH_3)_6]^{3+}$ ion and Cr(II) complex, respectively, and the concentration of Cr(II) complex at the starting poing of the simulation ($T=0$) according to the equation, $[Co(III)]_{T=0}=(A/B)[Cr(II)]_{T=0}$.

Table 3. Apparent first-order rate constants at 25 °C for $[Cr(bipy)_3]^{2+}$ and $[Cr(phen)_3]^{2+}$ by simulation

Reductant	Run No.[a]	$[Co(NH_3)_6^{3+}]$ (mM)	k'_{obs} (s^{-1})
$[Cr(bipy)_3]^{2+}$	1— 5	0.275	0.115±0.003
	3—12	2.49	0.508±0.010
	2— 2	2.52	0.590±0.010
	2— 4	2.52	0.576±0.005
$[Cr(phen)_3]^{2+}$	28— 7	2.50	1.03
	27— 8[b]	4.98	1.84
	27—15	4.98	1.84
	29— 5	9.99	3.72

a) The numerals are the same as those given in the first columns of Tables 1 and 2. b) The conditions are the same as those of No. 27—15.

k_{obs} according to Eq. (4) do not agree with those obtained from k'_{obs} according to Eq. (8) (Table 4). This discrepancy is caused by the fact that concentrations of Co(III) (abscissa, Fig. 6) change during the course of the reaction. (The effective initial concentrations of Co(III) are plotted in Fig. 6). Thus, in order to obtain k_1 and k_2 accurately, it is necessary to simulate Eq. (9) directly. For this purpose, a simulator (Fig. 4) was constructed.

The machine equation for the simulator is expressed as follows:

Table 4. First- and second-order rate constants[a]

	Rate constant[b]	Reductant $[Cr(bipy)_3]^{2+}$	Reductant $[Cr(phen)_3]^{2+}$
From k_{obs} and Fig. 6 (lines 1 and 2)	k_1	165±8	300±10
	k_2	0.15±0.01	0.69±0.04
From k'_{obs} and Fig. 6 (lines 3 and 4)	k_1	200±10	321±10
	k_2	0.10±0.01	0.57±0.03
Averaged value	k_1	183±18	311±11
	k_2	0.12_5±0.02_5	0.63±0.06
From simulations for Eq. (9)[c]	k_1	180±3	310±6
	k_2	0.120±0.002	0.630±0.010

a) Data of k_{obs} and k'_{obs} at 25 °C for $[Cr(bipy)_3]^{2+}$ and $[Cr(phen)_3]^{2+}$ were taken from Tables 1, 2, and 3. b) k_1 in $M^{-1}s^{-1}$ and k_2 in s^{-1}. c) Taken with the analogue computer whose circuit is shown in Fig. 4.

$$\frac{dX}{dT}=\frac{K_1}{10R_1C_1}(A-X)(B-X)+\frac{K_2}{R_1C_1}(B-X) \quad (10)$$

where K_1 and K_2 are proportional to k_1 and k_2, respectively, and given by

$$k_1=\frac{\alpha\beta K_1}{10R_1C_1} \quad (11)$$

$$k_2=\frac{\beta K_2}{R_1C_1} \quad (12)$$

The examples of the simulation carried out with this circuit are shown by curve 3 in Fig. 5(a) and (b). The values* of k_1 and k_2 thus obtained under the various conditions were constant irrespective of the concentration of Co(III) at a given temperature as shown in Table 5.

The accuracy of each rate constant obtained by the above procedures was within *ca.* 2% in relative error (Tables 1, 2, 3, and 5).

Therefore, k_1 and k_2 are considered to be the rate constants for the second-order and the first-order reactions, respectively, and it is concluded that Eq. (9) is adequate as the rate law for the present systems.

Results and Discussion

It was found that satisfactory values of rate constants in the oxidation reaction of $[Cr(bipy)_3]^{2+}$ and of $[Cr(phen)_3]^{2+}$ complexes with $[Co(NH_3)_6]^{3+}$ complex (Tables 1 and 2) cannot be obtained by the usual graphical method of analysis. However, by means of simulation procedures with an analogue computer (Fig. 3(a) and (b)), the apparent rate constants of appropriate values could be obtained for the second-order and the first-order reactions (Tables 1, 2, and 3). Both curves 1 and 2 obtained by these simulations deviate from the observed points in the later stage of the reaction (Fig.

* The values of k_{obs} and k'_{obs}, obtained with the circuits for simulations of the second-order and first-order reactions, respectively, do not correspond to those of k_1 and k_2 obtained by simulating as the composite reaction, and differ significantly. The values of k_{obs} and k'_{obs} are dependent on and those of k_1 and k_2 independent of the concentration of Co(III) complex.

TABLE 5. RATE CONSTANTS k_1 AND k_2 FOR $[Cr(bipy)_3]^{2+}$ AND $[Cr(phen)_3]^{2+}$ BY SIMULATION PROCEDURES[a]

Reductant	Run No.[b]	Temp (°C)	k_1 ($M^{-1}s^{-1}$)	k_2 (s^{-1})
$[Cr(bipy)_3]^{2+}$	1— 5	25.4	180	0.120
	2— 2	25.1	180	0.120
	2— 4	25.1	180	0.120
	2—21	39.9	340	0.480
	2—25	39.9	347	0.492
	2— 8	20.3	146	0.0722
	2—12	20.1	144	0.0707
$[Cr(phen)_3]^{2+}$	28— 6[c]	24.8	306	0.630
	28— 7	24.8	312	0.627
	27— 8	25.1	310	0.630
	27—14	25.1	310	0.630
	27—15	25.1	311	0.630
	29— 5	25.1	310	0.630
	29— 6[d]	25.1	310	0.630
	29— 8	25.1	310	0.630
	29—30[e]	39.9	636	3.69
	29—33	39.8	636	3.69
	29—34[e]	39.8	615	3.69
	29— 9	19.7	241	0.338
	29—11	20.0	241	0.338

a) Simulations were carried out by means of Eq. (9). b) The numerals are the same as those given in Tables 1, 2, and 3 unless otherwise stated. c) Conditions the same as those of No. 28—7. d) Conditions the same as those of No. 29—5. e) Solution compositions the same as those of No. 29—33.

5(b)). This discrepancy might be mainly due to the formation of $[Cr(OH)_2(bipy)_2]^+$, since the value of pH increased to *ca.* 8.5 in the final solution of the reaction. This is supported by the fact that the absorption spectrum of the reaction product[8] coincides with $[Cr(OH)_2(bipy)_2]^+$,[11] and it changes to $[Cr(H_2O)_2(bipy)_2]^{3+}$[11] on acidification.[8] The value of T_∞ is calculated to be 99.38%, which is just the same as the observed value (Fig. 2), if we assume that *ca.* 81% of the Cr(III) products is $[Cr(OH)_2(bipy)_2]^+$ ($\varepsilon_{562.5nm}$= 35 $l \cdot mol^{-1} cm^{-1}$)[11] and the rest is $[Cr(bipy)_3]^{3+}$, whereas the value is obtained to be 99.66% if we assume the formation of $[Cr(H_2O)_2(bipy)^2]^{3+}$ instead of $[Cr(OH)_2(bipy)_2]^+$. Thus, the product present as a ligand-deficient species is considered to be either $[Cr(H_2O)_2(bipy)_2]^{3+}$ or $[Cr(OH)_2(bipy)_2]^+$. The formation of the ligand-deficient species is explained by either an acid hydrolysis or a base hydrolysis. The dissociation of $[Cr(bipy)_3]^{2+}$ *via* the base hydrolysis becomes predominant with increase in pH of the solution in the later stage of the reaction, although the base hydrolysis does not occur in the earlier stage of the reaction because of the acidity. Since the dissociation rate for the base hydrolysis is considered to be greater than that for the acid hydrolysis,[14] the consumption of $[Cr(bipy)_3]^{2+}$ becomes more marked in the later stage than in the earlier stage of the reaction. The deviation of the simulation curve from the observed plot in the later stage of the reaction (Fig. 5(b)) can thus be explained. The curve-fitting procedures were applied during the time in which 65—70% of the effective initial concentration of each Cr(II) complex undergoes change by the reaction. The values of the rate constants thus obtained would not be affected by the base hydrolysis.

The results obtained for the rate constants for the oxidation and dissociation of $[Cr(bipy)_3]^{2+}$ and $[Cr(phen)_3]^{2+}$ complexes are shown in Table 5. The excellent constancy of the rate constants obtained under a wide variety of $[Cr(NH_3)_6]^{3+}$ concentrations validates the assumed rate law (Eq. (9)). Since the reaction involves the processes of both second-order (k_1 path) and first-order (k_2 path), it seems that the reaction of $[Cr(bipy)_3]^{2+}$ with $[Co(NH_3)_6]^{3+}$ proceeds *via* the composite processes of the direct oxidation of the former with the latter (second-order) and the dissociation of the former into $[Cr(H_2O)_2(bipy)_2]^{2+}$ (first-order). Provided the oxidation of $[Cr(H_2O)_2(bipy)_2]^{2+}$ is more rapid than the dissociation of $[Cr(bipy)_3]^{2+}$ and the concentration of the former is very low, the dissociation process of $[Cr(bipy)_3]^{2+}$ becomes the rate-determining step for the oxidation of the dissociated species, and it follows that the rate of oxidation of $[Cr(H_2O)_2(bipy)_2]^{2+}$ with $[Co(NH_3)_6]^{3+}$ is first-order in $[Cr(bipy)_3]^{2+}$ and zero-order in $[Co(NH_3)_6]^{3+}$. Consequently, the most probable mechanisms of these reactions can be expressed as follows:

$$[Cr(bipy)_3]^{2+} + [Co(NH_3)_6]^{3+} \xrightarrow{k_1} [Cr(bipy)_3]^{3+} + Co^{2+} + 6NH_3 \quad (13)$$

$$[Cr(bipy)_3]^{2+} + 2H_2O \underset{k_3}{\overset{k_2}{\rightleftharpoons}} [Cr(H_2O)_2(bipy)_2]^{2+} + bipy \quad (14)$$

$$[Cr(H_2O)_2(bipy)_2]^{2+} + [Co(NH_3)_6]^{3+} \xrightarrow{k_4} [Cr(H_2O)_2(bipy)_2]^{3+} + Co^{2+} + 6NH_3 \quad (15)$$

Baker and Mehta[9] assumed the rate constant k_5 of the equation

$$[Cr(H_2O)_2(bipy)_2]^{2+} + [Cr(bipy)_3]^{3+} \underset{k_6}{\overset{k_5}{\rightleftharpoons}} [Cr(H_2O)_2(bipy)_2]^{3+} + [Cr(bipy)_3]^{2+} \quad (16)$$

to be of the order of 10^5 M^{-1} s^{-1}. Since both oxidants in the reactions of Eqs. (15) and (16) are the 'outer-sphere' type of complex and the reductant $[Cr(H_2O)_2(bipy)_2]^{2+}$ is the low-spin[8] type of complex, it is assumed that k_4 and k_5 are at least of the same order of magnitude. Further, the rate constant k_3 is assumed to be *ca.* 10^3 M^{-1} s^{-1} from equilibrium[15] and kinetic[7,9] data. Thus it is estimated that the rates of Eqs. (14) and (15) satisfy the relations

$$k_3[bipy] < k_4[Co(NH_3)_6{}^{3+}] \quad (17)$$

$$k_2[Cr(bipy)_3{}^{2+}] < k_4[Cr(H_2O)_2(bipy)_2{}^{2+}][Co(NH_3)_6{}^{3+}] \quad (18)$$

under the present experimental conditions. Thus the forward reaction of Eq. (14) is concluded to be the rate-determining step for the oxidation of the dissociated complex with $[Co(NH_3)_6]^{3+}$. The following should be taken into account in Eqs. (13), (14), and

(15): the effect of $[Cr(bipy)_3]^{3+}$ formed by the reaction of Eq. (13) on the oxidation of $[Cr(H_2O)_2(bipy)_2]^{2+}$ (k_5 path), and the effect of $[Cr(H_2O)_2(bipy)_2]^{3+}$ formed by the reaction of Eq. (15) on the oxidation of $[Cr(bipy)_3]^{2+}$ (k_6 path).

If the reaction of the k_5 path affects reaction (15), these reactions are regarded as competition reactions for the oxidation of $[Cr(H_2O)_2(bipy)_2]^{2+}$. Since $[Cr(bipy)_3]^{2+}$ is produced by the reaction of the k_5 path, the value of the rate constant k_2 becomes smaller with the decrease in the concentration of $[Co(NH_3)_6]^{3+}$. However, the results in Table 5 show a constancy of the rate constant k_2 in a wide range of $[Co(NH_3)_6]^{3+}$ concentrations, indicating that the effect of $[Cr(bipy)_3]^{3+}$ (k_5 path) on the dissociation (k_2 path) is negligible. This is explained by the relation

$$k_5[Cr(bipy)_3{}^{3+}] \ll k_4[Co(NH_3)_6{}^{3+}] \quad (19)$$

This holds in a large excess of $[Co(NH_3)_6]^{3+}$ as compared with $[Cr(bipy)_3]^{2+}$, since the relation $[Cr(bipy_3)^{3+}] \ll [Co(NH_3)_6{}^{3+}]$ also holds if we consider the formation of $[Cr(bipy)_3]^{3+}$ by the direct oxidation of $[Cr(bipy)_3]^{2+}$ (*cf.* Eq. (13)).

The effect of the oxidant $[Cr(H_2O)_2(bipy)_2]^{3+}$ on the reaction of Eq. (13) will be ruled out if the relation

$$k_6[Cr(H_2O)_2(bipy)_2{}^{3+}] \ll k_1[Co(NH_3)_6{}^{3+}] \quad (20)$$

holds under the present experimental conditions. The value of k_6 in Eq. (16) is estimated to be *ca.* 10 M^{-1} s^{-1} from the assumed value of k_5 and the values of the reversible half-wave potentials of $[Cr(bipy)_3]^{3+}$ and $[Cr(H_2O)_2(bipy)_2]^{3+}$ obtained polarographically by Baker and Mehta,[9] and the concentration of $[Cr(H_2O)_2(bipy)_2]^{3+}$ is estimated to be *ca.* 10^{-4} M since its formation predominantly takes place *via* the reaction of Eq. (15). Since the concentration of $[Co(NH_3)_6]^{3+}$ is at least *ca.* 10^{-3} M under the large excess of the oxidant and the value of k_1 is assumed to be at least of the order of 10^2 M^{-1} s^{-1},[6] the magnitude of the right-hand side of Eq. (20) amounts to at least *ca.* 100 times that of the left-hand side of the equation. Thus it seems that the backward reaction of Eq. (16) does not affect the reaction of Eq. (13).

The effect of the backward reaction of Eq. (16) (k_6 path) on the dissociation (k_2 path) can also be neglected for the reason that the relation

$$k_6[Cr(H_2O)_2(bipy)_2{}^{3+}] \ll k_2 \quad (21)$$

holds, because the value of k_2 is estimated to be of the order of 10^{-1} s^{-1}.[7,9] Thus the rate constant k_2 is not affected by the backward reaction of Eq. (16).

Equations (20) and (21) seem to hold similarly in the slight excess of $[Co(NH_3)_6]^{3+}$, since k_1 and k_2 remain constant in a wide concentration range (Table 5). It is concluded that the reaction of $[Cr(bipy)_3]^{2+}$ with $[Co(NH_3)_6]^{3+}$ proceeds *via* the processes of both the direct oxidation of the former with the latter (second-order k_1 path) and the dissociation of the former to $[Cr(H_2O)_2(bipy)_2]^{2+}$ (first-order k_2 path) followed by the rapid oxidation with $[Co(NH_3)_6]^{3+}$; and that Eq. (9) assumed experimentally is adequate for expressing the rate law of the present system. These relationships and the rate law might hold also for the system $[Cr(phen)_3]^{2+}$–$[Co(NH_3)_6]^{3+}$.

A comparison of the rate constants is shown in Table 6. The rate constants for the dissociation of $[Cr(bipy)_3]^{2+}$ have been reported[7,9] (k_2 in Table 6). The values coincide with each other, in spite of the different medium and different ionic strength, and both are greater than ours. Although the value reported by Candlin, Halpern, and Trimm[7] was obtained by a preliminary experiment and thus a detailed discussion is not possible, the greater value in perchlorate medium as compared with that in chloride medium may be interpreted as being due to a salt effect. Both k_{obs}[6] and k_2[7] in the perchlorate medium are about three times those in the chloride medium. These rate constants (k_{obs} and k_2) might be subjected to the salt effect to the same extent. A detailed discussion cannot be presented, since k_{obs} involves k_1. On the other hand, the result for k_2 obtained by Baker and Mehta[9] can be discussed somewhat in detail. They measured the rate of dissociation of $[Cr(bipy)_3]^{2+}$ by following polarographically the decrease in the diffusion current of $[Cr(bipy)_3]^{3+}$ coexisting in solution. They dealt with the reaction on the assumption that the forward re-

Table 6. Rate constants for $[Cr(bipy)_3]^{2+}$ and $[Cr(phen)_3]^{2+}$ systems

μ (medium)	Temp (°C)	k_{obs} (M^{-1} s^{-1})	k_1 (M^{-1} s^{-1})	k_2 (s^{-1})	Ref.
$[Cr(bipy)_3]^{2+}$					
0.11 (NaCl)	25	228	180	0.120	a)
0.10 ($NaClO_4$)	25			0.37[b]	7
0.5 (NaCl)	25			0.38[c]	9
0.096(NaCl)	25	180[d]			6
0.20 (NaCl)	25	250[d]			6
0.10 ($NaClO_4$)	24	690[d]			6
0.20 (NaBr)	23	600[d]			6
$[Cr(phen)_3]^{2+}$					
0.20 (NaCl)	25	373	310	0.630	a)

a) This work. Oxidation with $[Co(NH)_3)_6]^{3+}$. b) Oxidation with $[Co(PO_4)(NH_3)_5]$. c) Reduction of $[Cr(bipy)_3]^{3+}$ with $[Cr(bipy)_3]^{2+}$ followed polarographically. d) Rate data reported are not of the rate constants k_1's but of the apparent rate constants k_{obs}'s defined in the present paper, since the dissociation path in Ref. 6 was not taken into consideration.

action of Eq. (16) proceeds faster than both its backward reaction and the reaction in either direction in Eq. (14), in which the dissociation is the rate-determining step. The assumption should be valid for the reaction in the bulk of the solution. However, the rate constant for the dissociation (k_2) cannot be obtained polarographically unless the rate of diffusion of the depolarizer, $[Cr(bipy)_3]^{3+}$, to the surface of the dropping mercury electrode is greater than that of the reduction of $[Cr(bipy)_3]^{3+}$ with $[Cr(H_2O)_2(bipy)_2]^{2+}$ (Eq. (16)). Otherwise, the consumption of $[Cr(bipy)_3]^{3+}$ during the course of diffusion causes a depression in the concentration of the depolarizer on the electrode surface, leading to the overestimation of the decrease in the bulk concentration. In fact the rate of diffusion does not seem to be so great as that of the reduction of $[Cr(bipy)_3]^{3+}$ with $[Cr(H_2O)_2(bipy)_2]^{2+}$.[16] However, Baker and Mehta ignored the diffusion term leaving the kinetic term, making their treatment inconsistent. Thus, the value 0.38 s^{-1} they obtained must have been overestimated. The greater value, as compared with the present value, cannot be explained either by considering the difference in the ionic strength.

The increasing rates with increase in ionic radii for anions ($Cl^- < Br^- < ClO_4^-$) of the media are considered to be largely due to the salt effect (*cf.* k_{obs} in Table 6). However, the apparent rate constants (k_{obs}) involving the dissociation rate constant k_2 are not necessarily well suited for comparing with each other. A detailed discussion should be based on the rate constant k_1 obtained under various conditions of ionic strengths and media.

The second-order rate constant for $[Cr(phen)_3]^{2+}$ is *ca.* 1.7 times greater than that for $[Cr(bipy)_3]^{2+}$, although there is a difference in ionic strength (*cf.* k_1 in Table 6). The greater rate for $[Cr(phen)_3]^{2+}$ cannot be explained by the tunneling effect as in the case of the reaction of $[Co(NH_3)_6]^{3+}$ or $[Co(en)_3]^{3+}$ (en denotes ethylenediamine) with $[Cr(bipy)_3]^{2+}$,[6] because of the greater size of the phenanthroline complex as compared with the bipyridine complex. The greater reactivity is in accord with the results obtained by Ford-Smith and Sutin[17] and Sutin and Gordon,[18] who reported the rate constants for the systems Fe^{2+}–$[Fe(bipy)_3]^{3+}$ and Fe^{2+}–$[Fe(phen)_3]^{3+}$ in 0.5 M $HClO_4$ at 25.0 °C to be 2.7×10^4 M^{-1} s^{-1} [17,18] and 3.7×10^4 M^{-1} s^{-1},[17] respectively. The ratio of the rate constant reported for the phenanthroline complex to that for the bipyridine complex is *ca.* 1.4, which agrees with ours, if the difference in ionic strength for Cr(II) complexes is taken into consideration. The greater reactivity for $[Cr(phen)_3]^{2+}$ is ascribed to the effect of an electron on the metal t_{2g} orbital spreading itself around on the ligand π orbital through the π interaction. The reaction is facilitated in spite of the larger size of the complex. The reactivity for these systems is caused by the electron conductivity of the ligand in the π-conjugate complex. For a complex without π-conjugation, such as Cr^{2+}, the slow rate for the oxidation with $[Co(NH_3)_6]^{3+}$ *via* the outer-sphere mechanism (8.8×10^{-4} M^{-1} s^{-1}, μ=0.40, at 25.0 °C)[2] can be explained by the poor electron conductivity of the water molecule attached.

From the temperature dependence of the rate constants k_1 and k_2 and of the apparent rate constant k_{obs}, the activation parameters for $[Cr(bipy)_3]^{2+}$ and $[Cr(phen)_3]^{2+}$ systems were evaluated by transition-state theory according to:

$$k = \frac{kT}{h} e^{-\Delta H^{\neq}/RT} e^{\Delta S^{\neq}/R}$$

The results are shown in Table 7, together with those of other investigators. The activation parameters for k_{obs} are in excellent agreement with those obtained by Zwickel and Taube,[6] considering the difference in ionic strengths. It is concluded that the rate constants they obtanied correspond to the apparent rate constant (k_{obs}) defined in the present paper. Since the reaction proceeds in two paths as expressed by Eq. (9), the parameters for both paths should be obtained (Table 7).

Table 7. Kinetic and activation parameters for the reactions of $[Cr(bipy)_3]^{2+}$ and $[Cr(phen)_3]^{2+}$ with $[Co(NH_3)_6]^{3+}$ at 25 °C

μ (medium)	Reaction path	Rate constant (M^{-1} s^{-1})	$\Delta H^{\neq}$ (kcal/mol)	$\Delta S^{\neq}$ (e.u.)	$\Delta G^{\neq}$ (kcal/mol)	Ref.
$[Cr(bipy)_3]^{2+}$						
0.11(NaCl)	k_{obs}	228	10.3	−13	14.2	a)
0.20(NaCl)	k_{obs}	250	9.9	−14	14.1	6
0.05(NaCl)	k_{obs}	113	11.3	−10	14.3	6
0.01(NaCl)	k_{obs}	40	13.0	− 9	15.7	6
0.11(NaCl)	k_1	180	7.5	−23	14.4	a)
0.11(NaCl)	k_2	0.120[b]	17.2	− 5	18.6	a)
0.5 (NaCl)	k_2	0.38[b]	22.6[c]	+13[d]	18.1	9[e]
$[Cr(phen)_3]^{2+}$						
0.20(NaCl)	k_{obs}	373	11.5	− 8	13.9	a)
0.20(NaCl)	k_1	310	8.2	−20	14.2	a)
0.20(NaCl)	k_2	0.630[b]	21.2	+12	17.6	a)

a) This work. b) For k_2 paths, the rate constant is in s^{-1}. c) Value for the activation energy, E_a. d) The value was not reported by Baker and Mehta,[9] so it is cited from Ref. 14a. e) *Cf.* footnote c), Table 6.

It is reasonable to consider that a similar mechanism is operative for the oxidation of $[Cr(bipy)_3]^{2+}$ and of $[Cr(phen)_3]^{2+}$ (k_1 in Table 7), because activation enthalpies (7.5 kcal/mol and 8.2 kcal/mol) and activation entropies (−23 e.u. and −20 e.u.) obtained for respective complexes are of similar magnitude. However, as the activation entropies, $\Delta S^{\neq}$'s, for outer-sphere reactions are sensitive to the medium, the values obtained at different ionic strengths cannot be compared directly with each other. Nevertheless, the values of the activation entropies obtained for $[Cr(bipy)_3]^{2+}$ and $[Cr(phen)_3]^{2+}$ indicate that the total charges on the transition complexes are between +4 and +5.[19] Discussions should be carried out with the use of the thermodynamic activation parameters.

The greater activation enthalpy for the k_1 path of $[Cr(phen)_3]^{2+}$ as compared with that of $[Cr(bipy)_3]^{2+}$ (Table 7) is interpreted as being due to the greater stability in the ground state of the former.

It should be noted that the coincidence of the $\Delta G^{\neq}$ value calculated from the results by Baker and Mehta[9] with ours for the k_2 path occurs as a result of the cancellation of the overestimated $\Delta H^{\neq}$ and $\Delta S^{\neq}$ values. Although the overestimation of the activation parameters cannot be easily interpreted, it might be caused by a greater overestimation of the rate constant for the dissociation at a higher temperature, since the temperature dependence of the diffusion rate is not as significant as that of the reduction rate of $[Cr(bipy)_3]^{3+}$.

Conclusion

The oxidation reaction of $[Cr(bipy)_3]^{2+}$ and of $[Cr(phen)_3]^{2+}$ complexes with $[Co(NH_3)_6]^{3+}$ ion proceeds in two paths through the outer-sphere mechanism: direct oxidation of $[Cr(bipy)_3]^{2+}$ or $[Cr(phen)_3]^{2+}$ (second-order reaction); oxidation of $[Cr(H_2O)_2(bipy)_2]^{2+}$ or $[Cr(H_2O)_2(phen)_2]^{2+}$ formed by the dissociation of $[Cr(bipy)_3]^{2+}$ or $[Cr(phen)_3]^{2+}$, the dissociation (first-order reaction) being rate-determining for the oxidation of the dissociated complex. The rate constants of the paths for these complexes were obtained by means of analogue computer simulation procedures. The activation parameters for the direct oxidation and dissociation processes of each of these complexes were also obtained.

The authors wish to express their thanks to Professor Masaki Nakanishi of Ochanomizu University for his advice on the analogue computer. The investigation was supported in part by a grant from the Ministry of Education.

References

1) Presented in part at the Symposium on Coordination Chemistry, Fukuoka, Japan, Nov. 16, 1973.
2) A. Zwickel and H. Taube, *J. Amer. Chem. Soc.*, **83**, 793 (1961).
3) A. A. Vlcek, "Sixth International Conference on Coordination Chemistry," S. Kirschner, Ed., The MacMillan Co., New York, (1961), p. 590.
4) R. A. Marcus, *J. Phys. Chem.*, **67**, 853 (1963).
5) J. F. Endicott and H. Taube, *J. Amer. Chem. Soc.*, **86**, 1686 (1964).
6) A. M. Zwickel and H. Taube, *Discuss. Faraday Soc.*, **29**, 42 (1960).
7) J. P. Candlin, J. Halpern, and D. L. Trimm, *J. Amer. Chem. Soc.*, **86**, 1019 (1964).
8) R. Murray and G. M. Waind, "Proceedings of the Seventh International Conference on Coordination Chemistry," Stockholm (1962), p. 309.
9) B. R. Baker and B. D. Mehta, *Inorg. Chem.*, **4**, 848 (1965).
10) I. Fujita, T. Yazaki, Y. Torii, and H. Kobayashi, This Bulletin, **45**, 2156 (1972).
11) R. G. Inskeep and J. Bjerrum, *Acta Chem. Scand.*, **15**, 62 (1961).
12) T. R. Harkins and H. Freiser, *J. Amer. Chem. Soc.*, **77**, 1374 (1955).
13) M. Nakanishi, *Talanta*, **19**, 285 (1972).
14) F. Basolo and R. G. Pearson, "Mechanisms of Inorganic Reactions," John Wiley & Sons, Inc., New York, 2nd Ed., (1967), a) p. 150; b) pp. 145—151; c) p. 146.
15) J. M. Crabtree, D. W. Marsh, J. C. Tomkinson, R. J. P. Williams, and W. C. Fernelius, *Proc. Chem. Soc.*, **1961**, 336.
16) D. M. H. Kern, *J. Amer. Chem. Soc.*, **75**, 2473 (1953).
17) M. H. Ford-Smith and N. Sutin, *ibid.*, **83**, 1830 (1961).
18) N. Sutin and B. M. Gordon, *ibid.*, **83**, 70 (1961).
19) A. G. Sykes, "Kinetics of Inorganic Reactions,'. Pergamon Press, London, (1966), p. 154; J. Halpern, *Quart' Rev.* (London), **15**, 207 (1961).

Effects of Additives on Solid State Reaction. I. A Kinetic Study of the Effects of Halides of the Formation of $MgAl_2O_4$

Shiro SHIMADA, Ryusaburo FURUICHI, and Tadao ISHII
Department of Applied Chemistry, Faculty of Engineering, Hokkaido University, Sapporo 060

(Received July 9, 1973)

The mechanism for the promoting effects of additives on the formation of $MgAl_2O_4$ has been systematically discussed from the results of kinetic measurements. A mixture of MgO and α-Al_2O_3 powder containing 10 mol% additives (LiF, NaF, MgF_2, CaF_2, BaF_2, NaCl or $CaCl_2$) and that without additives were isothermally heated in N_2 atmosphere in the temperature ranges 670—1142 °C and 1190—1360 °C. The diffusion-controlled Jander's equation was applied to all kinetic data obtained. In the case of fluoride additives, it has been found that the promoting actions are in the order $LiF \geq NaF > BaF_2 > MgF_2 > CaF_2$ and that the cations of fluorides play an important role in accelerating diffusion. The same promoting mechanism seems to be applicable in the case of chloride additives.

Solid state reactions are affected by various factors such as impurities or additives, preparation history of reacting material and atmosphere.[1,2] The effect of additives on the solid state reaction in MgO–Al_2O_3 system has been investigated by several authors.[3-5] Little attention, however, has been paid to the effect of additives on the solid state reaction, no explanation being given on their actions from a kinetic viewpoint.

In this paper, the promoting actions of alkali and alkaline earth halides on the formation of $MgAl_2O_4$ were discussed on the basis of the kinetic data. It was examined whether a mechanism similar to that for $MgCl_2$[6] additive could be applied to other chlorides.

Experimental

Sample. α-Al_2O_3 samples were prepared by calcining active alumina (Merck Co., 99.9% pure) at 1300 °C for 2 hr in the air. MgO samples were prepared from $Mg(OH)_2$ (Kanto Chemical Co., G.R. grade) under the same conditions. The particle size of α-Al_2O_3 was microscopically estimated to be in the range 58—90 μ, with an average of 70 μ. The MgO was found to have an average particle size of 0.1 μ by electron-microscopic observation. Powders of MgO, α-Al_2O_3 and additive were well mixed in the molar ratio 1 : 1 : 0.1. The additives used were LiF, NaF, MgF_2, CaF_2, BaF_2, NaCl and $CaCl_2 \cdot H_2O$ and were stored in a desiccator with silica gel before experiments. The additives (Kanto, Wako or Morita Companies) were of G.R. grade. The mixtures were pressed into pellets at 150 kg/cm^2 except for $CaCl_2 \cdot H_2O$ additive. The powders of MgO, α-Al_2O_3 and $CaCl_2 \cdot H_2O$ were mixed in a dry box because of the hygroscopic nature of $CaCl_2 \cdot H_2O$. These powder mixtures were heated at 400 °C to dehydrate $CaCl_2 \cdot H_2O$ prior to the kinetic experiment.

Kinetic Measurements. Two furnaces, Pt- and SiC-electric furnaces, were used for the measurements. The Pt-furnace was used for MgO–Al_2O_3–additive (LiF, NaF, MgF_2, BaF_2, NaCl or $CaCl_2$) systems in the temperature range 670—1100 °C). The furnace was equipped with a fused-silica tube connected to the vacuum system in which static nitrogen pressure was kept at 300 mmHg. The SiC-furnace was used for MgO–Al_2O_3 and MgO–Al_2O_3–CaF_2 systems in the temperature range 1100—1360 °C. This was equipped with a mullite tube through which nitrogen was allowed to flow at a rate of 30 ml/min. Compact pellets were placed on a Pt-boat in the tube and then heated isothermally. The temperature was measured with a Pt-Pt13Rh thermocouple.

Conversion of $MgAl_2O_4$ was determined by measuring the amount of the remaining MgO or α-Al_2O_3 after the reaction. The MgO unreacted was dissolved in 1.0 M nitric acid. The procedure was applied to the samples in the experiments of MgO–Al_2O_3 system and MgO–Al_2O_3–additive (LiF, NaF, NaCl or $CaCl_2$) system. Before titration, $CaCl_2$ was removed by washing the sample with alcohol. The amount of unreacted α-Al_2O_3 was estimated from the quantitative X-ray analysis by using CaF_2 as an external standard. This method was applied to the samples obtained from the MgO–Al_2O_3–additive (MgF_2, CaF_2 or BaF_2) systems. The results are shown in Table 1, and a satisfactory agreement can be seen between the chemical analysis and X-ray method.

Table 1. Fractional conversion (%) of $MgAl_2O_4$ for MgO–Al_2O_3 system

Chemical analysis	X-Ray analysis
$\alpha = 23$	$\alpha = 24$
26	30
36	37
42	45
46	48
94[a]	93[a]

a) results for 10 mol % additive of NaF

Reaction in MgO–Al_2O_3–additive System by the use of Pellets of MgO and α-Al_2O_3 (Model experiments). MgO and α-Al_2O_3 pellets, *ca.* 1 mm thick, were obtained by heating the compressed powders of MgO and α-Al_2O_3 at 1300 °C for 3 hr in the air. The experiment was carried out in the temperature range 900—950 °C for 5 hr in a vacuum (10^{-1} mmHg). The samples were prepared by sandwiching the powders of additives *ca.* 0.1 mm thick (LiF, NaF, BaF_2, LiCl, NaCl or $CaCl_2$) between MgO and α-Al_2O_3 pellets. After the reaction, the chlorides adhering to the pellets were removed by washing with alcohol in order to observe the surfaces and to measure the weight change of the pellets.

DTA Experiments. DTA experiments on the MgO–Al_2O_3–NaF system were carried out in nitrogen atmosphere at a heating rate of 10 °C/min. The sample was a mixture of MgO, α-Al_2O_3 and NaF with mol ratio 1 : 1 : 0.1, its weight being 300 mg.

Results and Discussion

Formation Rate of $MgAl_2O_4$. The rate of reaction between reactant particles is generally governed by either phase-boundary process or diffusion process.[7] The equations for the diffusion-controlled reaction have

been given by Jander,[8] Serin-Ellickson,[9] Ginstling-Brounshtein,[10] and Carter.[11] Jander's equation is

$$[1-(1-\alpha)^{1/3}]^2 = kt \quad (1)$$

$$k = 2DC_0/R^2 \quad (2)$$

where α=fractional conversion, k=rate constant, t=reaction time, D=diffusion coefficient, C_0=concentration of reactant at the interface, and R=particle radius.

The formation rates of $MgAl_2O_4$ in MgO–Al_2O_3 system and MgO–Al_2O_3–additive systems are shown in Figs. 1 and 2. All the data were obtained from the pellet except for the $CaCl_2$ additive (Fig. 2-D). The ⊗ marks in Fig. 1-A indicate the α values for loosely packed powder mixtures of MgO and α-Al_2O_3 heated at 1190 °C. Little difference was observed in the α values between the loosely packed powders and the compacted pellets under these experimental conditions.

A part of the data given in Figs. 1 and 2 plotted according to Eq. (1) is shown in Fig. 3. It can be seen that the data can fit Jander's equation up to about α=70%. For MgO-Al_2O_3 mixtures (Fig. 3-B, ○ and

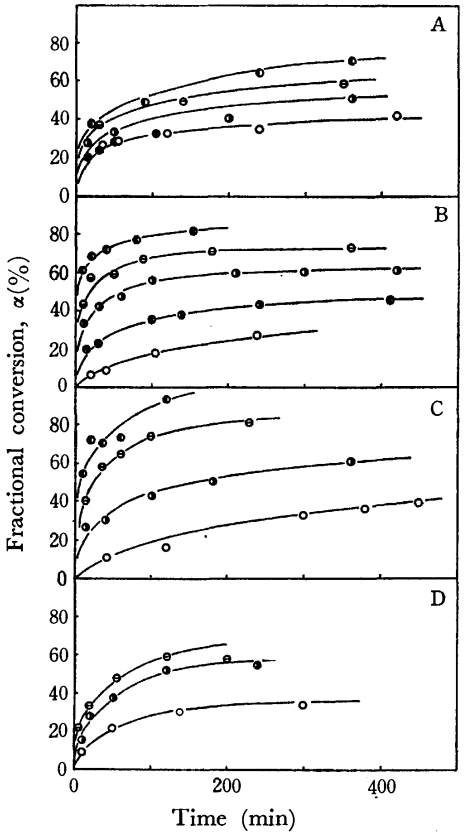

Fig. 1. Formation rate of $MgAl_2O_4$ for the MgO-Al_2O_3 and the MgO-Al_2O_3-alkali halide systems.
A: MgO-Al_2O_3 system
○: 1190 °C, ◑: 1240 °C, ⊖: 1295 °C, ◐: 1357 °C, ⊗: 1190 °C, results from the loosely packed powders
B: MgO-Al_2O_3-LiF system
○: 670 °C, ⊗: 714 °C, ◑: 753 °C, ⊖: 800 °C ◐: 850 °C
C: MgO-Al_3O_3-NaF system
○: 757 °C, ◑: 800 °C, ⊖: 840 °C, ◐: 870 °C
D: MgO-Al_2O_3-NaCl system
○: 965 °C, ◑: 1006 °C, ⊖: 1040 °C

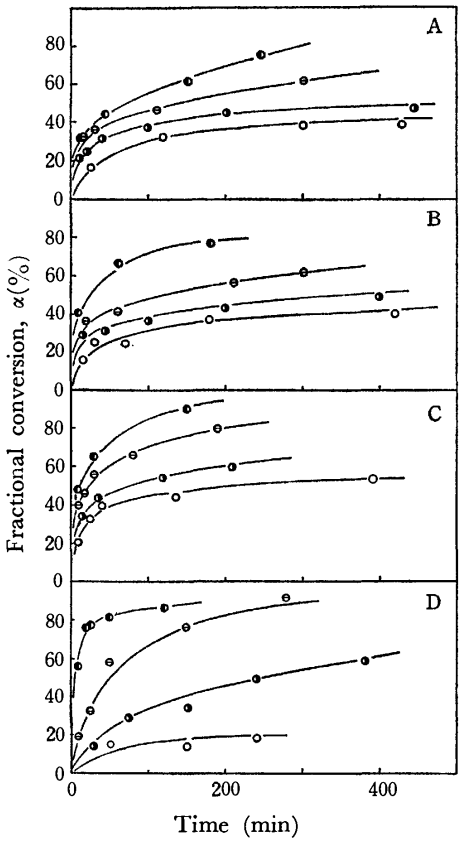

Fig. 2. Formation rate of $MgAl_2O_4$ for the MgO-Al_2O_3-alkaline earth halide system.
A: MgO-Al_2O_3-MgF_2 system
○: 985 °C, ◑: 1025 °C, ⊖: 1070 °C, ◐: 1100 °C
B: MgO-Al_2O_3-CaF_2 system
○: 1025 °C, ◑: 1056 °C, ⊖: 1100 °C, ◐: 1142 °C
C: MgO-Al_2O_3-BaF_2 system
○: 865 °C, ◐: 915 °C, ⊖: 960 °C, ◐: 990 °C
D: MgO-Al_2O_3-$CaCl_2$ system, the loosely packed powder samples
○: 860 °C, ◑: 900 °C, ⊖: 953 °C, ◐: 1003 °C

●) and those containing the fluoride additives (Fig. 3-A), the straight lines intersect the ordinate at kt values corresponding to α=20—30%. The fluoride additives seem to show larger intersecting values than those for non-additives systems. The straight lines of the chloride additives, however, fall approximately on the original point (Fig. 3-B). It seems that in the case of the fluoride additives, the initial formation of $MgAl_2O_4$ results from the reaction at the surface between the particles, and the subsequent reaction proceeds by the diffusion of the reactants through the $MgAl_2O_4$ layer formed. Abrupt change in slope was observed only for LiF additive system (Fig. 3—A, ○ and ●).

The rate constant k can be estimated from the slope of line in Fig. 3. The activation thermodynamic functions, ΔG^*, ΔH^*, ΔS^*, are calculated by

$$k = RT/Nh \exp(\Delta S^*/R) \exp(-\Delta H^*/RT) \quad (3)$$

where R=gas constant, T=absolute temperature, N=Avogadro's number, and h=Planck's constant. The transmission coefficient is assumed to be unity. The

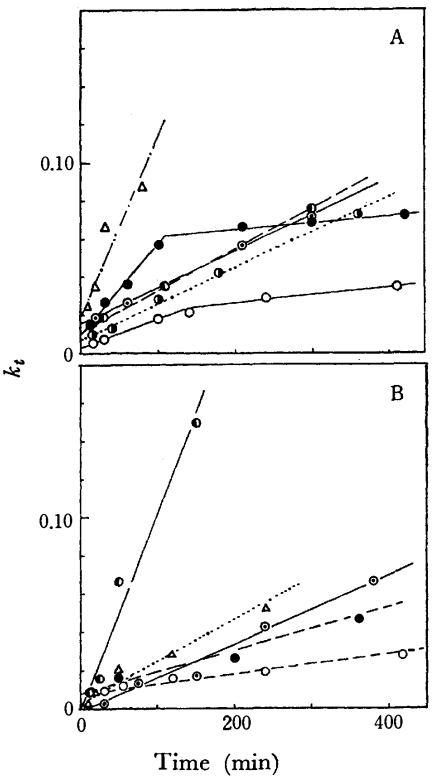

Fig. 3. Plots of k_t *vs.* t according to the Jander's equation.

A: ○: 714 °C, ●: 753 °C } LiF; ◑: 800 °C } NaF; ◐: 1070 °C } MgF_2; ⊙: 1100 °C } CaF_2; △: 960 °C } BaF_2

B: ○: 1190 °C, ●: 1240 °C } non-additive; △: 1006 °C } NaCl; ⊙: 900 °C, ◐: 953 °C } $CaCl_2$

values listed in Table 2 illustrate how greatly the formation reaction of $MgAl_2O_4$ is promoted by the presence of the additives. From the values for ΔG^*, the promoting actions of the additives can be represented by the sequences, LiF ≥ NaF > BaF_2 > $CaCl_2$ > NaCl > MgF_2 > CaF_2.

A comparison of the activation thermodynamic functions for the various additive systems with those for the non-additive system also shows that the additive systems give the values of ΔH^* and ΔS^* differing from those for non-additive system. This suggests that the diffusion mechanism in the additive systems differs from that in the non-additive system.

Halvac[12] studied the reaction of the powder compacts of α-Al_2O_3 and MgO in the air, in the temperature range 1000—1290 °C, and suggested that the formation rate of $MgAl_2O_4$ was controlled by either grain-boundary or volume diffusion step. The values of D in this temperature range have been calculated to be $D=10^{-12}$ 10^{-10} cm^2/s in the temperature range 1190—1360 °C, by assuming that $R=0.007$ cm, $C_0=1.0$[13] in Eq. (2). The value closely agrees with Halvac's. For LiF, NaF, BaF_2 and $CaCl_2$ additives, the values of D were also found to be $D=10^{-10}-10^{-8}$ cm^2/s in the temperature range 800—1000 °C, which was larger than the value of D for the non-additive system by a factor of 10^3—10^5, when D's at 800—1000 °C were corrected for 1190—1360 °C. The comparable values of D for the non-additive system therefore show that the grain-boundary or volume diffusion should be operative in the formation of $MgAl_2O_4$. On the other hand, the significant increase in the value of D in the case of LiF, NaF, BaF_2 and $CaCl_2$ additives indicates that these additives exert an enhancing action on the diffusion along grain-boundary or within bulk.

Model Experiment. The formation of $MgAl_2O_4$ in the systems with fluoride additives seems to consist of two stages; rapid reaction at the surface between the particles in the initial stage and diffusion in the later stage. In order to examine the rapid reaction at the surface, model experiments were carried out by using α-Al_2O_3 and MgO pellets between which the fluorides were placed.

Although the chloride additions showed no such rapid reaction at the surface, the interactions of chlorides with MgO or α-Al_2O_3 were examined by model experiments.

Fluoride: The model reaction on MgO–Al_2O_3–fluoride (LiF, NaF or BaF_2) systems was carried out at 950 °C for 5 hr in a vacuum.

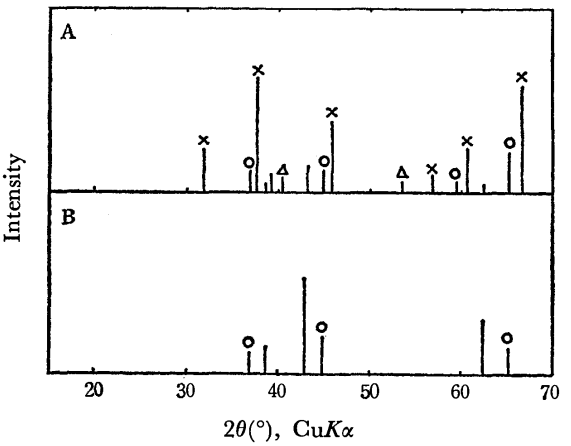

Fig. 4. X-ray diffraction patterns of the reaction surface of α-Al_2O_3 and MgO pellets in the MgO–Al_2O_3–LiF system.
Reaction temperature: 950 °C, time: 5 hr, in vacuum (10^{-1} mmHg).
A: α-Al_2O_3 pellet, B: MgO pellet
○: $MgAl_2O_4$, ×: $LiAl_5O_8$, △: MgF_2

Figure 4 shows the X-ray diffraction patterns of the surface of α-Al_2O_3 and MgO pellets obtained by the reaction in MgO–Al_2O_3–LiF system. We see that $LiAl_5O_8$ is formed on the surface of α-Al_2O_3 pellet (Fig. 4-A). Another two experiments showed that $NaAl_{11}O_{17}$ and $BaAl_2O_4$ were formed on the surface of α-Al_2O_3 pellet in the reaction of MgO–Al_2O_3–NaF system and MgO–Al_2O_3–BaF_2 system, respectively. $NaAl_{11}O_{17}$ was assumed to result from unreacted α-Al_2O_3 and $Na_2Al_2O_4$ formed from α-Al_2O_3 and NaF.[14] Thus, it can be concluded that the reaction of α-Al_2O_3 with fluoride results in the formation of aluminate.

Chloride: The model reactions of MgO–Al_2O_3–chloride ($CaCl_2$, LiCl or NaCl) systems were performed at 900—950 °C for 5 hr in a vacuum.

Table 2. Activation thermodynamic functions for formation reaction of $MgAl_2O_4$

Additive	React. temp. (°C)	k (min^{-1})	ΔG^* (kcal/mol)	ΔH^* (kcal/mol)	ΔS^* (cal/mol·deg)
non-additive	1190	3.80×10^{-5}	121	68	−36
	1240	8.50×10^{-5}	123		
	1295	1.48×10^{-4}	125		
	1357	2.75×10^{-4}	127		
LiF	670	4.00×10^{-5}	76	50	−28
	714	1.42×10^{-4}	78		
	753	4.70×10^{-4}	79		
	800	9.86×10^{-4}	80		
	850	1.60×10^{-3}	82		
NaF	757	5.17×10^{-5}	83	87	+3
	800	1.87×10^{-4}	83		
	840	1.37×10^{-3}	83		
	870	2.80×10^{-3}	83		
NaCl	965	3.97×10^{-5}	101	104	+3
	1006	1.77×10^{-4}	101		
	1040	4.65×10^{-4}	101		
MgF_2	985	3.50×10^{-5}	103	77	−21
	1025	8.50×10^{-5}	104		
	1070	2.13×10^{-4}	105		
	1100	4.87×10^{-4}	106		
CaF_2	1025	4.90×10^{-5}	105	67	−30
	1056	9.30×10^{-5}	106		
	1100	2.07×10^{-4}	108		
	1142	7.10×10^{-4}	109		
BaF_2	865	9.00×10^{-5}	91	60	−27
	915	2.50×10^{-4}	92		
	960	8.20×10^{-4}	94		
	990	2.00×10^{-3}	94		
$CaCl_2$	860	2.10×10^{-5}	92	113	+18
	900	1.82×10^{-4}	92		
	953	1.60×10^{-3}	91		
	1003	7.39×10^{-3}	90		

Table 3. Weight change of pellets of MgO and α-Al_2O_3 for the model reactions in the MgO-Al_2O_3-chloride systems

Additives	React. temp. (°C)	React. time (hr)	Melting point of additives[a] (°C)	Weight changes (mg) MgO[b]	Weight changes (mg) α-Al_2O_3[c]
$CaCl_2$	900	5.0	782	− 2	+ 5
$CaCl_2$	950	5.0	782	−21	+10
LiCl	940	5.0	610	− 4	+14
NaCl[d]	950	5.0	808	—	—
non-additive	960	5.0	—	0	0

a) From Ref. 15. b) weight loss of MgO pellets. c) Weight increase of α-Al_2O_3 pellets. Two pellets of MgO and α-Al_2O_3 could not be separated. The reacted surface of α-Al_2O_3 pellet obtained was exposed by polishing.

The weight changes of MgO and α-Al_2O_3 pellets and the melting point of additives are given in Table 3. The weight of MgO pellets is seen to decrease and that of α-Al_2O_3 pellets to increase. The X-ray diffraction patterns of the reacted surface of the pellets indicate that $MgAl_2O_4$ is formed only on the α-Al_2O_3 surface. These results suggest that molten chloride behaves as a vehicle, in which MgO is dissolved to disperse uniformly, and the molten phase containing MgO is transported into the α-Al_2O_3 particle which is an agglomerate of the crystallites.

Promoting Actions of Additives. *Fluoride*: From the results it seems that a large part of the cations of fluoride exists in the form of aluminate which is incorporated into $MgAl_2O_4$ layer. Thus, it is necessary to examine whether such cations exert an influence on the diffusion process.

The plots of log ($k_{additive}/k_{pure}$) for 1173 K against the electronegativity of cations[16] are shown in Fig. 5. The logarithmic ratios corrected for $T=1174$ K were calculated by means of Eq. (3) and the value of the thermodynamic functions in Table 2. The figure shows an exponential increase in the formation rate with the decrease in the electronegativity of cations. The activation enthalpy, ΔH^*, can be correlated with the electronegativity as shown in Fig. 6; the value of ΔH^* decreases linearly with the decrease in the electronegativity except for the NaF additive. It can be concluded

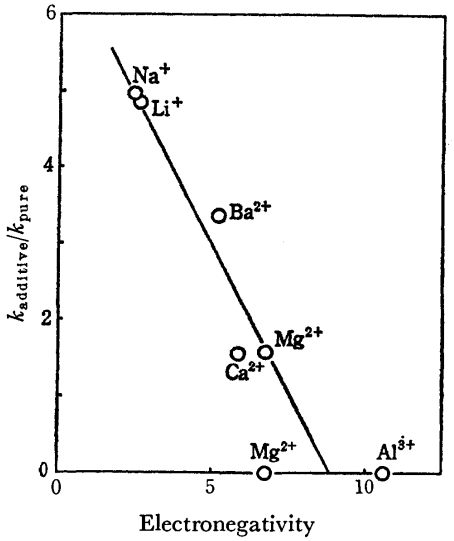

Fig. 5. Relationship between log ($k_{additive}/k_{pure}$) and the electronegativity of cations of fluorides.

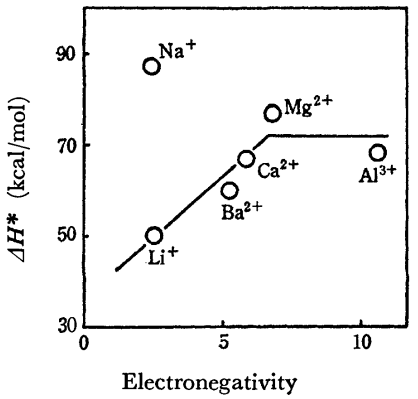

Fig. 6. Relationship between ΔH^* and the electronegativity of cations of fluorides.

that the cation of additives plays an important role in increasing the mobility of the Mg^{2+} or Al^{3+} ions and in lowering the energy required for diffusion.

The exceptional ΔH^* value of the NaF additive seems to be associated with the presence of liquid phase, since the DTA curves for MgO-Al_2O_3-NaF system showed an endothermic peak due to formation of liquid phase at near 800 °C. A similar relation between the large ΔH^* and the presence of liquid phase holds for the cases of $CaCl_2$ (ΔH^*=113 kcal/mol) and NaCl (ΔH^*= 104 kcal/mol) additives which are in liquid state at the reaction temperatures. The presence of liquid phase in the course of the reaction might be associated with the possitive value of ΔS^* of these additives (Table 2) which shows an activated state disordered more than the reactants.

Chloride: The same mechanism as that for the molten $MgCl_2$ may be applied to the other chloride additives since they are in liquid state at reaction temperatures. MgO particles may dissolve in the molten chloride, then they spread uniformly over the surface of α-Al_2O_3 particles and are transported to the inner part of α-Al_2O_3 particles consisting of the crystallites. In such cases, the value of C_0 in Eq. (2) is expected to be large and the diffusion distance reduced from the radius (R=70 μ) of α-Al_2O_3 particle to that (R=1—2 μ) of α-Al_2O_3 crystallites. However, such a reduction of distance would not occur in the non-additive system because of the absence of molten phase.

References

1) H. Schmalzried, *Ber. Dtsch. Keram. Ges.*, **42**, 11 (1965).
2) H. Schmalzried, "Reactivity of Solids," ed. by J. M. Mitchell, Schenectady (1968), p. 551.
3) I. S. Kainarskii and E. V. Degtyarava, *Zh. Prikl. Khim.*, **36**, 225 (1963).
4) H. Yanagida and M. Atumi, *J. Ceram. Assoc. Jap.*, **75**, 349 (1967).
5) V. A. Bron and M. I. Diesperova, *Chem. Abstr.*, **62**, 14213p (1966).
6) S. Shimada and T. Ishii, *Nippon Kagaku Kaishi*, **1972**, 1234.
7) K. J. Laidler, "Chemical Kinetics," McGraw-Hill, New York (1964), p. 316.
8) W. Jander, *Z. Anorg. Allg. Chem.*, **163**, 1 (1927).
9) B. Serin and R. J. Ellickson, *J. Chem. Phys.*, **9**, 742 (1941).
10) A. M. Ginstling and B. I. Brounshtein, *J. Appl. Chem.*, **23**, 1327 (1950).
11) R. E. Carter, *J. Chem. Phys.*, **34**, 2010 (1961).
12) J. Halvac, "Reactivity of Solids," ed. by De. Boer, Amsterdam (1960), p. 129.
13) The value of D calculated by assuming C_0=1.0 in Eq. (2) is approximately in agreement with that of D calculated from the Serin-Ellickson's equation ($1-\alpha=6/\pi^2\sum(1/n^2)\exp(-n^2\pi^2Dt/R^2)$.
14) J. Thery and D. Briancon, *Rev. Hautes. Temp. Refract.* **1**, 221 (1964).
15) G. J. Jang, "Molten Salts Handbook," Academic press, New York (1967), p. 5.
16) R. T. Sanderson, "Chemical Periodicity," Reinhold Publishing, New York (1960), p. 41.

Effect of Additive on Solid State Reaction. II. A Thermoanalytical Study of the Effect of Fluorides on the Formation of $MgAl_2O_4$ in Initial Stage

Shiro SHIMADA, Ryusaburo FURUICHI, and Tadao ISHII

Department of Applied Chemistry, Faculty of Engineering, Hokkaido University, Sapporo 060

(Received July 9, 1973)

The promoting actions of fluoride on the formation of $MgAl_2O_4$ in the initial stage have been studied by means of DTA and high-temperature X-ray diffraction techniques. LiF, NaF, MgF_2, CaF_2 and BaF_2 were used as additives. The three MgO-Al_2O_3-fluoride (LiF, NaF or BaF_2) systems showed similar DTA curves; an endothermic peak (peak-1) in the temperature range 660—800 °C, followed by an exothermic peak (peak-2) at 700—900 °C. The DTA curves for MgO-Al_2O_3-fluoride (MgF_2 or CaF_2) systems showed no thermal change. It was found that peak 1 corresponds to Reaction (2), $3MF+2Al_2O_3=3MAlO_2+AlF_3$, and peak 2 to Reaction (1), $3MgO+2AlF_3=3MgF_2+Al_2O_3$, and the formation of $MgAl_2O_4$. It was concluded that Reaction (2) takes place before the formation of $MgAl_2O_4$ and that AlF_3 resulting from Reaction (2) initiates the formation of $MgAl_2O_4$.

In the preceding paper[1] the promoting actions of fluorides and chlorides on the formation of $MgAl_2O_4$ were discussed from a kinetic viewpoint. Rate constants were obtained from isothermal experiments for determining the extent of promoting action. Some clues for the reaction mechanism such as a linear relation between the rate constant and electronegativity of cations of the halides were also obtained. However, it was not possible to see what kind of chemical reaction between the halide additives and reactants MgO and Al_2O_3 promotes the formation. DTA and high-temperature X-ray diffraction, both being non-isothermal techniques, are useful for clarifying the reaction over a wide temperature range and for finding the initiation temperature of the reaction. We have studied MgO–Al_2O_3–fluoride systems by the non-isothermal technique in order to find the chemical reaction between additive and reactant.

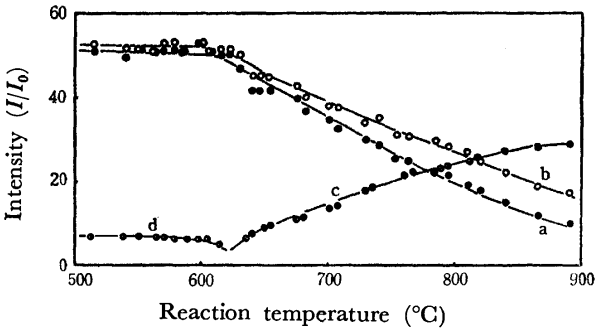

Fig. 1. High-temperature X-ray diffraction patterns of the reaction in MgO-Al_2O_3-LiF system. Molar mixing ratio: 1 : 1 : 0.2, Heating rate: 2—4 °C/min, in N_2 (300 mmHg).
a: α-Al_2O_3 (113), b: MgO (200), c: $MgAl_2O_4$ (400), d: LiF (200)

Experimental

Sample. α-Al_2O_3 and MgO samples were prepared by a method similar to that described.[1] The particle size of sample was smaller than 44 μ for α-Al_2O_3 and *ca.* 0.1 μ for MgO. The fluorides used as additive were LiF, NaF, MgF_2, CaF_2 and BaF_2.

DTA Experiments. DTA experiments were carried out with a Thermoflex 8001 type apparatus (Rigaku-Denki). Before heating the sample, the apparatus was evacuated to approximately 10^{-1} mmHg and then filled with N_2 of 300 mmHg to avoid the effect of water vapor in the air. Pt-Pt13Rh thermocouples were used for measuring the temperature, a heating rate of 10 °C/min being employed in all experiments. The sample weight was about 300 mg. α-Al_2O_3 of the same weight was taken as the standard material.

X-Ray Diffraction. A Geigerflex 2141 type diffractometer (Rigaku-Denki) was used for X-ray analysis of the samples obtained during DTA runs, the analysis being carried out with Ni-filtered Cu$K\alpha$, operation voltage 25 kV and current 10 mA. The fractional conversion of $MgAl_2O_4$ was determined by the quantitative X-ray analysis.[1]

High-temperature X-Ray Diffraction. A high-temperature A-4 type attachment (Rigaku-Denki) was used. The experiments were carried out in static N_2 of 300 mmHg at heating rate of 2—4 °C/min, operation voltage and current respectively 40 kV and 20 mA.

Results and Discussion

MgO-Al_2O_3-LiF System. The change of high-temperature X-ray diffraction intensities with the reaction temperature is shown in Fig. 1. Curve a: (113) line of α-Al_2O_3, Curve b: (200) of MgO, Curve c: (400) of $MgAl_2O_4$, Curve d: (200) of LiF. We see that $MgAl_2O_4$ begins to form simultaneously with the decrease of the reactants of MgO, α-Al_2O_3 and LiF near 630 °C, and that in the initial stage of the $MgAl_2O_4$ formation, the extent of the decrease in the X-ray intensity with temperature is larger for α-Al_2O_3 than for MgO. The shift of (200) diffraction line of LiF to the lower angle starts at a temperature near 400 °C. At 630 °C, the shift became 1°, and the diffraction line of $MgAl_2O_4$ appears. This shift indicates that LiF is strongly thermally expanded at the temperature of beginning of the formation of $MgAl_2O_4$.[2]

Figure 2 shows DTA curves (A: 1 : 1 : 0.2 mixture of MgO, Al_2O_3 and LiF in molar ratio) and X-ray diffraction patterns of the samples heated up to temperatures corresponding to points a and b on Curve A. The curve shows one endothermic peak 1 in the range 660—690 °C and one exothermic peak 2 in 690—750 °C. The cycles of heating and cooling of the sample for Curve A give endothermic and exothermic changes at 780—790 °C, respectively (Curve B). The samples containing LiF (0.5 molar ratio) showed DTA curves similar to Curves A and B. The DTA curves of MgO–LiF, Al_2O_3–LiF and MgO-Al_2O_3 systems, however, showed no thermal changes in the range 20—1000 °C except for the endothermic peak due to melting of LiF. It thus seems that only the ternary system of MgO,

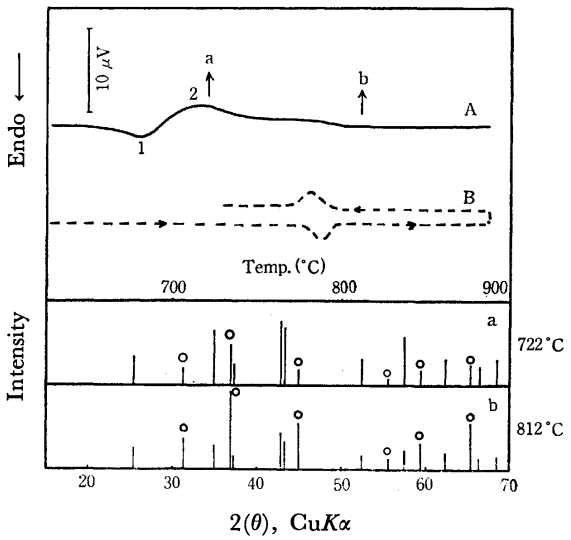

Fig. 2. DTA curve of the reaction in MgO-Al_2O_3-LiF system and X-ray diffraction patterns of the samples heated to a- and b-points. Heating rate: 10 °C/min, in N_2 (300 mmHg), sample weight: 300 mg.
A: 1 : 1 : 0.2 mixture of MgO, Al_2O_3 and LiF in molar ratio, B: heating and cooling cycle of sample for Curve A, ○: $MgAl_2O_4$

TABLE 1. THERMODYNAMIC DATA[a)]

$3LiF+2Al_2O_3=3LiAlO_2+AlF_3$	$\Delta H°=73$ kcal/mol
$3NaF+2Al_2O_3=3NaAlO_2+AlF_3$	$\Delta H°=76$ kcal/mol
$3MgF_2+4Al_2O_3=3MgAl_2O_4+2AlF_3$	$\Delta H°=111$ kcal/mol
$3CaF_2+4Al_2O_3=3CaAl_2O_4+2AlF_3$	$\Delta H°=210$ kcal/mol
$3BaF_2+4Al_2O_3=3BaAl_2O_4+2AlF_3$	$\Delta H°=$unknown
$MgO+2LiF=MgF_2+Li_2O$	$\Delta H°=30$ kcal/mol
$MgO+2NaF=MgF_2+Na_2O$	$\Delta H°=53$ kcal/mol
$MgO+CaF_2=MgF_2+CaO$	$\Delta H°=18$ kcal/mol
$MgO+BaF_2=MgF_2+BaO$	$\Delta H°=34$ kcal/mol
$3MgO+2AlF_3=3MgF_2+Al_2O_3$	$\Delta H°=-140$ kcal/mol
$MgO+2AlOF=MgF_2+Al_2O_3$	$\Delta H°=-243$ kcal/mol
$MgO+Al_2O_3=MgAl_2O_4$	$\Delta H°=-9.1$ kcal/mol

a) From Ref. 7.

Al_2O_3 and LiF shows peaks 1 and 2 (Curve A, Fig. 2). Peak 2 is probably related to the formation of $MgAl_2O_4$, since $MgAl_2O_4$ is formed at point a after peak 2 and $\Delta H°$ of this spinel formation is −9.1 kcal/mol (Table 1). At point b, a large amount of $MgAl_2O_4$ is also found to be formed. The reversible thermal changes of Curve B may be due to the formation of the liquid phase by the reaction in MgO–Al_2O_3–LiF system.

MgO–Al_2O_3–NaF System. Figure 3 shows the results of high-temperature X-ray analysis for the reaction of MgO–Al_2O_3–NaF system. The initiation of formation of $MgAl_2O_4$ is seen at 720 °C, a rapid increase in its amount with the rapid decrease in that of MgO and Al_2O_3 being observed. The temperature dependency leads to a large activation energy for the ΔH^* value formation of $MgAl_2O_4$. This is consistent with a ΔH^* value large (activation enthalpy).[1)] The thermal expansion of NaF is considered to be significant at 720 °C, since the large shift of diffraction line (200) to the

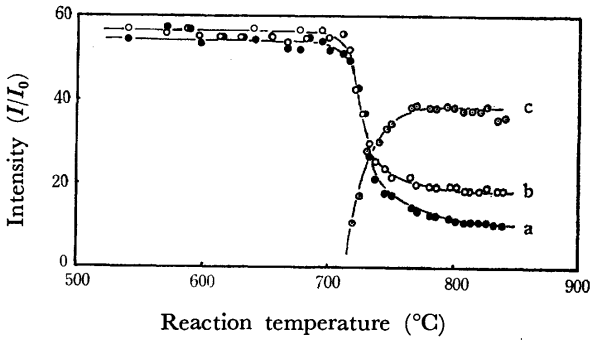

Fig. 3. High-temperature X-ray diffraction patterns of the reaction in MgO-Al_2O_3-NaF system. Molar mixing ratio: 1 : 1 : 0.2, Heating rate: 2—4 °C/min, in N_2 (300 mmHg).
a: α-Al_2O_3 (113), b: MgO (200), c: $MgAl_2O_4$ (400)

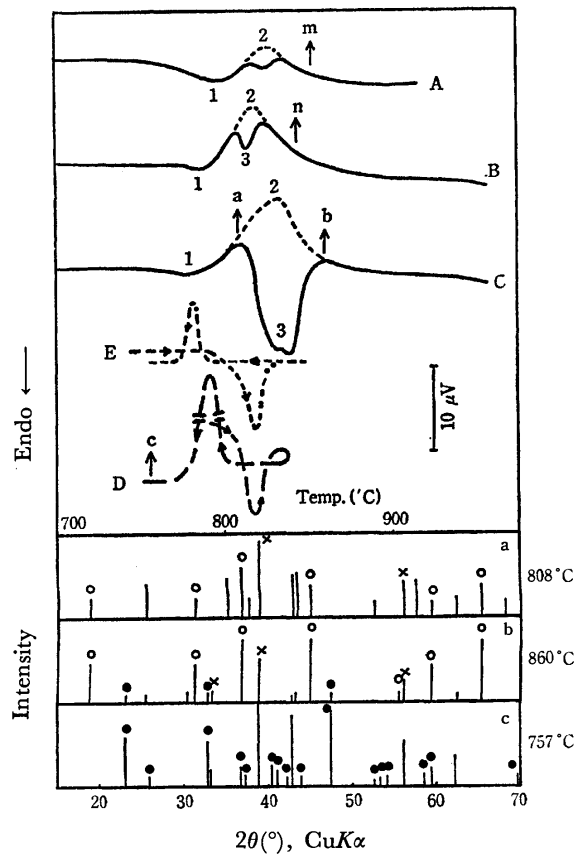

Fig. 4. DTA curves of the reaction in MgO-Al_2O_3-NaF system and X-ray diffraction patterns of the samples heated to a-, b- and c-points. Heating rate: 10 °C/min, in N_2 (300 mmHg), sample weight: 300 mg.
A: 1 : 1 : 0.1 mixture of MgO, Al_2O_3 and NaF in molar ratio, B: 1 : 1 : 0.2 mixture, C: 1 : 1 : 0.8 mixture, D: 1 : 1 mixture of MgF_2 and NaF in weight ratio, E: heating and cooling cycle of sample for Curve C
○: $MgAl_2O_4$, ×: NaF, ●: $NaMgF_3$
m: α=60%, n: α=55%

lower angle with temperature, similar to the case of LiF, was also observed for NaF.[3]

Figur 4 shows DTA curves and X-ray diffraction patterns of samples heated up to temperatures corresponding to points a, b and c on Curves C and D. The molar mixing ratios of MgO, Al_2O_3 and NaF for Curves A, B and C are: A, 1 : 1 : 0.1; B, 1 : 1 : 0.2; C, 1 : 1 : 0.8. Curve D was obtained from the 1 : 1 binary mixture (weight ratio) of MgF_2 and NaF, and Curve E from the sample used for Curve C after it had been heated up to 960 °C. Each curve of MgO–Al_2O_3–NaF systems shows an endothermic peak 1 in the range 760—795 °C and the overlap of an exothermic peak 2[4] with an endothermic peak 3. The DTA curves of binary systems such as MgO–NaF and Al_2O_3–NaF showed no thermal change except for the melting of NaF.

The fractional conversions of $MgAl_2O_4$ for the samples heated up to 852 °C (point m) on Curve A and up to 842 °C (point n) on Curve B were estimated to be α=60% and 55%, respectively. Comparable α values imply that the amount of $MgAl_2O_4$ produced does not necessarily depend on the amount of NaF added. The area of peak 2 seems to increase with the amount of NaF, suggesting peak 2 to contain another exothermic reaction in addition to $MgAl_2O_4$ formation. From X-ray diffraction patterns (Fig. 4), the presence of $NaMgF_3$, a complex compound formed from NaF and MgF_2,[5] is observed in addition to $MgAl_2O_4$ at point b on Curve C. Thus, it can be assumed that the exothermic peak 2 is due to the formation of $MgAl_2O_4$ and MgF_2. Peak 3 is considered to be due to the formation of liquid phase, since the cycles of heating and cooling of the sample for Curve C give endothermic and exothermic changes (Curve E). The two peak temperatures in Curve E are in agreement with those in Curve D obtained from MgF_2–NaF mixture, the temperatures being near the eutectic temperature of $NaMgF_3$ and NaF.[6] Thus, peak 3 might correspond to the melting of the mixture of $NaMgF_3$ and NaF. The results show that MgF_2 is formed in the MgO–Al_2O_3–NaF system, but not in the MgO–NaF system.

MgO–Al_2O_3–BaF_2 System. The results of high-temperature X-ray diffraction of this system are shown in Fig. 5. BaF_2 begins to decrease at *ca.* 680 °C (Curve d), and subsequently $MgAl_2O_4$ and $BaAl_2O_4$ begin to form near 700 °C (Curves c and e) with the simultaneous decrease of MgO and α–Al_2O_3 (Curves b and a). $BaAl_2O_4$ could be formed from the reaction of BaF_2 with α–Al_2O_3.

Figure 6 shows DTA curve (A: 1 : 1 : 0.5 mixture of MgO, Al_2O_3 and BaF_3 in molar ratio) and X-ray diffraction patterns of sample heated up to 870 °C (point a). Curve A shows similar thermal behaviors; a small endothermic peak 1, followed by an exothermic peak 2. DTA curves for the binary system of MgO–BaF_2 and Al_2O_3–BaF_2, however, showed no thermal change in the range 20—1100 °C. The cycles of heating and cooling of the sample for Curve A show no thermal change either. $MgAl_2O_4$ and $BaAl_2O_4$ were found to form at point a and the fractional conversion of $MgAl_2O_4$ was 63%. Thus peak 2 is related to the formation of $MgAl_2O_4$.

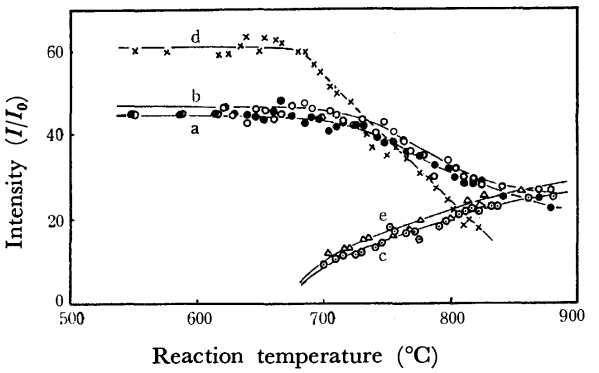

Fig. 5. High-temperature X-ray diffraction patterns of the reaction in MgO–Al_2O_3–BaF_2 system. Molar mixing ratio: 1 : 1 : 0.2, heating rate: 2—4 °C/min, in N_2 (300 mmHg).
a: α-Al_2O_3 (113), b: MgO (200), c: $MgAl_2O_4$ (400), d: BaF_2 (220), e: $BaAl_2O_4$ (112)

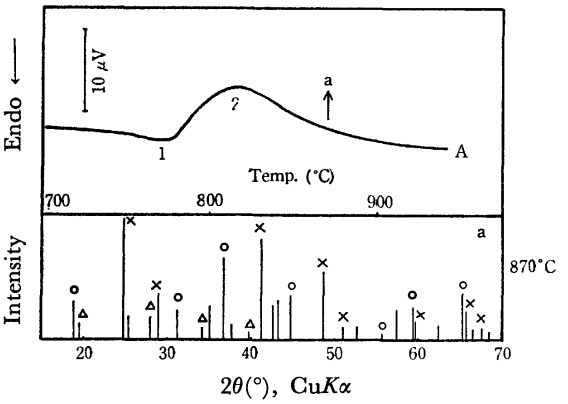

Fig. 6. DTA curve of reaction in MgO–Al_2O_3–BaF_2 system and X-ray diffraction patterns of the samples heated to a-point. Heating rate: 10 °C/min, in N_2 (300 mmHg), sample weight: 300 mg.
A: 1 : 1 : 0.5 mixture of MgO, Al_2O_3 and BaF_2 in molar ratio
△: $BaAl_2O_4$, ×: BaF_2, ○: $MgAl_2O_4$
a: α=63%

MgO–Al_2O_3–MgF_2 System. The high-temperature X-ray diffraction data are shown in Fig. 7. $MgAl_2O_4$ begins to form near 835 °C (Curve c) accompanied by the decrease of MgO, α-Al_2O_3 and MgF_2 (Curves b, a and d). The DTA curves in the MgO–Al_2O_3–MgF_2 and MgO–Al_2O_3–CaF_2 systems showed no thermal change in the range 20—1100 °C.

The Reaction of Fluorides with MgO and α-Al_2O_3. Peak 2 in Fig. 4 (MgO–Al_2O_3–NaF system) was found to correspond to the reaction, $MgO+Al_2O_3=MgAl_2O_4$ with $\Delta H°=-9.1$ kcal/mol, and to another extra exothermic reaction which seems to be MgF_2 formation from MgO and fluoride from the results of X-ray and DTA experiments. It was also found that the systems containing LiF (Fig. 2) and BaF_2 (Fig. 6) showed two peaks on the DTA curves similar to those of MgO–Al_2O_3–NaF system. Thus, peak 2 on the DTA curves of the systems containing LiF and BaF_2 is also assumed

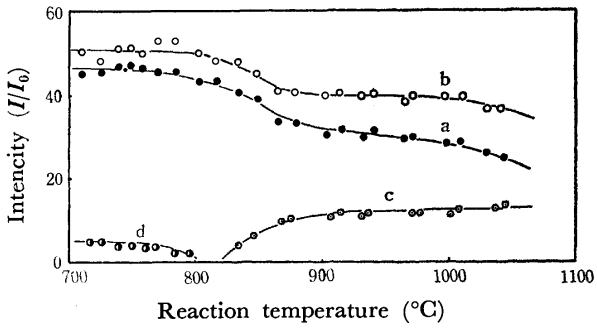

Fig. 7. High-temperature X-ray diffraction patterns of the reaction in $MgO-Al_2O_3-MgF_2$ system. Molar mixing ratio: 1 : 1 : 0.2, heating rate: 2—4 °C/min, in N_2 (300 mmHg).
a: α-Al_2O_3 (113), b: MgO (200), c: $MgAl_2O_4$ (400), d: MgF_2 (111)

to be due to the formation of MgF_2 and $MgAl_2O_4$, the latter being confirmed by X-ray analysis.

Three possible reactions, those of MgO with MF, AlOF or AlF_3, can be considered for MgF_2 formation (Table 1). However, the reactions of MgO with MF and AlOF can be excluded, since $\Delta H°$, the heat of the reaction of MgO with MF is positive, *viz.*, endothermic and experimental evidence for AlOF formation at temperatures below 1700 °C has not been reported.[8] Thus, it is reasonable to assume that MgF_2 is formed by the reaction

$$3MgO + 2AlF_3 = 3MgF_2 + Al_2O_3 \quad (1)$$

where AlF_3 is endothermally formed from Al_2O_3 and fluoride (Table 1). Thus the endothermic peak 1, which precedes peak 2, would be due to the reaction of α-Al_2O_3 with fluoride. On the other hand, the binary systems, Al_2O_3–fluoride, showed neither thermal changes in DTA curves nor X-ray diffraction lines of AlF_3. The results lead to an assumption that AlF_3 is formed from Al_2O_3 and fluoride in the presence of MgO in the temperature range 20—1000 °C. The reactions considered possible for peak 1 are as follows.

$$2Al_2O_3 + 3M^{I}F \xrightarrow{MgO} 3M^{I}AlO_2 + AlF_3 \quad (2)$$

$$4Al_2O_3 + 6M^{I}F \xrightarrow{MgO} 3M^{I}_2Al_2O_4 + 2AlF_3 \quad (2')$$

$$4Al_2O_3 + 3M^{II}F_2 \xrightarrow{MgO} 3M^{II}Al_2O_4 + 2AlF_3 \quad (3)$$

Formation of $M^{II}Al_2O_4$ was observed in the BaF_2–Al_2O_3–MgO system ($BaAl_2O_4$), and $NaAl_{11}O_{17}$, assumed to result from $M^{I}_2Al_2O_4$ ($Na_2Al_2O_4$) and Al_2O_3, was found in NaF–Al_2O_3–MgO system when NaF was sandwiched between MgO was Al_2O_3 pellets.[1]

AlF_3 was not found in any system examined directly by X-ray. This might be due to the small amount of fluoride additives and the easily occurring sublimation of AlF_3.[9] In order to examine the effects of AlF_3 resulting from Reaction (2)—(3), experiments were carried out for MgO–Al_2O_3–AlF_3 and MgO–AlF_3 system. Figure 8 shows DTA curves (A: MgO–Al_2O_3–AlF_3 system; B: MgO–AlF_3 system) and X-ray diffraction patterns. $AlF_3 \cdot H_2O$ used as starting material was subjected to dehydration in order to obtain anhydride AlF_3

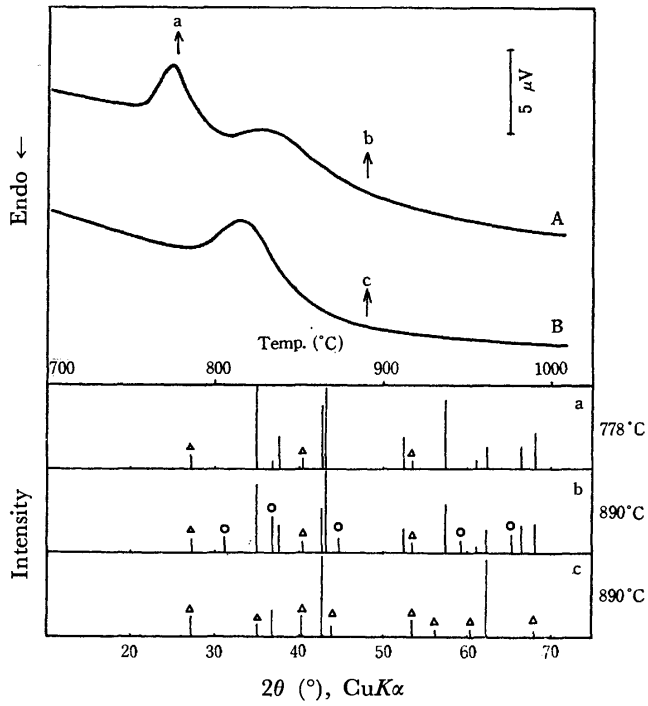

Fig. 8. DTA curves of the reaction in $MgO-Al_2O_3-AlF_3$ and $MgO-AlF_3$ systems, and X-ray diffraction patterns of the samples heated to a-, b- and c-points. Heating rate: 10°C/min, in N_2 (300 mmHg), sample weight: 300 mg.
○: $MgAl_2O_4$, △: MgF_2
a: α=0, b: α=32%

at 200—300 °C. MgO–AlF_3 system (Curve B) shows an exothermic peak due to Reaction (1) at 790—850 °C, since X-ray analysis indicated the formation of MgF_2 after this peak (point c). Curve A shows two exothermic peaks in the ranges 750—800 °C and 800—870 °C; the first corresponds to the exothermic peak on Curve B since only MgF_2 is formed at point a on Curve A; the second peak might be due to the formation of $MgAl_2O_4$, since $MgAl_2O_4$ was found to form at point b. It is thought that two exothermic peaks on Curve A can be associated with reaction of the exothermic peak 2 (Figs. 2, 4 and 6). The conversion of $MgAl_2O_4$ at point b (890 °C) was estimated to be α=32%. This

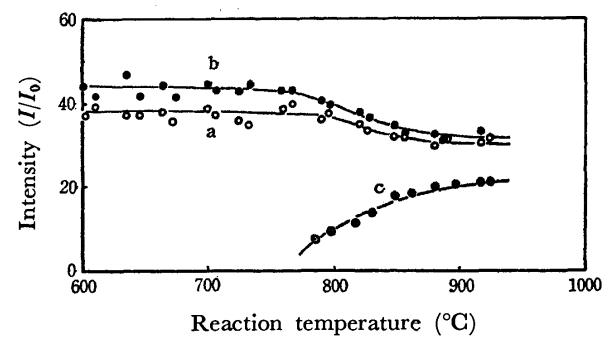

Fig. 9. High-temperature X-ray diffraction patterns of the reaction in $MgO-Al_2O_3-AlF_3$ system. Molar mixing ratio: 1 : 1 : 0.2, heating rate: 2—4 °C/min, in N_2 (300 mmHg).
a: α-Al_2O_3 (113), b: MgO (200), c: $MgAl_2O_4$ (400)

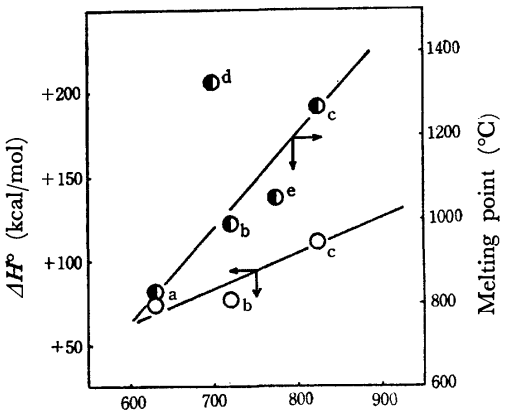

Fig. 10. Plots of $\Delta H°$ for the reactions in Table 1 and the melting points of fluorides *vs.* the initiation temperature of $MgAl_2O_4$ formation.
a: LiF, b: NaF, c: MgF_2, d: BaF_2, e: AlF_3

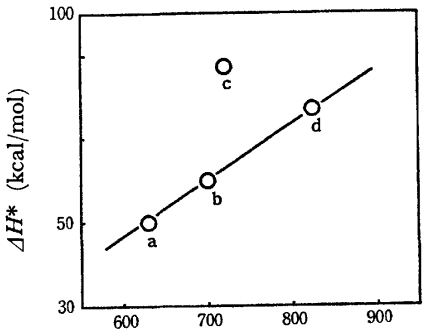

Fig. 11. Plots of activation enthalpy ΔH^* *vs.* the initiation temperatures of $MgAl_2O_4$ formation.
a: LiF, b: BaF_2, c: NaF, d: MgF_2

is comparable with $\alpha=20$—30%, the values corresponding to the rapid $MgAl_2O_4$ formation observed in the initial stage of isothermal experiments.[1] It seems from the data of MgO–Al_2O_3–AlF_3 (Fig. 9) that the presence of AlF_3 promotes the formation of $MgAl_2O_4$ as much as alkali and alkaline earth fluorides.

The formation of $MgAl_2O_4$ might be initiated by the presence of fluorides which form AlF_3 (Eqs. (2) and (3)), although each fluoride gives different initiation temperatures (Fig. 10). We see that the lower the value of $\Delta H°$ for Eqs. (2) and (3), the lower the initiation temperature of $MgAl_2O_4$ formation which can be determined by the high-temperature X-ray diffraction. We also see that the lower the melting point of the fluoride[10] except for point d (BaF_2), the lower the initiation temperature. This seems to be correlated to the strong thermal expansion of the crystalline lattices of LiF and NaF: the thermal vibration of these fluorides lattices is enhanced by the rise in temperature, and the exchange reaction between F^- and O^{-2} on the surface of α-Al_2O_3 and/or MgO particles occurs to form AlF_3. This might influence the surface of α-Al_2O_3 and MgO particles and causes the reaction between MgO and α-Al_2O_3 leading to the formation of $MgAl_2O_4$. The deviation of point d from the straight line (Fig. 10) cannot be explained at present.

The cations of fluoride play an important role in the enhancement of diffusion rate.[1] If the activation enthalpy (Table 2, Ref. 1) can be taken as a relative measure of the ease of the occurrence of reaction, it is expected that the smaller the activation enthalpy, the lower the initiation temperature of the formation of $MgAl_2O_4$. This is satisfied in Fig. 11 except for point c. Accordingly, it can be assumed that the initiation temperature of $MgAl_2O_4$ formation is lowered by the incorporation of Reactions (1), (2) and (3) with the reaction between MgO and α-Al_2O_3.

References

1) S. Shimada, R. Furuichi, and T. Ishii, This Bulletin, **47**, 2026 (1974).
2) The shift at 630 °C calculated by using the coefficient of expansion of LiF, $\alpha=3.4\times10^{-5}/K$[11] turned out to be 0.9°, which is comparable with the observed value.
3) The shift at 650 °C calculated by using $\alpha=3.6\times10^{-5}/K$[11], 1.0 was comparable with the observed value 0.7.
4) Peak 2 (dotted line) was drawn by assuming that it resulted from the reaction of $2AlF_3+3MgO=3MgF_2+Al_2O_3$ (Table 1).
5) A. F. Wells, "Structural Inorganic Chemistry," Oxford (1962), p. 360.
6) G. Gruve and H. Henne, *Z. Electrochem.*, **36**, 129 (1930).
7) Horigoshi Institute, "JANAF Thermochemical Tables," Vol. 1, 3 (1965).
8) M. Farber and H. L. Petersen, *Trans. Faraday Soc.*, **59**, 836 (1963).
9) P. J. Durrant and B. Durrant, "Advanced Inorganic Chemistry," Longman, London (1970), p. 570.
10) G. J. Jang, "Molten Salts Handbook," Academic Press, New York (1967), p. 2.
11) W. A. Wooster, "A Text-book on Crystal Physics," Cambridge (1938), p. 33.

The Thermal Deaquation-Anation Reactions of Aquopentamminechromium(III) Complexes in the Solid State

Kenzo NAGASE and Hiroko YOKOBAYASHI

Department of Chemistry, College of General Education, Tohoku University, Kawauchi, Sendai 980

(Received September 28, 1973)

The thermal deaquation-anation reactions of aquopentamminechromium(III) nitrate, chloride, bromide, and iodide in the solid state were investigated by the techniques of TG, DSC, X-ray powder diffraction analysis, and manometry. The first-order rate constants were obtained by isothermal kinetics. The activation enthalpies calculated from the first-order rate constants increased in the order: the nitrate(24.3) <the chloride(26.4) <the bromide(29.7) <the iodide(30.7 kcal/mol). The enthalpy changes by DSC were 12.3, 6.5, 6.3, and 7.0 kcal/mol for the nitrate, chloride, bromide, and iodide respectively. The slight deviation from the first-order kinetics was observed in cases of the nitrate and the chloride.

Although the deaquation-anation reactions of aquopentamminechromium(III) complexes in the solid state have been widely investigated by several workers, some problems still remain. The deaquation-anation reactions of aquopentamminechromium(III) complexes are, in general, represented by this equation:

$$[Cr(H_2O)(NH_3)_5]X_3 \longrightarrow [CrX(NH_3)_5]X_2 + H_2O$$

where X contains of nitrate, chloride, bromide, and iodide anions. The temperature of the initial weight-loss, which is taken as a measure of the thermal stability of the complex, was given by Wendlandt and Bear[1] as increasing in this order: the chloride <the nitrate <the bromide <the iodide. According to Tsuchiya and his co-workers,[2] though, the order is as follows:

the nitrate <the chloride <the bromide <the iodide

(40°) (60°) (68°) (70°C)

The thermal stabilities of the complexes depend on the variety of outer-sphere anions, and the order given by Tsuchiya *et al.* differs, of course, from that by Wendlandt and Bear.

Wendlandt and Bear[1] were the first to obtain the kinetic data of the deaquation-anation reactions of the aquopentamminechromium(III) complexes. They obtained the first-order rate constants by following the increase in the water vapor-pressure as a function of time at given temperature; the activation energies were thereby calculated to be 16, 18, 31, and 18 kcal/mol for the nitrate, chloride, bromide, and iodide respectively. Tsuchiya and his co-workers[2] also obtained the activation energies of the sulfate and sulfate in addition to those of the four complexes by non-isothermal methods, DTA or DTG curve analyses. The activation energies obtained by two groups of workers are in good agreement with one another except for those of the chloride.

Tsuchiya and his co-workers[2] discussed the mechanisms of the deaquation-anation reactions on the basis of the activation energies obtained and suggested that the bromide, sulfate, and sulfite, which have the larger activation energies, include, to some extent, the tendency of S_N1; this is attributed to the larger ionic radii of the bromide, sulfate, and sulfite anions. Their discussion seems reasonable, but the question remains of why the iodide, which contains the larger iodide anion has the smaller activation energy.

In the present paper, the deaquation-anation reactions of some aquopentamminechromium(III) complexes will be re-examined in order to explain the problems mentioned above.

Experimental

Materials. Aquopentamminechromium(III) nitrate[3] was prepared by the method in the literature and was recrystallized by adding a small amount of concentrated nitric acid to an aqueous solution of $[Cr(H_2O)(NH_3)_5](NO_3)_3$ below 20 °C. The chloride, bromide, and iodide were obtained by adding concentrated hydrochloric, hydrobromic, and hydriodic acid respectively to an aqueous solution of pure $[Cr(H_2O)(NH_3)_5](NO_3)_3$ below 20 °C. In each case, this process was repeated two times. The elemental analyses for N and H agreed with the calculated values within ±0.3%.

Measurements. The TG and DSC curves were simultaneously recorded with a Rigaku 8002 CS apparatus at a heating rate of 3 °C/min in a flowing-nitrogen atmosphere of 50 ml/min. Twenty milligrams of the powdered sample were placed in a crucible made from an aluminum sheet 0.1 mm thick. A lid of the same material rested inside the crucible. α-Alumina was used as the reference material. The heats of the deaquation-anation reactions were measured from the areas of the DSC curves. The instrument was calibrated in the sensitivity range of 2 millical/full-scale deflections, from the heat of transition of potassium nitrate, which appears at 128 °C with ΔH(transition) = 12.28 kcal/mol.

The X-ray diffraction patterns were measured with a Toshiba diffractometer ADG 101 equipped with a standard high-temperature sample holder in a vacuum. Copper-$K\alpha$ radiation with a nickel filter was used.

Pressure-time curves were obtained at a constant temperature with the apparatus reported in a previous paper.[4] The temperature of the furnace was kept within ±0.2 °C. The pressure was measured with a mercury manometer and cathetometer reading to 0.01 mm. About twenty milligrams of the sample in a Pyrex crucible were used in each measurement. The final water vapor-pressure became about 4 mmHg for $[Cr(H_2O)(NH_3)_5](NO_3)_3$. The procedure was as follows. A system about 300 ml in volume was previously evacuated for 1 hr by means of a rotary pump in order to remove any adsorbed gases. After the system was purged with N_2 gas, the reaction tube was taken out of a furnace

held at the required temperature. The sample was placed in the reaction tube, and then the reaction tube was again inserted in the furnace, which was immediately evacuated for 3 min. The system was closed by operating two stopcocks, and the change in the pressure with the time was measured.

Results

TG and DSC Studies. The DSC curves of the aquopentamminechromium(III) complexes gave a single endothermic peak in the 60—100 °C temperature region. It was found that a crystalline sample and a less crystalline sample of the nitrate gave different thermal stabilities, while the stability of the bromide and iodide were almost independent of their crystalline states, and that the chloride depended, to some extent, on its crystalline state. The corresponding weight-losses from the TG curves were 5.42(5.27), 5.48(5.27), 6.78(6.88), 4.55 (4.56), and 3.52(3.36%) for the nitrate[I], nitrate[II], chloride, bromide, and iodide respectively. Each calculated value of weight-losses is described in parentheses. The nitrate[I] is a crystalline sample which was prepared by the method described in the Experimental section, while [II] is a less crystalline sample which was prepared by adding a large amount of ethanol, all at once, to a saturated aqueous solution of $[Cr(H_2O)(NH_3)_5](NO_3)_3$. The X-ray diffraction patterns of both nitrates are given in Fig. 1, along with those of the nitrate[I] subjected to heat treatment. The temperatures of the initial weight-loss(t_i) and the enthalpy changes (ΔH) corresponding to the deaquation-anation reactions are summarized in Table 1, along with the data described previously.

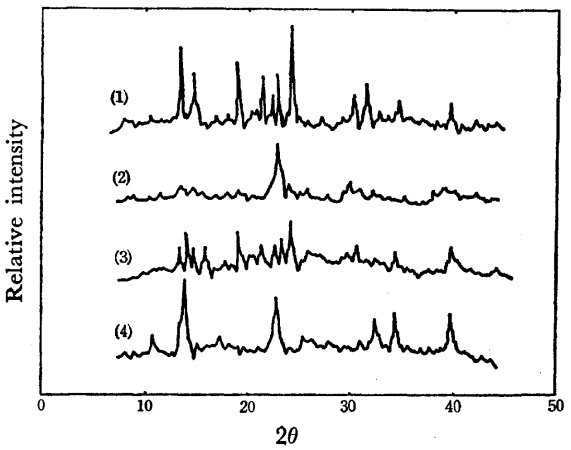

Fig. 1. X-ray diffraction patterns of $[Cr(H_2O)(NH_3)_5](NO_3)_3$ [I](line 1) and [II](2), and of the products after heating the nitrate[I] in a vacuum at 77 °C for 1 hr(3) and 3 hr(4).

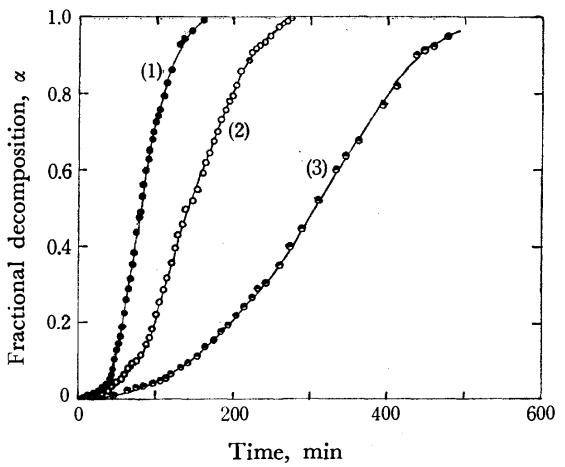

Fig. 2. Kinetic runs of $[Cr(H_2O)(NH_3)_5](NO_3)_3$[I] at (1) 86.5, (2) 81, and (3) 76 °C.

Kinetic Studies. The pressure-time curves of the complexes were obtained at various temperatures. The curves of the nitrate[I] and bromide are given, respectively, in Figs. 2 and 3, as examples, where α means the mol-ratio of liberated water to the complex.

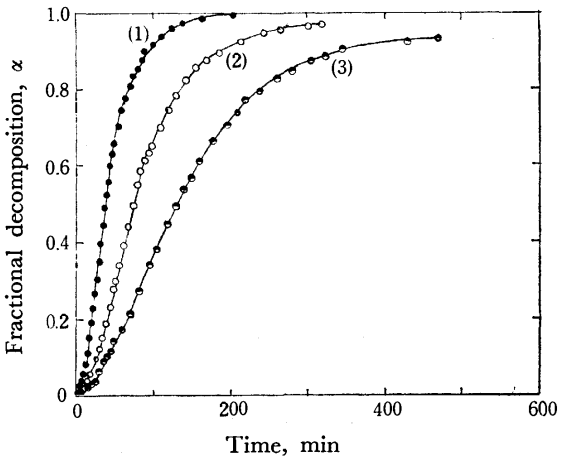

Fig. 3. Kinetic runs of $[Cr(H_2O)(NH_3)_5]Br_3$ at (1) 81, (2) 76, and (3) 70.8 °C.

Table 1. Temperatures of initial weight-loss(t_i) and enthalpy changes(ΔH) for deaquation-anation reactions of $[Cr(H_2O)(NH_3)_5]X_3$ in the solid state

X	t_i, °C		ΔH, kcal/mol		
	This work	Tsuchiya[2]	This work	Wendlandt[1]	Tsuchiya[2]
NO_3[I][a]	75	40	12.3	5.6	11.9
NO_3[II][b]	51		—		
Cl	56	60	6.5	6.1	6.1
Br	76	68	6.3	7.8	9.0
I	83	70	7.0	6.3	10.8

a) The crystalline sample, X-ray diffraction pattern(1) in Fig. 1. b) The less crystalline sample, X-ray diffraction pattern(2) in Fig. 1.

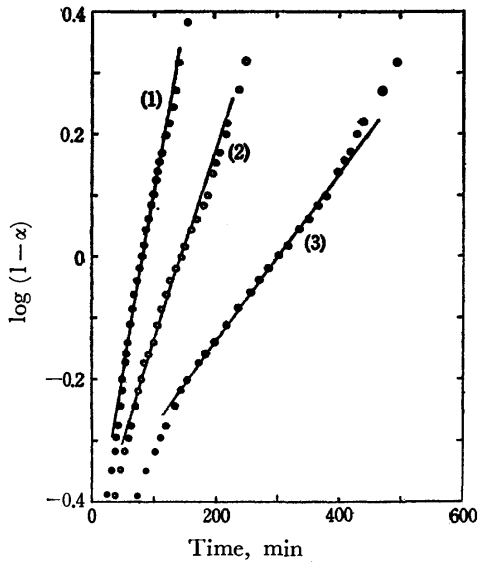

Fig. 4. Plots of log $(1-\alpha)$ *versus* time of $[Cr(H_2O)(NH_3)_5]Br_3$ at (1) 81, (2) 76, and (3) 70.8 °C. The rate constants obtained are a first-order.

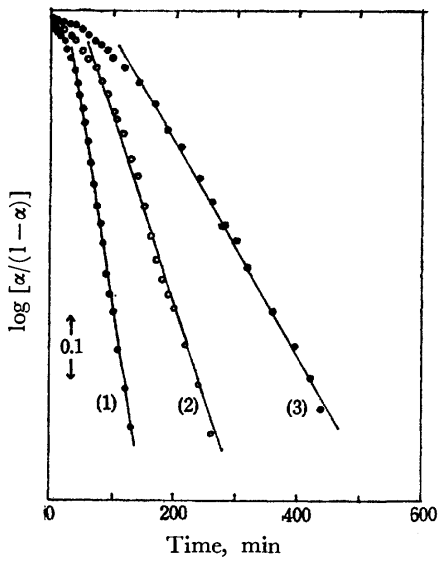

Fig. 5. Plots of log $[\alpha/(1-\alpha)]$ *versus* time of $[Cr(H_2O)(NH_3)_5](NO_3)_3$[I] at 86.5, (2) 81, and (3) 76 °C. The rate constants obtained are a second-order.

All the curves, except for those of the nitrate[I], were analyzed by means of the first-order rate equation: $\ln(1-\alpha)=-kt$. The first-order plots of $[Cr(H_2O)(NH_3)_5]Br_3$ are given in Fig. 4 as examples. The linear relations of $\ln(1-\alpha)$ *versus* the time were maintained in the rang of $0.1<\alpha<0.7$, $0.1<\alpha<0.7$, $0.2<\alpha<0.9$, and $0.2<\alpha<0.9$ for the nitrate[II], chloride, bromide and iodide, respectively. The curves of the nitrate[I] were analyzed by means of the Prout-Tompkins equation.[5] The plots of $\ln[\alpha/(1-\alpha)]$ *versus* the time for the nitrate[I] gave linear relations in the range of $0.1<\alpha<0.8$, as is shown in Fig. 5.

From the rate constants at various temperatures, the activation parameters were calculated. The rate constants(k), activation enthalpies ($\Delta H^{\ddagger}$), and activation entropies ($\Delta S^{\ddagger}$) obtained are presented in Table 2, along with those of the previous works.[1,2]

Discussion

The investigated deaquation-anation reactions of the aquopentamminechromium(III) complexes are essentially initiated by the substitution of an outer-sphere anion for a coordinated water molecule. The nitrate gives different thermal stabilities and shapes of kinetic runs between the crystalline sample and the less crystalline one. The former was dehydrated at temperatures higher than 24 °C, and the shape of the kinetic runs was sigmoidal. Since the reaction of the former gave an induction period and could be described by the $d\alpha/dt=k\alpha(1-\alpha)$ equation in the acceleration and decay periods, the reaction may be supposed to proceed through a nucleation and growth mechanism.[5,6] Therefore, the disagreement with the nitrate results reported in the previous works[1,2] may be due to the difference in the crystalline states of the samples used.

The activation enthalpies obtained from the first-order rate constants at various temperatures increased parallel to the increase in the temperatures of the initial weight-loss. The results differ from those of the previous works, as may be seen in Tables 1 and 2. Since the complexes containing larger anions have larger activation enthalpies, the reactions of the complexes investigated may proceed through the displacement mechanism(S_N2).[7] Although the reactions of the nitrate[II] and chloride have negative activation

Table 2. Rate constants(k), activation enthalpies($\Delta H^{\ddagger}$) and activation entropies($\Delta S^{\ddagger}$) for the deaquation-anation reactions of $[Cr(H_2O)(NH_3)_5]X_3$ in the solid state

X	$k\times10^4$, s^{-1} (°C)		$\Delta H^{\ddagger}$, kcal mol^{-1}				$\Delta S^{\ddagger}$, e.u.
	This work	Wendlandt[1]	This work	Wendlandt[1]	Tsuchiya[2] DTG	Tsuchiya[2] DTA	This work
NO_3[I]	1.21(81)[a]	1.86(85.4)	34.5	16	18	14	20.2
NO_3[II]	1.38(55)		24.3(25.1)[b]				−2.49
Cl	2.41(65)	10.0 (85)	26.4	18	28	25	−2.53
Br	2.43(76)	1.86(83.6)	29.7	31	38	36	9.2
I	1.61(82)	3.55(86.2)	32.7	18	—	19	15.4

a) The second-order rate constant, obtained from $kt=\ln[\alpha/(1-\alpha)]$. b) This value was obtained from the change of weight at constant temperature in a nitrogen atmosphere.

entropies, those of the bromide and iodide have positive values. The latter complexes may not form rigid activated complexes because of the larger ionic sizes of the entering outer-sphere anions.

The activation enthalpies obtained for the deaquation-anation reactions of the aquopentamminechromium(III) complexes are smaller than those for the deammonation-anation reactions of hexamminechromium(III) complexes:[7] $[Cr(NH_3)_6]Cl_3$, 30; $[Cr(NH_3)_6]Br_3$, 43; $[Cr(NH_3)_6]I_3$, 49 kcal/mol. This may be due to the smaller bond strength in $Cr-OH_2$ in the former complexes than those in $Cr-NH_3$ in the latter complexes.

It may be noted that, when the enthalpy changes obtained in this work are compared with the previous data, as in Table 1, there is an approximate agreement among them, only with a few exceptions. The data in the previous works were obtained by DTA. The values chloride, bromide, and iodide are similar to each other, while that of the nitrate is larger. This tendency has also been observed for the deaquation-anation reactions of aquopentamminecobalt(III) complexes.[8]

The authors wish to thank Nobuyuki Tanaka, Professor of Tohoku University, for his advice.

References

1) W. W. Wendlandt and J. L. Bear, *J. Inorg. Nucl. Chem.*, **22**, 77 (1965).
2) R. Tsuchiya, Y. Kaji, A. Uehara, and E. Kyuno, This Bulletin, **42**, 1881 (1969).
3) M. Mori, *Nippon Kagaku Zasshi*, **74**, 255 (1953).
4) M. Mori and R. Tsuchiya, This Bulletin, **32**, 467 (1959).
5) E. G. Prout and F. C. Tompkins, *Trans. Faraday Soc.*, **40**, 488 (1944).
6) A. Galway, "Chemistry of Solids," Chapman and Hall Ltd. (1967).
7) K. Nagase and N. Tanaka, This Bulletin, **46**, 2435 (1973).
8) W. W. Wendlandt, G. Dascenzo, and R. H. Gore, *J. Inorg. Nucl. Chem.*, **32**, 3404 (1970).

Studies on the Metal Complexes of Quinoxaline Derivatives. III.[1] Metal Chelates of 2-Quinoxalinecarboxylic Acid and Its *N*-Oxides

Yoshinori KIDANI, Kazuo OHIRA, and Hisashi KOIKE

Faculty of Pharmaceutical Sciences, Nagoya City University, Tanabe-dori, Mizuho-ku, Nagoya 467

(Received December 24, 1973)

Spectrophotometric measurements were carried out for the stability constants of the divalent metal chelates of 2-quinoxalinecarboxylic acid and copper, nickel, cobalt and zinc in a 5% aqueous ethanol solution. Successive stability constants, log K_1, of the copper, nickel, cobalt and zinc chelates were 3.30, 2.87, 2.83 and 2.80, respectively. The metal complexes were difficult to dissolve in water. Copper and cadmium afforded both 1 : 1 and 2 : 1 complexes, while other divalent metals such as nickel, cobalt, manganese, zinc and lead resulted in the 2 : 1 complex formation. From the results of IR and Far-IR spectral analyses it was found that the carboxyl group and the ring nitrogen group appear simultaneously in the chelate formation. Copper complexes of 2-quinoxalinecarboxylic acid 1- and 4-oxides, as well as its 1,4-dioxide were also studied.

Dutt *et al.*[2] attempted the use of 2-quinoxalinecarboxylic acid (2-QxCOOH) as a coprecipitant, since it forms water insoluble metal complexes with various divalent metals, as in the case of quinaldic acid. We reported[3] on the polarographic behavior of quinoxaline derivatives including 2-QxCOOH, and gave hypothesis that among the quinoxaline derivatives studied, the 2-QxCOOH is merged to form structural metal chelate compounds. Syntheses of copper, nickel, cobalt and zinc chelates with 2-QxCOOH were attempted and the stability constants of the metal chelates were determined in a 5% aqueous ethanol solution spectrophotometrically. In order to find the binding site of the metals, cadmium, manganese and lead chelates were also synthesized. Copper complexes of 2-QxCOOH 1- and 4-oxides, and 1,4-dioxide were prepared and examined by IR and Far-IR spectral analyses.

Experimental

Apparatus. Measurements were carried out with a Hitachi EPS-3T spectrophotometer, a Hitachi Model 139 spectrophotometer, a Nihon Bunko IRA-2 infrared spectrophotometer, a Nihon Bunko DS-701G infrared spectrophotometer, a Shimadzu IR 450 infrared spectrophotometer and a Hitachi-Horiba M-5 pH meter.

Reagents. 2-Quinoxalinecarboxylic acid was synthesized according to the method of Maurer and Boettger[4] and its *N*-oxides were prepared by Elina's method.[5] The ligand were recrystallized from EtOH and identified by melting point and elemental analyses. The other reagents used were of reagent grade.

Syntheses of Metal Complexes. Two parts of 0.1 M 2-QxCOOH EtOH solution and one part of a 0.1 M metal acetate aqueous solution were mixed in a 2 : 1 ratio and then heated on a water bath. On being cooled, precipitates were separated and removed and washed first in water and then in hot EtOH. The complexes obtained were dried at 90 °C under reduced pressure, chelates in the ratio 2 : 1 being prepared.

Aqueous solution of metal chloride and 2-QxCOOH EtOH solution were mixed in a 10 : 1 molar ratio, the precipitates deposited were washed with water and dried at 70 °C under reduced pressure. The 1 : 1 chelates of Cu and Cd were thus prepared.

Similarly, a EtOH solution of copper chloride was added to the EtOH solution each of 2-QxCOOH 1-oxide, 4-oxide and 1,4-dioxide in a 2 : 1 molar ratio and then heated. The mixture on being cooled, gave Cu complexes with the ratio 2 : 1. Elemental analyses of the complexes are shown in Table 1.

Measurements of Stability Constants. One ml of the 2.0×10^{-3} M 2-QxCOOH EtOH solution, and 5 ml of aqueous $(2.4-8.0)\times10^{-2}$ M metal chloride solution of Cu, Ni, Co and Zn were mixed together. To this mixture was added a

TABLE 1. ELEMENTAL ANALYSES OF METAL COMPLEXES

Formula	Analyses (%)					
	Calcd			Found		
	C	H	N	C	H	N
$(2\text{-QxCOO})_2Cu\cdot H_2O$	50.53	2.82	13.09	50.72	2.54	12.94
$2\text{-QxCOO}\cdot CuCl\cdot 2H_2O$	36.39	2.40	9.63	36.12	2.67	9.36
$(2\text{-QxCOO})_2Ni\cdot 2H_2O$	49.02	3.19	12.70	48.93	3.35	12.76
$(2\text{-QxCOO})_2Co\cdot 2H_2O$	48.99	3.19	12.70	48.77	3.06	12.79
$(2\text{-QxCOO})_2Zn\cdot 2H_2O$	48.29	3.14	12.51	48.06	2.97	12.41
$(2\text{-QxCOO})_2Cd\cdot 2H_2O$	43.70	2.93	11.28	43.70	2.85	11.32
$2\text{-QxCOO}\cdot CdCl\cdot H_2O$	31.50	2.04	8.07	31.34	2.22	8.01
$(2\text{-QxCOO})_2Mn\cdot 2H_2O$	49.44	3.22	12.81	49.16	3.14	12.60
$(2\text{-QxCOO})_2Pb\cdot H_2O$	37.72	1.93	9.80	37.83	2.11	9.93
$(2\text{-QxCOO 1-oxide})_2Cu\cdot 2H_2O$	45.05	3.36	11.68	45.23	3.39	11.79
$(2\text{-QxCOO 4-oxide})_2Cu$	56.84	3.18	14.73	56.73	3.16	14.88
$(2\text{-QxCOO 1,4-dioxide})_2Cu\cdot 2H_2O$	42.23	3.15	10.95	42.37	3.21	11.06

2 M KCl-HCl buffer of pH 1.40 to make the volume of the sample 20 ml. The absorptions were measured at each wavelength, and the ionic strength of the sample was kept at 0.1 with KCl. The measurements were carried out at 25 °C.

Results and Discussion

Stability Constants of Metal Chelates. A 5% aqueous ethanol solution of 2-QxCOOH shows a maximum absorption at 250 and 319.5 nm. However, the metal chelates have a maximum absorption at about 325 nm. The acid dissociation constant of the carboxylic acid group as measured by potentiometric method reported by Gum and Joullie[6] is 2.875. A spectrophotometric determination of the stability constants of the metal chelates was made according to the method of McConnell and Davidson.[7] When the divalent metal, M^{2+}, reacted with the ligand LH to give complex $L_nM_m^{2m-n}$, the stability constant $K_{m.n}$ is given as follows;

$$mM^{2+} + nLH \rightleftharpoons L_nM_m^{2m-n} + nH^+$$

$$K_{m.n} = \frac{[L_nM_m^{2m-n}][H^+]^n}{[M^{2+}]^m[LH]^n}$$

If the pH is maintained constant, the conditional stability constant, $K'_{m.n}$ is given by

$$K'_{m.n} = \frac{[L_nM_m^{2m-n}]}{[M^{2+}]^m[LH]^n}$$

When the total ligand concentration b remains constant and a total metal concentration a is added in very large excess of b, only one species, namely, the metal complex of $n=1$, can be taken into account, the linear relation falls between $b/(A-A_L)$ and $1/a^m$, where A and A_L are the total and ligand absorbances, respectively.

As an example, a 1 : 1 complex at pH 1.48 shows a straight line when $m=1$, and a curve when $m=2$. (Fig. 1).

Under these conditions, a 1 : 1 complex is usually the dominant form. The conditional stability constant, K', was calculated from the intercept and slope of the straight line, $b/(A-A_L)$ and $1/a$. From the $[H^+]$ and the dissociation constant, the successive stability constants log K_1 were obtained.

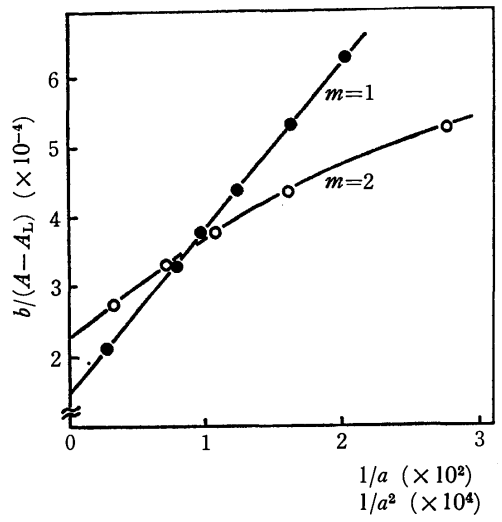

Fig. 1. Relationship between $b/(A-A_L)$ and $1/a^m$ of 2-QxCOOH-Cu complex at pH 1.48 in 5% aqueous EtOH.

The copper complex shows λ_{max} around 750 nm. Stability constants were determined using the method of Suzuki *et al.*[8] Table 2 gives a summary of the results obtained. In the case of the copper complex, the values measured in the ultraviolet region were recorded satisfactorily.

Table 2. Stability constants of 2-QxCOOH-metal chelates

Metal	λ_{max}(nm)	Analytical wavelength (nm)	pH	log K_1
Cu	326	341	1.48	3.29
Cu		748	1.48	3.31
Ni	325.5	342	1.45	2.87
Co	325	342	1.48	2.83
Zn	325	340	1.41	2.80

The values found for the stability constants of nickel, cobalt and zinc were about the same, but the stability constant log K_2 could not be measured, since precipitation takes place when a ligand is added in excess.

IR Spectral Analyses. Measurements of IR spectra (4000—600 cm^{-1}) were made by means of the KBr disk method. The 2-QxCOOH shows two broad bands, one at 2423 and the other at 1875 cm^{-1}. These bands are also observed in a heterocyclic carboxylic acid, such as picolinic acid and pyrazinecarboxylic acid at the same reading. Yoshida and Asai[9] explain that the bands result from the hydrogen bond formation between the ring nitrogen and the carboxyl groups. The two bands of 2-QxCOOH could be explained in the same way, since 2-QxCOOH potassium salt is not found in these hydrogen bonds.

On the other hand, the absorption bands due to the stretching of the carbonyl group appearing at 1740 and 1705 cm^{-1} in dioxane solution shift to 1750 and 1721 cm^{-1}, respectively. The band at a higher frequency is considered to be due to monomeric form without any hydrogen bond, while the other can be attributed to the intramolecular hydrogen bond formation.

Potassium salt of 2-QxCOOH shows asymmetric and symmetric stretching frequencies at 1618 and 1387 cm^{-1}, respectively.

IR Spectra of Metal Complexes. By a detailed examination of IR spectra of metal chelates of the various amino acids Condrate and Nakamoto[10] concluded that the increment of coordination character between the carboxyl group and metals shifts the asymmetric stretching vibration of the carboxyl group toward higher and the symmetric stretching vibration toward lower frequencies, resulting in a wider separation between the two absorption bands. By a similar argument of the metal chelates of picolinic and nicotinic acids, the following order was given among the metals for the increment of coordination charac-

TABLE 3. ASYMMETRIC AND SYMMETRIC ν_{COO} AND ΔE OF 2-QxCOOH METAL COMPLEXES (cm^{-1})

Compounds	$\nu_{asym COO}$	$\nu_{sym COO}$	ΔE
2-QxCOOK	1618	1387	231
$(2\text{-QxCOO})_2Cu\cdot 2H_2O$	1632	1360	272
$(2\text{-QxCOO})_2Ni\cdot 2H_2O$	1630	1363	267
$(2\text{-QxCOO})_2Co\cdot 2H_2O$	1630	1361	269
$(2\text{-QxCOO})_2Zn\cdot 2H_2O$	1626	1364	262
$(2\text{-QxCOO})_2Cd\cdot 2H_2O$	1628	1362	266
$(2\text{-QxCOO})_2Mn\cdot 2H_2O$	1610	1376	234
$(2\text{-QxCOO})_2Pb\cdot H_2O$	1593	1376	217
$2\text{-QxCOO}\cdot CuCl\cdot 2H_2O$	1677	1360	317
$2\text{-QxCOO}\cdot CdCl\cdot H_2O$	1655	1365	290

ters.[11]

$$Cu > Co > Ni > Zn$$

Table 3 shows the asymmetric and symmetric stretching frequencies of the carboxyl group together with the degree of separation (ΔE) between the two bands for the metal complexes of 2-QxCOOH.

As in the case of metal chelates of picolinic acid, ΔE obtained shows the same tendency of coordination character among the metals examined. The copper complex has a stronger coordination bond.

For the sake of comparison, the separation between the asymmetric and symmetric frequencies of the carboxyl group for sodium or potassium salts and copper complexes of acetic,[12] benzoic[13] and picolinic acids[14] is shown together with the dissociation constants of the carboxylic acid and stability constants (log K_1) of the copper chelates in Table 4.

The amount of separation found for copper complexes of picolinic acid and 2-QxCOOH is much greater than that of copper acetate and benzoate, the same tendency being observed for the potassium carboxylates.

The ΔE values obtained increase in the order picolinic, 2-quinoxalinecarboxylic, acetic and benzoic acids, corresponding to the stability constants of these carboxylates. From these ΔE values, we see that copper complex of 2-QxCOOH is more stabilized by the additional bond formation between the ring nitrogen and copper than copper benzoate and acetate, where bond formation is expected only between the carboxyl group and copper.

In spite of the fact that the dissociation constant of 2-QxCOOH is smaller than that of benzoic acid, the stability constants of the former with copper is larger, showing the chelate formation compensate for the gap in the dissociation constants.

The fact that asymmetric stretching of manganese and lead complexes of 2-QxCOOH appears in a lower frequency than that of the corresponding potassium salt leads to the conclusion that in these metal complexes the bond between the metal and carboxyl groups is ionic and the interaction between the metal and ring nitrogen is negligible.

Figure 2 illustrates the spectra of 1 : 1 and 2 : 1 copper complexes.

With regard to the two bands located at 1380 cm^{-1}, the 2 : 1 chelate shows a band of stronger intensity in the higher frequency region, while the 1 : 1 complex shows the reverse tendency. A similar phenomenon was observed for the cadmium chelate.

Far-IR of Metal Chelates. Measurements of Far-IR spectra (600—200 cm^{-1}) were made by means of the nujol mulls method. The metal complexes expected to form a chelate ring cause shortening of the bond

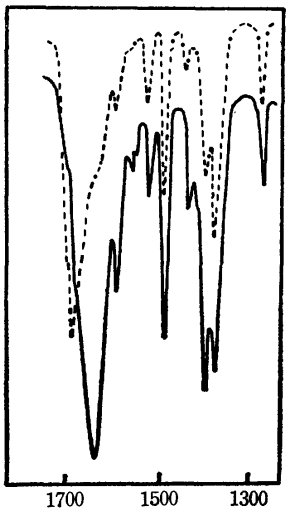

Fig. 2. IR spectra of 2-QxCOOH-Cu complexes.
----: $2\text{-QxCOO}\cdot CuCl\cdot 2H_2O$,
——: $(2\text{-QxCOO})_2Cu\cdot H_2O$

TABLE 4. CARBOXYLATE ASYMMETRIC AND SYMMETRIC STRETCHING FREQUENCIES, DIFFERENCES, pK_a AND COPPER COMPLEX STABILITY CONSTANTS (log K_1)

Compounds	$\nu_{asym COO}$	$\nu_{sym COO}$	ΔE	Ref.	pK_a	log K_1
Acetic acid-Na	1580	1422	158	12)		
-Cu	1590	1418	172	12)	4.55[a]	1.89[a]
Benzoic acid-Na	1555	1416	139	13)		
-Cu	1564	1408	156	13)	4.01[b]	1.6[b]
Picolinic acid-K	1608	1395	213	14)		
-Cu	1639	1350	289	14)	5.44[c]	8.6[c]
2-QxCOOH-K	1618	1387	231			
-Cu	1632	1360	272		2.875	3.30

a, b, c) These pK_a and log K_1 values were quoted from Refs. 15, 16 and 8, respectively.

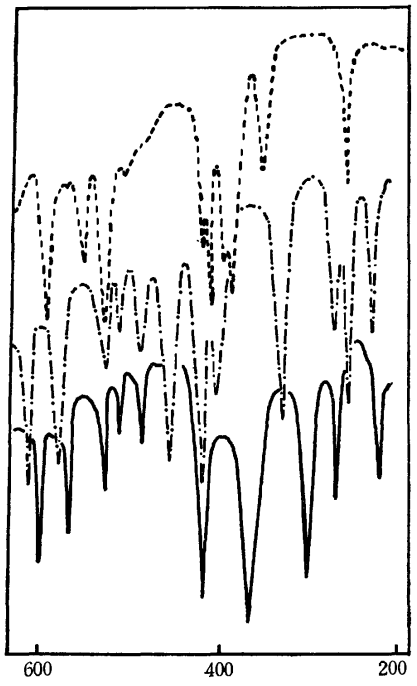

Fig. 3. Far-IR spectra of 2-QxCOOH and its metal complexes.
----: 2-QxCOOH, —·—: $(2\text{-QxCOO})_2Cu\cdot H_2O$,
——: $(2\text{-QxCOO})_2Ni\cdot 2H_2O$.

distance between metal–oxygen and metal–nitrogen to shift the stretching vibration of M–O and M–N toward higher frequencies.

The main peaks of 2-QxCOOH metal chelates are listed in Table 5. Absorption spectra of copper and nickel chelates of 2-QxCOOH are shown in Fig. 3.

According to the work of Taylor *et al.*[17] on lanthanide benzoate, out of and in plane rocking frequencies of carboxylate appear at 516—560 cm^{-1} and 390—425 cm^{-1}, respectively.

2-QxCOOH shows two bands at 546 and 392 cm^{-1} which, on chelation with metals, shift to around 550—580 cm^{-1} and 347—453 cm^{-1}, respectively, which is attributable to the stretching frequencies of metal-oxygen with combination of carboxyl rocking modes. These M–O stretchings take place at higher frequencies in the order Cu>Co>Ni>Zn. This correspond to the coordination character of the carboxyl group, namely, M–O bond in the copper chelate has stronger coordination character than the other metals examined. Billing *et al.*[18] investigated the copper metals of substituted quinoxaline derivatives and concluded that the band at 208—246 cm^{-1} is assigned to the stretching frequencies of M—N. From these values the bands around 326—257 cm^{-1} and 228—200 cm^{-1} are assigned to the M—N stretching. The first bands in particular show marked metal dependence on both absorbance and their shifts.

The 1 : 1 chelate shows a similar pattern of bands to that of the 2 : 1 chelate, indicating that the 1 : 1 chelate can assume a dimeric form including chlorine bridge.

Metal Chelates of 2-QxCOOH N-Oxides. The IR and Far-IR data of 2-QxCOOH *N*-oxides and their metal chelates are summarized in Table 6.

2-QxCOOH 4-oxide shows two broad bands around 2400 and 1900 cm^{-1} indicating hydrogen bond formation between the ring nitrogen and the carboxyl group, while in 2-QxCOOH 1-oxide and its 1,4-dioxide no such bands are observed. The stretching vibration of the carbonyl group shifts to higher frequencies in the order 2-QxCOOH 4-oxide, 1-oxide and 1,4-dioxide (Table 6). The band at 1702 cm^{-1} of 2-QxCOOH 4-oxide splits into two bands at 1722 and 1753 cm^{-1} in dioxane solutions, indicating non-existence of the hydrogen bond formation in 1-oxide and 1,4-dioxide.

The absorption bands of the *N*-oxide groups appeared at 1348—1378 cm^{-1} and those of the 2-QxCOOH 1,4-dioxide appeared in the higher frequency region, as in the case $\nu_{C=O}$.

The copper chelates of these ligands show $\nu_{asymCOO}$ at 1646—1667 cm^{-1}, ν_{symCOO} at 1368—1388 cm^{-1}

Table 5. Characteristic frequencies of 2-QxCOOH-metal complexes (cm^{-1})

2 : 1 Complexes							1 : 1 Complexes		Assignments
Cu	Ni	Co	Zn	Cd	Mn	Pb	Cu	Cd	
580	564	567	558	559	558	550	575	560	ν_{M-O}
453	366	382	357	355	359	347	432	351	
326	298	286	264	261	265	257	315	267	ν_{M-N}
228	221	214	205	207	202	205	211	200	

Table 6. Characteristic frequencies of 2-QxCOOH *N*-oxides and its copper complexes (cm^{-1})

2-QxCOOH 1-oxide		2-QxCOOH 4-oxide		2-QxCOOH 1,4-dioxide		Assignments
Ligand	Complex	Ligand	Complex	Ligand	Complex	
1710	1654	1702	1667	1721	1646	$\nu_{asymCOO}$
	1383		1388		1368	ν_{symCOO}
1372	1357	1348	1364	1378	1353	ν_{N-O}
	531		567		542	
	405		417		403	ν_{Cu-O}
	395				350	ν_{Cu-O}
			240			ν_{Cu-N}

and ν_{N-O} at 1353—1364 cm^{-1}. The lower frequency shift of $\nu_{asym COO}$ apparently indicates the bond formation between the carboxyl group and the copper atom. On the other hand, ν_{N-O} of 2-QxCOOH 4-oxide–copper complex shifts to higher frequency and those of 1-oxide and 1,4-dioxide–copper complexes shift to lower frequency.

We previously reported[1] that in Qx 1-oxide–cupric chloride complex the bond formation between copper and the ring nitrogen caused a ν_{N-O} higher frequency shift, and in Qx 1,4-dioxide–cupric chloride complex coordination of copper to the oxygen atom of *N*-oxide group a ν_{N-O} lower frequency shift. The coordination of copper to the ring nitrogen of 2-QxCOOH 4-oxide increases the double bond character of N–O bond to shift ν_{N-O} to a higher frequency. The other copper *N*-oxide complexes, namely, 1-oxide and 1,4-dioxide-copper coordination site of the ligands is the oxygen atom of *N*-oxide group, which causes lower frequency shifts of ν_{N-O}.

The fact that Qx 1,4-dioxide–cupric chloride complex dissociates into its components in aqueous solution[1] but not the 2-QxCOOH *N*-oxide-copper complexes can be explained by the increase in stabilization energy caused by the chelate ring formation in the latter.

Studies on the Far-IR spectra of these complexes were also made. The absorption peaks observed at 531—542 cm^{-1} and 403—407 cm^{-1} are assigned to the ν_{Cu-O} from the behavior of 2-QxCOOH–copper complex. The absorption peaks at 395 and 350 cm^{-1} of 2-QxCOOH 1-oxide and 1,4-dioxide are close to that of Qx 1,4-dioxide–cupric chloride complex at 397 cm^{-1},[1] and assigned to the Cu–O band between copper and the oxygen atom of the *N*-oxide group. The band due to Cu-O with the carboxyl oxygen of 2-QxCOOH 4-oxide copper complex is observed at a higher frequency than that of 1-oxide and 1,4-dioxide copper complexes.

This can be explained to be due to the fact that formation of the five-membered ring nitrogen, carboxyl oxygen and copper is more stable than that of the six-membered ring including oxygen atom of the *N*-oxide group. The same conclusion was also reported by Gupta *et al.*[19] concerning oxine and its *N*-oxide metal complexes.

2-QxCOOH 4-oxide–copper complex gives an absorption peak at 240 cm^{-1}, which is attributed to ν_{Cu-N} from the data of 2-QxCOOH–copper complex. IR and Far-IR analytical data indicate that 2-QxCOOH *N*-oxide–copper complexes forms the chelate ring as in the case of 2-QxCOOH complexes.

References

1) Y. Kidani, K. Ohira, and H. Koike, *Nippon Kagaku Kaishi*, **1974**, 690.
2) N. K. Dutt, G. S. Sanayal, and K. Nag, *Anal. Chim. Acta*, **41**, 331 (1968).
3) Y. Kidani, K. Ohira, and H. Koike, *Yakugaku Zasshi*, **93**, 157 (1973).
4) K. Maurer and B. Boettger, *Ber.*, **71**, 1383 (1938).
5) A. Elina, *Zh. Obshch. Khim.*, **25**, 161 (1955).
6) W. F. Gum and M. M. Joullie, *J. Org. Chem.*, **30**, 3982 (1965).
7) H. McConnell and N. Davidson, *J. Amer. Chem. Soc.*, **72**, 3164 (1950).
8) K. Suzuki, M. Yasuda, and K. Yamasaki, *J. Phys. Chem.*, **61**, 229 (1959).
9) S. Yoshida and M. Asai, *Chem. Pharm. Bull.* (Tokyo), **7**, 162 (1959).
10) R. A. Condrate and K. Nakamoto, *J. Chem. Phys.*, **42**, 2590 (1965).
11) Y. Kidani, M. Noji, and H. Koike, *Yakugaku Zasshi*, **93**, 1269 (1973).
12) Y. Kuroda, *Nippon Kagaku Zasshi*, **82**, 1624 (1961).
13) S. F. Pavkovic, *J. Inorg. Nucl. Chem.*, **33**, 1475 (1971).
14) M. Paris, G. Thomas, and J. C. Merlin, *Bull. Soc. Chim. Fr.*, **1961**, 707.
15) R. S. Kolet and J. E. Powell, *Inorg. Chem.*, **1**, 293 (1962).
16) M. Yasuda, K. Yamasaki, and H. Ohtaki, This Bulletin, **33**, 1067 (1960).
17) M. D. Taylor, C. P. Carter, and C. I. Wynter, *J. Inorg. Nucl. Chem.*, **30**, 1503 (1968).
18) D. E. Billing, A. E. Underhill, D. M. Adams, and D. M. Morris, *J. Chem. Soc. A*, **1966**, 902.
19) R. D. Gupta, G. S. Munku, A. N. Bhat, and B. D. Jain, *Aust. J. Chem.*, **23**, 1387 (1970).

Crystal Structure of Chloro-1-(2-thiazolylazo)-2-naphtholatopalladium(II) Dioxane Solvate

Masayasu KURAHASHI

Chemistry Division, National Research Institute for Metals, Meguro-ku, Tokyo 153

(Received Junuary 29, 1974)

The crystals of chloro-1-(2-thiazolylazo)-2-naphtholatopalladium(II) dioxane solvate, [PdCl(TAN)]·$C_4H_8O_2$, are orthorhombic and of space group Pbcm, with unit cell dimensions: $a=8.44(2)$, $b=30.97(4)$ and $c=6.82(2)$ Å and $Z=4$. The structure was determined by the heavy-atom method and refined by the least-squares procedure to give an R value of 0.097 for 1392 observed reflections. The crystallographic mirror plane normal to the c-axis coincides with the molecular plane of [PdCl(TAN)]. The 1-(2-thiazolylazo)-2-naphtholato group, *i.e.*, TAN, is a terdentate ligand; the phenolic oxygen atom, azo nitrogen atom and thiazole nitrogen atom are coordinated to the palladium atom to form two five-membered chelate rinsgs. The fourth coordination position is occupied by a chlorine atom.

Since Cheng and Bray used 1-(2-pyridylazo)-2-naphthol, "H-PAN", as an analytical reagent for metals in 1955,[1] a number of heterocyclic azo dyes have been prepared, their application to chemical analysis being studied by many researchers. 1-(2-Thiazolylazo)-2-naphthol (abbr. H-TAN) was found to be a useful and frequently used reagent for the spectrophotometric and titrimetric determination of metal ions as well as for their separation by solvent extraction techniques. In view of the lack of information on the structures of the metal chelate of H-TAN, a systematic X-ray investigation has been undertaken. This paper describes the structure of chloro-1-(2-thiazolylazo)-2-naphtholatopalladium(II) dioxane solvate.[2] This complex has been selected because its coordination configuration might be planar and it would differ from the configuration of iron(II)-, cobalt(II)- and nickel(II)-complexes. It is also of interest to see whether or not the thiazole sulfur atom takes part in the chelate ring formation.

Experimental

Green-colored and needle-like crystals were obtained by slow diffusion of aqueous palladium(II) chloride into dioxane solution of H-TAN. The crystal data are given in Table 1. The unit-cell dimensions were determined by oscillation and Weissenberg photographs.

From systematic absences, the space group was found to be Pbc2 or Pbcm, the latter being more probable from the positive result of intensity statistics for centrosymmetry.

TABLE 1. CRYSTAL DATA

$[PdCl(C_{13}H_8N_3OS)]\cdot C_4H_8O_2$
F. W. = 484.2
Orthorhombic
$a = 8.44\pm0.02$ Å
$b = 30.97\pm0.04$ Å
$c = 6.82\pm0.02$ Å
$V = 1783$ Å^3
$Z = 4$
$D_m = 1.8$ g·cm^{-3}
$D_x = 1.80$ g·cm^{-3}
$\mu = 111$ cm^{-1} (for Cu$K\alpha$)
Space group: Pbcm

The three dimensional data of hk(0—5) were collected from the equi-inclination Weissenberg photographs taken with Cu$K\alpha$ radiation. The intensities of reflections were measured visually by comparison with a standard scale, and corrected for the usual Lorentz and polarization factors. No absorption and extinction corrections were applied. The absolute scale of each layer were obtained at a later stage of refinement by correlation with the calculated values.

Structure Determination and Refinement

The positions of the palladium, sulfur, and chlorine atoms were readily deduced from three-dimensional Patterson maps. The Fourier synthesis of electron density phased on the positions of these heavy atoms revealed the location of the remaining atoms of the complex molecule. A difference synthesis was then carried out and 1,4-dioxane molecule was found to be trapped in the lattice. The structure thus obtained was refined by the block-diagonal least-squares method with the use of individual isotropic thermal factors. Unit weight was given to all the observed reflections. At the final stage of refinement, anisotropic temperature factors were introduced for all the non-hydrogen atoms and the R factor was reduced to 0.097 for 1392 non-zero reflections. The atomic scattering factors were taken from International Tables for X-ray Crystallography. The atomic coordinates and anisotropic thermal parameters along with their estimated standard deviations are given in Table 2, and the observed and calculated structure factors in Table 3*.

Description of the Structure and Discussion

The crystal consists of palladium(II)-complex and dioxane molecule. The bond lengths and angles are given in Table 4 together with their standard deviations. The thermal ellipsoids are shown in Fig. 1 with numbering of atoms.

The palladium(II)-complex is exactly planar, having a mirror symmetry fulfilling the requirement of the space group. The configuration around the palladium atom is square-planar. The 1-(2-thiazolylazo)-2-naphtholato group TAN is present as a terdentate

* Table 3 is kept as Document No. 7418 at the Chemical Society of Japan, 1—5, Kanda, Surugadai, Chiyoda-ku, Tokyo.

TABLE 2. ATOMIC PARAMETERS AND THEIR ESTIMATED STANDARD DEVIATIONS[a] ($\times 10^4$)
Temperature factors are of the form: $\exp[-(B_{11}h^2+B_{22}k^2+B_{33}l^2+B_{12}hk+B_{13}hl+B_{23}kl)]$

	x/a	y/b	z/c	B_{11}	B_{22}	B_{33}	B_{12}	B_{13}	B_{23}
Pd	1815(2)	1792(1)	2500(*)	113(2)	12(0)	349(6)	−6(1)	0(*)	0(*)
Cl	364(7)	1160(2)	2500(*)	127(8)	12(1)	461(26)	−12(4)	0(*)	0(*)
S	6974(7)	1663(2)	2500(*)	110(8)	15(1)	430(26)	1(4)	0(*)	0(*)
O(1)	34(22)	2233(5)	2500(*)	95(21)	16(2)	482(68)	−10(12)	0(*)	0(*)
N(1)	3047(24)	2316(6)	2500(*)	84(23)	15(3)	449(81)	−16(13)	0(*)	0(*)
N(2)	4670(27)	2260(7)	2500(*)	122(30)	22(4)	380(81)	−29(18)	0(*)	0(*)
N(3)	3975(23)	1519(6)	2500(*)	129(28)	10(2)	415(78)	17(13)	0(*)	0(*)
C(1)	2337(28)	2706(7)	2500(*)	130(34)	11(3)	414(97)	2(16)	0(*)	0(*)
C(2)	591(27)	2628(7)	2500(*)	172(38)	5(2)	448(98)	−1(14)	0(*)	0(*)
C(3)	−450(33)	3000(9)	2500(*)	113(34)	26(5)	226(82)	−1(21)	0(*)	0(*)
C(4)	184(34)	3378(9)	2500(*)	223(50)	16(4)	247(83)	13(22)	0(*)	0(*)
C(5)	1874(30)	3430(7)	2500(*)	73(26)	18(3)	366(89)	−7(17)	0(*)	0(*)
C(6)	2433(29)	3898(8)	2500(*)	192(42)	11(3)	332(87)	−19(18)	0(*)	0(*)
C(7)	4070(29)	3969(8)	2500(*)	275(56)	10(3)	313(88)	−13(20)	0(*)	0(*)
C(8)	5175(33)	3644(9)	2500(*)	167(42)	29(5)	157(75)	4(25)	0(*)	0(*)
C(9)	4609(28)	3222(8)	2500(*)	202(42)	7(2)	348(84)	−10(17)	0(*)	0(*)
C(10)	2824(31)	3135(8)	2500(*)	291(60)	8(2)	307(88)	−17(19)	0(*)	0(*)
C(11)	5141(27)	1854(7)	2500(*)	207(43)	7(2)	304(80)	−18(16)	0(*)	0(*)
C(12)	6350(36)	1151(9)	2500(*)	177(46)	26(5)	332(98)	53(26)	0(*)	0(*)
C(13)	4676(30)	1120(8)	2500(*)	136(36)	18(4)	292(85)	0(19)	0(*)	0(*)
O(2)	9295(22)	4657(6)	2500(*)	156(29)	16(2)	523(77)	41(14)	0(*)	0(*)
O(3)	6287(23)	5054(6)	2500(*)	180(31)	14(2)	559(83)	0(13)	0(*)	0(*)
C(14)	8371(24)	4641(6)	757(38)	210(33)	19(3)	483(83)	34(16)	−134(91)	−74(25)
C(15)	7252(23)	5043(6)	742(34)	193(33)	21(3)	477(89)	1(16)	114(86)	72(27)

a) Standard deviations are given in parentheses. * Parameter constrained by symmetry requirements.

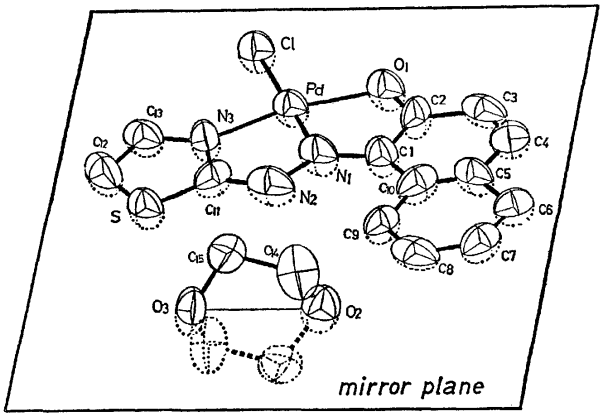

Fig. 1. Perspective drawing of [PdCl(TAN)] and dioxane.
The thermal ellipsoids are drawn at the 50% probability level. The diagram has been produced by the DEAM program.**

ligand; the phenolic oxygen atom, the azo nitrogen atom and the thiazole nitrogen atom are coordinated jointly to the palladium atom to form two five-membered chelate rings. The fourth coordination position is occupied by a chlorine atom. The feature of coordination of TAN to the palladium atom is quite common to those found in iron(II)-,[3] nickel(II)-[2] and copper(II)-TAN[2] chelates, although it is not the case with the configuration around the metal.

The structure of the palladium(II)-TAN chelate bears a close resemblance to that of the 1 : 1 copper(II)-PAN chelate observed in the crystals of $[Cu(PAN)\text{-}H_2O]\cdot ClO_4$.[4] Distances of Pd–Cl(2.31 Å), Pd–O(1) (2.03 Å) and Pd–N(2.01 Å) are all normal, but the central bond in the chelate, Pd–N(1)(1.93 Å), is slightly shorter than the normal Pd–N distance(2.02 Å). Bond angles around the palladium atom, O(1)–Pd–N(1) and N(1)–Pd–N(3), are compressed to 80° and 82°, respectively.

The crystal structure of H-TAN recently has been determined by the present author.[5] There are two crystallographically independent molecules in an asymmetric unit. Both molecules are in concordance with the chemical formula presented in Fig. 2a, although the details of their molecular structures differ from each other. A comparison of the structure of H-TAN with that of TAN in the form of [PdCl(TAN)] (Fig. 2) shows that both of the two ring systems of H-TAN attached to the central azo group are rotated by 180° around the two N–C single bonds in the case of chelate ring formation.

The crystal structure, as projected along the c-axis, is shown in Fig. 3 together with intermolecular distances less than 3.75 Å. Successive [PdCl(TAN)] molecules lie above one another along the c-axis to form columns. The interplanar distance is 3.41 Å. The molecular columns are held together by the van der Waals forces, constructing layers parallel to the (010) plane. Diox-

** A. Takenada, "Schematic Drawing of Crystal and Molecular Structures Containing Atomic Thermal Motions", APPLY 270/23—503—001, Tokyo, Fujitsu Ltd.

Table 4. Bond lengths and angles

Bond lengths (Å)		Bond angles (°)	
Pd-Cl	2.31(1)	Cl-Pd-O(1)	100(1)
Pd-O(1)	2.03(2)	Cl-Pd-N(3)	98(1)
Pd-N(1)	1.93(2)	O(1)-Pd-N(1)	80(1)
Pd-N(3)	2.01(2)	N(1)-Pd-N(3)	82(1)
S-C(11)	1.65(2)	C(11)-S-C(12)	92(1)
S-C(12)	1.68(3)	Pd-O(1)-C(2)	111(1)
O(1)-C(2)	1.31(3)	Pd-N(1)-N(2)	115(2)
N(1)-N(2)	1.39(3)	Pd-N(1)-C(1)	122(2)
N(1)-C(1)	1.34(3)	N(2)-N(1)-C(1)	123(2)
N(2)-C(11)	1.34(3)	N(1)-N(2)-C(11)	114(1)
N(3)-C(11)	1.42(3)	Pd-N(3)-C(11)	109(1)
N(3)-C(13)	1.38(3)	C(11)-N(3)-C(13)	111(2)
C(1)-C(2)	1.49(3)	N(1)-C(1)-C(2)	106(2)
C(1)-C(10)	1.36(4)	N(1)-C(1)-C(10)	137(2)
C(2)-C(3)	1.46(4)	C(2)-C(1)-C(10)	117(2)
C(3)-C(4)	1.32(4)	O(1)-C(2)-C(1)	121(2)
C(4)-C(5)	1.40(4)	O(1)-C(2)-C(3)	120(2)
C(5)-C(6)	1.51(4)	C(1)-C(2)-C(3)	119(2)
C(5)-C(10)	1.26(4)	C(2)-C(3)-C(4)	116(2)
C(6)-C(7)	1.42(4)	C(3)-C(4)-C(5)	122(3)
C(7)-C(8)	1.37(4)	C(4)-C(5)-C(6)	116(2)
C(8)-C(9)	1.41(4)	C(4)-C(5)-C(10)	124(3)
C(9)-C(10)	1.53(4)	C(6)-C(5)-C(10)	121(2)
C(12)-C(13)	1.40(4)	C(5)-C(6)-C(7)	118(2)
O(2)-C(14)	1.41(3)	C(6)-C(7)-C(8)	123(2)
O(3)-C(15)	1.46(3)	C(7)-C(8)-C(9)	117(2)
C(14)-C(15)	1.55(3)	C(8)-C(9)-C(10)	121(2)
		C(1)-C(10)-C(5)	123(2)
		C(1)-C(10)-C(9)	118(2)
		C(5)-C(10)-C(9)	120(2)
		S-C(11)-N(2)	128(2)
		S-C(11)-N(3)	113(2)
		N(2)-C(11)-N(3)	119(2)
		S-C(12)-C(13)	113(2)
		N(3)-C(13)-C(12)	112(2)
		O(2)-C(14)-C(15)	108(2)
		O(3)-C(15)-C(14)	111(2)

ane molecules are located between the layers of the chelate molecules.

Part of the calculation was carried out on the HITAC 5020F computer at the Computer Center of the National Aerospace Laboratory, using PAMI, HBLS-4 and SFR-5 programs in UNICS system.[6] The other calculations were performed on the NEAC 3100 computer at this Institute.

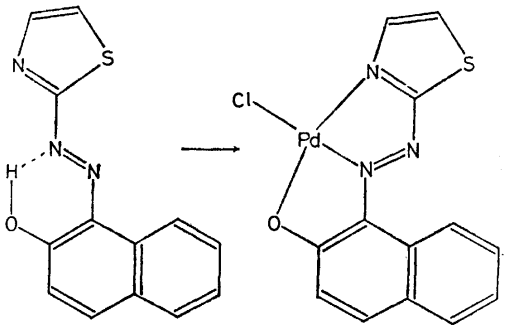

Fig. 2. Structure of [PdCl(TAN)] as compared with that of H-TAN.

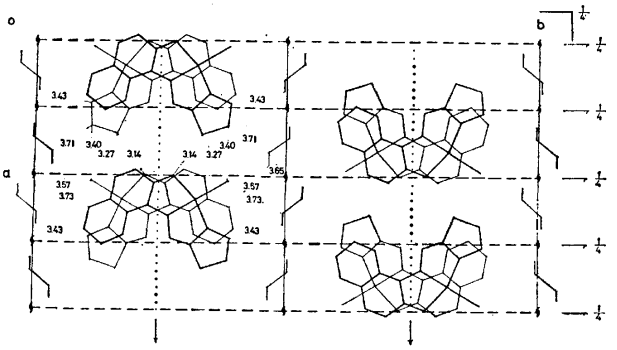

Fig. 3. The crystal structure projected along the *c*-axis.
Heavy lines indicate atoms at $z/c=1/4$, light line ones at $z/c=3/4$.

The author wishes to express his sincere thanks to Dr. A. Kawase for valuable discussions and advice.

References

1) K. L. Cheng and R. H. Bray, *Anal. Chem.*, **27**, 782 (1955).
2) A preliminary note; M. Kurahashi, *Chem. Lett.*, **1974**, 63.
3) M. Kurahashi, A. Kawase, K. Hirotsu, M. Fukuyo, and A. Shimada, This Bulletin, **45**, 1940 (1972).
4) S. Ooi, D. Carter, and Q. Fernando, *Chem. Commun.*, **1967**, 1301.
5) M. Kurahashi, *Chem. Lett.*, **1974**, 181.
6) "The Universal Crystallographic Computing System (I)", Japanese Crystallographic Association (1967).

The Mechanism of the Hydrolysis of Condensed Phosphates. I. The Solvent Effect on the Hydrolysis of Pyro- and Tripolyphosphates

Makoto WATANABE

Department of Industrial Chemistry, Chubu Institute of Technology, Matsumoto-cho, Kasugai-shi, Aichi 487

(Received March 28, 1974)

The hydrolysis of pyro- and tripolyphosphates was run in formic acid–water, acetic acid–water, dioxane–water, and water solvents with an initial concentration of 0.025 mol/l. The hydrolysis of both the phosphates followed first-order kinetics with respect to the concentration of the phosphate under all the conditions studied. The rate of the hydrolysis of both the phosphates in the formic acid–water and acetic acid–water solvents is slower, and that in dioxane–water solvent is faster, than in water. From the results, it has been concluded that, in the formic acid–water and acetic acid–water solvents, the nucleophilicity of the water molecule may decrease on account of the hydrogen bond of the water molecule with these acids, while, in the dioxane–water solvent, since the scission of the hydrogen bond between water molecules may occur by the interaction of the dioxane and the water molecules, the nucleophilicity of the water molecule may increase. The activation energy of the hydrolysis of the phosphates was 19—28 kcal/mol and increased with an increase in the pH value of a solution. The hydrolysis of pyro- and tripolyphosphates has been concluded to be a S_N2 reaction; the rate-determining step may be the nucleophilic attack of a water molecule on the phosphorus atom of the phosphates.

Many papers concerning the hydrolysis of condensed phosphates have been published during the last hundred years. The previous works on the hydrolysis of condensed phosphates have, however, been done chiefly for the purpose of determining the rate constant at a constant pH and of examing the effect of cations on the hydrolysis, rather than for studying the exact interaction of phosphates with the water molecule. It is well known that the hydrolysis of condensed phosphate in a several percent aqueous solution exhibits first-order kinetics with respect to the concentration of phosphate. The effect of the pyrophosphate concentration on the linearity of the rate plot was examined by Campbell and Kilpatrick.[1] In the present paper, the kinetics of the hydrolysis of pyro- and tripolyphosphates will be studied from the viewpoint of the nucleophilicity of a water molecule.

Experimental

Materials and Procedure. All the materials used other than the sodium tripolyphosphate were of a commercial grade. The sodium tripolyphosphate, I, was made by the method described in Reference[2] and was purified by recrystallization. The solvents employed in this experiment are listed in Table 1. When the solvent was water or aqueous dioxane, the pH of the solution was controlled with nitric acid and aqueous tetramethyl ammonium hydroxide by using a Hitachi-Horiba pH meter, F-5. The initial concentration of sodium pyro- and tripolyphosphate was 0.025 mol/l. About 25 ml of the solution was transferred to a test tube, and the tube was stoppered to prevent evaporation of the solvent. The test tube was then placed in water in a thermostat and the temperature was maintained at 30, 50, or 70±0.05 °C. A measured sample of the solution was withdrawn after the temperature of the solution in the test tube had reached the required temperature by using a microsyringe and spotted on to chromatograms. At measured intervals of time, further samples were similarly taken for quantitative chromatographic analysis. The pH of the solution was periodically measured. In the case of the formic acid–water and acetic acid–water solvents, the pH of the solution of the phosphates was not changed at any time, while in the case of the water and dioxane–water solvents, the pH of the solution was changed. Therefore, if they were in need of adjustment, enough tetramethyl ammonium hydroxide or nitric acid was added to bring them back to the proper pH. The pH adjustment was made within ±0.05 pH unit of the required value.

Table 1. Solvents used for the hydrolysis of pyro- and tripolyphosphates

Solvent	Symbol
35 vol% aqueous dioxane	S_1
25 vol% aqueous dioxane	S_2
15 vol% aqueous dioxane	S_3
Water	S_4
Formic acid–water	S_5
Acetic acid–water	S_6

Chromatography. One-dimensional paper-chromatographic separations were carried out by using filter paper of Toyo No. 51A of 2×50 cm. Samples of the phosphate solution (10 μl) were placed at the starting point of the filter paper and developed at 5 °C for 50 hr by using an acidic solvent; then the chromatograms were dried in an oven at 75 °C for more than 30 min. The acidic solvent was made by mixing 70 ml of isopropyl alcohol, 20 ml of 25% aqueous trichloroacetic acid, 10 ml of water, and 0.3 ml of 28% aqueous ammonia. The papers were then sprayed with a perchloric acid–molybdate solution, which had been made by mixing 200 ml of 5% aqueous ammonium molybdate, 10 ml of conc. hydrochloric acid, and 50 ml of 70% aqueous perchloric acid, and by then diluting the solution to 1000 ml with water. The paper was subsequently dried for about 10 min at 50 °C and exposed to ultraviolet rays until blue zones appeared.

Quantitative Analysis of Phosphates on Chromatograms. Every individual spot on the chromatogram was cut at the demarcation line and transferred to a 100-ml beaker. Ten milliliters of a 0.1 M-ammonium hydroxide solution were then added to the beaker. After one hr, the solution was transferred to a 25-ml volumetric flask together with 10 ml of wash water, and a 2-ml portion of Lucena-Conde and Prat's reagent[3] was added to the flask. The flask was heated in a boiling-water bath for one hr, subsequently cooled by placing it in a bath of cold water, and diluted to the mark with water. The absorbance of the blue solution was measured with a Hitachi 101 spectrophotometer at 830 nm. The absorbance of a reagent blank was deducted from each of the readings to give a net absorbance for each

phosphate fraction. The phosphorus content of each spot was expressed as a portion of the total phosphorus present as follows:

$$P(\%) = \frac{\text{Net absorbance for each fraction}}{\text{Sum of the net absorbances for each fraction}} \times 100$$

Results and Discussion

Order of Reaction and the pH Dependence of the Reaction Rate. The rate of the hydrolysis of pyro- and tripolyphosphates followed first-order kinetics with respect to the concentration of the phosphate under all the conditions studied. The pH dependences of the rate constant of pyro- and tripolyphosphates are shown in Figs. 1 and 2 respectively. In any solvent, the rate constant of the hydrolysis of pyro- and tripolyphosphates increases with a decrease in the pH of the solution. Therefore, the hydrolysis of the phosphates is an acid-catalyzed reaction, as has already been reported by many investigators.[1,4-9] There is a difference between the rate constants of the hydrolysis of pyro- or tripolyphosphate in different solvents at the same pH value. In a dioxane-water solvent, as the content of dioxane increases the rate constant of pyro- and tripolyphosphates increases at any pH value. On the other hand, in the formic acid- and acetic acid-water solvents the reaction rate is slow in comparison with that in the other solvents at the same pH and the difference in the rate constant between the acid solvent and dioxane–water or water solvent is larger at larger pH values (the concentrations of the formic acid at the pH values of 1.1, 1.9, and 2.5 are about 30, 10, and 3.2% respectively, while those of acetic acid at the pH values of 1.3, 1.9, and 2.5 are about 76, 61, and 30% respectively). This can reasonably be explained in terms of the difference in the nucleophilicity of the water molecule in each solution as follows: since formic acid or acetic acid combines with the water molecule by means of a hydrogen bond, the nucleophilicity of the water molecule for the phosphorus atom of phosphates may decrease, and since dioxane forms a hydrogen bond with the water molecule and since, consequently, the hydrogen bond between water molecules may be broken, the nucleophilicity of the water molecule for the phosphorus atom of phosphates may increase in the dioxane–water solvent. When the nucleophilicity of the water molecule decreases through the hydrogen bond with the acids, the hydrolysis of phosphate may become energetically disadvantageous because of the hydrogen-bond energy, and the approach of the water molecule to the phosphorus atom of phosphate may also be prevented. Accordingly, the activation energy and log A (A; frequency factor) were calculated by means of the Arrhenius plot, and the relation between these values and the reaction process of the hydrolysis of pyro- and tripolyphosphates was considered.

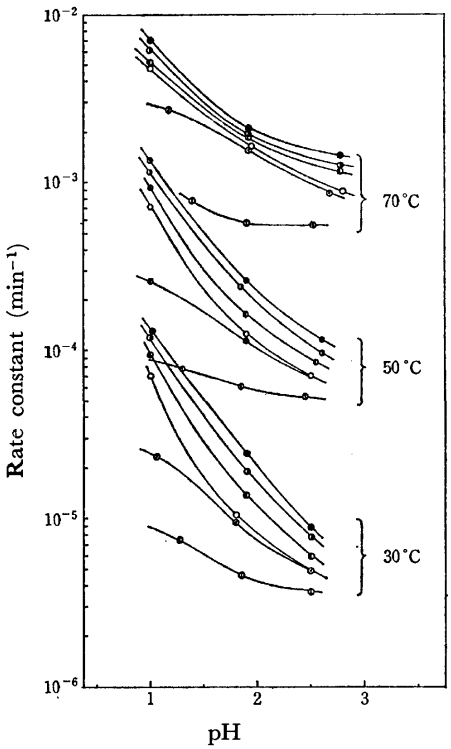

Fig. 1. pH dependence of rate constant of the hydrolysis of pyrophosphate.
●: S_1,[a] ◑: S_2, ◐: S_3, ○: S_4, ⊙: S_5, ⓘ: S_6
a) The symbol refers to Table 1.

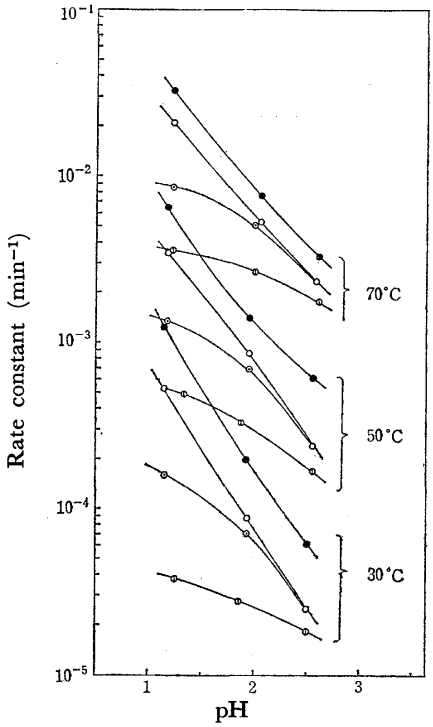

Fig. 2. pH dependence of rate constant of the hydrolysis of tripolyphosphate.
●: S_1,[a] ○: S_4, ⊙: S_5, ⓘ: S_6
a) The symbol refers to Table 1.

Activation Energy and log *A.* The activation energy and log A of the hydrolysis of pyro- and tripolyphosphates are listed in Tables 2 and 3 respectively. In any solvent, the activation energy of both the phosphates increases with an increase in the pH value. This tendency is in accordance with the results obtained by Van Wazer and his co-workers,[6] and the values of activation energy are similar to their results. The activation energy of both the phosphates is smaller in the dioxane–water solvent and larger in the formic

TABLE 2. ACTIVATION ENERGY, ΔE_A(kcal·mol^{-1}) AND log A(A: FREQUENCY FACTOR) OF THE HYDROLYSIS OF SODIUM PYROPHOSPHATE

pH=	1.5		2.0		2.5	
Solvent[a)]	ΔE_A	log A	ΔE_A	log A	ΔE_A	log A
S_1	21.2	11.0	23.8	12.5	26.8	14.3
S_2	22.0	11.5	24.6	12.9	26.8	14.2
S_3	23.9	12.7	26.0	13.8	27.6	14.7
S_4	26.2	14.1	27.3	14.6	28.4	15.1
S_5	26.6	14.3	27.5	14.7	28.4	15.1
S_6	24.6	12.5	24.8	12.5	25.8	13.2

a) Solvents refer to Table 1.

TABLE 3. ACTIVATION ENERGY, ΔE_A(kcal·mol^{-1}) AND log A(A: FREQUENCY FACTOR) OF THE HYDROLYSIS OF SODIUM TRIPHOSPHATE

pH=	1.5		2.0		2.5	
Solvent[a)]	ΔE_A	log A	ΔE_A	log A	ΔE_A	log A
S_1	19.0	10.4	21.0	11.3	22.1	11.8
S_4	20.9	11.4	22.5	12.1	24.5	13.0
S_5	21.3	11.4	22.9	12.3	24.5	13.0
S_6	23.1	12.2	24.0	12.7	24.6	12.9

a) Solvents refer to Table 1.

acid–water solvent than in water. In addition, the difference in the activation energy between water and the other solvents increases as the content of formic acid or dioxane increases. The results could be reduced to the formation or scission of the hydrogen bond of the water molecule with formic acid or dioxane respectively. In the acetic acid–water solvent, the hydrolysis of tripolyphosphate has the same solvent effect as that in the formic acid–water solvent, while the hydrolysis of pyrophosphate differs. The activation energy of the hydrolysis of pyrophosphate in the acetic acid–water solvent is smaller than that in water. Therefore, it can be concluded that the effect of entropy term is larger than that of the energy term for the rate of the hydrolysis of pyrophosphate in the acetic acid–water solvent. The compensation effect is valid between the activation energy and the entropy term under all the conditions studied.

Mechanism of Hydrolysis. According to the above results, the hydrolysis of pyro- and tripolyphosphates may be a dipole-dipole-type S_N2 reaction of the classification of Ingold and Hughes.[10] Since the hydrolysis of pyro- and tripolyphosphates is an acid-catalyzed reaction, the following reaction mechanism can be considered. In an acidic solution, a rapid equilibrium may be set up between the phosphate and hydrogen ion;

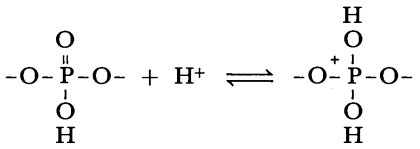

The phosphate ion on the right-hand side of the above equation may more readily accept the nucleophilic attack of the water molecule than the phosphate on the left-hand side. The rate-determining step of this reaction may be this next reaction;

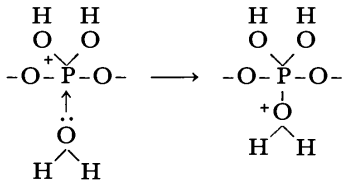

Thus, in an acidic solution, a rapider rate process of the hydrolysis of the phosphate may be given. The first-order kinetics of the hydrolysis of pyro- and tripolyphosphates with respect to the concentration of the phosphates can be reduced to the constancy of the activity of the water molecule because of the dilute nature of the concentration of the phosphates.

References

1) D. O. Campbell and M. L. Kilpatrick, *J. Amer. Chem. Soc.*, **76**, 893 (1954).
2) L. F. Audrieth, "Inorganic Syntheses," Vol. III, McGraw-Hill, New York (1950), p. 101.
3) F. Lucena-Conde and L. Prat, *Anal. Chim. Acta*, **16**, 473 (1957).
4) S. L. Friess, *J. Amer. Chem. Soc.*, **74**, 4027 (1952).
5) J. P. Crowther and A. E. R. Westman, *Can. J. Chem.*, **32**, 42 (1954).
6) J. R. Van Wazer, E. J. Griffith, and J. F. McCullough, *J. Amer. Chem. Soc.*, **77**, 287 (1955).
7) E. J. Griffith, *Ind. Eng. Chem.*, **51**, 240 (1959).
8) E. Karl-Kroupa, C. F. Callis, and E. Seifter, *ibid.*, **49**, 2061 (1957).
9) J. R. Van Wazer, E. J. Griffith, and J. F. McCullough, *J. Amer. Chem. Soc.*, **74**, 4977 (1952).
10) E. D. Hughes and C. K. Ingold, *J. Chem. Soc.*, **1935**, 244.

Autoxidation of Isobutyraldehyde

Shingo MIYAJIMA,* Takashi INUKAI, Hiroshi HARADA, Ryo YOSHIZAWA, Tadahiro HIRAI, Kazutoshi MATSUNAGA, and Masato HARADA

Research Laboratories, Chisso Corporation, Kamariya, Kanazawa-ku, Yokohama 236

(Received September 22, 1973)

The liquid phase autoxidation of isobutyraldehyde to peroxyisobutyric acid was investigated with ozone as an initiator. The selectivity of the peroxyacid increases with decrease in the amount of aldehyde converted per unit volume of reacting fluid, increase in the ozone feed rate, and decrease in temperature. A few percent of water in solvents increases the selectivity, although too much water brings about a reverse effect. Isopropyl alcohol, acetone, isopropyl formate, propane, propylene, carbon dioxide, and carbon monoxide are observed as by-products besides isobutyric acid. Purified peroxyisobutyric acid (97.2 wt%) was obtained by fractionally distilling the autoxidation product and some of its physical properties were determined. The utility of the peroxyacid as an epoxidizing agent is described.

Isobutyraldehyde is available as a by-product of the *n*-butyraldehyde production by the hydroformylation of propylene. However, little is known about its autoxidation to peroxyisobutyric acid.[1] This paper reports on the autoxidation of isobutyraldehyde in the liquid phase with ozone as an initiator.

Results and Discussion

Variations of the Selectivity of Peroxyisobutyric Acid (II) with Reaction Conditions. The influence of reaction conditions was investigated with a stirred flow reactor using ethyl acetate saturated with water at room temperature as a solvent. The autoxidation of isobutyraldehyde (I) involves the following two stages:

$$\underset{\text{I}}{{}^{i}\text{PrCHO}} + O_2 \rightarrow \underset{\text{II}}{{}^{i}\text{PrCO}_3\text{H}} \text{ (Rate, } R\text{)} \quad (1)$$

$${}^{i}\text{PrCHO} + {}^{i}\text{PrCO}_3\text{H} \rightarrow \underset{\text{IV}}{2\,{}^{i}\text{PrCO}_2\text{H}} \quad (2)$$

Formation of intermediate addition product (III) is known in the reactions of aliphatic saturated aldehydes with peroxyacids.[2-5]

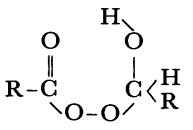

III

The amount of intermediate peroxide III (R=^{i}Pr) was estimated by NMR to be less than 0.05 mol/l. Thus, peroxyisobutyric acid (II) could be approximately estimated by iodometric titration, III being neglected. Isobutyric acid (IV) and unchanged I were determined by glpc after II had been reduced with dimethyl sulfide. The results are shown in Table 1, where

$$\text{Conversion of I} = \frac{\text{I converted (mol)}}{\text{I fed (mol)}} \times 100,$$

$$\text{Selectivity of II} = \frac{\text{II produced (mol)}}{\text{I converted (mol)}} \times 100$$

The variations of the selectivity of II with reaction conditions (conversion, feed concentration of I, ozone feed rate, and temperature) are summarized as follows: the selectivity increases with decreasing conversion of I (Runs 3, 2; 6, 5, 4; 14, 13), decreasing feed concentration of I (Runs 5, 2, 1), increasing ozone feed rate (Runs 9, 12, 3), and decreasing reaction temperature (Runs 14, 1).

White and Bailey[6] suggested that ozone attacks an aromatic aldehyde to form a transient intermediate peroxide, which decomposes to give radicals and initiates autoxidation.

$$\text{RCHO} + O_3 \rightarrow \text{X} \quad (3)$$

$$\text{X} \rightarrow n\text{R}'\cdot \quad (4)$$

Assuming that the initiation of the autoxidation of I occurs according to the above mechanism and the rate of reaction (3) is rapid enough to be represented by the feed rate of ozone (r),[7] we obtain

$$r_i = nr \quad (5)$$

where r_i is the rate of initiation. The general mechanism for autoxidation is

$$\text{R}'\cdot + \text{RCHO} \rightarrow \text{R}'\text{H} + \text{R}\dot{\text{C}}{=}\text{O} \quad (6)$$

$$\text{R}\dot{\text{C}}{=}\text{O} + O_2 \rightarrow \text{R-C}(=\text{O})\text{-O-O}\cdot \quad (7)$$

$$\text{R-C}(=\text{O})\text{-O-O}\cdot + \text{RCHO} \xrightarrow{k_p} \text{R-C}(=\text{O})\text{-OOH} + \text{R}\dot{\text{C}}{=}\text{O} \quad (8)$$

$$2\,\text{R-C}(=\text{O})\text{-O-O}\cdot \xrightarrow{k_t} \text{Non-radical products} \quad (9)$$

and the steady-state approximation leads to

$$\left[\text{R-C}(=\text{O})\text{-O-O}\cdot\right] = \left(\frac{nr}{k_t}\right)^{1/2} \quad (10)$$

Thus, the rate of the formation of II would be

$$\text{d[II]/d}t = R - k_2[\text{I}][\text{II}], \quad (11)$$

$$R = k_p\left[\text{R-C}(=\text{O})\text{-O-O}\cdot\right][\text{I}]$$

$$= k_p\left(\frac{nr}{k_t}\right)^{1/2}[\text{I}] = k_1 r^{1/2}[\text{I}] \quad (12)$$

where the rate of reaction (2) is assumed to obey second-order kinetics (rate constant, k_2).

* Present address: Department of Applied Chemistry, Faculty of Engineering, Toyo University, Kawagoe, Saitama 350.

Table 1. Autoxidation of I in ethyl acetate saturated with water[a)]

Run no.	Feed I		O_2	$O_3\times10^5$	Residence time	Temp.	Product mol/l			Conv. of I	Select. of II
	mol/l	mol/hr	mol/hr	mol/l·s[b)]	s	°C	I	II	IV	%	%
1	1.00	0.177	0.81	4.41	1630	10	0.35	0.59	0.02	65	91
2	2.00	0.306	1.21	6.32	1550	10	0.66	1.12	0.04	67	84
3	2.00	0.218	1.21	5.14	2670	10	0.45	1.26	0.19	78	81
4	3.00	0.585	1.21	4.90	1570	10	1.25	1.38	0.40	58	79
5	3.00	0.342	0.49	4.93	2240	10	0.95	1.40	0.40	68	68
6	3.00	0.333	1.21	4.96	2720	10	0.82	1.49	0.40	73	68
7	2.02	0.398	0.64	0.37	6010	10	0.58	1.12	0.14	71	78
8	2.03	0.410	0.51	0.94	5870	10	0.51	1.11	0.13	74	73
9	2.10	0.412	0.42	1.25	5400	10	0.47	1.20	0.19	78	74
10	2.00	0.104	0.49	1.58	5370	10	0.43	1.22	0.13	79	78
11	2.01	0.396	0.64	1.78	5650	10	0.38	1.22	0.20	81	75
12	2.00	0.122	0.49	2.01	4920	10	0.44	1.20	0.10	78	77
13	1.00	0.500	1.01	3.78	482	40	0.47	0.43	0.09	53	81
14	1.00	0.260	0.42	4.58	831	40	0.37	0.49	0.10	63	78
15	2.00	0.900	1.22	5.76	768	40	0.91	0.56	0.40	55	51

a) Autoxidation with a stirred flow reactor. b) Moles per unit volume of reacting fluid per unit time.

In the stirred flow reactor, the material balance for I or II at steady-state affords

$$F[\mathrm{I}]_0 = \{R+k_2[\mathrm{I}][\mathrm{II}]\}V + F[\mathrm{I}],$$
$$[\mathrm{I}]_0 - [\mathrm{I}] = \tau\{R+k_2[\mathrm{I}][\mathrm{II}]\} \quad (13)$$
$$0 = \{-R+k_2[\mathrm{I}][\mathrm{II}]\}V + F[\mathrm{II}],$$
$$[\mathrm{II}] = \tau\{R-k_2[\mathrm{I}][\mathrm{II}]\} \quad (14)$$

where $[\mathrm{I}]_0$ is the feed concentration of I, [I] and [II] are the concentrations of I and II in the product, respectively, F is the volumetric flow rate, and τ is the residence time. From Eqs. (13) and (14), we obtain

$$R = \frac{1}{2\tau}\{[\mathrm{I}]_0-[\mathrm{I}]+[\mathrm{II}]\} \quad (15)$$

$$k_2 = \frac{1}{2\tau[\mathrm{I}][\mathrm{II}]}\{[\mathrm{I}]_0-[\mathrm{I}]-[\mathrm{II}]\} \quad (16)$$

R values were estimated from Eq. (15) using the data listed in Table 1. Figures 1 and 2 show the $\log R$ *vs.* log[I]

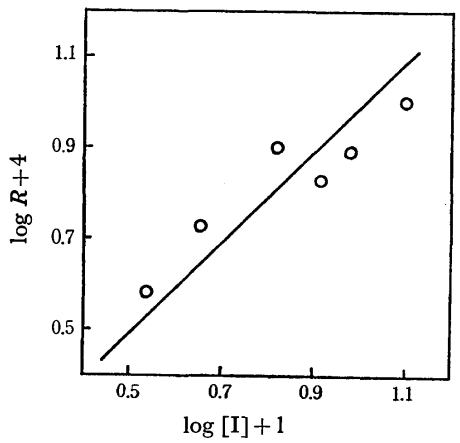

Fig. 1. Plot of $\log R$ *vs.* log [I]. r, $(4-6)\times10^{-5}$ mol/l·s; 10 °C.

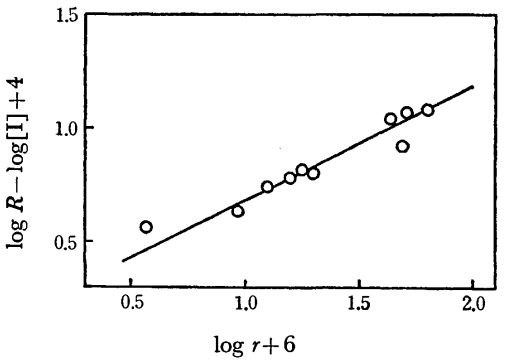

Fig. 2. Plot of $\log R-\log$ [I] *vs.* $\log r$. 10 °C.

Table 2. Rate data of the autoxidation of I in ethyl acetate saturated with water

Run no.	Temp. °C	$R\times10^4$ mol/l·s	$k_1\times10$ [l/mol·s]$^{1/2}$	$k_2\times10^4$ l/mol·s
1	10	3.8	1.6	0.9
2	10	7.9	1.5	1.0
3	10	5.3	1.6	1.0
4	10	10.0	1.1	0.7
5	10	7.7	1.2	1.1
6	10	6.7	1.2	1.0
7	10	2.1	1.9	0.4
8	10	2.2	1.4	0.6
9	10	2.6	1.6	0.7
10	10	2.6	1.5	0.6
11	10	2.5	1.6	0.8
12	10	2.8	1.4	0.7
			Av. 1.5	Av. 0.8
13	40	10.0	3.5	5.1
14	40	6.7	2.7	4.7
15	40	10.7	1.5	6.8
			Av. 2.6	Av. 5.5

(at approximately equal r) and the $\{\log R - \log[I]\}$ *vs.* $\log r$ relationships, respectively. Our data approximately satisfy Eq. (12). Constants k_1 and k_2 were evaluated from Eqs. (12) and (16), respectively, and are listed in Table 2.

Division of Eq. (14) by Eq. (13) and introduction of Eq. (12) give

$$\frac{[II]}{[I]_0-[I]} = \frac{\kappa-[II]}{\kappa+[II]} \tag{17}$$

where

$$\kappa = k_1 r^{1/2}/k_2 \tag{18}$$

Equation (17) expresses the dependence of the amount of II formed on that of I converted at various κ values. Figure 3 illustrates the [II] *vs.* $\{[I]_0-[I]\}$ curves calculated from Eq. (17) using κ values of 12 and 3. At the ozone feed rate of $(4—6)\times10^{-5}$ mol/l·s, the observed values of [II] and $\{[I]_0-[I]\}$ are also plotted in Fig. 3, in which the κ values are approximately 12 and 3 at 10° and 40 °C, respectively. The selectivity of II, defined as $[II]/\{[I]_0-[I]\}$, increases with decreasing $\{[I]_0-[I]\}$ at a constant κ, and with increasing κ at a constant $\{[I]_0-[I]\}$. Since a decrease in the conversion or the feed concentration of I leads to a decrease in $\{[I]_0-[I]\}$ and a lower reaction temperature or a higher feed rate of ozone leads to a larger κ value, all these effects result in an increase in the selectivity of II.

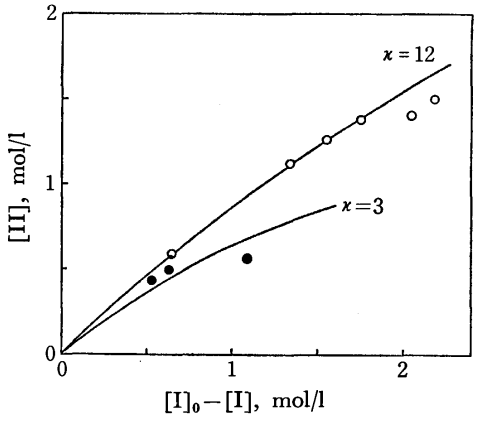

Fig. 3. [II] as a function of $[I]_0-[I]$.
Solid line, calculated from Eq. (17); ○, observed at 10 °C (r, $(4-6)\times10^{-5}$ mol/l·s); ●, observed at 40 °C (r, $(4-6)\times10^{-5}$ mol/l·s).

The values of k_1 and k_2 lack somewhat in constancy. This might be due to the difficulty of analysis and/or an over-simplification of the reaction kinetics. However, the above semi-quantitative treatment explains the results in spite of the complexity of the reaction.

Effect of Water. The effect of water was investigated by batchwise autoxidation. Figure 4 shows the yield of II as a function of water content in the solvent. A few percent of water in acetone increases the yield, although too much water brings about a reverse effect. The autoxidation in ethyl acetate saturated with water at room temperature[8] under similar reaction conditions as above gives II in about a 10% higher yield than that in anhydrous ethyl acetate.

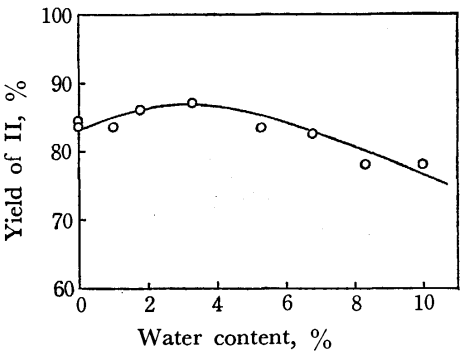

Fig. 4. Effect of water content in solvent on the yield of II.
Batch reactions at 40 °C; solvent, acetone; $[I]_0$, 1.00 mol/l; volume of reacting fluid, 200 ml; O_2, 0.52 l/min; O_3/O_2, 0.22 mmol/l; reaction time, 1.5 hr.

By-products. Besides IV, isopropyl alcohol and acetone were observed in 1—3% yields as by-products. They were identified through appropriate crystalline derivatives. When the autoxidation product was left to stand at 80—90 °C, their amounts of (particularly isopropyl alcohol) increased markedly. A possible pathway for the formation of these by-products is as follows:

$$II \rightarrow {}^{i}Pr\text{-}C(=O)(O\cdot) + \cdot OH \tag{19}$$

$${}^{i}Pr\text{-}C(=O)(O\cdot) \rightarrow {}^{i}Pr\cdot + CO_2 \tag{20}$$

$${}^{i}Pr\cdot + II \rightarrow {}^{i}Pr\text{-}OH + {}^{i}Pr\text{-}C(=O)(O\cdot) \tag{21}$$

$${}^{i}Pr\cdot + O_2 \rightarrow {}^{i}Pr\text{-}O\text{-}O\cdot \tag{22}$$

$${}^{i}Pr\text{-}O\text{-}O\cdot \rightarrow Me_2C{=}O + \cdot OH \tag{23}$$

A peak, the retention time of which agreed with that of isopropyl formate, was detected by glpc. This peak appeared in a comparable amount with that of isopropyl alcohol or acetone in the autoxidation in anhydrous ethyl acetate, but only in a trace amount in ethyl acetate saturated with water. On adding I to the autoxidation product, the intensity of this peak increased. Apparently, this was derived from the Baeyer-Villiger reaction of II with I.[9]

$$I + II \begin{cases} \xrightarrow{2\,IV} \\ \rightarrow IV + H\text{-}C(=O)\text{-}O\text{-}{}^{i}Pr \end{cases} \tag{24}$$

Isopropyl alcohol observed in the autoxidation in ethyl acetate saturated with water may have been partly derived from the hydrolysis of the formate. Carbon dioxide, carbon monoxide, propane, and propylene were detected by glpc in the exit gas. The formation of these by-products could be explained by Eqs. (20), (25), and (26).

$${}^{i}Pr\text{-}\dot{C}{=}O \rightarrow {}^{i}Pr\cdot + CO \tag{25}$$

$$2\,{}^{i}Pr\cdot \rightarrow CH_3CH_2CH_3 + CH_3CH{=}CH_2 \tag{26}$$

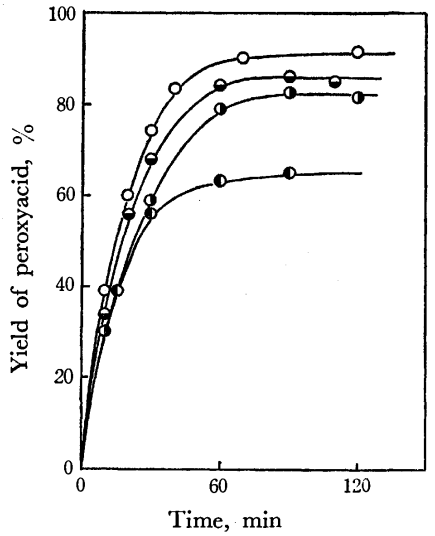

Fig. 5. Autoxidation of aldehydes.
Batch reactions at 40 °C; $[RCHO]_0$, 1.00 mol/l; solvent, ethyl acetate saturated with water (anhydrous ethyl acetate in the case of acetaldehyde); volume of reacting fluid, 200 ml; O_2, 0.52 l/min; O_3/O_2, 0.22 mmol/l; ○, isobutyraldehyde; ◒, *n*-butyraldehyde; ◑, propionaldehyde; ◐, acetaldehyde.

Comparison with Other Aldehydes. The autoxidation of I was compared with that of acetaldehyde,[10] propionaldehyde, and *n*-butyraldehyde. I gives peroxyacid in the highest yield (Fig. 5). This might be a reflection of the electron-donating nature of ^{i}Pr group, which would facilitate reaction (8), in view of preference for the attack of peroxy radicals on carbon-hydrogen bonds with the highest electron density.[11]

The solution of II, thus obtained, can be stored satisfactorily by addition of a small amount of stabilizer such as the sodium salt of a partially esterified polyphosphate.[12]

Epoxidation. The solution of II obtained by batchwise autoxidation was used for the epoxidation of cyclohexene. The rate constants are shown in Table 3 together with those by Frostick *et al.*,[13] who used peroxyacetic acid solution obtained by pyrolyzing α-hydroxyethyl peroxyacetate. Peroxyacid II can be used effectively as an epoxidizing agent.

Physical Properties of Peroxyisobutyric Acid (II). By fractional distillation under reduced pressure II was isolated from the autoxidation product. The purity was determined to be 97.2 wt% by iodometric titration. Some of the physical properties are listed in Table 4.

Table 3. Epoxidation of cyclohexene

Peroxyacid	Solvent	Temp. °C	$k\times10^6$ l/mol·s	$\Delta H^{\ddagger}$ kcal/mol	$-\Delta S^{\ddagger}$ e.u.
Peroxyisobutyric acid	EtOAc[a]	10	102	15.0	23.6
		25	412		
		40	1420		
Peroxyacetic acid[b]	EtOAc	0	20.2		
		15	104	16.9	16.2
		20	172		
		25	283		

a) Saturated with water. b) Ref. 13.

Table 4. Physical properties of II[a]

Bp	41.0 °C/30 mmHg
	(116—117 °C/760 mmHg)[b]
Mp	−30—−28 °C
d_4^{25}	1.049
Latent heat of vaporization	10.7 kcal/mol
	(13—65 mmHg)

a) 97.2 wt%. b) By extrapolation.

Experimental

All boiling points and melting points are uncorrected. NMR spectra were taken with a Varian A-60A spectrometer. Ozone was generated with a Nihon-Ozone 0-3-2 generator. Gas-liquid partition chromatographic data were obtained with a Hitachi K-23 gas chromatograph using helium as a carrier gas. Aldehydes were distilled under nitrogen just before use.

Autoxidation. Batch reactions were carried out in an all-glass cylindrical reactor having an external jacket as well as an internal coil for heat exchange. Oxygen containing ozone entered the reactor through a glass frit in the bottom and was vented through a Dry Ice condenser.

Continuous reactions were carried out in a glass vessel thermostatically controlled at a specified temperature. Under stirring, a solution of isobutyraldehyde was fed to the reactor into which oxygen containing ozone was dispersed through a glass frit in the bottom. The gas stream was vented through a Dry Ice condenser. Samples of the product stream, which overflowed, were chilled at once in a Dry Ice–acetone mixture and immediately subjected to analysis.

Analysis. α-Hydroxyisobutyl Peroxyisobutyrate (III, R=^{i}Pr): NMR spectrum was taken at −46 °C. Peroxide III (R=^{i}Pr) was estimated by comparing the peak area of $-O\diagdown\!\!\diagup O-C\!\!<^{H}$ proton (δ, 4.94) with that of the aromatic protons of mesitylene (δ, 6.75) as an internal standard.

Peroxyisobutyric Acid (II): A 1 ml sample was introduced into a flask containing 2 g of potassium iodide, 45 ml of water, 5 ml of acetic acid, 10 ml of chloroform, and a few pieces of Dry Ice. The liberated iodine was titrated with 0.1 M aqueous sodium thiosulfate solution to a colorless end-point.

Isobutyraldehyde (I) and Isobutyric Acid (IV): Dimethyl sulfide, 1 ml, was added dropwise to a 5 ml sample in a Dry Ice–acetone bath. The mixture was allowed to stand in an ice box for 15 min and analyzed by glpc on a Porapack Q column at 170 °C using benzene as an internal standard. Free IV in the reaction mixture was determined by subtracting II from the total IV found by glpc. Preliminary experiments showed that the reaction of dimethyl sulfide with II to yield dimethyl sulfoxide and IV was quantitative under the above conditions.

Identification of By-products. Glpc analysis (PEG 6000 column, 60 °C) of the autoxidation product, obtained by the ozone-initiated batchwise reaction in anhydrous ethyl acetate ($[I]_0$, 1.0 mol/l; 40 °C), showed three by-product peaks, x_1, x_2, and x_3. The retention times of x_1 and x_3 agreed with those of acetone and isopropyl alcohol, respectively. On decomposing the peroxyacid by heating the autoxidation product at 80—90 °C for 29 hr or by adding a small amount of cobaltic acetylacetonate and heating the mixture at 80—

90 °C for 30 min, the amounts of x_1 and x_3 (particularly x_3) increased markedly, while that of x_2 remained almost unaltered.

The retention time of x_2 agreed with that of isopropyl formate. When 80 ml of the autoxidation product was left to stand for 6.3 hr at 40 °C with 10 ml of I, the amount of x_2 increased by a factor of 4.5.

The autoxidation product, obtained with cobaltic acetylacetonate as an initiator ($[I]_0$, 1.0 mol/l; $[Co(acac)_3]$, 1.0×10^{-5} mol/l; 40 °C), decomposed spontaneously on being left to stand at room temperature. This was fractionally distilled with a 30 cm packed column (271 g).

Fraction	Head temp., °C	Wt., g
1	69.0—70.4	10.6
2	70.4—76.0	45.9
3	76.0—78.0	197.0

Acetone 2,4-dinitrophenylhydrazone (mp 122.5—123.5 °C) and isopropyl 3,5-dinitrobenzoate (mp 110—114 °C) were obtained from fractions 1 and 2, respectively. Mixture melting points with the authentic samples showed no depression.

Kinetic Measurements. To a solution of cyclohexene (210 ml), thermostated at a specified temperature, was added a solution of II (40 ml) stabilized by addition of a small amount of the sodium salt of a partially esterified polyphosphate. Ethyl acetate saturated with water at room temperature was used as a solvent. The initial concentrations of cyclohexene and II were $(2.93—5.85)\times10^{-1}$ and 1.31×10^{-1} mol/l, respectively. The reaction mixture was constantly agitated and the progress of the reaction was determined by analysis of II. The solution of II used in these measurements was prepared by the ozone-initiated batchwise autoxidation of I ($[I]_0$, 1.0 mol/l; 40 °C).

Isolation of Peroxyisobutyric Acid (II). A solution of I in anhydrous ethyl acetate (250 ml, 3.0 mol/l) was autoxidized at 5—16 °C (batchwise; O_2, 72 l/hr; O_3/O_2, 0.29 mmol/l). 2.3 molar solution of II was obtained after 70 min. A portion of this solution was distilled at 150 mmHg to remove most of the solvent, then at 30 mmHg to obtain crude II. This was purified by fractional distillation with a 30 cm packed column; bp 41 °C/30 mmHg. An all-glass apparatus was used, and a small amount of the sodium salt of a partially esterified polyphosphate was added before each distillation. Purified II, the purity of which was determined to be 97.2 wt% by iodometric titration, was stored in a Dry Ice box.

The authors thank Mr. Y. Ooe, Mr. I. Koga, Mr. T. Kakuhashi, and Mr. S. Kanno for their cooperation throughout this work.

References

1) J. Imamura, R. Wakasa, K. Kataoka, K. Kubota, S. Yamaguchi, and T. Saito have recently reported on the manufacturing process of peroxyisobutyric acid by the noncatalytic liquid phase autoxidation of isobutyraldehyde [*Bull. Japan Petrol. Inst.*, **13**, 273 (1971)].

2) P. S. Starcher, B. Phillips, and F. C. Frostick, Jr., *J. Org. Chem.*, **26**, 3568 (1961).

3) J. C. André, J. F. Large, X. Deglise, J. Lemaire, and M. Niclause, *Rev. Inst. Fr. Petrole Ann. Combust. Liquides*, **23**, 219 (1968).

4) T. Inukai and S. Kanno, Abstracts, Symposium on Oxidation Reactions of the Chemical Society of Japan, Osaka, November 1969, p. 8.

5) O. P. Yablonskii, M. G. Vinogradov, R. V. Kereselidze, and G. I. Nikishin, *Izv. Akad. Nauk SSSR, Ser. Khim.*, **1969**, 318; *Chem. Abstr.*, **70**, 114419u (1969).

6) H. M. White and P. S. Bailey, *J. Org. Chem.*, **30**, 3037 (1965).

7) Only a very small proportion of ozone was observed in the exit gas as long as I remained. As an example, in a batch autoxidation of I ($[I]_0$, 1.0 mol/l; volume of reacting fluid, 200 ml; O_2, 0.93 l/min; O_3/O_2, 0.564 mmol/l; 40 °C), the total ozone vented was less than 5% of the one introduced in 70 min until the reaction was virtually completed.

8) Analysis by Karl Fischer's method showed that ethyl acetate saturated with water at room temperature contains 3.1 wt% of water.

9) C. H. Hassall, "Organic Reactions," Vol. 9, ed. by R. Adams *et al.*, J. Wiley, New York, N. Y. (1957), p. 73.

10) Acetaldehyde was the only exception to the general observation that ethyl acetate saturated with water as a solvent gives a higher peroxyacid yield than anhydrous ethyl acetate.

11) J. A. Howard, "Free Radicals," Vol. 2, ed. by J. K. Kochi, J. Wiley, New York, N. Y. (1973), p. 1.

12) B. Phillips, P. S. Starcher, and B. D. Ash, *J. Org. Chem.*, **23**, 1823 (1959).

13) F. C. Frostick, Jr., B. Phillips, and P. S. Starcher, *J. Amer. Chem. Soc.*, **81**, 3350 (1959).

Application of Chemical Reactions on Thin-layer Chromatoplates. IV. Triterpenes

A. M. Osman, M. El-Garby Younes,* and Mrs. F. M. Ata
Department of Chemistry, Faculty of Science, University of Assiut, Assiut, Egypt, A.R.E.
(Received November 21, 1973)

Some specific reactions of triterpenoids had been performed on thin-layer chromatoplates. The reactions conducted were: oxidation with oxygen in K-*t*-butoxide, benzilic acid rearrangement, decarboxylation with lead tetraacetate, Wolff-Kischner reduction, reduction with sodium borohydride, reduction with lithium aluminium hydride, oxidation with chromium trioxide in pyridine and in acetic acid, oxidation with manganese dioxide in chloroform, methylene chloride and isopropyl alcohol, insertion of an oxygen atom in ring A of triterpenoids by the formation of acid anhydride and reduction by a modified Clemmensen method.

Previously,[1] we had carried out some chemical reactions characteristic of triterpenoids on thin-layer chromatoplates. Since we are working mainly on compounds belonging to this group, we decided to do more specific chemical reactions of triterpenes on thin-layer chromatoplates in order to serve in widenning the aspects of the technique and to overcome some difficulties encountered in our work on natural products. Besides the reactions carried out with amino-acids[2] on chromatoplates, also we had perfomed reactions characteristic of the monoterpenes.[3] Really, we found that the application of chemical reactions on chromatoplates solved several problems, particularly in the field of natural products.

Generally speaking, the reaction is carried out by mixing the substance under examination mostly in solution form, with the reactants within the area of a small spot at the starting line of a plate of an inert adsorbent. The mixture of reactants is then subjected to the favourable conditions and suitable length of time to simulate, as far as possible, the normal reaction conditions in the flask. The adsorbed layer is then treated in the normal manner as a chromatographic medium for the resolution of the components of the reaction mixture. Thus, development with a suitable solvent system enables the detection of the formed derivative or comparison with the expected material, spotted at the starting line immediately prior to development. Differentiation of the derivative from the starting material, if any remains, is always possible if the appropriate conditions are used.

Results and Discussion

Reactions involving oxidation of the triterpene ketones with oxygen in potassium *t*-butoxide at room temperature[4] to give the corresponding diosphenol, proceeded with difficulty, and most of the starting material was obtained unreacted (compound **1**, **2**, *cf.* Table 1), while the resulting diosphenol was obtained in a poor yield.

Benzilic acid rearrangement[5] of the diosphenol, was performed on the chromatoplate successfully for all the compounds tried, and the resulting α-hydroxy acids were obtained in a reasonable yield (**3**—**4** *cf.* Table 1).

Reactions of the α-hydroxy acids with lead tetraacetate in acetic acid[6] at room temperature was almost complete and smooth and the A-nor triterpenes were obtained in good yields.

Wolff-Kischner reduction of the triterpene ketones, proceeded under severe conditions and with difficulty, and the reacted materials were obtained in very poor yields, while most of the starting ketone remained unchanged.

Reduction of compounds (**8**—**10**, *cf.* Table 1) with sodium borohydride was performed easily with a good yield, while reduction with a suspension of lithium aluminium hydride in dry ether proceeded with difficulty and was incomplete, even by changing the experimental conditions,[3] for instance prolonging the time of exposure period.

Oxidation of compounds (**13**—**15** in Table 1) with chromium trioxide–pyridine at room temperature overnight was difficult, while oxidation with chromium trioxide–acetic acid at 50 °C for a few minutes proceeded smoothly with a good yield.

Oxidation of the hydroxy triterpenes (**13**—**18**; *cf.* Table 1) with manganese dioxide in different solvents[7] gave interesting reuslts and the yield changes according to the nature of the solvent. Using chloroform as a solvent the yield was poor, while by using methylene dichloride and isopropyl alcohol the oxidation reaction gave a better yield.

The formation of the triterpene anhydride[8] from the secodiacid (**19**; *cf.* Table 1) by heating at 100 °C for 2 hr with acetic anhydride proceeded with difficulty and a poor yield of the desired anhydride was formed, while most of the starting material was obtained unchanged.

Reduction of the keto-groups to methylene groups by a modified Clemmensen procedure[9] was proceeded smoothly under mild conditions using active zinc dust and acetic anhydride saturated with hydrogen chloride gas at 0 °C. The resulting methylene compounds were obtained in good yields (See experimental for compounds **8** and **20** in Table 1).

Conclusion: The results obtained in this study show that the application of chemical reactions of the triterpenoids on chromatoplates can afford reliable informations regarding the "preparation" of known derivatives and determining whether a given reaction can take place, all with the use of only negligible amounts of material.

* To whom inquires should be addressed.

Table 1

No. of compound	Starting material (R_f)	Reaction product (R_f)	Solvent system[a)]
	Oxidation with oxygen in K-*t*-butoxide		
1	Methyl 20(29)-dihydrobetulonate (0.68)	The corresponding diosphenol (0.43)	I
2	Methyl oleanonate (0.82)	Diosphenol (0.32)	I
	Benzilic acid rearrangment		
3	Methyl 2-hydroxy-ketoolean-1,12-dien-28-oate (0.58)	Methyl 2β-hydroxy-2α-carboxy-A-nor-olean-12-en-oate (0.09)	II
4	Methyl 2-hydroxy-3-keto-20(29)-dihydrolup-1-en-28-oate (0.57)	Methyl 2β-hydroxy-2α-carboxy-A-nor-20(29)-dihydrolup-28-oate (0.11)	II
	Decarboxylation with lead tetraacetate		
5	Methyl 2β-hydroxy-2α-carboxy-A-nor-olean-12-en-28-oate (0.09)	Methyl 2-keto-A-nor-olean-12-en-28-oate (0.63)	II
6	Methyl 2β-hydroxy-2α-carboxy-A-nor-20(29)-dihydrolup-28-oate (0.11)	Methyl 2-keto-A-nor-20(29)-dihydrolup-28-oate (0.57)	II
	Wolff-Kischner reduction		
7	Methyl 2-keto-A-nor-olean-12-en-28-oate (0.9)	A-Nor-olean-12-en-28-oic acid (0.64)	III
8	β-Amyrenone (0.18)	β-Amyrene (0.93)	IV
9	Methyl oleanonate (0.51)	Olean-12-en-28-oic acid (0.14)	II
	Reduction with sodium borohydride		
9	Methyl oleanonate (0.51)	Methyl oleanolate (0.27)	I
8	β-Amyrenone (0.94)	β-Amyrin (0.65)	V
10	Betulonic acid (0.92)	Betulinic acid (0.79)	V
	Reduction with lithium aluminium hydride		
11	Uvaol diacetate (0.93)	Uvaol (0.39)	V
12	Methyl 2α,3β-diacetoxy-urs-12-en-28-oate (0.8)	2α-Hydroxy-uvaol (0.3)	V
	Oxiation with CrO_3 and pyridine		
13	Methyl 2α-hydroxy-ursolate (0.3)	Diosphenol (0.8)	V
14	Eburicoic acid (0.17)	Did not react	
15	β-Amyrin (0.62)	β-Amyrenone (0.94)	V
	Oxidation with CrO_3 and acetic acid		
14	Eburicoic acid (0.12)	Corresponing ketone (0.73)	VI
13	Methyl 2α-hydroxy-ursolate (0.3)	Diosphenol (0.8)	V
	Oxidation with MnO_2 in chloroform		
15	β-Amyrin (0.31)	β-Amyrenone (0.61)	II
16	Lupeol (0.26)	Lupenone (0.62)	II
	Oxidation with MnO_2 in methylene dichloride		
17	Methyl oleanolate (0.16)	Methyl oleanonate (0.76)	I
18	Methyl maslinate (0.14)	Diosphenol (0.8)	V
	Oxidation with MnO_2 in isopropyl alcohol		
14	Eburicoic acid (0.16)	Corresponding ketone (0.94)	V
13	Methyl 2α-hydroxy-ursolate (0.3)	Diosphenol (0.8)	V
	Insertion of an oxygen atom in ring A		
19	2,3-Seco-urs-12-en-2,3,28-trioic acid 28-methyl ester (0.68)	The corresponding anhydride (0.96)	VII
	Modified Clemmensen reduction		
20	Euphone (0.41)	Euphadiene (0.95)	VIII
8	β-Amyrenone (0.17)	β-Amyrene (0.96)	IX

a) Solvent system: I:benzene–ether (9: 1), II: benzene, III: light petroleum–benzene (1: 1), IV: light petroleum–benzene (4: 1), V: benzene–ether (4: 1), VI: light petroleum–benzene (1: 4), VII: benzene–ether (1: 1), VIII: light petroleum–benzene (3: 2), IX: light petroleum–benzene (3: 1).

Experimental

Chromatoplates. These were prepared by slurring Kiesel gel G. (Merck) in water (1: 2 by weight) and applying manually onto plates (5×15 cm), followed by heating at 120 °C for 2 hr, then placed in a drying desiccator containing calcium chloride for drying. The development of the plates was done by placing them for 15 min in a tank containing iodine.

Oxidation with Oxygen in K-t-Butoxide. This reaction was performed by treating the ketonic triterpene spot in *t*-butyl-alcohol at the starting line of the chromatoplate with a saturated solution of potassium *t*-butoxide. The plate was then placed in a vacuum desiccator having a saturated atmosphere of *t*-butyl alcohol, the plate was evacuated from air and a stream of oxygen was then passed through for 2 hr. At the end of the reaction, the plate was dried in air prior to development.

Benzilic Acid Rearrangement. This reaction of the diospenols **3** and **4** (*cf.* Table 1) was achieved by treating the diosphenol spot in ethanol at the starting line of a chromatoplate with ethanolic KOH (10%). The plate was placed in a desiccator containing a saturated solution of the reagents and then heated at 70 °C for 5 hr after which the plate was cooled in air before chromatographic development.

Decarboxylation with Lead Tetraacetate. This reaction was performed by treating the α-hydroxy acid spot with a suspension of lead tetraacetate in acetic acid, the spotting of the reagent was continued for 10 min. The plate was placed in a desiccator containing acetic acid and the whole was maintained at 45 °C for 1 hr. After this period the spot was treated with ethylene glycol to destroy the excess of lead tetraacetate. The plate was dried and ready for chromatographic development.

Wolff-Kischner Reduction. This reaction was conducted on thin-layer chromatoplates by treating the triterpene ketonic spot under examination in ethanol with hydrazine hydrate (95%) and ethylene glycol. The plate was placed in a desiccator containing ethyl alcohol and ethyleneglycol, then the whole were heated at 150 °C in an oven for 2 hr, after this period the plate was cooled in air and a concentrated solution of ethanolic potassium hydroxide was applied on the reacting spot and heated again for extra 4 hr. At the end of this period the spot was cooled and acidified with sulfuric acid (1 M) prior to development.

Reduction with Sodium Borohydride. The ketone spot in methanol was treated with a suspension of sodium borohydride in water: methanol (5: 1) and the plate was heated as usual in the desiccator at 55 °C for 2 hr to give mainly the resultant alcohol after development.

Reduction with Lithium Aluminium Hydride. The reduction was performed by treating the ketone spot with a suspension of lithium aluminium hydride in dry ether at room temperature overnight prior to development.

Oxidation with Chromium Trioxide. (A) In Pyridine: The triterpene alcohol spot in pyridine was treated with chromium trioxide in pyridine and the plate was left in a desiccator containing pyridine for overnight. It showed that most of the starting alcohol remained unchanged.

(B) In Acetic Acid: The alcohol spot in acetic acid was treated with a solution of chromium trioxide in acetic acid and the chromatoplate in an atmosphere of acetic acid was heated at 50 °C for 15 min after which it was dried prior to development.

Oxidation with Manganese Dioxide. (A) In Chloroform: This reaction was performed by treating the triterpene alcohol spot n chloroform with manganese dioxide in chloroform and the plate was placed in a desiccator saturated with an atmosphere of chloroform and the whole was left at room temperature overnight after which the plate was dried in air prior to development.

(B) In Methylene Dichloride: The procedure is the same as that mentioned under method (A), except chloroform was replaced by methylene dichloride.

(C) In Isopropyl Alcohol: The reaction was performed as that under method (A), by replacing isopropyl alcohol instead of chloroform.

Formation of Acid Anhydride. The seco-diacid spot was treated with acetic anhydride and the plate was put in a desiccator containing acetic anhydride and the whole was heated at 100 °C for 2 hr, after which the plate was cooled prior to chromatographic development.

A Modified Clemmensen Reduction. This reaction was conducted on a tlc plate by treating the ketonic compound under examination at the starting line with a suspension of active zinc dust[9] in acetic anhydride. The plate was then placed in a vacuum desiccator containing a saturated atmosphere of acetic anhydride and the whole was cooled at 0 °C. Hydrogen chloride was passed into the desiccator until the space inside it became saturated with hydrogen chloride, then the whole system was left for 2 hr at 0 °C. The spot was treated with a solution of sodium carbonate and the plate was dried in air prior to development.

References

1) A. M. Osman, M. El-Garby Younes, and F. M. Ata, *U.A.R. J. Chem.*, **13** (3), 273 (1970).

2) M. El-Garby Younes, M. A. El-Maghraby, and Kh. M. Hassan, A manuscript had been accepted for publication in the 7th. Arab Scientific Conference, Cairo, September (1973) (in press).

3) M. El-Garby Younes and A. Mokhtar, *Z. Anal. Chem.* (West Germany), submitted for publication.

4) D. Lavie, E. Glotter, and Y. Shavo, *Tetrahedron*, **19**, 1377 (1963).

5) R. Hanna and G. Ourisson, *Bull. Soc. Chim. Fr.*, **1961**, 1945.

6) R. Hanna, C. Sandris, and G. Ourisson, *ibid.*, **1959**, (1454).

7) F. Sondheimer, O. Mancera, M. Urquiza, and G. Rosenkranz, *J. Amer. Chem. Soc.*, **77**, 414 (1955).

8) H. P. Stigg and Ch. Tamm, *Helv. Chim. Acta*, **43**, 1402 (1960).

9) M. Toda, M. Hayashi, Y. Hirata, and S. Yamamura, This Bulletin, **45**, 264 (1972).

Furano Compounds. XXII

M. Kanakalingeswara Rao and S. Rajagopal
Department of Chemistry, Regional Engineering College, Warangal, 506004 India
(Received November 21, 1973)

The synthesis of 2′,3′-diphenylfuranobenzoxanthones with the condensed benzene ring at the 5,6; 6,7; and 7,8 positions and with possible antifertility activity is recorded.

The first report on the use of polyphosphoric acid as an effective reagent for the condensation of phenols with benzoin to give 2′,3′-diphenylbenzofurans was made by us earlier.[1] Subsequently employing this method and various 1,3-dihydroxyxanthones in the place of phenols a number of 1-hydroxy-2′,3′-diphenylfurano[4′,5′: 3,4]xanthones carrying alkyl (methyl) substituents in various positions of the free benzenoid ring were synthesised and the results recorded.[2] The synthesis of these compounds was warranted on the basis that they may serve as potential antifertility agents due to the presence of 2,3-diphenylfuran moiety.

The beneficial influence of a naphthaleno nucleus on the antifertility activity is established by the observations of Carney *et al.*[4] on the enhanced activity of 2,3-diphenylnaphthofurans over 2,3-diphenylbenzofurans. This is further corroborated by Chawla *et al.*[3] who have shown that the antifertility activity of 3-(1-pyrrolidinoethoxyphenyl-2-phenyl)naptho[2,1-*b*]furan (A) (as hydrochloride) is ten times that of 2-phenyl-3-pyrrolidinoethoxyphenylbenzofuran (B).

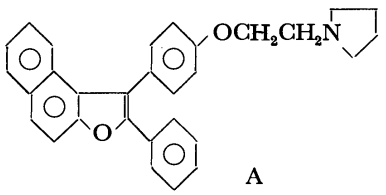

A

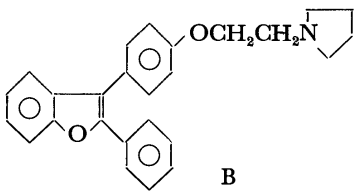

B

Hence the synthesis of various 2′,3′-diphenylfurano-[4′,5′: 3,4]benzoxanthones has been undertaken and the results recorded. Two angular and one linear benzoxanthones *viz.* 1,3-dihydroxy-5,6-benzoxanthone (I), 1,3-dihydroxy-7,8-benzoxanthone (II) as also 2,3-dihydroxy-6,7-benzoxanthone (III) have been used as the starting material. The xanthones (I) and (II) whose syntheses are recorded for the first time have been obtained by condensing phloroglucinol with 1-hydroxy-2-naphthoic acid (IV) in the case of I and 2-hydroxy-1-naphthoic acid (V) in the case of II in the presence of phosphorus oxychloride and zinc chloride (Grover, Shah, and Shah[5]). It may be added that in view of the easy decarboxylation of 2-hydroxy-1-naphthoic acid under the conditions employed for the preparation of xanthone, the reaction had to be carried out at room temperature for a longer period.

The hydroxyxanthones (I, II, and III) are then condensed with benzoin in the presence of polyphosphoric acid at 100—110 °C to yield the desired 2′,3′-diphenylfuranobenzoxanthones (VI—VIII). These compounds will be screened for their antifertility activity in due course.

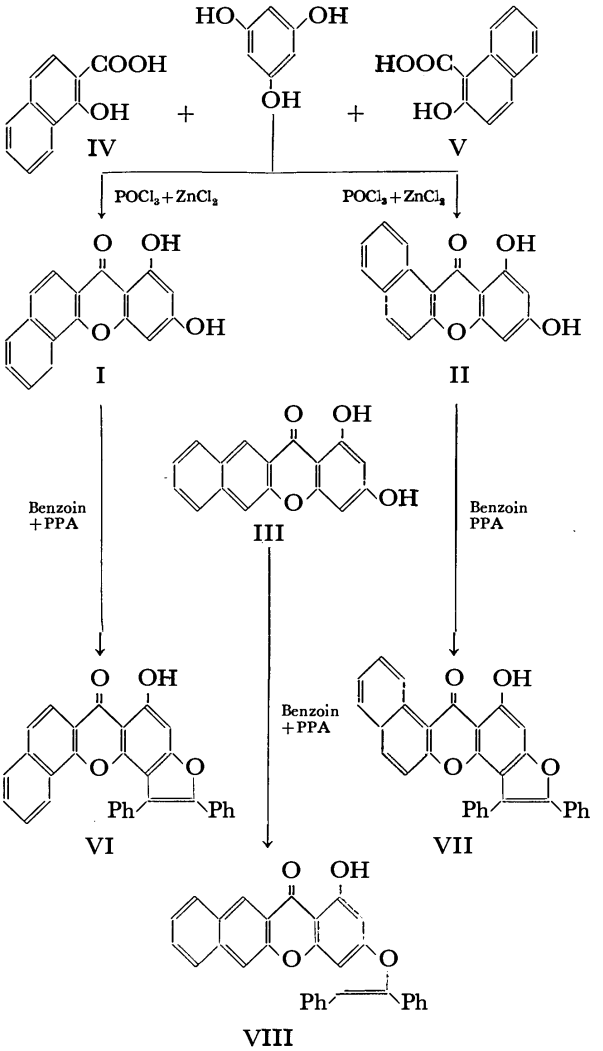

Experimental

IR Spectra were determined on a perkin-Elmer Model 221 spectrophotometer with sodium chloride prisim—in KBr disc.

1,3-Dihydroxy-5,6-Benzoxanthone (I). 1-Hydroxy-2-naphthoic acid (10 g), phloroglucinol (10 g), freshly fused zinc chloride (30 g) and phosphorus oxychloride (70 ml) were heated at 60—70 °C for 2 hr. The separated product was filtered, washed with dilute sodium bicarbonate solution

and with water. The xanthone crystallised from aqueous alcohol as yellow needles, mp 299—300 °C. Yield: 2.8 g. Found: C, 73.8; H, 4.2%. Calcd for $C_{17}H_{10}O_4$: C, 73.3; H, 3.6%. νCO: 1650 cm^{-1}, νOH: 3200 (broad) cm^{-1}.

1-Hydroxy-2',3'-diphenyl-5,6-benzo[4',5':3,4]furanoxanthone (VI). 1,3-Dihydroxy-5,6-benzoxanthone (2 g), benozin (2 g) were mixed and added in small portions to polyphosphoric acid (25 g of P_2O_5 and 12 ml of orthophosphoric acid) at 110 °C for 1 hr. The mixture was heated at 100—110 °C, with constant stirring for 4 hr. It was then cooled and poured into ice-water. The solid that separated was filtered, macerated with 5% aqueous sodium bicarbonate and again filtered. Purification of the crude product by chromatography over silica gel employing petroleum ether as the eluent gave compound (VI) which crystallised from benzene as shining needles, mp 212—213 °C. Yield: 0.06 g. Found: C, 81.5; H, 4.5%. Calcd for $C_{31}H_{18}O_4$: C, 81.9; H, 4.0%. νCO: 1645 cm^{-1}, No free OH absorption.

1,3-Dihydroxy-7,8-benzoxanthone (II). 2-Hydroxy-1-naphthoic acid (8 g), phloroglucinol (8 g) freshly fused zinc chloride (24 g) and phosphorus oxychloride (56 ml) were mixed together and kept at room temperature for 48 hr. The reaction mixture was poured into crushed ice and worked up as usual. The xanthone crystallised from aqueous alcohol as yellow needles, mp 271—272 °C. Yield: 2.5 g. Found: C, 69.6; H, 4.6%. Calcd for $C_{17}H_{10}O_4 \cdot H_2O$: C, 69.2; H, 4.7%. $\nu_{C=O}$: 1650 cm^{-1}. ν_{OH}: 3000, 3100 cm^{-1} (broad).

1-Hydroxy-7,8-benzo-2',3'-diphenyl[4',5':3,4]furanoxanthone (VII). A mixture of 1,3-dihydroxy-7,8-benzoxanthone (3 g), benzoin (3 g) were added to PPA (25 g of P_2O_5 and 14 ml of orthophosphoric acid) at 120 °C during 1 hr with stirring. The reaction mixture was heated for a further period of 5 hr at 100 °C and then poured into crushed ice. The crude substance was purified by chromatography over silicagel. Petroleum ether elution gave (VII) which crystallised from benzene as yellow shining needles, mp 245 °C. Yield: 0.1 g. Found: C, 81.7; H, 4.3%. Calcd for $C_{31}H_{18}O_4$: C, 81.9; H, 4.0%. $\nu_{C=O}$: 1645 cm^{-1}. No free OH absorption.

References

1) M. Kanakalingeswara Rao and S. Rajagopal, *Curr. Sci.*, **41**, 677 (1972).

2) M. Kanakalingeswara Rao and S. Rajagopal, *Ind. J. Chem.*, **11**, 708 (1973).

3) H. P. S. Chawla, P. K. Grover, Nitya Anand, V. P. Kamboj, and A. B. Kar, *J. Med. Chem.*, **13**, 54 (1970).

4) R. W. J. Carney, M. Hill, and W. L. Bencze, U.S. 3340276, 5 Sept. (1967).

5) P. K. Grover, G. D. Shah, and R. C. Shah, *J. Chem. Soc.*, **1955**, 3982.

NOTES

BULLETIN OF THE CHEMICAL SOCIETY OF JAPAN, VOL. 47(8), 2061—2062 (1974)

Substitution Effect in the Hydrogenation of Monoalkylbenzenes with Ruthenium Catalyst

Toshihisa YOSHIDA

Department of Natural Science, Faculty of Education, Saitama University, Shimo-Okubo, Urawa, Saitama 338

(Received November 5, 1973)

Synopsis. The influence of substituents on adsorption coefficients as well as rate constants can be understood from the rules of Horiuti-Polanyi and Taft. It is suggested that a nucleophilic adsorption of alkylbenzene and a nucleophilic surface reaction of the adsorbed alkylbenzene with the metal-hydride occur successively.

Various kinds of linear free energy relationship (LFER), such as the Hammett[1] and the Taft[2] equation, have been given in homogeneous reactions, but only the Horiuti-Polanyi rule[3] has been given in heterogeneous reactions. Recently, Kraus[4] pointed out that the equations of Hammett or Taft could be applied to some heterogeneous reactions over metals. The velocity constants k he used were obtained from experimental rate equations of Langmuir-Hinshelwood type, such as $k\prod_i K_i[A_i]/(1+\sum_j K_j[A_j])$.[5]

The object of the present work is to examine the influence of the substituents on the adsorption coefficients, K_i, as well as on the rate constants, k, in the hydrogenation of monoalkylbenzenes over ruthenium black catalyst.

Experimental

Materials. Alkylbenzenes (purity above 99%, Tokyo Kagaku Seiki Co. Ltd.); Ethanol and other reagents (G.R., Wako Pure Chem. Ind. Ltd.). Ruthenium black was prepared by the reduction of $RuCl_3 \cdot 3H_2O$ (Engelhard Ind. Inc.) with formaldehyde. It was washed 10 times with distilled water and stored in ethanol.

Apparatus and Procedure. The reaction vessel: 50 ml flask with cooler and sampling stopcock. After 4.85 mg of ruthenium black had been admitted into the reaction vessel, a given amount of substrate and solvent (ethanol) was added to make the total volume 20 ml under hydrogen atomosphere. Hydrogenation was carried out under a constant (atomospheric) pressure of hydrogen at 10—30 °C. The rate of hydrogenation was determined by measuring either amounts of absorbed hydrogen by a gas-buret or concentrations of the products by gas-liquid chromatography.

Results and Discussion

The initial rates of the benzene hydrogenation with the same catalyst can be expressed by the following rate equation.[6]

$$-\left(\frac{d[X]}{dt}\right)_0 = \frac{k_X K_X [X] P_H}{1+K_X[X]} \quad (1)$$

where [X] is the concentration of benzene and P_H is the pressure of hydrogen. It has been confirmed that the equation can also be applied to the hydrogenation of monoalkylbenzenes (–CH_3, –C_2H_5, –n-C_3H_7 and –i-C_3H_7). We can obtain respective values of k and K from the equation. For the competitive hydrogenation of monoalkylbenzenes A and B, we get

$$\frac{d[B]}{d[A]} = \frac{k_B K_B [B]}{k_A K_A [A]} \quad (2)$$

or

$$\frac{\log(1-X_B)}{\log(1-X_A)} = \frac{k_B K_B}{k_A K_A} \quad (3)$$

where X_A and X_B are conversions of substrates A and B, respectively. We can obtain respective values of k and K from the hydrogenation of single substrate,

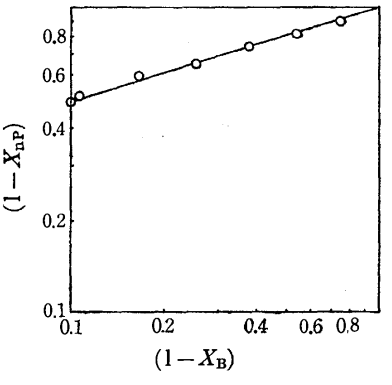

Fig. 1. Competitive hydrogenation between benzene (B) and n-propylbenzene (nP) at 30 °C in ethanol solvent.

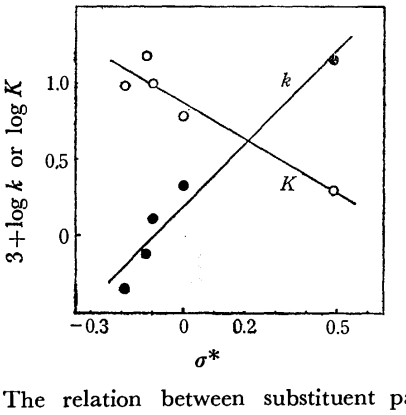

Fig. 2. The relation between substituent parameters (σ^*) and rate constants or adsorption constants at 20 °C in ethanol solvent.

taking the experimental ratios of kK from competitive hydrogenation of two substrates into consideration. The applicability of Eq. (3) in the case of the competitive hydrogenation of benzene and *n*-propylbenzene is shown in Fig. 1 and that of the Taft equation to rate constants k and the adsorption coefficients K in the hydrogenation of alkylbenzenes over ruthenium black in Fig. 2. It should be noted that the slopes of the two lines are opposite each other. That is, the reaction parameter k is positive ($\rho^*=2.05$), while adsorption parameter K is negative ($\rho^*=-1.17$). This can be understood on the basis of the Horiuti-Polanyi rule,[3] provided that the initial state of hydrogenation is the adsorption step of monoalkylbenzenes and that the attack of adsorbed hydrogen as a rate-determining step occurs in succession. The lower the value of σ^*, the higher the electron density in benzene nucleus. Thus, adsorbed alkylbenzene exists stably and surface reaction is retarded.

The negative reaction parameter thus obtained from the Taft plot of adsorption coefficients suggests that a nucleophilic adsorption occurs on the surface of ruthenium, as follows.

$$\text{Adsorption} \quad R + \overset{\delta+}{|}_{M} \longrightarrow R^{\delta+}|_{M} \qquad (4)$$

The positive reaction parameter between k and σ^* obtained suggests that a nucleophilic reaction of the adsorbed alkylbenzene complex with a metal-hydride occurs on the surface:

$$\text{Surface reaction} \quad R^{\delta+}|_{M} + H^{\delta-}|_{M} \rightarrow RH^{\delta-}|_{M} + {}^{\delta+}|_{M} \qquad (5)$$

The mechanism is similar to the nucleophilic type mechanisms proposed for other reactions; the hydrogenation of alkylbenzene over PtO_2[4,7] ($\rho^*=0.842$), the hydrogenolysis of chlorobenzenes over Pd-carbon[5] ($\rho^*=1.77$) and the homogeneous hydrogenolysis of organic halides with sodium bis(2-methoxyethoxy)aluminium hydride[5,8] ($\rho^*=4.0$).

In this experiment, the Taft plot is more favorable than the Hammett one, as was also pointed out by Kraus[4] who did not deal with adsorption coefficients. Recently, Simonikova *et al.*[9] have reported that the adsorption coefficients showed an opposite trend to the rate constants in heterogeneous hydrogenation of aliphatic ketones, in good agreement with out findings.

The author wishes to express his cordial thanks to Prof. Tominaga Keii, Tokyo Institute of Technology, for his advice and discussions.

References

1) L. P. Hammett, *Chem. Rev.*, **17**, 125 (1935); *J. Amer. Chem. Soc.*, **59**, 96 (1937).
2) R. W. Taft, *J. Amer. Chem. Soc.*, **75**, 4231 (1953).
3) J. Horiuti and M. Polanyi, *Acta Physicochim.* USSR., **2**, 505 (1935).
4) M. Kraus, *Advan. Catal.*, **17**, 75 (1967).
5) M. Kraus and V. Bažant, Proc. Intern. Congr. Catalysis 5th, 75—1073 (1972), Miami.
6) T. Yoshida, I. Iwamoto and T. Keii, *Kogyo Kagaku Zasshi* **71**, 1779 (1968).
7) H. A. Smith and E. F. H. Pennekamp, *J. Amer. Chem. Soc.*, **67**, 276 (1945).
8) M. Capka and V. Chavalovsky, *Collect. Czech. Chem. Commun.*, **34**, 2782 (1969).
9) J. Simonikova, A. Ralkova, and K. Kochloefl, *J. Catal.*, **29**, 412 (1973).

BULLETIN OF THE CHEMICAL SOCIETY OF JAPAN, VOL. 47(8), 2063—2064 (1974)

Molten-State Spectra of Anisyl-*p*-Benzoquinones[1)]

Jun-ichi AIHARA

Department of Chemistry, Faculty of Science, Hokkaido University, Sapporo 060

(Received February 7, 1974)

Synopsis. The absorption spectra of three anisyl-*p*-benzoquinones were observed in the molten state. Interestingly, only the *p*-anisyl isomer was found to form a self-complex in the molten state as in the solid state. Possible explanation was presented for this effect.

In the previous paper, we reported on dimorphism of anisyl-*p*-benzoquinones.[2)] These compounds are typical intramolecular charge-transfer compounds, in which the electron-donating anisyl moiety is directly bonded to *p*-benzoquinone with an electron affinity of 1.34 eV.[3)] Among them, *o*- and *p*-anisyl-*p*-benzoquinones were found to crystallize in two forms. Of these two isomers, one form is spectroscopically monomeric and another form exhibits an additional electronic transition on the low-energy side, which is missing in the solution spectrum. Such a transition was considered as due to intermolecular charge-transfer interactions. That is, there is supposedly a finite overlap between the donor orbital of one molecule and the acceptor orbital of the adjacent molecule in the crystal. Only one crystalline form of the *m*-anisyl isomer was monomeric.

In order to extend our understanding of the organic self-complex, we attempted to observe the absorption spectra of these compounds in the molten state. To the best of our knowledge, there have been no investigations of this kind except some visual observation of molten charge-transfer complexes.[4)]

Experimental

The experimental technique concerning spectrophotometry was described earlier.[5)] Instead of the powdered sample, a melt was sandwiched between two quartz plates. The apparent reflectance obtained by this method was quite similar to the transmittance of the sample. The reflectance from the interface between the sample and the quartz plate is negligible. Accordingly, the absorbance of the melt can be derived by applying Beer's law to the apparent reflectance. The relative absorbance was checked by comparing the ordinary solution spectra taken by this method and the transmission spectroscopy. The spectrum thus obtained is excellently reproducible unless the absorbance varies by two or more orders of magnitude within the energy range concerned.

The measurements were made at temperatures about 15 °C above the melting points. Fortunately, the present compounds have relatively low melting points; 64—65, 121 and 126—127 °C for *o*-, *m*- and *p*-anisyl-*p*-benzoquinones, respectively, in the stable form.[2)]

Results and Discussion

Figures 1—3 show the absorption spectra of *o*-, *m*- and *p*-anisyl-*p*-benzoquinones, respectively, in two fluid phases. Every solution spectrum displays an intramolecular charge-transfer band in the visible region. The absorption peaks are located at 25800, 27500 and 23800 cm^{-1} for *o*-, *m*- and *p*-anisyl isomers, respectively, in ethanol. On the other hand, the melts are yellowish, yellowish and red, respectively. The red melt of *p*-anisyl-*p*-benzoquinone is suggestive of the presence of the dimeric species. Actually, such visual observation is supported by the molten-state spectra of these compounds.

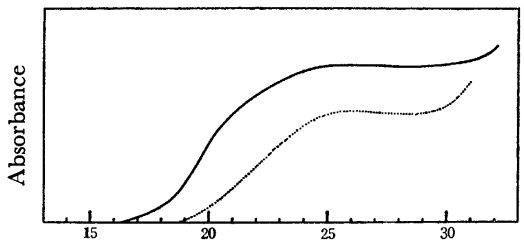

Fig. 1. Absorption spectra of *o*-anisyl-*p*-benzoquinone in ethanol (·····) and in the molten state (——).

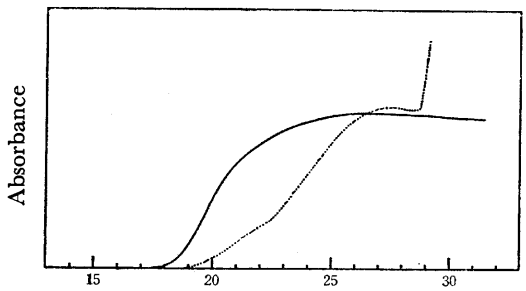

Fig. 2. Absorption spectra of *m*-anisyl-*p*-benzoquinone in ethanol (·····) and in the molten state (——).

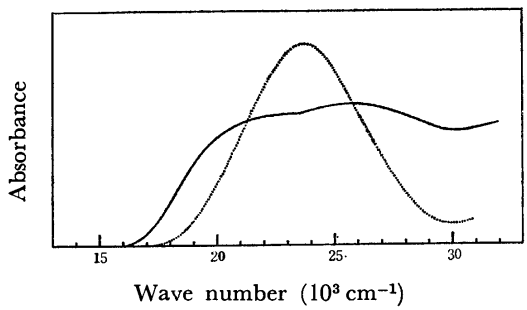

Fig. 3. Absorption spectra of *p*-anisyl-*p*-benzoquinone in ethanol (·····) and in the molten state (——).

The molten-state spectrum of the *o*-anisyl isomer closely resembles that of the *m*-anisyl isomer. The intermolecular interactions in the solid *o*-anisyl-*p*-benzo-

quinone are found to be effectively blocked by the fluidity of the melt. The molten-state spectrum of the *m*-anisyl isomer is a reproduction of the solid-state spectrum. Though these spectra are undoubtedly monomeric, they are somewhat different from the solution spectra in that the low-energy portions are considerably intensified.

In each spectrum, there is a round hump around 21000 cm^{-1}, which is energetically assignable to the n-π^* transition characteristic of the *p*-benzoquinones.[2,6] In the solution spectra of the *o*- and *p*-anisyl isomers, such an n-π^* transition overlaps totally with a more intense intramolecular charge-transfer band. However, the n-π^* transition is partially disclosed in an appropriate region of the solution spectrum of *m*-anisyl-*p*-benzoquinone, since the intramolecular band is much shifted to the higher-energy side for this isomer. The assignment of the hump to the n-π^* transition seems to be thus rationalized.

On the other hand, the absorption spectrum of the molten *p*-anisyl-*p*-benzoquinone is in marked contrast to the solution spectrum. From the viewpoint of the spectral shape, the presence of two different absorption bands is fairly obvious besides the missing n-π^* transition. The absorption peak around 25700 cm^{-1} corresponds well to the intramolecular transition in the solution spectrum. Since each band appears very smooth in the molten state, the break, *i.e.*, the inflection point, near 23500 cm^{-1} difinitely suggests that another absorption band is present on the low-energy side. In analogy with the solid-state spectrum, this band is assigned to the intermolecular charge-transfer transition.[2]

For *p*-anisyl-*p*-benzoquinone, the relative intensities of the intra- and inter-molecular charge-transfer bands are comparable to each other in the molten state as in the dimeric solid. Considering that, if the crystal is dimeric at all, the self-complex formation is attained to 100 percent in it, we might safely say that such a situation is almost preserved in the molten *p*-anisyl-*p*-benzoquinone. The association constant of this self-complex is extimated to be very large in the melt.

As was suggested in the previous paper,[2] the steric effect of the methoxy group might determine the optical behavior of the three anisyl-*p*-benzoquinones in condensed phases. This effect makes the dimer of the *p*-anisyl isomer the most stable of all. However, it is not sufficient to elucidate the monomeric aggregation of the *m*-anisyl isomer which is free from the steric hindrance. As was described above, the absorption peak of the intramolecular charge-transfer transition of the *m*-anisyl isomer is located at the highest energy in solution. This fact may reflect the weak donor ability of the *m*-anisyl isomer.

In summary, the intermolecular interactions of this kind are considered to be very weak, and are not always primary factors in determining the structure of the condensed phase.

References

1) Part II of "Organic Charge-Transfer Self-Complexes": Ref. 2 is hereafter referred to as Part I. This work was financially supported by Fuji Photo Film Co., Ltd.

2) J. Aihara, G. Kushibiki and Y. Matsunaga, This Bulletin, **46**, 3584 (1973).

3) A. L. Farragher and F. M. Page, *Trans. Faraday Soc.*, **62**, 3072 (1966).

4) P. R. Hammond and L. A. Burkardt, *J. Phys. Chem.*, **74**, 639 (1970).

5) G. Saito and Y. Matsunaga, This Bulletin, **44**, 3328 (1971).

6) E. A. Braude, *J. Chem. Soc.*, **1945**, 490.

BULLETIN OF THE CHEMICAL SOCIETY OF JAPAN, VOL. 47(8), 2065—2066 (1974)

The Absorption Spectra of the Electrochemically-generated Unstable Species of Tris(2,2′-bipyridine)cobalt(II) by Reflectivity Measurements at the Silver Electrode in Propylene Carbonate

Yuichi SATO

Toshiba Research and Development Center, Tokyo Shibaura Electric Co., Ltd., Komukai Toshiba-cho, Kawasaki 210

(Received September 3, 1973)

Synopsis. Tris(2,2′-bipyridine)cobalt(II) perchlorate gave a two-step reduction wave ascribed to $[Co(bipy)_3]^{2+} \xrightarrow{e} [Co(bipy)_3]^{+} \xrightarrow{2e} [Co(bipy)_3]^{-}$ at the Ag electrode in a propylene carbonate solution. The simultaneously-recorded reflectivity-potential curve showed a reflectivity decrease corresponding to each wave on the *i-E* curve. The absorption spectra due to the unstable reduction products, $[Co(bipy)_3]^{+}$ and $[Co(bipy)_3]^{-}$, were obtained by plotting the reflectivity change *vs.* the wavelengths.

In a previous paper,[1] we showed that the reflectivity measurement enabled one to obtain the spectra of unstable species generated during electrolysis, and that the method has successfully been used to detect the reduction products of the tris(2,2′-bipyridine)chromium(III) complex.

The present communication will extend the method to support the previous conclusion[2] that lower-valence complexes can be generated by the reduction of tris(2,2′-bipyridine)cobalt(II).

Experimental

The current-potential (*i-E*) and reflectivity-potential (R/R_0-*E*) curves were obtained in propylene carbonate (PC) by the same apparatus and method as were reported in the previous paper.[1] Tris(2,2′-bipyridine)cobalt(II) perchlorate, $[Co(bipy)_3](ClO_4)_2$, was prepared according to the literature.[3]

Results and Discussion

Figure 1 shows the *i-E* and R/R_0-*E* curves simultaneously obtained in a solution containing $[Co(bipy)_3](ClO_4)_2$. This complex gave a two-step reduction wave in the potential range between 0 and −2.0 V and the corresponding anodic wave. Upon the addition of free 2,2′-bipyridine to a solution containing the complex, the peak heights of the first and the second step were not affected; this shows that two steps may be concluded to be due to the reduction of the cobalt(II) complex itself and not to the reduction of the free bipyridine liberated from the complex. The peak potential of the first step is not affected, whereas that of the second one is shifted to more negative potentials with an increase in the concentrations of free bipyridine. This seems to be attributable to the substitution labile nature of the product—*viz.*, a dissociation of the ligand from the reduction product.[2] Such an instability could be avoided by the addition of a large excess of free ligands to the solution.

With the aid of the results obtained in an acetonitrile solution,[2] the first step in the cathodic scan seems to be ascribable to the one-electron reduction of;

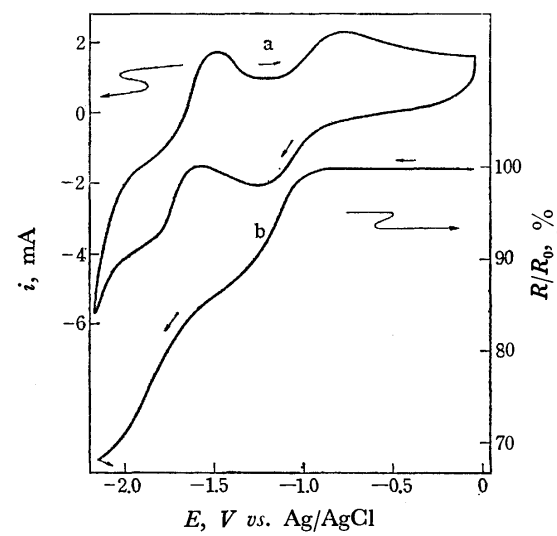

Fig. 1. The *i-E* (a) and R/R_0-*E* (b) curves of 0.5 mM $[Co(bipy)_3](ClO_4)_2$ at silver electrode in the presence of 20 mM 2,2′-bipyridine in 0.05 M $(C_2H_5)_4NClO_4$ of PC solution. Potential sweep rate was 440 mV/s and R/R_0 was measured at 630 nm.

$$[Co(bipy)_3]^{2+} + e \longrightarrow [Co(bipy)_3]^{+} \quad (1)$$

The peak potential difference between the first and the second cathodic peaks in a PC solution is about 0.65 V, nearly equal to the difference between the half-wave potentials of the first and the second reduction waves (0.66 V) obtained in an acetonitrile solution.[2] This fact suggests that the same electrode process as that in an acetonitrile solution occurs in the PC solution in the second process; namely:

$$[Co(bipy)_3]^{+} + 2e \longrightarrow [Co(bipy)_3]^{-} \quad (2)$$

Tanaka and Ogata[4] also pointed out that $[Fe(bipy)_3]^{2+}$ and $[Ni(bipy)_3]^{2+}$ in the PC solution showed almost the same polarographic waves due to the reduction into the low-valence states as those observed in the acetonitrile solution.

The simultaneously-recorded R/R_0-*E* curve is shown in Fig. 1 as Curve (b); only the cathodic process is shown. The correspondence between the *i-E* and R/R_0-*E* curves is very good; *i.e.*, the starting potentials of all the steps on the *i-E* and R/R_0-*E* curves are almost the same, and the first (−1.25 V) and the second peak potentials (−1.90 V) on the *i-E* curve correspond to the potentials where the reflectivity changes most dramatically, implying the formation of the reduced states at these potentials.

The reflectivity decrease is associated with the successive formation of two different types of reduction

products formed at each corresponding potential. The reflectivity decrease at the first wave is considered to be due to the formation of $[Co(bipy)_3]^+$. If this is true, and if Reaction (1) is reversible, the recovery of the reflectivity will be observed upon the oxidation of the reduction product. This was confirmed by measuring the R/R_0-t curve shown in Fig. 2. At first the potential was set at -1.35 V to produce $[Co(bipy)_3]^+$; then the potential was stepped to -0.70 V to oxidize the reduction product. During these operations, the recovery of the reflectivity at -0.70 V was clearly seen on the R/R_0-t curve, seeming to indicate the re-formation of $[Co(bipy)_3]^{2+}$ by the electro-oxidation.

The formation of $[Co(bipy)_3]^+$ is further supported by the absorption spectrum obtained. The reflectivity decrease observed at -1.35 V was plotted *vs.* the wavelength; it is shown in Fig. 3 as Curve (a). The observed reflectivity change is mainly due to the entities formed in the solution and not to the change in the optical properties of the silver electrode*; accordingly, plotting gives the absorption spectrum.

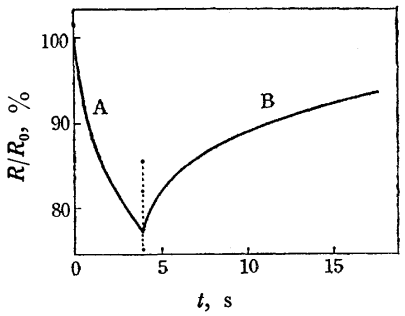

Fig. 2. The R/R_c-t curve of 0.5 mM $[Co(bipy)_3](ClO_4)_2$ in the presence of 20 mM 2,2′-bipyridine and 0.05 M $(C_2H_5)_4NClO_4$ in PC obtained at 630 nm.
Electrode potential was set at -1.35 V in region A and then stepped to -0.70 V in region B.

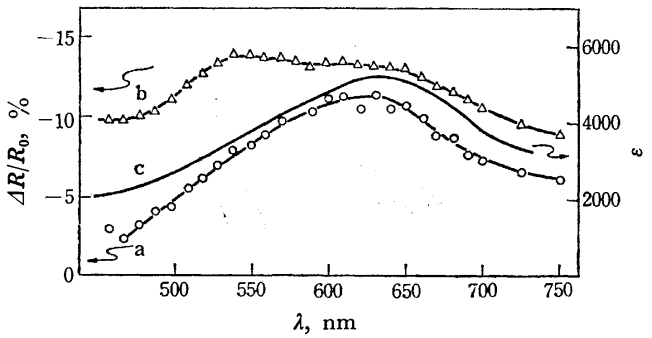

Fig. 3. Wavelength dependence of reflectivity decreases due to electrochemically generated species (a, b) and the absorption spectrum of $[Co(bipy)_3]^+$ in aqueous solution (c).[5] $\Delta R/R_0$ was obtained at varied wavelengths from R/R_0-E curve of the same solution as Fig. 1. $\Delta R/R_0$ of curve (a) was read at -1.35 V and curve (b), at -1.90 V.

* Even during the electrolysis, the decreased reflectivity was eliminated when the solution was stirred vigorously to remove the reduction product from the optical path.

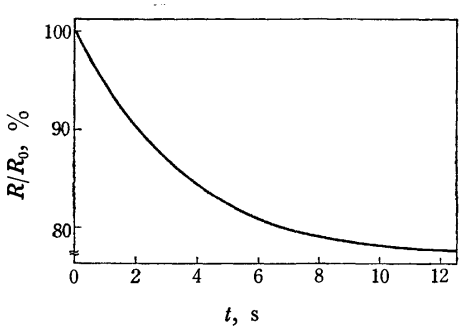

Fig. 4. The $\Delta R/R_0$-t curve measured at 630 nm at open circuit after electrolysis was carried out for 5 s at -1.90 V. Electrolytic solution contained 0.5 mM $[Co(bipy)_3](ClO_4)_2$, 20 mM 2,2′-bipyridine and 0.05 M $(C_2H_5)_4NClO_4$ in PC.

Curve (c) in Fig. 3 is the absorption spectrum of $[Co(bipy)_3]^+$ in an aqueous solution.[5] The curve obtained from the reflectivity measurement fairly well coincides with the reported curve.[5] The small difference in the position of the absorption maximum may be due to the difference in the medium used. Therefore, the reduction product at the first wave on the i-E curve may be concluded to be $[Co(bipy)_3]^+$, and the reflectivity measurement is proved to be a useful method for obtaining the absorption spectrum of the unstable species generated by the electrochemical method.

The absorption spectrum of the species formed at the potential of the second wave, which may be $[Co(bipy)_3]^-$, is given in Fig. 3 as Curve (b), where the difference in R/R_0 between the first and second steps in Fig. 1, (b) is plotted against the wavelength.[1] The bipyridine complex of Co(-I) has not yet been prepared, according to the author's knowledge, so this may be the first spectrum due to $[Co(bipy)_3]^-$.

The $\Delta R/R_0$-t curve was recorded at 630 nm at an open circuit after the electrolysis had been carried out at second wave for 5 s to produce $[Co(bipy)_3]^-$; then the electrolysis was turned off. The curve thus obtained is shown in Fig. 4. The $\Delta R/R_0$ at 630 nm decreased with the lapse of time. This means that $[Co(bipy)_3]^-$ was changed to a substance with an absorption at 630 nm; it may be $[Co(bipy)_3]^+$. That is, a proportionation reaction such as:

$$[Co(bipy)_3]^- + 2[Co(bipy)_3]^{2+} \longrightarrow 3[Co(bipy)_3]^+ \quad (3)$$

seems to occur, where $[Co(bipy)_3]^-$ is formed at -1.90 V and $[Co(bipy)_3]^{2+}$ is supplied from the bulk solution. For the confirmation of such a reaction, however, further detailed study will be required.

References

1) Y. Sato, *Chem. Lett.*, **1973**, 1027.
2) N. Tanaka and Y. Sato, This Bulletin, **41**, 2059 (1968).
3) F. H. Burstall and R. S. Nyholm, *J. Chem. Soc.*, **1952**, 3570.
4) N. Tanaka and T. Ogata, 19th Meeting of Polarographic Society of Japan, Sapporo (1973), No. 3B07 (p. 79).
5) G. M. Waind and B. Martin, *J. Inorg. Nucl. Chem.*, **8**, 551 (1958).

BULLETIN OF THE CHEMICAL SOCIETY OF JAPAN, VOL. 47(8), 2067—2068 (1974)

The Crystal Structure of Bis(1-(2-thiazolylazo)-2-naphtholato)nickel(II)

Masayasu KURAHASHI

Metal Chemistry Division, National Research Institute for Metals, Meguro-ku, Tokyo 153

(Received Junuary 29, 1974)

Synopsis. The crystals of bis(1-(2-thiazolylazo)-2-naphtholato)nickel(II), [Ni(TAN)$_2$], are triclinic with unit-cell dimensions: $a=12.38(6)$, $b=12.72(6)$, $c=8.41(4)$ Å, $\alpha=78.9(5)$, $\beta=95.0(5)$ and $\gamma=115.1(5)°$, $Z=2$, space group $P\bar{1}$. The TAN is terdentate, one nickel atom being surrounded octahedrally by two ligand anions in the *mer* configuration.

As part of studies on the structures of metal chelates of 1-(2-thiazolylazo)-2-naphthol (abbr. as H-TAN), the X-ray determination of bis(1-(2-thiazolylazo)-2-naphtholato)nickel(II), [Ni(TAN)$_2$], has been carried out.[1] The aim of the present investigation is to establish the configuration around the nickel atom. Two terdentate ligands in the complex were expected to be coordinated to the central metal atom as in the case of iron(II)-chelate, [Fe(TAN)$_2$];[2] however, the crystal of [Ni(TAN)$_2$] is not isomorphous with that of [Fe(TAN)$_2$] even though they are recrystallized from the same solvent (chloroform), the former giving diffuse diffraction spots. It was thus desirable to establish the structure of [Ni(TAN)$_2$]. It is of interest to compare the structure of this compound with that of the palladium(II)-TAN complex, [PdCl(TAN)],[3] since the electronic configuration is of d^8 for both metal ions.

Experimental

The crystals of [Ni(TAN)$_2$] were obtained by slow evaporation of a chloroform solution. Unit-cell dimensions were determined by the oscillation and Weissenberg photographs around the *a*-, *b*-, and *c*-axes. The density was measured by the flotation method in an aqueous NaI solution. The crystal data are shown in Table 1. Owing to the poor crystallinity of the specimens, the diffraction spots were markedly diffuse. With the use of Cu$K\alpha$ radiation, intensities of 795 independent non-zero reflections were determined visually from multiple film Weissenberg photographs of the layers (0—6)*kl*, *h0l*, and *hk*0. The usual Lorents and polarization factors were applied to the observed intensities, no correction being made as regards absorption effect. All the intensities were then placed on a common scale. Since there are two complex molecules in a unit cell, the space group $P\bar{1}$ was assumed. This was justified by the subsequent smooth refinement.

TABLE 1. CRYSTAL DATA FOR [Ni($C_{13}H_8N_3OS)_2$] (F.W.=567.3)

Triclinic, Space group $P\bar{1}$	
$a=12.38\pm0.06$ Å	$V=1177$ Å^3
$b=12.72\pm0.06$ Å	$Z=2$
$c=8.41\pm0.04$ Å	$D_m=1.55$ g·cm^{-3}
$\alpha=78.9\pm0.5°$	$D_x=1.60$ g·cm^{-3}
$\beta=95.0\pm0.5°$	$\mu=32.7$ cm^{-1} (for Cu$K\alpha$)
$\gamma=115.1\pm0.5°$	

Structure Determination and Refinement

The structure was determined by the heavy-atom method. The coordinates of the nickel and two sulfur atoms were deduced from the three dimensional Patterson maps. The remaining atomic positions were obtained by successive Fourier syntheses. The least-squares calculations were carried out with the use of isotropic temperature factors for all non-hydrogen atoms the *R* factor converging to 0.19. The anisotropic temperature factors were then applied to the nickel and two sulfur atoms, and the *R* index was improved to 0.16 after three cycles of refinement. The weighting scheme used was $w=1.0$ for $|F_o|\geqq11.0$, and $w=0.0$ for $|F_o|<11.0$. The diffraction data were so poor that no attempt was made to locate the hydrogen atoms. The structure thus obtained is chemically acceptable with satisfactory bond lengths and angles. The final atomic coordinates and thermal parameters of non-hydrogen atoms are shown in Table 2. The observed and calculated structure factors are listed in Table 3.*

Description of the Structure and Discussion

A perspective view of the molecule is shown in Fig. 1 along with the numbering of the atoms. The bond distances and angles are listed in Table 4 with their standard deviations. The TAN is present as a terdentate ligand; the thiazole nitrogen atom, the azo nitrogen atom adjacent to the naphthol ring and the phenolic oxygen atom are involved in chelate ring formation. The nickel atom is surrounded octahedrally by two ligand anions in the *mer* configuration. The features of the coordination of TAN to Ni(II)-, Fe(II)-, Pd(II)- and Cu(II)-atoms are common in their TAN-complexes. The configuration of [Ni(TAN)$_2$] coincides with that found in the crystals of [Fe(TAN)$_2$],[2] but differs from that of palladium(II)-chelate, [PdCl(TAN)],[3] or copper(II)-chelate, [Cu(TAN)($H_2O)_2$]$^+$,[3] in which the coordination configuration is square-planar or square-pyramidal, respectively. Both TAN anions are planar within the deviation ±0.2 Å. The bond angles of O–Ni–N(1), N(1)–Ni–N(3), O′–Ni–N′(1) and N′(1)–Ni–N′(3) are 80, 79, 80 and 76°, respectively, being fairly deviated from 90°. This is the characteristic feature which can be always seen in the TAN-complexes.

The crystal of Zn(II)–TAN chelate [Zn(TAN)$_2$] was found to be isostructural with that of [Ni(TAN)$_2$]. Both crystals have similar cell dimensions showing a

* Table 3 is kept as Document No. 7419 at the Chemical Society of Japan, 1-5, Kanda-Surugadai, Chiyoda-ku, Tokyo,

Table 2. Atomic parameters and their standard deviations[a)]

Atom	x/a	y/b	z/c	B	Atom	x/a	y/b	z/c	B
Ni	0.198(1)	0.397(1)	0.329(1)						
S	0.101(1)	0.065(1)	0.690(2)		S′	0.375(1)	0.450(1)	0.154(2)	
O	0.276(3)	0.471(3)	0.110(4)	6.8(8)	O′	0.347(3)	0.483(2)	0.436(3)	6.0(8)
N(1)	0.225(4)	0.268(3)	0.281(5)	7.0(10)	N′(1)	0.169(4)	0.528(3)	0.366(5)	7.9(11)
N(2)	0.195(3)	0.171(3)	0.383(5)	6.8(10)	N′(2)	0.084(3)	0.554(3)	0.316(5)	6.6(10)
N(3)	0.138(3)	0.279(3)	0.535(4)	4.8(9)	N′(3)	0.048(3)	0.374(3)	0.224(4)	4.7(9)
C(1)	0.281(4)	0.282(3)	0.136(5)	4.2(10)	C′(1)	0.258(4)	0.617(4)	0.437(5)	5.8(12)
C(2)	0.302(5)	0.397(4)	0.043(6)	7.5(14)	C′(2)	0.353(4)	0.579(4)	0.473(5)	5.3(11)
C(3)	0.374(5)	0.443(5)	0.899(6)	8.8(15)	C′(3)	0.463(4)	0.648(4)	0.557(6)	6.7(13)
C(4)	0.402(4)	0.368(4)	0.845(6)	7.0(13)	C′(4)	0.475(5)	0.746(5)	0.607(7)	9.6(17)
C(5)	0.369(4)	0.247(4)	0.929(5)	5.9(12)	C′(5)	0.390(4)	0.791(4)	0.560(5)	5.9(12)
C(6)	0.409(5)	0.163(4)	0.874(6)	8.4(15)	C′(6)	0.400(5)	0.886(4)	0.618(6)	7.5(14)
C(7)	0.377(5)	0.050(4)	0.970(6)	8.7(15)	C′(7)	0.309(5)	0.931(4)	0.578(6)	8.3(15)
C(8)	0.304(5)	0.996(5)	0.101(7)	10.2(17)	C′(8)	0.197(4)	0.867(4)	0.501(5)	5.8(12)
C(9)	0.277(4)	0.084(4)	0.159(6)	6.5(12)	C′(9)	0.184(5)	0.771(5)	0.439(6)	8.7(15)
C(10)	0.309(4)	0.201(3)	0.068(5)	4.7(11)	C′(10)	0.268(5)	0.718(4)	0.489(6)	6.9(13)
C(11)	0.147(4)	0.166(4)	0.534(5)	6.0(12)	C′(11)	0.990(4)	0.449(4)	0.248(5)	5.9(12)
C(12)	0.074(5)	0.161(5)	0.787(7)	9.0(16)	C′(12)	0.858(5)	0.337(4)	0.081(6)	8.2(15)
C(13)	0.091(5)	0.253(4)	0.686(6)	8.3(15)	C′(13)	0.938(5)	0.293(5)	0.146(7)	9.8(17)

Atom	B_{11}	B_{22}	B_{33}	B_{12}	B_{13}	B_{23}
Ni	0.015(1)	0.017(1)	0.049(2)	0.023(2)	−0.007(3)	−0.022(2)
S	0.011(2)	0.017(2)	0.039(4)	0.021(3)	0.018(4)	−0.001(4)
S′	0.011(2)	0.020(2)	0.032(4)	0.019(3)	−0.009(4)	−0.017(4)

The anisotropic temperature factors are of the form:
$\exp[-(B_{11}h^2+B_{22}k^2+B_{33}l^2+B_{12}hk+B_{13}hl+B_{23}kl)]$

a) E.s.d.'s in parentheses are in units of least significant digit.

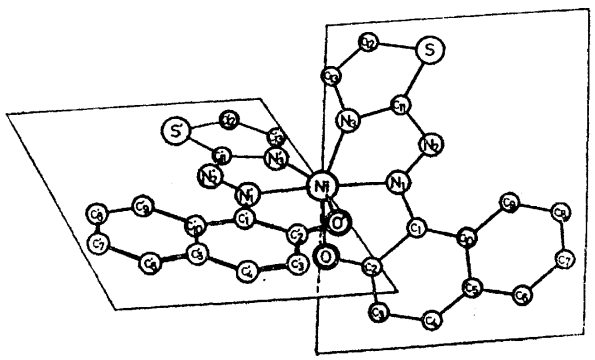

Fig. 1. Molecular structure of $[Ni(TAN)_2]$ and numbering of atoms.

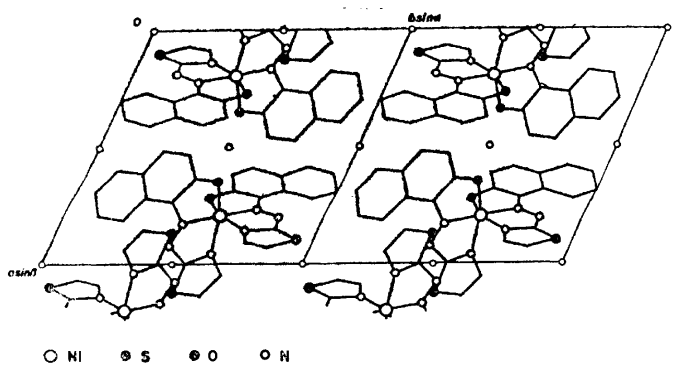

Fig. 2. The crystal structure of $[Ni(TAN)_2]$ as projected along the *c*-axis.

striking resemblance to each other in intensity distribution. It can thus be presumed that the molecular configuration of $[Zn(TAN)_2]$ is congruent with that of $[Ni(TAN)_2]$.

The crystal structure projected along the *c*-axis is shown in Fig. 2. No strong intermolecular interactions such as hydrogen bonding are observed in the structure. Since the positive charge of nickel(II) ion is neutralized by the coordination of the two bulky TAN ligands, the dominant force in the crystal should be essentially of the van der Waals type. Analogous packing of the chelate molecules can be observed in the crystals of $[Fe(TAN)_2]$ and $[Ni(TAN)_2]$, though vacant spaces are filled with solvent molecules in the former. Poor crystallinity of $[Ni(TAN)_2]$ might be related to the fact that some vacant spaces are retained in the crystal structure.

Table 4. Average bond distances and angles

Bond lengths (Å)		Bond angles (°)	
Ni-O	1.98(4)	O-Ni-N(1)	80(2)
Ni-N(1)	1.93(5)	N(1)-Ni-N(3)	78(2)
Ni-N(3)	1.97(4)	C(11)-S-C(12)	90(3)
S-C(11)	1.59(6)	Ni-O-C(2)	113(3)
S-C(12)	1.68(6)	Ni-N(1)-N(2)	124(3)
O-C(2)	1.32(6)	Ni-N(1)-C(1)	118(3)
N(1)-N(2)	1.26(6)	N(2)-N(1)-C(1)	117(4)
N(1)-C(1)	1.40(6)	N(1)-N(2)-C(11)	113(4)
N(2)-C(11)	1.47(6)	Ni-N(3)-C(11)	116(3)
N(3)-C(11)	1.48(6)	Ni-N(3)-C(13)	149(4)
N(3)-C(13)	1.43(7)	C(11)-N(3)-C(13)	95(4)
C(1)-C(2)	1.44(7)	N(1)-C(1)-C(2)	107(4)
C(1)-C(10)	1.42(8)	N(1)-C(1)-C(10)	120(4)
C(2)-C(3)	1.46(8)	C(2)-C(1)-C(10)	120(4)
C(3)-C(4)	1.33(8)	O-C(2)-C(1)	120(4)
C(4)-C(5)	1.42(8)	O-C(2)-C(3)	118(5)
C(5)-C(6)	1.43(8)	C(1)-C(2)-C(3)	122(5)
C(5)-C(10)	1.44(8)	C(2)-C(3)-C(4)	118(5)
C(6)-C(7)	1.43(8)	C(3)-C(4)-C(5)	121(5)
C(7)-C(8)	1.41(8)	C(4)-C(5)-C(6)	121(5)
C(8)-C(9)	1.41(8)	C(4)-C(5)-C(10)	124(5)
C(9)-C(10)	1.46(8)	C(6)-C(5)-C(10)	114(5)
C(12)-C(13)	1.31(8)	C(5)-C(6)-C(7)	119(5)
		C(6)-C(7)-C(8)	127(5)
		C(7)-C(8)-C(9)	114(5)
		C(8)-C(9)-C(10)	121(5)
		C(1)-C(10)-C(5)	115(5)
		C(1)-C(10)-C(9)	121(5)
		C(5)-C(10)-C(9)	124(5)
		S-C(11)-N(2)	129(4)
		S-C(11)-N(3)	121(4)
		N(2)-C(11)-N(3)	108(4)
		S-C(12)-C(13)	109(5)
		N(3)-C(13)-C(12)	122(5)

Some of the calculations were carried out on the HITAC 5020F computer at the Computer Center of National Aerospace Laboratory, using the UNICS system programs.[4)] The other calculations were made on the NEAC 3100 computer at this Institute.

The author is greatly indebted to Dr. A. Kawase of this Institute for helpful discussion and advice.

References

1) A part of this study was reported in a preliminary communication; M. Kurahashi, *Chem. Lett.*, **1974**, 63.

2) M. Kurahashi, A. Kawase, K. Hirotsu, M. Fukuyo, and A. Shimada, This Bulletin, **41**, 1940 (1972).

3) M. Kurahashi, *Chem. Lett.*, **1974**, 63; This Bulletin, **47**, 2045 (1974).

4) "The Universal Crystallographic Computing System (I)," Japanese Crystallographic Association (1967).

BULLETIN OF THE CHEMICAL SOCIETY OF JAPAN, VOL. 47(8), 2069—2070 (1974)

The Preparation of Mixed Cobalt(III) Complexes of *N,N*-Bis(2-aminoethyl)-glycine with the Carbonate or Oxalate Ion[1]

Syoji NAKASHIMA and Muraji SHIBATA

Department of Chemistry, Faculty of Science, Kanazawa University, Kanazawa 920

(Received February 20, 1974)

Synopsis. *mer*(N)- and *fac*(N)-[$CoCO_3$(*i*-dtma)] complexes have been prepared by the reaction of the tetradentate ligand with the $[Co(CO_3)_3]^{3-}$ complex. The corresponding [Coox(*i*-dtma)] complexes have been derived from the *mer*(N)-carbonato complex.

As to the cobalt(III) complex containing the tetradentate ligand *N,N*-bis(2-aminoethyl)glycine (abbreviated as *i*-DTMA) and the bidentate carbonate ion, two geometric isomers, *mer*(N) and *fac*(N), can possibly exist (Fig. 1). Of these, the *fac*(N) isomer has already been prepared by Schneider and Collman by means of a reaction between the [$CoCl_2$(*i*-dtma)] complex and lithium carbonate.[2] We have now succeeded in obtaining the second isomer, *mer*(N), by means of a reaction of the *i*-DTMA on the tricarbonatocobaltate(III) complex.

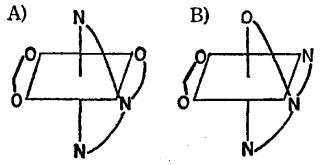

Fig. 1. Geometrical isomers of [$CoCO_3$(*i*-dtma)]
A: *mer*(N), B: *fac*(N).

The *i*-DTMA ligand was prepared from diethylenetriamine as a stock solution according to "Method B" described in the literature.[2] A proper quantity (0.1 mol) of the *i*-DTMA stock solution was added to a fresly prepared solution of potassium tricarbonatocobaltate (III) (0.1 mol),[3] and the mixture was stirred at room temperature for an hour. The resulting solution was charged on a column of a cation-exchange resin (Dowex 50WX8, Na-form). With careful washing with water, two bands, colored pink-violet and red-violet, descended the column, and the effluent was collected in two fractions. For convenience, these fractions were labeled "E-1" and "E-2". Each fraction was concentrated, and a small amount of a mixture of ethanol and ether was added to the concentrate; then the mixture was kept in a refrigerator. Very fine crystals were obtained from each concentrate. The complexes obtained from E-1 and E-2 were tentatively identified as *mer*(N) and *fac*(N) respectively, based on the order of elution.[4,5] The yields were about 6 g for *mer*(N) and about 9 g for *fac*(N). Found for *mer*(N): C, 29.40; H, 5.40; N, 14.56%. Calcd for [$CoCO_3$-($C_6H_{14}N_3O_2$)]·0.5H_2O: C, 29.18; H, 5.25; N, 14.58%. Found for *fac*(N): C, 30.05; H, 5.29; N, 15.07%. Calcd for [$CoCO_3$($C_6H_{14}N_3O_2$)]: C, 30.12; H, 5.06; N, 15.05%.

Two related complexes, *mer*(N), and *fac*(N)-[Coox(*i*-dtma)], were derived from the *mer*(N)-[$CoCO_3$(*i*-dtma)] complex. After the hydrolysis of the carbonato complex (10 g) by 60% $HClO_4$, a proper amount of potassium oxalate was added to the acid solution; then it was neutrallized with an aqueous solution of potassium hydroxide. After the removal of the precipitated material, the resulting solution was chromatographed in the same manner as the carbonato complexes. The two bands corresponding to the *mer*(N)- and *fac*(N)-isomers descended. The crystals of these isomers were obtained in the same manner as before. The yields were 3 g for *mer*(N) and 2 g for *fac*(N). Found for *mer*(N): C, 30.50; H, 4.71; N, 13.20%. Calcd for [Coox-($C_6H_{14}N_3O_2$)]·0.5H_2O: C, 30.39; H, 4.78; N, 13.29%. Found for *fac*(N): C, 31.12; H, 4.72; N, 13.73%. Calcd for [Coox($C_6H_{14}N_3O_2$)]: C, 31.28; H, 4.59; N, 13.68%.

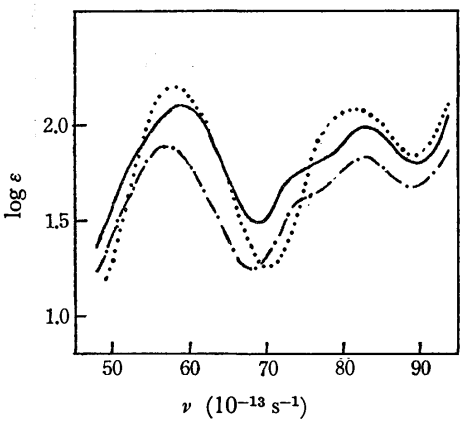

Fig. 2. Absorption spectra of *mer*(N)-[$CoCO_3$(*i*-dtma)] (——), *fac*(N)-[$CoCO_3$(*i*-dtma)] (·····) and *mer*-(*trans*)-[$CoCO_3$(gly)(NH_3)$_2$] (—·—).

The absorption spectra of the two carbonato complexes are shown in Fig. 2. The spectrum of the complex obtained from E-2 shows the first absorption band (ν_I) at 58.0×10^{13} s^{-1} (log ε=2.21) and the second band (ν_{II}) at 81.5×10^{13} s^{-1} (log ε=2.11). These values agree fairly with those for the known *fac*(N) complex (ν_I=58.5, ν_{II}=81.5).[2] From this it can be judged that this complex is the *fac*(N)-isomer. On the other hand, the spectrum of the complex obtained from E-1 shows the ν_I at 58.1×10^{13} s^{-1} (log ε=2.12) and the ν_{II} at 82.3×10^{13} s^{-1} (log ε=1.98). In addition, this spectrum exhibits a shoulder at *ca.* 74.5×10^{13} s^{-1} (log ε=1.7). A similar spectrum shape has been reported with the *mer*(*trans*)-[$Co(CO_3)$($gly(NH_3)_2$)] complex (*trans* refers to the two NH_3 groups).[6] The spectrum is included in Fig. 2. Although some hypso-

chromic shifts in the ν_I and ν_{II} bands can be seen in the present complex, the position of the shoulder scarcely shifts at all. From this similarity in spectrum, the present complex can be assigned to the *mer*(N)-isomer.

The PMR spectra of the same complexes are shown in Fig. 3. The E-1 or *mer*(N) complex shows a singlet at 3.75 ppm which has its origin in the methylene protons of the acetate group in the chelated *i*-DTMA, while the E-2 or *fac*(N) complex shows a quartet with the AB pattern at 3.80—4.25 ppm. These results confirm the assignments based on the absorption spectra.

As to the corresponding oxalato complex, the isomer obtained from the second fraction in chromatographic separation showed an absorption spectrum similar to that of the *fac*(N)-isomer of the carbonato complex except for hypsochromic shifts due to a higher ligand field: $\nu_I=57.9\times10^{13}\,s^{-1}$ (log $\varepsilon=2.19$), $\nu_{II}=82.6\times10^{13}\,s^{-1}$ (log $\varepsilon=2.25$). This fact indicates that this isomer has the *fac*(N) geometry. As to the isomer obtained from the first fraction, the gross features of the spectrum correspond well to those of the *mer*(N)-isomer of the carbonato complex except for the disappearance of a shoulder at *ca.* $74.5\times10^{13}\,s^{-1}$. Thus, this complex can be identified as the *mer*(N)-isomer.

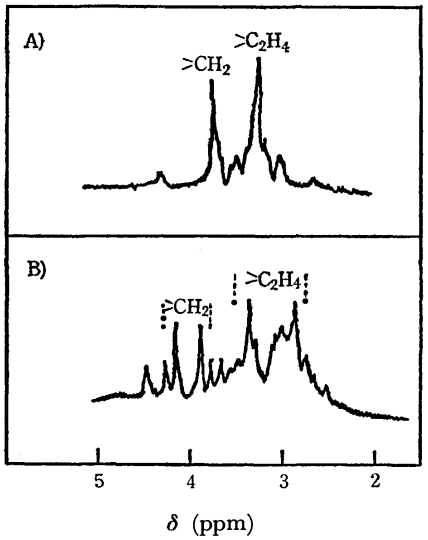

Fig. 3. PMR spectra of $[CoCO_3(i\text{-dtma})]$ (in D_2O, δ *vs.* DSS).
A: *mer*(N), B: *fac*(N).

In a previous paper,[7] it has been said that a cobalt (III) complex consisting of a five-membered α-aminoacidate ring, two NH_3 groups in the *trans* position, and a four-membered carbonate ring reveals a shoulder which may be considered to be one component of the split second absorption band. This remark can now be modified as follows: such a shoulder appears even though the two NH_3 groups and a NH_2 group of an α-aminoacidate ion are replaced by a diethylenetriamine backbone (NNN).

This work was supported in part by a grant from the Ministry of Education, to which the authors' grateful acknowledgements are made.

References

1) Presented at the 23rd Symposium on Coordination Chemistry, Fukuoka, Oct., 1973.
2) P. W. Schneider and J. P. Collman, *Inorg. Chem.*, **7**, 2010 (1968).
3) M. Shibata, *Nippon Kagaku Zasshi*, **87**, 771 (1966).
4) E. L. King and R. R. Walters, *J. Amer. Chem. Soc.*, **74**, 4471 (1952).
5) M. Mori, M. Shibata, and J. Azami, *Nippon Kagaku Zasshi*, **76**, 1003 (1955); M. Mori, M. Shibata, and M. Nanasawa, This Bulletin, **29**, 947 (1956); M. Mori, M. Shibata, and K. Hori, *ibid.*, **34**, 1809 (1961).
6) S. Kanazawa and M. Shibata, *ibid.*, **44**, 2424 (1971).
7) K. Nakai, S. Kanazawa, and M. Shibata, *ibid.*, **45**, 3544 (1972).

BULLETIN OF THE CHEMICAL SOCIETY OF JAPAN, VOL. 47(8), 2071—2072 (1974)

Miscibility of Lithium with Lithium Chloride and Lithium Chloride–Potassium Chloride Eutectic Mixture

Tsuyoshi NAKAJIMA, Ryohei MINAMI, Koichiro NAKANISHI, and Nobuatsu WATANABE

Department of Industrial Chemistry, Faculty of Engineering, Kyoto University, Yoshida, Sakyo-ku, Kyoto 606

(Received May 11, 1974)

Synopsis. The mutual solubilities of Li-LiCl and Li-LiCl-KCl systems were determined both in liquid-liquid and solid-liquid equilibrium regions. No critical solution temperature was observed for Li-LiCl system. The enthalpy of solution of LiCl in Li was estimated and compared with those for other alkali metal-alkali halides.

The phase diagrams and electric conductivity data for metal-salt systems are important information for the elucidation of the metal fog in molten salt electrolysis or the development of molten salt battery. Bredig *et al.*[1] have reported a number of phase diagrams for alkali metal–alkali halides systems and Pitzer[2] has given a theoretical analysis primarily based on the regular solution theory and the electronic nature of metal bonding. However, only a few data were obtained with lithium–lithium halides systems. In this work, the mutual solubilities of lithium–lithium chloride and lithium–lithium chloride–potassium chloride eutectic mixture systems were determined and a thermodynamic interpretation was given.

Experimental

The determination of solubilities between 294 and 850 °C were made by a static equilibration (saturation)-and-sampling method. The apparatus for the measurement of solubility of lithium in molten salt and the analytical methods were the same as those described previously.[3] An apparatus of the same type was used for the solubility measurement of salts in molten lithium. The amounts of chloride ion in the sample were determined with the Mohr method.

Furthermore, in order to determine the solubilities at temperature above 850 °C, differential thermal analysis was carried out using the molybdenum cell in which lithium and salts were sealed by means of electron beam welding. A Shimadzu Model DT-20B micro DTA apparatus was used.

Results and Discussion

Solubility Data. All the solubility data obtained in this work are shown in Table 1, and the phase diagram based on the data for lithium–lithium chloride system is given in Fig. 1. In the same figure, the data obtained by Bredig[1] and by Smirnov[4] for the solubility of Li in LiCl are also included. It is seen that our values are in good agreement with theirs. From the present measurement, the monotectic points for Li–LiCl system can be determined with reasonable accuracy. The monotectic temperature is estimated to be 608 °C which is about two degrees lower than the

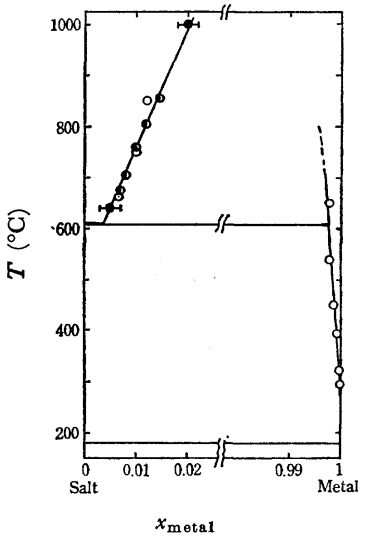

Fig. 1. Phase diagram of Li-LiCl system.
○ This work, ◐ Smirnov *et al*, ● Bredig *et al.*

TABLE 1. EQUILIBRIUM COMPOSITIONS IN Li-LiCl AND Li-LiCl-KCl EUTECTIC MIXTURE SYSTEMS

System	Li-LiCl		Li-LiCl-KCl eutectic	
Temp. (°C)	Salt rich phase (mole% metal)	Metal rich phase (mole% salt)	Salt rich phase (mole% metal)	Metal rich phase (mole% salt)
294		0.007		
322		0.019		
394		0.069		
450		0.14±0.02	0.083±0.002	0.098±0.001
540		0.21		
550			0.23±0.01	0.15±0.01
650		0.23±0.01	0.38±0.01	0.20
662	0.66±0.10[3]			
750	1.00±0.02		0.53±0.02	
850	1.22±0.01		0.65±0.03	

melting points of LiCl. The monotectic compositions are $X_{Li}=0.0045$ for salt-rich phase and $X_{LiCl}=0.0022$ for metal-rich phase (X: mole fraction). It is found that the mutual solubilities for Li–LiCl system are considerably smaller than those for Na–NaX or K–KX (X: halides) systems,[1] and accordingly their temperature coefficients are also very small. On the other hand, the mutual solubilities of Li–LiCl-KCl(eut. mixture) is still smaller than those for Li–LiCl system. This may be attributed to the fact that the equilibrium constant of the following equation, $Li+KCl \rightleftharpoons LiCl+K$, is 0.052.[5]

Critical Solution Temperature. Most of alkali (or alkali earth) metal-salt solutions are confirmed to exhibit an upper critical solution point at elevated temperatures.[1] One of the purposes of this work was to determine the critical point for Li–LiCl system. However, the upper critical solution temperature for this system could not be detected in spite of raising temperature of the system up to 1350 °C. This is higher than the boiling point of lithium metal. It may therefore be concluded that the present system has no upper critical point, though decisive observation could not be made.

Enthalpy of Solution of LiCl in Li. The plot of the logarithm of the solubility of solid LiCl in molten Li against the reciprocal of the absolute temperature are found to be linear within the experimental error, and the enthalpy of solution ΔH_{sol} of solid LiCl in molten Li was estimated to be about 14 kcal/mol. This is fairly small value when one compare this with those for NaCl in Na (20 kcal/mol)[6,7] or KCl in K (20 kcal/mol).[6,7] Since the enthalpy of solution ΔH_{sol} is the sum of the heat of fusion ΔH_f and the partial molar heat of mixture $\Delta \overline{H}_{mix}$, the ΔH_f values for these three salts are of comparable magnitude, this means that $\Delta \overline{H}_{mix}$ of LiCl in Li-LiCl solution is relatively smaller than those for Na-NaCl or K–KCl solution. This is rather unexpected result, because the cohesive energy of lithium metal is larger than those for Na or K metal and lithium is believed to be energitically unfavorable for the mixing with salt.

Excess Entropy. It is interesting to examine the sign and magnitude of the excess entropy of the present system. Since the mutual solubilities of, say, Na–NaCl system is larger than those of Li–LiCl, the excess free energy ΔG^E for Na–NaCl system should be positive and smaller in magnitude than that for Li–LiCl system. But they will be of comparable magnitude if comparison is made at the same lower temperature by extrapolation of the data for Na–NaCl system. Now ΔH^E for Na–NaCl is larger than that for Li–LiCl, then ΔS^E for Li–LiCl system will become smaller than that for Na–NaCl system. Possible contributions to the ΔS^E of metal-salt solutions were discussed by Pitzer[2] and the above result coincides with his analysis.

The authors thank to Toho Kinzoku Inc. for the manufacture of the molybdenum cells for DTA and to Kawasaki Jukogyo Inc. for the electron beam welding of them.

References

1) M. A. Bredig, "Molten Salt Chemistry," ed. by M. Blander, Interscience Publ. New York (1964), p. 367.
2) K. S. Pitzer, *J. Amer. Chem. Soc.*, **84**, 2025 (1962).
3) N. Watanabe, K. Nakanishi, and T. Nakajima, *Nippon Kagaku Kaishi*, **1974**, 401.
4) M. B. Smirnov and N. P. Podlesnyak, *Tr. Inst. Elektrokhim. Akad. Nauk SSSR, Ural'sk, Filial*, **14**, 14 (1970).
5) G. J. Janz, "Molten Salts Handbook," Academic Press (1967), p. 109.
6) M. A. Bredig, H. R. Bronstein, and Wm. T. Smith, Jr., *J. Amer. Chem. Soc.*, **77**, 1454 (1955).
7) J. W. Johnson and M. A. Bredig, *J. Phys. Chem.*, **62**, 604 (1958).

BULLETIN OF THE CHEMICAL SOCIETY OF JAPAN, VOL. 47(8), 2073—2074 (1974)

The Mass Spectra of Heteroaromatics. II.[1] Mass-spectral Fragmentation of 5-Nitro-2-furohydrazide Imide and Its N^2-Acyl Compounds[2]

Yasuhiko KATO

Department of Industrial Chemistry, Kyushu Institute of Technology, Tobata-ku, Kita-Kyushu 804

(Received May 17, 1973)

Synopsis. The high-resolution mass spectra of 5-nitro-2-furohydrazide imide and its N^2-acetyl, N^2-propionyl, and N^2-butyryl compounds have been examined. The major fragmentation pathways of the compounds were thus deduced.

It has been reported that the N^2-acyl derivatives of 5-nitro-2-furohydrazide imide (I) are cyclized to 5-alkyl-3-(5-nitro-2-furyl)-1,2,4-triazoles, with the release of a molecule of water, when heated at their melting points in a nitrogen stream.[3] In a continuation of a previous paper[1] concerning the mass-spectral fragmentation of the 1,2,4-triazoles, the mass spectra of I (R=H) and its N^2-acetyl (II, R=$COCH_3$), N^2-propionyl (III, R=COC_2H_5), and N^2-butyryl (IV, R=COC_3H_7) compounds have been examined in order to obtain information on the electron-impact reaction and in order to deduce the fragmentation pathways of the compounds.

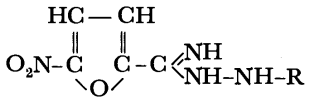

(I—IV)

Experimental

Measurement of the Mass Spectra. The high-resolution mass spectra were obtained with a Japan Electron Optics Laboratory Co., Ltd., JMS-OlSG-2 mass spectrometer, using the direct-inlet system. The operating conditions were as follows: ionizing energy, 75 eV; total emission current, 250 μA; accelerating voltage, 8 kV; ion multi., 1.5 kV (I and III) and 1.7 kV (II and IV); ion-source temperature, 200 °C; sample-vaporizing temperature, 100—120 °C (selected for each sample).

Samples. The samples used in this experiment were prepared by methods previously described.[4,5] IV; orange-yellow needles (recrystallized from methanol); mp 197—199 °C (decomp.).

Results and Discussion

The mass-spectral data of the compounds are shown in Table 1, while the major fragmentation paths are postulated in Schema 1 and 2.

5-Nitro-2-furohydrazide Imide (I). Compound I gave the most prominent molecular ion (M^+) (the base peak), with an *m/e* value of 170, reflecting its stability, caused by the resonance between the furan ring and its side chain at the 2 position. The distinct M–17 ion at *m/e* 153 is formed by the elimination of the ·OH radical from the M^+. This ion shows two modes of cleavage and may give ions at *m/e* 123 (Rel. int. 5%)[6] and *m/e* 96 (Ion composition, $C_4H_2NO_2$) by respectively, the loss of ·NO and HN=C=N-NH_2 fragments. The subsequent loss of HN, HCN, N_2, or ·N_2H from the *m/e* 123 ion would lead to the $(C_5H_4N_2O)^+$, $(C_4H_4N_2O)^+$, $(C_5H_5NO)^+$, and $(C_5H_4NO)^+$ ions at *m/e* 108, 96, 95, and 94. It may also be possible that the *m/e* 95 ion gives the *m/e* 94 ion by the loss of a ·H radical. On the other hand, the elmination of the

Table 1. Mass spectral data of the compounds, I—IV.

I (R=H)			II (R=$COCH_3$)			III (R=COC_2H_5)			IV (R=COC_3H_7)		
m/e	Ion composition[a]	Rel. int. %	*m/e*	Ion composition	Rel. int. %	*m/e*	Ion composition	Rel. int. %	*m/e*	Ion composition	Rel. int. %
170	$C_5H_6N_4O_3$	100	212	$C_7H_8N_4O_4$	98	226	$C_8H_{10}N_4O_4$	48	240	$C_9H_{12}N_4O_4$	55
153	$C_5H_5N_4O_2$	77	195	$C_7H_7N_4O_3$	25	209	$C_8H_9N_4O_3$	13	223	$C_9H_{11}N_4O_3$	16
139	$C_5H_3N_2O_3$	13	194	$C_7H_6N_4O_3$	25	208	$C_8H_8N_4O_3$	13	212	$C_7H_8N_4O_4$	13
138	$C_5H_2N_2O_3$	4	171	$C_6H_7N_2O_4$	25	197	$C_6H_5N_4O_4$	23	197	$C_6H_5N_4O_4$	20
108	$C_5H_4N_2O$	4	170	$C_5H_6N_4O_3$	100	180	$C_8H_{10}N_3O_2$	10	194	$C_7H_6N_4O_3$	21
	$C_5H_2NO_2$	4	154	$C_5H_6N_4O_2$	18	170	$C_5H_6N_4O_3$	100	170	$C_5H_6N_4O_3$	100
107	$CH_5N_3O_3$	9	153	$C_5H_5N_4O_2$	52	169	$C_5H_5N_4O_3$	6	153	$C_5H_5N_4O_2$	53
	C_5HNO_2	7		$C_5H_3N_3O_3$	36	153	$C_5H_5N_4O_2$	52	149	$C_6H_3N_3O_2$	16
96	$C_4H_2NO_2$	4	139	$C_5H_3N_2O_3$	29	149	$C_6H_3N_3O_2$	6			
	$C_4H_4N_2O$	3									
	$C_4H_6N_3$	5									
95	C_5H_5NO	5									
94	C_5H_4NO	18									

a) The high-resolution mass spectra of the compounds gave correct composition of all ions mentioned in the table, within the error of ±5 millimass units.

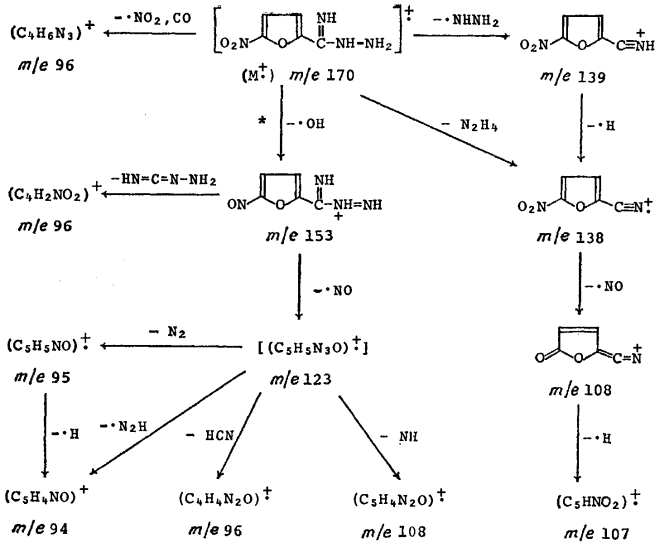

*; meta-stable ion observed

Scheme 1. Fragmentation of the compound, I.

$\cdot N_2H_3$ radical or N_2H_4 molecule from the M^+ gives distinct ions at *m/e* 139 and 138; the latter can be formed from the former by the loss of a ·H radical. The *m/e* 138 ion undergoes the elimination of an ·NO radical, followed by the loss of a ·H radical, thus giving the *m/e* 107 ion, which is consistent with the composition of C_5HNO_2.

Much as in the case of 3-(5-nitro-2-furyl)-1,2,4-triazoles,[1] the M^+ loses NO_2 and CO fragments by a one-step process to give an ion with the composition of $C_4H_6N_3$ at *m/e* 96.

N²-*Acyl Compounds (II, III, and IV).* In the spectra of II-IV, M^+ were also observed as intense peaks. In the first step of the fission of the M^+, as is shown in Scheme 2, there are four principal modes of elimination of the acyl groups:

(1) With the rearrangement of a hydrogen atom, the base peaks at *m/e* 170, which are consistent with the mass of the M^+ in I, result from the elimination of C_nH_{2n}-C=O (n=1, 2, and 3 respectively);

(2) the loss of an alkyl radical leads to the ion with *m/e* 197;

(3) the loss of an ·OH radical gives *m/e* 195 (II), *m/e* 209 (III), and *m/e* 223 (IV) ions respectively, and

(4) the elimination of an acyl group with the charge-transfer brings about *m/e* 43, 57, and 71 ions with 99, 50, and 43% intensities respectively, although the ion compositions have not been determined.

The ion at *m/e* 170 may be expected to show the same fragmentation as that of I, as is indicated in Scheme 1.

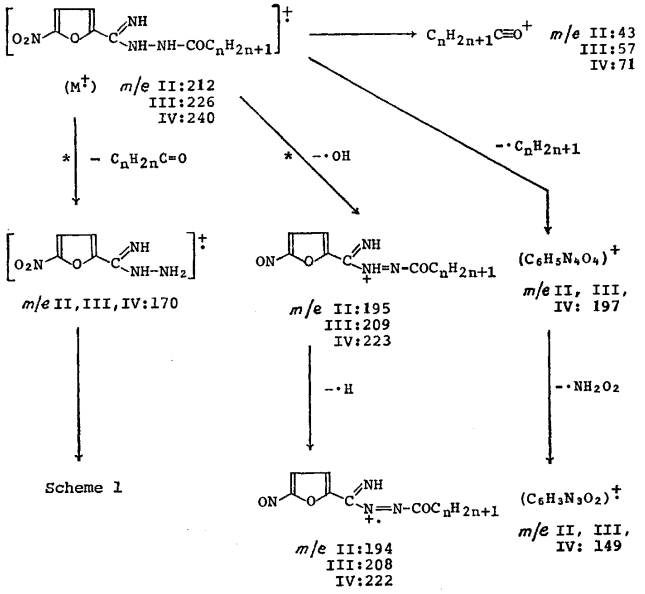

*; meta-stable ions observed

Scheme 2. Fragmentation of the compounds, II, III, and IV.

In addition to the four principal modes of fragmentation discussed above, there may exist some other fragmentation paths. Only in the case of Compound II, the ion at *m/e* 153 with the composition of $C_5H_3N_3O_3$ can be formed by the expulsion of the CH_3CONH_2 molecule from the M^+. In III, the NO_2 fragment is eliminated from the M^+, thus affording an ion at *m/e* 180, while in IV, the butyryl group of the M^+ is cleaved in the course of the McLafferty rearrangement to give the *m/e* 212 ion.

The author wishes to thank Dr. Y. Itagaki, the chief of the AID Application Laboratory of the Japan Electron Optics Lab. Co., Ltd., for the measurement of the mass spectra and for his useful suggestions.

References

1) Part I of this series: Y. Kato and I. Hirao, This Bulletin, **45**, 1876 (1972).

2) Presented at the 27th Annual Meeting of the Chemical Society of Japan, Nagoya, October 13, 1972.

3) The 25th Annual Meeting of the Chemical Society of Japan, Tokyo, October, 1971. Preprint, p. 511.

4) Y. Kato and I. Hirao, *Bull. Kyushu Inst. Technol.*, **No 15**, 57 (1965).

5) I. Hirao, Y. Kato, and H. Tateishi, This Bulletin, **45**, 208 (1972).

6) The composition of the *m/e* 123 ion was not determined.

BULLETIN OF THE CHEMICAL SOCIETY OF JAPAN, VOL. 47(8), 2075—2076 (1974)

Derivatives of Cyclic Disulfides. III.[1] A New Method of Deoxygenation of Thiolsulfinates and Thiolsulfonates with Inorganic Cyanide

Seizo TAMAGAKI, Hiroo HIROTA, and Shigeru OAE[2]

Department of Applied Chemistry, Faculty of Engineering, Osaka City University, Sugimoto-cho, Sumiyoshi-ku, Osaka 558

(Received November 21, 1973)

Synopsis. The reaction of rigid cyclic thiolsulfinates and thiolsulfonates such as 1,2-dithiaacenaphthene *S*-oxide and *S,S*-dioxide with inorganic cyanide afforded the corresponding reduced 1,2-dithiaacenaphthene, but not the open-chain *p*-tolyl benzenethiolsulfonate. This was explained by the proximity effect due to the rigidly confined S–S bond at peri-position of the naphthalene ring.

In the nucleophilic substitution reactions of atomic centers such as carbon, sulfur, and transition metal atoms, cyanide is known to show peculiar behavior as an excellent nucleophile.[3] It sometimes acts as a reducing agent and picks up oxygen, being oxidized to isocyanate despite its poor deoxygenative ability.[4] This was found to be the case in the reaction of 1,2-dithiaacenaphthene *S*-mono and *S,S*-dioxides.

The present investigation was undertaken to clarify the reaction of these disulfide derivatives, *i.e.*, thiolsulfinates, thiolsulfonates, and the related open-chain analogues with cyanide ion.

Results and Discussion

Many studies have been made on the heterolytic S-S bond cleavages of disulfides and their oxygenated derivatives by various types of nucleophiles. The S-S bond in disulfide undergoes facile scission by the action of CN^- to give the thiocyanate and the thiolate, while the thiolsulfonate gives the sulfinate and the thiocyanate.[5]

The reaction of *p*-tolyl benzenethiolsulfonate with sodium cyanide gives the products, which are identical with those reported[6] (Table 1). Cyanide ion simply attacks the S-S bond to afford sodium benzenesulfinate and *p*-tolylthiocyanate with no detectable amount of reduction product. On the other hand, a similar treatment of phenyl benzenethiolsulfinate with NaCN in MeOH at room temperature readily affords the transient sulfenate which subsequently reacts with the other partner, *i.e.*, thiocyanate, eventually giving the corresponding disulfide and NaOCN.

$$\mathrm{PhSO\text{-}SPh + CN^- \rightarrow PhSO^- + PhSCN \rightarrow}$$

$$\mathrm{PhSO\text{-}C(=N^-)\text{-}SPh \rightarrow PhSOCN + {}^-SPh \rightarrow PhS\text{-}SPh + OCN^-}$$

In contrast to the reaction of the open-chain *p*-tolyl benzenethiolsulfonate, 1,2-dithiaacenaphthene *S,S*-dioxide yields the reduced 1,2-dithiaacenaphthene when treated with NaCN in MeOH. This finding demonstrates that in the reduction of 1,2-dithiaacenaphthene *S,S*-dioxide the proximity effect due to the rigidly confined two sulfur atoms at peri-position is effectively in operation at the reduction stage where the oxygen atom of the sulfinate moiety and the carbon atom of the thiocyanate group are forced to approach each other sufficiently to react intramolecularly to form the intermediate(I) which upon the elimination of OCN^- gives the reduced disulfide. With regard to the elimination of OCN^- the above deoxygenation resembles the pathway for the formation of thiirane from the corresponding epoxide and SCN^-.[7]

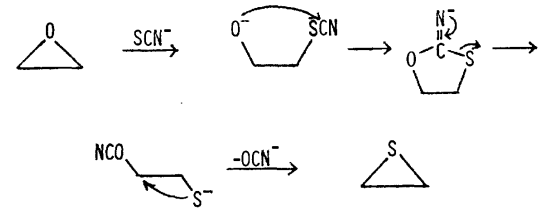

The fact that in the course of the reaction a spot due to 1,2-dithiaacenaphthene *S*-monoxide(M) was observed in thin layer chromatography supports the mechanism in which the reaction proceeds through the monoxide as a stable intermediate which in turn can be readily reduced to the corresponding disulfide in a good yield (Table I). The overall reaction pathway is outlined below.

Srivastava and Field reported that the alicyclic thiolsulfonate reacts with Na_2S to afford the trisulfide without giving any reduction product.[8]

However, with the rigidly confined thiolsulfonate even a reduction *via* the initial displacement reaction takes place smoothly, eventually producing the corresponding

TABLE 1. REACTION OF THIOLSULFINATES AND THIOLSULFONATES WITH NaCN[a] IN MeOH AT ROOM TEMPERATURE

Substrate	Reaction time	Reduced product	(%)	Other product (%)
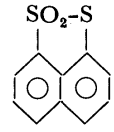	2 days	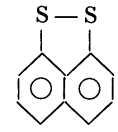	(48) (72)[c]	NaOCN[b]
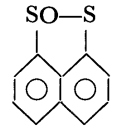	2 days	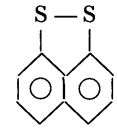	(83)	NaOCN
PhSO-SPh	0.5 hr	PhSSPh	(74)	NaOCN
$PhSO_2SPh$	1 hr	—		(Tol-S)$_2$ (9), Tol-SCN (24), $PhSO_2Na$ (86)

a) 1 equiv. of NaCN. b) Yields were not determined. c) 2 equiv. of NaCN.

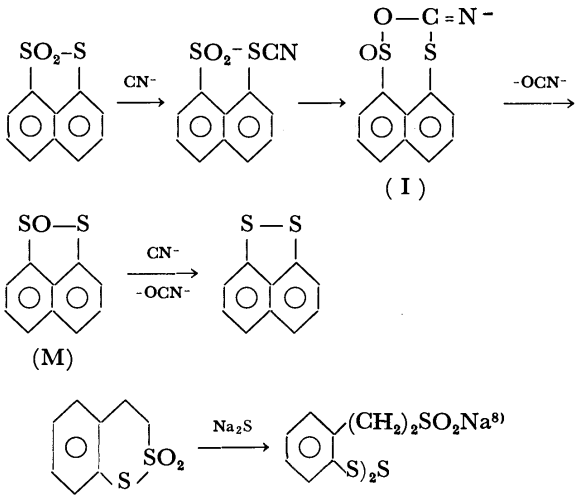

disulfide in an 86% yield. This would also show the characteristic aspect of this rigidly confined thiolsulfonate.

Comparing the reaction time for the open-chain compounds with that for the rigid cyclic analogues, we see that the latter is less reactive. This implies that the S-S bond rigidly confined at peri-positions of naphthalene nucleus should be less reactive toward an attack of nucleophile as compared with the open-chain compound. In fact the deoxygenation of 1,2-dithiaacenaphthene oxides by trimethyl phosphite is 100 times slower than that of phenyl benzenethiolsulfinate and the thiolsulfonate.[9]

Experimental

Materials. 1,2-Dithiaacenaphthene *S,S*-dioxide was prepared according to the reported procedure.[10] The monoxide was obtained in good yield either by the sodium metaperiodate oxidation of 1,2-dithiaacenaphthene or the deoxygenation of 1,2-dithiaacenaphthene *S,S*-dioxide with trimethyl phosphite; mp 82.5—83.5 °C.

Deoxygenation of Thiosulfinates and Thiosulfonates. Deoxygenation of 1,2-dithiaacenaphthene *S,S*-dioxide and *S*-monoxide by NaCN was carried out in MeOH at room temperature for 2 days. After the solvent was removed on a rotary evaporator, the preparative tlc using benzene afforded 1,2-dithiaacenaphthene. Identification of NaOCN was made by a comparison of its IR spectrum with that of the authentic sample(2240 cm^{-1}: C N).

References

1) Part II; S. Tamagaki, H. Hirota, and S. Oae, This Bulletin, **46**, 1247 (1973).
2) Responsible co-author: Department of Chemistry, University of Tsukuba, Sakura-mura, Niihari-gun, Ibaraki, 300-31, Japan.
3) R. L. Letsinger and R. R. Hautala, *Tetrahedron Lett.*, **1969**, 4205; E. W. Scott and J. R. Johnson, *J. Amer. Chem. Soc.*, **54**, 2549 (1932); S. Divald, M. C. Chun, and M. M. Joullié, *Tetrahedron Lett.*, **1970**, 777.
4) H. Tamura, *Kagaku*, (Kyoto), **27**, 920 (1972).
5) N. Kharasch, "The Chemistry of Organic Sulfur Compounds," Vol. 2, Pergamon Press Inc. (1966), p. 351.
6) S. Smiles and D. T. Gibson, *J. Chem. Soc.*, **125**, 176 (1924).
7) C. F. Allen and D. D. Mackay, "Organic Syntheses," Coll. Vol. 4, p. 233 (1963).
8) P. K. Srivastava and L. Field, *J. Org. Chem.*, **37**, 4196 (1972).
9) S. Tamagaki, H. Hirota, and S. Oae, unpublished data.
10) A. Zweig and A. H. Hoffman, *J. Org. Chem.*, **30**, 3997 (1965).

BULLETIN OF THE CHEMICAL SOCIETY OF JAPAN, VOL. 47(8), 2077—2078 (1974)

The Hydrolysis of Several Purine Nucleosides with Strong Hydrochloric Acid or Cation Exchange Resin

Yoshihisa SUZUKI

Central Research Laboratories, Ajinomoto Co., Inc., Suzuki-cho, Kawasaki 210

(Received November, 24, 1973)

Synopsis. The rates of hydrolysis were determined for several purine nucleosides with aq. HCl(0.1—4 M) or cation exchange resins(H-form) at 30 °C. The hydrolysis of adenosine with Diaion SK-1B is slower than guanosine while that with HCl is faster. This discrepancy was discussed.

Purine nucleosides are known to be susceptible to acid, giving nucleic bases and D-ribose. This property is based on the hydrolysis of the glycosidic bond. However, the treatment with cation exchange resin in the H-form has been found to be useful for the industrial isolation or purification of purine nucleosides.[1] This paper will describe their rates of hydrolysis with strong acids including cation exchange resins at room temperature.

Experimental

Materials. The guanosine, inosine, and adenosine used were commercial products of the Ajinomoto Co., Inc. Diaion SK-1B (Mitsubishi Chem. Ind. Ltd.), Duolite C-3 and Duolite ES-63 (Diamond Alkali Co.) were of 20—50 mesh and were conditioned to the H-form.

Paper Chromatography (PC). One-dimensional ascending PC was carried out on Toyo-Roshi No. 51A, the following two solvent systems being used: Solvent A, *n*-butanol-acetic acid-water(4 : 1 : 1); Solvent B, *n*-propanol-28% ammonia-water (20 : 15 : 3). Solvent A was used for the analysis of experimental runs involving inosine and adenosine (R_f, inosine 0.25, hypoxanthine 0.42, adenosine 0.46, adenine 0.58), and Solvent B, for guanosine (R_f, guanosine 0.50, guanine 0.41). The UV-absorbing spots of the samples and authentic standard references were cut off, together with their appropriate blanks, and eluted in 0.1 M HCl. The optical densities of the eluents at the wavelength of the maximum absorption of each component were measured. The percentages of the remaining original nucleosides and the nucleic bases thus produced were calculated from the optical densities.

Hydrolysis with HCl. Guanosine(0.1 g), inosine(0.25 g) or adenosine(0.25 g) was added to an Erlenmeyer flask which contained 50 ml of an HCl solution with a definite concentration (0.1—4.0 M) and kept at 30 °C. Each nucleoside was dissolved with vigorous stirring as soon as it was added. After the solution had been allowed to stand for a definite period (30 min-216 hr), it was cooled on an ice bath and neutralized with a cold NH_3 aqueous solution in order to stop the reaction. The resultant solution was analyzed with PC.

Hydrolysis with Cation Exchange Resins. Each nucleoside (0.3 g) was dissolved in a 0.15 M acetic acid solution(300 ml). Then, each wet resin(10 ml) was put into a stoppered Erlenmyer flask which contained the acetic acid solution described above. The resultant mixture was shaken for a definite period (20 min—48 hr) at 30 °C. The resin was filtered, washed with 20 ml of water, and then put into another Erlenmeyer flask which contained 50 ml of a 2 M NH_3 aqueous solution. After the mixture had been shaken for 30 min in order to elute the nucleoside and the base formed on the resin, the resin was put in a column and eluted with 350 ml of the 2 M NH_3 aqueous solution for complete elution. The eluates were then mixed and analyzed with PC. In the case of the experimental run using Duolite ES-63, 2M NaOH was used for the elution in place of the NH_3 aqueous solution because resin is not a strong cation-exchange resin.

Results and Discussion

Guanosine, inosine, and adenosine were hydrolyzed to give guanine, hypoxanthine, and adenine respectively. The decrease in the mole amount of nucleoside was equal to the amount of the nucleic base produced within the range of experimental error, and no side reaction was observed. In all the cases in the present study, first-order linear plots were obtained for the logarithm of the concentration of nucleoside with the reaction time. The observed first-order rate constants, k, were determined by the linear plots given by Eq. (1) or Eq. (2);

$$\ln([N_0]/[N]) = kt \quad (1)$$

$$\ln\{([N]+[B])/[N]\} = kt \quad (2)$$

where $[N_0]$ is the initial concentration of nucleoside, $[N]$ is the concentration of it at time t, and $[B]$ is that of the nucleic base.

On Diaion SK-1B, 93% of the guanosine or adenosine was adsorbed within 1 hr. It increased up to 97% within 6 hr. However, 50% and 47% of the inosine remained in the solution unadsorbed on the resin after the contact times of 6 hr and 16 hr respectively. This was because of the small pK_a value[2] of inosine(1.2) compared with that of guanosine(2.2) or adenosine(3.5). On Duolite ES-63, only 50% of the guanosine was adsorbed during the contact time of 48 hr, while the figure was above 95% within 1 hr on Duolite C-3. This was because of the small dissociation of the cation exchange group, phosphonic acid, in the former resin compared with that of methylenesulfonic acid in the latter.

More than 95% of the adsorbed substances were eluted in all the cases. There were some nucleic bases produced on the resin. The amount of the bases increased with the increase in the contact time, and the rate constants of hydrolysis were determined by Eq. (2).

Figure 1 shows the observed rate constants summarized with the acidity function, H_0. The acidity function represents, in short, the strength of the acidity of the solvent. The H_0 values of HCl solutions were determined from the literature.[3] Linear plots were obtained for the logarithm of the rate constant, log k,

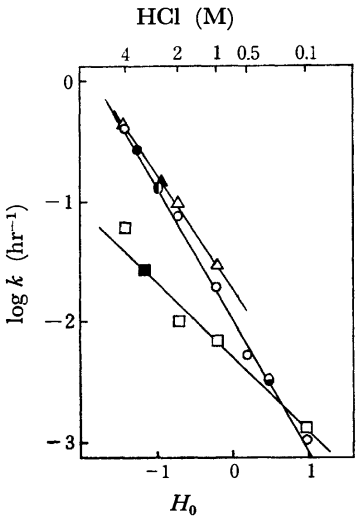

Fig. 1. Rate constants of acid hydrolysis for some purine nuclesides at 30 °C. The scale of the upper abscissa is given for convenience to compare the strength of cation exchange resins with that of HCl solutions. Adenosine with HCl (△) and with Diaion SK-1B (▲); guanosine with HCl (○), with Diaion SK-1B (●), with Duolite C-3 (◐) and with Duolite ES-63 (◒); inosine with HCl (□) and with Diaion SK-1B (■).

with the acidity function of H_0 from the experimental results for hydrolysis with an HCl solution. The results for hydrolysis with cation-exchange resins were placed on the lines corresponding with the individual nucleoside.

The rate constant with Diaion SK-1B for guanosine is equal to that with 3.2 M HCl. Hydrolysis with Duolite C-3 was equivalent to that with 2.5 M HCl. It is known that the hydrogen-ion concentration in cation-exchange regins is a few mol per liter. The above results are consistent with this knowledge, and the difference in the acid strength between Diaion SK-1B (sulfonic acid group, R–SO_3H) and Duolite C-3 (methylenesulfonic acid group, R–CH_2SO_3H) was quantitatively determined. The hydrogen-ion concentration in Duolite ES-63(phosphonic acid group, R–$P(O)(OH)_2$) was estimated to be equivalent to 0.3 M HCl from the rate of hydrolysis for guanosine, as above.

The hydrogen-ion concentration in Diaion SK-1B, as estimated from the rate constant for the acid hydrolysis of inosine, is in good agreement with that estimated from guanosine, while that estimated from adenosine is somewhat different from them. In relation to this estimation, a contradiction has been observed in this study in that hydrolysis with Diaion SK-1B for adenosine is slower than for guanosine, whereas hydrolysis with HCl is slightly faster. These facts strongly suggest that there is some difference between the position of the protonation in the acidic forms of adenosine (N-1)[4] and of guanosine (N-7).[5] This difference must affect the stereospecific binding of the nucleosides with the fixed cation-exchange group, the sulfonic acid in the resin, and the susceptibility of cleavage at the glycosyl bond. Therefore, the apparent values of the hydrogen-ion concentration were different between them. Jones and Robins[6] suspected that the position of the protonation in the acidic form of inosine was probably N-7, the same as that of guanosine.

In strong acid, the rate constant of hydrolysis for inosine is smaller than for guanosine, while the reversal is observed in 0.1 M HCl (Fig. 1). It is presumed that inosine will be hydrolyzed faster than guanosine in the weaker-acid or in the acidic pH region.

References

1) (a) Y. Suzuki and T. Nakamura, Japan. 71-3581, (b) Y. Suzuki, Y. Suzuki, and T. Nakamura, Japan. 73-28438.

2) W. E. Cohn, "The Nucleic Acids," Vol. I, ed. by E. Chargaff and J. N. Davidson, Academic Press, New York, N. Y. (1955), p. 217.

3) M. A. Paul and F. A. Long, *Chem. Rev.*, **57**, 1 (1957).

4) T. Nakajima and B. Pullman, *J. Amer. Chem. Soc.*, **81**, 3876 (1959).

5) M. Tsuboi, Y. Kyogoku, and T. Shimanouchi, *Biochim. Biophys. Acta*, **55**, 1 (1962).

6) J. W. Jones and R. K. Robins, *J. Amer. Chem. Soc.*, **85**, 193 (1963).

BULLETIN OF THE CHEMICAL SOCIETY OF JAPAN, VOL. 47(8), 2079—2080 (1974)

Preparation and Structures of Unsubstituted and Monofluorinated 2*H*(or 4*H*)-1,3,4-Benzoxadiazines

Peng Wai CHOW and Nobuo ISHIKAWA

Chemistry Department, University of Singapore, Singapore 10.

Department of Chemical Engineering, Tokyo Institute of Technology, Meguro-ku, Tokyo 152

(Received December 14, 1973)

Synopsis. Azo-coupling of diazomethane with benzenediazonium-2-oxide yielded 2*H*-1,3,4-benzoxadiazine while coupling of the same reagent with the monofluoro-substituted benzenediazonium-2-oxide derivatives gave the corresponding 4*H*-1,3,4-benzoxadiazines.

The preparation of 6,7,8-trifluoro-5-methoxycarbonyl-4*H*-1,3,4-benzoxadiazine by the reaction of 3,4,5-trifluoro-6-methoxycarbonylbenzenediazonium-2-oxide with diazomethane was previously reported.[1] An analogous reaction between a diazo-oxide and a substituted diazomethane was studied by Huisgen and Fleischman,[2] who observed the formation of 5,6,7,8-tetrachloro-2-phenyl-4*H*-1,3,4-benzoxadiazine from 3,4,5,6-tetrachlorobenzenediazonium-2-oxide and phenyldiazomethane.

No other report seems to have appeared on the heterocyclic system. We undertook to prepare unsubstituted 2*H*(or 4*H*)-1,3,4-benzoxadiazine and to confirm the effect of the electronegative halogen atoms of the benzene ring upon the stability of this heterocyclic compound.

For the purpose of preparing unsubstituted 2*H*(or 4*H*)-1,3,4-benzoxadiazine (**4** or **4a**), *o*-aminophenol (**1**) was reacted with *iso*-amyl nitrite to give 2-hydroxybenzenediazonium chloride (**2**),[3] from which elimination of a molecule of hydrochloric acid was effected with sodium carbonate.[4] On reaction with diazomethane, benzenediazonium-2-oxide (**3**) then afforded an oxadiazine compound, the result of diazo coupling followed by loss of nitrogen prior to ring cyclization.

The product, a fairly unstable yellow liquid, was assigned the structure 2*H*-1,3,4-benzoxadiazine (**4**), from infrared and nuclear magnetic resonance spectra. Thus, the IR absorptions at 2890 cm^{-1} and 2885 cm^{-1} were assigned to the methylene group, and those at 1360 cm^{-1} and 1250 cm^{-1} to C–N stretching vibrations and an ether linkage, respectively. The NMR spectrum, besides showing a complex multiplet at τ 2.27—3.35 due to the four aromatic protons, also revealed a singlet at τ 4.74, assigned to the methylene protons.[5]

On reacting with hydrogen over palladium catalyst, **4** afforded *o*-aminophenol (**1**) and methylamine, supporting the assignment of structure **4** for 2*H*-1,3,4-benzoxadiazine but not for 4*H*-compound (**4a**), since formation of these products is a consequence of hydrogenolysis during the course of reaction.

Introduction of a negative group such as fluorine atom in the benzene ring seemed to stabilize the 4*H*-1,3,4-benzoxadiazine compound rather than the 2*H*-compound, and we therefore attempted to prepare

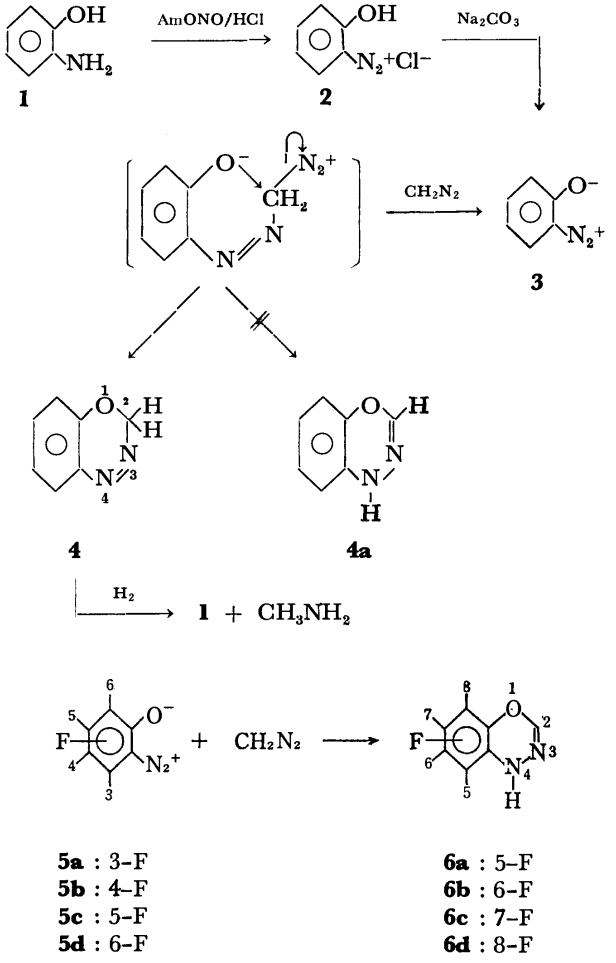

5a : 3-F
5b : 4-F
5c : 5-F
5d : 6-F

6a : 5-F
6b : 6-F
6c : 7-F
6d : 8-F

all species of hydro-1,3,4-benzoxadiazines which carry fluorine substituent in their benzene rings.

Coupling of the various monofluoro-substituted diazo-oxides (**5a**—**5d**) obtained from their respective fluoro-aminophenols by diazotization with aqueous sodium nitrite, gave fluorinated 4*H*-benzoxadiazines.

The compounds were obtained as stable crystals. The evidence for structures **6a**—**6d** for the fluorinated 4*H*-1,3,4-benzoxadiazines was readily deduced from their IR and NMR spectra. In line with the proposed structures, all the IR spectra showed absorptions which could be assigned to NH and C–N (Table 1). The NMR spectrum of **6d**, for example, also supported the structure, since the signal at τ 3.80, which was exchanged for deuterium oxide, could be assigned to a secondary amine, while the methine proton resonated as a singlet at τ 3.65.

In the azo-coupling of the fluoro-substituted diazo-oxide derivatives, preferable formation of the

Table 1. Preparation and properties of 4 and 6a—d

Compd. No.	Yield %	Mp °C (Bp °C/mmHg)	F Anal %		IR (cm^{-1})			
			Found	Calcd	CH_2	C-N	N-H	C=N
4	86	(58—59/2)	—	—	2885 2890	1360	—	—
6a	79	72.5—73.5	12.4	12.5	—	—	3420	1615
6b	94	73.5—74.5	12.5	12.5	—	—	3405	1630
6c	99	59	12.9	12.5	—	—	3410	1630
6d	99	83—83.5	12.6	12.5	—	—	3275	1645

4*H*-benzoxadiazines is expected, since the negative inductive effect of the fluorine atom is expected to make the oxadiazole ring somewhat acidic. The resulting intermolecular hydrogen bonding which combines N–H···N or N–H···O seems to stabilize the 4*H*-form and make the substances rather stable crystals.

Experimental

2H-1,3,4-Benzoxadiazine (4). Benzenediazonium-2-oxide (**3**) (3.90 g), prepared from *o*-aminophenol (**1**) by the reaction with isoamyl nitrite in hydrogen chloride saturated methanol and subsequent treatment of the resulting 2-hydroxybenzenediazonium chloride (**2**) with anhydrous sodium carbonate, was reacted with an excess of ethereal diazomethane at room temperature for 4 hr. The solvent was then evaporated. The crude product (4.23 g) was filtered through silica gel (20 g) in hexane. Evaporation of the solvent and subsequent distillation of the partially purified product gave pure benzoxadiazine **4** (3.80 g, 86%), bp 58—59 °C/2 mmHg. The yellow liquid, which turned reddish-brown when exposed to light, gradually decomposed at room temperature. Found: C, 60.8; H, 4.3; N, 20.3%. Calcd for $C_7H_6N_2O$: C, 62.7; H, 4.5; N, 20.9%. Mass spectrum: M^+ 134 (Calcd: 134).

Hydrogenolysis of 4. Benzoxadiazine **4** (1.32 g, 9.85 mmol) and 5% Pd/C catalyst (0.30 g) in ethanol (50 ml) were shaken in an atmosphere of hydrogen at room temperature and pressure. When the uptake of hydrogen had ceased (29.6 mmol), the catalyst was removed by filtration. The filtrate was heated to boiling in a water bath and the methylamine evolved was absorbed in ethanol (5 ml) maintained at about −5 °C. The filtrate was then evaporated and the resulting solid (0.86 g) was purified by sublimation *in vacuo* to give colorless crystals, mp 170—174 °C, which was undepressed on admixture with authentic *o*-aminophenol (**1**).

To the methylamine solution was added saturated ethanolic picric acid (5 ml), and the mixture was left at room temperature for 30 min, then heated in a water bath (5 min) and left to cool. The orange crystals deposited were purified by recrystallization from ethanol and confirmed to be methylamine picrate by IR and mixed mp.

Fluoro-4H-1,3,4-benzoxadiazine (6a—6d). The fluorobenzene diazonium oxides **5a—5d** were synthesized from the respective fluoro aminophenols, which in turn were prepared[6] from their corresponding nitro-derivatives by reduction with hydrogen gas over palladium catalyst. The diazo-oxides **5a—5d** thus obtained were then reacted with ethereal diazomethane in a similar manner.

As an example, 3-fluoro-2-aminophenol (1.50 g, 11.8 mmol), dissolved in water (32 ml) containing concentrated hydrochloric acid (5.5 ml), was converted into 6-fluorobenzenediazonium-2-oxide (1.51 g, 93%) with 5% aqueous sodium nitrite solution (18 ml, 13.0 mmol). This crude gummy product was treated with an excess of ethereal diazomethane and left at room temperature for 16 hr. The reaction mixture was filtered and the solvent evaporated to give a gum (1.5 g). This was extracted with boiling hexane, which was then evaporated leaving the benzoxadiazine **6a** (1.32 g, 79%) as yellow plates, mp 72.5—73.5 °C after crystallization from hexane followed by sublimation *in vacuo*. Found: C, 54.5; H, 3.4; N, 18.4; F, 12.4%. Calcd for $C_7H_5FN_2O$: C, 55.3; H, 3.3; N, 18.4; F, 12.5%. Mass spectrum: M^+ 152 (Calcd: 152).

References

1) S. Hayashi and N. Ishikawa, This Bulletin, **45**, 2909 (1972).
2) R. Huisgen and R. Fleischmann, *Ann.*, **623**, 47 (1959).
3) L. A. Kazitsyna, B. S. Kikot, B. V. Rassadin, and O. A. Rentov, *Zh. Obshch. Khim.*, **33**, 223 (1963).
4) B. S. Kikot, *ibid.*, **33**, 227 (1963).
5) A. Carrington and A. D. Mclachlan, "Introduction to Magnetic Resonance," Harper & Row, New York (1967).
6) P. Chow and N. Ishikawa, unpublished work.

BULLETIN OF THE CHEMICAL SOCIETY OF JAPAN, VOL. 47(8), 2081—2082 (1974)

The Reductive Amination of *d*-Camphor with the Methylamine and Carbon-13 NMR of the Reaction Products

Syun'ichi KIYOOKA and Kojiro SUZUKI

Department of Chemistry, Faculty of Literature and Science, Kochi University, Asakura, Kochi 780

(Received January 7, 1974)

Synopsis. The effects of catalysts (Raney Ni, 5% Pd-C, and PtO_2) in the title reactions have been discussed. The PtO_2 catalyst is excellent in reductive power and in selectivity. The CMR spectra of the reaction products (I, II, and III) are assigned, and the *N*-protonation shifts are further measured.

The reductive amination reactions using *d*-camphor and methylamine have not been investigated. The present paper reveals the reductive power and selectivity of some catalysts in the reactions. Generally, the reductive amination reactions of ketone with a primary amine are carried out in the presence of the Raney Ni catalyst and hydrogen, while the yields of the reactions are decreased by the sterically-enhanced bulkiness about the carbonyl groups and amino groups.[1] Raney Ni, 5% Pd–C, and PtO_2 were employed as catalysts. The reaction mixtures of methylamine and *d*-camphor, together with one of the three catalysts in an autoclave, were stirred at 120 °C for 24 hr. The basic oil obtained after the reaction was quantitatively analyzed by gas-chromatography. Three peaks appeared on the chromatogram. The structures of the three components (I, II, and III) were comfirmed by a comparison with the retention times of authentic samples (*N*-methylcamphorimine, *N*-methylbornylamine, and *N*-methylisobornylamine) prepared by known methods.[2-4]

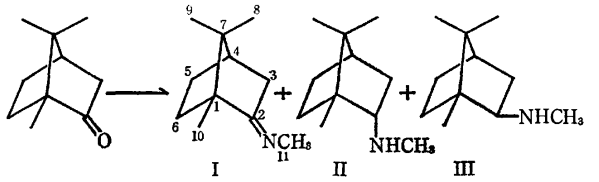

TABLE 1. THE CATALYTIC EFFECTS OF THE REDUCTIVE AMINATION

	Mixture yields (%)	Ratio of products (%)		
		I	II	III
Raney Ni	65	82.8	1.3	15.9
5% Pd-C	61	30.4	3.9	65.7
PtO_2	70	3.7	4.6	91.7
No catalyst	70	100.0		

Table 1 shows the yields and ratios of the products resulting from the effects of each catalyst. The remarkable differences in the reductive power of the catalysts were clarified. The reaction using the W-1 Raney Ni catalyst gave scarcely any Compounds II, and III, while the reaction using the PtO_2 catalyst gave mostly Compound III. Consequently, the PtO_2 catalyst is superior to the other catalysts in reductive powder and in selectivity, as shown by the ratios of the products of Compounds II and III, in the reductive amination reaction using ketones with sterically bulky groups, such as *d*-camphor. Similar results regarding the reductive power of the catalyst have been previously obtained by Goldberg and Lam.[5] As the reaction using no catalysts gave only Schiff base I, it may be assumed that the Schiff base was reduced to give Compounds II, and III in the reactions using catalysts. Moreover, the fact that Compound III was afforded as the main product means that the Schiff base was reduced by the *cis* addition of hydrogen from the endo side. Next, the ^{13}C NMR spectra of the three products in $CDCl_3$ and TFA (trifluoroacetic acid) were measured. Table 2 shows the observed chemical shifts, the multi-

TABLE 2. ^{13}C CHEMICAL SHIFTS ($\delta^{13}C$)[a] AND *N*-PROTONATION SHIFTS ($\Delta\delta^{13}C$)[b]

Compd		C-1	C-2	C-3	C-4	C-5	C-6	C-7	C-8	C-9	C-10	C-11
I	$\delta^{13}C$ in $CDCl_3$	53.6	183.5	35.2	43.9	27.5	32.1	47.1	*19.6	*19.1	11.3	39.3
	Off-resonance	s	s	t	d	t	t	s	q	q	q	q
	$\delta^{13}C$ in TFA	60.0	209.4	38.6	44.9	26.8	32.6	52.0	19.6	18.6	9.8	35.5
	$\Delta\delta^{13}C$	−6.4	−25.9	−3.4	−1.0	+0.7	−0.5	−4.9	0.0	+0.5	+1.5	+3.8
II	$\delta^{13}C$ in $CDCl_3$	48.3	69.2	38.3	45.2	27.4	37.0	46.6	*20.6	*20.5	12.0	35.3
	Off-resonance	s	d	t	d	t	t	s	q	q	q	q
	$\delta^{13}C$ in TFA	50.6	72.0	35.5	46.6	27.5	37.6	48.8	20.6	20.4	11.8	34.7
	$\Delta\delta^{13}C$	−2.3	−2.8	+2.8	−1.4	−0.1	−0.6	−2.2	0.0	+0.1	+0.2	+0.6
III	$\delta^{13}C$ in $CDCl_3$	48.6	65.6	37.6	45.0	27.5	28.4	48.4	*19.8	*18.7	14.3	36.0
	Off-resonance	s	d	t	d	t	t	s	q	q	q	q
	$\delta^{13}C$ in TFA	51.2	70.3	34.5	46.1	28.9	28.9	50.5	19.8	18.7	13.8	35.4
	$\Delta\delta^{13}C$	−2.6	−4.7	+3.1	−1.1	−1.4	−0.5	−2.1	0.0	0.0	+0.5	+0.6

a) ^{13}C chemical shifts are given in ppm from TMS and considered accurate to ±0.1 ppm. b) The plus and minus signs mean the upfield and downfield protonation shifts. * The asterisks designate pairs of shifts which have been assigned for consistency with other shift data, although there is a possibility that the assignments should be interchanged.

plicities observed in the off-resonance proton decoupled spectra, and the *N*-protonation shifts. The assignments of the ^{13}C signals of Compounds I, II, and III were decided with the aid of the CMR studies of norbornyl derivatives by Grutzner *et al*,[6] of camphor by Wenkert *et al*,[7] and of general substituent effects, the so-called α and β effects.[8]

Assignment of the ^{13}C NMR Spectra of N-*methylbornylamine II.* The 69.2 ppm resonance peak in the lowest field are immediately identified as C-2 attached to the methylamino group. The 45.2 ppm absorption appearing as a doublet in the off-resonance decoupled spectrum must be C-1 and C-7. Further, it is assumed, on the basis of the β effect of the substituent, that the line of C-1 is in a lower field than C-7. The lowest field peak at 38.3 ppm in the three triplet peaks when partially decoupled must belong to C-3, caused by a substantial downfield shift at positions β to the amino group. There are two absorptions, at 27.4 and 37.0 ppm, which appear as triplets', they must be C-5 and C-6. The C-6 is situated at positions β to the C-10 methyl group. The 35.3 ppm absorption appears as a quartet in the off-resonance decoupled spectrum and thus must be methyl carbon. The resonance line of methyl carbon agrees with the assignment given to the *N*-methyl groups.[9] The peak at 12.0 ppm was identified as C-10 according to Wenkert's work.[7] The remaining absorptions, at 20.5 and 20.6 ppm, must belong to C-8 and C-9. The assignment of C-8 and C-9 can not be decided on the basis of our present information. According to the general procedure described above, the ^{13}C chemical shifts of I and III have been assigned. The protonation-induced shifts are also shown in Table 2. It has been observed by Morishima *et al.*[10] that almost all the ^{13}C signals move to a higher field upon the *N*-protonation of some saturated amines. They concluded that, by the protonation of saturated amines, the C–H bond is polarized to produce the C^-–H^+ structure and that the electron on the hydrogen atom is transmitted through the carbon skeleton onto the positively-charged nitrogen atom. However, the observed protonation shifts of I, II, and III were downfield shifts at C-1, C-2, C-4, C-6, and C-7. It is especially notable that the protonation shift at C-2 of (I) was −25.9 ppm.

Experimental

General Procedure of Reductive Amination. To a 200-ml autoclave containing 20 g of *d*-camphor in 80 ml of a 30% methylamine-methanol solution, a catalyst (W-1 Raney Ni (5 g), 5% Pd-C (20 g), or PtO_2 (1.5 g)) was added. The autoclave was then filled with hydrogen at 60 kg/cm^2 (room temperature) and stirred magnetically at 120 °C for 24 hr. After cooling, 60 ml of 10% hydrochloric acid was added to the reaction mixture. The catalyst and the unreacted camphor were then filtered off. The filtrate was made strongly basic with 30% sodium hydroxide and extracted with ether, and the ethereal solution was dried over sodium hydroxide pellets. The evaporation of ether afforded a basic oil. The mixture oil was subsequently analyzed by gas chromatography. Four grams of the oil were chromatographed on 120 g of alumina. Elution with benzene afforded (I) (bp_{757} 203 °C), which was identified as *N*-methylcamphorimine (by means of infrared and PMR spectra). Further elution with a 10% ethanol-benzene solution yielded a mixture (bp 83—97 °C 10 mmHg), the identity of which were confirmed by comparing the retention times of the oily mixture on the gas chromatogram with those of *N*-methylbornylamine (II) (bp 89—96 °C/10 mmHg) and *N*-methylisobornylamine (III) (bp 82—83 °C 10 mmHg), both prepared by known methods.[3,4]

Gas-chromatographic Analysis. The gas chromatography was carried out with a Shimadzu GC-3AF Model apparatus. A $3\phi \times 2000$-mm stainless steel column was packed with THEED (15%) on Shimalite F (20—80 mesh). Nitrogen was used as the carrier gas. The column temperature was 100 °C. The percentages of the constituents of the oil were calculated from the areas of the peaks of the gas chromatogram.

CMR Spectral Measurement. All the ^{13}C spectra were obtained at natural abundance in 8-mmϕ tubes by means of a JNM-PS-100/PFT-100 spectrometer operating at 25.15 MHz (28 °C). The chemical shifts were determined with reference to the internal TMS from spectra taken with noise decoupling, which removed all the ^{13}C–H coupling. The repetition time of the pulse was 1—4 s. The numbers of scans were 1000—2000. Further, the off-resonance proton decoupling technique was applied to all samples. $CDCl_3$ and TFA were employed as the solvents. The concentrations of the samples were approximately 100 mg/ml.

References

1) W. S. Emerson, "Organic Reactions," Vol IV, Chapter 3 (1949).
2) M. O. Forster, *J. Chem. Soc.*, **71**, 193.
3) W. Hückel and P. Rieckmann, *Ann. Chem.*, **625**, 1 (1959).
4) M. O. Forster, *J. Chem. Soc.*, **75**, 941.
5) S. I. Goldberg and F. L. Lam, *J. Amer. Chem. Soc.*, **91**, 5113 (1969).
6) J. D. Grutzner, M. Jautelat, J. B. Dnece, R. A. Smith, and J. D. Roberts, *ibid.*, **92**, 7107 (1970).
7) E. Wenkert, A. O. Clouse, D. W. Cochran, and D. Doddrell, *Chem. Commun.*, **1969**, 1433.
8) J. B. Stothers, "Carbon-13 NMR Spectroscopy," Academic Press, New York (1972), p. 152.
9) G. C. Levy and G. L. Nelson, "Carbon-13 Nuclear Magnetic Resonance for Organic Chemists," Wiley-Interscience, New York (1972), p. 53.
10) I. Morishima, K. Yoshikawa, K. Okada, T. Yonezawa, and K. Goto, *J. Amer. Chem. Soc.*, **95**, 165 (1973).

BULLETIN OF THE CHEMICAL SOCIETY OF JAPAN, VOL. 47(8), 2083—2084 (1974)

^{13}C Nuclear Magnetic Resonance Spectra of Unsymmetrical Naphthyridines

Minoru HIROTA, Hideyuki MASUDA, Yoshiki HAMADA* and Isao TAKEUCHI*

Department of Applied Chemistry, Faculty of Engineering, Yokohama National University, Minami-ku, Yokohama 233

**Faculty of Pharmacy, Meijo University, Showa-ku, Nagoya 468*

(Received May, 21, 1974)

Synopsis. ^{13}C Nuclear magnetic resonance spectra of some naphthyridines were measured and the chemical shifts were compared with those theoretically calculated by an SCF-MO method of π-electron system. Fairly good linear relationship is observed between these values.

In the course of the investigations on the syntheses of naphthyridines and related compounds by modified Skraup reactions,[1] some naphthyridines were obtained and their ^{13}C NMR spectra were measured. The ^{13}C chemical shifts of the naphthyridines are shown in Table 1, together with the electron densities obtained by simple-LCAO and SCF(Pariser-Parr-Pople approximation) MO calculations.[2] The unambiguous assignment of the chemical shifts were obtained by the selective heteronuclear decoupling.

TABLE 1. ^{13}C CHEMICAL SHIFTS AND π-ELECTRON DENSITIES OF 1,X-NAPHTHYRIDINES

Compound	Position of C atom	Chemical shift Obsd./ppm	π-electron density Simple-LCAO	π-electron density SCF
1,5-Naphthyridine	2, 6	−22.55	0.8989	0.8464
	3, 7	+4.25	0.9929	1.0202
	4, 8	−8.81	0.9448	0.9506
	9, 10	−15.41	0.9582	0.9403
1,6-Naphthyridine	2	−26.26	0.8812	0.8034
	3	+5.99	1.0086	1.0572
	4	−7.06	0.9168	0.9331
	5	−24.39	0.8847	0.8294
	7	−18.42	0.9303	0.8698
	8	+4.83	1.0211	1.0380
	9	−21.92	0.9325	0.8597
	10	+6.38	1.0052	1.0601
1,7-Naphthyridine	2	−23.42	0.8951	0.8495
	3	+3.42	0.9927	1.0084
	4	−6.13	0.9346	0.9646
	5	+8.68	0.9973	1.0347
	6	−15.23	0.9487	0.9027
	8	−25.73	0.9088	0.8321
	9	−14.81	0.9606	0.9505
	10	−2.61	0.9774	0.9714
1,8-Naphthyridine	2, 7	−27.64	0.8827	0.8171
	3, 6	+5.70	1.0112	1.0516
	4, 5	−8.62	0.9218	0.9474
	9	−24.97	0.9123	0.8268
	10	+6.38	1.0035	1.0505

^{13}C Chemical shifts of aromatic hydrocarbons have been correlated approximately with the π-electron density by the following equation:[3]

$$\Delta\sigma_r = \alpha(q_r - 1)$$

where $\Delta\sigma_r$ is the chemical shift from benzene and α is a constant which is estimated to be 160 ppm by Lauterbur.[4] In order to examine the applicability of the equatoin to six-membered nitrogen heterocycles, the ^{13}C chemical shifts were plotted against the π-electron densities calculated by the SCF-MO method, and shown in Fig. 1. The full line in this figure illustrates the correlation line for $\alpha = 160$ ppm. The best fit value for this series of compounds was estimated to be about 140 ppm by the least-square calculation of the most appropriate slope of the correlation line as illustrated by the dotted line in the figure, and this value is close to the α value for aromatic hydrocarbons.

The observed and the theoretical spectra of 1,6- and 1,7-naphthyridines were given in Fig. 2. The theoretical spectra were calculated by the equation with the best fit parameters (See Fig. 1). Thus, the less elaborate π-electron calculation is proven to be

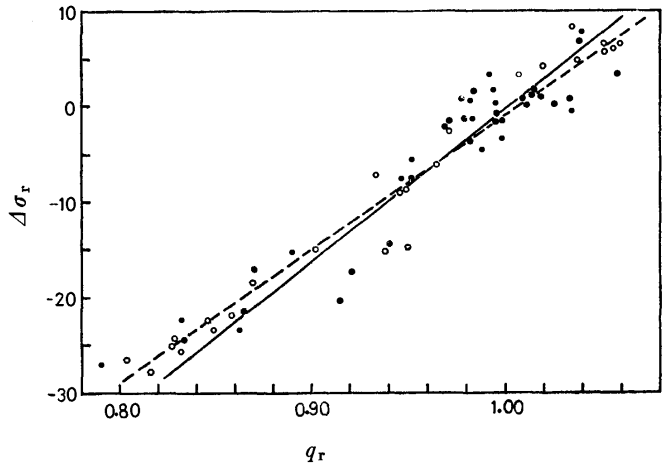

Fig. 1. ^{13}C Chemical shift *vs.* electron density plot. The full line in this figure corresponds to the equation $\Delta\sigma_r = 160\ (q_r - 1)$, and the broken line to the best fit equation $\Delta\sigma_r = 139.8\, q_r - 140.7$. The chemical shifts of naphthyridines investigated are illustrated by ○, and those of other six-membered aromatic nitrogen heterocycles by ●.

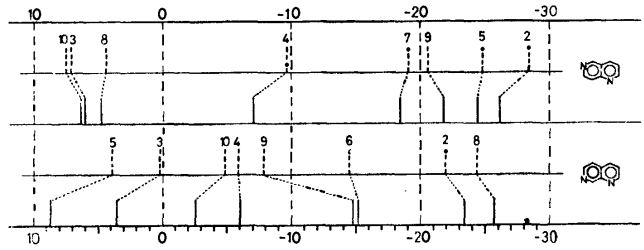

Fig. 2. Observed and calculated ^{13}C chemical shifts of 1,6- and 1,7-naphthyridines.

nearly as well useful as those including all valence shell electrons[5] to predict the ^{13}C chemical shifts of these heterocycles. The simple LCAO-MO calculation also predicts the ^{13}C chemical shifts of nitrogen heterocycles qualitatively. However, the correlation between the observed and the theoretical chemical shifts is poorer.

The authors are grateful to Dr. M. Imanari of the Japan Electron Optics Laboratories Co. for the measurement of ^{13}C NMR spectra.

References

1) Y. Hamada, I. Takeuchi, and M. Hirota, *Chem. Pharm. Bull. (Tokyo)*, **19**, 1751 (1971); *ibid.*, **22**, 485 (1974).
2) R. Pariser and R. G. Parr, *J. Chem. Phys.*, **21**, 767 (1953).
3) J. B. Stothers, *Quart. Revs.*, **1967**, 144.
4) P. C. Lauterbur, *Tetrahedron Lett.*, **1961**, 274.
5) The CNDO/2 calculations on symmetrical naphthyridines were compared with the ^{13}C chemical shifts in the following literature. A. C. Boicelli, R. Danieli and A. Mangini, *J. Chem. Soc. Perkin II*, **1973**, 1024.

Thermal Decay of the Colored Form in Photochromism of 2-Hydroxy-4-methoxytriphenylmethanol in *n*-Hexane

Sanyo HAMAI and Hiroshi KOKUBUN

Department of Chemistry, Faculty of Science, Tohoku University, Aramaki, Aoba, Sendai 980

(Received September 25, 1973)

It was found that, like 2-hydroxytriphenylmethanol (HM), 2-hydroxy-4-methoxytriphenylmethanol (HMM) shows photochromism as well as thermochromism. Photo- and thermochromism of HMM occur even in *n*-hexane, in which a photochemical irreversible reaction occurs for HM. In *n*-hexane solution of HMM, a three-stage thermal fading pattern was observed at room temperature and at lower temperatures, the pattern becoming a one-stage type at a higher temperature. Mechanical stirring of a sample solution caused a decrease in the concentration of the colored form in *n*-hexane at room and lower temperatures but not at a higher temperature. These phenomena are caused by the backward reaction on the wall of a sample cell including diffusion as the rate-determining step. In *n*-hexane–dimethoxyethane (or acetonitrile) mixed solvents, the first-order rate constant becomes smaller with increase in the dimethoxyethane (or acetonitrile) concentration. From a certain concentration, shaking of a cell causes no decrease in the concentration of the colored form.

2-Hydroxytriphenylmethanol (HM) is known to show thermochromism.[1] It also shows photochromism, its reaction being shown by the following scheme.[2]

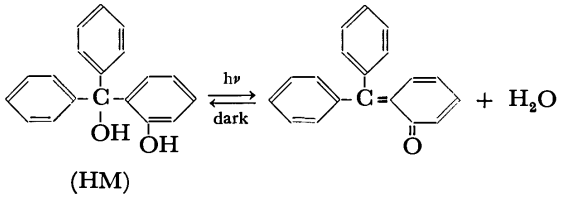

(HM)

Scheme 1.

At room temperature, HM shows photochromism in acetonitrile, ethyl ether, dimethoxyethane, benzene and 1,2-dichloroethane but only an irreversible reaction occurs in saturated hydrocarbon. Like HM, 2-hydroxy-4-methoxytriphenylmethanol (HMM) shows photochromism and thermochromism in these solvents. Photochromism occurs even in *n*-hexane, cyclohexane and methylcyclohexane, thermochromism being also observed in these solvents.

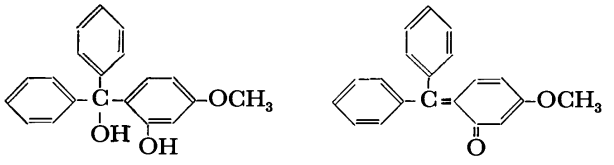

(HMM) (MF)

The behavior of the thermal decay of the colored form, *p*-methoxy-*o*-fuchsone (MF) in these hydrocarbon solvents is very curious differing from that in other solvents such as acetonitrile, ethyl ether. In order to make clear this curious behavior the thermal decay was followed under different conditions.

Experimental

Materials. 2-Hydroxy-4-methoxytriphenylmethanol was synthesized by the Grignard reaction of 2-hydroxy-4-methoxybenzophenone and phenylmagnesium bromide and purified by repeated recrystallization from an ether–*n*-hexane mixture and a methanol-water mixture after being treated with activated charcoal. *n*-Hexane, cyclohexane and methylcyclohexane were treated with fuming sulfuric acid diluted with concentrated sulfuric acid for a long time, washed with water, neutralized with an aqueous alkaline solution, treated with alkaline potassium permanganate, washed again with water, and then dried over calcium chloride. They were finally distilled over sodium wire. Acetonitrile was distilled over phosphorus pentoxide. Dimethoxyethane was dehydrated for several months over sodium-potassium alloy after evacuation.

The concentration of HMM was *ca.* 2×10^{-4} M in all the experiments.

Apparatus. A 6 W germicidal mercury lamp was used as a light source. The absorption spectrum was measured with a Hitachi EPS-3T spectrophotometer. The thermal decay was followed at 340 nm on the same instrument. Haake-FJ was used for temperature control.

Results

General Aspect of the Thermal Decay. MF appeared when the *n*-hexane solution of HMM was irradiated at 253.7 nm. The absorption spectrum of MF in *n*-hexane is shown in Fig. 1. The absorption maxima in *n*-hexane shift to shorter wavelength than those in acetonitrile or ethyl ether. In acetonitrile or ethyl ether an irreversible photo-product was formed in a small amount, but in saturated hydrocarbon the absorption spectrum after the termination of the thermal decay agreed almost completely with that of unirradiated HMM. The concentration of MF produced

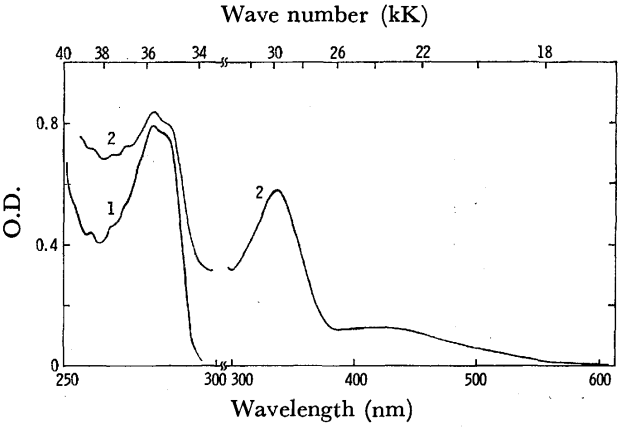

Fig. 1. Absorption spectrum of HMM in *n*-hexane.
1: Before irradiation, 2: After irradiation

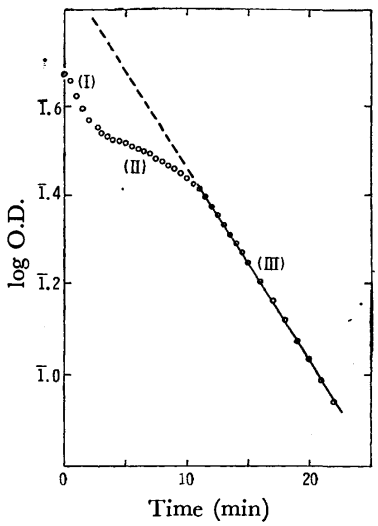

Fig. 2. Three-stage thermal decay of the colored form, MF, in *n*-hexane at 22 °C.

is the order of 10^{-5} M, water being also produced in the same concentration as in the case of HM (Scheme 1).

Mechanical stirring of a sample solution markedly decreases MF concentration. The thermal decay of MF was followed after the sample cell had been shaken. The decay rate decreased gradually after several minutes and became greater again approaching a constant value. The same phenomenon occurred each time the cell was shaken. The three-stage thermal decay after shaking is shown in Fig. 2. The decay pattern was identical within the optical density range of MF *ca.* 1.5—*ca.* 0.3 at 340 nm. The rate of decay of stage I is almost the same as that of III, the rate of stage II being smaller than that of I and III. A satisfactory first-order decay is seen at stage III. When a cell was shaken at stage III, a change was observed in which the rate constants at stages III and III′ agreed with each other fairly well (Fig. 3). The absorption spectrum is identical at any stage of the thermal decay. Consequently, no stable intermediate other than MF is involved in the thermal fading reaction in *n*-hexane. Oxygen would not be involved in it since the decay pattern was the same as that of the air saturated solution when the decay was followed after deoxygenation of the solution by bubbling nitrogen.

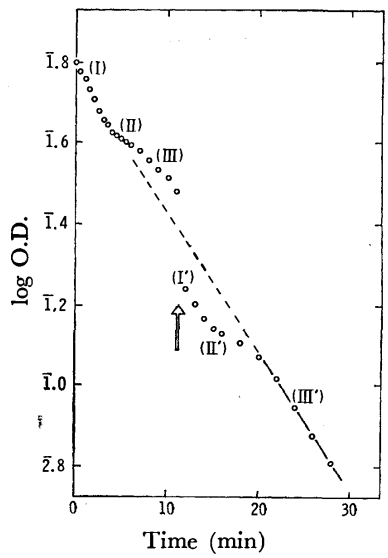

Fig. 3. Thermal decay of the colored form, MF, in *n*-hexane at 12 °C.
An arrow shows the point at which a sample cell was shaken.

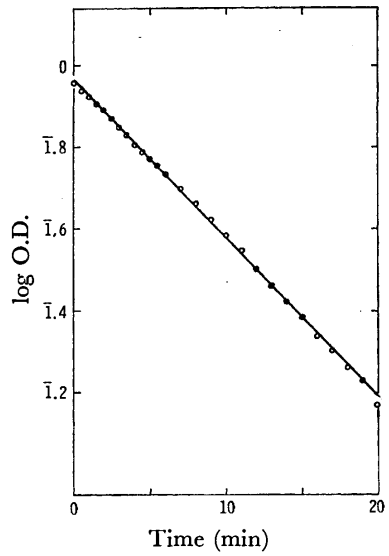

Fig. 4. One-stage thermal decay of the colored form, MF, in *n*-hexane at 36 °C.

Temperature Effect. The three-stage thermal fading pattern was observed at room temperature and lower temperatures, but at a higher temperature, *e.g.* at 36 °C, the pattern changed and an ordinary first-order decay was observed from the beginning (Fig. 4). Mechanical stirring of a cell in the course of decay does not accelerate the decrease of the concentration of MF. From the temperature dependence of the rate constant at III, the activation energy for the reaction was evaluated to be 1.7 kcal/mol, which agrees with the activation energy for the viscosity of *n*-hexane. Although the first-order decay was observed from the beginning at 28 °C, the decay pattern is a mixed type of the three-stage pattern and the ordinary first-order decay pattern (one-stage decay pattern), since shaking of a cell in the course of the decay slightly decreases the optical density of MF.

Addition Effect of Dimethoxyethane and Acetonitrile. The decay pattern of MF changes gradually from a three-stage to a one-stage type in the mixed solvent *n*-hexane–dimethoxyethane (or acetonitrile) with the increase of the dimethoxyethane (or acetonitrile) concentration. The decay rate constant also decreases at the same time. The relationship between the rate constant and the concentrations of dimethoxyethane and acetonitrile is shown in Fig. 5.

Thermal Decay in Water Saturated n-Hexane Solution. In acetonitrile or ethyl ether, the thermal decay rate constant of the colored form of HM or HMM is proportional to the concentration of the water added. However, in *n*-hexane saturated with water the decay pattern is the same as that in ordinary *n*-hexane, *i.e.*,

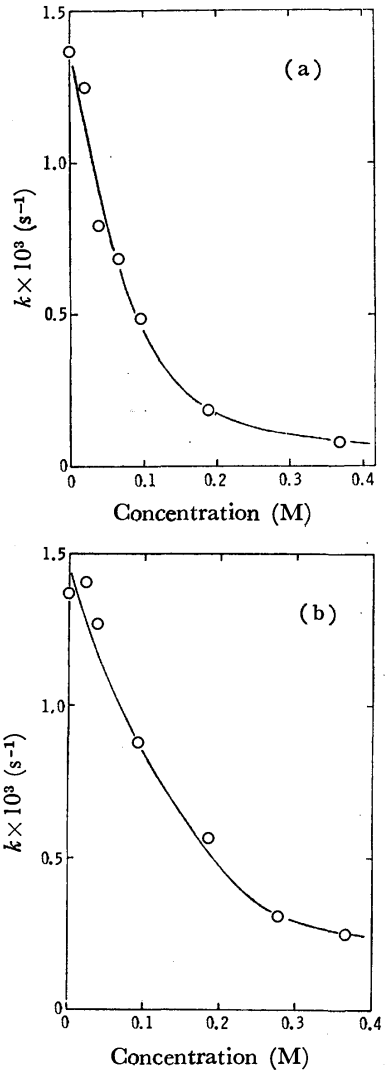

Fig. 5. (a) Dependence of the decay rate constant on the concentration of dimethoxyethane at 22 °C.
(b) Dependence of the decay rate constant on the concentration of acetonitrile at 22 °C.

the three-stage decay pattern changes to one-stage decay type with the rise of temperature. The rate constant 1.48×10^{-3} s^{-1} was nearly the same as that in ordinary *n*-hexane, 1.37×10^{-3} s^{-1}.

In the case of *n*-hexane solution saturated with water in a cell whose surface was damped with water, the decay pattern was the one-stage type and a shaking did not decrease the concentration of MF. This rate constant was about 1/20 as compared with a no-damped experiment.

Discussion

In *n*-hexane, the reaction mechanism of the thermal decay is quite different from that in acetonitrile and ethyl ether. The reaction system is never homogeneous. Dissolved water in cyclohexane or benzene does not exist as the associated forms such as dimer or trimer, but as a monomer.[3] It is highly probable that dissolved water in *n*-hexane exists as a monomer. Since the same decay pattern was observed in cyclohexane as well as *n*-hexane, the associated form of water would not be involved in the thermal fading reaction.

Adsorbed water on the surface of a quartz cell is considered to react with MF, but it is not clear whether MF is adsorbed or not. This is the diffusion-controlled reaction since the rate hardly changes with the concentration of dissolved water in *n*-hexane and a shaking of a cell accelerates the fading of MF. The concentration gradient on the surface of the cell is given by

$$\left(\frac{\partial c}{\partial x}\right)_{x=0} = \frac{{}^*c - {}^0c}{\sqrt{\pi Dt}}$$

where $\sqrt{\pi Dt}$ represents the thickness of the diffusion layer. The thickness of the diffusion layer depends on time in the system in which only diffusion occurs. Usually natural convection occurs because of the density gradient by the reaction on the surface, and then the thickness of the diffusion layer is constant after a certain period.[4] If we denote the thickness of the diffusion layer by δ, the concentration gradient is given by

$$\left(\frac{\partial c}{\partial x}\right)_{x=0} = \frac{{}^*c - {}^0c}{\delta}$$

Since the reaction on the surface is fast in comparison with diffusion, ${}^0c=0$. Thus the concentration gradient on the surface of the cell is expressed simply as follows.

$$\left(\frac{\partial c}{\partial x}\right)_{x=0} = \frac{{}^*c}{\delta}$$

Consequently, the rate formula for the thermal decay is

$$-\frac{dc}{dt} = D\frac{A}{V}\frac{c}{\delta} = kc$$

where A is the surface area in contact with solution and V is the volume of solution. A/V is equal to 4.25 cm^{-1} when 4 ml of solution is placed in a cell of 1 cm$\times$ 1 cm. For diffusion coefficient D, 10^{-5}—10^{-6} cm^2/s is taken, δ being *ca.* 10^{-3} cm, and for rate constant k, 10^{-2}—10^{-3} s^{-1} is taken. The reaction should be of first order. This satisfactorily elucidates the third stage of the three-stage decay. The diffusion coefficient for a molecule larger than a solvent molecule is given by Einstein's equation

$$D = \frac{kT}{6\pi r\eta}$$

where r is the radius of the diffusing molecule and η is the viscosity of the solvent. The activation energy for the thermal decay rate constant is, then, expected to agree with the activation energy for the viscosity of *n*-hexane. The former is 1.7 kcal/mol and the latter 1.76 kcal/mol, an excellent agreement being seen. Almost the same rate constants in water-saturated *n*-hexane and ordinary *n*-hexane are also understood in view of the diffusion-controlled reaction.

The forced convection by shaking of a cell remains at stage I of the three-stage decay. The convection decreases the thickness of the diffusion layer of MF. The decay is fast at this stage. At stage II, the forced convection gradually subsides and the thickness of the diffusion layer increases, the decay rate becoming small and finally the reaction is governed only by the dif-

fusion of MF. The change from stage II to stage III would be caused by the development of natural convection, which occurs by the accumulation of HMM in the vicinity of the cell surface with the progress of reaction. Natural convection reaches a steady state after a certain period, the thickness of the diffusion layer thus becoming constant and the first-order decay being observed. When compared with stage II the thickness of the diffusion layer decreases at stage III and the decay rate becomes great.

The decrease in diffusion coefficient due to the solvation by dimethoxyethane (or acetonitrile) molecules might make the rate decrease when dimethoxyethane (or acetonitrile) is added. The thermal decay rate decreases rapidly with the increase of the concentration of polar component and approaches a constant value. The switching of the reaction mechanism occurs at about 0.2 M for dimethoxyethane and about 0.3 M for acetonitrile. Above these concentrations, the thermal decay is governed by the one-stage type not controlled by diffusion. The reaction on the surface of a cell is inhibited and the reaction in solution may become the rate-determining step. The result of damped experiment shows that the reactivity of physically adsorbed water is of the same order as that of water in solution.

H. K. wishes to thank the Mitsubishi Foundation for financial support.

References

1) M. Gomberg and D. Nishida, *J. Amer. Chem. Soc.*, **45**, 190 (1923); S. T. Bowden and K. I. Beynon, *J. Chem. Soc.*, **1957**, 4244.

2) S. Hamai and H. Kokubun, *Z. Phys. Chem.* (Frankfurt), **88**, 211 (1974).

3) S. D. Christian and H. E. Affsprung, *J. Chem. Soc.*, **1963**, 1896; J. R. Johnson, S. D. Christian, and H. E. Affsprung, *J. Chem. Soc., A*, **1966**, 77.

4) H. A. Laitinen and I. M. Kolthoff, *J. Amer. Chem. Soc.*, **61**, 3344 (1939).

The Catalytic Activity of AgX-type Zeolite for the Isomerization of 1-Butene

Hiroshi SUGIHARA, Ling Yuan CHEN,* and Iwao YASUMORI

Department of Chemistry, Tokyo Institute of Technology, Ookayama, Meguro-ku, Tokyo 152

(Received January 5, 1974)

The catalytic activity of X-type zeolite exchanged by Ag^+ was studied for the isomerization of 1-butene. The activity gradually increased with the degree of exchange up to *ca.* 60%, whereafter it rose steeply. A good correlation was found between the activity and the number of acid sites of H_0 less than 3.3. Both preferences, that for the formation of *cis*-2-butene from 1-butene and that for the geometrical isomerization rather than the double-bond shift, indicated that the reaction proceeds *via* a carbonium-ion intermediate formed on an acidic site. In the region of exchange around 40%, however, the *cis*/*trans* ratio in the 2-butenes produced was less than unity and a change in the reaction mechanism was suggested. Treatment with H_2 enhanced the activity of exchanged zeolite by a factor of 10^2—10^3 without any change in the character of the reaction. These results were attributed to the formation of proton-X-zeolite by the replacement of Ag^+ with a proton. This conclusion was confirmed by the analysis of deuterium exchange during the isomerization on D_2-treated AgX.

Zeolites have been chosen as the subjects of many studies because of their well-defined structures and distinguished properties in adsorption and catalysis. Catalytic activities enhanced by the replacement of Na^+ by rare earth or alkaline earth cations have often been correlated to the protonic acidity.[1,2]

Transition-metal zeolites have also been studied recently.[3] The lack of a simple relationship between activity and acidity on them, however, necessitates precise studies of the state of the exchanged cation and its role in the reaction mechanism for each zeolite.

As for the exchange effect of the silver ion, Ward found, using the IR technique, that AgX-type zeolite differs from other zeolites with monovalent cations in having acid sites of mainly the Brönsted type.[4] Yates observed X-ray diffraction due to the (111) and (200) planes of metallic silver after the reduction of AgX by H_2.[5] Recently Tsutsumi and Takahashi found that silver particles were formed during the course of cumene cracking on AgY and concluded that the zeolite becomes decationated-form in which metallic silver was dispersed.[6]

This paper will report the results of our study on the nature of active sites on AgX, using the isomerization of 1-butene as a test reaction. The degree of ion-exchange by Ag^+ was extended to the range of 11—100%. The effect of treatment with H_2 on the catalytic activity was examined; the deuterium distribution in butenes was also determined for the reaction on the catalyst treated with D_2.

Experimental

Materials. AgX-type zeolites were prepared by immersing Linde Na 13X-zeolite, free of clay binder, in an aqueous solution of silver nitrate at room temperature for 12 hr. The amount of Na^+ exchanged by Ag^+ was determined by means of EDTA analysis.[7] Throughout this paper, the catalysts will be denoted by AgX, with the percentage of ion-exchange by Ag^+ in parentheses. The surface area of zeolite was evaluated from a Langmuir plot for nitrogen adsorption at 77 K. The X-ray diffraction pattern was recorded before and after the isomerization reaction; AgX-type zeolites were thus found to retain the original structures, irrespective of the degree of ion-exchange. The acidity of the catalysts was estimated from the adsorption of *n*-butylamine.[8] Methyl red ($pK_a=4.8$) and methyl yellow ($pK_a=3.3$) were used as indicators. Decationated X-zeolite, HX, was prepared by exchanging the Na^+ in the zeolite with NH_4^+ and by then heating to 350 °C under a vacuum.[9] The hydrogen (nominal purity, 99.9 mol%), deuterium (99.5 mol%), and 1-butene (containing less than 0.2 mol% of 2-butene) in a glass ampoule were obtained from the Takachiho Shoji Co. and were used without further purification.

Procedure. The reaction was studied using an apparatus which consisted of a reaction system of 440 ml combined with a circulation pump and a high-vacuum line. Samples were taken periodically from the reaction system and were analyzed by means of a reduced-pressure-type gas chromatograph[10] with a 16 m DMS-alumina column at room temperature. For kinetic measurements, 0.1 g of the catalyst was placed in the reaction vessel and the vessel was evacuated at 350 °C for 12 hr. After the subsequent degassing at the reaction temperature for 1 hr, 1-butene was admitted to the vessel to start the reaction. The pressure of 1-butene was maintained at 18 Torr in all the kinetic runs. In the treatment with H_2, 2.4×10^{-4} mol of hydrogen was introduced into the system and was circulated over the AgX catalyst at 150 °C for 1 hr. The amount of hydrogen consumed corresponded to a *ca.* 45% reduction of the Ag^+ to Ag^0, regardless of the degree of ion-exchange in zeolites. AgX treated similarly with D_2 was also used for the reaction. The distribution of deuterium in butene was determined by using a mass spectrometer, Hitachi RMU-5B. The isomerization of *cis*-2-butene and *trans*-2-butene was also examined on H_2-treated AgX (93.2%) and AgX (32.9%).

Results

The surface areas per unit of weight of dried catalysts are shown in Table 1. By taking into account the formular weight (NaX=13418, AgX(100%)=20719 and so on), the area per unit of weight of the zeolite framework was found to be almost independent of the degree of exchange and was estimated as 893 ± 35 m^2/g_{fr}. The surface area decreased when zeolite was exposed to 1-butene (2), but was recovered partly by a sub-

* Present address: Department of Technical Engineering, Cheng Kung University, Tainan, Taiwan, Republic of China.

TABLE 1. SURFACE AREAS OF ZEOLITES

Catalyst (% Na^+ exchanged)	Surface area (m^2/g_{dry}) (1)[a] Evacuation at 350 °C	(2) Reaction at 150 °C	(3) Contact with hydrogen at 150 °C	(4) Reaction at 150 °C
NaX	792	790	—	—
AgX (11.3%)	745	621	695	694
AgX (32.9%)	612	444	562	536
AgX (42.6%)	600	445	516	484
AgX (72.3%)	529	305	401	377
AgX (93.2%)	507	220	338	323
AgX (100%)	505	205	327	315

a) Number in parentheses shows the order of treatments.

sequent H_2-treatment (3). These changes may be attributed to the irreversible adsorption of 1-butene through the formation of the Ag^+–olefin complex,[11] thus blocking up the micropores of zeolite and its partial removal by hydrogen. This conclusion is supported by the finding that the decrease in the surface area becomes smaller when the zeolites are pretreated with hydrogen (4), since hydrogen reduces Ag^+ to Ag^0.[6]

Figure 1(a) illustrates the time course of 1-butene isomerization on AgX (93.2%) at 120 °C. The reaction did not have an induction period, and no product was detected other than 2-butenes. The reproducibility was satisfactory when the reaction temperature was kept below 150 °C. The rate of the disappearance of 1-butene was well expressed by the reversible first-order equation:

$$\log x_e/(x_e - x) = kt$$

were k represents the rate constant ($min^{-1}\,g^{-1}$), and where x and x_e denote the fraction of 2-butenes at time t and at equilibrium, respectively. The equilibrium compositions of three isomers were estimated from the literature.[12] The plots of this relation are shown in

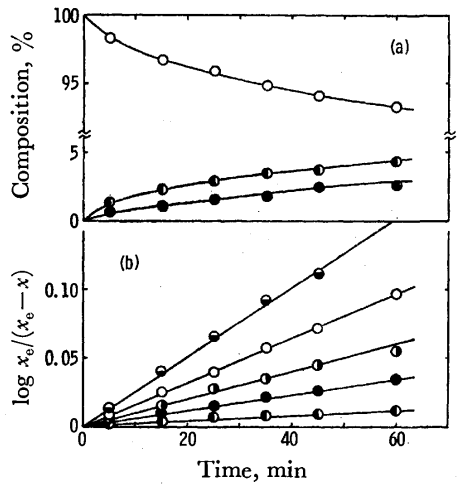

Fig. 1(a). Isomerization of 1-butene over AgX (93.2%) at 120 °C. ○, 1-butene; ●, *trans*-2-butene; ◐, *cis*-2-butene. 1(b). First-order plots for 1-butene isomerization. Reaction temperatures are 150, 140, 130, 120, and 100 °C in downward order.

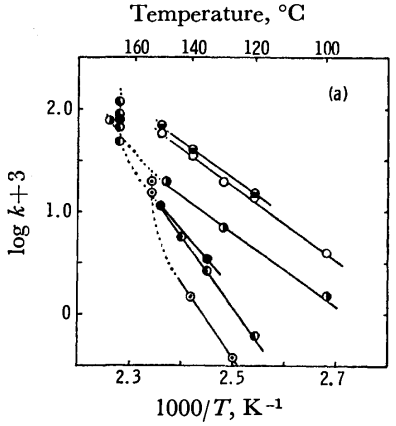

Fig. 2(a). Arrhenius plots for 1-butene isomerization over AgX. ⊙, AgX(11.3%); ◐, AgX(32.9%); ●, AgX(42.6%); ◑, AgX(72.3%); ○, AgX(93.2%); ◒, AgX(100%).

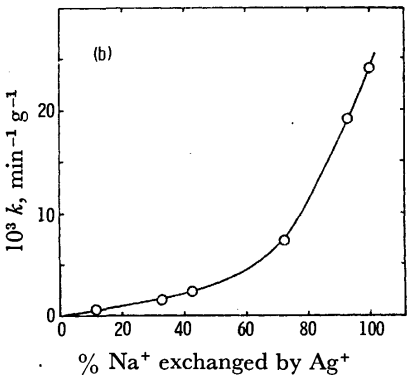

Fig. 2(b). Dependence of rate constants at 130 °C on the degree of ion-exchange.

Fig. 1(b) on AgX (93.2%) at temperatures ranging from 100 to 150 °C.

Effect of Ion-exchange. The dependence of the catalytic activity on the reaction temperature is given in Fig. 2(a). The broken lines indicate that the activity increases with repeated reactions above 150 °C. Figure 2(b) shows the first-order rate constants at 130 °C derived from these results. The activity increases gradually until the degree of exchange approaches 60% and rises steeply beyond that percentage. The energy of activation, as may be seen in Table 2, also changes abruptly at this degree of exchange. The initial ratio of the produced *cis*-2-butene to the *trans*-2-butene was larger than unity except in the case of AgX (42.6%) and increased with the temperature.

The results of acidity measurements are illustrated in Fig. 3. The total number of acid sites is linear with the degree of exchange, while strong acid sites of H_0 less than 3.3 increase drastically in number when the degree exceeds *ca.* 60%.

Effect of H_2-treatment. It was found that the silver particle was formed after the reaction at 200 °C, whereas this formation was not observed in the reaction below 100 °C. This fact suggests that olefins such as 1-butene can reduce AgX at high temperatures. Therefore, the effect of treatment with hydrogen as a reductant was examined.

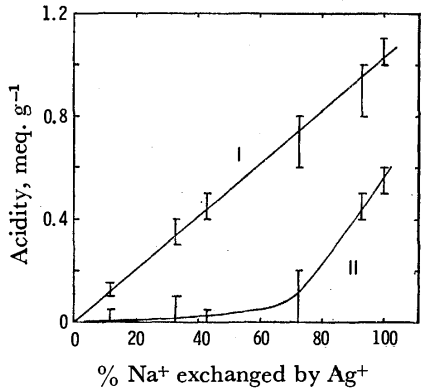

Fig. 3. Dependence of acidity on the degree of ion-exchange.
I, $H_0 \leqq +4.8$; II, $H_0 \leqq +3.3$ (H_0 is acidity function).

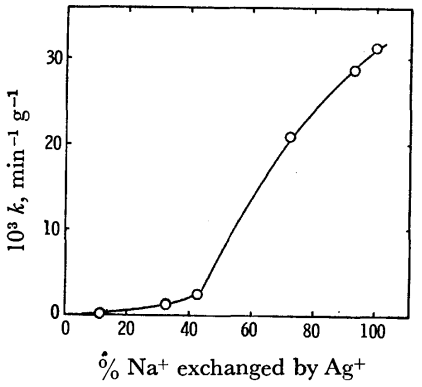

Fig. 4. Dependence of rate constants at 40 °C on the degree of ion-exchange over AgX pretreated with H_2.

Figure 4 shows the relationship between the rate constant and the degree of exchange for H_2-treated AgX. The abrupt increase in the activity begins at the degree of *ca.* 40%. The rate constants at 130 °C are greater than those for AgX without H_2-treatment by a factor of 10^2—10^3. The contribution of the formed silver particle to the activity may be negligible; a separate study of the silver powder catalyst has shown that the reaction became appreciable only above 350 °C. The energies of activation and the *cis*/*trans* ratios in the products are listed, together with the degrees of exchange, in Table 2. The ratio is less than unity for AgX (32.9%) as well as for AgX (42.6%).

Experiments with three butene isomers as the starting material provided the relative rate constants shown in the scheme below:[13]

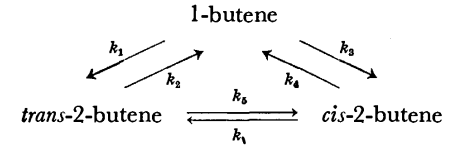

In the case of H_2-treated AgX (93.2%) at 72 °C, $k_1=12.8$, $k_3=17.3$, $k_4=3.5$, $k_5=2.1$, and $k_6=5.3$ were obtained by putting k_2 at unity, while $k_1=7.3$, $k_3=5.5$, $k_4=1.6$, $k_5=0.5$, and $k_6=1.1$ were obtained for H_2-treated AgX (32.9%) at 125 °C in a similar manner. On the reaction of 2-butenes, the treated AgX (93.2%) was evidently more active for the geometrical isomerization than for the double-bond shift. The preferential formation of *cis*-2-butene from 1-butene was also indicated. The treated AgX (32.9%) showed, on the contrary, a preference for the double-bond shift rather than for the geometrical isomerization and was active for the formation of *trans*-2-butene from 1-butene.

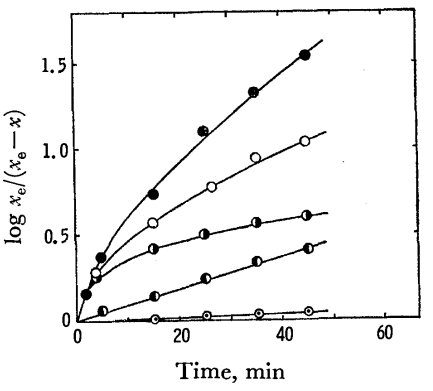

Fig. 5. First-order plots for 1-butene isomerization at 54 °C over AgX(100%) pretreated with H_2. Treatment temperature (⊙, 100 °C; ◐, 150 °C; ●, 250 °C; ○, 350 °C; ◑, 450 °C)

In Fig. 5, the effect of the treatment temperature on the activity is illustrated in terms of the first-order plot for the isomerization. The activity was raised slightly with H_2-treatment at 100 °C and became moderate and reproducible after treatment at 150 °C. When the treatment and the reaction were done alternately, the activity increased step by step and exceeded that of the decationated X-type zeolite, HX. When the temperature of treatment was higher than 250 °C, the initial rate became larger, but the degradation of activity occurred rapidly.

Parallel to this study of the activity, the X-ray diffraction of H_2-treated catalysts was examined. As the temperature of treatment was raised above 150 °C, a rapid growth of silver particles was recognized from the increase in the (111) and (200) diffraction intensities. The zeolite structure began to collapse above 250 °C and vanished completely after treatment at 450 °C.

Isotope Effect and Deuterium Distribution. In the case of treatment with D_2, the formation of HD as the result of exchange with surface hydrogen was negligible and the amount of deuterium atoms adsorbed on AgX (100%) was 9.30×10^{20} atom/g. This value was coincident with that of hydrogen atoms adsorbed when treated with H_2 under the same conditions. The initial rate constant for the isomerization of 1-butene at 56 °C was estimated to be 1.12×10^{-1} min^{-1} g^{-1}, compared with 1.67×10^{-1} min^{-1} g^{-1} over the H_2-treated catalyst; hence, the isotope effect was straightforward. The observed deuterium distribution is shown in Table 3. *trans*-2-butene, not quoted, had a distribution similar to that in *cis*-2-butene.

H_2- and D_2-treatment on AgX (32.9%) produced the rate constants of 1.10×10^{-1} min^{-1} g^{-1} and 1.00×10^{-1} min^{-1} g^{-1} respectively at 125 °C. The isotope effect appears to be small. The initial product by the isomerization of 1-butene on D_2-treated AgX (32.9%) consisted of 39% 2-butene-d_0 and 61% 2-butene-d_1.

Discussion

The preliminary experiment showed that the starting material, NaX, was inactive for the isomerization of 1-butene below 200 °C. As is evident from Fig. 2(b), the partial replacement of Na^+ by Ag^+ increases the activity, particularly when the degree of exchange exceeds 60%. There are several kinds of sites available to nonframework cations in zeolite: SI is at the center of the hexagonal prism; SII and SIII are in the sodalite cage; SIV faces the supercage, and SV is at the entrance into the supercage.[14] Shoemaker *et al.* determined the positions of the cation in AgY-type zeolite by means of X-ray diffraction and showed that all of the SI sites were occupied with silver ions.[15] Although the X-type zeolite differs from the Y-type in its Si/Al ratio and, consequently, in the number of cations, a similar site preference of Ag^+ is feasible. The preferential occupation of the interior sites, SI and SII and/or SIII, by Ag^+ is responsible for the slight increase in activity up to an exchange of *ca.* 60%. The cations which occupy the surface sites are expected to bring about a profound effect on the activity.

Table 2. Kinetic results of 1-butene isomerization on AgX-type zeolites

(a) Without H_2-treatment

Catalyst	Temperature range (°C)	*cis*/*trans* ratio	Energy of activation (kcal/mol)
AgX(11.3%)	127—141	1.4—1.6	34.2
AgX(32.9%)	120—144	1.8—2.1	31.9
AgX(42.6%)	135—150	0.7—0.9	29.2
AgX(72.3%)	100—150	1.3—1.7	16.4
AgX(93.2%)	100—150	1.8—2.1	16.4
AgX(100%)	120—140	1.9—2.1	16.4

(b) With H_2-treatment

Catalyst	Temperature range (°C)	*cis*/*trans* ratio	Energy of activation (kcal/mol)
AgX(11.3%)	125—183	1.3—1.7	15.4
AgX(32.9%)	77—125	0.3—0.8	13.4
AgX(42.6%)	71—144	0.4—0.7	13.4
AgX(72.3%)	27—86	1.3	11.2
AgX(93.2%)	40—83	1.2—1.5	11.0
AgX(100%)	40—83	1.5	11.1

The variation in the number of acid sites with the degree of exchange also reflects this location of cations. Exchanged zeolites with Ag^+ in the interior sites have only weak acid sites of H_0 between 3.3 and 4.8. Strong acid sites of H_0 less than 3.3 are observed on zeolites in which Ag^+ occupies the surface site. The correlation between the number of strong acid sites and the activity is remarkable when we combine Fig. 3 with Fig. 2(b). This result suggests that the isomerization on AgX proceeds on acidic sites.

cis-2-Butene was produced preferentially on all the AgX-type zeolites except AgX (42.6%). In the case of 2-butene, the geometrical isomerization was more rapid than the double-bond shift. These features are characteristic of the isomerization by a carbonium-ion mechanism on acidic sites. On the other hand, studies of basic catalysts have shown that, if the reaction proceeds *via* an allyl carbanion, much larger *cis*/*trans* ratios and higher selectivities toward the double-bond shift may be expected because of the restricted rotation of the intermediate.[16] The repetition of reactions above 150 °C or H_2-treatment on AgX enhanced the activity, accompanied by the formation of silver particles. However, the effect of H_2-treatment on the activity increase is larger than that of repeated reactions by a factor of 10^1—10^2. The H_2-treatment lowers the energy of activation (Table 2) and also shifts the threshold of the increase in the activity to a 40% exchange (Fig. 4); nevertheless, the features of the reaction are similar to those of the reaction on AgX without the treatment. The region of the degree of ion exchange, where the *cis*/*trans* ratio becomes anomalous and less than untiy, shifts to around 35% upon H_2-treatment. In this region, an alternative mechanism such as a hydrogen-switch seems to hold, where the double-bond shift is favored on the isomerization of 2-butene.[17]

Table 3. Deuterium distribution in products for 1-butene isomerization over D_2-treated AgX (100%) at 56 °C

Conversion (%)	1-butene				*cis*-2-butene			
	d_0	d_1	d_2	d_3	d_0	d_1	d_2	d_3
1	99.5	0.5	—	—	52.0	47.4	0.6	—
6	98.9	1.0	0.1	—	51.2	43.1	4.7	0.4
20	97.5	2.3	0.2	—	66.0	30.0	3.7	0.3
25	97.3	2.5	0.2	—	69.2	27.3	3.2	0.3
94	80.1	17.9	1.9	0.1	80.0	17.4	2.4	0.2

The deuterium distribution obtained by the use of D_2-treated AgX (100%) gives the following information (Table 3): the deuterium content in both 1-butene and *cis*-2-butene is 23% at 94% conversion, and the total number of deuterium atoms entering the butenes during the isomerization is estimated to be 7.80×10^{20} atom/g. Therefore, the finding that the number of deuterium atoms adsorbed upon D_2-treatment is 9.30×10^{20} atom/g predicts that the majority of deuterium atoms participate in the reaction. The result that the fraction of 2-butene-d_0 produced attained 50% even at 1% conversion requires some source of hydrogen. If the AgX (100%) treated with D_2 or H_2 is used for the isomerization of 1-butene and if a carbonium-ion mechanism is operative, the initial step in the formation of 2-butene may be supposed to be:

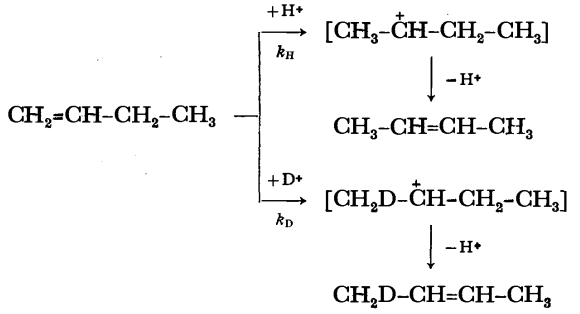

The ratio of rates on H_2- and D_2-treated catalysts can be given by:

$$V_H/V_D = k_H(n_H^0+n_H)/(k_Hn_H^0+k_Dn_D) \quad (1)$$

where n_H and n_D correspond to the numbers of hydrogen and deuterium atoms produced by the treatments, where n_H^0 is the number of hydrogen atoms existing in AgX before the treatment, and where k_H and k_D are rate constants. In a similar manner, the ratio of 2-butene-d_1/2-butene-d_0 produced in the reaction on D_2-treated AgX can be expressed by:

$$d_1/d_0 = k_Dn_D/k_Hn_H^0 \quad (2)$$

when the reaction is extrapolated to zero conversion. By substituting the observed values for V_H/V_D, d_1/d_0, n_H, and n_D in Eqs. (1) and (2), one can evaluate k_H/k_D to be 2.03 and n_H^0 to be 5.0×10^{20} atom/g. The latter value is comparable with the estimated total number of acid sites, 6.02×10^{20} site/g. This result strongly indicates that the acid sites in AgX are mainly of the Brönsted type and conforms to the finding of the IR study that AgX zeolite lacks Lewis acid sites.[4]

A similar analysis of the reaction on AgX (32.9%) gave a k_H/k_D ratio of 1.16 and an n_H^0 value of 2.3×10^{20} atom/g. The observed small isotope effect suggests that an alternative path is merged in the carbonium-ion mechanism. In the consideration of the tetrahedral geometry of SiOH on the surface, a hydrogen-switch mechanism[17] may be applicable to the reaction on AgX, with the degree of exchange around 35% expressed as follows:

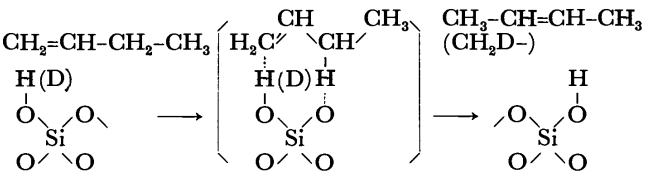

Since the surface hydrogen is protonic, the O–H bond may be thought to be weaker than the C–H bond. The rupture of the C–H bond is rate-determining, and there appears to be no direct isotope effect associated with the surface hydrogen. Accordingly, it is probable that the reaction proceeds by means of a simultaneous mechanism involving a hydrogen-switch and a carbonium-ion respectively, because 2-butene undergoes a *cis-trans* isomerization on this catalyst. This change in mechanism occurs in the limited range of ion exchange where Ag^+ would probably be located in the sodalite cage. This correlation between mechanism and structure requires further investigation.

The treatment with H_2 reduces silver ions into atoms, and an equivalent number of protons is produced. Since the number of acidic sites after treatment is, at most, three times as large as that before treatment, the remarkable increase in activity by a factor of 10^2—10^3 cannot be explained unless we introduce the increase in acid strength. Unfortunately, the acidity measurement is not possible because of the darkening of the treated AgX, but it seems reasonable to say that the distribution of acidic sites on the treated AgX became similar to that on the HX, spreading over a region of lower H_0 values. The H_2-treated AgX in the present study retains its crystal structure even though many of the Ag^+ ions are replaced with protons. As long as the H_2-treatment of AgX was performed at the relevant temperature, no water molecule was evolved and the Ag^+ ions remained as nonframework cations to maintain the zeolite structure. Protons with a strong acid strength are possibly stabilized in the structure.

References

1) P. B. Venuto, L. A. Hamilton, and P. S. Landis, *J. Catal.*, **5**, 484 (1966).
2) A. E. Hilschler, *ibid.*, **2**, 428 (1963); P. B. Weisz and V. J. Frilette, *J. Phys. Chem.*, **64**, 382 (1960); J. W. Ward, *J. Catal.*, **10**, 34 (1968).
3) CHR. Dimitrov and H. F. Leach, *ibid.*, **14**, 336 (1969); N. B. Cross, C. Kemball, and H. F. Leach, *J. Chem. Soc. A*, **1971**, 3315; K. Tsutsumi, S. Fuji, and H. Takahashi, *J. Catal.*, **24**, 8 (1972).
4) J. W. Ward, *ibid.*, **14**, 365 (1969).
5) D. J. C. Yates, *J. Phys. Chem.*, **69**, 1676 (1965).
6) K. Tsutsumi and H. Takahashi, This Bulletin, **45**, 2332 (1972).
7) H. Flaschka and F. Hudity, *Z. Anal. Chem.*, **137**, 104 (1952).
8) H. A. Benesi, *J. Phys. Chem.*, **61**, 970 (1957).
9) J. B. Uytterhoeven, P. Jacobs, K. Makay, and R. Schoonheydt, *ibid.*, **72**, 1768 (1968).
10) I. Yasumori and S. Ohno, This Bulletin, **39**, 1302 (1966).
11) J. L. Carter, D. J. C. Yates, P. J. Lucchesi, J. J. Elliott, and V. Kevorkian, *J. Phys. Chem.*, **70**, 1126 (1966).
12) E. F. Meyer and D. G. Stroz, *J. Amer. Chem. Soc.*, **94**, 6344 (1972).
13) W. O. Haag and H. Pines, *ibid.*, **82**, 387 (1960).
14) D. H. Olson, G. T. Kokotailo, and J. F. Charnell, *J. Colloid Interface Sci.*, **28**, 305 (1968).
15) G. R. Eulenberger, D. P. Shoemaker, and J. G. Keil, *J. Phys. Chem.*, **71**, 1812 (1967).
16) N. F. Foster and R. J. Cvetanovic, *J. Amer. Chem. Soc.*, **82**, 4272 (1960).
17) J. Turkevich and R. K. Smith, *J. Chem. Phys.*, **16**, 466 (1948).

Formation and Collapse of Mixed Monolayers of Trilaurin with Cholesterol and with Tristearin[1]

Masayuki NAKAGAKI and Noriaki FUNASAKI*

Faculty of Pharmaceutical Sciences, Kyoto University, Sakyo-ku, Kyoto 606

(Received January 24, 1974)

The surface pressure-area curves of mixed monolayers and the equilibrium spreading pressure of solid mixtures were measured at 25 °C for cholesterol and trilaurin as well as tristearin and trilaurin. The phase diagrams of these mixtures were obtained by the measurement of the melting point. From two curves, one representing the relation between the collapse pressure (if the mixed monolayer was not overcompressed) and the composition of mixed monolayer, and the other representing the relation between the equilibrium spreading pressure and the composition of solid mixture, it was shown that the compositions of the mixed monolayer and the solid mixture coexisting in equilibrium were obtained. It was found that when the mixed monolayer of cholesterol and trilaurin was compressed, pure trilaurin began to collapse and deposit, and that the mixed monolayer of tristearin and trilaurin was apt to be overcompressed. It was concluded on the basis of phase rule and thermodynamics for plane interfaces that the equilibrium spreading pressure is constant regardless of the composition of solid mixture if the solid mixture consists of two phases of mixed crystals, and that cholesterol and trilaurin form a regular solution in mixed monolayer.

The miscibility in a mixed monolayer can be discussed on the basis of the composition dependence of collapse pressure of the mixed monolayer.[2-4] A theoretical study has recently been reported on the equilibrium spreading pressure of mixed crystals.[5] In both processes, *i.e.*, when a lipid mixture forms a monolayer and when a mixed monolayer collapses and deposits a lipid mixture, a mixed monolayer and a lipid mixture coexist on the air-water interface. In order to clarify the coexisting state of a mixed monolayer and a bulk mixture, the phase rule[6] and thermodynamics of plane interface seem to be useful. However, a thorough study has not been reported yet.

In the present investigation, the collapse pressure of mixed monolayers of cholesterol and trilaurin as well as tristearin and trilaurin and also the equilibrium spreading pressure of these solid mixtures were measured and these results were discussed on the basis of the phase rule and thermodynamics of plane interface.

Experimental

Materials. Trilaurin and tristearin used in this work were the same as those used previously.[7] They were synthesized directly from the corresponding fatty acid chloride and glycerol and then purified by repeated recrystallization. Cholesterol (guaranteed grade, Wako Pure Chemicals, Ltd.) was recrystallized from ethanol.[8]

Measurement of Surface Pressure. The surface pressure-area curve of mixed monolayers of cholesterol and trilaurin as well as tristearin and trilaurin were drawn by measuring the surface pressure of the monolayer which was compressed at nearly constant speed.

Solid mixtures of cholesterol and trilaurin as well as tristearin and trilaurin were prepared by mixing the chloroform solutions of both components and evaporating the solvent gradually at room temperature. When this crystalline mixture was sprinkled gently onto a clean aqueous surface, the surface pressure increased and reached a constant value. When this was compressed to some extent and then kept at that area, the surface pressure once increased and then decreased to a value nearly equal to the original value. By averaging these two equilibrium values of surface pressure, the equilibrium spreading pressure, F_e, was determined. Although a part of the solid mixture spreads as a monolayer, the composition of the solid mixture does not vary, since the amount of mixture sprinkled was more than, at least, a hundred times as much as required to form the monolayer. The surface pressure was measured at 25±0.1 °C. Details of the measurement of surface pressure have been reported.[7]

Measurement of Melting Point. The solid was mixed in the same way as described above. The initial and final melting points of the solid mixture were measured with a Yanagimoto micro-melting point apparatus, SR-50, equipped with a polarization microscope.

Results

Surface Pressure-Area Curve. The relations between surface pressure F and mean area A of mixed monolayers of trilaurin with cholesterol and with tristearin are shown in Figs. 1 and 2, respectively. The kink-points (indicated by arrows) are the points at which the monolayers begin to collapse. The pressure and area

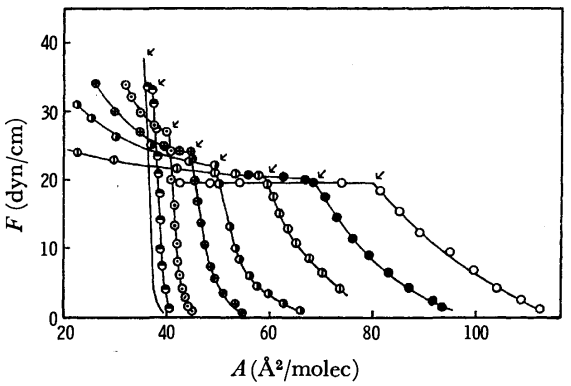

Fig. 1. The surface pressure-mean area curves of mixed monolayers of cholesterol and trilaurin of various mole ratios.
Cholesterol: trilaurin
—: 1:0, ◓: 9:1, ⊙: 4:1, ⊕: 2:1, ◑: 1:1, ◍: 1:2, ●: 1:5, ○: 0:1.

* Present address: *Kyoto College of Pharmacy, 5-Nakauchi-cho, Misasagi Yamashina, Higashiyama-ku, Kyoto 607.*

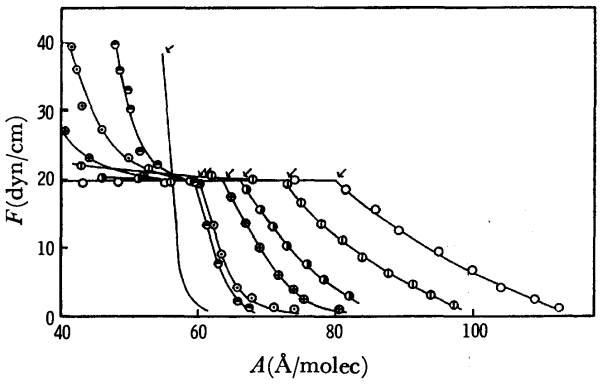

Fig. 2. The surface pressure-mean area curves of mixed monolayers of tristearin and trilaurin of various mole ratios.
Tristearin: trilaurin
—: 1: 0, ◓: 9: 1, ⊙: 4: 1, ⊕: 2: 1, ◑: 1: 1, ⓘ: 1: 2, ○: 0: 1.

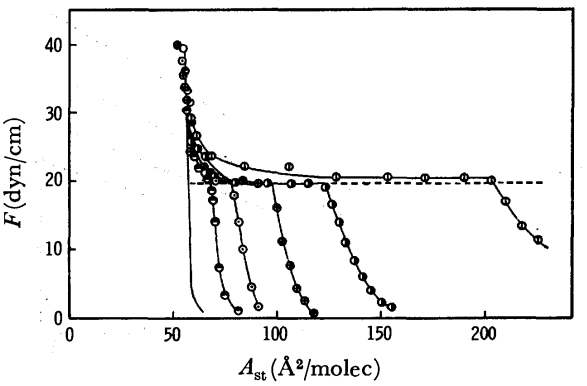

Fig. 4. The relation between surface pressure and area per molecule of tristearin for mixed monolayers of tristearin and trilaurin of various mole ratios.
Tristearin: trilaurin
—: 1: 0, ◓: 9: 1, ⊙: 4: 1, ⊕: 2; 1, ◑: 1: 1, ⓘ: 1: 2.
------: Collapse pressure of trilaurin.

of these points are collapse pressure F_c and collapse area A_c, respectively. The deposit formed by the collapse of a monolayer is expected to contain a component with lower collapse pressure in larger amount than one with a higher collapse pressure. In an extreme case, it is possible that only the former comes into the deposit, the latter remaining entirely in the monolayer. This might be clarified by dividing the area by the number of molecules of the component whose collapse pressure is higher, instead of the total number of initially spread molecules in the mixed monolayer, and by comparing the area thus obtained with the area per molecule in the pure monolayer of the component of higher collapse pressure. We see from Figs. 1 and 2 that the component with lower collapse pressure is trilaurin in both mixed monolayers. Instead of the mean area A, the area occupied by one molecule of cholesterol A_{ch}, and that occupied by one molecule of tristearin A_{st}, are plotted in Figs. 3 and 4, respectively. All the experimental values lies on one and the same curve (dotted line) at a pressure higher than collapse pressure regardless of the composition initially spread (Fig. 3). On the other hand, the collapse pressure is the same and equal to that of a trilaurin monolayer (dotted line) but the area at higher pressure varies with initial composition (Fig. 4).

Relation between Mean Area and Mole Fraction in the Mixed Monolayers. The relations between the mean area A at a given pressure and the mole fraction of trilaurin in the mixed monolayers x_1^s are given in Figs. 5 and 6, respectively. In these figures, the dotted line is calculated by the equation

$$A = x_1^s A_1 + x_2^s A_2 \qquad (1)$$

where x^s is the mole fraction in a monolayer, A the mean area per molecule, and subscripts 1 and 2 indicate the components. The experimental values of the area of mixed monolayer of tristearin and trilaurin agree with the values from Eq. (1) (Fig. 6), while the experimental values are smaller than the calculated values for the monolayer of cholesterol and trilaurin (Fig. 5).

Equilibrium Spreading Pressure and Collapse Pressure. Equilibrium spreading pressure was measured by gently sprinkling a large quantity of the crystalline mixture on the water surface. In the case of the mixture of tri-

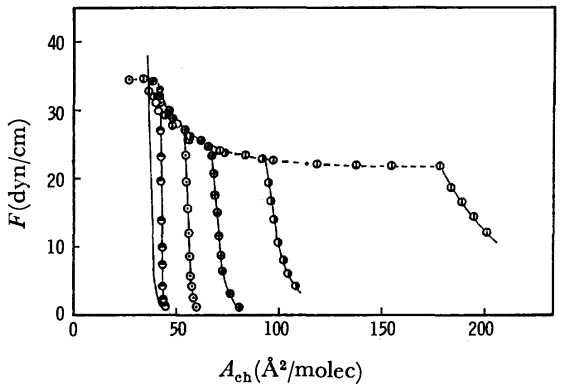

Fig. 3. The relation between surface pressure and area per molecule of cholesterol for mixed monolayers of cholesterol and trilaurin of various mole ratios.
Cholesterol: trilaurin
—: 1: 0, ◓: 9: 1, ⊙: 4: 1, ⊕: 2: 1, ◑: 1: 1, ⓘ: 1: 2.

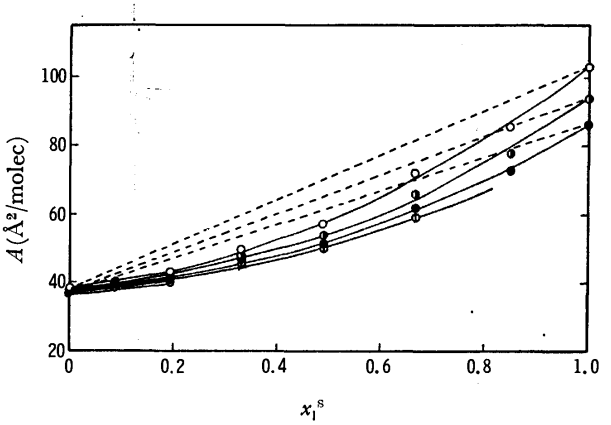

Fig. 5. The relation between mean area and mole fraction of trilaurin for mixed monolayers of cholesterol and trilaurin at various surface pressures.
------: Line calculated from Eq. (1).
F(dyn/cm)
○: 5, ◑: 10, ●: 15, ⓘ: 20, ◓: 27.5.

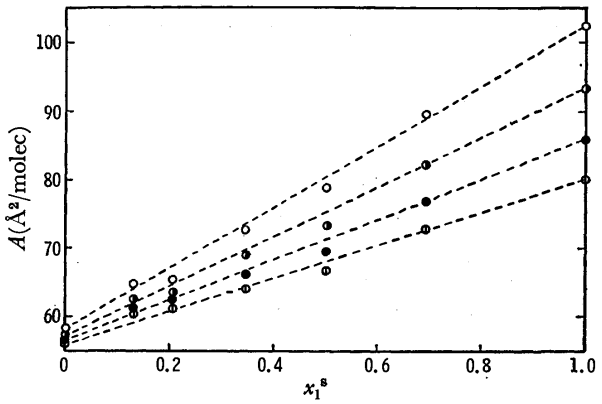

Fig. 6. The relation between mean area and mole fraction of trilaurin for mixed monolayers of tristearin and trilaurin at various surface pressures.
------: Line calculated from Eq. (1).
F(dyn/cm)
○: 5, ◑: 10, ●: 15, ⓕ: F_c.

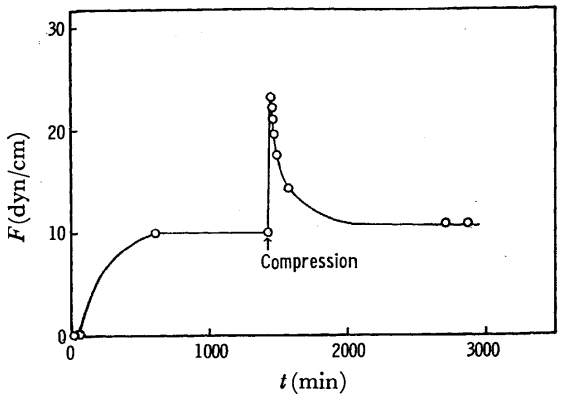

Fig. 7. Equilibrium spreading pressure of solid mixture of tristearin and trilaurin (1: 1).

stearin and trilaurin at the molar ratio of 1: 1, the surface pressure increased and reached a constant value (Fig. 7). When the monolayer in this state was compressed to some extent at the time indicated by an arrow, the pressure increased rapidly and returned

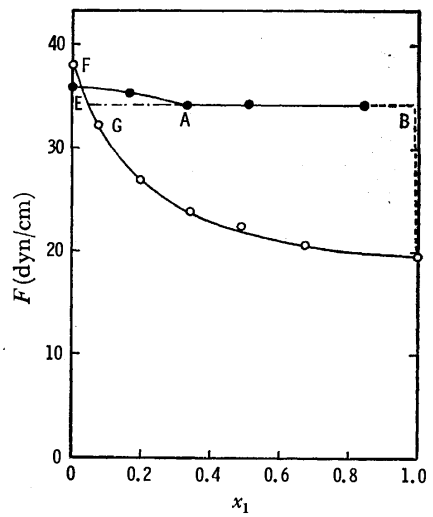

Fig. 8. Equilibrium spreading pressure and collapse pressure for mixed system of cholesterol and trilaurin.
●: $F_e-x_1^b$, ○: $F_c-x_1^s$.

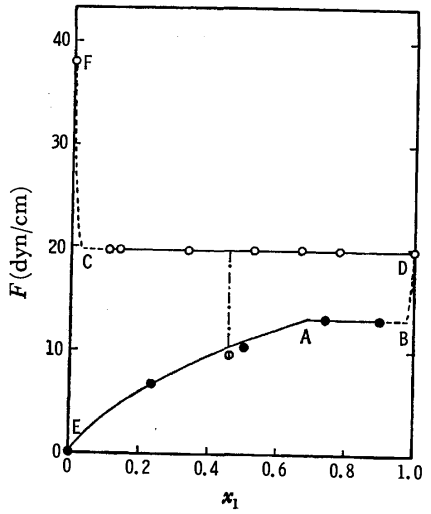

Fig. 9. Equilibrium spreading pressure and collapse pressure for mixed system of tristearin and trilaurin.
●: $F_e-x_1^b$, ○: $F_c-x_1^s$.

gradually to the original value. Equilibrium spreading pressure was determined as the mean value. It was thus confirmed that the crystal and the monolayer were in equilibrium. It took about one minute for trilaurin, about 30 min for cholesterol and more than 10 day for tristearin to return nearly to the original value after the monolayer had been compressed and kept at that area, while in mixed monolayer, it took about 30 min for the cholesterol–trilaurin system.

The relation between the equilibrium spreading pressure and mole fraction of trilaurin in solid mixture is shown by closed circles for cholesterol and trilaurin in Fig. 8 and for tristearin and trilaurin in Fig. 9. The composition of point B was uncertain, and the equilibrium spreading pressure near this point (shown by dotted lines) was not measured. The relation between the collapse pressure F_c, obtained from Figs. 1 and 2, and the mole fraction of trilaurin in the mixed monolayers x_1^s is also shown by open circles in Figs. 8

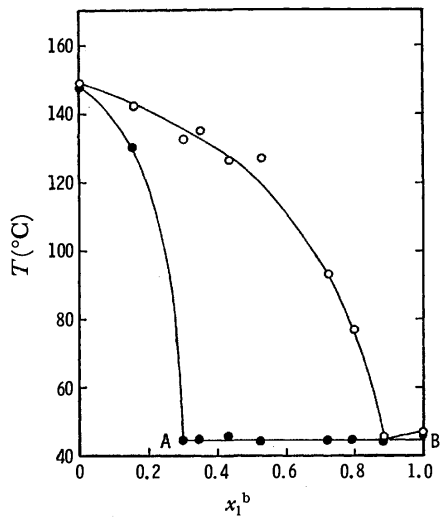

Fig. 10. The relation between melting points and mole fraction of trilaurin for a mixture of cholesterol and trilaurin.
●: Initial melting point, ○: Final melting point.

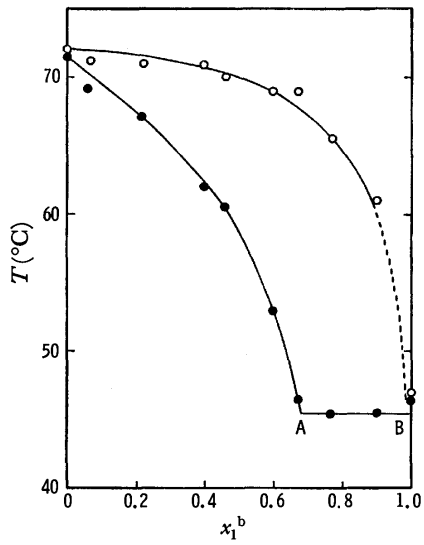

Fig. 11. The relation between melting points and mole fraction of trilaurin for a mixture of tristearin and trilaurin.
●: Initial melting point, ○: Final melting point.

and 9, respectively.

Melting Point of Solid Mixture. The melting points of solid mixtures for cholesterol and trilaurin and for tristearin and trilaurin are shown in Figs. 10 and11, respectively. Closed circles indicate the initial melting points and open circles the final melting points.

Discussion

Pressure-Area Curve. A_{ch} of mixed monolayer is larger than the area occupied by one molecule of cholesterol in its own monolayer (Fig. 3). The pressure-area curves of mixed monolayers at higher pressure than collapse pressure are on a single line regardless of the composition of initially spread monolayer. These two facts indicate that when the mixed monolayer collapses, only trilaurin deposits to solid and all the initially spread molecules of cholesterol remain in the monolayer, containing a part of trilaurin, and that the molar ratio of trilaurin to cholesterol in the monolayer depends only on the surface pressure regardless of the composition of the initially spread monolayer.

The mixed monolayer begins to collapse at the pressure equal to the collapse pressure of the trilaurin monolayer and after all the trilaurin molecules have deposited, *viz.*, the area A_{st} has reached the occupied area of the tristearin monolayer, the monolayer collapses again at the collapse pressure of the pure tristearin monolayer (Fig. 4). At a pressure lower than the collapse pressure, the mean area of the mixed monolayer agrees with the additivity of the area given by Eq. (1) (Fig. 6). Thus, it might be concluded that tristearin and trilaurin are completely immiscible in monolayer. However, the fact that the F-A_{st} curve varies with the composition of initially spread monolayer in the range from the first collapse pressure (equal to that of trilaurin monolayer) to the second collapse pressure (equal to that of tristearin monolayer), cannot be explained without taking the interaction between both components into account.

Equilibrium Spreading Pressure and Collapse Pressure. A phase diagram of cholesterol–trilaurin system is given in Fig. 8. The mixed monolayer exists at a surface pressure lower than the curve of collapse pressure (open circles), but mixed monolayer and solid coexist in the range between this curve and the curve of equilibrium spreading pressure (closed circles). If a horizontal line is drawn at a given surface pressure, its intersection with the curves of equilibrium spreading pressure and collapse pressure give mole fractions of trilaurin in the solid and in the monolayer, respectively, coexisting on the water surface. In this meaning, the curve of collapse pressure and that of equilibrium spreading pressure might be called monolayer and solidus lines, respectively, the latter being more generally called bulk phase line. It is seen that cholesterol, whose equilibrium spreading pressure is higher, is richer in the monolayer and trilaurin, whose equilibrium spreading pressure is lower, is richer in the solid phase. The mixed monolayers (Fig. 3) were those whose mole fraction of trilaurin was greater than x_1^G (Fig. 8), *viz.*, the mole fraction 0.06 of trilaurin at point G. In this range of composition, nearly pure trilaurin is expected to deposit, when the mixed monolayer is compressed. This agrees with the result given in Fig. 3. As expected, when the mixed monolayer was further compressed, the surface pressure increased and remained constant at about 34.2 dyn/cm, not increasing with further compression (Fig. 3). Further compression was not carried out, since the mixed monolayer had spread over the top of the trough.

The equilibrium spreading pressure is constant over the range of composition between A and B in Fig. 8. For interpretation, the phase rule for plane interface might be used. The number of freedom, ω, is given by[6]

$$\omega = c - \varphi - (\psi - s) + 2 \qquad (2)$$

where c is the number of components, φ is the number of the bulk phase, ψ is the number of interface phases and s is the number of types of interface. If the solid deposits over the range of composition between x^A and x^B is a mixture of two mixed crystals S^A, and S^B, whose compositions are x^A and x^B, respectively, and if A and W denote air and water, respectively, then c=4 (A, W, cholesterol and trilaurin), φ=4 (A, W, S^A and S^B) s=6 (A/W, A/S^A, A/S^B, W/S^A, W/S^B and S^A/S^B), and ψ=6 (one phase at each interface). Thus we get ω=2. Since temperature and pressure are kept constant, the surface pressure and composition of mixed monolayer should be constant irrespective of the composition of the solid mixture. The equilibrium spreading pressure is thus found to be constant in the range of composition between A and B in Fig. 8. Comparing this with the phase diagram of the bulk phase, it is found from Fig. 10 that the solids of the compositions of x^A and x^B coexist at 44.5 °C. If these compositions are considered nearly unvaried at temperatures below 44.5 °C, they correspond to compositions A and B (25 °C).

In the case of the tristearin–trilaurin system, the components were suspected of being immiscible in the

mixed monolayer (Figs. 4 and 6). However, it is not certain whether the monolayer is in equilibrium with the solid formed when the monolayer collapses, or not. The collapse pressure of tristearin monolayer is 38 dyn/cm, while the equilibrium spreading pressure is 0 dyn/cm (Fig. 9). This discrepancy may be due to the fact that the rate of collapse of the tristearin monolayer is low, so that its monolayer is apt to be overcompressed. Actually, the surface pressure decreased gradually with time and reached 1 dyn/cm after ten days, when the area of the tristearin monolayer was kept constant as soon as the monolayer began to collapse. Thus, the mixed monolayer of tristearin and trilaurin, also, has the possibility of being overcompressed. If the area of the mixed monolayer of tristearin and trilaurin at $x_1=0.406$ was kept constant as soon as the monolayer began to collapse, the surface pressure decreased (Fig. 9) down to the value ① after two days and did not decreased any more. The collapse pressure obtained from the pressure-area curves of the mixed monolayer of tristearin and trilaurin (Figs. 2 and 4) is too great to be in an equilibrium state. It cannot be concluded from the results (Figs. 4 and 6) that tristearin and trilaurin are immiscible in the mixed monolayer.

Since tristearin and trilaurin are completely miscible in the liquid state and partially miscible in the solid state (Fig. 11), it is unlikely that they are completely immiscible in the monolayer state. Therefore, the result showing the establishment of the additivity of the area (Fig. 6) should be interpreted as the ideal mixing in the monolayer.

The equilibrium spreading pressure is constant over the range from x_1^A to x_1^B (Fig. 9). This is interpreted to be due to the coexistence of the mixed crystals of the compositions x_1^A and x_1^B, corresponding to points A and B (Fig. 8) for the mixture of cholesterol and trilaurin. It is found that the compositions of points A and B (Fig. 9) are equal to those of points A and B (Fig. 11).

Thermodyndmic Treatment of the Equilibrium between Monolayer and Solid. Only trilaurin is deposited as a solid and the mixed monolayer is in equilibrium with the pure solid of trilaurin when the mixed monolayer of cholesterol and trilaurin collapses. Since the chemical potential of trilaurin in the mixed monolayer is equal to that in the solid, the following equation can be written according to Joos.[9]

$$\mu_1^{ob} = \mu_1^{os} + kT \ln \gamma_1^s x_1^s + F\bar{A}_1 \qquad (3)$$

where μ^0 is the standard chemical potential, γ the activity coefficient, x the mole fraction and $\bar{A}$ the partial molecular area. Superscripts b and s indicate a solid and a monolayer, respectively. For one-component system of trilaurin, we have

$$\mu_1^{ob} = \mu_1^{os} + F_{1c}A_{1c} \qquad (4)$$

with $x_1^s=1$, $\bar{A}_1=A_{1c}$ and $\gamma_1^s=1$. Substituting this equation into Eq. (3), we obtain the following equation for the surface activity coefficient of trilaurin γ_1^s.

$$\gamma_1^s = \frac{1}{x_1^s} \exp\left(\frac{F_{1c}A_{1c} - F\bar{A}_1}{kT}\right) \qquad (5)$$

From Fig. 1 we have $F_{1c}=19.4$ dyn/cm, and $A_{1c}=80.5$ Å^2/molec. The mole fraction of trilaurin in the mixed monolayer x_1^s at a given surface pressure is obtained from the curve of collapse pressure (Fig. 8). The value of $\bar{A}_1$ is obtained from the intercept of the tangent at the composition of x_1^s on the curve representing the relation between the mean area A and the mole fraction of the monolayer x_1^s under the given pressure. The right hand of Eq. (5) can be calculated at a given surface pressure. Proportionality holds between the logarithm of the surface activity coefficient of trilaurin γ_1^s and the square of the mole fraction of

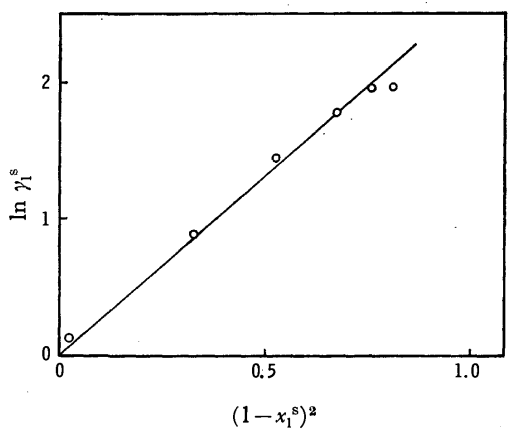

Fig. 12. The relation between the logarithm of surface activity coefficient of trilaurin and the square of mole fraction of cholesterol in mixed monolayer of cholesterol and trilaurin.

cholesterol in the monolayer $(1-x_1^s)^2$ (Fig. 12). If we denote proportionality constant by B/kT, we have

$$\ln \gamma_1^s = \frac{B}{kT}(1-x_1^s)^2. \qquad (6)$$

$B=1.58$ kcal/mol is obtained from Fig. 12. Equation (6) is the relationship expected from the theory of regular solution. Thus, it is concluded that cholesterol and trilaurin form a regular solution in the monolayer.

References

1) Presented at the 24th Colloquium on Colloid and Interface Chemistry, Gifu, October, 16, 1971.
2) D. J. Crisp, "Surface Chemistry," Supplement to Research, Butterworths, London (1949), p. 23.
3) G. L. Gaines, "Insoluble Monolayers at Liquid-Gas Interface," Interscience Publishers (1966), p. 281.
4) M. C. Phillips and P. Joos, *Kolloid-Z. Z. Polym.*, **238**, 499 (1970).
5) P. Joos, *J. Colloid Interfac. Sci.*, **35**, 215 (1971).
6) R. Defay, I. Prigogine, A. Bellemans, and D. H. Everett, "Surface Tension and Adsorption," Longmans, London (1966), p. 77.
7) M. Nakagaki, N. Funasaki, and K. Fujita, *Nippon Kagaku Zasshi*, **93**, 243 (1972).
8) M. Nakagaki and N. Funasaki, *ibid.*, **1972**, 1576.
9) P. Joos, *Bull. Soc. Chim. Belges*, **78**, 207 (1969).

Mechanism of Charge-transfer Polymerization. X. Flash Photolysis of the *N*-Vinylcarbazole–Pyromellitic Dianhydride System

Yasuhiko SHIROTA, Tamotsu TOMIKAWA,* Takashi NOGAMI, Kazuhiro TADA, Naoto YAMAMOTO,** Hiroshi TSUBOMURA,** and Hiroshi MIKAWA

Department of Applied Chemistry, Faculty of Engineering, Osaka University, Yamadakami, Suita, Osaka 565

(Received March 4, 1974)

The formation of transient *N*-vinylcarbazole cation-radical and pyromellitic dianhydride anion-radical was demonstrated for the *N*-vinylcarbazole-pyromellitic dianhydride-solvent system by means of flash spectroscopy. The transient decay process was found to be solvent-dependent. In 1,2-dichloroethane the decay of the anion-radical was of the first-order at initial stage ($t<100$ μs), and the second-order kinetics ($t>100$ μs) then followed. In acetonitrile the transient decay followed the second-order kinetics in the whole time region.

The photochemical reaction of *N*-vinylcarbazole (VCZ) in the presence of an electron acceptor is currently receiving great attention. The reaction involves cationic polymerization, radical polymerization or radical copolymerization with an electron-accepting monomer and cyclodimerization to give the *trans*-head-to-head cyclodimer, the reaction course being strongly solvent-dependent.[1] It has been postulated that these reactions are initiated by VCZ cation-radical formed by the photochemical electron transfer from VCZ to the electron acceptor, and the multi-reaction courses are explained in terms of the dual cationic and radical reactivity of the VCZ cation-radical.[1]

Recently, efforts have been made to elucidate the primary process of the above photochemical reactions. We demonstrated for the first time the formation of VCZ cation-radical and the anion-radical of the electron acceptor by means of flash spectroscopy for the VCZ–chloranil system in acetone, acetonitrile and methanol.[2] The formation of ion-radical species has since been confirmed successively for the VCZ–tetracyanobenzene[3] and VCZ–dimethyl terephthalate[4] systems by means of laser photolysis or conventional flash photolysis. However, only a few systems were studied as regards the photochemical primary process of the VCZ-electron acceptor system, not many studies being carried out on the effect of solvent on the transient decay.

As an extension of our studies on the photosensitized charge-transfer reaction of VCZ, we have investigated the flash photolysis for the VCZ–pyromellitic dianhydride (PMDA)–solvent system. 1,2-Dichloroethane and acetonitrile were selected as solvents: cationic polymerization of VCZ takes place in the former solvent, while the cyclodimerization of VCZ occurs in the latter solvent.[1] The transient absorption spectra and the transient decay process are described and discussed.

Experimental

Materials. *N*-Vinylcarbazole (VCZ) was purified and dried as described before.[2] Pyromellitic dianhydride (PMDA) (Wako Pure Chemical Ind., Ltd.) was recrystallized from anhydrous ethyl acetate and then sublimed twice *in vacuo*. 1,2-Dichloroethane was shaken with dilute aqueous sodium hydroxide, washed with water, dried over calcium chloride, refluxed with calcium hydride, and distilled immediately before use. Acetonitrile was refluxed over phosphorus pentoxide for more than 24 hr, distilled and then refluxed over anhydrous potassium carbonate and again distilled immediately before use.

Flash Spectroscopy. The concentrations of VCZ and PMDA for flash spectroscopy were mostly 3×10^{-4} M and 4×10^{-4} M, respectively. Freshly prepared solutions were degassed at 10^{-5} mmHg by means of several freeze-pump-thaw cycles and flashed at room temperature in a cylindrical silica cell with 20 cm path length and 1.5 cm diameter. The flash apparatus, a conventional one, was almost the same as that described by Yamamoto *et al.*[5] A stored electrical energy available for the flash was approximately 250 J, the half-duraction time of the flash being about 7 μs. The transient absorption spectra were photographed with a Narumi RM-23-I grating spectrograph with a Kodak high speed infrared film. A photoelectric recording system consisting of a R446 photomultiplier and a National type 501 oscilloscope was used. A filter solution composed of a glass plate and an aqueous solution of $NaNO_3$ (86 g in 500 ml solution) was inserted between the flash lamp and the reaction cell in order to ensure selective excitation of VCZ by the flash illumination (Fig. 1). In the case of the photoelectric recording of a transient decay, an aqueous solution of $CuSO_4\cdot5H_2O$ (80 g) and $NaNO_3$ (30 g) in 500 ml solution was used as a filter to obtain light of wavelength 330—620 nm. The electronic absorption spectra of the ground state molecule were taken with a Hitachi 124 spectrophotometer.

Results and Discussion

The VCZ–PMDA system forms a charge-transfer complex in the ground state, showing a charge-transfer absorption band (CT band) with a maximum at 490 nm (for the 1st CT band) in 1,2-dichloroethane. In the present flash photolysis, however, the donor-acceptor interaction in the ground state was negligible because of the low concentration of the solution (*ca.* 10^{-4} M order). Selective excitation of VCZ was possible as shown in Fig. 1.

Transient Spectra Obtained for the VCZ-PMDA–Acetonitrile System. The cyclodimerization of VCZ takes place to give *trans*-1,2-(9-dicarbazolyl)cyclobutane. The reaction mechanism is explained in terms of the intermediacy of VCZ cation radical formed by

* Present address: Mitsui Petrochemical Ind. Ltd., Iwakuni, Yamaguchi 740.

** Department of Chemistry, Faculty of Engineering Science, Osaka University, Toyonaka, Osaka 560.

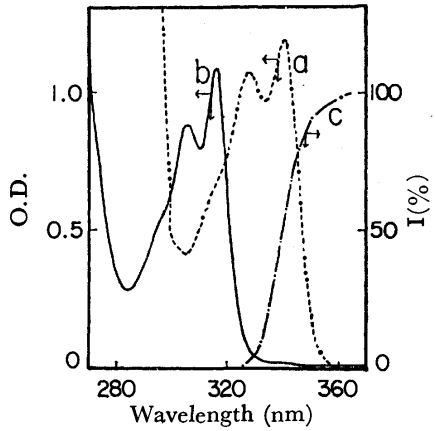

Fig. 1. The electronic absorption spectra of VCZ and PMDA in 1,2-dichloroethane and the transmittance of the filter solution used for the flash photolysis. (a) VCZ(3×10^{-4} M) (b) PMDA(4×10^{-4} M) (c) filter solution ($NaNO_3$ 86 g in 500 ml aqueous solution)

the photochemical electron transfer from VCZ to PMDA.[1] Flash excitation of VCZ in this system gave rise to a transient absorption spectrum consisting of two band systems, one in the wavelength region 550—700 nm with maxima at 665 and 615 nm, and the other in the wavelength region 700—850 nm with a maximum at 780 nm (Fig. 2). The former was identified as the PMDA anion-radical by comparison with the spectrum of the chemically prepared PMDA anion-radical.[6] The latter was assigned to the VCZ cation-radical by comparison with the spectrum of the authentic VCZ cation-radical generated by γ-ray irradiation in *sec*-butyl chloride glass at 77 K.[2] The absorption band of the VCZ cation-radical seems to more or less overlap with the absorption band of the PMDA anion-radical especially in the wavelength region around 615 nm. The transient absorption weakened more rapidly at around 615 nm than at 665 nm (Figs. 2 and 3). No transient absorption was obtained by the flash excitation of VCZ alone in acetonitrile. This indicates that the electron transfer occurred from the excited VCZ to PMDA to produce the VCZ cation-radical and the PMDA anion-radical.

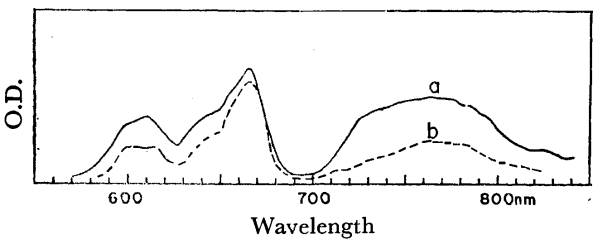

Fig. 2. The transient absorption spectra obtained by the flash photolysis for the VCZ(3×10^{-4} M)-PMDA (4×10^{-4} M)-acetonitrile system at room temperature. Delay time after flash excitation: (a) 4 μs (b) 59 μsec.

Transient Spectra Obtained for the VCZ-PMDA-1,2-Dichloroethane System. The cationic polymerization of VCZ occurs in preparatory scale reactions of this system. It has been proposed to be initiated by the VCZ cation-radical.[1] The formation of the transient VCZ cation-radical and PMDA anion-radical was likewise demonstrated by flash photolysis. The transient absorption spectra obtained by flash illumination are similar to those obtained in acetonitrile (Fig. 3). Confirmation of the occurrence of the electron transfer from VCZ to PMDA to produce the VCZ cation-radical and the PMDA anion-radical in acetonitrile and in 1,2-dichloroethane by means of flash spectroscopy provided direct evidence for the intermediacy of the VCZ cation-radical proposed for the photocyclodimerization and cationic photopolymerization of VCZ.

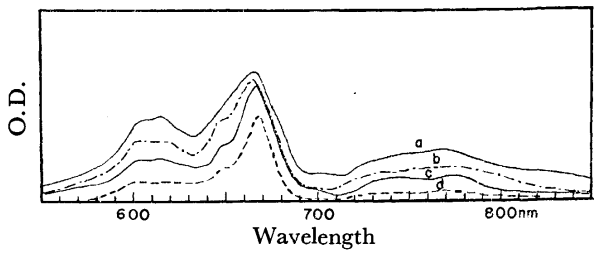

Fig. 3. The transient absorption spectra obtained by the flash photolysis for the VCZ(3×10^{-4} M)-PMDA (4×10^{-4} M)-1,2-dichloroethane system at room temperature. Delay time after flash excitation: (a) 3 μs (b) 23 μs (c) 53 μs (d) 105 μs.

Transient Spectra Obtained for the VCZ-1,2-Dichloroethane System. *N*-Vinylcarbazole generally undergoes radical polymerization by direct irradiation in the UV light in a high vacuum system in various solvents such as tetrahydrofuran, acetone, acetonitrile, *N*,*N*-dimethylformamide or dimethyl sulfoxide, the polymerization being suggested to be initiated by the excited triplet state of VCZ.[7,8] However, cationic photopolymerization of VCZ takes place in dichloromethane or in 1,2-dichloroethane even in the absence of an electron acceptor.[8] It has been suggested that the solvent, dichloromethane or 1,2-dichloroethane acts as an electron acceptor to the excited VCZ, the electron transfer occurring in these solvents from the excited VCZ to the solvent to produce the transient VCZ cation-radical which initiates the cationic polymerization of VCZ.[9] When VCZ alone was flash illuminated in 1,2-dichloroethane at room temperature, a transient absorption spectrum assignable to the VCZ cation-radical was obtained (Fig. 4), whereas no transient absorption was obtained in tetrahydrofuran, acetonitrile or *N*,*N*-dimethylformamide.[10] The results of flash photolysis support the mechanism of the VCZ cation-

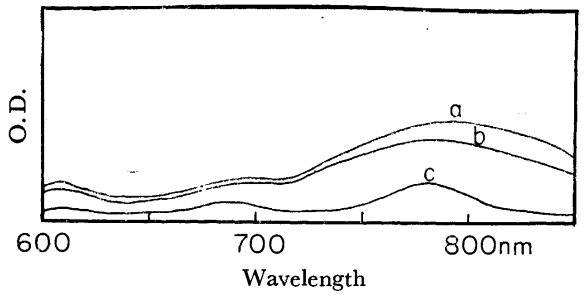

Fig. 4. The transient absorption spectra obtained by the flash photolysis for the VCZ(3×10^{-4} M)-1,2-dichloroethane system at room temperature. Delay time after flash excitation: (a) 5 μs (b) 28 μs (c) 60 μs.

radical initiation for the cationic photopolymerization of VCZ in 1,2-dichloroethane or in dichloromethane in the absence of an added electron acceptor.

Decay of the Transient Species. The transient decay followed by the photoelectric recording method was found to be solvent-dependent. In 1,2-dichloroethane, the decay of the PMDA anion-radical was of first-order at an initial stage ($t<100$ μs), followed by the second-order kinetics ($t>100$ μs). In contrast, the transient decay in acetonitrile followed the second-order kinetics for all the time intervals ($t>20$ μs). The oscilloscope traces for the decay of the PMDA anion-radical measured at the wavelength of the absorption maximum, 668 nm in 1,2-dichloroethane and 665 nm in acetonitrile, are shown in Figs. 5(a) and (b), and 6(a) and (b), respectively. The first-order and second-

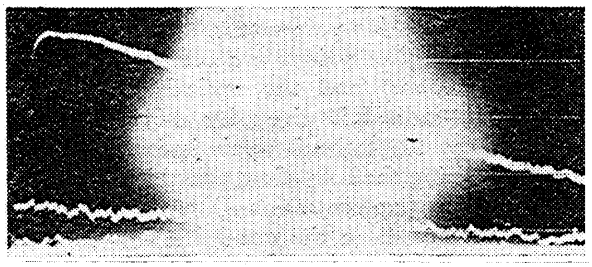

20 μs/div.

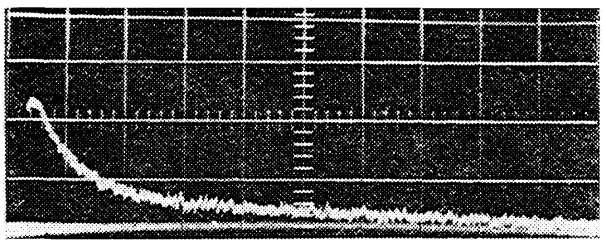

200 μs/div.

Fig. 5 (a) and (b). The oscilloscope traces for the decay of the transient PMDA anion-radical measured at 668 nm in 1,2-dichloroethane at around 20 °C. [VCZ] $=3\times10^{-4}$ M, [PMDA] $=4\times10^{-4}$ M. The vertical scale is 0.02 V/div.

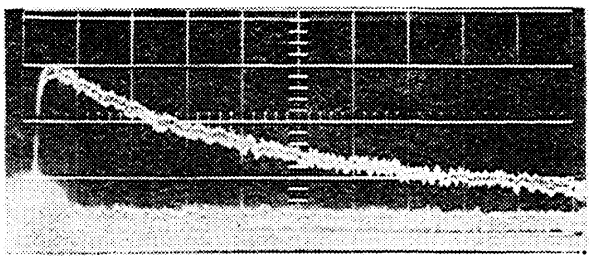

50 μs/div.

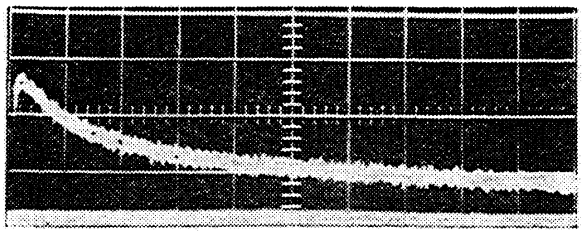

200 μs/div.

Fig. 6 (a) and (b). The oscilloscope traces for the decay of the transient PMDA anion-radical measured at 665 nm in acetonitrile at around 20 °C. [VCZ] $=3\times10^{-4}$ M, [PMDA] $=4\times10^{-4}$ M. The vertical scale is 0.02 V/div.

Table 1. Rate constants for the decay of the transient PMDA anion-radical produced in the VCZ–PMDA–solvent system at around 20 °C

Solvent	Wavelength (nm) measured	Rate constant
1,2-Dichloroethane	668	1.3×10^{4} s^{-1} ($t<100$ μs) $7.8\times\varepsilon_A-\times10^{5}$ M^{-1} s^{-1} ($t>100$μs)
Acetonitrile	665	$1.4\sim3.1\times\varepsilon_A-\times10^{5}$ M^{-1} s^{-1} (in all the time region measured, $t>20$ μs)

ε_A- represents the molar extinction coefficient of the PMDA anion-radiacl at each wavelength.

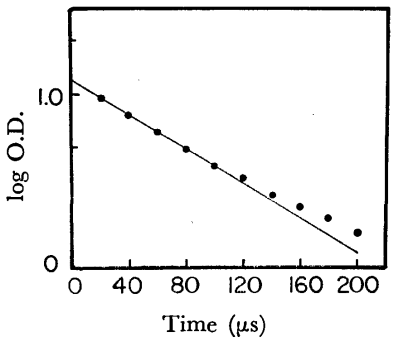

Fig. 7. The first-order plots for the decay of the transient PMDA anion-radical shown in Fig. 5(a) (in 1,2-dichloroethane).

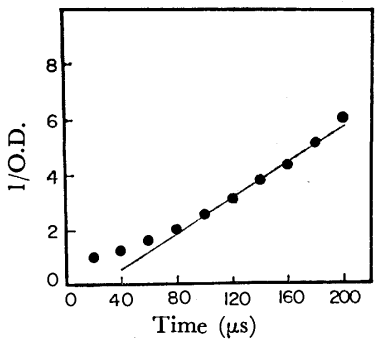

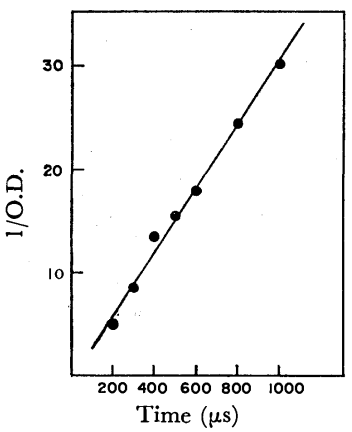

Fig. 8 (a) and (b). The second-order plots for the decay of the transient PMDA anion-radical shown in Figs. 5 (a) and (b), respectively (in 1,2-dichloroethane).

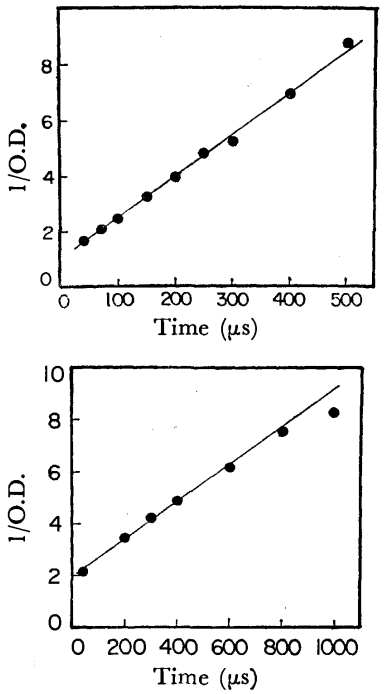

Fig. 9 (a) and (b). The second-order plots for the decay of the transient PMDA anion-radical shown in Figs. 6 (a) and (b), respectively (in acetonitrile).

order plots for the transient decay in 1,2-dichloroethane are shown in Figs. 7, and 8(a) and (b), respectively. The second-order plots for the transient decay in acetonitrile are shown in Fig. 9(a) and (b). Rate constants for the decay of the PMDA anion-radical obtained in each solvent are summarized in Table 1. Since the molar extinction coefficient of the absorption of the PMDA anion-radical is estimated to be at least 10000 at the wavelength of its absorption maximum,[6] it is indicated that the second-order decay occurred at a diffusion-controlled rate in each solvent. A similar transient decay has been observed for the triphenylene-PMDA system.[6]

The transient decay behaviors observed in the present systems can be explained by essentially the same kinetic treatment as described for the triphenylene-PMDA system. It is suggested that in acetonitrile possessing a high dielectric constant (37 at 20 °C) formation of the free ions are predominant by flash excitation, while in less polar 1,2-dichloroethane (dielectric constant: 10.37 at 25 °C) the ion pair is produced predominantly. The initial first-order decay followed by the final second-order decay process of the PMDA anion-radical in 1,2-dichloroethane is rationalized in terms of the initial very fast decay of the ion-pair, followed by the slower decay of the free ions. The photochemical primary process is given as in the following scheme of reactions.

$$D \xrightarrow{h\nu} D^*$$

$$D^* + A \xrightarrow{k_1} D^+A^- \text{ or } D^+ + A^-$$

$$D^+A^- \underset{k_{-3}}{\overset{k_3}{\rightleftharpoons}} D^+ + A^-$$

$$D^+A^- \xrightarrow{k_3} D + A$$

$$(D^+ + D \rightsquigarrow \text{Cyclodimer or Polymer})$$

The optical density of the absorption of the PMDA anion-radical is given by $\Delta D=\varepsilon_{A^-}[A^-]+\varepsilon_{D^+A^-}[D^+A^-]$, where ε_{A^-} and $\varepsilon_{D^+A^-}$ represent the molar extinction coefficients of the free ion and the ion-pair, respectively. In 1,2-dichloroethane the ion-pair D^+A^- is the predominant species, thus $\Delta D\simeq\varepsilon_{D^+A^-}[D^+A^-]$. Since the decay of D^+A^- is very fast, $k_3\gg k_2$ holds and the k_2 and k_{-2} terms can be neglected in the above scheme of reactions, and time-dependent behavior of the change in the optical density of the PMDA anion-radical in the initial decay stage would be given by $-d\Delta D/dt=k_3\Delta D$. When the ion-pair concentration rapidly decreases, essentially only ions are present (although in low concentrations) and the optical density of the PMDA anion-radical is given by $\Delta D\simeq\varepsilon_{A^-}[A^-]$. In the final decay stage the ion-pair is formed from D^+ and A^-, assuming the role of an unstable intermediate. The steady-state concentration $[D^+A^-]=k_{-2}/(k_2+k_3)\cdot[A^-]^2$ is obtained from the condition $d[D^+A^-]/dt=0$. Since $k_3\gg k_2$, the decay equation becomes $-d\Delta D/dt=(k_{-2}/\varepsilon_{A^-})(\Delta D)^2$. On the other hand, free ions are the predominant species in acetonitrile. Thus $\Delta D\simeq\varepsilon_{A^-}\cdot[A^-]$. The ion-pair equilibrium seems to be established very rapidly (within 20 μs) in acetonitrile. It is reasonable to assume that $k_2\gg k_3$, *viz.*, the ion-pair equilibrium is maintained during the decay process. In this case the concentration of D^+A^- would also be negligibly small. The second-order decay equation $-d\Delta D/dt=k_3(k_{-2}/k_2)(\Delta D)^2/\varepsilon_{A^-}$ is then obtained in acetonitrile. The first-order and the second-order rate constants for the decay of PMDA anion-radical in 1,2-dichloroethane and in acetonitrile (Table 1) represent k_3, k_{-2}, and $k_3(k_{-2}/k_2)$, respectively, in the above scheme of reactions (the absolute values of k_2, k_{-2}, and k_3 may differ with solvent).

References

1) K. Tada, Y. Shirota, and H. Mikawa, *Macromolecules*, **6**, 9 (1973).
2) Y. Shirota, K. Kawai, N. Yamamoto, K. Tada, T. Shida, H. Mikawa, and H. Tsubomura, This Bulletin, **45**, 2638 (1972).
3) Y. Taniguchi, Y. Nishina, and N. Mataga, *ibid.*, **46**, 1646 (1973).
4) M. Yamamoto, M. Ohoka, K. Kitagawa, S. Nishimoto, and Y. Nishijima, *Chem. Lett.*, **1973**, 745.
5) N. Yamamoto, Y. Nakato, and H. Tsubomura, This Bulletin, **39**, 2603 (1966).
6) Y. van P. Pilette and K. Weiss, *J. Phys. Chem.*, **75**, 3805 (1971).
7) Y. Shirota, K. Tada, M. Shimizu, S. Kusabayashi, and H. Mikawa, *Chem. Commun.*, **1970**, 1110.
8) K. Tada, Y. Shirota, and H. Mikawa, *J. Polym. Sci., Polym. Chem. Ed.*, **11**, 2961 (1973).
9) The lifetime of VCZ phosphorescence decreased appreciably with the addition of dichloroethane, but not that of VCZ fluorescence.[8]
10) Photoionization of VCZ by a double-photon process was not observed in the present flash photolysis.

Charge-transfer Interaction and Chemical Reaction. V. Reaction of *o*-Phenylenediamine with Chloranil

Takashi NOGAMI, Tadanori HISHIDA, Yasuhiko SHIROTA, Hiroshi MIKAWA, and Saburo NAGAKURA*

Department of Applied Chemistry, Faculty of Engineering, Osaka University, Yamadakami, Suita, Osaka 565
**Institute for Solid State Physics, The University of Tokyo, Roppongi, Minato, Tokyo 106*

(Received March 25, 1974)

The reaction of *o*-phenylenediamine with chloranil in ether was studied by measuring visible and ultraviolet absorption spectra at various temperatures between −78 °C and room temperature. Dehydrogenation of *o*-phenylenediamine by chloranil occurred, *o,o'*-diaminoazobenzene, 2,3-diaminophenazine and tetrachlorohydroquinone being produced as main reaction products. It was suggested that the reaction involves *o*-benzoquinone di-imine as an intermediate. For the sake of confirmation, *o*-benzoquinone di-imine was prepared by an independent method, and its reaction with *o*-phenylenediamine was examined. The difference in reactivity of isomeric phenylenediamines toward chloranil is discussed.

The reactions of chloranil (CA) with such aromatic amines as aniline, *s*-triaminobenzene, *m*-phenylenediamine, *p*-phenylenediamine, and *N,N*-dimethyl-*p*-phenylenediamine have been studied, special attention being paid to charge-transfer interaction.[1a-d] Spectrophotometric studies show that substitution reaction occurs for the *meta*-substituted derivatives of aniline in ether or acetone *via* inner complex (σ-complex) formed through outer complexes, while the reaction proceeds for the *para*-substituted derivatives in the mixed solvent, ether–isopropyl alcohol (3: 1), through ionic species produced from the outer complex. The difference in the reaction mechanism between the *m*- and *p*-substituted derivatives of aniline was explained in terms of the nonbonding electron density on the amino group.

The reaction of *ortho*-substituted derivatives of aniline with CA remains to be solved. We have studied spectrophotometrically the reaction between *o*-phenylenediamine (*o*-PD) and CA in ethyl ether. The results are given in this paper.

Experimental

Materials. Chloranil was purified by column chromatography (benzene–calcium carbonate) in order to eliminate acidic impurities,[2] and then recrystallized twice from acetone. *o*-Phenylenediamine was purified by repeated sublimation *in vacuo*.

Measurements. The ultraviolet and visible absorption spectra were measured with a Hitachi two-wavelength double beam spectrophotometer model 356 and also with a Hitachi 124 spectrophotometer. Donor and acceptor solutions were prepared separately and mixed together just before each measurement. For measurements at low temperatures, the sample was cooled with a dry-ice methanol mixture in a quartz Dewar vessel designed for spectroscopic measurements. The temperature was measured by a copper-Constantan thermocouple.

Isolation and Identification of the Reaction Products. *o*-Phenylenediamine (0.616 g) in 60 ml ether and chloranil (0.702 g) in 500 ml ether (the mole ratio, [*o*-PD]: [CA]= 2: 1) were mixed together at room temperature and kept for five days.[3] Precipitate (I) produced was collected by filtration, yield 0.175 g. The filtrate was evaporated to dryness under reduced pressure, 0.892 g of powder (II) being obtained. No component molecules were detected in I and II judging from their thin layer chromatograms. I and II were independently chromatographed on alumina (benzene–acetone mixed solvent as an elute). Three main fractions were collected, *i.e.*, a yellow eluent in I, a red one in II, and a colorless one in II. They were further purified by thin layer chromatography and identified as 2,3-diaminophenazine (DAP) (yellow eluent in I), *o,o'*-diaminoazobenzene (AB) (red eluent in II), and tetrachlorohydroquinone (TCHQ) (colorless eluent in II). The yields of DAP, AB, and TCHQ were respectively 10, 30, and 100% of theoretical values. In addition to the three main products, seven or more other minor products were formed. However, they were not identified because of small quantities and difficulty in purification. Identification of DAP and TCHQ was made by comparing their mass, IR and electronic absorption spectra with those of authentic samples. Electronic absorption spectra (in ethyl ether); DAP: λ_{max} 450 nm (ε=17000), 425 nm (ε=21000). TCHQ: λ_{max} 310 nm (ε=6600). Identification of AB was made by mass, IR and electronic absorption spectra and elemental analysis. Mass spectra; *m/e* 212 (M^+), 92 ($M^+-C_6H_4(NH_2)N_2$). IR spectra; 3430, 3350 cm^{-1} (NH stretching), 1560 cm^{-1} (N=N stretching). Electronic absorption spectra; λ_{max} 470 nm (ε=1580), 312 nm (ε=1580), 265 nm (ε=2170). Found: C, 67.39; H, 6.24; N, 26.37%. Calcd for $C_{12}H_{12}N_4$: C, 67.92; H, 5.66; N, 26.42%.

Synthesis of o-*Benzoquinone Di-imine.*[4] Freshly prepared lead dioxide[5] (350 mg) and anhydrous sodium sulfate (100 mg) baked beforehand for 30 min were added to an ether solution (30 ml) of *o*-PD (1.7 mg) under cooling with ice-salt and then vigorously stirred for five min. The solution was filtered, and the yellow filtrate was used directly. All the procedures were performed under anhydrous conditions. The yellow compound in the solution thus obtained seems to be spectroscopically of high purity, and is assigned to *o*-benzoquinone di-imine (*o*-BQDI), since the absorption spectrum of the yellow solution (λ_{max} 352 nm, ε=1300[6]) is similar to that of the corresponding isoelectronic *o*-benzoquinone.[7] *o*-BQDI obtained in ether solution was fairly stable only when kept below 0 °C in a dilute solution, but it was unstable in a concentrated solution because of its gradual conversion into AB. This prevented us from carrying out its isolation.

Results and Discussion

The reaction of *o*-PD with CA in ether at room temperature yielded AB, DAP, and TCHQ as main products.

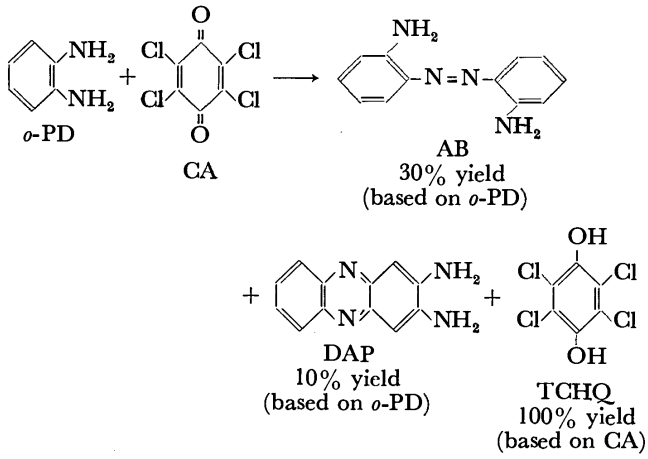

CA was quantitatively converted into TCHQ. This indicates that the dehydrogenation reaction of *o*-PD by CA occurs at first and the oxidized *o*-PD undergoes further reactions to yield AB and DAP.[8] The reaction course was followed by electronic absorption measurements under controlled temperature.

Spectroscopic Course of the Reaction in o-PD–CA System. After mixing an ether solution of *o*-PD (3.0×10^{-3} M) with one of CA (1.5×10^{-3} M) at −78 °C, the change of absorption spectra was measured at various temperatures. Figure 1 shows the spectral change measured below −50 °C. The 708 and 460 nm bands which appear immediately after mixing were assigned to the outer complex for the following reasons. (a) The 708 nm band is interpretated to be a charge-transfer (CT) band of the *o*-PD–CA complex from a comparison of its position with the CT band positions observed for the CA and trinitrobenzene complexes with several aromatic amines. (b) The intensities of both bands change parallel with temperature. Their intensities decrease monotonically with increasing temperature between −78 and −50 °C because of the decrease in the equilibrium constant of the outer complex.

Figure 2 shows the spectral change of the reaction system measured above −50 °C. The spectra measured at higher temperatures have new bands at 470 nm and around 360 nm[9] and show an isosbestic point at 590 nm. The bands are assigned to AB and *o*-BQDI, respectively. Figure 3 shows the time dependence of the absorption spectrum measured at room temperature ([*o*-PD]$=2.0\times10^{-3}$ M, [CA]$=1.0\times10^{-3}$ M). The intensity of the AB band at 470 nm increases slowly with time. The 430 nm band due to DAP appears about 13 hr after mixing. The 360 nm band was observed clearly only 6 hr after mixing. The increase of TCHQ band peaking at 310 nm could not be followed because of an overlap with the absorption of component molecules and reaction products.

Role of Outer Complex in the Reaction. It is of interest to see whether the outer complex takes part in the main reaction as a reaction intermediate or exists only in a side reaction. In this connection, Garbutt and Gerrard and Farrell and Ngo demonstrated by kinetic study that the outer complex directly takes part in the main reaction in the tricyanovinylation reaction of aniline and *N,N*-dimethylaniline with tetracyanoethylene.[10] We could not clarify the role of the outer complex in the present system, but it is probable that the reaction proceeds through the outer complex in view of the correspondence of the decrease of the outer complex band and the increase of AB band (Fig. 2).

o-Benzoquinone Di-imine as a Reaction Intermediate. The present result indicates that *o*-benzoquinone diimine (*o*-BQDI) can take part in the formations of AB and DAP as a reaction intermediate. For the sake of clarification, we attempted to prepare *o*-BQDI by another route and succeeded in obtaining *o*-BQDI fairly stably in an ether solution.[11] The absorption maximum of *o*-BQDI at 352 nm was found to be in good agreement with the shoulder around 360 nm appearing in the reaction of *o*-PD with CA.

o-BQDI alone produced AB, though very slowly. It was found that the addition of *o*-PD greatly accelerated the AB formation reaction. This indicates that AB is produced by the interaction between the

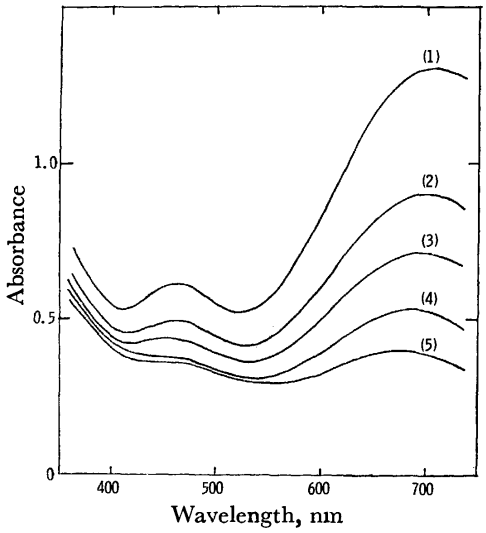

Fig. 1. The change of the outer complex bands with temperature in *o*-PD–CA system in ethyl ether. [*o*-PD]$=3.0\times10^{-3}$ M, [CA]$=1.5\times10^{-3}$ M.
(1) −78 °C, (2) −72 °C, (3) −65 °C, (4) −55 °C, (5) −50 °C.

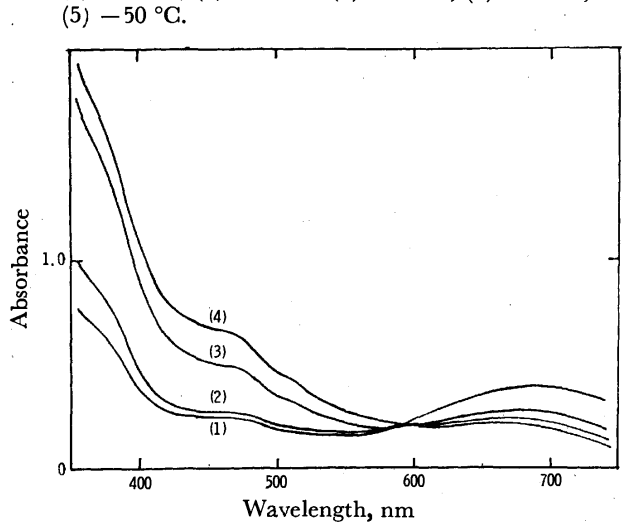

Fig. 2. Spectroscopic course of the reaction in *o*-PD–CA system in ethyl ether measured at several temperatures. [*o*-PD]$=3.0\times10^{-3}$ M, [CA]$=1.5\times10^{-3}$ M.
(1) −44 °C, (2) −31 °C, (3) −20 °C, (4) −7 °C.

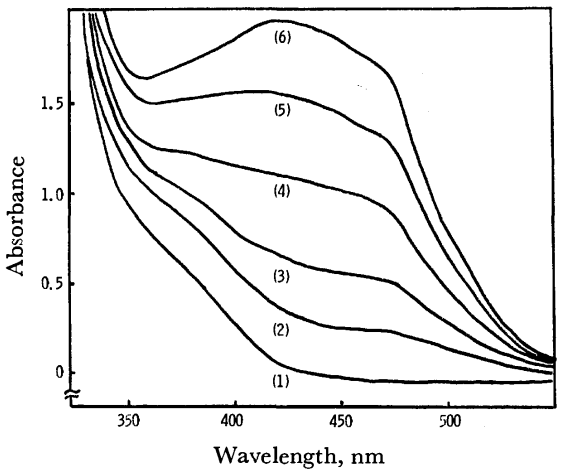

Fig. 3. Spectroscopic course of the reaction in o-PD–CA system in ethyl ether measured at room temperature. [o-PD]=2.0×10^{-3} M, [CA]=1.0×10^{-3} M.
(1) 5 min, (2) 1 hr, (3) 2 hr 26 min, (4) 6 hr 13 min, (5) 13 hr 15 min, (6) 21 hr after mixing.

intermediate o-BQDI and o-PD in the reaction of o-PD with CA. The time dependence of the absorption spectrum in o-BQDI–o-PD system in ethyl ether measured at room temperature is shown in Fig. 4. This figure shows that with the decreasing intensity

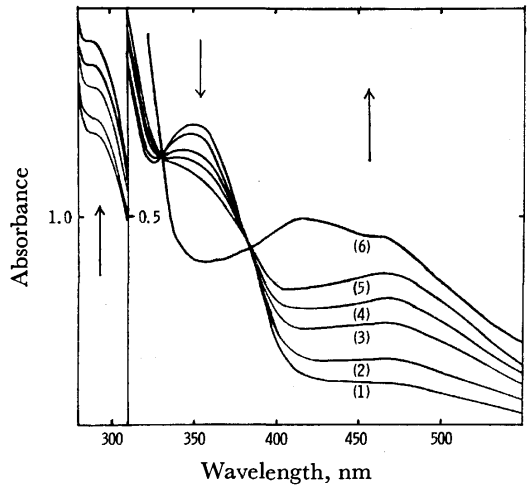

Fig. 4. Spectroscopic course of the reaction in o-BQDI–o-PD system in ethyl ether measured at room temperature. [o-BQDI]=3.8×10^{-3} M, estimated from the initial concentration of o-PD in the synthesis of o-BQDI, [o-PD]=9.5×10^{-4} M.
(1) 1 min, (2) 8 min, (3) 41 min, (4) 85 min, (5) 164 min, (6) 24 hr after mixing.

of the o-BQDI band at 352 nm, the intensity of AB band at 470 nm increases with the isosbestic point at 380 nm. It was found that DAP was produced when the solution of o-BQDI–o-PD system was left to stand for 24 hr. Thus, we can conclude that o-BQDI takes part in the reaction of o-PD with CA as an intermediate.

Reaction Scheme. The reaction scheme for the formation of AB, DAP, and TCHQ in the reaction of o-PD with CA might be shown as follows. The formation of AB through o,o'-diaminohydrazobenzene (HA) was suggested from its similarity with the reactions of p-benzoquinone di-imine with several aromatic amines.[12]

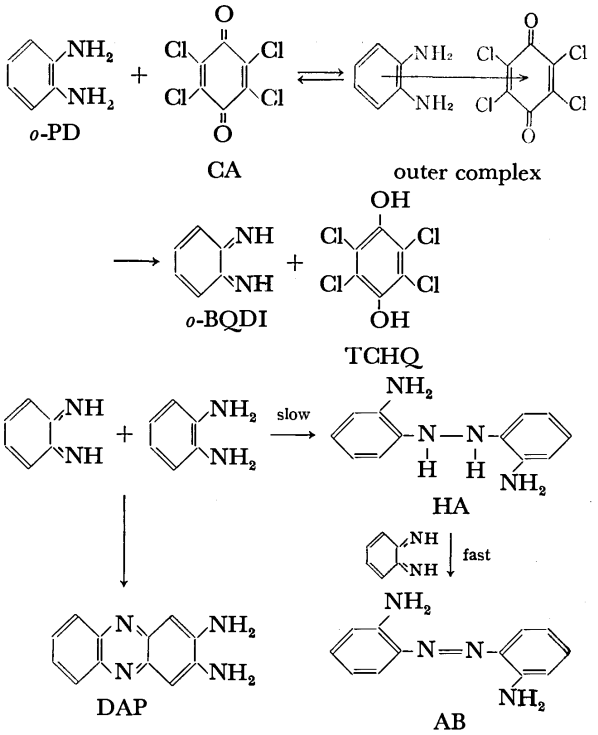

Details of the dehydrogenation process of o-PD by CA have not been clarified in the present study. The following two mechanisms have currently been accepted for the dehydrogenation mechanism by benzoquinone and its derivatives.[13] (1) Initial hydride ion abstraction from the donor compound D by CA to produce intermediate $D(-H)^+$ and CA semiquinone anion. (2) Initial electron transfer from D to CA to produce D cation radical and CA anion radical. In addition to these mechanisms, we considered a third one which involves semiquinone radical.[14] The possible reaction mechanisms can be described as follows:

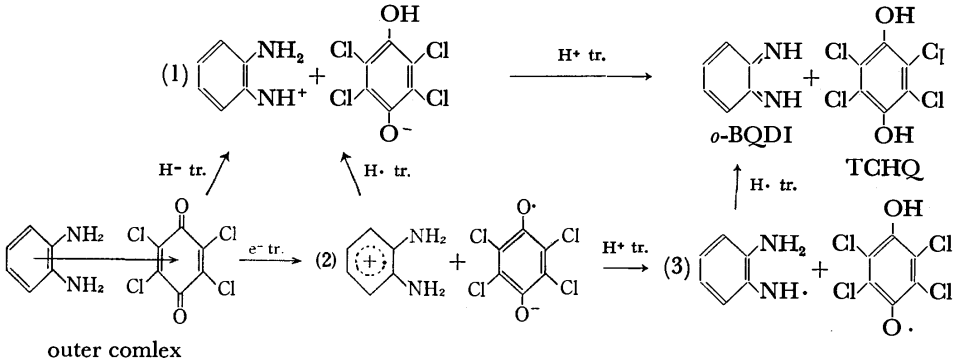

Spectrophotometrically, we could detect no transient species in the above scheme[15] probably due to the following reasons. (1) The reaction consists of the initial rate-determining formation of these intermediate species, followed by the rapid formations of *o*-BQDI and TCHQ. (2) The absorption bands of these intermediate species are covered with those of the reaction products and component molecules. (3) These species are too unstable in the presence of air to be detected by electronic absorption spectra.

Differences of Reactivity of Isomeric Phenylenediamines toward Chloranil. A series of studies on the reactions of CA with *o*-, *m*-, and *p*-phenylenediamines in ethyl ether[1a-d] lead to the conclusion that their reaction mechanisms differ from one another, although in all cases the outer complexes are involved as intermediates. Dehydrogenation reaction occurs for the *o*-PD–CA system, substitution reaction through inner complex for the *m*-PD–CA system, and formation of stable ion-pair salts *p*-PD^+CA^- and $(p\text{-PD})_2{}^+CA^-$ for the *p*-PD–CA system. The differences in the reactions can be explained by considering the following three competitive factors, (1) the electron-donating ability of the nonbonding electron on the amino group, (2) the facility of dehydrogenation of amino hydrogen, (3) the stability of the ion-pair salts. The nonbonding electron density on the amino nitrogen is larger in *m*-PD than in *o*-PD and *p*-PD.[1c] Thus, *m*-PD forms the inner complex with CA much easier, leading to the subsequent substitution reaction. In addition to the higher electron density on the amino nitrogen of *m*-PD, its dehydrogenation is less probable since the *m*-isomeric benzoquinone di-imine structure is impossible. The dehydrogenation reaction by CA is conceivable both in *o*-PD–CA and *p*-PD–CA systems. However, because of the stability of the ion-pair salts formed between *p*-PD and CA, salts formation reactions occur preferentially in the *p*-PD–CA system. We could not obtain the ion-pair salts in *o*-PD–CA and *m*-PD–CA systems using several solvents, showing the instability of the salts. Thus, the ion-pair salt is unstable and dehydrogenation occurs relatively easily for the *o*-PD–CA systems.[13] Reactivity factors are summarized in the Table 1. It should be noted that these discussions hold when one uses ethyl ether as a solvent.

TABLE 1. FACTORS REGULATING THE REACTIVITIES OF *o*-, *m*- AND *p*-PHENYLENEDIAMINES IN ETHYL ETHER

	Nonbonding electron density on amino nitrogen	Facility of dehydrogenation	Stability of ion-pair salt
o-PD	relatively small	large[a]	unstable
m-PD	relatively large[b]	small	unstable
p-PD	relatively small	large	stable[c]

a) This leads to the dehydrogenation reaction in the *o*-PD –CA system. b) This leads to the substitution reaction in the *m*-PD –CA system. c) This leads to the ion-pair salts formation in the *p*-PD –CA system.

References and Notes

1) a) Part I: T. Nogami, K. Yoshihara, H. Hosoya, and S. Nagakura, *J. Phys. Chem.*, **73**, 2670 (1969); b) Part II: T. Yamaoka and S. Nagakura, This Bulletin, **43**, 355 (1970); c) Part III: T. Nogami, T. Yamaoka, K. Yoshihara, and S. Nagakura, *ibid.*, **44**, 380 (1971); d) Part IV: T. Nogami, K. Yoshihara, and S. Nagakura, *ibid.*, **45**, 122 (1972).

2) T. Natuume, Y. Shirota, H. Hirata, S. Kusabayashi, and H. Mikawa, *Chem. Commun.*, **1969**, 289.

3) The reaction seemed to be completed in five days.

4) T. Nogami, T. Hishida, Y. Shirota, and H. Mikawa, *Chem. Lett.*, **1973**, 1019.

5) L. C. Newell and R. W. Maxon, "Inorganic Syntheses," Vol. 1, p. 45 (1939).

6) Estimated from the initial concentration of *o*-PD in the synthesis of *o*-BQDI.

7) H. Mason, *J. Amer. Chem. Soc.*, **70**, 138 (1948).

8) The oxidation of *o*-PD with AgO, (B. Ortiz, P. Villanueva, and F. Walls, *J. Org. Chem.*, **37**, 2748 (1972)), $FeCl_3$, (F. Ullmann and F. Mauthner, *Ber.*, **35**, 4302 (1902). F. Ullmann and J. Gnaedinger, *ibid.*, **45**, 3437 (1912)), lead tetraacetate, (K. Nakagawa and H. Onoue, *Tetrahedron Lett.*, **1965**, 1433. K. Nakagawa and H. Onoue, *Chem. Commun.*, **1965**, 396), and PbO_2 (R. Willstätter and A. Pfannenstiel, *Ber.*, **38**, 2350 (1905)), has been studied by several authors, AB, DAP and 1,4-dicyanobutadiene being reported as the reaction products.

9) This band appears as a shoulder because of the existence of a strong band below 350 nm.

10) S. Garbutt and D. L. Gerrard, *J. Chem. Soc. Perkin II*, **1972**, 782. P. G. Farrell and P. Ngo, *ibid.*, **1973**, 974.

11) R. Willstätter *et al.* postulated that they obtained *o*-BQDI, but their assignment was uncertain, see Ref. 8.

12) J. F. Corbett, *J. Chem. Soc., B*, **1969**, 818. J. F. Corbett and E. P. Gamson, *J. Chem. Soc. Perkin II*, **1972**, 1531, and papers cited therein.

13) E. A. Braude, L. M. Jackman, and R. P. Linstead, *J. Chem. Soc.*, 3548 (1954). E. M. Kosower, "Progress in Physical Organic Chemistry," ed. by S. G. Cohen, A. Streitwieser, Jr., and R. W. Taft, Interscience Publishers, N. Y. (1965), p. 81.

14) We considered this mechanism from our observation that the semiquinone radical is involved in the *p*-phenylenediamine–CA system in ether–isopropyl alcohol (3: 1) mixed solvent at low temperatures.

15) The absorption peak positions of semiquinone anion, CA anion radical and semiquinone radical are as follows: semiquinone anion: λ_{max} 330 nm; CA anion radical: λ_{max} 417, 455 nm; semiquinone radical: λ_{max} 395, 415, 435, 462 nm. Semiquinone anion was obtained by the reaction of equimolar ratios of TCHQ and KOH in ethanol. Dianion ($O\text{-}C_6Cl_4O^-$) was obtained (λ_{max} 350 nm) with the use of excess KOH.

16) It is well known that the *o*-, *m*-, and *p*-phenylenediamines show important differences in chemical properties, and that *o*-PD is distinguished by the facility with which it gives rise to condensation reactions to heterocyclic compounds. "Chemistry of Carbon Compounds," vol. III, ed. by E. H. Rodd, Elsevier Publishing Company, Amsterdam, Houston, London, New York (1954), p. 224.

Porous Structure Formed by the Decomposition of the Surface Product on ZnO Preserved in the Atmosphere

Mahiko NAGAO, Kunimitsu MORISHIGE, Toshie TAKESHITA, and Tetsuo MORIMOTO

Department of Chemistry, Faculty of Science, Okayama University, Tsushima, Okayama 700

(Received March 29, 1974)

The slow reaction of ZnO with CO_2 and water in the atmosphere is investigated by following the changes in both the surface area of the structure formed and the amounts of CO_2 and water evolved, by heating the product *in vacuo* at increasingly elevated temperatures. The results obtained show that ZnO reacts extremely gradually with CO_2 and water cooperatively in the atmosphere to produce an amorphous surface product with a composition approximate to $Zn_5(OH)_6(CO_3)_2$, and that this product is decomposed by heating *in vacuo* to release the CO_2 and water, leaving a porous structure on the ZnO. The surface area of the product was found to change upon heating: first it increases, passes a prominent maximum value at 200 °C, recovers the original value at 500 °C, and further decreases at higher temperatures; this reflects the initial growth and subsequent destruction of the porous structure. Furthermore, it was confirmed that the destruction of such a honeycomb-like structure is promoted by the adsorption of water.

Recently, it has become clear that ZnO chemisorbs water molecules to produce surface hydroxyl groups, on which a further physisorption of water occurs, and that the adsorption isotherm of water on ZnO reveals a sudden jump around the relative pressure of 0.2—0.3.[1-4] On the other hand, the chemisorption of CO_2 occurs on the dehydroxylated surface of ZnO, but not on the surface hydroxyl groups.[5] The chemisorption force of CO_2 is weaker than that of water, so the substitutional chemisorption of water for prechemisorbed CO_2 takes place on ZnO in contact with water vapor of 4.6 mmHg at 25 °C.[6] All these results are those obtained after equilibrating the system for several hours at most.

The present investigation is intended to examine the naturally-occurring reaction of ZnO with CO_2 and water present in the atmosphere for a much longer time. Another purpose of this work is to investigate the porous structure formed by heating the product *in vacuo* through the measurement of the surface area.

Experimental

Material. The original sample of ZnO used in this study was made by the Sakai Chemical Co. by burning Zn metal in air. The sample was stored in a bottle with a usual ground-glass stopper. The bottle was opened from time to time in order to use the sample for the measurements of the surface properties. The humidity in the laboratory varied within the range from 50 to 85%, the content of CO_2 in the atmosphere, from 0.030 to 0.041%, and the room temperature, from 5 to 32 °C.

Measurement of Surface Area. The specific surface area of ZnO was determined by applying the BET method to the N_2 adsorption data at −196 °C, in which the molecular area of N_2 was assumed to be 16.2 Å^2.

Determination of the Amounts of Water and CO_2 which Reacted with the ZnO Surface. The amounts of water and CO_2 which reacted with the ZnO surface were determined by analysing the gases evolved when the product was decomposed by heating at increasingly elevated temperatures. The sample from the stock bottle was first evacuated at room temperature for 10 hr in a vacuum of 10^{-5} Torr in order to remove the physisorbed molecules; then it was heated at 100 °C for 4 hr to permit the evolution of gases, which were introduced into a trap kept at −196 °C. The total gas volume of water and CO_2 condensed was determined volumetrically after evaporating at room temperature. The gas was recondensed at −78 °C and evacuated at the same temperature, which left water in the solid state; the volume of water was determined after reevaporation at room temperature as before. By subtracting the amount of water from the total gas volume, the amount of CO_2 could be obtained. Then the sample, was subjected to the next gas-evolution at 150 °C, and the determination of the CO_2 and water present was carried out in the same way. A similar set of procedures was repeated successively after each gas evolution at increasingly elevated temperatures up to 1100 °C. Mass-spectroscopic analysis showed that the gas evolved by heating the ZnO samples contained both CO_2 and water, and that the separation of them was accomplished by the above procedure. Thus, the amounts of CO_2 and water absorbed in ZnO during preservation in the atmosphere can be obtained by the summation of the gas volumes evolved at all the stages of heat treatment.

Differential Thermal Analysis. The apparatus used for the simultaneous measurements of the weight loss (TGA) and differential thermal analysis (DTA) was of the YGHD type made by the Rigaku Electric Co. The apparatus was operated in air, and the temperature was raised at the rate of 10 °C/min.

Results and Discussion

On the ZnO samples preserved for different periods of time in the atmosphere, the surface area was measured after degassing for 4 hr; they are plotted against the degassing temperature in Fig. 1. It can be seen from Fig. 1 that the surface area of the sample changes remarkably with the degassing temperature: it remains almost unchanged up to 150 °C, increases steeply to reach a maximum value at 200 °C, and decreases to recover the original value at 500 °C. A further decrease in surface area was observed upon heating at temperatures higher than 600 °C, suggesting the occurrence of sintering. Here, it should be noted that the longer the preservation period of the sample, the larger the maximum value of the surface area observed; the highest value obtained is about 2.3 times greater than the initial value, although the initial values are almost equal to one another irrespective of the preservation period of the sample.

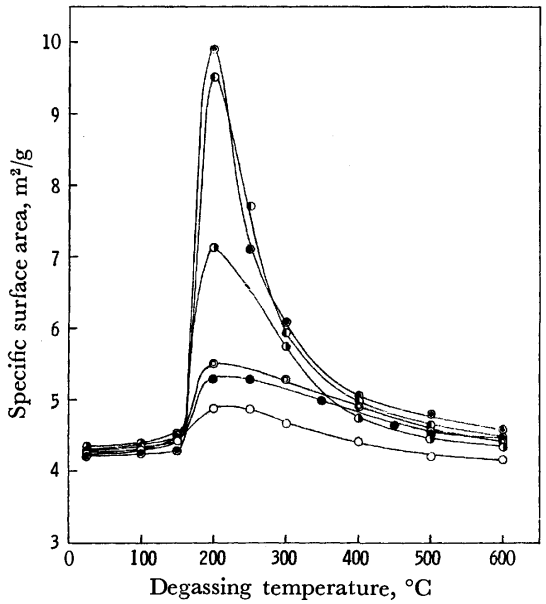

Fig. 1. Relation between specific surface area and degassing temperature on ZnO samples preserved for different periods: ○ 2, ● 30, ◎ 54, ◑ 60, ◐ 84, ◉ 90 months.

The amounts of water and CO_2 evolved are represented as functions of the heating temperature in Figs. 2 and 3 respectively, both expressed in the number of molecules expelled per 100 Å² of the initial surface of ZnO. It may be found from Figs. 2 and 3 that the evolution of CO_2 from ZnO reaches a maximum on heating at 200 °C, and is mostly finished by 300 °C, whereas the evolution of water occurs in two stages, corresponding to the two maxima at 200 and 300 °C,

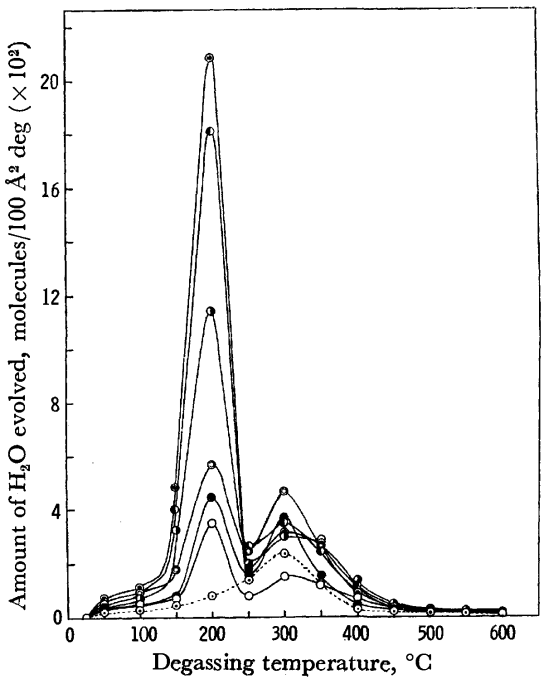

Fig. 2. Differential amount of water evolved against degassing temperature. Samples preserved for 2 (○), 30 (●), 54 (◎), 60 (◑), 84 (◐), 90 (◉) months. Dotted line means the desorption curve of chemisorbed water.

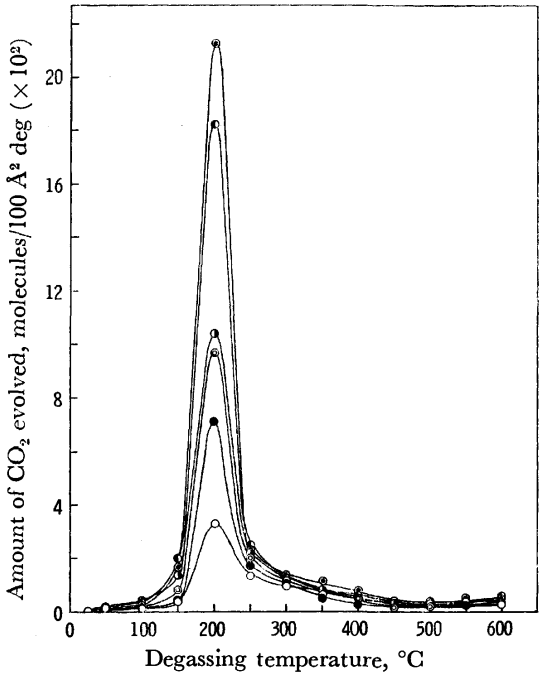

Fig. 3. Differential amount of CO_2 evolved against degassing temperature. Samples preserved for 2 (○), 30 (●), 54 (◎), 60 (◑), 84 (◐), 90 (◉) months.

and that the gas evolution increases gradually with the time of preservation.

A comparison of the results in Fig. 1 with those in Figs. 2 and 3 makes it possible to infer that the increase in the surface area of ZnO originates from the formation of pores after the evolution of gases. During the preservation of ZnO in the atmosphere, the surface layer will react with water and CO_2 cooperatively to produce a complicated compound; on subsequent heating *in vacuo*, the compound decomposes to recover the ZnO, accompanied by the evolution of water and CO_2, thus resulting in the formation of a porous structure, *i.e.*, presumably of a honeycomb-like structure, in the surface layer. The reaction of the surface layer will proceed more deeply with the time of preservation, so the depth of the honeycomb structure resulting from the decomposition will be increased. The increment of the surface area obtained can thus be considered to correspond to that of the inner wall in the honeycomb structure. The decrease in the surface area at temperatures higher than 200 °C will be due to the destruction of the honeycomb structure or the recrystallization of the wall in the structure upon heating.

TABLE 1. INTEGRATED VALUES OF CO_2 AND H_2O EVOLVED

Preservation period, month	CO_2 amount, molecules/100 Å²	H_2O amount, molecules/100 Å²	CO_2/H_2O	Number of ZnO layers
2	4.02	5.94	0.68	1.17
30	4.98	6.14	0.81	1.31
54	7.70	10.68	0.72	2.16
60	9.68	14.42	0.67	2.84
84	13.19	16.70	0.79	3.52
90	14.94	21.35	0.70	4.27

Table 1 gives the integrated values of water and CO_2 which are obtained from the data in Figs. 2 and 3. Though the numerical values of the ratio of CO_2 to water are widely dispersed, as is shown in Table 1, they approximate the 2: 3 ratio, suggesting the formation of $Zn_5(OH)_6(CO_3)_2$.[7] In order to ascertain more definitely the composition of the compound formed on the surface of ZnO in the atmosphere, an experiment was attempted: a few grams of ZnO, which had been newly prepared in our laboratory by burning metallic Zn in the atmosphere,[5] was allowed to react in a mixed gas of 760 mmHg CO_2 and 23 mmHg H_2O at room temperature. Though the reaction, when the ZnO sample was kept in a vessel containing one component of the mixed gas, did not proceed even after 3 months, all the ZnO sample was consumed in the mixed gas within 2 months to produce an amorphous product. This product was then subjected to differential thermal analysis; the results obtained are shown in Fig. 4. It may be found from Fig. 4 that the product decomposes in the temperature range from 230 to 260 °C, accompanied by heat absorption; the weight decrease amounts to 25.6%, which corresponds to the composition of $Zn_5(OH)_6(CO_3)_2$ (theoretical, 25.98%).[7]

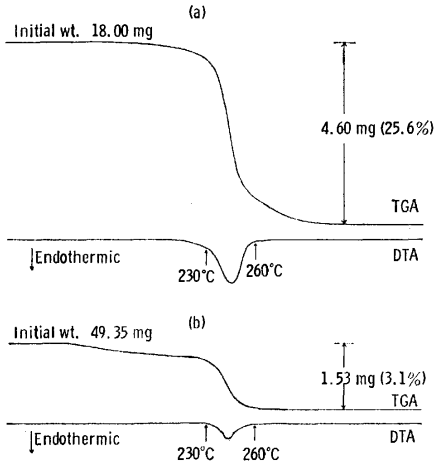

Fig. 4. DTA and TGA curves of ZnO samples. (a) completely converted sample, (b) partially modified sample in the atmosphere for 7 years.

In Fig. 4, the data on a sample preserved in the atmosphere are also added; the decomposition temperature of the sample is found to be the same as that of the completely-converted compound, which testifies that the two substances are the same, though the weight of the former is considerably smaller than that of the latter because of the smaller portion of the modified part in the former sample. These results indicate that the composition of the basic carbonate prepared from the reaction of ZnO in a gaseous atmosphere is $Zn_5(OH)_6(CO_3)_2$, though the product in this investigation was found to be amorphous by X-ray diffraction measurement.

It is interesting to consider why the second peak of water appears at 300 °C, as is shown in Fig. 2, contrary to the absence of the second peak in the case of CO_2. Undoubtedly, this peak area is included in the integration of the value of water in Table 1. In order to clarify this phenomenon, another test was made as follows. The ZnO sample, which had been treated at 450 °C *in vacuo* to remove most of the water and CO_2 absorbed, was exposed to saturated water vapor for 24 hr, degassed at room temperature for 12 hr, and then subjected to the analysis of water by means of the method described above. The results obtained are illustrated by the dotted line in Fig. 2. It shows that the position of the peak agrees well with that of the second peak of the other samples, and that the integrated value of water on this sample amounts to 8.2 OH's/100 Å^2. This indicates that the second peak of water originates from the chemisorbed water on ZnO. It may thus be reasonable to conclude that part of the water evolved by the decomposition of the complicated product is chemisorbed instantly on the ZnO surface newly developed.

Influence of Adsorbed Water on the Destruction of the Porous Structure. Figure 1 demonstrates that the porous structure formed on ZnO is destroyed by heating at temperatures higher than 200 °C. As has just been stated, part of the water evolved by the decomposition is presumably chemisorbed on the newly-formed surface. Here, it appears that the temperature at which the surface area sharply decreases, as is shown in Fig. 1, coincides with that corresponding to the second peak in Fig. 2; this suggests that the decrease in surface area is largely influenced by the adsorption of water. Figure 5 shows the data concerning the influence of adsorbed water upon the change in surface area. In this experiment, part of the 5-year sample was evacuated for 4 hr at 200 or 300 °C, subjected to the measurement of the surface area (Point 1 in Fig. 5), allowed to adsorb water at 25 °C in a vapor of 23 mmHg for 12 hr, and degassed at the same temperature for 4 hr in a vacuum of 10^{-5} Torr to remove the physisorbed water; then the second measurement of the surface area was carried out (Point 2). After the subsequent exposure of the sample to water vapor in the same way as before,

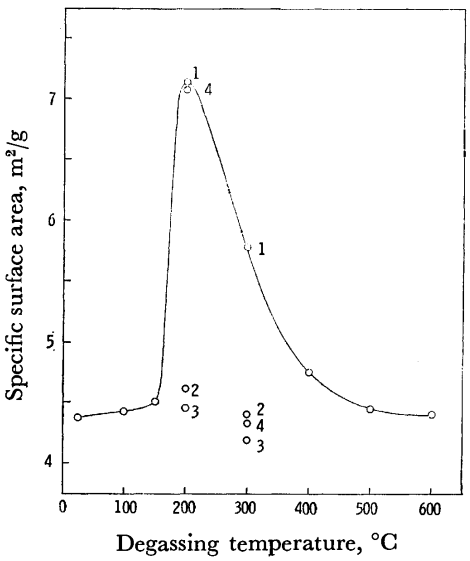

Fig. 5. Influence of adsorbed water upon the change in surface area of ZnO sample preserved for 5 years.

the third value of the surface area was obtained (Point 3). The final measurement of surface area was performed after the reevacuation of the sample at 200 or 300 °C for 4 hr (Point 4). In this series of measurements, the adsorption isotherms of N_2 were found to have no hysteresis, thus indicating the absence of pores with radii larger than about 15 Å.[8]

Figure 5 shows that the surface area of the 200 °C-treated sample drops after the chemisorption of water, but it recovers its original value after the subsequent desorption of the chemisorbed water. On the contrary, in the case of the 300 °C-treated sample, the surface area does not return to the original value even after the evacuation at 300 °C. Furthermore, it should be pointed out that, in both cases, the surface area of the samples covered with chemisorbed water is almost the same as that of the undecomposed sample. The nature of such an apparently similar result, however, is probably different depending on the treatment of the sample. The result obtained for the 200 °C-treated sample suggests that the pore radius in the honeycomb structure is so small as to lock out the adsorption of N_2 after the chemisorption of water on the inner surface of the structure. On the other hand, the walls of the honeycomb structure of the 300 °C-treated sample may be so delicate that they are ruptured and incorporated into the substrate crystals as a result of the adsorption of water, though they cannot be destroyed by the adsorption of N_2. This postulation seems feasible, since water has a large influence on the sintering of metal oxides.[9] However, it is not clear whether the destruction of the honeycomb structure occurs in the stage of water adsorption or in that of the subsequent heating to 300 °C. The reversibility of the surface area of the 200 °C-treated sample may reasonably be thought to be caused by the reinforcement of the pore wall due to the incomplete decomposition of the product.

In conclusion, we can roughly estimate the thickness of the surface layer of ZnO which reacted in the atmosphere. Assuming that, on the actual surface of ZnO, the (0001) and (10$\bar{1}$0) planes, both excellent in cleavage, appear in equal amounts, the average number of Zn atoms on the ZnO surfaces can be calculated to be 8.5/100 Å^2.[2] Since each molecule of water or CO_2 will react with each atomic pair of Zn and O on the crystal surface, as is expressed in the formula stated above, an average of 3.5 layers of Zn atoms on the ZnO crystal changes during a preservation of about 7 years. Thus, if half the atomic pairs of Zn and O in the surface layer is pulled out to form small pores, the depth of the pores will correspond to about 7 layers of the crystal planes.

References

1) T. Morimoto, M. Nagao, and F. Tokuda, This Bulletin, **41**, 1533 (1968).
2) T. Morimoto and M. Nagao, *ibid.*, **43**, 3746 (1970).
3) M. Nagao, *J. Phys. Chem.*, **75**, 3822 (1971).
4) T. Morimoto and M. Nagao, *ibid.*, **78**, 1116 (1974).
5) T. Morimoto and K. Morishige, This Bulletin, **47**, 92 (1974).
6) T. Morimoto and K. Morishige, submitted for the publication in *J. Phys. Chem.*
7) S. Ghose, *Acta Crystallogr.*, **17**, 1051 (1964).
8) S. J. Gregg and K. S. W. Sing, "Adsorption, Surface Area and Porosity," Academic Press, London and New York (1967).
9) H. E. Ries, Jr., *Advan. Catal.*, **4**, 87 (1952).

Resonace Raman Spectra of Acid-Base Indicators. II. Hydroxyarylazobenzene Derivatives

Yutaka SAITO, Bak-Kwang KIM, Katsunosuke MACHIDA, and Toyozo UNO

Faculty of Pharmaceutical Sciences, Kyoto University, Sakyo-ku, Kyoto 606

(Received April 13, 1974)

The effects of pH on resonance Raman spectra of several hydroxyarylazobenzene-type acid-base indicators have been investigated. All the compounds examined show the azo-type spectra in basic solutions, while the neutral solution spectra are the azo-type for *p*-hydroxyphenyl compounds and the quinoid-type for α- and β-hydroxynaphthyl compounds. The spectrum of Tropaeoline O changes complicatedly along with the protonation and deprotonation on the pH change.

The acid-base indicators containing azo group can be classified into two categories, the amino and the hydroxy derivatives. Recently, we have investigated the resonance Raman spectra of some important amino-azo-type acid-base indicators, and have shown that the spectral pattern reflects clearly the structure change accompanying the color change.[1] When the neutral solution of an aminoazo-type indicator is acidified to pH below the color change interval, the azo-type base form is protonated at the azo group and is transformed into the quinoid-type acid form. This transformation gives rise to the replacement of azo bands by quinoid bands in resonance Raman spectra along with the red shift of λ_{max} in visible absorption spectra. On the contrary, the color change of hydroxyazo-type acid-base indicators occurs mostly in the basic pH region, in such a way that λ_{max} shifts to red on addition of alkali to the neutral solution. The tautomerism between the azo and the quinoid forms is conceivable for the acid form. Extensive studies on visible and ultraviolet spectra of hydroxyarylazo compounds have shown that the tautomeric ratio varies widely depending on the nature of aromatic rings and substituents.[2-7] Accordingly, the color change of hydroxyazo-type indicators cannot be elucidated from such a simple correlation between λ_{max} and the structure as seen for amino-azo-type indicators for which the reddish color in acidic solutions is due to the quinoid form.[1] In this respect, it is of importance to clarify how the molecular vibrations of hydroxyazo derivatives are affected by the structure change underlying the color change.

In this paper, we report the resonance Raman spectra of several representative hydroxyphenyl- and hydroxynaphthylazobenzene derivatives, and discuss the structures of these compounds at various pH by referring to spectra of related compounds and deuteration effects.

Experimental

The hydroxyarylazobenzene derivatives taken up in this work were obtained from commercial sources, and were recrystallized several times from water or ethanol. In Table 1, the λ_{max} in the visible and ultraviolet absorption spectra and the color change intervals of these compounds are listed together with the abbreviations to be used in the text. The Raman spectra between 1800 and 1000 cm^{-1} were recorded on a JEOL S-1 laser Raman spectrophotometer by using the 488 nm excitation line of a coherent Ar^+ laser.

Each sample was sealed in a 1 mm capillary tube. The pH of aqueous solutions was adjusted by using 1 M HCl, 1 M NaOH and the phosphate and borate buffers. For the deuteration of active hydrogen atoms, the stock solutions of 1 M DCl and 1 M NaOD in heavy water were prepared and used as described in the previous paper.[1] Reagent grade ethanol and *n*-hexane were used as the solvents for SuI. The concentration dependence of Raman intensities was roughly surveyed for each compound, and the optimum concentration was found to fall between 10^{-2} and 10^{-4} M. The decomposition of samples due to the irradiation of the excitation beam was not detected except for the cases of AY in the neutral solution and SuI in 50% ethanol. The absorption spectra between 330 and 600 nm were recorded on a Shimadzu W-40 spectrophotometer.

Results and Discussion

p-Hydroxyphenylazo Derivatives. The resonance Raman spectra of HAS in neutral aqueous solution and

TABLE 1. ABSORPTION MAXIMA AND COLOR CHANGE INTERVALS

Compound	Abbr.	Absorption maximum (nm)		Color change interval (pH)
		Acid form	Base form	
p-Hydroxyazobenzenesulfonic acid	HAS	351	435	
m-Nitrobenzeneazosalicylic acid (Alizarine yellow GG)	AY	352	452	10.2—12.0[d]
p-(2-Hydroxy-1-naphthylazo)benzene (Sudan I)	SuI	475[a]	435[b]	
p-(4-Hydroxy-1-naphthylazo)benzenesulfonic acid (Orange I)	OrI	474	514	7.4—8.8[d]
p-(2-Hydroxy-1-naphthylazo)benzenesulfonic acid (Orange II)	OrII	484	455, 505[b]	10.9—11.9[e]
p-(2,4-Dihydroxy-phenylazo)benzenesulfonic acid (Tropaeoline O)	TrO	427[c]	491	11.1—12.7[d]

a) in EtOH. b) in 30% EtOH. c) The absorption maxima at pH 0.2 and 4.0 are at 440 and 380 nm, respectively. d) I. M. Kolthoff, "Acid-Base Indicators," The Macmillan Co., New York (1937), p. 147. e) Ref. 6.

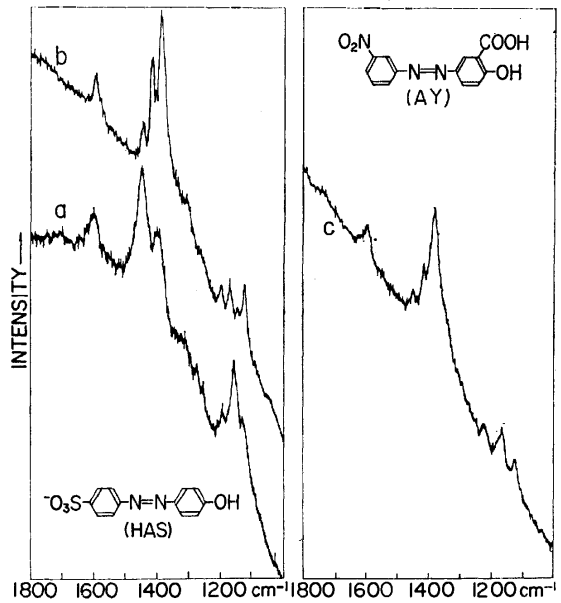

Fig. 1. Resonance Raman spectra of HAS and AY: (a) 1×10^{-2} M HAS in H_2O, slit width 27 cm^{-1}; (b) 1×10^{-3} M HAS in 0.5 M NaOH, slit width 14 cm^{-1}; (c) 1×10^{-3} M AY in 0.5 M NaOH, slit width 14 cm^{-1}.

of HAS and AY in 0.5 M NaOH are shown in Fig. 1. In all these spectra, several bands appear commonly in the region between 1600 and 1000 cm^{-1}, the strongest being near 1400 cm^{-1}. This spectral pattern is similar to those of *p*-phenylazophenol in methanol[8] and methyl-orange in water.[1,9] The strong band at 1445 cm^{-1} in Fig. 1a arises clearly from the stretching vibration of the *trans* N=N group, indicating that the monovalent anion of HAS exists dominantly as the azo form. This result is in agreement with the previous conclusions based on visible and ultraviolet spectra.[3,4] The assignment of the remaining bands was easily made as

Table 2. Observed frequencies and assignments for HAS and AY

HAS		AY	Assignments
H_2O	0.5M NaOH	0.5M NaOH	
1600 vw	1598 w	1597 w	Benzene ring
	1447 w	1450 w	Benzene ring
	1417 m	1415 m	Benzene ring
1445 s	1386 s	1382 s	N=N str.
1400 m			Benzene ring
1195 sh	1195 w	1223 w	Benzene ring
1150 m	1167 w 1145 vw	1167 m	C–N str.
1125 sh	1122 w	1123 w	Benzene ring

shown in Table 2 from analogy with the base form of methyl orange and related compounds.[1] The good correspondence of weak bands between HAS and AY in basic solutions shows that vibrations of the $-SO_3^-$, $-NO_2$, and $-CO_2^-$ groups do not participate in the resonance Raman effects of the hydroxyazo compounds treated in this work. The shift of the N=N stretching frequency from 1445 to 1386 cm^{-1} on going from the acid form to the base form of HAS indicates that the N=N bond order decreases on the deprotonation of the phenolic OH group. Accordingly, the divalent HAS anion can be described as a resonance hybrid

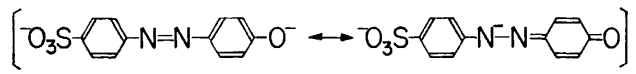

in which the contribution of the azo structure is predominant but that of the quinoid structure is not negligible. The red shift in the visible absorption on the deprotonation of azophenol derivatives may be related to this contribution of the quinoid structure.

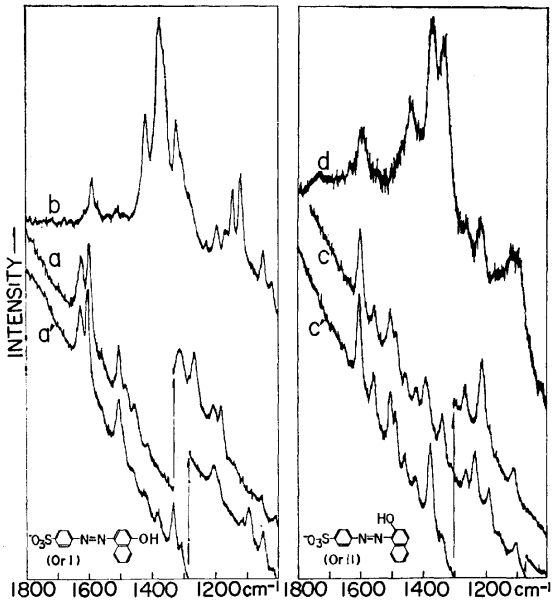

Fig. 2. Resonance Raman spectra of 1×10^{-3} M OrI and OrII: (a) OrI in H_2O, slit width 14 cm^{-1}; (a') OrI in D_2O, slit width, 14 cm^{-1}; (b) OrI in 0.5 M NaOH, slit width 27 cm^{-1}; (c) OrII in H_2O, slit width 14 cm^{-1}; (c') OrII in D_2O, slit width 14 cm^{-1}; (d) OrII in 0.5 M NaOH, slit width 27 cm^{-1}.

Hydroxynaphthylazo Derivatives. Figure 2 shows the resonance Raman spectra of hydroxynaphthylazobenzenesulfonic acids in neutral and basic solutions. In contrast to the case of HAS, the spectra of these naphthylazo derivatives undergo significant changes on the increase of pH from the neutral region to the basic region above the color change interval. In the resonance Raman spectrum of OrI in the neutral solution, there is no strong band around 1400 cm^{-1} assignable to the N=N stretching vibration. Instead, this spectrum shows medium to strong bands at 1629, 1508, and 1292 cm^{-1} in analogy with the previously reported spectra of *p*-aminoazobenzene derivatives in acidic solutions.[1] By referring to the latter case and also to the infrared spectra in the solid state,[10,11] most of the resonance Raman bands presently observed for OrI are assigned reasonably to vibrations of the quinoid form as shown in Table 3. Although OrI has a naphthalene ring in place of the benzene ring of *p*-aminoazobenzene derivatives, the spectral change on deuteration between 1400 and 1000 cm^{-1} of the former is quite analogous to that observed for the latter.[1] This result indicates that only the bands related to the structure C=N–NH–C are deuteration sensitive in both cases.

Table 3. Observed frequencies and assignments of the neutral solutions of OrI, OrII, and SuI

OrI		OrII		SuI		Assignments
H_2O	D_2O	H_2O	D_2O	EtOH	EtOD	
1629 m	1629 m					C=C str.
1603 m	1603 m	1601 s[a)]	1601 s[a)]	1608 s[a)]	1607 s[a)]	Benzene ring
1508 m	1506 m	1505 m	1504 m	1505 m	1500 m	Benzene ring
	1380 w	1390 m	1375 s	1396 m	1381 s	C-C str.
1292 w	1333 m	1262 w	1262 w	1270 vw	1263 w	C-N str.
1208 w	1205 m	1235 m	1210 s	1236 s	1213 s	N-N str.
	1095 w					N-D def.

a) Contributed also by the C=C stretching vibration.

The absence of the resonance Raman bands due to the azo form of OrI in the neutral solution seems at first sight to indicate that OrI exists exclusively as the quinoid form. There have been evidences from visible and ultraviolet spectra, however, for the existence of the azo form as the minor component in solutions of various 4-phenylazo-1-naphthol derivatives in polar solvents.[5)] The present result does not conflict with the visible and ultraviolet data since the quinoid form showing the λ_{max} near 480 nm should be much more sensitive to the resonance Raman effect by the 488 nm excitation than the azo form showing the λ_{max} near 420 nm.

The resonance Raman spectrum of OrII in the neutral solution resembles that of OrI in positions and relative intensities of several bands (see Table 3), suggesting that OrII takes the quinoid form predominantly in the neutral solution. OrII shows, however, a number of medium to weak bands which are not observed for OrI. The presence of these bands may be taken to reflect the structural difference between the *o*-quinoid and the *p*-quinoid rings, but it is also possible to attribute these bands of OrII, especially the medium band at 1390 cm^{-1}, to the azo form which may exist as the minor component. In order to clarify this point, we have recorded the resonance Raman spectra of SuI, for which the solvent effect on the visible and ultraviolet spectra has been studied in detail to discuss the tautomeric equilibrium between the azo and the quinoid forms.[5)] The result seems to support the assignment of the 1390 cm^{-1} band to the *o*-quinoid structure. If this band is due to the azo form, an appreciable increase of its relative intensity should occur on the change of solvent from ethanol to *n*-hexane, since the azo form is the major component in *n*-hexane but is not in ethanol according to the visible and ultraviolet spectra.[5)] As shown in Fig. 3, however, we observed no appreciable difference in the relative intensity of the 1396 cm^{-1} band between the ethanol and the *n*-hexane solutions of SuI.

In basic solutions, the hydroxynaphthyl derivatives show the same pattern of resonance Raman spectra as HAS, giving rise to the strong N=N stretching band around 1380 cm^{-1}; see Table 4. Accordingly, the base form of hydroxynaphthyl derivatives is the divalent anion existing as the resonance hybrid in which the contribution of the azo structure is predominant. The difference between OrI and OrII in the spectra of basic solutions is far less conspicuous than that in case of neutral solutions. This result reflects well the selective enhancement of the band intensities for vibrations of the chromophore group in the resonance Raman effect. It is expected that the vibrations of the C–N=N–C group are not practically affected by the position of the substituent on the aromatic ring, whereas the structure difference between the *o*-quinoid and the *p*-quinoid rings should give rise to appreciable differences in vibrational modes and frequencies.

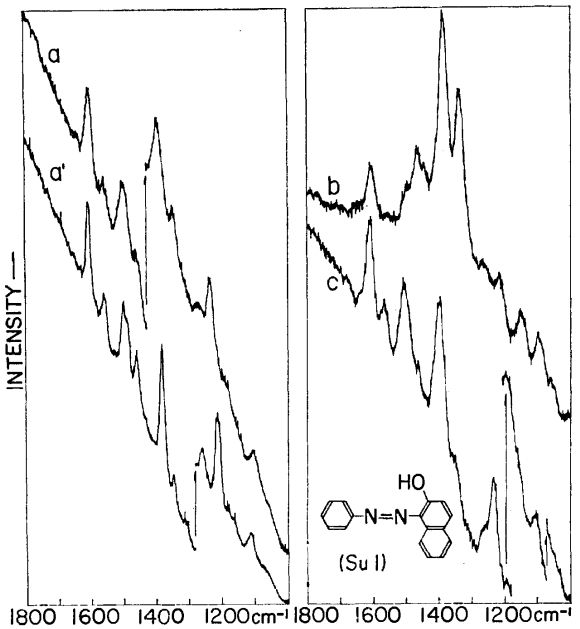

Fig. 3. Resonance Raman spectra of 1×10^{-3} M SuI: (a) in EtOH, slit width 27 cm^{-1}; (a') in EtOD, slit width 14 cm^{-1}; (b) in a 3:7 mixture of EtOH and 0.5 M NaOH, slit width 14 cm^{-1}; (c) in *n*-hexane, slit width 27 cm^{-1}.

Table 4. Observed frequencies and assignments for the basic solutions of OrI, OrII, and SuI

OrI	OrII	SuI	Assignments
1595 w	1595 w	1600 w	Ring vib.[a)]
1420 m	1440 w	1450 m[b)]	Ring vib.[a)]
1378 vs	1372 vs	1385 vs	N=N str.
1325 m	1345 s	1335 m	Ring vib.[a)]
1190 w	1215 w	1210 w	Ring vib.[a)]
1120 m	1125 w	1145 m	C–N str.

a) Vibrations due to the benzene or naphthalene ring.
b) Overlapped by the ethanol band.

Tropaeoline O. The visible and ultraviolet absorption spectrum of TrO changes in four steps on the pH

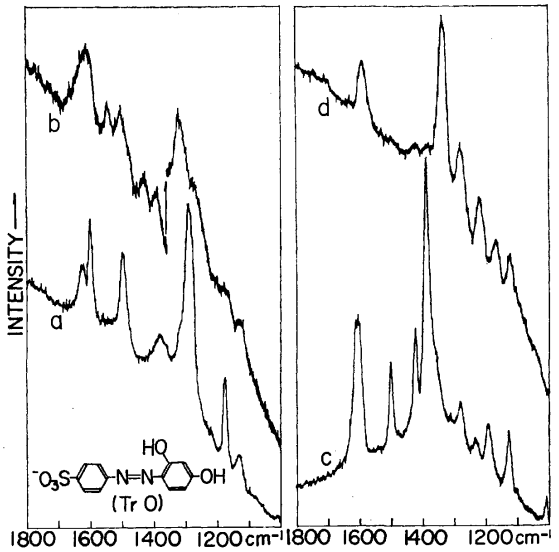

Fig. 4. Resonance Raman spectra of 1×10^{-3} M TrO: (a) in 1 M HCl, slit width 14 cm^{-1}; (b) in pH 4.0 buffer, slit width 27 cm^{-1}; (c) in pH 9.2 buffer, slit width 14 cm^{-1}; (d) in 1 M NaOH, slit width 14 cm^{-1}.

change of the solution from 1 M NaOH to 1 M HCl (see footnote,[c] Table 1). The resonance Raman spectra corresponding to these steps are different from one another as shown in Fig. 4. These spectral changes are thought to represent the stepwise protonation of TrO taking place according to Chart 1. The band assignments for the four spectra of TrO are summarized in Table 5. When dissolved in 1 M NaOH, TrO exists as the completely deprotonated trivalent anion and shows an azo-type resonance Raman spectrum in which the strongest band is observed at 1341 cm^{-1}. In analogy with the case of so far discussed monohydroxy compounds, the trivalent anion of TrO can be described as a resonance hybrid contributed mainly by the azo structure. The pattern of the resonance Raman spectrum of TrO in the pH 9.2 buffer solution is different from any of those already mentioned. This spectrum involves a number of bands attributable to the quinoid form of the divalent anion, *e.g.*, the strong

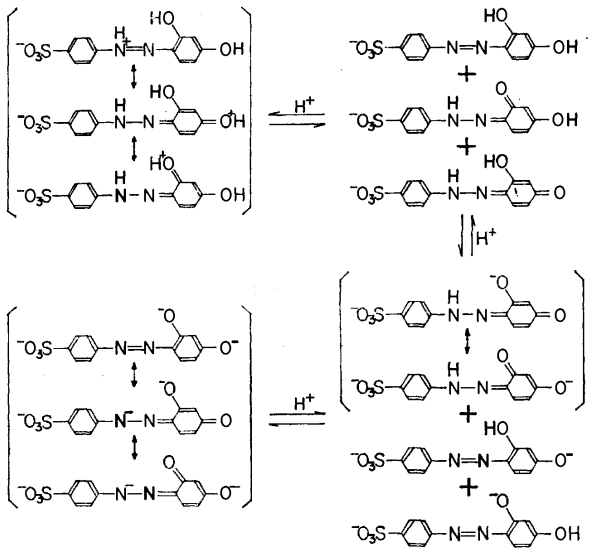

Chart 1

Table 5. Observed frequencies and assignments for TrO

1M HCl	pH 4.0 Buffer	pH 9.2 Buffer	1M NaOH	Assignments
1628 m	1610 s[a]	1618 s[b]		C=C str.
1601 s		1603 s[b]	1595 m	Benzene ring
1500 s	1500 m	1500 m		Benzene ring
1385 w	1390 w			C–C str.
		1387 vs	1341 vs	N=N str.
1290 vs	1320 s	1278 w		C–N str.(Quinoid)
			1282, 1221 m	Benzene ring
1175 m				N–N str.
		1193 w	1170 w	C–N str.(Azo)
1130 w	1130 sh	1130 m	1125 w	Benzene ring

a) Contributed also by the benzene ring vibration.
b) Measured with the slit width 6.8 cm^{-1}.

band at 1500 cm^{-1} and the weak band at 1278 cm^{-1}, of which the latter disappears on deuteration. The appearance of a very strong band at 1387 cm^{-1} in this spectrum suggests also that the azo form exists in an appreciable amount at pH 9. The resonance Raman spectrum of TrO in the pH 4 buffer solution is similar to those of the hydroxynaphthyl derivatives in neutral solutions, and is therefore due clearly to the quinoid form. It is not probable, however, that the monovalent anion of TrO takes the quinoid form exclusively in the pH 4 buffer solution, since the λ_{max} at pH 4 lies near 380 nm, where many azobenzene derivatives in the azo form show an absorption band.[2,3] The weakness of all the Raman bands in this spectrum indicates that the quinoid form is the less dominant tautomer at pH 4. In the solution in 1 M HCl, TrO shows strong resonance Raman bands at 1628, 1500, and 1290 cm^{-1} all attributable to the quinoid structure. On deuteration, the first two bands remain unchanged while the last disappears completely just as in case of the acid form of *p*-aminoazobenzene derivatives.[1] TrO in 1 M HCl is therefore described best as the zwitterionic resonance hybrid contributed mainly by the quinoid structure.

We wish to thank Professor Hisashi Tanaka for the use of the W-40 spectrophotometer in his laboratory, and Miss Kyoko Igarashi for her technical assistance.

References

1) K. Machida, B. Kim, Y. Saito, and T. Uno, This Bulletin, **47**, 78 (1974).
2) R. Kuhn and F. Bär, *Ann.*, **516**, 143 (1935).
3) J. N. Ospenson, *Acta Chem. Scand.*, **4**, 1351 (1950); *ibid.*, **5**, 491 (1951).
4) A. Burawoy and J. T. Chamberlain, *J. Chem. Soc.*, **1952**, 3734.
5) A. Burawoy, A. G. Salem, and A. R. Thompson, *ibid.*, **1952**, 4793.
6) J. B. Müller, L. Blangey, and H. E. Fierz-David, *Helv. Chem. Acta*, **35**, 2579 (1952).
7) E. Sawicki, *J. Org. Chem.*, **22**, 743 (1957).
8) H. Hacker, *Spectrochim. Acta*, **21**, 1989 (1965).
9) P. R. Carey, H. Schneider, and H. J. Bernstein, *Biochem. Biophys. Res. Commun.*, **47**, 588 (1972).
10) D. Hadži, *J. Chem. Soc.*, **1956**, 2143.
11) K. J. Morgan, *ibid.*, **1961**, 2151.

Interaction between Electron Donor and Acceptor: MINDO/2 Calculations on the Ammonia-I_2, Benzene-I_2 and Benzene-TCNE Systems

Toshiaki OHTA, Takashi FUJIKAWA, and Haruo KURODA

Department of Chemistry, Faculty of Science, The University of Tokyo, Hongo, Tokyo 113

(Received April 17, 1974)

The MINDO/2 method was applied to typical molecular complexes such as ammonia-I_2, benzene-I_2, and benzene-TCNE, these bimolecular systems being treated as single molecules. The intermolecular interaction energy was calculated as a function of intermolecular distance. Stable complex formation with a reasonable stabilization energy was predicted in the ammonia-I_2 system. It was predicted in the benzene-I_2 system for the axial model, but not for the resting model. However, the stabilization energy for the former was found to be too large. No stable conformation was found in the case of the benzene-TCNE system.

The concept of charge-transfer interaction between donor and acceptor in a molecular complex has been well established, but several problems concerning molecular complexes remain unclarified. The charge-transfer force has been considered to be of primary importance in stabilizing molecular complexes, and the conformations of complexes have often been discussed on the basis of the charge-transfer theory. However, several authors have pointed out the possibility that Coulomb and polarization forces play an important role in the complex formation.[1-4]

The intermolecular interaction has been treated most frequently by means of perturbation theory. However, in order to give quantitative prediction, an approach based on the molecular orbital method seems to have several advantages for carrying out numerical calculations. On the π-π complexes which involve polycyclic aromatic hydrocarbons as donor and tetracyanoethylene (TCNE) as acceptor, we have shown that their electronic spectra can be predicted by semi-empirical SCF-MO-CI calculations within the framework of the π-electron approximation by treating the bimolecular system as a single molecule.[5] However, in order to discuss the stabilization energy of a complex, this method seems inadequate since the contribution of σ- and/or n-electrons might not be negligible even in a typical π-π complex.

Wold[6] carried out an extended Hückel calculation on the benzene-TCNE complex, but failed to find any stable conformation. In the CNDO/2 calculation of the same complex, Chesnut and Wormer[7] predicted an extraordinarily deep potential minimum at an unreasonably short intermolecular distance.

As compared with the CNDO/2 method, the MINDO/2 method proposed by Bodor *et al.*[8] often gives better predictions as regards the heat of formations and ionization energies, at least, for relatively small organic molecules. The present paper reports on the results of MINDO/2 calculations of the ammonia-I_2, benzene-I_2, and benzene-TCNE systems. The purpose of this study is to elucidate the applicability and limitation of this type of calculation for studying the interaction between donor and acceptor molecules.

Method of Calculation

The MINDO/2 calculation was performed on a bimolecular system by the treatment as a single molecule. All empirical parameters except those related to the iodine atom were taken as proposed by Dewar and his collaborators.[8,9] For the iodine atom, we took only the 5s and 5p orbitals into account and determined the empirical parameters. For the CNDO/2 calculation, Whitehead[10] gave the core energies of 5s and 5p orbitals, U_{ss} and U_{pp}, and the one center Coulomb integral, F^0 for the iodine atom. We adopted these values with a slight modification. The one center exchange integral and electron repulsion integral can be expressed in terms of the Slater-Condon parameters, F^2 and G^1. The values of the Slater-Condon parameters have been given by Pople *et al.*[11] for the fluorine atom, but not for the iodine atom. The empirical values of F^2 and G^1 are usually estimated by means of spectroscopic data, but no such data were available for iodine. We therefore determined the empirical values of F^2 and G^1 of iodine in the following manner. F^2 and G^1 were first calculated non-empirically for the iodine and fluorine atoms by use of the Slater orbitals with the orbital exponents 1.90 and 2.60 for iodine and fluorine, respectively. The empirical values for iodine were then estimated so that their ratios to the non-empirical values are the same as the corresponding ratios in the fluorine atom. The ionization energy of the iodine 5s orbital was estimated by means of the equation given by Dewar *et al.*,[9] while the observed first ionization energy of the iodine atom was taken to be the 5p ionization energy. The iodine parameters thus obtained are listed in Table 1.

Table 1. Atomic parameters of iodine

U_{ss}	−76.905(eV),	U_{pp}	−67.202(eV)
F^0	9.448(eV),	F^2	4.077(eV)
G^1	6.526(eV),		
I_s	−26.743(eV),	I_p	−10.454(eV)
neutral atom energy			−305.010(eV)
ΔH_f for free atom			33.412(kcal)
Slater exponent			1.90

In MINDO/2 calculations, the following relation is assumed for the resonance integral:

$$\beta_{ij} = B_{ij} \times (I_i + I_j) \times S_{ij}, \quad (1)$$

where I_i and I_j are the ionization energies of the orbitals concerned, S_{ij} is the overlap integral, and B_{ij} is an empirical parameter. Ohno's approximation[12] is used

for the electron repulsion integral γ_{mn}, and the core-core repulsion integral CR_{mn} is estimated by means of the following equation,

$$CR_{mn} = \gamma_{mn} + (Z_m Z_n e^2/r_{mn} - \gamma_{mn})e^{-\alpha r_{mn}}, \quad (2)$$

where Z_m and Z_n are the core charges, r_{mn} is the distance between atoms m and n, and α is an empirical parameter.[13] Parameters B_{ij} and α are both characteristic of the kinds of atoms concerned. Their values had to be estimated for cases which involve iodine. We determined them by using I_2, HI, CH_3I, and ICN as the reference molecules so that the calculated heat of formations, equilibrium bond lengths and dipole moments of these molecules are in good agreement with the experimental values. The values of B_{ij} and α thus determined are listed in Table 2.

Table 2. Parameters α and B_{ij} for iodine

	I-H	I-C	I-N	I-I
α	0.78	1.403	1.22	0.40
B	0.60	0.52	0.58	0.88

The calculations were carried out for the bimolecular systems and for each constituent molecule. The intermolecular interaction energy ΔE was estimated by taking the difference between the total energy of the bimolecular system and the sum of the total energies of the isolated molecules.

The calculations were performed with a HITAC 5020E computer at the Computer Centre, the University of Tokyo, with our program.

Results and Discussion

Ammonia–I_2 Complex (n-σ type). As a typical example of n-σ complexes, we examined in detail the ammonia-I_2 system. We assumed a model (Fig. 1) in which the iodine molecule lies on the three-fold axis of the ammonia molecule, taking only the I–I distance, l, and N···I distance, z, as the variables specifying the conformation of the system. The bond distances and bond angles within the NH_3 moiety were fixed to be the same as those in the free ammonia molecule.[14]

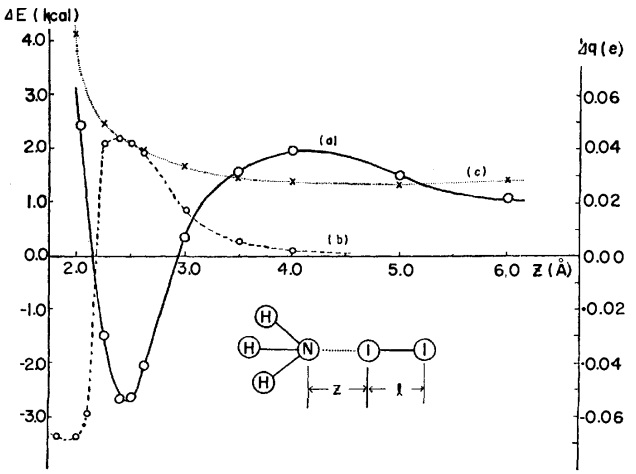

Fig. 1. Intermolecular interaction energy ΔE (a), net amount of charge transfer from NH_3 to I_2 Δq (b), and the decrease of the charge at N atom of ammonia, $-\Delta q_N$, (c) of the ammonia-iodine system as a function of the intermolecular separation, z(Å).

Although the actual structure of the ammonia–I_2 complex is not known, it should resemble the structure of the triethylamine–I_2 complex, where the I-I and N···I distances have been determined to be 2.83 and 2.27 Å respectively, from crystal structure data.[15] Thus we first carried out calculations for various z values assuming that l=2.8 Å. The results are shown in Fig. 1. On decreasing z from infinite, ΔE gradually increases and reaches a very broad maximum around 4 Å, and shows a well-defined minimum at z=2.5 Å with ΔE=−2.75 kcal/mol. Although the general shape of this energy curve is reasonable, the appearance of the repulsive region at $z>3$ Å is unexpected. A similar phenomenon appears also in other complexes. This seems to be a problem inherent to the present method of calculation.

Figure 1 also shows the net amount of charge transfer Δq, from ammonia to the iodine molecule, together with the decrease of the charge at N atom, $-\Delta q_N$, caused by the intermolecular interaction. While $-\Delta q_N$ is always positive and increases with decreasing N···I distance, the net amount of charge transfer shows a maximum at the distance corresponding to the minimum of the ΔE curve, and becomes negative in the region $z<2.2$ Å. This means that, at a short intermolecular distance, electron is transferred from iodine to ammonia, which results in the increase of the electron density at H atoms.

We next looked for the ΔE minimum by varying both l and z values. A minimum was found at z= 2.45 Å and l=2.67 Å, where ΔE was −7.5 kcal/mol. This seems to correspond to the stable conformation of the ammonia–I_2 complex. Figure 2 shows the dependence of ΔE and Δq on the I-I distance, for z= 2.45 Å. Since the lowest vacant orbital of the iodine molecule is an anitibonding σ-orbital, we can expect the I–I distance to increase with the amount of charge transfer. The relation between Δq and l shown in Fig. 2 is consistent with this expectation. The I–I distance in the free iodine molecule is 2.667 Å, while it is 2.83 Å in the triethylamin-I_2 complex, indicating

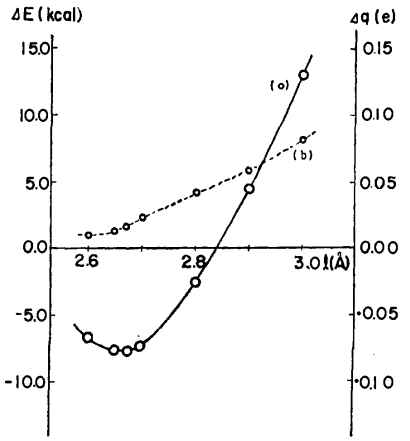

Fig. 2. Intermolecular interaction energy ΔE (a), and net amount of charge transfer Δq (b) of ammonia-iodine system as a function of the bond length of the iodine molecule, l(Å).

a relatively large charge transfer. As compared with the observed I–I distance in the triethylamine-I_2 complex, the l value 2.67 Å at the predicted ΔE minimum seems to be a little too small.

The heat of formation, dipole moment and other properties calculated for the predicted conformation of the ammonia-I_2 complex are summarized in Table 3 together with the corresponding experimental values. The calculated dipole moment is in reasonable agreement with the observed one. However, the amount of charge transfer, 1.8×10^{-2} electron, is quite small as compared with the ionic character of the complex estimated from the dipole moment by the conventional procedure without giving any allowance for the polarization effect.[16]

Table 3. Comparison of the calculated and experimental values of NH_3-I_2 complex

	Calcd	Exptl
μ(Debye)	4.5	6.1∼6.7[a]
$-\Delta E$(kcal/mol)	7.5	4.84[b]
Δq(e)	0.018	
z(Å)	2.45	
l(Å)	2.67	

a) Ref. 16. b) Ref. 25.

The calculated charge density for the stable conformation of the complex as well as for the ammonia molecule is shown in Fig. 3. As compared with the results of the calculation on the free molecule, the electron density in the complex is smaller by 0.039 at N atom, but larger by 0.007 at each H atom. A significant change is found in the I_2 part, where the density at the I atom directly contacting the N atom of ammonia decreases by 0.115, on the other hand, the density at the other I atom increases by 0.132. This means that a considerably large dipole moment has been induced in the I_2 molecule, making a significant contribution to the dipole moment of the complex.

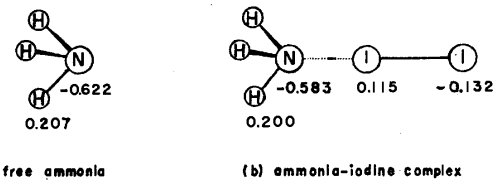

Fig. 3. Net charges of free ammonia (a) and the ammonia–iodine complex at the most stable configuration (b).

Several authors have recently pointed out the importance of the induced polarization in the observed dipole moments of molecular complexes.[1-3,17] The results of our calculation support the view.

Since the amount of charge transfer was calculated to be quite small, it seems of interest to examine the contribution of charge transfer in the stabilization energy of the complex. We estimated the contributions of different types of interaction by means of the approximations described in the Appendix, and found that the attraction energy due to the charge-transfer force is of primary importance for stabilizing the complex. The orbital energies of the molecular orbitals of the ammonia and iodine molecules are given in Table 4, and the contributions of different charge-transfer configurations to the intermolecular attraction energy in Table 5. The charge transfer from the highest occupied orbital of ammonia to the lowest vacant orbital of iodine makes the largest contribution, but there is an almost comparable contribution of a charge transfer from a deeper occupied orbital of ammonia. It should be noted that the contributions of back charge transfer are also quite significant.

Table 4. Energies of molecular orbitals

orbital	energy(eV)	orbital	energy(eV)
NH_3		C_6H_6[a]	
2e	4.91	$5e_2$	4.08
$3a_1$	3.21	$4e_1$	2.88
		4b(π)	2.66
$2a_1$	−10.45	4a	2.33
1e	−13.99	$4e_2$	2.19
$1a_1$	−35.58	3b	1.38
		$3e_2(\pi)$	0.42
I_2		$3e_1(\pi)$	−9.57
3a	0.26	$2e_2$	−10.01
		2b	−12.20
3s	−8.97	$2e_1$	−12.88
$2a(\pi)$	−12.1	$3a(\pi)$	−13.33
$2s(\pi)$	−15.4	1b	−14.82
1a	−25.6	2a	−17.61
1s	−36.8	$1e_2$	−20.67
		$1e_1$	−29.24
		1a	−38.53

a) Some higher orbitals less significant in the CT interaction have been omitted.

Table 5. Contribution of each component to the charge-transfer stabilization energy for NH_3-I_2 complex[a]

Donation			Back donation		
NH_3	I_2	energy(eV)	I_2	NH_3	energy(eV)
$2a_1$ →	3a	0.997	3s →	$3a_1$	0.425
1e →	3a	0.0	1a →	$3a_1$	0.098
$1a_1$ →	3a	0.601	1s →	$3a_1$	0.165
			$2a(\pi)$→	2e	0.010
			$2s(\pi)$ →	2e	0.006

a) Only the important components are listed in this table.

From the results of energy analysis described above, we can conclude that the prime effect in the ammonia–I_2 complex, *viz.*, stabilization of the system, is the charge-transfer force, but the net amount of charge transfer is small because of the significant contribution of the charge transfer from occupied orbitals of iodine to vacant orbitals of ammonia.

Benzene-I_2 Complex (π-σ type). For the benzene-I_2 complex, Mulliken[18] first proposed the resting model where the iodine molecule lies parallel to the benzene molecule. The model was considered doubtful from the analysis of infrared spectrum of the complex, which seemed to support the axial or oblique model.[19] How-

ever, it was realized later that the infrared spectrum does not provide any definite conclusion as regards the conformation of the benzene-I_2 complex.[20-22] In the crystals of the benzene-halogen complexes, the halogen molecules are oriented perpendicular to the molecular plane of benzene,[23] but the conformation of an isolated complex is not necessarily the same as the one found in the crystal of the molecular complex. Thus the actual conformation of the benzene-I_2 complex still remains unclarified.

We examined two models, axial and resting, in the present calculation (Fig. 4). Assuming the geometries of the benzene and iodine molecules to be the same as those of the free molecules, we varied the intermolecular distance z which is defined in Fig. 4.

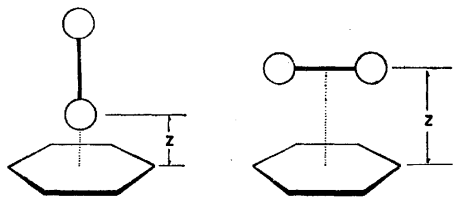

Fig. 4. Two models for the benzene–iodine complex: (a) axial model, (b) resting model.

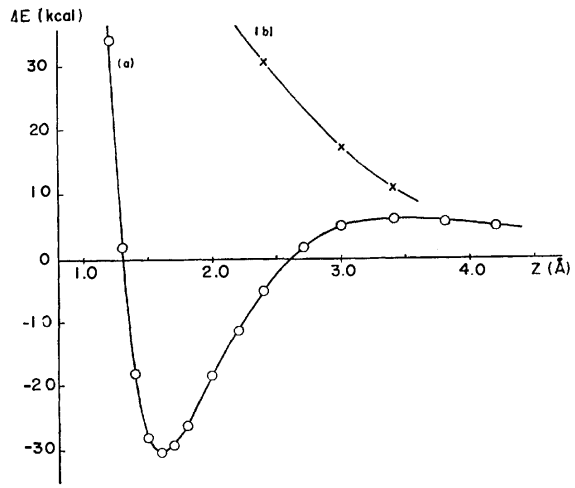

Fig. 5. Intermolecular interaction energy ΔE of the benzene-iodine system as a function of the intermolecular separation, z(Å).

The calculated ΔE is plotted against z in Fig. 5. The results indicate that the axial model is more stable than the resting model. It is also to be noted that a well-defined energy minimum is predicted in the former but not in the latter. The axial model is plausible for the benzene-I_2 complex. Quantitatively, however, our results confront serious problems. The z value at the energy minimum, 1.7 Å, is unreasonably short for the intermolecular separation between benzene and iodine, and the stabilization energy of the complex is predicted to be too large. The net amount of charge transfer from benzene to iodine is calculated to be -3.21×10^{-1} electron for the conformation corresponding to the energy minimum. This means that a considerable amount of charge is transferred from iodine to benzene and not from benzene to iodine, which is unreasonable. Thus it is hard to take the conformation at the ΔE minimum as the real structure of the benzene-I_2 complex.

The z-value dependence of the amount of charge transfer and dipole moment of the system is shown in Fig. 6. Δq is positive in the region $z>2.1$ Å, which first increases on decreasing z, reaches a maximum value, 3.72×10^{-2} electron, at $z=2.5$ Å, then steeply decreases to change its sign. The actual value of z for the axial model would be about 3.4 Å. Although the intermolecular interaction at this value is predicted to be repulsive, it seems worthwhile to examine the properties predicted for the conformation. The calculated dipole moment is 0.34 Debye, which is approximately one fifth of the observed value.[24] Even so, the ionic character of the complex corresponding to this calculated value of the dipole moment will be estimated as about 1.5%, if this dipole moment is attributed entirely to the charge transfer, but the amount of charge transfer actually obtained from the predicted electron densities is only 5.77×10^{-3} electron. The electron density is 6.994 at the iodine atom which is in direct contact with benzene, and 7.009 at the other iodine atom. This implies that a considerable polarization has been induced in the iodine molecule, which is of primary importance in the predicted dipole moment. The situation is more or less similar for other intermolecular distances.

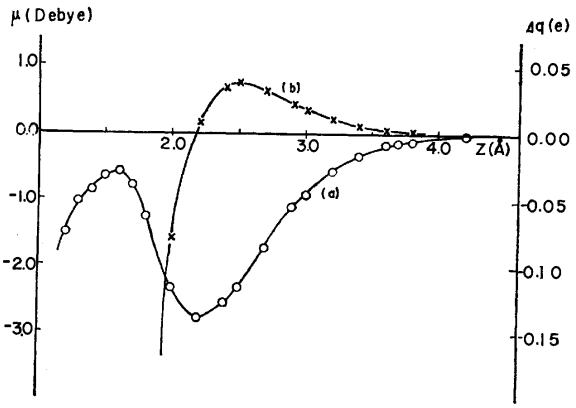

Fig. 6. Dipole moment μ (a) and net amount of charge transfer Δq from benzene to iodine (b) of the benzene-iodine complex as a function of z(Å).

The orbital energies of benzene and iodine are listed in Table 4. We estimated the contributions of various charge transfers for ΔE in the case of the conformation with $z=3.4$ Å. The results are shown in Table 6. One can see that the charge transfer from a lower π-orbital, $3a(\pi)$, of benzene to the lowest vacant orbital, $3a$, of iodine is of primary importance.

Benzene-TCNE Complex (π-π type). As an example of π-π complex we chosed the benzene-TCNE system. We assumed that the molecular planes of benzene and TCNE are parallel to each other, the center of the TCNE molecule being on the six-fold axis of benzene. The calculated interaction energy ΔE is plotted against the intermolecular distance z in Fig. 7.

Table 6. Contribution of each component to the charge-transfer stabilization energy for C_6H_6–I_2 complex[a)]

Donation			Back donation		
C_6H_6	I_2	energy(eV)	I_2	C_6H_6	energy(eV)
$3e_1(\pi)$ →	3a	0.0	3s →	4a	0.258
$3a(\pi)$ →	3a	4.193	1a →	4a	2.181
2a →	3a	0.355	1s →	4a	0.098
1a →	3a	0.765	$2a(\pi)$ →	$4e_1$	0.315
			$2s(\pi)$ →	$4e_1$	0.139
			$2a(\pi)$ →	$5e_2$	0.0
			$2s(\pi)$ →	$5e_2$	0.257

a) Only the important components are listed in this table.

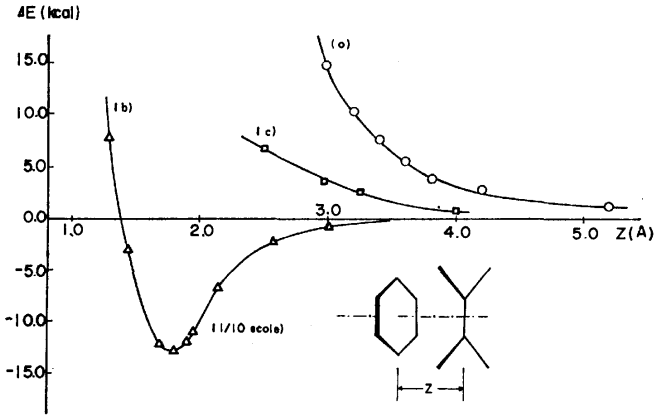

Fig. 7. Intermolecular interaction energy ΔE of the benzene–TCNE system from various methods. (a) MINDO/2 method in this work, (b) CNDO/2 method from Ref. 7, (c) extended Hückel method from Ref. 6.

The interaction between benzene and TCNE was predicted to be always repulsive. This result is quite different from that of the CNDO/2 calculation by Chesnut and Wormer,[7] and resembles the result of the extended Hückel calculation by Wold.[6]

We performed calculations on some other π-π complexes, but again failed to predict any stable conformation. Seemingly, the MINDO/2 calculation cannot give satisfactory results for a system consisting of weakly interacting π-donor and π-acceptor.

Conclusion

In the present study, we carried out MINDO/2 calculations on bimolecular systems composed of an electron donor and an electron acceptor. The calculation gave satisfactory results in the case of the ammonia–I_2 system, and succeeded in predicting the formation of a stable ammonia–I_2 complex. The dipole moment and other properties calculated for the predicted conformation of the complex were in reasonable agreement with the experimental results. The calculation was less successful for the benzene–I_2 system, where an unreasonably small intermolecular distance was predicted as the most stable conformation of the system. In the case of the benzene-TCNE system, the calculation completely failed to predict the formation of a stable complex.

Parametrization of MINDO/2 has been carried out for application on relatively small molecules. It gives good prediction as regards the heat of formation and ionization energy of various organic molecules, but it is not always suitable for calculations on a bimolecular system.

In MINDO/2 as well as in CNDO/2, the Slater atomic orbitals are used as the basis set with the Slater-Zener orbital exponents. This may be sufficient in calculations of small molecules, but not in those of bimolecular systems where the integrals between atoms with relatively large interatomic distance have significant contributions. This situation might not be so important for the ammonia–I_2 system, but seems to be of prime importance for the benzene-TCNE system.

While the MINDO/2 calculation fails to predict the stabilization of the benzene–TCNE complex, the CNDO/2 calculation gives an unreasonably large stabilization energy for the same complex. When we compare the two methods, the resonance integrals between the 2p orbitals of two carbon atoms are estimated to be more than twice as large in the CNDO/2 method as in the MINDO/2 method. As is known, the resonance integral between atoms with a large interatomic distance is usually markedly underestimated when the Slater AO's are used as the basis set. This can be improved by the use of the SCF–AO's. A possible way for the improvement of calculations on bimolecular systems, is to perform parametrization by use of the SCF–AO's as the basis set.

Appendix

In a molecular orbital approach on a bimolecular system, the physical nature of the intermolecular interaction cannot be understood straightfowardly. We will show an approximate way to separate the contributions of different types of interaction.

Let us express the Fock matrix of a bimolecular system composed of molecules A and B as follows.

$$\mathbf{F} = \begin{vmatrix} \mathbf{A}+\mathbf{A}' & \mathbf{C} \\ {}^t\mathbf{C} & \mathbf{B}+\mathbf{B}' \end{vmatrix} \tag{1}$$

where $\mathbf{A}$ and $\mathbf{B}$ are the SCF Fock matrices of the isolated molecules, $\mathbf{A}'$ and $\mathbf{B}'$ the perturbation matrices, $\mathbf{C}$ is the interaction matrix and ${}^t\mathbf{C}$ the transposed matrix of $\mathbf{C}$. The molecular orbital approach on the bimolecular system is to solve

$$\mathbf{FX} = \varepsilon\mathbf{X} \tag{2}$$

Any eigenvector $\mathbf{X}$ can be expressed in terms of the eigenvectors of $\mathbf{A}$ and $\mathbf{B}$ matrices as follows.

$$\mathbf{X} = \sum_{i=1}^{n} a_i \begin{bmatrix} \mathbf{a}_i \\ \mathbf{O} \end{bmatrix} + \sum_{j=1}^{m} b_j \begin{bmatrix} \mathbf{O} \\ \mathbf{b}_j \end{bmatrix} \tag{3}$$

where $\mathbf{a}_i$ ($i=1, 2, \cdots, n$) and $\mathbf{b}_j$ ($j=1, 2, \cdots, m$) are the eigenvectors of $\mathbf{A}$ and $\mathbf{B}$ matrices, respectively, and $\mathbf{O}$ and $\mathbf{O}'$ zero vectors of m and n rows, respectively.

Substituting Eqs. (1) and (3) into Eq. (2), we obtain

$$\begin{bmatrix} (\mathbf{A}+\mathbf{A})\sum_i a_i\mathbf{a}_i + \mathbf{C}\sum_j b_j\mathbf{b}_j \\ {}^t\mathbf{C}\sum_i a_i\mathbf{a}_i + (\mathbf{B}+\mathbf{B}')\sum_j b_j\mathbf{b}_j \end{bmatrix} = \varepsilon \begin{bmatrix} \sum_i a_i\mathbf{a}_i \\ \sum_j b_j\mathbf{b}_j \end{bmatrix} \tag{4}$$

from which the following equation can be derived.

$$\sum_i(\alpha_i-\varepsilon+\mathbf{A}')a_i\mathbf{a}_i + \mathbf{C}\sum_j b_j\mathbf{b}_j = 0 \quad (5)$$

and

$$^t\mathbf{C}\sum_i a_i\mathbf{a}_i + \sum_j(\beta_j-\varepsilon+\mathbf{B}')b_j\mathbf{b}_j = 0 \quad (6)$$

where α_i's are the eigenvalues of **A** matrix, and β_i's those of **B** matrix. Premultiplying Eq. (5) by $\mathbf{a}_k$ and Eq. (6) by $\mathbf{b}_l$, we get the following equations.

$$(\alpha_k-\varepsilon)a_k + \sum_i a_i\langle\mathbf{a}_k|\mathbf{A}'|\mathbf{a}_i\rangle + \sum_j b_j\langle\mathbf{a}_k|\mathbf{C}|\mathbf{b}_j\rangle = 0 \quad (7)$$

and

$$\sum_i a_i\langle\mathbf{b}_l|\mathbf{C}|\mathbf{a}_i\rangle + (\beta_l-\varepsilon)b_l + \sum_j b_j\langle\mathbf{b}_l|\mathbf{B}'|\mathbf{b}_j\rangle = 0 \quad (8)$$

These equations are reduced to the secular equation given below.

$$\begin{vmatrix} \alpha_1-\varepsilon+A'_{11} & A'_{12} \cdots\cdots & A'_{1n} & C_{11} & C_{12} \cdots\cdots & C_{1m} \\ A'_{21} & \alpha_2-\varepsilon+A'_{22} & & & C_{22} & \\ \vdots & \vdots & \vdots & \vdots & \vdots & \vdots \\ A_{n1} & \cdots\cdots\cdots & \alpha_n-\varepsilon+A'_{nn} & C_{n1} & \cdots\cdots\cdots & C_{nm} \\ C_{11} & C_{12} \cdots\cdots & C_{1n} & \beta_1-\varepsilon+B'_{11} & \cdots\cdots & B'_{1m} \\ & C_{22} & & B'_{21} & & \\ \vdots & \vdots & \vdots & \vdots & \vdots & \vdots \\ C_{m1} & \cdots\cdots\cdots & C_{mn} & B'_{m1} & \cdots\cdots & \beta_m-\varepsilon+B'_{mm} \end{vmatrix} = 0 \quad (9)$$

where $A'_{ik}=\langle\mathbf{a}_i|\mathbf{A}'|\mathbf{a}_k\rangle$, $B'_{il}=\langle\mathbf{b}_i|\mathbf{B}'|\mathbf{b}_l\rangle$, and $C_{ij}=\langle\mathbf{a}_j|\mathbf{C}|\mathbf{b}_j\rangle$. This is exactly the same as the secular equation which we have to solve in the molecular orbital calculation on the bimolecular system. When the interaction matrix **C** and the perturbation matrices **A'** and **B'** are sufficiently small, the solutions of Eq. (9) can be approximately given by the perturbation method as follows.

$$\varepsilon_i = \alpha_i + A'_{ii} + \sum_{k\neq i}\frac{A'^2_{ik}}{\alpha_i-\alpha_k} + \sum_j\frac{C_{ij}^2}{\alpha_i-\beta_j} + \cdots \quad (10)$$

and

$$\varepsilon_j = \beta_j + B'_{jj} + \sum_k\frac{C_{jk}^2}{\beta_j-\alpha_k} + \sum_{l\neq j}\frac{B'^2_{jl}}{\beta_j-\beta_l} + \cdots \quad (11)$$

where we have neglected higher order terms. The total energy of a closed-shell molecule is

$$E = 2\sum_i^{occ}\varepsilon_i - \sum_{i,j}^{occ}(2J_{ij}-K_{ij}) + \sum_{n,m}CR_{nm} \quad (12)$$

where J_{ij} is the Coulomb integral, K_{ij} the exchange integral, and $\sum_{n,m}CR_{nm}$ the sum of the core repulsion energy. Thus the intermolecular interaction energy ΔE, defined as the difference between the total energy of the bimolecular system and the sum of the total energies of the constituent molecules, can be expressed as follows.

$$\begin{aligned}\Delta E = {} & [2\sum_{i(A)}^{occ}A'_{ii} + 2\sum_{j(B)}^{occ}B'_{jj} - \sum_{i,j(A-B)}^{occ}(2J_{ij}-K_{ij}) \\ & + \sum_{i,i'(A)}^{occ}(2J_{ii'}-K_{ii'}) + \sum_{l,l'(B)}^{occ}(2J_{ll'}-K_{ll'}) + \sum_{n(A)}\sum_{m(B)}CR_{nm}] \\ & + 2\left[\sum_{i(A)}^{occ}\sum_{k(A)}^{vac}\frac{A'^2_{ik}}{\alpha_i-\alpha_k} + \sum_{j(B)}^{occ}\sum_{l(B)}^{vac}\frac{B'^2_{jl}}{\beta_j-\beta_l}\right] \\ & + 2\left[\sum_{i(A)}^{occ}\sum_{l(B)}^{vac}\frac{C_{il}^2}{\alpha_i-\beta_l} + \sum_{j(B)}^{occ}\sum_{k(A)}^{vac}\frac{C_{jk}^2}{\beta_j-\beta_k}\right] \end{aligned} \quad (13)$$

where $\sum_{i(A)}^{occ}$ stands for the summation over all occupied orbitals of the molecule A, and $\sum_{j(B)}^{occ}$ the corresponding summation for the molecule B. Roughly speaking, the terms in the first brackets give the contribution of the Coulomb and core repulsion energies, those in the second brackets give that of the induction energy and dispersion force, and those in the last brackets correspond to the charge transfer force. All of the integrals in Eq. (13) can be easily evaluated. As an example, C_{il} can be expressed as follows.

$$C_{il} = \sum_{r,s}a_{ir}b_{ls}F_{rs} \quad (14)$$

where a_{ir} is the coefficient of the atomic orbital r in the i-th molecular orbital of molecule A, b_{ls} the coefficient of the atomic orbital s in the l-th molecular orbital of molecule B, and F_{rs} is the element of the Fock matrix, which is given as follows in the MINDO/2 method.

$$F_{rs} = \beta_{rs} - \frac{1}{2}P_{rs}\gamma_{nm}$$

Thus, we can estimate the contribution of a charge-transfer configuration, CT($i\rightarrow l$),

$$\Delta E_{CT(i\rightarrow l)} = \frac{C_{il}^2}{\alpha_i-\beta_l}$$

by using the results of the molecular orbital calculations of the bimolecular system and those of the isolated molecules.

References

1) M. W. Hanna, *J. Amer. Chem. Soc.*, **90**, 285 (1968).
2) J. L. Lippert, M. W. Hanna, and P. J. Trotter, *ibid.*, **91**, 4035 (1969).
3) M. J. S. Dewar and C. C. Thompson Jr., *Tetrahedron, Suppl.*, **7**, 97 (1966).
4) W. C. Herndon and J. Feuer, *J. Amer. Chem. Soc.* **90**, 5914 (1968).
5) T. Ohta, H. Kuroda, and T. L. Kunii, *Theoret. Chim. Acta*, **19**, 167 (1970).
6) S. Wold, *Acta Chem. Scand.*, **20**, 2379 (1966).
7) D. B. Chesnut and P. E. Wormer, *Theoret. Chim. Acta*, **20**, 250 (1971).
8) N. Bodor. M. J. S. Dewar, A. Harget, and E. Hasellach, *J. Amer. Chem. Soc.*, **92**, 3854 (1970).
9) N. Baird and M. J. S. Dewar, *J. Chem. Phys.*, **50**, 1269 (1969).
10) M. A. Whitehead, "Sigma Molecular Orbital Theory," ed. by O. Sinanoglu and K. B. Wiberg, Yale University Press, New Haven and London (1970), p. 50.
11) J. A. Pople, D. L. Beveridge, and P. A. Dobosh, *J. Chem. Phys.*, **47**, 2026 (1967).
12) K. Ohno, Y. Tanabe, and F. Sasaki, *Theoret. Chim. Acta*, **1**, 378 (1963).
13) M. J. S. Dewar and G. Klopman, *J. Amer. Chem. Soc.*, **89**, 3089 (1967).
14) A. Almeningen and O. Bastiansen, *Acta Chem. Scand.*, **9**, 815 (1955).
15) O. K. Stroemme, *ibid.*, **15**, 407 (1961).
16) S. Kobinata and S. Nagakura, *J. Amer. Chem. Soc.*, **88**, 3905 (1966).
17) M. Manitone, *Theoret. Chim. Acta*, **11**, 119 (1968).
18) R. S. Mulliken, *J. Amer. Chem. Soc.*, **74**, 811 (1952).
19) E. E. Ferguson, *J. Chem. Phys.*, **25**, 577 (1956), **26**, 1357 (1957), *Spectrochim. Acta*, **10**, 123 (1957).
20) J. Collin and L. D'or, *J. Chem. Phys.*, **23**, 397 (1955).
21) E. E. Ferguson and F. A. Matsen, *J. Amer. Chem. Soc.*, **82**, 29 (1960).
22) H. B. Friedrich and W. B. Person, *J. Chem. Phys.*, **44**, 2161 (1966).
23) O. Hassel and K. O. Stroemme, *Acta Chem. Scand.*, **12**, 1146 (1958), **13**, 1781 (1959).
24) G. Kortüm and H. Walz, *Z. Elektrochem.*, **57**, 73 (1953).
25) H. Yada, J. Tanaka, and S. Nagakura, This Bulletin, **33**, 1660 (1960).

ESR Study on Fluorescein Semiquinone Radical

Shigeya NIIZUMA, Yoshiharu SATO, Shiro KONISHI, and Hiroshi KOKUBUN
Department of Chemistry, Faculty of Science, Tohoku University, Aoba, Aramaki, Sendai 980
(Received April 19, 1974)

The ESR spectrum of the fluorescein semiquinone radical (dianion form) produced by illumination of an alkaline aqueous solution of uranine and leuco-uranine at pH between 11 and 14 was observed and its hfs constants were determined by comparing the spectrum with those of the mono- and trianion forms of fluorescein semiquinone and those of eosin semiquinone reported by Leaver. Six protons in the xanthene ring were found to be comprised of three pairs of magnetically equivalent protons, which suggests a certain dynamic mechanism to average the coupling constants. From a temperature dependence of the line width, protonation to the -O⁻ group followed by deprotonation from the -OH group was proposed as a plausible mechanism.

When alkaline water-ethanol and water-2-propanol solutions of uranine (disodium salt of fluorescein) are illuminated with visible light, uranine is reduced to leuco-uranine *via* a half-reduced form (semiquinone radical).[1] The semiquinone, which is relatively stable in the alkaline solution, is also produced by uranine-sensitized photo-oxidation of leuco-uranine.[2] According to the investigations using the steady light as well as the flash illuminations, it was established that the radical is in ionic equilibrium as shown in scheme (I). The pK_a values of the mono- and dianions are reported to be 9.5 and >13,[3] respectively.

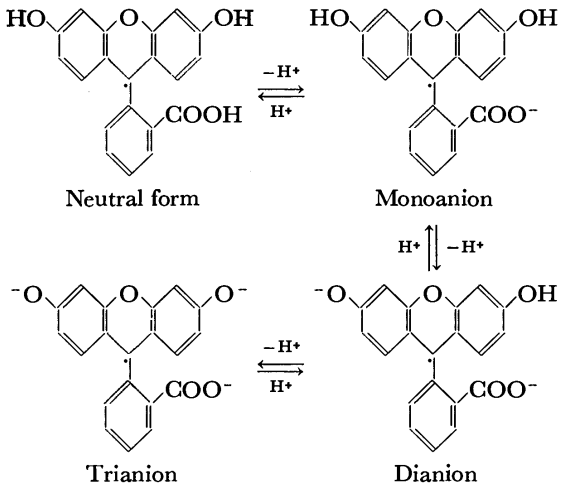

Scheme (I)

Therefore at the pH between 11 and 13, the semiquinone exists as the dianion form. From the kinetic study of the ESR signal of this radical, it was clarified that the signal intensity change after making the illumination off shows a typical second-order decay and the activation energy of disproportionation or recombination for this radical was found to be 10 to 12 kcal/mol.[4] Though a highly resolved ESR spectrum has ever been observed,[5,6] the analysis of hfs has not yet been performed sufficiently.

As to radicals containing one or more phenyl rings, for example benzophenone ketyl[7] and α-phenylbenzilidene malononitrile,[8] a steric and an electronic effect on rotation of the phenyl rings are recently treated as interesting problems. From this point of view, it will be interesting to analyse the hfs of the fluorescein semiquinone radical in detail in order to obtain the information about the rotation of the phenyl ring in this molecule.

By using the improved light source system, the more resolved spectrum than that in the previous report[4] has been detected. The results of the analysis of hfs and the signal behavior give the following information; (1) The radical species obtained at pH between 11 and 14 was the only one and was identified as a dianion. At the pH range from 9.5 to 10.5, the asymmetric spectra were obtained, which means in general that signals of two kinds of radicals superpose each other. No further analysis of these spectra was made. (2) The ESR spectrum of the radical identified as a dianion revealed that six protons in the xanthene frame consist of three pairs of magnetically equivalent protons. Therefore it is suggested that this molecule has a certain mechanism to make some pairs of protons equivalent magnetically. (3) Line broadening and narrowing occur reversibly with the temperature decrease and increase. The interpretation of these results was attempted. Two conceivable mechanisms are (a) the hindered rotation of the phenyl ring and (b) protonation to the -O⁻ group followed by deprotonation from the -OH group. The latter is more plausible.

Experimental

Materials. Uranine was prepared by treating fluorescein (Hikotaro Shudzui & Co., G. R. grade) with sodium carbonate in water and was recrystallized three times from ethanol. Leuco-uranine was obtained by reducing the above uranine with sodium amalgam in water and was used without further purification.

Procedures. The radical dianion was produced mainly by illuminating the aqueous solution of uranine (10^{-5}—10^{-4} mol/l) and leuco-uranine (10^{-3}—10^{-2} mol/l) mixture in an

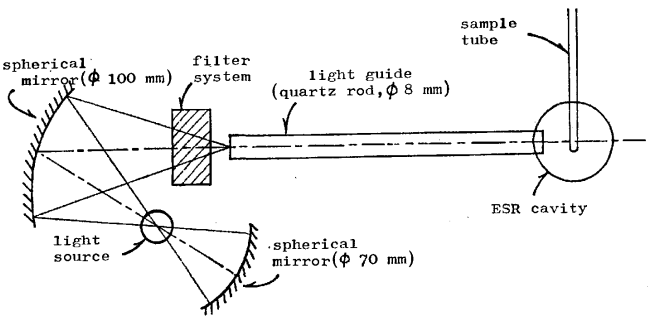

Fig. 1. The apparatus for the illumination system.

ESR sample tube placed in a cavity. pH of the solution was controlled with sodium hydroxide concentration. An Ushio super high-pressure mercury lamp (USH 500D) was used as a light source. The illuminating apparatus is shown in Fig. 1. Light was collected by two spherical mirrors, larger one (10 cm in diameter) being set to have a correct angle between the axis of incident light and that of reflected light and to focus the light on the front surface of a quartz light-guide. A filter system which consists of 1 cm water, a 1 cm cupric sulfate aqueous solution and a Toshiba VY-43 glass filter was placed between the mirror and the light-guide. This filter system transmits the visible light in the range from 430 to 600 nm. The wavelength of absorption maximum of uranine in alkaline aqueous solutions is 495 nm.

The temperature of the sample was controlled by inserting the doubly sealed quartz tube into a cavity and introducing cold nitrogen gas or hot air through the tube. A thermocouple was used to monitor the temperature in the tube.

Hyperfine splittings were determined using the signal of seven lines of Mn^{2+} in MgO as a standard. The separation between the third and fourth lines is 87.5 G.

A JEOL P-10 type ESR spectrometer (X band, 100 kHz modulation) was used. A NEAC 2200 MODEL 700 Electronic Computer in the Calculation Center of Tohoku University was used for the calculation of unpaired spin densities. For a simulation of ESR spectra, a JEOL JEC-6 Spectrum Computer was used.

Results and Discussion

ESR Spectra Obtained in the Solutions of Different pH Values. The ESR spectra obtained during photolysis of solutions of various pH values higher than 9.5 are shown in Fig. 2. The signals observed at pH values lower than 10.5 have a small S/N ratio because of a short lifetime of the radical and have an asymmetric line shape, which may be due to the superposition of signals from the mono- and dianions. At the pH range from 11 to 13, rather highly resolved spectra were detected. The di- and trianions might coexist at pH values greater than 14, but in fact similar spectra to those at pH range from 11 to 13 were observed with smaller intensity.

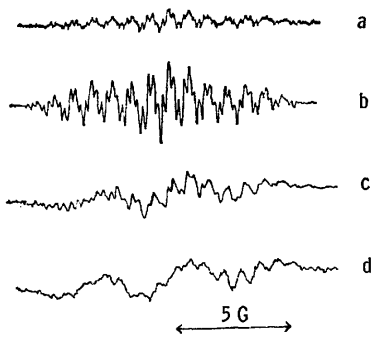

Fig. 2. ESR spectra of fluorescein semiquinone at pH> 14 (a), 12.3 (b), 10.5 (c), and 9.5 (d).

Simulation of ESR Spectrum and Determination of Coupling-Constants and Unpaired Spin Densities on Carbons. Figure 3(1) shows a typical spectrum of the dianion which is approximately the same as that obtained by Kimura *et al.*[5] in the γ-irradiated methanol solution of uranine. The arrow marked a indicates the center of the spectrum. When the modulation width is wide, the signal is a 1 : 2 : 1 triplet. As the modulation width becomes narrow, it splits into fifteen lines as a whole. Each component of the fifteen lines comprises seven or eight lines which are not well-resolved. The line shape of components marked a and b in Fig. 3(1) resembles each other: moreover both sides of marks a and b have a similar shape over a few gauss. The same relation hold between marks a and b'. (b' is the point at lower field half and not given in the figure.) Therefore the largest coupling exhibiting the triplet is taken as 3.287 G from the distance between a and b (or a and b'). The spectrum of a (or b) component (Fig. 4(1)) can be simulated satisfactorily by using four coupling constants of 0.220, 0.190, 0.170, and 0.090 G (Fig. 4(2)). This pattern is similar to the component of the triplet signal which has been obtained by photolysis of eosin in methanol-d_1[6] by Leaver (Fig. 4(3)). He reconstructed this pattern by using three protons of

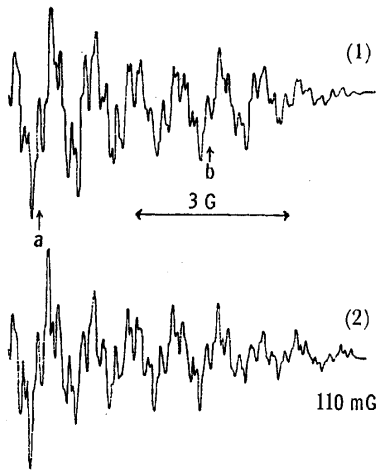

Fig. 3. ESR spectrum of the dianion in ethanol–aqueous solution (20 volume percent ethanol) at 44 °C (1) and its simulation (2).

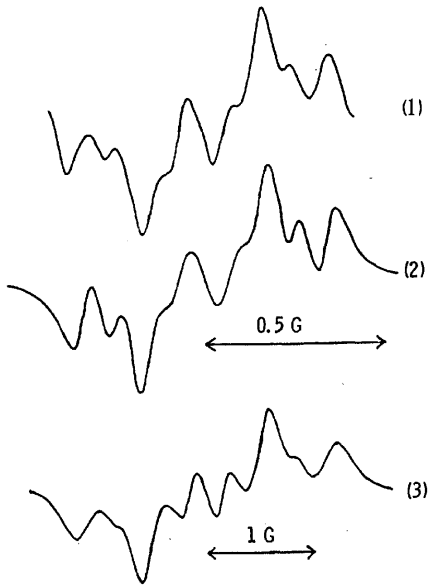

Fig. 4. a (or b) component of the fifteen lines (1), its simulation (2) and one component of the triplet spectrum of eosin semiquinone (3).

0.61 G and one proton of 0.29 G. The shape in Fig. 4(3) was assigned to that constructed with the coupling of four protons in the phenyl ring of eosin semiquinone.

The whole spectrum consisting of fifteen lines in Fig. 3(1) can be simulated by combining the four coupling constants, which produce the line shape in Fig. 4(1) with those of six protons in the xanthene ring, two of which are already estimated to be 3.287 G. As for the rest of the couplings, two of them are estimated to be 1.510 G and the other two 0.889 G. The coupling constants determined in this way are given in Table 1. The spectrum simulated with the aid of parameters in Table 1 is shown in Fig. 3(2).

Table 1. Coupling constants and unpaired spin densities

Position	Coupling const. Obsd(G)	Unpaired spin density Obsd[a)]	Calcd	Average
1	3.287	0.1133	0.1124	0.1120
8			0.1116	
2	1.510	0.0521	−0.0332	−0.0326
7			−0.0322	
4	0.889	0.0307	−0.0304	−0.0290
5			−0.0276	
13	0.220	0.0076	0.0098	
14	0.190	0.0066	0.0078	
15	0.170	0.0059	0.0028	
16	0.090	0.0031	0.0010	

a) $Q=29$ G was used.

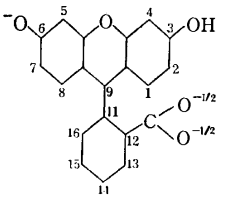

The unpaired spin densities calculated by McLachlan's method based on simple LCAO MO method are listed in the fourth column of Table 1. The following parameters were used in the calculation:

$$\alpha_{-O-} = \alpha + 2.0\beta \qquad \beta_{C-O-} = 0.6\beta$$
$$\alpha_{-OH} = \alpha + 2.5\beta \qquad \beta_{C-OH} = 0.7\beta$$
$$\alpha_{-O^{-1/2}} = \alpha + 2.25\beta \qquad \beta_{C-O^{-1/2}} = 0.8\beta$$
$$\alpha_{-O^{-}} = \alpha + 2.0\beta \qquad \beta_{C-O^{-}} = 0.8\beta$$

where α_i and β_{C-R} are respectively the Coulomb integral of C–i atom and exchange integral of C–R bond. As for McLachlan's parameter, $\lambda=1.0$ was used. Because of steric hindrance, the xanthene and phenyl rings cannot be in the same plane but incline to a considerable to extent each other. $\beta_{C_9-C_{11}}=\beta\cos^2\theta$ was added to the parameter for calculation, where θ is the angle between the axis of the p-orbital of C_9 and that of C_{11}. The calculated values listed in Table 1 are for $\theta\approx55°$. The agreement between the observed and the calculated values is rather good.

It is obvious from the pK values of the mono- and dianions determined by Lindqvist that the radical in question has the dianion form. This is also supported by the fact that the observed coupling value of the protons at the 1- and 8-positions (3.287 G) lies between those of the monoanion (3.39 G) and the trianion (2.89 G) reported by Leaver for methanol solutions. The tendency of decreasing coupling constants of the 1- and 8-positions with increasing negative charge of the radical implies that the unpaired electron migrates from the xanthene into the phenyl ring as the -OH groups at the 3- and 6-positions are replaced by the $-O^-$ groups.

If only the asymmetry of the molecule is taken into consideration, the coupling constant of the proton at the 1-position should differ slightly from that at the 8-position. A pair of protons at the 2- and 7-positions as well as a pair of those at the 4- and 5-positions should also have the different coupling constants due to the same reason. The differences in the calculated coupling constants of these pairs of protons are obviously beyond the simulation error. Therefore, a certain dynamic mechanism should be considered to explain the observed spectrum which shows the existence of three pairs of equivalent proton coupling constants.

Temperature Dependence of ESR Spectrum. The dynamic mechanisms conceivable are (a) the rapid hindered internal rotation of the phenyl ring about the C_9–C_{11} bond and (b) the isomerization reaction by protonation to the $-O^-$ group followed by deprotonation from the -OH group. The former is based on the assumption that the difference between the influences of $-O^-$ and -OH on the unpaired electron distribution in the xanthene ring is negligible and that although the substituted phenyl ring lowers symmetry of the spin distribution in the xanthene ring, the C_{2v} symmetry may be restored by a rapid rotation of the phenyl ring. At any rate, as the ESR spectrum of this radical suggests the existence of dynamic mechanism, the temperature effect on the ESR spectrum was investigated.

The low-field half of the ESR spectra measured at various temperatures using the mixture of ethanol and water (volume percent of water is 20) are given in Fig. 5(1). The line broadening is seen with the decrease of temperature and this change is reversible. Figure 5(2) shows the simulation of the above spectra obtained

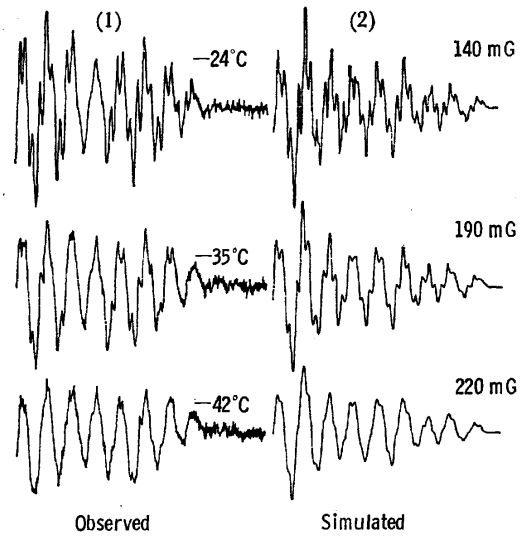

Fig. 5. ESR spectra of the dianion in an ethanol–aqueous solution (80 volume percent ethanol) at three different temperatures. Numbers in mG units are the line widths used for simulation.

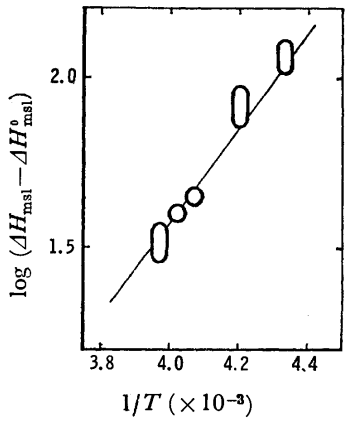

Fig. 6. Arrhenius plots for the increased portion of the line width used for simulation of the ESR spectra of the dianions in an ethanol-aqueous solution (80 volume percent ethanol).

from the same coupling constants as those used in simulating the spectrum of Fig. 3(1) and from the various line widths corresponding to various temperatures. Further, since the areas under the integrated curves of the ESR spectra at various temperatures are nearly constant, the change of the radical concentration is negligible.

Strictly speaking, the line width alternation ought to be detected, if the mechanism (a) or (b) is involved. But practically the line width broadening might be seen as a whole, because the semiquinone has three pairs of protons to commute their coupling constants each other and the differences in coupling constants of each pair are not so large. At the temperatures higher than room temperature, the line width converges to a constant value (100—110 mG; this is the half-width of Lorentzian line shape used for simulation). Therefore, as the observed line width, $1/T_{2,obsd}$ is given by Eq. (1),[9] the reciprocal of the increased portion of the line width associated with the temperature decrease was plotted against the reciprocal of the absolute temperature,

$$\frac{1}{T_{2,obsd}} = \frac{1}{T_2} + \frac{1}{\tau} \qquad (1)$$

where τ is the life time of one of the isomers in the mechanism (a) or (b) and T_2 is the transverse relaxation time when neither (a) nor (b) is involved. A straight line was obtained as shown in Fig. 6, which means Eq. (2) holds. From the slope of the line in

$$\frac{1}{\tau} = \frac{1}{\tau_0} \exp\left[-E/kT\right] \qquad (2)$$

Fig. 6, 6.3 kcal/mol is obtained as the activation energy E of the mechanism that brings the line broadening. The E values obtained for the various mixtures are listed in Table 2.

TABLE 2. ACTIVATION ENERGY OF THE ISOMERIZATION REACTION

Solvent (volume ratio)	Activation energy (kcal/mol)
EtOH: H_2O (4: 1)	6.3
EtOH: H_2O (1: 4)	6.5
EtOH: D_2O (4: 1)	6.2
EtOH: D_2O (1: 4)	7.2

Discussion on Coupling Constant Averaging Mechanism. If the hindered rotation of the $-COO^-$ substituted phenyl ring has any effect on the unpaired electron distribution in the xanthene ring, the interaction must be the steric hindrance between the $-COO^-$ group and the xanthene ring plane. As fluorescein and eosine molecules can change their structure from normal to lactone form under a suitable condition, the $-COO^-$ group might have a large influence on the distribution of the odd electron in the xanthene ring.

Next, considered was the line broadening by the isomerization reaction of protonation to the $-O^-$ group followed by deprotonation from the –OH group. The linewidth alternation due to a similar mechanism was found, for instance, in the ESR spectra of *p*-benzosemiquinone radical[9] and *trans*-biacetyl semidione radical.[10] If that is the case in our system, the life time required to average a pair of coupling constants can be estimated from the values in Table 1 and from the relation $\tau \ll 1/\gamma|a_i - a_j|$, where γ is a gyromagnetic ratio and a_i and a_j are a pair of coupling constants to be exchanged. The estimated life times are *ca.* 2.5×10^{-6} s, 2.0×10^{-6} s, and 6.7×10^{-6} s for the coupling constants of protons at the 1- and 8-positions, those at the 2- and 7-positions and those at the 4- and 5-positions, respectively. Therefore, the averaging may occur in order of 4- and 5-positions, 1- and 8-positions and 2- and 7-positions with the decrease of temperature. But the differences in the critical life time are not so large that the temperature range where the line broadening begins to appear may superpose each other.

According to Leaver, the proton coupling of the –OH groups was observed in the monoanion form while in our case the same ESR signal as that in H_2O was detected in D_2O. This fact means that the signal does not contain the coupling of the proton (or deuteron) in the –OH (or –OD) group. Moreover, taking the fact into account that the activation energy is too large for the rotational barrier of the phenyl ring, it seems reasonable to consider the protonation and deprotonation as a mechanism of averaging the proton coupling constants in the xanthene ring.

The proton concentration in the high pH solution where the fluorescein semiquinone radical has the stable form is extremely small. Therefore, the isomerization (protonation and deprotonation) of semiquinone must be altered as follows; at first semiquinone reacts with water molecule and then a proton transfers from water to the $-O^-$ group of the xanthene ring and immediately after that the –OH group on another side of the xanthene ring releases a proton. The activation energy of 6—7 kcal/mol may be responsible for the transfer of a proton from water to the radical.

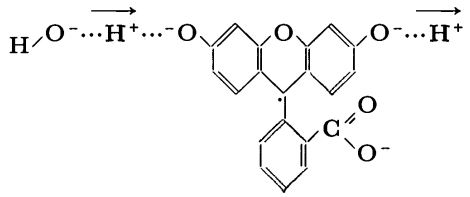

References

1) M. Imamura, This Bulletin, **31**, 962 (1958).
2) K. Uchida and M. Koizumi, *ibid.*, **35**, 1871 (1962).
3) L. Lindqvist, *Arkiv för Kemi*, **16**, 79 (1960).
4) M. Okuda, Y. Momose, S. Niizuma, and M. Koizumi, This Bulletin, **40**, 1332 (1967).
5) K. Kimura, T. Miwa, and M. Imamura, *ibid.*, **43**, 1329 (1970).
6) I. H. Leaver, *Aust. J. Chem.*, **24**, 753 (1971).
7) T. Takeshita and N. Hirota, *J. Chem. Phys.*, **51**, 2146 (1969).
8) R. Chang and R. D. Allendoerfer, *J. Phys. Chem.*, **76**, 3384 (1972).
9) J. E. Wertz and J. R. Bolton, "Electron Spin Resonance," McGraw-Hill, New York (1972), p. 198.
10) I. C. P. Smith and A. Carrington, *Mol. Phys.*, **12**, 439 (1967).
11) R. J. Pritchett, *ibid.*, **12**, 481 (1967).

A New Condensed Gas Calorimeter. Thermodynamic Properties of Solid and Liquid Dinitrogen Oxide

Tooru ATAKE and Hideaki CHIHARA

Department of Chemistry, Faculty of Science, Osaka University, Toyonaka 560

(Received June 3, 1974)

A new adiabatic calorimeter for use with condensed gases from 1.8 K to room temperature has been constructed. The heat capacity of solid and liquid dinitrogen oxide was measured between 1.9 and 184 K together with the vapor pressure above 146 K. The residual entropy was re-evaluated as 6.0 J K^{-1} mol^{-1}, which is now closer to R ln2, suggesting that the disorder of molecular end-for-end orientation is perfectly frozen in the solid state. The moments of lattice frequency spectrum were derived from low-temperature heat capacities and high-temperature vapor pressures. The anomalous increase of heat capacity below the triple point was interpreted as arising from thermal creation of orientational defects with the enthalpy of formation 10.8 kJ mol^{-1}. Other thermodynamic quantities determined are as follows: triple point of pure N_2O 182.407±0.002 K, heat of fusion 6 516±20 J mol^{-1}, entropy of fusion 35.7±0.1 J K^{-1} mol^{-1}, heat of vaporization at 184.81 K and 101.7 kPa 16 544± 20 J mol^{-1}, normal boiling point 184.74 K, translational zero-point energy 1.6±0.3 kJ mol^{-1}, Debye temperature corresponding to $3N$ degrees of freedom 141.0±1.0 K.

Dynamical properties of molecules in the solid state has attracted attention from experimental as well as theoretical points of view. Crystals of monatomic molecules have been studied by a variety of methods and their properties are rather well understood. The crystals of linear molecules have librational degrees of freedom which add some complexity to what has been known for monatomic crystals. In particular, α-CO and N_2O crystallize in a modified fcc lattice in which a molecular axis is oriented along one of the body diagonals in such a way that molecular quadrupole interaction determines the arrangement. Furthermore, there is a possibility of head-to-tail disorder, which has been considered to be at least partially frozen-in at low temperatures, as inferred from the existence of the residual entropy ($\approx R \ln 2$) determined by Giauque *et al.*[1,2] In 1964, however, Melhuish and Scott[3] calculated the Curie temperatures for the order-disorder transitions associated with molecular reorientation in solid CO and N_2O from evaluation of electrostatic energies, and they suggested that the transitions were to be expected at 5 and 11 K, respectively. Because these transition points were lower than the lowest temperature (about 15 K) from which Giauque *et al.*[1,2] started measurements of the heat capacities, attempts were made to locate the transition by extending the measurements on carbon monoxide to lower temperatures (down to 2.5 K) by the authors and J. A. Morrison and their coworkers in 1966.[4,5] Although no additional phase transition was found, the residual entropy of carbon monoxide was re-evaluated as 3.3±0.8 J K^{-1} mol^{-1}, which was significantly different from the value of $R \ln 2 = 5.76$ J K^{-1} mol^{-1}. In 1968, Pitzer *et al.*[6] examined kinetics of the order-disorder transition by tunneling mechanism and found the rate of transition to be unobservably slow. In 1969, Burford and Graham[7] further extended the heat capacity measurements on carbon monoxide down to about 0.8 K but failed to find an anomaly. For decisive explanation of the residual entropy of solid carbon monoxide, therefore, more investigation is still required. In the case of dinitrogen oxide, which is analogous to carbon monoxide in many respects, the calculated Curie temperature for the order-disorder transition is higher by a factor of 2. Therefore, more precise calorimetry below 15 K seemed to be in order. This paper reports the measurements of heat capacity and related thermodynamic properties of dinitrogen oxide and the results are analyzed in detail. In the course of this investigation, we found unusually large 'premelting' tail of the heat capacity below the triple point, which will be interpreted in terms of defect formation in the solid.

Descriptions will be presented of the new adiabatic calorimeter for use with condensed gases which works between 1.8 K and room temperature. Some modifications and improvements of the measuring system over the earlier model[4,8] will also be described.

Experimental

Calorimeter and Cryostat. A cryostat and an adiabatic calorimeter for condensed gases have been newly designed and constructed. The sectional plan of the apparatus is shown in Fig. 1. A feature of the cryostat is that it has two refrigerant containers of cascade type E, (inside volume of 430 cm^3) and I (1 770 cm^3), above the calorimeter vessel A, the adiabatic mantle B and the thermal sink C. The two containers are made of heavy brass and may be loaded with different refrigerants depending on the temperature region to work with. For the measurements from 2.6 to 13 K, the container E is filled with liquid helium which, by a single charging, lasts about twenty hours, as long as there is solid hydrogen in the container I. For the measurements in the lowest temperature region down to 1.8 K, both containers are filled with liquid helium in which case the refrigerant lasts about ten hours. The inner jacket H is soldered vacuum-tight to the hydrogen container I with Wood's alloy but the radiation shield D is only thermally anchored to the container E because the space inside H is a common vacuum. Both H and D are made of copper whereas the outer jacket J is made of brass. All the tubes a—f are made of SUS-27 stainless steel and have outside diameters of 10—16 mm and wall thickenss of 0.15 mm. The entire cryostat can be evacuated through the tubes c and f and maintained in a vacuum better than 1×10^{-4} Pa during measurements. The calorimeter is cooled by breaking the vacuum with small amount of helium exchange gas down to about 15 K. Below

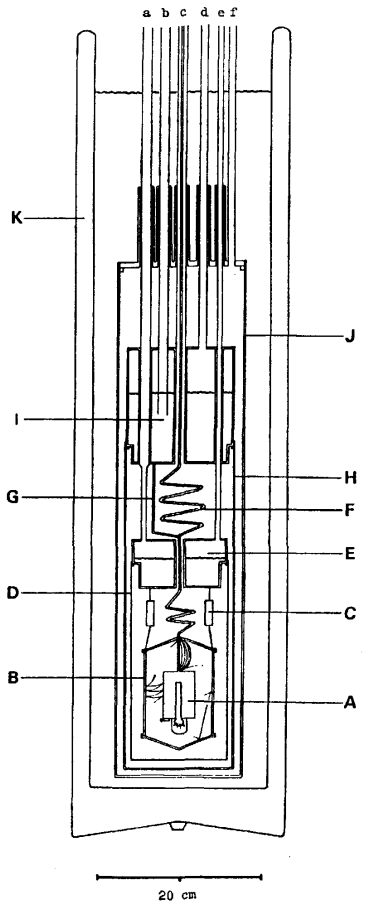

Fig. 1. The calorimeter assembly. A, Calorimeter vessel; B, Adiabatic mantle; C, Thermal sink; D, Radiation shield; E, Refrigerant container; F, Sample filling tube; G, Thermal shunt; H, Inner jacket; I, Refrigerant container; J, Outer jacket; K, Liquid nitrogen Dewar; a and b, Refrigerant transfer tubes; c, Inner jacket evacuation tube; d and e, Refrigerant evacuation tubes; f, Outer jacket evacuation tube.

about 15 K, the calorimeter is cooled only by heat conduction through the electrical leads. The sample filling tube F (German silver, 1 mm in outside diameter, 0.1 mm in wall thickness, 163 cm in length) connects the calorimeter vessel A to the external gas handling system (see Fig. 3). The filling tube is thermally anchored to the bottom of the container I by way of a short insert of copper wire (G in Fig. 1), over the length of which a Manganin heater is wound to prevent the gas from condensing at the cold spot. This thermal shunt is used when measurements are made in the lowest temperature region, where the sample has negligible vapor pressures, to keep minimum the heat leak into the calorimeter through the tube. Manganin heaters (B.S. # 36) are also closely wound non-inductively over the entire length of the filling tube except the portions inside the mantle B and above the top of the cryostat, and the heater wires are varnished to the tube with glyptal lacquer (G.E. adhesive No. 7031). The heaters are wound in seven separate parts and the temperature of each part is monitored and measured with a Constantan *vs.* Chromel-P thermocouple. Four lower parts of the filling tube may be at so low a temperature that a thermocopule would not have a sufficient sensitivity and therefore the parts are also equipped with carbon resistors (nominal value of 10 Ω, Allen-Bradley Co.) to use in the

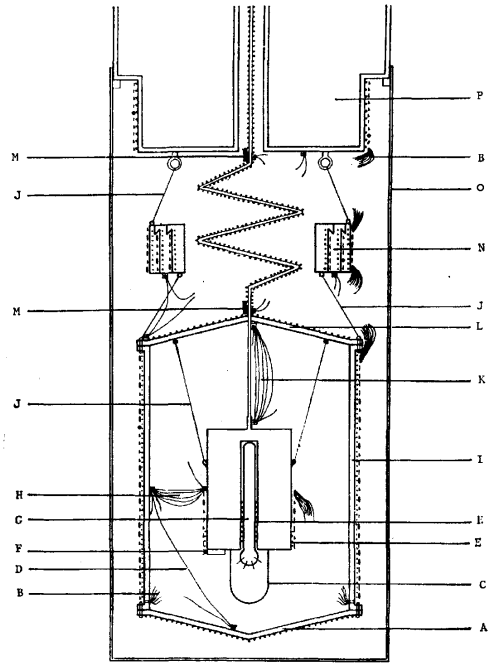

Fig. 2. The lower part of the cryostat. ------, Lead wires; ·····, Heater wires; A, Adiabatic mantle (Bottom); B, Lead wires; C, Radiation shield; D, Difference thermocouple between side and bottom; E, Calorimeter heater; F, Germanium thermometer; G, Platinum thermometer; H, Difference thermocouple between side and calorimeter; I, Adiabatic mantle (Side); J, Nylon cord; K, Difference thermocouple between top and calorimeter; L, Adiabatic mantle (Top); M, Carbon thermometer and thermocouple; N, Thermal sink; O, Radiation shield; P, Refrigerant container.

low temperature region. The electrical leads are double silk-insulated B.S. # 36 copper and are in good thermal contact with the refrigerant containers I and E at their bottoms.

Figure 2 shows the lower part of the cryostat. The copper thermal sink N is of three year-ring shaped construction for securing good thermal contact between the wires and the rings. The calorimeter vessel (gold, 44 cm^3 in volume, 75 g in net weight) has eight vanes for the inside thermal uniformity. A platinum resistance thermometer G is cast into the reentrant well with Wood's alloy and a germanium resistance thermometer F is fitted into a copper sheath which is soldered to the bottom of the vessel. The calorimeter heater E (150 Ω, B.S. # 36 KARMA wire, Driver-Harris Co.) is wound around the lower part of the vessel and also around the lower part of the platinum thermometer. The copper adiabatic mantle consists of three parts whose temperatures are monitored and controlled separately as described in the earlier paper.[8] The filling tube from the calorimeter vessel is soldered to the top L to ensure good control of its temperature. All the electrical leads between the calorimeter vessel and the terminal box outside the cryostat have soldered connections only at the bottom of the side of the mantle I.

External Equipments for Gas Handling. The gas handling apparatus external to the cryostat is schematically shown in Fig. 3. It consists of three manometers, a calibrated flask of about 5 dm^3 capacity, and traps for sample distillation. The sample gas from a cylinder or a sealed flask is desiccated

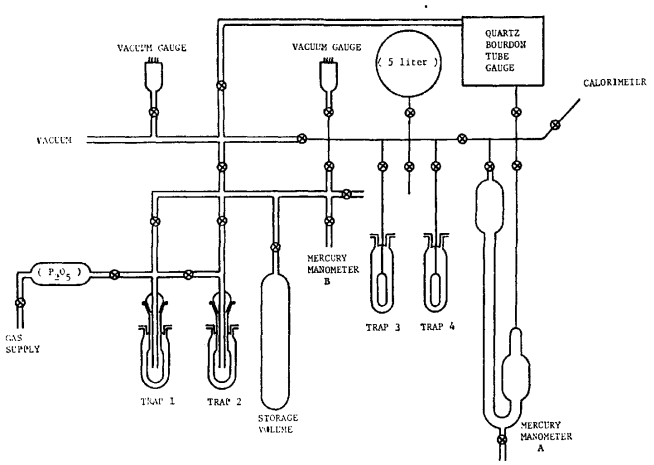

Fig. 3. The gas handling apparatus.

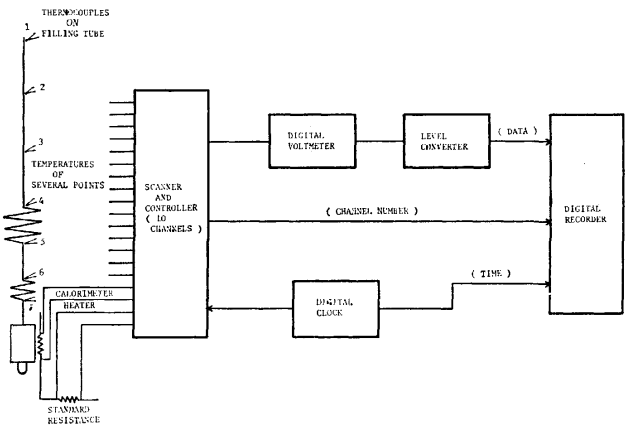

Fig. 4. The data acquisition system.

over P_2O_5 or other desiccants before condensing in trap 1 or 2. The traps 1 and 2 are used for purification by distilling the gas back and forth between the two. The pressure during the distillation is monitored with the mercury manometer B. The gas is then transferred to either trap 3 or 4 depending on the amount of the sample gas. The traps are of special design with a buffer space surrounding the sample container. This space is useful for a fine control of the temperature: a low-melting liquid may be put into this space while the entire trap is immersed in liquid nitrogen or in a cooled empty Dewar vessel (not shown). The condensed gas in trap 3 or 4 is then slowly evaporated into the 5 dm^3 flask (thermostated) and after standing for a sufficient length of time the pressure of the gas is carefully determined with the manometer A or with the quartz Bourdon gage (Texas Instruments Inc., Model 144-01). The dead space volume was determined by using helium as the working gas in advance. The amount of the specimen used for calorimetry is derived from two determinations of the gas before and after the filling into the calorimeter vessel. A small amount of the gas can be taken out into an appendix tube (not shown) for analysis.

In the earlier stage of the present study, the pressure was read on the mercury manometer A and in the later stage, it was determined with the Bourdon gage. The mercury manometer is so designed that it requires no corrections for the capillary depression and causes only small change in the dead space volume. The precision of the manometer is limited to ± 7 Pa, determined by the precision of the standard scale (stainless steel) and of the verniers of the travelling telescopes. The Bourdon gage, on the other hand, has an advantage that the measured volume can be kept constant. This is particularly helpful when measuring the vapor pressures and the heat capacities at the same time.

When measuring heat of vaporization, the calibrated flask is also used as a storage volume of the gas evaporated from the calorimeter vessel. During heat input, the pressure is controlled manually to within ± 150 Pa by adjusting a stopcock, being monitored with the Bourdon gage.

Electrical Measurements. The outputs from the seven thermocouples for measuring the temperature gradient along the length of the filling tube and also the potential and the current across the calorimeter heater are recorded on the automatic data acquisition system, the block diagram of which is shown in Fig. 4. The system consists of a scanner (TR-7216-20S and TR-7513, Takeda Riken Industry Co., Ltd.), a digital integrated voltmeter (3450A, Hewlett-Packard), a digital clock (TR-7414), and a digital printer (TR-6196) which records the time, the channel number, and the outputs of the digital voltmeter. The nominal sensitivity is better than ± 1 μV on the 100 mV range. The method of temperature measurements with platinum and germanium resistance thermometers is the same as that described in the earlier papers.[4,8,9]

Temperature Scales. The platinum resistance thermometer for the present calorimeter (Model 8164, Leeds & Northrup Co.) is the one calibrated on the IPTS-48 and the NBS-55 temperature scales at the U.S. National Bureau of Standards. Therefore, the temperature scale has been converted to the IPTS-68 by using the NEAC-2200-500 computer system at Computer Center of Osaka University.

The germanium scale (used below 13.81 K) was fixed by using a different method for each of the three temperature regions: (a) the 1958 ^{4}He vapor pressure temperature scale below 4.2 K, (b) the ^{4}He gas thermometric temperature scale between 4.2 and 13.81 K (for this purpose the calorimeter was used as a gas thermometer), (c) the IPTS-68 above 13.81 K (the germanium thermometer was compared with the platinum thermometer). The germanium resistance thermometer used in the early stage of this investigation bears the laboratory designation, the germanium thermometer α, and the one used in the later stage the germanium thermometer γ. The germanium thermometer γ (CR-1000, Cryocal Inc.) is of better quality (smaller size and higher sensitivity) than the α (MHSP-2401, Minneapolis-Honeywell Regulator Co.). The following two functions were examined for computer fitting by the method of least squares,

$$\log_{10} R = \sum_{i=1}^{b} A_i T^{i-a}, \tag{1}$$

$$\log_{10} R = \sum_{i=1}^{b} A_i (\log_{10} T)^{i-a}, \tag{2}$$

where R is the resistance in ohm and A_i's are constants. The best fit for germanium thermometer α was obtained by employing the formula:

$$\log_{10} R = \sum_{i=1}^{10} A_i T^{i-2}. \tag{3}$$

The ten coefficients are listed in Table 1, together with the sum of deviations, and the deviation plot is given in Fig. 5. In the second series of the heat capacity measurements of dinitrogen oxide, the α has been replaced by the germanium thermometer γ, which was calibrated by comparison with the resistance of the α. However, below 4.2 K the γ was recalibrated on the 1958 ^{4}He vapor pressure temperature scale, and for this purpose this condensed gas calorimeter was used as a vapor pressure thermometer. In this case, the formula

Table 1. The ten coefficients for the germanium resistance thermometer α.[a,b]

i	A_i	i	A_i
1	−0.072 215 608 7	6	0.028 195 779 8
2	6.182 766 499 5	7	−0.002 509 593 5
3	−2.434 412 857 7	8	0.000 137 184 0
4	0.884 287 351 4	9	−0.000 004 205 8
5	−0.199 832 886 2	10	0.000 000 055 3

a) Calibration formula:
$\log_{10} R=\sum_{i=1}^{10} A_i\ T^{i-2}$

b) Sum of deviations of the 27 calibration points:
$\sum_{i=1}^{27}(\log_{10} R_i(\text{calcd})-\log_{10} R_i(\text{obsd}))^2=0.000\ 428\ 87$

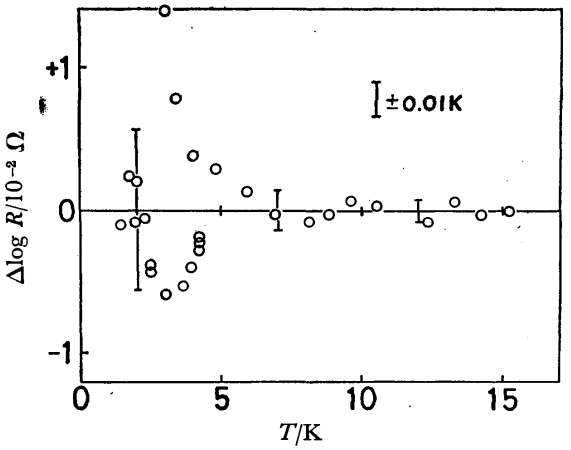

Fig. 5. The deviation plot for the germanium thermometer α fitted to the formula: $\log_{10} R=\sum_{i=1}^{10} A_i \cdot T^{i-2}$.

best fit between 1.7 and 15 K was determined as

$$\log_{10} R = \sum_{i=1}^{10} A_i T^{i-4}. \quad (4)$$

The ten coeffiecients and the sum of deviations are given in Table 2, and the deviation plot is shown in Fig. 6. Apparently, the γ scale is much closer to the measured calibration points than the α scale. Below 4.2 K, especially, the γ scale is more accurate than the α scale.

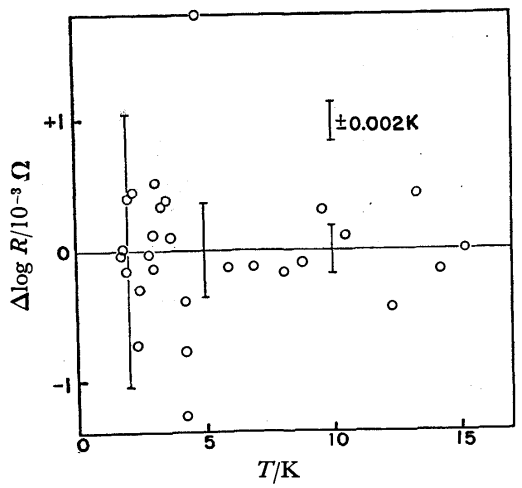

Fig. 6. The deviation plot for the germanium thermometer γ fitted to the formula: $\log_{10} R=\sum_{i=1}^{10} A_i\ T^{i-4}$.

Table 2. The ten coefficients for the germanium resistance thermometer γ.[a,b]

i	A_i	i	A_i
1	−9.904 502 823 5	6	0.341 814 300 2
2	19.518 944 667 3	7	−0.037 495 567 9
3	−14.398 844 122 6	8	0.002 528 407 9
4	10.255 492 344 7	9	−0.000 093 484 3
5	−2.093 324 956 6	10	0.000 001 443 3

a) Calibration formula:
$\log_{10} R=\sum_{i=1}^{10} A_i\ T^{i-4}$

b) Sum of deviations of the 28 calibration points:
$\sum_{i=1}^{28}(\log_{10} R_i(\text{calcd})-\log_{10} R_i(\text{obsd}))^2=0.000\ 007\ 91$

Material. The sample of dinitrogen oxide in 1 liter flasks at 101 kPa was purchased from Takachiho Kagaku Kogyo Co., Ltd., and its stated purity was 99.9 mol%. Dried over P_2O_5, the dinitrogen oxide was distilled twice by means of the traps 1—4 in Fig. 3. The final purity was 99.999 mol% as determined by the fractional melting method during the calorimetry. Gas-chromatographic and mass-spectrographic analyses showed no detectable impurities. The quantities of the purified dinitrogen oxide used for the calorimetry were determined by the *P-V-T* measurements, corrected for non-ideality of the gas by using published values of the second virial coefficients:[10] 0.426 5±0.001 6 mol in the first series and 0.180 0±0.003 0 mol in the second series. In the second series, however, the runs 1 and 2 were carried out on the sample of the amount of 0.200 7±0.000 5 mol.

Calorimetry. In the first series of the calorimetry on dinitrogen oxide, the germanium thermometer α was used and the pressure was measured with the mercury manometer, which caused the rather large uncertainties of the present results. In the second series, the germanium thermometer γ was used and the pressure was measured with the quartz Bourdon gage.

At high temperatures, the filling tube temperatures were so adjusted that the calorimeter may be the coldest in order to prevent distillation of the specimen out of the calorimeter.

No helium gas was introduced into the calorimeter vessel for heat exchange. The time for thermal equilibrium within the calorimeter vessel was a few seconds in the lowest temperature region, one minute at about 20 K, and a few minutes at about 50 K, increasing to ten or more minutes above 100 K.

In the region below about 10 K, the adiabatic condition between the calorimeter and the mantle was controlled manually because the sensitivity of the thermocopules was not sufficient to energize the automatic control device.[8]

Results

Heat Capacity. The heat capacity of dinitrogen oxide was measured between 1.9 and 184 K. The temperature rise by a single heat input was 0.3—0.5 K below 10 K, about 1 K below 30 K, and about 2 K above 30 K. Because the liquid phase exists over only 2.4 K temperature interval, a single temperature rise was chosen as about 1 K in this region. Corrections to the heat capacity were necessary above 140 K for vaporization of the solid or the liquid and other accompanying effects. Other quantities relevant for heat capacity computation were evaluated in the following

TABLE 3. HEAT CAPACITY OF DINITROGEN OXIDE
1 mol N_2O=44.012 8 g, IPTS-68

T/K	C_P/J K^{-1} mol^{-1}
Series I	
(Run 1)	
2.676	0.014 2
3.002	0.020 5
3.414	0.029 9
3.824	0.041 4
4.260	0.057 5
4.755	0.078 8
5.306	0.108 2
5.881	0.148 4
6.437	0.195 8
6.969	0.252 3
7.454	0.314 8
7.887	0.380 1
8.315	0.448 0
8.768	0.534 1
9.261	0.635 0
9.787	0.765 3
10.352	0.924 3
10.979	1.113 0
11.650	1.329 4
(Run 2)	
2.935	0.018 9
3.355	0.027 9
3.762	0.038 8
4.202	0.054 2
4.688	0.072 3
5.173	0.098 5
5.650	0.129 2
6.110	0.163 8
6.567	0.207 4
7.028	0.258 7
7.481	0.317 0
7.920	0.381 0
8.353	0.451 5
8.802	0.536 1
9.274	0.638 6
9.775	0.764 5
10.329	0.905 7
(Run 3)	
3.017	0.020 9
3.447	0.030 2
(Run 4)	
3.078	0.021 5
3.487	0.032 6
3.895	0.043 8
4.339	0.058 3
(Run 5)	
11.582	1.306 2
12.105	1.511 4
12.725	1.766
13.342	2.054
13.970	2.343
(Run 6)	
11.647	1.336 2
12.257	1.578 9
12.871	1.830
13.491	2.121
14.125	2.431
14.795	2.800
15.509	3.221
16.290	3.682
17.163	4.275
18.130	4.936
19.215	5.720
20.305	6.544
21.272	7.299
22.148	8.000
(Run 7)	
11.675	1.354 7
12.374	1.629 5
13.062	1.922
13.755	2.261
14.467	2.624
15.203	3.040
15.957	3.490
16.744	3.984
17.650	4.605
18.650	5.309
19.658	6.045
(Run 8)	
20.886	7.006
21.911	7.817
22.948	8.654
24.011	9.519
25.114	10.424
26.356	11.437
27.718	12.563
29.064	13.655
30.374	14.701
31.731	15.78
33.133	16.85
34.491	17.88
35.824	18.84
(Run 9)	
30.436	14.74
31.997	15.97
33.524	17.13
35.033	18.24
36.537	19.32
38.152	20.43
39.866	21.57
41.598	22.65
43.378	23.71
45.198	24.75
47.069	25.77
49.003	26.77
51.050	27.79
52.018	28.16
(Run 10)	
50.375	27.41
52.383	28.35
54.468	29.28
56.481	30.11
58.433	30.87
60.332	31.59
61.769	32.11
63.471	32.68
65.184	33.23
66.894	33.74
68.604	34.25
70.316	34.72
72.047	35.22
73.815	35.69
75.625	36.16
77.478	36.62
79.358	37.09
81.249	37.52
83.134	37.94
(Run 11)	
82.159	37.71
84.241	38.19
86.295	38.62
88.321	39.07
90.322	39.47
92.301	39.86
94.260	40.19
96.195	40.61
98.111	41.03
(Run 12)	
96.473	40.62
98.436	40.98
100.419	41.36
102.404	41.66
104.372	42.01
106.325	42.42
108.274	42.81
110.225	43.22
112.159	43.54
114.080	43.85
116.005	44.20
117.936	44.52
(Run 13)	
118.749	44.57
120.936	44.83
123.228	45.44
125.873	45.92
128.812	46.53
131.789	47.04
134.878	47.64
138.008	48.25
141.181	48.87
144.437	49.55
(Run 14)	
147.686	50.19
150.933	50.93
154.174	51.67
157.408	52.38
160.634	53.19
163.841	53.99
167.025	54.85
170.194	55.46
172.864	56.27
175.018	56.85
177.132	57.57
179.199	58.14
181.097	58.74
(fusion)	
183.215	76.79
184.241	77.43
(Run 15)	
183.096	76.45
183.993	76.46
Series II	
(Run 1)	
72.756	35.37
74.656	35.90
76.611	36.39
78.563	36.93
80.517	37.32
82.485	37.82
84.448	38.28
86.560	38.75
88.823	39.18
(Run 2)	
163.421	53.62
167.246	54.58
171.131	55.63
174.742	56.56
177.929	57.58
180.558	58.29
(fusion)	
183.062	76.19
(Run 3)	
1.907	0.004 6
2.193	0.007 7
2.570	0.010 9
2.988	0.018 2
3.400	0.026 2
3.830	0.038 2
4.248	0.053 5
4.655	0.069 3
(Run 4)	
3.453	0.027 9
3.957	0.043 0
4.491	0.062 2
5.009	0.087 3
(Run 5)	
184.427	78.00

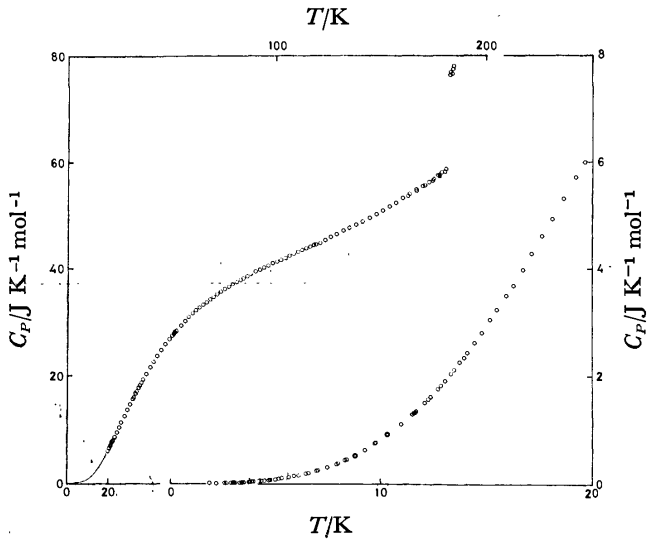

Fig. 7. Molar heat capacity of dinitrogen oxide.

way. The density of solid N_2O has been reported only at two temperatures (molar volume 27.0 cm^3 at 20 K and lattice constant a_0=0.566 nm at −190 °C);[11,12] therefore the densities at other temperatures were estimated by linear extrapolation to higher temperatures. The liquid densities were obtained by smoothing the published data.[13] The heat capacity of the gas of dinitrogen oxide was calculated from the spectroscopic data: fundamental frequencies of 1 277 cm^{-1}, 589 cm^{-1} (doubly degenerate) and 2 224 cm^{-1}. The values of the second virial coefficient were taken from literature;[10] however, they had to be extrapolated to below 197 K. The overall correction amounted to at most about 5% of the total input energy. In the first series of measurements, the calorimeter vessel contributed about 40% of the total heat capacity at all temperatures measured. The heat capacity values thus obtained are C_s under the saturated vapor pressures but the difference between C_s and C_P is negligibly small because the pressures are low and the C_s data are presented as C_P.

Table 4. Smoothed heat capacity values of dinitrogen oxide at rounded temperatures
1 mol N_2O=44.012 8 g, IPTS-68

T/K	C_P/J K^{-1} mol^{-1}	Deviation[a] /%
3	0.019	
5	0.089	
10	0.822	
15	2.918	
20	6.309	+0.16
30	14.40	+0.56
40	21.65	−0.84
50	27.25	+0.13
60	31.47	+0.54
70	34.64	+0.52
80	37.23	+0.62
90	39.41	+0.25
100	41.28	+0.36
110	43.07	+0.28
120	44.86	+0.47
130	46.70	+0.81
140	48.63	+0.86
150	50.70	+0.63
160	52.95	+0.45
170	55.48	+0.32
180	58.28	+0.39
185	77.50	+0.28

a) Deviation=[C_P(Blue and Giauque)−C_P(This)] ×100/C_P(This)

The heat capacity values of dinitrogen oxide without curvature corrections are given in Table 3 and plotted in Fig. 7. The smoothed values at rounded temperatures are given in Table 4, where comparisons are shown with the results by Blue and Giauque[2] in terms of deviations. Blue and Giauque's results are systematically larger than the present results but the differences are probably within the combined limits of errors. A more sensitive comparison can be made by use of equivalent Debye temperature Θ_D, whose temperature dependence for $5N$ degrees of freedom is shown in Fig. 8. We shall discuss the shape of the

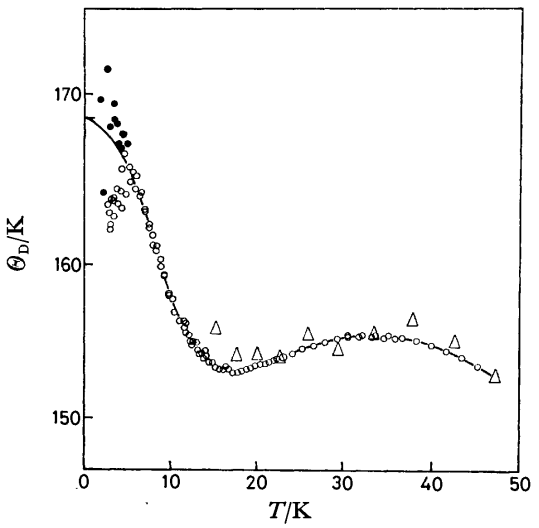

Fig. 8. The Debye characteristic temperatures of dinitrogen oxide derived from the measured heat capacities, assuming $5N$ degrees of freedom. ○, This research (measured with the germanium thermometer α and the platinum thermometer); ●, This research (measured with the germanium thermometer γ); △, R.W. Blue and W.F. Giauque (1935).

Θ_D curve in a later section but here focus our attention on the low temperature end of the curve. Apparently, there is a systematic difference between the results using the germanium thermometer α and those using γ. Since the γ scale is much closer to the measured calibration points than the α scale as is evident from a comparison of Tables 1 and 2, and Figs. 5 and 6, we would place more weight upon the results using the γ thermometer. The results of the two series agree with each other above 3.7 K. The scatter of the present results is much smaller than that of the results by Blue and Giauque: at most ±3% at 4 K, ±1% at 10 K, ±0.1% above 20 K, and ±0.5% above 170 K where the vapor pressure of dinitrogen oxide becomes

TABLE 5. THE HEAT OF FUSION OF DINITROGEN OXIDE

Amount of sample	Temperature interval	Heat input	(Corrections) $\int C_p dT$	Heat of vaporization	ΔH_f
mol	K	J	J	J	J·mol^{-1}
0.426 5	182.210 0—184.294 6	2 864.77	99.87	4.96	6 511
0.200 7	181.626 9—183.820 8	1 368.43	65.97	12.26	6 521
				average	6 516±20
				Blue and Giauque (1935)	6 541

TABLE 6. THE DATA OF FRACTIONAL MELTING OF DINITROGEN OXIDE

Fraction melted	Temperature	Vapor Pressure
	K	kPa
0.169	182.404 2	87.96
0.302	182.404 8	87.96
0.435	182.405 2	87.91
0.568	182.405 3	87.91
0.702	182.405 8	87.91
0.835	182.406 0	87.99
(1.000)	(182.406±0.002)	

The triple point of pure dinitrogen oxide: 182.407± 0.002 K. Clusius *et al.* (1930) 182.4 K; Blue and Giauque (1935) 182.26 K.

TABLE 7. THE HEAT OF VAPORIZATION OF DINITROGEN OXIDE

Starting point (T/K, P/kPa)	Final point (T/K, P/kPa)	Corrected heat input (ΔE/J)	Amount of evaporated N_2O (Δn/mol)
T_1: 184.413 2	T_2: 184.667 3	ΔE: 1 096.05	Δn: 0.065 361 5
P_1: 99.356	P_2: 100.854		
T_1: 184.800 3	T_2: 184.816 2	ΔE: 1 070.96	Δn: 0.064 708 0
P_1: 101.705	P_2: 101.777		
T_1: 184.674 5	T_2: 184.684 1	ΔE: 1 066.27	Δn: 0.064 493 1
P_1: 100.925	P_2: 100.947		

average ΔH_v=16 544±20 J mol^{-1} at 184.81 K

Blue and Giauque (1935)
ΔH_v=16 564±13 J·mol^{-1} at 184.59 K.

significantly high.

Fusion. The curve of the heat capacity of solid dinitrogen oxide shows an upward trend near the triple point (see Fig. 7). However, fusion itself occurs over a narrow range of 0.002 5 K (see Table 6) and therefore the latent heat of fusion was determined in the ususal manner, excluding the premelting portion of the heat capacity. The two series of measurements of heat of fusion are summarized in Table 5 together with the value of Blue and Giauque.[2] The mean value of the heat of fusion of dinitrogen oxide obtained was 6 516±20 J mol^{-1}, which is considerably smaller than the value of Blue and Giauque.[2] The rather large uncertainty in the present value comes from an error in determination of the amount of specimen used in the calorimetry. The triple point temperatures and the amount of impurities were evaluated from fractional melting experiment (see Table 6). The triple point of pure dinitrogen oxide thus determined was 182.407±0.002 K, and the amount of liquid-soluble, solid-insoluble impurities was estimated as 0.001 mol%. The triple point of the dinitrogen oxide used in this calorimetry was 182.406±0.002 K.

Heat of Vaporization. The heat of vaporization of dinitrogen oxide was measured during the second series of calorimetry in the manner as described in the preceding section. The results are summarized in Table 7, showing higher precision than for the heat of fusion because of more precise determination of the amount of the specimen evaporated. The heat of vaporization of dinitrogen oxide was obtained as 16 544±20 J mol^{-1} at 184.81 K and 101.7 kPa, which is again smaller than the value of Blue and Giauque[2] but agrees within the combined limits of error.

Vapor Pressures. The vapor pressures of solid and liquid dinitrogen oxide were measured concurrently with the heat capacity measurements. The results given in Table 8 were fitted to the Antoine equation as follows by the method of least squares;

a) 146 K—182.4 K (triple point): solid

$$\log_{10}(P/\text{Pa}) = -1\,270.42/T + 8.955\,644 - 0.000\,941\,21\,T, \quad (5)$$

b) 182.4 K (triple point)—185 K: liquid

$$\log_{10}(P/\text{Pa}) = -886.293/T + 9.803\,215. \quad (6)$$

Deviations from Eqs. (5) and (6) are also included in Table 8. The normal boiling point of dinitrogen oxide was evaluated as 184.74 K from Eq. (6). From the temperature dependences of vapor pressure described above, the heat of vaporization can be obtained by Clapeyron-Clausius equation: $dP/dT=\Delta H_v/T\Delta V_m$. The results calculated by use of this formula agree with the heat of vaporization determined by calorimetry to within ±0.5%. The molar volume of the gas was evaluated by applying the correction for non-ideality using the second virial data.[10]

Thermodynamic Functions. The thermodynamic functions of dinitrogen oxide were calculated from the smoothed heat capacity values and other data described above and are given in Table 9. The contribution of the heat capacities below the lowest temperature 1.9 K was estimated by a smooth extrapolation, which however was negligibly small.

Table 8. Vapor pressure of dinitrogen oxide

T/K	P/kPa	Deviation $\log_{10}(P_{obsd}/P_{smoothed})$
	(Solid)	
146.071	1.765	0.000 95
149.301	2.698	0.000 10
152.566	4.060	−0.001 37
155.781	5.990	−0.001 32
159.034	8.746	−0.000 71
162.234	12.478	−0.000 90
165.447	17.600	−0.000 59
168.603	24.340	−0.000 54
171.784	33.333	−0.000 53
171.783	33.324	−0.000 60
173.945	40.996	−0.000 49
176.091	50.096	−0.000 41
178.174	60.556	−0.000 44
180.222	72.686	−0.000 25
181.973	84.675	−0.000 11
181.758	83.133	−0.000 06
182.210	86.459	0.000 07
161.506	11.618	0.002 69
165.335	17.488	0.001 76
169.155	25.829	0.001 20
173.105	37.940	0.000 50
173.115	37.958	0.000 31
176.369	51.462	0.000 17
179.489	68.199	0.000 17
181.626	82.243	0.000 22
181.627	82.243	0.000 19
	(Liquid)	
184.295	98.650	−0.000 01
182.405	87.909	−0.000 27
182.408	87.920	−0.000 27
184.875	102.141	−0.000 01
182.617	89.083	−0.000 14
183.813	95.802	−0.000 13
183.822	95.838	−0.000 22
184.660	100.805	−0.000 14
183.577	94.469	−0.000 01
184.410	99.356	−0.000 08
184.413	99.356	−0.000 01
184.667	100.854	−0.000 12
183.821	95.914	0.000 17
182.482	88.500	0.000 60
183.643	94.899	0.000 23
184.679	100.973	0.000 10
184.089	97.475	0.000 14
182.407	87.976	0.000 02
182.407	87.969	0.000 01
183.937	96.548	−0.000 01
183.937	96.553	−0.000 02
184.917	102.419	0.000 09
184.800	101.705	0.000 07
184.816	101.777	−0.000 03
184.674	100.925	−0.000 00
184.684	100.947	−0.000 16

Table 9. Thermodynamic functions of dinitrogen oxide

T/K	$(S°-S_0°)$ / J K^{-1} mol^{-1}	$(H°-H_0°)/T$ / J K^{-1} mol^{-1}	$-(G°-H_0°)/T$ / J K^{-1} mol^{-1}
	(Solid)		
10	0.255 6	0.195 7	0.060
20	2.215	1.669	0.546
30	6.294	4.558	1.736
40	11.467	7.958	3.509
50	16.93	11.28	5.65
60	22.29	14.31	7.98
70	27.39	17.00	10.39
80	32.19	19.37	12.82
90	36.70	21.48	15.22
100	40.95	23.37	17.58
110	44.97	25.08	19.89
120	48.79	26.65	22.14
130	52.46	28.12	24.34
140	55.99	29.52	26.47
150	59.41	30.86	28.55
160	62.76	32.17	30.59
170	66.04	33.46	32.58
180	69.29	34.76	34.53
182.4	70.07	35.08	34.99
	(Liquid)		
182.4	105.79	70.80	34.99
184.8	106.80	70.88	35.92
	(Real gas)		
184.8	196.32	160.40	35.92

Analysis and Discussion

Orientational Disorder. The residual entropy is defined as the difference between the calorimetric and the statistical entropies and represents apparent failure of the third law of thermodynamics. The current interpretation of the residual entropy is based on one of three possibilities; (1) anomaly in the heat capacity exists below the lowest measured temperature, (2) degeneracies of the spin-rotation interaction are partially removed in the crystal lattice, and (3) the solid is in non-equilibrium state which is frozen-in at the lowest temperature attained.

Since Giauque *et al.*[1,2] reported the existence of residual entropy in carbon monoxide and dinitrogen oxide and presented an interpretation that the entropy arose from head-to-tail disorder of molecular arrangement, a number of papers were published to identify its origin with either (1) or (3). Thus, Melhuish and Scott[3] calculated electrostatic energies of some molecular crystals and suggested that the Curie temperatures for dipole orientation in CO and N_2O would be 5 and 11 K, respectively. Because these temperatures were lower than 15 K from which Giauque *et al.*[1,2] started heat capacity measurements, attempts were made to extend the measurements on CO to lower temperatures.[4,5] The results were, however, inconclusive; no additional phase transition was observed down to 2.5 K. Later experiments by Burford and Graham[7] went as far down as 0.8 K without detecting any anomalies either. Although there still remains a

possibility that the experimental temperatures were not low enough to see the removal of the residual entropy, odds are in favor of the 'freezing-in' interpretation. In the mean time, Pitzer *et al.*[6] considered the kinetics of the order-disorder transition in solid carbon monoxide by a tunneling mechanism and showed that the rate of transition was too small to produce a heat capacity anomaly.

The situation is quite analogous in the case of dinitrogen oxide which has a very small dipole moment of 0.55×10^{-30} Cm and the same crystal structure as the low-temperature form of carbon monoxide. Because the calculated Curie temperature of dinitrogen oxide was higher by a factor of 2, a greater chance was to be expected to observe a heat capacity anomaly. However, the experimental heat capacity curve is quite normal down to 1.9 K as shown in Fig. 7 and in the following section. We consider that this is due to 'freezing-in' of the end-for-end reorientational motion below the triple point partly because the potential barrier hindering such motion may be as high as 4000 K, as estimated from the libration frequency of 70 cm^{-1}, and partly because it would be hardly conceivable to be unable to find a rotational transition down to 1.9 K if we were dealing with the perfect equilibrium state.

TABLE 10. THE ENTROPY OF DINITROGEN OXIDE.

Contribution	$S°$/J K^{-1} mol^{-1}
The calorimetric entropy	
0K——2K (smooth extrapolation)	0.002
2K——182.41K (graphical)	70.07
Fusion (6 516/182.41)	35.72
182.41 K——184.81 K (graphical)	1.01
Vaporization (16 544/184.81)	89.52
The entropy of actual gas at 184.81 K	196.32±1.0
The entropy of ideal gas at 184.74 K	196.8 ±1.0
The statistical entropy	
S (trans.)	145.99
S (rot.)	55.87
S (vib.)	0.96
The statistical entropy at 184.74 K	202.8
The residual entropy	6.0 ±1.0
Blue and Giauque (1935)	$S_0°=4.8$

The residual entropy of dinitrogen oxide was re-evaluated by using the present calorimetric results and recent molecular constants. The details of calculation is given in Table 10 which gives $S_0=6.0\pm1.0$ J K^{-1} mol^{-1}, very close to $R\ln2=5.76$ J K^{-1} mol^{-1}. Therefore, it appears that molecular reorientation has become frozen somewhere between the triple point and 1.9 K but exactly where it occurs is not known. The measurements of heat capacity were carried out quite normally: Nowhere slow equilibration phenomenon was observed as was in the case of ice.[14]

Lattice Frequency Spectrum. Very little is known about the lattice frequency spectrum of molecular crystals having internal degrees of freedom. Simple ionic crystals (*e.g.* NaCl), covalent crystals (*e.g.* Ge), metals and other monatomic crystals (*e.g.* Ar) have been studied and the shape of their frequency spectra is rather well known. Molecular crystals may be characterized by small force constants for intermolecular interaction, compared with other types of solids. Such characteristics should manifest themselves in the vibrational spectrum of the solids. We shall examine this by an analysis of the low-temperature heat capacities through Debye temperature cruve and moments of lattice frequency spectrum of N_2O.

The Debye temperature curve converted from the measured heat capacity values for $5N$ degrees of freedom is given in Fig. 8. Very shallow, broad minimum is a feature of molecular crystals in contrast to the cases of ionic and covalent crystals. The feature should more clearly be seen by deriving the even moments $\mu_n(\nu)$ of the lattice vibration spectrum. To do this, contributions from translational modes of vibration were extracted from measured heat capacity values by subtracting intramolecular and libration contributions. Here we used frequency values 1 293, 590, and 2 240 cm^{-1} for intramolecular vibrations and 70 (E), 83 (T), and 126 cm^{-1} (T) for librations. The C_p–C_v corrections were negligibly small below 25 K. The procedure for calculating the moments were the same as in the previous paper.[8] Moments of different order n may be compared by deriving $\nu_D(n)$,

$$\nu_D(n)=\left[\frac{1}{3}(n+3)\mu_n\right]^{1/n} \quad (n>-3). \tag{7}$$

This is plotted as a function of n in Fig. 9. Points have also been included in Fig. 9 that correspond to $\nu_D(-3)$ (from $\Theta_0=141.0\pm1.0$ K), $\nu_D(0)$ (from $\Theta_\infty{}^S=141$ K), and $\nu_D(1)$ (from E_z; see following subsection). The ν_D functions for other values of n were not obtained because of poor convergence of expansion formulae. Figure 9 shows that there is a flat region for low n where there is a deep minimum in the case of NaCl or other strongly ionic crystals. This is the portion where contributions from low-frequency end of the spectrum are the largest. A difference in vibrational properties between ionic (covalent) and molecular crystals lies, therefore, in the fact that vibrational modes are more condensed into the low-frequency portion of the spectrum in molecular crystals.

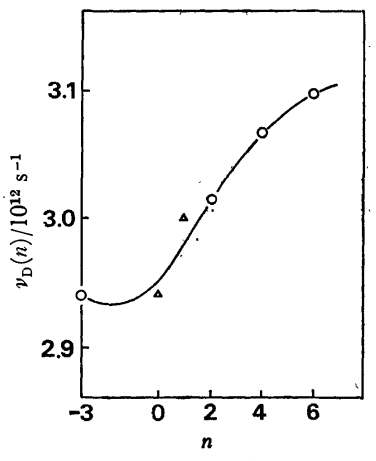

Fig. 9. Plot of $\nu_D(n)$ against n for solid dinitrogen oxide. △, from approximate calculation (see in text).

Zero-point Properties. Some of the properties of solid N_2O at 0 K will be summarized here.

Θ_0 was obtained from a plot of C/T^3 *vs.* T^2 as 141.0 ± 1.0 K for $3N$ degrees of freedom. If one uses 'translational' heat capacity curve for $5N$ degrees of freedom, Θ_0 becomes 167.4 ± 1.0 K.

Static lattice energy was derived by analysis of the vapor pressure data which were fitted to the formula[15]

$$\ln(PT^{3/2}) = (a/T) + b. \quad (8)$$

The static lattice energy E_0 is related to a through

$$aNk \doteq E_0' = E_0 - E_{z,\mathrm{lib}}, \quad (9)$$

where $E_{z,\mathrm{lib}}$ is the zero-point librational energy. The slope of a graph of $\ln(PT^{3/2})$ against T^{-1} gives E_0' a value of 25.91 kJ mol^{-1}. A small correction to this value must be made for the effect of defect formation in the neighborhood of the triple point,[15] which leads to a revised value of 26.0 kJ mol^{-1}. $E_{z,\mathrm{lib}}$ can be evaluated approximately from the librational frequencies as 1.15 kJ mol^{-1}; therefore $E_0=27.2$ kJ mol^{-1}.

The total zero-point energy E_z may be obtained as the difference between the static lattice energy E_0 and the heat of sublimation at 0 K which is 24.21 kJ mol^{-1}. Thus, $E_z=3.0$ kJ mol^{-1} of which 1.85 kJ mol^{-1} is the translational zero-point energy $E_{z,\mathrm{trans}}$. $E_{z,\mathrm{trans}}$ can also be obtained from $\nu_D(1)$. By smooth interpolation of Fig. 10, one obtains $E_{z,\mathrm{trans}}=1.34$ kJ mol^{-1} which is some 0.5 kJ mol^{-1} smaller but is in reasonable agreement with the value derived from E_0 and $\Delta H_v°$. The discrepancy probably comes from the uncertainty in the value of E_0.

Premelting Phenomenon. As is evident from Fig. 7, the heat capacity of solid N_2O tends to increase with a positive curvature from about 120 K to the triple point. We may call this phenomenon 'premelting' although it does not actually correspond to liquid formation. Similar tendency has been noted in a number of low-melting metals and some molecular crystals. It has been customary to account for the effect in terms of formation of vacancies in the crystalline lattice.

Other possibilities such as anharmonicity of the lattice vibration cannot be ruled out in general; but this is rather unlikely for the following reasons. Taking solid argon as an example, the anharmonicity, if any, appears in such a way that the heat capacity increases to a smaller extent than expected for a Debye solid, *i.e.*, the Debye temperature becomes gradually higher as the temperature is increased from about 40 K.[16] This means that the resultant heat capacity curve should never show a positive curvature after it has passed the Θ_D minimum. Moreover, the volume expansivity of argon shows the same trend as the heat capacity below the triple point. In the case of dinitrogen oxide, contributions from librational freedom of motion makes a similar analysis of the Θ_D curve much less meaningful but nevertheless it is quite reasonable to assume that some kind of defect formation is progressively excited as the triple point is approached.

Now by assuming that separated lattice imperfections are thermally created and their equilibrium concentration is determined by the Boltzmann factor, one obtains an excess ΔC_p of the heat capacity

$$\Delta C_p = \frac{\Delta H_s^2}{RT^2} \exp(\Delta S_s/R) \exp(-\Delta H_s/RT), \quad (10)$$

and the enthalpy of defect formation ΔH_s derived from a plot of $\log(T^2\Delta C_p)$ *vs.* $1/T$. The excess heat capacity was estimated by taking differences between the observed and the 'normal' heat capacity; the latter was obtained by smooth extrapolation from about 50 K upwards. The value of ΔH_s thus obtained is 10.8 ± 0.6 kJ mol^{-1}, corresponding to 45% of the heat of sublimation 24.2 kJ mol^{-1} at 0 K.

There is no direct experimental evidence that enables us to fix the type of imperfections. The equilibrium concentration of the imperfection at the triple point is only 2%; therefore very precise diffraction methods would only help to elucidate the nature of imperfections. The only clue we have at present is the magnitude of ΔH_s and its comparison with other relevant properties.

It is interesting to compare N_2O with iso-structural α-N_2 and α-CO. The low-temperature α-phase of nitrogen has an approximate space group Pa3 ($P2_13$ to be exact) and the α-phase of CO is also of Pa3. In this structure, the molecular centers are arranged at the lattice points of the fcc unit cell and the molecules are directed toward one of four equivalent body diagonals of the cell. By X-ray and nuclear quadrupole resonance studies of the high-temperature β-phase of N_2 (hexagonal), the molecules were shown to precess about the c-axis with an angle of precession 55°. This precession angle is exactly equal to the angle which a molecule makes with the c-axis in the α-phase. To visualize the mechanism of the phase transition at 35.61 K in N_2, the molecules undergo a precessional oscillation about the crystallographic axes and, as the temperature is increased, some molecules reorient themselves into another body-diagonal direction. In connection with such a phase transition, the heat capacity of nitrogen also shows an upward curvature below the transition point besides the similar phenomenon observed below the triple point.[17] An interpretation of the low-temperature tail of the transition is one by what might be called 'orientational defect', *i.e.*, some molecules are disoriented from their normal direction or some undergo reorientational motion. Application of Eq. (10) to the excess heat capacity of N_2 below its transition point leads to a value of 2 kJ mol^{-1} for the enthalpy of formation of an orientational defect. This value is not accurate because the heat capacity measurements were not closely spaced. However analogous treatment for the case of CO, for which more appropriate data are available,[4,5] gives $\Delta H_s=3$ kJ mol^{-1} or 38% of the heat of sublimation at 0 K.

We would thus like to propose that the pre-melting excess of heat capacity in N_2O mainly arises from thermal creation of orientational defects with the enthalpy of formation 10.8 kJ mol^{-1}. It is very likely that 'positional' defects or vacancies are also present at the same time, which probably accompany a heat effect of some 16 kJ mol^{-1} or more and are not seen in the present analysis.

For diatomic and pseudo-diatomic molecules, N_2, CO, and C_2H_2, the transition temperature T_c is determined by quadrupole interaction as inferred from close correla-

tion between T_c and Θ^2/R^5 where Θ is the molecular quadrupole moment and R is the nearest neighbor distance. In the case of triatomic molecules, N_2O and CO_2, repulsive interaction is so large as to push T_c to above the triple point but not too far above, because orientational disorder is in fact a pre-transition effect.

References

1) J. O. Clayton and W. F. Giauque, *J. Amer. Chem. Soc.*, **54**, 2610 (1932).
2) R. W. Blue and W. F. Giauque, *ibid.*, **57**, 991 (1935).
3) M. W. Melhuish and R. L. Scott, *J. Phys. Chem.*, **68**, 2301 (1964).
4) T. Shinoda, T. Atake, H. Chihara, Y. Mashiko, and S. Seki, *Kogyo Kagaku Zasshi*, **69**, 1619 (1966).
5) E. K. Gill and J. A. Morrison, *J. Chem. Phys.*, **45**, 1585 (1966).
6) R. F. Curl, Jr., H. P. Hopkins, Jr., and K. S. Pitzer, *ibid.*, **48**, 4064 (1968).
7) J. C. Burford and G. M. Graham, *Can. J. Phys.*, **47**, 23 (1969).
8) T. Atake and H. Chihara, *J. Chem. Thermodynamics*, **3**, 51 (1971).
9) T. Shinoda, H. Chihara, and S. Seki, *J. Phys. Soc. Japan*, **19**, 1637 (1964).
10) H. L. Johnston and H. R. Weimer, *J. Amer. Chem. Soc.*, **56**, 625 (1934).
11) W. Heuse, *Z. Phys. Chem.*, **A147**, 266 (1930).
12) L. Vegard, *Z. Phys.*, **71**, 465 (1931).
13) A. J. Leadbetter, D. J. Taylor, and B. Vincent, *Can. J. Chem.*, **42**, 2930 (1964).
14) a) O. Haida, T. Matsuo, H. Suga, and S. Seki, *Proc. Japan Acad.*, **48**, 489 (1972); b) O. Haida, H. Suga, and S. Seki, *ibid.*, **49**, 191 (1973).
15) a) L. S. Salter, *Trans. Faraday Soc.*, **59**, 657 (1963); b) H. Chihara and N. Nakamura, This Bulletin, **41**, 1787 (1968).
16) R. H. Beaumont, H. Chihara, and J. A. Morrison, *Proc. Phys. Soc.*, **78**, 1462 (1961).
17) W. F. Giauque and J. O. Clayton, *J. Amer. Chem. Soc.*, **55**, 4875 (1933).

Magnetic Property and Electronic Structure of Tris(2,2′-bipyridine) Complexes of Manganese in Low Oxidation States

Motomichi INOUE, Ken-ichi HARA, Tatsuo HORIBA, and Masaji KUBO
Department of Chemistry, Faculty of Science, Nagoya University, Chikusa, Nagoya 464
(Received June 7, 1974)

The magnetic susceptibilities of tris(2,2′-bipyridine)manganese complexes, $[Mn(bpy)_3]\cdot 2THF$ and $Li[Mn(bpy)_3]\cdot 4THF$ (THF: tetrahydrofuran), have been determined over a temperature range of 1.6—320 K. The susceptibility of $Li[Mn(bpy)_3]\cdot 4THF$ can be explained with a radical ion model, in which three 2,2′-bipyridine radical ions are coordinated to a manganese(II) ion. A similar model is applicable to $[Mn(bpy)_3]\cdot 2THF$ as well. The presence of antiferromagnetic interaction indicates the formation of a weak covalent bond between manganese and bipyridine. This can be elucidated consistently by the molecular orbital theory.

A number of the so-called zerovalent transition metal complexes of 2,2′-bipyridine, $[M(bpy)_3]$, have been prepared.[1] Varieties of experimental studies including those of magnetic moment,[1] ESR,[2] optical spectra,[3,4] and IR spectra[5] have been carried out on the complexes at room temperature in an attempt to obtain information about the valency of central metals. However, no definite conclusions have been obtained as yet. The temperature dependence of magnetic susceptibility is expected to give a valuable information about the oxidation state of central metals in these complexes. In our previous paper,[6] we have briefly reported that the magnetic susceptibility of $[Mn(bpy)_3]\cdot 2THF$ and $Li[Mn(bpy)_3]\cdot 4THF$ suggests the presence of a divalent manganese ion coordinated by 2,2′-bipyridine radical ions. In this paper, we present a more detailed discussion on the magnetic property and the electronic structure of the manganese complexes.

Experimental

The materials were prepared by methods reported by Herzog and Schmidt.[7,8] $[Mn(bpy)_3]\cdot 2THF$ was obtained from a tetrahydrofuran solution as deep brown needle crystals. Calcd: Mn, 8.2%; THF, 21.6%. Found: Mn, 8.0%; THF, 22.4%. The observed effective magnetic moment, $\mu_{eff}=4.1_3$ B.M. (290 K), of $[Mn(bpy)_3]\cdot 2THF$ agrees with the value, 4.1_0 B.M., reported for the crystals of $[Mn(bpy)_3]$.[7] Deep red crystals of $Li[Mn(bpy)_3]\cdot 4THF$ were separated from a tetrahydrofuran solution. Calcd: Mn, 6.7%; THF, 35.2%. Found: Mn, 6.3%; THF, 33.2%. The effective magnetic moment, $\mu_{eff}=3.6_3$ B.M., at 290 K agrees with the value, 3.7_1 B.M., described in the literature.[8]

The susceptibility was determined in the temperature range of 1.6—20 K by means of a Hartshorn bridge operating at 90 Hz with a field strength equal to about 10 Oe. Iron(III) alum was employed as a standard. Between 4.2 and 320 K, the susceptibility was determined by use of a magnetic balance already described.[9] The two different methods yielded data agreeing with each other within about ±2%. Each sample was sealed in a quartz cell with ambient helium because the compounds were very sensitive to atmospheric oxygen and moisture.

The molar susceptibilities were corrected for diamagnetic contributions (10^{-6} emu/mol) from 2,2′-bipyridine (−93) and THF (−55).[10] The contributions from manganese and lithium ions are negligible. The temperature-independent paramagnetism of manganese ions was disregarded because it is expected to be negligibly small in comparison with the observed susceptibility.

Results

Figures 1—4 show the observed susceptibility. The magnetic susceptibility of $Li[Mn(bpy)_3]\cdot 4THF$ does not obey the Curie-Weiss law in the temperature range investigated (see Fig. 1). On the other hand, that of $[Mn(bpy)_3]\cdot 2THF$ conforms to the Curie-Weiss law

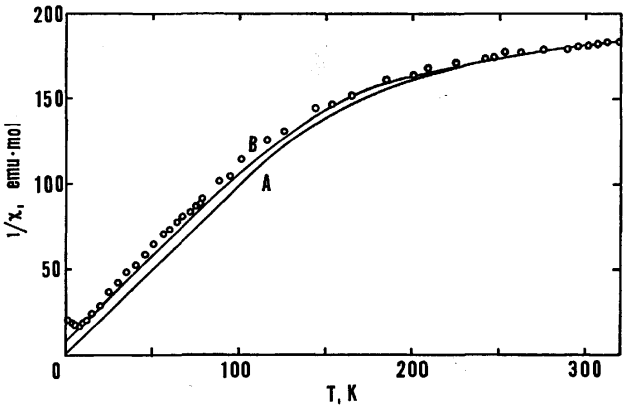

Fig. 1. Reciprocal magnetic susceptibility of $Li[Mn(bpy)_3]\cdot 4THF$. Curve A shows theoretical susceptibility calculated by Eq. (2) with $g=2.00$, $J/k=-180$ K, and $a=1.0$. Curve B represents susceptibility based on Eq. (6) with $g=2.00$, $J/k=-175$ K, $a=1.0$, and $\theta=-8$ K.

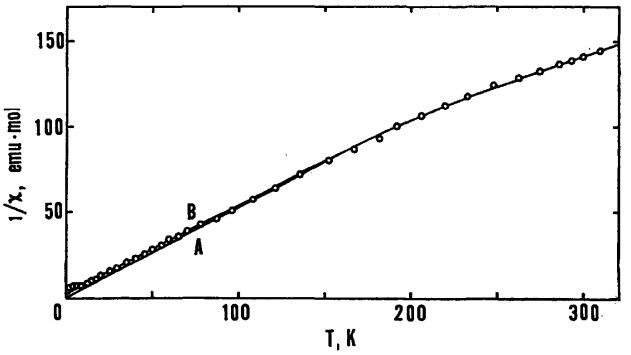

Fig. 2. Reciprocal magnetic susceptibility of $[Mn(bpy)_3]\cdot 2THF$. Curve A shows theoretical susceptibility calculated by Eq. (7) with $g=2.00$, $J/k=-200$ K, and $a=1.0$. Curve B represents modified susceptibility which takes into account magnetic interaction between complex molecules ($g=2.00$, $J/k=-200$ K, $a=1.0$, and $\theta=-4$ K).

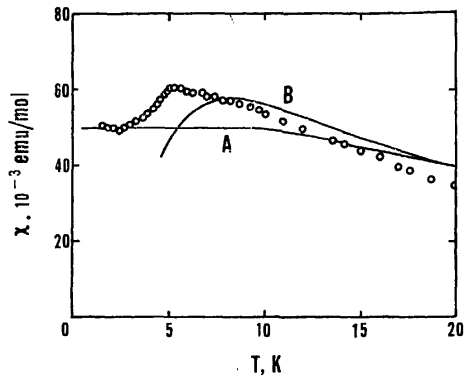

Fig. 3. Magnetic susceptibility of Li[Mn(bpy)$_3$]·4THF in a low temperature range and the theoretical susceptibility for the zero-field splitting. Curves A and B show the average susceptibility and the parallel susceptibility, respectively.

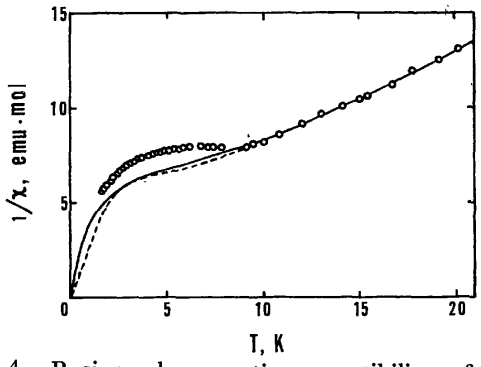

Fig. 4. Reciprocal magnetic susceptibility of [Mn(bpy)$_3$]·2THF in a low temperature range and the theoretical susceptibility for the zero-field splitting. The solid and broken curves show the average susceptibility and the parallel susceptibility, respectively.

fairly well between 20 and 160 K as is shown in Fig. 2. From the Curie constant, the magnetic moment was evaluated as $\mu=3.9$ B.M. It is noticeable that the susceptibility deviates from the Curie-Weiss law above about 160 K.

Discussion

The results of X-ray crystal analyses carried out on [Ti(bpy)$_3$], [V(bpy)$_3$], and [Cr(bpy)$_3$] have shown that each metal atom has a distorted octahedral coordination of six nitrogen atoms from three bipyridine molecules.[11] Therefore, the crystals of the manganese complexes are presumed to consist of discrete distorted octahedral units.

If the formula [Mn^{-1}(bpy^0)$_3$]$^-$ is assumed for Li[Mn(bpy)$_3$]·4THF, *i.e.*, if "excess electrons" are localized only on manganese, the central metal has a $3d^8$ configuration, in which a $^3A_2$ term lies lowest in an octahedral crystal field. The deviation from the Curie-Weiss law in the high temperature range cannot be explained theoretically on the basis of the crystal field, because the *g*-value of the $^3A_2$ term is independent of temperature. Interpretation is infeasible also by contribution from the temperature-independent paramagnetism given by $8N\beta^2/10Dq$.[12] Assuming that

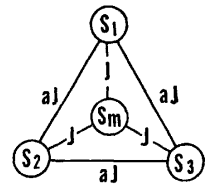

Fig. 5. Radical ion model. S_m and S_i ($i=1, 2, 3$) represent the spin quantum numbers of manganese and bipyridines, respectively. J and aJ denote exchange integrals.

$10Dq\sim7000$ cm^{-1}, the paramagnetism is roughly estimated to be 3×10^{-4} emu/mol. This value is too small to interpret the deviation from the Curie-Weiss law. For these reasons, we have proposed a radical ion model,[6] in which three bipyridine ions are coordinated to a divalent manganese ion instead of neutral ligands coordinating to a monovalent negative manganese (see Fig. 5). This model represents an extreme case of excess electrons distributed only on the ligands. For this model, the susceptibility can be derived from the following Hamiltonian,

$$\mathcal{H} = -2J\sum_{i=1}^{3}\mathbf{S}_m\cdot\mathbf{S}_i - 2aJ\sum_{\langle1,2,3\rangle}\mathbf{S}_i\cdot\mathbf{S}_j + g\beta\mathbf{H}(\mathbf{S}_m+\sum_{i=1}^{3}\mathbf{S}_i) \quad (1)$$

where apart from obvious notations, J and aJ represent exchange integrals and $\langle1,2,3\rangle$ denotes all pairs among $\mathbf{S}_1$, $\mathbf{S}_2$, and $\mathbf{S}_3$. Because $S_m=5/2$ in high spin manganese(II) complexes and $S_1=S_2=S_3=1/2$, the zero-field magnetic susceptibility is given by

$$\chi = \frac{2Ng^2\beta^2}{kT}\left[\frac{1+5x^4+10x^{7-3a}+14x^{10}+28x^{13-3a}+30x^{18}}{3+5x^4+10x^{7-3a}+7x^{10}+14x^{13-3a}+9x^{18}}\right] \quad (2)$$

where $x=\exp(J/kT)$. If the *g*-value is assumed to be equal to 2.00, the observed susceptibility can be reproduced by the theoretical equation with $a=1.0$ rather than with $a=0$ or 0.5 as reported in our previous paper.[6] Curve A in Fig. 1 represents the theoretical curve with $a=1.0$ and $J/k=-180$ K, showing a fairly good agreement with the observed data except for a low temperature range. Evidently, the disagreement is related to the anomaly at about 6 K. A broad maximum of susceptibility at the temperature (see Fig. 3) is attributable to a slight splitting of the degenerate ground level (triplet state) in a distorted coordination octahedron. The susceptibilities due to this zero-field splitting have been formulated as[13]

$$\chi_{\parallel} = \frac{2Ng_{\parallel}^2\beta^2}{kT}\left[\frac{\exp(-D/kT)}{1+2\exp(-D/kT)}\right] \quad (3)$$

$$\chi_{\perp} = \frac{2Ng_{\perp}^2\beta^2}{kT}\left[\frac{1-\exp(-D/kT)}{1+2\exp(-D/kT)}\right] \quad (4)$$

$$\chi_{av} = \frac{1}{3}(\chi_{\parallel}+2\chi_{\perp}) \quad (5)$$

where $\chi_{\parallel}$ and $\chi_{\perp}$ are the parallel and perpendicular susceptibilities, respectively, χ_{av} is the average susceptibility, and D denotes the zero-field splitting constant. Curve A in Fig. 3 shows χ_{av} calculated with $g=2.00$ and $D/k=40$ K. The curve exhibits no maximum and consequently does not explain the observed data. If only the parallel susceptibility is taken into account, the observed curve can be reproduced fairly

well by Eq. (3) with $g=2.00$ and $D/k=12$ K (see Fig. 3). An alternative explanation is conceivable for the behavior at about 6 K. The magnetic behavior might involve magnetic interaction between complex ions at very low temperature. If interaction between complex ions is much weaker than that within an ion, Eq. (2) can be modified as

$$\chi = \frac{2Ng^2\beta^2}{k(T-\theta)}[F(x)] \qquad (6)$$

where θ denotes the Weiss constant that takes into account the interaction between complex ions,[14] and $F(x)$ stands for the expression bracketed in Eq. (2). As shown in Fig. 1, curve B calculated by Eq. (6) with $g=2.00$, $J/k=-175$ K, and $\theta=-8$ K reproduces very well the observed curve at temperatures above about 6 K.

The magnetic moment, $\mu=3.9$ B.M., of $[Mn(bpy)_3]\cdot 2THF$ indicates that the ground state is a quartet ($\mu=3.87$ B.M.). When three bipyridine anions are coordinated to a manganese(III) ion ($S_m=2$ and $S_1=S_2=S_3=1/2$), a doublet state (1.73 B.M.) lies lowest in contradiction to the experimental result. If two bipyridine anions and a neutral bipyridine molecule are coordinated to a divalent manganese ion, *i.e.*; $S_m=5/2$, $S_1=S_2=1/2$, and $S_3=0$, the ground state is a quartet. In this case, the theoretical susceptibility is formulated as

$$\chi = \frac{Ng^2\beta^2}{4kT}\left[\frac{10+35x^5+35x^{7-2a}+84x^{12}}{2+3x^5+3x^{7-2a}+4x^{12}}\right] \qquad (7)$$

This formula reproduces the observed curve excellently with $g=2.00$, $J/k=-200$ K, and $a=1.0$ as shown in Fig. 2, except for a very low temperature range. If excess electrons are localized only on manganese, the metal has a $3d^7$ configuration, in which a $^4T_1$ level lies lowest in a weak octahedral field, whereas a ^2E level represents the gound state in a strong field. As the theoretical magnetic moment of the $^4T_1$ term shows temperature dependence owing to spin-orbit coupling,[15] it is possible to explain the observed curve qualitatively. However, the absolute value of the spin-orbit coupling constant, $\zeta=4170$ cm^{-1} ($\lambda=-1390$ cm^{-1}), for the best fit[6] is much greater than 239—402 cm^{-1} normally observed for manganese.[12] These suggest that the radical ion model is applicable to the so-called zero-valent manganese complexes as well. A magnetic anomaly appearing below about 10 K is due probably to the zero-field splitting of the ground level ($S=3/2$), which yields theoretical susceptibilities given by[13]

$$\chi_{\parallel} = \frac{Ng_{\parallel}^2\beta^2}{4kT}\left[\frac{1+9\exp(-2D/kT)}{1+\exp(-2D/kT)}\right] \qquad (8)$$

$$\chi_{\perp} = \frac{5Ng_{\perp}^2\beta^2}{4D}\left[\frac{1-\exp(-2D/kT)}{1+\exp(-2D/kT)}\right] \qquad (9)$$

The solid and broken curves in Fig. 4 represent the average susceptibility ($g=2.00$ and $D/k=10$ K) and the parallel susceptibility ($g=2.00$ and $D/k=4.8$ K), respectively; they show a good agreement with the observed curve. Magnetic interaction between complex molecules also may contribute to the aforementioned anomaly at low temperature. Equation 7 can be modified by introducing the Weiss constant in the same manner as for Eq. (6). Curve B in Fig. 2 shows modified susceptibility calculated with $g=2.00$, $J/k=-200$ K, and $\theta=-4$ K. It reproduces the observed curve excellently.

The radical ion model can explain the magnetic susceptibilities of the manganese complexes consistently, indicating that the excess electrons are localized for the most part on the ligands rather than on the central metal in agreement with the results of optical spectra.[3] However, the presence of antiferromagnetic interaction ($J<0$) suggests also the formation of weak covalent bonds between bipyridine anions and a manganese(II) ion. Therefore, the radical ion model has been treated by the molecular orbital theory for coordination compounds. The molecular orbital scheme has been proposed for tris(2,2'-bipyridine) complexes.[16,17] Figure 6 shows an energy diagram associated with 3d orbitals in a D_3 field. The bonding σ levels of the complex are completely filled with electrons from the σ orbitals of the ligands. When manganese in $[Mn(bpy)_3]^0$ is in a divalent high-spin state, the degenerate σ^* levels are occupied by two electrons from the $d\gamma$ orbitals of a manganese ion. The π level is filled with three electrons from $d\varepsilon$ orbitals of manganese and two electrons from the antibonding π orbitals of bipyridine ions, leading to a $\sigma^{12}\pi^5\pi^{*0}\sigma^{*2}$ configuration as shown in

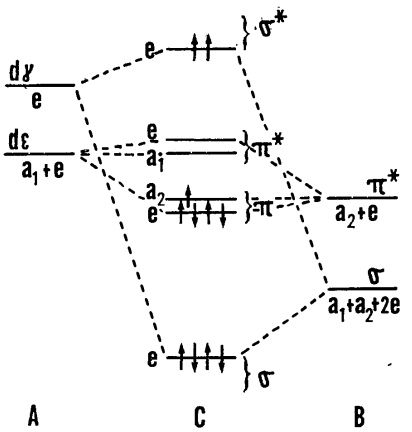

Fig. 6. Energy diagram of $[Mn(bpy)_3]^0$. A: 3d orbitals of a manganese ion. B: Combined orbitals of bipyridines. C: Molecular orbitals of the complex. The σ levels associated with the s and p orbitals of the metal are not shown.

Fig. 6. Because the π, π^*, and σ^* orbitals are orthogonal to one another, the ground state is a quartet ($\mu=3.87$ B.M.) in conformity with the observed magnetic moment. If the central metal has a valence of 3, the ground state has a $\sigma^{12}\pi^6\pi^{*0}\sigma^{*1}$ configuration ($\mu=1.73$ B.M.) in contradiction to the experimental result. A $\sigma^{12}\pi^6\pi^{*1}\sigma^{*0}$ configuration corresponding to a low-spin manganese(II) complex also conflicts with the observed moment. For the ground state having the configuration $\sigma^{12}\pi^5\pi^{*0}\sigma^{*2}$, the first excited state has a $\sigma^{12}\pi^4\pi^{*1}\sigma^{*2}$ configuration, which yields a total spin quantum number and degeneracy consistent with those derived from Eq. (1) for the radical ion model. The spin multiplicity of higher excited states also is in conformity with that for the radical ion model. In the molecular orbital

system of $[Mn(bpy)_3]^-$, the σ^* level is occupied by two electrons from the $d\gamma$ orbitals of a manganese(II) ion while the π level is filled with six electrons from the $d\varepsilon$ orbitals of manganese and the π^* orbitals of bipyridine ions, leading to a $\sigma^{12}\pi^6\pi^{*0}\sigma^{*2}$ configuration (μ=2.83 B.M.). Excited states, *i.e.*, $\sigma^{12}\pi^5\pi^{*1}\sigma^{*2}$ (S=2), $\sigma^{12}\pi^4\pi^{*2}\sigma^{*2}$ (S=3), and $\sigma^{12}\pi^3\pi^{*3}\sigma^{*2}$ (S=4), have magnetic moments and degeneracies consistent with those based on the radical ion model. Strictly speaking, energy separation between *a* and *e* levels should be taken into account. However, this does not affect essentially the foregoing discussion, especially when the energy separation is very small in comparison with the π-π^* separation.

As discussed above, the magnetic properties of the manganese complexes can be interpreted consistently by the molecular orbital theory as well as by the radical ion model involving antiferromagnetic interaction. This indicates that weak $d\pi$-π^* bonds are formed between manganese and bipyridine but that excess electrons are mostly localized in the antibonding π orbitals of bipyridine rather than in the orbitals of manganese. The π-π^* energy separation can be approximated with the value of $4|J|$ or $5|J|$ expressing an energy separation between the ground state and the first excited state in the radical ion model (see Eqs. (2) and (7)). The value may be nearly equal to an energy difference between the π^* of bipyridine anions and the $d\varepsilon$ of a manganese ion, because the π^* and $d\varepsilon$ orbitals are suspected to interact with each other only to a small extent.

References

1) S. Herzog and R. Taube, *Z. Chem.*, **2**, 208 (1962).
2) E. König, *Z. Naturforsch.*, **19a**, 1139 (1964).
3) Y. Kaizu, T. Yazaki, Y. Torii, and H. Kobayashi, This Bulletin, **43**, 2068 (1970).
4) E. König and S. Herzog, *J. Inorg. Nucl. Chem.*, **32**, 585, 601 (1970).
5) Y. Saito, J. Takemoto, B. Hutchinson, and K. Nakamoto, *Inorg. Chem.*, **11**, 2003 (1972).
6) K. Hara, M. Inoue, T. Horiba, and M. Kubo, *Chem. Lett.*, **1974**, 419.
7) S. Herzog and M. Schmidt, *Z. Chem.*, **2**, 24 (1962).
8) S. Herzog and M. Schmidt, *Z. Chem.*, **3**, 392 (1963).
9) M. Inoue, S. Emori, and M. Kubo, *Inorg. Chem.*, **7**, 1427 (1968).
10) G. Foëx, "Constantes Sélectionées, Diamagnétisme et Paramagnétisme," Masson, Paris (1957).
11) G. Albrecht, *Z. Chem.*, **3**, 182 (1963).
12) J. S. Griffith, "The Theory of Transition Metal Ions," Cambridge University Press, London (1961), pp. 280, 437.
13) B. N. Figgis, *Trans. Faraday Soc.*, **56**, 1553 (1960).
14) M. Inoue, M. Kishita, and M. Kubo, *Inorg. Chem.*, **6**, 900 (1967); K. Hara, M. Inoue, S. Emori, and M. Kubo, *J. Magn. Resonance*, **4**, 337 (1971).
15) B. N. Figgis and J. Lewis, "Progress in Inorganic Chemistry," vol. 6, ed. by F. A. Cotton, Interscience, New York, N. Y. (1964), p. 37.
16) R. Taube and S. Herzog, *Z. Chem.*, **2**, 225 (1962).
17) I. Hanazaki and S. Nagakura, This Bulletin, **44**, 2312 (1971).

The Estimation of Rate Constants in Systems of Linear and Nonlinear Differential Equations Using the Polynomial-approximated Least Squares-error and Iterative Search Technique

Katsutoshi OHKUBO, Hiroyuki SAKAMOTO, and Kohji TSUCHIHASHI

Department of Synthetic Chemistry, Faculty of Engineering, Kumamoto University, Kurokami, Kumamoto 860

(Received October 1, 1973)

A new technique is proposed for estimating the rate constants in systems of linear or nonlinear differential equations, using a polynomial approximation of the observed concentrations of species participating in the reaction and an iterative search technique. The method is implemented by minimizing the errors of the concentrations (of species), as computed by the theoretical equations derived from the linear differential equations or by the trapezoidal averaging simulation, relative to those calculated by the polynomial approximation. The present technique requires the concentrations (at the initial reaction stage) of s-2 species (the s species takes part in the reaction). Two kinetic example, A⇄B⇄C and S+E⇄ES→E+P, have been used to illustrate and develop the present technique.

The estimates of the rate constants in systems of linear or nonlinear differential equations have hitherto been performed by means of such numerical methods as the Runge-Kutta integration,[1] the Marquardt method,[2] and Taylor's series expansions.[3] These methods require, however, precision fits to very dense data and much computation time.

The new technique proposed in this paper is based on a polynomial-approximated least squares-error method and an iterative search technique. This technique for estimating the rate constants requires the time-dependence of the concentrations of species participating in the reaction. In order to illustrate and develop the present technique, the following two kinetic examples are used:

Example I

$$\mathrm{A} \underset{k_2}{\overset{k_1}{\rightleftharpoons}} \mathrm{B} \underset{k_4}{\overset{k_3}{\rightleftharpoons}} \mathrm{C} \qquad (1)$$

The example depicted by Eq. (1) represents a reaction like the Cannizzaro reaction, which can be described by linear differential equations:

$$\mathrm{RCHO} \overset{\mathrm{OH^-}}{\rightleftharpoons} \mathrm{R\text{-}\underset{\underset{\mathrm{O^-}}{|}}{\overset{\overset{\mathrm{H}}{|}}{C}}\text{-}OH} \rightleftharpoons \mathrm{R\text{-}\overset{\overset{\mathrm{O}}{\|}}{C}\text{-}OH} + \mathrm{H^-} \qquad (1')$$

(R=alkyl group; OH^-=base catalyst)

Example II

$$\mathrm{S} + \mathrm{E} \underset{k_2}{\overset{k_1}{\rightleftharpoons}} \mathrm{ES} \xrightarrow{k_3} \mathrm{E} + \mathrm{P} \qquad (2)$$

where S=substrate; E=enzyme; ES=enzyme-substrate complex, and P=product. The classical enzyme model depicted by Eq. (2) is used for a representative reaction described by nonlinear differential equations.

Method of Computation

First Example. The three-variable, four-rate constant isothermal model illustrated by Eq. (1) can be described by the following differential equations on the basis of the law of mass action:

$$\mathrm{d(A)}/dt = -k_1(\mathrm{A}) + k_2(\mathrm{B}) \qquad (\mathrm{A})_0 \neq 0 \qquad (3a)$$

$$\mathrm{d(B)}/dt = k_1(\mathrm{A}) - (k_2+k_3)(\mathrm{B}) + k_4(\mathrm{C}) \qquad (\mathrm{B})_0 = 0 \qquad (3b)$$

$$\mathrm{d(C)}/dt = k_3(\mathrm{B}) - k_4(\mathrm{C}) \qquad (\mathrm{C})_0 = 0 \qquad (3c)$$

where the parentheses denote the concentrations, typically in M units, and where the subscript zeros stand for the initial concentrations of the species.

The time dependence of (A), (B), or (C) is obtained from Eqs. (3a—c) as:

$$(\mathrm{A})_{t,\mathrm{calcd}} = k_2k_4(\mathrm{A})_0/b + C_1e^{\delta_1 t} + C_2e^{\delta_2 t} \qquad (4a)$$

$$(\mathrm{B})_{t,\mathrm{calcd}} = k_1k_4(\mathrm{A})_0/b - (C_1+C_2)e^{\delta_1 t} - (C_2+C_4)e^{\delta_2 t} \qquad (4b)$$

$$(\mathrm{C})_{t,\mathrm{calcd}} = k_1k_3(\mathrm{A})_0/b + C_3e^{\delta_1 t} + C_4e^{\delta_2 t} \qquad (4c)$$

where $\delta_1 = -a+\sqrt{a^2-b}$; $\delta_2 = -a-\sqrt{a^2-b}$; $a=(k_1+k_2+k_3+k_4)/2$; $b=k_1k_3+k_2k_4+k_1k_4$; $C_1=((k_2k_4-b)\delta_2-bk_1)(\mathrm{A})_0/b(\delta_1-\delta_2)$; $C_2=((b-k_2k_4)\delta_1+bk_1)(\mathrm{A})_0/b(\delta_1-\delta_2)$; $C_3=\delta_2k_1k_3(\mathrm{A})_0/b(\delta_1-\delta_2)$, and $C_4=\delta_1k_1k_3(\mathrm{A})_0/b(\delta_2-\delta_1)$.

Second Example. The classical enzyme model represented by Eq. (2) can be described by means of the following nonlinear differential equations:

$$\mathrm{d(S)}/dt = -k_1(\mathrm{S})(\mathrm{E}) + k_2(\mathrm{ES}) \qquad (\mathrm{S})_0 \neq 0 \qquad (5a)$$

$$\mathrm{d(E)}/dt = -k_1(\mathrm{S})(\mathrm{E}) + (k_2+k_3)(\mathrm{ES}) \qquad (\mathrm{E})_0 \neq 0 \qquad (5b)$$

$$\mathrm{d(ES)}/dt = k_1(\mathrm{S})(\mathrm{E}) - (k_2+k_3)(\mathrm{ES}) \qquad (\mathrm{ES})_0 = 0 \qquad (5c)$$

$$\mathrm{d(P)}/dt = k_3(\mathrm{ES}) \qquad (\mathrm{P})_0 = 0 \qquad (5d)$$

The trapezoidal averaging technique will no be adopted for solving Eqs. (5a—d). Three increments, $D(i)$ (i=1—3), are first defined as:

$$D(1) = k_1(\mathrm{S})(\mathrm{E})\Delta t; \quad D(2) = k_2(\mathrm{ES})\Delta t; \quad D(3) = k_3(\mathrm{ES})\Delta t \qquad (6)$$

The increments at the reaction time t, $D(i)_t$, are, then, defined by the use of those at $t-\Delta t$ and $t+\Delta t$, $D(i)_{t-\Delta t}$ and $D(i)_{t-\Delta t}$ respectively:

$$D(i)_t = (D(i)_{t-\Delta t}+D(i)_{t+\Delta t})/2 \quad (D(i)_{-\Delta t}=D(i)_0=0) \qquad (7)$$

where Δt indicates a very small time-interval. The average $D(i)$ values, $D(i)_{\mathrm{av}}$, are represented by:

$$\begin{aligned} D(i)_{\mathrm{av}} &= (D(i)_t+D(i)_{t+\Delta t})/2 \\ &= (D(i)_t+(2D(i)_t-D(i)_{t-\Delta t}))/2 \\ &= 1.5D(i)_t - 0.5D(i)_{t-\Delta t} \end{aligned} \qquad (8)$$

From Eqs. (5a—d), (6), and (8), the average increments of components (C_s) (s=number given for the component), $D(C_s)_{\mathrm{av}}$, are written by:

$$D(\mathrm{S})_{\mathrm{av}} = -D(1)_{\mathrm{av}} + D(2)_{\mathrm{av}};$$
$$D(\mathrm{E})_{\mathrm{av}} = -D(1)_{\mathrm{av}} + D(2)_{\mathrm{av}} + D(3)_{\mathrm{av}};$$
$$D(\mathrm{ES})_{\mathrm{av}} = D(1)_{\mathrm{av}} - D(2)_{\mathrm{av}} - D(3)_{\mathrm{av}};$$
$$D(\mathrm{P})_{\mathrm{av}} = D(3)_{\mathrm{av}} \quad (9)$$

The concentration of C_s at t, $(C_s)_{t,\mathrm{calcd}}$, is evaluated by means of:

$$(C_s)_{t,\mathrm{calcd}} = (C_s)_0 + \sum^{v} D(C_s)_{\mathrm{av}} \Delta t \quad (v\Delta t = t) \quad (10)$$

In the evaluation of the concentrations of the components participating in Reaction (1) or (2), the rate constants, k_i (i=1—4 in Reaction (1) and i=1—3 in Reaction (2)), are supplied by:

$$k_i = \min k_i + \sum^{m} 10^{(\gamma-\beta)} \min k_i, \quad \gamma = \mathrm{gauss}\left[\frac{m-1}{9\alpha}\right]$$
$$(m = 1, 2, 3, \cdots, \beta = 0, 1, 2, \cdots, \alpha = 10^{\beta}) \quad (11)$$

where min k_i=lower limit of k_i ($1.0\times10^{\delta}$; δ=integral constant); γ=integral number; β=integral constant; α=parameter determining the significant figures for k_i (*viz.*, k_i=(β+1) significant figures at $\alpha=10^{\beta}$). If the rate constant, k_i, is to be supplied in the range of 1.0×10^{-5}—1.0×10^{2} under the conditions of k_i=2 significant figures (β=1 and α=10), m=5400 is required, because $m=9\alpha$ can change the k_i value from $1.0\times10^{\delta}$ to $1.0\times10^{\delta+1}$. As a matter of course, the range of the value for each rate constant (k_i) can be controlled separately in compliance with the desired conditions.

On the other hand, the observed concentration of the s-th component at t, $(C_s)_{t,\mathrm{given}}$, is expressed by the following algebraic polynomial:

$$(C_s)_{t,\mathrm{given}} = a_n t^n + a_{n-1} t^{n-1} + \cdots + a_1 t + a_0 \quad (12)$$

where a_n (n=0, 1, 2, ···) denotes a coefficient. This polynomial approximation can be performed by the least squares-error analysis of the observed concentrations of C_n at t=0, 1, 2, 3, —, n (n corresponds to the n subscript of a_n in the highest order term of Eq. (12)).

The best set of rate constants is, then, selected from the set satisfying the following F function by means of the iterative search technique (see below):

$$\varepsilon_{p,s} = |(C_s)_{t,\mathrm{calcd}} - (C_s)_{t,\mathrm{given}}|/(C_s)_{t,\mathrm{given}} \quad (13a)$$

$$F = \text{minimize} \sum_{s=1}^{s-1} \sum_{p=1}^{p} \varepsilon_{p,s} \quad (13b)$$

where p is the number of the check points used for the calculation of the F function. In order to cancel the orders of the $(C_s)_{t,\mathrm{calcd}}$ and $(C_s)_{t,\mathrm{given}}$ values, the relative error defined by Eq. (13a) is more useful than the squares error under $(C_s)_{t,\mathrm{given}} \neq 0$. In the reaction system involving s components (s=1—3 in Reaction (1) or s=1—4 in Reaction (2)), the concentrations of the two components can be evaluated from the material balance.

The iterative search technique is carried out by the following procedure: one of the rate constants, k_j (j=1, 2, 3, ···, or j), is repetitively changed in turn with fixed $k_{i(i\neq j)}$ values (k_i=originally estimated or those assumed for the first run), until the set of k_i (i=1, 2, 3, —, and i) values which satisfy the condition described by Eq. (13b) is made identical. This technique requires about 20 s (by FACOM 230-60 computer) for the first example as the computation time for one iteration run under the conditions of p=1, i=4, m=5400, and α=100 (β=2).

In order to obtain reliable k_i values using the above iteration technique, the following factors should be taken into consideration:

(a) During each run of the iteration, the selected k_i group satisfying the F function should not include the lower or upper limit value of k_i. In order to avoid this problem, the k_i values should be supplied over a fairly wide range, or an automatic widening procedure for the range of k_i values should be included in the computation.

(b) If the preliminary estimate of k_i differs by 10^2 or more from the true values, the present technique requires two or three more iterations to obtain reliable values as compared with the case in which the orders of the k_i values are very close to the true ones. It is desirable, therefore, to estimate the order of k_i originally under the condition of the k_i=1 significant figure.

It should also be stressed here that check points ($p \geqq i$ are desirable) should be given at the initial early stage of the reaction, because the polynomials of Eq. (12) become more precise at $t\rightarrow0$:

$$\lim_{t\to0} \varepsilon_{p,s} = \lim_{\substack{n\to\infty \\ t\to0}} |(C_s)_{t,\mathrm{calcd}} - (C_s)_{t,\mathrm{given}}|/(C_s)_{t,\mathrm{given}} \approx 0 \quad (14)$$

However, the check point should not always be selected at an initial short time of the reaction, since the polynomials defined by Eq. (12), in which n is sufficiently large, can reproduce the time-conversion curve of $(C_s)_{t,\mathrm{given}}$ obtained from the experiments within the limits of experimental error. The accuracy of the rate constants estimated by the present technique is directly dependent on that of the polynomials and is almost independent of the check point number, so long as the check points ($p \geqq i$) are reasonably selected at suitable reaction times.

Computation Results and Discussion

First Example. Table 1 shows the given kinetic data obtained from Eqs. (4a—c) with the following specifications: k_1=0.3, k_2=0.1, k_3=0.6, k_4=0.2, $(\mathrm{A})_0$=10.0, and $(\mathrm{B})_0=(\mathrm{C})_0=0$. We will thus use the simulated concentrations as the given kinetic data, because we can easily compare the estimated rate constants ($k_{i,\mathrm{estimated}}$) with the originally known ones ($k_{i,\mathrm{given}}$) in order to check the accuracy of computations. Using the concentrations of C at t=0, 1, 2, 3, ···, n, the coefficients of a_n (n=0, 1, 2, ···, n) in Eq. (12) were evaluated by the least squares-error analysis. The time dependence of the $(C_s)_{t,\mathrm{given}}$ (s=3) values under n=2, 3, 4, 5, 6, and 10 is shown in Fig. 1. As Fig. 1 indicates, the higher the order (n) of the polynomial, the more precise the approximation becomes. Moreover, the check points should be taken from those near t=1.0, because the $(C_s)_{t,\mathrm{given}}$ (s=3) values are evaluated more accurately at $t\approx1.0$ (for instance, see Table 3). Therefore, we will use the $(C_s)_{t,\mathrm{given}}$ (s=3 and $0\lesssim t\lesssim1.0$) values evaluated by the following polynomial (n=10) approximation:

Table 1. Given kinetic data for first example

t[a)]	(A) $s=1$	(B) $s=2$	(C) $s=3$
0	10.00000	0.00000	0.00000
1	7.50707	1.87874	0.61419
2	5.75746	2.50819	1.73435
3	4.49108	2.66806	2.84087
4	3.55796	2.66279	3.77925
5	2.86353	2.60857	4.52790
6	2.34394	2.54764	5.10843
7	1.95401	2.49372	5.55227
8	1.66095	2.44990	5.88914
9	1.44050	2.42563	6.14387
10	1.27460	2.38930	6.33609
11	1.14972	2.36928	6.48100
12	1.05571	2.35412	6.59018
13	0.98493	2.34267	6.67240
14	0.93163	2.33404	6.73433
15	0.89151	2.32753	6.78096
16	0.86130	2.32263	6.81607
17	0.83855	2.31894	6.84251
18	0.82143	2.31616	6.86241
19	0.80853	2.31407	6.87740
20	0.79882	2.31249	6.88869
21	0.79151	2.31131	6.89718
22	0.78601	2.31042	6.90358
23	0.78186	2.30974	6.90840
24	0.77874	2.30924	6.91202
25	0.77639	2.30885	6.91475
26	0.77462	2.30857	6.91681
27	0.77329	2.30835	6.91836
28	0.77229	2.30819	6.91952
29	0.77153	2.30807	6.92040
30	0.77096	2.30797	6.92106

a) Arbitrary time unit.

$$(C_s)_{t,\text{given}}(s=3) = 4.1951\times10^{-9}t^{10} - 2.7882\times10^{-7}t^{9} + 8.2055\times10^{-6}t^{8} - 1.4329\times10^{-4}t^{7} + 1.6659\times10^{-3}t^{6} - 1.3737\times10^{-2}t^{5} + 8.2424\times10^{-2}t^{4} - 3.5191\times10^{-1}t^{3} + 8.9409\times10^{1}t^{2} + 1.7822\times10^{-3}t + 3.6863\times10^{-8} \quad (15)$$

The $(C_s)_{t,\text{given}}$ values required in Eq. (13a) are supplied from those (at $t=0.7$, 0.8, 0.9, and 1.0) calculated by Eq. (15), and the check points, (p,t), are taken to be: $(p, t)=(1, 0.7)$, (2, 0.8), (3, 0.9), and (4, 1.0). Table 2 lists the $k_{i,\text{estimated}}$ values obtained from Eq. (15) and the following polynomial form of Eq. (4c):

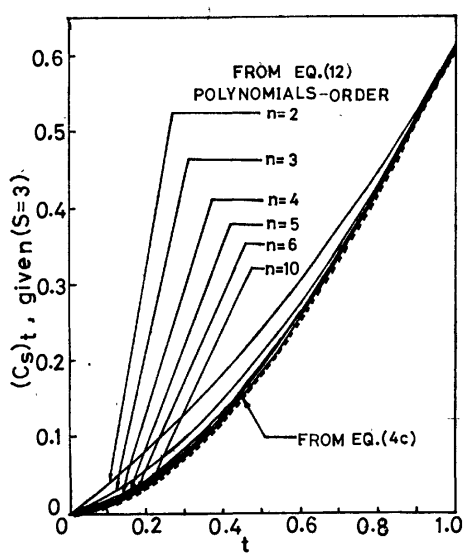

Fig. 1. Plots of $(C_s)_{t,\text{given}}$ $(s=3)$ *vs.* t.

$$(C_s)_{t,\text{calcd}}(s=3) = k_1k_3(\text{A})_0/b + C_3(1+\delta_1t+\delta_1^2t^2/2+\cdots+\delta_1^nt^n/n!+\cdots) + C_4(1+\delta_2t+\delta_2^2t^2/2+\cdots+\delta_2^nt^n/n!+\cdots) \quad (16)$$
$$(n=2, 3, 4, 5, \text{and } 6)$$

where the notations, b, C_3, C_4, δ_1, and δ_2, are the same as in Eq. (4c). We will here define the following series of errors, ε_k and $\varepsilon_{\max}$, in order to check the accuracy of estimated rate constants; they are also shown in Table 2:

$$\varepsilon_k = \sum_i\varepsilon_i = \sum_i|k_{i,\text{estimated}}-k_{i,\text{given}}|/k_{i,\text{given}} \quad (17)$$
$$(i=1, 2, 3, 4)$$

$$\varepsilon_{\max} = \sum_p\varepsilon_{p,3} + \sum_i\varepsilon_i \quad (18)$$
$$(p=1, 2, 3, 4;\ i=1, 2, 3, 4)$$

As can be seen from Table 2, the polynomials containing the high-order terms give reliable rate constants.

Let us compare the $k_{i,\text{estimated}}$ values given by Eq. (4c) with those given by Eq. (16) $(n=6)$ under the conditions of $(\text{A})_0=10.05$, and $(\text{B})_0=(\text{C})_0=0$ (the check points of (p,t) are the same as those mentioned above). The computation results are: $k_1=0.28$ (0.28); $k_2=0.046$ (0.050); $k_3=0.60$ (0.60); $k_4=0.20$ (0.20), and $\sum_p\varepsilon_{p,3}(\%)=0.844$ (0.922), where the values in parentheses are those evaluated by means of the polynomial $(n=6)$ of Eq. (16). Thus, both method give almost

Table 2. Estimates of rate constants for first example
$((\text{A})_0=10.0;\ (\text{B})_0=(\text{C})_0=0)$

		k_i				$\varepsilon_{p,3}$ (%)				$\sum_p\varepsilon_{p,3}$ (%)	ε_k (%)	$\varepsilon_{\max}$ (%)
		k_1	k_2	k_3	k_4	$\varepsilon_{1,3}$	$\varepsilon_{2,3}$	$\varepsilon_{3,3}$	$\varepsilon_{4,3}$			
Exponential function, Eq. (4C)		0.30	0.10	0.60	0.20	—	—	—	—	—	—	—
Polynomial approximation, Eq. (16)	$n=2$	0.22	3.4×10^4	0.59	0.09	7.17	3.63	0.001	3.73	14.5	>200	>214.5
	$n=3$	0.33	0.055	0.56	0.09	2.12	1.18	0.005	1.46	4.77	116.7	121.5
	$n=4$	0.30	0.15	0.60	0.20	0.52	0.30	0.038	0.528	1.39	50.0	51.39
	$n=5$	0.30	0.089	0.60	0.20	0.096	0.065	0.001	0.107	0.269	11.0	11.27
	$n=6$	0.30	0.097	0.60	0.20	0.013	0.011	0.009	0.006	0.039	3.0	3.039

In all cases, $k_i=2$ significant figures and iteration=3

TABLE 3. 10^3 $(C_4)_{t,\text{given}}$ VALUES EVALUATED BY TRAPEZOIDAL SIMULATION AND POLYNOMIALS

$10t$	Simulation[a]	Polynomial						
		$n=1$	$n=2$	$n=3$	$n=4$	$n=5$	$n=6$	$n=10$
1	0.0000	2.2170	1.7985	1.5269	1.3401	1.2023	1.0946	0.54248
2	1.0000	4.4340	3.6900	3.2326	2.9288	2.7105	2.5434	1.7204
3	2.9550	6.6510	5.6745	5.1074	4.7444	4.4903	4.2999	3.4102
4	5.1860	8.8680	7.7520	7.1421	6.7660	6.5099	6.3221	5.4732
5	7.6840	11.085	9.9225	9.3269	8.9737	8.7400	8.5722	7.8464
6	10.370	13.302	12.180	11.652	11.348	11.153	11.016	10.449
7	13.190	15.519	14.543	14.109	13.872	13.725	13.624	13.223
8	16.120	17.736	16.992	16.687	16.528	16.432	16.367	16.123
9	19.120	19.953	19.535	19.377	19.299	19.253	19.223	19.114
10	22.170	22.170	22.170	22.170	22.170	22.170	22.170	22.170

a) $\Delta t=0.10$

the same estimates for the rate constants.

Second Example. The given kinetic data, such as the $(C_s)_{t,\text{given}}$, for the classical enzyme model were also simulated with the specifications of $(S)_0=1.00$, $(E)_0=0.10$, $k_1=k_2=k_3=1.0$, and $\Delta t=0.10$ (shown in part in Table 3). In this section, we will try to estimate the best set of rate constants using only the concentrations of the product (P). The coefficients (a_n) of Eq. (12) were estimated similarly by means of least squares-error analysis of the (P) values at $t=0$, 1, 2, 3, —, and n. Table 3 lists the $(C_s)_{t,\text{given}}$ $(s=4)$ values $(0\leqq t\leqq 1.0)$ as evaluated by the polynomial functions $(n=1$, 2, 3, 4, 5, 6, and 10). As can be seen from Table 3, the lower the order (n) of the polynomial term, the more markedly the $(C_4)_{t,\text{given}}$ values differ from those of the simulation. It is also noticeable that the $(C_4)_{t,\text{given}}$ values become inaccurate as $t\to 0$, because the rate of the formation of P, $(d(P)/dt)_t$ does not increase monotonously during the initial short stage (*i.e.*, $(d(P)/dt)_{t\ 0}\simeq 0$). Therefore, we will use the $(C_4)_{t,\text{given}}$ values at $t=0.8$, 0.9, and 1.0 for computing the $\varepsilon_{p,s}$ $(s=4)$ values: that is, the check points, (p,t), are taken to be $(p,t)=(1, 0.8)$, $(2, 0.9)$, $(3, 1.0)$. Then, we will estimate the best sets of the k_i group using the $(C_4)_{t,\text{given}}$ values as evaluated by means of the polynomials $(n=1$—$10)$ and the $(C_4)_{t,\text{calcd}}$ values given by the trapezoidal simulation. Thus, the method of the k_i estimation in the Second Example is different from that in the First Example.

The iterative search technique gives the $k_{i,\text{estimated}}$ values for Second Example shown in Table 4. It may be seen from Table 4 that the higher the order of the polynomials used for the $(C_4)_{t,\text{given}}$ evaluation, the lower the errors of $\sum_p \varepsilon_{p,4}$ and ε_k. It may be deduced, therefore, that the accuracy of the $(C_4)_{t,\text{given}}$ values presented in Table 3 directly influences the estimation of the best k_i values.

The present technique used for Second Example can now be shown to be useful for estimating the rate constants in more detail.

In order to check the variation in the k_i estimation with the change in the initial specifications, such as, the concentrations of species and the Δt value,[4] the estimates of the rate constants were performed again with the specifications of $(S)_0=1.01$, $(E)_0=0.1$, and $\Delta t=0.10$, using the $(C_4)_{t,\text{given}}$ values $(t=0.8$, 0.9, and 1.0) obtained from the polynomial $(n=10)$ in Table 3. The computed results are: $k_1=1.0$, $k_2=1.0$, $k_3=$

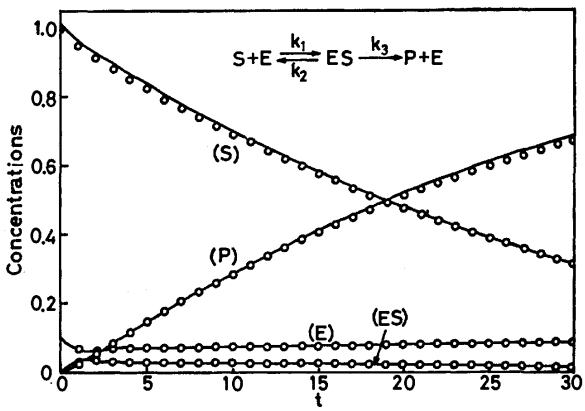

Fig. 2. Computer simulation of second example.
(circle point: given data; solid curve: predicted ones)

TABLE 4. ESTIMATED RATE CONSTANTS $((S)_0=1.0$ AND $(E)_0=0.1)$

n	k_i			$\varepsilon_{p,4}$ (%)			$\sum_p \varepsilon_{p,4}$(%)	ε_k(%)	$\varepsilon_{\max}$ (%)
	k_1	k_2	k_3	$\varepsilon_{1,4}$	$\varepsilon_{2,4}$	$\varepsilon_{3,4}$			
1	1.1	1.2	1.0	5.27	0.503	3.50	9.27	30.0	39.27
2	1.0	0.89	1.0	3.30	0.08	2.25	5.63	11.0	16.63
3	1.0	0.93	1.0	2.23	0.03	1.42	3.68	7.0	10.68
4	1.0	0.95	1.0	1.63	0.008	1.01	2.65	5.0	7.65
5	1.0	0.96	1.0	1.24	0.034	0.807	2.08	4.0	6.08
6	1.0	0.97	1.0	1.01	0.006	0.604	1.62	3.0	4.62
10	1.0	1.0	1.0	0.047	0.008	0.000	0.055	0.0	0.055

In all cases, $k_i=2$ significant figures, iteration=2, and computation time=2 min.

1.0, and $\sum_p \varepsilon_{p,4}=0.20\%$. The above $k_{i,\text{estimated}}$ values give the time-conversion curves of (S), (E), (ES), and (P) shown in Fig. 2. As may be seen from Fig. 2, we can easily predict the time dependence of the intermediate concentration by simulating the reaction using the estimated rate constants.

The authors wish to express their thanks to Professor Stephen Mazur of the University of Chicago for his valuable discussions and critical reading.

References

1) For instance, R. W. Southwork and S. L. Deleeuw, "Digital Computation and Numerical Method," McGraw-Hill, New York (1965), p. 420.

2) D. W. Marquardt, *J. Soc. Ind. Appl. Math.*, **11**, 431 (1963).

3) I. G. Darvey, S. J. Prokhovnik, and J. F. Williams, *J. Theoret. Biol.*, **11**, 459 (1966).

4) In regard to the effect of Δt on the k_i estimation, see K. Ohkubo, K. Tsuchihashi, and H. Sakamoto, This Bulletin, **47**, 579 (1974).

The Crystal Structure of the 2:1 Complex of Pyromellitic Dianhydride with *trans*-4-Methylstilbene

Toshiko KODAMA and Shigekazu KUMAKURA*

The Institute of Industrial Science, The University of Tokyo, Roppongi, Minato-ku, Tokyo 106
**Department of Chemistry, Faculty of Science and Engineering, Saitama University, Shimookubo, Urawa 338*

(Received December 26, 1973)

The 2:1 complex of pyromellitic dianhydride with *trans*-4-methylstilbene crystallizes in the Cc space group with four pyromellitic dianhydride molecules and two *trans*-4-methylstilbene molecules in a unit cell with dimensions of $a=12.780$, $b=7.446$, $c=15.050$ Å, and $\beta=91.09°$. In addition to the clearly-defined Laue spots, diffuse streaks elongated perpendicular to the molecular layers were observed with a half period of the b^* axis of the reciprocal lattice. The structure was solved from a three-dimensional $|E|^2$ Patterson synthesis and was refined by a block-diagonal least-squares method to the final R value of 0.13 for the visually-estimated 703 reflections. Refinement was difficult, however, because of the large correlation between parameters caused by the disorder. The crystal is built up of molecular layers stacked parallel to the $(10\bar{2})$ plane and is disordered in the stacking arrangement of the molecular layers. The pyromellitic dianhydride molecule and one of the benzene rings of the *trans*-4-methylstilbene molecule are alternately stacked plane-to-plane in infinite columns along $[10\bar{2}]$. The ethylene group of the *trans*-4-methylstilbene molecule joins the two columns. The molecular arrangement of the component molecules resembles those observed in the anthracene, pyrene, and perylene complexes with pyromellitic dianhydride and presents a striking contrast to that of the *trans*-stilbene complex. The interplanar distances range from 3.25 to 3.56 Å, smaller than that of the *trans*-stilbene complex.

The crystal structure of the equimolar charge transfer (CT) complex between pyromellitic dianhydride (PMDA) and *trans*-stilbene (STB) has been determined.[1] The crystal-structure analysis of the 2:1 pyromellitic dianhydride-*trans*-4-methylstilbene (ME-STB) complex was undertaken in order to study the CT interaction by comparing the molecular arrangement of the donor and acceptor molecules with those of a series of complexes of PMDA.[1-3]

Experimental

Red crystals of the complex grown from an ethyl acetate solution were kindly supplied by Professor Taku Matsuo of Kyushu University. The crystals cleave easily into thin plates and are sensitive to atmospheric moisture. The crystals are monoclinic, and the systematic absences, hkl (when $h+k$ is odd) and $h0l$ (when l is odd), are consistent with the C2/c or Cc space group (Cc was proved to be the true space group at a stage of the refinement). The lattice parameters were determined from zero-layer back-reflection Weissenberg photographs around the b and c axes. The crystal density was determined by flotation in trichloroethylene-chloroform mixture. The crystal data are:

$C_{15}H_{14}\cdot 2C_{10}H_2O_6$ F.W.=630.5

Monoclinic

$a = 12.780 \pm 0.008$ Å

$b = 7.446 \pm 0.005$ Å

$c = 15.050 \pm 0.004$ Å

$\beta = 91.09 \pm 0.04°$

$U = 1432$ Å^3

$D_m = 1.48$ g·cm^{-3}

$z = 2$

$D_x = 1.48$ g·cm^{-3}

Space group: Cc

On oscillation photographs around the b axis, well-defined sharp spots appeared in the k th layer lines ($k=0, 1, 2, \cdots$), whereas diffuse spots drawn out into streaks perpendicular to the b^* axis appeared in the $k+1/2$th layer lines, as is shown in Fig. 1. From Weissenberg photographs around the b axis (Fig. 2), the streaks were found to be elongated along $[10\bar{2}]$ in the reciprocal space.

The specimens with dimensions of $0.15\times0.23\times0.11$ mm and $0.17\times0.21\times0.13$ mm were used for the intensity measurements around the b and c axes respectively. The intensity data were recorded on multiple-film equi-inclination Weissenberg photographs around the b axis up to the 5th layer and around the c axis up to the 10th layer using Cu$K\alpha$ radiation. The intensities were estimated visually by a comparison with a time-calibrated intensity strip prepared from a well-defined sharp spot. 703 independent reflections were collected. The usual Lorentz, polarization, and spot shape correc-

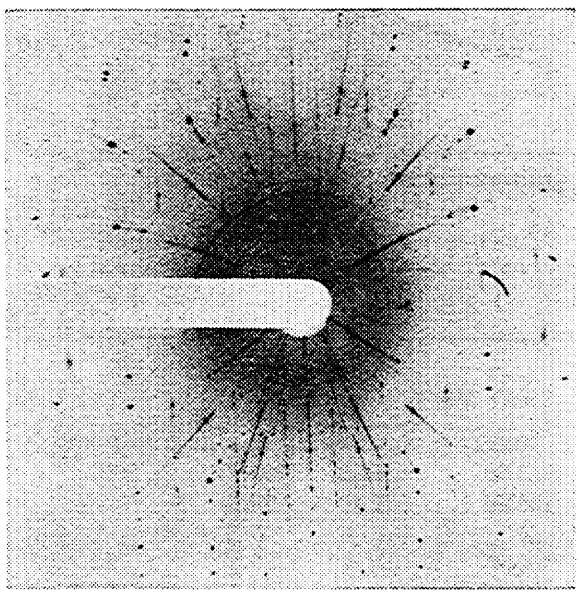

Fig. 1. Oscillation photograph around the b axis taken by Cu$K\alpha$ radiation

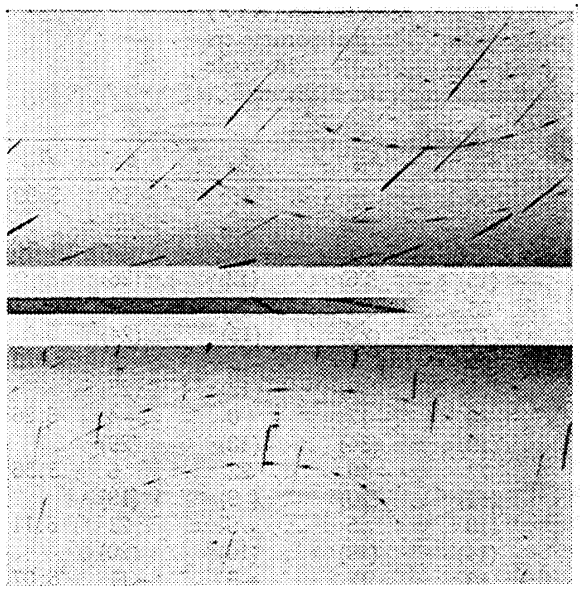

Fig. 2. Weissenberg photograph of the 3/2th layer around the *b* axis taken by the equi-inclination method using Cu$K\alpha$ radiation

tions were applied, but the absorption correction was neglected in view of the small size of the specimens.

Structure Determination

The layer structure of molecules parallel to $(10\bar{2})$ was indicated by the characteristic features that the cleavage plane is $(10\bar{2})$ and that the $20\bar{4}$ reflection and its higher-order reflections give strong X-ray intensities with thermal diffuse scattering and fall off uniformly in intensity. An $N(z)$ test based on the $h0l$ reflections indicated the crystal structure to be hypercentric. Therefore, the C2/c space group was assumed. Since only four PMDA molecules and two ME–STB molecules exist in a unit cell, they must be located at some kind of special positions.

A three-dimensional Patterson synthesis using $|E|^2$ as the coefficient was calculated using the complete set of observed data. The structure of the PMDA molecule was found to have a center of symmetry, thus accounting for the predominant peaks. The atomic coordinates of the PMDA molecule thus determined, combined with appropriate individual isotropic temperature factors, gave an R value of 0.45 for all the reflections.

A Fourier synthesis showed the ME–STB molecule to be located along the two-fold axis parallel to the *b* axis and to extend over a range of twice the *b* length-that is, over the twice repetition unit $b'=2b$ along the *b* axis; in other words, the two benzene rings of the ME-STB molecule were found to be overlapped at the same area in a scale of *b* units. It is necessary to measure the intensities of the diffuse reflections in order to determine the structure of the true unit cell of the crystal, but we did not undertake to do so because of the many atomic parameters in comparison with the small number of diffuse reflections and because of the poor quality of the crystals. Therefore, the average structure in the scale of *b* units along the *b* axis was determined in the present work. Assigning the C2/c space group to the crystal, the asymmetric unit of the structure consists of one-half of a PMDA molecule and a quarter of a ME–STB molecule. In the ME–STB molecule there is only one methyl group attached to the C(4) or the C(4′) position, so a quarter of a ME–STB molecule is a quasi-asymmetric unit.

After another Fourier synthesis, the atomic coordinates were refined by means of the block-diagonal least-squares procedure using a program written by Dr. Ashida. The structure data based on the C2/c space group gave an R value of 0.23. The difference synthesis showed several extra peaks around the benzene ring of the ME–STB molecule. Therefore, refinement based on the Cc space group, starting from a model with two independent benzene rings, was carried out; an R value of 0.15 was thus obtained. Since the R value was significantly lower, and since only simple patterns with low peak heights appeared on the difference synthesis, Cc was found to be the correct space group. Because of the parameter interaction, the positional and thermal parameters of one benzene ring of the ME–STB molecule were fixed, while those of the other were refined at each stage of the refinement. After three cycles of refinement using anisotropic temperature factors, the R value was lowered to 0.118, but there were several absurd bond lengths, from 1.1 to 1.6 Å, in the benzene rings of the ME–STB molecule. At each stage of the refinement, the R value shifted up and down. Therefore, refinement was done again by adjusting the positional parameters so as to give plausible bond lengths before each cycle of refinement. The R value gradually fell to 0.13. The weighting scheme for the least-squares procedure was: 0.5 for $|F_o|<5.0$ and 1.0 for $|F_o|\geq 5.0$. The topography of the final difference synthesis is flat within the range of ± 0.7 eÅ^{-3}. The final atomic and thermal parameters are listed in Table 1. A complete list of the observed and calculated structure factors is deposited at the Chemical Society of Japan.[4] The atomic scattering curves were taken from the International Tables for X-ray Crystallography.

Description and Discussion of the Structure

Crystal Structure. The projection of the structure viewed along the *a* axis is shown in Fig. 3. One of the possible positions of the methyl carbon atom is indicated by dotted lines. In view of the stacking disorder to be described later, it seemed that the position is on either the C(7) or the C(7′) position. The crystal is built up of molecular layers stacked parallel to $(10\bar{2})$. The component molecules are alternately stacked plane to plane in infinite columns along $[10\bar{2}]$. Each unit of the structure, namely, a PMDA molecule or one half of a ME–STB molecule, is surrounded by six others in a quasi-hexagonally close-packed array.

The molecular arrangement and intermolecular contacts of the component molecules in the column are shown in Figs. 4 and 5. The arrangement is quite

TABLE 1. FINAL ATOMIC COORDINATES ($\times 10^4$) AND THERMAL PARAMETERS ($\times 10^4$) (Estimated standard deviations are shown in parentheses. Thermal parameters are in the form of $\exp[-(h^2\beta_{11}+k^2\beta_{22}+l^2\beta_{33}+hk\beta_{12}+hl\beta_{13}+kl\beta_{23})]$. Isotropic temperature factors equivalent to the given anisotropic temperature factors, B_{eq}, are also shown in the last column.)

Atom	x/a	y/b	z/c	β_{11}	β_{22}	β_{33}	β_{12}	β_{13}	β_{23}	B_{eq}
C (11)	−350	−1857	63	125	217	55	56	−36	15	5.99
	(23)	(35)	(19)	(36)	(72)	(14)	(36)	(16)	(29)	
C (12)	−946	−380	365	56	162	71	−65	−10	22	4.56
	(17)	(33)	(17)	(15)	(58)	(15)	(26)	(12)	(26)	
C (13)	−547	1433	255	64	63	85	−25	−26	−20	4.43
	(17)	(30)	(17)	(16)	(46)	(17)	(23)	(13)	(24)	
C (14)	−1960	−274	829	52	299	59	−15	−5	−8	5.13
	(17)	(40)	(16)	(16)	(76)	(14)	(37)	(12)	(27)	
C (15)	−1356	2616	665	130	105	88	−17	0	−4	6.26
	(26)	(34)	(22)	(27)	(59)	(19)	(34)	(18)	(29)	
O (11)	−2588	−1448	961	81	220	72	−46	22	6	5.56
	(13)	(24)	(12)	(13)	(45)	(11)	(20)	(9)	(19)	
O (12)	−2250	1516	940	77	150	110	5	9	21	6.11
	(13)	(24)	(14)	(13)	(24)	(14)	(19)	(10)	(20)	
O (13)	−1387	4142	721	53	203	113	17	−9	−11	6.07
	(12)	(23)	(14)	(10)	(43)	(14)	(18)	(10)	(21)	
C (11′)	411	1752	−100	43	143	45	−59	1	18	3.35
	(14)	(29)	(13)	(13)	(55)	(12)	(21)	(10)	(20)	
C (12′)	963	283	−369	46	120	41	−31	−5	1	3.12
	(15)	(29)	(14)	(12)	(47)	(10)	(22)	(10)	(20)	
C (13′)	601	−1384	−313	65	176	38	−6	−13	39	3.86
	(17)	(33)	(15)	(15)	(58)	(10)	(24)	(10)	(21)	
C (14′)	1982	215	−732	70	292	55	−16	−9	11	5.34
	(18)	(38)	(17)	(19)	(76)	(14)	(31)	(13)	(30)	
C (15′)	1404	−2600	−626	66	156	41	−2	−15	−15	3.83
	(17)	(31)	(15)	(16)	(55)	(11)	(24)	(11)	(23)	
O (11′)	2592	1374	−956	65	215	121	−8	−14	64	6.66
	(12)	(25)	(14)	(12)	(49)	(16)	(21)	(11)	(23)	
O (12′)	2222	−1632	−911	77	190	66	2	−23	−41	5.08
	(12)	(23)	(11)	(12)	(42)	(10)	(19)	(9)	(18)	
O (13′)	1470	−4189	−735	143	263	49	21	−2	−12	6.54
	(16)	(25)	(12)	(19)	(50)	(10)	(26)	(11)	(18)	
C (1)	11	7591	2513	85	290	26	−26	−5	−29	4.78
	(54)	(51)	(54)	(31)	(120)	(17)	(106)	(19)	(80)	
C (2)	−753	8956	2809	26	324	16	3	−46	32	3.45
	(33)	(68)	(30)	(21)	(131)	(16)	(39)	(17)	(36)	
C (3)	−552	602	2731	52	257	65	−52	−11	19	5.00
	(36)	(74)	(33)	(30)	(140)	(28)	(54)	(24)	(50)	
C (4)	373	1401	2380	123	115	57	73	−29	0	5.25
	(28)	(59)	(30)	(50)	(110)	(28)	(56)	(32)	(50)	
C (5)	1076	269	2111	91	121	48	−12	32	51	4.33
	(32)	(62)	(28)	(39)	(114)	(24)	(53)	(25)	(45)	
C (6)	962	8274	2135	83	571	16	−47	16	−91	6.52
	(36)	(71)	(32)	(34)	(201)	(18)	(72)	(20)	(52)	
C (7)	−78	5751	2734	358	697	73	9	−72	−48	15.15
	(36)	(55)	(30)	(48)	(143)	(13)	(54)	(20)	(27)	
C (1′)	106	2346	2373	135	208	26	15	−25	24	5.27
	(39)	(66)	(52)	(52)	(113)	(30)	(90)	(31)	(50)	
C (2′)	−783	1681	2664	106	162	37	−89	−5	−2	4.62
	(38)	(66)	(29)	(43)	(125)	(23)	(58)	(25)	(43)	
C (3′)	−963	−123	2686	61	256	28	20	−19	32	4.07
	(32)	(70)	(25)	(30)	(131)	(19)	(51)	(20)	(43)	
C (4′)	−130	−1389	2489	158	279	44	47	−28	−32	6.83
	(80)	(72)	(60)	(68)	(134)	(23)	(109)	(33)	(86)	
C (5′)	882	−675	2271	81	300	32	−40	25	−66	4.95
	(35)	(72)	(29)	(39)	(157)	(21)	(61)	(24)	(46)	
C (6′)	999	1169	2236	13	89	55	53	11	−79	2.60
	(24)	(54)	(27)	(18)	(97)	(22)	(33)	(16)	(38)	
C (7′)	399	4409	2316	217	634	53	−142	−27	−6	11.01
	(39)	(66)	(37)	(27)	(115)	(13)	(40)	(17)	(28)	

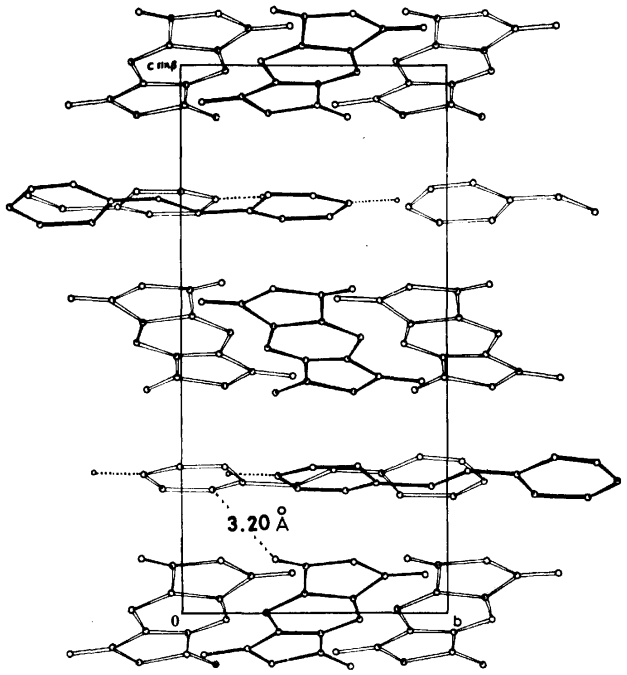

Fig. 3. The projection of the crystal structure viewed along the *a* axis. The molecules in thick lines are related to those in thin lines by the symmetry operation of C-face center.

different from that of the STB complex,[1] which is shown in Fig. 6. The long axes of the component molecules are perpendicular to each other in the ME–STB complex, whereas they are parallel in the STB complex. Thus, the molecular arrangement of the component molecules was shown to be easily

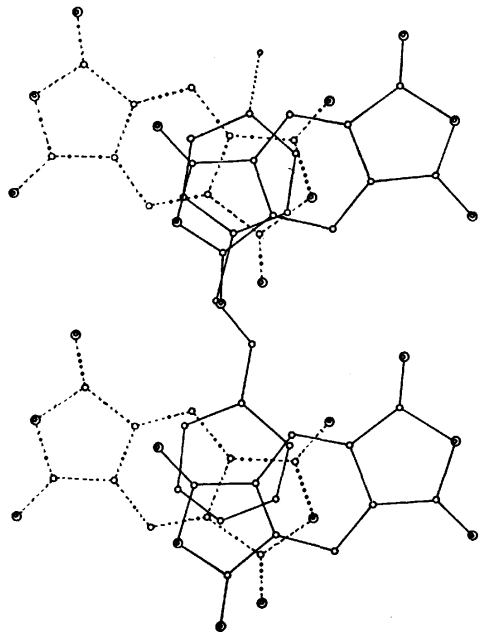

Fig. 4. The molecular arrangement of the component molecules of the PMDA-ME-STB complex projected perpendicular to the plane ($10\bar{2}$). The benzene ring planes of the ME-STB molecule contact the PMDA molecules in solid and dotted lines on both sides.

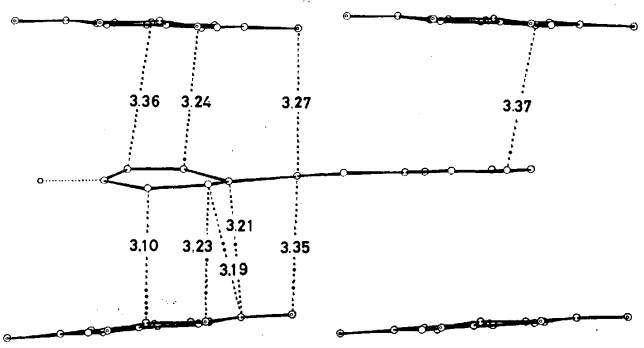

Fig. 5. Intermolecular contacts between PMDA and ME-STB with intermolecular distances shorter than 3.40 Å in Å units.

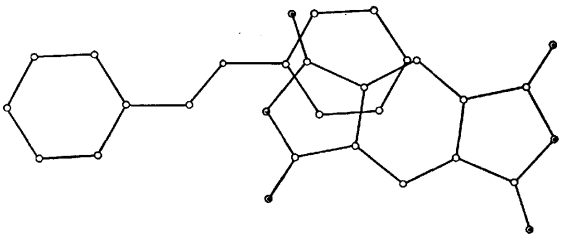

Fig. 6. The molecular arrangement of the component molecules of the PMDA-STB complex.

changed in the crystalline state by the slight geometrical difference between the ME–STB and the STB molecules. The difference in the molecular ratio of the component molecules between the 2:1 PMDA–ME–STB complex and the equimolar PMDA-STB complex corresponds to the difference in the molecular stacking; in the ME–STB complex both sides of the benzene ring planes of the ME-STB molecule are in contact with PMDA molecules, whereas in the STB complex only one side of the ring is in contact with a PMDA molecule. Because of the distinct difference in the overlapping geometry, the stacking axis of the component molecules is approximately perpendicular to the PMDA plane in the ME–STB complex, but is inclined about 39° against the PMDA plane in the STB complex. The ethylene group of the ME-STB molecule

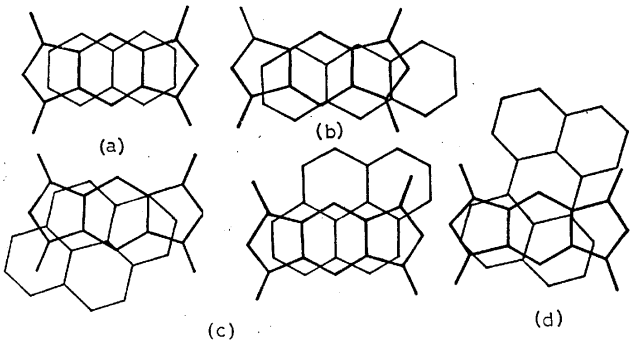

Fig. 7. The molecular arrangements of the component molecules of the complexes of PMDA with (a) naphthalene,[6] (b) anthracene,[2] (c) pyrene,[3] and (d) perylene.[2] Two independent molecular arrangements exist in PMDA-pyrene complex as shown in the figure.

of the ME-STB complex lies halfway between two columns and joins them, but that of the STB molecule of the STB complex lies within a column.

No theoretical consideration of the molecular arrangement of the component molecules of a series of CT complexes containing PMDA as an acceptor has hitherto been reported, but considerations of complexes containing maleic anhydride as an acceptor have been reported by Kobayashi *et al.*[5] The most stable molecular arrangements predicted in view of the CT interaction are consistent with those experimentally found in complexes of PMDA with perylene[2] and pyrene[3] (as is shown in Fig. 7). In view of the CT interaction, the molecular arrangement of the ME-STB complex seems to be more stable than that of the STB complex.

The PMDA molecule is planar within the maximum deviation of 0.007 Å of the atoms from the mean molecular plane. Moreover the benzene ring plane formed by C(1),···C(6) and that formed by C(1'),··· C(6') of the ME-STB molecule are planar within the maximum deviations of 0.01 and 0.06 Å respectively. The three molecular planes are expressed by the following equations, in the order mentioned above:

$$0.416x - 0.071y + 0.907z = 0.024 \quad (1)$$

$$0.41x - 0.01y + 0.91z = 3.39 \quad (2)$$

$$0.27x + 0.03y + 0.96z = -3.56 \quad (3)$$

where x, y, and z are coordinates (in Å) with respect to the a, b, and c crystal axes respectively. The (2) plane makes angles of 4.1 and 4.4° with the planes of the PMDA molecules within a column, with the average interplanar distances of 3.42 and 3.41 Å. The (3) plane makes angles of 10.7 and 9.7° with the planes of the PMDA molecules within a column, with the average interplanar distances of 3.52 and 3.56 Å.

The average intermolecular distances, the angles between the overlapping planes, and the C=O bond lengths of the CT complexes containing PMDA as an acceptor are shown in Table 2. The average intermolecular distance between the component molecules of the STB complex is the longest. The C=O bond lengths of a series of the complexes containing PMDA as an acceptor seem to tend to be shorter as the average intermolecular distances between the component molecules become longer.

The bond lengths and angles of the component molecules are shown in Figs. 8 and 9; they are also listed, along with the standard deviations, in Table 3. The ME-STB molecule is not planar, and the two benzene rings of the ME-STB molecule are twisted

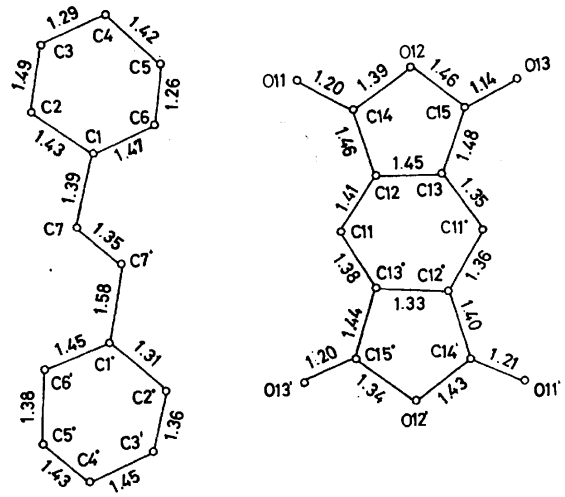

Fig. 8. Bond lengths (Å).

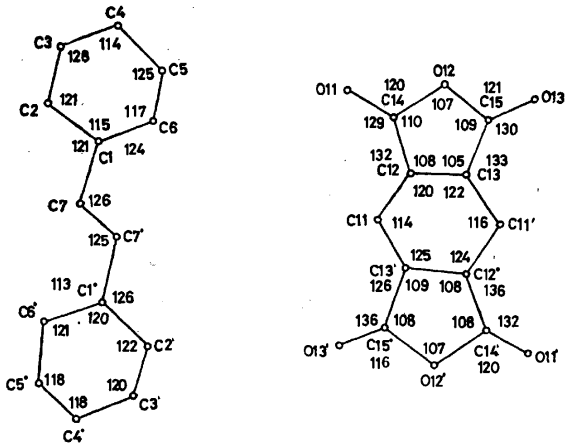

Fig. 9. Bond angles (degrees).

with an angle of 9°. A detailed structural discussion of the component molecules cannot be done because of the large standard deviations.

Description of the Disordered Crystal Structure. The observed diffuse reflections with indices of $k+1/2$ are elongated along [10$\bar{2}$]; that is, they are perpendicular to the molecular layers. Therefore, they can be explained if we assume that the stacking sequence of the molecular layers contains such mistaken layers that are shifted from the normal positions by half the $b'(b'=2b)$ axis. One of the models of the disordered crystal structure of this complex is shown schematically in Fig. 10. Although the inter-layer arrangement of the component molecules remains practically unchanged,

TABLE 2. THE AVERAGE INTERMOLECULAR DISTANCES, THE ANGLES BETWEEN THE OVERLAPPING PLANES AND THE C=O BOND LENGTHS OF THE CHARGE TRANSFER COMPLEXES CONTAINING PMDA AS AN ACCEPTOR

Donor	STB	ME-STB		Pyrene (110 K)		Perylene
Average interplanar spacing (Å)	3.58	3.41 3.56	3.42 3.25	3.33	3.30	3.33
Angle between the molecular planes (°)	4.8	4.4 9.7	4.0 10.7	1.34	1.18	0.82
C=O Bond length (Å)	1.181 1.188 ±0.009	1.20 1.20 ±0.04	1.14 1.12	1.197 1.191 ±0.006	1.195 1.190	1.23 1.18 ±0.01

Table 3. Bond lengths and angles and their standard deviations

PMDA			
C(11)–C(12)	1.41(0.04)Å	C(13′)–C(11)–C(12)	114(1)°
C(11)-C(13′)	1.38(0.04)	C(11)-C(12)-C(13)	120(2)
C(12)–C(13)	1.45(0.04)	C(11)–C(12)–C(14)	132(2)
C(12)–C(14)	1.46(0.04)	C(13)–C(12)-C(14)	108(2)
C(13)-C(15)	1.48(0.05)	C(12)-C(13)-C(11′)	122(1)
C(13)-C(11′)	1.35(0.03)	C(12)-C(13)–C(15)	105(2)
C(14)–O(11)	1.20(0.04)	C(15)–C(13)–C(11′)	133(2)
C(14)–O(12)	1.39(0.04)	C(12)-C(14)–O(11)	129(2)
C(15)-O(12)	1.46(0.04)	C(12)-C(14)-O(12)	110(2)
C(15)–O(13)	1.14(0.04)	O(11)–C(14)–O(12)	120(2)
C(11′)–C(12′)	1.36(0.04)	C(13)–C(15)-O(12)	109(1)
C(12′)-C(13′)	1.33(0.04)	C(13)–C(15)–O(13)	130(3)
C(12′)-C(14′)	1.40(0.04)	O(12)–C(15)–O(13)	121(3)
C(13′)–C(15′)	1.44(0.04)	C(14)–O(12)–C(15)	107(2)
C(14′)–O(11′)	1.21(0.04)	C(13)–C(11′)-C(12′)	116(1)
C(14′)-O(12′)	1.43(0.04)	C(11′)-C(12′)-C(13′)	124(2)
C(15′)-O(12′)	1.34(0.03)	C(11′)–C(12′)–C(14′)	136(1)
C(15′)-O(13′)	1.20(0.04)	C(13′)-C(12′)–C(14′)	108(2)
		C(11)–C(13′)–C(12′)	125(2)
		C(11)–C(13′)–C(15′)	126(2)
		C(12′)-C(13′)-C(15′)	109(2)
		C(12′)-C(14′)–O(11′)	132(2)
		C(12′)-C(14′)–O(12′)	108(2)
		O(11′)-C(14′)–O(12′)	120(2)
		C(13′)–C(15′)–O(12′)	108(1)
		C(13′)-C(15′)–O(13′)	136(2)
		O(12′)-C(15′)–O(13′)	116(2)
		C(14′)–O(12′)-C(15′)	107(2)
ME-STB			
C(1)-C(2)	1.43(0.11)	C(2)–C(1)–C(6)	115(3)
C(1)–C(6)	1.47(0.09)	C(7)–C(1)–C(2)	121(4)
C(1)–C(7)	1.39(0.13)	C(7)–C(1)–C(6)	124(6)
C(2)–C(3)	1.49(0.10)	C(1)–C(2)–C(3)	121(7)
C(3)–C(4)	1.29(0.08)	C(2)–C(3)–C(4)	128(4)
C(5)–C(6)	1.26(0.09)	C(3)–C(4)–C(5)	114(3)
C(4)-C(5)	1.42(0.08)	C(4)–C(5)–C(6)	125(4)
C(7)-C(7′)	1.35(0.18)	C(1)–C(6)–C(5)	117(5)
C(1′)–C(7′)	1.58(0.12)	C(1)–C(7)–C(7′)	126(14)
C(1′)–C(2′)	1.31(0.11)	C(7)–C(7′)–C(1)	125(9)
C(1′)–C(6′)	1.45(0.10)	C(2′)–C(1′)–C(6′)	120(3)
C(2′)–C(3′)	1.36(0.09)	C(7′)–C(1′)–C(2′)	126(5)
C(3′)–C(4′)	1.45(0.12)	C(7′)–C(1′)–C(6′)	113(6)
C(4′)–C(5′)	1.43(0.13)	C(1′)–C(2′)–C(3′)	122(5)
C(5′)–C(6′)	1.38(0.08)	C(2′)–C(3′)–C(4′)	120(4)
		C(3′)–C(4′)–C(5′)	118(3)

and although, moreover, the PMDA molecules are stacked regularly, the ethylene groups of the ME–STB molecules are randomly exchanged by the methyl groups and the hydrogens attached to C(4) of the neighboring ME–STB molecules. Since approximately equal electron densities were observed at the C(7) and C(7′) positions, the –CH=CH– ethylene groups are probably exchanged not only by the $-CH_3\cdots H-$ atomic groups, but also by the $-H\cdots CH_3-$ atomic groups which correspond to the upside-down arrangement of the ME–STB molecules. Such a random arrangement is probable because the forces between the layers are weaker than the forces within each layer and because the sizes of the –CH=CH– and $-CH_3\cdots H-$ atomic groups are similar. Such a geometric resemblance is considered to play an important role in the present type of disorder. No similar type of disorder was observed in the crystal of the PMDA–STB complex, which possesses no methyl group.

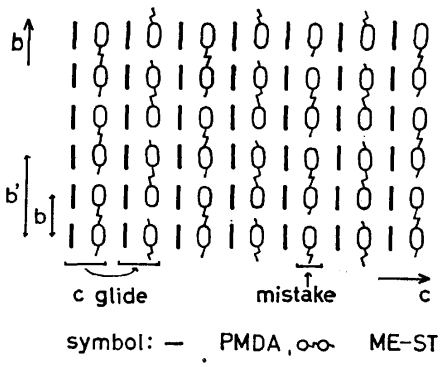

Fig. 10. Diagram showing the arrangement of molecules parallel to (100) described one of the models of the disordered structure.

The calculations were carried out on the HITAC 5020E computer at the Computer Centre of the University of Tokyo. The authors wish to express their thanks to Professor Yoshihiko Saito, the University of Tokyo, and Professor Fumiyuki Marumo, Tokyo Institute of Technology, for their helpful discussions.

References and Notes

1) T. Kodama and S. Kumakura, This Bulletin, **47**, 1081 (1974).

2) J. C. A. Boeyens and F. H. Herbstein, *J. Phys. Chem.*, **69**, 2160 (1965).

3) F. H. Herbstein and J. A. Snyman, *Phil. Trans. Roy. Soc.* (London), **A264**, 635 (1969).

4) The complete data of the F_o-F_c table are kept as Document at the office of the Bulletin of the Chemical Society of Japan. (Document No. 7421)

5) T. Kobayashi, S. Iwata, and S. Nagakura, This Bulletin, **43**, 713 (1970).

6) J. C. A. Boeyens and F. H. Herbstein, *J. Phys. Chem.*, **69**, 2153 (1965).

The Protonation of the TCNQ Anion Radical by Hydrogen Chloride

Akihiko YAMAGISHI and Masahiro SAKAMOTO*

Department of Chemisty, Faculty of Science, Hokkaido University, Sapporo 060

(Received January 5, 1974)

The kinetics of the protonation of sodium salt of 7,7,8,8-tetracyanoquinodimethane (Na^+TCNQ^-) by hydrogen chloride in alcohols and acetonitrile was investigated, using a stopped-flow apparatus. In methanol, the protonation rate is first-order in HCl and second-order in Na^+TCNQ^-, while in ethanol, the rate is one-half-order in HCl and second-order in Na^+TCNQ^-. The protonation rate in acetonitrile is first-order in HCl, but it deviates from second-order in Na^+TCNQ^-. These results are interpreted in terms of the rapid formation of a protonated intermediate in the initial stage of the reaction, according to $TCNQ^- + H^+ \rightleftharpoons HTCNQ\cdot$. The reversibility of this reaction is well demonstrated by the second-order dependence of the rate on Na^+TCNQ^-. The rate is also compared with the protonation rate of semiquinones, such as sodium salts of *p*-chloranil and 2,3-dicyano-1,4-benzoquinone, from the view point of the difference in reactivity between carbon and oxygen acids.

The kinetics of the protonation of aromatic radical anions by alcohols or water has been studied by several research groups.[1-5] Radical anions are protonated according to this stoichiometry:

$$2Ar^- + 2ROH = ArH_2 + Ar + 2RO^- \quad (1)$$

in which ArH_2 is the dihydroproduct of the parent hydrocarbon. On the basis of this stoichiometry, this mechanism of the protonation reaction was proposed by Paul, Lipkin, and Weissman:[6]

$$Ar^- + ROH \longrightarrow ArH\cdot + RO^- \quad (2)$$

$$ArH\cdot + Ar^- \longrightarrow ArH^- + Ar \quad (3)$$

$$ArH^- + ROH \longrightarrow ArH_2 + RO^- \quad (4)$$

The protonation of sodium naphthalenide (Na^+N^-) by water in tetrahydrofuran (THF) was found to proceed through this mechanism.[1] It implies that the proton-transfer reaction (2) is followed by the rapid electron-transfer reaction (3) due to the electron-accepting property of NH· being higher than N^-. There are, however, many aromatic radical anions whose protonations do not follow the above mechanism. Studies of the protonation of sodium perylenide (Na^+Pe^-) in THF by alcohols have revealed that the species to be protonated is a dianion, $2Na^+Pe^{2-}$, instead of Na^+Pe^-, although the dianion is present in a small amount. In the protonation of sodium and potassium anthracenides (Na^+A^- and K^+A^-) by alcohols in THF and dimethoxyethane (DME), the nature of the ion pairs profoundly affects their reactivity of protonation.[4,5] Protonation by methanol and ethanol proceeds through the protonation of Na^+A^- and K^+A^-. On the other hand, the participation of dianion of anthracene, $2Na^+A^{2-}$, is observed in the protonations by *t*-BuOH. In a word, the solvation and reduction states drastically affect the reactivity of the anion radicals and determine the main reaction paths.

Our work, described in this paper, is concerned with the protonation reaction of the 7,7,8,8-tetracyanoquinodimethane (TCNQ) anion radical by hydrogen chloride in alcohols and acetonitrile. $TCNQ^-$ is a weaker base than the ion radicals as has been mentioned above, it is stable in protonic solvents like alcohols and water. The first point we focus our attention on is the reversibility of Reaction (2). We expect that $TCNQ^-$ accepts a proton reversibly because of its weak basicity. The reversibility of Reaction (2) enables us to estimate the thermodynamically-defined basicity strength of $TCNQ^-$. The second point is to obtain the rate constant of Reaction (2) in order to compare it with the rate constants of the protonation of semiquinones. $TCNQ^-$ seems to accept a proton on a carbon atom,[7] while semiquinones are protonated on oxygen atoms, leading to hydroquinones. As far as diamagnetic molecules are concerned, it has been reported in several examples that the limiting rate of proton transfer to carbon acids is generally below the diffusion-controlled limit characteristic of oxygen and nitrogen acids.[8-10] We attempted to examine the validity of this rule in the scope of radical anions.

Experimental

Na^+TCNQ^- was prepared by reducing TCNQ with NaI in acetonitrile. The salt was dried *in vacuo*. Sodium salts of *p*-chloranil (QCl_4) and 2,3-dicyano-1,4-benzoquinone ($Q(CN)_2$) were prepared in a similar way. *p*-Phenylenedimalononitrile (H_2TCNQ) was prepared from Na^+TCNQ^- according to Method C as described by Acker and Hertler.[7] Tetraethylammonium chloride of a C.P. grade was used without purification. The methanol (MeOH) and ethanol (EtOH) were purified by distillation in the presence of CaO, using about a 30 cm distillation column. The acetonitrile (MeCN) was distilled after refluxing in the presence of P_2O_5 and K_2CO_3 successively. The water contents were determined by the Karl Fischer method; 0.5 mg/ml (MeOH), 4.3 mg/ml (EtOH) and 0.3 mg/ml (MeCN). Dried hydrogen chloride gas evolved by the reaction between concentrated sulfuric acid and concentrated hydrochloride acid was absorbed into these solvents. Stock solutions of these acid solutions (about 0.1 M) were kept in a refrigerator. The concentration of HCl was determined by titration with an 0.1 M NaOH aqueous solution.

The reaction was studied at 25 °C, utilizing a rapid-scan stopped-flow spectrophotometer, Union Giken Model 1300. The reaction was investigated under air dried by $CaCl_2$ and P_2O_5 successively. The progress of protonation was usually monitored by the absorbance at 840 nm (λ_{max} of Na^+TCNQ^-).

* Present address: Ebetsu City Office, Takasago, Ebetsu.

Results

Stoichiometry of the Protonation Reaction. Throughout this work, we assume that Na^+TCNQ^- dissociates completely into free ions in the solvents used. This assumption has not been verified experimentally, but it seems to be reasonable considering that the dielectric constants of these solvents are high and that these are all known as strong ion-solvating solvents. Figure 1

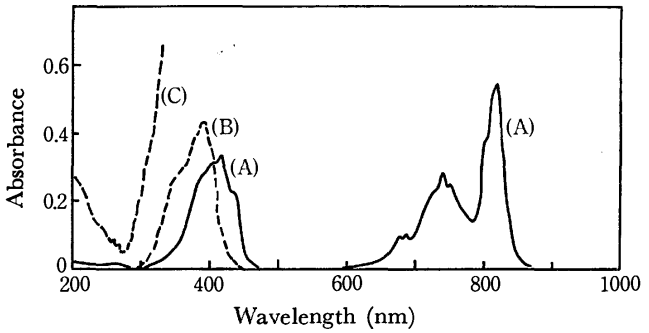

Fig. 1. Spectral change of Na^+TCNQ^- in MeCN when mixed with HCl solution.
(A) $[Na^+TCNQ^-]_0 = 1.32 \times 10^{-5}$ M, (B) $[Na^+TCNQ^-]_0 = 1.32 \times 10^{-5}$ M, [HCl] = 8.0×10^{-4} M. (C) $[Na^+TCNQ^-]_0 = 4.32 \times 10^{-4}$ M, [HCl] = 8.0×10^{-3} M (25 °C). ——: Na^+TCNQ^-, ------: $Na^+TCNQ^- + HCl$

shows the spectral change in Na^+TCNQ^- in MeCN when the Na^+TCNQ^- solution is mixed with the HCl solution. With the disappearance of the absorption due to $TCNQ^-$, the new peaks in 340—450 nm appear, they coincide with the spectra of TCNQ.[7] When a more concentrated solution of Na^+TCNQ^- is acidified, additional peaks are observed at 258, 264, and 270 nm. Comparing the spectra of H_2TCNQ in MeCN, these peaks are assigned to H_2TCNQ. Using the extinction coefficients of ε_{840} ($TCNQ^-$) 43300, ε_{395} (TCNQ) 63600,[7] and ε_{270} (H_2TCNQ) 300, which is approximately determined in this work, the initial concentration of Na^+TCNQ^-, and the final concentrations of TCNQ and H_2TCNQ were calculated

Table 1. Stoichiometry of reaction in MeCN at 25 °C

Run A)	Na^+TCNQ^-	initial	1.32×10^{-5}M
	TCNQ	final	6.60×10^{-6}M
Run B)	Na^+TCNQ^-	initial	4.20×10^{-4}M
	TCNQ	final	2.10×10^{-4}M
	H_2TCNQ	final	*ca.* 2×10^{-4}M

(Table 1). In EtOH and MeOH similar results were obtained except that the UV absorption due to H_2TCNQ was not observed. In the experiment where H_2TCNQ is dissolved in EtOH *in vacuo*, H_2TCNQ is found to have a broad peak at 309 nm in addition to several small peaks in the 250—270 nm region. At the present stage, it is uncertain why the H_2TCNQ product is not observed in alcoholic solvents. The reason may lie in the interaction of H_2TCNQ with alcohols in an acidic medium. The number of protons consumed in the reaction was determined in MeOH, using thymol blue as the proton indicator. We obtained 1.1 ± 0.2 as the ratio of protons consumed per $TCNQ^-$. Thus, the over-all stoichiometry of the reaction may be written as follows:

$$2Na^+TCNQ^- + 2HCl = TCNQ + H_2TCNQ + 2NaCl \quad (5)$$

which is identical with Eq. (1).

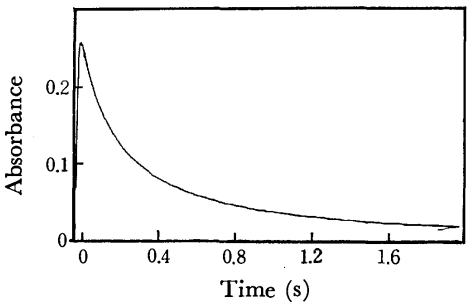

Fig. 2a. The decay of absorbance at 840 nm due to Na^+TCNQ^- during the reaction with HCl in MeOH.

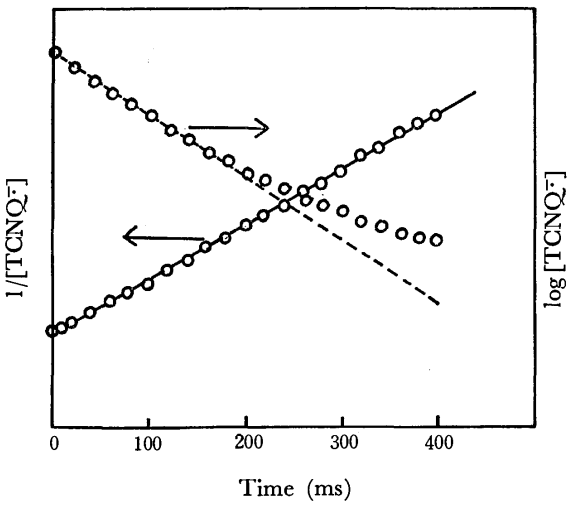

Fig. 2b. Plots of $1/[TCNQ^-]$ *vs.* time and $\log[TCNQ^-]$ *vs.* time in MeOH at 25 °C.
$[Na^+TCNQ^-]_0 = 7.60 \times 10^{-6}$ M, $[HCl] = 4.30 \times 10^{-4}$ M

Reaction in MeOH. The decay of $TCNQ^-$ was followed by mixing the MeOH solution of Na^+TCNQ^- with the MeOH solution of HCl. Even under the $[Na^+TCNQ^-] \gg [HCl]$ condition (Fig. 2a), the reaction is not first-order. As is shown in Fig. 2b, the decay of $TCNQ^-$ is second-order with respect to $TCNQ^-$. The apparent second-order rate constant increases linearly with the concentration of HCl (Table 2). The rate of protonation may, therefore, be written as:

$$\frac{d[TCNQ^-]}{dt} = -k_{obs}[TCNQ^-]^2[H^+] \quad (6)$$

The change in the spectra in 330—530 nm with the time (Fig. 3) shows the existence of the isosbestic point at 394 nm. This implies that the amount of intermediates accumulated in the course of the reaction, if any, is too small to give any disturbance to the condition:

TABLE 2. k_{obs} VALUES AT VARIOUS HCl CONCENTRATIONS IN MeOH AT 25 °C

Na^+TCNQ^-/M	HCl/M	$k_{obs}/M^{-2}s^{-1}$
7.60×10^{-6}	1.08×10^{-4}	1.73×10^{8}
7.60	2.15	1.66
7.60	4.30	1.64
7.60	8.60	1.40
7.60	21.5	1.48

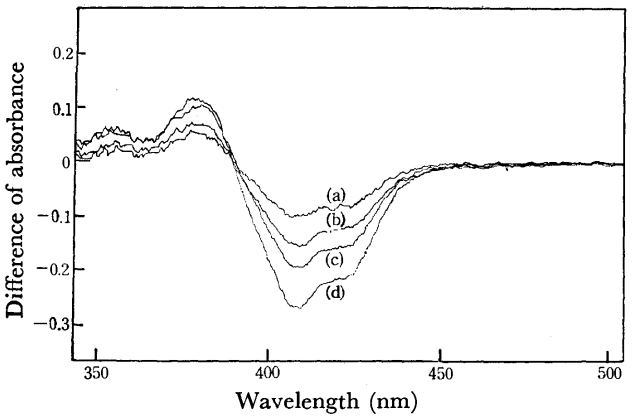

Fig. 3. Rapidly-scanned difference spectra for the system of Na^+TCNQ^- and HCl in MeOH.
(a) is the difference between the initial absorbance and the one 25 ms after mixing; (b) 50 ms after mixing; (c) 100 ms after mixing; (d) 500 ms after mixing. Scan speed 5 ms/300 nm. $[Na^+TCNQ^-]_0$ 8.23×10^{-6} M. [HCl] 1.50×10^{-3} M.

$$[TCNQ^-] + 2[TCNQ] = [TCNQ^-]_0$$

in which $[TCNQ^-]_0$ is the initial concentration of $TCNQ^-$. There are three possibilities conceivable for the origin of the second-order dependence of the rate on $TCNQ^-$. The species to be protonated is (i) a dianion, $TCNQ^{2-}$, which is produced by this reaction:

$$2TCNQ^- \rightleftharpoons TCNQ + TCNQ^{2-} \quad (7)$$

(ii) a dimer anion, $(TCNQ^-)_2$, which is produced by this reaction:

$$2TCNQ^- \rightleftharpoons (TCNQ^-)_2;\ K \quad (8)$$

or (iii) a $TCNQ^-$, and there exists a reversible reaction to form a protonated intermediate:

$$TCNQ^- + H^+ \underset{k_2}{\overset{k_1}{\rightleftharpoons}} HTCNQ^\cdot \quad (9)$$

$$HTCNQ^\cdot + TCNQ^- \xrightarrow{k_3} HTCNQ^- + TCNQ \quad (10)$$

The (i) possibility can be discarded because the addition of TCNQ has no effect on the protonation rate (Table 3). If Reaction (7) worked, TCNQ would retard the reaction rate, decreasing the concentration of $TCNQ^{2-}$.

TABLE 3. EFFECT OF TCNQ ON THE RATE OF PROTONATION REACTION IN MeOH AT 25 °C

Na^+TCNQ^-/M	HCl/M	TCNQ/M	$k_{obs}/M^{-2}s^{-1}$
8.23×10^{-6}	1.50×10^{-3}	0.00×10^{-5}	1.76×10^{8}
8.23	1.50	2.27	1.83
8.23	1.50	4.54	1.76

If the (ii) assumption is correct, the k_{obs} in Eq. (6) is equal to $k\cdot K$, where k is the protonation rate of $(TCNQ^-)_2$ by the proton and where K is an equilibrium constant of (8). Using $k_{obs}=1.5\times10^8\ M^{-2}\ s^{-1}$ and $k=10^{10}\ M^{-1}\ s^{-1}$, the lower limit of K is estimated to be $10^{-2}\ M^{-1}$. On the other hand, assuming that the extinction coefficient of $(TCNQ^-)_2$ at 643 nm is 33600,[11] the upper limit of K may be estimated to be $10\ M^{-1}$ from the electronic spectra. Therefore, the (ii) possibility can not be denied on the basis of only the kinetic results. However, in the case of sodium anthracenide, it is indicated that the $(A^-, Na^+)_2$ dimer is relatively unreactive.[4] The result in MeCN also supports the (9) and (10) mechanisms, as will be mentioned later. Thus, it seems that the (iii) possibility is most plausible at the present stage. From the first-order dependence of the rate on HCl, the reaction which follows Reaction (10) to produce a stable product may be concluded to be very fast. Applying the stationary state condition to $HTCNQ^\cdot$ in (9) and (10), we obtain the following rate equation:

$$\frac{d[TCNQ^-]}{dt} = -\frac{2k_1k_3[TCNQ^-]^2[H^+]}{k_2+k_3[TCNQ^-]} \quad (11)$$

in which H^+ is introduced as a proton source instead of HCl based on the results for the EtOH system.[12] Under this condition:

$$k_2 \gg k_3[TCNQ^-] \quad (12)$$

Eq. (11) becomes identical to the observed rate expression (6), leading to $k_{obs}=2k_1k_3/k_2$. Equation (11) predicts that the rate will deviate from the second-order dependence on $TCNQ^-$ at a sufficiently high concentration of $TCNQ^-$. This actually happens in the MeCN system. However, no deviation from Eq. (6) was observed up to $[Na^+TCNQ^-]=1.22\times10^{-4}$ M in MeOH, making it possible to conclude that $k_2/k_3 > 1.22\times10^{-4}$ M.

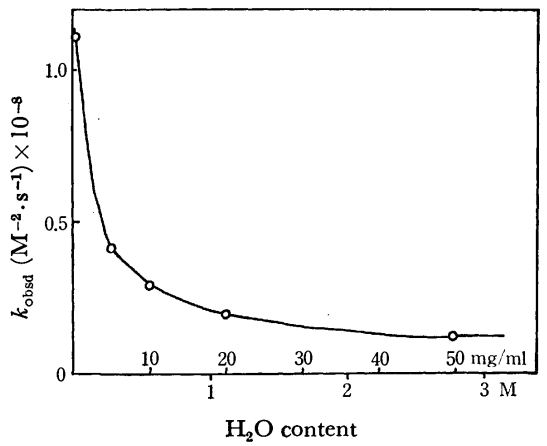

Fig. 4. Effect of H_2O on k_{obs} in MeOH at 25 °C. $[Na^+TCNQ^-]_0$ 2.8×10^{-6} M, [HCl] 1.07×10^{-2} M.

The small amount of water was found to reduce the k_{obs} value to a remarkable extent, although the mechanism is not altered (Fig. 4). We may ascribe this water effect to the solvation of the proton by water molecules:

$$H^+(MeOH)_n + mH_2O \rightleftharpoons nMeOH + H^+(H_2O)_m \quad (13)$$

which results in the leftward shift of the (9) equilibrium. The solvation of H^+ by water is reported to occur even in a small amount of water.[13] Since the electron-transfer reaction (10) is thought to be diffusion-controlled and little affected by the water content, the change in the k_{obs} value with water reflects the change in the equilibrium constant of Reaction (9) with the water content.

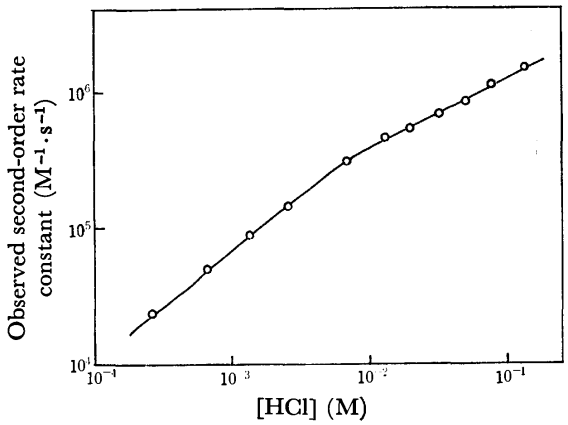

Fig. 5. Dependence of the second-order rate constant on HCl concentration in EtOH at 25 °C.
$[Na^+TCNQ^-]_0$ 6.81×10^{-6} M.

Reaction in EtOH. The decay of $TCNQ^-$, mixed with HCl in ethanol, is found to be second-order with respect to the $TCNQ^-$ concentration. However, the second-order rate constant is not always linearly dependent on the HCl concentration (Fig. 5). In the range of [HCl] larger than 10^{-2} M, the rate equation is written as:

$$\frac{d[TCNQ^-]}{dt} = -k_{obs}[TCNQ^-]^2[HCl]^{1/2} \qquad (6')$$

rather than as Eq. (6). The one-half-order dependence of the rate on the HCl concentration can best be interpreted by assuming a rapid equilibrium in EtOH:

$$HCl \rightleftharpoons H^+ + Cl^-;\ K \qquad (14)$$

and by assuming, in addition, that the dissociated proton H^+, but not HCl, is a protonating reagent. The free proton concentration is $[H^+]=K^{1/2}[HCl]^{1/2}$, supposing that the degree of dissociation is very small. From the plot in Fig. 5, the k_{obs} corresponding to $2k_1k_3/k_2$ in Eq. (6) and the equilibrium constant of (14), K, are estimated to be $1\pm0.2\times10^8$ $M^{-1}s^{-1}$ and $2.4\pm0.8\times10^{-3}$ M respectively.[14] This conclusion is confirmed by the fact that tetraethylammonium chloride is found to suppress the protonation rate, as is shown in Table 4.[15]

Table 4. The effect of tetraethylammonium chloride on the rate of protonation reaction in EtOH

Na^+TCNQ^-	HCl	Tetraethyl-ammonium chloride	k_{obs}[a]
1.28×10^{-5}M	1.8×10^{-2}M	0 M	$1.86\times10^5M^{-1}s^{-1}$
1.28	1.8	0.031	1.63
1.28	1.8	0.15	0.709
1.28	1.8	0.30	0.446

a) Temperature 15 °C, water content 8 mg/ml.

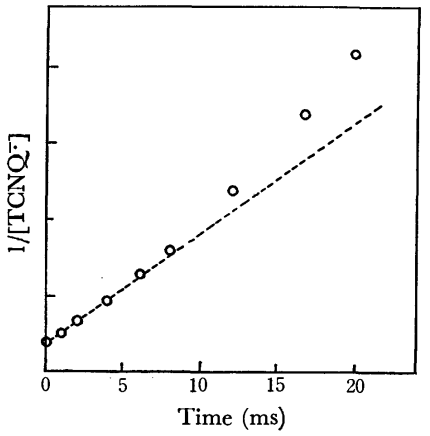

Fig. 6. Plot of $1/[TCNQ^-]$ *vs.* time for the reaction of $TCNQ^-$ with HCl in MeCN.
$[Na^+TCNQ^-]_0$ 4.12×10^{-5} M, [HCl] 1.08×10^{-3} M at 25 °C.

Reaction in MeCN. We studied the protonation reaction in MeCN with the purpose of obtaining the forward rate constant, k_1, in Reaction (9) directly. Since MeCN seems to solvate H^+ less effectively than alcohols, the backward rate constant, k_2, in (9) is expected to become smaller in MeCN than in alcohols. Consequently, the observed rate expression may approach:

$$\frac{d[TCNQ^-]}{dt} = -2k_1[TCNQ^-][H^+]$$

This rate law has been obtained in the case of the protonation of sodium naphalenide in THF.[1] As Fig. 6 shows, the decay of $TCNQ^-$ during the reaction with HCl is found to deviate from the second-order dependence on $TCNQ^-$. We consider that, at least in the initial stage, $TCNQ^-$ is protonated according to the (9) and (10) mechanism, keeping the condition of $k_2\approx k_3$ [$TCNQ^-$]. By integrating Eq. (11) under the condition of $[H^+]\gg[TCNQ^-]$, we obtain:

$$\frac{1}{2k_1[H^+]}\ln\frac{[TCNQ^-]_0}{[TCNQ^-]} + \frac{k_2}{2k_1k_3[H^+]}\left(\frac{1}{[TCNQ^-]} - \frac{1}{[TCNQ^-]_0}\right) = t$$

In order to obtain k_1 and k_2/k_1k_3 from the observed decay curve, we draw a group of straight lines on the (x, y) plane as expressed by:

$$\frac{2.3}{t}\log\frac{[TCNQ^-]_0}{[TCNQ^-]}\cdot x + \frac{1}{t}\left(\frac{1}{[TCNQ^-]} - \frac{1}{[TCNQ^-]_0}\right)\cdot y = 1$$

using a pair of $\frac{2.3}{t}\log\frac{[TCNQ^-]_0}{[TCNQ^-]}$ and $\frac{1}{t}\left(\frac{1}{[TCNQ^-]} - \frac{1}{[TCNQ^-]_0}\right)$ at various values of t for a constant $[H^+]$.

The common point (x_0, y_0), through which a group of straight lines pass gives the desired values of $1/2k_1$ and $k_2/2k_1k_3$. An example is shown in Fig. 7, leading to the results tabulated in Table 5. It should be noted that, if the dimer anion mechanism (possibility (ii) in MeOH) worked, the deviation from a second-order dependence on $TCNQ^-$ would be interpreted as the

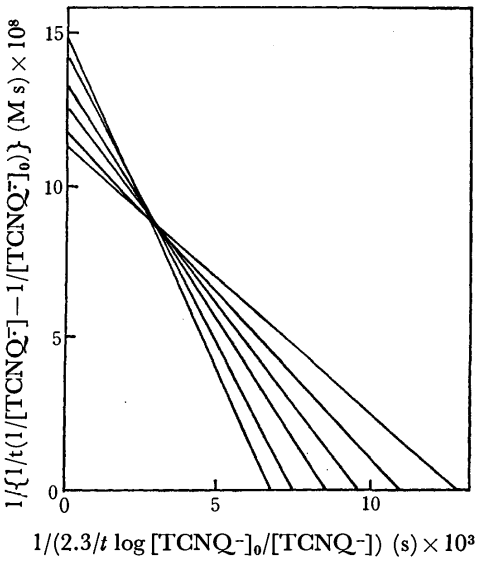

Fig. 7. Plots of a group of straight lines according to $\frac{2.3}{t}\log\frac{[TCNQ^-]_0}{[TCNQ^-]}\cdot x+\frac{1}{t}\left(\frac{1}{[TCNQ^-]}-\frac{1}{[TCNQ^-]_0}\right)\cdot y=1$ for various values of t.

TABLE 5. k_1 AND k_1k_3/k_2 VALUES IN MeCN AT 25 °C

Na^+TCNQ^-/M	HCl/M	$k_1/M^{-1}s^{-1}$	$k_1k_3/k_2/M^{-2}s^{-1}$
4.12×10^{-5}	5.40×10^{-4}	3.3×10^5	1.1×10^{10}
4.12	10.8	2.1	1.3
4.12	21.6	1.9	2.3
4.12	36.0	2.0	2.3

result of the participation of the direct protonation of $TCNQ^-$ (Reaction (9)). If this were the case, the deviation from second-order would appear at lower concentrations of $TCNQ^-$, since Reaction (8) would be predominant at higher concentrations of $TCNQ^-$. However, the fact is that the deviation was observed at higher concentrations of $TCNQ^-$, but not at lower concentrations. In this way, the possibility of a dimer mechanism could be dismissed. The magnitude of k_1 is about four orders below the diffusion-controlled rate constant.

In order to compare the k_1 value with the protonation rate of semiquinones, in which protonation occurs on oxygen atoms, we tried to obtain the reaction rates of protonation, $Na^+QCl_4^-$ and $Na^+Q(CN)_2^-$. Unfortunately, the decay of these semiquinones is too fast for us to analyse the kinetics of the protonation reaction. Therefore, the lower limits of k_1 and k_1k_2/k_3 were roughly estimated from the half-life of the decay curves of semiquinones, assuming that the decay curves are completely first-order or completely second-order respectively. The results are shown in Table 6. These values indicate that the protonation rates of semiquinones by free protons are more than one order larger than that of $TCNQ^-$.

TABLE 6. THE LOWER LIMIT OF RATE CONSTANTS OF PROTONATION OF QCl_4^- AND $Q(CN)_2^-$ IN MeCN AT 25 °C

Q^-/M	HCl/M	$t_{1/2}$ s	$k_1/M^{-1}s^{-1}$	$(k_1k_2/k_3)/M^{-2}s^{-1}$
		for QCl_4^-		
5×10^{-6} a)	4.10×10^{-5}	*ca.* 4×10^{-3}	$>3\times10^6$	$>5\times10^{11}$
2	8.10	*ca.* 2	>3	>15
2	16.1	*ca.* 0.8	>2	>20
		for $Q(CN)_2^-$		
5×10^{-6} b)	3.60×10^{-5}	*ca.* 2×10^{-3}	$>5\times10^6$	$>1\times10^{12}$

a) estimated, using $\varepsilon_{445}=9\times10^3$. b) estimated, using $\varepsilon_{465}=5\times10^3$.

Discussion

The reversibility of the initial step of the protonation:

$$TCNQ^- + H^+ \underset{k_2}{\overset{k_1}{\rightleftharpoons}} HTCNQ\cdot;\quad K_b \qquad (9)$$

is well demonstrated by the second-order dependence of the rate on the concentration of $TCNQ^-$. If the backward rate of the above reaction were forbidden, the rate would be first-order in $TCNQ^-$ as far as the decay of $TCNQ^-$ is monitored. As the final product of the protonation of $TCNQ^-$ is H_2TCNQ (I), $HTCNQ\cdot$ seems to have the (II) structure.

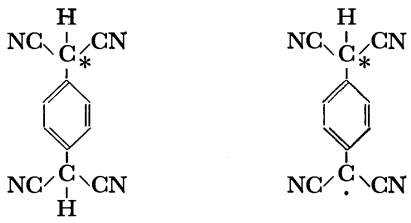

Therefore, the reversible protonation reaction (9) takes place on the carbon atom, C*. The magnitude of the equilibrium constant, K_b, can be estimated by assuming that the electron-transfer reaction (10) is diffusion-controlled. This assumption is reasonable, since Reaction (10) is more favoured from the energetic point of view than the exchange reaction:

$$TCNQ^- + TCNQ^* \rightleftharpoons TCNQ + TCNQ^{*-}$$

whose rate constant is known to be about $10^9\ M^{-1}s^{-1}$.[7] Table 7 gives the estimated values of K_b, assuming that $k_3=10^{10}\ M^{-1}\ s^{-1}$. The variation in K_b for various kinds of solvents is interpreted consistently in terms of the proton-solvating capacity of these solvents. Alcoholic solvents give K_b values of the same order. The

TABLE 7. THE ESTIMATED VALUE OF THE EQUILIBRIUM CONSTANT K_b FOR $TCNQ^- + H^+ \rightleftharpoons HTCNQ\cdot$ AT 25 °C

Solvent	H_2O/mg/ml	K_b/M^{-1} a)
MeOH	0.46	7.9×10^{-3}
MeOH	5.0	2.0
MeOH	10.0	1.5
MeOH	20.0	0.97
MeOH	50.0	0.62
EtOH	4.3	5±1
MeCN	0.3	1700±600

a) estimated from the observed k_1k_3/k_2 values, assuming $k_3=10^{10}M^{-1}s^{-1}$.

large value of the K_b in MeCN is due to the poor solvating capacity of MeCN. The water effect in MeOH implies that H_2O is the strongest solvating solvent for the proton.

A comparison of the k_1 value for the protonation of $TCNQ^-$ in MeCN with the lower limit of k_1 for QCl_4^- and $Q(CN)_2^-$ indicates that the k_1 for $TCNQ^-$ is more than one order smaller than that for semiquinones. We can not conclude that the smaller k_1 value for $TCNQ^-$ is characteristic of the protonation on a carbon atom in ion radicals, since a comparison between carbon and oxygen acids should be made for the limiting rate of protonation, which is obtained by extrapolating the rate to the limit of an infinite K_b. However, at the present stage of investigation it is meaningful to consider what factor of $TCNQ^-$ makes the protonation rate smaller than for semiquinones. At least three factors must be taken into consideration as determining the rate of protonation: (i) electron density of the atom on which protonation takes place, (ii) the localization energy caused by the protonation, and (iii) the steric hindrance in the vicinity of the proton-accepting atoms. In addition, another assumption (iv) may be introduced—that, in a transition state of protonation, a proton-accepting atom has an anionic character.

Table 8. Electron and spin densities of C* of $TCNQ^-$ and oxygen atom of QCl_4^-.

	Electron density	Spin density	Ref.
$TCNQ^-$	1.17−1.24	0.29−0.24	a)
QCl_4^-		0.213±0.010	b)

a) D. A. Lowitz, *J. Chem. Phys.*, **46**, 4698 (1967).
b) Y. Iida, This Bulletin, **44**, 1271 (1971).

At the initial stage of the reaction, where H^+ approaches anion radicals from an infinite distance, electostatic interaction may be predominant. The electron and spin densities of C* in $TCNQ^-$ are thus compared in Table 8 with those of the oxygen atom in QCl_4^-. There seems to be no remarkable difference in these quantities between $TCNQ^-$ and QCl_4^-. As H^+ comes closer to anion radicals, a localization of the odd π-electron takes place, together with a change in the electronic state of the C* atom into C^-. We regard the instability of the C^- state is the main factor for the protonation of $TCNQ^-$ being slower than that of semiquinones. In order to make this point clear, we roughly estimated the energy produced by the changes in electronic state (i) $=C<+e$ to $-C^-<$ and (ii) $=O+e$ to $-O^-$. Using the values given by Hinze and Jaffe,[16] the energies produced for (i) and (ii) are calculated to be 1.57 and 2.01 eV respectively. Thus, the C^- state is less stable by 0.44 eV than the O^- state. Assuming a small difference in π-localization energy between $TCNQ^-$ and semiquinones, the slower rate for the protonation of $TCNQ^-$ is attributable to the unstable character of the carbon anion. This circumstance is expected to hold similarly in diamagnetic molecules.

The authors wish to thank Professor Masatoshi Fujimoto for his continuous encouragement and Dr. Hiroshi Kashiwagi for his profitable suggestions.

References

1) S. Bank and B. Bockrath, *J. Amer. Chem. Soc.*, **93**, 430 (1971).
2) S. Hayano and M. Fujihira, This Bulletin, **44**, 1496 (1971).
3) G. Levin, C. Sutphen, and M. Szwarc, *J. Amer. Chem. Soc.*, **94**, 2652 (1972).
4) A. Rainis, R. Tung, and M. Szwarc, *ibid.*, **95**, 659 (1973).
5) E. R. Minnich, L. D. Long, J. M. Ceraso, and J. L. Dye, *ibid.*, **95**, 1061 (1973).
6) D. E. Paul, D. Lipkin, and S. I. Weissman, *ibid.*, **78**, 116 (1956).
7) D. S. Acker and W. R. Hertler, *ibid.*, **84**, 3370 (1962).
8) M. Eigen, *Angew. Chem.*, **75**, 489 (1963).
9) J. Stuehr, *J. Amer. Chem. Soc.*, **89**, 2826 (1967).
10) P. J. Dynes, G. S. Chapman, E. Kebede, and F. W. Schneider, *ibid.*, **94**, 6356 (1972).
11) R. H. Boyd and W. D. Phillips, *J. Chem. Phys.*, **43**, 2927 (1965).
12) Another possibility is that HCl is an attacking agent and that in MeOH most of HCl is present as an undissociated form. This is unlikely, however, because the dissociation constants of HCl in MeOH is considered to be larger than 10^{-4} M (See Ref. 15).
13) R. G. Bates, *J. Electroanal. Chem.*, **29**, 1 (1971).
14) In this estimation, the curve in Fig. 5 is regarded as a smooth curve whose slope changes gradually from 1 to 1/2.
15) The dissociation constants of HCl in alcohols, K, recently reported are $10^{-4.26}$ M (MeOH) and $10^{-4.21}$ M (EtOH) at 25 °C (A. P. Dreshkov, V. A. Drozdov and N. A. Kolchin, *Zhur. Fiz. Khim.*, **40**, 2150 (1966)). In this work, we conclude K (MeOH) is larger than 10^{-3} M and that K (EtOH) is about $10^{-2.7}$ M. These discrepancies may arise from the presence of water in our solvents.
16) J. Hinze and H. H. Jaffe, *J. Amer. Chem. Soc.*, **84**, 540 (1962).

The Mechanism for the Sulfonation of Olefins with a Sulfur Trioxide-Dioxane Complex[1)]

Masuzo NAGAYAMA, Osamu OKUMURA, Seiji NODA, Hiroshi MANDAI, and Akira MORI

Central Research Laboratories, Lion Fat & Oil Co., Ltd., Hirai, Edogawa-ku, Tokyo 132

(Received January 10, 1974)

The rates for the sulfonation of 1-dodecene with the sulfur trioxide-dioxane complex were measured spectrophotometrically. A bimolecular process occurred in this reaction, the rate being proportional to [1-dodecene] [SO_3-dioxane]. Furthermore, the stereochemistry of the initial products of the sulfonation reaction between *cis* or *trans*-2-butene and the sulfur trioxide-dioxane complex was studied. An equimolar amount of sulfur trioxide-dioxane (1 : 1) was added to *cis*- or *trans*-2-butene in chloroform to give the sultone, (I) or (II); (I) 1.5(q), 4.7—5.1(m), J_{AB} 7.9, J_{BC} 8.0, J_{CD} 6.0 Hz; (II) 1.5(q), 4.2—4.6(m), J_{AB} 6.8, J_{BC} 5.4, J_{CD} 6.8 Hz. These results indicate that the 2,3-butanesultones were produced stereospecifically from the corresponding 2-butene isomers. Similarly, the sulfonation of *cis*- or *trans*-2-pentene with sulfur trioxide-dioxane gave the corresponding 2,3-pentanesultones.

The sulfonation reaction of olefins, in particular long chain aliphatic α-olefins, with sulfur trioxide is utilized widely, even on a commercial scale, today. The reaction mechanism for the sulfonation of aliphatics, however, is scarcely known, although that of aromatic hydrocarbons has been extensively investigated.[2)] Some reports have been published on the mechanisms for the sulfonation of aliphatic olefins, these reports suggest that a four-membered ring sultone is formed *via* a zwitter-ion intermediate.[3-5)] However, no experimental proof for such an intermediate has been described, nor has any kinetic study about the sulfonation of aliphatic compounds been done.

In this paper, we wish to report on kinetic studies of the reaction between 1-dodecene and the sulfur trioxide-dioxane complex and a stereochemical studies of the sulfonation products of *cis*- and *trans*-2-butenes and *cis*- and *trans*-2-pentenes with the sulfur trioxide–dioxane complex.

Experimental

Experimental Procedure. *Kinetic Studies of the Sulfonation*: Kinetic experiments were carried out by the stopped-flow method* using a rapid scanning-type spectrophotometer (Hitachi Model RSP-2). In order to determine the rate of sulfonation, 1-dodecene and the SO_3-dioxane (1 : 1) complex were mixed in a mixing cell (path length, 1 cm); the decay curve in the absorbance appearing on an oscilloscope at 240 nm was used.

Three different molar ratios of 1-dodecene to SO_3-dioxane were taken: 1.05 : 1; 1 : 1; 1 : 1.5. A 0.2 M solution of 1-dodecene in ethylene dichloride and a 0.2 M solution of SO_3-dioxane in the same solvent were mixed at 25 °C, and then the absorbance was measured up to 500 ms after mixing. For the identification of the reaction products, the NMR spectra were measured.

Stereochemical Studies of the Sulfonation: Each of the *cis* and *trans* isomers of 2-butene and 2-pentene was allowed to react with a SO_3-dioxane (1 : 1) complex in chloroform at 0 °C for one hr, after which the 220 MHz or 100 MHz NMR spectra of the reaction mixture were measured at −5 °C. One half of the reaction mixture was then hydrolyzed with water and neutralized wih an excess of sodium hydroxide to give white crystals. To the other half of the reaction mixture were added two equivalents of aniline, and the mixture was allowed to stand for 24 hr and then neutralized to give crystals, which were recrystallyzed from aqueous ethanol (50 : 50). These crystals were subjected to NMR spectral analysis.

Reagents. The 1-dodecene——99.5% in purity by glc, prepared by the polymerization of ethylene——was dried over metallic sodium and distilled before use. The dioxane——a commercial product of a reagent grade——was dried over metallic sodium and distilled before use. The ethylene dichloride and chloroform——commercial materials of a reagent grade——were dried over P_2O_5 and distilled. The *cis*-2pentene (95.5%), *trans*-2-pentene (99.8%), *cis*-2-butene (98.3%) and *trans*-2-butene (98.0%)——all commercial materials——were used as received. The purity in parentheses were determined by glc.

Results and Discussion

Kinetic of the Reaction between 1-Dodecene and the SO_3-Dioxane Complex. The reaction product between 1-dodecene and the SO_3-dioxane complex in the initial stage was identified[6)] as a β-sultone** by 100 MHz NMR analysis.

The molar extinction coefficients (ε) at 240 nm were measured for SO_3-dioxane, 1-dodecene and β-sultone. Lambert-Beer's law held in each case and the values of ε were found to be as follows.

	$\varepsilon_{240\,nm}$ (l/mol·cm)
SO_3-dioxane	6.63
1-dodecene	1.37
C_{12}-β-sultone	2.72
ethylene dichloride	0.00272

The $\varepsilon_{240\,nm}$ value of ethylene dichloride is so much smaller than those of SO_3-dioxane, *etc.* that the total absorbances *versus* x is given by:

$$Abs_{240\,nm} = 6.63(a-x) - 1.37(b-x) + 2.72x$$

The reaction rate equation can be expressed as follows.

* Immediately after the 1-dodecene and SO_3-dioxane complex were mixed, measurement of the UV absorbance (at 240 nm) was started *versus* time.

** β-Sultone was stable to heat (no change in the NMR spectrum in 10 min at 65 °C) but was decomposed in a short time in the presence of a relatively weak base, for example, upon addition of a small amount of CD_3OD.

$$dx/dt = k_{n+m}(a-x)^n(b-x)^m$$

where

k_{n+m}: rate constant of the $(n+m)$th-order reaction
n,m: integer
a: initial concentration of the SO_3-dioxane complex
b: initial concentration of 1-dodecene
x: concentration of the reacted SO_3-dioxane (=that of the formed β-sultone)

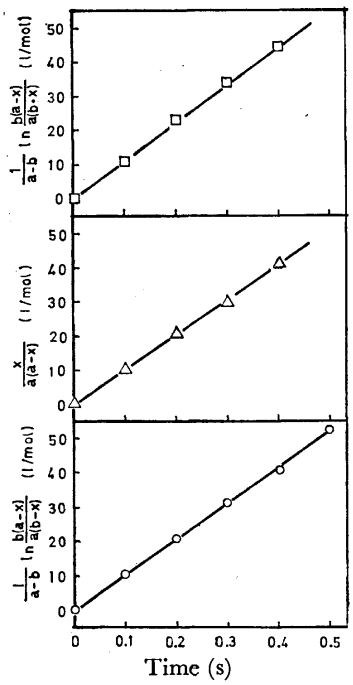

Fig. 1. The second-order type plots for different molar ratios of 1-dodecene to SO_3-dioxane at 25 °C.

An electrophilic addition reaction by SO_3 seems applicable in the first stage of this reaction; much as in the sulfonation of aromatic hydrocarbons.[7,8] The formation of sulfonic acid anhydride was not found here unlike the case of aromatic hydrocarbons; hence, the reaction is likely to become simpler thus, $m=1$. Besides, a straight line was obtained in the case of the second-order plot; $1/(a-b)\cdot\ln b(a-x)/a(b-x)$ *versus* time (Fig. 1). Therefore, in the molar ratios of 1-dodecene to the SO_3-dioxane complex from 1.05: 1 to 1: 1.5, the reaction is first-order with respect to both [α-olefin] and [SO_3] and second order as a whole. The second-order rate constant (k_2) was determined as follows from the figure.

$$k_2 = (1.1\pm0.1)\times10^2\ \mathrm{l\,mol^{-1}\,s^{-1}}\ (\text{at } 25°C)$$

This value is smaller by a factor of 10^3 than the rate constant of the sulfonation of an α-olefin in a thin-film reactor with gaseous SO_3.[9]

Stereochemical Studies. The kinetic studies showed that (1) the reaction between an α-olefin and SO_3 yields a β-sultone in the initial stage, and (2) the reaction is second-order and first order with respect to α-olefin and SO_3 respectively. Now, to see whether SO_3 undergoes a step-by-step addition to the α-olefin *via* a zwitter-ion or a concerted reaction, stereochemical studies of the reaction of SO_3 with *cis* and *trans* isomers of 2-butene and 2-pentene were undertaken.

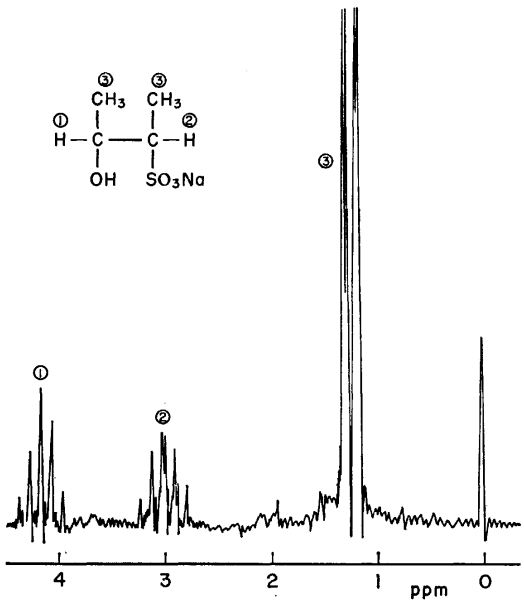

Fig. 2. The NMR spectrum of 3-hydroxybutane-2-sulfonate derived from *cis*-2-butene in D_2O at 25 °C, internal standard DSS.

The NMR spectra of the hydrolyzed products from *cis*- and *trans*-2-butene were exactly the same, as is shown in Fig. 2, demonstrating them to be 3-hydroxybutane-2-sulfonate. Found: S, 18.0 (*cis*); 18.3 (*trans*)%; Calcd for $C_4H_9O_4SNa$: 18.2%. Furthermore, from either *cis*- or *trans*-2-butene, we could isolate sodium 3-anilinobutane-2-sulfonate as white crystals (Table 1). Found: S, 12.7 (*cis*); 13.0 (*trans*)%; Calcd for $C_{10}H_{14}O_3SNa$: 12.7%. Therefore, the initial sulfonation products from both *cis*- and *trans*-2-butene must be the four-membered ring 2,3-sultone and not the six-membered ring 4,5-dimethyl-1, 3-dioxa-2,6-dithiacyclohexane-2,2,6,6-tetraoxide ("carbyl sulfate").[6,10]

Table 1. Chemical shifts (ppm) from the internal standard DSS and assignment of aniline derivatives of 2,3-sultones

Assignment		Chemical shift (ppm) *cis*	Chemical shift (ppm) *trans*
H-C-SO_3Na		3.20	3.20
H-C-NH-C_6H_5		4.16	3.88
CH_3		1.25	1.38
C_6H_5	*o*-, *p*-	6.86	6.86
	m-	7.30	7.30

It is noteworthy that the IR spectrum of the anilinobutane sulfonate obtained from *cis*-2-butene was superimposable upon that from the *trans* isomer, whereas the NMR spectra of these two samples exihibited different chemical shifts due to the H-C-NHC_6H_5 methine group, as is shown in Table 1. This difference will be discussed in some detail later in this paper.

We next studied the stereochemistry of the reaction products of *cis*- and *trans*-2-butene with the SO_3-dioxane complex by means of 220 MHz NMR analysis (Fig. 3). The NMR spectra of the products from the

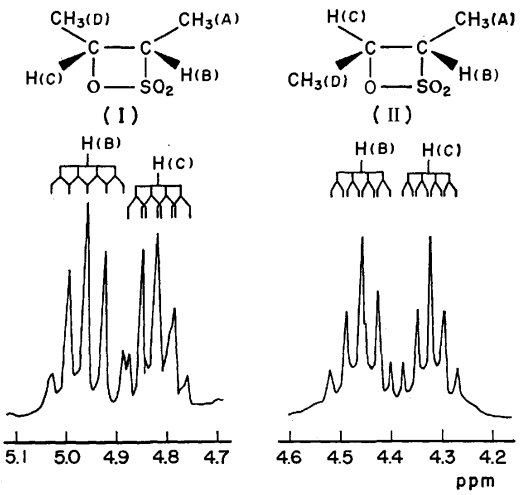

Fig. 3. The methine region of the 220 MHz NMR spectra of *cis*-butane sultone and *trans*-butane sultone derived from *cis*- and *trans*-2-butene in $CHCl_3$ at −5 °C, internal standard TMS.

isomeric olefins both showed an ABM system with a quartet at 1.5 ppm and a multiplet at 4.7—5.1 ppm for the *cis*, while it showed a quartet at 1.5 ppm and a multiplet at 4.2—4.6 ppm for the *trans*, and no other peak was found. It follows that the 2,3-sultones were produced stereospecifically from the corresponding 2-butene isomers.

Similarly, the sulfonation of *cis*- and *trans*-2-pentene with the SO_3–dioxane complex gave the corresponding 2,3-sultones.

Even in a non-complex system (an equimolar amount of SO_3 was added to *cis*- or *trans*-2-butene in chloroform at 0 °C), the stereospecific formation of *cis*- and *trans*-2,3-butanesultone was observed and a minor amount of products as yet unidentified was obtained.

The chemical shifts for two methines of the 2,3-sultone derived from *cis*-2-butene appeared at a lower field than those of the 2,3-sultone derived from *trans*-2-butene. It is almost certain that the former sultone has a *cis* configuration, while the latter has a *trans*, because, in the *cis*-sultone, the two methine hydrogen atoms are likely to be pushed toward the O–SO_2 side as a result of the repulsion by two methyl groups; as a result, the resonance signal would appear at a lower field, as was indeed observed.

The above-mentioned differences between the NMR spectra of the aniline adducts can be ascribed to the *threo* and *erythro* configuration. Aniline attacks the carbon atom bonded to oxygen by the S_N2 mechanism, and the *threo* configuration is formed from the *cis*-sultone, whereas the *erythro* is formed from the *trans*, as is shown in Scheme 1. An examination of the molecular models indicates that the sulfonate and anilino groups are so large that the rotation about the C–C axis bearing these groups is restricted. Also, the *gauche*-disposed NH-C_6H_5 and CH_3 groups undergo mutual repulsion to take such a conformation as (a') and (b') and no isomerization was observed. These findings also suggest that the 2,3-sultones were produced stereospecifically.

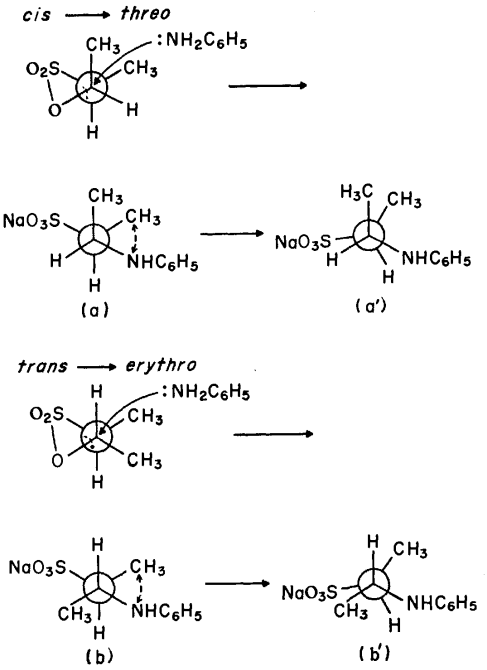

Scheme 1.

These results contain two possible mechanisms; one is that SO_3 forms a ring perfectly in a concerted reaction, while the other is that a zwitter-ion is once formed. However, the sultone ring is formed much faster than the rotation of C_1–C_2, which is minimized by the dipolar attractive force (Scheme 2). In this case, dioxane merely weakens the reactivity of SO_3; rather, it behaves as a polar solvent to make the zwitter-ion stable. Consequently, it seems more difficult to consider a zwitter-ion intermediate in the case of the non-complex system.

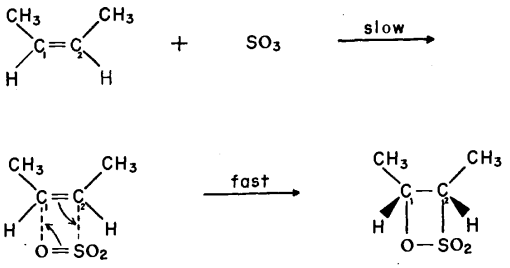

Scheme 2.

The authors wish to thank Dr. Morishima of Kyoto University for his cooperation in taking 220 MHz NMR spectra. Thanks are due to Professor Dr. Kumada of Kyoto University for his valuable advice throughout our experiment.

References

1) Preliminary communication; M. Nagayama, O. Okumura, S. Noda, and A. Mori, *Chem. Commun.*, **1973**, 841.

2) E. Gilbert, "Sulfonation and Related Reactions," Interscience Publishers, New York, N. Y. (1965), p. 31.

3) F. G. Bordwell and M. L. Peterson, *J. Amer. Chem. Soc.*, **81**, 2002 (1959).

4) I. L. Knunyants and G. A. Sokolski, *Angew. Chem. Internat. Edn.*, **11**, 583 (1972).
5) C. M. Suter, P. B. Evans, and J. M. Kiefer., *J. Amer. Chem. Soc.*, **60**, 538 (1938).
6) A. Mori, M. Nagayama, M. Aoki, and K. Yaguchi, *Kogyo Kagaku Zasshi*, **74**, 706 (1971).
7) D. R. Vicary and C. N. Hinshelwood, *J. Chem. Soc.*, **1939**, 1372.
8) H. Cerfontain, M. A. Telder, and L. Vollbracht, *Rec. Trav. Chim.*, **83**, 1103 (1964).
9) T. Miyauchi, T. Kikuchi, T. Ogoshi, R. Susuki, and H. Kataoka, *J. Chem. Eng. Jap.*, **4**, 44 (1971).
10) A. Mori, M. Nagayama, K. Yaguchi, and M. Aoki, *Kogyo Kagaku Zasshi.*, **74**, 710 (1971).

A Study of the Recoil Labeling of Fluothane with ^{82}Br during Neutron Irradiation

Hiroshi KUDO, Terutomi MOGI, and Kiyoshi HOIZUMI

Japan Atomic Energy Research Institute, Tokai-mura, Ibaraki-ken 319-11

(Received January 14, 1974)

1,1,1-Trifluoro-2-chloro-2-bromoethane labeled with ^{82}Br (fluothane-^{82}Br) was purely separated from neutron-irradiated fluothane by means of a gas-chromatographic technique. The maximum radiochemical yield of fluothane-^{82}Br was 38.3% when the target material was irradiated with neutrons to nvt of 3.4×10^{16} n·cm^{-2}. Of the many organic species produced by the recoil events following the radiative neutron capture and subsequent (I.T.) processes, $CF_3{}^{82}Br$ and $CF_3CHBr{}^{82}Br$ were also identified. In order to elucidate the mechanism of recoil labeling, the scavenger effects were examined in the $CF_3CHClBr$–Br_2 system, Br_2 being used as a radical scavenger. The "high-energy" yields of $CF_3CHCl{}^{82}Br$ thus estimated were approximately 3.6 to 4.8%. It was suggested that most of the ^{82}Br-labeled species were formed through the "thermal" processes including the reaction of ^{82}Br with the organic radicals produced by the radiolysis of the parent fluothane.

Fluothane (1,1,1-trifluoro-2-chloro-2-bromoethane) is a volatile anesthetic, and its metabolism has attracted much interest in biological research.[1] Fluothane labeled with radioisotopes has been used for the investigation of the behavior of anesthetics *in vivo*. Carbon-14 labeled fluothane has been synthesized starting with chloroacetic-1-^{14}C acid and used for the studies of metabolism.[2,3]

The aim of the present work is to investigate the feasibility of the recoil labeling of fluothane with ^{82}Br during neutron irradiation. The method is expected to be convenient for preparing labeled compounds with short-lived radioisotopes. Several factors leading to the preparation of fluothane-^{82}Br, determined by means of a gas chromatographic analysis, will be described in this article.

Fluothane is, on the other hand, an interesting substance in the fields of recoil and radiation chemistry, because C–H, C–F, C–Cl, C–Br, and C–C bonds coexist in a molecule. To compare the reactivity to a recoil atom among different kinds of chemical bonds may give important information for elucidating the mechanism of recoil labeling. The fundamental chemical behavior of ^{82}Br recoil atoms produced in neutron-irradiated fluothane will be discussed, with emphasis laid on the radiation and scavenger effects as well as on the reactivity of recoil atoms.

Experimental

1,1,1-Trifluoro-2-chloro-2-bromoethane (fluothane) from Takeda Chemical Industries, containing 0.01% of thymol, was purified at room temperature by means of a vacuum line with an approximate pressure of 10^{-3} mmHg. The vaporized portion of the material, the vapor pressure of which was 242 mmHg at 20 °C, was condensed in a cold trap. No impurity was observed in the gas chromatogram for the material thus trapped, although trace amounts of signals considered to be due to impurities[4] were observed in the mass spectrum even after the purification. The target material, 5 or 10 μl of liquid fluothane, or a mixture of it with bromine (0.5—70% Br_2 by molar ratio), was sealed in a 0.3—0.5 ml quartz ampoule *in vacuo* (0.9×10^{-3} mmHg) and then irradiated in the T-pipe of the JRR-4 reactor of the Japan Atomic Energy Research Institute, operated at 2.5 MW, at an ambient reactor temperature ~50 °C. The thermal neutron flux at the irradiation position was 2.8×10^{13} n·cm^{-2} s^{-1}, with an approximate γ-ray dose rate of 0.8×10^{8} rad·hr^{-1}. The neutron-irradiated samples were left in the cooling water of the reactor for more than 24 hr. A γ-ray irradiation facility with 45 kCi of ^{60}Co sources was utilized when the target materials were exposed to γ rays for the study of radiolysis. Ten microliters of liquid fluothane sealed in the same way as in the neutron irradiation were exposed to ^{60}Co γ-rays at room temperature (dose, 2.1×10^{21} and 1.0×10^{22} eV·g^{-1}).

The irradiated sample was directly introduced into a radio-gas chromatograph by means of a specially-designed ampoule breaker,[5] so that both the gaseous and the liquid substances were injected successfully into the column. Organic species labeled with ^{82}Br were separated by a gas-chromatographic set-up consisting of a thermal conductivity detector (TCD) and a glass column 2.5 m in length and with an inner diameter of 5 mm, packed with dioctyl phthalate (20% on chromosorb W, 60—80 mesh). Helium was used as the carrier gas at the flow rate of 120 ml·min^{-1}. The temperature at the TCD was 115 °C, while that of the glass column was kept at 60 °C. The latter was gradually raised to 110 °C after the signal of fluothane was observed.

The radioactivity of ^{82}Br of the gases leaving the TCD was detected using a single-channel pulse-height analyzer with a NaI(Tl) detector (well-type, 1.75″$\phi\times$2″). The radioactivity signals were registered both on a ratemeter, feeding a signal to a two-channel recorder, and on a digital printer. In the determination of the product yields, the radioactivities adsorbed both on potassium ferrocyanides (for inorganic products) and on activated carbons (for organic products), placed before and after the gas-chromatographic column, were measured.

In identifying the chromatographically-separated species, a gas chromatograph and mass spectrometer (GC-MS) from the Japan Electron Optics Laboratory, at Miyagi University of Education, was used. When the neutron-irradiated sample was analyzed by means of the GC-MS, the sample was stored in a vessel filled with ice for more than 3 months before analysis.

Results and Discussion

In neutron-irradiated fluothane, more than 20 organic products labeled with ^{82}Br, including fluothane-^{82}Br ($CF_3CHCl{}^{82}Br$), $CF_3{}^{82}Br$, and $CF_3CHBr{}^{82}Br$, were found. The gas chromatogram, of both the radioactivity and the mass signals, of fluothane irradiated

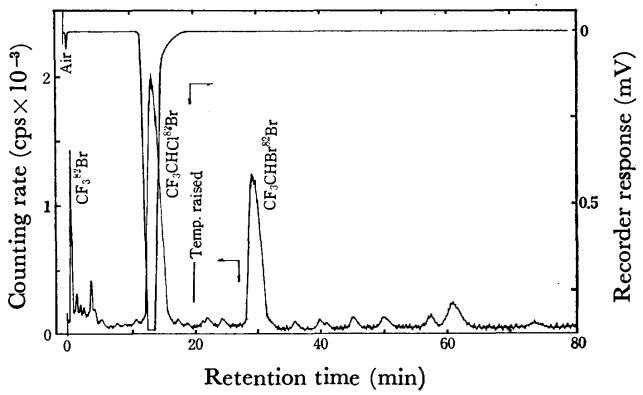

Fig. 1. Gas chromatograms of fluothane irradiated for 30 s in the JRR-4 reactor. The temperature of the gas chromatographic column was kept at 60 °C, although it was raised gradually up to 110 °C after the signal of $CF_3CHClBr$ was observed.

for 30 s in the JRR-4 reactor is illustrated in Fig. 1, where a 10 μl portion of the neutron-irradiated sample was subjected to analysis. Of the many radioactivity peaks, $CF_3CHCl^{82}Br$ showed the highest emergence. None of the mass peaks except for fluothane was found in the chromatogram, within the limits of detection.

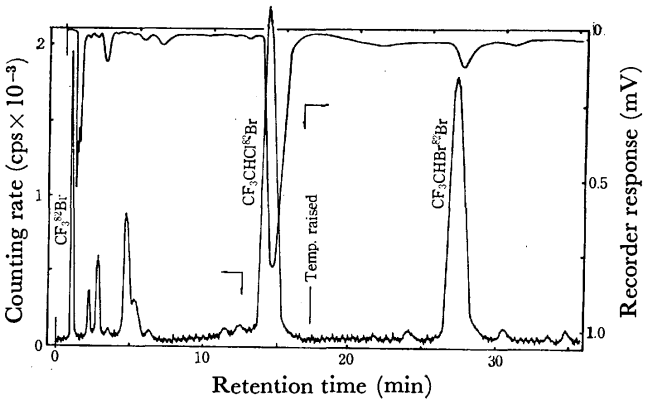

Fig. 2. Gas chromatograms of fluothane irradiated for 20 min in the JRR-4 reactor. The separation condition was identical with that of Fig. 1.

Figure 2 shows the gas chromatogram of fluothane irradiated with neutrons for 20 min. In this case, a 5 μl portion of the sample was subjected to analysis. The pattern of the radioactivity signal was identical with that in Fig. 1, while a few additional peaks were seen in the mass signal. Separation was performed by means of the gas chromatograph under the same conditions as in the previous case. Additional mass peaks were observed in the sample irradiated for more than 2 min, and the intensity increased with an increase in the irradiation time. The results suggest the occurrence of the radiolysis of the parent fluothane.

In order to examine the radiation effect, fluothane was exposed to ^{60}Co γ-rays at doses of 2.1×10^{21} and 1.0×10^{22} eV·g^{-1}. These γ-ray doses corresponded to the doses given the target material irradiated in the reactor for 25 min and 2 hr respectively. Various peaks of the radiolytic products from fluothane appeared in the gas chromatograms for both cases of

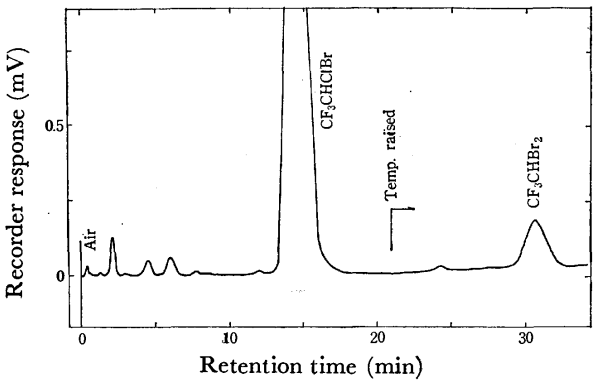

Fig. 3. Gas chromatogram of fluothane irradiated with ^{60}Co γ-rays to dose of 1.0×10^{22} eV/g. Only the liquid portion of the sample was subjected to the analysis.

γ-irradiation, although the intensities of all the peaks except for that of the parent fluothane were rather small in the former case. The pattern of the gas chromatogram for the latter case, illustrated in Fig. 3, was comparable enough with that of Fig. 2. The separation conditions of the gas chromatograph were identical with those of neutron-irradiated samples. It is noticeable that the radiolysis of fluothane is more sensitive to the irradiation in the reactor than to exposure to ^{60}Co γ-rays. This may be explained in terms of the internal radiation effect due to the recoil particles, such as ^{38}Cl, ^{80m}Br, ^{80}Br, ^{82m}Br, and ^{82}Br itself, produced in the neutron-irradiated sample. Details of the study of the radiolysis will be discussed elsewhere.[6]

The chemical distribution of ^{82}Br-labeled species resulting from the recoil processes in fluothane was investigated as a function of the irradiation time in the reactor. The radiochemical yields of the inorganic and organic products, including $CF_3CHCl^{82}Br$, are plotted against the irradiation time in Fig. 4. The overall organic yield increased abruptly around the irradiation time of 2 min and then reached a plateau at 95%, while the inorganic yield decreased from 32.6 to 5.5% in the same range of irradiation times. The yield of

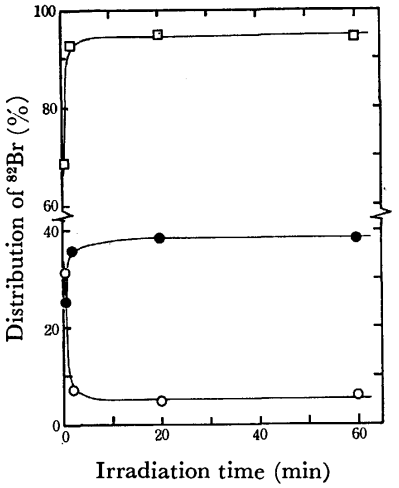

Fig. 4. Radioactivity yields of ^{82}Br-labeled products as a function of the irradiation time in the reactor. □, Overall organic products; ○, inorganic products; ●, $CF_3CHCl^{82}Br$.

$CF_3CHCl^{82}Br$ was about 26% for the target irradiated for less than 30 s; it increased to 38% at irradiation times above 2 min. Table 1 is a list of the detailed yields of the ^{82}Br-labeled products in neutron-irradiated fluothane. It is noteworthy that the yield of $CF_3CHBr^{82}Br$ was as high as 25% in the target irradiated for more than 2 min. The change in the chemical distribution of ^{82}Br-labeled species was investigated as a function of the elapsed time between 25 and 170 hr after the neutron-irradiation, but little change was observed when the irradiated samples were stored below room temperature. The results shown in Fig. 4 and Table 1 are the mean values of the experimental data, without any particular correction.

Table 1. Chemical distribution of ^{82}Br-labeled species in neutron-irradiated $CF_3CHClBr$ as a function of the irradiation time

Irradiation time	Fractional yield, %				
	Inorganic species	Organic species			
		$CF_3{}^{82}Br$	$CF_3CHCl{}^{82}Br$	$CF_3CHBr{}^{82}Br$	Others
10 s	32.6	1.1	27.4	17.9	21.0
30 s	31.4	1.2	25.6	18.5	23.3
2 min	7.3	1.1	35.8	26.6	29.2
20 min	5.0	2.3	38.3	24.7	29.7
1 h	6.2	2.9	37.9	25.5	27.5
5 h	5.2	2.8	19.9	25.6	46.5

Bromine-82 is produced by both the radiative neutron capture of Br and the isomeric transition (I.T.) of the resulting ^{82m}Br. By the time the ^{82m}Br nuclei with a half-life of 6.1 min have decayed, 90% of the surviving ^{82}Br (35.34 hr half-life[7]) will have come from the isomeric transition and 10% directly from the (n, γ) activation.[8] The primary recoil event of the ^{82}Br recoil atom is almost always followed by the Auger effect, since the 0.06 MeV transition of ^{82m}Br to its ground state has an internal conversion coefficient of 382.[8,9] Several studies have shown that, in the liquid phase, the organic yields from the converted isomeric transition process occurring in bromine nuclides are higher than the organic yields from the (n, γ) recoil processes.[10-13] The relatively high yield of $CF_3CHCl^{82}Br$ obtained in this experiment may be attributed to the contribution of the (I.T.) process. In this article, however, the problems involving the difference in the primary recoil events are not discussed in detail.

Two chemical processes are, on the whole, involved in the mechanism of recoil labeling: a high-energy (or "hot") process and a thermal process including radical reactions. In order to estimate the ratio of a high-energy process to the thermal processes, the scavenger effect was examined in connection with the chemical distribution of ^{82}Br-labeled products in neutron-irradiated fluothane, in which Br_2 was used as the radical scavenger. As is shown in Fig. 5, typical scavenger curves were obtained for the $CF_3CHClBr$–Br_2 system irradiated for 30 s in the reactor. By extrapolating the almost linear portion of the curves to the zero bromine concentration, 4.8±0.5% of $CF_3CHCl^{82}Br$ was estimated to be produced through the "high-energy" process. As is listed in Table 2, the "high-energy" yield of $CF_3CHCl^{82}Br$ estimated for the 20 min-irradiated target was 3.6±0.5%. A small difference in the "high-energy" yield was observed between the 30 s- and 20 min-irradiated targets. This difference was also found in the "high-energy" yields of $CF_3CHBr^{82}Br$: 4.0±0.5 and 2.4±0.5% for the targets irradiated for 30 s and 20 min respectively. If the "high-energy" yield estimated from the scavenger curve represents the yield due to a hot-atom reaction, it should be rather constant, independent of the irradiation time. The difference in the "high-energy" yield thus obtained may be correlated with the caging effect which is expected in the reaction of bromine atoms in the condensed phase. Because of this effect, the radical scavenger is considered to be inhibited in some portion from reacting with the thermalized ^{82}Br atoms. The decrease in the "high-energy" yield in a longer irradia-

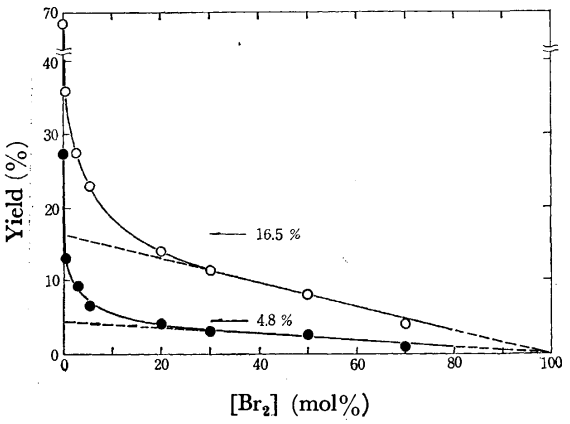

Fig. 5. Radioactivity yields of ^{82}Br-labeled product in the $CF_3CHClBr$–Br_2 system irradiated for 30 s in the JRR-4 reactor. ○, Overall organic products; ●, $CF_3CHCl^{82}Br$.

Table 2. Contribution of "thermal" and "high-energy" processes to the radiochemical yield of ^{82}Br-labeled species produced in neutron-irradiated $CF_3CHClBr$

Irradiation time	Radiochemical yield,[a] %					
	Overall organic		$CF_3CHCl^{82}Br$		$CF_3CHBr^{82}Br$	
	Y_t	Y_h	Y_t	Y_h	Y_t	Y_h
30 s	53.1±2.5	16.5±1.0	20.8±1.5	4.8±0.5	14.5±1.0	4.0±0.5
20 min	83.0±2.5	12.0±1.0	34.7±1.5	3.6±0.5	22.3±1.5	2.4±0.5

a) The Y_t and Y_h denote the "thermal" and "high-energy" yields, which were estimated from the scavenger curves obtained for the $CF_3CHClBr$–Br_2 system.

tion may be attributed to the contribution of the radiolytic organic radicals produced in the reaction zone.

At least, it can be pointed out that the high-energy yield of $CF_3CHCl^{82}Br$ is larger than that of $CF_3CHBr^{82}Br$. The high-energy yield of $CF_3{}^{82}Br$ is undoubtedly smaller than 1.1%, judging from the data listed in Table 1. Hardly any of the labeled product caused by ^{82}Br-for-F substitution was observed in this experiment. As a result, the order of the high-energy yields may be described as: $CF_3CHCl^{82}Br > CF_3CHBr^{82}Br > CF_3{}^{82}Br$ (>^{82}Br-for-F substituted species). This suggests that the high-energy reaction of ^{82}Br recoil atoms with $CF_3CHClBr$ has a close relation with the bond strength in the molecule, because the bond dissociation energies of the individual bond in $CF_3CHClBr$ should be in the order of: C–Br<C–Cl<C-C<C–H<C–F.[14]

The abrupt increase in the overall organic yield at the irradiation time of around 2 min may be explained in terms of the thermal reactions of ^{82}Br with organic radicals. When the target material was irradiated for less than 30 s, the bulk concentration of the radiolytic organic radicals should be quite low, judging from the fact that hardly any mass signals of organic species except for fluothane were observed in the gas chromatogram in Fig. 1. In this case, the thermalized ^{82}Br atom should give rise to an inorganic compound, probably forming $H^{82}Br$, $Cl^{82}Br$, or $Br^{82}Br$, although we have not yet identified them. On the other hand, in the case of the irradiation for more than 2 min, the concentration of the organic radicals produced by the radiolysis of the parent molecules might be sufficiently high in the vicinity of the ^{82}Br recoil atoms, so that the thermalized ^{82}Br atom could react with those radicals to form organic compounds *via* shorter diffusion paths. In fact, the increase in the thermal yield of the overall organic products between 30 s- and 20 min-irradiation, 29.9%, is comparable with decrease in the inorganic yield of 26.4%, within the limits of experimental error.

Through the present study of the chemical behavior of ^{82}Br recoil atoms produced in neutron-irradiated fluothane, several factors which determine the chemical distribution of the ^{82}Br-labeled species were elucidated. Recoil labeling was revealed to be a feasible method for the preparation of fluothane-^{82}Br; some technical information related to the practical preparation will be reported in a forthcoming journal.[5]

The authors wish to express their thanks to Professor Shinich Sasaki and Dr. Hidetsugu Abe of Miyagi University of Education for permitting the use of the gas chromatograph and mass spectrometer (GC-MS). The authors would also like to thank Dr. Hiroshi Amano and Mr. Takashi Moriya of the Japan Atomic Energy Research Institute for their useful suggestions and discussions.

References

1) E. R. Larsen, "Fluorine Chemistry Review," Vol. 3, ed. by P. Torrant, Marcel Dekker, New York, London (1967), p. 1.

2) R. A. Van Dyke, M. B. Chenoweth, and E. R. Larsen, *Nature*, **204**, 471 (1964).

3) R. A. Van Dyke and M. B. Chenoweth, *Biochem. Pharmacol.*, **14**, 603 (1965).

4) E. N. Cohen, J. W. Belleville, H. Budzikiewicz, and D. H. Williams, *Science*, **141**, 899 (1963). In the literature, fluothane is reported to contain C_4-compounds, *e.g.*, 1,1,1,-4,4,4-hexafluoro-2,3-dichlorobutene, as an impurity.

5) K. Hoizumi, T. Mogi, and H. Kudo, *J. Labelled Compounds*, in press.

6) K. Hoizumi, T. Moriya, T. Mogi, H. Kudo, H. Abe, and S. Sasaki, to be published.

7) C. M. Lederer, J. M. Hollander, and I. Perlman, "Table of Isotopes," 6th ed., John Wiley, New York (1968).

8) J. F. Emery, *J. Inorg. Nucl. Chem.*, **27**, 903 (1965).

9) O. U. Anders, *Phys. Rev. B*, **138**, 1 (1965).

10) E. G. Bohlman and J. E. Willard, *J. Amer. Chem. Soc.*, **64**, 1342 (1942).

11) J. A. Merrigan, J. B. Nicholas, and E. P. Rack, *Radiochim. Acta*, **6**, 94 (1966).

12) J. A. Merrigan, W. K. Ellgren, and E. P. Rack, *J. Chem. Phys.*, **44**, 174 (1966).

13) D. R. Urch, "MTP International Review of Science, Inorganic Chemistry Series One," Vol. 8, ed. by A. G. Maddock, Butterworth, London (1972), p. 149.

14) J. A. Kerr, *Chem. Rev.*, **66**, 465 (1966) and R. T. Sanderson, "Chemical Bonds and Bond Energy," Academic Press, New York (1971). Although the particular bond dissociation energies for the individual chemical bond in the CF_3-CHClBr molecule have not been reported in the literstures, it is not grossly in error to consider that the bond strength is in the order of C–Br<C-Cl<C-C<C–H<C–F.

A Shock-tube Investigation of Ignition in Ethylene-Oxygen-Argon Mixtures

Yoshiaki HIDAKA, Tsuyoshi KATAOKA, and Masao SUGA

Department of Chemistry, Faculty of Science, Ehime University, Bunkyo-cho, Matsuyama 790

(Received January 21, 1974)

The ignition of ethylene-oxygen mixtures highly diluted with argon was studied in a shock tube by monitoring the emission from CH* and C_2* or OH*. The measurements covered the temperature range of 1400—2100 K at the C_2H_4/O_2 ratios of 0.33—1.00. From the observation of the CH*, C_2*, and OH* emissions, a mechanism for the production of chemiluminescent species upon ethylene oxidation was briefly discussed, and from the observation of the induction period of the CH* emission, the following equation was found:

$$\log \tau_{CH}[O_2] = -11.45 + 27.5 \times 10^3/4.58T$$

in units of s mol l^{-1}, the rate-determining step being $C_2H_3+O_2 \rightarrow C_2H_3O+O$.

About fifteen years ago, one of the present authors studied the oxidation of ethylene in the temperature range from 700 to 1000 K by the "admission method" and found an apparent activation energy of about 30 kcal/mol.[1]

Since that time, the shock tube has been adopted as a very important tool for studying ignition processes and the shock-tube oxidation of ethylene has been studied by several investigators, for it allows gases to be heated rapidly and homogeneously so that wall effects and diffusion may be neglected. White[2] has reported that the induction period of the oxidation depends on both the ethylene and oxygen concentrations at small ratios (0.0025—0.01) of ethylene to oxygen in the temperature range from 1100 to 2200 K, using the interferometrical method. In this case, the total order was about one and the estimated activation energy was 17.3 kcal/mol. Gay *et al.*[3] have also observed the induction period at higher ratios (0.1—1.5) of C_2H_4/O_2 in the temperature range from 1500 to 2300 K; they found 24 kcal/mol to be the apparent activation energy. On the other hand, by monitoring both the infrared emission from CO and CO_2 and the CH* visible emission, Homer and Kistiakowsky[4] have obtained the activation energy of 17.1 kcal/mol at C_2H_4/O_2 ratios of 0.17—0.5 in the temperature range from 1500 to 2300 K.

In the present paper, we wish to report the results of simultaneous observations of CH* and C_2* or OH* emissions and wish to interpret the observed emission profiles. Another purpose of this paper is to determine the apparent activation energy of ethylene oxidation by means of measurements with the induction period of the CH* emission in a shock tube.

Experimental

Apparatus and Procedure. The shock tube used in these experiments was composed of a stainless steel tube 4.3 cm in inner diameter. The tube was divided into two sections, that is, the driver section, B (129 cm in length), and the test section, A (250 cm in length), separated by a diaphragm, D_i of polycarbonate or polyester film 25—70 μ thick punctured by a spring-located needle, N. The outline of the apparatus is shown in Fig. 1.

The velocity of the shock waves was measured by using two barium titanate gauges, G_2 and G_3. The G_1 gauge,

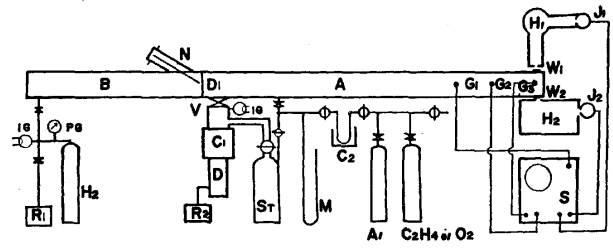

Fig. 1. Schematic diagram of apparatus.

located at a distance of 210 cm from the diaphragm, D_i, was used for starting the sweep of the synchroscope, S. Both distances, G_1—G_2 and G_2—G_3, were 15 cm. The incident shock speeds were recorded in order to evaluate the reflected shock temperatures.

The quartz windows, W_1 and W_2, located 1 cm from the reflecting plate, could be used to monitor the CH* emission and the C_2* or OH* emission simultaneously during the reaction. At one window, W_1, the measurement of the CH* emission was made using a Hilger prism monochromator, H_1 (with a half-width of 20 Å) equipped with a Hamamatsu R-300 photomultiplier, J_1. At the other window, W_2, the measurement of the OH* or C_2* emission was made using a Rico-MC-20 grating monochromator, H_2 (with a half-width of 25 Å), equipped with a Hamamatsu R-300 photomultiplier, J_2.

The out-put voltages from the gauges (G_2 and G_3) and the photomultipliers (J_1 and J_2) were recorded simultaneously on an Iwatsu DS-5158 A dual-beam synchroscope, S. The time response was better than 1 μs.

The driver section, B, was evacuated until the pressure was about 10^{-3} Torr by means of a rotary pump, R_1, before admitting the driver gas. On the other hand, the test section, A, and the gas sampling system could be evacuated until 1×10^{-5} Torr by the pumping system which included a 2 inch oil-diffusion pump, D, with a liquid nitrogen trap, C_1; the evacuation was checked by means of a cold cathode ionization gauge, IG. The test section, A, of the shock tube was always checked to a pressure of 1×10^{-4} Torr before filling it with a reaction mixture, and the shock was fired within 2 min after isolation from the pumping system, because it has a residual leak at the rate of 2×10^{-4} Torr per minute.

The inner wall of the test section, A, and especially the inner surfaces of the windows (W_1 and W_2) were cleaned after each run with a dry cloth in order to remove any unvolatile products. Also, the reaction mixtures were prepared manometorically and stored in a stainless steel storage vessel, ST (volume, *ca.* 30 l). The line and storage were flushed with argon before the preparation of the mixtures.

The other accessories of this apparatus and the method of operation were similar to those reported in an earlier publication.[5]

Materials. The ethylene, oxygen, and argon used were obtained from commercial cylinders; the purities were 99.99%, 99.9%, and 99.99% respectively. The driver gas was 99.9% pure-grade hydrogen. All the gases were used without further purification except for passing them through a dry ice trap, C_2.

Samples. The compositions of the reaction mixtures were (1% C_2H_4, 1% O_2, 98% Ar), (1% C_2H_4, 2% O_2, 97% Ar), and (1% C_2H_4, 3% O_2, 96% Ar), and the initial pressures of the reaction mixtures used were about 50 Torr and 100 Torr. Each shock-run was denoted a or b for the initial pressures of 50 Torr and 100 Torr, and 1, 2, and 3 for the oxygen concentrations of 1%, 2%, and 3% respectively. For example, 3a corresponds to the initial pressure of 50 Torr and the oxygen concentration of 3%.

Results and Discussion

The reflected shock temperatures were calculated from the measured incident shock velocities, using the three conservation equations and the ideal equation of a state assuming a thermal equilibrium.

Interpretation of Observed Emission Profiles. In the present experiments, we observed the C_2* emission at 5165 Å, the CH* emission at 4515 Å, and the OH* emission at 3067 Å. The CH* emission intensity observed using a Rico-MC-20 grating monochromator was about 1.4 times that observed using a Hilger prism monochromator at 4315 Å. In addition, the Hamamatsu R-300 photomultiplier has a different response of intensity according to the wavelength, that is, it is 100 at 3067 Å, 85 at 4315 Å, and 52 at 5165 Å. These values were applied in order to correct the emission intensities which were directly obtained from the observed emission profiles, as is shown in Fig. 2.

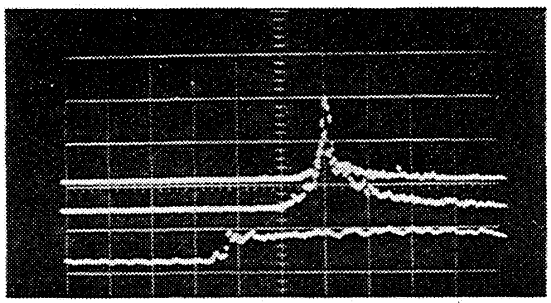

Fig. 2. Comparison of time history of CH* emission using the prism monochromator and OH* emission using the grating monochromator,
T_5=1506 K, P_5=1495 Torr, sweep=50 μs/div..
Upper trace: OH* emission at 3067 Å using grating monochromator, gain=0.05 V/div.
Middle trace: CH* emission at 4315 Å using the prism monochromator, gain=0.1 V/div.
Lower trace: G_3 signal.

The following characteristics were obtained from the emission profiles of each run:

1. The maximum emission intensity of OH* was considerably smaller than those of CH* and C_2*, showing a ratio of emission intensity of about 10 (CH*): 10 (C_2*): 1 (OH*); it was not distinguishable from noises, especially in the range of lean oxygen.

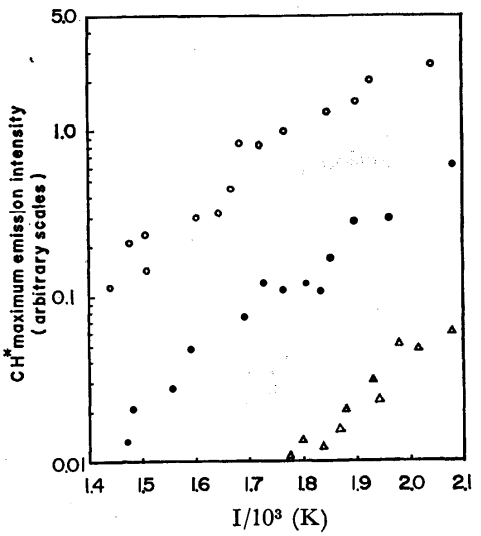

Fig. 3. Comparison of CH* maximum emission intensity of series a at various temperatures.

2. The maximum intensity of the CH* emission decreased extremely at both a lowering of the temperature and a decrease in the O_2 concentration, as is shown in Fig. 3; the OH* emission showed similar behavior.

3. The maximum intensity of the C_2* emission shows no clear dependence on the O_2 concentration, unlike the CH* and OH* emissions.

4. The onset of emission was qualitatively observed to be in the order of: CH*, C_2*, and OH*.

Several reaction mechanisms have been proposed by Gaydon[6] and Hand and Kistiakowsky[7] for the formation of CH* in hydrocarbon flames, *e.g.*;

$$C_2 + OH \longrightarrow CH^* + CO \quad (1\text{-}1)$$
$$C_2H + O_2 \longrightarrow CH^* + CO_2 \quad (1\text{-}2)$$
$$C_2H + O \longrightarrow CH^* + CO \quad (1\text{-}2')$$

The present experimental results indicate that the CH* emission arises mainly from Reactions (1-2) and (1-2′) rather than from (1-1), because of the great dependence of the O_2 concentration on the CH* emission; the onset of emission was observed in the order of: CH*, C_2*, and OH*.

Secondly, as to the production of C_2* in hydrocarbon flames, several reactions have been considered by Ferguson,[8] Miller and Palmer,[9] and Gaydon and Wolfhord,[10] *e.g.*;

$$CH + CH \longrightarrow C_2^* + H_2 \quad (1\text{-}3)$$
$$C + CH \longrightarrow C_2^* + H \quad (1\text{-}4)$$
$$CH_2 + C \longrightarrow C_2^* + H_2 \quad (1\text{-}5)$$
$$C_2O + C \longrightarrow C_2^* + CO \quad (1\text{-}6)$$

As CH_2 and C_2O may not be produced during C_2H_4 oxidation, the C_2* emission may arise from (1-3) and (1-4).

The production of OH* in hydrocarbon flames has been explained by this reaction:

$$CH + O_2 \longrightarrow CO + OH^* \quad (1\text{-}7)$$

for which evidence has been reported.[6,11]

The intensity of OH* emission was greatly dependent on the O_2 concentration, just like the CH* emission, and the intensity of the OH* emission was weak as compared with the intensities of CH* and C_2*. This implied that OH* emission may arise from Reaction (1-7); thus, Reaction (1-3) or (1-4) and Reaction (1-7) should be competitive reactions which consume the ground-state CH, while Reaction (1-2) or (1-2′) and Reaction (1-7) are also competitive reactions which consume oxygen.

It seemed that it would be very interesting to know exactly the process of the onset of emission in order to discuss the reaction mechanism. The order of the onset of emission was, qualitatively, the CH*, C_2*, and OH* emissions, as has been described above. However, we cannot discuss the reaction mechanism in detail on the basis of the CH*, C_2*, and OH* order of emission onset because of the complexity of the phenomena of the CH*, C_2*, and OH* emissions.

Induction Period. Table 1 summarizes the experimental conditions of the four groups of runs and the results of the measurement of the induction period, τ_{CH}, which is defined as the time lag between the reflected shock arrival and the onset of the CH*-emission signal. Figure 4 shows the plot of log τ_{CH} *versus* 1/T for three experimental groups, 3a, 2a, and 1a. It can readily be seen that the values of log τ_{CH} in Groups 3a, 2a, and 1a fall on a single linear line, indicating the effect of oxygen on the induction period. Figure 5 shows the plotting of log $\tau_{CH}[O_2]$ *versus* 1/T for four groups of experiments, 3a, 2a, and 1a, and 1b; all the points fit a single line. The temperature coefficient of the induction period can be obtained from the slope of the line drawn in Fig. 5. Consequently, over the temperature and concentration ranges covered by the present experiments, the induction period for the

TABLE 1. EXPERIMENTAL CONDITIONS AND INDUCTION PERIODS

Series	Shock No.	T_5 K	P_1 Torr	P_5 Torr	τ_{CH}* μs	Series	Shock No.	T_5 K	P_1 Torr	P_5 Torr	τ_{CH}* μs
3a	3001	1443	50.1	1386	93	2a	2020	1898	50.0	2074	19
	3004	1677	50.6	1760	30		2022	1960	50.8	2206	15
	3005	1600	50.4	1633	35		2024	1469	49.9	1411	152
	3006	1645	49.8	1684	30		2025	1588	50.8	1618	74
	3007	1633	50.3	1682	36		2027	1937	50.0	2135	15
	3008	1508	50.2	1486	68		2028	1924	50.4	2237	14
	3009	1506	50.6	1495	63		2030	1726	50.1	1809	35
	3010	1474	50.7	1450	79		2031	1799	50.6	1941	27
	3013	1508	50.3	1489	80		2033	1480	50.3	1440	150
	3014	1811	49.7	1938	14		2035	2081	50.2	2372	8
	3016	1664	51.0	1752	26		2036	1555	50.3	1553	77
	3018	1582	50.1	1596	49		2038	1847	50.3	2005	16
	3019	1597	47.0	1518	41						
	3020	1459	50.2	1412	108	1a	1001	1774	50.0	1841	53
	3021	1575	50.1	1561	45		1002	1786	50.0	1890	44
	3022	1534	50.9	1547	68		1004	1981	50.4	2213	22
	3024	1422	49.8	1347	108		1006	1786	50.2	1894	42
	3027	1720	50.9	1839	19		1007	1868	50.5	2039	32
	3029	1735	50.1	1834	24		1008	1860	50.8	2038	28
	3030	2042	51.3	2374	6		1010	1809	51.1	1957	38
	3031	1844	50.1	2005	10		1011	1929	50.7	2144	21
	3032	1924	49.8	2118	8		1013	1779	51.1	1921	44
	3034	1766	50.2	1886	15		1014	1769	51.1	1904	41
	3035	1806	50.2	1947	16		1015	1880	50.0	2038	25
	3036	1675	50.1	1739	22		1016	2007	50.2	2245	16
	3038	1841	50.5	2016	12		1018	1939	51.8	2207	18
	3039	1716	51.1	1840	22		1020	2009	50.3	2254	18
	3040	1897	50.8	2120	10		1021	1837	50.2	1979	36
							1022	2077	49.1	2304	13
2a	2002	1830	51.3	2018	20		1023	1804	50.6	1941	42
	2003	1733	49.8	1809	27						
	2005	1729	50.0	1811	28	1b	1125	1716	100.0	3566	34
	2006	1852	50.0	2001	15		1126	1629	101.3	3344	49
	2007	1765	49.8	1858	31		1127	1751	100.6	3693	28
	2009	1693	50.5	1771	40		1129	1846	93.8	3721	18
	2011	1804	49.6	1970	25		1130	1679	101.6	3507	50
	2012	1756	50.0	1851	37		1131	1596	100.0	3202	55
	2015	1797	51.6	1975	22		1133	1694	101.2	3538	44
	2016	1723	50.1	1803	36		1134	1797	99.6	3803	23
	2017	1827	49.6	1945	23		1135	1634	101.1	3350	62

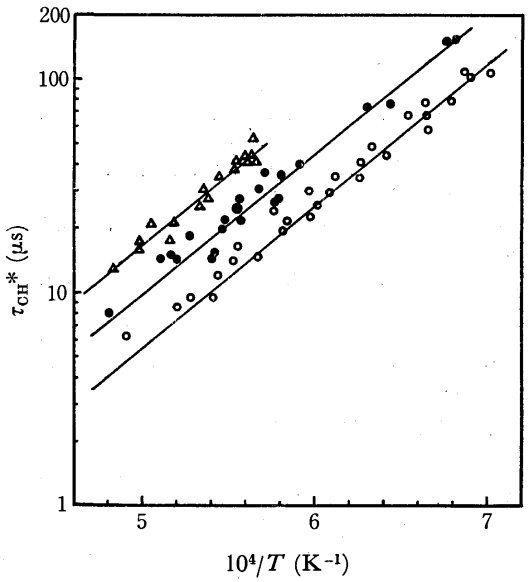

Fig. 4. A plot of log τ_{CH}* *versus* $1/T$ for three reaction mixtures at initial pressure of about 50 Torr.
○: 3% O_2+1% C_2H_4, ●: 2% O_2+1% C_2H_4,
△: 1% O_2+1% C_2H_4.

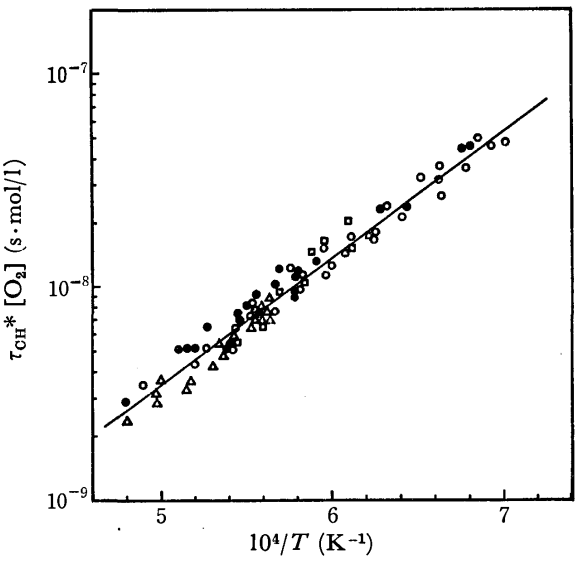

Fig. 5. A plot of log τ_{CH}*[O_2] *versus* $1/T$ for three reaction mixtures.
Initial pressure of about 50 Torr,
○: 3% O_2+1% C_2H_4, ●: 2% O_2+1% C_2H_4,
△: 1% O_2+1% C_2H_4.
Initial pressure of about 100 Torr,
□: 1% O_2+1% C_2H_4.

CH* emission can be represented as:

$$\log \tau_{CH}[O_2] = -11.45 + 27.5 \times 10^3/4.58T$$

in units of s mol l^{-1}.

White,[2] examining very lean mixtures (fuel/oxygen—0.1), observed that the induction periods before any detectable heat release from the C_2H_4–O_2 and C_2H_2–O_2 reactions were similar to each other in the temperature range from 1100 to 2200 K and led to an essentially common activation energy of 17.3 kcal/mol. Gay *et al.*,[3] using C_2H_4/O_2 ratios of 0.1—1.5, reported that the induction period and the intensity of chemiluminescence from CH* were similar in magnitude to those found in the C_2H_2–O_2 reaction, especially at the higher temperatures of 1800—2100 K. At lower temperatures, towards 1500 K, the induction periods were significantly greater than in the case of C_2H_2; the results gave an activation energy 24 kcal/mol larger than the 17 kcal/mol found for C_2H_2–O_2. They detected quite large concentrations of acetylene during the course of the C_2H_4–O_2 reaction and proposed the following tentative schemes:

	ΔH (kcal/mol)	
$C_2H_3 + O_2 \longrightarrow C_2H_3O + O$	+27	(2-1)
$O + C_2H_4 \longrightarrow C_2H_3 + OH$	+3	(2-2)
$OH + C_2H_4 \longrightarrow C_2H_3 + H_2O$	−14	(2-3)
$C_2H_3 + O_2 \longrightarrow 2CO + H_2 + H$	−67	(2-4)
$C_2H_3 + O_2 \longrightarrow C_2H_2 + HO_2$	+5	(2-5)
$C_2H_3O + M \longrightarrow C_2H_2 + OH + M$	+30	(2-6)
$C_2H_3O + O_2 \longrightarrow 2CO + H_2O + H$	−100	(2-7)
$C_2H_3 + M \longrightarrow C_2H_2 + H + M$	+41	(2-8)
$H + C_2H_4 \longrightarrow C_2H_3 + H_2$	+1	(2-9)

To satisfy the higher activation energy, they suggested that the rate-determining step was (2-1), the endothermicity being 27 kcal/mol.

On the other hand, Homer and Kistiakowsky[4] reported an activation energy of 17 kcal/mol and the rate-determining step of:

$$H + O_2 \longrightarrow OH + O \qquad (2\text{-}10)$$

at lower ratios of C_2H_4/O_2. They then proposed that the C_2H_4–O_2 reaction, in its early stages, consists mainly of the pyrolysis to the C_2H_2 and H_2 above 1800 K. They have also suggested the existence of some value larger than 24 kcal/mol controlling the ethylene-oxidation mechanism involving such intermediates as have been postulated by Gay *et al.*

The measurement of the induction period in the shock tube has been undertaken in the hope that it would offer a convenient method elucidating an activation energy and would be able to suggest a rate-determining step. The value of the apparent activation energy obtained from the present experiment is 27.5 kcal/mol at 1400—2100 K, the value of Gay *et al.* is 24 kcal/mol at 1500—2300 K, and our previous work[1] has shown the value of 30 kcal/mol in the range of 700—1000 K in spite of the difference in method. The variation in the apparent activation energy with the temperature has also been considered.[12] Since a rate-determining step in an elementary reaction will vary with the temperature and the composition, the difference in these values can be understood. As has been mentioned above, White and Homer *et al.* have reported an activation energy of about 17 kcal/mol at lower ratios of C_2H_4/O_2, and Gay *et al.* have reported an activation energy of 24 kcal/mol at higher ratios of C_2H_4/O_2. The value of activation obtained from the present experiment at higher ratios of C_2H_4/O_2 is 27.5 kcal/mol. Hence, it seems that, in the C_2H_4 oxidation, Reaction (2-10) is predominant at lower ratios of C_2H_4/O_2 and

Reaction (2-1) is predominant at higher ratios of C_2H_4/O_2. Considering the schemes proposed by Gay *et al.*, it may be supposed that the reaction:

$$C_2H_3 + O_2 \longrightarrow C_2H_3O + O \qquad (2\text{-}1)$$

is the rate-determining step for ethylene oxidation under our experimental conditions. Since Reaction (2-1) is endothermic, the activation energy of Reaction (2-1) should be larger than its endothermicity (27 kcal/mol).[13] The apparent activation energy obtained, 27.5 kcal/mol, satisfies the above relation. Therefore, the apparent activation energy, 27.5 kcal/mol, obtained from our measurements seems reasonable.

The authors would like to thank Professor H. Yamamura of Hiroshima University for his interest and helpful discussions, and be also grateful to Mr. H. Fujimoto and Mr. S. Doi for the assistance of observations done partly in the present experiment.

References

1) M. Suga, This Bulletin, **31**, 515 (1958).
2) D. R. White, "Symp. Combust. 11th," The Combustion Institute, Pittsburgh (1967), P. 147.
3) I. D. Gay, G. P. Glass, R. D. Kern, and G. B. Kistiakowsky, *J. Chem. Phys.*, **47**, 313 (1967).
4) J. B. Homer and G. B. Kistiakowsky, *J. Chem. Phys.*, **47**, 5290 (1967).
5) Y. Hidaka, K. Saito, and H. Yamamura, *J. Sci. Hiroshima Univ., Ser., A-II*, **32**, 291 (1968).
6) A. G. Gaydon, "The Spectroscopy of Flames," Willey (1957), p. 160.
7) C. W. Hand and G. B. Kistiakowsky, *J. Chem. Phys.*, **37**, 1239 (1962).
8) R. E. Ferguson, *J. Chem. Phys.*, **23**, 2085 (1955).
9) W. J. Miller and H. B. Palmer, "Symp. Combust. 9th," Academic Press (1963), p. 90.
10) A. G. Gaydon and G. H. Wolfhord, *Proc. Roy. Soc. Ser. A*, **213**, 366 (1952).
11) R. P. Porter, A. H. Clarke, W. E. Kaskan, and W. G. Browne, "Symp. Combust. 11th," The Combustion Institute, Pittsburgh (1967), p. 907.
12) C. N. Hinshellwood, "The Kinetics of Chemical Change," The Clarendon Press, Oxford (1955), p. 55.
13) N. N. Semenov, "Some Problems of Chemical Kinetics and Reactivity," Vol. 1, Pergamon, New York, (1959).

The Temperature Dependence of the *G*-Values of Nitrogen from the Gas-phase γ-Radiolysis of C_3-Hydrocarbons in the Presence of Nitrous Oxide

Kiyoshi OKAZAKI, Rei YUGETA, Ken-ichi KOWARI, and Shin SATO

Department of Applied Physics, Tokyo Institute of Technology, Ookayama, Meguro-ku, Tokyo 152

(Received March 6, 1974)

The *G*-values of nitrogen from the gas-phase γ-radiolysis of the C_3-hydrocarbons (propane, propylene, and cyclopropane) in the presence of nitrous oxide have been measured at the temperatures from −35 to 150 °C. The *G*-values increased with an increase in the pressure of N_2O and were saturated at about 4 mol% of N_2O. The saturated values, $G(N_2)_{max}$'s showed characteristic temperature dependences. In propane, they scarcely changed with the temperature and stayed at around 2 G_e. Here G_e is the *G*-value of electrons estimated from the *W*-value of the hydrocarbon. In propylene, the $G(N_2)_{max}$ changed from G_e at −35 °C to about 2 G_e at 150 °C, while in cyclopropane it changed from G_e at −35 °C to 4.5 G_e at 100 °C. Possible reaction mechanisms to explain these results have been discussed.

Nitrous oxide is a well-known electron scavenger.[1,2] When a hydrocarbon is γ-irradiated in the presence of a small amount of nitrous oxide, nitrogen is one of the main products and its formation can be explained by the mechanism initiated by the electron capture of nitrous oxide. The quantitative measurement, however, shows that the *G*-value of nitrogen is always larger than the *G*-value of scavenged electrons. This fact is now one of the most persistent problems in the study of hydrocarbon-radiolysis.[3-7]

In a previous paper,[7] we showed that the *G*-value of nitrogen from the N_2O-1-butene system is strongly dependent upon the temperature as well as on the total dose and the dose rate, and that these effects make the problem more complex. The present paper will report the results obtained with the C_3-hydrocarbons (propane, propylene, and cyclopropane), with which we can make experiments at lower temperatures at the same pressures.

Experimental

The experimental procedure was the same as that reported previously.[7] The temperature of −35 °C was obtained by mixing ice and $CaCl_2$ in a Dewar flask. The temperature lasted (within ±5 °C) long enough for the γ-irradiation, usually three hours.

Results

Figure 1 shows the temperature dependence of the $G(N_2)$'s from the three C_3-hydrocarbons-N_2O systems. Figure 2 shows the $G(H_2)$'s obtained simultaneously with the $G(N_2)$'s. The pressure of hydrocarbons is always around 600 Torr, and the dose rate is 1.3×10^{13} eV ml^{-1} s^{-1}. In order to elucidate the reaction mechanisms, the effects of several additives were also studied. The results are summarized in Table 1.

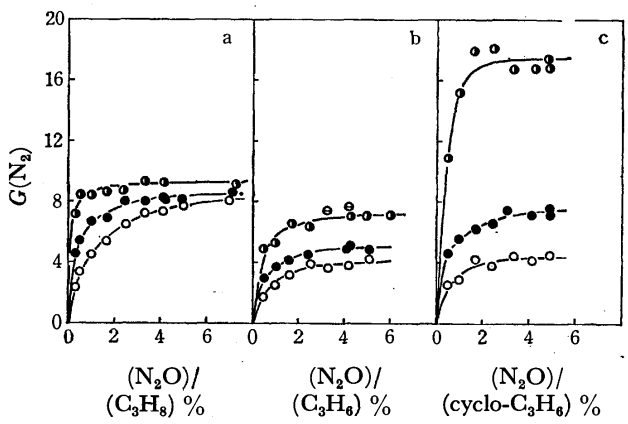

Fig. 1. The temperature dependence of the $G(N_2)$'s from C_3-hydrocarbons in the presence of nitrous oxide. a: propane, b: propylene, c: cyclopropane; ○: −35 °C, ●: 0 °C, ◑: 100 °C, ⊖: 150 °C.

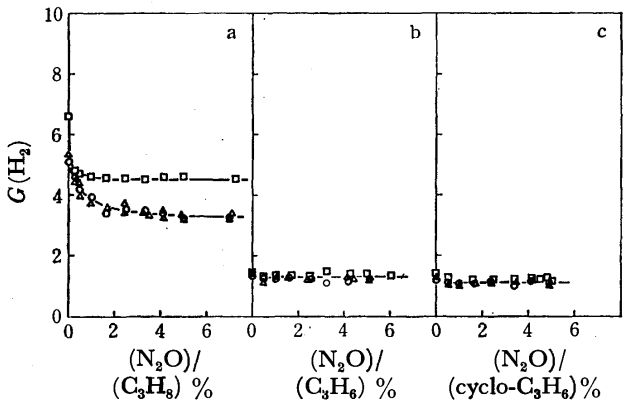

Fig. 2. The temperature dependence of the $G(H_2)$'s from C_3-hydrocarbons in the presence of nitrous oxide. a: propane, b: propylene, c: cyclopropane; ○: −35 °C, △: 0 °C, □: 100 °C.

Table 1. The effects of the additives on the $G(N_2)$'s from the 4 mol% N_2O-C_3 hydrocarbon systems at 0 °C

	$G(N_2)$				
	N_2O only	SF_6 0.03 mol %	CO_2 4 mol %	NH_3 4 mol %	CH_3OH 4 mol %
Propane	8.2	0.2	4.4	4.4	20.6
Propylene	5.0	0.3	3 8	4.4	11.1
Cyclopropane	5.9	0.2	3.8	4.4	27.1

Discussion

The electrons generated by γ-rays in a high-pressure hydrocarbon will be thermalized very quickly. According to the measurement of Warman and Sauer[8] using a microwave technique, 0.2 Torr of *n*-hexane is high enough to thermalize electrons in a few microseconds. In the present experiment, all the samples contain 600 Torr of C_3-hydrocarbons. The precursor of the nitrogen measured above must be thermalized electrons.[9]

Warman and Fessenden suggested that the electron capture by N_2O occurs through the third-body reaction:[10]

$$e^- + N_2O + M \longrightarrow N_2O^- + M \qquad (1)$$

However, the formation of N_2O^- ions is doubted by many researchers. One of the reasons is that N_2O^- ions have not been observed in the mass-spectrometric study at low pressures of N_2O.[11] The reaction might be:

$$e^- + N_2O \xrightarrow{(+M)} N_2 + O^- \qquad (2)$$

The present experiment cannot specify the reaction.

In a previous paper,[7] we proposed this reaction:

$$N_2O^- + SF_6 \longrightarrow N_2O + SF_6^- \qquad (3)$$

to explain the fact that a very small amount of SF_6 can inhibit the formation of nitrogen from the N_2O-hydrocarbon systems. However, according to the recent paper of Bansal and Fessenden,[12] the electron capture of SF_6 is extremely fast (2×10^{-7} cm^3 mol^{-1} s^{-1}). If this is true, the inhibition effect can be explained simply by the competition of N_2O and SF_6 for thermalized electrons.

In the following discussion, we will assume that N_2O^- ions, even if produced, react much as do O^- ions. When O^- (or N_2O^-) ions are produced in propane, the following reaction will occur very readily:

$$O^- + C_3H_8 \longrightarrow OH^- + C_3H_7 \qquad (4)$$

The rate of Reaction (4) has been reported to be 9.3×10^{-10} cm^3 mol^{-1} s^{-1}.[13] Since the OH^- ions thus formed are stable ions as far as they are not neutralized (the neutralization time at the dose rate used here is estimated to be 10^{-3} s), the following addition reaction may occur:

$$OH^- + N_2O \longrightarrow OHN_2O^- \qquad (5)$$

This reaction has been proposed by Parkes[14] on the basis of the mass-spectrometric observation that the principal product in the N_2O-C_2H_6 system is the mass 61, OHN_2O^-.

In our propane case, therefore, the main neutralization reaction may be:

$$OHN_2O^- + C_3H_8^+ \longrightarrow N_2 + C_3H_7 + 2OH \qquad (6)$$

If this mechanism is correct, we can understand the $G(N_2)\simeq 2G_e$ relation, which should be independent of the temperature examined. If NH_3, the dipole moment of which is larger than that of N_2O, is present, Reaction (5) will be interrupted by the clustering of NH_3 on the OH^- ion. This is in accord with the observation that the addition of NH_3 to the N_2O-hydrocarbon system decreased the $G(N_2)_{max}$'s to G_e, as shown in Table 1.

When propylene is the substrate, there are two possible processes in the reaction of O^- ions, because they are mono-radicals:

$$CH_3CH{=}CH_2 + O^- \longrightarrow \dot{C}H_2CH{=}CH_2 + OH^- \qquad (7)$$

$$\searrow\ CH_3\dot{C}H\text{-}CH_2\text{-}O^- \qquad (8)$$

Process (8) may be a third-body reaction, and the product ions may not contribute to the formation of nitrogen. By analogy to the reactions of monoradicals with olefins, Process (7) will have a certain amount of activation energy, while the activation energy of Process (8) may be nearly zero. Taking these reactions into account, the temperature dependence of the $G(N_2)_{max}$ in propylene may be expressed as follows:

$$\frac{G(N_2)_{max}}{G_e} = 1 + \frac{A\exp(-E_7/RT)}{1+A\exp(-E_7/RT)}$$

Here, E_7 represents the activation energy of Process (7). A is the ratio of the pre-exponential factors of Processes (7) and (8). The curve shown in Fig. 3 is drawn by assuming that $E_7=4.7$ kcal mol^{-1} and $A=2.8\times10^2$. These values are not unreasonable for a radical reaction.[15]

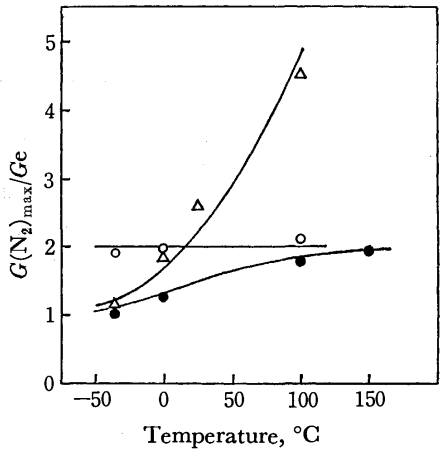

Fig. 3. The temperature dependence of the $G(N_2)_{max}$'s
○: propane, ●: propylene, △: cyclopropane.

In the case of cyclopropane, much more speculation has to be undertaken, because very few reports have been published on the reactions of cyclopropane. The results described above obviously show the chain decomposition of N_2O. One possible chain reaction is as follows:

$$O^- + \text{cyclo-}C_3H_6 \longrightarrow CH_2O^- + C_2H_4 \qquad (9)$$

$$CH_2O^- + N_2O \longrightarrow CH_2O + N_2 + O^- \qquad (10)$$

The apparent activation energy for the formation of nitrogen was calculated to be 3.6 kcal mol^{-1} by using this equation:

$$G(N_2)_{max}/G_e = 1 + A_9\exp(-E_9/RT)$$

Here, A_9 and E_9 are the pre-exponential factor and the activation energy of Process (9) respectively.

The addition of CO_2 to the 4 mol% N_2O-C_3-hydrocarbon systems reduced the $G(N_2)$'s to around G_e, irrespective of the C_3-hydrocarbons. Such an effect

has already been reported by Warman;[5] it may be interpreted in terms of this reaction:

$$O^- \text{ (or } N_2O^-) + CO_2 \longrightarrow CO_3^- (+N_2) \qquad (11)$$

The effect of CH_3OH on the $G(N_2)$'s is obviously different from those of other additives. In the radiolysis of pure methanol, it has already been recognized that, when N_2O is added to the system, nitrogen is produced in a chain reaction.[16] Although CH_3OH has been used as a positive ion-interceptor in the liquid-phase radiolysis, its effect is obviously not so simple in the gas-phase.

References

1) G. Scholes and M. Simic, *Nature*, **202**, 895 (1964).
2) S. Sato, R. Yugeta, K. Shinsaka, and T. Terao, This Bulletin, **39**, 156 (1966).
3) W. J. Holtslander and G. R. Freeman, *Can. J. Chem.*, **45**, 1661 (1967); *J. Phys. Chem.*, **71**, 2562 (1967).
4) S. J. Rzad and J. M. Warman, *ibid.*, **72**, 3013 (1968).
5) J. M. Warman, *ibid.*, **71**, 4066 (1967).
6) G. R. A. Johnson and J. L. Redpath, *Trans. Faraday Soc.*, **66**, 861 (1970).
7) K. Okazaki, R. Yugeta, and S. Sato, This Bulletin, **46**, 2066 (1973).
8) J. M. Warman and M. C. Sauer, Jr., *J. Chem. Phys.*, **52**, 6428 (1970).
9) By using the equation proposed for the thermalization of electrons in *n*-hexane, the thermalization time at 600 Torr is estimated to be 10^{-10} s, while the lifetime in the presence of N_2O, which captures electrons, can be calculated to be longer than 10^{-4} s.[10]
10) J. M. Warman and R. W. Fessenden, *J. Chem. Phys.*, **49**, 4718 (1968).
11) J. L. Moruzzi and J. T. Dakin, *ibid.*, **49**, 5000 (1968).
12) K. M. Bansal and R. W. Fessenden, *ibid.*, **59**, 1760 (1973).
13) D. K. Bohme and F. C. Fehsenfeld, *Can. J. Chem.*, **47**, 2715 (1969).
14) D. A. Parkes, *J. Chem. Soc. Faraday I*, **68**, 2103 (1972).
15) J. A. Kerr and A. F. Trotman-Dickenson, "Progress in Reaction Kinetics," Vol. 1, ed. by G. Porter, Pergamon Press, Oxford (1961), p. 105.
16) M. Meaburn and F. W. Mellows, *Trans. Faraday Soc.*, **61**, 1701 (1965).

The Estimation of the *G*-Values for the Ionization and Excitation of Noble Gases Irradiated by 100 keV Electrons

Shin SATO, Kiyoshi OKAZAKI, and Shin-ichi OHNO*

Department of Applied Physics, Tokyo Institute of Technology, Ookayama, Meguro-ku, Tokyo 152

**Japan Atomic Energy Research Institute, Tokai-mura, Ibaraki 319-11*

(Received March 7, 1974)

The binary-encounter collision theory has been applied to the calculation of the *G*-values for the ionization and excitation of noble gases irradiated by 100 keV electrons. The *G*-values obtained were as follows in the order of He, Ne, Ar, Kr, and Xe: 2.27, 2.19, 2.81, 3.20, 3.45 for *G*(electrons), 0.85, 1.55, 1.92, 1.64, 1.51 for *G*(singlet states), and 0.17, 0.07, 0.13, 0.23, 0.39 for *G*(triplet states). The method of the calculation and the significance of the results were discussed.

One of the most attractive and challenging problems for radiation chemists is the non-empirical calculation or prediction of the *G*-values of products from the compounds they are concerned with. Such a calculation, however, has not been carried out except for helium gas, because there are too many unknown factors and not-established procedures. Even if the factors and the procedures are properly approximated, laborious calculations have to be performed. The calculation for helium was carried out by Erskine,[1] Miller,[2] and Platzman.[3] Since then, several calculations for the degradation spectra in a number of media were carried out, and some of the results were compared with the experimental data obtained largely in metallic media.[4] Recently, Alkhazov has recalculated the degradation spectrum of non-relativistic electrons in helium and discussed the yields of ionization and excitations.[5] This calculation may be the most detailed one for helium at present. His method, however, cannot be applied to other compounds, because several experimental values, which are known only for a limited number of gases, are used. From the point of view of radiation chemists, a more general method which is applicable to a variety of compounds is desirable even though the results are less accurate.

One of the present authors has recently shown[6] that, if the binary-encounter collision theory and the procedure for calculating the degradation spectrum of electrons are combined, the *G*-values of ionization and excitations can be calculated for practically all of the molecules. As an example, he showed the calculation for helium and the hydrogen molecule,[7] the results of which were in reasonable agreement with those estimated from the experimental work. This calculation was so laborious when it is applied to more complex atoms that we wrote a program for an electronic computer and carried out the calculations for the noble gases from He to Xe. The present paper will report the details of the calculation and will attempt to ascertain the limitations of this method.

Method of Calculation

Cross Sections for Ionization and Excitations. The most difficult problem in the calculation of the degradation spectrum of a high-energy electron is the accurate formulation of the cross sections for various energy-loss processes, especially when the energy of electrons is lower than 100 eV. However, if the binary-encounter collision theory is assumed to be applicable to any incident electron, the formulation is rather straightforward. Such a formulation has already been summarized by Vriens and reported in detail.[8] For the present purpose, the final expressions will be satisfactory.

According to the symmetrical model for the collision of a high-energy electron with an atomic electron, the energy loss of the incident electron may be estimated by means of the collisional cross section, where we ignore the radiative energy loss:

$$\sigma_E = \sigma_{E,dir} + \sigma_{E,exc} = \frac{\pi e^4}{T+I_i+E_i}\left[\left(\frac{1}{E^2}+\frac{4E_i}{3E^3}\right) + \left\{\frac{1}{(T+I_i-E)^2}+\frac{1}{3(T+I_i-E)^3}\right\}\right] \quad \text{(I)}$$

for $T+I_i-E \geq 0$. Here, σ_E is the differential cross section per unit of energy for the energy loss (E) of the incident electron with the energy T, while E_i and I_i are, respectively, the average kinetic energy and the binding energy of the atomic electron under consideration. If the atomic electron is in the outermost shell of the atom, I_i is the ionization potential of the atom (I). The first term in the square bracket on the right-hand side of Eq. (I) corresponds to the direct excitation, and the second term, to the excitation induced by the exchange between the incident electron and an atomic electron. In the formulation of Vriens, there is another term, called "interference." This term results from the difference in the scattering angle between the direct and the exchange excitations. In the present calculation, though, we ignore it because the estimation is somewhat arbitrary when it is taken into account in the calculation[9] and because the contribution of this term to the whole calculation is very small, as will be shown later.

By using Eq. (I), we can derive the total ionization cross section per atomic electron:

$$Q_{ion} = \frac{1}{2}\int_{I_i}^{T}\sigma_E dE = \int_{I_i}^{(T+I_i)/2}\sigma_E dE = \int_{I_i}^{T}\sigma_{E,dir}dE = \frac{\pi e^4}{T+I_i+E_i}\left[\left(\frac{1}{I_i}-\frac{1}{T}\right)+\frac{2E_i}{3}\left(\frac{1}{I_i^2}-\frac{1}{T^2}\right)\right] \quad \text{(II)}$$

The factor of 1/2 has to be introduced because we cannot distinguish the origin of the scattered electron, whether it is originally the incident electron or the atomic electron.

For the cross sections of excitations, we use the following formula according to the treatment of Vriens.[10] Here, E_s and E_t are the energies of the lowest singlet and triplet levels respectively:

$$Q_{singl} = Q_{de} + \frac{1}{2}Q_{ee};\ Q_{tripl} = \frac{1}{2}Q'_{ee} \qquad \text{(III)}$$

Here,

$$Q_{de} = \int_{E_s}^{I} \sigma_{E,dir} dE$$

$$= \frac{\pi e^4}{T+I+E_i}\left[\left(\frac{1}{E_s}-\frac{1}{I}\right)+\frac{2E_i}{3}\left(\frac{1}{E_s^2}-\frac{1}{I^2}\right)\right]$$

for $T \geq I$, and

$$Q_{de} = \int_{E_s}^{T} \sigma_{E,dir} dE$$

for $I > T \geq E_s$. When $T < E_s$, Q_{de} is set equal to zero.

$$Q_{ee} = \int_{E_s}^{I} \sigma_{E,exc} dE$$

$$= \frac{\pi e^4}{T+I+E_i}\left[\left(\frac{1}{T}-\frac{1}{T+I-E_s}\right)+\frac{2E_i}{3}\left\{\frac{1}{T^2}-\frac{1}{(T+I-E_s)^2}\right\}\right]$$

for $T \geq I$, and similarly

$$Q_{ee} = \int_{E_s}^{T} \sigma_{E,exc} dE$$

for $I > T \geq E_s$. When $T < E_s$, Q_{ee} is set equal to zero.

$$Q'_{ee} = \int_{E_t}^{I} \sigma_{E,exc} dE$$

for $T > I$ and

$$Q'_{ee} = \int_{E_t}^{T} \sigma_{E,exc} dE$$

for $I > T \geq E_t$. When $T < E_t$, Q'_{ee} is set equal to zero. These equations are very tentative, as Vriens has already mentioned, and should be replaced by better equations when they become available.

Stopping Power. In the present paper, we consider the energy loss resulting in the atomic excitation or ionization. Therefore, the stopping power of the medium which consists of a single kind of atom may be expressed as follows:

$$S(T) = N\left\{\sum_i n_i \int_{I_1}^{(T+I_1)/2} E\sigma_E dE + n\left(\int_{E_s}^{I} E\sigma_E dE + \frac{1}{2}\int_{E_t}^{E_s} E\sigma_{E,exc} dE\right)\right\} \qquad \text{(IV)}$$

for $T \geq I$. Here, $S(T)$ is the stopping power, N is the number of atoms in a unit volume, n_i is the number of electrons in the i-th shell, and n is the number of electrons in the outermost shell. When the energy of the incident electron is smaller than I, the first term in Eq. (IV) disappears and the upper limit of the second integral should be replaced by T. Similarly, when $T < E_s$, the first and second terms dissappear and the E_s in the third integral should be replaced by T.

Degradation Spectrum. When a high-energy electron with the energy of T_0 passes through a medium, various types of ionizations take place and secondary electrons are ejected, the energies ranging from zero to T_0-I. If the kinetic energy of the secondary electrons thus produced is higher than I, they will induce another ionization. From the point of view of the medium, there is a spectrum of the electrons which have a wide range of kinetic energies. Such a spectrum is called a degradation spectrum. Spencer and Fano may have been the first to discuss the quantitative method for the calculation of the degradation spectrum.[11] Schneider and Cormack also investigated the method and performed the calculation for helium.[12] This method was used by Oda and Nishimura to obtain the degradation spectrum produced by ^{60}Co-γ rays in water.[13] Klots and Wright have also carried out the calculation on a simple atomic model and investigated the assumption of the continuous slowing-down which is involved in the calculation.[14] The method used here is essentially the same as that used by Oda and Nishimura.

On the assumption of a continuous slowing-down, the degradation spectrum of the incident electron may be expressed in this form:

$$y_1(T) = 1/S(T) \qquad \text{(V)}$$

On the way to the formation of this spectrum, the secondary electrons are ejected. To describe the degradation spectrum of these secondary electrons, it is more convenient to modify the differential cross section of ionization as follows:

$$\sigma(T_1T_2) = \frac{\pi e^4}{T_1+I_1+E_i}\left\{\left(\frac{1}{(T_2+I_1)^2}+\frac{4E_i}{3(T_2+I_1)^3}\right)+\left(\frac{1}{(T_1-T_2)^2}+\frac{4E_i}{3(T_1-T_2)^3}\right)\right\} \qquad \text{(VI)}$$

Here, $\sigma(T_1T_2)$ is the differential cross section for the production of the secondary electron with the energy of T_2 in the collision between the incident electron with the energy of T_1 and an atomic electron in the i-th shell. Therefore, the degradation spectrum of the secondary electrons may be expressed in this form:

$$y_2(T) = \frac{N}{S(T)}\sum_i n_i \int_T^{1/2(T_0-I_1)} \int_{2T_2+I_1}^{T_0} y_1(T_1)\sigma(T_1T_2)dT_1dT_2 \qquad \text{(VII)}$$

Here, the upper limit of the first integral, $1/2(T_0-I_i)$, comes from the fact that the electrons having energies higher than this value are counted as primary. Similarly, the degradation spectrum of tertiary electrons is expressed as follows:

$$y_3(T) = \frac{N}{S(T)}\sum_i n_i \int_T^{1/4(T_0-3I_1)} \int_{2T_2+I_1}^{1/2(T_0-I_1)} y_2(T_1)\sigma(T_1T_2)dT_1dT_2 \qquad \text{(VIII)}$$

Similar equations may be constructed for the electrons ejected in the later steps.

The total degradation spectrum is obviously the sum of the above spectra:

$$y(T) = \sum y_m(T) \qquad \text{(IX)}$$

In the actual calculation, this series rapidly converges, and the sum of the first five terms is probably accurate enough, but in the following calculation we took the sum of the six terms.

G-Values of Excitation and Ionization. Once $y(T)$ is obtained, the calculation of the yields of excitation and ionization per incident electron is straightforward

if we use the total cross section for each process:

$$N_s = Nn_i\int_{T_s}^{T_0} y(T)\cdot Q_s(T)\mathrm{d}T \qquad (X)$$

$$= Nn_i\int_{T_s}^{T_0} T\cdot y(T)\cdot Q_s(T)\mathrm{d}\ln T \qquad (XI)$$

Here, N_s is the number of the species produced in the s process, T_s is the threshold energy of the incident electron for the s process, and $Q_s(T)$ is the total cross section. According to the expression used by Platzman,[3] the results thus obtained can be shown, as they will be later, in the $T\cdot y(T)\cdot Q_s(T)$ *vs.* ln T plots, so that the area under the curve of $T\cdot y(T)\cdot Q_s(T)$ is proportional to the yield of the s process. Thus, we can estimate the G-values of each process by means of the equation:

$$G_s = \frac{100N_s}{T_0} \qquad (XII)$$

Constants Used for Calculation

In order to carry out the calculation, we have to know the constants which appear in the equations, the singlet and triplet excitation energies of the atom under consideration (E_s and E_t), the binding energies of the atomic electrons (I_i),[15] and their kinetic energies (E_i). Tables 1 and 2 summarize the values of E_s, E_t, and I_i used. The minimum I_i value for an atom is the ionization potential of the atom, for which the spectroscopic values may be better than those obtained by the technique of ESCA using X-rays.

TABLE 1. THE LOWEST SINGLET AND TRIPLET LEVELS (eV)

Atom	E_s	E_t
He	21.2	19.8
Ne	16.8	16.7
Ar	11.8	11.6
Kr	10.6	10.0
Xe	9.6	8.5

TABLE 2. THE BINDING ENERGY OF ELECTRON, I_i (eV)

Shell	He	Ne	Ar	Kr	Xe
1s	24.581	867	3203	14326	34561
2s		45	320	1921	5453
2p		21.559	246	1701	4943
3s			25	289	1145
3p			15.755	219	968
3d				89	679
4s				24	208
4p				13.996	147
4d					63
5s					18
5p					12.127

Since we have no experimental data for E_i, we have to calculate them. For the noble gases from He to Kr[16] and later for Xe and Rn atoms,[17] Hartree-Fock SCF wave functions based on the single zeta Slater-type function for each electron have been reported. The value of E_i, therefore, may be calculated by using this equation:

TABLE 3. THE KINETIC ENERGY OF ELECTRON, E_i (eV)

Shell	He	Ne	Ar	Kr	Xe
1s	38.74	1265	4169	16884	38090
2s		37.59	169.6	789.9	1796
2p		112.8	667.3	3492	8445
3s			18.19	133.7	383.1
3p			32.27	294.5	897.2
3d				643.0	2412
4s				15.55	83.11
4p				23.18	151.3
4d					232.7
5s					12.29
5p					16.75
Total kinetic energy	77.48	3282	12911	64934	164238
−(Total energy)[a]	77.00	3456	14217	74211	195223

a) Ref. 16 and 17

$$E_i = -\frac{1}{2}\int\phi_i\nabla^{*2}\phi_i\mathrm{d}\tau \qquad (XIII)$$

Table 3 summarizes the calculated values. According to the virial theorem, the total kinetic energy should be equal to the −(total energy) of the atom. The calculated total kinetic energy and the total energy reported[16,17] are compared in Table 3. The agreement is satisfactory for the present calculation.

Results

Figures 1 and 2 show the $y(T)$ and $T\cdot y(T)\cdot Q_s(T)$ *vs.* ln T plots obtained with helium. Figure 2 is very similar to that presented by Platzman.[3]

Table 4 summarizes all of the G-values obtained in the present calculation. All the integrations were carried out by means of a computer, HITAC 8700, with a mesh of $(0.5)^{1/40}$ for the energy. With the increase in mesh, the G-values obtained decreased slightly. In the case of He, the G-value of ionization obtained with the mesh of $(0.5)^{1/80}$ was 2.26; this value agreed within 0.3% with the G-value listed in Table 4.

As has been stated in the previous section, a calculation including the interference term in the cross section

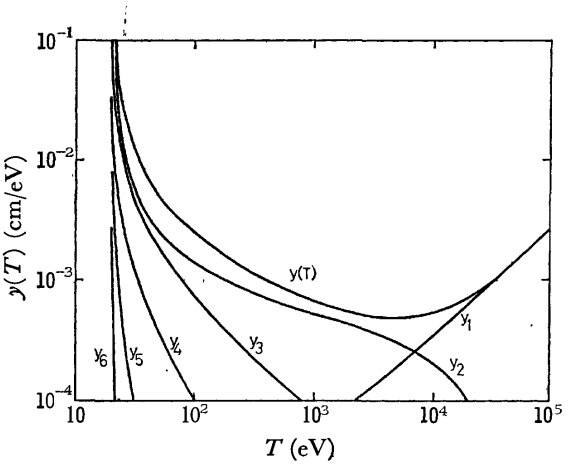

Fig. 1. Slowing-down spectrum in He.

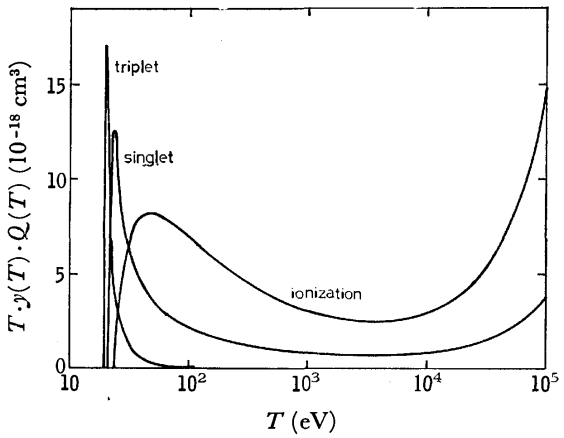

Fig. 2. Contribution of different portions of the electron slowing-down spectrum to the ionization and excitation in He.

TABLE 4. THE G-VALUES OF EXCITATIONS AND IONIZATIONS

	He	Ne	Ar	Kr	Xe
Excitation					
singlet	0.85	1.55	1.92	1.64	1.51
triplet	0.17	0.07	0.13	0.23	0.39
Ionization					
shell					
1s	2.27	0.0038	0.00062	0.000031	0.0000043
2s		0.100	0.0081	0.00040	0.000086
2p		2.06	0.065	0.0024	0.00048
3s			0.25	0.0042	0.00066
3p			2.19	0.025	0.0032
3d				0.35	0.016
4s				0.17	0.0061
4p				1.78	0.038
4d					0.37
5s					0.27
5p					2.03

was also carried out. The G-value of ionization in He was 2.25. The difference from the G-value listed in Table 4 is within 1%.

The degradation spectra in Ne, Ar, Kr, and Xe are shown in Fig. 3. All of the spectra are alike, though there are small differences in the energy region lower than 100 eV. This difference might play an important role in a radiation-induced chemical reaction when these gases are used as the solvents.

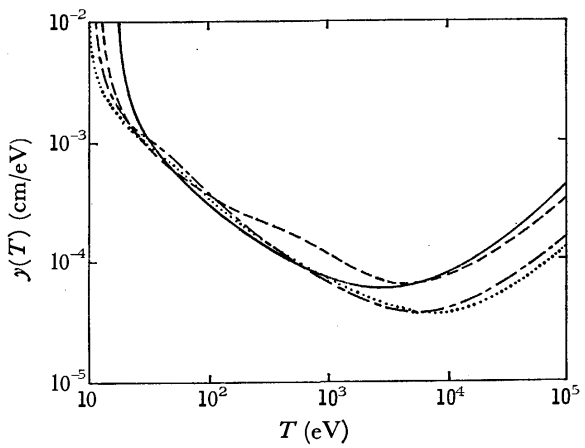

Fig. 3. Slowing-down spectra in Ne (——), Ar (----), Kr (-·-·-), and Xe (·····).

Figures 4 to 7 show the $T \cdot y(T) \cdot Q_i(T)$ *vs.* ln T plots for Ne, Ar, Kr, and Xe. They clearly show that the

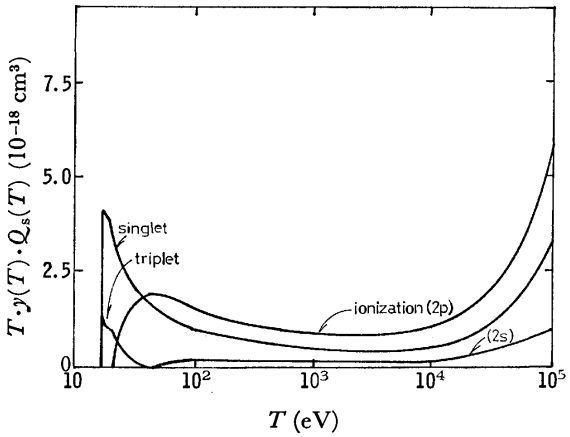

Fig. 4. Contribution of different portions of the electon slowing-down spectrum to the ionization and excitation in Ne.

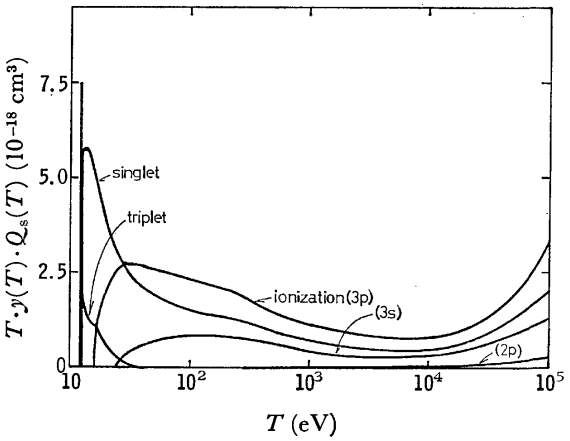

Fig. 5. Contribution of different portions of the electron slowing-down spectrum to the ionization and excitation in Ar.

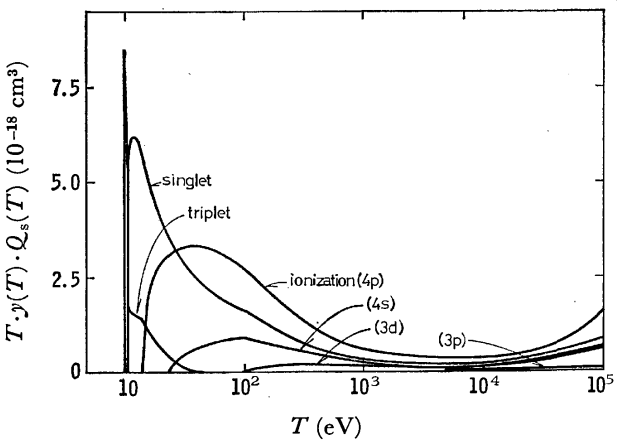

Fig. 6. Contribution of different portions of the electron slowing-down spectrum to the ionization and excitation in Kr.

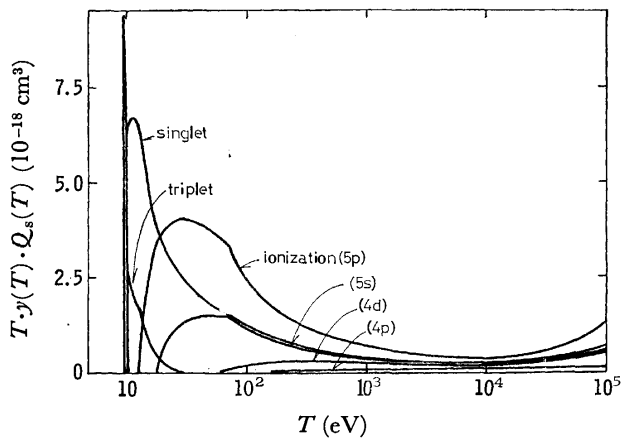

Fig. 7. Contribution of different portions of the electron slowing-down spectrum to the ionization and excitation in Xe.

ionizations from the inner shells become more important with an increase in the atomic number. Consequently, in order to estimate the G-values of electrons, we have to consider the Auger effect. For example, an excited Ar ion with the ejection of the 2p electron has energy enough for the auto-ionization:

$$Ar^+(2p) \longrightarrow Ar^{5+} + 4e^- \qquad (1)$$

To calculate the total G-value of electrons, the ionization from the 2p shell in Ar should be taken as corresponding to $5e^-$. Here, the yield of the fluorescence, which is often observed with the Auger effect, is ignored. For such a calculation, we need exact data for the multiple-ionizations of the noble gases. Most of the data we need are not available. Therefore, the G-values of electrons were estimated by using a tentative equation:

$$G(e^-) = \sum_i f_i G_i(M^+) \qquad (XIV)$$

Here, f_i is the largest integer which satisfies the equation:

$$I_i/I \geq \sum_{x=1}^{f_i} x \qquad (XV)^{18)}$$

and $G_i(M^+)$ is the G-value of the $M^+(i$-th shell) ion. Table 5 shows the results, together with the W-values calculated from the G-values and the W-values reported previously.[3,5] We believe that the agreement is satisfactory.

It may be worthwhile to notice here that the G-values of the electrons calculated here do not contain any contribution from the Hornbeck-Molnar process:[19]

$$M^* + M \longrightarrow M_2^+ + e^- \qquad (2)$$

Here, M* represents the excited state of a noble gas.

TABLE 5. THE G-VALUES OF ELECTRONS AND THE W-VALUES OBTAINED THEORETICALLY AND EXPERIMENTALLY

Atom	Theoretical			Experimental[3]
	present work		others	
	G_e	W	W	W
He	2.27	44.05	46.5[2]	42.3
			46.45±1.0[6]	
Ne	2.19	45.66		36.3
Ar	2.81	35.59		26.4
Kr	3.20	31.25		24.2
Xe	3.45	28.99		22.0

Discussion

For fast collisions ($T \geq 10^4$ eV), it is well known that the binary-encounter collision theory is an approximation to the Bethe theory,[8,20] because the model used for the binary-encounter collision theory can deal only with close collisions, not with distant collisions. However, since the energy distribution of secondary electrons is mainly determined by the close collisions, the binary-encounter collision theory may not be a bad approximation for the estimation of the degradation spectrum. On the other hand, the Bethe theory, although it is a quantum mechanical treatment, cannot properly estimate the close collisions within the Born approximation. Moreover, special treatment has to be applied to take the exchange effect into account.[20]

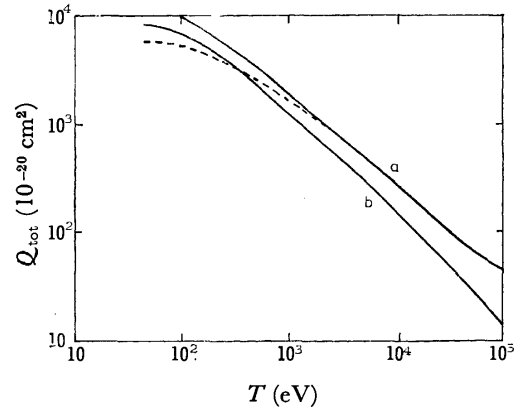

Fig. 8. Comparison of the total inelastic scattering cross sections derived from the Bethe theory (a) and from the binary-encounter collision theory (b). Broken line is experimental.

Figure 8 shows a comparison of the total inelastic scattering cross sections as calculated by the two theories for helium. Although, in the calculation of the degradation spectrum, the absolute value of the total inelastic scattering cross section does not directly affect the final result, the comparison of these values may be worthwhile in order to compare the two theories.

The a curve in Fig. 8 was drawn by using the Bethe asymptotic cross section theoretically estimated by Inokuti *et al.*:[21]

$$Q_{tot} = \frac{1}{\beta^2}\left\{1.410\left[\ln\left(\frac{\beta^2}{1-\beta^2}\right) - \beta^2\right] + 15.118\right\} \times 10^{-20}\ \text{cm}^2 \qquad (XVI)$$

Here, β is the ratio of the velocity of the incident electron and the velocity of light. The b curve was drawn by means of the equation used for the present calculation:

$$Q_{tot} = \sum_i n_i Q_{ion} + n(Q_{singl} + Q_{tripl}) \qquad (XVII)$$

Obviously, the present method underestimates the cross sections, especially at higher energies. On the other

hand, the Bethe asymptotic cross section deviates from the experimental value at lower energies of the incident electron and gives too high values.[22] The total inelastic scattering cross section obtained by the binary-encounter collision theory seems to compensate itself between higher energies and lower energies.

For noble gases other than He and Ne,[23] no theoretical cross sections are obtained by the Bethe theory. However, experimental values for 0.1—2.7 MeV electrons have been reported in the forms of M^2 and C in the following equation:[24]

$$Q = 4\pi\left(\frac{\hbar}{mc}\right)^2 (M^2 x_1 + C x_2) \qquad \text{(XVIII)}$$

Here, $4\pi(\hbar/mc)^2 = 1.874 \times 10^{-20}$ cm^2 and

$$x_1 = \beta^{-2} \ln [\beta^2/(1-\beta^2)] - 1, \quad x_2 = \beta^{-2}$$

Table 6. Comparison of the binary-encounter collision theory with the experiment in the total inelastic scattering cross section of electrons at the energy of 10^5 eV

Atom	$Q_{tot} \times 10^{20}$cm^2 calculated	$Q_{tot} \times 10^{20}$cm^2 experimental
He	13.62	45.09
Ne	132.0	107.6
Ar	106.2	225.3
Kr	145.2	305.9
Xe	143.6	433.5

In Table 6, the total inelastic scattering cross sections of the electrons at the energy of 10^5 eV as calculated by the binary-encounter collision theory are compared with the experimental values. Obviously, most of the cross sections calculated are smaller than the experimental values. In the case of Ne, though, the binary-encounter collision theory predicted a cross section larger than the experimental value. This anomaly seems to result from the overestimation of $E_i(2p)$. The discrepancy in the cross section shown in Table 6 as an example may be one of the most serious shortcomings of the present calculation, although this discrepancy is not directly reflected in the final G-values.

Table 7. The ratios of the G-value of excitation and the G-value of electrons

Atom	$G_{exc}/G(e^-)$
He	0.45
Ne	0.74
Ar	0.73
Kr	0.59
Xe	0.55

We believe that the G-values of ionization, at least the relative values of each process, shown in Table 4 are reliable; however, the G-values of excitations are much less reliable. Platzman assumed $G_{exc}/G(e^-) = 0.4$ for all noble gases.[3] The ratios calculated by the present method are listed in Table 7. The reliability of these ratios may be discussed in comparison with the experimental data for the mixture of noble gases, in which such Penning ionization as:

Table 8. The sum of $G(e^-)$ and G_{exc}. Comparison with the value calculated from Klots' data

Atom	present	Klots' data
He	3.29	3.50~3.66
Ne	3.81	3.98~4.01

$$He^* + Ar \longrightarrow He + Ar^+ + e^- \qquad (3)$$

occur. Such data, however, are not abundant. By using the α particles from ^{239}Pu as the exciting source. Klots measured the W-values of a mixture of two noble gases. From his data,[25] the G-values of the excited states of He and Ne can be estimated; they are shown in Table 8. The calculated G-values of excitations are not so bad as had been expected.

In conclusion, we would like to summarize two of our conclusions of the present calculation, points which are often overlooked by experimental radiation chemists, including us: 1) the ionization from inner shells cannot be ignored even in the molecules composed of atoms with low atomic numbers, and 2) the yields of the forbidden states, the triplet states in the present calculation, are very much dependent upon the $y(T)$ at low energies; *i.e.*, the yield greatly depends on the solvent in which the chemical reactions are taking place.

The authors are indebted to Professor Kazuo Hisatake and Dr. Yoshihiko Hatano for their valuable discussions.

References

1) G. A. Erskine, *Proc. Roy. Soc., Ser. A*, **224**, 362 (1954).
2) W. F. Miller, *Bull. Amer. Phys. Soc.*, **1**, 202 (1956).
3) R. L. Platzman, *Int. J. Appl. Radiation and Isotopes*, **10**, 116 (1961).
4) R. T. L. McGinnie, *Natl. Bur. Stands. Circular*, No. 597 (1958).
5) G. D. Alkhazov, Ioffe Institute of Physics and Technology, Preprint FTI-108, 52 (1968), Argonne National Laboratory Trans., 774 (1969).
6) S. Ohno, *Chem. Lett.*, **1973**, 817.
7) S. Ohno, Conference of Radiation Chemistry, Nagoya, Preprint, p. 150 (1973).
8) L. Vriens, "Case Studies in Atomic Collision Physics I," ed. by E. W. McDaniel *et al.*, North-Holland, Amsertdam (1969), p. 335.
9) L. Vriens, *Proc. Phys. Soc.*, **89**, 13 (1966).
10) L. Vriens, *Phys. Rev.*, **141**, 88 (1966).
11) L. V. Spencer and U. Fano, *ibid.*, **93**, 1172 (1954).
12) D. O. Schneider and D. V. Cormack, *Radiation Res.*, **11**, 418 (1959).
13) N. Oda and F. Nishimura, *Bull. Tokyo Inst. Tech.*, No. 54, 137 (1963).
14) C. E. Klots and H. Wright, *Int. J. Radiat. Phys. Chem.*, **2**, 191 (1970).
15) K. Siegbahn *et al.*, "ESCA Atomic, Molecular and Solid State Structure Studied by Means of Electron Spectroscopy," Nova Acta Regiae Societatis Scientarum Upsaliensis, Ser. IV, Vol. 20, (1967).
16) E. Clementi and D. L. Raimondi, *J. Chem. Phys.*, **38**, 2686 (1963); E. Clementi, *I. B. M. J. Res. Develop.*, **9**, 2 (1965).
17) M. Synek and G. E. Stungis, *J. Chem. Phys.*, **42**, 3068 (1965).
18) Eq. (XV) corresponds to the assumption that the ioniza-

tion potential of $M^{(n-1)+}$ is equal to n times the ionization potential of M. This assumption is roughly correct for Ne^{n+} ($n \leq 6$) and Ar^{n+} ($n \leq 8$).

19) J. A. Hornbeck and J. P. Molnar, *Phys. Rev.*, **84**, 621 (1951).

20) M. Inokuti, *Rev. Mod. Phys.*, **43**, 297 (1971).

21) M. Inokuti, Y.-K. Kim, and R. L. Platzman, *Phys. Rev.*, **164**, 55 (1967).

22) B. L. Schram, F. J. DeHeer, M. J. van der Wiel, and J. Kistemaker, *Physica*, **31**, 94 (1965).

23) F. F. Rieke and W. Prepejchal, *Phys. Rev.*, **A6**, 1507 (1972).

24) R. P. Saxon, *ibid.*, **A8**, 839 (1973).

25) C. E. Klots, *J. Chem. Phys.*, **46**, 3468 (1967).

Linear Free Energy Relationships in Heterogeneous Catalysis. XII.[1] Interpretation of the Catalytic Activity of Decomposition of Hydrogen Peroxide over Nickel Oxide on the Basis of Oxidation Power Distribution

Toshio UCHIJIMA and Yukio YONEDA

Department of Synthetic Chemistry, Faculty of Engineering, University of Tokyo
Hongo, Bunkyo-ku, Tokyo 113

(Received November 10, 1972)

Kinetic studies have been carried out on the heterogeneous decomposition of hydrogen peroxide over several nickel oxide catalysts calcined at different temperatures. Kinetic parameters such as reaction order and apparent activation energy depend somewhat on the reaction conditions, but show practically no change with catalyst. The catalytic activity changes with calcination temperature, becoming minimum at 550 °C and maximum at 600 °C. The trend does not change with pretreatment of the catalyst, resembling the behavior of surface excess oxygen having a relatively higher oxidation power. Thus the distribution of oxidation power is closely related to catalytic activity for the decomposition of hydrogen peroxide. We therefore applied the regional analysis assuming that the surface excess oxygen represents active sites for catalysis, and a specific regional activity corresponds to each regional oxygen. It was found that the fifth region (the range of free energy change of adsorption of oxygen being from −11.1 to −12.6 kcal/mol) markedly contributes to the reaction rate, and the calculated rates agree with the observed ones. The nature of the active site was discussed as regards pretreatment of the catalyst.

Of the reactions studied extensively on various catalytic materials including heterogeneous and homogeneous systems,[2] the catalytic decomposition of hydrogen peroxide is one of the most typical. Investigations were carried out with several metal oxide catalysts, aimed at understanding the catalysis on the basis of semiconductive properties,[3] activity order,[4] and the correlation between catalytic activities and the amounts of excess oxygen.[5,6] The amounts of excess oxygen are valuable for account for the catalytic activities of pure or doped, supported or unsupported chromium oxides[5] and the γ-irradiated nickel oxides.[6] Such correlation is reasonable in this reaction, since hydrogen peroxide acts as a reducing reagent as well as an oxidizing one.

A large number of metal oxides have more or less heterogeneous surfaces, certain parts of which contribute to catalysis as active sites. We developed a method to determine the distribution of oxidation power on the oxide surfaces, and applied it to a series of nickel oxide catalysts.[7] In the present study, we measured the catalytic activities for hydrogen peroxide decomposition in an aqueous solution under various reaction conditions using the same lots of nickel oxide catalysts. We found that they possess a similar pattern against the calcination temperature as in the surface excess oxygen of relatively higher oxidation power. This suggests that the distribution of oxidation power is closely related to catalytic activity for the decomposition of hydrogen peroxide. Regarding the regional surface excess oxygen as an active site having a specific activity characteristic of the respective region, the catalytic activities were analyzed by the regional analysis method[8] to estimate the most effective region for catalysis. The nature of the active site was discussed in reference to the fact that pretreatment such as reduction or oxidation affects the catalytic activities, giving rise to deactivation during the course of catalysis.

Experimental

Catalysts and Reagents. The same lots of catalysts as described previously,[7] *i.e.*, a series of pure nickel oxide and Li_2O-doped catalysts, were used. The oxidation power distribution of these oxides has been determined by the aqueous reduction method using hydrazine and KI(pH x) systems.[7] 30% hydrogen peroxide containing no stabilizer (Mitsubishi-Edogawa Co., Ltd.) was used. All the other reagents were commerical products of G.R. grade.

Procedures. The reaction rates of hydrogen peroxide decomposition were determined by following the pressure changes due to oxygen gas evolved, with a conventional reactor of constant volume (about 150 ml). The hydrogen peroxide solution (50 ml) was introduced into the reactor containing a weighed amount of catalyst at a constant temperature (within ±0.2 °C). The speed of stirring was chosen so as to provide a state in which true reaction rate was obtained but not the diffusion-controlled one. The reaction was carried out at temperatures 10—50 °C and concentrations 0.1—10 mol/l H_2O_2. In some cases, pure hydrogen peroxide solution was used without any additives, and in other cases, the solution buffered with potassium hydroxide or sodium tetraborate solution in the pH range 6—11.5.

When necessary, the catalysts were pretreated *in vacuo* or in oxygen gas of 1 atm at 300 °C in the reactor, and their effects on catalytic activities were examined.

Results

Reaction Order. The reaction curves can be analyzed on the basis of a certain reaction order except for their initial unsteady parts. The reaction orders for hydrogen peroxide were also obtained by varying its initial concentration. These values depend largely on the type of solution (additives or pH) and the conditions of pretreatment whereas they are mostly constant among the catalysts except for a few cases. The mean values of reaction order are given in Table 1. For

TABLE 1. REACTION ORDERS OF DECOMPOSITION OF HYDROGEN PEROXIDE UNDER VARIOUS CONDITIONS (30°C)

Reaction orders were obtained from analysis of the reaction curves (method 1) and also by varying the initial concentration of hydrogen peroxide (method 2).

Catalyst pretreatment	Solution	Reaction order[a]	
		Method 1	Method 2
Untreated	No additives	0.4	0.4[b]
Untreated	0.1 N KOH	0.6	—
Untreated	0.005 N $Na_2B_4O_7$	0.6	0.6[c]
Evacuated at 300°C	No additives	0.1[d]	—

a) Unless otherwise stated, the mean values are listed since variation among catalysts is relatively small. b) Ni-2-350-8. c) Ni-2-500-8. d) For Ni-2-600-8 and Ni-2-700-8 only, the reaction follows the order of 0.5 during the first run but gives the value of 0.1 after the second run.

example, the values of the untreated catalysts are 0.57—0.62 in a solution buffered with 0.005 mol/l sodium tetraborate. The only exception is the case of the first run on Ni-2-600-8 and Ni-2-700-8, subjected previously to evacuation at 300 °C, which yield much higher values than the others. The cause of this anomaly is not clear.

Table 1 also shows good agreement between the values obtained by the two independent methods. The kinetic curve would accompany the effect due to the changes of pH and the deactivation of catalysts during reaction. Both effects may compensate each other, yielding the agreement.

The reaction orders are reasonably lower than unity in all the cases and the reduced state is accompanied by the much lower order as compared with the oxidized one.

Dependency on pH. The decomposition rate of hydrogen peroxide varies with pH, where pH was controlled with potassium hydroxide or sodium tetraborate-potassium hydroxide solution. The additives affect the reaction rate not only through the pH changes but also through other effects possibly due to complex formation. In 1 mol/l H_2O_2 solution, addition of 10^{-5} M potassium hydroxide retards the rate slightly, while a remarkable accelerating effect is found above 10^{-4} M. A satisfactory linear relationship exists between log(rate) and log(H^+) in the concentration range 10^{-4}—10^{-1} M potassium hydroxide, yielding a value of −0.17 as the order with respect to (H^+). Similarly, pH was changed from 8.7 to 9.5 by the addition of potassium hydroxide to the solution buffered with sodium tetraborate of constant concentration. Analysis of the results gives a value of −0.31. Retardation of the reaction by hydrogen ion is in line with the well-examined case in homogeneous metal ion-catalyzed systems.[2]

A comparison of the system containing potassium hydroxide as an additive with that containing sodium tetraborate and potassium hydroxide each with the same pH shows that the rate of the latter is much lower. This suggests that the added ion blocks the active sites according to its coordination tendency.

TABLE 2. VARIATION OF CATALYTIC ACTIVITY DUE TO VARIOUS PRETREATMENTS OF CATALYST

Catalyst; Ni-2-350-8. Temperature; 30°C. Solution; 1 mol/l H_2O_2 solution

Pretreatment	Initial rate (10^{-2} mol/min·g)
Untreated	0.83
Evacuated at 200°C for 1 hr	2.23
Evacuated at 300°C for 1 hr	3.04
Treated with oxygen of 600 mmHg at 300°C for 14 hr after evacuation at 300°C for 9 hr.	0.61

Pretreatment Effects and Deactivation during Catalysis. Variation of catalytic activity due to pretreatment such as evacuation and oxidation at high temperature, which is comparable with the case of untreated catalysts, is shown in Table 2. The catalytic activity is largely enhanced after evacuation at high temperature. By oxidation of the evacuated catalyst in one atmospheric oxygen at 300 °C, the activity decreases to a level slightly lower than that of the untreated catalyst.

After the first run was completed on the catalyst evacuated at 300 °C using an unbuffered 1 mol/l H_2O_2 solution, 5 ml of 10 mol/l H_2O_2 solution was added and the reaction was then repeated under the same conditions. The variation of catalytic activity during these repeated runs is presented in Fig. 1. The activity declines gradually with each run and approaches a certain level which is approximated to the value of the fully oxidized catalyst. This might help clarify the nature of active sites.

Effects of Catalyst Variations. Catalyst activity, plotted against calcination temperature (a) and the amount of the doped lithium (b), is shown in Fig. 2. The results are obtained on the untreated catalysts using a 1 mol/l H_2O_2 solution with no additives at 25 °C. The curves show a complex dependency on

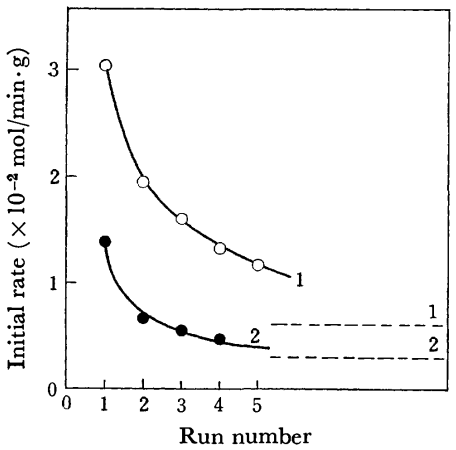

Fig. 1. Deterioration of the catalytic activities during repeated runs
The catalysts are pretreated at 300 °C *in vacuo* for 1 hr. Dotted lines show the rates over the fully oxidized catalysts.
Solution; 1.0 mol/l H_2O_2, Temperature; 30 °C, 1; Ni-2-350-8, 2; Ni-2-450-8

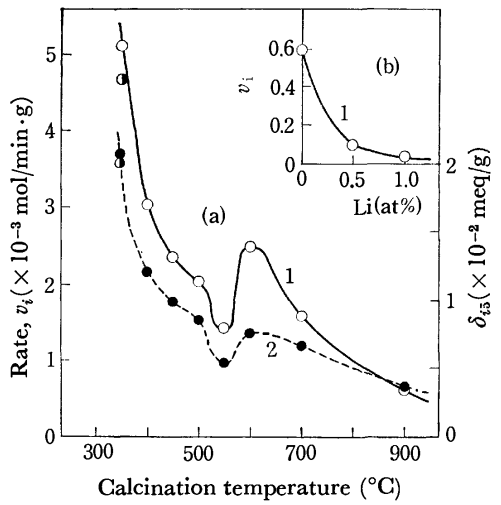

Fig. 2. Dependency of the catalytic activity on the calcination temperature (a) and the lithium content (b) of nickel oxide
Solution; 1.0 mol/l H_2O_2, Reaction temperature; 25 °C
Curve 1 shows the reaction rate, v_i, and curve 2 the amount of the surface excess oxygen of the fifth region, δ_{i5}. The values of the catalyst calcined for 16 hr are marked as ◑.

the calcination temperature characterized by a minimum at 550 °C and a maximum at 600 °C. As the lithium content is increased, the activity decreases monotonously. This is in line with the case of surface excess oxygen with relatively higher oxidation power, *e.g.*, the regional oxygen given as a difference between the ones measured by the KI (pH 10.8) and KI (pH 11.3) methods, which is also plotted in Fig. 2. Similar curves were obtained for both calcination temperature and lithium content under other reaction conditions such as in a buffered or unbuffered solution on the pretreated or untreated catalysts. The absolute values differ largely according to the reaction conditions.

The activation energies are obtained on several catalysts using a solution buffered with sodium tetraborate at temperatures 30—50 °C. The results are summarized in Table 3. The catalyst variations do not seem to affect activation energy, addition of lithium oxide having little effect.

Table 3. Apparent activation energies for decomposition of hydrogen peroxide over some nickel oxides
Solution; 0.1 mol/l H_2O_2, 0.005 mol/l $Na_2B_4O_7$.

Catalyst	Activation energy (kcal/mol)
Ni-2-350-8	17.2
Ni-2-500-8	17.5
Ni-2-600-8	16.8
Ni-2-900-8	16.8
Ni-2-Li-0.5-900-8	16.1

Discussion

In order to account for the catalytic activity of metal oxides for oxidation catalysis, a number of parameters such as dissociation pressure of oxide,[9] enthalpy change of formation of oxide,[10] homomolecular isotope exchange of oxygen,[11] reducibility of oxide[12] and excess oxygen[5,6] have been extensively examined. The surface of most metal oxides has been generally accepted to be of more or less heterogeneous distribution. In oxidation catalysis, however, such heterogeneity has not been introduced explicitly into quantitative analysis of catalytic activity except for a few studies.[9] The distribution of oxidation power represents the amount[7] of surface excess oxygen as a function of its oxidation power, which can be determined on the basis of oxidation-reduction equilibrium with a certain reducing reagent in an aqueous phase. It is interesting to examine whether catalytic activity can be accounted for by this oxidation power distribution, and if so to what extent.

As shown in Fig. 2, the catalytic activity of nickel oxide catalysts for the decomposition of hydrogen peroxide shows a complex curve against calcination temperature, and a monotonously decreasing curve against lithium oxide content. Since these relations are very similar to the behaviors in the surface excess oxygen of relatively higher oxidation power, the distribution of oxidation power is closely related to the catalytic activity for the decomposition of hydrogen peroxide. The regional analysis method[8] was applied assuming that the surface excess oxygen of oxides represents their active site for catalysis and a specific regional activity corresponds to each regional oxygen. The catalytic activity of the i-th catalyst, v_i (mol/min·g), can be represented by

$$v_i = \sum_j v_{0j} \times \delta_{ij} \qquad (1)$$

where v_{0j} (mol/min·meq) denotes the specific activity characteristic of surface excess oxygen of the j-th region (suffix 0 indicates its independency of the type of catalyst) and δ_{ij} (meq/g) the amount of surface excess oxygen of the j-th region of the i-th catalyst. Surface excess oxygen over these catalysts has been classified experimentally into six regions.[7] Each region is defined by the free energy change of adsorption of oxygen (ΔG) as follows.

Region 1; $-\Delta G = 141.5—29.9$ kcal/mol.
Region 2; $-\Delta G = 29.9—19.8$ 〃
Region 3; $-\Delta G = 19.8—14.6$ 〃
Region 4; $-\Delta G = 14.6—12.6$ 〃
Region 5; $-\Delta G = 12.6—11.1$ 〃
Region 6; $-\Delta G < 11.1$ 〃

For the lithium-doped nickel oxides, the fifth and sixth regions could not be determined separately and had to be excluded. Since Eq. (1) holds, consequently, over nine kinds of the pure nickel oxide catalysts, a set of probable values of v_{0j} corresponding to six regions can be estimated by means of the method of least squares. However, the degree of freedom for analysis is too small and the treatment provides too erroneous results. Thus, regional analysis is applied to all the possible combinations from two to five regions combining some

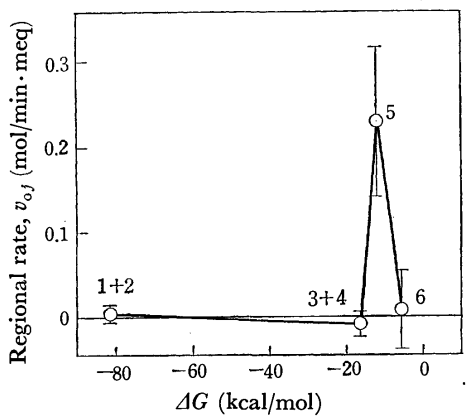

Fig. 3. Correlation between the regional rate calculated by Eq. (1) and the mean free energy change of the respective region.
Numerals in the Figure mean the numbers of regions. The range of errors is also shown.

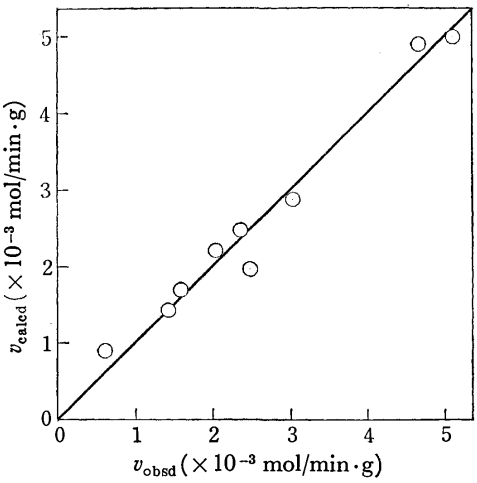

Fig. 4. Comparison of the rates calculated by Eq. (1), v_{calcd}, with the observed ones, v_{obsd}.

neighboring regions. From these the most acceptable one is picked to provide a solution having tolerable errors as well as reasonable physical meaning. In Fig. 3, the regional rates are plotted against the free energy changes of adsorption of oxygen. The result corresponds to such combination of regions as 1+2, 3+4, 5 and 6, and shows that the fifth region ($-\Delta G=$ 11.1—12.6) has a marked contribution to the reaction rate. The overall rates calculated with the above results by means of Eq. (1) are plotted against the observed ones in Fig. 4. A good agreement is observed.

Since oxidation power distribution implies the energy distribution of surface oxygen over the fully oxidized catalysts, the distribution should be caused by the difference of the energy states of adsorption sites for oxygen, *i.e.*, probably bare metal ion, which will be caused by the removal of surface oxygen. Oxidation power distribution corresponds also to discrimination of the energy states of bare metal ion sites. The fifth region provides the largest contribution to catalytic activity, but it is not clear whether the actual active site during catalysis is the surface oxygen or the bare metal ion.

The reaction mechanism of the decomposition of hydrogen peroxide over the oxide catalysts is not known, but information on the homogeneous system catalyzed by ferrous or ferric ion can be referred to.[2] The decomposition of hydrogen peroxide is initiated by the formation of HO_2 or OH radical by oxidation or reduction with ferric or ferrous ion, and proceeds through radical chain mechanism. Ferrous ion catalyzes the decomposition much more effectively than ferric ion, and the same final steady state having a particular ferrous/ferric ratio is obtained, regardless of whether the initial feed is ferrous or ferric ion. As shown in Fig. 1, the catalytic activity of nickel oxide increases markedly by prior evacuation at high temperature, and decreases gradually towards the final constant value with repetition of reaction. Contrarily, the fully oxidized catalyst shows about the same catalytic activity as in the catalyst which underwent no pretreatment. The nickel oxide shows a much higher catalytic activity in the reduced state than in the oxidized state.

Dependency of catalytic activity of these nickel oxides on calcination temperature is not altered by any pretreatment. Therefore, in the light of regional analysis, it will be assumed that both the bare nickel ion and the surface excess oxygen catalyzes the decomposition of hydrogen peroxide more effectively as long as they belong to the fifth region, the former being much more active than the latter. Since the mode of catalytic activity in the pretreatment is similar to that of the ferrous/ferric ion catalyzed system, the catalytic reaction and deterioration of the active sites over the nickel oxide follow a similar mechanism to that in the homogeneous system.

The catalytic activity of lithium-doped nickel oxide decreases monotonously with the amount of lithium added. We might suggest that this tendency is in parallel to the summed surface excess oxygen of the fifth and sixth regions, and the activation energy does not differ from that of the other pure nickel oxides. These facts also give evidence to the usefulness of oxidation power distribution for understanding the catalytic activity of oxide catalysts.

The authors wish to express their sincere thanks to Dr. Y. Saito for his helpful discussions and to Mr. N. Nojiri for his kind help in the course of this experiment. The reagent was supplied by the Mitsubishi-Edogawa Co., Ltd. The work was partly defrayed by a Grant in Aid of The Kawakami Foundation.

References

1) Part XI of this series: T. Uchijima, Y. Ishida, N. Uemitsu, and Y. Yoneda, *J. Catal.*, **29**, 60 (1973).
2) J. Weiss, *Advan. Catal.*, **4**, 343 (1952); J. H. Baxendale, *ibid.*, **4**, 31 (1952).
3) I. Matsuura, Y. Kubokawa, and O. Toyama, *Nippon Kagaku Zasshi*, **81**, 1209 (1960).
4) A. B. Hart and R. A. Ross, *J. Catal.*, **2**, 251 (1963).
5) J. Deren, J. Haber, A. Podgorecka, and J. Burzyk, *ibid.*, **2**, 161 (1963); J. Deren and J. Haber, *ibid.*, **4**, 22 (1965); M. Nachman, I. Maxim, and T. Braun, *J. Phys. Chem. Solids*, **20**, 307 (1961).

6) I. Maxim and T. Braun, *ibid.*, **24**, 537 (1963); T. Yamashina and M. Sano, This Bulletin, **38**, 1801 (1965).
7) T. Uchijima, M. Takahashi, and Y. Yoneda, *J. Catal.*, **9**, 403 (1967).
8) Y. Yoneda, *ibid.*, **9**, 51 (1967).
9) G. K. Boreskov, V. V. Popovsky, and V. A. Sazonov, Proc. Intern. Cong. on Catalysis, 4th Moscow, 33 (1968); W. M. H. Sachtler, G. J. H. Dorgelo, J. Fahrenfort, and R. J. H. Voorhoeve, *ibid.*, 4th Moscow, 34 (1968).
10) Y. Morooka and A. Ozaki, *J. Catal.*, **5**, 116 (1967); Y. Morooka and A. Ozaki, *ibid.*, **7**, 23 (1967).
11) G. K. Boreskov, *Advan. Catal.*, **15**, 285 (1964).
12) W. M. H. Sachtler and N. H. DeBoer, Proc. Intern. Cong. on Catalysis, 3rd Amsterdam, **1**, 252 (1964).

Interactions of 1-Substituted 2,4-Dinitrobenzenes with Methoxide and Hydroxide Ions in Dimethyl Sulfoxide with a Rapid Scan Spectrophotometer

Yoshinori HASEGAWA
College of General Education, Tohoku University, Kawauchi, Sendai 980
(Received January 7, 1974)

The interactions of *m*-dinitrobenzene and 1-substituted 2,4-dinitrobenzenes with sodium methoxide in methanolic dimethyl sulfoxide were studied with a rapid scan spectrophotometer. A similar study of 1-substituted 2,4-dinitrobenzenes with sodium hydroxide in aqueous dimethyl sulfoxide was carried out. Except for a few cases, the first transient colored-complexes of 3-substituted 2,6-dinitrocyclohexadienates were observed at initial stages before the complete formation of second colored-complexes having the π-electronic structures of 1,3-dinitropentadienyl anion.

In the interactions of aromatic dinitro compounds with nucleophiles, the initial formation of the kinetically-favored colored-complexes has been detected before the appearance of the thermodynamically-stable colored-complexes.[1,2] In the methoxide additions to *m*-dinitrobenzene and 2,4-dinitroanisole, thermodynamically-stable 1-methoxy-2,4-dinitrocyclohexadienate and 1,1-dimethoxy-2,4-dinitrocyclohexadienate, respectively, were detected by NMR and visible spectroscopy, but no kinetically-favored colored-complexes were detected.[3]

Studies have been made on the interactions of *m*-dinitrobenzene and 1-substituted 2,4-dinitrobenzenes with sodium methoxide in methanolic dimethyl sulfoxide (DMSO) with a rapid scan spectrophotometer. In order to extend the preceding study on the interactions of 1-substituted 2,4-dinitrobenzenes with sodium hydroxide,[1] the spectral changes of the DMSO solutions of some 1-substituted 2,4-dinitrobenzenes in the presence of sodium hydroxide have also been given.

Experimental

The dinitrobenzenes used are presented in Table 1. 2,4-Dinitrophenyl phenyl ether and 2,4-dinitrophenyl *p*-nitrophenyl ether were prepared according to Bost and Nicholson[4] and were recrystallized from methanol. Commercial dinitrobenzenes were purified by recrystallization or distillation.

Methanol was used for spectrophotometry. Sodium methoxide solutions were prepared by the reaction of clean sodium with methanol. Concentrations were determined by titration with a standard acid. DMSO was dried with calcium hydride and fractionated under reduced pressure.

A Hitachi rapid scan spectrophotometer RSP-2 was used to measure visible absorption spectra at various stages of a reaction path in solution. The mixing cell having a path length of 1.0 cm was controlled at 25 °C with a thermocirculater. Details of the apparatus and measurement were given in a previous paper.[1]

Results and Discussion

Interactions of m-*Dinitrobenzene and 2,4-Dinitroanisole with Sodium Methoxide.* When *m*-dinitrobenzene (6.4×10^{-5} M) was mixed with excess sodium methoxide (2.3×10^{-2} M) in DMSO-methanol (98/2, v/v), two colored-species having absorption maxima at 525 and 605 nm appeared 32 ms after mixing. 1/3 s after mixing, the first colored-species (λ_{max}=605 nm) disappeared and formation of the second (λ_{max}=525 nm) was complete. The second colored-species has been assigned to 1-methoxy-2,4-dinitrocyclohexadienate.[3a] It is known that the methoxide complexes having the π-electronic structures of 1,5-dinitropentadienyl anion in media rich in DMSO show longer wavelength bands in the range 585—640 nm.[1,5] The first colored-species is assigned to 1-methoxy-2,6-dinitrocyclohexadienate.

Spectra of 2,4-dinitroanisole in the presence of sodium methoxide showed the first (λ_{max}=560 nm) and second (λ_{max}=505 nm) colored-species, attributed to 1,3-dimethoxy-2,6-dinitrocyclohexadienate and 1,1-dimethoxy-2,4-dinitrocyclohexadienate, respectively.

Interactions of 2,4-Dinitrofluorobenzene, 2,4-Dinitrochlorobenzene, 2,4-Dinitrophenyl Phenyl Ether and 2,4-Dinitrophenyl p-*Nitrophenyl Ether with Sodium Methoxide.* All the solutions of these nitro compounds, containing sodium methoxide in a large excess, finally showed spectra similar to the spectrum of 1,1-dimethoxy-2,4-dinitrocyclohexadienate due to further reaction of methoxide ion with the resulting product of 2,4-dinitroanisole. In order to observe only the spectra of the colored-species formed from sodium methoxide and the nitro compounds, spectral measurements were carried

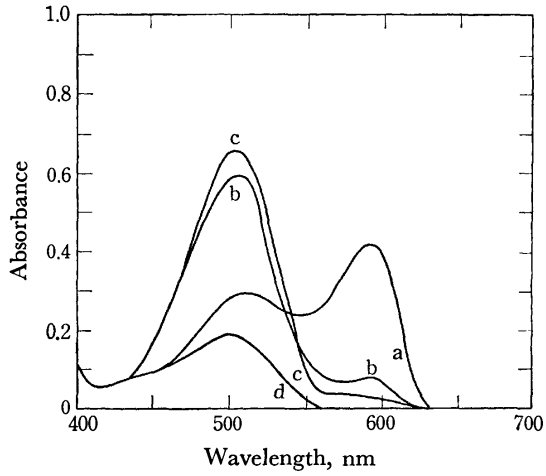

Fig. 1. Spectra observed with the DMSO solution containing 2,4-dinitrochlorobenzene (1.7×10^{-3}M), sodium methoxide (2.3×10^{-4} M) and methanol (2% by volume). Times measured after mixing: a, 30 ms; b, 1/3 s; c, 5 s; d, 30 s.

out under conditions where the concentration of the nitro compounds was several times larger than that of sodium methoxide.

The spectra observed with the DMSO solution containing 2,4-dinitrochlorobenzene (1.7×10^{-3} M), sodium methoxide (2.3×10^{-4} M) and methanol (2% by volume) are shown in Fig. 1. The first colored-species having an absorption peak at 590 nm appeared at initial stages and disappeared several seconds after mixing. Afterward the second colored-species having a peak at 505 nm gradually disappeared. The first colored-species is 1-methoxy-3-chloro-2,6-dinitrocyclohexadienate (**1**; X=Cl, Y=OMe). The second colored-species can be assigned to 2,4-dinitrocyclohexadienate which has the same π-electronic structures as 1,3-dinitropentadienyl anion of type **2** or **3** (X=Cl, Y=OMe).

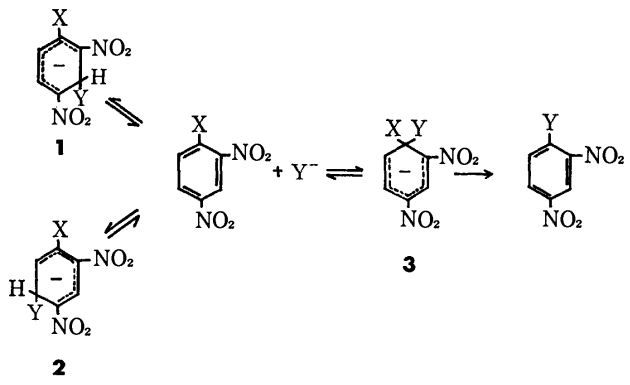

According to Crampton *et al.*,[6] the second colored-species should be ascribed to 1-methoxy-2,4-dinitro-5-chlorocyclohexadienate (**2**; X=Cl, Y=OMe).[1]

Spectra of 2,4-dinitrofluorobenzene, 2,4-dinitrophenyl phenyl ether and 2,4-dinitrophenyl *p*-nitrophenyl ether in the presence of sodium methoxide showed similar changes in the range 450—650 nm. The absorption maxima are listed in Table 1.

Interaction of 2,4-Dinitrotoluene with Sodium Methoxide. Spectra of 2,4-dinitrotoluene in the presence of sodium methoxide are shown in Fig. 2. At 3 s after mixing, the absorption bands initially observed at 530 and 600 nm disappeared and the bands at 410 and 650 nm remained. The bands at 530 and 600 nm are assigned to 2,4-dinitrocyclohexadienate of type **2** or **3** (X=CH_3, Y=OMe) and to 1-methoxy-3-methyl-2,6-dinitrocyclohexadienate (**1**; X=CH_3, Y=OMe), respectively. According to Pollitt and Saunders,[7] the bands at 410 and 650 nm are assigned to 2,4-dinitrobenzyl anion produced from 2,4-dinitrotoluene by loss of a proton.

Interactions of 2,4-Dinitrobenzoic Acid, 2,4-Dinitrobenzenesulfonic Acid, 2,4-Dinitrophenyl Thiocyanate and 2-(2,4-Dinitrophenylthio)benzothiazole with Sodium Methoxide. The absorption maxima of the colored-species obtained are listed and assigned in Table 1.

Interactions of 2,4-Dinitrophenyl Phenyl Ether, 2,4-Dinitrophenyl p*-Nitrophenyl Ether, 2,4-Dinitrophenyl Thiocyanate and 2-(2,4-Dinitrophenylthio)-benzothiazole with Sodium Hydroxide.* The spectra observed with the DMSO solution containing 2,4-dinitrophenyl phenyl ether (4.9×10^{-5} M), sodium hydroxide (2.3×10^{-3} M) and water (2% by volume) are shown in Fig. 3. The first colored-species having an absorption peak at 580 nm appeared at initial stages and disappeared within a minute. After the complete disappearance of the first colored-species, the second colored-species having a peak at 520 nm remained and then gradually disappeared. As the peak of the second colored-species decreased in intensity, the intensities of two peaks at 375 and 430 nm increased. The first and second colored-species are assigned to 1-hydroxy-3-phenoxy-2,6-dinitrocyclohexadienate (**1**; X=OPh, Y=OH) and to 2,4-dinitrocyclohexadienate of type **2** or **3** (X=OPh, Y=OH), respectively. The bands at 375 and 430 nm are due to 2,4-dinitrophenoxide ion.[1]

Spectra of 2,4-dinitrophenyl *p*-nitrophenyl ether, 2,4-dinitrophenyl thiocyanate and 2-(2,4-dinitrophenylthio)benzothiazole in the presence of sodium hydroxide

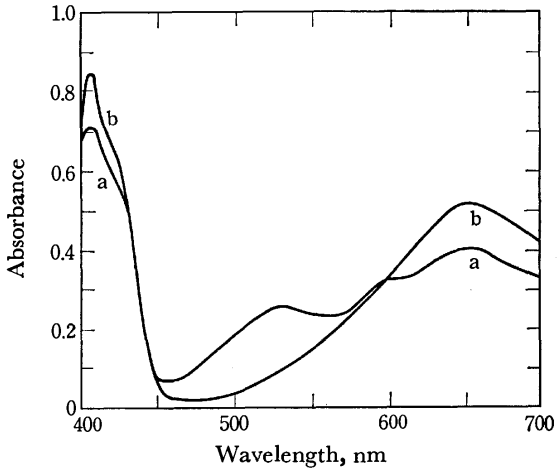

Fig. 2. Spectra observed with the DMSO solution containing 2,4-dinitrotoluene (4.0×10^{-5} M), sodium methoxide (5.9×10^{-3} M) and methanol (0.5% by volume) Times measured after mixing: a, 28 ms; b, 3 s.

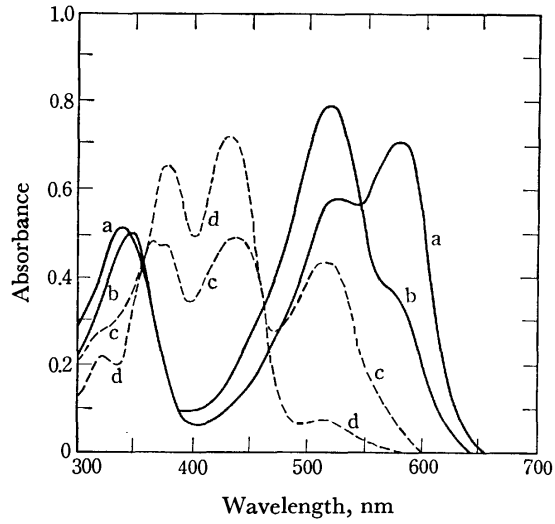

Fig. 3. Spectra observed with the DMSO solution containing 2,4-dinitrophenyl phenyl ether (4.9×10^{-5} M), sodium hydroxide (2.3×10^{-3} M) and water (2% by volume). Times measured after mixing: a, 1/3 s; b, 10 s; c, 4 min; d, 20 min.

Table 1. Visible absorption maxima (nm)

X	Y: OH[a] complex, Type 1	Y: OH[a] complex, Type 2 or 3	Y: OMe[b] complex, Type 1	Y: OMe[b] complex, Type 2 or 3
H	615[c]	535[c]	605	525
F	565[c]	505[c]	570	500
Cl	600[c,d]	510[c,d]	590	505
OMe	565[c]	505[c]	560	505
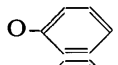	580	520	570	515
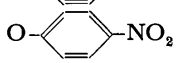	590	515	580	505
CH_3	Not observed	Not observed	600[e]	530[e]
COO^-	650[f]	550[f]	590	530
SO_3^-	Not observed	520	Not observed	520
SCN	600	480	590	485
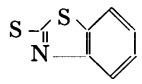	605	510	595	510

a) In DMSO–H_2O (98/2, v/v). b) In DMSO–MeOH (98/2, v/v). c) Ref. 1. d) In DMSO–H_2O (90/10, v/v). e) In DMSO–MeOH (99.5/0.5, v/v). f) In DMSO–H_2O (99/1, v/v).

showed similar changes. The absorption maxima of the colored-species are listed in Table 1.

Interactions of 2,4-Dinitrobenzoic Acid, 2,4-Dinitrobenzenesulfonic Acid and 2,4-Dinitrotoluene with Sodium Hydroxide. The absorption maxima of the colored-species obtained are listed in Table 1. In the presence of sodium hydroxide, 2,4-dinitrotoluene has bands at 410 and 650 nm attributed to 2,4-dinitrobenzyl anion, giving no hydroxide complex.

Substituent Effect on 2,6-Dinitrocyclohexadienate. We see from Table 1 that the substituents such as F and Cl except COO^- at 3-position shift the absorption bands of both 1-methoxy-2,6-dinitrocyclohexadienate and 1-hydroxy-2,6-dinitrocyclohexadienate towards blue. In contrast, the spectra of 4-substituted 2,6-dinitroanisole with methoxide ion show that the substituents such as F and Cl shift the band of 1,1-dimethoxy-2,6-dinitrocyclohexadienate towards red,[5b] and that electron-withdrawing substituents such as CF_3 shift it towards blue.[5b] The substituents at 3-position may produce a blue shift by twisting the nitro-groups from the planes of the rings, as described by Pollitt and Saunders in their studies on the Janovsky reaction.[7]

The author thanks Professor T. Abe for valuable suggestions.

References

1) Recent reviews and references are cited in: Y. Hasegawa and T. Abe, This Bulletin, **46**, 2756 (1973).

2) M. R. Crampton and H. A. Khan, *J. Chem. Soc. Perkin Trans. II*, **1972**, 1173. M. R. Crampton, M. A. El Ghariani, and H. A. Khan, *ibid.*, **1972**, 1178. M. R. Crampton and H. A. Khan, *ibid.*, **1972**, 2286. M. R. Crampton and H. A. Khan, *ibid.*, **1973**, 710. H. Wennerström and O. Wennerström, *Acta Chem. Scand.*, **26**, 2883 (1972).

3) a) M. R. Crampton and V. Gold, *J. Chem. Soc., B*, **1966**, 498; b) M. R. Crampton and V. Gold, *ibid.*, **1966**, 893; c) R. Foster and C. A. Fyfe, *Tetrahedron*, **21**, 3363 (1965); d) R. Foster, C. A. Fyfe, P. H. Emslie, and M. I. Foreman, *ibid.*, **23**, 227 (1967); e) W. E. Byrne, E. J. Fendler, J. H. Fendler, and C. E. Griffin, *J. Org. Chem.*, **32**, 2506 (1967).

4) R. W. Bost and F. Nicholson, *J. Amer. Chem. Soc.*, **57**, 2368 (1935).

5) a) F. Millot and F. Terrier, *Bull. Soc. Chim. France*, **1969**, 2692; b) F. Terrier and F. Millot, *ibid.*, **1970**, 1743; c) F. Terrier and M. P. Simonnin, *ibid.*, **1971**, 677; d) F. Terrier, J. C. Hallé, and M. P. Simonnin, *Org. Magn. Resonance*, **3**, 361 (1971).

6) M. R. Crampton, M. A. Ghariani, and H. A. Khan, *Tetrahedron*, **28**, 3299 (1972).

7) R. J. Pollitt and B. C. Saunders, *J. Chem. Soc.*, **1965**, 4615.

Thermochemical Studies on Platinum-Olefin Complexes. I

Manabu SENŌ, Kazutoshi IWAMOTO, and Teruzo ASAHARA
Institute of Industrial Science, The University of Tokyo, Minato-ku, Tokyo 106

(Received February 5, 1974)

Using a twin-type calorimeter, the enthalpy changes of solutions and reactions with aqueous KCN solution of Zeise's salts, $K[PtCl_3(olefin)]$, were measured. As ligand olefins, ethylene, propylene, 1-butene, 1-pentene, and 1-hexene were employed. It was estimated from a thermochemical analysis that the order of strength of platinum-olefin bonding is as follows; $K[PtCl_3(C_3H_6)] \gtrsim K[PtCl_3(C_2H_4)] \gtrsim K[PtCl_3(1\text{-}C_6H_{12})] \gtrsim K[PtCl_3(1\text{-}C_4H_8)] \gtrsim K[PtCl_3(1\text{-}C_5H_{10})]$. This order was compared with the data of infrared spectra and both the results coincide with each other.

In 1953, the nature of the bonding between an olefinic ligand and platinum atom in Zeise's salt, $K[PtCl_3(olefin)]$, was first interpreted by Chatt and Duncanson,[1] by applying the model for the bonding between Ag(I) and olefin ligands proposed by Dewar.[2] According to their model, besides a molecular μ-bond formed between the filled olefin π-molecular orbital and one of the vacant $5d6s6p^2$ platinum hybrid orbitals, the overlap between the vacant olefinic antibonding π^*-molecular orbital and one of the filled 5d6s platinum hybrid atomic orbitals was considered as an addition bonding to account for the stability of these metal-olefin complexes. Since then, theoretical and experimental studies on this metal-olefin bonding have been made through measurements of IR,[3] UV,[4] and NMR.[5] In order to get a further information, it would be useful to measure the enthalpy changes of the reactions (1) and (2).

$$K_2PtCl_4(c) + \text{olefin}(g) \longrightarrow K[PtCl_3(\text{olefin})](c) + KCl(c) \quad (1)$$

$$[PtCl_4]^{2-}(s) + \text{olefin}(g) \longrightarrow [PtCl_3(\text{olefin})]^-(s) + Cl^-(s) \quad (2)$$

Notations (c), (s), and (g) refer to crystalline, solvated and gaseous state, respectively. The calorimetric measurements of heats of reactions (1) and (2) with water-soluble olefins such as $CH_2{=}CH(CH_2)_nNH_3^+$ were carried out by Denning *et al.*[6] and Orchin,[7] but no measurement was yet done on Zeise's salts having simple olefins such as ethylene and propylene as ligands. The aim of this paper is to present the result of this measurement.

Experimental

Synthesis of $K[PtCl_3(olefin)]$. $K[PtCl_3(C_2H_4)]$, $K[PtCl_3(C_3H_6)]$, and $K[PtCl_3(1\text{-}C_4H_8)]$ were prepared from K_2PtCl_4 according to the method described by MacNevin *et al.*[8] The products were recrystallized twice from an aqueous 3% HCl solutions and the purity was checked by elemental analysis. $K[PtCl_3(1\text{-}C_5H_{10})]$ and $K[PtCl_3(1\text{-}C_6H_{12})]$ were prepared as follows; 5 g of K_2PtCl_4 was dissolved in 50 ml of an aqueous 3% HCl solution and stirred with introducing 1-pentene or 1-hexene for a few weeks in a sealed flask. After filtering, the filtrate was concentrated under low pressure and cooled to get yellow crystals. The crystals were washed with cold water and recrystallized twice from an aqueous 3% HCl solutions and the purity was checked by elemental analyses.

Calorimetric Measurements. A twin-type microcalorimeter, Tokyo Rico Type TCC-65, was used for the following calorimetric measurements. All the measurements were carried out at 25 °C. Anderson reported the next reaction.[9]

$$K[PtCl_3(C_2H_4)](c) + 4KCN(s) \longrightarrow K_2Pt(CN)_4(s) + C_2H_4 + 3KCl(s) \quad (3)$$

The reaction in an aqueous KCN solution proceeds rapidly and quantitatively at room temperature. The next reaction is also known to proceed in an aqueous KCN solution.

$$K_2PtCl_4(c) + 4KCN(s) \longrightarrow K_2Pt(CN)_4(s) + 4KCl(s) \quad (4)$$

Here, the following reaction schemes are supposed for convenience of construction of thermodynamic cycles.

$$K_2PtCl_4(c) + 4CN^-(s) \xrightarrow{\Delta H_I} 2K^+(s) + [Pt(CN)_4]^{2-}(s) + 4Cl^-(s) \quad (I)$$

$$K[PtCl_3(\text{olefin})](c) + 4CN^-(s) \xrightarrow{\Delta H_{II}} K^+(s) + [Pt(CN)_4]^{2-}(s) + 3Cl^-(s) + \text{olefin}(g) \quad (II)$$

$$K_2PtCl_4(c) \xrightarrow{\Delta H_{III}} 2K^+(s) + [PtCl_4]^{2-}(s) \quad (III)$$

$$K[PtCl_3(\text{olefin})](c) \xrightarrow{\Delta H_{IV}} K^+(s) + [PtCl_3(\text{olefin})]^-(s) \quad (IV)$$

$$KCl(c) \xrightarrow{\Delta H_V} K^+(s) + Cl^-(s) \quad (V)$$

By combining reactions (I), (II), and (V), we got

$$K_2PtCl_4(c) + \text{olefin}(g) \xrightarrow{\Delta H_1} K[PtCl_3(\text{olefin})](c) + KCl(c) \quad (1)$$

$$\Delta H_1 = \Delta H_I - \Delta H_{II} - \Delta H_V \quad (5)$$

By combining reactions (I), (II), (III), (IV), and (V), we got

$$[PtCl_4]^{2-}(s) + \text{olefin}(g) \xrightarrow{\Delta H_2} [PtCl_3(\text{olefin})]^-(s) + Cl^-(s) \quad (2)$$

$$\Delta H_2 = \Delta H_I - \Delta H_{II} - \Delta H_{III} + \Delta H_{IV} \quad (6)$$

The heats of Reactions (1) and (2) can be obtained from (5) and (b) by using measured values for Reactions (I)—(V).

Heats of Solution. The heat of solution of potassium chloride was measured when an accurately weighed sample (about 37.7 mg) of potassium chloride (guaranteed reagent) was dissolved in 50 ml of pure water in the microcalorimeter. The sample was dried beforehand to constant weight by heating under high vacuum. The heat of solution of potassium tetrachloroplatinate was measured when about 49.8mg (1.2×10^{-4} mol) of potassium tetrachloroplatinate was dissolved in 40 ml of an aqueous 3% HCl solution. Potassium tetrachloroplatinate was used after twice recrystallization.

The heats of solution of $K[PtCl_3(olefin)]$ was determined when about 1.2×10^{-4} mol of $K[PtCl_3(olefin)]$ was dissolved in 40 ml of an aqueous 3% HCl solutions in the microcalorimeter.

Heats of Reactions. An aqueous KCN solution used hereafter was prepared by dissolving about 800 mg of KCN (guaranteed reagent) into 40 ml of pure water. The heat of reaction between potassium tetrachloroplatinate and the aqueous KCN solution was measured when about 200 mg (4.8×10^{-4} mol) of K_2PtCl_4 was put into the KCN solution and reacted. The heats of reaction between $K[PtCl_3(olefin)]$ and the aqueous KCN solution was measured when about 4.8×10^{-4} mol of $K[PtCl_3(olefin)]$ was put into the KCN solutions and reacted in the microcalorimeter.

Results and Discussion

The enthalpy change of potassium chloride at 25 °C was measured thirty times, and the average $\Delta\bar{H}_V$ and the dispersion σ^2 of measured values ΔH_V were determined as follows.

$$\Delta\bar{H}_V = 4.490\ \text{kcal}\cdot\text{mol}^{-1}$$

$$\sigma^2 = 1/(30-1)\sum(\Delta H_V-\Delta\bar{H}_V)^2 = 0.07748$$

We adopted this σ^2 value as a mother dispersion of heat measurements. On the other hand, as the standard value of the heat of solution of potassium chloride at 25 °C was reported to be 4.146 kcal·mol^{-1}, we corrected the measured values by using this standard value.[10]

The corrected values of the enthalpy changes of solutions of complexes are shown in Table 1 and the enthalpy changes of complexes with an aqueous KCN solution were given in Table 2. The enthalpy changes of reactions (1) and (2) were calculated by using Eqs. (5) and (6) from these values and listed in Table 3.

Let's consider the following thermodynamic cycles to get an information for the bond strength of Pt-olefin in gaseous state.

Table 1. Enthalpy changes of solution of complexes

Molecular formula of complexes	Enthalpy changes of solution ΔH_{III} or ΔH_{IV} (kcal·mol^{-1})
K_2PtCl_4	12.6±0.2
$K[PtCl_3(C_2H_4)]$	10.2±0.2
$K[PtCl_3(C_3H_6)]$	10.5±0.2
$K[PtCl_3(1\text{-}C_4H_8)]$	10.4±0.2
$K[PtCl_3(1\text{-}C_5H_{10})]$	10.9±0.2
$K[PtCl_3(1\text{-}C_6H_{12})]$	10.8±0.2

Table 2. Enthalpy changes of reactions of complexes with aqueous KCN solution

Molecular formula of complexes	Enthalpy changes of reactions ΔH_I or ΔH_{II} (kcal·mol^{-1})
K_2PtCl_4	−87.8±0.3
$K[PtCl_3(C_2H_4)]$	−79.3±0.4
$K[PtCl_3(C_3H_6)]$	−77.0±0.6
$K[PtCl_3(1\text{-}C_4H_8)]$	−80.7±0.4
$K[PtCl_3(1\text{-}C_5H_{10})]$	−79.2±0.4
$K[PtCl_3(1\text{-}C_6H_{12})]$	−80.8±0.5

Table 3. Enthalpy changes of Reactions (1) and (2)

Olefin	ΔH_1 (kcal·mol^{-1})	ΔH_2 (kcal·mol^{-1})
Ethylene	−12.6±0.5	−10.9±0.6
Propylene	−14.9±0.7	−13.2±0.7
1-Butene	−11.3±0.5	−9.3±0.6
1-Pentene	−12.7±0.5	−10.2±0.6
1-Hexene	−11.1±0.7	−8.8±0.7

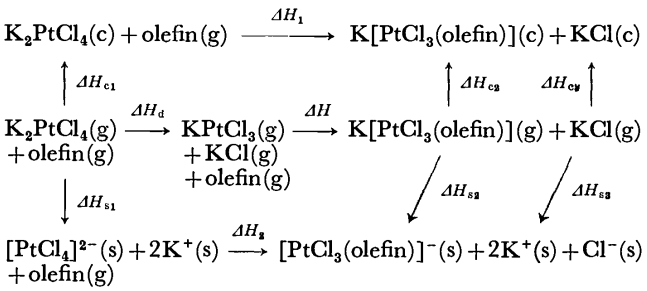

$$\Delta H = \Delta H_1 + \Delta H_{c1} - \Delta H_{c2} - \Delta H_{c3} - \Delta H_d$$
$$= \Delta H_2 + \Delta H_{s1} - \Delta H_{s2} - \Delta H_{s3} - \Delta H_d \qquad (7)$$

Here, ΔH_{c1}, ΔH_{c2}, and ΔH_{c3} are enthalpy changes of crystallization, and ΔH_{s1}, ΔH_{s2}, and ΔH_{s3} are enthalpy changes of electrolytic dissolution of K_2PtCl_4, KCl, and $K[PtCl_3(olefin)]$, respectively. ΔH_{c1}, ΔH_{c3}, ΔH_{s1}, ΔH_{s3} and ΔH_d are independent of olefin. By collecting these olefin-independent terms, Eq. (7) is rearranged as follows.

$$\Delta H = \Delta H_1 - \Delta H_{c2} + \Delta H'$$
$$= \Delta H_2 - \Delta H_{s2} + \Delta H''$$

where

$$\Delta H' = \Delta H_{c1} - \Delta H_{c3} - \Delta H_d$$
$$\Delta H'' = \Delta H_{s1} - \Delta H_{s3} - \Delta H_d$$

The value of ΔH_{c2} is the lattice energy of $K[PtCl_3(olefin)]$ and the value of ΔH_{s2} contains the dissociation energy of $K[PtCl_3(olefin)]$ and the solvating energies of resulting ions, K^+ and $[PtCl_3(olefin)]^-$. It would be tentatively assumed that these values are not influenced by the kind of olefin to a greater extent. Under this assumption, we get the following strength order of platinum-olefin bonds.

$$K[PtCl_3(C_3H_6)] \gtrsim K[PtCl_3(C_2H_4)] \gtrsim K[PtCl_3(1\text{-}C_6H_{12})]$$
$$\gtrsim K[PtCl_3(1\text{-}C_4H_8)] \gtrsim K[PtCl_3(1\text{-}C_5H_{10})]$$

We may compare this result with that of infrared spectrum. Sorzano[11] reported that the band of 491 cm^{-1} in $K[PtCl_3(C_2H_4)]$ is assigned to the Pt-‖ stretching vibration. Some authors[3,12] assigned the 1526 cm^{-1} band to the C=C stretching vibration. Recently, Hiraishi[13] assigned the 1250 cm^{-1} band to this mode by considering the Raman spectrum, and assigned the 1526 cm^{-1} band to the C–H scissoring vibration. The values of the infrared spectra of various complexes measured in the present investigation are listed in Table 4. It is seen from this table that the frequency of Pt-‖ stretching vibration in the propylene complex is higher than that in the other complexes. The higher the frequency of Pt-‖ stretching vibration is,

Table 4. Infrared data of $K[PtCl_3(olefin)]$

Molecular formula	Pt-|| stretching vib. cm^{-1}	C=C stretching vib. cm^{-1}	
$K[PtCl_3(C_2H_4)]$	490	1250	1526
$K[PtCl_3(C_3H_6)]$	495	1245	1506
$K[PtCl_3(1\text{-}C_4H_8)]$	490	1250	1504
$K[PtCl_3(1\text{-}C_5H_{10})]$	492	1252	1501
$K[PtCl_3(1\text{-}C_6H_{12})]$	490	1251	1500

the stronger the bonding is and, therefore, the bonding between platinum-propylene is considered to be stronger than the others. Moreover, it is known that the C=C stretching vibration shifts to lower frequencies upon coordination to the Pt atom. According to Hiraishi, the C=C stretching vibration is in a region near 1250 cm^{-1}. This band is 1250 cm^{-1} in the case of the ethylene complex and 1245 cm^{-1} in the case of the propylene complex. These values mean that propylene coordinates to the Pt atom stronger than ethylene. These results coincide with our data of calorimetric measurements.

References

1) J. Chatt and L. A. Duncanson, *J. Chem. Soc.*, **1953**, 2939.
2) M. J. S. Dewar, *Bull. Soc. Chim. Fr.*, **1951**, C71.
3) S. I. Shupack and M. Orchin, *J. Amer. Chem. Soc.*, **85**, 902 (1963).
4) S. I. Shupack and M. Orchin, *J. Chem. Soc.*, **1964**, 586.
5) P. D. Kaplan and M. Orchin, *Inorg. Chem.*, **4**, 1393 (1965); R. Cramer, *ibid.*, **4**, 445 (1965). T. Ibusuki and Y. Saito, *Chem. Lett.*, **1973**, 1255.
6) a) R. G. Denning, F. R. Hartley, and L. M. Venanzi, *J. Chem. Soc., A*, **1967**, 324. b) R. G. Denning, F. R. Hartley, and L. M. Venanzi, *ibid.*, **1967**, 328. c) F. R. Hartley and L. M. Venanzi, *ibid.*, **1967**, 330. d) R. G. Denning and L. M. Venanzi, *ibid.*, **1967**, 336.
7) J. R. Joy and M. Orchin, *ibid.*, **1959**, 305.
8) A. Giddings, W. MacNevin, and A. Foris, *Chem. Ind.* (London), **1958**, 557.
9) J. S. Anderson, *J. Chem. Soc.*, **1934**, 971.
10) G. Somsen, J. Coops, M. W. Tolk, *Rec. Trav. Chim. Pays-Bas*, **82**, 231 (1963).
11) J. P. Sorzano and J. P. Fackler, *J. Mol. Spectrosc.*, **22**, 88 (1967).
12) M. J. Grogan and K. Nakamoto, *J. Amer. Chem. Soc.*, **88**, 5454 (1966).
13) J. Hiraishi, *Spectrochim. Acta*, **25A**, 749 (1969).

Heat Capacity of Nematogenic *N*-*p*-Ethoxybenzylidene-*p'*-butylaniline between 14 and 375 K

Michio Sorai, Teruo Nakamura,* and Syûzô Seki
Department of Chemistry, Faculty of Science, Osaka University, Toyonaka, Osaka 560

(Received April 24, 1974)

The heat capacity of a low-temperature liquid crystal EBBA (*N*-*p*-ethoxybenzylidene-*p'*-butylaniline) of 99.75% (mol) purity was measured in the range 14—375 K with an adiabatic calorimeter. The melting point T_m was 305.62 K, and the enthalpy and entropy of fusion 27.09 kJ mol^{-1} and 88.71 J K^{-1} mol^{-1}, respectively. The temperature of mesomorphic transition T_c from nematic to isotropic liquid was 349.08 K, and the enthalpy and the entropy changes due to the mesomorphic transition were 1.553 kJ mol^{-1} and 4.524 J K^{-1} mol^{-1}, respectively. Excess heat capacity due to the mesophase transition, C(excess), is represented by $C(\text{excess}) \sim \varepsilon^{-0.7}$ in the range $10^{-4} < \varepsilon < 10^{-1.5}$, where $\varepsilon \equiv |T - T_c|/T_c$. This implies that the mesomorphic transition of EBBA can be regarded as of critical phenomena, characterized by a second-order rather than a first-order nature.

Liquid crystals are recently being reinvestigated both experimentally and theoretically. Studies on thermotropic liquid crystals are mainly devoted to elucidating the relationship between molecular geometry and liquid crystallinity and to clarifying the mechanism of mesomorphic transition based on the intermolecular forces and the order of molecular arrangements. The revival has been partially promoted by recent development in the industrial application of liquid crystals.

From a thermodynamic point of view the study of liquid crystals is interesting in the sense that a cooperative phase transition can be realized even in a liquid state. Thermodynamic quantities such as heat capacity, enthalpy, entropy, and free energy provide useful information on the energetic aspects inherent to a mesophase transition and are indispensable for understanding of the mesophase transition.

Compared with thermal analytic studies, precise calorimetric investigations are extremely scarce, which is partly due to the simplicity of thermal analyses. Mesophase transitions can be estimated qualitatively by simple thermal analyses, but quantitative information can be obtained only by significant calorimetric measurements.

As an extension of previous studies[1-4] we deal in this paper with the heat capacity of *N*-*p*-ethoxybenzylidene-*p'*-butylaniline (EBBA), which is known to exhibit a nematic mesophase in the range 36—80 °C.[5-7] The heat capacity of a more simple compound in this homologous series, MBBA (*N*-*p*-methoxybenzylidene-*p'*-butylaniline), has been measured by Mayer *et al.*[8] and Shinoda *et al.*[9] We have determined the heat capacity of OHMBBA, an *o*-hydroxy analog of MBBA, and found a glassy state of the nematic phase.[2,3] We attempted to establish a glassy liquid crystalline state for EBBA without success, though a glass transition phenomenon was found in many compounds of this homologous series.[4]

The order of mesomorphic transitions in liquid crystals is a current problem. We have attempted to analyze the mesophase transition from nematic to isotropic liquid in terms of critical phenomena.

* Present address: Department of Chemistry, Faculty of Science, Osaka City University, Sugimoto-cho, Osaka 558.

Experimental

Material. The nematogenic substance EBBA was prepared by the usual condensation reaction of *p*-butylaniline (Wako Pure Chemical Industries, Ltd.) with *p*-ethoxybenzaldehyde (Tokyo Kasei Kogyo Co., Ltd.) in ethanol. The product was recrystallized twice from ethanol and then twice from *n*-hexane. Found: C, 81.14; H, 8.30; N, 4.98%. Calcd for $C_{19}H_{23}NO$: C, 81.10; H, 8.24; N, 4.98%.

Thermal Analysis. Differential thermal analysis (DTA)[10] was carried out between −170 and 100 °C for a preliminary study of the thermal behavior of EBBA, about 500 mg of specimen being used.

Heat Capacity Measurement. The heat capacity of EBBA was measured with an adiabatic calorimeter[11] in the range 14—275 K. The all-gold calorimeter cell of approximately 35 cm^3 internal volume contained 17.8685 g (0.0634983 mol) of EBBA. The empty space was filled with helium gas at 1 atm pressure and room temperature to aid the heat transfer. A platinum resistance thermometer has been calibrated based on IPTS-68 scale.

Results and Discussion

Thermal Behavior. The thermal behavior of EBBA is illustrated in Fig. 1. A heating curve at the rate 2.5 K min^{-1} is shown by run 1. Melting point T_m of the stable crystal is 32.5 °C and the transition point T_c from nematic to isotropic liquid is 79.5

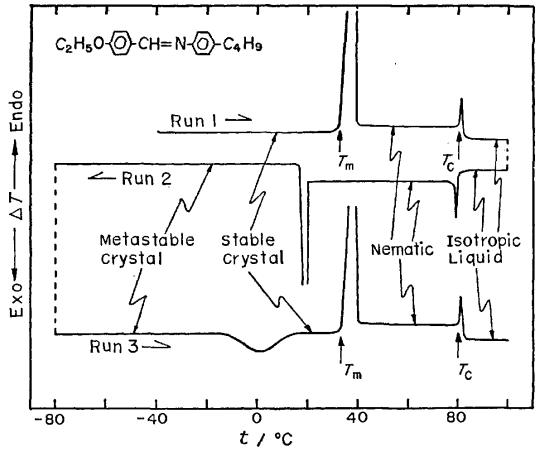

Fig. 1. DTA curves for EBBA.

TABLE 1. HEAT CAPACITY OF *N*-*p*-ETHOXY-BENZYLIDENE-*p'*-BUTYLANILINE (Molecular Weight 281.4013.)

T/K	C_p/J K^{-1} mol^{-1}	T/K	C_p/J K^{-1} mol^{-1}	T/K	C_p/J K^{-1} mol^{-1}	T/K	C_p/J K^{-1} mol^{-1}
(Crystal)		86.111	142.79	226.323	312.93	334.975	580.97
14.519	10.332	88.570	146.22	229.678	317.94	336.285	583.96
15.417	12.133	91.353	149.92	233.991	323.40	338.469	590.88
16.297	13.473	94.199	153.66	238.581	329.47	339.491	595.68
17.184	15.302	96.983	157.36	243.116	335.84	340.629	601.27
18.085	16.984	99.711	160.84	247.594	342.01	342.240	609.25
19.033	18.865	101.900	163.56	252.019	348.89	343.315	613.46
20.044	20.991	104.855	167.31	256.388	355.19	343.909	619.94
21.126	23.199	107.758	170.88	261.008	362.60	344.382	623.43
22.298	25.542	110.613	174.31	265.868	370.04	345.269	629.94
23.505	28.239	113.423	177.77	269.472	376.37	345.970	638.01
24.739	30.838	116.191	181.22	275.260	384.84	346.661	657.66
26.050	33.634	118.918	184.67	279.849	392.21	347.346	673.87
27.439	36.709	121.676	187.63	284.673	399.73	348.013	701.15
28.896	39.910	124.603	191.10	289.419	408.56	348.632	825.96
30.629	43.736	128.095	195.00	294.101	417.27	349.041	2592.7
32.571	48.086	132.004	199.67	298.718	431.16	T_c=349.08 K	
34.509	52.388	135.853	204.31	302.568	548.86	(Isotropic Liquid)	
36.538	56.781	139.643	208.51	304.319	1586.0	349.493	931.81
38.998	61.882	143.378	212.79	305.240	10639	349.522	613.20
41.782	67.824	147.061	217.08	305.453	35171	350.976	598.21
44.448	73.539	151.051	221.79	T_m=305.62K		351.425	592.90
46.990	78.661	154.553	225.62	(Nematic Liquid Crystal)		351.892	591.21
49.449	83.530	158.327	230.35	306.455	781.74	352.992	589.31
51.842	87.946	162.413	235.27	308.325	537.58	353.670	585.60
54.189	92.449	166.807	240.09	310.425	539.22	355.073	588.31
54.914	93.594	171.252	244.74	312.594	541.86	355.919	586.06
57.430	98.213	175.748	249.68	314.837	544.24	358.464	586.48
59.829	100.42	180.185	255.40	317.071	548.23	361.576	585.12
62.127	106.39	184.561	260.33	318.381	550.93	364.965	585.58
64.451	110.26	188.881	265.74	319.295	552.38	368.344	589.53
66.805	114.15	193.149	270.35	322.061	554.74	371.719	588.27
69.082	117.67	197.351	276.24	322.214	554.49	(Supercooled Nematic	
71.284	121.27	201.500	280.81	325.907	561.61	Liquid Crystal)	
73.425	124.46	205.615	286.05	326.423	561.96	298.910	526.70
75.522	127.52	209.680	291.55	329.634	568.68	300.138	528.96
77.704	130.95	213.693	296.03	330.399	570.02	301.977	530.60
79.215	132.93	218.314	302.51	331.864	572.82	304.415	533.38
81.567	136.43	223.209	308.97	334.077	579.26	306.844	535.42
83.862	139.73						

°C. The values of T_m and T_c are approximately the same as those previously given.[5-7] A cooling curve of the isotropic liquid at the rate $-2\sim-500$ K min^{-1} is shown by run 2. Within this range the isotropic liquid was transformed into the nematic phase at the same temperature T_c without indication of thermal hysteresis. The sample in nematic state was supercooled to 20 °C at which temperature it crystallized into a metastable crystalline form. The cooling rate -500 K min^{-1} was not great enough attaining a glassy state of liquid crystal.[1-4] A heating curve at the rate 2.5 K min^{-1} is shown by run 3. The metastable crystal was irreversibly transformed into a stable one with heat evolution between -15 and 15 °C. Once stabilized, the thermal behavior remained the same as that shown by run 1.

Heat Capacity. The results of calorimetric measurements have not been converted into molar heat capacity under the saturation vapor pressure C_{sat}, due to the lack of data on density, vapor pressure, and heat of vaporization. The present results (Table 1, Fig. 2) correspond approximately to the molar heat capacity at constant pressure C_p, although a minor effect of vaporization of the specimen into the narrow empty space of the calorimeter cell might be included in the liquid state.

The temperature of the triple point and a concentration of impurity involved in the sample were evaluated from a series of temperature measurements with various fractions of the sample in the liquid state (Table 2). The values obtained closely follow the Mastrangelo-Dornte equation,[12] derived by assuming the formation of solid solution, rather than the ideal solution equation based on Raoult's law. The variation of temperature with the fraction melted could be represented by

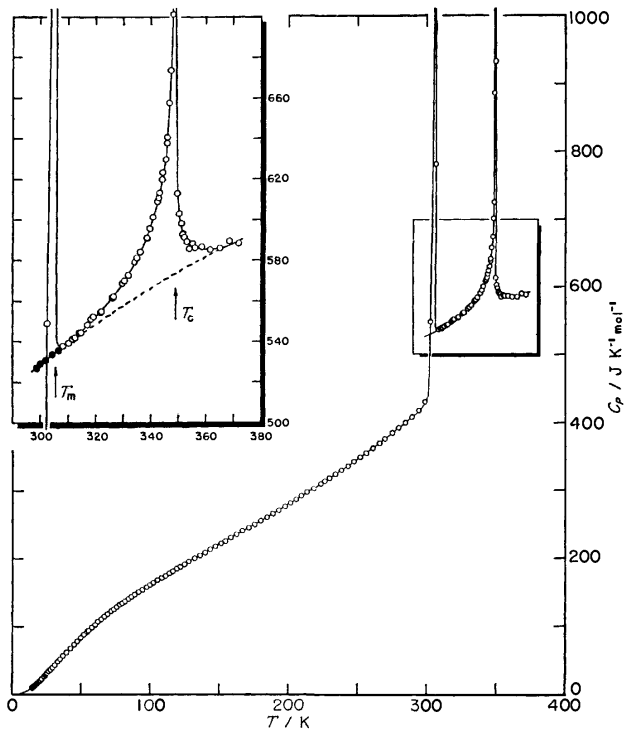

Fig. 2. Molar heat capacity of EBBA. Solid circles correspond to the heat capacity of supercooled nematic phase. Broken line indicates a normal heat capacity which separates the excess heat capacity due to phase transition from the total C_p.

Table 2. Melting temperature of EBBA

Fraction melted (F)	Osberved T/K	Calculated T/K
0.1999	305.403	305.403
0.3287	305.503	305.502
0.4592	305.552	305.550
0.5245	305.566	305.566
0.5903	305.577	305.578
0.6562	305.583	305.589
0.7219	305.595	305.597
0.7878	305.602	305.604
0.8536	305.611	305.610
0.9194	305.622	305.616
Triple point of sample		305.621
Triple point of pure EBBA		305.688

$$T = 305.6876 - 0.06928/(0.04388+F),$$

where F is the fraction melted. The most probable numerical values were determined by computer-iteration. The melting point of EBBA could be derived from the value of triple point by means of Clausius-Clapeyron's equation if the data of molar volume were available for both solid and liquid states. Lack of such data prevented us from making the evaluation and the triple point is approximately regarded as equal to melting point. The concentration of impurity was determined to be 0.25 mol percent.

The thermodynamic functions of EBBA were calculated from heat capacity data and the calorimetric enthalpies of fusion and mesomorphic transition (Table 3). Values are given for heat capacity $C_p°$, entropy $S°$, enthalpy function $(H°-H_0°)/T$, and the Gibbs energy function $-(G°-H_0°)/T$, at selected temperatures. The values at 5 and 10 K were estimated by means of an effective frequency-distribution method.[13]

Table 3. Thermodynamic functions of *N-p*-ethoxybenzylidene-*p'*-butylaniline in the standard state

T/K	$C_p°$ / J K^{-1} mol^{-1}	$S°$ / J K^{-1} mol^{-1}	$(H°-H_0°)/T$ / J K^{-1} mol^{-1}	$-(G°-H_0°)/T$ / J K^{-1} mol^{-1}
		Crystal		
5	(0.5354)	(0.179)	(0.134)	(0.045)
10	(4.0435)	(1.398)	(1.044)	(0.354)
15	11.282	4.302	3.164	1.137
20	20.806	8.815	6.352	2.463
25	31.396	14.583	10.291	4.292
30	42.392	21.276	14.722	6.554
35	53.406	28.640	19.463	9.176
40	64.182	36.478	24.383	12.095
45	74.563	44.642	29.387	15.255
50	84.467	53.015	34.404	18.611
60	102.75	70.062	44.299	25.763
70	119.19	87.156	53.843	33.313
80	134.18	104.064	62.961	41.103
90	148.10	120.681	71.656	49.025
100	161.22	136.971	79.963	57.008
110	173.57	152.920	87.916	65.004
120	185.83	168.549	95.566	72.983
130	197.28	183.875	102.949	80.926
140	208.92	198.928	110.109	88.819
150	220.55	213.737	117.082	96.655
160	232.36	228.339	123.910	104.429
170	243.43	242.764	130.621	112.143
180	255.17	256.998	137.202	119.796
190	266.95	271.105	143.716	127.389
200	279.16	285.106	150.180	134.926
210	291.91	299.028	156.619	142.409
220	304.63	312.891	163.048	149.843
230	318.35	326.726	169.494	157.232
240	331.46	340.548	175.966	164.582
250	345.76	354.365	182.468	171.897
260	360.98	368.219	189.038	179.181
270	377.14	382.139	195.699	186.440
273.15	381.75	386.540	198.965	187.575
280	392.44	396.125	202.446	193.679
290	409.64	410.184	209.282	200.902
298.15	429.09	421.788	216.148	205.640
300	466.02	424.455	216.339	208.116
		Nematic Liquid Crystal		
310	538.89	528.586	311.940	216.646
320	552.52	545.887	319.222	226.665
330	569.36	563.124	326.524	236.600
340	598.24	580.644	334.053	246.591
		Isotropic Liquid		
350	606.54	598.596	342.239	256.357
360	585.81	615.197	349.101	266.096
370	589.05	631.267	355.517	275.750

Enthalpy and entropy of fusion are listed in Table 4 together with changes due to mesomorphic transition.

Mesomorphic Transition. As in the case of OHMBBA,[3] the present mesomorphic transition is

characterized by a remarkable effect of pretransition. The effect, which results from easy fluctuation of the orientational order parameter in the vicinity of T_C, is obviously reflected in a large tail of the heat capacity curve below the transition point T_C. Recently, Goren *et al.*[14] measured the proton spin-lattice relaxation time of this compound in a wide temperature range and found that fluctuation of the order parameter is predominant around the mesomorphic transition point. The present result obtained from the heat capacity measurements is quite compatible with that of their nuclear magnetic resonance experiment.

The excess heat capacity, C(excess), due to the mesophase transition was determined by subtracting a normal heat capacity, C_p(normal), from the experimental one, C_p. The following quadratic equation was assumed for C_p(normal):

$$C_p(\text{normal}) = -2.6387\times10^{-3}T^2+2.6284T-22.214,$$

which corresponds to a curve passing through the three experimental C_p points at 300.138, 304.415, and 364.965 K. The enthalpy and entropy of transition were determined by integrating the C(excess) with respect to T and ln T, respectively (Table 4).

Table 4. Enthalpy and entropy of transition for EBBA

Transition	T / K	ΔH / kJ mol^{-1}	ΔS / J K^{-1} mol^{-1}
Crystal→Nematic (T_m)	305.62[a]	27.09	88.71
Nematic→Isotropic Liquid (T_C)	349.08	1.553	4.524

a) Melting point for the pure material T_m°=305.69 K.

With a differential scanning calorimeter (DSC) Smith and Gardlund[7] determined the enthalpy of mesophase transition to be 523 J mol^{-1}, which amounts to only one third of the present calorimetric value. A shortcoming inherent to thermal analysis with DSC is inability to detect a mild thermal change occurring gradually. In a mesomorphic transition, the contribution from the pretransitional region to ΔH is considerably large. In the DSC method, however, only a truncated part of a heat-capacity peak is detected. The large discrepancy between the DSC method and the present calorimetric measurement is therfore attributable to the underestimation of ΔH in the former method.

The order of phase transition provides useful information on the nature of transition. Except for the smectic-A to nematic (S_AN) transition[15,16] all other mesomorphic transitions are believed to be of first-order. No paper seems to have appeared dealing with the examination of the order of the nematic to isotropic liquid (NI) transition. It was difficult to decide whether the NI transition of EBBA is first-order or not, since, we have not measured the heat capacity in a cooling direction to examine the existence of thermal hysteresis, and the enthalpy of transition was too small to detect a latent heat.

We attempted to analyze the NI mesomorphic transition according to the treatment of critical phenomena.[17-19] If C(excess) is varied with the critical-point exponents α' and α for $\varepsilon(\equiv|T-T_C|/T_C)$, when $T\to T_C\pm0$, by

$$C(\text{excess}) \sim \varepsilon^{-\alpha'} \quad \text{for } T < T_C$$

and

$$C(\text{excess}) \sim \varepsilon^{-\alpha} \quad \text{for } T > T_C,$$

linearity is expected in the vicinity of the critical point T_C in a log C(excess) *versus* log ε plot (Fig. 3). We see that there is a linear region ($10^{-1.5}>\varepsilon>10^{-4}$) for both $T<T_C$ and $T>T_C$. The critical-point exponents were determined to be $\alpha'=\alpha=0.7$ as the slopes of these straight lines. This implies that the present NI transition can be treated as a critical phenomenon fulfilling apparently a scaling relation $\alpha'=\alpha$. The NI transition in EBBA can be characterized by a second-order phase transition rather than a first-order one, though the numerical value of 0.7 seems to be rather large as compared with the values obtained for typical critical phenomena such as the gas-liquid or the ferromagnetic critical phenomena.

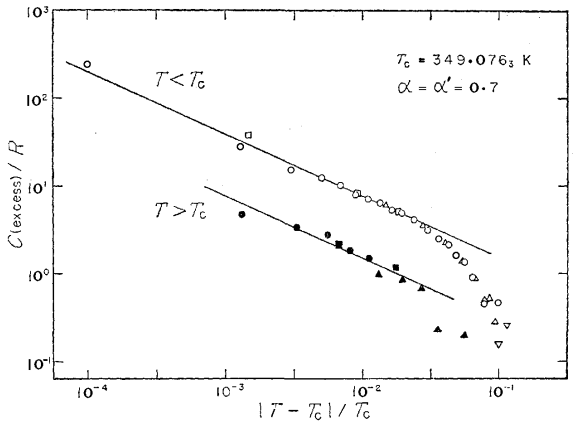

Fig. 3. Variation of excess heat capacity, C(excess), due to mesomorphic transition with the reduced temperature. Different symbols indicate different series of measurements.

McMillan[20] proposed a theory for the S_AN phase transition based on a simple microscopic model for the intermolecular interaction potential. One of the most interesting features of his theory is its prediction that the S_AN transition can be of first or second order, depending on the magnitude of the molecular interaction constants. Although this theoretical argument cannot be directly applied to the NI transition, it is very likely that the order of the NI transition depends on the nature of molecular interaction.

Existing chemical or physical impurity is also a dominant factor to control the transition behavior. High concentration of these impurities generally brings about (i) appreciable reduction of "a first-order character" in an intrinsic first-order phase transition[21] and (ii) incompleteness of the critical-exponent description for ideal critical phenomena.[22,23] We cannot determine whether a 0.25 mol percent concentration of chemical impurity is high enough to violate the intrinsic nature of the present NI transition or not, or what the physical impurity in a mesomorphic transition occurring in a liquid state is. Although a liquid crystalline state is characterized by an ordered trend of molecular

orientation, no regularity such as a lattice structure in crystal exists. Lattice defects or vacancies therefore do not belong to physical impurity in a liquid crystalline state. Only the physical impurity to bring about a significant effect in the vicinity of T_c may be the heterophase fluctuation. The mechanism of a mesomorphic transition, occurring cooperatively in a liquid state, should be understood in terms of the fluctuation of order parameter as well as the intermolecular interaction.

References

1) K. Tsuji, M. Sorai, and S. Seki, This Bulletin, **44**, 1452 (1971).
2) M. Sorai and S. Seki, *ibid.*, **44**, 2887 (1971).
3) M. Sorai and S. Seki, *Mol. Cryst. Liq. Cryst.*, **23**, 299 (1973).
4) M. Sorai, T. Nakamura, and S. Seki, International Conference on Liquid Crystals, Bangalore, December 3—8 (1973).
5) H. Kelker and B. Scheurle, *Angew. Chem.*, **81**, 903 (1969).
6) J. B. Flannery and W. Hass, *J. Phys. Chem.*, **74**, 3611 (1970).
7) G. W. Smith and Z. G. Gardlund, *J. Chem. Phys.*, **59**, 3214 (1973).
8) J. Mayer, T. Waluga, and J. A. Janik, *Phys. Lett.*, **41A**, 102 (1972).
9) T. Shinoda, Y. Maeda, and H. Enokido, The 24th Annual Meeting of the Chemical Society of Japan, April 1st (1971), Osaka; The 8th Japanese Calorimetry Conference, Nov. 29th (1972), Okayama.
10) H. Suga, H. Chihara, and S. Seki, *Nippon Kagaku Zasshi*, **82**, 24 (1961).
11) H. Suga and S. Seki, This Bulletin, **38**, 1000 (1965).
12) S. V. R. Mastrangelo and R. W. Dornte, *J. Amer. Chem. Soc.*, **77**, 6200 (1955).
13) M. Sorai and S. Seki, *J. Phys. Soc. Japan*, **32**, 382 (1972).
14) S. D. Goren, C. Korn, S. B. Marks, and R. Potashnik, *Chem. Phys. Lett.*, **24**, 249 (1974).
15) J. W. Doane, R. S. Parkes, B. Cvikl, D. L. Johnson, and D. L. Fishel, *Phys. Rev. Lett.*, **28**, 1694 (1972).
16) B. Cabane and W. G. Clark, *Solid State Commun.*, **13**, 129 (1973).
17) L. P. Kadanoff, W. Götze, D. Hamblen, R. Hecht, E. A. S. Lewis, V. V. Palciauskas, M. Rayl, J. Swift, D. Aspnes, and J. Kane, *Rev. Mod. Phys.*, **39**, 395 (1967).
18) M. E. Fisher, *Rept. Progr. Phys.*, **30**, 615 (1967).
19) P. Heller, *ibid.*, **30**, 731 (1967).
20) W. L. McMillan, *Phys. Rev.*, **A4**, 1238 (1971); *ibid.*, **A6**, 936 (1972).
21) J. Frenkel, "Kinetic Theory of Liquids," Oxford University Press, London (1947), Chap. VII.
22) B. M. McCoy and T. T. Wu, *Phys. Rev. Lett.*, **21**, 549 (1968); *Phys. Rev.*, **176**, 631 (1968).
23) B. M. McCoy, *Phys. Rev. Lett.*, **23**, 383 (1969).

An X-Ray Diffraction Study of the Structure of Hydrated Copper(II) Ion in a Copper(II) Perchlorate Solution

Hitoshi OHTAKI and Masunobu MAEDA

Laboratory of Solution Chemistry, Faculty of Engineering, Tokyo Institute of Technology, O-okayama, Meguro, Tokyo 152

(Received March 13, 1974)

The structure of hydrated copper(II) ion was determined by means of the X-ray diffraction of a 3.55 M copper(II) perchlorate solution. The radial distribution curve showed that the copper(II) ion has a distorted octahedral structure with six water molecules. Four water molecules occupy the equatorial sites of the octahedron at a distance of 1.94±0.02 Å from the Cu(II) ion and the other two water molecules at the axial sites are 2.43±0.03 Å distant from the central ion.

A number of X-ray investigations have been carried out on crystal structures of various copper(II) complexes, and anisotropic electron distributions of copper(II) have been observed in many complexes of Cu(II).[1-3]

X-Ray crystal studies of copper(II) hydrates disclosed the fact that the Cu^{2+} ion coordinated to six water molecules possesses a distorted octahedral configuration. Four water molecules are located at the equatorial positions with the Cu–O bond distance of 1.94—2.16 Å, and the other two water molecules are at the axial positions with the Cu–O distance of 2.2—2.5 Å.[4-8]

The distortion in the structure of hydrated copper(II) ion has also been observed in aqueous solution by Shapovalov and Radchenko,[9] who carried out X-ray diffraction measurements of an aqueous copper(II) sulfate solution, and determined that the Cu^{2+} ion is surrounded by six water molecules, four of which lie at a distance of 2.15 Å from the central ion and the other two occupy the opposite ends of the axis of the octahedron at a distance of 2.5 Å from the ion.

The present paper deals with an X-ray diffraction study of a copper(II) perchlorate solution, and the results are compared with those obtained for the sulfate solution.[9]

Experimental

Preparation and Analysis of Copper(II) Perchlorate Aqueous Solution. Copper(II) perchlorate was prepared by dissolving copper(II) oxide of p.a. quality (Wako Pure Chemicals Co.) in a hot perchloric acid and was recrystallized twice from water. A copper(II) perchlorate solution was prepared by dissolving the copper(II) perchlorate crystals in water containing a small amount of perchloric acid in order to prevent the hydrolysis of Cu^{2+} ion.

The concentration of Cu^{2+} ion in the sample solution was determined by means of electrodeposition of copper on a platinum gauze electrode. The amount of perchlorate ion was determined by an acid-base titration of a perchloric acid effluent obtained by passing an aliquot of the solution through a cation-exchanger column (Dowex 50W-X12) of the H^+ form. The concentration of hydrogen ion was determined from the relation, $[H^+]=[ClO_4^-]-2[Cu^{2+}]$. The density of the solution was measured with a pycnometer. The composition of the sample solution is given in Table 1.

Measurements and Treatment of X-Ray Diffraction Intensities. X-Ray diffraction measurements were carried out with an X-ray diffractometer (JEOL Co., Tokyo).[10]

Table 1. Composition of the sample solution (in g atoms/l)

Cu	3.550
Cl	7.357
O	69.86
H	81.12

The surface of the solution thermostated at 25±1 °C was irradiated with a divergent beam of MoKα radiation (λ= 0.7107 Å) emitted from a Philips PW210500 Mo X-ray tube.

The diffraction was measured at discrete points between θ=1 and 70°, where θ is half the scattering angle. Three different slit combinations, with divergent slits 1/12°, 1/4°, and 1°, were used. The diffracted intensities were measured as times used for preset 40000 counts (which contain a statistical error of 0.5%) at angular intervals of 0.125° in the low angle range θ=1—6° with a combination of a 1/12° divergent slit, 0.25° in the intermediate range θ=3—20° with a 1/4° divergent slit, and 0.5° in the high angle range θ=16—70° with a 1° divergent slit. The whole angle range was scanned twice in order to examine the reproducibility of the results. The intensities measured at the same angle usually agreed within 2%.

The measured intensities with the three different slit combinations were corrected for background radiation and were normalized to the intensities obtained with a 1° divergent slit by comparing them with those measured in the overlapping regions. The normalized intensities were corrected for absorption in the solution and polarization in the solution and in the monochromator and then scaled to absolute intensities in such a way that the asymptote became equal to the sum of the calculated coherent and incoherent intensities at high scattering angles (θ>50°). The scaling factor thus calculated agreed with that calculated by the method of Krogh-Moe[11] and Norman[12] within less than 1% accuracy.

Intensities $i(s)$ due to combinations of any pairs of atoms were evaluated from the scaled intensities $I(s)$ after correction of the independent atom- and incoherent-scattering according to the equation

$$i(s) = I(s) - \sum_i n_i[(f_i(s)+\Delta f_i')^2 + (\Delta f_i'')^2 + \Phi(s)\cdot I_i^{inco}(s)] \quad (1)$$

where s denotes $4\pi\sin\theta/\lambda$ (λ=0.7107 Å), n_i the number of atom i, $f_i(s)$ the scattering factor of atom i at angle s, $\Delta f_i'$ and $\Delta f_i''$ the real and imaginary parts, respectively, of the anomalous dispersion, and $\Phi(s)$ the fraction of the incoherent radiation reaching the counter. The reduced intensities $i(s)$ thus evaluated are shown in Fig. 1 in the form of $s\cdot i(s)$ *vs.* s.

The coherent scattering factors of Cu, Cl, and O were taken from Cromer and Waber,[13] and those of H from the

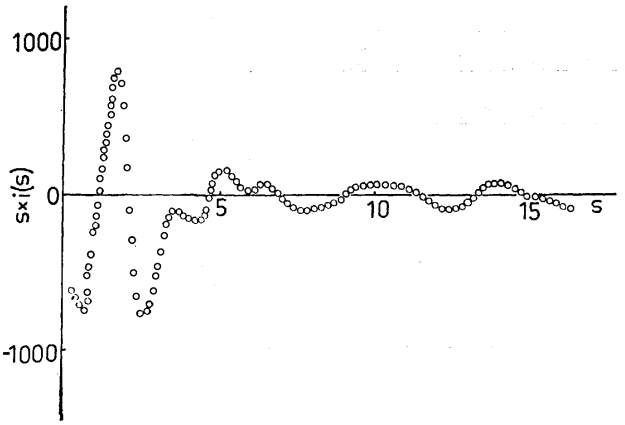

Fig. 1. The reduced intensities $i(s)$ multiplied by s as a function of s. For clarity not all of the experimental points are shown.

International Tables.[14] The incoherent scattering factors for Cu were those given by Cromer and Mann,[15] those for Cl and O by Cromer[16] and those for H by Compton and Allison.[17] The incoherent scattering factors were corrected by the Breit-Dirac factors. The values used for anomalous dispersion were taken from Cromer and Lieberman.[18]

Results and Discussion

The radial distribution curve $D(r)$ was calculated from the reduced intensity data $i(s)$ according to Eq. (2). The calculations were carried out with the help of the computer program KURVLR specially written for the analysis of X-ray diffraction data in solution.[19]

$$D(r) = 4\pi r^2\rho_0 + 2r\pi^{-1}\int_0^{s_{max}} s\cdot i(s)\cdot M(s)\cdot\sin(sr)\mathrm{d}s \qquad (2)$$

Here ρ_0 denotes the average scattering density of the solution in electron unit and the modification function $M(s)$ was chosen to be

$$\sum_i n_i f_i(0)^2/\sum_i n_i f_i(s)^2 \exp(-0.01s^2).$$

The $D(r)$ function thus calculated showed spurious peaks in the range less than 1 Å, which has no relation with any interatomic distance. These spurious peaks were eliminated by the Fourier inversion of the $D(r)$ function below 1 Å on the assumption that the $D(r)$ function below 1 Å consisting of contributions only from the O-H bonds within H_2O and the Cl-O bonds within ClO_4^-.

Figure 2(a) shows the final radial distribution function $D(r)$ thus calculated. It shows four peaks at around 1.4, 1.95, 2.4, and 3 Å. The peak at around 1.4 Å is due to the Cl–O bonds within ClO_4^-, that at 1.95 Å can be attributed to the bonds between Cu and O at an equatorial position within the hydrated Cu^{2+} ion, and the one at 2.4 Å is due to both the axial Cu–O bond within the hydrated Cu^{2+} ion and the O–O contact within ClO_4^-.

The distances and the numbers of equatorial and axial Cu-O bonds were determined from the residual peaks after subtraction of the contributions from the Cl–O and O-O contacts at 1.43 and 2.43 Å, respectively, within ClO_4^- ion and the O-H bond at 1.01 Å within H_2O. The theoretical peak shapes for the

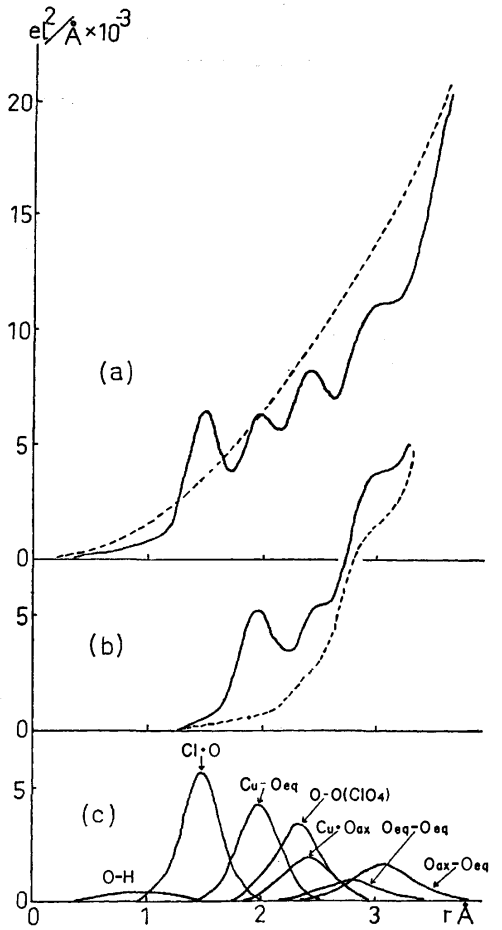

Fig. 2. (a) The radial distribution curve. The broken curve denotes $4\pi r^2\rho_0$. (b) The full curve gives the difference between $D(r)$ and the calculated peak shapes for the Cl–O and O–O atom pairs within ClO_4^-, and the broken curve the residual distribution function obtained by subtraction of the theoretical peak shapes shown in (c) from the $D(r)$ curve. (c) The calculated peak shapes with the parameters given in Table 2.

Cl–O, O–O, and O–H contacts were evaluated as follows.

Theoretical intensities caused by any i-j atom pair can be calculated by

$$i(s) = \sum_i\sum_j n_{ij} f_i(s) f_j(s) \frac{\sin(r_{ij}s)}{r_{ij}s} \exp(-b_{ij}s^2) \qquad (3)$$

where n_{ij}, r_{ij}, and b_{ij} represent the frequency factor, the distance, and the temperature factor, respectively, of the interaction between any atoms i and j.

The values of r, b, and n for the Cl–O and O–O pairs[10] and those for the O–H bond are given in Table 2.

The theoretical intensities thus calculated were converted into atomic pair distribution functions by means of the Fourier integration with Eq. (2). The calculated functions are reproduced in Fig. 2(c). Figure 2(b) gives the residual radial distribution curve (full line) obtained by subtracting these peaks from the $D(r)$ curve. Three peaks still remain at the positions 1.94, 2.43, and 3 Å. The area under the peak at 1.94 Å was estimated with a planimeter. The number of

Table 2. Final parameter values for the copper(II) ion coordinated to six water molecules, perchlorate ion, and water molecule

	r(Å)	b	n
$Cu(H_2O)_6^{2+}$			
$Cu-O_{eq}$	1.94	0.002	4
$Cu-O_{ax}$	2.43	0.005	2
$cis-O_{eq}-O_{eq}$	2.74	0.01	4
$O_{ax}-O_{eq}$	3.11	0.01	8
ClO_4^-			
Cl-O	1.43	0.001	4
O-O	2.34	0.002	6
H_2O			
O-H	1.01	0.001	2

water molecules around Cu was evaluated to be about four, which corresponds to the number of Cu-O bonds in an equatorial plane. The area under the peak at 2.43 Å, which may correspond to the number of bonds between Cu and water molecules at the axial coordination sites, was difficult to estimate, since contributions from atom pairs at longer distances were overlapped. The broad peak ranging from 2.7 to 3.2 Å is ascribable to both the equatorial O–O contacts at *cis*-position and the contacts between axial and equatorial oxygens within the distorted octahedron of the hydrated copper(II) ion.

From the results, it was assumed that the Cu^{2+} ion is bound by six water molecules and the length of four Cu–O bonds in the plane is 1.94 Å and that of the other two along the axis is 2.43 Å. The values of r, b, and n were evaluated for four kinds of atom pairs (the equatorial Cu–O, the axial Cu–O, the *cis*-contacts of the equatorial O–O and the equatorial O–axial O) within $Cu(H_2O)_6^{2+}$. They are given in Table 2, together with the values for the Cl-O and O–O pairs within ClO_4^- and for the O-H pair within H_2O.

In order to see if the proposed structure and the values of the parameters given in Table 2 can satisfactorily explain the experimental data, the theoretical peaks were calculated with the parameters according to Eqs. (3) and (2) (the calculated peaks for the interactions within $Cu(H_2O)_6^{2+}$ are shown in Fig. 2(c)). The peaks were subtracted from the residual curve (full line, Fig. 2(b)) which had been obtained by subtraction of the contributions of ClO_4^- from the $D(r)$ curve. The curve thus obtained (broken line, Fig. 2(b)) gives a smooth curve with no dominant peak in the region less than 2.8 Å. The broad peak remaining at around 2.9 Å may be due to the contacts between oxygen atoms of water molecules and oxygen atoms of ClO_4^-.[10,20,21]

It is thus concluded that the copper(II) ion, which is coordinated to six water molecules in the first coordination sphere, has a distorted octahedral structure with the values of the parameters given in Table 2.

Shapovalov and Radchenko[9] obtained 2.15 and 2.5 Å as the distrances from Cu to O occupying an equatorial and an axial site, respectively, in the sulfate solution. These distances are greater than the corresponding ones, 1.94 ± 0.02 Å and 2.43 ± 0.03 Å, we found in the perchlorate solution. The uncertainties of the distances were estimated from the shape of the distribution curve in Fig. 2(b).

The present work was supported by the Ministry of Education.

References

1) W. E. Hatfield and R. Whyman, *Transition Metal Chem.*, **5**, 47 (1969); *Chem. Abstr.*, **71**, 108519f (1969).
2) B. J. Hathaway and D. E. Billing, *Coord. Chem. Rev.*, **5**, 143 (1970).
3) B. J. Hathaway and P. G. Hodgson, *J. Inorg. Nucl. Chem.*, **35**, 4071 (1973).
4) H. Montgomery and E. C. Lingafelter, *Acta Crystallogr.*, **20**, 659 (1966).
5) N. V. Mani and S. Ramaseshan, *Z. Kristallogr.*, **115**, 97 (1961).
6) J. Fischer and R. Weiss, *Acta Crystallogr.*, **B29**, 1958 (1973).
7) J. Fischer, R. Elchinger, and R. Weiss, *ibid.*, **B29**, 1967 (1973).
8) S. Ray, A. Zalkin, and D. H. Templeton, *ibid.*, **B29**, 2748 (1973).
9) I. M. Shapovalov and I. V. Radchenko, *Russ. J. Struct. Chem.*, **12**, 705 (1972).
10) H. Ohtaki, M. Maeda, and S. Ito, This Bulletin, **47**, 2217 (1974).
11) J. Krogh-Moe, *Acta Crystallogr.*, **9**, 951 (1956).
12) N. Norman, *ibid.*, **10**, 370 (1957).
13) D. T. Cromer and J. T. Waber, *ibid.*, **18**, 104 (1965).
14) "International Tables for X-Ray Crystallography," Kynoch Press, Birmingham (1962), Vol. III.
15) D. T. Cromer and J. B. Mann, *J. Chem. Phys.*, **47**, 1892 (1967).
16) D. T. Cromer, *ibid.*, **50**, 4857 (1969).
17) A. H. Compton and S. K. Allison, "X-Ray in Theory and Experiments," van Nostrand, New York, (1935).
18) D. T. Cromer and D. Lieberman, *J. Chem. Phys.*, **53**, 1891 (1970).
19) G. Johansson and M. Sandström, *Chem. Scripta*, **4**, 195 (1973).
20) K. Michelsen, *Acta Chem. Scand.*, **6**, 1289 (1952).
21) G. Johansson and H. Ohtaki, *ibid.*, **27**, 643 (1973).

Kinetics of Multidentate Ligand Substitution Reactions. XVII.* Substitution Reactions of Diethylenetriaminepentaacetate (DTPA) with Aminopolycarboxylate Complexes of Nickel(II) and Cobalt(II)

Mutsuo KODAMA

Department of Chemistry, College of General Education, Hirosaki University, Bunkyo, Hirosaki 036

(Received March 20, 1974)

The kinetics of the substitution reactions of DTPA with *N*-(2-hydroxyethyl)iminodiacetate (HIDA) and *N*-(2-hydroxyethyl)ethylenediamine-*N,N',N'*-triacetate (EDTA-OH) complexes of nickel(II) and EDTA-OH and 2,2'-ethylenedioxydi(ethylamine)-*N,N,N',N'*-tetraacetate (GEDTA) complexes of cobalt(II) were studied systematically by employing the polarographic technique. The reaction of ethylenediaminetetraacetate (EDTA) with the nitrilotriacetate (NTA) complex of nickel(II) in an alkaline medium was also studied. All the substitution reactions were found to have a common reaction mechanism. They were first-order with respect to DTPA or EDTA and also first-order with respect to the 1 : 1 ratio metal(II) complex of HIDA, NTA, EDTA-OH, or GEDTA. From a comparison of the observed rate constants with those estimated on the basis of the proposed reaction intermediate, the detailed reaction mechanism and the steric effect of the DTPA anion on the reaction rates were studied. The DTPA anion had practically no effect on the rates of the substitution reactions of the aminopolycarboxylate complexes of metal (II) ions.

Previously,[1] the present author studied the kinetics of the substitution reaction of DTPA with the nickel(II)–NTA complex and discussed the effect of the protonation of the DTPA anion on its reaction rate. However, no detailed reaction mechanism was investigated in that paper. He also studied the kinetics of the substitution reactions of cyclohexane-1,2-diamine-*N,N,N',N'*-tetraacetate(CyDTA) with the aminopolycarboxylate complexes of zinc(II) and cobalt(II), and discussed the nature of the steric effect of the CyDTA anion on their reaction rates.[2] Consequently, in order to understand more precisely the nature of the steric effect of the entering group on the rate of the substitution reaction involving an aminopolycarboxylate complex, it seems to be necessary and important to conduct a kinetic study of the substitution reaction involving DTPA. This paper will describe a kinetic study of the substitution reactions of DTPA with the nickel(II)–HIDA and –EDTA-OH and cobalt(II)–EDTA-OH and –GEDTA complexes, using the polarographic technique. The substitution reaction of EDTA with the nickel(II)–NTA complex in an alkaline solution will also be studied in this paper, and its reaction rate will be compared with those of the DTPA reactions.

Experimental

Reagents. The methods of preparing and standardizing the nickel(II) and cobalt(II) nitrate solutions were given previously.[3] The EDTA, DTPA, EDTA-OH, and GEDTA used in this study were recrystallized as their acids from their aqueous solutions. The preparation and recrystallization of the acid form of HIDA were also given previously.[4] All the other chemicals used were of an analytical reagent grade and were used without further purification.

Apparatus and Experimental Procedures. The apparatus and experimental procedures employed were the same as those given previously.[2] In this study, no buffer reagent was used, because all the sample solutions always contained a large excess of uncomplexed HIDA, NTA, EDTA-OH, or GEDTA, and had enough buffer capacity over the entire pH range covered ($8.30<$pH<9.00 in the HIDA system, $9.00<$pH<10.00 in the NTA system, $9.00<$pH<10.40 in the EDTA-OH system, and $9.40<$pH<10.40 in the GEDTA system). All the kinetic measurements were conducted under experimental conditions where all the reactions could be treated as pseudo first-order reactions. The rate of the substitution reaction was determined by measuring the change in the dissolution wave-height due to the uncomplexed DTPA or EDTA. The ionic strength of the sample solution was adjusted to 0.30 by adding an appropriate amount of $NaClO_4$.

Results and Discussion

The substitution reactions of DTPA with the nickel(II)–HIDA and cobalt(II)–GEDTA complexes and the reaction of EDTA with the nickel(II)–NTA complex showed kinetic behavior quite similar to that of the reaction of DTPA with the nickel(II)–NTA complex.[1] This fact suggests that the reaction mechanism for the above reactions can be formulated as:

$$MX_2^{(2-2m)+} \rightleftharpoons MX^{(2-m)+} + X^{m-} \quad \text{(a) in a rapid equil.}$$

$$MX^{(2-m)+} + \begin{cases} HY^{1-n} \overset{k_H}{\rightleftharpoons} MY^{2-n} + HX^{1-m} & \text{(b)} \\ Y^{n-} \overset{k_0}{\rightleftharpoons} MY^{2-n} + X^{m-} & \text{(c)} \end{cases} \quad \text{rds}$$

corresponding to Relation (1):

$$k_{ap}^{+} = \frac{[\mathrm{Me(II)}] \times \left(k_0 + k_H \cdot \frac{[H^+]}{K_n}\right)}{(\alpha_H)_Y \cdot \left(1 + \frac{K_2 \cdot [X]_f}{(\alpha_H)_X}\right)} \qquad (1)$$

where k_{ap}, [Me(II)], and K_n are, respectively, the pseudo first-order rate constant, the metal(II) concentration, and the fifth dissociation constant of diethylenetriaminepentaacetic acid or the fourth dissociation constant of ethylenediaminetetraacetic acid; all the other symbols used have their usual meanings.[2] The k_0 and k_H values for the above reactions were determined from the intercepts and slopes of the linear relations between $k_{ap}^{+} \times (1 + K_2 \cdot [X]_f/(\alpha_H)_X)(\alpha_H)_Y/[\mathrm{Me(II)}]$ and $[H^+]$; they are listed in Tables 1 and 2.

* Part XVI: M. Kodama, This Bulletin, **47**, 1430 (1974).

Table 1. Substitution rate constants of Ni(II) complexes
μ=0.30, 25°C

System	Rate constant		Log rate constant ratio		
			Obsd		
	k_0	k_H	k_0	k_H	Calcd[a]
NTA[7]	3×10^{-5}	—	−7.76	—	−7.58
NTA-EDTA	1.5×10^{3}	2.33×10^{2}	0	0	0
NTA-DTPA[1]	9.1×10^{2}	3.06×10^{2}	−0.22	+0.12	0
HIDA-DTPA	1.1×10^{5}	1.50×10^{4}	1.87	1.81	2.08
EDTA-OH-DTPA	2.3×10^{-3}	3.76×10^{-3}	−4.82	−4.80	−5.14

a) Calculated on the basis of the Gly reaction mechanism.

Table 2. Substitution rate constants of Co(II) complexes
μ=0.30, 25°C

System	Rate constant		Log rate constant ratio		
			Obsd		
	k_0	k_H	k_0	k_H	Calcd[a]
EDTA-OH	2.1×10^{1}	3.8	0	0	0
GEDTA	1.0×10^{4} [b]	2.0×10^{3}	2.70	2.72	2.60

a) Calculated on the basis of the Gly reaction mechanism. b) Less accurate.

In the substitution reactions involving metal(II)-EDTA-OH complexes, the pseudo first-order rate constant, k_{ap}^{+}, was 1) proportional to the metal(II) concentration, 2) independent of the initial concentration of DTPA, and also 3) independent of the concentration of uncomplexed EDTA-OH. Furthermore, the plot of the k_{ap}^{+} value multiplied by $(\alpha_H)_Y/[Me(II)]$ against $[H^+]$ gave a linear relation with an intercept of a finite value (Fig. 1). These facts imply that the substitution reactions of DTPA with the metal(II)-EDTA-OH

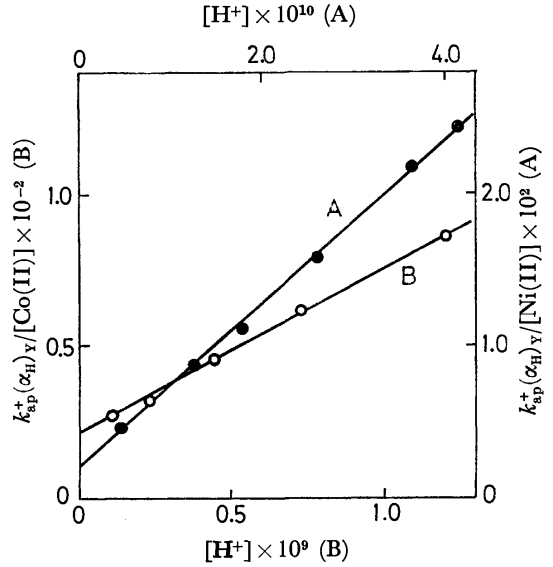

Fig. 1. The plot of $k_{ap}^{+}\times(\alpha_H)_Y/[Me(II)]$ against $[H^+]$
μ=0.30, 25 °C
A) Ni(II) system
$[Ni(II)]=18.2$ mM, $[EDTA\text{-}OH]_f=18.2$ mM, $[DTPA]_i=1.82$ mM
B) Co(II) system
$[Co(II)]=6.37$ mM, $[EDTA\text{-}OH]_f=21.0$ mM, $[DTPA]_i=0.546$ mM

$$k_{ap}^{+}=\frac{[Me(II)]}{(\alpha_H)_Y}\cdot\left(k_0+k_H\cdot\frac{[H^+]}{K_n}\right) \quad (2)$$

complexes proceed through (b) and (c), corresponding to Relation (2):
Therefore, the k_0 and k_H values were estimated from the intercepts and slopes of the straight lines in Fig. 1; they are listed in Tables 1 and 2.

As was discussed in connection with the dissociation[5] and substitution reactions[6] of the ethylenediaminemonoacetate (EDMA) complex of nickel(II), the entering group in the ligand substitution reaction just assists the dissociation of the leaving group without effecting any change in the detailed dissociation mechanism. Previously,[3] the present author established that the nickel(II)-NTA complex dissociates through the Gly reaction intermediate, in which the leaving NTA anion is bonded to the nickel(II) ion through the glycinate chelate ring (Gly mechanism). Therefore, it is natural to believe that the substitution reaction of the nickel(II)-NTA complex with EDTA also proceeds through a Gly mechanism.[2,7,8] If the Gly mechanism can be assumed for the reaction of the nickel(II)-NTA complex with EDTA, the rate constant ratio between the dissociation reaction of the nickel(II)-NTA complex,[9] and its substitution reaction with EDTA should be $1:10^{7.58}$. The above rate constant ratio was calculated with the aid of the $k=k_{rds}K_AK_LK_{st}K_{elec}/K_{MX}$ relation[2,10] by using the K_A value of $10^{9.27}$, the K_{st} ratio of 2, and the K_{elec} ratio of $10^{2.0}$. The observed ratio was $1:10^{7.76}$ (Table 1). The good agreement between the observed and calculated ratios supports the above Gly-mechanism explanation, suggesting that the EDTA anion had practically no steric effect on its substitution reaction with the nickel(II)-NTA complex. As is illustrated in Table 1, the k_0 and k_H values for the reaction of DTPA with the nickel(II)-NTA complex can also be understood in terms of a simple

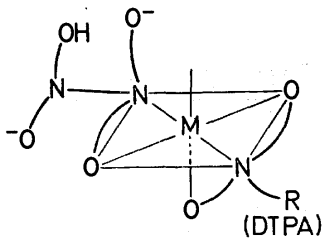

Fig. 2. A possible intermediate for the substitution reaction of DTPA with metal(II)-EDTA-OH complex, $[Me^{II}(EDTA\text{-}OH)(DTPA)]^{-n}$

Gly mechanism. The k_0 and k_H values of the substitution reaction of DTPA with the nickel(II)–HIDA complex can also be understood by assuming the Gly mechanism. The rate constant ratio between the DTPA reactions with the nickel(II)–HIDA and –NTA complexes estimated on the basis of the Gly mechanism was $1 : 10^{2.08}$, and the good agreement with the observed k_0 ratio of $1 : 10^{1.87}$ or the k_H ratio of $1 : 10^{1.82}$ (Table 1). Similarly, the k_0 and k_H values of the reaction of DTPA with the nickel(II)–EDTA-OH complex could also be understood by assuming the Gly reaction mechanism (the reaction intermediate in Fig. 2). The rate constant ratio between the nickel(II)–NTA and –EDTA-OH systems, as calculated on the basis of the proposed reaction mechanism, was $1 : 10^{-5.14}$. The observed k_0 and k_H ratios were $1 : 10^{-4.80}$ and $1 : 10^{-4.81}$ respectively. The agreement between the observed and calculated ratios can be regarded as satisfactory. As was mentioned above, the rates of the DTPA reactions studied could be understood by assuming the Gly reaction mechanism. This evidently implies that, irrespective of its large molecular size, the entering DTPA anion exerts practically no steric effect on the rate of its substitution reaction with the aminopolycarboxylate complex of nickel(II). The result obtained in the kinetic study of the DTPA substitution reactions of cobalt(II)–EDTA-OH and –GEDTA complexes proved the above conclusion to be true. Since the cobalt(II) complex shows kinetic behavior quite similar to that of the nickel(II) complex,[11] one can safely assume the Gly reaction mechanism for the DTPA reactions of the cobalt(II)–EDTA-OH and –GEDTA complexes. On the basis of the Gly mechanism, the rate constant ratio between the EDTA-OH and GEDTA systems could be estimated to be $1 : 10^{2.60}$. The observed k_0 and k_H ratios were $1 : 10^{2.70}$ and $1 : 10^{2.72}$ respectively. The agreement between the calculated and observed ratios can be regarded as satisfactory (Table 2). The conclusion that the DTPA anion has no practical effect on its substitution reaction rates could also be confirmed by an examination of the molecular model. A close examination of the molecular model revealed that, for all the DTPA system, the glycinate reaction intermediate in which the leaving aminopolycarboxylate and entering DTPA anions are, respectively, bonded to the metal(II) ion through the glycinate and iminodiacetate chelate rings could be formed without any difficulty. This can be ascribed chiefly to the free bond rotation of the DTPA and aminopolycarboxylate anions involved in the substitution reactions.

References

1) M. Kodama, This Bulletin, **42**, 2532 (1969).
2) M. Kodama and K. Hagiya, *ibid.*, **46**, 3151 (1973).
3) M. Kodama, H. Nunokawa, and N. Oyama, *ibid.*, **44**, 2387 (1971).
4) M. Kodama, K. Namekawa, and T. Horiuchi, *ibid.*, **47**, 2011 (1974).
5) M. Kodama and N. Oyama, *ibid.*, **44**, 2849 (1971).
6) M. Kodama, Y. Fujii, and T. Ueda, *ibid.*, **43**, 2085 (1970).
7) M. Kodama and T. Ueda, *ibid.*, **43**, 419 (1970).
8) M. Kodama, S. Karasawa, and T. Watanabe, *ibid.*, **44**, 1815 (1971).
9) M. Kimura, *Nippon Kagaku Zasshi*, **89**, 1209 (1967).
10) D. B. Rorabacher and D. W. Margerum, *Inorg. Chem.*, **3**, 382 (1964).
11) M. Kodama, T. Sato, and S. Karasawa, This Bulletin, **45**, 2757 (1972).

Differential Thermal Analysis of Some Tervalent Metal Chelates of 1,5-Dialkylpentane-2,4-dionates*

Isao YOSHIDA, Hiroshi KOBAYASHI, and Keihei UENO

Department of Organic Synthesis, Faculty of Engineering, Kyushu University, Hakozaki, Higashi-ku, Fukuoka 812

(Received April 16, 1974)

In connection with the purification of metal chelates by zone refining, thermal properties of the following β-diketone chelates of tervalent cobalt(III), aluminum(III), iron(III), manganese(III), and chromium(III) were investigated by differential thermal analysis (DTA). The β-diketones used in this study were heptane-3,5-dione, nonane-4,6-dione, 2,6-dimethylheptane-3,5-dione, 2,8-dimethylnonane-4,6-dione, 2,2,6,6-tetramethylheptane-3,5-dione, and tridecane-6,8-dione. Metal chelates of the alkyl substituted pentane-2,4-diones showed a lower melting- and higher decomposition temperature in comparison with the pentane-2,4-dionates. Discussion is given on the effects due to the structures of the alkyl substituents upon thermal properties of the hexacoordinate metal chelates.

The criteria for thermal properties of the samples which are to be subjected to zone melting process are the moderate melting temperature convenient for the operation, as well as the thermal durabilty and less volatility under prolonged heating at a molten state. Most of metal chelate compounds, however, decompose prior to melting with a few exceptions:[1,2] Metal oxinates belong to a group of metal chelates of the highest thermal stability; however, they are not found in a stable molten form because of their high melting points.[3,4] Although pentane-2,4-dionates are also regarded as thermally stable and low melting chelates, only the chromium(III),[5] beryllium(II)[6] and aluminum(III)[7] chelates were reported to give melts durable under prolonged heating. Fluoro-substituted pentane-2,4-dionates show lower melting temperatures than the pentane-2,4-dionates,[8,9] but the electron-withdrawing effect of the fluoroalkyl groups decreases the thermal stability of the metal chelates.[10,11] On the other hand, a large number of alkyl-substituted pentane-2,4-dione chelates of copper(II) were reported to melt in a lower temperature region and to be enough stable to melt without decomposition.[12-14]

In the continuation of the previous reports[15,16] on the thermal properties of some bivalent metal chelates of a range of β-diketones, this paper reports on the same aspects of some tervalent metal chelates of the following 1,5-dialkylpentane-2,4-diones.

The β-diketones chosen in this serial study are heptane-3,5-dione(or dipropionylmethane, DNPM), nonane-4,6-dione(or di-*n*-butyrylmethane, DNBM), 2,6-dimethylheptane-3,5-dione(or diisobutyrylmethane, DIBM), 2,8-dimethylnonane-4,6-dione (or diisovalerylmethane, DIVM), 2,2,6,6-tetramethylheptane-3,5-dione(or dipivaloylmethane, DPVM), and tridecane-6,8-dione(or di-*n*-caproylmethane, DNCM), and metal ions are cobalt(III), aluminum(III), iron(III), manganese (III), and chromium(III).

Melting, decomposing and some additional phase transition temperatures were determined by DTA measurements in the air and nitrogen atmosphere. Both melting and pyrolytic degradation reaction gave endothermic DTA peaks. The former peak was characterized as follows: 1) The peak position was reproducible upon repeated DTA runs of a sample. 2) Atmosphere did not affect the position and shape of the peak. 3) IR, UV, and visible spectra were identical on the samples before and after the DTA run. 4) After the endotherm, the base line returned to the same level as before. An endotherm which did not satisfy either of the above qualifications, was regarded as that due to the degradation reactions.[15]

Experimental

Synthesis of 1,5-dialkylpentane-2,4-diones[17] and their cobalt(III) chelates[18] were reported in our previous papers. Pentane-2,4-dione and all of the inorganic reagents were obtained commercially, and used without any further purifications. Analytical results and solvents used for recrystallization of the following metal chelates are summarized in Table 1.

Aluminum(III) Chelates. Tris(acetylacetonato)aluminum(III), $Al(AA)_3$, was prepared according to a standard method.[19] $Al(DIBM)_3$, $Al(DIVM)_3$, and $Al(DPVM)_3$ were prepared according to the modified Jones' method.[20] To a 50 ml of 3M-sodium hydroxide aqueous solution containing 1.25 g (0.003 mol) of aluminum nitrate nonahydrate was added 0.01 mol of each ligands. White precipitate was obtained immediately. These were collected by filtration, and then recrystallized from appropriate solvents which are listed in Table 1. DNPM, DNBM, and DNCM chelates could not be obtained by the above methods.

Iron(III) Chelates. To a 10 ml of an aqueous methanol solution containing 1.35 g (0.003 mol) of ferric nitrate hexahydrate was added 0.01 mol of a ligand, and then 6 ml of 2.5M-sodium hydroxide solution was added dropwise under vigorous stirring. AA, DIBM, DIVM, and DPVM gave red-orange solid, while DNPM, DNBM, and DNCM red-orange oil, respectively. Solid chelates were collected by filtration, and then recrystallized from appropriate solvents as listed in Table 1. The oily product was extracted with chloroform, and the chloroform extract was eluted from silica gel and alumina columns, each 10 cm long, successively. The eluate was evaporated, to give an oily liquid chelate.

Manganese(III) Chelates.[21] To 20 ml of an aqueous methanol was added 0.54 g of manganese(II) chloride tetrahydrate and 0.11 g of potassium permanganate. The resulting solution was adjusted to pH 6—7 by the addition of 0.8 M ammonium hydroxide. Then 0.01 mol of a ligand was added into the solution with vigorous stirring. Dark brown precipitate was afforded with AA, DIBM, DIVM,

* Contribution No. 330 from the Department of Organic Synthesis, Kyushu University.

Table 1. Analytical results of chelates

Complex	Molecular formula	Found C%	Found H%	Calcd C%	Calcd H%	Recrystallization solvent
$Al(AA)_3$	$C_{15}H_{21}O_6Al$	55.46	6.59	55.55	6.48	Ethanol
$Al(DIBM)_3$	$C_{27}H_{45}O_6Al$	65.80	9.22	65.87	9.14	Ethanol+Water
$Al(DIVM)_3$	$C_{33}H_{57}O_6Al$	68.68	9.94	68.77	9.89	Ethanol+Water
$Al(DPVM)_3$	$C_{33}H_{57}O_6Al$	68.81	9.93	68.77	9.89	Ethanol+Water
$Fe(AA)_3$	$C_{15}H_{21}O_6Fe$	51.20	6.08	51.17	5.96	Methanol+Water
$Fe(DNPM)_3$	$C_{21}H_{33}O_6Fe$	57.78	7.79	57.71	7.55	
$Fe(DNBM)_3$	$C_{27}H_{45}O_6Fe$	61.86	8.60	62.23	8.64	
$Fe(DIVM)_3$	$C_{33}H_{57}O_6Fe$	65.36	9.46	65.49	9.42	Methanol+Water
$Fe(DNCM)_3$	$C_{39}H_{69}O_6Fe$	68.03	10.14	67.96	10.01	
$Fe(DIBM)_2(CH_3O)$	$C_{19}H_{33}O_5Fe$	57.14	8.31	57.41	8.31	Methanol
$Fe(DPVM)_2(CH_3O)$	$C_{23}H_{41}O_5Fe$	61.16	9.22	60.97	9.05	Methanol+Ethyl Acetate
$Mn(AA)_3$	$C_{15}H_{21}O_6Mn$	51.20	6.08	51.17	5.96	Benzene+Petr. Ether
$Mn(DNPM)_3$	$C_{21}H_{33}O_6Mn$	56.85	7.54	57.83	7.57	
$Mn(DNBM)_3$	$C_{27}H_{45}O_6Mn$	62.36	8.67	62.33	8.65	
$Mn(DIBM)_3$	$C_{27}H_{45}O_6Mn$	61.97	8.46	62.33	8.65	Methanol+Water
$Mn(DIVM)_3$	$C_{33}H_{57}O_6Mn$	65.71	9.60	65.59	9.43	Methanol+Water
$Mn(DPVM)_3$	$C_{33}H_{57}O_6Mn$	65.49	9.49	65.59	9.43	Methanol
$Cr(AA)_3$	$C_{15}H_{21}O_6Cr$	51.63	6.15	51.62	6.01	Benzene+Petr. Ether
$Cr(DNPM)_3$	$C_{21}H_{33}O_6Cr$	57.73	7.55	58.21	7.62	
$Cr(DIBM)_3$	$C_{27}H_{45}O_6Cr$	62.41	8.86	62.69	8.70	Acetone+Water
$Cr(DPVM)_3$	$C_{33}H_{57}O_6Cr$	65.81	9.55	65.91	9.48	Acetone+Water

and DPVM. The solid precipitate was collected by filtration, and then recrystallized from an appropriate solvent. DNPM and DNBM gave oily chelates. These were extracted with benzene from the reaction mixture. After the extract was evaporated, the oily residue was dissolved again in an ether–methanol mixture. Then the solution was purified by elution in a similar manner to that for the oily iron(III) chelates. Manganese(II) acetylacetonate was prepared according to a standard method.[22]

Chromium(III) Chelates.[23] To 20 ml of an aqueous methanol solution containing 1.3 g (0.003 mol) of chromium nitrate hexahydrate and 7 g of urea was added 0.01 mol of a ligand. Then mixture was maintained at about 95 °C for 10 hr with stirring. AA, DIBM, and DPVM afforded solid precipitate. These were collected by filtration, and then recrystallized from an appropriate solvent. The remaining ligands gave oily products, which were hardly purified except $Cr(DNPM)_3$. The last chelate, $Cr(DNPM)_3$, was purified in a similar manner to those for the manganese(III) chelates.

Measurements. DTA curves were recorded on a Rigaku Denki Thermoflex 8001 in the air and nitrogen atmosphere. A hermetic-sealed sample holder was used for volatile and sublimable chelates; otherwise a pressure-capped one was used.** Procedure of the thermoanalysis was the same as described previously.[15]

Evolved ligand vapor upon the pyrolysis of a metal chelate was identified by means of gas-liquid chromatography by direct injection of the metal chelate as a solution into the GC vaporizing port maintained at 300 or 370 °C, or by injection of the solution of a vapor condensate upon the pyrolysis in a sealed tube at 300 °C for 10 min. Some of the vapor condensate were also identified by infrared spectral comparison as a carbon tetrachloride solution. IR spectra were measured on a JASCO-DS-403G spectrophotometer.

** Details of the two types of sample holders were given in the previous paper.[15]

Results and Discussion

Cobalt(III) Chelates. Figure 1 shows DTA curves of the cobalt(III) chelates measured in nitrogen atmosphere. $Co(DNPM)_3$, $Co(DIVM)_3$, and $Co(DPVM)_3$ show definite melting points, all of which are assignable to the reversible endotherms (A). The remaining solid

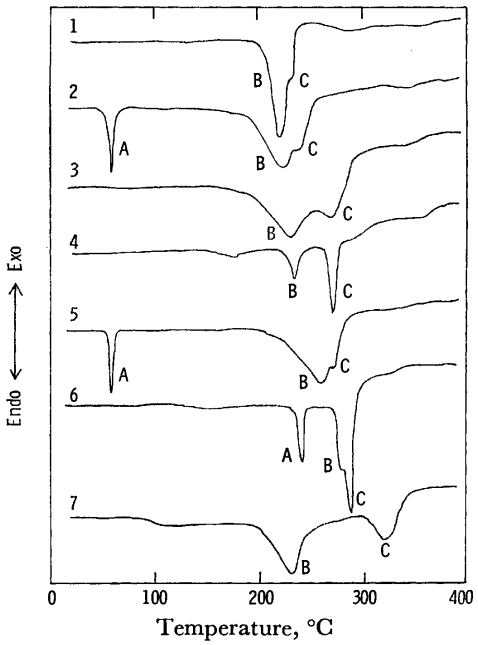

Fig. 1. DTA curves of the cobalt(III) chelates obtained in nitrogen atmosphere at heating rate of 10 °C/min. 1, $Co(AA)_3$; 2, $Co(DNPM)_3$; 3, $Co(DNBM)_3$; 4, $Co(DIBM)_3$; 5, $Co(DIVM)_3$; 6, $Co(DPVM)_3$; 7, $Co(DNCM)_3$.

chelates, $Co(AA)_3$ and $Co(DIBM)_3$, decompose without showing any melting peak. All the chelates show two irreversible endotherms (B) and (C) above 200 °C.

Green tris-β-diketonato cobalt(III) chelates turn to blood-red or pink solid after DTA scanning up to the temperature of the first irreversible endotherm (B). Figure 2 shows, as an example, IR spectra of the cobalt-DNPM chelates before and after the above transition. The latter, differing from the former, rather resembles that of the cobalt(II) chelate of the same ligand, $Co(DNPM)_2 \cdot H_2O$.[18] When the present cobalt(III) chelate was heated above the peak (B) temperature, the evolution of the free ligand was confirmed. The irreversible endotherm (B) is, therefore, considered due to a thermal degradation accompanied by the reduction of the central metal ion, to give an anhydrous cobalt(II) β-diketonate, which may become hydrated subsequently by atmospheric moisture.

The last peak (C) is presumably due to the decomposition of the resulting bis(β-diketonato)cobalt(II).

Aluminum(III) Chelates. The aluminum(III) chelates are highly volatile, and DTA curves were, therefore, obtained by use of a hermetic-sealed sample holder in nitrogen atmosphere. The results are shown in Fig. 3.

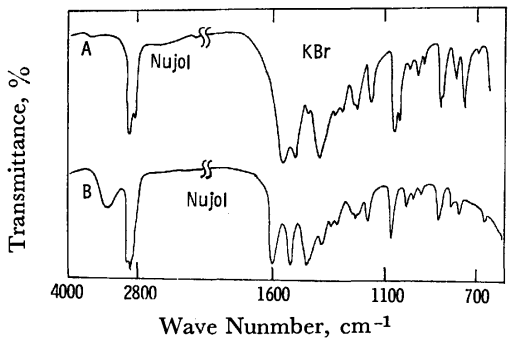

Fig. 2. IR spectrum of $Co(DNPM)_3$, A, and of the product from pyrolysis of the above chelate at 230 °C, B.

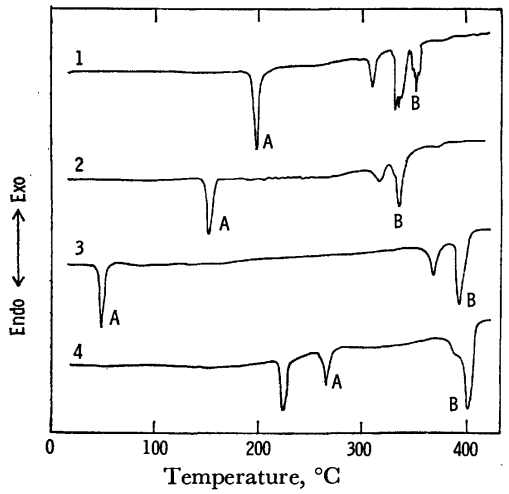

Fig. 3. DTA curves of the aluminum(III) chelates obtained in nitrogen atmosphere at heating rate of 10 °C/min.
1, $Al(AA)_3$; 2, $Al(DIBM)_3$; 3, $Al(DIVM)_3$; 4, $Al(DPVM)_3$.

In a temperature range below 300 °C, $Al(AA)_3$, $Al(DIBM)_3$, and $Al(DIVM)_3$ show single endothermic peaks (A), which agree well with their melting points. The peaks (A) were reproducible in the repeated DTA runs, being ascribable to the melting process. On the other hand, $Al(DPVM)_3$ shows two endothermic peaks in the same temperature region and that at the higher temperature is related to the melting points.[19] Irreversible endotherms (B) above 300 °C were probably due to the thermal degradation of the chelates, except $Al(AA)_3$. Endotherms (B) due to thermal degradation of $Al(AA)_3$ was probably accompanied by different kind of endotherms such as due to vaporization of the molten chelate.

Iron(III) Chelates. Analytical and IR data show that the DIBM and DPVM chelates of iron(III) have the composition of $FeL_2(CH_3O)$,[24] where L denotes the anionic ligand. Thermal behaviors of the two chelates are, therefore, not comparable to those of the other chelates of ML_3 form.

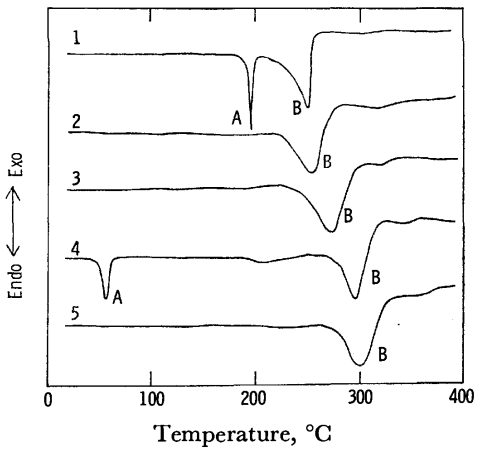

Fig. 4. DTA curves of the iron(III) chelates obtained in nitrogen atmosphere at heating rate of 10 °C/min.
1, $Fe(AA)_3$; 2, $Fe(DNPM)_3$; 3, $Fe(DNBM)_3$; 4, $Fe(DIVM)_3$; 5, $Fe(DNCM)_3$.

Figure 4 shows the DTA curves of the ML_3-type iron(III) chelates obtained in nitrogen atmosphere. $Fe(DIVM)_3$ and $Fe(AA)_3$ show reversible endotherms at 57 and 199 °C, respectively, which are related to their melting points. The corresponding endotherms of $Fe(DNCM)_3$ and $Fe(DNBM)_3$ occur below room temperature, which can not be detected on our DTA apparatus. The irreversible broad endotherms (B) at a higher temperature region are related to thermal decomposition. The melting process of $Fe(AA)_3$ chelate is immediately followed by a thermal degradation, indicating its poor thermal stability in a molten state. The decomposition temperature of the iron(III) chelates seemed to increase with the increasing size of alkyl substituents as observed in the case of cobalt(III) chelates.

Manganese(III) Chelates. DTA curves of manganese(III) chelates measured in nitrogen atmosphere are shown in Fig. 5. Reversible endotherms (A) of the $Mn(DIBM)_3$, $Mn(DIVM)_3$, and $Mn(DPVM)_3$ are ascribable to their melting processes. $Mn(AA)_3$ shows

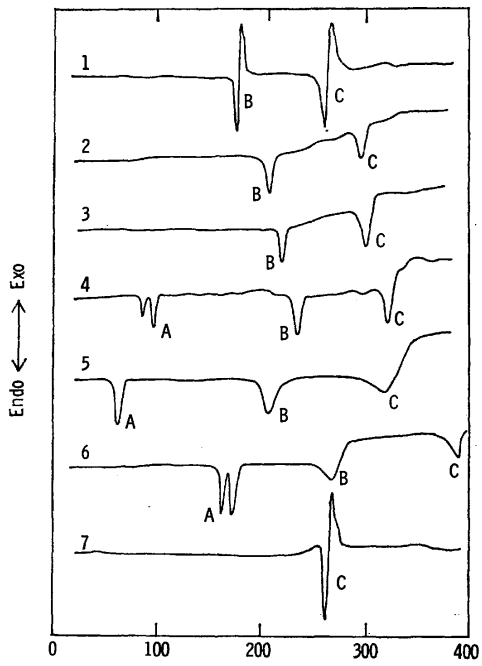

Fig. 5. DTA curves of the manganese(III) and manganese(II) chelates obtained in nitrogen atmosphere at heating rate of 10 °C/min. 1, $Mn(AA)_3$; 2, $Mn(DNPM)_3$; 3, $Mn(DNBM)_3$; 4, $Mn(DIBM)_3$; 5, $Mn(DIVM)_3$; 6, $Mn(DPVM)_3$; 7, $Mn(AA)_2$.

two irreversible endotherms immediately followed by exotherms. DTA characteristics of the second inflection (C) at 250—260 °C[22] seems quite similar to those observed on manganese(II) acetylacetonate, $Mn(AA)_2$, DTA curve of which was obtained separately, as shown in Fig. 5. When the $Mn(AA)_3$ was heated slightly above the first inflection (B) temperature, the resulting product showed an IR spectrum quite resembled that of $Mn(AA)_2$, and the evolution of acetylacetone was also confirmed upon the above thermal process.

The remaining manganese(III) chelates also liberate the ligand molecules when heated up to the peak (B) temperature. Thus the endotherms (B) can be ascribed to the reductive degradation from the tris(β-diketonato)-manganese(III) to the bis(β-diketonato)manganese(II), just so as observed in the cobalt(III) chelates.

The irreversible endotherms (C) at a higher temperature region may be due to the pyrolytic decomposition of the manganese(II) chelates which resulted at the endotherms (B).

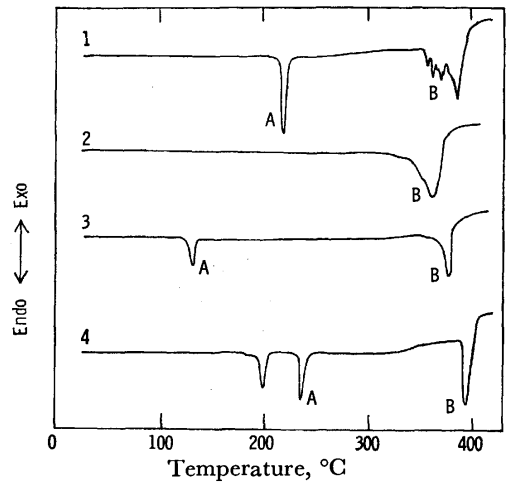

Fig. 6. DTA curves of the chromium(III) chelates obtained in nitrogen atmosphere at heating rate of 10 °C/min. 1, $Cr(AA)_3$; 2, $Cr(DNPM)_3$; 3, $Cr(DIBM)_3$; 4, $Cr(DPVM)_3$.

Chromium(III) Chelates. Figure 6 shows the DTA curves of the chromium(III) chelates measured with a hermetic-sealed sample holder in nitrogen atmosphere. $Cr(AA)_3$ and $Cr(DIBM)_3$ show reversible endotherms (A), which are related to their melting process. On the other hand, $Cr(DPVM)_3$ shows two reversible endotherms at about 200 °C, of which an endotherm at the higher temperature is ascribed to its melting process.[19]

In a higher temperature region, each chromium(III) chelate shows an irreversible endotherm (B). This was due to their decomposition process.

Table 2 summarizes the melting- and decomposition temperatures of the present chelates determined by DTA method. $Al(AA)_3$, $Cr(AA)_3$, and $Fe(AA)_3$ show characteristic melting points, respectively. The last acetylacetonate is, however, not very durable in the molten form. $Co(AA)_3$ and $Mn(AA)_3$ decompose prior to melting.

If one considers the thermal stability of a compound in terms of its pyrolytic decomposition temperature, the thermal stability of the pentane-2,4-dionates decreases in the order of Cr(III)>Al(III)>Fe(III)>Co(III)>Mn(III) so far as studied. A similar tendency in the thermal stability of pentane-2,4-dionates of the same tervalent metal ions was also observed by a different

Table 2. Melting- and decomposition temperature (°C) of chelates

Ligand	Co(III)		Al(III)		Fe(III)		Mn(III)		Cr(III)	
	mp	dp	mp	dp	mp	dp	mp	dp	mp	dp
AA	a	222	197	330—350	191	250	a	174	216	360—380
DNPM	59	224	b, c		b	254	b	209	b	370
DNBM	b	230	b, c		b	272	b	220	b, c	
DIBM	a	232	154	330	d		85—96	234	132	376
DIVM	58	259	50	393	57	295	63	237	b, c	
DPVM	240	286	266	402	d		163—171	269	236	400
DNCM	b	232	b, c		b	300	b, c		b, c	

a) Decomposed prior to melting. b) Oily liquid at room temperature. c) Not obtained as pure chelates. d) Not obtained as ML_3 composition.

method.[25] The present 1,5-dialkylpentane-2,4-dione chelates gave the same order of the thermal stability in respect to the kind of the central metal ion.

Regarding to the structures of β-diketones, one can see a general trend that the branched-alkyl derivatives afford metal chelates of higher melting temperatures than that of the linear-alkyl substituted ligands: DNPM, DNBM, and DNCM give liquid chelates with an exception of $Co(DNPM)_3$, while DIBM, DIVM, and DPVM solid chelates at room temperature.

For the cobalt(III) chelates, thermal stability increased in the order of AA<DNPM<DNBM< DIBM<DNCM<DIVM<DPVM, which agreed with the order of bulkiness of alkyl substituents. Similar tendencies were also obtained for the other tervalent metal chelates. The thermal stabilities of the present chelates are, therefore, considered to be partly due to the electron releasing effect of the alkyl groups. Such effect increases the basicity of the ligand oxygen atoms to form increasingly stable metal-oxygen bonding,[18] and this kind of thermodynamic stabilization effect was also observed with some bivalent metal chelates.[15] On the other hand, kinetic destabilization effect by the alkyl substituents such as observed in the copper(II) and palladium(II) chelate[15] was unlikely to operate on the present octahedral hexacoordinate chelates.

As described before, the pyrolytic degradation of the manganese(III) and cobalt(III) chelates is accompanied by the reduction of the central metal ion from tervalent to bivalent and the liberation of the free ligand.[26,27] Although the stoichiometry of the whole scheme of the reaction is unknown at this moment, it is most likely that the metal-oxygen bonding in the tervalent metal chelates may be homolytically cleaved at the endotherm (B) to form the bivalent metal chelates, meanwhile the liberated ligand radical regenerates as the ligand molecule through hydrogenation processes such as hydrogen-abstraction from neighboring matrix or disproportionation with other radical.

Such radical termination processes are usually exothermic, and the exothermic branch of the inflection (B) on the DTA curve of $Mn(III)(AA)_3$ might be an indication of such a kind of process. The other DTA curves lack apparent exotherms subsequent to the endotherms (B), and this might possibly result from that the exotherms overlaps on the endotherms or diffuse widely.

Similar pyrolytic reduction reaction was observed also in $Fe(III)(AA)_3$,[28] and these facts seem to suggest that the pyrolytic reduction occurs in the chelate of such a metal ion that in the bivalent state can also form a stable chelate of the same ligand. Although an LCAO-MO calculation on the tervalent metal pentane-2,4-dionates[29] might provide an explanation for the ease with which $Mn(III)(AA)_3$ could be reduced to $Mn(II)(AA)_2$, a consistent understanding is not attained for the reason why these particular metal ions are labile to be reduced in the tris(β-diketonato)metal chelates.

References

1) H. Kaneko and K. Ueno, *Talanta*, **13**, 1525 (1966).
2) H. Kaneko, H. Kobayashi, and K. Ueno, *ibid.*, **14**, 1403 (1967).
3) R. G. Charles, *Anal. Chim. Acta*, **27**, 474 (1962).
4) W. W. Wendlandt and G. R. Horton, *Anal. Chem.*, **34**, 1908 (1962).
5) W. C. Fernelius and J. E. Blanch, "Inorganic Syntheses," Vol. 5, McGraw-Hill Inc., New York, (1957), p. 130.
6) A. Arch and R. C. Young, *ibid.*, Vol. 2, (1946), p. 19.
7) R. C. Young, *ibid.*, Vol. 2, (1946), p. 25.
8) R. C. Fay and T. S. Piper, *J. Amer. Chem. Soc.*, **85**, 500 (1963).
9) M. L. Morris, R. W. Moshier, and R. E. Sievers, *Inorg. Chem.*, **2**, 411 (1963).
10) H. F. Holtzclaw, Jr., A. H. Carlson, and J. P. Collman, *J. Amer. Chem. Soc.*, **78**, 1838 (1956).
11) R. L. Belford, A. E. Martell, and M. Calvin, *J. Inorg. Nucl. Chem.*, **2**, 11 (1956).
12) K. G. Hampton, T. M. Harris, and C. R. Hauser, *J. Org. Chem.*, **30**, 61 (1965).
13) R. Levine, J. A. Conroy, J. T. Adams, and C. R. Hauser, *J. Amer. Chem. Soc.*, **67**, 1510 (1945).
14) J. T. Adams and C. R. Hauser, *ibid.*, **67**, 284 (1945).
15) I. Yoshida, H. Kobayashi, and K. Ueno, *J. Inorg. Nucl. Chem.*, **35**, 4061 (1973).
16) I. Yoshida, Y. Oono, H. Kobayashi, and K. Ueno, This Bulletin, **45**, 175 (1972).
17) I. Yoshida, H. Kobayashi, and K. Ueno, *ibid.*, **45**, 1411 (1972).
18) I. Yoshida, H. Kobayashi, and K. Ueno, *ibid.*, **45**, 2768 (1972).
19) G. S. Hammond, D. C. Nonhebel, and Chin-Hua S. Wu, *Inorg. Chem.*, **2**, 73 (1963).
20) M. M. Jones, *J. Amer. Chem. Soc.*, **81**, 3188 (1959).
21) R. G. Charles, "Inorganic Syntheses," Vol. 7, McGraw-Hill Inc., New York, (1963), p. 183.
22) R. G. Charles, *ibid.*, Vol. 6, (1960), p. 164.
23) W. C. Fernelius and J. E. Blanch, *ibid.*, Vol. 5, (1957), p. 130.
24) Chin-Hua S. Wu, G. R. Rossman, H. B. Gray, G. S. Hammond, and H. J. Schugar, *Inorg. Chem.*, **11**, 990 (1972).
25) R. G. Charles and M. A. Pawlikowski, *J. Phys. Chem.*, **62**, 440 (1958).
26) J. von Hoene, R. G. Charles, and W. M. Hickam, *ibid.*, **62**, 1098 (1958).
27) R. G. Charles, W. M. Hickam, and J. von Hoene, *ibid.*, **63**, 2084 (1959).
28) N. Tanaka, private communication; Y. Iwanami, Master Thesis, Tohoku Univ., 1970.
29) D. W. Barnum, *J. Inorg. Nucl. Chem.*, **22**, 183 (1961).

ESR Studies of the Triplet State Dimers of the Salicylaldehyde Schiff Base Complexes of Copper(II) in Toluene and in Chloroform

Makoto CHIKIRA, Hiroshi YOKOI, and Taro ISOBE

Chemical Research Institute of Non-Aqueous Solutions, Tohoku University, Katahira, Sendai 980

(Received February 1, 1974)

The ESR spectra of triplet-state dimers have been obtained for various bidentate and quadridentate salicylaldehyde Schiff base complexes of copper(II) in frozen solutions. The spectra have been analysed on the basis of the previously-obtained results concerning the non-coaxial g and fine-structure tensors. The results indicate that the angles between the $g_{\parallel}$ axis and the copper-copper axis of the dimers for the quadridentate Schiff base complexes are considerably smaller than those for the bidentate ones. Each of the actually-measured ESR spectra, however, consisted of two mutually-overlapping spectra; one is due to dimers (M_2), and the other, to monomers (M). The equilibrium constant for $2M \rightleftharpoons M_2$ has been estimated by comparing the ESR spectral intensities of the two species. The factors which govern the dimer formations have been discussed in some detail.

In our previous paper,[1] it has been revealed, through computer simulations of the triplet ESR spectra that the dimeric structure of Bis-(*N*-salicylidenemethylaminato)copper(II) in toluene is similar to that in its γ-form crystals,[2] and that it is necessary to take into account the non-coincidence of the principal axes of the g tensor with those of the fine-structure tensor in order to estimate such dimeric structures. A considerable number of copper(II) chelates are known to have dimeric structures in crystals such as those shown schematically in Fig. 1. Hatfield and his co-workers extensively studied the magnetic interaction within the dimers of this type by means of ESR and magnetic susceptibility measurements.[3] The factors which govern the dimer formations, the nature of the dimerization forces, and the mechanisms of the spin-exchange interaction within the dimers, however, have not yet been established in full detail. In order to study these problems, we systematically measured the ESR spectra of various salicylaldehyde Schiff base complexes of copper(II) in toluene and in chloroform, and discussed the influence of various substituent groups at the iminoic nitrogens and in the phenyl-rings on the dimer formation and dimeric structure.

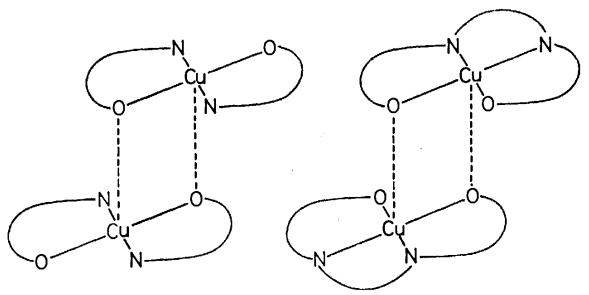

Fig. 1. Schematic illustrations of dimeric structure.

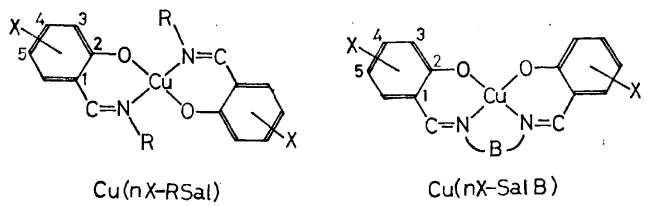

Cu(nX-RSal) Cu(nX-SalB)

Fig. 2. Schematic illustrations of salicylaldehyde Schiff base complexes of copper(II). Following abbreviations were made respectively.
X: Me–, CH_3–; MeO–, CH_3O–
R: Me, CH_3; Et, C_2H_5; n-Pr, C_3H_6
B: en, C_2H_2; pn, $(CH_3)CHCH_2$; bn, $(CH_3)CHCH(CH_3)$; ibn, $(CH_3)_2CCH_2$

Experimental

The salicylaldehyde Schiff base complexes of copper(II) with the general formulae of Cu(nX-RSal) and Cu(nX-SalB) (see Fig. 2) were prepared, where X, R, and B are the generalized ring, nitrogen, and bridging group substituents respectively, and where n represents the position of X in the phenyl ring. These complexes were obtained by refluxing salicylaldehyde or X-substituted salicylaldehyde copper(II) complexes with the appropriate amines or diamines in ethanol. The methyl-substituted salicylaldehyde was synthesized by Duff's reaction.[4] The other salicylaldehyde derivatives were commercially obtained.

The toluene and chloroform were purified according to the usual method,[5] and the chloroform was used immediately after the purification. The ESR of the quadridentate Schiff base complexes in chloroform solutions were measured at 77 K after the frozen solutions had been crushed to fine powders according to a method described previously.[6]

Results and Discussion

The Magnetic Parameters and the Dimeric Structure. The g and A values observed for the monomers of the salicylaldehyde Schiff base complexes of copper(II) were not changed greatly with the substituents ether at the iminoic nitrogens or in the phenyl rings. These magnetic parameters for the bidentate salicylaldehyde Schiff base complexes of copper(II) are in the range of $2.23 > g_{\parallel} > 2.21$, $2.06 > g_{\perp} > 2.04$, and $0.0195\ cm^{-1} > |A_{\parallel}| > 0.0185\ cm^{-1}$, while those for the quadridentate ones are in the range of $2.20 > g_{\parallel} > 2.18$, $2.06 > g_{\perp} > 2.04$, and $0.0215\ cm^{-1} > |A_{\parallel}| > 0.0205\ cm^{-1}$.

The ESR spectra of Cu(5Br–MeSal) and Cu(3Me-Salpn) in toluene are shown in Fig. 3. The magnetic parameters of the triplet-state dimers are defined in Fig. 3 as has been previously described,[1] and their values are tabulated in Table 1. The values of g_1 and g_2 are defined from the centers of the so-called full-field perpendicular and parallel lines respectively. The A_1 and A_h values express the hyperfine-splittings of the low-field and high-field parallel lines respec-

tively. The D_1 and D_2 values express the observed fine-structure splittings of the perpendicular and parallel lines respectively. As Table 1 shows, the magnetic parameters of the triplet dimers do not change markedly with the substituents. The line shapes and the magnetic parameters of the bidentate Schiff base complexes are characterized by the non-coaxial g and fine-structure tensors; that is, $(A_{\parallel}/2)>A_1>A_h$, and $g_2<g_{\parallel}$. Therefore, the dimeric structures of the bidentate complexes are considered to be similar to those of Cu(MeSal) in γ-form crystals, where the angle between the $g_{\parallel}$ axis and the copper-copper axis is about 30°.[1] On the other hand, the triplet-state dimers of the quadridentate Schiff base complexes show the typical ESR line shapes for the indication of the near co-axial g and fine-structure tensors; that is, A_1 and A_h are almost equal to the $A_{\parallel}/2$ of the monomers, while g_2 is almost equal to the $g_{\parallel}$ of the monomers.

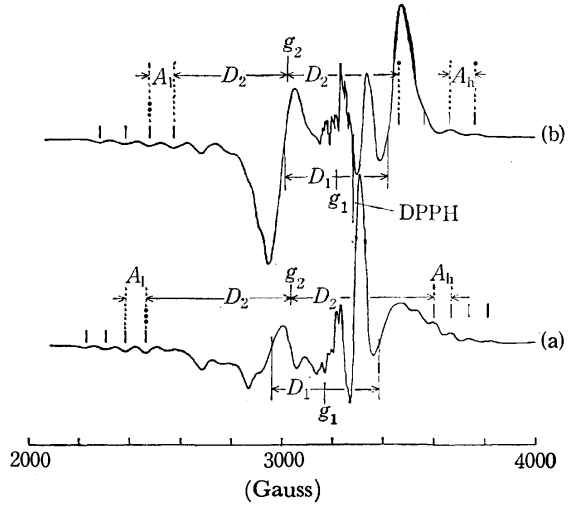

Fig. 3. ESR spectra of 77 K frozen toluene solutions of a) Cu(5Br-MeSal), b) Cu(3Me-Salpn).

Table 1. Magnetic parameters of triplet dimers

Ligand	g_1	g_2	A_1	A_h	D_1	D_2	Frequency (MHz)
			(gauss)				
MeSal	2.069	2.170	79	65	409	563	9220
3Me-			83		400		9224
4Me-	2.065	2.172	79	66	414	565	9293
5Me-	2.07	2.170	80	67	400	568	9285
5Br-	2.073	2.174	80	70	420	566	9288
EtSal	2.061	2.171	79	68	390	564	9135
5Br-	2.066		80		405		9182
nPrSal		2.171	75	67		563	9324
Salen		2.180	100	100		432	9139[a]
Salpn	2.042	2.190	100	100	380	428	9327
		2.185	103	103		434	9329[a]
3Me-	2.050	2.184	99	100	408	444	9230
4Me-		2.188	100	100		420	9249
5Me-	2.052		100		380		9284
5Br-	2.052		100		400		9211
Salbn		2.186	100	100		423	9210

a) Medium; chloroform. All the other data were obtained in frozen toluene solutions.

It is well known that Cu(Salen) has a dimeric structure in crystals similar to that of Cu(MeSal).[2,7] There are two possible explantions for the near coincidence between the principal axes of the g and fine-structure tensors. One is that the dimeric structure in the frozen solutions is so different from those in the crystals of Cu(Salen) or Cu(MeSal) that the $g_{\parallel}$ axis almost coincides with the copper-copper axis. The other is that, although the dimeric structure similar to that found in the crystals of Cu(Salen) is retained even in frozen solutions, the so-called pseudo-dipole interaction whose principal axes coincide with those of the g tensor cancels the effect of the non-coaxial g and fine-structure tensors in the spin-dipole interaction.

The magnitudes of the pseudo-dipole and spin-dipole interaction can be estimated from Eqs. (1) and (2), where J is the energy difference between a triplet state and a singlet state, and where r is the distance between the two copper ions.

$$D_{\text{pseudo}} = \frac{-1}{8} J \left\{ \frac{1}{4} (g_{//}-2)^2 - (g_{\perp}-2)^2 \right\} \qquad (1)^{8}$$

$$D_{\text{dd}} = \frac{-0.65 g_2^2}{r^3} \qquad (2)^{9}$$

The J value for the dimers of Cu(Salen) in crystals had been estimated at 5 cm^{-1}.[10] From this J value and the magnetic parameters for the triplet dimers of Cu(Salen), that is, $g_{\parallel}=g_2=2.19$, $g_{\perp}=2.05$, and $r=3.5$ Å, D_{pseudo} and D_{dd} can be estimated at -0.0041 and -0.0700 cm^{-1} respectively. It is clear that the obtained value of D_{pseudo} is too small to cancel the effect of the spin-dipole interaction. It may be concluded, therefore, that the first explanation is more reasonable than the second one in this case. It has been reported that the dimeric structure of $Cu(Etacest)_2$ in toluene is also different from that in crystals,[11] where Etacest is the anion of ethylacetoacetate. These facts indicate that the dimeric structures in crystals are often different from those in solutions: the dimeric structures in crystals depend to a greater or lesser degree upon the ways of molecular packing. The polymorphism of Cu(MeSal) is regarded as an example of such phenomena.

Two papers have appeared during the preparation of our report concerning the triplet-state dimers of the salicylaldehyde Schiff base complexes of copper(II) in solutions.[10,12] In both papers, the parameters of the spin Hamiltonian tensors were estimated on the basis of the computer simulations of the ESR spectra only for $\Delta M=2$ transitions. Toy *et al.* estimated the copper-copper distance and the angle between the $g_{\parallel}$ axis and the copper-copper axis for the Cu(Salen) dimers in chloroform at 4.55 Å and $40\pm5°$ respectively.[12] However, it is evident from the results of our computer simulation previously described that the spectral patterns for the $\Delta M=1$ transitions of Cu(Salen) cannot be reproduced by the use of such non-coaxial g and spin-dipole interaction tensors. On the other hand, Hatfield *et al.* concluded that the principal axes of the g and fine-structure tensors are coincident with each other. This conclusion is in accord with our results. However, they had previously assumed that the dimeric

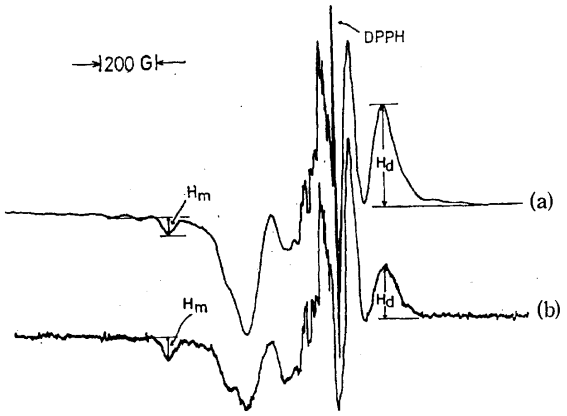

Fig. 4. Concentration dependence of ESR spectra of Cu(Salpn) in toluene at 77 K. a) 3.1×10^{-3} M, b) 0.5×10^{-3} M.

structure of Cu(Salen) in crystals is retained in frozen chloroform solutions, and had estimated the contribution of the spin-dipole interaction to the observed fine-structure splittings at 0.036 cm^{-1}.[13] This value seems too small to agree with the value calculated from Eq. (2). A further detailed report on the relation between the dimeric structure and the relative orientations of the g and fine-structure tensors will soon be published.

The Equilibrium between Dimers and Monomers. In order to obtain quantitative information on the effects of various substituents on the dimer formations, we have estimated the equilibrium constants for $2M \rightleftharpoons M_2$, where M and M_2 represent monomer and dimer species respectively. In our previous paper, we have already presented the following relation:[11]

$$2Q^2 + qQ = Kq^2c^\circ \tag{3}$$

where the equilibrium constant, K, is expressed as follows:

$$K = \frac{[M_2]}{[M]^2} \tag{4}$$

where c° is the initial concentration of a complex and where the Q and q values are defined as:

$$Q = \frac{H_d}{H_m} = q\frac{[M_2]}{[M]} \tag{5}$$

H_d and H_m in Eq. (5) are the peak heights of certain absorption lines due to the dimers and monomers respectively in the first derivative ESR spectra, as is shown in Fig. (4) in the case of Cu(Salpn) in toluene. It may reasonably be supposed that the magnitude of the spin exchange interaction within the present dimers is much smaller than the thermal energy at 77 K. Then, we can derive Eq. (6):

$$\frac{I_d}{I_m} = \frac{2[M_2]}{[M]} \tag{6}$$

where I_d is the total integrated intensities of the ESR spectra due to the dimers, and I_m, the total of those due to the monomers, respectively. I_d and I_m were obtained as has been described previously.[11]

The plots of $(2q^2+qQ)/q^2$ *vs.* c° for the toluene solutions of Cu(MeSal), Cu(EtSal), Cu(nPrSal), and Cu(Salpn) are shown in Figs. 5 and 6. Since the magnetic parameters of the triplet dimers of the salicylaldehyde Schiff base complexes of copper(II) do not change markedly with the substituents, it may reasonably be supposed that the q values do not change with the substituents. Then, we can estimate the values of K using the Q values obtained from the ESR spectra measured at only one concentration. The K values thus obtained for other salicylaldehyde Schiff base complexes by the use of the q values determined for Cu(MeSal) and Cu(Salpn) are listed in Tables 2 and 3. The salicylaldehyde Schiff base complexes of copper(II) employed here are soluble in many coordinating solvents, such as methanol, ethanol, and pyridine. However, the ESR signals due to the triplet dimers were not observed in these solutions. In general, the K values of the quadridentate complexes are much larger than those of the bidentate ones. The chloroform solutions of the bidentate complexes did not exhibit any signals due to triplet dimers, but those of the quadridentate ones did, though the spectral intensities due to the dimers were very weak as compared with those due to the monomers.

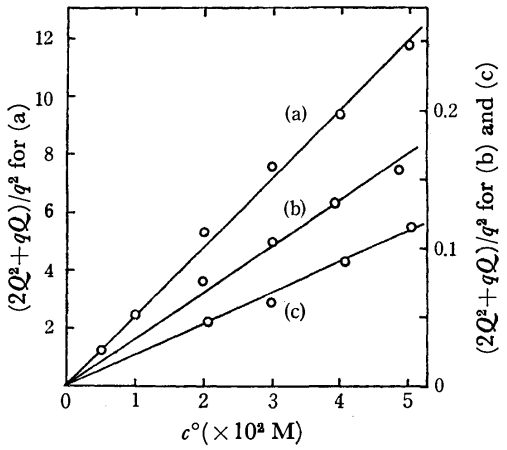

Fig. 5. The plot of $(2Q^2+qQ)/q^2$ *vs.* c° for the 77 K frozen toluene solutions. (q=2.0)
a) Cu(MeSal), b) Cu(EtSal), c) Cu(*n*PrSal)

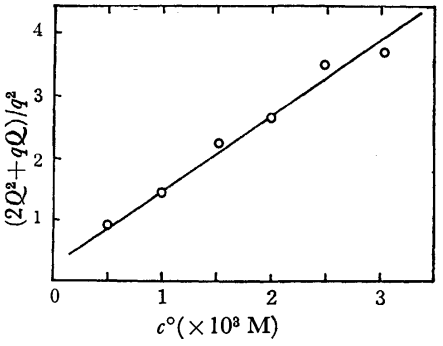

Fig. 6. The plot of $(2Q^2+qQ)/q^2$ *vs.* c° for the 77 K frozen toluene solutions of Cu(Salpn). (q=4.0)

Table 2 indicates the variation in the K values with the substituents at the iminoic nitrogens. In the case of the bidentate complexes, it is clear that the more bulky the substituent at the iminoic nitrogen becomes, the less the K value becomes. When the R in Fig. 2 was replaced by the isopropyl or *tert*-butyl group, no signals due to the triplet-state dimers could be detected.

Table 2. The dependence of the K values on the substituent groups at the iminoic nitrogens of salicylaldehyde Schiff bases

	Toluene	Chloroform
Cu(MeSal)	2.4×10^2	0
Cu(EtSal)	3.2	0
Cu(nPrSal)	2.3	0
Cu(Salen)	—[a]	41
Cu(Salpn)	1.3×10^3	28
Cu(Salbn)	1.1×10^3	0
Cu(Salibn)	7.8×10^2	0

a) Cu(Salen) is scarcely soluble in toluene.

Table 3. The dependence of the K values on the substituent groups at the phenyl rings of the salicylaldehyde Schiff bases

X	MeSal	Salpn		Salen
	Toluene	Toluene	Chloroform	Chloroform
H	2.4×10^2	1.3×10^3	28	41
3Me	21	1.2×10^4	28	24
4Me	4.7×10^2	2.4×10^2	49	1.2×10^2
5Me	1.8×10^2	6.6×10^3	54	54
5Br	2.3×10^3	3.2×10^4	71	—[b]
3MeO	0	—[c]	8.4×10^2	1.3×10^3
5MeO	2.1×10^3	—[c]	94	76

a) The q values for bidentate Schiff base complexes were put equal to that for Cu(MeSal) (2.0), and those for quadridentate ones, to that for Cu(Salpn) (4.0) in toluene. b) Cu(5Br-Salen) is scarcely soluble in chloroform. c) The spectral patterns correspond to crystalline powders were obtained.

On the other hand, when the R was replaced by proton, no evidence for the dimer formation could be obtained because of the low solubility of the complex in toluene. The K values for the quadridentate complexes in toluene were not changed by the methyl groups at the ethylene bridge. When the iminoic nitrogens were bridged with the trimethylene group, however, no signals due to the triplet-state dimers could be detected. These experimental facts suggest that the dimer formations are inhibited by the direct steric hindrance of bulky substituents near the first coordination sphere and/or by the tetrahedral deformation of coordination due to such bulky substituents.

Table 3 indicates the changes in the K values with substituents in the phenyl rings. We may clearly recognize large differences between the bidentate and quadridentate complexes in the effect of substituents in the phenyl rings on the K values. The 3-methyl and 3-methoxy groups of the bidentate complexes severely inhibited the dimer formation, whereas those of the quadridentate ones did not. For instance, the K values of Cu(3MeO-Salpn) and Cu(3Me-Salpn) become larger than those of the unsubstituted complexes. It should be further noticed that the influence of the substituents on the K values are markedly dependent upon the solvents. For instance, the K values for the toluene solutions of Cu(3Me-Salpn) and Cu(5Me-Salpn) were considerably larger than that of Cu(Salpn), whereas those of the chloroform solutions of the former did not increase so much as that of the latter. It may naturally be supposed that toluene molecules have a strong affinity for the phenyl rings of the complexes rather than for the copper ions and coordinating atoms. It seems likely that the dependence upon solvents for such changes in the influence of substituents in the phenyl rings is to be attributed to the changes in solvation. These experimental results suggest that the phenyl rings of the salicylaldehyde Schiff bases play an important role in determining the dimer formation. These estimations are further supported by the fact that no ESR signals of the triplet dimers were observed for a toluene solution of *N*, *N'*-ethylenebis(4-amino-3-penten-2-ono)copper(II) at 77 K. Recently, Yokoi indicated that the K values of bis(*t*-butylacetoacetato)copper(II) and Cu(Etacest)$_2$ change markedly with slight changes in the properties of the solvents.[14] Thus, it seems natural that the K values change greatly with a slight change in the properties of the substituents and the solvents.

Conclusion

In the solutions of various Schiff base complexes of copper(II), the K values for $2M \rightleftharpoons M_2$ depend on many delicate factors, although the triplet-state ESR spectral patterns do not change markedly with the substituents. It was also revealed that the dimeric structure of the quadridentate Schiff base complexes in frozen solutions is different from that of Cu(Salen) in crystals. These facts, besides similar results previously obtained, suggest that the dimerization force must be weak, and that the forces are generated not only by the coordination of the oxygen atoms to the apical positions of adjacent complexes, as is shown schematicaly in Fig. 1, but also by the wholly-molecular electric dipole or dispersion interaction between the monomeric halves in the dimers. It may be expected, accordingly, that the dimeric structures of these types of complexes change sensitively with the nature of such dimerization forces and with their environments.

References

1) M. Chikira and T. Isobe, This Bulletin, **45**, 3006 (1972).
2) D. Hall, S. V. Sheat, and T. N. Waters, *J. Chem. Soc., A*, **1968**, 460.
3) W. E. Hatfield, *Inorg. Chem.*, **11**, 216 (1972), and the references therein.
4) J. C. Duff, *J. Chem. Soc.*, **1941**, 547.
5) "Techniques of Chemistry, Organic Solvents," 3rd ed. by J. A. Riddick and W. B. Bunger, John Wiley & Sons, Inc., (1970), Chapter V.
6) M. Chikira, T. Kawakita, and T. Isobe, This Bulletin, **47**, 1283 (1974).
7) D. Hall and T. N. Waters, *J. Chem. Soc.*, **1960**, 2644.
8) B. Bleaney and K. D. Bowers, *Proc. Roy. Soc. Ser. A*, **214**, 451 (1952).
9) R. L. Belford, N. D. Chasteen, H. So, and R. E. Tapscott, *J. Amer. Chem. Soc.*, **91**, 4657 (1969).
10) T. Lund and W. E. Hatfield, *J. Chem. Phys.*, **59**,

885 (1973), and the references therein.
11) H. Yokoi and T. Isobe, This Bulletin, **46**, 447 (1973).
12) A. D. Toy, M. D. Hobday, P. D. W. Boyed, and T. D. Smith, *J. Chem. Soc., Dalton*, **1973**, 1259.
13) G. O. Carlisle and W. E. Hatfield, *Inorg. Nucl. Chem. Lett.* **6**, 633 (1970).
14) H. Yokoi, This Bulletin, **47**, 497 (1974).

The Chemistry of Protactinium. XI. A Study of the Solvent Extraction of Protactinium(IV) Reduced with Europium(II) from a Perchloric Acid Solution, Using Thenoyltrifluoroacetone as the Extractant

Isamu KAWASUJI, Akiko SATO, and Shin SUZUKI

The Research Institute for Iron, Steel and Other Metals, Tohoku University, Katahira, Sendai 980

(Received February 19, 1974)

Europium(II) was found to be an excellent reductant for reducing protactinium in microquantities to the tetravalent state. The behavior of Pa(IV) in the perchloric acid solution was investigated by the TTA–benzene extraction method. It was found that the $PaOH^{3+}$ ion existed predominantly in a 0.03—3 M perchloric acid solution at the ionic strength of 3. The reaction of TTA extraction may proceed as:

$$PaOH^{3+} + 4HA = PaA_4 + H_2O + 3H^+$$

or

$$PaOH^{3+} + 4HA = Pa(OH)A_3(HA) + 3H^+$$

The distribution ratio of Pa(IV) in the system using Eu(II) as the reductant is about ten times as large as that in the system using Cr(II) as the reductant. It was considered that a non-extractable complex may be formed between Pa(IV) and Cr(III), while such a complex may not be formed when Eu(II) is used as the reductant.

Chromium(II) has been used for reducing protactinium in microquantities to the tetravalent state. Guillaumont[1] investigated the behavior of Pa(IV) reduced with Cr(II) in a perchlorate solution by means of the TTA–benzene extraction method and showed that Pa^{4+} was gradually hydrolyzed to $Pa(OH)_3^+$ in the pH range from −0.3 to 3.0 at the ionic strength of 3. Mitsuji[2] also investigated the behavior of Pa(IV) reduced with Cr(II) in a perchlorate solution by means of TTA–benzene extraction in the pH range from 0.4 to 1.1 at the ionic strength of 0.5; he suggested that $Pa(OH)_2^{2+}$ was the most probable ionic species in the perchlorate solution. However, in a previous report[3] we ourselves suggested that a multi-nuclear complex between Pa(IV) and Cr(II) or Cr(III) might be formed, because the distribution ratio of Pa(IV) decreased with an increase in the concentration of Cr(II). We also tried to measure the absorption spectra of Pa(IV), but could not find any influence of Cr(II) on it.

In the present experiment, we tried to use another reagent to reduce the protactinium in place of Cr(II); Eu(II) was found to be an excellent reductant. The standard oxidation-reduction potential of Pa(IV)–Pa(V) has been reported to be about −0.25 V,[4] and that of Eu(II)–Eu(III), −0.43 V.[5]

After ^{233}Pa in a perchloric acid solution was reduced to the tetravalent state by means of a liquid zinc amalgam in the presence of Eu(III), the oxidation state of protactinium was examined by the co-precipitation method with thorium fluoride reported by Mitsuji[6] and it was found that the complete reduction of $^{233}Pa(V)$ was readily attained. The chemical behavior of the $^{233}Pa(IV)$ thus obtained in the perchloric acid solution was investigated by the solvent extraction method, using TTA as the extractant.

In order to examine the difference in the extraction behavior of Pa(IV) caused by the difference in reductant between Cr(II) and Eu(II), experiments were also carried out on the extraction behavior of Pa(IV) reduced with Cr(II) under the same conditions as in the case of Eu(II).

Cr(II)[1,3] was extracted from a perchloric acid solution with TTA–benzene, but Eu(II) was not extracted from a 0.03—3 M perchloric acid solution at the ionic strength of 3. Therefore, Eu(II) can not act as a "holding reductant" in the organic phase. The present authors tried to measure the stability of the Pa(IV)–TTA chelate in the benzene solution by means of spectrophotometric measurements.

Experimental

Reagents. ^{231}Pa was purified by a method reported previously,[7] and its radiochemical purity was certified by α- and γ-ray spectrometry. The concentration of protactinium in the ^{231}Pa solution was determined as Pa_2O_5 by gravimetry and by the absolute α-counting method. These two results agreed well within the limits of experimental error, so we could confirm that there was no contamination by non-radioactive impurities. ^{233}Pa was prepared by the method reported by Suzuki and Inoue.[7]

The extraction behavior of Cr(II) and Eu(II) was examined by the use of ^{51}Cr and ^{152}Eu respectively as the tracers. The radiochemical purity of ^{51}Cr or ^{152}Eu was certified by γ-ray spectrometry.

The lithium perchlorate was prepared by the method reported by Biedermann and Ciavatta.[8] The water used was purified by distillation, followed by ion-exchange treatment. TTA and the other reagents used in this experiment were of the highest purity.

Apparatus. Both the reduction and the extraction of protactinium were carried out in the reduction apparatus described in a previous report.[9] For the solvent extraction procedure, an Iwaki universal mechanical shaker, Model V-S, was used. The α-ray spectra were measured with an ORTEC silicon surface-barrier detector (active area: 450 mm^2; resolution: 30 KeV), coupled with a Tōshiba 4096-channel pulse-height analyzer. The α-ray counting was carried out by measuring the area of its energy peak and the counting efficiency of the detector with reference to the IAEA standard α-ray source ($^{239}Pu+^{241}Am+^{244}Cm$). The γ-ray spectra were measured with an ORTEC Ge(Li) coaxial detector (volume: 57 cc; resolution: 1.97 KeV), coupled with a Tōshiba 4096-channel pulse-height analyzer. For the γ-ray energy calibration, the IAEA standard γ-ray sources-^{60}Co,

^{57}Co, ^{137}Cs, ^{241}Am, ^{54}Mn, and ^{22}Na- were used. For the on-line data analysis, a Tōshiba TOSBAC-40 mini-computer was used. A Hitachi Model SP-3 well-type NaI(Tl) scintillation probe coupled with a Kōbe Kōgyō Model SA-250 scaler was used for the γ-activity measurements. For measuring the absorption spectrum, a Hitachi Model EPS-3 recording spectrophotometer and a 1 cm quartz cell were used.

Procedure. The Co-precipitation with Thorium Fluoride: Four milliliters of a perchloric acid solution of ^{233}Pa(V) containing a definite amount of Eu(III) were introduced into a reduction apparatus and thoroughly deoxygenated by bubbling with argon gas which had been passed through a dilute sulfuric acid solution of ammonium metavanadate. By shaking the reduction apparatus for about 15 min, the protactinium and europium were reduced with a freshly-prepared liquid zinc amalgam. After the amalgam had been excluded from the apparatus, 2 ml portions of a 0.05 M thorium chloride solution and of a 0.7 M potassium fluoride solution, which had been thoroughly deoxygenated, were added and thorium fluoride was precipitated. Then, the precipitate was separated by centrifuging the mixture for 3 min at 3000 rpm. The γ-activities of both the solution and the precipitate were measured, and the co-precipitation ratio was calculated.

The Absorption Spectra of the Pa(IV)-TTA Chelate: A sulfuric acid solution of ^{231}Pa was reduced by shaking with a liquid zinc amalgam for about 6 hr. After the ^{231}Pa(IV) had been extracted by shaking with a 0.5 M TTA-benzene solution for 10 min, the ^{231}Pa(IV)-TTA chelate in the organic phase was introduced into the quartz cell and the absorption spectrum was immediately measured with reference to a 0.5 M TTA-benzene solution.

The ^{233}Pa(IV) Extraction: Ten milliliters of a perchloric acid solution of ^{233}Pa(V) containing a definite amount of Eu(III) were reduced with a liquid zinc amalgam. Then, the solvent extraction of Pa(IV) was carried out by shaking it with 10 ml of TTA-benzene solution for 10 min. We had confirmed previously that the equilibrium was established sufficiently in that time. After the two phases had been completely separated, an aliquot of each phase was placed in a polyethylene test tube and its γ-radioactivity was counted. The distribution ratio(D) was calculated by means of the usual equation:

$$D = \frac{\gamma\text{-activity per ml of the organic phase}}{\gamma\text{-activity per ml of the aqueous phase}} \quad (1)$$

As Cr(II) was extracted with TTA, we needed to correct the concentration of the TTA-benzene solution resulting from the co-existence of Cr(II). Therefore, the TTA extraction was carried out after ^{51}Cr had been added to the ^{233}Pa solution, and the distribution ratios of Cr(II) and Pa(IV) were obtained at the same time by measuring their γ-radioactivities at the characteristic energy peaks of 319.8 KeV and 311.9 KeV respectively. The concentration of TTA was corrected by means of a method reported previously.[3]

The ionic strength was kept constant by the use of lithium perchlorate. All the experiments were carried out in an argon atmosphere at room temperature, 20—23 °C.

Results

The Co-precipitation with Thorium Fluoride. The co-precipitation of ^{233}Pa(IV) was almost complete in the presence of more than 10^{-3} M of europium, as is shown in Fig. 1. This means that protactinium can be reduced quantitatively to the tetravalent state on a tracer scale by the addition of europium. On the other hand, the co-precipitation of Pa(V) was about 15% when the concentration of europium was less than 3×10^{-4} M; this value then increased with an increase in the europium concentration when the concentration of europium was higher than 3×10^{-4} M; this was because of the contribution of Pa(V) co-precipitated with europium fluoride.

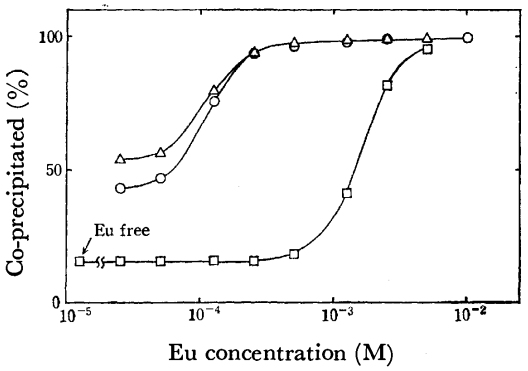

Fig. 1. Relation between Eu concentration and % co-precipitated with ThF_4
△: ^{233}Pa in 0.05 M $HClO_4$ reduced with Zn(Hg),
○: ^{233}Pa in 1 M $HClO_4$ reduced with Zn(Hg),
□: ^{233}Pa(V) in 0.3 M $HClO_4$.

The TTA Extraction of Europium. The extraction behavior of Eu(II) and Eu(III) was investigated using ^{152}Eu as a tracer. They were not extracted at all by the TTA-benzene solution from a perchloric acid solution when the acid concentration was 0.03—3 M at the ionic strength of 3.

The Stability of the Pa(IV)-TTA Chelate. The absorption spectra of the Pa(IV)-TTA chelate in benzene are shown in Fig. 2. The molar extinction coefficients at the main peaks of 730, 840, and 1980 nm were 1.50×10^3, 1.24×10^3, and 7.0×10^2 respectively. The molar extinction coefficient of the Pa(V)-TTA chelate was 1.76×10^4 at the characteristic peak of 418 nm. The stability of the Pa(IV)-TTA chelate was calculated on the basis of the decreasing rates of the intensities of the absorption peaks of the Pa(IV)-TTA chelate and the increasing rate of that of the

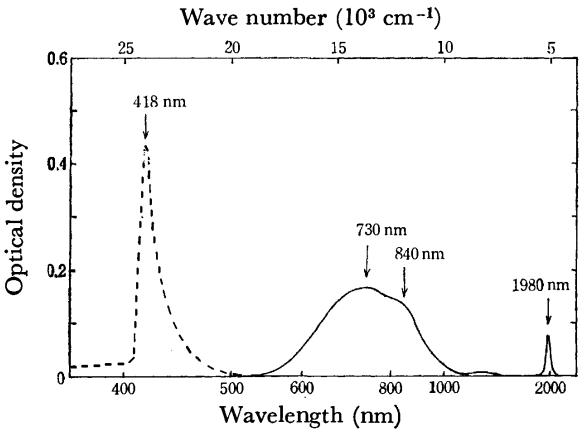

Fig. 2. Absorption spectra of Pa(IV)-TTA and Pa(V)-TTA chelates in benzene
----: Pa(V)-TTA chelate, ——: Pa(IV)-TTA chelate.

Pa(V)–TTA chelate as a function of the time. The oxidation rate of the Pa(IV)–TTA chelate was about 1%/hr, as is shown in Fig. 3. Therefore, we can confirm that Pa(IV) in a benzene solution is stable enough for us to carry out experiments without any effects of re-oxidation as long as all the atmospheric oxygen is excluded.

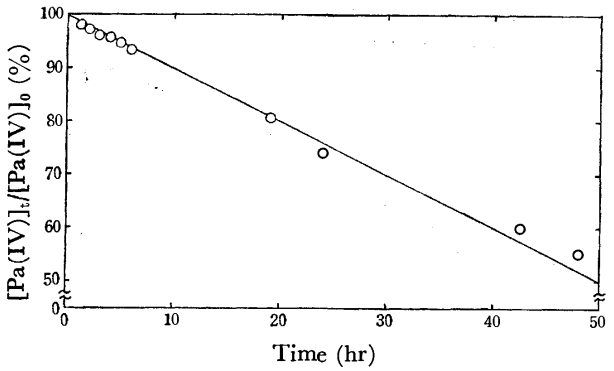

Fig. 3. Oxidation rate of Pa(IV)–TTA chelate in benzene

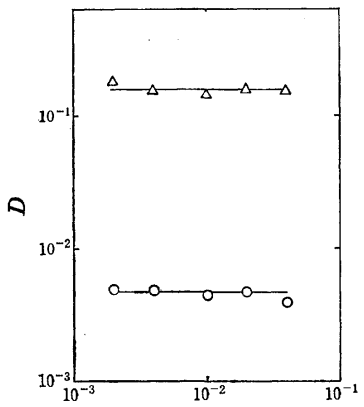

Fig. 4. Effect of Eu concentration on extraction of Pa(IV).
△: Org. phase: 0.04 M TTA-benzene, Aq. phase: I=2, 1 M $HClO_4$
○: Org. phase: 0.003 M TTA-benzene, Aq. phase: I=3, 0.1 M $HClO_4$

The Influence of the Europium Concentration on the TTA Extraction of Pa(IV). As is shown in Fig. 4, the log-log plot of the distribution ratio of Pa(IV) and the concentration of europium is constant within the limits of experimental error. This means that europium does not affect the TTA extraction of Pa(IV).

It is very useful that the performance of the reduction of Pa(V) can be checked by means of the color change of the solution. The absorption maxima of Eu(II) in the 1 M perchloric acid solution were at 250 nm ($\varepsilon = 2.6\times10^3$) and 322 nm ($\varepsilon = 7\times10^2$), and the color of the solution was yellow. About 2×10^{-2} M of europium is needed to observe the effective reduction of europium to the divalent state.

The Relation between the Distribution Ratio and the TTA Activity. The activity of TTA in the benzene phase at equilibrium is calculated from its initial concentration by means of the following equations:

$$\frac{(HA)_i}{(HA)_f} = 1.02 + \frac{10^{-8}}{(H^+)} \quad (2)\ [10]$$

$$f_{HA} = 1 - 0.25(HA)_f^{0.48} \quad (3)\ [11]$$

where f_{HA} is the activity coefficient of TTA in benzene; $(HA)_f$, the final concentration in benzene when equilibrated with an equal volume of an aqueous phase, and $(HA)_i$, the initial concentration.

When the perchloric acid concentration is 0.03—3 M at the ionic strength of 3, the log-log plot of the distribution ratio and the activity of TTA in benzene show a linear relationship, with a slope of 4 over a wide range of TTA activity, as is shown in Fig. 5.

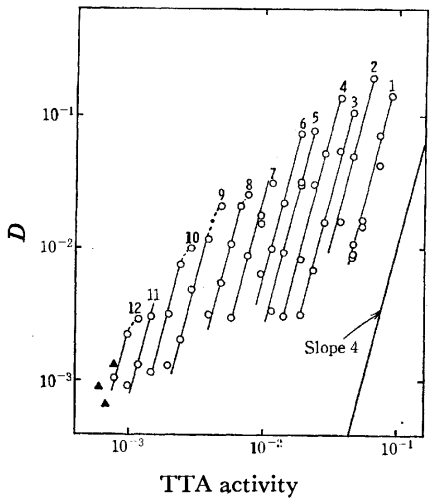

Fig. 5. Dependence of distribution ratio on TTA activity in benzene.
1: 3.0 M $HClO_4$, 2: 2.0 M $HClO_4$, 3: 1.5 M $HClO_4$, 4: 1.0 M $HClO_4$, 5: 0.7 M $HClO_4$, 6: 0.5 M $HClO_4$, 7: 0.3 M $HClO_4$, 8: 0.2 M $HClO_4$, 9: 0.1 M $HClO_4$, 10: 0.07 M $HClO_4$, 11: 0.05 M $HClO_4$, 12: 0.03 M $HClO_4$, ▲: 0.02 $HClO_4$; $[HClO_4]+[LiClO_4]=3.0$ M, $[Eu]=10^{-2}$ M.

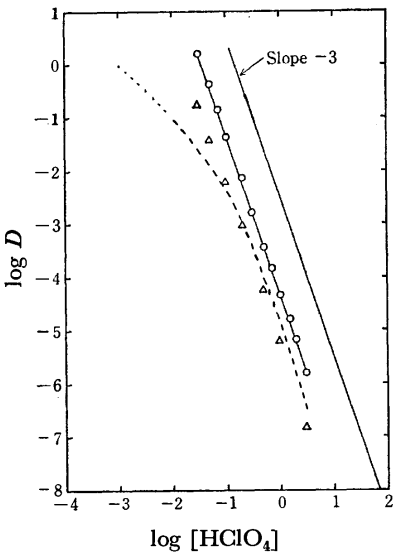

Fig. 6. Dependence of distribution ratio on $HClO_4$ concentration.
○: reduced with Eu(II), △: reduced with Cr(II), ----: by Guillaumont; TTA activity=5×10^{-3} M.

The Relation between the Distribution Ratio and the Perchloric Acid Concentration. The log-log plot of the distribution ratio and the perchloric acid concentration shows a linear relationship, with a slope of −3, as is shown in Fig. 6. The distribution ratios were calculated from the results shown in Fig. 5, and their values were normalized at the TTA activity of 5×10^{-3} M.

The relation between the distribution ratio of Pa(IV) reduced with Cr(II) and the perchloric acid concentration was examined under the conditions described above. The distribution ratio of Pa(IV) reduced with Cr(II) was about 1/10, compared to that of Pa(IV) reduced with Eu(II), as is shown in Fig. 6. The results obtained by Guillaumont[1] are also shown by a broken line in Fig. 6.

Discussion

The TTA Extraction of Pa(IV). From the results shown in Figs. 5 and 6, the equation for the TTA extraction reaction can be written as:

$$PaOH^{3+}(aq.) + 4HA(org.) = PaO_p(OH)_qA_{4-2p-q}(HA)_r(org.) + (1-p-q)H_2O + 3H^+(aq.) \quad (4)$$

where HA and A^- are used to denote the TTA molecule and the dissociated TTA anion respectively. If the coefficient of water represented in Eq. (4) is not negative, and if the oxygen which does not coordinate with Pa(IV) in the aqueous phase does not coordinate with Pa(IV) in the organic phase, we can say that:

$$p = 0,\ q = 0 \text{ or } 1 \quad (5)$$

Therefore, Eq. (4) may be rewritten as:

$$PaOH^{3+}(aq.) + 4HA(org.) = PaA_4(org.) + H_2O + 3H^+(aq.) \quad (6)$$

or

$$PaOH^{3+}(aq.) + 4HA(org.) = Pa(OH)A_3(HA)(org.) + 3H^+(aq.) \quad (7)$$

The Difference between the Distribution Ratio Obtained by This Experiment and That Obtained by Guillaumont.[1] The distribution ratio obtained by Guillaumont becomes lower than that obtained by the present authors as the acidity decreases. This may be caused by two factors. One is the incomplete reduction of Pa(V); that is, the distribution ratio of Pa(IV) is higher than that of Pa(V) when the acidity is lower than 1 M at the ionic strength of 3.[1,12] The other is due to the Cr(II)-TTA chelate; its low distribution ratio, which is known by the fact that the aqueous phase is the yellow color of Cr(II)–TTA chelate after extraction, leads to the incomplete correction of the concentration of the TTA–benzene solution, because its correction was done on the supposition that the Cr(II)–TTA chelate is extracted quantitatively into the benzene phase.

The Chromium-Protactinium Complex. The distribution ratio of Pa(IV) in the system using Eu(II) as the reductant is about ten times as large as that in the system using Cr(II) as the reductant, as is shown in Fig. 6. Moreover, the distribution ratio of Pa(IV) decreases with an increase in the concentration of chromium, as has been reported previously.[3] One of the most reliable explanations of the above facts is the possibility that a multi-nuclear complex between Pa(IV) and Cr(II) or Cr(III) is formed. Taube *et al.*[13,14] reported that, when $Co(III)(NH_3)_5X$ (X is a ligand; *i.e.* Cl^-, Br^-, or H_2O) was reduced with Cr(II), a bridged activated complex for an electron-transfer reaction like $[Co(NH_3)_5\text{-}X\text{-}Cr]$ was found. This reaction proceeds by means of an inner-sphere reaction mechanism. It has been established that when the actinoid ions are reduced with Cr(II) some binuclear intermediates are found. For instance, a 1 : 1 cationic complex[15] $[O\text{–}Np\text{–}O\text{–}Cr(H_2O)_5]^{4+}$ was formed, and this inner sphere complex was fairly stable because of a sufficiently slow substitution reaction on Cr(III) when Np(VI) was reduced with Cr(II) in a perchloric acid solution; the binuclear intermediate[16] was also found in the investigation concerned with the reduction of U(VI) with Cr(II).

From the above facts, it may be considered that the Cr(III)–Pa(IV) complex, with the structure mentioned above, may be formed when Pa(V) is reduced with Cr(II) and that the complex is difficult to extract by an extractant. On the contrary, Pa(IV) forms no cationic complexes with Eu(III), because the ligand within the coordination sphere of Eu(III) is not so substitutional inert as that of Cr(III).

A part of the expenses for this investigation has been defrayed by a grant-in-aid from the Ministry of Education.

References

1) R. Guillaumont, *Bull. Soc. Chim. Fr.*, **1968**, 162.
2) T. Mitsuji, This Bulletin, **41**, 115 (1968).
3) I. Kawasuji and S. Suzuki, *ibid.*, **47**, 104 (1974).
4) M. Haïssinsky and E. Pluchet, *J. Chem. Phys.*, **59**, 608 (1962).
5) H. N. McCoy, *J. Amer. Chem. Soc.*, **58**, 1577 (1936).
6) T. Mitsuji, This Bulletin, **40**, 2822 (1967).
7) S. Suzuki and Y. Inoue, *ibid.*, **39**, 490 (1966).
8) G. Biedermann and L. Ciavatta, *Acta Chem. Scand.*, **15**, 1347 (1961).
9) T. Mitsuji, This Bulletin, **40**, 2091 (1967).
10) A. M. Poskanzer and B. M. Foreman, *J. Inorg. Nucl. Chem.*, **16**, 323 (1961).
11) E. L. King and W. H. Reas, *J. Amer. Chem. Soc.*, **73**, 1804 (1951).
12) R. Guillaumont and G. Bouissières, *Bull. Soc. Chim. Fr.*, **1964**, 2098.
13) H. Taube, H. Myers, and R. L. Rich, *J. Amer. Chem. Soc.*, **75**, 4118 (1953).
14) H. Taube and H. Myers, *ibid.*, **76**, 2103 (1954).
15) J. C. Sullivan, *Inorg. Chem.*, **3**, 315 (1964).
16) T. W. Newton and F. B. Baker, *ibid.*, **1**, 368 (1962).

X-Ray Diffraction Studies of Aqueous Solutions of Cadmium Perchlorate and Sodium Tetraiodocadmate

Hitoshi OHTAKI, Masunobu MAEDA, and Satoshi ITO

Laboratory of Solution Chemistry, Faculty of Engineering, Tokyo Institute of Technology, O-okayama, Meguro-ku, Tokyo 152

(Received March 13, 1974)

X-Ray diffraction measurements were carried out for aqueous solutions of cadmium perchlorate and sodium tetraiodocadmate. X-Ray scattering data showed that the hydrated Cd^{2+} ion is coordinated to six water molecules, the distance between Cd^{2+} and H_2O being 2.31 ± 0.02 Å, and that the CdI_4^{2-} complex has a tetrahedral configuration with a Cd–I distance of 2.79 ± 0.01 Å. The tetrahedral structure of the CdI_4^{2-} complex was confirmed by Raman spectroscopy.

X-Ray diffraction for investigation of crystal structures was extended to the analysis of the structures of fused salts and pure liquids.[1-4] Its application to electrolytic solutions of relatively high concentration has since been undertaken to determine the structures of ionic species such as hydrated metal ions,[5-9] metal halide complexes[10-16] and polymerized hydrolysis species of metal ions.[17-22]

The structures of hydrated alkali metal,[5] alkaline-earth metal,[6] and transition-metal ions from Mn^{2+} to Zn^{2+} ions[7-9] were investigated in aqueous solutions of chloride, nitrate and sulphate ions.

Few studies, however, seem to have been made on the hydrated cadmium ion. The study by Bol *et al.*[9] of an aqueous cadmium nitrate solution, in which they showed that a cadmium ion is bound to six water molecules with the Cd–OH_2 distance 2.289 Å, appears to be the only case.

A number of equilibrium studies have been made on the cadmium iodide complexes in aqueous solution with various experimental techniques,[26] the results of which are consistent with the formation of only mononuclear complexes of CdI^+, CdI_2, CdI_3^-, and CdI_4^{2-}. From Raman spectroscopic measurements[27-29] it was found that CdI_4^{2-} has a tetrahedral configuration (T_d symmetry) in aqueous solution and organic solvents.

As far as we know, no X-ray diffraction measurement has been carried out for a study of the structures of the cadmium iodide complexes in aqueous solution.

In the present work we deal with aqueous cadmium perchlorate and sodium tetraiodocadmate solutions, the latter being also examined by Raman spectroscopy.

Experimental

Preparation and Analysis of Sample Solutions. Cadmium perchlorate was prepared by dissolving cadmium oxide in dilute perchloric acid and recrystallizing the cadmium perchlorate twice from water. The crystals thus prepared were dissolved in water containing a small amount of perchloric acid in order to prevent the hydrolysis of the Cd^{2+} ions.

The concentration of cadmium ion in the solution was determined both by gravimetry as $CdSO_4$ and by titration with EDTA. The results obtained by the two methods agreed within 0.2%. The perchlorate content of the solution was determined by using a column of cation exchange resin (Dowex 50 W-X12) of the hydrogen form. The hydrogen-ion concentration was calculated from the relation, $[H]^+ = [ClO^-_4] - 2[Cd^{2+}]$.

The cadmium iodide solution in which the tetraiodocadmate ion was predominant was prepared by the addition of NaI to a CdI_2 solution. The amount of NaI to be added was estimated from the distribution of cadmium iodide complexes calculated from the stability constants given by Leden.[30]

The total amount of cadmium in the cadmium iodide test solution was determined by EDTA titration, that of iodide being determined gravimetrically as AgI. The concentration of sodium ion was estimated from the material balance of ions in the solution. The density of the solutions was measured with a pycnometer. The composition of the solutions investigated is given in Table 1.

TABLE 1. COMPOSITIONS OF THE SOLUTIONS (in g atoms/l)

	Cadmium perchlorate soln.	Cadmium iodide soln.
Cd	2.920	2.246
I	—	11.39
Cl	6.303	—
Na	—	6.899
O	66.02	30.60
H	81.15	61.21

X-Ray Scattering Measurements. The X-ray diffractometer (JEOL Co., Tokyo) used is so designed that diffraction patterns are obtained from the free surface of the solution and that the X-ray tube and detector move symmetrically in a direction opposite the horizontal axis at the surface of the solution, *i.e.*, the Bragg–Brentano geometry is applied. The sample solution is contained in a flat glass tray, diameter 40 mm and depth 10 mm, covered tightly with a Teflon-coated stainless steel cover with a beryllium window for X-rays to protect the solution from evaporation and contamination. A LiF focusing monochromator is placed between a receiving slit and scintillation counter. A pulse-height analyzer is used for further monochromatization.

MoKα radiation ($\lambda=0.7107$ Å) was used, a Philips PW210500 X-ray tube being employed. The scattered intensity was measured at discrete points (about 200 points in all) between $\theta=1°$ and 70°, where 2θ is the scattering angle. The time required to accumulate 40000 counts was measured at angular intervals; 0.125° to $\theta=6°$, 0.25° to 20° and 0.5° to 70°. Three slit combinations, with 1/12°, 1/4° and 1° divergent slits, were employed. The whole angle range was scanned twice in order to detect the variation of measured intensities during the course of continuous operation. The variation was usually less than 2% of the measured intensities

and the intensities measured at each angle were averaged. The intensities for each slit combination were corrected for background radiation, determined by placing a lead plate just behind the receiving slit, and were normalized to the intensities measured with the 1° divergent slit from the data of overlapping regions.

The amount of incoherent radiation passing through the monochromator was estimated from the spectrum of the X-ray and the resolving power of the monochromator. It was also measured with a zirconium filter at large scattering angles. The Zr filter was first placed between the X-ray tube and the solution and the scattered intensity was measured. It was then placed between the solution and the detector and another measurement was carried out at the same scattering angle.

Raman Spectroscopic Measurements. Raman spectra for the tetraiodocadmate solution were measured with a JEOL Laser Raman Spectrophotometer JRS-Sl and a Shimadzu Laser Raman Spectrophotometer R-2D with use of the 4880 Å excitation line of Ar.

The composition of the sample solution was the same as that of the solution used for the X-ray measurements except that it contained ClO_4^- ion as an internal standard (A_1 line of ClO_4^-).

Treatment of X-Ray Intensity Data

The measured intensities were corrected for polarization in both the sample solution and monochromator and for absorption of the sample, and were scaled to absolute intensities (electron units) by comparing the asymptote with the sum of the calculated coherent and incoherent radiations at large scattering angles ($\theta \gtrsim 50°$). The scale factors thus calculated agreed within 1% with those calculated by the method of Norman[31] and Krogh-Moe.[32]

The scattering factors for Cd, I, Cl, Na, and O were taken from Cromer and Waber,[33] and those for H from the International Tables.[34] The values used for the incoherent scattering were those given by Cromer and Mann[35] for Cd and Na, by Cromer[36] for I, Cl, and O, and by Compton and Allison[37] for H. The incoherent scattering values were corrected by the Breit-Dirac factors. The values used for anomalous dispersion were taken from Cromer and Liberman.[38]

The reduced intensities $i(s)$ due to interatomic interactions in the system were evaluated from the measured intensities $I(s)$ which had been corrected for polarization and absorption, and also for scaling to electron unit, by subtracting intensities due to component atoms. The calculations were made by the equation

$$i(s) = I(s) - \sum_i n_i[(f_i(s)+\Delta f_i')^2 + (\Delta f_i'')^2 + \Phi(s)\cdot I_i^{\mathrm{inco}}(s)] \quad (1)$$

where s represents $4\pi\sin\theta/\lambda$ (λ=0.7107 Å), n_i the number of atom i, $\Delta f_i'$ and $\Delta f_i''$ the real and imaginary parts of the anomalous dispersion, respectively, $\Phi(s)$ the fraction of the incoherent radiation reaching the counter.

All the calculations were referred to a stoichiometric volume of a solution containing one cadmium atom. The reduced intensities $i(s)$ thus calculated are shown in Fig. 1 after being multiplied by s.

The radial distribution curves $D(r)$ were calculated

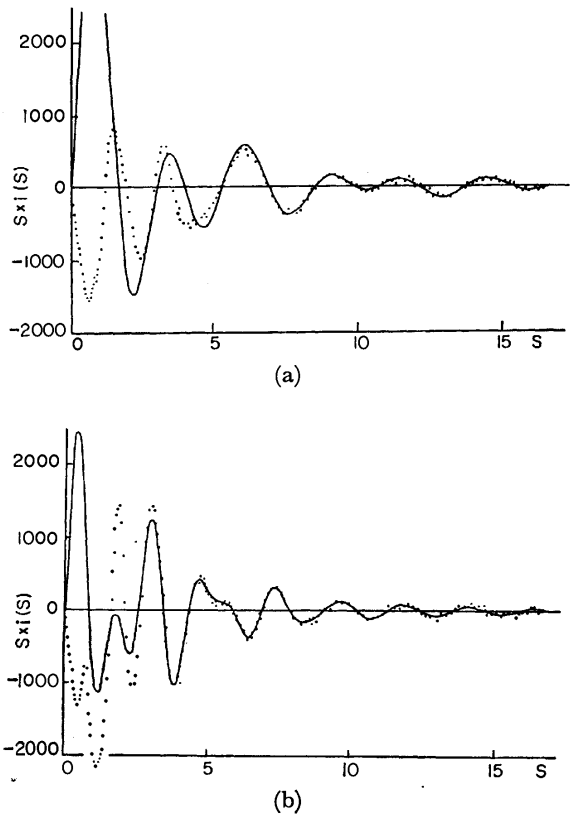

Fig. 1. Values $s\cdot i(s)$ for the two solutions as a function of s. Full circles are experimental points and full curves are calculated with the parameters given in Tables 2 and 4.
(a) the cadmium perchlorate solution, (b) the sodium tetraiodocadmate solution.

from the intensity curves by the integral formula

$$D(r) = 4\pi r^2\rho_0 + 2r\pi^{-1}\int_0^{s_{max}} s\cdot i(s)\cdot M(s)\cdot\sin(rs)\mathrm{d}s \quad (2)$$

where ρ_0 denotes the average scattering density of the sample in electron unit, the modification function $M(s)$ being chosen to be $(f_{Cd}^2(0)/f_{Cd}^2(s))\exp(-0.01s^2)$.

The calculated radial distribution curve showed small spurious peaks in the range less than 1 Å, which can not be related to any interatomic distance. Thus the reduced intensities were corrected for spurious peaks by means of the Fourier inversion of the radial distribution curve below 1 Å by taking into account the contributions from water and the perchlorate ion.

Theoretical intensities due to interatomic interactions were calculated by

$$i(s) = \sum_i\sum_j n_{ij}f_i(s)f_j(s)\frac{\sin(r_{ij}s)}{r_{ij}s}\exp(-b_{ij}s^2) \quad (3)$$

where $f_i(s)$ and $f_j(s)$ denote the scattering factors of atoms i and j, respectively, and n_{ij}, r_{ij}, and b_{ij} represent the frequency factor, the distance and the temperature factor of the interaction between any atoms i and j, respectively.

The calculations were carried out with the help of the KURVLR program specially compiled for the analysis of X-ray diffraction data by Johansson and Sandström.[39]

Analysis of Intensity Data and Results

Cadmium Perchlorate Solution. The radial distribution curve $D(r)$ is shown in Fig. 2(a). Two distinct peaks are seen at around 1.4 and 2.3 Å. The former peak is attributed to the Cl-O bonds within the perchlorate ion, which has been confirmed by several investigators.[17,40,41] The latter might be due to the Cd–O bonds within the hydrated cadmium ion, as expected from X-ray diffraction data for the crystal[42] and cadmium nitrate solution,[9] and contains a contribution from the O–O contact within ClO_4^- ion which has a tetrahedral structure. The distance and frequency factor of the Cd–O bond within the hydrated cadmium ion were estimated from the residual peak after subtraction of the O–O contribution from the second peak according to the following procedures. The theoretical intensities due to the O–O contact within ClO_4^- ion were calculated by means of Eq. (3) assuming that $r_{O-O}=2.33$ Å (which corresponds to $\sqrt{8/3}\times 1.43$ Å), $n_{O-O}=6$ and $b_{O-O}=0.002$. The theoretical peak corresponding to the O-O contact was evaluated by the Fourier inversion of the theoretical intensities according to Eq. (2) and was subtracted from the second peak. The area under the residual peak was estimated by a graphical technique with use of a planimeter and was correlated with the number of oxygen atoms around cadmium n_{Cd-O} by the relation $A_{Cd-O}=2x_{Cd}n_{Cd-O}Z_{Cd}Z_O$.[2] Here A_{Cd-O} denotes the area under the peak of the $D(r)$ curve caused by the Cd-O interaction, x_{Cd} the concentration of the cadmium ion, and Z_{Cd} and Z_O the atomic numbers of Cd and O, respectively. The frequency factor n_{Cd-O} thus evaluated was about six, and the Cd–O distance was found to be 2.31 ± 0.02 Å. The temperature factor for the Cd–O bond was estimated to be 0.002 from the peak shape.

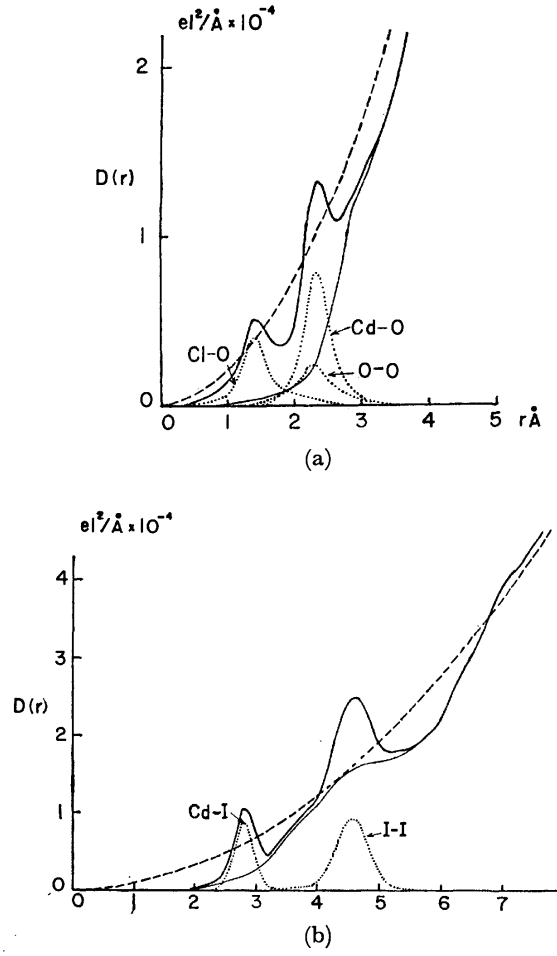

Fig. 2. Radial distribution curves $D(r)$ for the two solutions. The thick curves give $D(r)$ functions, the smooth brocken curves $4\pi r^2\rho_0$ functions, and the thin curves the difference curves obtained by subtraction of the theoretical peaks (dotted curves) from the $D(r)$ functions. The theoretical peaks (dotted curves) are calculated with the parameters listed in Tables 2 and 4.
(a) the cadmium perchlorate solution, (b) the sodium tetraiodocadmate solution.

The values for r, b, and n for the Cd–O bond within the cadmium hydrate and for the Cl–O and the O–O contacts within the tetrahedral perchlorate ion are given in Table 2.

Table 2. Final parameter values for the cadmium ion coordinated to six water molecules and the perchlorate

	r(Å)	b	n
Cd-O	2.31	0.002	6
Cl-O	1.43	0.001	4
O-O	2.33	0.002	6

The peaks calculated with these values were compared with those of the radial distribution curve (Fig. 2(a)). Subtraction of the calculated peaks from the radial distribution curve gives a smooth curve in the region less than 2.8 Å. This shows that the values of the parameters are reasonable and that other interatomic distances within the hydrated cadmium ion are ruled out. The intensities calculated with the parameters are also compared with the observed intensities (Fig. 1(a)). The agreement is satisfactory except in the low s region where contributions from the intermolecular atom pair interactions to the intensities are significant.

The residual curve obtained by subtraction of the calculated peaks from the residual distribution curve shows a very broad peak over the range 2.7—3.4 Å. If we assume that the hydrated cadmium ion possesses a regular octahedron, the distance between adjacent oxygen atoms should be 3.27 Å, which may be consistent with the present results. However, the configuration of water molecules around a cadmium atom could not be determined from the radial distribution curve, since the broad peak would be due to not only the contribution from the O-O contact within the hydrated cadmium ion, but also to contributions from the O-O distances between a ClO_4^- ion and a water molecule[40] and also from other atom pairs of longer distances.

The Cd–O distance 2.31 Å found in the present work is close to the values found in the crystal of

TABLE 3. LEAST SQUARES REFINEMENT FOR THE CADMIUM TETRAIODIDE SOLUTION

		$2.5<s<16.5$	$3<s<16.5$	$5<s<16.5$	$7<s<16.5$
A.	r_{Cd-I}	2.784 ±0.004	2.782 ±0.003	2.787 ±0.003	2.788 ±0.003
	b_{Cd-I}	0.0016±0.0005	0.0036±0.0006	0.0043±0.0006	0.0043±0.0007
	n_{Cd-I}	3.18 ±0.08	3.8 ±0.1	4.2 ±0.2	4.2 ±0.4
	r_{I-I}	4.556 ±0.005	4.568 ±0.005	4.551 ±0.007	4.544 ±0.013
	b_{I-I}	0.054 ±0.004	0.031 ±0.003	0.029 ±0.004	0.041 ±0.007
	n_{I-I}	11.6 ±0.5	7.4 ±0.4	8 ±2	17 ±6
		$3<s<16.5$	$4.5<s<16.5$	$6<s<16.5$	$8<s<16.5$
B.	r_{Cd-I}	2.790 ±0.002	2.787 ±0.003	2.786 ±0.003	2.790 ±0.004
	b_{Cd-I}	0.0050±0.0014	0.0037±0.0010	0.0045±0.0017	0.0007±0.0041
	b_{I-I}	0.023 ±0.002	0.021 ±0.001	0.024 ±0.002	0.030 ±0.004

$Cd(NH_4)_2(SO_4)_2 \cdot 6H_2O$[43] and in the cadmium nitrate solution,[9] which are 2.28 Å on the average and 2.289 Å, respectively.

Sodium Tetraiodocadmate Solution. The radial distribution curve $D(r)$ is shown in Fig. 2(b). It shows two prominent peaks in the region less than 6 Å. The peak at around 2.8 Å can be ascribed to the Cd-I bonds, and that at about 4.6 Å to the distance between iodide ions within the tetraiodocadmate complex. The ratio between these two distances is in good agreement with that expected for a tetrahedral structure. The number of iodide ions coordinated to a cadmium ion was estimated to be about four from the area under the peak at around 2.8 Å according to graphical procedure. It was not possible to determine the number of pairs of the adjacent iodide ions within the cadmium iodide complex, since other long-range interactions largely contribute to the peak at around 4.6 Å.

In order to confirm the structure of the CdI_4^{2-} complex deduced from the radial distribution curve and to refine the distances, analysis of the reduced intensity curve was carried out by means of a least squares method. For each pair of the Cd–I and I–I interactions three parameters were introduced, distance r, temperature factor b, and frequency factor n. These parameters were allowed to change so that the error square sum $U=\sum s^2(i(s)-i_{calc}(s))^2$ becomes a minimum, where $i(s_{calc})$ denotes the intensity theoretically calculated by means of Eq. (3). Different subsets of the intensity data were used for the refinement in order to detect errors in the refined parameters caused by a contribution to the intensity by the intermolecular interactions and experimental errors contained in the data. The least squares calculations were carried out by means of PUTSLR,[39] the generalized least squares program for X-ray diffraction of solution.

Two types of refinement (A and B) were carried out. The calculated results are summarized in Table 3.

In type A, all the six parameters for the Cd–I and the I–I interactions were allowed to change simultaneously. The frequency factor of the Cd–I bond is close to four, which is the value expected from the CdI_4^{2-} complex in any sets of data over the various s regions except the set of data in the region $2.5<s<16.5$ in which large contributions are included.

The ratio between the I–I and the Cd–I distances is about 1.63, which corresponds to $\sqrt{8/3}$ for the complex of the tetrahedral configuration.

The frequency factor n_{I-I} of the I–I pair was not definitely determined by the least squares method; n_{I-I} fell in the range $6<n_{I-I}<23$ when the standard deviations were taken into account (see Table 3).

In type B a tetrahedral structure was assumed, and the Cd–I distance and the two temperature factors for the Cd–I and I–I contacts were refined. The refined parameters are almost the same as those in type A.

TABLE 4. FINAL PARAMETER VALUES FOR THE TETRAHEDRAL CADMIUM TETRAIODIDE COMPLEX

	r(Å)	b	n
Cd–I	2.79	0.004	4
I–I	4.56	0.025	6

The distances and temperature factors for the Cd–I and I–I contacts for the CdI_4^{2-} complex are listed in Table 4, a tetrahedral structure of the complex being assumed. The assumption was supported by Raman spectroscopic measurements.

The observed intensities are compared with the calculated ones in Fig. 1(b) with use of the parameters in Table 4. It is seen that the agreement is satisfactory except at the low-angle part of the curve where the intermolecular interactions significantly contribute to the $s \cdot i(s)$ curve.

The calculated Cd–I and I–I peaks with use of the parameters given in Table 4 are compared with the radial distribution curve in Fig. 2(b). The residual curve obtained by subtraction of the calculated peaks from the radial distribution curve shows a broad peak in the range 4—5.5 Å. The peak is so broad that it can not be due to the interaction of any one kind of pairs of atoms, but to various kinds of interactions; one of them might be H_2O-H_2O interactions in bulk water.

A Raman spectrum of the CdI_4^{2-} solution is reproduced in Fig. 3, along with the resolved bands on a horizontal background. It shows four bands at around 36, 47, 110, and 145 cm^{-1}. The polarization measurements indicate that the strong band at 110 cm^{-1} is polarized and the other three bands are depolarized. This suggests that the CdI_4^{2-} complex has T_d symmetry. These results are in good agreement with those obtained by means of the Raman effect in which a tetrahedral structure was proposed for the CdI_4^{2-} complex.[27-29]

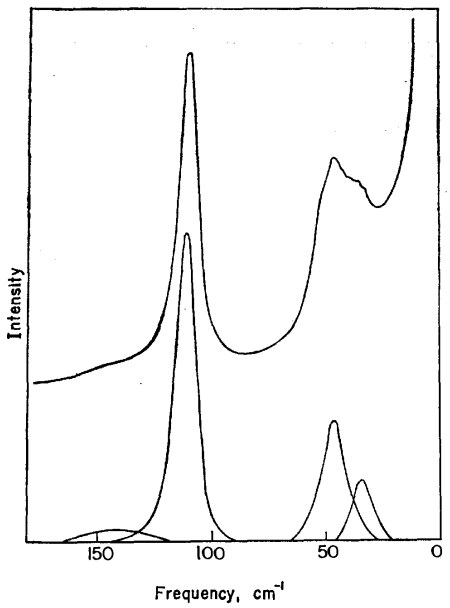

Fig. 3. A Raman spectrum of the CdI_4^{2-} solution, with resolved bands based on the horizontal background.

The authors express their sincere thanks to Prof. Georg Johansson, the Royal Institute of Technology, Stockholm, for his helpful advice throughout this work.

The present work was financially supported by the Ministry of Education.

References

1) K. Furukawa, *Rep. Progr. Phys.*, **25**, 395 (1962).
2) R. F. Kruh, *Chem. Rev.*, **62**, 319 (1962).
3) H. A. Levy and M. D. Danford, "Molten Salt Chemistry," Ed. by M. Blander, Wiley, New York (1964), Chapter 2.
4) C. J. Pings, "Physics of Simple Liquids," Ed. H. N. V. Temprley, G. S. Rushbrooke and J. S. Rowlinson, North-Holland Pub. Co., Amsterdam (1968), p. 387.
5) R. M. Laurence and R. F. Kruh, *J. Chem. Phys.*, **47**, 4758 (1967).
6) J. N. Albright, *ibid.*, **56**, 3783 (1972).
7) I. M. Shapovalov and I. V. Radchenko, *Russ. J. Struct. Chem.*, **12**, 705 (1971).
8) I. M. Shapovalov, I. V. Radchenko, and M. K. Lesovitskaya, *ibid.*, **13**, 721 (1972).
9) W. Bol, G. J. A. Gerrits, and C. L. van Panthaleon van Eck, *J. Appl. Crystallogr.*, **3**, 486 (1970).
10) D. L. Wertz and R. F. Kruh, *J. Chem. Phys.*, **50**, 4313 (1969).
11) D. L. Wertz and R. F. Kruh, *Inorg. Chem.*, **9**, 595 (1970).
12) D. L. Wertz, R. M. Laurence, and R. F. Kruh, *J. Chem. Phys.*, **43**, 2163 (1965).
13) G. W. Brady, *ibid.*, **29**, 1371 (1958).
14) D. L. Wertz and R. F. Kruh, *ibid.*, **50**, 4013 (1969).
15) F. Gaizer and G. Johansson, *Acta Chem. Scand.*, **22**, 3013 (1968).
16) D. L. Wertz and J. R. Bell, *J. Inorg. Nucl. Chem.*, **35**, 137, 861 (1973).
17) G. Johansson and H. Ohtaki, *Acta Chem. Scand.*, **27**, 643 (1973).
18) G. Johansson, *ibid.*, **25**, 2787, 2799 (1971).
19) O. E. Esval, Thesis, Univ. North Carolina (1962).
20) G. Johansson and Å. Olin, *Acta Chem. Scand.*, **22**, 3197 (1968).
21) H. A. Levy, D. Danford, and P. A. Agron, *J. Chem. Phys.*, **31**, 1458 (1959).
22) M. Åberg, *Acta Chem. Scand.*, **24**, 2901 (1970).
23) G. W. Brady, M. B. Robin, and J. Varimbi, *Inorg. Chem.*, **3**, 1168 (1964).
24) M. D. Lind, *J. Chem. Phys.*, **46**, 2010 (1967).
25) G. W. Brady, *ibid.*, **33**, 1079 (1960).
26) L. G. Sillén and A. E. Martell, "Stability Constants," Spec. Publ. No. 17 and Supplement No. 1, Spec. Publ. No. 25, The Chemical Society, London, 1971.
27) M. L. Delwaulle, *Bull. Soc. Chim. Fr.*, **1955**, 1294.
28) J. A. Rolfe, D. E. Sheppard, and L. A. Woodward, *Trans. Faraday Soc.*, **50**, 1275 (1954).
29) J. E. Davies and D. A. Long, *J. Chem. Soc., A*, **1968**, 2054.
30) I. Leden, *Z. Phys. Chem., A* **188**, 160 (1941).
31) N. Norman, *Acta Crystallogr.*, **10**, 370 (1957).
32) J. Krogh-Moe, *ibid.*, **9**, 951 (1956).
33) D. T. Cromer and J. T. Waber, *ibid.*, **18**, 104 (1965).
34) International Tables for X-Ray Crystallography, Kynoch Press, Birmingham 1962, Vol. III.
35) D. T. Cromer and J. B. Mann, *J. Chem. Phys.*, **47**, 1892 (1967).
36) D. T. Cromer, *ibid.*, **50**, 4857 (1969).
37) A. H. Compton and S. K. Allison, "X-Rays in Theory and Experiment," van Nostrand, New York, 1935.
38) D. T. Cromer and D. Lieberman, *J. Chem. Phys.*, **53**, 1891 (1970).
39) G. Johansson and M. Sandström, *Chem. Scripta*, **4**, 195 (1973).
40) K. Michelsen, *Acta Chem. Scand.*, **6**, 1289 (1952).
41) G. Johansson, *ibid.*, **25**, 2787 (1971).
42) H. Montgomery and E. C. Lingafelter, *Acta Crystallogr.*, **20**, 728 (1966).

Polarographic Study of Catalytic Reduction of Tris(2,2′-bipyridine)-copper(II) in the Presence of Nitrite Ion

Kazuyoshi TANAKA and Kunio NAKANO

Department of Chemistry, College of Science, Rikkyo University, Nishi-Ikebukuro, Toshima-ku, Tokyo 171

(Received December 19, 1973)

The rigorously derived equation for a catalytic current was applied to the evaluation of the rate constant for the oxidation reaction of bis(2,2′-bipyridine)copper(I) by nitrite ion by use of a computer and subroutine program for the curve-fitting method. This method made it possible to calculate the rate constant from low limiting current in the presence of nitrite ion. The rate in acetate buffer solutions has first-order dependence on each reactant and hydrogen ion, and the apparent rate constant is 1×10^6 M^{-2} s^{-1} at 25 °C.

A polarographic catalytic process can be schematically represented by

$$O + ne \longrightarrow R \quad (1)$$

$$R + Z \longrightarrow O \quad (2)$$

This refers to a post-electron transfer chemical reaction (2) which regenerates the original electrochemical species O. The reaction must be pseudo-unimolecular with respect to species R, when the oxidizing agent Z is present at a high and constant concentration at the electode surface. The theoretical equations describing a catalytic current have been developed by several workers[1-4] and derived on the assumption that a steady state at the dropping mercury surface set up by the combination of diffusion and chemical reaction, *i.e.*, a linear diffusion approximation concerning the concentration gradient at the electrode surface has been made. These equations should be used to evaluate a rate constant for a fast chemical reaction, such as the oxidation of titanium(III) by chlorate ion.[5] However, there are many slow reactions which cause a smaller catalytic current, such as the oxidation of titanium(III) by hydroxylamine,[6] and vanadium(II) by chlorate ion[7] and by vanadium(IV).[8]

Koutecky[9,10] has treated the diffusion problem using a more rigorous expanding sphere approximation and proposed a theoretical expression for the catalytic current. Since this equation is complicated and its application is very tedious to evaluate a rate constant, the graphical treatment of the equation has been carried out for some systems.[1,9] However, the curve-fitting method developed recently by use of a computer has been available for solving the equation, and, in the present work, this method was employed for determining the rate constant for the oxidation reaction of copper(I) by nitrite ion.

Experimental

Materials. Copper(II) stock solution was prepared by dissolving recrystallized $CuSO_4\cdot2H_2O$ into the redistilled water and its concentration was determined by measuring the second diffusion current in ammonia-ammonium chloride solutions compared with that of standard copper(II) solution which was made from high purity copper metal(99.999%). The weighed amount of reagent grade 2,2′-bipyridine was dissolved into an acetic acid solution and then the buffer solution was made by adding sodium acetate, which was also used as a supporting electrolyte. Sodium nitrite solution was prepared by dissolving an appropriate amount of reagent grade chemicals in the water.

Apparatus and Procedure. A Yanagimoto polarograph Model P-8 was used to record the polarograms. Catalytic current appeared when sodium nitrite solution was injected into acetate buffered solution containing 2,2′-bipyridine with a micropipet. Ionic strength was kept 0.2 M throughout the present work. All the pH values were measured by a Toa Dempa pH meter Model HM-5A.

Results and Discussion

Evaluation of Rate Constant. Koutecký and Cizek[10] have proposed the theoretical equation for the catalytic current

$$\frac{i}{i_d} = \Psi(\chi) + \xi[\Theta(\chi) - 0.78680\Psi(\chi)] = \Psi(\chi) - \xi\Phi(\chi) \quad (3)$$

and

$$\Psi(\chi) = e^{-\chi}\sum_{i=0}^{\infty} a_i\chi^i \quad (4)$$

$$\Theta(\chi) = e^{-\chi}\sum_{i=0}^{\infty} a_i r_i\chi^i \quad (5)$$

$$\xi = \sqrt{\frac{12D}{7r_1^2}}\,t^{1/6} \quad (6)$$

where i and i_d are the experimentally observed instantaneous currents for the reduction of species O in the presence and in the absence of Z, respectively. The parameter, ξ, corresponds to the function involving the diffusion coefficient, D, drop time, t, and mercury drop radius, r_1, at $t=1$ s, and in the present work the value of ξ was found to be 0.187. The parameter, a_i, is a complicated gamma function, whose values for $i=0$ to 15 are tabulated in the literature,[10] and the values of $\Phi(\chi)$ corresponding χ are also listed. The parameter, χ, in above equation is related to the apparent second-order rate constant, k_{app}, with respect to each reactant.

$$\chi = k_{app}C_z t \quad (7)$$

where C_z denotes the concentration of oxidizing agent, Z, nitrite ion in the present work. The rate constant can be evaluated from this equation if the consumed amount of Z by the chemical reaction is negligibly small, and if an appreciable change of the concentration of Z takes place, another theoretical equation derived on the basis of the stoichiometric consideration[11] must be applied to obtain the rate constant.

The evaluation of χ from the observed value of i/i_d

was made as follow: equation (3) was simplified by the first assumption that the term $\xi\Phi(\chi)$ could be neglected. This is verified by our experimental results as mentioned below. In the course of the calculation an approximate value of χ, which is given in Koutecký's Table,[9] is necessary to solve the function $\Phi(\chi)$ by use of a subroutine programs for the curve-fitting method. Thus, a more accurate value of χ can be obtained and used to evaluate the term $\Phi(\chi)$ by using the value in the table on the assumption that a linearity of $\Phi(\chi)$ with χ holds in the narrow range. Using this trial $\Phi(\chi)$ and the observed value of ξ, the value of χ is recalculated by use of Eq. (3) until the consistent value can be obtained. In the present work, one or two cycles were sufficient to define the value of χ within experimental error. This method is very convenient to evaluate the rate constant from the low value of i/i_d.

Kinetic Results. The typical polarograms are shown in Fig. 1. The two reduction waves with a polarographic maximum in the absence of nitrite ion appeared and it is concluded from their half-wave potentials that the first wave corresponds to the one-electron reduction of $Cu(bipy)_3^{2+}$ to $Cu(bipy)_2^{1+}$ and the second wave to that of $Cu(bipy)_2^{1+}$ to copper metal. The polarographic behavior of these species has been studied systematically by Onstott and Laitinen.[12] The first wave was increased by adding nitrite ion, indicating the catalytic current. When nitrite ion was in sufficiently high concentration compared with that of copper(II) ion, the first wave became larger than the second one, showing that the catalytic nature is specific to the first wave. The maximum at rising portion of the second wave increased with increasing concentration of copper(II) ion. The maximum suppressor was not used in this experiment, because the substance adsorbed on the mercury electrode would disturb the reaction layer at the electrode surface and make the experimental data inaccurate. However, the presence of this maximum and the large catalytic wave caused a narrow plateau of the first wave and made it difficult to measure the limiting current. Thus, it is necessary in the present system to evaluate the rate constant from the comparably small limiting current, *i.e.*, the low value of i/i_d.

Values of the catalytic current obtained at various concentrations of nitrite ion are presented in Table 1.

Table 1. Apparent rate constants of the oxidation of copper(I) by nitrite ion in acetate buffer solution of 1.94×10^{-4} M Cu(II)+1×10^{-2} M bipy, at 25 °C

pH	$[NO_2^-]$ mM	$-E$ V *vs.* SCE	i μA	i/i_d	k_{app} $M^{-1}s^{-1}$
4.1	—	0.160	0.510	—	—
	21.8	0.150	2.070	4.059	(141)[a]
4.8	21.8	0.175	0.984	1.853	23.9
	43.7	0.170	1.440	2.812	30.2
	84.9	0.175	2.046	3.853	(31.3)[a]
5.0	21.8	0.187	0.760	1.407	12.8
	43.7	0.182	0.965	1.770	10.6
	84.9	0.180	1.254	2.322	10.7
5.3	21.8	0.184	0.608	1.160	3.64
	43.7	0.190	0.724	1.382	4.40
	84.9	0.190	0.852	1.626	4.15
	163.5	0.190	1.050	2.004	3.86

a) Parenthesized values of k were calculated by using the simplified equation as described in this article.

The value of secondly difined χ' is about 10% larger than that of the first one and little differences can be observed between χ' and χ'', or χ'' and χ''' for a given condition, where χ'' and χ''' are thirdly and fourthly defined values of χ. In the case of $\chi>10$, Eq. (4) diversed and a finite value of χ could not be given by the present method. This was caused by using only the sixteen values of a_i involved in the function $\Phi(\chi)$. In this case, the value of k_{app} shown in the parenthesis was calculated from the simplified equation proposed by Koutecký[9] and corrected by employing the value of $\xi\Phi(\chi)$ in order to obtain a more accurate value. As shown in Table 1, though the half-wave potentials obtained in the presence of nitrite ion is thought to shift slightly to a more negative potential compared

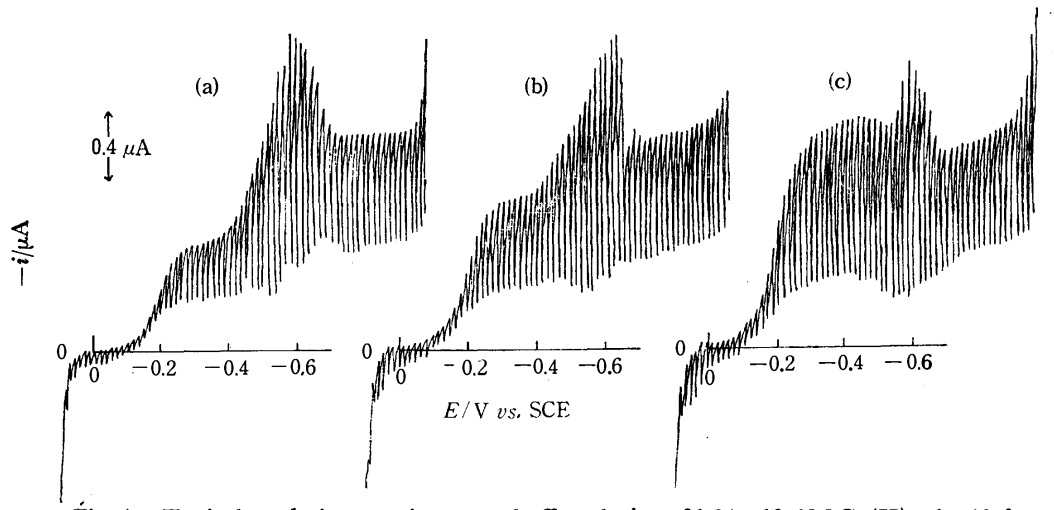

Fig. 1. Typical catalytic waves in acetate buffer solution of 1.94×10^{-4} M Cu(II)+1×10^{-2} M bipy, pH 5.3. The concentrations of nitrite ion are (a) 0, (b) 4.37×10^{-2}, (c) 1.63×10^{-1} M.

with that of the wave in the absence of oxidizing agent, no significant effect was observed.

Taking into account relative inaccuracy of the experimental data, it was concluded that almost consistent values of rate constants at the same pH value could be obtained. This supports the validity that the present method is useful to evaluate the rate constant from the small catalytic current, *i.e.*, $i/i_d<3$. The rate constants obtained under the condition of low nitrite ion concentration from 7.95 to 21.8 mM were 22.9 ± 1.6 $M^{-1}s^{-1}$ at pH 4.90. In this calculation, Eq. (3) was used provided that the change in nitrite ion concentration consumed by the chemical reaction could be practically neglected. This condition was comfirmed by the presence of at least twenty times larger amount of nitrite ion than that of copper(II), though the consistent value could not be obtained in the presence of 3.99 mM nitrite ion. The rate constants are much smaller than those of the oxidation reaction of bis(2,2'-bipyridine)copper(I) by oxygen and hydrogen peroxide.[13]

Effects of Drop-time and Bipyridine. The effect of the corrected height of mercury reservoir, h_{corr}, or the effect of drop time, on the limiting currents is seen in Fig. 2. Since the limiting current in the absence of

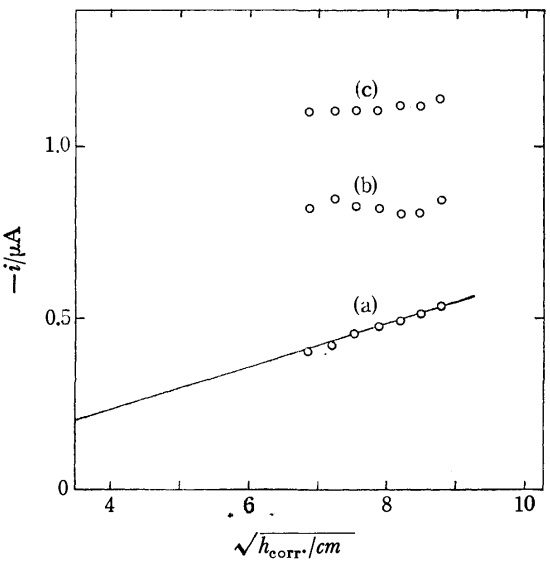

Fig. 2. Dependence of limiting currents on the corrected height of mercury reservoir in the acetate buffer solution of 1.94×10^{-4} M Cu(II) $+1\times10^{-2}$ M bipy, pH 5.3. The concentrations of nitrite ion are (a) 0, (b) 8.49×10^{-2}, (c) 1.65×10^{-1} M.

nitrite ion is linearly proportional to the square root of h_{corr}, it is diffusion-controlled. On the other hand, the limiting current in the presence of 0.163 M nitrite ion was independent of h_{corr}, indicating the dominant contribution of catalytic nature to total current. The apparent rate constant was found to be 4.06 ± 0.19 $M^{-1}s^{-1}$ at pH 5.28. Though the wave is essentially of catalytic nature, the small variation of the limiting currents observed in the presence of 0.0849 M nitrite ion is likely to result from the adsorption of depolarizer or bipyridine on mercury electrode.

The effect of 2,2'-bipyridine concentration on the rate constans is shown in Table 2. This shows that

Table 2. Apparent rate constants at various concentrations of 2,2'-bipyridine in acetate buffer solution of 1.94×10^{-4} M Cu(II) at pH 5.2

bipy mM	$[NO_2^-]$ mM	$-E_{1/2}$ V*vs.* SCE	i μA	i/i_d	k_{app} $M^{-1}s^{-1}$
1.28	—	0.142	0.486	—	—
	21.8	0.144	0.550	1.132	2.93
	43.7	0.145	0.640	1.317	3.69
2.18	—	0.166	0.490	—	—
	21.8	0.160	0.596	1.216	4.91
	43.7	0.160	0.670	1.367	4.35
	84.9	0.156	0.846	1.727	4.89
5.13	—	0.175	0.490	—	—
	21.8	0.165	0.600	1.224	5.21
	43.7	0.170	0.722	1.473	5.78
	84.9	0.174	0.910	1.857	5.97
	163.5	0.172	1.142	2.331	5.47

the value of rate constant increased somewhat with increasing bipyridine concentration and approached the consistent value obtained at 1×10^{-2} M bipyridine. Since the wave in 1.28×10^{-3} M bipyridine was poorly defined and the limiting current became inaccurate, it was not clear from the present data that bipyridine participated in the chemical reaction. Futhermore, the considerably low rate constant could not be explained. However, the shift of the half-wave potentials in the absence of nitrite ion corresponded to the dissociation of one bipyridine molecule in the electrode reaction, which could be substantiated by the reported value of the half-wave potential for the system of copper(II) and bipyridine.[12]

Catalytic Reaction Mechanism. In view of the above results the electrode reaction scheme can be written as

$$Cu(bipy)_3^{2+} \xrightarrow[-bipy]{+1e} Cu(bipy)_2^{1+} \xrightarrow[-2bipy]{+1e} Cu(0) \qquad (8)$$
$$\uparrow \qquad\qquad\qquad \downarrow +NO_2^-$$

This shows that the catalytic current due to nitrite ion is concerned only with the first wave and is quite indifferent to the second wave which corresponds to the reduction current of copper(I) to amalgamated copper metal. The value of rate constant decreased about 15% with a two-hold increase of copper(II) concentration. Further reaction between copper(I) and products of nitrite ion must be considered, and if the reaction product is bis(2,2'-bipyridine)copper(II), this species would undergo the electroreduction and cause the increase of catalytic current. Though the oxidation product of copper(I) is not clear from the present data, the rate law for the chemical reaction can be represented as

$$-\frac{d[Cu(bipy)_2^{1+}]}{dt} = k_{app}[Cu(bipy)_2^{1+}][NO_2^-]. \qquad (9)$$

Neverthless, it is not necessary that the rate corresponds to the increment of tris(2,2'-bipyridine)copper(II). A plot of $\log k_{app}$ against $\log [H^+]$ was approximately linear and yields a best straight line of slope 1.19 ± 0.04, from which it can be deduced that the rate has

also first-order dependence with respect to hydrogen ion, *i.e.*, $k_{app}=k'_{app}[H^+]$, and the value of k'_{app} is *ca.* $1\times10^6\ M^{-2}s^{-1}$ at 25 °C. This suggests that the equilibrium between nitrite ion and nitrous acid exists and nitrous acid should participate in the chemical oxidation. Nitrous acid is, in general, a more powerful oxidizing agent than nitrite ion.[14] Though the reaction is thought to be non-complementary, there is insufficient information about the reaction stoichiometry and the possibility that nitrite ion acts as a two-equivalent oxidizing agent to copper(I).

Reference

1) P. Delahay and G. Stiethl, *J. Amer. Chem. Soc.*, **74**, 3500 (1952).
2) S. L. Miller, *ibid.*, **74**, 4130 (1952).
3) D. M. H. Kern, *ibid.*, **75**, 2473 (1953).
4) Z. Pospisil, *Collect. Czech. Chem. Commun.*, **18**, 337 (1953).
5) J. Koryta and J. Tenygl, *ibid.*, **19**, 839 (1954).
6) M. Petek, T. E. Neal, R. L. McNeely and R. W. Murry, *Anal. Chem.*, **45**, 32 (1973).
7) K. Tanaka and K. Nakano, *J. Electroanal. Chem.*, **48**, 399 (1973).
8) J. W. Olver and W. Ross, Jr., *J. Phys. Chem.*, **66**, 1699 (1962).
9) J. Koutecký, *Collect. Czech. Chem. Commun.*, **18**, 311 (1953).
10) J. Koutecký and J. Cizek, *ibid.*, **21**, 1063 (1956).
11) J. Koutecký, *ibid.*, **22**, 160 (1957).
12) E. I. Onstott and H. A. Laitinen, *J. Amer. Chem. Soc.*, **72**, 4724 (1950).
13) I. Pecht and M. Anbar., *J. Chem. Soc. A*, **1968**, 1902.
14) W. M. Latimer, "Oxidation Potentials," 2nd ed. Prentice-Hall, N. J. (1952), p. 90.

Formation of Cubic Molybdenum Carbide by the Carbonization of MoO_3 with Plasma Arc and Properties of the Products

Osamu MATSUMOTO, Michio SAITO, and Takashi YOSHINO

Department of Chemistry, College of Science and Engineering, Aoyama Gakuin University, Chitosedai, Setagaya-ku, Tokyo 157

(Received March 8, 1974)

The formation of cubic molybdenum carbide (α-MoC_{1-x}) by the carbonization of MoO_3 with graphite by heating with argon plasma arc was studied. α-MoC_{1-x} including a small amount of hexagoanl η-MoC_{1-x} was formed. By the carbonization of mixture of MoO_3 and TiO_2 with graphite, a cubic solid solution of Mo–Ti–C system was formed. Chemical and X-ray analyses showed that the cubic form is defective in carbon content. The density of the cubic form was in agreement with that determined by means of X-ray diffraction. The products were found to be superconductors, the transition temperature varying with composition. The highest transition temperature 11.7 K was obtained for $Mo_{0.95}TiO_{0.05}C_{0.75}$.

A high temperature phase of composition MoC with a hexagonal unit cell is known to exist. Recently, a cubic modification (α-MoC_{1-x}) has been found. The cubic molybdenum carbide is stable above 2200 °C and decomposes into hexagonal η-MoC_{1-x} and graphite below 2200 °C.[1] Thus rapid quenching from high temperatures is necessary to obtain cubic α-MoC_{1-x}.

Cubic α-MoC_{1-x} has been prepared by quenching MoC, prepared by melting a mixture of molybdenum and carbon, from higher temperatures.[2-5] The products could not be obtained as a stoichiometric or complete single phase. The cubic form is always defective in carbon content, the maximum carbon content being given to be 40 atomic %. MoC forms the extended cubic solid solution with various carbide such as TiC, ZrC, NbC, TaC, and WC.[6,7]

α-MoC_{1-x} and cubic MoC–TiC solid solution are superconductors. The superconducting transition temperature of α-MoC_{1-x} is reported to be from 12.5 to 14.3 K.[2-4,7] It is the highest among the known transition temperatures for carbides. The transition temperature of MoC–TiC solid solution decreased with increasing TiC content.[7]

The authors have studied the formation of carbides such as ZrC,[8,9] TiC,[10] and NbC,[11] by the carbonization of respective oxides with graphite by heating with a plasma arc. α-MoC_{1-x} and cubic solid solution of Mo–Ti–C system were obtained by the carbonization of respective oxides with graphite. The products are confirmed and their properties such as density and superconducting transition temperature are described in this paper.

Experimental

Materials. MoO_3 (purity above 98%, Japan Heavy Metal Co.), TiO_2 (rutile type powder, purity above 99.5%, Toho Titanium Mfg. Co.) and graphite (spectroscopic grade, Tokai Electrode Co.) were mixed at the desired molar ratio (C/MoO_3, $C/(MoO_3+TiO_2)$). About one gram of the mixture was pressed into a tablet. Purified argon was used as plasma gas.

Apparatus. The plasma arc furnace and heating procedure are the same as described previously.[9] The temperature of the surface of the tablet under the plasma was measured with a micropyrometer (PYRO-WERK). An ADG-101 type X-ray diffractometer (Tokyo Shibaura Electric Co.) was used for identifying the products. Gaseous products were identified with a GLC-550 gas chromatograph (Yanagimoto Mfg. Co.).

Experimental Procedure. Temperature of the sample in the plasma arc was about 3000 °C, higher than the melting point of α-MoC_{1-x}. Heating was continued for 3 min. The plasma arc was then stopped and the melt was quenched.

The products were investigated by X-ray diffraction and chemical analysis. Chemical analyses of molybdenum and titanium were carried out by the redox titration method. Carbon content was determined by a combustion method. The density of the product was measured picnometrically at 25 °C using water as a reference liquid. The superconducting transition temperature of products was measured with a 21 Hz mutual inductance bridge.[12] Temperature was measured with a germanium thermometer calibrated against a superconducting standard and the vapour pressure of hydrogen.

Results and Discussion

Confirmation of Products. By quenching the MoO_3-graphite mixture from the melt, a silver white metallic cake was obtained on the graphite hearth anode. Chemical analysis data and crystal structures of the cake formed on the graphite anode with various C/MoO_3 values are given in Table 1. The product obtained at $C/MoO_3=3.9$ (sample No. 1) was hexagonal η-MoC_{1-x}, while the products obtained at $C/MoO_3=4.0$ and 4.3 (sample Nos. 2 and 3) were

Table 1. Chemical and X-ray analysis data of $Mo_xTi_yC_z$

Sample No.	Composition of $Mo_xTi_yC_z$			$\sum$ (Mo, Ti, C) (wt %)	Crystal Structure
	x	y	z		
1	0.71	—	0.29	99.1	hex.
2	0.63	—	0.37	100.9	cub.+hex.
3	0.54	—	0.46	100.1	cub.+hex.
4	0.56	0.005	0.44	100.1	cub.+hex.
5	0.57	0.011	0.43	100.2	cub.
6	0.56	0.020	0.42	100.0	cub.
7	0.54	0.030	0.43	100.3	cub.
8	0.51	0.050	0.44	100.1	cub.
9	0.48	0.081	0.44	100.0	cub.
10	0.44	0.12	0.44	100.0	cub.
11	0.41	0.15	0.44	100.2	cub.

α-MoC_{1-x} containing a small amount of η-MoC_{1-x}. The maximum atomic ratio of combined carbon to molybednum was 0.84 in the product obtained at $C/MoO_3=4.3$ (sample No. 3). It was found that pure α-MoC_{1-x} was not prepared by the carbonization of MoO_3 with graphite.

MoC forms an extended cubic solid solution with TiC. The MoC–TiC cubic solid solution was formed by the carbonization of a mixture of MoO_3 and TiO_2 with graphite by heating with a plasma arc. MoO_3, TiO_2 and graphite were mixed in desired molar ratios to form cubic solid solution with various compositions (Table 1). The hexagonal phase disappeared and a single cubic phase was obtained in the products containing Ti more than 1 atomic %.

The sum of Mo, Ti, and C contents of the products exceeded 100 wt% except for $Mo_{0.71}C_{0.29}$. It seems that oxygen contained in the products is small in each case.*

CO was the only detectable gaseous product by gaschromatography. The carbonization reaction of oxide can be carried out almost completely at high temperatures.

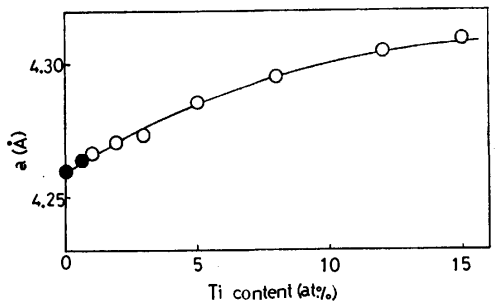

Fig. 1. a of cubic phase *vs.* Ti content.
● cubic+hexagonal, ○ cubic

Properties of Products. Lattice Parameter and Density of Cubic Phase: The relation between the lattice parameter of the cubic phase (a) in the product and the Ti content is shown in Fig. 1. The lattice parameter gradually increased with increasing Ti content.

The relation between the density of product at 25 °C and the Ti content is shown in Fig. 2. The density decreased with increasing Ti content. In the case of the single cubic phase, the density agreed with that determined by means of X-ray diffraction, if we assume that the Mo position in cubic lattice is substituted by Ti and the C position is vacant.

From the changes of the lattice parameter and density caused by the addition of Ti, it seems that Ti added in Mo–C system replaces the Mo atom in the Mo–C lattice and stabilizes the cubic form.

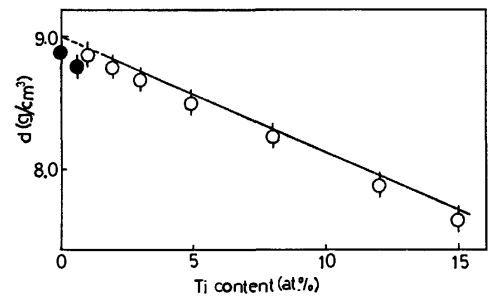

Fig. 2. Density *vs.* Ti content.
—— X-ray density, ○ measured density
● cubic+hexagonal, ○ cubic

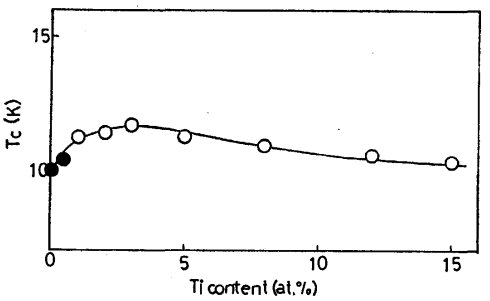

Fig. 3. T_c *vs.* Ti content.
● cubic+hexagonal, ○ cubic

Superconducting Transition Temperature: The relation between the superconducting transition temperature (T_c) of the product and the Ti content is shown in Fig. 3. η-MoC_{1-x} is normal down to 4.2 K. T_c of the mixture of α-MoC_{1-x} and η-MoC_{1-x} is 10.45 K, being somewhat lower than the value given in the literature.[2-4,7] With increasing Ti content T_c increased up to 11.7 K (3 at%), and then decreased. The values were about 2 degrees lower than those obtained by Willens *et al.*[7] If the major part of the curve is extrapolated to pure α-MoC_{1-x}, the resulting temperature becomes about 13 K. This is nearly equal to that of cubic MoC.

T_c of the cubic single phase of Mo–Ti–C system increased with increasing Ti content up to 3 atomic % Ti. As the Ti content was lower than 5 at%, T_c of Mo–Ti–C system was higher than that of the mixture of α-MoC_{1-x} and η-MoC_{1-x}. Thus it seems that the stabilization of the cubic phase of Mo–C system by a small amount of Ti raises T_c.

In the case of niobium and tantalum carbides, the

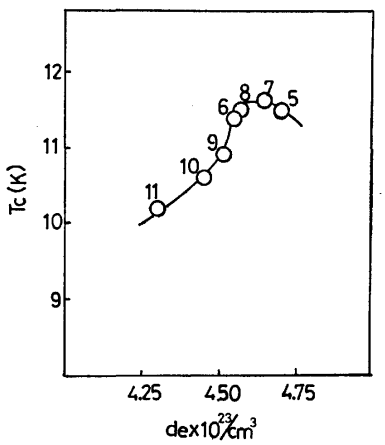

Fig. 4. T_c *vs.* de.
Numbers in this figure represent those of the sample in Table 1.

* In NbC formation by the carbonization of Nb_2O_5, the oxygen content in the product was 0.008 wt. % by radioactivation analysis.[11]

defficiecy of carbon site in the cubic lattice remarkably lowers T_c.[11,13] However, α-MoC_{1-x} and cubic MoC–TiC solid solution which are nonstoichiometric show high superconducting transition temperature. The relation between T_c and the electron density (de)** [14] of cubic Mo–Ti–C system is shown in Fig. 4. The addition of Ti to Mo–C system changes the electron density of the cubic lattice. T_c was maximum at about $4.6\times10^{23}/cm^3$ of de. The tendency is similar to that for various NaCl type compounds.[15,16]

The oxygen contained in the carbide or nitride in a small amount lowers T_c.[15] The oxygen content of the products formed in this study was found to be small. Thus it seems that T_c of Mo–C and Mo–Ti–C systems is affected by the crystal structure and the electron density.

The authors wish to thank Professor N. Kitamura and Mr. Y. Inada, Department of Physics, Aoyama Gakuin University, for their suggestions as regards the superconducting transition temperature measurement.

** The electron density was defined as

$$de = \frac{p\sum c_i N_i}{a^3}$$

where p is the number of atoms per unit cell, c_i and N_i are the fractional concentration and the valence electron of ith component, respectively, and a is the lattice parameter.

References

1) E. Rudy, St. Windish, A. J. Stosick, and J. R. Hoffman, *Trans. AIME*, **239**, 247 (1967).
2) L. E. Toth, V. H. Zackay, M. Wells, J. Olson, and E. R. Parker, *Acta Met.*, **13**, 379 (1965).
3) L. E. Toth, E. Rudy, J. Johnston, and E. R. Parker, *J. Phys. Chem. Solids*, **26**, 517 (1965).
4) R. H. Willens and E. Buchler, *Trans. AIME*, **236**, 171 (1966).
5) R. H. Willens and E. Buchler, *Appl. Phys. Lett.*, **7**, 25 (1965).
6) B. T. Matthias, E. A. Wood, E. Corenzwit, and V. B. Bala, *J. Phys. Chem. Solids*, **1**, 188 (1956).
7) R. H. Willens, E. Buchler, and B. T. Matthias, *Phys. Rev.*, **159**, 327 (1967).
8) O. Matsumoto and T. Miyazaki, *Denki Kagaku*, **39**, 388 (1971).
9) O. Matsumoto and T. Miyazaki, *High Temp. Sci.*, **5**, 40 (1973).
10) O. Matsumoto and M. Saito, *Denki Kagaku*, **41**, 742 (1973).
11) In press. O. Matsumoto, and M. Saito, *High Temp. Sci.*, "Formation of Niobium Carbide by the Carbonization of Nb_2O_5 with an Argon Plasma Arc and some Properties of Products."
12) T. B. Reed, H. C. Gatos, W. J. Lafender, and J. D. Roddy, *AIME Met. Soc. Conf.*, **19**, 71 (1962).
13) A. L. Giorgi, E. G. Szklarz, E. K. Strom, A. L. Brown, and B. T. Matthias, *Phys. Rev.*, **125**, 837 (1962).
14) N. Pessal and J. K. Hulm, *Physics*, **2**, 311 (1966).
15) N. Pessal, R. E. Gold, and H. A. Johansen, *J. Phys. Chem. Solids*, **29**, 19 (1968).
16) V. H. Zackay, M. F. Merrian, and K. M. Ralls, "Superconductivity and Phase Diagram" in "Phase Diagram," ed. by A. M. Alper, Vol. III, p. 87, Academic Press, New York (1970).

An X-Ray Investigation of the Structures of the Tetrachloro- and Tetrabromoaurate(III) Ions in Aqueous Solution

Masunobu MAEDA, Hitoshi OHTAKI, and Georg JOHANSSON*

Department of Electrochemistry, Tokyo Institute of Technology, O-okayama, Meguro-ku, Tokyo 152
**Department of Inorganic Chemistry, Royal Institute of Technology, S-100 44 Stockholm 70, Sweden*

(Received May 25, 1974)

The structures of the $AuCl_4^-$ and the $AuBr_4^-$ complexes in aqueous solutions have been determined from X-ray scattering measurements on concentrated solutions of tetrachloroauric and tetrabromoauric acids. Both the tetrachloroaurate(III) and the tetrabromoaurate(III) complexes were found to have a square planar symmetry. The values obtained for the interatomic distances within the complexes are: Au-Cl, 2.29_1 Å; *cis*-Cl-Cl, 3.24 Å; *trans*-Cl-Cl, 4.58 Å; Au-Br, 2.43_2 Å; *cis*-Br-Br, 3.44 Å; *trans*-Br-Br, 4.86 Å.

Gold(III) is known to combine with chloride, bromide and iodide ions to form stable complexes of the type AuX_4^- in acid solutions.[1] A square planar model for the structures of the $AuCl_4^-$ and the $AuBr_4^-$ ions in aqueous solutions has been found to be consistent with Raman spectroscopic measurements.[2] In the solid state the $AuCl_4^-$ and the $AuBr_4^-$ complexes have been shown by X-ray scattering,[3-6] Raman and IR measurements[7,8] to have a square planar structure.

As a preliminary to an investigation of the structures of the mixed halide complexes of gold(III) in aqueous solutions more detailed information was needed on the structures of the $AuCl_4^-$ and the $AuBr_4^-$ complexes in solution. For this purpose X-ray scattering measurements have been carried out on concentrated auric chloride and bromide solutions containing the $AuCl_4^-$ and the $AuBr_4^-$ complexes.

Experimental

Preparation and Analysis of Sample Solutions. A solution of tetrachloroauric acid was prepared by dissolving metallic gold of 99.99% purity in *aqua regia* and removing the nitric acid by repeated evaporation with hydrochloric acid.

Gold was determined gravimetrically as metallic gold after reduction with hydrazine sulphate. Chloride was determined gravimetrically as AgCl after reduction of the gold with hydrazine sulphate. The hydrogen-ion concentration was calculated from the relation $[H^+]=[Cl^-]-3[Au^{3+}]$.

A solution of tetrabromoauric acid was prepared by dissolving metallic gold in a mixture of hydrobromic acid and hydrogen peroxide. The analysis of the solution was made by the same procedure as used for the tetrachloroauric acid solution.

The density of a solution was determined with a pycnometer.

The compositions of the solutions investigated are given in Table 1.

TABLE 1. COMPOSITIONS OF THE SOLUTIONS (in g-atom·l^{-1})

	Tetrachloroaurate soln.	Tetrabromoaurate soln.
Au	3.133	2.766
Br	—	12.78
Cl	13.61	—
O	38.78	36.76
H	81.77	77.99

X-Ray Scattering Measurements. The diffractometer used was the same as that described in a previous paper.[9] Mo$K\alpha$ radiation ($\lambda=0.7107$ Å) was used for the measurements. The slit-openings were 1/12°, 1/4° and 1°. A LiF focusing monochromator was placed between the receiving slit and the scintillation counter. Further monochromatization was obtained by means of a pulse-height discriminator. The scattered intensity was measured at discrete points between $\theta=1°$ and 70°, where 2θ is the scattering angle. Points were taken at angular steps of 0.1° in θ up to $\theta=20°$, and 0.25° to $\theta=70°$. The number of counts collected at each angle corresponded to a standard deviation in the measured intensities of about 0.3%. To check long-time variations in the measured intensity, the measurements at each slit combination were made repeatedly. For each slit-opening the measured intensities after corrections for background radiation (about 0.90 counts per second) were recalculated to a common slit width through the use of measurements in overlapping regions. The amount of incoherent radiation passing through the monochromator was estimated from the spectrum of the X-ray tube and the resolving power of the monochromator as described previously.[9,10] It was also estimated experimentally by comparing, at a high angle ($\theta=65°$), intensity measurements obtained when a zirconium filter was placed between the tube and the sample with corresponding measurements with the same filter placed between the sample and the scintillation counter.

All measurements were carried out in a room thermostated at 25±2 °C.

Treatment of Intensity Data

The measured intensities were corrected for polarization in the sample and in the monochromator, and were normalized to correspond to the sum of the calculated coherent and incoherent scattering in the high-angle region ($\theta\gtrsim50°$) for a unit of volume of solution containing one gold atom. The normalization factors calculated in this way agreed within less than 1% with those calculated by the method of Norman[11] and Krogh-Moe.[12]

The scattering factors used for Au, Br, Cl, and O were those given by Cromer and Waber.[13] For H the values given by Stewart *et al.*[14] were used. Values for the incoherent scattering were those given by Cromer and Mann[15] for Au, by Cromer[16] for Br, Cl, and O, and by Compton and Allison[17] for H. The incoherent scattering was corrected for the Breit-Dirac factor.

Anomalous dispersion corrections were taken from Cromer and Liberman's paper.[18]

TABLE 2. OBSERVED INTENSITY VALUES AS A FUNCTION OF $s=4\pi \sin\theta/\lambda$.
$I(s)$ = observed intensities after normalization, $i(s)$ = reduced intensities (corrected for low-frequency additions to the intensity curves).

1) Tetrachloroaurate System

s	$I(s)$	$i(s)$	s	$I(s)$	$i(s)$	s	$I(s)$	$i(s)$
0.401	5958	−2058.0	2.339	4833	−783.9	4.248	3362	−84.8
0.432	6279	−1721.3	2.369	4849	−724.5	4.278	3322	−100.5
0.463	6580	−1404.4	2.400	4868	−662.7	4.308	3296	−103.5
0.494	6854	−1112.4	2.430	4884	−602.9	4.337	3253	−122.3
0.525	7156	−791.4	2.461	4907	−537.5	4.367	3212	−140.0
0.555	7350	−577.3	2.491	4925	−477.2	4.397	3170	−155.7
0.586	7501	−404.2	2.522	4947	−412.8	4.427	3132	−173.8
0.617	7481	−401.6	2.552	4963	−354.4	4.457	3112	−171.8
0.648	7607	−251.7	2.583	4987	−288.2	4.487	3065	−196.4
0.679	7497	−335.1	2.614	4999	−235.3	4.517	3032	−207.5
0.710	7467	−338.3	2.644	5015	−178.0	4.547	3001	−216.3
0.740	7378	−398.5	2.675	5053	−98.6	4.576	2966	−230.4
0.771	7281	−466.4	2.705	5013	−97.8	4.606	2940	−234.7
0.802	7233	−484.2	2.736	5022	−48.3	4.636	2920	−234.2
0.833	7125	−560.6	2.766	5012	−17.3	4.666	2887	−246.0
0.864	7102	−551.8	2.797	5016	26.4	4.695	2859	−253.9
0.895	6999	−621.2	2.827	5018	67.7	4.725	2825	−268.0
0.925	6889	−696.6	2.857	5009	98.0	4.755	2810	−262.9
0.956	6932	−619.1	2.888	4998	126.9	4.785	2786	−266.8
0.987	6856	−659.4	2.918	4998	165.0	4.814	2761	−272.3
1.018	6769	−710.3	2.949	4986	191.5	4.844	2744	−269.8
1.049	6697	−745.1	2.979	4964	207.8	4.874	2721	−273.8
1.079	6637	−767.2	3.010	4973	254.7	4.903	2709	−267.7
1.110	6618	−747.8	3.040	4948	267.6	4.933	2681	−277.3
1.141	6599	−728.2	3.070	4945	301.7	4.963	2679	−260.2
1.172	6573	−713.9	3.101	4935	329.0	4.992	2657	−264.1
1.203	6555	−692.0	3.131	4936	366.1	5.022	2655	−248.4
1.233	6518	−687.9	3.162	4901	367.3	5.051	2647	−239.1
1.264	6501	−664.4	3.192	4911	413.1	5.081	2626	−242.5
1.295	6494	−630.4	3.222	4876	414.6	5.111	2624	−227.0
1.326	6478	−604.2	3.253	4861	434.8	5.140	2634	−200.1
1.357	6471	−569.6	3.283	4848	455.9	5.170	2617	−200.1
1.387	6441	−557.1	3.313	4841	483.7	5.199	2617	−182.8
1.418	6422	−533.9	3.344	4822	499.7	5.229	2609	−174.5
1.449	6392	−520.3	3.374	4782	493.8	5.258	2611	−155.8
1.480	6385	−483.9	3.404	4742	487.2	5.288	2612	−139.5
1.510	6335	−490.1	3.434	4697	475.2	5.317	2617	−118.0
1.541	6289	−492.3	3.465	4673	484.1	5.346	2615	−104.0
1.572	6202	−535.1	3.495	4621	465.0	5.376	2610	−93.5
1.603	6138	−555.4	3.525	4584	460.6	5.405	2618	−69.9
1.633	6055	−593.8	3.555	4529	437.7	5.435	2632	−40.8
1.664	5946	−657.6	3.586	4478	417.8	5.464	2620	−38.3
1.695	5833	−725.1	3.616	4430	400.8	5.493	2632	−11.0
1.725	5714	−799.2	3.646	4366	368.1	5.523	2643	15.2
1.756	5565	−902.8	3.676	4326	358.5	5.552	2648	34.9
1.787	5451	−971.4	3.706	4259	322.4	5.581	2651	52.5
1.818	5345	−1032.1	3.737	4200	293.4	5.610	2646	61.4
1.848	5256	−1076.4	3.767	4135	258.1	5.640	2658	87.2
1.879	5149	−1137.8	3.797	4081	233.5	5.669	2665	108.7
1.910	5101	−1140.1	3.827	4018	198.8	5.698	2655	112.1
1.940	5028	−1168.3	3.857	3970	180.2	5.727	2663	134.1
1.971	4966	−1185.1	3.887	3911	148.9	5.757	2663	147.6
2.002	4916	−1190.0	3.917	3863	128.8	5.786	2665	163.4
2.032	4864	−1196.9	3.947	3819	113.2	5.815	2641	152.5
2.063	4834	−1181.3	3.978	3774	94.6	5.844	1640	165.3
2.094	4808	−1162.7	4.008	3704	51.8	5.873	2640	178.1
2.124	4783	−1142.8	4.083	3671	46.0	5.902	2652	203.1
2.155	4787	−1094.6	4.068	3609	10.5	5.931	2634	197.6
2.185	4787	−1050.4	4.098	3578	4.9	5.960	2631	206.9
2.216	4801	−992.1	4.128	3526	−20.6	5.989	2620	208.4
2.247	4792	−956.7	4.158	3502	−20.1	6.018	2601	202.1
2.277	4793	−909.7	4.188	3452	−44.2	6.047	2613	226.8
2.308	4802	−858.6	4.218	3408	−63.5	6.149	2557	212.9

Table 2. (Continued)

s	$I(s)$	$i(s)$	s	$I(s)$	$i(s)$	s	$I(s)$	$i(s)$
6.221	2525	210.4	10.666	1113	−35.1	14.232	689	12.9
6.293	2481	194.6	10.727	1110	−26.8	14.278	686	14.6
6.365	2419	160.7	10.788	1110	−16.6	14.323	684	17.3
6.437	2355	148.8	10.848	1103	−13.3	14.368	678	15.7
6.509	2302	127.2	10.910	1093	−12.5	14.413	670	11.5
6.581	2220	102.8	10.971	1096	1.1	14.457	666	11.3
6.652	2172	76.7	11.031	1091	6.2	14.502	663	12.6
6.724	2105	49.8	11.091	1085	9.4	14.546	654	7.9
6.795	2079	19.8	11.151	1079	13.6	14.589	655	12.3
6.866	2029	−6.2	11.211	1071	14.9	14.633	650	11.0
6.937	1997	−30.6	11.271	1061	14.6	14.676	641	5.9
7.008	1965	−52.9	11.330	1062	24.5	14.719	639	7.8
7.079	1938	−69.4	11.389	1048	20.1	14.762	639	11.8
7.149	1904	−81.3	11.448	1042	22.8	14.804	636	12.7
7.220	1867	−95.5	11.507	1039	29.0	14.846	624	4.0
7.290	1841	−100.3	11.565	1028	27.0	14.888	624	8.0
7.361	1805	−114.8	11.623	1022	29.7	14.929	615	2.4
7.431	1777	−121.8	11.682	1007	23.2	14.970	610	0.5
7.501	1756	−121.5	11.739	999	24.4	15.011	607	0.7
7.570	1739	−118.3	11.797	998	30.9	15.052	604	1.2
7.640	1726	−110.9	11.854	982	23.8	15.092	600	1.1
7.710	1717	−100.8	11.911	972	22.0	15.132	595	−0.7
7.779	1705	−93.3	11.968	961	19.4	15.172	593	−0.2
7.848	1692	−86.7	12.025	950	15.9	15.212	588	−1.7
7.917	1687	−72.8	12.081	937	10.5	15.251	584	−2.9
7.986	1690	−51.0	12.138	932	13.2	15.290	582	−1.5
8.055	1679	−42.9	12.194	919	8.4	15.328	578	−2.9
8.123	1679	−25.0	12.294	908	5.1	15.367	573	−4.5
8.192	1680	−5.8	12.305	895	−0.6	15.405	572	−2.5
8.260	1669	1.0	12.360	886	−1.9	15.442	566	−5.1
8.328	1667	16.1	12.415	874	−6.7	15.480	564	−5.1
8.396	1665	31.2	12.470	870	−4.4	15.517	559	−7.0
8.464	1653	36.3	12.525	855	−11.7	15.554	556	−6.8
8.532	1647	47.4	12.579	852	−8.0	15.590	555	−5.7
8.599	1638	54.9	12.633	833	−19.5	15.626	550	−7.8
8.667	1624	57.9	12.687	827	−19.5	15.662	548	−7.2
8.734	1609	58.3	12.741	820	−19.9	15.698	539	−13.4
8.801	1589	54.8	12.794	811	−21.9	15.733	540	−10.0
8.868	1586	67.8	12.847	802	−24.8	15.768	541	−6.6
8.934	1563	60.1	12.900	798	−22.3	15.803	534	−10.6
9.001	1555	67.1	12.953	787	−26.4	15.838	531	−11.1
9.067	1527	54.7	13.005	782	−25.5	15.872	534	−6.2
9.133	1503	46.1	13.057	778	−22.9	15.906	531	−6.3
9.199	1484	41.2	13.109	771	−23.8	15.939	531	−3.9
9.265	1456	28.5	13.161	764	−24.6	15.972	527	−5.8
9.331	1438	24.6	13.212	761	−21.7	16.005	522	−8.7
9.396	1417	18.3	13.263	754	−23.7	16.038	522	−6.5
9.461	1403	18.7	13.314	751	−20.3	16.070	522	−3.9
9.526	1388	17.0	13.365	746	−19.9	16.102	520	−4.5
9.591	1354	−3.3	13.415	741	−18.8	16.134	519	−2.7
9.656	1338	−5.3	13.465	743	−11.2	16.166	519	−0.5
9.721	1311	−18.2	13.515	738	−11.3	16.197	514	−4.0
9.785	1295	−21.7	13.565	732	−11.3	16.227	516	0.1
9.849	1276	−27.4	13.614	732	−6.8	16.258	512	−1.6
9.913	1260	−30.5	13.663	718	−14.6	16.288	515	2.9
9.977	1245	−32.8	13.712	720	−8.5	16.318	508	−1.5
10.040	1230	−34.9	13.761	717	−5.4	16.348	509	1.3
10.104	1220	−32.3	13.809	718	0.2	16.377	509	2.6
10.167	1203	−37.2	13.857	715	2.6	16.406	506	2.0
10.230	1186	−42.0	13.905	714	6.5	16.434	501	−1.2
10.293	1180	−36.0	13.952	709	5.7	16.463	505	3.7
10.356	1164	−40.4	14.000	708	9.9	16.491	500	1.2
10.418	1156	−36.0	14.047	698	4.7	16.518	501	4.0
10.480	1143	−37.9	14.093	695	5.8	16.546	500	4.3
10.542	1132	−37.8	14.140	690	5.7	16.573	499	5.1
10.604	1123	−35.3	14.186	689	9.2			

Table 2. (Continued)

2) Tetrabromoaurate System

s	$I(s)$	$i(s)$	s	$I(s)$	$i(s)$	s	$I(s)$	$i(s)$
0.401	14224	1252.5	2.369	8493	−370.0	4.337	4840	−547.2
0.432	14159	1216.3	2.400	8470	−323.2	4.367	4737	−613.2
0.463	14276	1363.7	2.430	8423	−301.3	4.397	4662	−650.8
0.494	14255	1375.8	2.461	8369	−286.7	4.427	4605	−671.3
0.525	14134	1289.7	2.491	8359	−228.5	4.457	4519	−721.6
0.555	14092	1283.7	2.522	8300	−219.5	4.487	4454	−750.6
0.586	13967	1197.9	2.552	8249	−203.5	4.517	4403	−766.2
0.617	13775	1047.0	2.583	8224	−161.8	4.547	4327	−807.5
0.648	13703	1018.1	2.614	8215	−104.5	4.576	4286	−814.2
0.679	13430	791.5	2.644	8181	−73.0	4.606	4227	−838.6
0.710	13264	674.2	2.675	8209	20.8	4.636	4183	−849.6
0.740	13144	603.6	2.705	8131	7.2	4.666	4172	−826.9
0.771	12833	344.9	2.736	8123	64.0	4.695	4132	−834.3
0.802	12750	315.2	2.766	8079	84.2	4.725	4104	−829.3
0.833	12481	100.7	2.797	8072	140.7	4.755	4088	−813.3
0.864	12364	40.3	2.827	8091	222.5	4.785	4074	−795.7
0.895	12115	−150.3	2.857	8104	297.0	4.814	4062	−776.1
0.925	12004	−202.4	2.888	8098	352.7	4.844	4064	−743.7
0.956	11690	−454.5	2.918	8071	387.0	4.874	4042	−734.7
0.987	11451	−632.0	2.949	8113	489.5	4.903	4059	−687.1
1.018	11181	−838.3	2.979	8138	574.9	4.933	4093	−623.7
1.049	10880	−1073.7	3.010	8147	642.7	4.963	4097	−589.9
1.079	10560	−1328.1	3.040	8196	751.4	4.992	4116	−541.3
1.110	10307	−1513.5	3.070	8195	808.3	5.022	4165	−463.5
1.141	10043	−1709.7	3.101	8196	867.7	5.051	4177	−421.9
1.172	9783	−1901.4	3.131	8204	933.0	5.081	4230	−340.6
1.203	9480	−2133.7	3.162	8176	961.9	5.111	4269	−274.0
1.233	9202	−2342.0	3.192	8162	1004.2	5.140	4289	−225.8
1.264	8959	−2513.6	3.222	8141	1039.3	5.170	4322	−164.7
1.295	8706	−2696.1	3.253	8103	1056.7	5.199	4370	−89.5
1.326	8466	−2865.5	3.283	8040	1048.8	5.229	4401	−32.3
1.357	8272	−2981.5	3.313	7975	1037.5	5.258	4440	33.8
1.387	8048	−3140.2	3.344	7870	987.0	5.288	4504	124.7
1.418	7874	−3241.1	3.374	7800	970.4	5.317	4525	171.8
1.449	7729	−3314.1	3.434	7580	856.0	5.346	4578	251.1
1.480	7607	−3362.6	3.465	7493	820.7	5.376	4599	297.3
1.510	7475	−3421.7	3.495	7361	739.3	5.405	4622	345.9
1.541	7352	−3470.9	3.525	7269	698.4	5.435	4666	415.1
1.572	7302	−3448.2	3.555	7181	660.6	5.464	4684	458.3
1.603	7256	−3420.6	3.586	7094	623.6	5.493	4681	480.0
1.633	7224	−3378.5	3.616	6992	570.7	5.523	4705	529.1
1.664	7222	−3306.0	3.646	6869	496.8	5.552	4720	568.3
1.695	7258	−3196.9	3.676	6788	463.9	5.581	4734	606.9
1.725	7272	−3108.8	3.706	6696	419.3	5.610	4732	628.8
1.756	7367	−2940.3	3.737	6614	384.0	5.640	4702	623.0
1.787	7415	−2818.0	3.767	6508	325.2	5.669	4698	642.3
1.818	7548	−2611.5	3.797	6416	279.6	5.698	4679	646.4
1.848	7663	−2423.1	3.827	6338	246.9	5.727	4657	648.2
1.879	7790	−2222.9	3.857	6251	204.6	5.757	4637	651.2
1.910	7952	−1987.5	3.887	6161	159.8	5.786	4613	649.9
1.940	6085	−1781.4	3.917	6070	112.7	5.815	4585	644.7
1.971	8211	−1582.5	3.947	5957	43.5	5.844	4524	606.1
2.002	8339	−1382.3	3.978	5884	13.9	5.873	4490	595.0
2.032	8413	−1234.9	4.008	5811	−16.4	5.902	4495	586.0
2.063	8475	−1100.8	4.038	5726	−59.4	5.931	4404	552.7
2.094	8557	−945.7	4.068	5625	−118.9	5.960	4360	530.7
2.124	8610	−821.2	4.098	5541	−160.9	5.989	4317	509.0
2.155	8631	−728.1	4.128	5440	−221.1	6.018	4258	471.6
2.185	8616	−671.4	4.158	5366	−254.5	6.047	4187	422.5
2.216	8619	−596.8	4.188	5260	−320.7	6.149	4027	335.4
2.247	8628	−516.3	4.218	5171	−370.6	6.221	3904	263.8
2.277	8580	−493.5	4.248	5102	−400.0	6.293	3737	146.3
2.308	8559	−443.8	4.278	4995	−468.4	6.365	3627	85.2
2.339	8517	−415.4	4.308	4903	−522.1	6.437	3475	10.9

Table 2. (Continued)

s	$I(s)$	$i(s)$	s	$I(s)$	$i(s)$	s	$I(s)$	$i(s)$
6.509	3327	−76.9	10.849	1676	82.6	14.323	917	−16.2
6.581	3199	−146.9	10.910	1663	85.5	14.368	915	−12.3
6.652	3070	−208.8	10.971	1637	75.4	14.413	904	−17.9
6.724	2971	−261.5	11.031	1618	72.0	14.457	898	−19.1
6.795	2903	−307.7	11.091	1602	71.6	14.502	885	−26.1
6.866	2838	−338.7	11.151	1583	67.7	14.546	882	−24.0
6.937	2804	−357.7	11.211	1566	65.1	14.589	884	−16.7
7.008	2770	−365.0	11.271	1546	60.6	14.633	869	−26.5
7.079	2744	−357.7	11.330	1520	48.7	14.676	870	−20.8
7.149	2719	−343.0	11.389	1502	45.2	14.719	855	−30.4
7.220	2705	−318.3	11.448	1470	26.7	14.762	856	−24.3
7.290	2708	−276.2	11.507	1448	18.5	14.804	842	−33.3
7.361	2705	−241.8	11.565	1423	7.5	14.846	840	−30.8
7.341	2719	−190.8	11.623	1403	0.7	14.888	839	−26.9
7.501	2726	−147.9	11.682	1379	−10.4	14.929	832	−29.5
7.570	2743	−94.8	11.739	1360	−16.1	14.970	829	−28.5
7.640	2753	−49.2	11.797	1334	−29.7	15.011	818	−34.5
7.710	2772	3.9	11.854	1323	−27.6	15.052	818	−29.8
7.779	2784	50.5	11.911	1292	−46.3	15.092	822	−22.0
7.848	2795	95.4	11.968	1282	−44.1	15.132	817	−22.6
7.917	2797	130.2	12.025	1258	−56.0	15.172	813	−22.7
7.986	2796	162.0	12.081	1238	−64.9	15.212	813	−19.1
8.055	2771	169.0	12.138	1224	−66.7	15.251	806	−21.6
8.123	2754	183.9	12.194	1219	−60.6	15.290	806	−17.9
8.192	2722	183.4	12.249	1204	−65.0	15.328	802	−17.4
8.260	2684	175.4	12.305	1187	−69.8	15.367	806	−10.5
8.328	2643	165.3	12.360	1174	−72.1	15.405	803	−9.0
8.396	2602	154.8	12.415	1165	−70.6	15.442	801	−7.7
8.464	2551	133.2	12.470	1163	−62.8	15.480	804	−0.8
8.532	2494	105.3	12.525	1159	−56.3	15.517	801	−0.2
8.599	2455	95.4	12.579	1149	−56.2	15.554	796	−1.8
8.667	2402	69.7	12.633	1149	−46.1	15.590	793	−1.0
8.734	2356	52.1	12.687	1142	−42.4	15.626	784	−6.5
8.801	2319	42.4	12.741	1135	−40.4	15.662	795	7.7
8.868	2263	13.7	12.794	1142	−23.6	15.698	799	14.5
8.934	2223	0.6	12.847	1137	−18.7	15.733	791	10.4
9.001	2185	−11.5	12.900	1139	−8.2	15.768	792	14.4
9.067	2154	−17.1	12.953	1137	−8.8	15.803	786	11.1
9.133	2109	−37.0	13.005	1137	8.4	15.838	787	15.1
9.199	2067	−53.9	13.057	1131	10.6	15.872	785	16.2
9.265	2031	−64.8	13.109	1128	16.8	15.906	779	13.2
9.331	1999	−72.2	13.161	1127	24.4	15.939	777	13.9
9.396	1965	−82.5	13.212	1119	24.4	15.972	777	17.8
9.461	1936	−88.1	13.263	1117	31.4	16.005	773	15.6
9.526	1904	−96.5	13.314	1111	33.3	16.038	766	11.7
9.591	1883	−94.9	13.365	1104	33.9	16.070	765	13.4
9.656	1857	−98.7	13.415	1100	38.3	16.102	759	10.3
9.721	1822	−111.2	13.465	1091	36.7	16.134	763	17.1
9.785	1800	−112.3	13.515	1080	33.8	16.166	759	15.9
9.849	1789	−101.2	13.565	1078	39.6	16.197	755	14.2
9.913	1761	−108.6	13.614	1064	33.2	16.227	756	17.4
9.977	1758	−91.3	13.663	1055	31.4	16.258	753	16.9
10.040	1750	−78.4	13.712	1049	32.4	16.288	752	18.6
10.104	1742	−66.4	13.761	1036	26.4	16.318	744	13.0
10.167	1726	−62.7	13.809	1028	25.0	16.348	740	11.5
10.230	1729	−40.4	13.857	1017	21.4	16.377	739	12.6
10.293	1724	−26.6	13.905	1006	16.6	16.406	738	13.8
10.356	1717	−15.7	13.952	992	9.9	16.434	733	11.1
10.418	1720	6.2	14.000	985	9.2	16.463	725	5.2
10.480	1715	19.0	14.047	969	−1.1	16.491	726	8.6
10.542	1715	36.8	14.093	968	4.5	16.518	717	1.8
10.604	1707	46.5	14.140	957	−0.1	16.546	720	6.8
10.666	1701	57.2	14.186	948	−2.5	16.573	715	3.5
10.727	1702	75.2	14.232	941	−4.7			
10.788	1685	75.1	14.278	937	−2.4			

The measured intensities, $I(s)$, corrected for polarization and normalized to correspond to the stoichiometric unit of volume were used to calculate the reduced intensities, $i(s)$, according to the formula:

$$i(s) = I(s) - \sum_i n_i[(f_i(s)+\Delta f_i')^2+(\Delta f_i'')^2 + \Phi(s)\cdot I_i^{\mathrm{Inco}}(s)] \quad (1)$$

Here $s=4\pi\sin\theta/\lambda$, n_i represents the number of atoms "i" in the stoichiometric unit of volume, f_i is the scattering factor, $\Delta f_i'$ and $\Delta f_i''$ are the real and the imaginary parts of the anomalous dispersion correction, $\Phi(s)$ is the fraction of the incoherent radiation reaching the counter, and $I_i^{\mathrm{inco}}(s)$ is the total incoherent radiation of an atom "i".

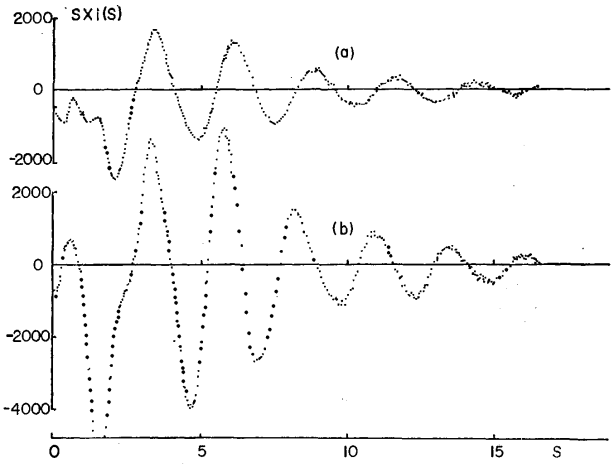

Fig. 1. Observed $s\cdot i(s)$ values for the chloride and the bromide solutions given as a function of $s=4\pi\sin\theta/\lambda$

The reduced intensities, $i(s)$, multiplied by s are shown in Fig. 1 and in Table 2. From these values, the radial distribution curves, $D(r)$, were calculated according to the expression:

$$D(r) = 4\pi r^2\rho_0 + 2r\pi^{-1}\int_0^{s_{\max}} s\cdot i(s)\cdot M(s)\cdot\sin(rs)\mathrm{d}s \quad (2)$$

where ρ_0 denotes the average scattering density of the sample in electron units. The modification function, $M(s)$, was chosen to be $(f_{\mathrm{Au}}^2(0)/f_{\mathrm{Au}}^2(s))\exp(-0.01s^2)$. Spurious peaks below 1 Å in the distribution functions, which could not correspond to interatomic distances, were used to correct the reduced intensity curves for low-frequency additions.

Theoretical intensities due to interatomic interactions were calculated from Eq. (3).

$$i(s) = \sum_i\sum_j f_i(s)f_j(s)\frac{\sin(r_{ij}s)}{r_{ij}s}\exp(-b_{ij}s^2) \quad (3)$$

where r_{ij} is the distance between two atoms "i" and "j", $f_i(s)$ and $f_j(s)$ are the scattering factors, and b_{ij} is the temperature factor corresponding to the interaction between the "i" and "j" atoms.

All calculations were carried out with the use of the KURVLR program.[19]

Analysis of the Intensity Data

The intensity data were first analyzed by means of the radial distribution functions (Fig. 2) calculated

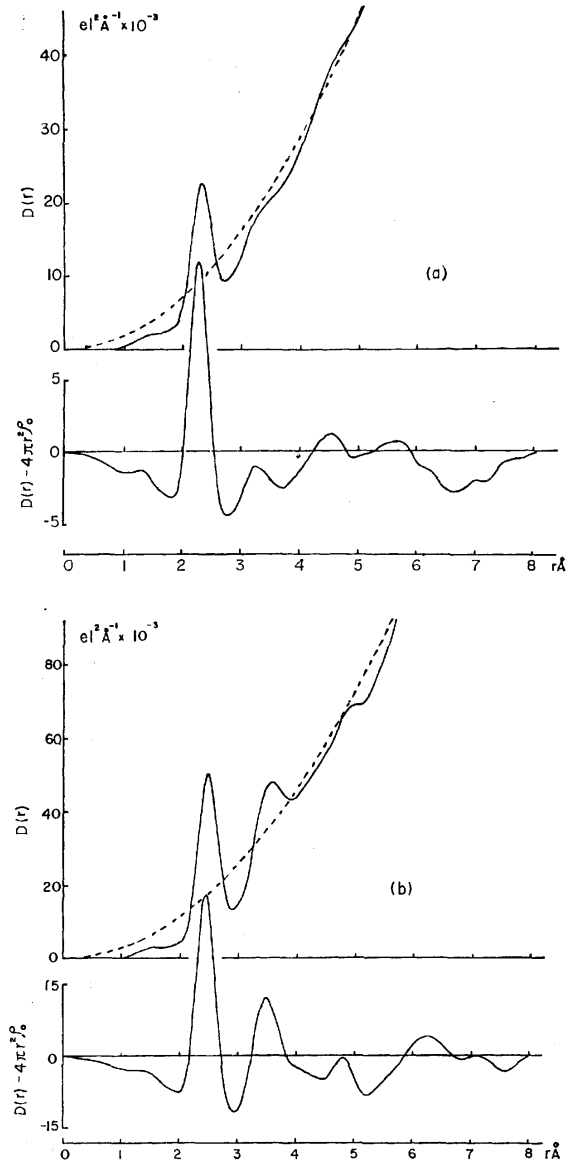

Fig. 2. Radial distribution curves, $D(r)$ and $D(r)-4\pi r^2\rho_0$
(a) The chloride solution. (b) The bromide solution

according to Eq. (2). Distances of gold-halogen and halogen-halogen atoms within a complex were determined from the corresponding peak positions in the distribution functions. The number of such interactions could be roughly estimated from the areas under the peaks.

The first pronounced peak in the radial distribution function (RDF) occurs at 2.3 Å for the chloride solution and 2.4_5 Å for the bromide solution. These peaks can be identified as corresponding to Au-Cl and Au-Br distances within the complexes, since in crystal structure determinations of $KAuCl_4$[6] and of $AuCl_3$,[5] for example, the Au-Cl distances within the planar $AuCl_4^-$ complexes have been found to be around 2.3 Å. Two more pronounced peaks occur in the RDF for the bromide solution: at 3.4 Å ($\simeq\sqrt{2}\times 2.45$ Å) and 4.9 Å ($=2\times 2.45$ Å). Corresponding peaks are present also for the chloride solution but are relatively much smaller.

These two peaks can be identified as Br–Br or Cl–Cl interactions. They occur at distances expected for a planar $AuBr_4^-$ or $AuCl_4^-$ complex. No other marked peaks, which can be related to intramolecular interactions, are present in the RDF functions. The RDF-s therefore are consistent with a square planar symmetry for the $AuCl_4^-$ and the $AuBr_4^-$ complexes.

Refinement of the Structures

In order to get more precise values for the structures of the complexes the influence of intermolecular interactions must be estimated or eliminated. This was done by adjusting the parameter values, derived from the RDF-functions, by means of a least squares procedure in which a minimum was sought for the function

$$\sum_{s_{min}}^{s_{max}} w(s)[i(s)_{obs}-i(s)_{calc}]^2.$$

Intermolecular interactions give their largest contributions to the reduced intensities, $i(s)$, at low s values, while intramolecular interactions are the main contributors at the larger s values. With only intramolecular interactions included for $i(s)_{calc}$ it was found that when the least squares refinements were carried out for different values of s_{min} the resulting parameter values did not show any systematic variations with the chosen s_{min} value for $s_{min}>2.5$ Å^{-1}. It was concluded, therefore, that the intermolecular interactions had a negligible influence on the results, if $i(s)$ values for $s<2.5$ Å^{-1} were excluded from the refinements. Consequently only intensity values for $2.6<s<16.5$ were used for the subsequent least-squares refinements.

The weighting factors, $w(s)$, were chosen to give approximately equal contributions to the least-squares error sum from each experimental $i(s)$ value. For each intramolecular interaction included for the calculation of $i(s)_{calc}$ three parameter values could be refined: the distance, r_{ij}, the temperature factor, b_{ij} and a frequency factor, n_{ij}. Various restrictions on the allowed variations of the values of the parameters could be imposed in the calculations in order to retain a given symmetry during a refinement.

Table 3. Summary of the results of the least-squares refinements

	$AuCl_4^-$	$AuBr_4^-$
A.	$r_{Au-Cl}=2.288[2]$Å	$r_{Au-Br}=2.422[4]$Å
	$b_{Au-Cl}=0.0011[4]$Å^2	$b_{Au-Br}=0.0016[6]$Å^2
	$n_{Au-Cl}=3.5[2]$	$n_{Au-Br}=4.0[2]$
B.		$r_{Au-Br}=2.431[3]$Å
		$b_{Au-Br}=0.0012[3]$Å^2
		$n_{Au-Br}=3.9[1]$
		$r_{Br-Br}=3.44[1]$Å
		$b_{Br-Br}=0.003[1]$Å^2
		$n_{Br-Br}=4.1[2]$
C.	$r_{Au-Cl}=2.291[2]$Å	$r_{Au-Br}=2.432[3]$Å
	$b_{Au-Cl}=0.003[2]$Å^2	$b_{Au-Br}=0.0017[10]$Å^2
	$b_{Cl-Cl}=0.004[2]$Å^2	$b_{Br-Br}=0.006[2]$Å^2
D.	conc.$=2.8[1]$M (=90[4]%)	conc.$=2.72[5]$M (=98[2]%)
	$r_{Au-Cl}=2.291[2]$Å	$r_{Au-Br}=2.433[2]$Å
	$b_{Au-Cl}=0.002[2]$Å^2	$b_{Au-Br}=0.0012[5]$Å^2
	$b_{Cl-Cl}=0.002[2]$Å^2	$b_{Br-Br}=0.006[1]$Å^2

A. Only Au–Cl or Au–Br interactions were included for $i(s)_{calc}$. The distance, the temperature factor and the frequency factor were refined.

B. In this refinement, which could be carried out only for the bromide solution, the Au-Br and the Br–Br interactions were refined independently. The bromide atoms were assumed to be arranged in a square, the size of which was varied in the refinement.

C. The $AuCl_4^-$ and the $AuBr_4^-$ complexes were assumed to form planar squares with the Au atom at the center of the square. The gold-halide distance, the corresponding temperature factor and a temperature factor for the halide-halide interactions were refined.

D. In addition to the parameters used in the previous refinement the concentration of the complexes was varied.

As shown by the results in Table 3 the different restrictions imposed on the refinements do not lead to any significant differences in the resulting parameter values. The independent refinement of the Au–Br and the Br–Br interactions in (B) leads to a ratio between these distances of $3.44/2.431=1.41$ which is close to the expected value of $\sqrt{2}=1.414$ for a square planar complex. In addition the number of Au–Br and of Br–Br interactions per Au atom does not differ significantly from the value of four expected for a AuX_4^- complex. The refinement of the concentration of the AuX_4^- complex in D does not lead to any significant difference from the analytically determined concentration of gold in the solution (Table 1), which indicates that all gold is bonded in AuX_4^- complexes.

Table 4. Final parameter values from the least-squares refinements

$AuCl_4^-$	$AuBr_4^-$
$r_{Au-Cl}=2.291[3]$Å	$r_{Au-Br}=2.432[3]$Å
$b_{Au-Cl}=0.002[2]$Å^2	$b_{Au-Br}=0.0012[5]$Å^2
$b_{Cl-Cl}=0.003[2]$Å^2	$b_{Br-Br}=0.006[2]$Å^2
$n_{Au-Cl}=3.6[2]$	$n_{Au-Br}=3.9[1]$

The best parameter values and the corresponding standard deviations are given in Table 4. The standard deviations are those calculated in the least-squares refinements and do not include possible systematic errors. As judged from the agreement between results obtained when intensities from different s ranges were used for the refinements such systematic errors are probably small and do not exceed the given standard deviations.

To check the calculations the parameter values given in Table 4 were used to calculate peak shapes for the intramolecular interactions. These are compared in Fig. 3 with the radial distribution curves. Subtraction of the calculated peaks from these curves leads to smooth background curves with no indications of residual intramolecular interactions. The $s\cdot i(s)_{calc}$ values are compared in Fig. 4 with the $s\cdot i(s)_{calc}$ values. The differences between observed and calculated values shown in the same figure show that the complexes

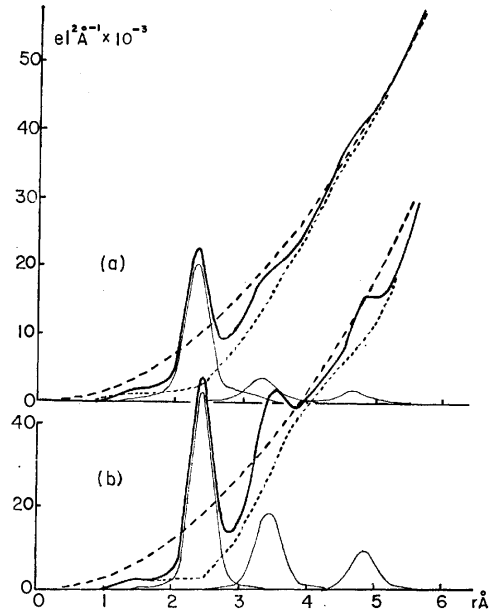

Fig. 3. Comparison between radial distribution curves and peak shapes calculated for the interactions in the AuX_4^- ions using the parameters in Table 4. The difference between the distribution curve and the calculated peaks is shown by the dashed line.
(a) The chloride solution. (b) The bromide solution.

assumed are sufficient to reproduce the observed intensities except for s values below about 3 $Å^{-1}$, where intermolecular interactions can be expected to become important.

The Au-Cl and the Au–Br distances found here for the complexes in solution (Table 4) are similar to those found in crystals in which $AuCl_4^-$ and $AuBr_4^-$ ions have a planar configuration. In crystals of $Cs_2AgAuCl_6$[3] and $RuAuCl_4$[5] the Au–Cl distances have been reported to be about 2.30 and 2.28 Å, respectively. Somewhat longer distances, 2.42 Å, have been reported for crystals of $Cs_2AuAuCl_6$.[3] Other values for the distances ranging from 2.20 to 2.37 Å with an average value of 2.28_6 Å have been found in $KAuCl_4$.[6] Values ranging from 2.25 to 2.34 Å, with an average value of 2.29_0 Å, have been found in crystals of $AuCl_3$, which contain the dimer Au_2Cl_6.

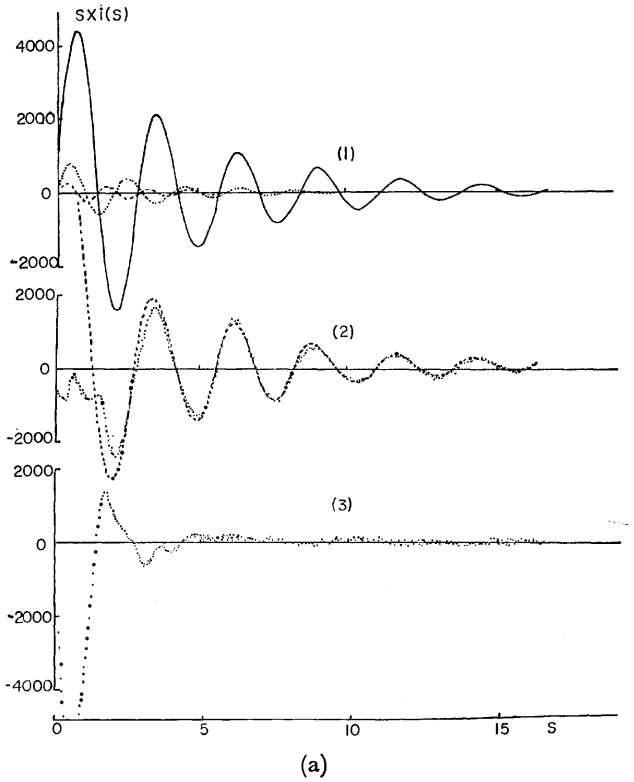

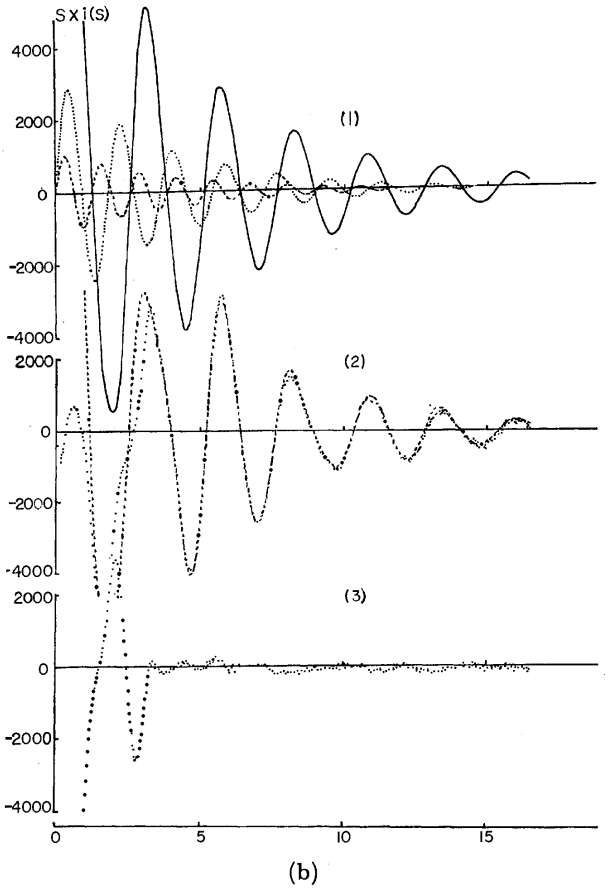

Fig. 4. Observed and calculated $s \cdot i(s)$ values for the chloride solution (a) and the bromide solution (b).
(1) Calculated $s \cdot i(s)$ values for the interactions within an AuX_4^- ion: Au-X full drawn line, *cis*-X-X dotted line and *trans*-X-X dashed line.
(2) Comparison between observed $s \cdot i(s)$ value (dots) and calculated $s \cdot i(s)$ values (dashed line).
(3) Difference between observed and calculated $s \cdot i(s)$ values.

The temperature factors found for the complexes in solution are small and correspond to root mean square values for the variations of the distances of about 0.02 Å for the gold-halide and about 0.03 Å for the halide-halide distances. This indicates a regular arrangement of the atoms in the complexes with no structural differencies between the distances.

This work was carried out at the Institute of Technology in Stockholm and was supported by the Swedish Natural Science Research Council. Computer time was made available by the Computer Division of the National Swedish Office for Administrative Rationaliza-

tion and Economy. We thank Dr. Derek Lewis for revising the English text.

References

1) L. G. Sillén and A. E. Martell, Stability Constants, Spec. Publ. No. 17 and Supplement No. 1, Spec. Publ. No. 25, The Chemical Society, London, 1964 and 1971.
2) H. Stammreich and R. Forneris, *Spectrochim. Acta*, **16**, 363 (1960).
3) N. Elliott and L. Pauling, *J. Amer. Chem. Soc.*, **60**, 1846 (1938).
4) E. G. Cox and K. C. Webster, *J. Chem. Soc.*, **1936**, 1635.
5) J. Strähle and H. Bärninghausen, *Z. Naturforsch.*, *B*, **25**, 1186 (1970).
6) M. Bonamico and G. Dessy, *Acta Crystallogr.*, **B29**, 1735 (1973).
7) D. M. Adams and H. A. Gebbie, *Spectrochim. Acta*, **19**, 925 (1963).
8) A. Sabatini, L. Sacconi, and V. Schettino, *Inorg. Chem.*, **3**, 1775 (1964).
9) G. Johansson, *Acta Chem. Scand.*, **20**, 553 (1966).
10) F. Gaizer and G. Johansson, *ibid.*, **22**, 3013 (1968).
11) N. Norman, *Acta Crystallogr.*, **10**, 370 (1957).
12) J. Krogh-Moe, *ibid.*, **9**, 951 (1956).
13) D. T. Cromer and J. T. Waber, *ibid.*, **18**, 104 (1965).
14) R. F. Stewart, E. K. Davidson, and W. T. Simpson, *J. Chem. Phys.*, **42**, 3175 (1965).
15) D. T. Cromer and J. B. Mann, *ibid.*, **47**, 1892 (1967).
16) D. T. Cromer, *ibid.*, **50**, 4857 (1969).
17) A. H. Compton and S. K. Allison, "X-Rays in Theory and Experiment," van Nostrand, New York (1935).
18) D. T. Cromer and D. Lieberman, *J. Chem. Phys.*, **53**, 1891 (1970).
19) G. Johansson and M. Sandström, *Chemica Scripta*, **4**, 195 (1973).

Atomic Absorption Spectrophotometric Determination of Rare Earths (Y, Eu, Gd, Dy, Ho, and Er) in Single Crystals of Magnetic Garnets and Sulfides

Kohei AMETANI

RCA Research Laboratories, Inc., Zushi-machi, Machida-shi, Tokyo 194-02

(Received June 13, 1974)

Atomic absorption spectrophotometric studies were carried out on single-crystal rare-earth magnetic garnets, $(R_1,R_2)_3(Fe,Ga)_5O_{12}$, where R_1 and R_2 are Y, Eu, Gd, and Er, and sulfides RCr_3S_6, where R is Y, Gd, Dy, Ho, and Er. A method using lanthanum chloride to suppress the interference effects of other elements was demonstrated for the atomic-absorption determination of rare earths. Lanthanum chloride is much better than alkaline metal chlorides (NaCl, KCl, and CsCl) and chelating agents (EDTA·2Na and EDTA·$2NH_4$) for removing the interference effects of foreign elements from the yttrium measurement. Similar results with lanthanum chloride are observed with other rare earths. Experimental results for various samples are also presented. The present method has been utilized for several years in our laboratories to analyse rare earths in newly prepared materials.

Atomic absorption spectrophotometry (AAS), as an important analytical tool, can be used to determine more than 60 elements which are major and minor constituents of cements, metals, alloys, glass, agricultural materials, and minerals, *etc.* In the case of rare earths, however, several workers[1-6] have studied the atomic absorption behavior, but very little in the way of applications has been published, presumably because sensitivity is poor in the air-acetylene flame which is routinely used. The rare earths are not totally dissociated in this flame. In a higher temperature flame, such as nitrous oxide-acetylene, the rare earths are generally dissociated but in many cases they are easily ionized and affected by other elements of the compound. Therefore, the determination of rare earths by AAS technique has usually been performed in the presence of easily ionized elements such as alkaline metals[6-8] and lanthanum,[9] so that the sensitivity of rare earths is increased and the interference of associated elements is overcome. In the present work, to establish a condition for the determination of rare earths in single crystals of magnetic garnets $(R_1,R_2)_3(Fe,Ga)_5O_{12}$, ($R_1$ and R_2=Y, Eu, Gd, and Er), and sulfides RCr_3S_6 (R=Y, Gd, Dy, Ho, and Er), we first studied the yttrium absorption in the presence of the following agents; compounds of easily ionized elements (NaCl, KCl, CsCl, and $LaCl_3$) and chelating agents (EDTA·2Na and EDTA·$2NH_4$). Among these agents, it was found that lanthanum chloride is most effective in removing the interference effects of other elements from the yttrium measurement. The usefulness of lanthanum chloride, in contrast with other agents, is demonstrated in the results given in Table 1 for a measurement of 50 ppm yttrium in the presence of foreign elements. Similar results are obtained for other rare earths with lanthanum chloride. Therefore, a method using lanthanum chloride is proposed for the atomic-absorption determination of rare earths which are a major component in crystals of the above-mentioned garnets and sulfides and the results for various samples are presented.

The garnets are dissolved in hydrochloric acid and the sulfides are dissolved in nitric acid. Hydrochloric acid is then used to acidify the sample solution because the atomic absorption of rare earths is reduced in the presence of nitric acid[5,6] and nitrate anions.[5] This acidification for the sulfide analyses is performed after the removal of nitric acid by evaporation with hydrochloric acid. In the case of zirconium and calcium rare-earth silicates,[9] however, rare earths were determined in a nitric acid and lanthanum nitrate medium. In order to demonstrate the applicability of this method for the analyses of individual single crystals a maximum sample weight of 20 mg was used.

Experimental

Apparatus. The atomic absorptions were measured in a nitrous oxide-acetylene flame using a Hitachi Model 208 atomic absorption spectrophotometer and Westinghouse hollow-cathode lamps. The following analytical lines were used; Y, 410.2 nm; Eu, 459.4 nm; Gd, 368.4 nm; Dy, 421.2 nm; Ho, 410.4 nm; Er, 400.8 nm.

Reagents. (1) Standard rare earth solutions: Rare-earth chloride hexahydrates were dissolved in deionized water and standardized by chelatometry using EDTA (1 mg rare earth/ml). These solutions were stocked as 0.1 M hydrochloric acid solution and working solutions were prepared by diluting the stock solutions. (2) Other solutions: Chlorides, except for gallium, as well as sodium and ammonium salts of EDTA were dissolved in deionized water to make the required concentration. Gallium solutions were prepared by dissolving high-purity gallium (99.99%) in nitric acid, removing the excess nitric acid by evaporation with hydrochloric acid, and then dissolving the residue in deionized water. Reagents used were of analytical reagent grade.

Results

Measurements of Yttrium Atomic Absorption in Several Matrices. The effects of several agents on the yttrium atomic absorption are shown in Fig. 1. Agents which increase the yttrium absorption are sodium chloride, potassium chloride, and lanthanum chloride, while the chelating agents decrease the yttrium absorption. In the case of cesium chloride, yttrium absorption was enhanced at lower concentrations of cesium chloride but gradually decreased with increasing cesium chloride concentration.

The effect of these agents in removing the interference of foreign elements from the yttrium absorption

Table 1. Measurement of 50 ppm yttrium in different matrices

Foreign[a] element (ppm)	No Agent (0.1 M HCl)		Agents added[b]					
			NaCl		$LaCl_3$		EDTA·2Na	
	found (ppm)	error (%)	found (ppm)	error (%)	found (ppm)	error (%)	found (ppm)	error (%)
Fe 50	52.3	+ 4.6	55.0	+10.0	49.2	−1.6	50.1	+ 0.2
Ga 500	57.7	+15.4	51.4	+ 2.8	50.0	0	50.3	+ 0.6
Gd 500	38.3	−23.4	42.4	−15.2	53.2	+6.4	16.5	−67.0
Fe 50, Ga 500, Gd 500	37.2	−25.6	43.5	−13.0	51.3	+2.6	25.8	−48.4

a) Elements were added as chloride. b) Solutions were adjusted to 0.1 M hydrochloric acid and the concentration of agents added was 2,000 ppm for both standards and samples.

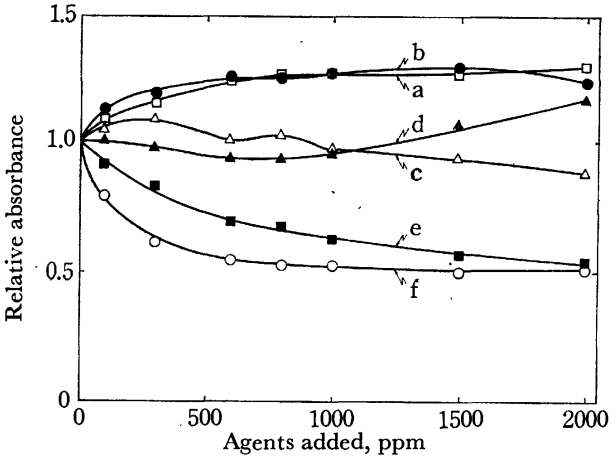

Fig. 1. Effect of several agents on yttrium atomic absorption in 0.1 M hydrochloric acid solution.
(a) NaCl, (b) KCl, (c) CsCl, (d) $LaCl_3$, (e) EDTA·2Na, (f) EDTA·$2NH_4$. Y: 50 ppm.

measurement was examined by adding 2000 ppm of agents to both of the yttrium-standard and the sample solutions. Foreign elements, such as iron, gallium, and gadolinium, were added as chlorides to the sample solutions. Typical results are summarized in Table 1, where sodium chloride and lanthanum chloride are chosen as the enhancement agent for yttrium absorption and EDTA disodium salt for the reducing agent. For comparison, measurements of the solution without the agents are also shown. In the solutions without agents all the foreign elements interfered with the yttrium measurement. Sodium chloride significantly reduced the interference effect of gallium but was not effective for iron and gadolinium. EDTA was useful in the presence of iron and gallium, but the yttrium absorption was greatly reduced by the coexistence of gadolinium. In the lanthanum chloride matrix, the yttrium measurements were generally satisfactory although a small enhancement by gadolinium remained. In comparison with the above-mentioned agents, lanthanum chloride seemed to be the most effective agent for removing the interference effects by foreign elements from the yttrium measurement. Furthermore, lanthanum chloride did not reduce the yttrium absorption as shown in Fig. 1. Therefore, in the work which follows, the measurement of rare earths is performed in the presence of lanthanum chloride with concentrations as high as 10000 ppm.

Effect of Lanthanum Chloride on Rare Earth Atomic Absorptions. As shown in Fig. 2, the absorption of rare earths was enhanced with an increase of lanthanum chloride concentration. For example, comparing the absorption for a solution containing 5000 ppm of lanthanum chloride to one without this agent, the following increased ratios of absorption are observed: Y 1.32, Eu 2.22, Gd 1.51, Dy 1.58, Ho 1.42, and Er 1.22.

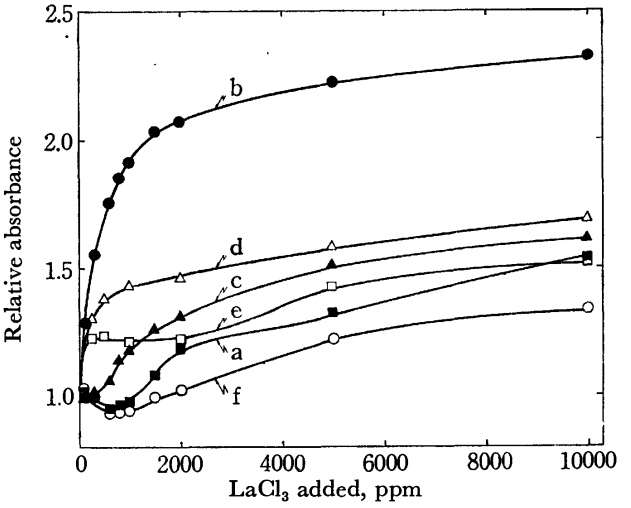

Fig. 2. Effect of lathanum chloride on atomic absorptions of rare earths in 0.1 M hydrochloric acid solution.
(a) Y 50 ppm, (b) Eu 50 ppm, (c) Gd 500 ppm, (d) Dy 50 ppm, (e) Ho 50 ppm, (f) Er 50 ppm.

As a demonstration of the usefulness of lanthanum chloride in removing the interference effects of foreign elements from the rare earth measurements, the results of yttrium and europium are tabulated by comparing with the results obtained without lanthanum chloride in Table 2. The matrix matching is the same between standard and sample solutions with respect to the concentrations of lanthanum chloride and hydrochloric acid. As seen from Table 2, the results with lanthanum chloride are much better than without. For the measurement of yttrium, the interference effect of gadolinium is overcome by the use of 5000 ppm of lanthanum chloride, although a small effect of gadolinium does remain if only 2000 ppm is used, as shown previously in Table 1. It was observed that lanthanum chloride,

Table 2. Comparison of measurements for yttrium and europium with and without lanthanum chloride added.

Analyte	Foreign[a] element (ppm)	Sample Solution: No $LaCl_3$ (0.1 M HCl) found (ppm)	error (%)	5,000 ppm $LaCl_3$[b] found (ppm)	error (%)
Y 50 ppm	Cr 50	64.5	+29.0	49.0	−2.0
	Fe 50	52.3	+ 4.6	49.9	−0.2
	Ga 500	57.7	+15.4	49.3	−1.4
	Ba 50	51.7	+ 3.4	50.1	+0.2
	Gd 500	38.3	+23.4	51.0	+2.0
	Cr 50, Ba 50	68.6	+37.2	49.5	−1.0
	Fe 50, Ga 500, Gd 500	37.2	−25.6	49.6	−0.8
Eu 50 ppm	Fe 100	50.6	+ 1.2	49.8	−0.4
	Ga 2500	90.4	+80.8	49.8	−0.4
	Gd 2500	77.0	+50.4	49.6	−0.8
	Er 100	55.0	+10.0	50.0	0
	Fe 100, Ga 500, Gd 500, Er 100	73.6	+47.2	49.9	−0.2
	Ga 2500, Gd 2500	91.4	+82.8	49.2	−1.6

a) Elements were added as chloride. b) The concentration added the was same between standards and samples, and solutions were adjusted to 0.1 M hydrochloric acid.

for concentrations between 5000 and 10000 ppm, suppresses the interference effects of foreign elements. It was also confirmed that the concentration of gallium and gadolinium can be increased up to 1000 ppm for the measurement of yttrium in the lanthanum chloride matrix. At concentrations higher than 1000 ppm of gallium and gadolinium, the interference effects of these elements were not suppressed by the addition of lanthanum chloride.

In the case of europium, the usefulness of lanthanum chloride is more striking than for yttrium. The error in the europium measurement is about 50 to 80% in the presence of gadolinium or gallium for solutions without lanthanum chloride, but is only 1 to 2% with its addition. Similar effects with lanthanum chloride were observed in measuring other rare earths such as gadolinium, dysprosium, holmium, and erbium. The error in the measurement of the rare earths due to the effects of all the foreign elements examined for the garnet and sulfide analyses was reduced to within 1 to 2% in the 5000 ppm of lanthanum chloride matrix, while the interference effects in solutions without this agent remained. Therefore, it is concluded that the present method using lanthanum chloride is useful for the measurement of rare earths in the presence of several foreign elements.

Analysis of Samples. Analyses were performed for a mixture of oxides with a known composition prior to the analysis of the actual samples. Results are given

Table 3. Results of mixed oxides analysis

Sample[a]	Analyte	wt% calcd	wt% obsd	R[b]
1	Y	35.34	35.2	1.2
2	Y	30.98	30.7	0.3
	Eu	5.88	5.9	0.1
3	Y	26.91	26.6	0.9
	Gd	11.90	11.7	0.3
4	Eu	15.71	15.4	0.1
	Er	34.58	34.8	0.3
5	Gd	46.60	47.1	0.6

a) Oxides were mixed with the following mole ratio;
1, 3.0 Y_2O_3: 3.8 Fe_2O_3: 1.2 Ga_2O_3
2, 2.7 Y_2O_3: 0.3 Eu_2O_3: 3.7 Fe_2O_3: 1.3 Ga_2O_3
3, 2.4 Y_2O_3: 0.6 Gd_2O_3: 4.0 Fe_2O_3: 1.0 Ga_2O_3
4, 1.0 Eu_2O_3: 2.0 Er_2O_3 : 4.3 Fe_2O_3: 0.7 Ga_2O_3
5, 3.0 Gd_2O_3: 5.0 Ga_2O_3
b) Difference between the maximum and minimum observed values.

in Table 3 for yttrium, gadolinium, europium, and erbium determinations, where oxides of rare earths are mixed with iron and gallium oxides. All the oxides have a purity of at least 99.9%. Twenty mg of the mixtures were dissolved in concentrated hydrochloric acid and the sample solutions were diluted to an appropriate concentration of analytes. The final sample solutions were adjusted to 0.1 M hydrochloric acid and 5000 ppm of lanthanum chloride. The same adjustment was carried out for the standards and the atomic absorptions were then measured. Each value shown in Table 3 is an average of at least three atomic absorption measurements of the same sample solution. The difference between the maximum and minimum observed values is shown in the "R" column. In all cases the tabulated results in Table 3 agree, within 1 to 2%, with the calculated values, and this technique is applicable to the analysis of rare earths.

The results for single crystal magnetic-garnet and sulfide samples are shown in Table 4, where sample weights from 10 to 20 mg were used. The garnets, except for $Gd_3Ga_5O_{12}$, were flux grown by Wada and Harada of these Laboratories while the sulfides were grown by Takahashi and Yamada,[10] also of these Laboratories, using chemical vapor transport. The $Gd_3Ga_5O_{12}$ sample was obtained from Lambda/Airtron. The garnets were dissolved in concentrated hydrochloric acid and the solutions were diluted to an appropriate concentration of analytes. Sulfides were dissolved in concentrated nitric acid containing bromine and the excess nitric acid was removed by evaporation with hydrochloric acid, and the solutions were then diluted. The final solutions in both cases were adjusted to 0.1 M hydrochloric acid and 5000 ppm of lanthanum chloride. The standard solutions were adjusted to similar hydrochloric acid and lanthanum chloride concentrations. Each value shown in Table 4 is the average of three atomic absorption measurements for the same sample solution. As shown in Table 4, the results are generally in good agreement with the calculated values. The measurement of other components in the garnets, such as iron and gallium, was performed

Table 4. Results of single crystals analysis

Sample intended composition	Analyte	wt% calcd	wt% obsd	$R^{a)}$
$Y_3Fe_{3.8}Ga_{1.2}O_{12}$	Y	35.34	35.2	1.0
$Y_{2.7}Eu_{0.3}Fe_{3.7}Ga_{1.3}O_{12}$	Y	30.98	30.6	0.2
	Eu	5.88	5.7	0.1
$Y_{2.5}Eu_{0.5}Fe_{3.7}Ga_{1.3}O_{12}$	Y	28.22	27.9	0.2
	Eu	9.65	9.6	0.0
$Y_{2.4}Gd_{0.6}Fe_{3.7}Ga_{1.3}O_{12}$	Y	26.77	26.2	0.2
	Gd	11.84	12.3	0.3
$Eu_3Fe_4GaO_{12}$	Eu	48.45	48.4	0.1
$Eu_2ErFe_{4.3}Ga_{0.7}O_{12}$	Eu	31.92	31.1	0.4
	Er	17.57	17.9	0.1
$EuEr_2Fe_{4.3}Ga_{0.7}O_{12}$	Eu	15.71	15.4	0.2
	Er	34.58	34.7	0.3
$Gd_3Ga_5O_{12}$	Gd	46.60	46.9	1.4
YCr_3S_6	Y	20.33	20.0	2.2
$GdCr_3S_6$	Gd	31.10	30.9	3.8
$DyCr_3S_6$	Dy	31.81	31.6	0.4
$HoCr_3S_6$	Ho	32.13	29.0	0.4
$ErCr_3S_6$	Er	32.44	31.9	0.3

a) Difference between the maximum and minimum observed values.

in a separate experiment, and the resultant data supported these results. For the sulfide analyses, the observed wt% values were sometimes lower than the calculated values, because of white insoluble materials (mostly silica) in the dissolution of samples.[10] In the case of $HoCr_3S_6$ a remarkably large amount of such insoluble residues were found. The values presented in Table 4 are not corrected for the insoluble residues. In another experiment, a chromium and sulfur analysis indicated that the rare earth content observed in this work was in agreement with the stoichiometric amount expected for the intended composition.[10]

The results of Table 2 to 4 substantiate the usefulness of this measurement method for the determination of rare earths in magnetic garnets $(R_1,R_2)_3(Fe,Ga)_5O_{12}$ (R_1 and R_2=Y, Eu, Gd, and Er), and sulfides RCr_3S_6 (R=Y, Gd, Dy, Ho, and Er). This method, therefore, has been utilized in our laboratories for the analysis of rare earths in newly prepared materials, using, at times, only 2 mg of a sample.

The author would like to express his sincere appreciation to Drs. Bernard Hershenov and Fumio Okamoto of these Laboratories for critical reading of the manuscript and helpful suggestions. He is also indebted to Drs. Yasuo Wada and Tatsuo Takahashi, and Messrs. Shigeo Harada and Osamu Yamada of these Laboratories for providing samples.

References

1) M. D. Amos and J. B. Willis, *Spectrochim. Acta*, **22**, 1325 (1966).
2) D. C. Manning, *At. Abs. Newslett.*, **5**, 127 (1966).
3) R. J. Jaworowski, R. P. Weberling, and D. J. Bracco, *Anal. Chim. Acta*, **37**, 284 (1967).
4) N. Shifrin, A. Hell, and J. Ramírez-Muñoz, *Appl. Spectrosc.*, **23**, 365 (1969).
5) A. M. Szaplonczay, *Analyst*, **97**, 29 (1972).
6) R. W. Cattrall and S. J. E. Slater, *Anal. Chim. Acta*, **56**, 143 (1971).
7) M. Satō, H. Matsui, and T. Matsubara, *Bunseki Kagaku*, **20**, 856 (1971).
8) T. Ishizuka, Y. Uwamino, and H. Sunahara, *ibid.*, **22**, 1450 (1973).
9) J. C. Van Loon, J. H. Galbraith, and H. M. Aarden, *Analyst*, **96**, 47 (1971).
10) T. Takahashi, K. Ametani, and O. Yamada, *J. Crystal Growth*, **24/25**, 151 (1974).

The Effect of Pressure on the Diels-Alder Reaction[1)]

Kazuyoshi SEGUCHI, Akira SERA, and Kazuhiro MARUYAMA
Department of Chemistry, Faculty of Science, Kyoto University, Sakyo-ku, Kyoto 606
(Received August 24, 1973)

The effect of pressure on the Diels-Alder reaction was investigated. The observed activation volume was found to have a significant correlation with the activation free energy of the reaction. A correlation diagram between the activation volume and the activation free energy was proposed. By this diagram, the position of the transition state in the Diels-Alder reaction was discussed, and the activation volume was suggested to be a good diagnostic probe for the position of the transition state. The importance of the contribution of the volume contraction resulting from secondary orbital interaction to the apparent activation volume was pointed out.

There has been only a little concern in the literature about the position of the transition state in an organic reaction along its reaction coordinate.[2)] In this respect, investigators have used the postulates of Hammond[3)] and of Swain and Thornton,[4)] the ρ-value,[5-7)] the kinetic isotope effect,[7)] Brönsted's α-value,[2)] and some quasi-thermodynamic parameters[8)] for the examination of the relative positions of the transition states. Although the Diels-Alder reaction is exothermic, its transition state has been believed to resemble the product in a geometric sense. Moreover, the Diels-Alder selectivity-reactivity relationship[9)] has been understood unsatisfactorily. It is, therefore, of great importance to ascertain the relative position of the transition state for the Diels-Alder reaction.

The present paper will be concerned with experimental evidence for the displacement of the position of the transition state along the reaction coordinate in the Diels-Alder reaction. For this purpose, the activation volume of the reaction (Eq. (1)[10)]) was employed as a new parameter:

$$-RT(\partial \ln k/\partial P)_T = \Delta V^{\ddagger} \quad (1)$$

It is well-known that the Diels-Alder reaction is a typical bimolecular, concerted, cleanly second-order reaction, and that it is almost insensitive to solvent change.[11)] In the present instance, the observed changes in the values of $\Delta V^{\ddagger}$ are referred to differences in the structural term, $\Delta_1 V^{\ddagger}$.[12)] This will make discussion rather simple, because one can eliminate the contribution of the solvation term, $\Delta_2 V^{\ddagger}$,[12)] in $\Delta V^{\ddagger}$, which occasionally introduces a puzzling effect on $\Delta V^{\ddagger}$.

Results and Discussion

The effects of the pressure on several Diels-Alder reactions have been investigated in order to elucidate the reaction mechanisms.[13-16)] We examined representative Diels-Alder reactions under pressures in the range from 1 to 900 kg/cm². *n*-Butyl chloride was employed as the solvent to make it possible to compare the present data with others, and because of the availability of its compressibility data.[17)] Typical rate plots at various pressures are shown in Fig. 1 for the reaction of 2,3-dimethylbutadiene with dimethyl fumarate. Since the plots of log *k* against the pressure showed a good linearity for all the reactions examined (for example, see Fig. 1), the activation volumes were calculated by Eq. (1) using the least-squares fit of the data to the following linear expression:

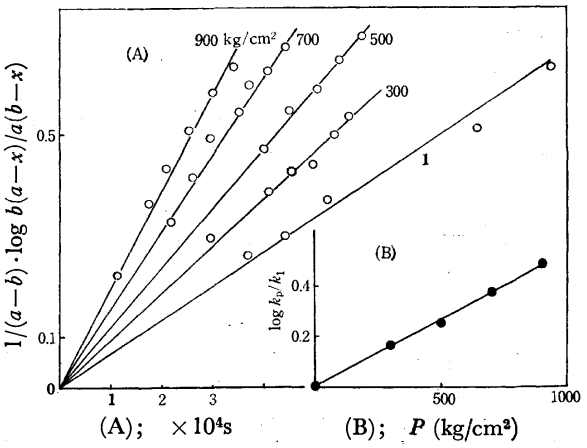

Fig. 1. (A): Rate plots under pressure for the reaction of 2,3-dimethylbutadiene with dimethyl fumarate.
(B): Plot of log k_p/k_1 against pressure for the same reaction.

$$\ln k = a + bP \quad (2)$$

The observed values of the activation volume ($\Delta V_c^{\ddagger}$) were corrected by means of the following equation to give those of the molal concentration basis ($\Delta V_x^{\ddagger}$), taking into account the compressibility of the solvent (κ_0):[17,18)]

$$\Delta V_x^{\ddagger} = \Delta V_c^{\ddagger} - \kappa_0 RT \quad (3)$$

The volume change of the reaction was estimated from measurements of the partial molal volumes of the reactants and the product.

Correlation of Activation Free Energy with Activation Volume. The apparent values of the rate constants, the activation volumes, and the volume changes in the Diels-Alder reactions are tabulated in Table 1. Although several reactions in Table 1 are known to give isomeric product mixtures, we referred to the apparent values of the activation volumes and the volume changes of the reactions because a) the difference in the activation volumes between the *endo*- and the *exo*-isomer producing processes ($\delta\Delta V^{\ddagger}=\Delta V^{\ddagger}_{exo}-\Delta V^{\ddagger}_{endo}$) were found to be quite small[19)] and b) in addition, the volume difference between the *endo*- and the *exo*-adducts has been reported to be negligible as well.[16a)] In the reactions where maleic anhydride was employed as a dienophile, $\delta\Delta V^{\ddagger}$ must be taken into account.[19)] In these cases, however, low *exo*: *endo* isomer ratios were usually found (1: 99 or less). Accordingly, the apparent values of $\Delta V^{\ddagger}$ could safely be

Table 1. Volume parameters for the Diels-Alder reaction in *n*-butyl chloride

Reaction No.	Diene–Dienophile	Temp. (°C)	Rate Constant (l/mol s)	$\Delta V^{\ddagger}$ (cm³/mol)	ΔV (cm³/mol)	Ref.
	Acyclic Dienes					
1	1-Methoxybutadiene–MA[a]	35	9.34×10^{-4} [b]	−45.4	−34.9	16c
2	2,3-Dimethylbutadiene–MA[a]	30	3.54×10^{-4}	−41.3	−36.3	
3	Isoprene–MA[a]	35	1.68×10^{-4} [b]	−38.0	−36.8	16b
4	2,3-Dimethylbutadiene–dimethyl fumarate	40	6.60×10^{-6}	−32.9	−37.2	
5	2,3-Dimethylbutadiene–*n*-butyl acrylate	40	2.14×10^{-7}	−29.6	−36.4	
6	2,3-Dimethylbutadiene–methyl acrylate	40	1.84×10^{-7}	−30.2	−37.0	
	Cyclic Dienes					
7	Cyclopentadiene–dimethyl fumarate	30	1.32×10^{-3}	−32.7	−36.7	
8	Cyclohexadiene-1,3–MA[a]	35	5.24×10^{-4} [b]	−37.2[d]	−30.3[d]	16a
9	Cyclopentadiene–dimethyl acetylenedicarboxylate	35	5.64×10^{-4} [b,c]	−30.2[e]	−33.9[e]	16a
10	Cyclopentadiene–methyl acrylate	40	5.30×10^{-5}	−30.1	−35.7	
11	1,2,3,4-Tetrachlorocyclopentadiene–methyl acrylate	40	1.89×10^{-5}	−24.6	−33.2	
12	Cyclopentadiene–cyclopentadiene	40	3.97×10^{-6}	−23.7	−33.0	

a) Maleic anhydride. b) The reported values were corrected for k_2 in l/mol s for comparison. c) Calculated from data at other temperatures. d) In methylene chloride. e) In ethyl acetate.

used as a mechanistic probe of the reaction.

It can be clearly seen in Table 1 that a reaction with a larger rate constant is associated with a more negative activation volume. The activation volume of a particular reaction may be determined by several factors;[20] nevertheless, the activation free energy was shown to have a good correlation with the activation volumes. This relationship is shown in Fig. 2 for the reactions of cyclic and acyclic dienes respectively. The observed correlation of these two classes of dienes are not identical, but are separated in a rather parallel manner. In general, an acyclic diene is thought to be an equilibrating mixture of *s-cis* and *s-trans* isomers; the former will react as an effective diene with a given dienophile.[21] This means that the inherent rate for the *s-cis* isomer must be larger than the observed rate. The intervention of this *cis-trans* equilibration must be responsible for the separated trend shown in Fig. 2.

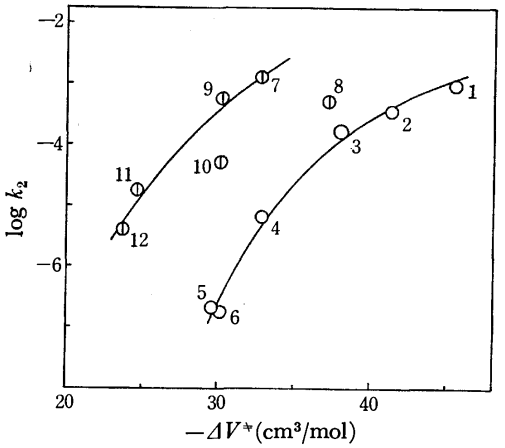

Fig. 2. Correlation of log k_2 with activation volume for the Diels-Alder reaction: numerals correspond to reaction numbers in Table 1; ○, acyclic diene; ⊕, cyclic diene.

An alternative explanation may be that the separated trend is caused by the $\Delta V^{\ddagger}$ term instead of the $\Delta F^{\ddagger}$ term. The geometry of a molecule is responsible for the magnitude of the partial molal volume of the molecule. The reaction of an acyclic diene with methyl acrylate, for example, necessarily proceeds through a monocyclic transition state, while that of a cyclic diene with the same dienophile must have a bicyclic transition state. Consequently, the differences in geometry in both the starting materials and the transition states may result in the differences in the activation volumes, which are responsible for the two separated lines in Fig. 2. However, this seems unlikely because the separated lines under consideration do not coalesce even if $\Delta F^{\ddagger}$ is plotted against $\Delta V^{\ddagger}/\Delta V$, a parameter indicating only the degree of progress for a given reaction and having no relation with the geometry of the reacting molecules and their transition states (see below).

The problem of symmetry in the Diels-Alder transition state is still unsettled. However, theoretical[22] and experimental[16a,23] evidence seems to indicate that, in most of the reactions, a concerted transition state is preferred. In this discussion, we will deal with the present Diels-Alder reactions as concerted cycloaddition reactions.[24] The basic assumption is that the volume of addends in the Diels-Alder reaction decreases monotonously along the reaction coordinate except in special cases (a strong CT-complexing, large secondary orbital interaction, a highly dipolar transition state, *etc.*). In other words, the volume profile along the reaction coordinate may have no extremum, as is depicted in Fig. 3. Furthermore, the structural term, $\Delta_1 V^{\ddagger}$, has been considered to reflect the extent of bond formation.[25] Accordingly, the value of the activation volume ($\Delta V^{\ddagger}$) may safely be anticipated to be a parameter in scrutinizing the relative position of the transition state.

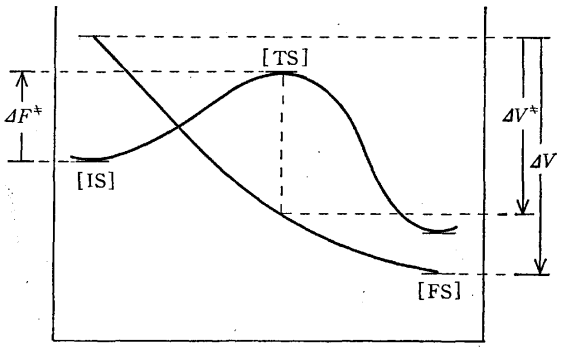

Fig. 3. A schematic diagram of free energy and volume changes for the Diels-Alder reaction: [IS] denotes an initial state, [TS] a transition state, and [FS] a final state.

As is illustrated in Fig. 3, a Diels-Alder reaction characterized by a more negative activation volume may be expected to have a more product-like transition state in respect to the molal volume (and probably to the structure). From an inspection of Table 1, it seems that this interesting concept is equivalent to saying that the transition state for the more reactive Diels-Alder reaction (lower activation free energy) must have a more product-like structure in the sense of the molal volume, and *vice versa*. In Fig. 4 a schematic energy diagram of this generalization for a more reactive (H) and a less reactive (C) Diels-Alder reactions is illustrated, together with the volume parameter. It should be mentioned, however, that the activation volumes of the reactions in which maleic anhydride (MA) was used as a dienophile are more negative than anticipated (see Table 1). The reason for this will be discussed in the succeeding paragraph.

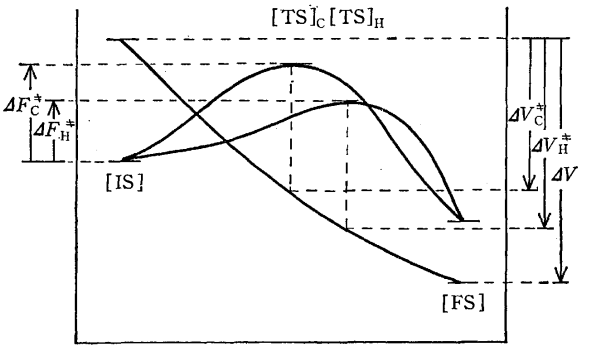

Fig. 4. A shematic diagram of free energy and volume changes for a hot (H) and a cold (C) Diels-Alder reactions: [IS] denotes an initial state, [TS] a transition state, and [FS] a final state. Subscripts H and C correspond to the hot and cold reactions.

Volume Contraction Due to Secondary Orbital Interaction. Recent investigations of the pressure effect on the Diels-Alder reactions revealed that the activation volume of the reaction consisted not only of the structural term, $\Delta_1 V^{\ddagger}$, but also of the volume contraction in the transition state due to secondary orbital interaction, $\Delta_s V^{\ddagger}$.[16,19] The value of $\Delta_s V^{\ddagger}$ is inevitably positive. While the importance of the secondary orbital interaction in [4+2] cycloaddition reactions seems to have been established, the degree of the interaction has scarcely been taken into consideration. When the value of $\Delta_s V^{\ddagger}$ is large, there is a possibility that the molal volume profile of the reaction has the minimum in Fig. 3. Hence, the value of $\Delta_s V^{\ddagger}$ must be estimated in order to discuss the position of the transition state.

Recently we reported that, in the reactions of cyclopentadiene with various dienophiles, the *exo*: *endo* product ratio is correlated to $\delta\Delta V^{\ddagger}$ (which is equal to $\Delta_s V^{\ddagger}$).[19] This correlation enables us to estimate the values of $\Delta_s V^{\ddagger}$ when *exo*: *endo* ratios are given. For most of the dienophiles $\Delta_s V^{\ddagger}$ was estimated to be negligible (0~1.0 cm^3/mol), while in the reactions with MA the estimated value attained nearly 5 cm^3/mol;[26] too large to be ignored. Hence, some of the observed $\Delta V^{\ddagger}$ values listed in Table 1 were corrected in order to give $\Delta V^{\ddagger}_{\text{corrected}}$, taking into account the provisionally assumed value of $\Delta_s V^{\ddagger}$, 4.0 cm^3/mol, for the reactions with MA.

In addition to the correction mentioned above, further revision was made. The use of the $\Delta V^{\ddagger}/\Delta V$ ratio as a parameter indicating the position of the transition state is more suitable than that of $\Delta V^{\ddagger}$ itself. The application of the $\Delta V^{\ddagger}/\Delta V$ parameter with regard to the activation free energy-activation volume relationship may cancel out any possible volume increase or decrease caused by subtle differences in the molecular structures of reagents and/or transition state species. Thus, the revised correlation of the activation free energy with $(\Delta V^{\ddagger}/\Delta V)_{\text{corrected}}$ is presented in Fig. 5. The correlation shown strongly supports the concept now under discussion.

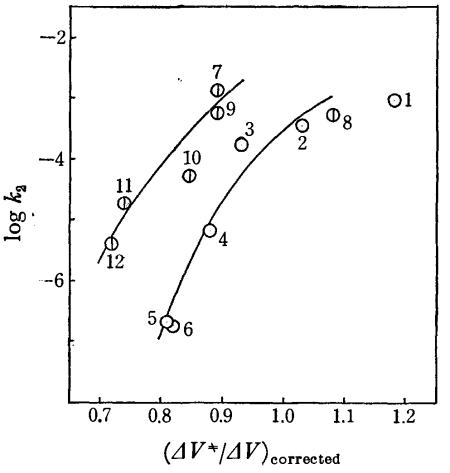

Fig. 5. Correlation of log k_2 with $\Delta V^{\ddagger}/\Delta V$ for the Diels-Alder reaction: numerals correspond to reaction numbers in Table 1; ○, acyclic diene; ⊕, cyclic diene.

However, this parameter should not be used if the solvation term ($\Delta_2 V^{\ddagger}$) is too large to be ignored. The reaction of methoxybutadiene with MA is typical; the activation volume of this reaction is abnormally negative and is dependent on the solvent (−32~−52 cm^3/mol).[16c] This contribution of the solvation term

can be estimated from the solvent dependence of $\Delta V^{\ddagger}/\Delta V$. The values of $\Delta V^{\ddagger}/\Delta V$ and $(\Delta V^{\ddagger}/\Delta V)_{corrected}$ are presented in Table 2 for the reactions of methoxybutadiene[16c] and isoprene[16b] with MA. The $\Delta V^{\ddagger}/\Delta V$ is solvent-dependent for the reaction of MA–methoxybutadiene, as expected, while that for the reaction of MA–isoprene is solvent-independent within the limits of experimental error. Actually, $(\Delta V^{\ddagger}/\Delta V)_{corrected}$ is anomalous for the former reaction, as is shown in Fig. 5 (point number 1). This anomaly is undoubtedly due to the highly dipolar transition state of the reaction.[16c] The other anomaly shown in Fig. 5 is the deviation of the reaction of cyclohexadiene-1,3 with MA (point number 8), which shows a rather larger $(\Delta V^{\ddagger}/\Delta V)_{corrected}$ value than expected. The reason for this is not yet fully understood. Possibly both the specificity of the solvent, dichloromethane (Table 2), and the geometric peculiarity of the reaction (a six-membered diene→bicyclo[2.2.2]-transition state) may be responsible for the observed anomaly.

Table 2. Solvent dependence of $\Delta V^{\ddagger}/\Delta V$ and $(\Delta V^{\ddagger}/\Delta V)_{corrected}$[a]

Solvent	Methoxybutadiene–MA	Isoprene–MA
Acetonitrile	0.99 (0.86)[a]	1.09 (0.97)[a]
Nitromethane	1.52 (1.38)	1.06 (0.93)
1,2-Dichloroethane	1.44 (1.30)	1.04 (0.93)
n-Butyl chloride	1.30 (1.18)	1.03 (0.92)[c]
Dimethyl carbonate	1.68 (1.55)	1.07 (0.96)[c]
Acetone	—	1.09 (0.98)
Dichloromethane	—	1.20 (1.07)
Zeroelectrostriction	1.18 (1.00)[b]	1.08 (0.97)

a) $(\Delta V^{\ddagger}/\Delta V)_{corrected}$ is given in parenthese. b) Estimated value from $\Delta V^{\ddagger}=-32$ cm³/mol and $\Delta V=-28$ cm³/mol. c) Calculated using ΔV in ethyl acetate.

In the reaction of isoprene with MA as well as in the other reactions under consideration, the solvation term may thus be thought to be negligible. Ideally, the value of $\Delta V^{\ddagger}/\Delta V$ at zeroelectrostriction should be referred to. However, the values of $\Delta V^{\ddagger}$ and ΔV at zeroelectrostriction are not so reliable.

The proposed reaction characteristics for the Diels-Alder reactions (Fig. 4) may allow us to scrutinize the selectivity-reactivity relationship of the reactions. The details will be reported elsewhere.[27]

Experimental

The NMR spectra were recorded on a JEOL PS-100 spectrometer, using TMS as the internal standard. The chemical shifts were expressed in δ-values. The analytical determination by glc was performed on a JEOL JGC-20K. The preparative glc was performed on a JEOL JGC-1100. The following stainless steel columns were used: A, 2m PEG 20M (5%); B, 1m Apiezon Grease L (5%); C, 1m PEG 20M (1%); D, 3m TCEP (7%); E, 2m Silicone QF-1 (7%).

Materials. 2,3-Dimethylbutadiene,[28] cyclopentadiene,[29] and 1,2,3,4-tetrachlorocyclopentadiene-1,3[30] were prepared by the reported procedures. The other dienophiles and solvents were commercial materials and were purified when necessary. The following Diels-Alder adducts were prepared by the usual methods: 4-carbomethoxy-2,3-dimethylcyclohexene-1, bp 114—115 °C/27 mmHg; 4-carbobutoxy-2,3-dimethylcyclohexene-1, bp 118—118.5 °C/5 mmHg; *trans*-4,5-dicarbomethoxy-2,3-dimethylcyclohexene-1, bp 131—132 °C/5 mmHg; 1,2-dimethylcyclohex-1-ene-4,5-dicarboxylic anhydride, mp 78—79 °C; *trans*-2,3-dicarbomethoxy-5-norbornene, bp 104—105 °C/4 mmHg. The *exo* and *endo* isomers of 2-carbomethoxy-5-norbornene were prepared by the reaction of cyclopentadiene with methyl acrylate and were separated by glc (column D); NMR spectrum, the *exo* isomer, 3.63 (CO_2CH_3); the *endo* isomer, 3.57 (CO_2CH_3). The *exo* and the *endo* isomers of 2-carbomethoxy-1,4,5,6-tetrachloro-5-norbornene were prepared by the reaction of 1,2,3,4-tetrachlorocyclopentadiene-1,3 with methyl acrylate and were separated by glc (column E); NMR spectrum, the *exo* isomer, 3.83 (CO_2CH_3); the *endo* isomer, 3.78 (CO_2CH_3). 2-Carbomethoxy-1,4,5,6,7,7-hexachloro-5-norbornene was prepared by the reaction of hexachlorocyclopentadiene with methyl acrylate; bp 140—145 °C/7 mmHg. The glc and NMR indicated the presence of a single product. NMR spectrum; 3.65 (CH), 2.60—2.76 (CH_2), 3.82 (CO_2CH_3).

High-Pressure Apparatus. The basic design of the pressure apparatus is essentially identical with that described by Whalley.[31] The high-pressure vessel was immersed in a thermostatted-bath, and the temperature was controlled within ±0.03 °C. The high-pressure hydroaulic liquid used was Silicon Oil KF-96 (200 cs, Shin-etsu Chem. Ind.).

Kinetics and Analysis. Stock solutions of a diene and a dienophile in *n*-butyl chloride were prepared and stored in a freezer. Aliquots were taken from the stock solutions and mixed for each kinetic run. The kinetic solution was transferred into a reaction vessel (20 cm³ glass syringe) and pressurized. Reactions were carried out at five fixed pressures (1, 300, 500, 700, 900 kg/cm²). Analysis was done by glc by means of a comparison of the peak areas or heights on a chromatogram. The initial concentrations of the dienes and the dienophiles, the column specifications and the internal standards for quantitative glc analyses are shown in Table 3.

Table 3. Data for kinetic measurement

Reaction No.[a]	Initial concentration (×10 M) Diene	Initial concentration (×10 M) Dienophile	Glc column[b]	Glc internal standard
2	1.28~2.88	1.36	B	*p*-bromo-*t*-butylbenzene
4	1.13	1.58~1.91	A	dimethyl benzylmalonate
5	4.89~5.31	8.82~11.0	A	ethyl phenylacetate
6	8.91~11.6	21.3~31.3	A	methyl phenylacetate
7	0.506	0.203~0.502	C	diethyl adipate
10	0.503	4.82~7.48	B	2,4-dichlorotoluene
11	2.33	2.20	C	2-carbomethoxy-1,4,5,6,7,7-hexachloro-5-norbornene
12	14.8~16.6	—	A	*p*-chlorotoluene

a) Reaction number cited corresponds to that in Table 1. b) See Experimental part.

Each reaction studied was cleanly second-order and gave only a single product or a mixture of *exo-endo* isomeric products. Although a small amount of a by-product (cyclopentadiene dimer) appeared in the reaction of cyclopentadiene with

methyl acrylate (reaction No. 10), the use of an excess of dienophile depressed the formation of this dimer. The second-order rate constants were calculated by the usual second-order rate expression.[32]

Partial Molal Volume. The technique employed for the determination of the partial molal volumes of liquid samples was the dilatometric method of Hyne and his coworkers.[33] For solid samples, the pycnometric method[34] was employed and calculations were made for the apparent partial molal volumes.

The present work has been supported in part by a Grant-in-aid for Scientific Research from the Ministry of Education.

References

1) Organic Reaction under High Pressure XII. Part XI, A. Sera, C. Yamagami, and K. Maruyama, This Bulletin, **46**, 3864 (1973).
2) J. E. Leffler and E. Grunwald, "Rates and Equilibria of Organic Reaction," John Wiley & Sons, Inc., New York (1963), p. 156.
3) G. S. Hammond, *J. Amer. Chem. Soc.*, **77**, 334 (1955).
4) C. G. Swain and E. R. Thornton, *ibid.*, **84**, 8177 (1962).
5) a) G. A. Olah, *Accounts Chem. Res.*, **4**, 240 (1971); b) G. A. Olah and S. Kobayashi, *J. Amer. Chem. Soc.*, **93**, 6864 (1971).
6) F. G. Bordwell, W. J. Boyle, Jr., and C. Yee, *ibid.*, **92**, 5926 (1970).
7) F. G. Bordwell and W. J. Boyle, Jr., *ibid.*, **93**, 511, 512 (1971).
8) a) M. H. Abraham, *J. Chem. Soc., Perkin* II, **1972**, 1343; b) P. Haberfield, *J. Amer. Chem. Soc.*, **93**, 2091 (1971).
9) T. Inukai and T. Kojima, *J. Org. Chem.*, **35**, 1342 (1970).
10) W. J. leNoble, "Progress in Physical Organic Chemistry," Vol. 5, ed. by A. Streitwieser, Jr. and R. W. Taft, Jr., Interscience Publishers Inc., New York (1967), p. 207.
11) J. Sauer, *Angew. Chem.*, **79**, 76 (1967).
12) In general, an activation volume of a particular reaction is considered to consist of the structural term ($\Delta_1 V^*$) and the solvation term ($\Delta_2 V^*$). The former represents an inherent volume change of reacting molecules resulting from changes in interatomic distances during an activation process, while the latter does a corresponding volume change due to interactions between solvent molecule(s) and a transition state species, see M. G. Evans and M. Polanyi, *Trans. Faraday Soc.*, **31**, 875 (1935). In the present instance, $\Delta_1 V^*$ is the dominant term because the solvent effect on the reaction is negligible except special cases (for example, the reaction of methoxybutadiene with maleic anhydride is a typical one, see text).
13) C. Walling and H. J. Schugar, *J. Amer. Chem. Soc.*, **85**, 607 (1963).
14) a) C. Walling and J. Peisach, *ibid.*, **80**, 5819 (1958); b) C. Walling and D. D. Tanner, *ibid.*, **85**, 612 (1963).
15) a) R. Raidstric, R. H. Sapiro, and D. H. Newitt, *J. Chem. Soc.*, **1939**, 1770; b) C. A. Stewart, Jr., *J. Amer. Chem. Soc.*, **94**, 635 (1972).
16) a) R. A. Grieger and C. A. Eckert, *ibid.*, **92**, 2918, 7149 (1970); b) *Trans. Faraday Soc.*, **66**, 2579 (1970); c) *Ind. Eng. Chem. Fundam.*, **10**, 369 (1971).
17) P. W. Bridgeman, *Proc. Amer. Acad. Arts Sci.*, **68**, 8 (1932).
18) K. E. Weale, "Chemical Reactions at High Pressures," E. and F. N. Spon Ltd., London (1967), Chap. 6.
19) K. Seguchi, A. Sera, and K. Maruyama, *Tetrahedron Lett.*, **1973**, 1585.
20) Although both ΔV^* and ln k are dependent on temperature, corrections by temperature coefficient was ignored because $(\partial \Delta V^*/\partial T)_P$ is unknown. However, as observed in the dimerizations of isoprene and of cyclopentadiene, the higher the temperature is, the more negative the activation volume becomes.[14] Accordingly the correlation trend shown in Fig. 2 will be, we believe, almost insensitive to temperature.
21) The equilibrium constant for isoprene was reported to be $K_{(cis/trans)}=0.03$ or less, see a) J. G. Aston, G. Szasz, H. W. Woolley, and F. G. Brickedde, *J. Chem. Phys.*, **14**, 67 (1946); b) W. B. Smith and J. L. Massingill, *J. Amer. Chem. Soc.*, **83**, 4301 (1961).
22) R. Hoffmann and R. B. Woodward, *ibid.*, **87**, 2046 (1965); L. Salem, *ibid.*, **90**, 543, 553 (1968); C. Trindle, *ibid.*, **92**, 3251, 3255 (1970); N. D. Epiotis, *ibid.*, **94**, 1924 (1972).
23) S. W. Benson and J. A. Benson, *ibid.*, **84**, 152 (1962); **86**, 259 (1964); C. Gauter, U. Scheideggar, and J. D. Roberts, *ibid.*, **87**, 2771 (1965); M. Taagepera and E. R. Thornton, *ibid.*, **94**, 1168 (1972).
24) A referee pointed out the importance of the role of "stage(s)" in the mechanistic feature of the reaction: R. B. Woodward and T. Katz, *Tetrahedron*, **5**, 70 (1959). We think that, in the simultaneous two bond formation process, the presence of a small secondary activation process (asymmetric transition state in the concerted addition) would give no serious effect on the volume profile of the reaction.
25) C. A. Eckert, *Ann. Rev. Phys. Chem.*, **23**, 239 (1972).
26) $\Delta_s V^*$ was estimated to be 2.5 cm^3/mol for the MA reactions giving 99.5% *endo* isomer judging from the proposed correlation.[19] However, because of the possible two-fold interaction between two carbonyl groups in MA and cyclopentadiene π-electrons, the volume contraction for MA reactions was assumed to be a little less than 5.0 cm^3/mol.
27) The authors express their gratitudes to referees for their helpful discussions.
28) C. E. Rehberg, "Organic Syntheses," Coll. Vol. IV, p. 33 (1963).
29) R. B. Moffett, *ibid.*, Coll. Vol. IV, p. 238 (1963).
30) E. T. McBee, R. K. Meyers, and C. F. Baranaukag, *J. Amer. Chem. Soc.*, **77**, 86 (1955).
31) E. Whalley, "Advances in Physical Organic Chemistry," Vol. 2 ed. by V. Gold, Academic Press, London (1964), p. 93.
32) A. A. Frost and R. G. Pearson, "Kinetics and Mechanism," John Wiley & Sons, Inc., New York (1953).
33) H. S. Golinkin, I. Lee, and J. B. Hyne, *J. Amer. Chem. Soc.*, **89**, 1307 (1967); C. Yamagami, A. Sera, and K. Maruyama, This Bulletin, **47**, 881 (1974).
34) A. Weissberger, "Technique of Organic Chemistry," 2nd Ed., Vol. 1, Part 1, Chap. 4, Interscience Publishers Inc., New York (1949).

Reaction of Sulfilimine and Sulfonium Ylide with Hydroxide or Methoxide Ion in Methanol

Naomichi FURUKAWA, Toshiaki MASUDA, Masatoshi YAKUSHIJI, and Shigeru OAE

Department of Applied Chemistry, Faculty of Engineering, Osaka City University, Sumiyoshi-ku, Osaka 558

(Received October 27, 1973)

The reactions of dialkyl and alkyl aryl *N*-*p*-tosylsulfilimines with hydroxide or methoxide in methanol afforded either *S*-substitution products or Pummerer type products or a mixture of both, their distribution being dependent on the structure of the sulfilimine. From the results of analyses, the mechanisms of the formation of these products are discussed. A similar alkaline methanolysis of sulfonium ylides was also investigated.

Cram and his co-workers investigated the hydrolysis of methyl *p*-tolyl *N*-*p*-tosylsulfilimine with sodium hydroxide in methanol to afford the corresponding sulfoxide in a high yield and suggested the reaction to proceed *via* the nucleophilic attack of hydroxide anion on *S*(III) atom.[1] We found that a similar alkaline treatment of cyclic *N*-*p*-tosylsulfilimines gave α-methoxysulfides as the main product without forming any detectable amount of the corresponding sulfoxides.[2] The marked difference in the mode of reaction by the change of the sulfilimine is of interest, and deserves further investigation with various sulfilimines in order to clarify the nature of the two reactions, the substitution on *S*(III) atom and the Pummerer type rearrangement. We have carried out the alkaline hydrolyses of various sulfilimines with both hydroxide and methoxide in methanol.

Results and Discussion

Reaction of Dialkyl or Alkyl Aryl N-p-*Tosylsulfilimines with Potassium Hydroxide in Methanol.* The reaction was carried out as follows: A mixture of a *N*-*p*-tosylsulfilimine with 20 mol excess of potassium hydroxide in methanol was kept for 24 hr at room temperature. The products were then isolated and identified by comparing their IR and NMR spectra with those of authentic samples. The yields of products are summarized in Table 1. The scheme of the reaction is as follows.

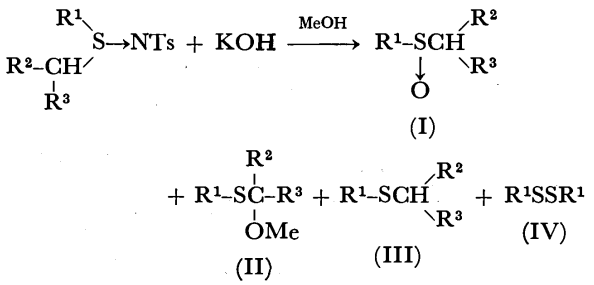

TABLE 1. REACTION OF DIALKYL OR ALKYL ARYL *N*-*p*-TOSYLSULFILIMINES WITH POTASSIUM HYDROXIDE IN METHANOL FOR 24 hr AT ROOM TEMPERATURE

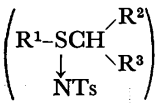

Sulfilimines			Products and yields			
R^1	R^2	R^3	I	II	III	IV
Me	H	H	56	—		
n-Pr	H	H	trace	45		
n-Bu	H	H	trace	41		
Ph	H	H	98	trace	trace	—
Ph	H	Me	27	45	trace	trace
p-$MeOC_6H_4$	H	Me	52	38	trace	ttace
Ph	H	Et	26	42	6	8
Ph	H		32	65	—	
Ph	$-CH_2CH_2-$[a]		96	—	—	
Ph	Me	Me	3	53	10	21
Ph	H	Ph[b]	9	44	12	16

a) This reaction was carried out by refluxing methanol for 24 hr. b) A trace amount of benzaldehyde was detected.

Reaction of Diaryl N-p-*Tosylsulfilimines with Potassium Hydroxide in Methanol.* Diphenyl *N*-*p*-tosylsulfilimine did not react even under refluxing with its alkaline methanol solution for 48 hr. However, *o*- or *p*-nitrophenyl phenyl *N*-*p*-tosylsulfilimine gave *o*- or *p*-nitroanisole in a quantitative yield as shown below.

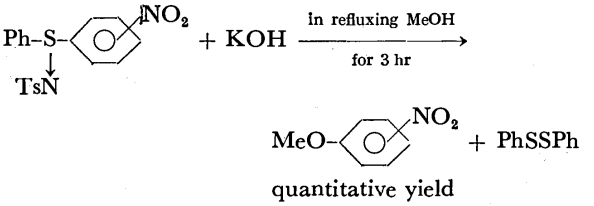

Reaction of Alkyl Phenyl N-p-*Tosylsulfilimines with Sodium Methoxide in Methanol.* The reactions of alkyl phenyl *N*-*p*-tosylsulfilimines with sodium methoxide were carried out in methanol at 40—50 °C for 20—35 hr. The distributions of products are summarized in Table 2.

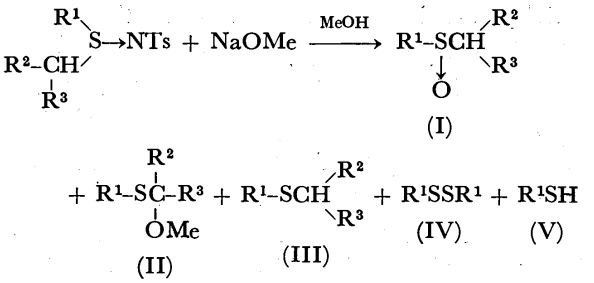

The following results were obtained. 1) The treatment of dimethyl, methyl phenyl and cyclopropyl phenyl sulfilimines with potassium hydroxide in methanol gave

Table 2. Reaction of alkyl phenyl *N*-*p*-tosylsulfilimines with sodium methoxide in methanol

$\left(R^1\text{-}SCH(R^2)(NTs)R^3\right)$

Sulfilimines			Reaction conditions		Products and Yields (%)				
R^1	R^2	R^3	Time (hr)	Temp. (°C)	I	II	III	IV	V
Ph	H	H	35	50	trace	9	70	—	trace
Ph	H	Me[a]	35	50	trace	62	22	—	5
Ph	Me	Me	35	50	trace	25	trace	61	10
Ph	Me	Me[b]	20	40	trace	32	trace	19	trace
Ph	H	Ph[c]	35	50	trace	58	trace	34	4

a) Phenyl vinyl sulfide was isolated in 5% yield. b) 42% sulfilimine was recovered. c) Benzaldehyde was obtained in 20% yield.

only the substitution products, *i.e.*, the corresponding sulfoxide. 2) A similar treatment of sulfilimines having α-ethyl, *n*-propyl or *i*-propyl groups gave both the sulfoxides and the Pummerer type rearranged products (α-methoxysulfides). The yield of the Pummerer type rearranged product increased in expense of the substitution product, the sulfoxide, with increasing bulkiness of alkyl substituents. 3) In the reactions with methoxide ion, however, the major products were the Pummerer type rearranged products and the reduced sulfides. 4) Diphenyl *N*-*p*-tosylsulfilimine did not react even under treatment with potassium hydroxide in refluxing methanol for 48 hr, while *o*- or *p*-nitrophenyl phenyl *N*-*p*-tosylsulfilimines reacted with potassium hydroxide readily affording unexpectedly either the *o*- or *p*-nitroanisole quantitatively. Thus, except for diaryl *N*-*p*-tosylsulfilimines, most sulfilimines react smoothly in alkaline methanol giving either the *S*(III)-substitution products or the Pummerer type rearrangement products or both. Both steric and electronic effects appear to control the reaction paths. In the case of nucleophilic attack on *S*(III) atom, *viz.*, route (1), the steric hindrance of alkyl group in the approach of hydroxide ion on *S*(III) atom plays an important role. Thus the yield of the sulfoxide in the series of alkyl phenyl sulfilimines, $\left(PhSCH(R^2)(NTs)R^3\right)$, falls in the order: Me(R^2,R^3; H,H)≫Et (R^2,R^3; H,Me)~*n*-Pr (R^2,R^3; H, Et)>*i*-Pr (R^2,R^3; Me,Me). This postulate also explains the higher reactivity of methyl phenyl sulfilimine as compared to cyclopropyl phenyl derivative and the lack of reactivity of diphenyl derivative. Since the Pummerer type rearrangement (2) is known to proceed *via* an E_1CB process the rate of the reaction depends on the stability of the postulated intermediate (A). Apparently (A) formed during the Pummerer rearrangement is stabilized mostly by the *S*(II) atom bonded to the α-carbon atom since the cyclopropylmethyl phenyl derivative afforded the corresponding cyclopropyl-α-methoxymethyl phenyl sulfide and not the ring enlargement or fission products. However the intermediary carbonium ion (A) could be stabilized further by the alkyl or aryl group attached to the α-carbon, thus yielding the Pummerer type products from alkyl phenyl *N*-*p*-tosylsulfilimines, $\left(PhSCH(R^2)(NTs)R^3\right)$, in the order: *i*-Pr ($R^2$,$R^3$; Me,Me)>$PhCH_2$ (R^2,R^3; H,Ph)~Et (R^2,R^3; H,Me)~*n*-Pr (R^2,R^3; H,Et)≫Me (R^2,R^3; H,H), which is in line with the order of ability to stabilize the carbonium ion by hyperconjugation.

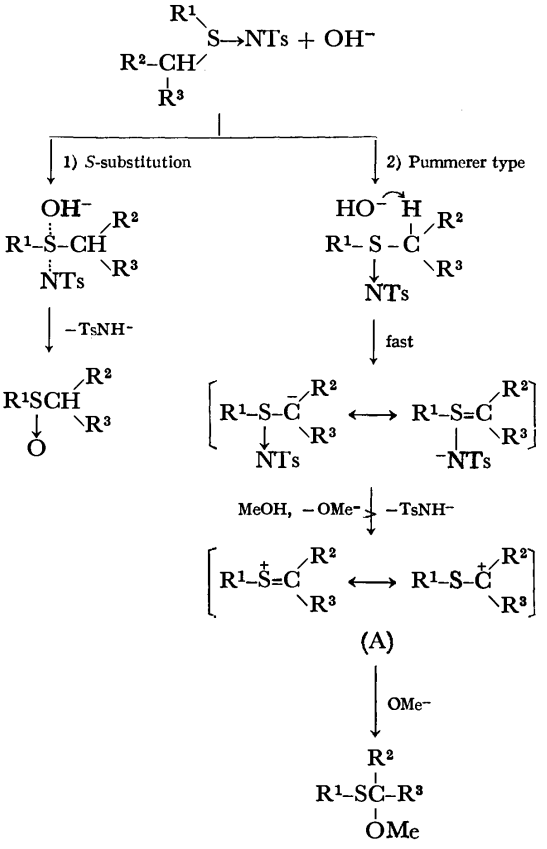

Apparently *o*- or *p*-nitroanisole is formed *via* an aromatic S_N reaction of the corresponding sulfilimine by the attack of methoxide anion on the phenyl carbon atom, with phenylsulfenamide as leaving group. When methoxide ion is used instead of hydroxide, the exchange of methoxide with NTs group might take place to form the alkoxy sulfonium salt from which both the Pummerer rearrangement and the reduction take place

analogously as in the case of alkoxy sulfonium salt[3] as shown below.

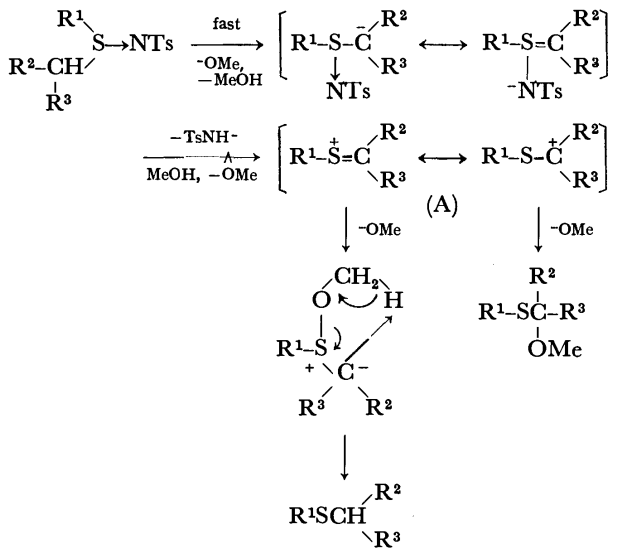

Reaction of Sulfonium Ylide with Potassium Hydroxide in Methanol. The hydrolysis of the sulfonium ylide with hydroxide proceeds *via* an entirely different route from that of the sulfilimine. When methyl *p*-tolyl or benzyl bis(methoxycarbonyl)sulfonium methylides or methyl phenyl bis(phenylsulfonyl)sulfonium methylide was refluxed with an excess potassium hydroxide in methanol, quantitative formation of *p*-toluenethioacetic acid or bis(phenylsulfonyl)methyl phenyl sulfide and benzyl methyl ether or dimethyl ether was observed, while the diphenyl derivative gave diphenyl sulfide in a poor yield.

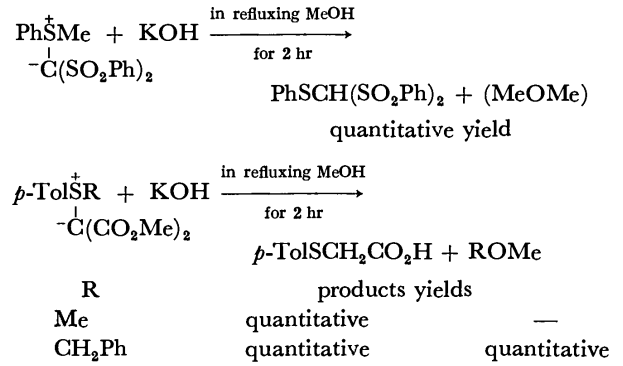

R	products yields	
Me	quantitative	—
CH_2Ph	quantitative	quantitative

The mechanism completely differs from that of the corresponding sulfilimine, the attacking site by methoxide being the α-carbon atom in this case. Although the mechanisms of all these reactions are by no means unambiguously clarified, our results indicate that the reactions of trivalent sulfur compounds are very sensitive to the minor change in the structure of both the attached substituents on the trivalent sulfur atom and the attacking bases.

Experimental

Materials. Methanol was purified by the standard procedure. Potassium hydroxide was of special grade. Sodium methoxide, sulfides and disulfide were prepared by the usual procedures. α-Methoxysulfides were prepared by the reaction of the corresponding α-chlorosulfides[4] with sodium methoxide in methanol. Sulfoxides were prepared by treating the corresponding sulfides with hydrogen peroxide in acetic acid;[5] (PhS- ; bp 137—138 °C/1 mmHg).

p-Toluenethioacetic acid was synthesized by first dissolving *p*-toluenethiol in an excess of aqueous sodium hydroxide, into which was then added a slight excess of chloroacetic acid; mp 93—94 °C (lit,[6] 94.0—94.4 °C).

Preparation of Starting Materials. All the *N*-*p*-tosylsulfilimines were prepared as usual by the reaction of the corresponding sulfides with Chloramine-T.[7]

(PhS- ; mp 135.0—135.5 °C; Found: C, 60.11; H, 5.47; N, 4.36%. Calcd for $C_{16}H_{17}NS_2O_2$: C, 60.12; H, 5.33; N, 4.39%.)

(PhSCH$_2$- ; mp 117.5—118.0 °C; Found: C, 61.19; H, 5.82; N, 4.22%. Calcd for $C_{17}H_{19}NS_2O_2$: C, 61.22; H, 5.71; N, 4.20%.)

All the sulfonium ylides were synthesized by the reaction of the corresponding sulfides with diazo-compounds in the presence of copper sulfate catalyst.[8]

($PhS^{+}Me$; $^{-}C(SO_2Ph)_2$ decomp. 160.5—161.5 °C; Found: C, 57.14; H, 4.27%. Calcd for $C_{20}H_{18}O_4S_3$: C, 57.42; H, 4.31%.)

(*p*-Tol$S^{+}Me$; $^{-}C(CO_2Me)_2$ mp 137—138 °C) (*p*-Tol$S^{+}CH_2Ph$; $^{-}C(CO_2Me)_2$ mp 154—155 °C)

Reaction of Dialkyl or Alkyl Aryl N-p-*Tosylsulfilimines with Potassium Hydroxide or Sodium Methoxide in Methanol.* About 10 mmol of each of the *N*-*p*-tosylfulfilimines was reacted with 20 mol excess of potassium hydroxide or sodium methoxide in methanol (40 ml). The reaction mixture was then neutralized with a 10% aqueous hydrochloric acid and the products were extracted with chloroform except in the case of dialkyl derivatives. In the case of dialkyl derivatives, after the solvents were evaporated, the products were extracted from the residue with chloroform. The products obtained were separated by chromatography through a silica-gel packed column and identified by comparing their IR and NMR spectra with those of authentic samples. The yields and products are given in Tables 1 and 2, respectively. In all the reactions, the corresponding *p*-tosylamide was obtained quantitatively.

Reaction of o- *or* p-*Nitrophenyl Phenyl* N-p-*Tosylsulfilimine with Potassium Hydroxide in Methanol.* About 10 mmol of *o*- or *p*-nitrophenyl phenyl *N*-*p*-tosylsulfilimine was heated with 20 mol excess of potassium hydroxide in refluxing methanol for 3 hr. The reaction solution was then poured into a large amount of water and acidified with 10% aqueous hydrochloric acid and the products were extracted with chloroform. The products obtained were separated by column chromatography and identified by comparing their IR and NMR spectra with those of authentic samples. Yields of *o*- or *p*-nitroanisole, *p*-tosylamide and diphenyl disulfide were quantitative.

Reaction of Bis(methoxycarbonyl)sulfonium Methylides or Bis(phenylsulfonyl)sulfonium Methylide with Potassium Hydroxide in Methanol. About 20 mmol of each of the sulfonium ylides was heated with 20 mol excess of potassium hydroxide for 2 hr in refluxing methanol (80 ml). The reaction solution was then neutralized with 10% aqueous hydrochloric acid

and the products were separated by passing the chloroform extract through a silica-gel packed column. The products obtained were identified by comparing their IR and NMR spectra with those of authentic samples. In all the reactions yields of bis(phenylsulfonyl)methyl phenyl sulfide, *p*-toluenethioacetic acid and benzyl methyl ether were quantitative.

References

1) J. Day and D. J. Cram, *J. Amer. Chem. Soc.*, **87**, 4398 (1968); D. R. Rayner, D. M. von Scritz, J. Day, and D. J. Cram, *ibid.*, **90**, 2721 (1968); D. J. Cram, J. Day, D. R. Rayner, D. M. von Scritz, D. J. Duchamp, and D. C. Garwood, *ibid.*, **92**, 7369 (1970).

2) H. Kobayashi, N. Furukawa, T. Aida, K. Tsujihara, and S. Oae, *Tetrahedron Lett.*, **1971**, 3109.

3) C. R. Johnson and W. G. Phillips, *J. Org. Chem.*, **32**, 1026 (1967); C. R. Johnson, J. C. Sharp, and W. G. Phillips, *Tetrahedron Lett.*, **1967**, 5299; C. R. Johnson and W. G. Phillips, *J. Amer. Chem. Soc.*, **91**, 682 (1969).

4) D. L. Tuleen and R. H. Benett, *J. Heterocycl. Chem.*, **1969**, 6115.

5) A. C. Cope, D. E. Morrison, and L. Field, *J. Amer. Chem. Soc.*, **72**, 59 (1950).

6) D. J. Pasto, D. McMillan, and T. Murphy, *J. Org. Chem.*, **30**, 2688 (1965).

7) K. Tsujihara, N. Furukawa, K. Oae, and S. Oae, This Bulletin, **42**, 2631 (1969).

8) W. Ando, T. Yagihara, S. Tozune, and T. Migita, *Tetrahedron Lett.*, **1969**, 1979.

The Ionic Reaction in the Chlorophosphonation of Alkylbenzenes

Toshihiro OKADA, Yoshiki OKAMOTO, and Hiroshi SAKURAI

The Institute of Scientific and Industrial Research, Osaka University, Suita, Osaka 565

(Received December 17, 1973)

The chlorophosphonation of toluene, *p*-xylene, ethylbenzene, and diphenylmethane gave methyldiphenylmethanes; 2,4′,5-trimethyldiphenylmethane and ethyl-1,1-diphenylethanes; and *p*-benzyltriphenylmethane respectively as the main products. Isopropylbenzene gave α-methylstyrene, 4-methyl-2,4-diphenylpentene-1, 4-methyl-2,4-diphenylpentene-2, and 1,1,3-trimethyl-3-phenylindane, in addition to the ordinary chlorophosphonated products. Those diphenylmethane derivatives may be formed by the electrophilic attack of the benzylic cations, presumably resulting from electron transfer from the benzylic radicals to phosphorus trichloride with the participation of the oxygen or oxy radical, upon toluene, *p*-xylene, ethylbenzene, or diphenylmethane. α-Methylstyrene may be formed by the elimination of a proton from the intermediate 1,1-dimethylbenzyl cation, resulting from isopropylbenzene in a manner similar to that above. Diphenylpentene and phenylindane derivatives may be formed by the acid-catalyzed dimerization of α-methylstyrene.

Jensen and Noller[1] reported that, on chlorophosphonation, toluene gave only a 12.8% yield of benzylphosphonic acid, ethylbenzene gave 11% of 2-phenylethylphosphonic acid, and diphenylmethane gave 2% of diphenylmethylphosphonic acid. Isbell and Wadsworth[2] reported that isopropylbenzene failed to react at all. Also, in our previous investigation of the chlorophosphonation of *n*-alkylbenzene,[3] it was found that the yield of the α-substituted product was abnormally lower than that to be anticipated from the inductive effect alone, in comparison with other isomers.

In the present paper, the chlorophosphonation of alkylbenzenes has been investigated in order to elucidate the reason for this anomalous behavior in the reactivity of the benzylic C-H bond of alkylbenzene.

Results and Discussion

The chlorophosphonation was performed on each alkylbenzene for 3 hr in the temperature range of −15—0 °C, with a 5-fold mole excess of phosphorus trichloride, by the control of the flow rate of oxygen gas. The products were isolated by vacuum distillation after the slipping of the phosphorus oxychloride and unreacted material. The isolated products were esterified with ethanol–triethylamine, followed by analysis with glc.

Toluene gave methyldiphenylmethanes (I) and diethyl benzylphosphonate (II) in the ratio of 50.0: 1.0; the isomer distribution of I was found by glc analysis to consist of 43.6% *o*-, 5.8% *m*-, and 50.6% *p*-isomers. This isomer distribution was similar to that of the benzylation of toluene with benzyl chloride catalyzed with aluminum trichloride in nitromethane.[4] *p*-Xylene gave 2,4′,5-trimethyldiphenylmethane (III) and diethyl *p*-methylbenzylphosphonate (IV) in the ratio of 3.2: 1.0. Ethylbenzene gave ethyl-1,1-diphenylethane (V), diethyl 1-, and diethyl 2-phenylethylphosphonate in the ratio of 12.5: 1.0: 2.0. The isomer distribution of V consisted of 6.6% *o*-, 2.1% *m*-, and 91.3% *p*-isomers. Styrene could not be detected. Diphenylmethane gave *p*-benzyltriphenylmethane (VI) and a trace amount of diphenylmethylphosphonic dichloride. Isopropylbenzene gave 1,1,3-trimethyl-3-phenylindane (VII) and diethyl 2-phenylpropylphosphonate as the main products in the ratio of 0.7: 1.0. Trace amounts of α-methylstyrene (VIII), 4-methyl-2,4-diphenylpentene-1 (IX), 4-methyl-2,4-diphenylpentene-2 (X), and diethyl 1-methyl-1-phenylethylphosphonate were also obtained.

TABLE 1. EFFECT OF SOLVENT ON THE ISOMER DISTRIBUTIONS AND YIELDS OF DIMERS OF VIII

Solvent	Yield (%)	Products (mol%)		
		IX	X	VII
PCl_3	20.8[a]	89.8	9.9	0.3
$POCl_3$	54.1[a]	29.2	68.6	2.2
PCl_3+POCl_3	38.3[a]	31.4	68.2	0.4
$POCl_3+H_3PO_4$	quant.[b]	trace	trace	100

a) Isolated yield. b) By glc.

The dimerization of VIII might give VII, IX, and X with an acid-catalyzed reaction.[5] The isomer distributions of VII, IX, and X obtained by the dimerization of VIII and with the participation of phosphorus trichloride, phosphorus oxychloride, a mixture of phosphorus trichloride and phosphorus oxychloride, or phosphorus oxychloride containing a small amount of phosphoric acid are given in Table 1. The phosphorus trichloride-catalyzed dimerization of VIII gave IX predominantly, while phosphorus oxychloride gave X as the major product and IX as a minor product. On the other hand, when a small amount of protic acid was added to phosphorus oxychloride, VIII dimerized to give VII only. The isomer distribution of the dimers obtained in the chlorophosphonation of isopropyl benzene was similar to that obtained in the last case. This similarity suggests that the dimerization of VIII which occurs during the chlorophosphonation is catalyzed effectively with protic acid, resulting from the hydrolysis of phosphorus trichloride or phosphorus oxychloride with the moisture in the reaction mixtures.

Mechanism. Mayo, Durham, and Griggs[6] have presented good evidence for the following sequence in the chlorophosphonation of cyclohexane:

$$RH + Cl\cdot \longrightarrow R\cdot + HCl \quad (1)$$

$$R\cdot + PCl_3 \longrightarrow \dot{R}PCl_3 \quad (2)$$

$$R\dot{P}Cl_3 + O_2 \longrightarrow RPCl_3OO\cdot \quad (3)$$

$$RPCl_3OO\cdot + PCl_3 \longrightarrow RPOCl_2 + POCl_3 + Cl\cdot \quad (4)$$

$$RPCl_3OO\cdot + PCl_3 \longrightarrow R\cdot + 2POCl_3 \quad (5)$$

However, the formation of I, III, V, VI, and VIII can not be explained only in terms of the radical substitution or disproportionation of R· in reaction (1) or (5), because the isomer distribution of I or V implies that they are formed *via* the electrophilic attack of the benzylic cation on the aromatic nucleus.

The addition of a small amount of iodine, a radical scavenger, to the reaction mixture of toluene and phosphorus trichloride inhibited the formation of both I and II. Moreover, by the reaction of toluene with di-*t*-butyl peroxide at 110 °C, in the presence of an equivalent amount of phosphorus trichloride, I and II were given in the ratio of 5.0: 1.0 without any bibenzyl. These facts, therefore, suggest that the benzyl radical is involved as an intermediate in the process of the formation of I.

A possible mechanism to account for the formation of I can be proposed. The benzyl chloride formed by

$$R\cdot + O_2 \longrightarrow ROO\cdot \quad (6)$$

$$ROO\cdot + PCl_3 \longrightarrow RO\cdot + POCl_3 \quad (7)$$

$$RO\cdot + RH \longrightarrow ROH + R\cdot \quad (8)$$

$$ROH + PCl_3(POCl_3) \longrightarrow RCl + HP(O)Cl_2 \quad (9)$$

the sequence of radical reactions (6)—(8) and a successive ionic reaction (9),[6] may react with toluene by means of the catalytic action of phosphorus trichloride or phosphorus oxychloride as a Lewis acid, thus giving I. However, this possibility can be eliminated on the basis of the following two facts: benzyl chloride could not be detected in the reaction mixture and, after a mixture of benzyl chloride and toluene with phosphorus trichloride or phosphorus oxychloride had been allowed to stand for at least 24 hr at room temperature, no I could be detected in the mixture.

The UV-irradiation of a mixture of benzyl chloride and toluene with phosphorus trichloride under degassed conditions gave neither bibenzyl nor I, but small amounts of unidentified products, although the irradiation of the same mixture without phosphorus trichloride gave bibenzyl in an appreciable yield, indicating the formation of the benzyl radical. These findings suggest that the presence of oxygen or an oxy radical is also required for the formation of I.

When the temperature of the chlorophosphonation of toluene was raised from −15—0 °C to 65—75 °C, the combined yield of I and II was reduced to one-third. This negative temperature effect is not incompatible with the idea that a thermally unstable phosphoranyl intermediate radical may be present in this process.[20]

The formation of I from toluene, like the formation of III, V, VI, and VIII from the other alkylbenzenes, can be explained by the following scheme, Scheme 1.

The intermediate peroxide radical (XI) may react with phosphorus trichloride to give alkylphosphonic dichloride, phosphorus oxychloride, and atomic chlorine (Path 1) or the alkyl radical and two mol of phosphorus oxychloride (Path 2), as presented by Mayo *et al.*[6] Competing with these reactions, however, the radicals of a low ionization potential, such as the benzyl radical,[7] may transfer an electron to the phosphorus trichloride–oxygen complex, thus resulting in the benzylic cation or the ionic complex $[C_6H_5\overset{+}{C}R_1R_2\dot{P}Cl_3\text{-}OO^-]$. A subsequent ionic reaction of the benzylic cation with the alkylbenzenes may give I, III, V, or VI. Isopropylbenzene gave VIII and its dimers, IX, X, and VII, but not isopropyl-2,2-diphenylpropane, which would be derived from the electrophilic attack of the 1,1-dimethylbenzyl cation on isopropylbenzene. The formation of VIII may be explained by the elimination of a proton from the methyl groups of the 1,1-dimethylbenzyl cation. The dimerization of VIII gives IX, X, and VII by means of the catalytic action of phosphorus trichloride and phosphorus oxychloride con-

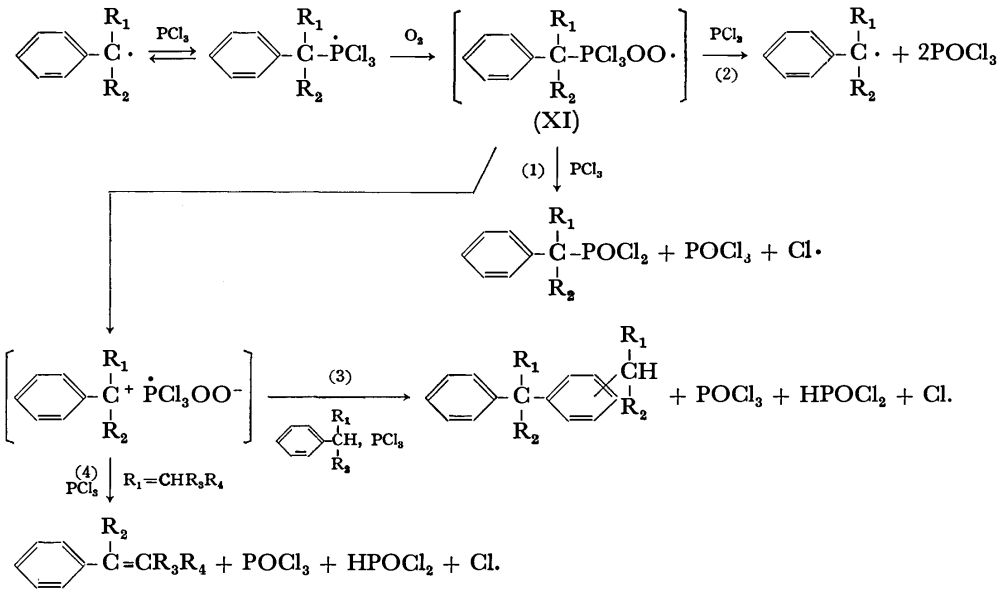

Scheme 1.

taining a small amount of acid. Ethylbenzene gave only V without the elimination of a proton from the 1-methylbenzyl cation. The difference in their behavior may result from differences in the stabilities or electrophilicities of their intermediate cations. Thus, Path 4 may be favorable for the more stable and less electrophilic 1,1-dimethylbenzyl cation, whilst the competing Path 3 may be favorable for the less stable and more electrophilic 1-methylbenzyl cation.

The mechanism proposed involves an intermediate complex, which then undergoes an ionic process to give the products. The formation of such similar complexes has been postulated for the reaction of benzoyl peroxide with tertiary amines or tertiary phosphine,[8] and for the inhibitation of the polymerization of acrylonitrile, vinyl chloride, or butyl acrylate with dimethylaniline.[9]

Recently, the formation of diphenylmethane derivatives by the thermal decomposition of benzoyl peroxide in toluene in the presence of boron trifluoride has also been reported.[10] In this case, a similar mechanism may be applied.

Experimental

All the boiling points are uncorrected. The NMR spectra were obtained at 100 MHz on a JNM-TS-100 spectrometer, with TMS as the internal reference. The mass spectra were obtained on a Hitachi RMU-6 or RMU-7 spectrometer with a direct inlet. The GC–MS were obtained on a Hitachi RMS-4 spectrometer. The gas-chromatographic analyses were done using a Shimadzu GC-3AF on a 3 m×3 mmϕ column packed with 5% Ucon LB 550X on Shimalite W, Mixed Nitrate on C-22,[11] or 10% Benton 34 on Neopack 1A. The preparative work was done using a Hitachi 023 on a 1 m×12 mmϕ column packed with 10% Benton 34 on Neopack 1A.

All the reagents used in this study were commercially available and were purified in all cases except that of di-*t*-butyl peroxide by distillation until found to be at least 99% pure by glc.

General Procedure of Chlorophosphonation. A mixture of alkylbenzene (0.2 mol) and phosphorus trichloride (1.0 mol) was placed in a reaction vessel equipped with a gas inlet and an outlet tube protected from moisture by a drying tube. Dry oxygen was bubbled into the mixture at a flow rate of 100 ml/min and at a temperature of −15—0 °C for 3 hr. After the removal of a large portion of the unreacted material and the phosphorus oxychloride, the residue was distilled *in vacuo*. The yields and boiling points of the products are given in Table 2.

Table 2. Yields of products in the chlorophosphonation of alkylbenzenes

Starting Material	Yield (g)	Bp °C/mmHg
Toluene	4.8	80—113/0.8
p-Xylene	7.8	96—121/1.0
Ethylbenzene	4.5	66— 86/0.1
Diphenylmethane	4.6	180/0.1
Isopropylbenzene	4.5	80—119/0.2

Analysis. The products were treated with ethanol-triethylamine, followed by distillation *in vacuo*, except for the products obtained from the reaction of diphenylmethane. The distillates were identified by a comparison of their retention times in glc with those of authentic samples, prepared by the methods to be described below. The products obtained from the reaction of diphenylmethane were identified with the data from the NMR and mass spectra of each component as follows; *p*-benzyltriphenylmethane; NMR(CCl_4): δ 3.85 (s, 2H, methylene), 5.40 (s, 1H, methine), 6.94 and 7.06 (19H, phenyl), MS: *m/e* 334 (M^+). Diphenylmethylphosphonic dichloride; NMR(CCl_4): δ 4.73 (d, 1H, J_{PCH} 20.0 Hz, methine), 7.30 (m, 10H, phenyl), MS: *m/e* 167 (M^+-121). Also, the two products, IX and X, obtained from the reaction of isopropylbenzene were identified with the data from the NMR on each component fractionated by a preparative glc and GC–MS as follows; 4-methyl-2,4-diphenylpentene-1 (IX); NMR(CCl_4): δ 1.20 (s, 6H, methyl), 2.80 (s, 2H, methylene), 4.75 (d, 1H, J 2.0 Hz, vinyl), 5.10 (d, 1H, J 2.0 Hz, vinyl), 7.16 (10H, phenyl), GC–MS: *m/e* 236 (M^+). 4-Methyl-2,4-diphenylpentene-2 (X); NMR(CCl_4): δ 1.21 (d, 3H, J 5.0 Hz, methyl), 1.44 (s, 6H, methyl), 6.00 (qui, 1H, J 5.0 Hz, vinyl), 7.13 (m, 10H, phenyl), GC–MS: *m/e* 236 (M^+).

Authentic Samples. The following diethyl alkylphosphonates were prepared by the Arbuzov reaction of alkyl bromides with triethyl phosphite,[12] or by the Michaelis-Becker reaction of alkyl bromides with diethyl sodium phosphite;[12] diethyl benzylphosphonate[13] (II bp 121—122 °C/3 mmHg), diethyl *p*-methylbenzylphosphonate[14] (IV bp 134—135 °C/3 mmHg), diethyl 1-phenylethylphosphonate[13] (bp 120—121 °C/0.7 mmHg), diethyl 2-phenylethylphosphonate[13] (bp 154—156 °C/6 mmHg), and diethyl 2-phenylpropylphosphonate (bp 120—122 °C/0.5 mmHg). Diethyl 1-methyl-1-phenylethylphosphonate[15] was prepared by the reaction of diethyl 1-lithio-1-phenylethylphosphonate with methyl iodide (bp 92—93 °C/0.1 mmHg). The diphenylmethane derivatives were prepared by the Friedel-Crafts reaction of alkylbenzenes with their corresponding α-chloro derivatives.[4] *m*- And *p*-isopropyl-2,2-diphenylpropane[16] were prepared by the Friedel-Crafts reaction of 2,2-diphenylpropane[17] with isopropyl alcohol (bp 96—99 °C/0.1 mmHg). 1,1,3-Trimethyl-3-phenylindane (VII) was prepared by the dimerization reaction of α-methylstyrene in the presence of sulfuric acid.

The Chlorophosphonation of Toluene in the Presence of Iodine. Three grams of iodine were added to a mixture of toluene (0.2 mol) and phosphorus trichloride (1.0 mol). The chlorophosphonation was then performed in the same manner as in the general procedure. Glc analysis showed no detectable amount of a product.

The Thermal Decomposition of Di-t-butyl Peroxide[18] in a Mixture of Toluene and Phosphorus Trichloride. A mixture of phosphorus trichloride (0.3 mol), toluene (0.3 mol), and di-*t*-butyl peroxide (1.0 mol) was refluxed for 5 hr. After the removal of a large portion of the unreacted material, the residue was treated with a solution of ethanol–triethylamine. Glc analysis showed I and II in the ratio of 5.0: 1.0; the isomer distribution of the former consisted of 45.1% *o*-, 5.9% *m*-, and 49.0% *p*-isomers. When a mixture of toluene and di-*t*-butyl peroxide was refluxed in the absence of phosphorus trichloride, only bibenzyl was obtained.

The Reaction of Benzyl Chloride and Toluene in the Presence of Phosphorus Trichloride or Phosphorus Oxychloride. A mixture of benzyl chloride (0.1 mol), toluene (0.1 mol), and phosphorus trichloride (1.0 mol) or phosphorus oxychloride (1.0 mol) was stirred under a nitrogen atmosphere at room temperature for 4.5 hr. Glc analysis showed no detectable amount of a product.

Photochemical Reaction of Benzyl Chloride in Toluene.[19] A mixture of toluene (4 g) and benzyl chloride (3 g) in a

Pyrex tube was irradiated with a high-pressure mercury arc at room temperature for 24 hr. The formation of bibenzyl alone was observed by glc. When phosphorus trichloride (7 g) was added to the mixture, and it was then irradiated in the same manner as above, neither bibenzyl nor I could be detected.

Dimerization Reaction of α-Methylstyrene. *a)*: A mixture of VIII (12 g) and phosphorus trichloride (13.7 g) was allowed to stand for 40 hr, protected from atmospheric moisture by a drying tube. After the removal of the VIII and the phosphorus trichloride by means of an aspirator, dimers were obtained by vacuum distillation (yield, 2.5 g; bp 86—98 °C/0.2 mmHg).

b): Phosphorus oxychloride (15 g) was used in place of phosphorus trichloride, and the reaction was carried out in a manner similar to that in *a)* (yield, 6.5 g; bp 84—98 °C/0.2 mmHg).

c): A mixture of phosphorus trichloride (7 g) and phosphorus oxychloride (7.5 g) was used in place of phosphorus trichloride, and the reaction was carried out in a manner similar to that in *a)* (yield, 4.5 g; bp 89—103 °C/0.5 mmHg).

d): A mixture of VIII (2 g), phosphorus oxychloride (60 g), and phosphoric acid (2 g) was allowed to stand for 15 hr. After the distillation of the phosphorus oxychloride, the solution was washed with water and extracted with ether. Glc analysis showed only VII.

References

1) W. L. Jensen and C. R. Noller, *J. Amer. Chem. Soc.*, **71**, 2384 (1949).
2) A. F. Isbell and F. T. Wadsworth, *ibid.*, **78**, 6042 (1956).
3) Y. Okamoto and H. Sakurai, *J. Japan Oil Chemists' Soc.*, **20**, 573 (1971).
4) G. A. Olah, S. J. Kuhn, and S. H. Flood, *J. Amer. Chem. Soc.*, **84**, 1688 (1962).
5) A. Švob, DJ. Deur-Šiftar, and V. Jarm, *J. Chromatog.*, **38**, 326 (1968).
6) F. R. Mayo, L. J. Durham, and K. S. Griggs, *J. Amer. Chem. Soc.*, **85**, 3156 (1963).
7) "Handbook of Chemistry and Physics," 54th ed. by R. C. Weast, Published by The Chemical Rubber Co., Cleaveland. Ohio, E-73 (1973).
8) M. Imoto, "Yukihanno no Riron," II, Kyoritutosyo, Tokyo (1961) p. 451.
9) M. Imoto, *ibid.*, II, p. 498.
10) G. A. Razuvaev, N. A. Kartshova, and L. S. Bogvslaskaya, *Zh. Organ. Khim.*, **2**, 1372 (1966).
11) W. W. Hanneman, C. F. Spencer, and J. F. Johnson, *Anal. Chem.*, **32**, 1386 (1960).
12) G. M. Kosolapoff, "Organic Reaction," Vol. 6, John Wiley & Sons, Inc, New York. London, (1960) p. 273.
13) F. Kagan, R. D. Birknmeyer, and R. E. Strube, *J. Amer. Chem. Soc.*, **81**, 3026 (1959).
14) B. P. Lugovkin and B. A. Arubzov, *Dok. Akad. Nauk S S S R*, **59**, 1301 (1959).
15) Y. Okamoto and H. Sakurai, *J. Japan Oil Chemists' Soc.*, **20**, 821 (1972).
16) E. I. Dupont de Nemours & Co., Brit. 753384 (1956).
17) A. Schneider, U. S. 2742512 (1956).
18) E. H. Farmer and C. G. Moor, *J. Chem. Soc.*, **16**, 131 (1951).
19) G. Porter and F. J. Wright, *Trans. Farady. Soc.*, **51**, 1469 (1955), G. Porter and E. Starchan, *ibid.*, **54**, 1595 (1958).
20) J. I. G. Cadogan, "Advances in Free-radical Chemistry," Vol. 2, (1967), p. 203.

Photochemical Reactions of Some 1-Aryl-1,2-propanediones[1)]

Yoshiro OGATA and Katsuhiko TAKAGI

Department of Applied Chemistry, Faculty of Engineering, Nagoya University, Chikusa-ku, Nagoya 464

(Received January 7, 1974)

Irradiation of four 1-aryl-1,2-propanediones (Ia—Id) with over 300 nm light in 2-propanol gives reduction products identified to be the corresponding pinacols or hydrols formed by the reduction at the aroyl (but not acetyl) oxygen. The products from 1-(*o*-tolyl)-1,2-propanedione (Id) can also be accounted for by the initial hydrogen abstraction from *ortho* methyl by the aroyl carbonyl oxygen. Their photoreactivities are discussed as regards their electronic emission spectra and triplet configuration.

Sometimes one of the two carbonyls in unsymmetrical α-dicarbonyl compounds is selectively photoreduced,[2,3)] *e.g.*, unsymmetrical benzils are photoreduced at a carbonyl with a stronger electron-withdrawing group.[4)] The product is not always determined by the hydrogen abstraction with excited diketone, because the 1,2-hydrogen migration from the resulting ketyl radical being sometimes significant.[5,6)] Intramolecular H abstraction reactions might be utilized to see which of the two carbonyls really abstracts a H atom on the basis of sterically favorable proximity. The intramolecular H transfer is specific as revealed by the fact that the 1,5-shift predominates over the 1,6-shift, particularly in acyclic ketones which are photoreduced with 100% γ-H abstraction.[7)]

Cyclization of 1-(*o*-tolyl)-1,2-propanedione to 2-hydroxy-2-methylindanone (V) on irradiation has been reported by Bishop and Hamer.[8)] They preferred a mechanism *via* benzocyclobutanol to that *via* photoenol (VIII).[8b,c)] We have obtained some evidence for a six-membered transition state (1,5-shift) followed by 1,2-shift, *e.g.*, trapping of the intermediary enol(VII) with dimethyl acetylenedicarboxylate (DADC) as shown below.

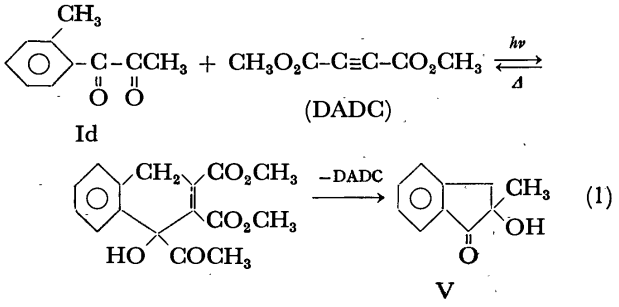

(1)

From their interest in the photoreduction behavior of alkyl aryl α-diketones, the authors present some results on the correlation of photoreactivity with electronic configuration.

Results and Discussion

Irradiation of α-Diketones. 1-Aryl-1,2-propanediones (Ia—Id) were irradiated in dilute 2-propanol or ethyl ether with UV light filtered with Pyrex (>300 nm).

Ia was photoreduced at the benzoyl oxygen but not the acetyl oxygen. A reduction dimer, 1,2-diacetyl-1,2-diphenylethanediol (IIa, 10%) was obtained. The major product was benzoic acid (23%) which seems

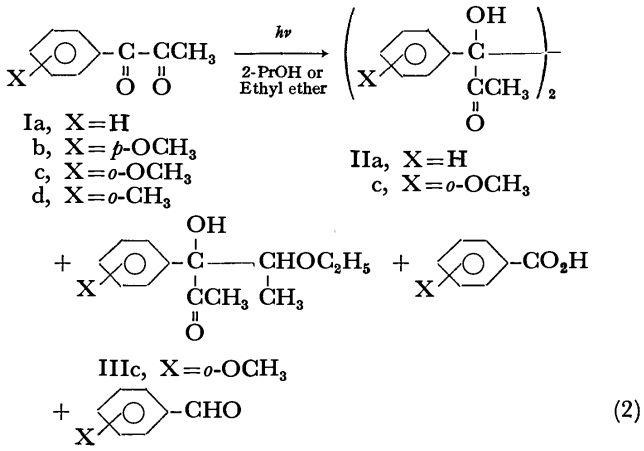

(2)

to be derived from benzoyl radical *via* photodecomposition. In the case of *p*-methoxy derivative (Ib), a complex mixture consisting of more than five components was obtained. The major product was *p*-anisaldehyde (*ca.* 40%) along with a small amount of *p*-anisic acid, all attempts for isolation of other components in a pure form being unsuccessful. The photodecomposition rate was *ca.* 5 times as slow as that of Ia. Photochemical behavior of Ic (*o*-OCH_3) is quite different from that of Ia and Ib. It is smoothly reduced in ether to a dimer (IIc, 550 mg) and a 1:1 adduct of ether (IIIc, 100 mg) along with a trace of *o*-anisic acid. The yield including all recovered materials becomes 90%. There is no product which is reduced at the acetyl oxygen or cyclized by the intramolecular reduction to benzofuran derivative (IV).

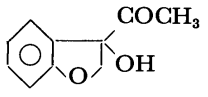

IV

Photolysis of 1-(o-Tolyl)-1,2-propanedione (Id). The photocyclization of Id to indanone (V) was reported by Bishop and Hamer, who assumed either a mechanism involving hydrogen abstraction of *o*-CH_3 hydrogen by acetyl oxygen or a presumed intermediate (VI) which then expanded to V.[8b)]

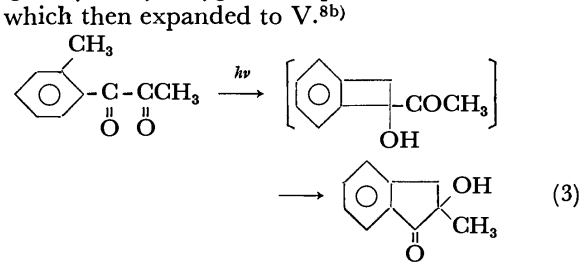

(3)

We postulated an alternative mechanism involving an enol intermediate for the photocyclization of Id on the basis of trapping of intermediary enol, VII.[9]

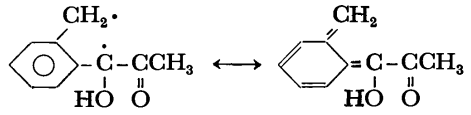

VII

The change of UV spectrum of Id in degassed cyclohexane on irradiation with 366 nm light (Fig. 1) illustrates the gradual disappearance of Id (λ_{max} 257 nm) with a simultaneous increase in V (λ_{max} 242 and 250 nm). The two isosbestic points at 253 and 297 nm indicate the stoichiometry for the conversion Id→V without accumulation of intermediates such as enols (VII and VIII).

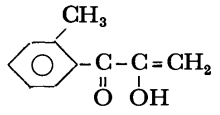

VIII

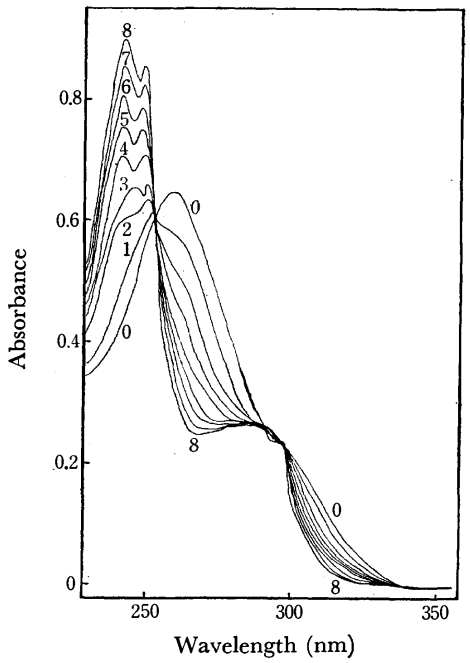

Fig. 1. UV absorption of 1-(*o*-tolyl)-1,2-propanedione in cyclohexane in a 1 cm square cell, degassed and sealed, followed by successive irradiation.
(0) Before irradiation, (1) after 30 s of irradiation, (2) after 60 s, (3) after 90 s, (4) after 135 s, (5) after 160 s, (6) after 200 s, (7) after 250 s, (8) after 300 s.

The quantum yields in various solvents for the disappearance of Id and the formation of V determined independently by glc and UV are given in Table 1.

If there is accumulation of enols (VII and/or VIII) liable to return to the starting diketone as evidenced with 1-phenyl-1,2-alkanedione,[10,11] quantum yields for the disappearance of Id estimated by means of glc at 180 °C (the injection temperature) would be lower than those by UV spectrometry at an ambient temperature. No appreciable difference can be seen between the

Table 1. Quantum yields for disappearance of Id and formation of V in various solvents[a]

Solvent	Quantum yield for disappearance of Id	Quantum yield for formation of V
Ethyl ether	0.46 (0.44)	0.25
Cyclohexane	0.57 (0.57)	0.51
Benzene	0.62 (0.61)	0.54
Acetonitrile	0.53 (0.51)	0.42
Ethanol	0.66 (0.51)	0.43

a) Degassed solutions of *ca.* 10^{-2}M diketone were irradiated to 50—70% conversion by 366 nm light. Ferrioxalate actinometry was used. Estimation by glc technique using propiophenone as an internal standard. Values in brackets are estimated from the measurement of disappearance of α-diketone $n\pi^*$ absorption around 400 nm.

yields from glc and UV (Table 1), suggesting no accumulation of enol although there may be the enol of short life. The stoichiometry of the photocyclization of Id to V was also confirmed by similar quantum yields for the disappearance of Id to those for the formation of V. However, the value of the quantum yield (0.57 in cyclohexane) is small in view of the quantum efficiency of over 0.9 for the population of α-diketones at its lowest triplet. Thus, the efficiency for the intersystem crossing of S→T with benzil is known to be 0.92[12] and other aliphatic α-diketones have values 0.95—0.98.[13] Photoenolization might be expected to play a role for the triplet energy dissipation, since the emissive efficiency is generally *ca.* 0.1.[14]

α-Diketons with α-hydrogen undergo facile photoenolization followed by thermal decomposition, which tends to lower apparent yields. Variation in solvent polarity does not affect the efficiency of disappearance of Id and formation of V (Table 1). The solvent effect was also observed with 1-phenyl-1,2-alkanediones,[10,11] *i.e.*, quantum yields for disappearance of diketones tends to be slightly higher in wet acetonitrile than in benzene.

This is contrast to the Type II photoenolization and photocyclization of aromatic monoketones,[15] which are influenced by solvent polarity, especially by a hydrogen bonding on account of the suppression of reversal hydrogen shift from 1,4-biradical to the original ketone. However, since the hydrogen exchange with solvent is difficult for semidione radical IX, as judged by no incorporation of deuterium into V,[8a] the reformation of Id and formation of product V should be too fast to exchange the proton of the hydroxy group with solvent.

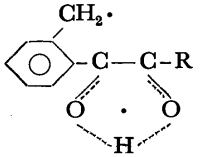

IX

The biradical seems to resist the hydrogen exchange by the intramolecular hydrogen bonding (IX).

Table 2. Absorption and emission spectra of α-diketones[a)]

Ar in Ar-COCOCH$_3$	abs λ_{max}^{EPA} (nm) (A)[b)]	abs λ_{max}^{IP} (nm)	phos λ_{max}^{EPA} (nm) (P)[c)]	phos λ_{max}^{IP} (nm)	$A-P$[d)] (cm^{-1})	ΔE_{ST}[f)] (cm^{-1})	E_T[e)] (kcal/mol)
	396	537	525	537	6300	1800	54.4
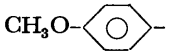	410	405, 410	520	527	5200	2100	55.0
	386	—	508	511	6200	300	56.3
	382	400	508	540	5800	900	56.3

a) Absorption spectra were measured at room temperature and emission spectra at 77 K in EPA (ether-isopentane-alcohol, 5: 5: 2, in vol.) and IP (isopentane). b) A: absorption maximum in EPA (cm^{-1}). c) P: phosphorescence maximum in EPA (cm^{-1}). d) The energy difference between the absorption and phosphorescence maxima. e) Value obtained from phosphorescence maxima. f) The energy difference between the fluorescence and phosphorescence maxima in EPA.

The formation of V can reasonably be explained by the following Scheme.[9)]

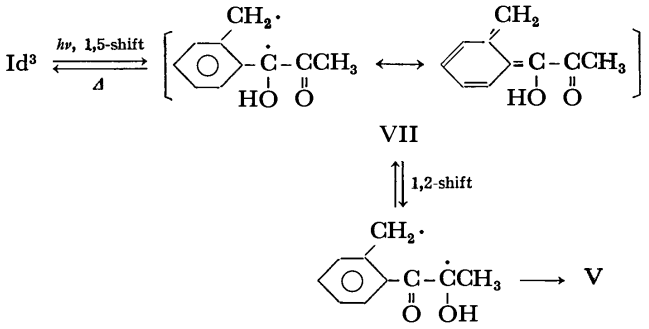

Scheme 1.

However, an alternative direct 1,6-hydrogen shift can not completely be excluded.

Configuration of the Lowest Triplet State of α-Diketones. The configurational analysis of α-diketones in their excited states was performed in a similar way to that in our previous procedures.[4)] The results are compiled in Table 2.

Phosphorescence spectra of α-diketones generally show a broad peak; hence we make use of their emission maxima at the lowest triplet energies instead of their 0-0 bands. Their energy diagrams are illustrated in Fig. 2.

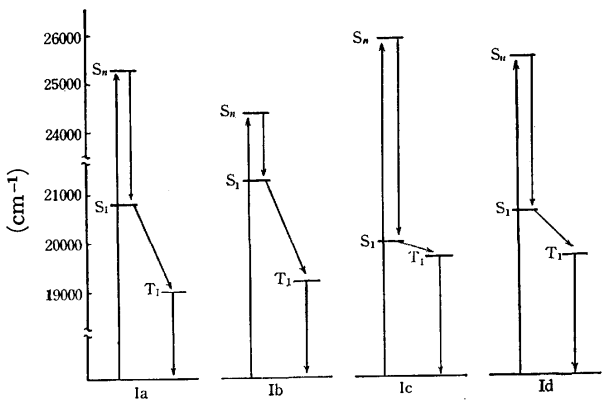

Fig. 2. Energy diagrams of α-diketones.

The $n\pi^*$ absorption maximum shifts hypsochromically (below 400 nm) as the dihedral angle between the planes of two carbonyl groups of α-diketone increases from 0 to 90°, and bathochromically (over 400 nm) as the angle increases from 90 to 180°.[16)]

Two carbonyls of 1-phenyl-1,2-propnedione (Ia) with its $n\pi^*$ at 396 nm is orthogonally twisted.[17)] The situation is the same with those for Ic and Id, since they have their $n\pi^*$ absorptions at 386 and 382 nm, respectively. An aromatic ring and a carbonyl attached to it tend to be coplanar because of the resonance between the groups. The large energy difference between the absorption and phosphorescence maxima (A–P) in EPA is ascribed to the recovery of coplanarity at the excited triplet.[17)] Judging from Table 2 and Fig. 2, the large value of (A–P) of Ic (6200 cm^{-1}) and Id (5800 cm^{-1}) similar to that of Ia (6300 cm^{-1}) seems to be due to the recovery of coplanarity of carbonyls. The coplanarity of carbonyls favors the hydrogen abstraction *via* a six-membered transition state in view of the proximity of *o*-methyl to benzoyl oxygen. α-(*o*-Tolyl)acetone, a monoketone analogue of Id, was found to yield the corresponding pinacol but not indenes.[9)] The reduction to pinacol in spite of the proximity of *ortho*-methyl to the acetyl oxygen is explained by the small ability of intramolecular hydrogen abstraction of acetyl oxygen *via* 1,6-shift.

The observed difference of photochemical behavior between Ib (*p*-OCH_3) and Ic (*o*-OCH_3) remains obscure. The trend where the *p*-methoxy substrate is easily photodecomposed was observed in the photolysis of *p*-methoxybenzil and *p*-methoxyacetophenone, *i.e.*, *p*-methoxybenzil is photodecomposed as easily as unsubstituted benzil, but the yield of the reduction is much lower,[4)] whereas, the *ortho*-substituted α-diketone, *o*-benzyloxyphenylglyoxalate, is photoreducible intramolecularly.[18a,b,c)] This difference in behavior of *p*- and *o*-methoxy-substrates can be explained by the difference in their lowest triplets, *i.e.*, $\pi\pi^*$ in the former and $n\pi^*$ in the latter. The lowest triplet levels for all these α-diketones (Ia—Id) have $n\pi^*$ character, since the phosphorescence maxima shift bathochromically with the change of solvent from EPA to isopentane (IP). Thus, the different behavior of Ic among Ia—Id should

be explained by the mixing of $n\pi^*$ triplet level with $\pi\pi^*$ or CT.

The energy difference between the lowest singlet and the triplet (ΔE_{ST}), a measure of the behavior in the intersystem crossing for singlet to triplet,[18d] seems to reflect their photochemical behavior since this type of carbonyl reduction occurs by way of triplet; *i.e.*, Ia (H) and Ib (p-OCH_3), which are more easily photodecomposed to acid and aldehyde, exhibit higher values of ΔE_{ST} ($>1800\ cm^{-1}$), while Ic (o-OCH_3) and Id (o-CH_3), which are mainly photoreduced, show a lower ΔE_{ST} ($<900\ cm^{-1}$). However, all these ΔE_{ST} are estimated to be within several kcal/mol which is negligible for a discussion of the intersystem crossing.

Experimental

All NMR spectra were taken in CCl_4 solution with TMS as an internal standard on a JEOL, C 60 HL. Mass spectra were recorded on a Hitachi RMS-4 at 70 eV ionizing voltage.

Materials. 1-Phenyl-1,2-propanedione (Ia) was prepared by oxidation of α-phenylacetone with selenium oxide.[19] 1-(p-Anisyl)-1,2-propanedione (Ib) was prepared by the reaction of *trans*-anetole with a mixture of mercuric oxide and mercuric acetate in aqueous acetic acid.[20] 1-(o-Anisyl)-1,2-propanedione (Ic): o-Methoxyisonitrosopropiophenone was prepared by reacting o-methoxypropiophenone with n-butyl nitrite passing through dry HCl, mp 133—134 °C (lit,[21] 132 °C). The oxime was converted by heating with aqueous H_2SO_4 to give a yellow liquid. It has IR band at 2830 (OCH_3), 1710 (aliph. C=O), 1660 (arom, C=O), and 760 cm^{-1} (*ortho* substituent); NMR: τ 2.2—3.2 (m, 4H, phenyl), 6.28 (s, 3H, OCH_3), and 7.69 (s, 3H, $COCH_3$). 1-(o-Tolyl)-1,2-propanedione (Id) was obtained by nitrosation of o-methylpropiophenone similarly to Ic, mp 106—108 °C, followed by conversion into the diketone by heating with H_2SO_4, bp 128—137 °C/20 mmHg.

Quantum Yields. A cyclohexane solution of *ca.* 10^{-4} and 10^{-2} M α-diketone in 1 cm square cells were degassed by three freeze-pump-thaw-cycles. Irradiation was carried out with a 300 W high-pressure mercury vapor lamp using a Corning color filter (7—51) to isolate 366 nm light. Ferrioxalate actinometry was used. Total light intensity on the 9×25 mm unmasked area of a reaction cell was estimated to be 2.1×10^{15} quanta/s.

Products from 1-Phenyl-1,2-propanedione (Ia). A 2-propanol solution (100 ml) of the diketone (700 mg) was irradiated for 6 hr until its original yellow color had disappeared, and the two products were collected by a column packed with silica gel. The first eluted product, mp 131.5—132 °C (lit,[22] mp 118.5 °C) (10% yield) was 1,2-diacetyl-1,2-diphenylethanediol (IIa). It has the following spectral properties: IR peak at 3450 (OH) and at 1700 cm^{-1} (aliph. C=O); NMR: τ 2.90 (m, 10H, phenyl), 4.52 (s, 2H, OH), 7.77 (s, 6H, $COCH_3$); Mass *m/e* 149 ($M^+/2$); UV: λ_{max}^{MeOH} 258—270 nm (an isolated phenyl ring). The second eluted product was identified to be benzoic acid (130 mg, 23%) from its IR data and mp.

Products from 1-(p-Anisyl)-1,2-propanedione (Ib). A 2-propanol solution (100 ml) of the diketone (1.01 g) was irradiated with over 300 nm light passing through a Pyrex filter; 64% of the starting diketone was recovered in spite of the long irradiation (24 hr). The glc analysis of the irradiated solution shows the presence of more than five products, in which p-anisaldehyde was a major product and confirmed by tlc, IR and UV. A small amount of p-anisic acid (5.4%) was detected.

Products from 1-(o-Anisyl)-1,2-propanedione (Ic). A dilute ethereal solution (120 ml) of the diketone (912 mg) was irradiated through a Pyrex filter to 90% conversion for 7 hr. Separation by column chromatography afforded three components. A major product was a pinacol (IIc, 550 mg); NMR: τ 3.0 (m, 8H, phenyl), 4.67 (s, 2H, OH), 6.34 (s, 6H, OCH_3), and 7.90 (s, 6H, $COCH_3$). The second product was a monoalcohol (IIIc, 100 mg); NMR: τ 3.0 (m, 7H, phenyl), 5.84 (s, 1H, OH), 6.25 (s, 3H, OCH_3), 6.74 (q, 2H, OCH_2CH_3), 8.00 (s, 3H, $COCH_3$), 8.78 (d, 3H, $OCH-CH_3$) and 9.05 (t, 3H, OCH_2CH_3). The NMR spectrum, however, did not clearly show the signal of ethoxy methine proton expected to appear at τ *ca.* 6.0 hidden by the signal of methoxy methyl and ethoxy methylene protons. The third product in a small amount was o-anisaldehyde on the basis of NMR: τ 2—3 (m, 4H, phenyl), 7.40 (s, 3H, methyl), and 0.03 (s, H, aldehyde).

Products from 1-(o-Tolyl)-1,2-propanedione (Id). A 2-propanol solution (120 ml) of the diketone (862 mg) was irradiated for 3 hr to complete the conversion and the three products were collected by a column packed with silica gel. The first eluate was the starting diketone (1.6%). The second eluate (12.6%) (mp 97—99 °C) was identified to be o-toluic acid, since it has the same spectra (IR and UV) as those of the authentic sample. The third eluate (mp 53.0—54.5 °C) was 2-hydroxy-2-methylindanone (V, 75%).[8a]

All preparative scale irradiation was conducted using UV light (>300 nm) from a high pressure mercury lamp (Halos HIP 300 W) in a Pyrex tube (ϕ 35×150 mm) under N_2 for 30 min prior to and during the irradiation.

Emission Studies. Emission studies were performed on a Hitachi MPF-2A Fluorescence Spectrophotometer with phosphorescence attachments. Fluorescence spectra were recorded at an ambient temperature using EPA (ether–isopentane–ethanol, 5:5:2 in volume) as a solvent and phosphorescence spectra were recorded at 77 K using the same solvent.

References

1) Contribution No. 202.
2) a) B. M. Monroe and S. A. Weiner, *J. Amer. Chem. Soc.*, **91**, 450 (1969); b) B. M. Monroe, S. A. Weiner, and G. S. Hammond, *ibid.*, **90**, 1913 (1968).
3) C. F. Koelsch and C. D. LeClaire, *J. Org. Chem.*, **6**, 516 (1941).
4) Y. Ogata, K. Takagi, and Y. Fujii, *ibid.*, **37**, 4026 (1972).
5) R. J. Prichett, *Mol. Phys.*, **12**, 481 (1967); *Chem. Abstr.*, **67**, 90276e (1967).
6) S. A. Weiner, E. J. Hamilton, Jr., and B. M. Monroe, *J. Amer. Chem. Soc.*, **91**, 6350 (1969).
7) a) P. J. Wagner, P. A. Kelso, and R. G. Zepp, *ibid.*, **94**, 7480 (1972); b) P. J. Wagner, *Accounts Chem. Res.*, **4**, 168 (1971).
8) a) R. Bishop and N. K. Hamer, *Chem. Commun.*, **1969**, 804; b) R. Bishop and N. K. Hamer, *J. Chem. Soc. C*, **1970**, 1193; c) N. K. Hamer and C. J. Samuel, *J. Chem. Soc. Perkin II*, **1973**, 1316.
9) Y. Ogata and K. Takagi, *J. Org. Chem.*, **39**, 1385 (1974).
10) R. G. Zepp and P. J. Wagner, *J. Amer. Chem. Soc.*, **92**, 7466 (1970).
11) N. J. Turro and T.-J. Lee, *ibid.*, **92**, 7467 (1970).
12) A. A. Lamola and G. S. Hammond, *J. Chem. Phys.*, **43**, 2129 (1965).

13) H. H. Richtol and F. H. Klappmeier, *ibid.*, **44**, 1519 (1966).
14) a) G. M. Almy and P. R. Gillette, *ibid.*, **11**, 188 (1943); b) H. H. Richtol and A. Belorit, *ibid.*, **45**, 35 (1966).
15) P. J. Wagner, *J. Amer. Chem. Soc.*, **89**, 5898 (1967).
16) K. Alder, H. K. Schaffer, H. Esser, H. Krieger, and R. Reubke, *Ann. Chem.*, **593**, 23 (1955).
17) T. R. Evans and P. A. Leermakers, *J. Amer. Chem. Soc.*, **89**, 4380 (1967).
18) a) S. P. Pappas, J. E. Alexander, and R. D. Zehr, Jr., *ibid.*, **92**, 6927 (1970); b) S. P. Pappas, B. C. Pappas, and J. E. Blackwell, Jr., *J. Org. Chem.*, **32**, 3066 (1967); c) S. P. Pappas and R. D. Zehr, Jr., *J. Amer. Chem. Soc.*, **93**, 7112 (1971); d) N. J. Turro, "*Molecular Photochemistry*," W. A. Benjamin, Inc., New York, N. Y. (1965), p. 25.
19) W. W. Hartman and L. J. Roll, "Organic Syntheses," Coll. Vol. III, p. 20 (1955).
20) R. Fusco and G. Caggianelli, *Farm. Sci. Etec.*, **3**, 125 (1948); *Chem. Abstr.*, **43**, 1741 (1949).
21) W. H. Hartung, J. C. Munch, E. Miller, and F. Crossby, *J. Amer. Chem. Soc.*, **53**, 4149 (1931).
22) T. Arai, *Denki Kagaku*, **30**, 175 (1962); *Chem. Abstr.*, **62**, 15760g (1965).

Nitration of Decamethylbiphenyl and 2,3,4,5,6-Pentamethyl-2′,3′,4′,5′,6′-pentachlorobiphenyl with Fuming Nitric Acid. Exclusive *Ortho* Orientation for the Side-chain Attack[1)]

Hitomi Suzuki, Osamu Yagiu, and Terukiyo Hanafusa

Department of Chemistry, Faculty of Science, Hiroshima University, Higashi-sendamachi, Hiroshima 730

(Received February 6, 1974)

Products obtained by the reaction of the title compounds with fuming nitric acid in dichloromethane were investigated. Decamethylbiphenyl gave 6,6′-bis(nitrooxymethyl)-2,2′,3,3′,4,4′,5,5′-octamethylbiphenyl or 2,6,6′-tris(nitrooxymethyl)-2′,3,3′,4,4′,5,5′-heptamethylbiphenyl as the major product, depending on the amount of nitrating agent. 2,3,4,5,6-Pentamethyl-2′,3′,4′,5′,6′-pentachlorobiphenyl similarly gave 6-nitrooxymethyl-2,3,4,5-tetramethyl-2′,3′,4′,5′,6′-pentachlorobiphenyl or 2,6-bis(nitrooxymethyl)-3,4,5-trimethyl-2′,3′,4′,5′,6′-pentachlorobiphenyl. Some plausible reaction sequences for the exclusive *ortho* attack on the alkyl side-chains of biphenyl systems have been suggested.

On treatment with fuming nitric acid at low temperature, polymethylbenzenes and their derivatives undergo side-chain nitrooxylation to give benzyl nitrates in good yields. The reaction is characterized by a peculiar orientation of the products and high positional selectivity. Substitution will preferentially occur into the side-chain *ortho* to the electron-withdrawing groups and *meta* to the electron-releasing groups.[2)] For a facile nitrooxylation there should be a pair of methyl groups situated *para* one another. In order to clarify the mechanism of the reaction, studies were extended to the unusual nitration of the biphenyl systems. So far no report has appeared on the nitration of fully alkylated biphenyl systems.

Decamethylbiphenyl (IV) was treated with five molar proportions of fuming nitric acid (d=1.5) in dichloromethane below 0 °C to give a light brown paste, which upon recrystallization from ligroin yielded a crystalline solid melting at 142—144 °C as the only product (*ca.* 70% yield). The compound has a molecular formula of $C_{22}H_{28}N_2O_6$ and shows strong infrared absorptions due to $-ONO_2$ at 1632, 1275, and 854 cm^{-1}; ^1H NMR peaks at δ 1.82, 2.28, 2.30, and 5.08 with relative areas 3:3:6:2. The peak at higher field (δ 1.82) corresponds to two *ortho* methyl groups. Signals of the methylene protons appear at a considerably high field (δ 5.08) as compared to those of ordinary benzyl nitrates (δ 5.5—5.8).[3)] This can be interpreted by the structure 6,6′-bis(nitrooxymethyl)-2,2′,3,3′,4,4′,5,5′-octamethylbiphenyl (V) and suggests a configuration in which one phenyl ring lies in a plane nearly perpendicular to that of another ring, each *ortho* methyl and nitrooxymethyl group lying above the adjacent ring and subjected to a diamagnetic shielding effect. Its identity was confirmed by comparison with an authentic specimen prepared from prehnitene by the sequence shown in Scheme 1. The alternative synthesis was initiated by the Ullmann condensation of iodoprehnitene (I). The resulting 2,2′,3,3′,4,4′,5,5′-octamethylbiphenyl (II) was bis-chloromethylated with chloromethyl methyl ether in the presence of anhydrous zinc chloride. The chloride (III) so obtained was converted into V by treatment with silver nitrate in acetonitrile. The possibility of the concurrent formation of other isomeric nitrates in a significant amount was rule out by comparison of ^1H NMR spectra of the crude product with those of authentic 5,5′-bis(nitrooxymethyl)-2,2′,3,3′,4,4′,6,6′-octamethylbiphenyl (XV) and 4,4′-bis(nitrooxymethyl)-2,2′,3,3′,5,5′,6,6′-octamethylbiphenyl (XVI), obtained from iodoisodurene and iododurene, respectively, by a similar sequence to that in Scheme 1. No peak could be observed in the region δ 5.6—5.7, ascribed to the absorptions of *meta* and *para* nitrooxymethyl groups.

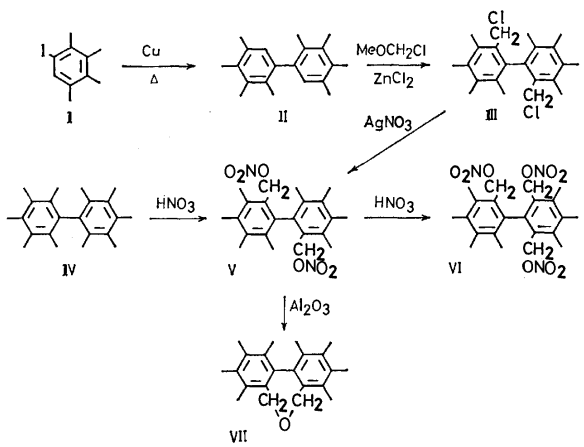

Scheme 1.

When the product mixture was placed on the top of an alumina column and eluted with light petroleum and diethyl ether, successively, large prisms with the composition $C_{22}H_{28}O$ (*m/e* 308) were obtained from the ether eluates in 42% yield. The compound exhibited ^1H NMR peaks at δ 2.04 (2 Me), 2.32 (4 Me), 2.40 (2 Me), 3.72 (2 CH, d; J_{gem}=12 Hz), and 4.82 (2 CH, d; J_{gem}=12 Hz); infrared band at 1036 cm^{-1} (C–O–C). These spectral data are consistent with the formulation of the product as 6,6′-(2-oxapropano)-2,2′,3,3′,4,4′,5,5′-octamethylbiphenyl (VII), which was obtained from V by the alumina-catalyzed ring closure during elution. A pair of *geminal* benzylic protons appear as a doublet

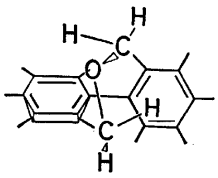

Fig. 1.

at a higher field (δ 3.72). This is ascribed to a greater diamagnetic shielding of the protons due to the induced ring current, suggesting the configuration shown in Fig. 1. Methylene signals of bisbenzyl ethers usually appear in the δ 4.6—4.9 region.[4]

With the use of a large excess of fuming nitric acid, the major isolable product was found to be 2,6,6′-tris(nitrooxymethyl)-2′,3,3′,4,4′,5,5′-heptamethylbiphenyl (VI), the structure of which was established by elemental analysis as well as by comparison of the spectra of related compounds. Isolation of VI as pure crystalline solid was difficult. Most of the product (80%) remained as non-crystallizable syrupy substance. This result is in contrast to the nitration of hexamethylbenzene under similar conditions to give predominantly 5,6-bis(nitrooxymethyl)-1,2,3,4-tetramethylbenzene.[5]

2,3,4,5,6-Pentamethyl-2′,3′,4′,5′,6′-pentachlorobiphenyl (X) was comparatively stable towards the action of cold fuming nitric acid in dichloromethane, but readily underwent side-chain nitrooxylation at room temperature to give a nitrate in 84% yield. The nitrate was identified as 6-nitrooxymethyl-2,3,4,5-tetramethyl-2′,3′,4′,5′,6′-pentachlorobiphenyl (XI) by direct comparison with the authentic sample prepared from 2,3,4,5-tetramethyl-2′,3′,4′,5′,6′-pentachlorobiphenyl (VIII) by chloromethylation to IX followed by treatment with silver nitrate in hot acetonitrile (Scheme 2).

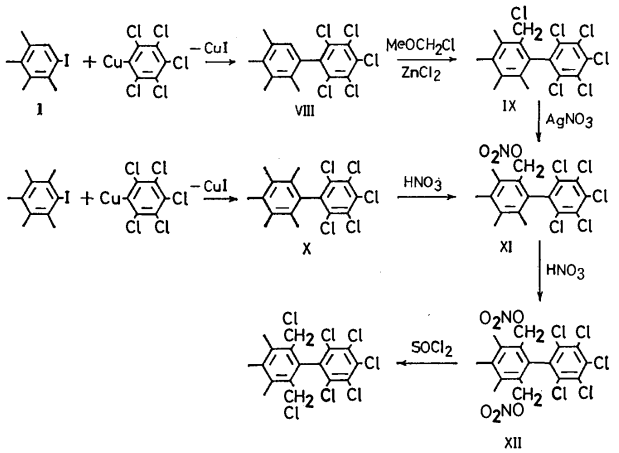

Scheme 2.

When either X or XI was treated with a large excess of fuming nitric acid in an ice bath and the mixture was left to stand for several hours, the temperature of the system being allowed to gradually rise to room temperature, the only product was 2,6-bis(nitrooxymethyl)-3,4,5-trimethyl-2′,3′,4′,5′,6′-pentachlorobiphenyl (XII), which was obtained almost quantitatively and resisted further reaction even on prolonged contact with the nitrating agent. Proof of the symmetrical structure of XII was obtained from the ^{1}H NMR spectrum which contained the expected sharp bands at δ 2.37, 2.43, and 5.17 in a 3:6:4 ratio of intensities. Thus, irrespective of the electronic nature of substituent groups on the opposite ring, the side-chain substitutions in the polymethylated biphenyl systems are found to occur exclusively on the methyl groups adjacent to the phenyl-phenyl bond. The nitrooxymethyl group is a versatile unit, and the present reaction provides an attractive entry into some polysubstituted biphenyls with functionalized substituents at *ortho* positions.

The exclusive *ortho* orientation for the side-chain attack might be rationalized as follows: electrophilic attack of nitronium ion on biphenyl (XVII) can theoretically lead to a mixture of four benzenium ions (XVIII to XXI) (Scheme 3). Although the attack

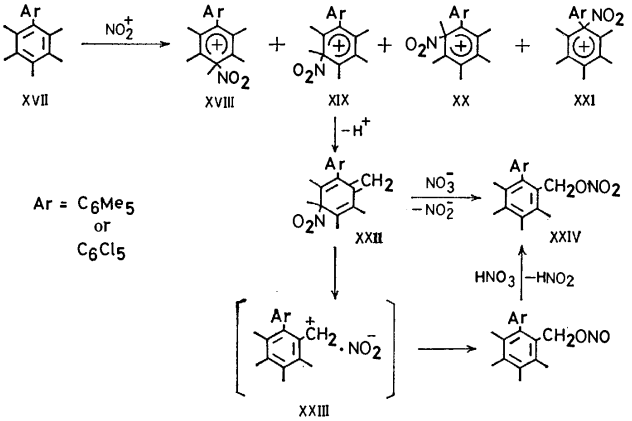

Scheme 3.

of nitronium ion at C_4 will be most favored with unsubstituted biphenyl due to the electromeric diffusion of positive charge into the adjacent ring, the ion XVIII can not enjoy such stabilizing effect, because it exists in a non-planar configuration to minimize the steric interaction of four *ortho* substituents. Contribution of ions XX and XXI is supposed to be much less important, since the access of the nitronium ion to the ring positions C_1 and C_2 to form these ions would undergo considerable steric hindrance. Thus, ion XIX in which the charge is most effectively dissipated by three methyl groups seems to be the most favored intermediate ion, from which the proton release would occur preferentially on the methyl group bonded to the more positively polarized ring carbon at the 6-position, giving a methylene cyclohexadiene (XXII). Heterolytic scission of the carbon-nitrogen bond in XXII will form a benzyl cation-nitrite ion pair (XXIII); recombination at benzylic carbon atom *via* carbon-oxygen bond followed by oxidation will afford the nitrate (XXIV). A possible alternative mechanism for the conversion of XXII into XXIV involves the attachment of the nitrate ion to the terminal methylene carbon of XXII, redistribution of electrons to regain the aromatic system, and concurrent departure of the nitro group as an anion, leading to the formation of XXIV.[6] It is not clear which course is actually followed.

Experimental

All melting points were determined with a hot-stage apparatus and are uncorrected. Infrared spectra were obtained as Nujol on a Jasco 402G spectrophotometer. ^{1}H NMR measurements were carried out in deuteriochloroform solutions on a Varian T-60 spectrometer at probe temperatures against internal tetramethylsilane.

Decamethylbiphenyl (IV)[7] was prepared by the Ullmann reaction of iodopentamethylbenzene and purified by chro-

matography on alumina with light petroleum as an eluant. Mp 259—262 °C.

2,3,4,5,6-Pentamethyl-2',3',4',5',6'-pentachlorobiphenyl (X). A Grignard reagent was prepared from magnesium (1.3 g) and hexachlorobenzene (14 g) in tetrahydrofuran (40 ml). Cuprous iodide (9.6 g) was added to this solution, and the mixture was stirred for some hours at room temperature. Iodopentamethylbenzene (13.7 g) was then added and the reaction mixture was heated under reflux for 8 hr and poured into water. The insoluble solid was filtered off and extracted with benzene with a Soxlhet extractor. The extract was concentrated and passed over alumina to give pentachlorobenzene from light petroleum eluates and X (5.1 g; 25.7%) from benzene eluates. Mp 276—278 °C.

Found: C, 51.02; H, 3.70%. Calcd for $C_{17}H_{15}Cl_5$: C, 51.49; H, 3.81%.

2,3,4,5-Tetramethyl-2',3',4',5',6'-pentachlorobiphenyl (VIII) was prepared in a similar manner from iodoprehnitene (I). Mp 281—283 °C.

Authentic specimens of nitrooxymethyl compounds XIII, XIV, and IX were prepared by essentially the same procedure involving chloromethylation of the respective biphenyls with chloromethyl methyl ether, followed by treatment of the chlorides with silver nitrate in acetonitrile. Physical properties of a series of polysubstituted biphenyls prepared in the context of the present work are summarized in Table 1.

6,6'-Bis(chloromethyl)-2,2',3,3',4,4',5,5'-octamethylbiphenyl (III). A mixture of 2,2',3,3',4,4',5,5'-octamethylbiphenyl (II; 0.30 g),[8] chloromethyl methyl ether (3 g), and anhydrous zinc chloride (0.04 g) was heated with stirring at 40—50 °C for 1 hr, and then poured into water to give III (0.28 g; 68%), which was crystallized from ligroin in the form of fine needles, mp 205—206 °C.

Found: C, 72.46; H, 7.65%. Calcd for $C_{22}H_{28}Cl_2$: C, 72.72; H, 7.77%.

By a similar treatment, 2,2',3,3',4,4',6,6'-octamethylbiphenyl[9] was converted into *5,5'-bis(chloromethyl)-2,2',3,3',4,4',6,6'-octamethylbiphenyl (XIII)*, mp 211—213 °C; 2,2',3,3',5,5',6,6'-octamethylbiphenyl[10] and 2,3,4,5-tetramethyl-2',3',4',5',6'-pentachlorobiphenyl (VIII) were converted into *4,4'-bis(chloromethyl)-2,2',3,3',5,5',6,6'-octamethylbiphenyl (XIV)*, mp 246—247 °C, and *6-chloromethyl-2,3,4,5-tetramethyl-2',3',4',5',6'-pentachlorobiphenyl (IX)*, mp 265—268 °C, respectively. VIII required an extended reaction period to obtain satisfactory conversion into IX.

XIII: Found: C, 72.84; H, 7.62%. Calcd for $C_{22}H_{28}Cl_2$: C, 72.72; H, 7.77%.

XIV: Found: C, 72.68; H, 7.82%. Calcd for $C_{22}H_{28}Cl_2$: C, 72.72; H, 7.77%.

IX: Found: C, 47.21; H, 3.19%. Calcd for $C_{17}H_{14}Cl_6$: C, 47.37; H, 3.27%.

6,6'-Bis(nitrooxymethyl)-2,2',3,3',4,4',5,5'-octamethylbiphenyl (V). A warm solution of silver nitrate (0.75 g) in acetonitrile (20 ml) was added all at once with stirring to a hot solution of III (0.31 g) in the same solvent (30 ml). The mixture was stirred with heating for several hours, silver chloride being separated by filtration. Evaporation of the solvent *in vacuo*, followed by crystallization of the residue

Table 1. Physical properties of some polysubstituted biphenyls

Compound		X	Y	Mp (°C)	^{1}H NMR Spectra (δ)
	II	H	H	138—140	1.97 (2 Me), 2.25 (6 Me), 6.88 (2 aromatic H)
	III	CH_2Cl	Me	205—206	1.86 (2 Me), 2.28 (2 Me), 2.32 (2 Me), 2.41 (2 Me), 4.28 (2 CH_2)
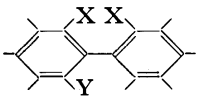	IV	Me	Me	259—262	1.80 (4 Me), 2.26 (4 Me), 2.30 (2 Me)
	V	CH_2ONO_2	Me	144—146	1.82 (2 Me), 2.28 (2 Me), 2.30 (4 Me), 5.08 (2 CH_2)
	VI	CH_2ONO_2	CH_2ONO_2	154—160	1.83 (Me), 2.27 (Me), 2.31 (3 Me), 2.35 (Me), 2.37 (Me), 5.07 (CH_2), 5.13 (2 CH_2)
	VII	CH_2OCH_2	Me	252—253	2.04 (2 Me), 2.32 (4 Me), 2.40 (2 Me), 3.72 (2 CH; J_{gem}=12 Hz), 4.82 (2 CH; J_{gem}=12 Hz),
		H	H	121—122	1.84 (4 Me), 2.21 (2 Me), 2.32 (2 Me), 6.96 (2 aromatic H)
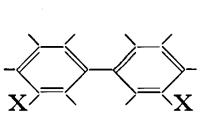	XIII	CH_2Cl	CH_2Cl	211—213	1.80 (2 Me), 1.92 (2 Me), 2.25 (2 Me), 2.43 (2 Me), 4.78 (2 CH_2)
	XV	CH_2ONO_2	CH_2ONO_2	178—179	1.83 (2 Me), 1.88 (2 Me), 2.26 (2 Me), 2.38 (2 Me), 5.67 (2 CH_2)
		H	H	136—138	1.74 (4 Me), 2.26 (4 Me), 6.99 (2 aromatic H)
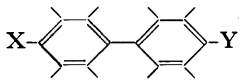	XIV	CH_2Cl	CH_2Cl	246—247	1.76 (4 Me), 2.35 (4 Me), 4.81 (2 CH_2)
	XVI	CH_2ONO_2	CH_2ONO_2	178—179	1.76 (4 Me), 2.33 (4 Me), 5.67 (2 CH_2)
	VIII	H	Me	281—283	2.16 (Me), 2.25 (2 Me), 2.38 (Me), 6.95 (aromatic H)
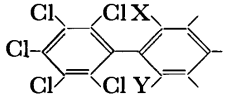	IX	CH_2Cl	Me	265—268	1.89 (Me), 2.27 (Me), 2.31 (Me), 2.40 (Me), 4.25 (CH_2)
	X	Me	Me	276—278	1.84 (2 Me), 2.24 (2 Me), 2.28 (Me)
	XI	CH_2ONO_2	Me	177—178	1.88 (Me), 2.32 (2 Me), 2.35 (Me), 5.16 (CH_2)
	XII	CH_2ONO_2	CH_2ONO_2	230—231 (decomp.)	2.37 (Me), 2.43 (2 Me), 5.17 (2 CH_2)
		CH_2Cl	CH_2Cl	292—294	2.35 (Me), 2.44 (2 Me), 4.24 (2 CH_2)

from hot ligroin gave V as white prisms (0.22 g; 62%), mp 144—146 °C; slightly soluble in cold ligroin and readily soluble in chloroform.

Found: C, 63.24; H, 6.61%. Calcd for $C_{22}H_{28}N_2O_6$: C, 63.45; H, 6.78%.

The above procedure applied to XIII, XIV, and IX gave *5,5'-bis(nitrooxymethyl)-2,2',3,3',4,4',6,6'-octamethylbiphenyl (XV)*, mp 140—141 °C; *4,4'-bis(nitrooxymethyl)-2,2',3,3',5,5',6,6'-octamethylbiphenyl (XVI)*, mp 178—179 °C; and *6-nitrooxymethyl-2,3,4,5-tetramethyl-2',3',4',5',6'-pentachlorobiphenyl (XI)*, mp 177—178 °C, respectively.

XV: Found: C, 63.77; H, 6.90%. Calcd for $C_{22}H_{28}N_2O_6$: C, 63.45; H, 6.78%.

XVI: Found: C, 63.48; H, 6.65%. Calcd for $C_{22}H_{28}N_2O_6$: C, 63.45; H, 6.78%.

XI: Found: C, 44.39; H, 3.12; N, 3.25%. Calcd for $C_{17}H_{14}Cl_5NO_3$: C, 44.62; H, 3.08; N, 3.06%.

Procedure for Nitration of Fully Substituted Biphenyls. A mixture of a biphenyl (IV or X; 0.005 mol) and dichloromethane (10 ml) was vigorously stirred and fuming nitric acid (d=1.5; 1.6 g) in the same solvent (5 ml) was added dropwise at −5 to 0 °C to give a dark brown solution. The mixture was allowed to stand at room temperature for several hours, during the course of which the initial dark color faded to light yellow. It was then poured into water and the organic layer was thoroughly washed with water. Evaporation of the solvent left a light brown paste (in the case of IV) or a white crystalline solid (in the case of X), which was inspected by IR, ^1H NMR, or thin-layer chromatography. Nitrates were obtained by crystallization of the crude product from a mixture of dichloromethane and light petroleum, and identified by their spectra and elemental analyses, or by direct comparison with the authentic specimens.

Chromatography on alumina of the crude nitration product obtained from IV gave unchanged material and nitrooxymethyl compounds from light petroleum eluates, and a cyclic ether VII (42%) from diethyl ether eluates. Recovery of nitrooxymethyl compounds was very unsatisfactory.

VI: Found: C, 56.29; H, 5.78; N, 8.59%. Calcd for $C_{22}H_{27}N_3O_9$: C, 55.34; H, 5.70; N, 8.80%.

IR: 1624, 1274, and 857 cm^{-1} ($-ONO_2$).

VII: Found: C, 85.47; H, 9.09%. Calcd for $C_{22}H_{28}O$: C, 85.66; H, 9.15%.

XI: Found: C, 44.52; H, 3.11; N, 3.08%. Calcd for $C_{17}H_{14}Cl_5NO_3$: C, 44.62; H, 3.08; N, 3.06%.

IR: 1632, 1277, and 855 cm^{-1} ($-ONO_2$).

XII: Found: C, 39.46; H, 2.55; N, 5.28%. Calcd for $C_{17}H_{13}Cl_5N_2O_6$: C, 39.37; H, 2.53; N, 5.40%.

IR: 1632, 1276, and 842 cm^{-1} ($-ONO_2$).

We are grateful to the Ministry of Education of Japan for financial support of this work.

References

1) The Reaction of Polysubstituted Aromatics. Part XXXVI; Part XXXV: H. Suzuki and T. Hanafusa, *Synthesis*, **1974**, 432.

2) H. Suzuki and K. Nakamura, This Bulletin, **44**, 227 (1971).

3) H. Suzuki and K. Nakamura, *ibid.*, **43**, 473 (1970); H. Suzuki, *ibid.*, **43**, 481 (1970).

4) H. Suzuki, K. Nakamura, and M. Takeshima, *ibid.*, **44**, 2248 (1971).

5) H. Suzuki, *ibid.*, **43**, 879 (1970).

6) K. Nakamura, *ibid.*, **44**, 133 (1971).

7) V. A. Koptyug, A. P. Krysin, and M. I. Gorfinkel, *Izv. Sib. Otd. Akad. Nauk SSSR, Ser. Khim. Nauk*, **1967**, 61; *Chem. Abstr.*, **69**, 67002v (1968).

8) P. B. D. de la Mare, E. A. Johnson, and J. S. Lomas, *J. Chem. Soc.*, **1965**, 6893.

9) A. E. Knauf and R. Adams, *J. Amer. Chem. Soc.*, **55**, 4704 (1933).

10) E. Marcus, W. M. Lauer, and R. T. Arnold, *ibid.*, **80**, 3742 (1958).

Aromatic Nucleophilic Substitution. III.[1] Meisenheimer Complexes in the Reactions of 1-(*N*,*N*-Dialkylamino)-2,4-dinitronaphthalenes with Sodium Methoxide

Shizen SEKIGUCHI, Katsuo SHINOZAKI, Tetsuo HIROSE
Kohji MATSUI, and Kiyoshi SEKINE
Department of Synthetic Chemistry, Gunma University, Tenjincho, Kiryu, Gunma 376

(Received February 6, 1974)

The intermediates in the reaction of 1-(*N*,*N*-dimethylamino)-2,4-dinitronaphthalene (**9**) with sodium methoxide have been studied in the mixtures of DMSO and CH_3OH. The NMR spectra of the equimolar mixture of **9** and sodium methoxide indicate that **9** and a 1,1-disubstituted Meisenheimer complex coexist immediately after mixing, and that nearly all **9** changed into the Meisenheimer complex 15 min after mixing. The addition of 2 mol of sodium methoxide to 1 mol of **9** gave no 1,1,3,3-tetrasubstituted 2,4-dinitronaphthalene Meisenheimer complex. 1-Piperidino- or 1-(*N*-methyl-*N*-*n*-butylamino)-2,4-dinitronaphthalene reacted with sodium methoxide to give a similar Meisenheimer complex.

Many Meisenheimer complexes have been prepared by nucleophilic attack on polynitroaromatic compounds, the reactions being extensively studied and the results reviewed in detail.[2]

In the nucleophilic substitution reaction of 1-ethoxy-2,4-dinitronaphthalene (**1**) with primary amines, Orvik and Bunnett[3] confirmed the presence of the Meisenheimer complex (**2**, hereinafter referred to as σ complex) during the course of reaction by means of the kinetics and visible spectra as shown in Eq. (1). We reported on the presence of σ complexes (**4**) in the

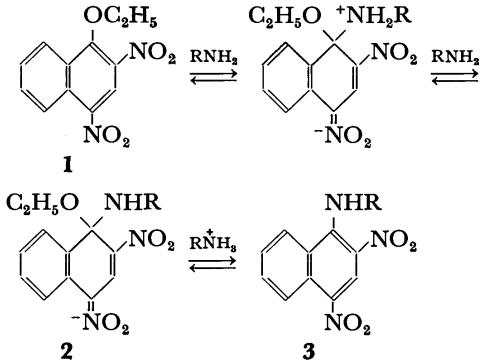

(1)

reactions of **1** or 1-ethoxy-2,4,5-trinitronaphthalene (**5**) with secondary amines by NMR measurement:[1] Only

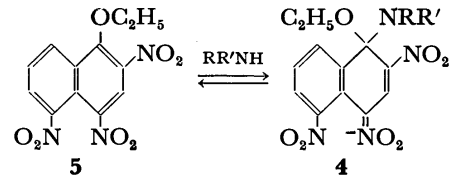

(2)

a few papers have appeared on the reactions of amino-substituted polynitromaromatic compounds with sodium or potassium alkoxides.

Crampton and Gold[4] reported that 1-(*N*,*N*-dimethylamino)-2,4,6-trinitrobenzene (**6**) reacted with CH_3ONa to give a 1,3-disubstituted Meisenheimer complex (**7**) and that addition of excess CH_3ONa produced dianion (**8**).

We have carried out the reactions of 1-(*N*,*N*-dialkylamino)-2,4-dinitronaphthalenes with CH_3ONa in DMSO–CH_3OH mixture and found that 1,1-disubstituted σ complexes were formed but no 1,3-disubstituted σ

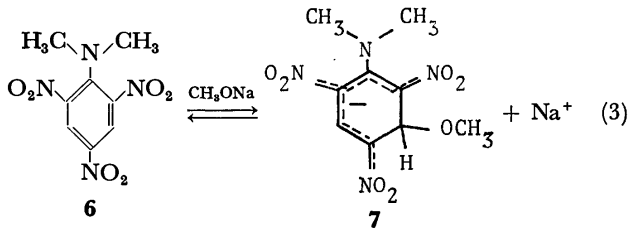

(3)

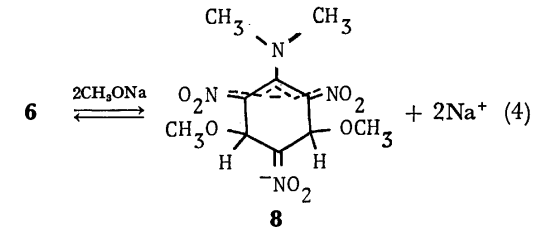

(4)

complex, and that the reactions give an easy method for the preparation of 1,1-disubstituted naphthalene σ complexes containing both an alkoxyl- and a dialkylamino groups at C-1:

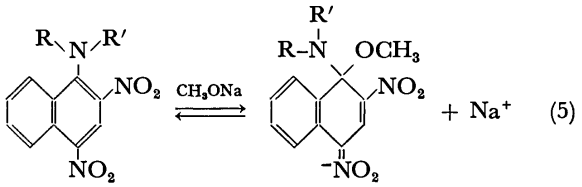

(5)

This paper reports on the presence of σ complexes in the reactions of 1-(*N*,*N*-dialkylamino)-2,4-dinitronaphthalenes with CH_3ONa.

Results and Discussion

*Reaction of 1-(*N,N*-Dimethylamino)-2,4-dinitronaphthalene (9) with Sodium Methoxide.* The addition of methanolic CH_3ONa to a solution of **9** in DMSO (**9** 2.19×10^{-5} mol/l, CH_3ONa 2.05×10^{-1} mol/l) gave a red species (λ_{max} 351, 264, and 518 nm). Not only the shape but also the positions and intensities of these bands are similar to those of 1,1-disubstituted polynitronaphthalene σ complexes.[1,2]

The NMR spectra of the reaction system are shown in Fig. 1. Immediately after methanolic CH_3ONa was added to **9** in DMSO (0.20 ml) (CH_3ONa 1.68×10^{-4}

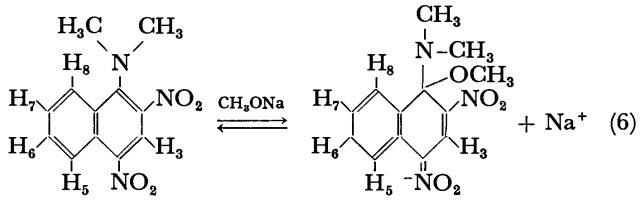

9 **10**

mol, **9** 1.68×10^{-4} mol), to which a small amount of CH_3OH had been added so that the volume ratio (DMSO/CH_3OH) was 1.5, the H_3 band intensity of **9** (δ 8.61, Fig. 1A, 1B) decreased, and, at the same time,

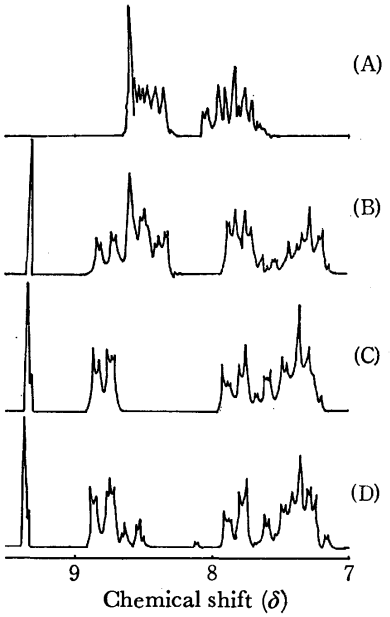

Fig. 1. NMR spectra relevant to the reaction of **9** with CH_3ONa: (A) **9** before addition of CH_3ONa; (B), (C), and (D) immediately, *ca.* 15 min, and 24 hr, respectively, after addition of CH_3ONa.

its band position was shifted to δ 9.32, attributed to H_3 of **10**.[1,4] A new multiplet appeared at δ 7.33, attributed to H_6 and H_7 of **10** (Fig. 1B).[1,4] The calculation of band intensity indicates the presence of the H_3 band of **9**, which overlaps the H_8 band (d, δ 8.79) of **10**. Thus, the spectrum (Fig. 1B) indicates that compounds **9** and **10** coexist in this reaction system. The bands at δ 8.45 (Table 1) disappeared 15 min after mixing (Figs. 1B and 1C). Even 1 hr after mixing, the spectrum of the system was the same as that in Fig. 1C. After 24 hr a part of **10** decomposed to **9** since bands attributed to **9** appeared (Fig. 1D).[5]

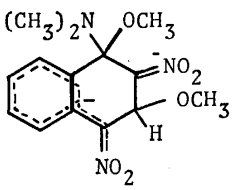

11

When two mol of CH_3ONa had been added to one mol of **9** under similar conditions, the same spectrum as that in Fig. 1C was obtained. In the case of **9**, therefore, no dianion such as **11**, which is similar in structure to **8**, was produced. When the solvent ratio was varied, the chemical shift of each proton band of **10** was substantially the same in both cases (Table 1). The results and the large shift of each proton band position in the conversion of **9** into **10** indicate that the intermediate in the reaction of **9** with CH_3ONa is not a charge transfer complex, but a σ one.[6-8]

Reaction of 1-Piperidino-2,4-dinitronaphthalene (12) with Sodium Methoxide. The addition of methanolic CH_3ONa to a solution of **12** in DMSO (**12** 2.39×10^{-5} mol/l, CH_3ONa 2.39×10^{-2} mol/l) gave a red species (λ_{max} 352, 361, and 517 nm). The spectrum was similar in shape, position and intensity to that of the complex in the reaction of **9** with CH_3ONa.

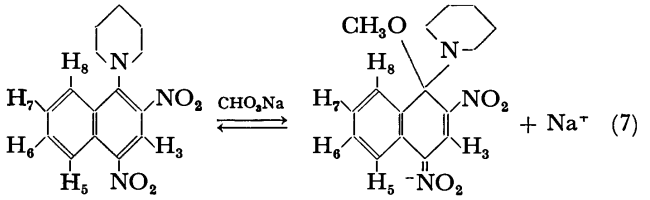

12 **13**

The NMR spectra of the reaction system are shown in Fig. 2[9] [**12** 1.83×10^{-4} mol, CH_3ONa 1.83×10^{-4} mol, DMSO/CH_3OH 0.62 ml (4.2/1)].

The time-dependent change of the spectrum of the reaction system differs from that in the reaction of **9** with CH_3ONa. Immediately after mixing, the H_3 bands of **12** and **13** appeared at δ 8.65 and 9.31, respectively (Figs. 2A and 2B). The H_8, H_5, and $H_{6,7}$ bands of **12** appeared at δ 8.78, 7.71, and 7.29, respectively, besides the bands of the aromatic protons of **12** (Fig. 2B). These results indicate that **12** and **13** coexist immediately after mixing. Twenty-four hours after mixing, nearly all **12** changed into **13** (Fig. 2C). Calculation of band intensity indicates that 43 hr after mixing a part of **13** decomposes to **12**.[5]

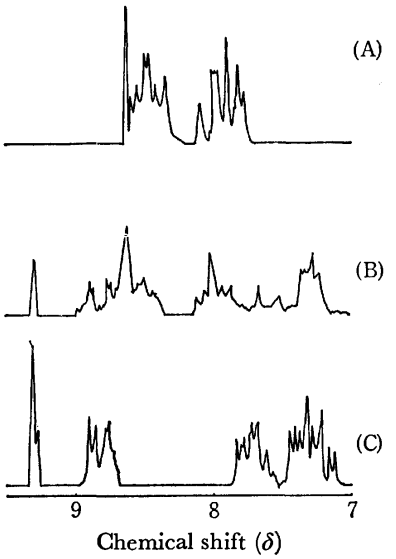

Fig. 2. NMR spectra relevant to the reaction of **12** with CH_3ONa: (A) **12** before addition of CH_3ONa; (B) and (C) immediately and 24 hr, respectively, after addition of CH_3ONa.

TABLE 1. RELEVANT NMR DATA

Compound	H_3	H_8	H_5	$H_{6,7}$	Solvent ratio $\frac{DMSO}{CH_3OH}$ (vol.)
9	8.61 (s)	8.45 (m)		7.85 (m)	DMSO[b]
10	9.32 (d)	8.79 (d)	7.79 (d)	7.33 (m)	1.5
	9.31 (d)	8.80 (d)	7.65 (d)	7.23 (m)	4.4
12	8.60 (s)	8.47 (d)		7.92 (m)	DMSO[b]
13	9.23 (s)	8.78 (d)	7.71 (m)	7.29 (m)	4.3
14	8.65 (s)	8.50 (m)		7.94 (m)	DMSO[b]
15	9.31 (s)	8.83 (m)	7.61 (m)[c]	7.21 (m)	4.5

a) Chemical shifts were described in δ values relative to TMS. b) NMR spectra were measured in DMSO only. c) The doublets were split into multiplets by long range coupling.

Reaction of 1-(N-Methyl-N-n-butylamino)-2,4-dinitronaphthalene (14) with Sodium Methoxide. As in the reaction of **9** or **12** with CH_3ONa, the addition of methanolic CH_3ONa to a solution of **14** in DMSO (**14**, 2.47×10^{-5} mol/l; CH_3ONa, 2.47×10^{-1} mol/l) gave a red species (λ_{max} 349, 364, and 516 nm). The spectrum was also similar to that obtained in the reaction of **9** or **12** with CH_3ONa.

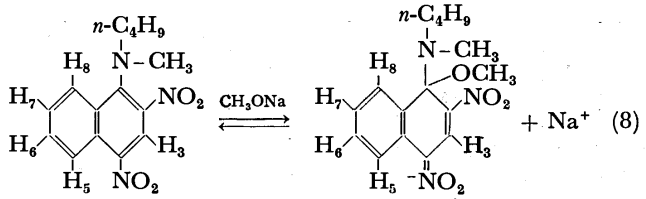

14 **15**

The NMR spectra of the reaction system are shown in Fig. 3[9] [**14** 1.79×10^{-4} mol, CH_3ONa 1.79×10^{-4} mol, DMSO/CH_3OH 0.24 ml (4.5/1)]. Only the bands attributed to the aromatic protons of **15** appeared immediately after mixing (Figs. 3A and 3B). The spectrum did not substantially change 24 hr after mixing, but a part of **15** decomposed to **14** 43 hr after mixing (Fig. 3C).[5]

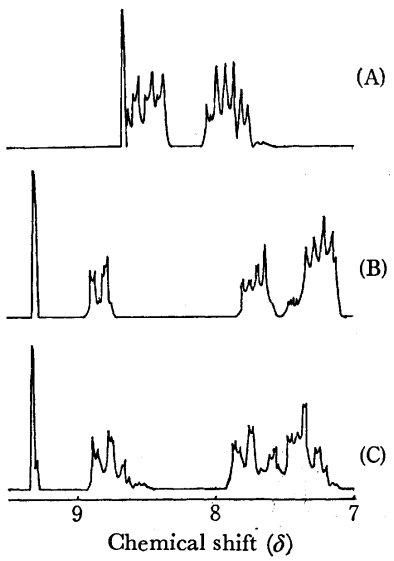

Fig. 3. NMR spectra relevant to the reaction of **14** with CH_3ONa: (A) **14** before addition of CH_3ONa; (B) and (C) immediately and 43 hr, respectively, after addition of CH_3ONa.

It is thus concluded that a 1,1-disubstituted naphthalene σ complex is formed in the reaction of 1-(*N,N*-dialkylamino)-2,4-dinitronaphthalene with CH_3ONa. Bunnett and Zahler[10] stated that the formation of an anion by the dissociation of a complex depends upon the stability of the anion: the ease of anion separation decreases in the order alkoxide ions>amide ions.

The fact that no nucleophilic substitution by methoxide ion took place confirms the interpretation of Bunnett and Zahler. For the sake of confirmation relevant NMR spectral data are included in Table 1.

Experimental

NMR spectra were recorded on a Varian A-60D spectrometer. Visible spectra were measured on a Hitachi-124 UV-VIS spectrophotometer. Compounds **9**, **12**, and **14** were prepared according to the method given previously.[1]

References

1) Part II, S. Sekiguchi, T. Itagaki, T. Hirose, K. Matsui, and K. Sekine, *Tetrahedron*, **29**, 3527 (1973).

2) a) T. J. de Boer and I. P. Dirkx in "The Chemistry of the Nitro and Nitroso Groups," Part I, H. Feuyer, Ed., Interscience, New York, N.Y. (1969), p. 487; b) J. Miller, "Aromatic Nucleophilic Substitution," Elsevier, New York, N.Y. (1968).

3) J. A. Orvik and J. F. Bunnett, *J. Amer. Chem. Soc.*, **92**, 2417 (1970).

4) M. R. Crampton and V. Gold, *J. Chem. Soc., B*, **1966** 893.

5) The decomposition might be caused by a trace of water remaining almost invariably in dried DMSO.

6) W. E. Byren, E. J. Fendler, J. H. Fendler, and C. E. Griffin, *J. Org. Chem.*, **32**, 2506 (1967).

7) a) G. A. Russell and E. G. Janzen, *J. Amer. Chem. Soc.*, **84**, 4153 (1962); b) G. A. Russell, E. G. Janzen, and E. T. Strom, *ibid.*, **86**, 1807 (1964).

8) G. Fraenkel, R. E. Carter, A. McLachlan, and J. H. Richards, *ibid.*, **82**, 5846 (1960).

9) Reaction rates change with concentration, structure of substrate and nucleophile, and solvent. In the present work time intervals in NMR measurements were arbitrary and the reaction rates could not be compared. Stress is made on the confirmation of σ complexes.

10) J. F. Bunnett and R. E. Zahler, *Chem. Rev.*, **49**, 273 (1951).

Base-induced Reactions of 2-Substituted 2-Bromodimedones

Tadahiro WAKUI, Yoshio OTSUJI, and Eiji IMOTO

Department of Applied Chemistry, College of Engineering, University of Osaka Prefecture, Sakai-shi, Osaka 591

(Received February 12, 1974)

The reactions of 2-substituted 2-bromodimedones with various bases were studied. The behavior of the dimedones changed with the base and substituent attached to the dimedones. Treatment of 2-alkyl-2-bromodimedones (**1a** and **1b**) with a weak nucleophilic base such as sodium acetate afforded 2-alkyl-4,4-dimethyl-2-cyclopenten-1-ones (**2a** and **2b**), 2-alkyl-5,5-dimethyl-3-oxo-1-cyclopentene-1-carboxylic acids (**3a** and **3b**), 2-alkyl-5,5-dimethylcyclohexane-1,3-diones (**4a** and **4b**) and carbon monoxide. A similar treatment of 2,2-dibromodimedone (**7**) with the weak nucleophilic base gave 2,3-dibromo-4,4-dimethyl-2-cyclopenten-1-one (**8**), 2-bromo-5,5-dimethylcyclohexane-1,3,4-trione (**9**) and 2-bromodimedone (**10**). However, the reactions of **1a** and **7** with a strong nucleophilic base such as sodium ethoxide gave mainly the open-chain products, ethyl 3,3-dimethyl-5-oxoheptanoate (**5a**) and diethyl 3,3-dimethylglutarate (**11**). On treatment of **1a** with silver acetate, a debrominative dimerization occurred to produce the dimer **6**. The mechanisms of these reactions were discussed.

The preparation of substituted cyclopentenones has drawn considerable attention. One available method is the conversion of cyclohexane-1,3-dione derivatives into cyclopentenones. Spencer and co-workers[1,2] reported that the thermolysis of 2-acetoxy-2-alkylcyclohexane-1,3-diones gives carbon monoxide and 2-alkylcyclopentenones. However, an application of this method is limited because of the difficulty to prepare the acetoxydiones. Büchi and Egger[3] found that 2-chloro-2-(2-pentynyl)-cyclohexane-1,3-dione can be converted into 2-(2-pentynyl)-2-cyclopenten-1-one in an 80% yield upon treatment with sodium carbonate. Since 2-chlorocyclohexane-1,3-dione derivatives are readily accessible, this base-induced ring contraction seems to have a wide applicability, provided that the ring contraction is a general reaction. We recently found that the chemical behavior of 2-bromocyclohexane-1,3-diones varied remarkably with the nature of the base employed and also with the substituent attached to the diones. This paper deals with a systematic study on the reactions of 2-substituted 2-bromodimedones with various bases.

Results and Discussion

Reaction Products. The reactions of 2-substituted 2-bromodimedones with various bases were carried out in tetrahydrofuran (THF) or in ether, and the products were isolated and then characterized. The products isolated are summarized in Table 1.

The reaction of 2-bromo-2-methyldimedone (**1a**) with an equivalent of sodium acetate in THF under reflux afforded 2,5,5-trimethyl-2-cyclopenten-1-one (**2a**), 2,4,4-trimethyl-3-oxo-1-cyclopentene-1-carboxylic acid (**3a**) and 2-methyldimedone (**4a**). A similar reaction of 2-bromo-2-butyldimedone (**1b**) with sodium acetate gave the corresponding products, **2b**, **3b**, and **4b**. Evolution of CO was observed during the course of these reactions.

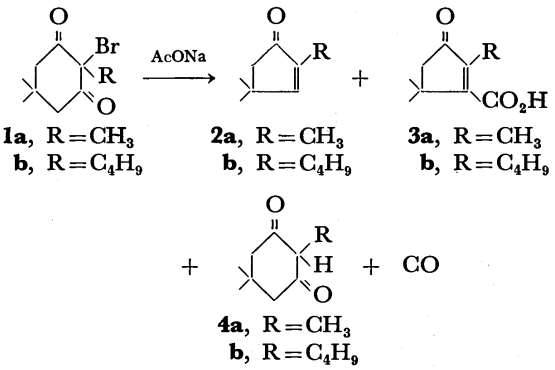

1a, R=CH_3 **2a**, R=CH_3 **3a**, R=CH_3
b, R=C_4H_9 **b**, R=C_4H_9 **b**, R=C_4H_9

4a, R=CH_3
b, R=C_4H_9

However, when **1a** was treated with two equivalents

Table 1. Reactions of 2-substituted 2-bromodimedones with bases in THF

Compd	Base	Reaction time, hr	Products (Yield, %)			
			Cyclopentenone	Cyclopentenone-carboxylic acid		Others
1a	AcONa	4	**2a** (21)	**3a** (37)		**4a** (7.5)
1b	AcONa	4	**2b** (35)	**3b** (15)		**4b** (5.3)
1a	C_2H_5ONa[a]	5	**3a** (5.6)		**5a** (64)	**4a** (9)
1a	*t*-C_4H_9ONa	5	**2a** (12)			**4a** (34)
1a	AcOAg	5	**2a** (17)	**3a** (10)	**6** (53)	**4a** (7.5)
1a	AcOAg	18	**2a** (19)	**3a** (3)	**6** (22)	**4a** (9)
7	AcONa	4	**8** (25)		**9** (16)	**10** (32)
7	Na_2CO_3	4	**8** (16)		**9** (10)	**10** (25)
7	$C_2H_5CO_2Na$	4	**8** (15)		**9** (13)	**10** (28)
7	C_2H_5ONa	5			**11** (38)	**10** (35)
7	AcOAg	5	**12** (24)			**10** (41)

a) The reactions were carried out in ether instead of THF.

of sodium ethoxide, ethyl 3,3-dimethyl-5-oxoheptanoate (**5a**) was obtained as a major product along with small amounts of **2a** and **4a**.

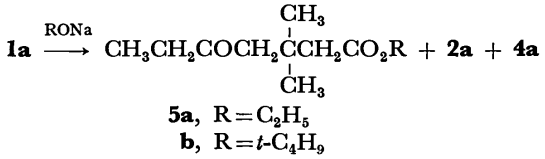

5a, R=C_2H_5
b, R=t-C_4H_9

Treatment of **1a** with an equivalent of sodium t-butoxide gave **2a** and **4a**, but t-butyl ester (**5b**) could not be isolated. The reaction of **1a** with an equivalent of silver acetate in THF yielded a small amount of a dimeric product (**6**) along with **2a**, **3a** and **4a**.

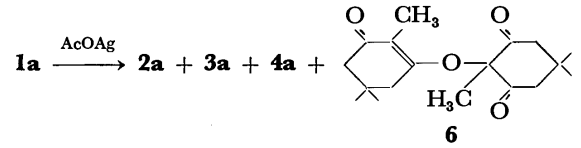

6

The reaction of 2,2-dibromodimedone (**7**) with various bases was then examined. Treatment of **7** with an equivalent of weak bases, such as sodium acetate, sodium propionate and sodium carbonate, in THF afforded 2-bromodimedone (**10**), 2,3-dibromo-4,4-dimethyl-2-cyclopenten-1-one (**8**) and 2-bromo-5,5-dimethylcyclohexane-1,3,4-trione (**9**). The reaction of **7** with two equivalents of sodium ethoxide in ether gave **10** and diethyl 3,3-dimethylglutarate (**11**). The reaction of **7** with an equivalent of silver acetate in THF yielded **10** and 2-bromo-4,4-dimethyl-2-cyclopenten-1-one (**12**).

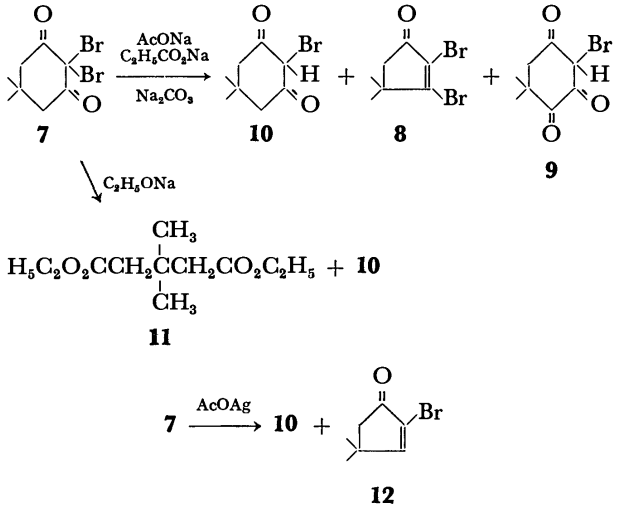

11

12

Determination of the Structures of the Products. The structures of the cyclopentenones **2a**, **2b**, **8**, and **12** were readily established from their IR and NMR spectra which exhibited absorptions and signals characteristic of the assigned structures (see Experimental): the IR and NMR spectral data of **2a** obtained in this investigation were identical with those reported.[1]

The structures of the cyclopetenonecarboxylic acids **3a** and **3b** were established by their IR, NMR, and UV spectra. The IR spectrum (KBr) of **3a** showed multiple absorptions characteristic of a carboxyl group at 3300—2500 cm^{-1}, carbonyl absorptions at 1710 and 1670 cm^{-1}, and an absorption due to the C=C bond at 1620 cm^{-1}. The NMR spectrum ($CDCl_3$–DMSO-d_6) of **3a** exhibited a singlet signal due to six protons of the two methyl groups at the 5-position at δ 1.34, and a singlet signal due to three protons of the methyl group at the 2-position at δ 1.88, a singlet signal due to two protons of the methylene function at the 4-position at δ 2.32, and a broad singlet signal due to one proton of the carboxyl group at the 1-position at δ 6.15. The UV spectrum of **3a** in 95% ethanol showed an absorption maximum at 243 nm (ε 9800), indicating that **3a** has a cyclopentenone skeleton.[4] These data are consistent with the structure assigned to **3a**. Similar spectral data were obtained for **3b**, confirming the assingned structure: the IR spectrum (KBr) showed absorptions at 3300—2600 (multiplet), 1710, 1680, and 1620 (C=C) cm^{-1}. The NMR spectrum (CCl_4) exhibited a singlet signal at δ 1.36 (six protons of the two methyl groups at the 5-position), multiplet signals at δ 0.8—2.3 (nine protons of the butyl group at the 2-position), a singlet signal at δ 2.32 (two protons of the methylene group at the 4-position) and a broad singlet signal centered at δ 9.1 (one proton of the carboxyl group at the 1-position). The UV spectrum in 95% ethanol showed an absorption maximum at 244 nm (ε 9300).

The IR and NMR spectral data of the dimer **6** obtained in this investigation were identical with those reported.[1] Additional evidence for the assigned structure was obtained from the fact that a mild treatment of **6** with aqueous hydrochloric acid afforded quantitatively 2-methyldimedone (**4a**). As a result of this chemical reaction, a fragment peak appeared at m/e 153 (corresponding to just a half of the molecule) in the mass spectrum. The structure of **9** was confirmed by a color reaction with ferric chloride, which demonstrated the enolizable property of the substance, and by the IR and NMR spectra. The structures of the esters **5a** and **11** were confirmed by comparison of the retention times in vpc with those of authentic samples.

Mechanistic Interpretation. From the results obtained we see that the kind and distribution of the products produced by the reactions of 2-bromodimedones with bases depend largely on the nature of the base as well as the substituent attached at the 2-position of dimedones.

The reactions of 2-alkyl-2-bromodimedones, **1a** and **1b**, with bases are discussed first. The yields of cyclopentenones **2a** and **2b** were high in the reactions with a weak nucleophilic base such as sodium acetate. The production of **2a** and **2b** was accompanied by the formation of cyclopentenonecarboxylic acids **3a** and **3b** and debrominated dimedones **4a** and **4b**. When **1a** was allowed to react with sodium ethoxide which possesses a relatively high nucleophilicity, an attack of ethoxide ion on a carbonyl carbon in the substrate predominated to produce mainly the open-chain product, **5**. The proposed mechanisms which qualitatively accomodate these results are represented in Schemes 1 and 2: since experimental difficulty in the separation of the products prevented a quantitative determination of the product distribution, the proposed

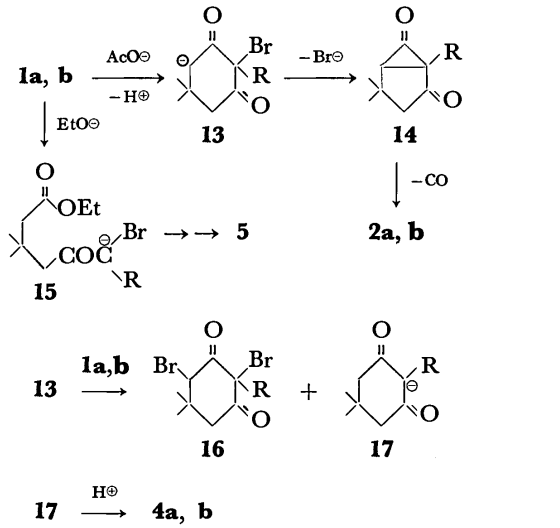

Scheme 1.

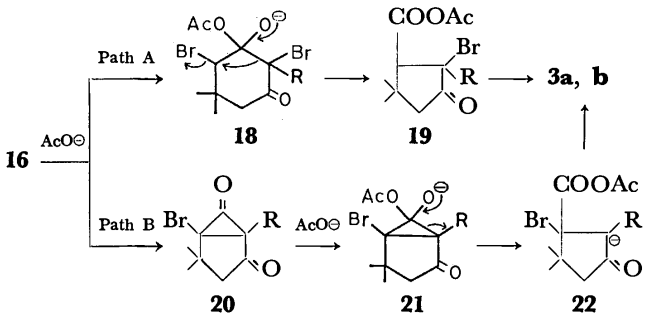

Scheme 2.

mechanisms might be inconsistent with the results given in Table 1.

A base of low nucleophilicity abstracts a proton from an active methylene group of **1a**, **b** to form carbanion **13**, which is then transformed into cyclopropanone intermediate **14** by elimination of bromide ion. The 1,3-elimination of hydrogen bromide of this sort has been postulated in the Favorskii rearrangement of α-bromoketones.[5] Decarbonylation from **14** affords the cyclopentenone **2a**, **b** (Scheme 1). The stabilized carbanion **13** would also react with **1a**, **b** to form the dibromide **16** and the carbanion **17** which on protonation yields **4a**, **b**. The transfer of bromonium ion from **1a**, **b** to **13** is possible, since bromine in **1a**, **b** is activated by the two adjacent carbonyl groups.

Two paths can be considered for the formation of **3a**, **b** (Scheme 2). Path A is a semibenzylic-type rearrangement[6] induced by an attack of base to the carbonyl carbon of **16** to form an intermediate **19** which is readily converted into **3a**, **b** by the dehydrobromination and the hydrolysis. Path B is the base-induced Favorskii-type rearrangement of **16** to produce **3a**, **b** through an intermediate **22**. We prefer path A to path B from the following considerations: (a) The reaction of **1a** with *t*-butoxide, which is a bulky strong base, exclusively affords **2a** without formation of **3a**. This result can be interpreted by assuming that a larger steric interaction between a substituent at the 2-position of **16** and base hinders an attack of the base on the carbonyl carbon of **16**. (b) If path B were to be taken, a compound produced by the decarbonylation from **20** should be obtained. However, such a product could not be isolated.

A possible mechanism for the reactions of **7** with weak bases is outlined in Scheme 3. In these reactions cyclohexane-1,3,4-trione (**9**) was obtained, but not 2-bromo-5,5-dimethyl-3-oxo-1-cyclopentene-1-carboxylic acid (**3c**, R=Br in **3**). This is understandable from the fact that 2-monosubstituted dimedone such as **27** which is a precursor of **3c** exists predominantly in the enol form such as **28**. The attack of weak bases on the enolized carbonyl carbon would be difficult. Consequently, the pathway leading to **3c** is prohibited, and **28** might be transformed into **9** through complex pathways involving oxidation.

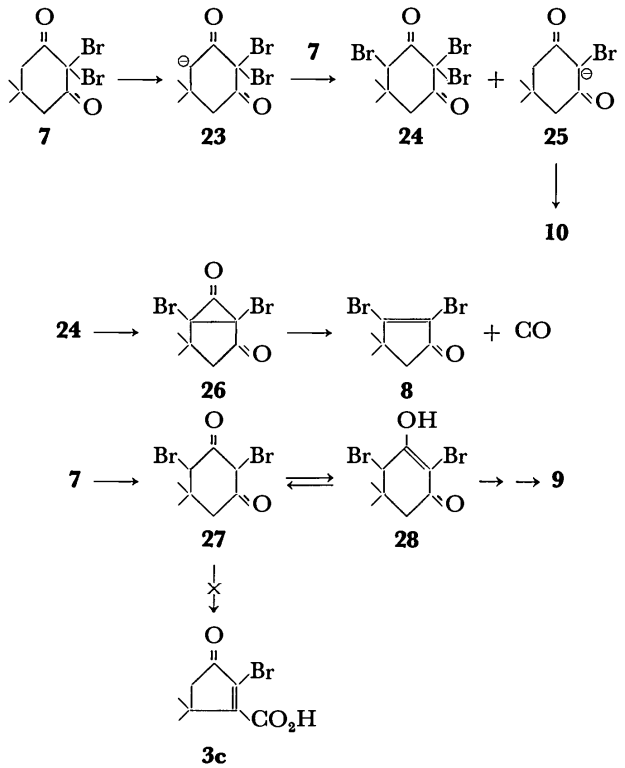

Scheme 3.

An unusual reaction took place with the use of silver acetate. The reaction of **1a** with silver acetate gave the dimeric product **6**, whose yield increased with reaction time. However, the mechanism for the formation of **6** is yet uncertain. The reaction of **7** with silver acetate afforded the monobromocyclopentenone **12**. This may be accounted for by a strong affinity of silver ion to bromide ion, which promotes the formation of the cyclopropanone **29** from **23**.

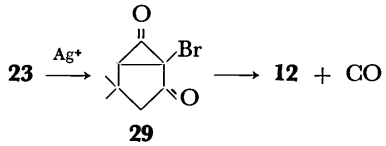

Experimental

2-Bromo-2-methyldimedone (1a). Bromine (16.0 g, 0.1 mol) was added gradually to a stirred mixture of 15.4 g

(0.1 mol) of 2-methyldimedone (**4a**)[7] and 11.8 g (0.1 mol) of AcONa in 120 ml of $CHCl_3$–H_2O (6: 1) below 5 °C. The mixture was stirred for 1 hr, and the $CHCl_3$ layer was then separated. The aqueous layer was extracted with 50 ml of $CHCl_3$. The combined $CHCl_3$ solutions were dried (Na_2SO_4) and evaporated under reduced pressure. Recrystallization of the residue from $CHCl_3$–CCl_4 (1: 3) gave 19.5 g (84%) of **1a**; mp 102—104 °C. IR(KBr): 1720 and 1695 cm^{-1} (C=O). NMR($CDCl_3$) δ 1.12 (s, 6H, two CH_3's), 1.82 (s, 3H, CH_3–C(Br)–) and 2.70 (s, 4H, $-CH_2-C(Br)-CH_2-$).

Found: C, 46.52; H, 5.37%. Calcd for $C_9H_{12}O_2Br$: C, 46.37; H, 5.62%.

2-Bromo-2-butyldimedone (1b). Bromination of 2-butyldimedone[7] by a method similar to that described above gave **1b** in 78% yield; mp 97—99 °C; IR(KBr) 1710 and 1700 cm^{-1} (C=O).

Found: C, 52.46; H, 6.62%. Calcd for $C_{12}H_{19}O_2Br$: C, 52.38; H, 6.96%.

Reaction of 1a with AcONa. A mixture of 1.0 g (4.3 mmol) of **1a** and 0.37 g (4.5 mmol) of anhydrous AcONa in 60 ml of THF was refluxed for 4 hr. The reaction mixture was poured into water, neutralized with 1 M HCl, and extracted with two 30 ml portions of ether. The combined ether extracts were washed with 5% Na_2CO_3, dried and evaporated to leave an oil. Distillation of the oil gave 0.11 g (21%) of (**2a**); bp 160—165 °C. IR (film): 1700 (C=O) and 1640 cm^{-1} (C=C). NMR (CCl_4): δ 1.19 (s, 6H, two CH_3's at the 4-position), 1.65 (d, J=1 Hz, 3H, **CH_3**–C=CH–), 2.12 (s, 2H, –**CH_2**–), and 6.92 (q, J=1 Hz, 1H, **H**–C=C–CH_3).

Found: C, 77.68; H, 9.58%. Calcd for $C_8H_{12}O$: C, 77.38; H, 9.74%.

Chromatography of the oil on silica-gel with $CHCl_3$ gave 50 mg (5%) of unchanged **1a**.

The Na_2CO_3 solution was neutralized with 1 M HCl and extracted with ether. The extract was dried over Na_2SO_4, and evaporated. The residue was chromatographed on silica-gel with benzene–CCl_4 (1: 3). The earlier fractions gave 0.27 g (37%) of 5,5-dimethyl-2-methyl-3-oxo-1-cyclopentene-1-carboxylic acid (**3a**), which upon recrystallization from $CHCl_3$ afforded an analytical sample of mp 189—191 °C. Mass spectrum: *m/e* 168 (M^+), 140, 125, and 124.

Found: C, 64.53; H, 7.41%. Calcd for $C_9H_{12}O_3$: C, 64.27; H, 7.19%.

The latter fractions in the chromatography afforded 50 mg (7.5%) of **4a**, mp 160—162 °C (lit,[7] mp 162—163 °C).

Found: C, 70.33; H, 8.92%. Calcd for $C_9H_{14}O_2$: C, 70.10; H, 9.15%.

Reaction of 1b with AcONa. A mixture of 0.8 g (2.9 mmol) of **1b** and 0.25 g (3.0 mmol) of AcONa in 50 ml of THF was refluxed for 4 hr. The reaction mixture was worked up as described above and separated into two fractions. From the neutral fraction, an oil was obtained after evaporation of the ether. Distillation of the oil gave 0.17 g (35%) of 2-butyl-4,4-dimethyl-2-cyclopenten-1-one (**2b**); bp 65—70 °C/3 mmHg. IR (film): 1730 (C=O) and 1630 cm^{-1} (C=C). NMR (CCl_4): δ 1.20 (s, 6H, two CH_3's), 0.7—2.3 (m, 9H, $-CH_2CH_2CH_2CH_3$), 2.16 (s, 2H, –CO**CH_2**C(CH_3)–), and 6.97 (m, 1H, >C=C**H**–). Mass spectrum: *m/e* 166 (M^+), 151, 138, and 109.

Found: C, 79.41; H, 10.76%. Calcd for $C_{11}H_{18}O$: C, 79.47; H, 10.91%.

The oily material obtained from the Na_2CO_3-soluble fraction was triturated with ice-water. The solid thus precipitated was separated into 0.03 g (5.3%) of **4b**, mp 152—153 °C (lit,[7] mp 155 °C) and 0.09 g (15%) of 2-butyl-5,5-dimethyl-3-oxo-1-cyclopentene-1-carboxylic acid (**3b**) by fractional recrystallization from benzene–CCl_4 (1: 3). An analytical sample of **3b** was prepared by recrystallization from $CHCl_3$; mp 159—162 °C. Mass spectrum; *m/e* 210 (M^+), 182, 166, 153.

Found: C, 68.33; H, 8.98%. Calcd for $C_{12}H_{18}O_3$: C, 68.54; H, 8.63%.

Reaction of 1a with EtONa. A suspension of 1.0 g (4.3 mmol) of **1a** and 0.58 g (8.6 mmol) of EtONa in 100 ml of dry ether was heated under reflux for 5 hr. The reaction mixture was poured into 50 ml of water and neutralized with 1 M HCl, the ether layer then being separated. The aqueous layer was further extracted twice with 30 ml portions of ether. The ether solutions were combined, washed with 5% Na_2CO_3, dried over Na_2SO_4, and the ether was evaporated. The residual oil was distilled to give 0.47 g (64%) of ethyl 3,3-dimethyl-5-oxoheptanoate (**5a**); bp 73—75 °C/1 mmHg. IR (film): 1735 (sh) and 1730 cm^{-1} (C=O). NMR ($CDCl_3$): δ 1.13 (s, 6H, $(CH_3)_2$C–), 1.20 (t, J=6.0 Hz, 3H, –$COCH_2$–**CH_3**), 1.25 (t, J=7.0 Hz, 3H, –$COOCH_2$**CH_3**), 1.90 (s, 2H, –**CH_2**–), 2.40 (s, 2H, –**CH_2**–), 4.12 (q, J=6.0 Hz, 2H, –CO**CH_2**–CH_3), and 4.20 (q, J=7.0 Hz, 2H, –COO**CH_2**CH_3). Mass spectrum: *m/e* 200 (M^+), 172, 156, 146, 130, 87, 83, 43, and 29.

Found: C, 65.55; H, 9.82%. Calcd for $C_{11}H_{20}O_3$: C, 65.97; H, 10.07%.

Vpc analysis of the residual oil indicated that the oil contained 30 mg (5.6%) of 2,4,4-trimethyl-2-cyclopenten-1-one (**2a**). The aqueous Na_2CO_3 solution was neutralized with 1 M HCl, and extracted with ether. The ether extract was dried over Na_2SO_4 and evaporated. The residue was recrystallized from $CHCl_3$ to give 60 mg (9%) of **4a**.

Reaction of 1a with t-BuONa. A mixture of 0.8 g (3.4 mmol) of **1a** with 0.4 g (3.7 mmol) of *t*-BuONa in 50 ml of anhydrous THF was heated under reflux for 5 hr. The reaction mixture was poured into 40 ml of water, neutralized with 1 M HCl and then extracted with two 30 ml portions of ether. The ether extracts were washed with 5% Na_2CO_3, dried and evaporated to leave a tarry material which could not be purified. However, vpc analysis indicated that the tar contained 50 mg (12%) of **2a**. Work-up of the aqueous Na_2CO_3 solution gave 0.18 g (34%) of **4a**.

Reaction of 1a with AcOAg. A mixture of 1.0 g (4.3 mmol) of **1a** and 0.75 g (4.5 mmol) of AcOAg in 40 ml of THF was refluxed with stirring for 5 hr. The reaction mixture was separated into two fractions, *i.e.*, neutral and Na_2CO_3 soluble fractions, by a method similar to that described above. Fractional distillation of the oil obtained from the neutral fraction gave first 90 mg (17%) of **2a**. Trituration of the residue of this distillation gave the solid, which upon fractional recrystallizations from hexane–CCl_4 (5: 1) yielded 0.2 g (20% of unchanged **1a** and 0.06 g (5.3%) of the dimer (**6**).[1] Compound **6** melted at 168—169 °C. IR(KBr): 1725, 1710, 1635, and 1610 cm^{-1}. NMR ($CDCl_3$): δ 1.00—1.17 (m, 12H, four CH_3's), 1.60 (s, 3H, CH_3C(–)–O–), 1.75 (t, J=2 Hz, 3H, **CH_3**–C=C–CH_2–), 2.04 (q, J=2 Hz, 2H, –**CH_2**–C=C–CH_3), 2.23 (s, 2H, –C=C(CH_3)CO**CH_2**–), and 2.81 (m, 4H, two of –CO**CH_2**C(CH_3)$_2$–). Mass spectrum: *m/e* 153 (M—153, 30%), 151 (30), 136 (15), 125 (10), 109 (20), 98 (50), and 83 (100).

Found: C, 70.34; H, 8.52%. Calcd for $C_{18}H_{26}O_4$: C, 70.56; H, 8.55%.

Work-up of the Na_2CO_3 soluble fraction gave 0.07 g (10%) of **3a** and 0.05 g (7.5%) of **4a**.

When the reaction of 1.0 g (4.3 mmol) of **1a** with 0.75 g (4.5 mmol) of AcOAg was carried out for 18 hr, 0.1 g (19%) of **2a**, 0.02 g (3%) of **3a**, 0.27 g (22%) of **6** and 0.06 g (9%) of **4a** were isolated.

Hydrolysis of **6**. A solution of 0.1 g (0.3 mmol) of **6** in 30 ml of dioxane-water mixture (1: 1) containing 6 M HCl was heated at 80 °C for 3 hr, and then evaporated to dryness under reduced pressure. Recrystallization of the residue from $CHCl_3$ gave 0.09 g (90%) of **4a**.

2,2-Dibromodimedone (7). This compound was prepared by the bromination of dimedone with two equivalents of Br_2 in 77% yield; mp 144—145 °C, (lit,[8] mp 144—146 °C). IR(KBr): 1720 and 1730 cm^{-1}. NMR ($CDCl_3$): 1.05 (s, 6H), and 3.05 (s, 4H).

Found: C, 32.22; H, 3.45%. Calcd for $C_8H_{10}O_2Br_2$; C, 32.25; H, 3.38%.

Reaction of 7 with AcONa. A mixture of 1.5 g (5 mmol) of **7** and 0.45 g (5.5 mmol) of anhydrous AcONa in 60 ml of THF was stirred under reflux for 4 hr. The reaction mixture was separated into two fractions. An oily material obtained from the neutral fraction was chromatographed on silica-gel with hexane-CCl_4 (5: 1) to give 0.33 g (25%) of 2,3-dibromo-4,4-dimethyl-2-cyclopenten-1-one (**8**). An analytical sample of **8** was obtained by recrystallization from hexane; mp 85—86 °C. IR(KBr): 1702 (C=O), and 1570 cm^{-1} (C=C). NMR (CCl_4); δ 1.50 (s, 6H, two CH_3's at the 4-position) and 2.70 (s, 2H, $-CO\mathbf{CH_2}C(CH_3)_2-$). Mass spectrum: *m/e* 270, 268, 266 (1: 2: 1); 255, 253, 251 (1: 2: 1); 227, 225, 223 (1: 2: 1); 189, 187 (1: 1); 161, 159 (1: 1); 133, 131, (1: 1).

Found: C, 31.28; H, 2.98%. Calcd for $C_7H_8OBr_2$; C, 31.38; H, 3.01%.

Another oily material obtained from the Na_2CO_3 soluble fraction was partly solidified on being left to stand overnight in a refrigerator. The solid was separated by filtration and then recrystallized from CCl_4-$CHCl_3$ (2: 1) to give 0.35 g (32%) of **10**: mp 169—172 °C (lit,[8] mp 175—176 °C). IR (KBr): 1620 cm^{-1} (C=O).

Found: C, 43.62; H, 5.13%. Calcd for $C_8H_{11}O_2Br$: C, 43.86; H, 5.06%.

A mixture-melting point test of **10** with its authentic sample showed no depression. The filtrate was chromatographed on silica-gel with $CHCl_3$-CCl_4 (3: 1) to give 0.19 g (16%) of 2-bromo-5,5-dimethylcyclohexane-1,3,4-trione (**9**); mp 188—190 °C. IR(KBr): 3200, 1690, 1665, 1650, and 1620 cm^{-1}. NMR (DMSO-d_6): δ 1.16 (s, 6H, two CH_3's at the 5-position), 2.82 (s, 2H, $-CO\mathbf{CH_2}C(CH_3)_2-$) and 6.02—6.25 (broad s, 1H, $-CO-\mathbf{CH}Br-CO-$). Mass spectrum: *m/e* 234, 232 (1: 1), and 220, 218 (1: 1).

Found: C, 41.20; H, 3.66%. Calcd for $C_8H_9O_3Br$: C, 41.23; H, 3.89%.

Reaction of 7 with Na_2CO_3 and with C_2H_5COONa. The reactions were carried out under conditions similar to those described above. The isolated products are given Table 1.

Reaction of **7** *with EtONa*. A mixture of 1.5 g (5.0 mmol) of **7** and 0.68 g (10 mmol) of EtONa in 60 ml of dry ether was stirred at reflux temperature for 5 hr. The reaction mixture was separated into two fractions, *i.e.*, neutral and Na_2CO_3-soluble fractions. An oil obtained from the neutral fraction was distilled under reduced pressure to give 0.41 g (38%) of diethyl 3,3-dimethylglutarate (**11**); bp 82—84 °C/3 mmHg. IR (film); 1735 cm^{-1} (C=O). NMR (CCl_4): δ 1.08 (s, 6H, two CH_3's at the 3-position), 1.24 (t, J=7.0 Hz, 6H, two of $COOCH_2\mathbf{CH_3}$), 2.35 (s, 4H, CH_2's at the 2- and 4-positions), 4.12 (q, J=7.0 Hz, 4H, two of $COO\mathbf{CH_2}CH_3$).

Found: C, 61.37; H, 9.06%. Calcd for $C_{11}H_{20}O_4$: C, 61.11; H, 9.32%.

The retention time of **11** in vpc was the same as that of the authentic sample.[9] A solid obtained from the Na_2CO_3-soluble fraction was recrystallized from CCl_4-$CHCl_3$ (2: 1) to give 0.38 g (35%) of 2-bromodimedone (**10**).

Reaction of 7 with AcOAg. A mixture of 1.5 g (5 mmol) of **7** and 0.84 g (5 mmol) of AcOAg in 50 ml of THF was stirred at reflux temperature for 5 hr. The reaction mixture was separated into two fractions. An oily material obtained from the neutral fraction was chromatographed on silica-gel with CCl_4 to give 0.23 g (24%) of 2-bromo-4,4-dimethyl-2-cyclopenten-1-one (**12**), which upon recrystallization from hexane showed mp 67—68 °C. IR(KBr): 1710 (C-O) and 1585 cm^{-1}. NMR(CCl_4): δ 1.26 (s, 6H, two CH_3's at the 4-position), 2.27 (s, 2H, $-CO\mathbf{CH_2}C(CH_3)_2-$), and 7.42 (s, 1H, $-CBr=\mathbf{CH}-$). Mass spectrum: *m/e* 190, 188 (1: 1), 175, 173 (1: 1); 147, 145 (1: 1); 110.

Found: C, 44.43; H, 4.51%. Calcd for C_7H_9OBr: C, 44.47; H, 4.80%.

From the Na_2CO_3-soluble fraction, 0.45 g (41%) of **10** was obtained.

References

1) T. A. Spencer, A. L. Hall, C. Fordham, and V. Reyn, *J. Org. Chem.*, **33**, 3369 (1968).

2) T. A. Spencer, S. W. Baldwin, and K. K. Schmiegel, *ibid.*, **30**, 1294 (1965).

3) G. Büchi and B. Egger, *J. Org. Chem.*, **14**, 2021 (1971).

4) M. Sutter and E. Schlittler, *Helv. Chim. Acta*, **32**, 1855 (1949).

5) (a) A. S. Kende, "Organic Reactions," Vol. 11, p. 261 (1960). (b) R. B. Loftfield, *J. Amer. Chem. Soc.*, **72**, 632 (1950); (c) F. G. Bordwell and R. G. Scamehorn, *ibid.*, **90**, 6751 (1968).

6) (a) J. M. Conia and J. Salaun, *Bull. Soc. Chim. Fr.*, **1964**, 1957; (b) C. Rappe and L. Knutsson, *Acta Chem. Scand.*, **21**, 163 (1967).

7) R. D. Desai, *J. Chem. Soc.*, **1932**, 1079.

8) E. Guclriniece, G. Vanags, and L. Mazklake, *Zh. Obshch. Khim.*, **30**, 2379 (1960); *Chem. Abstr.*, **55**, 10312c (1961).

9) J. C. Bardhan, S. K. Banerji, and M. K. Bose, *J. Chem. Soc.*, **1935**, 1127.

p-(3,4-Diphenyl-1,3-cyclopentadien-1-yl)phenyltropylium Perchlorate. An Intermediate in the Synthesis of [5.6.7]Quinarene System[1,2]

Kazuko TAKAHASHI, Shunsuke TAKENAKA,* Yoriko KIKUCHI, Kahei TAKASE, and Tetsuo NOZOE**

Department of Chemistry, Faculty of Science, Tohoku University, Aramaki-aza-Aoba, Sendai 980

(Received February 18, 1974)

Attempt was made to dehydrogenate *p*-(3,4-diphenyl-1,3-cyclopentadien-1-yl)phenyltropilidene, prepared by treating *p*-tropylphenyllithium or *p*-tropylphenylmagnesium bromide[3] with 3,4-diphenylcyclopent-2-enone, to 3″,4″-diphenyl-1-cycloheptatrienylidene-4-cyclopentadienylidene-2,5-cyclohexadiene, 10,11-diphenyl[5.6.7]quinarene. The resulting blue pigment showed spectral properties in line with those of *p*-(3,4-diphenyl-1,3-cyclopentadien-1-yl)phenyltropylium ion, [5.6.7]quinarenium ion, carrying a delocalized positive charge (VII′), but not those of expected cross-conjugated hydrocarbon.

The chemistry of fulvalene has been developed[4] and shown to be of greate theoretical interest.[5] The chemistry of polycyclic cross-conjugated π-systems such as I,[2,6] II or III having an inserted *p*-quinoid structure between the two dipole centers of heptafulvene, sesquifulvalene or calicene would also be of interest in connection with its aromatic nature. We have used the name "quinarene"[7] for the sake of convenience to designate this type of polycyclic cross-conjugated hydrocarbon possessing quinoid structure inserted between the two rings of fulvalene (fulvene) type structure. The ring size is shown in brackets; II being [5.6.7]-quinarene, III [3.6.5]quinarene and I [1.6.7]quinarene.[2] Numbering systems (I, II, III) are given for the structures.

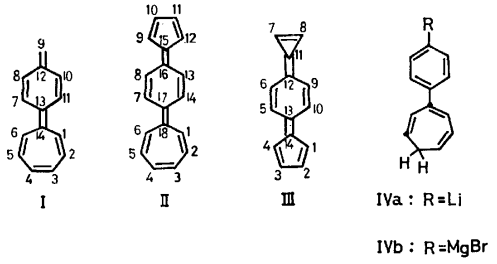

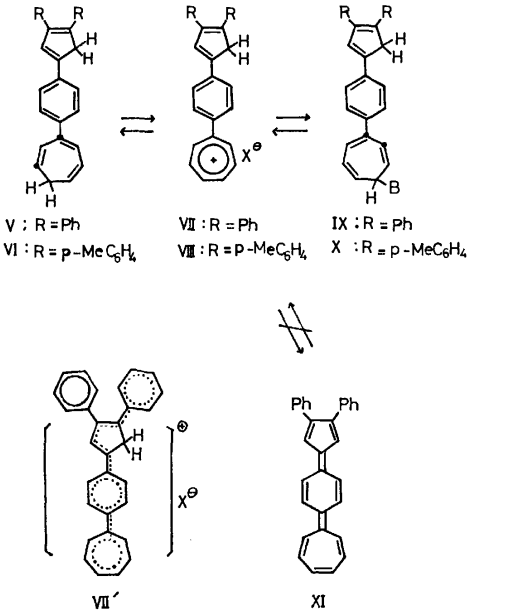

Chart 1.

PPP-type SCF-π-MO calculation[8] suggests that the quinarene (II) should have aromatic character (E_R/π) analogous to sesquifulvalene. In order to determine the ground-state properties of II, the synthesis of 10,11-diphenyl[5.6.7]quinarene (XI) was undertaken.

We reported on a convenient synthetic method of *p*-tropylphenylcarbinol derivative by the reaction of *p*-tropylphenyllithium (IVa) with alkyl or aryl ketones.[2] The reaction was developed for the synthesis of the compounds of type II.

Results and Discussion

Treatment of IVa or the corresponding Grignard reagent (IVb) with 1.7 mol equivalents of 3,4-diphenylcyclopent-2-enone[9] in ether at room temperature followed by hydrolysis with 2 M sulfuric acid gave yellow needles (V), mp 125—126 °C in 33.5% yield. V has no OH band in its IR spectrum and contains one additional singlet methylene proton resonance at 3.84 ppm besides a triplet (at 2.31 ppm) and a doublet (at 2.72 ppm) tropyl[3] methylene proton resonance in NMR spectrum, indicating that the dehydration of primarily formed carbinol had occurred to afford the hydrocarbon (V). V in dichloromethane was allowed to react with 2.5 mol equivalents of triphenylmethyl perchlorate resulting in an intensely blue solution, from which perchlorate VII was isolated as blue black needles in 88% yield. Di-*p*-tolyl derivative (VI), obtained by the treatment of IV with 3,4-di-*p*-tolylcyclopent-2-enone, also afforded blue black needles (VIII)[10] on reaction with triphenylmethyl salt. VII turned to the original tropilidene (V) on lithium aluminum hydride reduction in ether. Perchlorate (VII) was immediately converted into a yellow 3- and 2-aryl-7-ethoxytropilidene (IX: B=OEt) on treatment with sodium bicarbonate in the presence of ethanol, from which salts of the cation (VII) were regenerated by the action of acids such as hydrogen bromide, hydrogen chloride, trifluoroacetic acid, or perchloric acid. The chemical

* Present address: Department of Applied Chemistry, Osaka University, Suita 565.

** Present address: No. 811, 2-5-1, Kamiyoga, Setagaya-ku, Tokyo.

Table 1. Solvent effects on the electronic absorptions of 10, 11-diaryl[5.6.7]-quinarenium ions (VII and VIII)

nm (log ε)	CH_3CN	$MeCO_2H$	HCl-MeOH	CH_2Cl_2	$CHCl_3$	CF_3CO_2H
VII	543 (4.2)	550 (4.2)	548 (4.3)	630 (4.3)	617 (4.2)	627 (4.3)
X=ClO_4	352 (4.1)	354 (4.1)	352 (4.1)	364 (4.1)	364 (4.0)	482 (3.9)[a]
	273 (4.3)	—	270 (4.3)	275 (4.2)	276 (4.2)	365 (4.0)
VIII	556 (4.3)	565 (4.2)	565 (4.3)	650 (4.4)	640 (4.3)	639 (4.0)
X=ClO_4	357 (4.1)	358 (4.2)	358 (4.1)	365 (4.2)	371 (4.2)	490 (4.3)[a]
	276 (4.2)	—	270 (4.3)	275 (4.4)	275 (4.3)	350 (4.0)

a) Absorption maxima of dications formed by a protonation at the 5-membered ring of VII and VIII.

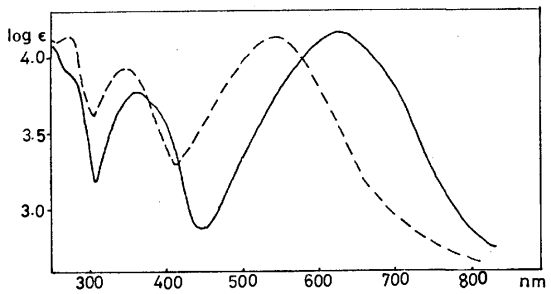

Fig. 1. Electronic absorption spectra of 10,11-diphenyl-[5.6.7]quinarenium ion (VII): (——) in $CHCl_3$, and (------) in CH_3CN.

properties as well as elemental composition of VII ($C_{30}H_{23}ClO_4$) were in line with the *p*-(3,4-diphenyl-1,3-cyclopentadien-1-yl)phenyltropylium ion structure.

However, there is some doubt as to the structure of pigment (VII), as seen from its electronic spectra. The longest wavelength absorption maximum of VII at 543—550 nm in such solvents as acetonitrile, acetic acid, or methanol–hydrochloric acid (violet solutions) shows a large bathochromic shift to 617—630 nm when the solvent is changed to chloroform, dichloromethane, or 9: 1 mixed solvent of chloroform and trifluoroacetic acid (blue solutions) (Table 1 and Fig. 1). The absorption maximum of VII at an extraordinary longer wavelength region of 630 nm is conspicuous as compared with the absorption maxima of phenyltropylium ion[11,12] at 385 nm and *p*-biphenylyltropylium ion at 415 nm. On the other hand, molecular orbital calculation for diphenyl derivative of [5.6.7]quinarene[8] using the variable bond length SCF-π-MO-CI procedure predicted the lowest singlet transition energies of XI to be 2.09 eV: f=2.96. The observed absorption maximum (630 nm) of VII and molecular orbital

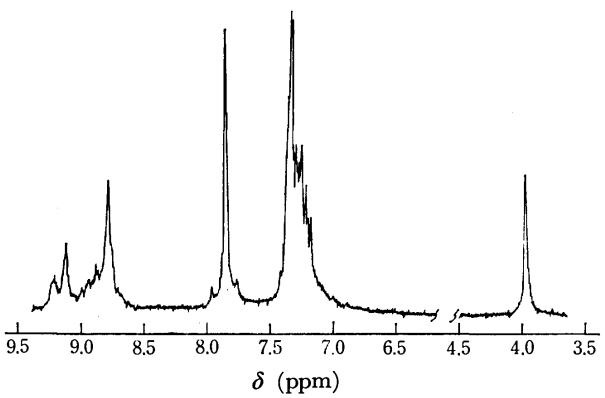

Fig. 2. NMR spectrum of 10,11-diphenyl[5.6.7]quinarenium ion (VII) in a 9: 1 mixture of $CHCl_3$ and CF_3CO_2H.

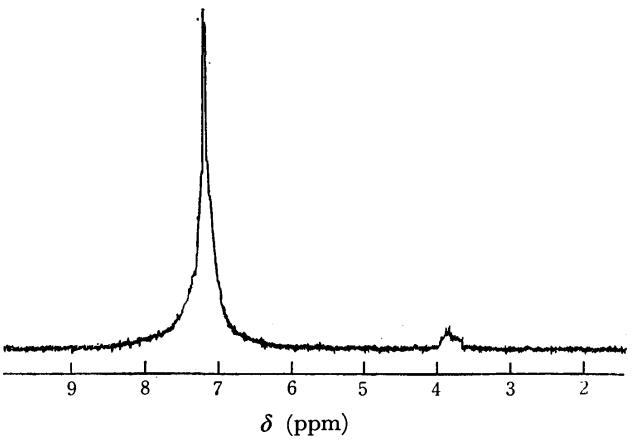

Fig. 3. NMR spectrum of 10,11-diphenyl[5.6.7]quinarenium ion (VII) in $CHCl_3$ at +30 °C.

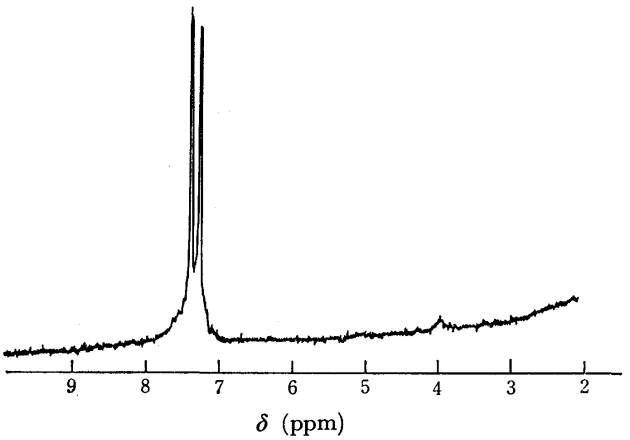

Fig. 4. NMR spectrum of 10,11-diphenyl[5.6.7]quinarenium ion (VII) in $CHCl_3$ at −30 °C.

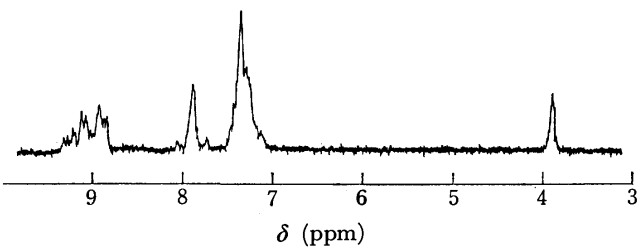

Fig. 5. NMR spectrum of 10,11-diphenyl[5.6.7]quinarenium ion (VII) in liq. SO_2.

calculation would be reasonable if cation (VII) is capable of existing as an equilibrium mixture with quinarene-type hydrocarbon (XI) in chloroform or dichloromethane solution.

NMR spectral studies of VII, however, exclude the possibility of the equilibrium. A deep blue solution of VII in chloroform containing 10% of trifluoroacetic acid shows a multiplet at 8.90 ppm (6H, tropylium ion), AB-type triplet at 7.80 ppm (4H, benzene ring), a multiplet at 7.20 ppm (11H, benzene ring and an olefinic proton of 5-membered ring) and a singlet at 3.96 ppm (2H, methylene), indicating that VII is the structure of the blue pigment (Fig. 2). In non-acidic, pure chloroform, the presumed equilibrium between VII and XI would favor deprotonated species XI. However, the solution showed a small and broad singlet at 3.9—4.0 ppm attributed to the methylene group of the 5-membered ring of VII, besides a broad peak at around 7.20 ppm, at +30 °C (Fig. 3), and two sharp peaks at −30 °C (Fig. 4) where all 7- and 6-membered ring protons appear together, no signal at lower field being observed. Moreover the solution of VII in liq. SO_2, having violet color (λ_{max} at 552 nm) analogous to the acetonitrile solution, showed a spectrum of Fig. 5 clearly attributable to the cation (VII).

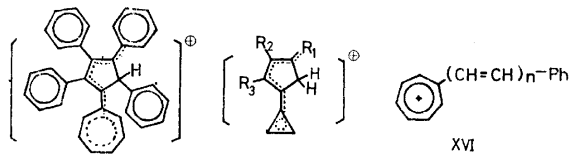

XIII XV XVI

Chart 2.

TABLE 2. CALCULATED TRANSITION ENERGIES OF 10,11-DIPHENYL[5.6.7]QUINARENE (XI) AND 10,11-DIPHENYL [5.6.7]QUINARENIUM ION (VII) COMPARED WITH THE OBSERVED SPECTRUM OF VII IN CHLOROFORM

Calculated				Experimental
XI		VII		VII (X=ClO_4)
ΔE (eV)	f	ΔE (eV)	f	ΔE (eV) (logε)
2.00	0.004 (y)	2.02	0.79	2.02 (4.2)
2.08	0.008 (y)	2.52	0.008	
2.09	2.96 (z)	3.10	0.57	3.40 (4.0)
3.33	0.06 (z)	3.45	0.27	
3.81	0.00 (y)	3.60	0.003	

It was concluded that both violet- and blue-colored solutions contain a single species having structure VII excluding the presumed equilibrium with XI. The absorption maximum of VII at a longer wavelength region of 630—617 nm might be due to the contribution of structure VII′ carrying a delocalized positive charge all over the molecule. Prinzbach and his co-workers observed a similar bathochromic effect[13-15] of the conjugated acids XIII and XV as compared with the corresponding cross-conjugated hydrocarbons, sesquifulvalene (XII) and calicene (XIV). Jutz and Voithenleitner[16] presented further examples of the long conjugated tropylium ion derivatives (XVI), stating that XVI (n=3) and XVI (n=4) have absorption maximum at 592 nm in chloroform (539 nm in acetonitrile) and at 646 nm in chloroform (582 nm in acetonitrile), respectively. These values are in fair agreement with the spectral characteristics of VII, if the bathochromic effect of a benzene ring is equivalent to about 1½ ethylenic links.[17]

The calculated electronic spectral data of VII are summarized in Table 2, where the calculated values for VII, rather than those for XI, are in good agreement with the observed values. The deprotonation of VII with a base such as diisopropylamine or pyridine has not been successful so far.

Experimental

Mps and bps are uncorrected. The instruments used for spectral measurements are Shimadzu IR-27-G spectrophotometer (IR), Varian Associates A-60 and HA-100 spectrometers (NMR, TMS as internal standard) and Hitachi EPS-2U spectrometer (UV).

Preparation of 3-[p-(3,4-Diphenyl-1,3-cyclopentadien-1-yl)-phenyl]tropilidene (V). *a)* To a solution of *p*-tropylphenyllithium[1] (10.0 mmol) in ether (40 ml), prepared from *p*-tropyliodobenzene (4.0 g, 13.6 mmol) and *n*-butyllithium (30.0 mmol), was added dropwise a solution of 3,4-diphenylcyclopent-2-enone (2.58 g, 11.1 mmol) in ether (100 ml) with stirring at room temperature. After being stirred for 5 hr, the mixture was hydrolyzed with 2M-H_2SO_4 and extracted with ether. The combined organic solution was washed (satd. $NaHCO_3$ soln.), dried (Na_2SO_4), and concentrated. The residual yellow semi-solid was chromatographed on an alumina column with light petroleum-benzene as an eluent. The chromatographic fractions from light petroleum-benzene (1: 1) were recrystallized from ether to give V (1.29 g, 33.6%) as yellow needles, mp 125—126 °C; ν_{max} (KBr) 3050, 2930, 1600, 1500, 1440, 1370, 1200, 1070, 1030, 912, 891, 822, 759, 697 cm^{-1}; δ (CCl_4) 7.39 (4H, s, benzene), 7.26 (5H, s, benzene), 7.15 (5H, s, benzene), 6.96 (1H, s, 5-membered ring) 6.60—6.05 (3H, m, tropyl), 5.65—5.15 (2H, m, tropyl), 3.84 (2H, s, 5-membered methylene), 2.72 (4/5H, d, J=7.0 Hz, tropyl methylene), 2.31 (6/5H, t, J=6.8 Hz, tropyl methylene); λ_{max} ($CHCl_3$) nm (log ε) 303 (4.25), 375 (4.57). Found: C, 93.59; H, 6.56%. Calcd for $C_{30}H_{24}$: C, 93.71; H, 6.29%.

b) To a solution of *p*-tropylphenylmagnesium bromide[1] (7.7 mmol) in THF (25 ml), prepared from *p*-tropylbromobenzene (2.4 g, 9.7 mmol) and Mg-ribbon (1.236 g, 9.7 mmol), was added a solution of 3,4-diphenylcyclopent-2-enone (1.96 g, 8.4 mmol) in THF (30 ml) with stirring at room temperature. After being stirred for 5 hr, the mixture was worked up as above to give V (1.19 g, 31%).

Preparation of 4-Hydroxy-3,4-di(p-tolyl)-2-cyclopentenone. To a suspension of 4,4′-dimethylbenzil (12.5 g, 51.3 mmol) in acetone (10 ml) was added 33% NaOH solution (0.5 ml) and the red solution was stirred for 30 min at room temp. After addition of another NaOH solution (33%, 1.5 ml), the mixture was refluxed for 2 hr and then poured into hot water (50 ml). The crude product (10.3 g, 72.4%) which separated was washed with ether and recrystallized from benzene to give 4-hydroxy-3,4-di(*p*-tolyl)-2-cyclopentenone as colorless needles, mp 171 °C; ν_{max} (KBr) 3440, 2920, 1680, 1590, 1515, 1410, 1333, 1267, 1212, 1183, 1060, 980, 864, 831, 818, 734 cm^{-1}; δ ($CDCl_3$) 7.25 (8H, m, benzene), 6.56 (1H, s, 5-membered ring), 3.51 (1H, s, OH), 2.94, 2.79, (each 1H, AB-q, J=19.0 Hz); λ_{max} (MeOH) nm (log ε)

399 (4.40), 220 (4.37). Found: C, 81.64; H, 6.59%. Calcd for $C_{19}H_{18}O_2$: C, 81.98; H, 6.52%.

Preparation of 3,4-Di(p-tolyl)cyclopent-2-enone. To a warmed mixture (50 °C) of red phosphorus (3.4 g), 58% hydriodic acid (1.8 ml) and acetic acid (30 ml) was added 4-hydroxy-3,4-di(*p*-tolyl)-2-cyclopentenone (3.2 g, 11.5 mmol). The mixture was stirred for 2 hr at 80 °C and then filtered to remove phosphorus. The filtrate was added to cooled 10% $NaHSO_3$ solution and extracted with ether. After removal of the ether, the residue was distilled *in vacuo* affording the crude product (2.32 g, 76.8%), which was recrystallized to colorless needles, mp 109 °C; ν_{max} (KBr) 2950, 1680, 1590, 1510, 1270, 1190, 935, 813 cm^{-1}; δ ($CDCl_3$) 7.45, 7.12, (each 2H, J=8.2 Hz, benzene), 7.05 (4H, s, benzene), 6.72 (1H, d, J=1.5 Hz, 5-membered ring), 4.57 (1H, ddd, J=7.3, 2.5, 1.5 Hz, benzyl), 3.10 (1H, dd, J=18.5, 7.3 Hz, methylene), 2.37 (1H, dd, 18.5, 2.5 Hz, methylene), 2.29 (3H, s, methyl), 2.25 (3H, s, methyl); λ_{max} (MeOH) nm (log ε) 295 (4.31), 220 (4.18). Found: C, 86.91; H, 7.05%. Calcd for $C_{19}H_{18}O$: C, 86.98; H, 6.91%).

3-[p-(3,4-Di-p-tolyl-1,3-cyclopentadien-1-yl)phenyl]tropilidene (VI). To a solution of *p*-tropylphenyllithium[1] (5.0 mmol) in ether (20 ml) was added dropwise a solution of 3,4-di(*p*-tolyl)cyclopent-2-enone (1.57 g, 6.0 mmol) in ether (80 ml) with stirring at room temperature. After being stirred for 5 hr at the same temp., the resulting mixture was worked up as for V and the residual oil was chromatographed on silica gel column with 5% benzene in *n*-hexane as an eluent. The later chromatographic fraction was recrystallized from light petroleum to give VI (0.94 g, 45.5%) as pale yellow needles, mp 156 °C; ν_{max} (KBr) 3020, 1505, 810, 764, 718 cm^{-1}; δ (CCl_4) 7.37 (4H, s, benzene), 7.17—6.81 (8H, m, tolyl), 6.97 (1H, s, 5-membered ring), 6.46—6.05 (3H, m, tropyl), 5.60—5.18 (2H, m, tropyl), 3.73 (2H, s, 5-membered methylene), 2.68 (1/5H, d, J=7.0 Hz, tropyl methylene), 2.30 (9/5H, t, J=6.8 Hz, tropyl methylene), 2.26 (3H, s, methyl), 2.32 (3H, s, methyl); λ_{max} (MeOH) nm (log ε) 370 (4.51), 298 (4.22), 275 (4.19), 238 (4.35). Found: C, 93.43; H, 6.97%. Calcd for $C_{32}H_{28}$: C, 93.16; H, 6.84%.

p-(3,4-Diphenyl-1,3-cyclopentadien-1-yl)phenyltropylium Perchlorate (VII). To a solution of tropilidene (V) (0.20 g, 0.52 mmol) in dichloromethane (9 ml) was added triphenylmethyl perchlorate (0.45 g, 1.30 mmol) with stirring. After being stirred for 3 hr, the precipitate was filtered and washed with ether to give crude VII (0.22 g, 88%). Recrystallization from acetic acid gave blue black needles, mp>300 °C; ν_{max} (KBr) 3030, 1600, 1517, 1500, 1477, 1260, 1200, 1090, 917, 829, 758, 697 cm^{-1}; δ (10% CF_3CO_2D in $CDCl_3$) 9.25—8.70 (6H, m, tropylium), 7.77 (4H, s, benzene), 7.40—7.17 (10H, m, benzene), 3.98 (2H, s, methylene); λ_{max} ($CHCl_3$) nm (log ε) 617 (4.24), 363 (4.02), 276 sh (4.16). Found: C, 74.27; H, 4.97%. Calcd for $C_{30}H_{23}ClO_4$: C, 74.58; H, 4.85%.

p-(3,4-Di-p-tolyl-1,3-cyclopentadien-1-yl)phenyltropylium Perchlorate (VIII). Tropilidene (VI) (0.30 g, 0.73 mmol) in dichloromethane (5 ml) was treated with triphenylmethyl perchlorate (0.50 g, 1.46 mmol) as for VII to give crude VIII (0.25 g, 67.3%). Recrystallization from acetic acid afforded blue black needles, mp>300 °C; ν_{max} (KBr) 3003, 1590, 1508, 1490, 1260, 1200, 1090, 917, 813, 765 cm^{-1}: δ (10% CF_3CO_2D in $CDCl_3$) 9.34—8.77 (6H, m, tropylium), 7.84 (4H, s, benzene), 7.34—6.97 (8H, m, benzene), 3.90 (2H, s, methylene), 2.37 (3H, s, methyl), 2.31 (3H, s, methyl); λ_{max} ($CHCl_3$) nm (log ε) 640 (4.32), 371 (4.16), 281 (4.27). Found: C, 75.27; H, 5.44%. Calcd for $C_{32}H_{27}ClO_4$: C, 75.21; H, 5.33%.

Reduction of VII with Lithium Aluminum Hydride. To a suspension of tropylium ion (VII: X=BF_4) (0.10 g, 0.2 mmol) in ether (8 ml) was added dropwise a solution of $LiAlH_4$ (24.5 mg, 0.64 mmol) in ether (3 ml). The solution was stirred for 2 hr at room temperature. Water was then added to decompose the excess reagent and the precipitate was filtered. The precipitate and the filtrate were separately extracted with ether, and the combined extract was evaporated. The residue (82 mg) was chromatographed on a silica gel column and eluted with benzene(3%)-hexane. Yellow needles (30 mg, 37%) obtained showed IR spectrum identical with that of V.

Reaction of VII with Ethanol in the Presence of Sodium Bicarbonate. To a suspension of VII (0.10 g, 0.21 mmol) in chloroform (30 ml) and ethanol (3 ml) was added satd. $NaHCO_3$ soln. (30 ml). The mixture was then shaken vigorously and a yellow chloroform layer was separated, washed (satd. NaCl soln.) and dried (Na_2SO_4). Evaporation of the solvent gave IX: B=OEt (80 mg, 88%) as a yellow powder, mp 108—110 °C; ν_{max} (KBr) 3021, 2857, 1597, 1502, 1441, 1372, 1200, 1109, 912, 889, 820, 757, 696 cm^{-1}; δ ($CDCl_3$) 7.45 (4H, s, benzene), 7.25 (10H, m, benzene), 7.00 (1H, s, 5-membered ring), 6.70—6.05 (m, tropyl), 5.80—5.45 (m, tropyl), 3.85 (2H, s, 5-membered methylene), 3.65 (4/5H, q, J=6.9 Hz, ethyl), 3.51 (6/5H, q, J=6.9 Hz, ethyl), 3.50 (1H, m, methine), 1.26 (6/5H, t, ethyl), 1.23 (9/5H, t, ethyl); λ_{max} ($CHCl_3$) nm (log ε) 275 sh, 290 sh, 370 (4.27).

Reaction of VIII with Ethanol in the Presence of Sodium Bicarbonate. Tropylium perchlorate(VIII) (0.20 g, 0.39 mmol) in chloroform (50 ml) and ethanol (5 ml) was treated with $NaHCO_3$ as above to give X: B=OEt (0.16 g, 90%) as a yellow powder; δ (CCl_4) 7.37 (4H, s, benzene), 7.05 (9H, m, tolyl and 5-membered ring), 6.40—5.90 and 5.80—5.30 (5H, m, tropyl), 3.75 (2H, s, methylene), 3.62 (4/5H, q, J=6.9 Hz, ethyl), 3.58 (6/5H, q, J=6.9 Hz, ethyl), 3.50 (1H, m, methine), 2.32 and 2.16 (each 3H, tolyl methyl), 2.92 (6/5H, t, J=6.9 Hz, ethyl), 2.90 (9/5H, t, J=6.9 Hz, ethyl).

Reaction of IX with Hydrogen Bromide. Dry hydrogen bromide was introduced to a solution of IX: B=OEt (80 mg, 0.186 mmol) in benzene (5 ml). The blue black precipitate was then collected by filtration, washed (with benzene) and dried *in vacuo*, affording VII: X=Br (60 mg, 70.0%). Recrystallization from acetic acid gave blue needles, mp 180 °C (decomp.). Found: C, 77.23; H, 4.99%. Calcd for $C_{30}H_{23}Br$: C, 77.75; H, 5.00%.

Reaction of IX with Hydrogen Chloride. Dry hydrogen chloride was introduced to a solution of IX: B=OEt (100 mg, 0.23 mmol) in benzene (5 ml). The reaction mixture was worked up as above to give a blue black powder of VII:X=Cl (87 mg, 87%), which was recrystallized from acetic acid to give blue black needles, mp 150 °C (decomp.). Found: C, 85.38; H, 5.27%. Calcd for $C_{30}H_{23}Cl$: C, 86.00; H, 5.53%.

The authors express their hearty thanks to Professor T. Nakajima and Dr. H. Yamaguchi for the MO calculation. The work was carried out with financial support from the Ministry of Education and Sankyo Co., Ltd.

References

1) Presented in part at the 20th Annual Meeting of the Chemical Society of Japan, Tokyo, April 2, (1967), *Abstr.* p. 491. For reviews see *Kagaku to Kogyo*, **20**, 64 (1967); **22**, 72 (1969); **23**, 1547 (1970); *Pure Appl. Chem.* **28**, 239 (1971).

2) Part II of Cyclic Cross-conjugated Hydrocarbons Having Inserted *p*-Quinoid Ring. Part I: K. Takahashi,

S. Takenaka, and T. Nozoe, *Tetrahedron*, **30**, 2191 (1974).

3) When no notation is given, tropyl or tropilidene indicates 3-substituted cycloheptatriene containing 10—20% of 1-substituted isomer. Detailed components of each compound are given in NMR spectrum.

4) H. Prinzbach, D. Seip, L. Knothe, and W. Faisst, *Ann. Chem.*, **698**, 34 (1966); H. Prinzbach, D. Seip, and G. Englert, *ibid.*, **698**, 57 (1966); H. Prinzbach and H. Knofel, *Angew. Chem.*, **81**, 900 (1969); H. Prinzbach and L. Knothe, *ibid.*, **79**, 620 (1967); E. D. Bergman and I. Agranat, *Chem. Commun.*, **1965**, 512; W. M. Jones and R. S. Pyron, *J. Amer. Chem. Soc.*, **87**, 1608 (1965); M. Ueno, I. Murata, and Y. Kitahara, *Tetrahedron Lett.*, **1965**, 2976; I. Murata, M. Ueno, Y. Kitahara, and H. Watanabe, *ibid.*, **1966**, 1831; Y. Kitahara, I. Murata, M. Ueno, K. Sato, and H. Watanabe, *Chem. Commun.*, **1966**, 180; H. Prinzbach, D. Seip, and U. Fisher, *Angew. Chem.*, **77**, 621 (1965); *Helv. Chim. Acta*, **50**, 1669, 1692 (1967); A. S. Kende and P. T. Izzo, *J. Amer. Chem. Soc.*, **87**, 4162 (1965); A. S. Kende, P. T. Izzo, and P. T. MacGregor, *ibid.*, **88**, 3359 (1966).

5) M. J. S. Dewar and G. J. Gleicher, *Tetrahedron*, **21**, 3423 (1965); T. Nakajima, S. Kohda, A. Tajiri, and S. Karasawa, *ibid.*, **23**, 2189 (1967); A. Y. Meyer, *Theor. Chim. Acta*, **8**, 178 (1967); H. Yamaguchi, T. Nakajima, and T. L. Kunii, *ibid.*, **12**, 349 (1968); H. Yamaguchi, T. Terasaka, and T. Nakajima, *ibid.*, **18**, 255 (1970).

6) K. Takahashi, N. Hirata, and K. Takase, *Tetrahedron Lett.*, **1970**, 1285.

7) The name "quinarene" was proposed by T. Nozoe at the 19th Annual Meeting of the Chemical Society of Japan, Tokyo, April 2, (1966) and at the International Symposium of Nonbenzenoid Aromatic Compounds, Sendai, August 24, (1970).

8) The SCF orbitals were calculated by T. Nakajima and H. Yamaguchi.

9) T. A. Geissman and C. F. Koelsch, *J. Org. Chem.*, **3**, 489 (1938).

10) Chemical and physical properties of VIII appeared to be strikingly similar to those of VII (see Experimental).

11) C. Jutz and F. Voithenleitner, *Chem. Ber.*, **97**, 29 (1964).

12) K. Takahashi, This Bulletin, **40**, 1462 (1967).

13) H. Prinzbach, D. Seip, L. Knothe, and W. Faisst, *Ann. Chem.*, **698**, 42 (1966); H. Prinzbach and H. Knofel, *Angew. Chem.*, **81**, 900 (1969).

14) H. Prinzbach and U. Fisher, *Helv. Chim. Acta*, **50**, 1680 (1967); H. Prinzbach and E. Woischnik, *ibid.*, **52**, 2472 (1969).

15) H. Prinzbach and L. Knothe, *Angew. Chem.*, **79**, 620 (1967); H. Prinzbach, L. Knothe, and A. Dieffenbach, *Tetrahedron Lett.*, **1969**, 2093.

16) C. Jutz and F. Voithenleitner, *Chem. Ber.*, **97**, 1590 (1964).

17) E. S. Stern and C. J. Timmons, "Electronic Absorption Spectroscopy in Organic Chemistry," Edward Arnold Ltd., London (1970), p. 127.

Studies on Cyclic Dipeptides. II.[1] Isomerization among *cyclo*-(-4-Hydroxyprolyl-4-hydroxyprolyl-)s and a Novel Conversion of D-*allo*-Hydroxyproline to L-Hydroxyproline[2]

Chikahiko EGUCHI and Akio KAKUTA

Central Research Laboratories, Ajinomoto Co., Inc., Suzuki-cho, Kawasaki-ku, Kawasaki 210

(Received March 26, 1974)

The isomerization among *c*-L-Hyp-L-Hyp (**1**), *c*-L-Hyp-D-*a*Hyp (**2**) and *c*-D-*a*Hyp-D-*a*Hyp (**3**) has been examined in ethanolic sodium ethoxide at 25—78 °C as well as in aqueous solutions at 75—250 °C. At equilibrium state, **1** was predominant and **2** was not found at all in the reaction mixture. By the use of this isomerization reaction and the difference of solubility between **1** and **3**, **3** could be converted almost quantitatively to **1**. The mixture of **1** and **3** was obtained in good yield directly from D-*a*Hyp or L-Hyp by heating in water or ethylene glycol. **1** was hydrolyzed quantitatively to L-Hyp by acid. Thus, L-Hyp was obtained with the yield of 59% from D-*a*Hyp by combination of preparation, isomerization and acid hydrolysis of cyclic dipeptide.

In our previous work,[1] we have determined the thermodynamic constants (K, $\Delta G°$, $\Delta H°$, and $\Delta S°$) of the *cis-trans* isomerization of cyclic dipeptides and found that, for *c*-Pro-Pro type of cyclic dipeptides, *e.g.*, *c*-Pro-Pro, *c*-Hyp-Hyp, only the *cis*-isomer occurs at equilibrium. This finding suggested a new method of obtaining L-Hyp from D-*a*Hyp, which involves an application of the isomerization reaction among *cyclo*(-4-hydroxyprolyl-4-hydroxyprolyl-)s. Our further study conducted on this suggestion is a subject of this paper.

So far, the interconversion between L-Hyp and D-*a*Hyp has been made by three methods: (A) heating an aqueous solution of the amino acid in the presence of excess barium hydroxide at 200 °C for several hours,[3] (B) treating the amino acid with excess acetic anhydride in refluxing glacial acetic acid,[4] and (c) heating an aqueous solution of the amino acid at 200 °C for 2 hr.[5] The method of obtaining L-Hyp from D-*a*Hyp is important to our new process to synthesize L-Hyp from D-Glu.[5] However, the reaction mixture at equilibrium state contained about 50% of L-Hyp in method (A), about 25% of L-Hyp in method (B), and about 55% of L-Hyp in method (C). Thus, it was not efficient to obtain L-Hyp from D-*a*Hyp by these methods. By our present method, on the other hand, the reaction mixture at equilibrium state contains about 97% of L-Hyp, therefore, L-Hyp is very easily obtained from D-*a*Hyp as will be described below.

Results and Discussion

Isomerization among c-L-*Hyp*-L-*Hyp* ***(1)***, c-L-*Hyp*-D-a*Hyp* ***(2)***, *and* c-D-a*Hyp*-D-a*Hyp* ***(3)***. The *cis-trans* isomerization among **1**, **2**, and **3** (Scheme 1) has been examined in 0.1 M ethanolic sodium ethoxide at three temperatures, 25, 50, and 78 °C. A part of the results is shown in Fig. 1. It was found that **2** is very rapidly isomerized to **1** and **3**. For example, when the isomerization was started from **2** at 25 °C, after only two min **2** was not found at all in the reaction mixture any more. Thus, under these conditions, the isomerization among *cis*-isomers (**1** and **3**) and *trans*-isomer (**2**) was actually equivalent to the isomerization between only two *cis*-isomers. The equilibrium constants (K) between **3** and **1** were determined at 25, 50, and 78 °C,

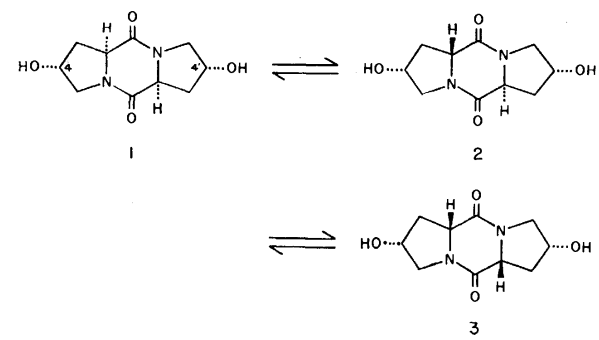

Scheme 1.

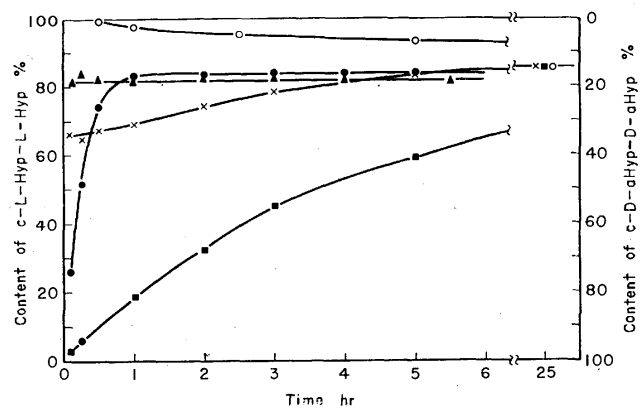

Fig. 1. Contents of *c*-L-Hyp-L-Hyp and *c*-D-*a*Hyp-D-*a*Hyp in the isomerization mixture in 0.1 M ethanolic sodium ethoxide: (○), **1** (starting material), 25 °C (reaction temperature); (×), **2**, 25 °C; (■), **3**, 25 °C; (●), **3**, 50 °C; (▲), **3**, 78 °C.

and then the thermodynamic constants ($\Delta H°$ and $\Delta S°$) of this isomerization were obtained by plotting $\log K$ against $1/T$ and by adopting the least-squares method. The results are summarized in Table 1.

Table 1. Thermodynamic constants for the equilibrium, *c*-D-*a*HYP-D-*a*HYP (**3**) ⇌ *c*-L-HYP-L-HYP (**1**)

$K_{298} = 5.94$	(85.6% of **1**)
$K_{323} = 5.10$	(83.6% of **1**)
$K_{351} = 4.43$	(81.6% of **1**)
$\Delta G_{323} = -1.04 \pm 0.01$ kcal/mol	
$\Delta H° = -1.15 \pm 0.2$ kcal/mol	
$\Delta S° = -0.29 \pm 0.3$ e.u.	

The conformation of the diketopiperazine (DKP) ring of **3** is probably similar to that of **1**, which is a boat form with C^{α}–C^{β} bond in the pyrrolidine ring setting at the quasi-equatorial position of the DKP ring.[1,6-8] The enthalpy difference between **1** and **3** is considered to be due to intramolecular dipole-dipole interactions. The vector sum of the dipole moments of two amide groups in the DKP ring is considered to be oriented along the perpendicular direction of the DKP ring. In **1**, both dipole moments of the C–O bonds on the two pyrrolidine rings are directed opposite to that of the amide groups. While, in **3**, the two C–O dipoles are oriented along the same direction with the net dipole of the amide groups.

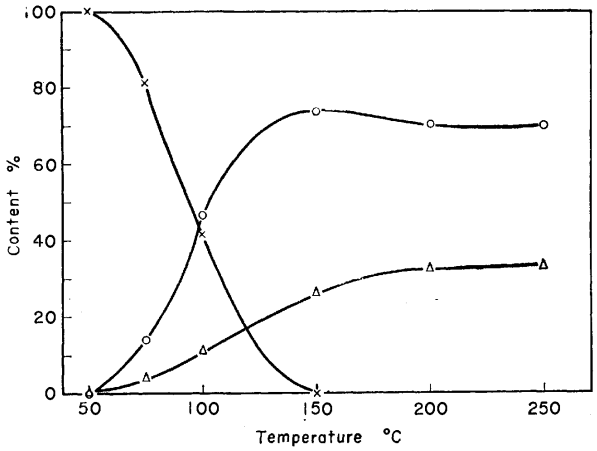

Fig. 2. Contents of *c*-L-Hyp-L-Hyp (○), *c*-L-Hyp-D-*a*Hyp (×), and *c*-D-*a*Hyp-D-*a*Hyp (△), in the isomerization mixture: starting material, 10% aqueous solution of **2**; heating time, 2 hr.

The isomerization experiment was also carried out in an aqueous solution in the temperature range of 75—250 °C. The results of the experiment in which the reaction was started from **2** are shown in Fig. 2. When an aqueous solution of **2** was heated for 2 hr at 150 °C, **2** was completely isomerized into a mixture of 74% of **1** and 26% of **3**. On the other hand, when an aqueous solution of **1** or **3** was heated, **2** was not found at all in the reaction mixture at any temperature. The equilibrium mixture at 250 °C contained 71% of **1** and 29% of **3**.

Almost Quantitative Conversion of 3 to 1. The solubility of **1** in ethanol or water is lower than that of **3**, so **1** and **3** are easily separated by fractional crystallization. Thus almost quantitative conversion of **3** to **1** may be accomplished by letting the isomerization reaction and the fractional crystallization proceed simultaneously in one vessel.

The compound, **3** (181 mg) was heated in 0.1 M ethanolic sodium ethoxide (2 ml) for 15 min at 78 °C, so that it was completely dissolved. The solution was cooled slowly to room temperature for 4 hr under stirring. The crystals thus produced were filtered, washed with absolute ethanol. The mother liquor was immediately neutralized with hydrochloric acid. The contents of **1** and **3** in the crystals, those in the washing solution and those in the mother liquor were analyzed by glc (Expt. No. 1 in Table 2). The crystals were shown to be pure **1** (78% yield). The ratio of **1** to **3** in the mother liquor was found to be equal to the ratio of the equilibrium at room temperature, so the equilibrium between **1** and **3** is considered to be established in the solution before the end of the reaction. As shown in Fig. 1, only about 83% of **3** would be able to be converted to **1** if only the equilibrium reaction between **1** and **3** at room temperature was used. However, 97% of **3** could, in fact, be converted to **1** in our experiment as shown in Table 2 (Expt. No. 1). These results show that the isomerization and the fractional crystallization simultaneously took place in practice.

A mixture of 58% of **3** and 42% of **1** in crystalline states could also be converted to 96% of **1** and 4% of **3** on the whole as shown in Table 2 (Expt. No. 2). During this experiment, which is different from the case of Expt. No. 1, there were always some amount of crystals remaining in the solution.

By this method, any mixture composed of **1**, **2**, and **3** would be converted almost quantitatively to **1** in one vessel.

One-step Preparation of Cyclic Dipeptide from the Amino Acid. A cyclic dipeptide is known to be prepared by heating the corresponding amino acid in ethylene glycol, however, no detailed examination has yet been made on the composition of the product, that is, the

Table 2. Conversion of *c*-D-*a*Hyp-D-*a*Hyp (**3**) to *c*-L-Hyp-L-Hyp (**1**)

Expt. No.	Substrate	Composition of cyclic dipeptide[a]				
			Product			
		Starting material	Crystal	Washing solution	Mother liquor	Total
1[b]	**1** (mg)	0.0	141.9	8.1	25.4	175.4
	3 (mg)	181.0	0.0	0.2	5.2	5.4
	[**1**]/[**3**]	0/100	100/0	98/2	83/17	97/3
2[c]	**1** (g)	2.84	5.10	1.28		6.38
	3 (g)	3.96	0.04	0.21		0.25
	[**1**]/[**3**]	42/58	99/1	86/4		96/4

a) The amounts of cyclic dipeptides were estimated by glc. b) The solution of cyclic dipeptide in 0.1 M ethanolic sodium ethoxide (2 ml) was heated at 78°C for 15 min and cooled to room temperature for about 4 hr. c) The solution of cyclic dipeptides in 0.1 M ethanolic sodium ethoxide (43.6 ml) was treated in a similar manner to Expt. No. 1.

Table 3. One-step preparation of cyclic dipeptides from the corresponding amino acid by heating

Compd	Reaction condition[a]	Cyclic dipeptides, %[b]		
		Yield	Composition	
L-Hyp	A	88	**1**	70
			3	30
D-*a*Hyp	A	90	**1**	72
			3	28
L-*a*Hyp	A	87	**8**	71
			10	29
DL-Hyp + DL-*a*Hyp[c]	A	84	(**1** + **8**)	35
			(**3** + **10**)	15
			(**4** + **6**)	50
D-*a*Hyp	B	87	**1**	77
			3	23
L-Pro	B	80	(**11** + **12**)	100

a) A: a 20—25% solution of amino acid in water was heated at 260—290°C for 4 hr. B: a 5—10% solution of amino acid in ethylene glycol was refluxed for 7—10 hr. b) The content was estimated by glc. c) A mixture of equal amounts of DL-Hyp and DL-*a*Hyp.

amounts of *cis*- and *trans*-isomers.[9,10] In the course of the present studies, it was found that cyclic dipeptides can be formed even in an aqueous solution (instead of ethylene glycol) directly from the amino acid at high temperature in good yield. We therefore examined, in the next step, the composition of *cis*- and *trans*-isomers in such products. The results are shown in Table 3 for the case of 4-hydroxyproline and proline heated in an aqueous solution or ethylene glycol.

The composition of cyclic dipeptides produced by heating an aqueous solution of L-Hyp or D-*a*Hyp was found to be equal to that in the equilibrium of the isomerization between **1** and **3** at the same temperature. Pure **1** was easily obtained by the recrystallization of these cyclic dipeptides mixture from ethanol or water.

When a mixture of equal amounts of DL-Hyp and DL-*a*Hyp was heated in an aqueous solution, only the *cis*-isomers were formed. This *cis*-isomer mixture contained 50% of racemic modification of **1** and **3**, and 50% of racemic modification of *c*-L-Hyp-L-*a*Hyp (**4**) as shown in Table 3. Therefore, three isomerization reactions, *i.e.*, the reaction shown in Scheme 1, the reaction among *c*-D-Hyp-D-Hyp (**8**), *c*-D-Hyp-L-*a*Hyp (**9**) and *c*-L-*a*Hyp-L-*a*Hyp (**10**) (the enantiomeric reaction of Scheme 1), and the reaction among *c*-L-Hyp-L-*a*Hyp (**4**), *c*-L-Hyp-D-Hyp (**5**), *c*-D-*a*Hyp-D-Hyp (**6**), and *c*-D-*a*Hyp-L-*a*Hyp (**7**) (Scheme 2), occurred and

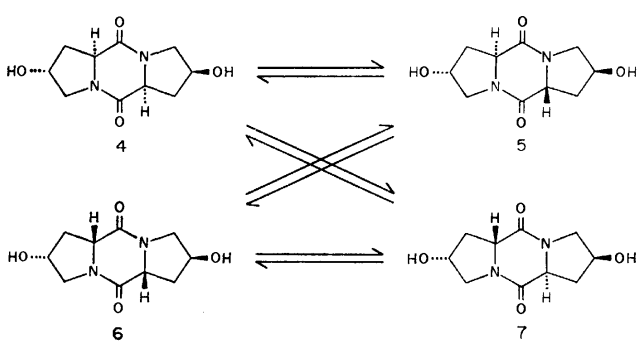

Scheme 2.

independently reached the equilibrium without mutual intersection.

By refluxing in ethylene glycol, L-Pro was coverted to optically inactive *c*-Pro-Pro,[10] which was found in the present studies to be racemic form, *i.e.*, equimolar mixture of *c*-L-Pro-L-Pro (**11**) and *c*-D-Pro-D-Pro (**12**), but not to be *meso* form, *c*-L-Pro-D-Pro (**13**).

Acid Hydrolysis of Cyclic Dipeptides. In order to obtain L-Hyp from D-*a*Hyp through cyclic dipeptide, **1** should be hydrolyzed into L-Hyp in its last step. Therefore, it is desirable that no racemization takes place in this procedure. It was reported, however, that the amino acids produced by acid hydrolysis of cyclic dipeptides were in general partially racemized.[11,12] We therefore made a slightly more detailed examination on this point.

Table 4. Acid hydrolysis of cyclic dipeptides

Compd	Reaction condition[a]	Amino acid, %		
			Yield[b]	Degree of racemization[c]
1	A	L-Hyp	97.4	2.1
		D-*a*Hyp	2.1	
2	A	L-Hyp	52.6	52.1
		D-*a*Hyp	48.2	
3	A	L-Hyp	3.3	3.3[d]
		D-*a*Hyp	96.4	
11	A	Pro	101.9	3.1[e]
14[f]	B	Ala	99.4	1.9[e]
15[g]	C	Val	69.9	1.2[e]

a) A: a 5% solution of cyclic dipeptide in 6 M hydrochloric acid was heated for 14 hr at 110°C in an open vessel B: a 0.5% solution of cyclic dipeptide in 6 M hydrochloric acid was similarly heated. C: a 0.3% solution of cyclic dipeptide in 6 M hydrochloric acid was similarly heated in a closed vessel. b) The analyses were carried out by amino acid analyzer. c) [D]/[L+D]. d) [L]/[L+D]. e) The analyses were performed by the method of Halpern and Westley (Refs. 15 and 16). f) *c*-L-Ala-L-Ala (**14**). g) *c*-L-Val-L-Val (**15**).

The *c*-Pro-Pro type of cyclic dipeptides were hydrolyzed under acidic condition and then the degree of racemization during hydrolysis was examined. The results are shown in Table 4. When a solution of the cyclic dipeptide in 6 M hydrochloric acid was heated for 14 hr at 110 °C, the degree of racemization was about 2—3%. This value is not so much larger than that found for other peptides.[13,14] Therefore, cyclic dipeptides are not necessarily considered to be easily racemized under acidic condition. Pure L-Hyp was easily obtained by recrystallization of crude L-Hyp produced by hydrolysis of **1**.

Conversion of D-a*Hyp to* L-*Hyp.* On the basis of our examination so far described, it has now been made clear that, by combination of isomerization and hydrolysis of cyclic dipeptide, L-Hyp could be readily obtained from D-*a*Hyp or any mixture of D-*a*Hyp and L-Hyp. Actually L-Hyp was obtained in 59% yield from D-*a*Hyp by the procedures. Here, the preparation of cyclic dipeptides was made in an aqueous solution by heating and the isomerization was made

in ethanolic sodium ethoxide. L-Hyp was also very easily obtained in 50% yield from D-*a*Hyp by combination of preparation of cyclic dipeptides by heating in ethylene glycol and acid hydrolysis of cyclic dipeptides. These procedures have been also applied to the conversion of L-*a*Hyp to D-Hyp with practically the same yield in the conversion of D-*a*Hyp to L-Hyp, as expected.

Experimental

All melting points are uncorrected. IR spectra were recorded in KBr disk on a Jasco Model IR-S Infrared Spectrophotometer. NMR spectra were measured in DMSO-d_6 solution with a Varian Spectrometer T-60 using TMS as internal standard. Mass spectra were obtained using a Hitachi RMU-6E Mass Spectrometer. Optical rotations were measured with a Jasco Model DIP-SL automatic polarimeter. The thin layer chromatography (tlc) was carried out on Merck silica gel 60 using the following solvent systems: (A) chloroform: methanol: acetic acid: water=68: 28: 1: 3; (B) *n*-butanol: acetic acid: water=4: 1: 1. The analyses of amino acid were carried out using a Hitachi KLA-3B Automatic Amino Acid Analyzer (column size, 50×0.9 cm; resin, Hitachi Type 2612; column flow rate, 60 ml/hr; buffer, citrate (0.2 N) pH 3.25; temperature, 55 °C). Glc analyses were performed using a Hewlet Packard 402 High Efficiency Gas Chromatogram equipped with FID and a 4 ft×1/4 in. i.d. glass column packed with 5% QF-1 on Chromosorb G (AW-DMC), 80—100 mesh.

Preparation of Cyclic Dipeptides. The physical constants of *c-Pro-Pro* type of cyclic dipeptides are summarized in Table 5.

c-L-*Hyp*-L-*Hyp* (*1*) and *c*-L-*Pro*-L-*Pro* (*11*) were prepared by the method of Kapfammer and Matthes.[17] *c*-L-*Pro*-D-*Pro* (*13*) was prepared by the method of Siemion.[6]

c-L-*Hyp*-D-*aHyp* (*2*). A mixture of D-*allo*-hydroxyproline methyl ester hydrochloride (6.90 g, 39.0 mmol) and equimolar triethylamine in 30 ml of chloroform was added at −5 °C with vigorously stirring to a mixture of *N*-carbobenzoxy-L-hydroxyproline (10.1 g, 38.0 mmol), methyl chloroformate (4.10 g, 38.0 mmol) and equimolar triethylamine in 100 ml of chloroform. The mixture was stirred at 0 °C for 4 hr and washed with water, 2 M hydrochloric acid, water, saturated sodium bicarbonate and water. The chloroform solution was dried over sodium sulfate. Evaporation gave *N*-carbobenzoxy-L-hydroxyprolyl-D-*allo*-hydroxyproline methyl ester (4.90 g) in 33% yield as oil. This dipeptide ester was hydrogenated in methanol solution at atmospheric pressure in the presence of 10% Pd-C (50 mg) for 10 hr and the filtrate was evaporated. Water (10 ml) was added to the residue and the aqueous solution was passed through an ion exchange column carrying 5 ml of IR·120 resin (acid form) to remove substrates positive for ninhydrin test. The passed solution was decolorized with active charcoal and evaporated to dryness under

TABLE 5. PHYSICAL CONSTANTS OF *c*-PRO-PRO TYPE OF CYCLIC DIPEPTIDES

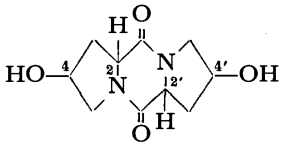

Compound	Configuration				°C Mp,	$[\alpha]_D^{28}$ (*c* 1.0, H_2O)	R_t[a] min	R_f[b]	Found (%)[c]		
	C_2	C_2'	C_4	C_4'					C	H	N
c-L-Hyp-L-Hyp[d]	S	S	R	R	248—249	−152.7	16.7	0.71	53.20	6.36	12.35
c-D-Hyp-D-Hyp	R	R	S	S	248—250	+153.9	16.7	0.71	53.09	6.27	12.49
c-D-*a*Hyp-D-*a*Hyp	R	R	R	R	220—221	+ 65.5	14.2	0.59	53.20	6.37	12.60
c-L-Hyp-D-*a*Hyp	R	S	R	R	210—211	− 18.5	18.2	0.63	53.09	6.24	12.28
c-L-Hyp-L-*a*Hyp	S	S	R	S	192—193	−113.3	14.2	0.63	53.27	6.19	12.53
c-L-Hyp-D-Hyp	S	R	R	S	275—276	0	21.2	0.68	52.88	6.23	12.11
c-D-*a*Hyp-L-*a*Hyp	R	S	R	S	240—241	0	16.6	0.59	53.04	6.17	12.38

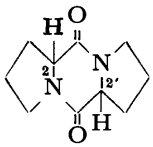

Compound	Configuration		Mp, °C	$[\alpha]_D^{24}$ (*c* 1.0, H_2O)	R_t[e] min	R_f[f]	Found (%)[g]		
	C_2	C_2'					C	H	N
c-L-Pro-L-Pro[h]	S	S	143—144	−149.5	9.0	0.62	61.60	7.20	14.36
c-D-Pro-D-Pro	R	R	141—143	+147.5	9.0	0.62	61.68	7.27	14.25
racemi *c*-Pro-Pro	S (R)	S (R)	149—150	0	9.0	0.62	61.60	7.30	14.50
c-L-Pro-D-Pro[i]	S	R	193—195	0	10.2	0.60	62.00	7.23	14.40

a) Retention time of the trimethylsilyl derivative of cyclic dipeptide in glc (220 °C; He gas, 80 ml/min). b) R_f value of tlc using solvent system A. c) Calcd for $C_{10}H_{14}O_4N_2$: C, 53.09; H, 6.24; N, 12.38%. d) Mp 245—246 °C, $[\alpha]_D^{19}$ −153.4 °C (c 2.05, H_2O) (Ref. 17); $[\alpha]_D$ −153 ° (Ref. 18). e) Retention time of unmodified cyclic dipeptide in glc (192 °C; He gas, 80 ml/min). f) R_f value of tlc using solvent system B. g) Calcd for $C_{10}H_{14}O_2N_2$: C, 61.83; H, 7.27; N, 14.42%. h) Mp 146 °C, $[\alpha]_D^{19}$ −147.2 ° (*c* 2.13, H_2O) (Ref. 17); mp 143 °C, $[\alpha]_D^{20}$ −151.15 ° (*c* 0.867, H_2O) (Ref. 19). i) Mp 179—181 °C (Ref. 6).

reduced pressure. The residue was recrystallized from ethanol–ether to give 1.22 g (5.40 mmol) of **2** in 43% yield from dipeptide ester: IR 3380 (OH), 1655 and 1625 (C=O) cm^{-1}; NMR δ 1.6—2.2 (4H), 3.40 (4H), 4.2—4.5 (4H) and 5.16 (2H).

c-L-*Hyp*-L-*aHyp* (**4**), *c*-L-*Hyp*-D-*Hyp* (**5**) and *c*-D-*aHyp*-L-*aHyp* (**7**) were prepared in a similar manner to that of **2**. **4**: IR 3350 (OH), 1632 and 1645 (C=O) cm^{-1}; NMR δ 1.9—2.4 (4H), 3.39 (4H), 4.2—4.6 (4H) and 5.10 (2H). **5**: IR 3334 (OH) and 1630 (C=O) cm^{-1}; NMR δ 1.8—2.2 (4H), 3.4 (4H), 4.0—4.5 (4H) and 5.22 (2H). **7**: IR 3390 (OH) and 1635 (C=O) cm^{-1}; NMR δ 1.5—2.0 (4H), 3.40 (4H), 4.0—4.6 (4H) and 5.20 (2H).

c-D-*aHyp*-D-*aHyp* (**3**). Thionyl chloride (5.45 g, 45.8 mmol) was added to a solution of D-*aHyp* (5.00 mg, 38.2 mmol) in 50 ml of methanol at —5 °C. The mixture was refluxed for 2 hr and evaporated under reduced pressure. Anhydrous ammonia was bubbled into a chloroform solution (50 ml) of the dried residue at 0 °C. After filtration of ammonium chloride, the filtrate was concentrated below 40 °C under reduced pressure. The resulting syrup was allowed to stand at room temperature for two weeks. Water (10 ml) was added and the aqueous solution was treated with IR-120 resin (acid form) and active charcoal in a similar manner to that of **2**. The residue was recrystallized from ethanol to give 3.67 g (16.2 mmol) of **3** in 85% yield: IR 3380 (OH) and 1645 (C=O) cm^{-1}; NMR δ 2.1—2.5 (4H), 3.35 (4H), 4.2—4.5 (4H) and 5.00 (2H); mass spectrum *m/e* 226 (M^+), 198, 140, 112 and 86. Differences among **1**—**10** were not found in mass spectra.

c-D-*Pro*-D-*Pro* (**12**) was prepared from D-Pro in a similar manner to that of **3**.

Racemic c-Pro-Pro. An equimolar mixture of **11** (0.219 g, 1.13 mmol) and **12** (0.219 g, 1.13 mmol) in ethanol was recrystallized to yield racemic *c*-Pro-Pro (0.277 g, 1.43 mmol, 63%).

Isomerization in 0.1 M Ethanolic Sodium Ethoxide. A solution of *c*-D-*a*Hyp-D-*a*Hyp (**3**) (50.0 mg, 0.221 mmol) in absolute ethanol (3.57 ml) was allowed to stand at 50.0±0.1 °C. The isomerization started immediately after 0.85 ml of 0.520 M ethanolic sodium ethoxide was poured into the solution. After 5 min, 0.44 ml of the solution was taken out and rapidly poured into 0.095 ml of 0.5 M hydrochloric acid. The slightly acidic solution was immediately evaporated to dryness under reduced pressure. The residue was further dried *in vacuo* over potasium hydroxide and was heated with *N,O*-bis(trimethylsilyl)acetamide (0.5 ml) and dry pyridine (0.5 ml) for 5 min at 80 °C. The mixture was injected directly into gas liquid chromatogram. The contents of **1**, **2** and **3** were analyzed. The mixture was composed of 26.1% of **1** and 73.9% of **3**. **2** was not detectable. The samplings were done at different times. The following results were obtained: 52.8% of **1** at 15 min, 74.3% of **1** at 30 min, 83.3% of **1** at 1 hr, 83.6% of **1** at 3 hr, 83.7% of **1** at 4 hr, 83.4% of **1** at 5 hr, and 83.6% of **1** at 8 hr. From the isomerization using **1** as a starting material, the following results were obtained at the same temperature: 83.6% of **1** at 3 hr, 83.7% of **1** at 4 hr, and 83.4% of **1** at 8 hr. The isomerizations were similarly carried out at 25.0±0.1 °C and 78.0±0.1 °C by use of **1**, **2** and **3**. The time required for reaching the equilibrium between **1** and **3** was about 20 hr at 25 °C, 2 hr at 50 °C and 0.5 hr at 78 °C.

Isomerization in Aqueous Solution. A solution of *c*-L-Hyp-D-*a*Hyp (**2**) (50 mg, 0.22 mmol) in water (0.5 ml) was sealed in a small glass tube and heated at 100 °C for 2 hr. The tube was immediately cooled and opened. One-eighth of the resulting clear solution was taken out and evaporated under reduced pressure. The residue was treated in a similar manner to that described in the isomerization in ethanolic sodium ethoxide. The product was composed of 46.8% of **1**, 42.0% of **2** and 11.2% of **3**. In a similar manner, the isomerizations were carried out at 50, 75, 100, 150, 200 and 250 °C by use of **1**, **2** and **3**.

Conversion of c-D-aHyp-D-aHyp (3) to c-L-Hyp-L-Hyp (1). The reaction condition and the results are shown in Table 2. The following results were obtained for the crystals in Table 2, Expt. No. 1: mp 243—245 °C; $[\alpha]_D^{25}$ −153.2° (*c* 1.00, H_2O); Found: C, 53.30; H, 6.32; N, 12.40; Na, 0.041%. Calcd for $C_{10}H_{14}O_4N_2$: C, 53.09; H, 6.24; N, 12.38%. The following analytical results were also obtained for the crystals in Table 2, Expt. No. 2: mp 245—247 °C; $[\alpha]_D^{28}$ −150.1° (*c* 1.00, H_2O).

Preparation of c-L-Hyp-L-Hyp (1) from D-aHyp. (*A*) A solution of D-*a*Hyp (15.0 g, 115 mmol) in water (80 ml) was heated at 250—270 °C for 4 hr. The mixture was passed through an ion exchange column carrying 15 ml of IR-120 resin (acid form) to remove substrates positive for ninhydrin test. The passed solution was decolorized with active charcoal and evaporated to dryness under reduced pressure. The residue was further dried *in vacuo* over phosphorus pentoxide. The residue weighed 11.6 g and, by the results of glc analyses, was composed of 72% of **1** and 28% of **3**. A solution of 10.0 g of the cyclic dipeptide mixture thus obtained in 0.1 M ethanolic sodium ethoxide (70.0 ml) was heated by stirring at 78 °C for 30 min. The solution was cooled by gently stirring to room temperature for 4 hr. The crystals thus produced were filtered, washed with cooled absolute ethanol and dried *in vacuo* to give 7.54 g (33.4 mmol) of **1** in 68% yield from D-*a*Hyp: mp 247—249 °C; $[\alpha]_D^{24}$ −152.0° (c 1.00, H_2O); Found: C, 53.08; H, 6.26: N, 12.34%. Calcd for $C_{10}H_{14}O_4N_2$: C, 53.09; H, 6.24; N, 12.38%.

(*B*) A solution of D-*a*Hyp (30.0 g, 229 mmol) in ethylene glycol (500 ml) was heated under refluxing for 10 hr. The mixture was evaporated under reduced pressure. Water (150 ml) was poured into the residue. The aqueous solution was similary treated with IR-120 resin and active charcoal, and evaporated. By the results of glc analyses, the residue contained 22.3 g (99 mmol, 87%) of cyclic dipeptides composed of 77% of **1** and 23% of **3**. This residue was recrystallized from water to give 14.8 g (65.5 mmol) of **1** in 57% yield: mp 248—249 °C; $[\alpha]_D^{28}$ −155.3° (c 1.00, H_2O); Found: C, 53.00; H, 6.26; N, 12.41%. Calcd for $C_{10}H_{14}O_4N_2$: C, 53.09; H, 6.24; N, 12.38%.

Preparation of c-D-Hyp-D-Hyp (8) from L-aHyp. A solution of L-*a*Hyp (7.85 g, 59.9 mmol) in water (70 ml) was heated at 270—290 °C for 2 hr and was similarly treated with IR-120 resin. By the results of glc analyses, the passed solution contained 5.89 g (26.1 mmol, 87%) of cyclic dipeptides composed of 71% of **8** and 29% of *c*-L-*aHyp*-L-*aHyp* (**10**). The passed solution was decolorized with active charcoal, concentrated and cooled. The crystals thus produced were filtered, washed with cold water and dried *in vacuo* to give 3.68 g (16.3 mmol) of **8** in 54% yield: mp 248—250 °C; $[\alpha]_D^{28}$ +153.9° (c 1.17, H_2O); Found: C, 53.09; H, 6.27; N, 12.49%. Calcd for $C_{10}H_{14}O_4N_2$: C, 53.09; H, 6.24; N, 12.38%. IR 3290 (OH), 1655 and 1635 (C=O) cm^{-1}. NMR δ 1.9—2.1 (4H). 3.32 (4H), 4.1—4.7 (4H) and 5.05 (2H).

Hydrolysis of c-L-Hyp-L-Hyp (1). A solution of **1** (5.00 g, 22.1 mmol) in 6 M hydrochloric acid (100 ml) was heated for 14 hr at 110 °C. The contents of amino acids in the mixture were analyzed by automatic amino acid analyzer. L-Hyp (5.65 g, 43.1 mmol, 97.4% yield) and D-*a*Hyp (0.12 g, 0.93 mmol, 2.1% yield) were formed. The mixture was evaporated under reduced pressure. The residue was dissolved in water (30 ml) and the aqueous solution was

applied to an ion exchange column carrying 100 ml of IR-120 resin (acid form). The resin was washed with water and the absorbed amino acids were eluted with 0.2 M ammonium hydroxide. The elute was decolorized with active charcoal and concentrated under reduced pressure. Ethanol was poured into the residue to yield precipitates. The precipitates were filtered, washed with ethanol and dried *in vacuo* to give 5.03 g (38.4 mmol) of L-Hyp in 87% yield: mp 276—277 °C; $[\alpha]_D^{29}$ —76.0° (c 1.01, H_2O); Found: C, 45.92; H, 6.75; N, 10.84%. Calcd for $C_5H_9O_3N$: C, 45.80; H, 6.92; N, 10.68%.

The authors wish to express their thanks to Prof. Masamichi Tsuboi and Prof. Naoki Inamoto in University of Tokyo for their valuable suggestions, and to Dr. Takehiko Ichikawa, Dr. Yuji Iwashita and Dr. Masatsune Kainosho for many helpful discussions.

References

1) Part I: (a) C. Equchi and A. Kakuta, The 6th Symposium on Structural Organic Chemistry, October 12, Fukuoka (1973), p. 109 of the Proceeding. (b) C. Equchi and A. Kakuta, *J. Amer. Chem. Soc.*, **96**, 3985 (1974).

2) The abbriviations for amino acids and peptides recommended by the IUPAC-IUB Commision on Biochemical Nomenclature, *J. Biol. Chem.*, **247**, 977 (1972), have been used throughout. In addition: Hyp=*trans*-4-hydroxyproline, *a*Hyp=*cis*-4-hydroxyproline, *c*=*cyclo*.

3) H. Leuchs and H. Felser, *Ber.*, **41**, 1726 (1908).

4) D. S. Robinson and J. P. Greenstein, *J. Biol. Chem.*, **195**, 383 (1952).

5) C. Eguchi and A. Kakuta, This Bulletin, **47**, 1704 (1974).

6) I. Z. Siemion, *Ann. Chem.*, **748**, 88 (1971).

7) J. Vičar, M. Buděšinsky, and K. Blaha, *Collect. Czech. Chem. Commun.*, **38**, 1940 (1973).

8) P. E. Young, V. Madison, and E. R. Blout, *J. Amer. Chem. Soc.*, **95**, 6142 (1973).

9) H. F. Scott, J. B. Larkin, L. B. Rockland, and M. S. Dunn, *J. Org. Chem.*, **12**, 490 (1947).

10) J. P. Li and J. H. Biel, *J. Heterocycl. Chem.*, 307, (1968).

11) P. A. Levene and R. E. Steiger, *J. Biol. Chem.*, **86**, 703 (1930).

12) P. A. Levene, A. Rothen, R. E. Steiger, and M. Osaki, *ibid.*, **86**, 723 (1930).

13) J. M. Manning and S. Moore, *ibid.*, **243**, 5591 (1968).

14) E. Bayer, E. Gil-Av, W. A. König, S. Nakaparksin, J. Oro, and W. Parr, *J. Amer. Chem. Soc.*, **92**, 1738 (1970).

15) B. Halpern and J. W. Westley, *Biochem. Biophys. Res. Commun.*, **19**, 361 (1965).

16) W. A. Bonner, *J. Chromatogr. Sci.*, **10**, 159 (1972).

17) J. Kapfammer and A. Matthes, *Z. Phys. Chem.*, **223**, 43 (1933).

18) A. Chemizard and S. Pavid, *Bull. Soc. Chim. Fr.*, **1**, 184 (1966).

19) E. Abderhlden and H. Nienburg, *Ferment Forschung*, **13**, 573 (1933).

A Photochemical Reaction of Lupan-3-one

Hiroshi HIROTA, Takahiko TSUYUKI, Yoshiaki TANAHASHI, and Takeyoshi TAKAHASHI

Department of Chemistry, Faculty of Science, The University of Tokyo, Bunkyo-ku, Tokyo 113

(Received April 8, 1974)

Lupan-3-one (**5**) was irradiated in *n*-hexane under an argon atmosphere using a high pressure mercury lamp. Besides three seco compounds, namely 10α-(2-formylethyl)-5β-isopropenyl-des-A-lupane (**6**), 10α-(2-carboxyethyl)-5β-isopropyl-des-A-lupane (**8**), and 10α-(2-carboxyethyl)-5β-isopropenyl-des-A-lupane (**9**), two seco-nor compounds, 10α-(carboxymethyl)-5β-isopropyl-des-A-lupane (**7**) and lactone of 10α-(carboxymethyl)-5α-hydroxy-5β-isopropyl-des-A-lupane (**10**), have been isolated and their structures have been determined. NMR signals of **10** were examined using Eu(fod)$_3$-d_{27} as a shift reagent.

In previous papers[1] we reported the photochemical reaction of friedelin (**1**), in which seco-nor products such as 5α-ethyl-10β-(formylmethyl)-des-A-friedelane (**2**) and 10β-(carboxymethyl)-5α-ethyl-des-A-friedelane (**3**) were obtained as abnormal products together with a normal product, 10β-(2-carboxyethyl)-5α-ethyl-des-A-friedelane (**4**). In connection with this observation, a formation of seco-nor derivatives was examined in a photo-reaction of lupan-3-one (**5**), bearing a 3-oxo-4,4-dimethyl moiety in the A ring. We wish to describe the isolation and structure determination of compounds (**6**—**10**) which were obtained by the photolysis of lupan-3-one (**5**) in *n*-hexane. Among these products, the seco-acid (**8**) had been obtained in about 50% yield by the photolysis of **5** in a mixture of water and acetic acid.[2]

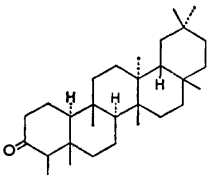

1

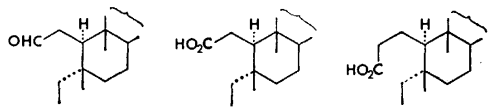

2 3 4

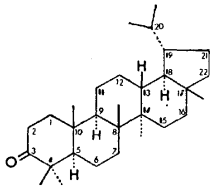

5

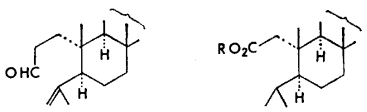

6 7 R=H 7a R=Me

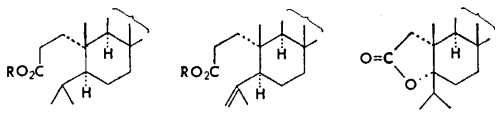

8 R=H 8a R=Me 9 R=H 9a R=Me 10

A solution of lupan-3-one (**5**) in *n*-hexane was irradiated at room temperature under an argon atmosphere for about 6.5 hr using a 100 W high pressure mercury lamp to give a complex reaction mixture, which was separated by silica gel column and thin layer chromatographies into hydrocarbon, aldehyde, ketone, lactone, and acid fractions.

From the aldehyde fraction, only one compound, $C_{30}H_{50}O$ (M^+ *m/e* 426) was isolated. This substance showed the presence of one olefinic methyl (δ 1.72), two olefinic protons (δ 4.65 and 4.85, each multiplet) and an aldehydic proton (δ 9.75, t, J=2 Hz) in NMR spectrum and exhibited characteristic IR absorption bands at 2720, 1735 (–CHO), 1640 and 895 cm^{-1} (–C=CH$_2$). Thus, the aldehyde was inferred to be 10α-(2-formylethyl)-5β-isopropenyl-des-A-lupane (**6**) and the structure was also supported by the fragmentation pattern of the mass spectrum.

The isolation of an unsaturated aldehyde with an isopropenyl group rather than an isopropylidene group in the photolysis of lupan-3-one (**5**) is unexpected. Since the well-documented photo-cleavage of cyclohexanones leads to a δ-unsaturated aldehyde by α-cleavage followed by transfer of a hydrogen atom from a δ-carbon (C-5 in the case of lupan-3-one (**5**)) *via* a six-membered ring transition state (reaction pathway "a"), the resulting unsaturated aldehyde from lupan-3-one (**5**) should be 10α-(2-formylethyl)-5-isopropylidene-des-A-lupane (**11**). The formation of the unsaturated aldehyde (**6**) with an isopropenyl moiety could be explained by α-cleavage of **5** followed by an abstraction of a hydrogen atom of $C_{(4)}$–CH_3 by the acyl radical through an eight-membered ring transition state (reaction pathway "b").[3] Although the occurrence of the reaction pathway "a" seems to be more likely than that of the path "b" in lupan-3-one (**5**), the aldehyde (**11**) was not obtained in the photolysate. However, the absence of the aldehyde (**11**) does not always mean that the path "a" did not occur at all,

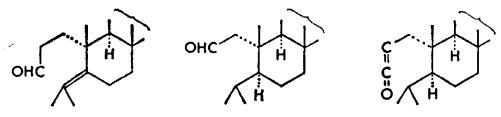

11 12 13

because the aldehyde (**11**) could further react photochemically or thermally.

The ketone fraction was shown to be lupan-3-one (**5**) and the recovery was about 12%.

The carboxylic acid fraction showed three spots on tlc. A compound with the highest R_f value had molecular formula $C_{29}H_{50}O$, which was confirmed by high resolution mass spectrometry, and showed IR absorption band at 1705 cm^{-1}. This acid was converted into the methyl ester (IR 1740 cm^{-1}; NMR δ 3.64 ($-CO_2C\underline{H}_3$) and 2.37 (2H, s, $-\underset{|}{C}-C\underline{H}_2-CO_2CH_3$); M^+ *m/e* 444). From these findings, the original acid could be formulated as 10α-(carboxymethyl)-5β-isopropyl-des-A-lupane (**7**). This acid with one carbon atom less than lupan-3-one (**5**) is corresponding to the photochemically unusual carboxylic acid (**3**) obtained by the photochemical reaction of friedelin (**1**) in *n*-hexane. Although in the case of lupan-3-one (**5**), the seco-nor aldehyde (**12**) was not isolated, the formation of the acid (**7**) was explicable by the oxidation of the seco-nor aldehyde (**12**), which could be produced by the autoxidation of the ketene (**13**) during a subsequent separation work-up after the irradiation, as stated elsewhere.[1]

The remaining two carboxylic acids were converted into their methyl esters and separated by tlc. A methyl ester with higher R_f value was identical with an authentic specimen (**8a**), which was prepared by photochemical reaction of lup-20(29)-en-3-one (**14**) in methanol followed by hydrogenation. Thus, the original acid was identified to be 10α-(2-carboxyethyl)-5β-isopropyl-des-A-lupane (**8**) and the spectral data were identical with those of tetrahydrocanaric acid.[2]

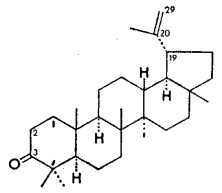

14

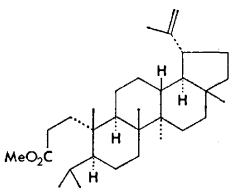

21

The other methyl ester with lower R_f value showed characteristic IR and NMR spectra due to an isopropenyl group. On hydrogenation, the methyl ester gave a saturated methyl ester, which was identical with 5β-isopropyl-10α-(2-methoxycarbonylethyl)-des-A-lupane (**8a**). The carboxylic acid, therefore, was formulated as 10α-(2-carboxyethyl)-5β-isopropenyl-des-A-lupane (**9**) and the formation could be explained by the oxidation of the unsaturated aldehyde (**6**) during work-up.

A lactone was isolated from the fraction between the ketone and the carboxylic acids by preparative tlc and recrystallized from chloroform-methanol. IR and NMR spectral data and the molecular formula, $C_{28}H_{48}O_2$, given by high resolution mass spectrometry, indicate the presence of a γ-lactone group with one carbon atom less than the original ketone (**5**). Fragment ions at *m/e* 191 ($C_{14}H_{23}$) and 205 ($C_{15}H_{25}$) correspond to species **15** and **16**, respectively, showing the presence of the intact rings D and E (and C).[4] The NMR spectrum showed the presence of an isolated methylene (δ 2.41, 2H, br.s) at the α-position to the carbonyl group and the absence of a hydrogen atom on the carbon atom adjacent to the ethereal oxygen atom.

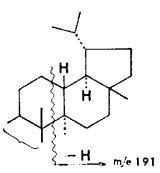

15

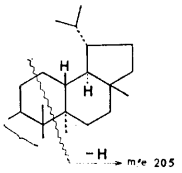

16

NMR measurements using Eu(fod)$_3$-d_{27} as a shift reagent were applied in order to determine the structure of the lactone. The result was summarized in Fig. 1. A spectrum obtained in a mixture of Eu(fod)$_3$-d_{27} and the lactone in a molar ratio of 1.33: 1 in deuteriochloroform solution, was given in Fig. 2. In addition to the isopropyl group at C-19, the presence of a new isopropyl group was clearly shown. On irradiation of the signal around δ 5.3, two pairs of doublets due to two methyl protons (δ 3.54, J=7 Hz and δ 2.46, J=7 Hz) changed into two singlets. Judging from a large degree of the shift, one of the isopropyl groups must be located fairly near the carbonyl group. These observations suggest that the lactone could be represented by structure (**10**).

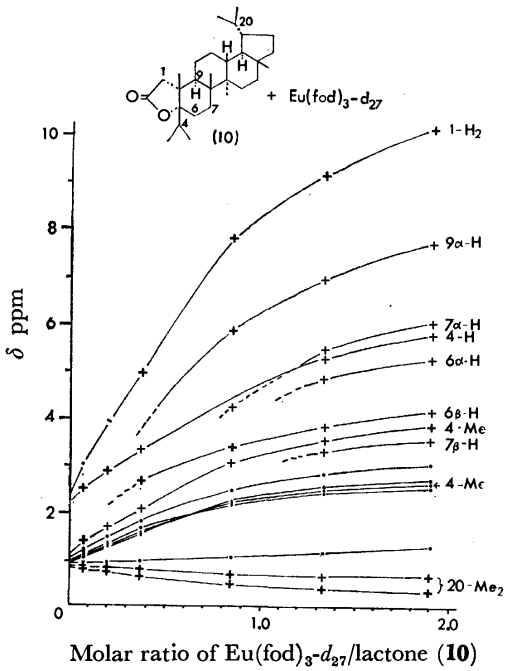

Fig. 1. Molar ratio of Eu(fod)$_3$-d_{27}/lactone (**10**) *vs.* chemical shift.

From the fact that two methylene protons adjacent to the carbonyl carbon were shifted with the largest slope and with nearly the same degree (see Figs. 1 and 2), it is considered that Eu(fod)$_3$-d_{27} is associated with the carbonyl group (and the ethereal oxygen) and located almost on a plane which bisects the methylene group at C-1. One proton (q, J=10.5 and 5.5 Hz) showing the second largest slope was assigned to 9α-(axial)-proton from the degree of shift (Figs. 1 and 2). These assignments, therefore, lead to the conclusion

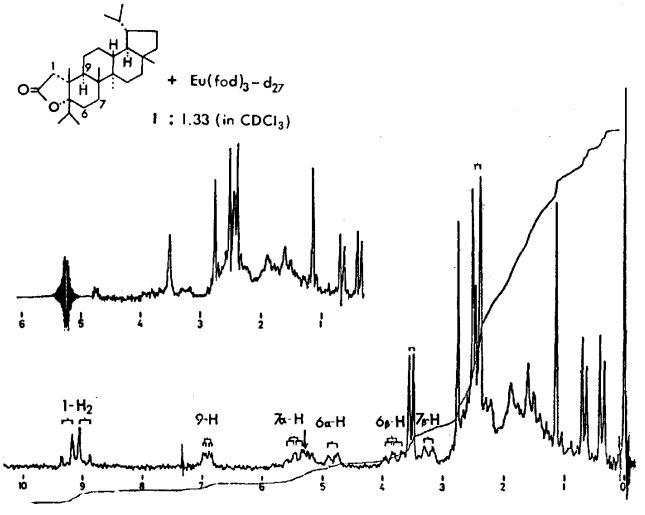

Fig. 2. NMR spectra.

that the ring juncture A/B is *cis* and then the C-5 isopropyl group is situated in β-side. The other stereochemistries are not compatible with the spectral data including pseudo-contact shift experiments. For example, a proton at C-9 of a *trans*-lactone (a C-5 epimer of **10**) would scarecely suffer the induced paramagnetic shift. Thus, the conformation of the lactone molecule is established as **17**. This conformation (**17**) could also explain a small shift of two methyl protons of 19α-isopropyl group. The remaining four protons (7α-, 6α-, 6β-, and 7β-) at ring B, which showed fairly large shifts, could be assigned as shown in Fig. 2 from the degree of the pseudo-contact shift and from the results of decoupling experiments (Figs. 1 and 2).

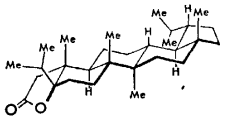

17

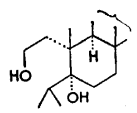

18

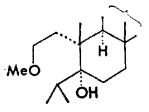

19

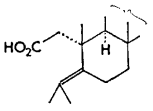

20

The lactone (**10**) was reduced with lithium aluminium hydride in tetrahydrofuran to the corresponding diol (**18**), which in turn was coverted into the monomethyl ether (**19**) with methyl iodide and silver oxide in dimethylformamide.[5] The spectral data of these two derivatives could be explicable by their proposed structures. These observations furnish further evidence for the presence of the lactone structure in **10**.

It is most likely that the lactone (**10**) may be derived from 10α-carboxymethyl-5-isopropylidene-des-A-lupane (**20**), which was undetectable in the photo-reaction products of lupan-3-one (**5**) in *n*-hexane, although the formation of the unsaturated seco-nor acid (**20**) could hardly be explained. The elucidation of the mechanism is under way.

Experimental

IR spectra were measured using a Hitachi EPI-G2 spectrometer. NMR spectra were taken on a Hitachi R-20B (60 MHz) or a JEOL-PS-100 spectrometer (100 MHz) in deuteriochloroform solution containing tetramethylsilane as an internal standard. High resolution mass spectra were measured using a Hitachi RMH-2 or RMU-7M mass spectrometer operating at 70 eV. Measurements of low resolution mass spectra were carried out using a Hitachi RMU-6-Tokugata mass spectrometer with a direct inlet system operating at 70 eV unless otherwise stated. Gas chromatographic (glc) analyses were performed on a Shimadzu gas chromatograph model GC-4APF. For column chromatography Wakogel C-200 (Wako Pure Chemical Industries) and Activated Alumina (mesh 200—300, Showa Chemical Co.) were used. Thin layer chromatography (tlc) was carried out on Kieselgel G (E. Merck, Darmstadt) in 0.25 mm thickness. All melting points were determined on a hot block and reported uncorrected.

n-Hexane (extra pure grade, Wako Pure Chemical Industries) was found to contain 2-methylpentane, 3-methylpentane, and methylcyclopentane, but no unsaturated hydrocarbons as impurities by GC-MS examination (column: DC-550, 1m; oven temperature 10 °C). Any coloration with concentrated sulfuric acid was not observed.

The purity of the starting material, lupan-3-one (**5**) was checked by glc (column: OV-1 (2%); 270 °C and OV-17 (2%), 300 °C), tlc, and MS. And the absence of any compound with one carbon atom less than lupan-3-one (**5**) was confirmed.

Photochemical Reaction of Lupan-3-one (5). Lupan-3-one (**5**; 500 mg) was dissolved completely in dry *n*-hexane (750 ml) and the solution in a Pyrex vessel was then irradiated for about 6.5 hr at room temperature using a 100 W high pressure mercury lamp under an argon atmosphere.

Isolation and Characterization of the Reaction Products. After the solvent was distilled off under reduced pressure, the reaction products were roughly separated by silica gel (100 g) column chromatography into hydrocarbon, aldehyde, ketone, lactone, and carboxylic acid fractions. Each fraction was further separated and purified by repetition of column and/or preparative thin layer chromatography.

Elution with petroleum ether gave a mixture (about 20 mg) of hydrocarbons, which showed more than three spots on tlc (10% $AgNO_3$-SiO_2). Further examination of the mixture was not effected.

Successive elution with petroleum ether–benzene (1: 1) afforded about 80 mg of a crude aldehyde (**6**). However, the aldehyde was so liable to decompose gradually in contact with air and rapidly on silica gel and alumina, that column chromatographic separations on silica gel and then on alumina could give only about 20 mg of the aldehyde (**6**).

Upon continued elution with benzene, a ketone (about 60 mg) was obtained, which was identified by direct comparison of the IR and MS data with those of the starting material, lupan-3-one (**5**).

Although further elution with benzene–ether (10: 1) was continued, good separation was not obtained. A mixture (about 180 mg) of γ-lactone (**10**), carboxylic acids (**7**), (**8**), and (**9**) and other unknown minor compounds was eluted at the same time. The main four compounds were recorded in their order of elution. Since it was difficult to separate these compounds completely, further separation was accompanied with a considerable extent of loss. Repetition of column and thin layer chromatographic separations, though

these methods were not so effective for the separation of the fraction obtained above, could afford about 20 mg of pure γ-lactone (**10**) and about 15 mg of pure seco-nor acid (**7**). A mixture of the remaining two carboxylic acids with the lowest and the second lowest R_f values was treated with diazomethane in ether to give a mixture of their methyl esters (**8a**) and (**9a**). The mixture was separated into **8a** and **9a**. Each weighed about 15—20 mg.

10α-(2-Formylethyl)-5β-isopropenyl-des-A-lupane (6): An amorphous solid, IR (KBr disk) 2720, 1735, 1640, and 895 cm^{-1}; NMR δ 1.72 (CH_2=Ç-C$\underline{H}_3$), 4.65, 4.85 (each m, C$\underline{H}_2$=Ç-), and 9.75 (t, J=2 Hz, -C$\underline{H}$O), 0.76, 0.82, 0.88, 0.95, 1.05, and 1.10 (other methyl protons); MS *m/e* (relative intensity %) 426 [3; $M^+(C_{30}H_{50}O)$], 411 [3; $(M-15)^+$], 383 [5; $(M-43)^+$], 369 [5; $(M-57)^+$], 345 [12; $(M-81)^+$], 327 [15; $(M-99)^+$], 231 (17), 205 (37), 191 (61), and 81 (100).

10α-(Carboxymethyl)-5β-isopropyl-des-A-lupane (7): An amorphous solid, IR (Nujol mull) 3400—2500 (br) and 1705 cm^{-1}; MW 430.3805, Calcd for $C_{29}H_{50}O_2$: 430.3808; MS *m/e* (%) 430 (13; M^+), 387 (16), 371 (6), 370 (4), 259 (8), 231 (10), 205 (16), 191 (31), and 95 (100).

5β-Isopropyl-10α-(methoxycarbonylmethyl)-des-A-lupane (7a): The above carboxylic acid (**7**; 15 mg) was treated with diazomethane and the methyl ester (**7a**; 12 mg) was obtained. An oil, IR (neat) 1740 cm^{-1}; NMR δ 2.37 (2**H**, s), 3.64 (3H, s), and other methyl protons; 0.75 (s), 0.83 (s), 0.91 (s), 1.05 (s), 0.75 (d, J=6.5 Hz), 0.82 (d, J=6.5 Hz), 0.84 (d, J=6.5 Hz), and 0.93 (d, J=6.5 Hz); MS *m/e* (%) 444 [23; $M^+(C_{30}H_{52}O_2)$], 401 (20), 371 (18), 370 (29), 205 (23), 191 (31), 178 (18), 177 (21), and 95 (100).

5β-Isopropyl-10α-(2-methoxycarbonylethyl)-des-A-lupane (8a): Mp 139—140 °C (recrystallized from chloroform-methanol); IR (KBr disk) 1745 cm^{-1}; MW 458.4130, Calcd for $C_{31}H_{54}O_2$: 458.4121; MS *m/e* (%) 458 (11; M^+), 443 (6), 415 (11), 371 (12), 253 (23), 231 (19), 209 (21), 205 (25), 191 (40), 137 (80), and 109 (100).

5β-Isopropenyl-10α-(2-methoxycarbonylethyl)-des-A-lupane (9a): An amorphous solid, IR (KBr disk) 1745, 1640, and 890 cm^{-1}; NMR δ 0.75 (3H, s), 0.76 (3H, d, J=7 Hz), 0.83 (3H, d, J=7 Hz), 0.84 (3H, s), 0.94 (3H, s), 1.08 (3H, s), 1.72 (3H, s), 2.25 (2H, m), 3.63 (3H, s), ~4.6 (1**H**, m), and ~4.8 (1H, m); MS *m/e* (%) 456 [5; $M^+(C_{31}H_{52}O_2)$], 441 (3), 425 (2), 413 (5), 375 (47), 369 (13), 231 (24), 205 (32), 191 (52), and 109 (100), (Ionization potential: 30 eV).

The methyl ester (**9a**; 10 mg) in methanol (30 ml) was hydrogenated in the presence of 10% palladium-carbon at room temperature overnight to afford **8a** quantitatively. This ester (**8a**) was identical (IR, NMR, and tlc) with a specimen mentioned above and also with an authentic specimen, prepared by photochemical reaction of lup-20(29)-en-3-one (**14**) in methanol followed by hydrogenation (*vide infra*).

Lactone of 10α-(Carboxymethyl)-5α-hydroxy-5β-isopropyl-des-A-lupane (10): A white crystal, mp 245—246 °C with sublimation; IR (KBr disk) 1775, 1455, 1390, 1385, 1375, 1280, 1245, 995, 950, and 945 cm^{-1}; MW 428.3652, Calcd for $C_{29}H_{48}O_2$: 428.3652; MS *m/e* (%; fragment composition, determined by high resolution mass spectrometry) 428 (2; $C_{29}H_{48}O_2$), 413 (3; $C_{28}H_{45}O_2$), 400 (1; $C_{28}H_{48}O$), 385 (95; $C_{26}H_{41}O_2$), 357 (24; $C_{25}H_{41}O$), 205 (15; $C_{15}H_{25}$), 191 (33; $C_{14}H_{23}$), and 69 (100; C_5H_9); NMR δ 0.77 (3H, d, J=7 Hz), 0.79 (3H, s), 0.87 (3H, d, J=7 Hz), 0.95 (3H, s), 1.03 (6H, d, J=7 Hz), 1.12 (3H, s), 1.16 (3H, s), and 2.41 (2H, br.s). The data using Eu(fod)$_3$-d_{27} were shown in Figs. 1 and 2.

Reduction of Lactone of 10α-Carboxymethyl-5α-hydroxy-5β-isopropyl-des-A-lupane (10) with Lithium Aluminium Hydride. A mixture of the lactone (**10**; 45 mg) and lithium aluminium hydride (about 30 mg, in large excess) in tetrahydrofuran (10 ml) was heated under reflux for 8.5 hr. Usual work-up gave a crystalline product, which was purified by preparative tlc to afford 5α-hydroxy-10α-(2-hydroxyethyl)-5β-isopropyl-des-A-lupane (**18**; 20 mg). Mp 221—222 °C (recrystallized from chloroform-methanol); IR (KBr disk) 3500—3150 (br), 1070, and 990 cm^{-1}; NMR (sparingly insoluble in $CDCl_3$) δ 3.4—3.8 (2H, m); MS (no molecular ion was observed at any of the measured ionization potential at 70, 25, and 20 eV.) *m/e* (%) 389 [7; $(M-43)^+$], 371 [100; $(M-43-18)^+$], 333 [24; $(M-99)^+$], 205 (22), 191 (40), and 111 (100).

Methylation of 5α-Hydroxy-10α-(2-hydroxyethyl)-5β-isopropyl-des-A-lupane (18). A mixture of the diol (**18**; 40 mg), methyl iodide (1 ml), silver oxide (200 mg) and dimethylformamide (5 ml) was stirred at room temperature for 21 hr. After usual treatment, 5α-hydroxy-5β-isopropyl-10α-(2-methoxyethyl)-des-A-lupane (**19**; 25 mg) was obtained by preparative tlc. Mp 168—169.5 °C (recrystallized from chloroform-methanol); IR (KBr disk) 3600—3300 (br), 1110, 1040, and 995 cm^{-1}; NMR δ 3.34 (3H, s), 4.12 (1H, br.s, O$\underline{H}$); MS (the molecular ion (*m/e* 446) was not observed at any of the measured ionization potential at 70, 20, and 15 eV.) *m/e* (%) 403 [10; $(M-43)^+$], 385 [4; $(M-43-18)^+$], 371 [100; $(M-43-33)^+$], 347 (26; $(M-99)^+$], 315 (27), 205 (26), and 191 (48); Found: C, 80.44; H, 12.29%. Calcd for $C_{30}H_{54}O_2$: C, 80.65; H, 12.18%.

Photochemical Reaction of Lup-20(29)-en-3-one (14) Followed by Hydrogenation. A solution of lup-20(29)-en-3-one (**14**; 400 mg) in methanol (700 ml) was irradiated using a 100 W high pressure mercury lamp under a nitrogen atmosphere for 16.5 hr at room temperature. After the solvent was removed, the reaction products were separated by silica gel column chromatography to afford 5β-isopropyl-10α-(2-methoxycarbonylethyl)-des-A-lup-20(29)-ene (**21**; about 100 mg) as a main product. IR (neat) 1750, 1645, and 890 cm^{-1}; NMR δ 3.65 (3H, s) and 4.50—4.75 (2H, m); MS *m/e* (%) 456 [43; M^+ ($C_{31}H_{52}O_2$)], 441 (22), 413 (16), 373 (9), 369 (30), 203 (77), and 189 (100).

Then, a mixture of the methyl ester (**21**; 40 mg) and 5% palladium-carbon (20 mg) in methanol was stirred under a hydrogen atmosphere at 50 °C for one day. After filtration, the reaction mixture was subjected to preparative tlc using a mixture of petroleum ether-benzene-chloroform (4:1:1) as an eluent. The main product (**8a**; 25 mg) was obtained as crystals.

The authors wish to thank Dr. Hiroshi Satoh and Dr. Yoshiaki Katoh of Naka Works, Hitachi Ltd. and Dr. Kazuyuki Aizawa of Department of Agricultural Chemistry, this University, for the measurements of high resolution mass spectra.

References

1) R. Aoyagi, T. Tsuyuki, M. Takai, T. Takahashi, F. Kohen, and R. Stevenson, *Tetrahedron*, **29**, 4331 (1973), and the references cited therein.

2) R. M. Carman, *Aust. J. Chem.*, **18**, 1493 (1965).

3) K. Kojima, K. Sakai, and T. Tanabe, *Tetrahedron Lett.*, **1969**, 3399.

4) H. Budzikiewicz, J. M. Wilson, and C. Djerassi, *J. Amer. Chem. Soc.*, **85**, 3688 (1963).

5) H. G. Walker, Jr., M. Gee, and M. McCready, *J. Org. Chem.*, **27**, 2100 (1962).

Sulfur-containing Polymers. XIII.[1] The Synthesis and Properties of Soluble Polydithiocarbamates

Norio KOBAYASHI, Akiko OSAWA, and Tamotsu FUJISAWA

Sagami Chemical Research Center, Nishi-Ohnuma, Sagamihara, Kanagawa 229

(Received April 15, 1974)

Polydithiocarbamates have been synthesized by the polycondensation of di-K or di-Na bisdithiocarbamates based on secondary diamines with bischloromethylated aromatics in *N,N*-dimethylformamide. The polymers obtained in good yields had inherent viscosities up to 0.66. The polymers derived from 1,3-di-4-piperidylpropane were soluble in organic solvents, such as dichloromethane and chloroform, and gave transparent, tough films from the solution. These polymers decomposed upon UV irradiation, with the liberation of carbon disulfide. The photopolymerization of methyl methacrylate in the presence of the polymer has also been studied.

The facile condensation of Na or K dithiocarbamates with alkyl halides is well known and has been extensively studied.[2] This reaction has been employed to introduce a dithiocarbamate side chain into polymers. Some of these polymers can serve as the backbone for photografting and as photosensitive resin.[3,4] However, the condensation reaction has not been extended to the preparation of high molecular-weight linear polymers. Although Zochniak has prepared polydithiocarbamates by the polycondensation of di-Na alkylene bisdithiocarbamates with bischloromethylated diphenyl ether, the polymers are insoluble in organic solvents.[5] This presents a major obstacle to the solution characterization of the products.

We have been interested in the polymers containing photosensitive groups in the main chain.[6-8] In the course of our studies, it was found that fairly high molecular-weight polydithiocarbamates (**3**) with good solubility characteristics can be prepared from di-K or di-Na bisdithiocarbamates based on secondary diamines (**1**) and bischloromethylated aromatics (**2**).[9] This paper will describe the synthesis and properties of the polydithiocarbamates. Their photochemical behavior will also be discussed in some detail.

Results and Discussion

Synthesis. The bisdithiocarbamate salts, **1**, were prepared from secondary diamines, carbon disulfide, and alkali metal hydroxides [Eq. (1)]. Their structures were confirmed as dibenzyl derivatives, (**4**) and (**5**). The polycondensation of **1** with **2** proceeds according to Eq. (2). The polymer formation was carried out by

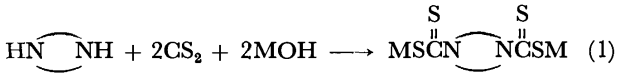

(1)

1a: M=K, 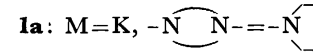

b: M=Na, 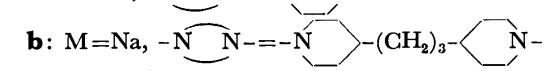

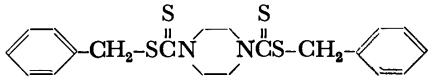

4

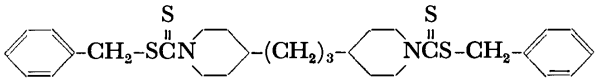

5

(2)

stirring an equimolar mixture of **1** and **2** in *N,N*-dimethylformamide (DMF) for 1 hr at room temperature followed by heating the mixture up to 110 °C over a 30 min period. The polymer which was precipitated

Table 1. Preparation of polydithiocarbamates (**3**)

Polymer No.	1	2 -Ar-	Yield (%)	Softening point (°C[a])	Dec. point (°C[b])	η_{inh}
3a	a		83	251—254 (dec.)	271	0.43[c]
3b	a		83	202—208	278	0.54[c]
3c	a	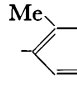	90	285—293 (dec.)	274	0.41[c]
3d	a		91	242—248 (dec.)	282	0.54[c]
3e	a	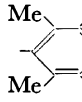	91	>300	295	0.38[c]
3f	b		95	167—178	277	0.63[d]
3g	b		98	141—150	286	0.53[d]
3h	b	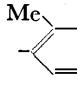	94	173—185	276	0.66[d]
3i	b		95	162—178	273	0.47[d]
3j	b	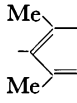	90	258—266	273	0.60[d]

a) Determined by a hot-stage microscope. b) Determined by DTA (heating rate 10 °C/min). c) Measured in methanesulfonic acid (0.5 g/100 ml, 30 °C). d) Measured in TCE (0.5 g/100 ml, 30 °C).

during the reaction was washed with water and methanol and dried at 50 °C under a vacuum. Using different combinations of **1** and **2**, a variety of different polymers with novel backbone structures were prepared. Table 1 contains a listing of these polymers, together with a partial compilation of their properties. Polymers were obtained in good yields regardless of the combinations of **1** and **2**. The inherent viscosities of the polymers ranged from 0.38 to 0.66, indicating that these polymers were of a fairly high molecular weight.

Other solvents, such as benzene–water, chloroform–water, and *sym*-tetrachloroethane (TCE), can also be used in the polycondensation; however, they usually give polymers with low inherent viscosities. The prominent feature of DMF may be attributed to its ability to increase the nucleophilicity of anions and to activate halogenated compounds by forming ionic complexes.[10]

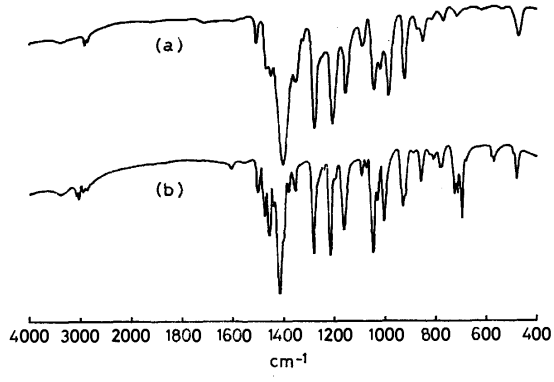

Fig. 1. The IR spectra of (a) polymer **3a** and (b) model compound **4** (KBr disks).

The polymers showed essentially the same results of elemental analyses as polydithiocarbamates. The IR spectra of the **3a**—**3e** polymers (piperazine polymers) were virtually identical and compared favorably with that of the corresponding model compound, **4** (Fig. 1). The bands at 1280, 990, and 930 cm^{-1} are characteristic of the dithiocarbamate group and are assigned to ν_{C-N}, $\nu_{C=S}$, and ν_{C-S}, respectively. It is interesting to note that the band at 1470 cm^{-1} due to the polar C–N partial double bond[11] is not so intense. On the other hand, the IR spectra of the **3f**—**3j** polymers (dipiperidylpropane polymers) and the model compound **5** displayed an intense absorption of $\nu_{C=N}$ at 1480 cm^{-1}. The NMR spectra provided further support for the assigned polymer structures; these polymers showed a triplet, centered at $\delta\sim3.1$ ($J=12$ Hz), for the four axial *N*-methylene protons, a broad signal centered at δ 5.1—5.2 for the four equatorial *N*-methylene protons, and a singlet at δ 4.5—4.6 for the four benzylic protons. As is shown in Fig. 2, the NMR spectrum of the **3f** polymer is quite similar to that of **5**.

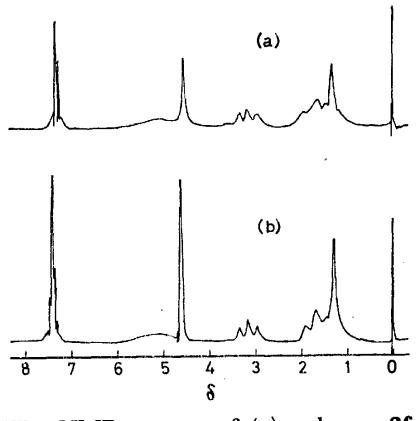

Fig. 2. The NMR spectra of (a) polymer **3f** and (b) model compound **5** ($CDCl_3$–TMS).

General Properties. The softening points of the piperidylpropane polymers lie below those of the corresponding piperazine polymers and tend to increase with an increase in the number of methyl substituents per unit. The introduction of symmetrical 1,4-phenylene ring structures into the polymer chain also increases the softening point. All the polymers decomposed on heating above 270 °C. The decomposition was exothermic, according to DTA.

The piperazine polymers were soluble in methanesulfonic acid and insoluble in organic solvents, whereas the dipiperidylpropane polymers were soluble in dichloromethane, chloroform, TCE, and *m*-cresol in addition to methanesulfonic acid, and the resulting polymer solutions gave transparent, tough films when cast upon a glass plate. This made possible an investigation of the photochemical properties of the polymers.

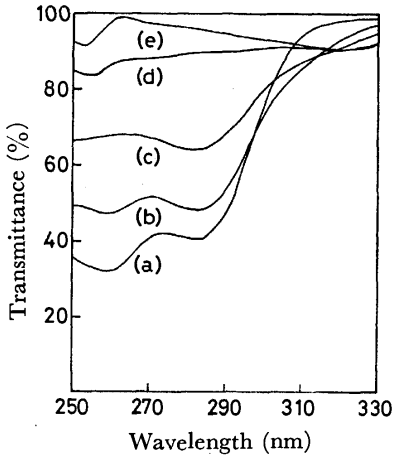

Fig. 3. UV spectral changes of polymer **3j** with irradiation in chloroform solution. Irradiation time; (a) 0, (b) 1, (c) 3, (d) 15, and (e) 110 min.

Photochemical Properties. When polymer films were exposed to the UV light from a 450 W high-pressure mercury lamp, they decomposed with a noticeable color change. The photolysis of the **3j** polymer was followed by means of the UV and IR spectra in an appropriate solvent. Figure 3 depicts the changes in the UV spectra on irradiation. The unirradiated sample showed two bands at 260 and 283 nm assignable to the S–C=S conjugation and the N–C=S conjugation, respectively.[12] These bands decreased in intensity with time and finally disappeared, while two new bands appeared. The band in the 252—255 nm range showed a shift to a shorter wavelength with continued exposure; it was unaccounted for. The band at approximately 320 nm coincided in position with that of carbon disulfide. The formation of carbon disulfide

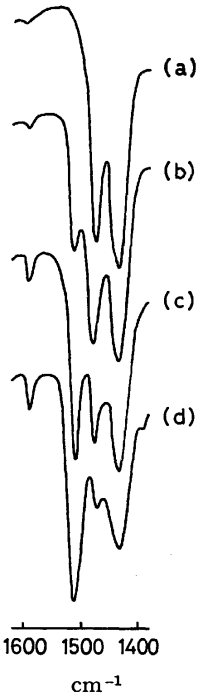

Fig. 4. IR spectral changes of polymer **3j** with irradiation in dichloromethane solution. Irradiation time; (a) 0, (b) 4, (c) 11, and (d) 25 hr.

was confirmed by the IR spectra. As is shown in Fig. 4, a new band attributable to carbon disulfide appeared on irradiation at 1510 cm^{-1}. The intensity of the band increased with a decrease in the intensity of C=N band at 1480 cm^{-1}. From the spectral evidence and the precedents for the photolysis of non-polymeric analogues,[13,14] the following scheme for the photolysis of **3j** may be assumed:

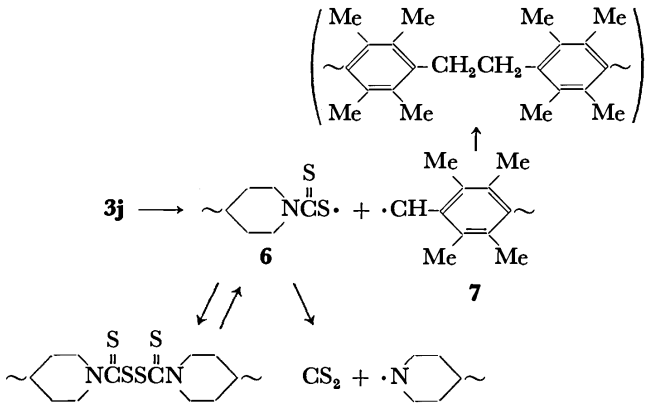

The initial photochemical step involves the formation of a dithiocarbamoyl radical (**6**) and a benzyl radical (**7**). The former either dimerizes to a thiuram disulfide or dissociates to carbon disulfide and an amino radical.[15] The **7** radical may dimerize to give a bibenzyl derivative, but this point is not clear.

Photopolymerization of Methyl Methacrylate (MMA). In view of the above results and the known tendency of dithiocarbamate to initiate the photopolymerization of vinyl monomers,[3,13,16] we expected that a new type of block copolymers could be obtained by using the **3** polymer as the initiator of the vinyl polymerization. Chloroform solutions containing MMA and **3j** were irradiated in a Pyrex tube (frozen and vacuum sealed) at room temperature. A linear relationship was noticed between the polymer yield and the reaction time. The IR spectra of the polymers obtained were identical with that of poly MMA, but the UV spectra exhibited characteristic absorption of **3j** at 259 and 283 nm, showing that some units of **3j** were incorporated in the polymer. Table 2 shows the effect of **3j** on the polymerization of MMA, the polymerization time being 2 hr. The molecular weights of the polymers were determined viscometrically in toluene at 30 °C with the aid of the relation, $[\eta]=7.0\times10^{-5}\,M^{0.71}$, given by Stanley.[17] Compared to the polymerization without additives, the polymerization in the presence of **3j** gave a polymer with a lower molecular weight in higher yield. Thus, it may be concluded that **3j** functions not only as an initiator but also as a chain-transfer agent. A similar observation has been reported for benzyl diethyldithiocarbamate.[3] The ratio of the **3j** unit and the MMA unit in the polymer (m: n), as estimated on the basis of sulfur analysis, was 1: 64.[18] This means that each polymer molecule contains about 11 units of **3j**. Furthermore, the ratio of the durene unit and the MMA unit obtained from the NMR spectrum[19] was 1: 72. These values are indicative of the block character of the copolymer.

Experimental

Instrumentation. The following instruments were used in this study: a Hitachi EPI-G3 grating infrared spectrophotometer, a Varian T-60 NMR spectrometer, a Hitachi EPS-3 recording spectrophotometer, and an AGNE TGD-1500 thermal balance.

Materials. 2,5-Bis(chloromethyl)-*p*-xylene and 4,6-bis-(chloromethyl)-*m*-xylene were prepared by the reaction of the corresponding xylene with formaline and hydrochloric acid.

Table 2. Photopolymerization of MMA

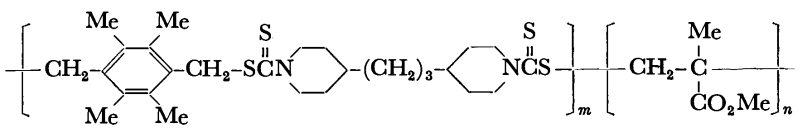

MMA (mol/l)	**3j** (mol[a]/l)	Polymer Yield (%)	$[\eta]$[b]	MW $\times10^{-5}$	S anal. (%)	n/m[c]	m per molecule
2.83	0	1.0	0.60	3.47	—	—	—
2.83	9.6×10^{-3}	14.5	0.21	0.79	1.85	64	11.4

a) Based on recurring unit. b) Measured in toluene at 30 °C. c) Estimated from sulfur analysis.

2,5-Bis(chloromethyl)-*p*-xylene; mp 134 °C (lit,[20] mp 132—134 °C). 4,6-Bis(chloromethyl)-*m*-xylene; mp 98—99 °C (lit,[21] mp 99 °C). Piperazine, 1,3-(di-4-piperidyl)propane, α,α′-dichloro-*p*-xylene, -*m*-xylene, and 3,6-bis(chloromethyl)-durene were used as received. MMA was purified by distillation in the usual manner.[22]

Di-K Piperazine-N,N′-*biscarbodithioate (1a).* To a solution of 8.6 g of piperazine and 13.1 g of potassium hydroxide in 200 ml of ethanol was added dropwise a solution of 15.2 g of carbon disulfide in 40 ml of ether below 10 °C; the mixture was then stirred for 1 hr. The solid product was used for a subsequent reaction after one reprecipitation from water into acetone, followed by drying at 80 °C under a vacuum. The yield was 23.2 g.

Di-Na 1,3-Di-4-piperidylpropane-N,N′-*biscarbodithioate (1b).* To a stirred solution of 21.0 g of 1,3-(di-4-piperidyl)propane and 9.0 g of sodium hydroxide in 200 ml of ethanol was added dropwise a solution of 15.2 g of carbon disulfide in 40 ml of ether below 10 °C after which the mixture was stirred for 1 hr. The mixture was then filtered into a large volume of ether. The white precipitate was used for a subsequent reaction after one reprecipitation from ethanol into ether, followed by drying at 80 °C under a vacuum. The yield was 36.0 g.

Dibenzyl Piperazine-N,N′-*biscarbodithioate (4).* A solution of 6.28 g of **1a** in 150 ml of water was mixed with a solution of 5.07 g of benzyl chloride in 50 ml of chloroform. The mixture was stirred vigorously for 3 hr under reflux. The chloroform layer was then separated, washed with water, dried over anhydrous magnesium sulfate, and concentrated to give 7.85 g (94%) of **4**; mp 122—123 °C (from benzene-*n*-hexane). The IR spectrum is shown in Fig. 1.

NMR ($CDCl_3$); δ 4.33 (s, 8H), 4.70 (s, 4H), 7.48 (m, 10H).

Found: C, 57.42; H, 5.13; N, 6.59; S, 30.66%. Calcd for $C_{20}H_{22}N_2S_4$: C, 57.38; H, 5.30; N, 6.69; S, 30.63%.

Dibenzyl 1,3-(Di-4-piperidyl)propane-N,N′-*biscarbodithioate (5).* A mixture of 8.13 g of **1b**, 5.07 g of benzyl chloride, 150 ml of water, and 50 ml of chloroform was refluxed for 3 hr with vigorous stirring. From the reaction mixture, 10.4 g of an oily product was obtained after the same work-up as above. The product was treated with 100 ml of ether to give 8.90 g (82%) of **5**; mp 122—124 °C (from ethanol). The NMR spectrum is shown in Fig. 2.

Found: C, 64.40; H, 6.89; N, 5.17; S, 23.84%. Calcd for $C_{29}H_{38}N_2S_4$: C, 64.16; H, 7.06; N, 5.16; S, 23.62%.

Polycondensation. The polycondensation of **1** with **2** was carried out in DMF. The results are summarized in Table 1. The following is a typical example. A mixture of 2.03 g of **1b**, 1.16 g of 3,6-bis(chloromethyl)durene, and 30 ml of DMF was stirred for 1 hr at room temperature and then heated up to 110 °C over a 30 min period. The mixture was cooled and kneaded with 50 ml of methanol. The solvents were decanted. This treatment was repeated until the polymer solidified completely. The polymer was filtered with suction, washed with water and methanol, and dried at 50 °C under a vacuum. The yield of the **3j** polymer was 2.33 g (90%).

NMR ($CDCl_3$); δ 0.8—2.0 (m, 16H), 2.33 (s, 12H), 3.12 (t, J=12 Hz, 4H), 4.50 (s, 4H), ~5.1 (broad signal, 4H).

The polymer was purified by two reprecipitations from chloroform into methanol and was then used for analysis and photolysis.

Found: C, 62.35; H, 7.61; N, 5.25; S, 24.57%. Calcd for $(C_{27}H_{40}N_2S_4)_n$: C, 62.26; H, 7.74; N, 5.38; S, 24.62%.

Photolysis of 3j. Irradiations were carried out with a 450 W high-pressure mercury lamp (Ushio UM-452) centrally situated in a water-cooled Pyrex cold-finger. A chloroform solution of **3j** (1.1×10^{-5} mole-based on the repeating unit/l) was irradiated in a 1 cm quartz cell at a distance of 60 cm from the lamp. The UV spectral measurements were made immediately after the removal of the sample from the exposure unit. The results are shown in Fig. 3.

A dichloromethane solution of **3j** (*ca.* 6×10^{-3} mol-based on the repeating unit/l) was irradiated in a 0.1 mm NaCl closed cell at a distance of 20 cm from the UV lamp. The IR spectral changes around 1500 cm^{-1} are shown in Fig. 4.

Photopolymerization of MMA. A solution of 0.05 g of **3j** and 3 ml of MMA in 10 ml of chloroform was placed in a Pyrex tube, 2 cm in diameter. The tube was degassed under a vacuum by the usual freezing and thawing technique and then sealed. The tube was irradiated at a distance of 40 cm from the UV lamp. After a given interval the mixture was concentrated under reduced pressure, dissolved in acetone, and filtered into a large volume of methanol. The yield was calculated from the weight of the polymer obtained in the dry state. Viscosity measurements were made in toluene with a Ubbelohde viscometer at 30 °C. The IR spectra of the polymers were identical with that of poly MMA. The UV spectra exhibited the weak absorptions at 259 and 283 nm characteristic of **3j**.

References

1) Part XII: N. Kobayashi, A. Osawa, and T. Fujisawa, *Chem. Lett.*, **1973**, 1315.

2) E. E. Reid, "Organic Chemistry of Bivalent Sulfur," Vol. 4, Chemical Publishing, New York, (1962), pp. 235—237.

3) M. Okawara, H. Yamashina, K. Ishiyama, and E. Imoto, *Kogyo Kagaku Zasshi*, **66**, 1383 (1963).

4) M. Okawara, K. Morishita, and E. Imoto, *ibid.*, **69**, 761 (1966).

5) A. Zochniak, *J. Polym. Sci., Polym. Chem. Ed.*, **10**, 3101 (1972).

6) N. Kobayashi and T. Fujisawa, *Macromolecules*, **5**, 106 (1972).

7) N. Kobayashi and T. Fujisawa, *J. Polym. Sci. A-1*, **10**, 1233, 3165 (1972).

8) N. Kobayashi, A. Osawa, and T. Fujisawa, *J. Polym. Sci., Polym. Chem. Ed.*, **11**, 553, 2099 (1973).

9) Poly(ethylene *N*-aryldithiocarbamates), which dissolve in *o*-cresol or DMF, have been obtained by the reaction of *N*-arylethylenimines with carbon disulfide, but their intrinsic viscosities were only 0.02—0.05. See A. P. Sineokov, F. N. Gladysheva, and V. S. Etlis, *Khim. Geterotsikl. Soedin.*, **1970**, 611.

10) S. Yoneda, I. Morishima, K. Fukui, and Z. Yoshida, *Kogyo Kagaku Zasshi*, **68**, 1074, 1077 (1965).

11) G. D. Thorn and R. A. Ludwig, "The Dithiocarbamates and Related Compounds," Elsevier Publishing, New York, (1962), pp. 43—44.

12) M. J. Janssen, *Rec. Trav. Chim. Pays-Bas*, **79**, 454 (1960).

13) M. Okawara, T. Nakai, K. Morishita, and E. Imoto, *Kogyo Kagaku Zasshi*, **67**, 2108 (1964).

14) A. O. Fitton, J. Hill, M. Qutob, and A. Thompson, *J. Chem. Soc. Perkin I*, **1972**, 2658.

15) The decomposition of dithiocarbamoyl radical into carbon disulfide: T. Ferington and A. V. Tobolsky, *J. Amer. Chem. Soc.*, **80**, 3215 (1958).

16) M. Okawara, K. Morishita, E. Imoto, M. Ori, and T. Nakai, *Kogyo Kagaku Zasshi*, **69**, 761, 766 (1966).

17) E. L. Stanley, "Analytical Chemistry of Polymers," Part 1, ed. by G. M. Kline, Interscience, New York, N. Y. (1959), p. 14.

18) The estimation was based on the assumption that the numbers of durene unit and 1,3-dipiperidylpropane unit are equal. This assumption was supported by the NMR spectrum.

19) The ratio was calculated from the area ratio of methyl proton of durene residue (δ 2.33) and *O*-methyl proton (δ 3.62).

20) K. Murao, S. Tanimoto, and R. Oda, *Kogyo Kagaku Zasshi*, **66**, 1538 (1963).

21) J. Braun and J. Nelles, *Ber.*, **67**, 1094 (1934).

22) K. Taniyama, "Textbook of Polymer Experiment," Vol. 9, ed. by S. Kambara, Kyoritsu Shuppan, Tokyo, (1959), p. 141.

Chemical Studies on Tuberactinomycin. VII.[1] Synthesis of γ-Hydroxy-β-lysine[2]

Tateaki WAKAMIYA, Tadashi TESHIMA, Ichiro KUBOTA,*
Tetsuo SHIBA, and Takeo KANEKO**
Department of Chemistry, Faculty of Science, Osaka University, Toyonaka, Osaka 560
(Received June 7, 1974)

γ-Hydroxy-β-lysine is a new basic amino acid isolated from the hydrolyzates of antitubercular peptides, tuberactinomycin A and N. In order to confirm the structure and establish the stereochemistry of the amino acid, two diastereoisomers of γ-hydroxy-DL-β-lysine were synthesized by Arndt-Eistert synthesis *via* β-hydroxyornithine. Synthetic *erythro* and *threo* isomers were found to be identical spectroscopically and chromatographically with the corresponding forms obtained from the antibiotics respectively.

The isolation and the structural determination of γ-hydroxy-β-lysine in antitubercular peptides tuberactinomycin A and N[3] were reported in the previous paper.[4] Two different stereoisomers of the amino acid were obtained depending on acid reagent and reaction condition for the hydrolysis. The complete hydrolysis of the peptides by heating with hydrochloric acid gave *threo*-γ-hydroxy-β-lysine, while the partial hydrolysis with concentrated sulfuric acid at room temperature afforded the *erythro* isomer.[4] Our stereochemical investigation on *N,O*-acyl migration reaction of vicinal hydroxy amino acid revealed that the *threo* form of this amino acid was a genuine configuration in the intact molecules of tuberactinomycins, since the treatment with concentrated sulfuric acid caused an epimerization of the configuration at carbon atom carrying the hydroxyl group.[1,5] This paper presents a total synthesis of both isomers of the amino acid in order to confirm the conclusion of the structural and stereochemical studies.

In our synthetic plan, β-hydroxyornithine is required as an important intermediate which is subjected to the homologation to γ-hydroxy-β-lysine through Arndt-Eistert reaction. The synthesis of β-hydroxyornithine was carried out as follows (Scheme 1). Coupling of phthalimide with acrolein gave 3-phthaliminopropionaldehyde (III), which was then condensed with malonic acid to yield 5-phthalimino-2-pentenoic acid (IV).[6] Acid IV was esterified to benzyl ester V with benzyl alcohol and *p*-toluenesulfonic acid in benzene. From the coupling constant of 16 Hz for olefinic protons in its NMR spectrum, the benzyl ester V thus obtained was indicated to be a *trans* form. The ester V was allowed to react with mercuric acetate in methanol to give benzyl 2-acetoxymercuri-3-methoxy-5-phthaliminopentanoate (VI). A conversion of 2-acetoxymercuri compound VI to 2-bromomercuri derivative with potassium bromide followed by bromination gave benzyl 2-bromo-3-methoxy-5-phthaliminopentanoate (VII) in a good yield. A direct amination of VII in alkaline medium should be avoided in view of possible cleavage of phthalyl group to phthalamic acid derivative.[7] Since a substitution of phthalimino group into α-carbon atom of VII with potassium phthalimide failed, the compound VII was converted to an azide derivative with sodium azide in aqueous dimethylformamide and then hydrogenated to N^{δ}-phthalyl-β-methoxyornithine (VIII) using palladium on charcoal as a catalyst. The amino acid VIII thus obtained was a mixture of two diastereoisomers. One of them was easily crystallized as hydrochloride from ethanolic solution, while another isomer was crystallized as free base from the mother liquor on addition of triethylamine.

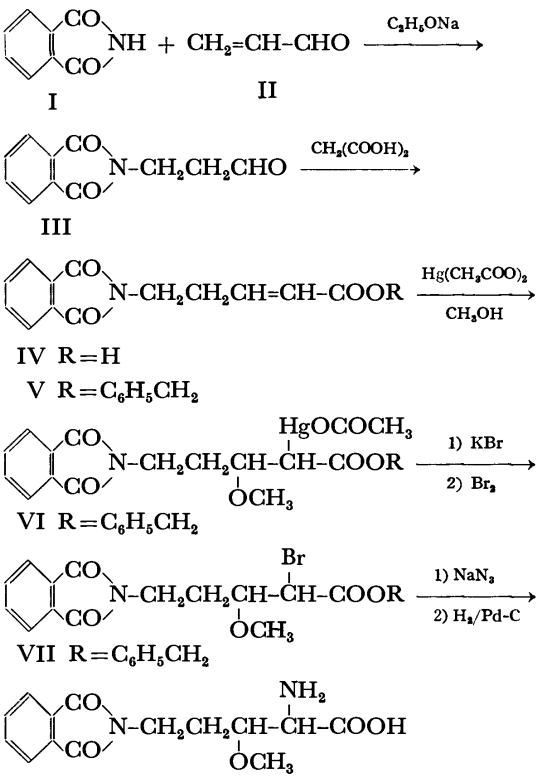

VIIIa, *erythro* as hydrochloride
b, *threo* as free base

Scheme 1.

In order to determine the configuration of these products, the NMR study for oxazolidone derivative of β-hydroxy-α-amino acid was applied.[8] Thus VIII was hydrolyzed to β-hydroxyornithine (IX) with hydrobromic acid in the presence of anisole. The amino acid IX was then benzyloxycarbonylated in aqueous sodium hydroxide solution to afford the oxazolidone

* Present address: Department of Agricultural Chemistry, Nagoya University, Chikusa-ku, Nagoya 464.
** Present address: Shiseido Laboratory, Nippa-cho, Kohoku-ku, Yokohama 223.

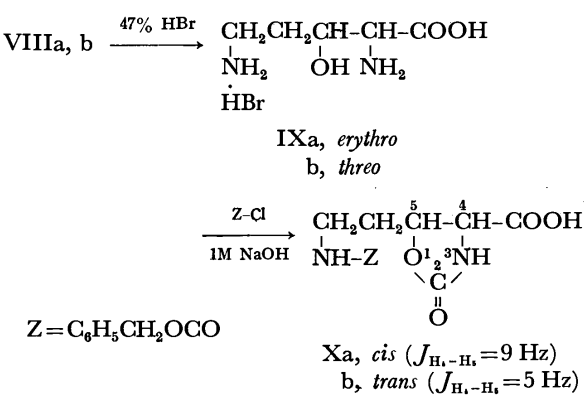

Scheme 2.

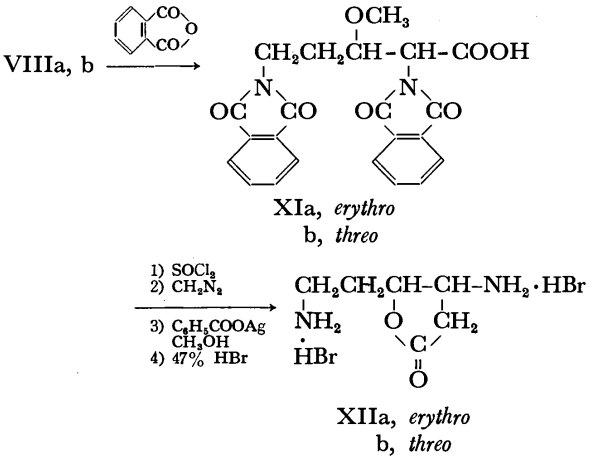

Scheme 3.

derivative X (Scheme 2). Oxazolidone compounds derived from β-hydroxy-α-amino acids may possess a fixed structure of nearly planar five-membered ring. Therefore, the coupling constants of *cis* and *trans* isomers will be distinguishable. In fact, the coupling constants of vicinal protons on the ring of several oxazolidone derivatives are converged at around 9 Hz in *cis* configurations and at 5 Hz in *trans* ones as far as tested.[8] Actually, the coupling constant between C-4 and C-5 protons was measured to be 9 Hz in Xa and 5 Hz in Xb. Consequently, the configurations of Xa and Xb were assigned to *cis* and *trans* forms which should have been derived from *erythro* and *threo* compounds respectively. Therefore, the configurations of VIIIa and VIIIb must be *erythro* and *threo* forms respectively. In general, a so-called hydroxymercuration, an addition reaction of mercuric acetate to an olefin in methanol, is known to proceed by *trans* addition preferentially.[9] However, since the following bromination induced racemization at α-carbon atom more or less,[9,10] the fact is not unreasonable that the product VII and hence VIII were mixtures of the diastereoisomers.

For Arndt-Eistert synthesis, each isomer of VIII was then phthalylated respectively to N^{α},N^{δ}-diphthalyl-β-methoxyornithine (XIa) (XIb) with phthalic anhydride either by fusion method or by heating in dioxane. Use of ethoxycarbonylphthalimide as phthalylation reagent[11] did not give satisfactory result, because of a possible cleavage of N^{δ}-phthalyl group to phthalamic acid derivative during the reaction under a basic condition.

According to the usual manner of Arndt-Eistert reaction, diphthalyl acid XI was converted to an acid chloride and then to diazoketone which was rearranged to N^{β},N^{ϵ}-diphthalyl-γ-methoxy-β-lysine methyl ester in methanol using silver benzoate. Without isolation of the ester, the product was immediately hydrolyzed with hydrobromic acid in the presence of anisole. Eventually, both desired isomers of γ-hydroxy-DL-β-lysine were obtained starting from VIIIa and VIIIb respectively as their lactone (XIIa) (XIIb) dihydrobromide (Scheme 3).

Since the configurations of the asymmetric carbon atoms are known to be maintained through Arndt-Eistert synthesis involving Wolff rearrangement reaction, the final product XIIa prepared from *erythro* compound XIa can be assigned to *erythro* form and XIIb from XIb to *threo* form. The lactone XIIa dihydrobromide synthesized here was completely identical with *erythro*-γ-hydroxy-L-β-lysine lactone dihydrobromide obtained by *N,O*-acyl migration with concentrated sulfuric acid from tuberactinomycin A and N, in IR, NMR spectra, thin-layer chromatogram, and paper electrophoresis. Another isomer XIIb was also identified with *threo*-γ-hydroxy-L-β-lysine lactone obtained from the hydrochloric acid hydrolyzates of tuberactinomycin A and N in all respects.

The synthesis of γ-hydroxy-β-lysine by the usual Arndt-Eistert reaction *via* acid chloride could not always give good yields. This defect seems to be due to an undesirable formation of chloroketone which may be produced from diazoketone and hydrogen chloride in the reaction course. Actually, mixed crystals composing of the diazoketone and the chloroketone was readily precipitated in the case of *erythro* compound and purification of the diazoketone by recrystallization of the mixed crystals was made extremely difficult. By this reason, an improved method for preparation of the diazoketone was attempted by application of mixed carbonic-carboxylic acid anhydride method.[12] This method afforded a satisfactory result in yield of the product compared with the acid chloride method (Scheme 4). However, partial racemization occurred through the reaction particularly in *threo* isomer. Therefore, for the preparation of *erythro*-γ-hydroxy-β-lysine, Arndt-Eistert synthesis *via* the mixed anhydride procedure serves as a fairly good synthetic process, though

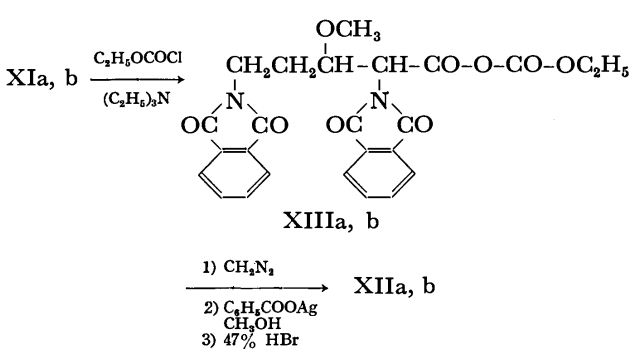

Scheme 4.

the purification of the *threo*-isomer was shown to be difficult even after repetition of recrystallization. However, the mixed anhydride method could be improved for diazoketone synthesis, if a prevention of the partial racemization becomes feasible for instance by choice of protection of α-amino group or by use of an adequate amine like *N*-methylmorpholine in place of triethylamine.

In attempt of an interconversion of diastereoisomers of γ-hydroxy-β-lysine, an epimerization of γ-carbon atom of the amino acid was investigated. As shown in

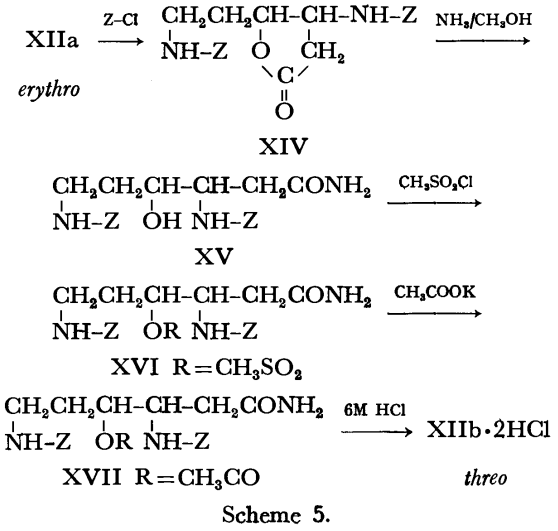

Scheme 5.

Scheme 5, synthetic *erythro*-γ-hydroxy-DL-β-lysine lactone XIIa was benzyloxycarbonylated to N^{β},N^{ϵ}-dibenzyloxycarbonyl-*erythro*-γ-hydroxy-DL-β-lysine lactone (XIV) which was then converted to its amide XV. Otherwise, the reverse lactonization proceeded very easily when free hydroxy acid was attempted to be obtained. Hydroxyl group of the amide XV was mesylated with methanesulfonyl chloride in pyridine. When this *O*-mesyl compound XVI was treated with potassium acetate in absolute ethanol, substitution of acetoxyl group was accompanied by an inversion of the configuration on γ-carbon atom. Through hydrolysis of γ-acetoxy derivative XVII thus prepared with 6 M hydrochloric acid, *threo*-γ-hydroxy-DL-β-lysine lactone (XIIb) dihydrochloride was obtained. This conversion was also confirmed by identity of XIIb with natural *threo*-γ-hydroxy-L-β-lysine from the antibiotics on thin-layer chromatogram and IR spectra.

From the result of this synthetic study, not only the assignment of the chemical structure of the new natural amino acid in tuberactinomycins to γ-hydroxy-β-lysine, was assured, but also the relationship between the stereoisomers of the amino acid was clearly established.

Experimental

All melting points are uncorrected. The IR spectra were obtained in nujol mull with a Nihon Bunko IR-S spectrophotometer. The NMR spectra were obtained with a Varian T-60 spectrometer (60 MHz). Tetramethylsilane (TMS) was used as an internal reference in deuterochloroform and deuteromethanol solution, and as an external reference in the case of deuterium oxide solution. Thin-layer chromatography was carried out by the ascending method on silica gel G using a developing solvent of phenol–water–28% ammonium hydroxide (30: 10: 0.6). Paper electrophoresis was carried out at 750 volt and 10 mA for 1.5 hr on Toyo Roshi No. 51 filter paper using a buffer solution of pyridine–acetic acid–water (30: 4: 966).

Benzyl 5-Phthalimino-2-pentenoate (V). To a suspension of 5-phthalimino-2-pentenoic acid[6] (36.9 g, 0.150 mol) in 220 ml of benzene, there were added benzyl alcohol (26.0 g, 0.241 mol) and *p*-toluenesulfonic acid monohydrate (2.16 g, 11.4 mmol). The mixture was heated under reflux and the liberated water was removed azeotropically by means of Dean and Stark distilling receiver. After water had been no longer distilled off, the reaction mixture was permitted to cool to room temperature. Clear benzene solution was washed with sodium hydrogencarbonate solution and then water. Organic layer was dried over anhydrous sodium sulfate and evaporated *in vacuo*. Oily residue was triturated in petroleum ether under cooling to deposit crystals, yield 38.3 g (76%). Recrystallization from methanol gave prisms, mp 57—58 °C.

Found: C, 71.58; H, 5.20; N, 4.15%. Calcd for $C_{20}H_{17}O_4N$: C, 71.63; H, 5.11; N, 4.18%.

Benzyl 2-Bromo-3-methoxy-5-phthaliminopentanoate (VII). To a solution of V (63.0 g, 0.188 mol) in 500 ml of methanol, mercuric acetate (89.9 g, 0.282 mol) was added. The clear reaction mixture was stirred at room temperature for four days. The colorless crystals of 2-acetoxymercuri-3-methoxy derivative (VI) precipitated were filtered, yield 86.0 g. To the suspension of the above crystals VI in 500 ml of acetone, a solution of potassium bromide (41.8 g, 0.351 mol) in 75 ml of water was added on stirring. A clear solution thus obtained was concentrated *in vacuo*. A residue obtained was dissolved in water and then extracted with chloroform. The organic layer was dried over anhydrous sodium sulfate and concentrated to 200 ml *in vacuo*. To the chloroform solution containing 2-bromomercuri derivative a solution of bromine (28.0 g, 0.175 mol) in 50 ml of chloroform was added dropwise at 50 °C. The precipitate of mercuric bromide was filtered off and the filtrate was washed with aqueous sodium hydrogencarbonate and then water. It was dried over anhydrous sodium sulfate and concentrated *in vacuo*. Residual oil was triturated with petroleum ether to make powder, yield 66.1 g (78.7%). Recrystallization from benzene gave needles, mp 112—114 °C.

Found: C, 56.73; H, 4.55; N, 3.15; Br, 17.64%. Calcd for $C_{21}H_{20}O_5NBr$: C, 56.51; H, 4.52; N, 3.14; Br, 17.91%.

*N^{δ}-Phthalyl-β-methoxy-*DL*-ornithine (VIII).* To a suspension of sodium azide (24.5 g, 0.377 mol) in 60 ml of dimethylformamide and 20 ml of water, a solution of VII (11.2 g, 0.025 mol) in 20 ml of dimethylformamide was added dropwise at 50 °C for 30 min. The solution was stirred at the same temperature overnight. The reaction mixture was diluted with water, saturated with sodium chloride, and then extracted with ethyl acetate. The extract was dried over anhydrous sodium sulfate and evaporated *in vacuo*. Residual oil was dissolved in a mixture of 30 ml of methanol and 2 ml of concentrated hydrochloric acid. Catalytic hydrogenation was carried out by passing a slow stream of hydrogen gas through the above solution added with 5% palladium on charcoal as a catalyst until the IR absorption band of the azide group disappeared in the reaction mixture. After filtration of catalyst, the filtrate was concentrated *in vacuo*. The residue was dissolved in water and extracted with ether several times. Aqueous layer was again concentrated *in vacuo*, and the residue was dissolved in ethanol. An addition

of ether precipitated *erythro* isomer VIIIa as hydrochloride. Recrystallization from aqueous ethanol and ether gave needles, yield 1.30 g (15.8%), mp 221 °C (decomp.).

Found: C, 50.92; H, 5.37; N, 8.55; Cl, 11.12%. Calcd for $C_{14}H_{17}O_5N_2Cl$: C, 51.15; H, 5.21; N, 8.52; Cl, 10.79%.

The filtrate of VIIIa was concentrated *in vacuo* and the residue was dissolved in a small amount of ethanol. On addition of triethylamine and then ether to the solution, precipitate of a free amino acid was formed. It was filtered and washed with ethanol. Recrystallization from aqueous ethanol gave needles of *threo* isomer VIIIb, yield 1.10 g (15.1%), mp 214—215 °C (decomp.).

Found: C, 57.43; H, 5.53; N, 9.65%. Calcd for $C_{14}H_{16}O_5N_2$: C, 57.53; H, 5.52; N, 9.59%.

erythro-*β-Hydroxy*-DL-*ornithine Hydrobromide (IXa)*. A solution of VIIIa (1.00 g, 3.04 mmol) in 30 ml of 47% hydrobromic acid was heated under reflux in the presence of 15 ml of anisole for 20 hr. Hydrolyzate was extracted with benzene and aqueous layer was concentrated *in vacuo*. Crystalline residue was recrystallized from aqueous ethanol and ether, yield 0.46 g (66%). Recrystallization was repeated from aqueous ethanol for analysis, mp 230 °C (decomp.).

Found: C, 26.58; H, 5.85; N, 12.15; Br, 34.70%. Calcd for $C_5H_{13}O_3N_2Br$: C, 26.21; H, 5.72; N, 12.23; Br, 34.89%.

threo-*β-Hydroxy*-DL-*ornithine Hydrobromide (IXb)*. Hydrolysis of VIIIb (1.00 g, 3.42 mmol) was similarly carried out as for the *erythro* isomer to obtain IXb, yield 0.59 g (75%). Recrystallization from aqueous ethanol gave needles, mp 110—111 °C.

Found: C, 25.47; H, 6.02; N, 11.77; Br, 33.49%. Calcd for $C_5H_{13}O_3N_2Br \cdot 1/2H_2O$: C, 25.22; H, 5.92; N, 11.77; Br, 33.56%.

cis-*5-(2-Benzyloxycarbonylaminoethyl)-2-oxazolidone-4-carboxylic Acid (Xa)*. To a solution of IXa (0.28 g, 1.22 mmol) in 5 ml of 1 M sodium hydroxide, benzyloxycarbonyl chloride (0.50 g, 2.93 mmol) was added at 0 °C and the mixture was stirred for 30 min at the same temperature. After stirring at room temperature for 3 hr, the reaction mixture was extracted with ether and an aqueous layer was acidified with hydrochloric acid. Oily product formed was extracted with ethyl acetate and an organic layer was dried over anhydrous sodium sulfate. It was concentrated *in vacuo* to obtain the oily residue which was triturated with petroleum ether and then ether to yield crystals. Recrystallization from ethyl acetate and petroleum ether gave needles, yield 0.15 g (43.0%), mp 139—140 °C (decomp.). NMR: δ 4.33 (d, H-4, $J_{4-5}=9$ Hz).

Found: C, 54.63; H, 5.33; N, 8.98%. Calcd for $C_{14}H_{16}O_6N_2$: C, 54.54; H, 5.23; N, 9.09%.

trans-*5-(2-Benzyloxycarbonylaminoethyl)-2-oxazolidone-4-carboxylic Acid (Xb)*. *trans*-Oxazolidone derivative Xb was obtained from IXb (1.00 g, 4.37 mmol) as in the preparation of Xa, yield 0.80 g (59.0%). It was recrystallized from ethyl acetate and petroleum ether, mp 103—105 °C. NMR: δ 4.08 (d, H-4, $J_{4-5}=5$ Hz).

Found: C, 54.24; H, 5.30; N, 9.06%. Calcd for $C_{14}H_{16}O_6N_2$: C, 54.54; H, 5.23; N, 9.09%.

N^{α},N^{δ}-*Diphthalyl*-erythro-*β-methoxy*-DL-*ornithine (XIa)*. To a solution of VIIIa (1.00 g, 3.04 mmol) in methanol, triethylamine was added in excess and the mixture was concentrated *in vacuo*. Crystalline residue was suspended in anhydrous dioxane and phthalic anhydride (0.50 g, 3.38 mmol) was added. The suspension was refluxed at 130—135 °C for 30 hr, and then the clear solution was concentrated *in vacuo*. Residual oil was dissolved in sodium hydrogencarbonate solution and extracted with ethyl acetate. Aqueous layer was acidified with 6 M hydrochloric acid and extracted with ethyl acetate for several times. Ethyl acetate layer was washed with water and dried over anhydrous sodium sulfate. It was concentrated *in vacuo* and the oily residue was dissolved in a small amount of methanol. Crystals formed were filtered and recrystallized from methanol, yield 1.00 g (72.1%), mp 188—189 °C.

Found: C, 58.07; H, 4.82; N, 6.09%. Calcd for $C_{22}H_{18}O_7N_2 \cdot 2H_2O$: C, 57.64; H, 4.84; N, 6.11%.

After drying over phosphorus pentoxide at 80 °C for 36 hr under reduced pressure, elemental analysis was repeated.

Found: C, 62.13; H, 4.40; N, 6.67%. Calcd for $C_{22}H_{18}O_7N_2$: C, 62.56; H, 4.30; N, 6.63%.

N^{α},N^{δ}-*Diphthalyl*-threo-*β-methoxy*-DL-*ornithine (XIb)*. The mixture of VIIIb (1.00 g, 3.42 mmol) and phthalic anhydride (0.76 g, 5.13 mmol) was heated at 150—160 °C for 1 hr. The melting product was cooled to room temperature and the residue was treated with ether. Insoluble material was recrystallized from methanol, yield 1.03 g (71.3%), mp 214—215 °C.

Found: C, 62.43; H, 4.36; N, 6.58%.

Mixed Anhydride of N^{α},N^{δ}-*Diphthalyl*-erythro-*β-methoxy*-DL-*ornithine with Ethoxycarbonic Acid (XIIIa)*. To a solution of XIa (0.43 g, 1.02 mmol) in 5 ml of anhydrous dioxane and 10 ml of anhydrous ether, triethylamine (0.13 g, 1.29 mmol) and then ethoxycarbonyl chloride (0.12 g, 1.12 mmol) were added on ice cooling. After stirring for 30 min at 0 °C and then at room temperature for several hours, petroleum ether was added to the reaction mixture. Precipitate was filtered and washed rapidly with water. It was dried over phosphorus pentoxide in vacuum desiccator, yield 0.42 g (84.9%). Recrystallization from dioxane and petroleum ether gave needles, mp 160—161 °C.

Found: C, 60.50; H, 4.62; N, 5.57%. Calcd for $C_{25}H_{22}O_9N_2$: C, 60.73; H, 4.49; N, 5.67%.

Mixed Anhydride of N^{α},N^{δ}-*Diphthalyl*-threo-*β-methoxy-ornithine With Ethoxycarbonic Acid (XIIIb)*. To a solution of XIb (0.84 g, 1.99 mmol) in 4 ml of dimethylformamide, triethylamine (0.23 g, 2.28 mmol) and ethoxycarbonyl chloride (0.24 g, 2.20 mmol) were added under ice cooling. After stirring at 0 °C for 1 hr, 20 ml of anhydrous ether and 100 ml of petroleum ether were added. Precipitate formed was filtered and washed rapidly with water. It was dried over phosphorus pentoxide in vacuum desiccator, yield 0.76 g (78%). Recrystallization from ethyl acetate and petroleum ether gave prisms, mp 143—144 °C.

Found: C, 60.67; H, 4.56; N, 5.74%. Calcd for $C_{25}H_{22}O_9N_2$: C, 60.73; H, 4.49; N, 5.67%.

erythro-*γ-Hydroxy*-DL-*β-lysine Lactone Dihydrobromide (XIIa)*. *a)* via *Acid Chloride*: A solution of XIa (1.50 g, 3.55 mmol) in 15 ml of thionyl chloride was refluxed for 30 min. Thionyl chloride was thoroughly removed by evaporation *in vacuo* with anhydrous benzene. Residual oil was dried over sodium hydroxide in vacuum desiccator. Acid chloride thus obtained was dissolved in 70 ml of anhydrous benzene and added to a solution of diazomethane in ether on ice cooling for 2.5 hr. After stirring at room temperature for 3 hr, the reaction mixture was kept in a refrigerator. Pale yellow precipitate (0.90 g, 56%) obtained was suspended in methanol and a solution of silver benzoate (0.20 g, 0.87 mmol) in 1 ml of triethylamine was added. After stirring in the dark overnight, insoluble material was filtered off. Filtrate was concentrated *in vacuo* and oily residue was dissolved in ethyl acetate. Insoluble material formed again was filtered off and filtrate was washed with dilute hydrochloric acid and then water. Organic layer was dried over anhydrous sodium sulfate and concentrated *in vacuo*. Oily residue obtained was dissolved in 20 ml of 47% hydrobromic acid containing 7 ml

of anisole. It was heated under reflux for 20 hr. Aqueous layer was separated from organic layer and washed with benzene several times. Aqueous solution was concentrated *in vacuo* and the residue was crystallized from a small amount of ethanol. It was recrystallized from 94% ethanol and ether, yield 60 mg (9.7%), mp 217—219 °C (decomp.).

Found: C, 23.56; H, 4.67; N, 9.14; Br, 52.02%. Calcd for $C_6H_{14}O_2N_2Br_2$: C, 23.54; H, 4.61; N, 9.16; Br, 52.23%.

b) via *Mixed Anhydride*: A solution of XIIIa (1.07 g, 2.53 mmol) in 50 ml of anhydrous dioxane was added to a 0.1 mol solution of diazomethane in ether on ice cooling. After stirring at 0 °C for 6 hr and allowing to stand overnight at room temperature, the reaction mixture was concentrated *in vacuo* to obtain pale yellow oily residue of diazoketone in a quantitative yield. To a solution of the diazoketone in methanol, a solution of silver benzoate (0.10 g, 0.44 mmol) in triethylamine was added. Subsequent treatments were carried out as mentioned in a), yield 0.25 g (37.8%), mp 217—219 °C (decomp.).

threo-*γ-Hydroxy*-DL-*β-lysine Lactone Dihydrobromide (XIIb)*. *a)* via *Acid Chloride*: When the reaction of acid chloride of XIb and diazomethane was carried out at room temperature in a similar procedure to that in preparation of XIIa, crystalline diazoketone could not be isolated. Then the reaction mixture was warmed at 40 °C for removal of excess diazomethane and evaporated *in vacuo*. The oily residue thus obtained was immediately used for subsequent rearrangement and hydrolysis. From XIb (0.47 g, 1.11 mmol) 80 mg of *threo* isomer XIIb (23.5%) was obtained, mp 220—229 °C (decomp.).

Found: C, 23.64; H, 4.61; N, 9.19; Br, 52.12%. Calcd for $C_6H_{14}O_2N_2Br_2$: C, 23.54; H, 4.61; N, 9.16; Br, 52.23%.

b) via *Mixed Anhydride*: By mixed anhydride method as mentioned in the preparation of XIIa, *threo* isomer XIIb was obtained from XIIIb (0.65 g, 1.54 mmol), yield 0.14 g (34%). It was recrystallized from 94% ethanol and ether, mp 205—212 °C (decomp.).

N^{β},N^{ε}-*Dibenzyloxycarbonyl*-erythro-*γ-hydroxy*-DL-*β-lysine Lactone (XIV)*. To an aqueous solution of XIIa (0.11 g, 0.36 mmol), sodium carbonate (0.27 g, 2.55 mmol) and benzyloxycarbonyl chloride (0.15 g, 0.87 mmol) were added at 0 °C. After stirring at 0 °C for 30 min and then at room temperature for 4 hr, the reaction mixture was acidified with dilute hydrochloric acid. Oily product formed was extracted with ethyl acetate and organic layer was dried over anhydrous sodium sulfate. It was concentrated *in vacuo* and the residual oil was treated with petroleum ether. Finally, the oil was dissolved in ethyl acetate. Addition of petroleum ether yielded crystals, yield 95 mg (64%). Recrystallization from ethyl acetate and petroleum ether gave needles, mp 79—81 °C.

Found: C, 63.78; H, 5.89; N, 6.71%. Calcd for $C_{22}H_{24}O_6N_2$: C, 64.06; H, 5.87; N, 6.79%.

N^{β},N^{ε}-*Dibenzyloxycarbonyl*-erythro-*γ-hydroxy*-DL-*β-lysine Amide (XV)*. A solution of XIV (80 mg, 0.19 mmol) in methanol was saturated with ammonia. After keeping at room temperature in a pressure bottle for 3 days, methanol was evaporated *in vacuo* to obtain crystals, yield 80 mg (96%). Recrystallization from methanol gave needles, mp 197—198 °C.

Found: C, 61.69; H, 6.44; N, 9.69%. Calcd for $C_{22}H_{27}O_6N_3$: C, 61.52; H, 6.34; N, 9.79%.

N^{β},N^{ε}-*Dibenzyloxycarbonyl*-O-*methanesulfonyl*-erythro-*γ-hydroxy*-DL-*β-lysine Amide (XVI)*. To a suspension of XV (0.10 g, 0.23 mmol) in 2 ml of pyridine, methanesulfonyl chloride (0.10 g, 0.87 mmol) was added. After stirring overnight, the reaction mixture was poured into ice-cold water. The aqueous solution was saturated with sodium chloride and extracted with ethyl acetate. Organic layer was washed with saturated sodium chloride solution and dried over anhydrous sodium sulfate. It was concentrated *in vacuo* and the residual oil was purified by silica gel column chromatography. Elution with chloroform gave a pure mesylate XVI, yield 60 mg (51%). It was recrystallized from ethyl acetate and petroleum ether, mp 106—107 °C.

Found: C, 54.37; H, 5.72; N, 8.49; S, 6.65%. Calcd for $C_{23}H_{29}O_8N_3S$: C, 54.42; H, 5.76; N, 8.28; S, 6.32%.

Conversion of erythro *Amide (XVI) to* threo *Lactone (XIIb)*. To a solution of XVI (30 mg, 0.06 mmol) in anhydrous ethanol, potassium acetate (0.20 g, 2.04 mmol) was added. The reaction mixture was heated under reflux for 10 hr, and then concentrated *in vacuo*. The residue was dissolved in water and extracted with ethyl acetate. Organic layer was concentrated *in vacuo* after drying over anhydrous sodium sulfate. The oily residue obtained was hydrolyzed with 6 M hydrochloric acid. Hydrolyzate was extracted with ethyl acetate and aqueous layer was evaporated *in vacuo* to obtain crystals of XIIb, yield 5 mg (39%).

References and Notes

1) Part VI: T. Wakamiya, and T. Shiba, *J. Antibiotics*, in press.

2) Presented at the 26th Annual Meeting of the Chemical Society of Japan, Tokyo, April, 1972; p. 1275 and the 28th Annual Meeting, Tokyo, April, 1973; p. 1849.

3) A. Nagata, T. Ando, R. Izumi, H. Sakakibara, T. Take, K. Hayano, and J. Abe, *J. Antibiotics*, **21**, 681 (1968); R. Izumi, T. Noda, T. Ando, T. Take, and A. Nagata, *ibid.*, **25**, 201 (1972).

4) T. Wakamiya, T. Shiba, and T. Kaneko, This Bulletin, **45**, 3668 (1972).

5) T. Wakamiya, Y. Tarumi, and T. Shiba, *Chem. Lett.*, **1973**, 233.

6) B. R. Baker, R. E. Shaub, M. V. Querry, and J. H. Williams, *J. Org. Chem.*, **17**, 77 (1952).

7) J. C. Sheehan, and J. G. Whitney, *J. Amer. Chem. Soc.*, **85**, 3863 (1963); C. H. Stammer, and R. G. Weeb, *J. Org. Chem.*, **34**, 2306 (1969).

8) S. Futagawa, T. Inui, and T. Shiba, This Bulletin, **46**, 3308 (1973).

9) H. E. Carter and H. D. West, Org. Syn., Coll. Vol. 3, 813 (1965); H. O. House, "Modern Synthetic Reactions," 2nd Ed., W. A. Benjamin, Inc., (1972) p. 387.

10) M. L. Wood, R. J. Madden, and H. E. Carter, *J. Biol. Chem.*, **117**, 1 (1937).

11) G. H. L. Nefkens, G. I. Tesser, and R. J. F. Nivard, *Rec. Trav. Chim. Pays-Bas*, **79**, 688 (1960).

12) D. S. Tarbell, and J. A. Price, *J. Org. Chem.*, **22**, 245 (1957); B. Penke, J. Czombos, L. Baláspiri, J. Petres, and K. Kovács, *Helv. Chim. Acta*, **53**, 1057 (1970); M. A. Ondetti, J. Pluščec, E. R. Weaver, N. Williams, E. E. Sabo, and O. Kocy, "Chemistry and Biology of Peptides (Proc. of the 3rd American Peptide Symposium)," Ann Arbor Science Publishers Inc., (1972) p. 525.

Nucleosides. XXI.[1] Preparative Routes to Nucleosides Derived from 4-Amino-4-deoxy-β-D-glucopyranose[2]

Frieder W. LICHTENTHALER, Peter Voss, and Gerd BAMBACH
Institut für Organische Chemie, Technische Hochschule Darmstadt, 61 Darmstadt, Germany
(Received January 14, 1974)

Four-step syntheses for the 4′-amino-4′-deoxy-β-D-glucopyranosyl nucleosides of adenine (**7**), uracil (**12**) and cytosine (**16**) from a readily accessible galactose derivative (**2**) are described, in overall yields of 41—47%. The reaction sequence, used, involved (i) stannic chloride catalyzed nucleosidations of **2** with the bis-trimethylsilyl derivatives of N^6-benzoyladenine, uracil and N^4-acetylcytosine, (ii) displacement of the 4′-sulfonyloxy groups in **3**, **10**, and **15** by azide, (iii) de-*O*-benzoylation and (iv) hydrogenation. An alternate route to **12** and **16**, comprising nucleosidation of tetraacetyl-4-acetamido-4-deoxy-D-glucopyranose (**20**) *via* the classical Hilbert-Johnson approach proved feasable, yet inferior with respect to yields and accessibility of educts. The structures and configurations assigned followed from the synthetic route as well as from spectroscopic data, particularly from the acetyl resonances of the peracetylated nucleosides **9**, **14**, and **18**, which are in excellent agreement with those of the respective glucosyl- and 3-acetamido-3-deoxy-glucosyl analogs (Table).

The aminoacyl-4-aminohexosyl-cytosine antibiotics gougerotin and blasticidin S, both elaborated by streptomyces species found in Japan,[3,4] have been the subject of intense chemical and biochemical investigations,[5] the main stimulus stemming from their inhibition of protein biosynthesis at the peptide chain elongation stage.[6] As a result, the structures of these antibiotics have been unequivocally established,[7] total synthesis for both have been advanced[16,17] and their structure-activity relationships have been assessed on the basis of the presently available structural analogs.[18] However, number and variety of the structural types being rather limited, these minimal functional group and spatial requirements for inhibition of transpeptidation[18] need to be further substantiated in order to elicit persuasive conclusions with respect to the molecular architecture of the ribosomal binding site. To provide this corroborative evidence, the synthesis of a systematic series of structural analogs, modified in nucleobase, aminosugar unit and aminoacid component, was deemed essential, which on biological evaluation are more likely to produce results of biological significance than previous studies, mainly directed towards the total syntheses of the natural products.[19] By consequence, synthetic work on purine and pyrimidine nucleosides derived from 4-amino-4-deoxy-hexoses was initiated.[15,20] In this paper, we present the results of our synthetic studies on 4′-amino-4′-deoxy-β-D-glucopyranosyl nucleosides, providing with the synthesis of **7** the first purine nucleoside in this series, as well as preparative procedures for the respective uracil (**12**) and cytosine nucleosides (**16**), that are alternate or considerably improved over those already known.[14,15,21]

Choice of Methods. Of the newer nucleosidation procedures available,[22] the most recently advanced[23] "Friedel-Crafts catalyzed trimethylsilyl procedure" was considered the most propitious for the preparation of pyrimidine as well as purine nucleosides[1] allowing utilization of a per-*O*-acyl-glycose rather than the 1-halide. As the sugar precursor to be nucleosidated, a suitably blocked derivative of 4-amino-4-deoxy-D-glucopyranose, *e.g.* its pentaacetate **20**, might be surmised to provide a very direct access to 4-aminoglucosyl nucleosides. However, whilst this approach can be realized as shown by the conversion of **20** to **19** (*vide infra*), it appears to be of limited general applicability for several reasons; *e.g.* the educt is encumbered by conceivable ring contraction to the pyrrolidinose form during nucleosidation and difficulties may arise in removing an *N*-acetyl group in purine nucleosides. Hence, a more suitable starting sugar for Friedel-Crafts catalyzed *N*-glycosidations was required and found in 1-*O*-acetyl-2,3,6-tri-*O*-benzoyl-4-*O*-mesyl-α-D-galactopyranose (**2**), readily accessible in crystalline form and good yield (79%) from its methyl glycoside **1**[24] by acetolysis in the presence of boron trifluoride-etherate.[25]

Adenine Nucleosides (3—9). When 1-*O*-acetyl-2,3,6-tri-*O*-benzoyl-4-*O*-mesyl-α-D-galactose (**2**) was allowed to react with a slight excess of *N*-benzoyl-*N*,9-bis(trimethylsilyl)adenine in the presence of stannic chloride (12 hr/60 °C in dichloroethane), the protected nucleoside **3** could be isolated by a simple workup procedure in reasonable yield (59%). Subsequent removal of the *O*- and *N*-benzoyl groups with sodium methoxide/methanol afforded the highly crystalline 4′-*O*-mesyl-derivative **4**. Of the two compounds, **3** and **4**, respectively, **3** was found to give a more uniform reaction mixture when subjected to azidolysis with sodium azide in hexamethyl phosphoric triamide (8 hr/80 °C). The protected azidonucleoside **5** formed in this way was directly debenzoylated, to afford in an overall yield (**3**→**6**) of 78% the 4′-azidoglucosyl-adenine **6**. Subsequent hydrogenation over 10% palladium on carbon proceeded smoothly to give in the form of colorless prisms the desired 4′-amino-4′-deoxy-β-D-glucopyranosyl-adenine (**7**)—the hitherto first purine nucleoside of a 4-aminohexose. It was further characterized by its 4′-acetamido derivative **8** as well as its peracetate **9**, each clearly exhibiting the NMR characteristics required for the *gluco*-configuration (*cf.* Table).

Of particular relevance in this context appears to be the overall yield for the four step reaction sequence **2**→**3**→**5**→**6**→**7**, which is 42%, and, hence, may be the method of choice for the preparation of other 4-amino-hexosyl-purines, should their synthesis be required.

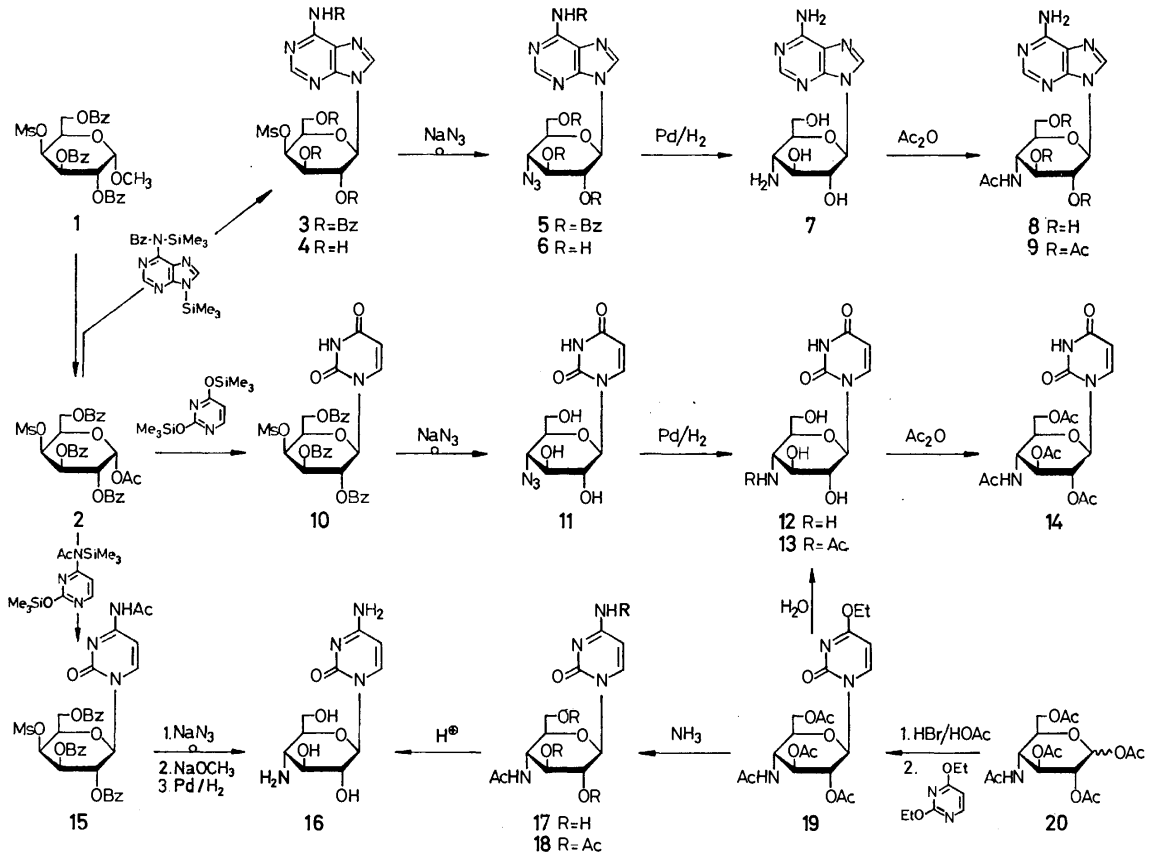

Uracil Nucleosides (10—14). Whilst stannic chloride catalyzed nucleosidations of 1-*O*-acetyl-2,3,5-tri-*O*-benzoyl-D-ribofuranose with silylated pyrimidines may readily be performed at room temperature,[23] it was found advantageous to use somewhat more forcing conditions (12 hr, 60 °C) for the *N*-glycosidation of *O,O*-bis(trimethylsilyl)uracil with the hexose derivative **2**, particularly when performing the reaction on rather larger scale. In this way, a crystalline product was obtained in 83% yield, comprising according to tlc an approximate 10: 1 mixture of the *β*-nucleoside **10** and a second component, most probably the N^3-isomer. The latter, however, was readily removed by recrystallization to afford the protected galactosyl-uracil **10** in a yield of 71%. Displacement of the mesyloxy group in **10** by sodium azide in hexamethyl phosphoric triamide (5 hr, 80 °C) followed by de-*O*-benzoylation with sodium methoxide gave the 4'-azidoglucosyl nucleoside **11** (72%). The subsequent hydrogenation over 10% palladium on carbon readily afforded 4'-amino-4'-deoxy-*β*-D-glucosyl-uracil **12** (81%), which was further characterized by an amorphous *N*-acetate (**13**) and its crystalline tetraacetyl derivative **14**.

Prior to the availability of the "Friedel-Crafts catalyzed silyl procedure" we had followed another approach for the preparation of the pyrimidine nucleosides **13** and **18**,[15] which expectedly gave inferior results with respect to accessibility of the starting sugar and the yield in the nucleoside synthesis: nucleosidation of peracetylated 4-aminoglucosyl bromide *via* the classical Hilbert-Johnson procedure.[26] Accordingly, 4-acetamido-1,2,3,6-tetra-*O*-acetyl-4-deoxy-D-glucopyranose (**20**) in the form of a sirupy 9: 1 *α*/*β*-mixture,[27] was converted into the corresponding 1-bromo sugar by treatment with 40% hydrogen bromide in glacial acetic acid, which *in situ* was reacted with diethoxypyrimidine. The ethoxypyrimidinone nucleoside **19** was readily obtained from the reaction mixture, yet the yield was far from satisfactory (36%, based on **20**). The subsequent hydrolysis with methanolic hydrochloric acid, however, proceeded smoothly affording **13** in 84% yield.

In comparing the preparative utility of the three synthetic routes by which 4-aminoglucosyl-uracil now has been prepared, the four step conversion of **2** into **12** in a 41% overall yield appears to be an appreciable improvement over the alternate five step sequence from the much less accessible galactosyl-uracil (overall yield: 31%[21]). The classical Hilbert-Johnson approach **20**→**19**→**13**→**12**, however, is expectedly inferior to either one of the two others.

Cytosine Nucleosides (15—18). Whilst a conversion of galactoside **1** into nucleoside **15** *via* the glycosyl bromide of **1** and its condensation with N^4-acetylcytosine has already been described,[14] the high yield (95%) reported for the two steps was based on the pyrimidine precursor, and amounts to only 47% when based on the more precious sugar component. A superior procedure appears to be the nucleosidation of the acetolysis product of **1** with N^4,*O*-bis(trimethylsilyl)-N^4-acetylcytosine in the presence of stannic chloride (12 hr/60 °C in dichloroethane) affording crystalline **15** with a yield of 85% in the nucleosidation step **2**→**15** (62% from **1**). Since the conversion **15**→**16** is readily accomplished by the three step sequence azidolysis→deacetylation→hydrogenation,[14] 4'-amino-

4′-deoxy-β-D-glucosyl-cytosine can now be prepared from a readily accessible galactose derivative (**2**) in an overall yield of 47%.

An alternate route to **16**, elaborated earlier, proved to be of less preparative utility (21% overall yield): the classical Hilbert-Johnson nucleosidation of 4-amino-glucose peracetate (**20**→**19**) followed by aminolysis to **17** and de-*N*-acetylation (**17**→**16**). Nevertheless, a sample prepared in this way, which was subsequently *N*-acylated with BOC-blocked sarcosyl-seryl-azide[15] has provided the first biologically active analogue[31] of the nucleoside antibiotic gougerotin.

Structural and Configurational Assignments. Whilst the mode of preparation in itself provides conclusive proof for structure and configuration of the nucleosides described, corroborative evidence is readily derived from NMR data. However, except for the anomeric proton (*cf.* Table 1), the chemical shifts and coupling patterns of the pyranoid ring protons are not extractable from 60 MHz spectra without extensive decoupling. Much more conveniently, the configurations are ascertained by the chemical shifts of the acetyl resonances of per-acetylated nucleosides on the basis of the "acetyl resonance rule" elaborated for cyclitols,[32] hexopyranoses[33] and hexopyranosyl nucleosides.[33,34] As is apparent from the data collected in Table 1, neither one of the glucopyranosyl nucleosides (II—III), their 3′-amino-analogs (V—VII) or their 4′-amino counterparts (**9**, **14**, **18**, and **19**) exhibited signals attributable to an axially oriented acetoxy group (below τ 7.95 in DMSO-d_6). Equally distinct is the presence of an equatorial acetamido function in the 3′-aminoglucosyl nucleosides V—VII as well as their 4′-amino analogs, appearing as a signal in the τ 8.20—8.24 range, nicely separated from the others. Noteworthy is also the low field resonances for the cytosine nucleosides III and VI, originating from the N^4-acetyl group in the aglycon, as well as the highfield signals, at τ 8.30 and 8.31

Table 1. NMR-Data in DMSO-d_6 and rotations of peracetyl-β-D-glucopyranosyl-nucleosides

Sugar moiety	R[a]		Chemical shifts in τ units[b] H-1′	a-OAc	e-OAc 6′-OAc	e-NHAc	$[\alpha]_D$ (solvent, °C)
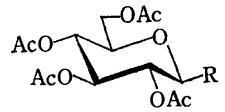	U	(I)	4.03	—	7.98 (2) 8.04 8.08	—	+4 (MeOH, 23)[c]
	U(O⁴-Et)	(II)	3.98	—	7.99 (2) 8.04 8.12	—	+36 ($CHCl_3$, 26)[d]
	C(N⁴-Ac)	(III)	3.94	—	7.88[e] 7.97 (2) 8.02 8.11	—	+38 ($CHCl_3$, 23)[d]
	A(N⁶-Bz)	(IV)	?	—	?	—	+6 ($CHCl_3$, 10)[f]
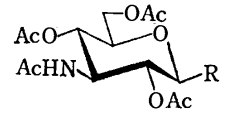	U	(V)	4.01	—	7.98 8.02 8.11	8.23	−9 ($CHCl_3$, 24)[g]
	C(N⁴-Ac)	(VI)	3.97	—	7.89[e] 8.00 8.12	8.23	+12 (MeOH, 23)[g]
	A	(VII)	3.91	—	8.00 8.03 8.30	8.24	−36 ($CHCl_3$, 24)[h]
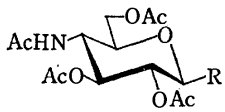	U	(**14**)	4.15	—	8.00 8.06 8.10	8.21	+11 (MeOH, 23)
	U(O⁴-Et)	(**19**)	4.02	—	7.99 8.03 8.14	8.20	+46 (MeOH, 23)
	C(N⁴-Ac)	(**18**)	3.09	—	7.89[e] 8.01 8.05 8.09	8.23	+28 (DMF, 23)
	A	(**9**)	3.98	—	8.03 (2) 8.31	8.22	+6 ($CHCl_3$, 20)

a) Abbreviations used = uracilyl-1; U(O⁴-Et) = 4-ethoxypyrimidinonyl-1; C(N⁴-Ac) = N⁴-acetylcytosinyl-1; A = adeninyl-9; A(N⁶-Bz) = N^6-benzoyladeninyl-9. b) Except for compound VI (P. Emig, Techn. Hochschule Darmstadt, unpublished results) the NMR data for I—III, V and VII are derived from Ref. 33. c) T. Ueno, Techn. Hochschule Darmstadt, unpublished results. d) G. E. Hilbert and E. F. Jansen, *J. Amer. Chem. Soc.*, **58**, 60 (1936). e) N⁴-Acetyl resonance of the cytosine moiety. f) N. Yamaoka, K. Aso, and K. Matsuda, *J. Org. Chem.*, **30**, 149 (1965). g) S. Takei and Y. Kuwada, *Chem. Pharm. Bull.*, **16**, 944 (1965). h) J. Beranek, H. A. Friedman, K. A. Watanabe, and J. J. Fox, *J. Heterocycl. Chem.*, **2**, 188 (1965).

respectively, for the adenine derivatives VII and **9** (*cf.* Table 1). Those clearly arise from the 2'-acetoxy resonances, being in the range of diamagnetic shielding by the purine moiety, since similar upfield shifts have been observed for other purine nucleosides with an equatorial pyranoid 2'-acetoxy function.[33] In the pyrimidine nucleosides, this diamagnetic shielding is expectedly[33] lower, giving rise to resonances that are only shifted by approximately 0.1 ppm towards higher field (τ 8.08—8.14).

The results clearly demonstrate that examination of the acetyl resonances in DMSO-d_6 provides a reliable, convenient method for configurational assignments in the hexopyranosyl nucleoside field, when taking into consideration the predictable shielding effects by purine and pyrimidine nucleobases. Converse conclusions reached by Cushley *et al.*[35] have later been shown[36] invalid, being based, in part, on incorrect configurational assignments.

Whilst configuration and conformation of the sugar moiety may readily be elicited from NMR data, the orientation of nucleobase to the sugar is less clear. An attempt was made to obtain some, though admittedly limited information on this from the rotational values of the peracetylated nucleosides. Since replacement of an acetoxy by an acetamido group does not substantially affect rotations,[37] the sign and magnitude of the nucleosides in the Table 1 would be excepted to be at least very similar, if the sugar-nucleobase orientations are identical. However, as is clearly apparent from the data in the Table, they vary within too wide a range as to allow even limited conclusions on this matter.

Experimental

Melting points were determined on a Bock Monoskop, and are uncorrected. Spectra were recorded on Perkin-Elmer 125 (IR), Perkin-Elmer 137 (UV), and Varian A-60A (NMR) instruments.

Thin layer chromatography (tlc) on Kieselgel F_{254} plastic sheets (Merck, Darmstadt) was used throughout to monitor the reactions and to ascertain the purity of the products; developers employed (A) ethyl acetate–chloroform (1:1); (B) ethyl acetate–ethanol–water (15:2:1). The spots were visibilized by UV, by iodine vaporing, or by spraying with 80% aqueous sulfuric acid and charring at 110 °C for 5 min. Column chromatography was carried out on silica gel of 70—230 mesh ("Kieselgel 60", Merck, Darmstadt).

1-O-Acetyl-2,3,6-tri-O-benzoyl-4-O-mesyl-α-D-galactopyranose (2). To a solution of 30.0 g (51 mmol) of methyl 2,3,6-tri-*O*-benzoyl-4-*O*-mesyl-α-D-galactopyranoside (**1**)[28] in 600 ml of acetic anhydride 30 ml of BF_3–etherate in ether was added, and the mixture was heated to 60 °C for 12 hr, followed by gradually stirring into ice–water (3 l). After 2 hr, the solution was neutralized by careful addition of solid $NaHCO_3$, and subsequently extracted with two 500 ml portions of dichloromethane. The organic phase was dried over Na_2SO_4 and evaporated to dryness to yield a residue, which after charcoal treatment in methanol (500 ml), was recrystallized from the minimum amount of methanol: 24.2 g (79%), mp 143—144 °C; $[\alpha]_D^{20}$ +92° (*c* 1, $CHCl_3$); NMR ($CDCl_3$) τ 1.8—2.8 (m, 15, $3C_6H_5$), 3.35 (narrow [4 Hz] m, H-1), 4.12 (narrow m [4 Hz], H-2 and H-3), 4.41 (m [4 Hz], 1, H-4), 6.90 (s, 3, OMs), 7.83 (s, 3, OAc).

Found: C, 58.42; H, 4.63; S, 5.16%. Calcd for $C_{30}H_{28}O_{12}S$: C, 58.82; H, 4.61; S, 5.22%.

Adenine Nucleosides (3—9). 9-(2',3',6'-Tri-O-benzoyl-4'-O-mesyl-β-D-galactopyranosyl)-N⁶-benzoyladenine (3): To a solution of 3.0 g (4.9 mmol) of 4-*O*-mesylgalactose **2** in 1,2-dichloroethane (75 ml) was added 6 g of molecular sieve[38] and 1.5 ml of stannic chloride. After 30 min standing 2.0 g (5.2 mmol) of N^6-benzoyl-N^6,9-bis(trimethylsilyl)adenine[39,40] was added and the mixture was heated to 60 °C for 12 hr under careful exclusion of moisture. The molecular sieve was removed and the solution, after dilution with dichloromethane (75 ml), was extracted with aqueous sodium bicarbonate (2×100 ml) and washed with water (2×100 ml). Drying (Na_2SO_4) and evaporation to dryness followed by repeated reevaporations from methanol, left a sirup, which was crystallized by dissolving in benzene (120 ml), removal of some insoluble material, and gradual addition of cyclohexane (*ca.* 100 ml): 2.3 g (59%) of a colorless, amorphous product, uniform by tlc (A); $[\alpha]_D^{20}$ −17° (*c* 1, $CHCl_3$); NMR ($CDCl_3$) τ 1.26 and 1.52 (two 2 H-s, H-2 and H-8), 1.8—2.8 (broad m, 20, $4C_6H_5$), 3.65 (m, 2, H-1' and H-4'), 6.83 (s, 3, OMs).

Found: C, 60.45; H, 4.26; N, 8.83; S, 3.97%. Calcd for $C_{40}H_{33}N_5O_{11}S$: C, 60.67; H, 4.20; N, 8.85; S, 4.05%.

9-(4'-O-Mesyl-β-D-galactopyranosyl)adenine (4): To 1.0 g of tetrabenzoyl derivative **3** in methanol (20 ml) was added 1 ml of 5 M methanolic sodium methoxide with cooling, and the mixture was stored in a refrigerator overnight. The crystals, which had separated, were filtered off (0.35 g). From the mother liquor a second crop (0.1 g) was obtained by deionization with a strongly acidic ion exchange resin (Merck I), evaporation to dryness and trituration with little methanol. Both fractions were recrystallized from little water: 0.28 g (58%) of **4** as needles of mp 216—218 °C (decomp.); $[\alpha]_D^{20}$ +9° (*c* 0.6, H_2O); NMR (DMSO-d_6) τ 6.67 (s, 3, OMs).

Found: C, 37.97; H, 4.68; N, 18.49; S, 8.41%. Calcd for $C_{12}H_{17}N_5O_7S$: C, 38.30; H, 4.57; N, 18.66; S, 8.53%.

9-(4'-Azido-4'-deoxy-β-D-glucopyranosyl)adenine (6): To a solution of 10.0 g (12.6 mmol) of galacto-mesylate **3** in hexamethyl phosphoric acid triamide (50 ml) was added sodium azide (4.2 g, 5 molar equiv.) and the mixture was heated to 80 °C with vigorous stirring for 8 hr, followed by pouring into ice–water (2 l). The precipitate was collected, washed with water and subjected to treatment with activated carbon in methanol (150 ml). Evaporation to dryness, filtration with water and drying gave 9-(2',3',6'-tri-*O*-benzoyl-4'-azido 4'-deoxy-β-D-glucopyranosyl)-N^6-benzoyladenine (**5**) as an amorphous, colorless product (9.0 g), showing only traces of an impurity (tlc in A). Due to difficulties encountered in crystallization attempts from the usual solvents, the product was directly subjected to debenzoylation with sodium methoxide (4 ml of a 5 M methanolic solution) in methanol (100 ml) by storing for 24 hr at ambient temperature. Some product had crystallized and was isolated after standing overnight in a refrigerator: 2.60 g (60%) of mp 231—233 °C (decomp.). The mother liquor was deionized (Merck I resin) and evaporated to dryness *in vacuo* to give, from a concentrated methanolic solution, a second crop (0.77 g) Total yield on crude **6**: 3.37 g (78%); mp 229—231 (decomp.). For analytical data, a 200 mg portion was recrystallized from a small amount of water; mp 236—238 °C (decomp.); $[\alpha]_D^{20}$ +46° (*c* 1, dimethylformamide); IR (KBr) N_3 at 2100 cm^{-1}; NMR (DMSO-d_6 + D_2O) τ 1.84 and 1.99 (two 1 H-s, H-2 and H-8), 4.67 (d, 1, $J_{1,2}$=8.5 Hz, H-1').

Found: C, 39.00; H, 4.39; N, 32.98%. Calcd for $C_{11}H_{14}N_8O_4 \cdot H_2O$: C, 38.82; H, 4.74; N, 32.93%.

9-(4'-Amino-4'-deoxy-β-D-glucopyranosyl)adenine (7): To a

prehydrogenated suspension of 500 mg 10% Pd/C in water (100 ml) was added a solution of 2.0 g (6.3 mmol) of azido-nucleoside **6**, and the hydrogenation was continued. After 2 hr, tlc in B showing the absence of starting material, the catalyst was removed followed by concentration to dryness and several reevaporations from methanol, which induced crystallization: 1.70 g (90%) of **7**, crystallizing with 1 mol of methanol in colorless prisms, decomposing from 200 °C on, after sintering around 160 °C; $[\alpha]_D^{20}$ +12° (*c* 1, H_2O).

Found: C, 43.67; H, 6.00; N, 25.54. Calcd for $C_{11}H_{16}N_6O_4 \cdot CH_3OH$: C, 43.90; H, 6.14; N, 25.60%.

9-(4'-Acetamido-4'-deoxy-β-D-glucopyranosyl)adenine (8): To a stirred suspension of **7** (100 mg) in methanol (10 ml) was added 1 ml of acetic anhydride, giving gradually a clear solution. After 5 hr at room temperature (tlc in B showed the reaction to be complete), the mixture was evaporated to dryness followed by two reevaporations from ethanol. The residue was filtered with ethanol to give **7** as a hygroscopic (after drying over P_2O_5), solid product, containing 1 mol of acetic acid; NMR (D_2O) τ 1.63 and 1.83 (two 1 H-s, H-2 and H-8), 4.33 (d, 1, $J_{1',2'}$=9 Hz, H-1'), 7.86 (s, 3, acetic acid of crystallization), 7.91 (s, 3, NHAc).

Found: C, 44.94; H, 5.55; N, 21.39%. Calcd for $C_{13}H_{18}N_6O_5 \cdot CH_3COOH$: C, 45.22; H, 5.57; N, 21.10%.

9-(4'-Acetamido-2',4',6'-tri-O-acetyl-4'-deoxy-β-D-glucopyranosyl) adenine (9): To a pyridine solution (2 ml) of **8** (100 mg) was added 1 ml of acetic anhydride with cooling and stirring and the mixture was then kept at room temperature for 3 hr. Concentration to dryness *in vacuo* (finally 0.1 mm, bath temperature 25 °C), followed by reevaporations from water and ethanol–water (1: 1) gave a sirup which on trituration with ether solidified. Filtration afforded 100 mg (63%) of an amorphous product, uniform by tlc (in B); $[\alpha]_D^{20}$ +6° (*c* 1, $CHCl_3$); NMR (DMSO-d_6) τ 1.60 and 1.80 (two 1 H-s, H-2 and H-8), 2.00 (d, 1, J=8 Hz, 4'-NH), 2.71 (s, 2, 6-NH_2), 3.98 (d, 1, $J_{1',2'}$=9 Hz, H-1'), 4.25 (t, 1, $J_{1',2'}=J_{2',3'}$= 9 Hz, H-3'), 5.88 (m, 4, H-4', H-5', and 6'-CH_2), acetyl resonances *cf.* Table 1.

Found: C, 49.00; H, 5.56; N, 17.89%. Calcd for $C_{18}H_{24}N_6O_8$C: 49.14; H, 5.21; N, 18.10%.

Uracil Nucleosides. 1-(2',3',6'-Tri-O-benzoyl-4'-O-mesyl-β-D-galactopyranosyl)uracil (10): To a solution of 20.0 g (32.7 mmol) of 4-*O*-mesyl-galactose **2** in 1,2-dichlorethane was added 40 g of molecular sieve,[38] followed, after standing for 30 min, by the addition of stannic chloride (10 ml) and *O,O*-bis(trimethylsilyl)uracil[39,41] (11.0 g, 1.3 molar equiv.). The mixture was heated to 60 °C for 12 hr, and subsequently treated with saturated sodium bicarbonate solution (2×500 ml) and water (2×500 ml). The organic layer was dried (Na_2SO_4), concentrated to dryness and reevaporated twice from methanol. The residue was dissolved in hot ethanol (150 ml), from which it crystallized: 18.4 g of product, mp 189—190 °C, that, according to tlc in B, was contaminated with approximately 10% of another product (N^3-isomer) of lower R_f-value. The latter, being scarcely soluble in ethanol, was removed by one recrystallization from this solvent, affording 15.5 g (71%) of **10** as needles of mp 204—206 °C (lit,[21] 207—208 °C); UV (MeOH) and NMR data ($CDCl_3$) correlated well with those reported by Kondo and Goto[21] for their product, obtained by another route.

Found: C, 57.87; H, 4.19; N, 4.26; S, 4.71%. Calcd for $C_{12}H_{28}N_2O_{12}S$: C, 57.83; H, 4.25; N, 4.22; S, 4.82%.

1-(4'-Azido-4'-deoxy-β-D-glucopyranosyl)uracil (11): A mixture of 12.0 g (18 mmol) of mesyl-nucleoside **10**, 6.6 g (5 molar equiv.) of sodium azide and 45 ml of hexamethyl phosphoric triamide was stirred at 80—90 °C for 5 hr, followed by pouring into ice-water (1 l). The solid precipitate was filtered off, dried over P_2O_5 and directly subjected to de-*O*-benzoylation by dissolution in methanol (110 ml), containing 5 ml of 5 M methanolic sodium methoxide, and storage at room temperature overnight. The mixture was then deionized by a strongly acidic resin (Merck I) and evaporated to dryness, followed by several reevaorations from 1: 1 methanol–water, which induced crystallization. Filtration with methanol yielded 3.3 g (72%) of **11** as colorless crystals of mp 226—228 °C (decomp.); lit,[21]: 226 °C (decomp.).

1-(4'-Amino-4'-deoxy-β-D-glucopyranosyl)uracil (12): *A. Form Azidonucleoside 11 by Hydrogenation*:[42] To a prehydrogenated suspension of 500 mg 10% Pd/C in 1: 1 water–ethanol (100 ml) was added 2.0 g (6.8 mmol) of azide **11** in 20 ml of water, and the hydrogenation was continued. After 3 hr, tlc in B showing the absence of starting material, the catalyst was removed followed by evaporation to dryness *in vacuo*. Trituration of the residue with ethanol gave a crystalline product, which was filtered after standing in a refrigerator overnight: 1.52 g (81%) of colorless crystals, mp 241—243 °C (decomp.); mp, UV (MeOH), NMR (D_2O) and analytical data corresponded well with those reported for a product from another route.[21]

B. From 4'-Acetamido-nucleoside 13 by Deacetylation: A solution of sirupy **13** (680 mg, 2.15 mmol) in 4 M hydrochloric acid was refluxed for 3 hr, followed, after cooling down, by deionization with a strongly basic resin (Merck III), which was thoroughly washed on removal. The filtrate was subjected to charcoal treatment and subsequently evaporated to dryness, yielding a residue which crystallized on several reevaporations from ethanol. Filtration with ethanol and recrystallization from the same solvent gave 410 mg (65%) of **12** as colorless crystals, identical in all respects with the product described under A.

1-(4'-Acetamido-4'-deoxy-β-D-glucopyranosyl)uracil (13): *A. From Ethoxypyrimidinone-Nucleoside 20 by Hydrolysis*: A solution of 750 mg (1.5 mmol) of **20** in 8% methanolic hydrochloric acid (30 ml) was kept at ambient temperature for 24 hr followed by concentration *in vacuo* and repeated reevaporations of the residue from methanol. The yellowish sirup was purified on a silica gel column by elution with methanol to yield, after drying for 2 hr at 60 °C and 0.1 mm, 476 mg of amorphous **13** (84%), homogeneous by tlc (B), $[\alpha]_D^{23}$ +8° (*c* 1, CH_3OH); the product could not be crystallized from the usual solvents.

Found: C, 45.64; H, 5.52; N, 13.10%. Calcd for $C_{12}H_{17}N_3O_7$: C, 45.71; H, 5.44; N, 13.33%.

B. De-O-acetylation of Tetraacetate 14: To a solution of 440 mg (1 mmol) of **14** in methanol (15 ml) was added 0.2 ml of N methanolic sodium methoxide and the mixture was kept overnight at ambient temperature. Deionization with Dowex 50 (H^+) and concentration to dryness followed by repeated reevaporations from ethanol left a sirup, which was subjected to a small silica gel column and eluted with methanol. After evaporation to dryness *in vacuo* (finally 0.1 mm): 240 mg (76%) of **14** a colorless sirup, identical with respect to tlc (in B), IR and NMR data with the product described under A.

1-(4'-Acetamido-2',3',6'-tri-O-acetyl-4'-deoxy-β-D-glucopyranosyl)uracil (14): To aminoglucosyl-uracil **12** (430 mg, 1.5 mmol) in pyridine (10 ml) was added with stirring 4 ml of acetic anhydride. After 15 hr at ambient temperature, the clear solution was evaporated to dryness *in vacuo* (finally 0.1 mm) followed by coevaporations with water, water–ethanol (1: 1) and ethanol. The resulting sirup was dissolved in a small amount of methanol from which **14** crystallyzed gradually. Filtration after standing overnight in a refrigerator and drying at 60 °C/0.1 mm for 3 hr afforded 470 mg (68%) of

14 as colorless crystals of mp 260—263 °C (decomp.)[43]; $[\alpha]-$ +11° (*c* 1, CH_3OH); NMR (DMSO-d_6) τ 1.35 (s, 1, uracil-NH), 2.01 (broad d, 1, 4'-NH), 2.07 and 4.31 (two 1 H-d, $J_{5,6}$=8.5 Hz, H-5 and H-6), 4.15 (m, 1, H-1'), acetyl resonances *cf.* Table.

Found: C, 48.79; H, 5.15; N, 9.49%. Calcd for $C_{18}H_{23}N_3O_{10}$: C, 48.98; H, 5.25; N, 9.52%.

Treatment of *N*-acetyl derivative **13** with pyridine–acetic anhydride and processing of the mixture in a manner analogous to the one described above gave compound **14** in 74% yield.

*1-(4'-Acetamido-2',3',6'-tri-*O*-acetyl-4'-deoxy-β-*D*-glucopyranosyl)-4-ethoxypyrimidin-2-one (19)*: A solution of 2.30 g (5.9 mmol) of sirupy 1,2,3,6-tetra-*O*-acetyl-4-acetamido-4-deoxy-D-glucopyranose (**20**, α/β-ratio 9: 1)[27] in 40% HBr in glacial acetic acid (15 ml) was kept at ambient temperature for 3 hr. The mixture was then diluted with chloroform (200 ml) and extracted successively with cold water (2×100 ml), saturated sodium bicarbonate solution (2×100 ml) and water, followed by drying of the organic phase (Na_2SO_4). After filtration, the solution was added to 4.0 g (4 molar equiv.) of 2,4-diethoxypyrimidine and the solvent was removed *in vacuo*. The resulting mixture was then heated for 12 hr on a water-bath at 60 °C. After cooling down, *n*-hexane (200 ml) was added, resulting in a brownish precipitate. The hexane, containing the excessive diethoxypyrimidine, was removed by decantation, followed by another *n*-hexane extraction and discoloration of the residue in benzene solution with activated charcoal. Addition of *n*-hexane to the filtrate till beginning turbidity and standing in a refrigerator gave a first crop of crude **20**, successive further additions of *n*-hexane to the respective mother liquors a second and third. Recrystallization of the combined fractions by dissolution in the minimum amount of methanol and addition of water afforded 1.07 g (36%) of **20**, mp 118—120 °C (after sintering around 110 °C); $[\alpha]_D^{23}$ +46° (*c* 1, CH_3OH), +59° (*c* 1, $CHCl_3$); NMR (DMSO-d_6) τ 1.81 and 3.93 (two 1 H-d, $J_{5,6}$=7.5 Hz, H-5 and H-6), 2.10 (d, 1, $J_{4',NH}$=9 Hz, NH), 4.02 (m, 1, halfwidth 9 Hz, H-1'), 4.68 (m, 2, H-3' and H-2'), 5.63 and 8.71 (2H-q and 3H-t, J=7 Hz, OCH_2CH_3), 5.9 (m, 4, H-4', H-5', and 6'-CH_2), acetyl resonances *cf.* Table 1; acetyl resonances in $CDCl_3$ at τ 7.93, 7.97, 8.02, and 8.04.

Found: C, 50.99; H, 6.03; N, 8.90%. Calcd for $C_{20}H_{27}N_3O_{10}$: C, 51.17; H, 5.80; N, 8.95%.

*Cytosine-Nucleosides (15—18). 1-(2',3',6'-Tri-*O*-benzoyl-4-*O*-methanesulfonyl-β-*D*-galactopyranosyl)-*N*⁴-acetylcytosine (15)*: To a stirred solution of 4-*O*-mesyl-galactose **2** (4.8 g, 7.8 mmol) in sieve-dried 1,2-dichlorethane (150 ml) was added molecular sieve[38] (5 g), tin tetrachloride (2.4 ml), and, after 15 min, 1.65 g (1.1 molar equiv.) of N^4,*O*-bis(trimethylsilyl)-N^4-acetylcytosine,[39] and the mixture was kept in a bath at 60 °C for 12 hr. After dilution with 300 ml of 1,2-dichloroethane the solution was extracted with saturated sodium hydrogen carbonate (2×200 ml) followed by washing with water (2×200 ml). The organic phase was dried (Na_2SO_4), and evaporated to dryness *in vacuo*, yielding a solid mass that was filtered and thoroughly washed with ethanol: 4.7 g (85%) of **15** as colorless needles, mp 266—268 °C (decomp.) and $[\alpha]_D^{23}$ +38.6° (*c* 1, dimethylformamide). The product was identical with respect to tlc (in A), IR and NMR with a sample prepared by another route.[14]

*1-(4'-Acetamido-4'-deoxy-β-*D*-glucopyranosyl)cytosine (17)*: A solution of ethoxypyrimidinone-nucleoside **19** (2.70 g, 5.46 mmol) in methanol, saturated with ammonia (150 ml), was heated in a pressure bottle for 22 hr at 95 °C. After treatment with charcoal, the mixture was concentrated to dryness followed by several reevaporations from methanol. The solid residue was recrystallized from methanol: 1.13 g (66%) of **17** as colorless crystals of mp 290—292 °C (decomp.) and $[\alpha]_D^{23}$ +34° (*c* 1, H_2O). The product was identical with a sample prepared by *N*-acetylation of **16** with acetic anhydride in methanol, for which mp 317—319 °C (decomp.) and $[\alpha]_D^{26}$ +32° (*c* 1, H_2O) have been reported.[14]

*1-(4'-Amino-4'-deoxy-β-*D*-glucopyranosyl)cytosine (16)*: A solution of 4'-acetamido-nucleoside **17** (540 mg, 1.72 mmol) in 4 M hydrochloric acid was refluxed for 4 hr, followed, after cooling, by deionization with a strongly basic resin (Merck III), which was thoroughly washed on removal. The filtrate was subjected to charcoal treatment and then evaporated to dryness, giving a sirupous residue that gradually crystallized on repeated reevaporations from methanol. Recrystallization from the same solvent afforded 320 mg (69%) of **16** of mp 210 °C and $[\alpha]_D^{23}$ +15° (*c* 1, H_2O).

A sample prepared from mesylate **15** *via* azidolysis, deacylation and hydrogenation[14] had mp, UV, and IR data duplicating those above.

*1-(4'-Acetamido-2',3',6'-tri-*O*-acetyl-4'-deoxy-β-*D*-glucopyranosyl)-*N*⁴-acetylcytosine (18)*: *N*-Acetyl derivative **17** (1.0 g) in 1:1 pyridine–acetic anhydride (1:1) was kept overnight at ambient temperature, followed by evaporation to dryness *in vacuo* (finally 0.1 mm). Trituration of the residue with ethanol induced crystallization to give, after recrystallization from the same solvent 1.1 g (72%) of **18** as needles of mp 295 °C (decomp.); $[\alpha]_{23}^{D}$ +28.1° (*c* 1, dimethylformamide); lit.,[14] mp 293—294 °C; $[\alpha]_{25}^{D}$ +27°; NMR (DMSO-d_6) τ −0.84 (s, 1, N^4-H), 1.56 and 2.75, (two 1 H-d, $J_{5,6}$=7 Hz, H-6 and H-5), 2.18 (d, 1, $J_{4',NH}$=9 Hz, C-4'-NH), 3.90 (m, 1, H-1'), acetyl resonances *cf.* Table 1.

Grateful acknowledgment is made to the Deutsche Forschungsgemeinschaft and to the Fonds der Chemischen Industrie for persevering support of this research and to the Japan Society for the Promotion of Science for granting a visiting professorship (to F. W. L.) at Keio University, Yokohama, providing the quietude for writing this work.

References

1) Part XX: F. W. Lichtenthaler, P. Voss, and A. Heerd, *Tetrahedron Lett.*, **1974**, 2141.

2) Portions of this work have been presented at the Meeting of the Chemical Society Carbohydrate Group, Brighton, April 1972, and the Second Symposium on the Chemistry of Nucleic Acid Components, Liblice, CSSR, Sept. 1972.

3) T. Kanzaki, E. Higashide, H. Yamamoto, M. Shibata, N. Nakazawa, H. Iwasaki, T. Takewaka, and A. Miyake, *J. Antibiotics* (Tokyo), **15A**, 83 (1962); T. Ikeuchi, F. Kitame, M. Kikuchi, and N. Ishida, *ibid.*, **25**, 548 (1972).

4) S. Takeuchi, K. Hirayama, K. Ueda, H. Sakai, and H. Yonehara, *J. Antibiotics* (Tokyo), **11A**, 1 (1958); T. Tsuruoka and T. Niida, Meiji Seika Kenkyu Nempo, 23 (1963).

5) R. J. Suhadolnik, "Nucleoside Antibiotics," Wiley-Interscience, New York (1970), p. 170ff.

6) S. Pestka, *Ann. Rev. Microbiol.*, **25**, 520 (1971).

7) Unlike Blasticidin S, the structure of which was early confirmed by X-ray analysis,[8] there has been a special fascination with respect to the gradual evolvement of the correct structure for gougerotin,[9-16] requiring two corrections[10,12] before being finalized by partial[13-15] and total syntheses.[16]

8) S. Onuma, Y. Nawata, and Y. Saito, This Bulletin,

39, 1091 (1966).
9) H. Iwasaki, *Yakugaku Zasshi*, **82**, 1380 (1962).
10) J. J. Fox, Y. Kuwada, K. A. Watanabe, T. Ueda, and E. B. Whipple, *Antimicrobial Agents Chemother.*, **1964**, 518.
11) F. W. Lichtenthaler and P. Heidel, *Angew. Chem.*, **80**, 441 (1968); *Angew. Chem. Int. Ed. Engl.*, **7**, 458 (1968).
12) J. J. Fox, Y. Kuwada, and K. A. Watanabe, *Tetrahedron Lett.*, **1968**, 6029.
13) H. Paulsen, K. Propp, and K. Heyns, *ibid.*, **1969**, 683.
14) K. A. Watanabe, M. P. Kotick, and J. J. Fox, *J. Org. Chem.*, **35**, 231 (1970).
15) F. W. Lichtenthaler, G. Trummlitz, G. Bambach, and I. Rychlik, *Angew. Chem.*, **83**, 331 (1971); *Angew. Chem. Int. Ed. Engl.*, **10**, 334 (1971).
16) K. A. Watanabe, E. A. Falco, and J. J. Fox, *J. Amer. Chem. Soc.*, **94**, 3272 (1971).
17) T. Kondo, H. Nakai, and T. Goto, *Tetrahedron*, **29**, 1801 (1973); H. Yonehara and N. Otake, *Antimicrobial Agents Chemother.*, **1965**, 855.
18) F. W. Lichtenthaler and G. Trummlitz, *Fed. Eur. Biochem. Soc. Lett.*, **38**, 237 (1974).
19) J. J. Fox and K. A. Watanabe, *Pure Appl. Chem.*, **23**, 475 (1971).
20) F. W. Lichtenthaler, T. Ueno, and P. Voss, This Bulletin, **47**, 2304 (1974).
21) T. Kondo and T. Goto, *Agric. Biol. Chem. Japan*, **35**, 625 (1971).
22) W. W. Zorbach, *Synthesis*, **1970**, 329.
23) U. Niedballa and H. Vorbrüggen, *Angew. Chem.*, **82**, 449 (1970); *Angew. Chem. Int. Ed. Engl.*, **9**, 461 (1970).
24) Although the direct utilization of 1-alkoxy derivatives of a blocked sugar was reported to be feasable in nucleosidations with $TiCl_4$, $SnCl_4$, and BF_3 as catalyst,[25] the methyl galactoside **1**, under a variety of conditions, could not be induced to react with bis-trimethylsilyl derivatives of uracil, *N*-acetyl-cytosine or *N*-benzoyl-adenine.
25) For other BF_3-catalyzed acetolyses *cf.* F. W. Lichtenthaler, J. Breunig, and W. Fischer, *Tetrahedron Lett.*, **1971**, 2825.
26) J. Pliml and M. Prystas, *Advances Heterocyclic Chem.*, **8**, 115 (1968).
27) Prepared by boron trifluoride or sulfuric acid catalyzed acetolysis of methyl 4-acetamido-2,3,6-tri-*O*-acetyl-4-deoxy-α-D-glucopyranoside[28] and subsequent separation from 4-acetamido-1,2,3,5,6-penta-*O*-acetyl-4-deoxy-α-D-glucofuranose which can be obtained as needles of mp 96 °C and $[\alpha]_D^{23}$ +18° (*c* 1, $CHCl_3$).[29] This finding is in contrast to previous reports,[30] that acetolysis of methyl 4-amino-4-deoxy-α-D-glucoside and its *N*-acetyl compound exclusively yield pyranose peracetate anomers (**20**).
28) E. J. Reist, R. R. Spencer, D. F. Calkins, B. R. Baker, and L. Goodman, *J. Org. Chem.*, **30**, 2312 (1965).
29) F. Bambach, Dissertation, Technische Hochschule Darmstadt, Nov. 1971.
30) E. J. Reist, D. E. Gueffroy, R. W. Blackford, and L. Goodman, *J. Org. Chem.*, **31**, 4025 (1966).
31) J. Černá, F. W. Lichtenthaler, and I. Rychlik, *Fed. Eur. Biochem. Soc. Lett.*, **12**, 45 (1971).
32) F. W. Lichtenthaler and P. Emig, *Carbohyd. Res.*, **7**, 121 (1968).
33) F. W. Lichtenthaler, G. Bambach, and P. Emig, *Chem. Ber.*, **102**, 994 (1969).
34) F. W. Lichtenthaler and H. Zinke, *J. Org. Chem.*, **37**, 1612 (1972).
35) R. J. Cushley, K. A. Watanabe, and J. J. Fox, *J. Amer. Chem. Soc.*, **89**, 394 (1967).
36) F. W. Lichtenthaler, G. Bambach, and U. Scheidegger, *Chem. Ber.*, **102**, 986 (1969).
37) A. C. Richardson and K. A. McLauchlan, *J. Chem. Soc.*, **1962**, 2499; F. W. Lichtenthaler and H. K. Yahya, *Chem. Ber.*, **100**, 2389 (1967).
38) Grade 4 Å of 2 mm pearls (Merck, Darmstadt).
39) T. Nishimura and I. Iwai, *Chem. Pharm. Bull.* (Tokyo), **12**, 352 (1964).
40) I. Iwai, T. Nishimura, and B. Shimizu, *Synth. Proc. Nucl. Acid Chem.*, **1**, 135 (1968).
41) I. Iwai, T. Nishimura, and B. Shimizu, *ibid.*, **1**, 388 (1968).
42) In adaption of the procedure used by Kondo and Goto.[21]
43) If not dried thoroughly, the product melts lower, *i.e.* at 255—260 °C (decomp.), as reported in the preliminary communication.[15]

Nucleosides. XXII.[1] Pyrimidine Nucleosides of 4-Amino-4-deoxy-β-D-galactopyranose

Frieder W. LICHTENTHALER, Tamio UENO,[2] and Peter Voss
Institut für Organische Chemie, Technische Hochschule Darmstadt, 61 Darmstadt, Germany

(Received January 14, 1974)

In a four step sequence from 1-*O*-acetyl-2,3,6-tri-*O*-benzoyl-4-*O*-mesyl-α-D-glucose (**4**), 4′-amino-4′-deoxy-β-D-galactosyl-cytosine (**1**) was synthesized, involving stannic chloride catalyzed nucleosidation with bis(trimethylsilyl)-N^4-acetyl-cytosine, azidolysis of the 4′-sulfonyloxy group, deblocking and reduction (overall yield: 48%). An alternate, though preparatively less satisfactory approach was used for the preparation of the uracil analogue **2**, which started from β-D-glucosyl-cytosine or uracil (**9** or **15**) and proceeded *via* standard blocking and deblocking reactions to the 4′-*O*-mesylglucosyl-uracil (**20**) and was concluded by azidolysis (**20**, **21**), removal of protecting groups and reduction. Structural and configurational assignments evolved from the mode of preparation as well as from spectroscopic data, most conveniently from the acetyl resonances of the peracetylated nucleosides **8** and **24**, which are in accord with those of their galactosyl and 3-acetamido-3-deoxy-galactosyl counterparts (Table).

Because of the unique structural features associated with the aminoacyl-aminohexosyl-cytosine group of antibiotics, considerable attention has been given to an assessment of their structure-activity relationships.[3] The variety of analogs modified in the carbohydrate portion being rather limited, it was of interest to evaluate analogs for their biological relevance, which have a "1,4-*cis*-arrangement" of nucleobase and amino-acid component, *i.e.* 4-aminogalacto-configuration in the sugar unit, rather than the 1,4-*trans*-disposition present in gougerotin and blasticidin S. We have, by consequence, initiated studies towards a preparatively satisfactory access to 4-amino-galactosyl-pyrimidine nucleosides **1** and **2**, the results being subject of this communication.

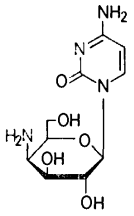

1

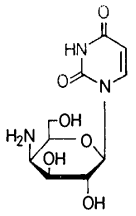

2

In design, the synthetic scheme was based upon the efficient preparation of 4-amino-4-deoxy-D-galactose and derivatives by a route involving direct displacement of a 4-mesyloxy group by azide ion in a suitably blocked D-glucose derivative.[4] Nevertheless, when utilizing this route for the preparation of 4-amino-galactosyl nucleosides, several synthetic possibilities remain with respect to the stage at which the aglycon is preferably introduced:

(i) Nucleoside synthesis with an *a priori* prepared 4-aminosugar derivative, *e.g.* with tetra-*O*-acetyl-4-acetamido-4-deoxy-D-galactopyranose by the fusion method or the Friedel-Crafts catalyzed silyl procedure.

(ii) Nucleosidation at the outset, *e.g.* conversion of the respective glucopyranosyl nucleoside *via* a series of reactions into a suitably blocked 4′-*O*-mesylate followed by azidolysis, deblocking and reduction.

(iii) Introduction of the nucleobase at some intermediate stage, *e.g.* at that of a suitably blocked 4-*O*-mesyl-glucose.

Since certain preliminary experiments with the first approach, which might be surmised to be the most direct one, presented some preparative complications when employing the stannic chloride catalyzed silyl nucleosidation,[5,6] the second and third reaction path was deemed more appropriate and used for the preparation of **1** and **2**.

Cytosine Nucleosides. A 4-*O*-mesyl-glucose derivative suitable for nucleosidation *via* the Friedel-Crafts catalyzed silyl procedure[5,6] proved to be 1-*O*-acetyl-2,3,6-tri-*O*-benzoyl-4-*O*-mesyl-α-D-galactopyranose (**4**), obtained from its readily accessible methyl glycoside **3**[4] by boron trifluoride catalyzed acetolysis.[7] When reacted in dichloroethane with N^4-acetyl-bis(trimethylsilyl)-cytosine in the presence of stannic chloride (12 hr, 60 °C), crystalline nucleoside **5** was obtained in high yield (81%). The secondary C-4′-mesyloxy function in **5** was readily displaced by sodium azide in hexamethylphosphoric triamide (20 hr, 80 °C), to afford the blocked azidogalactosyl nucleoside. Subsequent de-*O*-benzoylation by methanolic ammonia to the free azido-nucleoside **7**, followed by hydrogenation over palladium-on-charcoal then yielded the desired 4′-amino-4′-deoxy-β-D-galactosyl-cytosine (**1**) as an analytically and chromatographically pure sirup, that could not be induced to crystallize, yet gave a crystalline tetraacetyl derivative (**8**). The yields in this four-step sequence from **4** *via* **5**, **6**, and **7** to **1** being consistently high, the overall yield amounts to a quite satisfactory 48%.

In addition, a number of new crystalline derivatives of β-D-glucopyranosylcytosine (**9**) were prepared and although they could not directly be utilized for the synthesis of **1** (yet of **2**, see below), are placed on record as readily accessible, preparatively useful intermediates. Thus, selective benzoylation of the N^4-amino function in the nucleobase was readily achieved by refluxing **9** with benzoic anhydride in methanol, to afford highly crystalline **10** in 74% yield, further characterized as its tetra-*O*-acetyl derivative. By treatment with benzaldehyde/zinc chloride, **9** as well as **10** were converted into their 4′,6′-*O*-benzylidene derivatives **11** and **12**, respectively, the conversion **9**→**11**, however, proceeding

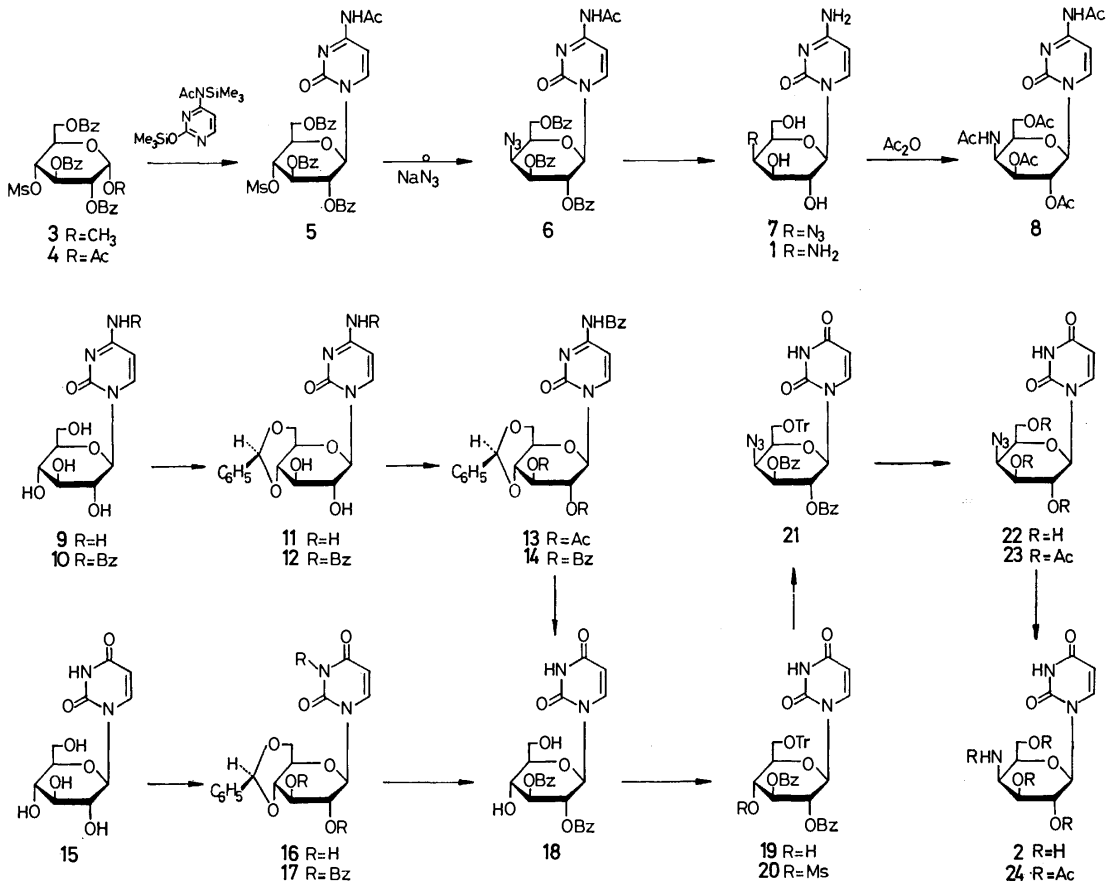

rather sluggishly due to the low solubility of the educt in the reaction mixture. Subsequent acylation of **12** with acetic anhydride or benzoyl chloride in the presence of pyridine proceeded smoothly to afford the 2′,3′-di-*O*-acyl derivatives **13** and **14**. However, as expected from the ready hydrolytic deamination of N^4-acylated cytosine and cytidine derivatives,[8,9] a de-*O*-acetalization in benzylidene-nucleosides **11**—**14** cannot be achieved without concomitant removal of the benzoylamido-function to yield the respective uracil nucleosides. Thus, brief treatment of **14** with 80% acetic acid at 80—90 °C, gave in an 81% yield 2′,3′-di-*O*-benzoyl-β-D-glucosyluracil (**18**), identical with the same product prepared by another route (*cf.* below).

Uracil Nucleosides. In analogy to the efficacious four-step preparation of **1** from 4-*O*-mesyl-glucose (**4**), for a synthesis of 4-aminogalactosyluracil (**2**) the nucleosidation of **4** with bis(trimethylsilyl)uracil followed by introduction of the 4′-amino function must be considered to be the most appropriate and should be feasible without complications. Yet, prior to this, we had followed approach (ii) for a synthesis of **2**, comprising eight steps from readily accessible[10] β-D-glucopyranosyl-uracil (**15**). The conversion of **15** into its 2′,3′-di-*O*-benzoyl derivative (**18**) was readily accomplished by treatment with benzaldehyde/zinc chloride (to **16**), acylation with benzoyl chloride/pyridine to the N^3,2′,3′-tribenzoyl derivative **17** and deacetalization with 80% acetic acid (1 hr, 80 °C) to **18**, which was also obtained from the cytosine nucleoside **18** (*vide supra*). Subsequent tritylation of the primary hydroxyl function in **18**, followed by mesylation gave the key intermediate **20**, suitably blocked for an ensuing S_N2-displacement of its 4′-mesyloxy function by sodium azide in HMPT (20 hr, 90 °C). Deblocking in **21** by treatment with sodium methoxide/methanol and, subsequently, with 80% acetic acid afforded the free azidogalactosyl nucleoside **22**. Due to difficulties in crystallizing **22**, it was directly hydrogenated to yield 4′-aminogalactosyl-uracil (**2**) as an amorphous substance. The peracetyl derivatives of **22** and **2**, however, were obtained in crystalline, readily characterizable form, as was the case with all other intermediates in the conversion of **15** into **2** over eight steps. Not unexpected, though, the preparative utility of the reaction sequence **15**→**2** is considerably inferior to the four-step approach employed in the cytosine series for the synthesis of **1**.

Structural and Configurational Assignments. Since well-defined synthetic procedures have been used throughout as well as readily characterizable starting materials (**4**, **9**, and **15**, respectively), the structures and configurations of the newly synthesized nucleosides already follow from the mode of preparation. Sustaining evidence is furnished by NMR data, most conveniently from the acetyl resonances in $CDCl_3$ or DMSO-d_6 of the peracetylated nucleosides. As is clearly apparent from the empirical principles laid down in the "acetyl resonance rule",[11,12] hexopyranosyl nucleosides with axial *O*-acetyl substituents give a larger separation of signals in the 8 τ range than *e.g.* glucosyl derivatives[13] with an equatorial orientation of groups.

Table 1. Relevant NMR-data in DMSO-d_6 and $CDCl_3$, and rotations of peracetyl-β-D-galactopyranosylpyrimidines

Sugar moiety	R[a]		DMSO-d_6[b] H-1′[c]	a-OAc	e-OAc 6′-OAc a-NHAc	e-NHAc	$CDCl_3$[b] H-1′[c]	a-OAc	e-OAc 6′-OAc a-NHAc	e-NHAc	$[\alpha]_D$ (solvent, °C)
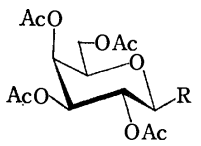	U	(I)	3.96	7.83	8.00 8.06 8.10	—	3.83	7.80	7.95 7.99 (2)	—	+32 (CH_3OH, 22)[e]
	U(O⁴-Et)	(II)	4.03	7.83	8.02 8.06 8.10	—	3.89	7.81	7.93 8.00 (2)	—	+59 ($CHCl_3$, 21)[f]
	C	(III)	3.94	7.82	8.01 8.06 8.10	—	3.87	7.82	7.97 8.02 8.04	—	+48 (CH_3OH, 23)[e]
	C(N⁴-Ac)	(IV)	3.81	7.82	7.88[d] 8.02 8.06 8.10	—	3.92	7.80	7.73[d] 7.97 8.01 8.03	—	?
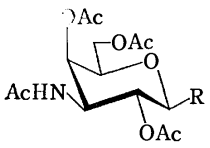	U	(V)	4.08	7.84	8.02 8.09	8.23	3.90	7.81	7.97 8.00	8.08	+35 (CH_3OH, 23)[g]
	U(O⁴-Et)	(VI)	3.91	7.82	8.02 8.12	8.22	3.84	7.80	7.97 8.00	8.08	+80 (CH_3OH, 23)[g] +87 ($CHCl_3$, 23)[g]
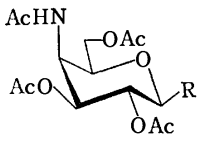	U	(**24**)	4.06	—	8.02 8.05 (2) 8.08	—	3.91	—	7.94 7.97 (2) 8.02	—	+14 (CH_3OH, 23)
	C(N⁴-Ac)	(**8**)	3.91	—	7.88[d] 8.02 (2) 8.08 8.10	—	3.86	—	7.71[d] 7.95 (2) 7.99 8.02	—	+16 ($CHCl_3$, 20)

a) Abbreviations used: U = uracilyl-1; U(O⁴-Et) = 4-ethoxypyrimidinonyl-1; C = cytosinyl-1; C(N⁴-Ac) = N^4-acetyl-cytosinyl-1. b) Except for some values in $CDCl_3$ (G. Bambach, Diplomarbeit, Techn. Hochschule Darmstadt, 1968) the NMR data for compounds I—VI are derived from Ref.[11] c) Observed as doublets with $J_{1',2'} = 8$—9 Hz. d) N^4-Acetyl resonance of the cytosine moiety. e) F.W. Lichtenthaler, G. Bambach, and P. Emig, *Chem. Ber.*, **102**, 1003 (1969). f) G. E. Hilbert, *J. Amer. Chem. Soc.*, **59**, 330 (1937). g) F. W. Lichtenthaler, G. Bambach, and U. Scheidegger, *Chem. Ber.*, **102**, 991 (1969).

In DMSO-d_6 and in $CDCl_3$, the peracetylated galactosyl-nucleosides I—IV as well as their 3′-aminoanalogs V[14] and VI show one distinct lowfield resonance in the 7.80—7.85 τ range (*cf.* Table), clearly attributable to the axial C-4′-acetoxy group. The 4′-aminogalactosyl-pyrimidines **8** and **24**, however, were expectedly devoid of a resonance within the axial range, since acetamido resonances of axial orientation fall together with those for equatorial and C-6′-signals.[11] Equally distinct is the presence of an equatorial acetamido function in 3′-aminogalactosyl nucleosides V and VI, appearing at τ 8.08 in $CDCl_3$, yet at 8.23 in DMSO-d_6, the separation from the equatorial acetoxy groups being larger by about 0.1 ppm in the more polar solvent, undoubtedly due to different solvation of the acetamido group. This solvent effect is also observed—yet in reverse direction—with the N^4-acetyl resonances of the cytosine nucleosides IV and **8**, exhibiting lowfield resonances at τ 7.88 in DMSO-d_6, yet at 7.73 and 7.71, resp., in $CDCl_3$. Worthy of note with all nucleosides in the Table 1 is also the appearance of an acetyl resonance in the upper equatorial range (τ 8.09—8.10 in DMSO-d_6) which is to be assigned to the respective 2′-acetoxy resonances, being in the range of diamagnetic shielding by the nucleobase.

The rotational values for the peracetylated nucleosides, which should be similar in sign and magnitude, if the sugar-nucleobase orientations are identical, show a considerably better conformity as their glucoanalogs.[13] Although farreaching conclusions may not be drawn therefrom, it is interesting to note that the ethoxypyrimidinone nucleosides II and VI have the highest rotational values (+59 and +87° in chloroform, *cf.* Table 1), whilst, curiously, the 4′-aminogalacto derivatives exhibit the lowest.

Experimental

Melting points were determined on a Bock Monoskop, and are uncorrected. Spectral measurements were effected with Perkin-Elmer 125 (IR), Perkin-Elmer 137 (UV), and Varian A-60A (NMR) instruments. Thin layer chromatography on Kieselgel F_{254} plastic sheets (Merck, Darmstadt) was used to monitor the reactions and to ascertain the purity of the reaction products; developers employed (A) benzene–ethyl acetate (4:1); (B) benzene–ethyl acetate–methanol (12:7:1); (C) ethyl acetate–ethanol–water (15:2:1). The spots were visivalized by UV light, by iodine vaporing or by spraying with 80% aqueous sulfuric acid and charring at 110 °C for 5 min. Column chromatography was carried out on silica gel 70—230 mesh ("Kieselgel 60", Merck,

Darmstadt).

1-O-Acetyl-2,3,6-tri-O-benzoyl-4-O-mesyl-α-D-glucopyranose (**4**). To a solution of 10.0 g (17 mmol) of methyl 2,3,6-tri-*O*-benzoyl-4-*O*-mesyl-α-D-glucopyranoside (3)[4] in acetic anhydride (200 ml) was added 20 ml of ethereal BF_3-etherate and the mixture was kept at 60 °C for 12 hr, followed by pouring into ice-water under vigorous stirring. The aqueous phase was decanted several times to be replaced by new ice-water. After 2 hr, chloroform (500 ml) was added and the organic phase was separated, dried over Na_2SO_4 and evaporated to dryness. The residue, after charcoal treatment in hot methanol (150 ml), was crystallized gradually on standing at ambient temperature and was collected after standing overnight in a refrigerator: 5.9 g (47%), mp 175—178 °C, after sintering from 150 °C on; $[\alpha]_D^{20}$ +126° (*c* 1, $CHCl_3$); NMR ($CDCl_3$) τ 3.40 (d, 1, $J_{1,2}$=3.5 Hz, H-1), 3.86 (t, 1, $J_{2,3}=J_{3,4}$=10 Hz, H-3), 4.53 (q, 1, J=3.5 Hz and 10 Hz, H-2), 4.77 (t, 1, $J_{3,4}=J_{4,5}$=10 Hz, H-4), 7.08 (s, 3, OMs), 7.84 (s, 3, OAc).

Found: C, 59.09; H, 4.63; S, 5.39%. Calcd for $C_{20}H_{28}O_{12}S$: C, 58.82; H, 4.61; S, 5.22.

Cytosine Nucleosides (1, 5—14). *N⁴-Acetyl-1-(2',3',6'-tri-O-benzoyl-4'-O-mesyl-β-D-glucopyranosyl)cytosine* (**5**): To a solution of 3.0 g (4.9 mmol) of mesylate **4** in 1,2-dichloroethane (100 ml) was added 6 g of molecular sieve,[18] stannous tetrachloride (1.5 ml) and, after 15 min, 1.65 (1.1 molar equiv.) of *N⁴,O*-bis(trimethylsilyl)-*N⁴*-acetyl-cytosine[19] and the mixture was heated to 60° for 12 hr. Subsequently, 750 ml of dichloromethane was added and the solution was extracted with two 200 ml portions of saturated $NaHCO_3$-solution,[20] followed by washing with water (2×200 ml). The organic phase was dried (Na_2SO_4), and evaporated to dryness *in vacuo*, to leave a crystalline residue which was filtered and thoroughly washed with ethanol: 2.8 g (81%) of crystals; mp 240—241 °C (decomp.); $[\alpha]_D^{20}$ +24° (*c* 1.2, dimethylformamide); uniform by tlc (D); λ_{max}^{MeOH} 233, 283, and 330 nm.

Found: C, 57.63; H, 4.48; N, 5.85; S, 5.46%. Calcd for $C_{34}H_{31}N_3O_{12}S$: C, 57.87; H, 4.43; N, 5.96; S, 5.54%.

N⁴-Acetyl-1-(4'-azido-2',3',6'-tri-O-benzoyl-4'-deoxy-β-D-galactopyranosyl)cytosine (**6**): A suspension of 2.3 g (3.1 mmol) of mesyl derivative **5** and sodium azide (1.0 g, 5 molar equiv.) in hexamethylphosphoric acid triamide (20 ml) was heated at 80 °C for 20 hr with vigorous stirring. The yellow mixture, containing some undissolved sodium azide, was poured into ice-water (100 ml), and the crystalline, colorless precipitate was filtered off: 1.8 g (88%) of the crude, chromatographically homogenous (tlc in A) product which was used for the ensuing reactions. A small amount was recrystallized from chloroform-methanol to give the analytical sample of mp 228 °C (decomp.) and $[\alpha]_D^{20}$ +121° (*c* 1, $CHCl_3$); NMR ($CDCl_3$) τ 0.33 (s, 1, NH), 2.0—3.0 (m, 17, H-5, H-6 and 3 C_6H_5); 3.77 (m, 1, H-1'), 8.13 (s, 3, NHAc).

Found: C, 60.65; H, 4.30; N, 12.75%. Calcd for $C_{33}H_{28}N_6O_9$: C, 60.74; H, 4.43; N, 12.87%.

1-(4'-Azido-4'-deoxy-β-D-galactopyranosyl)cytosine (**7**): To a suspension of **6** (1.6 g, 2.5 mmol, of crude product as described above) in methanol (20 ml) was added, with stirring, 0.1 ml of sodium methoxide solution, prepared from 1 g of sodium and 10 ml of methanol. A clear solution was not obtained, since product (**7**) started to precipitate immediately. After 3 hr stirring and standing overnight at ambient temperature, the precipitate was filtered (500 mg, 61%). Deionization of the filtrate and evaporation to dryness afforded a second crop (120 mg, 15%) of crude product, homogeneous by tlc (in C), which was used for hydrogenation (s. below).

A 150 mg portion was recrystallized from little methanol (standing for 1—2 days due to slow crystallization) to give the analytical sample of mp 180—182 °C (effervesc.); $[\alpha]_D^{20}$ −34° (*c* 1, H_2O); NMR (D_2O) τ 2.28 and 3.90 (two d, 1, $J_{5,6}$=7.5 Hz, H-6 and H-5), 4.36 (d, 1, $J_{1,2}$=8 Hz, H-1'), other protons give complex multiplets.

Found: C, 39.98; H, 5.00; N, 27.94%. Calcd for $C_{10}H_{14}N_6O_5$: C, 40.27; H, 4.73; N, 28.18%.

1-(4'-Amino-4'-deoxy-β-D-galactopyranosyl)cytosine (**1**): To a prehydrogenated suspension of 10% Pd/C (100 mg) in water (30 ml) was added 450 mg of crude azido-nucleoside **7**, and the hydrogenation was continued. After 2 hr, tlc (in C) showing the absence of starting material, the catalyst was removed and the filtrate was evaporated *in vacuo* (bath temperature below 25 °C) to give 380 mg (89%) of **1** as a sirup, that could not be induced to crystallization from the usual solvents. The analytical sample was dried at 0.1 mm for 12 hr.

Found: C, 43.95; H, 6.14; N, 20.14%. Calcd for $C_{10}H_{16}N_5O_5$: C, 44.11; H, 5.92; N, 20.58%.

N⁴-Acetyl-1-(4'-acetamido-2',3',6'-tri-O-acetyl-4'-deoxy-β-D-galactopyranosyl)cytosine (**8**): Sirupy **1** (250 mg) was refluxed for 30 min in 1:1 pyridine-acetic anhydride, followed by evaporation to dryness *in vacuo* (finally 0.1 mm). The remaining sirup was subjected to purification on a silica gel column (2×20 cm) with ethyl acetate. The residue, obtained after concentration of the eluate, was dissolved in ethyl acetate (3 ml) and precipitated by addition of ether: 380 mg (86%); mp 174—177 °C, after sintering from 165 °C on; $[\alpha]_D^{20}$ +16° (*c* 1, $CHCl_3$); NMR (DMSO-d_6) τ 0.87 (s, 1, cytosine-NH), 1.54 and 2.73 (two 1 H-d, $J_{5,6}$=7.5 Hz, H-6 and H-5); 1.86 (d, 1, $J_{4',NH}$=10 Hz, C-4'-NH), 3.91 (m, 1, H-1'), 4.63 (narrow (6 Hz) m, 2, H-2' and H-3'), 5.5 (broad m (25 Hz), 2, H-4' and H-5'), 5.95 (m, 2, CH_2), acetyl resonances *cf.* Table.

Found: C, 49.64; H, 5.27; N, 11.63%. Calcd for $C_{20}H_{26}N_4O_{10}$: C, 49.79; H, 5.39; N, 11.62%.

N⁴-Benzoyl-1-(β-D-glucopyranosyl)cytosine (**10**): To solution of 5.0 g (0.18 mol) of 1-(β-D-glucopyranosyl)cytosine (**9**)[22] in methanol (500 ml) was added 4.2 g (1 molar equiv.) of benzoic anhydride and the mixture was refluxed. After 1 and 3 hr, respectively, another molar equiv. of benzoic anhydride was added, followed by additional 4 hr of reflux. Filtration and evaporation to dryness *in vacuo* left a white residue, which was thoroughly extracted with ether for removal of benzoic acid and excessive benzoic anhydride. The ether-insoluble residue (3.2 g, mp 173—177 °C) was recrystallized twice from ethanol to yield 2.55 g (74%) of **10** as colorless prisms of mp 191—192 °C; $[\alpha]_D^{20}$ +28° (*c* 1, dimethylformamide).

Found: C, 54.06; H, 4.99; N, 11.12%. Calcd for $C_{17}H_{19}N_3O_7$: C, 54.11; H, 5.08; N, 11.14%.

N⁴-Benzoyl-1-(tetra-O-acetyl-β-D-glucopyranosyl)cytosine: A solution of 200 mg of **10** in 1:1 pyridine-acetic anhydride (10 ml) was kept at ambient temperature overnight followed by concentration to dryness and several reevaporations from ethanol. The solid residue was recrystallized from ethanol to give needles (150 mg, 52%) of mp 248—252 °C; NMR ($CDCl_3$) τ 7.93, 7.95, 8.01, and 8.03 for acetoxy resonances.

Found: C, 55.51; H, 4.94; N, 7.75%. Calcd for $C_{25}H_{27}N_3O_{11}$: C, 55.62; H, 4.99; N, 7.70%.

1-(4',6'-O-Benzylidene-β-D-glucopyranosyl)cytosine (**11**): Anhydrous zinc chloride (4.0 g) and 2.5 g (9.2 mmol) of glucosylcytosine (**9**) in 20 ml of benzaldehyde were stirred at ambient temperature until completely dissolved (5 days). The mixture was then stirred into ice-water (400 ml) and the crystalline product was filtered off. Recrystallization from methanol gave 1.4 g (42%) of **11**, decomposing from 270 °C on,

$[\alpha]_D^{20}$ −48° (*c* 1, $CHCl_3$).

Found: C, 56.43; H, 5.20; N, 11.60%. Calcd for $C_{17}H_{19}N_3O_6$: C, 56.50; H, 5.30; N, 11.63%.

N^4-*Benzoyl-1-(4′,6′-O-benzylidene-β-D-glucopyranosyl)cytosine* (**12**): A mixture of zinc chloride (1.2 g), **10** (1.2 g, 3.2 mmol) and benzaldehyde (12 ml) was stirred overnight at room temperature followed by pouring into ice-water (200 ml) with vigorous stirring. *n*-Hexane (200 ml) was added whereafter the product started to crystallize. Filtration, washing with cold ethanol and recrystallization from methanol afforded 850 mg (61%) of colorless prisms of mp 245—248 °C; $[\alpha]_D^{20}$ −11° (*c* 1, dimethylformamide).

Found: C, 61.86; H, 4.96; N, 9.01%. Calcd for $C_{24}H_{23}N_3O_7$: C, 61.93; H, 4.98; N, 9.03%.

N^4-*Benzoyl-1-(2′,3′-di-O-acetyl-4′,6′-O-benzylidene-β-D-glucopyranosyl)cytosine* (**13**): A solution of **12** (465 mg, 1 mmol) in 1:1 pyridin-acetic anhydride (10 ml) was kept for 2 hr at 80 °C and subsequently stirred into ice-water (150 ml). The crystalline solid was filtered off after 1 hr and recrystallized from ethanol: 360 mg (65%) of **13** as colorless needles; mp 262—264 °C; $[\alpha]_D^{20}$ −37° (*c* 1, $CHCl_3$).

Found: C, 60.98; H, 5.02; N, 7.62%. Calcd for $C_{28}H_{27}N_3O_9$: C, 61.20; H, 4.95; N, 7.65%.

N^4-*Benzoyl-1-(2′,3′-di-O-benzoyl-4′,6′-O-benzylidene-β-D-glucopyranosyl)cytosine* (**14**): Benzoyl chloride (2.0 ml) was added to 1.18 g (2.5 mmol) of **12** in pyridine (40 ml) and the mixture was heated to 80 °C for 6 hr. Since starting material could still be detected by tlc (in B), another 2.0 ml of benzoyl chloride was added followed by heating to 100 °C for 5 hr. The mixture was then evaporated to dryness *in vacuo* (finally 0.1 mm) and the residue was dissolved in chloroform (150 ml) followed by washings, successively, with 1 M NaOH, water, 2 M HCl and again water. Drying over Na_2SO_4 and removal of the solvent left a residue which was recrystallized from ethanol: 1.32 g of **14** as colorless prisms; mp 271—273 °C; $[\alpha]_D^{20}$ −26° (*c* 1, $CHCl_3$).

Found: C, 67.43; H, 4.92; N, 5.96%. Calcd for $C_{38}H_{31}N_3O_9$: C, 67.46; H, 5.06; N, 6.21%.

Uracil Nucleosides (**2**, **15**—**24**). *1-(4′,6′-O-Benzylidene-β-D-glucopyranosyl)uracil* (**16**): A suspension of 10.0 g (36.4 mmol) of 1-(β-D-glucopyranosyl)uracil (**15**)[10] and 11 g of freshly molten zinc chloride in 115 ml of benzaldehyde was shaken for 30 hr. The resulting clear solution was stirred into ice water (700 ml), from which was decanted after 1 hr of vigorous stirring. The viscous sirup was brought to crystallization by trituration with petroleum ether, filtered off and recrystallized from methanol: 4.5 g (72%) of **16** as colorless needles, uniform by tlc (C); mp 282—284 °C; $[\alpha]_D^{22}$ −10° (*c* 1, dimethylformamide).

Found: C, 56.54; H, 5.21; N, 7.85%. Calcd for $C_{17}H_{18}N_2O_7$: C, 56.35; H, 5.01; N, 7.73.

1-(2′,3′-Di-O-benzoyl-4′,6′-O-benzylidene-β-D-glucopyranosyl)-N^3-benzoyluracil (**17**): To a suspension of 9.2 g (25.4 mmol) of **17** in pyridine (360 ml) was added with cooling 30 ml of benzoyl chloride and the mixture was stirred at ambient temperature for 24 hr. After removal of pyridine by evaporation (1 mm, bath temperature 50 °C), the brownish residue was taken up in chloroform and washed, successively, with N sodium carbonate, water, 0.1 M hydrochloric acid, and water. Treatment with activated carbon, drying over Na_2SO_4 and removal of chloroform *in vacuo* left a residue, which crystallized on solution in little hot chloroform and addition of methanol. Recrystallization from methanol afforded 10.1 g (59%) of colorless prisms; mp 217—219 °C; $[\alpha]_D^{22}$ +3.7° (*c* 1, chloroform).

Found: C, 67.63; H, 4.42; N, 4.19%. Calcd for $C_{38}H_{30}N_2O_{10}$: C, 67.65; H, 4.48; N, 4.15%.

1-(2′,3′-Di-O-benzoyl-β-D-glucopyranosyl)uracil (**18**): *A. From* **17** *by Removal of* N-*Benzoyl and* O-*Benzylidene Groups*: A solution of **17** (9.15 g, 13.5 mmol) was refluxed in 80% aqueous acetic acid for 9 hr and the mixture was subsequently taken to dryness *in vacuo* (1 mm), followed by several reevaporations from ethanol-water to remove the benzaldehyde formed. The residue crystallized on trituration with ether and was recrystallized by dissolution in little hot ethanol and addition of ether until turbidity: 4.0 g (61%) of **18**; tlc in A; mp 158—161 °C; $[\alpha]_D^{22}$ +47° (*c* 1, ethanol); τ (DMSO-d_6) 1.9—2.8 (11H-m, H-6 and $2C_6H_5$), 3.91 (1H-d, J=8.5 Hz, H-1′).

Found: C, 60.01; H, 4.73; N, 5.89. Calcd for $C_{24}H_{22}N_2O_9$: C, 59.75; H, 4.60; N, 5.81%.

B. From Cytosine Nucleoside **14** *by Simultaneous De-O-benzylidenation and Hydrolytic Deamination*: A solution of **14** (1.60 g, 2.4 mmol) in 80% acetic acid (80 ml) was heated to 80—90 °C for 1 hr, and subsequently filtered upon addition of charcoal. Evaporation to dryness and trituration of the residue with ethanol gave a solid mass, which was filtered and recrystallized from ethanol-ether (as above), to yield 1.13 g (81%) of **18** as colorless needles, identical in mp, rotation, tlc (A) and IR data with the product obtained above.

1-(2′,3′-Di-O-benzoyl-6′-O-trityl-β-D-glucopyranosyl)uracil (**19**): To a solution of 1.82 g (3.7 mmol) of **18** in pyridine (30 ml) was added 4.0 g (4 molar equiv.) of trityl chloride[23] and the mixture was stirred for 3 days at ambient temperature. Filtration, evaporation to dryness followed by several reevaporations from ethanol-water gave a sirup, which was disolsved in chloroform. Washing with water, drying over Na_2SO_4 and evaporation *in vacuo* left a sirup, which was transfered to a silica gel column (2×20 cm) and eluted with chloroform until the effluent was free of UV active material.[24] The product (**19**) was then eluted with ethyl acetate, followed by evaporation of the eluate to dryness and trituration of the residue with methanol, which induced crystallization. Recrystallization from ethanol-*n*-hexane afforded 2.1 g (78%) of tlc pure (A) crystals of mp 171—173 °C and $[\alpha]_D^{25}$ +46° (*c* 1, $CHCl_3$).

Found: C, 71.16; H, 4.98; N, 4.10%. Calcd for $C_{43}H_{36}N_2O_9$: C, 71.26; H, 5.01; N, 3.87%.

1-(2′,3′-Di-O-benzoyl-4′-O-mesyl-6′-O-trityl-β-D-glucopyranosyl)uracil (**20**): To a solution of 1.90 g (2.6 mmol) of the trityl derivative **19** in pyridine (60 ml) was added under cooling (0 °C) 1.3 ml (7 molar equiv.) of methanesulfonyl chloride and the mixture was kept in a refrigerator (5 °C) for 24 hr, followed by stirring into ice-water (50 ml). The resulting precipitate was filtered off, washed with water and subjected to purification by chromatography on silica with chloroform. Removal of solvent from the eluate and recrystallization of the residue from ethanol-*n*-hexane gave 1.42 g (66%) of **20** as prisms of mp 152—154 °C; $[\alpha]_D^{25}$ +89° (*c* 1, $CHCl_3$).

Found: C, 65.53; H, 4.58; N, 3.38%. Calcd for $C_{44}H_{38}N_2O_{11}S$: C, 65.82; H, 4.47; N, 3.49%.

1-(4′-Azido-2′,3′-di-O-benzoyl-4′-deoxy-6′-O-trityl-β-D-galactopyranosyl)uracil (**21**): A mixture of 1.20 g (1.5 mmol) of mesylate **20** and 390 mg of sodium azide (4 molar equiv.) in hexamethyl phosphoric triamide (50 ml) was heated at 90 °C for 24 days, followed by evaporation to dryness *in vacuo* (1 Torr). The sirup was dissolved in ethyl acetate, which was repeatedly washed with water and dried over Na_2SO_4. Removal of the solvent, and purification of the sirup by chromatography on a silica gel column (2×20 cm) with chloroform. The residue obtained on evaporation to dryness of the appropriate eluate, crystallized on trituration with ethanol. Recrystallization from the same solvent yielded 0.88 g (78%) of **21** as colorless prisms; mp 226—227 °C; $[\alpha]_D^{25}$ −37° (*c* 1,

$CHCl_3$).

Found: C, 68.92; H, 4.75; N, 9.52%. Calcd for $C_{43}H_{35}N_5O_8$: C, 68.88; H, 4.71; N, 9.34%.

1-(4'-Azido-2',3',6'-tri-O-acetyl-4'-deoxy-β-D-galactopyranosyl)-uracil (23): To azidogalactoside **21** (750 mg, 1 mmol) in methanol (70 ml) was added 0.5 ml of 4% methanolic sodium methoxide, followed by storage in a refrigerator (5 °C) for 2 days. After neutralization with acetic acid, the mixture was taken to dryness *in vacuo* and the residual sirup was heated in 30 ml of 80% acetic acid for 1 hr (80 °C). Evaporation to dryness *in vacuo*, followed by several reevaporations from ethanol gave a sirup, which upon solution in water was extracted twice with ether. The aqueous phase was evaporated to dryness and the residual **22**, resisting crystallization, was refluxed in acetic anhydride (20 ml) containing potassium acetate (200 mg) for 2 hr. The dark solution was poured in water followed by several extractions with 1:1 chloroform–ethyl acetate. The combined extracts, after drying over Na_2SO_4, were taken to dryness and the solid mass remaining was recrystallized from ethanol, involving charcoal treatment: 285 mg (68%) of **23** as colorless crystals of mp 225—226 °C; $[\alpha]_D^{25}$ −40° (*c* 0.5, dimethylformamide), IR (KBr) cm^{-1} 2154; N_3; NMR (DMSO-d_6) τ −1.73 (broad s, 1, NH) 2.51 (d, 1, $J_{5,6}$=8.5 Hz, H-6), 4.04 (d, 1, $J_{1',2'}$=9.0 Hz, H-1'), 4.29 (d, 1, $J_{5,6}$=8.5 Hz, H-5), 4.36 (dd, 1, J=3 and 9 Hz, H-3'), 4.79 (t, 1, J=9 Hz, H-2'), 7.93, 7.97, and 8.06 (three 3H-s, acetyl resonances).

Found: C, 44.98; H, 4.55; N, 16.41%. Calcd for $C_{16}H_{19}N_5O_9$: C, 45.18; H, 4.50; N, 16.47%.

1-(4'-Amino-4'-deoxy-β-D-galactopyranosyl)uracil (2): To blocked azidogalactosyl-uracil **21** (800 mg, 1.1 mmol) in methanol (80 ml) was added 2 ml of N sodium methoxide/methanol. After being stood at 5 °C for 2 days, the mixture was neutralized with acetic acid followed by evaporation to dryness. After treatment with 80% acetic acid (30 ml) for 1 hr at 80 °C, to effect complete detrytilation, the mixture was evaporated to a sirup, which upon solution in water was extracted twice with ether for removal of methyl benzoate and tritanol. The aqueous layer was taken to dryness, repeatedly reevaporated from ethanol to yield a viscous sirup of **22**, not amenable to crystallization. It was dissolved in 1:1 methanol–water (50 ml) and added to a prehydrogenated suspension of Pd/C in water (200 mg in 20 ml). After 2 hr the hydrogen uptake was complete (tlc in C), the catalyst was filtered off and the filtrate taken to dryness. Solving the residue in warm ethanol (70—80 ml), removal of some insoluble material, and concentration to a volume of about 30 ml afforded after longer standing (1—2 day) 94 mg (67%) of **2** as an amorphous, hygroscopic, ninhydrin-positive product; another 25 mg was isolated by concentration of the mother liquor; mp 155—158 °C, $[\alpha]_D^{23}$ +45° (*c* 0.2, MeOH).

Found: C, 43.73; H, 5.70; N, 15.12. Calcd for $C_{10}H_{15}N_3O_6$: C, 43.96; H, 5.53; N, 15.38.

1-(4'-Acetamido-2',3',6'-tri-O-acetyl-4'-deoxy-β-D-galactopyranosyl)uracil (24): A solution of 200 mg of azidotriacetate **23** in 50 ml of methanol saturated with ammonia was stored in a refrigerator (5 °C) overnight, followed by evaporation to dryness and hydrogenation of the residue in water (50 ml) in the presence of Raney-Nickel T4 catalyst[25] (1 ml). After 2 hr, tlc (C) showing the absence of starting material, the catalyst was removed by filtration and the filtrate was evaporated to dryness *in vacuo*. *N*-Acetylation of the sirupous residue with acetic anhydride (0.5 ml) in 20 ml of methanol (5 hr, 25 °C) and evaporation to dryness with subsequent reevaporations from methanol afforded a sirup, pure by tlc (C), yet resistant to crystallization from the usual solvents.[26] Treatment with 1:1 pyridine–acetic anhydride (20 ml) for 12 hr at ambient temperature, removal of solvents *in vacuo* (finally 0.1 mm), yielded a sirup, which was dissolved in ethyl acetate and extracted with water (3×10 ml). The aqueous extracts were washed with ethyl acetate (2×10 ml) and the combined ethyl acetate solutions were evaporated to dryness. The remaining residue was applied to a silica gel column (2×20 cm) and first eluted with chloroform for removal of impurities, subsequently with ethyl acetate to yield the product. Evaporation of the eluate gave a sirup which crystallized on dissolution in little methanol and addition of benzene: 124 mg (59%) of crystals, pure by tlc (C); mp 165—168 °C after sintering from 145 °C on; $[\alpha]_D^{23}$ +14° (*c* 1, CH_3OH); NMR (DMSO-d_6) τ −1.36 (s, 1, uracil-NH), 1.90 and 4.22 (two d, 1, $J_{5,6}$=8.5 Hz, H-6 and H-5), 1.92 (d, 1, $J_{4',NH}$=9 Hz, C-4'-NH), 4.06 and 4.67 (two m, 1 and 2, ABX system for H-1' and H-2'/H-3'), 5.5 (m, 2, H-4' and H-5'), 6.00 (m, 2, 6'-CH_2); acetyl resonances *cf.* Table 1.

Found: C, 48.89; H, 5.18; N, 9.40%. Calcd for $C_{18}H_{23}N_3O_{10}$: C, 48.98; H, 5.25; N, 9.52%.

Support of this work by the Deutsche Forschungsgemeinschaft and the Fonds der Chemischen Industrie is gratefully acknowledged.

References

1) Part XXI: F. W. Lichtenthaler, P. Voss, and G. Bambach, This Bulletin, **47**, 2297 (1974).

2) Experiments Technische Hochschule Darmstadt 1967/68. Present address: Pesticide Research Institute, Kyoto University, Kyoto.

3) F. W. Lichtenthaler and G. Trummlitz, *Fed. Eur. Biochem. Soc. Lett.*, **38**, 227 (1974).

4) F. W. Lichtenthaler and P. Heidel, *Angew. Chem.*, **80**, 441 (1968); *J. Org. Chem.*, **39**, 1457 (1974).

5) U. Niedballa and H. Vorbrüggen, *Angew. Chem.*, **82**, 449 (1970); *Angew. Chem. Int. Ed. Engl.*, **9**, 461 (1970).

6) F. W. Lichtenthaler, A. Heerd, and K. Strobel, *Chem. Lett*, **1974**, 449.

7) For other BF_3-catalyzed acetolyses *cf.* F. W. Lichtenthaler, J. Breunig, and W. Fischer, *Tetrahedron Lett.*, **1971**, 2825.

8) D. M. Brown, A. R. Todd, and S. Varadarajan, *J. Chem. Soc.*, 2384 (1956).

9) H. G. Khorana, A. F. Turner, and J. P. Vizsolyi, *J. Amer. Chem. Soc.*, **83**, 686 (1961).

10) G. E. Hilbert and T. B. Johnson, *ibid.*, **52**, 4489 (1930).

11) F. W. Lichtenthaler, G. Bambach, and P. Emig, *Chem. Ber.*, **102**, 994 (1969).

12) F. W. Lichtenthaler and H. Zinke, *J. Org. Chem.*, **37**, 1612 (1972).

13) For comparison *cf.* Table in Ref. 1.

14) Findings that the axial 4'-acetoxy resonances of uracil nucleoside V and its 5,6-dihydrouracil derivative appear at τ 8.03 and 8.11, respectively,[15] have been clearly disproved on the basis of an unambigously synthesized compounds.[16] This not only proved the alleged two independent syntheses[17] to be incorrect, but more importantly invalidated the conclusions reached on the basis of the erroneous acetyl resonances.[15]

15) R. J. Cushley, K. A. Watanabe, and J. J. Fox, *J. Amer. Chem. Soc.*, **89**, 394 (1967).

16) F. W. Lichtenthaler, G. Bambach, and U. Scheidegger, *Chem. Ber.*, **102**, 986 (1969).

17) K. A. Watanabe and J. J. Fox, *J. Org. Chem.*, **31**, 211 (1966).

18) Grade 4 Å of 2 mm pearls (Merck, Darmstadt).

19) T. Nishimura and I. Iwai, *Chem. Pharm. Bull.* (Tokyo), **12**, 352 (1964).

20) For a rapid removal of the relatively stable N^4-trimethylsilyl group, treatment with sodium bicarbonate solution is employed. Also, due to the low solubility of **5** in dichloromethane, the use of large amounts of this solvent is imperative to prevent separation of the product with the SnO_2 formed.

21) Obtained[22] as a chromatographically uniform (tlc in A), amorphous product of mp 135—140 °C; lit,[22]: 197—199 °C.

22) G. E. Hilbert and E. F. Jansen, *J. Amer. Chem. Soc.*, **58**, 60 (1936).

23) When using equimolar amounts of trityl chloride, the reaction is still incomplete after 5 days.

24) With chloroform, only trityl chloride is eluted.

25) S. Nishimura, This Bulletin, **32**, 61 (1959).

26) The presence of 1-(4′-acetamido-4′-deoxy-β-D-galactopyranosyl)uracil, was ascertained by an NMR spectrum in D_2O, showing the anomeric proton as a 9 Hz-d at τ 4.43 and the acetamido resonance at τ 7.89.

Conformational Analysis About N-N Bond by NMR Spectroscopy: *N'*-Sulphonyl Derivatives of *N*-Aminoimides of Anthracene-Citraconic Anhydride and Naphthalene-Maleic Anhydride Adducts

S. M. VERMA, O. SUBBA RAO, and K. O. P. SINHA
Department of Chemistry, Banaras Hindu University, Varanasi-221005, India
(Received February 4, 1974)

A series of *N',N'*-disulphonyl and *N'*-sulphonyl-*N'*-acetyl derivatives of *N*-amino-9,10-dihydroanthracene-9,10-*endo*-α-methyl-α,β-succinimide and *N*-amino-1,2,3,4-tetrahydro-1,4-etheno/ethano-naphthalene-2,3-*exo*/*endo*-dicarboximides with a benzo ring in the cage-moiety were prepared and their NMR spectra were studied. Shielding constants of the substituents provide evidence for the non-eclipsed conformations of the *N'*-substituents with the ring carbonyls. The preferred conformations of *N'*-sulphonyl-*N'*-acetyl derivatives are explained on steric grounds. In *N'*-tosyl-*N'*-acetyl derivatives the tosyl group takes up a fixed conformation about *N'*-SO_2 bond in which the aryl part of the tosyl group projects away from the cage-moiety.

Preferred conformations about N–N bond in systems of type I have been reported with the help of a cage-moiety which does not possess symmetry about the plane of the succinimidyl ring.[1-4] Nonplanar conformations about the N–N' bond in *N',N'*-diacetyl-*N*-amino-1,2,3,4-tetrahydro-1,4-etheno/ethano-naphthalene-2,3-*endo*/*exo*-dicarboximides have been used to assign *endo*/*exo*-configurations to the Diels-Alder adducts.[5] A study has been made of the steric and electronic effects of a sulphonyl substituent at the *exo*-cyclic nitrogen of the *N*-aminocamphorimide[6] leading to the synthesis and conformational study of a series of *N'*-sulphonyl derivatives of *N*-amino-9,10-dihydroanthracene-9,10-*endo*-α-methyl-α,β-succinimide (II) and *N*-amino-1,2,3,4-tetrahydro-1,4-ethano/etheno-naphthalene-2,3-*endo*/*exo*-dicarboximides (III and IV) with a cage benzo ring.

Torsional barriers to rotation about N–N bond ($\Delta G^{\ddagger}$ of the order of 23 kcal/mol) have been reported in *N',N'*-dimesyl and *N'*-mesyl-*N'*-acetyl-*N*-aminocamphorimides.[6] The NMR spectra of the compounds at 45 °C gave further support for the non-planar ground states in *N',N'*-disulphonyl and *N'*-sulphonyl-*N'*-acetyl-*N*-aminoimide systems. Variable temperature NMR spectra have provided evidence for some slow conformational changes in the molecule in solution. The general spectral pattern in nitrobenzene was similar to that observed in $CDCl_3$.

Results and Discussion

N',N'-Dimesyl Compounds (IIb and IIIc). The NMR spectra of compounds IIb and IIIc (Fig. 1) in $CDCl_3$ are similar and show two sharp singlets of equal

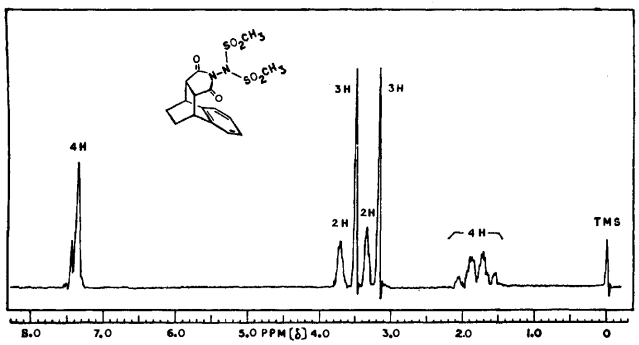

Fig. 1. 60 MHz NMR spectrum of *N',N'*-dimesyl-*N*-amino-1,2,3,4-tetrahydro-1,4-ethanonaphthalene-2,3-*endo*-dicarboximide (IIIc) in $CDCl_3$ at 45 °C.

TABLE 1. NMR SPECTRAL[a] DATA OF COMPOUNDS IIa—IIf

Compound	δR_1	δR_2	$\delta 9$	$\delta 10$	$\delta 11$	$\delta 12$	$\delta 1$—8
IIa	(s, 3H) 3.50	—	(d, 1H) 5.10	(s, 1H) 4.75	(s, 3H) 1.28	(d, 1H) 3.08	—
IIb	(ds, 3H) 3.37; 1:1; 18 Hz	(ds, 3H) 3.37; 1:1; 18 Hz	(d, 1H) 4.93	(s, 1H) 4.58	(s, 3H) 1.28	(d, 1H) 2.90	(m, 8H) 7.45
IIc	(s, 3H) 3.45	(s, 3H) 0.95	(d, 1H) 4.90	(s, 1H) 4.57	(s, 3H) 1.28	(d, 1H) 2.88	(m, 8H) 7.44
IId	(s, 3H) 2.47; (m, 4H) 7.60	(s, 1H) 6.66	(d, 1H) 4.80	(s, 1H) 4.41	(s, 3H) 1.17	(d, 1H) 2.75	(m, 8H) 7.60
IIe	(bs, 3H) 2.50; (m, 4H) 7.66	(bs, 3H) 2.50; (m, 4H) 7.66	(d, 1H) 4.83	(s, 1H) 4.50	(s, 3H) 1.23	(d, 1H) 2.78	(m, 8H) 7.66
IIf	(s, 3H) 2.46; (m, 4H) 7.63	(s, 3H) 0.80	(d, 1H) 4.93	(s, 1H) 4.61	(s, 3H) 1.37	(d, 1H) 2.97	(m, 8H) 7.63

a) The NMR spectra of all the compounds (Tables 1 and 2) were recorded in $CDCl_3$ except IIa which was recorded in pyridine and IIIb, IIIe, and IVb which were recorded in nitrobenzene. The total number of protons and the multiplicity of the bands are indicated in brackets. In case of multiplicity due to slow rotation, the ratio of the intensity of downfield to upfield and the separation in Hz are indicated. s=singlet, t=triplet, q=quartet, m=multiplet, ds=double singlet, nm=narrow multiplet, bs=broad singlet. TMS was used as internal reference.

TABLE 2. NMR SPECTRAL[a] DATA OF COMPOUNDS IIIa—IIIg AND IVa—IVd

Compound	δR_1	δR_2	$\delta(1+4)$	$\delta(2+3)$	$\delta(9+10)$	$\delta(5-8)$
IIIa	(m, 1H) 3.90	(m, 1H) 3.90	(m, 2H) 3.66	(m, 2H) 3.16	(q, 4H) 1.79	(nm, 4H) 7.33
IIIb	(s, 3H) 3.56	—	(m, 2H) 3.76	(m, 2H) 3.41	(q, 4H) 1.62	—
IIIc	(ds, 3H) 3.32; 1:1; 20 Hz	(ds, 3H) 3.32; 1:1; 20 Hz	(m, 2H) 3.71	(m, 2H) 3.34	(q, 4H) 1.80	(m, 4H) 7.40
IIId	(s, 3H) 3.43	(s, 3H) 0.80	(m, 2H) 3.72	(m, 2H) 3.40	(q, 4H) 1.81	(m, 4H) 7.40
IIIe	(s, 3H) 2.48	—	(m, 2H) 3.78	(m, 2H) 3.43	(q, 4H) 1.65	—
IIIf	(bs, 3H) 2.53; (m, 4H) 7.50	(bs, 3H) 2.53; (m, 4H) 7.50	(m, 2H) 3.73	(m, 2H) 3.33	(q, 4H) 1.75	(m, 4H) 7.50
IIIg	(s, 3H) 2.47; (q, 4H) 7.81	(s, 3H) 0.70	(m, 2H) 3.78	(m, 2H) 3.51	(q, 4H) 1.81	(nm, 4H) 7.34
IVa	(m, 1H) 4.41	(m, 1H) 4.41	(m, 2H) 4.60	(t, 2H) 3.03	(m, 2H) 6.67	(m, 4H) 7.44
IVb	(s, 3H) 3.50	(m, 1H) 2.41	(m, 2H) 4.80	(m, 2H) 3.38	(m, 2H) 6.41	—
IVc	(ds, 3H) 3.58; 1:4; 4 Hz	(ds, 3H) 2.20; 1:4; 5 Hz	(m, 2H) 4.72	(t, 2H) 3.26	(m, 2H) 6.80	(m, 4H) 7.45
IVd	(bs, 3H) 2.53; (m, 4H) 7.73	(bs, 3H) 2.53; (m, 4H) 7.73	(m, 2H) 4.61	(t, 2H) 3.09	(m, 2H) 6.75	(m, 4H) 7.73

a) Refer to footnote, Table 1.

intensity for the two mesyl groups with an internal chemical shift of 20 Hz. The other cage proton resonances are given in Tables 1 and 2. The spectra are temperature dependent and the two mesyl proton signals move closer as the temperature is raised.

The structure of the *exo*-cyclic trivalent nitrogen atom is assumed to be nearly planar, since the sulphonyl group is as efficient as a carbonyl group for the delocalization of the nitrogen lone-pair electrons.[7] The possibility of slow rotation about N′–SO_2 bond is discarded since the free rotation about this bond is possible with effective and continuous $p\pi$-$d\pi$ delocalization.[7,8] Hence, slow rotation about N–N′ bond could be the only possible explanation for the observed multiplicity.

Non-planar conformations about the N-N′ bond similar to tetraacyl hydrazines, could explain the large $\Delta\nu$=20 Hz between the two mesyl signals as compared to the $\Delta\nu$=5.7 Hz of *N*′,*N*′-dimesyl-*N*-aminocamphorimide.[6] In the proposed conformation (V and Fig. 1) the mesyl group *syn* to the cage-moiety is shielded by the cage benzo ring, whereas the mesyl group *anti* to the cage-moiety appears at the normal position. Non-bonding repulsions between the ring carbonyls and the sulphonyl groups and also some steric factors could make the N–N′ bond torsional barrier sufficiently high.

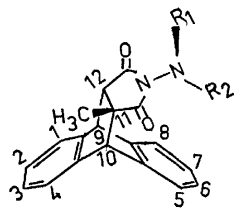

II

Compd.	R_1	R_2
IIa	SO_2CH_3	H
IIb	SO_2CH_3	SO_2CH_3
IIc	SO_2CH_3	$COCH_3$
IId	$SO_2C_6H_4\cdot CH_3$-*p*	H
IIe	$SO_2C_6H_4\cdot CH_3$-*p*	$SO_2C_6H_4\cdot CH_3$-*p*
IIf	$SO_2C_6H_4\cdot CH_3$-*p*	$COCH_3$

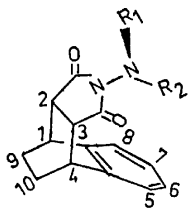

III *endo**

Compd.	R_1	R_2
IIIa	H	H
IIIb	SO_2CH_3	H
IIIc	SO_2CH_3	SO_2CH_3
IIId	SO_2CH_3	$COCH_3$
IIIe	$SO_2C_6H_4CH_3$-*p*	H
IIIf	$SO_2C_6H_4CH_3$-*p*	$SO_2C_6H_4CH_3$-*p*
IIIg	$SO_2C_6H_4CH_3$-*p*	$COCH_3$

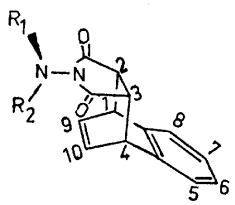

IV *exo*

Compd.	R_1	R_2
IVa	H	H
IVb	SO_2CH_3	H
IVc	SO_2CH_3	$COCH_3$
IVd	$SO_2C_6H_4CH_3$-*p*	$SO_2C_6H_4CH_3$-*p*

N′,N′-*Ditosyl Compounds (IIe, IIIf, and IVd).* The *N*′,*N*′-ditosyl compounds show, in their NMR spectra, a slightly broad singlet of 6H intensity near δ 2.50 for the two tosyl-methyl protons, whereas the monotosyl compounds show a sharp singlet (width at half height 1.5 Hz) for its tosyl methyl protons (Tables 1 and 2).

* The prefixes *endo* and *exo* are used in the sense that substituents on the same side of the bicyclo[2.2.2]octene ring as the benzene ring are *endo*, those on the other side are *exo*.

The broadness of the singlet (width at half height 3 Hz) observed for the two tosyl-methyl groups may be due to hindered rotation about the N–N′ bond. A preferred conformation about the N–N′ bond in these compounds could give two signals for the two tosyl-methyl groups as in *N′,N′*-dimesyl compounds IIb and IIIc, but the appearance of a broad singlet indicates that the two tosyl-methyl protons lie away from the effective magnetic zone of the cage-moiety.

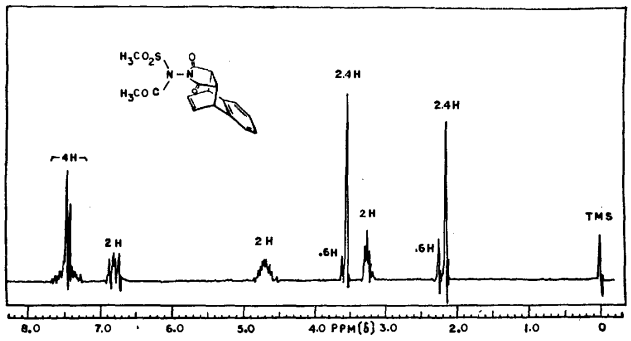

Fig. 2. 60 MHz NMR spectrum of N′-mesyl-N′-acetyl-N-amino-1,2,3,4-tetrahydro-1,4-ethylenonaphthalene-2,3-*exo*-dicarboximide (IVc) in $CDCl_3$ at 45 °C.

N′-Suphonyl-N′-acetyl Derivatives (IIc, IIf, IIId, IIIg, and IVc). The NMR spectrum of *N′*-mesyl-*N′*-acetyl compound (IVc) in $CDCl_3$ (Fig. 2) shows along with other normal resonances (Table 2), two singlets for mesyl protons and two singlets for acetyl protons.

The splitting of the mesyl and acetyl proton signals in the spectrum indicates the possibility of two conformations due to the restricted rotation about the N–N′ bond. In the two different conformations the mesyl protons experience different magnetic environments and therefore, appear as a pair of singlets. The conformer in which the acetyl group lies *syn* to the cage-moiety, while the bulkier mesyl group lies *anti*, is predominant (Fig. 2).

Compounds IIc and IIId in $CDCl_3$ exhibit different patterns in their NMR spectra. Each compound shows a singlet of 3H intensity for the mesyl protons at a normal position ($\delta \approx 3.43$) and another singlet of 3H intensity for the acetyl protons at a shielded position ($\delta \approx 0.80$). As in the case of compound IVc, restricted rotation about N–N′ bond could also be expected in IIc and IIId. Appearance of the acetyl signal with 3H population at the shielded position indicates that the conformation (VI and VII) in which the acetyl group lies *syn* to the cage-moiety is preferred.

The NMR spectrum of each of the *N′*-tosyl-*N′*-acetyl compounds IIf and IIIg in $CDCl_3$ shows two sharp singlets, one for the tosyl-methyl protons and the other for the acetyl protons, along with other proton resonances (Tables 1 and 2).

The spectral features of these compounds are very much similar to *N′*-mesyl-*N′*-acetyl analogues IIc and IIId. They also take up preferred conformations of types VI and VII in which the less bulkier acetyl group is *syn* to the cage-benzo ring.

The tosyl group does not have any shielding effect on the cage-moiety protons. Shielding of the cage protons by the *N′*-benzoyl group has been reported in the case of *N′*-benzoyl-*N′*-acetyl derivatives of *N*-amino-[2.2.1]bicycloheptene-2,3-*endo*-dicarboximide[2] and *N*-aminocamphorimide.[6] This observation indicates that the aryl part of the tosyl group projects away from the cage-moiety (VIII).

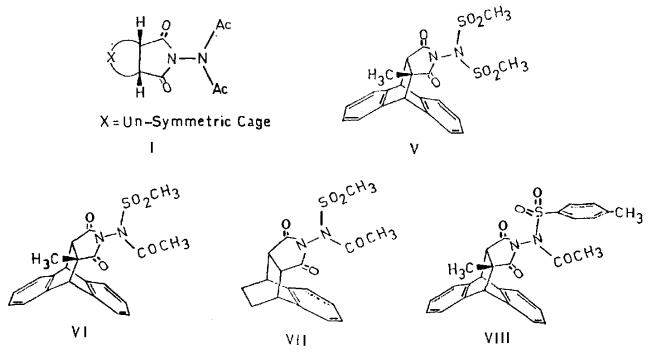

Experimental

NMR spectra were recorded on a Varian A-60D spectrometer equipped with a variable temperature controller (Model No. V-6040). IR spectra were recorded for Nujol mulls on a Perkin-Elmer-257 spectrophotometer. NMR spectral data are given in Tables 1 and 2, and IR spectral data, melting points and elemental analyses of all the compounds in Table 3.

1,2,3,4-Tetrahydro-1,4-ethenonaphthalene-2,3-endo/exo-*dicasboxylic anhydrides* were obtained by the method of Takeda *et al.*[9] The *endo*-isomer on refluxing with hydrazine hydrate[10] (4 mol) in ethanol medium in the presence of animal charcoal gave the reduced product, 1,2,3,4-tetrahydro-1,4-ethanonaphthalene-2,3-*endo*-dicarboximide (IIIa). The *exo*-isomer was reacted with equimolecular amount of hydrazine hydrate in ethanol medium at room temperature to give the *N*-aminoimide (IVa). The two *N*-aminoimides were recrystallized from ethanol and gave benzal derivatives with benzaldehyde which showed a characteristic one proton singlet near δ 9.0.

*N′-Monomesyl and N′,N′-Dimesyl Derivatives of N-Amino-9,10-dihydroanthracene-9,10-*endo-*α-methyl-α,β-succinimide*[4] *and N-Amino-1,2,3,4-tetrahydro-1,4-ethanonaphthalene-2,3-*endo-*dicarboximide IIIa (IIa, IIb, IIIb, and IIIc).* The compounds were prepared by heating the corresponding *N*-aminoimide with mesyl chloride (2 mol) in the presence of pyridine on a water bath for about 2 hr. The reaction mixture was then washed with water, filtered, dried and recrystallized from a mixture of ethanol and ethyl acetate. The product thus obtained was a mixture of both *N′*-monomesyl and *N′,N′*-dimesyl derivatives. *N′,N′*-Dimesyl derivatives were soluble in cold chloroform and were separated from the mixture.

N′-Monomesyl Derivative (IVb). This was prepared by heating *N*-amino-1,2,3,4-tetrahydro-1,4-ethenonaphthalene-2,3-*exo*-dicarboximide (1 mol) with mesyl chloride (2 mol) in the presence of a few drops of pyridine on a water bath for about 2 hr. The product was recrystallized from ethanol and was found to be exclusively a monomesyl derivative.

N′-Mesyl-N′-acetyl Derivatives (IIc, IIId and IVc). The compounds were prepared by heating the corresponding *N′*-monomesyl derivative with acetic anhydride in the presence of pyridine on a water bath for 2—3 hr. The reaction mixture was then treated with water, filtered, dried and recrystallized from ethanol.

N′-Monotosyl-N-aminoimides (IId and IIIe). The compounds were prepared by heating equimolar amounts of *N*-aminoimide and tosyl chloride in the presence of pyridine on a water bath for about 2—3 hr and were recrystallized

Table 3. Mps, elemental analyses and IR[a] data

Compound	Mp °C	Elemental analyses Found C%	Found H%	Calculated C%	Calculated H%	IR ν_{max} (cm^{-1})
IIa	290	62.53	4.52	62.82	4.71	3240m, 1790w, 1725s, 1160s, 760m
IIb	225	54.56	4.22	54.78	4.35	1800w, 1730s, 1165s, 770m
IIc	237	62.07	5.01	62.27	4.71	1790w, 1740s, 1170s, 760m
IId	226	68.06	4.92	68.12	4.80	3170m, 1790w, 1740s, 1590m, 1165s, 755m
IIe	280	64.35	4.43	64.70	4.57	1810w, 1750s, 1595w, 1175s, 770w
IIf	257	66.83	4.66	67.20	4.80	1800w, 1740s, 1595w, 1165s, 760w
IIIa	227—230	69.02	5.66	69.42	5.78	3315m, 3260w, 1690s, 1610w
IIIb	245—247	55.92	4.87	56.25	5.00	3255m, 1805w, 1730s, 1158s, 760w
IIIc	214—217	48.54	4.38	48.24	4.52	1808w, 1750s, 1176s, 756m
IIId	198—200	56.12	5.01	56.35	4.97	1806w, 1745s, 1728s, 1170s, 760m
IIIe	240—242	63.24	5.32	63.63	5.05	3240m, 3210m, 1805w, 1746s, 1734s, 1608w, 1180s, 765w
IIIf	250—253	60.83	4.65	61.09	4.73	1810w, 1750s, 1600m, 1188s, 1180s
IIIg	202—205	63.46	4.97	63.01	5.02	1808w, 1748s, 1730s, 1598w, 1180s, 760w
IVa	185—187	69.60	5.33	70.00	5.00	3325m, 3260m, 3200m, 1778m, 1695s, 1620m, 760m
IVb	206—208	56.28	4.32	56.60	4.40	3270m, 1800w, 1733s, 1335s, 1154s, 760m
IVc	196—197	56.59	4.56	56.66	4.44	1800w, 1730s, 1180s, 760m
IVd	176—177	61.12	4.20	61.31	4.38	1814w, 1755s, 1600m, 1175s, 1158s, 748w

a) All IR spectra were recorded in Nujol. m=medium, s=strong and w=weak.

from ethanol.

N′-*Tosyl*-N′-*acetyl Derivatives (IIf and IIIg)*. The compounds were acetylated with acetic anhydride as in the case of IIc, IIIc, and IVb.

N′,N′-*Ditosyl Derivatives (IIe, IIIf, and IVd)*. The compounds were prepared by heating *N*-aminoimide (1 mol) with tosyl chloride (2 mol) in the presence of a few drops of pyridine on a water bath for about 3 hr. The product was then washed with water, dried and recrystallized from ethanol.

The authors thank Prof. G. B. Singh for his keen interest in the study. One of the authors (O.S.R.) is grateful to U.G.C. for the award of a Research Fellowship.

References

1) a) B. H. Korsch and N. V. Riggs, *Tetrahedron Lett.*, **1966**, 5897; b) N. V. Riggs and S. M. Verma, *Aust. J. Chem.*, **23**, 1913 (1970).

2) S. M. Verma and C. Koteswara Rao, *Tetrahedron*, **28**, 5029 (1972).

3) a) S. M. Verma and R. Prasad, *J. Org. Chem.*, **38**, 1004 (1973); b) S. M. Verma and O. Subba Rao, *Aust. J. Chem.*, **26**, 1963 (1973).

4) S. M. Verma and K. O. P. Sinha, *Ind. J. Chem.*, **11**, 1138 (1973).

5) S. M. Verma, O. Subba Rao, and C. Koteswara Rao, *Tetrahedron Lett.*, **1973**, 1639.

6) S. M. Verma and R. Prasad, *J. Org. Chem.*, **38**, 3745 (1973).

7) F. G. Bordwell and G. D. Cooper, *J. Amer. Chem. Soc.*, **74**, 1058 (1952).

8) R. M. Moriarty, *Tetrahedron Lett.*, **1964**, 509.

9) K. Takeda, K. Kitahonoki, M. Sugiura, and Y. Takano, *Chem. Ber.*, **95**, 2344 (1962).

10) A. Furst, R. C. Berlo, and S. Hooton, *Chem. Rev.*, **65**, 51 (1965).

Dielectric Studies of *ortho*- and *para*-Bromoanisoles and β-Bromophenetole in the Liquid State

Alpana GHATAK, Arati DAS, and Subir Kr. ROY

Optics Department, Indian Association for the Cultivation of Science, Calcutta 32, India

(Received February 8, 1974)

Complex dielectric permittivities in *ortho*- and *para*-bromoanisoles and β-bromophenetole in the liquid state have been measured in 1.6, 3.17, and 3.49 cm microwave regions at different temperatures. The dielectric data were analysed in terms of molecular and intramolecular relaxation times. The values of methoxy group relaxation times and its contribution to total polarization obtained in the liquid bromoanisoles have been compared to the corresponding values in dilute solutions reported in literatures. Activation energy for dielectric relaxation and viscous flow in all the cases have also been obtained in all the liquids.

From studies of dielectric relaxation in anisole and dimethoxy benzenes in the liquid state Vaughan *et al.*[1] reported that the relaxation time of methoxy group rotation τ_2 and its contribution C_2 to total polarization are about 3 ps at 20 °C and 0.2 respectively excepting in the case of *o*-dimethoxy benzene where $C_2=0.7$. Garg and Smyth[2] extended the investigation in liquid anisole at still higher frequency region and reported the similar values of τ_2 and C_2. These values of τ_2 and C_2 in anisole and *p*-dimethoxy benzene in dilute solutions reported by different workers[3-5] are found to be 7—9 ps at 20 °C and 0.7 respectively, while in *p*-bromoanisole in dilute solution though the τ_2 value is 9 ps at 20 °C, the C_2 is only 0.2 as reported by Farmer and Walker.[4] So it appears that the methoxy group relaxation time and its contribution C_2 in anisole or dimethoxy benzene in dilute solution are larger than their values in pure liquids. Garg and Smyth[2] suggested that the reduction in the contribution of C_2 of the methoxy group rotation from its value in solution to the liquid state might be due to some restraint in the C–O bond as a result the methoxy group rotation in anisole is not completely free but hindered.

It will be interesting to study how the methoxy group rotation τ_2 and its contribution C_2 in haloanisoles in the liquid state, compare with the corresponding values in dilute solutions published in literatures. The present paper reports the results of investigation on dielectric relaxation of *o*-bromo and *p*-bromoanisoles and β-bromophenetole in the liquid state together with a discussion of the results.

Experimental

Pure samples of *o*-bromoanisole, *p*-bromoanisole and β-bromophenetole were dried with fused calcium chloride and then subjected to fractional distillation. The proper fraction was then distilled under reduced pressure before use in the investigation. The experimental arrangement for measurement of dielectric permittivity ε', dielectric loss ε'', static dielectric constant ε_0, refractive index n_D, viscosity η, and density d at different temperatures were the same as described in an earlier paper.[6] The accuracy in the measurements of ε' and ε'' were about 2 and 5% respectively.

Results

The experimentally obtained values of ε' and ε'' at different wave lengths and at different temperatures together with ε_0 at 1 MHz at different temperatures are given in Table 1 and the viscosity η, density d and refractive index n_D at different temperatures are given in Table 2. Cole-Cole arc plots (some shown in Fig. 1) were drawn with the dielectric data. The high frequency dielectric constant ε_∞ and the distribution parameter α were obtained as usual from the arc plots. The large values of distribution parameter and also the nonlinear plots of ε' *vs.* $\varepsilon''\omega$ indicated the presence of more than one relaxation mechanism in all the liquids. The dielectric data were therefore analysed in terms of two relaxation processes by a straightforward analytical method developed by Kastha[7] and applied successfully by others.[8-10] The values of relaxation times for

Table 1. Values of ε', ε'' and ε_0

Compound	Temp. °C	$\lambda=1.62$ cm		$\lambda=3.17$ cm		$\lambda=3.49$ cm		ε_0
		ε'	ε''	ε'	ε''	ε'	ε''	
o-Bromoanisole	30	3.27	0.97	3.68	1.41	3.91	1.62	8.96
	50	3.35	1.11	3.79	1.55	4.18	1.82	8.68
	70	3.42	1.28	3.96	1.76	4.20	1.91	8.36
	85	3.45	1.33	4.01	1.91	4.39	2.04	8.14
p-Bromoanisole	30	2.97	0.67	3.32	1.16	3.46	1.27	7.40
	50	2.99	0.89	3.35	1.43	3.47	1.53	7.12
	70	3.05	0.90	3.53	1.44	3.67	1.52	6.82
	85	3.04	0.99	3.63	1.54	3.73	1.62	6.56
β-Bromophenetole	40	3.12	0.84	3.48	1.30	3.66	1.34	7.04
	55	3.23	0.95	3.69	1.34	3.86	1.42	6.69
	70	3.32	1.04	3.88	1.40	4.00	1.45	6.28
	85	3.44	1.06	4.02	1.34	4.19	1.37	6.00

TABLE 2. VALUES OF α, η, d, n_D^2 AND ε_∞

Compound	Temp. °C	Distribution parameter α	Viscosity η (cP)	Density d (g/cm^3)	Square of refractive index n_D^2	ε_∞
o-Bromoanisole	30	0.175	1.998	1.500	2.46	2.94
	50	0.159	1.353	1.481	2.43	2.88
	70	0.140	1.002	1.455	2.40	2.84
	85	0.059	0.839	1.437	2.37	2.80
p-Bromoanisole	30	0.095	1.499	1.482	2.43	2.76
	50	0.090	1.150	1.457	2.40	2.66
	70	0.084	0.910	1.438	2.37	2.64
	85	0.080	0.769	1.421	2.35	2.56
β-Bromophenetole	40	0.126	2.420	1.409	2.39	2.82
	55	0.116	1.726	1.392	2.37	2.81
	70	0.115	1.325	1.372	2.35	2.77
	85	0.112	1.003	1.356	2.32	2.74

TABLE 3. VALUES OF τ_1, τ_2, C_1, $\Delta H\tau_1$, $\Delta H\tau_2$, $\Delta H\eta$ AND μ

Compound	Temp. °C	$\tau_1 \times 10^{12}$ (s)	$\tau_2 \times 10^{12}$ (s)	C_1	$\Delta H\tau_1$ (kcal/mol)	$\Delta H\tau_2$ (kcal/mol)	$\Delta H\eta$ (kcal/mol)	Dipole moment μ (D)
o-Bromoanisole	30	48.9	10.9	0.63	2.28	2.22	3.45	2.15
	50	37.2	8.7					
	70	28.7	7.7					
	85	22.6	6.2					
p-Bromoanisole	30	33.7	7.3	0.85	2.02	2.72	2.70	1.98
	50	24.9	5.6					
	70	23.5	4.2					
	85	19.2	3.2					
β-Bromophenetole	40	33.0	9.8	0.65	2.01	2.16	3.54	2.02
	55	28.5	8.5					
	70	22.8	7.1					
	85	20.6	5.6					

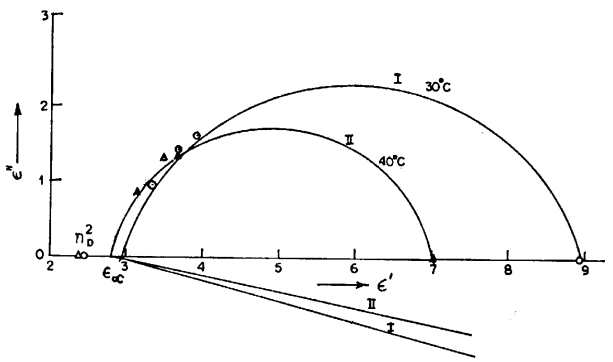

Fig. 1. Cole-Cole plot of *o*-bromoanisole at 30 °C (Curve I, ⊙) and *β*-bromophenetole at 40 °C (Curve II, △).

molecular orientation τ_1 and group rotation τ_2 and weight factor C_1 for molecular orientation are included in Table 3. The activation energies for dielectric relaxation by molecular orientation $\Delta H\tau_1$ and group rotation $\Delta H\tau_2$ were obtained from the slopes of the straight line plots of log $T\tau$ *vs.* $1/T$ and the activation energy for viscous flow $\Delta H\eta$ were obtained from the graphs of log η *vs.* $1/T$. The values of $\Delta H\tau_1$, $\Delta H\tau_2$, and $\Delta H\eta$ are included in Table 3.

Discussion

It can be seen from Table 3 that the molecular and intramolecular relaxation times as also the distribution parameter α in all the liquids decrease with increase of temperature as is generally observed.

The value of molecular relaxation time τ_1=49 ps at 30 °C in *o*-bromoanisole appears much larger than the value of τ_1=33.7 ps at the same temperature in *p*-bromoanisole. But the reduced relaxation time τ_1/η of the two molecules are of the same order (≈23 ps) of magnitude, showing thereby that the two isomeric molecules are of the same size.

o-Bromoanisole. A comparison of molecular relaxation time τ_1 of *o*-bromoanisole and *o*-dimethoxy benzene both in the liquid state, shows that the molecular relaxation time $\tau_1 \simeq$49 ps at 30 °C in the former molecule obtained in the present investigation is almost the same as that of 48.5 ps at 25 °C in the latter reported by Vaughan *et al.*[1] This is consistent with the sizes of the two molecules.

The contribution of methoxy group rotation C_2 in *o*-bromoanisole in the liquid state is only about 0.37 as against the value 0.7 in the case of *o*-dimethoxy benzene in the liquid state. The former molecule having C–Br bond moment of about 1.55 D as against O-CH_3 bond moment of ≈1.3 D in the latter molecule, has total moment larger than the latter molecule. So the ratio of group moment component to the total moment which is a measure of C_2 is expected to be larger in the latter molecule.

The contribution of the methoxy group rotation C_2 in *o*-bromoanisole can be calculated from the consideration of total moment and methoxy group moment of the molecule. The O–CH_3 bond has a moment of about 1.3 D making an angle 55° with the direction of C–O bond in the benzene ring. The component of the O-CH_3 bond moment perpendicular to the direction of C–O bond, which is responsible for methoxy group rotation is

$$\mu_2 = 1.3\text{D} \times \sin 55° = 1.06\text{D}$$

and the total moment of the molecule μ_1 can be obtained by the vector sum of C–Br bond moment and component of O–CH_3 bond moment along the C–O axis and is given by

$$\begin{aligned}\mu_1^2 &= (1.55)^2 + (1.3\cos 55°)^2 \\ &\quad + 2 \times 1.55 \times 1.3 \cos 55° \cdot \cos 60° \\ &= 3.92 \\ \mu_1 &= 1.99\text{D}\end{aligned}$$

This value of 1.99 D agrees fairly well with the experimentally obtained value of 2.15 D.

Now $$C_2 = \left(\frac{\mu_2}{\mu_1}\right)^2 = \left(\frac{1.06}{1.99}\right)^2 = 0.30$$

So theoretically calculated value of C_2=0.30 compares reasonably well with the experimentally obtained value of C_2=0.37.

p-*Bromoanisole.* The value of molecular relaxation time τ_1=33.7 ps and group relaxation time τ_2=7.3 ps at 30 °C as also the contribution from methoxy group rotation C_2=0.15 obtained in the liquid *p*-bromoanisole, agree fairly well with the values of τ_1=31 ps τ_2=7 ps at 25 °C and C_2=0.2 in *p*-bromoanisole in dilute solution of *p*-xylene reported by Farmer and Walker.[4] The similarity in dielectric behaviour of *p*-bromoanisole in pure liquid and dilute solution suggests that the dipole-dipole interaction is not very effective in the liquid state of the molecule.

Comparison of the Relaxation Time of Methoxy Group Rotation in Pure Liquid and Dilute Solution. The relaxation time of methoxy group rotation in *o*-bromo- and *p*-bromoanisole in the liquid state obtained in the present investigation are of the same order of methoxy group rotation (7—9) ps reported in anisole and substituted anisoles in dilute solutions reported by Farmer and Walker[4] and Klages and Krauss[5] but larger than the value of about 3 ps of the methoxy group rotation in anisole and dimethoxy benzenes in liquid state reported by Vaughan *et al.*[1] and Garg and Smyth.[2] So it appears that the methoxy group rotation in molecules containing only methoxy group as substituent is less hindered in the liquid state than in anisole in dilute solution or in haloanisoles either in the liquid state or in solutions. This is supported by the fact that the activation energy of methoxy group rotation in anisole in liquid state as reported by Garg and Smyth[2] is only 1.5 kcal/mol which is much smaller than the value of 2.6 kcal/mol for methoxy group rotation in anisole in dilute solution in *p*-xylene calculated from the data of Farmer and Walker[4] and also from the values of 2.2—2.6 kcal/mol (Table 3) for methoxy group rotation in the bromo-anisoles in liquid state obtained in the present investigation.

The larger value of the methoxy group rotation of anisole in benzene or *p*-xylene solution than in the pure liquid may be due to the formation of a weak bond between the π-electron of the solvent molecule and hydrogen atom of the methoxy group. Similar bond formation in 1,2-dichloroethane and benzene has been reported by Chitoku and Higasi.[11]

β-Bromophenetole. The reduced molecular relaxation time τ_1/η of β-bromophenetole at 40 °C is about 14 ps which is smaller than the value τ_1/η=23 ps at 30 °C in bromoanisoles. Thus the β-bromophenetole molecule appears to be a little bit smaller than the molecules of bromoanisoles.

The group relaxation time τ_2=9.8 ps at 40 °C in this case is larger than the methoxy group rotation in anisole in dilute solution or haloanisoles in liquid state. This value of τ_2=9.8 ps at 40 °C is also larger than the relaxation time of ethoxy group rotation τ_2=4 ps at 40 °C in the liquid state reported by Bhattacharyya *et al.*[8] which is consistent with their sizes.

The contribution of group rotation C_2 here is only −0.32 as against the value of C_2=0.63 in ethoxy group rotation in phenetole. The substitution of Br-atom in the ethoxy group might increase hindrance and thus reduces the value of C_2 in the present case.

Activation Energy. The activation energy of dielectric relaxation by molecular orientation in all the liquids are of the same order (2.1 kcal/mol) and each is smaller than the corresponding activation energy for vicous flow as usually observed.

The activation energy for molecular relaxation $\Delta H\tau_1$=2.1 kcal/mol in *p*-bromoanisole in liquid state obtained in the present investigation is about the same as the value of $\Delta H\tau_1$=2.07 kcal/mol obtained for *p*-bromoanisole in dilute solution, calculated from the data of Farmer and Walker.[4] This shows that the dipolar interaction are almost the same in the liquid *p*-bromoanisole and its solution in *p*-xylene as mentioned earlier.

The activation energy of group rotation in the liquid ($\Delta H\tau_2$=2.2 kcal/mol) and in solution ($\Delta H\tau_2$=1.9 kcal/mol) calculated from the data of Farmer and Walker[4] are also compatible.

It can be seen from Table 2 that the values of n_D^2 in all the liquids are less than the respective values of ε_∞. This indicates the presence of a high frequency absorption region as suggested by Poley.[12] This 'Poley absorption' has been generally explained as due to torsional molecular librations in potential minima of fluctuating interaction field of the neighbouring molecules.[13]

The authors wish to express their sincere thanks to Dr. S. B. Roy for his guidance and to Professor G. S. Kastha for his keen interest.

References

1) W. E. Vaughan, S. B. W. Roeder, and T. Provder, *J. Chem. Phys.*, **39**, 703 (1963).
2) S. K. Garg and C. P. Smyth, *ibid.*, **46**, 373 (1967).

3) E. Forest and C. P. Smyth, *J. Amer. Chem. Soc.*, **86**, 3474 (1964).
4) D. B. Farmer and S. Walker, *Can. J. Chem.*, **47**, 4645 (1969).
5) G. Klages and G. Krauss, *Z. Naturforsch*, **26a**, 1272 (1971).
6) A. Hasan, A. Das (nee' Pal), and A. Ghatak, This Bulletin, **44**, 322 (1971).
7) G. S. Kastha, *Ind. J. Phys.*, **42**, 223 (1968).
8) J. Bhattacharyya, A. Hasan, S. B. Roy, and G. S. Kastha, *J. Phys. Soc. Japan*, **28**, 204 (1970).
9) G. S. Kastha, B. Dutta, J. Bhattacharyya, and S. B. Roy, *Ind. J. Phys.*, **43**, 14 (1969).
10) A. Hasan, A. Das, and A. Ghatak, *ibid.*, **45**, 558 (1971).
11) K. Chitoku and K. Higasi, This Bulletin, **40**, 773 (1967).
12) J. Ph. Polęy, *Appl. Sci. Res.*, **B4**, 337 (1955).
13) J. B. Birks and J. Hart, "Progress in Dielectic," Vol. 3, Heywood & Company Ltd., London (1961), p. 90.

NOTES

BULLETIN OF THE CHEMICAL SOCIETY OF JAPAN, VOL. 47 (9), 2319—2320 (1974)

Dye Sensitized Photo-oxidation of Diphenylamine

W. R. BANSAL, S. PURI, and K. S. SIDHU*
Physical Chemistry Laboratories, Punjabi University, Patiala, India

(Received October 22, 1973)

Synopsis. Evidence is presented to show that excited O_2 ($1\sum_g^+$, $1\Delta_g$) is an intermediate in the dye (methylene blue, rose bengal, eosin) sensitized oxidation of diphenylamine which yeilds *N*-phenyl-*p*-benzoquinonimine. The relative rates in different solvents are reported and a mechanism is suggested.

Evidence has been presented for the non-participation of O_2 ($^1\sum_g^+$ or $^1\Delta_g$) in the ketone or dye sensitized oxidation of a number of aliphatic amines and *N*-substituted anilines.[1-3] In the benzophenone sensitization of diphenylamine (DPA) diphenyl nitroxide formed through triplet DPA in the presence of oxygen is reported[4] while in the absence of oxygen 4-(*N*-phenylamino)-phenyl-diphenylmethanol has been identified.[5] Sensitization of DPA which is apparently quite complex[2] thus has appeared to fall in line with general mechanistic features of other similar amines. We report here the isolation of a unique product in its oxidation sensitized by methylene blue, rose bengal and eosin (all known for initiating reactions through their triplet states[6]) along with other kinetic features suggesting the participation of first excited singlet state of oxygen.

Experimental

All reagents were BDH grade and were purified by repeated crystallization and fractional distillation. The dyes had their maxima in spectrograde methanol in the visible at; methylene blue 645 nm; rose bengal 550 nm, eosin 515 nm. Photolysis assembly consisted of a white light bulb, a 320 nm cut off glass filter and a pyrex cell (50 mm dia × 10 mm) maintained at 26±2 °C in an air thermostat. Oxygen concentrations were varied by maintaining different partial pressures of it in the cell. Mixtures of dry nitrogen and oxygen at a total pressure of one atmosphere were used for the purpose. The reaction mixture after evaporation of the solvent was fractionated by column chromatography over alumina with benzene as eluent. The brown product after crystallization from petroleum ether was identified as *N*-phenyl-*p*-benzoquinonimine (PBQ) by mp 101—102 °C (reported 101.5 °C); identity of its IR in KBr with the reported spectrum and understandable NMR in CS_2.[7] PBQ on hydrolysis with 10^{-2} M HCl at 65 °C gave aniline and *p*-quinone which were identified by UV spectra after chromatographic separation. The product yields in these runs were kept between 2.4 and 3.0% in order to avoid any secondary products through secondary photolysis. In the kinetic runs the monitoring was done at 448 nm where PBQ has a maximum in alcohols with blank as reference on a Hilger and Watt spectrophotmeter.

Hydrogen peroxide was shown to have no reaction with DPA in alcohols at the concentrations examined. To solutions of hydrogen peroxide (0.3 M) in excess and DPA (0.05 M) in alcohol-water mixtures in the ratio 5: 1, varying amounts of NaOCl (0.2 M) were added dropwise from the burette. After the instantaneous reaction at 26 °C the reaction mixture was double diluted with water and extracted with ether. The ether layer was evaporated and column chromatographed. The yields were kept below 8.0% and no attempt was made to carry the reaction to completion because of the observed further oxidation of PBQ at larger concentrations. NaOCl alone gave a different mixture of products.

Results and Discussion

In the photolysis of 5.0×10^{-4} to 1.0×10^{-2} M of DPA with 3.0×10^{-5} to 7.5×10^{-4} M of the dye, time study and UV/visible spectra demonstrated PBQ to be a primary product. Unlike previous studies increase in oxygen concentration increased the extent of reaction.[3c] The relative reaction rates in different solvents were CH_3OH=1.00, C_2H_5OH=0.78, *iso*-C_3H_7OH=0.55, *n*-C_4H_9OH=0.69, CH_3CN=0.78, CH_3OH–H_2O(9: 1)=1.68, CH_3OH–H_2O(8: 2)=2.76, CH_3OH–H_2O(7: 3)=3.95. Viscosity effect decreasing the rates is apparent in alcohols. In isopropanol an additional decrease appears because of the availability of easily abstractable tertiary hydrogen. The effect of water cannot be a pure dielectric effect in view of the rate in acetonitrile. The life time of singlet oxygen is also less in water.[8] It appears, therefore, that water is stabilizing some of the intermediate radical species. A very likely course for the reaction is;

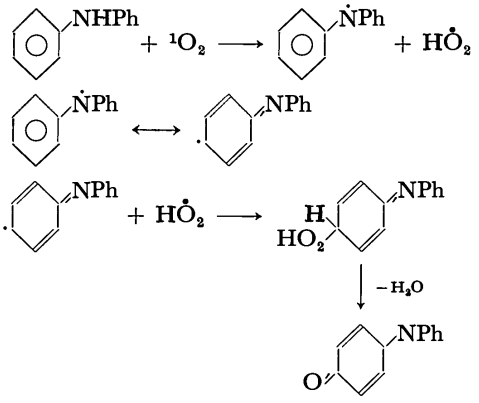

There exist the possibilities of (a) intial hydrogen abstraction from N–H by the triplet dye and (b) direct attack of singlet O_2 at the *para* position as proposed in the photo-oxidation of phenols.[9,10] However, both of these require a hydrogen abstraction by the inter-

* To whom correspondence be addressed.

mediate peroxy radical mechanisms and in view of the low concentration of the substrate as compared to the solvent and bond strengths of N–H and *tert*-C–H (in isopropanol)[11] the rate in isopropanol should be higher. On the contrary the rate is higher in methanol. Also H_2O_2 is a product which militates against these possibilities.

A specific search for tetraphenyl hydrazine did not detect it. This is evidence of the greater stability of the conjugated structure of the radical. The reaction sequence is helped by the resonance stabilization of the radical as expected.

To further substantiate the participation of singlet oxygen, these species were generated chemically by the well-known reaction of $NaOCl+H_2O_2$.[12,13] In alcohols with similar concentrations of DPA, PBQ was formed with parallel kinetic features (*cf.* effect of solvents).

It is thus established that excited $O_2(^1\Sigma_g^+, {}^1\Delta_g)$ is an intermediate in the dye sensitized oxidation of diphenyl amine which proceeds through hydrogen abstraction by $^1O_2$.

We thank UGC and CSIR for the award of fellowships (to W.R.B. and S.P.) and financial assistance. We also thank Regional Research Laboratory, Hyderabad for the NMR spectra.

References

1) M. Santhanam and V. Ramakrishnan, *Chem. Commun.*, **1970**, 344.

2) H. Shizuka, Y. Takayama, I. Tanaka, and T. Morita, *J. Amer. Chem. Soc.*, **92**, 7270 (1972).

3) a) R. F. Bartholomew and R. S. Davidson, *Chem. Commun.*, **1970**, 1174. b) R. F. Barholomew and R. S. Davidson, *J. Chem. Soc., C*, **1971**, 2342. c) R. F. Bartholomew and R. S. Davidson, *ibid., C*, **1971**, 2347. d) R. F. Bartholomew, R. S. Davidson, and M. J. Howell, *ibid., C*, **1971**, 2864.

4) M. Santhanam and V. Ramakrishnan, *Indian J. Chem.*, **8**, 374 (1970).

5) C. Pac, H. Sakurai, and T. Tosa, *Chem. Commun.*, **1970**, 1311.

6) K. Gollnick, "Advances in Photochemistry," ed. by W. A. Noyes, Jr., G. S. Hammond, J. N. Pitts, Jr., Interscience Publishers, Vol. 6, (1968), p. 1.

7) a) R. Lantz and J. Gascon, *Bull. Soc. Chim. Fr.*, **1959**, 1161. b) H. J. Teuber and W. Schmidtke, *Chem. Ber.*, **93**, 1257 (1960).

8) P. B. Merkel and D. R. Kearns, *J. Amer. Chem. Soc.*, **94**, 1029 (1972).

9) K. Pfoertner and D. Boese, *Helv. Chem. Acta*, **53**, 1553 (1970).

10) I. Saito, S. Kato, and T. Matsuura, *Tetrahedron Lett.*, **1970**, 239.

11) G. Glockler, *Discuss Faraday Soc.*, **10**, 26 (1951).

12) C. S. Foote and S. Wexler, *J. Amer. Chem. Soc.*, **86**, 3879, 3880 (1964).

13) T. Yamase, H. Kokado, and E. Inoue, This Bulletin, **45**, 726 (1972).

BULLETIN OF THE CHEMICAL SOCIETY OF JAPAN, VOL. 47 (9), 2321—2322 (1974)

The Crystal and Molecular Structure of Dimeric [3-(Salicylideneamino)-1-propanolato(2−)]copper(II)

Peter J. NASSIFF,* E. R. BOYKO, and Loren D. THOMPSON

Contribution from the Department of Chemistry, Providence College, Providence, R. I., 02908 U.S.A.

(Received May 4, 1974)

Synopsis. The crystal structure of dimeric[3-(salicylideneamino)-1-propanolato(2−)]copper(II) has been determined by X-ray diffraction. The two copper atoms are square planar with a separation of 3.021(4) Å and are bridged with aliphatic oxygens. The unusually low antiferromagnetism, explained by superexchange, has been correlated with the Cu-O-Cu angles of similar complexes.

Tridentate Schiff bases which contain an alcoholic side chain occasionally form 1 : 1 copper(II)-ligand complexes which have unusually low antiferromagnetic moments.[1,2] At room temperature the moments for these compounds lie between 0.3 and 0.7 BM, compared to the more usual values which are in the range 1.1 to 1.7 BM. The title compound, abbreviated $[Cu(3\text{-PrO}\cdot Sal)]_2$, is of this type; molecular weight measurements indicate a dimer.[1]

Three possible dimeric structures have been discussed in the literature.[3] These involve bridging with the aliphatic oxygens, I, bridging with the phenolic oxygens, II, or a combination of both, III. Infrared studies strongly favor structure I.[3] It is clear that a crystal structure determination is desirable, and this is the purpose of the present work.

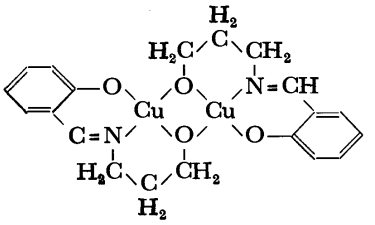

I

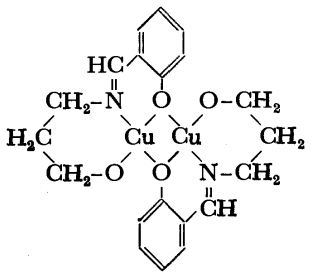

II

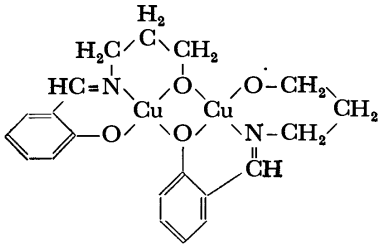

III

Experimental

Bis[3-(Salicylideneamino)-1-propanolato(1-)]copper(II) was converted into $[Cu(3\text{-PrO}\cdot Sal)]_2$ by refluxing in DMF for 5 hr (52% yield). Violet crystals were crystallized from DMF. Found: Cu, 26.51; C, 50.02; H, 4.70; N, 6.50%.[4] Calcd for $Cu(C_{10}H_{11}NO_2)$: Cu, 26.40; C, 49.89; H, 4.60; N, 5.81%.

The smaller crystals were plates having a predominant (100) face, and examination under polarized light showed that extensive twinning occurs. A crystal of dimensions $0.5\times0.5\times0.1$ mm in which a small amount of twinning could be seen around the edges was mounted for X-ray investigation.

Crystal data: $Cu_2C_{20}H_{22}N_2O_4$; Monoclinic, space group $P2_1/c$, $a=9.018(5)$,[5] $b=10.810(4)$, $c=10.233(5)$ Å, $\beta=106.62(9)°$, $D_m=1.667$, $D_x=1.673$, $Z=2$, $F(000)=984$. Absorption for Ni-Kα radiation, 37.0 cm^{-1}.

Using Ni-Kα radiation, multiple-film equi-inclination Weissenberg photographs were taken for the layers *h0l* to *h5l*. Because of the twinning problem, the same crystal was then used to obtain the *hk*0 and *hll* zones. The intensities were visually estimated, and no corrections for absorption or extinction effects were made. Standard treatment of the data produced 860 observed independent structure factors.

Structure Determination

Space group considerations require the dimer to have a center of symmetry which coincides with one in tke unit cell. A Patterson synthesis produced the approximate location of the copper atom, and an electron density map was computed employing the signs determined from its coordinates. An outstanding feature of the map was a large peak in a position which would correspond to a bridging oxygen. Assuming that this was a bridging oxygen, and that the dimer for the most part was expected to be planar, the electron density map for the plane determined by the copper and oxygen positions and the center of symmetry of the dimer was calculated. The observed regions of high electron

TABLE 1. FINAL POSITIONAL AND THERMAL PARAMETERS FOR $[Cu(3\text{-PrO}\cdot Sal)]_2$

Atom	X	Y	Z	B, Å
Cu	0.0675(2)	0.0935(3)	0.4233(2)	2.81(4)
O1	0.0875(12)	−0.0758(14)	0.4813(11)	3.06(24)
O2	0.1989(14)	0.0680(15)	0.3106(12)	3.68(27)
N	0.0411(13)	0.2657(17)	0.3898(12)	2.25(26)
C1	0.2687(16)	0.1574(20)	0.2599(15)	2.18(30)
C2	0.2414(16)	0.2853(20)	0.2691(15)	2.31(31)
C3	0.3162(20)	0.3702(22)	0.2055(17)	3.16(36)
C4	0.4167(20)	0.3349(23)	0.1364(18)	3.34(37)
C5	0.4443(18)	0.2159(20)	0.1255(16)	2.72(33)
C6	0.3719(20)	0.1172(23)	0.1818(18)	3.47(38)
C7	0.1210(20)	0.3313(24)	0.3244(18)	3.46(39)
C8	0.0759(22)	−0.3350(24)	0.5632(19)	3.94(43)
C9	0.2162(25)	−0.2551(30)	0.5766(22)	5.19(51)
C10	0.2007(17)	−0.1625(21)	0.4718(16)	2.40(31)

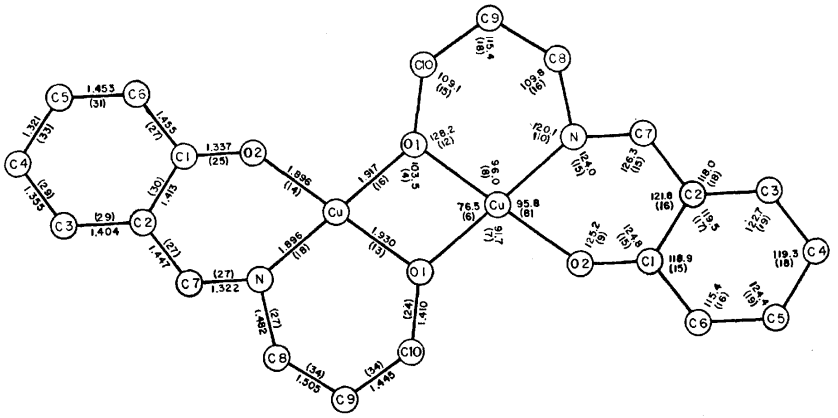

Fig. 1. Bond distances and bond angles of $[Cu(3\text{-}PrO\cdot Sal)]_2$.

density in this plane were interpreted on the basis of isomer I, and a full trial structure developed.

The structure was then refined by the block-diagonal least-squares technique with isotropic thermal parameters. After several cycles, 25 strong reflections with low Bragg angles had calculated structure factors well exceeding the observed values. These reflections were suspected of suffering from absorption or extinction effects and were removed from the refinement process which was then continued until convergence to an R value of 0.132. The R value for all observed structure factors was 0.136. An anisotropic treatment of the copper atom reduced R slightly and produced no significant shifts in the atomic coordinates. Consequently, the refinement process was considered complete. Table 1 lists the final atomic coordinates and thermal parameters.

Discussion

The bond distances and angles of the final structure are shown in Fig. 1; there are no short intermolecular contacts. The structure is that which has been proposed by Miners and Sinn on the basis of infrared studies.[3] The dimer may be considered to be approximately planar with the exception of C9 which is 0.72 Å out of the least-squared plane of the other atoms. A better description, however, is provided by the use of two planes which have a dihedral angle of 11°. The first plane is determined by the Cu, N, O1, C7, and C8 atoms and is restricted to go through the center of symmetry of the dimer at 0 0 1/2. The maximum deviation of the atoms used in the determination is 0.05 Å. Atoms C9 and C10 are out of this plane by 0.84 and 0.25 Å, respectively. The second plane is determined by atoms C1 through C6 and the phenolic oxygen, O2. The maximum deviation of those atoms from the plane is 0.02 Å. The two benzene rings are stepped with an interplanar distance of 0.50 Å.

Our results are compared in Table 2 with two previously reported copper(II) alkoxy-bridged dimer complexes with ligands prepared by the addition of acetylacetone to 2-amino-1-ethanol (EIA) and 3-amino-1-propanol (PIA).[6] It is seen that the Cu–Cu separations are similar.

The magnetic susceptibility of the series can be correlated with the Cu–O–Cu angle.[8] Relatively large Cu–Cu separations rule out direct interactions. Consequently the principal path for magnetic interaction is the mechanism of superexchange through the Cu–O–Cu bridge.[9] The values of the singlet-triplet energy level splitting, $2J$, may be calculated by using the Bleaney-Bowers equation for exchanged-coupled copper(II) dimers. With $g=2.10$ and $N\alpha=6\times10^{-5}$, the resulting values are listed in Table 2. The value of $2J$ for $[Cu(PIA)]_2$ is based only on the room temperature magnetic susceptibility. $[Cu(EIA)]_4$ is a tetramer and is considered magnetically normal. The values of $2J$ show the same trend as previously reported,[8] *i.e.*, an increasing negative $2J$ with increasing Cu–O–Cu bond angle.

Table 2. Magnetic and structural properties of alkoxy-bridged copper(II) dimers

Compound	Cu–Cu distance, Å	Cu–O–Cu angle	$2J$, cm^{-1}
$[Cu(EIA)]_4$[a]	3.006(8)	97.8(8)	0
$[Cu(3\text{-}PrO\cdot Sal)]_2$[b]	3.021(4)	103.5(4)	− 890[c]
$[Cu(PIA)]_2$[a]	3.026(6)	106.4(6)	−1100[d]

a) Ref. 6. b) Present authors. c) Magnetic susceptibility measurement from Ref. 7. d) Magnetic susceptibility measurement from Ref. 6.

References

1) S. Yamada, Y. Kuge, and K. Yamanouchi, *Inorg. Chim. Acta*, **1**, 139 (1967).

2) M. Kato, Y. Muto, H. B. Jonassen, K. Imai, and A. Harano, This Bulletin, **41**, 1864 (1968).

3) J. O. Miners and E. Sinn, *ibid.*, **46**, 1457 (1973). Additional references concerning bridged structures can be found here.

4) Copper analysis performed in this laboratory. Carbon, hydrogen, and nitrogen analysis performed by Galbraith Laboratories, Knoxville, Tenn.

5) Numbers in paretheses here and elsewhere are estimated standard deviations in units of the last digit.

6) J. A. Bertrand and J. A. Kelley, *Inorg. Chim. Acta*, **4**, 203 (1970).

7) K. V. Fischer, M. S. Thesis, Dept. of Chemistry, Providence College, Providence, R. I. (1972).

8) D. L. Lewis, W. E. Hatfield, and D. J. Hodgson, *Inorg. Chem.*, **11**, 2216 (1972).

9) J. B. Goodenough, "Magnetism and the Chemical Bond", Interscience, New York, N.Y. (1963), p. 180 ff.

BULLETIN OF THE CHEMICAL SOCIETY OF JAPAN, VOL. 47, 2323—2324 (1974)

The Mechanism of the Reduction of Tosylhydrazones with B_2H_6 and with $NaBH_4$ in Aprotic Solvents

S. CACCHI, L. CAGLIOTI, and G. PAOLUCCI
Istituto Chimica Organica, Via Castro Laurenziano 9, Roma, Italy

(Received May 4, 1973)

Synopsis. Cyclohexanone tosylhydrazone was reduced with $NaBH_4$ and B_2H_6 in aprotic solvents; results indicate that the reduction affords cyclohexyl-tosylhydrazine or an equivalent organometallic adduct confirming the mechanism previously proposed by us in the case of $NaBH_4$ in protic solvents.

The reduction of tosylhydrazones of aldehydes and ketones with reducing hydrides such as B_2H_6, $LiAlH_4$ and $NaBH_4$[1] constitutes an efficient method for conversion of carbonyls to CH_2 under mild conditions. The reactions can be carried out in either protic ($NaBH_4$)[2,3] or aprotic solvents ($NaBH_4$, B_2H_6, and $LiAlH_4$).[2,4,5]

As far as the mechanism of the reaction is concerned, we have demonstrated[6] that in protic solvents the treatment of tosylhydrazones with $NaBH_4$ leads to tosylhydrazines followed by subsequent thermal decomposition to TsH, N_2 and Alkanes.

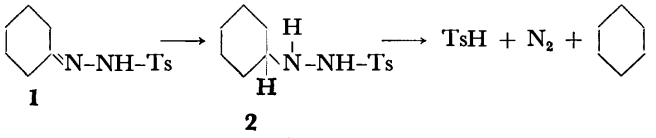

1 2

In aprotic solvents, it has been shown [4,8] that the reaction of tosylhydrazones with $LiAlH_4$ and B_2H_6 proceeds in two steps: reduction to an intermediate compound followed by decomposition of the intermediate.

The mode of action of $LiAlH_4$ and B_2H_6 towards C=N bonds,[9] and other considerations, induced us to postulate the formation of intermediary organometallic compounds, whose oxidation level is identical to that of a substituted tosylhydrazine. With B_2H_6 as reducing agent, this conclusion is well substantiated by the observation that no hydrogen is evolved during the first step of the reaction and that the intermediate compound contains all the theoretical nitrogen. The following mechanism[10] is proposed:

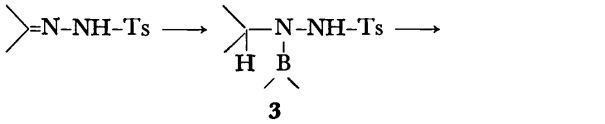

3

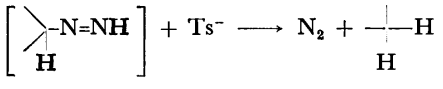

4

In order to complete our work, and to confirm our previous conclusions, this report presents results obtained upon reduction of cyclohexanone tosylhydrazone (**1**), with B_2H_6 and with $NaBH_4$ in aprotic solvents. Cyclohexanone tosylhydrazone (**1**) was chosen for study since the corresponding 1-cyclohexyl-2-tosylhydrazine (**2**) is well characterized and readily obtainable by reduction of **1** with $NaBH_4$ in protic solvents.[6]

From reduction of **1** with B_2H_6 in THF solution at room temperature, pure **2** in 55—60% yield was obtained.

These results substantiate the mechanism previously proposed for the reduction of tosylhydrazones with diborane: the reduction occurs at the C=N double bond to give an intermediate compound (**3**) which contains the fundamental skeleton of alkyltosylhydrazines.

Then, this intermediate decompose to alkanes *via* an unstable[7] alkyl diimide.

Compound **1** has been submitted to reduction with $NaBH_4$ in different aprotic solvents: ether–tetrahydrofuran (6: 1), 1,2-dimethoxyethane, diglyme and the course of the reaction was examined by thin layer chromatography. Compound **2** was isolated after reduction of **1** in ether–tetrahydrofuran (10—15%), 1,2-dimethoxyethane (50—55%) and diglyme (70—75%). The low yield in ether–tetrahydrofuran apparently results from the slow reduction rate in this solvent which allows decomposition of the intermediate (**2**).

The above results indicate that the reduction of **1** in aprotic solvent affords **2**, or an equivalent organometallic adduct that leads to the formation of **2** when treated with water or when subjected to thin layer chromatography.

However, when the action of the reducing agent is complete (excess hydride is neutralized by addition of acetone) the fundamental skeleton of **2** is present in the molecule. Thus the results obtained with B_2H_6 and $NaBH_4$ in aprotic solvents confirm our previous conclusions and are analogous to those observed with $NaBH_4$ in protic solvents.

Finally, it is noteworthy that the reduction of tosylhydrazones, at least with B_2H_6, and $NaBH_4$ in protic and aprotic solvents, leads to the formation of a substituted tosylhydrazines (or equivalent organometallic adducts (**3**)) as the first product. Subsequent elimination of Ts^- leads to the formation of an alkyl diimide (**4**), which decomposes rapidly to N_2 and alkane. One of the two hydrogens of the resulting CH_2 takes its origin from the reducing hydride, the second one from the NH originally present in the tosylhydrazone (B_2H_6 and $NaBH_4$) or from water added during the working up of the reaction mixture ($LiAlH_4$).

The experimental results reported by Djerassi and coworkers[11] are in perfect agreement with the mechanism proposed by us. With regard to the reaction pathway of tosylhydrazones with $NaBH_4$, a different mechanism has been suggested.[12] This mechanism is

in contrast with our experimental data and with our conclusions.

Experimental

1-Cyclohexyl-2-tosylhydrazine from Reduction of Cyclohexanone Tosylhydrazone with B_2H_6. A solution of compound **1** (1 g, 3.75 mmol) in diglyme (20 ml) was treated at room temperature with excess of B_2H_6 (5.5 mmol) in THF (5 ml). After 15 min, the mixture was poured into a large excess of water and the resulting precipitate was filtered. Compound **2** (850 mg) was obtained, mixed with variable amounts of boron-containing compounds. This material was treated three-four times with aqueous methanol in the cold and passed through a column of Kieselgel (10-fold) in CH_2Cl_2 solution to obtain pure **2** (55—60%) identified by comparison with an authentic sample.[6]

1-Cyclohexyl-2-tosylhydrazine from Reduction of Cyclohexanone Tosylhydrazone with $NaBH_4$. To a solution of **1** (1 g, 3.75 mmol) in diglyme (20 ml), 300 mg (7.94 mmol) of $NaBH_4$ were added and the solution was maintained at room temperature for 10 min. Acetone (20 ml) was added and then (30 s) H_2O (200 ml). The resulting precipitate of crude **2** (810 mg) was recrystallized from CH_2Cl_2–hexane to give **2** in 70—75% yield.

In a parallel experiment, 1 g of **1** in diglyme (20 ml) and 300 mg of $NaBH_4$ were mixed, and in a few seconds, acetone (20 ml) and H_2O (200 ml) were added to the solution. No **2** was obtained. When 1,2-dimethoxyethane was used as solvent, the reaction time was prolonged to 20 min in order to obtain a good yield.

We wish to thank C.N.R. for financial support (Contract N°72.00048.03).

References

1) The reaction can be performed also with another modified borohydride: see R. O. Hutchins, B. E. Maryanoff, and C. A. Milewski, *J. Amer. Chem. Soc.*, **93**, 1793 (1971).

2) L. Caglioti and P. Grasselli, *Chem. Ind.* (London), **1964**, 153.

3) A typical experiment has been described: see L. Caglioti, "Organic Syntheses," Vol. 52, p. 122 (1972).

4) L. Caglioti and P. Grasselli, *Chim. Ind.* (Milan), **46**, 799 (1964).

5) L. Caglioti and M. Magi, *Tetrahedron*, **19**, 1127 (1963).

6) L. Caglioti and P. Grasselli, *Chim. Ind.* (Milan), **46**, 1492 (1964).

7) D. J. Cram and J. S. Bradshaw, *J. Amer. Chem. Soc.*, **85**, 1108 (1963); E. M. Kosower, H. C. Pih-Kuei, and T. Tsuji, *ibid.*, **91**, 2325 (1969).

8) L. Caglioti, *Ric. Sci.*, **34** (I), 41 (1964).

9) Both B_2H_6 and $LiAlH_4$ are reported to reduce C=N to CH–NH by hydrolysis of intermediate of the type CH–N(–B)– and analogous organoaluminium compounds: H. Feuer and B. Vincet, *J. Amer. Chem. Soc.*, **84**, 3771 (1962); H. C. Brown and C. P. Garg, *ibid.*, **86**, 1085 (1964); R. F. Nystrom and W. G. Brown, *ibid.*, **70**, 3738 (1948); J. B. Billman and K. W. Tai, *J. Org. Chem.*, **23**, 537 (1958); H. C. Brown and B. S. Subba Rao, *J. Amer. Chem. Soc.*, **82**, 681 (1960); M. F. Hawthorne, *Tetrahedron*, **17**, 117 (1962); S. Also and N. G. Gaylord, "Reduction with Complex Metal Hydrides," Interscience Publisher, New York, (1956).

10) For a summary paper of previous work: L. Caglioti, *Tetrahedron*, **22**, 487 (1966).

11) M. Fisher, Z. Pelah, D. H. Williams, and C. Djerassi, *Chem. Ber.*, **98**, 3236 (1965).

12) J. Fried and J. A. Edwards, "Organic Reactions in Steroid Chemistry," Vol. 1, Van Nostrand Reinhold Company (1972), p. 176.

BULLETIN OF THE CHEMICAL SOCIETY OF JAPAN, VOL. 47(9), 2325—2326 (1974)

Stereochemistry of Ionic Thiol Addition to Acetylenic Ketones

Mohamed Tawfik OMAR and Mohamed Nabih BASYOUNI

Chemistry Department, Faculty of Science, Ain Shams University, Abbassia, Cairo, Egypt

(Received September 4, 1973)

Synopsis. Piperidine-catalysed addition of thiols to benzoyl- and *p*-chlorobenzoyl-phenylacetylenes in benzene gave a mixture of (*E*)- and (*Z*)-1-aryl-3-arylthio-3-phenyl-2-propen-1-ones. However, in methanol or aqueous 1,4-dioxane only the (*Z*)-isomers were obtained. Configurational assignments to the isomers were based on NMR, UV, and IR spectroscopy.

Although the nucleophilic thiol addition to acetylenes[1-3] has been studied no reports seem to deal with such addition to acetylenic ketones. The present publication describes the nucleophilic addition of thiols to benzoyl- and *p*-chlorobenzoyl-phenylacetylenes. The work was undertaken primarily to elucidate the stereochemistry of the mono-adducts for such addition, and also to study the effect of solvents on these additions.

Piperidine-catalysed addition of *p*-bromophenyl thiol to benzoyl-Ia and *p*-chlorobenzoyl-Ib-phenylacetylenes in benzene gave a mixture of (*E*)*-1-aryl-3-*p*-bromophenylthio-3-phenyl-2-propen-1-ones IIa and IIb, and their (*Z*)*-isomers IIIa and IIIb, respectively. The ratio of the (*E*)- to the (*Z*)-isomers in both cases was about 1:3.

The structures of IIa and IIb and IIIa and IIIb were confirmed by analytical data, electronic and infrared spectra. Their configurational assignments were based primarily on electronic spectroscopy since the absorption maxima of III are shifted slightly towards the red with intensification when compared with the corresponding II isomers. This indicates that IIa and IIb have the (*E*)-configuration, whereas IIIa and IIIb have the (*Z*)-configuration. This is consistent with the *cis-trans* relationship[4] on the one hand and *cis-* and *trans-*chalcones[5] on the other. Further confirmation for these configurational assignments was gained from infrared spectroscopy. $\nu_{C=O}$ of the (*E*)-isomers II are at a relatively higher value than those of the corresponding (*Z*)-isomers III. The configurational assignments to IIa and IIIa were confirmed by studying their NMR spectra. This was based on the deshielding effect caused by a phenyl group on a *β-cis* olefinic proton relative to a *trans* proton,[6] a feature characteristic of a number of styrene derivatives.[7,8] According to our data (Table 1), no vinyl proton signal for IIIa can be observed; apparently, it is hidden in the multiplet of aromatic protons, and must acquire the (*Z*)-configuration.

Isomer IIIa was identical with the product obtained by treating *cis*-(H/Ph)-*β*-bromochalcone[9] with *p*-bromophenylthiolate at 0 °C. The authentic sample is the (*Z*)-isomer since similar reactions are known to proceed with retention of configuration.[10]

When the addition of *p*-bromophenyl thiol to Ia or Ib was conducted in methanol or aqueous 1,4-dioxan, only the (*Z*)-isomers III were obtained in a nearly quantitative yield.

The investigation was extended to include the addition of other thiols such as benzyl-, *p*-tolyl-, and phenylthiols to Ia and Ib. In the case of the two latter thiols, when the addition was conducted in benzene a mix-

TABLE 1. ACTION OF THIOLS ON Ia AND Ib

Thiol	Product	Melting point	Yield %	Formula	Found (%) C	H	S	Calcd (%) C	H	S
A	IIa	95—97	20	$C_{21}H_{15}BrSO$	63.9	3.9	8.2	63.8	3.8	8.1
	IIIa	167—169 Yellow	70 (90)	$C_{21}H_{15}BrSO$	64.0	3.8	8.0	63.8	3.8	8.1
	IIb	85—86	30	$C_{21}H_{14}BrClSO$	58.7	3.4	7.5	58.7	3.3	7.45
	IIIb	153—155 Yellow	65 (98)	$C_{21}H_{14}BrClSO$	58.8	3.3	7.5	58.7	3.3	7.45
B	IIc	70—72	20	$C_{21}H_{16}SO$	79.8	5.1	10.2	79.7	5.1	10.1
	IIIc	105—107 Yellow	70 (95)	$C_{21}H_{16}SO$	79.9	5.2	10.1	79.7	5.1	10.1
	IId	97—98	25	$C_{21}H_{15}ClSO$	71.2	4.3	9.0	71.1	4.25	9.1
	IIId	121—122 Yellow	70 (98)	$C_{21}H_{15}ClSO$	71.0	4.2	9.2	71.1	4.25	9.1
C	IIe	78—90	25	$C_{22}H_{18}SO$	80.1	5.5	9.7	80.0	5.45	9.7
	IIIe	174—176 Yellow	70 (94)	$C_{22}H_{18}SO$	79.9	5.3	9.9	80.0	5.45	9.7
	IIf	89—91	20	$C_{22}H_{17}ClSO$	72.5	4.8	9.1	72.4	4.7	8.7
	IIIf	129 Yellow	75 (96)	$C_{22}H_{17}ClSO$	72.4	4.9	9.0	72.4	4.7	8.7
D	IIIg	132—134 Yellow	80 (95)	$C_{22}H_{18}SO$	80.1	5.5	9.9	80.0	5.45	9.7
	IIIh	110 Yellow	85 (95)	$C_{22}H_{17}ClSO$	72.5	4.8	8.8	72.4	4.7	8.7

A=*p*-Bromophenyl thiol, B=Phenyl thiol, C=*p*-Tolyl thiol, D=Benzyl thiol.
Yields in parentheses are those obtained in methanol or aqueous 1,4-dioxan.

* The nomenclature of *cis/trans* isomers used herein follows the IUPAC 1968 Tentative Rules, Section E, Fundamental Stereochemistry, *J. Org. Chem.*, **35**, 2849 (1970).

Table 2. Spectral data for compounds II and III

Compound	Electronic spectra λ_{max} (nm)	ε_{max}	λ_{max} (nm)	ε_{max}	λ_{max} (nm)	ε_{max}	Infrared spectra $\nu_{C=O}$ (cm^{-1})
IIa[a]	210	17925	230	16595	332	12945	1645
			264	12445			
IIb	208	16460	250	22790	332	12200	1647
IIc	212	18325	256	13845	330	13435	1645
IId	210	17720	264	24285	335	13280	1643
IIe	220	22060	257	15860	332	16620	1645
IIf	220	18955	263	10660	336	15660	1645
IIIa[b]	210	20220	224	18200	334	17860	1620
			266	14490			
IIIb	210	18800	266	14950	336	17895	1620
IIIc	212	18930	259	14185	335	19445	1620
IIId	212	18540	265	14345	338	19590	1622
IIIe	210	23880	258	17550	335	22430	1620
IIIf	210	19250	263	13755	339	18915	1620
IIIg	212	19320	258	12660	340	18015	1620
IIIh	211	17640	264	12050	336	17895	1620

a) $\tau(CDCl_3)$ 3.58 (1H, singlet), 2.2—2.8 (14H, multiplet).
b) $\tau(CDCl_3)$ 1.8—2.9 (15H, multiplet)

ture of (*E*)- and (*Z*)-isomers IIc—f and IIIc—f, respectively, was obtained; benzyl thiol, however, yielded only the (*Z*)-isomers IIIg and IIIh with either of the two ketones. In methanol or aqueous 1,4-dioxan, only the (*Z*)-isomers III were obtained in a nearly quantitative yield.

The structures of IIb—f and IIIb—h were confirmed by analytical data, electronic and infrared spectra. Their stereochemical configurations were established by analogy of their electronic spectra with those of IIa and IIIa, respectively. Furthermore, $\nu_{C=O}$ of the (*E*)-isomers are of a higher frequency than those of the (*Z*)-isomers.

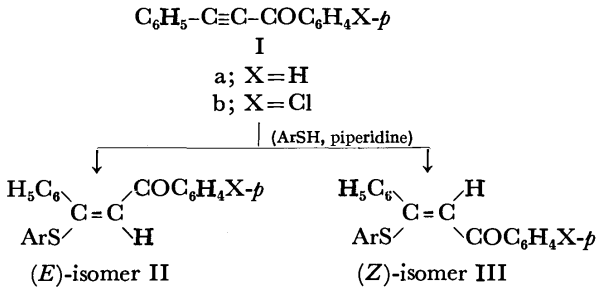

a; Ar=*p*-bromophenyl, X=H
b; Ar=*p*-bromophenyl, X=Cl
c; Ar=phenyl, X=H
d; Ar=phenyl, X=Cl
e; Ar=*p*-tolyl, X=H
f; Ar=*p*-tolyl, X=Cl
g; Ar=benzyl, X=H
h; Ar=benzyl, X=Cl

Experimental

All melting points are not corrected. Infrared and electronic spectra were measured on a Unicam SP 1200 spectrophotometer (KBr discs) and Beckmann DK 1 spectrophotometer (in methanol), respectively. NMR spectra (in $CDCl_2$) were determined on a Varian T 60 instrument using TMS as an internal reference. Light petroleum refers to the fraction of bp 60—80 °C, unless otherwise stated.

(E)-*IIa—f and* (Z)-*IIIa—h 1-Aryl-3-arylthio-3-phenyl-2-propen-1-ones.* To a solution of the ketone (0.004 mol) and phenyl-, *p*-tolyl-, *p*-bromophenyl, or benzyl-thiol (0.004 mol) in benzene (5 ml) was added two drops of piperidine and the solution was allowed to stand at room temperature overnight. Crystallization of the filtered solid products from benzene-light petroleum gave the (Z)-*Title compounds.* Evaporation of the mother-liquors at room temperature gave a solid residue which was fractionally crystallized from the same solvent to give an additional amount of the (*Z*)-isomers besides the (*E*)-*Title compounds.*

When methanol was used as a solvent, a quantitative yield of the (*Z*)-isomers was obtained immediately. However, in the case of aqueous 1,4-dioxan they were obtained after being left to stand overnight. The results are shown in Table 1.

(Z)-*IIIa.* To a cold solution (0 °C) of *cis*-(H/Ph)-*β*-bromo-chalcone[9] (0.5 g) in ethanol (10 ml) was added dropwise an alcoholic solution of sodium *p*-bromophenyl thiolate (0.4 g). After 1 hr at 0 °C the precipitated product was filtered off and crystallized from benzene–light petroleum to give (Z)-*3-p-bromophenylthio-1,3-diphenyl-2-propen-1-one* IIIa in yellow needles, mp 167—169 °C. Found: C, 63.9; H, 3.6; S, 8.2%. Calcd for $C_{21}H_{15}BrSO$: C, 63.8; H, 3.8; S, 8.1%.

References

1) J. Reppe and co-workers, *Ann.* **601**, 111 (1956).
2) W. E. Truce "Organic Sulphur Compounds," Vol. I, Karasch, ed. Pergamon Press, New York, N. Y. (1961), Chapter 12, p. 113.
3) W. E. Truce and D. L. Goldhamer, *J. Amer. Chem. Soc.*, **81**, 5795 (1959).
4) F. A. Miller in H. Gilman "Organic Chemistry," Vol. III, John Wiley & Sons, Inc., New York, N. Y. (1953), Chapter 2, p. 168.
5) W. BruceBlack and R. E. Lutz, *J. Amer. Chem. Soc.*, **77**, 5134 (1955).
6) C. N. Bonwell and N. Sheppard, *Mol. Phys.*, **3**, 351 (1960); L. M. Jackman and R. H. Wiley, *J. Chem. Soc.*, **1960**, 2881.
7) G. H. Schmid and M. Heinola, *J. Amer. Chem. Soc.*, **90**, 3466 (1968).
8) R. C. Fahey and C. Shubert, *ibid.*, **87**, 5172 (1965).
9) E. Pergmann, *J. Chem. Soc.*, **1936**, 402.
10) D. E. Jones, R. O. Morris, C. A. Vernon, and R. F. M. White, *ibid.*, **1960**, 2349; E. Angeletti and F. Montanari, *Boll. Sci. Fac. Chim. Ind. Bologna*, **16**, 140 (1958).

BULLETIN OF THE CHEMICAL SOCIETY OF JAPAN, VOL. 47 (9), 2327—2328 (1974)

Reaction of Methylcyclopentane and *n*-Hexane over Evaporated Platinum Film Catalysts

J. R. ANDERSON* and Kin'ya SHIMOMURA**
School of Physical Sciences, Flinders University, Adelaide, Australia

(Received June 8, 1973)

Synopsis. In the reaction of *n*-hexane and methylcyclopentane over polycrystalline platinum films evaporated in a ultrahigh vacuum condition, the initial distribution of reaction products varied with the reaction temperature and the hydrogen/hydrocarbon ratio. The effect of the reaction conditions was interpreted as depending on the possible reaction mechanisms cited.

Since hydrogenolysis of saturated hydrocarbons accompanied by skeletal isomerization over evaporated platinum films was first reported by Anderson and his collaborators, extensive studies have shown the reaction to involve a simple C–C bond shift or the use of an adsorbed carbocyclic intermediate.[1]

We have carried out the reaction of methylcyclopentane and *n*-hexane over unoriented platinum films evaporated in a ultrahigh vacuum in order to study the effect of the reaction conditions on the initial distribution of C_6 reaction products.

From methylcyclopentane, two classes of C_6 reaction products were obtained: (1) 2- and 3-methylpentane and *n*-hexane, (2) C_6 cyclic products (cyclohexane and benzene). The proportion of C_6 cyclic products decreased with increasing hydrogen/methylcyclopentane ratio, while this also caused the proportion of the methylpentanes to increase. Changing the reaction temperature from 240 to 310 °C caused a decrease in the proportion of the methylpentanes and an increase in that of *n*-hexane.

The possible existence of a diadsorbed σ-complex and an adsorbed π-complex (allyl type) in the reaction of saturated hydrocarbons has been suggested mechanistically.[2]

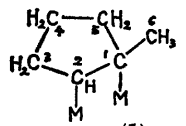

(1)

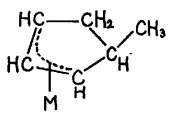

(2)

These intermediates in the hydrogenolysis of methylcyclopentane were also shown to occur over Al_2O_3-supported platinum catalysts.[3] In the present case, at a higher hydrogen ratio the probability of formation of (2) could be favoured since (2) requires only one free metal site, whereas (1) requires two sites and their geometrical distributions suitable for the structure and orientation of the methylcyclopentane molecule to be adsorbed in the positions C_1–C_2 and C_5–C_1 for *n*-hexane formation, on the surface covered predominantly with hydrogen.

The hydrogenolytic ring opening modes including diadsorbed species in the positions C_2–C_3, C_4–C_5, and C_3–C_4 for the formation of 2-methylpentane and 3-methylpentane, which might be compatible with the occurrence of (2), could also be taken into consideration in conjunction with the hydrogen/methylcyclopentane ratio. It has been proposed that the direction of hydrogenolysis of methylcyclopentane is determined by the correlation between the electron density distribution in the hydrocarbon molecule and the electron affinity of the metal atom or ion.[4] Hydrogen, chemisorbed over platinum, could exist in two forms—M^+–H^- and M^-–H_2^+ on the surface and an increased hydrogen coverage favours the proportion of hydrogen chemisorbed in the form of H_2^+.[5] This tendency could cause a decrease in the electron acceptability of platinum to increase the proportion of adsorption occurring at the positions C_2–C_3, C_4–C_5, and C_3–C_4 in conformity with the higher negative charge distribution in the methylcyclopentane molecule. However, this reaction mode does not appear dominant because the above-mentioned correlation between the electron distribution among these carbon atoms and the electronegativity of platinum is not reflected in the experimental result where the ratio of 2-methylpentane/3-methylpentane produced remains almost constant with changing ratio of hydrogen.

A possible mode of aromatization of methylcyclopentane which might alternatively occur has been presented.[6]

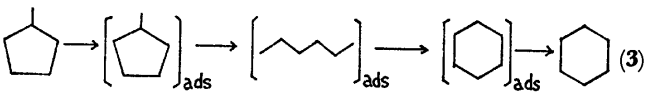

(3)

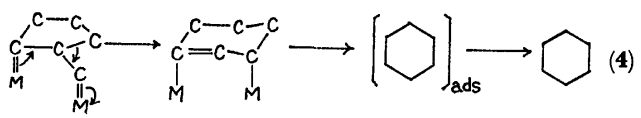

(4)

These mechanisms could probably take place in parallel with the formation of (1) and (2) for ring opening. The fact that at a higher hydrogen ratio the proportion of *n*-hexane and C_6 cyclic products showed a concurrent decrease suggests less preferential occurrence of (3) than (4), in which the formation of 1,3-diadsorbed intermediate would be suppressed at a higher hydrogen coverage on the surface to decrease ring enlargement by a bond-shift process *via* this intermediate.

Higher reaction temperatures apparently favour the formation of a diadsorbed σ-complex to produce *n*-hexane probably by reducing the covering effect of adsorbed hydrogen.

* Present address: CSIRO., Division of Tribophysics, University of Melbourne, Parkville, Victoria, Australia 3052.
** Present address: 6th Division, National Chemical Laboratory for Industry, 2-19-19, Mita, Meguro-ku, Tokyo 153.

Table 1. Effects of reaction temperature and hydrogen/reactant ratio on the initial product distributions

Reactant	Reaction temperature (°C)	Hydrogen/ reactant ratio	Total conversion (%)	Lower molecular products (%)[a]				C_6 products (%)[a]			
				C_1—C_4	*i*-P	*n*-P	Cp	2-&3-Mp	Mcp	*n*-H	C_6 cyclics
n-Hexane	275	7/1	2.50	1.6	trace	5.0	0.8	10.1	65.2	—	17.3
	275	3/1	0.61	1.9	trace	8.1	2.4	18.6	33.2	—	35.8
	275	1/1	0.17	17.8	trace	29.3	9.2	23.8	trace	—	19.7
	240	7/1	0.90	5.5	trace	10.4	1.1	34.3	36.2	—	12.4
	275	7/1	2.50	1.6	trace	5.0	0.8	10.1	65.2	—	17.3
	310	7/1	3.35	11.8	0.3	13.9	3.5	16.4	20.3	—	33.8
Methylcyclopentane	275	7/1	1.11[b]	1.9	0.4	1.0	2.4	74.7	—	19.5	trace
	275	3/1	0.50	trace	trace	trace	1.5	49.8	—	24.8	22.5
	275	1/1	0.31	2.0	0.6	1.0	2.7	22.4	—	33.1	38.8
	240	7/1	1.49	2.3	0.3	0.4	trace	77.6	—	19.4	trace
	275	7/1	1.11[b]	1.9	0.4	1.0	2.4	74.7	—	19.5	trace
	310	7/1	1.69	6.7	0.6	1.9	trace	54.2	—	34.2	2.5

a) *i*-P, *n*-P: isopentanes, *n*-pentane, Cp: cyclopentane, 2- and 3-Mp: 2:-methylpentane plus 3-methylpentane, Mcp: methylcyclopentane, *n*-H: *n*-hexane, C_6 cyclics: cyclohexane plus benzene.
b) Reaction time: 35 min.

From *n*-hexane, three classes of C_6 products were obtained: (1) 2- and 3-methylpentane, (2) methylcyclopentane, (3) C_6 cyclic products. The proportion of methylcyclopentane increased with an increasing ratio of hydrogen/*n*-hexane, while this also caused the proportion of the methylpentanes to decrease. Increasing reaction temperature in the range 240—310 °C caused the proportion of C_6 cyclic products to increase and the proportion of methylpentanes and methylcyclopentane to decrease.

According to the proposed mechanism for the isomerization and dehydrocyclization of hexanes,[6] the first step of *n*-hexane could be expressed as

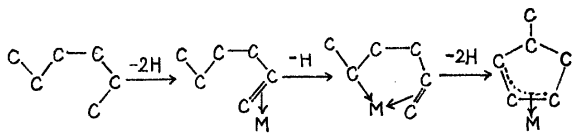

(5)

The results could be accounted for if the effect of increasing the hydrogen concentration strongly increases the rate of desorption of the π-allyl adsorbed C_5 species (*cf.* reaction (5)), and if this effect is more important than the effect of an increased hydrogen concentration on the rate of ring opening in the π-allyl adsorbed species.

It was found that the lower the hydrogen/*n*-hexane ratio in the reactant, the greater the tendency for the formation of lower molecular weight hydrogenolysis products. This was very pronounced when the reactant ratio was 1/1. This is probably because a low hydrogen/hydrocarbon ratio favours the retention of adsorbed hydrocarbon residues on the surface, so that a greater chance for carbon-carbon bond rupture occurs.

Aromatization of *n*-hexane could be explained by a proposed mechanism[7] which proceeds *via* a direct C_6 ring formation or a C_5 ring formation followed by enlargement to a C_6 ring by two-site adsorption. The experimental facts could be explained by a retardation of the third step in reaction scheme (3) with an increasing hydrogen/*n*-hexane ratio and by promotion of both the third and fourth steps in reaction scheme (3) with increasing reaction temperature.

Experimental

The reaction system is similar to the one reported previously,[8] which consists of a bakeable reaction system and a gas handling line. A platinum filament, made of 0.1 mm diameter platinum wire wound on 0.2 mm diameter tungsten wire of a hair-pin type, was pretreated for outgassing and melting, accompanied by a slight evaporation, at a heating electric current up to 7 A in a separate bell-jar system. After the filament was spot-welded in a Pyrex glass reaction vessel, evaporation was carried out within 10^{-9} Torr at 275 °C for about an hour. The reaction mixture of hydrogen, purified by a heated palladium thimble in a separate purification system, and hydrocarbon, evaporated from a liquid nitrogen-cooled trap in the gas handling line of 10^{-6} Torr, was made in a reservoir whose pressure was measured with a capsule dial gauge. The reactant and products were collected in a trap cooled with liquid nitrogen and analysed by gas chromatography.[9] The maximum extent of reaction 45 min after the introduction of a reaction mixture was about 3%.

References

1) J. R. Anderson and B. G. Baker, "Chemisorption and Reactions on Metallic Films," ed. by J. R. Anderson, Academic Press, London (1971), Vol. 2, p. 162.
2) J. J. Rooney, *J. Catal.*, **2**, 53 (1963).
3) V. V. Voronin, Kh. M. Minachev, and I. I. Levitskii, *Izv. Akad. Nauk SSSR, Ser. Khim.*, **1968**, 1753.
4) A. M. Gyul'maliev, I. I. Levitskii, Kh. M. Minachev, and I. V. Stankevich, *ibid.*, **1972**, 2475.
5) I. I. Levitskii, Kh. M. Minachev, and A. M. Boganov, *ibid.*, **1973**, 762.
6) Y. Barron, G. Maire, J. M. Muller, and F. G. Gault, *J. Catal.*, **5**, 428 (1966).
7) E. F. G. Herington and E. K. Rideal, *Proc. Roy. Soc. Ser. A*, **184**, 434 (1945).
8) J. R. Anderson and R. J. Macdonald, *J. Catal.*, **13**, 345 (1969).
9) J. R. Anderson, R. J. Macdonald, and Y. Shimoyama, *ibid.*, **20**, 147 (1971).

BULLETIN OF THE CHEMICAL SOCIETY OF JAPAN, VOL. 47 (9), 2329—2330 (1974)

Adsorption of Aniline Derivatives on Platinum Electrode in Aqueous Alkaline Solution

Yoshiharu MATSUDA,* Yukio ISHIKAWA, and Hideo TAMURA

*Department of Industrial Chemistry, Faculty of Engineering, Yamaguchi University, Tokiwadai, Ube 755
Department of Applied Chemistry, Faculty of Engineering, Osaka University, Yamadakami, Suita 565

(Received September 21, 1973)

Synopsis. In the adsorption of aniline derivatives on Pt electrode, a linear relation was observed between the chemical shift of the *m*- and *p*-amino protons and the inhibiting effect on the anodic oxidation of methanol. However, *o*-alkylanilines and chloroanilines showed deviations due to steric hindrance and strong interactions, respectively.

Earlier papers[1,2] pointed out that the adsorption phenomena in the electrode-solution interphase is possibly related to the overvoltage of the electrochemical reaction on the electrode. The influence of the structures of some organic compounds on the adsorption has also been reported[3,4] with reference to corrosion inhibitors. Cox and his co-workers[5] reported on the relationship between the NMR chemical shift of the amino protons of the aromatic inhibitors and the corrosion-inhibiting effect on iron in hydrochloric acid. Furthermore, some works[6-8] have referred to the inductive effects of the anchoring groups in organic compounds in connection with corrosion inhibition. The mechanism[3] of the adsorption of organic compounds containing nitrogen was investigated with reference to the iron in acids and with reference to the platinum in an aqueous alkaline solution.[9] Previous reports suggested a strong inhibition of chloro-substituted alkylamines[10,11] and allyl halides.[12]

The nitrogen atoms of organic amines and pyridine homologues can occupy anchoring positions on the adsorption on the platinum electrode in an aqueous alkaline solution, because of their strong electronegativity. However, the halogen atoms in organic compounds are also electronegative, and they may also be expected to occupy the anchoring positions. The purpose of this work is, then, to clarify the mechanism of the adsorption of the aniline derivatives on the platinum electrode in aqueous alkaline solution. The adsorption of the aniline derivatives on the electrode is estimated by measuring the influence on the peak current of the current-potential curves in the anodic oxidation of methanol.

Experimental

The sodium hydroxide, methanol, and aniline were guaranteed reagents by the Japanese Industrial Standards. The *m*- and *p*-chloroanilines, *o*-, *m*-, and *p*-methylanilines, *p*-ethylaniline, 2,4-dimethylaniline, *N*-methylaniline, and *N,N*-dimethylaniline were also guaranteed reagents, while the *o*-ethylaniline was an extra pure reagent made by the Wako Pure Chemical Ind. Co., Ltd. The purity of these reagents was detected by ascertaining one peak on the gas chromatograms. The carbon tetrachloride used in NMR measurements was a spectrometric-grade reagent made by the Nakarai Chemicals Co., Ltd.

The electrolytic cell and the instrument used for the potential sweep voltammetry were identical with those previously described.[13] The test electrode was a platinum plate with dimensions of $1\times1\times0.05$ cm^3; it was pretreated as in the previous work.[13] The electrolyte solution was deoxygenized by bubbling argon gas for 10 min before electrolysis.

The adsorption of aniline derivatives on the platinum electrode was estimated by measuring the influence of the peak current of methanol added to the electrolyte solution on the potential-current curves by single-sweep voltammetry.[13,14] The inhibition of the anodic oxidation of methanol as a measure of the adsorption was calculated by using Eq. (1):

Degree of the inhibiting eflect

$$= [(i_0-i)/i_0] \times 100\ (\%) \qquad (1)$$

where i_0 is the current on the electrode in the solution without the aniline derivatives and where i is that in the solution with the aniline derivatives. The NMR spectra of the aniline derivatives in carbon tetrachloride were measured on a JNM 3H-60 spectrometer (Nippon Denshi Co., Ltd.), with tetramethylsilane as the internal standard.

Results and Discussion

In the single-sweep voltammetry, the potential of the test electrode was initially maintained at −400 mV (*vs.* Hg/HgO/1 M KOH) for 15 min and was then swept anodically, at the rate of 100 mV/s, in aqueous solutions of potassium hydroxide containing aniline and methanol. The anodic current peaks were observed at about −140 mV on the current-potential curve for the aqueous solution of 1 M potassium hydroxide containing 0.5 mol/l methanol. These peaks were caused by the adsorption and electro-oxidation of methanol. This process was irreversible, and a linear relation was observed between the peak potentials and the logarithms of the potential sweep rate in the range from 0.001 to 0.4 V/s.

We also measured the influence of the concentration of aniline in 1 M aqueous potassium hydroxide containing 0.5 mol/l methanol on the degree of the inhibiting effect of the anodic oxidation of methanol, as is shown in Table 1. From these results, the proper concentration of the aniline derivatives for the test was determined to be 5×10^{-4} mol/l. The peak potential for the anodic oxidation of methanol was shifted in the anodic direction according to the addition of aniline; it was −85 mV (*vs.* Hg/HgO/1 M KOH) in an aqueous solution containing 1 M potassium hydroxide, 0.5 mol/l methanol, and 5×10^{-4} mol/l aniline. With regard to the accuracy of the inhibiting effect (percent), the standard deviation for five measurements was 1.3 percent in the solution cited above. However,

Table 1. Inhibiting effect of aniline on the anodic oxidation of methanol in aqueous potassium hydroxide. (concentration: 1 M KOH, 0.5 M CH_3OH), 25°C.

Concentration of aniline M	Inhibiting effect %
10^{-2}	95.5
5×10^{-3}	89.3
10^{-3}	85.0
5×10^{-4}	72.4
10^{-4}	64.0
5×10^{-5}	42.0
10^{-5}	33.1
5×10^{-6}	16.7
10^{-6}	8.8

these peak potentials were almost constant with the variation in the concentration of methanol in the range from 0.01 to 1 mol/l.

The mechanism of the adsorption of aniline derivatives on the platinum electrode is presumed to be related to the variation in the electron densities, and it probably has some relation with the chemical shift of the NMR spectra of these derivatives. For example, in these experiments, the chemical shifts of the amino protons of aniline and *p*-chloroaniline were observed at 6.69 and 6.61 ppm respectively. In this case, it was found from the spectra that the chemical shift of the amino protons was displayed at a field 0.08 ppm lower than that in aniline as a result of the introduction of the chloro-substituent. Similarly, the chemical shift of the amino proton of *p*-chloroaniline was in a lower magnetic field because of the strong electrophilicity of the chlorine atom. Figure 1 shows the relations between these chemical shifts of the amino protons of the aniline derivatives and the inhibiting effect on the anodic current of methanol in aqueous potassium hydroxide resulting from the adsorption of the derivatives on the electrode.

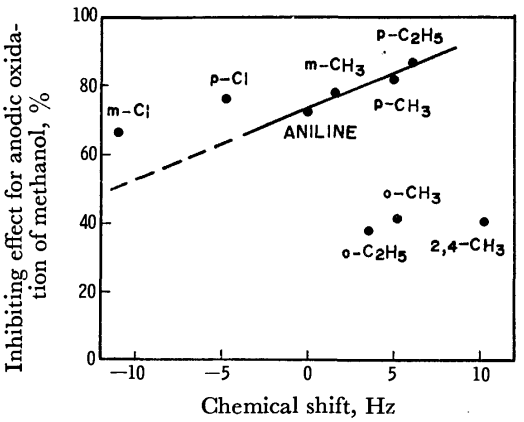

Fig. 1. Chemical shift of the amino protons of aniline derivatives plotted against the inhibition of the anodic oxidation of methanol. 25 °C.

As has been reported in previous reports,[5-9] the adsorption of the organic compounds containing nitrogen is related to the variation in the electron densities around the nitrogen atoms caused by the effects of resonance and hyperconjugation and by the inductive effect. In Fig. 1, a linear relation may be observed between the chemical shifts of the amino protons and the inhibiting effect of the anodic oxidation of methanol with regard to the *p*- and *m*-alkylanilines. However, the steric hindrance of the *o*-alkylanilines to the anchoring nitrogen atom gave large deviations from the linear relation shown in Fig. 1. In the case of the additions of 5×10^{-4} mol/l *N*-methylaniline and *N,N*-dimethylaniline, the inhibiting effects were 23.0 and 9.3% respectively. These low effects probably depend on the strong steric hindrance to nitrogen atoms in the molecules.

Furthermore, the deviations of the chloroanilines were observed in the direction opposite from that shown in Fig. 1; this phenomenon suggests some direct combination of the chlorine atom with the electrode. These results correspond with the previous experimental results [10-12] that the inhibiting effect of chlorinated alkylamines and allyl halides on the corrosion of iron is stronger than that of the corresponding alkylamines and allyl compounds.

The results suggest that there is a linear relation between the chemical shifts of the amino protons of *m*- and *p*-alkylanilines and the inhibiting effect of the aniline derivatives on the anodic oxidation of methanol on a platinum electrode in an aqueous alkaline solution, but *o*-alkylanilines and chloroanilines showed deviations from this relation. The anchoring site of these derivatives should be the nitrogen atom, but some steric hindrance was observed with the *o*-alkylanilines and some strong interactions were observed on *m*- and *p*-chloroanilines respectively.

The authors wish to express their thanks to Dr. Yoshiki Ohshiro for his helpful discussion and encouragement throughout the course of this work.

References

1) N. Isgarishev and S. Berkmann, *Z. Elektrochem.*, **28**, 40 (1923).
2) S. Glasstone, *Trans. Faraday Soc.*, **21**, 36 (1925).
3) N. Hackerman and A. C. Markides, *Ind. Eng. Chem.*, **46**, 523 (1954).
4) N. Hackerman, *Corrosion*, **18**, 332t (1962).
5) P. F. Cox, R. L. Every, and O. L. Riggs, Jr., *ibid.*, **20**, 299t (1965).
6) F. M. Donahue and K. Nobe, *J. Electrochem. Soc.*, **112**, 886 (1965).
7) H. Tamura, Y. Matsuda, and M. Iijima, *Kogyo Kagaku Zasshi*, **72**, 1077 (1969).
8) J. Vosta and J. Eliasek, *Corros. Sci.*, **11**, 223 (1971).
9) Y. Matsuda and H. Tamura, *Electrochimica Acta*, **14**, 427 (1969).
10) Y. Matsuda, Y. Kinuhata, M. Okahara, S. Komori, and H. Tamura, *Corros. Sci.*, **10**, 179 (1970).
11) H. Tamura, Y. Matsuda, Y. Kinuhata, M. Okahara, and S. Komori, *Kogyo Kagaku Zasshi*, **73**, 438 (1970).
12) S. Nakagawa and G. Hashizume, *Denki Kagaku*, **38**, 831 (1970).
13) H. Tamura, Y. Matsuda, and C. Iwakura, *Kogyo Kagaku Zasshi*, **71**, 1141 (1968).
14) K. Sasaki, I. Izumi, K. Ohashi, T. Uemura, and S. Nagaura, *Nippon Kagaku Zasshi*, **87**, 918 (1966).

BULLETIN OF THE CHEMICAL SOCIETY OF JAPAN, VOL. 47 (9), 2331—2332 (1974)

The Dissociation of Carbon Monoxide in an Induction-coupled Argon Plasma Jet

Yukio NISHIMURA,* Takeyoshi TAKENOUCHI,* and Wataru SAKAI**

*Research Institute of Industrial Science, Kyushu University, Hakozaki, Higashi-ku, Fukuoka 812

**Department of Organic Synthesis, Faculty of Engineering, Kyushu University, Hakozaki, Higashi-ku, Fukuoka 812

(Received October 2, 1973)

Synopsis. The major products were solid carbon, CO_2 and O_2. As the inside diameter of the probe decreased, the concentration of O_2 in the quenched gas increased and that of CO_2 decreased. The product distribution was independent of the argon-flow rate.

For many high-temperature chemical reactions, the distribution of the final products is determined by the quenching step. One of the techniques used to quench reacting high-temperature gas streams is placing them in contact with a cold wall[1-5] by, for example, passing them through a small-diameter, water-cooled tube. Baddour and Iwasyk have studied the reactions of elemental carbon with hydrogen above 2800 K, using this quenching method.[1] A similar method of quenching has been also applied to the synthesis of nitrogen fluorides[2] and of hydrogen cyanide.[3]

The present work, using small silica tube as a quenching apparatus, was undertaken in order to examine the effects of the operating conditions on the quenching conditions and on the distribution of the final products, when carbon monoxide was decomposed in the induction-coupled argon plasma jet at 1 atm.

Experimental

Materials. The argon used in this work was a high-purity cylinder gas (above 99.99% purity), while the carbon monoxide was commercially obtained from the Seitetsu Kagaku Co. (above 99.0% purity).

Apparatus and Procedures. The apparatus and procedures were similar to those used in previous papers.[6,7] Carbon monoxide was charged into the plasma jet counter-currently. The quenching of the decomposed products was done by means of small water-cooled silica tubes (which we shall hereafter name "probes"). The distance between the probe inlet and the induction coil was 0.5 cm. The mean temperature of the gas at the probe inlet was estimated by a method previously reported.[8] In this estimation, the hot gas was assumed to be composed of argon only, since it was difficult to ascertain precisely the composition of the hot gas at the probe inlet and since argon accounted for more than 93% of the hot gas under the conditions used in this work.

Results and Discussion

Table 1 shows the effects of the inside diameters of probes on the decomposition results and the mean temperatures of gas at the probe inlet. The major products are solid carbon, molecular oxygen, and carbon dioxide. Most of the carbonaceous species formed by the dissociation of carbon monoxide are transformed to solid carbon in the quenching step. As is clear from Table 1, the mean temperature of the gas at the probe inlet reaches 7500—8100 K; it is within the limits of experimental error independent of the inside diameter of the probe with a given outside diameter. Thermodynamic calculations of the carbon-oxygen system with a composition of C/O=1.0 at 1 atm have suggested that the partial pressures of molecular oxygen and carbon dioxide are less than 10^{-4} atm above 2500 K.[9] Therefore, it is certain that molecular oxygen and carbon dioxide are formed mainly in the quenching process. It is considered that the cooling rate in the probe with an inside diameter of 1 mm is greater than those in the other two probes.[4,8] Table 1 shows that, as the cooling rate increases, the amount of carbon dioxide formed decreases and that of molecular oxygen increases. Table 1 also shows that the conversion of carbon monoxide decreases with a lowering of cooling rate; this result suggests that the reproduction of carbon monoxide occurs in the quenching process.

Figure 1 shows the effects of the argon-flow rates on the conversions of carbon monoxide and the mean temperatures of gas at the probe inlet. Figures 2 and 3 indicate the variations in the quenched-gas compositions with the argon-flow rates. At a given power

TABLE 1. EFFECT OF PROBE INSIDE DIAMETERS ON DISSOCIATION OF CO

Ar: 1.07±0.01/min, CO: 0.044±0.003 l/min, Power input: 7.60±0.02 kW

Outside diameter of probe: 15 mm

Inside diameter (mm)	Conversion (%)[a]	Solid carbon (%)[a]	Compn. of quenched gas (vol%)			Temp.[b,c] (K)
			CO	O_2	CO_2	
1	37.2±2.8	34.9±2.8	76.9±2.2	20.3±2.3	2.8±0.5	8100
3	31.5±2.1	26.8±2.7	80.8±2.0	12.9±1.9	6.3±0.4	8000
5	32.9±2.1	28.1±2.2	80.3±1.5	14.0±1.4	5.7±0.2	7500

a) Carbon base.

b) The mean temperature of gas at the probe inlet which was estimated from the heat balance based on the temperature of the probe exit gas and the temperature rise of water which cooled the probe.[8]

c) Maximum experimental error: ±700 K.

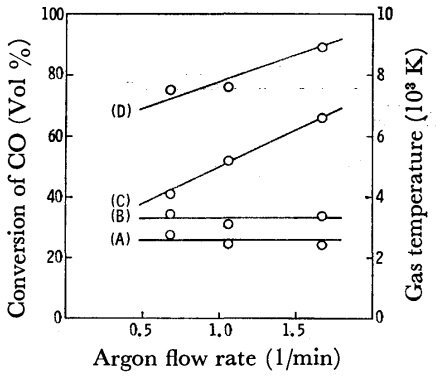

Fig. 1. Effect of argon flow rate on conversion of CO and mean temperature of gas at the probe inlet (I.D. of probe: 3 mm, O.D. of probe: 15 mm, CO: 0.044+ 0.003 l/min).
(A) and (B): Conversion of CO at 4.62±0.02 kW and 8.65±0.02 kW, respectively.
(C) and (D): Mean temperature of gas at the probe inlet at 4.62±0.02 kW and 8.65±0.02 kW, respectively.

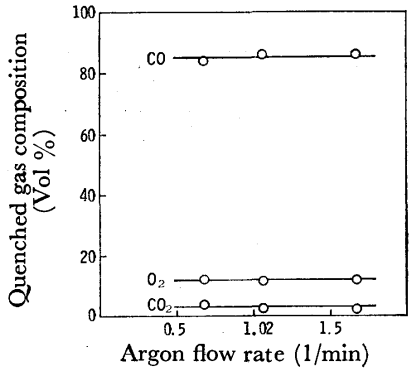

Fig. 2. Variation of quenched gas composition with argon flow rate at 4.62±0.02 kW (other conditions are the same as that of Fig. 1).

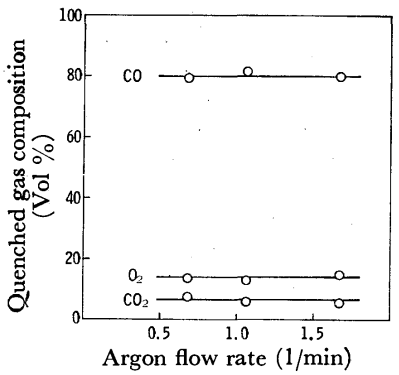

Fig. 3. Variation of quenched gas composition with argon flow rate at 8.65±0.02 kW (other conditions are the same as that of Fig. 1).

input, the mean temperature of the gas at the probe inlet becomes higher as the argon-flow rate increases, but the conversion of carbon monoxide and the composition of the quenched gas are almost independent of the argon-flow rate. It has been reported by Sundstrom and DeMichiell that the rate of quenching is greater at a higher mass flow rate in the case of the same initial gas temperature.[4] However, when the initial gas temperature is low at a given mass flow rate, it has been assumed that the decomposed products are cooled to the quenching temperature in a time shorter than when the initial gas temperature is high.[4,8] That is, when the argon-flow rate is increased, the increase in the rate of quenching is cancelled out by the rise of the initial gas temperature; apparently, then, the quenching temperature does not depend on the argon-flow rate. Therefore, it may be considered that the conversion of carbon monoxide and the composition of the quenched gas are almost independent of the argon-flow rate.

At a given argon-flow rate, as is clear from Figs. 2 and 3, both the conversion of carbon monoxide and the concentration of carbon dioxide in the quenched gas increase slightly with an increase in the power input. The mean temperature of gas at the probe inlet at 8.65 kW is higher than that at 4.62 kW. Thus, the situation in the quenching step is similar to that described above. However, one may say that, at a given argon flow rate, the dissociation of carbon monoxide at a high power input gives a quenched gas in which the concentration of carbon dioxide is higher than does the dissociation of carbon monoxide at a low power input.

References

1) R. F. Baddour and J. M. Iwasyk, *Ind. Eng. Chem. Process Des. Develop.*, **1**, 169 (1962).
2) B. R. Bronfin and R. N. Hazlett, *Ind. Eng. Chem. Fundam.*, **5**, 472 (1966).
3) B. R. Bronfin, "Advances in Chemistry Series 80," ed. by R. F. Gould, American Chemical Society Publications, Washington, D. C. (1969), p. 423.
4) D. W. Sundstrom and R. L. DeMichiell, *Ind. Eng. Chem. Process Des. Develop.*, **10**, 114 (1971).
5) P. R. Ammann and R. S. Timmins, *A.I.Ch.E.J.*, **12**, 956 (1966).
6) Y. Nishimura, K. Takeshita, and W. Sakai, *Sekiyu Gakkai Shi*, **15**, 299 (1972).
7) Y. Nishimura and W. Sakai, *High Temp. High Press.*, **5**, 183 (1973).
8) Y. Nishimura, A. Satoh, and W. Sakai, *Bull. Japan Petrol. Inst.*, **15**, 12 (1973).
9) Y. Nishimura, unpublished data.

BULLETIN OF THE CHEMICAL SOCIETY OF JAPAN, VOL. 47 (9), 2333—2334 (1974)

The Crystal Structure of Tetraiodo-*p*-benzoquinone

Hayao KOBAYASHI, Takaaki DANNO, and Ichimin SHIROTANI*

Department of Chemistry, Faculty of Science, Toho University, Narashino, Chiba 275

**The Institute for Solid State Physics, The University of Tokyo, Roppongi, Minato-ku, Tokyo 106*

(Received December 20, 1973)

Synopsis. The crystals of tetraiodo-*p*-benzoquinone-(iodanil) are monoclinic, with a space group of $P2_1/c$ and with $a=7.630(1)$, $b=5.268(1)$, $c=14.222(2)$ Å, $\beta=113.07(2)°$, and $Z=2$. The iodanil molecules are stacked to form columns along the b axis, with an interplanar distance of 3.694 Å.

The crystals of iodine molecules have been reported to be metallic under high pressure (>200 kbar).[1] On the other hand, those of tetraiodo-*p*-benzoquinone (iodanol) are still semiconductive up to 500 kbar. However, the pressure dependence of the electrical resistivity of the powder crystals of iodanil is quite large (10^{12} Ωcm at 1 bar and 10^{-1} Ωcm at 500 kbar[2]). Considering the simplicity of the molecular structure, such a large change in conductivity seems noteworthy.

The crystals of iodanil were subjected to X-ray structure analysis in order to obtain structural information.

Experimental

The iodanil was prepared by the reaction of bromanil with NaI and KI and was crystallized from an ethylacetate solution. The crystal data are; $C_6I_4O_2$, F.W. 611.7, monoclinic, $a=7.630(1)$, $b=5.268(1)$, $c=14.222(2)$ Å, $\beta=113.07(2)°$, $U=525.9$ Å^3, $D_x=3.862$ gcm^{-3}, $Z=2$, Space group $P2_1/c$. The intensities were collected on a Rigaku automated four-circle diffractometer with Mo$K\alpha$ radiation monochromated by a graphite crystal. The shape of the crystal used was parallelpiped, with dimensions of $0.17\times0.16\times0.09$ mm. The $\omega-2\theta$ scan technique was employed. Data were recorded for 1683 independent reflections up to $2\theta=60°$, of which 831 were observed.

Determination of the Structure and Discussion

The structure was solved by means of three-dimensional Patterson maps. The atomic parameters were refined by the block-diagonal least-squares method. The R-value was reduced to 0.069. The positional and thermal parameters are listed in Table 1.

TABLE 1. THE FINAL ATOMIC PARAMETERS AND THEIR ESTIMATED STANDARD DEVIATIONS ($\times10^4$)

Temperature factor=exp $[-(h^2B_{11}+k^2B_{22}+l^2B_{33}+2hkB_{12}+2hlB_{13}+2klB_{23})]$

Atom	X	Y	Z	B_{11}	B_{22}	B_{33}	B_{12}	B_{13}	B_{23}
I(1)	2962	3683	2015	240	384	50	−69	3	−15
	3	4	1	4	7	1	5	1	2
I(2)	−2155	4245	1096	264	418	63	45	54	7
	3	4	1	4	8	1	5	2	3
O	3785	−434	725	129	396	46	−1	2	−86
	21	34	12	32	79	10	42	14	23
C(1)	2052	−215	392	122	202	28	−30	0	16
	28	40	14	40	75	10	45	17	24
C(2)	1065	1576	822	163	182	34	−28	20	8
	30	40	14	45	74	11	48	18	25
C(3)	−785	1825	502	131	247	35	−10	22	10
	29	43	15	42	86	12	48	18	26

The iodanil molecules are stacked at equal intervals to form columns parallel to the b axis (Figs. 1a and 1b). The interplanar distance is 3.694 Å. Since no short contact can be observed, the intermolecular interaction between iodanil in the same column seems to be weak. The mode of overlapping is illustrated in Fig. 2. The least-squares plane of iodanil is:

$$-0.3000X-0.7060Y+0.6416Z=0.0,$$

where X, Y, and Z are coordinates (in Å) referred to the a, b, and c* crystal axes respectively. The deviations of atoms from this plane are:

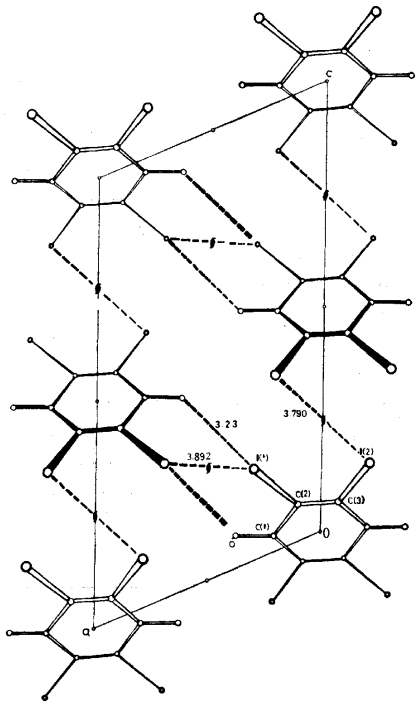

Fig. 1a. Projection of the structure along the b axis.

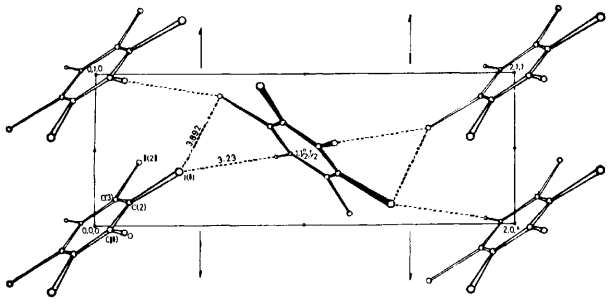

Fig. 1b. The structure viewed along [201].

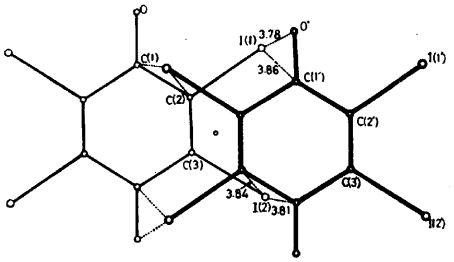

Fig. 2. Nearest-neighbour packing.

I(1), −0.019; I(2), 0.017; O, 0.025; C(1), 0.005; C(2), −0.003; C(3), 0.007 Å.

Few intermolecular short contacts are observed (Figs. 1a and 1b). The interatomic distances, which are shorter than the sum of the van der Waals radii, are as follows:

$I(1^{i})\cdots I(2^{ii})$, 3.790(3); $I(2^{i})\cdots I(1^{ii})$, 4.181(3); $I(1^{i})\cdots I(1^{iii})$, 3.892(4); $I(1^{i})\cdots O^{iii}$, 3.23(2) Å,

where the figures in parentheses are the standard deviations and where i, ii, and iii indicate the following equivalent positions:

i, x, y, z; ii, $-x, -0.5+y, 0.5-z$; iii, $1.0-x, 0.5+y, 0.5-z$.

The bond lengths and angles are given in Fig. 3; they show a strong quinoid character in iodanil. The mean bond length of C(1)–C(2) and C(1)–C(3′) is 1.50 Å (C(3′) is the atom associated with C(3) (Table 1) by a center of symmetry) and C(2)–C(3) is 1.31 Å. The corresponding values of chroranil are 1.490 and 1.344 Å respectively.[3] C(2)–I(1) (2.069 Å) is slightly longer than C(3)–I(2) (2.030 Å).

The visible absorption spectra of the vacuum-deposited thin films on quartz gave two broad maxima (330 and 380 mμ), wheras only one maximum (320 mμ) was observed in the spectra of the benzene solution (7×10^{-5} M). The infrared spectra showed that the C=O stretching frequencies in iodanil are 1665 and 1652 cm^{-1} in solution (carbon tetrachloride) and in a crystalline solid (KBr disks and Nujol mulls) respectively. For chloranil it is 1686 cm^{-1} in a chloroform solution and 1674 cm^{-1} in the crystalline state.[4] The magnitudes of the shift of the C=O stretching frequencies are almost equal to each other, while the shift is only 2 cm^{-1} in *p*-benzoquinone.[4] A crystal-structure analysis of chloranil has revealed that there is one unusually short contact between carbon and oxygen atoms (r(C···O)=2.85 Å).[4] In iodanil crystals O···I(1) is 0.32 Å shorter than the van der Waals radii (Figs. 1a and 1b), which may be noteworthy in this regard.

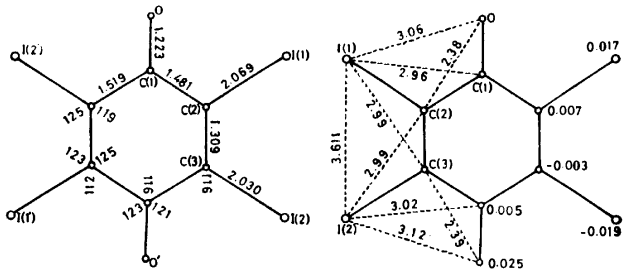

Fig. 3. Geometry of the iodanil molecule.
a) Bond lengths and angles, σ(C–I)=0.02 Å, σ(remaining bonds)=0.03 Å, σ(angle)=1.5—2.0 °.
b) Deviation from the best plane of iodanil and the values for some non-bonded distances.

The large electrical conductivity under high pressure indicates that the interatomic distances between adjacent molecules may be extremly reduced. The contact of O···I and I···I (Figs. 1 and 3) would be important for electric conduction. More information on molecular arrangement under high pressure would be desirable.

References

1) B. M. Riggleman and H. G. Drickamer, *J. Chem. Phys.*, **38**, 2721 (1962). A. S. Balchan and H. G. Drickamer, *ibid.*, **34**, 1948 (1961).
2) A. Onodera, I. Shirotani, H. Inokuchi, and N. Kawai, *Chem. Phys. Lett.*, **25**, 296 (1974).
3) K. J. Weperen and G. J. Visser, *Acta Crystallogr.*, **B28**, 338 (1972).
4) S. C. C. Shirley, G. A. Jeffrey, and T. Sakurai, *ibid.*, **15**, 661 (1962).

BULLETIN OF THE CHEMICAL SOCIETY OF JAPAN, VOL. 47 (9), 2335—2336 (1974)

The Photosensitized Isomerization of 2-Butenes by Sensitizers Adsorbed on Porous Vycor Glass

Kiyoshi OTSUKA and Akira MORIKAWA

Department of Chemical Engineering, Tokyo Institute of Technology, Ookayama, Meguro-ku, Tokyo 152

(Received December 26, 1973)

Synopsis. The triplet-triplet energy transfer from ketones adsorbed on the Vycor glass to 2-butenes was rapid enough for us to neglect the transfer to the surface when the transfer is exothermic. Different photoisomerization mechanisms were suggested for different groups of sensitizers.

The photochemical behavior of electronically-excited molecules adsorbed on the solid surface is considerably different from that in the gas or solution phase.[1]

The photosensitized *cis-trans* isomerizations of olefins have been studied in detail in a homogeneous system; these studies have led to a considerable increase in our understanding of the triplet-triplet energy transfer mechanism.[2] However, the mechanism of the photoisomerization by the electronically-excited molecules adsorbed on the solid surface has not yet been well understood.

In this brief note, we intend to report on a study of the *cis-trans* photoisomerization of 2-butenes using various kinds of adsorbed molecules as sensitizers and to discuss the effect of the adsorption on the reaction.

Experimental

Adsorbent. A porous Vycor glass plate (30×9×1 mm, Corning 7930, surface area of 144 m²/g) used as an adsorbent is transparent in the ultraviolet region down to about 200 nm. Its transparency and large surface area are advantageous for the UV-spectra measurement of the adsorbed molecules and for the kinetic investigation of the sensitized isomerization. Prior to every run of the experiments, the glass was calcined with dried air in a reactor and degassed at 650 °C *in vacuo* for 2 hr.

Materials. The compounds used as sensitizers were extra pure reagents obtained from Tokyo Kasei Kogyo Co., Ltd., or Wako Pure Chemical Industries, Ltd. The sulfur dioxide was an anhydrous product of Matheson Chemical Co.

Procedure. The photoisomerization of 2-butenes was carried out using a closed gas-circulation apparatus capable of achieving a vacuum down to 10^{-6} Torr. Vycor glass plates on which sensitizers has been adsorbed with a coverage of 0.25 at most were irradiated by means of a Toshiba H-400-P medium-pressure mercury lamp. The light was filtered by passing it through a 1 cm path of water and one of the following glass filters: (1) Corning 7—54 (transparent 230—410 nm), (2) Toshiba UV-29 (transparent >270 nm), and (3) Toshiba UV-35 (transparent >320 nm). The choice of filter depends on the sensitizers used for exciting the molecules to their lowest singlet states. The adsorption of sensitizers and the photoisomerization of 2-butenes were carried out at room temperature.

Results and Discussion

The Vycor glass plate degassed at temperatures lower than 600 °C catalyzed the thermal isomerization of butenes, while it became negligible at 650 °C.

Upon irradiation, the adsorbed acetone, methylethyl ketone, pyrazine, acetophenone, biacetyl, nitrobenzene, and sulfur dioxide sensitized the photoisomerization of 2-butenes without any double-bond migration. Without irradiation, the isomerization did not occur on the Vycor glass where one of those compounds has been adsorbed; this was checked before and after carrying out the photosensitized isomerization. The adsorbed benzene, toluene, naphthalene, phenol, aniline, and *p*-dichlorobenzene could catalyze the *cis-trans* isomerization as well as the double-bond migration appreciably. However, irradiation increased the rate of *cis-trans* isomerization only.[3]

The simplest general scheme for a sensitized *cis-trans* photoisomerization over the solid surface is given by Eqs. (1)—(7), by analogy with the homogeneous reaction,[4] where $^0S(a)$, $^1S(a)$, and $^3S(a)$ are the adsorbed

$$^0S(a) \xrightarrow{h\nu} {}^1S(a) \quad (1)$$

$$^1S(a) \longrightarrow {}^0S(a) \quad (2)$$

$$^1S(a) \longrightarrow {}^3S(a) \quad (3)$$

$$^3S(a) \xrightarrow{\text{surface}} {}^0S(a) \quad (4)$$

$$^3S(a) + t\text{-}{}^0B(a) \longrightarrow {}^0S(a) + X^*(a) \quad (5)$$

$$^3S(a) + c\text{-}{}^0B(a) \longrightarrow {}^0S(a) + X^*(a) \quad (6)$$

$$X^*(a) \longrightarrow \alpha \cdot t\text{-}{}^0B(a) + (1-\alpha) \cdot c\text{-}{}^0B(a) \quad (7)$$

sensitizers in the ground, lowest singlet, and lowest triplet states respectively, and where c-$^0B(a)$ and t-$^0B(a)$ are adsorbed *cis-* and *trans*-2-butene in the ground states respectively. $X^*(a)$ represents an unspecified common intermediate which produces *trans*-2-butene with a probability of α.

Starting from 100% of *cis*-2-butene, the initial rate of *trans* isomer formation, R_0, can be written as follows;

$$R_0 = \alpha I_0 \phi_{isc} \cdot [c\text{-}{}^0B]/(k_4/k_6 + [c\text{-}{}^0B]) \quad (8)$$

where I_0 is the light intensity absorbed by a sensitizer on the Vycor glass, and where ϕ_{isc} is the quantum yield of intersystem crossing for the sensitizer. I, the relative light intensity adsorbed by a sensitizer, was calculated by the combination of the UV-absorption spectra of the adsorbed sensitizer with the radiative intensity distribution of the arc and the transmission of the combined filters. The relative quantum yields of *cis* to *trans* isomerization (R_0/I) for the sensitizers obtained at an initial *cis*-2-butene pressure of 50 Torr are plotted against the lowest triplet energies (E_T) of the sensitizers in Fig. 1.[5]

The relative quantum yields for ketones and pyrazine[6] increased sharply at an E_T value of about 77 kcal/mol, which is very close to that of 2-butenes.[11] This shows that the triplet-triplet energy-transfer mech-

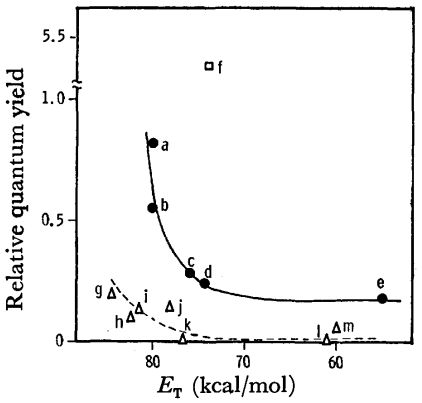

Fig. 1. The relative quantum yield as a function of the triplet energy of the sensitizers.
a, methyl-ethyl-ketone; b, acetone; c, pyrazine; d, acetophenone; e, biacetyl; f, sulfur dioxide; g, benzene; h, toluene; i, phenol; j, *p*-dichlorobenzene; k, aniline; l, naphthalene; m, nitrobenzene.

anism must be favored when the triplet state of a sensitizer has a higher energy than that of 2-butenes. In this case, X*(a) represents the adsorbed 2-butene in the triplet state.

It has been shown that the triplet-triplet energy transfer occurs upon every collision if the transfer is exothermic in the gas phase.[12] This is valid also for stilbene and piperylene in the solution phase.[4] On the solid surface, however, since adsorbed triplet molecules are always in contact with the surface, the energy dissipation to the surface, Eq. (4), may compete effectively with Eq. (5) or (6). To examine this, the pressure effect on the rates of photoisomerization was studied with acetone as a sensitizer. The relation between the initial rates of *trans*-2-butene formation and the pressures of *cis*-2-butene is shown in Fig. 2. The rates do not depend on the pressure. The coverage of adsorbed 2-butenes was confirmed to be less than unity when the pressure was lower than about 300 Torr. These results show that Reaction (6) is fast enough for us to neglect the (4) process in this case.

The fairly high isomerization yield for biacetyl, even though its triplet energy is as low as 54.9 kcal/mol,[13]

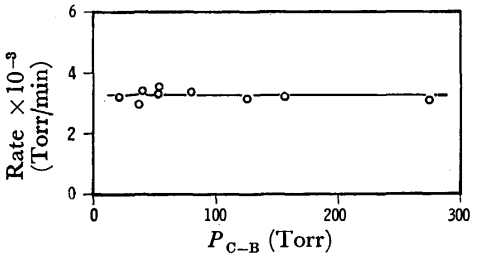

Fig. 2. The effect of pressure of *cis*-2-butene on the rate of photoisomerization.

implies that a different intermediate is produced. Presumably, the Schenck mechanism[14] predominates in this case.

Naphthalene, benzene, and its derivatives showed low quantum yields compared to those of ketones, as may be seen in Fig. 1. The correlation between the quantum yield and E_T is not so clear as that found for ketones. If the energy transfer from the excited singlet state to the surface occurs rapidly, the low isomerization yield may be attributed to the inefficient triplet formation of sensitizers.[15] On the other hand, if this process is not competitive with the intersystem crossing, it is conceivable that the low isomerization yield may be caused by a relatively faster triplet energy transfer to the surface than to 2-butenes.

The isomerization yield for sulfur dioxide was extremely high compared to those of the other compounds examined. A rough estimation of the absolute quantum yield gave about 5 for this compound. This high quantum yield suggests that the reaction proceeds *via* a chain mechanism.

Additional study is still needed before the role of adsorption can be clarified definitively for the above sensitized photoisomerization. However, we would like to stress that the mechanisms on the surface are quite different among the groups of sensitizers.

References

1) C. H. Nicholls and P. A. Leermakers, *Advan. Photochem.*, **8**, 315 (1971).

2) For a review see N. J. Turro, "Molecular Photochemistry," Benjamin, New York, (1967), p. 178.

3) Irradiation with the light of wavelength about 250 nm to the bare surface caused the isomerization to some extent, and its rate was proportional to the intensity of incident light. In the cases of benzene, toluene, phenol, and *p*-dichlorobenzene as sensitizers, the light of this wavelength region was included. However, more than 90% of incident light was absorbed by the sensitizers, and the contribution from the bare surface to the total reaction can be neglected.

4) G. S. Hammond, J. Saltiel, A. A. Lamola, N. J. Turro, J. S. Bradshaw, D. O. Cown, R. C. Counsell, V. Vogt, and C. Dalton, *J. Amer. Chem. Soc.*, **86**, 3197 (1964).

5) The contributions of thermal isomerization in the cases of naphthalene, benzene, and its derivatives were subtracted from the total reaction rates.

6) ϕ_{isc} for these compounds can be taken as unity. This is valid for acetone,[7] acetophenone,[8] biacetyl,[9] and pyrazine[10] in the liquid phase.

7) R. A. Borkman and D. R. Kearns, *J. Chem. Phys.*, **44**, 945 (1966).

8) A. A. Lamola and G. S. Hammond, *ibid.*, **43**, 2129 (1965).

9) P. S. Engel and B. M. Monroe, *Advan. Photochem.*, **8**, 302 (1971).

10) S. H. Jones and T. L. Brewer, *J. Amer. Chem. Soc.*, **94**, 6310 (1972).

11) a) J. H. Moore, Jr., *J. Phys. Chem.*, **76**, 1130 (1972); b) G. P. Semeluk and R. D. S. Stevens, *Can. J. Chem.*, **49**, 2452 (1971).

12) R. B. Cundall, Progress in Reaction Kinetics, ed. G. Porter, Vol. 2, New York, Pergamon Press, (1967), p. 166.

13) W. G. Herkstroeter, A. A. Lamola, and G. S. Hammond, *J. Amer. Chem. Soc.*, **86**, 4537 (1964).

14) a) G. O. Schenck and R. Steinmetz, *Bull. Soc. Chim. Belges*, **71**, 781 (1962); b) N. C. Yang, J. I. Cohen, and A. Shani, *J. Amer. Chem. Soc.*, **90**, 3264 (1968).

15) The intersystem crossing efficiencies of naphthalene and benzene derivatives were shown to be less than unity; benzene (0.25), toluene (0.53), and naphthalene (0.68) by K. Sandros, *Acta Chem. Scand.*, **23**, 2815 (1969).

BULLETIN OF THE CHEMICAL SOCIETY OF JAPAN, VOL. 47 (9), 2337—2338 (1974)

The Molecular Structure of Boron Triiodide as Determined by Gas Electron Diffraction

Hironobu KAKUBARI,* Shigehiro KONAKA, and Masao KIMURA**
Department of Chemistry, Faculty of Science, Hokkaido University, Sapporo 060
(Received January 21, 1974)

Synopsis. The B–I distance of BI_3 was determined to be 2.118±0.005 Å. A modified Schomaker-Stevenson rule holds for the boron-halogen bond lengths of the boron trihalides except for the fluoride. The B–F distance is much shorter than the value predicted by the rule.

Previously one of the present authors (S.K.) and co-workers reported the molecular structures of BF_3,[1] BCl_3,[2] and BBr_3[3] as determined by gas-phase electron diffraction. The present note will report on the molecular structure of BI_3 as determined by the same method, aiming at a comparison of the boron–halogen bond distances.

The sample was obtained commercially and was purified by sublimation before use. Diffraction photographs were taken with a high-temperature nozzle under the following experimental conditions: camera length, 123.9 mm; accelerating voltage, about 42 kV; beam current, 0.06 μA; exposure time, 240 s; nozzle temperature, about 60 °C. The scale factor was determined by using the diffraction pattern of carbon disulfide. The data covered the $6<s<26$ Å^{-1} range.[4] The measurement of the scattering intensities and the reduction of the molecular intensities were carried out by our usual procedure.[5] Three plates were selected for analysis. The dots in Fig. 1 typify the observed molecular intensities.

The structure was determined by the least-squares method.[5] In the analysis, a planar equilibrium structure with D_{3h} symmetry was assumed. The B–I bond distance, which contributes little to the total intensity,

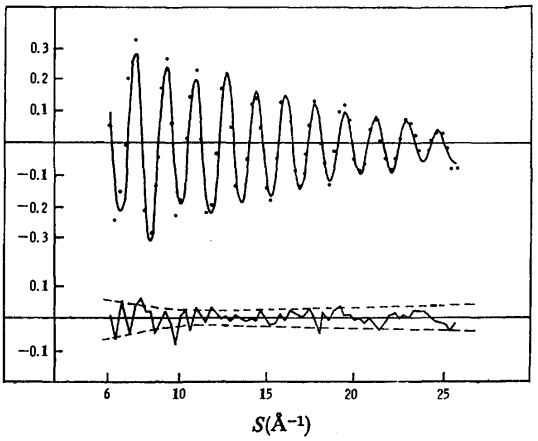

Fig. 1. The observed (dots) and theoretical (solid curve) molecular intensities and the differences. The broken line shows the estimated uncertainty in the intensity measurement.

Table 1. The structure of BI_3 (in Å units)[a]

	B–I	I···I
r_g	2.118±0.005	3.662±0.008

a) The B–I distance was calculated from the observed I···I distance. The errors represent the limits of error.

was constrained to have an r_a distance calculated from the I···I distance by taking the shrinkage effect into account.[6] The B–I mean-amplitude was fixed at the value evaluated at 60 °C, 0.059 Å, using the force filed proposed by Cyvin.[7] The Hartree-Fock and the Thomas-Fermi-Dirac elastic scattering factors for B and I respectively,[8] and the Thomas-Fermi inelastic scattering factors,[9] were used.[10] The interatomic distances thus derived are shown in Table 1. The I···I mean amplitude and the index of resolution were determined to be 0.078±0.006 Å and 0.63±0.05 respectively. The errors indicate the limits of error, which include both the random error and the systematic error due to the uncertainty in the scale factor. The corresponding theoretical intensity curve and the differences from the observed intensities are shown in Fig. 1. The observed index of resolution, 0.63, is unexpectedly small in our ordinary experimental experience,[11] and the I···I mean amplitude is smaller than the calculated value, 0.089 Å. One of the most probable causes of these discrepancies seems to be the extraneous background due to scattering from impurities produced by reactions with moisture, nozzle materials, and grease, and also by thermal decomposition during the loading and heating of the sample in the high-temperature nozzle. At a nozzle temperature of about 60 °C, HI and I_2 are thought to be the main impurities contributing to the background scattering. In order to examine the influence of these impurities on the results, the data were analyzed by assuming mixtures in various ratios of BI_3 and HI or I_2 by the use of known structures for the latter molecules.[12,13] In the cases of mixtures of BI_3 and I_2, the index of resolution increased with an increase in the amount of mixed I_2, becoming about unity in the case of a mixture of 50% I_2 in mole fraction. On the other hand, the standard deviations for the I···I distance and its mean amplitude increased approximately proportionally to the amount of mixed I_2 and became, for a 50% mixture, about three times as large as those in the case of pure BI_3. Those results indicate that no significant amount of I_2 is present in the sample gas. For mixtures of BI_3 and HI, the index of resolution increased linearly with an increase in the amount of HI, for instance, from 0.63 in the case of pure BI_3 to 0.96 in the case of a mixture containing 60% HI, while the other parameters and their standard deviations remained practically the same

* Present address: Oki Electric Industry Co., Ltd., Higashiasakawa, Hachioji, Tokyo.
** To whom correspondence should be addressed.

as the quoted results. The amount of HI mixing in the sample gas is not known. However, the injected gas can hardly be considered to contain 50% or more impurities. There seems to be another unknown background spreading over the inner scattering region. In any case, this extraneous scattering has no influence on the resulting I···I distance and its mean amplitude. The discrepancy between the experimental and calculated I···I mean amplitudes remains unexplained.

Table 2. Comparison of the observed and calculated bond lengths (in Å units).

Molecules	Obsd.[a] r_g(B−X)	Sum of covalent radii[b] r_B+r_X	$(r_B+r_X)-r_g$(B−X)	Electronegativity correction $0.06\lvert\chi_B-\chi_X\rvert$
BF_3[c]	1.313 (1)	1.53	0.22	0.12
BCl_3[d]	1.742 (4)	1.80	0.06	0.06
BBr_3[e]	1.893 (5)	1.95	0.06	0.05
BI_3[f]	2.118 (5)	2.14	0.02	0.03

a) The numbers in parentheses represent the limits of error to the last significant figures.
b) Ref. 15. c) Ref. 1. d) Ref. 2. e) Ref. 3.
f) The present study.

Table 2 compares the observed bond lengths, r_g, the sums of the covalent radii, r_B+r_X, the differences, $(r_B+r_X)-r_g$, and modified Schomaker-Stevenson correction terms proportional to the differences in electronegativity, $0.06|\chi_B-\chi_X|$, for boron trihalide molecules.[14] The observed B–X bond lengths, except for the fluoride, can be reproduced by this equation with a correction term for bond ionicity, while the B–F bond length is much shorter than the value predicted by the equation. This extra shortening of the B–F bond seems to reflect a larger amount of double-bond character in the B–F bond.[15]

The authors are grateful to Professor Takao Iijima for his helpful advice. The computation was carried out on the FACOM 230-60 of the Hokkaido University Computing Center.

References

1) K. Kuchitsu and S. Konaka, *J. Chem. Phys.*, **45**, 4342 (1966).
2) S. Konaka, Y. Murata, K. Kuchitsu, and Y. Morino, This Bulletin, **39**, 1134 (1966).
3) S. Konaka, T. Ito, and Y. Morino, *ibid.*, **39**, 1146 (1966).
4) The original intensity data were deposited with the Chemical Society of Japan (Document No. 7420).
5) S. Konaka and M. Kimura, This Bulletin, **43**, 1693 (1970).
6) $r_a(B-I)=(1/\sqrt{3})r_a(I\cdots I)+0.0035$ Å.
7) S. J. Cyvin, *Acta Chem. Scand.*, **13**, 334 (1959).
8) M. Kimura, S. Konaka, and M. Ogasawara, *J. Chem. Phys.*, **46**, 2599 (1967); M. Ogasawara, S. Konaka, and M. Kimura, *ibid.*, **50**, 1488 (1969).
9) R. F. Pohler and H. P. Hanson, *ibid.*, **42**, 2347 (1965); C, Tavard, D. Nicolas, and M. Rouault, *J. Chim. Phys.*, **64**, 540, 555 (1967).
10) In the range beyond $s=6$ Å^{-1} no appreciable difference has been found between the scattering factors of an iodine atom based upon the statistical atomic potential and the relativistic-Hartree-Fock-Slater or Hartree-Fock atomic potential; see, *e.g.*, M. Kimura, S. Konaka, K. Kashiwabara, and M. Nagashima, *Chem. Phys. Lett.*, **18**, 540 (1973).
11) The index of resolution for the patterns of CS_2 taken in the present experiment was 0.88 ± 0.02.
12) HI: N. B. Hannay and C. P. Smith, *J. Amer. Chem. Soc.*, **68**, 171 (1946); E. D. Palik, *J. Chem. Phys.*, **23**, 217 (1955).
13) I_2: T. Ukaji and K. Kuchitsu, This Bulletin, **39**, 2153 (1966).
14) The covalent radii and electronegativity values are cited in L. Pauling, "The Nature of the Chemical Bond," Cornell University Press (1960).
15) Ref. 14. See also, W. Gordy, W. V. Smith, and R. F. Trambarulo, "Microwave Spectroscopy," John Wiley & Sons, Inc. (1953).

BULLETIN OF THE CHEMICAL SOCIETY OF JAPAN, VOL. 47 (9), 2339—2340 (1974)

Simple Mechanical Model Calculations of the Elastic Constants and Normal Frequencies of the $NaNO_2$ Crystal

Akio YAMAMOTO, Yuji SHIRO,* and Hiromu MURATA

Department of Chemistry, Faculty of Science, Hiroshima University, Higashisenda-machi, Hiroshima 730
**Shinonome Branch School, Faculty of Education, Hiroshima University, Shinonome-3-chome, Hiroshima 734*

(Received February 18, 1974)

Synopsis. The optically-active vibration was analyzed for the $NaNO_2$ crystal on the basis of a simple mechanical model. Force constants which interpret fairly well both the observed elastic constants and the vibrational frequencies of the optically-active modes were determined.

In connection with the phase-transition phenomena, many investigators have taken part in the determination of the elastic constants[1] and in the spectroscopic study[2] of the crystal. In the present work, the elastic constants and the eigenfrequencies of the optically-active modes were calculated using a simple mechanical model.

The space symmetry of the sodium nitrite crystal is Im2m in the ferroelectric phase, and the cell constants are a_0=3.569 Å, b_0=5.563 Å, and c_0=5.348 Å.[3] Since two formula units are present in this crystallographic cell, the original lattice vector, **a**, has been transformed into a conventional lattice vector, $\mathbf{a}'=(\mathbf{a}+\mathbf{b}+\mathbf{c})/2$, in order to obtain the primitive unit cell in the vibrational analysis.[2a] The vibrational analysis was performed on the basis of the GF-matrix method,[4] in which vibrationally-induced dynamical effects[5] are implicitly neglected. In addition to the ordinary potential parameters of the NO_2 group, thirteen short-range interaction parameters were taken into account, as is illustrated in Fig. 1.

The elastic constants were microscopically calculated by the method established by Shiro.[6] In order to obtain the best fit, the potential parameters were

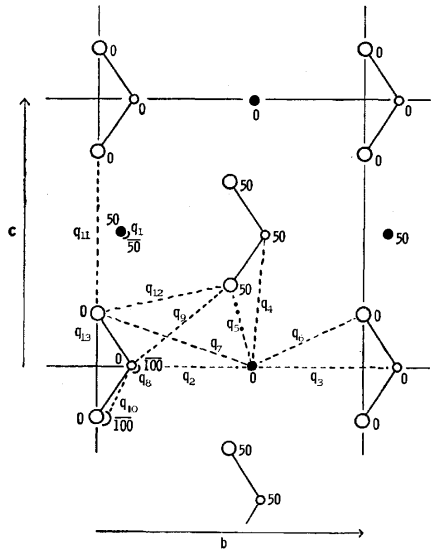

Fig. 1. Short-range interactions in $NaNO_2$ crystal. The heights of atoms are expressed in units of $100/a_0$.
●, Na; ○, N; ○, O.

Table 1. Internal coordinates and force constants in $NaNO_2$

Coord.	NO.	Distance[a]	Pair	Force	Constant[b]
R	2	1.247	N O	6.946	K
q_1	1	3.569	Na Na	0.008	f_1
q_2	1	2.579	Na N	0.041	f_2
q_3	1	2.985	Na N	0.047	f_3
q_4	4	3.236	Na N	0.035	f_4
q_5	4	2.472	Na O	0.154	f_5
q_6	2	2.534	Na O	0.210	f_6
q_7	2	3.420	Na O	0.025	f_7
q_8	1	3.569	N N	0.008	f_8
q_9	4	3.212	N O	0.019	f_9
q_{10}	4	3.781	N O	0.010	f_{10}
q_{11}	1	3.289	O O	0.023	f_{11}
q_{12}	4	3.358	O O	0.018	f_{12}
q_{13}	2	3.569	O O	0.008	f_{13}
ϕ	1	(115°)	O N O	0.567	H
			O O	2.723	F
			(R, R')	0.595	P[c]

a) Distance in Å. b) Force constant in mdny/Å.
c) Correction term.

Table 2. Observed and calculated elastic constants (10^{10} dyn/cm^2) and contribution (%) of potential terms in $NaNO_2$

	Obsd[a]	Calcd	K	f_1	f_2	f_3	f_4	f_5	f_6	f_7	f_8	f_9	f_{10}	f_{11}	f_{12}	f_{13}	H	F	p
C_{11}	30.05	39.27	0	0	28	2	0	2	14	32	0	8	0	0	13	0	0	0	0
C_{21}	12.60	10.16	1	0	−10	3	−5	57	24	−12	0	31	0	0	13	0	−1	−1	0
C_{22}	54.79	54.07	0	0	0	0	21	52	2	0	0	4	0	19	0	0	0	1	0
C_{31}	10.60	33.30	0	0	−8	2	−3	46	20	−10	0	25	0	0	29	0	−1	−1	0
C_{32}	9.30	11.25	0	0	0	0	18	71	2	0	0	6	0	0	2	0	0	1	0
C_{33}	62.37	63.03	0	5	0	0	7	43	1	0	5	3	5	0	3	10	0	0	0
C_{44}	10.73	9.62	0	0	0	0	49	10	0	0	0	1	0	0	11	0	0	0	0
C_{55}	9.93	11.59	0	0	0	0	5	1	0	0	0	35	0	0	54	0	0	0	0
C_{66}	5.53	5.51	0	0	0	0	0	8	27	2	0	37	0	0	26	0	0	0	0

a) Ref. 1.

refined by the least-squares method with reference to the observed elastic constants[1c] and the vibrational frequencies[2c] complementally.

The best set of force constants was determined to be as is shown in Table 1. The observed[1c] and calculated elastic constants are compared in Table 2. Obviously, the observed elastic constants other than the C_{31} are reproduced fairly well. The contribution (%) of the potential parameters to the calculated elastic constants is also listed in Table 2. It is difficult on the basis of this model only to explain the relatively small value of the observed C_{31}, since the C_{31} constant is found to be considerably coupled with the C_{11} and C_{21} constants.

Table 3. Observed and calculated frequencies (cm^{-1}) of sodium nitrite crystal

Sym.		Obsd[a]	Calcd	Assignment[b]
A_1	ν_{11}	1330	1328	NO str.
	ν_{12}	826	821	ONO angle def.
	ν_{13}	217	235	transl (b).
A_2	ν_{21}	117	156	rot (b).
B_1	ν_{31}	242	209	rot (c).
	ν_{32}	169	124	transl (a).
B_2	ν_{41}	1316	1316	NO str.
	ν_{42}	286	248	rot (a).
	ν_{43}	160	151	transl (c).

a) Ref. 2(c). b) str, stretching; def, deformation; transl (a), translational(along the direction parallel to the a axis); rot (a), rotational (around the *a* axis).

The vibrational modes of the crystal have the following irreducible representations: $\Gamma=3A_1+A_2+2B_1+3B_2$. The calculated eigenfrequencies and the tentative assignments are given in Table 3. The observed frequencies cited here are the ones corrected by Tsuboi *et al.*[2c] to exclude conventionally the dynamical effects.[5] The simple Urey-Bradley force field has been found to give a somewhat poor agreement with the observed frequencies in a water-type molecule; therefore, we have introduced the correction term, p, between the stretching coordinates.[7] It is shown in Table 3 that the calculated frequencies reproduce the observed ones fairly well. Further investigations will, however, be required on the basis of some elaborated models, for a rigorous treatment is essential for the satisfactory explanation of the other dynamical properties.[2e] The degrees of the contribution of the potential parameters are considered to be independent of those from the elastic constants; therefore, the resulting force constants, which were obtained with reference to both properties complementally, seem to be reliable, at least in this idealized but simple model. The force constants obtained here may become a measure of the interatomic interactions due to repulsive forces.

The calculations were carried out on the TOSBAC 3400 TOPS 14 electronic computer at the Computing Center of Hiroshima University. The authors wish to express their thanks to Mr. Masaru Ohsaku of their laboratory for his useful suggestions.

References

1) a) K. Hamano, K. Negishi, M. Marutake, and S. Nomura, *Japan. J. Appl. Phys.*, **2**, 83 (1963); b) G. Hauret and A. Gharbi, *C. R. Acad. Sci. Paris, Ser. B*, **271**, 1072 (1970); c) K. Ota, Y. Ishibashi, and Y. Takagi, *J. Phys. Soc. Japan*, **29**, 1545 (1970).

2) a) E. V. Chisler and M. Shur, *Phys. Stat. Sol.*, **17**, 163 (1966); b) M. K. Barnoski and J. M. Ballantyne, *Phys. Rev.*, **174**, 946 (1968); c) M. Tsuboi, M. Terada, and T. Kajiura, presented at the Symposium on Molecular Structure, Tokyo, October (1968); d) Y. Luspin and J. P. Chapelle, *C. R. Acad. Sci. Paris, Ser. B*, **269**, 263 (1970); e) J. Sakurai, R. A. Cowley, and G. Dolling, *J. Phys. Soc. Japan*, **28**, 1426 (1970).

3) M. I. Kay and B. C. Frazer, *Acta Crystallogr.*, **14**, 56 (1961).

4) T. Shimanouchi, M. Tsuboi, and T. Miyazawa, *J. Chem. Phys.*, **35**, 1597 (1961).

5) R. Frech and J. C. Decius, *ibid.*, **54**, 2374 (1971).

6) Y. Shiro and T. Miyazawa, This Bulletin, **44**, 2371 (1971).

7) T. Shimanouchi, *Pure Appl. Chem.*, **7**, 131 (1963).

BULLETIN OF THE CHEMICAL SOCIETY OF JAPAN, VOL. 47 (9), 2341—2342 (1974)

Mössbauer Spectroscopic Studies of Iron(II) and Iron(III) 1-Nitroso-2-naphtholate Complexes

Mitsuko TAKADA* and Hirotoshi SANO**

Department of Chemistry, Faculty of Science, Tokyo Metropolitan University, Fukazawa, Setagaya-ku, Tokyo 158

(Received May 2, 1974)

Synopsis. The anomalous Mössbauer parameters of iron(II) 1-nitroso-2-naphtholate complex are interpreted by assuming the presence of iron(III) and iron(II) complex species. Partial oxidation of iron(II) by 1-nitroso-2-naphthol is suggested.

Iron 1-nitroso-2-naphtholate complexes known in analytical chemistry are used as the dye "Naphthol Green Y".[1] However, there are not many structural studies on these complexes except for the work by Stukan *et al.*[2] on bis (1-nitroso-2-naphtholato)iron(II) by means of the Mössbauer effect. They reported that bis(1-nitroso-2-naphtholato)iron(II) shows a quadruplet in the Mössbauer spectrum. A component doublet of the spectrum has parameters similar to those for the spectrum of other planar iron complexes, while the quadrupole splitting of the second doublet is similar to that of high-spin iron(II) compounds, although the isomer shift is anomalously more negative than that of the latter. The reason for the appearance of a quadruplet has not so far been clarified.[3] Since no Mössbauer spectroscopic data have been given of tris-(1-nitroso-2-naphtholato)iron(III), we examined the Mössbauer spectroscopic character of these complexes.

Dark colored crystallites of tris(1-nitroso-2-naphtholato)iron(III) were prepared from iron(III) trichloride hexahydrate and 1-nitroso-2-naphthol both in ethanol or in acetic acid.[1] The products were identified as $Fe(C_{10}H_6NO_2)_3$ by elemental analysis. The molar magnetic susceptibility observed by the Gouy method was 2.09 ± 0.7 B.M. at room temperature, indicating low-spin ($S=1/2$) iron(III) state. Mössbauer spectra were measured against a ^{57}Co(Pt) source moving with constant acceleration at room temperature. A typical Mössbauer spectrum is shown in Fig. 1a. The isomer shift is 0.19 mm/s with respect to metallic iron, the quadrupole splitting being 2.12 mm/s at 78 K. The large quadrupole splitting suggests an octahedral structure with a peripheral configuration.

Optimum conditions for the preparation of a stoichiometric iron(II) 1-nitroso-2-naphtholate complex were studied.[4] An ethanol solution saturated with potassium 1-nitroso-2-naphtholate was prepared by adding a concentrated potassium hydroxide solution to an ethanol solution of 1-nitroso-2-naphthol. The mixture was allowed to stand for one day at room temperature. The resulting blue-green crystallites were filtered and washed with water and ethanol. All the procedures were carried out under nitrogen. Found: Fe, 8.67; C, 55.90; H, 3.53; N, 6.54%. Calcd for $KFe(C_{10}H_5NO_2)_3 2H_2O$: Fe, 8.63; C, 55.65; H, 3.43; N, 6.49%. Magnetic susceptibility measurements indicate that the compound is diamagnetic ($S=0$). A Mössbauer spectrum is shown in Fig. 1b. The isomer shift is 0.22 mm/s and the quadrupole splitting is 0.86 mm/s at 78 K. The fairly large quadrupole splitting suggests an octahedral structure with peripheral configuration as in tris(1-nitroso-2-naphtholato)iron(III).

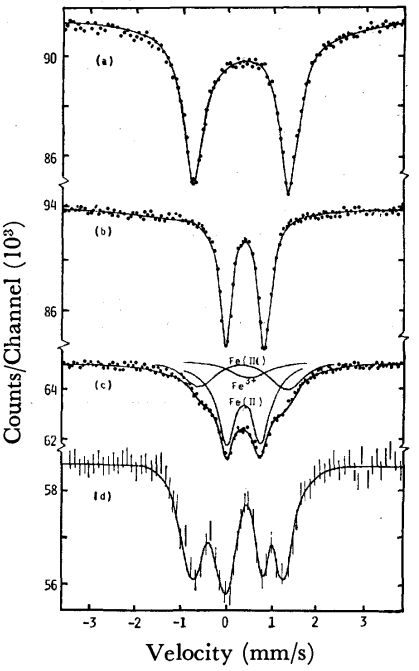

Fig. 1. Mössbauer spectra at 78 K of (a) tris(1-nitroso-2-naphtholato)iron(III), (b) potassium tris(1-nitroso-2-naphtholato)ferrate(II), (c) bis(1-nitroso-2-naphtholato)iron [containing iron(II) and iron(III) species]. (d) Spectrum of bis(1-nitroso-2-naphtholato)iron at 80 K, reproduced from Ref. 4.

The low values of isomer shift found in the tris-(1-nitroso-2-naphtholato)iron(III) and potassium tris(1-nitroso-2-naphtholato)ferrate(II) indicate the low-spin iron(III) and iron(II) states, respectively, which are consistent with the magnetic measurements. The results could be ascribed to the back-donation of non-bonding $3d_{t2g}$ electrons of iron to the π^* orbitals of the ligands through nitrogen and oxygen atoms.

Dark green crystallites were obtained by mixing iron(II) dichloride tetrahydrate and 1-nitroso-2-naphthol in a 1:2 mole ratio in ethanol under nitrogen. The elemental analysis gives a reproducible result, but always higher iron content as compared with the calculated value for $Fe(C_{10}H_6NO_2)_2H_2O$ and lower

* Present address: Japanese Patent Office, Kasumigaseki, Chiyoda-ku, Tokyo.

** To whom all correspondence should be addressed.

values for carbon and hydrogen. The apparent molar susceptibility was 3.70 B.M. at room temperature. The Mössbauer spectrum (Fig. 1c) could be decomposed into two doublets and a small singlet assigned to tris(1-nitroso-2-naphtholato)ferrate(II), tris(1-nitroso-2-naphtholato)iron(III), and high-spin iron(III) species, respectively. The results suggest that some iron(II) species are oxidized to iron(III) species probably by 1-nitroso-2-naphthol, as in the reaction of this reagent with cobalt(II) species,[5] giving tris(1-nitroso-2-naphtholato)iron(III) and some inorganic iron(III) species. The quadruplet consisting of two doublets seems similar to the spectrum reported by Stukan *et al.* in the values of isomer shift and quadrupole splitting.[2] Earlier data on some salicylaldehyde and salicylaldoxime iron(II) chelates[2,6] were found by De Vries *et al.* to be erroneous in the interpretation of Mössbauer parameters of what were believed to be pure iron(II) compounds.[7] The result on bis(1-nitroso-2-naphtholato)iron may also be interpreted by assuming oxidation of iron(II) species in the preparation of the material, since the obtained potassium tris(1-nitroso-2-naphtholato)ferrate(II) is stable in air at room temperature.

A part of this work was carried out at Ochanomizu University.

References

1) M. Ilinski and G. von Knorre, *Ber.*, **18**, 699, 2728 (1885); F. C. Mathers, *J. Amer. Chem. Soc.*, **30**, 209 (1909); G. von Knorre, *Ber.*, **20**, 283 (1887).

2) R. A. Stukan, V. I. Gol'danskii, E. F. Makarov, and E. G. Ruchadse, *Zh. Strukt. Khim.*, **8**, 239 (1965).

3) V. I. Gol'danskii and R. H. Herber (ed.), Chemical Applications of Mössbauer Spectroscopy, Academic Press, New York, 1968, p. 286.

4) H. Iimura, *Research Repts. Fac. Eng. Gifu Univ.*, **1**, 41 (1951).

5) I. M. Kolthoff and E. Jacobsen, *J. Amer. Chem. Soc.*, **79**, 3677 (1957); C. M. Callahan, W. C. Fernelius, and B. P. Block, *Anal. Chim. Acta*, **16**, 101 (1957).

6) K. Burger, L. Korecz, I. B. A. Manuaba, and P. Mag, *J. Inorg. Nucl. Chem.*, **28**, 1673 (1966).

7) J. L. K. F. De Vries, J. M. Trooster, and E. de Boer, *Chem. Commun.*, **1970**, 604.

BULLETIN OF THE CHEMICAL SOCIETY OF JAPAN, VOL. 47 (9), 2343—2344 (1974)

The Conversion Reaction of Alkali 4-Hydroxyisophthalates into Hydroxybenzoic Acids

Koki OTA

Department of Chemistry, Kyushu Institute of Technology, Tobata-ku, Kitakyushu-shi 804

(Received October 8, 1973)

Synopsis. When alkali 4-hydroxyisophthalates are heated with phenol or alkali phenolates, *p*-hydroxybenzoic acid is formed from potassium salts and salicylic acid is formed from sodium salts preferentially.

Although the Kolbe-Schmidt reaction has long been studied from the synthetic point of view, the complete elucidation of this reaction mechanism has not yet been given and 4-hydroxyisophthalic acid (4-OIP) has been regarded as an unimportant by-product, because its yield was extremely poor.

In a preceding paper,[1] though, it was reported that 4-OIP was formed in a good yield when the rearrangement of monopotassium *o*-hydroxybenzoate (SA–K) to dipotassium *p*-hydroxybenzoate (POB–K_2) was investigated in detail by means of microthermal analyses.

4-OIP may be the dominant product which holds the key to the Kolbe-Schmidt reaction scheme. Therefore, the thermal behavior of 4-OIP under various conditions was examined.

Experimental

Samples. The disodium, trisodium, dipotassium, and tripotassium 4-hydroxyisophthalates (4-OIP–Na_2, –Na_3, –K_2, and –K_3) were prepared as has been reported previously[1] from commercial 4-OIP (Tokyo Kasei Kogyo, Ltd.).

Methods. The reader should refer to the previous paper[1,2] for a description of the methods and the apparatus. When the experiment was carried out at increased pressures, a tubular resistance[3] was connected to the apparatus in order to maintain the sample vessel at 3.85 atm.

Results and Discussion

Rostron *et al.*[4] have proposed the following scheme for the reaction of 4-OIP–K_3 with potassium phenolate (PhOK),

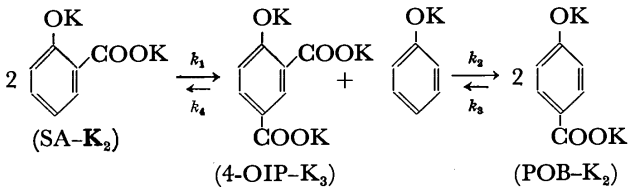

This reaction was at first re-investigated by using a mixture of 4-OIP–K_3 and PhOK (4-OIP–K_3: PhOK = 1 : 1) at 300 °C under a N_2 atmosphere. As PhOK reacts with CO_2, this reaction in a CO_2 atmosphere was not examined.

The amount of evolved gases (PhOH+CO_2) leads to a decrease in the sample; this decrease was evaluated by subtracting the product's weight from the anhydrous sample's weight, as has been described in the previous paper.[1] PhOK is fairly stable in a N_2 atmosphere, even at elevated temperatures.

Table 1. Reactions of 4-OIP–K_3 with PhOK or PhOH at 300°C[a]

Atmospheric condition	Decrement[b] (%)	Purity[c] (%)	Composition of acids (mol%)		
			POB[d]	SA[e]	4-OIP[f]
With PhOK					
N_2 stream[g]	10.9	94.1	6	0	94
N_2 stream	13.2	89.1	16	16	68
N_2 3.85 atm[g]	10.0	90.0	3	0	97
N_2 3.85 atm	14.1	91.8	16	6	78
With PhOH					
N_2 stream	3.6[h]	94.2	22	18	60
N_2 3.85 atm	2.4[h]	83.3	41	14	45
CO_2 stream	3.1[h]	95.0	23	18	59
CO_2 3.85 atm	5.0[h]	80.7	32	13	55

a) Reaction period = 10 s (Raised the temperature continuously at the rate of 10°C/min from 30°C to the fixed temperature). b) (Decrease in weight/Original weight) × 100. c) [K salts of the total acid/(The product—PhOK)] × 100. d) *p*-Hydroxybenzoic acid. e) Salicylic acid. f) 4-Hydroxyisophthalic acid. g) The sample was sealed into a small Al vessel to suppress the evolution of gases. h) (Decrease in weight/Original weight of 4-OIP–K_3) × 100.

As is shown in Table 1, a mixture is converted into POB and SA with an increase in the decrement, regardless of the variation in the N_2 pressure. The rate of conversion decreases in this order: $k_2 > k_4$. The conversion of 4-OIP–K_3 is affected more remarkably in the presence of PhOH than in the presence of PhOK, as was revealed by the previous results.

On the bases of these results, we carried out the reaction of 4-OIP–K_3 with PhOH under N_2 and CO_2 (Table 1). As expected, the conversion took place more rapidly in the presence of PhOH and the yield of POB was higher than that of SA. 4-OIP–K_3 itself was very stable upon heating in the absence of PhOK or PhOH and was more stable than 4-OIP–K_2 at 300 °C, as is shown in Table 2.

It seems that the formation of a large amount of 4-OIP conflicts with the poor yield of 4-OIP obtained from the same reaction carried out in an autoclave.[5]

This can be explained as follows: the fair amounts of both 4-OIP–K_2 and –K_3 produced are consumed in their interaction with the PhOH which is simultaneously formed and can not be removed from an autoclave. Therefore, the reaction of 4-OIP–K_2 with PhOH was examined under N_2 or CO_2 (PhOH/4-OIP–K_2 = 1.2 mol/mol). The results are shown in Table 3.

The conversion of 4-OIP–K_2 into POB and SA was

Table 2. Thermal stabilities of 4-OIP-K_2 and -K_3 at 300°C and those of 4-OIP-Na_2 and -Na_3 at 320°C[a]

Reactant	Atmospheric condition	Decrement[b] (%)	Purity[c] (%)	Composition of acids (mol%) POB[d]	SA[e]	4-OIP[f]
4-OIP-K_2	N_2 stream	13.1	86.4	38	13	49
	N_2 3.85 atm	17.5	80.4	45	8	47
	CO_2 stream	18.2	87.8	32	13	55
	CO_2 3.85atm	18.7	81.3	33	11	56
4-OIP-K_3	N_2 stream	4.6	97.1	6	6	88
	N_2 3.85 atm	2.9	96.0	8	6	86
	CO_2 stream	4.8	94.5	6	8	86
	CO_2 3.85atm	3.0	93.3	5	1	94
4-OIP-Na_2	N_2 stream	24.8	88.9	13	17	70
	N_2 3.85 atm	25.0	80.2	15	18	67
	CO_2 stream	23.7	94.3	11	20	69
	CO_2 3.85atm	21.2	86.6	9	24	67
4-OIP-Na_3	N_2 stream	3.8	92.1	11	21	68
	N_2 3.85 atm	12.6	73.4	17	19	64
	CO_2 stream	5.4	91.2	10	26	64
	CO_2 3.85atm	11.3	78.0	11	26	63

a), b), c), d), e), f), See Table 1.
Every K in Eq. c) is replaced by Na in the case of Na salts.

Table 3. Reactions of 4-OIP-K_2 with PhOK or PhOH at 300°C[a]

Atmospheric condition	Decrement[b] (%)	Purity[c] (%)	Composition of acids (mol%) POB[d]	SA[e]	4-OIP[f]
With PhOK					
N_2 stream	21.5	88.1	48	12	40
N_2 3.85 atm	21.1	96.6	52	11	37
N_2 3.85 atm[g]	24.4	72.7	44	46	10
With PhOH					
N_2 stream[g]	17.2[h]	84.3	55	7	38
N_2 3.85 atm[g]	18.6[h]	78.1	85	5	10
CO_2 stream[g]	17.7[h]	89.2	54	8	38
CO_2 3.85 atm[g]	15.8[h]	84.0	90	3	7

a), b), c), d), e), f), g), See Table 1.
h) (Decrease in weight/Original weight of 4-OIP-K_2) $\times 100$.

found to occur much more effectively in the presence of PhOH in a closed system than in the absence of PhOH. The reaction proceeded greatly and the 4-OIP-K_2 was almost completely converted into POB under increasing pressures. This suggests that a rather large quantity of PhOH remains in the reaction system and contributes to the formation of POB.

The reaction of 4-OIP-K_2 with PhOK instead of PhOH was carried out under N_2; the results are shown in Table 3. This reaction proceeded more rapidly than the reaction in the absence of PhOH (Table 2). Especially, the reaction with PhOK in a closed Al vessel resembled that with PhOH under the same conditions, but the compositions of the acids formed were different.

The thermal stabilities of 4-OIP-Na_2 and 4-OIP-Na_3 were examined at 320 °C (Table 2). 4-OIP-Na_2 was slightly more stable than 4-OIP-Na_3; this relation was the reverse of that of the corresponding potassium salts (4-OIP-K_2<4-OIP-K_3). The effects of the differences in atmosphere and pressure were hard to recognize in the conversion of both sodium salts into SA and POB.

Table 4. Reactions of both 4-OIP-Na_2 and 4-OIP-Na_3 with PhONa or PhOH at 340°C[a]

Reactant	Atmospheric condition	Decrement[b] (%)	Purity[c] (%)	Composition of acids (mol%) POB[d]	SA[e]	4-OIP[f]
4-OIP-Na_2	With PhONa[i]					
	N_2 3.85 atm[g]	24.0	85.3	9	45	46
	With PhOH[j]					
	N_2 3.85 atm[g]	21.8[h]	80.7	10	45	45
	CO_2 3.85atm[g]	20.9[h]	81.8	9	53	38
4-OIP-Na_3	With PhONa[i]					
	N_2 3.85 atm[g]	22.0	80.1	18	37	45
	With PhOH[j]					
	N_2 3.85 atm[g]	12.8[h]	68.5	12	43	45
	CO_2 3.85atm[g]	12.1[h]	75.0	10	55	35

a), b), c), d), e), f), g), h), See Table 1, and also c), h), See Tables 2 and 3 (K is replaced by Na).
i) PhONa/4-OIP-$Na_{2(3)}$ = 1.2 mol/mol. j) PhOH/4-OIP-$Na_{2(3)}$ = 1.6 mol/mol.

The results of the reaction of 4-OIP-Na_2 with PhOH or sodium phenolate (PhONa) and that of 4-OIP-Na_3 with PhOH or PhONa are shown in Table 4. As may be seen in Table 4, both 4-OIP-Na_2 and -Na_3 were markedly converted into SA in the presence of PhOH or PhONa at 340 °C under an elevated gaseous pressure.

In conclusion, the difference in the orientation between PhOK and PhONa in the Kolbe-Schmidt reaction—that is, at high temperatures PhOK and PhONa give POB and SA respectively—may be caused by the difference in the degree of conversion between 4-OIP-K_α and 4-OIP-Na_α (α=2, 3).

The author wishes to thank Dr. Manabu Senō, Tokyo University, for his advice and Dr. Tetsuro Seiyama, Kyushu University, for his encouragement.

References

1) K. Ota, This Bulletin, **46**, 3617 (1973).
2) K. Ota, *Nippon Kagaku Kaishi*, **1974**, 1697.
3) K. Ota, *Yuki Gosei Kagaku Kyokai Shi*, **31**, 766 (1973).
4) A. J. Rostron and A. M. Spivey, *J. Chem. Soc.*, **1964**, 3092.
5) K. Ota, I. Yuji, and I. Hirao, *Yuki Gosei Kagaku Kyokai Shi*, **26**, 992 (1968) and related papers.

BULLETIN OF THE CHEMICAL SOCIETY OF JAPAN, VOL. 47 (9), 2345—2346 (1974)

The Synthesis of Methoxylated Aromatic Carotenoids

Nobuhisa OKUKADO

Department of Chemistry, Faculty of Science, Kyushu University, Higashi-ku, Fukuoka 812

(Received December 21, 1973)

Synopsis. Four methoxylated aromatic carotenoid derivatives (IVa—d) were prepared by the condensations of the ylids derived from the phosphonium salts (Ia—d) with didehydrocrocetindial (II) followed by partial hydrogenation of the acetylenic bond.

Since aromatic carotenoid hydrocarbons had been isolated from a sea sponge "*Reniera japonica*",[1] the natural occurrence of aromatic carotenoids with oxygen functions such as hydroxyl or methoxy groups on their aryl end-groups has been expected. In fact, phenolic carotenoids were isolated from "*Streptmyces mediolani*" in 1969,[2] but the presence of pigments containing methoxylated aryl end-groups has not so far been reported. In this paper, the synthesis and characterization of 3,3'- and 4,4'-dimethoxyisorenieratene (IVa and IVb), 4,4'- and 5,5'-dimethoxyrenierapurpurin (IVc and IVd), and their 15,15'-didehydro compounds (IIIa—d) will be described.

Syntheses were carried out according to the $C_{10}+C_{20}+C_{10}$ building principle.[3] Wittig reactions of didehydrocrocetindial (II) with the appropriate methoxylated trimethylbenzylidenetriphenylphosphoranes prepared from the corresponding phosphonium salts (Ia—d) gave 15,15'-didehydro compounds (IIIa—d), which were then converted to all-*trans* pigments (IVa—d) by partial hydrogenation and isomerization during purification under diffused light.

The structures and configurations of IVa—d were ascertained by analytical and spectral studies, as is shown in Tables 1 and 2. The facts that IVa—d exhibited the highest UV λ_{max}, with a wavelength 21—23 nm longer and with a higher intensity than those of the corresponding 15,15'-didehydro compounds (IIIa—d), and that IVa—d did not show any *cis*-peak in their UV spectra evidently suggest that IVa—d has the all-*trans* configuration.[4] This was also supported by the IR spectra of IVa—d, which showed a sharp singlet at 962—965 cm^{-1} due to CH out-of-plane deformation vibrations.[5]

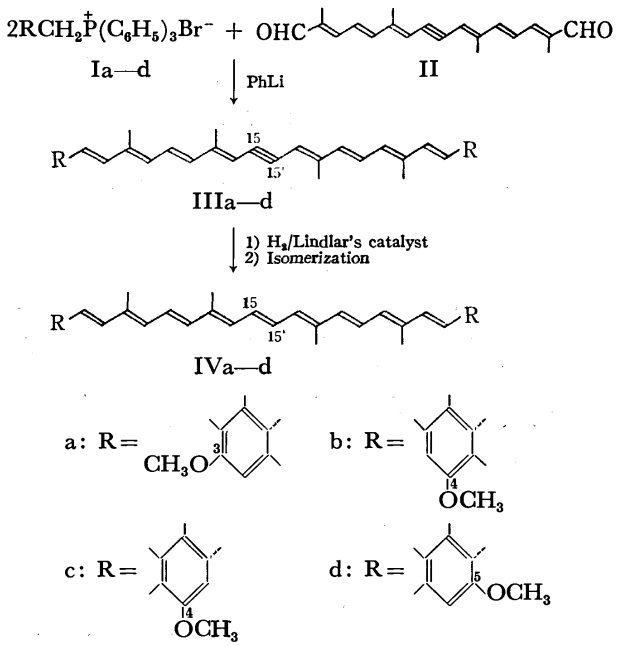

When the highest λ_{max} of IVa—d were compared with those of the parent non-substituted compounds, isorenieratene[1b] [IV, R=2,3,6-$(CH_3)_3C_6H_2$-, λ_{max}, 466 nm (C_6H_6)] and renierapurpurin[1c] [IV, R=2,3,4-$(CH_3)_3C_6H_2$-, λ_{max}, 486 nm (C_6H_6)], the bathochromic effect of methoxy groups was observed only in IVa, in which the substituents are located at *para* positions to the polyene chain. The IVd and IVb pigments, which contain methoxy groups at positions *ortho* or *meta* to the chain respectively, absorbed at a wavelength location 3—4 nm lower than the corresponding parent compounds. This apparently shows that the chromophore systems of these pigments are more distorted than those of the corresponding parent compounds because of the steric interference between the polyene chain

TABLE 1. MELTING POINTS, YIELDS, ELEMENTAL ANALYSES, UV, AND IR DATA OF IIIa—d AND IVa—d

Compound	Mp (°C)	Yield (%)	Found C(%)	Found H(%)	Highest $\lambda_{max}^{C_6H_6}$ nm (log ε)	IR (cm^{-1}) Ar-OCH_3	IR (cm^{-1}) -CH=CH-
IIIa	199	57[a]	85.32	8.53[b]	448 (4.95)	1121	962
IIIb	198—200	69	86.10	8.64[b]	441 (4.91)	1120	960
IIIc	242	74	85.95	8.85[b]	464 (4.94)	1120	960
IIId	235—236	64	85.43	8.67[b]	459 (5.04)	1120	962
IVa	227—230	57	85.55	9.09[c]	469 (5.07)	1122	965
IVb	231	66	85.19	9.12[c]	463 (5.09)	1121	965
IVc	216—218	51	85.32	8.83[c]	486 (5.08)	1123	963
IVd	225—228	64	85.27	8.87[c]	482 (5.08)	1120	962

a) Yields for IIIa—d were calculated based on didehydrocrocetindial. b) Calcd for $C_{42}H_{50}O_2$: C, 85.96; H, 8.59%. c) Calcd for $C_{42}H_{52}O_2$: C, 85.67; H, 8.90%.

Table 2. NMR data of IIIa—d and IVa—d

Compound	Chemical shifts of methyl protons[a] (δ in ppm; $CDCl_3$)					
	C-9,9'-	C-13,13'-	Aryl-			Methoxy-
IIIa	2.08 (2) [b]	2.14 (2)	2.14 (2) [c]	2.23 (2)	2.29 (2)	3.81 (2)
IIIb	2.09 (2)	2.11 (2)	2.15 (4)	2.27 (2)		3.80 (2)
IIIc	2.07 (2)	2.11 (2)	2.18 (2)	2.20 (2)	2.25 (2)	3.85 (2)
IIId	2.09 (2)	2.13 (2)	2.16 (2)	2.30 (4)		3.80 (2)
IVa	2.09 (2)	2.00 (2)	2.17 (2)	2.24 (2)	2.32 (2)	3.82 (2)
IVb	2.08 (2)	1.98 (2)	2.16 (4)	2.27 (2)		3.81 (2)
IVc	2.08 (2)	2.00 (2)	2.19 (2)	2.21 (2)	2.26 (2)	3.86 (2)
IVd	2.07 (2)	1.98 (2)	2.16 (2)	2.29 (4)		3.80 (2)

a) Besides the methyl signals described here, the NMR spectra of IIIa—d showed a singlet at δ 5.75—5.76 ppm assignable to 14,14'-protons and a complex multiplet in the region of δ 6.10—7.00 ppm due to the other olefinic and aromatic protons, but the spectra of IVa—d exhibited only a complex multiplet in the δ 6.10—7.00 ppm region due to all olefinic and aromatic protons. b) Values in parenthesis show number of methyl groups. c) The signal was overlapped with that of C-13, 13'-methyls.

and the newly-introduced substituents or because of the increase in the steric effect of 5,5'-standing methyl groups by the buttressing effect of 4,4'-standing methoxy groups. However, the methoxy groups at positions *meta* to the chain in IVc caused no appreciable change in the absorption maximum.

Experimental

All the melting points are uncorrected. The UV spectra were taken with a Hitachi EPS-3T spectrometer. The IR spectra were recorded from KBr pellets, using a Hitachi 215 infrared spectrometer. The NMR spectra were measured with a Hitachi R-22 spectrometer at 90 MHz, using tetramethylsilane as the internal standard.

Preparations of Methoxytrimethylbenzyltriphenylphosphonium Bromides (Ia—d). These were prepared from the corresponding benzyl alcohols[6] according to the method described by Cooper *et al.*[7] Ia, colorless prisms, mp 225 °C. Found: C, 68.82; H, 6.18%. Calcd for $C_{29}H_{30}BrOP$: C, 68.91; H, 5.98%. Ib, colorless prisms, mp 240 °C. Found: C, 68.56; H, 6.08%. Ic, colorless prisms, mp 229—230 °C. Found: C, 68.79; H, 5.88%. Id, colorless prisms, mp 249 °C. Found: C, 68.92; H, 6.22%.

Preparations of 15,15'-Didehydro Compounds (IIIa—d). A typical example is as follows: to a stirred suspension of phosphonium bromide (Ia, 1.5 g) in absolute ether (30 ml), was added an ethereal solution of phenyllithium (*ca.* 1 M, 5 ml) over a 5 min period under an atmosphere of nitrogen. The mixture was then stirred for 1 hr at room temperature, and methylene chloride (0.3 ml) was added to decompose the excess of phenyllithium. After 10 min, a solution of didehydrocrocetindial (II, 250 mg) in methylene chloride (15 ml) was added, and the mixture was stirred under reflux for 5 hr. The mixture was then diluted with methanol (70 ml) and allowed to stand overnight in an ice-box. The precipitate was subsequently collected; several recrystallizations from a mixture of methylene chloride and ethanol gave IIIa (280 mg) as orange prisms. The yields, melting points, elemental analyses, and UV, IR, and NMR spectral data of IIIa—d are given in Tables 1 and 2.

Preparations of All-trans Carotenoids (IVa—d). A typical example is as follows: IIIa (30 mg) was dissolved in toluene (45 ml) and hydrogenated at 25 °C in the presence of the Lindlar catalyst[8] (65 mg) and quinoline (0.3 ml) until a 1.2-molar equivalent of hydrogen (1.4 ml) was consumed. The catalyst was filtered and washed with benzene. The combined filtrate was concentrated under reduced pressure, petroleum benzine (20 ml) was added to the residue, and the mixture was allowed to stand overnight in an ice-box. The crystallized product was collected, and several recrystallizations from a mixture of chloroform and ethanol gave IVa (17 mg) as purple crystals. The yields, melting points, elemental analyses, and UV, IR, and NMR spectral data of IVa—d are given in Tables 1 and 2.

The author wishes to express his deep gratitude to Professor Masaru Yamaguchi and Professor Tamotsu Yoshino of this department for their many helpful discussions and suggestions during this work.

References

1) a) M. Yamaguchi, This Bulletin, **30**, 111, 979 (1957); **31**, 739 (1958). b) M. Yamaguchi, *ibid.*, **31**, 51 (1958). c) M. Yamaguchi, *ibid.*, **33**, 1560 (1960).

2) F. Arcamone, B. Camerino, E. Cotta, G. Franceschi, A. Grein, S. Penco, and C. Spalla, *Experientia*, **25**, 241 (1969); F. Arcamone, B. Camerino, G. Franceschi, and S. Penco, *Gazz. Chim. Ital.*, **100**, 581 (1970).

3) O. Isler, H. Gutmann, H. Lindlar, M. Montavon, R. Rüegg, G. Ryser, and P. Zeller, *Helv. Chim. Acta*, **39**, 463 (1956).

4) O. Isler, H. Lindlar, M. Montavon, R. Rüegg, and P. Zeller, *ibid.*, **39**, 249 (1956).

5) K. Lunde and L. Zechmeister, *J. Amer. Chem. Soc.*, **77**, 1647 (1955).

6) S. Odate, N. Okukado, and M. Yamaguchi, *Mem. Fac. Sci., Kyushu Univ., C*, **6**, 93 (1968); N. Okukado, *ibid.*, **9**, 39 (1974).

7) R. D. G. Cooper, J. B. Davis, and B. C. L. Weedon, *J. Chem. Soc.*, **1963**, 5637.

8) H. Lindlar, *Helv. Chim. Acta*, **35**, 446 (1952).

BULLETIN OF THE CHEMICAL SOCIETY OF JAPAN, VOL. 47 (9), 2347—2348 (1974)

Organic Photochemical Reactions. XXII.[1] The Photoaddition of Methyl Pyruvate to Methyl-substituted Olefins

Kensuke SHIMA, Teruo KAWAMURA, and Koji TANABE

Department of Industrial Chemistry, Faculty of Engineering, Miyazaki University, Miyazaki 880

(Received January 21, 1974)

Synopsis. The irradiation of methyl pyruvate (III) and several methyl-substituted olefins (I) in acetonitrile gives allylic ethers (IV) as well as oxetanes (V) and alcohols (VI). Quenching studies suggest that IV and V are formed from the triplet state of methyl pyruvate, while VI is produced from the excited singlet state.

We have recently described a novel photoreaction in which biacetyl adds to methyl-substituted olefins, such as 2,3-dimethyl-2-butene (Ia), 2-methyl-2-butene (Ib), α-methylstyrene (Ic), and 2-ethoxypropene (Id), to afford allylic ethers (II).[2] We now find that the formation of allylic ethers is not confined to biacetyl, but is also applicable to methyl pyruvate (III), the simplest α-ketoester.[3]

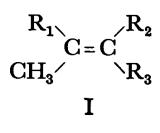

I

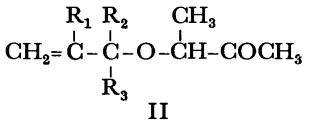

II

$CH_3COCO_2CH_3$

III

a, $R_1=R_2=R_3=CH_3$
b, $R_1=R_2=CH_3$, $R_3=H$
c, $R_1=C_6H_5$, $R_2=R_3=H$
d, $R_1=OC_2H_5$, $R_2=R_3=H$

The irradiation of a solution of methyl pyruvate and 2,3-dimethyl-2-butene using a 300 W high-pressure mercury arc filtered through an *n*-hexane solution of naphthalene yielded IVa, VIa-1, and VIa-2. No detectable amounts of oxetanes were isolated in this photoreaction, as was the case with biacetyl and Ia. Furthermore, large amounts of alcohols (VIa-1 and VIa-2), the products expected from the hydrogen abstraction of Ia by excited III, were obtained. Similarly, the irradiation of methyl pyruvate and 2-methyl-2-butene gave IVb, Vb, and VIb. The major products from the irradiation of methyl pyruvate with α-methylstyrene and 2-ethoxypropene were the Vc and Vd oxetanes respectively. No detectable amounts of allylic ethers and alcohols were isolated in these reactions. These 1:1 adducts were isolated by preparative vpc and by distillation.

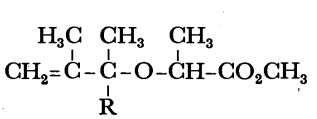

IVa, R=CH_3
IVb, R=H

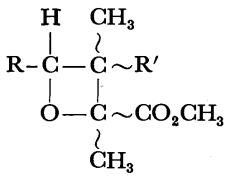

Vb, R=R′=CH_3
Vc, R=H, R′=C_6H_5
Vd, R=H, R′=OC_2H_5

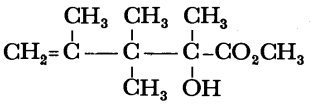

VIa-1

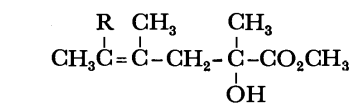

VIa-2, R=CH_3;
VIb, R=H

Table 1 shows the yields and ratios of oxetanes to allylic ethers for these reactions. The formation of IV and V is quenched by the presence of 1,3-cyclohexadiene or 2,3-dimethyl-1,3-butadiene. The Stern-Volmer plots are linear in benzene and acetonitrile.[4] On the other hand, the formation of VI is not quenched at all by large amounts of these triplet quenchers. From this observation, it is evident that VI is formed from an excited singlet state of methyl pyruvate. These results are very interesting because it has been reported that the rate of the hydrogen abstraction from an excited singlet carbonyl compound is slow.[5]

Table 1. Product yields in the photoreaction of III with Ia—Id

Olefin	Product yield, %			Ratio of V/IV
	IV	V	VI	
Ia	21	—	74	0 (0)
Ib	24	15	25	0.61 (0.41)
Ic	—	50, 27	—	(1.8)
Id	—	54, 46	—	(2.1)

Experimental

General. The NMR spectra were recorded on a Hitachi Perkin-Elmer R-20 or on a JEOL JNM-100 spectrometer in CCl_4. The infrared spectra were obtained on a JASCO IRA-1 infrared spectrophotometer. The mass spectra were obtained on a Hitachi Perkin-Elmer RMU-60 mass spectrometer. The vapor-phase chromatographic analyses were run on a Shimadzu gas chromatograph, GC-3BF or GC-2C.

The following materials were prepared by the previously-reported procedures: 2,3-dimethyl-2-butene (Ia),[6] 2-methyl-2-butene (Ib),[7] 2-ethoxypropene (Id),[8] methyl pyruvate (III),[9] 2,3-dimethyl-1,3-butadiene,[10] and 1,3-cyclohexadiene.[11]

Irradiation of Methyl Pyruvate (III) with 2,3-Dimethyl-2-butene (Ia). A solution of III (10.2 g) and Ia (8.4 g) in acetonitrile was irradiated for 120 hr using a 300 W high-pressure mercury arc filtered through an *n*-hexane solution of naphthalene under nitrogen at room temperature. Vpc (PEG 6000, 150 °C) showed the starting materials plus four products with a relative ratio of the peak areas of 21: 5: 29: 45. After the evaporation of the low-boiling fractions, a fraction boiling at 105—125 °C/30 mmHg (5.0 g) was collected; residues, 1.1 g. These products were separated by preparative vpc on a 3 m PEG 6000 column (140 °C).

The first component was identified as 1,1,2-trimethyl-2-propenyl 1′-carbomethoxyethyl ether (IVa): bp 82 °C/25

mmHg; *m/e* 186 (M^+), 171, 127, and 87 (base); IR 1755, 1640, and 1125 cm^{-1}; NMR δ 1.22 (3H, s), 1.25 (3H, d, $J=7$ Hz), 1.27 (3H, s), 1.73 (3H, s), 3.63 (3H, s), 3.80 (1H, q, $J=7$ Hz), and 4.89 (2H, m). Found: C, 64.19; H, 10.04%. Calcd for $C_{10}H_{18}O_3$: C, 64.49; H, 9.74%.

Due to its instability, the second component was neither isolated nor identified.

The third component was identified as methyl 2-hydroxy-2,3,3,4-tetramethyl-4-pentenoate (VIa—l): bp 101 °C/25 mmHg; *m/e* 186 (M^+), 168, 127, 104, and 43 (base); IR 3590, 1740, and 1640 cm^{-1}; NMR δ 1.14 (6H, s), 1.29 (3H, s), 1.76 (3H, s), 3.10 (1H, s, OH), 3.70 (3H, s), and 4.70—4.92 (2H, m). Found: C, 64.26; H, 9.58%. Calcd for $C_{10}H_{18}O_3$: C, 64.49; H, 9.74%.

The fourth component was identified as methyl 2-hydroxy-2,4,5-trimethyl-4-hexenoate (VIa-2): bp 107 °C/22 mmHg; *m/e* 186 (M^+), 168, 127, 104, and 83 (base); IR 3530 and 1735 cm^{-1}; NMR δ 1.33 (3H, s), 1.64 (9H, s), 2.44 (2H, s), 2.99 (1H, s, OH), and 3.70 (3H, s). Found: C, 64.56; H, 9.72%. Calcd for $C_{10}H_{18}O_3$: C, 64.49; H, 9.74%.

Irradiation of Methyl Pyruvate (III) with 2-Methyl-2-butene (Ib). A mixture of III (10.2 g) and Ib (7.0 g) in acetonitrile was irradiated for 250 hr. After the removal of the unreacted materials, a fraction boiling at 83—99 °C/30 mmHg (7.6 g) was collected; residues, 4.0 g. Vpc analysis (PEG 6000, 120 °C) showed five products with a relative ratio of peak areas of 24: 27: 15: 25: 9. These products were separated by preparative vpc on a 3 m PEG 6000 column at 125 °C.

The first component was identified as 1,2-dimethyl-2-propenyl 1′-carbomethoxyethyl ether (IVb): bp 75 °C/19 mmHg; *m/e* 172; IR 1755, 1650, and 1120 cm^{-1}; NMR δ 1.20 (3H, d, $J=7$ Hz), 1.29 (3H, d, $J=7$ Hz), 1.70 (3H, s), 3.62 (3H, s), 3.85 (2H, q, $J=7$ Hz), and 4.60—4.88 (2H, m). Found: C, 62.67; H, 9.31%. Calcd for $C_9H_{16}O_3$: C, 62.76; H, 9.36%.

The second component proved to be an inseparable mixture of two products (areas, *ca.* 40: 60). The minor product was assumed to be VII from the NMR data of the hydrogenation product of this component. The structure of the major one has not yet been determined.

The third component was identified as 2,3,3,4-tetramethyl-2-carbomethoxyoxetane (Vb); bp 89 °C/23 mmHg; *m/e* 172; IR 1745 and 980 cm^{-1}; NMR δ 0.99 (3H, s), 1.12 (3H, s),

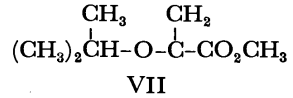

VII

1.16 (3H, d, $J=7$ Hz), 1.44 (3H, s), 3.67 (3H, s), and 4.34 (1H, q, $J=7$ Hz). Found: C, 62.60; H, 9.23%. Calcd for $C_9H_{16}O_3$: C, 62.76; H, 9.36%.

The fourth component was identified as VIb: bp 93 °C/20 mmHg; *m/e* 172; IR 3500 and 1735 cm^{-1}; NMR δ 1.32 (3H, s), 1.55—1.82 (6H, m), 2.16—2.46 (2H, m), 2.93 (1H, s, OH), 3.72 (3H, s), and 4.85—5.40 (1H, m). Found: C, 62.51; H, 9.34%. Calcd for $C_9H_{16}O_3$: C, 62.76; H, 9.36%.

The fifth component is an alcohol, but its exact structure remains undetermined.

Irradiation of Methyl Pyruvate (III) with α-Methylstyrene (Ic). After a 120 hr irradiation of a mixture of III (10.2 g) and Ic (23.6 g) in acetonitrile, a fraction boiling at 112—115 °C/4 mmHg (1.9 g) was obtained; residues, 0.9 g. The products were analyzed and separated by vpc using a 3 m Silicone DC 550 column at 190 °C. The relative ratio of the peak areas of the two major peaks was 27: 50.

The first component was identified as 2,*t*-3-dimethyl-2-carbomethoxy-3-phenyloxetane (Vc-1): bp 104 °C/4 mmHg; *m/e* 220; IR 1745 and 990 cm^{-1}; NMR δ 1.61 (3H, s), 1.64 (3H, s), 3.15 (3H, s), 4.20 (1H, d, $J=5$ Hz), 5.23 (1H, d, $J=5$ Hz), and 6.90—7.40 (5H, m). Found: C, 70.61; H, 7.50%. Calcd for $C_{13}H_{16}O_3$: C, 70.89; H, 7.32%.

The second component was identified as 2,*c*-3-dimethyl-2-carbomethoxy-3-phenyloxetane (Vc-2): mp 68.5—69 °C; IR 1750 and 982 cm^{-1}; NMR δ 1.27 (3H, s), 1.57 (3H, s), 3.83 (3H, s), 4.20 (1H, d, $J=5$ Hz), 4.96 (1H, d, $J=5$ Hz), and 7.05—7.35 (5H, m). Found: C, 70.65; H, 7.35%. Calcd for $C_{13}H_{16}O_3$: C, 70.89; H, 7.32%.

Irradiation of Methyl Pyruvate (III) with 2-Ethoxypropene (Id). A solution of III (10.2 g) and Id (8.6 g) in acetonitrile was irradiated for 300 hr. After the removal of the unreacted materials, a fraction boiling at 98—123 °C/15 mmHg (3.1 g) was collected; residue, 1.8 g. The vpc analysis (DNP, 3 m, 150 °C) of the distillate showed one major peak. The product, isolated by preparative vpc, was identified as a mixture of 2,*t*-3- and 2,*c*-3-dimethyl-2-carbomethoxy-3-ethoxyoxetane (Vd-1 and Vd-2) from the NMR spectra (ratios, *ca.* 6: 5): bp 103 °C/18 mmHg; NMR, Vd-1 δ 1.22 (3H, t, $J=7$ Hz), 1.41 (3H, s), 1.50 (3H, s), 3.46 (2H, q, $J=7$ Hz), 3.68 (3H, s), 4.07 (1H, d, $J=6$ Hz), and 4.36 (1H, d, $J=6$ Hz); Vd-2 δ 1.10 (3H, t, $J=7$ Hz), 1.46 (3H, s), 1.58 (3H, s), 3.37 (2H, q, $J=7$ Hz), 3.68 (3H, s), 4.07 (1H, d, $J=6$ Hz), and 4.62 (1H, d, $J=6$ Hz). Found: C, 57.19; H, 8.66%. Calcd for $C_9H_{16}O_4$: C, 57.43; H, 8.57%.

References

1) Part XVII, H.-S. Ryang, K. Shima, and H. Sakurai, *J. Amer. Chem. Soc.*, **93**, 5270 (1971); Part XVIII, Y. Nagao, K. Shima, and H. Sakurai, *Chem. Lett.*, **1972**, 147; Part XIX, T. Kubota, K. Shima, and H. Sakurai, *Chem. Lett.*, **1972**, 343; Part XX, Y. Nagao, K. Shima, and H. Sakurai, This Bulletin, **45**, 3122 (1972); Part XXI, H.-S. Ryang, K. Shima, and H. Sakurai, *J. Org. Chem.*, **38**, 2860 (1973).

2) H.-S. Ryang, K. Shima, and H. Sakurai, *Tetrahedron Lett.*, **1970**, 1094; *J. Amer. Chem. Soc.*, **93**, 5270 (1971); *J. Org. Chem.*, **38**, 2860 (1973).

3) It was also found that dimethyl oxomalonate photochemically adds to isobutene and 2-butenes to give such allylic ethers. This result will be reported elsewhere. Recently, Carless has reported that such allylic ethers are also produced by the photoreaction of acetone with Ia; H. A. J. Carless, *J. Chem. Soc., Chem. Commun.*, **1973**, 316.

4) $\Phi_0/\Phi=1+k_q\tau[Q]$; $k_q\tau$ in benzene 91 for IVa; 189 for IVb (quencher: 1,3-cyclohexadiene). $k_q\tau$ in benzene 28.5 for IVa; 51.6 for IVb; 46 for Vb (quencher: 2,3-dimethyl-1,3-butadiene).

5) P. J. Wagner, *J. Amer. Chem. Soc.*, **88**, 5672 (1966).

6) I. Shurman and C. E. Boord, *ibid.*, **55**, 4930 (1933).

7) F. C. Whitmore, C. S. Rowland, S. N. Wrenn, and G. W. Kilmer, *ibid.*, **64**, 2970 (1942).

8) M. A. Dolliver, T. L. Gersham, G. B. Kistiakowsky, E. A. Smith, and W. E. Vaugham, *ibid.*, **60**, 440 (1938).

9) A. Weissberger and C. J. Kibler, "Organic Syntheses," Coll. Vol. III, p. 610 (1955).

10) R. Adams and E. W. Adams, "Organic Syntheses," Coll. Vol. I, p. 459 (1941); C. F. H. Allen and A. Bell, *ibid.*, Coll. Vol. III, p. 312 (1955).

11) C. S. Marvel and G. E. Hartzell, *J. Amer. Chem. Soc.*, **81**, 448 (1959).

BULLETIN OF THE CHEMICAL SOCIETY OF JAPAN, VOL. 47 (9), 2349—2350 (1974)

Functionalization of *trans*-Decalin. I. Synthesis of 1-Oxo-*trans*-decalin-4a, 6-carbolactone

Sigeru TORII, Tsuyosi KUNITOMI, and Tsutomu OKAMOTO

Department of Industrial Chemistry, School of Engineering, Okayama University, Okayama 700

(Received February 25, 1974)

Synopsis. The synthesis of 4a-carbomethoxy-*cis*- and *trans*-Δ^6-octalin-1-ones (**2a** and **2b**), 4a-carboxy-*trans*-Δ^6-octalin-1-one (**3b**), and 1-oxo-*trans*-decalin-4a,6-carbolactone (**5**) from the adduct of 3-carbomethoxy-2-cyclohexen-1-one with butadiene was described.

Although the combinations of some alicyclic β-methyl-α,β-unsaturated ketones with butadienes were unsuccessful,[1] alicyclic β-carbomethoxy-α,β-unsaturated ketone such as 3-carbomethoxy-2-cyclohexen-1-one (**1**) was found to be a reactive dienophile. A similar reaction has been observed in the β-carboxy-α-butenolide system.[2] Thus, the cycloaddition of **1** with butadiene was investigated as a means of preparing functionalized *trans*-decalins (**4** and **5**), which would provide a synthetic intermediate for the preparation of sesquiterpenoids. The starting compound (**1**)[3] was prepared from readily available 1-carbomethoxycyclohexene[4] by oxidation with selenium dioxide[3] followed by treatment with the Jones reagent[5] in dichloromethane.

The Diels-Alder reaction of **1** with butadiene at 130—140 °C in a sealed tube exclusively afforded the *cis* adduct (**2a**) in 55% yield. However, when the reaction was carried out above 155 °C, a mixture of *cis*- and *trans*-adducts (**2a** and **2b**) was obtained in a *ca.* 3:1 ratio. Hydrolysis of **2a** with a wet ethanolic potassium hydroxide solution gave the corresponding acids (**3a** and **3b**) in a 1:4 ratio. Separation of the *trans* isomer (**3b**), a white crystals, mp 138 °C, was performed by column chromatography on silica gel, followed by recrystallization from water. Reaction of **3b** with diazomethane provided a pure specimen of **2b**. During the course of recrystallization from hot water, isomerization of the *cis* isomer (**3a**) into **3b** took place. The structures of **2a** and **2b** were comfirmed by means of elemental analyses and spectral data. Their NMR spectra showed differences such as a three-proton singlet at δ 3.58 (*trans* isomer) and 3.65 (*cis* isomer), both due to the methyl ester protons, and also a two-proton broad singlet at δ 5.50 (*cis* isomer) and 5.58 (*trans* isomer).

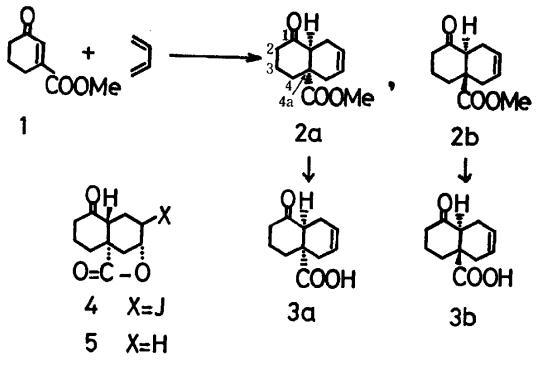

Iodolactonization[6] of **3b** gave a lactone iodide (**4**) in 95% yield, mp 119 °C. Reduction of **4** with tri-*n*-butyltin hydride[7] afforded a keto lactone (**5**) in 80% yield, mp 104 °C. The structures of **4** and **5** were confirmed by their elemental analyses and spectral data. Characteristic carbonyl bands of **4** were seen at 1770 (iodolactone carbonyl) and 1708 (ketone carbonyl) cm^{-1}, whereas those of **5** appeared at 1762 (lactone carbonyl) and 1715 (ketone carbonyl) cm^{-1}, indicating that both decalin-1-ones have a γ-lactone function.

Experimental

All the melting points are uncorrected. The IR spectra were recorded on a Hitachi EPI-S2 spectrophotometer. The NMR spectra were observed with Hitachi R-24 and/or R-22 spectrometers. Mass spectral analyses were carried out on a Hitachi RMS-4 mass spectrometer, ionizing at the order of 70 eV.

3-Carbomethoxy-2-cyclohexen-1-one (1). A mixture of 3.33 g (30 mmol) of selenium dioxide and 3.50 g (25 mmol) of 1-carbomethoxy-1-cyclohexene[4] in 35 ml of dioxane was stirred at 70—80 °C for 18—20 hr and at 90 °C for 3 hr. The precipitate was filtered and washed with 20 ml of dichloromethane. The combined filtrates were concentrated in a rotary evaporator. The residue, a reddish-brown viscous oil, was taken up in ether–*n*-hexane (4:1). The mixture was stirred for some minutes, after which the organic layer was separated. Removal of the solvent gave crude 3-carbomethoxy-2-cyclohexen-1-ol. Without further purification, a solution of the crude alcohol in 50 ml of dichloromethane was treated with 12 ml of a chromic acid solution[5b] with vigorous stirring for 25 min under nitrogen atmosphere at 0 °C. After being left to stand for a few minutes, the organic layer was separated. The aqueous layer was washed with 30 ml of dichloromethane. The combined extracts were washed with water and dried (Na_2SO_4). The solvent was concentrated and the residue was taken up in ether and the insoluble material was filtered off. The filtrate was concentrated in a rotary evaporator to afford a brown oil. The crude oil was purified by column chromatography on silica gel with *n*-hexane–dichloromethane (2:1), which eluted 0.89 g (23%) of **1**; bp 126—128 °C/8 mmHg; IR (Neat) 1725 (ester C=O), 1685 (conj. ketone), 1628 (C=C) cm^{-1}; NMR (CCl_4) δ 1.97—2.71 (m, 6H, CH_2), 3.78 (s, 3H, CH_3O), 6.59 (m, 1H, HC=C). Found: C, 62.24; H, 6.53%. Calcd for $C_8H_{10}O_3$: C, 62.33; H, 6.54%.

4a-Carbomethoxy-cis-Δ^6-octalin-1-one (2a). A mixture of 462 mg (3.0 mmol) of 3-carbomethoxy-2-cyclohexenone (**1**), 1 mg of 2,5-di-*tert*-butylhydroquinone, and 1.35 ml of butadiene in 1 ml of benzene was charged in a sealed tube. The tube was allowed to stand in an oil bath at 130—140 °C for 3 day. The mixture was then poured into 15 ml of methanol. The precipitate was filtered and washed with methanol. The combined filtrates were concentrated in a rotary evaporator. The residue was purified by chromatography on a

silica gel column with dichloromethane-*n*-hexane (1:3), which eluted 343 mg (54.9%) of **2a**, mp 78.0—78.5 °C, bp 111—114 °C/1 mmHg; IR (Neat) 1725 (ester C=O), 1715 (ketone C=O) cm^{-1}; NMR ($CDCl_3$) δ 1.83—2.46 (m, 10H, CH_2), 3.00 (broad, d, 1H, CHC=O), 3.65 (s, 3H, CH_3O), 5.50 (broad s, 2H, HC=C); MS (*m/e*) 208 (M^+). Found: C, 69.20; H, 7.72%. Calcd for $C_{12}H_{16}O_3$: C, 69.21; H, 7.74%.

A mixture of *cis*- and *trans*-adducts (**2a** and **2b**) (3:1) was obtained when the sealed tube was heated above 155 °C for 3 day.

4a-Carboxy-trans-Δ^6-*octalin-1-one (3b)*. To a stirred solution of 112 mg (2.0 mmol) of potassium hydroxide in 1 ml of water was added a solution of 250 mg (1.2 mmol) of **2a** in 2 ml of ethanol. After stirring at room temperature for 15—20 hr, the solution was heated at 60 °C for 2 hr and then concentrated. The residual solution was acidified with 10% aqueous hydrogen chloride and extracted with chloroform. The extracts were washed with brine and dried (Na_2SO_4). Removal of the solvent gave 210 mg of crude acids (**3a** and **3b**) (*ca.* 1:4). The crude product was chromatographed over silica gel (Wako Gel C-200). Elution of the column with dichloromethane gave 80 mg of a mixture of **3a** and **3b** (*ca.* 1:1) as an oil. The following elution with dichloromethane-ethyl acetate (4:1) gave 110 mg (48% yield) of **3b** as a white crystals, mp 138.0 °C (from water); IR (Nujol) 3400—2500 (COOH), 1723 (C=O), 1682 (COOH) cm^{-1}; NMR ($CDCl_3$) δ 1.55—2.53 (m, 10H, CH_2), 2.66 (m, 1H, CHC=O), 5.69 (broad s, 2H, CH=C), 10.93 (s, 1H, COOH). Found: C, 68.20; H, 7.40%. Calcd for $C_{11}H_{14}O_3$: C, 68.02; H, 7.27%.

4a-Carbomethoxy-trans-Δ^6-*octalin-1-one (2b)*. Mp 71.5—73.0 °C, bp 83—86 °C/0.02 mmHg, obtained by treatment of **3b** with diazomethane: IR (Nujol) 1724 (ester C=O), 1712 (ketone C=O) cm^{-1}; NMR ($CDCl_3$) δ 1.67—2.67 (m, 10H, CH_2), 2.83 (m, 1H, CHC=O), 3.58 (s, 3H, CH_3O), 5.58 (broad s, 2H, HC=C). Found: C, 69.38; H, 7.89%. Calcd for $C_{12}H_{16}O_3$: C, 69.21; H, 7.74%.

1-Oxo-trans-*decalin-4a,6-carbolactone (5)*. To a stirred solution of 160 mg (0.82 mmol) of **3b** in 5 ml of 0.5 M aqueous sodium bicarbonate was added a mixture of 317 mg (1.25 mmol) of iodine and 1.33 g (8.0 mmol) of potassium iodide in 3 ml of water for 5 min under cooling in an ice-water bath. The flask was covered with a black napkin and stirring was continued for 24 hr at room temperature. The reaction mixture was extracted with ether. The extracts were washed with aqueous sodium thiosulfate and saturated aqueous sodium carbonate and dried (Na_2SO_4). Removal of the solvent gave 250 mg (95%) of the iodolactone (**4**), mp 119 °C, as a white crystal (from *n*-hexane-benzene, 2:3): IR (Nujol) 1770 (lactone C=O), 1708 (C=O) cm^{-1}; NMR ($CDCl_3$) δ 1.74—3.04 (m, 11H), 4.47—4.88 (m, 2H, HCI, HC–O). Found: C, 41.42; H, 4.15%. Calcd for $C_{11}H_{13}O_3I$: C, 41.27; H, 4.09%.

To a solution of 250 mg of **4** in 5 ml of dry benzene was added 450 mg (1.55 mmol) of tri-*n*-butyltin hydride dropwise with stirring for 5 min at 5 °C under nitrogen atmosphere. Stirring was continued for 48 hr at room temperature and the solvent was removed in a rotary evaporator to afford 128 mg (80% yield) of **5**, a columnar crystals, mp 104 °C (from benzene-*n*-hexane, 3:2): IR (Nujol) 1762 (γ-lactone C=O), 1710 (C=O) cm^{-1}; NMR ($CDCl_3$) δ 1.68—2.43 (m, 13H, CH_2, CH), 4.73 (t, 1H, HC–O); MS (*m/e*) 194 (M^+). Found: C, 68.25; H, 7.25%. Calcd for $C_{11}H_{14}O_3$: C, 68.02; H, 7.27%.

References

1) a) R. Robinson and J. Walker, *J. Chem. Soc.*, **1935**, 1530. b) R. M. Acheson, *ibid.*, **1952**, 3415. c) Reported diene additions to α-methylcyclenones gave adducts in poor yields: L. W. Butz and A. W. Rytina, *Org. Reactions*, **5**, 153 (1949). An improved method has recently been reported: I. Nagakura, S. Maeda, and Y. Kitahara, *Yuki Gosei Kagaku Kyokai Shi*, **31**, 251 (1973).

2) S. Torii, T. Oie, H. Tanaka, J. D. White, and T. Furuta, *Tetrahedron Lett.*, **1973**, 2471.

3) 3-Carbomethoxy-2-cyclohexen-1-one was prepared from 1-cyanocyclohexene: M. Mousseron, R. Jacquier, and A. Fontaine, *C. R. Acad. Sci. Paris*, **235**, 1512 (1952). Improvement in its preparation is presented.

4) S. J. Rhoads, J. K. Chattopadhyay, and E. E. Waali, *J. Org. Chem.*, **35**, 3352 (1970); E. J. Moriconi and P. H. Mazzocchi, *ibid.*, **31**, 1372 (1966).

5) a) G. H. Rasmusson, H. O. House, E. F. Zaweski, and C. H. DePuy, "Organic Syntheses," Vol. 42, p. 36 (1962); b) H. C. Brown, C. P. Garg, and K. T. Liu, *J. Org. Chem.*, **36**, 387 (1971).

6) H. O. House, S. G. Boots, and V. K. Jones, *ibid.*, **30**, 2519 (1965); H. O. House, D. G. Melillo, and F. J. Sauter, *ibid.*, **38**, 741 (1973).

7) G. J. M. van der Kerk, J. G. Moltes, and J. G. A. Luijten, *J. Appl. Chem.*, **7**, 356 (1957).

BULLETIN OF THE CHEMICAL SOCIETY OF JAPAN, VOL. 47 (9), 2351—2352 (1974)

The Diazo-coupling Reaction of Phenol in Organic Solvents. The Isomer Ratio

Hideo YAMADA, Yōji HASHIDA, Shizen SEKIGUCHI, and Kohji MATSUI

Department of Synthetic Chemistry, Faculty of Engineering, Gunma University, Tenjincho, Kiryu, Gunma 376

(Received March 11, 1974)

Synopsis. The *ortho*: *para*-ratios in the reaction of phenol with benzenediazonium fluoroborate have been investigated in organic solvents. It has been found that the *o*/*p* ratios in protic solvents were smaller than those in aprotic solvents. The results were interpreted in terms of the difference in solvation toward the phenolate ion.

In diazo-coupling reactions, it is known[1] that the ratio of the isomers depends upon various factors, such as the structures of the diazo and coupling components, the pH values of the media, the reaction temperatures, and the catalysts. In a previous paper,[2] we reported that the rate of the reaction of 2-naphthol with benzene diazonium salt was markedly affected by the solvent. Thus, in the diazo-coupling reaction of phenol, the isomer ratio can be expected also to be influenced by the solvents, as has been reported for the other aromatic electrophilic substitutions.[3,4] However, the effect of solvents on the isomer ratios has not been studied systematically in connection with this reaction. This paper will report the *ortho*: *para*-ratios for the diazo-coupling reactions of phenol with benzenediazonium salt in organic media.

Experimental

Materials. Commercial phenol and triethylamine were purified by distillation prior to use. The benzenediazonium fluoroborate was prepared by the usual method and were dried over phosphorus pentoxide.

Solvents. The solvents used were purified by the usual methods.[5]

Syntheses of Azo-compounds. The *p*-hydroxyazobenzene,[6] *o*-hydroxyazobenzene,[6] and 2,4-bis(phenylazo)phenol[7] were prepared by the usual procedure. Their purities were checked by observing their melting points, by elemental analyses, and by thin-layer chromatography. The optical properties of these azo-compounds are shown in Table 1.

TABLE 1. OPTICAL PROPERTIES OF AZO-COMPOUNDS

Azo-compound	Mp (°C)	λ_{max}(nm)	ε[a]
2-Hydroxyazobenzene	83—83.5	322	19100
4-Hydroxyazobenzene	154—155	346	25300
2,4-Bis(phenylzao)phenol	130—131	335	44700

a) In methanol.

Measurements of the Product Distributions. The product distributions were measured spectrophotometrically by the method described below. To 100 ml of a solution of phenol (0.471 g, 5×10^{-3} M) and triethylamine (1.52 g, 1.5×10^{-2} M) in an appropriate solvent, we added finely-powdered benzenediazonium fluoroborate (0.960 g, 5×10^{-3} M) at 0 °C. The reaction mixture was stirred for a few hours after the diazonium salt had been dissolved, and the reaction mixture was concentrated; then the azo-compounds thus produced were separated by silica gel thin-layer chromatography, using a mixture of *n*-hexane and acetone (20: 1, v/v) as the developing solvent. From the thin-layer chromatogram each azo-compound was extracted and diluted to a definite volume with methanol; its extinction was measured spectrophotometrically.

Results and Discussion

As has been reported[6] for the coupling reaction in water, phenol gave *o*-, *p*-, and 2,4-di-substituted[8] products even in the reactions in organic solvents. The product distributions in various solvents are given in Table 2.

TABLE 2. PRODUCT DISTRIBUTIONS FOR THE REACTION OF PHENOL WITH BENZENEDIAZONIUM FLUOROBORATE (0 °C)

No.	Solvent	(Molar comp. of) product (%)			
		o-	*p*-	2,4-di-	$o/p\times100$
1	Water	0.7	99.1	0.2	0.7
2	Methanol	1.2	97.5	1.3	1.2
3	Methanol[a]	1.4	98.3	0.3	1.4
4	2-Propanol	1.6	98.4	—[b]	1.7
5	Phenol	3.2	96.8	—[b]	3.3
6	*t*-Butanol	4.3	89.9	5.8	4.8
7	Acetone	3.2	93.1	3.6	3.5
8	Tetrahydrofuran	3.6	96.3	—[b]	3.8
9	Acetonitrile	3.8	91.5	4.7	4.2
10	Dimethylsulfoxide[c]	4.6	90.7	4.7	5.0
11	Nitromethane	4.7	93.1	2.2	5.0
12	Dioxane	5.2	93.2	1.6	5.6
13	Dimethylformamide	6.5	88.7	4.8	7.3
14	Pyridine	6.7	86.7	6.6	7.7

a) Pyridine was used as a base (see Experimental Section). b) The product ratio could not be measured by the method of T.L.C., because of the formation of unknown by-product. c) At 20 °C.

In diazo-coupling reactions, many examples are known[1] in which the isomer ratio depends upon the base used and upon its concentration. To examine the effect of bases on isomer ratios, the reaction was carried out in methanol in the presence of triethylamine and/or pyridine; however, these bases scarcely affected the *o*/*p* ratio at all (No. 2, 3).

As can be seen from Table 2, the solvents do have significant effects on the isomer ratio, even though every value of the *o*/*p* ratio is small: in pyridine and DMF, the yields of the *o*-isomer were greater than that in water by a factor of about ten. The solvents employed can be divided into two groups: the protic (No. 1—6)

and aprotic solvents (No. 7—14).

In the protic solvents, the *o*/*p* ratios were small; however, within a series of protic solvents with similar structures, the yield of the *o*-isomer increased with a decrease in the solvent polarity in this order: H_2O< MeOH<*i*-PrOH<*t*-BuOH.

On the contrary, in the aprotic solvents there was no significant correlation between the *o*/*p* ratio and the solvent polarity. However, as a whole, in the aprotic solvents higher yields of the *ortho*-substituted derivatives were obtained than in the protic solvents.

In the ordinary electrophilic substitutions of monosubstituted benzenes, many factors have been suggested[9] as affecting the *o*/*p* ratio; however, little is known about the effect of solvents on the isomer distribution. Therefore, it was of interest to consider the solvent effect on the isomer ratio in this reaction.

One of the most important factors of the solvent effect in this reaction is considered to be the influence on the reactivities of the reaction components by solvation. According to the selectivity relationship,[10] the difference in yields between *ortho*- and *para*-products is also assumed to increase as the reactivity of the reagent decreases;[11,12] this concept is consistent with the results described above. It was pointed out in a previous work[2] that, in the diazo-coupling reaction of 2-naphthol, the reactive species of the substrate is the naphtholate ion, even in organic solvents, and that the reaction is remarkably enhanced in dipolar aprotic solvents, presumably because of the decrease in the solvation of the naphtholate ion in these solvents.[2] A similar relation between the reactivities of the substrates and the kind of solvent is considered to hold for the reaction of phenol; therefore, the coupling reaction of benzenediazonium salt with phenol is considered to proceed more rapidly in dipolar aprotic solvents than in protic solvents. Therefore, the finding that, in this reaction, relatively high *o*/*p* ratios were obtained in the aprotic solvents is quite reasonable. Furthermore, the tendency for, in protic solvents, the *o*/*p* ratio to increase with a decrease in the solvent polarity may be ascribed to a decrease in solvation in the less polar solvent, which thus increases the reactivity of the phenolate ion. Thus, the increased reactivity of the phenolate ion leads to a decrease in selectivity.

On the other hand, it is also known[10] that the *o*/*p* ratio of the aromatic electrophilic substitution is governed by the steric effect of the substituents of the substrates. The change in the *o*/*p* ratio described above may be also explained by assuming that the steric effect of the $-O^-$ group varies with the solvents, as has been pointed out by several authors.[4,13] For example, the total bulkiness of the $-O^-$ group may be larger in protic solvents than in aprotic solvents, for the $-O^-$ group is considered to be strongly solvated in protic solvents by means of the general hydrogen-bonding. The bound solvent molecules would interfere with the *ortho*-substitution.

Either of the two concepts may explain our results satisfactorily, but it is difficult to conclude at present which of the effects plays the leading role; the isomer ratios are probably affected by the combined action of both the effects.

References

1) H. Zollinger, "Azo and Diazo Chemistry," Interscience Publishers, New York (1961), p. 253.
2) Y. Hashida, H. Ishida, S. Sekiguchi, and K. Matsui, This Bulletin, **47**, 1224 (1974).
3) L. M. Stock and A. Himoe, *Tetrahedron Lett.*, **1960**, 9.
4) A. Campbell and D. J. Shields, *Tetrahedron*, **21**, 211 (1965).
5) J. A. Riddick and W. B. Bunger, "Organic Solvents," Wiley-Interscience, New York, (1970), Chapter 5.
6) E. Bamberger, *Ber.*, **33**, 3188 (1900).
7) E. Bamberger, *ibid.*, **35**, 1606 (1902).
8) 2,4-Disubstituted product has been reported to be produced from the reaction of *p*-substituted product with diazonium salt [Kishimoto, *et al.*, *Kogyo Kagaku Zasshi*, **71**, 1195 (1968)]. Therefore, it may be reasonable that *o*/*p* ratio should be calculated from the *o*/*p*+2,4-disubstituted compound. However, there was no serious difference between *o*/*p* and *o*/*p*+2,4-substituted derivative.
9) R. O. C. Norman and R. Taylor, "Electrophilic Aromatic Substitution in Benzenoid Compounds," Elsevier Publishing Co., Amsterdam (1965), p. 301.
10) L. M. Stock and H. C. Brown, "Advance in Physical Organic Chemistry," Vol. 1, ed. by V. Gold, Academic Press., London (1963), p. 35.
11) P. B. D. de la Mare and J. H. Ridd, "Aromatic Substitution," Butterworths Scientific Publications, London (1959), p. 83.
12) R. O. C. Norman and G. K. Radda, *J. Chem. Soc.*, **1961**, 3610.
13) W. J. Le Nobel, *J. Amer. Chem. Soc.*, **85**, 1470 (1963).

The Isomerization of Purine Nucleosides in a Dilute Alkaline Solution

Yoshihisa SUZUKI and Setsuko YATABE

Central Research Laboratories, Ajinomoto Co., Inc., Suzuki-cho, Kawasaki 210

(Received January 24, 1974)

A further study of the isomerization of inosine (**1a**) in a dilute alkaline solution has revealed the formation of α-pyranosyl isomer (**4a**) and its β-isomer (**3a**). Adenosine (**1b**) was isomerized at 130 °C for 12 hr at pH 10, giving α-furanosyl (**2b**) (2% yield), β-pyranosyl (**3b**) (11%), and the α-pyranosyl isomer (**4b**) (0.8%), respectively; 65% of the **1b** also remained. 9-β-D-Ribopyranosyl-6-mercaptopurine (**3c**) was prepared through this reaction from the corresponding β-furanoside (**1c**). Arabinosyl or xylosyl purine nucleosides were also isomerized, whereas neither 2′-deoxy nor 2′-substituted nucleoside showed any clear evidence of isomerization. In conclusion, the purine base and the 2′-hydroxyl anion are essential to the alkaline isomerization of nucleosides. By means of NMR, both **4a** and **4b** were found to have a 1C conformation, while **3a** and **3b** have a C1 conformation.

The isomerization of inosine (**1a**) in a dilute alkaline solution (pH 10), giving 9-β-D-ribopyranosyl hypoxanthine (**3a**), has been reported in the preceding paper.[1] This paper will describe the isolation of 9-α-D-ribopyranosyl hypoxanthine (**4a**) from the same mixture as that described in the preceding paper, and will further describe the isomerization of adenosine (**1b**) and other purine nucleosides under the standard conditions at 130 °C for 6 hr at pH 10 (Chart 1).

The action of alkali on some purine nucleosides was examined by Jones *et al.*[2] in 1 M NaOH at 100 °C for 1 hr; they found that **1a** was extremely stable under their conditions and that **1b** gave two degraded compounds (adenine and 4,5,6-triaminopyrimidine) and one deaminated nucleoside, **1a**. Garret and Mehta[3] examined the solvolysis of adenine nucleosides in 0.05—1.0 M NaOH at 60—80 °C and obtained similar products. Neither of these groups, however, found any isomerization. On the basis of what we found, it does not occur under their conditions (pH values over 13 and temperatures below 100 °C); a more diluted alkali and a temperature higher than 100 °C are essential for isomerization.

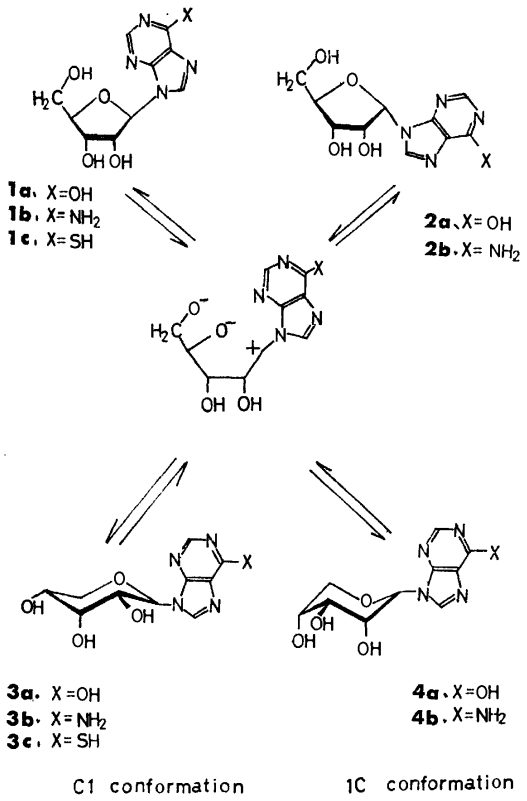

Chart 1.

The action of alkali on pyrimidine nucleosides was examined by Jones *et al.*[4] under the same conditions as with purine nucleosides; they found that thymidine is quite stable, that some amounts of urea and ammonia are formed from uridine, and that a considerable degree of deamination takes place for cytidine. These pyrimidine nucleosides did not show any clear evidence of isomerization even under the conditions where the isomerization of purine nucleosides takes place. On the other hand, an isomerization of an abnormal pyrimidine nucleoside, pseudouridine, was found in acid and in alkali by Chambers *et al.*[5]

Although both α- and β-pyranosyl anomers of pseudouridine were illustrated in the C1 form by Thomasz *et al.*,[6] the α-pyranosyl anomers of adenosine (**4b**) and **4a** were found to be in the 1C conformation, and their β-pyranosyl anomers, to be in the C1 form.

These alkaline isomerizations will be useful for the synthesis of various analogs of nucleic acid components.

Results and Discussion

Identification of 4a. Under the standard conditions, **1a** was treated in a KOH aqueous solution. The reaction mixture was fractionated by use of a column of Diaion SK1B-S, as is illustrated in Fig. 1. The I-1 and I-2 fractions are assignable to **3a** and **1a** respectively on the basis of our previous study.[1]

The I-4 fraction was found by means of tlc to be a mixture of hypoxanthine and 5-amino-1-β-D-ribofuranosyl-4-imidazolecarboxamide (AICA-riboside); this is consistent with our previous results. The new fraction, I-3, which was not clearly detected in the previous experiments,[1] was found to be a mixture of two other components: hypoxanthine and another compound which is similar to **1a** in its behavior in tlc and UV spectroscopy. The former is suspected to be a degraded product of the latter in the isolation procedure. The latter reacts with the orcinol reagent; therefore, its ribose moiety is intact. This compound was separated from hypoxanthine by means of the acetylation of the ribose moiety, followed by the extraction of the acetylated compound with dichlormethane and then deacetylation.

Table 1. The analytical data on the four isomers of 9-ribosyl adenine

Compound	R_f[a]	Mp[b] (°C)	UV maximum 0.1 M HCl	UV maximum H_2O	UV maximum 0.1 M NaOH	$[\alpha]_D$ in H_2O[c]	NMR[d] H-1′	$J_{1'2'}$/Hz
A-1	0.37	142—3 278—82[e]	257	259.5	260	−61.7 (*c*, 0.4)	5.79 d	0—1
A-2	0.32	249	257.5	260	260	−37 (*c*, 0.4)	5.74 d	8—9
A-3	0.46	130—1 225—6[e]	259	260	260	+21.5 (*c*, 1.1)	6.3 d	5.2
A-4	0.46	234—5	257.5	260	260	−59 (*c*, 0.2)	5.9 d	6.1
4b	—	—	—	—	—	— —	—	—
3b	—	254[9] 250—4[12]	258.5[12]	—	260	−37 (*c*, 0.6)[9] −32.4 (*c*, 0.28)[12]	5.72 d[12]	9.0[12]
2b	—	201[11]	257[10]	259[10]	260[10]	+24 (*c*, 0.65)[11]	6.38 d[10]	4.8[10]
1b	—	233—4[10]	257[10]	259[10]	—	−60.4 (*c*, 1.0)[10,11]	6.02 d[10]	5.9[10]

a) Tlc in solvent system *n*-BuOH-AcOH-H_2O (4 : 1 : 1). b) For the compound crystallized from water and uncorrected. c) At room temperature. d) DMSO-d_6. e) For the compound crystallized from ethanol and uncorrected.

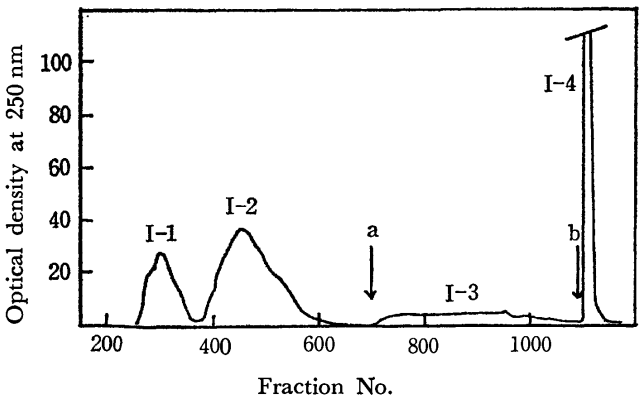

Fig. 1. The elution of UV-absorbing compounds contained in alkaline-treated inosine from the Diaion SK1B-S column with water followed 0.1 M NH_4Cl(a) and 0.1 M NH_4OH(b).
I-1 : 9-β-D-Ribopyranosyl hypoxanthine (**3a**).
I-2 : Inosine (**1a**).
I-3 : 9-α-D-Ribopyranosyl hypoxanthine (**4a**) and hypoxanthine.
I-4 : AICA-riboside and hypoxanthine.

The compound now in question has been found to be **4a** in the following way: On the thin-layer plate this compound gave a spot between those of **1a** and **3a**. On paper chromatography (PC), the acid hydrolysate gave one UV-absorbing spot (the R_f value agreed with that of authentic hypoxanthine), and also one positive spot with a periodate reagent (the R_f value agreed with that of authentic D-ribose). The UV spectrum was similar to that of **1a**, and after acid hydrolysis it came into accord with that of authentic hypoxanthine. These facts suggested that the compound was 9-α-D-ribosyl hypoxanthine. The optical rotation in water was −50°. Martinez *et al.*[7] reported the amounts of the optical rotation of four isomers of arabinosyl adenine. By comparison with their data, this compound was assumed to be α-pyranoside rather than α-furanoside because the latter is expected to have an opposite sign or at least a levorotatory value smaller than the −50° actually observed. The measurements of the NMR spectra supported this assumption. When the compound is acetylated, the signals in CD_3OD display the acetylation shifts for H-2′, 3′, and 4′. This fact means that three hydroxyl groups are attached, at C-2′, 3′, and 4′ respectively, and that the ribose ring has a pyranosyl structure. Signals appeared at 4.01 δ (J_{AB}=14 Hz, J_{AX}=2 Hz) and 4.28 δ (J_{AB}=14 Hz, J_{BX}=2 Hz), indicating that two protons of H-5′ and one proton of H-4′ are in the *gauche* relation around the C-4′—C-5′ bond. Thus, the pyranose ring was determined to have the 1C conformation. The small value of $J_{1'2'}$ (0—1 Hz) also explains well that the compound is the α-pyranoside in the 1C conformation.[8]

Thus, α-pyranoside of inosine has been found in the reaction mixture; therefore, the concomitant formation of α-furanoside is considered to be probable. However, this was not satisfactorily detected by the column chromatography. Presumably the amount is too small to be detected.

Identification of Four Isomers of Adenosine. **1b** was treated at 130 °C for 12 hr in a KOH aqueous solution whose pH was kept at 9—10. The reaction mixture gave three major spots on the thin-layer plate, as has been reported before.[1] They were suspected to be adenine, unreacted **1b**, and the β-pyranosyl isomer (**3b**) on the basis of the known results in the case of inosine. The reaction products were fractionated by a column of Dowex-1 with an eluting reagent of 25% methanol (Fig. 2). Four fractions were obtained, but adenine was not eluted from the column. Each of the four compounds from the four fractions were confirmed to be adenine nucleosides through some analytical tests such as orcinol reaction, UV spectrometry, and acid hydrolysis. The results of the individual identifications are summarized in Table 1 in comparison with the known data in the literature. In spite of a lack of available data on **4b** in the literature, the optical rotation datum of A-1 made it reasonable to identify it as **4b**, in comparison with the data on 9-D-arabinopyranosyl adenine.[1,7]

The conformations of the pyranosyl anomers (**3b** and **4b**) were determined on the basis of the chemical

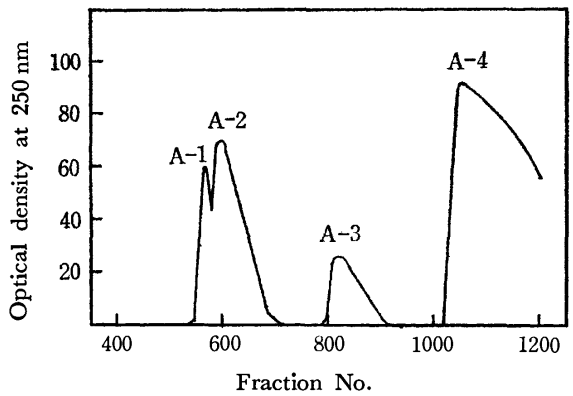

Fig. 2. The elution of UV-absorbing compounds contained in alkaline-treated adenosine from theD owex-1 column with 25% methanol.
A-1 : 9-α-D-Ribopyranosyl adenine (**4b**).
A-2 : 9-β-D-Ribopyranosyl adenine (**3b**).
A-3 : 9-α-D-Ribofuranosyl adenine (**2b**).
A-4 : 9-β-D-Ribofuranosyl adenine (adenosine, **1b**).

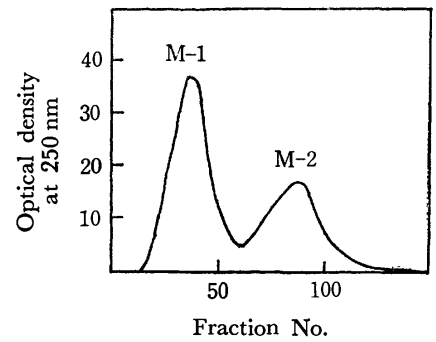

Fig. 3. The elution of UV-absorbing compounds contained in alkaline-treated 9-β-D-ribofuranosyl-6-mercaptopurine from the Dowex-50 W column with water.
M-1 : 9-β-D-ribopyranosyl-6-mercaptopurine (**3c**).
M-2 : 9-β-D-ribofuranosyl-6-mercaptopurine (**1c**).

shifts in the NMR spectra in DMSO-d_6. An NMR signal of **3b** attributable to the anomeric proton appears at 5.74 δ, and the coupling constant, $J_{1'2'}$, is found to be 8—9 Hz. Since such a large coupling constant could only be expected for an axial-axial interaction between the protons on C-1′ and C-2′, **3b** was unambigously identified as β-ribopyranoside in the C1 conformation as was determined by Pan *et al.*[12] On the other hand, the 1C conformation of **4b** was corroborated on the basis of the signals of two protons for H-5′ after acetylation. The H-5′ and H-4′ protons appear as ABX-type signals at 4.04 δ (J_{AB}= 14 Hz, J_{AX}=2 Hz) and 4.38 δ (J_{AB}=14 Hz, J_{BX}= 2 Hz).

Isolation of ***1a*** *from Alkaline-treated* ***3a***. The isomerization of **3a** to give **1a** was confirmed. The reaction mixture which was obtained by heating **3a** at 150 °C for 6 hr at pH 10 was subjected to column chromatography on a Dowex-50W column. Subsequent elution with 0.001 M NH_4Cl gave two UV-absorbing fractions; the first one is considered to be the unreacted starting material, and the second, **1a**. The crystals obtained from the latter fraction were identified as **1a** on the basis of the R_f value on the tlc and the X-ray diffraction pattern of its anhydrous α-crystal form.[13]

*Preparation of 9-β-D-Ribopyranosyl-6-mercaptopurine (**3c**).* **3c** was obtained through the isomerization of **1c**. The products were fractionated by column chromatography on a Dowex-50W column (Fig. 3). The two UV-absorbing fractions (M-1 and M-2) were obtained upon elution with water. The first was assigned to **3c**, and the second, to the original **1c**, on the basis of an analogy with the fractionation of alkaline-treated inosine. The mobilities of these two fractions on tlc supported these assignments. It is empirically established that the β-pyranosyl isomer shows a little less mobility than that of the corresponding β-furanosyl one on tlc and PC in the *n*-butanol–acetic acid–water (4 : 1 : 1) solvent system. From the M-1 fraction, needle crystals were obtained. The UV spectrum of this compound was found to be similar to that of **1c**. The results of elementary analysis and mass spectrometry after trimethylsililation were consistent with what would be expected for **3c**. An NMR signal of **3c** attributable to the anomeric proton appears at 5.62 δ, with a large coupling constant, $J_{1'2'}$, of 9 Hz; this can be explained unambigously by the fact that **3c** is β-pyranoside in the C1 conformation.

Alkaline Treatment of Various Nucleosides. Tables 2 and 3 summarize the reaction products of various nucleosides with alkali. All the reaction mixtures of adenosine, guanosine, and xantosine gave three major UV-absorbing spots on the chromatograms corresponding to the base, β-pyranoside, and unreacted β-furanoside. Usually too few of the α-isomers of these nucleosides were produced for their spots to be given clearly on the chromatograms.

1a and **1c** exhibit more complicated reactions. They are cloven at C-2 of the purine ring, giving 5-amino-4-imidazolecarboxamide (AICA) derivatives as has been reported in the previous paper. The AICA derivatives are detectable by means of the NBDF-reagent,[1] giving a purple-red color on the chromatogram. Isomerization was observed in competition with these degrading reactions. The substitution also took place in the case of **1c**, giving **1a**.

9-β-D-Arabinofuranosyl adenine and 9-β-D-xylofuranosyl hypoxanthine are also considered to isomerize in alkali in a way similar to that of purine ribonucleosides on the basis of the presence of a characteristic UV-absorbing spot located a little lower than that of the original furanoside on the chromatogram. A change in the sugar moiety from ribose to arabinose or from ribose to xylose of the purine nucleoside does not exert any significant effect on the isomerization.

However, the substitution of the sugar 2′-hydroxyl group serves to prevent the isomerization. 2′-*O*-Methyladenosine gave only adenine and no other UV-absorbing products under the same conditions as when adenosine gives its β-pyranoside. 2′-Deoxyinosine is hydrolyzed completely and gives a large amount of hypoxanthine and a small amount of a NBDF-reagent-positive compound. The latter is considered to be AICA-2′-deoxy-riboside from the fact that λ_{max} in 0.1

TABLE 2. THE REACTION PRODUCTS OF ALKALINE TREATED PURINE NUCLEOSIDES[a]

Nucleoside	R_f[b]	Yield(%)[c]	Products
Inosine	0.35	3	Hypoxanthine
	0.31[i]	17	AICA[d]-riboside
	0.22	64	SM[e] **1a**
	0.22	0.7	α-Inosine(P)[f] **4a**
	0.19	11	Inosine(P) **3a**
Adenosine	0.56	20	Adenine
	0.46	58	SM **1b**
	0.46	2	α-Adenosine **2b**
	0.37	0.8	α-Adenosine (P) **4b**
	0.32	10	Adenosine(P) **3b**
6-MP[g]-riboside	0.51[j]	—	AITCA[h]
	0.42[j]	—	AITCA-riboside
	0.30[i]	—	AICA-riboside
	0.27[j]	—	SM **1c**
	0.22[j]	—	6-MP-riboside(P) **3c**
	0.19	—	Inosine
Guanosine	0.24	12	Guanine
	0.19	71	SM
	0.14	8	Guanosine(P)
Xantosine	0.32	2	Xanthine
	0.20	78	SM
	0.13		Xantosine(P)
Arabinosyl adenine	0.56	2	Adenine
	0.39	85	SM
	0.26	13	Arabinosyl adenine(P)
Xylosyl hypoxanthine	0.35	5	Hypoxanthine
	0.27[i]	24	AICA-xyloside
	0.20	47	SM
	0.11	24	Xylosyl hypoxanthine(P)
Inosine(P)	0.41[i]	trace	AICA
	0.34	1	Hypoxanthine
	0.32[i]	1	AICA-riboside
	0.27[i]	22	AICA-riboside(P)
	0.22	5	Inosine
	0.19	68	SM

a) Treated in aq. KOH (pH 10) at 130 °C for 6 hr except adenosine (12 hr) and guanosine (additional 4 hr at 140 °C). b) UV-absorbing spots on tlc. Solvent system, *n*-butanol–acetic acid–water (4 : 1 : 1). c) See experimental section. d) 5-Amino-4-imidazolecarboxamide. e) Starting material remained. f) Pyranoside. g) Mercaptopurine. h) 5-Amino-4-imidazolethiocarboxamide. i) Purple-red color development by NBDF reagent. j) Circle white spot appeared by NBDF reagent.

TABLE 3. THE REACTION PRODUCT OF ALKALINE TREATED SOME NUCLEOSIDES[a]

Nucleoside	R_f[b]	Yield(%)[c]	Products
2'-Deoxyinosine	0.40[f]	trace	2'-Deoxy-AICA-riboside
	0.36	71	Hypoxanthine
2'-Deoxyguanosine	0.31	75	SM[d]
	0.26	—	Guanine
	0.18	trace	Unknown
	0.11	trace	Unknown
2'-*O*-Methyl-adenosine	0.75	90	SM
	0.63	4	Adenine
Ip[e]-inosine	0.80[f]	30	Ip-AICA-riboside
	0.70	17	SM
	0.39[f]	trace	AICA
	0.34	1	Hypoxanthine
	0.32[f]	trace	AICA-riboside
	0.25	—	Inosine
	0.23[f]	trace	Unknown
AICA-riboside	0.40[f]	1	AICA
	0.31[f]	87	SM
Uridine	0.55	2	Uracil
	0.38	52	SM
Cytidine	0.55	—	Uracil
	0.38	—	Uridine
	0.34	—	SM
Thymidine	0.70	trace	Thymine
	0.63	84	SM

a) Treated in aq. KOH (pH 10) at 130 °C for 6 hr except uridine (12 hr), thymidine (13 hr), AICA-riboside (42 hr) and Ip-inosine (additional 11 hr at 160 °C at pH 10.5). b) UV-absorbing spots on tlc. Solvent system, *n*-butanol–acetic acid–water (4 : 1 : 1). c) See experimental section. d) Starting material remained. e) 2',3'-isopropylidene. f) Purple-red color development was observed with NBDF reagent.

M NaOH (267.5 nm) is similar to that of AICA-riboside (268 nm) and unlike that of AICA (278.5 nm) and from the fact that the presence of deoxysugar was proved by the method of Buchanan.[14] 2'-Deoxyguanosine was more stable than 2'-deoxyinosine, and no evidence of isomerization was observed. Some guanine and a trace amount of an unknown compound were obtained. 2',3'-Isopropylidene-inosine gave several spots (Table 3); however, none of them was considered to be responsible for the isomerization.

The isomerization was also significantly affected by a change in the base moiety from purine to pyrimidine or from purine to imidazole. Thymidine was found to be resistant against alkali, and even when the reaction period was prolonged up to 12 hr, no spot was observed except that of the starting material and a trace of thymine. Uridine was less resistant than thymidine; however, no UV-absorbing products could be detected except uracil. No effect was found even under more severe conditions (1 M KOH, 140 °C, 6 hr). In the case of cytidine, deamination followed by hydrolysis at the glycosyl bond was dominantly observed under the standard conditions, so that chromatography revealed three UV-abosorbing compounds corresponding to uridine, uracil, and cytidine. AICA-riboside was also resistant against alkali; even when it was reacted for 42 hr, the only reaction product was found to be AICA. The above four nucleosides showed no evidence of isomerization, even though the starting pH of the solution was changed from 10 to 8 or 12.

Reaction Mechanism. The available information concerning the alkaline isomerization of usual nucleosides is insufficient for us to determine clearly its reaction mechanism. One of the most important pieces of information is that the isomerization takes place only for 2'-hydroxypurine nucleosides. The C-2' hydroxyl group is known to be the most acidic hydroxyl group of the three OH groups in the ribofuranoside.

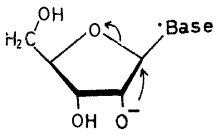

Chart 2. C-2′ Oxyanion participation of β-nucleoside for cleavage of sugar ring at C-1′.

It is supposed that the formation of the carbonium ion at C-1′ is facilitated by the anchimeric assistance[15] of an ionized hydroxyl group at C-2′, and that then the isomerization proceeds (Chart 2). The final equilibrium state of the four isomers and the rate of the reaction are not known.

Garret *et al.*[3] reported that adenosine and 2′-deoxyadenosine in an alkaline solution (pH higher than 13) have almost equal rates of hydrolysis at the glycosyl bond. Therefore, it may be supposed that the oxyanion participation affects only the cleavage of the sugar-ring bond at C-1′, while it does not affect that of the glycosyl bond.

The dissociation constant, pK_a, of the ribose moiety in nucleosides is approximately 12, and the isomerization in question is dependent on the pH of the solution. The optimum pH is between 7 and 12, about 10.[16] This pH range results from the competition among several parallel and sequential reactions, and outside this pH range these concomitant reactions occur in preference to isomerization. It has not been demonstrated whether or not the rate of isomerization would depend on the concentration of the hydroxyl ion, because parallel reactions, for example, hydrolysis, disturb the system.

It has not yet been explained why pyrimidine nucleosides do not isomerize, while purine nucleosides do.

Experimental

Materials and Equipment. The **1a**, **1b**, guanosine, and AICA-riboside used were commercial products of the Ajinomoto Co., Inc. The xantosine, uridine, cytidine, and 9-β-D-arabinofuranosyl adenine used were reagents of the Nutritional Biochem. Corp. The 2′-deoxyinosine and 2′-deoxyguanosine were obtained from Sigma Chemicals. The 2′,3′-isopropylideneinosine and 9-β-D-xylofuranosyl hypoxanthine were supplied by Dr. Akihiro Yamazaki of this department. The **3a** and **1c** were prepared according to the method described in the preceding paper[1] and according to the method of J. J. Fox *et al.*[17] respectively. The **1b** was methylated by the method of Martin *et al.*[18]; however, the separation of 2′-*O*-methyladenosine from the 3′-isomer by this method was unsatisfactory. It was, though, achieved with a method similar to that described by Gin *et al.*[19] The pHs of the solutions were measured at room temperature. The NMR spectra were recorded at 100 MHz with a Varian XL-100 spectrometer, using TMS as the internal standard. The melting points were measured by the use of a Yanagimoto MP-S2 apparatus and are uncorrected.

PC and Tlc. One-dimensional ascending PC on Toyo-Roshi No. 51A for quantitative analysis, and tlc on DC-Fertigplatten Cellulose F for qualitative analysis, were both carried out in the *n*-butanol–acetic acid–water (4 : 1 : 1) solvent system. Whichever chromatography was used, paper or thin-layer, similar R_f values were obtained for the same compounds. A paper or a plate was thrice developed if necessary to separate the components completely on the chromatogram. The components of the reaction mixture were detected on the paper or plate by two methods: (a) absorption in UV light, and (b) color development with a NBDF reagent[1] for the detection of diazotizable amines.

Conditions of Alkaline Treatment. The compound was dissolved in aq. KOH (1.5—4 g/dl), and the pH was adjusted to 10. Unless otherwise stated, a solution was heated at 130 °C for 6 hr in a sealed stainless steel tube on an oil bath. Adenosine and AICA-riboside were reacted for 12 hr and 42 hr respectively. The tube was removed from an oil bath after 2—3 hr, and the decreased pH of the solution was corrected to 10. The pH was corrected two times 2 hr and 6 hr after heating for adenosine and six times, at six-hour intervals, for AICA-riboside. Guanosine was subjected to further heating for 4 hr at 140 °C in addition to that under the standard conditions. In the cases of some nucleosides, several different conditions were also employed where the initial pH of the solution was changed. Two solutions (pH 9.6 and 11.3) of AICA-riboside were heated at 130 °C for 42 hr, and two solutions (pH 8.6 and 11.5) of cytidine, at 130 °C for 6 hr. Uridine was heated at 140 °C for 6 hr in 1 M KOH.

Determination of the Yields of the Products. Samples of the reaction mixtures were made up to appropriate volumes with water and submitted to PC. The spots of the samples and available authentic references, which were developed on the same paper with the samples, were cut off, together with their appropriate blanks, and eluted in 0.1 M HCl. The optical density of the eluent at the wavelength of the maximum absorption of each component was measured. The percentage of the remaining original material and the products, which were obviously identified as known compounds by means of the R_f values and UV spectra, were calculated from the optical density of the spots of the samples, which were compared with that of each authentic standard reference. The percentages of the products were converted into those of the original compound by the use of the equivalent mole ratio. The yields in Tables 2 and 3 were obtained by this procedure except in the cases of **4a**, **2b**, and **4b**. The yields of these three compounds were roughly calculated from the optical density of the individual fraction, and the molar extinction coefficients were assumed to be 12,000. The recovery yields of **1a** and **1b** were corrected by the subtraction of the above yields of **4a** and **2b** respectively because they are not separable on PC.

*Isolation of **4a**.* **1a** (5 g) was dissolved in 125 ml of 0.2 M KOH and heated at 130 °C for 2 hr. A few drops of 1M KOH were added to correct the pH of the solution to 10.0. After the reaction had been continued for another 4 hr, the mixture was made acid (pH 2) with conc. HCl and applied to a column (28 cm × 3 cm) of Diaion SK1B-S (H-form, 50—100 mesh). The column was eluted with 7 l of water. Each 20-ml fraction was collected. The first and second UV-absorbing peaks were obtained within 7 l. When an eluting reagent was changed to 3.9 l of 0.1 M NH_4Cl, a third peak was obtained. It was composed of two components on tlc, the one was hypoxanthine (R_f 0.35), and the other, a compound closely resembling inosine (R_f 0.22). A fourth, obtained by the use of an eluting reagent of 0.1 M ammonia, was a mixture of hypoxanthine and AICA-riboside (R_f 0.31). The fractions between No. 718 and No. 1,080 in the third peak were collected, neutralized with 1 M NaOH, and concentrated *in vacuo*. The resultant solution was applied to a column (30 cm × 0.7 cm) of granular activated carbon (Tsurumi-Coal GVA-80) in order to eliminate

inorganic salts passing through the column. The column was then eluted with a solvent mixture (1 : 1) of ethanol and 20% aq. ammonia. The eluate was concentrated *in vacuo* to dryness. The residue was dissolved in a small portion of pyridine and added to the same volume of acetic anhydride for acetylation. After refluxing for 1 hr, the solution was allowed to stand for 30 min at room temperature. To the solution some portion of ethanol was added and then it was evaporated *in vacuo*. The addition of ethanol to the solution and the evaporation of the resultant mixture were repeated several times, and finally it was evaporated to dryness. The residue was extracted with CH_2Cl_2, and the extract was evaporated to dryness, giving an acetylated compound. This compound was dissolved into ammonia-saturated methanol for deacetylation. The solution was then allowed to stand overnight and concentrated *in vacuo* to dryness. The resultant solid was extracted with $CHCl_3$ in order to remove the acetamide. The remaining solid was dried for analysis. (a) R_f on tlc. (thrice-developed) 0.39, for control inosine 0.43 and β-pyranoside 0.33. (b) UV_{max}; 249.2 nm in 0.1 M HCl, 248.2 nm in H_2O, and 253.9 nm in 0.1 M NaOH, for control, inosine corresponds to 249.9 nm, 249.2 nm and 254.5 nm respectively. (c) Components of acid hydrolysate: The compound was refluxed for 1.5 hr in 4 M H_2SO_4 followed by neutralization with $Ba(OH)_2$ and filtration of the resultant $BaSO_4$. UV_{max}; the values of 249.5 nm, in 0.1 M HCl and 264.5 nm in 0.1 M NaOH agreed with those of hypoxanthine. PC; an UV-absorbing spot, R_f 0.35 (hypoxanthine). A positive spot with a periodate reagent, R_f 0.33 (D-ribose). (d) Optical rotation. $[\alpha]_D^{20}$ −50° (c, 0.2, water). (e) NMR. (DMSO-d_6) δ 8.09 (H-2), 8.32 (H-8), 5.75 (H-1′, d, $J_{1'2'}$=0—1 Hz), 3.7—4.0 (broad, m); the acetylated compound (CD_3OD), δ 4.01 (J_{AB}=14 Hz, J_{AX}=2 Hz) and 4.28 (J_{AB}=14 Hz, J_{BX}=2 Hz) for two protons of H-5′.

Four Isomers of Adenosine. **1b** (5 g) was dissolved in 120 ml of 0.005 M KOH at 60 °C and heated in a sealed tube at 130 °C for 2 hr. The pH of the solution varied from 10.0 to 9.4 during the reaction period. A few drops of 1 M KOH were added to correct the pH to 10.0, and then the reaction was continued for another 4 hr. The pH of the solution decreased again to 8.9. After the pH adjustment, the reaction was continued for 6 hr more. When the reaction mixture was submitted to tlc, three major UV-absorbing spots were obtained (R_f 0.56, 0.46, 0.32). Then the reaction mixture was neutralized with conc. HCl and submitted to a column (36 cm×3 cm) of Dowex-1, X-4, (OH-form, 200—400 mesh). The column was eluted with 25% (w/v) methanol. Each 4-ml fraction was collected. Four UV-absorbing fractions were obtained. The first fraction (from No. 551 to No. 580), the second (from No. 581 to No. 700), the third (from No. 795 to No. 910), and the fourth (from No. 1,011 to No. 1,200) were severally concentrated to dryness *in vacuo*, and the residues were recrystallized from water. Two of them (A-1 and A-3) were finally crystallized from ethanol. The results of the analysis are summarized in Table 1. Pieces of the four compounds were individually hydrolyzed in 6 M HCl at 80 °C for 1 hr. The four hydrolysates all showed, on PC, one UV-absorbing spot (R_f 0.56) (adenine) and one positive spot (R_f 0.33) with a periodate reagent (D-ribose). NMR: Compound A-**1** (DMSO-d_6), δ 8.18(H-2), 8.39(H-8), 7.26(NH_2-6), 5.79(H-1′, d, J_{AB}=14 Hz); an acetylated compound ($CDCl_3$), δ 4.04 (J_{AB}=14 Hz, J_{AX}=2 Hz) and 4.38(J_{AB}=14 Hz, J_{BX}=2 Hz) for two protons of H-5′.

*Isomerization of **3a**.* **3a** (10 g) was dissolved in 250 ml of 0.15 M KOH to give a solution with a pH of 10. When the solution was heated at 150 °C for 3 hr, the decreased pH (8.4) of the solution was corrected to 10 with 13 ml of 1 M KOH. After further heating for 3 hr, the reaction mixture was acidified to pH 4 with 1 M HCl and submitted to a column (53 cm×3.1 cm) of Dowex 50W X-4 (H-form, 100—200 mesh). The column was washed with 2 l of water, and then eluted with 0.001 M NH_4Cl. Each 20-ml fraction was collected. The first UV-absorbing fraction was obtained from No. 260 to No. 370, and the second, from No. 450 to No. 590. The latter fraction was concentrated *in vacuo* until 3 ml and cooled for crystallization overnight. Subsequent recrystallization from water gave 50 mg (dried in a desiccator) of needle crystals. PC: R_f 0.23. UV_{max}: 250 nm in 0.1 M HCl, 249 nm in H_2O, 254 nm in 0.1 M NaOH. The X-ray (Cu$K\alpha$) diffraction pattern: α-form of inosine.[12]

*Preparation of **3c**.* To 50 ml of 0.01 M KOH, **1c** (1 g) was added and the pH was adjusted to 10.2 with a few drops of 1 M KOH. The solution was heated in a sealed tube at 130 °C for 6 hr. The reaction mixture was neutralized with 1 M HCl, concentrated *in vacuo* to 10 ml, and submitted to a column (40 cm×1.3 cm) of Dowex-50W (H-form, 50—100 mesh). The column was eluted with 1.6 l of water. Each 10-ml fraction was collected. The first and second UV-absorbing peaks appeared from No. 20 to No. 60 and from No. 61 to No. 110 respectively. The first fractions were concentrated *in vacuo* until 2 ml and then allowed to stand in an ice box overnight for crystallization. The precipitated crystals were filtered and recrystallized from water. Needle crystals were thus obtained (47 mg). Found: C, 41.90; H, 4.32; N, 19.56%; Calcd for $C_{10}H_{12}N_4O_4S \cdot 0.2\,H_2O$: C, 42.25; H, 4.23; N, 19.72%. Mp 232—233 °C. UV_{max}; 317.5 nm at pH 7. Mass: M^+ 500 (trimethylsililated). NMR (DMSO-d_6): δ 5.62 (H-1′, d, $J_{1',2'}$=9.0 Hz), 1.14 (SH-6).

We wish to thank Dr. Masatsune Kainosho and Dr. Akihiro Yamazaki in this department for their valuable suggestions. We are also indebted to Professor Dr. Masamichi Tsuboi of Tokyo University for reading the manuscript.

References

1) Y. Suzuki, This Bulletin, **47**, 898 (1974).
2) A. S. Jones, A. M. Mian, and R. T. Walker, *J. Chem. Soc.*, 692 (1966).
3) E. R. Garret and P. J. Mehta, *J. Amer. Chem. Soc.*, **94**, 8542 (1972).
4) A. S. Jones, A. M. Mian, and R. T. Walker, *J. Chem. Soc. C*, **1966**, 1784.
5) R. W. Chambers, V. Kurkov, and R. Shapiro, *Biochem.*, **2**, 1192 (1963).
6) M. Tomasz, Y. Sanno, and R. Chambers, *ibid.*, **4**, 1710 (1965).
7) A. P. Martinez, W. W. Lee, and L. Goodman, *J. Org. Chem.*, **34**, 92 (1969).
8) T. D. Inch, "Annual Reports on NMR Spectroscopy," Vol. 5A, ed. by E. F. Mooney, Academic Press, London and New York (1972), p. 305.
9) M. Viscontini and S. Huwyler, *Helv. Chim. Acta*, **43**, 782 (1960).
10) K. Onodera, S. Hirano, and F. Masuda, *Carbohyd. Res.*, **4**, 263 (1967).
11) R. S. Wright, G. M. Tener, and H. G. Khorana, *J. Amer. Chem. Soc.*, **80**, 2004 (1958).
12) Y. H. Pan, R. K. Robins, and L. B. Townsend, *J. Heterocyclic Chem.*, **4**, 246 (1967).

13) Y. Suzuki and N. Nagashima, This Bulletin, **43**, 1600 (1970).
14) J. G. Buchanan, *Nature*, **168**, 1091 (1951).
15) S. Winstein and E. Grunwald, *J. Amer. Chem. Soc.*, **70**, 828 (1948).
16) Y. Suzuki, This Bulletin, **47**, 2469 (1974).
17) J. J. Fox, I. Wempen, A. Hampton, and I. L. Doerr, *J. Amer. Chem. Soc.*, **80**, 1669 (1958).
18) D. M. G. Martin, C. B. Reese, and G. F. Stephenson, *Biochem.*, **7**, 1406 (1968).
19) J. B. Gin and C. A. Dekker, *ibid.*, **7**, 1413 (1968).

Alkylation of Phenols. II. The Selective Formation of Thymol from *m*-Cresol and Propylene with a γ-Alumina Catalyst

Masahiro NITTA, Kazuo AOMURA, and Katsumi YAMAGUCHI

Faculty of Engineering, Hokkaido University, Sapporo 060

(Received February 16, 1974)

The alkylation of *m*-cresol with propylene was carried out over a γ-alumina catalyst in a flow system under atmospheric pressure. It was found that the composition of the thymol mixture thus obtained was greatly *ortho*-rich. It was also observed that the catalytic activity varied with the temperature and the atmosphere for the calcination of the catalyst, whereas the selectivity for thymol formation was almost constant at about 90% at the reaction temperature of 250 °C. It has been established that thymol can be obtained selectively by vapor-phase alkylation over a commercial γ-alumina catalyst under appropriate reaction conditions. Furthermore, the active sites of γ-alumina for this reaction were investigated by the poisoning technique with acids and bases. It was suggested that, for the alkylation, the Lewis-acid sites (surface aluminum) and the adjacent acid sites (surface hydroxyl) are necessary. The mechanism of the alkylation on those sites is also discussed.

In the first part of this series the present authors reported their results on the vapor-phase alkylation of *m*-cresol with propylene over supported metal sulfate catalysts.[1] It was shown that the activity of the catalyst depended on the catalyst acidity, and that the selectivity of the catalyst for thymol formation seemed to be affected by the surface structure of the catalyst. However, experimental research to obtain thymol in higher yields has been required, because thymol is the raw material of an important perfumery, menthol.

On the other hand, it is well known that γ-Al_2O_3 has acidity[2-5] and promotes the reaction of phenol with alcohols;[6,7] recently the structure and orientation of phenols chemisorbed on γ-Al_2O_3 have been reported.[8] No method of synthesizing thymol using this catalyst is found in the literature. It is, therefore, of particular interest to examine the activity and selectivity of γ-Al_2O_3 for the said reaction.

The present paper will describe the results on the γ-Al_2O_3 catalyst, which shows quite a good thymol selectivity. Descriptions will also be given of the active sites of the catalyst for the alkylation, as well as discussions of the reaction mechanism.

Experimental

Materials. Commercial *m*-cresol was vacuum-distilled under an atmosphere of nitrogen; the purity was estimated to be over 99.5% by means of gas chromatography. Propylene, with a purity of over 99%, was obtained from the Mitsubishi Petrochemical Co., Ltd.

Catalyst. AE-11-type γ-Al_2O_3 obtained from the Nishio Industries Co., Ltd., was used. The alumina was pellected, crushed, and sized in 10—20 mesh, and then it was heat-treated before reaction at a temperature between 250 and 900 °C for 3 hr in an atmosphere of nitrogen, oxygen, hydrogen, or air. When the calcination temperature was below 500 °C, the catalyst was heated in a glass tube reactor, while when it was above 500 °C, it was calcined in a crucible in the air.

Analysis. The liquid products obtained were analyzed by gas chromatography (GC) and identified by a comparison of their chromatograms with those of authentic samples. The conditions for the analysis have been described in a previous report (Part I).[1] The analysis of the gaseous products was done by another GC with a column containing DMF on Chromosorb AW (8 m, 0 °C).

Measurement of the Surface Properties. The surface acidity of the catalyst was determined by the usual titration method with *n*-butylamine and Hammett indicators and by the color change of *p*-phenylenediamine.[9] The specific surface area of the catalyst was measured by the BET method using the N_2 adsorbate. The X-ray powder diffraction patterns of the catalyst was taken using filtered copper $K\alpha$ radiation.

Apparatus and Procedure. The same continuous-flow apparatus as has been described in Part I was used. The reaction was carried out in the same manner as has been described in Part I. In the experiments to investigate the poisoning effect of the acid or base agent, the reagent was introduced into the catalyst bed before the reaction. After the injection, the carrier gas was made to flow for 30 min; the alkylation reaction was then carried out.

The activity of the catalyst was expressed in terms of the conversion of *m*-cresol; it was taken at the highest conversion, which usually occurred after 1 or 2 hr of process time.

The selectivity of the catalyst defined as below did not change with the process time, except at the start of the reaction:

$$\text{Selectivity} = \frac{\text{thymol}}{(\text{thymol isomers}) - (\text{unknown})} \times 100 \ (\%)$$

Results and Discussion

The material balance of the reaction of *m*-cresol and propylene was first investigated at the reaction temperature of 250 °C using γ-Al_2O_3 calcined at 300 °C in an N_2 stream. Over 90% of the reacted propylene was obtained in the form of alkylates. All of the *m*-cresol was recovered in the liquid product. Some of the lost propylene would be consumed by the polymerization and cracking to produce other hydrocarbons. Practically, propane was detected in the exhaust gas. The products obtained in this alkylation, except at higher reaction temperatures, are as follows:

The influence of *iso*-thymol on the results below 300 °C could be neglected because its amount almost held constant at about 2% of all the alkylates. There was also an unknown peak at the end of the gas chromatogram; it was estimated to be a polyalkylate (U) such as 2,6-diisopropyl-5-methylphenol. The amount of U did not exceed 10%* of all the alkylates.

* We assumed the relative mole sensitivity of U to be the same as that (0.78) of thymol isomers to *m*-cresol.

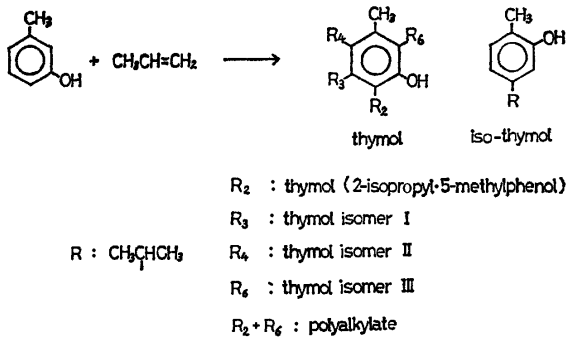

Both the methyl and hydroxyl groups in benzene nuclei are known to have a *para*/*ortho* orientation effect; most of the products may be, therefore, considered to be *ortho* and *para* isomers with respect to the hydroxyl of *m*-cresol. In the present case, however, the *ortho* alkylates, *i.e.*, thymol and III, were formed in much excess, as will be shown below (Fig. 1).

The catalytic activity changes gradually with the process time, as is shown in Fig. 1. This method of activity change is similar to that observed in the alkylation by zeolite catalysts,[10,11] but not in that by metal sulfate catalysts.[1] This may be due to the existence of an induction period and the catalyst aging.

Surprisingly, in many runs, the selectivity of the γ-Al_2O_3 catalyst for thymol formation had the high value of about 90%, much more than that of the metal sulfate catalyst.[1] In the case of the liquid-phase reaction using a protonic acid catalyst or the Friedel-Crafts catalyst, the thymol selectivity is about 70%.[12]** In addition, those catalysts have the disadvantage of the corrosion of reaction facilities. In this process, the problem does not exist. It can, consequently, be accepted that γ-Al_2O_3 is the most suitable catalyst for the selective formation of thymol.

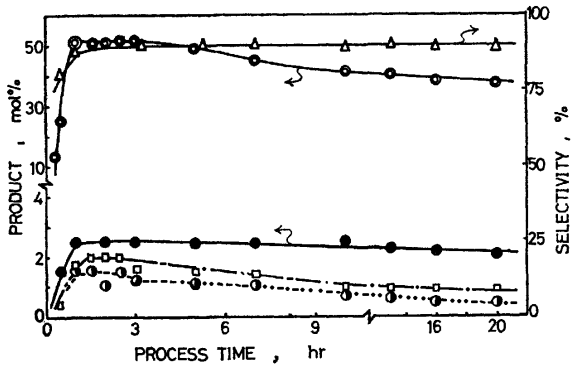

Fig 1. Activity and selectivity changes with process time.
Conditions: W/F=19.5 g·hr/mol, reaction temp=250 °C, propylene/*m*-cresol=1.0 mol/mol. Catalyst: γ-Al_2O_3 calcined at 300 °C. ◎: thymol, ◑: I, □: II, ●: III, △: thymol selectivity.

** Kolka *et al.* have obtained *o*-alkylphenol selectively in the presence of aluminum phenoxide-type catalyst in liquid phase.[13] For example, in the reaction of phenol and ethylene, 2-ethylphenol and 2,6-diethylphenol selectivities were 68% and 29% respectively (using the same selectivity as we defined here).

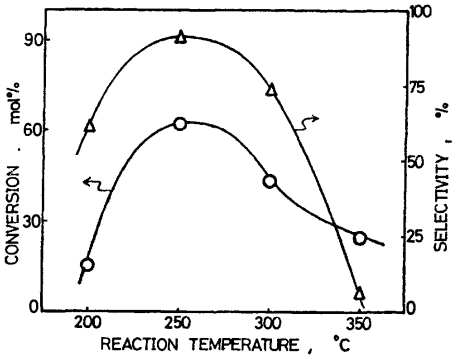

Fig. 2. Effect of reaction temperature on conversion and selectivity.
Conditions: W/F=19.5 g·hr/mol, propylene/*m*-cresol=1.0, calcination temp=400 °C.
○: conversion of *m*-cresol, △: thymol selectivity.

The effects of the reaction conditions on the catalytic activity and selectivity were investigated in detail using the γ-Al_2O_3 calcined at 300 and 400 °C. Furthermore, the active sites and reaction mechanism were discussed.

Effect of the Reaction Temperature. The effect of the reaction temperature on the selectivity of thymol formation was investigated with the γ-Al_2O_3 calcined at 400 °C under a constant contact time (W/F) and a constant mole ratio of reactants. The results are shown in Fig. 2. The optimal reaction temperature was 250 °C. At temperatures higher than 250 °C, the conversion of *m*-cresol decreased with the rise in the temperature. This is attributed to a side reaction, such as the polymerization of the alkylating agent. Further, the selectivity of thymol formation also decreased suddenly because of the formation of many unknowns in addition to U. Many of the unknwons may be alkylates with secondary alkylating agents which are produced by the above side reactions of propylene, or transalkylates. However, the amount of the unknwons was below 10%, as is shown by the single symbol in the right top of Fig. 3.

Figure 3 shows the relation between the reaction temperature and the product distribution. The increase in *iso*-thymol at higher temperatures indicates the occurrence of isomerization or disproportionation.

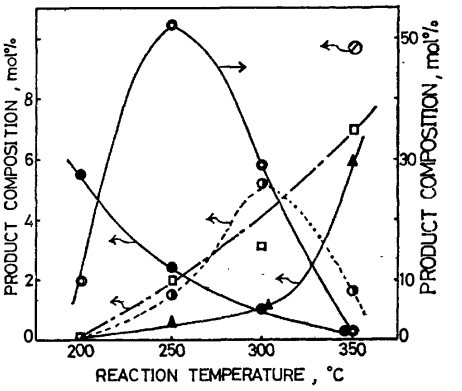

Fig. 3. Relation between reaction temperature and product composition.
Conditions are the same as in Fig. 2.
▲: *iso*-thymol, other symbols are defined in Fig. 1.

Thymol isomer III seems to be unstable energetically and transforms into other thymol isomers at higher temperatures.

Effect of the Contact Time. As an indication of contact time, we used W/F, defined as follows:

$$W/F = \frac{\text{catalyst weight (g)}}{\text{feed rate of reactants (mol/hr)}}$$

The effect of W/F on the convresion of *m*-cresol and on the thymol formation are presented in Fig. 4. The largest conversion was obtained at $W/F \approx 40$. Above this W/F value, there was no noticeable change in the conversion or in the selectivity. The thymol selectivity was constant; it was maintained at a high value of 90% except at low contact times.

At low contact times, thymol and III were formed predominantly and the formation of I and II was very small. With higher contact times, however, the formation of III decreased, while those of thymol, I and II increased. Finally, at $W/F > 20$ the yield of thymol became almost constant. The isomerization of thymol (cyclohexane solution) was carried out using a nitrogen carrier instead of propylene under the same conditions as the alkylation. The resulting products were *m*-cresol, isopropylphenol, I and II, and the unknowns including U. It is, consequently, almost certain that the isomerization and the disproportionation of thymol and III take place during the reaction. It was difficult to estimate the equilibrium composition of thymol isomers in the present experiment because of the unknowns produced.

Effect of Mole Ratio of Reactants. The conversion of *m*-cresol increased with the increase in propylene in the reactant mixture, as is shown in Fig. 5. The thymol selectivity did not change with the mole ratio of propylene to *m*-cresol, whereas *iso*-thymol and U increased. From the standpoint of selective thymol formation, the optimal mole ratio is 1.0.

From these results, the reaction conditions were so chosen that the conversion was large and the thymol selectivity was the highest. The optimal conditions

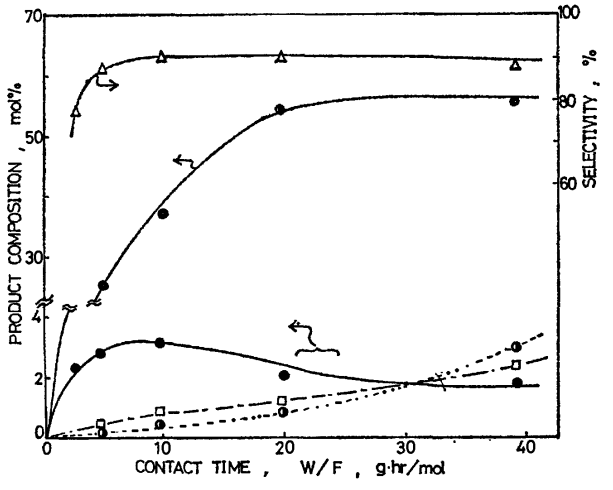

Fig. 4. Effect of change of contact time.
Conditions: reaction temp=250 °C, propylene/*m*-cresol=1.0, calcination temp=300 °C.
Symbols are defined in Figs. 1 and 2.

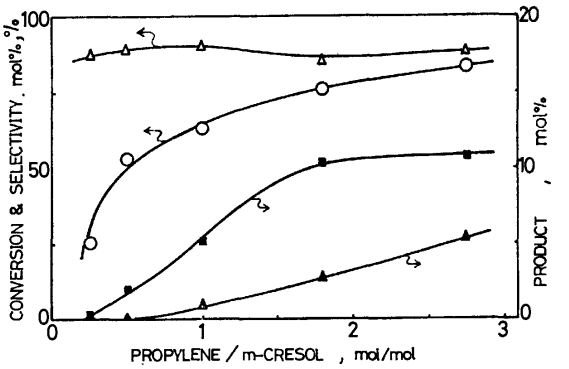

Fig. 5. Effect of mole ratio of reactants (propylene/*m*-cresol).
Conditions: W/F=19.5 g·hr/mol, reaction temp=250 °C, calcination temp=300 °C. ▲: *iso*-thymol, ■: unknown (polyalkylate). Other symbols are defined in Fig. 2.

are as follows:

W/F = 19.5 (g·hr/mol)

Reaction temperature=250 °C

Propylene/*m*-cresol=1.0 (mol/mol)

Further investigations of the active sites of the catalyst have been made under the above conditions.

Catalyst Activation. In general, the activity of solid oxide catalysts changes appreciably with the conditions for activating the catalyst—for example, the calcination temperature and the calcination atmosphere. Therefore, the activity and selectivity of γ-Al_2O_3 have been investigated over a wide range of calcination temperatures between 250 and 900 °C. The results are shown in Fig. 6. Thymol was produced selectively on every catalyst calcined between 250—900 °C. No anomalous product distribution was observed over 250—900 °C, but the activity changed appreciably. For the catalyst calcined at 250 °C, the low activity may be due to the incomplete desorption of materials, such as CO_2 and H_2O, which covered the active sites on the catalyst surface. The results of the physical-property measurements for the catalyst calcined at 900 °C re-

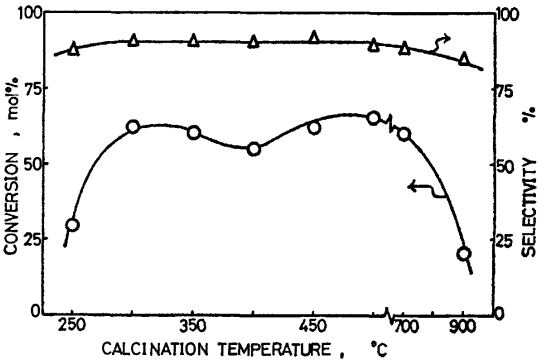

Fig. 6. Activity and selectivity of γ-Al_2O_3 catalyst calcined at various temperatures.
Conditions: calcination atmosphere=$N_2 \leqq 500$ °C, air>500 °C, reaction temp=250 °C, propylene/*m*-cresol=1.0, W/F=19.5 g·hr/mol.
Symbols are defined in Fig. 2.

Table 1. Influence of calcination atmosphere of γ-Al_2O_3

Atmosphere[a]	Conversion[b] (mol%)	Selectivity (%)
Air	47	89
N_2	63	90
H_2	56	90
O_2	0.4	75

a) Calcination temp=300 °C; 3 hr b) Conditions: W/F=19.5 g·hr/mol, temp=250 °C, propylene/*m*-cresol=1.0.

vealed that the crystal form of alumina changed from the γ to the θ type and that the surface area decreased from 154 to 84 m^2/g. These facts suggest that the differences in the surface structure among aluminas of different calcination temperatures may sensitively result in the differences in the nature of active sites. Such an effect of the calcination temperature on the surface properties of alumina has also been found in studies of the acidity.[5,14] Therefore, the activity changes with the calcination temperatures may be related to the acidity of the catalyst.

The influence of the calcination atmosphere was next examined. The results are summarized in Table 1. It was found that the catalytic activity of γ-Al_2O_3 varied with the change in the calcination atmosphere. In particular, the activity almost completely disappeared on calcining at 300 °C in an oxygen stream. The activity decrease due to the calcination in the air can apparently be explained by the influence of oxygen in the air. However, the comparison of the X-ray diffraction patterns and the surface area gave little information about the differences in the crystal form of the catalyst calcined in N_2, O_2, H_2, and air. When the catalyst was recalcined at 250 °C for 1 hr in a nitrogen stream after having been calcined at 300 °C for 3 hr in an oxygen stream, the catalytic activity and selectivity were restored to the standard level of N_2 calcination. It may, therefore, be considered that, on the sample calcined in oxygen, the adsorbed oxygen molecules would cover the active sites for alkylation.

Effect of Acid and Base Addition. It has been shown that, in addition to acid sites, basic sites exist on the surface of alumina.[15] By masking either acidic sites or basic sites it is possible to discern which sites are effective in the isopropylation of *m*-cresol. Before the reaction various acid and base reagents were added to the catalyst in the reaction system at 250 °C and their effects were examined. The results are shown in Table 2. Neither the activity nor the selectivity was changed by the addition of acidic reagents. On the other hand, basic reagents poisoned the catalyst. With the increase in the strength (pK_a value) of the added base the activity fell. Aniline, which is a weaker base, has little effect on the activity. This implies that a weak poison adsorbs reversibly on alumina; that is, the reactant molecules replace the preadsorbed poison molecules. On the contrary, the catalyst was completely deactivated by the addition of stronger bases, such as benzylamine and *n*-butylamine. The alkylation activity decreased with the increase in the amount of the base added, and the depressed activity was restored little with the process time. Therefore, the strong bases are considered to be irreversible poisons. The catalyst partially poisoned with a strong base produced only *ortho* alkylates, *i. e.*, thymol and III (60 mol% and 40 mol% respectively), though the conversion was low. Consequently, it may be concluded that the active sites promoting the isopropylation of *m*-cresol are mainly the acid sites on the γ-Al_2O_3 catalyst.

Catalyst Acidity. It is possible to confirm the existence of the Lewis-type acid sites on γ-Al_2O_3 by means of the coloration of *p*-phenylenediamine. The observed dark violet coloration of this reagent on the alumina indicates the presence of electron-acceptor sites (Lewis-acid sites in the most general sense), because its color is based on the cation radical formed from the reagent.[9] It is supposed that γ-Al_2O_3 also has weak Brönsted-type acid sites.[3] From the above results, a correlation can be expected to be seen between the activity and the acidity of each catalyst. We then tried to determine the total amount of the surface acid sites using the method of amine titration

Table 2. Effect of the addition of acidic and basic reagents

Reagent	Amount of addition (mmol)	pK_a	Conversion[a] (mol%)	Selectivity (%)	Product composition[b] (mol%) of thymol			
					Thymol	III	I	II
None	—	—	63	90	52	2.2	1.5	2.0
HCl (36%)	10	—	59	89	48	2.2	1.5	1.6
CH_3COOH	10	4.7	55	90	46	2.8	0.8	1.2
CO_2	10	—	57	89	47	2.9	1.1	1.4
H_2O	10	15.5	59	89	48	2.5	1.5	1.8
Aniline	10	4.6[c]	55	90	49	1.6	0.5	1.0
N,*N*-Diethylaniline	1	6.5[c]	42	92	37	1.7	0.3	0.8
N,*N*-Diethylaniline	10	6.5[c]	12	78	9.3	2.3	0	0.2
Benzylamine	1	9.4[c]	0.5	60	0.3	0.2	0	0
n-Butylamine	1	10.6[c]	0.4	60	0.2	0.2	0	0

a) Conditions: Temp=250 °C, W/F=19.5 g·hr/mol, propylene/*m*-cresol=1.0. b) Other products are *iso*-thymol (~1%) and an unknown(~5%). c) pK_a of the conjugated acid form.

with the Hammett indicators. However, it was very difficult to determine accurately the acidity by this method, because the catalysts were very sensitive to moisture in cooling after the calcination and in the weighing of the sample. It was, therefore, impossible to find a direct correlation between the acidity and the activity.

General Discussion

The experimental results showed that the γ-Al_2O_3 catalyst used in the present work has a considerably high selectivity for thymol formation. This seems to suggest that there are some merits of the orientation effect of reactants on the γ-Al_2O_3 surface, at least under the present experimental conditions. Thus, the model for the surface sites on alumina and that for the adsorbed state of *m*-cresol, both proposed by Medema,[5] Peri,[2,3] and Taylor,[8] can favorably be used to discuss the active sites and the reaction mechanism in the present work.

Small numbers of aluminum ions exposed to the surface as a result of the condensation of surface hydroxyl groups form L acid sites on the calcined γ-Al_2O_3. In addition, small numbers of hydroxyl ions of several types persist on the alumina surface even after the calcination at high temperatures; they form B acid sites. Taylor *et al.* showed that phenols form a strongly chemisorbed aluminum phenoxide on γ-Al_2O_3 at 300 °C. They concluded that the cresol molecule is oriented with its aromatic ring almost coplanar with the surface, but is tilted upward so that the *para* position is further from the surface than the *ortho* position. On the other hand, Cvetanovic *et al.*[16] have shown that there are two different sites on the alumina surface for the chemisorption of olefin. They considered that this is an intrinsic property of alumina catalysts. Further, they have suggested that one of the two types of adsorption sites may be Brönsted-type acid centers, and that olefin molecules adsorbed on the sites of this type could transform so as to have the character of chemisorbed carbonium ions.

Based on the above-mentioned surface models proposed by the previous workers and the results of the present work, the alkylation of *m*-cresol with propylene over γ-Al_2O_3 can be pictured as follows:

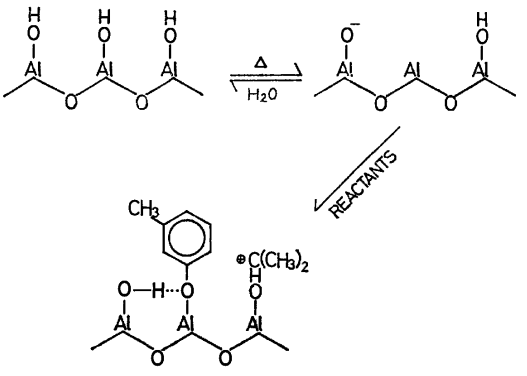

That is, if *m*-cresol is adsorbed on the L acid sites and if propylene is adsorbed on the neighboring B acid sites, most of the isopropylcarbonium ions will subsequently attack the *ortho* positions (2 and 6 in the following picture) of the adsorbed *m*-cresol, because these positions are closer to the surface.

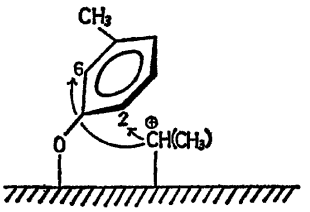

However, the attack on the 6-position must be subjected to steric hindrance by the methyl group of the adsorbed *m*-cresol. Consequently, propylene may add preferably to the 2-position, and thymol is formed selectively. Kolka also explained the high selectivity of the liquid-phase *ortho* alkylation in terms of the intermediate formation of aluminum phenoxide.[13]

The poisoning action of a strong base appears to be closely related to the irreversible adsorption on active sites. The bonding of the base with aluminum or hydroxyl is much stronger because the nitrogen atom in the base molecule is more basic than the oxygen atom in the *m*-cresol molecule or the double bond in the propylene molecule.

References

1) M. Nitta, K. Yamaguchi, and K. Aomura, This Bulletin in press.
2) J. B. Peri and R. B. Hannan, *J. Phys. Chem.*, **64**, 1526 (1960).
3) J. B. Peri, *ibid.*, **69**, 231 (1965).
4) E. P. Parry, *J. Catal.*, **2**, 371 (1963).
5) J. Medema, J. G. Van Bokhoven, and A. E. T. Kuiper, *ibid.*, **25**, 238 (1972).
6) E. Briner, W. Pluss, and H. Paillard, *Helv. Chim. Acta*, **7**, 1046 (1924).
7) L. H. Klemn and D. R. Taylor, *J. Org. Chem.*, **35**, 3216 (1970).
8) D. R. Taylor and K. H. Lundlum, *J. Phys. Chem.*, **76**, 2882 (1972).
9) N. Okuda, *Nippon Kagaku Zasshi*, **82**, 1290 (1961).
10) P. B. Venuto, L. H. Hamilton, P. S. Landis, and J. J. Wise, *J. Catal.*, **4**, 81 (1966).
11) T. Yashima, N. Hara, H. Ahmad, and K. Yamazaki, *ibid.*, **16**, 273, (1970); **17**, 151 (1970); **26**, 303 (1972).
12) S. H. Patinkin, and B. S. Friedman, "Friedel-Crafts and Related Reactions", Vol. II, Part I, ed by G. A. Olah, Interscience Publishers, New York (1964), p. 1.
13) A. J. Kolka, J. P. Napolitano, A. H. Filbey, and G. G. Ecke, *J. Org. Chem.*, **22**, 642 (1957).
14) K. Tanabe, "Solid Acids and Bases," Kodansha-Tokyo, Academic Press, New York (1970), p. 45.
15) G. M. Schwab, and H. Kral, Proc. Intern. Congr. Catalysis, 3rd, Amsterdam, I. No. 20 (1964).
16) R. J. Cvetanovic and Y. Amenomiya, *Advan. Catal.*, **17**, 103 (1967).

Reactions in the Adsorbed Layer: Hydrogenation of Acetone on Nickel Catalysts

Hisashi MIYATA, Mitsuhiko MINOBE,* and Yutaka KUBOKAWA

Department of Applied Chemitsry, University of Osaka Prefecture, Mozu-Umemachi, Sakai, Osaka 591

(Received November 26, 1973)

The hydrogenation of acetone adsorbed and the dehydrogenation of isopropanol adsorbed on silica-supported nickel catalyst have been studied by following the changes of hydrogen pressure and the reaction products as well as the IR spectra of adsorbed species. It was found that the formation of isopropanol proceeds *via* a precursor composed of acetone and hydrogen. The activation energies of hydrogenation of acetone adsorbed and of dehydrogenation of isopropanol adsorbed were 11—13 and 4—8 kcal/mol, respectively. The activation energy of the desorption was 13 kcal/mol for isopropanol and 19 kcal/mol for acetone. From the results the potential energy change during the hydrogenation of acetone was determined.

Although a number of investigations have been made on the hydrogenation of acetone on nickel catalysts, in most cases the nature of the adsorbed species on the catalysts as well as the energy relation for the reaction was deduced on the basis of the kinetics of the reaction. They can be elucidated more precisely by measurements of the hydrogenation of adsorbed acetone. Work along this line was carried out[1-3] with some decomposition reactions. As an extension of this work, hydrogenation of acetone adsorbed on nickel catalyst has been investigated by an infrared technique as well as by the analysis of reaction products.

Experimental

Materials. The 15 wt% Ni-SiO_2 catalyst was prepared by impregnation of silica gel (30—50 mesh) with an aqueous solution of $Ni(NO_3)_2 \cdot 6H_2O$. The supported salt was dried at 100 °C and heated at 400 °C in the air. The catalyst samples were reduced in 100 Torr hydrogen at 400 °C for 60 hr and degassed at the same temperature for 3 hr. The equilibrium amount of hydrogen adsorbed after the reduction was 1.8 cm^3/g at 0 °C and 20 Torr hydrogen. For spectroscopic experiments, Aerosil (Degussa) supporting 6.5 wt% nickel was prepared by impregnation with a nickel nitrate solution. The slurry was dried at 100 °C in the air and heated in a vacuum at 300 °C. The silica-salt mixture was pressed into a disk of 20 mm diameter. Before adsorption of acetone, the disk was heated in hydrogen at 350 °C for 6 hr and degassed at the same temperature.

Acetone and isopropanol (Tokyo Chemical Industry) were dried in a vacuum over a degassed molecular sieve, degassed by freeze-pump-thaw cycles and stored over the molecular sieve. Cylinder hydrogen was purified by diffusing through an electrically heated palladium thimble.

Apparatus and Procedures. A closed circulation system, equipped with Töpler pump and a mercury diffusion pump, was used for desorption experiments. The rate of hydrogen uptake by the catalyst adsorbed acetone was determined manometrically. The experiments of dehydrogenation of isopropanol adsorbed were carried out as follows: Using either liquid N_2 traps or a Töpler pump and a diffusion pump, the desorbed amounts of hydrogen as well as of condensable gases such as acetone, isopropanol, and propane were determined as a function of time, the rate of desorption being obtained. Details were described previously.[1-4] During the rate measurements the temperature of the catalyst was lowered abruptly and the temperature dependence of the rates at the same amount adsorbed was obtained. The desorption products were analyzed by gas-chromatography with the use of a column with 3 m silica gel or 2 m molecular sieve for methane and hydrogen and with a 2 m PEG 1500 column for the other products. Similar desorption experiments were carried out under circulation of hydrogen over the catalyst. In this case the desorption system was kept shut and only the condensable desorption products were analyzed.

The IR cell was the same as that used previously.[5] All the spectra were recorded at room temperature with a Hitachi EPI-G2 grating infrared spectrophotometer with a spectral slit width 2.8 cm^{-1} at 1000 cm^{-1}.

Results and Discussion

Hydrogenation of Acetone Adsorbed. The IR spectra of acetone adsorbed on the nickel catalyst at 25 °C showed bands at 1700 cm^{-1} (ν(C=O)), 1420, 1370 ($\delta(CH_3)$), and also around 3000 cm^{-1} (ν(CH)).[6] When hydrogen was admitted into the catalyst with adsorbed acetone at room temperature, the spectra changed gradually, hydrogen uptake occurring simultaneously. With increasing time of contact with hydrogen, the band due to the carbonyl group became

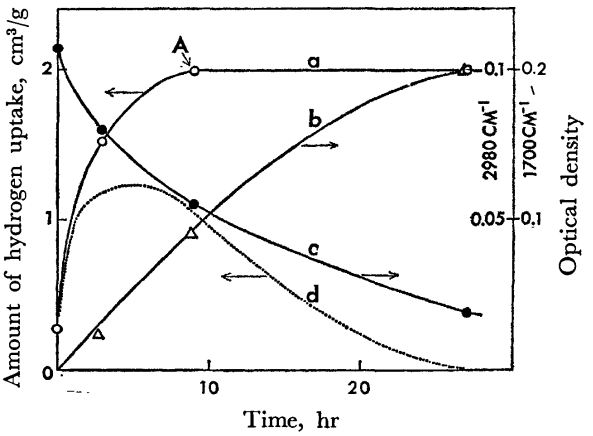

Fig. 1. Changes in the intensities of the bands and in the amount of hydrogen uptake: (a) amount of hydrogen uptake; (b) band intensity at 2980 cm^{-1}; (c) band intensity at 1700 cm^{-1}; (d) amount of the precursor. The amount of acetone adsorbed at 25 °C and hydrogen pressure were 1.75 cm^3/g and 20 Torr, respectively.

* Present address: Chemical Planning Department, Kyowa Hakko Kogyo Co., Ohtemachi, Chiyoda-ku, Tokyo 100

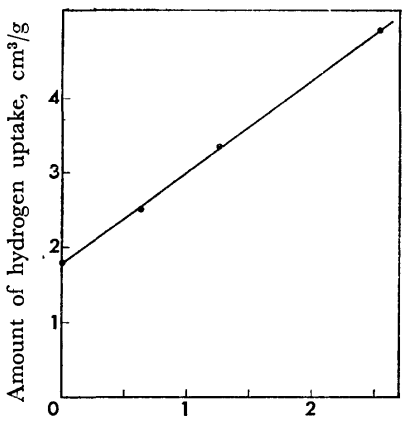

Fig. 2. Hydrogen uptake by the acetone-covered surface. Temp, 20 °C. The amount of catalyst and the equilibrium pressure of hydrogen were 6.67 g and 20 Torr, respectively.

weak, while a new band at 2980 cm^{-1} was intensified. The new band is attributable to ν(CH) of isopropanol.[7] The results are shown in Fig. 1. After 8 hr the amount of hydrogen uptake appears to attain a saturation value, while the intensities of the bands at 1700 and 2980 cm^{-1} still change. Such a phenomenon suggests that during the hydrogenation of acetone adsorbed, hydrogen adsorption of a certain type takes place to form an intermediate. In other words, the formation of isopropanol proceeds *via* a precursor composed of acetone and hydrogen. The amount of hydrogen uptake at the saturation (point A, Fig. 1) increased with increasing amount of acetone adsorbed. The increase in the amount of hydrogen uptake is 1.2 times as much as the amount of acetone adsorbed (Fig. 2).[8] Such a constant ratio suggests the formation of the precursor. A similar phenomenon was reported by Akhtar and Tompkins[9] who suggested that on the Pt surface containing adradicals such as $-NH_2$, -OH, and $-CH_3$, hydrogen is molecularly adsorbed on the adradicals (possibly by H-bonding). It was found that the intensity of the band at 2980 cm^{-1} was proportional to the amount of adsorbed isopropanol in the range 0.6—1.5 cm^3/g.[10] Assuming that the amount of hydrogen uptake at the saturation corresponds to the intensity of the band observed at 2980 cm^{-1} after 25 hr, it is possible to estimate the amount of the precursor which has a maximum (curve d, in Fig. 1).

It can be seen that an instantaneous hydrogen uptake is followed by a slow uptake. Taking account of the practical absence of hydrogen uptake without adsorbed acetone, it is concluded that the instantaneous uptake is due to the hydrogen adsorption between acetone molecules[12] and the slow uptake to the formation of isopropanol as well as of the precursor. The activation energy of the slow hydrogen uptake increased from 11 to 13 kcal/mol with the progress of uptake in the range 0.3—0.8 of the fraction of hydrogenated acetone. The rate of hydrogen uptake varied in proportion to the square root of hydrogen pressure in the range 20—100 Torr.

Dehydrogenation of Isopropanol Adsorbed. In order to obtain information on the energy changes for the dehydrogenation of isopropanol, the following experiments were carried out. After the hydrogenation of adsorbed acetone at 0 °C was completed, hydrogen was removed from the reaction vessel. The temperature of the catalyst was then raised stepwise to 20, 50, and 100 °C. The products are shown in Table 1. In the temperature range below 50 °C the hydrogen evolved amounted to 80% of the total hydrogen uptake, while a negligible evolution was observed for acetone as well as isopropanol. This suggests that acetone as well as isopropanol is adsorbed more strongly than hydrogen.

The rates of evolution of hydrogen were measured at 20 and 0 °C with various amounts of isopropanol adsorbed. The value of E for the hydrogen evolution (Rate$\propto\exp(-E/RT)$) increased from 4 to 8 kcal/mol with increasing fraction of dehydrogenated isopropanol from 0.1 to 0.3. It appears that the rate of dehydrogenation of isopropanol adsorbed is equal to the evolution rate of hydrogen, since the observed rate of hydrogen evolution was much larger than that for the catalyst with only adsorbed hydrogen.

In order to obtain energetic information on the hydrogenation of acetone, the dehydrogenation of isopropanol adsorbed was carried out in the presence of hydrogen circulating over the catalyst. The results of experiments in which the temperature of the catalyst was raised stepwise are shown in Fig. 3. Evolution of acetone as well as isopropanol began at 50 °C, showing a maximum at 100 °C and then decreased. Figure 4 shows the results of experiments at a constant temperature. The evolution rate of the products decreased with a decrease in the amount of isopropanol adsorbed. Dependence of the rate of evolution of the products upon hydrogen pressure was determined by abruptly changing the pressure during the course

Table 1. Dehydrogenation of isopropanol adsorbed

Temp range °C	Products,[a] $cm^3/g\times10^2$						Remaining amount,[b] cm^3/g	
	A	IPA	C_3H_8	CH_4	H_2O	H_2	A	H_2
0	—	0.09	—	—	0.11	57.3	2.51	3.96
0— 20	0.45	1.17	—	—	0.27	121.2	2.50	2.73
20— 50	18.4	3.87	0.30	4.68	1.89	190.2	2.25	0.748
50—100	86.2	0.35	1.39	33.6	7.32	158.8	1.26	—

a) A, Acetone; IPA, isopropanol. The temperature of the catalyst was kept constant for 2 hr at each step of temperature rise. b) The remaining amount is expressed as acetone+H_2, *e.g.*, at 0 °C isopropanol remained 2.51 and hydrogen 1.45 cm^3/g. Above 50 °C most of the hydrogen formed arises from the decomposition of acetone adsorbed.

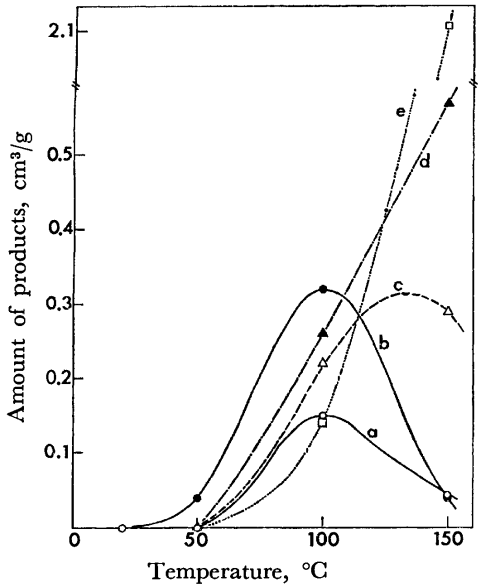

Fig. 3. Dehydrogenation of isopropanol adsorbed: (a) acetone; (b) isopropanol; (c) propane; (d) water; (e) methane. The amount of acetone adsorbed at 0 °C and hydrogen pressure were 2.51 cm³/g and 20 Torr, respectively.

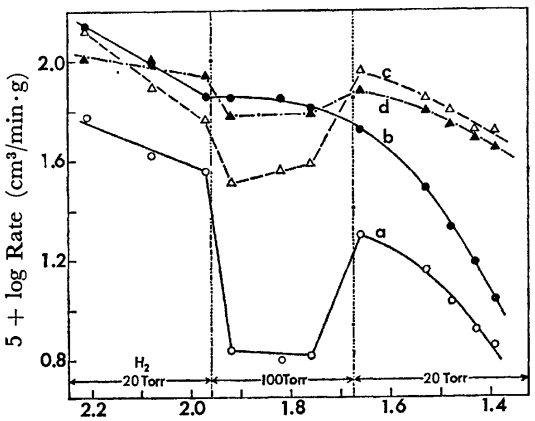

Fig. 4. Dehydrogenation of isopropanol adsorbed at 100 °C. Symbols are the same as for Fig. 3.

of dehydrogenation. The rate of evolution of acetone changes inversely proportional to P_H, while that of isopropanol is independent of P_H (Fig. 4).

The temperature dependence of the rate of evolution for isopropanol and for acetone was determined from the results shown in Fig. 5. The values of E at 1.95 cm³/g of the amount of isopropanol adsorbed are calculated to be 26.8 for acetone and 13.3 kcal/mol for isopropanol. Another experiment at 4.2 cm³/g of the amount of isopropanol adsorbed gave the activation energies 22.5 and 13.3 kcal/mol, respectively. It is seen that the value of E for acetone evolution changes with the remaining amount of isopropanol but that for isopropanol is nearly constant.

Dependence of the rates of evolution of the products upon the amount of isopropanol adsorbed was examined over a wide range of adsorbed amounts. The rate of evolution of propane changes slightly with

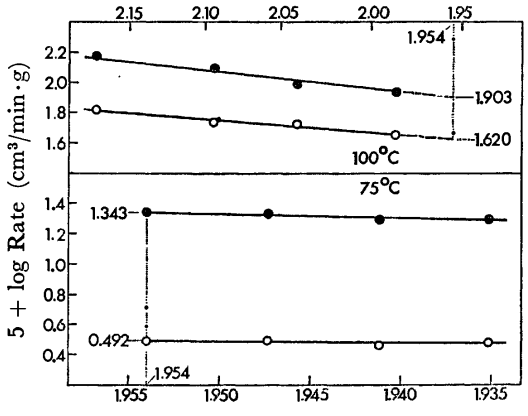

Fig. 5. Change in the rates of evolution of the products with temperature. During the measurements the temperature was changed abruptly from 100 to 75 °C, the rates at 1.954 cm³/g being compared. Hydrogen pressure, 20 Torr. Symbols are the same as for Fig. 3.

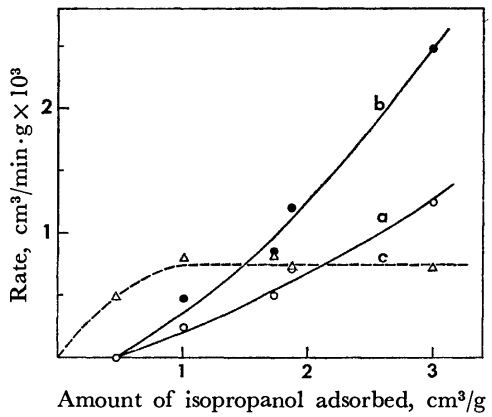

Fig. 6. Change in the rates of evolution of the products with the amount of isopropanol adsorbed. Symbols are the same as for Fig. 3. The temperature and hydrogen pressure were 100 °C and 20 Torr, respectively.

increasing amount adsorbed, while that of isopropanol markedly increases (Fig. 6). Such a behavior suggests that propane is formed from a strongly adsorbed species.

Potential Energy Change During the Hydrogenation of Acetone. Taking into account the results given in Table 1 and Fig. 1, it seems that the hydrogen uptake by the catalyst with adsorbed acetone and its reverse reaction, *i.e.*, hydrogenation of acetone adsorbed and dehydrogenation of isopropanol adsorbed[13] are much faster than the desorption of acetone as well as isopropanol at around 100 °C, where the dehydrogenation experiments were carried out. It appears that the equilibrium is established for the dehydrogenation and its reverse reaction. Since hydrogen is adsorbed between the acetone molecules, it would be expected that the acetone adsorption is independent of hydrogen adsorption. Hence

$$k_4\theta_A\theta_H'^2 = k_{-4}\theta_{IPA}(1-\theta_H')^2, \quad (1)$$

where $\theta_H'=1$ corresponds to a saturated amount of hydrogen adsorbed between acetone molecules; the rate constants refer to the following steps:

$$\begin{array}{ccccc} A(g) & & H_2(g) & & IPA(g) \\ k_1\uparrow & & k_2\uparrow\downarrow k_{-2} & & k_3\uparrow \\ A(a) & + & 2H(a) & \underset{k_{-4}}{\overset{k_4}{\rightleftharpoons}} & IPA(a) \end{array}$$

where A, H_2, and IPA represent acetone, hydrogen, and isopropanol, respectively. Since adsorption equilibrium is established for hydrogen, we have

$$k_{-2}P_H(1-\theta_H')^2 = k_2\theta_H'^2, \quad K = k_{-2}/k_2 \tag{2}$$

Substitution of equation (2) into equation (1) gives

$$\theta_A = k_{-4}\theta_{IPA}/k_1KP_H. \tag{3}$$

Hence, the evolution rates of isopropanol and acetone, R_{IPA} and R_A, are given by

$$R_{IPA} = k_3\theta_{IPA} \tag{4}$$

$$R_A = k_1\theta_A = k_1k_{-4}\theta_{IPA}/k_4KP_H. \tag{5}$$

In the case where θ_{IPA} is independent of hydrogen pressure, R_{IPA} becomes independent of P_H and R_A inversely proportional to P_H, in agreement with the results described above. Such a pressure independence of θ_{IPA} suggests that during the experiments such as shown in Fig. 6 the values of $\theta_{IPA}/(\theta_A+\theta_{IPA})$ are always close to unity, although θ_{IPA} as well as θ_A decrease with progress of the reaction. The pressure dependence of R_A as well as R_{IPA} would support the assumption that equilibrium is established for the hydrogenation and dehydrogenation reaction.

According to Eqs. (4) and (5), the temperature dependence of k_3 and k_1k_{-4}/k_4K is the same as that of R_{IPA} and R_A, which are 13.3 (E_3) and 22.5—26.8 kcal/mol (E_A), respectively. When Eqs. (4) and (5) hold, the value of R_{IPA}/R_A should be constant at a constant hydrogen pressure, irrespective of the amount of isopropanol adsorbed. Such a prediction was confirmed by experiments (Fig. 6, $R_{IPA}/R_A=1.98$ at 20 Torr hydrogen). The activation energy (E_4) of 11—13 kcal/mol for the hydrogen uptake corresponds to the temperature dependence of k_4. The activation energy (E_{-4}) of 4—8 kcal/mol for the evolution of hydrogen from isopropanol adsorbed corresponds to the temperature dependence of k_{-4}. Schuit and Reijen[14] investigated the adsorption isotherms of hydrogen on a silica supported nickel catalyst similar to the one we used. By applying their results to the present system, the coverage of hydrogen during the course of dehydrogenation of isopropanol at 100 °C and 20 Torr hydrogen is estimated at 0.7. Their results show that the heat of adsorption at $\theta=0.7$ is 16 kcal/mol.[15] Thus the temperature dependence (E_2) of K is estimated as -16 kcal/mol. From the relationship $E_A=E_1+E_{-4}-E_4-E_2$, the value of E_1 for k_1 can be calculated. The values of E_4 and E_{-4} vary with the progress of dehydrogenation. $E_4=12$ and $E_{-4}=4$ are obtained from the values at the fraction of hydrogenated acetone of 0.8. Combining these values with $E_A=27$, the value of E_1 for k_1 is obtained as 19 kcal/mol. Figure 7 shows the energy values as the change of potential energy during the course of reaction. The activation energies of adsorption of acetone, hydrogen, and isopropanol are neglected.

Strictly speaking, Fig. 7 is valid only in the case where the fraction of hydrogenated acetone is 0.8. In the case where the fraction of hydrogenated acetone is small, it is expected that the value of E_{-4} becomes larger than 8, although other quantities such as E_1, E_3, and E_4 do not change a great deal.

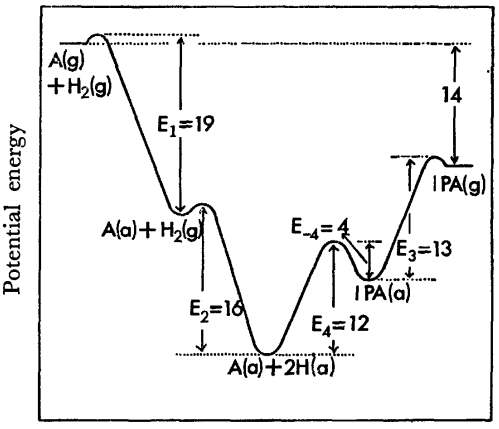

Fig. 7. Potential energy diagram for acetone hydrogenation. Figures indicate the potential energy in kcal/mol. The amount of isopropanol adsorbed and hydrogen pressure were 2.0 cm³/g and 20 Torr, respectively.

References

1) Y. Kubokawa and H. Miyata, "Proceedings of the Third International Congress on Catalysis," Vol. 2, North-Holland Publishing, Amsterdam (1965), p. 871.

2) Y. Kubokawa, H. Miyata, and M. Minobe, *J. Catal.*, **12**, 317 (1968).

3) Y. Kubokawa and H. Miyata, *J. Phys. Chem.*, **72**, 356 (1968).

4) Y. Kubokawa, This Bulletin, **33**, 546, 550, 555, 739, 747, 936 (1960); *J. Phys. Chem.*, **69**, 2676 (1965).

5) H. Miyata, Y. Toda, and Y. Kubokawa, *J. Catal.*, **32**, 155 (1974).

6) G. Dellepiane and J. Overrend, *Spectrochim. Acta*, **22**, 593 (1966).

7) C. Tanaka, *Nippon Kagaku Zasshi*, **83**, 521 (1962).

8) The results in Fig. 2 were obtained with a catalyst differing from the one used in IR studies. Similar results were obtained with Aerosil supported nickel catalyst as well as unsupported nickel catalyst.

9) M. Akhtar and F. C. Tompkins, *Trans. Faraday Soc.*, **67**, 2461 (1971).

10) No simple relationship appears between the intensity of the carbonyl band and the surface concentration of acetone, since there are two types of adsorbed species, *i.e.*, associatively and coordinately adsorbed species for acetone adsorption as reported by Young and Sheppard.[11]

11) R. P. Young and N. Sheppard, *J. Catal.*, **20**, 333 (1971).

12) C. L. Herbo, *J. Chim. Phys.*, **47**, 454 (1950).

13) Since only the products appearing in the gas phase have been examined (Fig. 6), it is impossible to distinguish isopropanol from its precursor. Consequently, in the following discussion IPA(a) refers to the state of isopropanol adsorbed as well as of its precursor.

14) G. C. A. Schuit and L. L. van Reijen, *Advan. Catal.*, **10**, 243 (1958).

15) In the presence of acetone adsorbed, θ appears to differ from 0.7. According to Schuit and Reijen,[14] the heat of adsorption does not change markedly with coverage. It seems unlikely, therefore, that the above conclusion is affected seriously by a different θ value.

The Magnetic Properties of Verdazyl Free Radicals. VI. ESR Studies of Pairs and Triads† of the Symmetrical Triphenylverdazyl Radical in the 1,3,5-Triphenylbenzene Matrix

Nagao AZUMA, Hiroaki OHYA-NISHIGUCHI, Jun YAMAUCHI*, Kazuo MUKAI**, and Yasuo DEGUCHI

Department of Chemistry, Faculty of Science, Kyoto University, Sakyo-ku, Kyoto 606

(Received February 22, 1974)

Single-crystal ESR studies have been carried out on symmetrical triphenylverdazyl (TPV) doped in a diamagnetic 1,3,5-triphenylbenzene (TPB) crystal at room temperature. There have appeared seven pairs of fine-structure absorptions in addition to the hyperfine splittings. Three out of the seven pairs have been assigned as zero-field splittings due to radical pairs, while the other three pairs have been identified as from radical triads. The six fine structure tensors have been determined through the angular variation of the resonance-field separations. The structures of the pairs and triads of TPV were discussed on the basis of the fine structure tensors, the crystal structures of TPB and TPV, and the spin distribution in the radical molecule, assuming that the unit cell of the mixed crystal with the radical concentration of less than 11.1% is identical with that of the host crystal, TPB. Within the limits of the X-ray examination, this assumption was found to be reliable. It was found that the molecular planes in each species are almost parallel to the *bc*-plane and that all the *C*-phenyl rings lie in the *c*-direction.

Recently, the present authors have reported the temperature dependence of the ESR linewidth, the *g*-value shift, and the magnetic susceptibility of the powdered sample of symmetrical triphenylverdazyl (TPV) and have concluded from these data, the crystal structure, and the spin distribution that this radical solid is subjected to the magnetic phase-transition from the short-range ordered state to the long-range ordered one at about 1.7 K.[1,2] In order to clarify the magnetic properties of the TPV solid in more detail, single-crystal experiments are highly desirable. For this investigation, it would be a reasonable step to study the magnetic behavior of the radical pair or triad of TPV, since they are magnetic unit systems containing interacting spins. However, it is difficult in general to investigate precisely the magnetic dipolar and exchange interactions of the radical pair in the solid of the stable neutral radical at any temperature, because of the above interactions between the given two spins and the surrounding spins, which cause the work to be desperately complicated. In the rather fortunate case in which the species is defined well by some evidence, one can study the spin-spin interactions in the radical pair by making a certain portion of the radical diluted in a suitable diamagnetic crystal. This method is different from that employed in the case of the thermally-excited triplets[3] or the radical pairs caused by the irradiation.[4,5] In fact, the dilution method was applied to nitroxide radicals which possess a fairly localized electron spin.[6,7]

On the other hand, Wiersma and Kommandeur have pointed out that even a *D*-parameter depends largely upon the magnitude of the spin delocalization.[4] Therefore, it is also of particular interest to study the dipolar coupling tensor of a radical pair with delocalized spins and, in turn, to compare the tensor with that expected for the hypothetical radical pair with localized spins. The TPV radical not only has a delocalized spin,[1] by which its enormous stability can be understood, but its molecular structure is also well known,[8] so that this radical is an adequate example for the study of the effect of the spin delocalization on the magnetic properties.

By the way, the spin structure or the interaction between the spins and the lattice in the ordered state of TPV solid has not yet been made clear. For the purpose of clarifying this spin-lattice interaction, the study of the anisotropic dipolar interactions in the radical pair of TPV, its derivatives,[9] and its analogues[10] may be a possible approach, for the dipolar interaction Hamiltonian contains the scalar product of the spin and the vector distance, while the single-spin vector in the monoradical molecule has little interaction with the vector distance.

This paper will describe mainly the fine-structure tensors of the TPV radical pairs in the 1,3,5-triphenylbenzene (TPB) matrix in order to present the fundamental data for the above-mentioned studies as well as the investigation of these magnetic entities themselves. Besides, the possible TPV radical triads will also be discussed on the basis of the radical concentration, the ESR signal intensity, and the crystal structures of TPB and TPV.

The Crystal Structures of TPB and TPV. These structures were investigated by Farag[11] and Williams[8] respectively; they are shown in Figs. 1 and 2. It should be remarked that the molecular geometry of TPV is similar to that of TPB: Each configuration

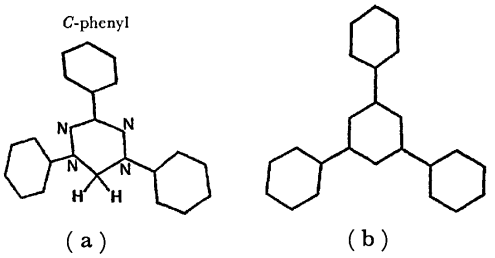

(a) (b)

Fig. 1. Molecular structures of the TPV radical (a)[8] and diamagnetic TPB matrix (b).[11]

† "Triad" means a three-membered radical cluster in which the exchange interaction energy should be much less than that of the ordinary chemical bond. We will refer to it as a "radical triad" in this text.

* The Institute for Chemical Research, Kyoto University, Uji, Kyoto 611.

** Department of Chemistry, Faculty of Science, Ehime University, Matsuyama, Ehime 790.

of the three substituted phenyl rings of both the compounds is antipropellar in the crystalline state. Some molecular flexibility of the compounds may be encountered because of the bending and twisting freedom about the bonds connecting with the rigid ring systems. Furthermore, it should be noted that the large and intense diffused X-ray spots corresponding to thermal vibrations affecting the (200) planes of TPB signify that all the bonds in these planes are stronger than those normal to them[11] and that the elastic constant along the *a*-direction, which is almost normal to the molecular planes, as may be seen from Fig. 2, is naturally smaller than the others.[12] This fact may be favorable to accommodate the guest molecule, TPV, with a molecular thickness slightly different from that of the host molecule, TPB. In the meantime, Kuhn and Trischmann have reported a Debye-Scherrer X-ray photograph with sharp lines from the equi-molecular mixed crystal of TPB and TPV,[13] which may indicate a uniform mono-phase crystal. Therefore, it is expected, in the low-concentration region, that the guest molecules, TPV, can be doped substitutionally in the host, TPB, crystal without any drastical crystal distortion, as will be described in detail in a later section. Thus, the TPV molecules in the TPB matrix will be able to form radical pairs and triads with certain concentrations.

TPB is an orthorhombic crystal with the crystal parameters of $a=7.47$, $b=19.66$, $c=11.19$ Å, and $z=4$; the space group is $Pna2_1$.[11] The molecules inclined from the *bc*-plane by $\pm 11°$ are stacked face-to-face and form two zigzag chains along the *a*-axis. The chains are related to each other by the twofold screw axis parallel to the *c*-axis. Since the interchain distance is longer than 10 Å, not only the nearest-neighboring but also the second-nearest-neighboring molecules can be found in the same chain, separated by 4.90 and 7.47 Å respectively. For the present purpose, it is safe to confine our consideration to one chain. The angle in the zigzag chain, which is bisected by the *bc*-plane, is about 100°, so that the radical pairs in the chain can be expected to be related to each other by the plane of symmetry parallel to the *bc*-plane. The most probable direction of the N-N bonds in the radical pair has been considered to be parallel to the *ac*-plane if the local symmetry around the radical pair is the same as that of the host crystal, since the crystal distortion of that orientation would be the smallest among those of the three possible orientations. The above arguments would also hold in the case of the radical triads.

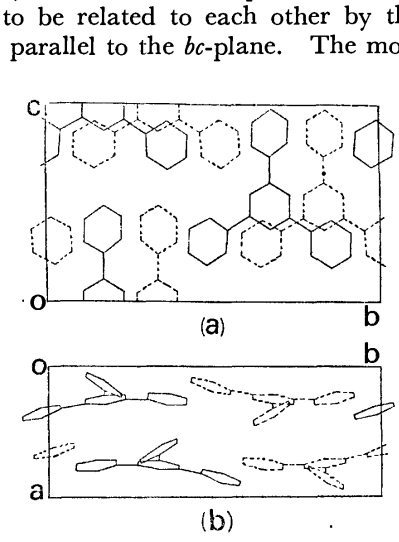

Fig. 2. Molecular packing of the host crystal, TPB.[11] (a) and (b) were projected along the crystallographic *a*- and *c*-axis, respectively.

Experimental

The TPV prepared by the method of Kuhn and Trischmann[13] was identified by the melting point, by studying the ESR spectrum in a solution, and by elementary analysis. The values obtained were in good agreement with those in the literature.[13] Commercial TPB was recrystallized from an ethereal solution; the results of the elementary analysis were satisfactory. The TPV and TPB (3 : 7 in weight) were dissolved together in an ether solvent and then slowly evaporated under nitrogen gas, thus giving small crystals. Then, the sample crystals of a suitable size were recrystallized again from the ethereal solution under a nitrogen gas flow for three days. Judging from the elementary analysis for carbon and nitrogen, the sample crystals contained TPV of 11.1% (Found: C, 92.15; N, 2.10%). More diluted crystals and reference crystals of pure TPB were also prepared by the same procedure.

The mixed and reference crystals were compared with each other, observing their crystal forms and cleavages, measuring their interfacial angles, and by the polarizing microscope technique. The X-ray diffraction spectra of the powdered samples were also compared with each other in the region from 7 to 40 degrees in 2θ, using Cu$K\alpha$ radiation.

The crystals used in the ESR measurements were mounted on the end of a synthesized polymer rod in various orientations by means of the goniometer. The ESR spectra about each of three mutually-perpendicular axes were obtained at room temperature by rotation at 5° intervals, using a JEOLCO JES-ME3X X-band spectrometer, equipped with a 100 kHz field modulation for the first derivatives and with an 80 Hz one for the second derivatives. The magnetic field was calibrated by the hyperfine splittings of Mn^{2+} in MgO.

The powdered sample containing 11.1% TPV exhibited the ESR absorptions characteristic of the randomly-oriented triplets. The half-field absorptions ($g=4$, $\Delta m_s=\pm 2$) were also observed in the powdered sample with a radical concentration of 11.1%, but no $\Delta m_s=\pm 2$ absorption was detected in the more diluted sample with a radical concentration of less than 3%.

Results and Spectral Analyses

Crystallography. When we compared the mixed crystals with the reference TPB crystals, no difference between them was detected, except for their colors, within the limits of our experimental error. This fact clearly indicates that the unit cell of the mixed crystal is identical macroscopically with that of the host crystal. Using the polarizing microscope, the samples were identified as single crystals. The sample crystal was of a trigonal form elongated along the *a*-axis and also showed an imperfect cleavage normal to that axis.[11] The faces parallel to the *a*-axis were (011) and (01$\bar{1}$) planes, and the interfacial angle was 59 degrees.

The mixed crystal with a radical concentration of less than 3% was studied by means of the ESR

technique in order to clarify the orientation of the TPV molecules. For the rotation about the *a*-axis, the crystal exhibited a symmetrical single line with the small angular dependent peak-to-peak width of 12 gauss. For the rotation about the *b*- and *c*-axis, the resonance lines varied with the rotation of the crystal; the maximum number of the lines was 18, at which the over-all width of the resonance field spread to about 100 gauss. On the other hand, the ESR spectrum of TPV in solution gave nine lines with the hyperfine coupling constant of 6 gauss due to the almost-equivalent four nitrogen nuclei. These facts indicate that the angular dependent lines are attributable to the hyperfine splittings due to the nitrogen nuclei in the isolated radical, and that no radical oligomer has any significant population. It may also reasonably be deduced that this fairly planar π-radical can occupy at least two sites and that its molecular plane is nearly parallel to the *bc*-plane.

ESR Spectra. Figure 3 shows some typical ESR spectra of the 11.1% single crystal. The intense central peak in Fig. 3(A) and nine sharp peaks in Fig. 3(B) are due to the hyperfine interactions of the isolated radicals. Each of the absorption pairs with the resonance-field separation of d_{I} and d_{I}' in Fig. 3(A) is results from two differently-oriented species. The fine structure lines in Fig. 3(B) are broader than those in Fig. 3(A). Their linewidths, proportional to the over-all width of the central lines, are probably due to the hyperfine structure broadening, which indicates that the orientation of the molecules in the pairs and triads of TPV is similar to that of the isolated radicals.

The angular variations of the observed splittings denoted by d_{I}, d_{II}, *etc.* in Fig. 3 are shown in Fig. 4. The rectangular coordinate system a'b'c' was chosen so as to avoid the overlap of the spectral lines in the orthorhombic crystal system *abc*. The relationship between the two right-hand systems is given by the following equation:

$$\begin{bmatrix} a \\ b \\ c \end{bmatrix} = \begin{bmatrix} 1 & 0 & 0 \\ 0 & \cos\alpha & -\sin\alpha \\ 0 & \sin\alpha & \cos\alpha \end{bmatrix} \begin{bmatrix} a' \\ b' \\ c' \end{bmatrix}, \quad \alpha = -59.2^\circ \qquad (1)$$

where α is the angle measured from the *b*- to the b'-axis, equalling the interfacial angle between (011) and (01$\bar{1}$) planes.

Spectral Analysis of the Triplet. Under the conditions of (I) $g\beta H \gg |D|$, $|E|$ and (II) small *g*-anisotropy, the zero-field splittings of the triplet species can be analyzed by the approximate method described by Itoh.[14] Recently, this method has been successfully employed by Takizawa *et al.*[6] in the case of a radical pair in a matrix. The (I) assumption is considered to be valid in the present case, because the maximum value of the zero-field parameters is estimated to be less than 300 gauss from the angular variation of the splittings shown in Fig. 4. On the other hand, the *g*-values of the organic free radicals are usually almost isotropic and close to the free electron *g*-value. In fact, the *g*-value of TPV is found to be almost isotropic and to be very close to 2.0033. Therefore, the second assumption (II) is also reliable in the present case. We

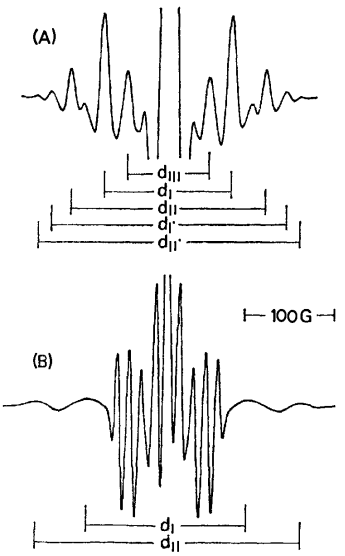

Fig. 3. Tracings of the ESR spectra from a single crystal of the diluted TPV radical. (A) *c*//**H**, the second derivative; (B) *a*//**H**, the second derivative.

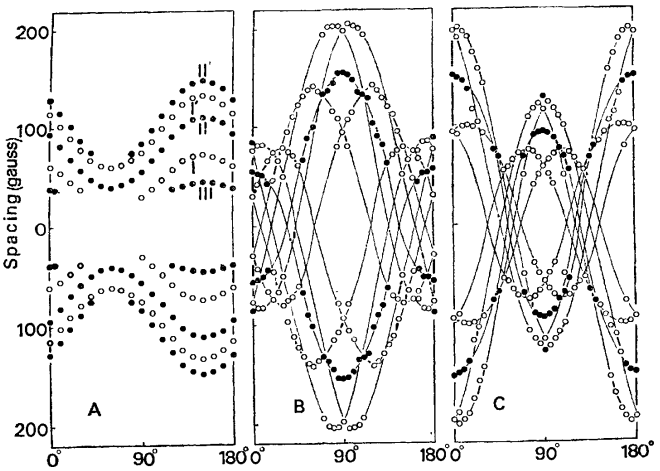

Fig. 4. Angular variations of the resonance-field separations. The numbers on the *abscissa* indicate the rotation angles. The separation, *d*, is represented by the term of *spacing*. The number of *zero* on the *ordinate* corresponds to the central field of the pairing resonance field. A, B, and C were obtained by rotations about the a'-, b'-, and c'-axis, respectively.

can thus introduce the following spin Hamiltonian:

$$\mathrm{H} = g\beta\mathbf{S}\cdot\mathbf{H} + \mathbf{S}\cdot\tilde{\mathbf{D}}\cdot\mathbf{S}, \qquad (2)$$

where $\mathbf{S}=\mathbf{S}_1+\mathbf{S}_2$, and where the subscripts 1 and 2 indicate the respective radicals forming the radical pair. The other symbols have the usual meanings. The second term in Eq. (2) is the perturbing Hamiltonian. The second-order perturbation theory gives the following resonance-field separation of the doublet splitting in the case of a-axis rotation:

$$\begin{aligned} d &= 3(g_e/g)(D'_{zz}) \\ &= 3(g_e/g)(D'_{bb}\cos^2\theta + D'_{bc}\sin 2\theta + D'_{cc}\sin^2\theta) \text{ (gauss)}, \end{aligned} \qquad (3)$$

where g_e is the free electron *g*-value and where D'_{ij}

Table 1. Observed fine structure tensors of the pairs and triads of TPV radical

Name	Principal values[a]	Direction cosines with respect to *abc* system[b]			D[c] E[c]
Radical pairs					
I_a	±102.3	0.8550	0.5183	0.0182	153.5
	∓47.6	0.0617	−0.0667	−0.9959	3.5
	∓54.7	−0.5150	0.8526	−0.0891	
I_b	±101.9	0.8543	−0.5196	−0.0149	152.8
	∓47.2	−0.0586	−0.0678	−0.9960	3.7
	∓54.6	0.5165	0.8517	−0.0884	
II	±99.4	0.9999	0.0046	0.0091	149.5
	∓74.2	0.0091	0.0118	−0.9999	24.5
	∓25.2	−0.0046	0.9999	0.0117	
Radical triads					
I_a'	±66.9	0.9814	0.1920	−0.0017	100.3
	∓44.8	−0.0043	0.0127	−0.9999	11.4
	∓22.1	−0.1919	0.9814	0.0133	
I_b'	±66.2	0.9863	−0.1605	0.0377	99.3
	∓45.1	0.0430	0.0298	−0.9987	12.0
	∓21.2	0.1591	0.9866	0.0364	
II′	±72.5	0.9999	−0.0044	0.0165	109.0
	∓49.8	0.0165	0.0016	−0.9999	13.5
	∓22.7	0.0043	1.0000	0.0015	

a) The alignment of the principal values is; D_{ZZ}, D_{XX}, and D_{YY}. The values were measured in gauss. Experimental errors in the values from I_a to I_b' were ±2.0 gauss. As for II′, an approximation which was described in the text was made. b) Experimental errors in directions were ±2°. c) The parameters were represented by an absolute value (in gauss).

(i,j=a, b, c) is the ij-component of the dipolar coupling tensor, $\tilde{\mathbf{D}}$, defined by the abc-system. The θ angle is measured from the b-axis to the external field, $\mathbf{H}$. For the rotation about the other two axes, the separation, d, is also described by Eq. (3) with the cyclic replacement of the subscripts. By applying the least-squares method to Eq. (3), the components of the dipolar coupling tensor can be completely determined by means of the abc-system. Then, the resulting tensor is diagonalized, giving the principal values and their directions. The zero-field parameters are given by:

$$D = 3D_{ZZ}/2 = D_{ZZ} - (D_{XX}+D_{YY})/2,$$
$$E = (D_{XX}-D_{YY})/2, \tag{4}$$

where D_{KK} (K=X, Y, Z) represents the principal value. The results of the analysis are shown in Table 1.

Spectral Analysis of the Quartet. One can analyze the spectra due to the quartet state by the procedure employed in the case of the triplet state. As is well known, the spin Hamiltonian is given by Eq. (2), but $\mathbf{S}=\mathbf{S}_1+\mathbf{S}_2+\mathbf{S}_3$, where the subscripts show the radicals in the radical triad. By employing the assumptions introduced in the last section and the second-order perturbation theory, the energy levels in terms of the Zeeman coordinate system, xyz, are obtained:

$$E(\pm 3/2) = (\pm 3/2)g\beta H + \varepsilon \pm \gamma,$$
$$E(\pm 1/2) = (\pm 1/2)g\beta H + \varepsilon' \pm \gamma',$$

where:

$$\varepsilon = (3/4)(3D_{zz}+D_{xx}+D_{yy}),$$
$$\varepsilon' = (1/4)\{D_{zz}+7(D_{xx}+D_{yy})\},$$
$$\gamma = \{24(D_{zx}^2+D_{yz}^2)+3(D_{xx}-D_{yy})^2+12D_{xy}^2\}/8g_e\beta H,$$
$$\gamma' = \{-24(D_{zx}^2+D_{yz}^2)+3(D_{xx}-D_{yy})^2+12D_{xy}^2\}/8g_e\beta H.$$

For the $\Delta m_s=\pm 1$ transition, the three resonance fields are given by:

$$H(1/2-3/2) = (g_e/g)(H_o-\delta-\delta'),$$
$$H(-1/2-1/2) = (g_e/g)(H_o+\delta'') = (g_e/g)H_o(1+\delta''/H_o), \tag{5}$$
$$H(-3/2--1/2) = (g_e/g)(H_o+\delta-\delta'),$$

where:

$$\delta = 2D'_{zz} - (D'_{xx}+D'_{yy}),$$
$$\delta' = 6(D'_{zx}^2 + D'_{yz}^2)/H_o,$$
$$\delta'' = (3/4)\{8(D'_{zx}^2+D'_{yz}^2) - (D'_{xx}-D'_{yy})^2 - 4D'_{xy}^2\}/H_o, \tag{6}$$

and where H_o stands for the resonance field of the free electron. The resonance-field separation, d, is as follows:

$$d = H(-3/2--1/2) - H(1/2-3/2)$$
$$= 2(g_e/g)(2D'_{zz}-D'_{xx}-D'_{yy})$$
$$= 6(g_e/g)D'_{zz}, \tag{7}$$

where we used this relationship: $D'_{xx}+D'_{yy}+D'_{zz}=0$. The $\tilde{\mathbf{D}}_{xyz}$-tensor in terms of the Zeeman coordinate system is represented by means of the $\tilde{\mathbf{D}}_{abc}$-tensor, which is defined by the rectangular coordinate system fixed in a crystal, using a unitary matrix, $\tilde{\mathbf{U}}$:

$$\tilde{\mathbf{D}}_{xyz} = \tilde{\mathbf{U}}^{-1}\cdot\tilde{\mathbf{D}}_{abc}\cdot\tilde{\mathbf{U}}. \tag{8}$$

When the crystal is rotated about the a-axis which coincides with the y-axis, and when the external field, $\mathbf{H}$, makes an angle, θ, with the b-axis, $\tilde{\mathbf{U}}$ is represented by:

$$\tilde{\mathbf{U}} = \begin{bmatrix} 0 & 1 & 0 \\ -\sin\theta & 0 & \cos\theta \\ \cos\theta & 0 & \sin\theta \end{bmatrix}. \tag{9}$$

By using Eqs. (7)—(9), d is given by:

$$d = 6(g_e/g)(D'_{bb}\cos^2\theta + D'_{bc}\sin 2\theta + D'_{cc}\sin^2\theta). \tag{10}$$

Eq. (10) is similar to Eq. (3) used in the case of the triplet. Therefore, we can analyze the spectra due to the quartet state using Eq. (10), to which the same procedure as that employed in the last section is applied.

As for the (−1/2—1/2) transition, let us put the second-order term given by Eq. (6) on the far right-hand side in Eq. (5). The δ''/H_o ratio is estimated roughly to be 1/100 at most in the case of H_o=3000, D=200 gauss, and $|E|<|D|$, so that the angular variation of the absorption is restricted within ±30 gauss from the central resonance field. Hence, the absorption is hard to detect in the radical triad in a matrix because of its overlap with the much more intense absorptions due to the isolated radicals.

The results of the analysis are also shown in Table 1, in which the indices from I to II′ correspond to the same subscripts and to the indices in Figs. 3 and 4 respectively. The subscripts, a and b, stand for the

sites occupied by the radical oligomers. The directions obtained in the a'b'c'-system were transformed to those with respect to the orthorhombic one, *abc*, by using Eq. (1). In the case of the zero-field splitting, II', we could measure $d_{II'}$ only in two directions about the b'-axis and in only one about the c'-axis because of the quite weak absorption intensities in addition to the broader linewidths. However, the following approximation was taken based on the angular variations of the other splittings as well as the $d_{II'}$ obtained: the absorption lines of II' are overlapped with those of I_a' and I_b', at least in the vicinity of each summit in Figs. 4-B and 4-C. The directions obtained by such an approximation may be more reliable than the principal values.

Discussion

Discrimination of Radical Triad from Radical Pair. In the chain containing the radical molecules with a moderate concentration, **c**, the probabilities making the radical triad, the radical pair, and the isolated radical are $3\mathbf{c}^3(1-\mathbf{c})^2$, $2\mathbf{c}^2(1-\mathbf{c})^2$, and $\mathbf{c}(1-\mathbf{c})^2$ respectively. When **c** is 0.11, the ratios of the triad to the isolated radical and to the pair give 0.036 and 0.165 respectively. Therefore, the observation of the radical triad is possible by the usual ESR technique, using a rather bulky single crystal with a suitable radical concentration. The observed intensity ratio, $\Sigma I_{triad}/\Sigma I_{pair}$, is about 0.12 after the correction for the absorption from the (−1/2—1/2) transition. This value is quite close to the calculated one, provided that the signal intensities are proportional to the concentrations of the species along with a common proportionality constant.†† This result supports our assignment of the radical oligomers. Other evidence for the identification will be discussed later.*

Structure of the Radical Pair. The $\tilde{\mathbf{D}}$-tensors of I_a and I_b satisfy the aforementioned symmetry within the limits of experimental error. The angles between the *a*-axis and each z-axis in these radical pairs are both 31°, which is close to the angle of 40° deduced from the intrachain angle of the host crystal. The $\tilde{\mathbf{D}}$-tensors, I_a and I_b, can, therefore, be attributed to the radical pairs which are formed from the TPV molecules located as nearest-neighbors to each other in the host crystal. On the other hand, the x-axis coincides approximately with the *c*-axis. This implies that one of the substituted phenyl rings is almost in the *c*-direction; this is consistent with the crystal structure of TPB, in view of the molecular geometry of TPV. However, we can not definitely decide the orientation of the *C*-phenyl rings (see Fig. 1) on the basis of the $\tilde{\mathbf{D}}$-tensor alone, as will be discussed in later section.

The *D*-parameter of II is the same as those of I_a and I_b, but the three principal axes coincide with the orthorhombic crystal axes within the limits of experimental error. The absorption intensity ratio of I_{II}/I_{I_a} is about 3/4. These results were reproduced using another sample of a (1 : 4) mixture, so this species is an intrinsic radical pair in the TPV-TPB system. The structure of this radical pair, based on the $\tilde{\mathbf{D}}$-tensor, is as follows: both of the molecular planes in this pair are parallel to the *bc*-plane, and the *C*-phenyl rings are in the *c*-direction; the second molecule is just above the first molecule, the distance between them being about *a*/2. This structure implies that the molecules in this pair have; (i) a planar geometry or (ii) a plane of symmetry. The first possibility, (i), is alternative evidence for the planar geometry of the TPV molecule, although Williams has revealed it by means of X-ray diffraction.[8] As for the second possibility, (ii), we would like to present the following facts: the symmetrically-substituted verdazyls seem to possess a plane of symmetry in their crystalline state.** In fact, TPV itself has a pseudo- or almost-mirror plane.[8]***

Radical Triad. The $\tilde{\mathbf{D}}$-tensors of I_a' and I_b' in Table 1 have the same symmetry as that of the tensors of I_a and I_b within the limits of experimental error. The *a*-axis and each of the z-axes in the former make angles of 10°, which is one-third of that in the latter. The above results suggest that the $\tilde{\mathbf{D}}$-tensors of I_a' and I_b' ought to be attributed to the radical triads. If it were not for the radical triad, one should presume another radical pair with an intermolecular distance less than that of the pair, I_a, without the third radical molecule on either side of the latter pair causing the deformation of the pair. A similar comment can be made on the I_b and II radical pairs. On the other hand, the directions of the $\tilde{\mathbf{D}}$-tensor, II', are also similar to those of the tensor, II. The tensor of II' can also be attributed to the radical triad for the same reason. All the results may be consistent with the structures of the radical triads proposed in Fig. 5; each triad is formed by adding one radical molecule to each aforementioned radical pair to the position obtained by the *a*-transla-

†† When both the electron-spin-exchange interactions in the radical oligomers are antiferromagnetic, and when a linear alignment of the spins in the radical triad is taken, the more reasonable signal intensity ratio, I_{triad}/I_{pair} $(=r)$, can be given by:

$$r = 3\mathbf{c}^3(1-\mathbf{c})^2\chi_q\{2\mathbf{c}^2(1-\mathbf{c})^2\chi_t\}^{-1}$$
$$= 15\mathbf{c}\{3+\exp(2|J_t|/kT)\}[8\{2+\exp(3|J_q|/2kT)+\exp(5|J_q|/2kT)\}]^{-1},$$

where χ_q and χ_t are the magnetic susceptibilities due to the quartet and triplet states respectively. J_q and J_t stand for the exchange integrals in the radical triad and the pair respectively. *T* and *k* have the usual meanings. When one puts $\mathbf{c}=0.11$, $T=300$ K, and $-J_q/k=-J_t/k=10$, 50, 100 K into the equation, the ratios give 0.203, 0.189, and 0.172 respectively. The exchange integrals, $|J/k|$'s, in the present radical oligomers are supposed to be from ten to a few score degrees. Therefore, the approximation ($r=3\mathbf{c}^3(1-\mathbf{c})^2/2\mathbf{c}^2(1-\mathbf{c})^2$ $(=0.165$ for $\mathbf{c}=0.11)$) mentioned in the text is considered to be a tolerable one.

* The possibility of the observation of the radical tetrad was not discussed, because the ratio of the tetrad to the triad is about 1/10.

** Two symmetrical verdazyls have a plane of symmetry (Ref. 15).

*** Note that Fig. 1(a) was not projected along the normal of the molecular plane.

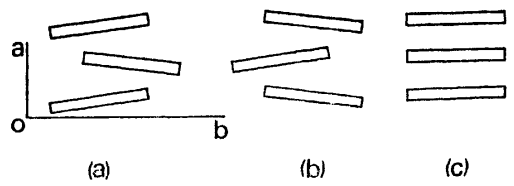

Fig. 5. Schematic drawings of chemical structures of the proposed radical triads projected along the *c*-axis. (a), (b), and (c) correspond to the radical triads I_a', I_b', and II', respectively. Oblongs stand for the sections of the idealized molecular planes.

tion of that occupied by the first molecule in the pair.

The absorption-intensity ratio, $I_{II'}/(I_{I_a'}+I_{I_b'})$, is very close to the $I_{II}/(I_{I_a}+I_{I_b})$ ratio. This suggests the following mechanism for the formation of the radical oligomer in the TPV-TPB system. There are two types of positions occupied by the first radical molecule; (A) one is one of the four general positions determined originally by the host molecules in the unit cell, and (B) the other is a special one. The positions occupied by one kind of radical oligomer are all of the same type, that is, A-A or B-B and A-A-A or B-B-B for the radical pairs and triads respectively. This mechanism also may explain the observation of only three $\tilde{\mathbf{D}}$-tensors for the radical triads. The letters correspond to the subscripts in Table 1. On the basis of the above consideration, we expect that the B-B-B type stacking may be a meta-stable packing of the host and the guest molecules. Actually, a molecular packing very similar to this type has been found in the 1,3,5-triphenyl-6-methylverdazyl crystal.[15]

The spin multiplicity of the fine structure defined by the resonance-field separation, d_{III}, is not clear at present, although the signal intensity can be explained well b assuming a radical triad containing one TPB molecule in its structure rather than presuming a second-nearest-neighboring radical pair.

$\tilde{D}$-Tensor Calculation with Spin Densities. The calculation of the dipolar coupling tensors of the proposed radical pairs is made in order to clarify the orientation of the *C*-phenyl rings in the pairs and in order to examine the effect of the spin delocalization on the $\tilde{\mathbf{D}}$-tensor. The parameters, *D* and *E*, of radical pairs have already been calculated by several authors[4,16] on the basis of the molecular orbital theory. Although the present method is essentially the same as theirs, the principal values and their directions are both obtained by our method. The spin Hamiltonian which is considered to be valid for the radical pair is given by:

$$H_D = \sum_{i,j} g^2\beta^2\rho_i\rho_j\{\mathbf{S}_1\cdot\mathbf{S}_2/r_{ij}^3 - 3(\mathbf{S}_1\cdot\mathbf{r}_{ij})(\mathbf{S}_2\cdot\mathbf{r}_{ij})/r_{ij}^5\}, \quad (11)$$

where ρ_i and ρ_j are the π-spin densities on the *i* atom in the first molecule, 1, and on the *j* atom in the second molecule, 2, and where $\mathbf{r}_{ij}$ is the vector distance connecting *i* to *j*. The Hamiltonian, Eq. (11), is rewritten in a matrix form by means of the total spin, $\mathbf{S}=\mathbf{S}_1+\mathbf{S}_2$:

$$H_D = \mathbf{S}\cdot\tilde{\mathbf{D}}\cdot\mathbf{S},$$

where the symmetrical tensor is:

$$\tilde{\mathbf{D}} = \begin{bmatrix} D_{xx} & D_{xy} & D_{xz} \\ D_{xy} & D_{yy} & D_{yz} \\ D_{xz} & D_{yz} & D_{zz} \end{bmatrix}, \quad (12)$$

and where:

$$D_{mm} = (1/2)g^2\beta^2\sum_{i,j}\rho_i\rho_j(r_{ij}^2-3m_{ij}^2)/r_{ij}^5, \quad (m=x, y, z),$$

$$D_{mn} = (1/2)g^2\beta^2\sum_{i,j}\rho_i\rho_j(-3m_{ij}n_{ij})/r_{ij}^5,$$

$$(m, n=x, y, z; \text{ but } m\neq n).$$

The $\tilde{\mathbf{D}}$-tensor given by Eq. (12) can be calculated in an arbitrary rectangular coordinate system if the structure of the radical pair and the spin distribution are known, followed by diagonalization. However, we use an alternative method in which the Zeeman system is employed and in which only the *zz*-component is used:

$$D'_{zz} = (1/2)g\beta\sum_{i,j}\rho_i\rho_j(r_{ij}^2-3z_{ij}^2)/r_{ij}^5$$

$$= (1/2)g\beta\sum_{i,j}\rho_i\rho_j(1-3\cos^2\theta_{ij})/r_{ij}^3, \quad (13)$$

where θ_{ij} is the angle between the vector, $\mathbf{r}_{ij}$, and an applied field, $\mathbf{H}$. Putting Eq. (13) into Eq. (3), we obtain:

$$d = (3/2)g_e\beta\sum_{i,j}\rho_i\rho_j(1-3\cos^2\theta_{ij})/r_{ij}^3, \quad (14)$$

By employing Eq. (14), the diagonalized $\tilde{\mathbf{D}}$-tensor is obtained by the procedure described in the section on spectral analyses.

The results of the calculation are shown in Table 2, together with the directions of the *C*-phenyl rings. When the calculation was carried out, the spin densities were taken from Ref. 1. The vector distances were deduced from the host crystal for the I_1 and I_2 radical pairs. As for the II_1 and II_2 pairs, the distances have been estimated from the structures in which the first molecules are the same as those in the I_1 and I_2 pairs, while the second molecules are obtained by the *a*/2-translation of the first molecules. In the table, the $\tilde{\mathbf{D}}$-tensor of I_a in Table 1 is close to the I_1 rather than to the I_2. This result suggests that the *C*-phenyl rings in the I_a and I_b radical pairs are in the *c*-direction, which is consistent with our expectation. II_1 also explains II; this indicates again the orientation of the *C*-phenyl rings in the radical pair of II along the *c*-axis. The discrepancy between the observed and the calculated $\tilde{\mathbf{D}}$-tensors depends mainly on the difference between the true and the presumed vector distances. However, the results of the calculation may not only support our assignment of the radical pairs with the proposed structure, but also suggest that the $\tilde{\mathbf{D}}$-tensors due to the proposed radical triads can not be explained by assuming the radical pairs with *C*-phenyl rings differently oriented from those in the I_a, I_b, and II pairs.

In order to compare the *D*-parameters observed and calculated above with that expected from a point-spin approach, we estimated the latter to be 240 gauss by using the relation: $D=(3/2)g\beta/r^3$.[17] On the other hand, the *D*-parameters observed and calculated by our method are 150 and 130 gauss respectively. This

Table 2. Calculated dipolar coupling tensors of the proposed radical pairs

Name[a]	Principal values[d]	Direction cosines with respect to *abc* system			D[e] E[e]
I_1	±85.5	0.9065	0.4219	0.0142	128.2
	∓49.2	−0.0249	0.0199	0.9995	6.5
	∓36.3	−0.4214	0.9064	−0.0285	
I_2[b]	±68.1	0.7638	0.6430	0.0557	102.2
	∓39.2	−0.6173	0.7530	−0.2277	5.2
	∓28.9	−0.1884	0.1396	0.9721	
II_1	±120.3	0.9989	0.0432	0.0168	180.4
	∓73.6	−0.0171	0.0079	0.9998	13.5
	∓46.6	−0.0430	0.9990	−0.0086	
II_2[c]	±119.4	0.9967	0.0359	0.0728	179.2
	∓72.2	0.0048	0.8699	−0.4932	12.5
	∓47.2	−0.0811	0.4919	0.8669	

a) The capital letters correspond to those in Table 1. I_1 and II_1; *C*-phenyl rings are in the *c*-direction. b) An alternative candidate for radical pair I_a; the respective *C*-phenyl rings lie in the [011] and [01$\bar{1}$] directions. c) Another candidate for radical pair II; the *C*-phenyl rings lie in the [01$\bar{1}$] direction. d) The order of the principal values is the same as that in Table 1. The values were measured in gauss. e) Refer to the last footnote in Table 1.

large discrepancy of 90 gauss may indicate that the point-spin approach to the radical pair with the delocalized spins is a very rough approximation.

The authors would like to acknowledge the encouragement of Professors Hideo Takaki, Kazuhiko Ishizu, and Mamoru Mekata and of their other collaborators in the laboratories. They are also grateful to Professors Yoshihiko Saito and Fumiyuki Marumo of the University of Tokyo for offering them a chance to determine the crystal structures of other verdazyls.

References

1) N. Azuma, J. Yamauchi, K. Mukai, H. Ohya-Nishiguchi, and Y. Deugchi, This Bulletin, **46**, 2728 (1973).
2) to be published.
3) D. B. Chesnut and W. D. Phillips, *J. Chem. Phys.*, **35**, 1002 (1961); D. B. Chesnut and P. Arthur, Jr., *ibid.*, **36**, 2969 (1962); D. D. Thomas, A. W. Merkl, A. F. Hildebrandt, and H. M. McConnell, *ibid.*, **40**, 2588 (1964); M. A. Marechal and H. M. McConnell, *ibid.*, **43**, 497 (1965); M. J. Hove, B. M. Hoffman, and J. A. Ibers, *ibid.*, **56**, 3490 (1972).
4) D. A. Wiersma and J. Kommandeur, *Mol. Phys.*, **13**, 241 (1967).
5) Y. Kurita, *J. Chem. Phys.*, **41**, 3926 (1964).
6) O. Takizawa, J. Yamauchi, H. Ohya-Nishiguchi, and Y. Deguchi, This Bulletin, **46**, 1991 (1973).
7) Y. Deguchi, *ibid.*, **34**, 910 (1960); A. Nakajima, *ibid.*, **46**, 1129 (1973).
8) D. E. Williams, *Acta Crystallogr.*, **B29**, 96 (1973).
9) K. Mukai, N. Azuma, H. Shikata, and K. Ishizu, This Bulletin, **43**, 3958 (1970).
10) N. Azuma, K. Mukai, and K. Ishizu, *ibid.*, **43**, 3960 (1970).
11) M. S. Farag, *Acta Crystallogr.*, **7**, 117 (1954).
12) S. Chandra and M. P. Hemkar, *ibid.*, **A29**, 25 (1973).
13) R. Kuhn and H. Trischmann, *Monatsh. Chem.*, **95**, 457 (1964).
14) K. Itoh, "Jikken Kagaku Koza," ed. by the Chemical Society of Japan, Maruzen, Tokyo (1967), Vol. 13, p. 153.
15) to be published.
16) D. D. Thomas, H. Keller, and H. M. McConnell, *J. Chem.* Phys., **39**, 2321 (1963).
17) H. van Willigen and S. I. Weissman, *Mol. Phys.*, **11**, 175 (1966).

Electronic Spectra of Perylene Crystals

Jiro TANAKA, Tohru KISHI, and Masashi TANAKA
Department of Chemistry, Faculty of Science, Nagoya University, Chikusa, Nagoya 464
(Received March 20, 1974)

The electronic absorption and emission spectra of α and β forms of perylene have been investigated. The low-temperature spectra have been studied with the (001) plane, and a detailed vibrational analysis is presented. The reflection measurements with the (001) plane and the (110) or (1$\bar{1}$0) plane are carried out, and the Kramers-Kronig transformation is carried out in order to obtain the absorption coefficient. The results present reasonable evidence for the existence of the intermolecular CT transition in the 27000 cm^{-1} region. The emission spectra at 4.2 K present several novel features of the mechanism of a monomer-like emission of the α-crystal.

Since the absorption and fluorescence of perylene have been investigated on two crystalline forms of perylene,[1] many papers have apperared on this and related problems.[2-6] Detailed spectroscopic investigations of this system will still be of great value, because they will provide a unique chance to examine the conditions of the excimer formation in molecular crystals.[7] The intermolecular CT band between the same entity in a neat crystal is still a problem of dispute[8]; however, the CT band of 9,10-dichloroanthracene[9] has recently been confirmed by the electroreflectance experiment of Abbi and Hanson.[10]

In the present paper, we will report a further spectroscopic investigation of perylene crystals by using somewhat elaborate methods. First, the low-temperature absorption spectra at 1.6 K and 4.2 K of the α and β forms of perylene are measured by the transmission method, using a medium spectrograph. Then, the crystalline reflection spectra are recorded and the Kramers-Krnoig transformation is used to calculate the absorption spectra. By the latter method the spectra along a different crystalline direction which has not been measured in the previous paper can be obtained, and further discussions of the CT state and of hypochromism are presented. The emission spectra at 4.2 K are also photographed, and the Stokes shifts of fluorescence are discussed in connection with the crystal structure and intermolecular interactions.

Experimental

The perylene used was a product of Theodor Schuchardt of W. Germany. It was recrystallized, and then further purification was carried out by means of column chromatography. The α crystal for the transmission measurement was obtained by a sublimation method, and it was not difficult to obtain crystals about 5 mm × 5 mm with a thickness of less than 1 μ. The thin crystal of the β form was rather difficult to obtain, but it could be grown from a solution of 90% benzene and 10% toluene. For the transmission measurement the crystal was polished with benzene until it showed retardation of about 300 mμ of a yellow colour. The crystals for the absorption measurement at a low temperature were mounted between thin quartz disks and then covered with a black mask with a pin-hole. The light penetrated through the pin-hole, with a diameter of less than 1 mm, and the pin-hole was placed on the uniformly thick part of the crystal. The crystals were placed in the holder in the direction in which the polarization effect of the grating spectrograph was not serious. The holder was then placed in the double quartz Dewar vessel and immersed in liquid helium.

The set-up of apparatus for absorption and emission measurements is shown in Fig. 1. The spectrograph used was a Shimadzu GE-100 apparatus, with a Bausch-Lomb grating of dispersion of 8.3 Å/mm. The light source for the absorption measurement was a tungsten lamp containing iodine of 100 W. A high-pressure mercury lamp of 250 W combined with a Toshiba DV-1 filter was used for the excitation of fluorescence. The fluorescence was either photographed by means of the spectrograph or was photo-electrically recorded by means of a Carl-Zeiss spectrofluorometer. For the measurement at 1.6 K, the helium Dewar was pumped out and the temperature was measured by means of the vapour pressure of helium.

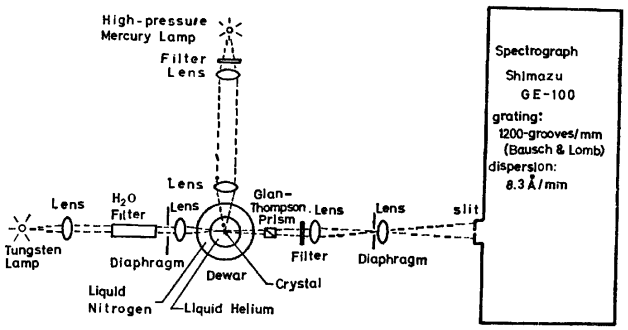

Fig. 1. The optical system for spectral measurement.

The reflection spectra are recorded with (001) and (110) or (1$\bar{1}$0) planes of α and β forms by means of a system which will be described in a separate paper.[11] Although the transmission measurements are confined along the a- and b-axes of α and β crystals, the reflection data are obtained with the other direction, perpendicular to the ab plane.

Results and Discussion

Low-temperature Absorption Spectra of α-Perylene. The low-temperature absorption spectra of the α-crystal at 1.6 K show clear vibrational structures in the beginning of the band series. The absorption band along the b-axis shows a particularly close resemblance to that of the solution (Fig. 2), while the band shape and intensities are greatly changed along the a-axis (Fig. 3). The 0–0 band origins are certainly confirmed along the a- and b-axes, and the Davydov splitting is determined as 820 cm^{-1}. The band systems are assigned with reference to the solution band system as is shown in Table 1. The band width is much broader along the a-axis, and the width of the 0–0 band at 1.6 K was 300 cm^{-1} for the a-axis and 190 cm^{-1} for the b-axis. The width in the *n*-hexane solution was smaller than 10 cm^{-1}, which may be a typical pattern

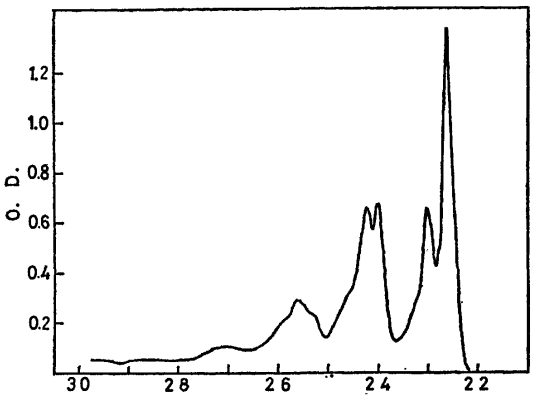

Fig. 2. Absorption bands of perylene in EPA solution at 77 K.

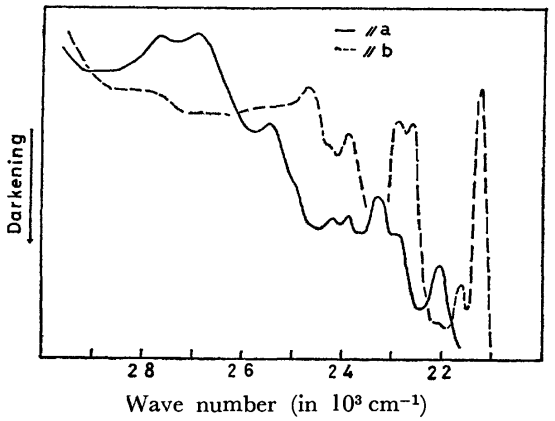

Fig. 3. Polarized absorption spectra of α crystal at 1.6 K.

of the Shpolskii effect.[12] At higher vibrational levels the band widths are much broader for the a- and b-axes; this may be induced by the effect of other types of transitions near-by or overlapping.

Above 26000 cm^{-1} the band becomes very broad and it may be supposed that the band in this region is composed of transitions of a different character rather than of vibrational progressions of a unique electronic origin. The intermolecular CT transition, which has been suspected because of its weak intensity, is found in this spectra in the 26500—29000 cm^{-1} region. There have been several discussions of the presence of the CT band, because only a weak and broad band was found at room temperature in an earlier paper.[1] One of the criticisms of the CT mechanism is based on the calculation of the vibronic structure of the coupled dimer,[3,4] but the broad character of the band at very low temperatures can not be reasonably explained by this mechanism because each vibronic band is clearly resolved in the 21000—25000 cm^{-1} region. Therefore, the overlapping of the intermolecular CT band and the vibrational progressions of the first $^1B_{2u}$-type transition seem the most reasonable explanations of the anomalous

Table 1. Absorption bands of perylene at 21000—29000 cm^{-1} region

Solution		α-Form						
(cm^{-1})	$\Delta\nu$	a-axis	$\Delta\nu$	b-axis	$\Delta\nu$	~c-axis	$\Delta\nu$	$\Delta\nu_{ab}$
22630	(0)	22050	(0)	21230	(0)	21800	(0)	820
22960	(+330)			21640	(+410)			
23340	(+710)							
23960	(+1330)	22950	(+900)	22620	(+1390)			330
24240	(+1610)	23320	(+1270)	22850	(+1620)	23200	(+1400)	470
25250	(+2620)	23910	(+1860)	23840	(+2590)	23600	(+1800)	70
25600	(+2970)	24210	(+2160)	24260	(+3030)			
25900	(+3270)							
27100	(+4470)	25500	(+3450)	24740	(+3510)	24800	(+3000)	
		26900	(+4850)					
		27700	(+5650)					

Solution		β-Form						
(cm^{-1})	$\Delta\nu$	a-axis		b-axis		~c-axis		$\Delta\nu_{ab}$
22630	(0)	21640	(0)	20810	(0)	21500	(0)	830
22960	(+330)	22070	(+430)	21180	(+370)			
23340	(+710)			21650	(+840)			
		22440	(+800)	22160	(+1350)			280
23960	(+1330)	23120	(+1480)	22360	(+1550)	23000	(+1500)	760
24240	(+1610)			22730	(+2690)			
				22970	(+2160)			
		23700	(+2060)	23500	(+2690)			
25250	(+2620)	23950	(+2310)	23750	(+2940)			
25600	(+2970)			24100	(+3290)			
25900	(+3270)					24500	(+3000)	
27100	(+4470)			25500	(+4690)	26200	(+4700)	

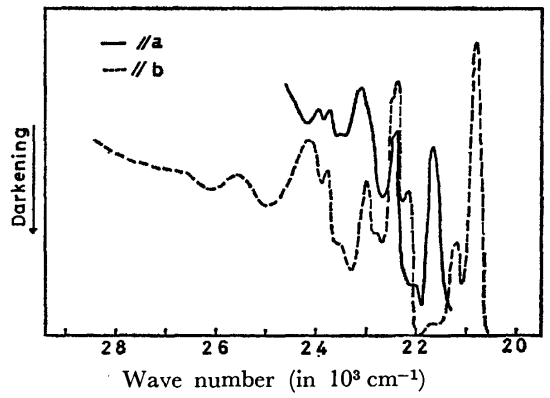

Fig. 4. Polarized absorption spectra of β crystal at 1.6 K.

band shape.

Low-temperature Absorption Spectra of β-Perylene. The spectra photographed at 1.6 K with the (001) plane are shown in Fig. 4. The 0–0 band origin and the details of the vibrational structures were clearly resolved. The Davydov splitting is 830 cm^{-1}, of nearly the same magnitude as the α crystal. In an earlier paper[1] a much larger value was assigned for this splitting, but it should be corrected because the 0–0 band origin has now been clearly confirmed.

The vibrational progressions of the b-axis spectra are nicely correlated with the solution spectra, since the band shape is nearly regular. On the other hand, the band shape is rather anomalous along the a-axis, and the band width for the a-axis is broader than for the b-axis. For instance, the half-width of the 0–0 band is 290 cm^{-1} for the a-axis and 180 cm^{-1} for the b-axis. The pattern of vibrational progression along the a-axis is also modified from the solution band. There are several reasons for this change; one is the change in Franck-Condon factors from the free molecule to the molecule in the crystal, which means that the vibrational mode in the excited state involves a significant anisotropy. Another possible effect may be due to the CT transition or band-to-band transition along the direction of the stacking of the molecule. Although the intensities of these transitions may be quite small, they may be influential upon the a-axis band in causing hypochromism or broadening. In this respect, several weak humps around the 28000—31000 cm^{-1} region may be suspected as CT bands, because these bands were enhanced under high pressures.[13]

Two more characteristics of the low-temperature spectra of the α and β crystals are that the Davydov splitting for higher vibrational progressions are rather small, while the band splitting is not proportional to the intensity of each vibronic band. The assignment of band splitting with higher levels was rather difficult; it appears thereby that the intramolecular vibrational coupling is much stronger than the excitonic interaction between adjacent molecules in the crystalline lattice. At any rate, the weak coupling scheme must be used to analyse the perylene crystalline spectra rather than the intermediate or strong coupling, because the band splittings were found at all vibronic levels.

Reflection Spectra of α and β Perylene. The reflection measurement has several advantages over the transmission method; for instance, the thick crystal can be used to determine the polarization direction with more than two crystalline faces, and the intensity of a very strong band can be determined rather accurately.

The reflectivities of the α and β forms are shown in Figs. 5 and 6. The Kramers-Kronig transform of the reflectivity gave the absorption spectra shown in Figs. 7 and 8. The spectra are taken with the (001) and ($\bar{1}$10) planes of the α crystal and with the (001) and (110) planes of the β crystal. Although the direction perpendicular to the (001) plane is not exactly coincident with the c-axis, it is in nearly the same direction. The spectra show several interesting properties which have not been recognized in earlier transmission measurements on the (001) plane.

The first absorption region of the α crystal, at 20000—28000 cm^{-1}, can be recorded for all three directions.

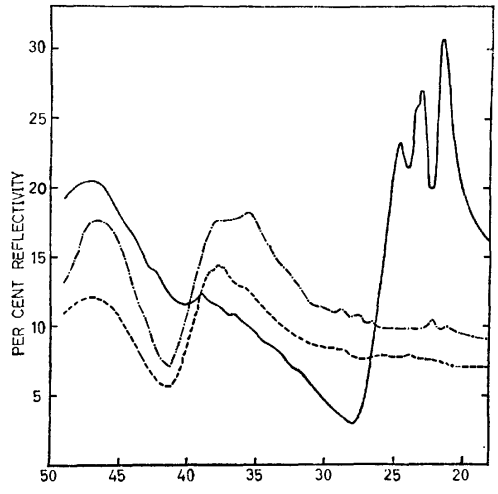

Fig. 5. Reflectivity of α crystal at room temperature.
—— a-axis, —·— b-axis, —— c-axis.

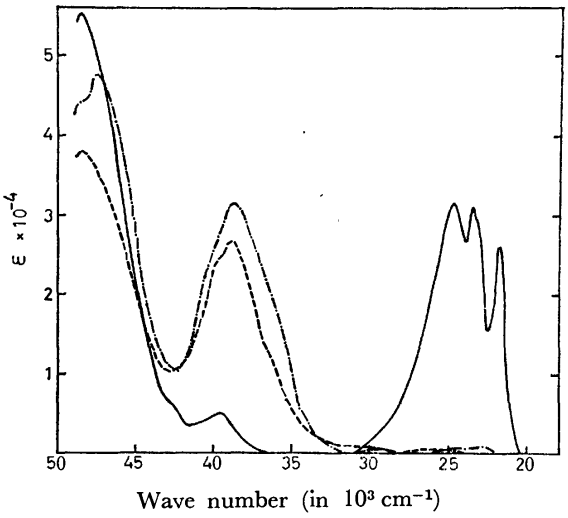

Fig. 6. Absorption spectra of α crystal obtained from Kramers-Kronig transformation.
---- a-axis, —·— b-axis, —— c-axis.

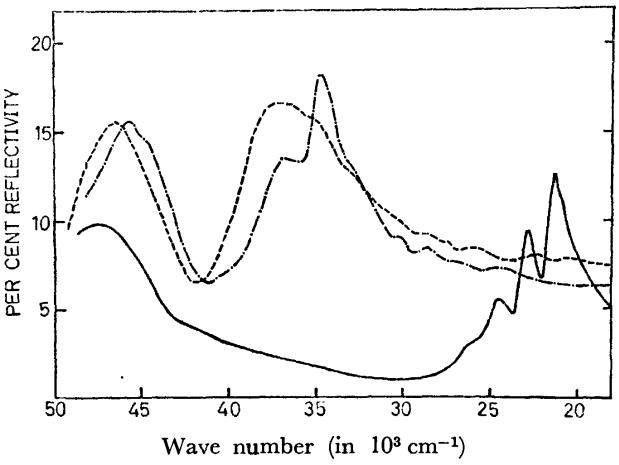

Fig. 7. Reflectivity of β crystal at room temperature.
—— a-axis, —·— b-axis, —— c-axis.

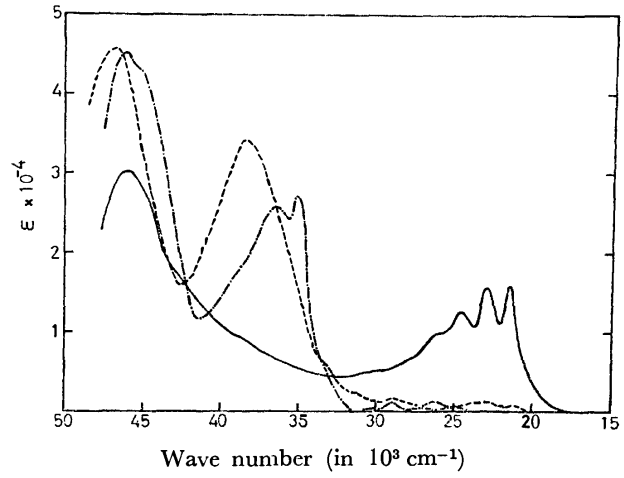

Fig. 8. Absorption spectra of β crystal at room temperature.
—— a-axis, —·— b-axis, —— c-axis.

It is quite interesting that the spectrum along the c-axis is nearly in agreement with the powder state spectra in KBr disk measured by Offen and Beardslee;[13] this result is reasonable since the intensity is strongest along this axis. The absorption curves obtained by reflection for the $^1B_2$ and the CT bands of the a- and b-axes were not accurate enough as compared with the transmission results. The c-axis spectrum of the β-crystals shows vibrational progressions which resemble those of the solution spectra; this may imply that the whole band in this region is of a unique character. On the other hand, the c-axis band of the α crystal is in marked contrast; there the vibrational progressions higher than 23500 cm^{-1} are greatly changed from their regular shape.

Theoretically, the energy levels of a molecular crystal should conform to the group theoretical splitting, and the levels must be the same for the a- and c-axes bands in a monoclinic crystal. Therefore, the band positions should be coincident for the a- and c-axes if the same electronic transition is involved. Actually, this prediction is almost in accord with the first several vibronic levels when we compare the band positions of the a-axis obtained by the transmission method with the c-axis band based on the reflection data. Moreover, the band shape of the c-axis spectrum is in accord with neither the a-axis spectrum nor the theoretical curve of Witkowskii *et al.*[4]

On the other hand, a similar change in band shape has been observed in the case of the mixing of the CT state with the molecular exciton state. The CT transition may cause such an anomaly; for instance, the c-axis band of 9,10-dichloroanthracene is changed from the regular band shape in solution. In this crystal, the CT transition with the out-of-plane polarization has been found along the particular crystalline direction (a-axis);[9] the presence of such a CT state influences the shape of the in-plane transitions along the c-axis. Therefore, the marked change in the α perylene spectra along the c-axis in this range may be regarded as another token of this type of mixing, indicating the existence of the CT transition in the 26000—28000 cm^{-1} region of the a-axis. The enhancement of the 25000 cm^{-1} band of α perylene under high pressure has been reasonably explained by the CT mechanism.[13]

Direct evidence for the existence of the CT state with the (001)-plane reflection spectra was rather difficult to obtain because of the weak intensity of the bands along the a-axis. In spite of this difficulty, though, several weak bands were observed with the a- and b-axes of the α and β-form crystals in this region. It may be said that the detection of a weak CT transition is rather difficult by the reflection method unless the crystal structure is mostly favoured; a negative result with dibenzoselenophene[14] may be understood by this reasoning.

The second absorption region at 33000—42000 cm^{-1} is due to the short-axis polarized transition of the $^1B_{3u}$ type, and the absorption shape is different for the α and β crystals. The absorption spectra transformed from the reflection data for the α form gave a pattern similar to that of the transmission result, but the β form spectrum was somewhat different from the earlier transmission result. Along the a-axis band of the β crystal, a vibrational progression resembling that of the solution was observed. A Davydov splitting of the same sign and magnitude as the calculated value given in the previous paper was found with the β crystal.

The higher energy transition in the 44000—53000 cm^{-1} region in a solution is confirmed to be composed of several long- and short-axes polarized bands. This was also found by Fuke, Kaya, and Nagakura[15] independently.

In the light of the present results, it is quite interesting that the dimer spectra in a rigid solution found by Ferguson[3] showed a band shape similar to that of the a-axis band of the α crystal. Since the average of intensities with three crystalline axes is more or less the same as that of the solution spectrum, it appears that the dimer or its aggregates in a rigid solution may have a much more symmetrical or specific structure than in crystals, because the hypochromism and the anomaly of the band shape is rather pronounced.

Fluorescence Spectra of α and β Perylene. At 4.2 K the excimer fluorescence of the α form does not appear; instead, a monomer-like emission is observed. In an earlier investigation the effect of the re-absorption of the crystalline surface on the shape of the fluorescence

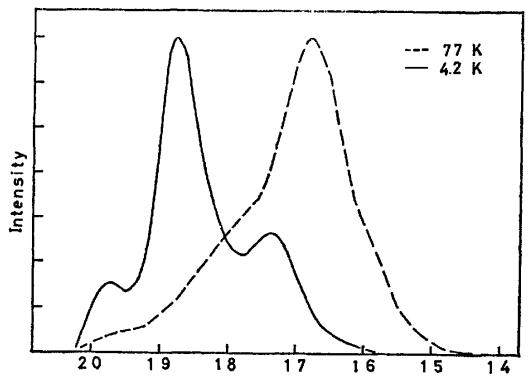

Wave number (in 10^3 cm^{-1})

Fig. 9. Emission spectra of α crystal at 4.2 K.

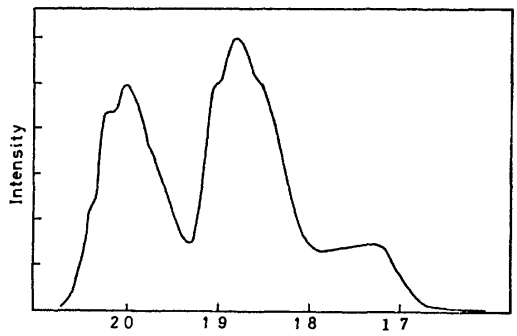

Wave number (in 10^3 cm^{-1})

Fig. 10. Emission spectra of β crystal at 4.2 K.

was not properly taken into account;[5] therefore, a detailed band analysis is undertaken in this study. The fluorescence spectra of α and β perylene are illustrated in Figs. 9 and 10, where the results at 4.2 K are presented. No essential difference in spectra were found at 1.6 K and 4.2 K. The spectra are recorded on a Carl-Zeiss fluorometer.

In the photograph of β emission at 1.6 K, very sharp lines are observed, and the 0–0 band origin is assigned at 20517 cm^{-1}. The vibrational progressions are tabulated in Table 2, together with the values found in a solution. The Stokes shift in a solution is only 30 cm^{-1}, while the corresponding value for the β crystal is 293 cm^{-1}.

The α-form emission at 77 K shows the peak of the excimer band at 16850 cm^{-1}, but weak components at 19000—20000 cm^{-1} are also observed. Inoue *et al.*[6] showed, by time-resolving spectroscopy, that these results are due to a monomer-like emission.

The photographs at 4.2 K and 1.6 K show only broad emission bands, situated at 19800, 18750, and 17400 cm^{-1}. The band origin was not clearly ascertained since no fine structure could be detected at the beginning of the first band. The Stokes shift was estimated as about 1000—1400 cm^{-1}, significantly larger than that of the β crystal.

It has been suggested in an earlier paper[1] that the intermolecular approach of two molecules in the excited state is essential for the excimer formation. This point seems to be substantiated by the following investigations. At 4.2 K in the α crystal, the excimer emission is absent, but there still remains a significant red

Table 2. Sharp emission lines of β-perylene crystal

β-Crystal (cm^{-1})	$\Delta\nu$	*n*-Hexane solution[12] $\Delta\nu$
20517	(0)	0
20496	(−21)	
20473	(−44)	
20408	(−109)	
20333	(−184)	
20182	(−335)	−357
20145	(−372)	
19389	(−1128)	−1104
19314	(−1203)	
19283	(−1234)	
19212	(−1305)	−1298
19144	(−1373)	−1375
18939	(−1577)	−1578

shift of the emission band. The shift is certainly larger than the monomer emission band of the β crystal. This may imply that the levels in the α crystal are split by the excitonic interaction at the distance of the ground-state configuration or that the shift of the level is accompanied by a slight distortion of the structure. The lower energy level will be forbidden in a strict D_{2h} symmetry, but the band is actually observed to the red of the 0–0 absorption band; this may suggest a deformation of the paired molecule from the parallel arrangement. In other words, the intermolecular interaction is much larger for the α-form than for the β-form even at 4.2 K.

The emission spectrum of the perylene dimer[3] in a rigid solution is reported to have a maximum at 18280 cm^{-1}, and the band shape at 20 K is composed of the excimer type and a monomer-like band of the α crystal. The crystalline bands are 500 cm^{-1} higher in energy than that found for the dimer. This finding suggests that the excitonic and charge-resonance interaction will be easier for the dimer in a rigid solution than in crystals.

In the earlier paper the monomer-like emission of the α-form at 4.2 K was simply called a monomer band, and it was considered it was nearly the same in character as the β-form emission band. As a matter of fact, the level is significantly shifted; therefore, the previous interpretation of this level must be revised so as to involve a different character rather than the Franck-Condon excitonic state.

Recently Inoue *et al.*[6] claimed that the excimer formation from the Franck-Condon excited state competes with the process of the relaxation to a monomer-like emission level. The discrimination of the monomer-like emissive level of the α crystal from the Franck-Condon excited level will be important for any further analysis of the excimer process.

The red shift of the excimer emission of the α-form at 77 K may be estimated to be as large as 9000 cm^{-1} if we take the origin of the CT band at 26000 cm^{-1}. Therefore, such a large shift can be explained only when the distortion of molecules in the excited state is allowed to move to a closer distance than in a crystal

at 4.2 K[1,16] where the interaction of the charge-resonance state with the excitonic state will be very much larger than for the above-mentioned deformed configuration.

Concluding Remarks. The existence of the CT state in neat molecular crystals is a problem of interest, and evidence of such a state obtained by an accurate spectral study has been presented for perylene crystals. The polymorphism of the crystal has been shown to be of great help for such an investigation. Although the reflection method in crystalline spectroscopy is very powerful, its limitation for weak transitions has been presented. The combination of reflection with the transmission method will give the most reliable results in determining the polarization character. The investigation of the CT state in neat molecular crystals will still be a challenging problem, and the critical condition for observing such a band must be sought in further studies.

Although the geometry of the excimer state is still not known, it has been found that the shape and position of the emission band are greatly dependent on the relative orientation of molecules in the crystal. Further investigation will elucidate the structure of the excimer state in a crystal or in a fluid solution.

References

1) J. Tanaka, This Bulletin, **36**, 1237 (1963).
2) R. M. Hochstrasser, *J. Chem. Phys.*, **40**, 2559 (1964).
3) J. Ferguson, *ibid.*, **44**, 2677 (1966).
4) A. Witkowski and M. Z. Zgierski, *Chem. Phys. Lett.*, **9**, 336 (1971); *Phys. Stat. Sol. (b)*, **46**, 429 (1971).
5) K. Kawaoka and D. R. Kearns, *J. Chem. Phys.*, **45**, **147** (1966).
6) A. Inoue, K. Yoshihara, T. Kasuya, and S. Nagakura, This Bulletin, **45**, 720 (1972).
7) B. Stevens, *Spectrochim. Acta*, **18**, 439 (1962).
8) D. M. Hanson, *Crit. Rev. Solid State Sci.*, **3**, 243 (1973).
9) J. Tanaka and M. Shibata, This Bulletin, **41**, 34 (1968).
10) S. C. Abbi and D. M. Hanson, *J. Chem. Phys.*, **60**, 319 (1974).
11) J. Tanaka, S. Muramatsu, and M. Tanaka, to be published.
12) M. M. Valdman and R. I. Personov, *Opt. Spectrosc.*, **19**, 296 (1965).
13) H. W. Offen and R. A. Beardslee, *J. Chem. Phys.*, **48**, 3584 (1968).
14) G. A. Gerhold and L. B. Clark, *ibid.*, **54**, 3102 (1971).
15) K. Fuke, K. Kaya, and S. Nagakura, Presented at Symposium on Molecular Structure (1972), Sendai.
16) J. N. Murrell and J. Tanaka, *Mol. Phys.*, **7**, 363 (1964).

Microwave Spectrum, Structure and Dipole Moment of Ethanethiol. I. *Trans* Isomer

Michiro HAYASHI, Hisae IMAISHI, and Kazunori KUWADA
Department of Chemistry, Faculty of Science, Hiroshima University, Higashi-sendamachi, Hiroshima 730
(Received December 10, 1973)

The microwave spectra of *trans*-ethanethiol and its isotopic species were measured. The r_s structure of the *trans* isomer was determined from the observed moments of inertia. The *trans* isomer has a symmetrical CH_3 group, the parameters for the CH_2SH part of the molecule being approximately equal to those of methanethiol. The C-C bond length, found to be 1.529±0.006 Å, is close to that of propane. The angle α(CCS), obtained as 108°34′ ±19′, is much smaller than that of analogous molecules. Discussion is given for this anomalously small α(CCS) angle. From the Stark shifts, the dipole moment of the *trans* isomer was determined to be $\mu_a = 1.058 \pm 0.023$, $\mu_b = 1.146 \pm 0.002$ and $\mu_{total} = 1.560 \pm 0.032$ D, an angle of 28°46′ being made with the bisector of the α(CSH) angle inclining towards the ethyl group. Since the dipole moment of methanethiol makes an angle of 18°30′ with the bisector of the α(CSH) angle, the increase of the angle with the bisector for ethanethiol was concluded to arise from the induction moment of the ethyl group. A brief description is given for the spectra due to the *gauche* isomer.

From an interest in the internal rotation of completely asymmetric molecules, we investigated the microwave spectra of ethanethiol. The rotational spectra of ethanethiol might be influenced by two modes of internal rotation, one relating to the CH_3 group and the other to the SH group. If the barrier to the internal rotation of the SH group is sufficiently high, the rotational isomers can be observed. Actually we could observe two groups of strong spectra belonging to the ground states of the *trans* and *gauche* isomers, as well as several groups of weak spectra belonging to the vibrationally excited states.

Kadzhar, Abbasov, and Imanov[1] reported on the microwave spectra of two isotopic species of *trans*-ethanethiol. Schmidt and Quade[2] studied the normal species of *trans*-ethanethiol.

A part of our studies on the microwave spectra of ethanethiol, was reported[3] but publication of details was postponed until the spectra of a sufficient number of isotopic species necessary for determining the r_s structure of *trans*-ethanethiol were obtained.

As regards the *gauche* isomer, several strong spectra with Stark effects characteristic of the *a*-type *R* brnach transitions were observed for the normal and seven deuterated species. For the normal and CH_3CD_2SH species, the transitions of types $(J+1)_{1J+1} \leftarrow J_{1J}$ and $(J+1)_{1J} \leftarrow J_{1J-1}$ exhibited doublet structures with several MHz spacings, each component of the doublet having identical Stark shifts. The transitions of types $(J+1)_{0J+1} \leftarrow J_{0J}$, $(J+1)_{2J} \leftarrow J_{2J-1}$ and $(J+1)_{2J-1} \leftarrow J_{2J-2}$ were observed as singlets. For the CH_3CH_2SD and two of the CH_3CHDSH species, all the *a*-type transitions were observed as singlets.

For the CH_2DCH_2SH species, there are two different molecular forms expected for the *trans* isomer, (designated as *s*-CH_2DCH_2SH and *a*-CH_2DCH_2SH species, where "*s*-" and "*a*-" refer to the symmetric and asymmetric forms, respectively, with respect to the molecular plane). There are three different molecular forms expected for the *gauche* isomer, one of which corresponds to the *s*-CH_2DCH_2SH species for the *trans* isomer and the other two to the *a*-CH_2DCH_2SH species.

For these three CH_2DCH_2SH species for the *gauche* isomer, similar doublet structures were observed for the species corresponding to the *s*-CH_2DCH_2SH species of the *trans* isomer, while only singlets were observed for the other two species corresponding to the *a*-CH_2DCH_2SH species of the *trans* isomer.

The splittings of the transitions vanish for the CH_3CH_2SD species whose reduced moment of inertia around the internal rotation axis of the SH group increases, and only the singlets were observed for the species expected to have non-equivalent *gauche* minima of the internal rotation potential. Thus these spectra can be confirmed to belong to the *gauche* isomer and the doublet structures can be considered to arise from the tunnelling effect through the barrier between two *gauche* minima.

For the four species having non-equivalent *gauche* minima, the *c*-type *Q* and *R* branch transitions could also be assigned.

For the other four species, the rotational constant *A* cannot be obtained from the *a*-type transition frequencies alone since the *gauche* isomer is still a nearly symmetric top molecule. Splittings of the transitions prevent an accurate determination of the *B* and *C* rotational constants unless a theoretical analysis of the internal rotation is carried out.

In the present paper, we deal with the r_s structure and the dipole moment of the *trans* isomer alone.

Experimental

Commercial normal species of ethanethiol was purified by gas chromatography. CH_3CH_2SD was prepared from sodium ethanethiolate and D_2O.[4] CH_2DCH_2SH, CH_3CHDSH and CH_3CD_2SH were prepared from the corresponding S-ethyl thiuronium bromides prepared from CH_2DCH_2Br, CH_3CHDBr and CH_3CD_2Br, respectively, with thiourea.[5]

The spectra of ^{34}S and ^{13}C species were measured with a sample of ethanethiol containing these species in natural isotopic abundance.

Measurements were carried out in the frequency region 8.4—34 GHz with conventional Stark modulation spectrometers with 100 kHz square- and sine-wave modulation. The $2_{12} \leftarrow 1_{01}$ transition appearing around 42500 MHz was also measured for four of the isotopic species. Measurements were usually made on an oscilloscope at dry ice temperature, a strip-chart recorder being used for the measurements for ^{34}S and ^{13}C species.

Rotational Spectra of the *Trans* Isomer

Spectra belonging to the *trans* isomer of ethanethiol were observed as singlets, indicating that the barrier to the internal rotation of the CH_3 group is relatively high. Both *a*- and *b*-type transitions could be easily assigned, for the normal and deuterated species (Table 1). For ^{34}S and two ^{13}C species, most of the *a*-type transitions were obscured under strong spectra of the normal species since the measurements were made in natural abundance. In order to ascertain the present assignments, the measurements were extended to the $2_{12}\leftarrow1_{01}$ transitions around 42500 MHz which exhibited characteristic Stark patterns.

As the influence of the centrifugal distortion seems to be small, the rotational constants were determined by a least-squares analysis from all the observed frequencies (Table 1) so as to fit a modified rigid rotor expression which includes only the $D_J[J(J+1)]^2$ term of the centrifugal distortion formula. The rotational constants and the moments of inertia are shown in Tables 2 and 3, respectively.

The quantities ΔP_c shown in the table are quite reasonable for all the isotopic species,[6] confirming the present assignments of transitions.

Table 1. Observed frequencies in the ground state of *trans*-ethanethiol (MHz)

Transition	CH_3CH_2SH	$CH_3CH_2{}^{34}SH$	$CH_3{}^{13}CH_2SH$	$^{13}CH_3CH_2SH$	CH_3CH_2SD	CH_3CHDSH	CH_3CD_2SH	*s*-CH_2DCH_2SH[b]	*a*-CH_2DCH_2SH[c]
$1_{10}\leftarrow1_{01}$	23534.74	23544.86	22861.60	23466.05	22453.49	20171.84	17584.02	23816.87	21199.14
$2_{11}\leftarrow2_{02}$	24150.41	24137.90	23496.00	24053.03	23067.61	20829.78	18253.62	24350.76	21791.18
$3_{12}\leftarrow3_{03}$	25096.12	25047.69	24471.04	24953.56	24011.40	21845.33	19292.47	25167.95	22701.27
$4_{13}\leftarrow4_{04}$	26397.46	26297.96	25815.45	26191.11	25312.11	23252.52	20740.42	26287.76	23955.89
$5_{14}\leftarrow5_{05}$	28088.18	27921.00	27565.62	27796.69	27004.85	25095.70	22648.45	27735.72	25590.01
$6_{15}\leftarrow6_{06}$	30208.45	29953.36	29766.28	29807.28	29130.76	27425.63	25074.03	29542.17	27643.49
$7_{16}\leftarrow7_{07}$	32802.59	32437.20	32463.40	32263.60	31735.72	30296.20	28076.27	31741.71	30161.06
$1_{11}\leftarrow0_{00}$	33298.74	33115.06	32550.94	—[a]	31858.44	29728.53	26966.74	32958.10	30628.27
$2_{12}\leftarrow1_{01}$	43062.09	42685.31	42240.57	42450.99					
$3_{03}\leftarrow2_{12}$	8716.32	—[a]	9248.88	—[a]	—[a]	11630.19	13728.20	—[a]	9924.98
$4_{04}\leftarrow3_{13}$	19878.92	18942.05	20371.70	18668.50	19503.83	22645.46	24566.49	16555.95	20689.26
$5_{05}\leftarrow4_{14}$	31242.40	30060.79	—[a]	29694.05	30493.81	33849.30		27114.14	31639.84
$1_{01}\leftarrow0_{00}$	10367.48	—[a]			10006.44	10198.73	10034.57	—[a]	10008.63
$2_{02}\leftarrow1_{01}$	20723.42	—[a]			20001.77	20381.77	20049.57	19322.66	—[a]
$2_{12}\leftarrow1_{11}$	20131.34	19722.17			19412.65	19755.19	19416.73	18806.19	19437.49
$2_{11}\leftarrow1_{10}$	21339.12	20885.84			20615.56	21039.41	20719.07	19856.42	20596.43
$3_{03}\leftarrow2_{02}$	31055.56	—[a]			29971.81	30028.39	30028.39	28962.11	29977.35
$3_{13}\leftarrow2_{12}$	30189.56	—[a]			29110.76	29623.06	29113.60	28204.22	29148.58
$3_{12}\leftarrow2_{11}$	32001.21	—[a]			30915.50	31549.32	31067.12	29779.28	30887.08
$3_{22}\leftarrow2_{21}$	31102.95	—[a]			30021.34	30596.20	30102.07	—[a]	30025.63
$3_{21}\leftarrow2_{20}$	31149.49	30499.87			30069.63	30658.32	30175.39	29032.42	30073.57

a) Overlapped with another transition. b) "*s*-" refers to the symmetric form with respect to the molecular plane. c) "*a*-" refers to the asymmetric form with respect to the molecular plane.

Table 2. Observed rotational constants (MHz) of *trans*-ethanethiol[a]

Species	*A*	*B*	*C*	$D_J\times10^3$ (MHz)[b]	R. M. S.[c] (MHz)
CH_3CH_2SH	28416.89 (0.74)	5485.77 (0.09)	4881.92 (0.10)	−4.68 (4.09)	0.22
$CH_3CH_2{}^{34}SH$	28330.19 (0.58)	5367.00 (0.07)	4785.13 (0.07)	−5.06 (3.33)	0.21
$CH_3{}^{13}CH_2SH$	27706.34 (0.49)	5466.02 (0.06)	4844.68 (0.06)	0.29 (5.69)[d]	0.19
$^{13}CH_3CH_2SH$	28212.58 (0.56)	5322.41 (0.05)	4746.32 (0.05)	−10.05 (3.25)[d]	0.22
CH_3CH_2SD	27156.24 (0.90)	5304.38 (0.10)	4702.68 (0.11)	−3.52 (4.58)	0.26
CH_3CHDSH	24950.46 (0.65)	5420.40 (0.08)	4778.38 (0.08)	−4.26 (3.40)	0.19
CH_3CD_2SH	22275.58 (0.81)	5342.61 (0.09)	4691.45 (0.09)	−2.56 (6.73)	0.23
s-CH_2DCH_2SH	28387.68 (0.78)	5095.38 (0.09)	4570.42 (0.10)	−3.13 (4.05)	0.24
a-CH_2DCH_2SH	25914.08 (0.88)	5294.10 (0.10)	4714.56 (0.10)	−5.52 (4.60)	0.26

a) Figures in parentheses indicate the uncertainty calculated from 2.5 times the standard deviations. b) Coefficient of the $[J(J+1)]^2$ term of centrifugal distortion contributions. c) Indicates root mean square deviation between the calculated and observed transition frequencies by use of solved rotational constants. d) The D_J value could not be determined satisfactorily for lack of a sufficient number of observed frequencies.

TABLE 3. OBSERVED MOMENTS OF INERTIA (amu·Å²) OF *trans*-ETHANETHIOL[a]

Species	I_a	δ[b]	I_b	δ[b]	I_c	δ[b]	P_c[c]	ΔP_c
CH_3CH_2SH	17.78435(46)	0.07726	92.12490(156)	0.44172	103.52003(201)	0.45573	3.19461(129)	——
$CH_3CH_2{}^{34}SH$	17.83878(36)	0.07732	94.16352(128)	0.44531	105.61381(163)	0.46011	3.19425(105)	−0.00036(167)
$CH_3{}^{13}CH_2SH$	18.24045(31)	0.07503	92.45775(108)	0.43743	104.31558(133)	0.45581	3.19131 (87)	−0.00330(156)
$^{13}CH_3CH_2SH$	17.91315(35)	0.07626	94.95247 (94)	0.43834	106.47744(116)	0.45239	3.19409 (77)	−0.00052(150)
CH_3CH_2SD	18.60994(61)	0.09200	95.27519(185)	0.46272	107.46555(239)	0.46112	3.20979(154)	0.01518(201)
CH_3CHDSH	20.25518(52)	0.07804	93.23585(129)	0.43843	105.76313(170)	0.45337	3.86395(110)	0.66934(170)
CH_3CD_2SH	22.68745(82)	0.07988	94.59347(162)	0.43883	107.72277(204)	0.45457	4.77907(137)	1.58446(188)
s-CH_2DCH_2SH	17.80266(48)	0.08151	99.18314(179)	0.44655	110.57552(229)	0.44375	3.20514(147)	0.01053(196)
a-CH_2DCH_2SH	19.50199(65)	0.07595	95.46016(187)	0.43988	107.19473(243)	0.45205	3.88370(157)	0.68910(203)

a) Conversion factor is 505376 MHz·amu·Å². Figures in parentheses indicate the uncertainty attached to the last significant figures estimated from 2.5 times the standard deviations. Only the effect of uncertainty in measured frequencies is taken into account. b) $\delta = I_{obsd} - I_{calcd}$. I_{calcd} is calculated on the basis of the structure shown in Table 4. c) $P_c = (I_a + I_b - I_c)/2$. d) $\Delta P_c = (P_c)_{isotopic} - (P_c)_{parent}$.

The r_s Structure of the *Trans* Isomer

Our data are sufficient to determine the r_s coordinates of all the atoms in the *trans* isomer by the substitution method. The *trans* isomer possesses a plane of symmetry perpendicular to the *c*-axis, so that the isotopic substitution of an atom in this plane would leave $P_c(=(I_a + I_b - I_c)/2)$ unaltered if the molecule is rigid. If such were the case, one of the three moments of inertia of the isotopic species would be calculated from the other two. Any two of the three moments of inertia would be sufficient for calculation of the x_a and x_b coordinates of the atom by the following specialized Kraitchman equation for the in-plane atom.

$$\left.\begin{aligned} |x_a| &= [(\Delta I_b/\mu)(1+\Delta I_a/(I_a{}^0 - I_b{}^0))]^{1/2} \\ |x_b| &= [(\Delta I_a/\mu)(1+\Delta I_b/(I_b{}^0 - I_a{}^0))]^{1/2} \\ |x_c| &= 0 \\ \Delta I_g &= I_g - I_g{}^0,\ \mu = \Delta m M/(M+\Delta m) \end{aligned}\right\} \quad (1)$$

where M is the molecular weight of the parent species, Δm is the mass increment of the substituted atom in the isotopic species and $I_g{}^0$ and I_g indicate the g-th moment of inertia for the parent and isotopic species, respectively.

However, since isotopic substitution of such an atom usually alters P_c slightly, the computed coordinates will depend on which pair of moments is used, or whether all three moments are used in the Kraitchman equation.

In order to check the dependence of the computed coordinates on the choice of the moments, the following five different cases were compared. a) All the three moments were used equally in the following general Kraitchman equation.

$$\left.\begin{aligned} |x_a| &= [(\Delta P_a/\mu)(1+\Delta P_b/(I_a{}^0 - I_b{}^0))(1+\Delta P_c/(I_a{}^0 - I_c{}^0))]^{1/2} \\ |x_b| &= [(\Delta P_b/\mu)(1+\Delta P_c/(I_b{}^0 - I_c{}^0))(1+\Delta P_a/(I_b{}^0 - I_a{}^0))]^{1/2} \\ |x_c| &= [(\Delta P_c/\mu)(1+\Delta P_a/(I_c{}^0 - I_a{}^0))(1+\Delta P_b/(I_c{}^0 - I_b{}^0))]^{1/2} \\ P_a &= (-I_a + I_b + I_c)/2,\ P_b = (I_a - I_b + I_c)/2 \\ P_c &= (I_a + I_b - I_c)/2,\ \Delta P_g = P_g - P_g{}^0,\ \text{g=a, b and c} \end{aligned}\right\} \quad (2)$$

where $P_g{}^0$ and P_g indicate the quantities P_g for the parent and isotopic species, respectively. In this case the x_c coordinate, which should be zero from the symmetry, can also be calculated if $\Delta P_c > 0$, but will be disregarded. b) All the three moments were used but ΔP_c was set to zero. c) ΔI_a and ΔI_b were used in the specialized Kraitchman equation (1). d) ΔI_c and ΔI_b were used assuming $\Delta P_c = 0$. e) ΔI_a and ΔI_c were used assuming $\Delta P_c = 0$.

The coordinates calculated in the five cases were in good agreement with each other for the two C atoms and the S atom within estimated uncertainty of the observed moments of inertia. Therefore, the averages of the five values were used for the r_s coordinates of these atoms.

However, the difference in the coordinate values for the five cases was found to exceed the estimated experimental uncertainty for the hydrogen atom in the SH group and for the in-plane hydrogen atom (H_s) in the CH_3 group. Since $\Delta P_c > 0$, the apparent x_c coordinates in case a) can be calculated for these atoms. They are 0.130 and 0.107 Å, respectively, and indicate the serious influence of the zero point energy contribution to the coordinates of these atoms.

Since the x_b coordinate of H_s is small, the serious influence of the zero point energy is not surprising and makes it impossible to calculate from the expreimental data for this coordinate. Then, this coordinate is considered to be better determined from other coordinates by the use of some special assumptions such as the first moment equation and so on.

However, even for the x_a coordinate of H_s and the x_a and x_b coordinates of the hydrogen atom in the SH group which are not so small and for which the solutions of the Kraitchman equation can be regarded to be reliable, the half differences between the largest and smallest values of the coordinates for the five cases $(|x_{max}| - |x_{mix}|)/2$ are calculated to be 0.00219, 0.00447 and 0.00565 Å, respectively, while the uncertainties are 0.00114, 0.00174 and 0.00324 Å, respectively. The structural parameters such as r(SH), α(CSH), $r(CH_s)$, $\alpha(CCH_s)$ and $\alpha(H_aCH_s)$, which are related to these coordinates will then strongly depend on the choice of the moments of inertia.

The same situation was reported for ethyl choride[7] by Schwendeman and Jacobs, and for propane[8] by Lide. Taking the above into account, case a) was used for the r_s coordinate of the hydrogen atom in

Table 4. Atom coordinates (Å)[a] and the structural parameters of *trans*-ethanethiol

Atom	x_a	x_b	x_c
H (SH)	1.76920 (142)	0.92278 (287)	0.0
S	1.02635 (128)	−0.17049 (715)	0.0
C (CH_2)	−0.58101 (412)	0.68306 (319)	0.0
C (CH_3)	−1.69064 (137)	−0.36850 (593)	0.0
H (CH_2)	−0.65758 (274)	1.31230 (285)	±0.88703 (219)
H_s (CH_3)	−2.66712 (93)	0.12609 (1155)	0.0
H_a (CH_3)	−1.61659 (155)	−1.00514 (250)	±0.88425 (326)

Skeleton		CH_2 group		CH_3 group	
r(SH)	1.322 Å (0.006)	r(CH)	1.090 Å (0.003)	$r(CH_s)$	1.095 Å (0.006)
r(SC)	1.820 Å (0.005)	α(SCH)	109°26′ (30′)	$r(CH_a)$	1.092 Å (0.005)
r(CC)	1.529 Å (0.006)	α(HCC)	110°14′ (33′)	$\alpha(CCH_s)$	109°40′ (34′)
α(CSH)	96°13′ (23′)	α(HCH)	108°54′ (22′)	$\alpha(CCH_a)$	110°35′ (29′)
α(CCS)	108°34′ (19′)			$\alpha(H_sCH_a)$	108°53′ (49′)
				$\alpha(H_aCH_a)$	108° 7′ (33′)

a) Figures in parentheses are 99% reliability intervals attached to the last significant figures.

the SH group and the x_a coordinate of the H_s atom. The x_b coordinate of the H_s atom was then determined from the first moment equation.

As for the hydrogen in the CH_2 group, two independent sets of r_s coordinates are available from the observed moments of inertia for CH_3CHDSH and CH_3CD_2SH species.

For the substituted atom in CH_3CD_2SH species whose coordinates satisfy relations $(x_a)_1=(x_a)_2$, $(x_b)_1=(x_b)_2$ and $(x_c)_1=-(x_c)_2$, where 1 and 2 designate the substituted atom number, the Kraitchman equation can be written as

$$\left.\begin{aligned} |x_a| &= [(\Delta P_a/\mu)(1+\Delta P_b/(I_a^0-I_b^0))]^{1/2} \\ |x_b| &= [(\Delta P_b/\mu)(1+\Delta P_a/(I_b^0-I_a^0))]^{1/2} \\ |x_c| &= [\Delta P_c/2\Delta m]^{1/2},\ \mu=2\Delta mM/(M+2\Delta m) \end{aligned}\right\} \quad (3)$$

Actually, the two sets of computed coordinates were found to be in good agreement within experimental uncertainty in spite of the expected large difference of the zero point energy contributions between the two species. The averages of the two sets of the coordinate values were then used for the r_s coordinates of this atom.

Since no other isotopic species useful for determining the coordinates of the H_a atom in the CH_3 group is available at present, the influence of the zero point energy to these coordinates cannot be evaluated from a unique solution of the general Kraitchman equation (2) alone.

Coordinates of the atoms and structural parameters are given in Table 4.

It is seen that a slightly asymmetric CH_3 structure was obtained from the above procedures though it is within the range of uncertainties for the structural parameters.

Completion of the determination of the structure of *trans*-ethanethiol is of interest since it is desirable to know to what extent the structure correlations found in the analogous molecules are applicable.

Comparison of the structural parameters of the CH_2SH part of *trans*-ethanethiol with those of methanethiol[9] reveals that r(SC) remains unchanged between them, while those of both ethane- and methanethiol are definitely greater than that of dimethyl sulfide (1.802±0.002 Å).[10]

r(SH) and α(CSH) of ethanethiol are essentially equal to those of methanethiol within experimental error.

A comparison of the structural parameters of the CH_2 part of the molecule with those of ethyl halides,[7,11] propane[8] and ethylsilane[12] is given in Table 5.

r(CC) of ethanethiol has a value between that of ethylsilane and those of ethyl chloride and bromide, being roughly equal to that of propane.

The value 108°34′ obtained for α(SCC) of ethanethiol is abnormally small compared with the value for α(XCC) (X=Cl, Br, Si and C) of analogous molecules, for which they are always larger than tetrahedral. On the other hand, the value 108°54′ obtained for α(HCH) is smaller than tetrahedral.

The following angular constraint can be imposed on sp^3 hybrids for the present case if each hybrid is orthonormal or localized.[13] That is, the α(HCH) angle should be larger than tetrahedral if the α(XCC) angle is smaller than tetrahedral.

This is approximately valid for CH_3CH_2X molecules except *trans*-ethanethiol (Table 5). On the other hand, though this rule is valid for the α(HCC) and α(HCX) angles of all the molecules listed, the α(HCX) angle of *trans*-ethanethiol is the largest, except that of propane for which these two angles should be equal for the sake of symmetry.

This anomalous feature found in *trans*-ethanethiol can be easily explained if the ethyl group is tilted in the molecular plane towards the lone pair electrons of the S atom.

When the tilt angle is assumed to be equal to that of methanethiol and of dimethyl sulfide (2°30′), the α(CCS) and α(HCS) angles of ethanethiol are considered to contain contributions in amounts of −2°30′ and +1°15′ respectively. In order to compare these angles with those of other molecules having the non-tilted ethyl group, the corrected angle values should be used.

Table 5. Comparison of the structural parameters of *trans*-ethanethiol with those of similar molecules[a)]

	CH_3CH_2SH	CH_3SH	CH_3CH_2Cl	CH_3CH_2Br	$CH_3CH_2CH_3$	$CH_3CH_2SiH_3$
CSH						
r(SH) (Å)	1.322(0.006)	1.332(0.010)				
r(SC) (Å)	1.820(0.005)	1.819(0.005)				
α(HSC)	96°13′ (23′)	96°30′ (30′)				
CCH_2X						
r(CH) (Å)	1.090(0.003)	1.092(0.010)[b)]	1.089(0.010)	1.087(0.010)	1.096(0.002)	1.097(0.002)
r(CC) (Å)	1.529(0.006)		1.520(0.003)	1.518(0.004)	1.526(0.002)	1.540(0.002)
α(CCX)	108°34′ (19′)	109°11′ [b)]	111° 2′ (8′)	111° 2′ (15′)	112°24′ (12′)	113°11′ (12′)
α(HCH)	108°54′ (22′)	109°45′ (30′)[b)]	109°12′ (30′)	109°54′ (30′)	106° 6′ (12′)	105°46′ (24′)
α(HCC)	110°14′ (33′)		111°36′ (30′)	112°15′ (30′)	109°34′[c)]	110°10′[c)]
α(HCX)	109°26′ (30′)		106°41′[c)]	105°25′ (30′)	109°34′[c)]	108°45′[c)]
CH_3C						
$r(CH_s)$ (Å)	1.095(0.006)		1.091(0.010)[d)]	1.093(0.010)[d)]	1.089(0.009)	1.093(assumed)[f)]
$r(CH_a)$ (Å)	1.092(0.005)				1.094[e)]	1.093(0.002)
$\alpha(CCH_s)$	109°40′ (34′)		110°26′[e)]	110° 4′[e)]	111°48′ (1°)	111°57′ (1°)
$\alpha(CCH_a)$	110°35′ (29′)				110°36′[e)]	111° 2′ (30′)
$\alpha(H_sCH_a)$	108°35′ (49′)		108°30′ (30′)[d)]	108°52′ (30′)[d)]	108° 6′[e)]	107°15′ (1°)
$\alpha(H_aCH_a)$	108° 7′ (33′)				107°18′[e)]	106°59′ (30′)

a) Figures in parentheses indicate 99% reliability intervals. b) Parameters for the CH_3 group, that is, $r(CH)_{ave}$, $\alpha(H_sCS)$, and $\alpha(H_aCS)$, respectively, where $\alpha(H_sCS)$ was calculated from $\alpha(H_aCS)$. c) Calculated by the present authors from the reported coordinates. d) Averaged values given by the original authors. e) The uncertainty is not described by the original authors. f) Assumed to be equal to $r(CH_a)$ by the original authors.

Table 6. Stark coefficents and dipole moment of *trans*-ethanethiol[a)]

Transition	M	$\Delta\nu/E^2\times10^4$ MHz/(V/cm)^2 Obsd	Calcd	Range of E (V/cm)
$1_{10}\leftarrow1_{01}$	1	4.757(0.06)	4.873	20→ 200
$2_{11}\leftarrow2_{01}$	1	0.578(0.01)	0.568	200→ 450
	2	1.042(0.02)	1.041	100→ 450
$1_{11}\leftarrow0_{00}$	0	0.954(0.02)	0.894	100→ 450
$2_{12}\leftarrow1_{01}$	0	−0.225(0.001)	−0.223	200→ 600
	1	0.041(0.001)	0.032	200→1000
$1_{01}\leftarrow0_{00}$	0	0.645(0.007)	0.646	200→ 300
$2_{02}\leftarrow1_{01}$	1	−0.894(0.002)	−0.073	300→ 700
$2_{12}\leftarrow1_{11}$	0	−0.488(0.02)	−0.471	100→ 300
	1	4.044(0.05)	4.040	50→ 120
$2_{11}\leftarrow1_{10}$	0	0.142(0.001)	0.140	400→ 700
	1	−4.420(0.5)	−4.342	50→ 120

$\mu_{total}=1.560$ D (0.032), $\mu_a=1.058$ D (0.023), $\mu_b=1.146$ D (0.022)

a) Figures in parentheses indicate the uncertainty calculated from 2.5 times the standard deviations.

They are 108°34′+2°30′=111°4′ and 109°26′−1°15′=108°11′ for α(CCS) and α(HCS), respectively, which are plausible as values expected from angles of similar molecules.

Dipole Moment

The electric dipole moment and its components for the parent species were quantitatively determined by Stark-effect measurements of eight *a*- and *b*-type rotational transitions. Two Stark components of different M values could be resolved for some of the transitions. Before and after the measurements, the electric field was calibrated using the OCS molecule as a standard.[14] The results are given in Table 6.

Since the molecule is a slightly asymmetric top having a relatively large μ_a dipole component, some transitions used for the Stark-effect measurements exhibit fast Stark shifts due to the first-order effect. On the other hand, in the relatively higher range of applied field strength, the frequency shift $\Delta\nu$ changes linearly against the squares of the field strength E^2 within experimental error for all the transitions used, so that the fourth-order effect[15] might not be noticeable. Analysis of the present Stark-effect measurements is possible by the usual second-order perturbation treatment with the appropriate first-order corrections,[16] but the method by direct diagonalization of the energy matrices[17] was used in order to make calculation with an electronic computer easier. As the J quantum number for the transitions used is at most 2, the energy matrices were truncated at $J=4$ after confirming that the truncation error was negligible.

The theoretical Stark coefficients are shown in Table 6 where $\Delta\nu/E^2$ is the value at the field strength 200 V/cm. Agreement is very good for both *a*- and *b*-type transitions.

The obtained dipole moments are $\mu_a=1.058\pm0.023$, $\mu_b=1.146\pm0.022$ and $\mu_{total}=1.560\pm0.032$ D.

The dipole moment of *trans*-ethanethiol determined by microwave spectroscopy can be compared with the value 1.33 D obtained by dielectric constant measurement[18] in the gaseous state. The reported values for methanethiol by microwave spectroscopy and dielectric constant measurement are 1.532 D[9] and 1.26 D,[19] respectively. The values obtained by the former measurement are larger for both molecules,

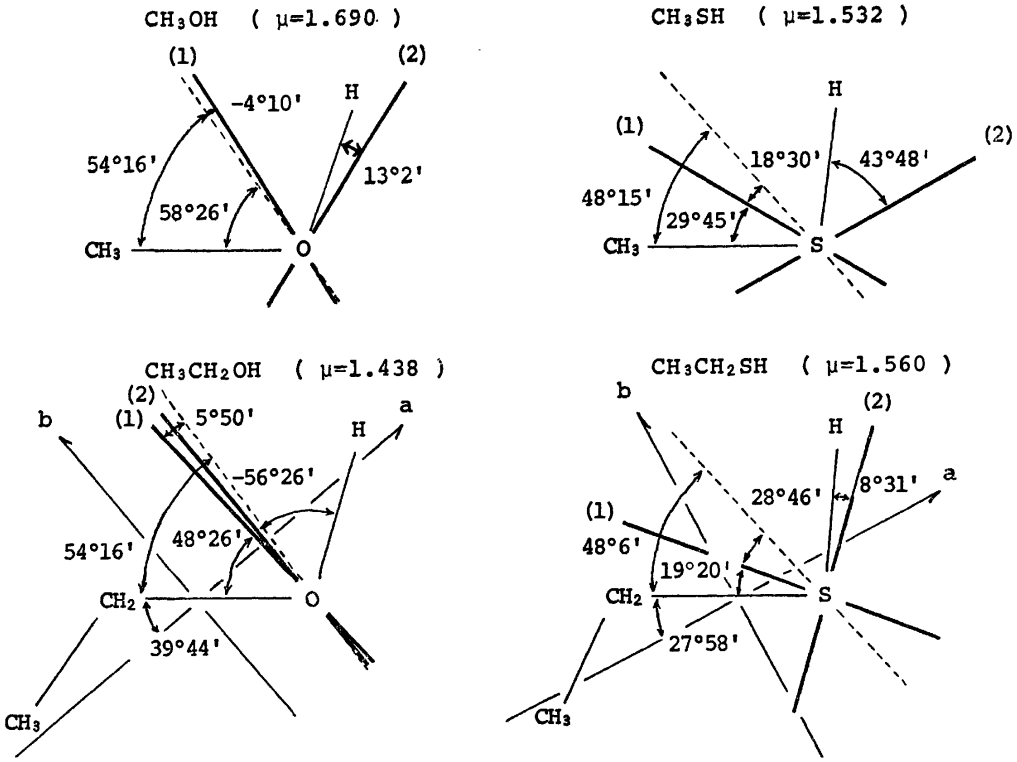

Fig. 1. Directions of the dipole moments for CH_3SH, CH_3CH_2SH, CH_3OH, and CH_3CH_2OH.
—— Direction of the dipole moment.
---- Bisector of the angle CXH, X=O, S.
←— The principal inertial axis.

From the dipole components obtained, the dipole moment of *trans*-ethanethiol is inclined by either 47°18′ or 132°42′ against the *a*-principal inertial axis (Fig. 1). Usually the direction of the dipole moment can be determined uniquely if a comparison is made between the isotopic species. However, for *trans*-ethanethiol, the rotation of the principal axes due to the isotopic substitution is estimated to be too small when compared with the experimental error limit for the available isotopic species.

In order to find the correct direction of the dipole moment, a comparison was made between methanethiol, ethanethiol, methanol[20] and ethanol.[21] The reported values of the CXH angles of these molecules are 96°30′ 96°13′, 108°32′ and 108°32′, respectively. The possible directions of the dipole moment in the molecule are designated as (1) and (2) in Fig. 1, the dotted line indicating the bisector of the CXH angle.

The CS and CO bonds are found to make angles of 27°58′ and 39°44′, respectively, with the *a*-axis for *trans*-ethanethiol and ethanol from the structure analysis. Direction (1) then makes angles of 29°45′, 19°20′, 58°26′ and 48°26′ with the CX bonds of methanethiol, ethanethiol, methanol and ethanol, respectively, which correspond to the angles 17°30′, 28°46′, −4°10′ and 5°50′ against the bisectors, respectively.

Direction (2) makes angles of 43°48′, 8°31′, 13°2′ and −56°26′ with the XH bonds, respectively. A regularity can be found for direction (1) in the angles with the CX bonds and with the bisectors of the CXH angles. No such regularity can be found for direction (2). Since both of the two possible directions for ethanol are almost parallel to the bisector of the COH angle, this strongly suggests that the correct direction of the dipole moments for this series of molecules can be regarded as (1) which is more parallel to the bisector of the CXH angle than (2).

The angle between the dipole moment and the bisector of the CXH angle increases by about 10° when the methyl group is replaced by the ethyl group for both mercaptan and alcohol. The dipole moments of the present series are considered to consist of the C–X and X–H bond moments and the moment along the bisector of the CXH angle which is produced by the long pair electrons on the atom X. The directions of these moments are considered to be from H to X for the X–H bond moment, from C to X for the C–X bond moment and from X to the outside of the CXH angle for the lone pair moment. Thus, if the lone pair moment and the X–H bond moment remain unchanged on replacement of the alkyl group, the above change in direction of the dipole moment indicates that the apparent C–X bond moment increases as the methyl group is replaced by the ethyl group. This is similar to the so-called inductive effect for the case of alkyl halides.[22]

If the X–H and lone pair moments between methane- and ethanethiol and between methanol and ethanol are assumed to be equal, the C–X bond moments of the ethyl group are calculated to be larger than those of the methyl group by about 0.36 and 0.33 D, re-

spectively.

The authors would like to thank Dr. Chi Matsumura and Dr. Harutoshi Takeo, Government Chemical Industrial Research Institute, for the use of their spectrometer and for their kind assistance in measuring the spectra due to the ^{13}C and ^{34}S species of ethanethiol.

References

1) Ch. O. Kadzhar, A. A. Abbasov, and L. M. Imanov, *Opt. Spectrosc.* (USSR) (English Transl.), **24**, 334 (1968).
2) R. E. Schmidt and C. R. Quade, *Bull. Amer. Phys. Soc.*, **II 17**, 657 (1972).
3) M. Hayashi, H. Imaishi, K. Ohno, and H. Murata, This Bulletin, **44**, 872 (1971).
4) A. Murray, III and D. L. Williams, Organic Syntheses with Isotopes, Part II, Interscience, New York (1958), p. 1341.
5) *ibid.*, p. 1340.
6) D. R. Herschbach and V. W. Laurie, *J. Chem. Phys.*, **40**, 3142 (1964).
7) R. H. Schwendeman and G. D. Jacobs, *ibid.*, **36**, 1245 (1962).
8) D. R. Lide, Jr., *ibid.*, **33**, 1514 (1961).
9) T. Kojima and T. Nishikawa, *J. Phys. Soc. Japan*, **12**, 680 (1957); T. Kojima, *ibid.*, **15**, 1284 (1960).
10) L. Pierce and M. Hayashi, *J. Chem. Phys.*, **35**, 479 (1961); H. Dreizler and H. D. Rudolph, *Z. Naturforsch.*, **17a**, 712 (1962).
11) C. Flanagan and L. Pierce, *J. Chem. Phys.*, **38**, 2963 (1963).
12) H. D. Petersen, Thesis, The University of Notre Dame (1961).
13) W. H. Flygare, *Science*, **140**, 1179 (1963).
14) J. S. Muenter, *J. Chem. Phys.*, **48**, 4544 (1968).
15) J. S. Muenter and V. M. Laurie, *ibid.*, **45**, 855 (1966).
16) S. Golden and E. B. Wilson, Jr., *ibid.*, **16**, 699 (1948).
17) L. N. Gunderova and N. M. Posdeev, *Opt. Spectrosc.* (USSR) (English Transl.), **24**, 132 (1970); R. Peter, and H. Dreizler, *Z. Naturforsch.*, **20a**, 301 (1965); H. Imaishi, M. Hayashi, and H. Murata, *J. Sci. Hiroshima Univ.*, **AII 37**, 171 (1973).
18) E. C. E. Hunter and J. R. Partington, *J. Chem. Soc.*, **1932**, 2812.
19) C. P. Smyth, "Dielectric Behavior and Structure," McGraw-Hill, Co., Ltd., New York (1955), p. 298.
20) E. V. Ivash and D. M. Dennison, *J. Chem. Phys.*, **21**, 1804 (1953); D. G. Burkhard and D. M. Dennison, *Phys. Rev.*, **84**, 408 (1951).
21) M. Takano, Y. Sasada, and T. Satoh, *J. Mol. Spectrosc.*, **26**, 157 (1968).
22) I. Miyagawa, *Nippon Kagaku Zasshi*, **75**, 1061 (1954).

The Ion-exchange Behavior of Some Cations on Crystalline Zirconium Phosphate

Yoshitsugu HASEGAWA* and Isao TOMITA

Department of Chemistry, Faculty of Science, Tokyo Kyoiku University, Bunkyo-ku, Tokyo 112

(Received January 30, 1974)

The distribution coefficients of Ag^+, Tl^+, K^+, NH_4^+, Mg^{2+}, Ca^{2+}, Sr^{2+}, Ba^{2+}, Co^{2+}, Zn^{2+}, Y^{3+}, and Ce^{3+} have been determined on a crystalline zirconium phosphate ion-exchanger in chloride solution media, and the affinity sequences are presented. pH titration curves and X-ray powder diffraction data were obtained for calcium and barium ions. The ion-exchange capacity of the exchanger for barium ions was found to be 4.4 meq/g, but the X-ray powder patterns were rather unusual as compared to those of other ions studied previously.

Extensive investigations have been made of the crystalline zirconium phosphate ion-exchanger, $Zr(HPO_4)_2 \cdot H_2O$ (c-ZrP). Studies of the exchanger at lower loadings have mainly been concerned with the distribution coefficients (K_d) of alkali metal ions and their pH dependence.[1,2] In the first half of the present study, the measurement of K_d values was extended to monovalent cations, such as Ag^+, K^+, Tl^+, and NH_4^+, alkaline earth cations, and some polyvalent cations such as Co^{2+}, Zn^{2+}, Y^{3+}, and Ce^{3+}.

On the other hand, studies of the ion-exchange at higher loadings include pH titrations on the exchanger for alkali or alkaline earth metal ions and X-ray studies of cation-replaced exchangers as well as of the original hydrogen-form.[3-7] With regard to the uptake of alkaline earth metal ions onto c-ZrP, Clearfield and Smith have shown that strontium ions can be sorbed, but barium ions are not taken up from acidic media.[4] Harvie and Nancollas have given the pH titration curve for calcium-hydrogen exchange.[5] Dyer *et al.* have reported that the barium form of c-ZrP was prepared.[6] Further, Alberti *et al.* have shown that hydrolysis starts at a 10% conversion of barium ions.[7]

In the second half of this paper, the results of detailed examination of the pH titration curves for barium ions as well as of the X-ray diffraction patterns of the metal ion-replaced solid are given.

Experimental

The crystalline zirconium phosphate (c-ZrP) was prepared by refluxing a gelatinous precipitate in 6.7M phosphoric acid for 120 hr, as has been reported previously.[2] The resulting crystalline solid was an extremely fine powder, and after drying it was made into tablets under a pressure of about 4200 Kg/cm^2 and then sieved to a grain size of 100—200 mesh.

Distribution Coefficients. The batch distribution coefficients were measured at 25 °C by equilibrating a weighed amount of c-ZrP with known volumes of suitable solutions, followed by analysis of the supernatant liquid. The ratio of volume to the solid weight was usually 100 ml/g.

For all the metal concentrations studied, the exchange reaction attained to equilibrium within 6 hr. The determination of the batch distribution coefficients was made after the reaction mixtures had been shaken for at least 24 hr.

Chemical analyses included the use of such radioisotopes as ^{110m}Ag, ^{133}Ba, ^{89}Sr, ^{60}Co, ^{65}Zn, ^{90}Y, and ^{144}Ce as isotopic tracers. The yttrium-90 tracer was prepared from its parent, ^{90}Sr, using the c-ZrP column as an example of the practical application of the exchanger. For the determinations of potassium, magnesium, and calcium, atomic-absorption photometry was employed. The thallium and ammonium were determined colorimetrically by the use of rhodamine B[8] and the Nessler reagent[9] respectively.

For some cations, the values of the distribution coefficients were determined as a function of the acidity.

pH Titration. A 250 mg portion of c-ZrP was placed in contact at 25 °C with 50 ml of a solution $CaCl_2 + Ca(OH)_2$. The ratio of chloride to hydroxide was varied for each run, keeping the total calcium concentration at 0.1 N. After equilibration, the pH of the supernatant was measured with a glass electrode. Since the solubility of calcium hydroxide is rather low, the amount of hydroxide used was limited up to about 6 meq/g of c-ZrP. The experiment with the barium solution was performed in a similar way. In this case, the barium-ion content in the supernatant was determined by EDTA titration. The solid phase obtained at the neutralization point was analyzed for Zr, P, and Ba.

X-Ray Powder Diffraction. The X-ray powder patterns of the exchangers taken during the titration were obtained with Ni filtered copper X-rays using a Geigerflex (Rigaku Denki Co., Ltd.).

Results and Discussion

Affinity series. Table 1 gives the values of the distribution coefficients, K_d, for several ions on the hydrogen-form of c-ZrP. For Zn^{2+} ions, the initial pH of the solution was set at 4.12 in order to suppress hydrolysis. The sorption of monovalent cations increases in the following order:

$$Ag^+ < NH_4^+ < K^+ \simeq Tl^+$$

As compared with the affinity of these ions on a gelatinous zirconium phosphate,[10] less sorption of silver ion is found. The affinity increases with an increase in the crystal radii except for the ammonium ion.

For alkaline earth cations, the sequence is as follows:

$$Mg^{2+} < Sr^{2+} < Ca^{2+} < Ba^{2+}$$

The series of these ions on a gel has been reported by Amphlett *et al.*[10]:

$$Mg^{2+} < Ca^{2+},\ Sr^{2+} < Ba^{2+}$$

Separation factors calculated from the $\alpha_{M_1}^{M_2} = K_d(M_2)/K_d(M_1)$ relation are rather constant and give a value of about 1.46 for a pair of adjacent alkaline earth cations in the sequence.

* Present address: Department of Industrial Chemistry, Tokyo University of Agriculture and Technology, Koganei, Tokyo 184

TABLE 1. DISTRIBUTION COEFFICIENTS (K_d values) FOR CATIONS WITH INITIAL CONCENTRATION OF 1×10^{-3} N

ion	pH of solution		K_d
	initial	final	
Ag^+	5.10	3.68	30
NH_4^+	5.30	3.11	63
K^+	5.85	3.07	94
Tl^+	5.20	3.51	110
Mg^{2+}	5.50	3.01	90
Ca^{2+}	5.55	3.00	190
Sr^{2+}	5.88	3.00	130
Ba^{2+}	5.85	2.97	280
Co^{2+}	5.60	2.93	230
Zn^{2+}	4.12	2.94	340
Y^{3+}	5.35	2.96	$\sim5.7\times10^3$
Ce^{3+}	5.30	3.39	$\sim3.6\times10^4$

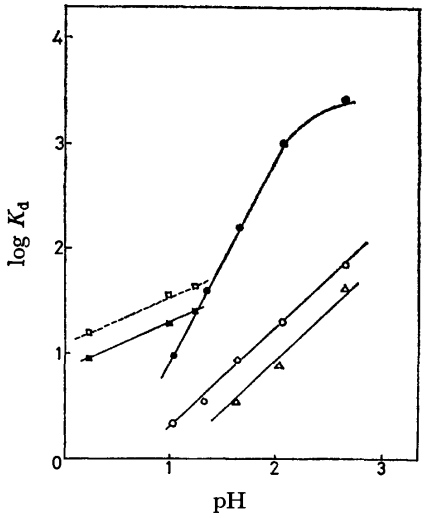

Fig. 1. Distribution coefficients for some cations on c-ZrP at different acidities
○: Ba^{2+}, △: Co^{2+}, ●: Ce^{3+}, ■: Rb^+, □: Cs^+
(total metal ion concentration is 1.0×10^{-3} N)

For other polyvalent cations, the K_d values increase in the order shown in Table 1:

$$Co^{2+} < Zn^{2+} < Y^{3+} < Ce^{3+}$$

This sequence is identical with that reported by Ahrland *et al.* for a gelatinous zirconium phosphate.[11]

When the values of K_d are plotted as a function of pH, straight lines are obtained (see below). Hence, the affinity sequences obtained may hold in the acidic media.

One of the possible factors which determine the distribution coefficients on the crystalline zirconium phosphate ion-exchanger might be the formation of a stable, less soluble phosphate of polyvalent cations.

In Figs. 1 and 2, the logarithmic values of the distribution coefficients are plotted against the pH. In the cases of Ba^{2+} and Co^{2+} ions whose concentrations are 1×10^{-3} N in the initial solutions, straight lines with a slope of nearly unity were obtained. For Ce^{3+}, the slope was about 2 up to the pH value of 2, beyond

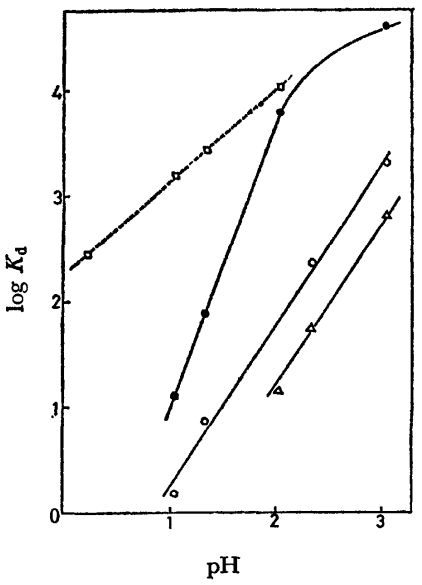

Fig. 2. Distribution coefficients for some cations on c-ZrP at different acidities
○: Ba^{2+}, △: Co^{2+}, ●: Ce^{3+}, □: Cs^+
(total metal ion concentration is 1.0×10^{-5} N)

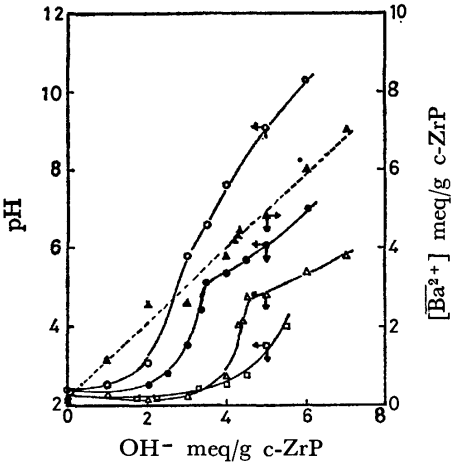

Fig. 3. pH titration curves
□: titrant $CaCl_2+Ca(OH)_2$. (the ratio of solution volume to exchanger weight is 200 (ml/g))
Others: titrant $BaCl_2+Ba(OH)_2$. (the ratio of solution volume to exchanger weight is 100 (ml/g))
reaction time, ○: 6 hr, ●: 24 hr, △: 6 days.
▲: Ba^{2+} content in the exchanger $[\overline{Ba^{2+}}]$ calculated for 6 days samples.

this point a serious deviation from the straight line resulted. For the metal-ion concentrations of 1.0×10^{-5} N, the log K_d *vs.* pH plots again exhibit straight lines for these ions, with slopes of somewhat higher values for each case. The slopes are certainly correlated with the charge of the sorbed cations, but no quantitative explanation can be made on the basis of the data given here, because they were not based upon the constant loading of exchanging ions along the curves.[12,13]

pH Titrations. The results of the pH titrations for Ca^{2+} and Ba^{2+} are given in Fig. 3. The titration curve for Ca^{2+} agreed with those given by Harvie and Nancollas and by Alberti *et al.*[5,7]

In the barium titration, the dependence of the pH of a supernatant on the time was determined at three different compositions (see Fig. 4). It is inferred that the neutralization reaction proceeds in two steps: that is, at an earlier stage the reaction takes place on a surface of the exchanger, and then the diffusion of the cations into the exchanger proceeds gradually. Under those experimental conditions, it took about four days to reach equilibrium. In Fig. 3 the titration curves at different reaction times and the barium-ion contents in the exchanger calculated from those in the supernatants of 6-day sample are shown. The titration curves show that the ion-exchange capacity of c-ZrP for barium ions is equal to 4.4 meq/g (corresponding to 66% of the total exchange capacity) and that the reaction time between 50 and 66% of exchange is quite long.

Beyond 66% of exchange, the exchanger itself is hydrolyzed and the phosphates of barium and zirconium hydroxide are precipitated.

The exchanger at 66% of exchange was stored on a saturated sodium chloride solution, then placed in contact with *ca.* 1 N hydrochloric acid and warmed on a water bath for two days. After cooling, the suspension was centrifuged. The barium ions in the supernatant were analyzed by EDTA titration, and the zirconium and phosphate were analyzed as has been described previously.[14] Found: Zr 22.2%, PO_4^{3-} 42.3%, Ba^{2+} 20.4 and H_2O 10.3% (weight loss at 120 °C). These data correspond to the $ZrBa_{0.67}H_{0.67}(PO_4)_2 \cdot 2.39H_2O$ formula. The barium content is lower than that calculated from the supernatant in the pH titration. This suggests that the barium ion is held strongly in the exchanger. The phosphate ion was not detected in the supernatant.

X-Ray Studies. X-Ray powder patterns of the exchanger at different titration stages are shown in Fig. 5. The first reflection of c-ZrP was detectable in the diffractograms up to a 5 meq/g addition of OH^-. In the diffraction patterns of the ignited exchanger, the peaks of zirconium pyrophosphate resulting from c-ZrP were found up to 5 meq/g. Moreover, exchanger at 10 meq/g showed the peaks to be those of zirconium oxide.

In conclusion, in 0~66% of exchange, the mixture of c-ZrP and its barium form, and at 66% of exchange the $ZrBa_{0.67}H_{0.67}(PO_4)_2 \cdot nH_2O$ phase was present, while beyond 67% of exchange the complex mixtures including the hydrolysis product were present.

The crystalline zirconium phosphate is known to have a layered structure and to contain a zeolitic cavity between the layers, and the expansion of the interlayer distance is caused by an uptake of cations.[15,16] According to Clearfield *et al.* the opening to the cavity permits only the cations with a 2.6Å diameter to diffuse into the crystal lattice unless c-ZrP swells considerably. Hence, the ionic radius of sorbed cations has a significant effect on the ion-exchange capacity of c-ZrP. However, as has been shown above, the ion-exchange capacity for barium ions is equal to 4.4 meq/g, which is equal to that for lithium and ammonium ions.[14,17]

In Table 2, the interplanar spacing (*d* values) of the Ca^{2+} and Ba^{2+} ion-replaced exchangers are shown. For the Ca^{2+} ion-replaced exchanger, an increase in the interlayer distance (7.6→10.05Å) was observed, as had been expected from the previous works. On the

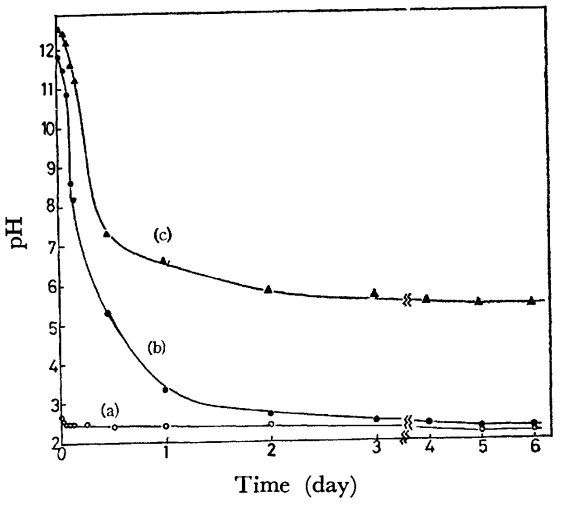

Fig. 4. The dependence of pH of supernatants on time
a 0, b 3, c 6 meq/g OH^- addition

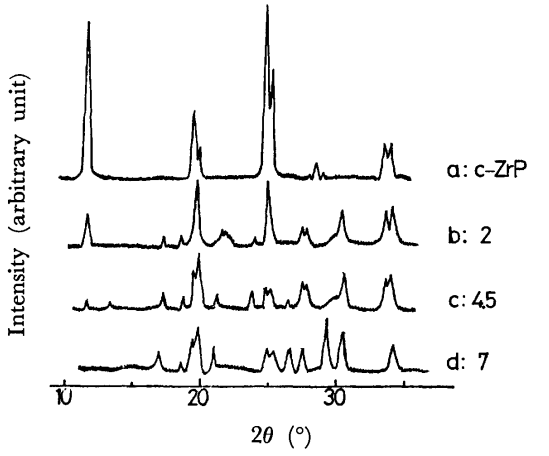

Fig. 5. Schematic diagrams of X-ray diffraction patterns. Numerals correspond to those of abscissa in Fig. 3.

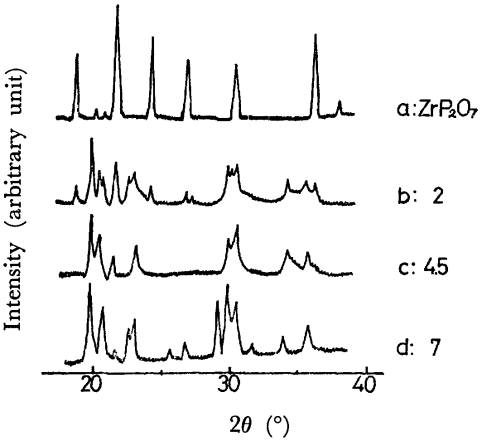

Fig. 6. Schematic diagrams of X-ray diffraction patterns for ignited samples. Numerals correspond to those of abscissa in Fig. 3.

TABLE 2. *d*-VALUES OF CALCIUM AND BARIUM FORMS OF c-ZrP (A)

Ca-ZrP	Ba-ZrP
10.05 s	7.69 vw
5.01 m	5.13 vw
4.58 s	4.51 m
4.48 s	3.72 vw
4.11 s	3.56 m
3.93 s	3.23 w
3.75 s	3.01 vw
3.19 s	2.94 m
3.13 m	2.65 m
3.06 w	2.63 m
2.76 w	1.90 vw
2.65 s	1.73 vw
2.61 m	1.71 vw
2.06 vw	
1.96 vw	
1.87 vw	

other hand, for the Ba^{2+} ion-replaced exchanger, no change in the interlayer distance was observed.

The above results should be further considered in terms of the behavior of hydrated water molecule during exchange; an investigation along this line is needed. It should be worthwhile, also, to mention how much the press treatment influences the exchange behavior.

The authors wish to express their sincere thanks to Professor Kozo Nagashima of Tokyo Kyoiku University for his valuable suggestions and constant encouragement throughout this work. They also wish to express their gratitude to Professor Shuji Abe of Tokyo University of Agriculture and Technology for his ready permission for use of the university facilities.

References

1) J. Albertsson, *Acta Chem. Scand.*, **20**, 1689 (1966).
2) Y. Hasegawa and I. Tomita, This Bulletin, **43**, 3011 (1970).
3) A. Clearfield and G. D. Smith, *J. Colloid Interface Sci.*, **28**, 325 (1968).
4) A. Clearfield and G. D. Smith, *J. Inorg. Nucl. Chem.* **30**, 327 (1968).
5) S. J. Harvie and G. H. Nancollas, *ibid.*, **32**, 3923 (1970).
6) A. Dyer, D. Leigh, and F. T. Ocon, *ibid.*, **33**, 3141 (1971).
7) G. Alberti, U. Constantino, and M. Pelliccioni, *ibid.*, **35**, 1327 (1973).
8) H. Onishi, This Bulletin, **30**, 567 (1957).
9) D. F. Boltz, "Colorimetric Determination of Nonmetals," Interscience Publishers Inc., N. Y. (1958).
10) C. B. Amphlett, L. A. McDonald, and M. J. Redman, *J. Inorg. Nucl. Chem.*, **6**, 220 (1958).
11) S. Ahrland, J. Albertsson, A. Oskarsson, and A. Niklasson, *ibid.*, **32**, 2069 (1970).
12) S. Ahrland and J. Albertsson, *Acta Chem. Scand.*, **18**, 1861 (1964).
13) H. Sekino and I. Tomita, This Bulletin, **46**, 1005 (1973).
14) Y. Hasegawa and H. Aoki, *ibid.*, **46**, 836 (1973).
15) A. Clearfield and G. D. Smith, *Inorg. Chem.*, **8**, 431 (1969).
16) A. Clearfield, W. L. Duax, A. S. Medina, G. D. Smith, and J. R. Thomas, *J. Phys. Chem.*, **73**, 3424 (1969).
17) A. Clearfield and J. Troup, *ibid.*, **74**, 314 (1970).

Metal Complexes of Amino Acids. VI.[1] μ-L-Aspartato and μ-L-Glutamato Complexes of Cobalt(III)

Takaji YASUI, Hiroshi KAWAGUCHI, Zenjiro KANDA, and Tomoharu AMA

Faculty of Arts and Sciences, Kochi University, Asakura, Kochi 780

(Received June 20, 1974)

Some binuclear and trinuclear complexes containing μ-L-aminocarboxylato ligands, $(+)_D$- and $(-)_D$-$[en_2Co(OCOCH(NH_2)(CH_2)_nCOO)Co(OH_2)en_2](ClO_4)_4$, $(+)_D$-$[en_2Co(OCOCH(NH_2)(CH_2)_nCOO)Co(NH_3)_5](ClO_4)_4$, and $(+)_D$- and $(-)_D$-$[en_2Co\{(OCOCH(NH_2)(CH_2)_nCOO)Co\ en_2\}_2](ClO_4)_5$ ($n=1$ for L-aspartato and $n=2$ for L-glutamato), have been newly prepared. The structure and vicinal CD effect of these complexes were discussed on the basis of their absorption, ^{13}C NMR and CD spectra data. Their geometrical structures were assigned as *cis* to the μ-L-aminocarboxylato-OH_2 binuclear complexes (with respect to the β-COO or γ-COO end of μ-aminocarboxylato bridge and the aquo ligand), and as *trans* to the di-μ-L-aminocarboxylato trinuclear complexes (with respect to the β-COO or γ-COO ends of two μ-aminocarboxylato bridges).

In the previous paper[1] we reported the study on the formation and preparations of the binuclear and trinuclear complexes containing μ-aminocarboxylato ligand, $[(NH_3)_5Co(OCORNH_2)Co\ NO_2(acac)_2]ClO_4$ and $[en_2Co\{(OCORNH_2)Co\ NO_2(acac)_2\}_2]ClO_4$. In these complexes the μ-aminocarboxylato ligand is the bidentate which bridged two cobalt(III) ions with the COO and NH_2 ends.

In the present paper, the preparations of some new binuclear and trinuclear complexes containing L-aspartato or L-glutamato as the μ-aminocarboxylato ligand are reported. The complexes isolated are characterized on the basis of their elemental analyses, visible and ultraviolet absorption, CD, and ^{13}C NMR spectra.

Experimental

Preparation of Starting Materials—L-Aspartato and L-Glutamato-bis(ethylenediamine)cobalt(III) Complexes. $(+)_D$-$[Co(L\text{-}asp)en_2]ClO_4\cdot 2H_2O$, $(-)_D$-$[Co(L\text{-}asp)en_2]ClO_4\cdot H_2O$, $(+)_D$- and $(-)_D$-$[Co(L\text{-}glu)en_2]ClO_4$ were prepared and separated by the same method as that of Legg and Steele.[2] Elemental analyses and $[\alpha]_D$ values of these complexes are listed in Table 1.

Preparation and Separation of μ-L-Aspartato Binuclear Complexes—$(+)_D$-$[en_2Co(L\text{-}asp)Co(OH_2)en_2](ClO_4)_4\cdot H_2O$ (abbreviation: $(+)_D$-μ-L-asp-OH_2). An aqueous solution containing 1.78 g (0.004 mol) of $(+)_D$-$[Co(L\text{-}asp)en_2]ClO_4\cdot 2H_2O$ ($[\alpha]_D=+445°$) and 3.10 g (0.006 mol) of $[Co(OH_2)_2en_2](ClO_4)_3$ in 40 ml of water was gradually evaporated almost to dryness at 50—55 °C on a water-bath. The residue was dissolved in 15—20 ml of water, and the solution was repeatedly evaporated to dryness. The final residue was dissolved in about 100 ml of water and then the solution was loaded on a SP-Sephadex cation-exchange column (C-25, Na-form, 3.6 cm × 70 cm). The red band adsorbed was developed with 0.1—0.3 N aqueous solution of $NaClO_4$. Each band which splitted from the red band was eluted in the order of orange-yellow ($[Co(L\text{-}asp)en_2]^+$), orange ($[Co(L\text{-}aspH)en_2]^{2+}$), pinkish-red ($[Co(OH_2)_2en_2]^{3+}$), and orange (μ-L-asp-$OH_2$ binuclear complex ion) bands. The latest orange eluate was concentrated by using a vacuum evaporator at 35—40 °C, and the deposited $NaClO_4$ was filtered off. After repeating the evaporation of the solution and the removal of $NaClO_4$, finally the solution was completely dried, and a large amount of absolute ethanol was added to the residue. The complex which remained as orange powder was collected by filtration and washed with absolute ethanol and then ether. Recrystallization of the complex was carried out by adding a small amount of $NaClO_4$ and ethanol to a concentrated solution and by allowing to stand the mixture in a refrigerator overnight. The complex deposited as reddish-orange crystals was filtered, washed with ethanol and then ether, and dried in a vacuum desiccator at room temperature. The yield was about 0.7 g. The complex obtained was readily soluble in water, and sparingly soluble in methanol and acetone, but insoluble in ethanol and ether.

$(-)_D$-$[en_2Co(L\text{-}asp)Co(OH_2)en_2](ClO_4)_4\cdot H_2O$. This complex was prepared by the same method as used for the $(+)_D$-isomer, except for using $(-)_D$-$[Co(L\text{-}asp)en_2]ClO_4\cdot 2H_2O$ ($[\alpha]_D=-315°$) instead of $(+)_D$-$[Co(L\text{-}asp)en_2]ClO_4\cdot H_2O$.

$(+)_D$-$[en_2Co(L\text{-}asp)Co(NH_3)_5](ClO_4)_4\cdot H_2O$ (abbr.: $(+)_D$-μ-L-asp-NH_3). To an aqueous solution containing 2.25 g (0.005 mol) of $(+)_D$-$[Co(L\text{-}asp)en_2]ClO_4\cdot 2H_2O$ ($[\alpha]_D=+445°$) in 10 ml of water was added 2.4 g (0.005 mol) of $[Co(NH_3)_5(OH_2)](ClO_4)_3\cdot H_2O$, and the mixture was gradually evaporated almost to dryness at 50—55 °C on a water-bath. The residue was dissolved in 10 ml of water, and the solution was evaporated again. The final residue was dissolved in 10 ml of water, and the solution was loaded on a SP-Sephadex cation-exchange column (C-25, Na-form, 3.6 cm × 70 cm). The adsorbed band splitted into five bands in sweeping with 0.3 N aqueous solution of $NaClO_4$. The eluate from the third band was concentrated to about 5 ml by using a vacuum evaporator at 35—40 °C, and a large amount of ethanol was added to the concentrated solution. The μ-L-aspartato binuclear complex which deposited as a pinkish-orange powder was filtered, and washed with a mixture of water–methanol (1 : 3) mixture, methanol and then ether. Recrystallization was carried out by adding a small amount of methanol to the concentrated solution and by keeping in a refrigerator overnight. The pinkish-orange complex was obtained as needle crystals. The yield was 1.2 g.

Preparation and Separation of μ-L-Glutamato Binuclear Complexes—$(+)_D$-$[en_2Co(L\text{-}glu)Co(OH_2)en_2](ClO_4)_4\cdot 2H_2O$ (abbr.: $(+)_D$-μ-L-glu-OH_2). This complex was obtained by a procedure similar to that of the $(+)_D$-μ-L-aspartato binuclear complexes, except for using 2.3 g (0.0045 mol) of $[Co(OH_2)_2en_2](ClO_4)_3$ and 1.27 g (0.003 mol) of $(+)_D$-$[Co(L\text{-}glu)en_2]ClO_4$ ($[\alpha]_D=+348°$) instead of $(+)_D$-$[Co(L\text{-}asp)en_2]ClO_4\cdot 2H_2O$. The yield was about 0.8 g. The reddish-orange complex was readily soluble in water, sparingly soluble in methanol and acetone, but insoluble in ethanol and ether.

$(-)_D$-$[en_2Co(L\text{-}glu)Co(OH_2)en_2](ClO_4)_4\cdot 2H_2O$. This $(-)_D$-isomer was obtained by the same procedure as that for $(+)_D$-isomer, except for using $(-)_D$-$[Co(L\text{-}glu)en_2]ClO_4$ in-

stead of $(+)_D$-[Co(L-glu)en_2]ClO_4.

$(+)_D$-[en_2Co(L-glu)Co(NH_3)$_5$](ClO_4)$_4\cdot H_2O$ (abbr.: $(+)_D$-μ-L-glu-NH_3). To an aqueous solution containing 2.4 g (0.005 mol) of [Co(NH_3)$_5$(OH_2)](ClO_4)$_3\cdot H_2O$ in 20 ml of warm water was added 2.12 g (0.005 mol) of $(+)_D$-[Co(L-glu)en_2]ClO_4 ($[\alpha]_D=+348°$). The solution was gradually evaporated to dryness at 60—65 °C on a water-bath. The residue was dissolved in 5—10 ml of water, and the solution was evaporated again. This procedure was repeated six or seven more times. Finally the residue was dissolved in 100 ml of warm water, and the solution was loaded on a SP-Sephadex cation-exchange column (C-25, Na-form, 3.6 cm × 70 cm). The elution and the isolation of the complex were performed by the same way as the case of $(+)_D$-[en_2Co(L-asp)Co(NH_3)$_5$](ClO_4)$_4\cdot H_2O$. The crude complex obtained was recrystallized from a minimum amount of water by adding a small amount of ethanol to the concentrated solution and by keeping in a refrigerator overnight. The yield was 0.2 g.

Preparations and Separations of Di-μ-L-aspartato and -L-glutamato Trinuclear Complexes—$(+)_D$-[en_2Co{(L-asp)Co en_2}$_2$](ClO_4)$_5\cdot 5H_2O$ (abbr.: di-μ-L-asp). To an aqueous solution of 0.82 g (0.006 mol) of [Co(OH_2)$_2$$en_2$]($ClO_4$)$_3$ containing in 20—30 ml of water was added 1.31 g (0.003 mol) of $(+)_D$-[Co(L-asp)en_2]$ClO_4\cdot 2H_2O$ ($[\alpha]_D=+445°$). The solution was evaporated to dryness at over 80 °C on a steam-bath. The residue was dissolved in about 10 ml of water and evaporated again. This procedure was repeated two more times. Finally the residue was dissolved in 50 ml of water, and the solution was loaded on a SP-Sephadex cation-exchange column (C-25, Na-form, 3.6 cm × 50 cm), and the adsorbed band was developed with 0.1—0.3 N aqueous solution of $NaClO_4$. Each band splitted was eluted in the order of orange-yellow ([Co(L-asp)en_2]$^+$), orange ([Co(L-aspH)en_2]$^{2+}$), pinkish-red ([Co(OH_2)$_2$$en_2$]$^{3+}$), pinkish-red ([$en_2$Co(L-asp)Co($OH_2$)$en_2$]$^{4+}$), and reddish-orange (di-μ-L-asp trinuclear complex ion) bands. The latest eluate was concentrated by using a vacuum evaporator and the deposited $NaClO_4$ was filtered off. After repeating the procedure of the evaporation of the solution and the removal of an excess of $NaClO_4$, finally the solution was completely evaporated to dryness, and a large amount of methanol was added to the residue until the deposited $NaClO_4$ disappeared. The reddish-orange complex deposited as needle crystals was filtered and washed with methanol and then acetone. Recrystallization was carried out from a minimum amount of warm water by adding a few drops of saturated solution of $NaClO_4$, and by keeping in a refrigerator for 2—3 hours. The yield was 1.1 g.

$(-)_D$-[en_2Co{(L-asp)Co en_2}$_2$](ClO_4)$_5\cdot 5H_2O$. The $(-)_D$-isomer was prepared by the same method as used for the $(+)_D$-isomer.

$(+)_D$- and $(-)_D$-[en_2Co{(L-glu)Co en_2}$_2$](ClO_4)$_5\cdot nH_2O$ (n= 4 and 5 for $(+)_D$- and $(-)_D$-isomers) (abbr.: $(+)_D$- and $(-)_D$- di-μ-L-glu). These complexes were prepared by a similar way to that used for the $(+)_D$-di-μ-L-asp trinuclear complex, except for using 1.03 g (0.002 mol) of [Co(OH_2)$_2$-en_2](ClO_4)$_3$ and 1.70 g (0.004 mol) of $(+)_D$-[Co(L-glu)en_2]-ClO_4 ($[\alpha]_D=+348°$)/and $(-)_D$-[Co(L-glu)en_2]ClO_4 ($[\alpha]_D=-409°$) instead of $(+)_D$-[Co(L-asp)en_2]$ClO_4\cdot 2H_2O$. The reddish-orange complexes were obtained as needle crystals. The yields were about 0.7 g.

Measurements. The absorption spectra were obtained by using a Hitachi Model EDS-3T spectrophotometer. The CD measurements were made by a JASCO Model ORD/UV-5 spectrophotometer with CD attachment. The ^{13}C NMR spectra were recorded on a JEOL MH-100 spectrometer with pulsed Fourier transform/proton noise-decoupled mode. The samples used for the ^{13}C NMR measurements were converted perchlorate to the chloride to obtained higher solubility in D_2O. An external benzene was used as a standard signal.

The chemical shifts (ppm) in the figures are shown by adopting chemical shift of benzene down field of 128.50 ppm from that of TMS.[3]

Results and Discussion

Elemental analyses and CD data for the μ-L-amino-carboxylato binuclear and trinuclear complexes are listed in Table 1.

Absorption Spectra. The absorption curves of the L-asp mononuclear ([Co(L-asp)en_2]$^+$), μ-L-asp binuclear and di-μ-L-asp trinuclear complexes are shown in Fig. 1. In Figs. 2, 4 and 5, the residual absorption curves for the μ-L-asp-OH_2 and μ-L-asp-NH_3 binuclear complexes, and di-μ-L-asp trinuclear complex are shown. The absorption spectra of these complexes indicate almost analogous absorption curve each other, although their intensities are different (Fig. 1). However, the residual curve for the trinuclear complex (Fig. 5) shows quite different behavior from those for the binuclear complexes (Figs. 2 and 4), and consists of two splitted bands in the first band region. Such split for the trinuclear complex coincides with the absorption behavior which generally appears in the *trans(O)*-[Co O_2N_4] type complexes.[4,5] Therefore, it can be concluded that the di-μ-L-asp trinuclear complex obtained in the present study takes the *trans(O)* structure with respect

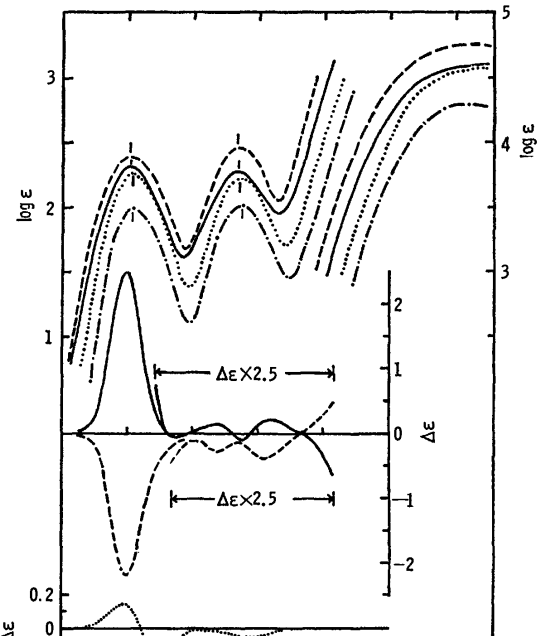

Fig. 1. Absorption and CD curves of L-asp complexes. Absorption curves: —·—, [Co(L-asp)en_2]$^+$; ——, [en_2Co(L-asp)Co(OH_2)en_2]$^{4+}$; ·····, [en_2Co(L-asp)-Co(NH_3)$_5$]$^{4+}$; ----, [en_2Co{(L-asp)Co en_2}$_2$]$^{5+}$. CD curves: (1) ——, $(+)_D$-[Co(L-asp)en_2]$^+$; (2) ----, $(-)_D$-[Co(L-asp)en_2]$^+$; (3) ·····, 1/2{(1)+(2)}.

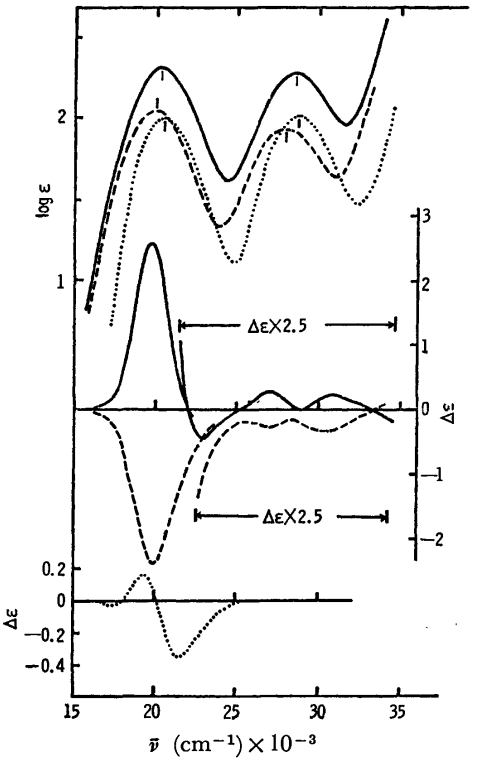

Fig. 2. Absorption, CD and their residual curves for μ-L-asp-OH_2 binuclear complex.
Absorption curves: (1) ——, $[en_2Co(L\text{-asp})Co(OH_2)en_2]^{4+}$; (2) ·····, $[Co(L\text{-asp})en_2]^+$; (3) ----, (1)—(2).
CD curves: (1) ——, $(+)_D$-$[en_2Co(L\text{-asp})Co(OH_2)en_2]^{4+}$; (2) ----, $(-)_D$-$[en_2Co(L\text{-asp})Co(OH_2)en_2]^{4+}$; (3) ·····, (1)—{$(+)_D$-$[Co(L\text{-asp})en_2]^+$}.

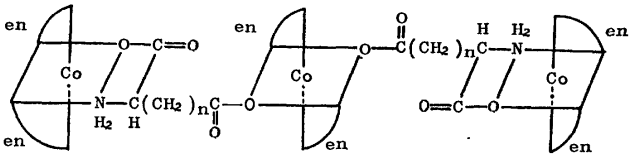

Fig. 3. The structure of di-μ-L-asp ($n=1$) or di-μ-L-glu ($n=2$) trinuclear complex.

to the two β-carboxyl groups of the μ-L-aspartato ligands, as shown in Fig. 3. On the other hand, the residual curve for the μ-L-asp-OH_2 binuclear complex does not indicate such splitted band as observed for the trinuclear complex. In addition the first and second band maxima (502 and 358 nm) in the residual curve appear at the positions corresponding to the *cis(O)*-[Co O_2N_4] type complexes.[5,6] Therefore, it is reasonable to conclude that this binuclear complex takes the *cis* structure with respect to the β-carboxyl group of the μ-L-aspartato and the coordinated OH_2 (Fig. 6). The same conclusions can also be obtained for the corresponding μ-L-glutamato complexes.

Circular Dichroism Spectra. Gillard *et al.* prepared the $(+)_D$- and $(-)_D$-$[Co(L\text{-glu})en_2]ClO_4$ by the reaction between $[Co\ CO_3en_2]ClO_4$ and L-glutamic acid, and showed that the $(+)_D$-isomer produces more preferentially than the $(-)_D$-isomer.[7,8] They have also determined that the absolute configutation of the $(+)_D$-isomer is Λ-form by the X-ray analysis.[9]

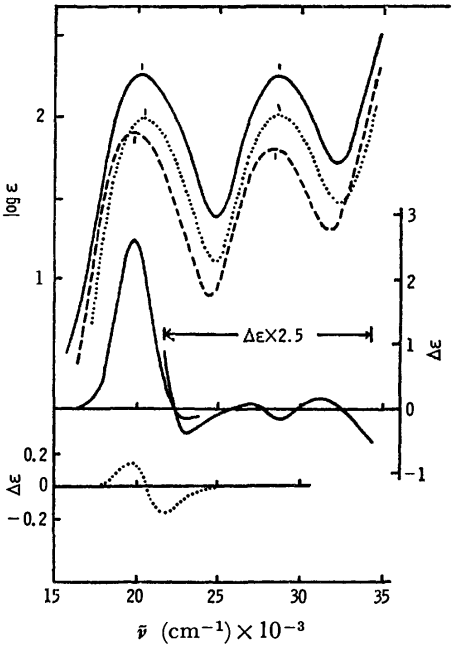

Fig. 4. Absorption, CD and their residual curves for μ-L-asp-NH_3 binuclear complex.
Absorption curves: (1) ——, $[en_2Co(L\text{-asp})Co(NH_3)_5]^{4+}$; (2) ·····, $(+)_D$-$[Co(L\text{-asp})en_2]^+$; (3) ----, (1)—(2).
CD curves: (1) ——, $(+)_D$-$[en_2Co(L\text{-asp})Co(NH_3)_5]^{4+}$; (2) ·····, (1)—{$(+)_D$-$[Co(L\text{-asp})en_2]^+$}.

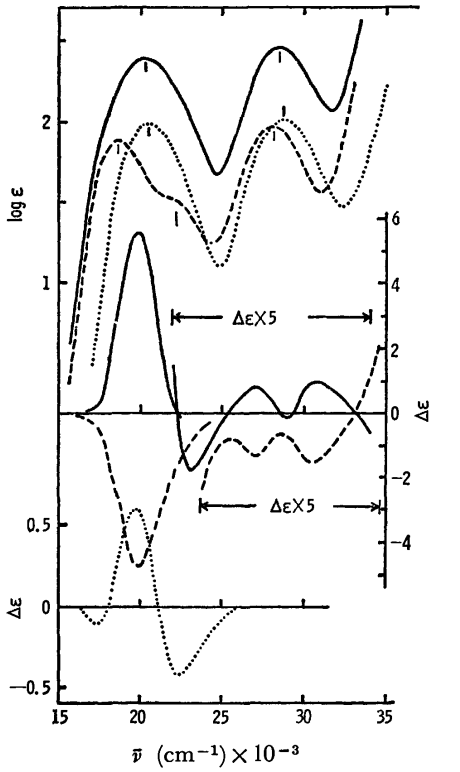

Fig. 5. Absorption, CD and their residual curves for di-μ-L-asp trinuclear complex.
Absorption curves: (1) ——, $(+)_D$-$[en_2Co\{(L\text{-asp})Co\ en_2\}_2]^{5+}$; (2) ·····, $(+)_D$-$[Co(L\text{-asp})en_2]^+$; (3) ----, (1)—(2)×2.
CD curves: (1) ——, $(+)_D$-$[en_2Co\{(L\text{-asp})Co\ en_2\}_2]^{5+}$; (2) ----, $(-)_D$-$[en_2Co\{(L\text{-asp})Co\ en_2\}_2]^{5+}$; (3) ·····, (1)—2{$(+)_D$-$[Co(L\text{-asp})en_2]^+$}.

Table 1. Elemental analyses and CD data

Complexes	$[\alpha]_D$ (°)	C, % Found (Calcd)	H, % Found (Calcd)	N, % Found (Calcd)	$\tilde{\nu}_{ext}$, 10^3 cm^{-1} ($\Delta\varepsilon$) First Band	Second Band
$(+)_D$-$[Co(L\text{-asp})en_2]ClO_4\cdot 2H_2O$	+445	21.79 (21.55)	5.87 (5.66)	15.44 (15.71)	19.92(+2.476) 23.53(−0.014)	27.03(+0.055) 28.70(−0.042) 30.77(+0.072)
$(-)_D$-$[Co(L\text{-asp})en_2]ClO_4\cdot H_2O$	−315	22.14 (22.46)	5.45 (5.43)	16.33 (16.38)	19.92(−2.190)	26.90(−0.106) 30.40(−0.160)
$(+)_D$-$[Co(L\text{-glu})en_2]ClO_4$	+348	25.50 (25.50)	5.62 (5.48)	16.61 (16.53)	19.96(+2.470) 23.26(−0.087)	26.81(+0.036) 28.70(−0.060) 31.00(+0.060)
$(-)_D$-$[Co(L\text{-glu})en_2]ClO_4$	−409	25.54 (25.50)	5.58 (5.48)	16.42 (16.53)	19.61(−2.207)	27.30(−0.231) 29.85(−0.261)
$(+)_D$-$[en_2Co(L\text{-asp})Co(OH_2)en_2]$-$(ClO_4)_4\cdot 2H_2O$	+220	15.19 (15.31)	4.81 (4.61)	13.48 (13.40)	19.80(+2.571) 22.99(−0.191)	26.88(+0.110) 30.77(+0.089)
$(-)_D$-$[en_2Co(L\text{-asp})Co(OH_2)en_2]$-$(ClO_4)_4\cdot H_2O$	−166	15.74 (15.61)	4.72 (4.49)	13.43 (13.66)	20.00(−2.396)	27.03(−0.114) 30.50(−0.156)
$(+)_D$-$[en_2Co(L\text{-glu})Co(OH_2)en_2]$-$(ClO_4)_4\cdot 2H_2O$	+166	16.45 (16.34)	4.98 (4.76)	13.02 (13.20)	19.92(+3.000) 22.99(−0.204)	27.03(+0.444) 28.60(−0.070) 30.80(+0.080)
$(-)_D$-$[en_2Co(L\text{-glu})Co(OH_2)en_2]$-$(ClO_4)_4\cdot 2H_2O$	−222	16.44 (16.34)	4.96 (4.76)	13.24 (13.20)	19.80(−2.620)	27.20(−0.160) 30.40(−0.180)
$(+)_D$-$[en_2Co(L\text{-asp})Co(NH_3)_5]$-$(ClO_4)_4\cdot 3H_2O$	+211	10.77 (10.60)	4.65 (4.68)	15.36 (15.46)	19.80(+2.645) 23.00(−0.103)	26.81(+0.074) 28.41(−0.030) 31.00(+0.094)
$(+)_D$-$[en_2Co(L\text{-glu})Co(NH_3)_5]$-$(ClO_4)_4\cdot H_2O$	+161	12.40 (12.22)	4.68 (4.56)	15.68 (15.84)	19.92(+2.584) 23.00(−0.159)	27.03(+0.029) 28.70(−0.061) 31.00(+0.061)
$(+)_D$-$[en_2Co\{(L\text{-asp})Co\ en_2\}_2]$-$(ClO_4)_5\cdot 5H_2O$	+265	17.06 (17.32)	5.17 (4.95)	14.06 (14.14)	19.88(+5.566) 22.99(−0.376)	27.03(+0.170) 28.82(−0.041) 30.77(+0.205)
$(-)_D$-$[en_2Co\{(L\text{-asp})Co\ en_2\}_2]$-$(ClO_4)_5\cdot 5H_2O$	−236	17.28 (17.32)	5.00 (4.95)	14.19 (14.14)	19.90(−4.716)	27.10(−0.270) 30.50(−0.320)
$(+)_D$-$[en_2Co\{(L\text{-glu})Co\ en_2\}_2]$-$(ClO_4)_5\cdot 4H_2O$	−217	18.99 (18.91)	5.12 (5.06)	14.12 (14.04)	19.88(+5.854) 22.99(−0.311)	26.67(+0.124) 28.57(−0.124) 31.00(+0.156)
$(-)_D$-$[en_2Co\{(L\text{-glu})Co\ en_2\}_2]$-$(ClO_4)_5\cdot 5H_2O$	−283	18.61 (18.67)	5.23 (5.14)	13.77 (13.86)	19.69(−4.911)	26.90(−0.364) 30.10(−0.347)

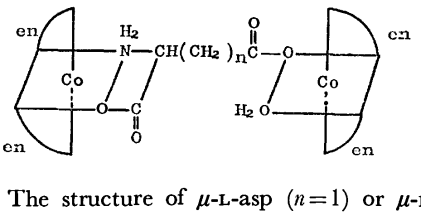

Fig. 6. The structure of μ-L-asp ($n=1$) or μ-L-glu ($n=2$) binuclear complex.

Recently, Buckingham *et al.* have demonstrated from the kinetical and thermodynamical studies that there is no substantial preference for the formation of one diastereomer relative to the other in the $[Co(L\text{-glu})en_2]^+$ complex ion.[10] The complete separation of the $(+)_D$- and $(-)_D$-isomers of L-aspartato-bis(ethylenediamine)-cobalt(III) complexes was performed by Legg *et al.*,[2,11] and Kojima and Shibata.[12]

The CD curves of the mononuclear, binuclear and trinuclear L-aspartato complexes are shown in Figs. 1, 2, 4 and 5, and those of L-glutamato complexes are shown in Fig. 7. The absolute configurations of the mononuclear complexes for the $(+)_D$- and $(-)_D$-isomers are assigned respectively as Λ- and Δ-form from the sign of the main CD band in the first band region (in Fig. 1).[13] The μ-L-asp binuclear and di-μ-L-asp trinuclear complexes indicate the CD curves of similar type to those of the L-asp mononuclear complexes. This suggests that the CD bands of these binuclear and trinuclear complexes arise from the contributional CD effect of the mononuclear complex. The same discussion can also be made for the L-glutamato complexes.

The residual CD curves which were obtained by subtracting the CD curve of the mononuclear complex from that of each binuclear and trinuclear complex are shown in Figs. 2, 4, 5 and 7. These residual curves mean that the CD band of the mononuclear complex is intensified by the coordination of another cobalt(III) complex ion to the free β- or γ-carboxyl group of the

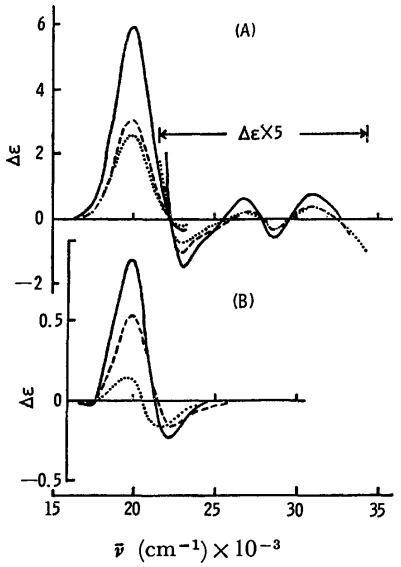

Fig. 7. CD and its residual curves for $(+)_D$-μ-L-glu complexes.
(A) (1) ·····, $[en_2Co(L\text{-}glu)Co(NH_3)_5]^{4+}$; (2) ----, $[en_2Co(L\text{-}glu)Co(OH_2)en_2]^{4+}$; (3) ——, $[en_2Co\{(L\text{-}glu)Co\ en_2\}_2]^{5+}$. (B) ·····, (1)—$\{(+)_D\text{-}[Co(L\text{-}glu)\text{-}en_2]^+\}$; ----, (2)—$\{(+)_D\text{-}[Co(L\text{-}glu)en_2]^+\}$; ——, (3)—$\{(+)_D\text{-}[Co(L\text{-}glu)en_2]^+\}$.

former complex, and that no configurational change of the original mononuclear complex occurs in the preparing process of the binuclear and trinuclear complexes. The almost symmetrical curves of the main CD bands for the $(+)_D$- and $(-)_D$-isomers of the binuclear and trinuclear complexes with μ-L-aspartato also support the complete retention of the configuration in the original mononuclear complex.

The intensities of these residual CD bands increase in the order of the μ-L-aa-NH_3, μ-L-aa-OH_2 binuclear and di-μ-L-aa trinuclear complexes. The residual CD band of the μ-L-aa-OH_2 binuclear complex indicates lower intensity of about half as compared with that of the trinuclear complex. This suggests that the former complex consists of the equivalent mixture of the two diastereomers (Λ(L)-Λ and Λ(L)-Δ).

^{13}C Nuclear Magnetic Resonance Spectra. The ^{13}C NMR patterns of some $(+)_D$-L-aspartato complexes are shown in Fig. 8. Two kinds of resonance signals which appear in the low magnetic field (176.55—186.98 ppm) correspond to the carbon atoms of the two carboxyl groups (α- and β-carboxyl groups) in the L-aspartato. Of these signals, the ones at the lower field side exhibit hardly change in chemical shift, but the ones at the higher field side do the considerable different chemical shift among the mononuclear and μ-L-asp complexes. The change of the chemical shift in the carboxyl group can be related to the change of its chemical environment. Quirt *et al.* have demonstrated from the pH titration study for the various amino acids that the carbon resonance of the carboxyl group indicates large shift with pH change.[11] The signal of 179.32 ppm in the $(+)_D$-$[Co(L\text{-}asp)en_2]^+$ ion shifts to higher field side (176.55 ppm) when its solution was acidified with D_2SO_4, and contrarily to lower field side (183.83 and 184.43 ppm) in the binuclear and

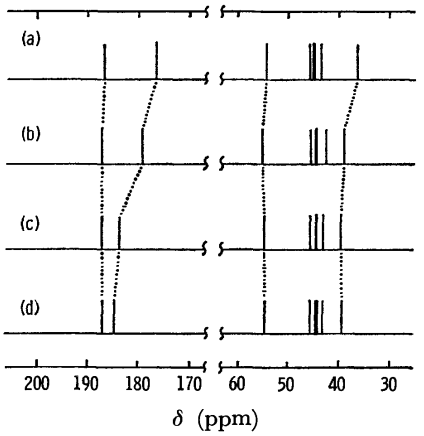

Fig. 8. ^{13}C NMR patterns of $(+)_D$-L-asp complexes in D_2O: (a) $[Co(L\text{-}aspD)en_2]^{2+}$ (acidified with D_2SO_4), (b) $[Co(L\text{-}asp)en_2]^+$, (c) $[en_2Co(L\text{-}asp)Co(NH_3)_5]^{4+}$, (d) $[en_2Co\{(L\text{-}asp)Co\ en_2\}_2]^{5+}$.

trinuclear complexes. The former shift can be related to the protonation of the free β-carboxyl group and the latter ones to the coordination of the β-carboxyl group to the cobalt(III) ion. The signals at the lower field side exhibit nearly constant chemical shift (186.74—187.35 ppm) for all the L-aspartato complexes. This result suggests that these signals can be assigned to the carbon atoms of the α-carboxyl groups which take the same coordination form in these complexes.

The carbon signals of methin and methylene of L-aspartato, and of ethylenediamine appear at the positions of about 55, 36—40, and 43—46 ppm, respectively. The change of the chemical shift is also observed in the methylene carbon of the protonated mononuclear complex. More detailed discussion relating to the ^{13}C NMR of these complexes will be made in the successive study.

References

1) Part V of this series: T. Yasui, T. Ama, H. Morio, M. Okabayashi, and Y. Shimura, This Bulletin, in press.
2) J. I. Legg and J. Steele, *Inorg. Chem.*, **10**, 2177 (1971).
3) L-R. F. Johnson and W. C. Jankowski, "Carbon-13 NMR Spectra", John Wiley & Sons, Inc., New York (1972).
4) T. Yasui, J. Hidaka, and Y. Shimura, This Bulletin, **39**, 2417 (1966).
5) N. Matsuoka, J. Hidaka, and Y. Shimura, *ibid.*, **40**, 1868 (1967).
6) T. Yasui, J. Fujita, and Y. Shimura, *ibid.*, **42**, 2081 (1969).
7) J. H. Dunlop, R. D. Gillard, and N. C. Payne, *J. Chem. Soc. A*, **1967**, 1469.
8) R. D. Gillard, R. Maskill, and A. Pasin, *ibid.*, **1971**, 2268.
9) R. D. Gillard, N. C. Payne, and G. B. Robertson, *ibid.*, **1970**, 2579.
10) D. A. Buckingham, J. Dekkers, A. M. Sargeson, and L. G. Marzilli, *Inorg. Chem.*, **12**, 1207 (1973).
11) W. E. Keyes and J. I. Legg, *J. Amer. Chem. Soc.*, **95**, 3431 (1973).
12) Y. Kojima and M. Shibata, *Inorg. Chem.*, **12**, 1009 (1973).
13) A. J. McCaffery and S. F. Mason, *Mol. Phys.*, **6**, 359 (1963).
14) A. R. Quirt, J. R. Lyerla, Jr., I. R. Peat, J. S. Cohen, W. F. Reynolds, and M. H. Freedman, *J. Amer. Chem. Soc.*, **96**, 570 (1974).

Layered Compounds. XVIII[1]. Synthesis of a Paracyclophane Containing the 1,2,3,4,5-Hexapentaene Group and the Stereochemistry of Its Formation

Taichi NEGI, Takahiro KANEDA, Hiroshi MIZUNO, Toshihiro TOYODA, Yoshiteru SAKATA, and Soichi MISUMI

The Institute of Scientific and Industrial Research, Osaka University, Suita, Osaka 565

(Received September 28, 1973)

Novel cyclic 1,2,3,4,5-hexapentaene compounds were synthesized from cyclic diyne-diol IX *via* diallene-dibromide X in order to study transannular electronic interaction. A diallene-dibromide Xc-I obtained from a diyne-diol isomer IXc-I was debrominated with active zinc to give cyclic hexapentaene IIc, whereas the other diallene-dibromide Xc-II derived from the second diyne-diol isomer IXc-II was not. The X-ray crystallographic analysis of the dibromide Xc-I was then carried out, and the *s-trans* structure was assigned to the dibromide. On the basis of this result, the stereochemistry of the transformation from diyne-diol to the hexapentaene group was discussed. The electronic spectrum of a cyclophane IIa containing the hexapentaene group showed a transannular π-electronic interaction between the benzene ring and the hexapentaene group, unlike those of the other hexapentaene derivatives, IIc and XV.

In the previous paper we reported that the electronic spectra of [*m.n*]paracyclophadiynes (I) show remarkable transannular interaction between the benzene nucleus and the diacetylenic unit as the numbers of the bridge methylene chains, *m* and *n*, decrease.[2] However, the absorption band of the diacetylene unit is partially submerged into the strong short-wavelength band of the benzene chromophore. Accordingly, the spectra have been mainly interpreted in terms of the long-wavelength band of the latter chromophore. For the clearer elucidation of the transannular electronic interaction between two different chromophores, a distinct observation of the absorption bands due to both chromophores is desirable. For that purpose, we have undertaken to study a paracyclophane IIa containing a benzene nucleus and a 1,2,3,4,5-hexapentaene group which shows a characteristic, strong absorption band in a longer wavelength region than that of the former chromophore.[3]

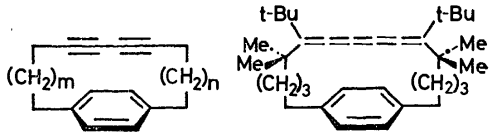

I IIa

The present paper deals with the syntheses and properties of IIa and related compounds and discusses stereochemical process concerning the formation of the 1,2,3,4,5-hexapentaene group from 2,4-butadiyne-1,6-diol derivatives *via* an intermediate diallene-dibromide like X. Three cumulenic compounds, IIa, IIb, and IIc, are the first cyclic 1,2,3,4,5-hexapentaene derivatives except for some annulenes having a formal hexapentaene group.[4]

Results and Discussion

Synthesis. The syntheses of the cyclic hexapentaenes IIa, IIb, and IIc, are outlined in Schemes 1 and 2. By the reaction of the bis-Grignard compound of the dichloride IV with pivaloyl chloride in the presence of copper powder and cuprous chloride,[5] a diketone VIIa was obtained in a low yield (14%), along with a large amount of olefinic compounds. The syntheses of the diketones VIIb and VIIc were achieved *via* two steps from acid chlorides V and XI respectively. Thus, two diketones, VI and 2,2,13,13-tetramethyl-3,12-tetradecanedione, which were obtained from V and XI in 87 and 65% yields respectively, were subjected to methylation with sodium amide and methyl iodide to give VIIb and VIIc in 53 and 37% yields respectively. This methylation process needs to be repeated to give good yields of VII. The reaction of the highly-branched diketone VII with ethynylmagnesium bromide[6] was barely completed after 7—10 days at 35 °C to afford a 68—80% yield of a diyne-diol VIII. Such a slow reaction is obviously caused by the bulkiness around the α-carbon atoms adjacent to the carbonyl group, because an unbranched ketone XVI gives a 61% yield of a diyne-diol XVII even under the mild conditions of room temperature for 4 hr. The intramolecular oxidative coupling reaction of the diyne-diol VIII was carried out by the use of a high-dilution technique to give cyclic monomers, IXa and IXc, in 13 and 32% yields respectively.[7] On the other hand, the oxidative coupling of VIIIb afforded a cyclic dimer IXb (34% yield) in place of the cyclic monomer, probably because of internal steric hindrance in the monomer. By column chromatography with silica gel, each of the cyclic monomers IXa and IXc were separated into two isomers, a meso and a racemic, distinguishable by means of the IR spectra.

Both isomers of IXc, the first-eluted one IXc-I and the second-eluted one IXc-II, were individually treated with phosphorus tribromide[8a] to derive diallene-dibromides Xc-I and Xc-II respectively. By the debromination of Xc-I with active zinc powder,[8a] followed by chromatography with neutral alumina, a cyclic hexapentaene IIc was obtained as pale greenish yellow crystals in a 71% yield, whereas the same treatment of Xc-II gave no product with a spectrum characteristic of the hexapentaene group. On the other hand, upon debromination reaction with methylmagnesium iodide,[8b] both Xc-I and Xc-II afforded the desired compound IIc. This reaction sequence from the diyne-diol IXc to IIc is of particular interest with regard to the stereochemistry in the reaction mechanism, which will be discussed below.

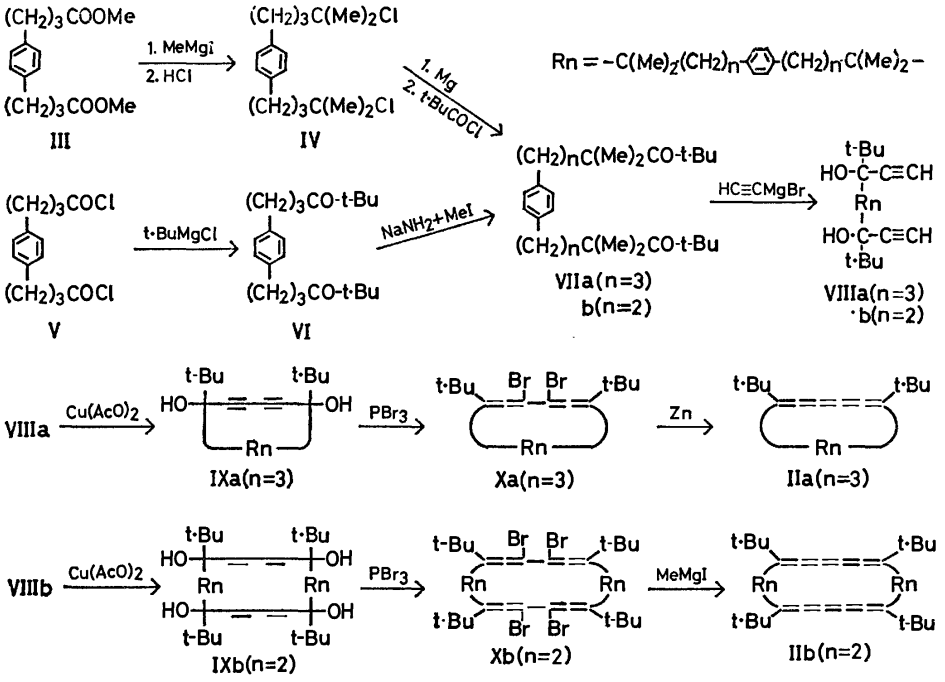

Scheme 1.

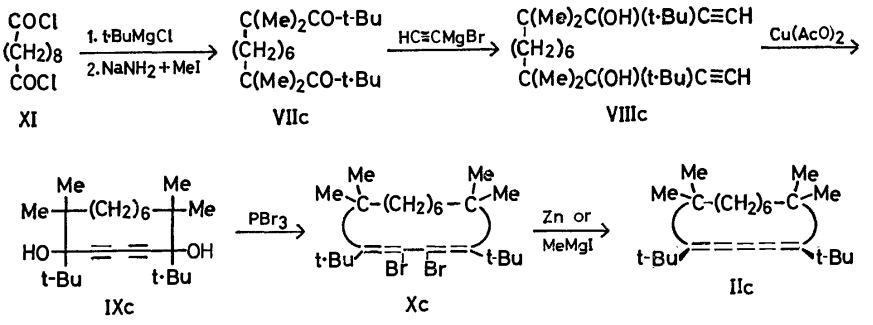

Scheme 2.

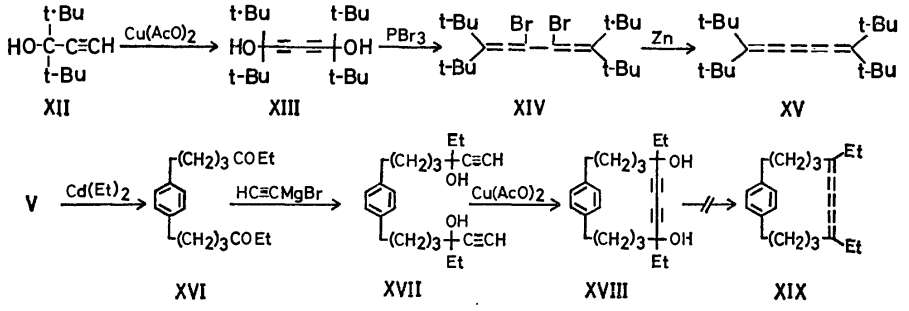

Scheme 3.

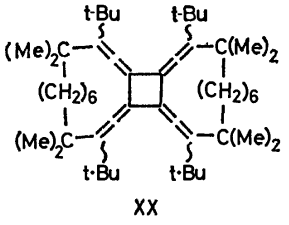

XX

Upon melting (146—147 °C), IIc immediately solidified to give white crystals with a mp of 280—282 °C. On the basis of the elemental analysis, the mass spectrum, and the UV spectrum of tetrakis(di-*tert*-butylvinylidene)cyclobutane,[8c] this product is assumed to be a dimer XX, the configuration of which has not yet been determined.

The debromination of diallene-dibromide Xa obtained in a 62% yield through the same treatment of IXa as in the case of IXc, was carried out by the active zinc method above-stated to give the desired cyclic hexapentaene IIa as a greenish yellow oil. Also, by debromination with methylmagnesium iodide, the

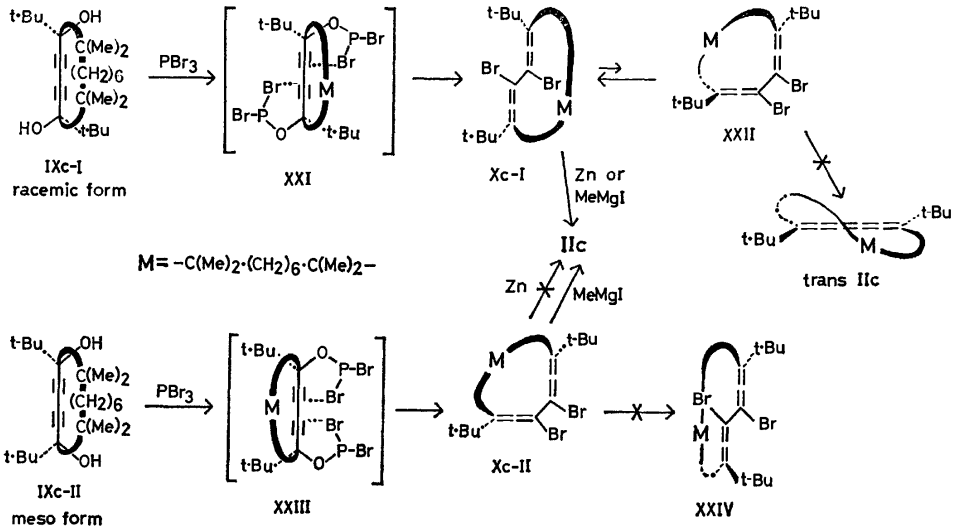

Scheme 4.

tetraallene-tetrabromide Xb derived from IXb gave a cyclic bishexapentaene IIb as greenish yellow crystals, which showed an electronic spectrum characteristic of the hexapentaene group. Tetra-*tert*-butyl-1,2,3,4,5-hexapentaene XV[8c] was prepared *via* the synthetic route shown in Scheme 3 for spectral reference.

In preliminary experiments, the preparation of a simpler cyclic hexapentaene XIX from XVIII was attempted by the following methods: 1) phosphorus diiodide,[9] 2) phosphorus tribromide in pyridine,[10] 3) phosphorus tribromide followed by active zinc, 4) stannous chloride-hydrogen chloride,[11] and 5) methylmagnesium bromide, but all the methods failed to give XIX.

Crystal Structure of Diallene-dibromide Xc-I. The diallene-dibromide Xc-I obtained from the first-eluted diyne-diol IXc-I is considered as an important key substance for clarifying the reaction mechanism for the well-known formation of the hexapentaene group from the diyne-diol derivative, as will be described below. In order to determine the geometrical structure of Xc-I and then to elucidate the stereochemical course of the formation of the hexapentaene IIc, X-ray crystallographic analysis was carried out.

The diallene-dibromide Xc-I was crystallized from ethyl acetate as colorless columns.

Crystal data: $C_{26}H_{42}Br_2$, Mol wt=514.4, triclinic, $a=9.662$, $b=16.761$, $c=8.306$ Å; $\alpha=88.12°$, $\beta=92.30°$, $\gamma=92.73°$; $V=1341.9$ Å^3; $D_m=1.267$, $D_x=1.273$ gcm^{-3}; $Z=2$, Space group $P\bar{1}$.

The crystal selected for data collection was of the approximate dimensions of $0.13\times0.10\times0.23$ mm and was mounted with the c-axis coincident to the ϕ-axis of the goniostat. The intensity data were collected with $2\theta<55°$ on a fully-automatic Hilger four-circle diffractometer using Zr-filtered Mo-Kα radiation and the ω-2θ scan technique. The intensities of 1863 independent reflections were recorded as observed. However, when the intensity of a standard reflection, $\bar{5}1\bar{1}$, was measured every 10 reflections, an obvious decay was discernible. Accordingly, the intensities of the observed reflections were corrected with the Lorentz and polarization factors after a decay correction corresponding to the decay curve of the $\bar{5}1\bar{1}$ reflection. No absorption corrections were made.

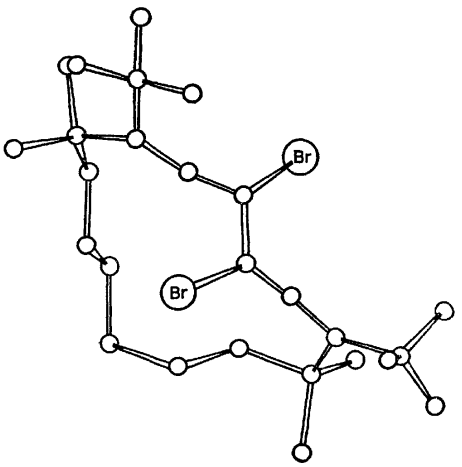

Fig. 1. Crystal structure of diallene-dibromide Xc-I.

A three-dimensional Patterson synthesis was first computed, and the positions of the bromine atoms were deduced. All the carbon atoms were revealed after successive Fourier synthesis. Although the structure of this dibromide was partially disordered, the essential features of the molecule are shown in Fig. 1 with a final R index of 0.113. The figure clearly shows that the two bromine atoms are positioned in the manner of the *s-trans* form around the sp^2-sp^2 single bond and that the two *tert*-butyl groups are in the *cis* configuration with respect to the plane containing the two bromine atoms.

All the calculations were performed on a NEAC-700 computer at the Computation Center of Osaka University by the use of the following programs: PSSFR-5* and HBLS-IV.**

* T. Sakurai, The Universal Crystallographic Computing System (I), p. 18, The Crystallographic Society of Japan, 1967.

** T. Ashida, The Universal Crystallographic Computing System-Osaka, p. 55, The Computation Center, Osaka University, 1973.

Stereochemical Aspect of the Formation of Hexapentaene. The stereochemistry of the reaction sequence from cyclic diyne-diol IXc to cyclic hexapentaene IIc is given in Scheme 4. The bromination of IXc with phosphorus tribromide is presumed to proceed in a stereospecific manner *via* a bis-dibromophosphite ester, XXI or XXIII, as a cyclic transition state,[13] since the halogenation of acetylenic alcohol with thionyl chloride[12] or phosphorus tribromide[13] has been well established or illustrated to follow the S_Ni' mechanism.

Thus, *s-trans*-diallene-dibromide Xc-I should be derived from the racemic form of the diyne-diol IXc-I *via* the bis-dibromophosphite ester XXI, whereas its *s-cis* conformer XXII seems to be hardly producible at all, for it is considerably strained, according to an examination with the Stuart-Briegleb molecular model. Similarly, the *s-cis*-dibromide Xc-II should be formed from the meso form of the diyne-diol IXc-II through the bis-dibromophosphite ester XXIII, and the corresponding *s-trans* conformer XXIV can not be yielded because of its highly strained system.***

As is shown in Fig. 1, X-ray crystallographic analysis assigned the *s-trans* structure of Xc-I to the diallene-dibromide which was obtained from the first-eluted diyne-diol IXc-I. Accordingly, this result demonstrates that the diyne-diol IXc-I is of the racemic form, whereas the second-eluted diyne-diol IXc-II must be of the meso form. Since *trans*-IIc, in which two *t*-butyl groups are bonded in the *trans* form to the hexapentaene group, can not at all expect to exist because of the short bridged chain, the debromination product IIc should have the *cis* configuration. Consequently, the fact that IIc is obtained from Xc-I by debromination with zinc powder, but not from Xc-II, clearly indicates that the debromination proceeds through the *trans* elimination mechanism. On the other hand, the debromination with methylmagnesium iodide might proceed by a mechanism other than E2 elimination, because both Xc-I and Xc-II afforded IIc by the reaction.

Electronic Spectra. Figure 2 records the electronic spectra of cyclic hexapentaenes as well as that of an open-chain analogue, tetra-*t*-butylhexapentaene XV. The spectrum of IIc is very similar to that of the reference compound XV. On the other hand, the hexapentaene cyclophane IIa shows a red shift of the longest wavelength band by 8 nm than the corresponding band of IIc, besides a slight change of the bands in the 220—270 nm region. A Stuart-Briegleb molecular model demonstrates that both cyclic hexapentaenes, IIc and IIa, are strainless and in similar steric environments around the hexapentaene group. Accordingly, it may be concluded that the red shift of the longest wavelength band of IIa is caused by transannular π-electronic interaction between the benzene ring and the 1,2,3,4,5-hexapentaene group. The longest wavelength bands of cyclic bis-hexapentaene IIb appear near the band positions of IIc, hence, such an interaction is hardly discernible.

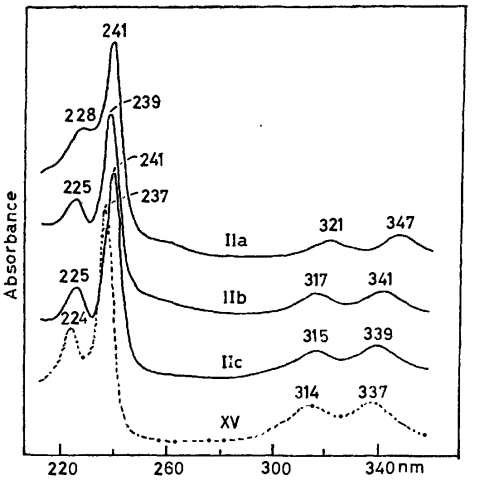

Fig. 2. Electronic spectra of cyclic cumulenes and tetra-*t*-butyl hexapentaene in ether.

Experimental

The melting points are uncorrected. The UV, IR, NMR, and mass spectra were measured on a Hitachi EPS-3T autorecording spectrophotometer, a Hitachi EPI-G2 spectrometer a Hitachi R-20 spectrometer, and a Hitachi RMU-7 spectrometer respectively.

p-*Bis(4-hydroxy-4-methylpentyl)benzene.* Into a solution of methylmagnesium iodide, prepared from magnesium (14 g, 0.58 mol) and methyl iodide (81 g, 0.57 mol) in 300 ml of ether, a solution of the diester III[14] (20 g, 0.072 mol) in 100 ml of ether was added over a period of 1.5 hr with stirring at reflux. The mixture was refluxed for 2 hr with stirring and then poured into a dilute sulfuric acid. The diol thus precipitated was collected, washed well with water, and dried. The filtrate was extracted with ether, followed by the usual work-up. After removing the solvent, the residue was chromatographed on 50 g of silica gel, using ether-petroleum ether (2 : 3) as an eluent, to yield white crystals. The total yield of the desired diol was 18 g (90%).

For analysis, a small amount of the sample was recrystallized from toluene to yield white crystals, mp 121—122 °C. Found: C, 77.73; H, 10.92%; Mol wt, 278 (mass spectrometry). Calcd for $C_{18}H_{30}O_2$: C, 77.65; H, 10.86%; Mol wt, 278. IR (KBr disk): 3280, 1510, 1190, and 826 cm^{-1}. NMR ($CDCl_3$), δ: 7.07 (s, 4H), 2.59 (t, 4H), 1.65~1.5 (m, 8H), 1.32 (s, 2H), and 1.20 ppm (s, 12H).

p-*Bis(4-Chloro-4-methylpentyl)benzene (IV).* Into an ice-cooled mixture of the above diol (52 g), 100 ml of methanol, and 2 l of petroleum ether, a current of hydrogen chloride was passed for 6 hr with stirring. The upper organic layer of the mixture was then separated, washed with concd sulfuric acid, and allowed to stand overnight over sodium carbonate. The subsequent concentration of the solution gave colorless plates (44 g, 75%).

For analysis, a small amount of the sample was recrystallized from petroleun ether to yield colorless plates, mp 49—51 °C. Found: C, 68.44; H, 9.18; Cl, 22.42%. Calcd for $C_{18}H_{28}Cl_2$: C, 68.56; H, 8.95; Cl, 22.49%.

p-*Bis (4,4,6,6-tetramethyl-5-oxoheptyl)benzene (VIIa).* To magnesium (0.60 g, 0.025 mol) in 50 ml of dry ether, a solution of the dichloride IV (4.0 g, 0.013 mol) in 50 ml of ether was added dropwise in a 1.5 hr period with stirring under a nitrogen atmosphere. A mixture of copper powder

*** Although the diallene-dibromides are also considered to yield by a "two-step mechanism" through a monodibromophosphite ester as a cyclic transition state, one may reach stereochemically the same result.

(1.5 g), cuprous chloride (2.4 g), freshly-prepared pivaloyl chloride (2.7 g, 0.022 mol), and 100 ml of ether in an alternative flask was cooled in an ice-salt bath, and into the mixture the above Grignard solution, filtered through glass-wool, was added dropwise over a period of 1 hr with vigorous stirring under a nitrogen atmosphere. Stirring was then continued for 4 hr at room temperature, after which the reaction mixture was poured into a dilute hydrochloric acid and the organic layer was separated. The aqueous layer was extracted with ether. The combined etherial solution was washed successively with dilute hydrochloric acid, a sodium bicarbonate solution, and water, and then dried over magnesium sulfate. After the solvent had been removed, the residue was chromatographed on 50 g of alumina, using ether–petroleum ether (1 : 3) as an eluent, to yield a colorless solid (0.63 g, 14% based on pivaloyl chloride).

For analysis a small amount of the sample was recrystallized from petroleum ether to yield colorless plates, mp 66—67 °C. Found: C, 80.95; H, 11.27%; Mol wt, 414 (mass spectrometry). Calcd for $C_{28}H_{46}O_2$: C, 81.10; H, 11.18%; Mol wt, 414. IR (KBr disk): 1674 cm^{-1} (C=O).

p-Bis (5-t-butyl)-5-hydroxy-4,4-dimethyl-6-heptynyl) benzene (VIIIa). To a solution of ethynylmagnesium bromide,[6] prepared from magnesium (31 g, 1.3 mol), ethyl bromide (140 g, 1.3 mol), and 1 l of dry tetrahydrofuran, a solution of the diketone VIIa (5.0 g, 0.012 mol) in 100 ml of tetrahydrofuran was added dropwise over a period of 30 min. The mixture was stirred for a week at 30—35 °C with the passage through of a slow stream of acetylene. After the addition of dilute sulfuric acid and salting-out, the mixture was extracted with ether. The ether extract was washed successively with dilute sulfuric acid, a sodium bicarbonate solution, and water, and then dried over magnesium sulfate. After the solvent had been removed, the residue was chromatographed on 120 g of silica gel, using ether–petroleum ether (1 : 4), to give a colorless oil (3.8 g, 68%); IR (neat), 3560 (OH) and 3305 cm^{-1} (C≡CH); NMR (CCl_4), δ: 7.00 (s, 4H), 2.5 (m, 4H), 2.33 (s, 2H), 1.8—1.5 (m, 10H), and 1.15 and 1.09 ppm (d, 30 H).

5,10-Di-t-butyl-4,4,11,11-tetramethyl-6,8-[14]paracyclophadiyne-5,10-diol (IXa). The intramolecular oxidative coupling of the bisethynyl compound VIIIa was accomplished in a manner similar to that previously reported.[2b] Into a mixture of 30 g of anhydrous cupric acetate and 1.5 l of pyridine, a solution of VIIIa (3.0 g) in 2 l of oxygen-free ether was added dropwise over a period of three days at 50 °C with vigorous stirring under a nitrogen atmosphere. After the addition, the reaction was continued for another day. The reaction mixture was then poured into a cold dilute sulfuric acid, and the organic layer was separated. The aqueous layer was extracted with ether, and the combined ethereal solution was washed well with dilute sulfuric acid, a sodium bicarbonate solution, and water successively, and dried over anhydrous magnesium sulfate. The solvent were removed under reduced pressure, and the residue was chromatographed on 120 g of silica gel to yield two compounds.

The first compound (230 mg, 7.7%) was eluted with ether–petroleum ether (1 : 2). It was confirmed to be the cyclic monomer IXa-I. For analysis, a small amount of the sample was recrystallized from carbon tetrachloride–petroleum ether, colorless needles, mp 161 °C. Found: C, 82.52; H, 10.76%. Mol wt, 464 (mass spectrometry). Calcd for $C_{32}H_{48}O_2$: C, 82.70; H, 10.41%. Mol wt, 464. UV (cyclohexane): λ_{max} 214, 220, 225, 247, 260, 265, 268, and 274 nm. IR (KBr disk): 3580, 3470, 1511, 1393, 1384, 1367, 1290, 1220, 1205, 1069, 1051, 980, 927, and 800 cm^{-1}.

The second substance (170 mg, 5.7%) was eluted with ether–petroleum ether (1 : 1). It was confirmed to be the cyclic monomer IXa-II. For analysis, a small amount of the sample was recrystallized from carbon tetrachloride–petroleum ether, white crystals, mp 175.5—176 °C. Found: C, 82.85; H, 10.64%; Mol wt, 464 (mass spectrometry). UV (cyclohexane): λ_{max} 214, 221, 226, 247, 260, 265, 267, and 273 nm. IR (KBr disk): 3570, 3480, 1506, 1385, 1366, 1297, 1227, 1208, 1195, 1124, 1074, 1053, 1040, 1006, 998, 983, 932, 884, and 803 cm^{-1}.

7,8-Dibromo-5,10-di-t-butyl-4,4,11,11-tetramethyl-5,6,8,9-[14]-paracyclophatetraene (Xa). A mixture of the diyne-diol IXa (100 mg, 0.22 mmol), phosphorus tribromide (1 g, 3.7 mmol), and 50 ml of dry benzene was stirred at 50 °C for 3 hr under a nitrogen atmosphere. The reaction mixture was then poured into ice–water and extracted with ether. The ethereal solution was washed successively with dilute hydrochloric acid, a sodium carbonate solution, and water, and then dried over anhydrous magnesium sulfate in a dark and cold room. The solvent was removed under reduced pressure, and the residue was recrystallized from chloroform–methanol to yield a white solid (93 mg, 62%).

For analysis, a small amount of the sample was recrystallized from chloroform–methanol, white crystals, mp 145—146 °C. Found: C, 65.16; H, 7.61%; Mol wt, 590 (mass spectrometry). Calcd for $C_{32}H_{46}Br_2$: C, 65.08; H, 7.85%; Mol wt, 590. UV (cyclohexane): λ_{max} 232 nm (ε 45300).* IR (KBr disk): 1938, 1510, 840, 685, and 654 cm^{-1}.

5,10-Di-t-butyl-4,4,11,11-tetramethyl-5,6,7,8,9-[14]paracyclophapentaene (IIa). A mixture of diallene-dibromide Xa (50 mg, 0.085 mmol) and 5 g of active zinc powder[8a] in 50 ml of dry ether was stirred for three days at room temperature under a nitrogen atmosphere. The reaction mixture was filtered through a short column of silica gel to remove the zinc under a nitrogen atmosphere. The filtrate was then concentrated under reduced pressure, and the residue was chromatographed on 20 g of silica gel, using petroleum ether as an eluent and under a nitrogen atmosphere, to give a greenish yellow oil; MS (*m/e*), 430 (M^+), 373 (M−Bu-*t*) and 316 (M−2Bu-*t*); NMR (CCl_4), δ: 6.90 (s, 4H), 2.7—2.4 (m, 4H), 1.4 (m, 8H), and 1.27 and 1.25 ppm (d, 30H); UV: Fig. 2.

2,2,13,13-Tetramethyl-3,12-tetradecanedione. A mixture of freshly-prepared acid chloride XI (30 g, 0.13 mol), copper powder (25 g), cuprous chloride (50 g), and 300 ml of dry eth r was cooled in an ice-salt bath. Into the mixture a solution of *tert*-butylmagnesium chloride, prepared from magnesium (12 g, 0.49 mol) and *tert*-butyl chloride (45 g, 0.49 mol) in 300 ml of dry ether, was added dropwise over a period of 6 hr with vigorous stirring. Stirring was continued overnight at room temperature. Water was added to decompose the excess of the Grignard reagent, and the mixture was poured into dilute hydrochloric acid and then extracted with ether, followed by the usual work-up. After the solvent had been removed, the residue was chromatographed on 120 g of silica gel, using 5% ether–petroleum ether as an eluent, to yield colorless crystals (23 g, 65%).

For analysis, a small amount of the sample was recrystallized from *n*-hexane, colorless needles, mp 24—25 °C (lit,[15] bp 178—182 °C/1 mmHg). Found: C, 76.27; H, 12.46%. Calcd for $C_{18}H_{34}O_2$: 76.54; H, 12.13%. IR(neat): 1705 cm^{-1} (C=O).

2,2,4,4,11,11,13,13-Octamethyl-3,12-tetradecanedione (VIIc). A mixture of the above diketone (28 g, 0.099 mol) and sodium

* In the previous paper (Ref. 3) this value was erroneously reported as 45.3×10^4.

amide (40 g, 1.0 mol) in 300 ml of benzene was refluxed for 24 hr. To the cold mixture, methyl iodide (210 g, 1.5 mol) was added for 1 hr, after which the mixture was refluxed for 3 hr with stirring. Methanol was added to decompose the excess sodium amide, after which the reaction mixture was poured into dilute hydrochloric acid and extracted with ether, followed by the usual work-up. After the solvent had been removed, the residue was subjected to the above treatment for exhaustive methylation once again. The resulting product, obtained by removing the solvent, was chromatographed on 200 g of neutral alumina, using ether-petroleum ether (1 : 4) as an eluent, to yield white crystals (12 g, 37%).

For analysis, a small amount of the sample was recrystallized from *n*-hexane, colorless plates, mp 40—41 °C. Found: C, 77.91; H, 12.70%; Mol wt, 338 (mass spectrometry). Calcd for $C_{22}H_{42}O_2$: C, 78.04; H, 12.50%; Mol wt, 338. IR (KBr disk): 1670 cm^{-1} (C=O).

*3,12-Di-*t*-butyl-4,4,11,11-tetramethyl-1,13-tetradecadiyne-3,12-diol (VIIIc).* The ethynylation of the diketone VIIc was accomplished in a manner similar to that described for the preparation of VIIIa. From 11 g of the diketone VIIc we obtained 10 g (79%) of the diyne-diol VIIIc as a colorless oil after chromatography on 150 g of silica gel, using ether-petroleum ether (1 : 9); IR (neat), 3490 (OH) and 3310 cm^{-1} (C≡CH); NMR (CCl_4), δ: 2.34 (s, 2H) and 1.8—1.1 ppm (m, 44H: 1.75 (s), 1.3 (m), 1.18 (s), and 1.10 (s)).

*5,14-Di-*t*-butyl-6,6,13,13-tetramethyl-1,3-cyclotetradecadiyne-5,14-diol (IXc).* The intramolecular oxidative coupling of VIIIc was accomplished in a manner similar to that described for that of VIIIa except for the following conditions: anhydrous cupric acetate, 60 g; VIIIc, 5.0 g; reaction temperature, 60 °C; dropping period, five days. The residue obtained by removing the solvent was chromatographed on 200 g of silica gel to yield two compounds.

The first compound (980 mg, 20% yield) was eluted with ether-petroleum ether (1 : 20); it was the cyclic monomer IXc-I (racemic isomer). For analysis, a small amount of the sample was recrystallized from carbon tetrachloride, colorless needles, mp 202 °C (dec, in sealed tube). Found: C, 80.15; H, 11.67%; Mol wt, 388 (mass spectrometry). Calcd for $C_{26}H_{44}O_2$: C, 80.35; H, 11.41%; Mol wt, 388. UV (cyclohexane): λ_{max} 225, 236, 248, and 261 nm. IR (KBr disk): 3583, 1395, 1385, 1367, 1287, 1253, 1222, 1202, 1063, 1036, 1006, 980, and 925 cm^{-1}.

The second substance (620 mg, 12%) was eluted with ether-petroleum ether (1 : 9); it was the cyclic monomer IXc-II (*meso* isomer). For analysis, a small amount of the sample was recrystallized from carbon tetrachloride, white crystals, mp 142—143 °C. Found: C, 80.30; H, 11.58%; Mol wt, 388 (mass spectrometry). UV (cyclohexane): λ_{max} 224, 235, 248, and 261 nm. IR (KBr disk): 3580, 3450, 1392, 1382, 1370, 1288, 1220, 1205, 1082, 1043, 1005, 975, and 937 cm^{-1}.

*3,4-Dibromo-1,6-di-*t*-butyl-7,7,14,14-tetramethyl-1,2,4,5-cyclotetradecatetraene (Xc).* The bromination of diyne-diol IXc was accomplished in a manner similar to that described in the case of IXa.

From the first-eluted diyne-diol IXc-I (3.0 g, 7.7 mmol), phosphorus tribromide (10 g, 37 mmol), and 50 ml of dry benzene, we obtained 1.7 g (43%) of diallene-dibromide Xc-I as white crystals after chromatography on 30 g of silica gel using *n*-hexane. For analysis, a small amount of the sample was recrystallized from carbon tetrachloride-methanol, white crystals, mp 132—134 °C. Found: C, 60.73; H, 8.46; Br, 31.22%; Mol wt, 514 (mass spectrometry). Calcd for $C_{26}H_{42}Br_2$: C, 60.70; H, 8.23; Br, 31.07%; Mol wt, 514. UV (cyclohexane): λ_{max} 231 nm (ε 38700). NMR (CCl_4), δ: 1.28 and 1.37 ppm. IR (KBr): 1950, 1928, 1364, 1222, 1205, 1158, 974, 685, and 653 cm^{-1}.

From the second-eluted diyne-diol IXc-II (3.0 g), diallene-dibromide Xc-II was obtained by the method described above, white crystals, mp 134—135 °C (from carbon tetrachloride-methanol). Found: C, 60.89; H, 8.48; Br, 31.42%. UV(cyclohexane): λ_{max} 231 nm (ε 41700). NMR (CCl_4), δ: 1.28 and 1.38 ppm. IR (KBr): 1950, 1925, 1363, 1221, 1204, 1156, 972, 685, and 653 cm^{-1}.

*1,6-Di-*t*-butyl-7,7,14,14-tetramethyl-1,2,3,4,5-cyclotetradecapentaene (IIc). Debromination with Active Zinc*: The debromination of Xc was accomplished in a manner similar to that described for the preparation of IIa. From Xc-I (200 mg), active zinc powder (5 g), and 80 ml of dry ether, cyclic hexapentaene IIc was obtained by chromatography on 10 g of neutral alumina, using petroleum ether under a nitrogen atmosphere, as pale greenish yellow plates (98 mg, 71%), mp 146—147 °C. MS (*m/e*): 354 (M^+), 297 (M−Bu-*t*), and 240 (M−2Bu-*t*). NMR (CCl_4), δ: 1.45—1.2 ppm (m). UV: Fig. 2.

Diallene-dibromide Xc-II was treated with active zinc under conditions as like those described above as possible. However, no spectral evidence characteristic of IIc was observed.

Debromination with Methylmagnesium Iodide: To a solution of Xc-I (83 mg) in 25 ml of dry ether, we added a solution of methylmagnesium iodide, prepared from magnesium (6 g) and methyl iodide (35 g) in 100 ml of ether; the mixture was then stirred overnight at room temperature under nitrogen atmosphere. After the decomposition of the excess of the Grignard reagent with a saturated ammonium chloride solution, the mixture was extracted with ether and dried over anhydrous sodium sulfate. The etherial solution obtained by passing the mixture through a short column of silica gel under nitrogen showed the λ_{max}'s characteristic of IIc.

Similarly, Xc-II gave the same results upon the same treatment.

p-Bis(5,5-dimethyl-4-oxohexyl)benzene (VI). The alkylation of V was accomplished in a manner similar to that described for the preparation of 2,2,13,13-tetramethyl-3,12-tetradecanedione. From 20 g of fresh acid chloride V, which had been prepared from *p*-bis(3-carboxypropyl)benzene,[14] we obtained 20 g (87%) of the diketone VI as colorless crystals after chromatography on 150 g of silica gel using ether-petroleum ether (1 : 9).

For analysis, a small amount of the sample was recrystallized from petroleum ether, white crystals, mp 45—46 °C. Found: C, 79.85; H, 10.44%. Calcd for $C_{22}H_{34}O_2$: C, 79.95; H, 10.37%. IR (KBr disk): 1675 cm^{-1} (C=O).

p-Bis(3,3,5,5-tetramethyl-4-oxohexyl)benzene (VIIb). The methylation of the above diketone was accomplished in a manner similar to that described for the preparation of VIIc. From 15 g of the diketone VI we obtained 9.4 g (53%) of the diketone VIIb as colorless crystals after chromatography on 100 g of silica gel using ether-petroleum ether (1 : 4).

For analysis, a small amount of the sample was recrystallized from *n*-hexane, colorless needles, mp 79—80 °C. Found: C, 80.56; H, 11.25%; Mol wt, 386 (mass spectrometry). Calcd for $C_{26}H_{42}O_2$: C, 80.77; H, 10.95%; Mol wt, 386. IR (KBr disk): 1660 cm^{-1} (C=O).

*p-Bis(4-*t*-butyl-4-hydroxy-3,3-dimethyl-5-hexynyl)benzene (VIIIb).* The ethynylation of the diketone VIIb was accomplished in a manner similar to that described for the preparation of VIIIa. From 9 g of the diketone VIIb we obtained 8.2 g (80%) of the diyne-diol VIIIb as a colorless solid (mp 63—65 °C) after chromatography on 150 g of silica gel using ether-petroleum ether (1 : 9); IR (KBr disk):

3250 (OH) and 3300 cm^{-1} (C≡CH); NMR (CCl_4), δ: 6.97 (s, 4H), 2.8—2.4 (m, 4H), 2.37 (s, 2H), 2.1—1.6 (m, 6H), and 1.20 ppm (s, 30H).

Oxidative Coupling of VIIIb. The oxidative coupling of VIIIb was accomplished in a manner similar to that described for the case of VIIIa except for the following conditions: anhydrous cupric acetate, 40 g; VIIIb, 3.0 g; dropping period, seven days. The residue obtained by removing the solvent was chromatographed on 120 g of silica gel, using ether-*n*-hexane (1 : 1), to yield the cyclic dimer IXb as white crystals (1.0 g, 33%). For analysis, a small amount of the sample was recrystallized from carbon tetrachloride, colorless fine crystals, mp 240—241 °C. Found: C, 82.23; H, 10.40%; Mol wt, 865 (osmometry). Calcd for $C_{60}H_{88}O_4$: 82.51; H, 10.16%; Mol wt, 873. UV(cyclohexane): λ_{max} 214, 220, 224, 248, 260, 265, 268, and 274 nm.

Tetraallene-tetrabromide Xb. The bromination of XIb was accomplished in a manner similar to that described for the preparation of Xa except for the use of benzene-chloroform (10 : 1) as a solvent. From 200 mg of IXb, 97 mg (38%) of tetraallene-tetrabromide Xb was obtained as fine white crystals, mp 204—205 °C (from chloroform-methanol). Mol wt, Found: 1092 (osmometry). Calcd for $C_{60}H_{84}Br_4$: 1124. UV (cyclohexane): λ_{max} 222 and 231 nm. IR (KBr disk): 1924 cm^{-1} (C=C=C).

Cyclic Bis-hexapentaene IIb. The debromination of tetraallene-tetrabromide Xb with methylmagnesium iodide was accomplished in a manner similar to that described for the case of Xc. From 200 mg of Xb, 54 mg (58%) of cyclic bis-hexapentaene IIb was obtained as greenish yellow crystals, which showed a negative Beilstein's test and which were decomposed in the range of 180—200 °C, after chromatography on 10 g of neutral alumina using ether-petroleum ether (1 : 9). The UV spectrum of IIb is shown in Fig. 2.

3,8-Di-t-butyl-2,2,9,9-tetramethyl-4,6-decadiyne-3,8-diol (XIII). A mixture of di-*tert*-butyl ethynyl carbinol[16] (XII) (10 g) and anhydrous cupric acetate (30 g) in 400 ml of pyridine was stirred for 24 hr at 50 °C under a nitrogen atmosphere. The reaction mixture was poured into cooled dilute sulfuric acid and extracted with ether, followed by the usual work-up. The residue obtained by removing the solvent was chromatographed on silica gel using petroleum ether-ether (5 : 1) to yield 6.8 g (69%) of pale yellow crystals.

For analysis, a small amount of the sample was recrystallized from *n*-pentane-carbon tetrachloride, white crystals, mp 166 °C. Found: C, 78.83; H, 11.66%. Calcd for $C_{22}H_{38}O_2$: C, 78.98; H, 11.45%. IR (KBr disk): 3480 cm^{-1} (OH). NMR ($CDCl_3$), δ: 1.90 (s, 2H) and 1.17 ppm (s, 36H).

5,6-Dibromo-3,8-di-t-butyl-2,2,9,9-tetramethyl-3,4,6,7-decatetraene (XIV). The bromination of the diyne-diol XIII was accomplished in a manner similar to that described for the preparation of Xa. From 6 g of XIII, 85 g of phosphorus tribromide, and 100 ml of benzene we obtained 5.2 g (63%) of diallene-dibromide XIV as a white solid after recrystallization from chloroform-methanol. The further recrystallization of this solid gave white plates, mp 232—233 °C (sealed tube). Found: C, 57.53; H, 8.23; Br, 34.38%. Calcd for $C_{22}H_{36}Br_2$: C, 57.40; H, 7.88; Br, 34.72%. IR (KBr disk): 1937 cm^{-1} (C=C=C). UV (cyclohexane): λ_{max} 231 nm (ε 43500). NMR ($CDCl_3$), δ: 1.27 ppm (s).

1,1,6,6-Tetra-t-butylhexapentaene (XV). The debromination of XIV with active zinc was accomplished in a manner similar to that described for the case of Xa. From XIV (200 mg) and active zinc powder (3 g), 81 mg (62%) of the hexapentaene XV was obtained as yellow crystals, mp 182—184 °C (lit,[8c] mp 188—189 °C). NMR (CCl_4), δ: 1.29 ppm (s) (lit,[8c] 1.28 ppm (s) in $CDCl_3$). The UV spectrum of XV is shown in Fig. 2.

p-Bis(4-oxohexyl)benzene (XVI). A suspension of diethylcadmium,[17] prepared from magnesium (3.9 g, 0.16 mol), ethyl bromide (18 g, 0.17 mol), cadmium chloride (24 g, 0.13 mol), and 150 ml of ether, was cooled in an ice-salt bath. Into the mixture a solution of freshly-prepared acid chloride V (5.5 g, 0.019 mol) in 50 ml of benzene was added dropwise over a period of 20 min with vigorous stirring. The mixture was stirred for an hour and then for a further hour at room temperature. After the addition of dilute sulfuric acid and extraction with ether, followed by the usual work-up, the residue obtained by removing the solvent was chromatographed on 40 g of silica gel, using ether-petroleum ether (1 : 4), to give colorless needles (3.9 g, 74% from V).

For analysis, a small amount of the sample was recrystallized from carbon tetrachloride, colorless needles, mp 36—37 °C. Found: C, 78.82; H, 9.65%. Calcd for $C_{18}H_{26}O_2$: C, 78.79; H, 9.55%.

p-Bis(4-ethyl-4-hydroxy-5-hexynyl)benzene (XVII). The ethynylation of the diketone XVI was accomplished in a manner similar to that described for the preparation of VIIIa, but in this case the completion of the reaction required 4 hr. From 2.5 g of the diketone XVI, 1.8 g (61%) of the diynediol XVII was obtained as a pale yellow oil after chromatography on 50 g of silica gel using ether-petroleum ether (1 : 2), NMR (CCl_4), δ: 7.00 (s, 4H), 2.58 (t, J=7 Hz, 4H), 2.25 (s, 2H), 1.97 (s, 2H), 1.9—1.4 (m, 12H), and 0.98 (t, J=7 Hz, 6H).

4,9-Diethyl-5,7-[12]paracyclophadiyne-4,9-diol (XVIII). The intramolecular oxidative coupling of XVII was accomplished in a method similar to that described for the case of VIIIa except for the following conditions: XVII, 2.9 g; reaction temperature, 40 °C; dropping period, 4 days. The residue obtained by removing the solvent was chromatographed on 80 g of silica gel to yield two compounds.

The first compound (500 mg, 17%) was eluted with ether-petroleum ether (1 : 4), it was the cyclic monomer XVIII-I; colorless crystals (from carbon tetrachloride-petroleum ether), mp 155—156.5 °C. Mol wt, Found: 324 (mass spectrometry). Calcd for $C_{22}H_{28}O_2$: 324. UV (cyclohexane): λ_{max} 214, 221, 225, 250, 259, 266, and 273 nm. NMR ($CDCl_3$), δ: 7.12 (s, 4H), 2.7—2.5 (m, 4H), 2.1—1.4 (m, 14H), 1.60 (q, J=7 Hz), and 0.98 ppm (t, J=7 Hz, 6H). IR (KBr disk): 3340 cm^{-1} (OH).

The second substance (520 mg, 18%) was eluted with ether-petroleum ether (2 : 3); it was the cyclic monomer XVIII-II, white fine crystals (from carbon tetrachloride-petroleum ether), mp 156—158 °C. Mol wt, 324 (mass spectrometry). UV (cyclohexane): λ_{max} 214, 220, 225, 245, 259, 264, and 273 nm. NMR ($CDCl_3$), δ: 7.11 (s, 4H), 2.7—2.5 (m, 4H), 2.1—1.4 (m, 14H), 1.61 (q, J=7 H_2), and 0.97 ppm (t, J=7 Hz, 6H). IR (KBr disk): 3540, 3400, and 3340 cm^{-1} (OH).

The authors are greatly indebted to Dr. Hirozo Koyama of the Shionogi Research Laboratory, Shionogi & Co., Ltd., for X-ray crystallographic analysis, to Mr. Takuzo Fujino and Mr. Tsuneyo Shishido for microanalyses, and to Mr. Yoshio Takai for his NMR measurements. This research is supported by a grant-in-aid of the Ministry of Education, to which the authors' thanks are due.

References

1) Part XVII: N. Kannen, T. Umemoto, T. Otsubo, and S. Misumi, *Tetrahedron Lett.*, **1973**, 4537.

2) a) T. Matsuoka, Y. Sakata, and S. Misumi, *ibid.*, **1970**, 2549; b) T. Matsuoka, T. Negi, T. Otsubo, Y. Sakata, and S. Misumi, This Bulletin, **45**, 1825 (1972); c) T. Matsuoka, T. Negi, and S. Misumi, *Synth. Commun.*, **2**, 87 (1972).

3) T. Negi, T. Kaneda, Y. Sakata, and S. Misumi, *Chem. Lett.*, **1972**, 703.

4) J. Ojima, T. Katakami, G. Nakaminami, and M. Nakagawa, *Tetrahedron Lett.*, **1968**, 1115; K. Fukui, T. Okamoto, and M. Nakagawa, *ibid.*, **1971**, 3121; T. Katakami, S. Tomita, K. Fukui, and M. Nakagawa, *Chem. Lett.*, **1972**, 225.

5) C. J. Stehman, N. C. Cook, and F. C. Whitmore, *J. Amer. Chem. Soc.*, **71**, 1509 (1949); N. C. Cook and W. C. Percival, *ibid.*, **71**, 4141 (1949).

6) L. Skattebøl, E. R. H. Jones, and M. C. Whiting, "Organic Syntheses," Coll. Vol. 4, p. 792 (1963).

7) G. Eglinton and A. R. Galbraith, *J. Chem. Soc.*, **1959**, 889.

8) a) F. Bohlmann and K. Kieslich, *Chem. Ber.*, **87**, 1363 (1954); b) L. Skattebøl, *Tetrahedron Lett.*, **1965**, 2175; *Tetrahedron*, **21**, 1357 (1965): c) H. D. Hartzler, *J. Amer. Chem. Soc.*, **88**, 3155 (1966); *ibid.*, **93** 4527 (1971).

9) R. Kuhn and K. Wallenfels, *Ber.*, **71**, 783 (1938).

10) R. Kuhn and J. Jahn, *Chem. Ber.*, **86**, 759 (1953).

11) R. Kuhn and H. Krauch, *ibid.*, **88**, 309 (1955).

12) Y. R. Bhatia, P. D. Landor, and S. R. Landor, *J. Chem. Soc.*, **1959**, 24; S. R. Landor and R. Taylor-Smith, *Proc. Chem. Soc.*, **1959**, 154.

13) H. Fischer, "The Chemistry of Alkenes," ed. by S. Patai, Interscience Publishers, New York, N. Y. (1964), p. 1042, 1110.

14) D. J. Cram, N. L. Allinger, and H. Steinberg, *J. Amer. Chem. Soc.*, **76**, 6132 (1954).

15) A. D. Petrov, E. B. Sokolova, and C. L. Kao, *Zh. Obshch. Khim.*, **30**, 1107 (1960); *Chem. Abstr.*, **55**, 374 (1961).

16) W. J. Hickinbottom, A. A. Hyatt, and M. B. Sparke, *J. Chem. Soc.*, **1954**, 2529.

17) H. Gilman and J. F. Nelson, *Rec. Trav. Chim.*, **55**, 518 (1936).

Reaction of Chlorohydrocarbons. VI. Co-pyrolysis of Chloroethanes and Methanol on Activated Alumina

Kiyonori SHINODA

Toyama Technical College, Hongo, Toyama-shi, 930

(Received December 21, 1973)

Co-pyrolysis of chloroethanes and methanol on activated alumina was carried out in order to elucidate the reaction mechanism. The reaction rate was of first order in chloroethanes in the presence of excess methanol. A linear free energy relationship was found to exist between the reactivities of chloroethanes (at 230 °C) and Taft's σ^* constants. ρ^* values for reactions of RCH_3, RCH_2Cl and $RCHCl_2$ series were 0.24, 0.45 and 0.70, respectively. It could be assumed that a β-hydrogen of chloroethanes was abstracted by the nucleophilic attack of methanol, chlorine being removed at the same time. *E*2 reaction seems to dominate in co-pyrolysis of chloroethanes and methanol on activated alumina.

Chloroethylenes and methyl chloride are formed by co-pyrolysis of 1,1,2-trichloroethane and methanol on activated alumina.[1] Andrussow and Edler[2] reported that in the co-pyrolysis of 1,1,2,2-tetrachloroethane and methanol on activated alumina the reaction proceeds according to the following equation.

$$CHCl_2CHCl_2 + CH_3OH \rightarrow CHCl{:}CCl_2 + CH_3Cl + H_2O$$

Dehydrochlorination of 1,1,2-trichloroethane at high temperature is unfavorable for the formation of 1,1-dichloroethylene.[3] Elimination of hydrogen chloride from 1,1,2-trichloroethane on solid acids such as activated alumina, has a poor selectivity for 1,1-dichloroethylene.[4,5] In contrast, the 1,1/1,2 ratio in co-pyrolysis of 1,1,2-trichloroethane and methanol amounted to several times as high as that of ordinary pyrolysis.[1] Another merit of the reaction is that the dehydrochlorination of chloroethanes can proceed at a lower temperature.

The present investigation was undertaken to study co-pyrolysis of several different chloroethanes and methanol on activated alumina with a conventional flow type reactor. The relation between the molecular structure and the rate of the dehydrochlorination is discussed.

Experimental

Reagents. 1,1-Dichloroethane, 1,2-dichloroethane, 1,1,2-trichloroethane and 1,1,2,2-tetrachloroethane (Wako Pure Chemicals Co.) were of reagent grade and were used without further purification. 1,1,1-Trichloroethane was washed several times with water, and then dried with calcium chloride and fractionated. Pentachloroethane and 1,1,1,2-tetrachloroethane were prepared by the chlorination of trichloroethylene and 1,1,1-trichloroethane in the presence of ferric chloride as a catalyst, washed with aqueous sodium carbonate solution and then with water, and fractionally distilled; bp 161.5 °C for pentachloroethane and 129—130 °C for 1,1,1,2-tetrachloroethane.

Catalyst. 0.4 cm pellets of activated alumina (KH-A24, Sumitomo Chemical Co.) with surface area 200 m^2/g and 0.2% Na_2O content were used.

Apparatus. A flow type reaction system was used. A Pyrex reaction vessel, tube of length *ca.* 30 cm and diameter 2.6 cm was heated in a vertical electric furnace. The evaporator, a glass tube, was placed in an electrically wound vertical furnace. The reaction temperature was measured with a Chromel-Alumel thermocouple in a thermowell placed in the catalyst bed.

Procedure. 20 g of catalyst was placed in the middle of the reactor, the bed being supported by necking the reactor tube. The catalyst was heated in the air at 350 °C for 3 to 5 hr. While the reaction temperature was regulated, nitrogen gas was passed over the catalyst. A mixture of chloroethanes and methanol was then fed into the evaporator with a microfeeder and preheated to 200°C, the vapor being passed to the reactor. The time factor (W/F: g·hr/g-mol) was varied by adjusting the feed rate of each chlorinated ethane (F: g-mol/hr), the weight of the catalyst (W : g) being kept constant. The product gas stream entered a cooler and condensed in a water-ice trap. Organic products were separated from the water with a separating funnel.

Gas-chromatographic analyses were performed with a GC-5 type apparatus from Shimadzu Seisakusho. The column was Silicone DC 550 on Celite.

Results

Co-pyrolysis of chloroethanes and methanol on activated alumina proceeded as follows.

$$C_2H_{6-n}Cl_n + CH_3OH \rightarrow C_2H_{5-n}Cl_{n-1} + CH_3Cl + H_2O$$

The side reaction products were dimethyl ether and a dechlorinated product. Dimethyl ether was formed by the dehydration of methanol on the surface of activated alumina. The dechlorinated product was formed by the pyrolysis of higher chlorinated derivatives such as 1,1,1,2-tetrachloroethane and pentachloroethane. Hydrogen chloride was formed in a trace amount. Dimethyl ether and methyl chloride were not determined. In all runs, two chloroethanes were competitively pyrolyzed in order to check the balance of the volatile products such as vinyl chloride.

1,1-Dichloroethane and 1,1,1,2-tetrachloroethane were mixed with methanol at the mole ratio 0.107 : 0.142 : 1.00. W/F values were 305 and 403 for 1,1-dichloroethane and 1,1,1,2-tetrachloroethane, respectively. All other experiments were carried out with the chloroethanes to methanol mole ratio 0.5 : 0.5 : 3.0.

The design equation[6] for a catalytic flow reactor can be written as

$$W/F = \int_0^x dx/r \qquad (1)$$

The reaction rate r is of first order in each chloroethane. r is a function of conversion since the concentration of chlorinated ethane varies with conversion.

The final equation[7] is

$$\frac{W}{F} = \frac{2.303}{k} \times \log \frac{n_0}{n_0 - x} \qquad (2)$$

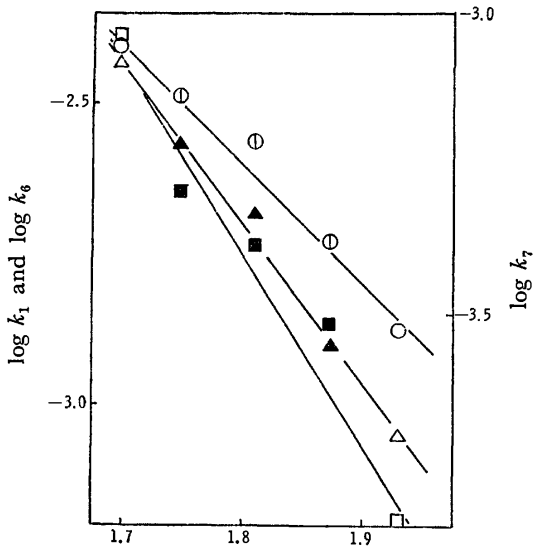

Fig. 1. Arrhenius plots for competitive pyrolysis of CH_3CHCl_2 and CH_2ClCCl_3.
W/F: 294, 305, 403 g·hr/g-mol
○, ⊕, —: $CH_3CHCl_2 \xrightarrow{k_1} CH_2 : CHCl$
△, —, ▲: $CH_2ClCCl_3 \xrightarrow{k_6} CHCl : CCl_2$
□, —, ■: $CH_2ClCCl_3 \xrightarrow{k_7} CH_2 : CCl_2$

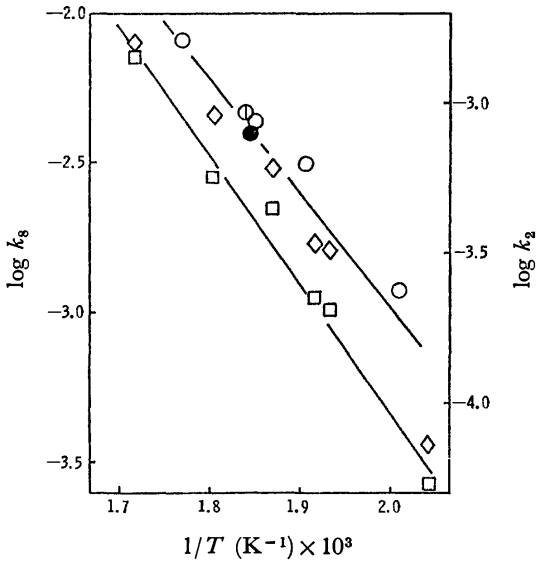

Fig. 2. Arrhenius plots for competitive pyrolysis of CH_2ClCH_2Cl and $CHCl_2CHCl_2$.
W/F: 147, 294, 588 g·hr/g-mol
—, □, —: $CH_2ClCH_2Cl \xrightarrow{k_2} CH_2 : CHCl$
(⊕), ◇(○), (●): $CHCl_2CHCl_2 \xrightarrow{k_8} CHCl : CCl_2$
The symbols in ( ) represent the values which were obtained from co-pyrolysis of 1,1,2-trichloroethane and 1,1,2,2-tetrachloroethane.

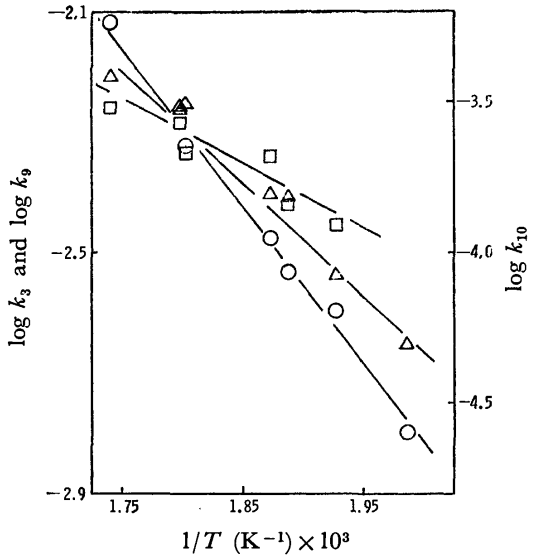

Fig. 3. Arrhenius plots for competitive pyrolysis of CH_3CCl_3 and $CHCl_2CCl_3$.
W/F: 294 g·hr/g-mol
○: $CH_3CCl_3 \xrightarrow{k_3} CH_2 : CCl_2$
△: $CHCl_2CCl_3 \xrightarrow{k_9} CCl_2 : CCl_2$
□: $CHCl_2CCl_3 \xrightarrow{k_{10}} CHCl : CCl_2$

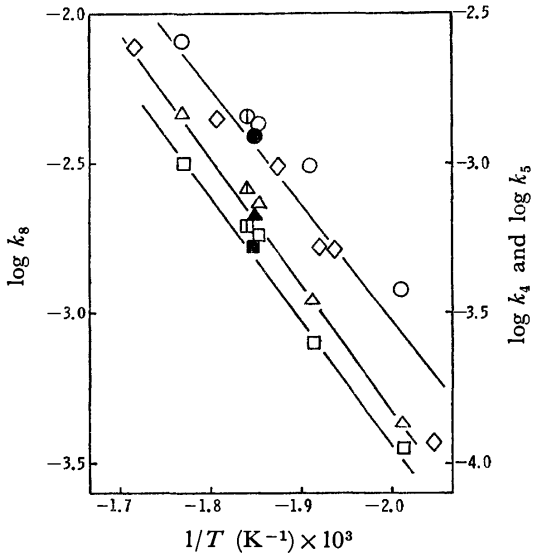

Fig. 4. Arrhenius plots for competitive pyrolysis of $CH_2ClCHCl_2$ and $CHCl_2CHCl_2$.
W/F: 147, 294, 588 g·hr/g-mol
△, △, ▲: $CH_2ClCHCl_2 \xrightarrow{k_4} CH_2 : CCl_2$
⊞, □, ■: $CH_2ClCHCl_2 \xrightarrow{k_5} CHCl : CHCl$
⊕, ○(◇), ●: $CHCl_2CHCl_2 \xrightarrow{k_8} CHCl : CCl_2$
The symbols in ( ) represont the values which were obtained from co-pyrolysis of 1,2-dichloroethane and 1,1,2,2-tetrachloroethane.

where n_0 is the initial concentration of chlorinated ethane and x is the amount of chlorinated ethylene formed.

The plots of $\log k$ against $1/T$ gave straight lines (Fig. 1). From the slopes of the straight lines, the activation energies for the dehydrochlorination of 1,1-dichloroethane and 1,1,1,2-tetrachloroethane were calculated to be 9100 and 12000 cal, respectively. In the case of 1,1,1,2-tetrachloroethane dechlorination, exchange of chlorine with hydrogen, took place besides the

TABLE 1. REACTION RATE CONSTANTS

Reaction type	Reaction rate constant (g-mol/g·hr)	Entropy of activation (cal/deg.)
$CH_3CHCl_2 \rightarrow CH_2 : CHCl$	$k_1 = 9.47 \exp(-9060/RT)$	−55.13
$CH_2ClCH_2Cl \rightarrow 1/2\,CH_2 : CHCl$	$k_2 = 7.36 \times 10^3 \exp(-17900/RT)$	−41.89
$CH_3CCl_3 \rightarrow CH_2 : CCl_2$	$k_3 = 3.38 \times 10^2 \exp(-12200/RT)$	−48.02
$CH_2ClCHCl_2 \rightarrow CH_2 : CCl_2$	$k_4 = 1.00 \times 10^5 \exp(-20200/RT)$	−36.71
$CH_2ClCHCl_2 \rightarrow CHCl : CHCl$	$k_5 = 1.67 \times 10^4 \exp(-18600/RT)$	−40.28
$CH_2ClCCl_3 \rightarrow CHCl : CCl_2$	$k_6 = 1.08 \times 10^2 \exp(-12000/RT)$	−50.30
$CH_2ClCCl_3 \rightarrow CH_2 : CCl_2$	$k_7 = 1.33 \times 10^2 \exp(-14000/RT)$	−49.88
$CHCl_2CHCl_2 \rightarrow 1/2\,CHCl : CCl_2$	$k_8 = 4.69 \times 10^4 \exp(-17600/RT)$	−38.23
$CHCl_2CCl_3 \rightarrow CCl_2 : CCl_2$	$k_9 = 2.30 \times 10 \exp(-9230/RT)$	−53.37
$CHCl_2CCl_3 \rightarrow CHCl : CCl_2$	$k_{10} = 1.58 \exp(-9700/RT)$	−58.69

elimination of hydrogen chloride. The rate of dechlorination was found to be smaller than that of dehydrochlorination.

The effect of the temperature on co-pyrolysis of 1,2-dichloroethane and 1,1,2,2-tetrachloroethane is shown in Fig. 2. The values indicated by symbol ○ were obtained from co-pyrolysis of 1,1,2-trichloroethane and 1,1,2,2-tetrachloroethane to confirm the reproducibility of the experiment. We see that the dehydrochlorination rate of 1,1,2,2-tetrachloroethane is greater than that of 1,2-dichloroethane. However, the activation energies showed no difference under the experimental conditions within the limits of error.

Figure 3 shows the Arrhenius plots of co-pyrolysis of 1,1,1-trichloroethane and pentachloroethane. Dechlorination of pentachloroethane took place concurrently with dehydrochlorination to some extent. The activation energies for the dehydrochlorination of 1,1,1-trichloroethane and pentachloroethane were 12200 and 9200 cal, respectively.

The Arrhenius plots for the competitive pyrolysis of 1,1,2-trichloroethane and 1,1,2,2-tetrachloroethane are shown in Fig. 4. The dehydrochlorinated products of 1,1,2-trichloroethane are 1,1-dichloroethylene, *cis*- and *trans*-1,2-dichloroethylene. The rate constant k_5 was a sum of the rates of the formation of *cis*- and *trans*-dichloroethylene. The ratio of 1,1-dichloroethylene to 1,2-dichloroethylene amounted to several times as high as that in ordinary pyrolysis.[1] However, the rate constants of the dehydrochlorination of 1,1,2-trichloroethane were considerably smaller than that of 1,1,2,2-tetrachloroethane. Activation energies for the formation of 1,1-dichloroethylene and 1,2-dichloroethylene were calculated from the slopes to be 20200 and 18600 cal, respectively.

Discussion

The reaction rate constants were obtained by means of the activation energies and intercepts of Arrhenius plots (Table 1). Since the reactivity seemed to be affected by the polar nature of the substituent, Taft's equation was applied to this heterogeneous catalysis.

$$\log k/k_0 = \rho^*\sigma^* \qquad (3)$$

where k/k_0 is the relative rate constant with respect to standard reaction (1,2-dichloroethane in this case),

TABLE 2. RELATIVE REACTIVITIES FOR CO-PYROLYSIS OF CHLOROETHANES AND METHANOL ON ACTIVATED ALUMINA AT 230 °C

Reaction site	Substituent	Relative reactivity
$-CH_3$	$-CCl_3$	13.71
	$-CHCl_2$	9.34
$-CH_2Cl$	$-CCl_3$	5.49
	$-CHCl_2$	1.14
	$-CH_2Cl$	1.00 (Standard)
$-CHCl_2$	$-CCl_3$	19.06
	$-CHCl_2$	8.90
	$-CH_2Cl$	1.46

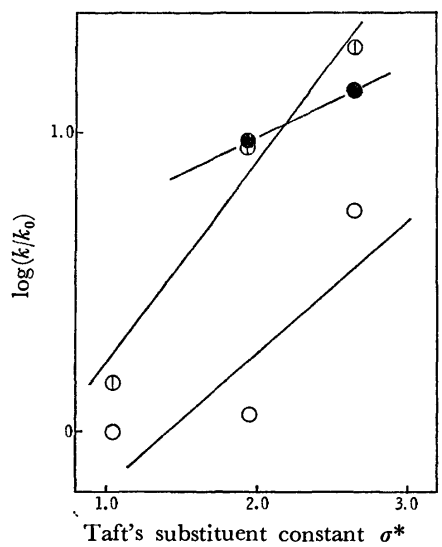

Fig. 5. Hammett plots for co-pyrolysis of chloroethanes and methanol.
●: $-CH_3$, ○: $-CH_2Cl$, ⓓ: $-CHCl_2$

and σ^* represents the alkyl substituent parameter which is a measure of the inductive effect.[8] Rate constants at 230 °C were calculated from the equations in Table 1. The relative reactivities obtained in the competitive co-pyrolysis of chloroethanes and methanol on activated alumina are given in Table 2. A linear free energy relationship was found to exist between the reactivities of chloroethanes and Taft's σ^* constants (Fig. 5). Values of ρ^* were calculated by the method

of least squares. ρ^* values for reactions of RCH_3, RCH_2Cl and $RCHCl_2$ series were 0.24, 0.45 and 0.70, respectively.

For the photochlorination and chlorine-sensitized photooxidation of chloroethanes, ρ^* values were negative, indicating an electrophilic reaction mechanism.[9-11] On the other hand, positive ρ^* values were observed for co-pyrolysis of chloroethanes and methanol on activated alumina.

For the formation of ethers from alcohols over alumina catalysts, Knözinger and Bühl observed a positive ρ^* value.[12] Adsorption of alcohol molecules on basic sites of alumina by hydrogen bonding through the hydrogen of the hydroxyl group generates incipient alkoxide anions.[13] Thus, it was suggested that a β-hydrogen of chloroethanes was abstracted by the nucleophilic attack of methanol, chlorine being removed at the same time. For example, the reaction scheme in the case of 1,1,2-trichloroethane can be given by the following equations.

$$CH_3OH \xrightarrow{\text{basic sites of alumina}} CH_3O^{\ominus} + H^{\oplus}$$

$$CH_3O^{\ominus} + \underset{\beta}{CHCl_2}\underset{\alpha}{CH_2Cl} \rightarrow \left[CH_3O^{\delta\ominus}\cdots H \quad H \;\; Cl{-}C{=}C{-}H \;\; Cl \quad Cl^{\delta\ominus} \right]$$

$$CH_3OH + CCl_2 : CH_2 + Cl^{\ominus}$$

$$H^{\oplus} + Cl^{\ominus} \rightarrow HCl$$

$$CH_3OH + HCl \xrightarrow{\text{activated alumina}} CH_3Cl + H_2O$$

Dechlorination occurred considerably with the pyrolyses of 1,1,1,2-tetrachloroethane and pentachloroethane. The acid sites of alumina seemed to play an important role in the elimination reaction. The reaction could proceed according to *E*1 on the acid sites and *E*2 on the basic sites of the catalysts. It was found that *E*2 reaction dominated in the co-pyrolysis of chloroethanes and methanol on activated alumina.

References

1) K. Shinoda, *Chem. Lett.*, **1973**, 877.
2) L. Andrussow and E. Edler, *Chem. Process Eng.*, **48**, 41 (1967).
3) K. Teramoto, M. Kitabatake, and T. Onouchi, *Kogyo Kagaku Zasshi*, **67**, 460 (1964).
4) I. Mochida, J. Take, Y. Saito, and Y. Yoneda, *J. Org. Chem.*, **32**, 3894 (1967).
5) A. Suzuki, K. Sakuma, and T. Onda, *Kogyo Kagaku Zasshi*, **74**, 1375 (1971).
6) S. Thyagarajan, R. Kumar, and N. R. Kuloor, *Ind. Eng. Chem., Process Des. Develop.*, **5**, 209 (1966).
7) Y. Kosaka and M. Hayata, *Kogyo Kagaku Zasshi*, **69**, 244 (1966).
8) M. S. Newman, "Steric Effects in Organic Chemistry," John Wiley & Sons, Inc. New York, N Y. (1956) p. 618.
9) W. Mack, *Tetrahedron Lett.*, **49**, 4993 (1967).
10) T. Migita, M. Kosugi, and Y. Nagai, This Bulletin, **40**, 920 (1967).
11) K. Shinoda, *Nippon Kagaku Kaishi*, **1973**, 542.
12) H. Knözinger and H. Bühl, *Z. Naturforsch. B.*, **24**, 290 (1969); H. Knözinger, *Angew. Chem., Int. Ed. Engl.*, **7**, 791 (1968).
13) J. R. Jain, and C. N. Pallai, *J. Catal.*, **9**, 322 (1967).

Effects of Substituents on the Formation of Acetals of 4-Substituted 1,3-Indandiones

Kazuo SAKANE, Yoshio OTSUJI, and Eiji IMOTO

Department of Applied Chemistry, College of Engineering, University of Osaka Prefecture, Sakai-shi, Osaka 591

(Received February 22, 1974)

Treatment of 4-nitro-1,3-indandione (**1**) with an equivalent of ethylene glycol in benzene in the presence of *p*-toluenesulfonic acid afforded 4-nitro-1,3-indandione-1-ethylene acetal (**2**), 3-ethylene acetal (**3**) and 1,3-bis-ethylene acetal (**4**). Kinetic studies revealed that **2** is a kinetically preferred product and **3** is a thermodynamically preferred product. However, the reaction of 4-acetamido-1,3-indandione (**5**) with ethylene glycol under similar conditions gave 4-acetamido-1,3-indandione-1-ethylene acetal (**6**) as a product both kinetically and thermodynamically controlled. Thioacetalization of **1** with an equivalent of 1,2-ethanedithiol afforded selectively 4-nitro-1,3-indandione-1-ethylene thioacetal (**9**).

The regioselective preparation of an acetal of polycarbonyl compounds is in general difficult.[1] From the need of monoacetals of 4-substituted 1,3-indandiones for our synthetic studies of azaacenaphthene derivatives, we studied the acetalization of 4-substituted 1,3-indandiones and found that the keto groups, where the acetalization takes place, are largely influenced by the substituents attached and alcohols used. The results are summarized and the mechanisms of the reactions are discussed in the present paper.

Results and Discussion

Reactions and Mechanisms. Treatment of 4-nitro-1,3-indandione (**1**) with an equivalent of ethylene glycol in benzene in the presence of *p*-toluenesulfonic acid afforded a mixture of 4-nitro-1,3-indandione-1-ethylene acetal (**2**), 4-nitro-1,3-indandione-3-ethylene acetal (**3**) and 4-nitro-1,3-indandione-1,3-bisethylene acetal (**4**). The reaction of **1** with a large excess of ethylene glycol under similar conditions gave only **4**. Products **2**, **3** and **4** were isolated by repeated fractional recrystallization.

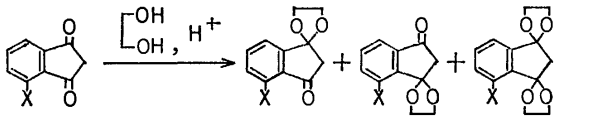

1; X=NO2 2; X=NO2 3; X=NO2 4; X= NO2

5; X= NHAc 6; X=NHAc 7; X=NHAc 8; X= NHAc

The yields of **2**, **3** and **4** varied with reaction time when the reaction of **1** with an equivalent of ethylene glycol was carried out in benzene in the presence of *p*-toluenesulfonic acid. The yields of **2**, **3** and **4** were determined by vpc analysis of the reaction mixture at appropriate time intervals.[2] The results are shown in Fig. 1. At an initial stage of the reaction, the yield of **2** was higher than that of **3**. Aftre a while, however, the situation was reversed and finally the yields of **2**, **3** and **4** approached constant values.

When **2** was refluxed in benzene in the presence of *p*-toluenesulfonic acid without ethylene glycol, **3** and **4** were obtained. A similar treatment of **3** yielded **2** and **4**. Variation of the yields of the products with reaction time for these reactions were followed by vpc analyses of the reaction mixtures. The results are shown in Figs. 2 and 3. The results indicate that the rate of disappearance of **2** is greater than that of **3**, and that **3** and **4** are produced from **2** at almost equal rates. The rates of formation of **2** and **4** from **3** are also almost equal.

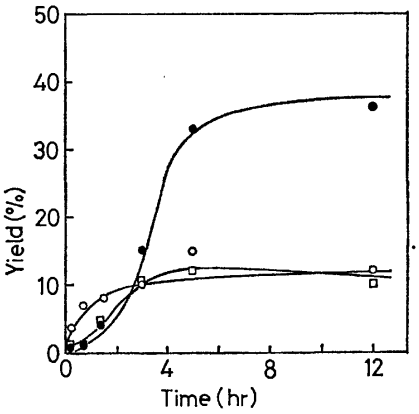

Fig. 1. Variation of the yields of the products with reaction time in the acid-catalyzed acetalization of **1** with ethylene glycol. A mixture of 5.7 g (0.03 mol) of **1**, 1.8 g (0.03 mol) of ethylene glycol and 0.3 g of *p*-TsOH·H_2O in 300 ml of benzene was refluxed. ○: **2**, ●: **3**, □: **4**.

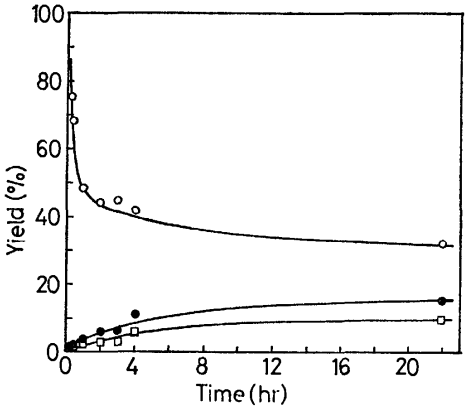

Fig. 2. Variation of the yields of the products with reaction time in the acid-catalyzed reaction of **2**. A mixture of 12.2 mg (0.052 mmol) of **2** and 1.0 mg of *p*-TsOH·H_2O in 1.0 ml of benzene was refluxed. ○: **2**, ●: **3**, □: **4**.

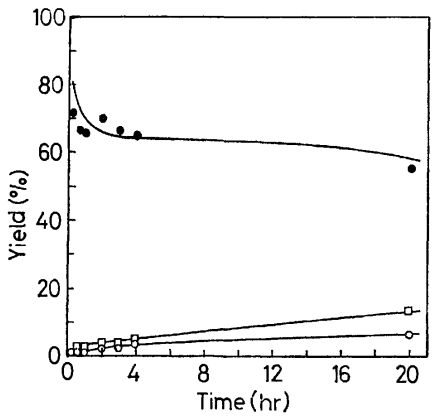

Fig. 3. Variation of the yields of the products with reaction time in the acid-catalyzed reaction of **3**. A mixture of 11.1 mg (0.047 mmol) of **3** and 1.0 mg of *p*-TsOH·H_2O in 1.0 ml of benzene was refluxed.
○: **2**, ●: **3**, □: **4**.

The results may be accounted for by assuming that the acid-catalyzed acetalization of **1** with ethylene glycol proceeds through the pathways represented in Scheme 1.[3] Since $k_1 > k_3$, the formation of **2** is favored over that of **3** at the initial stage of acetalization.

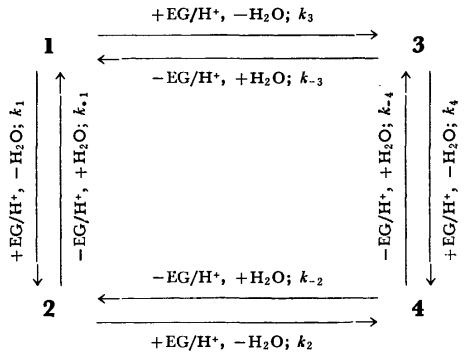

Scheme 1.

However, as a result of $k_{-1} > k_{-3}$ the yield of **3** becomes higher than that of **2** after a prolonged reaction, indicating that **3** is a thermodynamically controlled product; **3** is thermodynamically more stable than **2**.

As another example of acetalization, we studied the acid-catalyzed acetalization of 4-acetamido-1,3-indandione (**5**) with ethylene glycol. Treatment of **5** with an equivalent of ethylene glycol in benzene in the presence of *p*-toluenesulfonic acid gave 4-acetamido-1,3-indandione-1-ethylene acetal (**6**), accompanied by a black material which could not be purified. In this reaction, 3-ethylene acetal (**7**) and 1,3-bisethylene acetal (**8**) were not detected. Variation of the yield of **6** with reaction time is shown in Fig. 4. Treatment of **7** in benzene in the presence of *p*-toluenesulfonic acid afforded **5** and **6**. Variation of the yields of **5** and **6** with reaction time is shown in Fig. 5. The results suggest that **6** is a product which is both kinetically and thermodynamically preferable in the acetalization of **5**. The results also indicate that the acetal formation of 1,3-indandiones is strongly influenced by the substituents attached to the benzene ring in the diones; an

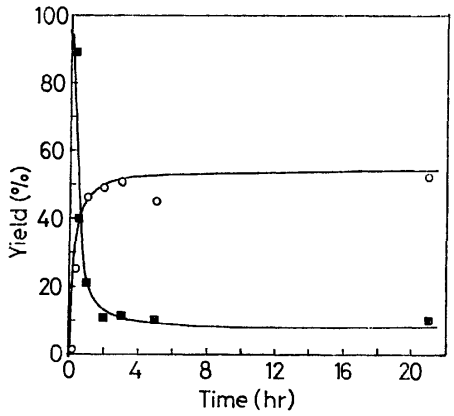

Fig. 4. Variation of the yields of the products with reaction time in the acid-catalyzed acetalization of **5**. A mixture of 50.9 mg (0.25 mmol) of **5**, 35.3 mg (0.57 mmol) of ethylene glycol and 5.3 mg of *p*-TsOH·H_2O in 5.0 ml of benzene was refluxed.
■: **5**, ○: **6**.

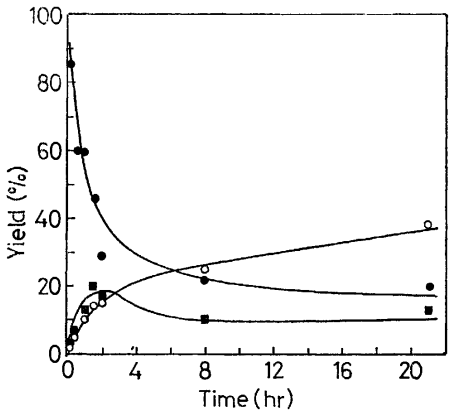

Fig. 5. Variation of the yields of the products with reaction time in the acid-catalyzed reaction of **7**. A mixture of 9.9 mg (0.04 mmol) of **7** and 1.0 mmg of *p*-TsOH·H_2O in 1.0 ml of benzene was refluxed.
■: **5**, ○: **6**, ●: **7**.

electron-withdrawing substituent such as a nitro group at the 4-position stabilizes 3-ethylene acetal, but an electron-releasing substituent at the same position stabilizes 1-ethylene acetal.[4] However, it must be borne in mind that in a kinetical sense, the carbonyl group at the 1-position is more reactive than the carbonyl group at the 3-position, irrespective of the nature of substituents.[5]

In contrast to ethylene acetals, ethylene thioacetals are relatively stable under the conditions of their formation; they are not easily hydrolyzed by mineral acids. Consequently, in the case of thioacetals, a predominant formation of the kinetically controlled products is to be expected: *i.e.*, thioacetalization of **1** would yield selectively 4-nitro-1,3-indandione-1-ethylene thioacetal (**9**). The reaction of **1** with an equivalent of 1,2-ethanedithiol in acetic acid in the presence of *p*-toluenesulfonic acid gave **9** in a 36% yield along with a small amount (1% yield) of 4-nitro-1,3-indandione-1,3-bisethylene thioacetal (**10**), but no 3-ethylene thioacetal (**11**). The reaction of **1** with a large excess

of 1,2-ethanedithiol gave only **10**. A high regioselectivity of this reaction may in part be attributed to a bulkiness of sulfur atoms besides an inherent high reactivity of the carbonyl group at the 1-position.

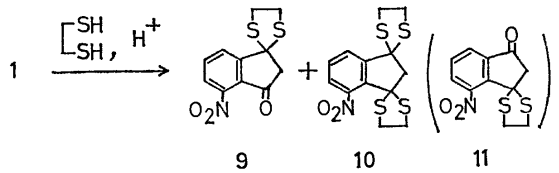

9 10 11

Characterization of the Products. The structures of the products were established by the sepctral properties and chemical modifications whereby the products can be interrelated. The relevant IR and NMR spectral data of compounds **1**—**9** and 4-acetamido-1,3-indandione-1-ethylene thioacetal (**12**) are listed in Table 1.

The 4-acetamido derivatives **5**, **7** and **8** were prepared respectively from the corresponding 4-nitro derivatives, **1**, **3** and **4**. Catalytic reduction of **1**, **3** and **4** over a Raney nickel to the corresponding amino derivatives followed by acetylation led to the formation of **5**, **7** and **8**, respectively. Compound **6** was obtained by the acetalization of **5**. The catalytic reduction of **9** over a Raney nickel gave 4-amino-1,3-indandione-1-ethylene thioacetal which was acetylated to yield **12**.

Let us compare the spectral properties of the 4-nitro derivatives with those of the corresponding 4-acetamido derivatives. The carbonyl band in the IR spectrum of 4-nitro-1-ethylene acetal **2** appeared at higher wavenumber than that of 4-acetamido-1-ethylene acetal **6** by 50 cm^{-1}. A similar shift of the carbonyl band was observed in a comparison of 4-nitro-1-ethylene thioacetal **9** with 4-acetamido-1-ethylene thioacetal **12**; *i.e.*, the carbonyl band of **9** appeared at higher wavenumber than that of **12** by 32 cm^{-1}. In contrast, the carbonyl band of 4-nitro-3-ethylene acetal **3** appeared at a wave number almost the same as that of 4-acetamido-3-ethylene acetal **7**.

Another difference in spectral properties between the 1-ethylene acetal (or the 1-ethylene thioacetal) and the 3-ethylene acetal was observed in the NMR spectra. For 1-ethylene acetal **6** and 1-ethylene thioacetal **12**, the signal due to the NH proton appeared at δ 10—11 ppm. On the other hand, the same signals appeared at higher fields, *i.e.*, δ 8—9 ppm, for 3-ethylene acetal **7** and 1,3-bisethylene acetal **8**. All these spectral properties can be interpreted by assuming that an intramolecular interaction exists between the NH and carbonyl groups in 4-acetamido-1-ethylene acetals and 4-acetamido-1-ethylene thioacetal.

Table 1. Spectral properties

Compd	νC=O (cm^{-1})	Compd	νC=O	NH (ppm)
1	1740 1710	**5**	1740 1705	10.08— 10.40
2	1740	**6**	1690	10.07— 10.70
3	1725	**7**	1722	8.03— 8.31
4	—	**8**	—	8.25— 8.90
9	1730	**12**	1698	10.14— 10.54

The chemistry and spectral properties described above are consistent with the assigned structures. Further evidence for the structure assignment was provided by the fact that 5-azaacenaphthene derivatives were synthesized from **2** and **9**.[6]

Experimental

Vpc analyses were carried out on a 063 Hitachi gas chromatograph with a column packed with 30% Silicone-grease on Celite 545 and tlc analyses with Wakogel B5.

4-Nitro-1,3-indandione-1-ethylene Acetal (2). A mixture of 1.9 g (0.01 mol) of 4-nitro-1,3-indandione (**1**),[7] 5.0 g (0.08 mol) of ethylene glycol and 0.1 g of *p*-toluenesulfonic acid monohydrate (*p*-TsOH·H_2O) in 75 ml of benzene was heated under reflux in a Dean-Stark trap for 2 hr, water formed during the reaction being continuously removed. The reaction mixture was then washed with two 20 ml portions of 5% Na_2CO_3. The aqueous layer was extracted with two 30 ml portions of benzene. All the benzene solutions were combined, washed twice with 100 ml of water, dried (Na_2SO_4) and then evaporated. The oily residue was recrystallized from $CHCl_3$–CCl_4 to yield 0.55 g (23%) of the crude **2**. Repeated fractional recrystallization from $CHCl_3$–CCl_4 gave an analytical sample of **2** as white crystals, mp 142—143 °C. IR (KBr): 1740 (C=O), 1539 (NO_2), and 1361 cm^{-1} (NO_2). NMR ($CDCl_3$): δ 3.04 (s, 2H, $-CO-CH_2C(O-)_2$), 4.12—4.50 (m, 4H, $-OCH_2CH_2O-$), and 7.92 ppm (s, 3H, aromatic H); Mass: *m/e* 235 (M^+), 219, 205, 192, 177, 161, 147, and 133.

Found: C, 56.22; H, 3.78; N, 5.88%. Calcd for $C_{11}H_9NO_5$: C, 56.17; H, 3.86; N, 5.96%.

4-Nitro-1,3-indandione-3-ethylene Acetal (3). A mixture of 5.7 g (0.03 mol) of **1**, 1.8 g (0.03 mol) of ethylene glycol and 0.3 g of *p*-TsOH·H_2O in 240 ml of benzene was heated under reflux in a Dean-Stark trap for 24 hr. The reaction mixture was worked up as described above. From the benzene solution, 5.3 g (76%) of crude **3** was obtained. Repeated fractional recrystallization from ethanol gave an analytical sample of **3** as white crystals, mp 134—136 °C. IR(KBr): 1725 (C=O), 1540 and 1362 cm^{-1} (NO_2). NMR ($CDCl_3$): δ 2.95 (s, 2H, $-COCH_2C(O-)_2$), 4.00—4.50 (m, 4H, $-OCH_2-CH_2O-$), and 7.52—8.30 ppm (m, 2H, aromatic H). Mass: *m/e* 235 (M^+), 207, 192, 175, 167, 161, 159, 149, 147, 145, 133, and 113.

Found: C, 55.98; H, 3.70; N, 5.92%. Calcd for $C_{11}H_9NO_5$: C, 56.17; H, 3.86; N, 5.96%.

Upon acidification of the Na_2CO_3 solution, 0.95 g (17%) of crude **1** was recovered.

4-Nitro-1,3-indandione-1,3-bisethylene Acetal (4). A mixture of 5.7 g (0.03 mol) of **1**, 7.2 g (0.12 mol) of ethylene glycol and 0.3 g of *p*-TsOH·H_2O in 200 ml of benzene was heated under reflux in a Dean-Stark trap for 48 hr. The reaction mixture was worked up as described above. Recrystallization of the residue obtained after evaporation of benzene from CCl_4–hexane gave 5.7 g (69%) of **4** as light pink crystals; mp 78—80 °C. IR (KBr): 1535 cm^{-1} (NO_2), no absorption appearing at the carbonyl region. NMR ($CDCl_3$): δ 2.49 (s, 2H, $(-O)_2CCH_2C(O-)_2$), 3.94—4.50 (m, 8H, two of

$-OCH_2CH_2O-$), 7.38—7.64 (m, 2H, aromatic H), and 7.75 ppm (dd, $J=6.4$ and 3.0 Hz, 1H, aromatic H). Mass: *m/e* 279 (M^+), 262, 249, 233, 207, 191, 177, 162, 161, 147 and 133.

Found: C, 55.95; H, 4.46; N, 4.89%. Calcd for $C_{13}H_{13}NO_6$: C, 55.91; H, 4.70; N, 5.02%.

4-Amino-1,3-indandione. A suspension of 3.8 g (0.02 mol) of **1** and *ca.* 10 g of a W-1 Raney nickel in 340 ml of ethanol was hydrogenated under atmospheric pressure at room temperature for 8 hr. The catalyst was separated and washed thoroughly with ethanol. The filtrate was evaporated to give a deep yellow solid. Recrystallization of the solid from ethanol gave 1.0 g (30%) of the amino compound as yellow needles; mp 203—205 °C. IR (KBr): 3455, 3340 (NH_2), 1720, 1685 (C=O), and 1620 cm^{-1}.

Found: C, 67.27; H, 4.30; N, 8.67%. Calcd for $C_9H_7NO_2$: C, 67.07; H, 4.38; N, 8.69%.

4-Acetamido-1,3-indandione (5). A solution of 100 mg (0.62 mmol) of 4-amino-1,3-indandione in 2 ml of acetic anhydride was heated at 80 °C for a few minutes. Evaporation of the solvent gave a dark brown oil. Recrystallization of the oil from CCl_4 gave 60 mg (55%) of **5** as yellow plates; mp 120—124 °C. IR (KBr): 3310 (NH), 1740, 1705, 1690 (C=O), and 1600 cm^{-1}. NMR ($CDCl_3$): δ 2.29 (s, 3H, $-COCH_3$), 3.28 (s, 2H, $-COCH_2CO-$), 7.58 (dd, $J=7.2$ and 1.7 Hz, 1H, aromatic H), 7.80 (t, $J=7.2$ Hz, 1H, aromatic H), 8.91 (dd, $J=7.2$ and 1.7 Hz, 1H, aromatic H), and 10.08—10.40 ppm (m, 1H, NH). Mass: *m/e* 203 (M^+), 161, 133, 87, and 43.

Found: C, 65.15; H, 4.22; N, 6.83%. Calcd for $C_{11}H_9NO_3$: C, 65.02; H, 4.46; N, 6.89%.

4-Acetamido-1,3-indandione-1-ethylene Acetal (6). A mixture of 0.5 g (2.5 mmol) of **5**, 0.6 g (8.1 mmol) of ethylene glycol, and 30 mg of *p*-TsOH·H_2O in 50 ml of benzene was heated under reflux in a Dean-Stark trap for 10 hr. The reaction mixture was worked up by a method similar to that for **2**. Recrystallization of the product from CCl_4-hexane gave 0.1 g (16%) of **6** as yellow crystals; mp 145—147 °C. IR(KBr): 3310 (NH), 1690 (C=O), 1610, and 1540 cm^{-1}. NMR ($CDCl_3$): δ 2.23 (s, 3H, $-COCH_3$), 2.97 (s, 2H, $-COCH_2C<^{O-}_{O-}$), 4.15—4.40 (m, 4H, $-OCH_2CH_2O-$), 7.25 (d, $J=7.7$ Hz, 1H, aromatic H), 7.65 (t, $J=7.7$ Hz, 1H, aromatic H), and 8.58 ppm (d, $J=7.7$ Hz, 1H, aromatic H). Mass: *m/e* 247 (M^+), 205, 177, 162, 149, 133, and 120.

Found: C, 62.85; H, 5.11; N, 5.87%. Calcd for $C_{13}H_{13}NO_4$: C, 63.15; H, 5.30; N, 5.67%.

4-Amino-1,3-indandione-3-ethylene Acetal. A suspension of 2.35 g (0.01 mol) of **3** was hydrogenated on a W-1 Raney nickel in 100 ml of dioxane over 3 hr. The crude product was recrystallized from $CHCl_3$–hexane to give yellow needles; mp 132—135 °C. IR(KBr): 3440, 3350 (NH_2), 1705 (C=O), and 1620 cm^{-1}. NMR($CDCl_3$): δ 2.79 (s, 2H, $-COCH_2C<^{O-}_{O-}$), 3.90—4.62 (m, 4H, $-OCH_2CH_2O-$), 6.77 (dd, $J=6.9$ and 2.1 Hz, 1H, aromatic H), and 6.91—7.42 ppm (m, 2H, aromatic H).

Found: C, 64.65; H, 5.50; N, 7.02%. Calcd for $C_{11}H_{11}NO_3$: C, 64.38; H, 5.40; N, 6.83%.

4-Acetamido-1,3-indandione-3-ethylene Acetal (7). A solution of 410 mg (2.0 mmol) of 4-amino-1,3-indandione-3-ethylene acetal in 10 ml of dry tetrahydrofuran (THF) was added to a stirred mixture of 300 mg (3.8 mmol) of acetyl chloride and 5 ml of pyridine in 5 ml of dry THF under cooling in an ice-water bath. The mixture was stirred at room temperature for 0.5 hr and then poured into 100 ml of water. The aqueous mixture was extracted with three 200 ml portions of CH_2Cl_2. The extract was washed with two 30 ml portions of water, dried over Na_2SO_4 and evaporated. Recrystallization of the solid from ethanol gave **7** as white needles quantitatively; mp 162—165 °C. IR(KBr) 3345 (NH), 1722, 1690 (C=O), and 1600 cm^{-1}. NMR ($CDCl_3$): δ 2.17 (s, 3H, $-COCH_3$), 2.83 (s, 2H, $-COCH_2C<^{O-}_{O-}$), 4.07—4.41 (m, 4H, $-OCH_2CH_2O-$), 7.42—7.61 (m, 2H, aromatic H), 8.00—8.30 (m, 1H, NH), and 8.69 ppm (dd, $J=5.8$ and 2.9 Hz, 1H, aromatic H). Mass: *m/e* 247 (M^+), 204, 188, 174, 162, 161, 149, 133, and 120.

Found: C, 62.98; H, 5.19; N, 5.58%. Calcd for $C_{13}H_{13}NO_4$: C, 63.15; H, 5.30; N, 5.67%.

4-Amino-1,3-indandione-1,3-bisethylene Acetal. A suspension of 2.8 g (0.01 mmol) of **4** was hydrogenated on a W-1 Raney nickel in 100 ml of dioxane over 7 hr. Recrystallization of the crude product from CCl_4-hexane gave 2.5 g (quantitative) of the amino compound as yellow needles; mp 132—134 °C. IR(KBr) 3100—3600 (NH_2) and 1620 cm^{-1}.

Found: C, 62.88; H, 5.82; N, 5.90%. Calcd for $C_{13}H_{15}NO_4$: C, 62.64; H, 6.07; N, 5.62%.

4-Acetamido-1,3-indandione-1,3-bisethylene Acetal (8). Acetylation of 4-amino-1,3-indandione-1,3-bisethylene acetal with acetyl chloride in the presence of pyridine in dry THF yielded crude **8**, which upon recrystallization from ethanol–$CHCl_3$ gave a pure sample as pale yellow crystals in 70% yield; mp 210 °C. IR(KBr): 3380 (NH), 1692 (C=O), and 1610 cm^{-1}. NMR ($CDCl_3$) δ 2.16 (s, 3H, $-COCH_3$), 2.53 (s, 2H, $-O>CCH_2C<^{O-}_{O-}$), 4.10—4.50 (m, 8H, $-OCH_2-CH_2O-$), 7.30 (t, $J=7.4$ Hz, 1H, aromatic H), 7.64 (d, $J=7.4$ Hz, 1H, aromatic H), and 8.25—8.92 ppm (m, 2H, NH plus aromatic H). Mass: *m/e* 291 (M^+), 263, 248, 247, 232, 219, 206, 205, and 191.

Found: C, 61.77; H, 5.75; N, 4.79%. Calcd for $C_{15}H_{17}NO_5$: C, 61.85; H, 5.88; N, 4.81%.

4-Nitro-1,3-indandione-1-ethylene Thioacetal (9). To a solution of 3.8 g (0.02 mol) of **1** in 140 ml of AcOH were added 1.9 g (0.02 mol) of 1,2-ethanedithiol and 2.0 g (0.01 mol) of *p*-TsOH·H_2O. The mixture was allowed to stand at room temperature overnight. Filtration of the mixture gave 60 mg (1%) of 4-nitro-1,3-indandione-1,3-bisethylene thioacetal (**10**), mp 202—205 °C, which showed no depression in the mixed melting-point test with the product obtained by the reaction of **1** with an excess 1,2-ethanedithiol. The filtrate was poured into 300 ml of water and extracted with three 50 ml portions of CH_2Cl_2. The extract was washed successively with two 300 ml portions of water, two 100 ml portions of 5% NaOH and two 200 ml portions of water. The CH_2Cl_2 solution was dried over Na_2SO_4 and then evaporated to give 2.7 g (51%) of crude monothioacetal **9**. The tlc analysis of this crude product indicated that the product consists of only **9**. Recrystallization from $CHCl_3$-hexane gave 1.9 g (36%) of **9** as pure yellow needles; mp 117—119 °C. IR (KBr): 1730 (C=O), 1530, and 1360 cm^{-1} (NO_2). NMR ($CDCl_3$): δ 3.48 (s, 2H, $-COCH_2C<^{S-}_{S-}$), 3.63 (m, 4H, $-SCH_2CH_2S-$), and 7.60—8.17 ppm (m, 3H, aromatic H).

Found: C, 49.32; H, 3.29; N, 5.03%. Calcd for $C_{11}H_9NO_3S_2$: C, 49.44; H, 3.40; N, 5.24%.

Upon acidification of the NaOH solution, 1.3 g (34%) of **1** was recovered.

4-Nitro-1,3-indandione-1,3-bisethylene Thioacetal (10). A mixture of 1.9 g (0.01 mol) of **1** and 10 ml of BF_3-etherate in 70 ml of AcOH was maintained at room temperature

overnight. The resulting solid was filtered, washed with water and then dried to give **10** as greenish yellow solid quantitatively; mp 205—207 °C. IR(KBr): 1520 and 1355 cm^{-1} (NO_2).

Found: C, 45.56; H, 3.78; N, 3.83%. Calcd for $C_{13}H_{13}NO_2S_4$: C, 45.49; H, 3.82; N, 4.08%.

4-Amino-1,3-indandione-1-ethylene Thioacetal. A suspension of 5.34 g (0.02 mol) of **9** was hydrogenated over a W-I Raney nickel in 100 ml of dioxane under atmospheric pressure at room temperature for 3 hr. The catalyst was removed by filtration. Evaporation of the filtrate left a yellow oil which was chromatographed on a neutral alumina. Elution with $CHCl_3$ gave 3.5 g (73%) of the amino compound as a pale yellow oil. IR (film): 3450, 3340 (NH_2), and 1670 cm^{-1} (C=O). The oil solidified upon distillation under reduced pressure; bp 200—210 °C/0.4 mmHg. Recrystallization from CCl_4–hexane gave an analytical sample as yellow needles; mp 94—99 °C.

Found: C, 55.56; H, 4.58; N, 5.77%. Calcd for $C_{11}H_{11}NOS_2$: C, 55.70; H, 4.64; N, 5.91%.

*4-Acetamido-1,3-indandione-1-ethylene Thioacetal (**12**).* Crude 4-amino-1,3-indandione-1-ethylene thioacetal was heated with excess Ac_2O on a water bath for 1 hr. After removal of AcOH and excess Ac_2O under reduced pressure, the residue was recrystallized from ethanol to yield **12** as light brown needles in 70% yield, mp 128—130 °C. IR (KBr): 3210—3280 (NH), 1698, and 1675 cm^{-1} (C=O). NMR ($CDCl_3$): δ 2.24 (s, 3H, $-COCH_3$), 3.49 (s, 2H, $-COCH_2-\overset{1}{C}<^{S-}_{S-}$), 3.62 (bs, 4H, $-SCH_2CH_2S-$), 7.50 (dd, $J=7.2$ and 1.7 Hz, 1H, aromatic H), 7.63 (t, $J=7.2$ Hz, 1H, aromatic H), and 10.14—10.54 ppm (m, 1H, NH).

Found: C, 55.71; H, 4.87; N, 5.12%. Calcd for $C_{13}H_{13}NO_2S_2$: C, 55.91; H, 4.70; N, 5.02%.

References

1) For example, C. Djerassi, "Steriod Reactions," Holden-Day, Inc., San Francisco (1963), pp. 3—5.

2) Recovery of **1** was not confirmed, since no peak due to **1** appeared in vpc ananysis of the reaction mixture.

3) Pathway through which **2** is directly transformed into **3** and *vice versa* are also possible. However, no evidence was obtained.

4) Origin of the effects of substituents on the stability of acetals is not clear. However, it seems that a dipole-dipole interaction between a substituent at the 4-position and a a carbonyl group at the 1- or 3-position is a predominant factor determining stability of the ethylene acetals.

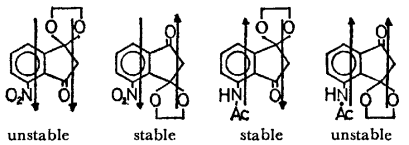

5) It has been reported that a less hindered carbonyl group of a diketone is selectively acetalized; D. D. Chapman, W. J. Musliner, and J. W. Gates, *J. Chem. Soc., C*, **1969**, 124.

6) K. Sakaen, Y. Otsuji, and E. Imoto, unpublished results.

7) V. Oskaja and G. Vanags, *Uch. Zap. Latv. Univ.*, **57**, 67 (1964); *Chem. Abstr.*, **63**, 13129a (1965).

Restricted Rotation Involving the Tetrahedral Carbon. X. Barriers to Rotation of Methyl Groups in 9-Methyltriptycene Derivatives.[1]

Mikio NAKAMURA, Michinori ŌKI, Hiroshi NAKANISHI,* and Osamu YAMAMOTO*

Department of Chemistry, Faculty of Science, The University of Tokyo, Tokyo 113

**National Chemical Laboratory for Industry, Shibuya, Tokyo 151*

(Received March 5, 1974)

Several 9-methyltriptycene derivatives have been synthesized and the PMR spectra examined at low temperatures. The compounds which have a methoxy or a methyl group at a peri position showed only broadening of methyl signals, whereas those with a chlorine at a peri position and another substituent at some other peri position showed a splitting of methyl signals. The compounds which have a halogen atom at a peri position are the intermediary cases in a sense that they show separation of the signal into two with 1 : 2 relative intensities but fail to show fine splittings. Activation parameters for the rotation were obtained by total line shape analysis. Substituent effects have been discussed.

Many studies have been made on restricted rotation about carbon-carbon single bonds by means of the variable temperature technique of high resolution NMR spectroscopy.[2] However, this method is only applicable to the 10^0-10^3 s^{-1} rates of exchange, and little is known about the rates of restricted rotation of methyl groups whose barriers to rotation are in the range 3.0 (ethane)—4.3 (neopentane) kcal/mol.[3] In order to detect the slow rotation of methyl groups of this kind, the temperature has to be so lowered that technical difficulties arise.

There are two cases as regards the restricted rotation of a methyl group, one of which is 9-methyl-9,9'-bifluorenyl (**1**) which shows line-broadening of the methyl at low temperatures as reported by Bartle *et al.*[4] Dave and Warnhoff observed a similar phenomenon with quaternary methyl groups of compound **2** and claimed that it must be attributed to the slow rotation of the methyl groups.[5] However, the observations deal only with line-broadening and lack a basis for claiming the restricted rotation. No report has appeared to show further evidence for the restricted rotation of methyl groups.[6] If the rotation of a methyl group is frozen, an ABC or AB_2 type signal is expected depending upon the substituent of the neighboring carbon. The situation is clear when Newman projections (**4** and **5**) are drawn. In the intermediary cases, a methyl group should show an unsymmetrical signal, since differences in chemical shifts between A and B and C are generally not the same.

Recently we were able to observe an unsymmetrical methyl signal at −133 °C with compound **3** and attributed it to the slow rotation of the methyl group on the NMR time scale.[7] We looked for examples showing distinct splitting of a methyl signal. Probable examples were 9-methyltriptycene derivatives,

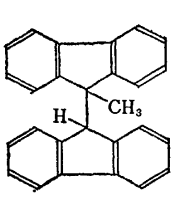

(**1**)

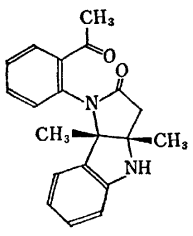

(**2**)

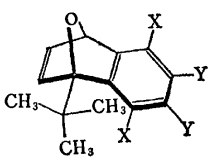

(**3**)

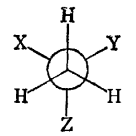

(**4**) ABC Type

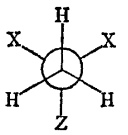

(**5**) AB_2 Type

since 9-*t*-butyltriptycene type compounds are known to possess extremely high barriers to rotation about the C_9–C_{Bu} bond,[8] and 9-chloromethyltriptycene has been reported to have a high barrier to internal rotation.[9]

Results and Discussion

9-Methyl-1,2,3,4-tetrachlorotriptycene (**8**) was prepared by treating 9-methylanthracene with tetrachlorobenzyne and its PMR spectrum was examined at low temperature. The compound gave no signals with fine structure even at −95 °C, though separation of the methyl signal into two with 2 : 1 relative intensities was observed. The results sugest that the methyl group rotates slowly enough to show different chemical shifts of two kinds of protons but the rotation is too fast to show fine splittings. It was thought that increasing the steric hindrance by introducing another substituent to another ring might increase the barrier.

9-Methyl-1,2,3,4,5,6,7,8-octachlorotriptycene (**10**) was similarly prepared. Its methyl signal showed a clear AB_2 type splitting at −65.4 °C and below, suggesting that the rotation in question is really slow on the

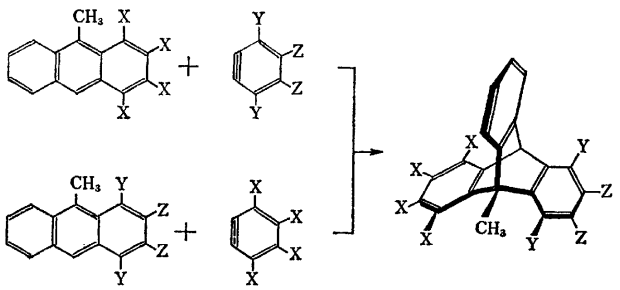

	X	Y	Z
(**6**)	H	OCH_3	H
(**7**)	H	CH_3	H
(**8**)	Cl	H	H
(**9**)	Br	H	H

	X	Y	Z
(**10**)	Cl	Cl	Cl
(**11**)	Cl	Br	Br
(**12**)	Cl	CH_3	H

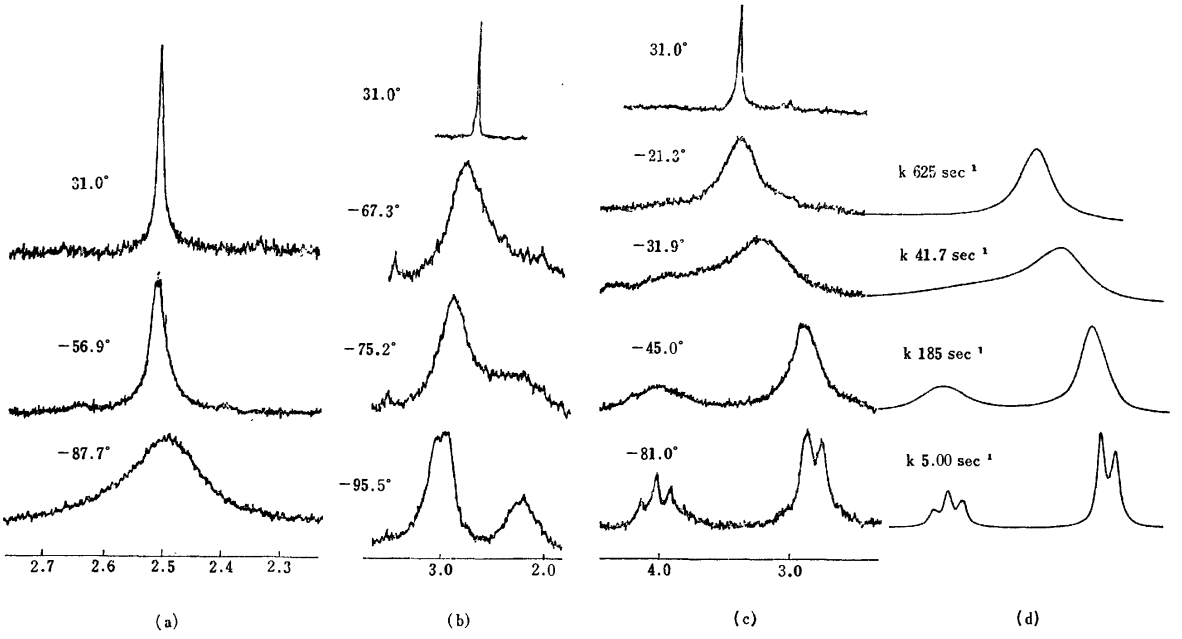

Fig. 1. Temperature dependence of PMR spectra of 9-methyltriptycenes and calculated spectra: (a) compound **6**, (b) compound **8**, (c) compound **11**, and (d) calculated spectra of compound **11**.

NMR time scale. The results imply that the substituents at peri positions play an important role in determining the rates of rotation. Various types of substituted 9-methyltriptycenes were prepared in order to obtain information on the effect of substituents at peri positions.

The methyl signals can be classified into three cases: (a) only line-broadening at low temperature, (b) separation of a methyl signal into two broad signals with relative intensities 1 : 2, and (c) appearance of a clear AB_2 type signal. Compounds **6** and **7** with one substituent other than a halogen atom at a peri position belong to (a), **8** and **9** with one halogen atom at a peri position to (b) and **10**, **11**, and **12** with a substituent at a peri position in addition to a halogen atom at another peri position to (c). Figure 1 shows the temperature-dependent PMR spectra of **6**, **8**, and **11** as typical examples.

The effect of a peri-substituent is important. The factor determining the barrier might not be van der Waals radius only: a methyl group which has a larger van der Waals radius than a chlorine seems to effect a smaller barrier. In order to discuss this point, exact knowledge of kinetic parameters or the chemical shift difference is necessary, because, if the latter is small, the coalescence temperature is low.

TABLE 1. PMR PARAMETERS OF METHYL PROTONS OF COMPOUNDS **8**—**12**

Compound	δ_A	δ_B	δ_C	$\delta_B-\delta_A$	J_{AB}
8	2.23	3.02	—	0.79	—
9	2.20	3.09	—	0.89	—
10	2.78	3.89	—	1.11	−12.6
11	2.71	4.07	—	1.36	−12.6[a]
12	2.72	2.82	3.53	—	−12

a) Assumed value.

The chemical shifts of protons of methyl groups were obtained with the use of LAOCOON MBYH program[10] for compounds **8**—**12**. The results are shown in Table 1. Since the difference in chemical shifts of protons B and C in compound **11**, as shown in a Newman projection **13**, was considered to be very small, the line shape was treated as an AB_2 pattern. The coupling constants were also obtained when possible. They are also given in Table 1. It was not possible to obtain geminal coupling constants of methyl protons in compounds **8** and **9**, since they showed no signal splitting. We could obtain three chemical shifts for the methyl protons of compound **12**, but estimation of the geminal coupling constants was difficult: the spectral lines were broad even at −90 °C due to the slow rotation taking place and further lowering of temperature caused precipitation.

Chemical shifts of methyl protons of compounds **6** and **7** could not be obtained by computation since they showed symmetrical signals, although broad, even at the lowest temperature attained (−90 °C). Thus the chemical shifts were estimated by making the following simple assumption. A chemical shift of the methyl group of 9-methyltriptycene in carbon disulfide is known to be δ 2.25. Since three protons

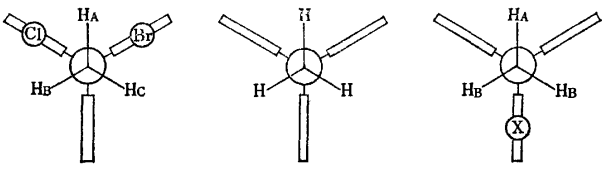

(**13**) (**14**) (**15**)

are located in the identical environment (**14**), it follows that the chemical shift of each proton should also be δ 2.25. If we extend this discussion to the substituted triptycenes in questions, the observed

Table 2. Calculated chemical shifts of methyl protons of compounds **6** and **7**

Compound	δ_{obs}[a)]	δ_A	δ_B	$\delta_B-\delta_A$
9-methyltriptycene	2.25	2.25	2.25	0
6	2.50	2.25	2.63	0.38
7	2.53	2.25	2.67	0.42

a) in CS_2 solution

chemical shift is the average of two identical chemical shifts of protons (H_B in **15**) in the neighborhood of the peri-substituent and a proton (H_A in **15**) far from the substituent. Since H_A is far from the substituent, we may tentatively assume that the chemical shift of H_A is very close to that of protons in 9-methyltriptycene, δ 2.25. Since the observed value is the weighted mean, we can calculate the chemical shift of H_B. The values thus obtained are given in Table 2.

The validity of the above assumption should be checked by seeing whether the assumption is valid for other compounds such as **8** and **9** whose chemical shifts of protons far from the substituents are δ 2.23 and 2.20, respectively (Table 1). Since these values agree with those obtained by the assumption to the extent of two significant digits, the assumption could be taken as valid for semi-quantitative discussion.

Comparison of the chemical shift differences ($\delta_B-\delta_A$) in Tables 1 and 2 shows that those compounds which exhibited line separation or splitting have larger values than those which showed only line broadening. The large difference in chemical shift caused by the halogen atom is one reason that we could detect the frozen rotation of the methyl group in compound **10**. We were lucky in a sense that a compound with a large difference in chemical shift of methyl protons was chosen as the first example.

We should know the activation parameters to discuss the substituent effect, since the difference in the chemical shift between compounds is not common. The observed line shapes were simulated by putting the parameters in Table 1 into INVERS EX II program. Some computed spectra are shown in Fig. 1 to demonstrate the agreement with the observed. The rate constants thus obtained were plotted against $1/T$. Linearity holds and activation energies are obtained. Substitution of these data into Eyring's equation affords kinetic parameters shown in Table 3.

Various kinetic parameters are used, depending upon the authors, for discussion of the barrier to rotation. We believe that the Arrhenius activation energy is the most appropriate for comparison since it is obtainable from the experimental results.

Activation energies can be classified into three categories, as in the case of the spectra. From the chemical shift difference of two kinds of protons and the fact that the signal at −90 °C was still symmetrical, *i.e.* −90 °C is still above the coalescence temperature, free energy of activation seems to be less than 8 kcal/mol for compounds **6** and **7**.[11] Thus compounds **6** and **7** form group (a) with a barrier less than 8 kcal/mol, compounds **8** and **9** form another group (b) with a barrier 9—10 kcal/mol, and **10**, **11**, and **12** form a third group (c) with a barrier greater than 12 kcal/mol.

As regards group (a), a comparison of the heights of signals at low temperature is possible to some extent. Since the difference in chemical shift of methyl protons in compounds **6** and **7** is almost the same, the coalescence temperature of the methyl protons should be higher for a compound having a higher barrier than one with a lower barrier. Though no coalescence was observed, it is reasonable to assume that the coalescence temperature is reflected in the height or the half-band width of signals: a broader signal is a reflection of a higher coalescence temperature. Since the half-height widths for **6** and **7** are 12 and 5 Hz at −90 °C, respectively, and relative heights are 1 : 1.4, the methyl compound (**7**) seems to possess lower barrier to rotation than the methoxy compound (**6**).

From the above discussion, effectiveness of substituents in monosubstituted methyltriptycenes for raising the barrier would be in the order

$$Br > Cl > OCH_3 > CH_3$$

This is in line with the van der Waals radii except for the methyl. Butterssing effects may be incorporated in chloro (**8**) and bromo (**9**) compounds, but the barrier in compound **7** is much smaller than expected.

This apparent reversal of the sequence could be explained by considering either one of the following factors or both. 1) Attractive interactions may exist between atoms having lone pair electrons and the methyl group at the 9-position, functioning to lower the ground state level for rotation and raising the barrier to rotation. This cannot be expected between two methyl groups, as in compound **7**. 2) The shape of a halogen atom might be considered spherically symmetrical, whereas a methyl group is tetrapodal. In compound **8**, the relation between the chlorine atom and the methyl group at the transition state of rotation does not differ from that at the ground state, whereas the situation is not the same for compound **7**. Two methyl groups, in a heavily compressed state such as in compound **7**, could not take a conformation in which a hydrogen atom in one methyl group can squeeze in the apertures made by two hydrogen atoms of

Table 3. Activation parameters for rotation of methyl groups (25 °C)

Compound	E_a (kcal/mol)	$\Delta H^{\neq}$ (kcal/mol)	$\Delta S^{\neq}$ (eu)	$\Delta G^{\neq}$ (kcal/mol)
8	9.2±0.4	8.6±0.4	−5.9±2.1	10.3±1.0
9	10.2±0.4	9.6±0.4	−2.1±2.0	10.2±1.0
10	14.1±0.6	13.5±0.6	9.8±3.0	10.6±1.0
11	13.0±0.3	12.4±0.3	3.4±1.3	11.4±0.6
12	12.7±0.3	12.1±0.3	3.0±1.4	11.2±0.7

another methyl. Thus the relation of the two methyls in space could be considered as a pair of gears. In the process where the methyl gear at position 9 rotates

ground state transition state

to reach the transition state, another methyl gear should rotate as well.[12] It is thus considered that effective van der Waals radius of the methyl group in heavily compressed cases is far less than the normal methyl and rather close to that of a carbon atom.

The barrier to rotation in compounds which carry substituents at two peri positions showed a tendency similar to that observed above, *viz.*, methyl compound (**12**) shows a lower barrier to rotation than the halogen compounds (**10** and **11**). The bromo compound (**11**) shows a lower barrier to rotation than that of the chloro compound (**10**). It is difficult to account for this from a mere consideration of the transition state. We attribute this to the rise of the ground state level due to the large size of the bromine atom.

Experimental

Syntheses. *1,2,3,4-Tetrachloro-9-methylanthracene.* To a vigorously stirred solution of methylmagnesium iodide, prepared from 7.1 g (0.05 mol) of methyl iodide and 1.3 g (0.053 mol) of magnesium, was added 13.2 g (0.04 mol) of 1,2,3,4-tetrachloroanthrone[13] at 0 °C. The reaction mixture was heated with stirring for 2 hr and cooled. The mixture was treated with concentrated hydrochloric acid and the organic layer separated. After drying the ethereal solution over sodium sulfate, the solvent was evaporated and the residue chromatographed on alumina. Elution with hexane followed by recrystallization from chloroform yielded pure yellow product, mp 171—172 °C, yield being 61% based on the anthrone. Found: C, 54.42; H, 2.40; Cl, 43.20%. Calcd for $C_{15}H_8Cl_4$: C, 54.59; H, 2.44; Cl, 42.97%. NMR ($CDCl_3$, δ): 3.27 (3H, s), 7.0—8.4 (4H, m), 8.67 (1H, s).

*1,4-Dimethoxy-9-methyltriptycene (**6**).* To a vigorously stirred solution of 3.47 g (0.02 mol) of 1-chloro-2,5-dimethoxybenzene and 1.92 g (0.01 mol) of 9-methylanthracene[14] in 20 ml of dry benzene was added a suspension of *ca.* 2 g (0.02 mol) of phenylsodium[15] in 20 ml of dry benzene over a period of 30 min under nitrogen. After being stirred for 5 hr below 20 °C, the reaction mixture was treated as above to give 1.97 g (60%) of colorless crystals, mp 238—239 °C, after recrystallization from benzene. Found: C, 84.09; H, 5.86%. Calcd for $C_{23}H_{20}O_2$: C, 84.12; H, 6.14%. NMR ($CDCl_3$-CS_2, δ): 2.50 (3H, s), 3.63 (3H, s), 3.72 (3H, s), 5.72 (1H, s), 6.37 (2H, s), 6.8—7.4 (8H, m).

*1,4,9-Trimethyltriptycene (**7**).* To a refluxing solution of 3.11 g (0.03 mol) of butyl nitrite and 2.20 g (0.01 mol) of 1,4,9-trimethylanthracene[16] in 20 ml of methylene chloride was added with stirring a solution of 1.78 g (0.013 mol) of anthranilic acid in 30 ml of purified acetone over a period of 3 hr. The reaction mixture was heated for 3 hr, cooled and evaporated *in vacuo*. The residue was taken up in hexane, washed with aqueous sodium bicarbonate and then with aqueous sodium chloride, and dried over sodium sulfate. After evaporation of the solvent, the residue was chromatographed on alumina. Elution with hexane afforded 2.16 g (73%) of pure **7**, mp 245—246 °C, after recrystallization from chloroform-methanol. Found: C, 93.40; H, 6.50%. Calcd for $C_{23}H_{20}$: C, 93.20; H, 6.80%. NMR ($CDCl_3$, δ): 2.48 (3H, s), 2.52 (3H, s), 2.60 (3H, s), 5.63 (1H, s), 6.6—7.5 (10H, m). The signal at 2.60 was assigned to 9-methyl protons since the signal showed line-broadening at low temperature.

*1,2,3,4-Tetrachloro-9-methyltriptycene (**8**),* mp 276 °C, was similarly prepared by treating 9-methylanthracene and butyl nitrite in methylene chloride with tetrachloroanthranilic acid[17] in purified acetone. The yield was 65%. Found: C, 62.16; H, 2.79; Cl, 34.99%. Calcd for $C_{21}H_{12}Cl_4$: C, 62.10; H, 2.98; Cl, 34.92%. NMR ($CDCl_3$, δ): 2.73 (3H, s), 6.03 (1H, s), 6.9—7.5 (8H, m).

*1,2,3,4-Tetrabromo-9-methyltriptycene (**9**),* mp 302 °C, was similarly prepared by treating 9-methylanthracene and butyl nitrite in methylene chloride with tetrabromoanthranilic acid[18] in purified acetone. The yield was 52%. Found: C, 43.52; H, 2.09; Br, 55.12%. Calcd for $C_{21}H_{12}Br_4$: C, 43.19; H, 2.07; Br, 54.74%. NMR ($CDCl_3$, δ): 2.75 (3H, s), 6.10 (1H, s), 6.9—7.6 (8H, m).

*1,2,3,4,5,6,7,8-Octachloro-9-methyltriptycene (**10**),* mp > 300°C, was prepared by treating 1,2,3,4-tetrachloro-9-methylanthracene and butyl nitrite in methylene chloride with tetrachloroanthranilic acid in purified acetone. The yield was 45%. Found: C, 46.57; H, 1.22; Cl, 52.06%. Calcd for $C_{21}H_8Cl_8$: C, 46.37; H, 1.48; Cl, 52.14%. NMR ($CDCl_3$, δ): 3.17 (3H, s), 6.75 (1H, s), 7.0—7.7 (4H, m).

*1,2,3,4-Tetrabromo-5,6,7,8-tetrachloro-9-methyltriptycene (**11**),* mp > 300 °C, was prepared by treating 1,2,3,4-tetrachloro-9-methylanthracene and butyl nitrite in methylene chloride with tetrabromoanthranilic acid in pure acetone. The yield was 35%. Although it was not possible to obtain satisfactory analytical data for this compound, probably because of poor combustibility, it gave no signals attributable to impurities in the PMR spectrum. The mass spectrum showed a peak at *m/e* 722 which corresponded to the molecular ion. NMR ($CDCl_3$, δ): 3.13 (3H, s), 6.78 (1H, s), 7.0—7.7 (4H, m).

*1,2,3,4-Tetrachloro-5,8,9-trimethyltriptycene (**12**),* mp 250.5—251.5 °C, was similarly prepared from 1,4,9-trimethylanthracene, butyl nitrite and tetrachloroanthranilic acid, the yield being 55%. Found: C, 63.56; H, 3.98; Cl, 32.48%. Calcd for $C_{23}H_{16}Cl_4$: C, 63.62; H, 3.71; Cl, 32.66%. NMR $CDCl_3$, δ): 2.53 (3H, s), 2.62 (3H, s), 2.98 (3H, s), 6.03 (1H, s), 6.65 and 6.75 (2H, AB quartet), 6.9—7.6 (4H, m). The signal at δ 2.98 was assigned to 9-methyl protons because of its broadening and splitting at low temperatures.

PMR Measurement and Calculation. PMR spectra at various temperatures were recorded on a Varian HA-100D spectrometer operating at 100 MHz by the usual field sweep method. In every case TMS was used as an internal reference and a lock signal. Compounds were dissolved in $CDCl_3$-CS_2 to make up *ca.* 3% solutions. The temperature was read by the method reported previously.[19] Calculations in spectral analysis and line shape analysis were performed with a FACOM 270/30 computer.

PMR Spectral Analysis. The chemical shifts and coupling constants of methyl protons were determined by computation using the LAOCOON MBYH program.[10] The line position of each signal was determined with a frequency counter. The analysis for compounds **10** and **11** was performed by assuming the spectral patterns to be of AB_2 type and spin coupling constant J_{AB} equal to J_{BB}. The rms errors

estimated were about 0.08 Hz, the calculated spectra agreeing with the observed ones. Spectral analysis of compound **12** was difficult since the signals due to the 9-methyl group were obscured by the aromatic methyl signals at the tail part of the higher field. However, when the coupling constants (J_{AB} and J_{BB}) were assumed to be -12.6 Hz, the spectra obtained agreed. Calculation of the PMR parameters for compounds **8** and **9** were performed by trial and error, taking the chemical shift as a variable and assuming geminal coupling constants to be -12.6 Hz.

Total Line Shape Analysis. The line shape analysis of temperature-dependent spectra of methyl protons was performed by the density matrix method, since the protons couple with each other. The principle of evaluation of density matrix equations to determine the rotational rates has been described.[20] Rotation of the methyl group corresponds to the exchange of three proton spins. The methyl group can rotate in two directions, clockwise and counter-clockwise. If one spin can exchange with two spins at different positions, the density matrix in general becomes very complex.[21-23] In the three spin system, two 9×9 dimension matrices and one 27×27 dimension matrix must be treated, making computation time-consuming. In the case of the rotation of a methyl group, however, the three spins are all protons, the transition probability in clockwise and counter-clockwise directions is the same, and the two mean life-times are also the same. Thus the damping term is not $(\boldsymbol{R}\rho\boldsymbol{R}-\rho)/\tau$ but

$$\frac{\boldsymbol{R}'\rho\boldsymbol{R}+\boldsymbol{R}\rho\boldsymbol{R}'-2\rho}{2\tau}$$

where $\boldsymbol{R}$ and $\boldsymbol{R}'$ are the exchange operators in the clockwise and counter-clockwise rotations, respectively, ρ is the density matrix operator, and τ the mean life time. The total density matrix equation is then

$$\frac{\mathrm{d}\rho}{\mathrm{d}t}=\frac{\boldsymbol{R}'\rho\boldsymbol{R}+\boldsymbol{R}\rho\boldsymbol{R}'-2\rho}{2\tau}+\frac{i}{\hbar}[\rho,\mathscr{H}]$$

By means of this equation, the coefficient matrix of the density operators for the three spin system can be divided into two 3×3 dimension matrices and one 9×9 dimension matrix, greatly reducing the calculation time.

A computer program was written along this line. For the calculation of theoretical spectra, chemical shifts and coupling constants as determined by spectral analysis were used. Natural line width was included in the calculation, taking advantage of the line width of bridge-head methine protons. The rates of rotation of methyl groups were determined by iteration method or visual fitting of the calculated spectra with the observed at various temperatures. Agreement between the theoretical and experimental spectra was excellent.

References

1) Preceding paper: M. Nakamura and M. Ōki, *Tetrahedron Lett.*, **1974**, 505. A preliminary report has been published: M. Nakamura, M. Ōki, and H. Nakanishi, *J. Amer. Chem. Soc.*, **95**, 7169 (1973).

2) M. Nakamura, M. Ōki, and H. Nakanishi, *Tetrahedron*, **30**, 543 (1974) and references cited therein.

3) J. R. During, S. M. Craven, and J. Bragin, *J. Chem. Phys.*, **52**, 2046 (1970).

4) K. D. Bartle, P. M. G. Davin, D. W. Jones, and R. L'Amie, *Tetrahedron*, **26**, 911 (1970).

5) V. Dave and E. W. Warnhoff, *Can. J. Chem.*, **50**, 2470 (1972).

6) While this manuscript was in preparation, the following paper appeared on the line separation of a methyl signal into two with 1 : 2 relative intensity. J. E. Anderson and D. I. Rawson, *Chem. Commun.*, **1973**, 830.

7) H. Nakanishi, O. Yamamoto, M. Nakamura, and M. Ōki, *Tetrahedron Lett.*, **1973**, 727.

8) a) M. Ōki and G. Yamamoto, *Chem. Lett.*, **1972**, 45. b) M. Ōki and M. Suda, This Bulletin, **44**, 1876 (1971).

9) a) N. M. Sergeyev, K. F. Abdulla, and V. R. Skvarchenko, *Chem. Commun.*, **1972**, 368. b) Y. K. Grishin, N. M. Sergeyev, O. A. Subbotin, and Y. A. Ustynyuk, *Mol. Phys.*, **25**, 297 (1973).

10) LAOCOON II by Castellano and Bothner-By was modified by O. Yamamoto. S. Castellano and A. A. Bothner-By, *J. Chem. Phys.*, **41**, 3863 (1964).

11) Trial calculation of the line shape of these compounds was performed, starting from the chemical shifts and the coupling constants. A 7.8 kcal/mol barrier to rotation was obtained for compound **6**. The barrier of compound **7** should be smaller than this value.

12) This does not mean that two methyl groups rotate synchronously. Even line-broadening was not observed for methyl protons at the peri position. Even at the ground state of rotation of 9-methyl group, the peri-methyl can rotate since the transition state for rotation such as **16** will not be of too high energy.

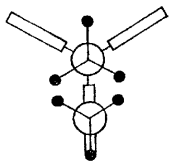

(**16**)

13) P. Kniel, *Helv. Chim. Acta*, **46**, 492 (1963).

14) R. LaLonde and R. Calas, *Bull. Soc. Chim. Fr.*, **1959**, 766.

15) G. Ehrhart, *Chem. Ber.*, **96**, 2042 (1963).

16) E. de. B. Barnett and J. A. Low., *Ber.*, **64**, 49 (1931).

17) V. Villiger and L. Blangey, *ibid.*, **42**, 3549 (1909).

18) H. Heaney, K. G. Mason, and J. M. Stechley, *J. Chem. Soc., C*, 567 (1971).

19) O. Yamamoto and M. Yanagisawa, *Anal. Chem.*, **42**, 1463 (1970).

20) O. Yamamoto and H. Nakanishi, *Tetrahedron*, **29**, 781 (1973).

21) C. S. Johnson, Jr., "Advances in Magnetic Resonance," Vol. 1, Academic Press, New York (1965), p. 33.

22) C. S. Johnson, Jr., *J. Mag. Res.* **1**, 98 (1969).

23) G. Binsch, *J. Amer. Chem. Soc.*, **91**, 1304 (1969).

Reactivity of *exo*- and *endo*-Tricyclo[3.2.1.$0^{2,4}$]octan-8-ylidenes and 7-Norbornenylidene

Shun-Ichi MURAHASHI,* Kazuo OKUMURA, Yusuke MAEDA, Akio SONODA, and Ichiro MORITANI

Department of Chemistry, Faculty of Engineering Science, Osaka University, Machikaneyama, Toyonaka, Osaka, 560

(Received March 9, 1974)

endo-Tricyclo[3.2.1.$0^{2,4}$]octan-8-ylidene (**2**) generated by the thermolysis of sodium salt of *endo*-tricyclo[3.2.1.$0^{2,4}$]octan-8-one tosylhydrazone (**5**) gave toluene (3.9%), cyclohepta-1,4-diene(**6**, 14%), cyclohepta-1,3-diene(**7**, 3.5%), bicyclo[3.3.0]octa-1,6-diene(**8**, 4.8%), bicyclo[3.3.0]octa-1,7-diene(**9**, 9.0%), and *endo*-tricyclo[3.2.1.$0^{2,4}$]-octane (**10**, 21%). In sharp contrast, *exo*-tricyclo[3.2.1.$0^{2,4}$]oct-8-ylidene (**1**) gave toluene (1.5%) and tricyclo-[5.1.$0^{2,3}$.$0^{1,7}$]oct-5-ene (**14**, 57%). The results indicate significant homoconjugative interaction between the p-orbital of the divalent carbon and the symmetric Walsh orbital of the cyclopropane. This is in line with the results of 7-norbornenylidene (**3**) in which the interaction between the divalent carbon and the carbon-carbon double bond stabilizes the nonclassical methylene. Thermolysis of sodium salt of 7-norbornenone tosylhydrazone (**18**) gave rise to cyclohexa-1,3-diene (3%), norbornene (6%), toluene (5%), spiro[2.4]hepta-4,6-diene (**19**, 10%), and bicyclo[3.2.0]hepta-1,6-diene (**21**, 56%).

Moss and Whittle reported the intramolecular reaction of 7-norbornanylidene to give norbornane (11 %), tricyclo[3.2.0.$0^{2,7}$]heptane (9.5%) and bicyclo[3.2.0]hept-1-ene (52%), and suggested the carbene to have normal geometry and a triplet ground state.[1] In constrast, Fisch and Pierce[2] reported bicyclo[3.3.1]-non-2-en-9-ylidene to be a singlet stabilized nonclassical methylene[3] with interaction between the carbenic bridge and the p-orbital of the double bond. In connection with this, the reactions of *exo*- and *endo*-tricyclo[3.2.1.$0^{2,4}$]octan-8-ylidene (**1** and **2**, respectively) and 7-norbornenylidene (**3**) are of interest, since significant homoconjugative interaction between the p-orbital of the divalent carbon and the symmetric Walsh orbital of the cyclopropane ring or the carbon-carbon double bond can be expected. Related cyclopropyl or olefinic homoconjugative participation at the developing carbonium ion center has been demonstrated,[4] kinetic results as well as extended Hückel calculations[5] on 8-tricyclo[3.2.1.$0^{2,4}$]octenyl cation indicating primary stabilization of the bridge cation from interaction with the cyclopropane ring rather than the double bond.[4]

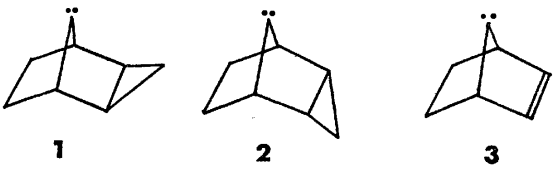

Fig. 1.

Results on the chemistry of **1** and **2** were reported by Freeman *et al.*[6] A report was made on results differing to some extent but clearly demonstrating the presence of tris-homocyclopropenyl interaction in *endo*-carbene **2**.[7] We also report results on carbene **3**, prepared from sodium salt. Moss *et al.* initially prepared it by thermolysis of lithium salt.[8] The overlapping of the vacant p-orbital of the divalent carbon with the p-orbital of the carbon-carbon double bond could be expected to stabilize sp^2 hybrid of the singlet state as in norbornenyl cation.[9]

Results and Discussion

endo-Tricyclo[3.2.1.$0^{2,4}$]octan-8-one tosylhydrazone (**4**) was converted into sodium salt **5** by treatment with sodium hydride in THF. Salt **5**, dried at 130° *in vacuo*, was placed in a flask connected with a trap cooled at 77 °K. The flask was promptly immersed into an oil-bath which had been preheated at 180°. The volatile products (65% yield) were collected in the receiver, and subjected to careful vpc analyses. The pyrolysate was revealed to consist of six hydrocarbons as shown in Scheme 1. The first, second, third, and fifth components were readily assigned to toluene (6.9%), cyclohepta-1,4-diene (**6**, 25%),[10] cyclohepta-1,3-diene(**7**, 6.3%),[10] and *endo*-tricyclo[3.2.1.$0^{2,4}$]octane (**10**, 38%),[11] respectively, by comparison of their IR NMR and mass spectra, and the retention times with those of an authentic sample. Both fourth and fifth components are highly unstable olefins, and their mass spectra show the molecular peak at *m/e* 106. The NMR spectrum of the former component (8.6%) shows the vinyl proton resonances at δ 5.42 (multiplet, H^a)[12] and 5.75 (broad singlet, 2H) as well as signals due to

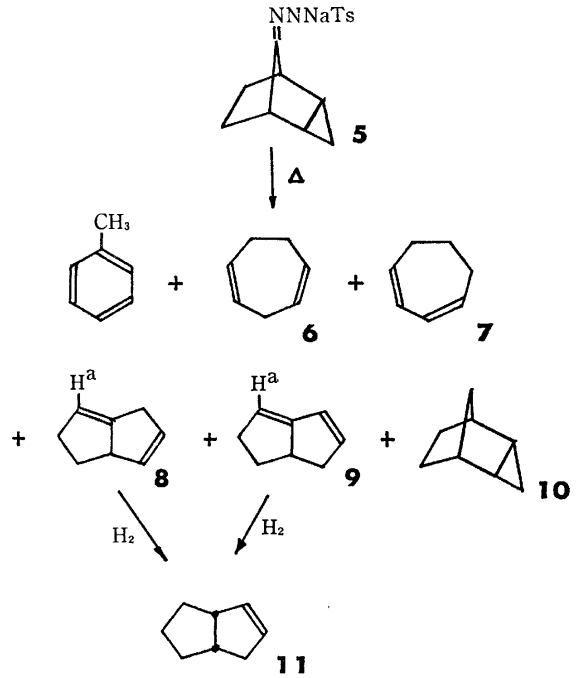

Scheme 1.

the methine proton at 3.45 (multiplet, H), double allylic protons at 2.77 (multiplet, 2H), the allylic protons at 2.34 (multiplet, 2H), and the methylene protons at 1.46 (triplet-doublet, 2H). The UV spectrum shows $\lambda_{max}^{n\text{-hexane}}$ 218 nm, indicating its non-conjugated olefin structure. Careful hydrogenation over palladium in carbon tetrachloride gave *cis*-bicyclo[3.3.0]oct-2-ene (**11**).[13] Thus, the structure was assigned to bicyclo-[3.3.0]octa-1,6-diene(**8**). On the other hand, the NMR spectrum of the fifth component (16% yield) shows signals arising from the vinyl protons at δ 5.27 (multiplet, H^a) and 6.23 (singlet, 2H), the methine proton at 3.0 (multiplet, H), the allylic protons at 2.83—1.89 (multiplet, 4H), and the methylene protons at 1.49 (triplet-doublet, 2H). The UV spectrum shows $\lambda_{max}^{n\text{-hexane}}$ 246 nm, indicating the existence of a conjugated diene moiety. Its hydrogenation gave **11** again. Thus, the structure was assigned to bicyclo[3.3.0]oct-1,7-diene (**9**).[14]

A similar vacuum pyrolysis of sodium salt **13** derived from *exo*-tricyclo[3.2.1.$0^{2,4}$]octan-8-one tosylhydrazone (**12**) gave hydrocarbons (60% yield), consisting of extremely unstable tricyclo[5.1.$0^{2,5}$.$0^{1,7}$]oct-5-ene (**14**, 95.5%) and toluene (2.5%). The NMR spectrum of **14** displays multiplets at δ 5.13 (vinyl proton, H^a), 3.0—2.4 (allylic and methine, 3H), 2.3—1.5 (cyclopropyl and methylene, 4H), 1.15—0.92 and 0.55—0.35 (cyclopropyl, 1H each). Careful hydrogenation of **14** at −30——20 °C over palladium black in carbon tetrachloride caused absorption of one equivalent of hydrogen to yield *trans*-tricyclo[5.1.$0^{2,5}$.$0^{1,7}$]octane (**15**), which was identical with a sample independently prepared by hydrogenation of *trans*-tricyclo[5.1.$0^{2,5}$,$0^{1,7}$]-oct-3-ene (**16**)[15] over palladium black in methanol. The molecular ion in the mass spectrum was found at *m/e* 108. The NMR spectrum consisted of three multiplets at δ 2.93—1.14 (10H), 0.64—0.24 (1H), and −0.22——0.46 (1H).

Pyrolysis of sodium salt **18** derived from 7-norbornenone tosylhydrazone (**17**) at 180° gave hydrocarbons

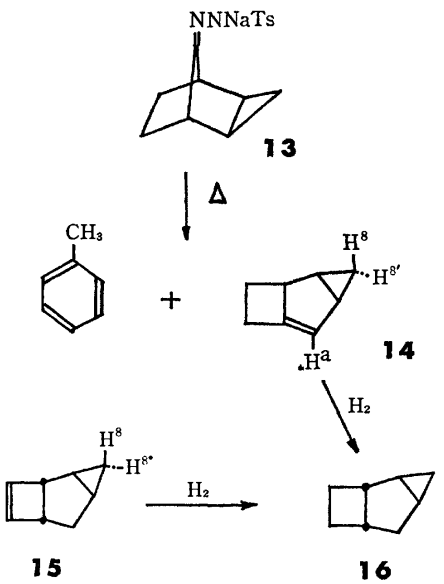

Scheme 2.

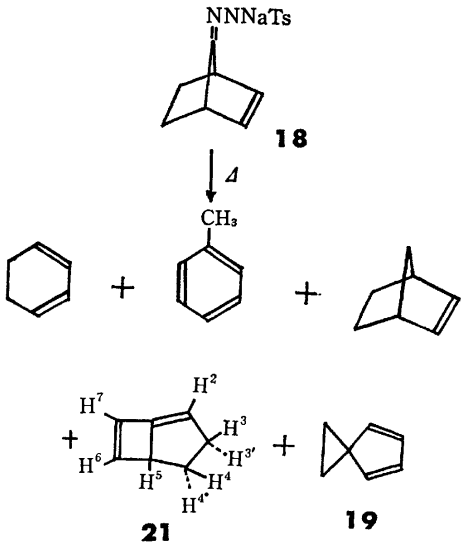

Scheme 3.

(80% yield),[16] which by careful vpc analyses was found to consist of five components in the ratio 3.7 : 8.0 : 70 : 5.7 : 12. The first, second, and fourth components were assigned to 1,3-cyclohexadiene, norbornene, and toluene, respectively, by comparison of their spectral data and the vpc retention times with those of the corresponding authentic sample. The structure of the fifth component was assigned to spiro[2.4]hepta-4,6-diene (**19**) by spectral comparison with an authentic sample.[17] For the sake of confirmation, **19** was converted into the TCNE adduct **20**. The NMR spectrum (acetone-d_6) includes signals due to the vinyl protons at δ 6.85 (triplet, 2H), the bridge protons at 3.88 (triplet, 2H), and the cyclopropyl protons at 1.05 (A_2X_2, 4H). The structure of the third, very unstable component was confirmed as follows. Hydrogenation over Pd-sponge gave bicyclo[3.2.0]pentane, which was identical with a sample prepared by hydrogenation of bicyclo[3.2.0]-hepta-2,6-diene.[18] The mass spectrum showed a molecular peak at *m/e* 92. The presence of three vinyl protons was indicated by the NMR spectrum (δ 6.67 doublet, 6.36 triplet, and 4.92 quartet). Thus, structure **21** or **22** can be considered. Double irradiation experiments showed that H_2 (δ 4.92) is not coupled to the vinyl protons, either H^6 (6.36) or H^7 (6.67), and coupled to methylene protons (H^3 and $H^{3'}$). This confirms the structure of bicyclo[3.2.0]hepta-1,6-diene (**21**) as the third component of the volatile products. Treatment of **21** with tetracyanoethylene at −78° gave rise to the TCNE-adduct, 8,8,9,9-tetracyanotricyclo[5.2.$0^{1,4}$.$0^{1,7}$]oct-2-ene (**23**). The structure of the adduct was firmly established by analysis of the IR (2260 cm^{-1}, C≡N), mass (*m/e* 220), and NMR spectra. The 100 MHz NMR spectrum ($CDCl_3$) showed absorption at δ 6.47 (H^3, doublet-doublet), 6.21 (H^2, doublet), 3.87 (H^7, multiplet), 3.63 (H^4, multiplet), 2.55 (H^5, $H^{5'}$, multiplet 2.30, and 1.80 (H^6, $H^{6'}$, multiplet). Double irradiation experiments showed that H^7 was coupled to H^6 and $H^{6'}$. Control experiments showed that norbornene, **19** and **21** are stable under the pyrolysis conditions in the presence of so-

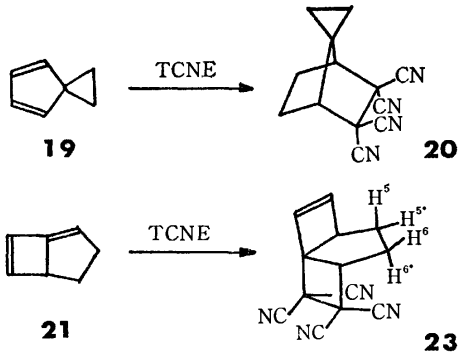

Fig. 2.

dium p-toluenesulfinate. When the pyrolysate left to stand at −20 °C, the diene **19** polymerized gradually, but other products remained unchanged.

The products of vacuum pyrolyses of **5**, **13**, and **18** are explained reasonably by assuming the intermediacy of free carbene.[1,2] However, the pyrolysis products of either **5** or **13** are different from those derived from decomposition of **5** and **13** prepared with sodium methoxide in diglyme.[6] Thus, tetracyclo[3.3.0^{2,8}.0^{4,6}]-octane, which is the main product of decomposition of **5** in diglyme, could not be detected among the products of the vacuum pyrolysis of **5**. Under the conditions of thermolysis in diglyme, two major reaction routes, a carbonium ion pathway as well as a carbene pathway, can be involved. Carbon-hydrogen and carbon-skelton rearrangements can be derived from a highly energetic cation.[19] Thus, no real chemical discrepancy between **1** and **2** can be pointed out. A favorable pathway of the reaction of **2** affording **6**—**10** can be envisioned as shown in Scheme 4. Dienes **8** and **9** can be formed by bond cleavage between C-1 and C-7 of a highly strained intermediate **24** derived from symmetrical interaction of the olefin-like cyclopropyl ring orbitals with the p-orbital of the divalent carbon. This resembles the behavior of bicyclo[3.3.1]nonen-9-ylidene[2] and indicates the nonclassical stabilization[3] of carbene **2**. It is noteworthy that tricyclo[5.1.0^{2,5}.0^{1,7}]oct-5-ene and its derivatives which can be formed *via* the 1,2-alkyl shift could not be detected among the products. Cycloheptadiene **6** can stem from cycloreversion[10] of **2** *via* the biradical intermediate **25**, accompanied by the release of a singlet carbon atom C_1. Analogous fragmentation and release of carbon atom were observed in quadricyclanylidene[20] and **3** forming cyclohexa-1,3-diene as a product. Diene **7** is an isomerization product of diene **6**.[10] Compound **10** is a hydrogen-abstraction product of carbene **2**, as norbornene arises from carbene **3**. The products from carbene **3** can be rationalized by Scheme 5. Diene **21** would arise *via* the 1,2-rearrangement (a) and diene **19** *via* the 1,2-rearrangement (b) followed by 1,5-sigmatropic rearrangement.[21] Preference of the formation of **21** to that of **19** indicates that **21** would arise fulfillment of the carbene π-bond interaction. The 1,2-rearrangement (a) of **3** finds analogies in carbonium ion chemistry.[9] It is noteworthy that the 1,3-insertion product, tricyclo[4.1.0.0^{3,7}]hept-4-ene[22] could not be detected among the reaction products;

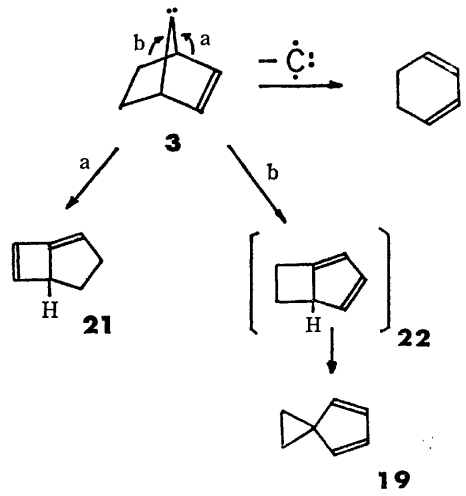

Scheme 5.

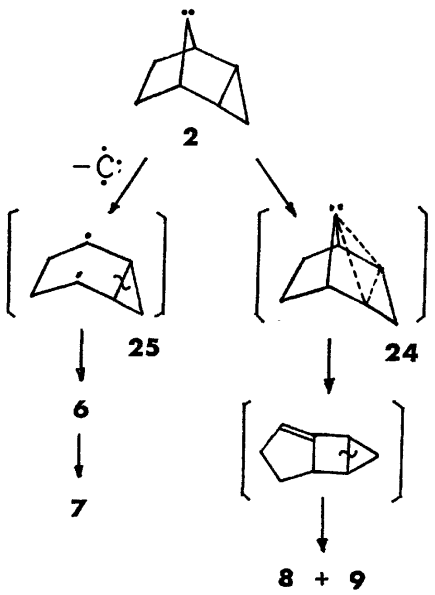

Scheme 4.

considerable 1,3-insertion products were obtained in the reaction of norbornanylidene.[1] This also suggests the presence of the carbene-π bond interaction in carbene **3**.

In sharp contrast, in the *exo*-carbene **1**, no participation of the cyclopropane ring can be observed to stabilize the carbenic center. The result was analogous to that of norbornanylidene which is suggested to have normal geometry and a triplet ground state.[1] Migration of C-7 (**26**) affording **14** is an exclusive pathway, which is presumably ascribed to steric reason.

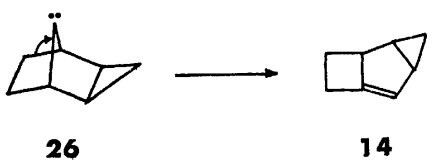

Fig. 3.

In brief, the presence of significant homoconjugative interaction between the p-orbital of the divalent carbon and either the symmetric Walsh orbital of the cyclopropane ring or the p-orbital of the carbon-carbon double bond can be demonstrated by comparative studies of the chemical reactivities of the carbenes **1**—**3** and norbornanylidene.

Experimental

All melting points are uncorrected. Infrared spectra were determined with a Hitachi 215 spectrometer, and NMR spectra with JNM-4H-100 with the use of internal tetramethylsilane. Mass spectra were taken on a Hitachi RSM-4 mass spectrometer. Vpc analyses were carried out on YANACO-550T and JEOL-20K.

endo-*Tricyclo[3.2.1.0^{2,4}]octan-8-one.*[11] Hydrolysis of 8,8-dimethoxy-*endo*-tricyclo[3.2.1.0^{2,4}]octane [bp 84°/9 mm Hg; NMR (CCl_4) δ 3.25 (s, 3H), 3.15 (s, 3H), 2.03 (m, 2H), and 1.72—0.56 (m, 8H)], with 3 M $HClO_4$ solution gave the ketone in 67% yield. IR (liquid film) 1760 cm^{-1} (C=O).

endo-*Tricyclo[3.2.1.0^{2,4}]octan-8-one* p-*Touenesulfonylhydrazone (4).* A mixture of *p*-toluenesulfonylhydrazine (2.1 g, 11 mmol) and the ketone (1.1 g, 8.6 mmole) in ethanol (55 ml) was stirred for 40 min at 65°C. Evaporation of ethanol, followed by washing with ether and methanol gave pure tosylhydrazone (2.4 g, 94%): mp 171.5—172 °C (decomp); IR (Nujol mull) 3210 (N-H), 1685 (s), 1600(s), 1350(s), 1314(s), 1180(s), 1095(m), 980(s), and 925(s) cm^{-1}; NMR ($CDCl_3$) δ 7.77 (AX, J=8 Hz, 2H), 7.24 (AX, J=8 Hz, 2H), 2.42 (broad s, 3H), and 1.8—0.6 (m, 10H).

Pyrolysis of the Sodium Salt (5) of endo-*Tricyclo[3.2.1.0^{2,4}]octan-8-one* p-*Touenesulfonylhydrazone (4).* To a suspension of sodium hydride (1 g, 21 mmol) prewashed with dry THF (10 ml) in a 200 ml-round flask was added a solution of tosylhydrazone **4** (5 g, 17 mmol) in THF (105 ml). The mixture was stirred under nitrogen until the evolution of hydrogen ceased. Evaporation of THF gave white powder. Further removal of THF under reduced pressure at 130 °C gave sodium salt **5**. The flask was bridged with glass tubing to a trap cooled at 77 K under reduced pressure (2 mmHg), when the salt was immersed into an oil bath preheated at 180 °C, spontaneous decomposition occurred to give the pyrolysate (1 g, 56%) in the trap. The pyrolysate was subjected to the vpc analysis (KF-96, injection temp 105 °C, detector temp 130 °C, colomun temp 60 °C). The vpc showed that six components were existent in the reaction mixture in the ratio 7 : 25 : 6 : 9 : 16 : 38, which was uncorrected for vpc detector response. The retention times of these products are 6, 11, 12, 16, 19, and 21 min, respectively. The first component was assigned to toluene, the second to cyclohepta-1,4-diene (**6**) [Mass *m/e* 94; NMR (CCl_4) δ 5.95—5.12 (m, 4H), 3.00—2.70 (m, 2H), and 2.35—2.14 (m, 4H); IR (liquid film) 1660 cm^{-1} (C=C)], the third to cyclohepta-1,3-diene (**7**) [Mass *m/e* 94; NMR (CCl_4) 5.84—6.65 (broad s, 4H) 2.55—2.16 (m, 4H), and 2.10—1.61 (m, 2H)], the sixth to *endo*-tricyclo[3.2.1.0^{2,4}]octane (**10**) [Mass *m/e* 108; IR (liquid film) 3080(m), 3030(s), 3015(s), 2960(s), 2880(s), 1480(m), 1455(m), 1440(m), 1315(s) 1250(w), 1175(w), 1150(w), 1120(m), 1075(w), 1040(m), 1015(w), 1000(m), 920(w), 900(w), 860(w), and 720(s) cm^{-1}]. Each product was collected by preparative vpc (KF-96, 20%, 6m). The extremely unstable fourth component collected in a receiver at —78° was assigned to bicyclo[3.3.0]oct-1,6-diene (**8**) according to the following data. Mass *m/e* 106; NMR (CCl_4) δ 5.54—5.32 (m, H), 5.81—5.70 (broad s, 2H), 3.75—3.27 (broad m, H), 2.87—2.71 (m, 2H), 2.62—2.12 (m, 2H), and 1.46 (d-t, $J_{H^4H^5}$=8 Hz, $J_{H^3H^4}$=10 Hz, 2H). Hydrogenation of the sample collected by vpc over palladium in carbon tetrachloride afforded a sample containing two products. Preative vpc (Ucon oil 20%, 2m, colomun temp 75 °C) of the main component gave *cis*-bicyclo[3.3.0]-oct-2-ene in a 65% yield. Mass *m/e* 108; NMR (CCl_4) δ 5.44 (m, 2H), 3.37—2.88 (m, H), 2.88—2.60 (m, H), 2.60—2.28 (m, H), 2.28—1.97 (m, H), and 1.97—0.71 (m, 6H). The minor product, mass *m/e* 106, was tentatively assigned to *cis*-bicyclo[3.3.0]oct-2,6-diene, which was probably derived from **8** *via* palladium induced 1,3-hydride site.[23] The fifth extremely unstable component was assigned to bicyclo-[3.3.0]oct-1,7-diene (**9**), [Mass *m/e* 106; NMR (CCl_4) δ 5.40—5.20 (m, H), 6.23 (broad s, 2H), 3.38—2.62 (broad m, H), 2.83—1.89 (m, 4H), and 1.49 (t-d, $J_{H^3H^4}$=11 Hz, $J_{H^4H^5}$=8 Hz, 2H)]. Hydrogenation over palladium-charcoal (5%) in carbon tetrachloride followed by preparative vpc gave *cis*-bicyclo[3.3.0]oct-2-ene in 69% yield along with *cis*-bicyclo[3.3.0]oct-2,7-diene, since hydrogenation of **8** gave the same product.

exo-*Tricyclo[3.2.1.0^{2,4}]octan-8-one.* To a suspension of Zn(Cu) (36 g) in dry ether (200 ml) was added freshly distilled methylene iodide (2 g) with stirring. To the mixture was added a solution of 7,7-dimethoxynorbornene(20 g) and and methylene iodide (80 g) with rigorous stirring at reflux for 1 hr. After stirring for 1 hr, a solution of 0.5 M HCl and ice was added. The usual work-up followed by distillation gave a mixture (10.2 g, 67—75°C/30 mmHg), which contained norbornen-7-one (8%), an unidentified product (16%), *exo*-tricyclo[3.2.1.0^{2,4}]octan-8-one (70%), and *exo*-8,8-dimethoxy-tricyclo[3.2.1.0^{2,4}]octane (6%). Mass *m/e* 168; IR (CCl_4 (liquid film) 3100 and 1020 cm^{-1} (cyclopropyl C-H); NMR (CCl_4) δ 3.03 (s, 6H), 2.06 (broad s, 2H), 1.7 (m, 2H), 1.30—1.15 (m, 4H), and 0.75 (m, 2H). Found: C, 71.28; H, 9.95%. Calcd for $C_{10}H_{16}O_2$: C, 71.39; H, 9.95%. Further fine distillation gave pure *exo*-tricyclo[3.2.1.0^{2,4}]octan-8-one (bp 75 °C/30 mmHg) in 32% yield. Mass *m/e* 122; IR (liquid film) 1775 cm^{-1} (C=O); NMR (CCl_4) δ 1.98 (broad s, 2H), 1.77 (broad s, 4H), 1.16 (d-d, $J_{H^2H^3}$=3.4 Hz, $J_{H^2H^{3'}}$=6.9 0.50 (d-t, $J_{H^3H^{3'}}$=6,9 Hz, $J_{H^2H^{3'}}$=6.9 Hz, H$^{3'}$), and 0.14 (d-t, $J_{H^3H^{3'}}$=6.9 Hz, $J_{H^2H^3}$=3.4 Hz, H^3). Found: C, 78.68; H, 8.36%. Calcd for $C_8H_{12}O$: C, 78.65; H, 8.23%. *exo*-8,8-Dimethoxytricyclo[3.2.1.0^{2,4}]octane can be quantitatively converted into the ketone on treatment with a small amount of acetic acid at ambient temperature for 8 hr.

exo-*Tricyclo[3.2.1.0^{2,4}]octan-8-one* p-*Touenesulfonylhydrazone (12).* *p*-Toluenesulfonylhydrazine (6 g, 32 mmol) was dissolved in a minimum amount of dry methanol, and *exo*-tricyclo[3.2.1.0^{2,4}]octan-8-one (4 g, 33 mmol) was added. The mixture was stirred under reflux for 30 hr. On standing, a precipitated colorless solid was collected by filtration. Recrystallization from methanol gave **12** (5 g, 53%). [Mp 165—166°; IR (Nujol mull) 3330 cm^{-1} (N-H); NMR (acetone-d_6) δ 7.88 (AX, J=9 Hz, 2H), 7.51 (AX, J=9 Hz, 2H), 3.2 (broad s, H), 2.45 (s, 3H), 2.3 (broad s, 2H), 1.6 (broad s, 4H), 1.05—0.95 (m, 2H), 0.16 (d-t, $J_{H^2H^3}$=6.55 Hz, $J_{H^3H^{3'}}$=6.7 Hz, H^3), and —0.33 (d-t, $J_{H^3H^{3'}}$=6.7 Hz, $J_{H^2H^{3'}}$=3.5 Hz, H$^{3'}$). Found: C, 62.16; H, 6.13; N, 9.76; S, 11.21%. Calcd for $C_{15}H_{18}N_2O_2S$: C, 62.04; H, 6.25; N, 9.65; S, 11.04%].

Pyrolysis of the Sodium Salt (13) of exo-*Tricyclo[3.2.1.0^{2,4}]octan-8-one* p-*Touenesulfonylhydrazone (12).* Vacuum pyrolysis of salt **13** prepared from sodium hydride (0.7 g, 15 mmol) and **12** (3.2 g, 11 mmol) gave the pyrolysate (0.7 g, 60%) in a cold trap. Vpc analysis (KF-96, 20%, 2m, 80 °C) showed that three components were contained in the ratio 2.5 : 2.2 : 95.3. The first component was assigned to toluene,

but the second component could not be identified. Preparative vpc (Ucon oil, 20%, 2m, 50 °C) gave an analytical sample of the extremely unstable third component, assigned to tricyclo[5.1.$0^{2,5}$.$0^{1,7}$]oct-5-ene (**14**) according to the following spectral data. Mass *m/e* 106, NMR(CCl_4) (at −20 °C) δ 5.20—5.08 (m, H), 3.00—2.40 (m, 3H), 2.30—1.50 (m, 4H), 1.03 (d-t, $J_{H^1H^8}=4.05$ Hz, $J_{H^8H^{8'}}=4.05$ Hz, H^8), and 0.44 (d-t, $J_{H^1H^8}=8.3$ Hz, $J_{H^8H^{8'}}=4.05$ Hz, $H^{8'}$)]. Hydrogenation **14** over palladium black at −30—20 °C in carbon tetrachloride gave tricyclo[5.1.$0^{2,5}$.$0^{1,7}$]octane (**15**), [Mass *m/e* 108; (CCl_4) 3080(m), 3045(m), 2950(s), 2875(s), 1730(w), 1460(m), 1380(w), 1338(w), 1300(w), 1250(w), 1120(w), 1080(w), 1030 (w), 1005(w), 980(w), 830(w), 810(m), 790(w), and 730(w); NMR (CCl_4) δ 2.93—1.14 (m, 10H), 0.43 (d-t, $J_{H^8H^{8'}}=$ 4.2 Hz, $J_{H^1H^8}=8.4$ Hz, H^8), and −0.34 (d-t, $J_{H^8H^{8'}}=4.2$ Hz, $J_{H^1H^{8'}}=4.2$ Hz, $H^{8'}$)], which was independently synthesized by hydrogenation of *trans*-tricyclo[5.1.$0^{2,5}$.$0^{1,7}$]oct-3-ene (98 mg) over palladium black in methanol.

7-Norbornenone p-*Toluenesulfonylhydrazone* (***17***). 7-Norbornenone was prepared by the method of Gassman and Rape[24] from 7,7-dimethoxybicyclo[2.2.1]hept-2-ene, [Bp 64.5 —65.5 °C/30 mmHg, IR (liquid film) 1860, 1790, and 1780 cm^{-1} (C=O); NMR (CCl_4) δ 0.9—2.5 (m, 4H), 2.75 (q, 2H), 6.5(t, $J=2.5$ Hz, 2H)]. A solution of *p*-toluenesulfonylhydrazine (2.2 g, 12 mmol) and 7-norbornenone (1.3 g, 12 mmole) in methanol (30 ml) was stirred at ambient temperature for 1 hr. Precipitated white crystals were collected and recrystallized from methanol to give **11** (2.7 g, 82%). [Mp 159—160 °C (decomp); IR (Nujol mull) 3230 (N-H), 1720(s), 1600(s), 1460(s), 1330(s), 1290(m), 1170(s), 1090(s), 1018(s), and 930(s). NMR (acetone-d_6) δ 7.73 (AX, $J=8$ Hz, 2H), 7.35 (AX, $J=8$ Hz, 2H), 6.55 (t, $J=2$ Hz, 2H), 3.6(m, 1H), 2.65—2.8 (m, 2H), 2.38(s, 3H), 1.6— 2.0 (m, 2H), and 1.0—1.3 (m, 2H). Found: C, 60.57; H, 5.96; N, 10.01%. Calcd for $C_{14}H_{16}N_2SO_2$: C, 60.85; H, 5.84; N, 10.13%].

Pyrolysis of the Sodium Salt (***18***) *of 7-Norbornenone* p-*Toluenesulfonylhydrazone* (***17***). Vacuum pyrolysis of salt **18** prepared from tosylhydrazone **17** (7.68 g, 28 mmol) and sodium hydride (0.16 g) gave volatile products (2 g) in the trap. Vpc analyses (di-*n*-decyl phthalate 2 m, column temp 60 °C, detecter temp 135 °C, injection temp 130 °C) showed that five components were contained in the reaction mixture in the ratio 1.0 : 2.2 : 19 : 1.5 : 3.3. The first component was assigned to 1,3-cyclohexadiene, the second to norbornadiene, and fourth to toluene. These compounds were collected by preparative vpc, and their structures were determined by comparison with those of authentic samples. The fifth component was assigned to spiro-[2.4]heptadiene-(**19**) which was identified by comparison of their NMR spec trum with that of an authentic sample. NMR (CCl_4) δ 7.45 (m, 2H), 6.05—5.75 (m, 2H), 1.52 (s, 4H); Mass *m/e* (species %) 92 (M^+, 100), 91 (M^+-1, 215), 65 ($M^+ + 1 - C_2H_4$, 37), 63($M^+ - C_5H_5$, 15). For confirmation of the stractural assignment, **19** was converted into the TCNE adduct. To a solution of tetracyanoethylene (692 mg, 5.4 mmol) in THF (20 ml) was added **19** (500 mg, 5.4 mmol) with stirring. After being stirred for 1 hr, precipitated white crystals were collected by filtration. Recrystallization from THF gave the adduct **20** (1.1 g, 90%). [Mp 217 °C (decomp); NMR (acetone-d_6) δ 6.85 (t, $J=2.5$ Hz, 2H), 3.88 (t, $J=2.5$ Hz, 2H), and 1.05 (A_2X_2, $\Delta\nu/J$ 2, 4H). Mass *m/e* 220(M^+). Found: C, 70.61; H, 3.70; N, 25.50%. Calcd for $C_{13}H_{18}N_4$: C, 70.89; H, 3.66; N, 25.44%]. The fourth component, highly polymerizable even at −20 °C, was assigned to bicyclo[3.2.0]hept-1,6-diene (**21**) as follows. Hydrogenation of a sample collected by vpc palladium-sponge in ether at −30° gave rise to bicyclo[3.2.0]heptane. Mass *m/e* 96; NMR (CCl_4) δ 2.7 (m, 2H), 2.4—1.7 (m, 4H), and 1.6— 1.2 (m, 6H). The NMR spectrum was identical with that of the sample prepared by hydrogenation of bicyclo[3.2.0]-hept-2,6-diene. Mass *m/e* (species, %) 92 (M^+, 100), 91($M^+ - 1$, 360), 73(620), 72(1900), 71(1000), 58(400), and 57(2900); NMR (CS_2, −60 °C) δ 6.67 (d, $J=1.5$ Hz, H^7), 6.36 (t, $J=2$ Hz, H^6), 4.92 (q, H^2), 3.6—3.0 (m, H^5), and 3.0—1.0 (m, 4H). To a solution of the pyrolysate in THF was added a solution of TCNE in THF at −60°. White crystalline material precipitated was collected and recrystallized from THF and acetone to give pure 8,8,9,9-tetracyanotricyclo[5.2.0]oct-2-ene (**23**). [Mp 154—155°; IR (Nujol mull) 2260(m), 1310(m), 1305(s), 1280(m), 1195(m), 1150(m), 905(m), 800(m), 785(s), 760(s), and 700(m) cm^{-1}; NMR($CDCl_3$) δ 6.47 (d-d, $J_{H^1H^2}=3$ Hz, H^2), 6.21(d, H^1), 3.87(d, H^8), 3.63 (m, H^3), 2.55(m. H^4, H^5), and 2.30 and 1.89(m, H^6, H^7). Found: C, 70.70; H, 3.70%. Calcd for $C_{13}H_8N_4$: C, 70.89; H, 3.66%].

Photolysis of the Sodium Salt (***18***) *of* p-*Toluenesulfonylhydrazone* (***17***). A solution of sodium salt (**18**, 30 mg) in THF (10 ml) was irradiated at −78 °C with a high pressure mercury arc for various periods of time with and without Pyrex filter. Aliquots were withdrawn periodically and examined by vpc.

References and Notes

1) R. A. Moss and J. R. Whittle, *Chem. Commun.*, **1969**, 341.

2) M. H. Fisch and H. D. Pierce, *ibid.*, **1970**, 503.

3) R. Gleiter and R. Hoffmann, *J. Amer. Chem. Soc.*, **90**, 5457 (1968).

4) H. Tanida, T. Tsuji, and T. Irie, *ibid.*, **89**, 1953. (1967); M. A. Batiste, C. L. Derup, R. E. Pincock, and J. Haywood-Farmer, *ibid.*, **89**, 1954 (1967).

5) R. Hoffmann, *Tetrahedron Lett.*, **1965**, 3819.

6) P. K. Freeman, R. S. Raghavan, and D. G. Kuper, *J. Amer. Chem. Soc.*, **93**, 5288 (1971).

7) Preliminary report, S. -I. Murahashi, K. Okumura, T. Kubota, and I. Moritani, *Tetrahedron Lett.*, **1973**, 4197.

8) R. A. Moss, U-H. Dolling, and J. R. Whittle, *ibid.*, 931 (1971).

9) S. Winstein, A. H. Lewin, and K. C. Pande, *J. Amer. Chem. Soc.*, **85**, 2324 (1963).

10) W. von E. Doering and W. R. Roth, *Tetrahedron*, **19**, 715 (1963); E. Vogel, K. H. Ott, and K. Gajek, *Ann. Chem.*, **644**, 172 (1961).

11) S. C. Clark, K. J. Frayne, and B. L. Johnson, *Tetrahedron*, **25**, 1265 (1969).

12) The signal at δ 5.42 is due to the vinyl proton of H^a. The C_2-H proton of bicyclo[3.2.0]hept-1-ene appears at δ 5.13.[1]

13) D. R. Stappand and R. F. Kleinschmidt, *J. Org. Chem.*, **30**, 3006 (1965).

14) G. N. Fickes and C. B. Rose, *J. Org. Chem.*, **37**, 2898 (1972).

15) W. R. Roth and B. Peltzer, *Ann. Chem.*, **685**, 56 (1965).

16) Irradiation of sodium salt **18** in THF gave toluene, which was identified by comparison of the retention time and mass spectroscopic data with those of an authentic sample. Control experiments showed that toluene could not be obtained by photolysis of either sodium *p*-toluenesulfinate or any products of thermally generated **3**.

17) K. Alder, H.-J. Ache, and F. H. Flock, *Chem. Ber.*, **93**, 1888 (1960).

18) W. G. Dauben and R. G. Cargill, *Tetrahedron*, **12**, 186 (1961).

19) K. B. Wiberg and J. M. Lavanish, *J. Amer. Chem. Soc.*, **88**, 5272 (1966); F. Cook, H. Shechter, J. Bayless, L. Friedman, R. L. Foltz, and R. Randall, *ibid.*, **88**, 3870 (1966).
20) P. B. Shelvin and A. P. Wolf, *Tetrahedron Lett.*, **1970**, 3987.
21) N. K. Hamer and M. Stubbs, *Chem. Commun.*, **1970**, 1013.
22) Tricyclo[4.1.0.$0^{3,7}$]hept-4-ene was reported as the product (1%) of **3** thermally generated from the lithium salt of **17**.[8] However, this was not detected among the products of **3** thermally generated from the sodium salt of **17**. There is not much discrepancy between the products from the sodium salt and the lithium salt; cyclohexa-1,3-diene (3.0%), norbornene (6.4%), **21** (56%), toluene (4.6%) and **19** (9.6%) *vs.* cyclohexa-1,3-diene (2.3%), norbornene (0.9 %), **21** (67%), toluene (1.6%), and **19** (6.9%).
23) G. V. Smith and J. R. Swoop, *J. Org, Chem.*, **31**, 3904 (1966); G. M. Green, R. N. Haszeldine, and J. Lindley, *J. Organometal. Chem*, **6**, 107 (1966).
24) P. G. Gassman and P. G. Rape, *J. Org. Chem.*, **29**, 160 (1960).

The One-electron Reduction of Carbonium Ions. VII. A Kinetic Study of the Reduction of the Aryl- and *n*-Alkyl-substituted Tropylium Ions with Cr(II)

Kunio OKAMOTO, Koichi KOMATSU, Masami FUJIMORI, and Sumio YASUDA

Department of Hydrocarbon Chemistry, Faculty of Engineering, Kyoto University, Sakyo-ku, Kyoto 606

(Received March 13, 1974)

A series of substituted phenyltropylium (I) and *n*-alkyltropylium ions (II) has been synthesized, and the kinetic measurements for the one-electron reduction of these ions have been carried out with Cr(II) in 10% HCl at 25 °C. A linear correlation is observed between the log k_2 values, for I (X-C_6H_4-$C_7H_6^+$, X=*p*-OH, *p*-OCH_3, *p*-CH_3, H, *p*-Cl, *p*-Br, *p*-CN, *m*-OCH_3) and for II (C_nH_{2n+1}-$C_7H_6^+$, $n=0$, 1—6), and the transition energy of the charge-transfer band of these ions, with pyrene as a donor. In addition, the values of log k_2 for I exhibit a good linear free-energy relationship with pK_{R^+} and also with the σ-value ($\rho=+1.31$), but not with σ^+. The *n*-alkyl group is shown to diminish the reducibility of the tropylium ion, and a slight alternation effect of the length of the *n*-alkyl chain on the k_2's is observed.

In previous papers of this series, we have reported on the chromous-ion reduction of some substituted tropylium[1a,b] and cyclopropenium ions.[1c] It was demonstrated that the reducibility of these carbonium ions depends mainly on the electron affinity of the respective cations and that it is also linearly correlated with their pK_{R^+} values.

In the present study, first, we have investigated the effect of substituents on the reducibility of the phenyltropylium ion. The problem with regard to the nature and extent of the electronic effect exerted by phenyl substituents upon the electronic state of a tropylium ring has aroused much interest[2,3] especially when it has been assumed that the plane of the phenyl ring makes a considerable dihedral angle with the seven-membered ring in the phenyltropylium system. Thus, Jutz and Voithenleitner[2] have synthesized a series of aryltropylium ions and discussed their pK_{R^+}'s and electronic spectra; Schuster and his coworkers[3] have carried out the HMO calculation of the various aryltropylium ions and compared the results with their electronic and NMR spectra. However, no systematic study of the chemical reactivity of aryltropylium ions seems yet to have been reported.

Secondly, we have also synthesized a series of *n*-alkyltropylium ions and examined the effect of the alkyl-chain length upon the properties and reducibility of these ions.

Results and Discussion

The salts of the aryltropylium ions (Ia—f, h·Y^-) were prepared according to the method of Jutz and Voithenleitner.[2] *p*-Cyanophenyltropylium perchlorate (Ig·ClO_4^-) is a new compound; it was synthesized by hydride abstraction from 7-(*p*-cyanophenyl)-1,3,5-cycloheptatriene, which in turn has been prepared from 7-(*p*-aminophenyl)-1,3,5-cycloheptatriene by the use of the Sandmeyer reaction.

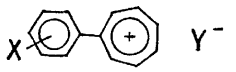

	X	Y
Ia	*p*-OH	BF_4
Ib	*p*-OCH_3	BF_4
Ic	*p*-CH_3	BF_4
Id	H	BF_4
Ie	*p*-Cl	ClO_4
If	*p*-Br	ClO_4
Ig	*p*-CN	ClO_4
Ih	*m*-OCH_3	ClO_4

The perchlorates of the *n*-alkyltropylium ions (II: C_nH_{2n+1}-$C_7H_6^+\cdot ClO_4^-$; $n=1-6$, 8, 12) were prepared, in part ($n=3,4,5,6,8$) for the first time, in a similar manner from 7-alkyl-1,3,5-cycloheptatrienes, which had themselves been synthesized by the reaction of alkylmagnesium bromides with 7-ethoxy-1,3,5-cycloheptatriene. The spectral and analytical data for II are listed in Table 1. It is of interest to note that the change in the mp's of these salts with the increase in the alkyl-chain length exhibits a tendency similar to that of *n*-alkylbenzenes, as is shown in Fig. 1.

The I and II ions are all readily soluble and quite stable in such polar solvents as acetonitrile and aqueous HCl except for II ($n=8,12$), which is hardly soluble in aqueous HCl (10%), though it dissolves rather more readily in a non-polar solvent, benzene.[4] Thus, the one-electron reduction was carried out for I and II ($n=1-6$) with Cr(II) in 10% HCl and for II ($n=8,12$) with zinc powder in acetonitrile. The respec-

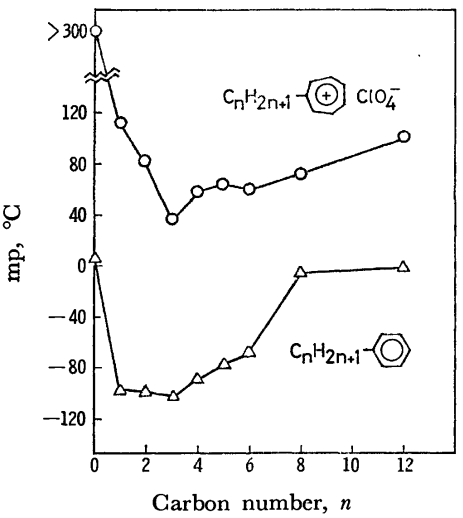

Fig. 1. The effect of the alkyl-chain length on mp's of alkyltropylium perchlorates and of alkylbenzenes. (Δ: mp's of alkylbenzenes, cited from G. Egloff, "Physical Constants of Hydrocarbons," Vol. III, Reinhold Publishing Co., N. Y. (1946))

Table 1. Physical properties and analytical data of *n*-alkyltropylium perchlorates

Substituent	mp °C	UV $\lambda_{max}^{10\%\ HCl}$ nm	UV (log ε)	Elemental analysis Found (Calcd) C%	H%
H-[a]	>300	273.5	(3.64)	—	—
CH_3-[b]	110.0—111.5	287	(3.68)	—	—
C_2H_5-[b]	84.0—84.3	292	(3.69)	—	—
C_3H_7-	36.0—41.1	296	(3.69)	51.59 (51.62)	5.58 (5.63)
C_4H_9-	65.0—66.3	297.5	(3.78)	53.44 (53.55)	6.10 (6.13)
C_5H_{11}-	72.5—73.9	297.5	(3.77)	55.54 (55.28)	6.58 (6.57)
C_6H_{13}-	64.3—65.2	298.5	(3.75)	56.69 (56.82)	6.85 (6.97)
C_8H_{17}-	77.9—79.5	297.5	(3.76)	59.21 (59.49)	7.64 (7.65)
$C_{12}H_{25}$-	99.0—100.0	298	(3.75)	63.43 (63.58)	8.75 (8.71)

a) H. J. Dauben, Jr., F. A. Gadecki, K. M. Harmon, and D. L. Pearson, *J. Amer. Chem. Soc.*, **79**, 4557 (1957). b) Ref. 1b.

tive tropylium ions gave the dimers of each substituted tropyl radical, *i.e.*, x,x'-disubstituted bitropyl, in almost quantitative yields without the formation of any by-product. The NMR spectra of the products indicated a typical pattern for a cycloheptatrienyl system, together with the signals corresponding to each substituents, in a manner similar to one that has previously been reported.[1b] The analytical and ultraviolet spectral data are shown in Table 4 (see Experimental).

A previous mechanistic study[5] indicated that the chromous ion (0.01—0.02 g-ion/l) in 10% HCl (2.9 M) is co-ordinated with the chloride ion and that, therefore, the one-electron reduction of the carbonium ion in this solvent would proceed effectively by way of the chloride-ion bridging between the two reagents. Thus, the kinetic measurements for the chromous-ion reduction of I and II (n=3—6) were carried out in 10% HCl, by the use of the flow method described previously,[5] to give the results listed in Table 2.

It has already been shown that the transition energy for the charge-transfer band observed between carbonium ions and a given electron donor (*e.g.*, pyrene) is correlated with the relative electron affinity of those cations[6] and also with the log k_2 for the chromous-ion reduction.[1] The I and II ions were also found to exhibit a charge-transfer band ($\nu_{C.T.max}$) with pyrene as the standard electron donor (Table 3); the correlation between log k_2 and the values of $\nu_{C.T.max}$ is reasonably good (Fig. 2) and seems to support the previous assumption[1] that the reducibility of these ions with Cr(II) can be regarded as a relative criterion of the electron affinity of the carbonium ion in solution.

With respect to the aryltropylium ions, I, the reducibility (log k_2) is also linearly related to the pK_{R^+} values, measured spectrophotometrically in 23% ethanol (Table 3), as is shown in Fig. 3. The electron-with-

Table 2. Second-order rate constants for the reaction of the aryl- and *n*-alkyltropylium ions with Cr(II) in 10% HCl at 25 °C

Substituent	Initial concn. R^+ 10^{-2} M	Initial concn. Cr(II) 10^{-2} M	k_2 $M^{-1}\cdot s^{-1}$	$k_{2\ average}$ $M^{-1}\cdot s^{-1}$
p-HO-C_6H_4-	0.470	1.10	63.3	64.3
	0.497	1.06	65.2	
	0.533	0.825	64.5	
p-CH_3O-C_6H_4-	0.458	1.09	60.3	62.1
	0.490	0.957	64.5	
	0.510	0.947	58.7	
	0.528	0.877	64.9	
p-CH_3-C_6H_4-	0.323	0.910	99.0	100
	0.470	1.27	94.2	
	0.503	1.23	108	
C_6H_5-[a]	0.426	0.857	140	144
	0.462	0.928	147	
p-Cl-C_6H_4-	0.248	0.549	230	237
	0.254	0.506	260	
	0.273	0.406	220	
p-Br-C_6H_4-	0.203	0.495	249	252
	0.204	0.438	283	
	0.208	0.536	256	
	0.223	0.484	221	
m-CH_3O-C_6H_4-	0.227	0.525	246	243
	0.211	0.502	240	
p-NC-C_6H_4-	0.0440	0.200	1470	1527
	0.0450	0.142	1580	
	0.0481	0.148	1530	
H-[a]	1.80	3.05	74.1	74.0
	2.05	3.75	73.8	
CH_3-[a]	1.99	4.12	11.1	11.1
	2.60	5.39	11.0	
	2.61	5.20	11.3	
C_2H_5-[a]	2.48	4.87	9.90	10.3
	2.50	5.22	9.80	
	2.60	5.22	11.1	
C_3H_7-	0.590	1.40	11.4	11.4
	0.590	1.44	11.4	
C_4H_9-	0.440	1.53	9.52	9.69
	0.511	1.36	9.86	
	0.950	2.43	9.70	
C_5H_{11}-	0.504	1.36	10.1	10.2
	0.514	1.53	10.6	
	0.574	1.22	9.79	
C_6H_{13}-	0.401	1.26	9.90	9.14
	0.520	1.33	9.12	
	0.635	1.20	8.39	

a) Ref. 1b.

drawing substituents accelerate the reaction rate, whereas the electron-donating groups decelerate it. Thus, the Hammett plot, shown in Fig. 4, gave a positive ρ-value (+1.31). The application of the σ-value[7] gave a better linear correlation (correlation coefficient, 0.980) than that of the σ^+-value[8] (correlation coefficient 0.815) as the substituent constant. This would imply that the *para*-substituent on the phenyl group does not

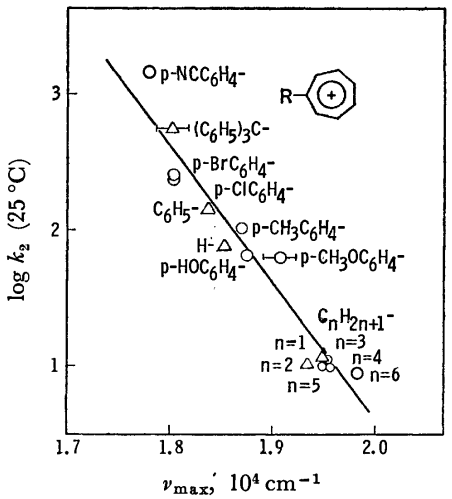

Fig. 2. The correlation of $\log k_2$ with C. T. transition energy (ν_{max}). (Δ: data from Ref. 1a)

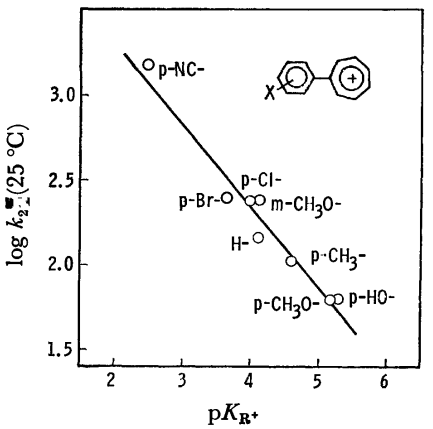

Fig. 3. The correlation of $\log k_2$ with pK_{R^+}.

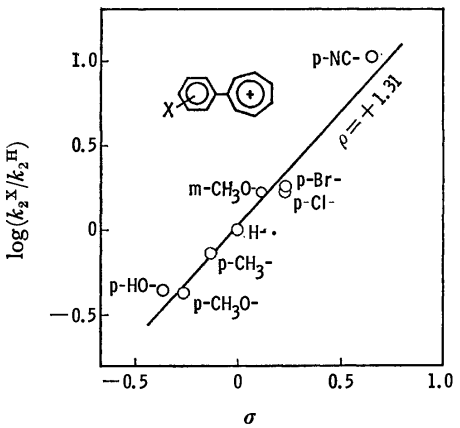

Fig. 4. The correlation of $\log k_2$ with Hammett σ.

Table 3. Results of the measurements of charge-transfer bands and pK_{R^+}'s of substituted tropylium ions

Substituent	$\log k_2$[a] (25 °C)	C. T. band[b] λ_{max} nm	C. T. band[b] ν_{max} 10^4 cm^{-1}	pK_{R^+} Obsd.[c]	pK_{R^+} Lit.[d]
p-HO-C_6H_4-	1.808	533	1.876	5.32	4.96
p-CH_3O-C_6H_4-	1.793	520—530	1.923—1.887	5.17	4.59
p-CH_3-C_6H_4-	2.002	535	1.869	4.61	4.17
C_6H_5-[e]	2.158	544	1.838	4.13	3.88
p-Cl-C_6H_4-	2.375	555	1.802	3.99	3.30
p-Br-C_6H_4-	2.402	555	1.802	3.65	3.25
m-CH_3O-C_6H_4-	2.386	560—570(sh)[f]		4.16	3.51
p-NC-C_6H_4-	3.184	560	1.786	2.51	—
H-[e]	1.869	540	1.852	4.30	4.7[g]
CH_3-[e]	1.046	513	1.949	[h]	
C_2H_5-[e]	1.013	512	1.953		
C_3H_7-	1.057	512	1.953		
C_4H_9-	0.986	511	1.957		
C_5H_{11}-	1.009	513	1.949		
C_6H_{13}-	0.961	504	1.984		

a) The logarithmic value of the averaged rate constant for the chromous-ion reduction of the respective tropylium ions. b) Measured in 1,2-dichloroethane with pyrene as an electron donor. c) Determined in 23% aqueous ethanol. d) Measured in 50% aqueous acetonitrile (Ref. 2). e) Data from Ref. 1b. f) A clear maximum was not observed. g) Determined by potentiometric titration in water (W. von E. Doering and L. H. Knox, *J. Amer. Chem. Soc.*, **76**, 3203 (1954). h) Not determined owing to the decomposition in aqueous media of pH> 1.

exert a strong conjugative effect across the phenyl group upon the tropylium ring in either the ground or transition state, in accord with the assumption that the phenyltropylium ion can not be coplanar, but the planes of phenyl and tropylium rings are twisted more than 45°.[2,3,9]

The results of the reduction of *n*-alkyltropylium ions, II, indicated that the introduction of the alkyl group into the tropylium ring brings about a decrease in the reducibility of the cation. The chain length of the *n*-alkyl substituent was found to have no remarkable effect upon the reducibility, but a slight alternation of $\log k_2$ is observed with the increase in the carbon number of the *n*-alkyl chain. A similar alternating effect is sometimes observed in the case of S_N2 reactions of *n*-alkyl halides.[10]

Experimental[11]

Materials. All the reagents employed were of a reagent-grade quality except when otherwise noted. The acetonitrile and ethyl acetate were refluxed and distilled over phosphorus pentoxide; acetonitrile, bp 81.5—81.7 °C; ethyl acetate, bp 77.0—77.4 °C. The 1,2-dichloroethane for the measurement of the charge-transfer band was dried and distilled over calcium chloride: bp 83.0—83.5 °C.

Aryltropylium ions, Ia-f, h, were prepared according to the method of Jutz and Voithenleitner.[2]

7-(p-Cyanophenyl)-1,3,5-cycloheptatriene was synthesized from 7-(*p*-aminophenyl)-1,3,5-cycloheptatriene[2] by reference to the preparation of *p*-tolunitrile reported by Clarke and Read[12] as follows. Into 25 ml of 20% HCl we dissolved 10.0 g (54.6 mmol) of 7-(*p*-aminophenyl)-1,3,5-cycloheptatriene by vigorous stirring at 60 °C for 10 min. To this turbid solution there was then slowly added, with ice-cooling,

a solution of 3.9 g (57 mmol) of sodium nitrite in 20 ml of water over a 5-min period with magnetic stirring. The mixture was subsequently stirred at 0 °C for 1.5 hr to give a dark brown solution, which was then neutralized with *ca.* 7 g of sodium carbonate. On the other hand, 60 ml of an aqueous solution of cuprous cyanide was prepared by the reaction of 8.8 g (180 mmol) of sodium cyanide with the aqueous solution of cuprous chloride which had been obtained from 1.72 g (68.9 mmol) of $CuSO_4 \cdot 5H_2O$ and 4.5 g (77 mmol) of NaCl upon the action of 3.6 g (35 mmol) of $NaHSO_3$ and 2.4 g (60 mmol) of NaOH in an aqueous medium. Into a stirred mixture of 50 ml of benzene-ether (4 : 1) and 60 ml of an aqueous solution of cuprous cyanide, a dark brown solution of the diazonium salt was added over a 30-min period with ice-cooling. The mixture was stirred at 0 °C for 40 min, at room temperature for 4 hr, and finally at 60 °C for 30 min. The mixture was then extracted with benzene and worked up in the usual way to give 6.1 g of a viscous, dark red oil, which was chromatographed over 130 g of silica gel (Nakarai, No. II-A, 100—200 mesh). From the fractions eluted with benzene we isolated, by the use of preparative tlc over silica gel (Merck, Kieselgel PF_{254}) with the same eluent, 1.070 g (5.54 mmol) of crude 7-(*p*-cyanophenyl)-1,3,5-cycloheptatriene, which was then further purified by vacuum distillation to give white crystals; 10.1% yield; bp 135 °C (bath tempreature)/0.05 mmHg; mp 68.5—73.8 °C; NMR, τ_{CCl_4} 2.5 (m, 4H, phenyl protons), 3.4 (t, 2H, $H^{3,4}$), 3.8 (m, 2H, $H^{2,5}$), 4.8 (d of d, 2H, $H^{1,6}$)), 7.2 (t, 1H, H^7).

Found: C, 87.13; H, 5.50%. Calcd for $C_{14}H_{11}N$: C, 87.01; H, 5.74%.

p-*Cyanophenyltropylium perchlorate (Ig·ClO_4^-)* was synthesized by the following procedures. To a solution of 0.735 g (3.85 mmol) of 7-(*p*-cyanophenyl)-1,3,5-cycloheptatriene in 2.4 ml of acetonitrile, we added 1.30 g (3.79 mmol) of triphenylmethyl perchlorate. The mixture was stirred at 60 °C for 15 min and at 80 °C for 3 min to give a dark red solution. Then, 25 ml of ethyl acetate was added and the solution was cooled to 0 °C. The glittering crystals which separated out were collected, washed successively with ethyl acetate and dry ether, and dried under reduced pressure to afford 1.021 g (3.50 mmol) of Ig·ClO_4^- as yellowish brown crystals; 92.4% yield. The crystals were then further recrystallized from acetonitrile-ethyl acetate; mp 212.5—212.8 °C (dec); ν_{max}^{KBr} 1090 (ClO_4^-), 1480 ($-C_7H_6^+$), 2240 cm^{-1} (–CN); $\lambda_{max}^{10\% HCl}$ 228.5 (ε, 33900), 270.5 (18200), 349 nm (17400); NMR, τ_{CF_3COOH} 0.6 (m, 6H, tropylium ring protons), 1.9 (s, 4H, phenyl protons).

Found: C, 57.66; H, 3.27%. Calcd for $C_{14}H_{10}NClO_4$: C, 57.64; H, 3.46%.

The 7-n-alkyl-1,3,5-cycloheptatrienes were prepared by the reaction of 7-ethoxy-1,3,5-cycloheptatriene with *n*-alkylmagnesium bromides following the procedures reported previously.[1b]

The Alkyltropylium perchlorates (II, n=3—6, 8, 12) were synthesized by hydride abstraction from the corresponding alkylcycloheptatrienes, following a previously-reported[1b] method. The melting points and ultraviolet-spectral and analytical data are given in Table 1.

One-electron Reduction of the Substituted Tropylium Ions. The Chromous-ion Reduction of Ia-h and II (n=3—6). Details of the procedures will be described below for the reduction of the *p*-chlorophenyltropylium ion (Ie) as a representative case. To a magnetically-stirred solution of 0.209 g (0.692 mmol) of Ie·ClO_4^- in 70 ml of 10% HCl, we added 3.5 ml (3.5 mmol) of a 1M solution of chromous chloride in 10% HCl by the use of a hypodermic syringe under an atmosphere of nitrogen. The solution was stirred for 5 min at room temperature, and then extracted with *n*-hexane and worked up in the usual way to give 0.140 g (0.347 mmol) of x,x'-di(*p*-chlorophenyl)bitropyl (x,x'-di(*p*-chlorophenyl)biscyclohepta-2,4,6-trien-1-yl) as a partially-solidified viscous oil; 100.3% yield; NMR, τ_{CDCl_3} 2.6 (m, 4H, phenyl protons), 3.1—3.5 (m, 3H, H^{3-6}), 4.4 (m, 2H, $H^{2,7}$), 7.8 (m, 1H, H^1). The chromous-ion reductions of Ia—d, If—h, and II (*n*= 3—6) were carried out in the same way to give the dimers in yields of 100—106%.

The Zinc Reduction of II (n=8, 12). To a magnetically-stirred solution of 0.0374 g (0.104 mmol) of *n*-dodecyltropylium perchlorate, II·ClO_4^- (*n*=12), in 2.1 ml of acetonitrile, there was added 0.0713 g (1.09 mg-atom) of zinc powder in a stream of nitrogen, after which the mixture was stirred for 10 min at room temperature. After the filtration of the reaction mixture, a 5-ml portion of water was added to the filtrate, which was then extracted with *n*-hexane and worked up in the usual way to give 0.0303 g (0.0582 mmol) of x,x'-di-*n*-dodecylbitropyl as a viscous oil; 106% yield; NMR, τ_{CCl_4} 3.4—4.1 (m, 3H, H^{3-6}), 4.9 (m, 2H, $H^{2,7}$), 7.9 (br, 3H, H^1 and $\rangle C-CH_2-$), 8.8 (s, 20H, $-(CH_2)_{10}-$), 9.2 (t, 3H, $-CH_3$). The zinc reduction of II (*n*=8) was conducted in the same

Table 4. Spectral and analytical data for x,x'-disubstituted bitropyls

Substituent	UV λ_{max}^{EtOH} nm	UV (log ε)	Element analysis Found (Calcd) C %	H %
p-HO-C_6H_4-	243.5	(4.31)	a)	
	288	(4.16)		
p-CH_3O-C_6H_4-	250	(4.42) b)		
	280	(4.22) b)		
p-CH_3-C_6H_4-	242	(4.54)	92.78	7.47
	280 (sh)	(4.12)	(92.77)	(7.23)
C_6H_5- c)	239	(4.57)	93.27	6.64
	280 (sh)	(4.10)	(93.37)	(6.63)
p-Cl-C_6H_4-	248	(4.58) b)	77.43	4.70
	280 (sh)	(4.21) b)	(77.42)	(5.00)
p-Br-C_6H_4-	250	(4.64) b)	63.60	4.11
			(63.44)	(4.10)
p-NC-C_6H_4-	259	(4.45)	86.39 d)	5.30
	280 (sh)	(4.37)	(87.47)	(5.24)
m-CH_3O-C_6H_4-	286	(4.16) b)	84.80	6.66
			(85.24)	(6.64)
C_3H_7-	254	(3.84)	90.01	9.78
			(90.16)	(9.84)
C_4H_9-	254.5	(3.88)	89.68	10.54
			(89.73)	(10.27)
C_5H_{11}-	255	(3.88)	89.48	10.37
			(89.37)	(10.63)
C_6H_{13}-	255	(3.87)	88.83	10.68
			(89.07)	(10.93)
C_8H_{17}-	255	(3.92)	88.50	11.60
			(88.60)	(11.40)
$C_{12}H_{25}$-	255	(3.79)	87.34	12.24
			(87.95)	(12.05)

a) Analyzed as the biscycloheptyl derivatives obtained by catalytic hydrogenation (see Experimental). b) Measured in chloroform as the solvent. c) Data from Ref. 1b. d) Satisfactory analytical data were not obtained owing to the instability of this compound.

way to give the dimer in a 95.0% yield.

The Analysis of the Di-substituted Bitropyls. The elemental analysis and ultraviolet spectroscopy were performed in the reduction products of Ic—h and II ($n=3$—6, 8, 12), which had been purified by preparative tlc over silica gel (Merck, Kieselgel PF_{254}). The results are listed in Table 4. In the cases of Ia and Ib, the reduction products were not stable enough for purification by tlc. Therefore, they were transformed to x,x'-di(*p*-methoxyphenyl)biscycloheptyl as follows and then analyzed. First, 0.548 g (1.49 mmol) of crude x,x'-di(*p*-hydroxyphenyl)bitropyl was catalytically hydrogenated over 1.0 g of palladium carbon (Nakarai, 5%) in 30 ml of dry methanol to give 0.320 g (0.845 mmol) of x,x'-di(*p*-hydroxyphenyl)biscycloheptyl; 56.7% yield. Then, 0.180 g (0.476 mmol) of the biscycloheptyl was methylated with 0.20 g (1.6 mmol) of dimethyl sulfate in alkaline aqueous ethanol, by reference to the method reported by Vyas and Shah.[13] The subsequent purification of the crude product by the use of preparative tlc afforded 0.102 g (0.251 mmol) of x,x'-di(*p*-methoxyphenyl)biscycloheptyl as a colorless oil; 52.7% yield; NMR, τ_{CCl_4} 3.2 (q, 8H, phenyl protons), 6.3 (s, 6H, methoxy), 7.5 (br, 4H, methine), 8.3 (br, 20H, methylene).

Found: C, 82.69; H, 9.37%. Calcd for $C_{28}H_{38}O_2$: C, 82.71; H, 9.42%.

The reduction product of Ib was also hydrogenated in the same way to give x,x'-di(*p*-methoxyphenyl)biscycloheptyl, which showed an infrared spectrum identical with that of the authentic sample described above.

Kinetic Measurements. The reaction rate of the chromous-ion reduction was measured in 10% HCl at 25.0± 0.2 °C by the use of a flow method reported previously.[5] The products were determined by ultraviolet spectroscopy, using the characteristic bands listed in Table 4.

Measurements of the Charge-transfer Bands with Pyrene. The charge-transfer spectrum was measured in 1,2-dichloroethane as has been reported previously.[1b] The concentrations of pyrene and of the tropylium salts were 0.2 M and 2×10^{-3} M respectively. Precautions were taken so that the sample solution was shielded from the room light, and the spectrum was measured immediately after the preparation of the sample.

Determination of pK_{R^+}*'s.* The previously-described spectrophotometric method[1b] was followed for the determination of pK_{R^+}'s for I in 23% ethanol. As for the cations, II, the pK_{R^+} values could not be measured because of the decomposition of II in an aqueous solution with pH> 1.

References

1) a) K. Okamoto, K. Komatsu, O. Murai, and O. Sakaguchi, *Tetrahedron Lett.*, **1972**, 4989. b) K. Okamoto, K. Komatsu, O. Murai, O. Sakaguchi, and Y. Matsui, This Bulletin, **46**, 1785 (1973). c) K. Okamoto, K. Komatsu, and A. Hitomi, *ibid.*, **46**, 3881 (1973).

2) C. Jutz and F. Voithenleitner, *Chem. Ber.*, **97**, 29 (1964).

3) P. Schuster, D. Vedrilla, and O. E. Polansky, *Monatsch. Chem.*, **100**, 1 (1969).

4) Dodecyltropylium perchlorate (II, $n=12$) has been studied as a surface-activating reagent which is effective in concentrated acid media; M. Abu-Hamidiyyah and K. J. Mysels, *J. Phys. Chem.*, **69**, 1466 (1965).

5) K. Okamoto, K. Komatsu, S. Tsukada, and O. Murai, This Bulletin, **46**, 1780 (1973).

6) H. J. Dauben, Jr. and J. D. Wilson, *Chem. Commun.*, **1968**, 1629; and the references cited therein.

7) D. H. McDaniel and H. C. Brown, *J. Org. Chem.*, **23**, 420 (1958).

8) H. C. Brown and Y. Okamoto, *J. Amer. Chem. Soc.*, **80**, 4979 (1958).

9) R. Hoffmann, R. Bissell, and D. G. Farnum, *J. Phys. Chem.*, **73**, 1789 (1969).

10) For recent examples, see J. J. Delpuech, *Bull. Soc. Chim. France*, **1966**, 1616; K. Okamoto, T. Kita, and H. Shingu, This Bulletin, **40**, 1908 (1967).

11) The melting points and boiling points are uncorrected. The elemental analyses were performed by the Microanalytical Center, Kyoto University, Kyoto. The infrared and ultraviolet spectra were recorded with a Hitachi spectrometer model 215 and with a Shimadzu spectrometer model UV-50M respectively. The NMR spectra were taken on a model R-24 spectrometer (60 MHz) with tetramethylsilane as the internal standard.

12) H. T. Clarke and R. R. Read, "Organic Syntheses," Coll. Vol. I, p. 514 (1941).

13) G. N. Vyas and N. M. Shah, "Organic Syntheses," Coll. Vol. IV, p. 837 (1963).

The One-electron Reduction of Carbonium Ions. VIII. The Reducibility of Hetero-substituted Tropylium Ions as Measured by the Competitive Reduction Method with Zinc Powder

Kunio OKAMOTO, Koichi KOMATSU, and Osamu SAKAGUCHI

Department of Hydrocarbon Chemistry, Faculty of Engineering, Kyoto University, Sakyo-ku, Kyoto 606

(Received March 13, 1974)

A series of hetero-substituted tropylium salts ($X\text{-}C_7H_6^+ \cdot Y^-$), including three new compounds, have been synthesized. Their relative reactivities in one-electron reductions with zinc powder have been determined by the use of a competitive-reaction method, which gave the following reactivity sequence: $CH_3O\text{-}C_7H_6^+$ ($k_{rel.}=0.0295$), $t\text{-}C_4H_9\text{-}C_7H_6^+$ (0.146), $CH_3S\text{-}C_7H_6^+$ (0.255), $C_7H_7^+$ (1.00), $C_6H_5\text{-}C_7H_6^+$ (2.50), $(C_6H_5)_3Si\text{-}C_7H_6^+$ (7.50), $Cl\text{-}C_7H_6^+$ (16.8), $CH_3OCO\text{-}C_7H_6^+$ (35.7), $NC\text{-}C_7H_6^+$ (163). The values of log $k_{rel.}$ for the $t\text{-}C_4H_9$-, H-, and $C_6H_5\text{-}C_7H_6^+$ ions exhibit a good linear relationship with those of log k_2 in the chromous-ion reduction. A linear correlation is also observed between log $k_{rel.}$ and the transition energy for the charge-transfer band of the respective cations, with pyrene as a donor. A plot of log $k_{rel.}$ against σ_p (for the ring substituent, X) gives a greater ρ-value (+4.0) than in the case of $X\text{-}C_6H_4\text{-}C_7H_6^+$ (+1.31), reflecting the influence of the direct substitution on the tropylium ring.

In earlier publications,[1] we have demonstrated that the "one-electron" reducibility (log k_2) for some of the substituted tropylium and cyclopropenium ions in the chromous-ion reduction is linearly correlated with the electron affinity, which was estimated from the transition energy for the charge-transfer bands of the respective cations, with pyrene as the donor. Also, with respect to substituted phenyltropylium ions, the existence of the Hammett linear free-energy relationship was demonstrated.[1d] We were, therefore, encouraged to extend these studies to the tropylium ions with a variety of hetero-substituents which are directly bonded to the seven-membered ring.

However, the previous method of the chromous-ion reduction is not applicable to the hetero-substituted tropylium ions because of the instability of these cations in "aqueous" media. Furthermore, acetonitrile, in which these cations are stable, is not a good solvent for chromous ion. Hence, we have attempted to estimate the relative reducibility of these substituted tropylium ions by the use of a competitive heterogeneous reduction with zinc powder in "anhydrous" acetonitrile. The use of zinc powder as a one-electron reductant for the carbonium ions has been well documented[2] since the first observation of the zinc reduction of the tropylium ion to give bitropyl reported by Doering and Knox.[2a] In addition, the formation of the radical species (tropyl radical) in the course of the zinc reduction of the tropylium ion has been proved by the radical-trapping technique.[3]

In this paper, the correlation of the reducibility of the hetero-substituted tropylium ions with the electron affinity and the substituent effect on the rates of reduction will be discussed by the use of the relative reduction rates as measured by the competitive-reduction method.

Results and Discussion

Syntheses of the Hetero-substituted Tropylium Ions. Among the perchlorates of the hetero-substituted tropylium ions, I-VIII, those of the chloro-[4] (III), methoxy[5] (VI), diethylamino-[6] (VII), and *t*-butylamino-[6] (VIII) derivatives were prepared according to the literatures. The cyano- (I), carbomethoxy-(II) and methylthiotropylium[4] (V) perchlorates were synthesized by hydride abstraction from the corresponding 3-substituted 1,3,5-cycloheptatrienes, which had been obtained from the 7-substituted derivatives[7] by thermal isomerization. The triphenylsilyltropylium perchlorate (IV) was synthesized in the same way from 7-triphenylsilyl-1,3,5-cycloheptatriene, which had itself been obtained by the reaction of 7-ethoxy-1,3,5-cycloheptatriene with triphenylsilyllithium.[8] Among these salts, I,[9] II, and IV are new compounds.

	X	Y
I	-CN	ClO_4
II	$-CO_2CH_3$	ClO_4
III	-Cl	ClO_4
IV	$-Si(C_6H_5)_3$	ClO_4
V	$-SCH_3$	ClO_4
VI	$-OCH_3$	ClO_4
VII	$-N(C_2H_5)_2$	ClO_4
VIII	$-NH\text{-}t\text{-}C_4H_9$	ClO_4
IX	$-C_6H_5$	BF_4
IX′	$-C_6D_5$	BF_4
X	-H	BF_4
XI	$-t\text{-}C_4H_9$	ClO_4

Previously, we have observed a homolytic dissociation of 7-triphenylmethyl-1,3,5-cycloheptatriene into the tropyl (cycloheptatrienyl) and triphenylmethyl radicals by means of ESR measurements at 60—95 °C.[10] Larrabee[11] has found that 7-triphenylstannic-1,3,5-cycloheptatriene undergoes a similar thermal cleavage at 160 °C and also reported on the fluxional behavior of the triphenylstannic group around the seven-membered ring on the basis of NMR measurements at 0—139 °C. The ease of these homolytic cleavages may be attributed to the considerable resonance-stabilization of the "symmetrical" tropyl radical.[12] However, in spite of the close similarity of the structure, 7-triphenylsilyl-1,3,5-cycloheptatriene does not exhibit such behavior. It does not show any evidence of bitropyl formation when heated at 200 °C, indicating the resistance of the C-Si bond to homolytic dissociation.

Competitive Reductions. First, the one-electron reduction of each single cation with an excess (twenty-fold of the theoretical amount) of zinc powder was

carried out in acetonitrile for ten minutes. An almost quantitative formation of the x,x'-disubstituted bitropyl was confirmed, except for the aminotropylium ions, VII and VIII, which were not reduced, but were recovered unchanged under these conditions. This indicates the exceptional stability due to electron donation by the amino group. The analytical and spectral data for x,x'-disubstituted bitropyls are tabulated in Table 2 (see Experimental).

Then, the competitive reduction was conducted as follows. Each pair of equal amounts of cations (R_A^+, R_B^+) was subjected to a competitive reduction in acetonitrile at 25 °C with zinc powder 1/4~1/2 of the theoretical amount required for the complete reduction of a single cation. The mixture of the coupling products of the radicals formed from both cations (R_A–R_A, R_A–R_B, R_B–R_B) was then extracted. The yield of each radical was determined from the weight of the coupling-product mixture and by NMR analysis.[13] In each case, the material balance of the reduction was found to be 90—105% from the UV analysis of the unchanged cation. When we assume the first-order dependence of the reaction rate on the cation concentration, the ratio of rate constants for the competing cations is expressed by the following equation:[14]

$$k_A/k_B=\log([R_A^+]/[R_A^+]_0)/\log([R_B^+]/[R_B^+]_0)$$

where $[R_A^+]_0$ and $[R_B^+]_0$ denote the initial concentrations of the R_A^+ and R_B^+ cations respectively. The application of this equation to the present case was justified by the linearity of the plot of $\log([R_A^+]/[R_A^+]_0)$ against $\log([R_B^+]/[R_B^+]_0)$ through the point of origin, with regard to each cation pair, as is shown in Figs. 1 and 2. From the slope of each straight line, the relative rate constant ($k_{rel.}$) for the zinc reduction of each cation was determined. The results are listed in Table 1, together with the charge-transfer maxima (*vide infra*) of the respective cations.

In order to compare the results obtained by the present method ($k_{rel.}$) with that determined from the homogeneous chromous-ion reduction (k_2), $\log k_{rel.}$ was plotted against $\log k_2$. A linear correlation with the slope of 0.98 has been observed, as is shown in Fig. 3. This result clearly indicates that, in spite of the heterogeneous condition, the present method gives reasonably correct relative values for the reducibility inherent in the carbonium ions.

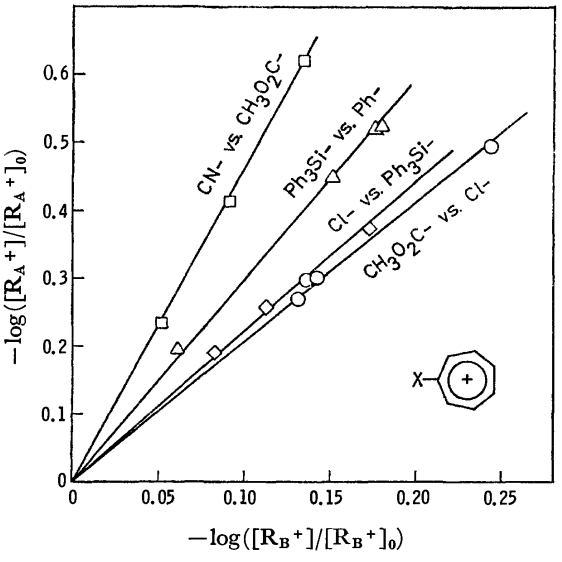

Fig. 1. Plot of $-\log([R_A^+]/[R_A^+]_0)$ *vs.* $-\log([R_B^+]/[R_B^+]_0)$ for the competitive reduction of NC–, CH_3OCO–, Cl–, $(C_6H_5)_3Si$–, and C_6H_5–$C_7H_6^+$ with Zn in CH_3CN at 25 °C.

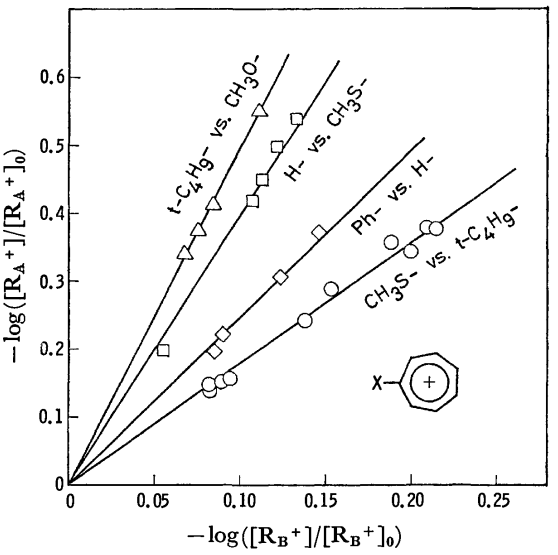

Fig. 2. Plot of $-\log([R_A^+]/[R_A^+]_0)$ *vs.* $-\log([R_B^+]/[R_B^+]_0)$ for the competitive reduction of C_6H_5–, H–, CH_3S–, *t*-C_4H_9–, and CH_3O–$C_7H_6^+$ with Zn in CH_3CN at 25 °C.

Table 1. Relative rate constants for the zinc reduction of hetero-substituted tropylium ions and absorptions of their charge-transfer spectra

Substituent	$k_{rel.}$[a]	log $k_{rel.}$	C. T. band[b]	
			λ_{max} nm	ν_{max} 10^4 cm^{-1}
CH_3O–	0.0295	−1.530	480	2.083
t-C_4H_9–	0.146	−0.836	508	1.969
CH_3S–	0.255	−0.594	510	1.961
H–	1.000	0.000	540	1.852
C_6H_5–	2.50	0.398	543	1.842
$(C_6H_5)_3Si$–	7.50	0.875	555	1.802
Cl–	16.8	1.225	580	1.724
CH_3OCO–	35.7	1.552	610	1.639
NC–	163	2.212	680	1.471

a) Determined by the competitive reduction in acetonitrile at 25 °C. b) Measured in 1,2-dichloroethane with pyrene as a donor.

The Correlation of log $k_{rel.}$ with the Charge-transfer Energy. In order to examine the correlation of the reducibility with the electron affinity, the values of log $k_{rel.}$ were plotted against the wave number corresponding to the maximum absorption at the charge-transfer spectrum (ν_{max}, see Table 1) of each substituted tropylium ion, with pyrene as the standard electron donor. A good linear correlation was obtained, as is shown in Fig. 4. Since, for a given donor molecule,

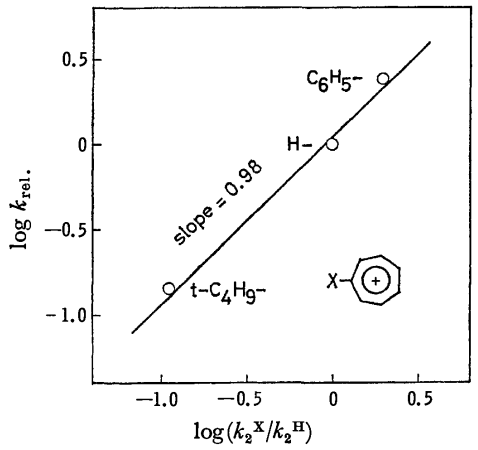

Fig. 3. Plot of $\log k_{rel.}$ measured by the competitive reduction *vs.* $\log(k_2^X/k_2^H)$ determined by the chromous-ion reduction.

the ν_{max} for the charge-transfer spectrum of a series of acceptors should correlate with the electron affinity of the acceptors,[15] this correlation (Fig. 4) clearly indicates that the reducibility of these cations is essentially regulated by the electron affinity inherent in the cation itself. Thus, the correlation[1] which holds for the alkyl- and aryl-substituted tropylium and cyclopropenium series has been successfully extended to a series of hetero-substituted tropylium ions.

The Correlation of log $k_{rel.}$ with Hammett's σ_p. The variation in the reactivity of substituted tropylium ions obviously reflects the influence of the electronic stabilization or destabilization caused by these substituents. In order to compare the substituent effect with that observed in the case of substituted phenyltropylium ions, the values of $\log k_{rel.}$ were plotted against Hammett's σ_p[16] (Fig. 5). The one-electron reducibility of the substituted tropylium ion thus measured is considered to be an average of the reactivity of the seven individual carbon atoms in the ring toward the reductant. Hence, the use of a single σ_p constant, though it includes both resonance and inductive electronic effects, may not be explicitly called for. This is perhaps one of the causes of the scatters in Fig. 5.[17] Thus, although we can not avoid such

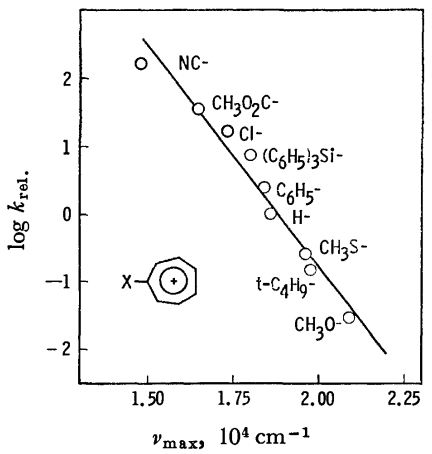

Fig. 4. Plot of $\log k_{rel.}$ *vs.* ν_{max} of the charge-transfer spectra.

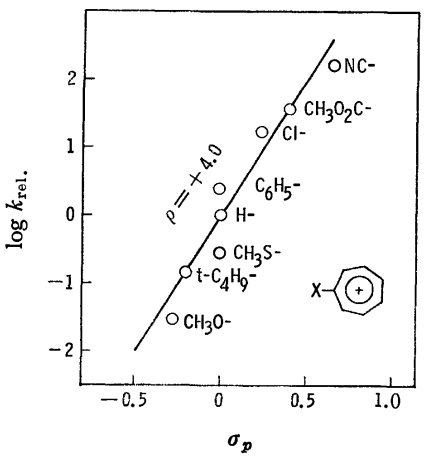

Fig. 5. Plot of $\log k_{rel.}$ *vs.* Hammett's σ_p.

a theoretical ambiguity, if we express the sensitivity to the substituent effect with the ρ-value it will amount to about +4.0. The increase in ρ-value, compared with that obtained in the case of a substituted phenyltropylium system (+1.31),[1d] is evidently caused by the direct transmission of the electronic effect of the substituent to the tropylium ring.

Experimental[18]

Materials. All the reagents employed were of a reagent-grade quality. The acetonitrile and ethyl acetate were refluxed and distilled over phosphorus pentoxide; acetonitrile, bp 80.5—81.1 °C; ethyl acetate, bp 75.5—76.5 °C. The carbon tetrachloride, chloroform and 1,2-dichloroethane were refluxed and distilled over calcium chloride; carbon tetrachloride, bp 75.0—75.5 °C; chloroform, bp 60.0—60.3 °C; 1,2-dichloroethane, bp 83.0—83.5 °C. The tetrahydrofuran (THF) was distilled over lithium aluminum hydride; bp 66.0—66.4 °C.

The chloro-[4] (III), methoxy-[5] (VI), diethylamino-[6] (VII), and *t*-butylamino-[6] (VIII) tropylium perchlorates were prepared by the methods reported in the literature; III, mp 175.0—176.0 °C (lit, mp 172—173 °C[4]), $\lambda_{max}^{CH_3CN}$ 232 nm (ε, 37200), 308 nm (9100) (lit, $\lambda_{max}^{CH_3CN}$ 232 nm (log ε, 4.57), 308 nm (3.96)[4]); VI, mp 107.0—107.5 °C (lit, mp 107 °C[5]), $\lambda_{max}^{CH_3CN}$ 232 nm (ε, 34700), 313 nm (11000) (lit, $\lambda_{max}^{CH_3CN}$ 232 nm (log ε, 4.54) 313 nm (4.04)[4]); VII, mp 68.0—72.0 °C (lit, mp 75—76 °C,[6]), $\lambda_{max}^{CH_3CN}$ 241 nm (ε, 20000) 335 nm (16300) (lit, $\lambda_{max}^{CH_3CN}$ 241 nm (log ε, 4.30), 335 nm (4.21)[6]); VIII, mp 111.5—112.0 °C (lit, mp 112—113 °C[6]), $\lambda_{max}^{CH_3CN}$ 239 nm (ε, 18400), 242.5 nm (18400), 333 nm (13000) (lit, $\lambda_{max}^{CH_3CN}$ 237 nm (log ε, 4.35), 330 nm (4.18)[6]).

The phenyl- (IX) and unsubstituted (X) tropylium fluoroborates and *t*-butyltropylium perchlorate (XI) were prepared by previously-reported methods.[1b]

Synthesis of Cyanotropylium Perchlorate (I). 7-Cyano-1,3,5-cycloheptatriene[2a] was heated in an evacuated ampoule at 175 °C for 1.5 hr and distilled under reduced pressure to give a mixture of 3- and 1-cyano-1,3,5-cycloheptatrienes; bp 86.5—90.0 °C/5 mmHg. To a solution of 3.498 g (29.8 mmol) of an isomeric mixture of cyanocycloheptatrienes in 7.7 ml of acetonitrile, we added 10.231 g (29.8 mmol) of triphenylmethyl (trityl) perchlorate. The mixture was magnetically stirred at 60 °C for 1 hr and then at 80 °C for 5 min; most of the crystals of trityl perchlorate thereby disappeared and the mixture turned dark red. After the addition of 26 ml of ethyl acetate, the mixture was cooled to 0 °C.

The pale yellow crystals that separated out were collected by filtration, washed successively with ethyl acetate and ether, and dried *in vacuo* to give 4.885 g (22.7 mmol) of I; 76.2% yield. For the analyses, I was purified by recrystallization from acetonitrile–ethyl acetate; mp 158.0 °C (decomposition with violent explosion); $\lambda_{max}^{CH_3CN}$ 293 nm (ε, 6610), 298 nm (6450); ν_{max}^{KBr} 3020, 2220, 1630, 1595, 1525, 1480, 1440, 1380, 1150—1080, 955, 940, 870, 740 cm^{-1}; NMR, τ_{CF_3COOH} 0.4 (s, tropylium ring protons).

Found: C, 44.34; H, 2.81%. Calcd for $C_8H_6NClO_4$: C, 44.57; H, 2.81%.

Synthesis of Carbomethoxytropylium Perchlorate (II). 7-Carbomethoxy-1,3,5-cycloheptatriene[7] was thermally isomerized at 175 °C for 1.5 hr to give a mixture of 3- and 1-carbomethoxy-1,3,5-cycloheptatrienes; bp 74.0—77.0 °C/3 mmHg. In 6.4 ml of acetonitrile, 3.509 g (23.4 mmol) of a mixture of carbomethoxycycloheptatrienes was allowed to react with 8.012 g (23.3 mmol) of trityl perchlorate with magnetic stirring at 60 °C for 6 min; the trityl salt disappeared almost instantaneously when the mixture was heated, and instead pale yellow crystals separated. After the addition of 24 ml of ethyl acetate, the mixture was cooled to 0 °C and then filtered to give 5.427 g (21.8 mmol) of II as pale yellow crystals; 93.4% yield; mp 143.0—143.3 °C (after recrystallization from acetonitrile–ethyl acetate); $\lambda_{max}^{CH_3CN}$ 225.5 nm (ε, 43000), 286 nm (4660); ν_{max}^{KBr} 3015, 2960, 1730, 1615, 1480, 1440, 1370, 1350, 1290, 1270, 1250, 1150—1070, 970, 940, 925, 870, 805, 760, 740, 680 cm^{-1}; NMR, τ_{CF_3COOH} 0.0 (m, 2H, tropylium ring protons), 0.5 (m, 4H, tropylium ring protons), 5.7 (s, 3H, methyl protons).

Found: C, 43.21; H, 3.58%. Calcd for $C_9H_9ClO_6$: C, 43.48; H, 3.65%.

Synthesis of Methylthiotropylium Perchlorate (V). To a magnetically-stirred solution of 10.356 g (58.1 mmol) of tropylium fluoroborate in 110 ml of 0.1 M HCl, we added 9.5 g of a 30% methanolic solution of methanethiol (58.7 mmol); a slightly exothermic reaction then took place, and the solution turned yellow. After stirring for 20 min at room temperature, the turbid solution was extracted with three 100-ml portions of ether, washed with 10% NaCl, and dried over $MgSO_4$. The ethereal solution, after evaporation and distillation, gave 4.309 g (31.2 mmol) of 7-methylthio-1,3,5-cycloheptatriene as a pale yellow oil; 53.6% yield; bp 74 °C/5 mmHg; NMR, τ_{CCl_4} 3.5 (t, 2H, $H^{3,4}$), 3.9 (m, 2H, $H^{2,5}$), 4.7 (d of d, 2H, $H^{1,6}$), 6.9 (t, 1H, H^7), 7.9 (s, 3H, methyl protons).

Found: C, 69.72; H, 7.42%. Calcd for $C_8H_{10}S$: C, 69.51; H, 7.29%.

A solution of 2.092 g (15.1 mmol) of the isomeric mixture of methylthiocycloheptatrienes (bp, 50.0—61.0 °C/4 mmHg), obtained by the thermal isomerization described above, in 10 ml of acetonitrile was added to a magnetically-stirred suspension of 5.205 g (15.2 mmol) of trityl perchlorate in 10 ml of acetonitrile over a 2-min period at room temperature. During the addition, the reaction temperature rose from 22.5 °C to 30.0 °C and all the trityl salt dissolved to give a dark red solution. After stirring for 15 min at room temperature, 100 ml of ethyl acetate was added and the mixture was cooled to 0 °C. The yellow crystals that thus separated out were collected, washed, and dried as has been described above to give 2.860 g (12.1 mmol) of V: 80.0% yield; mp 114.0—115.0 °C (lit, mp 114—115 °C[4]); $\lambda_{max}^{CH_3CN}$ 219.5 nm (ε, 23300), 260 nm (17000), 380 nm (19800) (lit, $\lambda_{max}^{CH_3CN}$ 258 nm (ε, 14800), 378 nm (17400)[4]); ν_{max}^{KBr} 3010, 2910, 1615, 1600, 1510, 1470, 1430, 1420(sh), 1370, 1325, 1280, 1235, 1225, 1120—1040, 845, 740 cm^{-1}.

Synthesis of 7-Triphenylsilyl-1,3,5-cycloheptatriene. To a stirred solution of 5.791 g (45.9 mmol) of 7-ethoxy-1,3,5-cycloheptatriene in 20 ml of THF, we added 130 ml of a THF solution of triphenylsilyllithium, prepared from 15.0 g (51.0 mmol) of triphenylsilyl chloride and 1.40 g (0.202 g-atom) of lithium according to the method of Gilman *et al.*,[8] by the use of a hypodermic syringe over a 25-min period at room temperature; the reaction temperature rose from 25.0 °C to 35.0 °C, and the dark reddish brown color of triphenylsilyllithium, which was, at the beginning, instantaneously discharged upon addition to the ethoxycycloheptatriene solution, began to remain during the course of addition. The dark brown mixture with white precipitates was stirred at room temperature for 2.5 hr and then left to stand overnight. Then, 150 ml of 10% HCl was cautiously added and the mixture was worked up in the usual way to give 17.5 g of a partially-solidified yellowish oil, from which, upon recrystallization from benzene, 0.451 g (0.836 mmol) of hexaphenyldisilane was separated as white crystals; mp 355—360 °C (lit, mp 361—362 °C[8]); the IR spectrum was identical with that of the authentic sample. The mother liquor was concentrated *in vacuo*, and the residual solid, upon recrystallization from ethanol, gave 3.338 g (9.53 mmol) of 7-triphenylsilyl-1,3,5-cycloheptatriene as white crystals; this compound begins to melt at 152 °C, but at 155 °C another solid, presumably the 3-triphenylsilyl isomer, appears, which eventually melts at 178 °C; NMR, τ_{CCl_4} 2.6 (m, 15H, phenyl protons), 3.4 (t, 2H, $H^{3,4}$), 3.7 (m, 2H, $H^{2,5}$), 4.8 (d of d, 2H, $H^{1,6}$), 8.2 (t, 1H, H^7).

Found: C, 85.48; H, 6.07%. Calcd for $C_{25}H_{22}Si$: C, 85.66; H, 6.33%.

The filtrate of the recrystallization, upon evaporation, gave 12.260 g of a yellowish solid, which was then chromatographed over 310 g of silica gel (Nakarai, No. II-A, 100—200 mesh). From the fractions eluted with *n*-hexane–benzene (9 : 1—6 : 1) we obtained a mixture of 0.163 g (0.898 mmol) of bitropyl and 0.340 g (0.131 mmol) of triphenylsilane; the composition was determined by the NMR analysis. From the fractions eluted with *n*-hexane–benzene(3 : 1) we isolated 4.654 g (13.3 mmol) of 7-triphenylsilyl-1,3,5-cycloheptatriene, whereas the following fractions, when eluted with *n*-hexane–benzene(2 : 1), gave 0.657 g (1.22 mmol) of hexaphenyldisilane after recrystallization from chloroform. In addition, the fractions eluted with benzene–ether (1 : 1) afforded 3.364 g (12.2 mmol) of triphenylsilanol after recrystallization from benzene; mp 152—155 °C (lit, mp 153—155 °C[8]).

Thus, the yields of each isolated product may be summarized as follows: bitropyl, 3.9%; 7-triphenylsilyl-1,3,5-cycloheptatriene, 47.5%; the tropylium ion, 21.2% (as determined from the UV spectrum of the aqueous layer); hexaphenyldisilane, 4.8% (based on triphenylsilyl chloride); triphenylsilane, 2.6% (*vide supra*); triphenylsilanol, 24.1% (*vide supra*).

7-Triphenylsilyl-1,3,5-cycloheptatriene was sealed in a Pyrex tube under a vacuum and heated at 200 °C for 30 min. The tlc analysis of the recovered sample indicated the presence of an isomeric mixture of triphenylsilylcycloheptatrienes, but no spot corresponding to bitropyl was detected.

Synthesis of Triphenylsilyltropylium Perchlorate (IV). 7-Triphenylsilyl-1,3,5-cycloheptatriene was thermally isomerized at 150 °C for 5 hr to give 3-triphenylsilyl-1,3,5-cycloheptatriene; NMR, τ_{CCl_4} 2.6 (m, 15H, phenyl protons), 3.1 (d, 1H, H^4), 3.7 (m, 2H, $H^{2,5}$), 4.5 (m, 2H, $H^{1,6}$), 7.7 (t, 2H, H^7). A suspension of 0.638 g (1.82 mmol) of the triphenylsilylcycloheptatriene and 0.634 g (1.85 mmol) of trityl perchlorate in 10 ml of acetonitrile was magnetically stirred at 55 °C for 30 min and then at 80 °C for 5 min to give a dark red solution. After the addition of 100 ml of ethyl acetate, the solution was cooled to 0 °C. The glittering, brownish

crystals that separated out were collected in the usual way to give 0.702 g (1.57 mmol) of IV; 86.0% yield. Recrystallization from acetonitrile–ethyl acetate gave a mp of 188.0 °C (decomposition with explosion); $\lambda_{max}^{CH_3CN}$ 218 nm (ε, 65000), 265 nm (sh) (6960), 271.5 nm (6800), 281 nm (6500); λ_{max}^{KBr} 3080, 3050, 3020, 1590, 1485, 1440(sh), 1430, 1380, 1265, 1240, 1190, 1160, 1120—1070, 1030, 1000, 940, 870, 750, 745(sh), 715, 700, 680 cm^{-1}; NMR, τ_{CH_3COOH} 0.5—0.8 (m, 6H, tropylium ring protons), 2.5 (s, 15H, phenyl protons).

Found: C, 66.80; H, 4.52%. Calcd for $C_{25}H_{21}SiClO_4$: C, 66.88; H, 4.72%.

Synthesis of Phenyl-d_5-tropylium Perchlorate (IX'). For the purpose of product analysis in the competitive reduction of IV and IX (*vide infra*), the phenyl-d_5 derivative of IX was synthesized from bromobenzene-d_5,[19] following the methods used for the preparation of IX;[1b] mp 152.0—153.0 °C (dec) (lit, mp for IX 151.0—152.0 °C[1b]); ν_{max}^{KBr} 3020, 3000, 2950, 2270, 2080, 1630, 1600, 1520, 1480, 1440, 1430, 1380, 1315, 1283, 1273, 1240, 1200, 1130—1000, 880, 860, 845, 830, 800, 790, 740 cm^{-1}; NMR, τ_{CF_3COOH} 0.6—0.9 (m, tropylium ring protons).

One-electron Reduction of the Substituted Tropylium Ions with Zinc Powder. To a magnetically-stirred solution of 0.500 g (2.01 mmol) of II in 20 ml of acetonitrile, we added 1.315 g (20.1 mg-atom) of zinc powder. The mixture was stirred for 10 min at room temperature under an atmosphere of nitrogen. The excessive zinc was then filtered off, and 40 ml of carbon tetrachloride and 40 ml of water were added to the filtrate, which was then worked up in the usual way to give 0.317 g (1.06 mmol) of x,x'-dicarbomethoxybitropyl as a viscous oil; 105.6% yield; NMR, τ_{CCl_4} 2.2—4.7 (m, 10H, olefinic ring protons), 6.1 and 6.2 (s, 6H, methyl), 8.0 (br, 2H, methine).

The Reductions of I, III, IV, V, VI, IX, and XI were carried out in the same way to give the disubstituted bitropyls in yields of 91—108%. The UV spectra and the results of the elemental analyses of all the products are tabulated in Table 2.

Under the same reaction conditions, 0.0557 g (0.239 mmol) of VII was allowed to react with 0.160 g (2.46 mg-atom) of zinc powder in 2 ml of acetonitrile. After filtration, 20 ml of ether was added to the filtrate and the white precipitates that separated were collected in the usual way to give 0.0503 g (0.216 mmol) of unchanged VII; 90.4% recovery. The ethereal filtrate gave 0.0015 g of an unidentified oily substance. An attempted reduction of VIII, with the same procedures, also resulted in a 106% recovery of VIII.

Table 2. Ultraviolet spectral and analytical data for x,x'-disubstituted bitropyls[a]

Substituent	UV		Elemental analysis	
	λ_{max}^{EtOH} nm	(ε)	Found (Calcd) C%	H%
CH_3O-	250.5	(6580)	79.08	7.50
	285	(5270)	(79.31)	(7.49)
CH_3S-	302	(8800)	70.06	6.84
			(70.02)	(6.61)
$(C_6H_5)_3Si$-	255.5	(11800)	85.73	6.10
	261	(11820)	(85.91)	(6.06)
	265(sh)	(11050)		
Cl-	261	(6800)	66.94	4.81
			(66.95)	(4.82)
CH_3O_2C-	223.5	(37100)	71.73	6.01
			(72.47)	(6.08)
NC-	263	(6340)	82.60	5.47
			(82.73)	(5.21)

a) As for the data for diphenyl-, di-*t*-butyl-, and unsubstituted bitropyls, see Ref. 1b.

Competitive Reductions. With respect to the competitive reduction of the I, II, III, IV, IX, and X cations the details of the procedures may be illustrated by the following description of a representative run for the competition of I and II. Into a 25-ml, four-necked flask equipped with a thermometer, a magnetic-stirring bar, and a nitrogen inlet and outlet, which had been immersed in a water bath thermostated at 25.0 °C, there was stirred a solution of 0.108 g (0.502 mmol) of I and 0.125 g (0.503 mmol) of II in 5.0 ml of acetonitrile. To this solution we then added 0.0169 g (0.259 mg-atom) of zinc powder, and the mixture was stirred under a nitrogen atmosphere for 10 min. The reaction appeared to be very fast, completing in less than 1 min, as indicated by the rapid disappearance of the zinc powder. The solution was evaporated under reduced pressure to give an oily solid, which was then extracted in five portions with 25 ml of carbon tetrachloride. The carbon tetrachloride solution was washed with three 35-ml portions of water, dried over $MgSO_4$, and evaporated to give 0.0626 g of a colorless oil, which was then analyzed by means of NMR as follows: regarding the product oil as a mixture of substituted bitropyls such as,

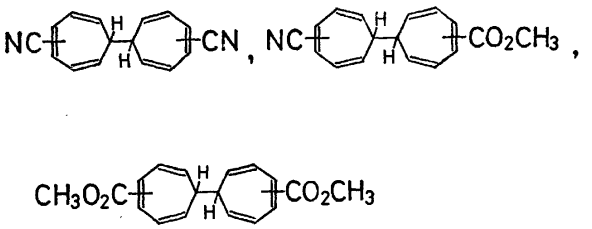

the molar ratio of the cyano- and carbomethoxytropyl groups was determined to be 3.32 : 1.00 from the relative values of the integrated intensities (average of 5 measurements) for the signals corresponding to the methyl protons and the total olefinic ring protons (H^{2-7}). From this molar ratio and the weight of the product mixture, the radical yield was calculated to be 77.2% for the reduction of I and 23.3% for the reduction of II. On the other hand, the residual solid from the carbon-tetrachloride extraction was dissolved in acetonitrile and subjected to UV analysis. The amounts of the unchanged cations, I and II, were determined to be 0.116 mmol (23.1% recovery) and 0.373 mmol (74.2% recovery) respectively by the use of the absorbance and the molar extinction coefficient of each cation at the wave lengths corresponding to the maximum absorptions of the individual cations, assuming the additivity of the absorbance of the respective cations at each wavelength. The results of the competitive reduction were treated as has been described above. For the competition of IV and IX, the phenyl-d_5 derivative (IX')[20] was employed instead of IX itself, so that the NMR analysis of the product ratio became more accurate by integrating the signals for phenyl protons which came from IV and the total of the olefinic ring protons.

With respect to the V, VI, X, and XI cations, exactly the same method was adopted except for the following procedures: after the reaction, 20 ml of 10% HCl was added to the reaction mixture, after which the products were extracted with ether, worked up, and analyzed as has been described above, while the unchanged cations were determined by UV analyses of the acidic aqueous layer.

The validity of the analytical methods described above is verified by the fairly good material balance (90—105%) obtained in each case.

Measurements of the Charge-transfer Bands with Pyrene. The charge-transfer spectra were measured in 1,2-dichloroethane as has been reported previously.[1b] The concentrations of the donor (pyrene) and of the acceptor (the substituted tropylium ion) were 0.1 M and 1×10^{-3} M respectively. The previously-described[1d] precautions were taken against the light, and the spectra were measured immediately after the preparation of the sample solution.

References

1) a) K. Okamoto, K. Komatsu, O. Murai, and O. Sakaguchi, *Tetrahedron Lett.*, **1972**, 4989. b) K. Okamoto, K. Komatsu, O. Murai, O. Sakaguchi, and Y. Matsui, This Bulletin, **46**, 1785 (1973). c) K. Okamoto, K. Komatsu, and A. Hitomi, *ibid.*, **46**, 3881 (1973). d) K. Okamoto, K. Komatsu, M. Fujimori, and S. Yasuda, *ibid.*, **47**, 2426 (1974).

2) For example, a) W. von E. Doering and L. H. Knox, *J. Amer. Chem. Soc.*, **79**, 352 (1957). b) R. Breslow and P. Gal, *ibid.*, **81**, 4747 (1959). c) K. Okamoto, K. Komatsu, and H. Shingu, This Bulletin, **42**, 3249 (1969). d) C. C. Price, M. Siskin, and C. K. Miao *J. Org. Chem.*, **36**, 794 (1971). Also, see the review by M. Siskin in E. S. Huyser, "Methods in Free Radical Chemistry," Vol. 3, M. Decker, Inc., New York, N. Y., (1972), p. 83.

3) K. Okamoto and K. Komatsu, This Bulletin, **47**, 1709 (1974).

4) E. Haug and B. Föhlisch, *Chem. Ber.*, **104**, 2324 (1971).

5) H. J. Dauben, Jr., F. A. Gadecki, K. M. Harmon, and D. L. Pearson, *J. Amer. Chem. Soc.*, **79**, 4557 (1957).

6) E. Haug and B. Föhlisch, *Chem. Ber.*, **104**, 2338 (1971).

7) The preparations of 7-cyano- and 7-carbomethoxy-1,3,5-cycloheptatrienes are reported in the literatures (Ref. 2a and W. Betz and J. Daub, *Chem. Ber.*, **105**, 1778 (1972), respectively, whereas 7-methylthio derivative was prepared by the reaction of the tropylium ion with methanethiol.

8) M. V. George, D. J. Peterson, and H. Gilman, *J. Amer. Chem. Soc.*, **82**, 403 (1960).

9) The charge-transfer spectrum of I has been reported (H. J. Dauben, Jr., and J. D. Wilson, *Chem. Commun.*, **1968**, 1629), but neither the synthetic method nor its property has been described.

10) K. Okamoto, K. Komatsu, T. Kinoshita, and H. Shingu, This Bulletin, **43**, 1901 (1970).

11) R. B. Larrabee, *J. Amer. Chem. Soc.*, **93**, 1510 (1971).

12) G. Vincow, H. J. Dauben, Jr., F. R. Hunter, and W. V. Volland, *ibid.*, **91**, 2823 (1969).

13) The probable error in the NMR analysis is less than 10%.

14) a) A. W. Francis, A. J. Hill, and J. Johnston, *ibid.*, **47**, 2211 (1925). b) C. K. Ingold and M. S. Smith, *J. Chem. Soc.*, **1938**, 905. c) S. L. Friess and A. Weissberger, "Technique of Organic Chemistry," Vol. III, p. 100, Interscience Publishers, Inc., New York, N. Y. (1953).

15) Ref. 1b and the references cited therein.

16) The values of σ_p were cited from D. H. McDaniel and H. C. Brown, *J. Org. Chem.*, **23**, 420 (1958), except that for $-CO_2CH_3$, which was cited from H. van Bekkum, P. E. Verkade, and B. M. Wepster, *Rec. Trav. Chim.*, **78**, 815 (1959).

17) When log $k_{rel.}$ is plotted against Brown's σ_p^+ (H. C. Brown and Y. Okamoto, *J. Amer. Chem. Soc.*, **80**, 4979 (1958)), the correlation is worse than that in Fig. 5. This may be a reflection of the fact that the extent of conjugation of the substituent with the seven-membered ring is not changed so much throughout the reaction path from the tropylium ion to the tropyl radical, whereas, from the definition, σ_p^+ is applicable to those reactions in which the conjugative interaction of the carbonium-ion center with the substituent arises and develops during the course from the ground state to the intermediate.

18) The melting points and boiling points are uncorrected. The elemental analyses were performed by the Microanalytical Center, Kyoto University, Kyoto. The infrared and ultraviolet spectra were recorded on a Hitachi model 215 and Shimadzu model UV-50M spectrometers repsectively. The NMR spectra were taken with a Hitachi model R-24 spectrometer with tetramethylsilane as the internal standard.

19) Bromobenzene-d_5 was prepared by bromination of benzene-d_6 (99.6%, CEA, France), according to the method of L. Gatterman and F. H. Wieland, "Die Praxis des organischen Chemikers," Walter de Gruyter & Co., Berlin (1961), p. 95.

20) The reducibility of IX′ was examined also by the use of the chromous-ion reduction method. It was indicated that the reducibility of IX was not affected by deuteration of the phenyl ring.

Synthetic Photochemistry. IV.[1] The Reaction of Betaines with Singlet Oxygen

Hitoshi TAKESHITA, Akira MORI, and Shumei OHTA

Research Institute of Industrial Science, Kyushu University, Hakozaki, Fukuoka 812

(Received March 14, 1974)

Singlet oxygen was allowed to react with three 3-hydroxypyridine derivatives, I, II, and III, in order to investigate its general behavior toward dipolar substrates. The occurrence of an easy C=C cleavage process to give furanones (V and XI) through the dioxetones was a characteristic feature. In addition, maleimides (IV and IX), oxamates (VIII, XII and XIV), and a carbamate (XIII) were isolated as highly oxidized products.

During the course of our studies of the photosensitized oxygenation of vinyl cyclopropane derivatives, we have noticed an indication which could better be interpreted in terms of the involvement of a dipolar intermediate in the formation of dioxetanes.[2]

Therefore, it seemed that it would be worthwhile to study the reaction with dipolar substrates, like betaines, to observe the structural effect on the dipolar intermediate. In addition, there seems to have been no report on the reaction of singlet oxygen with a betaine derivative, although there have been some reports on the photooxidation of a few related compounds. For example, the photooxidation of an indenone epoxide[3] or an epoxycyclopentenone[4] has been shown to give the products corresponding to that of pyrilium 3-oxide on oxygen, probably by a reaction of photo-excited substrates and ground-state oxygen; furthermore, the photooxidation of a thiopyrilium salt[5] gave several products, but the substrate was shown to be inert against singlet oxygen. In this paper, we would like to describe the results of the reaction of singlet oxygen carried out in both an aprotic solvent(chloroform) and a protic solvent(ethanol) with *N*-meth lp ridinium 3-oxide (I), *N*-benzylpyridinium 3-oxide(II) and their parent compound, 3-hydroxypyridine(III).

Results and Discussion

Oxidation of N-*Methylpyridinium 3-Oxide.* When a chloroform solution of I was irradiated by means of a 500-W tungsten lamp under an oxygen stream with catalytic amounts of methylene blue, two products, IV and V, were obtained in yields of 3.8 and 26% respectively. IV was identified as *N*-methylmaleimide,[6] while the structure of V was deduced as follows: The NMR spectrum [$\delta^{35°C}_{CDCl_3}$: 2.71(3H, s), 6.1—7.3 (3H, m) and 8.36 (1H, s) for Va; 2.79(3H, s), 6.1—7.3(3H, m) and 8.20(1H, s) for Vb; (a : b=2 : 1). $\delta^{35°C}_{(CD_3)_2SO}$: 2.5(3H, s), 6.49(1H, dd, J=6, 2 Hz), 6.65 (1H, t, J=2 Hz), 7.66(1H, dd, J=6 2 Hz) and 8.39 (1H, s) for Va; 2.70(3H, s), and 8.22(1H, s) for Vb, (a : b=5 : 1)] indicated the existence of a pair of stereoisomers and was characteristic of a formamide derivative;[7] in addition, the lactonic carbonyl frequencies in the IR spectrum were in the range for γ-butenolides. Thus, V is 5-(*N*-methylformamido)-2(5*H*)-furanone. The NMR at higher temperature showed the coalescence of the each signal due to the respective components [$\delta^{150°C}_{(CD_3)_2SO}$: 2.68(3H, s), 6.45 (1H, dd, J=6, 2 Hz), 6.62(1H, t, J=2 Hz), 7.56 (1H, dd, J=6, 2 Hz), and 8.28(1H, s)].

When the irradiations were performed in an ethanol solution, the products were different from those described above. The mixture was fractionated by silica-gel column chromatography to give four products, 3-hydroxy-*N*-methyl-α-pyridone (VI),[8] diethyl maleate, (VIIa), diethyl fumarate (VIIb), and ethyl *N*-methyloxamate (VIII).[9] Thus a solvent dependence on the product formation is observed.

Oxidation of N-*Benzylpyridinium 3-Oxide.* A chloroform solution of *N*-benzylpyridinium 3-Oxide (II) was similarly irradiated by means of a tungsten lamp. The reaction in this case was faster than that of I. From the mixture, *N*-benzylmaleimide (IX, 1%),[6] *N*-benzylformamide (X, 12%),[10] and 5-(*N*-benzylformamido)-2(5*H*)-furanone (XI, 9.3%) were isolated. IX and X were identical with authentic specimens prepared independently. XI again revealed a presence of a stereoisomeric pair of compounds in NMR at room temperature [δ_{CDCl_3}: 4.13(1H, d, J=16 Hz), 4.87 (1H, d, J=16 Hz), 6.0—7.3(3H, m), 7.27 (5H, br.), and 8.64 (1H, s) for XIa; 4.17(1H, d, J=16 Hz), 4.50(1H, d, J=16 Hz), 6.0—7.13(3H, m), 7.27 (5H, br.) and 8.40(1H, s) for XIb(a : b=2 : 1)] and coalescence at higher temperatures.

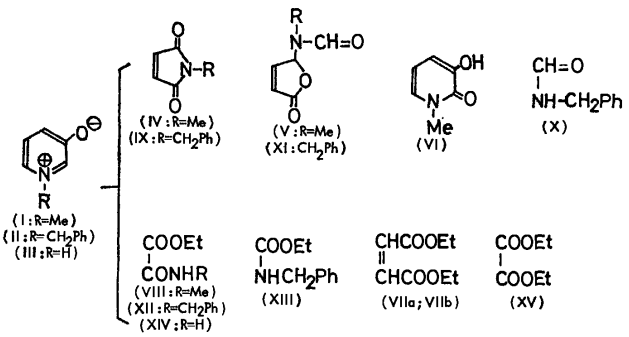

Chart 1.

The high-resolution mass spectrum of XI also supported the deduction of its structure; *i.e.*, the base peak was shown to correspond to $C_8H_8ON^+$, appearing at 134.06178 (Calcd: 134.06059), and arose from a cleavage of its C_5-N bond.

The oxidation of II in an ethanolic solution proceeded similarly to give the above three substances(2%, 21% and 14% yields respectively), together with two additional products, ethyl *N*-benzyloxamate(XII, 5.3%)[11] and ethyl *N*-benzylcarbamate(XIII, 8.7%),[12] which were identified by a direct comparison with an authentic specimen.

The Oxidation of 3-Hydroxypyridine(III). III is formally expressed in two tautomeric forms, IIIa and

IIIb, as has been illustrated.[13] Therefore, its behavior in reaction to singlet oxygen will be of interest in comparison with I and III. No oxidation in a chloroform solution has occurred; after irradiation for 160 hr, most of the starting material was recovered.

On the other hand, the oxidation performed in ethanol at 10—15 °C was shown to give diethyl maleate (VIIa), ethyl oxamate(XIV), and diethyl oxalate(XV) in low yields.

On the Pathways of Product Formations. As one sees, various types of products were formed. A technical difficulty in the isolation work-up of the products and the low yields almost throughout the reaction prevents detailed discussion; however, some of the interesting features should be noted.

Since a number of indoles and other chemiluminescent heterocycles has been shown to yield cleavage products by the action of ground-state oxygen, with the involvement of the intermediary dioxetanes formed *via* peroxy anions,[14] we have examined the reaction in the dark; no reaction with I and II has taken place. Therefore, the present C=C cleavage process must be solely photochemical, and the reactive species in the oxidation may be supposed to be the singlet oxygen, as in other dye-sensitized (by visible-light) photooxygenations.

The occurrence of the C=C cleavage process in both aprotic and protic solvents can be interpreted in terms of dioxetane formation, but the present "dipolar dioxetanes" might behave somewhat differently from those produced of ordinary substrates. The following explanation is based on this conception.

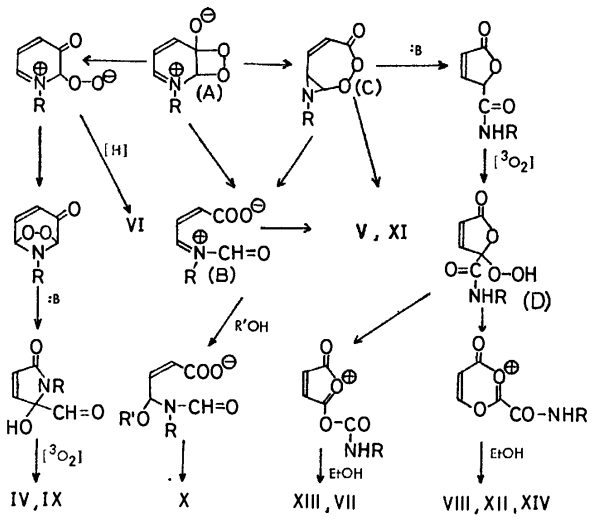

Chart 2.

The dioxetane (**A**), other than its ordinary fragmentation to **B**, can internally neutralize the separate charges by a rearrangement to **C**; it could equally possible be transformed into **B**. Once formed as a transient species, **B** could cause a lactonization (by an intramolecular path) or could form an amido-ether and an amido-alcohol (by an intermolecular path); the latter, derived by the addition of water, a trace of which should be present in the system, is thought to be responsible for the production of X. Since none of the maleimides (IV and IV), being stable under further reaction conditions, was converted into diethyl maleate (VIIa), their formation involves an independent path. Furthermore, the formamides (V and XI) were experimentally shown to be precursors of neither carbamate (XIII) nor oxamates (VIII, XII and XIV); hydroxy-α-pyridone, VI, was also shown to be inert under its formation conditions. Thus, among the remaining possibilities, we prefer to propose the formation of oxamates and maleate by a Baeyer-Villiger-type rearrangement of **D**, as a common intermediate which is probably formed by an action of the ground state oxygen. Further study along this line will be reported in the future.

Experimental

Photooxidation of N-*Methylpyridinium 3-Oxide (I).* a) I (2.0 g) was dissolved in chloroform (50 ml) and irradiated by means of a 500-W tungsten lamp in the presence of methylene blue under an oxygen stream for 73 hr at 10—15 °C. Then, after the removal of the solvent and the dye, the mixture was fractionated by silica-gel column chromatography to give IV (colorless crystals, 77 mg) (mp 92—94 °C (lit,[8] 90—92 °C)) and V (a colorless liquid, 674 mg) (Found: C, 50.90; H, 5.31; N, 10.46%. Calcd for $C_6H_7O_3N$: C, 51.06; H, 5.00; N, 9.93%. *ν*: 1800, 1770 and 1690 cm^{-1}).

b) I (5.05 g) was dissolved in ethanol (80 ml) and similarly irradiated at 0—5 °C. The silica-gel column chromatography of the mixture afforded VI (207 mg) as colorless needles (mp 134—134.5 °C (lit,[8] 130—131 °C)), found identical with an authentic sample by IR, NMR, and mixed-mp comparisons.

c) I (5.11 g) was irradiated in ethanol (80 ml) at 10—15 °C. A mixture of the products was then fractionated by silica-gel column chromatography to give VIIa (83 mg), VIIb (76 mg), and VIII (184 mg) (*δ* : 1.38(3H, t), 2.94 (3H, d, J=5.5 Hz), 4.34 (2H, q)). These three were found identical with independently-prepared samples by the IR and NMR spectral comparisons as well as by glc analysis.

Preparation of N-*Benzylpyridinium 3-Oxide (II).* III (10 g and benzyl chloride (13.3 g) were dissolved in *n*-propanol and refluxed for 8 hr. The mixture was then neutralized by passing it through anion-exchange resin (Amberlite IRA 401) to give hygroscopic crystals, (14.5 g, 74%), which gave the crystalline picrate (mp 185—187 °C (Found: C, 51.91; H, 3.29; N, 13.50%. Calcd for $C_{18}H_{14}O_8N_4$: C, 52.18; H, 3.41; N, 13.52%)).

Photooxidation of N-*Benzylpyridinium 3-Oxide (II).* a) II (2 g) was dissolved in chloroform (50 ml) and similarly irradiated. A mixture of the products was separated by silica-gel column chromotography to give IX (17 mg, colorless plates) (mp 71—72 °C (lit,[6] 67.7 °C) (*δ*: 4.60 (2H, s), 6.62 (2H, s), 7.25 (5H, s)) and X (180 mg, colorless needles) (mp 62—63 °C (lit,[10] 60—61 °C) (*δ*: 4.25(2H, d, J=7 8.15 (1H, s))), as identified by direct comparisons with independently-prepared samples (mixed-mp, IR and NMR spectra, and glc). The latter fraction of the chromatography yielded a colorless oil (220 mg) which was deduced to be XI (Found: mol. wt.=217.0781 (M^+). Calcd for $C_{12}H_{11}O_3N$: 217.0789. $\delta^{25°C}_{(CD_3)_2SO}$: 8.29(1H, s) for XIa and 8.60(1H, s) for XIb (a : b=1 : 6). $\delta^{100°C}_{(CD_3)_2SO}$: 8.55(1H, s). *ν*: 1800, 1700, 1620, and 1500 cm^{-1}).

b) Similarly, II (118 mg) was oxidized in ethanol at 10—15 °C to give IX (43 mg), X(300 mg), XI(330 mg), and

XII (118 mg, colorless needles) (mp 47—48 °C (lit,[11] 46—47 °C) (δ: 1.38(3H, t), 4.34(2H, q), 4.51(2H, d, J=6.2 Hz), ~1.3(1H, br.), and 7.32(5H, s))), (which was identified by means of a mixed-mp test as well as by spectral comparisons with an authentic sample), and XIII (172 mg, a colorless oil) (δ: 1.23(3H, t), 4.15(2H, q), 4.35(2H, q, J=6.2 Hz), 5.0(1H, br.), and 7.30(5H, s)), which was identical with an authentic sample (IR and MNR analysis).

Photooxidation of 3-Hydroxypyridine (III). III (1.0 g) was dissolved in ethanol (50 ml) and similarly irradiated at 10—15 °C. After 67 hr, the resulting mixture was chromatographed through a silica-gel column to give VIIa (17 mg), XIV (28 mg), and XV (25 mg). They were all found to be identical with authentic samples by IR and NMR spectral comparisons as well as by glc analysis.

Attempted Transformation of IV and IX under the Reaction Conditions. Authentic IV (200 mg) and IX (140 mg) were separately dissolved in ethanol (each 80 ml) and irradiated for 48 hr at room temperature under an oxygen stream with methylene blue. By the usual subsequent work-up, IV and IX were recovered quantitatively.

Further Oxidation of VI in an Ethanol Solution. VI (510 mg) was irradiated for 16 hr under an oxygen stream. Despite extensive fractionation by silica-gel column chromatography, no isolable product was obtained.

Further Oxidation of XI in Ethanol. XI (170 mg) was dissolved in ethanol (50 ml) and was irradiated for 21 hr under conditions similar to those of its formation. A careful fractionation of the reaction mixture by silica-gel column chromatography gave only the recovered XI quantitatively.

Attempted Autooxidation of I. I (500 mg) was dissolved in chloroform or ethanol, into which an oxygen stream was introduced for 84 hr at room temperature (with or without Methylene Blue). By a work-up similar to the one described above, unreacted I was recovered in a quantitative yield.

We wish to thank The Ministry of Education for its financial support.

References

1) Part III: H. Takeshita, A. Mori, and S. Itô, This Bulletin, **47**, 1678 (1974).
2) H. Takeshita, T. Hatsui, and H. Kanamori, *Tetrahedron Lett.*, **1973**, 1697.
3) H. H. Wasserman and D. L. Pavia, *Chem. Commun.*, **1970**, 1459.
4) E. F. Ullman and W. A. Henderson, Jr., *J. Amer. Chem. Soc.*, **89**, 4390 (1967).
5) Z. Yoshida, T. Sugimoto, and S. Yoneda, *Tetrahedron Lett.*, **1971**, 4259.
6) A. Piutti and E. Giustiniani, *Gazz. Chim. Ital.*, **26 I** 431 (1896).
7) A. J. R. Bourn and E. W. Randall, *J. Mol. Spectroscopy*, **13**, 29 (1964).
8) A. F. Bickel and J. P. Wibaut, *Rec. Trav. Chim. Pays-Bas*, **65**, 65 (1946).
9) O. Wallach and P. West, *Liebigs Ann. Chem.*, **184**, 57 (1876).
10) S. Sugasawa and H. Shigehara, *Yakugaku Zasshi*, **62**, 531 (1942).
11) J. Thiele, *Liebigs Ann. Chem.*, **376**, 239 (1910).
12) A. Hantzsch, *Chem. Ber.*, **31**, 177 (1898).
13) The following two tautomeric structures can be accounted:

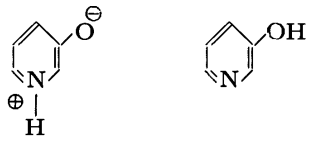

(IIIa) (IIIb)

14) *Cf.* F. McCapra and Y. C. Chang, *Chem. Commun.*, **1967**, 1011; F. McCapar, *Intern. Pure Appl. Chem.*, **1970**, 611.

Chemistry of α-Haloaldehyde. VI.* Reaction of 2-Chloro-2-methylpropanal with Benzoylacetonitrile in the Presence of Potassium Carbonate

Akira TAKEDA, Sadao TSUBOI, and Takashi SAKAI

Department of Synthetics Chemistry, School of Engineering, Okayama University, Tsushima, Okayama 700

(Received March 30, 1974)

The reaction of 2-chloro-2-methylpropanal with benzoylacetonitrile in aqueous K_2CO_3 has been studied. When 2-chloro-2-methylpropanal was added to a stirred suspension of benzoylacetonitrile in aqueous K_2CO_3, 2-hydroxy-3,3-dimethyl-4-cyano-5-phenyl-2,3-dihydrofuran (**7**) was obtained. The oxidation of **7** with CrO_3 gave α,α-dimethyl-β-cyano-γ-phenyl-$\Delta^{\beta,\gamma}$-butenolide (**8**). When benzoylacetonitrile was added to a suspension of 2-chloro-2-methylpropanal in aqueous K_2CO_3 stirred beforehand for 60 min, the reaction proceeded in a different manner to give the enol tautomer (**9b**) of 2,4-dibenzoyl-3-(α-hydroxyisopropyl)glutaronitrile (**9a**) at room temperature, and 2,2-dimethyl-3-(α-carbaminophenacyl)-4-cyano-5-phenyl-2,3-dihydrofuran (**11**) at 80—90 °C. The alkaline hydrolysis of the nitrile **9** conducted at 70 °C also afforded the amide **11**. The nitrile **9** eliminated one mol of benzoylacetonitrile on treatment with H_2SO_4 to afford 2,2-dimethyl-3-hydroxy-4-cyano-5-phenyl-2,3-dihydrofuran (**12**). Chromic acid oxidation of **12** gave 2,2-dimethyl-3-oxo-4-cyano-5-phenyl-2,3-dihydrofuran (**14**), which can be derived from bullatenone in two steps. Structures of compounds **11**, **12**, and **14**, which all possess 2,2-dimethyl-4-cyano-5-phenyl-2,3-dihydrofuran ring, have been confirmed and well correlated by both chemical transformations and spectral data.

The synthesis of bullatenone (2,2-dimethyl-3-oxo-5-phenyl-2,3-dihydrofuran) (**1**) has been carried out.[1,2] Studies on the reaction of 2-halo-2-methylpropanal (**2**)[3,4] with active methylene compounds show that in contrast to reactions under nonaqueous conditions, undergoing S_N2-type substitution at the α carbon of **2**, the enolate anion attacks the carbonyl carbon of **2** in aqueous media. It was thought that the base-catalyzed condensation of **2** with ethyl benzoylacetate in an aqueous solution of K_2CO_3 might turn out to be a new route for obtaining 3-hydroxydihydrofuran **3**, which is expected to be readily oxidized to bullatenone. However, it gave only α-benzoyl-β-benzoylethoxycarbonylmethyl-γ-butyrolactone (**4**).[4] It appears that the extraordinarily facile lactonization of the aldol-type product interrupted the formation of **3**. Such a breakdown could be evaded by starting from benzoylacetonitrile (**5**) in place of ester, since the aldol-type product in this case is incapable of lactonization. We report the result of the title reaction conducted under several basic conditions in aqueous media. Structural assignments were made based on spectral data and microanalysis.

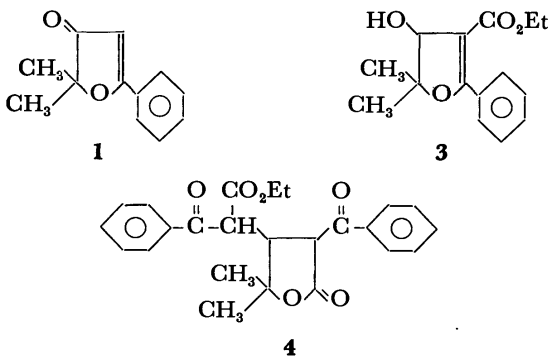

1 **3** **4**

Results and Discussion

When 2-chloro-2-methylpropanal (**2a**) was added to a stirred suspension of benzoylacetonitrile (**5**) in an aqueous solution of K_2CO_3, 2-hydroxy-3,3-dimethyl-4-cyano-5-phenyl-2,3-dihydrofuran (**7**) was obtained in a 72% yield. This indicates that a nucleophilic substitution occurred at the α carbon of **2a** to give the 1,4-dioxo compound **6** as an intermediate, which immediately tautomerized to the cyclic hemiacetal **7**. Compound **7** is more stable against heating as compared with the corresponding ester and resists ring-opening on distillation.[5] The oxidation of **7** with CrO_3 gave α,α-dimethyl-β-cyano-γ-phenyl-$\Delta^{\beta,\gamma}$-butenolide (**8**) in an 81% yield. NMR spectrum ($CDCl_3$) of **8** showed a simple pattern exhibiting a singlet at δ 1.55 ppm due to α,α-dimethyl protons and a multiplet (5H) at δ 7.2—8.0 ppm due to phenyl protons. Its IR spectrum showed characteristic bands at 2240 and 1830 cm^{-1} due to β-cyano-$\Delta^{\beta,\gamma}$-butenolide structure. The reaction sequence of the formation of compounds **7** and **8** is shown in Scheme 1.

The reaction proceeded quite differently when nitrile **5** was added to a suspension of **2a** in an aqueous solution of K_2CO_3, which was stirred beforehand for at least 60 min (Scheme 2). The reaction carried out in this way at room temperature gave the enol tautomer of 2,4-dibenzoyl-3-(α-hydroxyisopropyl)glutaro-

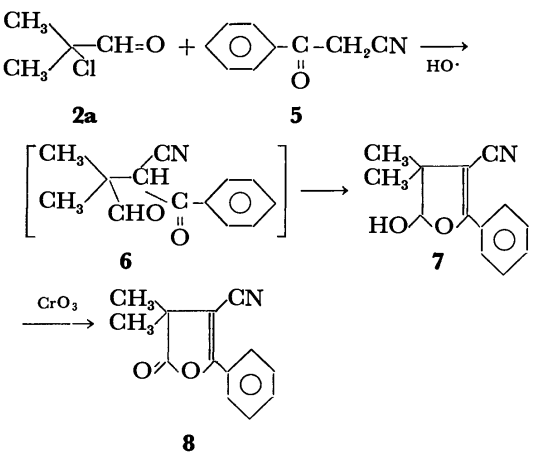

2a **5** **6** **7** **8**

Scheme 1.

* Presented at the 30th Annual Meeting of the Chemical Society of Japan, Higashi-Osaka, April 1, 1974.

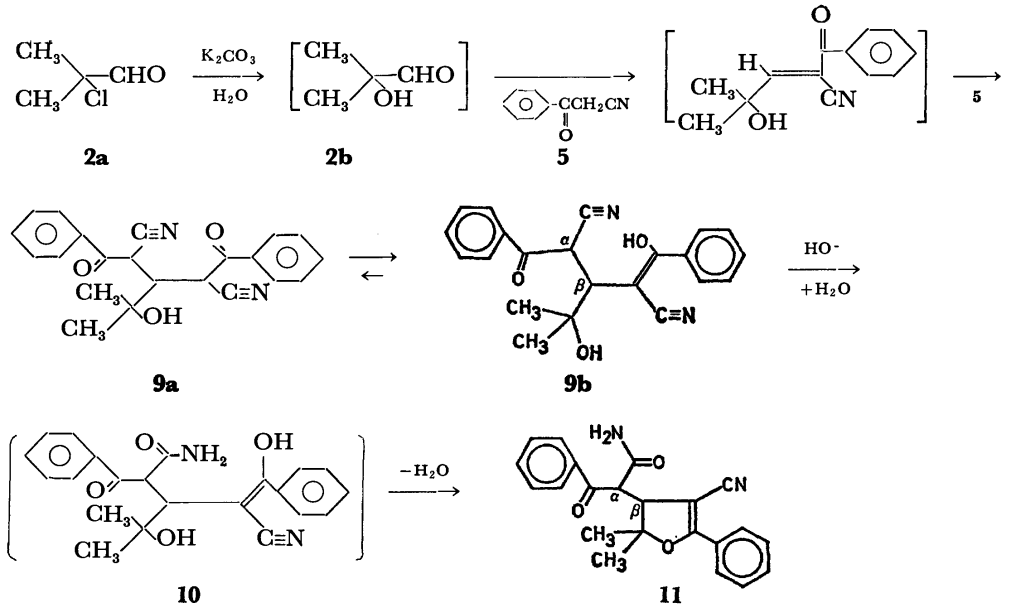

Scheme 2.

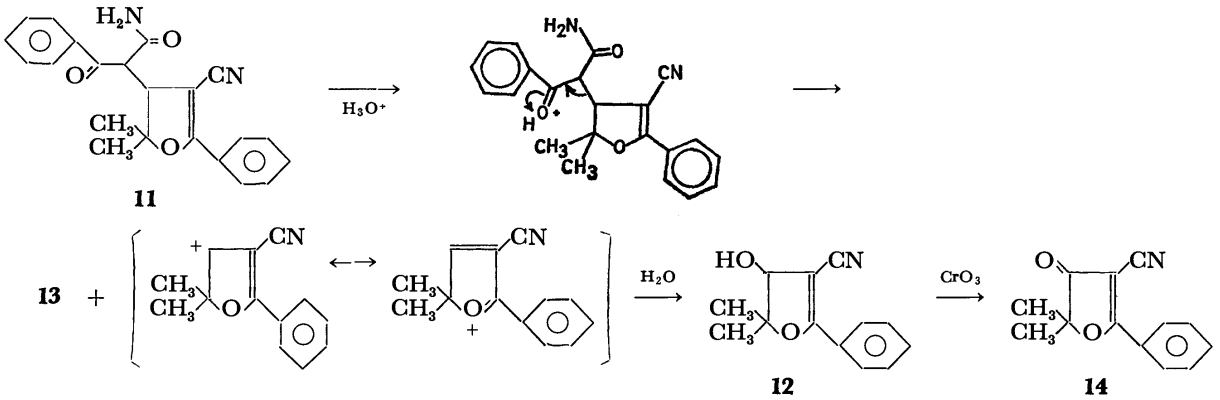

Scheme 3.

nitrile (**9**) in an 81% yield, whereas a similar reaction conducted at 80—90 °C afforded 2,2-dimethyl-3-(α-carbaminophenacyl)-4-cyano-5-phenyl-2,3-dihydrofuran (**11**) in a 48% yield together with a small amount of α-benzoyl-γ,γ-dimethyl-$\Delta^{\alpha,\beta}$-butenolide (11%).[5] NMR spectrum [$(CD_3)_2SO$] of the nitrile **9** exhibited two doublets at δ 3.11 and 4.21 ppm (1H each, J= 13 Hz, β-methine proton and α-methine proton), and singlets at 3.20 and 11.8 ppm (1H each, 2 OH), respectively. These signals indicate that one of two benzoyl groups of **9** has been enolized, since otherwise a more complex pattern due to three methine protons coupled to each other should be observed. On the other hand, NMR spectrum [$(CD_3)_2SO$] of the amide **11** showed two singlets at δ 1.01 and 1.40 ppm due to 2,2-dimethyl protons, and one singlet at δ 3.30 ppm due to amide protons. Signals due to two methine protons of this compound appeared at δ 5.02 ppm (d, 1H, J=11 Hz, β-methine proton) and 5.38 ppm (d, 1H, J=11 Hz, α-methine proton), respectively. The amide **11** can be prepared also by treating **9** with an aqueous solution of K_2CO_3 at 70 °C in an 88% yield. Since **9** does not show any tendency to cyclize to dihydrofuran structure, compound **11** is thought to be derived from amide **10**, which was produced from **9** by the saponification of its cyano group.

Treatment of **9** with concentrated H_2SO_4 caused elimination to yield 2,2-dimethyl-3-hydroxy-4-cyano-5-phenyl-2,3-dihydrofuran (**12**) and benzoylacetamide (**13**) in 69% and 78% yields, respectively. A probable mechanism of this acid-catalyzed elimination is given in Scheme 3. The chromic acid oxidation of **12** afforded 2,2-dimethyl-3-oxo-4-cyano-5-phenyl-2,3-dihydrofuran (**14**). This ketone has been prepared by an alternative way starting from bullatenone (**1**). The direct bromination of **1** gave 2,2-dimethyl-3-oxo-4-bromo-5-phenyl-2,3-dihydrofuran (**15**) in good yield (91%). The treatment of **15** with CuCN afforded **14** in a 24% yield.

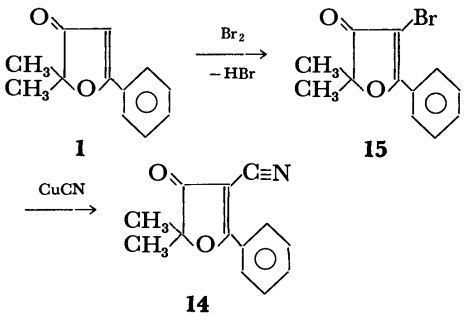

It is assumed that 2-hydroxy-2-methylpropanal (**2b**) acts as the real substrate of the reaction when nitrile **5** was added to **2a** treated beforehand with an aqueous solution of K_2CO_3, since 2-halo-2-methylpropanal promptly undergoes displacement of halogen to give **2b**.[6] The fact that the reaction of **2b** and **5** carried out at 60 °C in an aqueous solution of K_2CO_3 also gave **11** in a 55% yield supports the assumption.

Experimental

General. Melting points and boiling points are uncorrected. The infrared spectra were recorded on a Hitachi EPI-S2 model spectrophotometer. NMR spectra (60 MHz) were taken on a Hitachi R-24 model spectrometer, and MS spectra were obtained on a Hitachi RMS-4 model mass spectrometer. Analytical thin layer chromatography (tlc) was carried out using silica gel GF_{254} (E. Merck AG, Darmstadt). Preparative tlc was carried out on silica gel PF_{254} (E. Merck AG). Microanalyses were carried out by Mr. Eiichiro Amano of our laboratory. Starting materials such as 2-chloro-2-methylpropanal (**2a**),[7] 2-hydroxy-2-methylpropanal (**2b**)[8] were prepared by the procedures in literature.

2-Hydroxy-3,3-dimethyl-4-cyano-5-phenyl-2,3-dihydrofuran (7). To a solution of 4.8 g (0.0345 mol) of potassium carbonate in 12 ml of water was added 5 g (0.035 mol) of **5** at room temperature. To the resulting mixture was added 3.3 g (0.031 mol) of **2a** with ice bath cooling. The mixture was stirred at room temperature for 2 hr, and then at 60 °C for 3 hr. It was poured into a large amount of water and extracted with ether. The ethereal extract was washed several times with water and dried over Na_2SO_4. Removal of the solvent left 7 g of a brown oil which, on distillation, gave 4.8 g (72%) of **7**: bp 144—148 °C/0.16 mmHg; mp 75—76 °C (petroleum ether–benzene–ethanol); IR (nujol) 3420 (OH), 2200 (CN), 1615 (C=C), 1600 and 1575 cm^{-1} (benzene C=C); NMR ($CDCl_3$) δ 1.30 (s, 6H, $2CH_3$), 4.35 (broad s, 1H, OH), 5.60 (s, 1H, >CH(OH)), 7.26—8.02 (m, 5H, C_6H_5); MS (70 eV) *m/e* (rel. intensity) 215 (14, M^+), 200 (8, M^+-CH_3), 186 (43), 172 (9), 154 (14), 105 (100, PhCO), 77 (74, C_6H_5). Found: C, 72.59; H, 6.05; N, 6.81%. Calcd for $C_{13}H_{13}NO_2$: C, 72.54; H, 6.09; N, 6.51%.

α,α-Dimethyl-β-cyano-γ-phenyl-$\Delta^{\beta,\gamma}$-butenolide (8). To a mixed solution of 0.62 g (0.0029 mol) of **7** in 5 ml of aqueous 50% acetic acid was added 0.32 g (0.0032 mol) of chromium trioxide in several portions, with moderate cooling. The mixture was stirred for 2.5 hr at room temperature. The reaction mixture was diluted with 5 ml of water and then extracted with ether. The ethereal extract was washed with water and dried over Na_2SO_4. Removal of the solvent left 0.50 g (81%) of **8**: mp 95—95.5 °C (petroleum ether–benzene); IR (neat) 2240 (CN), 1830 (lactone C=O), 1640 cm^{-1} (conjugated C=C); NMR (CCl_4) δ 1.55 (s, 6H, $2CH_3$), 7.20—8.00 (m, 5H, C_6H_5); MS (70 eV) *m/e* (rel. intensity) 213 (50, M^+), 198 (85, M^+-CH_3), 184 (40, $M^+-C_2H_5$), 171 (34), 157 (8), 143 (8), 122 (31), 105 (100, PhCO), 77 (87, C_6H_5).

Found: C, 73.41; H, 5.08; N, 6.61%. Calcd for $C_{13}H_{11}NO_2$: C, 73.23; H, 5.20; N, 6.57%.

Enol Tautomer (9b) of 2,4-Dibenzoyl-3-(α-hydroxyisopropyl)-glutaronitrile (9a). To a solution of 2.5 g (0.017 mol) of potassium carbonate in 10 ml of water was added 1.85 g (0.017 mol) of **2a**. After the mixture was stirred for 1 hr at room temperature, 4.0 g (0.028 mol) of **5** was added and the stirring was continued for 17 hr. The semisolid material separated was collected by filtration and washed with 10% HCl and with ether successively to give 2.4 g (81%) of **9b**, white crystal: mp 178—178.5 °C (acetone); IR (KBr) 3300 (broad, OH), 2980, 2200 (CN), 1700 (m, C=O), 1630 (s, C=C, C=O), 1600 (w), 1350, 1240, 1050, 765, 700 cm^{-1}; NMR [$(CD_3)_2SO$] δ 1.33 (s, 3H, CH_3), 1.57 (s, 3H, CH_3), 3.11 (d, 1H, J=13 Hz, β-methine proton), 3.20 (broad s, 1H, OH), 4.21 (d, 1H, J=13 Hz, α-methine proton), 7.10—7.83 (m, 10H, $2C_6H_5$), 11.80 (broad s, 1H, enolic OH); MS (70 eV) *m/e* (rel. intensity) 343 (0.1), 342 (0.1). 317 (0.2), 302 (0.2), 198 (3), 197 (2.6), 172 (4.4), 149 (9), 145 (5), 122 (4), 105 (100, PhCO), 77 (79, C_6H_5).

Found: C, 73.39; H, 5.88; N, 7.47%. Calcd for $C_{22}H_{20}N_2O_3$: C, 73.32; H, 5.59; N, 7.77%.

2,2-Dimethyl-3-(α-carbaminophenacyl)-4-cyano-5-phenyl-2,3-dihydrofuran (11). (a) From 2a and 5. A mixed solution of **2a** (0.107 g, 0.001 mol) and potassium carbonate (0.138 g, 0.001 mol) in 1 ml of water was stirred for 30 min at room temperature. To the resulting suspension was added 0.145 g (0.001 mol) of benzoylacetonitrile. After being stirred at room temperature for 2 hr and at 80—90 °C for an additional 3 hr, the mixture was acidified with 10% HCl. After addition of a small amount of ether, the precipitated crystals of **11** (0.0445 g, 25%) were collected by filtration: mp 230 °C (THF); IR (KBr) 3450 (sharp, NH_2), 2230 (w, CN), 1685 (s, C=O), 1640 (m, C=C), 1604 and 1584 (benzene ring), 780, 700 cm^{-1}; NMR [$(CD_3)_2SO$] δ 1.01 (s, 3H, CH_3), 1.40 (s, 3H, CH_3), 3.30 (s, 2H, $CONH_2$), 5.02 (d, 1H, J=11 Hz, β-methine proton), 5.38 (d, 1H, J=11 Hz, α-methine proton), 7.30—8.30 (m, 10H, $2C_6H_5$); MS (70 eV) *m/e* (rel. intensity) 343 (0.2), 317 (3), 302 (8), 197 (3), 195 (6), 122 (33), 105 (100, C_6H_5CO), 77 (67, C_6H_5).

Found: C, 73.50; H, 5.63; N, 7.67%. Calcd for $C_{22}H_{20}N_2O_3$: C, 73.32; H, 5.59; N, 7.77%.

Tlc analysis (*n*-hexane : acetone, 1 : 1) of the residue (0.077 g) recovered from the filtrate showed three spots at R_f values 0.48, 0.57, and 0.66 (content ratio in wt, 12 : 42 : 23). Component with R_f value 0.57 and that with R_f value 0.66 were identified as **11** (23%)[9] and α-benzoyl-γ,γ-dimethyl-$\Delta^{\alpha,\beta}$-butenolide[5] (11% yield), respectively, by the identities of the spectral data with those of authentic samples.

(b) From 9b. A mixed solution of **9b** (0.067 g, 0.19 mmol) and potassium carbonate (0.068 g, 0.49 mmol) in water (1 ml) was stirred for 3 hr at 70 °C. After being acidified with 10% HCl, the mixture was extracted with ether. White crystals (0.031 g) precipitated were collected and identified as **11** by comparison of its IR spectrum with that of an authentic sample. From the ethereal layer, additional amount (0.040 g) of crude product with 70% purity by tlc analysis (*n*-hexane : acetone, 1 : 1) was obtained, total yield 88%.

(c) From 2b and 5. To a solution of 0.106 g (0.76 mmol) of potassium carbonate in 0.45 ml of water was added 0.11 g (0.76 mmol) of **5**. After the mixture was stirred for 1 hr, 0.081 g (0.76 mmol) of **2b** was added. It was stirred at room temperature for 2 hr, and at 60—65 °C for 3 hr, and then acidified with dilute HCl. The crude product was collected and washed with ether to give 0.15 g (55%) of **11**: mp 230 °C (acetone).

2,2-Dimethyl-3-hydroxy-4-cyano-5-phenyl-2,3-dihydrofuran (12). The nitrile **9** (0.24 g, 0.67 mmol) was dissolved in 6 ml of concd H_2SO_4. After being allowed to stand for one day at room temperature, the solution was poured into 50 ml of ice-water. The organic layer was extracted with ether and dried over $MgSO_4$. After removal of the solvent, residual semisolid (0.018 g) was obtained. Tlc analysis (*n*-hexane : acetone, 2 : 1) of this solid showed two spots at R_f values 0.07 and 0.26 (content ratio in wt, 44 : 56). Component with R_f value 0.07 was collected by preparative tlc and iden-

tified as benzoylacetamide (**13**), 78% recovery: mp 111—112 °C (acetone) (lit,[10] mp 112—113 °C). IR and NMR spectra were identical with those of the authentic sample obtained by the treatment of benzoylacetonitrile with concd H_2SO_4: IR (KBr) 3400 and 3170 (NH and enolic OH), 1670 and 1630 (C=O), 1595 and 1575 (benzene C=C), 1390, 800, 760, 690 cm^{-1}: NMR[11] [$(CD_3)_2SO$] δ 2.85 (broad s, NH_2), 3.99 (s, $-CH_2CO$), 5.88 (s, enolic >C=CH–), 7.30—8.18 (m, C_6H_5), 15.10 (broad s, enolic OH).

Component with R_f value 0.26 collected by preparative tlc was microdistilled at 150 °C under 0.05 mmHg with a bath, and identified as **12**, yield 69%: IR (neat) 3450 (OH), 2200 (CN), 1625 (C=C), 1575 (benzene C=C), 1495, 1115, 1070, 875, 820, 780, 695 cm^{-1}; NMR [$(CD_3)_2C=O$] δ 1.43 (s, 3H, CH_3), 1.50 (s, 3H, CH_3), 4.71 (d, 1H, J=8 Hz, OH), 4.85 (d, 1H, J=8 Hz, >CHOH), 7.40—8.10 (m, 5H, C_6H_5); MS (70 eV) *m/e* (rel. intensity) 215 (40, M^+), 188 (34), 156 (26), 141 (40), 128 (50), 105 (100), 77 (78), 59 (68).

Found: C, 72.70; H, 6.33; N, 6.31%. Calcd for $C_{13}H_{13}NO_2$: C, 72.54; H, 6.09; N, 6.51%.

*2,2-Dimethyl-3-oxo-4-cyano-5-phenyl-2,3-dihydrofuran (**14**).* *(a) From **12**.* To a mixture of 0.1 ml of 70% acetic acid and 0.04 g (0.4 mmol) of chromium trioxide was added 0.042 g (0.2 mmol) of **12** in several portions at 0 °C. The mixture was stirred for 2 hr at room temperature and then for 1 hr at 60 °C. The mixture was poured into 1 ml of water and the organic layer was extracted with ether, washed with water, and dried over $MgSO_4$. After removal of the solvent, 0.022 g of the residual oil was obtained. Tlc analysis (*n*-hexane : acetone, 2 : 1) of this oil showed two spots at R_f values 0.3 and 0.5 (content ratio in wt, 1 : 3). The component of R_f value 0.5 collected by preparative tlc was recrystallized from the mixed solvent of *n*-hexane and ether to give 0.017 g (40%) of **14**: mp 122—124 °C; IR (KBr) 2200 (CN), 1705 (C=O), 1590 (benzene ring), 1560 (C=C), 1395, 1215, 900 (C–O), 765 and 695 cm^{-1} (monosubstituted benzene); NMR ($CDCl_3$) δ 1.57 (s, 6H, $2CH_3$), 7.40—8.45 (m, 5H, C_6H_5); MS (70 eV) *m/e* (rel. intensity) 213 (22, M^+), 149 (10), 127 (100), 105 (11, C_6H_5CO), 77 (11, C_6H_5).

Found: C, 72.85; H, 5.28; N, 6.86%. Calcd for $C_{13}H_{11}NO_2$: C, 73.23; H, 5.20; N, 6.57%.

*(b) Synthesis from 2,2-Dimethyl-3-oxo-4-bromo-5-phenyl-2,3-dihydrofuran (**15**).* In a hood, a stirred suspension of 0.18 g (0.66 mmol) of **15** and 0.069 g (0.76 mmol) of cuprous cyanide in 1 ml of dry DMF was heated at 80 °C for 4 hr, and finally at 150 °C for 20 min. A solution of 2 g of ferric chloride in 4 ml of 5% HCl was added to the reaction mixture, which was then stirred for 20 min at 60 °C to decompose the complex. Ethereal extract of the organic layer was washed with water and dried over $MgSO_4$. After removal of the solvent, 0.146 g of a solid was obtained. Tlc analysis (*n*-hexane : acetone, 2 : 1) of this solid showed the presence of two spots at R_f values 0.42 and 0.49. Preparative tlc of the component with the R_f value 0.42 gave 0.034 g (24%) of a crystal, which was identified as **14** by comparison of IR spectrum with that of the authentic sample. The component with the R_f value 0.49 was collected similarly and identified as **15**.

*2,2-Dimethyl-3-oxo-4-bromo-5-phenyl-2,3-dihydrofuran (**15**).* To a stirred suspension of 0.38 g (2 mmol) of **1**[1] in 2 ml of water was added 0.51 g (3.2 mmol) of bromine dropwise at 80 °C. The mixture was stirred for 15 min at 90 °C. Removal of the solvent left 0.49 g (91%) of **15**: mp 66—67 °C (*n*-hexane): IR (KBr) 1700 (C=O), 1602 and 1583 (benzene ring), 1559 cm^{-1} (C=C); NMR ($CDCl_3$) δ 1.51 (s, 6H, $2CH_3$), 7.40—8.30 (m, 5H, C_6H_5); MS (70 eV) *m/e* (rel. intensity) 266 (68, M^+, 1Br), 187 (8, M^+-Br), 180 (22, $C_6H_5C{-}CBr$, 1Br), 129 (100, $C_6H_5C=C=C=O$).

Found: C, 53.97; H, 3.96%. Calcd for $C_{12}H_{11}O_2Br$: C, 53.95; H, 4.31%.

References and Notes

1) A. Takeda, S. Tsuboi, and T. Sakai, *Chem. Lett.*, **1973**, 425 (1973).

2) C. W. Brandt, W. I. Taylor, and B. R. Thomas, *J. Chem. Soc.*, **1954**, 3245. (b) W. Parker, R. A. Raphael, and D. I. Wilkinson, *ibid.*, **1958**, 3871.

3) A. Takeda, S. Tsuboi, and Y. Oota, *J. Org. Chem.*, **38**, 4148 (1973).

4) A. Takeda, S. Tsuboi, and T. Sakai, Fourth International Congress of Heterocyclic Chemistry, Abstracts, 213 (1973).

5) A. Takeda, S. Tsuboi, and T. Sakai, *J. Org. Chem.*, (*in press*): "Chemistry of α-Haloaldehydes. IV. Reaction of 2-Halo-2-methylpropanal with Acylacetates in the Presence of Base." Ethyl 2-hydroxy-3,3-dimethyl-5-phenyl-2,3-dihydrofuran-4-carboxylate, a cyclic hemiacetal related to the nitrile **7**, can be converted into 2,2-dimethyl-3-(ethoxycarbonyl)-4-phenyl-4-oxobutanal by distillation (bp 130 °C/0.1 mmHg). The latter compound, when kept at room temperature for several days, tautomerized to the cyclic hemiacetal. The stability of **7** is partly attributable to the conjugation of cyano group with the ring system.

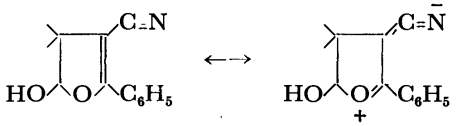

The butyrolactone **4**, on distillation, eliminates one mol of ethyl benzoylacetate releasing α-benzoyl-γ,γ-dimethyl-$\Delta^{\alpha,\beta}$-butenolide quantitatively: mp 65—66 °C; IR (nujol) 1750—1780 (lactone C=O), 1650 (benzoyl C=O), 1630 (C=C), 1598 and 1580 cm^{-1} (benzene C=C); NMR ($CDCl_3$) δ 1.58 (s, 6H, $2CH_3$), 7.70 (s, 1H, =C–H), 7.40—7.90 (m, 5H, C_6H_5).

6) The percentage of **2a** transformed into **2b** was found to be 90% in 15 min, 95% in 30 min, and 97% in 60 min.

7) C. L. Stevens and B. T. Gillis, *J. Amer. Chem. Soc.*, **79**, 3448 (1957).

8) R. Dworzak and J. Pierri, *Monats. Chem.*, **52**, 141 (1929).

9) Additional yield of **11**.

10) J. T. Abrams and F. S. Kipping, *J. Chem. Soc.*, **1934**, 1990.

11) This spectrum showed the existence of a mixture of keto and enol forms (1 : 1).

Reactions of Aryliminotriphenylphosphoranes with Sulfenes

Takayuki KAWASHIMA and Naoki INAMOTO

Department of Chemistry, Faculty of Science, The University of Tokyo, Hongo, Tokyo 113

(Received May 9, 1974)

Aryliminotriphenylphosphoranes reacted with methanesulfonyl, ethanesulfonyl and α-toluenesulfonyl chlorides in the presence of triethylamine to give 1 : 2 adducts [α-(*N*-alkanesulfonyl-*N*-arylsulfamoyl)alkylidenephosphoranes] and the decomposition products, instead of 1 : 1 adducts [α-(*N*-arylsulfamoyl)alkylidenephosphoranes). They were obtained under ice-cooling, the structure being of betaine type. In the case of methanesulfonyl chloride, isomeric 1 : 2 adduct [α-(*N*-arylsulfamoyl)methanesulfonylmethylenephosphorane] was also obtained. 2-Propanesulfonyl chloride gave *N*-triphenylphosphonio-*N*-arylsulfamate instead of expected adduct. In the absence of triethylamine, α-(*N*-arylsulfamoyl)alkyltriphenylphosphonium chlorides were obtained in good yields. Possible mechanisms of these reactions have been discussed.

In a previous paper,[1] we reported that reactions of arylimino- and acylmethylenetriphenylphosphoranes with benzenediazonium-2-carboxylate take place in a different manner. Ito *et al.*[2] reported the formation of alkanesulfonylmethylenephosphoranes (1 : 1 adduct) and episulfones or the decomposition products (*i.e.*, olefins) in the reactions of alkylidenephosphoranes with sulfene (CH_2=SO_2). Hamid and Trippett[3] obtained a similar 1 : 1 adduct in the reaction with phenylsulfene.

We have carried out the reactions of aryliminophosphoranes with sulfenes in order to compare them with reactions of alkylidenephosphoranes. Slightly different results were obtained.

Reactions with Unsubstituted Sulfene. When aryliminotriphenylphosphoranes (**1**) were allowed to react with two equivalents of sulfene generated from methanesulfonyl chloride (**2a**) and triethylamine at room temperature, *N*-aryl-*N*-methanesulfonylsulfamoylmethylenetriphenylphosphoranes (**3**), α-(*N*-arylsulfamoyl)-methanesulfonylmethylenetriphenylphosphoranes (**4**), which is an isomer of **3**, and triphenylphosphoniomethanesulfonate (**5**) were obtained in the yields shown in the following chart.

$$Ph_3P{=}N\text{-}Ar + 2\,MeSO_2Cl + 2\,Et_3N \rightarrow$$
1 **2a**

a, Ar=Ph
b, Ar=*p*-MeC_6H_4

$$Ph_3P{=}CHSO_2NAr\text{-}SO_2Me + Ph_3P{=}C(SO_2Me)SO_2NHAr + Ph_3\overset{+}{P}CH_2SO_3^-$$

	3	**4**	**5**
a	54%	38%	6%
b	38%	33%	16%

The structures of **3**, **4** and **5** were determined by elemental analyses, IR, NMR and MS spectra.

The NMR spectrum of **3a** showed a singlet peak at δ 3.20 ($MeSO_2$) and a doublet at δ 3.45 (J_{PCH} 12 Hz, disappeared by D_2O). The ^{31}P-NMR spectrum of **3b** exhibited a signal at δ_p −14.4 ppm (from 85% H_3PO_4 as an external standard). The data support the phosphorane structure (**3**), ruling out the exclusively cyclic structures **6** and **7**.

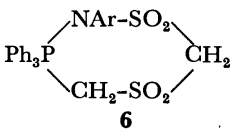

6

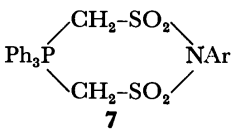

7

The IR spectra of **4** showed an NH absorption band at about 3300 cm^{-1}.

The structures are also supported by the following reactions. By chromatography on silica gel, **3a** was partially hydrolyzed to triphenylphosphine oxide (**8**) and bis(methanesulfonyl)anilide (**9**), mp 195—196 °C, which was in agreement with that of an authentic sample prepared from aniline and excess of **2a**. Reaction of **3b** with *p*-nitrobenzaldehyde gave the corresponding olefin (**10**) and **8** in 38 and 41% yields, respectively.

p-$NO_2C_6H_4$-CH=CH-SO_2-N(SO_2Me)-C_6H_4Me-*p*

10

The presence of NH group in **4b** was confirmed by *N*-methylation to the *N*-methyl derivative (**11**).

$Ph_3P{=}C(SO_2Me)\text{-}SO_2NMe\text{-}C_6H_4Me\text{-}p$

11

The spectral data and melting point of **5** were in agreement with those of an authentic sample prepared from methylenetriphenylphosphorane with sulfur trioxide according to the method of Nesmeyanov *et al.*[4]

Equimolar reaction of **1a** and sulfene also gave 1 : 2 adducts (**3a** and **4a**) at room temperature, but a 1 : 1 adduct (**12a**) by slow addition of **2a** under cooling with ice. However, **12a** could not be obtained in a pure state, because of easy hydrolysis in solution to **8** and methanesulfonylanilide (**13a**).

The MS spectrum of **12a** showed a parent peak at *m/e* 431. The absence of NH absorption band in the IR spectrum and the presence of a broad singlet at δ 4.30 (2H) in the NMR spectrum supported the betaine structure (**12a**) rather than a phosphorane structure (**12'a**).

$$Ph_3P{=}NPh + CH_2{=}SO_2 \rightarrow Ph_3\overset{+}{P}\text{-}\overset{-}{C}H_2SO_2NPh \xrightarrow{H_2O}$$
1a **12a**

$$Ph_3PO + MeSO_2NHPh \qquad Ph_3P{=}CHSO_2NHPh$$
8 **13a** **12'a**

Crude **12a** was allowed to react with sulfene to give 1 : 2 adducts **3a** and **4a** in 38 and 26% yields, respectively. The ratio of yield of **3a** to that of **4a** is 1.46, which is nearly equal to that in the above-mentioned 1 : 2 molar reaction (1.42). This indicates that **12a** is regarded as an intermediate in the formation of **3a** and **4a**.

Thus, the following mechanism is suggested.

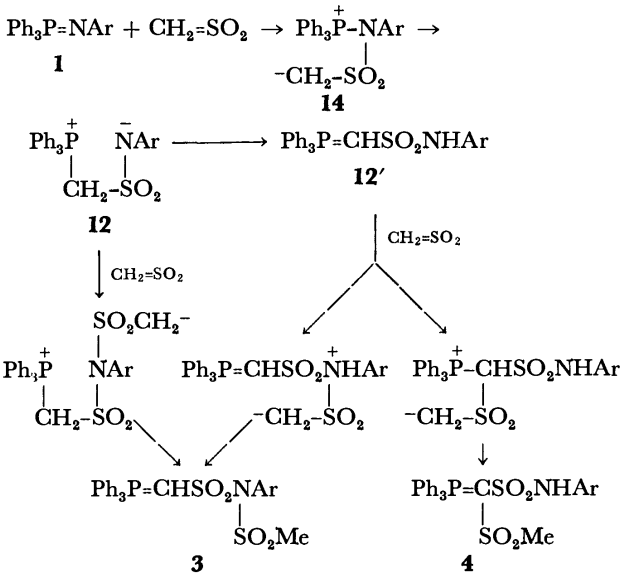

The first step is supported by the fact that benzoyliminophosphorane did not react with sulfenes, because of the low electron density on the nitrogen atom.

On the other hand, the ratio of yield of **3b** to that of **4b** was 1.15 in the case of **1b**. This value was inconsistent with an expectation (above 1.42) on the basis of the presence of electron-donating methyl group, but the yield of **5** from **1b** was larger than that from **1a**. It is thus suggested that **5** is formed by the hydrolysis of **3b** during the treatment.

No nucleophilic attack of the carbanion center in **14** on the nitrogen atom gave triphenylphosphine and thiaziridine 1,1-dioxide or Schiff's base. This is a different case from that of alkylidenephosphoranes having no α-hydrogen,[2] and might be attributed to a greater stabilization of betaine (**12**) than that of carbon analogues, because of more electronegative nitrogen.

Reactions with Monosubstituted Sulfenes. Reaction of **1b** with phenylsulfene, generated from α-toluenesulfonyl chloride (**2b**) and triethylamine, gave 1 : 2 adduct (**3c**) and a betaine (**15c**) in 26 and 44% yields, respectively. Chromatography of the residue gave α-toluenesulfonyl-*p*-toluidide (**13c**) and **8** in 66 and 24% yields, respectively.

$$\underset{\mathbf{1}}{Ph_3P{=}NAr} + 2\,RCH_2SO_2Cl + 2\,Et_3N \rightarrow \underset{\mathbf{2}}{}$$

a, Ar=Ph b, R=Ph
b, Ar=*p*-MeC_6H_4 c, R=Me

$$Ph_3P{=}CR{-}SO_2NAr{-}SO_2CH_2R + RCH_2SO_2NHAr$$
$$\mathbf{3} \qquad\qquad \mathbf{13}$$

c, Ar=*p*-MeC_6H_4, R=Ph;
d, Ar=Ph, R=Me

$$+\ Ph_3\overset{+}{P}{-}CHR{-}SO_3^- + Ph_3PO$$
$$\mathbf{15} \qquad\quad \mathbf{8}$$

c, R=Ph

Betaine (**15c**) precipitated from the filtrate on standing was insoluble in usual organic solvents, suggesting that it was formed during the treatment. Formation of **13c** and **8** also suggests that these compounds are hydrolyzed products of **3c**.

Thus, **3b** was heated in aqueous ethanol as a model compound, but was recovered unchanged. When hydrogen chloride gas was bubbled into **3b** in chloroform, **5** and **13b** (R=H, Ar=*p*-MeC_6H_4) were obtained almost quantitatively. Thus, it seems reasonable to consider that **5** or **15** and **13** are formed by acid-catalyzed hydrolysis of **3**, where acid is probably sulfonic acid produced during treatment. The first step is considered to be protonation at the α-carbon of **3b**, because the NMR spectrum of **3b** containing hydrogen chloride gas showed a doublet (δ 6.20, J_{PCH} 12 Hz) assignable to α-methylene protons of the corresponding phosphonium chloride, which is hydrolyzed easily because of the presence of positively charged phosphorus atom.

In the case of reaction of **1a** with methylsulfene, only 1 : 2 adduct (**3d**) was obtained in 34% yield as an identified product.

Reaction with Disubstituted Sulfene. Reactions of dimethylsulfene as a disubstituted sulfene with **1a** and **1b** gave only *N*-triphenylphosphonio-*N*-phenylsulfamate (**16a**) and -*N*-*p*-tolylsulfamate (**16b**) in 45 and 44% yields, respectively, as identified products.

$$\underset{\mathbf{1}}{Ph_3P{=}NAr} + Me_2C{=}SO_2 \rightarrow \underset{\mathbf{16}}{Ph_3\overset{+}{P}{-}NAr{-}SO_3^-}$$

a, Ar=Ph; b, Ar=*p*-MeC_6H_4

The structures were determined by elemental analyses, IR, ^1H- and ^{31}P-NMR spectra. The ^1H-NMR spectrum of **16b** showed A_2B_2 spin system (J 8.4 Hz) for four aromatic protons of *p*-tolyl group. The ^{31}P-NMR spectrum of **16a** showed a signal at δ_p −39 ppm, which is nearly equal to that of anilinotriphenylphosphonium chloride (δ_p −34 ppm[5]). However, **16** was stable against alkaline hydrolysis.

For the preparation of **16a**, **1a** was allowed to react with sulfur trioxide, but an isomeric betaine (**17**) was obtained in 58% yield. The alkaline hydrolysis gave sodium sulfanilate and **8**.

$$\underset{}{Ph_3P{=}NPh} + SO_3 \rightarrow \underset{\mathbf{17}}{Ph_3\overset{+}{P}{-}NHC_6H_4{-}SO_3^-{-}p}$$

The formation mechanism of **16** is obscure.

Reactions with Sulfonyl Chlorides in the Absence of Base. In the absence of triethylamine, reactions of iminophosphoranes (**1a,b**) with sulfonyl chlorides (**2a—c**) gave α-(*N*-arylsulfamoyl)alkyltriphenylphosphonium chlorides (**18**) in quantitative yields except for the case of **18c** (40% yield).

$$\underset{\mathbf{1}}{Ph_3P{=}NAr} + \underset{\mathbf{2}}{RCH_2SO_2Cl}$$

a, Ar=Ph a, R=H
b, Ar=*p*-MeC_6H_4 b, R=Ph

$$\underset{\mathbf{19}}{Ph_3\overset{+}{P}{-}NAr{-}SO_2CH_2R\ Cl^-}$$

$$\longrightarrow \underset{\textbf{18}}{Ph_3\overset{+}{P}\text{-}CHRSO_2NHAr\ Cl^-}$$

a, Ar=Ph, R=H
b, Ar=Ph, R=Ph
c, Ar=Ph, R=Me
d, Ar=*p*-MeC_6H_4, R=H

The spectral data showed evidence that these products have structure **18** instead of the expected structure **19**[6] which was synthesized from triphenylphosphine and the corresponding *N*-chloroamide. Their IR spectra showed very broad NH absorption bands at 2700—2810 cm^{-1}, and their NMR spectra exhibited signals due to methine or methylene protons coupling with phosphorus nucleus.

Reaction of **1a** with **2b** gave **18b** and anilinotriphenylphosphonium chloride in 46 and 28% yields, respectively, under conditions similar to those in the case of **2a**. Thus, the reaction mechanism is considered to be as follows.

$$\underset{\textbf{1}}{Ph_3P{=}NAr} + \underset{\textbf{2}}{RCH_2SO_2Cl} \rightarrow Ph_3\overset{+}{P}\text{-}NHAr\ Cl^- + RCH{=}SO_2$$

$$RCH{=}SO_2 \overset{\textbf{1}}{\rightarrow} Ph_3\overset{+}{P}\text{-}\overset{-}{C}HRSO_2NAr \rightarrow \underset{\textbf{20}}{Ph_3P{=}CRSO_2NHAr}$$

$$\textbf{20} + Ph_3\overset{+}{P}NHAr\ Cl^- \rightleftharpoons \underset{\textbf{18}\quad a,\ Ar=Ph;\quad b,\ Ar=p\text{-}MeC_6H_4}{Ph_3\overset{+}{P}\text{-}CHRSO_2NHAr\ Cl^-} + \textbf{1}$$

Namely, **1** acts also as a base to generate sulfenes from **2**. In the case of **2b**, the basicity of the phosphorane (**20**) is weak because of α-phenyl group and attainment of the equilibrium in the last step becomes slow.

These reactions are the first example of reaction of aryliminophosphoranes with sulfonyl chlorides and may be synthetically useful because of high yield and easy treatment.

Experimental

All melting and boiling points were uncorrected. IR and MS spectra were measured with a Hitachi EPI-G2 spectrophotometer and a Hitachi RMU-6L mass spectrometer, respectively. ^{1}H-NMR spectra were measured with Hitachi R-20B, R-24 and R-22 spectrometers using TMS as an internal standard. ^{31}P-NMR spectra were measured with Hitachi R-20-R-204-P and R-20B-R-204-PB spectrometers using 85% phosphoric acid as an external standard.

Materials. Aryliminotriphenylphosphoranes were prepared by the method of Horner and Oediger[7]: phenylimino- (**1a**), mp 128—131 °C, and *p*-tolyliminotriphenylphosphoranes (**1b**), mp 133—136 °C.

Methanesulfonyl, α-toluenesulfonyl and 2-propanesulfonyl chlorides were prepared by the procedures given in literature: methanesulfonyl,[8] bp 154—158 °C, α-toluenesulfonyl,[9] mp 92 °C, and 2-propanesulfonyl chlorides,[10] bp 80 °C/20 mmHg. Commercial ethanesulfonyl chloride and triethylamine were used without further purification.

*Reactions of Methanesulfonyl Chloride (**2a**) in the Presence of Triethylamine. a) With Phenyliminotriphenylphosphorane (**1a**)*: To **1a** (3.53 g, 10.0 mmol) and triethylamine (2.06 g, 20.3 mmol) in benzene (150 ml) was added dropwise **2a** (2.30 g, 20.2 mmol) in benzene (5 ml) with stirring at room temperature and the mixture was stirred overnight. The resulting precipitates were thoroughly washed with water and recrystallized from acetone to give **3a** (2.75 g, 54%), mp 198—199 °C(dec). IR (KBr): 1340, 1310 (*as*-SO_2), 1150 and 1130 cm^{-1} (*s*-SO_2); NMR ($CDCl_3$): δ 3.20 (s, 3H, SO_2Me), 3.45 (d, J_{PCH} 12 Hz, 1H, P=CH–, disappeared by D_2O), 7.0—7.2 (m, 5H, NPh), and 7.4—7.8 (m, 15H, Ph_3P).

Found: C, 61.42; H, 4.48; N, 2.82; S, 12.82%. Calcd for $C_{26}H_{24}NO_4PS_2$: C, 61.28; H, 4.75; N, 2.75; S, 12.58%.

Concentration of the mother liquor in the above recrystallization gave **4a**, mp 215—216 °C (dec) (from MeOH), yield 0.87 g. IR (KBr): 3300 (NH), 1335, 1285 (*as*-SO_2), 1150 and 1120 cm^{-1} (*s*-SO_2); NMR ($CDCl_3$): δ 2.98 (s, 3H, SO_2Me), 7.22 (s, 5H, NPh), and 7.38—7.73 (m, 15H, Ph_3P). No signal due to NH proton could be detected. HDO signal (1H) appeared at δ 4.65 by addition of D_2O.

Found: C, 61.28; H, 4.66; N, 2.59; S, 12.50%. Calcd for $C_{26}H_{24}NO_4PS_2$: C, 61.28; H, 4.75; N, 2.75; S, 12.58%.

From the filtrate of the reaction mixture, **5** precipitated on standing, mp 290—291 °C (from EtOH), yield 0.20 g (6%). IR (KBr): 1255 and 1240 cm^{-1} (SO_3^-); NMR (DMSO-d_6): δ 5.20 (d, J_{PCH} 13 Hz, 2H, CH_2), and 7.7—8.0 (m, 15H, Ph_3P).

Found: C, 63.97; H, 4.53; S, 9.06%; mol wt (Rast), 332. Calcd for $C_{19}H_{17}O_3PS$: C, 64.03; H, 4.81; S, 9.00%; mol wt, 356.

From the above filtrate, 1.07 g of **4a** was further obtained. Thus, the total yield of **4a** was 38%.

*b) With p-tolyliminotriphenylphosphorane (**1b**)*: A similar reaction using **1b** (5.50 g, 15 mmol), Et_3N (3.23 g, 32 mmol), and **2a** (3.65 g, 32 mmol) in benzene (200 ml) gave **3b** (3.00 g, 38%), **4b** (2.60 g, 33%), and **5** (0.86 g, 16%).

3b: mp 188—189 °C (dec) (from acetone); IR (KBr): 1340, 1300 (*as*-SO_2), 1160 and 1130 cm^{-1} (*s*-SO_2); ^{1}H-NMR ($CDCl_3$): δ 2.76 (s, 3H, C_6H_4Me), 3.21 (s, 3H, SO_2Me), 3.49 (d, J_{PCH} 12 Hz, 1H, P=CH–), 6.94 (s, 4H, C_6H_4Me), and 7.4—7.8 (m, 15H, Ph_3P); ^{31}P-NMR (DMF): δ_p −14.4 ppm; MS: *m/e* 523 (M^+).

Found: C, 61.65; H, 4.86; N, 2.38; S, 12.08%. Calcd for $C_{27}H_{26}NO_4PS_2$: C, 61.95; H, 4.95; N, 2.68; S, 12.24%.

4b: mp 194—195 °C (dec) (from benzene); IR (KBr): 3260 (NH), 1320, 1290 (*as*-SO_2), 1135 and 1125 cm^{-1} (*s*-SO_2); NMR ($CDCl_3$): δ 2.32 (s, 3H, C_6H_4Me), 2.95 (s, 3H, SO_2Me), 7.10 (m, 4H, C_6H_4), and 7.3—7.8 (m, 15H, Ph_3P). Signal due to NH proton was obscure.

Found: C, 62.19; H, 4.65; N, 2.82; S, 12.28%. Calcd for $C_{27}H_{26}NO_4PS_2$: C, 61.95; H, 4.95; N, 2.68; S, 12.24%.

*Reaction of **1b** with α-Toluenesulfonyl Chloride (**2b**) in the Presence of Triethylamine.* To a solution of **1b** (4.40 g, 12.0 mmol) and Et_3N (2.54 g, 25.2 mmol) in benzene (200 ml) was added dropwise **2b** (5.01 g, 25.8 mmol) in benzene (100 ml) and the mixture was stirred for 10 hr at room temperature. The resulting precipitates were washed with water and recrystallized from acetonitrile and then acetone to give **3c** (2.12 g, 26%), mp 177 °C (dec). IR (KBr): 1350, 1265 (*as*-SO_2), 1190 and 1165 cm^{-1} (*s*-SO_2); NMR ($CDCl_3$): δ 2.05 (s, 3H, C_6H_4Me), 4.30 (s, 2H, SO_2CH_2), 6.60 (s, 4H, NC_6H_4Me), and 6.8—8.0 (m, 25H, 5Ph).

Found: C, 69.41; H, 4.83; N, 1.77; S, 9.75%. Calcd for $C_{39}H_{34}NO_4PS_2$: C, 69.31; H, 5.07; N, 2.07; S, 9.49%.

On being left to stand the filtrate gave **15c** (2.26 g, 44%), mp 280—282 °C (dec) (from acetonitrile). IR (KBr): 1250 and 1230 cm^{-1} (SO_3^-); NMR (DMSO-d_6): δ 6.70 (d, J_{PCH} 14 Hz, 1H, CH), 7.3—7.5 (m, 5H, CHPh), and 7.6—8.0 (m, 15H, Ph_3P).

An analytically pure sample could not be obtained, but

the structure was supported by the spectral data.

The filtrate was chromatographed on silica gel. Elution with benzene, benzene-ether and ethyl acetate-ethanol gave unchanged **2b** (0.40 g), **13c** (2.07 g, 66%), mp 113—114 °C (from EtOH) (lit,[11] 113 °C), and **8** (0.81 g, 24%), mp 153 °C (lit,[12] 156 °C), respectively.

*Reaction of **1a** with Ethanesulfonyl Chloride (**2c**) in the Presence Triethylamine.* Triethylamine (1.97 g, 18.3 mmol), **1a** (3.07 g, 8.7 mmol) and **2c** (2.48 g, 18.3 mmol) in benzene (100 ml) were allowed to react in a similar way, except for cooling with ice. The resulting precipitates were mainly triethylamine hydrochloride. After the solvent was removed from the filtrate, the residue was treated with ethanol to precipitate **3d**, mp 178 °C (from benzene), yield 1.58 g (34%). IR (KBr): 1335, 1300 (*as*-SO_2), 1160 and 1150 cm^{-1} (*s*-SO_2); NMR ($CDCl_3$): δ 1.41 (t, J 8 Hz, 3H, $SO_2CH_2CH_3$), 1.84 (d, J_{PCCH} 12 Hz, 3H, =CMe), 3.65 (q, J 8 Hz, 2H, SO_2CH_2), and 7.3—7.6 (m, 20H, Ph).

Found: C, 62.82; H, 5.46; N, 2.57; S, 12.18%. Calcd for $C_{28}H_{28}NO_4PS_2$: C, 62.55; H, 5.25; N, 2.61; S, 11.93%.

*Reaction of 2-Propanesulfonyl Chloride in the Presence of Triethylamine. a) With **1a**:* To a solution of **1a** (3.54 g, 10 mmol) and triethylamine (2.10 g, 20.8 mmol) in benzene (100 ml) was added dropwise 2-propanesulfonyl chloride (2.87 g, 20.1 mmol) in benzene (5 ml), and the mixture was stirred for two days. The resulting triethylamine hydrochloride (2.08 g, 71%) was filtered off and the filtrate was evaporated. After addition of benzene, recrystallization of the insoluble part from ethanol gave **16a** (1.94 g, 45%), mp 178—180 °C. IR (KBr): 1270 cm^{-1} (SO_3^-); ^{31}P-NMR (DMF): δ_p −39 ppm.

Found: C, 66.45; H, 4.61; N, 3.13; S, 7.68%. Calcd for $C_{24}H_{20}NO_3PS$: C, 66.50; H, 4.65; N, 3.23; S, 7.40%.

*b) With **1b**:* Triethylamine (2 ml), **1b** (1.84 g, 5.01 mmol) and the chloride (1.44 g, 10.1 mmol) were allowed to react in benzene in a similar manner.

16b: yield 1.00 g (44%); mp 181—182 °C (from EtOH); IR (KBr): 1275 cm^{-1} (SO_3^-); NMR (DMSO-d_6): δ 2.16 (s, 3H, C_6H_4Me), 6.90, 7.04, 7.17, 7.30, (A_2B_2, J 8.4 Hz, 4H, C_6H_4Me), and 7.5—8.1 (m, 15H, Ph_3P).

Found: C, 67.02; H, 5.00; N, 3.21; S, 7.30%. Calcd for $C_{25}H_{22}NO_3PS$: C, 67.10; H, 4.90; N, 3.13; S, 7.17%.

*Equimolar Reaction of **1a** with Sulfene.* To a solution of **1a** (3.51 g, 9.95 mmol) and triethylamine (1.5 ml) in benzene (100 ml) was added dropwise **2a** (1.14 g, 10.0 mmol) in benzene (10 ml) with stirring under cooling with ice and the mixture was stirred for 4 hr. The resulting precipitates were washed with water and dried quickly over phosphorus pentoxide to give **12a** (4.27 g, 99.5%). IR (KBr): 1290, 1255, 1165, and 1140 cm^{-1} (SO_2); NMR ($CDCl_3$): δ 2.90 (s, 0.6H, impurity, $PhNHSO_2Me$), 4.30 (broad s, 2H, P-CH_2SO_2, disappeared by D_2O), 7.1 (s, 5H, NPh), and 7.5—7.9 (m, 15H, Ph_3P); MS: *m/e* 431 (M^+). Addition of D_2O resulted in increase of the signal at 2.90.

The pure sample could not be obtained, because of easy hydrolysis in solution by moisture to **8** and **13a**. Thus, it was used for reactions without further purification.

*Reaction of **12a**. a) With Hydrogen Chloride*: Into a solution of **12a** (1.66 g, 3.86 mmol) in absolute methanol (50 ml) was bubbled dry hydrogen chloride for 1 hr. The solvent was removed *in vacuo* and the residue was chromatographed on silica gel. Elution with chloroform-methanol (15 : 1) gave *N*-phenylsulfamoylmethylenetriphenylphosphonium chloride (1.07 g, 60%). The compound was recrystallized from ethanol. The spectra and melting point were in agreement with those of the sample obtained from **1a** and **2a**.

b) With Sulfene: To a suspension of **12a** (1.04 g, 2.4 mmol) and triethylamine (0.5 ml) in benzene (50 ml) was added dropwise **2a** (0.275 g, 2.4 mmol) in benzene (5 ml) and the mixture was stirred overnight. Washing of the resulting precipitates with water gave 0.30 g (0.59 mmol) of **3a**. Removal of the solvent from the filtrate and addition of ethanol afforded 0.49 g of precipitates, which were found to be a mixture of **3a** and **4a** by thin layer chromatography (tlc) and NMR spectrum. On the basis of the signal areas of methanesulfonyl protons in the NMR spectrum, the ratio of **3a** (δ 3.20) to **4a** (δ 2.98) was calculated to be 35/65. Thus, the total yields of **3a** and **4a** were 38 (0.47 g) and 26% (0.32 g), respectively.

*Wittig Reaction of **3b** with p-Nitrobenzaldehyde.* A mixture of **3b** (0.587 g, 1.12 mmol) and *p*-nitrobenzaldehyde (0.175 g, 1.15 mmol) in *o*-dichlorobenzene (50 ml) was heated at 150 °C for 32 hr under nitrogen. After filtration of precipitates and removal of the solvent from the filtrate, the residue was chromatographed on alumina. Fractions eluted with chloroform-benzene(3 : 5) gave 0.167 g (0.42 mmol, 38%) of **10**, mp 233—235 °C (from EtOH). IR (KBr): 1620 (C=C) 1510, 1370 (NO_2), 1350, 1330 (*as*-SO_2), 1160 and 1110 cm^{-1} (*s*-SO_2); NMR (DMSO-d_6): δ 2.35 (s, 3H, C_6H_4Me), 3.56 (s, 3H, SO_2Me), 7.32 (s, 4H, NC_6H_4Me), 7.71, 7.75 (2H), and 8.2—8.4 (m, 4H, $C_6H_4NO_2$); MS: *m/e* 396 (M^+).

Found: C, 48.78; H, 4.05; N, 6.81; S, 15.88%. Calcd for $C_{16}H_{16}N_2O_6S_2$: C, 48.48; H, 4.07; N, 7.07; S, 16.18%.

Elution with chloroform gave 0.129 g (0.46 mmol, 41%) of **8**.

*Methylation of **4b**.* Sodium hydride (45 mg) was added to a solution of **4b** (0.492 g, 0.94 mmol) in benzene (50 ml) and the mixture was stirred at room temperature for 1 hr. After addition of methyl iodide (1 ml), the mixture was refluxed overnight. After evaporation, the residue was washed with water and recrystallized from ethanol to give 0.345 g (68%) of **11**, mp 232—234 °C. IR (KBr): 1330, 1280 (*as*-SO_2), 1140 and 1120 cm^{-1} (*s*-SO_2); NMR ($CDCl_3$): δ 2.30 (s, 3H, C_6H_4Me), 2.95 (s, 3H, NMe), 3.30 (s, 3H, SO_2Me), 7.0—7.15 (m, 4H, C_6H_4Me), and 7.3—7.8 (m, 15H, Ph_3P); MS: *m/e* 537 (M^+).

Found: C, 62.29; H, 4.96; N, 2.43; S, 11.87%. Calcd for $C_{28}H_{28}NO_4PS_2$: C, 62.55; H, 5.25; N, 2.61; S, 11.93%.

*Preparation of **5**.* To a suspension of methyltriphenylphosphonium bromide (18 g, 50.4 mmol) in dioxane (80 ml) was added sodium hydride (1.5 g) under nitrogen, and the mixture was stirred for 1 hr. Filtration of sodium bromide and unchanged materials under nitrogen gave a solution of methylenetriphenylphosphorane. The solution was added dropwise to a suspension of sulfur trioxide-dioxane adduct[13] (14 g) in dioxane (80 ml) under nitrogen. The dioxane layer was separated off and the viscous liquid was chromatographed on silica gel. Elution with chloroform-methanol (15 : 1) gave 1 g (6%) of **5**, mp 290—291 °C (from EtOH).

*Reaction of **1a** with Sulfur Trioxide.* To a suspension of sulfur trioxide-dioxane adduct (10 g) in dichloromethane (30 ml) was added dropwise **1a** (8.39 g, 23.5 mmol) in dichloromethane (10 ml) and the mixture was stirred for 3 hr at room temperature. The resulting precipitates were recrystallized from methanol quickly, because of hygroscopic material, to give 5.955 g (58.4%) of **17** mp 276 °C (dec). IR (KBr): 2700 (NH) and 1230 cm^{-1} (SO_3^-); NMR ($HOCH_2CH_2OH$): 3.26, 3.40 (2H, half part of A_2B_2), 3.90, 4.0—4.6 (17H), and 4.70 ppm (broad s, 1H, NH), in low field from methylene signal of ethylene glycol.

Found: C, 66.54; H, 4.66; N, 3.07%. Calcd for $C_{24}H_{20}NO_3PS$: C, 66.50; H, 4.65; N, 3.23%.

*Hydrolysis of **3b**.* Into a solution of **3b** (0.53 g, 1.0 mmol) in chloroform (40 ml) was bubbled hydrogen chloride gas for 2 hr. After evaporation, the residue was chromatographed on silica gel to give **13b**, mp 101—102 °C (from EtOH) (lit,[14] 102.5 °C) with chloroform-methanol (19 : 1) and **5** with chloroform-methanol (5 : 1) almost quantitatively.

*Reactions of **1** with Sulfonyl Chloride (**2**) in the Absence of Triethylamine. a) Reaction of **1a** with **2a**:* A solution of **2a** (2.29 g, 2.01 mmol) in benzene (10 ml) was added dropwise to a solution of **1a** (7.05 g, 20.0 mmol) in benzene (100 ml) at room temperature under stirring and the mixture was stirred for 1 hr. The resulting precipitates were identified as **18a**, mp 122—124 °C (from acetone). Yield, quantitative. IR (KBr): 2700 (NH), 1350 and 1170 cm^{-1} (SO_2); NMR ($CDCl_3$): δ 5.86 (d, J_{PCH} 12 Hz, 2H, PCH_2SO_2), 7.15—8.0 (m, 20H, 4Ph), and 12.7 (very broad s, 1H, NH).

Found: C, 64.11; H, 5.17; N, 2.69; S, 6.93%. Calcd for $C_{25}H_{23}ClNO_2PS$: C, 64.17; H, 4.95; N, 2.99; S, 6.85%.

To **18a** (1.125 g, 24 mmol) in dichloromethane (50 ml) was added an excess of triethylamine, and the reaction mixture was subjected to silica gel dry column chromatography with ether after being stirred for 10 hr. Extraction of a part of R_f 0.6—0.8 with ether and recrystallization from ethanol gave 0.29 g (71%) of **13a**, mp 102 °C (lit,[14] 100.5 °C). Extraction of a part of R_f 0.2—0.5 with ethyl acetate gave 0.515 g (97%) of **8**.

*b) Reaction of **1a** with **2b**.* 1) A mixture of **1a** (3.56 g, 10.1 mmol) and **2b** (1.96 g, 10.3 mmol) was allowed to react similarly to give 3.83 g of precipitates. A part of the precipitates (1.60 g) was chromatographed on silica gel. Elution with chloroform-methanol (79 : 1) gave 1.07 g (46%) of **18b**, mp 150—151 °C (from ethanol-ether). IR (KBr): 2800 (NH), 1350 and 1160 cm^{-1} (SO_2); NMR ($CDCl_3$): δ 6.7—8.0 (m, 25H, 5Ph), 8.65 (d, J_{PCH} 16 Hz, 1H, P-CH-Ph), and 10.8 (very broad s, 1H, NH).

Found: C, 68.49; H, 4.86; N, 2.67; S, 5.99; Cl, 6.74%. Calcd for $C_{31}H_{27}ClNO_2PS$: C, 68.44; H, 5.00; N, 2.57; S, 5.89; Cl, 6.52%.

Elution of chloroform-methanol (3 : 1) gave 0.51 g (28%) of anilinotriphenylphosphonium chloride, mp 229—233 °C (lit,[15] 230—233 °C).

2) **1a** (3.55 g, 10.1 mmol) and **2b** (1.88 g, 9.87 mmol) were reacted in benzene (100 ml) for 3 days at room temperature to give **18b**, mp 150—151 °C, as precipitates quantitatively.

*Reactions of **1a** and **2c**.* **1a** (3.57 g, 10.1 mmol) and **2c** (1.31 g, 10.2 mmol) in benzene were allowed to react as in the case of **2a**. **18c** was obtained as precipitates, 1.97 g (40%), mp 180—185 °C (dec) (from acetone). IR (KBr): 2810 (NH), 1355 and 1170 cm^{-1} (SO_2); NMR ($CDCl_3$): δ 1.50 (d d, J_{PCCH} 18, J_{HH} 6 Hz, 3H, P-CHMe), 7.0—7.3 (m, 3H), 7.5—8.3 (m, 18H), and 11.75 (very broad s, 1H, NH). On addition of D_2O, the signal at δ 11.75 disappeared and double doublets at 1.50 changed to a doublet (J 18 Hz). Signal at 7.5—8.3 changed the peak area to 17H, indicating an overlap with methine proton.

Found: C, 64.81; H, 5.06; N, 2.71%. Calcd for $C_{26}H_{25}ClNO_2PS$: C, 64.79; H, 5.23; N, 2.91%.

*Reaction of **1b** and **2a**.* **1b** (3.657 g, 10.0 mmol) was allowed to react with **2a** (1.43 g, 9.98 mmol) as in the case of **2a** to afford **18d**, mp 166.7—168 °C (from acetone), quantitatively. IR (KBr): 2810 (NH), 1345 and 1165 cm^{-1} (SO_2); NMR ($CDCl_3$): δ 2.30 (s, 3H, C_6H_4Me), 5.91 (d, J_{PCH} 12 Hz, 2H, PCH_2SO_2), 7.01, 7.16, 7.50 (centered at 7.33) (A_2B_2, J 9 Hz, 3H, NC_6H_4Me), 7.6—8.2 (m, 16H, 3Ph and CH), and 10.57 (broad s, 1H, NH).

Found: C, 64.74; H, 5.31; N, 2.62%. Calcd for $C_{26}H_{25}ClNO_2PS$: C, 64.79; H, 5.19; N, 2.91%.

Acknowledgement is made to the Ministry of Education for financial support to one of the authors (N. I.). The authors thank Dr. Koh-ichi Yamada for assistance in part of the work.

References

1) T. Kawashima and N. Inamoto, This Bulletin, **45**, 3504 (1972).
2) Y. Ito, M. Okano, and R. Oda, *Tetrahedron*, **23**, 2137 (1967).
3) A. M. Hamid and S. Trippett, *J. Chem. Soc., C*, **1968**, 1612.
4) N. A. Nesmeyanov, S. T. Zhuzhlikova, and O. A. Reutov, *Dokl. Akad. Nauk SSSR*, **151**, 856 (1963).
5) M. Yoshifuji, *Yuki Gosei Kagaku Kyokaishi*, **28**, 177 (1970).
6) V. A. Shokol, L. I. Molyavko, and G. I. Derkach, *Zh. Obshch. Khim.*, **36**, 930 (1966).
7) L. Horner and H. Oediger, *Ann. Chem.*, **627**, 142 (1959).
8) P. K. Dutt, *J. Chem. Soc.*, **125**, 1463 (1924).
9) T. B. Johnson and J. A. Ambler, *J. Amer. Chem. Soc.*, **36**, 372 (1914).
10) S. Zuffanti, *ibid.*, **62**, 1044 (1940).
11) E. Fromm and J. de Seixas Palma, *Ber.*, **39**, 3308 (1906).
12) C. Screttas and A. F. Isbell, *J. Org. Chem.*, **27**, 2573 (1962).
13) C. S. Rondestvedt, Jr. and F. G. Bordwell, "Organic Syntheses," Coll. Vol. 4, p. 846 (1963).
14) C. S. Marvel, M. D. Helfrick, and J. P. Belsley, *J. Amer. Chem. Soc.*, **51**, 1272 (1929).
15) R. D. Partos and K. W. Ratts, *ibid.*, **88**, 4996 (1966).

Metal Phosphinylides and Phosphinothioylides. I. Formation of Metal Diphenylphosphinylides and Diphenylphosphinothioylides and the Reactions with Some Organic Halides and Aldehydes

Tateki Emoto, Hideyuki Gomi, Masaaki Yoshifuji, Renji Okazaki, and Naoki Inamoto

Department of Chemistry, Faculty of Science, The University of Tokyo, Hongo, Tokyo 113

(Received May 14, 1974)

Lithium diphenylphosphinylide or diphenylphosphinothioylide ([Ph_2PX]Li; X=O, S), prepared from diphenylphosphine oxide or sulfide and *n*-butyllithium, reacted with methyl iodide, acetaldehyde and benzaldehyde to give the corresponding phosphine oxides or sulfides in good yields, indicating the formation of C–P bond. Formation of [Ph_2PS]MgCl from diphenylphosphinothioyl chloride (**1**) and magnesium was confirmed by the similar reactions. When **1** was allowed to react with magnesium or sodium for a long time, diphenylphosphides ([Ph_2P]-M) were produced by desulfurization, together with [Ph_2PS]M (M=MgCl, Na). Reaction of **1** with [Ph_2PS]M gave tetraphenyldiphosphine disulfide through formation of P-P bond, while diphenylphosphinyl chloride and [Ph_2PO]M reacted through formation of P–O bond. The difference has been explained by soft-hard-acid-base concept.

Tetraphenyldiphosphine disulfide is prepared by the reaction of diphenylphosphinothioyl chloride (**1**) with an alkyl Grignard reagent. The reaction mechanism has been considered as follows.[1)]

$$\underset{\mathbf{1}}{Ph_2P(S)Cl} + RMgBr \longrightarrow \underset{\mathbf{2'}}{Ph_2P(S)MgBr} + RCl$$

$$\mathbf{2'} + \mathbf{1} \longrightarrow Ph_2P(S)\text{-}P(S)Ph_2 + MgClBr \qquad (1)$$

Phosphinothioylmagnesium bromide (**2'**) has been assumed as the intermediate,[1)] but there is no report on the direct formation of phosphinothioylmagnesium chloride (**2**) from **1** and magnesium. There are several reports[2,3)] on formation of metal diphenylphosphinylides by reaction of dialkyl phosphite with excess amounts of phenylmagnesium bromide[2)] and by reaction of diphenylphosphinyl chloride with sodium or magnesium.[3)]

Metal diphenylphosphinylides and diphenylphosphinothioylides have two reaction centers, that is, the phosphorus and the oxygen or sulfur atoms.

$$Ph_2P(X)\text{-}M \rightleftharpoons Ph_2P\text{-}X\text{-}M \qquad [X=O, S]$$

In this paper, such compounds are represented as [Ph_2PX]M. It has been reported that metal derivatives (M=Li, Na, K, MgCl) of dialkyl phosphites exist as $(RO)_2P$–O–M from the ^{31}P-NMR data.[4)] ^{31}P-NMR measurements of [Ph_2PX]M are under investigation and will be reported in the near future.

This paper describes formation of **2** and other metal diphenylphosphinothioylides by metallation of diphenylphosphine sulfide (**3b**) and by reaction of some metals with **1**, and comparison of their reactions with those of metal diphenylphosphinylides prepared by similar methods.

First, lithium derivatives (**4**) were prepared from diphenylphosphine oxide (**3a**) or sulfide (**3b**) and *n*-butyllithium in tetrahydrofuran (THF) at 0 °C.

$$\underset{\mathbf{3}}{Ph_2P(X)H} + n\text{-}Bu\text{-}Li \longrightarrow \underset{\mathbf{4}}{[Ph_2PX]Li}$$

a, X=O; b, X=S

Reactions of **4a** with methyl iodide, acetaldehyde and benzaldehyde gave methyldiphenylphosphine oxide (**5a**) (93%), α-hydroxyethyldiphenylphosphine oxide (**6a**) (95%), and α-hydroxybenzyldiphenylphosphine oxide (**7a**) (63%), respectively. Similar reactions of **4b** gave the corresponding sulfides (**5b, 6b** and **7b**) in 66, 81 and 63% yields, respectively.

In the case of reaction of **4b** with methyl iodide, methyl diphenylphosphinothionite could not be detected in the crude reaction mixture by means of NMR.

$$\underset{\mathbf{4}}{[Ph_2PX]Li} \xrightarrow{MeI} \underset{\mathbf{5}}{Ph_2P(X)Me}$$

$$\xrightarrow{RCHO} Ph_2P(X)CHOH\text{-}R$$

a, X=O
b, X=S

6, R=Me; **7**, R=Ph

In all cases, the reaction center seems to be the phosphorus atom.

Reactions of **1** with magnesium was carried out to prepare **2**. An equimolar mixture of **1** and magnesium was refluxed for 1 hr in THF. Treatment of the reaction mixture with water gave **3b** in 37% yield, indicating the formation of **2**.

Grignard-type reagent (**2**), prepared under the same condition, reacted with benzyl chloride, benzaldehyde and **1** to give benzyldiphenylphosphine sulfide (**8**), **7b** and tetraphenyldiphosphine disulfide (**9**) in 44, 31 and 36% yields, respectively. Formation of **9** from **1** and **2** supported the reaction (1).

$$\underset{\mathbf{1}}{Ph_2P(S)Cl} + Mg \xrightarrow[\text{refl. THF}]{1\text{ hr}} \underset{\mathbf{2}}{[Ph_2PS]MgCl}$$

$$\underset{\mathbf{3b}}{Ph_2P(S)H} \xleftarrow{H_2O} \underset{\mathbf{2}}{[Ph_2PS]MgCl} \xrightarrow[\mathbf{1}]{PhCHO} \underset{\mathbf{7b}}{Ph_2P(S)CHPh\text{-}OH}$$

$$\underset{\mathbf{8}}{Ph_2P(S)CH_2Ph} \xleftarrow{PhCH_2Cl} \qquad \longrightarrow \underset{\mathbf{9}}{Ph_2P(S)\text{-}P(S)Ph_2}$$

From the above results, it is expected that yields of **2** were below 50% under the above condition. Then, two equivalents of magnesium were used and the mixture was refluxed for 8—10 hr. Hydrolysis of the reaction mixture gave **3b** in only 0.6% yield, and produced **3a** and diphenylphosphinic acid in 77 and 14% yields, respectively, indicating the formation of $[Ph_2P]MgCl$ by desulfurization.

$$Ph_2P(S)Cl\ (\mathbf{1}) + 2\,Mg \xrightarrow[\text{refl. THF}]{\text{8—10 hr}} [Ph_2PS]MgCl + [Ph_2P]MgCl$$

$[Ph_2PS]MgCl \xrightarrow{H_2O} Ph_2P(S)H$ (**3b**)

$[Ph_2P]MgCl \xrightarrow{H_2O} Ph_2PH \xrightarrow{O_2} Ph_2P(O)H$ (**3a**) $\xrightarrow{O_2} Ph_2P(O)OH$

The formation of **3a** and diphenylphosphinic acid is attributed to successive oxidation of diphenylphosphine initially formed during treatment.

The desulfurization was also indicated by formation of **7a** (7.5%) and **7b** (18%) in reaction with benzaldehyde.

Reaction of **1** with excess amounts of sodium in toluene for 115 hr at room temperature gave **9** (3.8%) and diphenylphosphinic acid (30%) after hydrolysis. The formation of the latter also indicates occurrence of desulfurization.

$$Ph_2P(S)Cl\ (\mathbf{1}) + Na \xrightarrow[\text{in PhMe}]{\text{115 hr, r. t.}} [Ph_2PS]Na + [Ph_2P]Na$$

$[Ph_2PS]Na \xrightarrow{1} Ph_2P(S)\text{-}P(S)Ph_2$ (**9**)

$[Ph_2P]Na \xrightarrow{H_2O} \xrightarrow{O_2} Ph_2P(O)OH$

From the above results, it is suggested that reaction of **1** with the corresponding metal derivative ($[Ph_2PS]$-M) gives diphosphine disulfide, indicating the formation of P(S)-P(S) bond.

Reaction of diphenylphosphinyl chloride (**10**) with twice molar amounts of sodium was carried out in refluxed toluene for 5 hr. The resulting precipitates contained sodium diphenylphosphinylide (**11**) from result of hydrolysis, and reacted with **10** to give diphenylphosphinic acid in 55% yield.

$$Ph_2P(O)Cl\ (\mathbf{10}) + 2\,Na \rightarrow [Ph_2PO]Na\ (\mathbf{11}) \xrightarrow{\mathbf{10}} (Ph_2P(O)\text{-}OPPh_2)\ (\mathbf{12})$$

$$\xrightarrow{O_2} (Ph_2P(O)\text{-}O\text{-}P(O)Ph_2)\ (\mathbf{13}) \xrightarrow{H_2O} 2\,Ph_2P(O)OH$$

In this case, the crude product was found to contain diphenylphosphinic diphenylphosphonous anhydride (**12**) by IR and mass spectra. Therefore, the formation of diphenylphosphinic acid is attributed to oxidation[5] and hydrolysis of **12** during isolation and purification, because diphenylphosphinic anhydride (**13**) undergoes hydrolysis easily.[6]

Thus reaction of **10** with the corresponding metal derivative ($[Ph_2PO]M$) was found to afford the product through the formation of P–O–P(O) bond.

The difference in the reactions of $[Ph_2PX]M$ with $Ph_2P(X)Cl$ may be explicable in terms of soft-hard-acid-base.[7] The phosphorus and oxygen atoms of $[Ph_2PO]M$ are soft and hard, respectively, and the phosphorus atom of **10** is hard.[8] Thus, in the reaction of **11** with **10**, P–O–P(O) bond is formed. The phosphorus and sulfur atoms of $[Ph_2PS]M$ and also the phosphorus atom of **1** are all soft,[8] and moreover, tervalent phosphorus atom is more nucleophilic than sulfide anion.[9] Therefore, in the reaction of **2** with **1**, P(S)–P(S) bond is formed.

The following reactions support this consideration.[5,10]

$$Ph_2P(O)H \xrightarrow{Ph_2PCl} Ph_2P(O)\text{-}PPh_2\ ^{10)}$$

$$Ph_2P(O)H \xrightarrow[\mathbf{10},\ Et_3N]{Et_3N} Ph_2P\text{-}OP(O)Ph_2\ ^{5)}$$

One possible mechanism of desulfurization in preparation of $[Ph_2PS]M$ may be disproportionation as follows, because the reaction of **1** with magnesium in THF at 150 °C gave a small amount of diphenylphosphinodithioic acid.[11]

$$2[Ph_2PS]^- \longrightarrow Ph_2P^- + Ph_2P(S)S^-$$

In the preparation of $[Ph_2PS]M$ from **1** and metal, desulfurization took place by using excess amounts of metal or by heating for a long time. Therefore, the best method to prepare $[Ph_2PS]M$ is that from **3b** through hydrogen-metal exchange reaction, because of homogeneous and rapid reaction.

Experimental

All melting and boiling points are uncorrected. The IR spectra were recorded on Hitachi EPI-G2 spectrophotometer, NMR spectra were measured with Hitachi R-24 and R-20B spectrometers using TMS as an internal standard, and ^{31}P-NMR spectra were measured with a Hitachi R-20B spectrometer equipped with a phosphorus measurement unit R-204-PB (24.3 Hz) using 85% phosphoric acid as an external standard. Mass spectra were determined with Hitachi RMU-6L mass spectrometer. All reactions were carried out under nitrogen.

Materials. The following materials were prepared by the methods reported in the literature: diphenylphosphinothioyl chloride,[12] bp 155—157 °C/0.3 mmHg; diphenylphosphinyl chloride,[13] bp 155 °C/0.1 mmHg; diphenylphosphine sulfide,[14] mp 93—94 °C; diphenylphosphine oxide,[15] mp 45—48 °C. *n*-Butyllithium was used as 15% *n*-hexane solution.

*Reactions of Lithium Diphenylphosphinylide (**4a**).* *a) With Methyl Iodide*: A solution of **4a** prepared from diphenylphosphine oxide (**3a**) (2.66 g, 13.2 mmol) and *n*-butyllithium (13.2 mmol) in THF (50 ml) was stirred with methyl iodide (2.00 g, 14.0 mmol) in THF (10 ml) for 2.5 hr. After removal of THF, the residue was treated with water, and extracted with ether. After removal of ether from the dried extract, crude methyldiphenylphosphine oxide (**5a**) was recrystallized from *n*-hexane-benzene, mp 113.5—115 °C (lit,[16] 113—114 °C), yield 2.66 g (93%). NMR ($CDCl_3$): δ 2.02 (d, J_{PCH} 13.6 Hz, 3H, Me) and 7.3—8.0 (m, 10H, 2Ph); δ_P ($CHCl_3$): −29.7 ppm.

b) With Acetaldehyde: A solution of **4a** prepared from **3a** (2.11 g, 10.4 mmol) and *n*-butyllithium (11 mmol) in THF (60 ml) was stirred with acetaldehyde (0.66 g, 14.9 mmol) for 2 hr. Similar work-up gave α-hydroxyethyldiphenylphosphine oxide (**6a**) (2.54 g, 95%), mp 131—132 °C (from benzene). IR (KBr): 3150 (OH) and 1170 cm^{-1} (P=O); NMR ($CDCl_3$): δ 1.38 (d d, J_{PCCH} 15.4, J_{HH} 7.2 Hz, 3H, Me), 4.57 (q, J_{PCH} *ca.* 0 Hz, 1H, CH), 5.02 (s, 1H, OH), and 7.3—8.1 (m, 10H, 2Ph); δ_P ($CHCl_3$): −32.9 ppm.

Found: C, 68.31; H, 6.00%. Calcd for $C_{14}C_{15}O_2P$: C, 68.29; H, 6.14%.

c) With Benzaldehyde: A solution of **4a** prepared from **3a** (1.98 g, 9.4 mmol) and *n*-butyllithium (10.4 mmol) in THF (40 ml) was refluxed with benzaldehyde (1.7 g, 16 mmol) in THF (15 ml) for 1.5 hr. The reaction mixture was poured into a mixture of ice and hydrochloric acid, and ether was added. Evaporation of the ethereal layer gave α-hydroxybenzyldiphenylphosphine oxide (**7a**) (1.9 g, 63%), mp 172—174 °C (from ethanol) (lit,[3a] 176 °C). δ_P (DMF): −26.9 ppm.

*Reactions of Lithium Diphenylphosphinothioylide (**4b**).* *a) With Methyl Iodide*: To a solution of diphenylphosphine sulfide (**3b**) (5.01 g, 23 mmol) in THF (50 ml) was added dropwise *n*-butyllithium (24 mmol) in hexane under ice-cooling with stirring over 30 min. The mixture was stirred at room temperature for 30 min. To the solution was added dropwise 3.47 g (24.4 mmol) of methyl iodide in 10 ml of THF with stirring under ice-cooling, and the mixture was stirred for 2 hr at room temperature. After removal of THF, the residue was treated with water, and extracted with ether. Removal of the ether from the dried extract gave oily material. The NMR spectrum was quite the same with that of the distillate (**5b**), bp 170—171 °C/1 mmHg (lit,[17] 181 °C/1.5 mmHg), yield 3.52 g (66%). NMR (CCl_4): δ 2.07 (d, J_{PCH} 13.6 Hz, 3H, Me) and 7.2—8.0 (m, 10H, 2Ph); δ_P ($CHCl_3$): −35.9 ppm.

b) With Acetaldehyde: To a solution of **4b** prepared from **3b** (4.01 g, 18.4 mmol) in THF (50 ml) and *n*-butyllithium (19 mmol), acetaldehyde (0.83 g, 19 mmol) was added dropwise at room temperature and the mixture was stirred for 2 hr. Similar work-up gave oily materials, which solidified on standing to give **6b**, mp 84—86 °C (from *n*-hexane-ether), yield 3.91 g (81%). IR (KBr): 3300 (OH) and 590 cm^{-1} (P=S); NMR ($CDCl_3$): δ 1.30 (d d, J_{PCCH} 17, J_{HH} 7.2 Hz, 3H, Me), 2.87 (s, 1H, OH), 4.72 (d q, J_{PCH} 2.6, J_{HH} 7.2 Hz, 1H, CH), and 7.3—8.2 (m, 10H, 2Ph); δ_P ($CHCl_3$): −49.0 ppm.

Found: C, 64.16; H, 5.57%. Calcd for $C_{14}H_{15}OPS$: 64.10; H, 5.77%.

c) With Benzaldehyde: A solution of **4b** prepared from **3b** (2.14 g, 9.8 mmol) and *n*-butyllithium (10 mmol) in THF (50 ml) was stirred with benzaldehyde (1.78 g, 16.8 mmol) for 20 hr. Similar work-up gave colorless crystals, which were recrystallized from carbon tetrachloride to give **7b**, mp 121—122.5 °C, yield 1.99 g (63%). IR (KBr): 3250 (OH) and 610 cm^{-1} (P=S); NMR ($CDCl_3$); δ 3.92 (s, 1H, OH), 5.54 (d, J_{PCH} 1.8 Hz, 1H, CH), and 6.8—8.15 (m, 15H, 3Ph); δ_P ($CHCl_3$): −52.3 ppm.

Found: C, 70.39; H, 5.30; S, 9.95%. Calcd for $C_{19}H_{17}OPS$: C, 70.35; H, 5.29; S, 9.88%.

*Preparation of Diphenylphosphinothioylmagnesium Chloride (**2**) and the Hydrolysis.* *a) Shorter Reaction Time*: A mixture of diphenylphosphinothioyl chloride (**1**) (5.1 g, 20 mmol) and magnesium turnings (0.73 g, 30 mg atom) in THF (100 ml) was heated under reflux for 1 hr. The reaction mixture was decanted and the solution was evaporated *in vacuo*. After addition of ether to the residue, 10% aqueous ammonium chloride was poured into the ether solution, and the ether was removed from the dried ethereal layer. The residual oily material was crystallized with acetonitrile to give **3b** (1.6 g, 37%), mp 93—94 °C (lit,[14] 95—97 °C).

b) Longer Reaction Time: A mixture of **1** (4.5 g, 18 mmol) and magnesium turnings (875 mg, 36 mg atom) in THF (50 ml) was heated under reflux with vigorous stirring for 10 hr. Remaining magnesium (0.14 g, 6 mg atom) was removed by decantation and the solution was evaporated. The residue was dissolved in 50 ml of benzene and a small amount of water was added. The benzene layer was dried and removal of the benzene gave oily material, which was crystallized with ether to give diphenylphosphinic acid (0.56 g, 14%), mp 190—191 °C (lit,[18] 194 °C). After evaporation of the filtrate the residue was chromatographed on silica gel with dichloromethane to afford 2.8 g (77%) of **3a**, mp 46—48 °C (lit,[15] 51—54 °C), and 22 mg (0.6%) of **3b**, mp 92—93 °C.

*Reactions of **2**.* *a) With Benzyl Chloride*: A solution of **2** was prepared from **1** (5.1 g, 20 mmol), magnesium (0.5 g, 20 mg atom) and THF (60 ml) under a condition of shorter reaction time described above. To the solution was added benzyl chloride (2.6 g, 21 mmol) in THF (10 ml) at room temperature. After stirring for 20 min, the mixture was heated under reflux for 2 hr. After removal of THF, the residual oil dissolved in dichloromethane was dried with anhydrous sodium sulfate. After removal of the dichloromethane, the residual oil was mixed with a small amount of ethanol to precipitate benzyldiphenylphosphine sulfide (**8**) (2.7 g, 44%), mp 160—161 °C (from ethanol) (lit,[19] 162—163 °C).

b) With Benzaldehyde: 1) To a solution of **2** prepared by the same method described in a), was added dropwise benzaldehyde (2.12 g, 20 mmol) in THF (15 ml) at room temperature. After stirring for 1 hr, the mixture was heated gradually and then refluxed for 10 min. THF was removed, the residue was treated with 10% aqueous ammonium chloride, and extracted with dichloromethane. After evaporation of the dried extract, the residue was recrystallized from 2-propanol to give **7b** (2.0 g, 31%), mp 113—114 °C, which was identified by the IR spectrum.

2) A mixture of **1** (5.1 g, 20 mmol), magnesium (0.97 g, 40 mg atom) in 100 ml of THF was refluxed for 8 hr. After decantation, to the solution was added dropwise 2.1 g (20 mmol) of benzaldehyde in 10 ml of THF at room temperature, and the mixture was refluxed for 2 hr. The residue, which was obtained by a similar treatment to that described in 1), gave colorless crystals by addition of ether. The crystals were recrystallized from ethanol to give pure **7a** (0.49 g, 7.5%), mp 173—175 °C (lit,[3a] 176 °C). Standing of the ethereal filtrate gave 1.1 g (18%) of **7b**.

*c) With Diphenylphosphinothioyl Chloride (**1**)*: A mixture of **1** (7.9 g, 31 mmol), magnesium (0.82 g, 34 mg atom) and THF (60 ml) was refluxed for 1 hr. To the solution was added dropwise **1** (7.7 g, 30 mmol) in THF (40 ml) at room temperature. The mixture was refluxed for 6 hr. After filtration of magnesium chloride and removal of THF from the filtrate, the residual semi-solid was washed twice with water and extracted with dichloromethane. Removal of dichloromethane from the extract gave oily material, which crystallized by addition of a small amount of ethanol. The crystals were recrystallized from acetone-ethanol (9 : 1) to give **9** (4.7 g, 36%), mp 165—167 °C (lit,[20] 168.5 °C).

*Reaction of **1** with Sodium.* A solution of **1** (1.7 g, 6.8 mmol) in toluene (10 ml) was added dropwise to sodium (1.2 g, 52 mg atom) in toluene (10 ml) at room temperature, the mixture was stirred for 115 hr and poured into water,

The organic layer was evaporated after drying. Extraction with a small amount of acetonitrile gave diphenylphosphinic acid (4.4 g, 30%), mp 188—190 °C, as insoluble material. The acetonitrile solution gave a solid after evaporation. Recrystallization from ether gave **9** (56 mg, 3.8%), mp 167—168.5 °C.

*Reaction of Sodium Diphenylphosphinylide with Diphenylphosphinyl Chloride. (**10**).* To a suspension of sodium (0.97 g, 42 mg atom) in toluene (50 ml) was added dropwise **10** (4.9 g, 21 mmol) in toluene (50 ml), and the mixture was refluxed for 5 hr. Precipitates thus obtained were filtered off under nitrogen. Hydrolysis of a small amount of the precipitates gave **3a**. To a suspension of the dry precipitates (1.2 g), which contain an equimolar amount of sodium chloride, in xylene (25 ml) was added dropwise **10** (1.0 g, 4.2 mmol) in xylene (25 ml) at room temperature, and the mixture was refluxed for 12 hr. Treatment of the reaction mixture with water gave insoluble solid, which was identified as diphenylphosphinic acid (1.0 g, 55%) by IR. Evaporation of the organic layer gave white solid, which was found to be diphenylphosphinic acid mainly by IR. The IR spectrum showed a band at 960 cm^{-1} (P-O-P). The mass spectrum also showed the absence of tetraphenyldiphosphine dioxide (M^+, *m/e* 402) and the presence of diphenylphosphinic anhydride (M^+, *m/e* 418).

The author (N. I.) thanks the Ministry of Education for financial support.

References

1) N. K. Patel and H. J. Harwood, *J. Org. Chem.*, **32**, 2999 (1967).
2) B. B. Hunt and B. C. Saunders, *J. Chem. Soc.*, **1957**, 2413; R. C. Miller, C. D. Miller, W. Rogers, Jr., and L. H. Hamilton, *J. Amer. Chem. Soc.*, **79**, 424 (1957).
3) a) L. Horner, P. Beck, and V. G. Toscano, *Chem. Ber.*, **94**, 1317 (1961); b) L. Horner, P. Beck, and H. Hoffmann *ibid.*, **92**, 2088 (1959).
4) K. Moedritzer, *J. Inorg. Nucl. Chem.*, **22**, 19 (1961).
5) L. D. Quin and H. G. Anderson, *J. Org. Chem.*, **31**, 1206 (1966).
6) T. Emoto, R. Okazaki, and N. Inamoto, This Bulletin, **46**, 898 (1973).
7) R. G. Pearson and J. Songstad, *J. Amer. Chem. Soc.*, **89**, 1827 (1967).
8) R. F. Hudson, "Structure and Mechanism in Organophosphorus Chemistry," Academic Press, London (1965), p. 109.
9) *Idem.*, *ibid.*, p. 115.
10) J. McKechnie, D. S. Payne, and W. Sim, *J. Chem. Soc.*, **1965**, 3500.
11) Unpublished work.
12) L. Maier, *Helv. Chim. Acta*, **47**, 120 (1964).
13) W. M. A. Higgins, P. W. Vogel, and W. G. Craig, *J. Amer. Chem. Soc.*, **77**, 1864 (1955).
14) G. Petters, *ibid.*, **82**, 4751 (1960).
15) R. C. Miller, *J. Org. Chem.*, **24**, 2013 (1959).
16) G. Aksnes and L. J. Brudvik, *Acta Chem. Scand.*, **17**, 1616 (1963).
17) R. A. Zingaro and R. E. McGlothlin, *J. Chem. Eng. Data*, **8**, 226 (1963); D. Seyferth and D. E. Welch, *J. Organometal. Chem.*, **2**, 1 (1964).
18) "Inorganic Synthesis," Vol. 8, p. 71 (1966).
19) A. M. Aguiar, J. Beisler, and A. Mills, *J. Org. Chem.*, **27**, 1001 (1962).
20) W. Kuchen and H. Buchwald, *Chem. Ber.*, **91**, 2871 (1958).

Metal Phosphinylides and Phosphinothioylides. II.[1] Effects of Metals on the Reactions of [Ph_2PX]M with Benzaldehyde and *p*-Benzoquinone

Koshiro GODA, Hideyuki GOMI, Masaaki YOSHIFUJI, and Naoki INAMOTO
Department of Chemistry, Faculty of Science, The University of Tokyo, Hongo, Tokyo 113
(Received May 14, 1974)

Reactions of [Ph_2PO]M with benzaldehyde gave benzyl benzoate and benzyldiphenylphosphine oxide (**3**) in the case of M=Na, **3**, α-hydroxybenzyldiphenylphosphine oxide, benzyl alcohol, benzoin and benzil in the case of M=MgCl, and **3** in the case of M=ZnCl. Reactions of [Ph_2PX]M with *p*-benzoquinone gave 2,5-dihydroxyphenyldiphenylphosphine oxide or sulfide and *p*-hydroxyphenyl diphenylphosphinate in the cases X=O, S and M=Li, MgCl, Al, and 1,4-phenylene bis(diphenylphosphinate) or bis(diphenylphosphinothioate) in the cases X=O, S and M=FeCl. The reaction mechanisms have been discussed.

The formation of [Ph_2PX]M (X=O, S; M=Li, Na, MgCl) was reported in the preceding paper,[1] reactions of [Ph_2PO]Li or [Ph_2PS]M (M=Li, MgCl) with benzaldehyde giving α-hydroxybenzyldiphenylphosphine oxide or sulfide in good yields.

This paper describes the effects of metals on reactions of [Ph_2PO]M with benzaldehyde, and those on the reactions of [Ph_2PX]M (X=O, S) with *p*-benzoquinone.

Reactions with Benzaldehyde. When sodium diphenylphosphinylide (**2a**) prepared from diphenylphosphinyl chloride (**1a**) and two equivalents of sodium in tetrahydrofuran (THF) was allowed to react with benzaldehyde for 24 hr at room temperature and then for 2 hr at the refluxing temperature, benzyl benzoate (65%) and benzyldiphenylphosphine oxide (**3**) (7%) were obtained, instead of α-hydroxybenzyldiphenylphosphine oxide (**4**).

$$\underset{\mathbf{1a}}{Ph_2P(O)Cl} + 2\,Na \rightarrow \underset{\mathbf{2a}}{[Ph_2PO]Na} \xrightarrow{PhCHO} Ph_2P(O)CH_2Ph + PhCO_2CH_2Ph$$

3

A similar reaction of diphenylphosphinylmagnesium chloride (**5a**) with benzaldehyde gave **4** in only 6% yield, together with **3** (1%), benzyl alcohol (30%), benzoin (5%) and benzil (9%).

$$\underset{\mathbf{5a}}{[Ph_2PO]MgCl} + PhCHO \rightarrow \mathbf{3} + \underset{\mathbf{4}}{Ph_2P(O)CHPh\text{-}OH} + PhCH_2OH + PhCOCHOHPh + PhCOCOPh$$

The reaction of diphenylphosphinylzinc chloride (**6a**) with benzaldehyde gave only 8% of **3** as an isolated product.

Formation of **3** is explicable by the deoxygenation of intermediate anion (**7**) by diphenylphosphinylide anion as follows.

$$[Ph_2PO]^- + PhCHO \rightleftharpoons \underset{\mathbf{7}}{Ph_2P(O)CHPh\text{-}O^-} \xrightarrow{[Ph_2PO]^-} Ph_2P(O)O^- + \underset{\mathbf{8}}{Ph_2P(O)\bar{C}HPh} \xrightarrow{H^+} \mathbf{3}$$

The driving force may be due to the formation of stabilized anion (**8**).

In the case of **5a**, **3** was formed in a trace amount, the normal product (**4**) being also obtained. The result is attributable to the fact that the concentration of free anion (**7**) in this case was lower than that in the case of **2a**, due to the formation of the covalent magnesium derivative of **7**.

The formation of benzyl alcohol and benzoate is explained by an intermolecular hydride shift from **7** to benzaldehyde to give benzyloxide anion and benzoyldiphenylphosphine oxide (**9**). The mechanism is analogous to that in the Cannizzaro reaction.

$$\underset{\mathbf{7}}{Ph_2P(O)CHPh\text{-}O^-} + PhCHO \rightarrow \underset{\mathbf{9}}{Ph_2P(O)COPh} + PhCH_2O^- \xrightarrow{H^+} [Ph_2PO]^- + PhCOOCH_2Ph \quad PhCH_2OH$$

In the case of **5a** benzyl alcohol is produced due to a low concentration of free benzyloxide anion. However, in the case of **2a**, benzyl benzoate is formed through attack of free benzyloxide anion on the carbon atom of the carbonyl group in **9**, since diphenylphosphinylide anion is considered to be a good leaving group on the basis of the following decomposition.[2]

$$Ph_2P(O)CH_2OH \xrightarrow{OH^-} Ph_2P(O)CH_2O^- \rightarrow [Ph_2PO]^- + CH_2O$$

The formation of benzoin is considered to be analogous to benzoin condensation, indicating that diphenylphosphinylide anion behaves in a similar way to that of cyanide anion.

$$\underset{\mathbf{7}}{PhCH(O^-)\text{-}PPh_2} \rightarrow \underset{\mathbf{10}}{Ph\text{-}\bar{C}(HO)\text{-}PPh_2} \xrightarrow{PhCHO} PhC(OH)\text{-}CHPh\text{-}O^- \rightarrow Ph\text{-}C(O^-)\text{-}CHPh\text{-}OH \rightarrow PhCOCHOHPh + [Ph_2PO]^-$$

Benzil is formed through an attack of the anion (**10**) on the carbonyl carbon atom of **9**.

$$\underset{\mathbf{10}}{Ph\text{-}\bar{C}(OH)\text{-}P(O)Ph_2} + \underset{\mathbf{9}}{PhCOP(O)Ph_2} \rightarrow PhC(OH)\text{—}CPh\text{-}O^- \rightarrow PhC(OH)\text{-}COPh + [Ph_2PO]^- \rightarrow Ph\text{-}C(O^-)\text{-}COPh \rightarrow PhCOCOPh + [Ph_2PO]^-$$

An analogous formation of benzoin has recently been reported.[3]

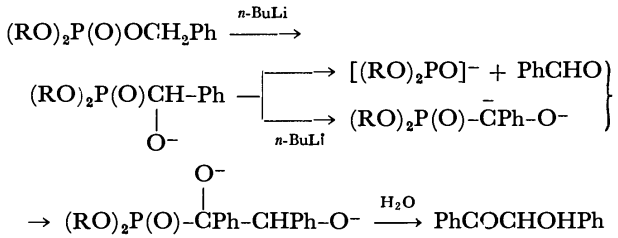

In conclusion, since the formation of **7** is reversible, long reaction time results in the formation of several abnormal products. The products depend on the extent of ionic character of the initial addition product (**7**), which depends on metal in $[Ph_2PO]M$.

Reactions with p-*Benzoquinone.* Reactions of $[Ph_2PX]M$ (X=O, S) with *p*-benzoquinone were carried out at room temperature in THF.

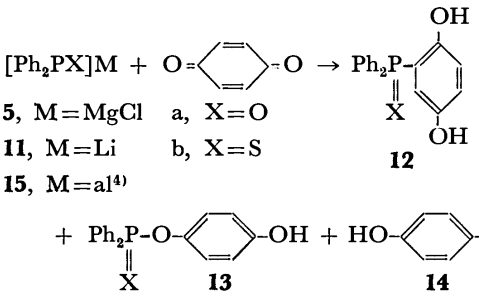

5, M=MgCl a, X=O
11, M=Li b, X=S
15, M=al[4]

12

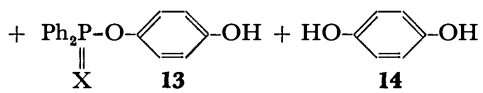

13 **14**

The reaction of lithium diphenylphosphinylide (**11a**) gave 2,5-dihydroxyphenyldiphenylphosphine oxide (**12a**) (20%), *p*-hydroxyphenyl diphenylphosphinate (**13a**) (18%) and hydroquinone (**14**) (33%).

The reaction of **5a** gave 17% of **12a**, 17% of **14**, and 8% of magnesium diphenylphosphinate.

The reaction of **15a** gave 8% of **13a**, 20% of **14** and compounds containing aluminum as the main product. A similar reaction of **15b** gave 9% of **13a** and similar aluminum-containing products as main products. The formation of **13a** indicates desulfurization during the course of the preparation of **15b**.[1] The above aluminum-containing compounds are considered to be a mixture of aluminum chelate of **12** and aluminum diphenylphosphinate, but attempts to isolate **12** were unsuccessful.

Reaction of **11b** gave also 30% of **12b**.

A reaction mixture of diphenylphosphinyl (**1a**) or diphenylphosphinothioyl chloride (**1b**) with reduced iron powder in THF reacted with *p*-benzoquinone to give 1,4-phenylene bis(diphenylphosphinate) (**17a**) or bis(diphenylphosphinothioate) (**17b**) by considerably fast reaction in 78 or 79% yield, respectively.

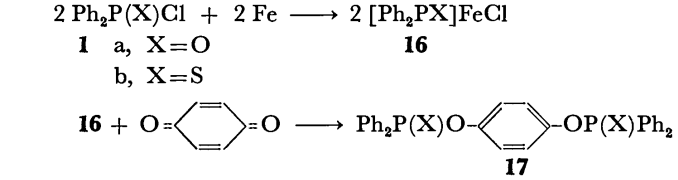

1 a, X=O b, X=S **16**

17

Solutions of **16** were pale green and the ^{1}H-NMR spectra could be measured without difficulty. Thus, the iron atom in **16** is considered to be bivalent.

Compounds **12** are considered to be formed through a nucleophilic addition to quinone nucleus, since diphenylphosphine oxide and sulfide give **12a**[5] and **12b** with *p*-benzoquinone, respectively. It is noteworthy that **12b** is formed in a better yield in the absence of any base than in the presence of base, isolation being very easy.

The formation of **13** and **14** is considered to be due to electron transfer mechanism.

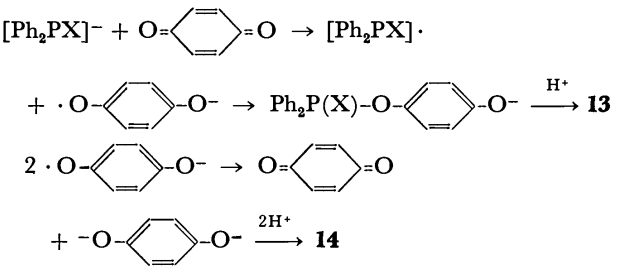

However, the following direct addition to the oxygen atom of quinone cannot be ruled out for the formation of **13**.

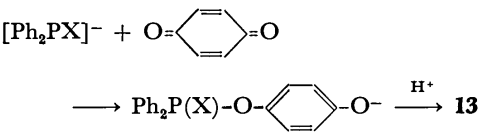

Since **16** did not react with benzyl chloride, acetaldehyde, diethyl disulfide, olefins, dienes, and naphthalene, it does not have an anionic character and does not generate free radicals under similar conditions.

Moreover, **16a** reacted with air to give iron diphenylphosphinate, which gave diphenylphosphinic acid after alkaline hydrolysis. It is suggested that the reactions proceed through an coordinate complex between **16** and quinone in a homolytic fashion without formation of free radicals.

Experimental

All melting and boiling points are uncorrected. IR and mass spectra were measured with a Hitachi EPI-G2 spectrophotometer and a Hitachi RMU-6L mass spectrometer, respectively. ^{1}H-NMR spectra were measured with Hitachi R-20B and R-24 spectrometers, using TMS as an internal standard. ^{31}P-NMR spectra were measured with Hitachi R-20-R-204-P and R-20B-R-204-PB spectrometers, using 85% phosphoric acid as an external standard.

Starting materials were prepared as described previously.[1] All the reactions were carried out under nitrogen.

Reactions of Benzaldehyde. *a) With* $[Ph_2PO]Na$ *(**2a**)*: A solution of **2a** was prepared from 2.27 g (9.6 mmol) of diphenylphosphinyl chloride (**1a**) and 0.47 g (20 mg atom) of sodium metal in 14 ml of THF at room temperature for 24 hr. To the filtrate was added 2.39 g (23 mmol) of benzaldehyde. The mixture was stirred for 24 hr at room temperature and then refluxed for 2 hr. The reaction mixture was poured into water and extracted with ether. The dried extract was evaporated and the residue was separated by dry column chromatography (DCC) on silica gel with ether to give 0.187 g (7%) of benzyldiphenylphosphine oxide (**3**) and 1.55 g (65%) of benzyl benzoate which was identified by the IR spectrum.

3: mp 190—192 °C (from ethanol) (lit,[6] 192—193 °C); NMR ($CDCl_3$): δ 3.6 (d, J_{PCH} 13.8 Hz, 2H, PCH_2), 7.15 (s, 5H, Ph), and 7.35—7.9 (m, 10H, 2Ph).

*b) With $[Ph_2PO]MgCl$ (**5a**)*: A mixture of 2.97 g (12.6 mmol) of **1a** and 0.568 mg (23.7 mg atom) of magnesium in THF (32 ml) was stirred at room temperature for 1 hr and then refluxed for 1 hr. To the filtrate was added 2.13 g (20 mmol) of benzaldehyde and the mixture was treated similarly. Separation by DCC gave 0.64 g (30%) of benzyl alcohol, 0.112 g (5%) of benzoin, 0.197 g (9%) of benzil, which were identified by the IR spectra, 0.227 g (6%) of α-hydroxybenzyldiphenylphosphine oxide, mp 172—174 °C (lit,[2b] 176 °C), and 34 mg (1%) of **3**, mp 190—192 °C, which were identified by the IR and NMR spectra.

*c) With $[Ph_2PO]ZnCl$ (**6a**)*: A mixture of 1.47 g (6.2 mmol) of **1a** and 0.954 g (15 mg atom) of zinc dust in 15 ml of THF was stirred at room temperature for 24 hr. To the solution was added 2.32 g (22 mmol) of benzaldehyde. The mixture was stirred for 24 hr at room temperature and then refluxed for 2 hr. After removal of unchanged zinc dust and THF, the residue was crystallized to give 0.813 g (60%) of diphenylphosphinic acid and 0.149 g (8%) of **3**, successively.

Reactions of p-*Benzoquinone.* *a) With $[Ph_2PO]Li$ (**11a**)*: A solution of **11a** was prepared from 1.53 g (6.5 mmol) of **1a** and 0.19 g (27 mg atom) of lithium metal in 15 ml of THF by stirring for 3 hr at room temperature and then heating for 1 hr, and decanted under nitrogen. To the solution was added 0.562 g (5.2 mmol) of *p*-benzoquinone in 15 ml of THF and the mixture was allowed to stand overnight. The resulting blue solution was poured into water, acidified with 2M hydrochloric acid, and extracted with chloroform and ethyl acetate, successively. The ethyl acetate extracts gave 0.19 g (33%) of hydroquinone (**14**) after evaporation, which was identified by comparison of IR and tlc with those of an authentic sample. The chloroform extracts were chromatographed on silica gel with chloroform to give two crystalline compounds. One was recrystallized twice from 95% ethanol to give **12a**, mp 218—220 °C, yield 0.341 g (20%). IR (KBr): 3150 (OH) and 1140 cm^{-1} (P=O); Mass: *m/e* 310 (M^+).

Found: C, 69.93; H, 5.06%. Calcd for $C_{18}H_{15}O_3P$: C, 69.67; H, 4.87%.

The other was recrystallized from benzene-methanol to give **13a**, mp 190—192 °C, yield 0.267 g (18%); IR (KBr): 3200 (OH) and 1218 cm^{-1} (P=O); NMR ($CDCl_3$): δ 6.75 (q, *J* 9 Hz, 4H) and 7.4—8.2 (m, 10H).

Found: C, 69.92; H, 4.85%. Calcd for $C_{18}H_{15}O_3P$: C, 69.67; H, 4.87%.

*b) With $[Ph_2PO]MgCl$ (**5a**)*: A solution of **5a**, prepared from 1.50 g (6.3 mmol) of **1a** and 0.257 g (11 mg atom) of magnesium in 15 ml of THF, was added to 0.545 g (5 mmol) of *p*-benzoquinone in THF (15 ml) and stirred for 14 hr at room temperature. The resulting greenish precipitates turned brown in the air. The precipitates were added to 2 M hydrochloric acid, but were not completely soluble. A small amount of methanol was then added for complete dissolution and the reaction mixture was treated with DCC on silica gel with ether. Each fraction was extracted with methanol to give 0.342 g (17%) of **12a**, 94 mg (17%) of **14**, mp 172—173 °C (identified by tlc and IR), and 0.124 g (8%) of magnesium salt, mp>300 °C, which was dissolved in 10% NaOH solution and neutralized with hydrochloric acid to give diphenylphosphinic acid after extraction with chloroform.

*c) With $[Ph_2PO]al$ (**15a**)*: A solution of **15a**, prepared from 1.65 g (7.0 mmol) of **1a**, 0.263 g (9.7 mg atom) of aluminum foil and 54 mg (0.2 mmol) of mercuric chloride in 15 ml of THF by heating for 6 hr, was added to 0.932 g (8.6 mmol) of *p*-benzoquinone in 15 ml of THF. The reaction mixture was chromatographed on silica gel after filtration to give 0.134 g (8%) of **13a** and 0.183 g (20%) of **14**. The precipitates (1.33 g) contained aluminum which was difficult to remove.

*d) With $[Ph_2PS]al$ (**15b**)*: A solution of **15b**, prepared from 1.89 g (7.5 mmol) of **1b**, 0.435 g (16 mg atom) of aluminum foil and 54 mg (0.2 mmol) of mercuric chloride in 15 ml of THF by heating for 3 hr, was added to 0.693 g (6.4 mmol) of *p*-benzoquinone in 15 ml of THF, and stirred for 15 hr at room temperature. After filtration of precipitates, the filtrate was chromatographed to give 47 mg (0.4 mmol) of recovered quinone and 0.221 g (9%) of **13a**. The precipitates (1.26 g) contained aluminum.

e) With Diphenylphosphine Sulfide: A mixture of 1.64 g (7.5 mmol) of the sulfide and 0.97 g (9.0 mmol) of *p*-benzoquinone in 50 ml of THF was stirred for one day at room temperature. After evaporation, a dark brown tarry substance was subjected to DCC on silica gel with chloroform to afford 1.71 g (70%) of **12b**, which was further purified by column chromatography on alumina with ethanol and recrystallized from ethanol-*n*-hexane, mp 148—149 °C. IR (KBr): 3320, 3275 (OH), and 640 cm^{-1} (P=S); NMR ($CDCl_3$): δ 6.12 (s, 1H, OH), 6.22 (d, J_{PCCH} 14.4 Hz, 1H), 6.8—6.9 (m, 2H), 7.2—7.85 (m, 10H, 2Ph), and 9.07 (s, 1H, OH); δ_p ($CHCl_3$): −37.2 ppm; Mass: *m/e* 326 (M^+).

Found: C, 66.30; H, 4.59%. Calcd for $C_{18}H_{15}O_2PS$: C, 66.25; H, 4.63%.

*f) With $[Ph_2PS]Li$ (**11b**)*: To a solution of **11b** prepared from diphenylphosphine sulfide (1.44 g, 6.6 mmol) in THF (50 ml) and *n*-butyllithium (7.7 mmol) was added dropwise 0.81 g (7.5 mmol) of *p*-benzoquinone in 20 ml of THF with stirring, and the mixture was stirred for one day at room temperature. After removal of THF, the residue was treated with 2 M hydrochloric acid, and extracted with chloroform. Removal of the chloroform from the dried extract gave a tarry product, which was subjected to column chromatography with ethyl acetate to give 0.646 g (30%) of **12b**. Crude **12b** was purified by DCC on silica gel with ether and recrystallized from chloroform-*n*-hexane, mp 155—157 °C. The NMR, IR, and mass spectral data were identical with those of a sample obtained in *e*).

*g) With $[Ph_2PO]FeCl$ (**16a**)*: A mixture of 1.48 g (6.3 mmol) of **1a** and 0.30 g (5.4 mg atom) of reduced iron powder in 15 ml of THF was stirred overnight. To the solution was added 0.338 g (3.1 mmol) of *p*-benzoquinone in 15 ml of THF and stirred for 30 min at room temperature. The resulting precipitates were filtered off. The filtrate was again filtered through alumina to remove diphenylphosphinic acid and the filtrate was evaporated. The residue was treated with ether. Insoluble part (**17a**) was recrystallized from 2-propanol, mp 210—212 °C, yield 1.24 g (78%). IR (KBr): 1235 (P=O), 1180 (Ph–O), and 920 cm^{-1} (P–O); NMR ($CDCl_3$): δ 7.25 (s, 4H) and 7.5—8.2 (m, 20H); δ_p ($CHCl_3$): −30.5 ppm.

Found: C, 70.38; H, 4.58%. Calcd for $C_{30}H_{24}O_4P_2$: C, 70.56; H, 4.74%.

The precipitates (0.287 g) were insoluble in organic solvents. When the precipitates were dissolved in 10% NaOH solution and neutralized with hydrochloric acid, diphenylphosphinic acid was obtained.

*h) With $[Ph_2PS]FeCl$ (**16b**)*: A reaction mixture of 1.55 g (6.1 mmol) of **1b** and 0.270 g (4.7 mg atom) of reduced iron powder in 15 ml of THF was added to 0.254 g (2.3 mmol) of quinone in 15 ml of THF and 1.00 g (79%) of **17b** was obtained, mp 220—221 °C (from 2-propanol). IR (KBr): 1170 (C–O), 1120 (P–Ph), 900 (P–O), and 550 cm^{-1} (P=S); NMR ($CDCl_3$): δ 6.9 (s, 4H) and 7.35—8.2 (m, 20H).

Found: C, 66.20; H, 4.22%. Calcd for $C_{30}H_{24}O_2P_2S_2$: C, 66.41; H, 4.46%.

One of the authors (N. I.) was granted financial support by the Ministry of Education.

References and Notes

1) For Part I see: T. Emoto, H. Gomi, M. Yoshifuji, R. Okazaki, and N. Inamoto, This Bulletin, **47**, 2449 (1974).

2) a) R. C. Miller, C. D. Miller, W. Rogers, Jr., and L. A. Hamilton, *J. Amer. Chem. Soc.*, **79**, 424 (1957); b) L. Horner, P. Beck, and V. G. Toscano, *Chem. Ber.*, **94**, 1317 (1961).

3) G. Sturtz and B. Corbel, *C. R. Acad. Sci. Paris, Ser. C*, **276**, 1807 (1973).

4) The structure of **15** is obscure in the case of aluminum. M is therefore represented as "al".

5) I. G. M. Campbell and I. D. R. Stevens, *Chem. Commun.*, **1966**, 505.

6) L. Horner, P. Beck, and H. Hoffmann, *Chem. Ber.*, **92**, 2088 (1959).

Anomeric Effect in Sulfur Heterocycles Carrying Sulfur Substituents[1]

Michinori Ōki, Tadashi Sugawara, and Hiizu Iwamura
Department of Chemistry, Faculty of Science, The University of Tokyo, Tokyo 113
(Received July 4, 1974)

Conformational analysis of 1,3,5-trithiane derivatives with sulfur-substituents was carried out with the aid of PMR spectra at various temperatures. 2-Phenylthio-1,3,5-trithiane exhibited the strong anomeric effect whereas 2-phenylthiothiane the moderate. This enhanced anomeric effect in trithiane derivatives was attributed to both the stabilization of the axial form and the destabilization of the equatorial form. *cis*-2,4-Bis(phenylthio)-1,3,5-trithiane was found to possess a diaxial conformation to a fair extent in support of the presence of the strong anomeric effect. Equilibration between *cis* and *trans* forms of 2,4-bis(phenylthio)-1,3,5-trithiane was carried out to show that the *trans* form was more stable than the *cis*. The barrier to inversion of *trans*-2,4-bis(phenylthio)-1,3,5-trithiane was obtained as *ca.* 11 kcal/mol.

Since the discovery of the fact, by Lemieux *et al.*,[2] that pyranose derivatives possessing such substituents as alkoxy, acyloxy, or halogen at 2-position prefer the substituent-axial conformation, the phenomenon has drawn attention of many investigators. This phenomenon is in sharp contrast with the free energy difference in cyclohexane derivatives in which the substituent equatorial conformation predominates. The effect which favors the axial conformation in pyranose and analogous sulfur systems has been recognized as the anomeric effect.

Whereas many reports have been published on this effect in oxane and 1,3-dioxane derivatives,[3] there has been only one report on the anomeric effect in sulfur analogs.[4] Since we have observed strong anomeric effect in benzoyloxy derivatives of thiane and analogs,[5] it must be of interest to see the effect in sulfur-substituted thiane and trithiane.

As to the conformational energy of sulfur-substituents, there are two factors to be considered. These are the bond length and the van der Waals radius. Comparison of these factors with the oxygen compound indicates that a longer C–S distance (1.81 Å) than that of the C–O (1.43 Å) tends to lessen and a larger van der Waals radius of sulfur (1.85 Å) than that of oxygen (1.40 Å) tends to enlarge the 1,3-diaxial interaction. As a consequence, the conformational free energy diference for the SH group (0.9 kcal/mol) is only a little larger than that for the OH (0.7 kcal/mol) in cyclohexane series.[6] There is another factor to be considered in sulfur heterocycles. The larger bond distance of the C–S may lessen the 1,3-diaxial interaction.

This paper reports discovery of strong anomeric effect in trithiane derivatives, compares the effect with another sulfur heterocycle, and discusses equilibria of disubstituted compounds.

Results and Discussion

Monosubstituted 1,3,5-Trithianes. Methylene and methine part of PMR spectra of 2-phenylthio-1,3,5-trithiane (**1**) in $CDCl_3$–CS_2 (1 : 1 v/v) both at room temperature and at −83 °C are shown in Fig. 1. At room temperature, methine and methylene signals are seen at δ 5.35, and 3.73 and 4.80, respectively, whereas at −83 °C, a pair of methine signals at δ 5.46, and 5.10, and a pair of AB signals (δ 3.55 and 5.15, J=14.4 Hz; δ 3.91 and 4.40, J=14.4 Hz) are found. The results must be interpreted on a basis that, while the exchange between two conformations is too fast at room temperature, that at −83 °C is slow enough to detect the respective conformations by means of NMR technique. The integrated intensities of these signals show that the population ratio of these isomers is 8.2±0.2.

The spectral features of the more stable isomer are showing up of the methine signal at lower field than the unstable conformer and larger difference in chemical shifts of the A and B protons. Indeed, the difference in chemical shifts of the AB signals amounts to 1.60 ppm and is much larger than that of 1,3,5-trithiane in $CDCl_3$ at −70 °C (0.75 ppm). In contrast to this feature, the difference in chemical shifts of AB signals of the less stable isomer is only 0.45 ppm which is a little smaller than the corresponding value of trithiane. These spectral features of two conformers should be clues to assign the conformation.

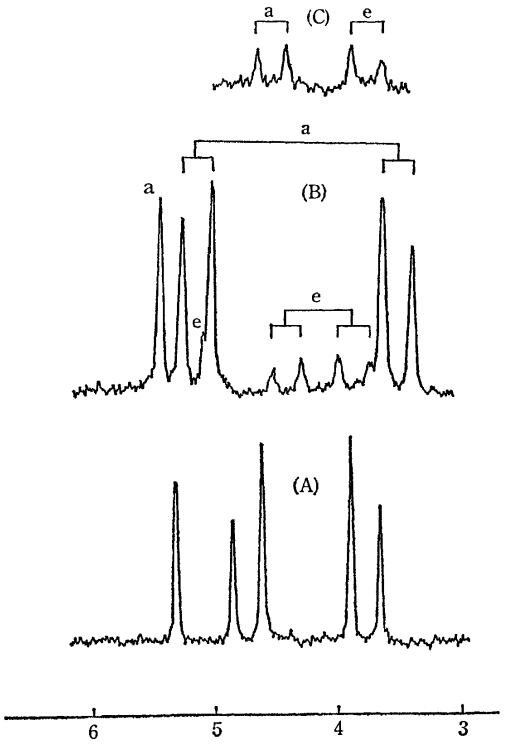

Fig. 1. PMR spectra of 2-phenylthio-1,3,5-trithiane [(A) at 34 °C and (B) at −83 °C] and that of 1,3,5-trithiane [(C) at −70 °C] in $CDCl_3$–CS_2 (1 : 1).

Higher field doublets of the respective AB signals may be assigned to the equatorial proton because equatorial protons are known to give a higher field signal than the axial in trimethyltrithianes.[7] Since 1,3,5-trithiane shows AB signals at δ 3.76 and 4.51 with coupling constant of 14.7 Hz, the equatorial proton of the more populated isomer shows a little up-field shift from the trithiane itself, whereas the axial proton a large low-field shift. As the difference in structure between 1,3,5-trithiane and **1**, the presence of phenylthio group instead of hydrogen can be taken as a major one. Since phenyl is a bulky group, it will not reside above the trithiane ring as one of the possible conformations of phenylthio-axial conformer requests: an assumption that conformations like **1a** only exist becomes a good approximation in the present discussion. Then a major factor which determines the chemical shifts of equatorial and axial protons in the axial isomer is the presence of an axial C–S bond. Likewise, in the phenylthio-equatorial conformer, the C–S bond exerts the major factor for determining the chemical shifts of the axial and equatorial protons. While three conformations are made by the rotation about the C_{ph}–S bond in this case, the phenyl group is located so distantly from the protons in question that its effect may be neglected.

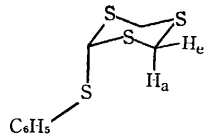

(**1a**)

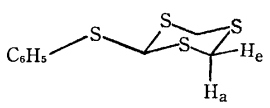

(**1e**)

Consideration of the standard molecular structure, the bond anisotropy of the C–S bond, and McConnell equation[8] reveals that, if there is an axial C–S bond, the axial proton (H_a) at 3-position from the C–S should be strongly deshielded, whereas the equatorial proton (H_e) should be relatively unaffected. Consequently, an increase in chemical shift difference is expected for the methylene protons from that of trithiane. This tendency compares with the observed value of an increase by 0.85 ppm. On the other hand, if there is an equatorial C–S bond, H_e should be unaffected whereas H_a should shift to the higher field slightly. As a consequence, the chemical shift difference should decrease slightly from that of trithiane. This tendency compares with the observed one of a decrease by 0.30 ppm. Thus the more stable isomer must be assigned to phenylthio-axial isomer (**1a**) and the less stable isomer to phenylthio-equatorial isomer (**1e**).

Above assignment is supported by the following fact. When the PMR spectrum of **1** is taken as a CD_3COCD_3 solution at −83 °C, population of the conformer which shows the smaller chemical shift difference increases and the ratio becomes 1.6±0.2 in favor of the isomer which gives larger chemical shift difference. These results indicate that the more polar form is the one which shows less chemical shift difference between protons of the AB type. Since the direction of the dipole in thioethers is known to be that of the lone pairs,[9] compound **1** is considered to be more polar if it takes the phenylthio-equatorial conformation (**1e**).[3] Then a conclusion is drawn that **1a** conformation is more stable and is consistent with that drawn by consideration of the chemical shift difference of the AB protons.

It may be argued that, because of the anisotropy of the C–S bond, the equatorial methine proton at the foot of the phenylthio group should appear at the higher magentic field than the axial, as are the other trithiane protons.[7] The following consideration, however, could give rationale to the apparent reversal of the chemical shifts of axial-equatorial methine protons.

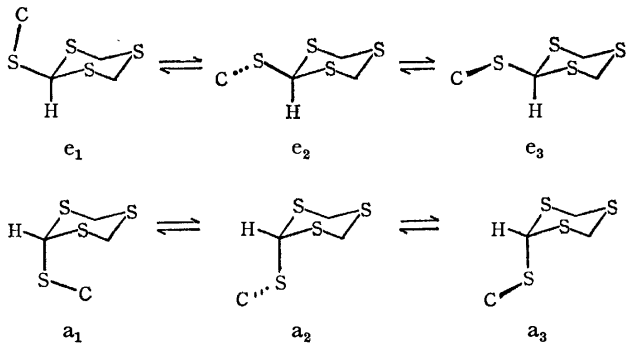

Three stable conformations (e_1, e_2, and e_3) made by the rotation about the S–$C_{trithiane}$ bond of the phenylthio-equatorial conformations may be considered. From the steric grounds, none of these conformations is very unstable and these contribute to a fair extent. On the other hand, the phenylthio-axial form includes other apparently stable conformations (a_1, a_2, and a_3) produced by the rotation about the S–$C_{trithiane}$ bond. As discussed earlier, however, a_1 conformation is considered to be unstable because of the steric effect of the phenyl group and contributes to a very limited extent, if any. Consideration of the dipole moments of the respective conformers reveals that e_1 is the least polar among the phenylthio-equatorial conformations and that there is no appreciable difference in polarity among the phenylthio-axial conformations. Thus, in non-polar media such as those we are discussing here, the e_1 form is the most populated species among **1e**, whereas the a_1 form will have scarce contribution.[10]

A plausible assumption is again that the chemical shift of the methine proton is mainly determined by the bond anisotropy of the C–S bond. Considered the bond anisotropy of the C–S bond, conformers e_2, e_3, a_2, and a_3 are the ones in which the methine proton suffers from the deshielding, whereas the methine proton in conformation e_1 and a_1 is relatively shielded. Then the phenylthio-equatorial form which exists mainly as e_1 should give the methine proton signal at the relatively high field, compared with the phenylthio-axial form which exists mainly as a_2 and a_3.

One may wonder why the apparently abnormal chemical shift of equatorial protons at the foot of the phenylthio group is not attributed to the effect of the phenyl group. However, that this is not the case is understood when the case of 2-methylthio-1,3,5-trithiane (**2**) is taken into account. This compound in $CDCl_3$–CS_2 showed a single peak for the methine proton

Table 1. Chemical shift differences between two methylene protons of 2-phenylthio-1,3,5-trithiane at various temperatures and equilibrium constants for the equilibrium **1a**⇌**1e**

in $CDCl_3$–CS_2 (1 : 1 v/v)							
T °C	63	49	33	15	2.5	−15	−35
$\Delta\delta$ ppm	0.84	0.88	0.92	0.99	1.03	1.08	1.19
K	1.8	1.9	2.1	2.4	2.6	3.2	4.1
T °C	−68	−75	−78	−83[a]			
$\Delta\delta$ ppm	a 1.60	1.60	1.61	1.60			
	e 0.49	0.50	0.48	0.49			
in CD_3COCD_3							
T °C	49	31	7	−83			
$\Delta\delta$ ppm	0.40	0.42	0.45	a 1.23			
				e 0.56			
K	1.1_7	1.2_2	1.3_2	1.6[b]			

a) Equilibrium constant is 8.2, judged from the integrated intensities. b) Obtained by direct integration.

Table 2. Chemical shift differences between two methylene protons of 2-methylthio-1,3,5-trithiane at various temperatures and equilibrium constants for the equilibrium **2a**⇌**2e**

in $CDCl_3$–CS_2 (1 : 1 v/v)							in CD_3COCD_3				
T °C	61	50	39	26	17.5	−83	T °C	46.5	29	14	−6	−83
$\Delta\delta$ ppm	0.84	0.86	0.88	0.92	0.94	a 1.56	$\Delta\delta$ ppm	0.37	0.37	0.39	0.40	a 1.11
						e 0.46						e 0.46
K	1.8	1.9	2.0	2.2	2.3	3.5[a]	K	1.1	1.1	1.2	1.2	1.2[a]

a) Otained by direct integration.

at δ 4.95 and a quartet for the methylene protons (δ 4.63 and 3.73, J=14.5 Hz), which split into a pair of singlets (δ 5.05 and 4.95) and a pair of quartets (δ 3.51 and 5.07, J=14.4 Hz; δ 3.99 and 4.45, J=14.4 Hz), respectively, at −83 °C. The ratio of integrated intensities was 3.0±0.2 in favor of the conformer which showed a large chemical shift difference between A and B protons of the AB quartet. The stable isomer may be assigned to the methylthio-axial conformer (**2a**) from the same ground as discussed earlier. This assignment is supported by a fact that the population ratio of these isomers is reduced to 1.1±0.1 when the spectrum is measured with CD_3COCD_3 solution at −83 °C; the less stable form is apparently more polar than the stable.[3] Taking this assignment into account, the axial proton at the foot of methylthio group is at the higher magnetic field than the equatorial.

(**2e**) (**2a**)

After the establishment of the assignment of conformations, determination of the difference in conformational energies will be worthy of study. The conformational energy may be obtained by applying the following equations and obtaining equilibrium constants (K) at various temperatures.

$$\Delta\delta_{obs} = N_a\Delta\delta_a + N_e\Delta\delta_e \quad (1)$$

$$K = \frac{N_e}{N_a} \quad (2)$$

where $\Delta\delta_{obs}$ is the observed chemical shift difference between A and B protons of the AB type after coalescence, $\Delta\delta_a$ and $\Delta\delta_e$ are those of axial and equatorial conformers, respectively, and N_a and N_e are the mole fractions of axial and equatorial conformers, respectively. A similar treatment would have been possible for the methine protons at 2-position, if the heavy overlap with the strong signal were not present. In order to make Eq. (1) valid, the chemical shift of each isomer should not vary at various temperatures. Measurements at various temperatures after splitting of the signals were thus carried out and the results are listed in Table 1. It will be seen that the chemical shift differences between −68 °C and −85 °C are essentially the same. The same tendency may be extended up to room temperature.* The chemical shift differences after coalescence of the two sets of AB signals are also listed in Table 1.

By the averaging process above the coalescence temperature, an equatorial proton of one conformer is converted to an axial proton of the other. Therefore the sign of $\Delta\delta_a$ and $\Delta\delta_e$ must be different. In the actual calculations $\Delta\delta_a$ was taken as positive and $\Delta\delta_e$ negative. The equilibrium constans thus obtained are shown in Table 1. From these data, ΔH and ΔS for the equilibrium **1a**⇌**1e** in $CDCl_3$–CS_2 were obtained as 1.3±0.1 kcal/mol and 3.0±0.5 eu, respectively. The conformational energy in acetone-d_6 can be obtained in the same manner: ΔH=0.4±0.1 kcal/mol and ΔS=1.0±0.3 eu. It can be pointed out that

* This method of determination of thermodynamic parameters can be checked by extrapolating the population ratio to low temperatures. The calculated value is 7.7±0.5 at −83 °C and this compares favorably with the observed ratio of 8.2±0.2

Table 3. Chemical shift difference between two methylene protons of *cis*-2,4-bis(phenylthio)-1,3,5-trithiane at various temperatures and equilibrium constants for the equilibrium **3aa**⇌**3bb** (1 : 1 $CDCl_3$-CS_2)

T°C	51	46.5	32	29	14	−6	−83
$\Delta\delta$ ppm	0.21	0.20	0.19	0.17	0.16	0.16	a 1.60
							e 0.27
K	0.34	0.33	0.32	0.30	0.29	0.29	0.3[a]

a) Obtained by direct integration.

ΔH is reduced by 0.9 kcal/mol in acetone-d_6, and this change can be attributed largely to the fact that conformer **1e** is stabilized in a high dielectric medium on the electric ground.

Similar treatment was made for 2-methylthio-1,3,5-trithiane. The results are listed in Table 2, which produce ΔH and ΔS, for the equilibrium **2a**⇌**2e** in $CDCl_3$–CS_2, of 0.9±0.1 kcal/mol and 1.0±0.5 eu, respectively. These parameters in acetone-d_6 are 0.1± 0.1 kcal/mol and 0.2±0.2 eu, respectively. Stabilization, to a large extent, of the polar conformer is observed again.

Disubstituted 1,3,5-Trithianes. Since the anomeric effect in 2-phenylthio-1,3,5-trithiane has been found to be fairly large, it will be interesting to see the effect of substitution by one more phenylthio group in 1,3,5-trithiane system. If 2,4-bis(phenylthio)-1,3,5-trithiane has a *cis* configuration, it will assume either a diequatorial (**3ee**) or a diaxial (**3aa**) conformation. In cyclohexane series, the diequatorial form is overwhelming because of a severe 1,3-*syn*-diaxial interaction, whereas the diequatorial form in 1,3,5-trithiane system is disfavored by the anomeric effect. The PMR spectrum of *cis*-2,4-bis(phenylthio)-1,3,5-trithiane (**3**) in $CDCl_3$–CS_2 showed a single peak for methine protons at δ 5.10 and a quartet for methylene protons at δ 3.98 and 4.17, J being 14.4 Hz. On cooling the solution

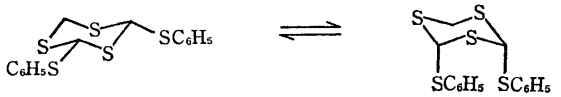

(**3ee**) (**3aa**)

down to −83 °C, however, the spectrum changed to show a pair of singlets at δ 4.92 and 5.38 and two sets of AB quartets (δ 3.88 and 4.15, J=14.4 Hz; δ 3.62 and 5.22, J=14.4 Hz). The results are best interpreted by assuming that the inversion of the ring is fast at room temperature but frozen at −83 °C on the PMR time scale to show the signals of both isomers (**3ee** and **3aa**) separately. The population ratio as determined by the integrated intensity was 3.2±0.3. From an analogy of the discussion given in the part of 2-phenylthio-1,3,5-trithiane, it will be natural to assume that an isomer which has two axial phenylthio groups should give further separation of the chemical shifts of the AB protons, because two C–S bonds are inserted axially. On the contrary, an isomer which has two equatorial phenylthio groups should show smaller separation of the chemical shifts than **1e**. Thus the isomer which gives $\Delta\delta$ of 1.60 ppm is assigned to **3aa** and the other to **3ee**, $\Delta\delta$ for the latter being 0.27 ppm. Then the diequatorial form **3ee** is favored over the diaxial form **3aa**. The chemical shifts and intensities of the methine protons at 2-position are consistent with this assignment: the signal at higher magnetic field is more intense than that at the lower field.

The change in population of **3ee** and **3aa** at various temperatures is tabulated in Table 3. The enthalpy change and entropy change for the equilibrium **3aa**⇌ **3ee** are estimated to be −0.2±0.1 kcal/mol and +1.0± 0.1 eu, respectively, from these results. Thus composition of **3** at 34 °C is 24.5% **3aa** and 75.5% **3ee**.

It is rather surprising to see that the diaxial form exists to a fair extent in **3**, in view of the results obtained with cyclohexane derivatives. In the cyclohexane series, a substituent of RS type generally shows the free energy difference of *ca.* 0.8 kcal/mol at room temperature, the equatorial form being favored.[6] Existence of 1,3-diaxial conformer **3aa** to a fair extent must then be a reflection of the strong anomeric effect and lessened 1,3-diaxial interaction because of the long distance of C–S bonds in this compound.

Barrier to Inversion of trans-*2,4-Bis(phenylthio)-1,3,5-trithiane.* It may be argued that the ring conformation of 1,3,5-trithiane with a phenylthio axial substituent might be altered from the normal chair as in the case of multisubstituted 1,3-dithiane series.[11] However, this possibility may not be taken as a serious one for the following reason.

Since it is well known that the inversion barrier of the six-membered rings is not largely affected by substituents if the ring structure is not deformed from the normal chair,[12] estimation of the inversion barrier of the system in question must lead help in diagnosing the ring conformation.

trans-2,4-Bis(phenylthio)-1,3,5-trithiane (**4**) was used for the investigation, because this compound should give easier analysis due to the high degree of symmetry. While **4** showed sharp singlets due to methylene (δ 4.37) and methine (δ 5.62) protons at 34 °C, the former split to two singlets (δ 5.52 and 5.69)** and the latter

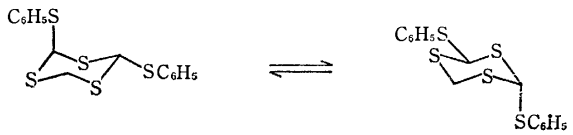

(**4**) (**4'**)

** The signal at the lower field is assigned to the axial, because the signal at the higher magnetic field is broader probably owing to the long range coupling. This anomaly, compared with other methine protons at the foot of phenylthio group in compounds examined here, may be attributed to the presence of an axial C–S bond at 3-position from the proton.

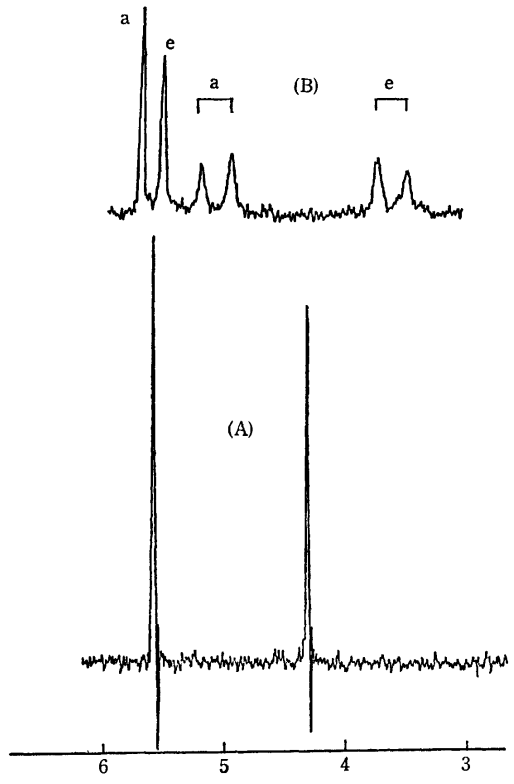

Fig. 2. PMR spectra of *trans*-1,3-bis(phenylthio)-1,3,5-trithiane in $CDCl_3$-CS_2 (1 : 1): (A) at 34 °C and (B) at −80 °C.

changed to an AB quartet (δ 3.70 and 5.09, J=15 Hz) at −80 °C. The methine protons showed coalesence of the signals at −61 °C, whereas the methylene protons at −46 °C. The free energy of activation for inversion was calculated to be 10.4 and 11.1 kcal/mol from methine and methylene protons, respectively, by putting these results into the following equations. Equation (3) was applied for the methine proton and Eq. (4) for the methylene protons. These data are in good agreement with the barrier (11.0 kcal/mol) to inversion of 1,3,5-trithiane.[13]

$$\Delta G_C^{*} = 4.57\ T_C(9.97+\log_{10} T_C/\Delta\nu) \quad (3)[14]$$

$$\Delta G_C^{*} = 4.57\ T_C(9.97+\log_{10} T_C/\sqrt{\Delta\nu^2+6J_{AB}{}^2}) \quad (4)[15]$$

cis-trans *Equilibration of 2,4-Bis(phenylthio)-1,3,5-trithiane.* In view of the fact that 1,3-diaxial form is present to a fair extent in *cis*-2,4-bis(phenylthio)-1,3,5-trithiane (**4**), equilibration between the *cis* and *trans* isomers of **4** will clear another aspect of the conformational energies of the phenylthio group in trithiane. In the *cis* isomer, both phenylthio groups will be either axial or equatorial, whereas one of the phenylthio groups is equatorial and the other axial in the *trans*.

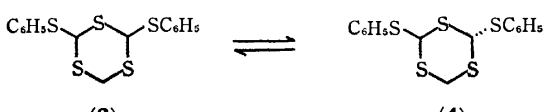

(**3**) (**4**)

The equilibration is carried out by heating the *cis*-isomer in $CDCl_3$ at 80 °C in the presence of benzoic acid as a catalyst. Equilibrium constant was obtained as 3.2 in favor of the *trans*. The same ratio of *cis* and *trans* isomers was obtained also by starting from the *trans*-isomer. Since the *trans* form has two degenerate conformations **4** and **4'**, these conformations must contribute to the same degree and the contributions are calculated to be 38% each. On the other hand, the equilibrium constant for **3aa**⇌**3ee** at 80 °C is calculated as 0.37 by using the thermodynamic parameters derived as before. Thus the equilibrium mixture of 2,4-bis(phenylthio)-1,3,5-trithiane at 80 °C must consist of 6% **3aa**, 18% **3ee**, 38% **4** and 38% **4'**. Although detailed discussion on the conformational and configurational equilibrium of *cis* and *trans* compounds is difficult because of the presence of many factors, the preference of the trans compound clearly indicates the presence of strong anomeric effect.

2-Phenylthiothiane. In order to discuss the strength of anomeric effect in 1,3,5-trithiane derivatives, conformational analysis of 2-phenylthiothiane (**5**) will afford the useful information. Thus study on this compound was undertaken. Compound **5** in $CDCl_3$ shows a near double doublet signal (J=7.5 and 3.0 Hz) for the methine proton at 2-position in the PMR spectrum at 34 °C to indicate that the phenylthio equatorial isomer exists to at least some extent. This result is in accordance with those obtained by Zefirov *et al.*[4] who reported that 2-phenylthiothiane exists as a mixture of 45% **5a** and 55% **5e** from the shapes of methine proton signals.

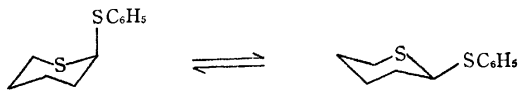

(**5a**) (**5e**)

On cooling the solution, the methine proton signal broadened considerably at −80 °C and was split into two peaks at −100 °C: one peak is a near triplet centered at δ 4.26 and the other an apparent double doublet centered at δ 3.89. The assignment is straightforward: the near triplet signal and the double doublet are assigned to **5a** and **5e**, respectively.[16] The relative intensity is 1.8±0.2 to 1 in favor of **5a**. From these data ΔH and ΔS are calculated as 0.2±0.1 kcal/mol and 0.4±0.2 eu, respectively. The results indicate that the axial isomer is more stable in terms of enthalpy but, because of unfavorable entropy change probably due to the steric effect in one of the rotational isomers, the equatorial isomer contributes to a fair extent at relatively high temperatures: 44% at 34 °C.

Comparison of the Anomeric Effect in Various Compounds. Three main factors are usually cited for the appearance of the anomeric effect. They are dipole-dipole interactions of the polar bonds,[17] repulsive lone-pair-lone-pair interactions of the heteroatoms,[18] and the resonance effect which involves overlap between the p-orbitals of the heteroatom and the back lobe of the orbital involved in forming the axial polar bond.[19] These three factors operate favorably in axial isomers but not in the equatorial.

It is quite natural to consider that these factors are enhanced when heteroatoms reside on both sides of the axial polar bond and these must cause the enhanced anomeric effect in 1,3,5-trithiane, compared with

thiane derivatives. There are reports which contradict this idea: the anomeric effect in 2-methoxy-1,3-dioxane is smaller than that in 2-methoxyoxane.[3] However, the phenomenon was later attributed to the puckering of 1,3-dioxane ring[20] and the short distance in 1,3-*syn*-axial interaction because the C–O bond is shorter than the C–C.[10]

Striking enhancement of the anomeric effect is observed by going from thiane to trithiane. This observation may be attributed to the destabilization of the equatorial form and/or the stabilization of the axial form in trithiane derivatives. In the axial form of 1,3,5-trithiane derivatives, the energy level may not be so high as that of the corresponding thiane derivatives because the 1,3-diaxial interaction is lessened to a considerable extent owing to the longer distance of the C–S bonds and a somewhat flattened conformation of trithiane.[21] In the equatorial form of 2-phenylthiothiane, the repulsive interaction between lone pairs of electrons belonging to two sulfur atoms in the ring and the substituent may be relieved to some extent by increasing the torsion angle about the C_{ring}–C_{subst} bond. However, this mode of relief is not possible for the trithiane derivative: the relief of repulsive interaction with one sulfur atom by increasing the torsion angle necessarily increases the repulsive interaction with another sulfur. Thus both factors seem to enhance the anomeric effect in trithianes.

Experimental

PMR Measurement. The PMR spectra were recorded on a Hitachi R 20B spectrometer equipped with a temperature variation accessory. Temperature was read by the chemical shift difference of methyl and hydroxy protons of methanol at the low temperature and those of ethylene glycol at room temperature or above.

*2-Phenylthio-1,3,5-trithiane (**1**)*, mp 123.0—123.5 °C, was prepared from 2-benzoyloxy-1,3,5-trithiane and benzenethiol as reported previously.[5]

*2-Methylthio-1,3,5-trithiane (**2**).* A solution of 2 g (9 mmol) of 2-benzoyloxy-1,3,5-trithiane[5] and 1.5 g (30 mmol) of methanethiol in 30 ml of chloroform was heated for 5 hr in a reaction vessel equipped with a Dry Ice condenser. Benzoic acid produced during the reaction was removed by passing the solution through a potassium carbonate layer and the solvent was evaporated to give crude products (95 %). Recrystallization from carbon tetrachloride–chloroform (1 : 1 v/v) gave a pure compound, mp 94—95 °C. Found: C, 26.27; H, 4.20%. Calcd for $C_4H_8S_4$: C, 26.06; H, 4.37%. PMR ($CDCl_3$, δ): 2.21 (s, 3H), 3.73 and 4.63 (q, 4H), 4.95 (s, 1H).

*2,4-Bis(phenylthio)-1,3,5-trithianes (**3** and **4**).* A solution of 4 g (0.01 mol) of *cis*-2,4-dibenzoyloxy-1,3,5-trithiane[5] and 3 g (0.03 mol) of benzenethiol in 50 ml of benzene was refluxed for 3 hr. Removal of benzoic acid followed by evaporation of the solvent gave an isomeric mixture of bis-(phenylthio) derivatives (95%). They were separated by chromatography on neutral alumina.

Elution with hexane–benzene(7 : 3) afforded the trans isomer which was purified by recrystallization from carbon tetrachloride, mp 97—99 °C. Found: C, 51.03; H, 3.82; 45.04%. Calcd for $C_{15}H_{14}S_5$: C, 50.80; H, 3.98; S, 45.21%. PMR ($CDCl_3$, δ): 4.33 (2, 2H), 5.61 (s, 2H), 7.2—7.6 (m, 10H).

Elution with benzene afforded the crude *cis* isomer which was purified by rechromatography. Found: C, 51.07; H, 4.39%. Calcd for $C_{15}H_{14}S_5$: C, 50.80; H, 3.98%. PMR ($CDCl_3$, δ): 4.03 and 4.18 (q, 2H), 5.09 (s, 2H), 7.2—7.6 (m, 10H).

Equilibration of cis- *and* trans-*2,4-bis(phenylthio)-1,3,5-trithianes.* A solution of 60 mg (0.16 mmol) of **3** and 50 mg (0.4 mmol) of benzoic acid in 0.4 ml of deuteriochloroform was heated in a sealed NMR sample tube at 80 °C. The process of equilibration could be monitored by the careful integration of methine proton signals of the respective isomers. It took 10 hr to reach the equilibrium.

The same equilibrium mixture was obtained by starting from the *trans* isomer (**4**). It took 20 hr to reach the equilibrium.

References

1) A preliminary report has been published: M. Ōki, T. Sugawara, and H. Iwamura, *Chem. Lett.*, **1973**, 997.

2) R. U. Lemieux, R. K. Kulling, H. J. Bernstein, and W. G. Schneider, *J. Amer. Chem. Soc.*, **80**, 6098 (1958).

3) E. L. Eliel and C. A. Giza, *J. Org. Chem.*, **33**, 3754 (1968); A. J. de Hoog, H. R. Buys, C. Altona, and E. Havinga, *Tetrahedron*, **25**, 3365 (1969); F. W. Nader and E. L. Eliel, *J. Amer. Chem. Soc.*, **92**, 3050 (1970).

4) N. S. Zefirov, V. S. Blagoveshchensky, I. V. Kazimirchik, and O. P. Yakovleva, *Zh. Org. Khim.*, **1**, 594 (1971).

5) T. Sugawara, H. Iwamura, and M. Ōki, This Bulletin, **47**, 1496 (1974).

6) J. A. Hirsch, "Table of Conformational Energies-1967," in "Topics in Stereochemistry", Vol. 1, ed. by N. L. Allinger and E. L. Eliel., Interscience Publishers, New York (1967), p. 199.

7) E. Campainge, N. F. Chamberlain, and B. E. Edwards, *J. Org. Chem.*, **27**, 135 (1962).

8) H. M. McConnell, *J. Chem. Phys.*, **27**, 226 (1957).

9) C. W. N. Cumper and S. Walker, *Trans. Faraday Soc.*, **52**, 193 (1956).

10) E. L. Eliel and F. Nader, *J. Amer. Chem. Soc.*, **91**, 2703 (1969).

11) E. L. Eliel and R. O. Hutchins, *ibid.*, **91**, 2703 (1969).

12) G. Eccleston, E. W. Jones, and W. J. O. Thomas, *J. Chem. Soc., B*, **1971**, 1551; J. B. Hendrickson, *J. Amer. Chem. Soc.*, **83**, 4537 (1961).

13) J. E. Anderson, *J. Chem. Soc., B*, **1971**, 2030.

14) E. L. Eliel, N. L. Allinger, S. J. Angyal, G. A. Morrison, "Conformational Analysis," Interscience Publishers, New York (1965), p. 154.

15) R. J. Kurland, M. B. Rubin, and W. B. Wise, *J. Chem. Phys.*, **40**, 2426 (1964); M. Ōki, H. Iwamura, and N. Hayakawa, This Bulletin, **37**, 1865 (1964).

16) A. Hassner and C. Heathcock, *J. Org. Chem.*, **29**, 1350 (1964).

17) J. T. Edward, *Chem. Ind.* (London), 1102 (1955).

18) R. O. Hutchins, L. D. Kopp, and E. L. Eliel, *J. Amer. Chem. Soc.*, **90**, 7174 (1968).

19) C. Romers, C. Altona, H. R. Buys, and E. Havinga, "Geometry and Conformational Properties of Some Five- and Six-Membered Heterocyclic Compounds Containing Oxygen or Sulfur," "Topics in Stereochemistry," Vol. 4, ed. by E. L. Eliel and N. L. Allinger., Interscience Publishers New York (1969), p. 77. Anomeric effect has also been considered from the standpoint of orbital interactions; see S. David, J. O. Eisenstein, W. J. Hehre, L. Salem, and R. Hoffmann, *J. Amer. Chem. Soc.*, **95**, 3806 (1973). See also L. Radom, W. J. Hehre, and J. A. Pople, *J. Amer. Chem. Soc.*, **94**, 2371 (1972).

20) A. J. de Kok and C. Ronners, *Rec. Trav. Chim. Pays-Bas*, **89**, 313 (1970).

21) H. T. Kaff and C. Ronners, *Acta Crystallogr.*, **20**, 490 (1960).

Die Rolle des Oxydationseffekts bei der Lithentwicklung

Tsuneo SUGA

Forschungslaboratorium der Konishiroku Photoindustrie AG, Hino-shi, Sakura-machi 1, Tokio 191

(Eingegangen am 4. März 1974)

Als Fortsetzung früherer Mitteilungen,[1,2] in welchen der Autor auf die oxydative Wirkung der Oxydationsprodukte des Hydrochinons bei der Lithentwicklung hinwies, wurde hier der Oxydationseffekt eingehender untersucht und der Mechanismus der Lithentwicklung diskutiert, obwohl einige Arbeiten[3-6] keinen Oxydationseffekt vertreten. Die Lithentwicklung hat eine beträchtliche Induktionsperiode, in der man keine Schwärzung bemerken kann. Durch physikalische Entwicklung, die der chemischen Entwicklung und dem Fixieren nachfolgte, bemerkte man eine sichtbare Schwärzung. Diese Versuchsmethode führte zu folgenden Ergebnissen. Während der Induktionsperiode konnte man das Wachstum von Entwicklungskeimen experimentell finden. Der Oxydationseffekt angesammelter Oxydationsprodukte auf die Entwicklungskeime wurde im Entwicklungsverlauf nach der Induktionsperiode als wirksam betrachtet. Während der Induktionsperiode wurde aber eine Oxydation der Entwicklungskeime durch die diffundierenden Oxydationsprodukte als Saumeffekt beobachtet. Durch die Feststellung des Oxydationseffekts ist die Folgerung über den Mechanismus der Lithentwicklung die gleiche wie in früheren Arbeiten, kann aber ausführlicher beschrieben werden.

Der Lithentwickler ist bekanntlich ein Hydrochinon-Alkali-Entwickler mit einer niedrigen Konzentration von Sulfitionen, bei dessen Behandlung ein Lithfilm einen bildscharfen Litheffekt zeigt. Zum Mechanismus der Lithentwicklung wurden bisher verschiedene Hypothesen[2] vorgeschlagen, von denen die auf einer Entwicklungsaktivität der Oxydationsprodukte des Hydrochinons beruhende besonders unterstützt werden kann. In früheren Arbeiten[1,2] weist der Autor auf die Wichtigkeit des Oxydationseffekts der Oxydationsprodukte sowie deren Beschleunigungseffekt über den Mechanismus der Lithentwicklung hin. Eine Reihe von gegenteiligen Arbeiten,[3-6] die keinen Oxydationseffekt bei der Lithentwicklung mitteilen, sind bis heute erschienen: Zwicky[3] fand keine Oxydation des latenten Bildkeimes durch die Phenidon-Hydrochinon-Entwicklung nach der Lithentwicklung. Die Versuche von Okutsu, Sakai und Iwano,[4,6] die den Einfluß der diffundierenden Oxydationsprodukte auf eine andere Emulsionsschicht suchten, zeigten keinen Oxydationseffekt. Die elektronenmikroskopischen Beobachtungen von Shiozawa und Sakai[5] zeigten ebenso keine Oxydation der Entwicklungskeime.

In der vorliengenden Arbeit wurde der Oxydationseffekt eingehender als früher untersucht, indem der Beschleunigungseffekt berichtet wurde.[2] In Zusammenfassung der Ergebnisse wurde eine Hypothese über den Mechanismus der Lithentwicklung diskutiert.

Experimentelles

Emulsion und chemische Entwicklung. Eine Chlorbromsilber-Emulsion, die 30 Mol% AgBr betrug und schwefelsensibilisiert wurde, wurde auf eine Unterlage gegossen. Für die chemische Entwicklung bei 20 °C dienten ein normaler Lithentwickler und dieser Lithentwickler mit Natriumsulfit. Einzelheiten der Materialien und der Versuchsdurchführung wurden in früherer Arbeit[2] beschrieben.

Physikalische Entwicklung. Die Probefilme, die zuerst chemisch entwickelt, fixiert und gewässert wurden, wurden dann in der Lüppo-Cramerschen Lösung 60 Sekunden bei 20°C physikalisch entwickelt. Sie enthielt pro Liter 10 g Metol (*N*-Monomethyl-*p*-aminophenolsulfat), 100 g Zitronensäure, 10 g Natriumzitrat und außerdem 10 g Silbernitrat, die kurz vor der Behandlung zugesetzt wurden.

Ergebnisse und Diskussion

Hydrochinonentwicklung hat eine ausgeprägte Induktionsperiode bis zur ersten sichtbaren Silberabscheidung, die in diesem Versuch etwa 45 Sekunden dauerte. Gegenwart von Sulfit verhindert bekanntlich die Bildung der Oxydationsprodukte des Hydrochinons unter Bildung von Hydrochinonsulfonsäure. Die Wirkung des Sulfites auf den Entwicklungsverlauf nach der Induktionsperiode wurde heir untersucht. Abb. 1 schildert den Einfluß der Sulfitkonzentration von 0, 10 und 30 g/l auf die Form der Schwärzungskurven von 60 und 90 Sekunden chemisch entwickelter Probefilme. Durch steigende Sulfitzusätze rückte der Fuß der Schwärzungskurven vor, indem er eine weiche Gradation zeigte. Die Ursache dafür wurde in voriger Arbeit[2] auf die oxydative Wirkung der Oxydationsprodukte mit Hilfe von Br^-- und H^+-Ionen zurückgeführt.

Innerhalb der Induktionsperiode kann man elektronenmikroskopisch die kleinsten Entwicklungskeime an Körnern beobachten. Pontius *et al.*[7] fanden elektronenmikroskopisch, daß sich die Entwicklungskeime ungefähr beim Endpunkt der Induktionsperiode in sichtbare fadenförmige Silberteilchen verändern. Von den Ent-

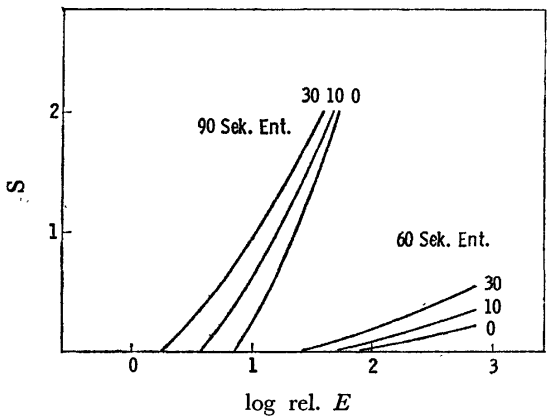

Abb. 1. Einfluß des Sulfites auf Lithentwicklungsvorgang nach der Induktionsperiode. Die Filme wurden 60 und 90 Sekunden bei Anwesenheit von 0, 10 und 30 g Natriumsulfit/l chemisch entwickelt.

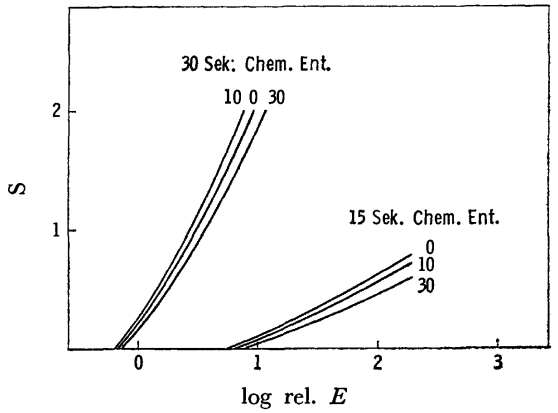

Abb. 2. Schwärzungskurven für physikalische Entwicklung von zuvor 15 und 30 Sekunden chemisch entwickelten Filmen in Entwicklern mit 0, 10 und 30 g Natriumsulfit/l.

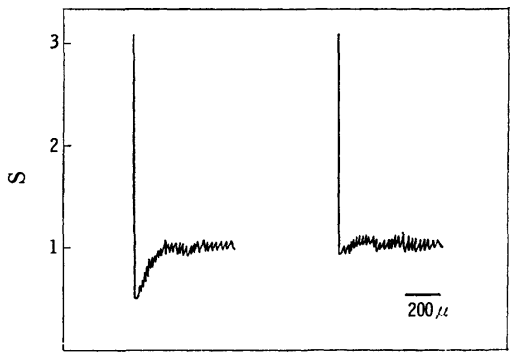

Abb. 3. Saumeffekt von chemischen Entwicklungskeimen während der Induktionsperiode an der scharfen Grenze zweier Flächen verschiedener Belichtung. Die Keime wurden sichtbar durch nachfolgende physikalische Entwicklung.
links: Lithentwickler
rechts: Lithentwickler + 30 g Natriumsulfit/l

wicklungskeimen während der Induktionsperiode nimmt man an, daß sie als physikalische Entwicklungskeime wirken. Nach Vorob'eva und Svirilov[8] beträgt die minimale Größe der Keime für die physikalische Entwicklung etwa 35 Å. Die Versuche, deren Engebnisse in Abb. 2 dargestellt sind, wurden folgendermaßen durchgeführt. Die belichteten Filmstreifen wurden kurze Zeit chemisch entwickelt, fixiert und gewässert, wobei man fast keine Schwärzung bemerkte. Hier sollen die Keime von der Lösungsphase umgeben werden. Bei der nachfolgenden physikalischen Entwicklung entstand eine Schwärzung, die sich mit der Lichtmengenzunahme erhöhte. In dieser Schicht beobachtete man elektronenmikroskopisch die kugelförmigen Silberteilchen. Abb. 2 zeigt Schwärzungskurven der physikalischen Entwicklung von Filmstreifen, die zunächst 15 und 30 Sekunden chemisch entwickelt worden waren. Daraus ist ersichtlich, daß sich mit zunehmender chemischer Entwicklungsdauer die Abscheidungsmenge des Silbers bei der physikalischen Entwicklung erhöhte. Diese Tatsache zeigt, daß sich die unsichtbaren Entwicklungskeime während der Induktionsperiode bei der Hydrochinonentwicklung vergrößern. Wie aus Abb. 2 ersichtlich ist, hatte Sulfit einen geringen Einfluß auf das Keimwachstum im Anfangsstadium der Lithentwicklung, während es im Entwicklungsverlauf nach der Induktionsperiode sehr wirksam war. Daher ist anzunehmen, daß sich die Oxydationsprodukte im Entwicklungsverlauf nach der Induktionsperiode wesentlich auf die Keime auswirken. Die Ursache dafür ist vermutlich ein Vorkommen von geringen Mengen an Oxydationsprodukten zu Beginn der Entwicklung oder eine irreversible Reaktion der Oxydationsprodukte mit Gelatine. Dieses Resultat entspricht dem von Charkoudian *et al.*,[9] die beobachteten, daß keine Spur von Semichinon im Anfangsstadium der Lithentwicklung durch ESR-Messungen vorkam.

An der entwickelten Grenzlinie zwischen schwächer und stärker belichteten Filmflächen bemerkt man eine Schwärzungserniedrigung, wie sie auch als Saumeffekt bezeichnet wird. Im Fall der Lithentwicklung nach der Induktionsperiode wurde schon mitgeteilt,[2] daß die Ursache hierfür auf die oxydative Wirkung der aus den stärker belichteten Stellen diffundierenden Oxydationsprodukte zurückgeführt werden kann. In der vorliegenden Arbeit wurde der Saumeffekt im Laufe der Induktionsperiode, in welcher sich die unsichtbaren Entwicklungskeime vergrößern, untersucht. Die nach der früheren Methode[2] unterschiedlich belichteten Filmflächen wurden 80 Sekunden chemisch entwickelt, wobei sich eine Schwärzung auf der stärker belichteten Fläche befand, jedoch keine auf der schwächer belichteten. Die Schicht wurde dann physikalisch entwickelt, um eine Schwärzung auf der schwächer belichteten Fläche hervorzubringen. Die mikrodensitometrischen Schwärzungsverteilungen zwischen beiden Flächen sind in Abb. 3 dargestellt. Im Fall der Lithentwicklung ist eine merkliche Schwärzungserniedrigung an der Grenze erkennbar, die sich durch Zusatz von Sulfit erheblich verringerte. Auf Grund dieser Tatsachen kann man folgern, daß im Anfangsstadium der Lithentwicklung die von Stellen hoher Schwärzung herausdiffundierenden Oxydationsprodukte auf die Bildkeime der schwächerer Belichtung oxydativ einwirken, um das Wachstum der Keime bei der Entwicklung zurückzuhalten, oder um die Keime zum Abbau zu führen. Dies entspricht einer Oxydation der Bildkeime, deren Möglichkeit aus Messungen von Redoxpotentialen der latenten Bildkeime und der umliegenden Lösung bereits gedeutet wurde.[2] Der exakte Nachweis, ob es sich um eine oxydative Hemmung der Entwicklung oder um einen Abbau von Keimen handelt, ist experimentell schwierig und nicht so bedeutungsvoll für den Mechanismus der Lithentwicklung. Eine vollständige Erklärung der Lithentwicklung ist noch nicht ausreichend, aber eine Hypothese dafür soll mit Hilfe der neuen Ergebnisse ausführlicher als früher wie folgt beschrieben werden. Im Anfangsstadium der Lithentwicklung ist das Wachstum der Entwicklungskeime elektronenmikroskopisch zu beobachten. Die entstandenen Oxydationsprodukte wirken sich währenddessen auf die Keime wenig aus. Im fortgeschritteneren Entwicklungsstadium während der Induktionsperiode sammeln sich die Oxydationsprodukte bei Abwesenheit von Sulfit an, so daß sie auf die Keime

zuerst oxydativ einwirken, um das Auswachsen zum sichtbaren Silber zu hemmen. Diese oxydative Hemmung im Entwicklungsverlauf nach der Induktionsperiode ist wahrscheinlich an den schwächer belichteten Stellen besonders stark. Die Keime an den stärker belichteten Stellen widerstehen der Oxydation und werden weiter entwickelt, wo eine Menge Oxydationsprodukte entstehen, und diffundieren einigen Abstand zu den benachbarten Körnern, in denen die stärker belichteten Bildkeime durch die Herabsetzung der Ladungsschranke beschleunigend entwickelt werden, und die schwächer belichteten durch die oxydative Hemmung oder durch den oxydativen Abbau hemmend entwickelt werden. Die Lithentwicklung gehört einem komplizierten Entwicklungssystem an, in dem die Oxydationsprodukte gleichzeitig zwei Rollen spielen, d.h. die Entwicklung zu beschleunigen und sie oxydativ zu hemmen, oder die Keime oxydativ abzubauen. Eine einheitliche Deutung, wie man sie bisher angenommen hat, wäre für die Diskussion der Lithentwicklung nicht ausreichend.

Obwohl einige Untersuchungen[3-6] keinen Oxydationseffekt bei der Lithentwicklung bemerken, wurde eine Oxydation der Entwicklungskeime durch Versuch bestätigt, was zur Vorstellung der Lithentwicklung von großer Bedeutung ist. Aus dieser Bestätigung des Oxydationseffekts kommt man auch diesmal mit Berücksichtigung der vorigen Ergebnisse der Emulsionseigenschaften[2] im Lithentwickler über die Entstehung des Litheffekts folgendermaßen zu derselben Erklärung wie zuvor:[1,2] Der Litheffekt ist abhängig von der Entwickelbarkeit der stärker belichteten Bildkeime und von der Oxydierbarkeit der schwächer belichteten. Eine richtige Balance dieser beiden Faktoren ist für einen guten Litheffekt wichtig.

Herrn Prof. Dr. K. Honda von der Universität Tokio möchte ich herzlichst für die Diskussion danken.

Literatur

1) T. Suga, *Intn. Congr. Photogr. Sci., Moscow*, C-16 (1970).
2) T. Suga, Dieses Bulletin, **45**, 3464 (1972).
3) H. Zwicky, *Photogr. Korresp.*, **107**, 151 (1971).
4) E. Okutsu, T. Sakai, und H. Iwano, *Nippon Shashin Gakkai Kaishi*, **36**, 95 (1973).
5) T. Shiozawa und T. Sakai, *ibid.*, **36**, 171 (1973).
6) E. Okutsu und H. Iwano, Soc. Photogr. Sci. Eng., Tokyo Symposium, A-3 (1973).
7) R. B. Pontius, R. G. Willis, und R. J. Newmiller, Intn. Congr. Photogr. Sci., Moscow, C-22 (1970).
8) T. N. Vorob'eva und V. V. Svirilov, *Zh. Nauch. Prikl. Fotogr. Kinematogr.*, **18**, 55 (1973).
9) J. Charkoudian, A. Ames, und A. Hoffman, *Photogr. Sci. Eng.*, **17**, 456 (1973).

The Methylation of Phenol and the Decomposition of Methanol on ZnO-Fe_2O_3 Catalyst

Takeshi KOTANIGAWA

Government Industrial Development Laboratory Hokkaido, Higashi-Tsukisamu, Toyohiraku, Sapporo 061-01

(Received March 23, 1974)

As a result of a series of studies, ZnO-Fe_2O_3 catalysts have been shown to promote the selective methylation (k_1) of phenol at the ortho position and also to promote the decomposition of methanol (k_2). The activation energies were determined to be 22±2 kcal/mol for the methylation and 27±3 kcal/mol for the decomposition. The selectivity factor ($S=k_1/k_2$) of the simultaneous reaction was determined for five types of catalysts in order to estimate the most favorable catalyst for the methylation. The selectivity factor of these catalysts decrease with the rise in the calcination temperature. For example, the S on the catalysts calcined at 500 °C is approximately at unity but the S on the catalysts calcined at 800 °C is at about 0.4. These results suggest that the calcination using the present catalysts should be controlled at a low temperature.

In the vapor-phase reaction on a solid catalyst, the selectivity for a desired product is said to be enormously affected by the pore structure of the catalyst.[1,2] However, there have been few experimental studies treating the effects of the pore structure on the selectivity for a desired reaction. Weisz *et al.*, however, reported the effects of pore sizes in the cracking of cyclohexane on a chromia-alumina catalyst.[3] Further, they reported the relations between the pore sizes and the selectivity for the dehydration of *iso*-butyl alcohol and *n*-butyl alcohol on a calcium alumino-silicate.[4]

The present author previously demonstrated that ZnO-Fe_2O_3 catalysts promoted the selective methylation of phenol at the ortho position and that it simultaneously promoted the decomposition of methanol.[5] Further, the relations between the preparative methods and the pore structures of the ZnO-Fe_2O_3 catalysts were studied.[6] In this paper, the present author will, therefore, discuss the relations between the preparative methods of the ZnO-Fe_2O_3 and the selectivity of the methylation of phenol to the decomposition of methanol on five types of ZnO-Fe_2O_3 catalysts.

Experimental

Apparatus and Reaction Conditions. A conventional flow-type reaction apparatus (reactor : Pyrex glass, 18 mm, i.d.) was used. A mixture of 1 mol of phenol and 5 mol of methanol was introduced into the vaporizer. The reaction vapors were carried with nitrogen gas onto the catalyst bed. The partial pressures of the phenol, methanol, and nitrogen gas in the reaction system were 0.105 atm, 0.515 atm, and 0.38 atm respectively. The time factor, W/F, was changed from 6 to 36 g-cat.h/mol-feed, and the reaction temperature was selected between 300 °C and 400 °C.

Analysis of the Reaction Products. The contents of the reaction products were quantitatively analyzed by means of gas chromatography. In the packed columns for gas chromatography, silicon oil DC 550 was used for analyzing aromatics, porapak Q was used for analyzing water and methanol in liquid products, and active charcoal was used for analyzing gaseous products.

Catalysts. The catalysts were prepared by the procedures reported in the previous paper.[6] These catalysts were analyzed as ZnO-$ZnFe_2O_4$ by means of X-ray analysis ($FeK\alpha$ radiation). All the experimental data were obtained using catalysts with particle sizes of 0.75 mm (average, 0.5—1.0 mm).

Results and Discussion

The physical properties of the catalysts are summarized in Table 1. These catalysts possess micropores of about 20 Å in addition to macropores (Table 1).

The reaction between phenol and methanol was carried out at 375 °C. The time factor was 14.4 g-cat. h/mol-feed, and the catalysts in the calcination at 500 °C were used. The results of the reaction are shown in Tables 2a and 2b. As may be seen in Tables 2a and 2b, the catalysts selectively catalyze the methylation at the ortho position of phenol and simultaneously catalyze the decomposition of methanol. In order to

Table 1. Physical properties of the ZnO-Fe_2O_3 catalysts in several preparations

Catalyst symbol	Starting materials (Zn-Fe)	Calcination temperature (°C)	Total pore volume (cm^3/g)	Surface area (m^2/g)	Pore[b] radius (Å)
A-5	O-O[a]	500	0.265	9.4	610
A-6	(Tableting)	600	0.294	7.5	720
A-7		700	0.276	5.8	960
A-8		800	0.192	5.3	1300
B-5	CO_3-O	500	0.442	35.0	150
B-6	(Extrusion)	600	0.418	18.8	250
B-7		700	0.373	15.0	290
B-8		800	0.308	5.5	700
C-5	O-OH	500	0.190	40.4	80
C-6	(Extrusion)	600	0.190	14.5	270
C-7		700	0.170	8.2	380
C-8		800	0.110	5.6	390
D-5	CO_3-OH	500	0.189	21.2	135
D-6	(Extrusion)	600	0.203	19.6	140
D-7		700	0.152	5.3	380
D-8		800	0.100	2.3	700
E-5	OH-OH	500	0.134	36.6	85
E-6	(Coprecipi-	600	0.126	12.6	175
E-7	tation)	700	0.058	3.3	215
E-8		800	0.013	—	—

a) Catalyst prepared from ZnO and Fe_2O_3. b) All catalysts have micropores of about 20 Å radius.

Table 2a. Reaction products in the reaction between phenol and methanol on various catalysts

Catalyst symbol	A-5	B-5	C-5	D-5	E-5
Phenol converted, mol%	16.4	21.3	55.9	26.5	54.0
Selectivity, %[a]					
o-Cresol	92.5	92.4	90.0	88.0	86.3
2,6-Xylenol	7.5	7.6	10.0	12.0	13.7
Methanol converted, mol%	27.3	26.8	52.8	28.0	43.7
Selectivity, %[b]					
Methylation	12.8	16.8	17.4	17.0	18.9
Decomposition	87.2	83.2	82.6	83.2	80.9

a) Defined by (mol of *o*-cresol or 2,6-xylenol per mol of converted phenol). b) Defined by (mol of methyl group in products or gaseous products per mol of converted methanol).

Table 2b. Compositions of gaseous products in the reaction between phenol and methanol over various catalysts

Catalyst symbol	A-5	B-5	C-5	D-5	E-5
Carbon dioxide, mol%	16.5	20.6	17.4	18.0	17.5
Hydrogen, mol%	56.4	51.6	60.8	58.9	59.7
Methane, mol%	23.9	20.9	12.3	14.5	15.2
Carbon monoxide, mol%	8.1	6.8	9.5	8.6	7.6

confirm the above results, the reaction between 2,6-xylenol and methanol was carried out on a (A-6) catalyst under the same reaction conditions. The experimental results showed that no methylphenol was produced. However, it was shown that methanol decomposed to form gaseous products similar to those shown in Table 2b. Therefore, it may be concluded that the overall reaction is a composite of the following two reactions:

$$\text{Phenol} + \text{Methanol} \xrightarrow{k_1} \begin{cases} o\text{-Cresol} \\ 2,6\text{-Xylenol} \end{cases} \quad (1)$$

$$\text{Methanol} \xrightarrow{k_2} \text{Gaseous products} \quad (2)$$

Phenol is consecutively consumed by Reaction (1), but methanol is consumed by Reactions (1) and (2).

In order to obtain available information on the preparative method of the most favorable catalyst, estimations of the individual rate constants were undertaken. For this purpose, the effects of the intraparticle diffusion on the observed rate should be clarified. The relation between the particle size and the activity of catalyst is shown in Fig. 1. The figure indicates that the effect of intraparticle diffusion is negligible. On the basis of this experimental result, the catalysts used for measuring the rate constant were crushed and sieved from 0.5 mm to 1.0 mm size.

The rate of the methylation was found to obey the following equation:

$$-\ln(1-f_p) = k_1(W/F) \quad (3)$$

where f_p is the conversion of phenol.

However, as methanol is consumed by both methylation and decomposition, the rate of Reaction (2) should be expressed by the net conversion (f_m) of the decomposition of methanol. Therefore, the rate of the decomposition satisfies the following equation:

$$-\ln(1-f_m) = k_2(W/F) \quad (4)$$

Arrhenius plots of k_1 and k_2 are given in Fig. 2, and the activation energies are summarized in Table 3.

The data summarized in Table 4 indicate that the activities of the catalysts used were not directly proportional to the surface area. Further, it may be suggested on the basis of Table 4 that the difference in the activities of these catalysts arises from the different starting materials and the various calcination tem-

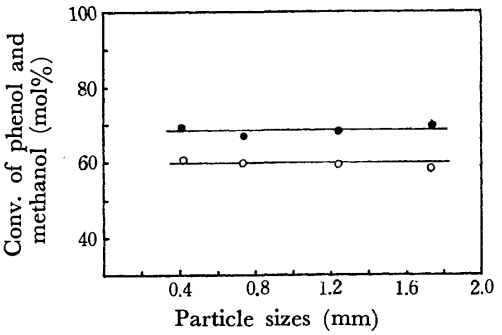

Fig. 1. Effects of particle sizes of the catalyst.
-○-: conversion of phenol
-●-: conversion of methanol
Conditions;
Reaction temp.; 375 °C
W/F; 35 g-cat. h/mol-feed
Reactants; methanol (5 mol)/phenol(1 mol)
Catalyst; A-5

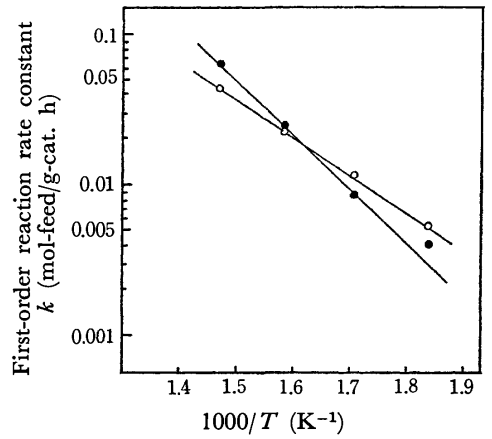

Fig. 2. Arrhenius plots of k_1 and k_2.
-●-: decomposition of methanol
-○-: conversion of phenol

Table 3. Activation energies of the methylation and the decomposition over the ZnO–Fe_2O_3 catalysts

Catalyst symbol	E_1 (kcal/mol)	$A_1\times10^{-6}$ (h^{-1})	E_2 (kcal/mol)	$A_2\times10^{-7}$ (h^{-1})
A-5	22.6	0.59	24.7	0.33
B-5	20.1	0.15	28.6	10.1
C-5	25.4	18.0	27.4	6.8
D-5	22.7	11.0	29.9	38.1
E-5	24.1	5.4	30.5	76.0

TABLE 4. FIRST-ORDER RATE CONSTANTS PER UNIT SURFACE AREA

Catalyst symbol	$k_1 \times 10^3$ (mol/m² h)	$k_2 \times 10^3$ (mol/m² h)
A-5	1.47	1.60
A-6	0.51	1.35
A-7	0.44	1.10
A-8	0.16	0.58
B-5	0.67	0.70
B-6	0.62	0.73
B-7	0.32	0.53
B-8	0.20	0.56
C-5	1.22	1.10
C-6	1.17	1.13
C-7	0.97	1.45
C-8	0.63	1.26
D-5	1.16	1.15
D-6	0.98	1.14
D-7	0.41	1.02
D-8	0.48	1.54
E-5	1.12	1.03
E-6	1.86	1.75
E-7	1.29	2.04
E-8	—	—

peratures. For example, although the (B) and (D) catalysts were both prepared from the one starting material of zinc carbonate (Table 1) and have nearly equal pore radii, the activities show a considerable difference, even at the same calcination temperature. The difference in the activities of the (B) and (D) catalysts may, therefore, be attributed to the difference in the starting material because the (B) catalyst was prepared from ferric oxide as the other starting material, while the (D) catalyst was prepared from ferric hydroxide. Moreover, the difference in the activities of the catalysts prepared from the same starting materials may be attributed to the difference in the calcination temperature. That is, the degree of the decrease in the rate of the methylation becomes considerably larger with the rise in the calcination temperature of the catalyst, while that of the decomposition is not so large.

These facts seem to indicate that the difference in the intrinsic activity of the catalysts resulted from the differences in the preparative method and in the calcination temperature.

According to Wheeler,[2] when the effects of the intraparticle diffusion is negligible, the selectivity factor (S) in a simultaneous reaction is defined as follows:

$$S = k_1/k_2 \qquad (5)$$

Since the rate constants in Table 4 were determined under negligible intraparticle diffusion, Eq. (5) was reasonably used for the estimation of the most favorable

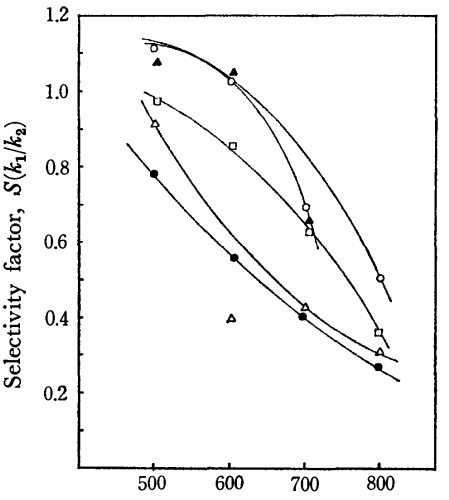

Fig. 3. Relations between the selectivity factor and the calcination temperature.
△: A, □: B, ○: C, ●: D, ▲: E.

catalyst. The effects of the calcination temperature on the selectivity factor are shown in Fig. 3. The Figure shows that the selectivity factor is considerably affected not only by the calcination temperature, but also by the preparative methods. The selectivity factors of the (A) and (D) catalysts (S_a and S_d) decrease considerably with the rise in the calcination temperature, but S_b and S_c are comparatively stable at temperatures below 600 °C. Although the decrease in the selectivity factor occurs with the disappearance of the active sites for the methylation and/or creation of the active sites for the decomposition, it may be said on the basis of Table 4 that when the calcination temperature is higher, the concentration of the active sites for the methylation is smaller.

Thus, it was concluded that the ZnO-Fe_2O_3 catalyst should be prepared at a low temperature. Further, it can be said that the catalysts for the methylation are effective in this order: (C), (E)>(B)>(D),(A).

The author is grateful to Mr. Mitsuyoshi Yamamoto for his assistance in the experiments.

References

1) J. M. Thomas and W. J. Thomas, "Introduction to the Principles of Heterogeneous Catalysis," Academic Press (1967).
2) A. Wheeler, "Advances in Catalysis III," 250, Academic Press (1951).
3) P. B. Weisz, V. J. Frilette, R. W. Maatman, and E. B. Mower, *J. Catal.*, **1**, 307 (1962).
4) P. B. Weisz and E. W. Swegler, *J. Phys. Chem.*, **59**, 823 (1955).
5) T. Kotanigawa, M. Yamamoto, K. Shimokawa, and Y. Yoshida, This Bulletin, **44**, 1961 (1971).
6) T. Kotanigawa and M. Yamamoto, *ibid.*, **47**, 954 (1974).

The Stability of Inosine in Acid and in Alkali

Yoshihisa SUZUKI

Central Research Laboratories, Ajinomoto Co., Inc., Suzuki-cho, Kawasaki 210

(Received November 30, 1973)

The rate constants of the decrease in inosine at several temperatures between 50 °C and 140 °C in water were determined over the pH range from 1 to 13. They can be expressed as a sum of four simultaneous bimolecular reactions. Their thermodynamic parameters were obtained.

For the industrial isolation of inosine from the fermentation broth, information about the stability of inosine in acid and in alkali is of importance to developing the process design for the maximum yield. The kinetics of the hydrolysis of some purine nucleosides,[1-4] such as adenosine and guanosine has been reported in a limited pH range, and that for psicofuranine,[5] over the whole pH range. However, no studies concerning inosine have been reported in the literature. The present paper deals with the pH profile of the rates of the decrease in inosine at several temperatures, and with the pH dependence on the yields of the products.

Experimental

Material and Equipment. The inosine used was a commercial product of the Ajinomoto Co., Inc. The pH of the solution was measured at room temperature with a Toa Dempa HM-5A pH meter. The UV absorbance was measured with a Hitachi spectrophotometer, Model 139.

Paper Chromatography (PC). One-dimensional ascending PC was carried out on Toyo-Roshi No. 51A, the following two solvent systems being used: Solvent A, *n*-butanol–acetic acid–water (4 : 1 : 1); Solvent B, distilled *i*-butyric acid–*n*-butanol–28% ammonia aq.–water (36 : 30 : 3 : 31). The papers were developed three times if necessary for the complete separation of the components on the chromatogram. The components of the reaction mixture were detected on the paper by means of UV absorption. Usually standard solutions of inosine and hypoxanthine(H) were spotted with the reaction mixture. Several spots corresponding with the products including the remaining inosine and the standards were cut off, together with their appropriate blanks, and eluted with 0.1 M HCl, and the absorbances of the eluates were measured at 250 nm. The concentration of each component in the reaction mixture was calculated from the absorbance compared with that of each standard reference. The standard solution of 9-*β*-D-ribopyranosyl hypoxanthine (Y) used was that of inosine because of their similarity. The absorbance of the spot corresponding with 5-amino-1-*β*-D-ribofuranosyl-4-imidazolecarboxamide(X) was corrected in terms of inosine by the use of their molecular extinction coefficients.

Acid Hydrolysis. Inosine was dissolved(3 w/v%) in aq. HCl with a definite concentration, and 25 ml of the resulting solution was sealed in a glass ampoule or a stainless steel tube. It was kept for a definite period on an oil-bath at a constant temperature. The resultant solution was diluted with water to 100 ml and analyzed by means of PC in Solvent A. Table 1 lists the conditions. A steel tube was used for each run over 100 °C and a glass ampoule for each below 80 °C except that a steel tube was used for No. 6 (at 70 °C).

Degradation in Neutral Buffer Solutions. The method used was the same as that to be described with alkaline degradation except that the solvents were phosphate buffer solutions. Table 2 lists the conditions. The following buffer solutions were used: B-1, B-2, B-3, M/2 KH_2PO_4-M/2 Na_2HPO_4 (95 : 5), (30 : 60), (5 : 95); B-4, B-5, M/15 KH_2PO_4-M/15 Na_2HPO_4 (90 : 10 , (40 : 60 .

Alkaline Degradation. Inosine was degraded in the same manner as has been described above in the case of acid hydrolysis except that the solvent was aq. NaOH instead of HCl and except that a steel tube was used throughout all the runs. Table 3 lists the conditions. The chromatogram in Solvent A with three-times development was exhibited in the preceding paper.[6] The spot corresponding with inosine(R_f 0.52) tends to be contaminated with an unknown pale-red spot (R_f 0.55), while that corresponding with Y(R_f 0.43) is not. Therefore, the amount of Y was determined by the use of the chromatogram in Solvent A. The chromatogram in Solvent B with two-times development indicates a clear separation of a pale-red spot(R_f 0.64) from that o:

TABLE 1. CONDITIONS AND OBSERVED FIRST-ORDER RATE CONSTANTS FOR THE ACID HYDROLYSIS OF INOSINE

Run	°C	[HCl] (M)	hr	Obsd. pH		10^2k (hr^{-1})		
				Init.	Final			
1a, b, c	50	0.175	3, 6, 10	1.1	1.3, 1.4, 1.4	3.66,	3.33,	3.75
2a, b, c	60	0.175	3, 4, 6	1.1	1.4, 1.4, 1.4	15.4,	14.8,	15.2
3a, b, c	70	0.175	1, 3, 4	1.1	1.2, 1.4, 1.4	50.5,	49.4,	50.1
4a, b, c	70	0.015	4, 6, 8	2.1	2.3, 2.4, 2.4	5.35,	5.40,	4.61
5a, b	70	0.002	24, 48	3.0	3.2, 3.3	0.647,	0.579	
6	70	0.0002	96	4.0	4.1	0.0845		
7a, b, c	80	0.015	4, 6, 8	2.1	2.5, 2.5, 2.5	15.3,	14.1,	14.2
8a, b, c	80	0.002	6, 8, 10	3.0	3.2, 3.2, 3.2	2.53,	2.35,	2.52
9a, b	100	0.015	1, 2	2.1	2.4, 2.5	112	88.5	
10a, b, c	100	0.002	2, 4, 6	3.0	3.3, 3.4, 3.4	24.8,	15.7,	13.4
11a, b	100	0.0002	12, 24	3.5	3.8, 3.8	2.89,	2.90	
12a, b, c	120	0.0002	2, 4, 6	3.9	3.9, 3.8, 3.8	20.3,	27.1,	23.3

Table 2. Conditions and observed first-order rate constants for the degradation of inosine in the neutral buffer solutions

Run	°C	Buffer	hr	Obsd. pH Init.	Obsd. pH Final	10^2k (hr^{-1})
13a, b	120	B-1	8, 16	5.4	5.2, 4.8	1.48, 2.53
14a, b	120	B-4	10, 16	6.0	5.3, 4.7	0.770, 1.02
15a, b	120	B-5	10, 16	7.0	6.5, 6.4	0.661, 0.775
16a, b	130	B-1	4, 8	5.4	5.0, 4.7	5.68, 5.88
17	130	B-4	6	6.0	4.8	2.95
18	130	B-5	10	7.0	6.2	1.88
19	130	B-3	24	8.0	7.1	3.12
20a, b	140	B-2	3, 6	7.1	6.9, 6.7	9.77, 12.0
21a, b	140	B-3	3, 6	8.0	7.5, 7.3	14.4, 10.2

Table 3. Conditions and observed first-order rate constants for the alkaline degradation of inosine

Run	°C	[NaOH] M	hr	Obsd. pH Init.	Obsd. pH Final	10^2k (hr^{-1})
22	100	0.019	16	8.1	8.0	2.74
23	100	0.060	16	8.9	8.8	8.35
24	100	0.095	16	9.7	9.4	13.5
25	100	0.120	16	11.0	10.0	17.5
26	100	0.151	16	11.9	11.6	15.1
27	100	0.500	16	13.2	13.0	21.7
28	120	0.002	8	7.1	6.8	5.23
29a, b	120	0.019	8, 16	8.1	7.9, 7.4	16.2, 11.8
30a, b	120	0.095	8, 16	9.7	9.4, 9.1	44.7, 34.8
31a, b	120	0.151	4, 8	11.9	11.4, 10.3	70.6, 66.6
c			16		9.9	62.5
32a, b	120	0.500	8, 16	13.2	12.9, 13.0	89.1, 112
33	130	0.095	4	9.7	9.4	103

inosine(R_f 0.55), whereas the mobility of Y is the same as that of inosine. Then, the total amounts of inosine and Y were determined by the use of the chromatogram in Solvent B; the subsequent subtraction of the amount of Y determined before gave that of inosine. The amounts of H and X were determined by means of PC in Solvent A.

Results and Discussion

Inosine (I) degrades in an acid solution, giving hypoxanthine (H) and D-ribose. On the other hand, in an alkaline solution a significant amount of a ring-opened or isomerized product, such as 5-amino-1-β-D-ribofuranosyl-4-imidazolecarboxamide (X) or 9-β-D-ribopyranosyl hypoxanthine (Y), is concomitantly produced, as has been described previously[6] (Chart 1). However, apparent first-order linear plots were obtained for the acid-catalyzed degradation, and even for the alkaline treatment.

Rates of the Decrease in Inosine. Tables 1, 2 and 3 show the conditions and observed first-order rate constants (k) corresponding to the regions for acid, for a neutral solution, and for alkali. A variation in the pH during the degradation was usually observed, and it was larger under alkaline conditions than in acid,

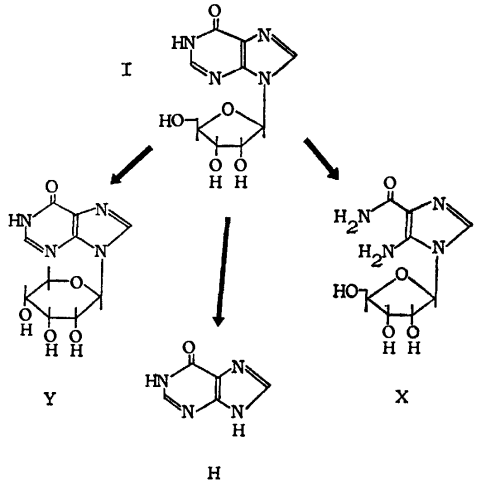

Chart 1

The longer the reaction time, the larger the variation in the pH. This variation, however, had a significant effect on the first-order rate constants. This is the reason why there are some differences in the rate constants in the corresponding experimental runs in Tables 2 and 3; for instance, between Experimental Runs No. 29a and No. 29b in Table 3 there is some difference in rate constant (16.2—11.8) resulting from the difference in the final pH (7.9—7.4). Such a variation in pH can be explained in terms of the production of considerable acid substances; for example, formic acid is released when inosine is cloven at C-2 in dilute alkali, giving X.

The observed first-order rate constant, k, at a constant pH was determined by the linear plots given by Eq. (2), which is derived from Eq. (1):

$$-d[I]/dt = k[I] \quad (1)$$

$$\ln([I_s]/[I]) = kt \quad (2)$$

where $[I_s]$ is the initial concentration of inosine and where [I] is its concentration after a certain time, t.

Figure 1 shows the profile of the overall rates of the decreases in inosine at several tempreatures. The rate is linearly dependent on the hydrogen-ion concentration in the 1—5 pH range, decreasing with an increase in the pH to a minimum of 6—7 and then

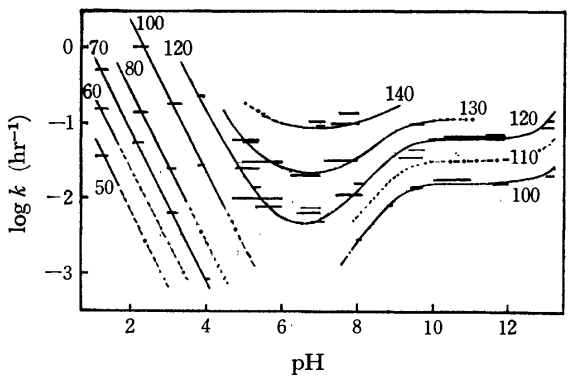

Fig. 1. Overall rate constants for the decrease of inosine in water at several temperatures (°C) as a function of pH.

Table 4. Catalytic rate constants for the decrease in inosine

Temp. °C	k_1 ($l \cdot mol^{-1} \cdot hr^{-1}$)[a]			
	$i=1$	$i=2$	$i=3$	$i=4$
50	6.48×10^{-1}	—	—	—
60	2.37	—	—	—
70	8.04	—	—	—
80	2.54×10	—	—	—
100	2.12×10^{2}	—	2.73×10^{-4}	6.26×10^{-2}
120	1.42×10^{3}	2.19×10^{6}	1.07×10^{-3}	4.41×10^{-1}
130	—	1.03×10^{7}	2.01×10^{-3}	—
140	—	4.48×10^{7}	—	—

a) Rate constants for specific hydrogen ion catalysis to uncharged species (k_1), for specific hydrogen ion catalysis to mono-anionic species (k_2), for water catalysis to mono-anionic species (k_3) and for hydroxyl ion catalysis to anionic species (k_4).

increasing with an increase in the pH in the pH range of 8—9. It is insensitive to the pH in the region pH of 10—12 and then seems to increase again with an increase in the pH. This profile is similar to that obtained for aspirin by Edwards[7] with the exceptions, that the minimum of the rate constant is in the neutral region and that has a smaller value. As will be shown below, the profile of this curve can be explained in terms of four bimolecular simultaneous reactions composed of those between uncharged inosine and hydrogen ions, anionic inosine and hydrogen ions, anionic inosine and water molecules, and anionic inosine and hydroxyl ions.

It is known that the acid-catalyzed hydrolysis of nucleosides giving nucleic bases and sugars can be explained in terms of a bimolecular reaction between nucleosides and hydrogen ions.[2] The mechanism of the reaction has also been discussed.[2] A decrease in the inosine in the acid solution in the present study can be simply explained by this reaction.

In the pH range of 1—5 plots of log k *vs.* pH show a linear relation with a slope of unity (Fig. 1), and the rates of the hydrogen ion-catalyzed reactions are given by Eq. (3):

$$-d[I]/dt = k[I] = k_1[H^+][I^\circ] \quad (3)$$

where k_1 is the catalytic rate constant for a specific hydrogen-ion catalysis and where $[I^\circ]$ is the concentration of the uncharged species of inosine, being equal to the total inosine [I] in this pH range. The intercepts, log k_1, at the several temperatures derived from the acid branch in Fig. 1 are given as k_1 in Table 4.

The Arrhenius plots according to the classical relation of the specific rate constant, k or k_1, are given by:

$$k_1 = A \cdot \exp(-E_a/RT) \quad (4)$$

The plots of log k_1 *vs.* $1/T$ were linear, and the activation energy, E_a and the frequency factor, A, were determined as is shown in Table 5 using Eq. (4), where R is 2 $cal \cdot deg^{-1} \cdot mol^{-1}$ and where T is $(273+t)$K.

In the pH region over 6 the dissociation of inosine to the anion (pK_a 8.75[8]) must be taken into consideration; that is,

$$[I^\circ] \rightleftharpoons [I^-] + [H^+] \quad (5)$$

$$[I^-]/[I^\circ] = K_a/[H^+] \quad (6)$$

$$[I] = [I^\circ] + [I^-] \quad (7)$$

where $[I^-]$ is the concentration of anionic inosine and where K_a is the ionization constant of the equilibrium given in Eq. (5). The plots of log k *vs.* pH in this region are not linear. However, a ready explanation can be found for this curve by employing other terms, including a water-catalytic reaction independent of both hydrogen and hydroxyl ions, in addition to a usual hydrogen-ion- or hydroxyl-ion-catalyzed reaction for anionic inosine. Such a solvent attack on a degradable species is known to be frequently acceptable. The observed rate expression in this region is given by Eq. (8):

$$-d[I]/dt = k[I] = k_2[H^+][I^-] + k_3[H_2O][I^-] + k_4[OH^-][I^-] \quad (8)$$

where k_2 and k_4 are the catalytic rate constants for hydrogen-ion and hydroxyl-ion catalysis respectively and where k_3 is that for water catalysis.

The isomerization or ring-cleavage is observed in this region besides usual hydrolysis, and three main UV-absorbing reaction products, illustrated in Chart 1, were found, along with several minor products, as has been described in a previous paper.[6] However, these three main reaction products seem not to correspond simply with the above three bimolecular reactions. This problem will be briefly discussed later. The complete mechanisms of these three reactions will be clarified in the future. In spite of the above uncertainty, Eq. (8) is useful in estimating the stability of inosine over a wide pH range with a view to obtaining information about the decrease in a marked compound.

The rate constants over the whole pH range can be expressed by a sum by Eq. (3) and Eq. (8). This resultant equation may be rearranged by the use of Eq. (6) and Eq. (7) as follows:

$$k = \frac{k_1[H^+]}{1+K_a/[H^+]} + \frac{k_2[H^+]+K_3[H_2O]+k_4[OH^-]}{1+[H^+]/K_a} \quad (9)$$

The term including k_1 predominates over the others below pH 5, the term including k_2 does so at pH 6—7, k_3 does so at pH 8—12, and k_4, over pH 13.

The k_3 value is easily obtained from the apparent first-order rate constant, k, by the use of Eq. (9) at pH 11, where k is completely independent of the pH (Fig. 1) and where the other three terms are negligible. The Arrhenius plots for k_3 are also easily obtained by the use of Eq. (4). The determination of k_2 and k_4 were not so simple because of the considerable influence from the other terms. They were obtained so as to fit with the observed values of the total rate constants, k, by the use of Eq. (9). The activational energy and the frequency factor for them were also obtained so as to get the best fit with the experimental data. These are summarized in Tables 4 and 5, where K_a is 1.8×10^{-9}.

The curves in Fig. 1 were drawn by the use of Eq. (9) and the constants in Tables 4 and 5; they show a good agreement with the observed values. The ioniza-

Table 5. Thermodynamic parameters for the decrease in inosine in four contributing reaction types

Reaction types[a)]	The activational energy E_a (kcal·mol^{-1})	The frequency factor A (hr^{-1})
1	27.9	3.7×10^{18}
2	49.0	2.6×10^{33}
3	20.0	1.2×10^{8}
4	28.6	2.8×10^{15}

a) Correspond to k_i (i=1—4).

tion of inosine for the cation and the dianion has little effect on the present study because their pK_a values are estimated[9)] to be 1.2 and 12.3 respectively. However, some disturbances are probable at both ends of our pH range; especially at the end of the alkaline region it is necessary to assume that [I$^-$] includes the dianion. It may be supposed that Eq. (9) gives a somewhat larger value if it is applied in the pH region below 1.

When the rate constants for acid hydrolysis are compared with those of guanosine as measured by Zoltewicz *et al.*,[3)] inosine is found to be hydrolyzed about 2 times faster than guanosine at 100 °C in the 1—4 pH range. This is consistent with our previous estimation[10)] that inosine would be hydrolyzed faster than guanosine in a weak acid, while it would be hydrolyzed slower in a strong acid.

Yields of Products. In the acid region the decrease in the mole amount of inosine was equal to amount of H produced, and no side-reaction was observed. On the other hand, in the alkaline region three major UV-absorbing products, H, X and Y, were obtained. The sum of these three products and the inosine remaining was often below 100% when a long reaction time was employed. This indicates the presence of other parallel or sequential degradations.

The representative pH dependences of the three major UV-absorbing products are exhibited in Fig. 2 in the case of 120 °C, corresponding to Experimental Runs No. 29—32. There is an optimum near pH 10 for the production of X and Y, while H increases with an increase in the pH. These convex curves for X and Y correspond with that calculated from the percentage for the mono-anionic species of inosine, as is shown in Fig. 2. The rate-determining term near pH 10 in Eq. (9) included k_5; this term represents a bimolecular reaction between the mono-anionic inosine and the water molecule. Therefore, the rate-determining step of such a reaction that produces X or Y must involve the attack of water on the mono-anionic inosine.

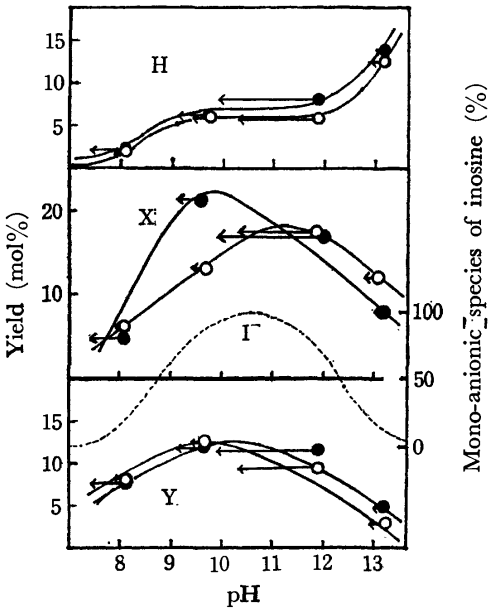

Fig. 2. Yields of UV-absorbing products at 120 °C, and a calculated curve of the development of mono-anionic inosine.
○: Reacted for 8 hr. ●: For 16 hr.
←: Variation in pH during the reaction.
H: Hypoxanthine.
X: 5-Amino-1-β-D-ribofuranosyl-4-imidazolecarboxamide.
Y: 9-β-D-Ribopyranosyl hypoxanthine.
I$^-$: Mono-anionic species of inosine.

The author wishes to thank Mr. Takashi Sato for his technical assistance.

References

1) H. Venner, *Z. Phys. Chem.*, **339**, 14 (1964).
2) R. Shapiro and S. Kang, *Biochemistry*, **8**, 1806 (1969).
3) J. A. Zoltewicz, D. F. Clark, T. W. Sharpless, and G. Grahe, *J. Amer. Chem. Soc.*, **92**, 1741 (1970).
4) R. Shapiro and M. Danzig, *Biochemistry*, **11**, 23 (1972).
5) E. R. Garrett, *J. Amer. Chem. Soc.*, **82**, 827 (1960).
6) Y. Suzuki, This Bulletin, **47**, 898 (1974).
7) L. J. Edwards, *Trans. Faraday Soc.*, **46**, 723 (1950).
8) P. A. Leven, H. S. Simms and L. W. Bass, *J. Biol. Chem.*, **70**, 243 (1926).
9) W. E. Cohn, "The Nucleic Acids," Vol. I, ed. by E. Chargaff and J. N. Davidson, Academic Press, New York, N. Y. (1955), pp. 217,459.
10) Y. Suzuki, This Bulletin, **47**, 2077 (1974).

The Reaction of α-Olefins and Epoxyalkanes with the Dimethyl Sulfide–Sulfur Trioxide Complex

Masuzo NAGAYAMA, Osamu OKUMURA, Katsumi YAGUCHI, and Akira MORI

Central Research Laboratories, Lion Fat & Oil Co., Ltd., Hirai, Edogawa-ku, Tokyo 132

(Received March 2, 1974)

2-Dimethylsulfonioalkane-1-sulfonates were formed by the reaction of α-olefins with the dimethyl sulfide-sulfur trioxide complex. The treatment of these products with alkali gave Δ^1-alkene-1-sulfonates quantitatively. In the reaction between 1,2-epoxyalkanes and the dimethyl sulfide-sulfur trioxide complex, 1-dimethylsulfoniomethyl-1-alkyl sulfate was formed exclusively. 1-Dimethylsulfonio-1-alkenes were quantitatively formed upon the treatment of these products with alkali. The chemical structures of these compounds have been established, and the reaction routes were discussed.

The reaction product from an α-olefin with sulfur trioxide *i.e.*, an α-olefin sulfonate, is considered to be the base material of a new anionic surface-active agent, and a mechanism for the reaction has been proposed.[1,2]

Furthermore, numerous reports have been published on the chemistry of sulfonation using sulfur trioxide-Lewis base complexes.[3,4] We have now obtained some interesting results when the dimethyl sulfide-sulfur trioxide complex was used as the sulfonating agent in the sulfonation of α-olefins and epoxyalkanes; we will report those results in this paper.

Results and Discussion

Reaction of α-Olefins with the Dimethyl Sulfide-Sulfur Trioxide Complex. Many studies have been carried out on the reaction between olefins and the sulfur trioxide-dioxane complex, particularly by Bordwell *et al.*[5-7] They considered that the zwitter ion was the initial sulfonation intermediate of this reaction; however, the zwitter ion has not actually been isolated. On the other hand we have ourselves proposed a new reaction mechanism in a previous paper.[4] An α-olefin was reacted with the sulfur trioxide-dimethyl sulfide complex, in ethylene dichloride at room temperature, to give a 2-dimethyl-sulfonioalkane-1-sulfonate (I) in a high yield. The structure of the product was established by IR and NMR spectroscopy.

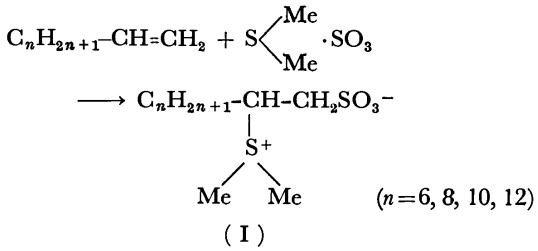

Sulfonium sulfonate internal salts have been synthesized either by the alkylation of mercaptoalkane sulfonates or by the addition of alkyl sulfides to sultones.[8] In the previous report, we established that the initial product of the reaction of α-olefin with sulfur trioxide is a β-sultone,[4] which immediately undergoes ring-opening by means of a nucleophilic reagent. It appears likely that the β-sultone is first formed in the present reaction also, and that it then reacts with dimethyl sulfide.

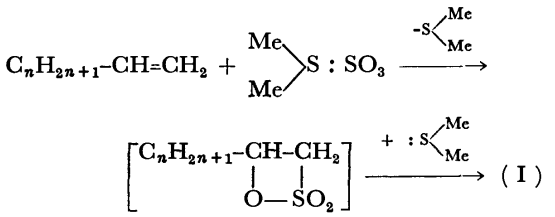

In fact, we confirmed that the reaction between C_{12}-β-sultone, prepared by the previous method,[1] and dimethyl sulfide proceeds more rapidly than the reaction between the olefin itself and dimethyl sulfide. Also, in the former case the same 2-dimethylsulfoniododecane sulfonate internal salt was obtained in an excellent yield. Consequently, it may be considered that the formation of β-sultone is the rate-determining step. These internal salts decomposed easily with alkali to form Δ^1-alkene-1-sulfonates quantitatively.

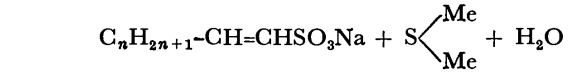

It is apparent that the α-hydrogen has become highly activated by both dimethylsulfonium and sulfonyloxy groups. The decomposed product was identified by means of the NMR spectra.

The decomposition rate was measured using a pH stat. It was dependent on the pH above 6, and consequently, this amphoteric surface active agent is unsuitable for use on the alkaline side. It was confirmed by NMR spectroscopy that the Δ^1-octene-1-sulfonate in the product obtained from 1-octene was a mixture of 61% *trans*-form and 39% *cis*-form, and this finding suggests that the alkaline decomposition proceeds by means of competitive E_2 and E_{1cb} processes.

From olefins of a shorter chain length, similar sulfonation and alkaline decomposition products were obtained, as is shown in Table 1. From this table, a rather clear correlation between the yields and the electron-donating power of the alkyl groups of the olefins can be observed.

Reaction of Epoxyalkanes with the Dimethyl Sulfide-Sulfur Trioxide Complex. An epoxyalkane reacted with the dimethyl sulfide-sulfur trioxide complex in ethylene dichloride to give a 1-dimethylsulfoniomethyl-1-alkyl sulfate(II) quantitatively. The structure of the product was established by IR and NMR spectroscopy.

TABLE 1. REACTION PRODUCTS OF LOWER OLEFINS WITH DIMETHYL SULFIDE-SULFUR TRIOXIDE COMPLEX

Olefin	Product	Yield %	Found % C	Found % H	Calcd % C	Calcd % H	Alkaline decomposed product
1-Butene	C_2H_5-CH-$CH_2SO_3^-$ (S+, CH_3, CH_3)	48	36.35	7.19	36.34	7.12	C_2H_5-CH=$CHSO_3Na$
Isobutene	CH_3, CH_3-C(H)-$CH_2SO_3^-$ (S+, CH_3, CH_3)	67	36.31	7.25	36.34	7.12	CH_3, CH_3-C=$CHSO_3Na$
Propylene	CH_3-CH-$CH_2SO_3^-$ (S+, CH_3, CH_3)	76	32.76	6.74	32.59	6.56	CH_3-CH=$CHSO_3Na$
Ethylene	CH_2-$CH_2SO_3^-$ [a] (S+, CH_3, CH_3)	trace	—	—	28.22	5.92	CH_2=$CHSO_3Na$

a) This product was not isolated, but identified by NMR spectrum, in reaction solution.

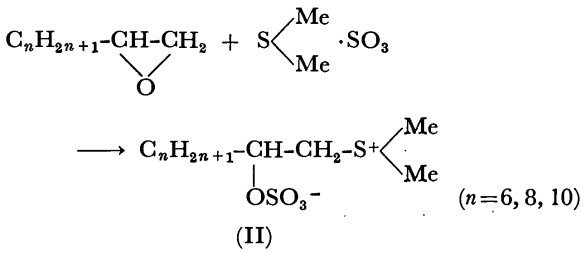

(II) (n=6, 8, 10)

G. E. Ham has reported that SO_3 is inserted into ethylene oxide to form ethylene sulfate.[9]

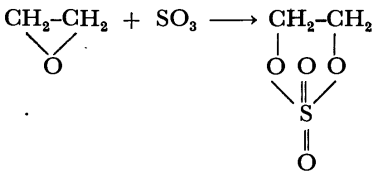

Therefore, the mechanism of this reaction may be considered to involve the initial formation of alkyl-substituted ethylene sulfate, followed by ring-opening by means of S_N2 process with dimethyl sulfide.

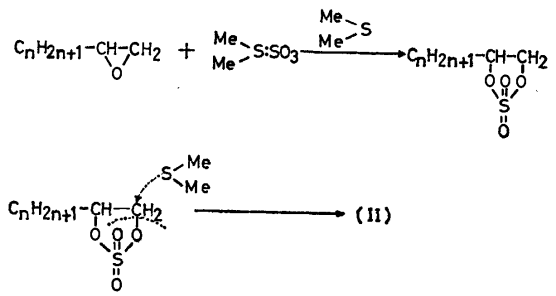

The 1-dimethylsulfoniomethyl-1-alkyl sulfate (II) can be easily decomposed in an alkaline medium to form Δ^1-alkenesulfonium salt quantitatively.

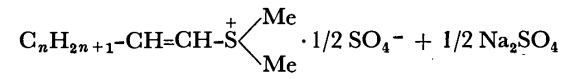

In this case, it was also confirmed by NMR spectroscopy that the decomposed product was a mixture of 70% *trans*-form and 30% *cis*-form for n=6. The decomposition rate was measured similarly with a pH stat. It was dependent upon the pH. For example, the decomposition rate constant (at pH=9.0) is 0.0599 min^{-1}, about 80 times larger than that of the sulfonium-sulfonate (I) type mentioned above.

Ethylene oxide reacted similarly with the dimethyl sulfide-sulfur trioxide complex quantitatively.

As well as with dimethyl sulfide, the reaction also proceeded with methyl ethyl sulfide and diethyl sulfide. However, the expected products were not obtained with ethyl hexyl sulfide, suggesting that a steric effect may be an important factor in this reaction.

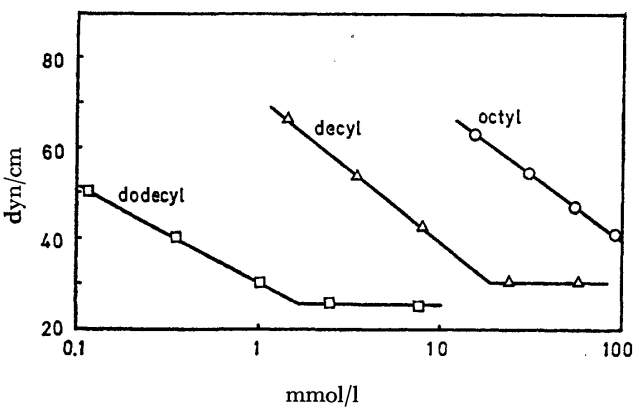

Fig. 1. Surface tension *versus* concentration of 1-dimethylsulfoniomethyl 1-alkyl (octyl, dodecyl) sulfate at 70 °C.

Surface-active Properties. 2-Dimethylsulfonioalkane-1-sulfonates have superior surface-active properties; Compound (I) with $n=8$ has an optimum surface activity, and its critical micelle concentration is 28 mmol/l and $\gamma_{cmc}=30$ dyn/cm. Its wetting power is 11 s at 25 °C, 40 mmol/l and its forming height is 170 mm at 25 °C, 40 mmol/l.

1-Dimethylsulfoniomethyl-1-alkyl sulfates (II) also show good surface activities. The correlation between their concentrations and surface tensions is shown in Fig. 1.

Experimental

Materials. The sulfur trioxide (liquid and stabilized, manufactured by the Nisso Kinzoku Co.) was used after distillation. The C_{10}–C_{16} olefins (manufactured by the Gulf Oil Co.) were purified by distillation. The C_8—C_{14} epoxyalkanes were prepared according to the method of Swern.[10] The ethylene, propylene, 1-butene, and isobutene (manufactured by the Wako Junyaku Co.) were used as received.

Reaction of α-Olefins with the Dimethyl Sulfide-Sulfur Trioxide Complex. The case of 1-dodecene will be described as a typical example. Dimethyl sulfide (0.6 M) was dissolved in 100 g of ethylene dichloride, and the mixture was cooled to −10 °C. When 0.5 M of sulfur trioxide, dissolved in 50 g of ethylene dichloride, was stirred, drop by drop, into the dimethyl sulfide solution, a white precipitate of dimethyl sulfide-sulfur trioxide complex was formed, with the evolution of heat. When 0.6 M of 1-dodecene was added to the reaction mixture, the reaction solution became transparent. A white precipitate was gradually formed while the reaction temperature was maintained at 55 °C for 3 hr. The product was cooled to 0 °C, filtered, and then recrystallized from ethanol. The yield was 52% on the basis of the sulfur trioxide. Found: C, 53.79; H, 9.60; S, 20.4%; Calcd for $C_{14}H_{30}S_2O_3$: C, 54.15; H, 9.74; S, 20.7%. IR (KBr-disk); 1200 ($\nu_{S=O}$) cm^{-1}, 1045 ($\nu_{S=O}$) cm^{-1}. NMR; 7.05 (s, 6H, $CH_3\rangle\overset{+}{S}-$), 6.63 (d, 2H, $-CH_2SO_3^-$), 6.20 (m, 1H, $\rangle CH-\overset{+}{S}\langle$).

Reaction of the C_{12} β-Sultone with Dimethyl Sulfide-Sulfur Trioxide Complex. C_{12} β-sultone (0.1 M), prepared by the previous method,[1] was dissolved in ethylene dichloride (100 g). To this solution, dimethyl sulfide (0.11 M) was added at 0 °C, and the mixture was stirred for 2 hr, a white precipitate was gradually formed, filtered and then recrystallized from ethanol. 26.4 g (85% yield) of 2-dimethylsulfoniododecane-1-sulfonate were thus obtained.

Reaction of the Epoxyalkanes with Dimethyl Sulfide-Sulfur Trioxide Complex. The following procedure for the reaction with 1,2-epoxydodecane is typical. The dimethyl sulfide-sulfur trioxide complex was prepared by the method described above. To one equivalent of this complex, we added equivalents of 1,2-epoxydodecane. A white precipitate was formed when the reaction product was aged at 45 °C for 25 hr. The reaction product was filtered and recrystallized from ethanol. The yield was 85% on the basis of the sulfur trioxide. Found: C, 51.74; H, 9.26; S, 19.7%: Calcd for $C_{14}H_{30}S_2O_4$: C, 51.50; H, 9.26; S, 19.6%. IR (KBr-disk); 1300, 1250, 1100 ($\nu_{S=O}$) cm^{-1}. NMR; 5.30 (m, 1H, $CH-OSO_3^-$), 7.02 (s, 6H, $-\overset{+}{S}\langle^{CH_3}_{CH_3}$), 6.33 (d, 2H, $-CH_2\overset{+}{S}\langle$).

Ethylene oxide was treated similarly to give 1-dimethylsulfonio ethane-2-sulfate in a 96% yield.

Measurements of Sulface-active Properties. The surface-active properties were measured by the JIS K-3362 method.

Measurements of the Decomposition Rates. The decomposition rate was measured at a given pH value in a pH stat(manufactured by the Toa Electronic Co., Model HS-1B). The amount of decomposed substances were calculated from those of the sodium hydroxide required to counterbalance the decrease in the pH with the progress of the reaction. The initial concentration of the substrate was 0.509 mmol/l; solvent, water; temperature, 48 °C; pH, 4.0—11.0.

References

1) A. Mori, M. Nagayama, M. Aoki, and K. Yaguchi, *Kogyo Kagaku Zasshi*, **74**, 706 (1971).
2) Presented at 20th Annual Meeting of the Oil Chemist's Society of Japan, Tokyo, 22, Nov. 1972.
3) E. Gilbert, "Sulfonation and Related Reactions," Interscience Publishers, New York, N. Y. (1965), p. 7.
4) M. Nagayama, O. Okumura, S. Noda, H. Mandai, and A. Mori, "Mechanism of Sulfonation of Olefins with Sulfur Trioxide-Dioxane Complex," This Bulletin in press.
5) G. G. Bordwell and M. L. Peterson, *J. Amer. Chem. Soc.*, **81**, 2002 (1957).
6) I. L. Knunyants and G. A. Sokolski, *Angew. Chem. Internat. Edn.*, **11**, 583 (1972).
7) C. M. Suter, P. B. Evans, and J. M. Kiefer, *J. Amer. Chem. Soc.*, **60**, 538 (1938).
8) Van R. Gaertner, U. S. 2813898 (1957).
9) G. E. Ham, U. S. 3045027 (1962).
10) D. Swern, G. N. Billen, and J. T. Scanlan, *J. Amer. Chem. Soc.*, **68**, 1504 (1946).

Phosphorimetric Investigation of Triplet-Triplet Energy Transfer in Fluid Solution

Takeshi TAKEMURA, Masayuki AIKAWA, and Hiroaki BABA

Division of Chemistry, Research Institute of Applied Electricity, Hokkaido University, Sapporo 060

(Received March 29, 1974)

The mechanism of triplet-triplet (T-T) energy transfer in fluid solution has been studied by means of phosphorimetry in the temperature range 0—60 °C with acetophenone as energy donor, 1,4-dibromonaphthalene as acceptor and isooctane, isopentane or carbon tetrachloride as solvent. From the temperature dependence of the energy transfer, α and k_{dif} could be evaluated separately, k_{dif} denoting the diffusion-controlled rate constant for the encounter of donor and acceptor molecules and αk_{dif} corresponds to the rate constant for the overall energy transfer reaction. The α values are 0.28 at 25 °C in isopentane and 0.43 at 21 °C in isooctane, indicating that the T-T energy transfer process is not strictly diffusion-controlled. The k_{dif} values are nearly equal to those predicted by a modified Debye equation.

In a previous paper,[1] it was suggested by means of laser pulse photolysis that the triplet-triplet (T–T) energy transfer process is not strictly diffusion controlled in fluid solution. The overall T-T energy transfer rate constant k_t can be expressed as $k_t=\alpha k_{dif}$, where k_{dif} is the diffusion-controlled rate constant. We calculated k_{dif} from the standard Debye equation,

$$k_{dif} = 8RT/3000\eta \quad (1)$$

and obtained an α value smaller than unity.

Since the study by Porter and Wilkinson,[2] considerable attention has been given to whether the T-T energy transfer is diffusion controlled or not.[1–9] In most cases, the question was discussed through a comparison of k_t with k_{dif} which was predicted either by Eq. (1) or by a slightly modified Debye equation, *i. e.*,

$$k_{dif} = 8RT/2000\eta \quad (2)$$

However, we cannot place much reliance on the results because of the assumptions involved in the evaluation of k_{dif}.

We have examined the mechanism of T-T energy transfer in a fluid solution without resort to theoretical prediction. The experiment was carried out with the aid of the donor and acceptor phosphorescence emissions observed in fluid solution. Since it is generally difficult to detect phosphorescence in a fluid solution, most studies on T-T energy transfer have been made by means of T-T absorption or analysis of photochemical products. However, in the former method the first order rate constant for triplet decay is difficult to determine, because an exciting flash of very high intensity is used; the latter method is not suitable for obtaining direct information on the energy transfer process.

Acetophenone was chosen as the energy donor and 1,4-dibromonaphthalene as acceptor, isooctane, isopentane and carbon tetrachloride being used as solvents. We utilized the fact that both acetophenone and 1,4-dibromonaphthalene show phosphorescence with an appreciable intensity even in a fluid solvent provided that the solvent is fully degassed.[1,10–12]

Experimental

Reagents of Wako Pure Chemical Industries, Osaka were used. Acetophenone was purified by high-vacuum distillation, and 1,4-dibromonaphthalene (DBN) by vacuum sublimation. Spectro-grade isooctane and carbon tetrachloride were used without further purification. Isopentane was passed through a silica gel column.

The sample solutions consisted of acetophenone of a constant concentration (1.0×10^{-2} M) and DBN of varying concentrations (10^{-5}—10^{-4} M), with isooctane, isopentane or carbon tetrachloride as solvent. Each of these solutions was degassed repeatedly (7 or 8 times) by freeze-thaw cycles until the phosphorescence intensity of acetophenone reached a maximum. A representative example of the effect of degassing on the phosphorescence intensity is shown in Fig. 1, in which the phosphorescence intensity of DBN in isooctane is plotted against the number of freeze-thaw cycles.

The phosphorescence spectra were measured at various temperatures between 0° and 60 °C with a Hitachi MPF-2A fluorescence spectrophotometer equipped with a temperature-controlled water bath. The donor phosphorescence spectra were corrected for spectral sensitivity of a monochromator-photomultiplier system using quinine sulfate and β-naphthol as standards. The donor phosphorescence quantum yields were determined by comparing the corrected phosphorescence spectra with a corrected fluorescence spectrum of quinine sulfate in 0.5 M sulfuric acid, which has a fluorescence quantum yield of 0.51. The acceptor phosphorescence spectra were uncorrected because of large correction errors involved over the insensitive spectral region of the photomultiplier. Thus, the relative intensities of the peak were used in the acceptor phosphorescence analysis.

The phosphorescence decay was measured by means of the second harmonic of a giant pulse ruby laser[1] or a xenon flash for excitation.

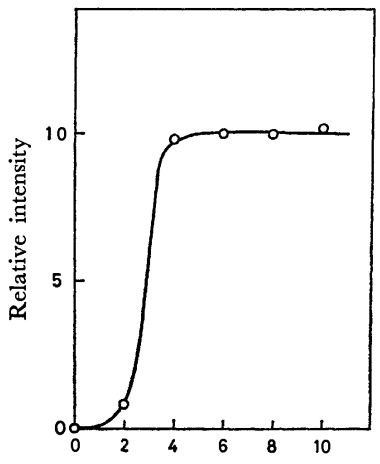

Fig. 1. Effect of degassing on the phosphorescence intensity of DBN in isooctane at room temperature.

Results

Changes in the phosphorescence spectrum of the acetophenone-1,4-dibromonaphthalene (DBN) system in isooctane at 25 °C caused by the increase of the concentration of DBN are shown in Fig. 2. In the absence of acetophenone no phosphorescence emission was observed from DBN upon excitation at 340 nm, which was adopted as the excitation wavelength throughout the T-T energy transfer experiments. The spectral changes are therefore regarded as due to the T-T energy transfer from acetophenone to DBN. Similar spectral changes were observed in isopentane and carbon tetrachloride at various temperatures (0—60 °C).

The Stern-Volmer plots for the quenching of the phosphorescence of acetophenone by DBN in isooctane at different temperatures are shown in Fig. 3, where ϕ_D^0 and ϕ_D are the quantum yields of the donor phosphorescence in the absence and presence of the acceptor, respectively, $[^1A]_0$ being the initial concentration of the acceptor in its ground state. The plot is linear for any temperature, the slope increasing with decreasing temperature. Stern-Volmer plots of essentially the same nature are obtained on changing the solvent from isooctane to isopentane or carbon tetrachloride (Figs. 4 and 5).

Under our experimental conditions of a weak excitation intensity and a low acceptor concentration, the reaction scheme involving the T-T energy transfer may be expressed as

$$^1D \longrightarrow {}^3D^* \tag{3a}$$

$$^3D^* \longrightarrow {}^1D \qquad k_1 \tag{3b}$$

$$^3D^* + {}^1A \longrightarrow (^3D^*...{}^1A) \qquad k_{dif} \tag{3c}$$

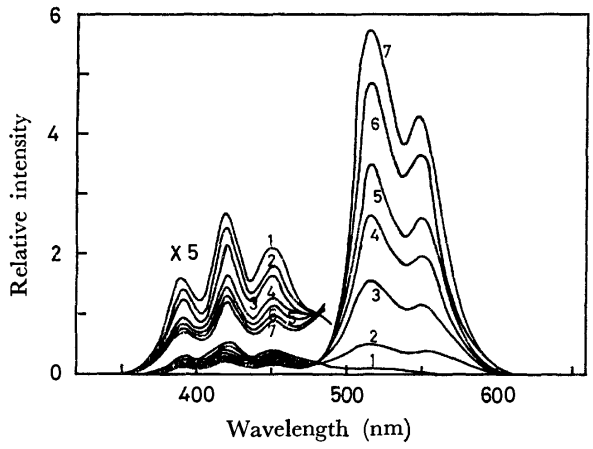

Fig. 2. Phosphorescence spectra (uncorrected for instrument response) of acetophenone-DBN system obtained by excitation at 340 nm in isooctane at 25 °C. The concentrations of DBN: (1) 0; (2) 0.12×10^{-4} M; (3) 0.25×10^{-4} M; (4) 0.74×10^{-4} M; (5) 0.98×10^{-4} M; (6) 1.23×10^{-4} M; (7) 1.47×10^{-4} M.

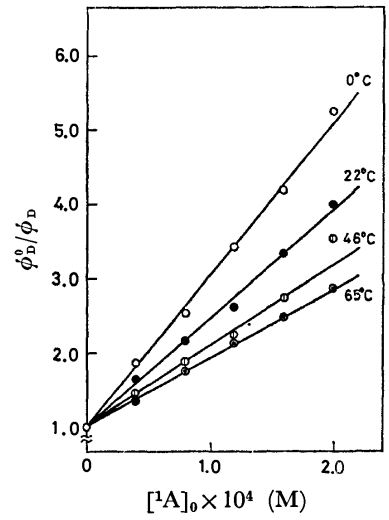

Fig. 3. Stern-Volmer plots for the quenching of the phosphorescence of acetophenone by DBN in isooctane at different temperatures between 0 and 65 °C.

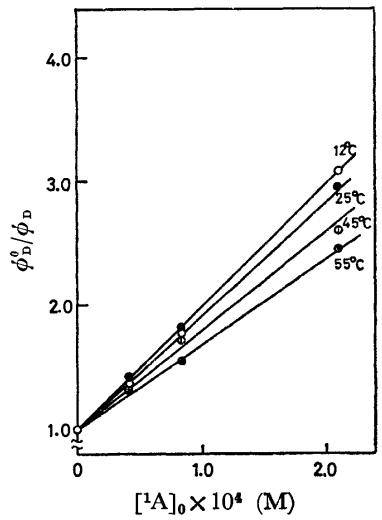

Fig. 4. Stern-Volmer plots for the quenching of the phosphorescence of acetophenone by DBN in isopentane at different temperatures between 12 and 55 °C.

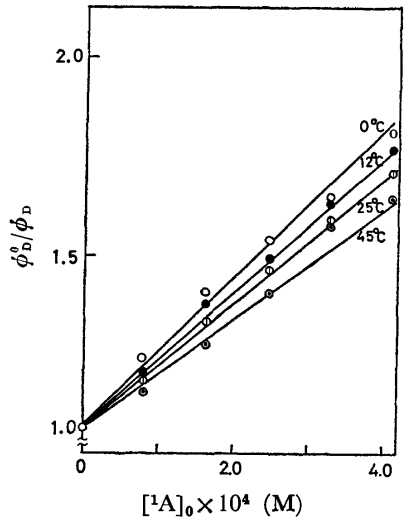

Fig. 5. Stern-Volmer plots for the quenching of the phosphorescence of acetophenone by DBN in carbon tetrachloride at different temperatures between 0 and 45 °C.

$$(^3D^*...^1A) \longrightarrow {}^3D^* + {}^1A \qquad k_{-dif} \qquad (3d)$$

$$(^3D^*...^1A) \longrightarrow (^1D...^1A) \qquad k_1' \qquad (3e)$$

$$(^3D^*...^1A) \longrightarrow (^1D...^3A^*) \qquad k_{et} \qquad (3f)$$

$$(^1D...^3A^*) \longrightarrow {}^1D + {}^3A^* \qquad (3g)$$

$$^3A^* \longrightarrow {}^1A \qquad (3h)$$

where $^3D^*$, ^1D and $^3A^*$, ^1A represent the excited triplet and ground singlet states of donor (D) and acceptor (A), respectively and k_1 and k_1' denote the sums of all unimolecular decay processes including both radiative and nonradiative transitions. The process expressed by (3c) corresponds to the encounter of a donor molecule in the triplet state and an acceptor molecule in the ground state; process (3d) represents the dissociation of the encounter complex, and (3f) the energy transfer from the donor to the acceptor.

We are here concerned with photostationary conditions. Since the concentrations of the encounter complexes ($^3D^*\cdots{}^1A$) and ($^1D\cdots{}^3A^*$) are considered to be very small as compared with those of the "free" triplet species $^3D^*$ and $^3A^*$, respectively, we can regard the donor and acceptor phosphorescence emissions as due exclusively to the free species. Furthermore, we may safely assume that $k_1' \ll k_{et}$. Thus it follows from the above reaction scheme that

$$\phi_D^0/\phi_D = 1 + \alpha k_{dif}\tau_0[^1A]_0 \qquad (4)$$

with

$$\alpha = \frac{k_{et}}{k_{-dif}+k_{et}} \qquad (4')$$

where $\tau_0(=1/k_1)$ is the phosphorescence lifetime of the donor in the absence of acceptor. α represents the probability that energy transfer occurs during the lifetime of the encounter complex. Equation (4) is compatible with the linear relations between ϕ_D^0/ϕ_D and $[^1A]_0$ (Figs. 3—5). Thus, from the slopes of the straight lines in these figures, the values of $\alpha k_{dif}\tau_0$ can be obtained for each temperature. The results given in Table 1 show that the quantity $\alpha k_{dif}\tau_0$ depends on the temperature.

TABLE 1. VALUES OF $\alpha k_{dif}\tau_0$ AT VARIOUS TEMPERATURES IN DIFFERENT SOLVENTS

Solvent	$\alpha k_{dif}\tau_0 \times 10^{-4}$, M^{-1}				
Isopentane		1.0 (12 °C)	0.9 (25 °C)	0.8 (40 °C)	0.7 (55 °C)
Isooctane	2.0 (0 °C)	1.5 (21 °C)	1.3[a] (25 °C)	1.2 (46 °C)	0.9 (65 °C)
Carbon tetrachloride	0.20 (0 °C)	0.18 (12 °C)	0.17 (25 °C)	0.16[a] (25 °C)	0.15 (45 °C)

a) Obtained from the sensitized acceptor phosphorescence.

Let us examine the spectral data concerning the sensitized acceptor phosphorescence. It can be shown that the following equation is derived from the reaction scheme:

$$\frac{1}{\phi_A} = \frac{1}{\theta}\left(1+\frac{1}{\alpha k_{dif}\tau_0[^1A]_0}\right) \qquad (5)$$

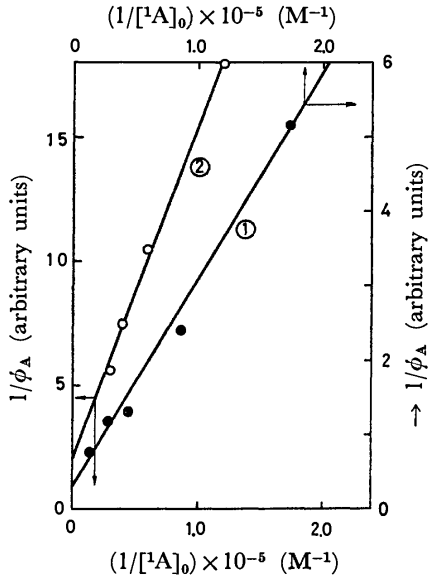

Fig. 6. Plots of $1/\phi_A$ *vs.* $1/[^1A]_0$ for acetophenone-DBN system in isooctane (1) and in carbon tetrachloride (2) at 25 °C.

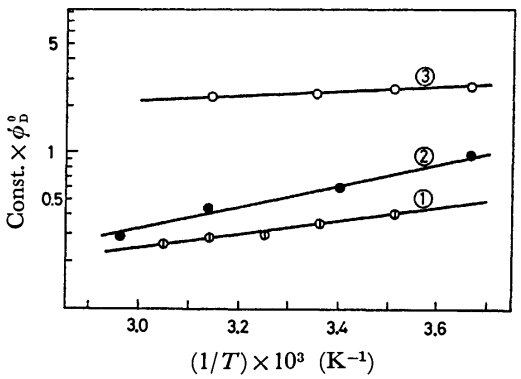

Fig. 7. Temperature dependence of ϕ_D^0 in various solvents: (1) isopentane, (2) isooctane; (3) carbon tetrachloride.

TABLE 2. DATA FOR THE DONOR PHOSPHORESCENCE IN THE ABSENCE OF THE ACCEPTOR IN VARIOUS SOLVENTS, AND THE VALUES OF ΔE_{flow} AND η OF THE SOLVENTS

Solvent	$\phi_D^0 \times 10^{4}$[a]	$\tau_0 \times 10^{6}$[a] s	ΔE kcal/mol	ΔE_{flow} kcal/mol	η[b] cP
Isopentane	0.95	0.63	1.8	1.5	0.225
Isooctane	2.7	1.6	2.8	2.1	0.504
Carbon tetrachloride	5.1		0.9	2.6	0.969

a) At 25 °C. b) At 20 °C, taken from Ref. 21.

where ϕ_A is the quantum yield of the sensitized acceptor phosphorescence and θ the fraction of triplet acceptor molecules which phosphoresce. Plots of $1/\phi_A$ against $1/[^1A]_0$ in isooctane and carbon tetrachloride at 25 °C give straight lines (Fig. 6). From the intercepts and slopes of these lines, we can obtain the values of $\alpha k_{dif}\tau_0$. The values were found to be in good agreement with those obtained from the quenching of the donor phosphorescence (*cf.* Table 1). This indicates

that the reaction scheme involving processes (3a)—(3h) describes satisfactorily the T-T energy transfer phenomenon in fluid solution.

Figure 7 shows the temperature dependence of ϕ_D^0. In each of the solvents a linear relation is found between log ϕ_D^0 and $1/T$.

Lifetimes of the donor phosphorescence at 25 °C in the absence of the acceptor are given in Table 2. The phosphorescence decay was found to be exponential in all the solvents.

Discussion

Evaluation of α and k_{dif}. Although we have obtained the values of $\alpha k_{dif}\tau_0$ at various temperatures from the slopes of the Stern-Volmer plots (Table 1), it is necessary to evaluate α and k_{dif} separately in order to establish whether the T-T energy transfer process is diffusion-controlled or not in a fluid solution.

On reference to Eq. (4') the changes in slope of the Stern-Volmer plots caused by temperature change are expressed as

$$y(T) = \frac{k_{et}}{k_{et}+k_{-dif}} k_{dif}\tau_0 \tag{6}$$

which is rewritten as

$$\frac{k_{dif}\tau_0 - y(T)}{y(T)} = \frac{k_{-dif}}{k_{et}} \tag{7}$$

We examine here the temperature dependence of the quantum yield of the donor phosphorescence in the absence of the acceptor, ϕ_D^0. From the fact that the phosphoressence decay is exponential, the donor lifetime τ_0 as defined in Eq. (4) is expressed in the form

$$\tau_0 = 1/(k_r+k_q),$$

where k_r denotes the rate constant for the radiative transition in the donor molecule, and k_q the sum of the rate constants for unimolecular and pseudo-unimolecular quenching processes of the donor; the latter quenching process might be caused by solvent molecules and by some quenching impurities. The quantum yield ϕ_D^0 is expressed in the form

$$\phi_D^0 = \phi_{ISC} k_r \tau_0 = \text{Const.} \times \tau_0,$$

where ϕ_{ISC} is the intersystem crossing quantum yield of the donor.

In a fluid solution, it can safely be assumed that $k_r \ll k_q$, so that $\tau_0 = 1/k_q$. In addition, it is recognized that the quenching constant k_q has a diffusion-controlled character.[13] Therefore k_q can be written as

$$k_q = \text{Const.} \times \exp(-\Delta E/RT) \tag{8}$$

where ΔE is an activation energy. Thus, ϕ_D^0 has the form

$$\phi_D^0 = \text{Const.} \times \exp(\Delta E/RT)$$

The foregoing considerations are supported by the fact that a linear relation exists between log ϕ_D^0 and $1/T$ in each of the solvents (Fig. 7). From the slopes of the straight lines, ΔE values are calculated to be 1.8, 2.8, and 0.9 kcal/mol, respectively, in isopentane, isooctane, and carbon tetrachloride as solvents. These values are approximately equal to the activation energies of flow, ΔE_{flow}, for the solvents except for the value in carbon tetrachloride. The data for ΔE and ΔE_{flow} are given in Table 2.

In view of these results we may assume that in a hydrocarbon solvent ΔE agrees with ΔE_{flow}. Thus it follows from Eq. (8) that $k_{dif}\tau_0$ is independent of temperature, since $k_q = 1/\tau_0$ and k_{dif} can be expressed as Const. $\times \exp(-\Delta E_{flow}/RT)$. The difference between the values of ΔE and ΔE_{flow} for carbon tetrachloride as a solvent cannot be explained from the present experimental data alone. It might be due to such a specific effect as an external heavy-atom effect of the solvent on the donor phosphorescence.

Let us now return to Eq. (7). k_{-dif} should show the same temperature dependence as k_{dif}. On the other hand, for the donor-acceptor pair under study, k_{et} would not appreciably vary with temperature. The right-hand side of Eq. (7) can then be written as

$$\frac{k_{-dif}}{k_{et}} = C \exp\left(-\frac{B}{RT}\right) \tag{9}$$

where C and B are constants. Even if k_{et} depends on temperature, Eq. (9) holds provided that k_{et} is assumed to be expressed by an Arrhenius type equation. Substitution of Eq. (9) into Eq. (7) gives

$$\frac{A-y(T)}{y(T)} = C \exp\left(-\frac{B}{RT}\right) \tag{10}$$

where A stands for $k_{dif}\tau_0$. If an appropriate value is inserted into A, a polt of $\log\{[A-y(T)]/y(T)\}$ against $1/T$ should yield a straight line.

Figure 8 shows the plots in question for different A values. It is seen that, when A equals 3.5×10^4 M^{-1} (the solid line), the plot gives a striaght line for acetophenone–DBN system in isooctane; from the slope of the line B is found to be 3.5 kcal/mol. A similar treatment of the same system in isopentane leads to $A=3.2\times10^4$ M^{-1} and $B=2.2$ kcal/mol.

By the use of $A(\equiv k_{dif}\tau_0)$ thus determined the values of α are immediately obtained (*cf.* Table 1), with the results shown in Table 3. It is seen that α is definitely smaller than unity. This shows that the T-T energy transfer is not diffusion-controlled under the present experimental conditions. Furthermore, α is found to decrease with increasing temperature. The lowering of the solvent viscosity accompanied by temperature

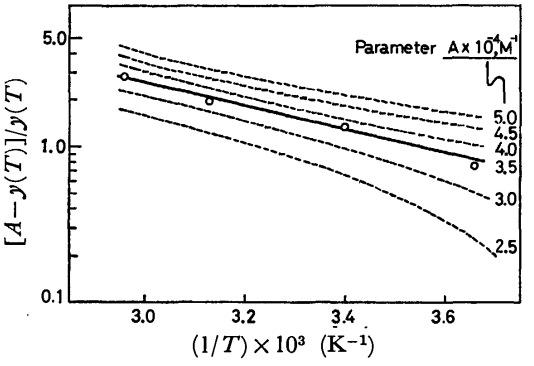

Fig. 8. Plots of $\log[A-y(T)]/y(T)$ *vs.* $1/T$ in isooctane solvent for different values of parameter A.

Table 3. Values of α at various temperatures in isopentane and isooctane

Solvent	α			
Isopentane	0.31 (12 °C)	0.28 (25 °C)	0.25 (40 °C)	0.21 (55 °C)
Isooctane	0.57 (0 °C)	0.43 (21 °C)	0.34 (46 °C)	0.26 (65 °C)

rise will increase the value of k_{-dif}, leaving k_{et} essentially unchanged. This causes a decrease in magnitude of α, since α is expressed as $1/(1+k_{-dif}/k_{et})$. In contrast, as temperature decreases, or the solvent viscosity increases, α becomes larger and tends to approach unity, so that the T-T transfer is reduced to a diffusion-controlled process. These statements are in agreement with the previous observations that T-T energy transfer is diffusion-controlled in solvents of relatively high viscosity,[3] but in less viscous solvents it is not strictly diffusion-controlled.[1,4]

Using the value of τ_0 shown in Table 2, we obtain $k_{dif}=5.1\times10^{10}$ M^{-1} s^{-1} in isopentane and 2.2×10^{10} M^{-1} s^{-1} in isooctane at 25 °C. These values differ from the k_{dif} values derived from the standard Debye equation (1), but agree well with the corresponding values predicted by the modified Debye equation (2). This is consistent with the results obtained by Osborne and Porter for T-T energy transfer in viscous solution.[3]

Estimation of k_{et}. From Smoluchowski's theory of the diffusion-controlled process,[14] the rate constant for the encounter of donor and acceptor molecules is given by[15-17]

$$k_{dif} = \frac{4\pi R_0 DN}{1000} \tag{11}$$

where R_0 is the sum of the radii of the donor and acceptor molecules in the encounter complex, D the sum of their respective diffusion coefficients D_d and D_a, and N is Avogadro's number. In this equation the transient term is neglected, since it is very small under present conditions of phosphorescence measurement.

The value $D=D_d+D_a$ was determined with the aid of the following relations:

$$\begin{aligned} D_d &= TC_d/\eta \\ D_a &= TC_a/\eta \end{aligned} \tag{12}$$

where C_d and C_a each are assumed to be a constant common to hydrocarbon solvents.[17] The C values, found in the literature,[18,19] for benzoic acid in toluene and for 1-bromonaphthalene in benzene were used, respectively, as C_d for acetophenone in isooctane and C_a for DBN in the same solvent.

By inserting the values of D determined in this way and k_{dif} obtained before into Eq. (11), R_0 in isooctane is calculated to be about 9 Å. The mean of the donor and acceptor radii ($R_0/2$) is somewhat greater than the mean of the radii estimated from the molar volumes of the donor and acceptor (3 Å).

On the basis of random-walk theory,[15,16] Wagner and Kochea gave the following relation:[4]

$$\frac{1-\alpha}{\alpha} = \frac{k_{-dif}}{k_{et}} = \frac{\xi}{k_{et}}\cdot k_{dif} \tag{13}$$

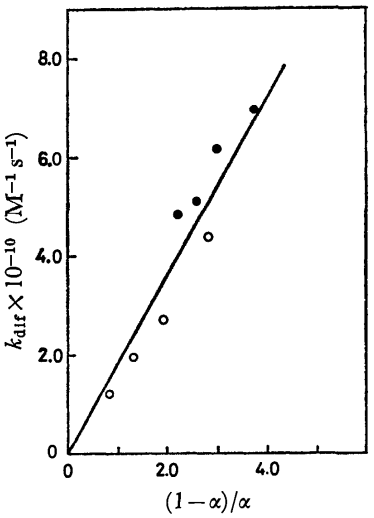

Fig. 9. Plots of k_{dif} *vs.* $(1-\alpha)/\alpha$: ○, in isooctane; ●, in isopentane.

with

$$\xi = \frac{3000}{2\pi NR_0^3} \tag{14}$$

The plot of k_{dif} against $(1-\alpha)/\alpha$ was found to give a straight line (Fig. 9). The value of k_{et}/ξ is determined to be 1.8×10^{10} M^{-1} s^{-1} from the slope of the line. By inserting the R_0 value into Eq. (14) ξ is found to be 1.1 M. We thus immediately obtain $k_{et}=2.0\times10^{10}$ s^{-1}. This k_{et} value, which corresponds to $R_0=9$ Å, is smaller by a factor of 10 than the value obtained in a mixed crystal.[20] This discrepancy may be understood by noting that the rate of T-T energy transfer should vary with the distance between donor and acceptor molecules,[22] and that the distance concerned is greater in the solution than in the mixed crystal.

References

1) T. Takemura, H. Baba, and M. Fujita, This Bulletin, **46**, 2625 (1973).
2) G. Porter and F. Wilkinson, *Proc. Roy. Soc. Ser. A*, **264**, 1 (1961).
3) A. D. Osborne and G. Porter, *ibid.*, **284**, 9 (1965).
4) P. J. Wagner and I. Kochevar, *J. Amer. Chem. Soc.*, **90**, 2232 (1968).
5) H. Labhart and D. Wyrsch, *Chem. Phys. Lett.*, **12**, 373, 378 (1971).
6) A. Yekta and N. J. Turro, *Mol. Photochem.*, **3**, 307 (1972).
7) J. B. Birks, *Chem. Phys. Lett.*, **2**, 417 (1968).
8) J. B. Birks, "Photophysics of Aromatic Molecules," Wiley-Interscience (1970).
9) C. A. Parker, "Photoluminescence of Solutions," Elsevier Publishing Company, Amsterdam (1968).
10) S. C. Tsai and G. W. Robinson, *J. Chem. Phys.*, **49**, 3184 (1968).
11) J. Langelaar, R. P. H. Rettschnick, and G. J. Hoytink, *ibid.*, **54**, 1 (1971).
12) W. D. K. Clark, A. D. Litt, and C. Steel, *J. Amer. Chem. Soc.*, **91**, 5413 (1969).
13) S. K. Lower and M. A. El-Sayed, *Chem. Rev.*, **66**, 199 (1966).
14) M. von Smoluchowski, *Z. Physik. Chem.*, **92**, 129 (1917).

15) A. Weller, *Z. Phys. Chem.*, (Frankfurt), **13**, 335 (1957).
16) R. M. Noyes, *Progr. Reaction Kinetics*, **1**, 131 (1961).
17) W. R. Ware and J. S. Novros, *J. Phys. Chem.*, **70**, 3246 (1966).
18) J. B. Lewis, *J. Appl. Chem.*, **5**, 228 (1955).
19) A. E. Stearn, E. M. Irish, and H. Eyring, *J. Phys. Chem.*, **44**, 981 (1940).
20) H. Baessler, G. Vaubell, and H. Kallman, *J. Chem. Phys.*, **53**, 370 (1970).
21) J. A. Riddick and W. B. Bunger, "Techniques of Chemistry," Vol. II, ed. by A. Weissberger, Wiley-Interscience, New York (1970).
22) D. O. Cowan and A. A. Baum, *J. Amer. Chem. Soc.*, **93**, 1153 (1971).

The Formation and Collapse of Mixed Monolayer of Triolein and Tricaprylin

Masayuki NAKAGAKI and Noriaki FUNASAKI*

Faculty of Pharmaceutical Sciences, Kyoto University, Sakyo-ku, Kyoto 606

(Received May 8, 1974)

The surface pressure-area curves of mixed monolayers of triolein and tricaprylin and the equilibrium spreading pressures of these liquid mixtures were measured at 25 °C. The surface pressures of the monolayers of the pure components, triolein and tricaprylin, did not vary when the monolayer was compressed below its collapse area, but the surface pressure of their mixed monolayers increased with the compression; the surface pressure at a zero area agreed well with the value of the equilibrium spreading pressure. From the two curves, the one representing the relation between the collapse pressure and the composition of the mixed monolayer, and the other representing the relation between the equilibrium spreading pressure and the composition of the liquid mixture, the compositions of the mixed monolayer and the liquid mixture coexisting in the equilibrium were obtained. Consequently, it was found that the component whose collapse pressure was lower was richer in the liquid mixture than in the mixed monolayer, while the other component, whose collapse pressure was higher, was poorer in the liquid mixture than in the mixed monolayer. It was concluded, on the basis of the phase rule and thermodynamics for a plane interface, that triolein and tricaprylin form a regular mixture in the monolayer as well as in a liquid.

Studies of the processes by which a lipid mixture forms a monolayer and a mixed monolayer collapses to deposit a lipid mixture on the water-air interface are important in that the biological membrane contains the lipid mixture as one of its main components. Theoretical and experimental studies have been reported of the collapse pressure of mixed monolayers[1-3] and the equilibrium spreading pressure of mixed crystals.[4]

In a previous paper,[5] the compositions of the monolayer and the solid, which is in equilibrium with the former, have been studied for the binary system of triglyceride and cholesterol, and the miscibility of these components in the monolayer state and the solid state has been discussed on the basis of the two-dimensional phase rule. Moreover, the overcompression of the monolayer has been discussed. The state of the monolayer and the solid in equilibrium could not, however, be explained thoroughly, because these mixtures were solids, so the rate was quite low to arrive at an equilibrium between a monolayer and a solid.

In this paper, the equilibrium spreading pressure and the collapse pressure for the binary system of triolein and tricaprylin were measured, because these substances are liquid at room temperature and are practically insoluble in water.

Experimental

The triolein and tricaprylin were purchased from the Sigma Chemical Company and were stored at −25 °C. The water and chloroform were twice distilled. A mixture of triolein and tricaprylin was produced by evaporating the solvent from a chloroform solution in which the triolein and tricaprylin had been completely mixed. The triolein and tricaprylin were miscible in the liquid state in any proportion examined. When about 20 mg of this liquid mixture was dropped onto a clean aqueous surface with an area of about 60 cm², the surface pressure immediately increased, reaching a constant value after a while. This surface pressure was determined as the equilibrium spreading pressure, F_e, and it was measured at various compositions of mixtures of triolein and tricaprylin. On the other hand, the mixed monolayer of triolein and tricaprylin was spread from their chloroform solution and the pressure-area curve of the mixed monolayer was determined. The surface pressure was measured at 25±0.1 °C using a surface through equipped with a vertical-type surface balance described previously.[6]

Results

Pressure-Area Curve. The surface pressure-area curves of mixed monolayers of triolein and tricaprylin are shown at various mole fractions of tricaprylin, x_c, in Fig. 1. The kink points shown by arrows in this figure indicate that the monolayers begin to collapse at these points. Therefore, the pressures and the areas of these points are the collapse pressure, F_c, and the collapse area, A_c, respectively. At surface pressures lower than the collapse pressure, the pressure-area curves of the monolayers of triolein (shown by open circles in Fig. 1) and tricaprylin (shown by closed circles) were examined to see whether or not they fit the following equation presented by Jura and Harkins:[7]

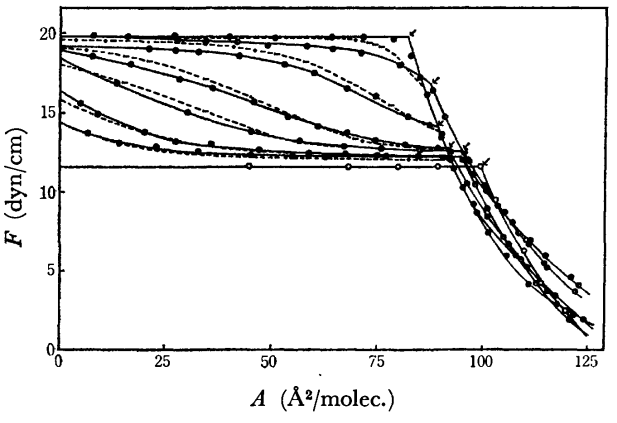

Fig. 1. The pressure-area curves of mixed monolayers of triolein and tricaprylin at various mole fractions of tricaprylin.
x_c, ○: 0, ◓: 0.200, ◑: 0.309, ◑: 0.520, ⊕: 0.668, ⊖: 0.866, ◐: 0.978, ●: 1.
- - - Theoretical curve from Eq. (3).

* Present address: Kyoto College of Pharmacy, 5-Nakauchi-cho, Misasagi Yamashina, Higashiyama-ku, Kyoto 607,

$$F = -\alpha \log A + \beta A + \gamma \quad (1)$$

It has been found that these curves can be represented by Eq. (1), with $\alpha=500$ dyn/cm, $\beta=1.57$ dyn molec./cm Å^2, and $\gamma=856.53$ dyn/cm for the triolein monolayer, and with $\alpha=400$ dyn/cm, $\beta=1.290$ dyn molec./cm Å^2, and $\gamma=679.64$ dyn/cm for the tricaprylin monolayer, respectively. It has, therefore, been concluded that the monolayer of each component is in the state of the liquid expanded film. At the area below their collapse areas (shown by arrows), the surface pressure of monolayers of the pure components, triolein and tricaprylin, are kept constant, but those of their mixed monolayers increase with the decrease in the area.

Equilibrium Spreading Pressure and Collapse Pressure. The equilibrium spreading pressure was determined as the time-independent surface pressure exerted when a excess of a liquid mixture of triolein and tricaprylin was dropped onto the clean aqueous surface. In the case of the mixture of triolein and tricaprylin with the molar ratio of 1 : 2, for example, the surface pressure increased rapidly when a drop of the mixture was placed on the surface, thereafter reaching a constant value, as is shown in Fig. 2. Moreover, when the film in this state was compressed to some extent at the time shown by an arrow, the pressure increased slightly, but it returned immediately to its original value. This is the equilibrium spreading pressure, F_e, at the composition of the liquid mixture. Thus, the relation between the equilibrium spreading pressure and the mole fraction of tricaprylin, x_c^b, in the liquid mixture was obtained; it is shown in Fig. 3 by closed circles. The relation between the collapse pressure, F_c, obtained from Fig. 1 and the mole fraction of tricaprylin, x_c^s, in the mixed monolayer is also shown in Fig. 3 by open circles.

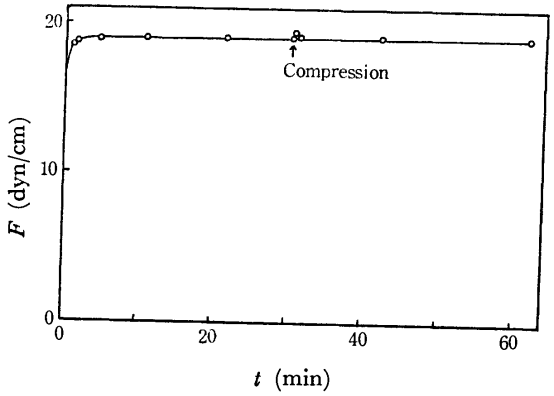

Fig. 2. The change of surface pressure with elapsed time in existence of the liquid mixture of triolein and tricaprylin (1 : 2).

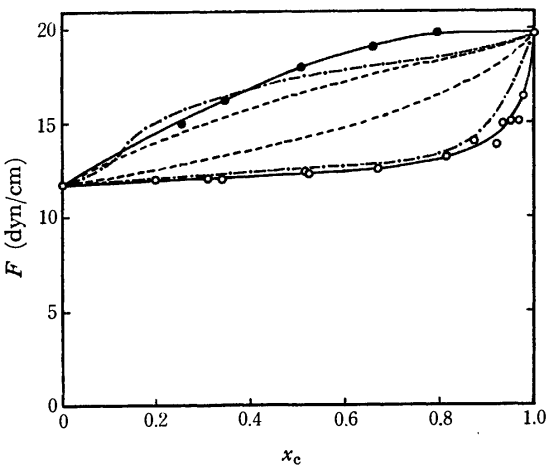

Fig. 3. Equilibrium spreading pressure and collapse pressure for the mixture system of triolein and tricaprylin.
●: $F_e-x_c^b$, ○: $F_c-x_c^s$.
- - - Curve calculated from Eq. (10) and Eq. (11) with $B^b=B^s=0$. -·-·- Curve calculated from Eq. (10) and Eq. (11) with $B^b=0.78$ kcal/mol and $B^s=1.13$ kcal/mol.

For the monolayers of both the pure components, triolein and tricaprylin, the collapse pressure was in good agreement with the equilibrium spreading pressure. For mixtures, however, the equilibrium spreading pressure varied continuously with the composition of the liquid mixtures, while the collapse pressure also varied with the composition of the mixed monolayer. The two curves, $F_e-x_c^b$ and $F_c-x_c^s$, did not agreed with each other, suggesting that the compositions of the liquid droplet and the monolayer are different from each other.

Discussion

Equilibrium Spreading Pressure and Collapse Pressure. Figure 3 shows the relation between the composition of a liquid mixture and that of the mixed monolayer coexisting at a given surface pressure. If a horizontal line is drawn at a given surface pressure in Fig. 3, the intersections of this line with the curve of the equilibrium spreading pressure (drawn through closed circles) and with the curve of the collapse pressure (drawn through open circles) give the mole fractions of tricaprylin in the liquid mixture and the mixed monolayer respectively. Therefore, it is found that tricaprylin, whose equilibrium spreading pressure is higher, is richer in the mixed monolayer than in the liquid mixture, while triolein, whose equilibrium spreading pressure is lower, is richer in the liquid mixture than in the mixed monolayer.

The facts in Fig. 3 show that both the equilibrium spreading pressure and the collapse pressure vary continuously, meaning that these components are miscible both in a liquid and in a monolayer. This can be concluded from the following. According to the phase rule for a plane interface,[8] the number of degrees of freedom for the surface phase, ω, is given by the Eq. (2):

$$\omega = c - \varphi - (\psi - s) + 2 \quad (2)$$

where c is the number of components, φ is the number of the bulk phases, ψ is the number of the interface phases, and s is the number of types of interfaces. When G, W and L designate air, water, and the liquid mixture of triolein and tricaprylin respectively, $c=4$, $\varphi=3$(G,W,L), $s=3$ (G/W, G/L, L/W), and $\psi=3$ (one phase at each interface). Then, ω is equal to the 3 from Eq. (2). As the temperature and pressure are

constant under the experimental conditions used in this study, it may be concluded that one more freedom is left. Therefore, the surface pressure can be varied continuously while the compositions of the liquid mixture and the mixed monolayer are fixed for each value of the surface pressure. This is the case when triolein and tricaprylin are miscible both in a liquid and in a monolayer. On the other hand, when both components are immiscible in either the liquid state or the monolayer state, the equilibrium spreading pressure or the collapse pressure must take a constant value, independent of the composition of the liquid mixture or of the mixed monolayer. This has been described in detail in a previous paper.[5]

The Pressure-Area Curve of the Monolayer in Equilibrium with Liquid Droplets. The interrelation between the pressure-area curve (Fig. 1) and the curves of the equilibrium spreading pressure and collapse pressure (Fig. 3) is illustrated schematically in Fig. 4. The left figure (a) of Fig. 4 corresponds to Fig. 3, while the NKLMP and NHIJP curves represent the equilibrium spreading pressure and the collapse pressure respectively. The right figure (b) of Fig. 4 corresponds to Fig. 1, while the BCDE curve represents the pressure-area curve of the mixed monolayer, whose mole fraction is x_2. In Fig. 4(b), the relation between the collapse pressure, F_c, and the collapse area, A_c, is given by the chained line, which is so drawn that it passes through the kink-points indicated by arrows in Fig. 1.

When the mixed monolayer at the mole fraction of x_2 is compressed along the BC curve, the monoalyer starts collapsing at the C point. At this point, it may be seen from Fig. 4(a) that the mixed monolayer at the mole fraction of x_2 coexists with a trace of the liquid mixture at the mole fraction of x_2^K. If the surface pressure is now increased further, the concentration of the 2 component (more stable against collapse) in the monolayer is increased by separating the liquid mixture further. At a certain point, *e.g.*, D in Fig. 4(b), the mixed monolayer of the composition of x_2^I and the liquid mixture of the composition of x_2^L coexist at the molar ratio of $(x_2-x_2^L)$ to $(x_2^I-x_2)$, as may easily be seen from Fig. 4(a). Finally, at the E point in Fig. 4(b), the liquid mixture of the composition of x_2 coexists with a trace of the mixed monolayer of the composition of x_2^J, as may be seen in Fig. 4(a). Since the area occupied by the liquid mixture is negligible, the mean molecular area at the E point, A^E, is obviously zero and the surface pressure in this state is the equilibrium spreading pressure of the liquid mixture whose composition is x_2.

Now, the CDE curve of Fig. 4(b) can be drawn theoretically as follows by calculating the area, A^D, corresponding to the point, D, at which the mixed monolayer of the surface pressure, F^D, coexists with the liquid mixture. The area actually occupied by one molecule in the monolayer is A^G, but only a fraction, $(x_2-x_2^L)/(x_2^I-x_2^L)$, of the initially-spread molecules remains in the monolayer. Since the area occupied by the liquid deposit can be neglected, the area divided by the total number of initially-spread molecules, A^D, is given by the following Eq. (3):

$$A^D = \frac{x_2-x_2^L}{x_2^I-x_2^L} \times A^G \tag{3}$$

The relation between the values of A^D calculated from Eq. (3) and various surface pressure values is shown by dotted lines in Fig. 1 as a function of the x_2 parameter, which is the mole fraction of the 2 component in the initially-spread monolayer. The calculated curves (dotted lines) are in good agreement with the curves obtained experimentally (solid lines).

Thermodynamic Treatment. The equilibrium between the mixed monolayer and the liquid mixture will be discussed here thermodynamically. Because the chemical potentials of the components, 1 and 2, in the liquid mixture are equal to those in the mixed monolayer in the equilibrium, the following two equations can be written according to Joos[9]:

$$\mu_1^{ob} + kT\ln\gamma_1^b x_1^b = \mu_1^{os} + kT\ln\gamma_1^s x_1^s + F\bar{A}_1 \tag{4}$$

$$\mu_2^{ob} + kT\ln\gamma_2^b x_2^b = \mu_2^{os} + kT\ln\gamma_2^s x_2^s + F\bar{A}_2 \tag{5}$$

where μ^0 is the standard chemical potential, γ is the activity coefficient, x is the mole fraction, and $\bar{A}$ is the partial molecular area. The superscripts, b and s, indicate the liquid mixture and the mixed monolayer respectively, while the subscripts, 1 and 2, indicate the components, 1 and 2 respectively. For one-component systems,

$$\mu_1^{ob} = \mu_1^{os} + F_{1c}A_{1c} \tag{6}$$

is derived for the 1 component from Eq. (4), with $x_1^b = x_1^s = 1$, and $\gamma_1^b = \gamma_1^s = 1$, while

$$\mu_2^{ob} = \mu_2^{os} + F_{2c}A_{2c} \tag{7}$$

is derived for the 2 component from Eq. (5). Assuming that the theory of regular solution applies to both the liquid mixture and the mixed monolayer, the activity coefficients can be replaced by using the following equations, which contain the B^b and B^s constants:

$$kT\ln\gamma_1^b = B^b(x_2^b)^2, \qquad kT\ln\gamma_1^s = B^s(x_2^s)^2 \tag{8}$$

$$kT\ln\gamma_2^b = B^b(x_1^b)^2, \qquad kT\ln\gamma_2^s = B^s(x_1^s)^2 \tag{9}$$

The substitution of these relations into Eqs. (4) and (5) yields:

$$kT\ln x_1^b + B^b(x_2^b)^2 + F_{1c}A_{1c} = kT\ln x_1^s + B^s(x_2^s)^2 + F\bar{A}_1 \tag{10}$$

and:

$$kT\ln x_2^b + B^b(x_1^b)^2 + F_{2c}A_{2c} = kT\ln x_2^s + B^s(x_1^s)^2 + F\bar{A}_2 \tag{11}$$

Therefore, the relation between x^s and x^b can be obtained by solving Eqs. (10) and (11) simultaneously, if the value of the partial molecular area, $\bar{A}$, is known as a function of the surface pressure, F, and if the values of the parameters, B, are assumed properly. If the values of the parameters, B^b and B^s, are assumed properly, the only unknown quantities in Eqs. (10) and (11) are x^s and x^b at a given surface pressure. The values of the partial molecular area, $\bar{A}$, should be obtained by drawing a tangent on the curve representing the relation between the mean area, A, and the mole fraction, x^s, of the monolayer at a given surface pressure. When A

was plotted against x^s on the basis of the data given in Fig. 1, a linear relationship between them was found to hold within the limits of experimental error. It was, therefore, concluded that the partial molecular area, $\bar{A}$, is equal to the molecular area of the pure component. For triolein, whose collapse pressure is relatively low, the following equation, previously presented, was used to obtain the value of the molecular area, by extrapolation, for a surface pressure higher than its collapse pressure:

$$F = -500 \log A + 1.547 A + 856.53. \quad (12)$$

When both B^b and B^s are set equal to zero, the values of x^s and x^b, as calculated from Eqs. (10) and (11), are as shown by dotted lines in Fig. 3. In this case, γ_1^s, γ_1^b, γ_2^s, and γ_2^b are all equal to one, according to Eqs. (8) and (9): their solutions are ideal both in the liquid mixture and in the mixed monolayer. They are considerably different from the experimental values. Next, when x^s and x^b are calculated from Eqs. (10) and (11) with $B^b = 0.78$ kcal/mol and $B^s = 1.13$ kcal/mol, the calculated results are as shown by chained lines in Fig. 3. These chained lines are fairly closed to the experimentally-found values. Therefore, it may be concluded that the mixture of triolein and tricaprylin can be treated like the regular solutions both in the liquid and in the monolayer states.

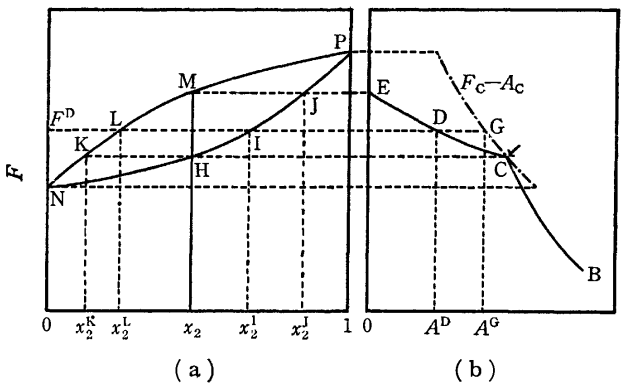

Fig. 4(a). The curve of equilibrium spreading pressure, NKLMP, and the curve of collapse pressure, NHIJP.
(b). Pressure-area curve, BCDE.
—·—·— Collapse pressure-collapse area curve.

References

1) D. J. Crisp, "Surface Chemistry," Supplement to Research, Butterworths, London (1949), p. 23.
2) G. L. Gaines, "Insoluble Monolayers at Liquid-Gas Interfaces," Interscience Publishers (1960), p. 281.
3) M. C. Phillips and P. Joos, *Kolloid-Z. Z. Polym.*, **238**, 499 (1970).
4) P. Joos, *J. Colloid Interface Sci.*, **35**, 215 (1971).
5) M. Nakagaki and N. Funasaki, This Bulletin, **47**, 2094 (1974).
6) M. Nakagaki, N. Funasaki, and M. Nishino, *Nippon Yakugaku Zasshi*, **90**, 1088 (1970).
7) G. Jura and W. D. Harkins, *J. Chem. Phys.*, **12**, 113 (1944).
8) R. Defay, I. Prigogine, A. Bellemans, and D. H. Everett "Surface Tension and Adsorption," Longmance, London (1966), p. 77.
9) P. Joos, *Bull. Soc. Chim. Belges*, **78**, 207 (1969).

Fourier Analysis of AC Polarography. Elimination of Non-Faradaic Effects and Determination of Kinetic Parameters for Cd(II)-Na_2SO_4 System

Michio HIROTA, Yoshio UMEZAWA, Hiroyuki KOJIMA,* and Shizuo FUJIWARA

Department of Chemistry, Faculty of Science, University of Tokyo, Hongo, Tokyo 113

(Received March 7, 1974)

The on-line Fourier analysis of the AC polarographic current was found to give accurate results for electrode kinetics provided that the compensation of the *iR* drop and of the non-faradaic current was attained: The *iR* drop was compensated by a *positive feedback technique*. The charging current was cancelled by addition of a *pseudo-charging current*, inverse in phase to the former. Both the phase angles and amplitudes of the fundamental and second harmonic AC responses for the system of Pb(II) in 1M $NaClO_4$ ($[H^+]=12$ mM) agreed with theoretical prediction. As an illustration, the kinetic parameters of Cd(II)-1 N Na_2SO_4 system have been determined to be $k_s=(0.20\pm0.03)$ cm/s and $\alpha=0.30$ $(0.27<0.30<0.35)$ from the second harmonic AC polarogram.

The on-line Fourier analysis of instantaneuos AC polarographic currents enable us to determine simultaneously the amplitudes and phase angles of the fundamental and second harmonic responses.[1] However, since no instrumental compensation of the *iR* drop and the non-faradaic current(charging current) was made, the values obtained showed significant departure from those predicted theoretically. Thus, it was necessary to improve the instrument in order to eliminate the *iR* drop and the non-faradaic current. The cell resistance decreases the intensity and shifts the phase angle of AC polarographic current, and the large capacitive current reduces the precision of the analog-to-digital(A/D) conversion of small faradaic currents.

In the present study, a simple circuit has been adopted in order to compensate the charging current due to double layer capacity. A *positive feedback technique*[2-4] was employed for compensation of the *iR* drop. The results for typical chemical systems are presented to show the applicability of the apparatus.

Experimental

Apparatus and Procedure. A block diagram of the apparatus is given in Fig. 1. It is similar to the one previously described[1] except for the addition of circuits of compensation for the *iR* drop and the charging current. An oscillator (Model SY-118, NF Circuit Design Block) was used. A frequency counter(Model 5326B, Yokogawa-Hewlett-Packard) was used as a trigger generator. A sinusoidal AC potential with small amplitude was superposed on the DC potential applied to the electrode. A dropping mercury electrode (DME) was used with a reference electrode (saturated calomel electrode(SCE), Yanagimoto Model MRP). The polarographic current was sampled during a single drop life and stored in the computer with an 8 bit A/D converter(JRA-5 of JEOLCO), which was connected to the potentiostat. The Fourier transformation was performed after the DC component of the polarographic current had been largely eliminated by shifting the zero level.

Compensation for Charging Current and iR Drop. The charging current was nearly compensated with the aid of a *pseudo-charging current*, inverse in phase to the charging current. It was supplied from the common signal source (oscillator) through the phase inverter and differential circuit, the output of this circuit thus being inverse in phase to the charging current. It was then added to the polarographic current at the amplifier. The amplitude of the output of the differential circuit was proportional to the frequency of the input AC potentials in the range 20 Hz~3 kHz. In order to stabilize the circuit, a resistance was connected in series with the input of the differential circuit. Figure 2 shows the effect of the compensation for the charging current of the Cd(II)-1 N Na_2SO_4 system. At a potential where the faradaic current was negligible, the amplitude of the pseudo-charging current was adjusted to minimize the observed polarographic current. When the *iR* drop is effectively compensated, the second harmonic response is not influenced by the charging current. The amplitude of the charging current varies with DC potentials at which polarographic currents are measured and with the area of the DME, which makes it difficult to completely eliminate the charging current at all potential regions. It is therefore desirable for measurement of the second harmonic AC current for the charging current to be eliminated in major part, in order to retain accuracy and precision of A/D conversion and digital calculations. For the measurement of the fundamental harmonic response, the present method of charging current compensation only lowers the base line of the capacitive component.

The *iR* drop compensation was fulfilled by the use of the positive feedback circuit reported by Smith and his co-

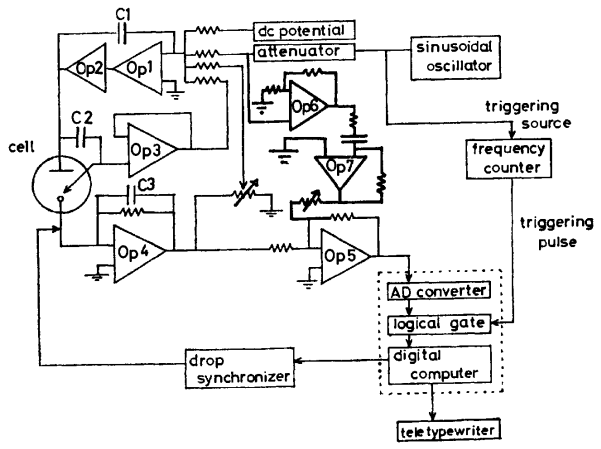

Fig. 1. The block diagram of the apparatus.
Operational amplifiers used are as follows;
Adder; Op1=Teledyne Philbrick(TP) 1029,
Op2=Philbrick/Nexus BQ 100.
Voltage follower; Op3=TP 1009.
Current follower; Op4=TP 1029.
Amplifier; Op5=TP Nexus 1024.
The circuit of the pseudo-charging current;
Op6=TP 1319, Op7=Burr Brown 3112/12C.

* Present address: Department of Chemistry, University of Texas, Austin, Texas, U.S.A.

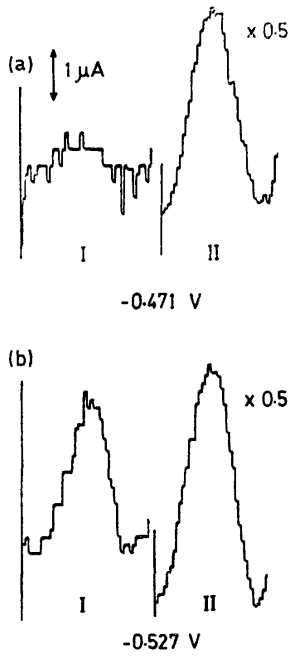

Fig. 2. The effect of the pseudo-charging current.
[Cd(II)]=0.49 mM, [Na_2SO_4]=1.0 N.
(a) charging current
(b) charging current with small faradaic current
I: with the pseudo-charging current
II: without the pseudo-charging current

workers:[2-4] The same amount of voltage as that of the *iR* drop was returned from the current follower to the adder *via* the variable resistance (Fig. 1). The small capacitances (C1, C2, C3=100 pF) were used to stabilize the circuit.

Measurement. The amplitude of the AC potential (ΔE) superposed on the DC potential was 5 mV or 15 mV, the frequency being adjusted to 27.9 or 173.6 Hz. The A/D converter began to sample 16 cycles of the AC polarographic current in 8 bit digital form 3.44 s after the time when the new drop started growing. The sampling method was similar to that reported previously.[5] The Fourier transformation was performed with a Fast Fourier Transform (FFT) program. The flow rate of mercury was 0.67 mg/s at the mercury column height of 40 cm. All the measurements were carried out at (25.0±0.5) °C. A computer simulation was performed using a HITAC 8800/8700 system at the Computer Centre, The University of Tokyo. A FORTRAN program from D. E. Smith was used to calculate the theoretical curves of the fundamental and the second harmonic responses.

All chemicals used were of analytical reagent grade. Water was distilled after deionization.

Results and Discussion

Figure 3 shows the reversible fundamental and second harmonic AC polarograms of Pb(II)–1M $NaClO_4$ ([H^+]=12 mM) system, where the tracings of the original instantaneous AC currents are also demonstrated for the sake of comparison.[6] The frequency and amplitude of the AC potential in this case were 27.9 Hz and 5 mV, respectively. The magnitude of resistance of the feedback for the *iR* drop was determined at the DC potential(arrow, Fig. 3(B)) so that the phase angle of the second harmonic response was made equal to the theoretical value.[7]* The solid lines indicate the reversible theoretical curves for the fundamental and the second harmonic responses which were calculated according to the expanding plane model by the following equations.

$$I(\omega t)=\frac{n^2F^2AC_0^*(\omega D_0)^{1/2}(\Delta E)}{4RT\cosh^2(j/2)}\sin(\omega t+\pi/4) \quad (1)$$

$$I(2\omega t)=\frac{n^3F^3AC_0^*(2\omega D_0)^{1/2}(\Delta E)^2\sinh(j/2)}{(4RT)^2\cosh^3(j/2)}\sin(2\omega t-\pi/4) \quad (2)$$

$$j=\frac{nF}{RT}(E_{DC}-E^r_{1/2}) \quad (3)$$

where $I(\omega t)$ and $I(2\omega t)$ represent the fundamental and the second harmonic AC currents, respectively. The other notations have their usual meanings.[1] D_0 was obtained experimentally from the average diffusion current by means of the Ilkovič equation. The electrode area A was obtained by

$$A=0.85\,m^{2/3}t^{2/3} \quad (4)$$

where m is the flow rate of mercury, t the drop time calculated from

$$t=(\text{waiting time})+\frac{(\text{sampling time})}{2} \quad (5)$$

where the waiting time was the quiescent time from the beginning of the drop growth to the data sampling, the sampling time being the time interval of the data sampling. The waiting time and sampling time were made to be 3.44 s and 0.57 s, respectively, so that 16 cycles of AC polarographic current were stored in the memory during the course of sampling time.

The cathodic peak of the second harmonic AC wave was higher than that of the anodic one, the peak intensity of the fundamental harmonic AC wave being slightly higher than that of the theoretical one (Fig. 3). The results are interpreted to be due to the effect of the spherical diffusion in which the reduced form is soluble in the DME.[8,9]

Departure of phase angles from theoretical values was less than ±1° in the regions (E_p±0.4) V for the fundamental harmonic AC polarogram, where E_p is the peak potential, and (E_p±0.1) V for the second harmonic AC polarogram. The results suggest that the circuit for the *iR* drop compensation works satisfactorily.

The effect of the amplitude of the applied AC potential was also examined. With the increase of amplitude of AC potential up to 15 mV, the half-width of the fundamental and the peak-to-peak separation of the second harmonic AC polarogram exceeded the theoretical values by 10%.

It is thus concluded that the apparatus can be used to obtain accurate values for the kinetic parameters of the electrode reactions.

* Cell resistance in the absence of the feedback circuit can be easily calculated from the measured vector components of the admittance for the electrolyte solution without depolarizer. However, this operation is less accurate than that mentioned above.

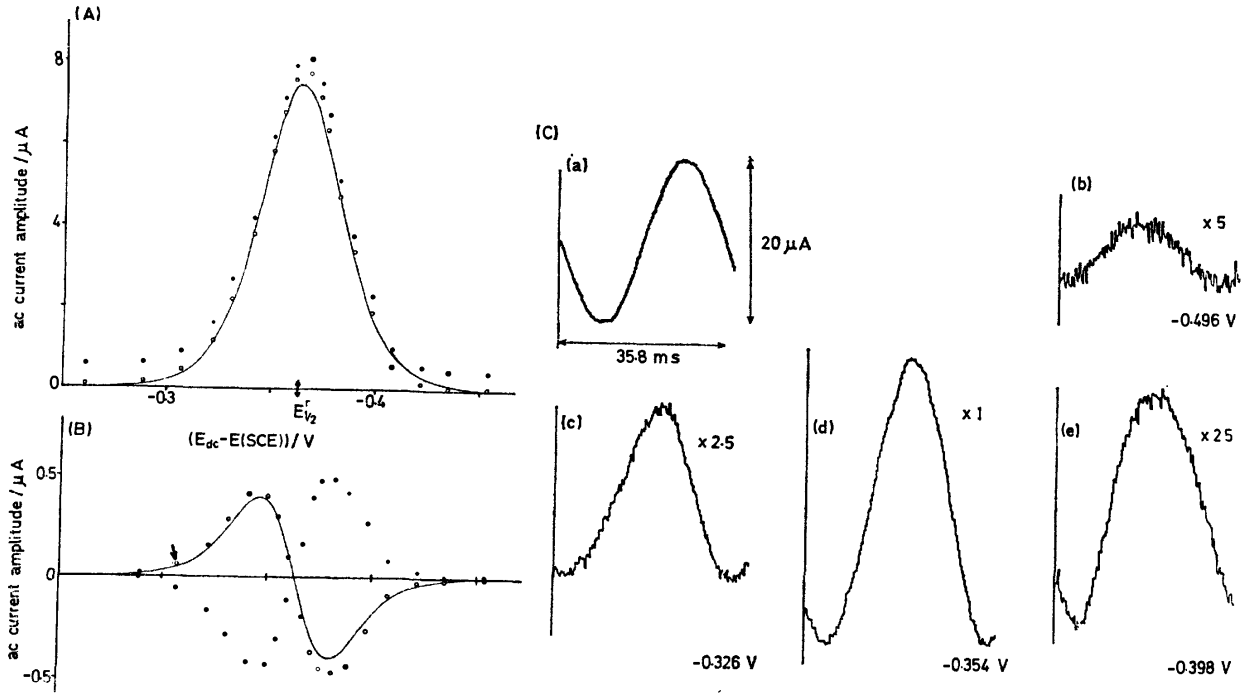

Fig. 3. The AC polarogram of lead(II).
$[Pb(II)]=0.83$ mM, $[NaClO_4]=1.0$ M, $[HClO_4]=12$ mM.
(A) fundamental harmonic AC polarogram. (B) second harmonic AC polarogram.
○ in-phase component ● quadrature component
—— theoretical curves of the in-phase component based on the expanding plane model
$n=2$, $D_0=1.07\times10^{-5}$ cm²/s, $A=0.016$ cm², $\Delta E=5$ mV, frequency=27.9 Hz.
(C) instantaneous AC current.
(a) dummy cell with 1 kΩ resistance. (b) charging current only. (c, d, e) faradaic currents of Pb(II)/Pb(Hg) and charging current.

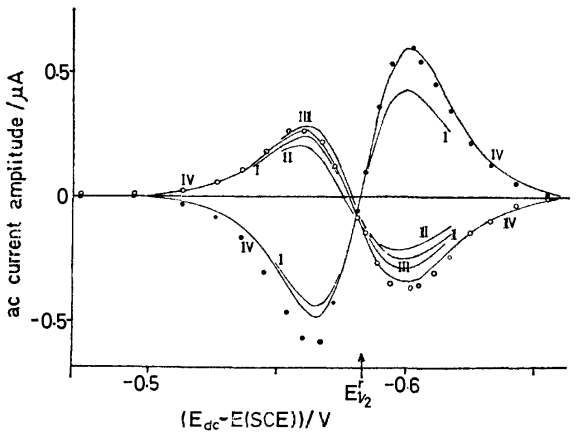

Fig. 4. The second harmonic AC polarogram of cadmium(II).
$[Cd(II)]=0.49$ mM, $[Na_2SO_4]=1.0$ N.
○ in-phase component ● quadrature component
—— theoretical curves based on the expanding plane model
$\alpha=0.30$
I: $k_s=0.20$ cm/s, II: 0.15 cm/s, III: 0.25 cm/s (II, III in-phase component only), IV: corrected for spherical diffusion on the curve I
$n=2$, $D_0=0.84\times10^{-5}$ cm²/s, $D_r=1.6\times10^{-5}$ cm²/s, $A=0.015$ cm², $\Delta E=5$ mV, frequency=173.6 Hz.

Figure 4 shows the second harmonic AC polarogram for the Cd(II)–1 N Na_2SO_4 system. The frequency and amplitude of the AC potential were 173.6 Hz and 5 mV, respectively. The kinetic parameters for this system were found to be (0.20±0.03) cm/s for k_s and 0.30(0.27 <0.30<0.35) for α by computer simulation.[7] The diffusion coefficient of the reduced form was taken from the works of Furman *et al.*[10] The solid lines (I—III) are theoretical curves calculated from the expanding plane model. Curve IV was calculated considering the effect of spherical diffusion at the stationary electrode[11] on curve I. The kinetic parameters for Cd(II)–1 N Na_2SO_4 system are in good agreement with those obtained by the phase-sensitive AC polarographic method.[4,11-13]

We are grateful to Dr. M. Nishiyama and Mr. K. Hayashida of Yanagimoto MFG. Co., Ltd. for their helpful discussions and advice concerning the construction of the apparatus.

References

1) H. Kojima and S. Fujiwara, This Bulletin, **44** 2158 (1971).
2) E. R. Brown, T. G. McCord, D. E. Smith, and D. D. DeFord, *Anal. Chem.*, **38**, 1119 (1966).
3) E. R. Brown, D. E. Smith, and G. L. Booman, *ibid.*, **40**, 1411 (1968).

4) E. R. Brown, H. L. Hung, T. G. McCord, D. E. Smith, and G. L. Booman, *Anal. Chem.*, **40**, 1424 (1968).
5) S. Fujiwara, M. Hirota, K. Sawatari, H. Kojima, and Y. Umezawa, This Bulletin, **47**, 499 (1974).
6) B. Breyer, *Rev. Polarog.*, **9**, 125 (1961).
7) T. G. McCord and D. E. Smith, *Anal. Chem.*, **40**, 289 (1968).
8) J. R. Delmastro and D. E. Smith, *ibid.*, **38**, 169 (1966).
9) T. G. McCord, E. R. Brown, and D. E. Smith, *ibid.*, **38**, 1615 (1966).
10) Average value was taken from (a) N. H. Furman and W. C. Cooper, *J. Amer. Chem. Soc.*, **72**, 5667 (1950) and (b) W. C. Cooper and N. H. Furman, *ibid.*, **74**, 6183 (1952).
11) T. G. McCord and D. E. Smith, *Anal. Chem.*, **41**, 131 (1969).
12) D. E. Glover and D. E. Smith, *ibid.*, **43**, 775 (1971).
13) D. E. Glover and D. E. Smith, *ibid.*, **44**, 1140 (1972).

A Polarographic Study of the Dissociation Reactions of the Ethylenediaminemonoacetatocobalt(II) (Co(II)-EDMA) and Ethylenediaminediacetatonickel(II) (Ni(II)-EDDA) Complexes

Mutsuo KODAMA

Department of Chemistry, College of General Education, Hirosaki University, Bunkyo, Hirosaki, Aomori 036

(Received March 20, 1974)

The rates and the mechanisms of the dissociation reactions of the Co(II)-EDMA complex in a phosphate buffer solution and the Ni(II)-EDDA complex in an ethylenediaminediacetate solution were studied by analyzing their kinetic waves by means of conventional DC polarography. The dissociation of the Co(II)-EDMA complex gave this rate law: $-d[Co(II)\text{-}EDMA]/dt=k_p\cdot[Co(edma)^+]\cdot[H_2PO_4]^-$. On the other hand, the dissociation of the Ni(II)-EDDA complex was found to proceed through a reaction mechanism which involves ligandolysis, corresponding to this rate law: $-d[Ni(edda)^0]/dt=k_0\times[Ni(edda)^0]$. On the basis of the relative rate constant, the detailed reaction mechanism was discussed. In the dissociation of the Co(II)-EDMA complex, the phosphate anion acts just as a proton donor. In the case of the Ni(II)-EDDA complex, the ligandolysis of the coordinated water has a profound effect on the dissociation rate of the $edda^{2-}$ anion from the nickel(II) ion.

Previously,[1] the present author determined the detailed dissociation mechanisms of the aspartate, iminodiacetate, and 2,2′-ethylenedioxydi(ethylamine)-*N*,*N*,*N*′,*N*′-tetraacetate complexes of cobalt(II) by studying the nature of the kinetic waves they gave. The Co(II)-EDMA complex in a phosphate buffer solution and the Ni(II)-EDDA complex in an ethylenediaminediacetate (EDDA) solution also gave kinetic waves due to their dissociations at the electrode surface. In this paper, the present author will study their dissociation reactions by examining the nature of the kinetic waves. The effect of the phosphate anion on the dissociation of the Co(II)-EDMA complex, and that of the ligandolysis of the coordinated water on the dissociation rate of Ni(II)-EDDA complex, will also be discussed.

Experimental

Reagents. The procedure used to prepare the standard nickel(II) and cobalt(II) nitrate solutions was described previously.[2] The preparation and purification of the acid form of EDMA were also given in a previous paper.[3] All the other chemicals used were of analytical reagent-grades and were used without further purification.

Apparatus and Experimental Procedures. All the polarographs used for the measurement of the DC current-voltage curves have been described previously.[2] The characteristic feature of the DME used in this study has also been described previously.[4] All the other apparatus and the experimental procedures employed have also been described previously.[2] The ionic strength of the sample solution was adjusted to 0.30 by adding an appropriate amount of pure sodium perchlorate. For the Co(II)-EDMA system, a phosphate buffer solution was used. In the case of the Ni(II)-EDDA system, no buffer reagent was used, because the sample solutions always contained a large excess of uncomplexed EDDA and had a sufficient buffer capacity ($5.40<pH<7.20$).

Results and Discussion

The Co(II)-EDMA complex in a phosphate buffer solution containing an excess of ethylenediaminemonoacetate (EDMA) gave a single wave which is kinetically-controlled in nature. From the effects of the solution pH and the concentration of the uncomplexed EDMA, $[X]_f$, on the limiting current, i_k, the kinetic wave can be ascribed to the dissociation of the Co(II)-EDMA complex at the electrode surface. As in the case of the aminopolycarboxylate complexes of cobalt(II),[1] the reaction mechanism was investigated with the aid of the relation employed by Koryta in his polarographic study of the dissociation of the nitrilotriacetate complex of cadmium(II).[5] As is shown by the results in Fig. 1, at given concentrations of uncomplexed EDMA, $[X]_f$, and phosphate, $[P]_f$, the plot of $i_k/(i_d-i_k)$ against $[H^+]\cdot(\alpha_H)_X^{1/2}/(\alpha_H)_P^{1/2}\cdot(1+K_2\cdot[X]_f/(\alpha_H)_X)$ invariably gave a linear relation passing through the point of origin. Furthermore, the plot of $i_k/(i_d-i_k)$ against $[H^+]\cdot(\alpha_H)_X^{1/2}/(\alpha_H)_P^{1/2}\cdot(1+K_2\cdot[X]_f/(\alpha_H)_X)\cdot[X]_f^{1/2}$ also gave a straight line passing through the point of origin (Fig. 1). Here, $(\alpha_H)_X$ and $(\alpha_H)_P$

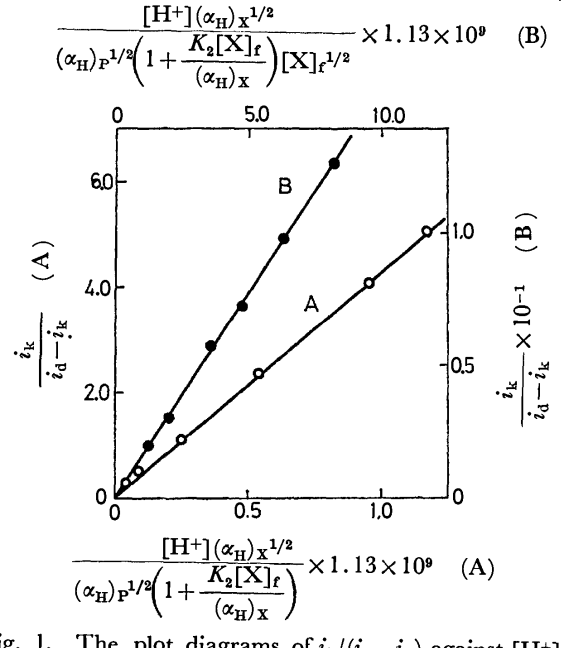

Fig. 1. The plot diagrams of $i_k/(i_d-i_k)$ against $[H^+]\cdot(\alpha_H)_X^{1/2}/(\alpha_H)_P^{1/2}\cdot(1+K_2\cdot[X]_f/(\alpha_H)_X)$ (A) and of that against $[H^+]\cdot(\alpha_H)_X^{1/2}/(\alpha_H)_P^{1/2}\cdot(1+K_2\cdot[X]_f/(\alpha_H)_X)\cdot[X]_f^{1/2}$ (B)
$\mu=0.3$, 25 °C
$[Co(II)]=0.74$ mM, $[P]_f=47.3$ M
(A) $[edma]_f=46.3$ mM
The pH ranged from 7.00 to 8.00.
(B) $[edma]_f$ ranged from 15 to 6.0 mM

Table 1. The phosphate anion effect on the $i_k/(i_d-i_k)$ ratio
$\mu=0.30$, 25 °C, pH=7.38
$[edma]_f=46.3$ mM, $[Co(II)]=0.74$ mM

$[P]_f$, mM	$\frac{i_k}{i_d-i_k}$	$\frac{i_k}{i_d-i_k}\cdot\frac{1}{[P]_f^{1/2}}$
46.3	2.36	11.0
92.6	3.35	10.9
138.9	4.10	11.0

are the (α_H) values of EDMA[6] and phosphoric acid respectively, and K_2, the second successive formation constant of the Co(II)-EDMA complex. When the other experimental conditions are kept constant, the $i_k/(i_d-i_k)$ value divided by $[P]_f^{1/2}$ was almost independent of the concentration of phosphate, $[P]_f$, (Table 1). Taking into consideration the fact that the cobalt(II) ions do not form a stable complex with the phosphate anion under the usual experimental conditions, the above facts suggest that the following reaction mechanism may operate for the kinetic wave of the Co(II)-EDMA system:

$$CoX_2^0 = CoX^+ + X^- \quad \text{in a rapid equilibrium}$$

$$CoX^+ + H_2PO_4^- \overset{k_p}{=} Co^{2+} + HX^0 + HPO_4^{2-} \quad \text{rate-determining step}$$

$$Co^{2+} + Hg + 2e^- = Co(Hg)$$

$$X^- = edma^-$$

corresponding to Relation (1):

$$\frac{i_k}{i_d-i_k}=0.886\cdot\sqrt{\frac{k_p\cdot t\cdot[H^+]^2\cdot(\alpha_H)_X\cdot[P]_f}{K_{CoX}\cdot(\alpha_H)_P\cdot K_2^P\cdot K_3^P\cdot[X]_f}}\,\frac{1}{1+\dfrac{K_2\cdot[X]_f}{(\alpha_H)_X}} \quad (1)$$

where K_{CoX} ($10^{8.30}$) is the formation constant of the 1 : 1-ratio Co(II)-EDMA complex and K_2^P and K_3^P, the second and third dissociation constants of phosphoric acid.[7] The k_p value was determined from the slope of straight line (A) given in Fig. 1; it is listed in Table 2. This value agreed well with that determined from the slope of the straight line (B) in Fig. 1, lending strong support to the above explanation.

Table 2. Dissociation rate constants
$\mu=0.30$, 25 °C

System	Rata constant
Co(II)-EDMA	$k_p=10^{8.33}$ ($M^{-1}s^{-1}$)
Ni(II)-EDDA	$k_o=10^{9.0}$ (s^{-1})

In the case of the Ni(II)-EDDA complex, the plot of $i_k/(i_d-i_k)$ against $(\alpha_H)_X^{1/2}[H^+]^{-1/2}$ (at a given concentration of uncomplexed EDDA, $[X]_f$) or $(\alpha_H)_X^{1/2}/[H^+]^{1/2}\cdot[X]_f^{1/2}$ yielded a straight line passing through the point of origin (Fig. 2). Here, $(\alpha_H)_X$ means the (α_H) value of EDDA. Since the $edda^{2-}$ anion forms only a 1 : 1-ratio complex with the nickel(II) ion, the above finding evidently implies that the reaction mechanism for the kinetic wave of the Ni(II)-EDDA system can be formulated as,

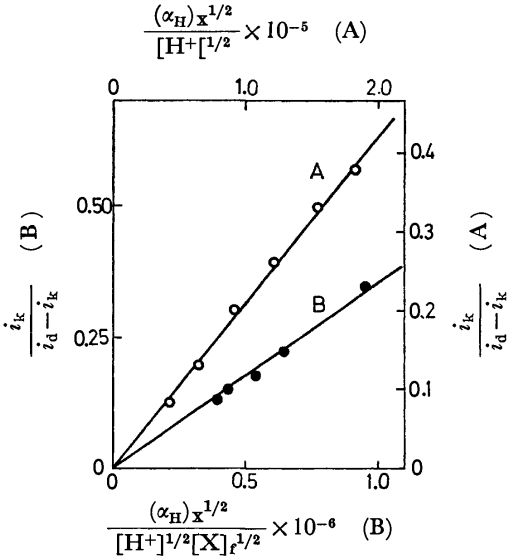

Fig. 2. The plot diagrams of $i_k/(i_d-i_k)$ against $(\alpha_H)_X^{1/2}/[H^+]^{1/2}$ (A) and of that against $(\alpha_H)_X^{1/2}/[H^+]^{1/2}\cdot[X]_f^{1/2}$ (B)
$\mu=0.30$, 25 °C
$[Ni(II)]=1.0$ mM
(A) $[edda]_f=30$ mM
The pH ranged from 5.20 to 6.50.
(B) $[edda]_f$ ranged from 10 to 50 mM.

$$NiX^0 \overset{k_0}{=} Ni(OH)^+ + HX^- \quad \text{rate-determining step}$$

$$Ni(OH)^+ + Hg + 2e^- = Ni(Hg) + OH^-$$

corresponding to Relation (2):

$$\frac{i_k}{i_d-i_k}=0.886\cdot\sqrt{\frac{k_0\cdot t\cdot(\alpha_H)_X\cdot K_{Ni(OH)}\cdot K_W}{K_{NiX}\cdot[H^+]\cdot[X]_f}} \quad (2)$$

where $K_{Ni(OH)}$ and K_{NiX}[7] are, respectively, the formation constants of the 1 : 1-ratio Ni(II)-OH and -EDDA complexes and K_w,[7] the ion product of water. The k_0 values estimated from the slopes of the straight lines, (A) and (B), in Fig. 2 agreed well with each other. This aggrement also supports the reaction mechanism proposed above. The $K_{Ni(OH)}$ value used in the estimation of k_0 was evaluated with the aid of this relation: $\log K_{Ni(OH)}=pK_w-pK^*$.[7]

Previously,[6] the present author reported that the Ni(II)-EDMA complex dissociates through the ethylenediamine-reaction intermediate. Since the cobalt(II) complex shows a kinetic behavior similar to that of the nickel(II) complex, it is not unreasonable to consider that the cobalt(II)-EDMA complex also dissociates through the ethylenediamine-reaction intermediate, by analogy with this. If the cobalt(II)-EDMA complex dissociates through the ethylenediamine-recation intermediate, the dissociation rate constant should be 10.0. This value was calculated by using the relation: $k=k_{rds}\cdot K_{Co\text{-}En}\cdot K_{st}\cdot K_{elec}/K_{CoX}$[6] and the k_{rds} estimated from the dissociation rate constant of a 1 : 1-ratio cobalt(II)-ammine complex[8] by making the correction for the rotational barrier around to C–N or C–C bond.[9] Here, $K_{Co\text{-}En}$ means the formation constant of a 1 : 1-ratio cobalt(II)-ethylenediamine complex. The observed rate constant, k_p, was $10^{7.30}$ times larger than that calculated. Previously,[10] Tanaka *et al.* determined

the rate constants of direct and proton-assisted dissociations of the cobalt(II)-EDTA complex. The rate constant for the proton-assisted dissociation is about $10^{7.0}$ times larger than that for the direct dissociation. Therefore, in view of the fact that the pK_2 value of EDMA is nearly identical with the pK_3 value of EDTA,[7] the fact that the k_0 value is $10^{7.30}$ times larger than the rate constant calculated on the basis of a simple ethylenediamine mechanism means that the $H_2PO_4^-$ anion acts just as a proton donor in the dissociation of the cobalt(II)-EDMA complex. This is also in full accord with the fact that the cobalt(II) ions do not form a stable complex with a phosphate anion.

The formation rate constant, k_f, of the 1 : 1-ratio Ni(II)-EDDA complex from $Ni(OH)^+$ and the $Hedda^-$ anion was estimated to be $10^{3.84}$ by employing the $k_f/k_0=K_{NIX}\cdot K_2/K_w\cdot K_{NI(OH)}$ relation, and the k_0 value of $10^{9.0}$. This value is nearly identical with the characteristic water-exchange rate of the aquo nickel(II) ion.[11] Since the outer-sphere association constant for the $Ni(OH)^+$—$Hedda^-$ system approximated by the Fuoss equation[12] is nearly equal to unity, the above fact means that the formation reaction of the 1 : 1-ratio complex, $Ni(edda)^0$, from $Ni(OH)^+$ and the $Hedda^-$ anion proceeds through a reaction mechanism in which the outer-sphere association between $Ni(OH)^+$ and $Hedda^-$ and the proton transfer from $Hedda^-$ to $Ni(OH)^+$ to give Ni^{2+} proceed verys rapidly; then, the slow dissociation of the coordinated water molecule from the nickel(II) ion is followed by the rapid formation of the Ni(II)-EDDA bond. The k_0 value determined in this study is much larger than the rate constant estimated on the basis of a simple ethylenediamine-reaction intermediate. This suggests that the ligandolysis of the coordinated water plays an important role in determining the dissociation rate of the nickel(II)-EDDA complex. That is to say, the hydroxide anion and the proton formed upon the dissociation of the coordinated water will effectively assist the dissociation of the $edda^{2-}$ anion from the nickel(II).

References

1) M. Kodama, This Bulletin, **46**, 3422 (1973).
2) M. Kodama, H. Nunokawa, and N. Oyama, *ibid.*, **44**, 2387 (1971).
3) Y. Fujii, E. Kyuno, and R. Tsuchiya, *ibid.*, **43**, 786 (1970).
4) M. Kodama, *ibid.*, **47**, 1434 (1974).
5) J. Koryta, *Collection Czecho. Chem. Commun.*, **24**, 3057 (1959).
6) M. Kodama and N. Oyama, This Bulletin, **44**, 2849 (1971).
7) L. G. Sillén and A. E. Martell, "Stability Constants of Metal-Ion Complexes," 2nd ed., The Chemical Society, London (1964).
8) D. B. Rorabacher, *Inorg. Chem.*, **5**, 1891 (1966).
9) D. W. Margerum, D. B. Rorabacher, and J. F. Clarke, Jr., *Inorg. Chem.*, **2**, 667 (1963).
10) a) N. Tanaka, H. Osawa, and M. Kamada, This Bulletin, **36**, 67 (1963). b) N. Tanaka and H. Ogino, *ibid.*, **40**, 867 (1967).
11) M. Eigen, *Ber. Bunsenges. Phys. Chem.*, **67**, 753 (1963).
12) R. M. Fuoss, *J. Amer. Chem. Soc.*, **80**, 5059 (1958).

Glass Formation in Multicomponent Phosphate Systems Containing TiO_2

Akira KISHIOKA, Masanori HABA,* and Michio AMAGASA

Department of Chemistry, Faculty of Science and Technology, Sophia University, Kioicho, Chiyoda-ku, Tokyo 102

(Received March 30, 1974)

Glass formation was investigated in the Na_2O-TiO_2-P_2O_5, K_2O-TiO_2-P_2O_5, BaO-TiO_2-P_2O_5, Na_2O-BaO-P_2O_5, and Na_2O-BaO-TiO_2-P_2O_5 systems. In the Na_2O-TiO_2-P_2O_5 system, glass containing up to 45.5 mol% TiO_2 was found to be formed at the composition of $Na_2O/P_2O_5=1$, whereas in the K_2O-TiO_2-P_2O_5 system the glass formation was observed in a narrow region along the composition of $K_2O/P_2O_5=1$ in a three-component diagram. In the BaO-TiO_2-P_2O_5 system, only the glass containing about 10 mol% TiO_2 as a maximum was obtained. In the Na_2O-BaO-TiO_2-P_2O_5 system, the region of glass formation extended with an increase of Na_2O up to 30 mol%. These results suggested that a certain amount of Na_2O is necessary for the formation of glass containing a large amount of TiO_2 in the presence of BaO. The three-component diagrams of the Na_2O-TiO_2-P_2O_5 and Na_2O-BaO-P_2O_5 systems indicated that the most favorable amount of Na_2O for the glass formation in this four-component system is 27 to 28 mol%.

The region for glass formation in a three-component diagram is determined by the role of cations in the glass structure. The conditions and the region for glass formation in ternary systems of borate, silicate, germanate, and tellurite have been studied in detail by Imaoka *et al.*[1,2] However, there have been few investigations of glass formation in multicomponent phosphate systems of three or more components. From the studies of three-component diagram for glass formation in these multicomponent systems, one may be able to get some information on the role of cations, especially of such intermediate ions as Ti^{4+}, in the glass structure. It may also be worthwhile to determine the most favorable conditions for the glass formation in multicomponent phosphate systems.

In this work, the regions for glass formation in the three-component diagrams were determined for three kinds of phosphate systems containing TiO_2—the Na_2O–TiO_2–P_2O_5, K_2O–TiO_2–P_2O_5, and BaO–TiO_2–P_2O_5 systems. Based on the results of these ternary phosphate systems containing TiO_2 and that of the Na_2O–BaO–P_2O_5 system, the conditions for the formation of the glasses containing maximum amounts of TiO_2 and BaO were investigated for the four-component system of Na_2O–BaO–TiO_2–P_2O_5.

Experimental

Preparation of Glass. The raw materials used were sodium dihydrogenphosphate dihydrate, sodium triphosphate, anhydrous sodium carbonate, potassium dihydrogenphosphate, anhydrous potassium carbonate, barium carbonate, titanium dioxide, and orthophosphoric acid (85%). All the chemicals except sodium triphosphate were of a reagent grade. Commercial reagent-grade sodium triphosphate was purified before use by recrystallization and dehydration. Mixtures of from two to four kinds of the raw materials were placed in platinum evaporating dishes. For the batch of Na_2O/P_2O_5 or $K_2O/P_2O_5=1$ in the Na_2O–P_2O_5 or K_2O–P_2O_5 two-component system, $NaH_2PO_4\cdot 2H_2O$ or KH_2PO_4 was used respectively. All the batches were about 15 g in weight.

Samples were heated in a Siliconit electric furnace BSH-1530 (Siliconit Konetsukogyo Co.) equipped with a platinum platinum-rhodium thermocouple with an automatic thermoelectric regulator. It took about 5 hr to heat them up to 1350 °C, and this temperature was kept for 1 hr. The melt was quenched by pressing with copper plate cooled with water. In the batches containing TiO_2 with more than 50 mol% P_2O_5, except for the composition in which the homogeneous glass was formed, the crystalline material was separated out in the melt. The homogeneity of the glass formed was immediately observed by the naked eye and under a microscope or a polarizing microscope. No phase separation of the melt itself was found in any of the systems.

The phosphate glass usually contains a small amount of water in its structure when prepared by dehydration and condensation.[3,4] In addition, the composition of the glass is varied by the loss of P_2O_5 during the heating, it depends on the conditions of preparation.[3] In the Na_2O-BaO-P_2O_5 system, the amount of the volatillization loss of P_2O_5 was in the range from 3.3 to 14.0 mol%. Taking these facts into account, all the diagrams for the glass formation were expressed in terms of the batch composition.

Examination of Chemical Durability. Glass grains (0.25—1 mm) of about 0.5 g were weighed and each portion was placed in a 100-ml Erlenmeyer flask. Then 25 ml of water, 25 ml of 35% HCl, and 25 ml of 10% NaOH were added separately into each flask, and they were stoppered. After having been shaken at speed of 80 strokes per minute in the thermostat at 25 °C for 1 hr, the weight loss (%) of each sample was determined.

Results and Discussion

The experimental results for the glass-forming region in each system are given in Figs. 1, 3, and 5—11. Figures 7—11 show the glass-forming region in the Na_2O–BaO–TiO_2–P_2O_5 four-component system. In the systems containing TiO_2, the glasses were colored purple or brown due to the titanium ion reduced. The chemical durabilities of the Na_2O–TiO_2–P_2O_5 and K_2O–TiO_2–P_2O_5 glasses are shown in Figs. 2 and 4.

Na_2O–TiO_2–P_2O_5 System (Fig. 1). A slight amount of glass was obtained in the system with more than 50 mol% P_2O_5. However, glass with a large amount of TiO_2 was obtained by decreasing the amount of P_2O_5 to less than 50 mol%. It may be seen in Fig. 1 that the system containing Na_2O and P_2O_5 in the ratio of unity is most favorable for formation of the glass with a high TiO_2 content. This fact may possibly be interpreted by associating the increase in the glass-forming ability of the Ti^{4+} ion with the ring-opening polymerization of sodium trimetaphosphate ($Na_3P_3O_9$).[5] The composition of the glass containing a maximal

* Present address: Meidensha Electric Mfg. Co., Ltd., Osaki, Shinagawa-ku, Tokyo 141

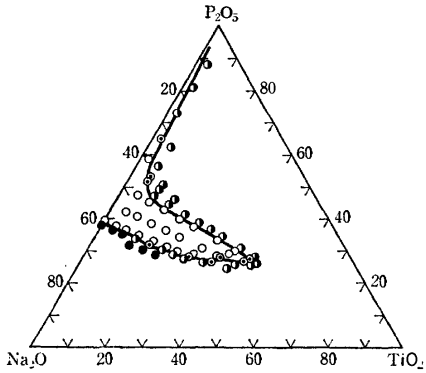

Fig. 1. Glass-forming region in Na_2O-TiO_2-P_2O_5 system
○: homogeneous glass, ⊙: trace amounts of crystal in glass, ◑: glass and crystal, ●: crystal.

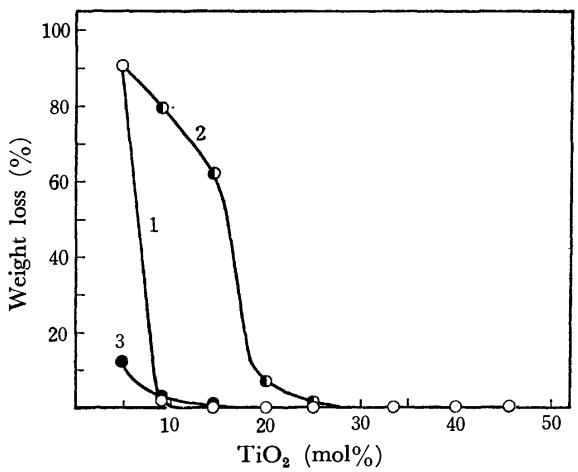

Fig. 2. Chemical durability of Na_2O-TiO_2-P_2O_5 glass ($Na_2O/P_2O_5=1$)
1 : water, 2 : 35% HCl, 3 : 10% NaOH.

quantity of TiO_2 is Na_2O: 27.3, TiO_2: 45.5, and P_2O_5: 27.3 mol%.

Figure 2 shows that the chemical durability of the glass is very much increased by increasing the amount of TiO_2. The glass containing more than 20 mol% TiO_2 is insoluble or only slightly soluble in either water, 35% HCl, or 10% NaOH.

K_2O-TiO_2-P_2O_5 System (Fig. 3). With respect to more than 50 mol% P_2O_5, the region of glass formation of this system is similar to that of the Na_2O-TiO_2-P_2O_5 system. As is shown with arrow marks in Fig. 3, the region of glass formation in the composition along the line of $K_2O/P_2O_5=1$ is narrow. This is a marked difference from the Na_2O-TiO_2-P_2O_5 system, it may be interpreted in terms of the formation of straight-chain molecules of potassium metaphosphate.[6]

Rao[7,8] reported a formation of glass in the K_2O-TiO_2 system. Under the experimental conditions in the present work, however, no homogeneous glass was obtained in the same system.

In the A and B regions in Fig. 3, the maximum concentrations of TiO_2 were about 38 mol% and 35 mol% respectively. The coloration in the glass was observed in only the A region. As is shown in Fig. 4,

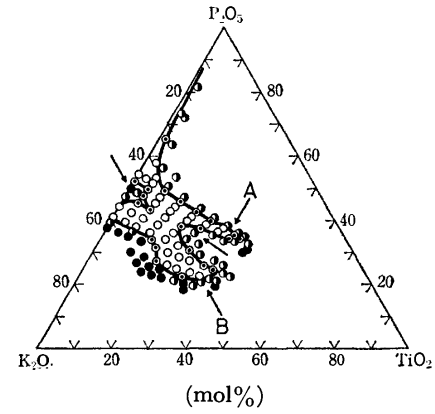

Fig. 3. Glass-forming region in K_2O-TiO_2-P_2O_5 system.
A; Region obtained the glass containing TiO_2 in the largest quantity in $K_2O/P_2O_5<1$
B: Region obtained the glass containing TiO_2 in the largest quantity in $K_2O/P_2O_5>1$

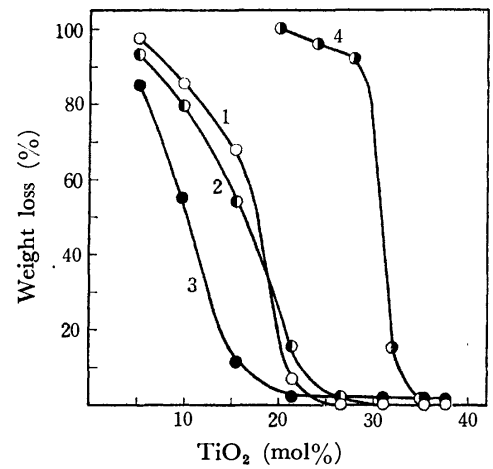

Fig. 4. Chemical durability of K_2O-TiO_2-P_2O_5 glass.
1: $K_2O/P_2O_5=0.83$, water, 2: $K_2O/P_2O_5=0.83$ 35% HCl, 3: $K_2O/P_2O_5=0.83$, 10% NaOH, 4: $K_2O/P_2O_5=1.67$, water.

the increase in the chemical durability of the glass formed in the system of K_2O-TiO_2-P_2O_5 was also observed with an increase in the TiO_2 content, as in the case of the NaO_2-TiO_2-P_2O_5 system

According to RaO,[7] the Ti^{4+} ion is able to act as a network former in silicate glass. The -P-O-Ti- linkage is probably formed in the phosphate glass. It seems that the increase in the chemical durability of the glass containing a large amount of TiO_2 results from the formation of such a linkage.

BaO-TiO_2-P_2O_5 System (Fig. 5). The homogeneous glass was obtained in the BaO-P_2O_5 system containing BaO up to approximately 58 mol%, but only about 10 mol% TiO_2 could be introduced in this glass at a maximum. This is very different from the glass formation in the NaO-TiO_2-P_2O_5 and K_2O-TiO_2-P_2O_5 systems (Figs. 1 and 3).

According to Kordes *et al.*,[9] the BaO-P_2O_5 glass is classified as a "normal glass" among the binary glasses of alkaline earth oxides and P_2O_5, and the Ba^{2+} ion has been regarded as a network modifier. However, the

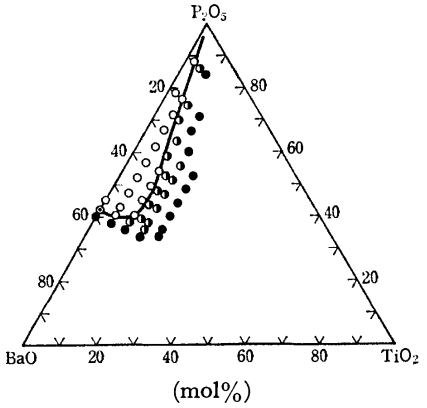

Fig. 5. Glass-forming region in BaO-TiO_2-P_2O_5 system.

electrostatic bond strength of the divalent Ba^{2+} ion, *i.e.*, the ratio of the charge number of the ion to its coordination number, is larger than that of the univalent Na^+ or K^+ ion. Thus it seems that BaO stabilizes the glass structure much more than Na_2O or K_2O in the phosphate glasses. The maximum content of TiO_2 in the Na_2O–TiO_2–P_2O_5 glass was found to be 45.5 mol% at $Na_2O/P_2O_5=1$, but that in the BaO–TiO_2–P_2O_5 glass only about 10 mol% at $BaO/P_2O_5=1$ (Figs. 1 and 5). The Ba^{2+} ion probably interferes with the introduction of the tetravalent Ti^{4+} ion into the glass structure.

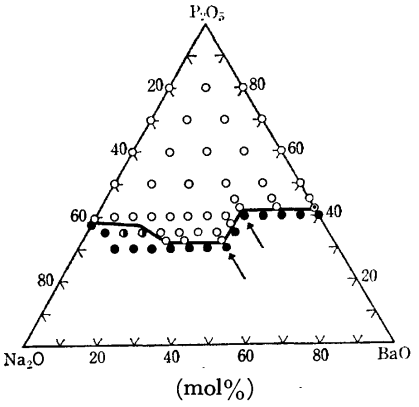

Fig. 6. Glass-forming region in Na_2O-BaO-P_2O_5 system.

Na_2O–BaO–P_2O_5 System (Fig. 6). This system consists of two kinds of network modifiers (Na_2O and BaO) and a network former (P_2O_5).

As is shown in Fig. 6, the glass is obtained over a considerably wide region. The lower limit of the P_2O_5 content in the glass formation is approximately 32 mol%. From the boundary curve in Fig. 6, it is known that the P_2O_5 content is constant in the regions of the Na_2O contents up to 20 mol%, 30—40 mol%, and 50—60 mol%, whereas the BaO content is constant in the region of 20 to 30 mol% Na_2O.

This shape of the boundary curve may possibly be interpreted as follows: the boundary of glass formation may be determined by the difference in the action between Na^+ and Ba^{2+} ions in the glass structure at the glass-forming limit. Thus, the increase in the Na_2O contents from 20 up to 30 mol% along the boundary (arrow marks in Fig. 6) seems to be the result of a break in the –P-O-P- linkage rather than of the substitution of the Ba^{2+} ion by the Na^+ ion. In the glass-forming boundary, the Ti^{4+} ion may be introduced quite easily into this glass when the Na_2O content is 20—30 mol%.

Na_2O–BaO–TiO_2–P_2O_5 System (Figs. 7—11). In order to observe the effect of Na_2O on the glass forma-

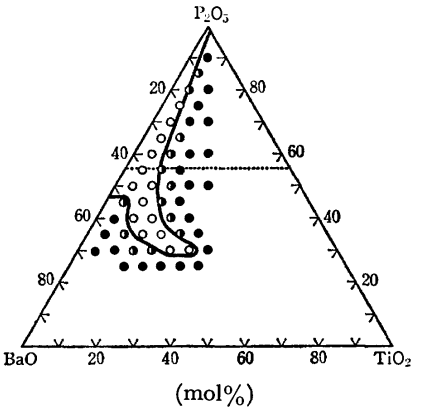

Fig. 7. Glass-forming region in Na_2O-BaO-TiO_2-P_2O_5 system containing 10 mol% Na_2O (dotted line represents P_2O_5 content is 50 mol%).

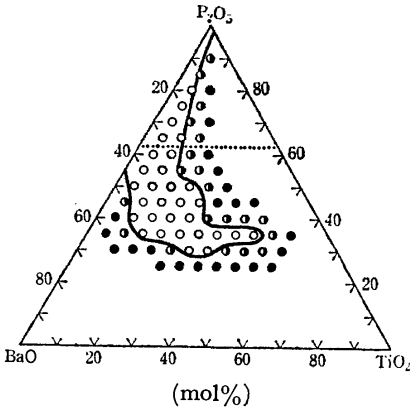

Fig. 8. Glass-forming region in Na_2O-BaO-TiO_2-P_2O_5 system containing 20 mol% Na_2O (dotted line represents P_2O_5 content is 50 mol%).

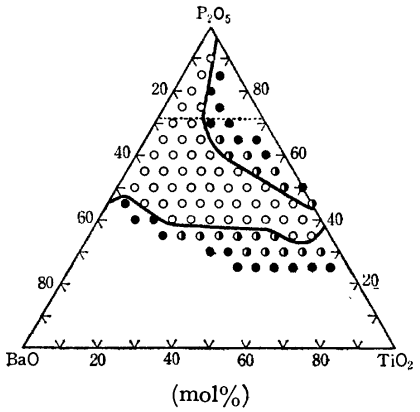

Fig. 9. Glass-forming region in Na_2O-BaO-TiO_2-P_2O_5 system containing 30 mol% Na_2O (dotted line represents P_2O_5 content is 50 mol%).

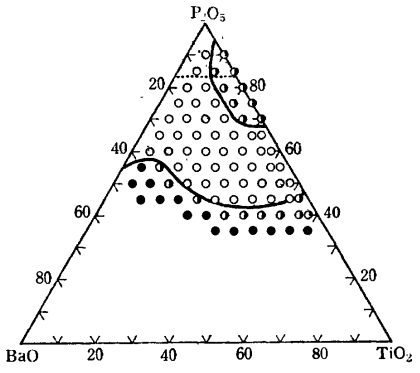

Fig. 10. Glass-forming region in Na_2O-BaO-TiO_2-P_2O_5 system containing 40 mol% Na_2O (dotted line represents P_2O_5 content is 50 mol%).

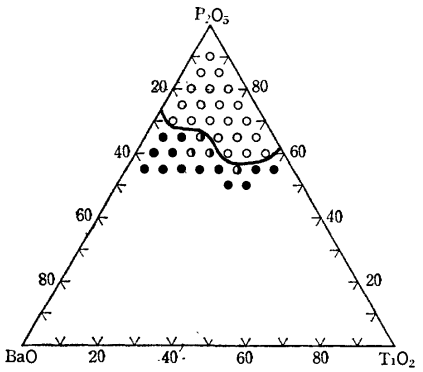

Fig. 11. Glass-forming region in Na_2O-BaO-TiO_2-P_2O_5 system containing 50 mol% Na_2O.

tion in the Na_2O–BaO–TiO_2–P_2O_5 system, the glass-forming region was studied for batches with different Na_2O contents (10, 20, 30, 40 and 50 mol%).

The results are shown in Figs. 7—11. The region in which the glass containing TiO_2 is formed extends up to 30 mol% of Na_2O. The decrease in the P_2O_5 content causes an increase in the TiO_2 content and a decrease in the BaO content in the glass. In addition, the tendency of the glass-forming region to be extended was observed in the system of up to 30 mol% Na_2O along with the compositions of the P_2O_5 contents of 27—28 mol%. The Ti^{4+} ion seems to be introduced easily into the glass structure at this amount of P_2O_5. The P_2O_5 content corresponds to the lower limit of the P_2O_5 contents in the Na_2O–TiO_2–P_2O_5 system (about 27 mol%). The glass-forming region in the Na_2O–BaO–TiO_2–P_2O_5 system (Figs. 7—11) extends to the boundary line in the Na_2O-TiO_2-P_2O_5 system (Fig. 1) when the Na_2O content is 27—28 mol%.

These results suggest that a certain amount of Na_2O is necessary for the formation of the glass containing a large amount of TiO_2 in the presence of BaO. This amount is probably in the range from 27 to 28 mol% Na_2O. Thus, it may be concluded that the Ti^{4+} ion is easily introduced into the glass when both Na_2O and P_2O_5 are 27—28 mol%; $Na_2O/P_2O_5 \approx 1$. These results also support the interpretation of the boundary of glass formation in the Na_2O–BaO–P_2O_5 system (Fig. 6).

The authors wish to thank Professor Hiroshi Fukutomi of the Tokyo Institute of Technology, and Associate Professor Koh Sakamoto of Kanazawa University, for their helpful advice

References

1) M. Imaoka, *Yogyo-Kyokai-Shi*, **67**, 364 (1959).
2) M. Imaoka, H. Kurakata, S. Tai, and H. Nonomiya, *ibid.*, **74**, 52 (1966).
3) H. Namikawa and M. Munakata, *ibid.*, **73**, 86 (1965).
4) A. Naruse, Y. Abe, and H. Inoue, *ibid.*, **76**, 36 (1968).
5) M. Nakagaki, H. Inoue, T. Fujie, and S. Ohashi, This Bulletin, **36**, 595 (1963).
6) J. R. Van Wazer, "Phosphorus and Its Compounds," Vol. 1, Interscience Publishers, New York (1964), p. 675.
7) Bh. V. J. Rao, *Phys. Chem. Glasses*, **4**, 22 (1963).
8) Bh. V. J. Rao, *J. Am. Ceram. Soc.*, **47**, 455 (1964).
9) E. Kordes, W. Vogel, and R. Feterowsky, *Z. Elektrochem.*, **57**, 282 (1953).

Properties and Configuration of Manganese(II), Cobalt(II), Nickel(II), Copper(II) and Zinc(II) Chelates of Acetoacetylferrocene

Hiromu IMAI and Tadamasa ŌTA*

Faculty of Engineering, Kansai University, Senriyama, Suita-shi, Osaka 564

(Received April 2, 1974)

Physical and chemical properties of manganese(II), cobalt(II), nickel(II), copper(II) and zinc(II) chelates of acetoacetylferrocene were investigated. The solubility decreased in the order $CHCl_3 > CH_2Cl_2 > C_6H_5Cl > C_6H_4(CH_3)_2 > C_6H_6$, the chelates being more soluble in pyridine. It was found from magnetic data that the configuration is octahedral for the aquo or pyridine adduct of manganese(II), cobalt(II) and nickel(II) chelates, square planar for anhydride of copper(II) chelate, distorted octahedral for its pyridine adduct, and quasi-tetrahedral for the anhydride of manganese(II) chelate. The d-d transition of electronic spectra was analysed by O_h symmetry for cobalt(II) and nickel(II) chelates, and by C_{2h} symmetry for copper(II) chelate. Assignment of the d-d transition for manganese(II) chelate was difficult.

It is of interest to investigate the behavior and properties of the chelates of acetoacetylferrocene ($C_5H_5FeC_5H_4COCH_2COCH_3$) in which the terminal methyl group in pentane-2,4-dione is replaced by a bulky ferrocenyl group. The bidentate ligand has been reported by several workers,[1-4] some of the first transition metal chelates being synthesized.[1-3] However, the properties and configuration of the chelates do not seem to have been reported. We wish to report on the solubility of the manganese(II), cobalt(II), nickel(II), copper(II) and zinc(II) chelates, and the configuration and assignment of the ligand field band of each chelate in the organic solvent and in the solid state.

Experimental

Synthesis of Ligand. The ligand was synthesized by the procedure described previously.[1]

Preparation of Chelates. Each chelate of manganese(II), cobalt(II), nickel(II), copper(II) and zinc(II) was prepared by the procedure reported previously.[1] The chelate obtained was dissolved in chloroform, and the filtrate was evaporated to a small volume under reduced pressure at room temperature. The chelate precipitated immediately on addition of four-fold petroleum ether to the concentrated solution. After being cooled overnight at about 0 °C, the precipitate was filtered, and washed thoroughly with petroleum ether.

Preparation of Pyridine Adduct. A solution obtained by dissolving 0.5 g of the chelate in 50 ml of pyridine was evaporated to about 10 ml under reduced pressure at room temperature. The pyridine adduct precipitated on addition of 40 ml of petroleum ether was filtered after being cooled overnight at about 0 °C, and washed thoroughly with petroleum ether.

Solubility Measurements. Excess chelate was added to 50 ml of various organic solvents which was warmed to 50 °C, and dissolved thoroughly. The resulting solution was allowed to stand at 25±0.1 °C for 3 hr, and then filtered. A 25 ml portion pipetted from this solution was evaporated completely under reduced pressure at room temperature. The solubility was measured by weighing the precipitated chelate.

Spectral Measurements. Solid reflectance spectra were measured with a Shimadzu QR-50 spectrophotometer with a diffuse reflectance attachment. Absorption spectra in ultraviolet and visible regions were measured with the same instrument. Infrared absorption spectra were measured with a Shimadzu IR-27G spectrophotometer on KBr pellets.

Molecular Weight Measurements. Molecular weights of the chelates were determined with a Shibayama recording cryoscope in bromoform, nitrobenzene, dioxane and dimethyl sulfoxide.

Magnetic Moment Measurements. The magnetic moment of the chelates in the solid state or in the organic solvent was measured by the Gouy method at room tempreature.

Results and Discussion

Solubility. The solubility of chelates reported[1] was determined in various organic solvents of different polarity. The results are given in Table 1.

Solubility decreases in the order $CHCl_3 > CH_2Cl_2 > C_6H_5Cl > C_6H_4(CH_3)_2 > C_6H_6$, which is in line with the decrease of polarity of solvent. All chelates, besides those given in Table 1, are soluble in pyridine, slightly soluble in methanol, ethanol and acetone, and almost insoluble in petroleum ether.

Composition of Chelates. It has been reported that the composition of the chelates (Table 1) is 2 : 1, other chelates except copper chelate being the bisaquo adduct.[1] When such chelates were recrystallized with a mixture of chloroform-petroleum ether, a change in color was recognized in manganese and zinc chelates. The results of elemental analysis and molecular weight determination are given in Table 2.

It was found that the water molecules coordinated to manganese and zinc chelates are dehydrated more easily than the bisaquo adduct of cobalt and nickel chelates.

The molecular weight agreed with the calculated one of the monomeric structure for other chelates except nickel. The molecular weight of the nickel chelate varies with the polarity of solvent, and has been found to be a monomer in bromoform (0.99D) or nitrobenzene (3.99D), and a dimer in dioxane (0.45D).

It is well known that bis(pentane-2,4-dionato)nickel(II) anhydride in the solid state has a trimeric structure, in which nickel(II) ion is octahedrally coordinated.[5] However, when a terminal methyl group in pentane-2,4-dione is replaced by a bulky ferrocenyl group, the steric hindrance among the substituents seems to prevent trimerization. Thus, the bisaquo adduct of the nickel chelate in a solvent such as dioxane

* Present address: Taiho Yakuhin Kogyo Co., Ltd., Kanda-tsukasa-cho, Chiyoda-ku, Tokyo.

Table 1. Solubility of chelates
L : FcCOCHCOCH$_3$, Temp. : 25±0.1 °C

Complexes	Solubility (g/100 ml)				
	$CHCl_3$	CH_2Cl_2	C_6H_5Cl	$C_6H_4(CH_3)_2$	C_6H_6
$MnL_2\cdot 2H_2O$	4.48	3.64	1.14	0.77	0.40
$CoL_2\cdot 2H_2O$	4.53	2.22	1.85	0.77	0.54
$NiL_2\cdot 2H_2O$	3.37	2.22	0.76	0.88	0.68
CuL_2	1.62	1.23	0.53	0.09	0.27
$ZnL_2\cdot 2H_2O$	3.11	1.21	1.20	0.48	0.56

Table 2. Elemental analysis and molecular weight
L : FcCOCHCOCH$_3$

Complexes	Mp (°C)	Elemental analysis C (%) Found	Calcd	H (%) Found	Calcd	Molecular weight Found (1)	Calcd (2)	(1)/(2)	Appearance
MnL_2	271—273	57.04	56.70	4.53	4.42	613[a]	593.2	1.03	Black-brown
						646[b]		1.09	
$CoL_2\cdot 2H_2O$		Previously reported.[1]				634[a]	633.2	1.00	
						628[a]		0.99	
						654[c]		1.03	
$NiL_2\cdot 2H_2O$		ditto				723[a]	633.0	1.14	Red-orange
						605[b]		0.96	
						1140[c]		1.80	
CuL_2		ditto				621[a]	601.8	1.03	Golden brown
						644[b]		1.07	
						609[c]		1.01	
ZnL_2	234—236	55.94	55.72	4.44	4.34	657[a]	603.6	1.08	Red-orange
						627[b]		1.04	
						630[d]		1.04	

The molecular weight was measured in the following solvents; a) bromoform, b) nitrobenzene, c) dioxane, d) dimethyl sulfoxide.

Table 3. Elemental analysis and molecular weight of pyridine adducts
L : FcCOCHCOCH$_3$, py : pyridine

Complexes	Mp (°C)	Elemental analysis C (%) Found	Calcd	H (%) Found	Calcd	N (%) Found	Calcd	Molecular weight Found (1)	Calcd (2)	(1)/(2)	Appearance
$MnL_2\cdot 2py$	267—270	61.06	60.74	4.85	4.84	4.11	3.73	726[a]	751.2	0.97	Brown
$CoL_2\cdot 2py$	186—187	60.21	60.42	4.56	4.81	3.61	3.71	729[a]	755.2	0.97	Yellow-orange
$NiL_2\cdot py\cdot H_2O$	190—192	56.90	57.11	4.71	4.79	1.83	2.02	694[b]	694.0	1.00	Orange
$CuL_2\cdot 2py$	197—199	60.31	60.05	4.55	4.78	3.39	3.69	708[c]	759.8	0.93	Brown
$ZnL_2\cdot 2py$	159—161	60.18	59.91	4.96	4.76	3.40	3.68	758[a]	761.6	1.00	Red-brown

The molecular weight was measured in the following solvents: a) dimethyl sulfoxide, b) nitrobenzene, c) dioxane.

with a low polarity is suggested to be similar in structure to the dimeric octahedral structure of bis(1,5-dialkyl-2,4-pentanediono)nickel(II) monohydrate.[6]

The results of elemental analysis and molecular weight measurement of the pyridine adducts are given in Table 3.

From the composition of the pyridine adducts, they were recognized to be monomeric in the solvents used. Thus, when the chelates (Table 2) were isolated from pyridine solution, the hexa-coordinate chelates of $ML_2\cdot 2py$ type were obtained from the bisaquo adduct of the cobalt chelate by ligand exchange reaction, and from the anhydride of the manganese, copper and zinc chelates by coordination of pyridine molecules. It is of interest that $NiL_2\cdot py\cdot H_2O$ chelate, in which one water molecule was replaced by a pyridine molecule, is obtained from the bisaquo adduct of the nickel chelate.

A black-brown bispyridine adduct of CuL_2 turned gradually golden brown on exposure to the air, while

Table 4. Magnetic moments
L : FcCOCHCOCH$_3$

Complexes	Magnetic moment BM (K) in solid state	Magnetic moment BM (K) in py	Complexes	Magnetic moment in solid state BM (K)
$MnL_2 \cdot 2H_2O$	5.94 (301)	5.52 (304)	$MnL_2 \cdot 2py$	5.64 (296)
MnL_2	4.32 (295)	5.79 (304)		
$CoL_2 \cdot 2H_2O$	4.89 (304)	4.77 (303)	$CoL_2 \cdot 2py$	4.75 (296)
$NiL_2 \cdot 2H_2O$	3.49 (302)	3.50 (302)	$NiL_2 \cdot py \cdot H_2O$	3.64 (296)
CuL_2	1.91 (296)	2.14 (306)	$CuL_2 \cdot 2py$	2.10 (293)

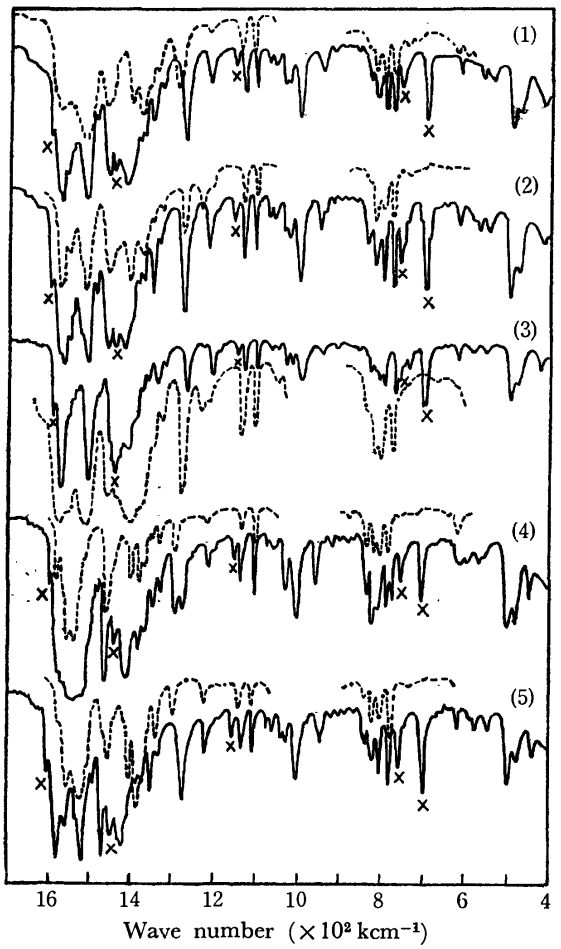

Fig. 1. IR Spectra.
——: (1) $MnL_2 \cdot 2py$, (2) $CoL_2 \cdot 2py$, (3) $NiL_2 \cdot py \cdot H_2O$, (4) $CuL_2 \cdot 2py$, (5) $ZnL_2 \cdot 2py$, ----: (1) MnL_2, (2) $CoL_2 \cdot 2H_2O$, (3) $NiL_2 \cdot 2H_2O$, (4) CuL_2, (5) ZnL_2, L: FcCOCHCOCH$_3$

other pyridine adducts were stable under the same conditions.

The presence of pyridine molecules in such chelates is also confirmed by IR spectra (Fig. 1).

The absorption bands assignable to pyridine are observed in the spectra of the adducts. Thus, the absorption of $\nu_{C=C}$ on the pyridine ring is observed at about 1595 cm^{-1}, but that of $\nu_{C=N}$ could not be confirmed because of the overlapping with the strong absorption band of the chelates $\nu_{C=O}$ appearing at about 1570 cm^{-1}. There is a tendency that the absorption of $\nu_{C=O}$ shifts slightly towards the low wave number side by the coordination of pyridine. The absorption of ring vibration and δ_{CH} of adjacent hydrogen on pyridine were recognized at about 1135, 750 and 695 cm^{-1}. The absorption of ν_{M-O} of the pyridine adduct shifted to the low wave number side in comparison with that of the anhydrous or hydrous chelates as follow; from 426 cm^{-1} to 418 cm^{-1} for $MnL_2 \cdot 2py$, from 419 cm^{-1} to 415 cm^{-1} for $CoL_2 \cdot 2py$, from 422 cm^{-1} to 418 cm^{-1} for $NiL_2 \cdot py \cdot H_2O$, from 450 cm^{-1} to 445 cm^{-1} for $CuL_2 \cdot 2py$ and from 438 cm^{-1} to 422 cm^{-1} for $ZnL_2 \cdot 2py$.

Magnetic Moments. The magnetic moments of each chelate measured in the solid state or in pyridine are given in Table 4.

a) Manganese Chelate: The magnetic moment of 5.94 BM in the solid state of $MnL_2 \cdot 2H_2O$ agreed with 6.02 BM of bis(pentane-2,4-dionato)manganese(II) dihydrate,[7] and also with 5.92 BM of the theoretical spin-only moment which indicates the octahedral structure of a high-spin type. As the moment of 5.52 BM in pyridine is close to 5.64 BM in the solid state of $MnL_2 \cdot 2py$, the bisaquo adduct is thought to change into the pyridine adduct in pyridine solution. The moment of 4.32 BM in the solid state of MnL_2 anhydride showed a slightly higher value than the theoretical value of n=3, being close to 4.55 BM of phthalocyanine manganese(II) chelate which is considered to have a quasi-tetrahedral structure rather than a square planar one.[8] In contrast, the anhydride in pyridine showed a moment of 5.79 BM which corresponds to that of $MnL_2 \cdot 2py$. From the above results, MnL_2 anhydride, which is considered to have a quasi-tetrahedral structure, has been found to change into an octahedral structure by the coordination of two pyridine molecules in pyridine.

b) Cobalt and Nickel Chelates: The magnetic moment of 4.75—4.89 BM in the solid state or in pyridine of $CoL_2 \cdot 2H_2O$, and in the solid state of $CoL_2 \cdot 2py$ is in the range 4.4—5.6 BM of all cobalt(II) complexes which indicates the octahedral structure. $NiL_2 \cdot 2H_2O$ in the solid state or in pyridine, and $NiL_2 \cdot py \cdot H_2O$ in the solid state showed a moment of 3.50 and 3.64 BM, respectively. The bisaquo adduct of the nickel chelate in chloroform also showed a moment of 3.50 BM. The values were slightly higher than 3.2 BM of bis(pentane-2,4-dionato)nickel(II) dihydrate[9] and 3.32 BM of hexaamminenickel(II) chloride[10] which have octahedral structures. Thus, the aquo or pyridine adduct of the cobalt and nickel chelates were found to have the octahedral structure.

c) Copper Chelate: The magnetic moment in the solid state of CuL_2 showed a higher value than the

Table 5. Absorption band and extinction coefficient
L : $FcCOCHCOCH_3$

Complexes	C_6H_6				$CHCl_3$			
	kcm^{-1}	log ε	kcm^{-1}	log ε	kcm^{-1}	log ε	kcm^{-1}	log ε
MnL_2	32.7	4.32	21.4	3.43	32.7	4.27	21.3	3.42
$CoL_2 \cdot 2H_2O$	31.4	4.36	21.6	3.42	32.7	4.14	21.4	3.30
$NiL_2 \cdot 2H_2O$	31.2	4.24	21.8	3.29	32.4	4.14	21.4	3.31
CuL_2	31.0	4.42	21.8	3.40	31.2	4.36	21.4	3.39
ZnL_2	32.8	4.33	21.6	3.34	32.5	4.26	21.3	3.32
$MnL_2 \cdot 2py$	32.6	4.31	21.7	3.48	32.7	4.30	21.6	3.42
$CoL_2 \cdot 2py$	31.5	4.34	21.7	3.34	33.3	4.30	21.8	3.52
$NiL_2 \cdot py \cdot H_2O$	30.2	4.08	22.0	3.13	32.4	4.20	21.8	3.39
$CuL_2 \cdot 2py$	30.9	4.52	21.7	3.42	31.0	4.53	21.4	3.50
$ZnL_2 \cdot 2py$	32.2	4.29	21.5	3.35	32.0	4.18	21.6	3.24

Table 6. Assignment of ligand field bands
L : $FcCOCHCOCH_3$

Complexes	Assignment	Absorption bands and extinction coefficient in $CHCl_3$		Absorption bands and extinction coefficient in py		Reflectance bands: Hydrate or anhydride	Reflectance bands: py adduct	The value obtained from Tanabe-Sugano diagram: aquo adduct	The value obtained from Tanabe-Sugano diagram: py adduct
		kcm^{-1}	ε	kcm^{-1}	ε	kcm^{-1}	kcm^{-1}	kcm^{-1}	kcm^{-1}
$MnL_2 \cdot 2H_2O$		(13.0)	400	(15.5)	300	(15.0)	(15.0)		
MnL_2		9.1	45	(15.0)	250	8.8			
$CoL_2 \cdot 2H_2O$[a]	$^4T_{1g}(P) \leftarrow {}^4T_{1g}(F)$					(19.4)		19.4	
	$^4A_{2g}(F) \leftarrow$	(14.5)	23	(18.2)	36	(14.5)	(18.0)	15.5	18.1
	$^4T_{2g}(F) \leftarrow$	8.7	11	9.8	10	8.8	9.5	8.7($10Dq$)	9.8($10Dq$)
$NiL_2 \cdot 2H_2O$[a]	$^1E_g(D) \leftarrow {}^3A_{2g}(F)$	(15.5)	29	(13.2)	6	(15.4)	(13.0)	15.1	13.1
	$^3T_{1g}(F) \leftarrow$	(14.2)	14	(15.5)	9	(14.2)	(15.3)	14.8	15.6
	$^3T_{2g}(F) \leftarrow$	8.9	9	10.0	9	8.9	10.0	8.9($10Dq$)	10.0($10Dq$)
CuL_2	A_g or $B_{2g}(D) \leftarrow B_{3g}(D)$			15.0	93		15.2		
	B_{2g} or $A_g(D) \leftarrow$	(16.0)	74			(16.3)			
	$A_g(D) \leftarrow$			(10.5)	25	(14.5)	(10.3)		

Values in parentheses are the wave numbers of shoulder absorptions. a) The following values were the most suitable for electron repulsion parameter B: 860 cm^{-1} for aquo adduct and 840 cm^{-1} for pyridine adduct of cobalt chelate; 850 cm^{-1} for aquo adduct and 730 cm^{-1} for pyridine adduct of nickel chelate.

theoretical spin-only moment of 1.73 BM, being in the range 1.9—2.0 BM of all copper(II) complexes which indicates the tetra-coordinate square planar structure. As the value of CuL_2 in pyridine agrees with 2.10 BM in the solid state of $CuL_2 \cdot 2py$, it is suggested that CuL_2 in pyridine changes into the distorted octahedral structure by the coordination of two pyridine molecules to the central copper(II) ion in planar on both side along z axis.

Electronic Spectra. The absorption bands of each chelate in 20—40 kcm^{-1} region are given in Table 5.

Two bands of 31—33 kcm^{-1} and 21—22 kcm^{-1} are due to the chelated carbonyl group and the charge transfer between cyclopentadienyl-iron atom, respectively. The former in benzene shifted slightly to the low wave number side than that in chloroform, and the latter, to the high wave number side. The wave numbers of both bands for the pyridine adduct were practically unchanged as compared with those of the corresponding anhydrous or hydrous chelate.

The absorption spectra in chloroform or pyridine, and the diffuse reflectance spectra of solid state in 8—20 kcm^{-1} region are shown in Fig. 2. Assignment of ligand field bands is given in Table 6.

a) Manganese Chelate: The very weak band at about 9 kcm^{-1} was observed in the spectra of MnL_2 in chloroform and in the solid state. The spectral pattern of the anhydride chelate in pyridine is close to that of bisaquo adduct measured in chloroform or pyridine (not given in Fig. 2(1)). Such spectral change is due to the formation of $MnL_2 \cdot 2py$. Although the structure of the anhydride and bisaquo or bispyridine adduct of this chelate was presumed from the magnetic data, the assignment of ligand field band was difficult.

b) Cobalt and Nickel Chelates: The spectra of the bisaquo adduct of cobalt and nickel chelates are very much similar to each other, and show a shoulder at 13—16 kcm^{-1}. The absorption or reflectance band of about 9 kcm^{-1} observed on spectra of both chelates in chloroform or in the solid state shifts about 10 kcm^{-1} in pyridine. The electronic spectra of both chelates confirmed to have an O_h symmetry from the magnetic data were analysed from the Tanabe-Sugano diagram[11] for d^7 and d^8 configurations with the use of the measured

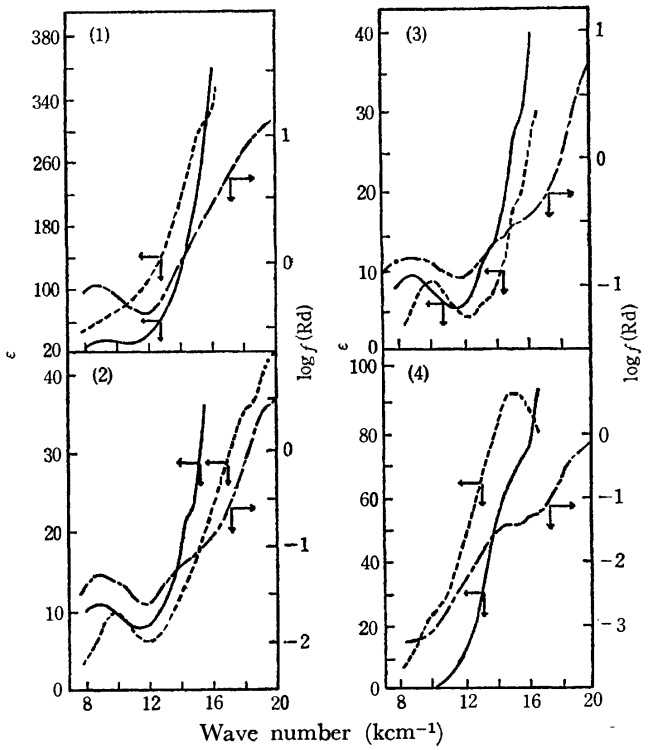

Fig. 2. Electronic spectra of each chelate.
Complexes: (1) MnL_2, (2) $CoL_2 \cdot 2H_2O$, (3) $NiL_2 \cdot 2H_2O$, (4) CuL_2, L: $FcCOCHCOCH_3$, ——: $CHCl_3$, ----: py, ——: Solid state

Table 7. β values

Complexes	B_0[a] cm^{-1}	β $(B/B_0)\%$
$CoL_2 \cdot 2H_2O$	1120	77
$CoL_2 \cdot 2py$	1120	75
$NiL_2 \cdot 2H_2O$	1080	79
$NiL_2 \cdot py \cdot H_2O$	1080	68

a) B. N. Figgis, "Introduction to Ligand Field," Interscience Publishers, New York (1966), p. 52.

crystal field stabilization energy 10 Dq of both chelates and the electron repulsion parameter B (Table 6). The wave number of ligand field bands measured is very close to the values obtained from this diagram, each band can be assigned as shown in Table 6. In order to investigate the partial covalent bonding in the coordination bond of both chelates from the above results, the B parameters were compared with the B_0 parameter of free ion of cobalt(II) and nickel(II).

The degree of covalent bonding $(1-\beta)$ for both chelates is estimated to be 20—30% from the results given inTable 7.

c) Copper Chelate: The absorption bands of CuL_2 in pyridine appeared at 15.0 and 10.5 kcm^{-1}. The sharp band of the former corresponds to the shoulder observed at 13—16 kcm^{-1} in chloroform and in the solid state, and the shoulder of the latter suggests the formation of a pyridine adduct which has a distorted octahedral structure. Although the transition of absorption bands for bis(pentane-2,4-dioato)copper(II) was assigned to D_{4h}[12-14] or D_{2h}[15] symmetry, it is considered that the C_{2h} symmetry used by Allene[16] is better for the chelate with a ligand such as acetoacetylferrocene (Table 6).

d) Zinc Chelate: Since all zinc(II) complexes have a tetrahedral or octahedral structure, ZnL_2 or $ZnL_2 \cdot 2H_2O$ might also have such structures.

References

1) H. Imai and Y. Yaehashi, *Nippon Kagaku Zasshi*, **91**, 452 (1970).
2) V. Weinmayer, *Naturwiss.*, **45**, 311 (1958).
3) C. J. Pederson and V. Weinmayer, U. S. 2875223 (1959).
4) I. I. Grandberg and A. N. Kost, *Zh. Obshch. Khim.*, **32**, 3025 (1962).
5) G. J. Bullen, *Nature*, **177**, 537 (1956), G. J. Bullen, R. Mason, and P. Pauling, *ibid.*, **189**, 291 (1961).
6) I. Yoshida, H. Kobayashi, and K. Ueno, This Bulletin, **45**, 1411 (1972).
7) D. P. Graddon and G. M. Mockler, *Aust. J. Chem.*, **17**, 1119 (1964).
8) L. Klemm and W. Klemm, *J. Prakt. Chem.*, **143**, 82 (1935), H. Senff and W. Klemm, *ibid.*, **154**, 73 (1935).
9) F. A. Cotton and J. P. Fackler, *J. Amer. Chem. Soc.*, **82**, 5005 (1960).
10) A. Earnshaw, "Introduction to Magnetochemistry," Academic Press Inc. (London) Ltd, Translation, H. Inokuchi, N. Ohigashi, and J. Aihara, "Jiki Kagaku Nyumon," Baifukan, (1970), p. 44.
11) Y. Tanabe and S. Sugano, J. *Phys. Soc. Japan*, **9**, 753, 766 (1954).
12) B. L. Belford, M. Calvin, and G. Belford, *J. Chem. Phys.*, **26**, 1165 (1957).
13) C. J. Ballhausen, "Introduction to Ligand Field Theory", McGraw-Hill Book Co. Inc. New York. (1962), p. 268.
14) B. N. Figgis, "Introduction to Ligand Field," Interscience Publishers, New York (1966), p. 316.
15) J. Ferguson, *J. Chem. Phys.*, **34**, 1609 (1961).
16) H. C. Allene, *ibid.*, **45**, 553 (1966).

Solvent Extraction Studies of the Hydrolysis of Antimony(III) in Tracer Concentrations

Hitoshi SHOJI,* Hisao MABUCHI, and Nobufusa SAITO

Department of Chemistry, Faculty of Science, The University of Tokyo, Hongo, Bunkyo-ku, Tokyo 113

(Received June 14, 1974)

The hydrolysis of antimony(III) ions was investigated through solvent extraction with dithizone-carbon tetrachloride solutions. In a 3 M (H, Na)ClO_4 solution, a tracer concentration of antimony(III) ($<10^{-8}$ M) was found in the form of a monovalent cation, $Sb(OH)_2^+$ or SbO^+, and a neutral species, $Sb(OH)_3$ or SbO(OH). The former is predominant in strongly acidic media, while the latter becomes abundant in the weakly acidic-to-neutral region. One of the constants of successive hydrolysis, $K_1=[Sb(OH)_2^+][Sb(OH)_3]^{-1}[H^+]^{-1}$, was calculated from the distribution ratios, giving the result: $\log K_1=1.23_6\pm0.06$. The chemical composition of the extracted species was estimated to be $Sb(HDz)_3$.

Antimony, with its typical amphoteric character, is located on the border between the metal and non-metal regions in the periodic table. Since both antimony(III) and antimony(V) ions easily hydrolyze in an aqueous solution, it is difficult to keep macro amounts of antimony ions stationary in any solution except in highly acidic media. For this reason, relatively little fundamental information is available on the chemical species of antimony in aqueous solutions, especially on their stability constants. In earlier works,[1-12] the solubility measurement was the main tool for studying these problems with some exceptions—for example, spectrophotometry, potentiometry, the measurement of diffusion coefficients, and the chemical analysis of precipitates. Since these techniques necessitated the use of macro amounts of antimony, there was always some ambiguity about the formation of polymerized species whose chemical composition is hard to determine.

We investigated the hydrolysis of antimony(III) through solvent extraction with dithizone, using radioactive tracers. Some reports suggest the reaction of antimony(III) ions with dithizone,[13-15] but no quantitative treatment of this reaction has ever been given. Our preliminary experiment showed that dithizone extracts antimony(III) in the form of dithizonate and that it is very suitable for the present research because of its rather high extractability and good reproducibility.

Experimental

Water. Tap water was deionized with a mono-bed-type ion exchanger and then distilled in an all-glass distilling apparatus.

Perchloric Acid. A G.R.-grade reagent was diluted with distilled water and purified with a dithiozone-carbon tetrachloride solution.

Sodium Perchlorate Solution. The solution was prepared from G.R.-grade sodium carbonate and the purified perchloric acid. After the reagents had been mixed, the resulting solution was purified by filtration, crystallization, and dithizone extraction.

Acetic Acid. G.R.-grade glacial acetic acid was diluted with distilled water. The dilute solution was purified by dithizone extraction.

Ammonia Water. G.R.-grade ammonia water was distilled and absorbed in distilled water.

Carbon Tetrachloride. A G.R.-grade reagent was distilled in an all-glass distilling apparatus, and a fraction with a boiling temperature of 76—78 °C was taken.

Dithizone Solution. The Merck product was purified according to the method by E. B. Sandell.[16] The purity of the dithizone in carbon tetrachloride was checked spectrophotometrically by examining the ratio of the optical density at 620 mμ to that at 450 mμ.[17]

Radioactive Tracers. Two kinds of radioactive antimony(III) tracers were prepared.

a) Sb-125: Carrier-free isotope was purchased from the Oak Ridge National Laboratory, U.S.A. Further purification was carried out to exclude a trace amount of tin, the target element of Sb-125 production, by extraction with isopropyl ether and anion ion-exchange chromatography.[18] The purified Sb(III)-125 was stocked in a carbon tetrachloirde solution of dithizone. The concentration of non-radioactive antimony in this solution was found by neutron-activation analysis to be below 10^{-8} M. This tracer was employed to study the behaviour of the tracer amount of antimony.

b) Mixture of Sb-122 and Sb-124: This mixture was produced through the neutron irradiation of antimony in the JRR-1 reactor at the Japan Atomic Energy Research Institute. The irradiated, highly pure antimony metal was dissolved in *aqua regia*, evaporated to dryness, redissolved in 3 M HCl, and finally purified by dithizone extraction to remove other interfering metal ions. After reduction with SO_2, the trivalent antimony was extracted with a dithizone solution. It was then back-extracted and stocked as a perchloric acid solution.

Measurement of the Distribution Ratio. In the case of a tracer amount of antimony, the stocked organic solution of Sb-125 was added to a carbon tetrachloride solution of dithizone. The organic phase thus prepared was mixed with a solution of (H, Na)ClO_4 and was then shaken at 25±0.5 °C until the partition equilibrium was attained. In the case of macro amounts of antimony, the purified antimony containing the radio-nuclides was initially in various acidities of perchloric acid. A fresh carbon tetrachloride solution of dithizone was added to the aqueous phase and was shaken in a way similar to that in the case of the tracer amount of antimony.

In both cases, after the equilibrium had been attained, an equal volume of each phase was pipetted into a test tube and subjected to the measurement of the γ-activity. Another portion of the aqueous phase was used for the measurement of the hydrogen ion concentration. The distribution ratio, D, is given by the radioactivity of the organic phase divided by that of the aqueous phase.

Measurement of Hydrogen Ion Concentration. As for acidic media (pH<2), the hydrogen ion concentration was deter-

* Present address: Department of Chemistry, Faculty of Science, Tokyo Kyoiku University, Otsuka, Bunkyo-ku, Tokyo 112.

mined by the titration method. In other cases it was determined by potentiometry. The emf measurement was carried out using a pH meter (Radiometer PHM-4 type) with a glass electrode at 25±0.5 °C as soon as possible after shaking. As reference solutions, mixtures of 0.01 M $HClO_4$ and $(x-0.01)$ M $NaClO_4$ were prepared for the x M (H, Na)ClO_4 solution series ($-\log [H^+]=2.00$).

Measurement of Radioactivity. A well-type NaI(Tl) scintillation counter was used. For Sb-125, the sum of γ-rays whose energies are higher than 200 keV was taken in order to eliminate the daughter Te-125m activity. For the mixture of Sb-122 and Sb-124, the total γ-rays were counted.

Results

(1) Time Necessary for the Partition Equilibrium. As is shown in Fig. 1, the partition of antimony(III) between two phases reaches equilibrium within five minutes. This proved to be true under any conditions, independent of the acidity, the concentration of antimony (up to 2×10^{-4} M), the concentration of dithizone, and the phase to which antimony was added initially.

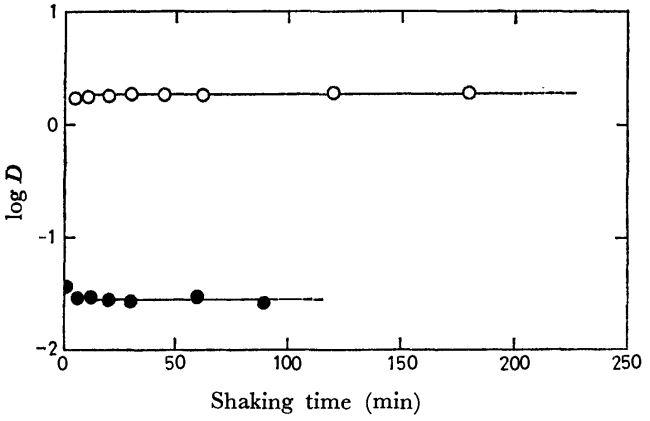

Fig. 1. The effect of shaking time on the distribution ratio in the back-extraction. ●: $[H^+]$ in the aqueous phase of 3.0 M (H, Na)ClO_4=1.5 M, $[H_2Dz]_{org}=2.5\times10^{-4}$ M. ○: $-\log [H^+]$ in the aqueous phase of 3.0 M (H, Na)ClO_4=3.5, $[H_2Dz]_{org}=3.1\times10^{-4}$ M.

(2) Effect of Acetate Buffer Solution. In the weakly acidic region ($-\log [H^+]>2$), an acetate buffer solution was employed for the adjustment of the hydrogen ion concentration in the aqueous phase. In order to study the effect of the acetate buffer on the distribution ratio, we varied the concentration of the acetate buffer from 3.0 to 0.008 M in the region of $-\log [H^+]=4-5$, where the distribution ratio is practically independent of $-\log [H^+]$. The results in the region are shown in Fig. 2. It may be seen that acetate concentrations less than 0.1 M have no effect on the distribution ratio.

(3) Dependence of the Distribution Ratio on the Antimony Concentration. Figure 3 shows the distribution ratios measured as a function of the antimony concentration in the tracer-amount region ($<10^{-8}$ M). No effect of the antimony concentration was observed for either 3.0 M perchloric acid media or a 3.0 M (H, Na)ClO_4 solution of $-\log [H^+]=4.6-4.8$. This

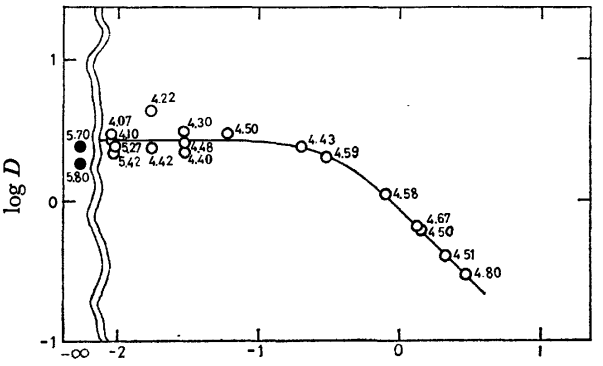

Fig. 2. The dependence of the distribution ratio on the total concentration of acetate buffer added. Each numerical value shows $-\log [H^+]$ in the aqueous phase after the equilibrium. ●: Without any acetate. The concentration of total salts was kept constant (3.0 M) by adding sodium perchlorate. $[H_2Dz]_{org}=3.0\times10^{-4}$ M.

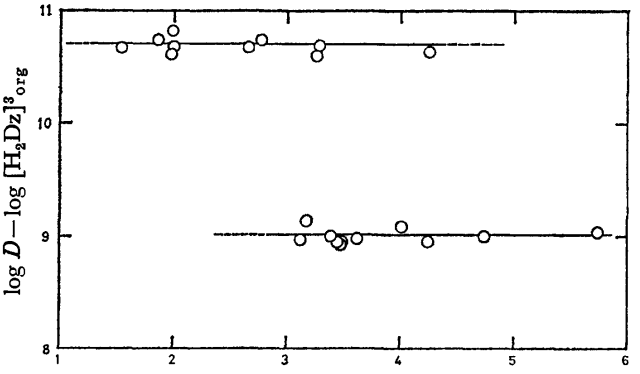

Fig. 3. The dependence of the distribution ratio on the tracer concentration of antimony(III) in the aqueous phase after the equilibrium. Upper group: $-\log [H^+]$ in the aqueous phase of 3.0 M (H, Na)-ClO_4=4.6−4.8. Lower group: Aqueous phase - - - 3.0 M $HClO_4$.

suggests that there is no difference in the polymerization number between the antimony species in the aqueous phase and those in the organic phase. Since it is improbable that any polymerized species are kept stable in both phases over such a wide range of antimony concentrations, we may safely assume that the monomers are the main species involved in the solvent extraction of tracer concentrations of antimony.

In the case of the 2×10^{-4} M antimony solution, the distribution ratio for the 0.5 M perchloric acid medium agreed well with that of the tracer amount of antimony, while a slightly higher value was obtained for the 0.06 M perchloric acid medium.

(4) Dependence of the Distribution Ratio on the Dithizone Concentration in the Organic Phase. The distribution ratio, D, was measured as a function of the dithizone concentration under various conditions. The results are shown in Figs. 4 and 5. From the figures we see that the slope of $\log D$ *versus* $\log [H_2Dz]_{org}$ is 3 in all cases, independent of the acid and antimony concentrations, where "H_2Dz" represents a neutral

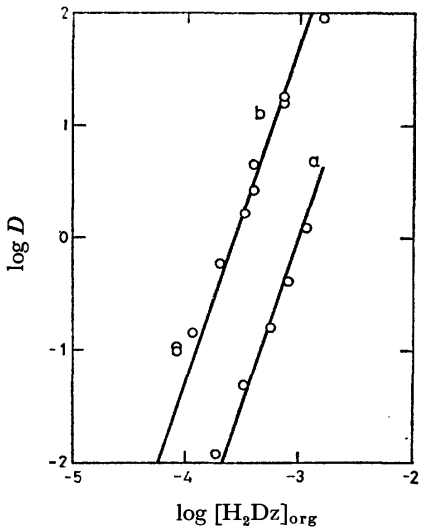

Fig. 4. The dependence of the distribution ratio on the concentration of dithizone in the organic phase. Tracer amount of antimony was used with Sb-125 as the tracer. a: Aqueous phase - - - 3.0 M $HClO_4$. b: $-\log[H^+]$ in the aqueous phase of 3.0 M (H, Na)ClO_4=4.2.

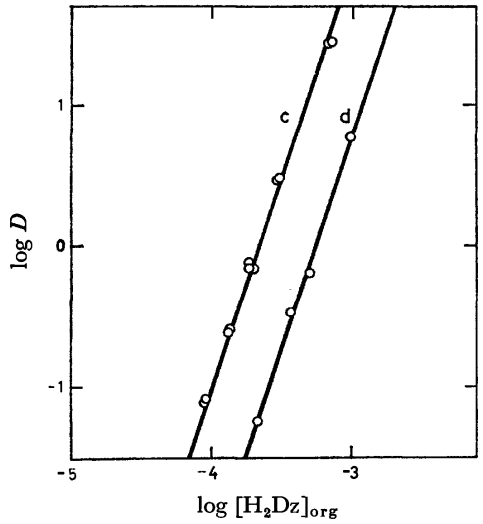

Fig. 5. The dependence of the distribution ratio on the concentration of dithizone in the organic phase. The initial concentration of antimony(III) in the aqueous phase was 2×10^{-4} M. Sb-124 was used as the tracer. c: Aqueous phase - - - 0.06 M $HClO_4$. d: Aqueous phase - - - 0.5 M $HClO_4$.

dithizone molecule.

The distribution ratio, D, is expressed as follows:

$$D=\frac{\sum_m[Sb(OH)_{3-m}(HDz)_m]_{org}}{\sum_p\sum_q[Sb(OH)_p(HDz)_q{}^{3-p-q}]}=\frac{\sum_m\{\bar{K}_m[Sb(OH)_3][H_2Dz]^m{}_{org}\}}{\sum_p\sum_q\{K_{p,q}[Sb(OH)_p{}^{3-p}][H^+]^{-q}[H_2Dz]^q{}_{org}\}},$$

where

$$\bar{K}_m=\frac{[Sb(OH)_{3-m}(HDz)_m]_{org}}{[Sb(OH)_3][H_2Dz]^m{}_{org}}$$

for this reaction:

$$Sb(OH)_3+m\cdot H_2Dz(org)=Sb(OH)_{3-m}(HDz)_m(org)+m\cdot H_2O,$$

and where

$$K_{p,q}=\frac{[Sb(OH)_p(HDz)_q{}^{3-p-q}][H^+]^q}{[Sb(OH)_p{}^{3-p}][H_2Dz]^q{}_{org}}$$

for this reaction:

$$Sb(OH)_p{}^{3-p}+q\cdot H_2Dz(org)=Sb(OH)_p(HDz)_q{}^{3-p-q}+q\cdot H^+.$$

In general, the slope of log D *versus* log $[H_2Dz]_{org}$, or that of $\partial\log D/\partial\log[H_2Dz]_{org}$, indicates the difference in the average number of monovalent dithizonate ions (HDz^-) attached to an antimony atom between the organic phase and the aqueous phase. The extracted species must be electrically neutral. It is generally accepted that the coordination number of antimony(III) is 4 or 6.[19-29] Therefore, we can reasonably assume that it does not exceed 6. Since HDz^- is a bidentate ligand, our results shown in Figs. 4 and 5 lead to the conclusion that only one kind of antimony species, *i.e.*, $Sb(HDz)_3$, exists in the organic phase without any adduct formation, and that the concentration of the Sb(III)-(HDz^-) complex species is negligibly low in the aqueous phase. Thus, D may be simplified as follows;

$$D=\frac{[Sb(HDz)_3]_{org}}{\sum_{n=0}^{6}[Sb(OH)_n{}^{3-n}]}=\frac{\bar{K}_3[Sb(OH)_3][H_2Dz]^3{}_{org}}{\sum_{n=0}^{6}[Sb(OH)_n{}^{3-n}]}$$

where

$$\bar{K}_3=\frac{[Sb(HDz)_3]_{org}}{[Sb(OH)_3][H_2Dz]^3{}_{org}}.$$

(5) Dependence of the Distribution Ratio on the Hydrogen Ion Concentration. In Fig. 6, we plot log $(D/[H_2Dz]^3{}_{org})$ for a tracer amount of antiomny as a function of $-\log[H^+]$. The slope is +1 for $-\log[H^+]<1$ and 0 for $-\log[H^+]=3-6$.

The distribution ratio of the previous section is expressed in terms of hydrolysis constants as follows:

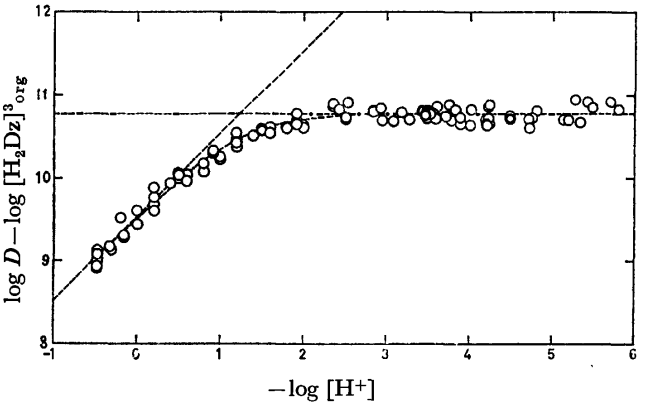

Fig. 6. The dependence of the distribution ratio on the hydrogen ion concentration. Aqueous phase - - - 3.0 M (H, Na)ClO_4. The best fitted theoretical curve based on the refined two constants is shown together with its two asymptotes.

$$D = \frac{\overline{K_3}[H_2Dz]^3_{org}}{\sum_{i=1}^{3}(K_i[H^+]^i)+1+\sum_{j=1}^{3}(K_j'[H^+]^{-j})}$$

where

$$K_i = \frac{[Sb(OH)_{3-i}^{i+}]}{[Sb(OH)_3][H^+]^i}$$

and

$$K_j' = \frac{[Sb(OH)_{3+j}^{j-}][H^+]^j}{[Sb(OH)_3]} .$$

The plot of log $(D/[H_2Dz]^3_{org})$ *versus* $-\log [H^+]$ in Fig. 6 indicates the presence of a neutral species, $Sb(OH)_3$ (or SbO(OH)), in the region of the long plateau and of a monovalent cation, $Sb(OH)_2^+$ (or SbO^+), in the acidic region where the slope is $+1$. Thus, the equation may be written in a simplified form for the present case:

$$\frac{D}{[H_2Dz]^3_{org}} = \frac{\overline{K_3}}{K_1[H^+]+1} ,$$

where

$$K_1 = \frac{[Sb(OH)_2^+]}{[Sb(OH)_3][H^+]} ;$$

(6) Estimation of the $\overline{K_3}$ and K_1 Constants. The approximate values of a set of $\overline{K_3}$ and K_1 constants were obtained by the graphical curve fitting method.[30,31]

We found:

$$\log \overline{K_3} = 10.77$$
$$\log K_1 = 1.25 .$$

These values were refined through computer work using a program based on a modified least-squares method.

The refined values are:

$$\log \overline{K_3} = 10.77_5 \pm 0.03$$
$$\log K_1 = 1.23_6 \pm 0.06 ,$$

where the uncertainties mean 3σ.

(7) Effect of Perchlorate and Chloride Ions. From Fig. 7, we can see that the distribution ratios at 0.1 M (H, Na)ClO_4 do not differ from those at 3.0 M (H, Na)ClO_4 over the range of $-\log [H^+]=1-4$. It can safely be said that perchlorate ions do not form any complex compounds with antimony(III), as is generally believed.

As for chloride ions, very little effect is seen in the region where $-\log [H^+]$ is nearly 4.5 (Fig. 8), while the effect is remarkable in the acidic media, as is shown in Fig. 9. Our preliminary experiment showed that the extraction behavior of the Sb(III)-Cl^-–H_2Dz system is very complicated and needs to be carefully studied. The details of this kind of investigation will be reported in a separate paper.

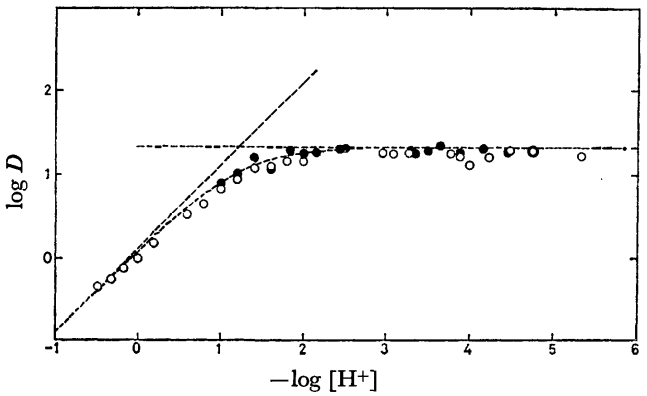

Fig. 7. The influence of the concentration of (H, Na)-ClO_4 media on the distribution ratio. ●: 0.1 M (H, Na)ClO_4. ○: 3.0 M (H, Na)ClO_4. $[H_2Dz]_{org}$ $=7.1\times10^{-4}$ M. The best fitted theoretical curve for all the data involving those other than presented here is shown together with its two asymptotes.

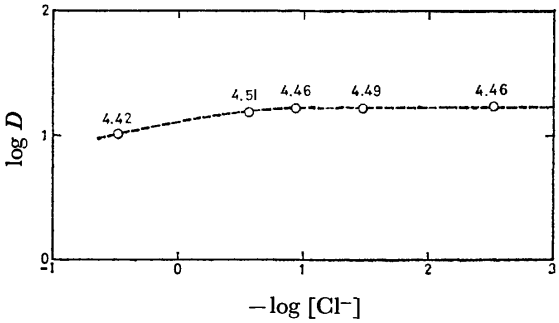

Fig. 8. The dependence of the distribution ratio on the concentration of the chloride ion. $[H_2Dz]_{org}=$ 7.1×10^{-4} M. The numerical data show $-\log [H^+]$ in the aqueous phase of 3.0 M (H, Na)(Cl, ClO_4).

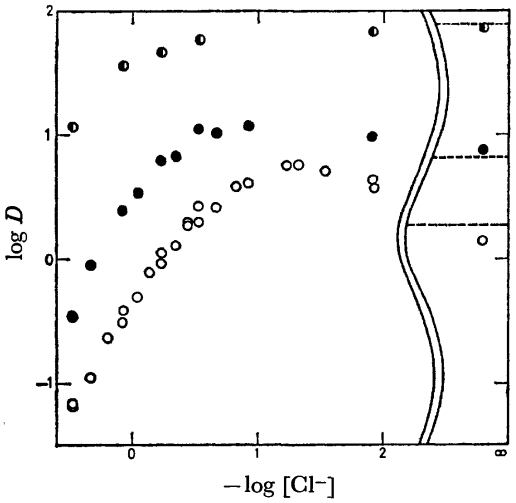

Fig. 9. The dependence of the distribution ratio on the concentration of the chloride ion. $[H_2Dz]_{org}=$ 1.16×10^{-3} M. Aqueous phase - - - 3.0 M (H, Na)(Cl, ClO_4). $[H^+]$: ○ 3.0 M, ● 0.6 M and ◐ 0.012 M. At the right side, the experimental points (as circles) and the calculated values using the refined constants (as broken lines) are also shown on the case without the chloride ion.

Discussion

In acidic and neutral aqueous solutions, a tracer concentration of antimony(III) was found to be present as a monovalent cation and a neutral species of mono-nuclear antimony. The former is predominant in acidic solutions, while the latter is abundant in the

weakly acidic and neutral regions. These results agree with the observations by Schuhmann,[1] Gayer *et al.*,[4] Faucherre,[5] Pitman *et al.*,[6] and Mishra *et al.*,[11] who studied the solubility of macro amounts of antimony(III) oxide, the equilibrium potential of antimony metal–water system, or spectrometry.

The divalent and trivalent cation of antimony(III) could not be detected in the present investigation. The hydrolysis constants given by Kasper from his solubility measurements suggest the existence of the divalent cation in the acidic region.[3] Jander and Hartmann describe the possibility of the coexistence of a small amount of the trivalent cation and the predominant monovalent one in the perchloric acid solution judging from the results of their high-voltage ionophoresis and diffusion studies.[9] Dawson *et al.* have also reported the existence of the trivalent cation together with the monovalent one in perchloric acid media on the basis of a solvent-extraction study using phenylfluorone.[10] Our present results did not confirm these observations.

The value of the hydrolysis constant, K_1, obtained in the present investigation ($\log K_1 = 1.23_6 \pm 0.06$) falls in the range of three published data: 1.59,[4] 1.42,[11] and 0.87.[6] Kasper's value ($\log K_1 = 11.8$) seems to be too large.[3]

No evidence of the existence of polymerized species was found in the aqueous media investigated for the concentrations of antimony(III) below 10^{-8} M. According to Jander and Hartmann, no soluble, polymerized species were observed in the solution from 16 M sodium hydroxide to 11 M perchloric acid for the antimony concentrations of 10^{-6}—10^{-5} M in the acidic, 0.4×10^{-6} M in the neutral, and 10^{-6}—10^{-3} M in the alkaline region.[9] Dawson *et al.* report that the polymerization of antimony(III) ions occurs in 0.4—4 M perchloric acid solutions with antimony concentrations greater than 1×10^{-4} M.[10] For the alkaline solution of antimony(III), Jander and Hartmann report the existence of only one species, very likely a hydrated monomer SbO_2^-, in a sodium hydroxide solution with a 10^{-6}—10^{-3} M antimony concentration (up to 9 M sodium hydroxide),[9] while Scholder and Merbeth describe a polymerized species, $Sb_6O_{10}^{2-}$, in a 2.5—8.3 M sodium hydroxide solution with a 10^{-2}—10^{-1} M antimony concentration, $Sb_4O_7^{2-}$ in a 8.3—16.1 M sodium hydroxide solution with a 10^{-1} M order of antimony, and SbO_2^- in a strongly alkaline solution with a 10^{-1} M order of antimony.[8] Meites and Schlossel report that antimony(III) ions exist in the forms of $Sb(OH)_4^-$ and $Sb_2O(OH)_4$ in a $(1-5)\times10^{-1}$ M sodium hydroxide solution of 2×10^{-5}—1×10^{-2} M antimony.[12]

Using the data of the present work and the literature,[32-40] we can compare the monomeric chemical species in aqueous media in the absence of special complexing anions among the ions with the oxidation number of +3 of nitrogen-group elements. The comparison is shown in Fig. 10. A similar comparison is made, in Fig. 11, between antimony(III) and antimony(V), using the constants from this work and the literature.[6,41] From these figures we see a regularity on hydrolysis as a function of the charge density.

It may be noted that the distribution ratio for the Sb(III)–H_2Dz system is independent of the total ion

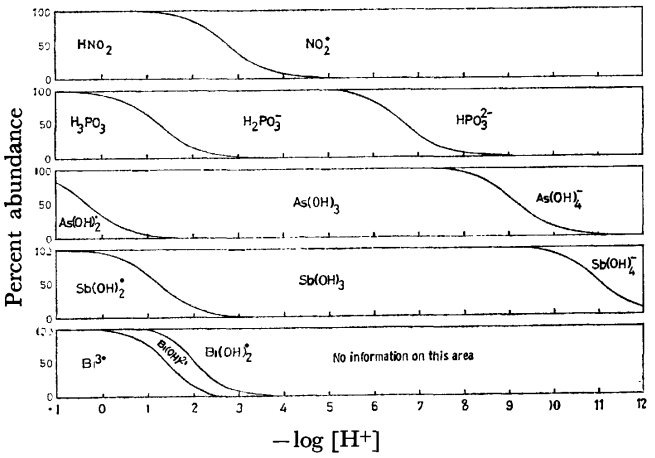

Fig. 10. Variation of the monomeric chemical species of the trivalent ion of the nitrogen group with the change of $-\log[H^+]$ value in the aqueous solution without any special complexing ligands.

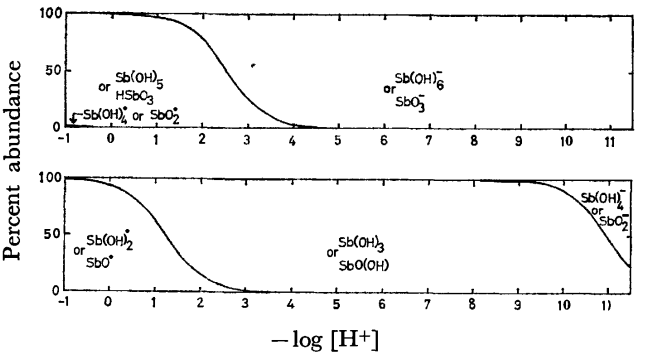

Fig. 11. The chemical species of the antimony(V) and antimony(III) ion in the aqueous solution without any special complexing ligands. Upper: Antimony(V). Lower: Antimony(III).

concentration, as is shown in Fig. 7. Sekine reports the presence of some effect in the case of the Zn-Amberlite LA-1 system.[42] Our results indicate that the number of hydrating water molecules is the same in both phases, or that the change in the water concentration is compensated for by the change in the activity coefficients of the chemical species involved.

In conclusion, it was found that antimony is one of the so-called dithizone metals[43] whose dithizonate has a stoichiometric composition of $Sb(HDz)_3$. The formation constant and one of the hydrolysis constants were obtained.

The authors are very grateful to Professor Tatsuya Sekine of the Science University of Tokyo for his valuable suggestions, especially with regard to the potentiometric measurements. The authors are also thankful to Professor Nagao Ikeda of Tokyo Kyoiku University for his kind support of this work. The authors wish to express their thanks to Professor Yukiyoshi Sasaki for his helpful suggestions, to Dr. Isao Okada for his valuable discussions, and to Dr. Shizu Tonomura and her colleagues in the Institute of Physical and Chemical Research for the absorptiometric measurements.

Calculations were carried out on the HITAC 5020

computer at the Computation Center of the University of Tokyo.

References

1) R. Schuhmann, *J. Amer. Chem. Soc.*, **46**, 52 (1924).
2) V. Bayerle, *Rec. Trav. Chim. Pays-Bas*, **44**, 514 (1925).
3) J. Kasper, Thesis, 1941, Johns Hopkins Univ., Baltimore, Md.
4) K. H. Gayer and A. B. Garrett, *J. Amer. Chem. Soc.*, **74**, 2353 (1952).
5) J. Faucherre, *Bull. Soc. Chim. Fr.*, **1954**, 253.
6) A. L. Pitman, M. Pourbaix, and N. de Zoubov, *Cebelcor Rapp. Tech.*, **1957**, No. 55.
7) P. N. Kovalenko, *Zh. Prikl. Khim.*, **31**, 1488 (1958).
8) R. Scholder and H. Merbeth, *J. Prakt. Chem.*, **5**, 260 (1958).
9) G. Jander and H. -J. Hartmann, *Z. Anorg. Allgem. Chem.*, **339**, 239, 248 and 256 (1965).
10) J. L. Dawson, J. Wilkinson, and M. I. Gillibrand, *J. Inorg. Nucl. Chem.*, **32**, 501 (1970).
11) S. K. Mishra and Y. K. Gupta, *Indian J. Chem.*, **6**, 757 (1968).
12) L. Meites and R. H. Schlossel, *J. Phys. Chem.*, **67**, 2397 (1963).
13) F. H. Burstall, G. R. Davies, R. P. Linstead, and R. A. Wells, *J. Chem. Soc.*, **1950**, 516.
14) J. K. Carlton and W. C. Bradbury, *Anal. Chem.*, **26**, 1226 (1954).
15) H. Pfeifer and H. Diller, *Z. Anal. Chem.*, **149**, 264 (1956).
16) E. B. Sandell, "Colorimetric Determination of Traces of Metals," second edition, Interscience Publishers Inc., New York (1950).
17) S. S. Cooper and M. L. Sullivan, *Anal. Chem.*, **23**, 613 (1951).
18) Y. Sasaki, This Bulletin, **28**, 615 (1955).
19) A. Berton, *C. R. Acad. Sci. Paris*, **207**, 625 (1938).
20) Y. Volmar and G. Goettelmann, *ibid.*, **215**, 417 (1942); **220**, 282 (1945).
21) S. Stahl, *Ark. Kem. Min. Geol.*, **17B**, No. 5, 1 (1943); *Chem. Zentr.*, **1944 I**, 342.
22) A. Byström and A. Westgren, *Ark. Kem. Min. Geol.*, **17B**, No. 2, 1 (1943); *Chem. Zentr.*, **1944 I**, 342.
23) A. Byström and K. A. Wilhelmi, *Nature*, **167**, 780 (1951).
24) N. Elliott, *J. Chem. Phys.*, **2**, 298 (1934).
25) R. W. Asmussen, *Z. Elektrochem.*, **45**, 698 (1939).
26) K. A. Jensen, *Z. Anorg. Allgem. Chem.*, **232**, 193 (1937); **252**, 317 (1944).
27) H. Yamatera, presented at the 6th annual meeting of the Chemical Society of Japan (1953).
28) J. Whitney and N. Davidson, *J. Amer. Chem. Soc.*, **69**, 2076 (1947); **71**, 3809 (1949).
29) N. Davidson, *ibid.*, **73**, 2361 (1951).
30) L. G. Sillén, *Acta Chem. Scand.*, **10**, 186 (1956).
31) F. J. C. Rossotti and H. Rossotti, "The Determination of Stability Constants," McGraw-Hill, New York (1961).
32) E. G. Vassian and W. H. Eberhardt, *J. Phys. Chem.*, **62**, 84 (1958).
33) I. M. Kolthoff, *Rec. Trav. Chim. Pays-Bas*, **46**, 350 (1927).
34) T. D. Farr, *TVA Chem. Eng. Rept.*, No. 8, p. 27 (1950).
35) E. M. Washburn and E. K. Strachan, *J. Amer. Chem. Soc.*, **35**, 681 (1913).
36) M. Randall, "International Critical Tables", Vol. VII, p. 242 (1930).
37) P. J. Antikainen and K. Tevanen, *Suomen. Kem.*, **34** B, 3 (1961).
38) F. Granér, Å. Olin and L. G. Sillén, *Acta Chem. Scand.*, **10**, 476 (1956).
39) Å. Olin, *ibid.*, **11**, 1445 (1957).
40) G. W. Goward, Thesis, Princeton, 1954, Univ. Mikrofilms 9414.
41) J. Lefevbre and H. Maria, *C. R. Acad. Sci. Paris*, **256**, 3121 (1963).
42) T. Sekine, *Acta Chem. Scand.*, **19**, 1526 (1965).
43) G. Iwantscheff, "Das Dithizon und seine Anwendung in der Mikro- und Spurenanalyse," Verlag Chemie, Weinheim (1958).

Intramolecular Hydrogen Bonding and Conformations of α,α-Dialkyl- and α-Alkyl-o-methoxybenzyl Alcohols

Akihiko YAMASHITA, Katsuo HARA, Shigeko AIZAWA, and Minoru HIROTA*

Department of Applied Chemistry, Faculty of Engineering, Yokohama National University, Minami-ku, Yokohama 233

(Received January 18, 1974)

The stable conformations of α-alkyl- and α,α-dialkyl-o-methoxybenzyl alcohols were deduced by measurement of their infrared and PMR spectra. Population of these conformations was estimated from the intensities of the O-H stretching bands of the free and the hydrogen-bonded species. The O-H chemical shifts at infinite dilution (δ^{∞}_{OH}) of the free and the hydrogen-bonded species were determined by plotting the δ^{∞}_{OH} values against population obtained from the infrared spectra. An anomalous behavior was observed with the α-alkyl-α-*t*-butyl alcohols, which might be due to a buttressing effect.

α,α-Di-*t*-butylbenzyl alcohol consists of a highly overcrowded molecule in which the rotation of the di-*t*-butylhydroxymethyl group around the $C_{sp^3}-C_{sp^2}$ bond is so slow as to make it possible to observe the hydrogen atoms of the 2 and 6 positions of the aromatic nucleus separately by PMR measurement.[1,2] This suggests that conformer I or a similar one predominates over conformer II.

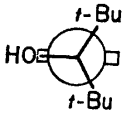

(I)

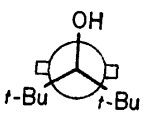

(II)

In relation to studies on the accelerating effect of the methoxy group upon the Grignard reaction between *o*-methoxyphenylmagnesium bromide and crowded ketones,[3] the conformations of the α,α-dialkyl-*o*-methoxybenzyl alcohols obtained were investigated by means of infrared and PMR spectroscopic measurements.

The two bulky *t*-butyl groups are expected to force the hydroxyl group nearer to the oxygen atom of the methoxy group than those of the unhindered dialkyl- and monoalkyl-benzyl alcohols in conformation I, causing a larger hydrogen bond shift of the O–H stretching absorption and a low field shift of the O-H proton signal.

Experimental

Preparation of Materials. All the α,α-dialkyl- and α-monoalkyl-benzyl alcohols were prepared by the addition of *o*-methoxyphenylmagnesium bromide to the corresponding ketones in tetrahydrofuran under nitrogen atmosphere. Some of the alcohols are new compounds and identified by elementary analyses, infrared and PMR spectra. The physical constants and the results of elementary analysis are given in Table 1.

Results and Discussion

The O-H stretching frequencies and molar absorptivities of α,α-dialkyl-*o*-methoxybenzyl alcohols[4] are given in Table 2, together with those of the monoalkyl substituted ones. A typical spectrum is illustrated in Fig. 1.

* To whom correspondences should be addressed.

The strength of the O-H···O hydrogen bond in these alcohols can be evaluated from the hydrogen bond shift $\Delta\nu$. The $\Delta\nu$ values are correlated with the length of hydrogen bond H···O by the following equation in which d is the H···O distance in cm.[5]

TABLE 1. PHYSICAL CONSTANTS AND ELEMENTARY ANALYSES OF NEW *o*-METHOXYBENZYL ALCOHOLS (o-$CH_3OC_6H_4CR_1R_2OH$)

R_1	R_2	Boiling point (°C/mmHg)	Calcd C(%)	Calcd H(%)	Found C(%)	Found H(%)
Me	Et	95/4	73.30	8.95	73.28	8.97
Me	*i*-Pr	110/5	74.19	9.34	74.07	9.11
Me	*t*-Bu	143.5/14	74.96	9.68	74.85	9.48
Et	Et	135/16.5	74.19	9.34	74.31	9.46
Et	*i*-Pr	112/6	74.96	9.68	74.74	9.60
Et	*t*-Bu	123/3	75.63	9.97	75.90	9.85
i-Pr	*i*-Pr	122/6	75.63	9.97	75.58	10.04
i-Pr	*t*-Bu	133/5	76.22	10.24	76.50	9.96
t-Bu	*t*-Bu	155/5	76.75	10.47	76.64	10.21

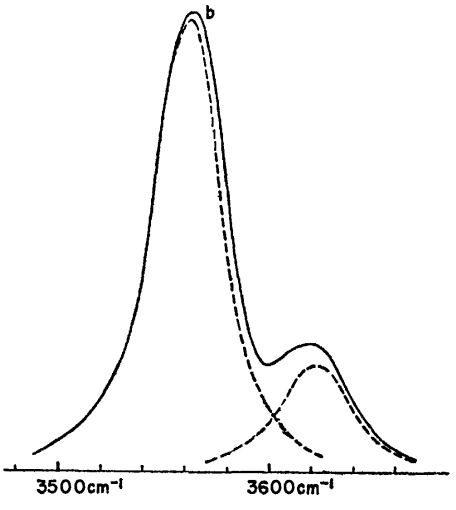

Wave number in cm^{-1}

Fig. 1. The O-H stretching absorption of α,α-dimethyl-*o*-methoxybenzyl alcohol. The broken lines in this figure show the dissolved absorption bands of the free and the hydrogen-bonded species. Thus the corrected absorptivity values were employed for calculating the $\varepsilon_b/(\varepsilon_f+\varepsilon_b)$ values when the overlap of the bands is serious.

TABLE 2. O-H STRETCHING ABSORPTIONS AND O-H CHEMICAL SHIFTS OF *o*-METHOXYBENZYL ALCOHOLS

No.	Substituent		O-H Stretching frequency in cm^{-1}			δ^{∞}_{OH} (ppm)	$\frac{\varepsilon_b}{\varepsilon_f+\varepsilon_b}$
	R_1	R_2	$\nu_f(\varepsilon_f)$[a]	$\nu_b(\varepsilon_b)$[a]	$\Delta\nu$		
1	H	Me	3620.3(50.9)	3583.5(36.8)	38.5	1.98	0.415
2	H	Et	3624.1(53.6)	3576.3(30.4)	47.8	1.70	0.375
3	H	*i*-Pr	3622.2(52.1)	3580.0(28.2)	42.2	1.72	0.355
4	H	*t*-Bu	3627.5(60.2)	3566.7(25.1)	60.8	1.80	0.310
5	Me	Me	3620.0(21.3)	3562.5(78.0)	57.5	3.37	0.821
6	Me	Et	3617.5(19.9)	3564.6(60.9)	52.9	3.15	0.813
7	Me	*i*-Pr	3620.9(16.6)	3560.1(66.8)	60.8	3.17	0.853
8	Me	*t*-Bu	3609.7(9.0)	3532.1(74.2)	77.6	—	0.943
9	Et	Et	3620.2(32.0)	3555.9(57.9)	64.3	2.84	0.734
10	Et	*i*-Pr	3621.4(28.4)	3550.1(53.5)	71.3	2.72	0.670
11	Et	*t*-Bu	3606.8(9.9)	3536.3(120.0)	70.5	5.24	0.942
12	*i*-Pi	*i*-Pr	3627.6(26.6)	3544.7(71.8)	82.9	2.74	0.730
13	*i*-Pi	*t*-Bu	3603.5(10.5)	3532.1(105.0)	71.4	5.60	0.951
14	*t*-Bu	*t*-Bu	3608.0(17.4)	3532.3(113.7)	75.7	5.57	0.947

a) Molar absorptivity in $l \cdot mol^{-1} \cdot cm^{-1}$.

$$\Delta\nu = \frac{250 \times 10^{-8}}{d} - 74$$

The larger $\Delta\nu$ value indicates that the stronger hydrogen bond exists in the methoxy-alcohol. Except for the case of *t*-butyl substituted ones, the $\Delta\nu$ value increases with the increase in the bulkiness of the alkyl group, indicating that the hydrogen bond is stronger when the α-alkyl groups are bulkier.** However, the population of hydrogen-bonded species is not proportional to the bulkiness of the substituent.

The free O–H bands of the tertiary alcohols of this class generally lie near 3620 cm^{-1}, and the O–H bands arising from the O–H···π hydrogen-bonded forms are located near 3600 cm^{-1}.[6,7] Thus, the higher frequency band might be assigned to the free hydroxyl group and the lower frequency one to the O–H···O hydrogen-bonded hydroxyl group, at least with the *o*-methoxybenzyl alcohols without *t*-butyl substituent at the α-position. No absorption band due to O–H···π interaction could be detected. The O–H···π hydrogen-bonded conformation might be rather unfavorable. This conclusion is apparently contrary to the findings on benzyl alcohols without *o*-methoxy substituent.[6,7] However, it can be rationalized in the following way. α,α-Dialkyl-*o*-methoxybenzyl alcohols exist as the equilibrium mixture of the hydrogen-bonded and the free O–O *syn-periplanar* conformer represented by III and IV, respectively. Thus, the II′ conformation of the

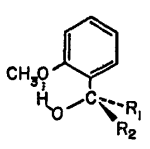

(III)

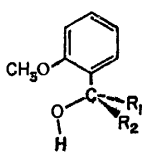

(IV)

o-methoxy-alcohols is by far less stable than the corresponding conformation of the parent benzyl alcohols due to the steric repulsion between the α-alkyl (R_1 in II′) and the *o*-methoxy groups. Thus, its contribution to the conformational equilibrium is not predominant. It is not certain whether IV or IV′ conformation gives rise to the free O–H absorption. However, the O–O *syn-periplanar* conformation IV seems somewhat less crowded when both of two substituents (R_1 and R_2) are alkyl groups. This is true especially when the alkyl groups are isopropyl and *t*-butyl.

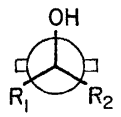

(II′)

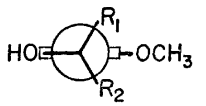

(IV′)

In the alcohols of α-monoalkyl series (Compounds 1—4), the proportion of the hydrogen-bonded species is lower even when the alkyl group is *t*-butyl. In these molecules, the H_α-OCH_3 *syn-periplanar* conformation V might be a stable conformation, since the benzyl hydrogen atom is much less bulkier than the alkyl substituent in the dialkyl series. This conformation would have a free O–H stretching absorption, if the bulkiest alkyl group occupies a position nearly perpendicular to the aromatic nucleus as shown in V.

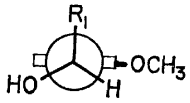

(V)

If we assume that the O–H chemical shift at infinite dilution δ^{∞}_{OH} is not affected by the nature of the alkyl substituent, the observed chemical shift (δ^{∞}_{OH}) should be linear with respect to the percentage of the hydrogen-bonded species. Hence, the chemical shift (δ^{∞}_{OH}) of the O–H···O hydrogen-bonded species and the free species might be obtained by extrapolating the observed δ^{∞}_{OH} *vs.* percentage plot. The O–H chemical

** The hydrogen-bonded O–H frequencies of the *t*-butyl substituted derivatives are lower than those of the other alcohols investigated, but the $\Delta\nu$ values are smaller because of their lower free O–H frequencies.

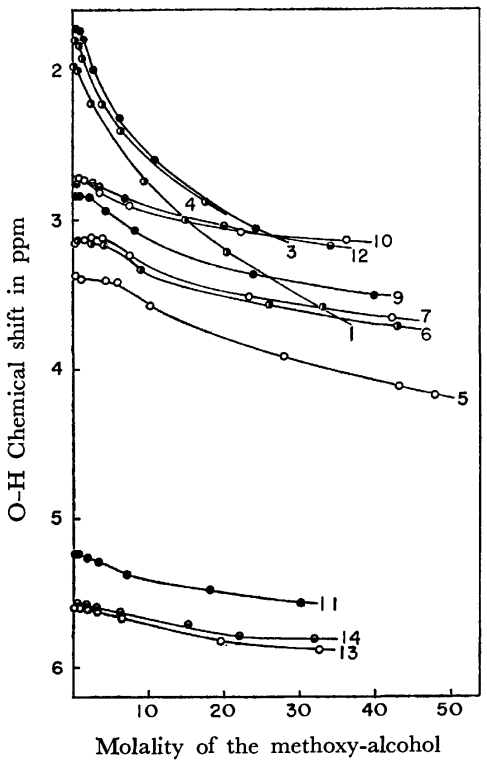

Fig. 2. The concentration dependence of the O-H chemical shifts of the *o*-methoxybenzyl alcohols.

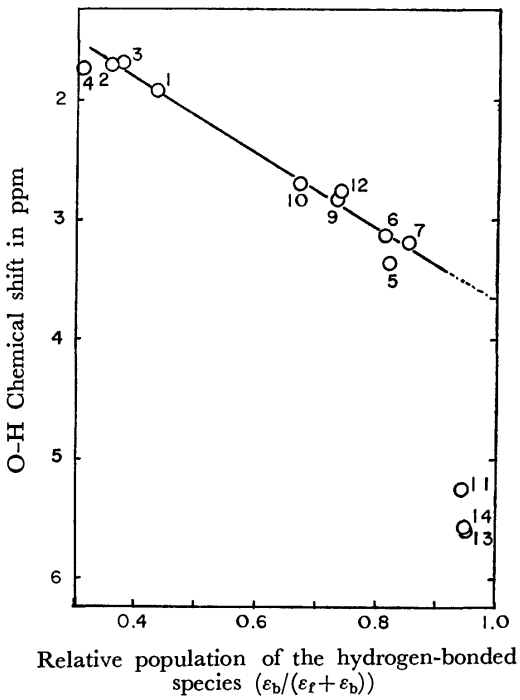

Fig. 3. The O-H chemical shift (δ^{∞}_{OH}) *vs.* the population of the hydrogen-bonded species $(\varepsilon_b/(\varepsilon_f+\varepsilon_b))$ plot.

values for the methoxy-benzyl alcohols were obtained from the O–H chemical shift *vs.* molality plot (Fig. 2) by extrapolating the δ^{∞}_{OH} values to zero concentrations. The δ^{∞}_{OH} values should be weighted mean values of the δ^{∞}_{OH}'s of the free and the intramolecularly hydrogen-bonded species of the alcohols. The proportion of the hydrogen-bonded species in these methoxy-alcohols, in turn, was estimated from the infrared spectral data. Thus, the intensity ratio $\varepsilon_b/(\varepsilon_f+\varepsilon_b)$ is taken as a measure for the proportion of the hydrogen-bonded species. Strictly speaking, the integrated intensities for the free and the hydrogen-bonded species should be estimated first, and the proportion should be derived with these values. However, the total molar absorptivity $(\varepsilon_f+\varepsilon_b)$ is constant through the series of alcohols without *t*-butyl group. Thus, the ratio $\varepsilon_b/(\varepsilon_f+\varepsilon_b)$ might be a suitable measure for the abundance of the intramolecularly hydrogen-bonded species. The plot δ^{∞}_{OH} *vs.* $\varepsilon_b/(\varepsilon_f+\varepsilon_b)$ is illustrated in Fig. 3 for the alcohols given in Table 2. Because of the broadening of the O–H signal in PMR spectra at lower concentrations, the δ^{∞}_{OH} value for α-methyl-α-*t*-butyl-*o*-methoxybenzyl alcohol could not be determined. The extrapolation gives the δ^{∞}_{OH} values for the free and the hydrogen-bonded species to be 0.63 ppm and 3.67 ppm, respectively. The δ^{∞}_{OH} value for the free form is lower than those reported by Ōki and Iwamura[8] for benzyl alcohols. The lower δ^{∞}_{OH} value can be interpreted by conformation IV in which the hydroxyl proton lies in the plane of the aromatic nucleus, opposite to the methoxy oxygen atom.

The plots of the alkyl-*t*-butyl alcohols (11, 13 and 14 in Fig. 3) deviate to the lower fields in the δ_{OH} scale from the line obtained by the mean square calculation excluding the plots of the *t*-butyl derivatives. The anomalous behavior of the *t*-butyl derivatives can be attributed to the buttressing effect which bends the aromatic carbon-benzyl carbon bond towards the methoxy group and forces the hydroxyl and methoxy oxygen atoms to approach closer than normal. Lowering of the free O–H frequencies in the *t*-butyl derivatives was not observed with α,α-di-*t*-butylbenzyl alcohol, and is peculiar to *o*-methoxybenzyl alcohols. The O–H···π interaction would not appear to be persistent in these alcohols carrying bulky alkyl groups. The lower O–H frequencies in overcrowded molecules have been observed in several cases.[9,10] Anet and Bavin[9] reported a similar frequency shift with some alcohols. However, the reason for it remains still unclarified.

The authors are grateful to Prof. M. Ōki, the University of Tokyo, for his valuable advice.

References

1) G. P. Newsereff and S. Sternhell, *Tetrahedron Lett.*, **1967**, 2539.
2) P. D. Bartlett, T. R. Steadman, T. T. Tidwell, and P. Weber, *ibid.*, **1970**, 2915.
3) M. Ōki, M. Hirota, H. Satonaka, and T. Hagiwara, *ibid.*, **1967**, 1785.
4) PMR spectra of *p*-substituted analogs: R. J. Quellette, D. L. Marks, and D. Miller, *J, Amer. Chem. Soc.*, **89**, 913 (1967).
5) L. P. Kuhn, ibid., 74, 2492 (1952).
6) M. Ōki, and H. Iwamura, This Bulletin, **35**, 1552 (1962).
7) M. Ōki and H. Iwamura, *ibid.*, **32**, 950 (1959).
8) M. Ōki and H. Iwamura, *ibid.*, **36**, 1 (1963).
9) F. A. L. Anet and P. M. G. Bavin, *Can. J. Chem.*, **34**, 1756 (1956).
10) A. R. H. Cole and P. R. Jefferies, *J. Chem. Soc.*, **1956**, 4391.

Reactions of Organoboranes with Ferric Chloride and Thiocyanate. Convenient Syntheses of Alkyl Chlorides and Thiocyanates from Olefins *via* Hydroboration

Akira ARASE, Yuzuru MASUDA, and Akira SUZUKI*

Kitami Institute of Technology, Kitami, Hokkaido 090

**Department of Applied Chemistry, Faculty of Engineering, Hokkaido University, Sapporo 060*

(Received March 13, 1974)

The reactions of trialkylboranes with ferric chloride and thiocyanate in an aqueous tetrahydrofuran solution give the corresponding alkyl chlorides and thiocyanates in good yields. It was found that two equivalents of ferric salts per alkyl group of organoborane are required, and not only the first alkyl group of trialkylborane but other alkyl groups are also used.

Many reports have appeared on new applications of organoboranes to the synthesis of various organic compounds.[1] Alkyl halide synthesis has also been reported. For example, the reaction of organoboranes with *N*-chlorodialkylamines gives the corresponding alkyl chlorides in 30—53% yields based on trialkylboranes.[2]

It was shown that concurrent polar and radical processes occur to give amine and alkyl chlorides, respectively, as follows.[3]

$$R_3B + R_2NCl \begin{cases} \xrightarrow{\text{polar}} RNR_2 + R_2BCl \\ \xrightarrow{\text{radical}} RCl + R_2BNR_2 \end{cases} \quad (1)$$

However, this reaction is unsuitable for efficient preparation of alkyl chlorides, since the four products are formed in approximately equal yields.

On the other hand, alkyl bromides and iodides are produced readily *via* organoboranes. For instance, the reaction of organoboranes with bromine in dichloromethane gives the corresponding alkyl bromides in yields exceeding 80% based on R_3B.[4,5] Treatment of trialkylboranes with bromine in the presence of sodium methoxide also gives the corresponding alkyl bromides in excellent yields,[6] the three alkyl groups in trialkylborane being almost consumed by the reaction.

Organoboranes similarly react with iodine in the presence of base to produce alkyl iodides in relatively good yields.[7] Alkyl iodides are synthesized by the reaction of organoboranes with allylic or benzylic iodides in tetrahydrofuran in the presence of air.[8]

Lane reported an interesting synthetic procedure for alkyl chlorides and bromides by the reaction between trialkylboranes and cupric halides in 43—92% yields based upon R_3B:[9]

$$R_3B + 2CuX_2 \rightarrow RX + R_2BOH + Cu_2X_2 + HX \quad (2)$$
$$(X=Br, Cl)$$

During the course of studies on oxygen-induced addition reactions of organoboranes with α,β-unsaturated carbonyl compound,[10] it was found that the above reactions are enhanced in the presence of the Fenton reagent (hydrogen peroxide–ferrous sulfate),[11] and that when ferrous chloride is used instead of sulfate in the Fenton reagent, alkyl chlorides are obtained in high yield from the corresponding organoboranes.[12] We wish to report herewith our results, since they differ from and have certain advantages over those given by Lane.[9]

Results and Discussion

Reaction of Trialkylboranes with Fenton Reagent (Ferrous Chloride–Hydrogen Peroxide). It was reported that organoboranes react smoothly with methyl vinyl ketone through a co-ordination process.[10a]

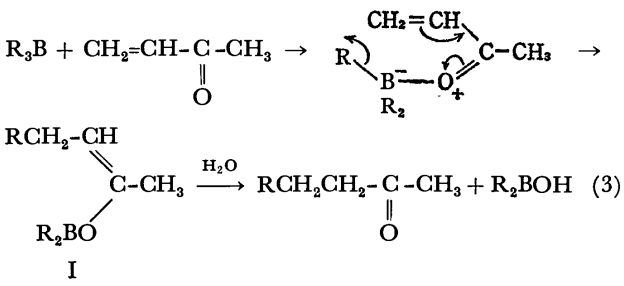

I

In the absence of water or other protonolyzing species, the reaction product seemed to be enol borinate (I). Actually, such an intermediate was found to be readily isolated by distillation under reduced pressure.[13] Intermediate (I) was rapidly hydrolyzed to ketone by addition of water. However, the mechanism (Eq. 3) was later revised and it was reported that the reaction should proceed through a radical-chain mechanism.[10] Brown and Kabalka[14] confirmed that oxygen acts as a powerful radical initiator.

In connection with this work, we examined the reactions with α,β-unsaturated ketones in the presence of hydrogen peroxide–iron salt (Fenton reagent), since the reagent is known to form hydroxy radicals and could be considered to act as a radical initiator. Tricyclohexylborane was treated with crotonaldehyde in aqueous tetrahydrofuran in the presence of hydrogen peroxide–ferrous chloride at 40 °C. The reaction mixture was analyzed by glpc. It was found that the expected 4-methyl-4-cyclohexylbutyraldehyde was obtained in 91% yield, based on the organoborane, in addition to which cyclohexyl chloride was also produced in 70% yield.[12] We have attempted to find the synthetic procedure of alkyl chlorides. The results of representative reactions are summarized in Table 1.

It was found that more than one single alkyl group in trialkylborane seem to be involved in this reaction, contrary to general aspects of the organoborane reaction, in which only one alkyl group is used as the alkyl source.

Reaction of Trialkylboranes with Ferric Chloride. In

Table 1. Reaction[a] of trialkylboranes with ferrous chloride-hydrogen peroxide

R_3B from olefin	Reaction time, hr	Product	Yield,[b] %
1-Hexene	48	1-Chlorohexane	168[c] (153)[d]
		2-Chlorohexane	15[c] (9)[d]
Cyclohexene	24	Chlorocyclohexane	183[c] (156)[d]
Cyclooctene	48	Chlorocyclooctane	180[c]

a) Carried out at 55 °C by using R_3B (8 mmol), $FeCl_2$ (48 mmol) and H_2O_2 (48 mmol). b) Based on the trialkylborane, R_3B used. c) Determined by glpc. d) Isolated by distillation.

Table 2. Reaction[a] of trialkylboranes with ferric chloride

R_3B from olefin	Reaction time, hr	Product	Yield,[b] %
1-Pentene	24	1-Chloropentane	177[c] (144)[d]
		2-Chloropentane	12[c] (6)[d]
1-Hexene	48	1-Chlorohexane	180[c] (162)[d]
		2-Chlorohexane	15[c] (12)[d]
1-Octene	48	1-Chlorooctane	165[c]
		2-Chlorooctane	12[c]
Cyclohexene	48	Chlorocyclohexane	219[c] (195)[d]
Cyclooctene	48	Chlorocyclooctane	81[c]

a) Carried out at 55 °C by using R_3B (8 mmol) and $FeCl_3$ (48 mmol). b) Based on the trialkylborane used. c) Determined by glpc. d) Isolated by distillation.

Table 3. Reaction[a] of trialkylboranes with cupric halides

R_3B from olefin	Cupric halide	Reaction time, hr	Product	Yield,[b] %
1-Hexene	$CuCl_2$	48	1-Chlorohexane	186[c]
			2-Chlorohexane	12[c]
Cyclohexene	$CuCl_2$	48	Chlorocyclohexane	186[c]
cis-2-Butene	$CuBr_2$	24	2-Bromobutane	165[c]
1-Pentene	$CuBr_2$	24	1-Bromopentane	216[c] (195)[d]
			2-Bromopentane	15[c] (12)[d]
1-Hexene	$CuBr_2$	48	1-Bromohexane	258[c] (234)[d]
			2-Bromohexane	12[c] (9)[d]
1-Octene	$CuBr_2$	48	1-Bromooctane	153[c]
			2-Bromooctane	9[c]
Cyclohexene	$CuBr_2$	48	Bromocyclooctane	249[c]
Cyclooctene	$CuBr_2$	48	Bromocyclooctane	24[c]

a) Carried out at 55 °C by using R_3B (8 mmol) and CuX_2 (48 mmol). b) Based on the trialkylborane used. c) Determined by glpc. d) Isolated by distillation.

the reaction of organoboranes with ferrous chloride-hydrogen peroxide, color change was observed. The brown color due to ferric ion gradually turned pale yellowish green, suggesting the reduction of Fe^{3+} ion to Fe^{2+} ion. Thus we examined the direct reaction between trialkylboranes and ferric chloride. The reaction proceeded smoothly. The results are given in Table 2. In the case of tricyclohexylborane, cyclohexyl chloride was obtained in a 219% yield based on tricyclohexylborane, indicating that not only the first and second alkyl groups in R_3B but also a part of the third alkyl group takes part in the reaction.

Table 4. Stoichiometric study of the reaction[a] of tricyclohexylborane with ferric chloride

$FeCl_3$, mmol	Product	Yield,[b] mmol (%)[c]
2.0	0.9	(11)
4.0	1.9	(24)
8.0	3.9	(49)
16.0	7.4	(93)
48.0	17.4	(219)

a) Carried out at 55 °C for 48 hr by using 8 mmol of tricyclohexylborane. b) Determined by glpc. c) Based on tricyclohexylborane.

Reaction of Trialkylboranes with Other Metal Halides. Other metal halides, including manganese chloride, cobalt chloride, cuprous chloride, cupric chloride, stannic chloride, mercuric chloride, ferrous bromide, cuprous bromide and cupric bromide, were examined as regards their activities in the reactions. Cuprous chloride-hydrogen peroxide, cupric chloride, cuprous bromide-hydrogen peroxide and cupric bromide were found to be powerful reactants. The results of the reactions of typical organoboranes with cupric chloride and bromide are summarized in Table 3.

Stoichiometric Study on the Reaction of Tricyclohexylborane with Ferric Chloride. In order to clarify stoichiometry in the reaction, we carried out reactions using tricyclohexylborane with various amounts of ferric chloride. The results are given in Table 4. We see that the use of two equivalents of ferric chloride for each equivalent of tricyclohexylboranes gave rise to an almost quantitative conversion of a single alkyl group into cyclohexyl chloride. Consequently, the reaction is considered to obey stoichiometry (Eq. 4), as pointed out by Lane[9] and Ainley and Challenger.[15] It was also observed that the use of 48 mmol of ferric chloride for 8 mmol of tricyclohexylborane gives 17.4 mmol of the product. Lane reported that a single alkyl group of a trialkylborane is converted into the corresponding alkyl halide in a reasonable length of time. However, our results demonstrate that not only the first alkyl group of the organoborane but also the second and third cyclohexyl groups react with ferric chloride (Eq. 5)

$$R_3B + 2FeCl_3 + H_2O \longrightarrow RCl + R_2BOH + 2FeCl_2 + HCl \quad (4)$$

$$R_3B + 6FeCl_3 + 3H_2O \longrightarrow 3RCl + B(OH)_3 + 6FeCl_2 + 3HCl \quad (5)$$

No mechanistic investigation was carried out for the reaction. However, the mechanism through an alkyl radical from organoborane by an electron transfer reduction of metal salts, proposed by Lane,[9] is apparently reasonable.

Reaction of Trialkylboranes with Ferric Thiocyanate. We attempted to extend the reaction to synthesize alkyl thiocyanates by using metal thiocyanates, instead of metal halides. Although potassium and cupric thiocyanates did not react smoothly with such trialkylboranes, the reaction with ferric thiocyanate gave the

Table 5. Reaction[a] of trialkylboranes with ferric thiocyanate

Exp. no	R_3B from olefin mmol	$Fe(NH_4)(SO_4)_2$ mmol	KSCN mmol	Product	Yield[b] mmol (%)	Bp, °C (mmHg)
	1-Butene					
1	1.7	10.2	30.6	1-BuSCN	3.8 (226)[c]	
				2-BuSCN	0.2 (14)[c]	
	2-Butene					
2	1.7	0	30.6	None		
3	1.7	10.2	30.6	2-BuSCN	3.7 (217)[c]	
4	8.5	51.0	153.0	2-BuSCN	17.0 (200)[d]	93(66)
	1-Hexene					
5	1.7	0	30.6	None		
6	1.7	10.2	30.6	1-HexSCN	3.9 (230)[c]	
				2-HexSCN	0.3 (17)[c]	
7	8.5	51.0	153.0	1-HexSCN	20.3 (239)[d]	110(17)
	Cyclohexene					
8	1.7	10.2	30.6	CyclohexSCN	3.4 (200)[c]	
				CyclohexNCS	0.3 (15)[c]	
9	8.5	51.0	153.0	CyclohexSCN	16.2 (191)[d]	85 (4)
				CyclohexNCS	0.6 (7)[d]	
	2-Methyl-2-butene					
10	1.7	10.2	30.6	3-Me-2-BuSCN	1.7 (98)[c]	

a) Carried out at 55 °C for 24 hr. b) Based on the trialkylborane employed. c) Determined by glpc. d) Isolated by distillation.

corresponding alkyl thiocyanates in good yields. When a mixture of ferric ammonium sulfate (6 equiv. to each organoborane) and potassium thiocyanate (18 equiv.) in water was gradually added to a solution of tricyclohexylborane in tetrahydrofuran and refluxed for 24 hr, formation of a mixture of cyclohexyl thiocyanate and cyclohexyl isothiocyanate was shown by glpc in yields of 200% and 15%, respectively, based on R_3B. Representative results of the reaction are summarized in Table 5. In the preparative scale experiments 4, 7 and 9, the products were readily separated by extraction with petroleum ether, followed by distillation.

Experimental

Materials. Commercial 1-pentene, 1-hexene, 1-octene, cyclohexene and cyclooctene were dried over Molecular Sieve-5A, and 30%-hydrogen peroxide, metal halides and thiocyanates(Wako Chemical Co.) were used. Ferrous chloride was used after analysis by the usual *o*-phenanthroline method.

Reaction between Trialkylboranes and Metal Halides. The following procedure for the preparation of cyclohexyl chloride is representative. A dry 50-ml flask equipped with a magnetic stirring bar, septum inlet and reflux condenser was flushed with nitrogen. The flask was charged under nitrogen with 8 mmol of tricyclohexylborane in 5 ml of dry THF and 48 mmol of ferric chloride in 10 ml of water. The reaction mixture was stirred at 55 °C for 48 hr. After the completion of the reaction, the lower aqueous layer was separated and extracted with ether. The combined upper layer and extracts were washed with saturated aqueous sodium chloride solution, and finally analyzed by glpc, demonstrating that cyclohexyl chloride was obtained in a yield of 219% based on tricyclohexylborane.

All the products were confirmed either by comparison with authentic samples or examination of analytical and spectral data in accordance with assigned structures.

Reaction of Trialkylboranes with Ferric Thiocyanate. The following procedure is representative. A 100-ml flask, fitted with the same equipment as mentioned above, was charged with 8.5 mmol of the tri-2-butylborane obtained by hydroboration of 2-butene with diborane. To the solution was slowly added 8 ml (51 mmol) of aqueous solution of ferric ammonium sulfate and 40 ml (153 mmol) of aqueous solution of potassium thiocyanate. The mixture was refluxed at 55 °C for 24 hr under stirring. After cooling, the reaction mixture was extracted with petroleum ether several times. The combined extracts were washed with water and dried over anhydrous magnesium sulfate, and then distilled at 93 °C under 66 mmHg. Thus, 17.0 mmol (200%) of 2-butyl thiocyanate were obtained in a pure state. All the products were identified by direct comparison with authentic samples.

References

1) (a) A. Suzuki, *Yuki Gosei Kagaku Kyokai Shi*, **28**, 288 (1970). (b) A. Suzuki, *ibid.*, **29**, 995 (1971). (c) H. C. Brown and M. M. Rogić, *Organometal. Chem. Syn.*, **1**, 305 (1972). (d) H. C. Brown and M. M. Midland, *Angew. Chem. Int. Ed. Engl.*, **11**, 692 (1972). (e) H. C. Brown, "Boranes in Organic Chemistry," Cornell Univ. Press, Ithaca, 1972.

2) J. G. Sharefkin and H. D. Banks, *J. Org. Chem.*, **30**, 4313 (1965).

3) A. G. Davies, S. C. W. Hook, and B. P. Roberts, *J. Organometal. Chem.*, **23**, C11 (1970).

4) C. F. Lane and H. C. Brown, *J. Amer. Chem. Soc.*, **92**, 7212 (1970).

5) C. F. Lane and H. C. Brown, *J. Organometal. Chem.*, **26**, C51 (1971).

6) H. C. Brown and C. F. Lane, *J. Amer. Chem. Soc.*, **92**, 6660 (1970).

7) H. C. Brown, M. W. Rathke, and M. M. Rogić, *J. Amer. Chem. Soc.*, **90**, 5038 (1968).
8) A. Suzuki, S. Nozawa, M. Harada, M. Itoh, H. C. Brown, and M. M. Midland, *ibid.*, **93**, 1508 (1971).
9) C. F. Lane, *J. Organometal. Chem.*, **31**, 421 (1971).
10) (a) A. Suzuki, A. Arase, H. Matsumoto, M. Itoh, H. C. Brown, M. M. Rogić, and M. W. Rathke, *J. Amer. Chem. Soc.*, **89**, 5708 (1967). (b) A. Suzuki, S. Nozawa, M. Itoh, H. C. Brown, E. Negishi, and S. K. Gupta, *Chem. Commun.*, **1969**, 1009. (c) G. W. Kabalka, H. C. Brown, A. Suzuki, S. Honma, A. Arase, and M. Itoh, *J. Amer. Chem. Soc.*, **92**, 710 (1970). (d) A. Suzuki, S. Nozawa, M. Itoh, H. C. Brown, G. W. Kabalka, and G. W. Holland, *ibid.*, **92**, 3503 (1970).
11) Presented at the 14th Symposium on Essential Oil and Terpene Chemistry of the Chemical Society of Japan, Kitami, September 5, 1970.
12) Presented at the Hokkaido Local Meeting of the Chemical Society of Japan, Tomakomai, August 7, 1971.
13) N. Miyaura, M. Harada, M. Itoh, and A. Suzuki, *Chem. Lett.*, **1973**, 1145.
14) H. C. Brown and G. W. Kabalka, *J. Amer. Chem. Soc.*, **92**, 714 (1970).
15) A. D. Ainley and F. Challenger, *J. Chem. Soc.*, **1930**, 2171.

Preparation of 1,7-Disubstituted Indan Derivatives and Their Application to the Synthesis of Tricyclic Heterocyclic Compounds

Kazuo SAKANE, Shinichi ODA, Eiichi HARUKI, Yoshio OTSUJI, and Eiji IMOTO

Department of Applied Chemistry, College of Engineering, University of Osaka Prefecture, Sakai-shi, Osaka 591

(Received March 22, 1974)

The Birch reduction of acenaphthene (**1**) followed by treatment of the reduction product with sodium ethoxide gave 2a,3-dihydroacenaphthene (**3**). The oxidation of **3** with hydrogen peroxide gave 2a,3,4,5-tetrahydroacenaphthene-4,5-diol (**5**). Further oxidation of **5** afforded various 1,7-disubstituted indan derivatives including 7-carboxyindan-1-acetic acid (**7**). Two tricyclic *N*-heterocyclic compounds, 3,3a-dihydrocyclopent[*de*]quinolin-2(1*H*)-one (**13**) and 3,3a-dihydrocyclopent[*de*]isoquinolin-1(2*H*)-one (**17**), were synthesized from **7**.

1,7-Disubstituted indan derivatives might be useful synthetic intermediates, since they can be converted into compounds of various structures. Rapoport and Pasky[1] synthesized the fused tricyclic compounds containing one six- and two five-membered rings, utilizing 1,7-disubstituted indan derivatives as key intermediates. However, their method of preparation involved a lengthy route starting from indene.

In this paper, we describe an alternative method for the preparation of 1,7-disubstituted indan derivatives and their application to the synthesis of tricyclic *N*-heterocycles, very rare type of compounds. Our method involves the Birch reduction of acenaphthene and an oxidative cleavage of the reduction product as key steps.

Results and Discussion

Preparation of 1,7-Disubstituted Indan Derivatives. The reduction of acenaphthene (**1**)* with calcium hexammine in ether and with a large excess of sodium in liquid ammonia gave 2a,3,4,5-tetrahydroacenaphthene.[2,3] However, we found that the Birch reduction of **1** by use of 2.3—2.4 molar equivalents of sodium in liquid ammonia afforded a mixture of 2a,5-dihydro- and 2a,3-dihydroacenaphthene (**2** and **3**) in a 90% yield. Treatment of the mixture with sodium ethoxide in ethanol gave **3** practically in a pure state. That the product obtained by the Birch reduction of **1** consists of a mixture of **2** and **3** is suggested from the fact that treatment of the reduction product with

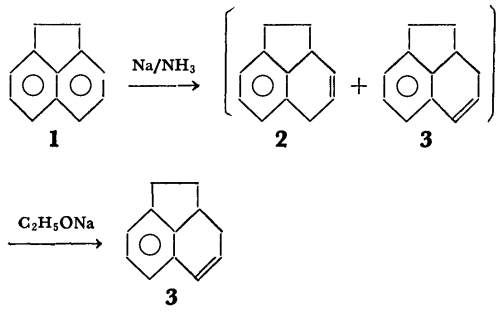

* The numbering system used for acenaphthene (**1**) is shown in the formula.

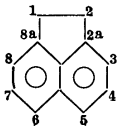

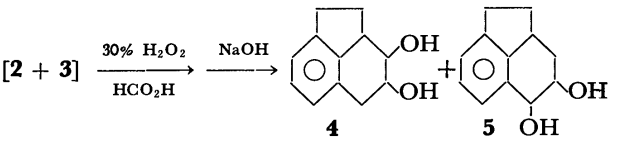

hydrogen peroxide in formic acid followed by hydrolysis gave a mixture of 2a,3,4,5-tetrahydroacenaphthene-3,4-diol (**4**) and 2a,3,4,5-tetrahydroacenaphthene-4,5-diol (**5**) which were separated by repeated recrystallization. The hydrogen peroxide oxidation of a pure sample of **3** afforded **5** in a 70% yield. The structures of **4** and **5** were confirmed by the fragmentation patterns in their mass spectra, which show the base peaks at *m/e* 130 and 146, respectively. These ions could be formed by the retro-Diels-Alder cleavage of the compounds, corresponding respectively to the loss of $C_2H_4O_2$ and C_2H_4O fragments.

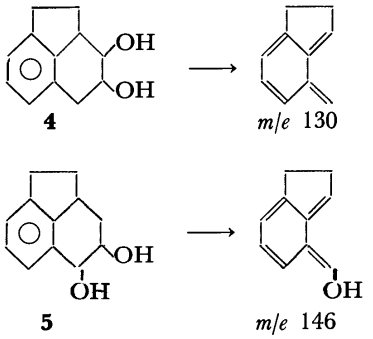

The oxidation of **5** with sodium metaperiodate in an aqueous ethanol gave 7-formylindan-1-acetaldehyde (**6**) in an 86% yield. The IR spectrum (film) of **6** showed carbonyl absorptions at 1690 and 1720 cm^{-1}. Its NMR spectrum (CCl_4) showed a multiplet at δ 9.9 due to an aliphatic aldehyde proton and a singlet at δ 10.2 due to an aromatic aldehyde proton. Treatment

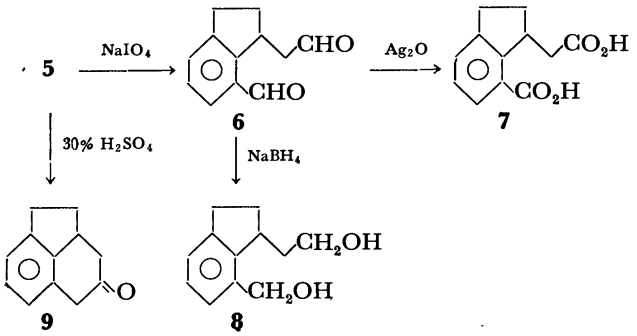

of **6** with silver oxide gave 7-carboxyindan-1-acetic acid (**7**) in an 88% yield. The dicarboxylic acid **7** has been synthesized starting from indene.[1] The reduction of **6** with sodium borohydride gave 1-(2-hydroxyethyl)-7-hydroxymethylindan (**8**) in a 78% yield. When **5** was refluxed in 30% sulfuric acid, 2a, 3,4,5-tetrahydroacenaphthen-4-one (**9**) was obtained in a 58% yield. IR spectrum (KBr) of **9** showed a carbonyl absorption at 1710 cm^{-1} and its NMR spectrum a singlet at δ 3.38 attributable to two methylene protons at C-5.

Synthesis of Heterocyclic Compounds. By the method of Rapoport and Pasky,[1] **7** was converted into 2,2a-dihydro-1-oxo-1H-cyclopent[*cd*]indene (**11**) *via* the lead salt (**10**). The transformation of **11** to its oxime **12**, followed by treatment with polyphosphoric acid

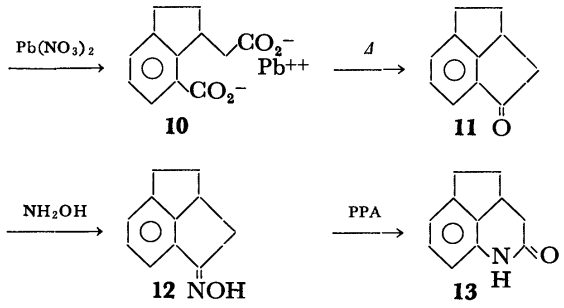

(PPA) afforded 3,3a-dihydrocyclopent[*de*]quinolin-2(1*H*)-one (**13**) in a 28% yield. The IR spectrum (KBr) of **13** showed absorptions at 3200, 1690 and 1630 cm^{-1} due to the amide group. The heterocyclic compound **13** was synthesized by Fuson and Veazey[4] from β-(*o*-nitrophenyl)glutaric acid. The melting point of **13** we obtained was in good agreement with theirs.[4]

We attempted to synthesize 3,3a-dihydrocyclopent-[*de*]isoquinolin-1(2*H*)-one (**17**), a structural isomer of **13**.

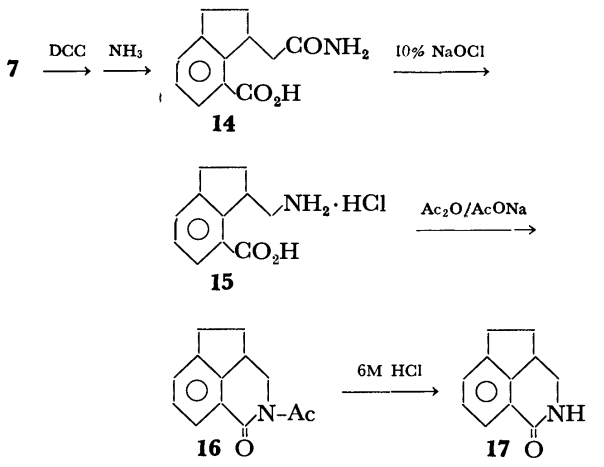

Treatment of **7** with *N,N'*-dicyclohexylcarbodiimide (DCC) followed by the addition of concentrated aqueous ammonia gave 7-carboxyindan-1-acetamide (**14**) in a 70% yield. The Hofmann rearrangement of **14** was carried out by use of sodium hypochlorite in an aqueous sodium hydroxide. Acidification of the rearranged product gave 7-carboxyindan-1-methylamine hydrochloride (**15**) which could not be purified. Treatment of the crude **15** with acetic anhydride containing sodium acetate afforded 2-acetyl-3,3a-dihydrocyclopent[*de*]isoquinolin-1(2*H*)-one (**16**) in a good yield. The IR spectrum (KBr) of **16** showed an amidecarbonyl absorption at 1690 cm^{-1} and no absorptions due to NH group, its NMR spectrum (CCl_4) a sharp singlet at δ 2.47 due to three methyl protons of the acetyl group, and its mass spectrum the parent peak at *m/e* 215. Hydrolysis of **16** with 6M hydrochloric acid gave a mixture of **17** (37%) and **15** (32%). The IR spectrum (KBr) of **17** showed absorptions characteristic of the amide group at 3200, 1670 and 1590 cm^{-1}, and its mass spectrum the parent peak at *m/e* 173.

Experimental

Birch Reduction of Acenaphthene (1). A solution of 40 g (0.26 mol) of **1** in 150 ml of dry ether was added rapidly to a stirred solution of 14 g (0.61 mol) of sodium in 400 ml of liquid ammonia at −70 °C, and the mixture was stirred for 3 hr at the same temperature. Excess ammonium chloride was added to this mixture, and ammonia was then evaporated at room temperature. Water and then ether were added to the residue. The ether layer was separated, washed with water, dried over Na_2SO_4, and then evaporated. The residual oil was distilled to yield 37 g of a pale yellow oil consisting of a mixture of **3** and **4**, bp 58—59 °C/0.15 mmHg. IR(film): 3020, 2940, 2840, 1600, 1460, 1435, 800, 760, 715, and 690 cm^{-1}. NMR(CCl_4): δ 1.3—2.0(1H, m), 2.1—2.7(2H, m), 2.7—3.1(2H, m), 3.0—3.5(2H, m), 5.7—6.1(1.6H, m), 6.5 (0.4H, dd, J= 10.0 and 3.0 Hz), and 6.65—7.15 ppm(3H, m).

2a,3-Dihydroacenaphthene (3). A solution of sodium ethoxide was prepared by adding 34.5 g (1.5 g-atom) of sodium to 500 ml of absolute ethanol. To this was added 46.8 g of the Birch reduction product, and the mixture was refluxed for 3 hr under nitrogen atmosphere. Most of the ethanol was removed, and then ice-water was added to the residue. The resulting mixture was extracted with ether. The ether solution was dried over Na_2SO_4 and evaporated. Distillation of the residue gave 42.1 g of **3** as a colorless oil, bp 73—74 °C/0.5 mmHg. The yield of **3** from **1** was 81%. IR(film): 3030, 2940, 2840, 1630, 1600, 1480, 1460, 1435, 800, 790, 750, and 690 cm^{-1}. NMR(CCl_4): δ 1.3—2.0 (2H, m, CH_2 at C-3), 2.1—2.7 (2H, m, CH_2 at C-2), 2.7—3.0(2H, m, CH_2 at C-1), 3.0—3.5(1H, m, CH at C-2a), 5.9(1H, bd, J= 10.0 Hz, vinyl proton at C-4), 6.5(1H, dd, J= 10.0 and 3.0 Hz, vinyl proton at C-5), and 6.65—7.15 ppm(3H, m, aromatic H).

2a,3,4,5-Tetrahedroacenaphthene-4,5-diol (5). To a stirred mixture of 30 g (0.19 mol) of **3** in 12 ml of 95% HCO_2H was added 26.5 g of 30% H_2O_2 at 20—25 °C. The reaction mixture was stirred for 1 hr at the same temperature, poured into 500ml of water, then extracted with $CHCl_3$. The $CHCl_3$ solution was washed with 10% $NaHCO_3$ solution, dried over Na_2SO_4, then evaporated to give a white solid. Since its IR spectrum(KBr) showed a carbonyl absorption due to the ester group at 1700 cm^{-1}, the solid was subjected to hydrolysis. To a stirred solution of the solid in 100ml of ethanol was added 65 ml of 20% NaOH solution under ice-cooling. The mixture was stirred for 5 hr at room temperature and diluted with 500 ml of water. The resulting brown solid was filtered, washed thoroughly with water to give 26 g (71%) of **5**. Recrystallization from benzene-ethanol gave pure **5** as white crystals, mp 138—139 °C. IR(KBr): 3320 cm^{-1}(OH). NMR($(CD_3)_2CO$): δ 1.3—1.9(2H, m), 2.65—3.0(2H, m), 3.0—3.5(1H, m), 3.85—4.3(3H, m), 4.55(1H, dd, J=5.6 and 3.1 Hz), and 7.2 ppm(3H, bs). Mass: *m/e* 190(M^+).

Found: C, 75.54; H, 7.58%. Calcd for $C_{12}H_{14}O_2$: C, 75.76; H, 7.42%.

Hydrogen Peroxide Oxidation of the Birch Reduction Product. The Birch reduction product (30 g) was treated with H_2O_2-HCO_2H and then with NaOH solution in the same manner as described above. The resulting mixture was extracted with $CHCl_3$. The extract was washed with water, dried over Na_2SO_4 and evaporated to give a brown viscous oil which was solidified upon treatment with CCl_4. The solid was collected by filtration to give 11.5 g of crude **4**, mp 130—137 °C. The crude **4** was recrystallized from benzene to give an analytical sample, mp 139—141 °C. IR(KBr): 3350 cm^{-1}(OH). NMR($(CD_3)_2CO$): δ 2.55—3.05(4H, m), 3.28(1H, m), 3.62(1H, m), 3.84—4.4(3H, m), and 6.75—7.15 ppm(3H, m). Mass: *m/e* 190(M^+).

Found: C, 75.62; H, 7.46%. Calcd for $C_{12}H_{14}O_2$: C, 75.76; H, 7.42%.

The CCl_4 filtrate was evaporated to give a brown viscous oil. Distillation of this oil gave yellow viscous oil of bp 140—150 °C/0.2 mmHg, which upon trituration with benzene yielded a white solid. The solid was recrystallized from $CHCl_3$ to give **5** as white crystals, mp 138—140 °C.

7-Formylindan-1-acetaldehyde (6). A soluiton of 12.8 g (0.06 mol) of sodium metaperiodate in 200 ml of water was added over 30 min to a stirred solution of 9.5 g (0.05 mol) of **5** in 200 ml of ethanol at 15—20 °C. Stirring was continued for 20 hr at room temperature, and most of the ethanol was evaporated under reduced pressure at room temperature. The resulting yellow oil was diluted with water, and extracted with CH_2Cl_2. The extract was washed with water, dried over Na_2SO_4 and evaporated. The resulting oil was distilled to afford 8.1 g (86%) of **6** as a colorless oil, bp 117—119 °C/0.3 mmHg, which upon standing in a refrigerator gave a white solid. IR(film): 1720(C=O) and 1690 cm^{-1}(C=O). NMR(CCl_4): δ 1.7—2.75(4H, m), 2.75—3.3(2H, m), 4.0—4.6(1H, m, CH at C-1), 7.3—7.9(3H, m, aromatic H), 9.9 (1H, m, aliphatic CHO), and 10.2 ppm(1H, s, aromatic CHO).

Found: C, 76.49; H, 6.57%. Calcd for $C_{12}H_{12}O_2$: C, 76.57; H, 6.43%.

The semicarbazone of **6** was prepared by the usual method and recrystallized from ethanol-water, mp 200—202 °C(decomp.).

Found: C, 55.71; H, 6.18; N, 28.04%. Calcd for $C_{14}H_{18}N_6O_2$: C, 55.61; H, 6.00; N, 27.80%.

7-Carboxyindan-1-acetic Acid (7). A solution of 210 ml of 1M NaOH solution was added over 30 min to a stirred mixture of 4.3 g (0.023 mol) of **6** and 17.6 g(0.134 mol) of $AgNO_3$ in 100 ml of 50% aqueous ethanol under cooling with an ice-water bath. After stirring for 30 min, air was passed into the stirred reaction mixture for 6 hr at room temperature. A black solid was separated by decantation and washed several times with 5% NaOH solution. All the aqueous solutions were combined and washed with ether. The aqueous solution was acidified with 6 M HCl to give a white solid which was separated, washed with water, and dried *in vacuo* to yield 4.6 g (88%) of **7**, mp 178—181 °C. An analytical sample of **7** was obtained by recrystallization from water-ethanol, mp 181—184 °C (lit,[1] mp 190—191 °C). IR(KBr): 3600—2500(OH), 1690(C=O), and 1670 cm^{-1} (C=O).

Found: C, 66.01; H, 5.31%. Calcd for $C_{12}H_{12}O_4$: C, 65.44; H, 5.49%.

1-(2-Hydroxyethyl)-7-hydroxymethylindan (8). To a solution of 500 mg(2.66 mmol) of **6** in 10 ml of ethanol was added 76 mg(2.0 mmol) of $NaBH_4$, and the reaction mixture was stirred at room temperature for 2 hr. The solvent was evaporated under reduced pressure, and the colorless viscous residue was added to ice-water and then extracted with CH_2Cl_2. The extract was washed with water, dried over Na_2SO_4, and evaporated to give a colorless viscous oil, which upon scratching with a spatula solidified to yield 400 mg (79%) of crude **8**. The crude solid was recrystallized from CCl_4 to yield white crystals, mp 54—56 °C. IR(KBr): 3200 cm^{-1} (OH). NMR($CDCl_3$): δ 1.3—2.3(4H, m), 2.6—3.0(2H, m), 3.0—3.4(1H, m), 3.55(2H, t, J=6.2 Hz, $-CH_2\mathbf{CH_2}OH$), 3.95(2H, bs, two of OH), 4.55(2H, s, Ar–$\mathbf{CH_2}OH$), and 7.05 ppm(3H, bs, aromatic H).

Found: C, 74.75; H, 8.36%. Calcd for $C_{12}H_{16}O_2$: C, 74.97; H, 8.39%.

2a,3,4,5-Tetrahydroacenaphthen-4-one (9). A mixture of 1.9 g (0.01 mol) of **5** and 200 ml of 30% aqueous H_2SO_4 was refluxed for 2 hr, cooled to room temperature, and then diluted with 150 ml of ice-water. The aqueous solution was extracted with ether, and the extract was washed with water, dried over Na_2SO_4, and evaporated. The resulting brown solid was sublimed at 100 °C under 0.5 mmHg to give 1.0 g (58%) of **9** as a white solid, mp 48—51 °C. IR(KBr): 1710 cm^{-1} (C=O). NMR(CCl_4): δ 1.2—3.3(7H, m), 3.38(2H, s, CH_2 at C-5), and 6.75—7.3 ppm(3H, m, aromatic H).

The oxime of **9** was prepared in the usual manner and purified by recrystallization from cyclohexane, mp 129—131 °C.

Found: C, 77.10; H, 6.95; N, 7.51%. Calcd for $C_{12}H_{13}NO$: C, 76.97; H, 7.00; N, 7.48%.

2,2a-Dihydro-1-oxo-1H-cyclopent[cd]*indene (11).* This was prepared from **7** *via* its lead salt (**10**) by the method of Rapoport and Pasky,[1] mp 59—61 °C (lit.[1] mp 63 °C).

2,2a-Dihydro-1-hydroxyimino-1H-cyclopent[cd]*indene (12).* This was prepared from 1.5 g (22 mmol) of hydroxylamine hydrochloride and 590 mg (3.7 mmol) of **11** by the usual method. The yield of **12** was quantitative. A pure sample was obtained by recrystallization from water-ethanol, mp 130—132 °C. IR(KBr): 1660 cm^{-1} (C=N).

Found: C, 76.04; H, 6.43; N, 8.08%. Calcd for $C_{11}H_{11}NO$: C, 76.27; H, 6.40; N, 8.09%.

3,3a-Dihydrocyclopent[de]*quinolin-2(1H)-one (13).* Polyphosphoric acid (PPA) was prepared by stirring a mixture of 12 g of 85% H_3PO_4 and 16 g of P_2O_5 at 130—140 °C for 2 hr, and then 1.8 g (14 mmol) of **12** was added at 80—100 °C. The reaction mixture was stirred at the same temperature for 15 min and then chilled. Ice-water was added to the reaction mixture until PPA was dissolved. The resulting solid was collected by filtration and recrystallized from *n*-hexane-$CHCl_3$ to give 500 mg (28%) of **13**, mp 163—164 °C (lit,[4] mp 163—164 °C). IR(KBr): 3200, 1690, 1630, 1605, 1490, 1330, and 770 cm^{-1}. NMR($CDCl_3$): δ 1.4—3.1(6H, m), 3.1—3.6(1H, 6.5—7.1(3H, m, aromatic H), and 9.1—9.5 ppm(1H, bs, NH).

Found: C, 76.33; H, 6.47; N, 8.04%. Calcd for $C_{11}H_{11}NO$: C, 76.27; H, 6.40; N, 8.09%.

7-Carboxyindan-1-acetamide (14). To a solution of 1.05 g (5.4 mmol) of *N,N'*-dicyclohexylcarbodiimide in 15 ml of dry dioxane was added 1.0 g (4.5 mmol) of **7**. The reaction mixture was allowed to stand at room temperature for 1.5 hr. The resulting *N,N'*-dicyclohexylurea was removed by filtration and the filtrate was evaporated under reduced pressure to give a pale yellow viscous oil; its IR spectrum showed absorptions characteristic of an acid anhydride at 1790 and 1720 cm^{-1}. A concentrated aqueous ammonia (30 ml) was added to the acid anhydride under ice-cooling. The mixture was allowed to stand at room temperature for 3 hr, warmed on a water bath for 30 min, and then extracted with CH_2Cl_2. The aqueous solution was acidified with concentrated HCl. The resulting solid was collected by filtra-

tion, washed with water and dried to give 700 mg(70%) of crude **14**, mp 194—200 °C. An analytical sample was obtained recrystallization from ethanol, mp 209—212 °C. IR(KBr): 3400, 3200, 1690, and 1650 cm^{-1}.

Found: C, 65.85; H, 6.08; N, 6.44%. Calcd for $C_{12}H_{13}NO_3$: C, 65.74; H, 5.98; N, 6.39%.

*7-Carboxyindan-1-methylamine Hydrochloride (**15**).* To a solution of 2.2 g (0.01 mol) of **14** in 30 ml of 10% aqueous NaOH solution was added 9.7 g of 10% aqueous sodium hypochlorite solution at room temperature. The reaction mixture was stirred at room temperature for 15 min, at 55 °C for 1 hr, and at 70—80 °C for 30 min. It was then washed with CH_2Cl_2. The aqueous solution was acidified to pH 1.0 with concentrated HCl. The acidified solution was again washed with CH_2Cl_2, and the resulting brown solid was collected by filtration. When the filtrate was concentrated to one-half its initial volume, a second crop of the solid was obtained. All the solids were combined and used without further purification for the preparation of **16**. The solids thus obtained weighed 2.1 g and decomposed at 230—240 °C. IR(KBr): 3100—2500, 1680, and 1630 cm^{-1}.

2-Acetyl-3,3a-dihydrocyclopent[de]*isoquinolin-1(2H)-one (**16**).* A mixture of 1.5 g of crude **15**, 900 mg of anhydrous AcONa, and 5 ml of Ac_2O was refluxed for 20 min. A large excess of 10% NaOH solution was added to the cooled mixture. The resulting mixture was heated for 15 min, and then extracted with ether. The ether extract was washed with $NaHCO_3$ solution, dried over Na_2SO_4, then evaporated to give 1.0 g (70%) of a pale yellow solid. Recrystallization of the solid from methanol-water gave an analytical sample of **15**, mp 74—76 °C. IR(KBr): 1690, 1600, 1370, 1300, 1235, 1225, and 755 cm^{-1}. NMR(CCl_4): δ 1.4—2.0(1H, m), 2.2—2.8(1H, m), 2.47(3H, s), 2.8—3.6(4H, m), 4.9(1H, dd, J= 10.0 and 4.0 Hz), and 7.1—7.8 ppm(3H, m). Mass: *m/e* 215(M^+).

Found: C, 72.49; H, 6.16; N, 6.46%. Calcd for $C_{13}H_{13}NO_2$: C, 72.54; H, 6.09; N, 6.51%.

3,3a-Dihydrocyclopent[de]*isoquinolin-1(2H)-one (**17**).* A mixture of 1.0 g (4.6 mmol) of **16** and 50 ml of 6 M HCl was refluxed for 2 hr, and then extracted with $CHCl_3$. During this operation a white solid appeared and was collected by filtration to yield 350 mg (32%) of **15**.

The $CHCl_3$ solution was washed with water, dried over Na_2SO_4, and then evaporated to give 300 mg (37%) of a brown solid. The solid was recrystallized from *n*-hexane–$CHCl_3$ to give **17** as white crystals, mp 150—152 °C. IR (KBr): 3200, 1670, 1610, 1595, 1490, 1400, 1350, 1320, 800, and 760 cm^{-1}. Mass: *m/e* 173(M^+).

Found: C, 76.37; H, 6.60; N, 8.05%. Calcd for $C_{11}H_{11}NO$: C, 76.27; H, 6.40; N, 8.09%.

References

1) H. Rapoport and J. Z. Pasky, *J. Amer. Chem. Soc.*, **78**, 3788 (1956).

2) H. Boer and P. M. Duinker, *Rec. Trav. Chim.*, **77**, 346(1958); *Chem. Abstr.*, **52**, 15485g(1958).

3) P. Lebeau and M. Picon, *Compt. Rend.*, **159**, 70 (1914); *Chem. Abstr.*, **8**, 3288 (1914).

4) R. C. Fuson and T. M. Veazey, *J. Amer. Chem. Soc.*, **76**, 1169 (1954).

A New Synthesis of 3-Alkyl-2-hydroxy-2-cyclohexen-1-ones[1]

Kikumasa SATO, Seiichi INOUE, and Masao ŌHASHI*

Department of Applied Chemistry, Faculty of Engineering, Yokohama National University, Minami-ku, Yokohama, 233
**Chemical Laboratory, Seimi Chemical Co., Ltd., Chigasaki, Chigasaki-shi, Kanagawa 253*

(Received April 10, 1974)

A New synthesis of 2-hydroxy-3-methyl-2-cyclohexen-1-one (Ia), a flavor component of coffee aroma, is described. The selenium dioxide oxidation of ethyl 1-methyl-2-oxocyclohexanecarboxylate (IIa) gave α-diketone (IIIa), which was then hydrolyzed and decarboxylated to afford Ia. The treatment of IIa with cupric chloride in 50% acetic acid also yielded Ia. The dimethyl sulfoxide oxidation of ethyl 3-bromo-1-methyl-2-oxocyclohexanecarboxylate (IV) afforded IIIa, along with 3-bromo-6-ethoxycarbonyl-2-hydroxy-6-methyl-2-cyclohexen-1-one (V). The halogenation of IIa produced dihalogeno ketoesters (VIa) (VIIa), which also yielded Ia in a pure state by means of a direct acidic hydrolysis or by a two-step hydrolysis using morpholine. Other allied compounds are also described.

A number of alkyl-substituted cyclic α-diketones possessing a characteristic caramel flavor is known.[2] 2-Hydroxy-3-methyl-2-cyclohexen-1-one (Ia) has been identified in coffee aroma[3] and is one of the degradation products of fructose.[4] Ia has been synthesized in low yields by a variety of methods.[5]

We have previously reported the synthesis of 3-methyl-2-cyclopenten-2-ol-1-one.[6] In this paper, these studies will be extended to the synthesis of 3-alkyl-2-hydroxy-2-cyclohexen-1-ones (I) from ethyl 1-alkyl-2-oxocyclohexanecarboxylate (II) as starting materials.

Ethyl 1-methyl-2-oxocyclohexanecarboxylate (IIa) can readily be prepared by the alkylation of ethyl 2-oxocyclohexanecarboxylate[7] with methyl iodide.[8a] Under the same conditions, the alkylation of ethyl 2-oxocyclohexanecarboxylate with ethyl or n-propyl iodide gave the corresponding II in a low yield. However, in the presence of dimethyl formamide, the enolate of the ketoester was easily alkylated to give (IIb) and (IIc), both in good yields.

The infrared spectrum of the compound II in the 6 μ region is unusual in that it consists of an unresolved envelope of absorption bands (see Experimental section), of which peaks at the normal ketone frequency (1710 cm^{-1}) but which has poorly-defined shoulders at higher frequencies (1720 and 1740 cm^{-1}). This implies that ethoxycarbonyl groups exist as mixtures of equatorial and axial conformers.[8b]

We have examined the following oxidations of II, using the key precursors of I: (1) selenium dioxide oxidation, (2) cupric chloride oxidation, (3) α-geminal halogenation, and (4) the DMSO oxidation of ethyl 3-bromo-1-methyl-2-oxocyclohexanecarboxylate (IV), which is easily obtained from IIa.

When IIa was refluxed with excess selenium dioxide in aqueous dioxane for 22 hr, 6-ethoxycarbonyl-2-hydroxy-6-methyl-2-cyclohexen-1-one (IIIa) was obtained in a 40% yield. Similarly, (IIIb) was also obtained from the ketoester IIb.

Compound IIIa could be readily converted into Ia (62.7%) by refluxing with 4M hydrochloric acid. The structure of Ia was assigned on the basis of its NMR, infrared, and ultraviolet spectra and the results of an elemental analysis. The NMR spectrum suggested that Ia was 100% enolized and that Ia exist as geometrical isomers, for we observed the methylene protons in the ethoxycarbonyl group showing two quartets (δ 4.15 and 4.17 ppm) in equal quantities.

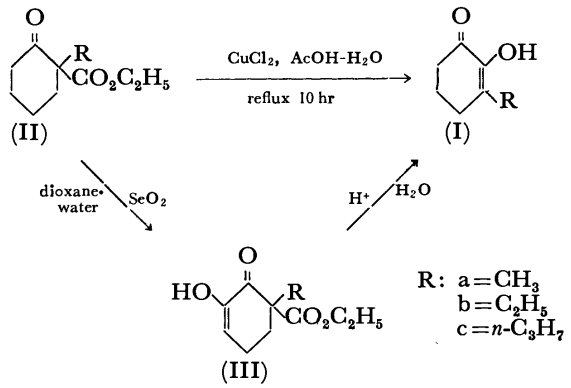

On the other hand, Compound Ia was also obtained directly in a rather low yield by the refluxing of IIa with cupric chloride in 50% aqueous acetic acid.

The gem-dihalogeno group α to the carbonyl of II seemed to be an attractive possibility as the ketone precursor.[9] Indeed, IIa was easily chlorinated in acetic acid at 40—45° in a high yield and was easily brominated in carbon tetrachloride to give the corresponding ethyl 1-alkyl-3,3-dihalogeno-2-oxocyclohexanecarboxylates, (VI) (VII).

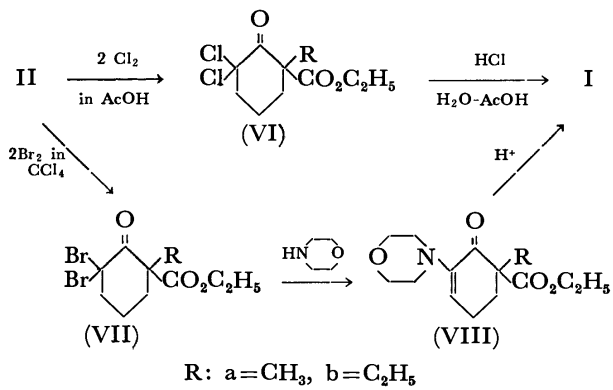

The NMR spectrum of VII in the region of the methylene protons in the ethoxycarbonyl group at an ordinary temperature peaks with two kinds of quartets (δ 4.15 and 4.17 ppm) equal in quantity. These two kinds of quartets are seemed due to axial and equatorial ethoxycarbonyl groups.

The dichloro ketoester (VIa) could be converted to Ia by hydrolysis and by subsequent decarboxylation.

When VIa was refluxed with dilute hydrochloric acid containing acetic acid, Ia was obtained in a 48% yield.

However, the direct acidic or basic hydrolysis of the dibromo ketoester (VIIa) gave mainly tarry materials; Ia was isolated in only a low yield.

On the other hand, the treatment of VIIa with morpholine,[10] followed by acidic hydrolysis, afforded Ia in a 59% yield.

Although the geminal dihalogeno compound has been shown to give the corresponding dimorpholino derivative upon treatment with morpholine,[10] an intermediate, ketoenamine (VIII), was isolated in this reaction in a 56% yield. The structure of VIII was assigned on the basis of its NMR, IR, and UV spectra and on the results of an elementary analysis.

The IR spectrum showed a conjugated double-bond absorption at 1620 cm^{-1}, and the NMR spectrum indicated the vinyl proton as a triplet (J=3.7 Hz) at δ 5.57 ppm.

The bromination of the IIa ketoester with an equimolar amount of bromine in carbon tetrachloride gave ethyl 3-bromo-1-methyl-2-oxocyclohexanecarboxylate (IV) in a good yield.

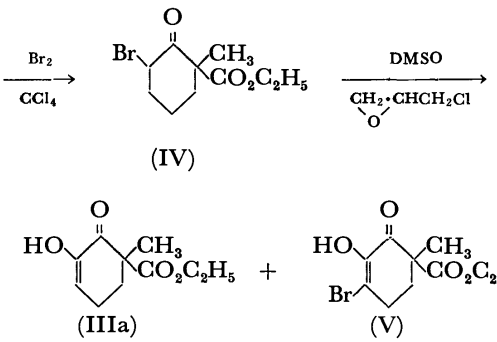

(IV)

(IIIa) (V)

The dimethyl sulfoxide oxidation of IV in the presence of epichlorohydrin as a scavenger for hydrogen bromide provided the enolate of α-diketone (IIIa), together with 3-bromo-6-ethoxycarbonyl-2-hydroxy-6-methyl-2-cyclohexen-1-one (V). The latter compound, V, seemed to be derived from the IIIa and bromine formed *in situ*.

This reaction contrasts with the fact that the DMSO oxidation of 2-bromo-5-ethoxycarbonyl-5-methylcyclopentanone in the presence of epichlorohydrin yielded 5-ethoxycarbonyl-2-hydroxy-5-methyl-2-cyclopenten-1-one exclusively.[6] Investigations are continuing into the DMSO oxidation of alicyclic α-haloketones.

Experimental

All the melting points and boiling points are uncorrected. The infrared spectra were recorded with a Hitachi Model EPI-S2 spectrophotometer, while the ultraviolet spectra were recorded with a Hitachi Model EPS-3T spectrophotometer. The NMR spectra were obtained on a JEOL Model C-60H spectrometer, with tetramethylsilane as the internal reference.

Materials. *Ethyl 2-oxocyclohexanecarboxylate* was prepared from cyclohexanone by the procedure of Synder.[7] *Ethyl 1-methyl-2-oxocyclohexanecarboxylate* was prepared by the method of Kötz.[8a]

Ethyl 1-Ethyl-2-oxocyclohexanecarboxylate (IIb). To a stirred suspension of sodium hydride (9.6 g, 0.2 mol as a 50% suspension in oil) in 300 ml of toluene, 34 g (0.2 mol) of ethyl 2-oxocyclohexanecarboxylate was added at 25°C, after which the mixture was stirred for 30 min. After the complete formation of the sodium salt, 10 ml of dimethyl formamide[11] and 34.3 g (0.22 mol) of ethyl iodide were dropped in at 25—30°C over a period of 15 min. The mixture was then refluxed with stirring for 3 hr. After cooling, the mixture was poured into 200 ml of water and the organic layer was separated. The water layer was extracted with ether, and the extract was combined with the organic layer. After washing with water and drying with magnesium sulfate, the solvent was distilled off. The residual oil (46 g) was distilled to give 33.3 g (84%) of IIb; bp 130—132°C/19 mmHg, n_D^{20}=1.4578. IR(neat): 1740, 1720 (C=O ester), 1710 (C=O) cm^{-1}. NMR(CCl_4): δ 0.80(3H, t, 7.0 Hz), 1.30 (3H, t, 7.0 Hz), 1.5—2.7 (10H, m), 4.18(2H, q, 7.0 Hz). Found: C, 66.77; H, 9.32%. Calcd for $C_{11}H_{18}O_3$: C, 66.64; H, 9.15%.

Ethyl 1-n-Propyl-2-oxocyclohexanecarboxylate (IIc). IIc was prepared according to the IIb procedure described above. Instead of ethyl iodide, *n*-propyl iodide (37.4 g (0.22 mol)) was used to give 35.2 g (83%) of IIc: bp 135—137 °C/14 mmHg, n_D^{20}=1.4573. IR(neat): 1740, 1720 (C=O ester), 1710 (C=O) cm^{-1}. NMR(CCl_4): δ *ca.* 0.95(3H, t, 7.0 Hz), 1.28 (3H, t, 7.0 Hz), 1.5—2.7(12H, m), 4.22(2H, q, 7.0 Hz). Found: C, 68.09; H, 9.89%. Calcd for $C_{12}H_{20}O_3$: C, 67.89; H, 9.50%.

6-Ethoxycarbonyl-2-hydroxy-6-methyl-2-cyclohexen-1-one (IIIa). A mixture of dioxane (100 ml), water (33 ml), selenium dioxide (4.4 g (0.04 mol)), and 3.68 g (0.02 mol) of IIa was stirred under reflux for 22 hr. After cooling, the deposited selenium was filtered off, the solvent was removed at reduced pressure, and the residue was extracted with ether. After drying, the ether was distilled and the resulting oil was distilled to give the crude product, IIIa: bp 92—106 °C/0.3 mmHg. Redistillation yielded 1.6 g (40%) of IIIa; bp 99—100 °C/0.3 mmHg. IR(neat): 3400 (O–H), 1730, 1680 (C=O), 1635 cm^{-1} (C=C). NMR(CCl_4): δ 1.25(3H, t, 7.0 Hz), 1.38(3H, s), 2.0—2.6(4H, m), 4.15 and 4.17(2H, q, 7.0 Hz), 6.0(1H, broad s), 6.55(1H, t, 3.0 Hz). UV max (EtOH): 283 nm (ε=8930). Found: C, 61.23; H, 7.23%. Calcd for $C_{10}H_{14}O_4$: C, 60.59; H, 7.12%.

6-Ethoxycarbonyl-6-ethyl-2-hydroxy-2-cyclohexen-1-one (IIIb). The preparation of IIIb was carried out according to the IIIa procedure described above. A mixture of dioxane (100 ml), water (33 ml), selenium dioxide (8.8 g(0.08 mol)), and IIb (8.0 g (0.04 mol)) was refluxed for 45 hr. A working-up of the reaction mixture yielded 3.0 g (35.4%) of IIIb: bp 110—111 °C/0.6 mmHg. IR(neat): 3400 (O–H), 1730, 1680 (C=O), 1635 cm^{-1} (C=C). NMR(CCl_4): δ 0.89(3H, t, 7.0 Hz), 1.23(3H, t, 7.0 Hz), 1.5—2.7(6H, m), 4.17 and 4.19(2H, q, 7.0 Hz), 6.10(1H, s), 6.75(1H, t, 3.0 Hz). UV-max(EtOH): 262 nm (ε=6390). Found: C, 61.93; H, 7.69%. Calcd for $C_{11}H_{16}O_4$: C, 62.25; H, 7.60%.

Ethyl 3,3-Dichloro-1-methyl-2-oxocyclohexanecarboxylate (VIa). Into a stirred solution of 9.2 g (0.05 mol) of IIa in 55 ml of acetic acid, chlorine(7.8 g(0.11 mol)) was bubbled at 45—50 °C over a period of 1 hr, and then the mixture was stirred for 2 hr (a vpc of the aliquot indicated a complete conversion to the dichlorinated material). The subsequent evaporation of the solvent gave a pale yellow liquid which was distilled to afford 12.5 g (99%) of VIa; bp 111—112 °C/0.45 mmHg, which was solidified in a cool place, mp 31—32 °C (petroleum ether). IR(KBr): 1730 (C=O), 1237 (C–O–C), 790 cm^{-1} (C–Cl). NMR(CCl_4): δ 1.24(3H, t, 7.0 Hz), 1.35(3H, t,

7.0 Hz), 1.5—2.9(6H, m), 4.05 and 4.07(2H, q, 7.0 Hz). Found: C, 47.22; H, 5.65; Cl, 28.16%. Calcd for $C_{10}H_{14}Cl_2O_3$: C, 47.45; H, 5.57; Cl, 28.01%.

Ethyl 3,3-Dibromo-1-methyl-2-oxocyclohexanecarboxylate (VIIa). Into a solution of 18.4 g (0.1 mol) of IIa in carbon tetrachloride (190 ml), we stirred a solution of 35.2 g(0.22 mol) of bromine in 10 ml of carbon tetrachloride at room temperature over a period of 50 min; the mixture was then warmed at 40—45 °C for 3 hr. The mixture was subsequently poured into 300 ml of ice–water, and the organic layer was washed with aqueous sodium bicarbonate and saturated aqueous sodium chloride. After drying and the removal of the solvent, the distillation of the residual pale yellow oil gave 31.6 g (92.4%) of VIIa; bp 130—131 °C/0.3 mmHg. The distillate solidified spontaneously, and recrystallization from petroleum ether afforded VIIa as colorless needles; mp 52 °C. IR(KBr): 1740, 1725 cm^{-1} (C=O); NMR(CCl_4): δ 1.30(3H, t, 7.0 Hz), 1.41(3H, s), 1.6—3.0(6H, m), 4.14 and 4.16(2H, q, 7.0 Hz). Found: C, 35.29; H, 4.18; Br, 46.54% Calcd for $C_{10}H_{14}Br_2O_3$: C, 35.12; H, 4.13; Br, 46.73%.

Ethyl 3,3-Dibromo-1-ethyl-2-oxocyclohexanecarboxylate (VIIb). The preparation of VIIb was carried out according to the procedure VIIa described above. From 9.9 g (0.05 mol) of IIb and 17.6 g (0.11 mol) of bromine, 16.5 g (93%) of VIIb were obtained; bp 138—142 °C/0.4 mmHg, mp 46—46.5 °C (petroleum ether). IR(KBr): 1730, 1715 cm^{-1} (C=O); NMR(CCl_4): δ 0.80(3H, t, 7.0 Hz), 1.30(3H, t, 7.0 Hz), 1.6—2.9(8H, m), 4.14 and 4.16 (2H, q, 7.0 Hz). Found: C, 37.63; H, 4.70%. Calcd for $C_{11}H_{16}Br_2O_3$: C, 37.11; H, 4.53%.

6-Ethoxycarbonyl-6-methyl-2-morpholino-2-cyclohexen-1-one (VIII). Into (17.4 g (0.2 mol) of morpholine, we stirred drop by drop, 6.8 g (0.02 mol) of VIIa. The mixture was then stirred at 35—40 °C for 3 hr. The removal of morpholine under reduced pressure yielded white crystals and orange oils. The crystals were filtered, washed with ether, and recrystallized from ethanol to give 6.4 g (94%) of morpholine hydrobromide; mp 201—202 °C (lit,[12] mp 202 °C). The filtrate was washed with water and dried over magnesium sulfate. After the removal of the ether, the residual oil was chromatographed on a silica gel column. Elution with benzene-ethanol (10 : 1) yielded 3.6 g (56.1%) of VIII: $n_D^{20}=1.5069$. IR(neat): 1725, 1690 (C=O), 1620 cm^{-1} (C=C); NMR(CCl_4): δ 1.20 (3H, t, 7.0 Hz), 1.24(3H, s), *ca.* 1.75 (2H, m), *ca.* 2.52 (6H, m), *ca.* 3.60(4H, m), 4.10(2H, q, 7.0 Hz), 5.57 (1H, t, 3.7 Hz); UVmax(EtOH): 301 nm ($\varepsilon=2710$). Found: N, 5.46%. Calcd for $C_{14}H_{21}NO_4$: N, 5.24%.

2-Hydroxy-3-methyl-2-cyclohexen-1-one (Ia). *a)*: A mixture of 1.5 g of IIIa and 20 ml of 4M-hydrochloric acid was heated with stirring for 4 hr. After cooling, the mixture was saturated with ammonium chloride and extracted with ether. The extract was dried and evaporated to dryness, giving a viscous oil which was solidified by standing in the cool box. Recrystallization from petroleum ether gave 0.60 g (62.7%) of Ia as colorless needles; mp 62—63 °C. (lit,[5d] mp 63 °C). IR(KBr): 3410(O–H), 1670 (C=O). 1645 cm^{-1}(C=C); NMR (CCl_4): δ 1.85(3H, s), 2.00(2H, m), 2.31(2H, m), 2.42(2H, m), 5.90(1H, s); UVmax(EtOH): 275 nm ($\varepsilon=10200$). Found: C, 67.06; H, 8.30%. Calcd for $C_7H_{10}O_2$: C, 66.65; H, 7.99%.

b): Into 17.4 g(0.2 mol) of morpholine, we stirred 6.8 g (0.02 mol) of VIIa, drop by drop. The mixture was then stirred at 35—40 °C for 3 hr. The subsequent evaporation of the excess morpholine yielded white crystals and orange oils. After the filtration of the crystals, the filtrate (5.0 g) was stirred with a 4M-hydrochloric acid solution for 1 hr at room temperature. A further 20 ml of conc. hydrochloric acid was added to the mixture, after which it was refluxed for 10 hr. Working up in a manner similar to that described above yielded 1.50 g (59.5%) of Ia; bp 70—80 °C/4 mmHg, mp 62 °C.

c): A mixture of 4.7 g (25.6 mmol) of IIa, 10.8 g(63.4 mmol) of cupric chloride, 40 ml of water, and 40 ml of acetic acid was stirred under reflux for 10 hr. After the copper compound has been filtered off, the solvent was removed under reduced pressure and extracted with ether. After drying and the removal of the ether, the distillation of the residual oil gave a pale yellow liquid (bp 80—90 °C/3 mmHg), parts of which solidified upon standing in a cool box. The precipitated crystals were separated, and recrystallization from petroleum ether gave 0.40 g (12.4%) of Ia; mp 60—62 °C.

d): A mixture of 6.3 g (25 mmol) of VIa, 50 ml of 5% hydrochloric acid, and 20 ml of acetic acid was refluxed with stirring for 46 hr. After cooling, the mixture was saturated with ammonium chloride and extracted with ether. After drying, the evaporation of the ether gave a viscous oil (3.8 g) which was subsequently distilled to give 1.50 g (47.6%) of Ia (bp 63—65 °C/3 mmHg), which was spontaneously solidified; mp 62—63 °C.

3-Ethyl-2-hydroxy-2-cyclohexen-1-one (Ib). *a)*: A mixture of 2.0 g of IIIb, 26 ml of 3M hydrochloric acid, and 8 ml of ethanol was refluxed with stirring for 20 hr., After cooling, a black oil was filtered off and the filtrate was extracted with chloroform. After the filtrate has been dried over magnesium sulfate, the evaporation of the solvent yielded a crude oil (0.60 g). The residual oil was distilled to give 0.40 g (30%) of Ib; bp 75—80 °C/6 mmHg; mp 29—30 °C (lit,[13] mp 29.5 °C). IR(KBr): 3410(O–H), 1670(C=O), 1650 cm^{-1} (C=C); NMR(CCl_4): δ 1.03(3H, t, 7.3 Hz), 1.6—2.7(8H, m), 5.89(1H, s); UVmax(EtOH): 276 nm ($\varepsilon=10800$). Found: C, 68.45; H, 8.57%. Calcd for $C_8H_{12}O_2$: C, 68.55; H, 8.63%.

b): Ib was prepared according to Procedure Ia Method *b)*, as described above. From 26.1 g (0.3 mol) of morpholine and 10.7 g (0.03 mol) of VIIb, we obtained 9.5 g of crude VIIIb, which was then hydrolyzed and decarbethoxylated to give 0.75 g (18%) of Ib; mp 29—30 °C. The infrared spectrum and the other chemical properties were identical with those of Ib presented above.

Ethyl 3-Bromo-1-methyl-2-oxocyclohexanecarboxylate (IV). To a stirred solution of 12.9 g (0.07 mol) of IIa in 140 ml of carbon tetrachloride, we added a solution of 11.5 g (0.072 mol) of bromine in 10 ml of carbon tetrachloride at 10 °C over a period of 80 min, and then we stirred the mixture for 5 hr. The resulting mixture was poured into water, and the organic layer was washed with aqueous sodium bicarbonate and aqueous sodium chloride. After drying and the removal of the solvent, the distillation of the residual oil gave 16.2 g (88.1%) of IV: bp 115—116 °C/1.2 mmHg. IR(neat) 1730, 1712 (C=O), 1260, 1160, 1024 cm^{-1} (C–O–C); NMR(CCl_4): δ 1.28(3H, t, 7.0 Hz), 1.32(3H, s), 1.6—2.7(6H, m), 4.23(2H, q, 7.0 Hz), 4.5—5.0(1H, m). Found: C, 45.61; H, 5.78; Br, 30.12%. Calcd for $C_{10}H_{15}BrO_3$: C, 45.64; H, 5.75; Br, 30.36%.

The Dimethyl Sulfoxide Oxidation of IV. A mixture of 10.5 g (0.04 mol) of IV, 3.7 g (0.04 mol) of epichlorohydrin, and 100 ml of DMSO was stirred at 69—72 °C for 8 hr. Then the DMSO was removed from the reaction mixture under reduced pressure, and the resulting oil was distilled to give 4.2 g (61%) of 1-bromo-3-chloro-2-propanol [bp 55—64 °C/0.7 mmHg, lit,[14] bp 92 °C/20 mmHg] and 6.6 g of an oil [bp 105—112 °C/0.7 mmHg]. The fractional distillation of the latter oil gave 2.0 g (25%) of IIIa [bp 105—108 °C/0.7

mmHg] and 3.5 g (33%) of V (bp 115—125 °C/0.7 mmHg), which was solidified spontaneously, subsequent recrystallization from petroleum ether afforded V as colorless crystals (mp 80—81 °C). IR(KBr): 3420 (O-H), 1715, 1675(C=O), 1640 cm^{-1}(C=C); NMR($CDCl_3$): δ 1.24(3H, t, 7.3 Hz), 1.44(3H, s), 1.70—3.0(4H, m), 4.16(2H, q, 7.3 Hz), 6.34(1H, s); UV_{max}(EtOH): 282.5 nm (ε=10200). Found: C, 43.84; H, 4.89%. Calcd for $C_{10}H_{13}BrO_4$: C, 43.34; H, 4.73%.

References

1) Presented in part at the 28th Annual Meeting of the Chemical Society of Japan, Tokyo, April, 1973.

2) A. O. Pittet, P. Rittersbacher, and R. Muralidhara, *J. Agr. Food. Chem.*, **18**, 929 (1970).

3) M. A. Gianturco, A. S. Giammarino, and R. G. Pitcher, *Tetrahedron*, **19**, 2051 (1963); M. A. Gianturco, A. S. Giammarino, and P. Friedel, *Nature*, **210**, 1358 (1966).

4) P. E. Shaw, J. H. Tatum, and R. E. Berry, *J. Agr. Food. Chem.*, **16**, 979 (1968).

5) a) C. Harries, *Ber.*, **35**, 1178 (1902); b) O. Wallach, *Ann. Chem.*, **414**, 314 (1918); c) O. Wallach and A. Weissenborn, *ibid.*, **437**, 180 (1924); d) W. N. Cumper, G. B. Leton, and A. I. Vogel, *J. Chem. Soc.*, **1965**, 2067.

6) K. Sato, S. Suzuki, and Y. Kojima, *J. Org. Chem.*, **32**, 339 (1967); K. Sato, Y. Kojima, and H. Sato, *ibid.*, **35**, 2374 (1970).

7) H. R. Synder, L. A. Brooks, and S. H. Shapiro, "Organic Syntheses," Coll. Vol. II, p. 531 (1943).

8) a) A. Kötz and A. Micheis, *Ann. Chem.*, **350**, 212 (1906); b) S. J. Rhoads, J. C. Gilbert, A. W. Decora, T. R. Garland, R. J. Spangler, and M. J. Urbigkit, *Tetrahedron*, **19**, 1625 (1963).

9) C. M. Leir, *J. Org. Chem.*, **35**, 3203 (1970).

10) M. Kerfant, *C. R. Acad. Sci. Paris*, **252**, 3457 (1961).

11) A large quantity of DMF decreases the yield of C-alkylated ketoester.

12) J. Gilbert and H. Gault, *Bull. Soc. Chim. Fr.*, **1965**, 2975.

13) Y. Abe, T. Harukawa, H. Ishikawa, and T. Miki, *Yakugaku Zasshi*, **72**, 1451 (1952).

14) L. Blanchard, *Bull. Soc. Chim. Fr.*, **41**, 824 (1927).

The Amination and Dimerization of Norbornadiene with Nickel, Palladium, and Rhodium Complexes

Jitsuo KIJI, Satoshi NISHIMURA, Susumu YOSHIKAWA, Eiichi SASAKAWA, and Junji FURUKAWA

Department of Synthetic Chemistry, Faculty of Engineering, Kyoto University, Kyoto 606

(Received May 1, 1974)

The reactions of norbornadiene in amine by the use of nickel, palladium and rhodium complexes have been studied in the presence of protic acid. A catalytic system of $Ni(COD)_2$ (**1**)-n-Bu_3P gives a mixture of 5-*exo*-(*o*-tolyl)-2-norbornene (**3**) and 5-*exo*-(*N*-amino)-2-norbornene (**4**). Bis(triphenylphosphine)(maleic anhydride)-palladium (**5**) gives 3-(*N*-amino)nortricyclene (**6**). Dichlorotetrakis(cyclooctene)dirhodium (**10**) gives a [2+4] cycloaddition product (**11**). All these reactions mechanisms are discussed from the point of view of an acid-promoted reaction on low-valent transition metal complexes.

The amination or telomerization of 1,3-dienes is of interest from the points of view of both synthetic chemistry and mechanistic study. It has been clarified that controlled amounts of some protic acids enhanced the reactions remarkably.[1] However, the transition metal-catalyzed addition of an amine to olefin or homo-conjugated diene has so far been lacking. Norbornadiene is here employed as the diolefinic substrate in order to determine whether or not the anchimeric participation of one double bond might result in a transition metal-catalyzed addition of amine similar to that observed for 1,3-dienes, if the amination is possible.

On the other hand, the dimerization of norbornadiene by transition metals has been extensively studied.[2] The normal products in an aprotic solvent are [2+2] or [4+2] cycloaddition compounds. Previous work in this laboratory has shown a novel dimerization of norbornadiene by some nickel catalysts in an amine, giving 5-*exo*-(*o*-tolyl)-2-norbornene as the major product.[3] This reaction is also explicable in terms of an acid-promoted dimerization on a zerovalent nickel complex. Consequently, we expected that the amination and the dimerization might occur competitively. It appeared to us that the reaction patterns can, to a great extent, be altered mainly by adjusting the acidity of the catalytic system or by controlling the amount of protic acid added. Accordingly, we undertook a study of the effect of added acid on the reaction. This paper will be concerned with a systematic investigation of the reactions of norbornadiene by several nickel-, palladium-, and rhodium complexes.

Results and Discussion

The polymerization of norbornadiene catalyzed by low-valent nickel or palladium complexes proceeded rapidly in an alcohol, but in an amine no appreciable polymerization occurred. The use of amine as a solvent was favorable for the reaction of norbornadiene. Consequently, under these conditions the dimerization and the amination occurred competitively when trifluoroacetic acid was added. Among the amines used, cyclic amines such as morpholine and piperidine gave the best results. Accordingly, these amines were used.

Nickel Catalysts. Bis(1,5-cyclooctadiene)nickel (**1**) was used in the presence of tri-*n*-butylphosphine. The reaction in morpholine or piperidine proceeded smoothly at 90 °C. Without trifluoroacetic acid, only the [2+2]cycloaddition compound (**2**) was formed in a *ca.* 60% yield.

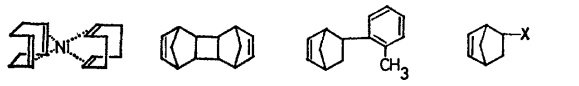

1 **2** **3** **4**

a: X=N O

b: X=N

A striking change in the reaction occurred when a small amount of trifluoroacetic acid (1 equiv. to Ni) was added to the system. The product (**2**) was no longer formed; instead 5-*exo*-(*o*-tolyl)-2-norbornene (**3**) was obtained as the sole dimeric product, accompanied by a small amount of 5-*exo*-(*N*-amino)-2-norbornene (**4**). The identifications of the products were based on the mass, infrared-, and NMR-spectra. The *endo* proton on the C-5 atom of **4** can couple only with two neighboring protons on the C-6 carbon atom, not with the bridge-head, giving a double doublet at 8.0 τ for **4a**. The spectral data of **3** have been reported previously.[3]

The further addition of the acid prevented the formation of **3**, but promoted that of **4**. These results are graphically shown in Fig. 1.

This reaction pattern is explicable in terms of a mechanism similar to that proposed in the dimerization

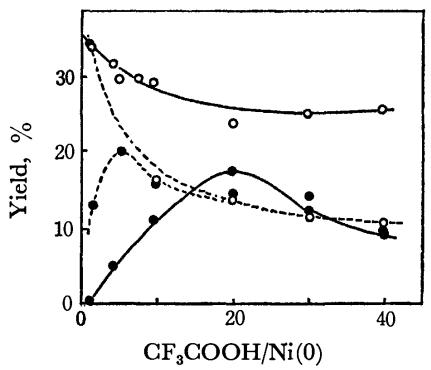

Fig. 1. Effect of [CF_3COOH] on the reaction by Ni at 90 °C.
(○), 5-*exo*-(*o*-Tolyl)-2-norbornene; (●), 5-*exo*-(N-amino)-2-norbornene.
(——), in morpholine; (·····), in piperidine.
Conditions: [$Ni(COD)_2$]=0.05 mmol, [n-Bu_3P]=0.2 mmol, [norbornadiene]=2 mmol; amine, 0.4 ml; 15 hr.

and amination of 1,3-dienes; a large amount of the added acid prevents the homolytic coupling of norbornadiene on the ligand-containing zerovalent nickel NiL_x, because the reaction of protic acid with the zerovalent nickel complex lies in the following equilibrium:[4]

$$HX + NiL_x \rightleftharpoons [HNiL_x]^+X^- \quad (1)$$

On the other hand, the first step in the amination appears to involve a metal-hydride initiated mechanism; metal-hydride adds to one of the carbon-carbon double bonds of norbornadiene. A similar reaction scheme was established in the reaction of 1,3-diene, which proceeds through a π-allyl intermediate.

It has already been reported in a previous paper[3] that the dimerization of norbornadiene in amine by the $(n\text{-}Bu_3P)_2NiBr_2$–$NaBH_4$ (1 : 1) system gives 5-*exo*-(*o*-tolyl)-2-norbornene. In this case, only the dimer was obtained, no appreciable amount of the reaction product of amine with norbornadiene being formed. The present results (Fig. 1) are consistent with the previous results, because the mixture of $(n\text{-}Bu_3P)_2NiBr_2$–$NaBH_4$ (1 : 1) is considered to give a system consisting of zerovalent nickel and an equimolar amount of hydrogen bromide (that is, the HX/Ni(0) ratio is unity); thus, the major product of the previous study is 5-*exo*-(*o*-tolyl)-2-norbornene.

Palladium Catalyst. Bis(triphenylphosphine)(maleic anhydride)palladium was effective in the reaction of norbornadiene with amines. The most marked difference in the catalysis between the palladium and nickel complexes lies in the reaction product. No dimeric product was formed; 3-(*N*-amino)nortricyclene was the sole reaction product. In this case, however, a higher temperature, 110 °C, was favorable for the desired reaction. The product was identified as

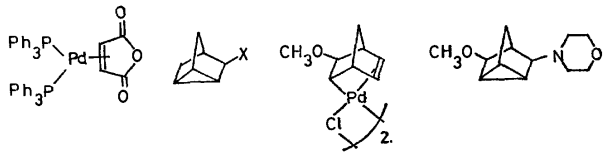

5 6 7 8

a: X= 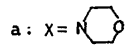

b: X= 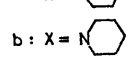

follows; the infrared spectrum has strong absorptions at 3080 and 805 cm^{-1} due to its nortricyclyl structure,[5] and no absorption due to olefinic protons is observed in its NMR spectrum.

In this catalytic system, trifluoroacetic acid plays an important role. No obvious reaction occurs without the added acid (Fig. 2). The added acid has a promoting effect on the formation of a palladium hydride. The equilibrium of Eq. 1 is applicable to the palladium complex also. However, in this case the equilibrium is considered to lie far to the right. This assumption is consistent with the fact that stable metal hydrides of the platinum group can be isolated.[6] Consequently, the coupling of norbornadiene no longer occurs on the palladium complex, but the reaction of the hydride

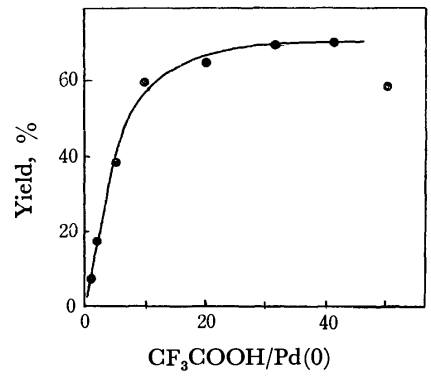

Fig. 2. Effect of [CF_3COOH] on the reaction by Pd at 110 °C.
Conditions: $Pd(PPh_3)_2(C_4H_2O_3)$, 0.015 mmol; norbornadiene, 2 mmol; piperidine, 0.4 ml; 5 hr.

with norbornadiene predominates; thus, a nortricyclyl palladium intermediate is formed. The addition of a large amount of the acid resulted in the formation of polymeric products. It is noteworthy that an acid-base reaction between the added acid and amine occurs competitively with the reaction of Eq. 1. Therefore, as the co-catalyst a quaternary ammonium salt such as piperidine hydrochloride can be used instead of the acid. However, its efficiency was far lower.

The stereochemistry of this amination is interesting to study. Complex **7**[7] was prepared for this purpose. When the pale-yellow complex **7** was added to morpholine, the complex turned black immediately. The gas-chromatographic analysis showed a single component(**8**). The presence of the infrared bands at 800 and 820 cm^{-1} indicated the formation of a derivative of nortricyclene. The chemical shift of the proton at C-5 (the carbomethoxy-bearing carbon) is very close to that of 3-carbomethoxynortricyclene.[8] From the spectral data, it may be concluded that the environment of the proton at the C-5 atom is not influenced by introducing the amino group at the C-3 atom. This fact indicates that the amino group is located in an *exo* configuration with respect to the methylene bridge. This stereochemistry suggests that the reaction of the amino group occurs in the opposite direction from the palladium atom. The reaction mechanism of this model compound seems to be applicable to the acid-promoted catalytic reaction with **5**. The only difference lies in the point that the intermediate in the catalytic reaction has a hydrogen atom instead of the methoxy group at the C-5 atom.

Rhodium Catalyst. As has been described above, the metal-hydride is an active species in the amination. From this point of view, hydridocarbonyltris(triphenylphosphine)rhodium (**9**) was used. However, the hydride was too stable to catalyze the amination.

$HRh(CO)(PPh_3)_3$ $[RhCl(C_8H_{14})_2]_2$ 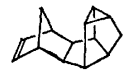

9 **10** **11**

The catalytic activity of dichlorotetrakis(cyclooctene)dirhodium (**10**) was low in reaction to the amination or

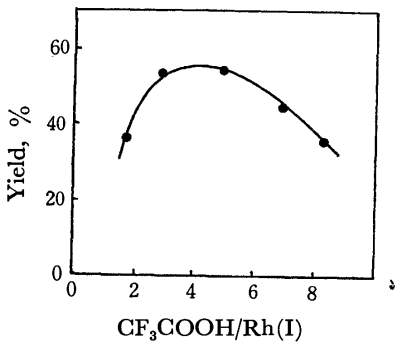

Fig. 3. Effect of [CF_3COOH] on the reaction by Rh at 110 °C.
Conditions: [$RhCl(COE)_2]_2$, 0.02 mmol; norbornadiene, 5.4 mmol; 8 hr.

dimerization in the presence of tri-*n*-butylphosphine and trifluoroacetic acid, and **4** was obtained in a low yield, accompanied by a small amount of the hydrogenation product of **4**. In the absence of the phosphine, however, **10** showed a specific activity for the formation of **11**. The identification of **11** was done by comparing its NMR spectrum with the reported one.[9] As is shown in Fig. 3, the yield was also influenced by the presence of acid. The maximum yield was realized when 4 equivalents of trifluoroacetic acid to **10** were added to the system. This catalytic system is characteristic in the point that **11** is selectively formed. The ordinary rhodium catalyst gives a mixture of dimers,[14] and the selectivity of **11** is not so high as in the present case. In this dimerization, the presence of amine has no effect on the reaction.

Experimental

Materials. Bis(1,5-cyclooctadiene)nickel,[10] dichlorobis(6-methoxybicyclo[2.1.1]hept-2-ene)dipalladium,[7] and bis(triphenylphosphine)(maleic anhydride)palladium,[11] hydridocarboxyltris(triphenylphosphine)rhodium,[12] and dichlorotetrakis(cyclooctene)dirhodium[13] were prepared according to the reported methods. Amines and norbornadiene were dried by the usual methods and, if necessary, distilled under an atmosphere of argon and stored over a Molecular Sieve 3 Å. Commercially-available trifluoroacetic acid and *n*-butylphosphine were used without further purification. Gas-chromatographic analyses were carried out on a Silicone DC 550 column on Celite 545 (3m, 150 °C), using tetralin as the internal standard.

Catalytic Reaction with Nickel Complex. All the reactions were carried out under an argon atmosphere in a sealed glass tube.

A. Without the Acid. In a glass tube (8 mm in diameter), 0.05 mmol of bis(1,5-cyclooctadiene)nickel was placed under an argon atmosphere, and then 0.2 mmol of Bu_3P, 0.4 ml of morpholine and 0.2 ml (2 mmol) of norbornadiene were added (in this order). The tube was sealed with a flame and heated without agitation at 90 °C for 15 hr. Subsequent gas-chromatographic analysis showed that the dimer (**2**) was formed in a 60% yield.

B. With the Acid. The following procedure is illustrative. To 0.05 mmol of $Ni(COD)_2$ in the glass tube was added 0.4 ml of morpholine containing 0.25 mmol (variable, as is shown in Fig. 1) of trifluoroacetic acid, 0.2 mmol of *n*-Bu_3P, and 0.2 ml of norbornadiene. The tube was sealed and heated without agitation at 90 °C for 15 hr. Subsequent gas-chromatographic analysis showed the formation of 5-*exo*-(*o*-tolyl)-2-norbornene, **3** (in a 30% yield) and **2**-*exo*-(*N*-morpholino)-2-norbornene, **4a** (in a 20% yield). The products were separated by gas-chromatography. The identification was based on the infrared, NMR, and mass spectra. The NMR spectrum ($CDCl_3$) showed peaks at 3.9, 4.1, (quartet), and 8.0 τ (double doublet). The yields under other conditions are shown graphically in Fig. 1.

*Catalytic Reactions with Palladium Complex (**5**).* The procedure was similar to those described above. The results are shown in Fig. 2. The infrared spectrum of **6a** showed strong absorptions at 800 and 810 cm^{-1} due to the nortricyclyl framework. The NMR spectrum ($CDCl_3$) showed multiplets centered at 8.0 (1H), 8.4 (1H), 8.9(1H), 8.2(2H), and 9.8 τ (4H).

*Reaction of **7** with Morpholine.* To 0.55 g (1 mmol) of **7** we added 4 ml of morpholine. The yellow complex, **7** immediately turned black. The solution was then stirred at room temperature for 5 hr. Subsequent gas-chromatographic analysis showed the formation of **8** in a 45% yield. The NMR spectrum has singlets at 8.7 (3H), 8.4 (1H), 8.0 (2H), and 6.6 τ (3H of methoxy group) and two multiplets centered at 7.7(4H, of morpholine) and 6.3 τ (4H of morpholine). The mass spectrum has a peak due to the molecular ion at *m/e* 209.

*Catalytic Reaction of the Rhodium Complex (**10**).* The reaction was carried out such as has been described above. The reaction conditions are shown in Fig. 3. The identification of the product (**11**) was based on the NMR spectrum.[9]

References

1) J. Kiji, K. Yamamoto, E. Sasakawa, and J. Furukawa, *Chem. Commun.*, **1970**, 770; *J. Organometal. Chem.*, in press.
2) F. D. Mango and J. H. Schachtschneider, "Transition Metals in Homogeneous Catalysis," ed. by G. N. Schrauzer, Marcel Dekker, New York, N. Y. (1971), p. 223.
3) S. Yoshikawa, K. Aoki, J. Kiji, and J. Furukawa, *Tetrahedron*, **30**, 405 (1974).
4) C. Tolman, *J. Amer. Chem. Soc.*, **92**, 4217 (1970).
5) J. D. Roberts, E. R. Trumbull, Jr., W. Bennett, and R. Armstrong, *ibid.*, **72**, 3116 (1950).
6) E. H. Brooks and F. Glockling, *J. Chem. Soc., A*, **1967**, 1030.
7) J. Chatt, L. M. Vallarino, and L. M. Venanzi, *J. Chem. Soc.*, **1957**, 1413.
8) J. K. Stille and L. F. Hines, *J. Amer. Chem. Soc.*, **92**, 1798 (1970).
9) G. E. Voecks, P. W. Jennings, G. D. Smith, and C. N. Caughlan, *J. Org. Chem.*, **37**, 1460 (1972).
10) M. F. Semmelhack, "Organic Reactions," Vol. 19, John Wiley and Sons, Inc., New York, N. Y., 1972, p. 115.
11) S. Takahashi, T. Shibano, and N. Hagihara, *Tetrahedron Lett.*, **1967**, 2451.
12) D. Evans, G. Yagupsky, and G. Wilkinson, *J. Chem. Soc. A*, **1968**, 2660.
13) L. Porri, A. Lionetti, G. Allegra, and A. Immirzi, *Chem. Commun.*, **1965**, 336.
14) The rhodium complex (**10**) has been used as a catalyst for the dimerization of norbornadiene. However, the complex **10** has no catalytic activity. In the presence of triphenylphosphine it gives a mixture of a varity of the dimers; N. Acton, R. J. Roth, T. J. Katz, J. K. Frank, C. A. Maier, and I. C. Paul, *J. Amer. Chem. Soc.*, **94**, 5446 (1972).

A New Method of Preparing Flavones

Akira KASAHARA, Taeko IZUMI, and Masatoshi OOSHIMA

Department of Applied Chemistry, Faculty of Engineering, Yamagata University, Yonezawa, Yamagata 992

(Received May 8, 1974)

The reaction of the sodium salt of 2′-hydroxychalcones with palladium(II) salt led to the formation of flavones, accompanied by a small amount of flavanones. The reaction proceeds *via* a phenoxypalladation, followed by the elimination of a hydridopalladium(II).

In the presence of palladium(II) salt, the reaction of the oxygen nucleophile with the carbon-carbon double bond has received wide attention.[1] Hosokawa *et al.*[2] have recently reported that the reaction of the sodium salt of 2-allylphenol with dichlorobis(benzonitrile) palladium in refluxing benzene proceeds *via* an intramolecular phenoxypalladation and gives 2-methylbenzofuran in a 31% yield. Independently of their work, we wish now to report that flavones (**1**) can be prepared in a high yield by the reaction of the sodium salt of 2′-hydroxychalcones (**2**) with lithium chloropalladite in a polar solvent, such as acetonitrile or ethanol. On the other hand, numerous reports of the synthesis of **1** have appeared in literature.[3] No direct cyclization of **2** into **1** is, however, known with the exception of the reaction of **2** with selenium dioxide in amyl alcohol or in xylene (the yields are not very good).[4]

Results and Discussion

At room temperature, the sodium salt of **2** was treated with lithium chloropalladite or with palladium(II) acetate in a polar solvent, such as acetonitrile or ethanol, to produce **1**, accompanied by a small amount of flavanone (**3**). For example, the reaction of 2′-hydroxychalcone (**2a**) with lithium chloropalladite in acetonitrile resulted in the formation of flavone (**1a**) (yield=75%) and flavanone (**3a**) (yield=6%). Similarly, 6-methoxy- and 7-methoxyflavone (**1d** and **1e**) were synthesized from the corresponding 2′-hydroxychalcones (**2d** and **2e** respectively). The reactions carried out are summarized in Table 1, and the usual conversions of **2** in the range of 40—90% were obtained. On the other hand, the reaction of **2a** with a combination of the palladium(II) catalyst and the copper(II) chloride co-catalyst gave **1a** (yield=62%) and **3a** (yield=16%). In the conversion of **2** to **1** with palladium(II) salt, no formation of the five-membered-ring product [benzylidenebenzofuran-3(2H)-one] was observed.

Usually, the addition of oxygen nucleophile to the carbon-carbon double bond of the olefin-palladium complex proceeds by the attack at the double bond on the side opposite from that facing the metal.[5] In addition, Henry *et al.*[6] have recently reported that the oxidation of deuterated cyclohexene by a mixture of palladium(II) chloride and copper(II) chloride in acetic acid gave products which were consistent with a *trans* acetoxypalladation, followed by a *cis* palladium(II)-hydride elimination. The reaction of **2** with palladium(II) salt, therefore, involves an intramolecular *trans* phenoxypalladation, followed by a *cis* palladium(II)-hydride elimination. On the other hand, the formation of **3** proceeds *via* a base-catalyzed cyclization of **2**.

Experimental

Materials. All the melting points are uncorrected. The following compounds were synthesized by the methods described in the literature: 2′-hydroxychalcone (**2a**),[7] 2′-hydroxy-4-methoxychalcone (**2b**),[8] 2′-hydroxy-3,4-methylenedioxychalcone (**2c**),[9] 2′-hydroxy-5′-methoxychalcone (**2d**),[10] 2′-hydroxy-4′-methoxychalcone (**2e**),[11] 2′-hydroxy-4,4′-dimethoxychalcone (**2f**),[12] and 2′-hydroxy-4,5′-dimethoxychalcone (**2g**).[13]

General Procedure for the Preparation of 1. A solution of 10 mmol of **2** in benzene (20 ml) was stirred with 10 mmol of sodium methoxide for 5 min at room temperature. To the mixture, lithium chloropalladite or palladium(II) acetate (10 mmol in 70 ml of solvent) was then added, after which the mixture was stirred at reaction temperature. After the resulting mixture had been filtered to remove the precipitated palladium metal, the filtrate was evaporated to dryness *in vacuo* to remove the solvent. The residue was poured into water and extracted with chloroform. The chloroform solution was washed with water, and then dried over anhydrous magnesium sulfate. After the evaporation of the solvent, the products were isolated by column chromatograph on silica gel. The first elution with benzene afforded the unreacted starting material (**2**), while the second elution and recrystallization from ethanol afforded the respective flavanones (**3**). Further elution with benzene-chloroform

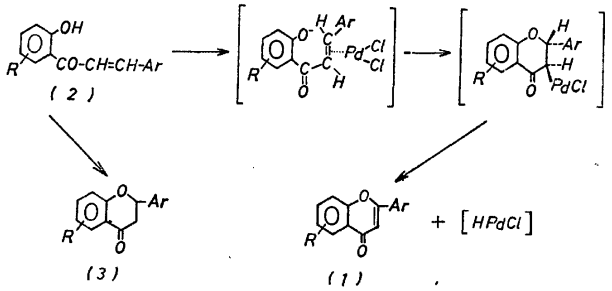

Fig. 1.

and recrystallization from benzene or ethanol afforded the respective flavones (**1**). The structures of the products were confirmed by mixed-melting-point determination with an authentic sample and by the observation of the IR and NMR spectra. The results are summarized in Table 1.

The authors would like to express their deep thanks to Mr. Hajime Baba of Yamagata University for his kind offering of the authentic samples, and to the Kawaken Fine Chemical Co., Ltd., for a gift of palladium chloride.

Table 1. The Reaction of 2'-hydroxychalcone (2) with palladium(II) salt

Substrate	Pd(II) salt	Solvent	Reaction temp.	Reaction time(hr)	Convn (%)[a]	Product	Mp °C (lit.)	Yield (%)
2a	Li_2PdCl_4	C_2H_5OH	room temp.	24	80	Flavone (**1a**)	96— 97 (97[b])	65
						Flavanone (**3a**)	75— 76 (76[c])	15
2a	Li_2PdCl_4	CH_3CN	room temp.	24	81	**1a**		75
						3a		6
2a	Li_2PdCl_4	CH_3CN	reflux	2	70	**1a**		55
						3a		15
2a	Li_2PdCl_4[d] $+CuCl_2$	CH_3CN	reflux	8	78	**1a**		62
						3a		25
2a	$Pd(OAc)_2$	CH_3CN	room temp.	48	40	**1a**		25
						3a		15
2a	$Pd(OAc)_2$	CH_3CN	reflux	2	65	**1a**		52
						3a		13
2b	Li_2PdCl_4	CH_3CN	room temp.	24	90	4'-Methoxyflavone (**1b**)	156—158 (157—158[e])	83
						4'-Methoxyflavanone (**3b**)	96— 97 (97[f])	7
2c	Li_2PdCl_4	CH_3CN	room temp.	24	87	3',4'-Methylenedioxyflavone (**1c**)	199—200 (200—201[e])	78
						3',4'-Methylenedioxyflavanone (**3c**)	127—128 (127[g])	9
2d	Li_2PdCl_4	CH_3CN	room temp.	24	90	6-Methoxyflavone (**1d**)	152—154 (154[h])	83
						6-Methoxyflavanone (**3d**)	140—142 (142[i])	7
2e	Li_2PdCl_4	CH_3CN	room temp.	24	85	7-Methoxyflavone (**1e**)	110—112 (110—111[j])	78
						7-Methoxyflavanone (**3e**)	90— 91 (91[k])	7
2f	Li_2PdCl_4	CH_3CN	room temp.	24	80	4',7-Dimethoxyflavone (**1f**)	142—143 (143—144[l])	72
						4',7-Dimethoxyflavanone (**3f**)	94— 95 (94— 95[m])	8
2g	Li_2PdCl_4	CH_3CN	room temp.	24	88	4',6-Dimethoxyflavone (**1g**)	192—194 (194—195[n])	82
						4',6-Dimethoxyflavanone (**3g**)	159—160 (160[o])	6

a) Conversion is defined as convn $\% = \frac{\text{mol (1+3)}}{\text{mol (2) charged}} \times 100$. b) T. S. Wheeler, "Organic Syntheses," Vol. 32, p. 72 (1952). c) A. Lowenbein, *Ber.*, **57**, 1515 (1924). d) In the reaction, 10 mmol of **2a**, 10 mmol of sodium methoxide, 2 mmol of Li_2PdCl_4, and 20 mmol of $CuCl_2 \cdot 2H_2O$ were used. e) K. v. Auwers and L. Auschutz, *Ber.*, **54**, 1543 (1921). f) A. Edelstein and S. v. Kostanecki, *ibid.*, **38**, 1507 (1905). g) S. Fujise and S. Sasaki, *Nippon Kagaku Zasshi*, **72**, 462 (1951). h) H. Simonis and D. Danischewski, *Ber.*, **59**, 2914 (1926). i) H. Simonis and C. Lear, *ibid.*, **59**, 2908 (1926). j) T. Emilewicz and S. v. Kostaneck, *ibid.*, **32**, 309 (1899). k) S. v. Kostanecki and M. L. Stoppani, *ibid.*, **37**, 1180 (1904). l) J. Tambor, *ibid.*, **49**, 1704 (1916). m) K. Juppen and S. v. Kostanecki, *ibid.*, **37**, 4161 (1904). n) A. T. M. Dunne, J. E. Gowan, J. Keane, B. M. O'Kelly, D. O'Sullivan, M. M. Rocke, P. M. Ryan, and T. S. Wheeler, *J. Chem. Soc.*, **1950**, 1252. o) S. v. Kostanecki and M. L. Stoppani, *Ber.*, **37**, 781 (1904).

References

1) a) J. Tsuji, "Advances in Organic Chemistry: Methods and Results," Vol. 6, ed. by E. C. Taylor and H. Wynberg, Interscience, New York (1969), p. 109. b) R. Jira and W. Freiesleben, "Organometallic Reactions," Vol. 3, ed. by E. I. Becker and M. Tsutsui, Wiley-Interscience, New York (1972), p. 1. c) M. Hancock, M. N. Levy, and M. Tsutsui, *ibid.*, Vol. 4, (1972) p. 1. d) P. M. Maitlis, "The Organic Chemistry of Palladium," Vol. 2, Academic Press, New York (1971), p. 77.

2) T. Hosokawa, K. Maeda, K. Koga, and I. Moritani, *Tetrahedron Lett.*, **1973**, 739.

3) S. Fujise, S. Hishida, S. Sasaki, H. Obara, and H. Uda, "Dai Yuki Kagaku," (Comprehensive Organic Chemistry), Vol. 14, ed. by M. Kotake, Asakura Shoten, Tokyo (1960), p. 1.

4) H. S. Mahel, H. S. Rai, and K. Venkatarman, *J. Chem. Soc.*, **1935**, 866; H. S. Mahel and K. Venkatarman, *ibid.*,

1936, 569.
5) a) M. Green and R. I. Hancock, *J. Chem. Soc. A*, **1967**, 2054. b) J. K. Stille and D. B. Fox, *J. Amer. Chem. Soc.*, **92**, 1274 (1970). c) J. K. Stille, D. E. James, and L. F. Hines, *ibid.*, **95**, 5062 (1973).
6) P. M. Henry and G. A. Ward, *ibid.*, **93**, 1494 (1971); *ibid.*, **94**, 7305 (1972).
7) W. Feuerstein and S. v. Kostanecki, *Ber.*, **31**, 710 (1898).
8) F. Herstein and S. v. Kostanecki, *ibid.*, **32**, 318 (1899).
9) W. Feuerstein and S. v. Kostanecki, *ibid.*, **32**, 315 (1899).
10) H. Simonis and S. Danischewski, *ibid.*, **59**, 2914 (1926).
11) K. v. Auwers and E. Risse, *ibid.*, **64**, 2216 (1931).
12) S. Fujise and H. Tatsuta, *Nippon Kagaku Zasshi*, **63**, 932 (1942).
13) G. N. Vyes and N. M. Shah, *J. Indian Chem. Soc.*, **28**, 75 (1957).

A New Synthesis of α,β-Unsaturated Carboxylic Esters. The Condensation of Ethyl Lithiotrimethylsilylacetate with Carbonyl Compounds

Hiroaki TAGUCHI, Katsuichi SHIMOJI, Hisashi YAMAMOTO, and Hitosi NOZAKI

Department of Industrial Chemistry, Faculty of Engineering, Kyoto University, Yoshida, Kyoto 606

(Received May 27, 1974)

The key step of the title synthesis involves the conversion of ethyl trimethylsilylacetate to the corresponding enolate, **1**, by treatment with lithium dicyclohexylamide in tetrahydrofuran at −78 °C. The condensation of **1** with aldehydes and ketones proceeds smoothly to afford the desired two carbon homologated unsaturated esters in excellent yields. The new process is extended with success to readily-enolizable carbonyl compounds and also to chalcone, which gives no trace of the Michael adduct in the present reaction.

In the conversion of carbonyl compounds to two carbon-homologated α,β-unsaturated carboxylic esters, the most frequently used method is that of Emmons-Wadsworth-Horner olefin synthesis involving the phosphonate carbanions.[1] However, this method has certain limitations with such carbonyl compounds as highly-hindered or readily-enolizable ketones, which are often inert to this type of carbanion,[2] and also with enones which are susceptible to the Michael addition.[1f]

The present paper will be concerned with a new method for the above transformation using ethyl lithiotrimethylsilylacetate, **1**, which affords α,β-unsaturated carboxylic esters, **2**, exclusively in high yields.

1 **2**

This method is based upon a recent development in silicon-substituted carbanion chemistry, the Peterson olefin synthesis.[3] It should be noted, however, that the polarization of the silicon-carbon bond gives rise to a slight anionic character of the carbon, which is much intensified by the directly-attached electron-withdrawing carbonyl group. Ethyl trimethylsilylacetate and similar compounds containing such a $SiCH_2CO$ moiety have been known to undergo a facile heterolysis of the silicon to the carbon bond with diluted acids, alkalis, or even with ethanol.[4] The activation of the silicon-carbon bond by the ester substituent allows condensations in the presence of a basic catalyst to yield β-trimethylsiloxycarboxylate.[5] The previously-proposed mechanism involving ethyl sodiotrimethylsilylacetate has been questioned, and the intermediacy of ethyl sodioacetate has been proposed, the base attack occurring on the silicon atom under the Si–CH_2–bond heterolysis to form an ester enolate ion.[6]

Rathke has prepared lithium ester enolates by treating the corresponding esters with lithium *N*-isopropylcyclohexylamide or lithium bis(trimethylsilyl)amide.[7] This method utilizing the highly-hindered lithium amide has also been successfully applied to the formation of the desired lithium ester enolate, **1**.

The treatment of ethyl trimethylsilylacetate with lithium dicyclohexylamide was performed in dry tetrahydrofuran at −78 °C for 10 min. The quenching of the resulting anion, **1**, with water, followed by gas-liquid partition chromatography (glpc) yielded a 95% recovery of the starting ester. The formation of the **1** anion was further verified by the transformation of carbonyl compounds to the two carbon homologated carboxylic esters in the yields summarized in Table 1.

Table 1. Conversion of carbonyl compounds into **2** using ethyl lithiotrimethylsilylacetate

R^1–CO–R^2	Yield of **2** (%)[a),b)]	Bp bath temp	*E*—*Z* ratio
Benzaldehyde	84	126 °C (2 mmHg)	3 : 1—9 : 1[c,e)]
Nonanal	81	148 °C (2 mmHg)	1 : 1[d)]
Cyclohexanone	95	132 °C (15 mmHg)	—
Cyclododecanone	94	155 °C (2 mmHg)	—
Cyclopentanone	81	120 °C (15 mmHg)	—
Chalcone	86	176 °C (0.5 mmHg)	7 : 3[d,g)]
Acetophenone	63	140 °C (4 mmHg)	2 : 1[d)]
Pinacolone	21	116 °C (12 mmHg)	[f)]
β-Ionone	82	150 °C (3 mmHg)	3 : 2[d)]

a) All products were characterized by spectroscopic methods and elemental analyses. b) Yields are based on material isolated by chromatography. c) Isomer ratio was variable according to the reaction condition. d) Determined by isolation ratio. e) Determined by glpc. f) The *Z* isomer was undetectable by NMR assay. g) The *E* configuration of C(4)—C(5) double bond is retained.

In Wittig-type reactions, cyclopentanone often fails to give the desired products because of its high degree of enolization.[2a,c] Proton-transfer reaction may occur faster than carbonyl addition, with the consequent risk of the isomerization of the resulting α,β-unsaturated esters and/or condensation reactions of the ketone enolate. Nevertheless, we obtain exclusively ethyl cyclopentylideneacetate in a good yield. The reaction mixture must be quenched at −25 °C in this case; otherwise, an appreciable amount (as high as 10%) of the isomerized, endo-olefinic β,γ-unsaturated ester is detected by NMR assay.

As expected, however, the condensation of lithium enolate, **1**, with highly-hindered pinacolone gave a poor yield of the desired adduct.

Few examples of the Wittig-Horner reaction of α,β-unsaturated ketones have been recorded. Only chalcone is known to react with the phosphonate carbanions to give a Michael and/or a Wittig-Horner product in low yields.[1f] We found that the lithium enolate, **1**, gave solely the expected normal product, ethyl 3,5-diphenylpenta-2,4-dienoate.

β-Ionylideneacetate is one of the important intermediates in the synthesis of vitamin A and its analogs.[8] The lithium enolate, **1**, proved to react with β-ionone smoothly to give the trienic ester.

In those instances where the formation of both *cis* and *trans* esters were possible, the isomer ratios are as given in Table 1. The stereochemistry was assigned on the basis of the NMR data; the shift values of the vinylic protons were diagnostic (for details, see the Experimental section).[10]

Experimental

The IR spectra were determined on a Shimadzu IR-27-G spectrometer; the UV spectra, on a Shimadzu MPS-50-L spectrometer; the mass spectra, on a Hitachi RMU-6L mass spectrometer; the glpc analyses, on a Yanagimoto GCG-550F, and the NMR spectra, on a JEOL C-60-H or Varian EM-360 spectrometer. The chemical shifts are given in δ, with TMS as the internal standard. The analyses were carried out by Mrs. Kiyoko Fujimoto, Prof. Kawanisi's Laboratory and by the staff at the Elemental Analyses Center of Kyoto University. All the experiments were carried out under an atmosphere of dry nitrogen, by preparative thin-layer chromatography (plc) on silica gel PF-254 plates(Merck) with benzene as an eluent, and by preparative column chromatography on silica gel Wakogel C-100 (Wako).

Preparation of Ethyl Trimethylsilylacetate. Ethyl trimethylsilylacetate was prepared by the method of Fessenden[9] in a 71% yield after distillation; bp 65 °C (68 mmHg).

*Generation of Ethyl Lithiotrimethylsilylacetate (**1**).* Dicyclohexylamine (365 mg, 2.00 mmol) was dissolved in dry tetrahydrofuran (10 ml). The solution was then cooled to −78 °C and treated with *n*-butyllithium dissolved in hexane (1.35 ml of 1.50 M solution). After it has been stirred for 15 min, a solution of ethyl trimethylsilylacetate (320 mg, 2.00 mmol) in dry tetrahydrofuran (1.0 ml) was added, drop by drop, at −78 °C, and the resulting solution was stirred at the same temperature for 10 min before the subsequent treatments to be described below.

*Quenching of Lithium Enolate, **1**, with Water.* A solution of **1** prepared from 320 mg (2.00 mmol) of ethyl trimethylsilylacetate was simply quenched with water at −78 °C. A subsequent glpc analysis of the organic layer with tetralin as an internal standard indicated a 95% recovery of the starting ethyl trimethylsilylacetate.

*Condensation of Lithium Enolate, **1**, with Aldehydes.* To a solution of **1** (1.20 mmol), a solution of the respective aldehyde (1.00 mmol) in dry tetrahydrofuran (1.0 ml) was added, drop by drop, at −78 °C. The reaction mixture was stirred at −78 °C for 1 hr, at −25 °C for 1 hr, and finally at 25 °C for 1 hr. Finely-ground sodium bisulfate monohydrate (0.22 g) was then added, and the mixture was stirred for 10 min. The solid was filtered off, and water was added to the filtrate. This solution was extracted with three 5-ml portions of ethyl acetate. The extracts were combined, dried, and evaporated *in vacuo* to yield an oily product, which was subsequently purified by plc.

*Ethyl (*E*) and (*Z*)-Cinnamate* were prepared from lithium enolate, **1** (1.20 mmol), and benzaldehyde (108 mg, 1.00 mmol). The crude product was purified by plc, thus furnishing 147 mg (84%) of ethyl cinnamate ((*E*) : (*Z*)=8 : 1). The isomers were separated on a 75 cm×3 mm 5% SE 30 on Chromosorb W column at 120 °C.

*Ethyl (*E*) and (*Z*)-2-Undecenoate* were prepared from **1** and nonanal (142 mg, 1.00 mmol). The resulting oil was chromatographed on a silica-gel thin-layer plate. The first band contained ethyl (*Z*)-2-undecenoate (51 mg, 24%): IR (neat) 1724, 1646, 1470, 1418, 1186, 1040, 822 cm^{-1}; NMR ($CDCl_3$) δ 0.68—1.04 (m, 3H), 1.05—1.75 (m, 12H), 1.24 (t, J=7, 3H), 2.57 (br d, 2H), 4.06 (q, J=7, 2H), 5.62 (d, J=9.3, 1H), 6.05 (d, J=9.3 Hz, t, J=6.3 Hz, 1H); mass *m/e* (%) 212 (17), 183 (3), 169 (32), 127 (81), 115 (32), 101 (28), 99 (100), 88 (42), 81 (42), 77 (33), 69 (39), 55 (72). The second band was ethyl (*E*)-2-undecenoate (128 mg, 58%): IR (neat) 1724, 1656, 1470, 1270, 1185, 1047, 985 cm^{-1}; NMR ($CDCl_3$) δ 0.70—1.08 (m, 3H), 1.09—1.85 (m, 12H), 1.28 (t, J=7 Hz, 3H), 2.18 (br t, 2H), 4.18 (q, J=7 Hz, 2H), 5.74 (d, J=15 Hz, 1H), 6.86 (t, J=7 Hz, d, J=15 Hz, 1H); mass *m/e* (%) 212 (2), 185 (3), 183 (2), 167 (42), 127 (8), 125 (33), 115 (20), 101 (71), 99 (34), 88 (44), 73 (64), 69 (47), 55 (100). (Found: C, 73.7; H, 11.4%).

*Condensation of Lithium Enolate, **1**, with Ketones.* To a solution of **1** (2.00 mmol), a solution of ketone (1.00 mmol) in dry tetrahydrofuran (1.0 ml) was added, drop by drop, at −78 °C. The resulting mixture was stirred at −78 °C for 1 hr, at −25 °C for 1 hr, and finally at 25 °C for 1 hr. Finely-ground sodium bisulfate monohydrate (0.40 g) was then added, and the mixture was stirred for 10 min. A subsequent work-up yielded an oil, which was purified by silica-gel chromatography, with benzene (plc) or hexane (column) as the eluent.

Ethyl Cyclododecylidenaecetate was prepared from **1** (20.0 mmol) and cyclododecanone (1.82 g, 10.0 mmol). The crude product was chromatographed over a 100-g silica gel column, thus furnishing 2.36 g (94%) of ethyl cyclododecylideneacetate as a colorless semisolid; bp 155 °C (bath temp, 2 mmHg); IR (neat) 1720, 1644, 1468, 1444, 1170, 1150, 1036 cm^{-1}; NMR (CCl_4) δ 1.24 (t, J=7 Hz, 3H), 1.20—2.00 (m, 18H), 2.21 (br t, J=7 Hz, 2H), 2.71 (br t, J=7 Hz, 2H), 4.06 (q, J=7 Hz, 2H), 5.63 (br s, 1H); mass *m/e* (%) 252 (27), 207 (36), 164 (60), 128 (100). (Found: C, 75.9; H, 11.1%).

Ethyl Cyclohexylideneacetate was prepared from **1** (2.00 mmol) and cyclohexanone (98.0 mg, 1.00 mmol). The liquid thus obtained was purified by plc thus furnishing 159 mg (95%) of ethyl cyclohexylideneacetate as an oil.

Ethyl cyclopentylideneacetate was prepared from cyclopentanone (84 mg, 1.00 mmol), the reaction being quenched by the addition of water at −25 °C. The liquid thus obtained was purified by plc, thus furnishing 125 mg (81%) of ethyl cyclopentylideneacetate as an oil: IR (neat) 1718, 1655, 1377, 1250, 1205, 1125, 1045, 860 cm^{-1}; NMR (CCl_4) δ 1.23 (t, J=7 Hz, 3H), 1.50—2.03 (m, 4H), 2.10—3.07 (m, 4H), 4.10 (q, J=7 Hz, 2H), 5.70 (s, 1H); mass *m/e* (%) 154 (88), 140 (50), 126 (80), 109 (100), 97 (32), 81 (85), 79 (64), 67 (96); Found: C, 70.3; H, 9.20%. Calcd for $C_9H_{14}O_2$: C, 70.1; H, 9.15%.

*Ethyl 3,5-Diphenylpenta-(2*E*,4*E*) and (2*Z*,4*E*)-dienoate* were prepared from **1** (2 mmol) and chalcone (108 mg, 1.00 mmol). The crude oil was purified by plc. The first band contained ethyl 3,5-diphenylpenta-(2*Z*,4*E*)-dienoate (72 mg, 26%): IR (neat) 1715, 1610, 1588, 1275, 1230, 1155, 1100, 1034, 964, 753, 690 cm^{-1}; NMR (CCl_4) δ 1.30 (t, J=7 Hz, 3H), 4.26 (q, J=7 Hz, 2H), 5.90 (s, 1H), 6.44 (d, J=16 Hz, 1H), 7.35 (d, J=16 Hz, 1H), 7.36 (m, 10H); UV λ_{max}^{EtOH} 314 nm (ε 833); mass *m/e* (%) 278 (18), 249 (3), 233 (11), 205 (100), 190 (8), 178 (6), 165(4), 137 (9), 105 (6), 101 (9), 91 (9), 89 (7), 77 (13). The second band was ethyl 3,5-diphenylpenta-(2*E*,4*E*)-dienoate (168 mg, 60%): IR (neat) 1712, 1610, 1590, 1275, 1230, 1155, 1100, 1034, 965, 753, 690 cm^{-1}; NMR (CCl_4) δ 1.04 (t, J=8 Hz, 3H), 4.02 (q, J=8 Hz, 2H), 6.06 (s, 1H), 6.33 (d, J=14 Hz, 1H) 7.04 (d, J=14 Hz,

1H), 7.30 (m, 10H); UV λ_{max}^{EtOH} 316 nm (ε 716); mass *m/e* (%) 278 (15), 249 (4), 233 (10), 205 (100), 190 (9), 178 (7), 165 (5), 127 (12), 115 (5), 101 (11), 91 (10), 89 (10), 77 (18).

Ethyl (E) and (Z)-3-Phenyl-2-butenoate were prepared from **1** (4 mmol) and acetophenone (240 mg, 2.00 mmol). The crude mixture was chromatographed on a silica-gel plate. The first band consisted of ethyl (*E*)-3-phenyl-2-butenoate (165 mg, 43%): IR (neat) 1710, 1628, 1447, 1346, 1273, 1170, 1044, 870, 767, 696 cm^{-1}; NMR ($CDCl_3$) δ 1.27 (t, J=7 Hz, 3H), 2.52 (d, J=2 Hz, 3H), 4.13 (q, J=7 Hz, 2H), 6.02 (m, 1H), 7.30 (m, 5H); mass *m/e* (%) 190 (63), 175 (4), 161 (32), 145 (100), 115 (56), 101 (10), 91 (28). The second band was ethyl (*Z*)-3-phenyl-2-butenoate (74 mg, 20%): IR (neat) 1715, 1640, 1443, 1375, 1230, 1160, 1045, 857, 768, 700 cm^{-1}; NMR ($CDCl_3$) δ 1.05 (t, J=7 Hz, 3H), 2.12 (d, J=2 Hz, 3H), 3.90 (q, J=7, 2H), 5.71 (m, 1H), 7.15 (m, 5H); mass *m/e* (%) 190 (68), 161 (40), 145 (100), 115 (70), 105 (17), 91 (30). A mixture of the (E) and (Z) isomers was analyzed. Found: C, 75.6; H, 7.52%. Calcd for $C_{12}H_{14}O_2$: C, 75.8; H, 7.42%.

Ethyl 3,4,4-Trimethyl-2-pentenoate was prepared from **1** (4.00 mmol) and pinacolone (200 mg, 2.00 mmol). The crude liquid was purified by plc, thus furnishing 67 mg (21%) of ethyl (*E*)-3,4,4-trimethyl-2-pentenoate: IR (neat) 1717, 1636, 1263, 1180, 1122, 1054, 868 cm^{-1}; NMR ($CDCl_3$) δ 1.10 (s, 9H), 1.23 (t, J=7, 3H), 2.08 (d, J=1, 3H), 4.00 q, J=7, 2H), 5.53 (d, J=1, 1H): mass *m/e* (%) 170 (20), 155 (66), 127 (54), 125 (70), 109 (50), 97 (100), 83 (36), 81 (36), 69 (31), 57 (36), 55 (74). Found: C, 70.7; H, 10.9%. Calcd for $C_{10}H_{18}O_2$: C, 70.5; H, 10.7%.

Ethyl (E) and (Z)-β-Ionylideneacetate were prepared from **1** (4.00 mmol) and β-ionone (384 mg, 2.00 mmol). The crude oil was purified by plc, thus furnishing 430 mg (82%) of ethyl β-ionylideneacetate ((*E*) : (*Z*)=3 : 2). The isomers were separated on a 75 cm×3 mm 5% SE 30 on Chromosorb W column at 170°. The first peak was ethyl (*Z*)-β-ionylideneacetate: IR (neat) 1710, 1610, 1450, 1376, 1230, 1155, 1053, 983, 842 cm^{-1}; NMR (CCl_4) δ 1.06 (s, 6H), 1.24 (t, J=7 Hz, 3H), 1.43—2.60 (m, 6H), 1.75 (s, 3H), 2.00 (s, 3H), 4.05 (q, J=7, 2H), 5.50 (br s, 1H), 6.42 (d, J=16 Hz, 1H), 7.52 (d, J=16 Hz, 1H); mass *m/e* (%) 262 (38), 247 (16), 233 (8), 217 (20), 201 (20), 189 (24), 173 (40), 159 (32), 133 (52), 119 (100), 105 (40), 91 (32). The second peak was ethyl (*E*)-β-ionylideneacetate: IR (neat) 1710, 1605, 1443, 1366, 1236, 1154, 1047, 970 cm^{-1}; NMR (CCl_4) δ 1.02 (s, 6H), 1.25 (t, J=7 Hz, 3H), 1.44—2.85 (m, 6H), 1.54 (s, 3H), 1.68 (s, 3H), 2.33 (s, 3H), 4.06 (q, J=7 Hz, 2H), 5.62 (br s, 1H), 6.00 (d, J=16 Hz, 1H), 6.43 (d, J=16 Hz, 1H); mass *m/e* (%) 262 (26), 247 (10), 233 (5), 217 (15), 201 (15), 189 (15), 173 (33), 159 (32), 133 (46), 119 (100), 105 (34), 91 (25). A mixture of the (*E*) and (*Z*) isomers was analyzed. Found: C, 78.1; H, 10.1%. Calcd for $C_{17}H_{26}O_2$: C, 77.8; H, 10.0%.

The authors acknowledge with pleasure the financial support by the Grant-in-aid administered by the Ministry of Education, Japanese Government.

References

1) (a) W. S. Wadsworth, Jr., and W. D. Emmons, *J. Amer. Chem. Soc.*, **83**, 1733 (1961); (b) H. Takahashi, K. Fujiwara, and M. Ohta, This Bulletin, **35**, 1498 (1962); (c) A. K. Bose and R. T. Dahill, Jr., *Tetrahedron Lett.*, **1963**, 959; *J. Org. Chem.*, **30**, 505 (1965); (d) J. Wolinsky and K. L. Erickson *ibid.*, **30**, 2208 (1965); (e) W. S. Wadsworth, Jr. and W. D. Emmons, "Organic Syntheses," Vol. 45, p. 441 (1965); (f) E. D. Bergmann and A. Solomonovici, *Tetrahedron*, **27**, 2675 (1971).

2) (a) E. J. Corey and J. I. Shulman, *J. Org. Chem.*, **35**, 777 (1970); (b) R. L. Sowerby and R. M. Coates, *J. Amer. Chem. Soc.*, **94**, 4758 (1972) and references cited therein; (c) see also, D. R. Coulson, *Tetrahedron Lett.*, **1964**, 3323.

3) (a) D. J. Peterson, *J. Org. Chem.*, **33**, 780 (1968); (b) T. H. Chan, E. Chan, and E. Vinokur, *Tetrahedron Lett.*, **1970**, 1137; (c) F. A. Carey and A. S. Court, *J. Org. Chem.*, **37**, 939, 1926 (1972); (d) D. Seebach, B-Th. Gröbel, A. K. Beck, M. Braun, and K. -H. Geiss, *Angew. Chem. Internat. Ed.*, **11**, 443 (1972); (e) C. Trindle, J-T. Hwang, and F. A. Carey, *J. Org. Chem.*, **38**, 2664 (1973); (f) F. A. Carey and O. Hernandez, *ibid.*, **38**, 2670 (1973); (g) H. Sakurai, K. Nishiwaki, and M. Kira, *Tetrahedron Lett.*, **1973**, 4193; (h) see also, D. J. Peterson, *Organometal. Chem. Rev. A*, **7**, 295 (1972).

4) (a) J. R. Gold, L. H. Sommer, and F. C. Whitmore, *J. Amer. Chem. Soc.*, **70**, 2874 (1948); (b) L. H. Sommer and N. S. Maras, *ibid.*, **72**, 1937 (1950).

5) L. Birkofer, A. Ritter, and H. Wieden, *Chem. Ber.*, **95**, 971 (1962).

6) C. Eaborn and R. W. Bott in "Organometallic Compounds of the Group IV Elements," Vol. 1, A. G. MacDiarmid, Ed., Dekker, New York, N. Y., (1968), p 1; L. Birkofer and A. Ritter, *Angew. Chem.*, **77**, 414 (1965).

7) M. W. Rathke, *J. Amer. Chem. Soc.*, **92**, 3222 (1970); M. W. Rathke and A. Lindert, *ibid.*, **93**, 2318 (1971); M. W. Rathke and J. Deitch, *Tetrahedron Lett.*, **1971**, 2953.

8) (a) C. von Planta, U. Shwieter, L. Chopard-dit-Jean, R. Ruegg, M. Kofler, and O. Isler, *Helv. Chim. Acta*, **45**, 548 (1962); (b) P. K. Korver, C. Kruk, P. J. van der Haak, J. L. Baas, and H. O. Huisman, *Tetrahedron*, **22**, 277 (1966); (c) G. Pattenden and B. C. L. Weedon, *J. Chem. Soc., C*, **1968**, 1984; (d) J. L. Olive and M. Mousseron-Canet, *Bull. Soc. Chim. Fr.*, **1969**, 3252.

9) R. J. Fessenden and J. S. Fessenden, *J. Org. Chem.*, **32**, 3535 (1967).

10) A preliminary account of this work has appeared: K. Shimoji, H. Taguchi, K. Oshima, H. Yamamoto, and H. Nozaki, *J. Amer. Chem. Soc.*, **96**, 1620 (1974).

X-Ray Photoelectron Spectroscopic Study of the Reaction of Evaporated Iron, Nickel, and Palladium with Nitric Oxide

Kosaku KISHI and Shigero IKEDA

Department of Chemistry, Faculty of Science, Osaka University, Toyonaka, Osaka 560

(Received December 14, 1973)

The reaction of the evaporated iron, nickel, and palladium with NO was investigated by X-ray photoelectron spectroscopy. On both iron and nickel larger part of NO dissociates to give two or more N(1s) and O(1s) photoelectron peaks which are ascribable to the surface oxide, nitride, and NO species. The proportion of these species is estimated roughly from the intensity ratios of the N(1s) and O(1s) peaks at 15 NO: 65 O: 20 N (iron) and 7 NO: 65 O: 28 N (nickel) when the metals are exposed to 5 Torr of NO gasfor 1 s, and 35 NO: 55 O: 10 N (iron) and 10 NO: 75 O: 15 N (nickel) when exposed to 10 Torr of NO for 10 min. On palladium the N(1s) for chemisorbed NO is observed. The N(1s) binding energies of the surface NO are compared with the N(1s) binding energies and the infrared NO frequencies of the corresponding transition metal nitrosyls.

The NO molecule has one electron in an antibonding π orbital and, in transition metal nitrosyls, bonds to a metal atom at various electronic states.[1] Two limiting species are linearly coordinated NO^+ and angularly coordinated (bent) NO^-. Chemisorbed NO on transition metals is expected to take various bonding and electronic structures. An electronic structure of NO has a significant resemblance to and yet a difference from CO and O_2 whose chemisorption has been widely investigated.

Infrared studies of NO adsorption on transition metals have been reported by Terenin and Roev,[2] Dunken and Hobert,[3] and Blyholder and Allen.[4] Two or more bands of NO stretching were observed for chemisorbed NO. These bands have been assigned to structures described as ionic, covalent, or coordinative[2] and discussed on correlating their frequencies to the extent of π back-bonding to NO.[4] Sachtler[5] has reported that NO partially dissociates on nickel and both chemisorbed NO and oxygen exist on the surface.

In the present paper, X-ray photoelectron spectroscopy (ESCA) is applied to observe the reaction of evaporated iron, nickel, and palladium in order to characterize the surface species and to check an existence of surface nitride.

Experimental

Metals were evaporated onto a stainless steel plate at 10^{-6} Torr as described elsewhere.[6] The evaporated metal film was exposed to the gas to be studied at room temperature after about 10 s from evaporation. After evacuation of the gas for 5 min, photoelectron spectra of the surface species formed were recorded. During the spectral measurement, the vacuum was maintained at 10^{-7} Torr.

NO gas was obtained from Takachiho Kagaku Kogyo.

Spectra were recorded in 0.1 eV steps on a KES-X2001 (Kokusai Electric Co.) electron spectrometer using Al$K\alpha$ (for nickel and palladium) and Mg$K\alpha$ (for iron) X-radiation. The binding energy reference is the Fermi level which is taken as the inflection point of the low-energy edge of the 4d band of palladium according to Baer *et al.*[7]

Results

When evaporated iron was exposed to NO at a pressure of 5 Torr for about 1 s, the broad N(1s) peaks were observed at the binding energies of 396.6 and 400.7 eV (Fig. 1-a). Both minimum and maximum counting rates (counts/5 s) are shown in parentheses in the figures. The O(1s) peaks were at 530.0 and around 533.0 eV (Fig. 2-a). The Fe($2p_{3/2}$) were at 707.0 and around 709.8 eV (Fig. 3-a). The chemical shift of the latter peak is about 2.8 eV from the former which is due to metallic iron.

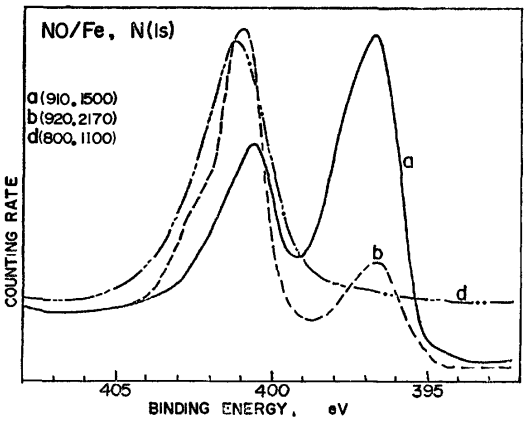

Fig. 1. N(1s) peaks from evaporated iron exposed to (a) 5 Torr of NO for about 1 s, (b) 10 Torr of NO for 10 min, (d) 10 Torr of NO for 10 min after exposure to 20 Torr of air for 5 min.

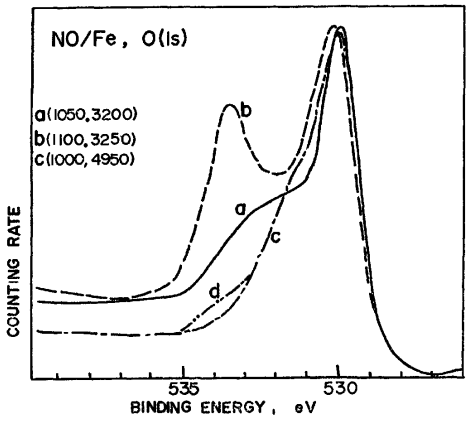

Fig. 2. O(1s) peaks from evaporated iron exposed to (a) 5 Torr of NO for about 1 s, (b) 10 Torr of NO for 10 min, (c) 20 Torr of air for 5 min, (d) 10 Torr of NO for 10 min after c.

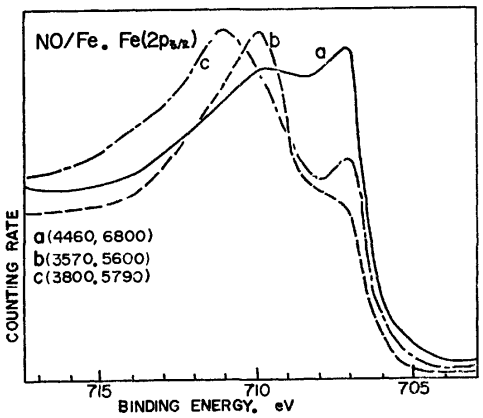

Fig. 3. $Fe(2p_{3/2})$ peaks from evaporated iron exposed to (a) 5 Torr of NO for about 1 s, (b) 10 Torr of NO for 10 min, (c) 20 Torr of air for 5 min.

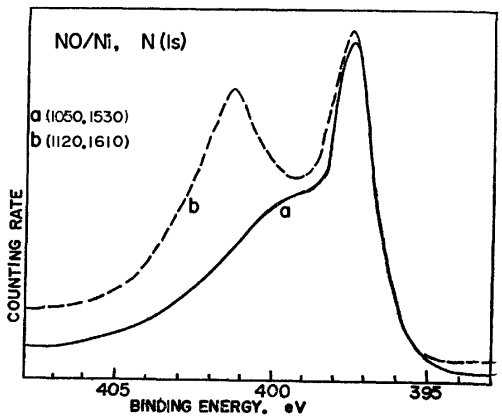

Fig. 4. N(1s) peaks from evaporated nickel exposed to (a) 5 Torr of NO for about 1 s, (b) 10 Torr of NO for 10 min.

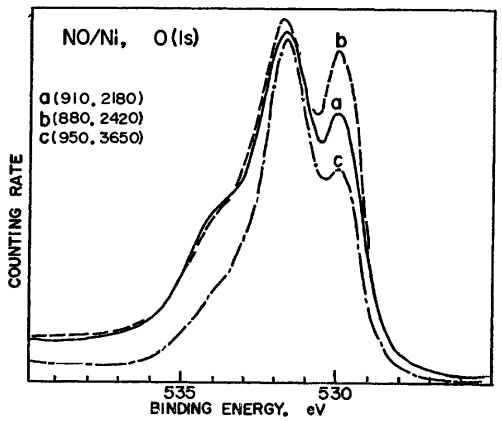

Fig. 5. O(1 s) peaks from evaporated nickel exposed to (a) 5 Torr of NO for about 1 s, (b) 10 Torr of NO for 10 min, (c) 20 Torr of air for 5 min.

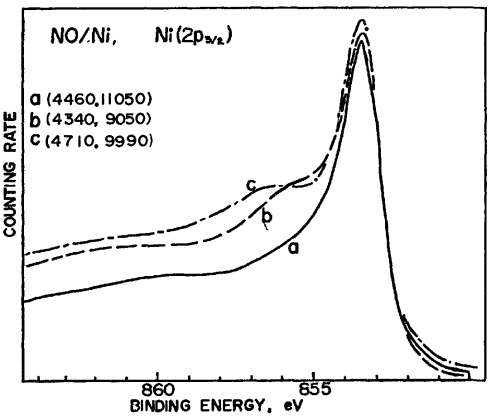

Fig. 6. $Ni(2p_{3/2})$ peaks from evaported nickel exposed to (a) 5 Torr of NO for about 1 s, (b) 10 Torr of NO for 10 min, (c) 20 Torr of air for 5 min.

Spectra b of Figs. 1 to 3 were recorded after evaporated iron was exposed to NO at a pressure of 10 Torr for 10 min. The N(1s) peaks are at 396.6 and 401.0 eV with a shoulder around 402.5 eV. The peak at 401.0 eV and the shoulder decreased in intensity with time during the spectral measurement while the 396.6 eV peak not at all. For example, the original 401.0 eV peak was depressed to one thirds after 1 hr. The N(1s), O(1s), and metal peaks (Figs. 1 to 3 for iron and 4 to 6 nickel) were recorded in this order within 1 hr. The 401.0 eV peak is considerably stronger in intensity than the 400.7 eV peak in Fig. 1-a. The O(1s) peaks are at 530.2 and 533.5 eV. The $Fe(2p_{3/2})$ peaks are at 707.0 and 710.0 eV. The 707.0 eV peak due to metallic iron is further depressed from that of spectrum a.

Spectra c of Figs. 2 and 3 were recorded after evaporated iron was exposed to air at a pressure of 20 Torr for 5 min. The intense O(1s) peak was observed at 530.0 eV with a shoulder around 531.7 eV. The $Fe(2p_{3/2})$ of oxidized iron shows a chemical shift of 4.0 eV from metallic iron which is 1.0 eV larger than when iron was exposed to NO. This surface oxide was subsequently exposed to NO at a pressure of 10 Torr for 10 min and spectra of Figs. 1 and 2 were recorded. The N(1s) electrons give only one broad peak at 401.3 eV and a weak O(1s) peak appeared at 533.7 eV. The above spectral data of N(1s) peaks are summarized in Table 1 with infrared data. The corresponding data of various compounds are also listed.

Spectra a of Figs. 4 to 6 were recorded after evaporated nickel was exposed to NO at a pressure of 5 Torr for about 1s. The N(1s) peaks are at 397.6 and around 400.2 eV. The O(1s) peaks are at 530.1, 531.7, and 533.3 eV. The $Ni(2p_{3/2})$ spectrum shows a peak at 853.5 eV due to metallic nickel and broad enhancement of intensity in the region from 854.8 to 859.5 eV as compared with the spectrum of unreacted nickel.

Spectra b of Figs. 4 to 6 were recorded after evaporated nickel was exposed to NO at a pressure of 10 Torr for 10 min. The N(1s) peaks are at 397.6 and 401.3 eV. Three O(1s) peaks are at the same binding energies as those in spectrum a. A shifted $Ni(2p_{3/2})$ peak is clearly shown at 855.9 eV; 2.4 eV from metallic nickel.

Spectra c of Figs. 5 and 6 were observed after evaporated nickel was exposed to air at a pressure of 20 Torr for 5 min. The binding energies of three O(1s) peaks are the same as those of spectra a and b. The chemical shift of $Ni(2p_{3/2})$ peak of oxidized nickel

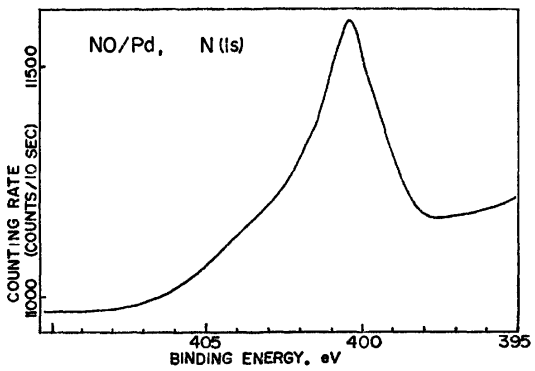

Fig. 7. N(1s) peaks from evaporated palladium exposed to 10 Torr of NO for 10 min.

is larger by 0.5 eV than that obtained when nickel was exposed to NO. After this surface oxide was subsequently exposed to NO at a pressure of 10 Torr for 10 min, no N(1s) peak could be detected even after counting the photoelectrons for 10 s/channel.

Figure 7 shows the N(1s) spectrum when evaporated palladium was exposed to NO at a pressure of 10 Torr for 10 min. The peak is at 400.4 eV and a very weak shoulder around 403.5 eV. The Pd 3d spectrum was the same in shape as that for unreacted palladium and no new peak was observed. The Pd($3p_{3/2}$) electrons give a strong peak at 532.7 eV and make the O(1s) peaks indistinct. The shape of Pd($3p_{3/2}$) peak is almost the same as that for unreacted palladium; indicating a low counting rate for O(1s) peaks.

When evaporated palladium was exposed to NO at a pressure of 5 Torr for about 1 s, the intensity of N(1s) peak at 400.4 eV was two thirds of that in Fig. 7 and the 403.5-eV shoulder could not be detected.

Discussion

The results for evaporated iron, nickel, and palladium reacted with NO show two or more N(1s) peaks (Table 1). The binding energy of N(1s) in NO_3^- or NO_2^- of $NaNO_3$(407.4 eV), $NaNO_2$ (404.1 eV), or of their transition metal compounds is much larger[8] than that obtained from the reaction of NO with the metals except the 403.5-eV peak in case of palladium. The N(1s) peaks from 400.2 to 402.5 eV for the surface species correspond in binding energy well with those in transition metal nitrosyls whose binding energies lie between 399.6 and 403.3 eV[8,9] and these peaks are, therefore, assigned to surface NO species.[10] The decrease in intensities of these peaks during spectra measurement is due to NO desorption occurred probably by evacuation or ejected electrons on the surface.

The N(1s) peaks at 396.6 eV for iron and 397.6 eV for nickel are smaller by 2.0 eV or more than that of NO^- in the metal nitrosyls. These peaks are reasonably assigned to the surface nitride since the N(1s) binding energies of VN and CrN are 397.2 and 396.6 eV, respectively.[8] The dissociation of NO on nickel has been reported.[4,5] The above results indicate that the dissociated nitrogen are in part present in the surface compounds on iron and nickel without recombining nitrogen molecule. From the N(1s) binding energies, the nitride-nitrogen is likely to be more ionic (negative) on iron than on nickel. This is similar to that the main oxygen species is smaller by 1.7 eV in binding energy of O(1s) peak (namely, more negative) on iron than on nickel when exposed to air. The absence of the nitride peak in case of palladium shows quite different reactivity to NO from nickel and indicates less stability of nitride or oxide on palladium surface at room temperature.

When iron and nickel were exposed to NO, the strongest O(1s) peak is at 530.0 eV in case of iron (Fig. 2) and at 531.7 eV in case of nickel (Fig. 5); being with the same binding energy as that obtained when each evaporated metal was exposed to air. In case of nickel exposed to air, the 531.7-eV peak does not correspond to the O(1s) of NiO (530.0 eV) and has been assigned to the surface oxide[11] or Ni_2O_3.[12] These facts also indicate that a large amount of oxygen anions are present on iron and nickel as a result of the dissociative reaction of NO.

When iron was preoxidized by air, the N(1s) due to

Table 1. Nitrogen 1s binding energies and NO stretching frequencies

Samples		N(1s) B. E., eV	ν(NO), cm^{-1}
$Na_2[Fe(NO)(CN)_5]2H_2O$		403.3[9]	1939[18]
$[FeCl(NO)(diars)_2](ClO_4)_2$		402.9	1865[15]
$[Fe(NO)(diars)_2](ClO_4)_2$		401.2, 399.6	1760[14]
$[FeCl(NO)(diars)_2]ClO_4$		400.0	1620[14]
$NiCl(NO)[P(C_6H_5)_3]_2$		399.8	1735[17]
$Ni(N_3)(NO)[P(C_6H_5)_3]_2$		399.6	
$RuCl(NO)_2[P(C_6H_5)_3]_2PF_6$		402.6, 400.2	1845, 1687[13]
VN		397.2[8]	
CrN		396.6	
Surface Species	NO/Fe	a) 400.7, 396.6 b) 401.0, 396.6 402.5	{1810[4] {1805[2] {1720 {1375
	NO/Ni	a) 400.2, 397.6 b) 401.3, 397.6	{ 1840[4] {1850[2] {(2205) {1735
	NO/Pd	400.4, (403.5)	1845, 1765[3]

a) NO exposure; 5 Torr for 1s. b) NO exposure; 10 Torr for 10 min.

the nitride could not be detected (Fig. 1-d). This indicates that the NO dissociation is effective on metal surfaces but not on the surface oxides.

The O(1s) peak at 533.5 eV in case b of Fig. 2 shows a fairly strong intensity and, under this reaction condition, the N(1s) peak at 401.0 eV is quite strong (case b of Fig. 1). Moreover, a weak O(1s) peak appeared at 533.7 eV (d of Fig. 2) with the appearance of the N(1s) peak at 401.3 eV (d of Fig. 1) when preoxidized iron surface was exposed to NO. These results indicate that the O(1s) at 533.5 eV and the N(1s) at 401.0 eV come from the same NO species. This is also affirmed by the counting rate ratio of the O(1s) and N(1s) peaks. The ratio of O(1s) peak to N(1s) peak in $NaNO_3$ is namely 1.2 per atom. In cases b of Figs. 1 and 2, the ratio is 1.25 for the O(1s) at 533.5 eV to the N(1s) at 401.0 eV.

In case of nickel, the O(1s) peak at 533.5 eV appears even when evaporated nickel was exposed to air (c of Fig. 5). This weak peak has been proposed as atomic oxygen adsorbed on nickel.[12]

In cases of iron, the ratio of NO to oxygen anion is derived approximately as 0.23 (case a) and 0.64 (case b), respectively, from the intensity ratio of the O(1s) peaks around 533 eV to the one at 530.0 eV of Fig. 2. This indicates that the initial reaction of NO with iron is, in larger part, the dissociative. Also from the intensity ratios of the N(1s) at 396.6 eV was the O(1s) at 530.0 eV in Figs. 1 and 2 and the counting ratio, 1.2, of O(1s) to N(1s), roughly 1/3 (case a) and 1/5 (case b) of nitrogen atoms formed by NO dissociation are estimated to remain on iron surface without recombining into molecular nitrogen. In other words, the proportion of the surface species is roughly, 15 NO: 65 O: 20 N in case a and 35 NO: 55 O: 10 N in case b.

In case of nickel, the corresponding values are roughly 7 : 65 : 28 (case a) and 10 : 75 : 15 (case b) which were estimated from the intensity ratio of the N(1s) at 400.2 eV (case a) or 401.3 eV (case b) for NO, the O(1s) at 530.1 eV plus the O(1s) at 531.7 eV for O, and the N(1s) at 397.6 eV for N.

When evaporated iron was exposed to air at a pressure of 20 Torr for 5 s, iron surface was oxidized nearly to Fe(III) as evidenced by the chemical shift, 4.0 eV, for Fe ($2p_{3/2}$) peak (Fig. 3-c) since that of Fe_2O_3 is 4.2 eV.[6] In case b of Fig. 3, the iron surface was oxidized by exposure to NO approximately to the same depth as in case c as shown by the similar intensity ratio of the two Fe($2p_{3/2}$) peaks which come from unreacted and oxidized iron in both cases. However, the chemical shift in case b is 3.0 eV and smaller by 1.0 eV than that in case c. This indicates that the iron atom on the surface is with higher electron densities in case b than in case c.

In case of nickel, the chemical shift of Ni($2p_{3/2}$) is also smaller when exposed to NO (2.4 eV in Fig. 6-b) than when exposed to air (2.9 eV in c). This also indicates that a surface nickel atom is with higher electron densities when reacted with NO than when oxidized with air.

Blyholder and Allen[4] have explained variations in NO stretching frequencies of the chemisorbed NO by the amount of charge in the second lowest π orbital of the Ni-N-O system, antibonding for the N-O bond but bonding for the Ni–N bond, which is depending on the number of metal atoms around the metal atom to which the chemisorbed NO is bound. In cases of iron and nickel, however, the surface oxygen and nitrogen anion as ligands are expected to take more important role in variations of NO stretching frequencies when considering the present photoelectron data, namely, the extent of surface oxidation and the proportions NO, O, and N on the surfaces. In $\{RuCl(NO)_2[P(C_6H_5)_3]_2\}PF_6$ complex, two different types of nitrosyls are bonded to the same metal atom;[13] linear equatorial nitrosyl (N(1s): 402.6 eV,[9] NO str. freq.: 1845 cm^{-1} [13]) and apical bent nitrosyl (400.2 eV, 1687 cm^{-1}). The surface compounds on the metal which have mixed ligands (NO, O, N) will also have various coordination geometries, coordination numbers, and electronic states. The metal atom surrounded by larger number of oxygen or nitrogen anions, especially oxygen, draws electrons from the NO to larger extent and gives higher binding energy of N(1s) peak and higher frequency of NO band as discussed below. Among the metal nitrosyls, bent nitrosyls (formally NO^-) generally show low binding energy of N(1s) peak and linear nitrosyls (NO^+) can show either low or high binding energy peak depending on the extent of π back-bonding from the metal.[9] The N(1s) binding energies are expected to be correlated with NO stretching frequencies in metal nitrosyls since the high positive charge on NO means less electrons on the orbital which is antibonding for the NO bond and, consequently, higher NO frequency. Such but rough correlations have been reported for many nitrosyl complexes.[9] For the iron complexes listed in Table 1, a good correlation is shown between the N(1s) binding energies and the NO stretching frequencies. The NO groups have been concluded to have relatively high positive charges in the upper two complexes and negative charges in the fourth complex. For the surface NO groups, the N(1s) of 401.0 eV and the NO str. freq. of 1720 cm^{-1} [4] correspond to the 401.2 eV[9] and the 1760-cm^{-1} [14] for $[Fe(NO)(diars)_2](ClO_4)_2$ and the 402.5 eV and the 1810-cm^{-1} to the 402.9 eV and the 1865 cm^{-1} [15] for $[FeCl(NO)(diars)](ClO_4)_2$. This means that the positive charges on NO groups increase and, namely, the π back donation to the NO decrease as NO oxidizes iron surface to larger extent as a result of dissociative reaction and the surface NO species increase in number.

The intensity of 401.0-eV peak is stronger than that of the 402.5 eV peak in case b of Fig. 1 while the the intensity of the 1720-cm^{-1} band is weaker than that of the 1810-cm^{-1} band for evaporated iron particles in an oil exposed to 10 Torr for NO 1 hr.[4] In the experiment by Terenin,[2] the 1805-cm^{-1} band shows approximately the same intensity as the 1735-cm^{-1} band for dispersed iron on alumina exposed to 20 Torr NO. This may suggest that the infrared bands were obtained the sample which was oxidized to larger extent by the dissociative reaction of NO and was bonded by larger number of NO species than the present photoelectron peaks were. The *trans*-[FeCl-

$(NO)(diars)_2](ClO_4)_2$ underwent decomposition in the X-ray beam, as evidenced by a gradual growth of a 400.4 eV peak at the expense of the 402.9 eV peak.[9] Such phenomenon also explains the intense 401.0 eV peak for the surface NO species.

The N(1s) binding energy for the chemisorbed NO on nickel is 400.2 eV (case a) and 401.3 eV (case b). The former value is near to that in $NiCl(NO)[P(C_6H_5)_3]_2$ (399.8 eV) and $Ni(N_3)(NO)[P(C_6H_5)_3]_2$ (399.6 eV,[9] Ni-N-O angle: 152.7°[16]). The NO frequency in $NiX(NO)[P(C_6H_5)_3]_2$ (X=Br, I) is 1735 cm^{-1}.[17] The weak 1735-cm^{-1} band for chemisorbed NO[2] seems to correspond to the surface NO species giving 400.2 eV peak. The low binding energy of N(1s) suggests a small negative charge on the surface NO. 401.3 eV peak in case b indicates less electron donation to NO from the nickel atom at higher oxidation state and is presumably associated with the NO giving the 1840-cm^{-1} band[4] (or 1850-cm^{-1} band[2]).

The low binding energy of N(1s) peak (400.4 eV) in case of palladium suggests that the surface NO groups bond to the palladium atom at very low oxidation state. This is in accord with the facts that the intense O(1s) peak was absent and no new peak for O (3d) due to oxidized palladium was detected. The surface NO may have small negative charge on it. Strongly chemisorbed NO on palladium supported on silica gives bands at 1845 and 1765 cm^{-1}.[3] However, the correspondence of the photoelectron peaks with the infrared bands is uncertain at present.

The authors wish to thank for the Ministry of Education for the financial support granted for this research.

References

1) Recent reviews, a) B. F. G. Johnson and J. A. McCleverty, *Progr. Inorg. Chem.*, **7**, 277 (1966), b) J. H. Swinehart, *Coord. Chem. Rev.*, **2**, 385 (1967), c) N. G. Connelly, *Inorg. Chim. Acta Rev.*, **6**, 47 (1972).

2) L. M. Roev and A. M. Terenin, *Optika Spektrosk.*, **7**, 756 (1959).

3) H. Dunken and H. Hobert, *Z. Chem.*, **3**, 398 (1963).

4) G. Blyholder and M. C. Allen, *J. Phys. Chem.*, **69**, 3998 (1965).

5) W. M. H. Sachtler, Actes Congr. Intern. Catalyse, 2nd, Paris (1960), p. 2197 (1961).

6) K. Kishi and S. Ikeda, This Bulletin, **46**, 341 (1973).

7) Y. Baer, P. F. Heden, J. Hedman, M. Klasson, C. Nordling, and K. Siegbahn, *Phys. Scr.*, **1**, 55 (1970).

8) D. N. Hendrickson, J. M. Hollander, and W. L. Jolly, *Inorg. Chem.*, **8**, 2642 (1969).

9) P. Finn and W. L. Jolly, *ibid.*, **11**, 893 (1972).

10) In order to check the energy references of Jolly *et al.* and of us, we measured the binding energy of N(ls) in $NaNO_3$ and KCN as common samples. Their binding energies are 407.4 (407.7) eV and 399.0 (398.7) eV, respectively. Our data are shown in the parentheses. This proves that a direct comparison of our data with those by Jolly *et al.* is possible without any correction.

11) G. Schön and S. T. Lundin, *J. Electron Spectrosc.*, **1**, 105 (1972/73).

12) K. S. Kim and R. E. Davis, *ibid.*, **1**, 251 (1972/73).

13) C. G. Pierpont, D. G. Van Derveer, W. Durland, and R. Eisenberg, *J. Amer. Chem. Soc.*, **93**, 4760 (1970).

14) W. Silerthorn and R. D. Feltham, *Inorg. Chem.*, **6**, 1662 (1967).

15) R. D. Feltham, listed in Ref. 9 as private communication to Prof. W. L. Jolly.

16) J. H. Enemark, *Inorg. Chem.*, **10**, 1952 (1971).

17) R. D. Feltham, *ibid.*, **3**, 116 (1964).

18) G. Paliani, A. Poletti, and A. Santucci, *J. Mol. Struct.*, **8**, 63 (1971).

Far Infrared Spectra and Internal Rotation of Ethyl Fluoride and Deuterated Species

Hiromu SUGETA, Yoshio ADACHI, and Tatsuo MIYAZAWA*

Institute for Protein Research, Osaka University, Yamada-kami, Suita, Osaka 565

(Received January 12, 1974)

Far infrared spectra were measured of ethyl fluoride CH_3CH_2F and deuterated species CH_3CD_2F, CD_3CH_2F, and CD_3CD_2F in the gaseous state. The potential barriers hindering the internal rotation were calculated with various models. Possibly because of isotope effects on structure relaxations due to torsional motion and to zero-point motion of other vibrational modes, the observed potential barriers are slightly different among isotopic molecules; the threefold barrier is lowered on the deuteration of the methyl group. The absorption intensities of the four isotopic species were also measured. The intensity of the torsional vibration of the methyl group is nearly doubled on deuteration of the methyl group but is reduced on deuteration of the methylene group. The observed intensity ratios among isotopic species were in good agreement with the ratios calculated with the intensity theory of our previous study.

In our previous study, infrared absorption intensities of torsion-rotation transitions of molecules with symmetric internal rotor were theoretically derived on the basis of torsion-rotation interactions and useful applications were discussed on absolute intensities, orientations of dipole transition moments, band types and deuteration effects.[1] According to the theory, the integrated absorption intensity of the internal-rotation vibration of methyl group [$-CH_3$] was expected to be nearly doubled on the deuteration of the methyl group [$-CD_3$].[1] In the present study, the far infrared spectra of deuterated ethyl fluoride [CH_3CD_2F, CD_3CH_2F, and CD_3CD_2F] were measured for the first time as well as ethyl fluoride [CH_3CH_2F], and experimental integrated intensities were compared with theoretical intensities.

As for the internal rotation of methyl groups, a number of data on barrier heights were accumulated by microwave spectroscopy[2] and far infrared spectroscopy.[3] The internal rotation barrier of ethyl fluoride [CH_3CH_2F] was previously determined as 3306 cal/mol (1156 cm^{-1}) by Herschbach with the microwave absorption spectroscopy.[4] The far infrared spectra of CH_3CH_2F were measured by Sage and Klemperer[5] and by Kinumaki and Kozuka,[6] and potential-barrier coefficients were estimated[5] as $V_3=1165$ and $V_6=-5$ cm^{-1}. In the present study, the internal-rotation potential for the four isotopic molecules were studied with various model calculations.

Experimental

The samples of ethyl fluoride [CH_3CH_2F] and deuterated species [CH_3CD_2F, CD_3CH_2F, and CD_3CD_2F] were prepared through tosyl esters from corresponding ethanols by the method of Edgell and Parts.[7] Ethanol [CH_3CH_2OH] and the perdeuterated species [CD_3CD_2OD] were obtained from commercial sources. The ethanol with the deuterated methylene group [CH_3CD_2OH] was prepared by the reduction of acetyl chloride with lithium aluminum deuteride. The ethanol with the deuterated methyl group [CD_3CH_2OH] was prepared by the reduction of CD_3COOD with lithium aluminum hydride. The samples for spectroscopic observations were dried over phosphorous pentoxide just before measurements.

Far infrared spectra were measured with a Hitachi FIS-3 Far Infrared Spectrophotometer and a 10 cm gas cell with polyethylene windows. The spectral slit width was 2—3 cm^{-1} and the frequency accuracy was estimated to be about ±0.5 cm^{-1}. The peak frequencies were calibrated with the absorption lines of water vapor.[8] The far infrared spectra observed for the four isotopic species are shown in Fig. 1. Mid infrared spectra were measured with a Hitachi Model-225 Infrared Spectrophotometer and a 10 cm gas cell with cesium iodide windows (gas pressure, 10 Torr). The infrared bands due to the C–H and/or C–D stretching vibrations of the four isotopic species are shown in Fig. 2.

Results on Peak Frequencies

The observed frequencies and assignments of internal-rotation transitions of ethyl fluorides are given in Table 1. The fundamental band ($1\leftarrow0$ transition) and two hot bands ($2\leftarrow1$ and $3\leftarrow2$ transitions) were observed for CH_3CH_2F and for CH_3CD_2F, while for CD_3CH_2F and CD_3CD_2F the fundamental band ($1\leftarrow0$) and three hot bands ($2\leftarrow1$, $3\leftarrow2$, and $4\leftarrow3$) were observed. The peak frequencies observed for CH_3CH_2F agreed with the values reported by Sage and Klemperer[5] within ±0.5 cm^{-1} but were slightly lower (by 0.6—1.3 cm^{-1}) than the values reported by Kinumaki and Kozuka.[6]

As for the symmetry index (σ) of the internal-rotation wave functions of ethyl fluoride, the selection rule of the infrared absorption allows $A_1\leftrightarrow A_2$ and $E\leftrightarrow E$ transitions for the vibrational transition $\Delta v=1$.[1,3] Accordingly, in principle, two peaks are expected for each transition $\Delta v=1$. However, in the present study, splitting into two peaks was not observed (Table 1). The $4A_1\leftrightarrow3A_2$ transition[5,6] and $4E\leftrightarrow3E$ transition[6] of CH_3CH_2F were not observed either, with the present experimental conditions.

Successive separations of hot bands usually increase with decreasing peak frequencies, although systematically anomalous cases have also been observed.[9] As shown in Table 1, for the four isotopic molecules of ethyl fluoride, systematic anomaly was not observed but for CD_3CH_2F some irregularity was found in successive separations of hot bands.

Internal Rotation Potential

The Hamiltonian for the internal rotation of a rigid

* Present address, Department of Biophysics and Biochemistry, Faculty of Science, University of Tokyo, Hongo, Bunkyo-ku, Tokyo 113.

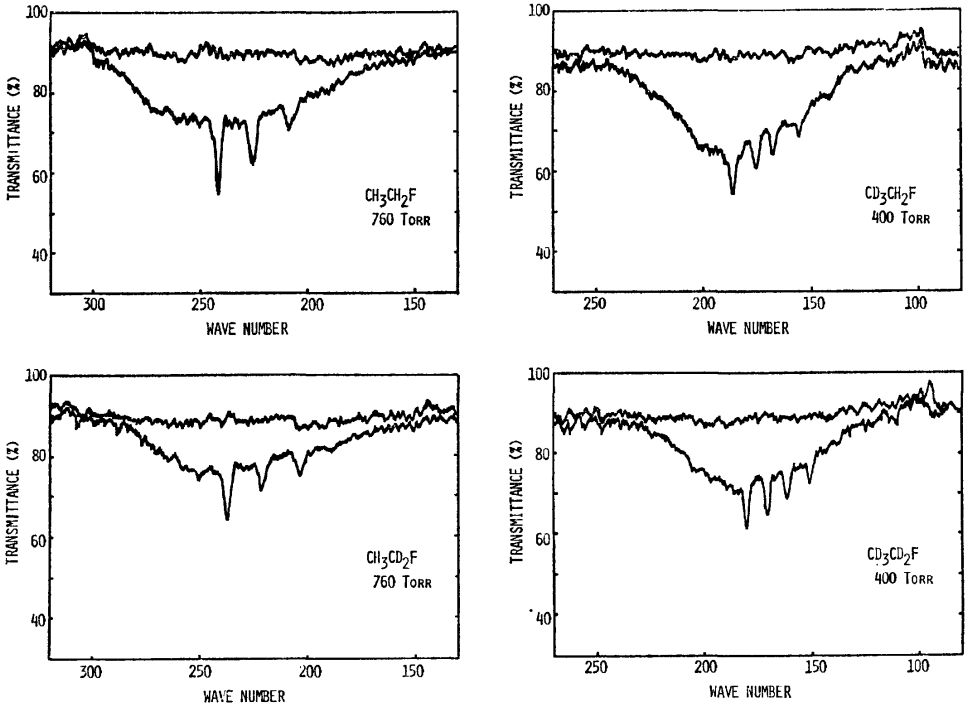

Fig. 1. Far infrared spectra of four isotopic species of ethyl fluoride in the gaseous state at 300 K (path length 10 cm).

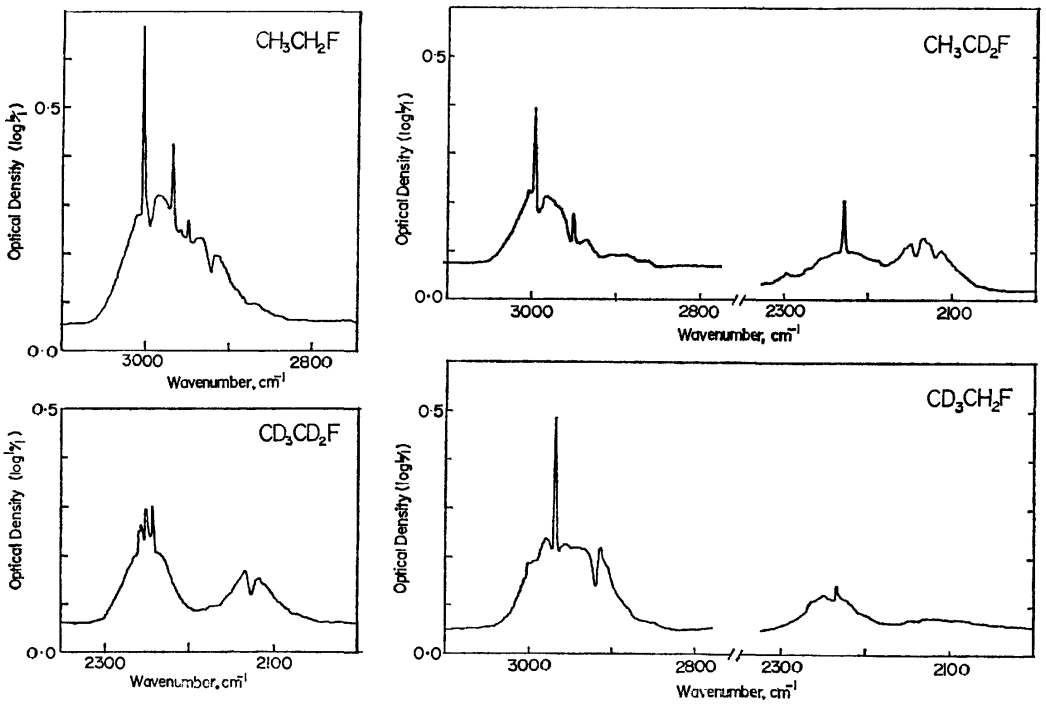

Fig. 2. Infrared spectra of four isotopic species of ethyl fluoride in the gaseous state at 300 K (path length 10 cm, gas pressure 10 Torr).

methyl group with respect to a rigid frame may be written as[10,11]

$$H = Fp_\alpha^2 + V_3(1-\cos 3\alpha)/2 + V_6(1-\cos 6\alpha)/2 + \cdots \quad (1)$$

where α is the internal-rotation angle ($\alpha=0$ for the staggered form), V_3 and V_6 are the threefold and sixfold barriers in the Fourier expansion of the potential energy, and F is equal to one-half of the inverse reduced moment of inertia. The F values for the four isotopic molecules were calculated, as given in Table 1, from molecular structure parameters reported by Nygaard.[12]

Calculation-I. In the rigid-top-rigid-frame model, the potential function may be taken common for all the isotopic molecules. In the first approximation, the threefold barrier (V_3) was taken into account but the sixfold barrier (V_6) was neglected. With the F values

Table 1. Observed frequencies (cm^{-1}) for torsional transitions of ethyl fluorides

Transition	CH_3CH_2F	Δ[a]	CH_3CD_2F	Δ[a]	CD_3CH_2F	Δ[a]	CD_3CD_2F	Δ[a]
1←0	242.2		237.7		186.4		180.7	
		16.5		16.4		10.9		9.3
2←1	225.7		221.3		175.5		171.4	
		17.3		17.4		7.7		9.5
3←2	208.4		203.9		167.8		161.9	
						12.4		10.9
4←3					155.4		151.0	
F (cm^{-1})[b]	6.460		6.174		3.771		3.501	

a) The separation (cm^{-1}) between the observed frequencies. b) Calculated from the structure of Ref. 12.

of Table 1, the potential barrier V_3 of ethyl fluoride molecule was calculated by the method of least squares, with reference to the observed transitions of the four isotopic species. Equal weight was given to each of the observed transitions in the least-squares treatment. Since splitting of the $A_1 \leftrightarrow A_2$ and $E \leftrightarrow E$ transitions was not observed in the present experimental conditions, the calculated transition frequencies were taken as the weighted average of the calculated $A_1 \leftrightarrow A_2$ (weight=1) and $E \leftrightarrow E$ (weight=2) transition frequencies.

The potential barrier was thus obtained as $V_3=1142$ cm^{-1}. The torsional frequencies calculated with this barrier are given in Table 2, together with deviations from the observed values. The calculated frequencies agree fairly well with the observed frequencies, although there are systematic deviations greater than experimental errors; the frequencies calculated for CH_3CH_2F or CH_3CD_2F molecules with the CH_3 group are lower than the observed frequencies whereas the frequencies calculated for CD_3CH_2F or CD_3CD_2F molecules with the CD_3 group are higher than the observed frequencies.

Calculation II. The sixfold barrier (V_6) as well as the threefold barrier (V_3) were taken common for all the isotopic molecules. These barriers were thus calculated as $V_3=1152\pm8$ and $V_6=-6\pm4$ cm^{-1}, with reference to the observed frequencies of the four isotopic molecules. The method of least squares was used in similar manners as Calculation-I, although the V_6 term was treated with the second-order perturbation method.

Calculated transition frequencies agreed with observed frequencies, slightly better than the results of Calculation-I. However, the systematic deviations for the CH_3- and CD_3-groups were little reduced.

Calculation-III. The use of common potential function for the isotopic molecules of ethyl fluoride results in systematic frequency deviations for the CH_3- and CD_3-groups. Accordingly, potential barriers were then calculated for each isotopic molecules, where the F values of Table 1 were used.

In Calculation-III, the three-fold barrier was taken into account but the sixfold barrier was neglected. For each isotopic molecule, the value of V_3 was calculated, as shown in Table 3, by the method of least squares. The V_3 values calculated for the CH_3- group are higher than those calculated for the CD_3- group. Agreements between the calculated and observed frequencies were much improved as compared with the case of Calcula-

Table 2. Calculated frequencies (cm^{-1}) of torsional transitions of ethyl fluorides

	Calcn-I $V_3=1141.6\pm4.2$[a]		Calcn-II $V_3=1151.6\pm7.5$[a] $V_6=-6.4\pm4.0$[a]	
	ν_{calcd}	δ[b]	ν_{calcd}	δ[b]
CH_3CH_2F				
1 ←0	242.1	−0.1	241.3	−0.9
2E←1E	225.1	−0.7	225.1	−0.6
2A←1A	225.0		225.0	
3A←2A	206.0	−3.3	206.8	−2.3
3E←2E	204.7		205.7	
4E←3E	183.6		185.2	
4A←3A	172.5		174.8	
(rmsd)		(1.9)		(1.5)
CH_3CD_2F				
1 ←0	237.1	−0.6	236.2	−1.5
2 ←1	220.8	−0.5	220.8	−0.5
3A←2A	202.6	−1.9	203.4	−1.1
3E←2E	201.7		202.6	
4E←3E	181.4		182.9	
4A←3A	172.8		174.8	
(rmsd)		(1.2)		(1.1)
CD_3CH_2F				
1 ←0	187.9	1.5	187.1	0.7
2 ←1	178.4	2.9	178.1	2.6
3 ←2	167.9	0.1	168.2	0.4
4E←3E	156.2	0.7	156.9	1.4
4A←3A	156.0		156.7	
5A←4A	143.5		144.6	
5E←4E	141.3		142.6	
6E←5E	128.0		129.6	
6A←5A	114.2		116.8	
(rmsd)		(1.7)		(1.6)
CD_3CD_2F				
1 ←0	181.4	0.7	180.6	−0.1
2 ←1	172.6	1.2	172.3	0.9
3 ←2	163.0	1.1	163.2	1.3
4E←3E	152.2	1.2	152.9	1.8
4A←3A	152.1		152.8	
5A←4A	140.4		141.4	
5E←4E	139.2		140.3	
6E←5E	126.3		127.7	
6A←5A	117.8		119.9	
(rmsd)		(1.1)		(1.2)
rmsd[c]		1.5		1.4

a) Errors are standard deviations (cm^{-1}) calculated by the method of least squares. b) $\delta=\nu_{calcd}-\nu_{obsd}$. c) Root-mean-squared deviation.

tion-I.

Calculation-IV. The sixfold barrier (V_6) as well as the threefold barrier (V_3) were calculated, as shown in Table 3, for each isotopic molecule by the method of least squares. The V_3 values calculated for the CH_3-group were systematically higher (by 30—35 cm^{-1}) than those calculated for the CD_3-group. The systematic variations of the calculated V_3 values possibly indicate the isotope effects on structure relaxations due to torsional motion and to zero-point motion of other vibrational modes.

For each isotopic molecule of ethyl fluoride, the agreements between the calculated and observed frequencies were improved, by the incorporation of the V_6 term, as compared with the case of Calculation-III. However, for the molecule of CD_3CH_2F, there are some noticeable frequency deviations for the 2←1 and 3←2 transitions. These deviations are due to the irregularity of successive separation of hot bands (Table 1). One of the origins for this irregularity may be ascribed to the Fermi resonance interaction between the second excited state of the torsional vibration and the first excited state of the skeletal C-C-F bending vibration. For the isotopic molecules of CH_3CH_2F, CH_3CD_2F, CD_3CH_2F, and CD_3CD_2F, the separations between the second excited torsional level and the ground level were calculated as 467.9, 459.0, 361.9, and 352.1 cm^{-1}, from the observed torsional transitions (Table 1). On the other hand, the separations between the first excited bending level and ground level were observed as the infrared bands[13] at 415, 409, 370, and 364 cm^{-1}. Accordingly, the separation between the second excited torsional level and the first excited bending level is smallest for CD_3CH_2F and some Fermi resonance effect may in fact be expected between these levels.

Calculation-V. The second excited torsional levels are perturbed by Fermi resonances whereas the first excited torsional levels are practically free from Fermi resonance interactions. Accordingly, from the observed fundamental transitions (1←0), the threefold barrier was calculated, as shown in Table 3, for each of the four isotopic molecules. The threefold barriers of the CH_3- group were calculated to be higher than those of the CD_3- group.

Calculation-VI. In Calculations III—V, the F values (Table 1) obtained by the microwave analyses[12] were used and the potential barriers were calculated for each isotopic molecule. Instead, the transition frequencies of the four isotopic molecules may also be reproduced by the least-square adjustments of F values for the four isotopic molecules and a common value of V_3. As shown in Table 4, the value of V_3 (1172± 14 cm^{-1}) thus calculated is higher than those of the Calculations-I—II whereas the values of F thus calculated are smaller than the F values from the microwave analyses. The attempt of determining the value of V_6 as well as V_3 and F values was not successful because of ill conditions for the least-squares adjustments.

Calculation-VII. The results of Calculations-I—VI imply that actual internal-rotation modes are accompanied with relaxations of the structures of the rotor and/or frame. Theoretical methods on non-rigid models were derived for the interpretation of microwave spectra by Kivelson[14] and by Kirtman.[15]

Table 3. The calculated frequencies and deviations (cm^{-1}) of torsional transitions of ethyl fluorides

	Calcn-III		Calcn-IV		Calcn-V	
CH_3CH_2F	$V_3=1153.4\pm8.3$		$V_3=1170.7\pm7.8$, $V_6=-11.4\pm4.4$		$V_3=1142$	
1 ←0	243.5	1.3	241.9	−0.3	242.2	0.0
2E←1E	226.4	0.7	226.4	0.7	225.1	(−0.6)
2A←1A	226.3		226.4		225.0	
3A←2A	207.4	−1.8	208.8	−0.3	206.0	(−3.2)
3E←2E	206.2		207.7		204.8	
4E←3E	185.0		187.7		183.7	
4A←3A	174.4		178.2		172.6	
rmsd		1.3		0.5		(1.9)
CH_3CD_2F	$V_3=1150.6\pm3.8$		$V_3=1157.7\pm6.2$, $V_6=-4.6\pm3.4$		$V_3=1147$	
1 ←0	238.1	0.4	237.4	−0.3	237.7	0.0
2 ←1	221.8	0.5	221.8	0.5	221.4	(0.1)
3A←2A	203.7	−0.8	204.2	−0.3	203.2	(−1.3)
3E←2E	202.8		203.4		202.3	
4A←3A	182.4		183.5		182.0	
4E←3E	174.1		175.6		173.6	
rmsd		0.6		0.4		(0.7)
CD_3CH_2F	$V_3=1126.8\pm6.9$		$V_3=1137.4\pm12.7$, $V_6=-6.8\pm6.8$		$V_3=1124$	
1 ←0	186.7	0.3	185.8	−0.6	186.4	0.0
2 ←1	177.1	1.6	176.8	1.3	176.9	(1.4)
3 ←2	166.6	−1.2	166.9	−0.9	166.4	(−1.4)
4E←3E	154.8	−0.7	155.6	0.1	154.6	(−0.9)
4A←3A	154.6		155.4		154.3	
5A←4A	142.2		143.4		141.9	
5E←4E	139.7		141.2		139.5	
6E←5E	126.6		128.3		126.4	
6A←5A	111.9		114.7		111.5	
rmsd		1.1		0.9		(1.1)
CD_3CD_2F	$V_3=1129.2\pm1.3$		$V_3=1126.5\pm2.3$, $V_6=1.6\pm1.2$		$V_3=1133$	
1 ←0	180.4	−0.3	180.6	−0.1	180.7	0.0
2 ←1	171.6	0.2	171.6	0.2	171.9	(0.5)
3 ←2	161.9	0.0	161.9	0.0	162.3	(0.4)
4E←3E	151.2	0.1	151.0	−0.1	151.5	(0.5)
4A←3A	151.0		150.9		151.4	
5A←4A	139.3		139.0		139.6	
5E←4E	138.0		137.7		138.4	
6E←5E	125.2		124.8		125.5	
6A←5A	116.1		115.5		116.6	
rmsd		0.2		0.1		(0.4)

In the present study, however, the empirical method by Ewig and Harris[16] was used for the interpretation of the far infrared spectra of ethyl fluorides.

The Hamiltonian for the internal rotation of a molecule with structure relaxations may be written in a one-dimensional approximation as,

$$H = p_\alpha F(\alpha) p_\alpha + V_3(1-\cos 3\alpha)/2 + V_6(1-\cos 6\alpha)/2 + \cdots \quad (2)$$

where $F(\alpha)$ is a function of the internal-rotation angle α (for the rigid model of Eq. (1), F is independent of α). The function $F(\alpha)$ may be evaluated with an *a priori* knowledge or an assumption on the molecular

Table 4. The calculated frequencies and deviations (cm^{-1}) of torsional transitions of ethyl fluorides [Calculation-VI][a)]

	CH_3CH_2F $F=6.298\pm0.109$		CH_3CD_2F $F=6.011\pm0.104$		CD_3CH_2F $F=3.569\pm0.061$		CD_3CD_2F $F=3.332\pm0.057$	
1 ←0	242.7	0.5	237.5	−0.2	185.7	−0.7	179.7	−1.0
2E←1E	226.2	0.4	221.7	0.4	176.7	1.2	171.4	0.0
2A←1A	226.1							
3A←2A	207.6	−1.4	204.1	−0.2	166.9	−0.9	162.3	0.4
3E←2E	206.7		203.5					
4E←3E	185.9		183.6		156.0	0.5	152.2	1.2
4A←3A	177.5		177.2		155.9		152.2	
5A←4A					143.9		141.0	
5E←4E					142.7		140.4	
6E←5E					129.5		127.9	
6A←5A					121.3		122.9	
rmsd		0.9		0.3		0.9		0.8

a) The threefold barrier was calculated to be $V_3=1172.6\pm14.0\ cm^{-1}$. The values of F are given in the unit of cm^{-1}. The overall rmsd was $0.8\ cm^{-1}$.

Table 5. The calculated frequencies and deviations (cm^{-1}) of torsional transitions of ethyl fluorides [Calculation-VII][a)]

	CH_3CH_2F $\bar{F}=6.027\pm0.117$ $\bar{V}_3=1211.3\pm17.3$		CH_3CD_2F $\bar{F}=6.001\pm0.105$ $\bar{V}_3=1174.0\pm14.9$		CD_3CH_2F $\bar{F}=3.615\pm0.153$ $\bar{V}_3=1161.4\pm36.2$		CD_3CD_2F $\bar{F}=3.532\pm0\cdot027$ $\bar{V}_3=1122.0\pm6.3$	
1 ←0	241.9	−0.3	237.5	−0.2	185.9	−0.5	180.5	−0.2
2E←1E	226.2	0.5	221.7	0.4	176.8	1.3	171.6	0.2
2A←1A	226.2							
3A←2A	208.5	−0.2	204.1	−0.2	166.8	−1.0	161.9	0.0
3E←2E	208.0		203.5					
4E←3E	188.0		183.6		153.7	0.2	151.0	−0.1
4A←3A	182.6		177.4		155.6		150.9	
5A←4A					143.4		139.0	
5E←4E					142.1		137.6	
6E←5E					128.8		124.7	
6A←5A					119.3		114.8	
rmsd		0.4		0.3		0.9		0.2

a) The values of $\bar{F}$ and $\bar{V}_3$ are given in the unit of cm^{-1}.

dynamics of the internal-rotation and other vibrational modes. The Hamiltonian in Eq. (2) may be transformed to the reduced θ representation,[16,17]

$$H=\bar{F}p_\theta^2+\bar{V}_3(1-\cos 3\theta)/2+\bar{V}_6(1-\cos 6\theta)/2+\cdots \quad (3)$$

on the basis of the following transformations.

$$\bar{F}^{-1/2}=(1/2\pi)\int_0^{2\pi}F(\alpha)^{-1/2}\,d\alpha \quad (4)$$

$$\theta=\bar{F}^{1/2}\int_0^{\alpha}F(\alpha')^{-1/2}\,d\alpha' \quad (5)$$

Here $\bar{F}$ is a constant independent of θ, and the transformation from α to θ is nonlinear. The angle θ has the same boundary condition as the internal-rotation angle α. The potential function $[\bar{V}(\theta)]$ of Eq. (3) is different from the potential function $[V(\alpha)]$ of Eq. (2), but these functions $\bar{V}(\theta)$ and $V(\alpha)$ have the same symmetry, same boundary condition, and same heights of the maxima and minima.[16,17]

For the four isotopic molecules of ethyl fluoride, sufficient knowledges were not available for evaluating the functions $F(\alpha)$. Therefore, the Hamiltonian H of Eq. (3) was used for determining empirically the kinetic-energy parameter $\bar{F}$ and the potential coefficients $\bar{V}_3$ and $\bar{V}_6$.

With Eq. (3), the values of $\bar{F}$ and $\bar{V}_3$ were calculated for each isotopic molecule, by the method of least squares, with reference to the observed transition frequencies. The $\bar{V}_6$ and higher terms were neglected. The calculated results are given in Table 5. Calculated transition frequencies agreed satisfactorily with observed frequencies. However, for the molecule of CD_3CH_2F, the frequency agreements were little improved, as compared with the case of Calculation-IV, possibly because of the limitation imposed by the effect of Fermi resonance.

As compared with the F values of the rigid model (Table 1), the $\bar{F}$ values calculated with Calculation-VII were smaller for the molecules of CH_3CH_2F, CH_3CD_2F, and CD_3CH_2F but larger for the molecule of CD_3CD_2F. Furthermore, as compared with the V_3 values of Calculation-III (Table 3), the $\bar{V}_3$ values calculated with Calculation-VII were higher for the molecules of CH_3CH_2F, CH_3CD_2F, and CD_3CH_2F but lower for the molecule of CD_3CD_2F. However, systematic deuteration effects were observed on the $\bar{V}_3$ values of the four isotopic molecules; the $\bar{V}_3$ values were lowered by deuteration of the methyl group ($\sim50\ cm^{-1}$) and also by the deuteration of the methylene group ($\sim40\ cm^{-1}$). The attempt of determining the value of $\bar{V}_6$ as well as

$\bar{V}_3$ and $\bar{F}$ was not successful because of ill conditions for the least-squares refinements.

Isotope Effects on Absorption Intensities of Torsional Bands

The absorption intensity of a torsional band may be calculated from molecular structure parameters and molecular dipole moment, with the theory previously reported by Sugeta and Miyazawa.[1] According to this theory, the molar integrated absorption intensity of the torsional transition ($\Delta v=1$) may be expressed as,

$$\int\alpha(\nu)\mathrm{d}\nu=\frac{N}{z}\frac{8\pi^3}{3h^2c}\times 4F^2|\boldsymbol{\mu}\times\boldsymbol{\rho}|^2\sum_{v,\sigma}[\exp(-E_{v,\sigma}/kT) -\exp(-E_{v+1,\sigma}/kT)]\times\frac{|\langle v+1,\sigma|p_\alpha|v,\sigma\rangle|^2}{E_{v+1,\sigma}-E_{v,\sigma}} \quad (6)$$

where v and σ are the vibrational quantum number and symmetry index, $E_{v,\sigma}$, is the eigenvalue of the state $v\sigma$, p_α is the angular momentum operator of the internal rotor along its symmetry axis, z is the partition function, N is the Avogadro number, and $\boldsymbol{\mu}$ is the dipole moment vector. The vector $\boldsymbol{\rho}$ is given by the moment of inertia of the internal rotor (I_α), the moment of inertia of the entire molecule (I_a, I_b, I_c), and the direction cosines of the internal-rotation axis (λ_a, λ_b, λ_c),

$$\tilde{\boldsymbol{\rho}}=[\lambda_aI_\alpha/I_a \quad \lambda_bI_\alpha/I_b \quad \lambda_cI_\alpha/I_c] \quad (7)$$

For the high-barrier harmonic approximation, Eq. (6) may be simplified as,[1]

$$\int\alpha(\nu)\mathrm{d}\nu\simeq(8\pi^3N/3h^2c)F|(\boldsymbol{\mu}\times\boldsymbol{\rho})|^2 \quad (8)$$

The theoretical absorption intensities of the torsional bands of the four isotopic species of ethyl fluoride were calculated, by the use of the molecular structure parameters[12] and dipole moment.[18] The results of Calculation-I were used for the intensity calculations. The theoretical intensities calculated with Eq. (6) are given for the four isotopic molecules in Table 6, where the summations in Eq. (6) were made up to the 4←3 transitions for CH_3CH_2F and CH_3CD_2F and up to the 6←5 transitions for CD_3CH_2F and CD_3CD_2F.

Table 6. Integrated absorption intensities[a] (and ratios[b]) of torsional bands of ethyl fluorides

Molecule	Experimental Intensity	Ratio	Calculated [Mathieu][c] Intensity	Ratio	Calculated [Harmonic][d] Intensity	Ratio
CH_3CH_2F	2.0_5		3.63		3.91	
CH_3CD_2F	1.1_5	0.5_5	2.27	0.62	2.45	0.63
CD_3CH_2F	3.8_0	1.8_5	6.29	1.73	6.62	1.69
CD_3CD_2F	2.7_5	1.3_5	4.09	1.12	4.32	1.10

a) In unit of $cm^{-2}\cdot atm^{-1}$, at 300 K. b) Relative to CH_3CH_2F. c) Calculated with Eq. (6). d) Calculated with Eq. (8).

On the deuteration of the methyl group, the theoretical intensities are nearly doubled (1.7—1.8 times), as discussed previously. This intensity enhancement is due to the twofold increase in the magnitude of the $\boldsymbol{\rho}$ vector, overcoming the decrease (to about one-half) in the F values. On the other hand, the theoretical intensities are reduced (to 0.6—0.7 times) on the deuteration of the methylene group. This intensity reduction is ascribed to the decrease in the magnitude of the $\boldsymbol{\rho}$ vector and in the F values.

The experimental absorption intensities were measured for the four isotopic species of ethyl fluoride and are given in Table 6. Experimental errors in the integrated intensities were estimated to be about 20%. In the far-infrared region, experimental determinations of absolute intensities were difficult with the present instrumental conditions, and accordingly the relative intensities among the four isotopic molecules were also calculated as shown in Table 6.

The experimental intensities were lower than the theoretical intensities [from Eq. (6)], because of instrumental limitations. However, as for the relative intensities among the four isotopic molecules, observed intensity ratios agreed fairly well with experimental intensity ratios. In particular, the observed changes of the absorption intensities on deuteration of the methyl group and methylene group confirmed the validity of the intensity theory previously reported.[1]

Theoretical values of the integrated absorption intensities of the torsional bands were also calculated with the high-barrier harmonic approximation [Eq. (8)]. As shown in Table 6, the intensity values calculated with Eq. (8) are appreciably higher than the values calculated with Eq. (6). Accordingly, for calculations of the absolute intensity values, Eq. (6) rather than Eq. (8) is to be used. However, the theoretical intensity ratios calculated with Eq. (8) agree closely with the ratios calculated with Eq. (6). With this harmonic approximation, evaluations of $F|(\boldsymbol{\mu}\times\boldsymbol{\rho})|^2$ in Eq. (8) are sufficient for calculating theoretical intensity ratios.

Discussion

For studying the effects of adjustable parameters (F, V_3, and V_6) on torsional transition frequencies, Jacobian elements have been calculated. For lower transitions, the values of $\delta\nu/\delta V_3$ are nearly constant so that a small increment in V_3 results in uniform shifts of transition frequencies. On the other hand, the values of $\delta\nu/\delta V_6$ significantly decrease for higher transitions so that a small increment in V_6 results in nonuniform shifts of transition frequencies. It may be remarked that the absolute values of $\delta\nu/\delta V_6$ are minimum for the 3←2 transitions of the CH_3 group and for the 4←3 or 5←4 transitions of the CD_3 group. These higher-transition frequencies are little subjected to the effect of the sixfold barriers, as noticed previously by Fateley and Miller.[19] The values of $\delta\nu/\delta F$ also decrease for higher transitions and an increment in F results in nonuniform shifts of transition frequencies.

In the present study on the four isotopic molecules of ethyl fluoride, systematic deviations between the observed and calculated frequencies were found in Calculations-I—II; the transition frequencies calculated for the molecules of CH_3CH_2F and CH_3CD_2F with the CH_3- group are lower than the observed frequencies whereas the frequencies calculated for the molecules of CD_3CH_2F and CD_3CD_2F with the CD_3-

group are higher than the observed frequencies. In Calculations-III—V, systematic variations among the barrier heights of isotopic molecules were found; the threefold barriers were lowered on the deuteration of the methyl group (from CH_3CH_2F to CD_3CH_2F and from CH_3CD_2F to CD_3CD_2F). In Calculation-VI, systematic variations among the apparent F values of isotopic molecules were found. Finally in Calculation-VII, systematic variations of the $\overline{V}_3$ values were also found; the $\overline{V}_3$ values were lowered by the deuteration of the methyl group and also by the deuteration of the methylene group. All these results indicate that the observed potential barriers hindering the internal rotation are slightly but definitely different among isotopic molecules, because of the structure relaxations due to torsional motion and to zero-point motion of other modes. This effect of deuteration on potential barriers of the methyl groups has also been found for other molecules.[20]

Recently some comments were made[16,21-23] on the physical meaning and spectroscopic determination of the V_6 terms of the internal-rotation potential and the 3α-dependent term of $F(\alpha)$ in Eq. (2).

$$F(\alpha) = F_0 + F_3 \cos 3\alpha + \cdots \quad (9)$$

In the least-squares refinements with reference to the observed transition frequencies,[16,22,23] the values of $4F_0V_6+F_3V_3$ may be estimated but the values of V_6 and F_3 may not be determined independent of each other. In the present non-rigid model of Calculation-VII, however, the internal-rotation angle α is transformed into the angle θ so that $\overline{F}$ is independent of θ and 3θ-dependent term vanishes [$\overline{F}_3=0$]. Then, the values of $\overline{F}$, $\overline{V}_3$, $\overline{V}_6$,$\cdots$in Eq. (3) may well be calculated by the method of least squares, if observed data of transition frequencies were sufficiently available.

In Calculation-VII, transition-frequency data of the present experimental study were not sufficient for the least-square adjustment of the three parameters $\overline{F}$, $\overline{V}_3$ and $\overline{V}_6$. For the molecule of CH_3CH_2F, the 4E←3E and 4A←3A transitions were observed by Kinumaki and Kozuka,[6] although their frequencies for lower transitions were systematically higher than those of the present study. These 4E←3E and 4A←3A transition frequencies were added to the present data of the 1←0, 2←1, and 3←2 transition frequencies, and the parameters $\overline{F}$, $\overline{V}_3$, and $\overline{V}_6$ were determined, as shown in Table 7, for the molecule of CH_3CH_2F. On the other hand, model calculations were made for the molecules of CD_3CH_2F and CD_3CD_2F, and it was found that the experimental data on the fundamental (1←0) through 5A←4A and 5E←4E or more preferably 6E←5E and 6A←5A transitions were required for calculating reliable values of $\overline{F}$, $\overline{V}_3$ and $\overline{V}_6$.

Table 7. Calculated frequencies and deviations (cm^{-1}) of torsional transitions of CH_3CH_2F.[a]

Transition	Observed	Calculated	Deviation
1 ←0	242.2	241.5	−0.7
2E←1E 2A←1A	225.7	226.7 226.6	1.0
3A←2A 3E←2E	208.4	209.6 208.4	0.4
4E←3E	189.6[b]	188.9	−0.7
4A←3A	178.4[b]	178.5	0.1

a) $\overline{F}=6.576\pm0.128\ cm^{-1}$, $\overline{V}_3=1168.4\pm7.5\ cm^{-1}$, $\overline{V}_6=-18.4\pm6.4\ cm^{-1}$, and rmsd$=0.7\ cm^{-1}$. b) Ref. 6.

After the present study was completed, high resolution far-infrared spectrum of C_2H_5F was reported by Tuazon *et al.*[24] and the dependence of the potential parameters V_3 and V_6 on changes in selected values of F was discussed.

Conclusion

In the present study, several types of calculations with various models were made for analyzing the far infrared spectra and for calculating potential barrier coefficients of the four isotopic molecules of ethyl fluoride, All those calculations indicate that the observed potential barriers hindering the internal rotation are slightly different among isotopic molecules, because of the small coupling between the internal-rotation mode and other vibrational modes. For more detailed determinations of the potential barriers, however, it is desirable to observe weak far-infrared bands due to transitions between higher excited torsional states and to analyze microwave spectra of higher excited torsional states.

It has been established that the absorption intensities of C–H stretching vibrations are reduced to about one half on deuteration. In the present study, the absorption intensities of the C–H stretching vibrations of ethyl fluoride were in fact found to decrease, as shown Fig. 2, on deuteration of the methyl and/or methylene group. On the other hand, it has been anticipated theoretically[1] that the absorption intensity of the torsional vibration of the CH_3 group is nearly doubled on deuteration of the methyl group but is reduced on deuteration of the methylene group. In the present study, the absorption intensity ratios of the torsional bands of the four isotopic molecules were in fact found to agree closely with the theoretical ratios, confirming the intensity theory previously derived.

Numerical calculations of the present study were carried out with a NEAC 2200—700 computer of Osaka University.

References

1) H. Sugeta and T. Miyazawa, This Bulletin, **46**, 2752 (1973).
2) W. Gordy and R. L. Cook, "Microwave Molecular Spectra," Interscience Publisher, New York (1970), Chap. 12.
3) K. D. Möller and W. G. Rothschild, "Far-Infrared Spectroscopy," Wiley-Interscience, New York (1971), Chap. 8.
4) D. R. Herschbach, *J. Chem. Phys.*, **25**, 358 (1956).
5) G. Sage and W. Klemperer, *ibid.*, **39**, 371 (1963).
6) S. Kinumaki and M. Kozuka, This Bulletin, **43**, 3933 (1970).
7) W. F. Edgell and L. Parts, *J. Amer. Chem. Soc.*, **77**, 4899 (1955).
8) K. N. Rao, C. J. Humphreys, and D. H. Rank, "Wavelength Standards in the Infrared," Academic Press, New York (1966), and also Reference 1, Chap. 9.
9) K. D. Möller and L. H. London, *J. Chem. Phys.*, **47**, 2505 (1967); L. H. London and K. D. Möller, *J. Mol. Struct.*, **2**, 493 (1968).

10) D. R. Herschbach, *J. Chem. Phys.*, **31**, 91 (1959).
11) W. G. Fateley and F. A. Miller, *Spectrochim. Acta*, **17**, 857 (1961).
12) L. Nygaard, *ibid.*, **22**, 1261 (1966).
13) Y. Adachi, H. Sugeta, and T. Miyazawa, Unpublished work.
14) D. Kivelson, *J. Chem. Phys.*, **23**, 2236 (1955).
15) B. Kirtman, *ibid.*, **37**, 2516 (1962).
16) C. S. Ewig and D. O. Harris, *ibid.*, **52**, 6268 (1970).
17) P. Meakin, D. O. Harris, and E. Hirota, *ibid.*, **51**, 3775 (1969).
18) J. Kraitchman, *ibid.*, **23**, 184 (1955).
19) W. G. Fateley and F. A. Miller, *Spectrochim. Acta*, **19**, 611 (1963).
20) [CH_3CHO, CD_3CHO, CD_3CDO] R. W. Kilb, C. C. Lin, and E. B. Wilson, Jr., *J. Chem. Phys.*, **26**, 1695 (1957); Ref. 21; [CH_3CFO, CD_3CFO] L. Pierce and L. C. Krisher, *ibid.*, **31**, 875 (1959); [CH_3COOH, CD_3COOH] L. C. Krisher and E. Saegebarth, *ibid.*, **54**, 4553 (1971); [CH_3COCH_3, CD_3COCD_3] R. Nelson and L. Pierce, *J. Mol. Spectrosc.*, **18**, 344 (1965); [$CH_3COCH_2CH_3$. $CD_3COCD_2CH_3$] L. Pierce, C. K. Chang, M. Hayashi, and R. Nelson, *J. Mol. Spectrosc.*, **32**, 449 (1969); [CH_3OH, CD_3OH, CH_3OD, CD_3OD] R. M. Lees, *J. Chem. Phys.*, **56**, 5887 (1972); Ref. 23; [CH_3NO, CD_3NO] D. Coffey, Jr., C. O. Britt, and J. E. Boggs, *J. Chem. Phys.*, **49**, 591 (1968); [CH_3CH_2Cl, CH_3CD_2Cl, CD_3CH_2Cl, CD_3CD_2Cl] W. G. Fateley, F. E. Kiviat, and F. A. Miller, *Spectrochim. Acta*, **26A**, 315 (1970); [CH_3NO_2, CD_3NO_2] E. Tannenbaum, R. J. Myers, and W. D. Gwinn, *J. Chem. Phys.*, **25**, 42 (1956).
21) C. E. Souter and J. L. Wood, *J. Chem. Phys.*, **52**, 674 (1970).
22) R. M. Lees, *J. Mol. Spectrosc.*, **33**, 124 (1970); *J. Chem. Phys.*, **59**, 2690 (1973).
23) R. M. Lees and J. G. Baker, *J. Chem. Phys.*, **48**, 5299 (1968).
24) E. C. Tuazon, S. Manocha, and W. G. Fateley, *Chem. Phys. Lett.*, **23**, 63 (1973).

Infrared Absorption Intensities of *trans*- and *cis*-Dichloroethylene

Kazutoshi TANABE and Shinnosuke SAËKI

National Chemical Laboratory for Industry, Honmachi, Shibuya-ku, Tokyo 151

(Received January 14, 1974)

Infrared absorption intensities of *trans*- and *cis*-dichloroethylene were measured in the vapor phase, and interpreted in terms of intensity parameters common to the isomers. In order to obtain L matrices, force constants common to the isomers were determined so as to attain the best fit between the observed and calculated frequencies of CHCl=CHCl, CDCl=CDCl and CHCl=CDCl. Using the L matrices thus obtained, intensity parameters were determined so as to attain the best fit between the observed and calculated intensities of CHCl=CHCl. As a result, the observed frequencies and intensities were satisfactorily represented in terms of the force constants and the intensity parameters common to the isomers.

In our serial studies on rotational isomerism,[1-3] the energy differences between the rotational isomers were evaluated by applying the absolute intensity method. This is quite a unique method, not requiring any temperature variation in experiment, hence it may give a very reliable value for an energy difference. But it has a great disadvantage that intensity parameters are assumed to be transferable between the rotational isomers concerned. The validity of this assumption can by no means be confirmed by any direct method.

In our serial studies on infrared absorption intensities,[4-6] intensity data were interpreted in terms of intensity parameters common to some molecular groups or molecular series. At least as far as the molecular series treated so far are concerned, it was concluded that intensity parameters are transferable among some molecular groups.

In this investigation, in order to confirm the transferability of intensity parameters in molecules containing double bonds, infrared absorption intensities of *trans*- and *cis*-dichloroethylene CHCl=CHCl measured in the vapor phase have been interpreted in terms of intensity parameters assumed as transferable between the isomeric molecules.

Experimental

Infrared absorption intensities of fundamental bands of *trans*- and *cis*-dichloroethylene CHCl=CHCl were measured in the vapor phase using Perkin-Elmer Model 421 grating spectrophotometer combined with a digital recorder.[7] The vapor phase spectra recorded are shown in Figs. 1(a) and 1(b). The commercial material of the extra pure grade was used without further purification. The observed spectrum of *trans* isomer shows that it contains at most 1% of *cis* isomer.

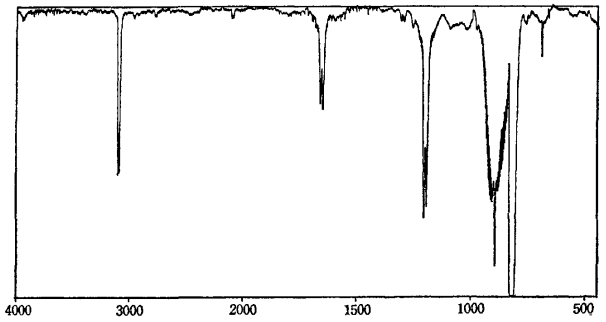

Wave number (cm^{-1})

Fig. 1(a). Vapor phase spectrum of *trans*-dichloroethylene.

Gas cells 5 or 10 cm thick with KBr or polyethylene windows were used, and measurements were made at least ten times at different sample pressures ranging from 5 to 100 mmHg. Since vibration-rotation fine structures were observed for some absorption bands, dry air was introduced as foreign gas into gas cells in order to pressurize up to 1 atm, and absolute band intensities were evaluated by applying the Wilson-Wells extrapolation technique. The plots of intensities against pressures for some absorption bands are shown in Fig. 2.

In order to integrate absorbance curves for obtaining absolute band intensities, encoded paper tapes punched out from the digital recorder were processed by using a FACOM

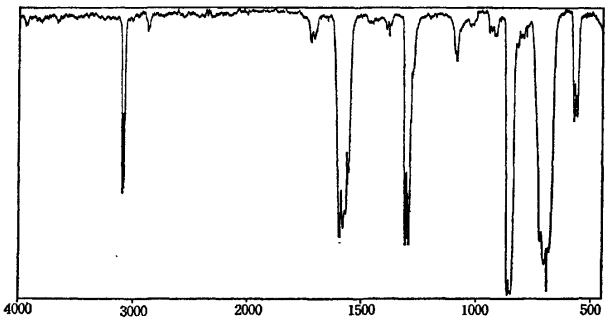

Wave number (cm^{-1})

Fig. 1(b). Vapor phase spectrum of *cis*-dichloroethylene.

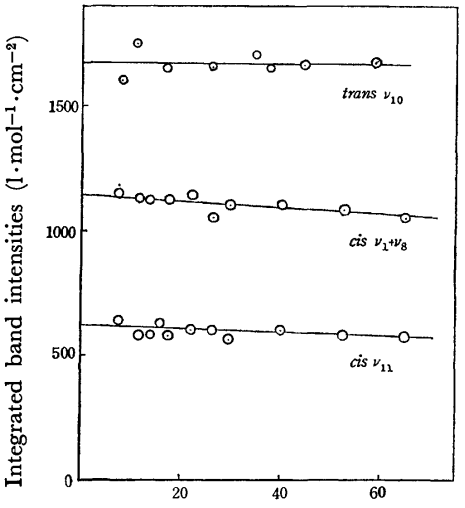

Pressure of dichloroethylene (mmHg)

Fig. 2. The Wilson-Wells extrapolation plot.

TABLE 1. OBSERVED AND CALCULATED INTENSITIES OF DICHLOROETHYLENE
(Unit: $l \cdot mol^{-1} \cdot cm^{-2}$)

		ν_{obsd} (cm^{-1})	A_{obsd}	Shimozawa, Wilson[8]		Dervil[9]		A_{calcd}
				A_{soln}[a]	A_{P-W}[b]	A_{soln}	A_{P-W}[b]	
trans	ν_9	3097	1200± 50	1632	1246			1183
	ν_{10}	1201	1700± 50	1452	1106			1862
	ν_6	898	4900±100	6620	5060			4881
	ν_{11}	826	9600±200			14000[c]	9470	8712
	ν_{12}	250	10± 5					25
	ν_7	227	100± 50					6
cis	ν_8	3087	1100± 50	1990	1524			1018
	ν_1	3086						123
	ν_2	1592	2200±300[d]					2656
	ν_9	1303	1800±100	2420	1850			310
	ν_3	1179	10± 5					23
	ν_{10}	857	5800±200			7150[e]	5845	5740
	ν_4	721	5700±200					2475
	ν_{12}	695						4569
	ν_{11}	569	600± 50					684
	ν_5	173	10± 5					21

a) Carbon tetrachloride solution. b) Gaseous intensities estimated by applying the Polo-Wilson's equation. c) Carbon disulfide solution. d) Owing to the overlapping with a combination band, the error is fairly large. e) *n*-Hexane solution.

TABLE 2. INTERNAL COORDINATES OF DICHLOROETHYLENE

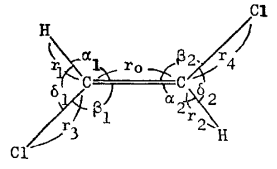

trans

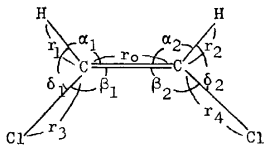

cis

r_0	CC stretching
r_1, r_2	CH stretching
r_3, r_4	CCl stretching
$(\alpha_1-\delta_1)/\sqrt{2}$, $(\alpha_2-\delta_2)/\sqrt{2}$	CCH bending
$(2\beta_1-\alpha_1-\delta_1)/\sqrt{6}$, $(2\beta_2-\alpha_2-\delta_2)/\sqrt{6}$	CCCl bending
π_1, π_2	Out-of-plane bending
τ	Torsion

TABLE 3. CONVERGED VALUES AND STANDARD DEVIATIONS OF FORCE CONSTANTS
(Unit: mdyn/Å, mdyn, or mdyn·Å)

F(CH)	5.15(0.03)
F(CC)	9.28(0.31)
F(CCl)	3.97(0.03)
E(CCH)	0.50(0.01)
F(CCCl)	0.88(0.02)
F(π)	0.25(0.00)
F(to)	0.62(0.01)
F(CH, CH')	−0.06(0.02)
F(CH, CC)	−0.16(0.10)
F(CH, CCH)	0.26(0.07)
F(CC, CCH)	0.28(0.08)
F(CC, CCCl)	0.20(0.12)
F(CCl, CCl')	0.12(0.03)
F(CCl, CCH)	−0.30(0.02)
F(CCl, CCCl)	0.39(0.02)
F(CCH, CCH')	0.00(0.01)
F(CCH, CCCl)	−0.04(0.02)
F(CCCl, CCCl')	−0.01(0.02)
F(π, π')	0.03(0.00)
F(π, to)	−0.07(0.00)

Model 270—30 electronic computer system. For the absorption bands below 500 cm^{-1}, the digital recording was not available, and their absorption intensities were estimated by using a planimeter.

Other experimental conditions for the intensity measurement are the same as described in our previous papers.[1-7]

Results and Discussion

The absolute intensities of fundamental bands of *trans*- and *cis*-dichloroethylene CHCl=CHCl measured in the vapor phase are listed in Table 1 with experimental errors. Although several papers were published on the vibrational frequencies of dichloroethylene, the absorption intensities for these isomeric molecules have received little attention.

Shimozawa and Wilson[8] measured the infrared absorption intensities of several fundamental bands of *trans*- and *cis*-dichloroethylene in carbon tetrachloride or carbon disulfide solution, and evaluated the gaseous band intensities by applying the Polo-Wilson's equation. The values estimated by them are in rather good accordance with the intensities obtained in this study, except for the ν_{10} band of *trans* isomer.

Dervil[9] measured the infrared absorption intensities of the *trans* ν_{11} and *cis* ν_{10} bands of dichloroethylene in hexane or carbon disulfide solution. The gaseous

TABLE 4. OBSERVED AND CALCULATED FREQUENCIES OF DICHLOROETHYLENE (cm^{-1})

			CHCl=CHCl			CDCl=CDCl				CHCl=CDCl		
			ν_{obsd}	ν_{calcd}	$\delta\nu$[a]	ν_{obsd}	ν_{calcd}	$\delta\nu$		ν_{obsd}	ν_{calcd}	$\delta\nu$
trans	1	A_g	3073	3082	9	2325	2319	−6	A′	3087	3090	3
	2		1585	1596	11	1570	1557	−13		2310	2301	−9
	3		1274	1260	−14	992	998	6		1574	1576	2
	4		852	858	6	765	752	−13		1241	1237	−4
	5		349	354	5	346	350	4		964	970	6
	6	A_u	898	898	0	660	655	−5		830	831	1
	7		227	224	−3	227	220	−7		776	774	−2
	8	B_g	763	765	2	657	656	−1		348	352	4
	9	B_u	3097	3098	1	2290	2282	−8		250	265	15
	10		1201	1218	17	916	913	−3	A″	830	834	4
	11		826	826	0	791	797	6		660	656	−5
	12		250	271	21	250	260	10		227	222	−5
cis	1	A_1	3086	3089	3	2325	2320	−5	A′	3078	3090	12
	2		1592	1602	10	1576	1563	−14		2306	2300	−6
	3		1179	1192	13	850	849	−1		1591	1582	−9
	4		721	720	−1	700	699	−1		1253	1251	−2
	5		173	160	−13	171	160	−11		957	966	9
	6	A_2	876	880	4	695	681	−14		788	780	−8
	7		406	405	−1	368	373	5		710	710	0
	8	B_1	3087	3091	4	2280	2280	−0		558	556	−2
	9		1303	1289	−14	1051	1052	1		175	160	−15
	10		857	859	2	766	755	−11	A″	817	819	2
	11		569	562	−7	540	550	10		584	584	−0
	12	B_2	695	701	6	558	541	−17		387	388	1

a) $\delta\nu = \nu_{calcd} - \nu_{obsd}$.

intensities estimated from her values by applying the Polo-Wilson's equation agree well with the present results. Hence the observed intensity data obtained in this study can be considered as reliable enough for the intensity computation.

In order to interpret these intensity data, it is necessary to obtain L matrices by the normal mode analysis. Concerning the vibrational frequencies of dichloroethylene, Bernstein *et al.*[10,11] pointed out the errors for the band assignments made by Wu,[12,13] Trumpy,[14] Herzberg,[15] or Pitzer *et al.*,[16] and reported the correct band assignment for *trans*- and *cis*-dichloroethylene CHCl=CHCl, CDCl=CDCl and CHCl=CDCl. However, the determination of force constants in dichloroethylene has received little attention, except for the out-of-plane vibrations studied by Pitzer *et al.*[16] or Dowling.[17]

In order to obtain L matrices as accurate as possible, force constants have been determined by the least-squares method so as to attain the best fit between the observed and calculated frequencies of *trans*- and *cis*-dichloroethylene CHCl=CHCl, CDCl=CDCl and CHCl=CDCl. Twenty force constants based on the internal coordinates given in Table 2 have been assumed as common to the *trans* and *cis* isomer, and their values have been refined from total seventy-two frequency data. As for the torsional coordinate, not τ(Cl–C–C–Cl), but the coordinate of the internal rotation type has been taken.

Previous authors pointed out that for substituted ethane or ethylene, it is necessary to introduce the *trans* interaction constant. Such an interaction constant may be required in the present case. However, since in this study, we examine whether we can explain the observed frequencies and intensities in terms of the force constants and the intensity parameters common to the isomeric molecules, the *trans* interaction constant has not been taken into account, and the determination of the common force constants has been carried out.

Converged values and standard deviations of the force constants are listed in Table 3, and the calculated normal frequencies are compared in Table 4 with the observed fundamental frequencies. The agreement between the observed and calculated frequencies is satisfactory on the whole, and the converged values of the force constants are all quite acceptable as compared with those of related molecules. A rather good agreement between the observed and calculated frequencies for the CCH bending vibrations may suggest that the *trans* interaction constant takes less significant role in representing the normal frequencies of dichloroethylene. Thus the L matrices obtained by this normal mode analysis can be considered as suitable enough for the intensity computation described below.

Using the L matrix data thus obtained, the intensity data given in Table 1 have been interpreted in terms of intensity parameters on the basis of the Gribov's valence-optical theory.[18,19] As for the intensity parameters for interpreting the intensity data of *trans*- and *cis*-dichloroethylene, the following assumption has been

TABLE 5. CONVERGED VALUES AND STANDARD DEVIATIONS OF INTENSITY PARAMETERS
(Unit : D, or D/Å)

μ_{CH}	0.80(0.01)
μ_{CCl}	−0.29(0.01)
$\delta\mu_{CH}/\delta r_{CH}$	0.14(0.04)
$\delta\mu_{CH}/\delta r_{CCl}$	−1.00(0.41)
$\delta\mu_{CH}/\delta\alpha_{CCH}$	0.12(0.05)
$\delta\mu_{CH}/\delta\beta_{CCCl}$	0.52(0.23)
$\delta\mu_{CCCl}/\delta r_{CCl}$	−3.57(0.21)
$\delta\mu_{CCCl}/\delta r_{CH}$	0.26(0.02)
$\delta\mu_{CCl}/\delta r_{CC}$	0.14(0.26)
$\delta\mu_{CCl}/\delta\beta_{CCCl}$	−0.26(0.14)
$\delta\mu_{CCCl}/\delta\alpha_{CCH}$	−0.28(0.07)

taken. That is, only bond moment derivatives have been taken where the bond moments and the internal coordinates are associated with the same carbon atoms, and the other bond moment derivatives have all been neglected.

The intensity parameters based on this assumption, as listed in Table 5, have been considered to take equal values between the *trans* and *cis* isomers, that is, they have been assumed as transferable. The values of these parameters have been refined by the least-squares method so as to attain the best fit between the observed and calculated band intensities and molecular dipole moment. Converged values and standard deviations of the intensity parameters are given in Table 5, and the calculated band intensities are compared in Table 1 with the observed intensities.

The agreement between the observed and calculated band intensities is rather satisfactory except for the ν_9 band of *cis*-dichloroethylene. The average difference between the calculated and observed intensities is about four times larger than the expreimental errors of the observed intensities. The accordance to such an extent is acceptable, taking into account the assumptions placed on the determination of the intensity parameters.

The converged values of the intensity parameters listed in Table 5 are all acceptable as compared with those of related molecules treated previously. Moreover, the determined values of the bond moments μ_{CH} and μ_{CCl} can well explain the observed molecular dipole moment of *cis*-dichloroethylene measured in the gaseous state ($\mu_{obsd}=1.90$ D, $\mu_{calcd}=1.899$ D). However, a comment has to be made on the values of μ_{CH} and μ_{CCl}.

In the case of chlorinated methanes[4,5] or ethanes,[6] μ_{CH} was converged to the values near 0.5 D, while μ_{CCl} was converged to −1.0 D. On the other hand, in the present case, μ_{CH} is relatively large, but the absolute value of μ_{CCl} is fairly small. The value of μ_{CH} is in rather good agreement with the one for ethylene (0.7 D).[20] The small value of μ_{CCl} might suggest that the non-bonded electron cloud on chlorine atoms in dichloroethylene may be attracted into π-electron cloud of the double bond.[21] Such a result will be confirmed by a quantum-chemical approach such as a CNDO technique.

In conclusion, the transferability of the intensity parameters in dichloroethylene may confirm that intensity parameters might be transferable in related molecules, and thus the absolute intensity method may reasonably be applied to the determination of an energy difference between the rotational isomers.

References

1) K. Tanabe, *Spectrochim. Acta*, **28A**, 407 (1972).
2) K. Tanabe and S. Saëki, *ibid.*, **28A**, 1083 (1972).
3) K. Tanabe, *ibid.*, to be published.
4) S. Saëki and K. Tanabe, *ibid.*, **25A**, 1325 (1969).
5) K. Tanabe and S. Saëki, *ibid.*, **26A**, 1469 (1970).
6) K. Tanabe and S. Saëki, This Bulletin, **45**, 32 (1972).
7) K. Tanabe, S. Saëki and M. Mizuno, *Bunseki Kagaku*, **18**, 1347 (1969).
8) J. T. Shimozawa and M. K. Wilson, *Spectrochim. Acta*, **22**, 1599 (1966).
9) E. Dervil, *C. R. Acad. Sci. Paris*, **264**, 168 (1967).
10) H. J. Bernstein and D. A. Ramsay, *J. Chem. Phys.*, **17**, 556 (1949).
11) H. J. Bernstein and A. D. E. Pullin, *Can. J. Chem.*, **30**, 963 (1952).
12) T-Y. Wu, *Phys. Rev.*, **46**, 465 (1934).
13) T-Y, Wu, *J. Chem. Phys.*, **5**, 392 (1937).
14) B. Trumpy, *Z. Phys.*, **98**, 672 (1935).
15) G. Herzberg, "Infrared and Raman Spectra of Polyatomic Molecules," D. Van Nostrand Company, Inc., New York (1945), p. 330.
16) K. S. Pitzer and N. K. Freeman, *J. Chem. Phys.* **14**, 586 (1946).
17) J. M. Dowling, *ibid.*, **25**, 284 (1956).
18) L. A. Gribov and E. M. Popov, *Opt. Spectrosc.*, **12**, 304 (1962).
19) L. A. Gribov, "Intensity Theory for Infrared Spectra of Polyatomic Molecules," Consultants Bureau, New York (1964).
20) E. M. Popov and L. A. Gribov, *Opt. Spectrosc.*, **12**, 396 (1962).
21) A. Pellegatti, J-C. Pieribattesti, and M. Bénard, *J. Chem. Phys.*, **68**, 1708 (1971).

The Polymorphism of Inosine. II. The Measurement of Solubilities in Water

Yoshihisa SUZUKI

Central Research Laboratories, Ajinomoto Co., Inc., Suzuki-cho, Kawasaki 210

(Received February 20, 1974)

The solubilities of anhydrous inosine crystals in the α-form and in the β-form in water were determined in the temperature range between 20 °C and 60 °C. The results may be formulated as follows:

α-form $\log S = 0.0190\,t - 0.065$

β-form $\log S = 0.0198\,t - 0.161$

These data indicate that the β-crystals are more stable than the α-crystals over the whole temperature range examined. However, the difference in solubility is too small to induce the transition without seed crystals in the β-form, so that the α-crystals themselves are practically stable in water. The rate of the transition from the α-form to the β-form varies in proportion to the amount of the seed β-crystals. At low temperatures the dihydrate form of inosine is more stable than both of these two anhydrous forms. The solubility may be formulated as follows:

dihydrate-form $\log S = 0.0314\,t - 0.276$

The polymorphism of anhydrous inosine crystals was briefly presented in the preceding paper.[1] The crystals in an orthorhombic system are called α-form, and those in a monoclinic system, β-form. The solubility data of inosine in water were reported for the α-form.[2] This paper will describe the solubilities in the two forms and the transition from the α-form to the β-form.

Experimental

Material. The inosine used was of a commercial A-grade of the Ajinomoto Co., Inc.

Preparation of the Crystals. *Inosine Dihydrate*: The commercial inosine was recrystallized in water at 5 °C.

Inosine Anhydrous in the α-Form: The commercial inosine was recrystallized in water at 40 °C. *Inosine Anhydrous in the β-Form*: The commercial inosine was recrystallized in water at 40 °C in the presence of the seed crystals in the β-form. The seed crystals were obtained as follows: the commercial inosine (1.2 g) was dissolved in a 70% (w/w) dimethyl sulfoxide solution (10 ml), after which the wall of the glass vessel was scraped with a glass rod at room temperature until the β-crystals has been nucleated.

Solubility Measurement. A sufficient amount of the crystals was mixed with water to make a slurry in tightly-capped glass bottles. The equilibrium was achieved by tumbling the bottles at a constant temperature (±0.2 °C) for 16 hr. The supernatant clear solutions were sampled with a cotton-filtered pipet, weighed, diluted to appropriate volumes, and submitted to the measurement of the UV absorbance in 0.1 M HCl at 250 nm. The concentrations of the inosine were calculated from the molar extinction coefficient of 11800 under the above conditions. The residues were filtered and examined by means of the X-ray powder diffraction method in order to confirm the crystal form of the solid phase.

α-β Transition in Water. *Analysis*: For a brief quantitative analysis of the mixture of the two forms, the relative peak heights of the X-ray diffraction patterns were compared. The intensity of the 8.37 Å line (I_α) and that of 7.59 Å line (I_β) were measured. The β-form content was defined as $\{I_\beta/(I_\alpha+I_\beta)\}\times 100\%$. The calibration curve was almost linear. *In the Presence of the Seed Crystals*: Inosine crystals in the α-form (10 g) were added to 100 ml of water to make a slurry at room temperature. About three grams of inosine were dissolved, and seven grams remained undissolved. After the inosine crystals in the β-form (0.7 g or 1.4 g) had been added, the slurry was tumbled on a shaker at 30 °C. The suspended residues were sampled at successive intervals for X-ray examination. *In the Absence of the Seed Crystals*: Inosine crystals in the α-form (100 g) were added to 100 ml of water. After the resultant slurry had been vigorously stirred at 95 °C for 24 hr, the residue was examined by means of the X-ray diffraction method.

α-β Transition on the Drying of the Dihydrate Crystals. The dihydrate crystals of inosine were dried in air at 60 °C overnight with a little portion of the seed crystals in the β-form or without them. The resultant crystals were examined by means of X-ray analysis.

Results and Discussion

Table 1 shows the solubilities of inosine in water. The logarithms of the solubilities are linear to the temperature and are expressed as follows:

$$\text{α-form:}\quad \log S = 0.0190\,t - 0.065 \qquad (1)$$

$$\text{β-form:}\quad \log S = 0.0198\,t - 0.161 \qquad (2)$$

where S represents the gram weight of inosine per 100 g of water and where t is the temperature (°C). These results show that inosine in the β-form is less soluble than that in the α-form, and that, therefore, the β-form is more stable than the α-form. Accordingly, it can be expected that the α-crystals will be transformed into the β-crystals in water. However, the difference in solubility between them is too small to induce the transition without the seed crystals in the β-form, so that the α-crystals themselves are practically stable in water. During the measurement of the solubility, the transition of the crystals in the residue was not observed. As two lines, represented by Eq. (1) and Eq. (2), cross at nearly 120 °C, the stability may be reversed beyond that temperature.

At low temperatures the dihydrate form of inosine is more stable than either of the two anhydrous forms. On the assumption that the same linear relation between log S and t as in Eq. (1) or Eq. (2) holds good, the solubility of the dihydrate form is expressed from the data in Table 1 as follows:

$$\text{dihydrate-form:}\quad \log S = 0.0314\,t - 0.276 \qquad (3)$$

Table 1. Solubilities of inosine in water[a)]

Temp. (°C)	S (g/100 g water)		
	Dihydrate[b)]	Anhydride	
		β-Form	α-Form
0	0.52	—	—
10	1.10	—	—
20	—	1.75	2.14
30	—	2.71	3.29
40	—	4.20	4.72
50	—	6.73	7.79
60	—	10.5	11.8

a) Average of two measurements with deviations within ±5% except for the data at 30 °C and 40 °C which are single. b) Solubilities are expressed in terms of anhydride.

where S represents the gram weight of inosine in terms of anhydride per 100 g of water. Two cross-points are obtained, the one formed by the two lines derived from Eq. (1) and Eq. (3), and the other, from those derived from Eq. (2) and Eq. (3). They represent the transition temperatures from the dihydrate-form to the α-form, and from the dihydrate-form to the β-form, respectively. The former is estimated to be about 17 °C, and the latter, about 10 °C. The dihydrate-form is stable below these temperatures.

The transition from the α-form to the β-form was observed when some seed β-crystals were added to a slurry of the α-crystals in water. The rate is in proportion to the amount of the seed β-crystals. When the amount of the seed β-crystals added was 20% of the amount of the α-crystals in the slurry, the transition was observed to begin a little after 1 hr, to be about half completed after 4 hr, and to be over completely within 20 hr. A slower rate was observed when the seed crystals were decreased to 10%. In this case, the transition was slightly observed after 6 hr, and it took 40 hr for the complete conversion. On the other hand, in the absence of the seed β-crystals a slurry of the α-crystals did not show any transformation, not even at 95 °C after 24 hr.

The addition of the seed β-crystals also has a significant influence on the drying of the dihydrate crystals in air. When the dihydrate crystals are dried in air with heating, they lose the water of crystallization with ease, giving anhydrous crystals in the α-form. However, they give the crystals in the β-form when some seed crystals in the β-form are mixed in before heating.

Inosine crystallizes usually in the α-form from an aqueous solution; this fact is consistent with the law of successive reactions proposed by Ostwald. However, the crystals in the β-form were found to be often directly obtainable from about a 70%(w/w) dimethyl sulfoxide solution without the seed β-crystals. Since the solubility gap between the two forms causes the transition, any difference in the solubility between them in a 70% dimethyl sulfoxide solution must be larger than that in water. This will be discussed in the next paper.

The author wishes to thank Mr. Takashi Sato for his technical assistance.

References

1) Y. Suzuki and N. Nagashima, This Bulletin, **43**, 1600 (1970).
2) Y. Suzuki, T. Toki, and T. Nakamura, Presented orally at 18th Annual Meeting of the Chemical Society of Japan, Osaka, 1965.

Polymorphism of Inosine. III. The Equilibrium for the Inosine–Dimethyl Sulfoxide–Water System

Yoshihisa SUZUKI and Kentaro HARA

Central Research Laboratories, Ajinomoto Co., Inc., Suzuki-cho, Kawasaki 210

(Received March 1, 1974)

The phase diagram for the inosine–dimethyl sulfoxide–water system was determined at 30 °C. Inosine in the α-form is more soluble than that in the β-form in aqueous DMSO. The difference in the solubilities between the two forms is small when the concentration of DMSO is below 50%. However, it becomes several times larger in 70% DMSO than in water. This is the reason why inosine in the β-form is often obtainable with ease from 70% DMSO in the absence of seed β-crystals, while it is with difficulty obtained only from water. When the concentration of DMSO becomes higher than 82%, a new solid phase is obtained. It consists of inosine with two mol of DMSO of crystallization. Inosine in the β-form is also obtainable with ease through the decomposition of these new crystals.

Inosine is usually crystallized in the α-form from water; only when some seed crystals in the β-form are present it is crystallized in the β-form. However, the crystals in the β-form are directly obtained without seed crystals when inosine is crystallized from 70% (w/w) aqueous dimethyl sulfoxide (DMSO) at 30 °C.[1] In order to explain the above fact, the equilibrium for the inosine–DMSO–water system was studied. There is a datum on the solubility of inosine in pure DMSO at 30 °C by Rosenthal.[2]

Results and Discussion

Figure 1 shows the phase diagram for the inosine–DMSO–water system at 30 °C, and in Fig. 2 the details are plotted with the experimental data in terms of the solubility of inosine per 100 g of aqueous DMSO.

The solubility of inosine in the α-form in aqueous DMSO is higher than that in the β-form over the whole range. Consequently, β-crystals are more stable than α-crystals in aqueous DMSO, as is the case in water. However, a notable distinction was found between the aqueous DMSO system and the water system. It is the difference in the solubility between the two forms. It increases with an increase in the DMSO, with a steep ascent beyond 50% DMSO, while it is small and constant below 50%. In 75% DMSO it reaches about six times that in water. This large difference in the solubility is sufficient to cause the quick transition from the α-form to the β-form without any seed crystals. This is the reason why inosine is crystallized in the β-form from the 70% DMSO solution, whereas it is crystallized in the α-form from water.

In high concentration of DMSO near 80%, a new solid phase was obtained. It was found to be inosine, with two mol of DMSO of crystallization. It appears consecutively on the line of the β-crystal phase, as is shown in the figures. The composition of the critical point is DMSO : water : inosine=75.0 : 16.1 : 8.9(Point A in Fig. 2). When the concentration of DMSO is higher than that value, the new solid phase is most stable.

These inosine crystals with the DMSO of crystallization are incongruent and are decomposed by pure water. This property suggests another new method for the direct preparation of β-crystals. When these new crystals are treated with a small portion of water or aqueous DMSO (below 80%), they are transformed into inosine anhydrous crystals in the β-form. It has been pointed out that there is a region where the new crystals are less soluble than α-crystals and more solu-

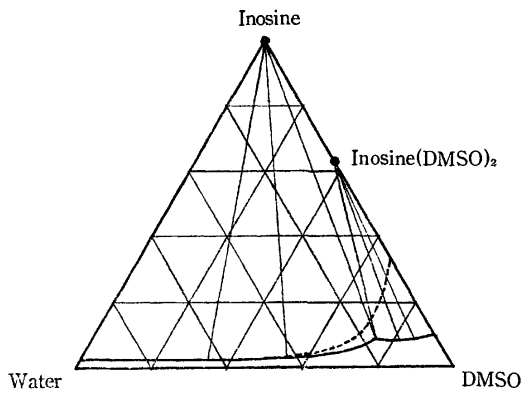

Fig. 1. Phase diagram for the inosine-dimethylsulfoxide-water system at 30 °C.

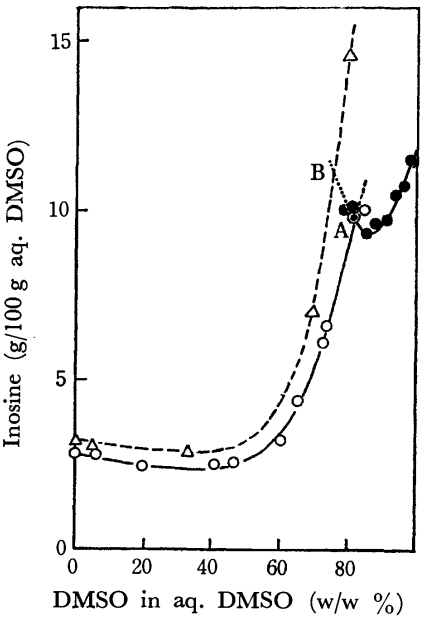

Fig. 2. Solubilities of inosine in aqueous dimethylsulfoxide at 30 °C.
△: Inosine in the α-form. ○: Inosine in the β-form.
: Inosine-dimethylsulfoxidate.

Table 1. X-Ray powder diffraction data of inosine-dimethylsulfoxidate

Inosine·(DMSO)$_2$	
d(Å)	I/I_0[a]
11.63	10
9.71	30
5.47	30
5.22	10
4.80	100
4.35	30
4.15	30
4.10	10
3.83	30
3.20	20

a) The scale is so chosen as to make the most intense line have the value 100.

ble than β-crystals. This region is shown between Point A and Point B in Fig. 2. When the new crystals are dissolved in this region, the β-crystals will be preferentially nucleated.

These new crystals are unstable in air and are gradually changed into β-crystals within a few days at room temperature, probably because of the influence of the humidity in the air. This transition of crystals in air is accelerated on heating.

Table 1 shows the X-ray powder diffraction data of these new crystals. It is of interest that inosine can be crystallized with two mol of DMSO of crystallization, while it is crystallized with the same moles of water of crystallization, and that DMSO is able to combine with inosine at room temperature, while water does so only at low temperatures.[1]

The solubility of inosine in pure DMSO reported by Rosenthal agreed with that for inosine in the α-form. However, it is obvious that the equilibrium is unstable and that inosine-dimethylsulfoxidate will be crystallized with a faint stimulation.

Experimental

Materials. The inosine used, of a commercial A-grade, was obtained from the Ajinomoto Co., Inc. The DMSO was of a reagent grade; its water content was checked by Karl Fischer titration.

Preparation of the Crystals. Inosine anhydrous crystals in the α-form and in the β-form were prepared according to the method reported in the preceding paper.[1] Inosine-dimethylsulfoxidate crystals were obtained as follows: inosine (12 g) was dissolved in DMSO (98%, 50 ml) with heating, after which mixture was stirred for two days at room temperature. The precipitated prism crystals were filtered, washed with ether, and analyzed immediately. Yield, 12 g; mp 88—89 °C. Found: C, 39.31; H, 5.69; N, 13.41%. Calcd for $C_{10}H_{12}N_4O_5\cdot(C_2H_6OS)_2$: C, 39.61; H, 5.70; N, 13.26%. Inosine content calculated from the optical density (250 nm in 0.1 M HCl) compared with the standard inosine, 64.0% (theoretical, 63.3%).

Solubility Measurements. A sufficient amount of the crystals selected among inosine-dimethylsulfoxidate and inosine in the α-form and in the β-form were mixed with aqueous DMSO to make a slurry in tightly-capped glass bottles. The equilibria were achieved by tumbling the bottles for 16 hr at 30 °C. Then, the mixtures were filtered by means of a glass filter. The UV absorbances at 250 nm in 0.1 M HCl were measured for the filtrates and the residues. The inosine contents were calculated from the molar extinction coefficient defined as 11,800 under the above conditions. The UV absorbances due to DMSO are negligible compared with those of inosine. The water contents in the solution phase were determined by Karl Fischer titration. The DMSO was determined by means of the difference. The residues on a filter were examined by the X-ray powder diffraction method in order to identify the crystal form.[3]

Decomposition of Inosine-dimethylsulfoxidate. (a) Inosine-dimethysulfoxidate (25 g) was added to aqueous DMSO (70%, 100 ml) to make a slurry. After the mixture had been shaken for 5 hr, it was left to stand overnight. The crystals suspended were filtered and identified by the X-ray method. (β-Form). (b) The crystals of inosine-dimethylsulfoxidate were precipitated according to the method described above. Immediately after the crystals had been removed from the mother liquor with a filter, they were washed with ether and left to stand in air for 3 hr at room temperature. Then, they are dried for 1 hr at 90 °C. They were identified by means of the X-ray method (β-Form).

The authors wish to thank Mr. Kunio Konno for his technical assistance.

References

1) Y. Suzuki, This Bulletin, **47**, 2549 (1974).
2) N. A. Rosenthal, Fr. 1468708 (1967).
3) Y. Suzuki and N. Nagashima, This Bulletin, **43**, 1600 (1970).

The Equilibria for the Inosine–Calcium Hydroxide–Water and Inosine–Strontium Hydroxide–Water Systems

Yoshihisa SUZUKI and Yasuichi NOMURA

Central Research Laboratories, Ajinomoto Co., Inc., Suzuki-cho, Kawasaki 210

(Received March 1, 1974)

Solubility data have been obtained for the inosine-$Ca(OH)_2$-H_2O and inosine-$Sr(OH)_2$-H_2O systems at 10 °C. Three different solid phases of the calcium salt of inosine were found in the former system. The first is the normal hemi-calcium salt, $(inosine)_2 \cdot Ca \cdot 2H_2O$; the second, an abnormal salt, $(inosine)_3 \cdot Ca \cdot 3H_2O$, and the third, another abnormal salt, $(inosine)_4 \cdot Ca \cdot 9H_2O$. The former two salts have stable regions in the system, while the last one does not. The system including $Sr(OH)_2$ is simple, and no other salt-formation was found except for that of normal hemi-strontium salt, $(inosine)_2 \cdot Sr \cdot 2H_2O$. The X-ray powder diffraction data of the above four salts are given. The solubilities of the two normal hemi-alkaline-earth-metal salts of inosine in water were determined at 10—60 °C and formulated as follows:

$$\text{Ca-salt, } \log S = 0.00406 \cdot t - 0.4725$$

$$\text{Sr-salt, } \log S = 0.00551 \cdot t - 0.4116$$

where S represents the gram weight of anhydrous salt per 100 g of water.

In order to contribute to the process design of the separation or the purification of inosine, the two systems were examined and the solubility data for some alkaline-earth metal salts of inosine were obtained. No information has been found in the literature.

Results and Discussion

The results of the determination for the systems are presented in Tables 1 and 2, along with the experimental conditions. The mole ratio for the salt-formation between inosine and alkaline-earth metal is expected to be 2 : 1, in view of the acid-base valence. However, the system including calcium hydroxide is complicated because of the formation of two additional abnormal calcium salts of inosine besides the normal salt expected. One of them is estimated to be composed of three mol of inosine per mol of calcium atom with three mol of water of crystallization, and the other, of four mol of inosine per mol of calcium atom with nine mol of water. Their crystal habits are both feathery and fine-needle-like, thus hindering the precise determination of the water of crystallization. The above two abnormal salts of inosine can be explained as molecular compounds between the normal salts and free inosine. The former salt has a stable region in the system, while the latter does not and is metastable through-out the range. Their X-ray powder diffraction patterns are

TABLE 1. THE EQUILIBRIUM FOR THE INOSINE-$Ca(OH)_2$-H_2O SYSTEM AT 10 °C

Exp. conditions[a] (g material/50 ml H_2O)			Solution phase (Weight %)		Solid phase[b]
I(α)[c]	$Ca(OH)_2$	Salt	Inosine	$Ca(OH)_2$	
lit.[e]	—	—	1.10	0	I2
2.0	—	A, 2.0	1.25	0.031	I2+C (m)
1.2	—	A, 1.0	1.18	0.030	C (m)
1.0	—	A, 1.0	0.860	0.034	C (m)
0.8	—	A, 1.0	0.678	0.052	C (m)
1.0[d]	—	B, 0.5+C, 0.5	0.803	0.029	I2+B
0.18	—	B, 1.0	0.667	0.028	B
—	—	B, 2.0	0.418	0.040	B
—	0.01	B, 1.0	0.455	0.063	B (m)
0.2	—	A, 1.0	0.748	0.048	A (m)
0.4	—	A, 1.0	0.691	0.046	A+C
0.11	—	A, 1.0	0.580	0.044	A (m)
0.11	—	A, 1.0+B, 1.0	0.422	0.044	A+B
—	—	A, 2.0	0.339	0.052	A
—	0.05	A, 2.0	0.389	0.137	A
—	0.08	A, 1.0	0.503	0.220	A
—	1.0	A, 1.0	0.658	0.330	A+$Ca(OH)_2$
0.15	1.0	—	0.296	0.240	$Ca(OH)_2$
lit.[f]	—	—	0	0.175	$Ca(OH)_2$

a) The equilibria were approached by dissolving the materials in water. b) I2: Inosine·$2H_2O$.
A: $(Inosine)_2 \cdot Ca \cdot 2H_2O$, B: $(Inosine)_3 \cdot Ca \cdot 3H_2O$, C: $(Inosine)_4 \cdot Ca \cdot 9H_2O$, m: metastable c) I(α): Inosine in the α-form.[1] d) I2 was used. e) Reference 1. f) The mean value: H. Bassett, *J. Chem. Soc.*, **1934**, 1270.

Table 2. The equilibrium for the inosine–$Sr(OH)_2$–H_2O system at 10 °C

Exp. conditions[a] (g material/50 ml H_2O)			Solution phase (Weight %)		Solid phase[b]
I(α)[c]	Sr8[b]	S[b]	Inosine	$Sr(OH)_2$	
lit.[e]	—	—	1.10	0	I2
2[d]	0.05	—	1.29	0.044	I2
2	—	2	1.61	0.092	I2+S
2[d]	—	2	1.56	0.091	I2+S
0.3	—	2	1.02	0.086	S
—	—	2	0.369	0.074	S
—	0.3	2	0.475	0.376	S
—	0.6	2	0.699	0.700	S
—	2	2	0.856	0.875	S+Sr8
0.2	2	—	0.405	0.733	Sr8
lit.[f]	—	—	0	0.57	Sr8

a) The equilibria were approached by dissolving the materials in water. b) I2: Inosine·$2H_2O$. S: $(Inosine)_2$·Sr·$2H_2O$, Sr8: $Sr(OH)_2$·$8H_2O$. c) I(α): Inosine in the α-form.[1] d) I2 was used. e) Ref. 1. f) C. Scheibler, *J. Pharm. Chim.*, **8**, 540 (1883).

Table 3. X-Ray powder diffraction data of some abnormal calcium salts of inosine

$(Inosine)_3$·Ca·$3H_2O$		$(Inosine)_4$·Ca·$9H_2O$	
d(Å)	I/I_0[a]	d(Å)	I/I_0[a]
15.00	90	10.05	100
8.76	5	7.56	40
8.08	40	6.00	10
7.44	100	5.73	20
7.11	5	5.28	20
6.13	40	5.13	5
4.93	70	5.04	25
4.40	40	4.97	20
4.23	30	3.88	20
4.04	70	3.75	20
3.90	30	3.58	20
3.28	20	3.50	20
3.24	20	3.36	30

a) The scale is so chosen as to make the most intense line have the value 100.

shown in Table 3; they are characteristic enough to enable us to distinguish these crystals from other crystals.

The system including strontium hydroxide is simple, and no other salt-formation was found except the normal hemi-strontium salt of inosine.

The normal hemi-calcium salt and hemi-strontium salt of inosine possess stable regions in the systems. They are both obtained in the mono-hydrate form with respect to one mol of inosine and a half of the alkaline-earth metal. Their X-ray powder diffraction patterns are similar (Table 4), and it may be supposed that they have almost the same crystal structure except for the unit-cell dimensions, which are controlled by the atomic size of the alkaline-earth metal. The crystal appearances are also similar, both being fine hard pillars.

Table 4. X-Ray powder diffraction data of normal alkaline-earth metal salts of inosine

$(Inosine)_2$·Ca·$2H_2O$		$(Inosine)_2$·Sr·$2H_2O$	
d(Å)	I/I_0[a]	d(Å)	I/I_0[a]
9.72	100	10.05	100
7.83	20	8.04	20
6.11	20	6.24	20
5.47	5	5.54	15
4.87	5	4.85	15
4.77	5	4.65	20
4.58	20	4.44	40
4.35	30	3.99	20
3.92	10	3.69	15
3.44	10	3.34	5
3.15	10	3.13	20
3.07	10	3.05	10

a) The scale is so chosen as to make the most intense line have the value 100.

Table 5. Solubilities of normal alkaline-earth metal salts of inosine in water

Temp. (°C)	S (g anhydrous salt/100 g water)	
	$(Inosine)_2$·Ca·$2H_2O$	$(Inosine)_2$·Sr·$2H_2O$
10	0.364	0.430
30	0.458	0.590
40	—	0.664
50	0.530	—
60	—	0.801

Table 5 shows the solubilities of these two normal hemi-alkaline-earth-metal salts of inosine in water. Each logarithm of the solubility is linear to the temperature; they are expressed as follows:

$$\text{Ca-salt} : \log S = 0.00406 \cdot t - 0.4725$$

$$\text{Sr-salt} : \log S = 0.00551 \cdot t - 0.4116$$

where S is the gram weight of anhydrous salt per 100 g of water. The solubility-behavior of these two salts is similar. They are less soluble than free inosine.[1]

The two phase diagrams plotted with the data in Tables 1 and 2 are roughly similar figures in spite of the difference in the salt-formation. This is confirmed when they are superimposed with the same co-ordinates. The inosine-contents in solution give nearly equal minima when the mole ratio of inosine and alkaline-earth metal is 2 : 1. They both gradually increase with an increase in the alkaline-earth metal hydroxide content from that point. They both also show a steep descent with an increase in the alkaline-earth metal hydroxide content from a point where the inosine and alkaline-earth metal salts of inosine share the solid phase. The solubilities of calcium- and strontium-hydroxide in water increase at the same slope with an increase in the addition of inosine.

On the other hand, there is one remarkable difference between these two systems. The solubility of inosine in water always begins to increase with an increase in the strontium hydroxide content. However, two cases are possible in the system concerning calcium hydroxide:

in the one case the addition of calcium hydroxide to a saturated aqueous solution of inosine causes an increase in the solubility of inosine, while in the other case it causes a decrease. These two cases are incompatible while the same solid phase (inosine dihydrate) is present in the system. A different solubility is acceptable when different solid phases (calcium salt of inosine, B and C in Table 1) appear in the system. Actually a decrease in the solubility is observed when calcium hydroxide is added to a saturated aqueous solution of inosine, because a decrease in the solubility produces a stable calcium salt of inosine, whereas an increase of that produces a metastable calcium salt.

Experimental

Materials. The inosine used, of a commercial A-grade, was obtained from the Ajinomoto Co., Inc.; the other materials were of a reagent grade.

Analysis. The inosine was determined with UV-absorbance at 250 nm in 0.1 M HCl, using the molar extinction coefficient of 11,800 under the above conditions. The calcium was determined by EDTA-titration with a BT indicator and strontium by displacement titration with EDTA-Mg, using BT. The chlorine was checked by the Volhard method. The X-ray powder diffraction patterns (CuK_α) were used for the identification of the solid phase in equilibrium. The degree of hydration of the crystals was determined by Karl Fischer titration.

Preparation of the Crystals. Normal Calcium Salt of Inosine (A): Two solutions were prepared; one was inosine (26.8 g) in 1/12 M NaOH (1.2 l), and the other, $CaCl_2 \cdot 2H_2O$ (7.35 g) in water (10 ml). The latter solution was gradually stirred into the former solution at 40 °C. After the subsequent mixture had been cooled to room temperature, the precipitated needle crystals were filtered and dried in air. Mp 265 °C (colored), 290—295 °C (decomp. with bubbling). Found: Ca, 6.78; H_2O, 5.33; Cl, 0.00%; $\varepsilon_{250\,nm}$ in 0.1 M HCl, 10,370. Calcd for $(C_{10}H_{11}N_4O_5)_2 \cdot Ca \cdot 2H_2O$: Ca, 6.56; H_2O, 5.90; Cl, 0%; ε, 10,370. *Abnormal Calcium Salt of Inosine (B)*: Two solutions were prepared; one was inosine (20.1 g) in 1/6 M NaOH (300 ml), and the other, $CaCl_2 \cdot 2H_2O$ (3.68 g) in water (5 ml). The latter solution was gradually stirred into the former at 60 °C. After the mixture had been stirred for 30 min at that temperature, the precipitated crystals were filtered and dried in air. Mp 249—51 °C (decomp. with darkening). Found: Ca, 4.50; H_2O, 6.61%; $\varepsilon_{250\,nm}$ in 0.1 M HCl, 10,590. Calcd for $(C_{10}H_{11}N_4O_5)_2 \cdot C_{10}H_{12}N_4O_5 \cdot Ca \cdot 3H_2O$: Ca, 4.77; H_2O, 6.03%; ε, 10,400.

Abnormal Calcium Salt of Inosine (C): Finely powdered $Ca(OH)_2$ (0.17 g) was dissolved in cold water (100 ml), and then inosine (3.4 g) was stirred into this solution at 5—10 °C. When a few fine crystals appeared, they were quickly filtered and dried in air. Mp 146 °C(began to melt), 156 °C(half-melted), and 164—167 °C(decomp. keeping white). Found: Ca, 3.22; H_2O, 12.59%: $\varepsilon_{250\,nm}$ in 0.1 M HCl, 9,940. Calcd for $(C_{10}H_{11}N_4O_5)_2 \cdot (C_{10}H_{12}N_4O_5)_2 \cdot Ca \cdot 9H_2O$: Ca, 13.5; H_2O; 12.74%; ε, 9,760. *Normal Strontium Salt of Inosine* In water (500 ml), $Sr(OH)_2 \cdot 8H_2O$(21.3 g) was dissolved at 60 °C, and then powdered inosine crystals (43 g) were stirred into this solution. After the mixture had been kept for 30 min at 60 °C, the precipitated crystals were filtered and dried in air. Mp 326—8 °C(decomp. with darkening and bubbling). Found: Sr, 13.3; H_2O, 5.3%; $\varepsilon_{250\,nm}$ in 0.1 M HCl, 9.680. Calcd for $(C_{10}H_{11}N_4O_5)_2 \cdot Sr \cdot 2H_2O$: Sr, 13.3; H_2O, 5.5%; ε, 9.620.

Determination of Equilibria. Definite amounts (see Tables 1 and 2) of materials selected from among inosine, its calcium salts and $Ca(OH)_2$, or inosine, its strontium salts and $Sr(OH)_2 \cdot 8H_2O$ were added to water (50 ml) in tightly-capped glass bottles. The equilibrium was achieved by tumbling the bottles for 16 hr on a water bath at 10 °C. Then, the mixtures were quickly filtered with a glass filter, and the solution and the solid were submitted to analysis.

Solubility Measurements of Normal Alkaline-earth Metal Salts of Inosine. A sufficient amount of normal calcuim- or strontium-salt of inosine was added to water in a tightly-capped glass bottle, and the bottle was tumbled for 16 hr at a constant temperature(10—60 °C). Then the mixture was quickly filtered, and the UV absorbance of the filtrate was measured. The residue was checked by X-ray analysis.

The authors wish to thank Mr. Takashi Sato for his technical assistance.

References

1) Y. Suzuki, This Bulletin, **47**, 2549 (1974).

A Study of the Inosine–Sodium Hydroxide–Water and Inosine–Potassium Hydroxide–Water Systems

Yoshihisa SUZUKI and Tadao TOKI

Central Research Laboratories, Ajinomoto Co., Inc., Suzuki-cho, Kawasaki 210

(Received March 27, 1974)

Solubility data have been obtained for the inosine-NaOH-H_2O and inosine-KOH-H_2O systems at 30 °C. Two different solid phases of the potassium salt of inosine ($C_{10}H_{11}N_4O_5 \cdot K \cdot H_2O$ and $C_{10}H_{11.5}N_4O_5 \cdot 0.5\,K \cdot 0.5\,H_2O$) were found in the latter system, while only one solid phase of the sodium salt of inosine ($C_{10}H_{11}N_4O_5 \cdot Na \cdot 2.5\,H_2O$) was found in the former system. The hemi-potassium salt of inosine is incongruent and is decomposed by pure water, whereas the mono-alkaline-metal salts are stable. The solubilities of the two mono-alkaline-metal salts of inosine in water were determined at 0—50 °C and formulated as follows:

$$\text{Na-salt, } \log S = 0.01359 \cdot t + 0.3997$$

$$\text{K-salt, } \log S = 0.00733 \cdot t + 1.6513$$

where S represents the gram weight of the anhydrous salt per 100 g of water. The X-ray powder diffraction data of the above three salts are given.

The equilibrium for the inosine—alkaline-earth metal hydroxide—water system was reported in the preceding paper.[1] This paper will describe the results for the inosine—alkaline metal hydroxide—water system. The solubilities of the alkaline metal salts of inosine in water were also determined.[2]

Results and Discussion

Table 1 shows the composition data in the solution phase for the inosine—sodium hydroxide—water system at 30 °C. The solubility of inosine increases linearly with an increase in the amount of sodium hydroxide until its mono-sodium salt is precipitated, and then it decreases with a steep slope until the mole ratio of inosine and sodium ion in the solution phase reaches 1 : 1. Thereafter, it increases again.

Table 2 shows the composition data in the solution phase and in the solid phase for the inosine—potassium hydroxide—water system at 30 °C. The solubility of inosine also increases with an increase in the quantity of potassium hydroxide with a slope nearly equal to that of sodium hydroxide until its mono-potassium salt is precipitated; thereafter it decreases a little until the mole ratio of inosine and potassium ion in the solution phase reaches about 2 : 3. Then, it increases again. However, on the way to the point where the mono-potassium salt begins to be precipitated, there is a clear region where the hemi-potassium salt of inosine is precipitated. Such a region is not found in the sodium hydroxide system.

The composition of the hemi-potassium salt of inosine can be explained as a molecular compound between one mole of the mono-potassium salt of inosine and one mole of free inosine. This salt is incongruent and is decomposed by pure water, because the region where this salt is stably present does not include the line on which the mole ratio of the inosine and the

Table 1. Composition data for the inosine–sodium hydroxide–water system at 30 °C

Run No.	Solution Phase (Weight %)		Solid Phase[a]
	Inosine	NaOH	
1	3.18	0	I(α)
2	5.81	0.243	I(α)
3	7.88	0.465	I(α)
4	11.72	0.849	I(α)
5	13.70	1.076	I(α) (metastable)
6	14.55	1.137	I(α) (metastable)
7	12.67	1.000	I(α)+S
8	12.87	1.040	I(α)+S
9	12.24	0.988	S
10	9.58	0.908	S
11	7.47	0.891	S
12	5.61	0.839	S
13	5.57	1.148	S
14	6.94	1.967	S
15	9.52	3.548	S

a) I(α): Inosine in the α-form, $C_{10}H_{12}N_4O_5$; S: Mono-sodium salt of inosine, $C_{10}H_{11}N_4O_5 \cdot Na \cdot 2.5H_2O$

Table 2. Composition data for the inosine–potassium hydroxide–water system at 30 °C

Run No.	Solution (Weight %)		Wet residue (Weight %)		Solid phase[a]
	Inosine	KOH	Inosine	KOH	
1	3.18	0	—	—	I(α)
2	19.04	2.44	69.90	0.905	I(α)
3	30.88	4.16	—	—	I(α)(m)
4	26.57	3.66	68.98	5.77	I(α)+K/2
5	27.22	4.36	70.53	7.98	K/2
6	33.24	6.48	69.95	8.37	K/2
7	38.70	7.89	72.70	11.69	K/2+K
8	36.04	7.76	77.52	16.14	K
9	34.36	8.81	73.98	15.94	K
10	33.92	11.89	76.13	16.83	K
11	36.26	14.82	71.65	16.73	K
12	40.19	17.31	76.99	17.62	K
13	42.94	20.14	75.22	18.08	K

a) I(α): Inosine in the α-form, $C_{10}H_{12}N_4O_5$; K/2: Hemi-potassium salt of inosine, $C_{10}H_{11.5}N_4O_5 \cdot 0.5K \cdot 0.5H_2O$; K: Mono-potassium salt of inosine, $C_{10}H_{11}N_4O_5 \cdot K \cdot H_2O$; m: metastable

Table 3. Solubilities of mono-alkaline-metal salts of inosine in water

Temp. (°C)	S (g, anhydrous salt/100 g water)	
	$C_{10}H_{11}N_4O_5 \cdot Na \cdot 2.5H_2O$	$C_{10}H_{11}N_4O_5 \cdot K \cdot H_2O$
0	2.57	43.2
5	—	50.8
10	3.35	55.4
30	6.47	74.6
50	12.22	100.5

Table 4. X-Ray powder diffraction patterns of alkaline metal salts of inosine

S[a]		K[b]		K/2[c]	
d(Å)	I/I_0[d]	d(Å)	I/I_0[d]	d(Å)	I/I_0[d]
7.31	10	7.11	20	10.10	20
6.92	40	6.28	20	8.35	50
5.72	10	5.37	15	6.76	30
5.50	50	5.20	10	6.13	100
5.16	50	4.75	10	4.77	40
5.01	90	4.65	30	3·88	60
4.48	90	4.27	100	3.68	30
4.21	40	4.05	20	3.56	25
3.82	50	3.87	15	3.52	30
3.75	100	3.58	30	3.10	40
3.41	40	3.41	50		
3.34	80	3.36	15		

a) Mono-sodium salt of inosine, $C_{10}H_{11}N_4O_5 \cdot Na \cdot 2.5H_2O$. b) Mono-potassium salt of inosine, $C_{10}H_{11}N_4O_5 \cdot K \cdot H_2O$. c) Hemi-potassium salt of inosine, $C_{10}H_{11.5}N_4O_5 \cdot 0.5K \cdot 0.5H_2O$. d) The scale is so chosen as to make the most intense line have the value 100.

potassium ion is 1 : (1/2).

On the other hand, the two mono-alkali-metal salts are stable in water. Table 3 shows the solubilities of these salts in water at 0—50 °C. Each logarithm of the solubility is linear to the temperature and is expressed as follows:

sodium-salt: $\log S = 0.01359 \cdot t + 0.3997$

potassium-salt: $\log S = 0.00733 \cdot t + 1.6513$

where S represents the gram weight of the salts per 100 g of water in terms of anhydride. No change in the solid phase was observed in the temperature range examined.

It is of interest that the alkaline metal salts of inosine examined in the present study show no similarity among each other with respect to solubility behavior and crystal structure, while the alkaline-earth metal salts of inosine do.[1] The solubility of the mono-potassium salt and that of the mono-sodium salt are quite different from each other. The former is ten times more soluble in water than the latter. On the other hand, the hemi-calcium salt and the hemi-strontium salt give solubilities nearly equal below a decimal point.[1] The hemi-alkaline-earth metal salts are both monohydrates, and their X-ray diffraction patterns are similar.[1] On the other hand, the mono-sodium salt possesses two and a half moles of water of crystallization, while mono-potassium salt possesses one mol of that; moreover, the X-ray diffraction patterns shown in Table 4 also indicate no resemblance.

There is another large difference between the two phase diagrams plotted with the data in Tables 1 and 2 in the mole ratios of inosine and alkaline metal ion at the point where mono-alkaline-metal salt begins to be precipitated. The ratios are 1 : 0.54 for the sodium hydroxide system and 1 : 0.98 for the potassium hydroxide system respectively. Because the latter value is very close to 1 : 1, it sometimes seems as if the mono-potassium salt of inosine were incongruent and were decomposed by pure water, especially when the salt possesses an impure composition.

Experimental

Materials. The inosine (α-form)[3] used was of a commercial A-grade of the Ajinomoto Co., Inc.,; the other materials were of a reagent grade.

Analysis. The inosine was determined by means of the UV absorbance at 250 nm in 0.1 M HCl using the molar extinction coefficient of 11,800 under the above conditions. The alkaline metal hydroxide was determined by titration with standard sulfuric acid, using a methyl red-bromcresol green indicator. The X-ray powder diffraction patterns (CuK_α) were used for the identification of the solid phase in equilibrium. The degree of hydration of the crystals was determined by Karl Fischer titration.

Preparation of the Crystals. *Mono-sodium Salt of Inosine*: Inosine (26.8 g) was dissolved in 1/2 M NaOH (200 ml) at 60 °C; then the solution was cooled at 10 °C. Precipitated thick prism crystals were filtered out and dried in air. Yield, 13 g; mp 198—202 °C. Found: Na, 6.90; H_2O, 13.5%; $\varepsilon_{250\,nm}$ in 0.1 M HCl, 9,450. Calcd for $C_{10}H_{11}N_4O_5 \cdot Na \cdot 2(1/2)H_2O$: Na, 6.87; H_2O, 13.4% ε, 9,440. *Mono-potassium Salt of Inosine*: Inosine (145 g) was dissolved in 22% aqueous KOH (180 g), and the solution was allowed to stand at 50 °C overnight with the addition of seed crystals. The seed crystals had previously been obtained by the rapid cooling of a little portion of that solution. The precipitated long prism crystals were filtered out, washed with 80% ethanol, and dried at 100 °C for 5 hr. Yield, 14 g; mp 163—6 °C. Found: K, 12.18; H_2O, 5.66%; $\varepsilon_{250\,nm}$ in 0.1 M HCl, 9,760. Calcd for $C_{10}H_{11}N_4O_5 \cdot K \cdot H_2O$: K, 12.06; H_2O, 5.55%; ε, 9,810. *Hemi-potassium Salt of Inosine*: Inosine (200 g) was dissolved at 80 °C in 12% aqueous KOH (240 g), after which the mixture was filtered with a glass filter in order to obtain a clear solution. When it was cooled to 50 °C, a very small amount of seed crystals was added; the mixture was then left to stand for two days at 50 °C. The seed crystals had previously been obtained by the rapid cooling of a little portion of that solution. The precipitated needle crystals were quickly filtered out, sandwiched between filter paper with pressure in order to remove the mother liquor completely, and then dried for 5 hr at 100 °C. Yield, 30 g; mp 172—5 °C. Found: K, 6.86; H_2O, 3.41%; $\varepsilon_{250\,nm}$ in 0.1 M HCl, 10,430. Calcd for $C_{10}H_{12}N_4O_5 \cdot C_{10}H_{11}N_4O_5 \cdot K \cdot H_2O$: K, 6.60; H_2O, 3.04%; ε, 10,660.

Determination of Equilibria. The equilibria were usually approached by dissolving the crystals in water or aqueous alkaline hydroxide at a constant temperature. In a few cases they were approached by cooling the supersaturated solution. The details in Table 1 show that the equilibria at 30 °C were approached by dissolving inosine in the α-form (Runs No. 1,3,7 and 11), by dissolving sodium salt of inosine

(No. 9,10 and 12—15), by dissolving the above two materials (No. 8), and by cooling the supersaturated solutions (No. 2,4,6 and 7). The supersaturated solutions were prepared by dissolving inosine in aqueous NaOH at 60 °C. Those in Table 2 show the results obtained by dissolving inosine in the α-form (Runs No. 1—3 and 5), by dissolving the hemi-potassium salt of inosine (No. 6), by dissolving the above two materials (No. 4), by dissolving the mono-potassium salt of inosine (No. 8—13), and by dissolving both hemi- and mono-potassium salts (No. 7). Those in Table 3 show the results obtained by dissolving the alkaline metal salts of inosine in water at a constant temperature (0—50 °C). It took 16 hr for the equilibrium to be reached by tumbling the bottles holding the mixture on a water bath at a constant temperature. The mixture in the bottles was quickly filtered with a glass filter, and the solutions and the residues were submitted to analysis.

The authors wish to thank Mr. Sukehiro Yamazaki for his technical assistance.

References

1) Y. Suzuki and Y. Nomura, This Bulletin, **47**, 2553 (1974).
2) A part of the results concerning the sodium salt of inosine was orally presented at the 18th Annual Meeting of the Chemical Society of Japan, Osaka, 1965.
3) Y. Suzuki and N. Nagashima, This Bulletin, **43**, 1600 (1970).

The Thermodynamic Properties of Tetraalkylammonium Halides in Acetone*

Masahiro IMURA, Hiroyasu NOMURA, Fumio KAWAIZUMI and Yutaka MIYAHARA

Department of Chemical Engineering, Faculty of Engineering, Nagoya University, Chikusa-ku, Nagoya-shi 464

(Received April 1, 1974)

The vapor-pressure depressions of solutions of four tetraalkylammonium halides in acetone were determined by means of a vapor-pressure osmometer. The experimental results were discussed by analyzing the relationship between the $h(=1000 \ln a_1/M_1m+1)$ function and the concentration. The following conclusions are obtained: tetraalkylammonium salts are dissociated in acetone, and the thermodynamic behavior of the dissociated species is described by the Debye-Hückel-Onsager limiting formula with sufficient accuracy, where the undissociated species are assumed to behave ideally.

Except for $(n\text{-Bu})_4\text{NCl}$, the dissociation constants determined by the present work are in good agreement with those found in the literature, which were determined conductometrically.

In our previous papers,[1,2] we presented the results of our thermodynamic study of solutions of various strong electrolytes in such solvents as acetone, methanol, ethanol, ethyl methyl ketone, and *N,N*-dimethylformamide. The activities of solvents in these solutions were determined by vapor-pressure osmometry, and the unusual behavior of the activity coefficients of solutes in the vicinity of infinite dilution derived from those of solvents was ascribed to existence of an association or a dissociation equilibrium.

In the present paper, the results of a similar study of solutions of a series of tetraalkylammonium salts in acetone will be presented.

Theoretical

In vapor-pressure osmometry, the activity of a solvent in the solutions, a_1, is related to the change in electrical resistance, Δr, of the thermistor by the following equation:

$$\Delta r = \frac{BrR}{\Delta H} \ln a_1 = K_e \ln a_1 \qquad (1)$$

where B is the thermistor-constant; r, the electrical resistance of the thermistor; R, the gas constant, and ΔH, the enthalpy change in the evaporation of the pure solvent. The proportional constant, K_e, is determined by measurement with a standard substance, the activity of which is known.

If the dissolved salt, MX, is dissociated into the ions, M^+ and X^-, as:

$$MX \rightleftharpoons M^+ + X^- \qquad (2)$$

the activities of undissociated salt and ions are related to the activity of the solvent by the Gibbs-Duhem equation as:

$$N_1 d\ln a_1 + m_2 d\ln a_2 + m_3 d\ln a_3 + m_4 d\ln a_4 = 0 \qquad (3)$$

where a_2, a_3, and a_4 are the activities of MX, M^+, and X^- respectively, N_1 is the mole-number of the solvent $(=1000/M_1)$, and m_2, m_3, and m_4 are the molalities of MX, M^+, and X^- respectively.

In order to calculate the activity of the solute from that of the solvent by using the Gibbs-Duhem equation, a function, h, defined as:

$$h = \frac{1000 \ln a_1}{M_1 m} + 1 \qquad (4)$$

is usually used. Here, m is the molal concentration of the added solute. The apparent activity of the added solute a_2', is given by the integration of h as:

$$\ln \frac{a_2'}{m} = -h - \int_0^m \frac{h}{m} dm \qquad (5)$$

The unusual behavior of the h/m function of strong electrolytes in organic solvents at an infinite dilution has been fully discussed in our previous papers.[1,2]

Experimental

The lowering of the vapor pressure of a solution was measured by means of a vapor-pressure osmometer, Hitachi-Perkin-meter, Type 115. When the concentrations of the solutions were in the range from *ca.* 1×10^{-3} to 30×10^{-3} mol/kg. solvent, the reading of the meter became stable within 5 min after the solution was dropped. As the standard substance for the determination of the K_e constant, a standard sample of benzyl supplied by Nissei Sangyo Co., Ltd., was used. The tetraalkylammonium salts used were $(n\text{-Pr})_4\text{NI}$, $(n\text{-Bu})_4\text{NCl}$, $(n\text{-Bu})_4\text{NI}$, and $(n\text{-Bu})_4\text{NBr}$. The former three were supplied by Nakarai Chemicals Co., Ltd., and the last one, by Tokyo Kasei Co., Ltd. The guaranteed pure-grade reagents were used without further purification. The acetone, solvent, used was obtained by drying and distilling the guaranteed pure-grade commercial product by the usual method. The measuring temperatures were 40.3 °C for all samples and furthermore, 43.8 and 33.3 °C for benzyl and $(n\text{-Bu})_4\text{NI}$.

Results and Discussion

As an illustration, the plots of Δr against m for $(n\text{-Bu})_4\text{NI}$ and benzyl, the standard sample, at the temperatures of 33.0, 40.3, and 43.8 °C are shown in Fig. 1. As may clearly be seen in Fig. 1, the plots of $(n\text{-Bu})_4\text{NI}$ do not fall on the straight lines of benzyl, the activity coefficient of which is believed to be unity. As has been reported in the previous paper,[1] Eq. (1) holds true under the conditions of thermodynamic equilibrium. The value of K_e empirically obtainable is, however, that of the steady state, which we will designate as K_s hereafter. The K_s/K_e ratio was examined for benzyl, the standard sample. K_e was obtained from the data of the heat of vaporization of the solvent, ΔH, and the noted value of the thermistor-constant, B. The results are shown in Table 1. As may be seen in Table 1, the values of the K_s/K_e ratio are nearly constant at these temperatures. On the basis of these

* Thermodynamic Properties of Ions in Nonaqueous Solvents. III.

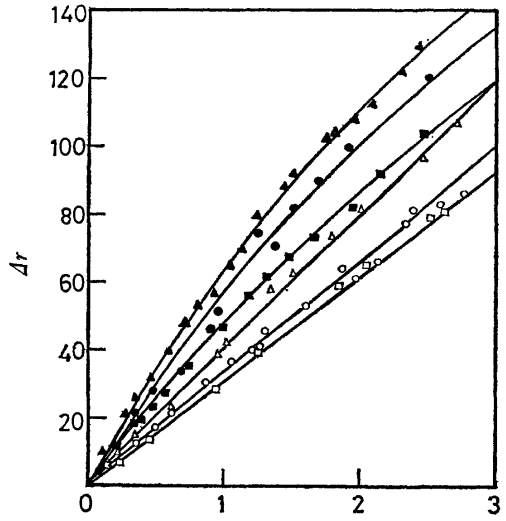

Fig. 1. Relationships between h and the concentration for benzil and $(n\text{-Bu})_4\text{NI}$ at three different temperatures.
□ benzil at 43.8 °C, ○ benzil at 40.3 °C,
△ benzil at 33.3 °C, ■ $(n\text{-Bu})_4\text{NI}$ at 43.8 °C,
● $(n\text{-Bu})_4\text{NI}$ at 40.3 °C, ▲ $(n\text{-Bu})_4\text{NI}$ at 33.3 °C

TABLE 1. K_s, K_e AND K_s/K_e AT THREE DIFFERENT TEMPERATURES

	33.3 °C	40.3 °C	43.8 °C
$K_s\times10^4$	7.11	5.79	5.38
$K_e\times10^4$	7.38	5.84	5.22
K_s/K_e	0.96	0.99	1.03

results, we assume that present results can be used as the thermodynamic standard values at all temperatures.

As has been reported in the previous papers,[1,2] the plots of h/m against m show the existence of dissociation when $\lim_{m\to0} h/m=-\infty$ and of association when $\lim_{m\to0} h/m=+\infty$. The plots of h/m *vs.* m are, however, not adequate for the curve-fitting to determine the activity coefficients, since the errors become larger when m approaches zero. In the present paper, therefore, the plots of h *vs.* m are used for this purpose.

In Fig. 2, the plots of h against m at 40.3 °C are shown. The value of h is, as may be seen in Figs. 2 and 3 in the $-1\leq h\leq0$ range, which shows the existence of a dissociation equilibrium.

According to the Gibbs-Duhem equation, the behavior of h at low concentrations may be formulated on the basis of the following assumptions:

(I) There exists neither dissociation nor association, and the activity coefficient of the solute is unity over all the concentration range. Then:

$$\ln a_1 = -\frac{m}{N_1} \tag{6}$$

and

$$\lim_{m\to0} h = 0 \tag{7}$$

(II) There exists a dissociation equilibrium. The activity coefficients of MX, M^+, and X^-, γ_2, γ_3, and

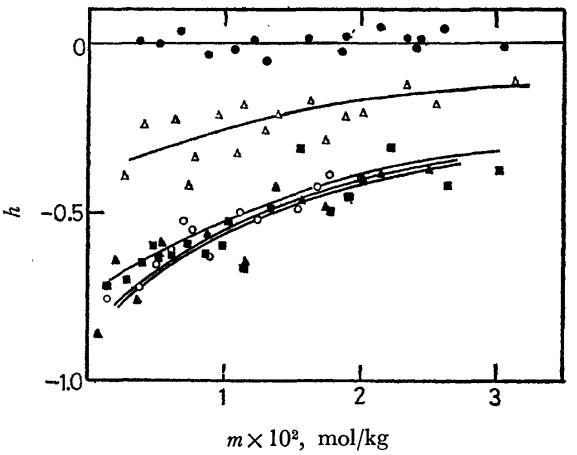

Fig. 2. Relationships between h and the concentration at 40.3 °C.
● benzil, ■ $(n\text{-Bu})_4\text{NBr}$, △ $(n\text{-Bu})_4\text{NCl}$
▲ $(n\text{-Bu})_4\text{NI}$ ○ $(n\text{-Pr})_4\text{NI}$

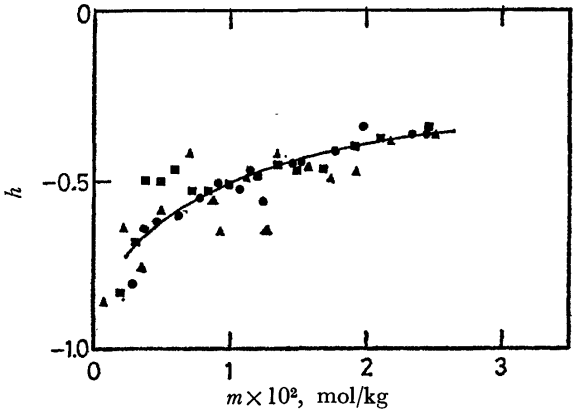

Fig. 3. Relationships between h and the concentration for $(n\text{-Bu})_4\text{NI}$ at three different tempertures.
■ at 43.8 °C, ▲ at 40.3 °C, ● at 33.3 °C

γ_4, are all unity. Then (see Appendix)

$$h = \frac{K-\sqrt{K^2+2mK}}{2m} \tag{8}$$

and:

$$\lim_{m\to0} h = -1 \tag{9}$$

where K represents a dissociation constant.

(III) The activity coefficient of MX, γ_2, is unity, while those of the dissociated ions, γ_3 and γ_4, obey the Debye-Hückel-Onsager limiting formula. Then (see Appendix):

$$h = \frac{1}{m}\left\{m_4 - \frac{2A(\sqrt{m_4})^3}{3}\sigma(x)\right\} \tag{10}$$

$$\sigma(x) = \frac{1}{x^3}\left\{(1+x)-2\ln(1+x)-\frac{1}{(1+x)}\right\} \tag{11}$$

$$x = Ba_0\sqrt{m} \tag{12}$$

$$m_4 = \frac{-K+\sqrt{K^2+4mK\gamma_\pm^2}}{2\gamma_\pm^2} \tag{13}$$

$$\ln\gamma_\pm = -\frac{A|Z_1Z_2|\sqrt{m_4}}{1+Ba_0\sqrt{m_4}} \tag{14}$$

(IV) The activity coefficient of the undissociated

molecule, γ_2, is also not unity. Then (see Appendix):

$$h = \frac{1}{m}\left\{\frac{1}{2}\beta_2 m_2^2 - \frac{2}{3}\beta_3 m_2^3 - m_4 + \frac{2A(\sqrt{m_4})^3}{3}\sigma(x)\right\} \quad (15)$$

$$\ln \gamma_2 = -\beta_2 m_2 + \beta_3 m_2^2 + \cdots \quad (16)$$

$$m_2 = m - m_4 \quad (17)$$

As may clearly be seen in Fig. 2, the (I) assumption is not satisfied in the present results. Most strictly speaking, the behavior of the solutes in solution must be analyzed on the basis of the (IV) assumption. In the present work, however, in order to determine the dissociation equilibrium constant, the curve-fitting was attempted by using Eq. (8) or (9) because of the difficulties in calculation and the obscurities of the parameters in Eq. (15) in their physical meanings. The calculations were carried out by means of a computer, HITAC 10. The calculated values of the dissociation constants obtained from either Eq. (8) or (10) are shown in Tables 2 and 3. The numerical values of a_0 appearing in Eqs. (12) and (14) are those of Evans *et al.*[3] obtained from the electric conductivity measurements. Table 4 shows the means errors for the h function, $|h_{exp}-h_{theor}|$.

Table 2. Dissociation constants K in acetone at 40.3 °C

	Eq. (8)	Eq. (10)
$(n\text{-Bu})_4$NCl	6.4×10^{-4}	5.5×10^{-4}
$(n\text{-Bu})_4$NBr	6.2×10^{-3}	4.5×10^{-3}
$(n\text{-Bu})_4$NI	5.6×10^{-3}	4.0×10^{-3}
$(n\text{-Pr})_4$NI	6.8×10^{-3}	4.4×10^{-3}

Table 3. Dissociation constants K of $(n\text{-Bu})_4$NI in acetone

	Eq. (8)	Eq. (10)
33.3 °C	5.4×10^{-3}	3.9×10^{-3}
40.3 °C	5.6×10^{-3}	4.0×10^{-3}
43.8 °C	4.6×10^{-3}	3.3×10^{-3}

Table 4. Mean errors for the h function ($=|h_{exp}-h_{theor}|$) in acetone at 40.3 °C

	Eq. (8)	Eq. (10)
$(n\text{-Bu})_4$NCl	0.042	0.041
$(n\text{-Bu})_4$NBr	0.053	0.048
$(n\text{-Bu})_4$NI	0.064	0.060
$(n\text{-Pr})_4$NI	0.032	0.030

As may be seen in Tables 2, 3, and 4, Eqs. (8) and (10) showed almost no significant difference in the values of the equilibrium constant and of h. Therefore, it can not be decided from the present results whether the activity coefficient of the undissociated molecule is unity or not.

Table 5 compares our values of the dissociation constant obtained from Eq. (10) and those found in the literature[4,5] obtained from the electric conductivity measurements. The agreement among them is satisfactory except for $(n\text{-Bu})_4$NCl.

Table 5. Comparison of the dissociation constants K by the present work with those by the conductometry

	Present work	Kraus *et al.*[4,5]	Evans *et al.*[3]
$(n\text{-Bu})_4$NCl	0.55×10^{-3}	2.28×10^{-3}	2.33×10^{-3}
$(n\text{-Bu})_4$NBr	4.5×10^{-3}	3.29×10^{-3}	3.51×10^{-3}
$(n\text{-Bu})_4$NI	4.0×10^{-3}	6.48×10^{-3}	6.45×10^{-3}
$(n\text{-Pr})_4$NI	4.4×10^{-3}	4.98×10^{-3}	5.75×10^{-3}

In the above comparison, the following two points were taken in consideration. First: in the electric conductivity measurements reported in the literature,[4,5] the concentration was given in terms of molarity, whereas that in our present result in terms of molality. The effect of this difference in the concentration on the final result is, however, considered not to be significant. Second: in Table 5, the measuring temperature of our present data is 40.3 °C, while that of the conductivity measurements is 25 °C. The effect of these temperature differences is also not taken into account since the temperature dependence of the equilibrium constant of the tetraalkylammonium salts in methanol reported by Kay *et al.*[6] is not very large.

Conclusion

Tetraalkylammonium salts dissolved in acetone are dissociated. The equilibrium constant of dissociation was determined on the assumption that the behavior of dissociated ions is represented by the Debye-Hückel-Onsager limiting formula. The extraordinarily small value in the equilibrium constant of $(n\text{-Bu})_4$NCl can not be explained at present.

References

1) H. Nomura, M. Ando, and Y. Miyahara, *Nippon Kagaku Zasshi*, **90**, 1222 (1969).
2) H. Nomura, M. Ando, and Y. Miyahara, *ibid.*, **91**, 840 (1970).
3) D. F. Evans, J. Thomas, J. A. Nadas, and S. M. A. Matersich, *J. Phys. Chem.*, **75**, 1714 (1971).
4) C. A. Kraus and M. J. McDowell, *J. Amer. Chem. Soc.*, **73**, 3293 (1951).
5) C. A. Kraus and M. B. Reynolds, *ibid.*, **70**, 1709 (1948).
6) R. L. Kay, D. F. Evans, and C. Zawoyski, *J. Phys. Chem.*, **69**, 4208 (1965).

Appendix

Derivation of Eq. (8): In the case of the (II) assumption, $a_2=m_2$, $a_3=m_3$, and $a_4=m_4$ as well as $m=m_2+m_4$ and $m_3=m_4$. The substitution of these relations into Eq. (3) gives, after integration:

$$\ln a_1 = -\frac{1}{N_1}(m+m_4) \quad (1a)$$

On the other hand, from the equation of the dissociation constant:

$$K = \frac{m\alpha^2}{1-\alpha} = \frac{m_4^2}{m-m_4} \quad (2a)$$

we obtain this relation:

$$m_4 = \frac{-K+\sqrt{K^2+4mK}}{2} \tag{3a}$$

On combining Eqs. (1a) and (3a) with Eq. (4), we obtain Eq. (8).

Derivation of Eq. (10): In the case of the (III) assumption, Eq. (3) reduces to:

$$N_1 \mathrm{d} \ln a_1 + \mathrm{d}m_2 + 2\mathrm{d}m_4 + 2m_4 \mathrm{d} \ln \gamma_\pm = 0 \tag{4a}$$

where $\gamma_\pm = (\gamma_3\gamma_4)^{1/2}$.

By substituting Eq. (13) in Eq. (4a) and intergrating the equation, we obtain:

$$\ln a_1 = -\frac{1}{N_1}\left\{m_2+2m_4-\frac{2A(\sqrt{m_4})^3}{3}\sigma(x)\right\} \tag{5a}$$

On combining Eq. (5a) with Eq. (4), we obtain Eq. (10).

Derivation of Eq. (15): we assume, for the activity coefficient, Eq. (16). Calculations similar to those for the derivation of Eq. (9) leads us to Eq. (15).

Photoelectron Spectra of Substituted Benzenes

Tsunetoshi KOBAYASHI and Saburo NAGAKURA

The Institute for Solid State Physics, The University of Tokyo, Roppongi, Minato, Tokyo 106

(Received April 25, 1974)

Photoelectron spectra were measured in the region between 6 and 21 eV for aniline, *N,N*-dimethylaniline, phenol, anisole, benzonitrile, acetophenone, nitrobenzene, and their methyl derivatives. The observed spectra were interpreted in terms of their MO's obtained by the CNDO/2 and EHMO methods, the methyl-substituent effect and the steric hindrance effect being considered. Both effects are essential for the reliable assignment of the observed photoelectron spectra. We found a general tendency that the interaction of the doubly degenerate highest occupied orbitals (e_{1g}) of the benzene ring with the highest occupied orbital of a substituent group is important for the interpretation of the observed lower energy (7~12 eV) bands. The only exceptional case is the nitrobenzenes in which the lowest vacant orbital of the substituent group is rather close to the highest occupied orbitals of the benzene ring and the interaction between them is important. The effects of the substituent groups upon the observed photoelectron spectra are classified into four types.

Photoelectron spectroscopy[1] developed in recent years gives direct information about occupied molecular orbital energies and is expected to be a useful tool to investigate the effect of substituent groups upon the electronic structures of parent hydrocarbons.

We have studied photoelectron spectra (PES) of various kinds of substituted benzenes and have already published the results of styrene and its methyl derivatives.[2] Steric hindrance of the α- or *ortho*-methyl group was found to have great effect on the PES of methyl-substituted styrenes, and the relation between the higher occupied π-orbital energies of styrene and the twist angle of the vinyl group was discussed from both experimental and theoretical points of view. Furthermore, some preliminary reports have been published on the PES of aniline, *N,N*-dimethylaniline, nitrobenzene, and their methyl derivatives.[3,4]

In this paper we intend to discuss systematically our results of PES obtained hitherto with substituted benzenes; phenol, anisole, benzonitrile, acetophenone, and their methyl derivatives being newly treated in addition to the molecules studied in the preliminary reports.[3,4] Main purposes of the present study are as follows: 1) to make assignments of lower energy bands in the PES of the substituted benzenes under consideration as reliably as possible, orbital energies calculated by the CNDO and EHMO methods and the effect of methyl-substituent group being considered; 2) to interpret systematically the observed PES in terms of the interaction between substituent groups and the benzene ring; 3) to clarify the correlation between the observed PES and the steric hindrance of methyl-substituent groups.

Baker *et al.*[5] measured the PES of aniline, *N,N*-dimethylaniline, *p*-toluidine, *N,N*-dimethyl-*p*-toluidine, phenol, and anisole with a relatively low-resolution magnetic deflection type photoelectron spectrometer. Thereafter, several works[6-11] on the PES of some of the compounds studied here have been published. They are discussed in comparison with our results in later parts of this paper.

Experimental and Calculation

2,4-Dimethylanisole and 2,6-dimethylanisole were synthesized according to Ref. 12 and isolated by column chromatography. All the samples were purified in usual ways and their purities were checked with the aid of gas chromatograms and NMR spectra.

The PES of these compounds were recorded on a JASCO model PE-1 photoelectron spectrometer and a newly constructed photoelectron spectrometer[2] with a sample inlet system which can be heated, if necessary, up to *ca.* 140 °C. HeI resonance line of 584 Å was used as excitation source and Xe gas as the internal standard for the calibration.

The CNDO/2[13] and the EHMO[14] calculations of these compounds were carried out by a FACOM 270—30 and a FACOM 230—60 computer at the Institute of Physical and Chemical Research. The geometrical structure of *N,N*-dimethylaniline was taken from Ref. 15 and the geometrical structures of the other compounds were taken from Refs. 16 and 17 or assumed based on the data given in these references.

Results and Discussion

Anilines. The PES of aniline, *o*-, *m*-, and *p*-toluidines, *N,N*-dimethylaniline, and *N,N*-dimethyl-*o*-, *m*-, and *p*-toluidines are shown in Fig. 1. The vertical ionization potentials, $I_v(J)$, of these compounds were obtained from the observed PES and are summarized in Table 1.

As is seen in Fig. 1 and Table 1, these aromatic amines commonly show three lower energy bands in the region from 7 eV to 11 eV. They are assigned to the ionizations from three π MO's, b_1 (like), a_2 (like), and b_1 (like),[3] which are caused by the interaction among the highest occupied doubly degenerate π orbitals, e_{1g}(S) and e_{1g}(A), (9.23 eV) of the ring and the lone pair (n) orbital of the corresponding alkylamine (9.7 eV[18] for methylamine and 8.5 eV[18] for trimethylamine). As is clearly seen in Fig. 2 which shows schematically the orbitals concerned, the first and third highest occupied π MO's are delocalized over both benzene ring and amino nitrogen atom, while the second highest occupied π MO is localized on the benzene ring. This assignment is supported by the fact that the first and third bands of aniline and toluidines shift much more by *N,N*-dimethylation than their second bands.

The shifts, $\Delta I_v(J)$ (J=1,2....), of the lowest three vertical ionization potentials of aniline and *N,N*-dimethylaniline by *o*-, *m*-, and *p*-methyl substitutions

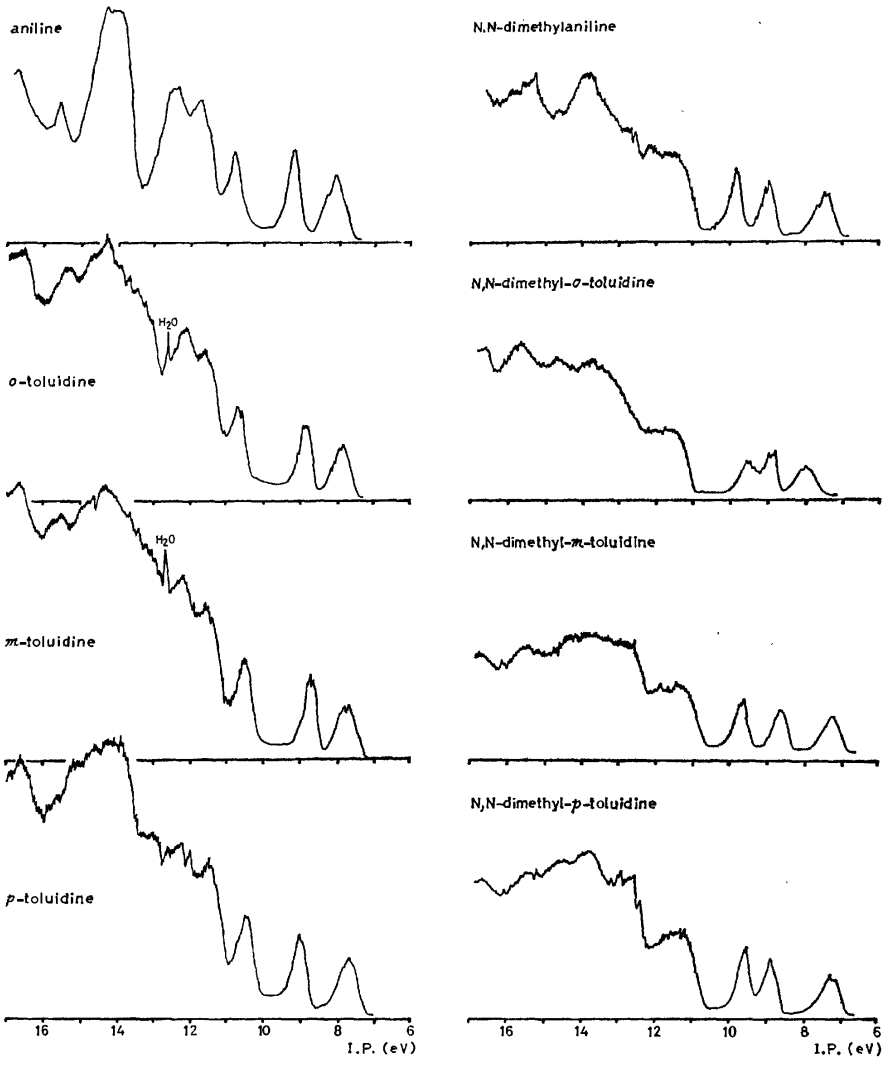

Fig. 1. Photoelectron spectra of anilines.

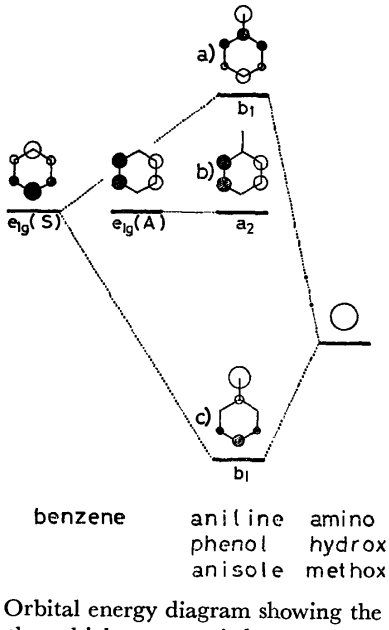

Fig. 2. Orbital energy diagram showing the correlation of the three highest occupied π orbitals of aniline (phenol or anisole) with the benzene e_{1g} π orbitals and a substituent lone pair orbital.

can be estimated by the aid of the following equation derived by the first-order perturbation theory.[19]

$$-\Delta I_v(J) = 0.0528 + 1.0110 \sum_{\zeta} (3C_{J\zeta}^2 + C_{J\tau}^2 + C_{J\tau'}^2)/3 \quad (1)$$

Here ζ denotes the position of methyl substitution, and τ and τ' the positions of the nearest neighbours to ζ. C_{Jk} is the coefficient of the k-th AO in the J-th π MO obtained by the CNDO/2 method. The vertical ionization potentials of methyl substituted anilines and *N,N*-dimethylanilines were estimated by considering those of the parent compounds and the $\Delta I_v(J)$ values thus obtained. The results are listed in Table 1 (in the parentheses).

As is seen in Table 1, the estimated values agree rather well with the observed ones except for the case of *N,N*-dimethyl-*o*-toluidine in which the estimated values of the first and third ionization potentials are smaller by 0.73 eV and greater by 0.17 eV than the corresponding observed ones, respectively, and, therefore, the estimated splitting between them (2.49 eV) is much larger than the observed value (1.59 eV). It is known[20-23] that the dimethylamino group of *N,N*-dimethyl-*o*-toluidine is twisted from the benzene ring

Table 1. Vertical ionization potentials ($I_v(J)$ in eV) of aniline, *N,N*-dimethylaniline, and their methyl derivatives[a,b]

	$I_v(J)$ (eV)			
J	1	2	3	4
Benzene[c]	9.23	11.67	12.32	13.97
Toluene[c]	8.85	9.34	11.43	
m-Xylene[c]	8.71	9.03	11.24	
Aniline	8.05	9.21	10.81	11.79
o-Toluidine	7.83	8.77	10.70	11.58
	(7.83)	(8.81)	(10.69)	
m-Toluidine	7.66	8.71	10.45	11.52
	(7.86)	(8.83)	(10.60)	
p-Toluidine	7.62	8.94	10.40	11.45
	(7.77)	(9.00)	(10.50)	
N,N-Dimethylaniline	7.37	8.96	9.80	11.63
N,N-Dimethyl-*o*-toluidine	7.92	8.78	9.51	11.57
	(7.19)	(8.57)	(9.68)	
N,N-Dimethyl-*m*-toluidine	7.24	8.63	9.61	11.18
	(7.22)	(8.58)	(9.66)	
N,N-Dimethyl-*p*-toluidine	7.27	8.86	9.55	11.37
	(7.15)	(8.75)	(9.60)	
Methylamine[d]	9.7	13.2	14.5	15.6
Dimethylamine[d]	8.9	12.6	13.3	13.8
Trimethylamine[d]	8.5	12.4	12.9	14.0

a) The values in the parentheses denote the ionization potentials estimated with the aid of Eq. (1). b) The $I_v(J)$'s of benzene, toluene, *m*-xylene, and some aliphatic amines are also tabulated in this table. c) Ref. 4. d) Ref. 18.

Table 2. Vertical ionization potentials ($I_v(J)$ in eV) of phenol, anisole, and their methyl derivatives[a,b,c]

	$I_v(J)$ (eV)			
J	1	2	3	4
Phenol	8.73	9.40	11.59	11.99
o-Cresol	8.48	9.08	11.42	11.67
	(8.48)	(9.01)	(11.49)	
m-Cresol	8.52	9.10	11.16	11.65
	(8.51)	(9.02)	(11.41)	
p-Cresol	8.38	9.25	11.14	11.68
	(8.38)	(9.18)	(11.34)	
2,4-Dimethylphenol	8.18	8.89	11.00	11.40
	(8.18)	(8.84)	(11.30)	
	[8.13]	[8.93]	[10.97]	
2,6-Dimethylphenol	8.26	8.78	11.13	11.51
	(8.28)	(8.66)	(11.45)	
	[8.23]	[8.76]	[11.25]	
Methanol[d]	10.96	12.62	15.21	15.64
Anisole	8.39	9.22	11.06	11.52
o-Methylanisole	8.24	8.93	10.92	11.37
	(8.16)	(8.83)	(10.95)	
m-Methylanisole	8·28	8.93	10.76	11.33
	(8.20)	(8.84)	(10.91)	
p-Methylanisole	8.18	9.11	10.75	11.34
	(8.09)	(9.01)	(10.84)	
2,4-Dimethylanisole	7.95	8.75	10.60	11.12
	(7.92)	(8.67)	(10.78)	
	[8.03]	[8.82]	[10.61]	
2,6-Dimethylanisole	8.51	8.71	9.87	11.31
	(8.00)	(8.48)	(10.89)	
	[8.09]	[8.64]	[10.78]	
Methyl ether[e]	10.04	11.91	13.43	14.2

a) See footnote a) for Table 1. b) The values in the square brackets are the I_v's estimated from those of the parent molecules and their mono-methyl derivatives. c) The $I_v(J)$ values of methanol and methyl ether are also given in this table. d) Ref. 25. e) Ref. 26.

plane by the steric hindrance effect of the *o*-methyl group. This twisting decreases the conjugation between the e_{1g}(S)-like π orbital of benzene ring and the nitrogen n orbital and, therefore, decreases the splitting between the first and third I_v's of *N,N*-dimethyl-*o*-toluidine.

In the preliminary report,[3] we estimated the lowest three I_v's of the hypothetical *N,N*-dimethyl-*o*-toluidine with no steric hindrance effect to be 7.41~7.48 eV, 8.69 eV, and 9.85~9.86 eV by adding the correction terms due to *N,N*-dimethylation to the corresponding values of *o*-toluidine. The splitting between the first and third ionization potentials thus obtained, 2.37—2.45 eV, is in good agreement with the value estimated with the aid of Eq. (1), 2.49 eV.

Concerning aniline, the splitting between the first and second bands is smaller than that between the second and third bands. The reverse is the case for *N,N*-dimethylaniline. This indicates that in the case of aniline, as is shown in Fig. 2, the benzene ring e_{1g} π orbitals are higher than the amino group n orbital, while, in the case of *N,N*-dimethylaniline, the relative height of both orbitals is reversed. This reversal is caused by the increase in the n orbital energy of the amino group by *N,N*-dimethylation. This means that the highest occupied and third highest occupied MO's of aniline are mainly contributed by e_{1g}(S) orbital of the ring and the n orbital on the nitrogen atom, respectively, while the reverse is the case for *N,N*-dimethylaniline. This is supported qualitatively by the CNDO/2 calculation.

The correlation diagram for the orbital energies of these aromatic amines obtained on the assumption of $\varepsilon=-I_v$ (Koopmans' theorem[24]) has already been shown in Fig. 1 of Ref. 3.

The PES of aniline, *N,N*-dimethylaniline, *o*-toluidine and *N,N*-dimethyl-*o*-toluidine have recently been reported by Maier and Turner[11] and their assignment of the three lower energy bands is consistent with that given in our preliminary report[3] and in the present paper.

Phenols and Anisoles. The PES of phenol, *o*-, *m*-, and *p*-cresols, 2,4- and 2,6-dimethylphenols, anisole, *o*-, *m*-, and *p*-methylanisoles, and 2,4- and 2,6-dimethylanisoles are shown in Fig. 3, and the observed $I_v(J)$'s of these compounds are summarized in Table 2.

Phenols and anisoles commonly show three lower energy bands in the region between 8 eV and 11.5 eV. This region corresponds to the ionization from the benzene e_{1g}(S) and e_{1g}(A) orbitals and from the n orbital on the oxygen atom of methanol (10.96 eV)[25] or methyl ether (10.04 eV).[26] Therefore, the lower three energy bands of phenols or anisoles are mainly related to the MO's caused by the interaction of the e_{1g}(S) and e_{1g}(A) orbitals of the ring with the oxygen

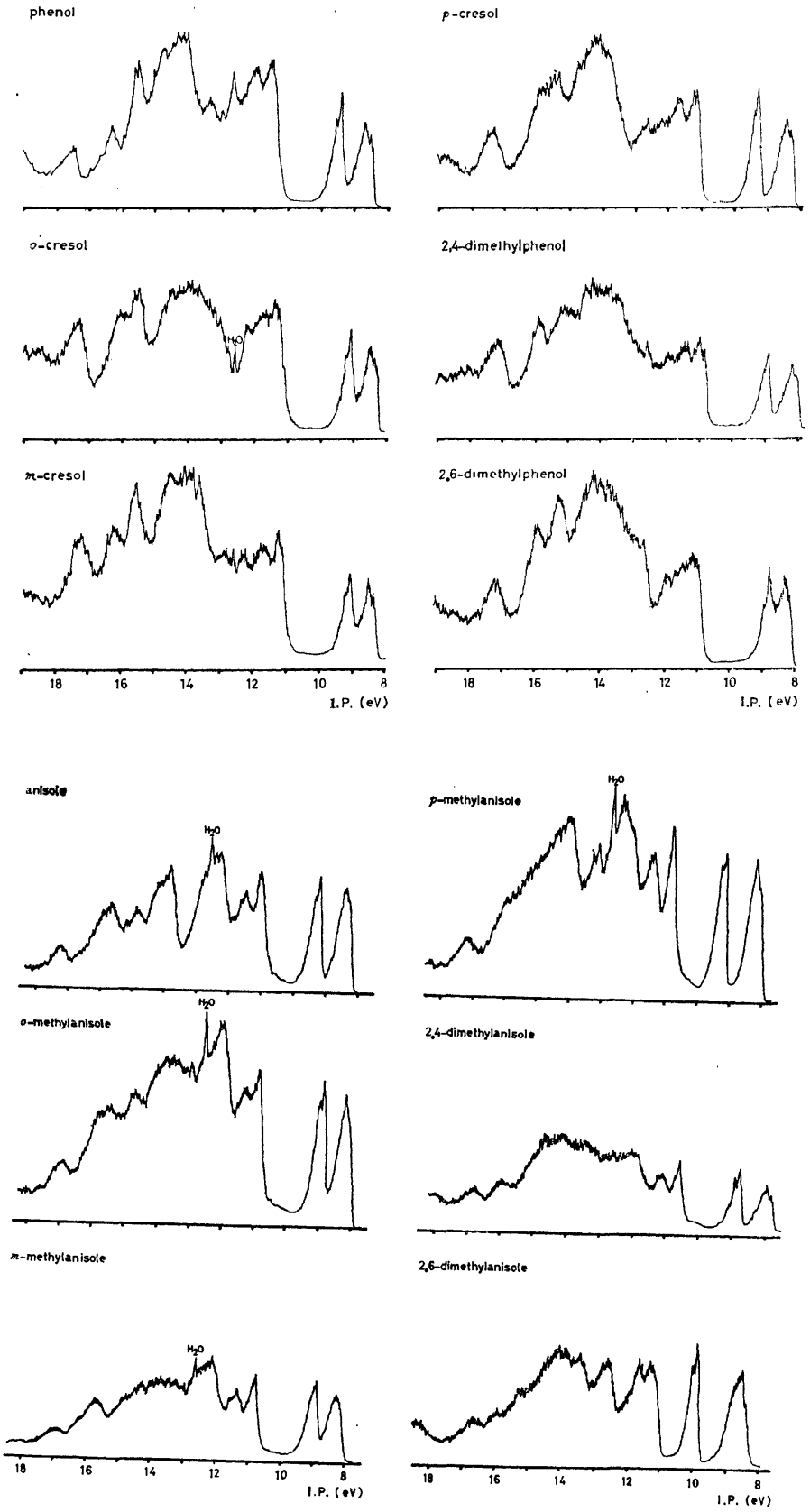

Fig. 3. Photoelectron spectra of phenols and anisoles.

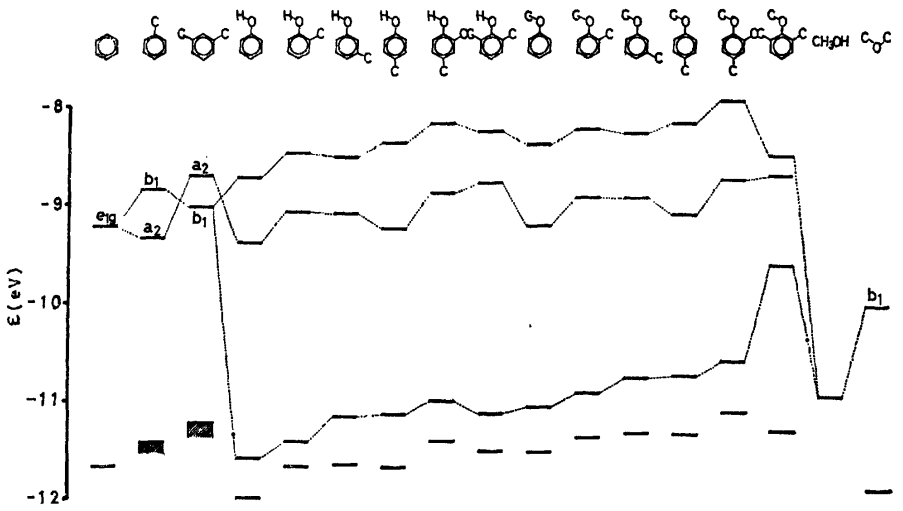

Fig. 4. Orbital energy diagram for the higher occupied orbitals of phenols and anisoles.

n orbital as schematically shown in Fig. 2. This qualitative scheme is supported by the CNDO/2 calculation. The observed orbital energy diagram estimated according to Koopmans' theorem[24] is shown in Fig. 4.

Now let us consider methyl substituent effects on the PES of phenol and anisole. The lowest three ionization potentials of some methyl substituted phenols and anisoles were estimated by two methods: one of them is to estimate the substituent effect by the aid of Eq. (1) and the other is to derive the ionization potentials of dimethyl derivatives from those of monomethyl derivatives and the parent molecules by assuming the additivity of the methyl substituent effect. The vertical ionization potentials of the methyl derivatives estimated by the aid of both methods are summarized in Table 2 (in the parentheses and the square brackets).

As is clearly seen in Table 2, the lowest three ionization potentials estimated by both methods are in good agreement with the observed values except for the case of 2,6-dimethylanisole. In particular, the agreement is better for the values estimated by the additivity rule.

The lowest and third lowest ionization potentials estimated by both methods for 2,6-dimethylanisole show large discrepancies from the observed values. The estimated values are for the planar molecule; in actuality, however, the methoxyl group of this molecule is considered to be twisted by around 90°[27,28] from the benzene ring plane because of the steric hindrance effect of the two *o*-methyl groups. This twisting decreases the conjugation between the ring π orbital and the oxygen n orbital. This is the reason why the observed lowest and third lowest ionization potentials are larger and smaller, respectively, compared with the corresponding values estimated for the hypothetical planar molecule.

The difference between the first and second ionization potentials is smaller for both phenol and anisole than that between the second and third ionization potentials. This is similar to the situation found for aniline and indicates that the highest occupied orbitals of phenol and anisole are mainly contributed by the ring e_{1g}(S) orbital.

The PES of phenol, *o*-cresol, 2,6-dimethylphenol, anisole, *o*-methylanisole and 2,6-dimethylanisole were reported recently by Maier and Turner.[11] The PES

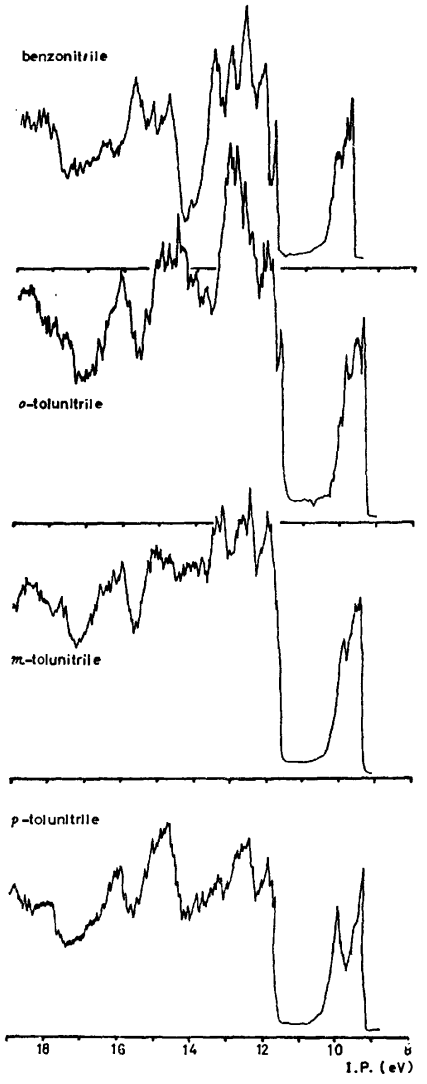

Fig. 5. Photoelectron spectra of benzonitriles.

of 2,6-dimethylanisole reported by them, however, is slightly different from ours: in their spectrum, the first band is too strong compared with the third band and an additional band appears around 9.20 eV. This additional band could not be observed for our sample which was purified by column chromatography and the purity of which was checked with gas chromatography and NMR spectrum. This band may be due to some impurities.

Benzonitriles. The PES of benzonitrile and *o*-, *m*-, and *p*-tolunitriles are shown in Fig. 5. The observed $I_v(J)$'s of benzonitriles are summarized in Table 3.

TABLE 3. VERTICAL IONIZATION POTENTIALS ($I_v(J)$ IN eV) OF BENZONITRILE AND ITS METHYL DERIVATIVES, AND ACETONITRILE[a)]

	$I_v(J)$ (eV)			
J	1	2	3	4
Benzonitrile	9.72	10.14	11.84	12.11
o-Tolunitrile	9.38 (9.49)	9.84 (9.75)	11.62	12.01 (12.01)
m-Tolunitrile	9.40 (9.51)	9.83 (9.75)	11.69	11.95 (11.91)
p-Tolunitrile	9.33 (9.39)	9.97 (9.92)	11.68	11.90 (11.83)
Acetonitrile[b)]	12.21	13.14		

a) See footnote a) for Table 1. b) Ref. 1.

According to the CNDO/2 and EHMO calculations, the occupied orbitals of benzonitrile are located in the following orders from the top, respectively: $b_1\pi$, $b_2\sigma$, $a_1\sigma$, $a_2\pi$.... and $a_2\pi$, $b_1\pi$, $a_1\sigma$, $b_2\sigma$..... Judging from the fact that the $e_{1g}(S)$ and $e_{1g}(A)$ orbitals of benzene are located at 9.23 eV while the highest occupied orbital of acetonitrile at 12.21 eV, we may safely assign the first and second bands of benzonitrile to two π($b_1\pi$ and $a_2\pi$) MO's mainly localized on the benzene ring.

Figure 6 shows the orbital energies determined from the observed ionization potentials by the aid of Koopmans' theorem.[24)] The observed first ionization potentials of *o*- and *m*-tolunitriles are similar to each other, but are larger than the corresponding value of *p*-tolunitrile. Furthermore, the second ionization potentials of *o*- and *m*-tolunitriles are smaller than that of the *p*-isomer. This tendency can be reproduced by the use of Eq. (1) on the assumption that the highest occupied π MO of benzonitrile is b_1 and the second one a_2. The ionization potentials obtained thus for *o*-, *m*-, and *p*-tolunitriles are in good agreement with the observed values as is shown in Table 3. Therefore the first and second bands of benzonitrile may be assigned to the ionizations from the $b_1\pi$ and $a_2\pi$ orbitals, respectively.

From the fact that the $b_1\pi$ orbital caused by the mixing with appropriate orbitals of the cyano group is located above the $a_2\pi$ orbital localized on the benzene ring, it is revealed that the highest occupied doubly degenerate orbitals of the ring interact more strongly with higher occupied orbitals of the cyano group than with lower vacant orbitals of the group. This scheme

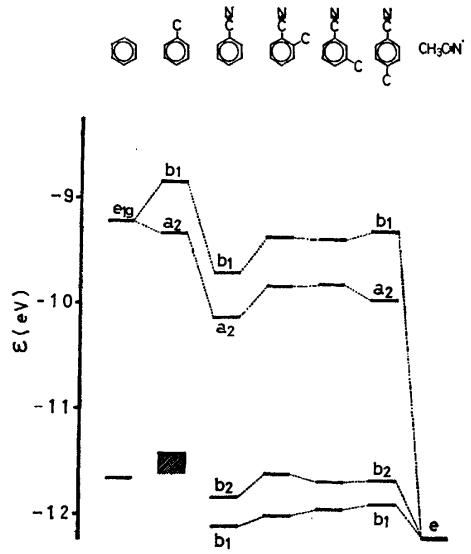

Fig. 6. Orbital energy diagram for the higher occupied orbitals of benzonitriles.

TABLE 4. VERTICAL IONIZATION POTENTIALS ($I_v(J)$ IN eV) OF ACETOPHENONE, *o*-, *m*-, AND *p*-METHYLACETOPHENONES, AND ACETONE[a)]

	$I_v(J)$ (eV)			
J	1	2	3	4
Acetophenone	9.37	9.55	9.77	11.91
o-Methylacetophenone	9.15 ((9.21))	9.32	9.44 ((9.47))	11.68
m-Methylacetophenone	9.14 ((9.23))	9.34	9.45 ((9.46))	11.69
p-Methylacetophenone	9.12 ((9.16))	9.36	9.56 ((9.60))	11.65
Acetone[b)]	9.72	12.6	13.4	13.9

a) The values in the double parentheses denote the ionization potentials estimated from the I_v data of acetophenone and benzonitriles on the assumption that the methyl-substitution effect upon the π orbitals of acetophenone is equal to that of benzonitrile. b) Ref. 29.

on the orbital interaction for benzonitrile is the same as for aniline, phenol, and anisole. There is a difference, however, between benzonitrile and aniline or phenol in the point that the first ionization potential of benzonitrile is greater than that of benzene, while the reverse is the case for aniline and phenol. This is due to the difference in the charge density on the benzene ring; the electron density on the ring is reduced by the electron-accepting group like the cyano group and is increased by the electron-donating group like amino or hydroxyl group.

Benzonitriles show commonly two sharp bands around 11.7~12.1 eV and this region is for the doubly degenerate π orbitals of the cyano group (for example, acetonitrile: 12.21 eV[1)]). Judging from the above assignment of the lowest energy band of benzonitrile, the higher energy band of the two sharp bands around 12 eV (the fourth lowest energy band) is due to the b_1-like π MO constructed by the bonding combination

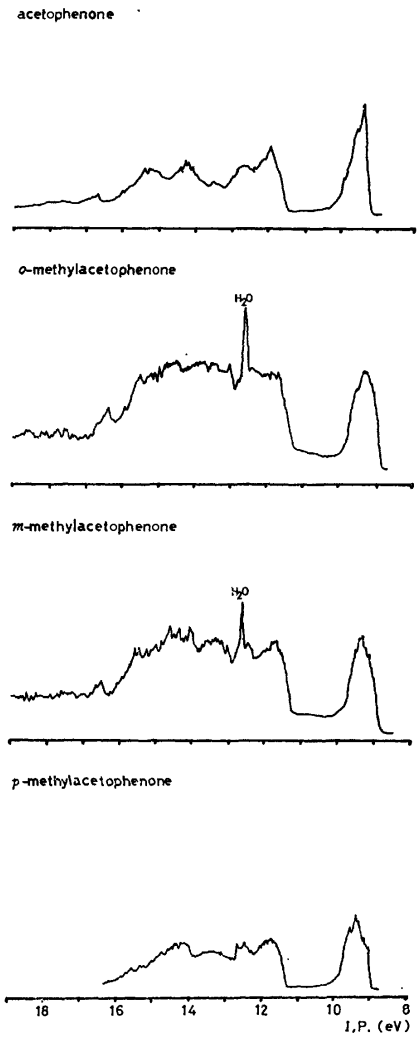

Fig. 7. Photoelectron spectra of acetophenones.

of the cyano group out-of-plane occupied π orbital and the ring e_{1g}(S)-type π orbital, and the other band (the third lowest energy band) is assigned to the ionization from the cyano group in-plane π orbital. The observed methyl-substitution effect on the former band supports this assignment; as is clearly seen in Table 3, the fourth ionization potentials of *o*-, *m*-, and *p*-tolunitriles estimated with the aid of Eq. (1) (the values in the parentheses in Table 3) are in excellent agreement with the observed values.

The PES of benzonitrile was recently assigned by Rabalais and Colton[9] on the basis of INDO and CNDO calculations, the assignment of the four lower energy bands being consistent with ours.

Acetophenones. The PES of acetophenone and *o*-, *m*-, and *p*-methylacetophenones are shown in Fig. 7. Their vertical ionization potentials are summarized in Table 4. Acetophenone has overlapped bands in the region of 9.3—9.8 eV. This region corresponds to the benzene e_{1g} orbital bands (9.23 eV) and the acetyl n orbital band (for example, acetone: 9.72 eV[29]). Therefore, it is quite natural to assign the overlapped bands to the acetyl n orbital and the benzene ring e_{1g}(S) and e_{1g}(A) orbitals perturbed by acetyl group π orbitals. The CNDO/2 calculation gives the following

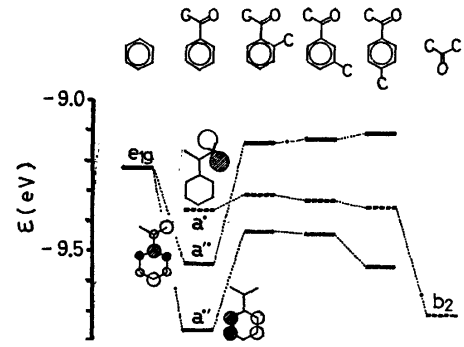

Fig. 8. Orbital energy diagram for the higher occupied orbitals of acetophenones.

order for the higher occupied orbitals of acetophenone: from the top, n, π, σ, and π. This order, however, is quite improbable in the point that the σ band is expected to appear in the 9.3—9.8 eV region.

Since the lowest energy peak at 9.37 eV is rather sharp, it is reasonable to assign this band to the acetyl n orbital. The second (9.55 eV) and third (9.77 eV) bands of acetophenone, which are due to the ionizations from π orbitals, change by the methyl substitution on the *o*-, *m*-, and *p*-positions with the same tendency as the first and second bands of benzonitrile, respectively. Therefore, by an analogy with the case of benzonitrile, the order of the π orbitals of acetophenone can be determined as shown in Fig. 8: namely, the π orbital localized on the ring (a″) is lower than the π orbital (a″) caused by the interaction of the ring π orbital with the highest occupied π orbital of the acetyl group.

Next, let us turn to the *o*-, *m*-, and *p*-methylacetophenones. The vertical ionization potentials from their π orbitals were estimated from the π $I_v(J)$ data of acetophenone and the benzonitriles on the assumption that the methyl-substitution effect upon the π orbitals of acetophenone is equal to that of benzonitrile: the results are given in Table 4 (in the double parentheses). The estimated values are in good agreement with the observed values for *o*-, *m*-, and *p*-methylacetophenones. It may be noticed that the a″ orbital of acetophenone is greatly pushed up by the methyl substitution while the a′ orbital is rather insensitive. Consequently, the highest and second highest occupied orbitals of acetophenone are reversed for the methyl substituted acetophenones. This is supported by the fact that the observed second ionization potentials of *o*-, *m*-, and *p*-methylacetophenones are almost constant and are close to the first ionization potential of acetophenone. The fact that these n ionization potentials are smaller than the corresponding value of acetone (9.72 eV) may be interpreted in terms of the electron migration from the benzene ring to the acetyl group and therefore the imcrement in the negative charge on the group.

Finally the orbital energy diagram estimated according to Koopmans' theorem[24] is shown in Fig. 8.

Nitrobenzenes. The PES of nitrobenzene, *o*-, *m*-, and *p*-nitrotoluenes, 2,4- and 2,6-dimethylnitrobenzenes, 2,4,6-trimethylnitrobenzene, and nitromethane are shown in Fig. 9. The vertical ionization potentials are summarized in Table 5. The correlation diagram

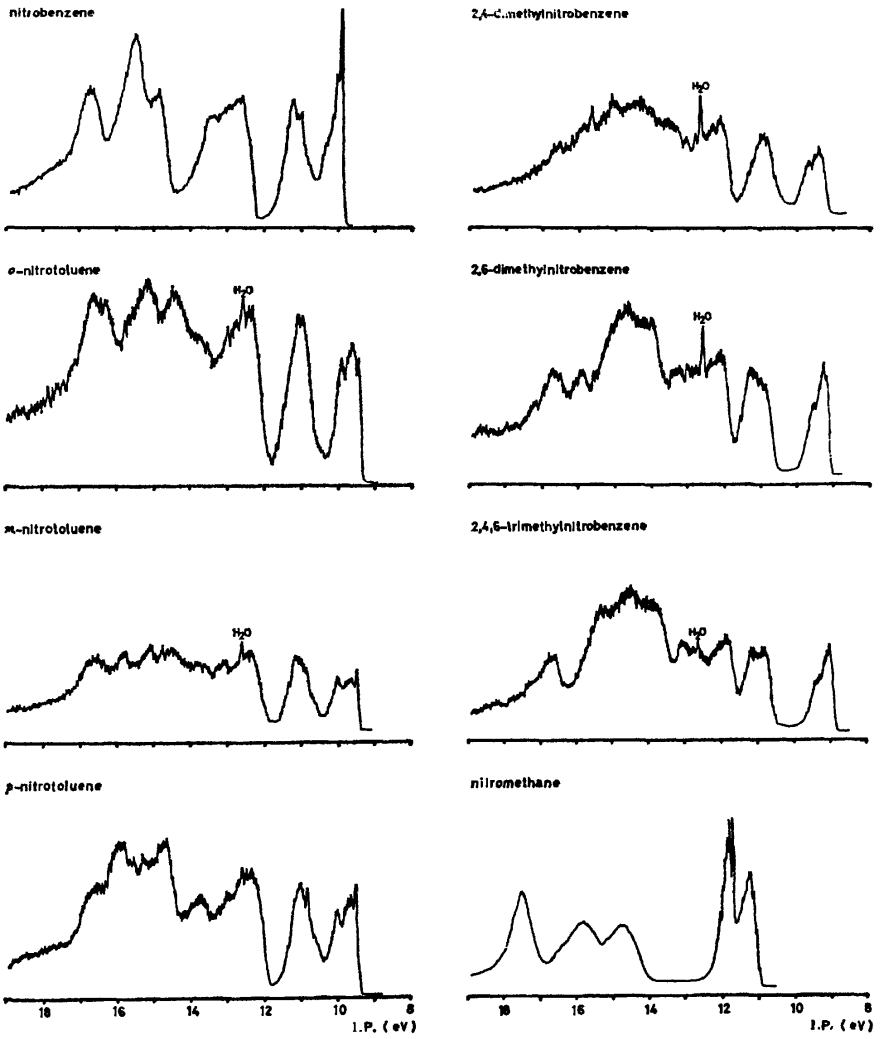

Fig. 9. Photoelectron spectra of nitrobenzenes and nitromethane.

Table 5. Vertical ionization potentials ($I_v(J)$ in eV) of nitrobenzene, its methyl derivatives, and nitromethane

	$I_v(J)$ (eV)				
J	1	2	3	4	5
Nitrobenzene	9.93	10.32	11.01	11.23	12.65
o-Nitrotoluene	9.63	9.90	10.98	11.09	12.43
m-Nitrotoluene	9.48	10.03	10.90	11.08	12.42
p-Nitrotoluene	9.52	10.01	10.84	11.01	12.36
2,4-Dimethyl-nitrobenzene	9.36	9.65	10.89		12.07
2,6-Dimethyl-nitrobenzene	9.17	9.57	10.87	11.20	12.10
2,4,6-Trimethyl-nitrobenzene	9.01	9.32	10.86	11.08	11.84
Nitromethane	11.29	11.71	14.76	15.80	17.49

for the orbital energies of these compounds obtained on the assumption $\varepsilon = -I_v(J)$ (Koopmans' theorem[24]) is shown in Fig. 10.

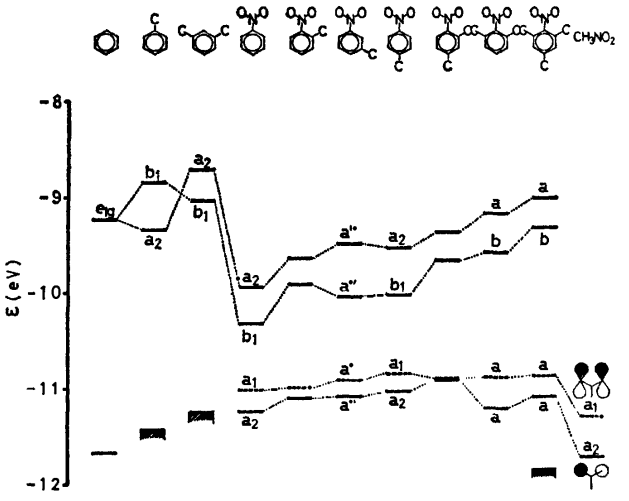

Fig. 10. Orbital energy diagram for the higher occupied orbitals of nitrobenzenes.

According to the EHMO calculation, the first and second bands can be correlated, respectively, with the $a_2\pi$ orbital corresponding to the e_{1g}(A) type π orbital of benzene and with the $b_1\pi$ orbital constructed by the combination of the lowest unoccupied orbital of the nitro group and the highest occupied e_{1g}(S) orbital of the benzene ring. These orbitals are schematically shown in Fig. 11. The prediction derived by the first-order perturbation theory on the basis of this assignment

can well explain the observed tendency shown in Fig. 10 that the difference between the first two vertical ionization potentials is larger for *m*-nitrotoluene than for *p*-nitrotoluene and is larger for 2,6-dimethylnitrobenzene than for 2,4,6-trimethylnitrobenzene.

It may be emphasized that in the case of nitrobenzenes the first band corresponds to a_2 (like) π orbital mainly localized on the benzene ring and the second band corresponds to the b_1 (like) π orbital, while the reverse is the case for the other molecules treated in the present paper. This characteristic of nitrobenzenes is due to the fact that the mixing of the ring $e_{1g}(S)$ orbital with the lowest vacant π orbital of the nitro group is predominant for nitrobenzenes, while, in the other cases, the occupied group π orbitals of the substituents mix more significantly with the benzene $e_{1g}(S)$-(like) orbital rather than the vacant group π orbital of the substituents.

From the spectral shape and the INDO calculation, Rabalais[8] assigned the first two bands of nitrobenzene to the $b_1\pi$ and $a_2\pi$ orbitals, respectively, but from the above discussion our assignment seems to be more reasonable.

Nitrobenzene and its methyl derivatives have commonly two bands in the range between 10.5 and 11.5 eV; lower energy bands around 10.9 eV and higher energy ones around 11.1 eV. From their positions and relative intensities, they are correlated with the 11.29 eV and 11.71 eV bands of nitromethane.[30] The third band of nitrobenzene at 11.01 eV is insensitive to the methyl substitution on the benzene ring and may be assigned to the a_1n orbital which is the nonbonding orbital in plane (see Fig. 11). The fourth band of nitrobenzene correlated with the 11.71 eV band of nitromethane is rather sensitive to the methyl substitution on a carbon atom of the benzene ring and may be due to the $a_2\pi$ orbital shown in Fig. 11. Further details of the assignment on the bands in the 10.5—12.0 eV region observed with nitromethane, nitrobenzene and its methyl derivatives are not described here, since they have been described in the previous paper[4]. Our assignments of the third and fourth bands are consistent with those by Rabalais.[8]

According to the first-order perturbation theory the splitting between the first two vertical ionization potentials of *o*-nitrotoluene should be similar to that of *m*-isomer. In reality, however, the former is significantly smaller than the latter. This abnormal result is easily understood if one remembers that in the case of *o*-isomer the conjugation between the benzene e_{1g}-like orbitals and the nitro group π orbitals is diminished by the twisting of the nitro group from the benzene ring plane: this twisting of $\sim 40°$ is caused by the steric hindrance of the *o*-methyl group.[4,31-40]

The second I_v of 2,4-dimethylnitrobenzene should be greater than that of 2,6-dimethylnitrobenzene according to the first-order perturbation theory but the reverse tendency was observed. This is also explained by the decreasing conjugation between the benzene $e_{1g}(S)$-like π orbital and the b_1 type vacant π orbital of the nitro group because of the additional twisting[40] of the nitro group from the benzene ring plane caused by the presence of two *o*-methyl groups.

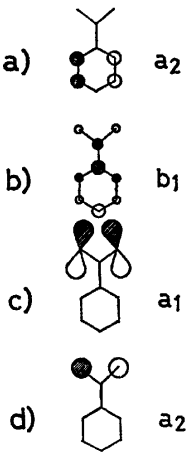

Fig. 11. Schematic representation of the higher occupied molecular orbitals of nitrobenzene.

TABLE 6. CLASSIFICATION OF SUBSTITUENT GROUPS

Character of substituent group	Case	Character of the H.O.[a]	Example
Electron donating	1	Mainly n	$-N(CH_3)_2$
	2	Mainly $e_{1g}(S)\pi$	$-NH_2$, $-OH$, $-OCH_3$
Electron accepting	3	$e_{1g}(S)\pi+S\pi$ (occupied)	$-CN$, $-COCH_3$
	4	$e_{1g}(A)\pi$	$-NO_2$

a) H.O. means the highest occupied orbital of a substituted benzene molecule, n the highest occupied nonbonding orbital of an electron-donating group, and $S\pi$(occupied) the highest occupied π orbital of an electron-accepting group.

PES of Substituted Benzenes and Classification of Substituent Groups. From the above discussion on the PES of substituted benzenes, the substituent groups under consideration can be classified into four categories as shown in Table 6.

Substituted benzenes with such electron-donating groups as OH, OCH_3, NH_2, and $N(CH_3)_2$ have lower first ionization potentials than benzene, because of the increasing electron density on the benzene ring. These substituent groups are divided into two cases, cases 1 and 2, in terms of the nature of the highest occupied MO's of substituted benzenes which are mainly constructed by the mixing of the highest occupied ($e_{1g}(S)$) MO of the ring with the highest occupied n orbital of the substituent group. Two cases are separated by the relative height of the e_{1g} MO to the n orbital. In case 1, the latter is located above the former and the highest occupied and third highest occupied MO's of the substituted benzenes are mainly contributed by the n orbital and the $e_{1g}(S)$ MO, respectively. In case 2, the reverse is the case concerning the relative height of the e_{1g} MO to the n orbital and also concerning the nature of the highest occupied and third highest occupied MO's.

Substituted benzenes with such electron-accepting groups as CN, $COCH_3$, and NO_2 have larger first π ionization potentials than benzene, because of the

decreasing electron density on the ring. From the consideration of the nature of their highest occupied π MO's, the electron-accepting groups are divided into two cases, cases 3 and 4.

In case 3, the highest occupied $e_{1g}(S)$ MO of the ring interacts mainly with the occupied π orbital of the substituent group and, therefore, both orbitals contribute to the highest occupied π orbital of the substituted benzene molecule. On the other hand, in case 4, the $e_{1g}(S)$ MO of the ring interacts mainly with the lowest vacant π orbital of the substituent group and the MO of the substituted benzene molecule obtained by this interaction is the second highest occupied MO: the highest occupied MO in this case is of the ring $e_{1g}(A)$ type.

The authors wish to thank Mr. Katsuyuki Yokota for his skillful assistance in the preparation of 2,4- and 2,6-dimethylanisoles. Their thanks are also due to Mr. H. Matsumoto, Japan Spectroscopic Co. for his kindness in putting the Jasco Model PE-1 spectrometer at their disposal at the initial stage of the present study.

References and Notes

1) D. W. Turner, C. Baker, A. D. Baker, and C. R. Brundle, "Molecular Photoelectron Spectroscopy," John Wiley and Sons, London (1970).
2) T. Kobayashi, K. Yokota, and S. Nagakura, *J. Electron Spectrosc.*, **3**, 449 (1973).
3) T. Kobayashi and S. Nagakura, *Chem. Lett.*, **1972**, 1013.
4) T. Kobayashi and S. Nagakura, *Chem. Lett.*, **1972**, 903.
5) A. D. Baker, D. P. May, and D. W. Turner, *J. Chem. Soc., B*, **1968**, 22.
6) M. J. S. Dewar and S. D. Worley, *J. Chem. Phys.*, **50**, 654 (1969).
7) H. Bock, G. Wagner, and J. Kroner, *Tetrahedron Lett.*, **1971**, 3713.
8) J. W. Rabalais, *J. Chem. Phys.*, **57**, 960 (1972).
9) J. W. Rabalais and R. J. Colton, *J. Electron Spectrosc.*, **1**, 83 (1972).
10) T. P. Debies and J. W. Rabalais, *ibid.*, **1**. 355 (1973).
11) J. P. Maier and D. W. Turner, *J. Chem. Soc. Faraday II*, **69**, 521 (1973).
12) G. S. Hiers and F. D. Hager, "Organic Syntheses," Coll. Vol. I, p. 58 (1956).
13) J. A. Pople and G. A. Segal, *J. Chem. Phys.*, **44**, 3289 (1966).
14) R. Hoffmann, *J. Chem. Phys.*, **39**, 1397 (1963).
15) L. V. Vilkov and T. P. Timasheva, *Dokl. Akad. Nauk S.S.S.R.*, **161**, 351 (1965).
16) "Interatomic Distances," Sp. Pub. No. 11, ed. by L. E. Sutton, The Chem. Soc., London (1958).
17) "Interatomic Distances," Sp. Pub. No. 18, ed. by L. E. Sutton, The Chem. Soc., London (1965).
18) A. B. Cornford, D. C. Frost, F. G. Herring, and C. A. McDowell, *Can. J. Chem.*, **49**, 1135 (1971).
19) E. Heilbronner, V. Hornung, F. H. Pinkerton, and S. F. Thames, *Helv. Chim. Acta*, **55**, 289 (1972).
20) I. Fischer, *Nature*, **165**, 239 (1950).
21) B. M. Wepster, *Rec. Trav. Chim. Pays-Bas*, **76**, 357 (1957).
22) H. B. Klevens and J. R. Platt, *J. Amer. Chem. Soc.*, **71**, 1714 (1949).
23) J. Burgers, M. A. Hoefnagel, P. E. Verkade, H. Visser, and B. M. Wepster, *Rec. Trav. Chim. Pays-Bas*, **77**, 491 (1958).
24) T. Koopmans, *Physica*, **1**, 104 (1934).
25) M. B. Robin and N. A. Kuebler, *J. Electron Spectrosc.*, **1**, 13 (1972).
26) S. Cradock and R. A. Whiteford, *J. Chem. Soc. Faraday II*, **68**, 281 (1972).
27) E. R. Clark and S. G. Williams, *J. Chem. Soc., B*, **1967**, 859.
28) M. J. Aroney, M. G. Cornfield, and R. J. W. Le Fèvre, *J. Chem. Soc.*, **1964**, 2554.
29) C. R. Brundle, M. B. Robin, N. A. Kuebler, and H. Basch, *J. Amer. Chem. Soc.*, **94**, 1451 (1972).
30) In view of the π electron attracting ability of the nitro group, we can understand the general tendency that the bands of nitromethane shift toward the lower energy side in nitrobenzenes. The CNDO/2 calculation predicts[4] that the first two bands of nitromethane may be assigned to the inoizations from the $a_2\pi$ orbital which has nonbonding character and a_1n orbital which is built by bonding type combination of the oxygen n orbitals.
31) H. Kofod, L. E. Sutton, P. E. Verkade, and B. M. Wepster, *Rec. Trav. Chim. Pays-Bas*, **78**, 790 (1959).
32) W. R. Remington, *J. Amer. Chem. Soc.*, **67**, 1838 (1945).
33) W. G. Brown and H. Reagan, *ibid.*, **69**, 1032 (1947).
34) B. M. Wepster, *Rec. Trav. Chim. Pays-Bas*, **76**, 335 (1957).
35) W. F. Forbes, *Can. J. Chem.*, **36**, 1350 (1958).
36) S. Nagakura, M. Kojima, and Y. Maruyama, *J. Mol. Spectrosc.*, **13**, 174 (1964).
37) C. P. Conduit, *J. Chem. Soc.*, **1959**, 3273.
38) A. Van Veen, P. E. Verkade, and B. M. Wepster, *Rec. Trav. Chim. Pays-Bas*, **76**, 801 (1957).
39) P. C. Lauterbur, *J. Chem. Phys.*, **38**, 1432 (1963).
40) J. Trotter, *Acta Crystallogr.*, **12**, 605 (1959).

Formation of Long-Lived Highly-Excited States of H, C, and N Atoms by Low-Energy Electron Impact on CH_3CN

Takemasa SHIBATA, Tsutomu FUKUYAMA, and Kozo KUCHITSU

Department of Chemistry, Faculty of Science, The University of Tokyo, Hongo, Bunkyo-ku, Tokyo 113

(Received May 8, 1974)

Long-lived excited states of hydrogen, carbon and nitrogen atoms (H**, C** and N**) produced by the electron bombardment of CH_3CN in the energy range from 20 to 100 eV were detected as H^+, C^+ and N^+ ions as a result of collisions with H_2O. The appearance potential of H^+ was observed to be about 3 eV lower than the threshold energy for He^+ formed from He** with H_2O (about 24.6 eV). The C^+ threshold energy was about the same as that for He^+, while that for N^+ appeared to be a few eV higher. This suggests that the H** species is mainly responsible for the formation of CH_3CN^- due to the electron bombardment of CH_3CN observed by Sugiura and Arakawa, at least in the energy region below the He** threshold energy.

Since the formation of long-lived highly-excited Rydberg states of atoms by electron impact was first observed by Čermák and Herman,[1] a number of investigations have been made on the formation mechanism and on the collision of such atoms with molecules.[2–6] The following three types of ionization processes of highly excited atoms (A**) in collisions with molecules (B or BC) are known:

$$A^{**} + B \longrightarrow A^+ + B + e \quad (1)$$

$$A^{**} + B \longrightarrow A^+ + B^- \quad (2)$$

$$A^{**} + BC \longrightarrow A^+ + B + C^- \quad (3)$$

The cross sections of these reactions have been estimated theoretically by Matsuzawa[7–9] and compared with experimental results.[4]

Recently, Sugiura and Arakawa[10] have observed the formation of a negative ion, CH_3CN^-, in a mixture of CH_3CN vapor and various rare gases by electron impact. They ascribed the formation of this ion to the reactions:

$$e + A \longrightarrow A^{**} + e \quad (4)$$

$$A^{**} + CH_3CN \longrightarrow A^+ + CH_3CN^-, \quad (5)$$

where A represents a He, Ne, Ar or Kr atom. This is an example of a reaction of type (2). Furthermore, they found that the CH_3CN^- ion was also produced from pure CH_3CN and that the CH_3CN^- intensity exhibited a second-order dependence with the gas pressure. Hence, they considered that the negative ion formation was due to the reactions:

$$e + CH_3CN \longrightarrow Y^{**} + Z + e \quad (6)$$

$$Y^{**} + CH_3CN \longrightarrow Y^+ + CH_3CN^-, \quad (7)$$

where Y** denotes an excited neutral fragment formed by the excitation of the electron to a high Rydberg state. The appearance threshold of CH_3CN^- was estimated to be 23.2±0.5 eV.

In the present study, the formation of the highly excited atoms, H**, C** and N**, from CH_3CN by the bombardment of electrons of 20—100 eV is reported. Among the three excited species, H** appeared at the lowest electron impact energy, while C** had nearly the same threshold energy as that of He**.

Experimental

The apparatus, which was described previously,[11,12] was evacuated to 2×10^{-6} Torr. The CH_3CN vapor was introduced into the excitation region (Fig. 1) through a multichannel orifice M and was subjected to electron impact. The total pressure of the vapor at the source S_1 was about 0.3 Torr. The filament was heated by a dc current of 6A operated at 5 V, and the electrons produced were accelerated by a voltage of from 20 to 100 V which was applied between the filament (measured at the low potential end) and electrode 3 in Fig. 1. The electron current measured at electrode 1 was 10—300 μA. The excited neutral species were separated from the accompanying ions by electrostatic potentials and were allowed to collide with the target H_2O molecules in the collision chamber C. The pressure of the H_2O target gas measured at the source S_2 was about 1 Torr. The ions produced in the collision chamber were measured by a quadrupole mass filter. The sample gas pressures were measured by oil manometers and Pirani gauges. In addition to H_2O, CH_3CN and CH_3OH were also used as target molecules.

The energy spread of the electrons was estimated to be a few eV. The energy scale was calibrated by measuring the He^+ ions formed under similar conditions from He**, *i.e.*, produced by the reactions:

$$e + He \longrightarrow He^{**} + e \quad (8)$$

$$He^{**} + H_2O \longrightarrow He^+ + H_2O + e \quad (9)$$

The appearance potential of He^+ formed from He** was assumed to be nearly equal to the inoization potential of He^+, 24.6 eV.[13]

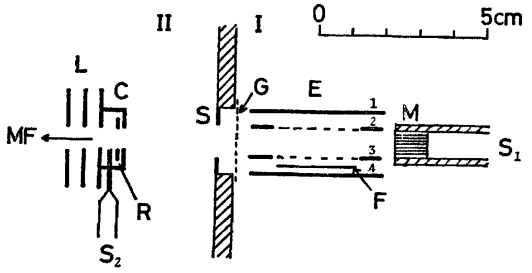

Fig. 1. Apparatus composed of Section I for producing long-lived highly-excited atoms by electron impact and section II, in which a collision chamber C and a mass filter MF are installed.
I: S_1, source of reactant molecules (CH_3CN); M, multichannel orifice; E, electron gun; F, tungsten filament; 1, electron trapping electrode; 2 and 3, exciting region; 4, repeller electrode; G, grid; S, slit. II: S_2, source of target molecule (H_2O); R, ion repeller electrode; L, ion lens system.

Results

The mass spectrum shown in Fig. 2 was obtained with H_2O as the target gas. Since the present study is concerned with the formation and ionization of H**, C** and N**, observed molecular ions, H_2O^+ *etc.*, were not analyzed in detail. The intensities of the H^+, C^+ and N^+ were found to be proportional to the electron current. In Fig. 3 the ion intensities divided by the electron currents are plotted as a function of the accelerating voltage. The intensities of H^+ and N^+ increased monotonically with increasing voltage, while the C^+ intensity curve had a shoulder at about 45 eV. The dependence of the H^+, C^+ and He^+ intensities on the electron accelerating voltage in the threshold region is shown in Fig. 4. The H^+ threshold appears to be about 3 eV lower than that for He^+, while the appearance potential of C^+ is nearly equal to the He^+ threshold.

The dependence of the ion intensities on the pressure of the target H_2O is shown in Fig. 5. The intensity I varies with the pressure p as

$$I \propto p \exp(-cp) \qquad (10)$$

This is demonstrated in Fig. 6, where $\log(I/p)$ values depend linearly on the gas pressure p. As discussed in Refs. 11 and 12, the behavior expressed by Eq. (10) can be accounted for as a result of the attenuation of the highly-excited atoms by collision with H_2O mole-

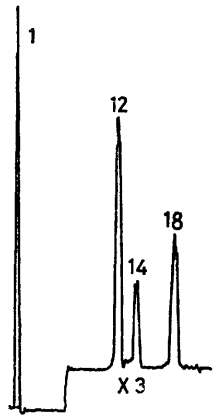

Fig. 2. Mass spectrum of the ions produced by collisions of highly-excited species from CH_3CN with H_2O. Electron accelerating voltage: 60 V, electron trap current: 200 μA, pressures of CH_3CN and H_2O: 0.13 and 0.4 Torr, respectively.

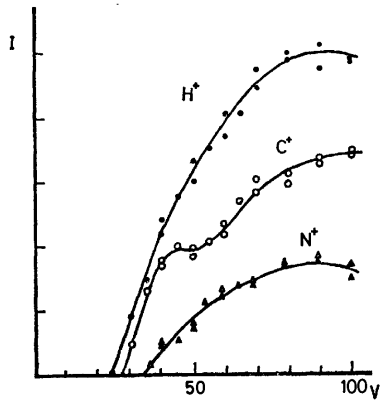

Fig. 3. Intensities of ions (in arbitrary units) divided by the electron trap current obtained for different electron accelerating voltages.

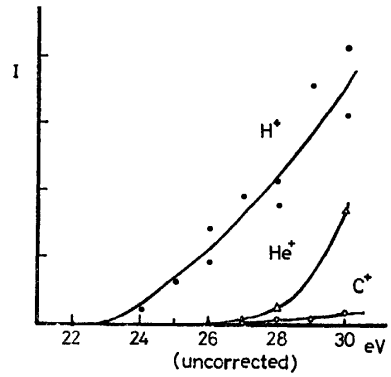

Fig. 4. Ion intensities (in arbitrary units) in the vicinity of threshold obtained for different electron bombardment energies.

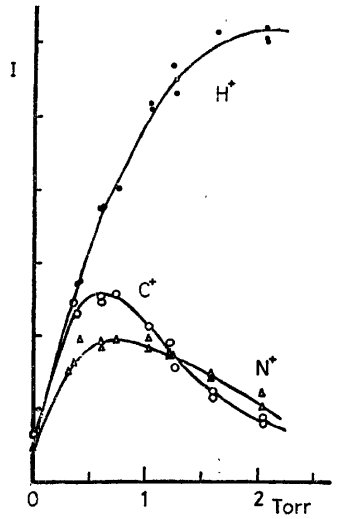

Fig. 5. Intensities of ions (in arbitrary units) plotted for different pressures of H_2O measured at S_2.

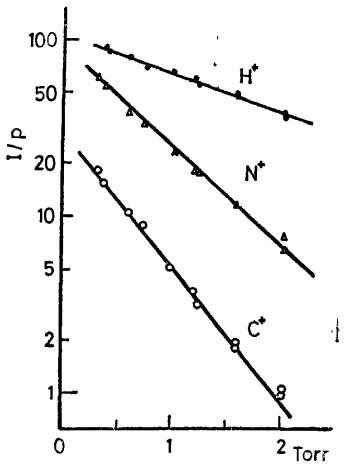

Fig. 6. Intensities of H^+, C^+ and N^+ displayed in Fig. 5 divided by the pressure p of H_2O measured at S_2 and plotted on a logarithmic scale as a function of p.

cules. The ion intensities do not tend to zero in the absence of target molecules, as shown in Fig. 5. This shows that the excited species can be ionized by collisions not only with the target gas but also with residual gases and/or the surface of the electrodes. The ion intensity varies with the pressure of the projectile molecule CH_3CN in a similar manner.

Ionization processes of the highly-excited atoms H**, C** and N** producing H^+, C^+ and N^+, respectively, were also observed when CH_3CN or CH_3OH was used as a target gas. The variations of the ion intensity, I, on the electron current and on the electron accelerating voltage were similar to those observed with H_2O as the target gas. The relation between I and the gas pressure p was also that given in Eq. (10).

Discussion

The uncorrected thresholds of H^+ and C^+ shown in Fig. 4 are shifted by about -1.4 eV with reference to that of He^+, as described in Experimental section, and compared with the appearance threshold of CH_3CN^- observed by Sugiura and Arakawa.[10] One can conclude that the essential part of the Y** species which they assumed in reactions (6) and (7) is H** at least in the range below the threshold of He**, since this species seems to be the only reactive species formed in this electron energy range. The C** and N** species can also contribute to molecular negative-ion formation at higher electron energies.

The threshold energy for H^+, which was thus estimated to be about 21.5 eV with a range of uncertainty of about 1.5 eV, seems to differ slightly from that for CH_3CN^- reported by Sugiura and Arakawa, 23.2 ± 0.5 eV; however, a more precise description of the threshold behavior requires a further critical experiment.

The shoulder appearing in the efficiency curve of C** suggests that the curve is composed of two separate efficiency curves which correspond to the C** species arising from the methyl and the nitrile carbon atoms in CH_3CN.

The authors are indebted to Drs. Toshio Sugiura and Kazuo Arakawa for helpful discussions and to Dr. Walter Shearer-Izumi for his critical reading of the manuscript.

References

1) V. Čermák and Z. Herman, *Coll. Czech. Chem. Comm.*, **29**, 253 (1964).
2) S. E. Kupriyanov, *Zh. Eksper. Teor. Fiz.*, **48**, 467 (1965).
3) S. E. Kupriyanov, *Khim. Vysok. Energii*, **6**, 304 (1972).
4) H. Hotop and A. Niehaus, *J. Chem. Phys.*, **47**, 2506 (1967).
5) R. S. Freund, *ibid.*, **54**, 3125 (1971).
6) K. C. Smyth, J. A. Schiavone, and R. S. Freund, *ibid.*, **59**, 5225 (1973).
7) M. Matsuzawa, *ibid.*, **55**, 2685 (1971).
8) M. Matsuzawa, *J. Phys. Soc. Jap.*, **32**, 1088 (1972).
9) M. Matsuzawa, *ibid.*, **33**, 1108 (1972).
10) T. Sugiura and K. Arakawa, "Recent Developments in Mass Spectroscopy," ed. by K. Ogata and T. Hayakawa, University of Tokyo Press, Tokyo (1970) p. 848.
11) T. Shibata, T. Fukuyama, and K. Kuchitsu, *Shitsuryo Bunseki*, **21**, 217 (1973).
12) T. Shibata, T. Fukuyama, and K. Kuchitsu, *Chem. Lett.*, **1974**, 75.
13) C. E. Moore, "Atomic Energy Levels," N. B. S. Circ. 467, Vol. I (1949).

Spectroscopic Studies on Some Ketimines

R. ABU-EITTAH and M. M. HAMED
Department of Chemistry, Faculty of Science, University of Cairo, Giza, Egypt
(Received June 20, 1973)

The electronic absorption spectra of some ketimines have been investigated using different solvents. Assignment of the obtained transitions was attempted. The *N*-substituted ketimines did not show a discrete band for the n—π^* transition as was obtained with the unsubstituted molecules. Molecular orbital calculations were carried out using the PPP variant of the SCF-MO theory. Agreement between the calculated and experimental transition energies was satisfactory.

The spectra of the ketimines are rarely found in the literature, though the spectra of the related compounds, anils or Schiff's bases, are common.[1] Kaplan[2] reported the spectra of some 4-alkyldiphenylketimine hydrochlorides. It was found that the unconjugated azomethine chromophore absorbs at higher energy than the corresponding carbonyl and thiocarbonyl chromophores.[3] The n→π^* transition for the >C=N– group is allowed but is symmetry forbidden for the carbonyls and thiocarbonyls.

Ultraviolet spectra of *N*-(diphenylmethylene) aniline were reported in different solvents.[4] The spectra of benzanils were found to be, essentially, a superposition of the spectra of the corresponding benzal and aniline parts of the molecule,[5] the azomethine group acted as an electron acceptor when linked to a phenyl group at its end.

Alexander *et al.*[6] investigated the solvent effects on the absorption spectra of *o*-, *m*-, and *p*-hydroxybenzylidenimines. Ebara[7] showed that the spectra of benzylideneanilines cannot be explained adopting the stilbene-type planar structure.

Different studies on some ketimines as ESR,[8] rate of hydrolysis,[9] complex formation with Cu(II) ion[10] and infrared spectra[11,12] are reported in the literature. Semi-empirical molecular orbital calculations were carried out on benzalaniline and some imines.[13,14]

In this work the spectroscopic behaviour of a series of ketimines, including halo and nitro ketimines, is investigated. Bands were assigned to transitions characteristic of specific chromophores in the molecules. To be more accurate, the extended PPP method of the SCF-MO theory was used to compute the energy of the lowest π→π^* transition.

Experimental

Solvents. Methanol and cyclohexane were purified by the conventional methods found in the literature.[15]

Compounds. 1,1-Diphenylmethylenimine was prepared by Grignard reaction between freshly distilled bromobenzene and phenylcyanide, where the complex was decomposed by absolute methanol.[16] The product was purified by vacuum distillation, n_D^{19} 1.6191. The other ketimines were prepared by condensing benzophenone and the corresponding aniline derivative till the calculated volume of water was collected.[17] Compounds were purified by repetitive crystallization. The compounds prepared were: *N*-(diphenylmethylene)aniline; *N*-(diphenylmethylene)-*ortho*-, *meta*-, and *para*-chloroanilines; *N*-(diphenylmethylene)-*p*-bromoaniline; *N*-(diphenylmethylene)-*ortho*-, *meta*-, and *para*-nitroanilines; *N*-(diphenylmethylene) *p*-methoxyaniline.

Melting points corresponded well to values reported in literature.

Apparatus. Spectra were scanned on a Beckmann DK-1 spectrophotometer using 1.0 cm fused silica cells.

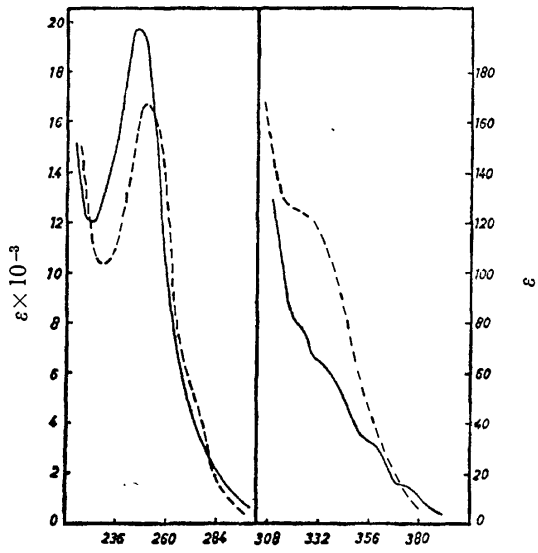

Fig. 1. Absorption spectra of 1,1-diphenylmethylenimine at room temperature.
—— in cyclohexane, ---- in methyl alcohol

Results and Discussion

Electronic Absorption Spectra. 1,1-Diphenylmethylenimine, N-*Phenyl and* p-*Methoxy Derivatives*: Figure 1 shows the absorption spectra of 1,1-diphenylmethylenimine (a) in polar and non-polar solvents. The extent of molecular coplanarity will be clearly reflected in its spectrum. If the distortion is maximum *i.e.*, the two benzene nuclei are perpendicular, the spectrum will be similar to that of *N*-benzylimine whereas if the distortion is slight the spectrum will be different than that of *N*-benzylimine. In benzophenone Jones[18] calculated 30° as the angle between the planes of the

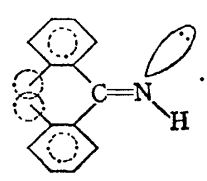

(a)

two benzene rings.

1,1-Diphenylmethylenimine is "π" isoelectronic with 1,1-diphenylethylene *i.e.* the $\pi \rightarrow \pi^*$ transitions of both compounds are expected to be energetically comparable. Korver[19] assigned the 260 nm band of 1,1-diphenylethylene to "styrene-conjugation" and the band around 230 nm to "phenyl-phenyl" interaction. Styrene[20] has O→O transition at ~290 nm, the blue shift of the O→O transition of 1,1-diphenylethylene is a result of steric hindrance.

The spectrum of 1,1-diphenylmethylenimine shows a weak shoulder (ε_{max}=65 in cyclohexane and 120 in methyl alcohol) at 332 nm in cyclohexane and at 323 nm in alcohol. The band shows a blue-shift in a polar solvent, and characteristic vibrational structures which are blurred in methanol, thus it may be assigned to an $n \rightarrow \pi^*$ transition. It was shown that 1,1-diphenylmethylenimine forms an n-σ charge transfer complex with iodine[21] which also supports this assignment.

In the UV region, 1,1-diphenylmethylenimine shows an intense assymetric band, with λ_{max} at 245 nm and a shoulder ~270 nm. The long wavelength shoulder is assigned to a transition corresponding to the $^1b_{2u} \leftarrow {}^1a_{1g}$ transition of benzene whereas the intense band is assigned to an intramolecular charge transfer transition. The donor site is a benzene nucleus, conjugated with the "π" system of the azomethine group, and the acceptor site is a free π-molecular orbital on the azomethine group. Evidences supporting this assignment will follow. The above way of transitions assignment is an approximate one, since with it, one is bisecting the same molecule to discrete chromophores. However, this approximation is not a crude one, especially if the separate chromophores are not coplanar.

Figure 2 shows the spectra of *N*-(diphenylmethylene)-aniline (b). The position and intensity of band maxima, in Figs. 1 and 2, are very much comparable. This

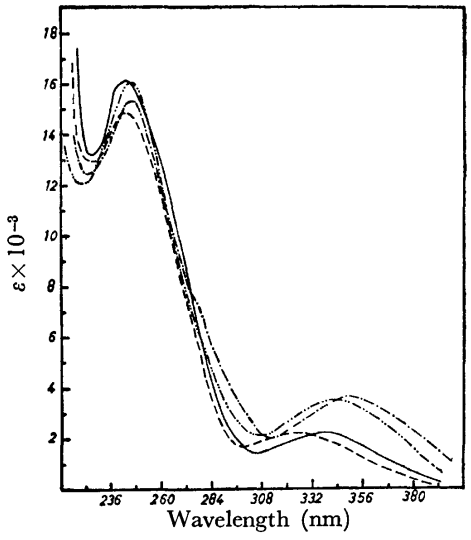

Fig. 2. Absorption spectra of *N*-(diphenylmethylene)-aniline.
—— in cyclohexane, ----- in methyl alcohol *N*-(diphenylmethylene)-*p*-methoxyaniline
-·-·- in cyclohexane, -·-·-·- in methyl alcohol at room temperature

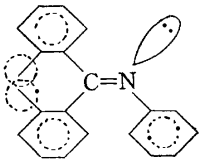

(b)

indicates that the π system of the *N*-phenyl ring is not conjugated with the π system of the >C=N– group and may be conjugated with "n" electrons on the nitrogen atom. If this is so, an $n \rightarrow \pi^*$ transition may overlap with the $\pi \rightarrow \pi^*$ band. The bands shown in Fig. 2 are all $\pi \rightarrow \pi^*$ transitions, the 338 nm band may correspond to the intense "a" band of stilbene.[22] The significant reduction of intensity is attributed to the non-coplanarity of the molecule. The 242 nm is assigned to an intramolecular charge transfer transition.

To confirm the above results, the spectra of *N*-(diphenylmethylene) *p*-methoxyaniline were investigated (Fig. 2). If "π" conjugation extends over the whole molecule, the $-OCH_3$ group will perturb all the π—π^* transitions, otherwise it will merely perturb the transitions localized on the benzene nucleus attached to it. Investigation of Fig. 2 indicates that the long wavelength band has been significantly red shifted and intensified on substitution by the $-OCH_3$ group whereas perturbation of the other transitions (at ~270 and 245 nm) is only slight. These results confirm that: the long wavelength transition is localized over the *N*-phenyl ring the "π" system of which is not in the same plane as the "π" system of the azomethine group. This is also confirmed by the fact that the band, ~245 nm, assigned to a charge transfer transition was not perturbed by $-OCH_3$ substitution. That is to say, the donor site is the same before and after $-OCH_3$ substitution. Anisole is of lower ionization potential than benzene, and if it were the donor, the energy of the charge transfer band would have been lowered than its value when benzene is the donor. In *N*-(diphenylmethylene) *p*-methoxyaniline, the anisole nucleus is not the donor, since its "π" system is not in the same plane as that of the acceptor site (C=N–). In Table 1 the values of the band maxima, molar extinction coefficient and oscillator strengths for the above molecules are given.

Table 1. Numerical values of the band maxima, molar extinction coefficients and the oscillator strengths of the absorption bands of some ketimines in cyclohexane

Compound	λ_{max} (nm)	ε_{max}	$f \times 10^3$
1,1-Diphenylmethylenimine	332	65	0.95
	~270*	3297	—
	245	19800	456
N-(Diphenylmethylene)-aniline	338	2160	61
	~270*	8000	—
	242	16100	523
N-(Diphenylmethylene)-*p*-Methoxyaniline	350	3659	103
	~270*	8000	—
	245	15300	760

* Shoulder.

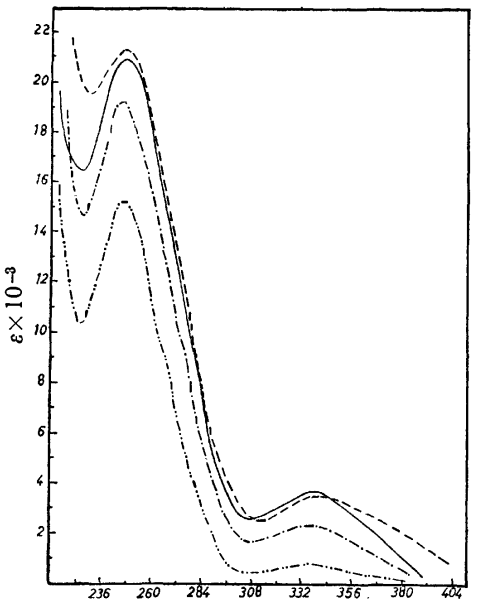

Fig. 3. Absorption spectra.
------ *N*-(diphenylmethylene) *o*-chloroaniline
-·-·- *N*-(diphenylmethylene) *m*-chloroaniline
----- *N*-(diphenylmethylene) *p*-chloroaniline
—— *N*-(diphenylmethylene) *p*-bromoaniline
in cyclohexane at room temperature

Halogenated Ketimines: Figure 3 shows the absorption spectra of *N*-(diphenylmethylene) *o*-chloroaniline in addition to the *meta* and *para* derivatives in cyclohexane. When the spectra were scanned in methanol, the long wavelength transition was slightly blue-shifted whereas the ~245 nm transition was red-shifted. The spectra are very much similar to those given in Figs. 1 and 2 indicating that the same types of electronic transitions are occurring. Chlorine substitution in the *N*-phenyl ring perturbed, mainly, the long wavelength transtion. This behaviour was also encountered with $-OCH_3$ substitution. Bands of the halogenated ketimines are assigned in a way similar to that of the previously studied ketimines. Bands of the *o*-chloro derivative are of lower intensity than those of the other, halo derivatives owing to steric hindrance in the former.

To confirm the above results the spectra of *N*-(diphenylmethylene) *p*-bromoaniline were studied (Fig. 3). Spectra of the *p*-chloro and *p*-bromo derivatives are very similar, yet one notices that though ionization potential of chlorobenzene differs from that of bromobenzene the band (248 nm) assigned to a charge transfer transition has the same λ_{max} for the two compounds. This indicates that the donor site is a benzene nucleus rather than the bromo or chlorobenzene nuclei. Rationalization of this point was given before. Numerical values of band maxima, molar extinction coefficients and oscillator strengths (Gaussian analysis was made to clarify the shape of the band and estimate its half width) of the absorption bands of halogenated derivatives are given in Table 2.

Nitroketimines: To investigate fairly the spectral properties of ketimines, the spectra of the nitro derivatives were studied. Figure 4 shows the spectrum of *N*-(diphenylmethylene) *o*-nitroaniline which is quite similar to that of *N*-(diphenylmethylene) aniline. This indicates that "π" conjugation does not extend over the >C=N– group and the nitrobenzene nucleus. Here again the nitro group, mainly, perturbed the long wavelength transition. The spectra of *p*-nitroketimine (Fig. 4) indicate many overlapping bands. More than one charge transfer transition can be obtained with this molecule and this reflects the large solvent effect on its spectra. In fact, *p*-nitroaniline possesses a symmetric charge transfer transition with an energy of 3.9 eV. The *p*-nitroketimine has a shoulder at —340 nm (3.6 eV), which appears more clearly in cyclo-

TABLE 2. NUMERICAL VALUES OF THE BAND MAXIMA, THEIR MOLAR EXTINCTION COEFFICIENTS AND THE OSCILLATOR STRENGTHS OF THE ABSORPTION BANDS OF HALOGENATED DERIVATIVES IN CYCLOHEXANE

Compound	λ_{max} (nm)	ε_{max}	$f\times10^3$
N-(Diphenylmethylene) *o*-chloroaniline	338	790	25
	~270*	6300	—
	246	15400	536
N-(Diphenylmethylene) *m*-chloroaniline	335	3200	57
	~270*	9700	—
	245	19200	711
N-(Diphenylmethylene) *p*-chloroaniline	338	2900	93
	~270*	8700	—
	248	17200	775
N-(Diphenylmethylene) *p*-bromoaniline	338	3700	100
	~270*	10800	—
	248	20800	949

* Shoulder.

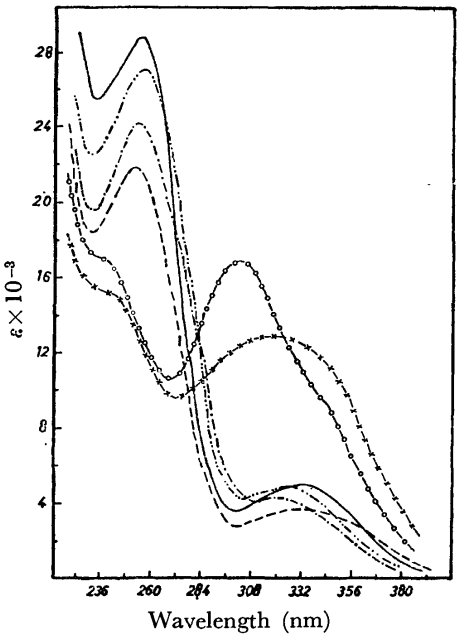

Fig. 4. Absorption spectra of *N*-(diphenylmethylene)-*o*-nitroaniline
—— in cyclohexane, ----- in methyl alcohol *N*-(diphenylmethylene) *m*-nitroaniline
------ in cyclohexane, ·---· in methyl alcohol *N*-(diphenylmethylene) *p*-nitroaniline
–o– in cyclohexane, –×– in methyl alcohol at room temperature

hexane, could very well be assigned to a charge transfer transition.

Figure 4 shows that the *ortho-* and *meta*-nitroketimines have similar spectra to each other which differ from that of the *para*-isomer. Moreover, the *para*-isomer has its first absorption maximum at a higher energy than those of the *ortho-* and *meta*-derivatives. The same results are found on investigating the spectra of nitroanilines. Resonance theory predicts that the *ortho-* and *para*-isomers should have similar spectra that differ from that of the *meta*-isomer. Godfrey and Murrell[23] calculated the energies of the first four transitions for *ortho-*, *meta-*, and *para*-nitroanilines using the localized-orbital model. Transitions were differentiated to locally-excited and charge-transfer ones. They found that the amino group *para-* to the nitro-group lowers the energy of the first charge transfer state but will have no effect on the energy of the second charge transfer state. On the other hand an amino-group *ortho-* or *meta-* to the nitro-group lowers the energy of the second charge transfer state three times as it does to the first charge transfer state. This goes along with experimental results.

The spectra of nitroketimines are comparable to those of nitroanilines and the lone pair of electrons on the nitrogen azomethine group will play the same role as that of the amino group in nitroanilines. Similarity of the spectra of the *ortho-* and *meta*-nitroketimines and their deviation from that of the *para* isomer are due to the lowering of the energy of the charge transfer states to different extents in the different isomers.

Localized-orbital model bisects the molecule to discrete chromophores, namely donor and acceptor,transition energies are better computed when the molecule is treated as one unit. Molecular orbital calculations were performed on 1,1-diphenylmethylenimine using the PPP[24] variant of the SCF-MO theory to investigate correspondence between the theoretical and experimental values of the energy of the first transition and to investigate how far the coplanarity of the molecule is distorted. The computed value of the energy of the first transition was found to be 4.2 eV (experimental value is 4.4 eV). The semi-empirical method of calculation accounted satisfactorily for the transition energy and showed that coplanarity of the molecule is not highly distorted. Table 3 gives the values of band maxima for the studied nitro derivatives.

Table 3. Numerical values of band maxima, molar extinction coefficients and oscillator strengths of studied nitro derivatives in cyclohexane

Compound	λ_{max} (nm)	ε_{max}	$f \times 10^3$
N-(Diphenylmethylene) *o*-Nitroaniline	332	5100	157
	~270*	15100	—
	251	28900	997
N-(Diphenylmethylene) *m*-Nitroaniline	326	4900	126
	~270*	14200	—
	257	27000	1236
N-(Diphenylmethylene) *p*-Nitroaniline	~340	9500	—
	302	17000	643
	~240*	17000	—

* Shoulder.

References

1) P. Nagy, *Szegedi Pedagog Foiskola Evkonyve*, **11**, 185 (1961); *Chem. Abstr.*, **60**, 125a (1964).
2) I. R. Kaplan, H. N. Parton, and J. Vanghan, *J. Amer. Chem. Soc.*, **75**, 4341 (1953).
3) J. J. Worman, G. L. Pool, and W. P. Jensen, *J. Chem. Educ.*, **47**, 709 (1970).
4) T. Kubota, M. Yamakawa, and Y. Mori, This Bulletin, **36**, 1552 (1963).
5) M. A. El-Bayoumi, M. El-Aasser, and F. A Halim, *J. Amer. Chem. Soc.*, **93**, 590 (1971).
6) P. W Alexander and R. J. Sleet, *Aust. J. Chem.*, **23**, 1183 (1970)
7) N. Ebara, This Bulletin, **33**, 534 (1960).
8) N. Toshima, H. Hirai, and S. Makishima, *Kogyo Kagaku Zasshi*, **72**, 184 (1969); *Chem. Abstr.*, **70**, 114378e, (1969).
9) J. B. Culbertson, *J. Amer. Chem. Soc.*, **73**, 4818 (1951).
10) A. Misono, T. Osa, and S. Koda, This Bulletin, **41**, 373 (1968).
11) P. L. Pickard and G. W. Polly, *J. Amer. Chem. Soc.*, **76**, 5169 (1954).
12) A. Perrier-Datin and M. L. Josien, *C. R. Acad. Sci. Paris*, **266**, 266 (1968).
13) G. Hohlneicher and W. Saenger, Quantum Aspects Heterocycl. Compounds Chem. Biochem., Proc. Int. Symp., 2nd. 1969 (Pub. 1970) 193, *Chem. Abstr.*, **75**, 124496j (1971).
14) D. R. Salahnb, *Theor. Chim. Acta*, **22**, 330 (1971).
15) A. I. Vogel, "Practical Organic Chemistry" Longmans, London (1956) 3rd. Ed.
16) P. L. Pickard and T. L. Tolbert, *J. Org. Chem.*, **26**, 4886 (1961).
17) A. W. Weston and R. J. Michaels, Jr., *J. Amer. Chem. Soc.*, **73**, 1381 (1951).
18) R. N. Jones, *ibid.*, **67**, 2127 (1945).
19) O. Korver, J. U. Veenland, and Th. J. de Boer, *Rec. Trav. Chim.*, **84**, 806 (1965).
20) W. W. Robertson, J. F. Music, and F. A. Matsen, *J. Amer. Chem. Soc.*, **72**, 5260 (1950).
21) R. Abu-Eittah and M. M. Hamed, This Bulletin, under publication.
22) H. Suzuki, *ibid.*, **33**, 381 (1960).
23) M. Godfrey and J. N. Murrell, *Proc. Roy. Soc. Ser. A*, **278**, 71 (1964).
24) J. A. Pople, *Proc. Phys. Soc., A*, **68**, 81 (1955).

Polarographic Behavior of Glycol Dimercaptoacetate

R. S SAXENA and S. K. BHATIA
Department of Chemistry, Malaviya Regional Engineering College, Jaipur, India
(Received November 20, 1973)

Polarographic behaviour of glycol dimercaptoacetate has been studied in 25% ethanol at d.m.e. in the pH range 1.56—11.56 in presence of 0.1 M KNO_3. In the acidic media, the current-voltage curves consist of three waves; a prewave due to the adsorption of anodic reaction product at the mercury drop surface, main anodic wave due to the electroxidation of -SH groups and a third wave at more positive potential due to the insoluble film formation on the electrode surface whose solubility depends on pH of the solution. In the alkaline media only two waves, a prewave and the main anodic wave, are observed. The effects of various factors such as different buffer, Hg-pressure, temperature, ethanol and depolarizer concentrations on the wave characteristics have been investigated. The electrode reaction is irreversible at higher pH but in acid media it is reversible and diffusion controlled involving a two electron transfer process, with the formation of $\begin{matrix}H_2COOCCH_2\text{-}S\\ \quad\quad\quad\

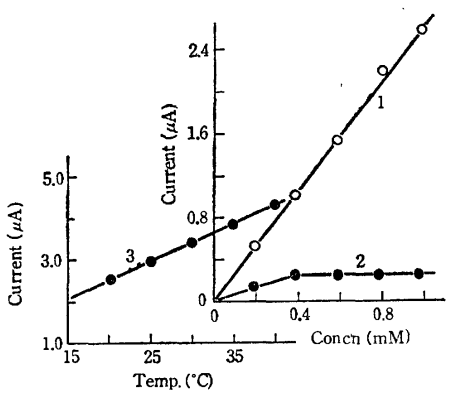

Fig. 2. Curve 1: Plot of i_d *vs.* [GDA], Curve 2: Plot of i_1 *vs.* [GDA], Curve 3: Plot of i_d *vs.* Temp.

the prewave, i_1, increases with [GDA] up to 0.4 mM above which it remains almost constant while i_2, i_3, and i_d vary linearly with [GDA] (0.2 to 1 mM). The mean values of diffusion current constant ($I=i_d/cm^{2/3}\cdot t^{1/6}$) and diffusion coefficient are 3.406 μA/mM/l/$mg^{2/3}\cdot s^{-1/2}$ and 6.60×10^{-6} cm^2/s respectively. These observations substantiate the diffusion controlled nature of the waves.

The total diffusion current (i_d) decreases with increase in ethanol percentage passing through a minimum in between 40—50% and then increases but the nature of the main wave remains the same.

Effect of $HgCl_2$ on Main Anodic Wave. Solutions containing GDA and $HgCl_2$ in proportions of 1:0, 1:0.5, and 1:1 were prepared. The insoluble mercury complex was removed by filtration and the filtrates were polarographed under identical conditions. In presence of increasing amounts of $HgCl_2$ the main anodic wave with decreased wave height was obtained; it disappeared completely, when GDA and $HgCl_2$ was present in 1:1 ratio. This shows the formation of 1:1 complex of GDA with Hg(II).

Mechanism of the Electrode Reaction. The electrooxidation of GDA (referred here as $R(SH)_2$) may involve (A) the formation of a disulphide, a four electron transfer Process (1) and (B) the formation of a mercuric-complex, a two electron transfer Process (2)

$$2R(SH)_2 \rightleftharpoons R\begin{<}S\text{-}S\\S\text{-}S\end{>}R + 4H^+ + 4e^- \quad (1)$$

$$R(SH)_2 + Hg \rightleftharpoons R\begin{<}S\\S\end{>}Hg + 2H^+ + 2e \quad (2)$$

Then the potential at every point on the wave should be given by

$$E = \text{Const.} - \frac{RT}{4F}\ln\frac{(i_d-i)^2}{i} \quad \text{(for reaction A)} \quad (3)$$

and

$$E = \text{Const.} - \frac{RT}{2F}\ln\frac{i_d-i}{i} \quad \text{(for reaction B)} \quad (4)$$

If the formation of a disulphide is involved (1), then the plot of $-E_{de}$ *vs.* $\log(i_d-i)^2/i$ should yield a straight line with slope 0.059/4 V. On the other hand, if Reaction (2) is involved, the plot of $-E_{de}$ *vs.* $\log i_d-i/i$ gives a straight line having a slope of 0.059/2 V.

It is observed that only the analysis corresponding to Eq. (4) yields a straight line with a slope of 0.031 V close enough to the theoretical slope of 0.029 V. Furthermore, it was found that the $E_{1/2}$ of the main wave was independent of [GDA]. This constancy of $E_{1/2}$ is characteristic of Eq. (4) and not of Eq. (3). This analysis indicates that the anodic reaction of GDA at d.m.e. occurs according to (2) and not to the formation of a disulphide.

If the reaction is reversible, then the mercury in the mercuric-GDA complex should be reversibly reducible at d.m.e. But on the contrary, the preceding experiments on the effect of added $HgCl_2$ show that the final product of the electrode reaction is an insoluble complex of mercury. It may, therefore, be concluded that the anodic wave is due to the formation of mercurous mercaptide $R\begin{<}S\text{-}Hg\\S\text{-}Hg\end{>}$ (soluble compound) which is unstable and changes into more stable mercuric complex and Hg.

$$R\begin{<}S\text{-}Hg\\S\text{-}Hg\end{>} \longrightarrow R\begin{<}S\\S\end{>}Hg + Hg$$

Adsorption Prewave. A steep depression in *E-t* curve was obtained for 1.0 mM GDA and 0.1 M KNO_3 at pH 4.80 in the potential range where the prewave appeared, showing the strong adsorption of the electrolysis product at d.m.e. A general theoretical treatment of adsorption waves (prewave) at the d.m.e. was first described by Brdicka who gave the expression for the average limiting current of the adsorption wave i_p.[9]

$$i_p = 0.85nFZm^{2/3}t^{-1/3} \quad (5)$$

in which i_p is expressed in ampere, Z is the maximum number of moles adsorbed per cm^2, m is the rate of mercury flow in g/s, t is the droptime in s, n and F have their usual significance. From Eq. (5), $Z=6.83\times10^{-10}$ mol/cm^2 *i.e.* 4.12×10^{14} molecule/cm^2 which corresponds to an area of 24.29 $Å^2$ per adsorbed molecule. Adsorption coefficient (ω) and molar adsorption energy (ϕ) are 1.445×10^4 and 31.2 kcal/g·mol, respectively, which are evaluated from the following equations:

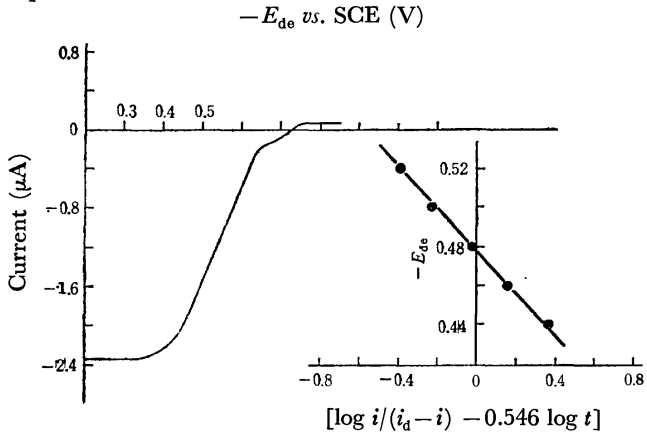

Fig. 3. (a) Polarograms for 1.0 mM GDA at pH= 11.56 (recorded by measureing current at the end of the drop life). (b) Plot of $-E_{de}$ *vs.* [log $i/(i_d-i)$ −0.546 log t]

$$\omega = \frac{2}{C_a} \exp \frac{n\Delta EF}{RT} \quad (6)$$

$$\phi = n\Delta EF + RT \ln \frac{2}{C_a V} \quad (7)$$

Where ΔE stands for the difference in half-wave potentials of the prewave and the main wave at concentration C_a at which adsorption and diffusion currents are equal and V is the molar volume of the particles.

Kinetic Parameters. The values of kinetic parameters are calculated at pH 11.56 from Koutecky's treatment[10] as extended by Meites and Israel.[11] For an irreversible anodic wave it follows:

$$E_{de} = -0.2412 + \frac{0.05915}{(1-\alpha)n} \log \frac{1.349K^{\circ}_{b.h}}{D_o^{1/2}} + \frac{0.0542}{(1-\alpha)n}\left[\log \frac{i}{i_d - i} - 0.546 \log t\right] \quad (8)$$

and

$$E^{\circ}_{1/2} = -0.2412 + \frac{0.05915}{(1-\alpha)n} \log \frac{1.349K^{\circ}_{b.h}}{D_o^{1/2}} \quad (9)$$

The plot of $[\log i/(i_d - i) - 0.546 \log t]$ *vs.* $-E_{de}$ yields a straight line (Fig. 3) whose slope is equated to $0.0542/(1-\alpha)n$ and the value of α is found to be 0.76. The intercept ($E^{\circ}_{1/2}$), obtained from the same plot, is substituted in Eq. (9) and the value of $K_{b,h}{}^{\circ}$ is calculated to be 2.6×10^{-9} cm/s.

The authors are thankful to C.S.I.R., New Delhi for the grant of a research fellowship to one of them (S.K.B.) and to Prof. R. M. Advani, Principal, for providing research facilities.

References

1) R. S. Saxena and U. S. Chaturvedi, *Electrochim. Acta*, **16**, 1107 (1971).
2) R. S. Saxena and K. C. Gupta, *J. Indian Chem. Soc.*, **47**, 101 (1970).
3) R. S. Saxena and Pratap Singh, *Z. Naturforsch.*, **24B**, 1520 (1969).
4) O. Grubner, *Chem. Listy*, **47**, 1133 (1953).
5) R. Zahradnik, *ibid.*, **49**, 1002 (1955).
6) R. Zahradnik, and L. Jensovsky, *ibid.*, **48**, 11 (1954).
7) J. Heyrovsky, "Principles of Polarography," Academic Press, New York (1966), p. 257.
8) M. Brezina and P. Zuman, "Polarography in Medicine, Biochemistry and Pharmacy," Interscience Publishers New York (1958), p. 472.
9) J. Herovsky and J. K. Kuta, "Principles of Polarography," Academic Press, New York (1966), p. 291.
10) L. Meites, "Polarographic Techniques," Interscience Publishers, New York (1965), p. 241.
11) L. Meites and Y. Israel, *J. Amer. Chem. Soc.*, **23**, 2903 (1961).

The Chemistry of α, *N*-Hydroxyamino Acids

Afzal AHMAD

Department of Chemistry, University of Islamabad, P.O. Box No. 1090, Islamabad, Pakistan

(Received February 4, 1974)

α,*N*-Hydroxyamino acids have been shown to be unstable compounds. They disproportionate into corresponding α-amino acids and α-oximino acids below pH 7. This has been suggested to be a general reaction in all mono-substituted hydroxylamines.

The chemistry of naturally occurring α-amino acids is well established and their biochemical importance is fully understood. Not enough is known, however, about the chemical behaviour of analogous *N*-hydroxyamino acids, which are now found to be present as parts of several natural products.[1-7]

During the course of investigations on the mechanisms of α-amino acid oxidation it was felt necessary to study the chemistry of α,*N*-hydroxyamino acids because of the conflicting reports in the available literature. They have been reported as weak acids without any significant basic properties,[2] and also as compounds giving acidic reaction in aqueous medium.[8] They are also described as amphoteric substances with isoelectric points between pH 6 and 7.[9] With ninhydrin they are reported to give yellow colors,[7] but have also been claimed to give blue or purple colors just like α-amino acids.[9]

Reasons for these discrepancies have now been determined. When α,*N*-hydroxyamino acids are paper chromatographed using the organic layer of *n*-butanol: acetic acid: water (40: 10: 50) as the irrigation solvent and the chromatograms developed with ninhydrin reagent, purple spots with long comet like tails appeared. The R_f values of these spots were found identical with those of the corresponding α-amino acids. When the chromatograms were sprayed with ammoniacal $AgNO_3$ or with triphenyltetrazolium chloride under appropriate conditions, only α,*N*-hydroxyaminopropionic acid and α,*N*-hydroxyaminoisobutyric acid were faintly detected, as black or pink spots. The R_f values of these two hydroxyamino acids were higher than those of the corresponding α-amino acids.

The appearance of long purple streaks on chromatograms and the partial or complete disappearance of α,*N*-hydroxyamino acids, strongly suggested that it was not the α,*N*-hydroxyamino acids which gave blue or purple colours with ninhydrin as reported, but that α,*N*-hydroxyamino acids had been spontaneously transformed to the corresponding α-amino acids during the process of chromatography. The complete identity of the R_f values of the ninhydrin positive products derived from α,*N*-hydroxyamino acids with authentic samples of the corresponding α-amino acids confirmed this transformation. The R_f values of α,*N*-hydroxyamino acids, of α-amino acids derived from the corresponding α,*N*-hydroxyamino acids on the chromatographic paper and of authentic α-amino acids are listed in Table 1. We have now been successful in separating α-amino acids as by-products of the syntheses of α,*N*-hydroxyamino acids.

Since the chromatographic solvent mixture did not contain any reducing agent, the formation of α-amino

Table 1

S. No.	α,*N*-Hydroxyamino acids (HAA)	Potentiometric Titration with 0.1 M NaOH		Paper chromatography in *n*-BuOH:AcOH:H_2O (40:10:50)		
		pK_1 (pK_2)	Isoelectric point $(pK_1+pK_2)/2$	R_f value of HAA	R_f value of α-amino acid derived from HAA	R_f value of authentic α-amino acids
1	CH_3-CH(NH$_2^+$OH)-COO$^-$	2.05 (5.75)	3.90	0.35	0.23	0.23
2	$CH_3 \cdot CH_2$-CH(NH$_2^+$OH)-COO$^-$	2.20 (5.65)	3.92	—	0.36	0.36
3	$CH_3 \cdot CH_2 \cdot CH_2$-CH(NH$_2^+$OH)-COO$^-$	2.35 (5.40)	3.88	—	0.51	0.51
4	$(CH_3)_2$CH-CH(NH$_2^+$OH)-COO$^-$	2.30 (5.80)	4.05	—	0.44	0.44
5	C$_6$H$_5$-CH$_2$-CH(NH$_2^+$OH)-COO$^-$	2.15 (5.20)	3.68	—	0.59	0.59
6	$(CH_3)_2$C(NH$_2^+$OH)-COO$^-$	2.08 (5.95)	4.01	0.46	0.39	0.39
7	C$_6$H$_4$(NH$_2^+$OH)-COO$^-$	2.45 (5.60)	4.03	—	0.60	0.60

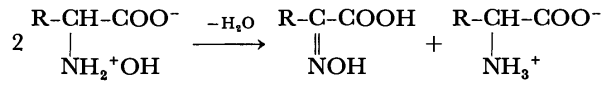

Fig. 1

acids from the corresponding α,*N*-hydroxyamino acids could most easily be explained by taking into consideration the possibility of a disproportionation reaction. The second product, therefore, could either be the corresponding α-nitroso acid or α-oximino acid formed by tautomerization of the nitroso compound (Fig. 1). The presence of α-oximino acids and of blue nitroso compounds on acid hydrolysis of α,*N*-hydroxyamino nitriles have now been demonstrated. The essential requirement of the disproportionation of α,*N*-hydroxyamino acids would be the formation of equimolar quantities of the corresponding α-amino acids and α-oximino acids. Confirmation of this fact came from the quantitative study.

α-Oximino acids, one of the products of disproportionation, have been shown to be unstable compounds in aqueous solutions, especially at higher temperatures and below pH 7. They decompose spontaneously to give lower homologous corresponding nitriles and CO_2[10]

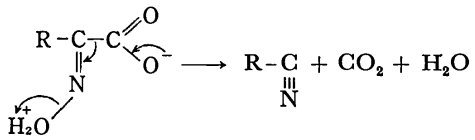

Fig. 2

(Fig. 2). Also since pK_2 ($-N^+H_2OH \rightleftharpoons -NHOH + H^+$) of an α,*N*-hydroxyamino acid is approximately 6 and that of the corresponding α-amino acid is 3—4 p*K* units higher, it is possible to titrate potentiometrically, a mixture of the two acids with standard alkali to a pH 7.5, which represents a complete titration of hydroxyamonium group of an α,*N*-hydroxyamino acid, whereas at this pH the ammonium group of the amino acid does not react with alkali at all. On addition of formaldehyde at pH 7.5, the pK_2 of the amino acid is sufficiently depressed to make possible the titration of the remaining α-amino acid with a reasonable sharp end point at pH 8.8. One such titration of a mixture of α,*N*-hydroxyaminopropionic acid and the corresponding α-amino acid (alanine) is shown in Fig. 3.

When known amounts of α,*N*-hydroxyamino acids were refluxed in aqueous solution under nitrogen atmosphere, corresponding α-amino acids and α-oximino

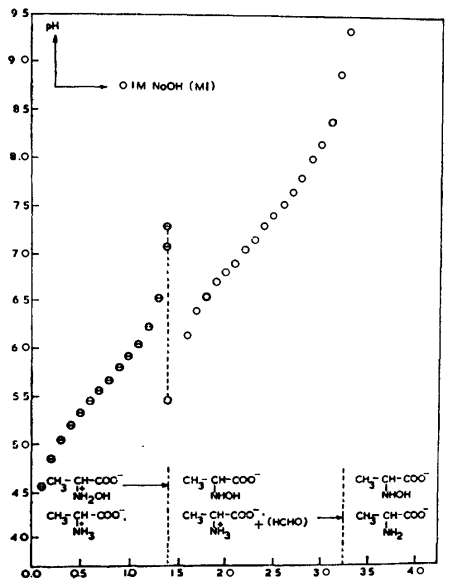

Fig. 3.

acids were obtained as primary products. Under these conditions α-oximino acids were decomposed to give lower nitriles and CO_2. With the exception of α,*N*-hydroxyamino-β-phenylpropionic acid and α,*N*-hydroxyaminoisovaleric acid, all other α,*N*-hydroxyamino acids gave almost equimolar yields of CO_2 (determined as $BaCO_3$) and the corresponding α-amino acids (Table 2). In general, yields of both α-amino acids and CO_2 were than theoretically expected on the basis of 100% disproportionation of the disappeared α,*N*-hydroxyamino acids. In the case of α,*N*-hydroxyaminophenylpropionic acid, the amount of CO_2 evolved was 43% more and phenylalanine formed was 49% less than expected on theoretical consideration based on 100% disproportionation. These differences were perhaps due to some other modes of decomposition in addition to disproportionation.

Since 5 out of 7 α,*N*-hydroxyamino acids studied gave almost equimolar quantities of CO_2 and the corresponding α-amino acids, it is reasonable to infer that two molecules of an α,*N*-hydroxyamino acid undergo mutual oxidation and reduction to give the corresponding α-amino acid and α-oximino acid as the primary products.

To explain the disproportionation, two mechanisms based on hydride shifts may be considered. Both are essentially alike as in one case nitrogen-linked hydrogen

Table 2

S. No.	α,*N*-Hydroxyamino acids (HAA)	HAA taken mg	HAA reacted mg (%)	α-Amino acid[a] formed mg (%)	$BaCO_3$[b] mg (%)
1	α,*N*-Hydroxyaminopropionic acid	36.00	18.15 (50.4)	8.28 (98.4)	18.0 (96.4)
2	α,*N*-Hydroxyaminobutyric acid	50.00	40.48 (81.0)	14.42 (76.1)	27.0 (74.4)
3	α,*N*-Hydroxyaminovaleric acid	55.00	55.00 (100.0)	18.14 (69.9)	40.0 (91.4)
4	α,*N*-Hydroxyaminoisovaleric acid	50.00	11.43 (22.9)	5.26 (97.6)	9.0 (100.0)
5	α,*N*-Hydroxyamino-β-phenylpropionic acid	50.00	50.00 (100.0)	12.25 (51.0)	41.0 (143.0)
6	α,*N*-Hydroxyaminoisobutyric acid	50.00	20.25 (40.5)	7.21 (76.0)	14.0 (77.0)
7	1-Hydroxyaminocyclohexane-1-carboxylic acid	50.00	40.46 (80.9)	11.45 (59.3)	16.0 (52.6)

a) Percentage of theoretical on the basis of (50/50) disproportionation of the reacted HAA. b) Percentage of theoretical on the basis of quantitative decomposition of α-oximino acid to nitrile and CO_2.

of one molecule of hydroxyamino compound shifts to the nitrogen of the other molecule of hydroxyamino compound as a hydride ion, whereas in the second case a hydrogen from the oxygen rather than the nitrogen of one molecule shifts to nitrogen of the other. (Scheme 1).

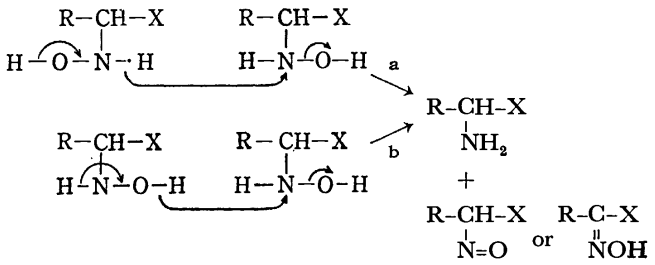

Scheme 1

The mechanism (b) seems to be more likely since -OH·····N and N-H·····O; types of hydrogen bonding have been shown to be preferential in solid hydroxylamine.[11]

It is now clear that the products obtained by Neelakantan and Hartung[9] and regarded as α,N-hydroxyamino acids and which were described as ninhydrin positive, reducing and amphoteric, were in fact mixtures containing α,N-hydroxyamino, α-amino and α-oximino acids. The reaction products were not carefully analyzed and their true nature was overlooked by them.

When α,N-hydroxyamino-β-phenylpropionic acid was synthesized, a small quantity of α-oximino-β-phenylpropionic acid was actually crystallized out from the reaction mixture. Similarly α-oximino acids in small amounts were found amongst the products of acid hydrolyzates of other α,N-hydroxyamino nitriles. A part of α-oximino acids was possibly lost by decomposition to lower homologous nitriles and CO_2 under the conditions. Amino acids were also found in every case. They were isolated by column chromatography of the crude mixtures by making use of cation and anion exchange resins.

It has now become possible to offer an explanation for the formation of α-amino acid, α-oximino acid, the lower homologous aldehydes and nitriles and the corresponding aliphatic acids as by-products of acid hydrolysis of α,N-hydroxyamino nitriles to give α,N-hydroxyamino acids. This is shown in Scheme 2. Two molecules of α,N-hydroxyamino compound undergo mutual oxidation and reduction to give one molecule each of an α-amino compound and an α-oximino compound. In case of α,N-hydroxyaminoisobutyronitrile and 1-hydroxyamino-1-cyanocyclohexane, which do not possess any hydrogen on α-carbon atoms, similar changes take place but instead of α-oximino compounds, blue nitroso compounds are generated which undergo gradual decomposition.[12]

It has also been observed that all α-oximino acids are quantitatively decomposed to give diphenylthiourea and CO_2 when refluxed for one minute with phenylisothiocyanate in benzene solution or when kept for one week at 40 °C. The possible mechanism of this reaction is shown in Scheme 3.

Analogous experiments with α,N-hydroxyamino acids, contrary to the earlier report,[9] failed to give any diphenylthiourea. But when the reflux time was increased to 5 min or more, a small quantity of diphenyl-

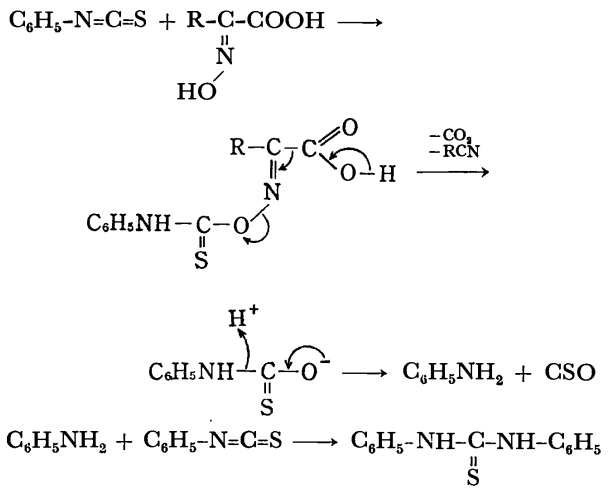

Scheme 3

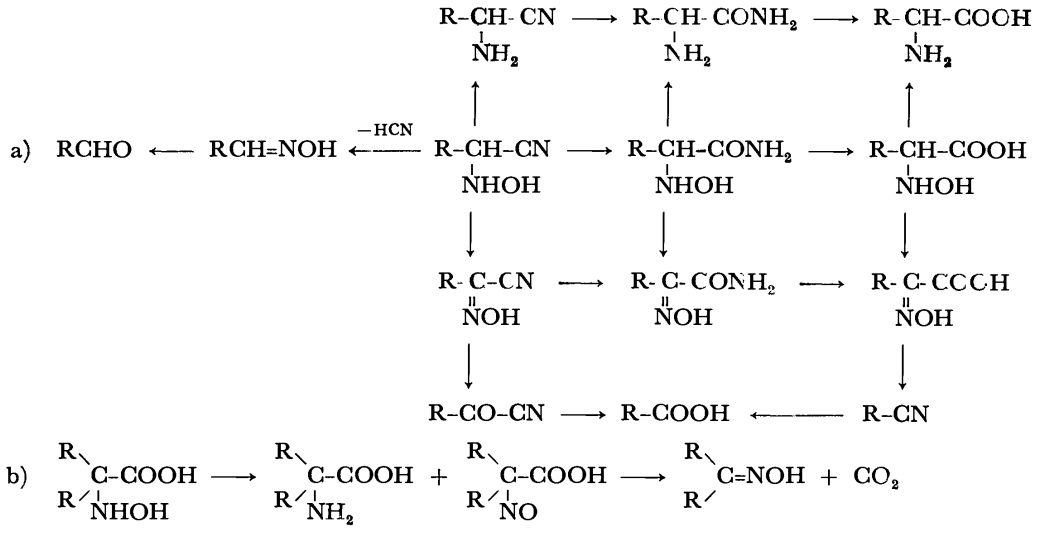

Scheme 2

thiourea did separate along with a major portion of another unidentified high melting product. It is likely that diphenylthiourea is formed from α-oximino acid which might have been produced by disproportionation of α,*N*-hydroxyamino acid. α,*N*-Hydroxyamino acids prepared by Neelakantan and Hartung yielding diphenylthiourea gives a further evidence in support of our observation that these products were in fact mixtures.

Treatment of α-halo acids with excess hydroxylamine gives rise to α-oximino acids.[13] With equimolar amounts of hydroxylamine, α,*N*-hydroxyamino acids are obtained in 50% yields.[2] The formation of α-oximino acids from α-halo acids and hydroxylamine, a reaction whose oddity has hitherto been ignored can now be explained on the basis of a disproportionation. It is now almost certain that hydroxyamino acid is a primary product which either disproportionates to give the corresponding α-amino acid and α-oximino acid or undergoes oxidation by a second molecule of hydroxylamine which is reduced to ammonia (Fig. 4).

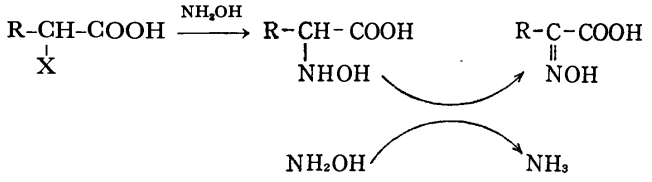

Fig. 4

It is interesting to note that not only α,*N*-hydroxyamino acids, but also hydroxylamine itself, and *N*-methyl and *N*-ethyl hydroxylamines have been reported to decompose in such a fashion[14] to give products whose origin can now be explained easily on the basis of a disproportionation reaction. *N*-Phenylhydroxylamine also gives products compatible with this interpretation.[15]

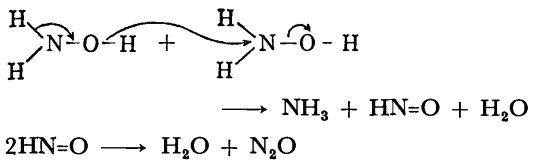

Fig. 5

Hydroxylamine when heated decomposes to give nitrous oxide, ammonia and water. The formation of these products can be explained in the following manner (Fig. 5). *N*-Methylhydroxylamine when distilled in the presence of alkali decomposes to give methylamine, ammonia and formic acid. *N*-Ethylamine under similar conditions gives ethylamine, acetic acid, acetaldehyde and ammonia (Fig. 6).

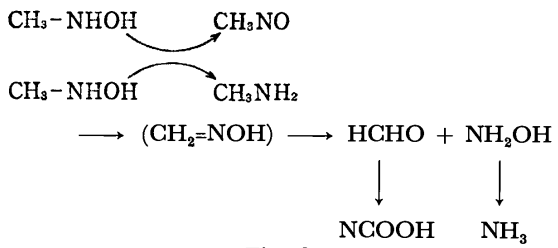

Fig. 6

It is therefore not difficult to infer that not only α,*N*-hydroxyamino acids but also other mono-*N*-substituted hydroxylamines are capable of undergoing disproportionation reactions. This likelihood is at present under investigation and the results will be communicated in a following publication.

Experimental

α,N-*Hydroxyamino Acids.*[16] Six α,*N*-hydroxyamino acids namely (α,*N*-hydroxyaminopropionic acid, α,*N*-hydroxyaminobutyric acid, α,*N*-hydroxyaminoisobutyric acid, α,*N*-hydroxyaminovaleric acid, α,*N*-hydroxyaminoisovaleric acid and 1-hydroxyaminocyclohexane-1-carboxylic acid) were prepared from the corresponding α,*N*-hydroxyaminonitriles by hydrolysis with concentrated hydrochloric acid.[7,9,17,18] When any one of α,*N*-hydroxyaminopropionitrile, α,*N*-hydroxyaminobutyronitrile, α,*N*-hydroxyaminovaleronitrile and α,*N*-hydroxyaminoisovaleronitrile was refluxed with concentrated hydrochloric acid for 5 hr, the reaction mixture was found to contain not only the expected α,*N*-hydroxyamino acid but also the corresponding α-amino acid, α-oximino acid, the lower homologous aldehyde and aliphatic acid. The aldehyde, the aliphatic acid and the oximino acid were separated by ether extraction of the acidic reaction mixture and the α,*N*-hydroxyamino acid was separated from the corresponding α-amino acid by cation and anion exchange resins. The quantity of oximino acid obtained was generally low but increased when the reaction mixture was allowed to stand at room temperature for a longer period before ether extraction.

α,N-*Hydroxyamino-β-phenylpropionic Acid.* α,*N*-Hydroxyamino-β-phenylpropionic acid was obtained from diethylbenzylmalonate.[19] Freshly cut sodium metal (2.3 g, 0.1 mol) was dissolved in absolute ethanol (150 ml) and diethylbenzylmalonate (25.0 g, 0.1 mol) was added, with cooling and stirring. Nitric oxide (generated by dropping conc. H_2SO_4 into a saturated aqueous solution of $NaNO_2$) was bubbled through the ethanolic reaction mixture for one hour. The yellow reaction product was kept overnight at 35 °C and then ethanol removed by evaporating at room temperature under reduced pressure to give a pale yellow slurry which was mixed with 20% aqueous NaOH (60 ml) and kept at 35 °C for 24 hr. The alkaline solution was then extracted with ether to remove any unchanged malonic ester. The solution was then acidified at 5 °C with 30% HCl, resulting in the separation of an oily product, which was extracted into ether. On removal of ether and warming the oily residue with concd HCl (50 ml) for 5 min, phenylpyruvic acid oxime (0.8 g), melting at 169—170 °C (decomp.) crystallized out. This was filtered off, and the filtrate evaporated to dryness. The residue was taken in water (20 ml) and treated with charcoal. The pale yellow clear solution obtained was passed through a column of cation exchange resin (Dowex 50W-X4, 200—400 mesh, H^+ form). After washing the column with water, the products were displaced with 2% aqueous ammonia. The effluent was collected into three fractions a, b, and c. The fraction (a) was strongly reducing towards ammoniacal $AgNO_3$. On evaporation to dryness at room temperature and reduced pressure this fraction yielded α,*N*-hydroxyamino-β-phenylpropionic acid (2.8 g, 15.5%), melting at 159 °C (decomp.) and identical in all respects with an authentic specimen.

The second fraction (b) on evaporation to dryness gave a mixture of α,*N*-hydroxyamino-β-phenylpropionic acid and phenylalanine. The third fraction (c) gave a strong ninhydrin positive reaction and on evaporation to dryness yeilded

phenylalanine (0.13 g), melting at 270..272 °C (decomp.), whose infrared spectrum was identical with an authentic specimen.

Paper Chromatography of α,N-Hydroxyamino Acids. Paper chromatography was carried out by the descending technique on 40 cm long Whatman No. 1 papers. One dimensional runs were performed using the organic layer of *n*-butanol: acetic acid: water (40: 10: 50 by volume) mixture as the solvent. The chromatograms were dried at 35 °C for 16 hr. α-Amino acids formed were detected by the conventional ninhydrin reagent. Reducing α,*N*-hydroxyamino acids were visualized either by spraying with ammoniacal $AgNO_3$ (1.0 g $AgNO_3$ in 100 ml water containing 15 ml 10 M ammonia), when α,*N*-hydroxyamino acids appeared as black spots or by spraying with a solution of triphenyltetrazolium chloride.[16] The dried chromatograms were first sprayed with 0.1% triphenyltetrazolium chloride in *n*-butanol saturated with water, dried once again, and resprayed lightly with a solution containing aqueous NaOH (10 M NaOH (10 ml)+ 95% ethanol (40 ml)+*n*-butanol (50 ml)). The presence of α,*N*-hydroxyamino acids was indicated by the immediate production of pink spots. The R_f values of α-amino acids were compared with those of markers of authentic samples applied to the same papers (Table 1).

Estimation of α-Amino Acid and the Corresponding α,N-Hydroxyamino Acid in the Presence of Each Other. A solution containing α,*N*-hydroxyaminopropionic acid (15.0 mg) and alanine (15.0 mg) in water (2 ml) in a 10 ml beaker, stirred by gently bubbling nitrogen gas, was potentiometrically titrated with 0.1 M NaOH. When the pH of the solution had reached to pH 7.5, the amount of alkali added corresponded to the quantity of the α,*N*-hydroxyaminopropionic acid. At this point 30% aqueous HCHO (1.0 ml), previously titrated with alkali to pH 7.5 was added, and the titration resumed with 0.1 M NaOH until pH rose to pH 8.8. The amount of alkali used in the second titration corresponded to the amount of alanine in the mixture. The plot of pH *versus* alkali added during the titration is shown in Fig. 3. Analogous results were obtained when other pairs of α-amino acids and the corresponding α,*N*-hydroxyamino acids were titrated in the same manner.

Disproportionation of α,N-Hydroxyamino Acids into Corresponding α-Amino Acids and α-Oximino Acids. The α,*N*-hydroxyamino acid (36 to 55 mg) was taken in water (10 ml) in a 25 ml two neck flask, supplied with water cooled condenser and a gas inlet. Nitrogen gas was passed first through a $Ba(OH)_2$ trap and then bubbled through the reaction mixture. CO_2 obtained by the decomposition of α-oximino acid was collected as $BaCO_3$ in a trap containing saturated $Ba(OH)_2$ solution and the reaction train was linked to a further baryta trap. All disproportionation experiments were conducted at reflux temperature over a period of 24 hr. $BaCO_3$ was carefully filtered off, washed with water and methanol before drying to a constant weight. From the weight of $BaCO_3$, the amount of α-oximino acid formed in the course of the reaction was determined.

The aqueous solution in the reaction flask was titrated potentiometrically against 0.1 M NaOH to pH 7.5. This titre was used to calculate the amount of unreacted α,*N*-hydroxyamino acid. At pH 7.5, 30% aqueous HCHO (2 ml, previously adjusted to pH 7.5 with NaOH) was added and the titration carried to pH 8.8. This second titre was taken as a measure of the amount of α-amino acid formed. Results are summarized in Table 2.

Reaction of α,N-Hydroxyamino-β-phenylpropionic Acid with Hydroxylamine. α,*N*-Hydroxyamino-β-phenylpropionic acid (1.0 g, 0.0055 mol) was dissolved in 5% aqueous NaOH (50 ml) containing $NH_2OH \cdot HCl$ (0.385 g, 0.0055 mol) and heated under reflux in a 100 ml reaction flask provided with a gas inlet and a water cooled condenser. Nitrogen gas was bubbled through the reaction mixture and the evolved ammonia was carried along with the nitrogen stream into a trap containing 0.1 M HCl (50 ml). After 12 hr the heating was discontinued and the acid solution in the trap was evaporated to dryness under reduced pressure to give ammonium chloride (0.2649, 91%). The alkaline solution in the reaction flask was cooled in ice and acidified with dil. H_2SO_4. A white material was precipitated out which on filtration, drying and recrystallization from dry benzene, was found identical with phenylpyruvic acid oxime (0.47 g, 46.8%).

Similar results were obtained when α,*N*-hydroxyamino-β-phenylpropionic acid was replaced by other α,*N*-hydroxyamino acids.

Reaction of α,N-Hydroxyamino Acid with Phenylisothiocyanate. α,*N*-Hydroxyaminobutyric acid (1.2 g, 0.01 mol) in dry benzene (50 ml) was mixed with freshly distilled phenylisothiocyanate (2 ml). After keeping at 40 °C for one week there was no sign of any reaction and α,*N*-hydroxyaminobutyric acid was separated unchanged. When the reaction was conducted at the reflux temperature for more than 5 min and the products analyzed, a less than 5% yield of diphenylthiourea was isolated along with an undetermined high melting white substance. Analogous results were obtained when other α,*N*-hydroxyamino acids were employed. α-Oximino acids, when treated with phenylisothiocyanate under identical conditions, almost quantitative yields of diphenylthiourea were obtained.

The author is grateful to Professor I. D. Spenser for helpful discussion during the course of this work.

References

1) E. A. Kaczka, C. O. Gitterman, E. L. Dulaney, and K. Folkers, *Biochemistry*, **1**, 340 (1962).
2) A. H. Cook and C. A. Slater, *J. Chem. Soc.*, **1956**, 4133.
3) J. D. Dutcher, *J. Biol. Chem.*, **171**, 321, 341 (1947).
4) A. J. Birch, R. A. Massy-Westropp, and R. W. Rickards, *J. Chem. Soc.*, **1956**, 3717.
5) T. Emery and J. B. Neilands, *J. Amer. Chem. Soc.*, **83**, 1626 (1961).
6) J. Turkova, O. Mikes, and F. Sorm, *Collect. Czech. Chem. Commun.*, **27**, 591 (1962).
7) G. A. Snow, *J. Chem. Soc.*, **1954**, 2588.
8) Von Miller and Ploche, *Ber.*, **26**, 1545 (1893).
9) L. Neelakantan and W. H. Hartung, *J. Org. Chem.*, **23**, 964 (1958).
10) A. Ahmad and I. D. Spenser *Can. J. Chem.*, **39**, 1340 (1961).
11) E. A. Meyers and W. N. Lipscomb, *Acta Crystallogr.*, **8**, 583 (1955).
12) E. Muller and H. Metzger, *Ber.*, **88**, 165, 1891 (1955).
13) A. Hantzsch and W. Wild, *Ann.*, **289**, 285 (1896).
14) C. Kjellin, *Svensk Kem. Tidskr.*, **33**, 213 (1921); *Chem. Abstr.*, **16**, 211.
15) Bamberger, *Ber.*, **27**, 1548 (1894).
16) A. Ahmad, This Bulletin, **47**, 1819 (1974).
17) W. V. Miller and J. Plochl, *Ber.*, **26**, 1545 (1893).
18) C. D. Hurd and J. M. Longfellow, *J. Org. Chem.*, **16**, 761 (1951).
19) W. Traube, *Ber.*, 2297 (1895).

Application of Chemical Reactions of Thin-Layer Chromatoplates. III.* Monoterpenes

M. EL-GARBY YOUNES** and A. MOKHTAR

Department of Chemistry, Faculty of Science, University of Assiut, Assiut, Egypt, A.R.E.

(Received February 15, 1974)

Some characteristic reactions of monoterpenoids were carried out on inert thin-layer chromatoplates under controlled conditions and the products of the reactions were compared with the expected substances on the same chromatogram. The reactions performed were: acetylation at 40 °C on silica gel and on alumina plates, saponification on silica gel and on alumina chromatoplates, benzoylation at 0 °C, dehydration with thionyl chloride, oxidation with chromium trioxide in acetic acid and in dry pyridine, formation of 2,4-dinitrophenylhydrazone derivatives, chloride formation, reduction with lithium aluminium hydride, reaction of *p*-toluenesulphonyl chloride with some monoterpene alcohols and a modified Clemmensen reaction on monoterpene ketones.

In the field of natural products the chromatoplate technique is used in detecting the components of natural mixtures and giving information useful for subsequent resolution of the mixtures on chromatographic columns. The technique is also used in following up the course of chemical reactions to its end point and consequently, a chemical reaction can be performed for the optimal length of the time and an improved yield of the end product could be obtained. The natural product chemist knows that, the amount of the material available for investigation and preparation of a derivative may be too minute to enable a conventional reaction in a conventional apparatus. Frequently, the desired derivative has a decisive value in elucidating the structure of the parent compound by comparing the obtained derivative with a known product. The chemist has encountered this handicap during his study of some natural products, which were available in only minute amounts, and yet required for their study the detection of certain functional groups and the preparation of certain derivatives. For this objective, we were interested in carrying out some chemical reactions on thin-layer chromatoplates and in making this technique broad enough to involve not only the application of some chemical reactions of triterpenes[1] and amino-acids,[2] but also most of those other fields of natural products, to show which reactions can or cannot proceed on chromatoplates.

Our aim in this work is to carry out some reactions of the monoterpenoids on the plates, in order to serve in widening the aspect of the technique and to overcome some difficulties encountered in our work on natural products.

Generally, the reaction is carried out by mixing the substance under examination, mostly in solution form, with the suitable reactants within the area of a small spot at the starting line of a chromatoplate on an inert adsorbent. The mixture of reactants is then subjected to the favorable conditions and suitable length of time to simulate, as far as possible, the normal reaction conditions in the flask. At the end of the reaction period a simplified "working up" may be necessary which is also performed within the confines of the spots. The adsorbed layer is then treated in the normal manner as a chromatographic medium for reaction of the components of the reaction mixture. Thus, development with a suitable solvent system enables the detection of the formed derivative and the comparison with the expected material, spotted at the starting line immediately prior to development. Differentiation of the derivative from the starting material, if any remains, is always possible if the appropriate conditions are used.

Results and Discussion

Reactions involving acetylation at 40 °C, proceeded smoothly and almost completely on both silica gel and alumina chromatoplates for monoterpene alcohols (compd. 1—2; *cf.* Table 1). We found that the acetylation reaction did not affect by changing the adsorbent.

Saponification of the monoterpene esters on silica gel chromatoplates was difficult and most of the esters remained unreacted, this is in contrast to saponification on alumina plates which proceeded successfully. This phenomena is in support to the saponification tried previously on triterpene esters.[1,4]

Benzoylation proceeded smoothly at 0 °C for the compounds investigated, and the benzoate derivatives were obtained in a good yield (Table 1).

Dehydration of monoterpene compounds containing tertiary hydroxyl groups with thionyl chloride and dry pyridine at 0 °C proceeded smoothly for compound 5 but gave poor yield for compound 6 (*cf.* Table 1), and no other products were detected on the plate.

Oxidation with chromium trioxide in acetic acid at 70 °C for 20 min was successful and the ketones were obtained in a reasonable yields. While oxidation with chromium trioxide in dry pyridine at room temperature overnight did not proceed.

Reaction of monoterpene aldehydes or ketones with 2,4-dinitrophenylhydrazine in acetic acid at room temperature for 2 hr on plates were proceeded smoothly and the 2,4-dinitrophenylhydrazone derivatives were obtained in a good yield.

The formation of monoterpene chlorides was achieved successfully by reacting the desired alcohols with thionyl chloride in dry benzene for 4 hr at room temperature. The chloride was obtained in a good yield.

Reduction with lithium aluminium hydride in dry ether was proceeded smoothly and the alcohols were

* For part II of this series see Ref. 2.

** To whom inquiries should be addressed.

Table 1

No. of compd.	Starting material (R_f)	Reaction product (R_f)	Solvent system[a]
Acetylation at 40 °C on silica gel plates			
1	Menthol (0.3)	Menthyl acetate (0.77)	I
2	Borneol (0.28)	Bornyl acetate (0.70)	I
Acetylation at 40 °C on alumina plates			
1	Menthol (0.22)	Menthyl acetate (0.65)	I
2	Borneol (0.20)	Bornyl acetate (0.60)	I
Saponification on silica gel plates			
3	Menthyl acetate (0.77)	Menthol (0.30)	I
4	Bornyl acetate (0.70)	Borneol (0.28)	I
Saponification on alumina plates			
3	Menthyl acetate (0.65)	Menthol (0.22)	I
4	Bornyl acetate (0.60)	Borneol (0.20)	I
Benzoylation			
1	Menthol (0.23)	Menthyl benzoate (0.66)	II
2	Borneol (0.26)	Bornyl benzoate (0.69)	I
Dehydration with thionyl chloride			
5	α-Terpineol (0.20)	Limonene (0.80)	III
6	Linalool (0.23)	Myrcene (0.94)	III
Oxidation with chromium trioxide in acetic acid			
1	Menthol (0.20)	Menthone (0.62)	III
2	Borneol (0.14)	Camphor (0.35)	III
Oxidation with chromium trioxide in pyridine			
1	Menthol	Did not react	
2	Borneol	Did not react	
Reaction with 2,4-dinitrophenylhydrazine			
7	Citral (0.54)	Citral 2,4-dinitrophenylhydrazone derivative (0.81)	IV
8	Fenchone (0.60)	Fenchone 2,4-dinitrophenylhydrazone derivative (0.80)	IV
9	Camphor (0.58)	Camphor 2,4-dinitrophenylhydrazone derivative (0.82)	IV
10	Citronellal (0.58)	Citronellal 2,4-dinitrophenylhydrazone derivative (0.90)	III
11	Menthone (0.68)	Menthone 2,4-dinitrophenylhydrazone derivative (0.89)	II
Chloride formation			
1	Menthol (0.20)	Menthyl chloride (0.71)	III
2	Borneol (0.14)	Bornyl chloride (0.90)	III
Reduction with lithium aluminium hydride			
8	Fenchone (0.68)	Fenchyl alcohol (0.38)	IV
11	Menthone (0.72)	Menthol (0.54)	IV
9	Camphor (0.56)	Borneol (0.28)	IV
Reaction with *p*-toluenesulphonyl chloride			
1	Menthol (0.3)	Menthyl *p*-toluenesulphonate (0.71)	I
2	Borneol (0.28)	Bornyl *p*-toluenesulphonate (0.68)	I
A modified Clemmensen reduction using zinc dust and dry ether at 0°			
11	Menthone (0.29)	Did not react	III
8	Fenchone (0.31)	Fenchone (0.87)	III
9	Camphor (0.35)	Did not react	III
A modified Clemmensen reduction using acetic anhydride			
11	Menthone (0.29)	Menthone (0.64)	III
9	Camphor (0.35)	Did not react	III
8	Fenchone (0.31)	Fenchane (0.87)	III

a) Solvent system: I=benzene–light petroleum (1:1), II=benzene–light petroleum (1:2), III=light petroleum, IV=benzene.

obtained in a good yield.

The reaction of the monoterpene alcohols with *p*-toluenesulphonyl chloride was difficult and most of the starting alcohols were obtained unchanged.

Since the monoterpenes are volatile and sensitive to high temperature, the reduction of the ketonic groups in the monoterpenes to methylene groups by the normal Clemmensen method was shown to be unsatisfactory. However, a modified procedure for Clemmensen reaction which was detected by Toda *et al.*[3] and carried out by us on monoterpene ketones was proceeded smoothly under very mild conditions and a reasonable yield for compounds 11 and 8 but not for compound 9 was obtained (see Experimental and Table 1). The reaction was achieved with active zinc dust in presence of either dry ether or acetic anhydride and hydrogen chloride gas at 0 °C for 2 hr. We found that when acetic anhydride was used it gave better results of the expected hydrocarbons than the dry ether, and no other products were detected on the plate.

Conclusion. As we have seen from the above discussion it appears that the application of chemical reactions of monoterpenoids on an inert chromatographic adsorbent, within the usual area of a spot can produce results comparable to those obtained in conventional reaction apparatus.

Experimental

Chromatoplates. Both the silica gel and the alumina plates were prepared by slurring Kiesel gel G. (Merck) or alumina grade II in water (1:2 by weight, and applied manually onto glass plates 5×12 cm), followed by drying at 120 °C for 2 hr. The development of the plates was achieved by placing them in a closed tank containing iodine.

Acetylation. (A) Acetylation at 40 °C on silica gel plates was performed by treating the monoterpene alcohol under examination at the starting line followed by treatment with an acetic anhydride–pyridine mixture (3:1), which was applied in the form of a spray over the chromatoplate. The latter was placed in a desiccator containing a saturated atmosphere of acetic anhydride, then heating the desiccator until the temperature reaches 40 °C for 2 hr. At the end of the reaction-period, the chromatoplate was freed from the reagents by standing at room temperature for 1 hr. The chromatoplate is then ready for chromatographic development.

(B) Acetylation at 40 °C on alumina plates was conducted exactly as mentioned in the previous procedure.

Saponification. (A) Saponification of the monoterpene esters on silica gel was conducted by treating the ester spot under examination with ethanolic potassium hydroxide (10%). The plate was then placed in a desiccator containing a saturated solution of potassium hydroxide and the desiccator was heated until the temperature reached 70 °C for 6 hr, after which the plate was cooled and ready for development.

(B) Saponification of the esters on alumina plates was performed in the same manner mentioned above.

Benzoylation. This reaction was done by treating monoterpene hydroxy compound spot, at the starting line of the chromatoplate, with a mixture of benzoyl chloride-pyridine (1:2) on the same spot. The chromatoplate was then placed in a desiccator saturated with the same mixture of benzoyl chloride-pyridine and the whole was cooled at 0 °C for 2 hr. At the end of the reaction period, the plate

was freed from the solvent and then was ready for development.

Dehydration. This reaction was performed by applying the substance under examination which contains a tertiary hydroxyl group (5 and 6 in Table 1), in the form of a solution at the starting line, followed by adding a mixture of thionyl chloride–pyridine (1:8) on the same spot. The plate was placed in a desiccator saturated with the same mixture,and the whole were cooled at 0 °C for 10 min. The plate was freed from the solvent by leaving it at room temperature for 1 hr prior to development.

Oxidation with Chromium Trioxide. *(A) In Acetic Acid*: This reaction was achieved by applying the alcohol under examination in the form of a solution at the starting line of the chromatoplate, followed by treating the alcohol spot with a solution of chromium trioxide–acetic acid (2%). After leaving the plate in a closed vessel containing saturated atmosphere of acetic acid, at room temperature for 50 min, the whole was heated at 70 °C for 20 min. The plate was then sprayed with methanol to destroy the excess of the oxidant and dried again in air prior to development.

(B) In Pyridine: A simple oxidation was performed by spotting the hydroxy compound at the starting line on the plate followed by treatment with a solution of chromium trioxide in dry pyridine. The plate was then placed in a desiccator saturated with dry pyridine and left standing at room temperature for overnight. The plate was then sprayed with methanol to destroy the excess of chromium trioxide and dried in air prior to development.

Chloride Formation.[4] This reaction was performed by treating the monoterpene alcohol spot under examination with a solution of thionyl chloride in dry benzene (50%). The plate was placed in a desiccator containing a saturated solution of thionyl chloride–benzene mixture and left standing at room temperature for 4 hr, after which it was dried in air prior to development.

Reduction with Lithium Aluminium Hydride. The carbonyl compound spot at the starting line of a chromatoplate, was treated with a suspension of lithium aluminium hydride in dry ether. The plate was then placed in a desiccator saturated with dry ether for 3 hr at 30 °C, after which the plate was freed from the solvent and the spot was acidified with sulphuric acid (1M) prior to chromatographic development.

Reaction with p-*Toluenesulphonyl Chloride.* This reaction was performed by treating the monoterpene alcohol spot at the starting line of a chromatoplate by a solution of *p*-toluenesulphonyl chloride in dry pyridine. The plate was then placed in a desiccator containing a saturated atmosphere of pyridine for 36 hr at room temperature. At the end of the reaction period, the chromatoplate was dried in air prior to development.

A Modified Clemmensen Reduction.[3] *(A) In Ether*: This reaction was achieved by treating the ketonic spot under examination at the starting line of a chromatoplate with a suspension of active zinc dust in ether. The plate was then placed in a vacuum desiccator containing a saturated atmosphere of dry ether and the whole was cooled at 0 °C. Hydrogen chloride gas was passed into the desiccator until the space inside it was saturated with the hydrogen chloride gas, then the whole system was left standing for 2 hr, at 0 °C. The spot was treated with a solution of sodium carbonate and the plate was dried in air prior to development.

(B) In Acetic Anhydride: The reaction was performed as mentioned under method (A) above, except dry ether was replaced by acetic anhydride.

References

1) A. M. Osman, M. El-Garby Younes, and F. M. Ata, *U.A.R. J. Chem.*, **13**, 273 (1970).

2) M. El-Garby Younes, M. El-Maghraby, and Kh. M. Hassan, A manuscript had been accepted for publication in the 7th Arab Scientific Conference, Cairo, September, 1973, in press.

3) M. Toda, M. Hayashi, Y. Hirata, and S. Yamamura, This Bulletin, **45**, 264 (1972).

4) M. H. A. E.-Gamal and M. B. E. Fayez, *Z. Anal. Chem.*, **226**, 408 (1967).

NOTES

BULLETIN OF THE CHEMICAL SOCIETY OF JAPAN, VOL. 47(10), 2591—2592 (1974)

Ionization Potentials of Radicals as Determined by the Unrestricted MINDO/2 Method[1]

Hiroshi ICHIKAWA and Michihiko OGATA

Hoshi College of Pharmacy, Ebara, Shinagawa-ku, Tokyo 142

(Received December 24, 1973)

Synopsis. The parametrization in the MINDO/2 theory has been applied to the unrestricted Hartree-Fock method to give the appropriate ionization potentials of various radicals.

A knowledge of the ionization potentials (IP's) of radicals is of importance when considering the various theories of molecular structures. This knowledge, for example, when combined with the electron-impact appearance potentials, yields useful information on the heats of formation of free radicals. In order to interpret the mass spectra of organic compounds it is necessary to know the IP's of various radicals, since, in the fragmentation of a molecular ion such as $[P\text{–}Q]\cdot^{+}\rightarrow P\cdot+Q^{+}$ or $[P\text{–}Q]\cdot^{+}\rightarrow P^{+}+\cdot Q$, the positive charge is indicated by Stevenson's rule[2] as remaining predominantly on the fragment with the lower IP.

From both the kinetic and mass spectroscopic methods it is difficult to get all the values of the IP's of the individual fragments.[3] Alternatively several molecular orbital (MO) theories can predict those values. As will be discussed, the CNDO/2[4] and INDO[5] theories provide unrealistic values. Therefore, the MINDO/2 theory,[6] which gives IP's for the closed-shell molecules close to those found experimentally, has been adopted in this study. However, the formal extension of the semi-empirical MO theory for closed-shell systems to open-shell systems involves a fundamental problem. The parameters in the original MO theory have been so adjusted as to give appropriate results for the closed-shell systems. This paper will discuss the adaptability of the unrestricted MINDO/2 method in the calculation of IP's, comparing those obtained by the CNDO/2, INDO, and experimental methods.

Method of Calculation

The calculations here are based on the unrestricted INDO methods of Pople *et al.*[5,7] The one-center integrals, the two-center repulsion integrals, the core-electron attractions, the one-electron resonance integrals, and the core-core repulsions were estimated as in the original MINDO/2 method,[6] where none of parameters were changed. Further details will not be repeated here. The bond-lengths (in Å) of the fragments are assumed to be as follows: C(sp^3)–C(sp^3), 1.54; C(sp^3)-C(sp^2, sp), 1.50; C–C, 1.35; C–O, C=N, 1.25; C=C(conj.), 1.40; C(sp)=O, 1.15; C–H,

TABLE 1. IONIZATION POTENTIALS[a] OF FRAGMENTS BY MEANS OF CNDO/2, INDO, AND MINDO/2 METHODS

Fragments[b]	CNDO/2		INDO		MINDO/2		Experiment[e]
	KIP[c]	DIP[d]	KIP	DIP	DIP	DIP	
CH_3	13.19(3.24)[f]	12.19(2.24)	13.13(3.18)	12.38(2.43)	10.51(0.56)	10.19(0.24)	9.95(0.03)[g]
CH_3CH_2	11.30(2.52)	10.10(1.32)	11.24(2.46)	10.20(1.42)	9.68(0.90)	9.05(0.27)	8.78(0.03)
$CH_3CH_2CH_2$	11.35(2.66)	9.97(1.28)	11.30(2.61)	10.11(1.42)	9.64(0.95)	8.87(0.18)	8.69(0.05)
$(CH_3)_2CH$	10.17(2.27)	8.82(0.92)	10.13(2.23)	8.92(1.02)	9.16(1.26)	8.30(0.40)	7.90(0.05)
$CH_3CH_2CH_2CH_2$	11.34(2.70)	9.87(1.23)	11.28(2.64)	10.01(1.37)	9.64(1.00)	8.76(0.12)	8.64(0.05)
$CH_3CH_2(CH_3)CH$	10.30(2.37)	8.80(0.87)	10.27(2.34)	8.93(1.00)	9.22(1.29)	8.22(0.29)	7.93(0.05)
$(CH_3)_3C$	9.39(1.97)	7.94(0.52)	9.38(1.96)	8.07(0.65)	8.77(1.35)	7.75(0.33)	7.42(0.05)
CH_2-CH=CH_2	10.81(2.65)	9.74(1.58)	10.61(2.45)	9.65(1.49)	9.65(1.49)	8.91(0.75)	8.16(0.03)
CH_2=C(CH_3)-CH_2	10.88(2.85)	9.68(1.65)	10.69(2.66)	9.59(1.56)	9.63(1.60)	8.77(0.74)	8.03(0.05)
$C_6H_5CH_2$	9.84(2.08)	8.75(0.99)	9.56(1.80)	8.54(0.78)	9.30(1.54)	8.52(0.76)	7.76(0.08)
CH≡C-CH_2	11.10(2.85)	10.18(1.93)	10.82(2.57)	10.03(1.78)	9.59(1.34)	9.01(0.76)	8.25(0.08)
CH_3(CN)CH	10.92(1.16)	9.89(0.13)	10.89(1.13)	9.95(0.19)	10.20(0.44)	9.52(−0.24)	9.76(0.1)
$NCCH_2CH_2$	11.83(1.98)	10.44(0.59)	11.77(1.92)	10.56(0.71)	10.36(0.51)	9.44(−0.41)	9.85(0.1)
$NC(CH_3)_2C$	10.08(0.93)	8.90(−0.25)	10.13(0.98)	9.05(−0.10)	9.76(0.61)	8.88(−0.27)	9.15(0.1)
$NCCH_2$	12.13(1.26)	11.24(0.37)	12.12(1.25)	11.34(0.47)	10.99(0.12)	10.41(−0.46)	10.87(0.1)
CHO	11.68(1.80)	11.45(1.57)	11.18(1.30)	11.00(1.12)	9.91(0.03)	9.80(−0.08)	9.88(0.05)
CH_3CHO	8.17(0.12)	7.26(−0.79)	7.63(−0.42)	6.85(−1.20)	8.14(0.09)	7.69(−0.45)	8.05(0.17)

a) In units of eV. b) The conformations were all set to be staggered. c) Koopmans' IP. d) Difference of the total energies between the ion and radical ($E_{ion}-E_{radical}$). e) Picked up from the data compiled by A. G. Harrison.[3] f) Difference between the calculated and experimental values. g) Experimental error.

1.09; O–H, 1.00; N–H, 1.02. The unpaired electron in each radical was assumed to occupy a 2p atomic orbital.

Results

Calculations were carried out for specific radicals (by the unrestricted methods) and ions (by the restricted methods). Table I shows the differences in total energies (DIP's) between the ion and the radical, the values of $-\varepsilon^{ho}$'s (KIP's) (where the ε^{ho}'s are the energies of the highest occupied MO's), and, in the last columns, the experimental values determined by the electron-impact method (with an error of *ca.* 0.1 eV). From Koopmans' theorem, the KIP value should be approximately equal to the IP value. It can be seen that the KIP values determined by the unrestricted CNDO/2 and INDO include an inconstant error of more than 3 eV in comparison with the experimentally-determined values. In the present method, the error is kept within 1.5 eV.

The CNDO/2 and INDO methods also yield DIP values with an inconstant error, though this error is considerably less than in the KIP values determined by the same methods. It is interesting that the difference between the DIP values and the corresponding experimental values becomes smaller as the number of substituents of the carbon atom of the radical center decreases.

Although the bond-lengths and the bond-angles have not been optimized, the DIP values obtained by the MINDO/2 method are far closer to the experimentally-determined values than those calculated by any other method. The difference between the DIP and the experimental values is relatively constant according as the type of radical, *i.e.*, *ca.* 0.25, 0.75, and −0.3 eV for alkyl radicals, unsaturated radicals, and radicals with an N or O atom respectively. This suggests that such a difference must be brought about by the inappropriate molecular geometries.

This research has been supported by a Grant-in-Aid from the Ministry of Education of Japan (877358). The computations[8] were all carried out on HITAC-8800/8700 computers at the Computer Centre of the University of Tokyo.

Reference

1) An MO approach to the interpretation of organic mass spectra. VII. Part VI, H. Ichikawa and M. Ogata, *Chem. Pharm. Bull.* (Tokyo), submitted for publication.

2) D. P. Stevenson, *Discuss. Faraday Soc.*, **10**, 35 (1951).

3) The experimental methods for determination of radical IP's and some values of measured IP's have been reviewed by A. G. Harrison (ed. by F. W. McLafferty, "Mass Spectrometry of Organic Ions," Academic Press, New York, 1963, Chapter 5).

4) J. A. Pople and G. A. Segal, *J. Chem. Phys.*, **44**, 3289 (1966).

5) J. A. Pople, D. L. Beveridge, and P. A. Dobosh, *ibid.*, **47**, 2026 (1970).

6) M. J. S. Dewar and E. Haselbach, *J. Amer. Chem. Soc.*, **92**, 590 (1967).

7) J. A. Pople and D. L. Beveridge, "Approximate Molecular Orbital Theory," McGraw-Hill, New York (1970).

8) The program of the restricted and unrestricted MINDO/2 method with the subprogram of energy-partition may be sent on request to one of the authors (H. I.).

BULLETIN OF THE CHEMICAL SOCIETY OF JAPAN, VOL. 47(10), 2593—2594 (1974)

Blue-colored Matter Appearing in an Alkaline Solution of Benzoin and Benzil in Aqueous Dimethyl Sulfoxide

Takehiro ABE and Masamoto IWAIZUMI*

College of General Education, Tohoku University, Kawauchi, Sendai 980

* *Chemical Research Institute of Non-Aqueous Solutions, Tohoku University, Katahira-2-chome, Sendai 980*

(Received January 16, 1974)

Synopsis. Blue-colored matter appearing in the alkaline solution of benzoin and benzil in aqueous dimethyl sulfoxide (DMSO) was confirmed to be a benzil anion-radical by visible and ESR spectroscopy.

The intensely purple-colored matter appearing during the course of the oxidation of benzoin to benzil in an alkaline alcoholic solution was confirmed by Ihrig and Caldwell[1] to be stable free radical with a Gouy-type magnetic balance. Although they assigned the colored matter to an aliphatic semiquinone such as benzil anion-radical (I), no evidence for the structure was given. The visible spectrum has not been given, since the matter is usually very labile.[2]

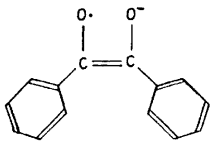

I

The colored matter can be more distinctly observed on addition of sodium hydroxide to a solution of benzoin and benzil in DMSO (blue) than in alcohol (purple). Benzil is an oxidizing agent appropriate for the formation of the colored matter.[1,3] We have investigated the colored species in DMSO by visible and ESR spectroscopy.

The blue species has bands at *ca.* 620 (shoulder), 650 and 720 nm (shoulder) in the visible region (Fig. 1). The disagreement in absorbance at 700 nm between the two measurements is due to the gradual disappearance of the blue matter. The solution resulting

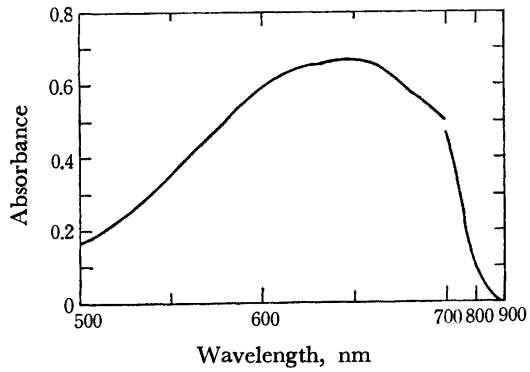

Fig. 1. The spectrum observed with the DMSO solution containing benzoin (5.5×10^{-4} M), benzil (6.3×10^{-4} M), sodium hydroxide (3.9×10^{-3} M) and 2%(v/v) water, at *ca.* 1 min after mixing.

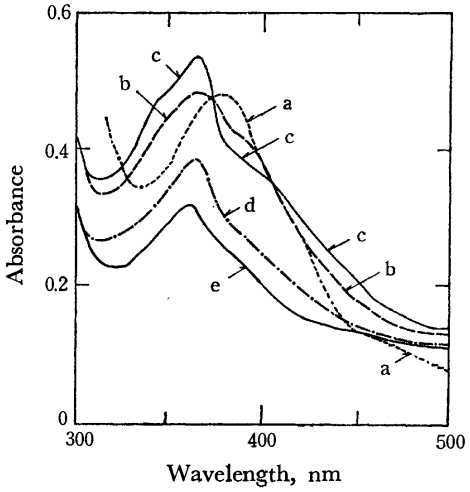

Fig. 2. The spectra observed with the DMSO solution containing benzoin (5×10^{-4} M), benzil (5×10^{-4} M), sodium hydroxide (3.9×10^{-3} M) and 2%(v/v) water. Time after mixing: a, 5 s; b, 30 s; c, 1 min; d, 8.3 min; e, 13.3 min.

from mixing shows an absorption peak at 380 nm at the initial stage and a peak at 359 nm later on (Fig. 2). The initial 380-nm band appeared before the appearance of the visible bands and disappeared with the increasing absorption intensities in the visible region, and it is therefore not due to the blue matter. On the other hand, the band at 359 nm seems to be ascribed to the blue matter, since the band decreased in intensity with the decreasing absorption intensities in the visible region.

The benzil anion-radical generated by electrolytic reduction in dimethylformamide solution[4] and by reduction with alkali metals in several solvents[5] is blue and purple, respectively. The benzil anion-radical produced in a γ-irradiated rigid solution in methyltetrahydrofuran at 77 K shows absorption bands at 650, 700 and 750 nm.[6] Thus the blue matter could be assigned to the benzil anion-radical.

The purple solution prepared by adding sodium hydroxide to a solution of benzoin and benzil in aqueous ethanol showed a very broad band with an absorption maximum at *ca.* 550 nm. The whole broad band shifted to the blue as compared with that of the blue DMSO solution. The difference in color between the blue DMSO solution and the purple ethanolic one seems to be due to a solvent effect.

The calculation made by Kawai[2] by the free-electron method predicts the peak position of 667 nm for radical I. The predicted position agrees closely with that observed in the present work.

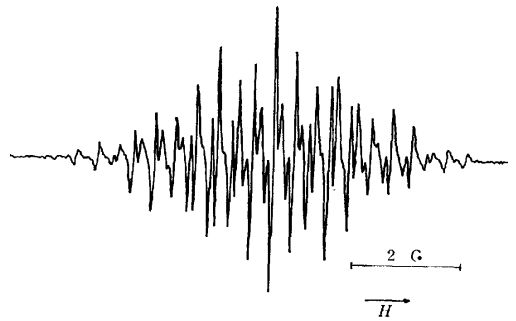

Fig. 3. The ESR Spectrum of the blue-colored species (the benzil anion-radical) produced by adding a drop of 4.9 M NaOH solution into the DMSO solution of benzoin (1×10^{-2} M) and benzil (1×10^{-2} M) in a thin sample tube open to the air at room temperature.

Table 1. Hyperfine splitting constants of the benzil anion-radical

Position	Splitting constants (G)		
	Present work	Ref. 4	Ref. 7
ortho	1.010	0.99	0.99
meta	0.368	0.36	0.37
para	1.123	1.12	0.99

The assignment of the benzil anion-radical for the blue matter can be confirmed by its ESR spectrum (Fig. 3), which is similar to that of the blue benzil anion-radical.[4] We see from Table 1 that the hyperfine splitting constants obtained from Fig. 3 agree closely with those reported for the benzil anion-radical.[4,7] Thus the blue matter can be confirmed to be the benzil anion-radical.

The DMSO solution of benzil in the presence of sodium hydroxide showed a band at 385 nm at the initial stage but no absorption bands in the visible region. In the DMSO solution of benzoin (1.5×10^{-3} M) and sodium hydroxide (3.9×10^{-3} M) in the absence of benzil, the blue-colored matter showing a visible spectrum similar to that shown in Fig. 1 appeared and disappeared later on. In this case the oxidation of benzoin proceeds owing to the presence of the oxygen dissolved in the solution.[3] It is thus evident that the blue matter is produced from benzoin. In the presence of benzil, however, it may also be produced by the reduction of benzil with benzoin.

Experimental

Commercial benzoin (G. R. Tokyo Kasei) was purified by recrystallization. Benzil (ultra-pure grade, Tokyo Kasei) was used. DMSO was dried with calcium hydride and fractionated under reduced pressure.

The electronic absorption spectra of the solutions were measured at room temperature with a Hitachi recording spectrophotometer EPS-3 having a path length of 1.00 cm, and with a Hitachi rapid scan spectrophotometer RSP-2 having a path length of 1.0 cm. Water was used as a reference. The ESR spectrum was measured with a Hitachi ESR spectrometer, Model 771, at 22 °C.

The authors are indebted to Professor Taro Isobe, Tohoku University, for his kind advice

References

1) J. L. Ihring and R. G. Caldwell, *J. Amer. Chem. Soc.*, **78**, 2097 (1956).
2) W. Kawai, *Kagaku*, **23**, 363 (1953).
3) L. Michaelis and E. S. Fetcher, Jr., *J. Amer. Chem. Soc.*, **59**, 1246 (1937).
4) R. Dehl and G. K. Fraenkel, *J. Chem. Phys.*, **39**, 1793 (1963).
5) N. L. Bauld, *J. Amer. Chem. Soc.*, **87**, 4788 (1965).
6) T. Shida and W. H. Hamill, *ibid.*, **88**, 3683 (1966).
7) G. R. Luckhurst and L. E. Orgel, *Mol. Phys.*, **7**, 297 (1963—1964).

BULLETIN OF THE CHEMICAL SOCIETY OF JAPAN, VOL. 47(10), 2595—2596 (1974)

Isomerization of 2-Pinene over Monohydrates of Metal Sulfates

Ryuichiro OHNISHI, Akira MATSUI, and Kozo TANABE*

Research Institute for Catalysis, Hokkaido University, Sapporo 060

* *Department of Chemistry, Faculty of Science, Hokkaido University, Sapporo 060*

(Received February 13, 1974)

Synopsis. Catalytic activity of the monohydrates of various metal sulfates for the isomerization of 2-pinene was found to be related to the infrared wave numbers of the rocking mode of the water of crystallization and the transition temperatures from the monohydrates to the anhydrates, but not to the electronegativity of metal ions.

The catalytic activity of various metal sulfates for some acid-catalyzed reactions is related to the electronegativity of the metal ions.[1-3] The activity as well as acidity of metal sulfates is known to change a great deal with amount of water of crystallization of sulfates.[4] Since the electronegativity values of metal ions are those of bare ions independent of water molecules, they can not necessarily be correlated with the activity of metal sulfates which contain various amounts of water of crystallization. If the amount of water of crystallization is kept constant for all sulfates, a more definite relationship is expected between the electronegativity and catalytic activity. However, the effect of water of crystallization on activity has not been taken into careful consideration. We have studied the isomerization of 2-pinene over *the monohydrates* of various metal sulfates. It was found that, contrary to expectation, there is no correlation of activity with electronegativity, but good correlation between activity and the strength of the coordination of water of crystallization to metal ion.

Experimental

Monohydrates of metal sulfates were prepared by first calcining the polyhydrates (guaranteed reagents, Kanto Chemical Co., except for $Cr_2(SO_4)_3 \cdot 4H_2O$, extra pure) at 120—130 °C, by sieving below 150 mesh after grinding to powder and then calcining for further 3 hr in air at temperatures chosen to obtain the monohydrates (Table 1). 2-Pinene was purified from turpentine oil (Wako Pure Chemical Co.) by distillation over sodium under a stream of nitrogen after separation by a preparative gas chromatograph (Perkin-Elmer F-21). All the reagents and catalysts were stored in sealed ampoules. The acidic properties of the catalysts were determined by the amine titration method with various Hammett indicators.[5] Specific surface area was obtained by applying the BET method to the adsorption isotherm of nitrogen at −196 °C.

The isomerization reaction was carried out in the temperature range 133—134 °C, except for nickel sulfate (109 °C), by stirring the reaction mixture in a cell containing 2.5—3.0 ml of 2-pinene and 0.5—1.0 g of catalysts in nitrogen atmosphere. The reaction products were analyzed by a gas chromatograph (Hitachi-Perkin-Elmer F-6D), with a 45 m capillary column of Ucon LB-550-X, after the catalyst had been removed by centrifuging.

Results and Discussion

The isomerization reaction of 2-pinene (I) gave mainly tricyclic monoterpene of 1,7,7-trimethyl-tricyclo[2.2.1.$0^{2,6}$] heptane (TTH, II), bicylic mono-

Reaction Scheme

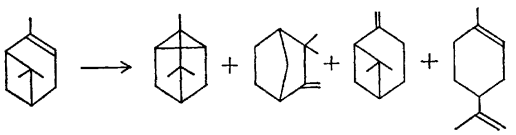

I II III IV V

Scheme 1.

TABLE 1. CATALYTIC ACTIVITY[a] AND SELECTIVITY[b] OF METAL SULFATES FOR ISOMERIZATION OF 2-PINENE

Sulfates	Calcination temp. (°C)	Mole of crystal water per mol of metal	Catalytic activity (mol% min^{-1} g^{-1})	Catalytic activity (mol% min^{-1} m^{-2})	Selectivity	Electronegativity[c]
Ni(II)	250	1.20	2.3	2.3×10^{-1}	0.74	9.0
Al(III)	250	1.33[d]	9.8×10^{-1}	8.2×10^{-1}	0.64	10.5
Mg(II)	250	1.10	6.0×10^{-1}	9.1×10^{-2}	0.71	6.0
Cr(III)	200	0.82[d]	4.6×10^{-1}	2.0	0.64	11.2
Co(II)	250	1.38	4.5×10^{-1}	7.4×10^{-1}	0.76	9.0
Cd(II)	150	1.02	1.2×10^{-1}	4.8×10^{-1}	0.67	8.5
Zn(II)	150	1.04	8.6×10^{-2}	3.2×10^{-1}	0.64	8.0
Ca(II)	150	0.33[d]	2.2×10^{-2}	7.9×10^{-3}	0.94[e]	5.0
Cu(II)	150	1.09	1.4×10^{-2}	1.3×10^{-2}	0.70	9.5
Mn(II)	150	1.09	8.7×10^{-3}	1.8×10^{-2}	0.73	7.5

a) Reaction temperature 133—134 °C except for 109 °C for Ni(II). b) Selectivity for formation of bicyclic monoterpenes [mol% of (II+III+IV)/mol% of I]. c) Quoted from Ref. 1. d) Monohydrates unstable. e) Unreliable because of small amount of products.

terpenes of camphene (III) and 2(10)-pinene (IV), and monocyclic monoterpene of *p*-mentha-1,8-diene (V) as shown in Scheme 1.

In order to see the selectivity of this reaction, mol% of 2-pinene remaining at reaction time t was plotted against mol% of camphene+TTH+2(10)-pinene or *p*-mentha-1,8-diene formed at time t, respectively. The plots gave straight lines in the region 100—20 mol% of 2-pinene as in nickel sulfate.[6] From the slope of the straight line, the selectivity for the formation of camphene+TTH+2(10)-pinene from 2-pinene was obtained (Table 1). The selectivity values do not vary much with the kind of sulfate.

Catalytic activity of metal sulfates expressed by initial rates per unit weight or unit surface area of catalyst is also given in Table 1. The catalysts are arranged in the order of activity per unit weight of catalyst. Either the activity per unit weight or unit surface area was found to have no correlation with the electronegativity of metal ions. The relation between activity per unit weight of catalyst and the acidic property is given in Table 2. A tendency is seen for the sulfates to have weaker acid strength or less acid amount to show less activity.

We have found that the order of activity per unit weight of catalyst agrees better with the order of the infrared wave number of rocking mode of the water of crystallization: Ni(933) > Mg(883) > Co, Cd(875) > Zn(870) > Cu(865 cm^{-1})[7] Ni(928) > Mg(889) > Co(875) > Zn(872) > Cu(865) > Mn(828 cm^{-1}).[8] This agrees also with the order of the temeratures at which the monohydrates are converted into anhydrates.[7]

Ni(420) > Mg(354) > Co, Zn(320) > Cu(270) > Mn(260) > Cd(205 °C).

The order of the temperatures and the wave numbers is considered to show the order of the bond strengths between the water of crystallization and the metal ions of the monohydrates, since, in the case of metal amine complex, Nakamoto[10] points out that the higher the NH_3 rocking frequency, the stronger the metal-nitrogen bond. The catalytic activity seems to be related with the bond strengths. The fact that the distances between the water of crystallization and the metal ions of the monohydrates measured by X-ray diffraction[9] are related to the activity supports the view:

$Ni(2.0_6) > Zn(2.1_5) > Co(2.1_7) > Mn(2.2_5$ Å).

However, the reason for the intensive properties such as transition temperature and wave number being correlated with the activity per unit weight and not with the activity per unit surface area has not been clarified.

TABLE 2. ACID PROPERTY OF MONOHYDRATES OF METAL SULFATES

Catalyst	Acid amounts ($\times 10^2$ mmol/g) at various acid strengths (pK_a's)				
	−3.0	+1.5	+3.3	+4.8	+6.8
Ni(II)	4.0	6.4	6.1	6.4	—
Al(III)	0	13	—	—	—
Mg(II)	2.2	2.2	2.5	2.5	6
Co(II)	0.67[a]				
Cd(II)	0	0	0.1	0.3	0.4
Zn(II)	0.5	1.6	1.7	2.0	3
Ca(II)	0	0.2	0.3	0.7	1.4
Cu(II)	0	0.4	0.4	0.4	1.6
Mn(II)	0	0.2	0.1	0.2	0.2

a) Quoted from a paper by R. Ohnishi, S. Ishikura, and K. Tanabe, *Nippon Kagaku Kaishi*, **1973**, 183. A value at $pK_a = 1.00$.

References

1) K. Tanaka and A. Ozaki, *J. Catal.*, **8**, 1 (1967).
2) M. Misono, Y. Saito, and Y. Yoneda, *ibid.*, **9**, 135 (1967); **10**, 88 (1968).
3) I. Mochida, A. Kato, and T. Seiyama, *ibid.*, **22**, 23 (1971).
4) T. Takeshita, R. Ohnishi, T. Matsui, and K. Tanabe, *J. Phys. Chem.*, **69**, 4077 (1965).
5) O. Johnson, *ibid.*, **59**, 827 (1955).
6) R. Ohnishi, K. Tanabe, S. Morikawa, and T. Nishizaki, This Bulletin, **47**, 571 (1974).
7) L. Ben-dor and R. Margalith, *Inorg. Chim. Acta*, **1**, 49 (1967).
8) H. R. Oswald, *Helv. Chim. Acta*, **48**, 600 (1965).
9) Y. Le Fur, J. Coing-Boyat, and G. Bassi, *C. R. Acad. Sci., Paris, Ser. C*, **262**, 632 (1966).
10) K. Nakamoto, "Infrared Spectra of Inorganic and Coordination Compounds," 2nd ed., John Wiley & Sons, New York (1970) p. 154.

BULLETIN OF THE CHEMICAL SOCIETY OF JAPAN, VOL. 47(10), 2597—2598 (1974)

The Basic Compound Produced in the γ-Radiolysis of Liquid Nitrogen Containing Hydrocarbons

Kaname Ishizaki and Shin Sato

Department of Applied Physics, Tokyo Institute of Technology, Ookayama, Meguro-ku, Tokyo 152

(Received April, 2, 1974)

Synopsis. The *G*-values of the basic compounds produced in the γ-radilysis of liquid nitrogen containing hydrocarbons have been measured by Conway's method. The concentration dependence of the *G*-values suggests that the basic compounds observed are the products of the reaction between nitrogen atoms and the hydrocarbon radicals eventually formed in the system.

In spite of the considerable number of studies, our understanding of the reactions of nitrogen atoms with hydrocarbons is limited.[1] One of the main reasons is that we have no proper method to produce nitrogen atoms.[2] A few years ago, our laboratory started to use the γ-radiolysis of liquid nitrogen to produce nitrogen atoms.[3] Since small hydrocarbons are soluble in liquid nitrogen, even though the solubilities are not very large, we could investigate a part of the complicated reactions of nitrogen atoms with hydrocarbons. Our concern at that time was mainly with the formation of hydrogen cyanide and nitrile compounds. During these studies, we recognized that there were some other products which were polymeric and basic in nature. We, therefore, tried to measure the *G*-values of these basic products, our results will be reported below. Unfortunately, however, we are still not successful in identifing these products.

Experimental

The dried high-purity nitrogen was purchased from the Japan Oxygen Co., Ltd., and was used after passing it through sulfuric acid. All the hydrocarbons and hydrochloric acid gas were supplied by the Takachiho Shoji Co. The Nessler reagent was the product of the Kishida Chemical Co.

The samples for γ-irradiation were prepared in almost the same way as has been described before; *i. e.*, the amount of the hydrocarbon is first measured by the *p-v* method, using an oil manometer, and the hydrocarbon is condensed in a glass sampling tube. Then, pure nitrogen is introduced into the tube at 77 K under the pressure a little higher than the atmosphere. The nitrogen is then easily liquified. The amount of the liquid is measured by the scale plotted on the sampling tube. At the top of the tube, a joint is connected by small springs which are easily dislocated if a sudden rise of pressure occurs inside the tube.

The γ-irradiation was carried out in a liquid nitrogen-Dewar flask with the dose rate of 0.65×10^6 R hr^{-1}, usually for one hour.

After irradiation, the sampling tube was again connected to a vacuum system and the inside was slowly pumped out at 77 K. Usually, two hours were taken for complete evacuation. After the evacuation, a small amount of hydrochloric acid gas was introduced into the tube and the tube was warmed up to room temperature. Then, the tube was opened to the atmosphere, and 1 ml of distilled water was poured into it. The aqueous solution thus prepared was subjected to the following analysis.

If nitrogen-containing products are present in the form of ammonia, amine, or imine, the amount may be measured by Conway's method.[4] A half ml of an aqueous solution is put into the outer section of a Conway vessel, and on the other edge of this section is put 1 ml of K_2CO_3 (30 g ml^{-1}). In the middle section of the Conway vessel, 1 ml of 1/400 M H_2SO_4 is placed. The vessel is then covered tightly with a greased lid and is gently moved in order to mix the product solution and the K_2CO_3 solution. The vessel is warmed in an oven at 38 °C for two hours. After having been cooled to room temperature, the solution in the middle part of the vessel is placed in a 10-ml measuring flask. 1 ml of Nessler reagent is poured into this solution, and then distilled water is added up to 10 ml. When nitrogen-containing products are present, the solution is slightly colored yellow. The absorption of this solution at 430 nm is measured with a Beckman spectrometer against a blank sample exactly 20 min after the Nessler reagent is poured into the solution. The calibration curve was obtained by using ammonia as the test substance. The lowest detectable concentration was 10^{-8} g ml^{-1}.

Results

All of the results are summarized in Fig. 1. From this figure, the following three conclusions may be drawn: 1) The *G*-values of basic compounds are saturated in the order of the solubilities of hydrocarbons in liquid nitrogen. In the case of ethane, the reported solubility is a 7.8×10^{-3} mole fraction,[5] although this value is not fully reliable.[6] 2) The concentration dependence of the *G*-values is very similar to that of the *G*-values of the hydrocarbons produced in the same system, while it is quite different from that of nitrile compounds. One example is shown in Fig. 2. 3)

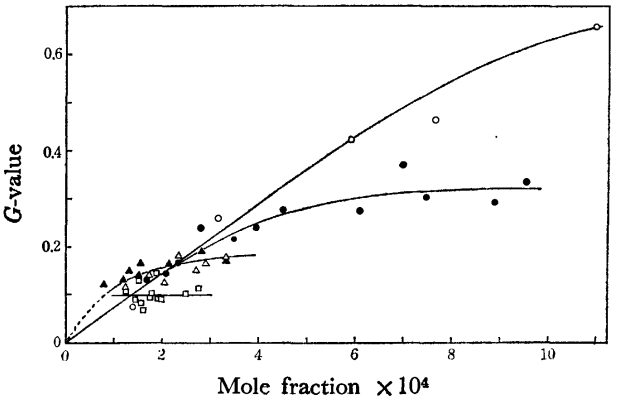

Fig. 1. *G*-Values of basic compounds as a function of the concentration of hydrocarbons.
○: ethane, ●: ethylene, △: propane, ▲: propylene, □: 1-butene.

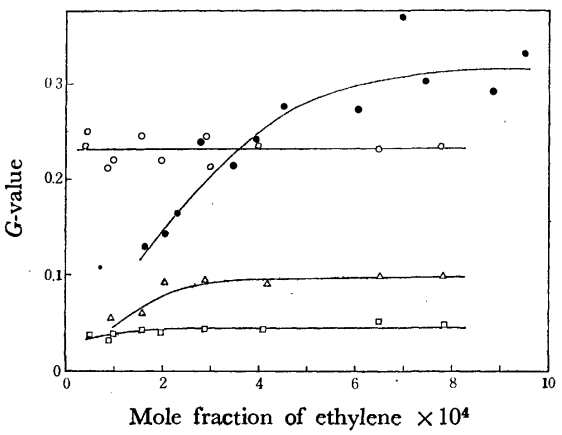

Fig. 2. *G*-Values of hydrogen cyanide (○), acetonitrile (□), acetylene ×10 (△), and basic compounds (●) from the liquid nitrogen solution of ethylene.

At the lowest concentration of hydrocarbons, the rate of formation of the basic compounds is faster for the larger hydrocarbons.

Discussion

In active nitrogen, the lowest excited state of the nitrogen molecule (A $^3\Sigma_u^+$) is known to be long in life (0.9 s). The formation of hydrocarbon radicals in the present system, therefore, may be due to this reaction:

$$N_2^*(^3\Sigma_u^+) + RH \rightarrow N_2 + R\cdot + H\cdot$$

In the case of olefins, the hydrogen atoms thus produced may add to the olefins:

$$R'CH{=}CH_2 + H\cdot \rightarrow R'CH\text{-}CH_3$$

These radicals may react with nitrogen atoms to produce basic compounds.

In the case of ethylene, a possible reaction mechanism for the formation of basic compounds may be described as follows:

$$N_2^* + C_2H_4 \rightarrow N_2 + C_2H_2 + H_2 \quad (1)$$

$$\searrow\ N_2 + C_2H_3\cdot + H\cdot \quad (2)$$

$$H\cdot + C_2H_4 \rightarrow C_2H_5\cdot \quad (3)$$

$$C_2H_3\cdot + C_2H_4 \rightarrow C_4H_7\cdot \quad (4)$$

$$RCH_2\cdot + \cdot N: \rightarrow RCH_2N: \ (R{=}CH_3 \text{ or } C_3H_5) \quad (5)$$

$$RCH_2N: \rightarrow RCH{=}NH \quad (6)$$

It is well known that an aliphatic imine such as RCH=NH polymerizes at room temperature and is easily hydrolyzed with water to aldehyde and ammonia. In fact, the aqueous solution we obtained in the present experiment showed the silver mirror reaction.

For the formation of nitrile compounds, we previously suggested the following reaction:

$$\cdot N: + RCH{=}CH_2 \rightarrow R\text{-}\overset{\overset{\curvearrowright}{\cdot}}{CH}\text{-}CH_2\cdot \rightarrow RCN + CH_3\cdot \quad (7)$$

$$\quad\quad\quad

BULLETIN OF THE CHEMICAL SOCIETY OF JAPAN, VOL. 47(10), 2599—2600 (1974)

ESR Spectra of Radicals during Photolysis of Chloranil in Solutions

Hiroshi YOSHIDA, Yoshihiko KAMBARA, and Bengt RÅNBY*

Faculty of Engineering, Hokkaido University, Kita-ku, Sapporo 060

(Received April 30, 1974)

Synopsis. ESR spectra were recorded during photolysis of chloranil in 2-propanol, ethanol, methanol and benzene at room temperature. The spectra observed from solution in alcohols are identified as due to neutral seqmiuinone radical. It is also suggested that excited chloranil abstracts a hydrogen from benzene.

Principal aims of this investigation are in the identification of electron spin resonance (ESR) spectra of short-lived intermediates formed during photolysis of chloranil (tetrachloro-*p*-benzoquinone) in alcohols and also in the confirmation by ESR method of the possibility that excited chloranil abstracts a hydrogen atom from benzene. Hales and Bolton observed a single line spectrum of 0.80 G width in the photolysis of chloranil in ethanol and methanol and attributed it to chloranil radical anion on the basis of its *g*-value.[1] Later, Wong *et al.* observed a spectrum of 0.58 G width from the 2-propanol solution and attributed it to neutral semiquinone radical of chloranil mainly on the basis of decay kinetics.[2] Identification of the spectra seems to be still uncertain because of the lack of hyperfine structure in it.

By a recent study of flash photolysis, optical absorption spectra attributable to both neutral semiquinone radical and radical anion were observed from the solution of chloranil in methanol.[3] One of the present author (H.Y.) and others studied short-lived intermediates during photolysis of *p*-benzoquinone and its methyl derivatives by ESR and found that both neutral radicals and radical anions are formed in alcohols.[4] These results also suggest the necessity of re-examination of the single line spectra observed from chloranil in alcohols. In addition, the flash photolysis study showed an interesting result that the neutral semiquinone radical is formed in the solution of chloranil in benzene, which is not believed to be a hydrogen donor. It may be worthwhile to detect ESR spectrum of the neutral radical to confirm this flash photolysis observation.

Experimental

All chemicals were analytical grade and used as received without further purification except that chloranil was recrystallized from chloroform.

ESR measurements were carried out at room temperature with a conventional X-band spectrometer (JEOL, Model JEX-ME) with a specially designed rectangular TE_{102} cavity during photolysis with light from a super-high pressure mercury arc (Philips, SP 500). Sample solutions were purged with helium gas to remove dissolved oxygen for at least half an hour, flowed through quartz flat cell in the cavity at a 4 ml/min and photolyzed with the light through a grid wall of the cavity.

Results and Discussion

Alcohol Solutions. Figure 1a shows a typical ESR spectrum observed from solution of chloranil in 2-propanol during photolysis. It is a single line spectrum without resolved hyperfine structure, as reported previously,[1] and its width (peak-to-peak width in derivative curve) is 0.55 G. The lifetime of the spectrum is shorter than the response time of the spectrometer used (0.3 s). No change is observed in the spectral shape and intensity by adding acetic acid to the solution. This fact strongly suggests that the spectrum is due to the neutral semiquinone radical rather than the radical anion, because radical anions are readily transformed to neutral radicals by protonation reaction in acidic solutions in the case of *p*-benzoquinone and its methyl derivatives.[4]

When chloranil is reduced by sodium methoxide in isopropanol, a stable single line spectrum of 0.43 G width is observed without light. It is attributed to the radical anion of chloranil. The intensity of the

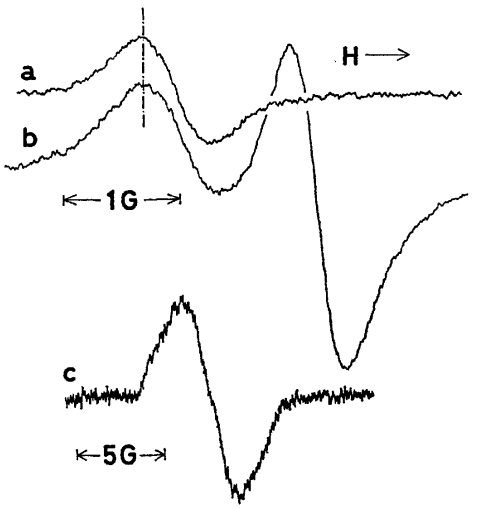

Fig. 1. ESR spectra observed at 20 °C during photolysis of solution of 1 mM chloranil (a) in isopropanol, (b) in 2-propanol with a small amount of sodium methoxide in it, and (c) in benzene. The vertical line gives a base for comparing the magnetic field position of the spectra (a) and (b) relative to each other. The signal curve (c) gives only the spectral shape and no information about the magnetic field position relative to that of (a) and (b).

* On leave from Royal Institute of Technology, Stockholm, as a visiting professor supported by Japanese Society for Promotion of Sciences during the period March—June, 1973.

spectrum is strong and depends on the concentration of methoxide. Figure 1b shows spectra recorded from the solution of chloranil in 2-propanol in the presence of low concentration of sodium methoxide during photolysis. The spectrum at lower field is the photo-induced unstable spectrum, which corresponds to that in Fig. 1a. The spectrum at higher field is the stable one just mentioned above. Coexistence of the two spectra during the photolysis indicates that the unstable spectrum is attributed to the neutral semiquinone radical formed by the hydrogen abstraction from solvent molecule by excited chloranil.

The *g*-value of the chloranil radical anion is smaller by 0.0008 than that of the corresponding neutral radical This contrasts to the absence of significant difference in *g*-value between radical anion and neutral radical formed from p-benzoquinone in ethanol (see the spectra in Fig. 1 of Ref. 4 and in 2-propanol.[2] Chlorine atoms having a large spin-orbit coupling constant may have caused a significant change in *g*-value, when the electronic state is modified by the attachment of a proton to the chloranil radical anion to form the neutral radical.

Observations are the same for the solution of chloranil in methanol or ethanol as solvent instead of 2-propanol. The unstable spectrum shows the width of 0.63 and 0.62 G in methanol and ethanol, respectively. The width of the stable spectrum is 0.49 G in methanol and 0.43 G in ethanol. The coexistence of the two spectra indicates that the photoinduced unstable spectrum is due to the neutral semiquinone radical in all alcohols examined.

As a conclusion, the ESR spectra observed during photolysis of chloranil in alcohols are due to the neutral radical regardless of which alcohol is used as solvent. This conclusion does not exclude the assignment of the optical absorption spectra observed by the flash photolysis study that they are due to both the neutral radical and the radical anion,[3] because the time scale of measurements is very much different between these two methods. It may be worth noting that the ESR spectrum of only the neutral radical is observed during photolysis of chloranil, while the spectra of both the neutral radical and the radical anion are simultaneously observed during the photolysis of benzoquinone and its methyl derivatives in the same solvents.

Benzene Solution. Figure 1c shows the spectrum observed from solution of chloranil in benzene during photolysis. The spectrum has a width of 3.4 G without resolved hyperfine structure, which is much wider than the spectrum of neutral semiquinone radical formed from chloranil in aprotic solvent of dioxane.[2] Although the reason why the present spectrum in benzene is so much wider is not known at this moment, it is suggested to be due to the neutral semiquinone radical, because the addition of acetic acid causes no change in the shape and intensity of the spectrum. The integrated intensity of the spectrum is comparable to or somewhat larger than that of the unstable spectrum observed from the alcohol solutions under the measuring conditions unchanged. The presence of dissolved oxygen reduces remarkably the efficiency of radical formation.

The above interpretation of the spectrum may raise a question what the excited chloranil abstracts a hydrogen atom from. Even if 5 vol% of isopropylbenzene is added as hydrogen donor into the solution, no increase is found in the intensity of the spectrum. The photolysis of chloranil in toluene gives the same spectrum as in the benzene solution, the intensity of which is also the same as in benzene. These results infer that the photochemical reactions involved are rather complex but the excited chloranil molecule abstracts a hydrogen atom from the benzene ring. The above interpretation is consistent with the previous flash photolysis study where transient optical absorption bands observed from the solution of chloranil in benzene were attributed to the neutral semiquinone radical.[3]

In addition to the main broad spectrum, spectra composed of several sharp hyperfine lines of 0.25 G width are traced from both the benzene and toluene solutions. However, the spectra are too weak to be recorded clearly. They are believed to be due to free radicals formed from solvent molecules, and their identification, if possible, may give an essential information of the reaction involved.

References

1) B. J. Hales and J. R. Bolton, *Photochem. Photobiol.*, **12**, 239 (1970).

2) S. K. Wong, L. Fabes, W. J. Green, and J. K. S. Wan, *J. Chem. Soc., Faraday Trans. I*, **68**, 2211 (1972).

3) K. Kawai, Y. Shirota, H. Tsubomura, and H. Mikawa, This Bulletin, **45**, 77 (1972).

4) H. Yoshida, K. Hayashi, and T. Warashina, *ibid.*, **45**, 3515 (1972).

BULLETIN OF THE CHEMICAL SOCIETY OF JAPAN, VOL. 47(10), 2601—2602 (1974)

The Crystal Structure of *dl*-Bi-1,4-dioxanyl

Akio FURUSAKI, Shunjiro MISUMI, and Takeshi MATSUMOTO

Department of Chemistry, Faculty of Science, Hokkaido University, Sapporo 060

(Received May 24, 1974)

Synopsis. The two forms of bi-1,4-dioxanyl (mp 157.5—158.0 °C and 133.5—134.0 °C), obtained by the photochemical reaction of 1,4-dioxane with acetophenone, have been assigned unequivocally to the *meso* and *dl* forms respectively by the X-ray method.

In the absence of copper ions, the photochemical reaction of 1,4-dioxane with *t*-butyl peracetate yielded two isomeric products ($C_8H_{14}O_4$), mp 157 °C and 132 °C.[1] From the results of microanalyses and molecular-weight determinations, it was inferred that one product was the *meso* form of bi-1,4-dioxanyl and the other was the *dl* form. It has recently been found in this laboratory that the same products, mp 157.5—158.0 °C and 133.5—134.0 °C, are obtained also by the photochemical reaction of 1,4-dioxane with acetophenone.[2] In order to assign unambiguously the configurations of these two products, an X-ray crystallographic analysis has been made on the product with the lower melting point.

The crystals are monoclinic, with four molecules in a unit cell of the dimensions; $a=12.198\pm0.004$, $b=4.645\pm0.002$, $c=14.660\pm0.004$ Å, and $\beta=93.56\pm0.07°$. These dimensions were measured on a single-crystal diffractometer using Cu$K\alpha$ radiation ($\lambda=1.54178$ Å). The calculated density is 1.395 g/cm^3. The systematic absences, hkl for $h+k=2n+1$ and $h0l$ for $l=2n+1$, showed that the space group was either Cc or C2/c. At the beginning of the study, the latter was assumed; this choice was confirmed later by successful refinement. A crystal with dimensions of about $0.1\times0.2\times0.5$ mm was used, and the intensity data were collected on a Rigaku automatic four-circle diffractometer using Cu$K\alpha$ radiation monochromatized with a LiF crystal. The intensities were corrected for the usual Lorentz and polarization factors, but not for either the absorption or the extinction effect. In the range of 2θ values up to 140°, 693 structure factor magnitudes above $2\sigma(F)$ were selected for the structural study.

The structure was solved by the symbolic addition procedure using 148 $|E|$ values above 1.30. Approximate positions of all non-hydrogen atoms were obtained from an *E*-map based on 143 phases. These atomic coordinates were refined by the block-diagonal-matrix least-squares method, at first with isotropic and then with anisotropic thermal parameters. A difference Fourier map yielded the locations of all 7 hydrogen atoms. Further least-squares refinement including these hydrogen atoms with isotropic temperature factors was carried out. In this refinement, the following weighting scheme was introduced:

$$W = 1/\{\sigma(F)^2 \exp(AX^2 + BY^2 + CXY + DX + EY)\}$$

where $X=|F_o|$ and $Y=\sin\theta/\lambda$. The coefficients, *A*, *B*, *C*, *D*, and *E*, are constants which have been determined from $(\Delta F)^2$ values. The *R* value reached 4.9%. The atomic parameters are listed in Table 1. The tables of the observed and calculated structure factors are preserved by the Chemical Society of Japan (Document No. 7422). The atomic scattering factors were taken from International Tables for X-ray Crystallography, Vol. III. All calculations were performed on a FACOM 230—60 computer at the Computer Center of Hokkaido University.

TABLE 1. THE FINAL ATOMIC PARAMETERS AND ESTIMATED STANDARD DEVIATIONS

(a) The non-hydrogen atoms

The parameters are multiplied by 10^5. The anisotropic temperature factors are defined as $\exp(-\beta_{11}h^2-\beta_{22}k^2-\beta_{33}l^2-\beta_{12}hk-\beta_{23}kl-\beta_{31}lh)$.

Atom	x/a	y/b	z/c	β_{11}	β_{22}	β_{33}	β_{12}	β_{23}	β_{31}
O(1)	40912(8)	25075(23)	4892(6)	576(6)	3719(40)	277(3)	−398(27)	515(21)	−140(7)
O(2)	38420(7)	1914(20)	22488(6)	384(4)	3428(36)	290(3)	−533(23)	278(20)	−15(6)
C(1)	45399(8)	26213(23)	21255(7)	375(6)	2466(41)	290(4)	−14(30)	48(24)	−6(8)
C(2)	49771(10)	25617(31)	11740(8)	436(7)	4023(56)	279(4)	−389(35)	332(28)	−14(9)
C(3)	34243(11)	348(30)	6160(8)	574(7)	3216(48)	316(5)	−137(34)	−24(27)	−167(9)
C(4)	29696(10)	1087(32)	15516(9)	396(6)	4037(57)	374(5)	−360(36)	103(30)	−79(9)

(b) The hydrogen atoms

The positional parameters are multiplied by 10^3.

Atom	x/a	y/b	z/c	B(Å^2)	Atom	x/a	y/b	z/c	B(Å^2)
H(1)	414(2)	431(4)	220(1)	1.2(3)	H(3-2)	283(2)	5(5)	14(1)	1.8(3)
H(2-1)	543(2)	89(5)	110(1)	1.6(3)	H(4-1)	250(2)	180(5)	159(2)	1.8(4)
H(2-2)	539(2)	426(5)	106(2)	2.2(4)	H(4-2)	256(2)	−158(6)	166(2)	2.2(4)
H(3-1)	386(2)	−174(5)	57(1)	1.5(3)					

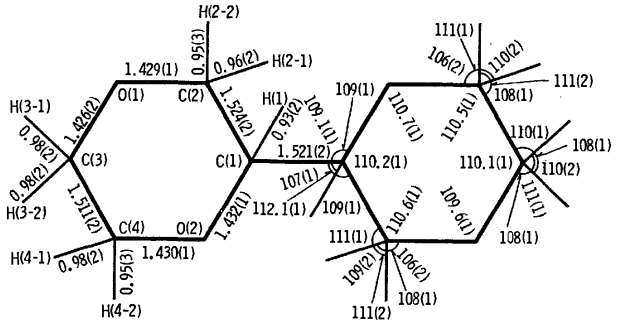

Fig. 1. The bond distances (Å) and angles (°).

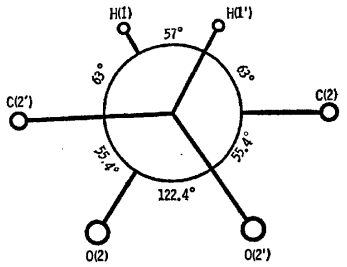

Fig. 2. The Newman projection along the C(1)-C(1′) bond.

As is shown in Fig. 3, the present molecule has the C_2 symmetry. Thus, out of the two crystalline forms of bi-1,4-dioxanyl, the one with the melting point of 133.5—134.0 °C is assigned to the *dl* form.

The bond distances and angles are given in Fig. 1. The dioxane rings in a molecule have normal chair-forms, with the C(1)–C(1′) bond oriented equatorially, and the molecule takes such a staggered conformation around the C(1)–C(1′) bond as is shown in Fig. 2.

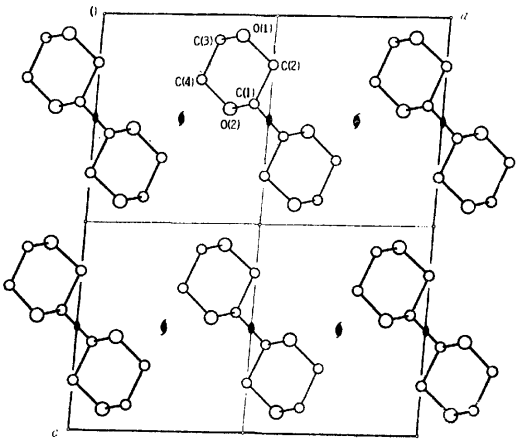

Fig. 3. The molecular arrangement viewed along the *b* axis.

This conformation, in which the largest groups, $C(2)H_2$ and $C(2')H_2$, are farthest from each other, is probably the most stable of the three possible staggered ones. The average of three independent C–C bond distances, 1.519 Å, is somewhat smaller than the normal distance for C–C, while the average of four C–O distances, 1.429 Å, is in good agreement with the standard value, 1.43 Å.

The crystal structure viewed along the *b* axis is shown in Fig. 3. The molecules are held together mainly by the van der Waals interactions.

References

1) G. Sosnovsky, *J. Org. Chem.*, **28**, 2934 (1963).
2) S. Misumi and T. Matsumoto, The 28th Annual Meeting of the Chemical Society of Japan, Tokyo, April, 1973; Preprint, Vol. III, p. 1559 (1973).

BULLETIN OF THE CHEMICAL SOCIETY OF JAPAN, VOL. 47(10), 2603—2604 (1974)

A Study on the Hydrolysis of Cadmium Ion in Aqueous 3M (Li)ClO_4 Solution

Haruo MATSUI* and Hitoshi OHTAKI

Department of Electrochemistry, Tokyo Institute of Technology, O-okayama, Meguro, Tokyo 152

(Received April 25, 1974)

Synopsis. The equilibrium constants of hydrolytic reactions of cadmium ion have been determined in a 3M (Li)ClO_4 aqueous medium at 25 °C as follows: log $*\beta_{1,1}=-10.3\pm0.1$ and log $*\beta_{1,2}=-9.13\pm0.01$.

Concerning the hydrolytic reactions of cadmium ion many authors reported the formation of mononuclear complexes.[1–6] The work by Biedermann and Ciavatta[7] was the only case in which polynuclear complexes were found. They prepared the solution by the addition of CdO powder to a slightly acidic 3M (Li)ClO_4 solution containing a suitable amount of $Cd(ClO_4)_2$, stirring the resulting mixture for about half a day. The supernatant was then subjected to titration. Schindler,[5] however, stated that a much longer time is required in order to establish an equilibrium between solid CdO (or $Cd(OH)_2$) and the aqueous phase which is saturated with hydroxo complexes of cadmium ions. Experiments we carried out for the preparation of test solutions containing hydrolyzed cadmium ions showed that a white precipitate is gradually formed after the CdO powder, turned white due to the formation of $Cd(OH)_2$ on the surface, has been removed from the solution which should be left to stand for at least ten days under agitation.

From these observations the question arose as to whether some polynuclear complexes really can be present as equilibrium species of hydrolyzed cadmium ions in solution. We have reexamined the procedure of Biedermann and Ciavatta[7] in order to confirm the formation of polynuclear complexes of hydrolyzed species of cadmium ions.

Experimental

Reagents and Apparatus. Cadmium perchlorate was prepared by dissolving CdO (99.99%, Mitsuwa Pure Chemicals Co., Osaka) in 1 : 1 $HClO_4$ (reagent grade). The purity of the cadmium oxide was checked by emission spectroscopy. The cadmium perchlorate was recrystallized twice from water.

Lithium perchlorate was prepared according to the method of Biedermann and Ciavatta.[7]

An Orion Digital pH Meter Model 801 was used in combination with a Beckman Glass Electrode No. 40498 and a Silver-Silver Chloride electrode.

A Metrohm E 211 A Type coulometer was employed as a current source for generation of hydrogen ions in a solution during the course of titration.

Preparation of Test Solutions. A small amount of CdO powder was added to 50 ml of a lithium perchlorate solution containing a suitable amount of $Cd(ClO_4)_2$, the total concentration of perchlorate ion being kept at 3M, and that of cadmium ion in the range 0.2261—1.401 M. The mixture was allowed to stand 3—7 days under agitation in nitrogen atmosphere and white precipitates formed were removed with a set of G-3 and G-4 glass filters. The filtrate was left to stand 7—20 days. When a precipitate was recognized in the solution, the solution was filtered again with the G-3 and G-4 glass filters. A twenty-five milliliter portion of the clear solution was used for emf measurements.

The method of measurement was essentially the same as those described previously.[8–10] All the measurements were carried out at 25.00 °C±0.01 °C. 3M (Li)ClO_4 was used as an ionic medium.

Results and Discussion

The results are given in Fig. 1 as the plot, Z *vs.* $-\log h$, where Z denotes the average number of hydrogen ions set free per cadmium atom and h the concentration of hydrogen ion at equilibrium. Since the Z values are low, the concentration of free cadmium ion (b) can approximately be made equal to the concentration of total cadmium (B) in preliminary calculations. Thus,

$$BZ = \sum_p \sum_q p[Cd_q(OH)_p{}^{(2q-p)+}] = \sum_p \sum_q p*\beta_{p,q}B^q h^{-p}$$

where

$$*\beta_{p,q} = [Cd_q(OH)_p{}^{(2q-p)+}][H^+]^p/[Cd^{2+}]^q.$$

Plots of Zh *vs.* h^{-1} gave a set of horizontal lines with intercepts dependent on B. A family of curves drawn according to a normalized function $y=x=f(\log x)$ fitted the Z *vs.* $-\log h$ plots. We thus conclude that the species formed are only the $CdOH^+$ and Cd_2OH^{3+}

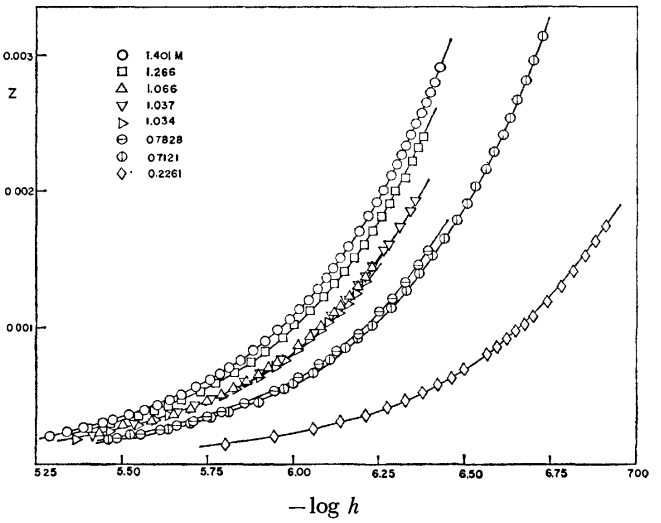

Fig. 1. The average number of hydrogen ion set free per cadmium atom Z plotted against $-\log h$. The solid lines show calculated curves using values finally obtained. The experimental data are available by request.

* Research fellow from the Government Industrial Research Institute of Nagoya, Kita-ku, Nagoya 462

complexes and the $Cd_4(OH)_4^{4+}$ complex proposed by Biedermann and Ciavatta was not formed.

The formation constants of the $CdOH^+$ and Cd_2OH^{3+} complexes were finally determined by means of a generalized least-squares method with the help of an electronic computer HITAC 8700. The values obtained were as follows:

$$\log {}^*\beta_{1,1} = -10.3 \pm 0.1$$
$$\log {}^*\beta_{1,2} = -9.13 \pm 0.01$$

These values agree with those reported by Biederamnn and Ciavatta ($\log {}^*\beta_{1,1} = -10.2 \pm 0.1$ and $\log {}^*\beta_{1,2} = -9.10 \pm 0.05$).

The maximum values of Z we obtained ($Z_{max} \approx 0.003$) were much lower than theirs ($Z_{max} = 0.01 \sim 0.02$). This suggests that the $Cd_4(OH)_4^{4+}$ complex and any other highly polymerized complexes, if formed at all, were unstable and precipitated and could not be present as equilibrium species of hydrolyzed cadmium ions in the solution.

References

1) C. Kullgren, *Z. Phys. Chem.*, **85**, 466 (1913).
2) N. Löfman, *Z. Anorg. Chem.*, **107**, 241 (1919).
3) Y. Marcus, *Acta Chem. Scand.*, **11**, 690 (1957).
4) K. H. Gayer and L. J. Wootner, *J. Phys. Chem.*, **61**, 364 (1957).
5) P. Schindler, *Helv. Chim. Acta*, **42**, 2736 (1959).
6) D. Dyrssen and P. Lumme, *Acta Chem. Scand.*, **16**, 1785 (1962).
7) G. Biedermann and L. Ciavatta, *ibid.*, **16**, 2221 (1962).
8) H. Ohtaki and G. Biedermann, This Bulletin, **44**, 1822 (1971).
9) H. Ohtaki and T. Kawai, *ibid.*, **45**, 1735 (1972).
10) T. Kawai, H. Otsuka, and H. Ohtaki, *ibid.*, **46**, 3753 (1973).

BULLETIN OF THE CHEMICAL SOCIETY OF JAPAN, VOL. 47(10), 2605—2606 (1974)

Phase Diagrams of the Binary Systems of Some Metal β-Diketonates[1]

Isao YOSHIDA, Hiroshi KOBAYASHI, and Keihei UENO

Department of Organic Synthesis, Faculty of Engineering, Kyushu University, Hakozaki, Higashi-ku, Fukuoka 812

(Received April, 30, 1974)

Synopsis. Phase diagrams of the binary systems consisting of some unchanged β-diketone chelates were determined. A combination of the chelate compounds which had the same coordination structures gave a mixed crystal system, and that of different coordination structures gave a eutectic system.

Separation of an impurity from a matrix compound by zone refining is governed by their solid-liquid phase diagram. A great number of phase diagrams have been determined on metals and inorganic and organic substances. However, those of metal chelate compounds are little known, and this is, in part, due to their thermal instabilities such as decomposition prior to melting.

We have prepared a certain range of metal 1,5-dialkylpentane-2,4-dionates which are stable enough in molten state without any decomposition, in connection with their application to zone refining.

This note is to report on the solid-liquid phase diagrams of binary mixtures consisting of such chelate compounds with common ligands.

Experimental

Materials. All the chelates were reported previously,[2,3] except $Zr(DNPM)_4$ and $Hf(DNPM)_4$, where DNPM stands for a dipropionylmethanate anion. The last two chelates were prepared by an addition of aqueous sodium carbonate into a water-methanol mixture containing the β-diketone ligand and a metal oxychloride (4 : 1 mole ratio of a ligand to a metal ion) until pH 6. Yellow tinged white precipitate was collected by filtration, then recrystallized from aqueous methanol to yield white needles. mp 59.0—60.0 °C, Found: C, 55.59; H, 7.24%. Calcd for $C_{28}H_{44}O_8Zr$: C, 56.09; H, 7.34%, λ_{max} in cyclohexane 272 nm, log ε_{max} 4.53. mp 54.0—55.0 °C, Found: C, 48.61; H, 6.61%. Calcd for $C_{28}H_{44}O_8Hf$: C, 48.96; H, 6.41%, λ_{max} in cyclohexane 272 nm, log ε_{max} 4.57.

Measurements. Temperatures of phase transitions were determined by differential thermal analysis method[4,5] with 3—6 mg of chelate samples of various compositions on a Rigakudenki Thermoflex 8001, α-alumina powder being used as a reference meterial. The heating rates were kept constant in the region of 10—15 °C/min. Electronic spectra were measured at room temperature with a Hitachi 124 double beam spectrophotometer in appropriate solvents.

Results and Discussion

A $Pd(DNBM)_2$-$Cu(DNBM)_2$ system forms mixed crystal over the entire range of compositions, as shown in Fig. 1. Binary systems which form mixed crystals are summarized in Table 1.

Figure 2 shows the eutectic phase diagram of a $Zr(DNPM)_4$-$Be(DNPM)_2$ system. Some other eutectic system are listed in Table 2.

Table 1. Binary systems for mixed crystal

Compound[a]	mp(°C)	Compound[a]	mp(°C)	Coord. Structure
$Al(AA)_3$	191	$Cr(AA)_3$	217	O_h-O_h[b]
$Rh(AA)_3$	260	$Cr(AA)_3$	217	O_h-O_h[b]
$Zr(DNPM)_4$	60	$Hf(DNPM)_4$	55	c)
$Pd(DNBM)_2$	134	$Cu(DNBM)_2$	161	D_{4h}-D_{4h}
$Pd(DIVM)_2$	136	$Cu(DIVM)_2$	162	D_{4h}-D_{4h}
$Fe(DIVM)_3$	51	$Co(DIVM)_3$	53	O_h-O_h

a) AA and DIVM stand for acetylacetonate and diisovalerylmethanate anions, respectively. b) Ref. 5. c) Archimedean antiprism-Archimedean antiprism.

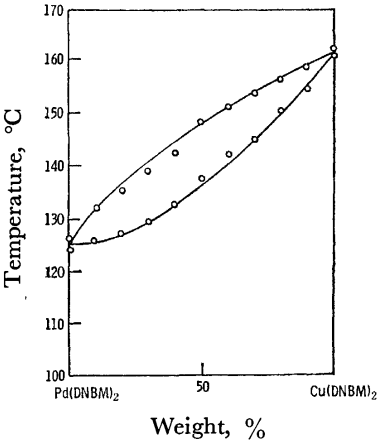

Fig. 1. Phase diagram of the binary system $Pd(DNBM)_2$-$Cu(DNBM)_2$, where DNBM stands for a dibutyrylmethanate anion.

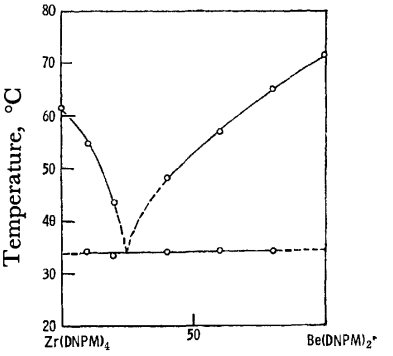

Fig. 2. Phase diagram of the binary system $Zr(DNPM)_4$-$Be(DNPM)_2$.

Absorption maxima of the π-π, d-d and d-π transitions in the present 1,5-dialkylpentane-2,4-dionates are essentially superimposable to those of the acetylacetonates with the same metal ions, respectively, though a

Table 2. Binary systems for eutectic

Compound(A)	mp(°C)	Compound(B)	mp(°C)	Eutectic Point		Coord. Structure
				mp(°C)	A%	
$Be(AA)_2$	110	$Cr(AA)_3$	217	98	83	T_d-O_h
$Be(AA)_2$	110	$Al(AA)_3$	195	97	72	T_d-O_h
$Zr(DNPM)_4$	60	$Be(DNPM)_2$	70	33	74	a
$Zr(DNPM)_4$	60	$Co(DNPM)_3$	53	32	60	b
$Fe(DIVM)_3$	51	$Cu(DIVM)_2$	162	49	98	O_h-D_{4h}
$Fe(DIVM)_3$	51	$Pd(DIVM)_2$	136	48	*ca.* 99	O_h-D_{4h}
$Be(DIVM)_2$	50	$Pd(DIVM)_2$	136	50	*ca.* 100	T_d-D_{4h}
$Be(DIVM)_2$	50	$Cu(DIVM)_2$	162	32	*ca.* 100	T_d-D_{4h}

a) Archimedean antiprism-T_d. b) Archimedean antiprism-O_h.

Table 3. Coordination and crystal structures of acetylacetonates

Compound	Cood. Structure	Crystal Structure					Reference
		a	*b*	*c*	*β*	Space Group	
$Co(AA)_3$	O_h	14.16	7.48	16.43	98	$P2_1/c$	7
$Al(AA)_3$	O_h	14.25	7.68	16.17	99	$P2_1/c$	8
$Rh(AA)_3$	O_h	13.94	7.51	16.43	98	$P2_1/c$	9
$Cr(AA)_3$	O_h	14.03	7.55	16.38	99	$P2_1/c$	8, 10
$Fe(AA)_3$	O_h	15.47	13.58	16.57		Pbca	11
$Cu(AA)_2$	D_{4h}	11.24	4.68	10.24	92	$P2_1/n$	12
$Pd(AA)_2$	D_{4h}	10.79	5.19	10.16	92	$P2_1/n$	13
$Be(AA)_2$	T_d	13.49	11.32	7.76	100	$P2_1$	14
$Zr(AA)_4$	a)	19.80	8.35	14.10	102	P2/c	15
$Hf(AA)_4$	a)						16

a) Archimedean antiprism.

few of them showing a slight increase in the ligand field due to the electronic effect of alkylsubstituents.[6] It is obvious, therefore, that the 1,5-dialkylpentane-2,4-dionates have the same coordination structures with those of the corresponding acetylacetonates. Coordination structures of the acetylacetonates are well known as listed in Table 3, as well as their crystal structures. The crystal structures therein seem to correlate with the coordination structures of the central metal ions, if the ligand is acetylacetonate anion in common.

Coordination structures of the present chelate compounds listed in Tables 1 and 2 are those presumed on the basis of the above presumption, except those of the acetylacetonates. One can readily notice that the combinations of chelates which form mixed crystals have the same coordination structures, and those forming eutectic have different ones.

In general, component substances of similar molecular structures afford a mixed crystal system of a substitution form. In the metal chelate compounds with a common ligand anion, the structural similarity requires not only the same coordination structure but also similar sizes of the central metal ions. Difference in ionic radii, 0.6 Å, between palladium(II) and copper (II) would be the largest among those of the combinations of metal ions which form metal chelates of the same coordination structures, and the chelates of these metal ions are still capable of forming a binary mixed crystal.

References

1) Contribution No. 333 from the Department of Organic Synthesis, Kyushu University.

2) I. Yoshida, H. Kobayashi, and K. Ueno, *J. Inorg. Nucl. Chem.*, **35**, 4061 (1973).

3) I. Yoshida, H. Kobayashi, and K. Ueno, This Bulletin, **47**, 2203 (1974).

4) M. J. Visser and W. H. Wallace, *Du Pont Thermogram*, **3**, 9 (1966).

5) H. Kaneko, H. Kobayashi, and K. Ueno, *Talanta*, **14**, 1403 (1967).

6) I. Yoshida, H. Kobayashi, and K. Ueno, This Bulletin, **45**, 2768 (1972).

7) V. M. Padmanabham, *Proc. Indian Acad. Sci.*, **47A**, 329 (1958). *Chem. Abstr.*, **52**, 17881h (1958).

8) E. A. Shugam and L. M. Shkolnikova, *Kristallografiya*, **1**, 478 (1956). *Chem. Abstr.*, **52**, 9708c (1958).

9) E. B. Parker and J. C. Morrow, *Acta Crystallogr.*, **21**, A147 (1966).

10) B. Morosin, *ibid.*, **19**, 131 (1965).

11) R. B. Roof, Jr., *ibid.*, **9**, 781 (1956).

12) E. G. Cox and K. C. Webster, *J. Chem. Soc.*, **1935**, 731.

13) E. A. Shugam, L. M. Shkolnikova, and V. V. Zelentsov, *Zh. Strukt. Khim.*, **7**, 128 (1966). *Chem. Abstr.*, **64**, 18555e (1966).

14) V. Amirthalingam, V. M. Padmanabham, and J. Shankar, *Acta, Crystallogr*, **13**, 201 (1960).

15) D. Grdenić and B. Matković, *ibid.*, **12**, 817 (1959).

16) E. M. Larsen, G. Terry, and J. Leddy, *J. Amer. Chem. Soc.*, **75**, 5107 (1953).

BULLETIN OF THE CHEMICAL SOCIETY OF JAPAN, VOL. 47(10), 2607—2608 (1974)

O–H Stretching Absorption and Conformation of the β-Methyl Derivatives of 1-Tetralol, 4-Chromanol, 4-Thiochromanol, and 4-Thiochromanol 1,1-Dioxide*

Kaoru HANAYA, Shinji ONODERA,** and Hideaki KUDO

Department of Chemistry, Faculty of Science, Yamagata University, Koshirakawa-cho, Yamagata 990

** *Chemical Research Institute of Non-Aqueous Solutions, Tohoku University, Katahira-2-chome, Sendai 980*

(Received November 29, 1973)

Synopsis. The conformation of eight benzyl alcohol derivatives has been examined by the measurements of OH stretching absorptions. Preference of the OH quasi-axial structure was shown.

The measurements of the OH stretching absorption bands of epimeric 1-tetralol, 4-chromanol, 4-thiochromanol, and 4-thiochromanol 1,1-dioxide were found to be useful for elucidation of their conformations and for estimation of their conformational free energies ($\Delta G°$).[1,2] A further study concerning OH conformation has been carried out for the epimers of the β-methyl derivatives of these compounds in carbon tetrachloride. The results are reported in this paper.

Results and Discussion

Table 1 shows the OH stretching absorption maxima of the β-methyl derivatives of 1-tetralol (**1**), 4-chromanol (**2**), 4-thiochromanol (**3**), and 4-thiochromanol 1,1-dioxide (**4**) together with their half-widths and intensities. We see that the OH absorption of the *cis*-epimers **1a, 2a, 3a,** and **4a** each shows a singlet band and the *trans*-epimers **1b, 2b, 3b,** and **4b** a doublet band. The lower frequency bands are stronger than the higher ones for the *trans*-epimers **1b** and **4b**, but weaker for **2b** and **3b**.

TABLE 1. ν_{OH} ABSORPTION MAXIMA OF THE β-METHYL DERIVATIVES OF 1-TETRALOL, 4-CHROMANOL, 4-THIOCHROMANOL, AND 4-THIOCHROMANOL 1,1-DIOXIDE

Compound[a)]	ν_{OH} (cm^{-1})	$\Delta\nu_{1/2}$ (cm^{-1})	ε
1a	3620	18	69
1b	3617	22	37
	3598	11	59
2a	3617	19	80
2b	3613	18	84
	3593	12	31
3a	3614	17	67
3b	3611	15	98
	3590	14	17
4a	3613.5	21	76
4b	3611	25	59
	3586	16	97

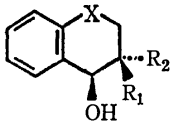

a) **1a** : X=CH_2, R_1=CH_3, R_2=H
1b : X=CH_2, R_1=H, R_2=CH_3
2a : X=O, R_1=CH_3, R_2=H
2b : X=O, R_1=H, R_2=CH_3
3a : X=S, R_1=CH_3, R_2=H
3b : X=S, R_1=H, R_2=CH_3
4a : X=SO_2, R_1=CH_3, R_2=H
4b : X=SO_2, R_1=H, R_2=CH_3

Referring to the preferred conformations of OH groups in 1-tetralol and 4-chromanols and their ν_{OH} bands,[2] the following consideration is given on the conformational equilibrium shown in Fig. 1. Since only a singlet band due to the axial OH group was observed for compounds **1a**, **2a**, **3a** and **4a**, it can be assumed that conformation A with the axial OH and equatorial CH_3 groups is decisively predominant over B.

Measurements for compounds **1b**~**4b** with *trans*-relation between the OH and CH_3 groups might be explained as follows. The axial OH conformation is usually predominant in such compounds if there is no other factor governing the conformation. The axial OH conformation, however, leads to the axial conformation of the CH_3 group as D, which will be unstable when X is a bulky group because of the steric repulsion with the CH_3 group. Thus, the 1,3-diaxial interaction between CH_3 and X would cause the preferential existence of the stable conformation C for **1b** and **4b** with bulky X. This is in line with the fact that a CH_3 group is more bulky than an OH group and has a larger conformational free energy than that of OH group in such a compound.[3] The "volume requirement" of the lone-paired electrons either on the oxygen atom in **2b** or the sulfur in **3b** will not cause sufficient 1,3-diaxial interaction for conversion of conformation. Such a small 1,3-diaxial interaction has been pointed out by Eliel and Knoeber[5] in their stereochemical study on *cis*-2-alkyl-4-butyl-1,3-dioxane, in which the axial conformation of the *t*-butyl group with a chair form was

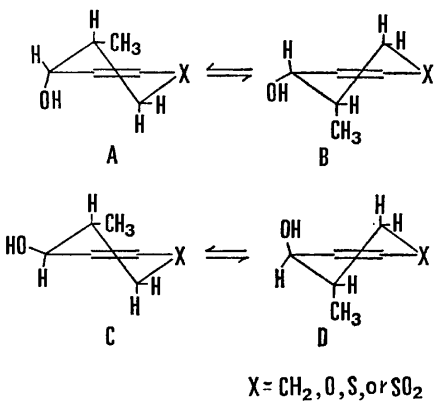

Fig. 1. Conformational equilibria for the β-methyl derivatives of 1-tetralol, 4-chromanol, 4-thiochromanol, and 4-thiochromanol 1,1-dioxide.

* A part of the study was presented at the 24th Annual Meeting of the Chemical Society of Japan, April, 2, 1971, Osaka.

Table 2. Temperature dependence of the OH stretching absorption band for *trans*-3-methyl-4-chromanol

Temperature °C	ν_{OH} cm^{-1}	ε_h	ν_{OH} cm^{-1}	ε_l	$\varepsilon_l/\varepsilon_h$
−20	3616	98	3588	35	0.35
0	3611	93	3588	35	0.37
23	3613	84	3592	31	0.37
55	3613	76	3591	32	0.42

Table 3. Temperature dependence of the OH stretching absorption band for *trans*-3-methyl-4-thiochromanol

Temperature °C	ν_{OH} cm^{-1}	ε_h	ν_{OH} cm^{-1}	ε_l	$\varepsilon_l/\varepsilon_h$
−23	3609	118	3588	18	0.15
0	3610	119	3588	22	0.19
23	3611	98	3590	17	0.17
55	3612	83	3591	17	0.21

predominant. They also suggested a small interaction between the *t*-butyl group and the sulfur atom in 5-*t*-butyl-4,6-dimethyl-1,3-dithiane on the basis of small conformational free energy.[6]

In order to confirm the conformational equilibrium (Fig. 1), the temperature dependence of the OH absorption was examined for **2b** and **3b** in the temperature range −23—55 °C. The results (Tables 2 and 3) indicate that the intensity of the lower frequency band increased with a rise in temperature for both **2b** and **3b**. This indicates that the stable form holds an axial OH conformation, supporting the above view. The $\Delta H°$ values were estimated to be 1.0 and 3.5 kcal·mol^{-1} for **2b** and **3b**, respectively.

Experimental

Materials. *cis*- and *trans*-2-Methyl-1-tetralols,[7] *cis*- and *trans*-3-methyl-4-chromanols[8] were prepared as reported. *cis*-3-Methyl-4-thiochromanol, *cis*- and *trans*-3-methyl-4-thiochroman ol1,1-dioxides were prepared by reduction with sodium borohydride or the Meerwein-Ponndorf reduction of the corresponding ketones. *trans*-3-Methyl-4-thiochromanol was prepared by the hydroboration-oxidation of 3-methyl-3-thiochromene.[9] *cis*-3-Methyl-4-thiochromanol (**3a**): mp 78—80 °C (lit.[9] 78—80 °C). *trans*-3-Methyl-4-thiochromanol (**3b**): mp 73—75 °C. Found: C, 66.40; H, 6.85%. Calcd for $C_{10}H_{12}OS$: C, 66.65; H, 6.71%. *cis*-3-Methyl-4-thiochromanol 1,1-dioxide (**4a**): mp 173—174.5 °C. Found: C, 56.75; H, 5.61%. Calcd for $C_{10}H_{12}O_3S$: C, 56.60; H, 6.70%. *trans*-3-Methyl-4-thiochromanol 1,1-dioxide (**4b**): mp 117—118 °C (lit.[10] 117—118 °C).

Instrumentation. The infrared spectra were measured with a Perkin-Elmer 125 or a JASCO DS-403G double beam grating high resolution infrared spectrophotometer. A KCl cell of 30 mm in optical length was used. The concentration of the solutions was *ca.* 0.005 mol/l in carbon tetrachloride, purified by distillation over phosphorus pentoxide. The band due to intermolecular hydrogen bonding was not observed at this concentration.

The authors wish to express their gratitude to Associate Professer Hiizu Iwamura, the University of Tokyo, for his valuable discussion and suggestions.

References

1) H. Iwamura and K. Hanaya, This Bulletin, **43**, 3901 (1970).
2) K. Hanaya, S. Onodera, S. Awano, and H. Kudo, *ibid.*, **47**, 509 (1974).
3) The conformational free energies ($-\Delta G°_{25}$) in the cyclohexyl derivatives are 1.7 and 0.6 kcal/mol for the methyl and hydroxyl groups, respectively.[4]
4) E. I. Eliel, *Angew. Chem.*, **77**, 784 (1965).
5) E. I. Eliel and M. C. Knoeber, *J. Amer. Chem. Soc.*, **90**, 3444 (1968).
6) R. O. Hutchins and E. I. Eliel, *ibid.*, **91**, 2703 (1969).
7) K. Hanaya, *Nippon Kagaku Zasshi*, **87**, 991 (1966).
8) K. Hanaya, This Bulletin, **43**, 442 (1970).
9) B. D. Tilak, H. S. Desai, C. V. Deshpande, S. K. Tain, and V. M. Vaidya, *Tetrahedron*, **22**, 7 (1966).
10) I. W. J. Still, and M. T. Thomas, *J. Org. Chem.*, **33**, 2730 (1968).

BULLETIN OF THE CHEMICAL SOCIETY OF JAPAN, VOL. 47(10), 2609—2610 (1974)

The Photoinduced Substitution Reaction of 4-Quinolinecarbonitrile

Norisuke HATA, Isao ONO, and Hiroshi SUZUKI

Department of Chemistry, College of Science and Engineering, Aoyama Gakuin University, Chitosedai, Setagaya-ku, Tokyo 157

(Received January 25, 1974)

Synopsis. The photochemical reactions of 4-quinolinecarbonitrile with alcohol (ethanol, 1-propanol, 2-propanol, or *t*-butyl alcohol) resulted in the substitution of the 1- and/or 2-hydroxyalkyl group at the 2-position of a quinoline nucleus.

As has been reported previously,[1-3] 2-quinolinecarbonitrile in alcoholic solvents undergoes a photochemical replacement of the cyano group at the 2-position of a quinoline nucleus by a hydroxyalkyl group in an atmosphere of oxygen, while, under a nitrogen atmosphere, a certain triazapentaphene is also produced in addition to the photosubstitution product. On the other hand, 3-quinolinecarbonitrile in methanol has been reported by Natsume and Wada to undergo the addition of methanol to afford 1,2-dihydro-2-hydroxymethylquinoline.[4] From the synthetic and mechanistic points of view, therefore, it is of interest to investigate whether 4-quinolinecarbonitrile is photochemically susceptible to the replacement of the cyano group by the hydroxyalkyl one or to the addition of alcohol to give 1,2-dihydro-2-hydroxyalkylquinoline.

4-Quinolinecarbonitrile[5] (0.5 g) dissolved in 350 ml of alcohol (ethanol, 1-propanol, 2-porpanol, or *t*-butyl alcohol) in a Pyrex vessel was irradiated with a 100W high-pressure immersion mercury lamp (Riko Kagaku Sangyo Co.) for 3 to 4 hr while oxygen was being bubbled in. After the removal of the solvent under reduced pressure, the residue was chromatographed on a slica-gel column by elution with dichloromethane to separate the products. As a result, as is shown in Table 1, white crystalline solids (Ia, Ic, Id, IIb, and IIc) and a colorless liquid (Ib) were isolated as the main products. The UV absorption spectra of these products were quite similar to that of 4-quinolinecarbonitrile; also, the IR spectra in KBr showed absorptions at 3200 cm^{-1} (O–H stretching), ~2900 cm^{-1} (aliphatic C–H stretching), and 2230 cm^{-1} (C≡N stretching).[6] The NMR spectra in $CDCl_3$ indicated the presence of a 1-hydroxyalkyl (Products Ia—Id) or 2-hydroxyalkyl group (Products IIb and IIc), which corresponds to the alcohol used as a reaction medium, at the 2-position of a quinoline nucleus.[7] In addition, the products were identified on the basis of the mass spectra[8] as well as by means of elemental analyses;

TABLE 1. ANALYTICAL DATA FOR THE PHOTOPRODUCTS

Solvent	Product 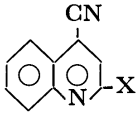	Mp (°C) Yield (%) Mass (M+)	NMR[a] (δ, ppm)	Elemental analysis Found (%)	Calcd (%)
Ethanol	(Ia) X=-CH(CH$_3$)OH	88 46 198	7.50—8.15 (m, 5H, aromatic) 5.00 (q, J=6.0 Hz, -C*H*(CH$_3$)OH) 3.85 (s, 1H, -O*H*)[c]	C 73.00 H 5.27 N 3.89	C 72.71 H 5.09 N 4.06 (for $C_{12}H_{10}N_2O$)
1-Propanol	(Ib) X=-CH(C$_2$H$_5$)OH	125—126[b] 24 212	7.41—8.30 (m, 5H, aromatic) 4.85 (q, J=4.8 Hz, 1H, -C*H*(OH)CH$_2$CH$_3$) 4.10 (s, 1H, -O*H*)[c] 1.45—2.30 (m, 2H, -CH(OH)C*H*$_2$CH$_3$) 0.99 (t, J=4.7 Hz, 3H, -CH(OH)CH$_2$C*H*$_3$)	$C_{13}H_{12}N_2O$[d]	
	(IIb) X=-CH(CH$_3$)CH$_2$OH	114—116 16 212	7.29—8.20 (m, 5H, aromatic) 3.96 (d, J=5.8 Hz, 2H, -CH(CH$_3$)C*H*$_2$OH) 2.90—3.50 (m, 1H, -C*H*(CH$_3$)CH$_2$OH) 1.35 (d, J=7 Hz, 3H, -CH(C*H*$_3$)CH$_2$OH)	$C_{13}H_{12}N_2O$[d]	
2-Propanol	(Ic) X=-C(CH$_3$)$_2$OH	110—111 25 212	7.45—8.25 (m, 5H, aromatic) 4.80 (s, 1H, -O*H*)[c] 1.65 (s, 6H, -C(C*H*)$_2$OH	C 73.20 H 5.73 N 13.00	C 73.58 H 5.66 N 13.21 (for $C_{13}H_{12}N_2O$)
	(IIc) X=-CH$_2$CH(CH$_3$)OH	100—103 19 212	7.34—8.22 (m, 5H, aromatic) 4.09—4.56 (m, 1H, -CH$_2$C*H*(CH$_3$)OH) 3.80 (s, 1H, -O*H*)[c] 1.34 (d, J=6.5 Hz, -CH$_2$CH(C*H*$_3$)OH)	C 73.31 H 5.73 N 13.23	C 73.58 H 5.66 N 13.21 (for $C_{13}H_{12}N_2O$)
t-Butyl alcohol	(Id) X=-CH$_2$C(CH$_3$)$_2$OH	94— 95 55 226	7.60—8.20 (m, 5H, aromatic) 4.10 (s, 1H, -O*H*)[c] 3.18 (s, 2H, -C*H*$_2$C(CH$_3$)$_2$OH) 1.32 (s, 6H, -CH$_2$C(C*H*$_3$)$_2$OH)	C 74.34 H 6.31 N 12.37	C 74.31 H 6.29 N 12.29 (for $C_{14}H_{14}N_2O$)

a) Measured in $CDCl_3$ solution using TMS as an internal standard. b) The picrate. c) Deuterium exchangeable. d) Estimated from the result of the mass analysis performed with a JEOL JMS-O1SG-2 mass spectrometer.

the analytical data are summarized in Table 1. The results definitely indicate that the 4-quinolinecarbonitrile in alcoholic solvents undergoes photochemically 1-hydroxyalkyl and/or 2-hydroxyalkyl substitution at the 2-position of a quinoline nucleus. Quite a similar photoreaction also occurred in an atmosphere of nitrogen.

The photoinduced-substitution reaction of 4-quinolinecarbonitrile is probably initiated by a hydrogen-atom abstraction from the alcoholic solvent by the ring nitrogen, just as in the case of 2-quinolinecarbonitrile.[3] It should be noticed that, in a 1- or 2-propanol solution, the product (IIb or IIc) arising from the β-hydrogen abstraction was obtained in addition to that from the α-hydrogen abstraction, quite unlike the case of 2-quinolinecarbonitrile. This could be interpreted as follows. In the case of 2-quinolinecarbonitrile, as has been discussed in a pervious paper,[3] the β-hydrogen abstraction from the alcohol hydrogen-bonded with the nitrogen of the quinoline nucleus is quite difficult because of the steric effect of a cyano group. On the other hand, such a steric hindrance does not exist in the case of 4-quinolinecarbonitrile, so the α- and β-hydrogen abstraction from 1- or 2-propanol by the ring nitrogen are considered to be possible, thus resulting in the IIb or IIc in addition to the Ib or Ic product.[9] In this respect, the present experimental results seem to support the idea that the photochemical hydroxyalkyl substitution reaction of 2- or 4-quinolinecarbonitrile in alcohol is initiated by a hydrogen-atom abstraction from the alcohol hydrogen-bonded with the nitrogen atom of the quinoline nucleus.[3]

References

1) N. Hata, I. Ono, and S. Ogawa, This Bulletin, **44**, 2286 (1971).
2) N. Hata, I. Ono, S. Matono, and H. Hirose, *ibid.*, **46**, 942 (1973).
3) N. Hata and T. Saito, *ibid.*, **47**, 942 (1974).
4) M. Natsume and M. Wada, *Tetrahedron Lett.*, **1971**, 4503.
5) The 4-quinolinecarbonitrile used in this expreiment was synthesized by treating 4-bromoquinoline with cuprous cyanide. I. Nakayama, *Yakugaku Zasshi*, **71**, 1391 (1951).
6) The UV absorption and the IR spectra were, respectively, determined with a Hitachi recording spectrophotometer EPS-3T and a JASCO infrared spectrophotometer IR-G.
7) The NMR spectra were measured with a Hitachi-Perkin Elmer NMR spectrometer R-20 at 60 MHz.
8) The mass spectra were obtained with a Hitachi RMU-6L or a JEOL JMS-OlSG-2 mass spectrometer.
9) However, such a remarkable difference between 2- and 4-quinolinecarbonitriles in the hydrogen abstraction reaction is also inferred to be due partly to the electronic effect of a cyano group.

BULLETIN OF THE CHEMICAL SOCIETY OF JAPAN, VOL. 47(10), 2611—2612 (1974)

The Determination of Ruthenium in a Sulfuric Acid Solution by Atomic Absorption Spectrophotometry

Reiko IWATA and Ikuei OGATA

National Chemical Laboratory for Industry, Honmachi, Shibuya-ku, Tokyo 151

(Received February 4, 1974)

Synopsis. The addition of sodium salts was found to make possible the determination of ruthenium in a sulfuric acid solution by atomic-absorption spectroscopy, something which is usually impossible because of the serious depressive interference of sulfuric acid.

We have recently synthesized a ruthenium complex which bears a polycyclic aromatic compound as a π-ligand and which is completely decomposable into a solution only with concentrated sulfuric acid. During the process of analyzing the ruthenium content by atomic absorption spectroscopy, we observed that sulfuric acid remarkably reduces the optical absorption of Ru. It has been reported that the atomic absorption of Ru is subject to various interferences; *e.g.*, Rowston and Ottaway[1] and Montford and Cribbs[2] have investigated the effects of various anions and cations, and Mallett *et al.*,[3] the mutual interference of noble metals. They eliminated the interferences through the addition of copper and cadmium sulphates[1] or uranium[2] as releasing agents. However, they studied only with aqueous and HCl solutions, and no reports have been made on the degree of interference encountered in a practical quantitative analysis of Ru in a sulfuric acid solution. Interference by H_2SO_4 has already been noted on other metals; it is generally eliminated by removing the sulfuric acid by vigorous fuming or by extraction with solvents. In the case of Ru, however, this technique could well cause a loss of Ru if the analysis were done by the inexperienced. The distillation of Ru as a volatile tetroxide is also recommended for the separation of Ru from complex mixtures, but it is troublesome and time-consuming, and a more direct approach would be advantageous.

After various studies, we would like to report here a very simple method in which sodium compounds are added to sample solutions.

The spectrophotometer used was a Techtron AA-100. Measurements were done with a fuel-rich air–acetylene flame[4] at a wavelength of 349.9 nm and a lamp current of 10 mA. The sample solutions used were prepared as follows: ruthenium acetylacetonate ($Ru(acac)_3$) was decomposed with concentrated acids, followed by the dilution of the resulting solutions to a Ru concentration of 50 ppm and also to stipulated values of the acid concentration. Acids of the Super-Special-Grade for precision analysis were used. The various foreign additives and acetylacetone used here were all of a reagent grade.

As may be seen in Fig. 1, which shows the interferences of H_2SO_4, HNO_3 and HCl, sulfuric acid remarkably suppressed the absorption of Ru; the absorbance was of the order of 0.01 even at a Ru concentration of 50 ppm. Therefore, the quantitative analysis of Ru in a sulfuric acid solution was practically impossible. Though not so large as H_2SO_4, nitric acid showed a fairly large suppressive effect. Further, during the process of decomposition by the boiling of $Ru(acac)_3$, $RuCl_3$, and other ruthenium-containing samples in concentrated HNO_3, a loss of Ru, presumably as a volatile oxide, was observed. Therefore, the use of HNO_3, which is generally used for atomic-absorption analysis as a less interferant acid, is undesirable in the case of Ru. Hydrochloric acid showed the least interference of the three.

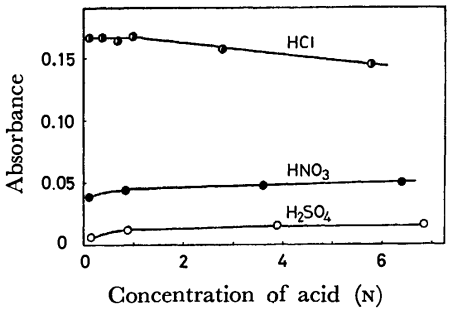

Fig. 1. Relations between interference and concentration of acids. Concentration of Ru: 50 ppm (in the cases of H_2SO_4 and HNO_3), 49 ppm (in the case of HCl).

When a large excess of acetylacetone to Ru was added to a sulfuric acid solution of Ru and the solution was allowed to stand at 50 °C, it gradually developed a pink color, indicating the formation of an acetylacetone chelate, while the absorbance increased. With the addition of 8 vol% of acetylacetone, about 5.6 times enhancement was observed in the 0.85 N H_2SO_4 solution of 48 ppm of Ru. Although the interference of H_2SO_4 can be removed in this way to a certain degree, the demerit is that this method requires a long time for the absorbance to become constant (about 10 hr).

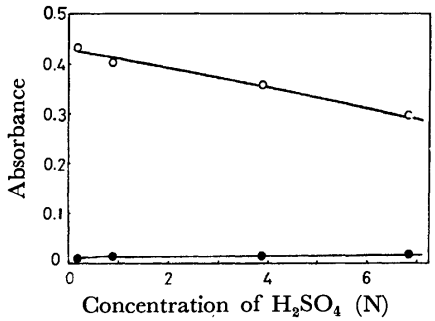

Fig. 2. Enhancement of atomic absorption of ruthenium by addition of sodium bicarbonate.
Concentration of Ru: 50 ppm. ●: without $NaHCO_3$, ○: with $NaHCO_3$ (25.2 mg/ml).

The further addition of $NaHCO_3$ to this solution containing acetylacetone in order to make the transformation of a sulfate into an acetylacetonate more efficient caused a further prominent increase of the absorbance. From the following experiments, however, it was found that this enhancement effect was not due to the formation of an acetylacetone chelate.

The addition of $NaHCO_3$ to the sample solution, even without acetylacetone, made the atomic absorption of Ru increase greatly as shown in Fig. 2. The same, but only a slight, effect of sodium salt has been reported in the case of the HCl solution of $H_2[RuCl_6]$ by Makarov and Kukushkin.[5] If the acid concentration was high, the degree of the enhancement decreased. The enhancement effect was smaller in a less interferant acid; *i.e.*, the magnitudes of the enhancement effect were in the order of $H_2SO_4 \gg HNO_3 > HCl$.

The study of the relation between the added amounts of $NaHCO_3$ and the enhancement effect revealed that the most appropriate amount of addition should be determined not on the basis of the concentration of the acid but on the basis of that of the $NaHCO_3$ in the solution. In a Ru solution of 50 ppm, it is over 4 mg/ml; especially, the range of 10–30 mg/ml is the most appropriate. When the amount of $NaHCO_3$ added was too large, the absorption tended to decrease. Further, as the amount added increases, a defective outcome develops since a separated salt attaches to the slit of the burner.

The relation between the kind of foreign additives and the enhancement effect was also studied. Table 1 shows a comparison on the basis of the relative ratio of absorbance, where the absorbance in the case of no foreign additive is defined as 1.0. Sodium compounds caused almost the same degree of enhancement, no matter what the counter anion was; this was also true in the cases of alkali and salt. Therefore, it can be seen that the enhancement is caused by Na. The effects of various sodium salts in aqueous and HCl solutions have been reported;[2] they are very complex and are not similar to those in our case of a sulfuric acid solution; some sodium compounds increased the absorbance, while some reduced it. A comparison of NaCl, $CoCl_2$, and $ZnCl_2$ showed that the higher the ionization potential of the metal, the lower the degree of relative enhancement. It is said that NH_4Cl is effective in suppressing the interference of H_2SO_4 in the determination of Mo,[6] but it caused only a very low enhancement in the case of Ru.

Table 1. Comparison of enhancement effect of foreign additives by relative ratio of absorbance[a]

Additive,[b] MX (0.3 m atom of M/ml)	Relative ratio of absorbance	Ionization potential M+ (eV)
none	1.0	
$NaHCO_3$	16.1	5.138
Na_2CO_3	16.3	
Na_2SO_4	16.2	
NaOH	16.0	
NaCl	15.9	
$CoCl_2$	6.5	7.86
$ZnCl_2$	4.9	9.391
NH_4Cl	2.2	

a) Ru 50 ppm in 0.9 N H_2SO_4. b) Additives were added in a solid state.

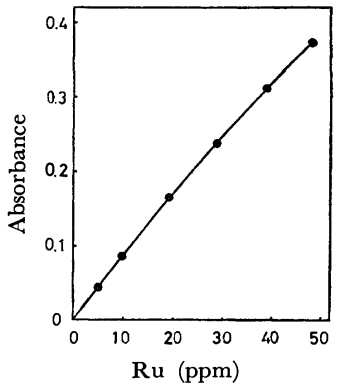

Fig. 3. Calibration curve of ruthenium in 1.48 N H_2SO_4 solution with 40 mg/ml of $NaHCO_3$ (Ru 349.9 nm, an air-acetylene flame).

Table 2. Analyses of ruthenium by atomic-absorption spectroscopy

Compound	Ru content (%) Found	Calcd
$[RuCl_2(C_6H_6)Me_2SO]_2$	30.3 29.5	30.79
$[RuCl_2(C_6H_6)PBu_3]_2$	22.1 21.7	22.34

Conditions for analysis are the same as in Fig. 3.

In order to confirm the practical applicability, a calibration curve was drawn by using the method in which a certain amount of $NaHCO_3$ is added to a sample solution containing H_2SO_4. It was a straight line until the Ru concentration was approximately 20 ppm, and a slight curve in the range over 20 ppm, as is shown in Fig. 3. Using this Ru calibration curve, satisfactory results were obtained in the analyses of some known ruthenium compounds, as is shown in Table 2.

We can conclude that, this is a simple and effective enough method to remove interference in the determination of Ru in a sulfuric acid solution with a large depressive interference.

References and Note

1) W. B. Rowston and J. M. Ottaway, *Anal. Lett.*, **3**, 411 (1970).

2) B. Montford and S. C. Cribbs, *Anal. Chim. Acta*, **53**, 101 (1971).

3) R. C. Mallett, D. C. G. Pearton, E. J. Ring, and T. W. Steele, *Talanta*, **19**, 181 (1972).

4) The use of a nitrous oxide-acetylene flame was improper because it made absorbance smaller.

5) D. F. Makarov and Yu. N. Kukushkin, *Zh. Anal. Khim.*, **24**, 1191 (1969).

6) K. Yasuda and N. Hasegawa, "Atomic Absorption Analysis," Kodansha, Tokyo (1972), p. 143.

BULLETIN OF THE CHEMICAL SOCIETY OF JAPAN, VOL. 47(10), 2613—2614 (1974)

Synthesis of 2,3,6-Trimethylbenzyl Alcohol

Tadashi KAWAI, Yasuo YAMAZAKI, and Shuei YUHASHI

Department of Industrial Chemistry, Faculty of Technology, Tokyo Metropolitan University, Fukazawa, Setagaya-ku, Tokyo 158

(Received February 26, 1974)

Synopsis. 2,3,6-Trimethylbenzyl alcohol was prepared by the Cannizzaro reaction of 2,3,6-trimethylbenzaldehyde; mp 83—85 °C. It was found that the substance regarded by Golivets *et al.* as 2,3,6-trimethylbenzyl alcohol is an eutectic mixture of 2,3,6- and 2,4,5-trimethylbenzyl alcohol.

In the condensation of 1,2,4-trimethylbenzene(1,2,4-TMB) with formaldehyde, bis(2,4,5-trimethylphenyl)-methane was formed as the main product, and a few asymmetric hexamethyldiphenylmethanes(HeMDPM) such as 2,3,6,2′,4′,5′-HeMDPM were formed as by-products.[1] As the routes for the formation of 2,3,6,-2′,4′,5′-HeMDPM, the reaction of 1,2,4-TMB with 2,3,6-trimethylbenzyl alcohol(2,3,6-TMBA) and/or the reaction of 1,2,4-TMB with 2,4,5-TMBA are considered. These TMBA's are formed a sprimary products in the condensation of 1,2,4-TMB with formaldehyde.

In order to obtain the starting materials for an investigation of this reaction scheme we attempted the synthesis of alcohols.

In the preparation of 2,4,5-TMBA(mp 83—84 °C) by the hydrolysis of monoacetoxymethyl-1,2,4-trimethylbenzenes obtained by the chloromethylation of 1,2,4-TMB and subsequent acetoxylation, Golivets *et al.*[2] isolated a substance (A) melting at 55—56 °C, which they regarded as 2,3,6-TMBA.

We also obtained a small amount of the substance (mp 54—55 °C) by the above reactions. However, from its IR and NMR spectra measurements, and mixed melting point test, it was suggested that the substance is not pure and that it might be an eutectic mixture of 2,3,6- and 2,4,5-TMBA.

We have applied the Cannizzaro reaction of 2,3,6-trimethylbenzaldehyde to the synthesis of 2,3,6-TMBA.

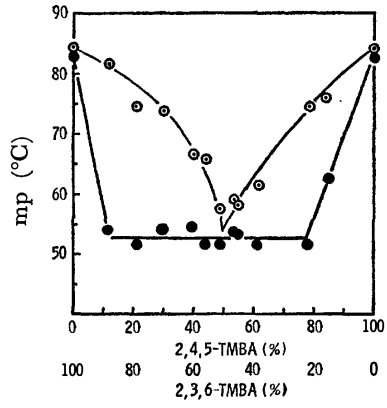

Fig. 1. Melting-point curve of 2,3,6-TMBA and 2,4,5-TMBA.

This was prepared by Lowe *et al.*[4] We obtained 2,3,6-TMBA as colorless needles, melting at 83—85 °C. For an estimation of its purity we attempted its hydrogenolysis[3] with a CoO-MoO_3-Al_2O_3 catalyst. The products obtained were tetramethylbenzenes(TeMB) and 1,2,4-TMB. The former consists of 1,2,3,4-: 98%, 1,2,4,5-: 1.1%, and 1,2,3,6-TeMB: 0.9%. The latter was formed by the dehydroxymethylation of the TMBA. Thus it was found that the purity of 2,3,6-TMBA obtained was 98%.

The IR spectrum of 2,3,6-TMBA showed a characteristic band assigned to two adjacent hydrogen systems at 805 cm^{-1}, and that of 2,4,5-TMBA three bands due to one adjacent hydrogen system in the 900—875 cm^{-1} regions. The IR spectrum of (A) showed two absorption bands in both regions. The NMR spectrum of (A) showed two absorptions at δ 4.52 and 4.39, assigned to the methylene hydrogens of 2,3,6- and 2,4,5-TMBA, respectively. The results suggest that (A) is a mixture of these alcohols.

We have made the melting-point curve of binary system of these alcohols. The eutectic mixture of the system consists of 2,3,6- (50%) and 2,4,5-TMBA (50%), melting at 53—54.5 °C. The melting point of the eutectic mixture agrees with that of (A).

Experimental

Hydrolysis of Monoacetoxymethyl-1,2,4-trimethylbenzenes: Monoacetoxymethyl-1,2,4-trimethylbenzenes (145 g, bp 105—108 °C/1 mmHg), prepared by acetoxylation of chloromethylated 1,2,4-TMB, KOH (46.9 g) and absolute methanol (295 ml) were refluxed with stirring for 2 hr. After cooling the separated crystal was collectd. White precipitate was formed by the dilution of the filtrate with twice its volume of water. By recrystallization of these solids from 30% methanol aqueous solution, white needles, 2,4,5-TMBA (mp 83—84 °C, 85 g, 63% yields) were obtained. White needles (substance (A)) (mp 54—55 °C, 1 g) were separated from the mother liquid.

A mixture of (A) and 2,4,5-TMBA showed no depression in melting point.

2,3,6-Trimethylbenzaldehyde: This was prepared by the method of Lowe *et al.* bp; 87—88 °C/1 mmHg (lit,[4] bp 111—114 °C/5 mmHg).

2,3,6-Trimethylbenzyl Alcohol: To a methanolic solution (75 ml) of KOH (50 g) was added a mixture of 2,3,6-trimethylbenzaldehyde (44 g) and formalin (37% concn., 29 ml) in methanol (30 ml) with stirring at 60 °C. After being kept at 60—70 °C for 3 hr, 90 ml of ice water was added. The yellowish solid was separated and recrystallized from 25% methanol aqueous solution. Colorless needles, 2,3,6-TMBA (mp 83—85 °C, 12 g), were obtained.

Found: C, 79.71; H, 9.41; O, 10.88%. Calcd for $C_{10}H_{14}O$: C, 79.95; H, 9.39; O, 10.65%.

References

1) T. Kawai and Y. Yamazaki, *J. Japan Petrol. Inst.*, **16**, 567 (1973).
2) G. I. Golivets, M. M. Dashyevskii, and I. V. Golivets, *Zh. Prikl. Khim.*, **41**, 148 (1968).
3) T. Kawai and Y. Yamazaki, *J. Japan Petrol. Inst.*, **16**, 749 (1973).
4) G. Lowe, F. G. Torto, and B. C. L. Weedon, *J. Chem. Soc.*, **1958**, 1855.

BULLETIN OF THE CHEMICAL SOCIETY OF JAPAN, VOL. 47(10), 2615—2616 (1974)

The Photochemistry of 3,3-Dialkoxy-1-phenylpropan-1-ones

Takehiko NISHIO and Hiromu AOYAMA

Department of Chemistry, Tokyo Kyoiku University, Otsuka, Tokyo 112

(Received March 6, 1974)

Synopsis. The irradiation of 3,3-dialkoxy-1-phenylpropan-1-ones (Ia-b) in a benzene solution afforded β-keto-esters (IIa-b), phenyl β-alkoxyvinyl ketones (IIIa-b), and tetrahydrofuranols (IVa-b).

The photoreaction of aliphatic ketones to give smaller ketones, olefins, and cyclobutanols has been widely studied.[1] It is well established that the reaction proceeds *via* γ-hydrogen abstraction to give 1,4-diradicals which can either cleave to olefins, ring closure to cyclobutanols, or return to starting materials. Recently, the ultraviolet irradiation of β-alkoxy ketones has been reported to give the tetrahydrofuranols as the major product.[2-4] They have been considered to arise *via* δ-hydrogen abstraction by excited carbonyl oxygen. We will report here on the photochemistry of 3,3-dialkoxy-1-phenylpropan-1-ones (Ia-b), which includes a new photooxidation (IIa-b) as well as photoelimination (IIIa-b) and δ-hydrogen abstraction (IVa-b).

The irradiation of 3,3-dimethoxy-1-phenylpropan-1-one (Ia) in a benzene solution with a high-pressure mercury lamp through a Pyrex filter under nitrogen for 20 hr gave methyl benzoylacetate (IIa) (35%), phenyl β-methoxyvinyl ketone (IIIa) (6.5%), and 3-phenyl-3-hydroxy-5-methoxy-tetrahydrofuran (IVa) (5%). Compounds IIa and IIIa did not show any H-abstraction under further irradiation and were recovered almost quantitatively. The structures of IIa[5] and IIIa[6] were confirmed by a direct comparison with their authentic samples. The structure of IVa was elucidated using its physical data and by elemental analysis. The NMR spectrum showed two doublets of a doublet at δ 2.23 (J=13.5, J=1.8 Hz, 1H at C-4) and δ 2.49 (J=13.5, J=3.5 Hz, 1H at C-4), two doublets at δ 4.06 and 4.26 (J=10 Hz, 2H at C-2), a doublet of a doublet at δ 5.19 (J=1.8, J=3.5 Hz, 1H at C-5), a singlet at δ 3.40 (3H, $-OCH_3$), a broad singlet at δ 3.90 (1H, –OH, exchangable with D_2O), and the multiplet at δ 7.15—7.65 (5H) due to the aromatic protons. The IR spectrum exhibited bands at 3500 cm^{-1} due to the hydroxy group and at 1100 cm^{-1} attributable to the ether group. The mass spectrum displayed prominent peaks at m/e 176 (M^+-H_2O), 164 ($M^+-CH_2{=}O$), 144 ($M^+-(H_2O+MeOH)$), and 115 ($M^+-(H_2O+MeOH+CHO)$).

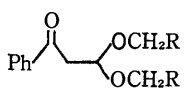

Ia R=H
Ib R=CH_3

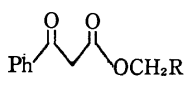

IIa R=H
IIb R=CH_3

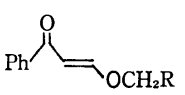

IIIa R=H
IIIb R=CH_3

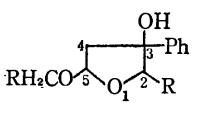

IVa R=H
IVb R=CH_3

Similarly, ethyl benzoyl acetate (IIb), phenyl β-ethoxyvinyl ketone (IIIb), and 2-methyl-3-phenyl-3-hydroxy-5-ethoxy-tetrahydrofuran (IVb) were obtained in 15, 15, and 6% yield respectively by the irradiation of 3,3-diethoxy-1-phenylpropan-1-one (Ib). The structures of IIb[5] and IIIb[7] were confirmed by a direct comparison with their authentic samples, while that of IVb was elucidated by means of its spectral data and by elemental analysis.

The formation of IIa-b is presumed to proceed through the oxidation of Ia-b by light. The formation of IIIa-b can be explained by the elimination of the alcohol.[8] On the other hand, the formation of IVa-b is considered to arise *via* δ-hydrogen abstraction by an excited carbonyl through a seven-membered ring transition state.

Experimental

All the boiling points are uncorrected.

The 3,3-dimethoxy-1-phenylpropan-1-one (Ia, bp 175—178 °C/20 mmHg (lit,[9] 111—111.5 °C/2 mmHg)) and 3,3-diethoxy-1-phenylpropan-1-one (Ib, bp 165—170 °C/20 mmHg (lit,[10] 111—112 °C/1 mmHg)) were prepared according to the methods of previous reports.

Irradiation of Ia. A solution of 1g of Ia in 150 ml of benzene was irradiated with a high-pressure merucry lamp through a Pyrex filter under nitrogen for 20 hr at room temperature. After irradiation, the benzene was evaporated *in vacuo*, and the residue was chromatographed on a silica gel column with benzene–ethyl acetate(50 : 1) to give 350 mg of methyl benzoyl acetate (IIa; bp 155—158 °C/20 mmHg (lit,[5] 152 °C/15 mmHg)), 65 mg of phenyl β-methoxyvinyl ketone (IIIa; bp 114—117 °C/2 mmHg (lit.[6] 135 °C/5—6 mmHg)), 50 mg of 3-phenyl-3-hydroxy-5-methoxy-tetrahydrofuran (IVa), and 50 mg of the recovered ketone.

3-Phenyl-3-hydroxy-5-methoxy-tetrahygrofuran (IVa): Bp 80 °C/2 mmHg. IR: ν_{max}^{film} cm^{-1}, 3500, 3050, 2830, 1600, 1492, 1100, 750, 690. Found: C, 67.77; H, 7.18%. Calcd for $C_{11}H_{14}O_3$: C, 68.02; H, 7.27%.

Irradiation of Ib. A solution of 1 g of Ib in 150 ml of benzene was irradiated under the same conditions as have been described above for 20 hr. After the removal of the solvent, the residue was chromatographed on a silica gel column with benzene–ethyl acetate (30 : 1) to give 150 mg of ethyl benzoylacetate (IIb; bp 152—158 °C/18 mmHg (lit.[5] 147 °C/11 mmHg)), 150 mg of phenyl β-ethoxyvinyl ketone (IIIb; bp 150—152 °C/20 mmHg (lit.[7] 156—158 °C/28 mmHg)), 60 mg of 2-methyl-3-phenyl-3-hydroxy-5-ethoxy-tetrahydrofuran (IVb), and 100 mg of the recovered ketone.

2-Methyl-3-phenyl-3-hydroxy-5-ethoxy-tetrahydrofuran (IVb): bp 93 °C/2 mmHg. IR: ν_{max}^{film} cm^{-1}, 3500, 3050, 1603, 1492,

1100, 750, 690. NMR: (δ in $CDCl_3$) 1.25 (t, 3H, J=9 Hz, methyl), 1.20 (d, 3H, J=6.5 Hz, methyl), 2.25 (d, 1H, J=13.5 Hz, methylene at C-4) and 2.63 (dd, 1H, J=13.5, J=5 Hz, methylene at C-4), 3.2—4.1 (m, 2H, methylene), 4.23 (q, 1H, J=6.5 Hz, methine at C-2), 5.23 (d, 1H, J= 5 Hz, methine at C-5), 7.2—7.65 (m, 5H, aromatic protons). When the signal of the methyl protons at δ 1.25 was irradiated, the signal of the methylene protons of the ethoxy group appeared as two doublets at δ 3.49 and 3.91 with the same coupling constant of 9 Hz. This phenomenon is considered to arise from the restriction of free rotation by the weak interaction of hydroxy and ethoxy groups. Mass spectrum: *m/e* 204 (M^+-H_2O), 178 ($M^+-CH_3CH{=}O$), 158 (M^+-H_2O+EtOH)), 115 ($M^+-(H_2O+EtOH+CH_3C{=}O)$). Found: C, 70.16; H, 8.09%. Calcd for $C_{13}H_{18}O_3$: C, 70.24; H, 8.16%.

References

1) P. J. Wagner and G. S. Hammond, *Advan. Photochem.*, **5**, 21 (1968).

2) D. J. Coyle, R. V. Peterosn, and J. Heicklen, *J. Amer. Chem. Soc.*, **86**, 3850 (1964).

3) P. Yates and J. M. Pal. *Chem. Commun.*, **1970**, 553.

4) L. M. Stephenson and J. L. Parlett, *J. Org. Chem.*, **36**, 1093 (1971).

5) S. I. Heilbron, "Dictionary of Organic Compounds," Vol. 1, Eyre and Spottiswoode, London, (1965), p. 356.

6) H. Shirahama and T. Matsumoto, This Bulletin **38**, 1293 (1965).

7) L. Panizz and M. S. Siene, *Gazz. Chim. Itali*, **73**, 335 (1943).

8) Coyle and his coworkers reported that the alcohol was eliminated *via* either four center reaction (A) or six-membered ring structure of the enol form of the ketone (B) in the photolysis of 4-methyl-4-methoxy-2-pentanone, *J. Amer. Chem. Soc.*, **86**, 3850 (1964).

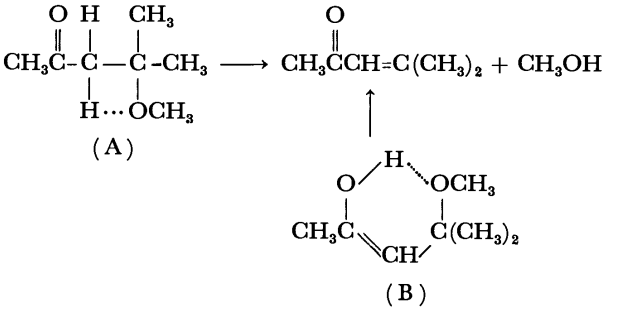

(A) (B)

9) E. E. Nifant'ev and S. D. Sokolov, *Zhur. Obschei Khim.*, **29**, 2570 (1959); *Chem. Abstr.*, **54**, 10930g (1960).

10) K. Bowden, E. A. Braude, and E. R. H. Jones, *J. Chem. Soc.*, **1946**, 945.

BULLETIN OF THE CHEMICAL SOCIETY OF JAPAN, VOL. 47(10), 2617 (1974)

The Stereoselective Reduction of Tropinone to Tropine

Yoshihiro HAYAKAWA and Ryoji NOYORI

Department of Chemistry, Faculty of Science, Nagoya University, Chikusa, Nagoya 464

(Received March 11, 1974)

Synopsis. The reduction of tropinone with diisobutylaluminum hydride in tetrahydrofuran at −78 °C leads to tropine selectively.

The sterochemistry of the reduction of tropinone (**1**) has been extensively studied.[1] The kinetically-controlled reduction with lithium aluminum hydride, sodium borohydride, or potassium borohydride afforded a mixture of tropine (**2**) and ψ-tropine (**3**), with a ratio between 28 : 72 and 55 : 44.[2,3] Although an increased proportion of **2** was obtained by the use of Meerwein-Pondorf-Verley reduction (the highest **2** : **3** ratio was 71 : 29), a prolonged reaction gave a mixture in which the unnatural isomer, **3**, was favored.[2] The **2** : **3** stereoisomeric composition after equilibrium had been reached was 11 : 88. The treatment of the ketone, **1**, or the α alcohol, **2**, with sodium metal in alcoholic solvents also led thermodynamically to the more stable β epimer, **3**. The treatment of **1** with zinc–hydriodic acid gave a mixture of **2**, **3**, and an over-reduction product, tropane, the ratio of **2** and **3** being 5 : 2.[4] The conversion of **1** to **2** with high stereoselectivity has thus been achieved only by catalytic reduction.[5] During the course of the development of a new tropane alkaloid synthesis[6,7] which requires a method for the *chemical* reduction of tropinone derivatives to the corresponding α alcohols, we have found that the use of diisobutylaluminum hydride in tetrahydrofuran solvent is suitable for this purpose. The present procedure was both highly efficient and selective; the tropine (**2**) thus obtained from **1** in a 95% yield was contaminated with only 3% of the epimer, **3**.

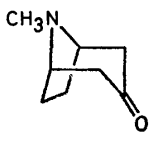

1

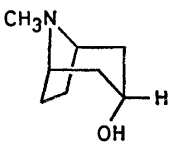

2

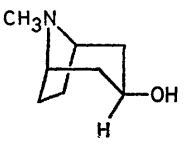

3

Experimental

*Reduction of Tropinone (**1**).* A solution of 1.0 g (7.0 mmol) of tropinone (**1**) (97% pure, Aldrich) in 45 ml of dry tetrahydrofuran was flushed with argon and cooled at −78 °C. Into the magnetically-stirred solution was then added 3.6 g (25 mmol) of diisobutylaluminum hydride (Alpha Inorganics) over a period of 20 min. The mixture was stirred at the same temperature for 17 hr and then quenched by adding 3 ml of water carefully ovre a 20-min period. The resulting voluminous gel was treated with 50 ml of ethyl acetate and filtered. The filter cake was washed with 100 ml of ethyl acetate. The combined organic solutions were concentrated *in vacuo* to give 1.2 g of a crude viscous oil, which consisted mainly of tropine (**2**) and ψ-tropine (**3**) (97 : 3 ratio, 95% combined yield). The isomeric ratio was determined by a comparison of the characteristic NMR signals due to the NCH_3 groups. The bulb-to-bulb distillation of the oil at 100—110 °C/0.1 mmHg (bath temperature) gave 0.869 g (89%) of a 97 : 3 mixture of **2** and **3** as a crystalline solid; mp 61—63 °C. A pure sample of **2** was obtained readily by recrystallization from benzene; mp and mmp 62—63 °C (lit,[8] 63—64 °C). IR ($CHCl_3$) 3600 and 3400 cm^{-1} (OH); NMR ($CDCl_3$, 100 MHz) δ 1.66 (br d, J= 13.5 Hz, 2H, equatorial protons at C(2) and C(4)), 1.9—2.3 (m, 7H, C(6)H_2, C(7)H_2, axial protons at C(2) and C(4), and OH), 2.28 (s, 3H, NCH_3), 3.25 (m, 2H, NCH), and 4.05 (br t, J=5.1 Hz, 1H, C<u>H</u>OH). The chromatography of the mother liquor of recrystallization on a column packed with neutral alumina (Merck, activity II—III) gave pure samples of **2** (1 : 20 methanol–ethyl acetate as the eluent) and **3** (1 : 10 methanol–ethyl acetate). The identity of the latter was established by a comparison of its physical properties with those of an authentic sample. Mp and mmp 106—108 °C (from *n*-hexane–benzene) (lit,[9] 108 °C); IR (CCl_4) 3600 and 3400 cm^{-1} (OH); NMR ($CDCl_3$, 100 MHz δ 1.5—1.9 (m, 6H, C(6)H_2, C(7)H_2, and equatorial protons at C(2) and C(4)), 1.9—2.2 (m, 2H, axial protons at C(2) and C(4)), 2.34 (s, 3H, NCH_3), 3.10 (br s, 1H, OH), 3.20 (m, 2H, NCH), and 3.88 (m, 1H, C<u>H</u>OH).

The support of this research by the Takeda Science Foundation is gratefully acknowledged.

References

1) Recent reviews of tropane alkaloids: G. Fodor, *Progr. Photochem.*, **1**, 491 (1968); G. Fodor in "Chemistry of the Alkaloids," ed. by S. W. Pelletier, Van Nostrand Reinhold, New York, N. Y. (1970), p. 431; G. Fodor in "The Alkaloids, Chemistry and Physiology," Vol. 13, ed. by R. H. Manske, Academic Press, New York, N. Y. (1971), p. 351.

2) A. H. Beckett, N. J. Harper, A. D. J. Balon, and T. H. E. Watts, *Tetrahedron*, **6**, 319 (1959).

3) R. Mirza, *Nature*, **170**, 630 (1952).

4) R. Willstätter and F. Iglauer, *Ber.*, **33**, 1170 (1900).

5) L. C. Keagle and W. H. Hartung, *J. Amer. Chem. Soc.*, **68**, 1608 (1946).

6) R. Noyori, S. Makino, Y. Baba, and Y. Hayakawa, *Tetrahedron Lett.*, **1974**, 1049.

7) R. Noyori, Y. Baba, and Y. Hayakawa, *J. Amer. Chem. Soc.*, **96**, 3336 (1974).

8) A. Orechoff and R. Konowalowa, *Ber.*, **67**, 1153 (1934).

9) R. Willstätter, *Ber.*, **29**, 936 (1896).

BULLETIN OF THE CHEMICAL SOCIETY OF JAPAN, VOL. 47 (10), 2618 (1974)

Electron Pairing Interaction and Electronic Spectra of Linear Polyene

Sadhan BASU

Department of Chemistry, University College of Science, Calcutta-9, India

(Received November 16, 1973)

Synopsis. Assuming the pairing interaction which arises in Hartree-Fock-Bogolyubov formulation in many-electron system, to be due to attraction between two electrons of opposite spin it has been shown that the longest wavelength singlet transition in linear polyenes will show convergence limit while the corresponding triplet transition will not.

In a previous communication[1] it has been shown that the convergence limit in the electronic spectra of linear polyene may be understood in terms of Δ_{i-i} (the pairing interaction) value in the Hartree-Fock-Bogolyubov (HFB) equation for many electron system. Since the Δ_{i-i} term is positive, it was assumed that it may be looked upon as attraction between a particle and a hole. If we are prepared to accept a non-classical conclusion, that is, there is residual attraction between electrons in a many electron system, then we may consider Δ_{i-i} to arise from attraction between electrons in states i and $-$i. The states i and $-$i have the same principal quantum number but one has the projection quantum number reversed in sign from the other. In spherical systems which are characterised by quantum numbers n, l, and m, the states i and $-$i differ from each other in the sign of m values. In linear polyene the good quantum number is n only (which appears in the electron-in-a-box calculation). Only way the states i and $-$i can differ from each other in these systems is by having spin $+1/2$ and $-1/2$. It is to be remembered, however, that HFB calculation do not take spin into account at any stage. We can only say that there is electron pairing in the same level of polyene, but to satisfy some basic requirements of the HFB theory, the two electrons must have opposite projection quantum number, which we consider to be spin. But this term does not arise from spin-spin interaction in any way. With this basic prescription we may analyse the electronic properties of linear polyenes in greater detail.

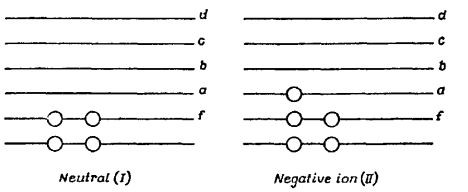

Fig. 1. Level scheme for neutral and mono-negative polyene.

Let us consider the level schemes for a neutral and a negatively charged polyene.

In the case (I) of Fig. 1 an electron from f (Fermi level) can go to a level c, such that $\varepsilon_c - \varepsilon_f \geq \Delta_{i-i}$ *i.e.* the low-lying excited levels cannot be populated as they are unable to break the pairing interaction. Therefore the minimum amount of energy which the system can take up is Δ_{i-i}, *i.e.* the spectrum should show convergence limit. In the case II on the other hand, the unpaired electron in level a, may be excited to any of the vacant levels as there is no pairing interaction to break. So these systems will not show any convergence limit. The same argument should hold for positive ions. We reached the same conclusion considering Δ_{i-i} as hole-particle interaction energy in the previous paper.

Let us consider the neutral molecule again. The two electrons in the level f have the spin $+1/2$ and $-1/2$. When one is excited to a level c, without changing the spin, we get a singlet state. For a triplet state excitation we have the electrons in f and c having the same spin, say $+1/2$. We may suppose that we have arrived at this state by electron transition from a virtual Fermi level having both the spins $+1/2$. In the HFB formulation there cannot be any pairing interaction between two electrons of the same spin in the virtual orbital. So the triplet transitions in linear polyenes will show no convergence limit. We may go over from the ground state to the virtual orbital by some type of spin-orbital interaction. Further when the energy difference $\varepsilon_f - \varepsilon_a$ becomes small, ε_a may be thermally populated by a triplet mechanism. So very large linear molecule may become paramagnetic and the magnetic moment increases with increasing temperature.[2]

This pairing interaction, however, fails to explain the convergence behaviour of cyanines for which hole-particle attraction model appears to be a better one.

References

1) S. Basu, This Bulletin, **47**, 735 (1974).
2) A. A. Berlin, G. A. Vinogradov, A. A. Ovchinnikov, *Int. J. Quantum Chem.*, **6**, 263 (1972).

BULLETIN OF THE CHEMICAL SOCIETY OF JAPAN, VOL. 47(10), 2619—2620 (1974)

Photochemistry of Acetophenone and Acetaldehyde in Ether Solvent —Formation of Diastereoisomeric Alcohols

Masao TOKUDA,* Miki HASEGAWA, Akira SUZUKI, and Mitsuomi ITOH

Department of Chemical Process Engineering, Faculty of Engineering, Hokkaido University, Sapporo 060

(Received March 26, 1974)

Synopsis. Irradiation of acetophenone and acetaldehyde in tetrahydrofuran or diethyl ether gave the following diastereoisomeric alcohols, 1-phenyl-1-(2-tetrahydrofuryl)-ethanol, 1-(2-tetrahydrofuryl)ethanol, 2-phenyl-3-ethoxy-2-butanol and 3-ethoxy-2-butanol.

Reports have been given on the steric effect in the addition reaction of the radical to the carbon-carbon double bond.[1,2] In order to investigate similar steric effects on the coupling reaction of unlike radicals, we isolated the diastereoisomeric alcohols obtained by the photochemical reaction of unsymmetric carbonyl compounds in ether solvent. Unsymmetric carbonyl compounds should provide a pair of radicals having asymmetrical radical centers when α hydrogen atom of diethyl ether or tetrahydrofuran (THF) is abstracted. A cross-coupling of these radicals should produce diastereoisomeric alcohols.

Irradiation of acetophenone in an excess of THF with 500 W high pressure mercury vapor lamp at room temperature for 8 hr gave diastereoisomeric alcohols **1a** (26%)[3] and **1b** (19%), *p*-(2-tetrahydrofuryl)acetophenone (4%), 2,2′-bitetrahydrofuryl and acetophenone pinacol in a 65% conversion. Diastereoisomeric alcohols could be separated by a preparative glpc and their structures were confirmed by spectral data and by means of dehydration. When each of these diastereoisomers was dehydrated with sulfuric acid–acetic acid solution,[4] both isomers (**1a, 1b**) were found to give an identical product (**5**) as in the following.

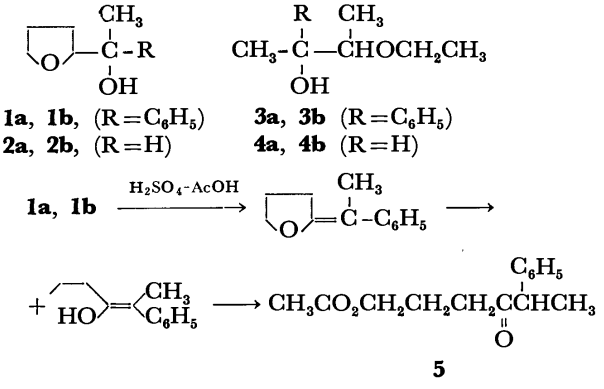

1a, 1b, (R=C_6H_5) **3a, 3b** (R=C_6H_5)
2a, 2b, (R=H) **4a, 4b** (R=H)

1a, 1b $\xrightarrow{H_2SO_4\text{-AcOH}}$ $\longrightarrow$

5

(1)

Methyl protons of **1a** and **1b** resonate at τ 8.61 and 8.42, respectively. An absorption of β-ring methylene of **1a** at τ 8.21 is shifted to a broad band at τ 8.0—9.0 in **1b**, indicating that some of the β-ring protons in **1b** lie over the plane of the aromatic ring. Accordingly, **1b** should correspond to conformation B and **1a** to A. Hydrogen bonded structures are suggested from the IR spectra of **1a** and **1b** and the NMR spectrum of 2-(2-tetrahydrofuryl)-2-propanol, which exhibits two methyl protons at different chemical shifts, *i.e.* τ 8.85 and 8.97.[5]

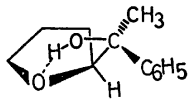

A

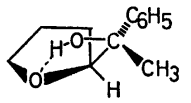

B

Irradiation of acetaldehyde in THF gave diastereoisomeric alcohols **2a** (23%) and **2b** (18%), and 2,2′-bitetrahydrofuryl. Diastereoisomers were separated by a preparative glpc, both isomers showing similar spectra in NMR.

Irradiation of acetophenone in diethyl ether gave diastereoisomeric alcohols **3a** (22%) and **3b** (22%), 1-phenylethanol (4%), 2,3-diethoxybutane (40%) in a 60% conversion. In this case, diastereoisomers could not be separated by glpc under various conditions. However, the NMR spectrum of a mixture of **3a** and **3b** indicates the presence of two isomers, exhibiting two singlets at τ 8.50 and 8.61, two doublets at τ 9.24 and 8.98 and two triplets at τ 8.81 and 8.92 attributable to the corresponding methyl protons. A mixture of **3a** and **3b** was treated with sulfuric acid-acetic acid to give a dehydration product (**6**) and a rearranged ketone (**7**).

3a, 3b $\xrightarrow{H_2SO_4\text{-AcOH}}$ $C_6H_5C(=CH_2)CH(CH_3)OC_2H_5$ + $C_6H_5CH(CH_3)C(=O)CH_3$ (2)

6 **7**

Irradiation of acetaldehyde in diethyl ether gave diastereoisomeric alcohols **4a** (20%) and **4b** (20%), 3-hydroxy-2-butanone (3%) and 2,3-diethoxybutane in a 70% conversion. The conformations of **4a** and **4b** could not be determined because of the spectral similarities of the isomers.

Most of the products obtained can be elucidated as combination products of the radicals resulting from a hydrogen abstraction by n-π^* excited carbonyls. A cross-coupling of the two radicals provides the diastereoisomeric alcohols. The isomeric ratio of these diastereoisomers is 1.0 when diethyl ether is employed as a hydrogen donor, and 1.4 and 1.3 when THF is used. Similar diastereoisomers were obtained in a nearly equal amount when β-keto esters were photolyzed in ether solvent.[6] In the case of acetophenone in THF, **1a** having conformation A predominates over **1b**. This might be explained from the point of view that an approach of nearly planar radicals *via* a sterically less hindered pathway should yield **1a** predominantly.

p-(2-Tetrahydrofuryl)acetophenone can be produced by a substitution reaction of tetrahydrofuryl radical to acetophenone.[7] A combination of acetyl and α-hydroxyethyl radical[8] should provide 3-hydroxy-2-butanone.

Experimental

Quantitative glpc analyses were carried out with an internal standard. All mps and bps are uncorrected.

Photochemistry of Acetophenone in THF. A mixture of acetophenone (0.01 mol) and THF (0.4 mol) in a quartz tube was cooled in water and externally irradiated with a 500 W high pressure mercury vapor lamp for 8 hr. Distillation and a preparative glpc (FFAP column; col. temp., 250°) of the irradiation mixture gave **1a**, **1b**, *p*-(2-tetrahydrofuryl)acetophenon and 2,2′-bitetrahydrofuryl.

1-Phenyl-1-(2-tetrahydrofuryl)ethanol (**1a**) has n_D^{23} 1.5344; IR(CCl_4) 3540, 3450 cm^{-1}; NMR(CCl_4) τ 8.61 (s, 3H), 8.21 (m, 4H), 7.54 (s, 1H), 5.9—6.9 (m, 3H), 2.8 (m, 5H); *m/e* 192(M^+), 121, 71. Found: C, 74.75; H, 8.33%. Calcd for $C_{12}H_{16}O_2$: C, 74.97; H, 8.39%.

The IR and mass spectra of **1b** are similar to those of **1a**. Diastereoisomer **1b** has n_D^{23} 1.5309; NMR(CCl_4) τ 8.42 (s, 3H) 8.0—9.0 (m, 4H), 7.58 (s, 1H), 5.9—6.5 (m, 3H), 2.7 (m, 5H). Found: C, 74.64; H, 8.38%.

p-*(2-Tetrahydrofuryl)acetophenone* was identified from spectral data: IR (CCl_4) 1760—2000 (characteristic absorption of *p*-substituted acetophenone), 1680 cm^{-1}; NMR(CCl_4) τ7.55 (s, 3H), 8.05 (m, 4H), 6.10 (m, 2H), 5.23 (t, 1H), 2.70 (d, 2H), 2.16 (d, 2H); *m/e* 190(M^+), 175, 147, 71, 43. Found: C, 75.48; H, 7.38%. Calcd for $C_{12}H_{14}O_2$: C, 75.76; H, 7.42%. 2,4-Dinitrophenylhydrazone, mp 169.0—170.5 °C.

Photochemistry of Acetaldehyde in THF. A preparative glpc of the irradiation mixture gave diastereoisomeric alcohols **2a**, **2b** and 2,2′-bitetrahydrofuryl.

1-(2-Tetrahydrofuryl)ethanol (**2a**) has n_D^{20} 1.4421; IR(CCl_4) 3560, 3440 cm^{-1}; NMR(CCl_4) τ 8.86 (d, 3H), 6.97 (s, 1H), 7.9—8.4 (m, 4H), 6.0—6.7 (m, 4H); *m/e* 101, 71, 45. Found: C, 61.85; H, 10.92%. Calcd for $C_6H_{12}O_2$: C, 62.04%; H, 11.03%.

The isomer **2b** has n_D^{20} 1.4060; NMR(CCl_4) τ 8.85 (d, 3H), 7.01 (s, 1H), 7.8—8.4 (m, 4H), 6.0—6.8 (m, 4H). Found: C, 61.88; H, 10.95.

Photochemistry of Acetophenone in Diethyl Ether. A preparative glpc (PEG 20M, 220 °C) of the irradiation mixture gave a mixture of diastereoisomers (**3a** and **3b**): IR(neat) 3470, 1110 cm^{-1}; NMR(CCl_4) τ 8.50 and 8.61 (s, 3H), 9.24 and 8.98 (d, 3H), 8.81 and 8.92 (t, 3H), 7.39 (s, 1H), 6.5 (m, 3H), 2.7 (m, 5H); *m/e* 194, 121, 73. Found: C, 74.02; H, 9.28%. Calcd for $C_{12}H_{18}O_2$: C, 74.30; H, 9.28%.

Photochemistry of Acetaldehyde in Diethyl Ether. A preparative glpc (PEG 20M, 120 °C) of the irradiation mixture gave the diastereoisomeric alcohols (**4a** and **4b**) and 3-hydroxy 2-butanone.

2-Hydroxy-3-ethoxybutane (**4a**) has bp 132 °C; n_D^{20} 1.4082; IR (CCl_4) 3560, 3470, 1115 cm^{-1}; NMR(CCl_4) τ 8.95 (d, 6H), 8.81 (t, 3H), 7.10 (s, 1H), 6—7 (m, 4H); *m/e* 73, 45. Found: C, 61.15; H, 11.75%. Calcd for $C_6H_{14}O_2$: C, 60.98; H, 11.94%.

The isomer **4b** has bp 125 °C; n_D^{20} 1.4112; IR(CCl_4) 3565, 3470, 1115 cm^{-1}; NMR(CCl_4) τ 8.90 (d, 6H), 8.78 (t, 3H), 7.07 (s, 1H), 6—7(m, 4H); *m/e* 73, 45. Found: C, 60.76; H, 11.72%.

*Dehydration of **1a** and **1b**.* Treatment of **1a** or **1b** (120 mg) with 0.15 ml of warm sulfuric acid-acetic acid solution[4] gave only 6-acetoxy-2-phenyl-3-hexanone (**5**): IR (CCl_4) 1735, 1715 cm^{-1}; NMR(CCl_4) τ 8.65 (d, 3H), 8.12 (s, 3H), 8.26 (q, 2H), 7.65 (t, 2H), 6.34 (q, 1H), 6.14 (t, 2H), 2.80 (5H); *m/e* 234, 129, 105, 87, 77. Found: C, 71.66; H, 7.53%. Calcd for $C_{14}H_{18}O_3$: C, 71.77; H, 7.74%.

*Dehydration of **3a** and **3b**.* Treatment of a mixture of **3a** and **3b** as mentioned above yielded 2-phenyl-3-ethoxy-1-butene (**6**) and 3-phenyl-2-butanone (**7**).

Product **6** has n_D^{20} 1.5092; IR(CCl_4) 1620, 910 cm^{-1}; NMR(CCl_4) τ 8.80 (t, 3H), 8.82 (d, 3H), 6.51 (q, 2H), 5.86 (q, 1H), 4.82 (s, 2H), 2.6—2.9 (m, 5H); *m/e* 161, 132, 117, 77, 73. Found: C, 81.60, H, 9.11%. Calcd for $C_{12}H_{16}O$: C, 81.77; H, 9.15%.

The other product **7** has n_D^{20} 1.5064; IR(CCl_4) 1715 cm^{-1}; NMR (CCl_4) τ 8.70 (d, 3H), 8.07 (s, 3H), 6.42 (q, 1H), 2.85 (m, 5H); *m/e* 148, 105. Found: C, 80.69; H, 8.32%. Calcd for $C_{10}H_{12}O$: C, 81.04; H, 8.16%.

References

1) M. Tokuda, Y. Yokoyama, T. Taguchi, A. Suzuki, and M. Itoh, *J. Org. Chem.*, **37**, 1859 (1972).

2) M. Tokuda, V. V. Chung, A. Suzuki, and M. Itoh, *Chem. Lett.*, **1972**, 405.

3) Yields are based upon the carbonyl compounds consumed.

4) E. W. Garbisch, Jr., *J. Org. Chem.*, **26**, 4165 (1961).

5) K. Shima and S. Tsutsumi, This Bulletin, **36**, 121 (1963)

6) M. Tokuda, M. Hataya, J. Imai, M. Itoh, and A. Suzuki, *Tetrahedron Lett.*, **1971**, 3133.

7) G. G. Wubbels, D. M. Tollefsen, R. S. Meredith, and L. A. Herwaldt, *J. Amer. Chem. Soc.*, **95**, 3820 (1973).

8) A. A. Lamola and N. J. Turro, "Energy Transfer and Organic Photochemistry," Interscience, New York, N. Y. (1969), p. 203.

BULLETIN OF THE CHEMICAL SOCIETY OF JAPAN, VOL. 47(10), 2621—2622 (1974)

The Preparation of 3,5-Dichloro-2,4,6-trifluorophenyl(cyclopentadienyl)-dicarbonyliron and Its Derivatives

Nobuo ISHIKAWA and Shuji IBUKI

Department of Chemical Engineering, Tokyo Institute of Technology, Ookayama, Meguro-ku, Tokyo 152

(Received March 18, 1974)

Synopsis. 3,5-Dichloro-2,4,6-trifluorophenyl(cyclopentadienyl)dicarbonyliron (**4**) was prepared by the nucleophilic substitution of *sym*-trichlorotrifluorobenzene with the (cyclopentadienyl)dicarbonyliron anion. One of the chlorine atoms of **4** was lithiated and the resulting lithio compound was hydrolyzed or carboxylated to give 3-chloro-2,4,6-trifluorophenyl(cyclopentadienyl)iron (**6**) or its 5-carboxylic acid (**7**) respectively.

A number of polyfluoroaryl(cyclopentadienyl)dicarbonylirons have recently been prepared by the nucleophilic substitution of a fluorine or other halogen atom of polyfluoro or monohalogenopolyfluoro aromatic compounds with the (cyclopentadienyl)dicarbonyliron anion.[1] For the preparation of further derivatives, however, polyfluoroaryliron compounds which carry other halogen atoms in addition to the fluorines on the aryl nucleus would seem to be more useful, because the halogen atom may be replaced by a functional group by means of the Grignard and similar reactions. As an example of such a kind of polyfluorohalogenoaryliron, bromotetrafluorophenyl(cyclopentadienyl)dicarbonyliron has been prepared by Cohen very recently.[2] We will here describe another compound of this type derived from *sym*-trichlorotrifluorobenzene (**1**).

The reaction between **1** and the iron complex anion, generated from the dimer of (cyclopentadienyl)dicarbonyliron and sodium amalgam, was carried out in tetrahydrofuran under a nitrogen atmosphere at −70 °C. At a higher temperature, only a tarry material resulted and no expected product was isolated, probably because of the formation of the (cyclopentadienyl)-dicarbonyliron dimer.[2]

In the usual nucleophilic reactions on *sym*-trichlorotrifluorobenzene, one or two fluorine atoms are replaced by the alkoxide ion or amines.[3,4] However, in the reactions between polyfluorohalogenobenzenes and the (cyclopentadienyl)dicarbonyliron anion, it is generally known that a chlorine or bromine atom is replaced in preference to a fluorine atom.[5] This can be explained by assuming that the elimination step of the halogen atom, and not the preceeding addition step of the anion, is the rate-determing step.[5] As expected, one chlorine atom of **1** was exclusively replaced by the (cyclopentadienyl)dicarbonyliron group to give 3,5-dichloro-2,4,6-trifluorophenyl(cyclopentadienyl)dicarbonyliron (**4**) in a yield of 14%.

The structure of **4** was evident from its ^{19}F NMR and mass spectra. In the ^{19}F NMR spectrum, two signals appeared, at +2.7 and +43.5 ppm,* in a 2 : 1 ratio of strength; those signals should be assigned to 2,6-F and 4-F respectively. These experimental values agree approximately with those calculated from the substituted shielding parameters of Bruce,[6] *i. e.*, +0.4 and +40.0 ppm. In the mass spectrum, *P* and *P*+2 peaks appeared at *m/e* 376 and 378 in a 100 : 65 ratio, as had been expected.

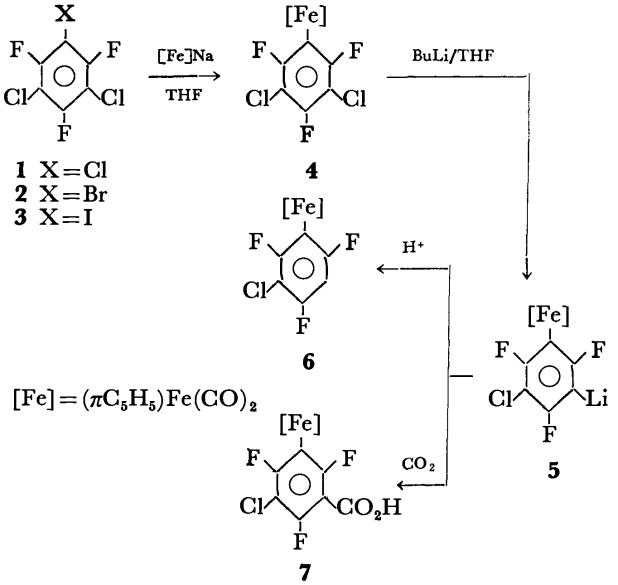

Bruce *et al.*[5] reported that the nucleophilic reactivity of the halogen atoms of polyfluorohalogenobenzenes towards the (cyclopentadienyl)dicarbonyliron anion increases in the order of Cl<Br<I. In order to have better yields, similar reactions with 3,5-dichloro-2,4,6-trifluorobromo- (**2**) and -iodobenzene (**3**) were examined. While a better yield (25%) was obtained from the bromo compound, **2**, the yield from the iodo compound, **3**, was poorer even than that from the chloro compound, **1**. We assumed that, while, in the cases of **1** and **2**, the elimination of the halogen atom is the rate-determining step, in the case of **3** it is the addition of the iron anion to the iodinated carbon atom.

The aryliron, **4**, is a very stable compound forming orange crystals; mp>200 °C (dec.); recrystallizable from various organic solvents including dimethylformamide. No chemical change occurred upon boiling in a methanolic solution either with sodium hydroxide or with concentrated hydrochloric acid for a long period. Concentrated sulfuric acid, however, hydrolyzed the C–Fe bond even at room temperature, giving 1,3-dichloro-2,4,6-trifluorobenzene.

One of the chlorine atoms of **4** could be lithiated with *n*-butyllithium in hexane–tetrahydrofuran, and from the resulting monolithio compound, **5**, 3-chloro-2,4,6-

* All ^{19}F NMR chemical shifts in this article are given in δ ppm from ext. CF_3CO_2H in tetrahydrofuran.

trifluorophenyl-(**6**) and 3-chloro-2,4,6-trifluoro-5-carboxyphenyl(cyclopentadienyl)dicarbonyliron (**7**) were derived by treatment with water and carbon dioxide respectively. The further lithiation of **6**, or dilithiation of **4**, to obtain a bifunctional aryliron compound was unsuccessful.

Experimental

*3,5-Dichloro-2,4,6-trifluorophenyl(cyclopentadienyl)dicarbonyliron (**4**).* A mixture of the dimer of (cyclopentadienyl)-dicarbonyliron (7.08 g, 20.0 mmol), 0.9% sodium amalgam (155 g, 60 mmol), and tetrahydrofuran (200 ml) was stirred for 1.5 hr at room temperature under a nitrogen atmosphere. The resulting solution of the (cyclopentadienyl)dicarbonyliron anion was cooled to −70 °C in a dry ice-acetone bath, into which a solution of *sym*-trichlorotrifluorobenzene (6.27 g, 26.7 mmol) in tetrahydrofuran (80 ml) was then added, drop by drop; the mixture was then gradually brought to room temperature, after which stirring was continued overnight. The tetrahydrofuran was evaporated at 0 °C under reduced pressure, and from the residue the product was extracted with benzene. The extract was passed through a column of activated alumina, and the first yellow band was eluted with benzene The eluate was concentrated to dryness to give a crude product of **4** (1.43 g, 14%). Recrystallization from tetrahydrofuran gave pale orange crystals, which gradually darkened and decomposed above 200 °C, without any definite melting or decomposing point. Found: C, 42.14; H, 1.30; Cl, 18.9; F, 15.3%. Calcd for $C_{13}H_5Cl_2F_3O_2Fe$: C, 41.42; H, 1.33; Cl, 18.8; F, 15.1%.

From the eluate of the second band, the dimer of (cyclopentadienyl)dicarbonyliron (3.60 g, 51%) was recovered.

1-Bromo-3,5-dichloro-2,4,6-trifluorobenzene and 1-iodo-3,5-dichloro-2,4,6-trifluorobenzene reacted in a similar manner to give **4** in yields of 25 and 12% respectively. In these cases, the dimer of (cyclopentadienyl)dicarbonyliron was also recovered in 56 and 79% yields.

*3-Chloro-2,4,6-trifluorophenyl(cyclopentadienyl)dicarbonyliron (**6**).* Into a solution of **4** (1.00 g, 2.66 mmol) in tetrahydrofuran (25 ml), a solution of *n*-butyllithium in hexane (2.39 M, 1.50 ml, 3.59 mmol) was added at −66 °C and stirred for 1 hr. The reaction mixture was thrown onto ice, and the resulting yellow precipitate (0.84 g, 92%) was collected by filtration. Recrystallization from *n*-hexane gave pale orange crystals; mp 151—153 °C. Found: C, 45.85; H, 1.76; F, 16.2%. Calcd for $C_{13}H_6ClF_3O_2Fe$: C, 45.59; H, 1.77; F, 16.6%. ^{19}F NMR*: 2-F, −1.1; 4-F, +41.5; 6-F, −0.5. Calcd:[6] 2-F, −1.8; 4-F, +37.9; 6-F, −1.7.

*3-Chloro-2,4,6-trifluoro-5-carboxyphenyl(cyclopentadienyl)dicarbonyliron(**7**).* Through a lithiated solution prepared as has been described above, carbon dioxide was bubbled in a course of 2 hr, with mechanical stirring. The reaction mixture was thrown onto ice water and made acidic with concd hydrochloric acid. Resulting yellow precipitate was collected by filtration and dissolved in a dilute aqueous solution of sodium hydroxide. After filtering to remove a small amount of an insoluble material, the carboxylic acid was reprecipitated with conc. hydrochloric acid to give **7** (0.87 g, 84%) as yellowish brown crystals; mp 181 °C (dec.). Found: C, 44.17; H, 1.61; F, 15.0%. Calcd for $C_{14}H_6ClF_3O_4Fe$: C, 43.50; H, 1.57; F, 14.8%. ^{19}F NMR*: 2-F, −4.2; 4-F, +40.8; 6-F −1.8. Calcd:[6] 2-F, −4.7; 4-F, +38.0; 6-F; −1.6.

References

1) N. Ishikawa and S. Hayashi, *Yuki Gōsei Kagaku Kyokai Shi*, **31**, 495 (1973).
2) S. C. Cohen, *J. Chem. Soc., Dalton Trans.*, **1973**, 553.
3) N. Ishikawa and I. Fujii, *Nippon Kagaku Zasshi*, **87**, 1089 (1966).
4) N. Ishikawa and T. Ogawa, *ibid.*, **88**, 1103 (1967).
5) M. I. Bruce and F. G. A. Stone, *J. Chem. Soc., A*, **1966**, 1837.
6) M. I. Bruce, *ibid.*, **1968**, 1459.

BULLETIN OF THE CHEMICAL SOCIETY OF JAPAN, VOL. 47(10), 2623—2624 (1974)

Determination of Conformations of Esters with the Use of Lanthanide Shift Reagents

Kazuhiko SAKAMOTO and Michinori ŌKI*

Department of Chemistry, Faculty of Science, The University of Tokyo, Tokyo 113

(Received March 30, 1974)

Synopsis. Lanthanide shift reagents have been used for diagnosis of *s-trans* and *s-cis* conformations of esters. By taking a ratio of lanthanide-induced shift of (H)CH_2C=O protons *vs.* [shift reagent]/[substrate] as a reference, relative ratio of (H)CH_2O- of the *s-trans* form has been found to be almost unity, whereas that of the *s-cis* *ca.* 0.5.

Following the discovery of Hinckley[1] a large number of papers[2] on the utility of the lanthanide shift reagents have been reported. Structures of organic oxygen compounds were investigated with the aid of shift reagents.[3] Interestingly, however, the use of shift reagents in determination of conformations of esters has not so far been reported to our knowledge.

Ester can take either *s-trans* or *s-cis* conformation in principle. Ordinary esters take *s-trans* conformation probably because of the steric and dipolar effects.[4] On the contrary, lactones of small ring size exist as *s-cis* conformation because of the steric requirements.[5] Thus a problem arises whether it is possible to take *s-trans* conformation for a mediumsized lactone or an analogous ring. Hetera-*p*-cyclophanes containing oxygen(s) in an ansa chain, which we have been interested in for some years,[6] is an example of this sort.

It has long been hoped that an infrared carbonyl stretching absorption could be used for diagonsis of the ester conformation. In reality, however, absorptions due to *s-cis* and *s-trans* conformations are so close with each other that they are almost useless for the purpose. Only careful examinations in the presence of both conformations proved to be usefull.[7]

Lanthanide shift reagents are one of the possibilities to solve this problem. If the lanthanide ion is located closely to the carbonyl oxygen, its effect on the ether methylene of the ester group should be different according to its conformation. We now wish to report a successful use of lanthanide shift reagents for determination of conformations of lactones and esters.

Simple esters are known to exist as *s-trans* conformation only[4] and γ-butyrolactone (**1**) must take *s-cis* conformation because of the steric requirement. Thus they were taken as typical examples of *s-trans* and *s-cis* conformations in the lanthanide-induced shift (LIS) measurements. 3-Isochromanone (**2**) was also included as an example of *s-cis* form of 6-membered rings.

PMR spectra of these compounds in deuteriochloroform were determined by adding various amounts of a shift reagent, molar ratio of the shift reagent to the substrate being 0—0.3. LIS was plotted against [L]/[S], where [L] and [S] are the molar concentrations

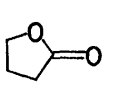

(**1**)

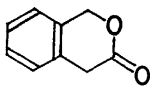

(**2**)

of the shift reagent and the substrate, respectively, to show good linearity. Relative slopes of the straight lines were obtained by taking that of protons at α-position to the carbonyl as a reference and are summarized in Table 1. Changing the shift reagent from Eu(fod)$_3$-d_{27} to Eu(dpm)$_3$ did not seem to give a significant change in the relative slopes. The LIS of the alcoholic methyl signals of methyl acetate was reported by Hart and Love, using Eu(dpm)$_3$.[8] The relative slope was calculated to be 0.96, which is in good agreement with the present datum.

Generally the ether oxygen in an ester group is inactive toward lanthanide shift reagent and preferred site of complexation is the carbonyl oxygen.[3,8,9] If small-sized lactones preferred to form complexes at the ether oxygen, differing from the general tendency of the esters, the relative slopes of the straight lines for the CH_2O would have been larger than unity. Data in Table 1 suggest that the site of complexation is the same for *s-cis* and *s-trans* conformations.

However, the differences in relative slopes concerned with the methylene groups alpha to the ether oxygen do exist; the relative slope of the straight line involving CH_2O group of *s-trans* conformation is almost 1, whereas that of *s-cis* conformation is *ca.* 0.5. In order to discuss the difference of the slopes quantitatively, many factors like pseudo-contact *vs.* contact interactions, symmetry of the anisotropy and the conformational uniformity may have to be considered[10] in the use of McConnell-Robertson equation.[11] Yet this change in relative slopes is distinct and must be useful in diagnosing the conformations of carboxylic esters, provided that they

TABLE 1. RELATIVE SLOPES OF STRAIGHT LINES OBTAINED FROM PLOTS OF LIS *vs.* [L]/[S] USING Eu(fod)$_3$-d_{27}[a]

Protons	$CH_3CO_2CH_3$	$CH_3CO_2C_2H_5$	$C_2H_5CO_2C_2H_5$	**1**	**2**
(H)CH_2C=O	1.00	1.00	1.00	1.00	1.00
(H)CH_2O-	0.90	1.02	1.03	0.51	0.49(0.54)
(H)CH_2CH_2O-		0.41	0.35	0.40	
(H)CH_2CH_2C=O			0.56		

a) Numericals in parentheses were obtained by using Eu(dpm)$_3$.

Table 2. Relative slopes of straight lines obtained with compounds 3, 4, and dioxa[n]paracyclophanes (5_n) using Eu(fod)$_3$-d_{27}[a]

Compound	$CH_2C{=}O$	CH_2O-	ArH	$ArCH_3$
3	1	1.0	0.59	—
4	1	0.97(1.0)	0.58(0.59)	0.37(0.39)
5_{11}	1	1.1	0.54	0.43
5_{12}	1	1.0	0.52	0.43
5_{13}	1	0.99	0.55	0.43
5_{14}	1	0.95	0.56	0.41
5_{15}	1	0.99	0.53	0.37
5_{16}	1	1.0(0.99)	0.57(0.55)	0.38(0.38)

a) Values in parentheses are those obtained by using Eu(dpm)$_3$.

exist as a single conformation. If an ester should exist as a mixture of *s-cis* and *s-trans* conformations and signals due to those conformations should not be resolved it would be natural to expect that an intermediary value between 0.5 and 1 is obtained.

Application of the above findings to complicated systems will be worthwhile to try. We had diester precursors (**3** and **4**) for preparations of hetera-*p*-carbophanes. Testing with these compounds will be worthy because several rotational isomers are possible due to the presence of a RCH_2CO_2R' group[12] and two ester groups are present. The results are shown in Table 2.

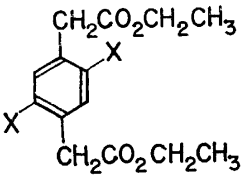

(**3**): X=H, (**4**): X=Me

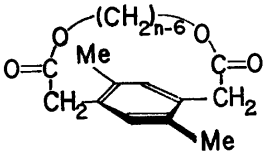

(5_n)

Relative slopes for the CH_2O group of these compounds are *ca.* 1.0. Doubtlessly, these esters exist as *s-trans* conformations. These observations are in conformity with the idea that the open chain esters take *s-trans* conformation usually and *s-cis* conformation is present in special cases only.[13] The results also suggest that the relative slope can be used in such complex esters also for diagnosis of the conformation.

It will be interesting to see the results applied to complex lactones. Dioxa[n]paracyclophanes (5_n)* show only a sharp C=O stretching band at *ca.* 1730 cm^{-1} which is not useful for determination of conformation. Since internal rotations of aromatic rings in the lower members of 5_n are known to be slow on the NMR time scale and rings are strained from the molecular model, a possibility exists that one or both of the ester groups assume *s-cis* conformation. The results of LIS measurements are also shown in Table 2. The relative slopes clearly suggest that these members take *s-trans* conformations irrespective to the ring size.

Usage of lanthanide shift reagents and relative slope of the straight lines obtained by plotting LIS against [L]/[S] of CH_2O signals are powerful tools in determination of conformations of esters. Eu(dpm)$_3$ and Eu(fod)$_3$-d_{27} gave almost the same numerical values. The slope values of methyl groups may be used as well as methylenes.

* *n* is the number of the members of the ansa chain.

Experimental

Syntheses. Syntheses of dioxa[n]paracyclophanes (5_n) will be reported elesewhere. γ-Butyrolactone (**1**) was of commercial origin and 3-isochromanone (**2**) was synthesized according to the method of literature.[14]

Diethyl 2,5-Dimethyl-1,4-phenylenediacetate (4). A mixture of 10 g (44 mmol) of 2,5-dimethyl-1,4-phenylenediacetic acid, 50 ml of ethanol, 100 ml of benzene, and a few drops of concentrated sulfuric acid was refluxed for several hours and worked up in a usual manner to give 9 g (71.8 %) of pale yellow crystals which were recrystallized from hexane-ether. Mp 55.5—56.5 °C. IR(KBr disk): 1725 cm^{-1} (ν_{CO}). NMR (CCl_4, δ,): 1.22 (6H, t); 2.23 (6H, s); 3.43 (4H, s); 4.04 (4H, q); 6.89 (2H, s). Mass spectrum: 278 (M^+). Found: C, 68.71; H, 7.91%. Calcd for $C_{16}H_{22}O_4$: C, 69.04; H, 7.97%.

Diethyl 1,4-Phenylenediacetate (3), mp 58.0—59.0 °C(lit,[15] mp 59 °C), was obtained similarly.

Measurement of Spectra. NMR spectra were recorded on a Hitachi R-20B spectrometer operating at 60 MHz. Shift reagents stocked over P_2O_5 were used.

References

1) C. C. Hinckley, *J. Amer. Chem. Soc.*, **91**, 5160 (1969).
2) A. F. Cockerill, G. L. O. Davies, R. C. Harden, and D. M. Rackham, *Chem. Rev.*, **73**, 535 (1973).
3) G. Montaudo, V. Liberando, S. Caccamese, and P. Maravigna, *J. Amer. Chem. Soc.*, **95**, 6365 (1973), and papers cited therein.
4) R. J. B. Marsden and L. E. Sutton, *J. Chem. Soc.*, **1936**, 1383; R. J. W. LeFevre and A. Sundaram, *ibid.*, **1962**, 3904; J. M. O'Gorman, W. Schand, Jr., and V. Schmacker, *J. Amer. Chem. Soc.*, **72**, 4222 (1950); J. K. Wilmshurst, *J. Mol Spectrosc.*, **1**, 201 (1957).
5) R. Huisgen and H. Ott, *Tetrahedron*, **6**, 253 (1959).
6) K. Sakamoto and M. Ōki, This Bulletin, **46**, 270 (1973); *Tetrahedron Lett.*, **1973**, 3989.
7) M. Ōki and H. Nakanishi, This Bulletin, **44**, 3148, 3419 (1971); *ibid.*, **45**, 1552, 1993 (1972).
8) H. Hart and G. M. Love, *Tetrahedron Lett.*, **1971**, 625.
9) O. Ceder and B. Beijer, *Acta Chem. Scand.*, **26**, 2977 (1972).
10) B. Bleaney, *J. Magnetic Resonance*, **8**, 91 (1972); B. Bleaney, C. M. Dobson, B. A. Levine, R. B. Martin, R. J. Williams, and A. V. Xavier, *Chem. Commun.*, **1972**, 791; J. M. Briggs, G. P. Moss, E. W. Randall, and K. D. Sales, *ibid.*, **1972**, 1180; G. E. Hawkes, D. Leibfritz, D. W. Roberts, and J. D. Roberts, *J. Amer. Chem. Soc.*, **95**, 1659 (1973); R. E. Cramer and R. Dubois, *Chem. Commun.*, **1973**, 936; K. Tori, Y. Yoshimura, M. Kainosho, and K. Ajisaka, *Tetrahedron Lett.*, **1973**, 1573.
11) H. M. McConnell and R. E. Robertson, *J. Chem. Phys.*, **29**, 1361 (1958).
12) M. Ōki and H. Nakanishi, This Bulletin, **44**, 3197 (1971).
13) M. Ōki and H. Nakanishi, *ibid.*, **43**, 2558 (1970).
14) G. A. Swan, *J. Chem. Soc.*, **1949**, 1720.
15) A. F. Titly, *ibid.*, **1928**, 2579.

BULLETIN OF THE CHEMICAL SOCIETY OF JAPAN, VOL. 47(10), 2625—2626 (1974)

Reaction of Polymethylbenzyl Cyanides with Fuming Nitric Acid. A New Route to Polysubstituted 3-Isochromanone Synthesis[1]

Hitomi SUZUKI and Terukiyo HANAFUSA

Department of Chemistry, Faculty of Science, Hiroshima University, Higashi-sendamachi, Hiroshima 730

(Received April 23, 1974)

Synopsis. Treatment of pentamethylbenzyl cyanide and bis(cyanomethyl)tetramethylbenzenes with fuming nitric acid in dichloromethane led to the regiospecific nitrooxylation of the methyl group adjacent to the cyanomethyl group, giving the corresponding benzyl nitrates in good yields. On acid hydrolysis, these nitrates were readily converted into 3-isochromanone derivatives.

Action of cold fuming nitric acid upon polymethylbenzenes leads to the formation of benzyl nitrates.[2] High regiospecificity for the side-chain attack offers a potential as a new entry into various types of benzylic compound. As part of our study concerned with this type of reaction, we report here a convenient preparation of certain polysubstituted 3-isochromanones (3,4-dihydro-1*H*-2-benzopyran-3-ones), useful intermediates for 3(2*H*)-isoquinolinone synthesis. Previously reported routes to 3-isochromanones involve the haloalkylation of phenylacetic acids,[3] the Baeyer-Villiger reaction of 2-indanones,[4] or the lactonization of *o*-acylphenylacetic acid derivatives.[5]

4,6-Bis(cyanomethyl)-1,2,3,5-tetramethylbenzene (I), readily obtained by chloromethylation of isodurene and subsequent treatment of the bis-chloride with sodium cyanide, underwent reaction with fuming nitric acid in dichloromethane at 0—5 °C, giving a high yield of a crystalline product, mp 172—173 °C with decomposition, which had a formula $C_{14}H_{15}N_3O_3$ and showed strong infrared bands due to CH_2ONO_2 group at 1645, 1624, 1286, and 870 cm^{-1}. The unaltered presence of cyano group was shown by the peak at 2245 cm^{-1}. The proton NMR spectrum of the product exhibited absorptions at δ 2.33 (s, 3H), 2.40 (s, 6H), 3.82 (s, 4H), and 5.65 (s, 2H). Loss of the lower-field methyl peak of I indicated that the methyl group flanked with cyanomethyl groups on both sides had been converted into a nitrooxymethyl group. These data are only compatible with the formulation of the product as 5-nitrooxymethyl-4,6-bis(cyanomethyl)-1,2,3-trimethylbenzene (II).

When an ethanolic solution of II was heated with dilute hydrochloric acid under gentle reflux, there were obtained white prisms with the composition $C_{14}H_{16}O_2$, mp 187—189 °C. This compound showed the infrared bands at 3200—2600 (OH), 1738, 1706 (C=O), 1220 (O–CO), 1010 (C–O), and 927 cm^{-1} (OH), and proton NMR peaks at δ 2.23 (s, 6H), 2.27 (s, 3H), 3.70 (s, 2H), 3.75 (s, 2H), and 5.34 (s, 2H). With aqueous alkali it went into solution and was again precipitated on acidification. From its mode of reaction and spectral data, therefore, the product was formulated as 6,7,8-trimethyl-3-isochromanone-5-acetic acid (III).

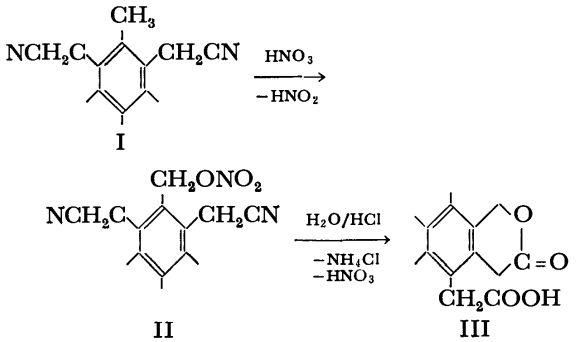

A similar treatment of 3,6-bis(cyanomethyl)-1,2,4,5-tetramethylbenzene gave 5-nitrooxymethyl-3,6-bis(cyanomethyl)-1,2,4-trimethylbenzene, which was then converted into 5,7,8-trimethyl-3-isochromanone-6-acetic acid. Pentamethylbenzyl cyanide offered an easy access to 5,6,7,8-tetramethyl-3-isochromanone over 2-cyanomethyl-3,4,5,6-tetramethylbenzyl nitrate. In every case side-chain nitrooxylation took place on the methyl group adjacent to the cyanomethyl group. 4,6-Bis-(cyanomethyl)-5-ethyl-1,2,3-trimethylbenzene could, potentially, afford a substance analogous to III. However, treatment of this cyanide with nitric acid followed by acid hydrolysis resulted in the formation of intractable gummy substance.

Like existing methods of preparation, our route to 3-isochromanone synthesis is also subject to limited application. It appears to be applicable only to some fully substituted benzyl cyanides carrying two methyl groups in *para* relationship. However, easy access to starting materials, satisfactory yield, and ease of manipulation would make this procedure still useful for some 3-isochromanone synthesis.

Experimental

Melting points are uncorrected. Proton NMR spectra were recorded at 60 MHz using deuteriochloroform as a solvent and TMS as an internal standard. IR spectra were obtained in Nujol with a Jasco 402G spectrophotometer. Satisfactory analyses were obtained for all new compounds.

Polymethylbenzyl cyanides were prepared from the corresponding chlorides by treatment with sodium cyanide in aqueous acetonitrile. Physical properties of benzyl cyanides, benzyl nitrates, and 3-isochromanones obtained in context with the present work are listed in Table 1. No attempt has been made to optimize the conditions.

Procedure for the Nitration of Benzyl Cyanides. A solution of nitric acid (d=1.5; 6.3 g) in dichloromethane (5 ml) was added with stirring to a suspension of benzyl cyanide (0.01 mol) in the same solvent (15 ml) cooled to −5—0 °C in a salt-ice bath. After addition, the mixture was allowed to warm and maintained at room temperature for several hours. It was then worked up by pouring into water, sep-

Table 1. Physical properties of some polysubstituted benzyl cyanides, benzyl nitrates, and 3-isochromanones

Compound	X	Y	Z	Mp (°C)	Proton NMR spectrum (δ)
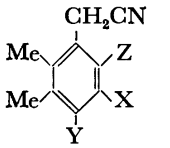	Me	Me	Me	113—115	2.18 (3Me), 2.26 (2Me), 3.52 (CH_2)
	CH_2CN	Me	Me	210—211	2.25 (Me), 2.34 (2Me), 2.42 (Me), 3.71 ($2CH_2$)
	CH_2CN	Me	Et	185—186	1.23 (Me), 2.27 (Me), 2.35 (2Me), 2.78 (CH_2), 3.72 ($2CH_2$)
	Me	CH_2CN	Me	269—270	2.34 (4Me), 3.73 ($2CH_2$)
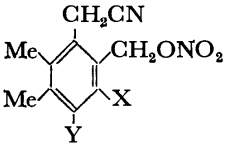	Me	Me	—	116—118	2.25 (2Me), 2.33 (2Me), 3.74 ($2CH_2$)
	CH_2CN	Me	—	177—178	2.33 (Me), 2.40 (2Me), 3.82 ($2CH_2$), 5.65 (CH_2)
	Me	CH_2CN	—	123—130	2.38 (2Me), 2.44 (Me), 3.72 (CH_2), 3.79 (CH_2), 5.62 (CH_2)
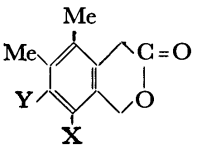	Me	Me	—	106—108	2.22 (2Me), 2.25 (2Me), 3.68 (CH_2), 5.37 (CH_2)
	CH_2COOH	Me	—	187—189	2.23 (2Me), 2.27 (Me), 3.70 (CH_2), 3.75 (CH_2), 5.34 (CH_2)
	Me	CH_2COOH	—	220—222	2.24 (2Me), 2.28 (Me), 3.69 (CH_2), 3.82 (CH_2), 5.37 (CH_2)

arating the organic layer, and evaporating the solvent to give a nitrate as crystalline solid or somewhat pasty cake. It was recrystallized from ethanol. Yields ranged from 67 to 85%.

Procedure for the Hydrolysis of 2-Cyanomethylbenzyl Nitrates to 3-Isochromanones. Dilute hydrochloric acid (10%; 10 ml) was added to a solution of benzyl nitrate (2.5 g) in ethanol (20 ml) and the mixture was heated under gentle reflux for several hours. The yellow solution was then evaporated under reduced pressure to give a residue, which was extracted and crystallized from aqueous ethanol to give 3-isochromanone as fine needles or plates. Yields ranged from 47 to 75%.

The use of concentrated acid led to the extensive formation of an alkali-soluble resin. 3-Isochromanones are readily soluble in ethanol, sparingly soluble in hot water, and almost insoluble in light petroleum.

References

1) The Reaction of Polysubstituted Aromatics. Part XXXVIII; Part XXXVII: H. Suzuki, H. Yoneda, and T. Hanafusa, This Bulletin, in press.

2) H. Suzuki and K, Nakamura, *ibid.*, **43**, 473 (1970); **44**, 227 (1971); H. Suzuki, K. Nakamura, and M. Takeshima, *ibid.*, **44**, 2248 (1971).

3) T. S. Stevens, *J. Chem. Soc.*, **1927**, 178; France Pat., M 4, 771 (1967); A. Arcoleo, T. Garofano, and M. C. Aversa, *Ann. Chim.* (Rome), **58**, 1116 (1968); U. S. Pat., 3480634 (1969); Japan Pat., 7006539 (1970); N. J. McCorkindale and A. W. McCulloch, *Tetrahedron*, **27**, 4653 (1971).

4) G. A. Swan, *J. Chem. Soc.*, **1949**, 1720; H, Hock, S. Lang, and G. Knauel, *Chem. Ber.*, **83**, 227 (1950).

5) M. Renson and L. Christiaens, *Bull. Soc. Chim. Belges*, **71**, 379 (1962); M. S. Newman and S. Mladenovic, *J. Amer. Chem. Soc.*, **88**, 4523 (1966): R. G. Hiskey and M. A. Harpold, *J. Org. Chem.*, **32**, 1986 (1967); O. C. Musgrave, R. Templeton, and H. D. Munro, *J. Chem. Soc., C*, **1968**, 250; J. M. Holland and D. W. Jones, *ibid.*, **1970**, 530.

BULLETIN OF THE CHEMICAL SOCIETY OF JAPAN, VOL. 47 (10), 2627—2628 (1974)

The Preparation of 1,5-Diaryl-3-Phenylsulfonylformazans from Phenylsulfonylacetarylamides and Their Arylazo Derivatives

A. Sami Shawali and A. L. Elansari*

Department of Chemistry, Faculty of Science, University of Kuwait, Kuwait

(Received February 22, 1974)

Synopsis Azo coupling of phenylsulfonylacetarylamides(I) in presence of NaOAc gives the hydrazones (II). In presence of NaOH (and not NaOAc) both I and II couple with diazonium salts to give the formazans (III). mechanism is suggested for the formation of III.

In a previous paper[1] we reported that phenylsulfonylacetanilide (Ia, X=H) afforded 2-phenylsulfonylglyoxalanilide arylhydrazones (II, X=H; Y≠H) upon treatment with diazonium salts in NaOAc buffered solution of EtOH. In this communication we present the results of a study of this reaction in presence of excess of NaOH and an extension of it to the arylhydrazones of type II.

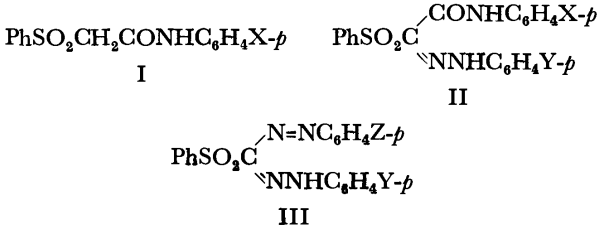

I II III

The treatment of Ia (X=H) with two equivalents of benzenediazonium ion in presence of sodium hydroxide gave a red crystalline product that was analyzed correctly for $C_{19}H_{16}N_4O_2S$. It was distinguished from Ia and IIa (X=Y=H) by the lack of the CONH bands in its IR spectrum. In addition, its electronic absorption spectrum in ethanol was quite different from that reported[1] for IIa (X=Y=H). It exhibits three maxima at 450 (log 3.85), 362 (log 4.25), and 285 (log 3.94) nm. These results suggest that the azo coupling of Ia with PhN_2^+ in presence of NaOH involves the concurrent hydrolytic cleavage of the phenylcarbamoyl group. This presumption was confirmed by the finding that similar treatments of the anilides Ib (X=Cl) and Ic (X=MeO) afforded products which were identical in every respect with that obtained from Ia (X=H). On the basis of these results, the product thus obtained was assigned the structure of 1,5-diphenyl-3-phenylsulfonylformazan (IIIa, Z=Y=H). Similar coupling of I with various diazonium ions yielded the corresponding symmetrically substituted formazans (IIIb—d) (Table 1).

When benzenediazonium chloride was added to IIa (X=Y=H) in NaOAc buffered solution of EtOH, the starting material IIa was recovered unchanged. However, when this coupling was repeated using excess of NaOH in place of NaOAc, IIIa (Y=Z=H) was obtained. The compound IIIa thus produced was identical with the sample obtained in the previous paragraph. Similar treatments of IIb (X=Cl, Y=H) and IId (X=MeO; Y=H) yielded IIIa. The mixture melting point of the three samples of IIIa prepared showed no depression.

The coupling of other hydrazones (IId—m) when similarly carried out with various diazotized arylamines gave the corresponding 3-phenylsulfonyl-1,5-diarylformazans (IIIe—i) in 26—50%. All formazans (IIIa—i) are new. They are intensely colored; exhibiting absorption bands above 400 nm (Table 2). Their electronic absorption spectral data are recorded in Table 2.

On the basis of the above considerations, we propose

Table 1. 2-Phenylsulfonylglyoxalarylamides arylhydrazones (IIa—m)

Compound No.	X	Y	Mp °C	Yield %	Formula	Sulfur, % Calcd	Sulfur, % Found	λ_{max}^{EtOH}, nm (log ε)
IIa	H	H	164	52	$C_{20}H_{17}N_3O_3S$	8.45	8.50	369 (4.43), 275 (3.85), 223 (4.18)
IIb	Cl	H	197	80	$C_{20}H_{16}N_3ClO_3S$[a]	7.74	7.59	369 (4.41), 278 (3.99), 233 (4.19)
IIc	MeO	H	161	48	$C_{21}H_{19}N_3O_4S$	7.83	7.80	368 (4.37), 275 (3.89), 228 (4.15)
IId	NO_2	H	259	92	$C_{20}H_{16}N_4O_5S$	7.69	7.56	374 (4.45), 274 (4.26), 216 (4.39)
IIe	Cl	Cl	243	78	$C_{20}H_{15}Cl_2N_3O_3S$[b]	7.15	7.09	365 (4.34), 282 (3.88), 233 (4.08)
IIf	MeO	Cl	192	82	$C_{21}H_{18}ClN_3O_4S$[c]	7.22	7.14	384 (4.40), 286 (3.94), 228 (4.15)
IIg	NO_2	Cl	260	69	$C_{20}H_{15}ClN_4O_5S$	6.98	7.00	378 (4.59), 224 (4.47)
IIh	MeO	MeO	152	86	$C_{22}H_{21}N_3O_5S$	7.29	7.17	364 (4.38), 278 (4.01), 228 (4.32)
IIi	Cl	MeO	175	77	$C_{21}H_{18}ClN_3O_4S$	7.22	7.13	380 (4.35), 287 (3.94), 226 (4.35)
IIj	NO_2	MeO	209	73	$C_{21}H_{18}N_4O_6S$	7.05	6.85	374 (3.17), 251 (4.28)
IIk	Cl	NO_2	266	89	$C_{20}H_{15}ClN_4O_5S$	6.98	6.80	371 (4.46), 312 (4.13), 218 (4.54)
III	MeO	NO_2	223	81	$C_{21}H_{18}N_4O_6S$	7.05	6.98	395 (4.35), 290 (4.17), 218 (4.33)
IIm	NO_2	NO_2	273	56	$C_{20}H_{15}N_5O_7S$	6.83	6.75	378 (4.15), 306 (3.81), 218 (4.20)

a) Calcd. C, 58.04; H, 3.39; Cl, 8.56%. Found: C, 58.10; H, 3.40; Cl, 8.60%. b) Calcd. C, 53.58; H, 3.37; Cl, 15.81%. Found: C, 53.40; H, 3.40; Cl, 15.71%. c) Calcd. C, 56.82; H, 4.08; Cl, 7.98%. Found: C, 56.60; H, 3.90; Cl, 7.90%.

* Taken in part from the M. Sc. Thesis of A. L. Elansari; University of Cairo, 1972, Egypt.

TABLE 2. 1,5-DIARYL-3-PHENYLSULFONYLFORMAZANS (IIIa—i)

Compound No.	Y	Z	Mp °C	Yield %	Method	Formula	Sulfur, % Calcd	Sulfur, % Found	Chlorine, % Calcd	Chlorine, % Found	λ_{max}^{EtOH} (log ε), nm
IIIa	H	H	148	49 35	A B	$C_{19}H_{16}N_4O_2S$	8.78	8.70			450 (3.85), 362 (4.25), 285 (3.94)
IIIb	Me	Me	201	42 40	A B	$C_{21}H_{20}N_4O_2S$	8.17	8.00			452 (4.31), 298 (4.06), 252 (4.12)
IIIc	Cl	Cl	203	23	A	$C_{19}H_{14}Cl_2N_4O_2S$	7.40	7.08	16.37	16.10	450 (4.33), 291 (4.18), 256 (4.16)
IIId	MeO	MeO	176	50	A	$C_{21}H_{20}N_4O_4S$	7.55	7.48			480 (4.35), 312 (3.97), 265 (4.10)
IIIe	Me	H	146	52	B	$C_{20}H_{18}N_4O_2S$	8.47	8.50			450 (3.80), 363 (4.30),
IIIf	Cl	H	143	28	B	$C_{19}H_{15}ClN_4O_2S$	8.04	8.00	8.88	8.70	450 (3.56), 360 (4.34),
IIIg	Cl	Me	201	52	B	$C_{20}H_{17}ClN_4O_2S$	7.75	7.62	8.58	8.40	450 (4.25), 292 (4.10), 254 (4.10)
IIIh	Cl	NO_2	220	36	B	$C_{19}H_{14}ClN_5O_4S$	7.22	7.10	7.98	8.10	445 (4.45), 318 (4.14), 249 (4.10)
IIIi	Me	NO_2	138	26	B	$C_{20}H_{17}N_5O_4S$	7.57	7.39			450 (3.60), 372 (4.39), 274 (3.90)

a) Calcd: C, 62.62; H, 4.40%. Found: C, 62.40; H, 4.35%. b) Calcd: C, 63.47; H, 4.79%. Found: C, 62.97; H, 4.65%.

the tentative mechanism represented in Scheme 1 for the formation of formazans from I and II. The fact that both I and II gave the same formazan when similarly treated with diazonium ion support the involvement of II as intermediate in the conversion of I into III. The base catalysed hydrolytic cleavage of the arylcarbamoyl group during azo coupling is very similar to the Japp-Klingemann reaction[2] of the hydrazones of ketones. Thus, the arylhydrazones of α-keto acids and the α-arylhydrazones of α,β-diketobutyric esters have been converted into formazans by coupling with diazonium ion in presence of NaOH. With the first type coupling causes decarboxylation, and with the second type an acetyl group is replaced.[3]

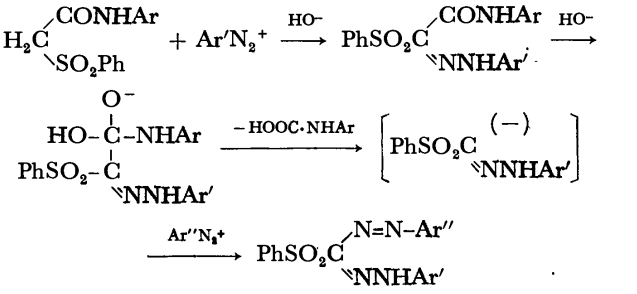

Scheme 1

Experimental

Melting points are uncorrected. Elemental analyses were performed at the Microanalytical Laboratories at the University of Cairo, Egypt. IR spectra were recorded on a Perkin Elmer 337 spectrophotometer. UV spectra were measured on a Beckman DK spectrophotometer.

Phenylsulfonylacetarylamides (Ia—d). To a solution of sodium benzenesulfinate (prepared by neutralising benzenesulfinic acid[4] (0.06 mol) in EtOH (50 ml) with 10% NaOH solution (25 ml)) was added a solution of the appropriate chloroacetarylamide (0.059 mol) in EtOH (50 ml). The mixture was refluxed for 4 hr and left overnight at room temperature. The precipitated product was collected, washed with water and finally recrystallized from dil. EtOH. The anilides, ($PhSO_2CH_2CONHC_6H_4X$-*p*) prepared are: (No., X, mp °C, yield %, Anal.): Ia, H, 138—139 °C, 60 (lit,[1] mp 139 °C); Ib, Cl, 152 °C, 50, Calcd for $C_{14}H_{12}ClNO_3S$: C, 54.28; H, 4.23; Cl, 11.40; S, 10.32%. Found: C, 54.30; H, 4.03; Cl, 11.35; S, 10.18%; Ic, MeO, 149 °C, 55, Calcd for $C_{15}H_{15}NO_4S$: C, 59.00; H, 4.94; S, 10.50%. Found: C, 58.90; H, 4.80; S, 10.60%; Id, NO_2; 210 °C, 70, Calcd for $C_{14}H_{12}N_2O_5S$: C, 52.49; H, 4.09; S, 10.01%. Found: C, 52.50; H, 4.00; S, 10.04%.

2-Phenylsulfonylglyoxalarylamides Arylhydrazones (IIa—m). These were prepared by coupling Ia—d with diazotized arylamines in sodium acetate buffered solution of ethanol following the procedure described earlier.[1] All compounds were recrystallized from acetic acid. The physical properties of the compounds prepared are listed in Table 1.

1,5-Diaryl-3-phenylsulfonylformazans (IIIa—i). *Method A*: To an ice-cold solution of I (0.005 mol) in EtOH (50 ml) was added a cold solution of sodium hydroxide (0.8 g) in water (5 ml) and the mixture was cooled to 0 °C. The resulting solution was treated with 0.01 mol of diazonium salt (prepared in the usual way)[1] with stirring, the temperature being kept below 5 °C. After all the diazonium salt solution had been added, the reaction mixture was stirred for additional 10 min and left overnight in refrigerator. The product precipitated was collected, washed with water and recrystallized from acetic acid. The symmetrically substituted formazans (IIIa—d) prepared by this way are listed in Table 2. The azo coupling of either Ia, Ib or Id with benzenediazonium chloride, when carried out in the same manner, gave IIIa in 40—50% yield as the only isolable product in each case. Mixed melting point of the three samples obtained showed no depression.

Method B: In this method the hydrazone II was coupled with an equivalent amount of the appropriate diazonium salt following the procedure described in method-A. The product obtained from coupling of either IIa, IIb or IId with benzendiazonium chloride proved to be identical in all respects with that obtained from coupling of Ia with two equivalent of the same diazonium salt according to method A. The mixed mp of the four samples of IIIa thus obtained was 148 °C. The unsymmetrically substituted formazans (IIIe—i) prepared by this way are listed in Table 2.

References

1) A. S. Shawali, M. I. Ali, and A. L. Elansari, *Tetrahedron*, **28**, 3805 (1972).

2) R. R. Phillips, "Organic Reactions," Vol. 10, ed. by R. Adams, Wiley, New York, N.Y. (1959), Chapter 2, p. 143.

3) M. Parmerter, *ibid.*, Vol. 10, Chapter 1, p. 4, and the references cited therein.

4) S. Kishnas and H. J. Singh, *J. Amer. Chem. Soc.*, **50**, 792 (1928).

BULLETIN OF THE CHEMICAL SOCIETY OF JAPAN, VOL. 47(10), 2629—2630 (1974)

ESR Study of γ-Irradiated Silk : Effect of Oxygen

Hisashi YOSHIOKA, Naoto KOIDE*, and Fukuji HIGASHIDE

Shizuoka College of Pharmacy, Oshika, Shizuoka, 422

* *Faculty of Education, Shizuoka University, Ohya, Shizuoka 422*

(Received May 14, 1974)

Synopsis. The ESR spectra of silk γ-irradiated in a vacuum showed a doublet at room temperature and at -196 °C. The doublet turns to a singlet at $g=2.006$ by admission of O_2. This is explained in terms of the formation of peroxide radicals.

ESR spectra of γ-irradiated proteins and polypeptides have been reported, the effect of O_2 being examined.[1,2] It is well-known that γ-irradiated polytetrafluoroethylene and polypropylene react with O_2 and form peroxide radicals.[3,4]

We report herewith on the ESR spectra of γ-irradiated silk and the effect of O_2.

Experimental

Raw silk, Japanese race Dōei×Kōhaku (spring 1974), was used. Silk fibroin was prepared by degumming with a 0.5% solution of Marseilles soap and rinsed thoroughly with Na_2CO_3 solution and deionized water. Oily matters were then extracted with ethyl ether with a Soxlet extractor.

Gamma-irradiation was carried out at a dose rate *ca.* 5×10^4 R/hr for 17—30 hr. ESR spectra were recorded at the X-band on a Japan Electron Optics Model JES-3BS.X spectrometer with 100 KHz field modulation.

Results and Discussion

The ESR spectrum of the silk fibroin, γ-irradiated in a vacuum at room temperature for 2 days and measured at room temperature, is shown in Fig. 1. It consists of a strong doublet and a weak background absorption. From the fact that about 50% amino-acid-residues are glycine, the doublet is thought to be attributed to

$$-NH-CO-\dot{C}H-NH-CO-$$

radicals formed at α-carbons of polymer main chains.[1,5]

The doublet turned to a singlet (Fig. 2-A) when the spectrum was measured one day after the admission of O_2 into the sample tube. The intensity of the singlet became only a few percent of that of the doublet. Thus most of the radicals were destroyed by O_2.

The spectrum became asymmetric at -196 °C due to an axially symmetric g-tensor. The values $g_\parallel=2.034$ and $g_\perp=2.002$ were calculated from the position of the peaks (Fig. 2-B). However, some uncertainty remains in the determination of the $g_\parallel$ value because of the weakness and broadness of the $g_\parallel$ peak. The values are almost equal to those of the peroxide radicals formed by the reaction of γ-irradiated polytetrafluoroethylene and polypropylene with O_2.[3,4] The results suggest that the peroxide radicals

$$-NH-CO-\underset{\displaystyle O-O\cdot}{\overset{\displaystyle |}{C}}H-NH-CO-$$

Fig. 1. ESR spectrum of γ-irradiated silk, measured at room temperature.

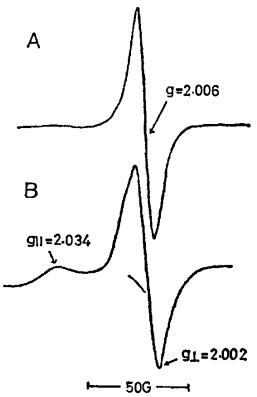

Fig. 2. ESR spectra of the peroxide radicals formed in γ-irradiated silk, measured at room temperature (A) and at -196 °C (B).

are formed in silk. Their molecular motion is considerably free at room temperature since it shows a singlet spectrum.

The doublet spectrum of γ-irradiated polyglycine does not turn to a singlet[1] in contrast to the above result. The difference is explained by assuming that the rate of the diffusion of O_2 into the solid is smaller than that of the decomposition of the peroxide radicals.[1] The glycine residues in silk are thought to exist in a coarse structure.

The ESR spectrum of silk γ-irradiated at -196 °C in the presence of O_2 showed no absorption due to the peroxide radicals when it was measured at -196 °C. However, when the temperature of the sample was elevated to -86 °C for a day, the formation of the radicals was observed. Thus the peroxide radicals are not formed at -196 °C.

The spectra of the raw silk did not differ from those of the silk fibroin.

The authors wish to express their thanks to Dr. Kunihiko Hasegawa for the experiments of γ-irradiation.

References

1) R. C. Drew and W. Gordy, *Radiation Res.*, **18**, 552 (1963).
2) T. Henriksen, *ibid.*, **32**, 892 (1967).
3) S. Siegel and H. Hedegraph, *J. Chem. Phys.*, **46**, 3904 (1967).
4) M. Iwasaki and Y. Sakai, *J. Polym. Sci., Part A-2*, **6**, 265 (1968).
5) W. Gordy and H. Shield, *Radiation Res.*, **9**, 611 (1958).

The Photoionization of Molecular and Crystalline Anthracene

Jun-ichi AIHARA* and Hiroo INOKUCHI
The Institute for Solid State Physics, The University of Tokyo, Roppongi, Tokyo 106
(Received January 12, 1974)

The photoionization efficiency curve of gaseous anthracene was examined by comparing it with the photoemission yield curve of solid anthracene. The direct ionization processes were found to dominate the two curves primarily. Some σ-valence orbitals of this compound were associated with considerably low ionization potentials. The cube law for the photoemission yield near the threshold was also established.

A considerable amount of effort has been devoted during the last decade to elucidate the ionization mechanism and the related valence-band structure of the organic crystal. The photoionization in the gas phase is an important phenomenon which provides a key to the electronic structure of the molecule; the solid-state ionization potential is, correspondingly, an important parameter governing the behavior of molecules in the solid state. Because of our great interest in the electronic behavior of polycyclic aromatics, anthracene and related molecules have recently been chosen for photoionization studies in the gas and solid phases.[1-11] In order to advance further the understanding of the molecular and solid-state photoionization, we attempted to measure the photoionization efficiency curve of molecular anthracene. In this article, we would like to examine the spectral response of the photoionization efficiency for this compound, and correlate the structure of the curve with that of the photoemission yield curve previously published.

Experimental

The photoionization efficiency (PIE) for the anthracene molecule was obtained as follows. The continuous flow of the anthracene vapor between the two electrodes was irradiated with a vacuum ultraviolet light. A 0.5 m vacuum monochromator was used under the same conditions as in Refs. 9 and 10. The light source was a hydrogen discharge tube. The photocurrent collected with the plate electrodes was arithmetically divided by the incident-light intensity. The spectral distribution thus defined is supposedly similar to that of the photoionization cross section,[12] since the vapor pressure employed was considerably lower than the saturated vapor pressure at room temperature. The synthetic anthracene was further purified and then used.

Results and Discussion

The PIE curve of the gaseous anthracene is shown in Fig. 1. The ionization efficiency increases gradually with an increase in the exciting photon energy, exhibiting several distinct breaks, *i.e.*, inflection points, in the observed energy region. The curve is composed of a series of smoothed-step functions of a photon energy. The various sharp bands characteristic of the PIE curve are not present. The possible autoionization peaks seem to be effectively suppressed for this compound. The smoothness of the curve can be phenomenally ascribed to the large molecular dimension of anthracene, since the PIE curves of simpler molecules generally display a more complex dependence on the photon energy.[13-18]

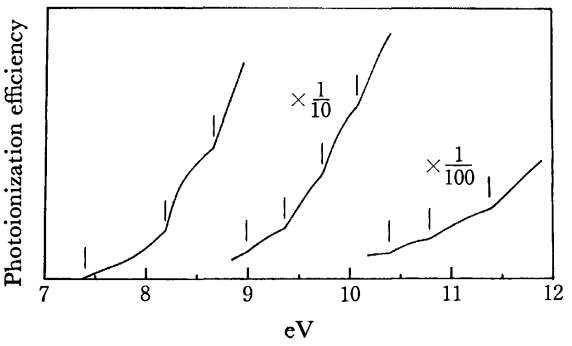

Fig. 1. Photoionization efficiency curve of the molecular anthracene. (Breaks are indicated by lines.)

This effect strongly suggests that, as for anthracene, most photoelectrons are emitted through the direct ionization processes. As long as the possibility of the autoionization processes can be ruled out, the breaks in the curve should correspond to the minimum energies needed to excite the ground-state molecule to the excited-state molecular cations. Every spacing between the adjacent two breaks is obviously too large to be explained in terms of vibrational levels. In other words, these breaks express the adiabatic ionization potentials associated with the lower-lying valence bands in the anthracene molecule.

The structure of the PIE curve is straightforwardly identified by comparing it with the external photoemission data on the crystalline anthracene. In 1963, Vilesov *et al.* carried out a photoemission study of the anthracene crystal and determined the valence-band structure from the kinetic energy distribution curves (EDC) of photoelectrons.[7] Furthermore, Kochi *et al.* observed the existence of several distinct breaks in the photoemission yield (PEY) curve.[10] The PEY curve itself is also a monotonously-varying function of the photon energy. The locations of the breaks in both phases are all listed in Table 1. The values in parentheses are given relative to the first ionization potential or to the threshold energy.

First of all, it is noteworthy that the breaks in the PIE curve are well reproduced in the PEY curve. The breaks in the PIE curve almost coincide with those in the PEY curve, if the threshold of the former curve is appropriately shifted to that of the latter one. The energy differences between the corresponding breaks

* Present address: Department of Chemistry, Faculty of Science, Hokkaido University, Sapporo 060.

TABLE 1. IONIZATION POTENTIALS OF ANTHRACENE (eV)

PIE[a]	PEY[b]	POL[c]	EDC[d]	PES[e]	TYPE[f]
7.40(0.00)	5.65(0.00)	1.75	0.0	7.40(0.00)	π
8.19(0.79)	6.40(0.75)	1.79	—	—	σ
8.65(1.25)	6.93(1.28)	1.72	1.2	8.52(1.12)	π
8.98(1.58)	7.18(1.53)	1.80	—	—	σ
9.35(1.95)	7.61(1.96)	1.74	1.8	9.16(1.76)	π
9.72(2.32)	7.83(2.18)	1.89	—	—	σ
10.07(2.67)	8.48(2.83)	1.59	2.6	10.13(2.73)	π
10.39(2.99)	—	—	—	10.21(2.81)	π
10.78(3.38)	—	1.7	3.4	10.7 (3.3)	σ
11.37(3.97)[g]	—	—	—	11.3 (3.9)	σ

a) From breaks in the photoionization efficiency curve. b) Ref. 10; from breaks in the photoemission yield curve. c) Polarization energy as defined by the difference between PIE and PEY. d) Ref. 7; from the kinetic energy distribution curves of photoelectrons. e) Ref. 2; from the photoelectron spectrum. f) The type of the valence orbital concerned. g) Note that this value was erroneously typewritten in Ref. 6.

are also listed in Table 1.

According to Lyons,[19] the ionization potential of the molecular crystal, I_c, is related to the gaseous ionization potential of the component molecule, I_g, by:

$$I_c = I_g - P, \qquad (1)$$

where P is the positive polarization energy of the crystal. This equation implies that the energy of the crystalline state can be described in terms of the molecular properties and the electrostatic polarization energy. This equation has often been applied to the explanation of the photoemission threshold energy of the molecular crystal.

However, the present results show that the energy difference between the corresponding breaks, which is considered the pertinent polarization energy, is almost preserved among the higher ionization potentials of the crystal. The polarization energy related to the first ionization potential is 1.75 eV. The energies for the first five ionization potentials are substantially the same. This means that the polarization energy is almost independent of the orbital symmetry of the molecular ion formed in the crystal. Several authors have calculated the polarization energy for the anthracene crystal.[20,21] The experimental polarization energy is, however, situated at the upper limit of the theoretical values (1.63 and 1.38 eV,[20] and 1.52 eV[21]). The accordance of the structures in the two curves gives further support to the first-mentioned aspect that both the PIE and PEY curves are primarily determined by the direct ionization processes, though different autoionization processes are possible for the different phases.[22-25]

Next, let us classify the breaks in the two curves. The assignment of the π-ionization potentials of anthracene has been completely established on the basis of recent molecular orbital calculations,[2-4] since these calculations are quite consistent with each other. These π-ionization potentials have all been identified by photoelectron (PE) spectroscopy.[2-4] Accordingly, breaks which correspond to such π-ionization potentials can readily be ascribed to the π-valence orbitals. However, additional breaks are also present in the PIE curve. They have no counterparts in the PE spectrum, the lower part of which comprises only photoelectrons ejected from π-valence orbitals. These breaks were necessarily attributed to the σ-valence orbitals, now that the locations of all the π-valence orbitals have been established with little doubt.

Here, it should be noted that the lowest σ-ionization potential of anthracene is as low as 8.19 eV. If one remembers the fact that the ionization potentials of n-alkanes converge to about 10 eV,[26] this value seems to be too small. The counterpart of the 8.19 eV break in the PIE curve is nevertheless found at 6.40 eV in the PEY curve. This break is found noticeably in the PEY curve obtained by Lyons and Morris.[27] Marchetti and Kearns also observed a PEY curve with a similar structure.[28] Such a common feature of the PEY curve appears to favor our interpretation of the 8.19 eV break in the PIE curve.

Why are these breaks undetected in the PE spectrum? The reason is presumably that such transitions induce appreciable ionization cross sections only when the photon energy does not much exceed the corresponding minimum ionization energies. This explanation is just the same one as Momigny and Lorquet presented for the photoionization of benzene.[29] Dewar *et al.* also suggested that there might be some missing bands, especially some bands related to the σ-valence orbitals, in the PE spectra of aromatic hydrocarbons.

The EDC curves of the solid species generally resemble the PE spectrum of the molecule.[7,10] Exceptionally, some trace of the 8.19 eV break is found, though it is not pronounced, in the EDC curves observed by Vilesov *et al.*[7] A shoulder is present between the first two peaks ascribed to the π-valence orbitals in some EDC curves. This is the most direct evidence for the presence of the valence orbital associated with it. The other σ-electron bands are substantially dissipated except for the higher-energy ones. Such an aspect of the σ-ionization potentials can be traced in Fig. 1, where the second step, beginning at 8.19 eV, is somewhat rounder, suggesting an abrupt decrease in the partial ionization cross section of the second transition with an increase in photon energies.

With the EDC data, we can estimate further the polarization energy of the crystal. The first σ-ionization potential which was clearly detected in the EDC curve of anthracene is located 3.4 eV above the first π-ionization potential.[7] On the other hand, the corresponding break in the PIE curve is found at 10.78 eV. Accordingly, the polarization energy concerned amounts to about 1.7—1.8 eV. This is almost the same value as that determined for lower ionization potentials. For the present, there is little evidence for the rearrangement of the molecule in the crystal, the occurrence of which was suggested in the carbon suboxide crystal.[31]

The above-mentioned results can be used to examine the threshold law for the photoemission from the organic solid. In general, the quantum efficiency of the photoemission near the threshold is very low and does not show any abrupt change.[8-10] Therefore, it is quite

difficult to determine the accurate photoemission threshold energy. This is in marked contrast to the distinct threshold behavior of the gaseous photoionization.[12]

However, the onsets of the transitions related to the higher ionization potentials are often easily distinguished as breaks in the PEY curve.[8,10] Supposing that the polarization energy is preserved among the first and higher ionization potentials, these breaks can be employed as a secondary standard in determining the actual threshold energy for the photoemission from the crystal. If the higher ionization potentials of the crystal could be identified by comparing the breaks in the PEY curve with those in the PIE curve, the threshold energy of the PEY curve would be the first ionization potential of the gaseous species minus the polarization energy associated with the higher ionization potentials. As has been mentioned above, the experimental threshold energy for the anthracene crystal satisfies these requirements, and so it can be regarded as the actual ionization potential of the crystal.

This fact verifies that the cube law for the photoemission threshold is valid for an organic crystal such as anthracene.[9,10] According to this law, the experimental threshold energy of anthracene (5.65 eV) can almost be reproduced by the extrapolated value of 5.68 eV.[10] This implies that the quantum efficiency of the photoemission near the threshold, $Y(h\nu)$, is adequately expressed as:

$$Y(h\nu) \propto (h\nu - E_{th})^3, \quad (2)$$

where E_{th} signifies the extrapolated threshold energy.

On the other hand, the threshold energy derived by Marchetti and Kearns (5.85—5.95 eV) seems to be somewhat larger,[28] probably because they did not take into account the discrete valence band structure and the related vibrational structure of the crystal in constructing their threshold law. Another power law was presented by Sworakowski.[32] According to his square-root law, the threshold energy must be 6.25 eV for the anthracene crystal. However, this law apparently retains the spectral behavior of the gaseous photoionization, since the photoionization efficiency of the gaseous molecule is approximately proportional to the square root of the energy difference between the threshold and the applied photon.[17,18] This aspect of the law is in contradiction to his theory, in which the escape probability and so on are also taken into consideration.[32] This is probably due to his density-of-state function which is not fit for the polycyclic aromatics.

In conclusion, the agreement between the structures of the PIE and PEY curves confirms the predominant direct ionization processes and the parallel valence-band structures in both phases. The parallel valence-band structures appear to characterize the organic molecular crystal and indicate that the whole valence-band structure of the solid is expressed in terms of molecular ionization potentials and a single polarization energy, as is suggested by Eq. (1). In this connection, the cube law for the photoemission threshold was established. It is noteworthy that the measurement of the PIE curve complements the PE spectroscopy well. A comparative study of these phenomena would be very helpful to a deeper understanding of the ionization mechanism in both gas and solid phases.

References

1) F. Brogli and E. Heilbronner, *Angew. Chem., Int. Ed. Engl.*, **11**, 538 (1972).
2) P. A. Clark, F. Brogli, and E. Heilbronner, *Helv. Chim. Acta*, **55**, 1415 (1972).
3) J. H. D. Eland, *Int. J. Mass Spectrom. Ion Phys.*, **9**, 214 (1972).
4) M. J. S. Dewar and D. W. Goodman, *J. Chem. Soc., Faraday Trans. II*, **68**, 1784 (1972).
5) R. Boschi and W. Schmidt, *Tetrahedron Lett.*, **1972**, 2577.
6) J. Aihara and H. Inokuchi, *Chem. Lett.*, **1973**, 421.
7) F. I. Vilesov, A. A. Zagrubskii, and D. Z. Garbuzov, *Fiz. Tver. Tela*, **5**, 2000 (1963) [*Sov. Phys.-Solid State*, **5**, 1460 (1964)].
8) M. Kochi, Y. Harada, and H. Inokuchi, This Bulletin, **40**, 531 (1967).
9) T. Hirooka, M. Kochi, J. Aihara, H. Inokuchi, and Y. Harada, *ibid.*, **42**, 1481 (1969).
10) M. Kochi, Y. Harada, T. Hirooka, and H. Inokuchi, *ibid.*, **43**, 2690 (1970).
11) T. Hirooka, K. Tanaka, K. Kuchitsu, M. Fujihira, H. Inokuchi, and Y. Harada, *Chem. Phys. Lett.*, **18**, 390 (1973).
12) D. W. Turner, "Determination of Organic Structures by Physical Methods," Vol. 2, ed. by F. C. Nachod and W. D. Phillips, Academic Press, New York, N. Y. (1962), Ch. 5.
13) W. A. Chupka and J. Berkowitz, *J. Chem. Phys.*, **51**, 4244 (1969).
14) B. Brehm, *Z. Naturforsch.*, **21a**, 196 (1966).
15) R. Botter, V. H. Dibeler, J. A. Walker, and H. M. Rosenstock, *J. Chem. Phys.*, **44**, 1271 (1966).
16) V. H. Dibeler and S. K. Liston, *ibid.*, **47**, 4548 (1967).
17) V. H. Dibeler and R. M. Reese, *J. Res. Natl. Bur. Std.*, **A68**, 409 (1964).
18) V. K. Potakov and O. A. Yuzhakova, *Dokl. Akad. Nauk SSSR*, **192**, 131 (1970); *Dokl. Phys. Chem.*, **192**, 364 (1970).
19) F. Gutman and L. E. Lyons, "Organic Semiconductors," John Wiley, New York, N. Y. (1967).
20) M. Batley, L. J. Johnston, and L. E. Lyons, *Aust. J. Chem.*, **23**, 2397 (1970).
21) A. Jurgis and E. A. Silinsh, *Phys. Status Solidi (b)*, **53**, 735 (1972).
22) J. C. Phillips, *Phys. Rev. Lett.*, **12**, 447 (1964).
23) Y. Onodera, *Phys. Rev.*, **B4**, 2751 (1971).
24) H. Aulich, B. Baron, and P. Delahay, *J. Chem. Phys.*, **58**, 603 (1973).
25) S. Yoshimura, *J. Phys. Soc. Japan*, **28**, 701 (1970).
26) D. F. Brailsford and B. Ford, *Mol. Phys.*, **18**, 621 (1970).
27) L. E. Lyons and G. C. Morris, *J. Chem. Soc.*, 5192 (1960).
28) A. P. Marchetti and D. R. Kearns, *Mol. Cryst. Liq. Cryst.*, **6**, 299 (1970).
29) J. Momigny and J. C. Lorquet, *Chem. Phys. Lett.*, **1**, 505 (1968).
30) M. J. S. Dewar, E. Haselbach, and S. D. Worley, *Proc. Roy. Soc. Lond., Ser. A*, **315**, 431 (1970).
31) U. Gelius, C. J. Allan, D. A. Allinson, H. Siegbahn, and K. Siegbahn, *Chem. Phys. Lett.*, **11**, 224 (1971).
32) J. Sworakowski, *Phys. Status Solidi (a)*, **13**, 381 (1972).

Effect of Alcohols on the Micelle Formation of Nonionic Surfactants in Aqueous Solutions

Nagamune NISHIKIDO, Yoshikiyo MOROI, Hiromoto UEHARA,* and Ryohei MATUURA

Department of Chemistry, Faculty of Science, Kyushu University, Fukuoka 812

(Received February 8, 1974)

The variation of critical micelle concentrations (CMC) of polyoxyethylene lauryl ethers having various ethylene oxide chain lengths $\bar{n}$($\bar{n}$=6, 11, 20, and 31) on addition of short chain alcohols to the surfactant aqueous solutions was determined at 20 °C. Thermodynamic quantities of micelle formation in methanol- and ethanol-water mixtures and in pure water were obtained in connection with the heat of micelle formation determined by direct calorimetry. Methanol and ethanol showed a CMC-increasing effect only, whereas the addition of *n*-propanol, *n*-butanol, and *n*-pentanol showed a CMC-decreasing effect. The overall CMC-increasing effect is interpreted as being mainly due to the fact that methanol and ethanol weaken the hydrophobic bond. However, the effect also has a secondary effect of lowering the CMC slightly on the polyoxyethylene portion of a surfactant. Several factors are suggested for explaining this secondary effect. The CMC-decreasing effect is explained by a decrease in the free energy of mixing resulting from the solubilization of alcohol molecules into the micelle.

The mechanism of micellization of nonionic surfactant in aqueous solution is analogous to that of ionic surfactant from the viewpoint that micellization is controlled by two opposing factors, the driving force for association and the factor preventing association.[1,2] However, detailed studies on the micelle formation of nonionic surfactants are few in number as compared with those of ionic surfactants.

We can gain useful information for clarifying the various factors governing micelle formation from a study of the effect of additives on the critical micelle concentration (CMC) of surfactant. In order to evaluate relative efficacies of protein denaturants weakening hydrophobic interaction, a convenient approach to assess their effects on the CMC of surfactants has been used.[3,4] Short chain alcohols, urea and guanidine salts are known to be denaturating agents, *viz.*, hydrophobic bond breakers. Their effect on the CMC of nonionic surfactants is of interest in view of protein denaturation.

The effect of alcohols on the CMC of ionic surfactants has been investigated extensively,[5] but not that of nonionic surfactants.[6-10] We have studied the effect of methanol, ethanol, *n*-propanol, *n*-butanol, and *n*-pentanol on the micelle formation of polyoxyethylene lauryl ethers having various mean ethylene oxide chain lengths. The CMC of polyoxyethylated surfactants in alcohol-water mixtures was determined by the surface tension method. Heats of micelle formation were obtained by direct calorimetric measurements.

Experimental

Materials. The surfactants used (Kao Soap Co., Ltd.) were polyoxyethylene lauryl ethers ($C_{12}H_{25}O(CH_2CH_2O)_{\bar{n}}H$, $\bar{n}$=6, 11, 20, 31, $\bar{n}$: the average number of ethylene oxide groups). The average chain lengths of the ethylene oxide adducts were determined from their hydroxyl values. The impurities, potassium acetate and polyethylene glycol, were checked by means of atomic absorption spectrophotometry and paper chromatography and found to be minute. Elementary analysis also showed that the samples were sufficiently pure. All the alcohols were thoroughly purified. Water was redistilled from alkaline permanganate solution and had 1.5×10^{-6} mho/cm specific conductance.

Method. The surface tension measurements were performed at 20 °C by the Wilhelmy method with a 22×22 mm glass plate and a Kyowa Electro Surface Balance. Before the measurement the plate was cleaned by heating in a chromic acid mixture for two hours and was washed thoroughly with water. Surfactant solutions were left to stand at the temperature of measurement for a day, preventing evaporation. It took about an hour to obtain equilibrium surface tension after the surfactant solution surface had been cleaned by suction with a fine glass capillary. The CMC was determined from sharp breaks in the surface tension *vs.* logarithm of concentration plots.[10] Precision of the CMC determinations was within ±7%. The CMC was also checked by the spectral method,[11] good agreement being found between the two methods.

The heats of micelle formation were obtained at 20 °C by the heat of dilution method according to Corkill *et al.*[12] with a modified Applied Electric Laboratory Microcalorimeter, Model CM-204S1.

Results and Discussion

Since alcohols are surface active, sharp breaks in the surface tension *vs.* logarithm of the surfactant concentration plots become uncertain with an increase in the concentration of the alcohol. Thus, the surface tension method was used up to *ca.* 8 mol/l alcohol concentration. Within this range well-defined CMC values could be obtained. A small minimum appeared near the CMC in the surface tension *vs.* concentration curve of $\bar{n}$=11, 20 and 31 in water. This may be due to the distribution of the ethylene oxide chain length of a surfactant molecule.[13] Surfactants used in this study might fall in the category of polydisperse materials defined by Gibbons,[14] but we believe that they have sufficient purity[15] for attaining the aim of the present work, since the appearance of the minimum in the surface tension-concentration curve is not remarkable and analytical result shows sufficient purity.

CMC in alcohol–water mixtures are shown in Figs. 1, 4, and 5 as a function of alcohol concentrations. Methanol and ethanol show only a CMC-incresing

* Present address: Department of Applied Chemistry, Faculty of Engineering, Kinki University, Kure.

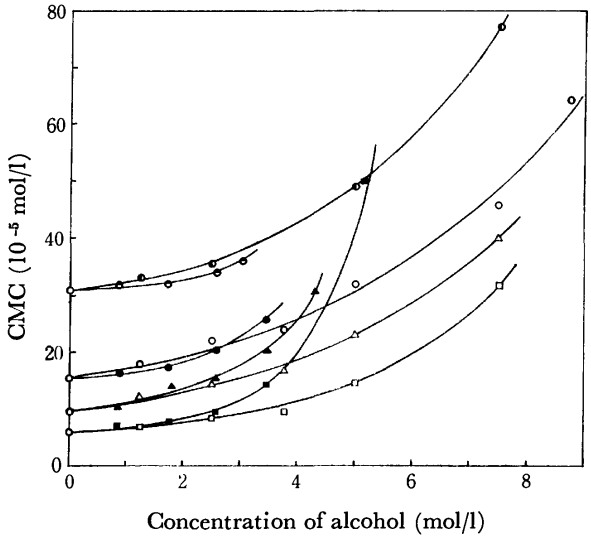

Fig. 1. The CMC's of $\bar{n}$=6, 11, 20 and 31 surfactants in methanol- and ethanol-water mixtures at 20 °C.
□: methanol, $\bar{n}$=6 ■: ethanol, $\bar{n}$=6
△: methanol, $\bar{n}$=11 ▲: ethanol, $\bar{n}$=11
○: methanol, $\bar{n}$=20 ●: ethanol, $\bar{n}$=20
◐: methanol, $\bar{n}$=31 ◓: ethanol, $\bar{n}$=31

effect (Fig. 1). *n*-Propanol shows a CMC-decreasing effect in the low concentration range for all $\bar{n}$'s and a CMC-increasing effect at higher concentration for $\bar{n}$=6 and 11 (Figs. 4 and 5), while *n*-butanol and *n*-pentanol show a CMC-decreasing effect (Figs. 4 and 5). However, the CMC-increasing tendency may be expected to appear in excess of the decreasing effects by more addition of these alcohols to the surfactant solutions in analogy with *n*-propanol. These results are in line with those for ionic surfactants.[16]

The CMC-increasing effect of methanol and ethanol is attributable to the increasing solvent power of these alcohol-water mixtures, if we neglect the solubilization of alcohols into the palisade layer of the micelle. At low concentrations of alcohols, ethanol behaves almost the same as methanol with respect to the efficiency of the CMC-increasing effect. With increasing concentrations, however, ethanol becomes much more effective than methanol.

In order to clarify the above behavior, the heats of micellization in methanol- and ethanol-water mixtures

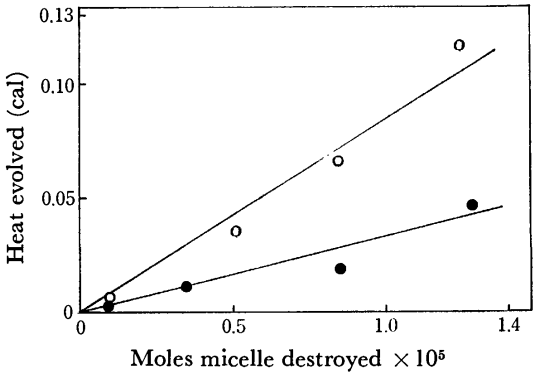

Fig. 2. The plots of heat evolved against moles of $\bar{n}$=31 surfactant demicellized at 20 °C in water (○) and 0.87 M ethanol (●).

are compared. The examples of measured heat of micellizatlon are shown in Fig. 2 with $\bar{n}$=31, in water and in 0.86 M ethanol. The abscissa represents the amount of micelle destroyed on dilution and the ordinate the observed heat change. The plot is almost linear and crosses close to the origin. Hence, within experimental error the assumption of Corkill *et al.*[12] is satisfied, *viz.* the heats of dilution of monomers and micelles are negligibly small as compared to the heat of micellization which is independent of concentration. The slope (Fig. 2) is the heat of micelle formation and equal to the standard enthalpy ΔH_m^0 with an opposite sign to that of the observed heat change.[12] The standard enthalpy ΔH_m^0 in conjunction with the standard free energy of micellization ΔG_m^0 gives the standard entropy ΔS_m^0. We take the pseudo-phase separation approach and get the following equations:[17,18]

$$\Delta G_m^0 = RT \ln X_c \quad (1)$$

$$\Delta S_m^0 = \frac{\Delta H_m^0 - \Delta G_m^0}{T} \quad (2)$$

where X_c is CMC expressed in mole fraction, since the CMC is small enough to replace activity by mole fraction. The solubilization of methanol and ethanol is considered to be negligible. Thus, the micelles in these short chain alcohol-water systems are single-component ones. The standard enthalpy ΔH_m^0 can be obtained in the above way (Fig. 2), and Eqs. (1)

Table 1. Thermodynamic quantities of micelle formation for surfactants of $\bar{n}$=6 and 31 in pure water, methanol- and ethanol-water mixtures at 20 °C

Additive	$\bar{n}$=6			$\bar{n}$=31		
	ΔH_m^0 kcal/mol	ΔS_m^0 e.u./mol	$\Delta G_m^0 \pm 0.06$ kcal/mol	ΔH_m^0 kcal/mol	ΔS_m^0 e.u./mol	$\Delta G_m^0 \pm 0.06$ kcal/mol
in water	7.8±1.6	54±5	−7.99	7.8±1.6	51±5	−7.03
1.25 M MeOH	4.5±0.9	42±3	−7.88	5.0±1.0	41±3	−6.95
3.75 M MeOH	3.0±0.6	36±3	−7.65	2.7±0.5	33±2	−6.83
7.50 M MeOH	−0.4±0.1	22±1	−6.91	−0.1±0.1	22±1	−6.40
0.43 M EtOH	4.1±0.9	41±3	−7.92	5.3±1.1	42±4	−7.01
0.86 M EtOH	2.2±0.5	34±3	−7.86	3.3±0.7	35±3	−6.99
2.58 M EtOH	0.6±0.1	28±1	−7.66	0.5±0.1	25±1	−6.91
5.16 M EtOH	−3.7±0.8	10±3	−6.62			

and (2) are valid for these systems, regarding the alcohol–water mixtures as solvents.

The values of ΔH_m^0 and ΔS_m^0 for representative methanol– and ethanol–water mixtures of $\bar{n}=6$ and 31 together with those in water are given in Table 1.

For the results in water, the large positive entropy ΔS_m^0 is responsible for the negative free energy ΔG_m^0 for micelle formation, since the enthalpy ΔH_m^0 is positive. Several causes for the positive entropy can be considered. Current views[18-28] are as follows. The ordered water around the hydrocarbon chains is released on micellization, contributing to the positive entropy. The gain in the conformational entropy of hydrocarbon chains may also give a positive value. Contribution of the change in solvation of hydrophilic chains is complicated. Desolvation of polyethylene oxide chains, which gives rise to a positive entropy change, has been proposed.[21-24] Elworthy and Florence[25,26] suggested that the mesh of polyethylene oxide chains in the micellar state can trap more solvent than the single chains in monomer, leading to a negative change. The negative contribution of the decrease of the configurational entropy of the flexible hydrophilic chains on micellization is also involved.

Studies on the dependence of ΔS_m^0 on the ethylene oxide content with the same hydrocarbon chains might elucidate the contribution of polyoxyethylene chains to ΔS_m^0. We have obtained the following data of ΔS_m^0 for various values of $\bar{n}$ in aqueous solution at 20 °C.

$\bar{n}$	6	11	20	31
ΔS_m^0 (e.u./mol)	54	54	50	51

It is seen that no essential difference of ΔS_m^0 in water exists among the surfactants having various oxyethylene chain lengths, so that we can consider that the contribution of polyoxyethylene chains is secondary. Thus, the large positive entropy ΔS_m^0 in water is considered to be primarily due to the loss of iceberg structure during the course of micellization. We see that the addition of methanol and ethanol to the surfactant aqueous solutions reduces the entropy ΔS_m^0, and the effectiveness of reducing ΔS_m^0 of ethanol becomes greater than that of methanol. At least qualitatively these alcohols primarily weaken the hydrophobic interactions, the important driving force for micellization, although other effects may also be involved.[29]

The difference in the effect of alcohol on ΔS_m^0 among various ethylene oxide chain lengths is ambiguous, but the effect on ΔG_m^0 displays the difference. In water and at constant concentrations of methanol and ethanol, ΔG_m^0 *vs.* $\bar{n}$ plots are almost linear. Thus, the gradient of the ΔG_m^0 *vs.* $\bar{n}$ plots is the free energy increment of the hydrophilic part of a surfactant in the process of micellization. The gradient $\Delta(\Delta G_m^0)/\Delta\bar{n}$ is plotted against the alcohol concentration in the solvent (Fig. 3). With increasing concentration of alcohols, the parameter $\Delta(\Delta G_m^0)/\Delta\bar{n}$ decreases rapidly, the rate being greater for ethanol than methanol. Alcohols might reduce the hydration of polyoxyethylene chains through the hydrogen bonding with water, but the interaction of alcohols with water is complicated.[30,31] According

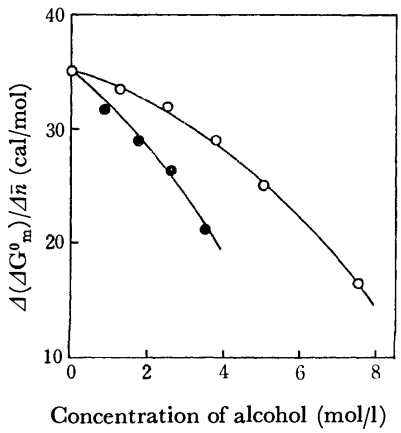

Fig. 3. $\Delta(\Delta G_m^0)/\Delta\bar{n}$ *vs.* methanol (●) and ethanol (○) concentration plots.

to Ray and Nemethy,[8] it is probable that alcohols have a solvent effect on the ethylene groups in the oxyethylene chains as well as the hydrocarbon chains of surfactants, since the ethylene groups may also be expected to increase the structual order in the surrounding water.

The CMC-increasing effect of methanol and ethanol is considered to contain two opposing factors: the primary effect on the hydrocarbon part, in which the alcohols weaken the hydrophobic bond, and lead to increasing the CMC; a secondary effect on the polyoxyethylene chains, which is a small effect of CMC-decreasing. The overall effect of methanol and ethanol is inclined towards raising the CMC.

Alcohols which have longer hydrocarbon chains than ethanol show a CMC-decreasing effect. The results are shown in Figs. 4 and 5 with $\bar{n}=6$ and 31, respectively. A similar behavior was obtained for $\bar{n}=11$ and 20. At low concentrations of alcohols, the CMC-decreasing effects are attributable to the penetration of alcohols into the palisade layer of the micelle, forming

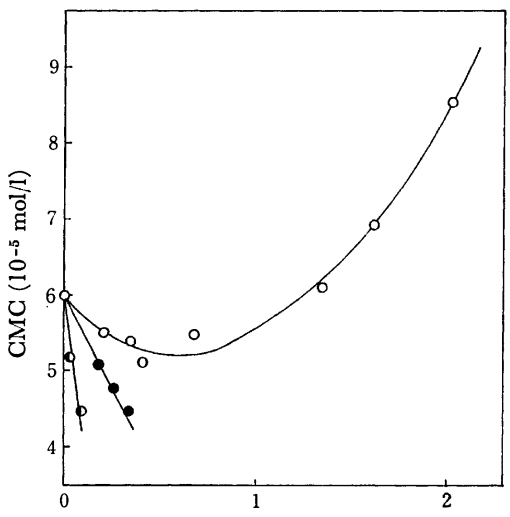

Fig. 4. The CMC's of $\bar{n}=6$ surfactant as a function of the concentrations of *n*-propanol (○), *n*-butanol (●) and *n*-pentanol (◐) at 20 °C.

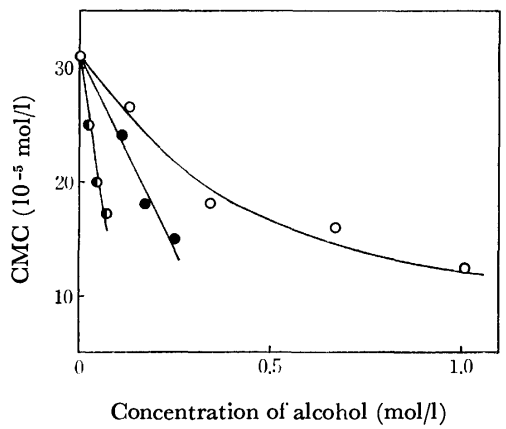

Fig. 5. The CMC's of $\bar{n}=31$ surfactant as a function of the concentrations of *n*-propanol (○), *n*-butanol (●) and *n*-pentanol (◐) at 20 °C.

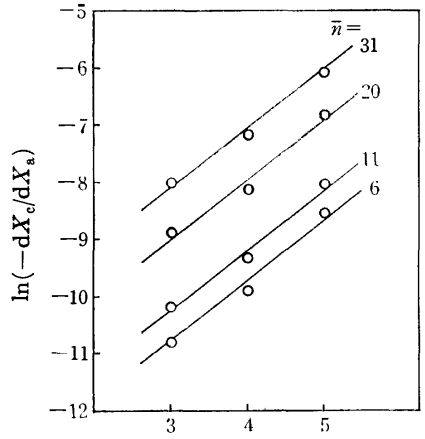

Fig. 6. The logarithm of the rate of change of the CMC with alcohol concentration, $\ln(-dX_c/dX_a)$ *vs.* the number of carbon atoms in alcohol, *m'*.

a mixed micelle.[16] At higher concentrations of *n*-propanol, the CMC-increasing effect overcomes the decreasing effect. This is due to the solvent effect as in the case of methanol and ethanol, although it is not seen in the case of *n*-butanol and *n*-pentanol. The CMC initially decreases linearly with alcohol concentration, which resembles closely the case of ionic surfactants (Figs. 4 and 5). The CMC-decreasing effects of alcohols have been explained by Shinoda in the case of ionic surfactants.[16] His view is herewith applied to the case of nonionic surfactants.

We take the phase separation model, equating the chemical potential of the surfactant molecule in the micelle phase to that in the bulk phase, assuming that the standard chemical potentials in water and alcohol–water system are approximately the same if the concentration of alcohols added is sufficiently low. We then have

$$\frac{X_c'}{X_c} = 1 - x; \quad x \ll 1 \tag{3}$$

where x is the mole fraction of alcohol in the mixed micelle, and X_c and X_c' are the CMC in the mole fraction unit in water and in the mixed solvent, respectively. Alcohols are considered to undergo partition between the micellar and bulk phase. The partition law is as follows.

$$\frac{X_a}{x} = K\exp\left(-\frac{m'\omega}{kT}\right); \quad X_a \ll 1 \tag{4}$$

where K is a constant, m' the number of carbon atoms in an alcohol, and ω the free energy change per methylene group transferred from water into the micelle phase. Near the CMC, the amount of solubilized alcohol is negligible. Thus, X_a can be put equal to the mole fraction of alcohol in the aqueous surfactant solution.

From Eqs. (3) and (4) we get

$$\ln\frac{X_c - X_c'}{X_a} = \ln X_c + \frac{m'\omega}{kT} - \ln K$$
$$= \ln X_c + 1.1m' - \ln K \tag{5}$$

where the value of ω is adopted to be $1.1\,kT$.[32,33]

This gives the relation between the logarithm of the rate of change of CMC with alcohol concentration, $\ln(-dX_c/dX_a)$, and the number of carbon atoms in alcohol, m'. The former, obtained from experimental data is plotted against the latter in Fig. 6. The values of the gradients of these plots are close to 1.1, the experimental data fitting Eq. (5) fairly well. The value of K obtained for each $\bar{n}$ is:

$\bar{n}$	6	11	20	41
K	1.57	1.51	0.64	0.55

It can be seen from Eq. (4) that x is inversely proportional to K when m' and X_a are fixed. We see that the surfactant with a larger oxyethylene chain length has a greater mole fraction of alcohol in mixed micelle. It seems that the surfactant solution with larger $\bar{n}$ solubilizes the alcohols to a greater extent. The result for *n*-propanol reflects the situation. At higher concentrations of alcohol, the CMC-increasing effect overcomes the CMC-decreasing effect on account of the increase of non-solubilized alcohol. It is seen that the CMC-increasing effect of *n*-propanol is more enhanced for the smaller $\bar{n}$, the CMC-decreasing effect prevailing for the larger $\bar{n}$ (Figs. 4 and 5). The results indicate that the CMC-decreasing effect (solubilization effect) increases with the increase of oxyethylene chain length. This conclusion agrees with Cohen's result in the case of *n*-heptanol.[34]

We express our hearty thanks to Kao Soap Co., Ltd. for the supply of nonionic surfactants.

References

1) T. Nakagawa and K. Kuriyama, *Nippon Kagaku Zasshi*, **78**, 1568 (1957).
2) D. C. Poland and H. A. Scheraga, *J. Phys. Chem.*, **69**, 2431 (1965).
3) W. Bruning and A. Holtzer, *J. Amer. Chem. Soc.*, **83**, 4865 (1961).
4) W. B. Gratzer and G. H. Beaven, *J. Phys. Chem.*, **73**, 2270 (1969).

5) B. D. Flockhart, *J. Colloid Sci.*, **12**, 557 (1957); S. H. Herzfeld, M. L. Corrin, and W. D. Harkins, *J. Phys. & Colloid Chem.*, **54**, 271 (1950); K. Shinoda, *J. Phys. Chem.*, **58**, 1136 (1954); M. F. Emerson and A. Holtzer, *ibid.*, **71**, 3320 (1967); K. Shirahama, M. Hayashi, and R. Matuura, This Bulletin, **42**, 1206 (1969); *etc.*
6) P. Becher, *J. Colloid Sci.*, **20**, 728 (1965).
7) L. Benjamin, *J. Colloid Interface Sci.*, **22**, 386 (1966).
8) A. Ray and G. Nemethy, *J. Phys. Chem.*, **75**, 809 (1971).
9) F. A. Green, *J. Colloid Interface Sci.*, **41**, 124 (1972).
10) P. Becher and S. E. Trifiletti, *ibid.*, **43**, 485 (1973).
11) A. Ray and G. Nemethy, *J. Phys. Chem.*, **75**, 804 (1971).
12) J. M. Corkill, J. F. Goodman, and J. R. Tate, *Trans. Faraday Soc.*, **60**, 996 (1964); J. M. Corkill, J. F. Goodman, P. Robson, and J. R. Tate, *ibid.*, **62**, 987 (1966); J. M. Corkill, J. F. Goodman, S. P. Harrold, and J. R. Tate, *ibid.*, **63**, 240 (1967).
13) E. H. Crook, D. B. Fordyce, and G. F. Trebbi, *J. Phys. Chem.*, **67**, 1987 (1963).
14) R. A. Gibbons, *Nature*, **200**, 665 (1963).
15) P. Becher, "Nonionic Surfactants," ed. by M. J. Schick, Marcel Dekker, New York, N.Y. (1967), p. 478.
16) K. Shinoda, T. Nakagawa, B. Tamamushi, and T. Isemura, "Colloidal Surfactants," Academic Press, New York (1963), p. 69.
17) D. G. Hall and B. A. Pethica, "Nonionic Surfactants," p. 516.
18) J. M. Corkill, J. F. Goodman, and S. P. Harrold, *Trans. Faraday Soc.*, **60**, 202 (1964).
19) L. Benjamin, *J. Phys. Chem.*, **68**, 3575 (1964).
20) C. McDonald, *J. Pharm. Pharmacol.*, **22**, 774 (1970).
21) K. W. Herrmann, *J. Phys. Chem.*, **66**, 295 (1962).
22) R. A. Hudson and B. A. Pethica, Proc. 4th Intern. Congre. Surface Activity, Brussels, **2**, 631 (1964).
23) H. Schott, *J. Pharm. Sci.*, **58**, 1521 (1969).
24) J. R. Bloor, J. C. Morrison, and C. T. Rhodes, *ibid.*, **59**, 387 (1970).
25) P. H. Elworthy and A. T. Florence, *Kolloid-Z.*, **195**, 23 (1964).
26) P. H. Elworthy and A. T. Florence, *J. Pharm. Pharmacol.*, **15**, 851 (1963).
27) M. J. Schick, *J. Phys. Chem.*, **67**, 1796 (1963).
28) E. H. Crook, G. F. Trebbi, and D. B. Fordyce, *ibid.*, **68**, 3592 (1964).
29) P. Mukerjee and A. Ray, *ibid.*, **67**, 190 (1963).
30) S. Y. Gerlsma, *Eur. J. Biochem.*, **14**, 150 (1970).
31) N. Laiken and G. Nemethy, *J. Phys. Chem.*, **74**, 3501 (1970).
32) I. J. Lin and P. Somasundaran, *J. Colloid Interface Sci.*, **37**, 731 (1971).
33) I. J. Lin, *J. Phys. Chem.*, **76**, 2019 (1972).
34) M. Cohen, *C. R. Acad. Sci. Paris*, **229**, 1074 (1949).

An Ultrasonic Method for Determination of the Volume Change Due to Internal Rotation in 1,2-Dichloroethane

Masakatsu Aoi and Kiyoshi Arakawa

Research Institute of Applied Electricity, Hokkaido University, Sapporo 060

(Received March 6, 1974)

A simple method for determining the volume change, ΔV, in conformational isomerism from sound velocity has been worked out from the theory of binary mixtures. The method was applied for obtaining the volume change due to internal rotation in 1,2-dichloroethane. The sound velocity was measured with an ultrasonic interferometer. The method was found useful.

The conformational equilibrium of halogenated ethanes has long been the subject of study from the viewpoint of molecular structure theory, the equilibrium between *trans* and *gauche* forms of 1,2-dichloroethane (DCE) having been clarified.[1-4] The energy difference between them is nearly zero in a liquid state,[1] while the ratio N_g/N_t in this state is 1.93 at room temperature, where N_g is the number of *gauche* molecules and N_t that of *trans* molecules.[3]

The molecular interaction in binary mixtures including DCE has been investigated by various methods such as the Raman effect, infra-red[2-5] and NMR[6] spectroscopy, and dielectric,[7-13] thermodynamic[14-20] and ultrasonic[21-25] methods.[26] However, the essential feature of the interactions between DCE and other compounds such as benzene has been a topic of controversy. Findenegg and Kohler[18,19] and Kiyohara and Arakawa[25] studied the DCE–benzene system by means of an ultrasonic method using theory of solutions, and Higasi *et al.*[12,13] by means of a dielectric method. Their conclusions did not agree.

In the above studies the volume change in conformational isomerism between *trans* and *gauche* forms of DCE[2,8,18,25] has not been taken into consideration, which seriously influences the determination of the magnitude of enthalpy difference ΔH and other thermodynamic quantities. This has been pointed out recently.[27-29]

Recent advancement in ultrasonic absorption technique made it possible to determine ΔV.[21] However, the determination is impossible when the frequency range does not cover the relaxation range of the system to be studied, the error being fairly large. ΔV has been usually neglected in studies of conformational equilibrium in which the assumption $(\Delta V/V)(C_p/\alpha) \ll \Delta H$ is valid.[21]

It has been reported[30] that the magnitude of $\Delta V/V$ in conformational isomerism for 1,1,2-trichloroethane (TCE) and other compounds in various solvents is 1—3%, but DCE was not included in the studies. We have undertaken to apply a simple method for obtaining ΔV from sound velocity on the basis of theory of solutions to DCE.

Method of Analysis

The solution of Percus-Yevick equation for binary liquid mixtures was given as follows.[31,32]

$$\frac{p}{kT} = \frac{1}{(1-\xi)^3}\left[(\rho_1+\rho_2)(1+\xi+\xi^2) - \frac{18}{\pi}\eta_1\eta_2(R_1-R_2)^2 \times \{R_1+R_2+R_1R_2(\eta_1R_1^2+\eta_2R_2^2)\}\right] \quad (1)$$

where R_i is the hard core diameter of i-th component, p pressure, T temperature, $\rho_i = N_i/V$ number density, $\eta_i = \pi\rho_i/6$, and ξ the volume fraction defined by

$$\xi = (\pi/6)(\rho_1R_1^3+\rho_2R_2^3). \quad (2)$$

We express here R_i as follows

$$R_1 = R,\ R_2 = R(1+\delta). \quad (3)$$

In actual cases of conformational equilibrium, δ is taken to be smaller than 0.1, thus Eq. (1) becomes

$$\frac{p}{kT} = \frac{1}{(1-\xi)^3}\left[\rho(1+\xi+\xi^2) - \frac{\pi}{2}x_1x_2R^3\rho^2\delta^2\left\{2+\frac{\pi}{6}R^3\rho + \delta\left(1+\frac{\pi}{6}R^3\rho(x_1+3x_2)\right) + \delta^2\left(\frac{\pi}{2}R^3\rho x_2\right) + \delta^3\left(\frac{\pi}{6}R^3\rho x_2\right)\right\}\right] \quad (4)$$

where $x_i = N_i/(N_1+N_2) = N_i/N$.

In order to obtain the isothermal compressibility κ_T defined by

$$\kappa_T = -\frac{1}{V}\left(\frac{\partial V}{\partial p}\right)_T = -\left(\frac{\rho}{N}\right)\left(-\frac{N}{\rho^2}\right)\left(\frac{\partial \rho}{\partial p}\right)_T = \frac{1}{\rho}\left(\frac{\partial \rho}{\partial p}\right)_T \quad (5)$$

Equation (4) is differentiated with respect to pressure, and we obtain

$$\frac{1}{kT} = \left(\frac{\partial \rho}{\partial p}\right)_T \frac{(1+2\xi)^2}{(1-\xi)^4}\left[1 - \frac{(\pi/2)x_1x_2R^3\rho\delta^2}{(1+2\xi)^2}\left\{4+2\xi+\frac{\pi}{2}R^3\rho + \delta\left(2+\xi+\frac{\pi}{2}R^3\rho(x_1+3x_2)\right) + \delta^2\left(\frac{3\pi}{2}R^3\rho x_2\right) + \delta^3\left(\frac{\pi}{2}R^3\rho x_2\right)\right\}\right]. \quad (6)$$

The magnitude of ξ is the order of 0.5, and

$$(\pi/6)R^3\rho < 1,\quad x_1x_2 \leqq 0.25.$$

Thus

$$(\pi/2)x_1x_2R^3\rho/(1+2\xi)^2 < 0.2,$$

$$4 + 2\xi + (\pi/2)R^3\rho < 8.$$

The second term in the bracket [ ] in Eq. (6) is much smaller than 0.02, and can be neglected in comparison with the first term, 1.

Thus we get

$$\frac{1}{kT} = \left(\frac{\partial \rho}{\partial p}\right)_T \frac{(1+2\xi)^2}{(1-\xi)^4}. \quad (7)$$

$\kappa_{T,0}$ which is attributed to repulsive forces only is

derived from Eqs. (5) and (7).

$$\kappa_{T,0} = \frac{1}{\rho kT}\frac{(1-\xi)^4}{(1+2\xi)^2} = \frac{\pi a^3}{6kT}\frac{(1-\xi)^4}{\xi(1+2\xi)^2}, \quad \delta<0.1 \tag{8}$$

Here, ξ is treated as follows

$$\xi = \frac{\pi}{6}(\rho_1 R_1^3+\rho_2 R_2^3) = \frac{\pi}{6}\frac{N_1R_1^3+N_2R_2^3}{V}$$
$$= \frac{\pi N(N_1R_1^3+N_2R_2^3)}{6V(N_1+N_2)} = \frac{\pi}{6}\rho\langle R_i^3\rangle = \frac{\pi}{6}\rho a^3,$$
$$\langle R_i^3\rangle \equiv a^3 \tag{9}$$

ξ is denoted by the "average hard core diameter" a, and indicates the "fraction of the hard core volumes of all molecules to whole volume of the mixture". Equation (8) is formally identical with the formula for a pure liquid derived by Reiss.[33]

Equation (1) is approximated as follows according to the above procedure.

$$\frac{p}{kT} = \left[\frac{1+\xi+\xi^2}{(1-\xi)^3}\right]\rho, \quad \delta<0.1 \tag{10}$$

This formula also agrees formally with that for a pure liquid,[33-36] ξ having the same expression and physical meaning as defined in Eq. (9).

It is necessary to consider the attractive forces, since the repulsive force only is considered in the above treatment. The average attractive potential is given by

$$-\langle U_N\rangle_{av.} = N\chi_0 = \Delta H_{vap.} - pV_{gas} = \frac{\text{const.}}{V^n} \tag{11}$$

where $\Delta H_{vap.}$ is enthalpy of vaporization and $n=1$ for van der Waals liquids.

The partition function for liquids is given by

$$Z = \left(\frac{2\pi mkT}{h^2}\right)^{3N/2} Q \exp(N\chi_0/kT) \tag{12}$$

where Q denotes the configurational integral.[17] It is well-known that

$$\left(\frac{\partial p}{\partial V}\right)_T = kT\left(\frac{\partial^2 \ln Z}{\partial V^2}\right)_T. \tag{13}$$

κ_T is obtained from Eqs. (5), (12), and (13) as follows.

$$\kappa_T = \left[-VkT\left(\frac{\partial^2 \ln Q}{\partial V^2}\right) - NV\left(\frac{\partial^2\chi_0}{\partial V^2}\right)\right]^{-1}$$
$$= \left[\frac{1}{\kappa_{T,0}} - \frac{2}{V}(\Delta H_{vap.}-RT)\right]^{-1}$$
$$= \left[\frac{RT}{V}\frac{(1+2\xi)^2}{(1-\xi)^4} - \frac{2}{V}(\Delta H_{vap.}-RT)\right]^{-1} \tag{14}$$

Adiabatic compressibility κ_S can be obtained from sound velocity, and isothermal compressibility κ_T from κ_S by means of the relation

$$\kappa_S = \frac{1}{\rho v^2}, \quad \kappa_T = \kappa_S + \frac{TV\alpha^2}{C_p} \tag{15}$$

where ρ is density in g/cm^3, v sound velocity, V molar volume of liquid, α thermal expansion coefficient, and C_p molar heat capacity.

When the values of κ_T and $\Delta H_{vap.}$ are substituted into Eq. (14), ξ can be evaluated, and we obtain the "average hard core diameter".

Thus, when the hard core diameter of one component in binary mixtures is known, that of another component is determined by Eq. (9).

Experimental

DCE (guaranteed reagent, Nakarai Chemicals Ltd.) was used with further purification.[37] Sound velocity was measured with an interferometer working at 3MHz.[25] Density was measured with a pycnometer. Measurements were carried out at 15—45 °C at 5 °C intervals. The temperature was controlled within ±0.05 °C. The results obtained were compared with the data in the literature (Table 1). The observed sound velocity agrees with the literature data, the accuracy being within 0.5 m/s.

Table 1. Comparison of observed values of sound velocity v (m/s) and adiabatic compressibility κ_S(10^{-12}cm^2/dyn) at 20 °C with literature values

	v	κ_S	Lit.
Obsd. value	1213.2	54.3_0	—
Lit. value	1213.4	54.2_1	18
	1213.2	54.2_3	19
	1213.5	54.2_0	25
		56.0	15

Results

The following values have been used in the calculation: α, 1.162×10^{-3} deg^{-1}; C_p, 129 J/mol deg; and $\Delta H_{vap.}$, 34.31 kJ/mol (Table 2). The value of N_g/N_t is taken to be 1.93 for DCE.[3]

The experimental values of κ_S and κ_T have been obtained from observed values of v. Values of hard core volume $\pi a^3/6$ have been determined from those of κ_T by Eq. (14) and are given in Table 3, the last row giving the average value of *trans* and *gauche* molecules.

Table 2. Thermodynamic parameters of DCE

Thermal expansion coefficient α (10^{-3} deg^{-1}), heat capacity C_p (J/mol deg), enthalpy of vaporization ΔH_{vap} (kJ/mol)

Temp. °C	α	C_p	ΔH_{vap}	Lit.
15—45	1.162			This work
20—40	1.132—1.190	129.0—131.5		15
20—40	1.183	130.1 (30 °C)		18
20—40	1.141—1.228	128.3—129.4		19
25—42			33.85—35.23	14
25			34.31	17

Table 3. Experimental and calculated results for DCE
v(m/s), κ_S and κ_T (10^{-12} cm^2/dyn), Hard core volume $\pi a^3/6$ (10^{-24} cm^3)

Temp °C	15	20	25	30	35	40	45
v	1232.6	1213.2	1194.6	1174.5	1155.4	1136.3	1116.9
κ_S	52.3_0	54.3_0	56.2_0	58.5_8	60.9_0	63.3_4	65.9_5
κ_T	76.0_1	78.5_6	81.0_9	83.9_4	86.8_4	89.8_6	93.0_6
$\pi a_3/6$	66.4_1	66.3_6	66.2_5	66.1_8	66.1_4	66.0_9	66.0_2

The hard core volume of *trans* molecule V_t has been determined from X-ray analysis of solid DCE,[38] in which all molecules are known to be in the *trans* state,[1] and also from other molecular structure data.[39,40] The value of V_t obtained from various sources is found to be 78.5×10^{-24} cm^3 per molecule.

V_g is estimated to be 59.8×10^{-24} cm^3 from Eq. (9), and $\Delta V/V_t$ 23.8% from the values of $\pi a^3/6$ and V_t.

Discussion

ΔV was not considered in previous studies owing to the lack of data.[2,8,18,25] Verma and others pointed out that the value of ΔV plays an important role in the determination of ΔH.[27] According to their estimation, if $\Delta V/V$ in methylcyclohexane increases from 0 to 10%, ΔH varies from 2.9 to 6.0 kcal/mol and other thermodynamic quantities also vary drastically.

In studies on dipolar and multipolar interactions in liquid state having various forms of isomers,[6] the influence of ΔV has often been neglected. The estimation of molecular interaction energy attributed to dipolar and quadrupolar fields is greatly affected by the estimation of ΔV. The difference of molecular volumes between various isomers affects the determination of molecular interaction energy a great deal. Thus the knowledge of ΔV in conformational isomerism is necessary to estimate ΔH and other thermodynamic variables exactly, and to explain the nature of the molecular interaction.

ΔV is determined by ultrasonic absorption technique.[21] However, determination is impossible when the frequency range of the apparatus does not cover the relaxation range of the system under investigation. In many cases conformational equilibrium was studied on the assumption,[21] $(\Delta V/V)(C_p/\alpha)\ll\Delta H$. In the case of DCE in liquid state, this does not hold since ΔH is nearly zero.[1]

The $\Delta V/V$ in conformational isomerism for TCE and other compounds in various solvents has been reported to be 1—3%,[30] but DCE was not included. The error is 50%.

In order to determine ΔV for liquid DCE, we should know the value of V_t. We can obtain V_t from the results of studies on solid DCE, in which all the molecules are known to be in the *trans* state.[1] The value of V_t can be obtained from X-ray analysis of solid DCE and other data.[38-40]

In solid DCE, the volume assigned to one molecule is found to be 106×10^{-24} cm^3 from its density.[38] Taking the magnitude of packing parameter to be 0.7405[41] (face-centered cubic), we estimate the value of V_t to be 78.5×10^{-24} cm^3. This value is regarded as an "equivalent" hard core volume of the molecule in a close-packed state.

On the other hand, DCE is assumed to be a rotational ellipsoid having a major axis of 6.90 Å and a minor axis of 4.68 Å from diffraction data.[38-40] The Cl–Cl distance estimated from X-ray data is 4.24 Å and the diameter of Cl atom 2.66 Å,[42] and we can thus estimate the major axis of the ellipsoid to be 6.90 Å. The minor axis is estimated from (1, 0, 0) projected surface, the most dense one.[38] V_t is thus calculated to be 79.1×10^{-24} cm^3 per molecule. This agrees with the value calculated from density. Thus the value 78.5×10^{-24} cm^3 is chosen for V_t.

The ratio N_g/N_t is also necessary for determining ΔV. The value is found from studies of molecular structure theory to be in the range 1.90—1.93 at room temperature.[1,3] We have used the value 1.93.[3] The fluctuation of ΔV for variation of N_g/N_t is very small, being of the order 0.1%.

The calculated hard core volume of DCE in the liquid state is held constant in the range 15—45 °C (Table 3), which shows the validity of the present method. It would be noted that the fraction N_g/N_t remains constant within the range of temperature in this study.

The value of $\Delta V/V_t$ is *ca.* 20%. The error is mainly due to the uncertainty in the determination of V_t. It is certain that the value for DCE is larger by one order than that for TCE, found to be 1—3% by Wyn-Jones *et al.*[30]

The authors thank Mr. Nobuo Takenaka for his help in carrying out this study.

References

1) S. Mizushima, "Structure of Molecules and Internal Rotation," Academic Press Inc., New York (1954), Chapt. I—III.
2) A. Wada, *J. Chem. Phys.*, **22**, 198 (1954).
3) A. Wada and Y. Morino, *ibid.*, **22**, 1276 (1954).
4) R. J. W. Le Fevre and B. J. Orr, *Aust. J. Chem.*, **17**, 1098 (1964).
5) N. Oi and J. F. Coctzee, *J. Amer. Chem. Soc.*, **91**, 2473, 2478 (1969).
6) R. J. Abraham, L. Cavalli, and K. G. R. Pachler, *Mol. Phys.*, **11**, 471 (1966); R. J. Abraham and K. G. R. Pachler, *ibid.*, **7**, 165 (1964).
7) A. Neckel und H. Volk, *Z. Elektrochem.*, **62**, 1104 (1958).
8) R. Fujishiro and K. Kimura, This Bulletin, **32**, 1237 (1959).
9) A. Abadie, C. Michel, et P. Mauret, *C. R. Acad. Sci. Paris, Ser. C*, **264**, 1433 (1967).
10) J. Crossley and S. Walker, *J. Chem. Phys.*, **48**, 4742 (1968).

11) J. Crossley and C. P. Smyth, *J. Amer. Chem. Soc.*, **91**, 2482 (1969).
12) K. Chitoku and K. Higasi, This Bulletin, **40**, 773 (1967).
13) A. Morita, H. Takahashi, and K. Higasi, *ibid.*, **45** 1045 (1972).
14) L. H. Ruiter, *Rec. Trav. Chim.*, **74**, 1131 (1955).
15) L. A. K. Staveley, W. I. Tupman, and K. R. Hart, *Trans. Faraday Soc.*, **51**, 323 (1955).
16) K. Amaya and R. Fujishiro, This Bulletin, **31**, 90 (1958).
17) J. H. Hildebrand and R. L. Scott, "The Solubility of Nonelectrolytes," Dover Publications Inc., New York, N.Y. (1964), 3rd Ed., Chapt. V.
18) G. H. Findenegg and F. Kohler, *Trans. Faraday Soc.*, **63**, 870 (1967).
19) E. Wilhelm, R. Schano, G. Becker, G. H. Findenegg, and F. Kohler, *ibid.*, **65**, 1443 (1969).
20) K. Arakawa and O. Kiyohara, This Bulletin, **43**, 975 (1970).
21) J. Lamb, "Physical Acoustics," Vol. 2A, ed. by W. P. Mason, Academic Press, New York, London, (1965), p. 203.
22) D. Sette, *J. Chem. Phys.*, **19**, 1337 (1951).
23) R. J. Fort and W. R. Moore, *Trans. Faraday Soc.*, **61**, 2102 (1965).
24) R. Fischer, H. Posch, und F. Kohler, *Monatsh. Chem.*, **96**, 1865 (1965).
25) O. Kiyohara and K. Arakawa, This Bulletin, **43**, 3037 (1970).
26) R. J. Fort and W. R. Moore, *Trans. Faraday Soc.*, **62**, 1112 (1966).
27) G. S. Verma, *Proc. Phys. Soc.*, **75**, 142 (1960); R. P. Singh, G. S. Darbari, and G. S. Verma, *J. Chem. Phys.*, **46**, 151 (1967).
28) R. O. Davies and J. Lamb, *Proc. Phys. Soc.*, **73**, 767 (1959).
29) E. Wyn-Jones and W. J. Orville-Thomas, "Molecular Relaxation Processes," Chem. Soc. Spec. Publ., No. 20 (1966), p. 209.
30) K. R. Crook, P. J. D. Park, and E. Wyn-Jones, *J. Chem. Soc., A*, **1969**, 2910; K. R. Crook and E. Wyn-Jones, *J. Chem. Phys.*, **50**, 3445 (1969); K. R. Crook, E. Wyn-Jones, and W. J. Orville-Thomas, *Trans. Faraday Soc.*, **66**, 1597 (1970); E. Wyn-Jones, *J. Mol. Struct.*, **6**, 65 (1970).
31) J. L. Lebowitz and J. S. Rowlinson, *J. Chem. Phys.*, **41**, 133 (1964).
32) J. L. Lebowitz, *Phys. Rev.*, **133 A**, 895 (1964).
33) H. Reiss, *Advan. Chem. Phys.*, **9**, 1 (1964).
34) H. Reiss, H. L. Frisch, and J. L. Lebowitz, *J. Chem. Phys.*, **31**, 369 (1959).
35) M. S. Wertheim, *Phys. Rev. Lett.*, **10**, 321 (1963); *J. Math. Phys.*, **5**, 643 (1964).
36) E. Thiele, *J. Chem. Phys.*, **39**, 474 (1963).
37) J. A. Riddick and W. B. Bunger, "Organic Solvents," Techniques of Chemistry, Vol. II, ed. by A. Weissberger, Wiley-Interscience, New York, N.Y. (1970), 3rd Ed., p. 776.
38) M. E. Milberg and W. N. Lipscomb, *Acta Crystallogr.*, **4**, 369 (1951).
39) J. Ainsworth and J. Karle, *J. Chem. Phys.*, **20**, 425 (1952).
40) L. Pauling, "The Nature of the Chemical Bond," Cornell University Press, New York, N.Y. (1960), 3rd Ed., Chapt. VII, XIII.
41) The value of V_t needed is that of the "equivalent" hard core volume in thermal motions which is statistically defined. Thus we chose the value of packing parameter to be 0.7405 for the closest packing in spite of the fact that the crystal form of solid DCE is known to be monoclinic.
42) The radius of Cl atom is assumed to be equal to that of K^+, 1.33 Å.[40]

The Circular Dichroism and Magnetic Circular Dichroism Spectra of Bis(stilbenediamine) nickel(II) Complexes

Sumio ARAKAWA, Tsunenori NOZAWA, and Masahiro HATANO
Chemical Research Institute of Non-Aqueous Solutions, Tohoku University, Sendai 980
(Received September 19, 1973)

The temperature dependence of the absorption and circular dichroism spectra for $[Ni((+)\text{-stien})_2](ClO_4)_2$ is indicative of the equilibrium between the square planar (yellow) and tetragonal (violet) species in acetone solutions. On the other hand, the square planar species is predominant in a methanol solution, even at room temperature, in the case of $[Ni(meso\text{-stien})_2](ClO_4)_2$. The Cl^- as a counter anion favored an equilibrium slightly displaced to the tetragonal species. The analysis of the CD and MCD bands suggests an ordering of the d-orbital energy levels of $d_{x^2-y^2} \gg d_{z^2} > d_{xz}, d_{yz} > d_{xy}$.

Despite considerable efforts, the spectra exhibited by d^8 square planar complexes are still imperfectly understood. It was only recently that some workers[1-4] have demonstrated the usefulness of magnetic circular dichroism (MCD) studies in obtaining spectroscopic information about the d^8 square planar complexes. The main features of the theory of the dispersion of MCD through absorption (AB) bands have previously been reviewed.[5-7] For AB bands which are too broad to assign, MCD is definitely superior, so the MCD spectra of $[Ni(meso\text{- and } (+)\text{-stien})_2]X_2$, where X=Cl and ClO_4, were measured in this study.

On the other hand, the optical rotatory dispersion and circular dichroism (CD) spectra for the violet and yellow forms of $[Ni((-)\text{-stien})_2]^{2+}$ have been measured by Lifschitz *et al.*[8] and Bosnich *et al.*[9] respectively. Bosnich and his colleagues analyzed the electronic structure of the yellow complexes and suggested an energy scheme.

It is well known[10] that Lifschitz's complexes with the general fomula of $[Ni(meso\text{-stien})_2]X_2$, where X is the anion of an organic acid, are present as equilibrium mixtures of the blue or violet and yellow forms under a variety of conditions.

In this study, we found that the equilibrium between the violet and yellow forms occurs more easily in an acetone solution of optically-active $[Ni((+)\text{-stien})_2](ClO_4)_2$, than in a methanol solution of optically-inactive $[Ni(meso\text{-stien})_2](ClO_4)_2$.

Experimental

Materials. The *meso*-stilbenediamine(*meso*-stien) (Calcd for $C_{14}H_{16}N_2$: C, 79.32; H, 7.61; N, 13.21%. Found: C, 79.16; H, 7.67; N, 12.58%) and (+)-stien ($[\alpha]_D = 185°$ (in ether)) were prepared by the methods of Irving and Parkins[11] and of Lifschitz and Bos[12] respectively. The $[Ni(meso\text{-stien})_2]Cl_2$ (Calcd for $NiC_{28}H_{32}N_4Cl_2$: C, 60.75; H, 5.83; N, 10.12%. Found: C, 60.81; H, 5.82; N, 9.98%), $[Ni(meso\text{-stien})_2](ClO_4)_2$ (Calcd for $NiC_{28}H_{32}N_4Cl_2O_8$: C, 49.34; H, 4.73; N, 8.22; Cl, 10.40%. Found: C, 49.19; H, 4.67; N, 8.15; Cl, 10.02%), and $[Ni((+)\text{-stien})_2](ClO_4)_2$ (Calcd for $NiC_{28}H_{32}N_4Cl_2O_8$: C, 49.34; H, 4.73; N, 8.22; Cl, 10.40%. Found: C, 49.21; H, 4.72; N, 8.25; Cl, 9.97%) were prepared by the method of Lifschitz, Bos, and Dijkema.[8]

Measurements. The CD and MCD measurements were made with a JASCO model 20A dichrograph equipped with an electromagnet. The magnetic field was set at 12500 G in the case of the MCD measurements. The electronic absorption spectra were measured by using a Hitachi EPS-3T recording spectrophotometer. The spectra at 0.8 °C were measured by using jacketed cells regulated with circulating water held at a constant temperature. The spectra at −75 °C were measured by the use of a quartz-Dewar designed in our laboratory. The temperatures were measured directly using a thermometer.

Results and Discussion

The Temperature Dependence of the AB and CD Spectra of Bis((+)-stien)nickel (II) Diperchlorate in an Acetone Solution. The temperature dependence of the AB spectrum for $[Ni((+)\text{-stien})_2](ClO_4)_2$ in an acetone solution is shown in Fig. 1. The AB bands at 22500, 11300, 18000, and 28000 cm^{-1} are denoted as AB bands—Y, V_1, V_2, and V_3 respectively. As the temperature of the $[Ni((+)\text{-stien})_2](ClO_4)_2$ acetone solution is raised, the intensity of the Y AB band increases, while that of the V_1 AB band decreases. The lack of isosbesticity and the variation in the intensity of the V_2 and V_3 bands may be due to experimental errors. It is well known that the V_1, V_2, and V_3 AB bands are attributable to the violet paramagnetic species, while the Y AB band is due to the yellow diamagnetic species. The temperature dependence and reversibility of the variation in intensity for each AB band lead us to expect the occurrence of the following equilibrium for $[Ni((+)\text{-stien})_2](ClO_4)_2$ in an acetone solution:

$$[Ni((+)\text{-stien})_2]^{2+} + 2S \rightleftarrows [Ni((+)\text{-stien})_2 \cdot 2S]^{2+} \quad (1)$$

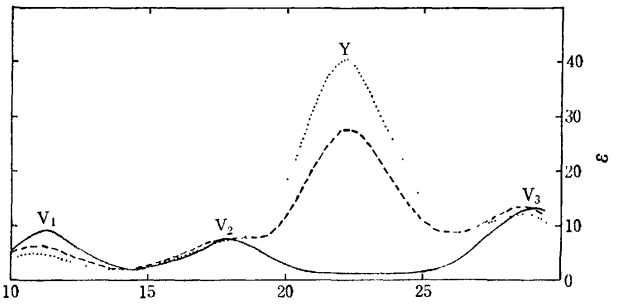

Fig. 1. AB spectra for $[Ni((+)\text{-stien})_2](ClO_4)_2$ in an acetone solution at +21 (·····), +0.8 (- - -), and −75 °C (——). Y and V denote the AB bands ascribed to the yellow and violet complexes, respectively.

where S is an acetone molecule. As the temperature increases, the equilibrium in Eq. (1) is shifted to the left side. Thus, the relative quantity of the violet species of the nickel(II) complex decreases with a rise in the temperature. It should be added that [Ni((+)-stien)$_2$]$^{2+}$ gives the violet species in a methanol solution, even at room temperature,[13] which means that methanol will coordinate to the [Ni((+)-stien)$_2$]$^{2+}$ much more strongly than will acetone.

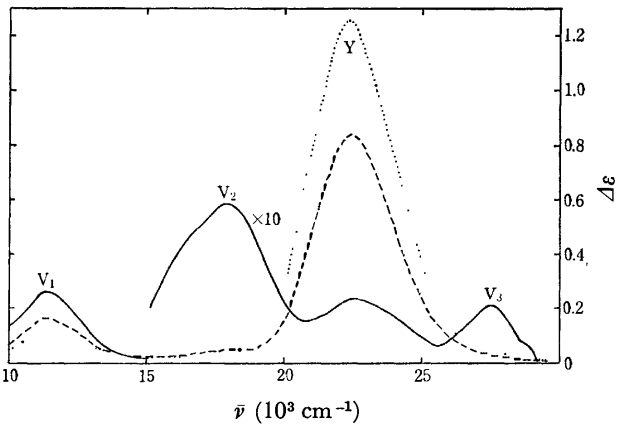

Fig. 2. CD spectra for [Ni((+)-stien)$_2$](ClO$_4$)$_2$ in an acetone solution at +21 (·····), +0.8 (-----), and −75 °C (——). Y and V denote the CD bands ascribed to the yellow and violet complexes, respectively.

The occurrence of the equilibrium discussed above was also confirmed by means of the CD spectra. In Fig. 2 the CD bands at 22500, 11400, 18000, and 27500 cm^{-1} are denoted as the Y, V_1, V_2, and V_3 CD bands respectively, corresponding to the AB bands.

First, it should be noted that the shape of the V_1, V_2, and V_3 CD bands are not symmetric, which suggests that they contain more than one transition. On the assumption of the octahedral (O_h) local symmetry of the complex, the V_1, V_2, and V_3 CD bands can be assigned to three spin-allowed d-d transitions $^3A_{2g}\rightarrow{}^3T_{2g}$, $^3A_{2g}\rightarrow{}^3T_{1g}$ (F), and $^3A_{2g}\rightarrow{}^3T_{1g}$ (P) respectively. However, in view of the facts that the violet complex [Ni((+)-stien)$_2$·2S]$^{2+}$ is presumably six-coordinated with the environment of *trans*-NiN$_4$O$_2$ with the two oxygen atoms furnished by acetone, and that these CD bands seem to contain more than one transition, the symmetry of the ligand field may be anticipated to be an octahedron elongated along the *z*-axis—namely, tetragonal (D_{4h}). The assignment of the CD bands can thus be examined as follows, assuming the D_{4h} symmetry. In this symmetry, the $^3T_{2g}$ and $^3T_{1g}$ levels of an octahedral complex split into $^3B_{2g}+{}^3E_g$ and $^3A_{2g}+{}^3E_g$ levels, respectively (see Fig. 3). According to Fig. 3, three CD bands, V_1, V_2, and V_3, can thus be assigned to spin-allowed transitions—$^3B_{1g}\rightarrow(^3E_g, {}^3B_{2g})$, $^3B_{1g}\rightarrow(^3A_{2g}, {}^3E_g)$, and $^3B_{1g}\rightarrow(^3E_g, {}^3A_{2g})$ respectively. The magnetic dipole forbidden transition, $^3B_{1g}\rightarrow{}^3A_{2g}$, in D_{4h} seems to appear as a shoulder in the V_2 and V_3 CD bands. This possibly implies that [Ni((+)-stien)$_2$·2S]$^{2+}$ contains lower symmetry components than does D_{4h}.

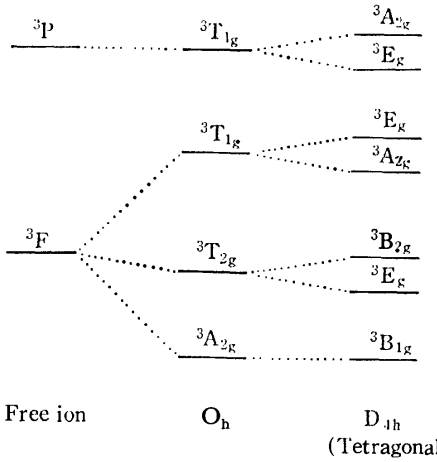

Fig. 3. Correlation diagram (Spin triplet only) for a d^8 ion in an octahedral (O_h) and tetragonal (D_{4h}) field.

Secondly, it should be noted that the shape of the Y CD band, which is characteristic of the yellow diamagnetic square planar complexes, is not symmetric. Although the Y CD band has already been assigned by Bosnich *et al.* for complexes of Ni(II) with (+)-propylenediamine,[9] we reassigned this CD band using the same line of reasoning as was employed. For the spin-paired Ni(II) complexes in a ligand field of approximately D_{4h} symmetry, three bands resulting from the $d_{xy}\rightarrow d_{x^2-y^2}$ ($^1A_{1g}\rightarrow{}^1A_{2g}$), $d_{xz}, d_{yz}\rightarrow d_{x^2-y^2}$ ($^1A_{1g}\rightarrow{}^1E_g$), and $d_{z^2}\rightarrow d_{x^2-y^2}$ ($^1A_{1g}\rightarrow{}^1B_{1g}$) transitions, may be expected in almost the same wave number region (Fig. 6). Only the first two transitions are magnetic-dipole allowed transitions. The Y CD band, centered around 22500 cm^{-1}, is situated on the higher-frequency side of the AB band (ν_{max}=22200 cm^{-1}). On the higher-frequency side of the Y CD band, its anisotropy factor ($\Delta\varepsilon/\varepsilon$) is about 0.03, while on the lower-frequency side, below 22200 cm^{-1}, it decreases below 0.03. This trend was also observed in other solvents such as nitromethane and ethylacetate.[15] This suggests that the apparently single Y CD band contains two transitions. The magnetic dipole-allowed transitions, $^1A_{1g}\rightarrow{}^1A_{2g}$ and $^1A_{1g}\rightarrow{}^1E_g$, are well-separated and give strongly negative and moderately negative CD bands respectively in the case of *trans*-[Co((−)-stien)$_2$Cl$_2$]ClO$_4$.[16] If we can assume that the similarity concerning the relative CD magnitudes with opposite signs will also be observed in the corresponding transitions for the square planar [Ni((+)-stien)$_2$](ClO$_4$)$_2$, it can be expected that the strongly positive and moderately positive CD bands are to be assigned to the $^1A_{1g}\rightarrow{}^1A_{2g}$ and $^1A_{1g}\rightarrow{}^1E_g$ respectively in the [Ni((+)-stien)$_2$]$^{2+}$ complex. The large amount of overlap between these transitions is believed to account for the apparently single band with a dissymmetric shape. This assignment suggests that the d_{xy} orbital lies below the degenerate d_{xz}, d_{yz} orbitals in the yellow diamagnetic species of [Ni((+)-stien)$_2$](ClO$_4$)$_2$.

MCD Spectra of Bis(stien)nickel(II) Complexes. Figure 4 shows the MCD spectra for the [Ni((+)-stien)$_2$](ClO$_4$)$_2$, along with its AB spectra. As was discussed in the previous section, both the yellow dia-

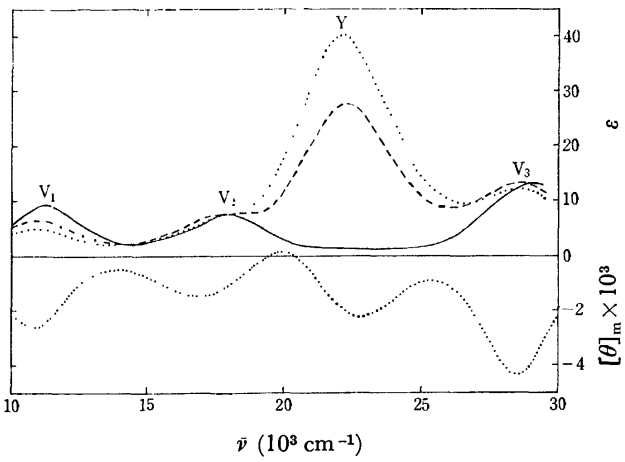

Fig. 4. AB and MCD spectra for [Ni((+)-stien)$_2$]-(ClO_4)$_2$ in an acetone solution at +21 (·····), +0.8 (------), and −75 °C (——). Y and V denote the AB bands ascribed to the yellow and violet complexes, respectively.

magnetic and violet paramagnetic species are present in an acetone solution at 21 °C. The temperature-variation studies of the AB and CD spectra in Figs. 1 and 2 indicate that the violet paramagnetic species is predominant in an acetone solution at −75 °C. The CD magnitude ($\Delta\varepsilon$) for the V_1 band, then, gives the approximate percentage of the violet paramagnetic species present. The calculation shows that the molar ratio of the violet paramagnetic species to that of the yellow diamagnetic species is 1 : 2 at 21 °C in an acetone solution. Hence, the MCD spectra in an acetone solution at 21 °C (Fig. 4) reveal that the MCD intensity of the V_3 band is about four times stronger than that of the negative band, Y.

Figure 5 shows the MCD spectrum for the [Ni-(*meso*-stien)$_2$](ClO_4)$_2$ in a methanol solution. Though methanol is a solvent which gives the violet species more preferably than acetone, the [Ni(*meso*-stien)$_2$](ClO_4)$_2$ in a methanol solution does not show any MCD due to the main violet species band (V_3) at around 27000 cm^{-1}. The most plausible reason why [Ni(*meso*-stien)$_2$](ClO_4)$_2$ tends to give the yellow species more easily than [Ni((+)-stien)$_2$](ClO_4)$_2$ seems to be a steric effect; that is, the axial phenyl group in the complexes will exert more steric hindrance toward the axial ligands than will the equatorial one. The molecular model and the X-ray analysis indicate that one of the phenyl groups in a *meso*-stien of the Ni(II) complex will be in an axial position, and the other in an equatorial position, relative to the NiN_4 plane in the [Ni(*meso*-stien)$_2$](ClO_4)$_2$, while both phenyl groups of (+)-stien in the [Ni((+)-stien)$_2$](ClO_4)$_2$ will be in equatorial positions in an energetically-favored form.[17]

It has been reported by Kobayashi[4] that the A term MCD in the diamagnetic yellow Ni(II) complex shows a normal A-term dispersion. If this is also the case for the yellow diamagnetic [Ni(*meso*-stien)$_2$](ClO_4)$_2$, the positive part for a normal A term will be nearly the positive peak at around 21500 cm^{-1}. Hence, three possibly B terms above, at and below the transition for the A term, are necessary to explain the experimental MCD curve for the [Ni(*meso*-stien)$_2$](ClO_4)$_2$ in Fig. 5. Thus, the MCD for [Ni(*meso*-stien)$_2$](ClO_4)$_2$ may be considered to consist of a normal A term with three possibly B terms with lower, the same, and higher transition energies. These MCD results suggest that the degenerate transition may be in the middle of the two nondegenerate transitions. This MCD assignment with the CD assignment for the yellow diamagnetic [Ni((+)-stien)$_2$](ClO_4)$_2$, as described in the previous

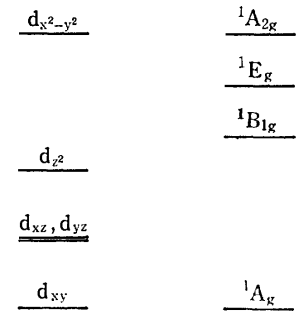

Fig. 6. Ordering of the d-orbital energy levels and the energy level diagram for a d^8 ion in a square-planar (D_{4h}) field.

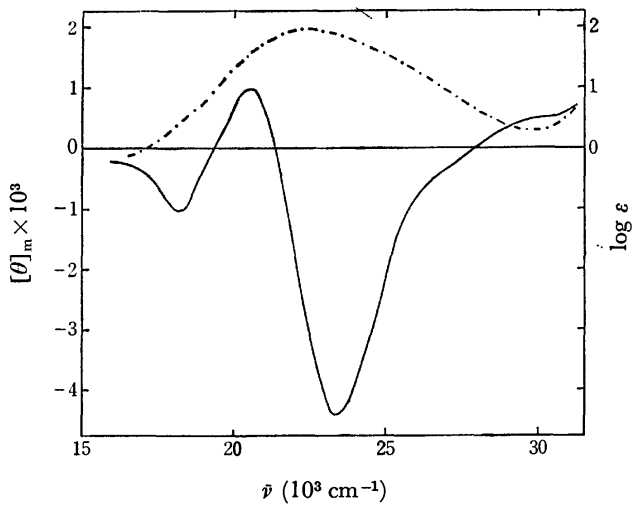

Fig. 5. AB (·····) and MCD (——) spectra for [Ni-(*meso*-stien)$_2$] (ClO_4)$_2$ in a methanol solution at room temperature.

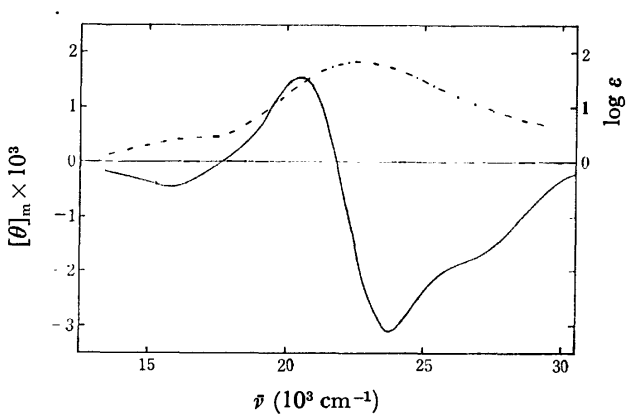

Fig. 7. AB (·····) and MCD (——) spectra for [Ni-(*meso*-stien)$_2$]Cl_2 in a methanol-water (4: 1) solution at room temperature.

section, implies an energy order of the d-orbital of $d_{z^2}>d_{xz}$, $d_{yz}>d_{xy}$. (Fig. 6)

The effect of counter anions on the equilibrium between the yellow diamagnetic and violet paramagnetic species was examined using [Ni(*meso*-stien)$_2$]-Cl_2, the MCD and AB spectra of which are shown in Fig. 7. Figure 7 indicates that the [Ni(*meso*-stien)$_2$]Cl_2 in a methanol-water solution has the violet paramagnetic species besides the yellow diamagnetic species, and that the ratio of the former to the latter is about 1 : 8. The existence of the violet paramagnetic species in the case of [Ni(*meso*-stien)$_2$]Cl_2 in a methanol-water solution at room temperature should be compared with the finding that [Ni(*meso*-stien)$_2$]$(ClO_4)_2$ has no violet paramagnetic species under the same conditions. This might be attributed to the greater bulkiness of ClO_4^- in comparison with that of Cl^-.

The authors wish to thank Professors Taro Isobe, Nobuyuki Tanaka, Kazuo Saito, and Junnosuke Fujita of Tohoku University for their useful discussions. A part of the expense for this work was defrayed by a grant from the Ministry of Education, to which the authors' thanks are due.

References

1) P. J. Stephens, A. J. McCaffery, and P. N. Schatz, *Inorg. Chem.*, **7**, 1923 (1968).
2) S. B. Piepho, P. N. Schatz, and A. J. McCaffery, *J. Amer. Chem. Soc.*, **91**, 5994 (1969).
3) Q. L. Looney and B. E. Douglas, *Inorg. Chem.*, **9**, 1955 (1970).
4) H. Kobayashi and B. K. Dasgkiewicz, This Bulletin, **45**, 2485 (1972).
5) A. D. Buckingham and P. J. Stephens, *Ann. Rev. Phys. Chem.*, **17**, 399 (1966).
6) P. N. Schatz and A. J. McCaffery, *Quart. Rev.*, **23**, 552 (1970).
7) D. Caldwell, J. M. Thorne, and H. Eyring, *Ann. Rev. Phys. Chem.*, **22**, 259 (1971).
8) I. Lifschitz and J. G. Bos, and K. M. Dijkema, *Z. Anorg. Allgem. Chem.*, **242**, 97 (1939).
9) B. Bosnich, J. H. Dunlop, and R. D. Gillard, *Chem. Commun.*, **1955**, 274.
10) W. C. Higginson, S. C. Nyburg, and J. S. Wood, *Inorg. Chem.*, **3**, 463 (1964).
11) M. N. Irving and R. M. Parkins, *J. Inorg. Nucl. Chem.*, **27**, 270 (1965).
12) I. Lifschitz and J. G. Bos, *Rec. Trav. Chim.*, **59**, 173 (1940).
13) I. Lifschitz and J. G. Bos, *ibid.*, **59**, 469 (1940).
14) C. Furlani and G. Sartori, *J. Inorg. Nucl. Chem.*, **8**, 126 (1958).
15) Unpublished data.
16) B. Bosnich and J. M. Harrowfield, *J. Amer. Chem. Soc.*, **94**, 3425 (1972).
17) B. C. Nyburg and J. S. Wood, *Inorg. Chem.*, **3**, 469 (1964).

The Solubility Study of Ion-pairs in Organic Solvents

Takejiro TAKAMATSU

Department of Chemistry, Faculty of Science, Kyoto University, Sakyo-ku, Kyoto 606

(Received January 5, 1974)

The solubilities of alkali picrates were measured in alcohols (13 species) and esters (19 species) at 25±0.2°C. It was found that the solubility data are well correlated with the solubility parameters of the solvents. It is also pointed out that the distribution ratios of the cesium picrate between the aqueous phase and the organic phase are apparently correlated with the solubility parameters of the extraction solvents.

In a previous paper,[1] it was reported that the solubilities of such ion-pairs as chloride, perchlorate, and tetraphenylborate salts of alkali metals and Ru(II)-(phen)$_3$ could be well correlated with the solubility parameters of solvents (δ_2). In the potassium halide systems,[2] the best linearity was found between the logarithmic solubilities (log S) and $(\delta_1-\delta_2)^2$, where δ_1, corresponding to the hypothetical solubility parameters of the ion-pairs, was calculated to be $(U/V)^{1/2}$, (U: lattice energy of the ionic crystal; V: molar volume).

In the present paper, the solubilities of alkali picrates in 13 alcohols and 19 esters and the distribution ratios of cesium picrate in liquid-liquid partition systems were measured at 25±0.2°. Both sets of data are discussed in relation to the solubility parameters of solvents from the empirical point of view.

Experimental

Reagents. All the reagents used here were of a reagent-grade purity. The organic solvents were purified mainly by distillation, as has been described before.[1] The alkali picrates (K-Pic, Rb-Pic, Cs-Pic) were synthesized as follows. Picric acid was neutralized by the corresponding alkali carbonates in an acetone–water (1:1) mixture. The resulting precipitates were filtered and washed with water several times. After being recrystallized in water, the precipitates were dried *in vacuo* for 5 day.

Solubilities. The solubility measurements of alkali picrates were performed as follows: 10 ml portions of the organic solvents were placed in test tubes equipped with ground stoppers which contained appropriate amounts of the precipitates of alkali picrates. After the test tubes had been tightly sealed with parafilm, the solubility equilibria were established by shaking them in a thermostat at 25±0.2°C for 10 day. The solubilities were then measured spectrophotometrically (λ_{max}=355 nm, ε_{max}=16110).

Extraction. The distribution of the cesium picrate was investigated as follows: 1 ml of a 2.0×10^{-5} M aqueous Cs_2SO_4 solution (containing ^{137}Cs as a tracer) and 4 ml of the 3.62×10^{-4} M aqueous sodium picrate (in alcohols) or 4 ml of the 2.42×10^{-2} M aqueous sodium picrate (in esters) were placed in polypropylene test tubes equipped with silicone rubber stoppers. After 5 ml of the organic solvent had then been added, the test tube was shaken vigorously for 10 min at 25±0.2°C. After the two phases had been separated by centrifugation, the distribution ratio was calculated as the ratio of the γ-radioactivities of the two phases. The γ-radioactivities were counted by using a well-type single-channel pulse-height analyzer (Osaka Dempa, Model LA-3T). Measurements in both the solubility study and the extraction study were repeated three times; the averages of the results are given in the table and figures.

Results and Discussion

Relation between log S and δ_2. The observed solubilities of alkali picrates in organic solvents are listed in Table 1, together with the solubility parameters of the solvents (δ_2). The logarithmic solubilities (log S) are shown in Figs. 1 and 2 as a function of δ_2

Table 1. Solubilities of alkali-picrate at 25 °C

Solvent	δ_2*)	(M)×10^5		
		K-Pic	Rb-Pic	Cs-Pic
Alcohols				
(1) methanol	14.50[a]	751	452	329
(2) ethanol	12.74	85.7	61.4	47.4
(3) 1-propanol	11.94	16.3	15.3	13.7
(4) 2-propanol	11.56	9.0	8.2	7.1
(5) 1-butanol	11.40	11.6	7.7	6.4
(6) isobutyl alcohol	11.19	4.8	5.1	4.6
(7) 2-butanol	11.05	3.3	3.0	2.5
(8) *n*-amyl alcohol	10.95	5.6	4.7	3.7
(9) isoamyl alcohol	10.79	4.1	3.0	2.5
(10) *tert*-amyl alcohol	10.21	1.5	1.1	0.7
(11) 1-hexanol	10.65	4.1	3.1	2.7
(12) 1-octanol	10.24	2.8	1.8	1.5
(13) 1-decanol	—	2.0	1.4	1.0
Esters				
(1) methyl formate	9.48[b]	1640	646	331
(2) ethyl formate	8.90	395	196	104
(3) propyl formate	8.69	165	90.2	50.2
(4) butyl formate	8.53	91.8	49.7	25.7
(5) methyl acetate	9.01	724	331	159
(6) ethyl acetate	8.58	186	76.0	32.7
(7) propyl acetate	8.41	123	48.8	20.7
(8) isopropyl acetate	8.07	73.2	27.1	11.9
(9) *n*-butyl acetate	8.31	69.1	27.9	12.7
(10) isobutyl acetate	8.13	56.5	21.2	9.8
(11) 2-butyl acetate	8.01	50.7	18.7	9.9
(12) isoamyl acetate	8.07	39.9	15.8	6.2
(13) ethyl butyrate	8.22	28.2	12.7	6.4
(14) *n*-amyl acetate	8.21	47.7	18.9	8.0
(15) *n*-octyl acetate	8.00	24.3	9.5	4.7
(16) 2-ethyl hexylacetate	7.81	18.3	7.8	3.8
(17) ethyl propionate	8.37	60.2	24.5	11.8
(18) benzyl acetate	9.49	43.2	22.5	13.1
(19) ethyl benzoate	9.40	62.6	28.7	17.0

a) Calculated by using ΔH_{25} values cited from the literature.[4] b) Calculated by using ΔH_{25} values estimated according to the Hildebrand rule.

*) $\delta_2=\left(\frac{\Delta H_{25}-RT}{V}\right)^{1/2}$

of the solvents. Although smooth correlations are obtained between log S and δ_2, a slight bending is observed for all the systems. Exceptional deviations from the curves are noticed in the two phenyl-substituted esters, *i.e.*, benzyl acetate and ethyl benzoate. The difference in slope was noticeable between the alcohol system and the ester system. Although no clear explanation can be given here, the difference may be due to the high δ_2 values of alcohols, which seem to be derived from the structural characteristics of alcohols, such as H-bonding.

Table 2. The calculated δ_1 values of ion-pairs

	r_c+r_a (Å)	U (kcal/mol)	V(ml)	δ_1
K-Pic	4.33	122.09	97.8	35.33
Rb-Pic	4.48	118.33	108.3	33.06
Cs-Pic	4.69	113.45	124.3	30.21

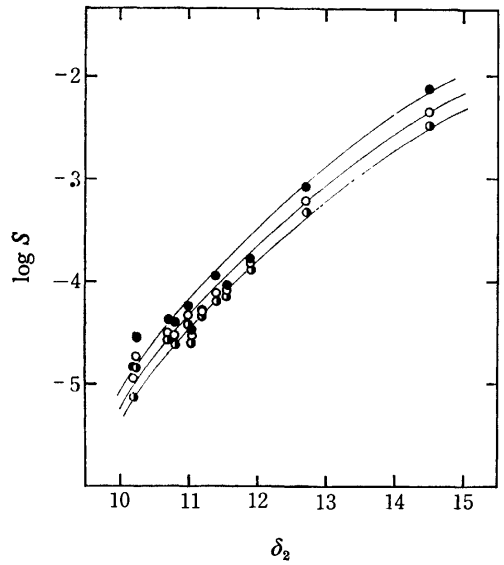

Fig. 1. The relation between log S and δ_2 in alcohol system.
(●): K-Pic, (○): Rb-Pic, (◑): Cs-Pic

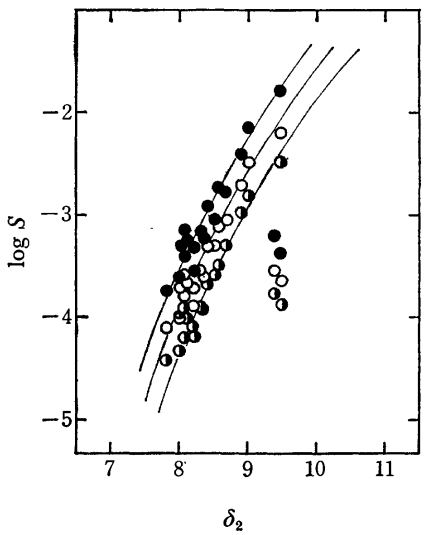

Fig. 2. The relation between log S and δ_2 in ester system.
(●): K-Pic, (○): Rb-Pic, (◑): Cs-Pic

Relation between log S and $(\delta_1-\delta_2)^2$. In order to find out a clearer correlation, the logarithmic solubilities (log S) were plotted against the difference in the solubility parameters of the solute and solvents as is shown in Figs. 3 and 4. The solubility parameters of the ion-pairs (δ_1) were approximated from the square root of the lattice-energy densities, $(U/V)^{1/2}$, as has been described in a previous paper.[2] In this calculation, 3.0 Å was used as the r_a value of the picrate anion.[3] The calculated values are shown in Table 2. As is shown in these figures, the plots, other than the two deviated plots in phenyl-substituted esters, give excellent straight lines.

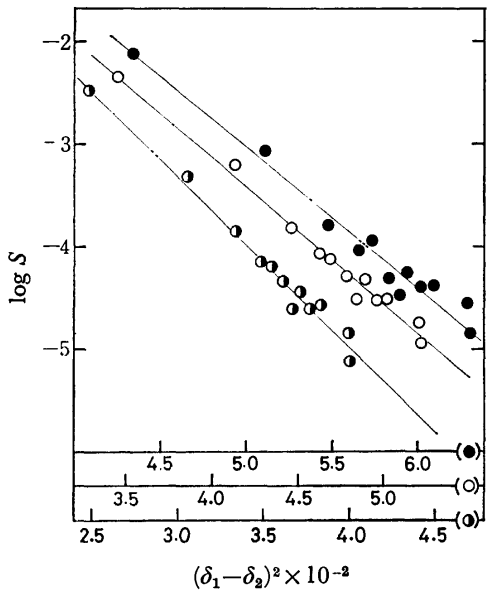

Fig. 3. The relation between log S and $(\delta_1-\delta_2)^2$ in alcohol system.
(●): K-Pic, (○): Rb-Pic, (◑): Cs-Pic

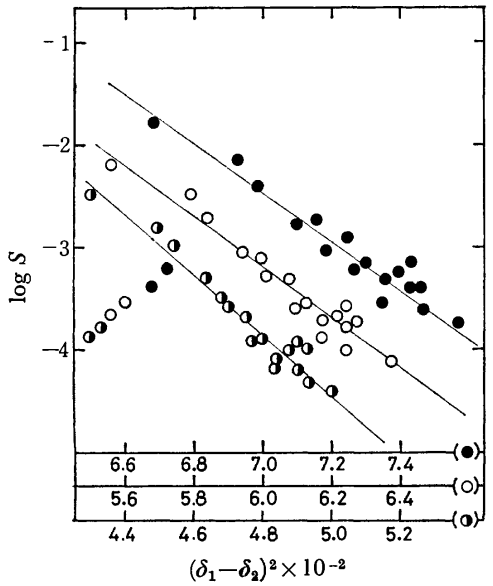

Fig. 4. The relation between log S and $(\delta_1-\delta_2)^2$ in ester sytem.
(●): K-Pic, (○): Rb-Pic, (◑): Cs-Pic

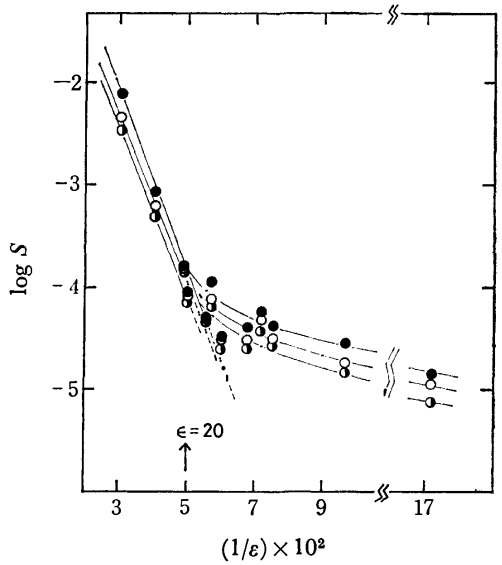

Fig. 5. The relation between log S and $1/\varepsilon$ in alcohol system.
(●): K-Pic, (○): Rb-Pic, (◑): Cs-Pic

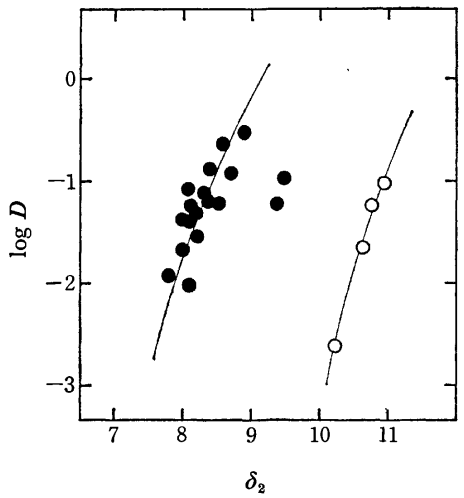

Fig. 6. The relation between log D and δ_2.
(○): alcohols, (●): esters

Relation between log S and 1/ε. In Fig. 5, for the sake of comparison one example of the plots between log S and the reciprocal of the dielectric constants ($1/\varepsilon$) of the solvents is shown in the alcohol system. Although a fairly good correlation is observed in the range of high dielectric constants ($\varepsilon \geq 20$), no lenear relationship holds in the range of low dielectric constants. The same pattern was also obtained in the ester system.

Relation between log D and δ_2. In Fig. 6, the logarithmic distribution ratios (log D) are plotted against the δ_2 values of the extraction solvents. The deviations of the solubility parameters, which are caused by the mutual solubilities of the two phases, are not taken into account here. However, it can be concluded that fairly good correlations hold between log D and δ_2.

Conclusion

In the ion-pair system whose cation and anion are bulky and possess quite a low charge density, the solubilities and the distribution ratios may both be predicted from the δ_2 values of the solvents, so long as one sort of solvent is used. However, no clear discussion with respect to the slopes of the plots is developed here because of the lack of data.

The author would like to express his thanks to Professor Taitiro Fujinaga and Dr. Mutsuo Koyama of Kyoto University for their helpful discussions and directions throughout the course of this study.

References

1) T. Takamatsu, This Bulletin, **47**, 1285 (1974).
2) T. Takamatsu, *ibid.*, **47**, 1287 (1974).
3) C. W. Davies, "The Conductivity of Electrolytes," 2nd ed., Chapman-Hall (1933).
4) J. A. Riddick and W. B. Bunger, "Techniques of Chemistry, Vol. 2, Organic Solvents," Wiley-Interscience, New York (1970).

The Electrochemical Reduction of Purine in Nonaqueous Solvents

Toshio YAO and Sōichirō MUSHA

Department of Applied Chemistry, College of Engineering, University of Osaka Prefecture, Mozuumemachi, Sakai 591

(Received February 18, 1974)

The electrochemical reduction of purine, which is the model compound for the reduction of the biologically-important purine bases, has been investigated in nonaqueous solvents (acetonitrile and DMF) by polarography, cyclic voltammetry, controlled potential electrolysis, and the ESR technique. In neutral solutions, purine is initially reduced in a one-electron, diffusion-controlled process at a fairly negative potential to produce an unstable radical anion, which then abstracts a proton from the parent purine to produce a free radical and an electroinactive purine anion. The free radical is quickly deactivated by fast dimerization to form a purine dimer and by a further one-electron reduction to produce, ultimately, 1,6-dihydropurine. The addition of various acids to purine solutions results in the appearance of a new, drawn-out wave at a more positive potential than the original purine reduction wave, which is attributed to the two-electron reduction of *N*-protonated purine species to produce 1,6-dihydropurine.

In recent years, the electrochemical reduction and oxidation of biologically-important compounds have been investigated with much interest. It is important to fully understand the redox behavior of these in considering the metabolism and analytical determination of biologically-important compounds. Recent works[1-3] have suggested a possible parallelism between the modes of electrochemical behavior and the biological transformation, *e.g.*, the enzymatic oxidation. It is also important, however, to fully investigate the electrochemical reduction behavior of biologically-important molecules, especially regarding those factors that influence the electron transfer processes, such as, *e.g.*, the pH.

A few works[4-6] have been done on purine itself and various purine derivatives in aqueous solutions. However, these works are due to the reduction of prototype purines. Consequently, the electrochemical reduction of purine, which is the model compound for the reduction of the biologically-important purine series, has been investigated in aprotic solvents on the basis of the idea that the information obtained in an inert solvent would reflect, more directly, the properties of purine itself and not its solvent-solute interaction. Another reason for investigating the purine reduction mechanism in nonaqueous solvents is to understand the properties and behavior of the anion free radical expected in a proton-poor medium.

Experimental

Chemicals. The purine (Sigma chemical company) was recrystallized four times from toluene. The acetonitrile was purified essentially by the method of Coetzee *et al.*[7] The dimethylformamide (DMF) was purified by the method of Hatano.[8] The moisture in the purified acetonitrile and DMF was determined by Karl-Fischer titration to be 0.01—0.02%. Tetraethylammonium perchlorate (TEAP) was used as the supporting electrolyte. TEAP was prepared following Fujinaga *et al.*,[9] and was recrystallized five times from distilled water before drying at 60 °C *in vacuo*. All the other reagents were of an extra-pure grade.

Apparatus. The polarographic curves were recorded using a Yanagimoto P-8 type Polarograph. Cyclic voltammograms were obtained with a versatile solid-state instrument constructed in this laboratory following the design of Goolsby and Sawyer.[10] The electrolysis cell consists of three electrodes. The reference electrode was constructed by dipping a coil of silver wire into a solution of 0.1 M $AgClO_4$ in solvents (acetonitrile or DMF)–0.1 M TEAP contained in a glass tube with a medium-porosity glass frit and salt bridge at one end. DME was used for the polarography ($m^{2/3}t^{1/6}=3.14$ $mg^{2/3}s^{1/6}$ in a 0.1 M TEAP–acetonitrile medium at −2.2 V *vs.* $Ag/AgClO_4$), and a hanging-drop mercury electrode (HDME) was used for cyclic voltammetry as the working electrode. A platinum wire served as the counter electrode. The ESR spectra were recorded on a Hitachi MES-4001 ESR spectrometer, and the sample was electrolyzed in the cavity of the ESR spectrometer. The temperature control of the samples was done by means of a Hitachi M-4602 variable-temperature accessory.

Procedure. A freshly-prepared sample solution which contained 0.1 M TEAP as the supporting electrolyte was placed in a cell. The dissolved oxygen was removed by bubbling with highly-purified nitrogen gas saturated with solvent vapor for about 15 min, and polarograms were recorded with nitrogen passing over the solution. All the experiments were carried out at 25.0±0.1 °C.

Results and Discussion

Polarography. The polarographic data for purine in various solvents are shown in Table 1. Purine is reduced at a very negative potential in aprotic solvents. The initial purine reduction wave is quite similar in both acetonitrile and DMF, but in the case of DMF the second wave appears at a more negative potential. In an aqueous solution, it is known[6] that purine exhibits two pH-dependent waves when in an acidic solution but none when in a neutral or alkaline solution, and that the first wave of these is attributable to a two-electron, diffusion-controlled process. The diffusion-current constant corrected for the change in viscosity obtained in nonaqueous solvents is about 1/4 that of the first wave obtained in an aqueous solvent; therefore, purine is initially reduced in a 1/2-electron process in aprotic solvents.

The limiting current of purine increases linearly with the concentration below 2 mM, as is shown in Fig. 1. The effect of the height of the mercury reservoir is shown in Fig. 2. The limiting current of purine is approximately proportional to $h^{1/2}$. The temperature

Table 1. Polarographic data for purine reduction in various solvents

Solvent	$E_{1/2}$, V	$E_{3/4}-E_{1/4}$ mV	I_d[d]	$\eta_{25°C}$	$I_d\eta^{1/2}$
CH_3CN	−2.16[a]	80	1.60	0.345	0.91
DMF	−2.38[b]	110	1.03	0.802	0.92
	−2.66[b]		0.22		0.20
H_2O	−0.691−0.083pH[c]	76	3.81	0.894	3.60
	−0.910−0.080pH[c]	89	5.67		5.36

a) V *vs.* Ag-$AgClO_4$ (0.1 M) electrode in CH_3CN. b) V *vs.* Ag-$AgClO_4$ (0.1 M) electrode in DMF. c) V *vs.* SCE (aqueous). d) Diffusion current constant.

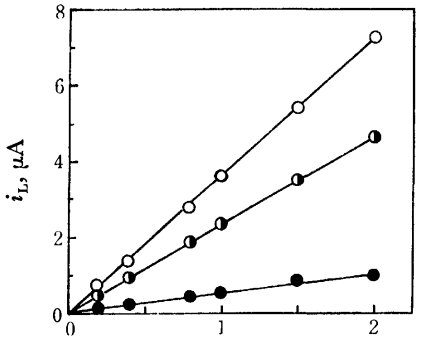

Fig. 1. Calibration curves of initial reduction waves of purine in acetonitrile (○) and DMF (◑: 1st wave, ●: 2nd wave).

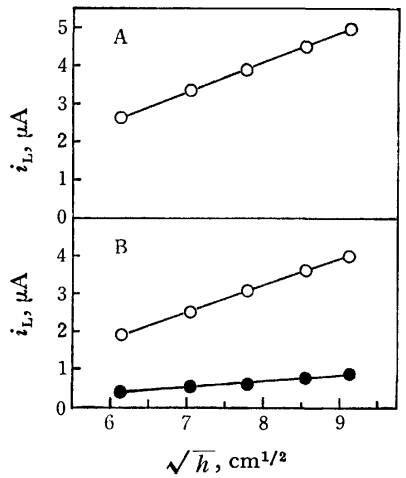

Fig. 2. Effect of the height of the mercury reservoir.
A: 1.0 mM purine in acetonitrile
B: 1.0 mM purine in DMF
(○: 1st wave, ●: 2nd wave)

coefficient of the limiting current of purine in acetonitrile is 1.2% per degree in the temperature range from 15 to 40 °C. These results show that the initial reduction wave of purine is diffusion-controlled in both acetonitrile and DMF.

Cyclic Voltammetry. The cyclic voltammograms are shown in Fig. 3. In the case of acetonitrile, purine first gives a cathodic peak corresponding to the polarographic wave, whose height is proportional to the concentration and the square root of the scan rate. However, on the return sweep, no anodic peak is seen until about −0.56 V (peak 3a), and a redox couple (peak 4a and 4c) on the positive-potential side of Peak 3a appears. In the case of DMF, a typical curve indicates a cathodic peak, followed by a reversible reduction step. However, the other voltammetric behavior for purine in DMF is similar to that in acetonitrile.

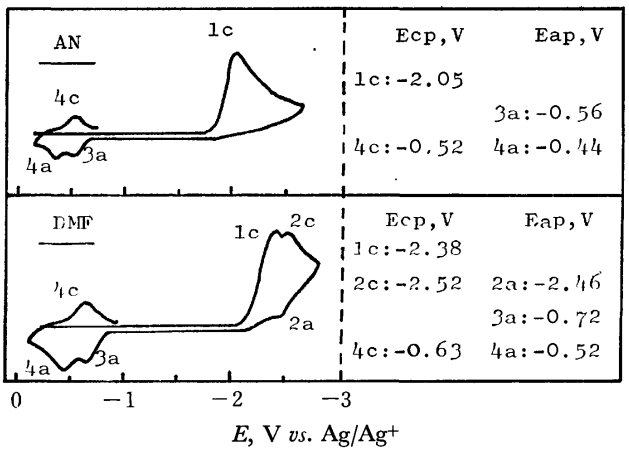

Fig. 3. Cyclic voltammogram of purine in aprotic solvents.
scan speed: 0.20 V/s

ESR Spectroscopy. The electrogenerated radical species of purine and the various biologically-important purine bases have not been detected[11] at room temperature. This is presumably because of the rapid dimerization of the radical anion of purines. There-

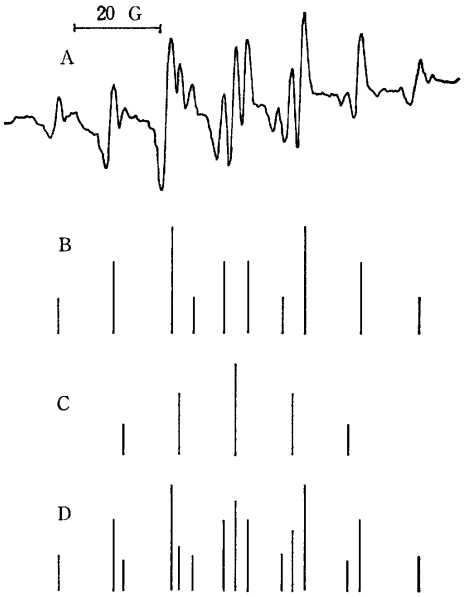

Fig. 4. A; Observed ESR spectrum obtained by controlled potential electrolysis at the potential of the first polarographic wave in DMF at −60 °C. B; calculated ESR spectrum of radical (1) with coupling constant A_H(6-Position) = 30.4 gauss and A_N(1 and 3-Position) = 12.7 gauss. C; calculated ESR spectrum of radical (2) with coupling constant A_N(1 and 3-Position) = 12.6 gauss. D; combined spectrum of B and C.

fore, the ESR technique at a low temperature was used to detect the electrogenerated radicals of purine. A typical ESR spectrum obtained by controlled potential electrolysis at the potential of the first polarographic wave in DMF at −60 °C is shown in Fig. 4A. The half-peak width of the hyperfine components is about 1.6 gauss, and the total width between the centers of the outermost observed lines is 41.0 gauss.

The results of the interpretation indicate that this spectrum consists of a combination of the hyperfine splitting of the two radical species shown below.

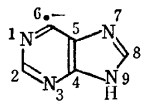

(1)

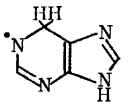

(2)

The spectrum (Fig. 4B) obtained by the use of Radical (1) is interpreted as deriving from the interaction of the unpaired electron with a proton (A_H=30.4 G) and an equivalent pair of the nitrogen nucleus (A_N=12.7 G). It may also be interpreted that the spectrum (Fig. 4C) obtained by the use of Radical (2) is attributable to the interaction of the unpaired electron with an equivalent pair of the nitrogen nucleus (A_N=12.6 G). The combined spectrum of B and C is shown in Fig. 4D; it is in good agreement with the observed ESR spectrum. The results of this ESR spectrum and the diffusion-current constant which corresponds to the 1/2-electron reduction wave indicate that purine is initially reduced in a one-electron process to produce an unstable radical anion, which then abstracts a proton from the parent purine to produce a free radical and an electro-inactive species.

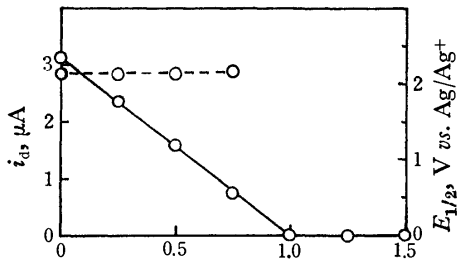

Fig. 5. Effect of strong base addition on polarograms of 1 mM purine in acetonitrile.
(——): i_d, (------): $E_{1/2}$

Effect of Base Addition. An acetonitrile solution of tetraethylammonium hydroxide (TEAH), which is a strong base in acetonitrile, was added to an acetonitrile solution of purine. The polarographic behavior of purine in the presence of TEAH is shown in Fig. 5. The presence of TEAH in the solution causes the wave-height of the original purine wave to decrease, approximately in proportion to the base concentration, and at a molar ratio of TEAH/purine ratio of about 1.0 the wave dissappears entirely. However, $E_{1/2}$ is constant in spite of the addition of TEAH. This behavior can be explained in terms of the production of an electro-inactive anion by a kind of acid-base reaction like that shown below:

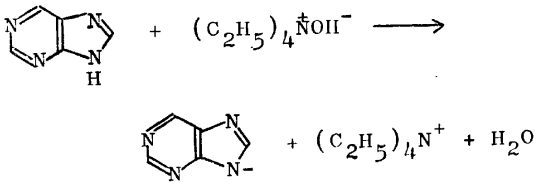

Effect of the Acid Addition. The various acids were added to both acetonitrile and a DMF solution of purine, and their effects on the polarograms were studied. In general, the addition of strong acid produces a new, drawn-out wave at a more positive potential than the original purine reduction wave.

On the addition of monochloroacetic acid to an acetonitrile solution of purine, a new wave appears at −1.89 V. With an increase in the acid/purine ratio, the wave-height of the new wave, that is approximately constant, in $E_{1/2}$ increases, and that of the original wave decreases, as is shown in Fig. 6. At a molar ratio of acid/purine higher than about 2.2, the new

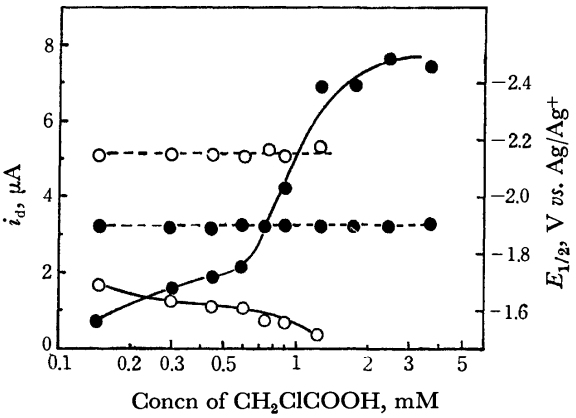

Fig. 6. Effect of monochloroacetic acid on the polarographic reduction of 0.6 mM purine in acetonitrile.
(——): i_d, (------): $E_{1/2}$
○: purine reduction wave, $E_{1/2}$=−2.16 V
●: purine-acid wave, $E_{1/2}$=−1.89 V

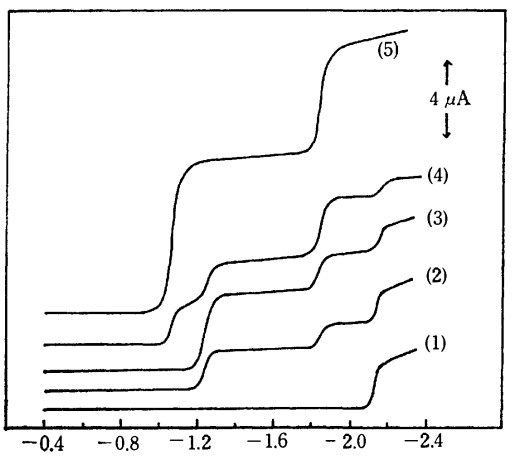

Fig. 7. Effect of $HClO_4$ concentration on polarograms of 0.6 mM purine in acetonitrile.
[$HClO_4$]/[purine] ratio: curve (1), 0; (2), 0.5; (3), 1.0; (4), 1.5; (5), 2.5

wave becomes constant, with a height that corresponds to that of the 2-electron reduction wave, and the original wave disappears. In the case of the addition of benzoic acid, the same behavior was observed.

The addition of a very strong acid, perchloric, results in the appearance of several waves at more positive potentials than the original purine wave, as is shown in Fig. 7. At a molar ratio of acid/purine lower than 1.0, two new waves appear at −1.24 and −1.84 V; their heights increase in proportion to the acid concentration. Perchloric acid present in a molar ratio of 1:1 decreases the height of the original wave to about 1/2 of the original value, and the wave at −1.24 V increases in height to nearly double the value of the original wave. A further increase in the perchloric acid concentration causes a new wave to appear at −1.07 V; its height increases until it is about 4 times the value of the original purine wave. However, the wave at −1.24 V and the original purine wave completely disappear at an acid/purine ratio of about 2.1, and the polarographic behavior is close to that observed for purine in unbuffered aqueous solutions. These results are consistent with a prior protonation of the purine molecule at one of the nitrogen atoms to give a species more easily reducible than the original purine wave. Consequently, the waves at −1.24 V and −1.07 V presumably contribute to the reduction of monoprotonated and diprotonated purine respectively. The presence of a weak acid, such as acetic acid and water, causes the half-wave potential of the original wave to shift to more positive values, also increasing its height until it is about 4 times that in dry acetonitrile. The polarographic behavior of purine in DMF in the presence of various acids is similar to that in

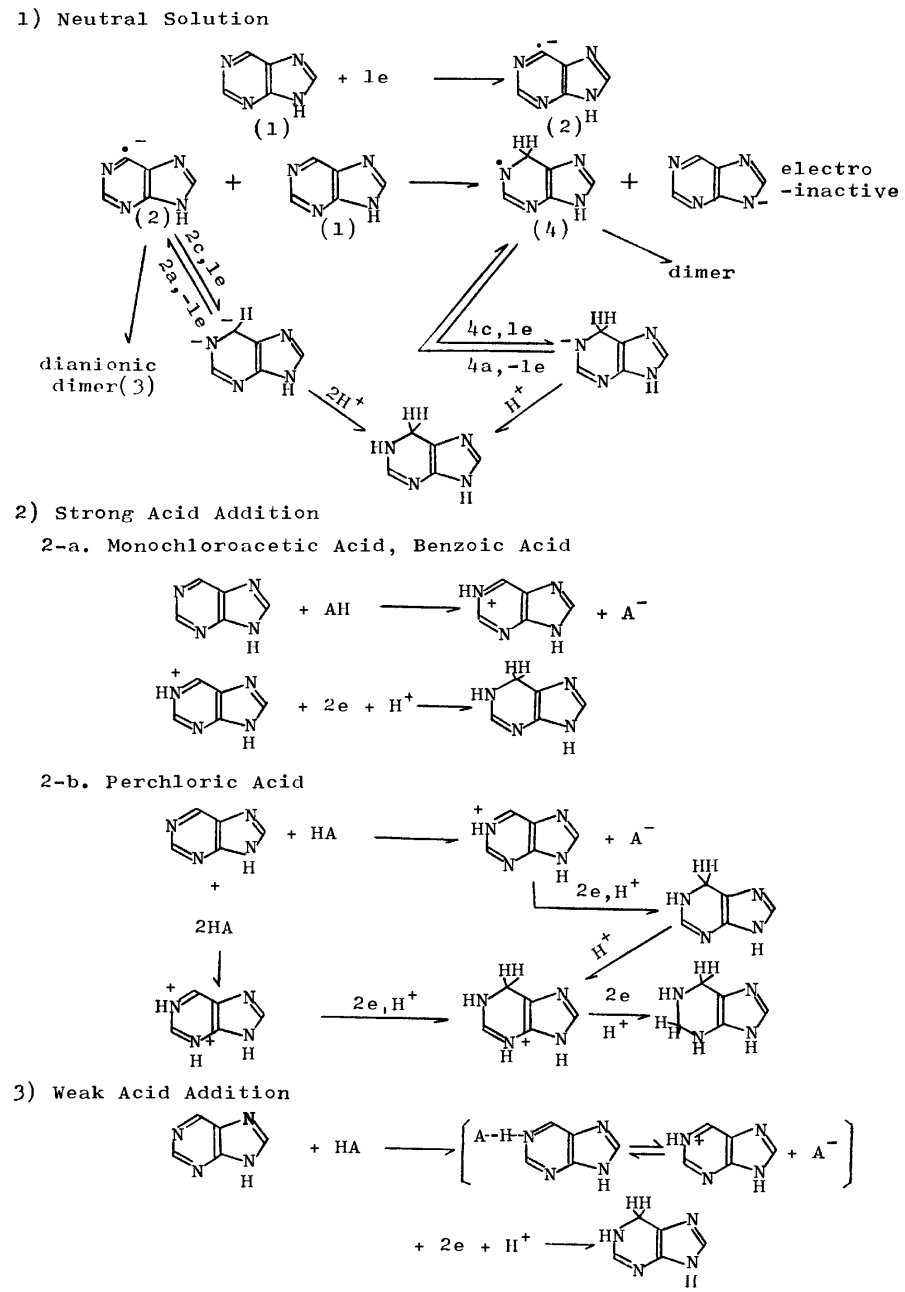

Scheme 1.

TABLE 2. CORRELATION OF POTENTIAL FOR THE PURINE REDUCTION WAVE WITH THE STRENGTH OF THE ADDED ACID

Acid added	pK_a^{aq}	$E_{1/2}$, V *vs.* Ag/Ag^+	
		Acetonitrile	DMF
Perchloric acid	a)	−1.07, −1.24, −1.84	−1.86+0.15 log[Acid]
Monochloroacetic acid	2.8	−1.89	−1.92+0.10 log[Acid]
Benzoic acid	4.2	−2.01	−2.02+0.10 log[Acid]
Acetic acid	4.8	−1.64+0.16 log[Acid]	−2.29+0.03 log[Acid]
Water		−2.11+0.09 log[Acid]	

a) Perchloric acid is completely dissociated in both acetonitrile and water.

acetonitrile in the presence of acetic acid and water.

The half-wave potentials of the purine reduction waves produced by adding the various acids are indicated in Table 2 in relation to the strengths of the added acids. The potential of the acid-produced purine reduction is more positive the stronger the acid added. The nature of the purine-acid species formed on acid addition is most probably a hydrogen-bonded or an ion-pair complex.

Mechanism of Purine Reduction. The mechanism presumed for purine reduction in acetonitrile and DMF at the mercury electrode is summarized in Scheme 1. In a neutral nonaqueous solution, purine undergoes a one-electron reduction to produce an unstable anion radical (2), which then abstracts a proton from the parent purine to produce a free radical (4) and an electro-inactive purine anion. The redox couple (peak 2c and 2a) which appears when DMF is used as the solvent, presumably corresponds to the further reduction of a solvated anion radical stabilized by the solvation with DMF, because this solvation effect prevents the fast dimerization reaction from producing the purine dianionic dimer (peak 3a). This is apparent from the fact that the line intensity of the ESR spectrum in the case of acetonitrile is smaller than that in the case of DMF. The three peaks (3a, 4a, and 4c) which appear at the positive potential above −0.7 V presumably correspond to the anions disappearing on addition of the acids. The unstable purine free radical (4) undergoes a fast dimerization to produce a purine dimer, but a part of that is further reduced almost instantaneously to produce the 6-hydropurine anion (peak 4c). When monochloroacetic acid and benzoic acid are present, a preprotonation reaction can occur, which is reduced in a two-electron process to produce 1,6-dihydropurine.[6] When perchloric acid is present, monoprotonated and diprotonated purine species are initially reduced in a two-electron process; this is followed by a further two-electron reduction to produce 1,2,3,6-tetrahydropurine.[6] The addition of weak acids produces an acid-base equilibrium between purine and acids, which equilibrium is reduced in a two-electron process.

References

1) G. Dryhurst, *J. Electrochem. Soc.*, **116**, 1097 (1969).
2) W. A. Struck and P. J. Elving, *Biochem.*, **4**, 1343 (1965).
3) G. Dryhurst and P. J. Elving, *J. Electrochem. Soc.*, **115**, 1014 (1968).
4) G. Dryhurst, *Talanta*, **16**, 855 (1969).
5) D. L. McAllister and G. Dryhurst, *J. Electroanal. Chem.*, **32**, 387 (1971).
6) D. L. Smith and P. J. Elving, *J. Amer. Chem. Soc.*, **84**, 1412 (1962).
7) J. F. Coetzee, G. P. Cunningham, D. K. McGuire, and G. R. Padmamabham, *Anal. Chem.*, **34**, 1139 (1962).
8) O. Hatano, *Bull. Chem. Rest. Non-aq. Soln. (Tohoku Univ.)*, **18**, 155 (1968).
9) T. Fujinaga, K. Izutsu, and K. Takaoka, *J. Electroanal. Chem.*, **12**, 203 (1966).
10) A. D. Goolsby and D. T. Sawyer, *Anal. Chem.*, **39**, 411 (1967).
11) J. E. O'Reilly and P. J. Elving, *J. Amer. Chem. Soc.*, **93**, 1871 (1971).

The Equilibria of Protonation Reaction of *N,N'*-Ethylenebis(salicylideneiminato)cobalt(II) and of Its Oxygenated Binuclear Complex by Perchloric Acid in Dimethyl Sulfoxide

Yuriko ABE* and Goro WADA

Department of Chemistry, Faculty of Science, Nara Women's University, Nara 630

(Received July 22, 1974)

Acid dependence of oxygen uptake by Co(II)salen in DMSO was studied. As the concentration of perchloric acid increases in the absence of O_2, Co(II)salen forms 1:1 and 1:2 protonated complexes, with the formation constants $K_1=8.3\times10^3$ M^{-1} and $K_2=1.6\times10^3$ M^{-1} measured spectrophotometrically by the linearity method. The oxygen uptake ratio n of Co(II)salen in the absence of acid is 0.5, indicating formation of a 2:1 O_2-bridged binuclear complex, with an immeasurably large formation constant K_3. The oxygenated complex is protonated by addition of acid with a formation constant $K_4=3.3\times10^5$ M^{-1} as observed again spectrophotometrically. When Co(II)salen is oxygenated in the presence of acid, n decreases considerably from 0.5 with increasing acid concentration. This is because the protonated Co(II)salen complexes are inert to oxygenation and both the rate of oxygenation of Co(II)salen and that of deoxygenation of oxygenated binuclear species are slow, as compared to the rapid processes of protonation.

In the last decade, much attention has been paid on the reversible oxygenation of some cobalt complexes by many investigators, especially on the reaction mechanisms and the electronic and the molecular structures of the oxygenated complexes,[1-3] because they have been taken as nice models for oxygen carriers in living systems. *N,N'*-Ethylenebis(salicylideneiminato)cobalt(II) (abbreviated as Co(II)salen below) was the first

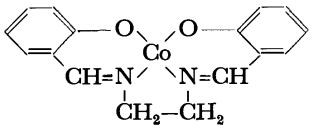

Co(II)salen

synthetic complex with a nature of reversible oxygenation,[4] which was mostly investigated in its solid state.[5] Recently, Floriani *et al.* found that Co(II)salen absorbs oxygen to form a binuclear complex Co(III)salen·O_2·-Co(III)salen in aprotic solvents such as dimethyl sulfoxide (DMSO) and *N,N*-dimethylformamide (DMF) at room temperature,[6] while Ochiai showed that Co(II)salen forms a 1:1 complex with an oxygen molecule at 77 K and that the stability of oxygenated species depends upon the ligand which is situated at the *trans* position with respect to the oxygen.[7,8] However, since the function of acid existing in the organic solvents towards the oxygenation reaction is not known yet to date, we investigated the thermodynamic equilibria among Co(II)salen, O_2, and hydrogen ion in DMSO in the present paper.

Experimental

Materials. The purification of commercial DMSO and the preparation of DMSO solution of perchloric acid was carried out according to our previous procedure.[9] Co(II)salen was prepared by a method in the literature.[10] Sodium perchlorate was recrystallized twice from aqueous solution and was used for the purpose of adjusting the ionic strength of DMSO solutions.

Oxygen Uptake Measurements. The volume of oxygen absorbed by Co(II)salen was measured by the use of a Warburg apparatus at 25 °C and an ionic strength 0.25 M, by dissolving a weighed amount of crystalline Co(II)salen into DMSO of a given ionic strength, under various partial pressures of oxygen.

Spectrophotometry. The optical absorbances of complexes were measured by a Hitachi spectrophotometer Model 101 and a Hitachi recording spectrophotometer Model EPS-3T with a quartz cell of 10 or 1 mm light path. In the case of complexes containing no oxygen, the measurements were performed under nitrogen atmosphere.

Results

Absorption Spectra and Formation Constants of Mono- and Di-Protonated Complexes. Figure 1 shows absorption spectra of Co(II)salen (Curve a) and of partly proto-

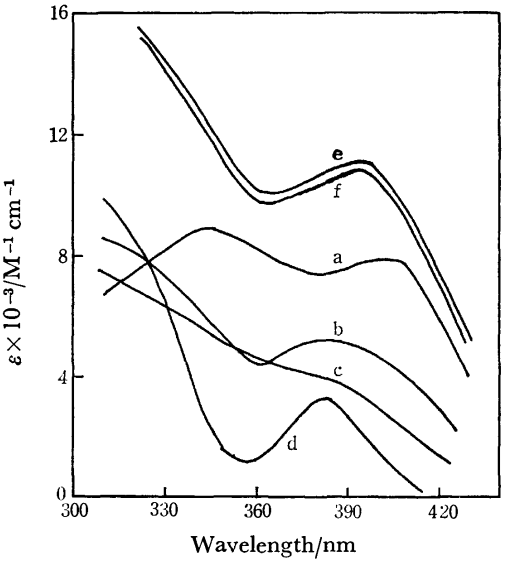

Fig. 1. Absorption spectra of Co(II)salen and its protonated and oxygenated species at $\mu=0.25$ M. (a) Co(II)salen, (b) $[Co(II)salen]_0=5.70\times10^{-4}$ M, $[HClO_4]_0=3.00\times10^{-4}$ M, (c) $[Co(II)salen]_0=5.70\times10^{-4}$ M, $[HClO_4]_0=2.00\times10^{-3}$ M, (d) Co(II)-salenH$^+$, (e) $(Co(III)salen)_2O_2$, (f) $[(Co(III)salen)_2O_2]_0=3.12\times10^{-4}$ M, $[HClO_4]_0=1.00\times10^{-4}$ M

* *Nee*: Yuriko Unno.

nated ones (Curve b for $[Co(II)salen]_0=5.70\times10^{-4}$ M and $[HClO_4]_0=3.00\times10^{-4}$ M and Curve c for $[Co(II)salen]_0=5.70\times10^{-4}$ M and $[HClO_4]_0=2.00\times10^{-3}$ M, where $[\ ]_0$ represents the total concentration). When acid concentration is lower than 3×10^{-4} M, an isosbestic point appears at 325 nm, indicating that there occurs a single species of protonated complex, although many curves between a and b passing the same isosbestic point are omitted in the figure. At higher acid concentrations, absorption spectrum gradually deviates from the isosbestic point because of probable occurrence of another protonated species.

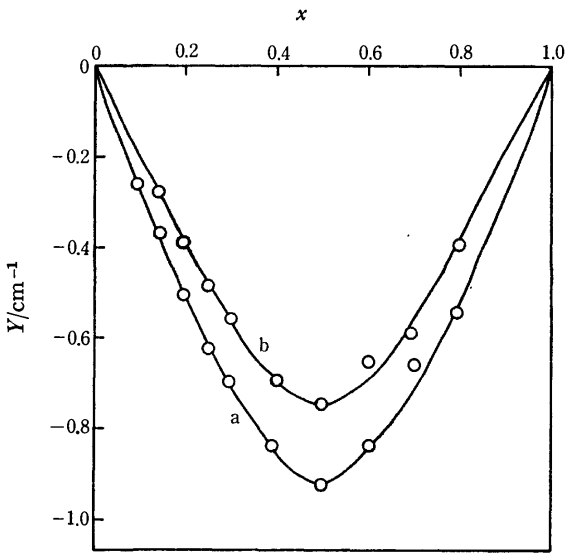

Fig. 2. Job's curves for Co(II)salen-$HClO_4$ system at 410 nm and $\mu=0.25$ M.
(a) $[Co(II)salen]_0+[HClO_4]_0=5.00\times10^{-4}$ M
(b) $[Co(II)salen]_0+[HClO_4]_0=4.00\times10^{-4}$ M

According to Job's curves of continuous variation for solutions of Co(II)salen and perchloric acid observed at 410 nm as shown in Fig. 2, minimum points are recognized at concentrations of $[Co(II)salen]_0=[HClO_4]_0$, proving formation of a 1 : 1 complex, namely monoprotonated complex Co(II)salenH$^+$, holding an equilibrium,

$$Co(II)\ salen + H^+ \rightleftarrows Co(II)\ salenH^+ \quad (1)$$

$$K_1 = \frac{[Co(II)\ salenH^+]}{[Co(II)\ salen][H^+]} \quad (2)$$

In Fig. 2, the values of Y as defined below are plotted against the mole fraction of Co(II)salen, $x=[Co(II)salen]_0/([Co(II)salen]_0+[HClO_4]_0)$ at two different total concentrations of Co(II)salen and acid.

$$\begin{aligned} Y &= \text{Absorbance} - \varepsilon_0[Co(II)\ salen]_0 \\ &= \varepsilon_0[Co(II)\ salen] + \varepsilon_1[Co(II)\ salenH^+] \\ &\quad - \varepsilon_0[Co(II)\ salen]_0 \\ &= (\varepsilon_1-\varepsilon_0)[Co(II)\ salenH^+] \end{aligned} \quad (3)$$

Here, ε_0 and ε_1 stand for the molar absorptivity of Co(II)salen and Co(II)salenH$^+$, respectively. By adopting our method[11] to Curves a and b in Fig. 2, the values of K_1 and ε_1 are calculated which are listed in Table 1, along with other related data. By using the value of K_1, the absorption spectrum of Co(II)salenH$^+$ can be obtained which is shown as Curve d in Fig. 1. The absorption spectrum of Co(II)salen (Curve a) exhibits two peaks at 345 and 405 nm, while the absorption spectrum of Co(II)salenH$^+$ (Curve d) appears generally below that of Co(II)salen at the wavelength range longer than the isosbestic point 325 nm, having a single peak at 383 nm.

Table 1. Formation constants and molar absorptivities of protonated Co(II)salen at $\mu=0.25$ M and 25 °C

Wavelength nm	K_1 M^{-1}	ε_1 $M^{-1}cm^{-1}$	K_2 M^{-1}	ε_2 $M^{-1}cm^{-1}$	Method
410	1.17×10^4	8.13×10^2	—	—	Job's
400	1.27×10^4	1.66×10^3	—	—	Job's
360	0.83×10^4	1.0×10^3	1.6×10^3	5.9×10^3	Linearity

At higher acid concentration, however, Curve c represents an absorption spectrum of a probable mixture of mono- and di-protonated Co(II)salen. When the apparent molar absorptivity of the mixture and the molar absorptivity of Co(II)salenH$_2^{2+}$ are expressed by ε and ε_2 respectively, the following relationship may be established.[11]

$$\varepsilon = \varepsilon_1 + \frac{1}{K_1}\frac{\varepsilon_0-\varepsilon}{[H^+]} + (\varepsilon_2-\varepsilon)K_2[H^+] \quad (4)$$

$$Co(II)\ salenH^+ + H^+ \rightleftarrows Co(II)\ salenH_2^{2+} \quad (5)$$

$$K_2 = \frac{[Co(II)\ salenH_2^{2+}]}{[Co(II)\ salenH^+][H^+]} \quad (6)$$

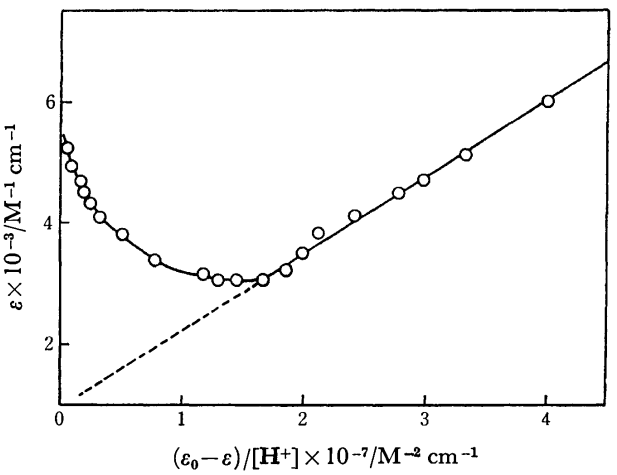

Fig. 3. Relationship between ε and $(\varepsilon_0-\varepsilon)/[H^+]$ at $[Co(II)salen]_0=5.50\times10^{-4}$ M, 360 nm, and $\mu=0.25$ M.

Therefore, a plot of ε against $(\varepsilon_0-\varepsilon)/[H^+]$ gives a straight line at sufficiently low hydrogen ion concentration as shown in Fig. 3, from whose slope and intercept, K_1 and ε_1 are obtained. At higher hydrogen ion concentration, however, the plot deviates from the linearity, caused by occurrence of the considerable amount of diprotonated species. At this range of hydrogen ion concentration, another linearity between ε and $\Delta\varepsilon(1+K_1[H^+])/K_1[H^+]^2$ must hold from the modification of Eq. (4), as follows:

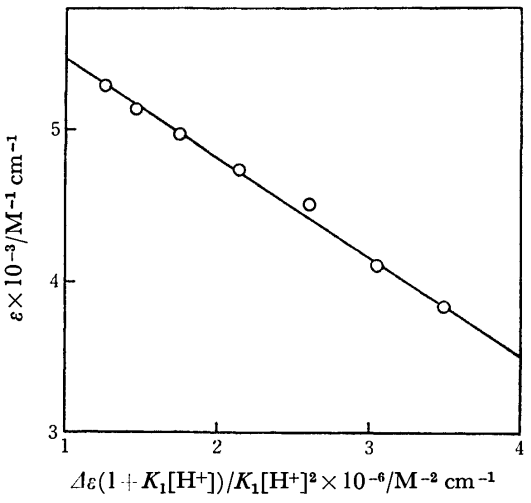

Fig. 4. Linear relationship between ε and $\Delta\varepsilon(1+K_1[H^+])/K_1[H^+]^2$ at $[Co(II)salen]_0=5.50\times10^{-4}$ M, 360 nm, and $\mu=0.25$ M.

$$\varepsilon = \varepsilon_2 - \frac{1}{K_2}\frac{\Delta\varepsilon(1+K_1[H^+])}{K_1[H^+]^2} \tag{7}$$

where $\Delta\varepsilon$ stands for the increment of ε caused by the occurrence of Co(II)salenH_2^{2+}. The linearity of Eq. (7) is shown in Fig. 4, from whose slope and intercept, K_2 and ε_2 are obtained. The values of K_1, K_2, ε_1, and ε_2 thus obtained are also listed in Table 1. The K_1 values from the two different methods agree with each other within experimental error.

Oxygen Uptake by Co(II)salen and Protonation of Oxygenated Complexes. The oxygen uptake by Co(II)-salen in the absence of acid in DMSO is very slow, the spectral change during the oxygenation being shown in Fig. 5. In the figure, it is seen that an absorption peak at 340 nm due to Co(II)salen gradually diminishes in the course of the oxygenation, while an alternative peak at 390 nm grows up due to the oxygenated species with an isosbestic point between the unoxygenated and oxygenated complexes at 325 nm. The mole ratio of

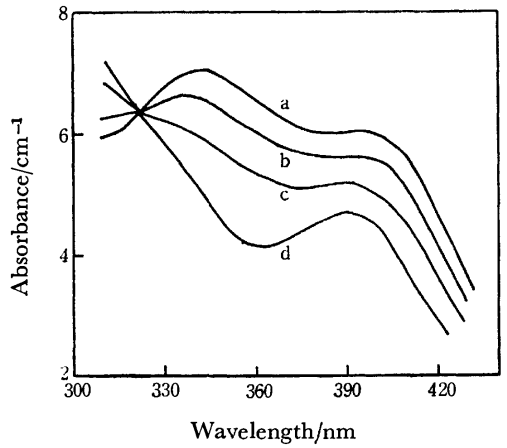

Fig. 5. Spectral change during the oxygenation of Co(II)salen at $[Co(II)salen]_0=8.20\times10^{-4}$ M in an atmospheric air at room temperature. Time after initiation of the reaction, (a) 11 min, (b) 87 min, (c) 300 min, (d) ∞

Table 2. Mole ratio n of O_2-uptake to the total Co-(II)salen under an atmospheric air at 25 °C

$[Co(II)salen]_0$ M	$[O_2$-uptake] M	n
5.16×10^{-3}	2.60×10^{-3}	0.50
1.00×10^{-2}	4.88×10^{-3}	0.48
1.28×10^{-2}	6.50×10^{-3}	0.51
1.42×10^{-2}	7.04×10^{-3}	0.50

oxygen uptake to the total Co(II)salen, n=[Absorbed O_2]/$[Co(II)salen]_0$ at infinite time is approximately 0.5 as listed in Table 2, which indicates the formation of a 2:1 complex as represented by $(Co(III)salen)_2O_2$ at room temperature. Thus, a chemical equilibrium is established as follows:

$$2Co(II)\ salen + O_2 \rightleftarrows (Co(III)\ salen)_2O_2 \tag{8}$$

$$K_3 = \frac{[(Co(III)\ salen)_2O_2]}{[Co(II)\ salen]^2[O_2]} \tag{9}$$

The equilibrium constant K_3 must be immeasurably large under the present condition, so large that the reaction could be regarded to be irreversible.[7,8]

When perchloric acid was added to binuclear oxygenated complex, a slight spectral change but no release of oxygen was observed. Therefore, it is deduced that the protonation of $(Co(III)salen)_2O_2$ must have occurred and quickly attained to an equilibrium.

$$(Co(III)\ salen)_2O_2 + H^+ \rightleftarrows (Co(III)\ salen)_2O_2H^+ \tag{10}$$

$$K_4 = \frac{[(Co(III)\ salen)_2O_2H^+]}{[(Co(III)\ salen)_2O_2][H^+]} \tag{11}$$

The equilibrium constant K_4 can be obtained by the method similar to the case of K_1 with ε_3, ε_4, and K_4 in place of ε_0, ε_1, and K_1 respectively and with ignoring the third term of the right-hand side in Eq. (4). The linearity of ε *vs.* $(\varepsilon_3-\varepsilon)/[H^+]$ is shown in Fig. 6 and the calculated data associated with the equilibrium 10 at 25 °C are as follows:

$$\left.\begin{aligned} K_4 &= 3.3\times10^5\ M^{-1} \\ \varepsilon_3 &= 1.11\times10^4\ M^{-1}\cdot cm^{-1} \\ \varepsilon_4 &= 9.80\times10^3\ M^{-1}\cdot cm^{-1} \end{aligned}\right\}\ \text{at 390 nm}$$

When Co(II)salen is oxygenated in the presence of perchloric acid, Reactions 1, 5, 8, and 10 might take

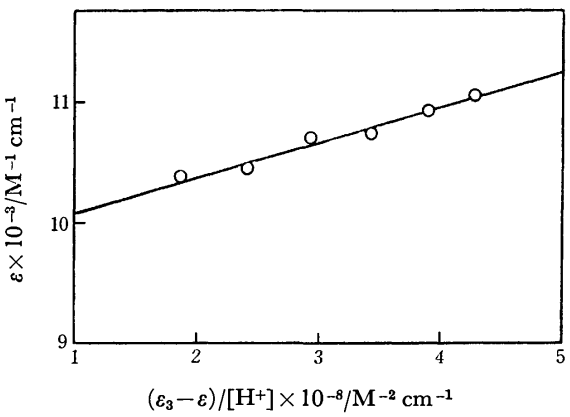

Fig. 6. Linear relationship between ε and $(\varepsilon_3-\varepsilon)/[H^+]$ at $[(Co(III)salen)_2O_2]_0=3.12\times10^{-4}$ M, 390 nm, and $\mu=0.25$ M.

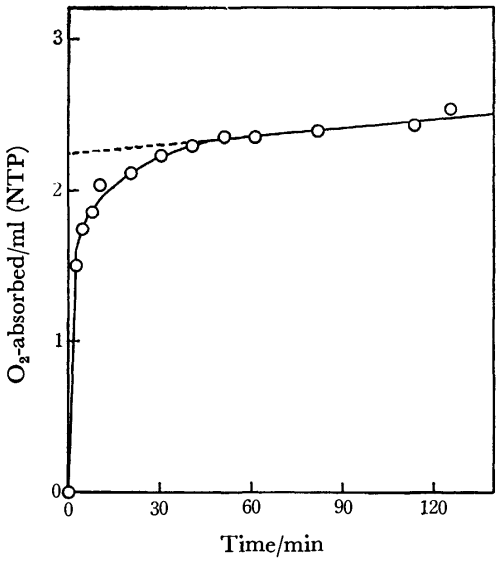

Fig. 7. Rate of oxygen uptake by Co(II)salen in the presence of perchloric acid under an atmospheric air at $[Co(II)salen]_0 = 1.00 \times 10^{-2}$ M, $[HClO_4]_0 = 2.19 \times 10^{-2}$ M, $\mu = 0.25$ M, and 25 °C.

place altogether, among which only Reaction 8 proceeds very slowly. The rate of oxygen uptake in the presence of acid is drawn in Fig. 7. The curve consists of two parts with a rapid uptake at earlier stage of the reaction, followed by a very slow uptake at later one. This means that the primary and the secondary protonation reactions of Co(II)salen (Reactions 1 and 5) quickly reach their equilibria without regard to the presence of oxygen and then, on the gradual progress of Reaction 8, the deprotonation reactions (backward reactions of 1 and 5) produce again Co(II)salen to be oxygenated. The protonated species themselves, Co(II)salenH$^+$ and Co(II)salenH_2^{2+}, are inert to oxygenation. The observed apparent oxygen uptake ratio n at earlier stage

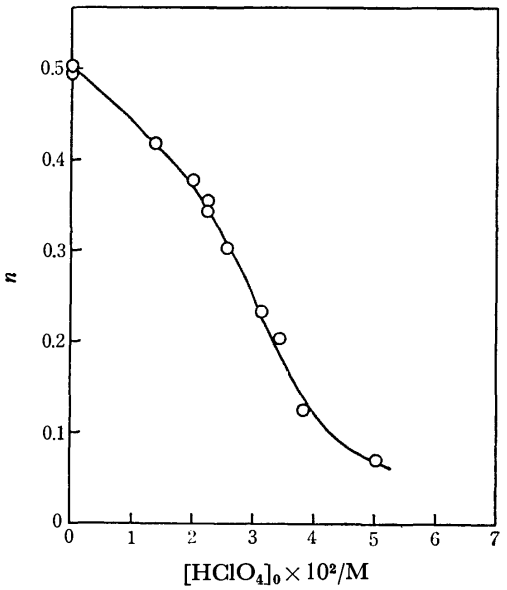

Fig. 8. Oxygen uptake ratio n, dependent upon acid concentration at $[Co(II)salen]_0 = 1.00 \times 10^{-2}$ M, $\mu = 0.25$ M, and 25 °C.

at various acid concentrations is represented in Fig. 8, in which n decreases with increasing acid concentration, being approximately expressed by a following equation, derived on the basis that the protonated species can not be oxygenated.

$$n = \frac{1}{2}\left(1 - \frac{K_1(1+K_2[H^+])[H^+][Co(II)\,salen]}{[Co(II)\,salen]_0}\right) \quad (12)$$

Discussion

The mono- and di-protonated Co(II)salen are produced according to the acid concentration. The protonation may take place at lone electron-pairs on oxygen atoms of Co(II)salen, resulting in weakening the electron donating ability of oxygen atom to Co(II) and consequently of Co(II) which might have reduced O_2 to O_2^-. Therefore, the protonated species must be inert to oxygenation as observed above.

The reducing ability of Co(II) is known to be affected by the basic nature of X at low temperature as expressed in the reaction,

$$\text{Co(II) salen}\cdot X + O_2 \rightleftarrows (O_2\text{Co(II) salen}\cdot X)^* \rightleftarrows O_2^-\cdot\text{Co(III) salen}\cdot X \quad (13)$$

the enthalpy of the reaction being in parallel with basicity of X in the order,[7] pyridine>DMSO>NCS^-> tetrahydrofuran > *N*, *N*-dimethylacetamide > CH_2Cl_2, where X coordinates with Co(II) at the site perpendicular to the salen plane. Thus, the basic nature of X assists Co(II)salen in reducing O_2 to O_2^-. Therefore, the inertness of the protonated species to the oxygenation is easily convinced by the fact that the proton is, say, of the least basic nature, although the attaching positions of X and H^+ are different to each other.

According to Ochiai,[8] the formation of 1 : 1 superoxo or 2 : 1 μ-peroxo complex by oxygen uptake depends upon the nature of solvent, ligand, and temperature. In our present case, the latter complex seems to be far more favored than the former in DMSO at room temperature, because of a considerably large negative free energy.[8]

The protonation of 2 : 1 μ-peroxo complex, (Co(III)-salen)$_2O_2$ (Reaction 10), occurs at the bridging O_2^{2-} on producing hydroperoxo ion, HO_2^-. The formation constants of protonated μ-peroxo binuclear cobalt complexes are compared as follows. The ammine, ethylenediamine, and cyano complexes in aqueous solutions maintain chemical equilibria with respective equilibrium constants,[12,13]

$$(NH_3)_5Co\text{-}O_2\text{-}Co(NH_3)_5^{4+} + H^+ \rightleftarrows (NH_3)_5Co\text{-}(O_2H)\text{-}Co(NH_3)_5^{5+} \quad (14)$$

$$\log K_{NH_3} = -1.2 \pm 0.2$$

$$(en)_2Co(NH_2)(O_2)Co(en)_2^{3+} + H^+ \rightleftarrows (en)_2Co(NH_2)(O_2H)Co(en)_2^{4+} \quad (15)$$

$$\log K_{en} = 0.8$$

$$(CN)_5Co\text{-}O_2\text{-}Co(CN)_5^{6-} + H^+ \rightleftharpoons (CN)_5Co\text{-}O_2(H)\text{-}Co(CN)_5^{5-} \quad (16)$$

$$\log K_{CN} = 10.5$$

while $\log K_{salen}$ for Co(II)salen in DMSO ($=\log K_4$ in Eq. (11)) has been found to be 5.5. Although the solvent used only for Co(II)salen was different from others, the order of K's, $K_{NH_3}<K_{en}<K_{salen}<K_{CN}$, agrees with the reverse order of electric charges on Co-complexes, $4+_{NH_3}>3+_{en}>0_{salen}>6-_{CN}$, indicating that the reactions are largely retarded or favored by Coulombic repulsive or attractive force between the Co-complex and H^+, respectively. The dielectric constant of DMSO is 46.7, being small as compared to that of water 78, but the effect of the smallness of dielectric constant of DMSO might be minute because the oxygenated Co(II)salen complex is chargeless. Consequently, the magnitude of K_4 for Reaction 10 seems to be reasonable.

In conclusion, the reactions considered in the present study are summarized below.

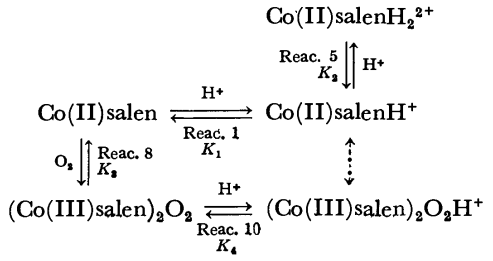

Since the protonating site differs from each other among Reactions 1, 5, and 10, all reactions lie in a line with the protonated species being inhibited for direct oxygenation or deoxygenation, as shown by a dotted arrow. Only Reaction 8 is very slow with an apparent decrease in oxygenation ratio in acid DMSO.

References

1) L. H. Vogt, Jr., H. M. Faigenbaum, and S. E. Wiberley, *Chem. Rev.*, **63**, 269 (1963).
2) S. Fallab, *Angew. Chem.*, **79**, 500 (1967).
3) A. G. Sykes, "Inorganic Reaction Mechanism," Progress in Inorganic Chemistry, Vol. 13, ed. by J. O. Edwards, Interscience Publishers, New York, (1970), p. 1.
4) T. Tsumaki, This Bulletin, **13**, 252 (1937).
5) M. Calvin, R. H. Bailes, and W. K. Wilmarth, *J. Amer. Chem. Soc.*, **68**, 2254 (1946).
6) C. Floriani and F. Calderazzo, *J. Chem. Soc., A*, **1969**, 946.
7) E. Ochiai, *J. Inorg. Nucl. Chem.*, **35**, 1727 (1973).
8) E. Ochiai, *ibid.*, **35**, 3375 (1973).
9) G. Wada, N. Yoshizawa, and Y. Sakamoto, This Bulletin, **44**, 1018 (1971).
10) R. H. Bailes and M. Calvin, *J. Amer. Chem. Soc.*, **69**, 1886 (1947).
11) G. Wada, This Bulletin, **41**, 882 (1968).
12) M. Mori and J. A. Weil, *J. Amer. Chem. Soc.*, **89**, 3732 (1967).
13) J. Simplicio and R. G. Wilkins, *ibid.*, **91**, 1325 (1969).

The Photochemical Reaction of Benzofuran Derivatives with Benzophenone or Benzaldehyde

Yoshiyuki KAWASE, Seiji YAMAGUCHI, Hirokazu OCHIAI, and Hisanori HORITA

Department of Chemistry, Faculty of Literature and Science, Toyama University, Gofuku, Toyama 930

(Received February 15, 1974)

The photochemical reaction of 2-methyl-, 2,3-dimethyl-, 2,3-butano-, and 2-hydroxymethyl-benzofuran with benzophenone gave the corresponding oxetanes in yields higher than, or comparable to, those in the case of unsubstituted benzofuran, but in lower yields than in the cases of 3-methyl- and 2-isopropyl-benzofuran. The oxetanes were also produced by the reaction of 2-methyl-, 2,3-dimethyl-, and 2,3-butano-benzofuran with benzaldehyde, but these yields were not so high because of their instability. The reaction of 2-methoxycarbonyl- and 2-cyano-benzofuran with benzophenone or benzaldehyde gave dimers of the benzofurans, as in the case of 2-phenylbenzofuran.

It has been reported that the photochemical reaction of furan derivatives with carbonyl compounds furnished the oxetanes;[1] also, a similar reaction of benzofuran with benzophenone or benzaldehyde furnished the oxetane, while benzofuran with acetone or acetophenone as well as 2-phenylbenzofuran with benzophenone or benzaldehyde furnished the cyclo-dimer of the benzofuran.[2] Now in the present experiments, the reaction of 2-, 3-, and 2,3-substituted benzofurans (**1**) with benzophenone (**2**) or benzaldehyde (**3**) was studied in order to investigate the effect of the substituents.

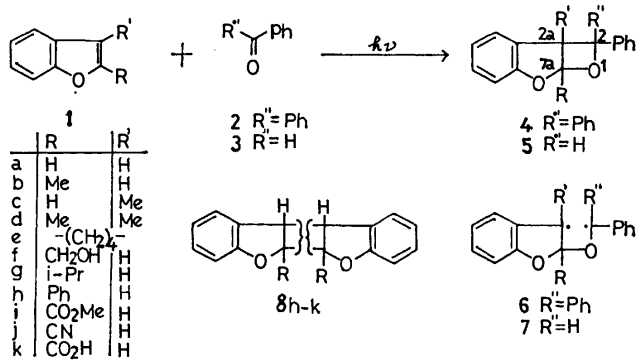

	R	R'
a	H	H
b	Me	H
c	H	Me
d	Me	Me
e	-(CH2)4-	
f	CH2OH	H
g	i-Pr	H
h	Ph	H
i	CO2Me	H
j	CN	H
k	CO2H	H

A benzene solution of a benzofuran derivative (**1a—j**) and benzophenone (**2**) or benzaldehyde (**3**) was irradiated for several hours by means of a 100 W high-pressure mercury lamp in a nitrogen atmosphere, the solvent was removed *in vacuo*, and the residual product was crystallized. In several cases, the reaction rate was checked by NMR spectroscopy. It was found that the reaction mixture contained only one kind of product and the starting materials, and that the yield of the product reached a maximum at about 20 hr irradiation in the case of **1a**, **b**, and **d** with **2**, while it reached a maximum at about 8 hr irradiation in the case of **1a**, **b**, and **d** with **3**. Therefore, the reaction was stopped at those times. The reaction of **1b**, **d**, **e**, and **f** with **2** furnished the corresponding oxetanes (**4b**, **d**, **e**, and **f**) in yields higher than, or comparable to, those in the case of benzofuran[2] (**1a**), but **1c** and **1g** furnished the oxetanes (**4c** and **4g**) in low yields only. In the case of the reaction of **1a—e** with **3**, a fairly large amount (about a 60% yield) of the oxetane (**5a—e**) was detected in the reaction mixture. However, not much of the pure product was isolated because of the instability of the oxetane; particularly the pure **5c** could not be isolated.

The structures of the oxetanes (**4** and **5**) were determined by elemental analyses and by spectroscopy (IR, NMR, and Mass), particularly by comparing their NMR data with those[2] of **4a** and **5a**. That is, the structures of **4b**, **4f**, **4g**, and **5b** were determined by means of the fact that the chemical shifts of 2a-H of **4b**, **4f**, **4g** (δ=4.56, 5.02, 4.82) and of **5b** (δ=3.83) were comparable with those of **4a** (δ=4.97) and **5a** (δ=4.12) respectively. Also, the structure of **4c** was determined by means of the chemical shift of 7a-H (δ=6.21) being comparable with that of **4a** (δ=6.50). Upon the basis of these data, the structure of **4d** was determined by means of the fact that the chemical shifts of 2a- and 7a-methyl hydrogen (δ=1.65 and 1.64) were comparable with those of **4c** and **4b** (δ= 1.40 and 1.61) respectively, while the structure of **5d** was determined by means of the fact that the shift of 7a-methyl hydrogen (δ=1.64) was comparable with that of **5b** (δ=1.75). Further, **4e** and **5e** were considered to have the structures shown in the chart by analogy to the cases of **4d** and **5d**. The configuration of the oxetanes (**5**) at the C_2-position has not yet been determined, but it seemed that the C_2-phenyl groups of **5a** and **5b** might be *cis* to the 2a-H, by analogy to the case of the oxetane produced from furan and benzaldehyde.[1g]

In the present reaction, the intermediate biradical, **6** or **7**, may be formed by the electrophilic attack of the oxygen radical of the excited triplet state of the carbonyl group, and the oxetane may be formed by the intra-molecular coupling of the biradical, as in the case of the reaction of furan derivatives with carbonyl compounds.[1] The alkyl groups (R and R') on the furan ring may facilitate the attack of the oxygen radical and increase the stability of the intermediate biradical; they may thus favor the formation of the oxetane. Indeed, in the reaction of the benzofuran derivative with benzophenone, the yields of the oxetane formation in the case of **4b**, **d**, and **e** are much higher than those of unsubstituted benzofuran. However, it seems necessary to consider the steric hindrance in order to explain the low yields of **4g** and **4c** and the yield of **4d** being lower than that of **4b**. In the reaction of the benzofuran derivative with benzaldehyde, the yield of the oxetane is not very high, and the oxetane is unstable on standing. It seems that these facts are

Table 1. The photo-chemical reaction

Starting compounds	Reaction time (hr)	Product (yield, %)	Mp °C (solvent[i])	NMR: δ (ppm) of H of R	R′	R″	solv.	Mass M^+ (m/e)
1a+**2**	20	**4a**(27[ii])	133—134[ii] (Me)	6.50[ii]	4.97[ii]		$CDCl_3$	300
1b+**2**	20	**4b**(79)	130—132 (Pe)	1.61	4.56		$CDCl_3$	314
1c+**2**	51	**4c**(2)	157—158.5 (Cy)	6.21	1.40		CCl_4	314
1d+**2**	20	**4d**(62)	193—194 (Cy)	1.65	1.43		$CDCl_3$	328
1e+**2**	20	**4e**(44)	174.5—176 (Cy)	2.75—0.90			$CDCl_3$	354
1f+**2**	20	**4f**(27)	164—165 (Ac)	3.83, 1.85	5.02		$CDCl_3$	330
1g+**2**	20	**4g**(6)	137.5—138.5 (Cy)	2.14, 1.03, 0.94	4.83		$CDCl_3$	342
1a+**3**	8	**5a**(30[iii])	96—97[iii] (Me)	6.60[iii]	4.12[iii] (J=3.4[iii])	5.45[iii]	$CDCl_3$	224
1b+**3**	8	**5b**(39)	78—81 (Pe)	1.75	3.83 (J=4.0)	5.32	CCl_4	238
1d+**3**	8	**5d**(42)	92—93 (Cy)	1.64	0.94	5.45	CCl_4	252
1e+**3**	8	**5e**(11)	83—84 (Me)	2.85—0.90		5.72	$CDCl_3$	iv)
1h+**2**	65	**8h**(1.5[v])	265—266[v] (Cl)		4.80[v]		$CDCl_3$	388
1h+**3**	12	**8h**(2[v])	265—266[v] (Cl)		4.80[v]		$CDCl_3$	388
1i+**2**	20	**8i**(2)	258—259 (Ac)	3.55	4.96		CF_3CO_2H	352
1i+**3**	20	**8i**(2)	258—259 (Ac)	3.55	4.96		CF_3CO_2H	352
1j+**2**	15	**8j**(27)	276.5—277.5 (Ac)					286
1j+**3**	15	**8j**(10)	276.5—277.5 (Ac)					286

i) Ac=acetone, Cl=chloroform, Me=methanol, and Pe=petroleum ether. ii) *Cf.* Ref. 2. Lit, mp 132 °C. iii) *Cf.* Ref. 2. Lit, mp 95—96 °C. iv) This was not detectable. v) *Cf.* Ref. 2. Lit, mp 279—280 °C.

due to the formation of the not-very-much-stabilized intermediate biradical, **7**; the stabilizing effect of the R and R′ groups is not great enough to improve the stability of **7**.

The reaction of 2-methoxycarbonyl- and 2-cyanobenzofuran (**1i** and **1j**) with **2** or **3** gave dimers (**8i** and **8j**) of the benzofurans in low yields, much as in the case of 2-phenylbenzofuran[2] (**1h**). The hydrolysis of **8i** as well as **8j** gave the same carboxylic acid, **8k** (**8**(R=CO_2H)). The structures of **8h**—**k** have not yet been established. In the reaction of **1i** and **1j** with **2** or **3**, it seems that the energy level of the excited benzofuran derivative is lowered by conjugation with the substituent, and **1i** and **1j** receive energy from the excited carbonyl compound to react with another molecule of **1i** and **1j**, the carbonyl compound having been used as a sensitizer.

Experimental

The melting points were not corrected; the IR spectra were measured on a Hitachi EPI-S spectrophotometer, the NMR spectra, on a JEOL JNM-C-60H (60 MHz) spectrometer, and the mass spectra, on a JEOL JMS-OIS spectrometer. The data are summarized in the tables.

Materials. The benzofuran[3] (**1a**), 2-methylbenzofuran[4] (**1b**), 3-methylbenzofuran[5] (**1c**), 2,3-dimethylbenzofuran[6] (**1d**), 2,3-butanobenzofuran[7] (**1e**), 2-benzofuranylmethyl alcohol[8] (**1f**), 2-phenylbenzofuran[9] (**1h**), methyl 2-benzofurancarboxylate[8] (**1i**), and 2-benzofurancarbonitrile[10] (**1j**) were prepared by the literature procedures. The 2-isopropylbenzofuran (**1g**) was prepared by the action of diethyl isopropylmalonate on salicylaldehyde, as will be reported later.

The Photochemical Reaction of the Benzofuran Derivative (1) with Benzophenone (2) or Benzaldehyde (3). A benzene solution of **1** and **2** or **3** (each 0.02 mol in 200 ml of benzene) was irradiated by means of a 100 W high-pressure mercury lamp through a Pyrex jacket (Rikosangyo Co.) in a nitrogen atmosphere at 20—25 °C for several hours, as is shown in the table. The solvent was then removed *in vacuo*, and the residual product was crystallized from the solvent shown in the table.

Table 2. Elemental analyses of the new compounds

Compound	Found (%) C	H	N	Formula	Calcd (%) C	H	N
4b	84.25	5.61		$C_{22}H_{18}O_2$	84.05	5.77	
4c	84.26	5.80		$C_{22}H_{18}O_2$	84.05	5.77	
4d	84.40	6.24		$C_{23}H_{20}O_2$	84.12	6.14	
4e	84.71	6.20		$C_{25}H_{22}O_2$	84.71	6.26	
4f	80.19	5.43		$C_{22}H_{18}O_3$	79.98	5.49	
4g	84.28	6.52		$C_{24}H_{22}O_2$	84.17	6.47	
5b	80.86	5.86		$C_{16}H_{14}O_2$	80.64	5.92	
5d	80.65	6.66		$C_{17}H_{16}O_2$	80.92	6.39	
5e	81.72	6.52		$C_{19}H_{18}O_2$	81.98	6.52	
8i	68.26	4.56		$C_{20}H_{16}O_6$	68.18	4.58	
8j	75.70	3.50	9.83	$C_{18}H_{10}O_2N_2$	75.51	3.52	9.79
8k	66.68	3.73		$C_{18}H_{12}O_6$	66.67	3.73	

The Hydrolysis of 8i. A mixture of **8i** (0.2 g), 50% aqueous potassium hydroxide (2 g), and methanol (2 ml) was refluxed for 3 hr. The reaction mixture was then treated as usual, and the product was crystallized from acetone to give 0.1 g (50%) of an acid, **8k**; mp 332 °C (decomp.), ν_{max}^{KBr} cm^{-1}: 3450—2510 (OH), 1712 (CO).

The Hydrolysis of 8j. A mixture of **8j** (0.5 g), 50% aqueous potassium hydroxide (6 g), and ethylene glycohol (5 ml) was heated at 100 °C for 8 hr. The reaction mixture was then diluted with water and acidified. The precipitates thus obtained were crystallized from acetone to give 0.15 g (26%) of **8k**, identical with the other sample.

References

1) a) G. O. Schenck, W. Hartmann, and R. Steinmetz, *Chem. Ber.*, **96**, 498 (1963); b) G. S. Hammond and N. J. Turro, *Science*, **142**, 1541 (1963); c) S. Toki, K. Shima, and H. Sakurai, This Bulletin, **38**, 760 (1965); K. Shima and H. Sakurai, *ibid.*, **39**, 1809 (1966); S. Toki and H. Sakurai, *Tetrahedron Lett.*, **1967**, 4119; d) J. Leitich, *ibid.*, **1967**, 1937; e) C. Rivas and E. Payo, *J. Org. Chem.*, **32**, 2918 (1967); f) M. Ogata, H. Watanabe, and H. Kano, *Tetrahedron Lett.*, **1967**, 533; g) G. R. Evanega and E. B. Whipple, *ibid.*, **1967**, 2163; E. B. Whipple and G. R. Evanega, *Tetrahedron*, **24**, 1299 (1968).

2) C. H. Krauch, W. Metzner, and G. O. Schenck, *Chem. Ber.*, **99**, 1723 (1966).

3) A. W. Burgstahler and L. R. Worden, "Organic Syntheses," Vol. 46, p. 28 (1965).

4) T. Abe and T. Shimizu, *Nippon Kagaku Zasshi*, **91**, 753 (1970).

5) W. R. Boehme, "Organic Syntheses," Coll. Vol. IV, p. 590, (1963).

6) E. Bisagni and R. Royer, *Bull. Soc. Chim. France*, **1962**, 925.

7) F. Ebel, *Helv. Chim. Acta*, **12**, 3 (1929).

8) B. I. Nurunnabi, *Pakistan J. Sci. Ind. Research*, **3**, 108 (1960) (*Chem. Abstr.*, **55**, 25903 (1961)).

9) S. Kawai, T. Nakamura, and N. Sugiyama, *Chem. Ber.*, **72**, 1146 (1939).

10) L. Roné and R. Royer, *Bull. Soc. Chim. France*, **1971**, 4329.

Acetoxythallation of Acetylenes and the Proto- and Halogenodethallation of the Products

Sakae UEMURA, Hideyuki TARA, Masaya OKANO, and Katsuhiko ICHIKAWA*

Institute for Chemical Research, Kyoto University, Uji, Kyoto 611

**Department of Hydrocarbon Chemistry, Faculty of Engineering, Kyoto University, Sakyo-ku, Kyoto 606*

(Received March 29, 1974)

The *trans* acetoxythallation of alkylphenylacetylene with $Tl(OAc)_3$ proceeds in acetic acid at 50—75 °C for 1—3 hr to give a mixture of two isomeric vinylthallium(III) compounds in 54—79% yields, 2-acetoxy-1-alkyl-2-phenyl- and 2-acetoxy-2-alkyl-1-phenylvinylthallium(III) diacetates [$C_6H_5C(OAc)=C(R)-Tl(OAc)_2$ (**1**) and $C_6H_5C(Tl(OAc)_2)=C(OAc)R$ (**2**), where R=Me, Et, *n*-Pr, and *n*-Bu]. Protodethallation of **1** and **2** in refluxing acetic acid occurs with retention of configuration to afford $C_6H_5C(OAc)=C(R)H$ (**3**) and $C_6H_5CH=C(OAc)R$ (**4**), respectively. The reaction of **1** and **2** with $NaBH_4$ in protic solvents at pH 6—7 also gives **3** and **4** with retention of configuration, where the hydrogen for replacement of thallium group comes almost completely (>98%) from the solvent. **1** and **2** are relatively stable to water and dilute HCl, while they readily give ketones in alkaline condition. Halogeno-, cyano-, and thiocyanodethallations of **1** is conducted by reactions with the corresponding copper(II) or (I) salts in acetonitrile to give $C_6H_5C(OAc)=C(R)X$ (X=I, Br, Cl, CN, and SCN) with retention of configuration. Bromodethallation of **1**(R=CH_3) by bromine gives $C_6H_5C(OAc)=C(CH_3)Br$ stereospecifically in pyridine (retention), while α,α-dibromopropiophenone is obtained in CS_2 and acetonitrile.

Oxymercuration and oxythallation of olefins give stable β-alkoxyalkylmercury and β-alkoxyalkylthallium compounds, respectively.[1,2] Oxymercuration of acetylenes affords the β-alkoxyvinylmercury compounds.[3] Although the reaction pathways through oxythallation of acetylenes were postulated in the hydration[4] and oxidation[5] reactions of acetylenes with thallium(III) salts, there has been no report on the successful isolation of oxythallated compounds (the oxythallates) of acetylenes by direct reaction between acetylenes and thallium (III) salts. Recently, Uemura *et al.*[6] and Sharma and Fellers[7] succeeded independently in isolating the oxythallates from alkylphenylacetylenes and dialkylacetylenes, respectively. The thallium group of oxythallates of olefins was replaced by halogens and pseudohalogens by use of the corresponding copper salts[8] and by hydrogen in the reduction with $NaBH_4$ in protic solvents.[9] Arylthallium compounds reacted similarly with such reagents to give aryl halides[10] and pseudohalides.[11] It seems worthwhile examining how the vinylic C–Tl bond of the oxythallates of acetylenes acts towards these reagents in order to compare the nature of the various kinds of C–Tl bonds. We report herewith on the preparation of the oxythallates of alkylphenylacetylenes and also the results of some reactions of the isolated vinylthallium compounds with acetic acid, $NaBH_4$, alkali, halogens, and copper halides, cyanide and thiocyanate.

Results and Discussion

Preparation of Acetoxythallated Compounds of Alkylphenylacetylenes, 1 and 2. Methyl-, ethyl-, *n*-propyl-, and *n*-butyl-phenylacetylenes reacted with $Tl(OAc)_3$ in acetic acid at 50—75 °C for 1—3 hr to give an isomeric mixture of 2-acetoxy-1-alkyl-2-phenylvinylthallium diacetate (**1**) and 2-acetoxy-2-alkyl-1-phenylvinylthallium diacetate (**2**) in 54—79% yield as in the following. The yield of products decreased with an increase in the bulkiness of the alkyl group. The isomer ratios (**1**:**2**) determined by treatment with $NaBH_4$ were 2.8—

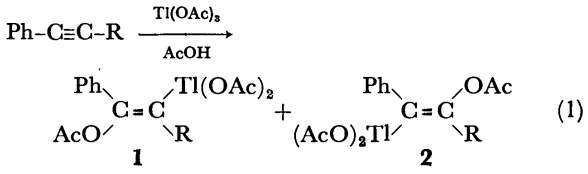

(1)

2.5 for Me, 1.9—1.8 for Et, *n*-Pr, and *n*-Bu. A mixture of **1** and **2** was isolated as white amorphous solids, stable in air and soluble in polar solvents, which were recrystallized from alcohols, acetone, CCl_4, 1,2-dichloroethane and benzene. Separation of each isomer was achieved by careful recrystallization from suitable solvents such as methanol, ethanol or diethyl ether. Each of the isomers **1** (R=Me), **1** (R=Et), and **2** (R=Et) was separated in a pure form, but it was not possible to separate either of **1** or **2** having the *n*-propyl or *n*-butyl group. The reaction conditions for the preparation of **1** and **2**, isolated yields, isomer ratios of **1** to **2**, melting points, and analytical data are summarized in Table 1.

The IR spectra (paraffin and hexachlorobutadiene mulls) of **1** and **2** showed strong absorption bands at 1760 and 1640 cm^{-1} due to vinyl ester group, $\nu_{C=O}$ and $\nu_{C=C}$ respectively, together with many bands in the acetate region [1600 (sh), 1560 (s), 1515 (s), 1420 (s, broad), and 1365 (m) cm^{-1}] which can be assigned to both the bridging and non-bridging acetate groups as has been discussed in the cases of aryl- and alkylthallium diacetates.[8,12]

Assignment of the structures of **1** and **2** was best carried out by NMR spectra (in CD_3OD). Coupling constants between Tl and the protons of the methyl or methylene group at allylic position in **1** were 976—1316 Hz, while those in **2** were 116—142 Hz. The values are quite reasonable considering the results reported by Maher and Evans in various organothallium compounds.[13] The aromatic ring protons were coupled with Tl in **2**, J_{Tl-o-H} and J_{Tl-m-H} being 126 and 64 Hz respectively, in contrast to the nearly singlet peak in **1**, showing that Tl was attached to the carbon α and β to phenyl group in **2** and **1**

TABLE 1. ACETOXYTHALLATION OF ALKYLPHENYLACETYLENES

Ph-C≡C-R R (mmol)	Tl-$(OAc)_3$ (mmol)	AcOH (ml)	Temp. (°C)	Time (hr)	Products, Yield (%)[a] 1+2	Ratio[b] 1/2	mp(d) (°C)	Analysis Found (Calcd) C	H
CH_3 20	10	10	65	1	75 (89)	2.5	1 169—171	36.28 (36.20)	3.40 (3.44)
CH_3 10	5	5	60	2	79 (87)	2.8	1+2 135—141	35.95 (36.20)	3.40 (3.44)
C_2H_5 20	10	10	65	2	70 (85)	1.8	1 133—135	37.75 (37.56)	3.72 (3.74)
							2 133—134	37.30 (37.56)	3.72 (3.74)
C_2H_5 20	10	10	60	3	71 (85)	1.8	1+2 104—114		
n-C_3H_7 20	10	10	65	3	66 (85)	1.9	1+2 120—126	38.73 (38.84)	4.23 (4.03)
n-C_4H_9 20	10	10	65	3	54 (73)	1.9	1+2 95—105	39.70 (40.06)	4.31 (4.30)

a) Based on $Tl(OAc)_3$ charged. Yields in parentheses were based on $Tl(OAc)_3$ consumed. b) Determined by hydrogenolysis with $NaBH_4$ in methanol.

respectively. The methyl protons of acetoxy group appeared as a doublet (J=13 Hz). This can be attributed to long-range coupling with Tl ($^6J_{Tl-H}$= 3.0 Hz was reported[14]) or through-space coupling with Tl. Since the coupling constant of 142 Hz (J_{Tl-CH_3}) in **2** (R=Me) agrees with that of 144 Hz between Tl on C_3 and methyl protons on C_2 in the 2-acetoxy-3-diacetoxythallium-*trans*-2-butene[7] where acetoxy (on C_2) and thallium (on C_3) are in *trans* position, we may assign the structure of **2** to the *trans*-acetoxythallate. From the NMR data and the structure of **2**, it seems reasonable to assign the structure of **1** as another *trans*-acetoxythallate. We also confirmed this configuration by protolysis and hydrogenolysis of **1**. Structures of **1** and **2** suggest that acetoxythallation proceeded completely in a *trans* fashion at least in the case of alkylphenylacetylenes. In contrast, Sharma and Fellers[7] obtained a mixture of *trans*- and *cis*-acetoxythallates from dimethylacetylene, but they observed at the same time the formation of only the *trans*-isomer from diethylacetylene. The bulkiness of substituent on acetylenes seems to affect the mode of addition of thallium-(III) salt to triple bond.

When the reaction mixture was refluxed for 2 hr in acetic acid after being kept at 65 °C for 1 hr, none of **1** and **2** was isolated, various organic products being obtained instead. Thus, from methylphenylacetylene, a mixture of 1-acetoxy-*trans*-1-phenylpropene [**3**(R=Me)], 2-acetoxy-*trans*-1-phenylpropene [**4**(R=Me)],

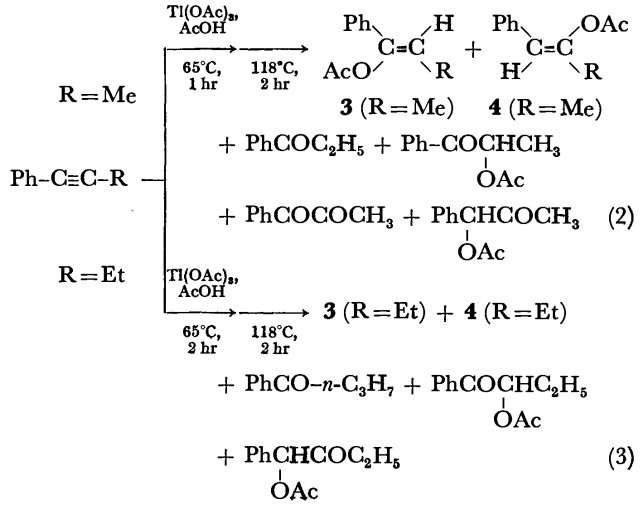

propiophenone, α-acetoxypropiophenone, 1-phenyl-1,2-propanedione, and 1-acetoxy-1-phenylacetone was obtained as shown below, **3** and **4** being the main products. Similarly, 1-acetoxy-*trans*-1-phenylbutene [**3**(R=Et)], 2-acetoxy-*trans*-1-phenylbutene [**4**(R=Et)], butyrophenone, acetoxybutyrophenone and 1-acetoxy-1-phenyl-2-butanone were the identified products from the reaction of ethylphenylacetylene. Here, **3** and **4** may be formed by protolysis of the intermediate acetoxythallates **1** and **2** by the solvent, while products other than **3** and **4** were found to be formed by the subsequent oxidation reaction of **3** and **4** with $Tl(OAc)_3$. In these reactions all of $Tl(OAc)_3$ was reduced to the thallium(I) salt, due partly to the oxidation of **3** and **4** and partly because of that of acetic acid solvent.[15]

From *t*-butylphenylacetylene (R=*t*-Bu) and diphenylacetylene (R=Ph), none of **1** and **2** was isolated by being stirred at 65 °C for 1—3 hr, and even under more drastic reaction conditions (at refluxing temperature for 4—24 hr) acetylenes were recovered almost quantitatively together with small amounts of the oxidation products. Several attempts to isolate **1** and **2** (or the methoxythallates) from the reaction of methylphenyl- or ethylphenylacetylenes with $Tl(OAc)_3$ in methanol solvent were unsuccessful under stirring at 25 °C for 5 hr, acetylenes being recovered in all cases. At refluxing temperature for 4 hr only the oxidation product, methyl 2-phenylpropionate,[16] was obtained in 50% yield from methylphenylacetylene as in the case of the reaction with $Tl(NO_3)_3$.[5]

Protodethallation of 1 and 2 by Acetic Acid. In order to confirm the possibility that various organic products (Eqs. (2) and (3)) were formed *via* the acetoxythallates of acetylenes, **1** or a mixture of **1** and **2** was heated in refluxing acetic acid for 2 hr. It was found that **1**(R=Me) gave **3**(R=Me) as the main product together with propiophenone, α-acetoxypropiophenone, and 1-phenyl-1,2-propanedione, while a mixture of **1**(R=Me) and **2**(R=Me) afforded **4**(R=Me) and 1-acetoxy-1-phenylacetone in addition to the four products. All the products were the same as those obtained directly from methylphenylacetylene. Similarly, a mixture of **1**(R=Et) and **2**(R=Et) gave the same products as those in Eq. (3), **3**(R=Et) and **4**(R=Et) being the main products. All the products other than **3** and **4** were formed by oxidation of **3** and **4** with $Tl(OAc)_3$; for example, **3**(R=Me) gave α-acetoxypropiophenone

as the main product together with small amounts of propiophenone and 1-phenyl-1,2-propanedione. A mixture of **3**(R=Me) and **4**(R=Me) afforded the above three compounds and 1-acetoxy-1-phenylacetone. A report was given on the α-acetoxylation and α,α-diacetoxylation (sometimes isolated as α-diketone) of ketones with $Tl(OAc)_3$ in acetic acid.[17] It was confirmed that propiophenone, butyrophenone, and phenylacetone reacted with $Tl(OAc)_3$ to give α-acetoxylated compounds and α-diketones (see Experimental). We might conclude that protolysis of **1** and **2** with acetic acid gives **3** and **4** followed by their subsequent oxidation with regenerated $Tl(OAc)_3$, and consequently that all the various products shown in Eqs. (2) and (3) were formed *via* acetoxythallation of acetylenes. The fact that *trans*-acetoxythallates gave exclusively **3** and **4** (where phenyl and alkyl are in *trans*-position) without formation of the *cis*-isomers indicates protodethallation to be completely stereospecific. In addition to the fact that proto- or halodemetallation and metal-metal exchange reaction of vinyl metal compounds (such metals as Hg, Sb, Sn, Li, and B) proceed electrophilically with retention of configuration,[18] deuteriodeboronation of vinylboron compounds by deuterioacetic acid[19] and also protolysis of vinylcopper compounds[20] proceed with complete retention of configuration. The results of protodethallation support the conclusion that acetoxythallation of alkylphenylacetylenes to form **1** and **2** proceeds completely in a *trans* fashion.

In contrast to facile protodethallation in acetic acid, **1** and **2** are stable in water and in aqueous HCl. For example, **1**(R=Me) gave **3**(R=Me) (5% yield), propiophenone (2%), α-acetoxypropiophenone (3%) together with methylphenylacetylene (4%) as the products only after refluxing for 3 hr. When **1**(R=Me) was treated with aqueous ethanol containing HCl (*ca.* 0.5 M) at 20 °C for 3 hr, hardly any reaction occurred. The almost quantitative protodethallation in acetic acid and the stability toward water and aqueous HCl seem to be a characteristic feature of the acetoxythallates of acetylenes. The alkoxythallates of olefins were solvolyzed with acetic acid and water to give oxidation products of olefins and no protodethallated compounds, while deoxythallation affording starting olefins occurred easily with aqueous ethanolic HCl.[8] It should be noted[21] that protolysis of various organoboranes proceeded smoothly by carboxylic acids with retention of configuration, but not by strong mineral acids, and that the unique effectiveness of carboxylic acids is attributed to the capability of boron of coordinating at the oxygen of the carbonyl group. We might assume that protolysis of vinylthallium compounds proceeds similarly to give **3** and/or **4** with

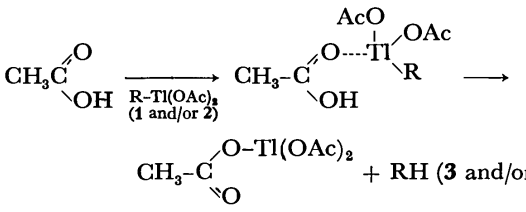

(4)

retention of configuration according to the following scheme, namely through coordination of thallium with the oxygen of the carbonyl group, and regenerated $Tl(OAc)_3$.

Table 2. Reaction of **1** and **2** with $NaBH_4$ in protic solvents at 0 °C for 1 hr

Tl compounds (mmol)			$NaBH_4$ (mmol)	Solvents (ml)	pH	Products and yield (%)[a]						
1 (R=Me)	**2**	**1**/**2** [b]				Methylphenylacetylene	**3**	**4** (R=Me)	**3D**	**4D**	Propiophenone	Phenylacetone
1	3	—	1.5	CH_3OH(20)	6— 7	3	85	0	—	—	trace	0
1	3	—	0.75	CH_3OH(20)	6— 7	3	69	0	—	—	trace	0
1+**2**	7.5	2.8	5	CH_3OH(40)	6— 7	3	66	24	—	—	trace	0
1+**2**	3.5	2.8	0.35	CH_3OH(30)	6— 7	3	18	8	—	—	trace	0
1	2	—	1	THF(20)+H_2O(20)	6— 7	4	84	0	—	—	trace	0
1+**2**	2	0.8	1	THF(10)+H_2O(10)	6— 7	4	42	53	—	—	trace	trace
1	3	—	0.75	CH_3OH(15)+3M-NaOH(5)	12—13	trace	trace	0	—	—	87[c]	0
1+**2**	2	0.8	0.5	CH_3OH(15)+3M-NaOH(5)	12—13	4	0	0	—	—	41	50
1	2	—	0	CH_3OH(15)+3M-NaOH(5)	12—13	trace	0	0	—	—	100	0
1+**2**	2	0.8	0	CH_3OH(15)+3M-NaOH(5)	12—13	3	0	0	—	—	41	12
1	5	—	2.5	CH_3OD(20)	6— 7	5	2	0	85	0	trace	0
1+**2**	5	0.8	2.5	THF(10)+D_2O(10)[d]	6— 7	3	1	1	39	47	trace	0
1	5	—	$NaBD_4$ 2.5	CH_3OH(20)	6— 7	2	90	0	<1	0	trace	0

a) Based on Tl compounds charged. b) Determined by NMR. c) 1-Phenylpropanol was obtained in 5% yield. d) React. Temp., 5 °C.

Hydrogenolysis of 1 and 2 by the Reaction with $NaBH_4$ in Protic Solvents. Hydrodemercuration of the oxymercurials of olefins by alkaline $NaBH_4$ reduction affording alcohols, ethers and amines *etc.* has been a current topic in the field of oxymetallation (solvomercuration-demercuration).[22,23] Oxymercuration of acetylenes and subsequent demercuration (*in situ*) by $NaBH_4$ gave ketones in an alkaline condition,[24] and enol acetates, enol ethers, and amines in a neutral condition.[25] The alkoxythallates of styrene were reduced by methanolic $NaBH_4$ especially in an alkaline condition to give styrene, α-alkoxyethylbenzenes and dialkylthallium salts, where styrene (the deoxythallation product) was the main product.[9] The hydrogen for replacement of thallium came from the solvent in contrast to the reduction of the oxymercurials of olefins where the hydrogen of $NaBH_4$ was used for hydrodemercuration.[23] In order to see how the thallium group of the oxythallates of acetylenes is replaced by hydrogen in the reaction with $NaBH_4$, **1** or a mixture of **1** and **2** was treated with $NaBH_4$ in various solvents such as methanol, aqueous methanol and aqueous THF at 0 °C for 1 hr. Some typical results are summarized in Table 2. In a neutral or slightly acidic condition (pH 6—7), **3**(R=Me) was obtained from **1**(R=Me) in a good yield together with a small amount of methylphenylacetylene (the deoxythallation product). Similarly a mixture of **1**(R=Me) and **2**(R=Me) was reduced to a mixture of **3**(R=Me) and **4**(R=Me) in methanol in more than 90% yield as shown in the following.

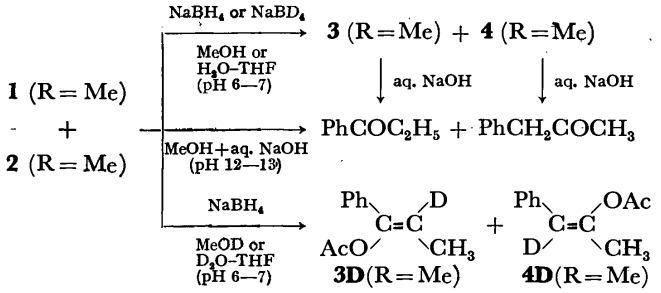

(5)

Since an isomer ratio of the products **3**(R=Me) and **4**(R=Me) was nearly the same as that of **1**(R=Me)/**2**(R=Me) determined by NMR, this reduction method was used for determining the ratios of **1** to **2** in the mixtures of the crude acetoxythallates of acetylenes (Table 1). In an alkaline condition (pH 12—13), **1**(R=Me) and a mixture of **1**(R=Me) and **2**(R=Me) afforded propiophenone and a mixture of propiophenone and phenylacetone, respectively, almost quantitatively. It was confirmed that **3**(R=Me) and **4**(R=Me) were readily hydrolyzed in this alkaline condition to propiophenone and phenylacetone respectively. It was also revealed that both **1**(R=Me) and **2**(R=Me) reacted with aqueous alkali to give the corresponding ketone even in the absence of $NaBH_4$ (Eq. (5)), the only difference being that the yield of **4** was lower in the absence of $NaBH_4$ than that in its presence. It is conceivable that **1** and **2** were solvolyzed in the reaction without $NaBH_4$ to the corresponding α-thallated ketones followed by hydrodethallation to give propiophenone and phenylacetone. Thus in the alkaline $NaBH_4$ reduction of **1** and **2**, both reaction routes would be operative.

When the reaction was carried out with $NaBD_4$ in methanol, hardly any deuterium incorporation was observed in the products, while the reaction with $NaBH_4$ in deuterated solvent such as MeOD or D_2O nearly completely gave the deuterated products, 1-acetoxy-2-deuterio-*trans*-1-phenylpropene (**3D**) and 2-acetoxy-1-deuterio-*trans*-1-phenylpropene (**4D**) (Eq. (5)). This shows that the hydrogen for replacement of thallium group came almost completely from the solvent and not from $NaBH_4$ as in the case of the reduction of the alkoxythallates of styrene.[9] In the reduction of arylthallium bis(trifluoroacetates) with $NaBH_4$ in ethanol, Herbert[26] pointed out that 2—8% of the hydrogen for replacement of thallium group to afford aromatic hydrocarbons came from $NaBH_4$. In the case of the reduction of the oxythallates of olefins and acetylenes, however, we could obtain only a small amount (at most 2% by NMR) of the deuterated products from the reaction with $NaBD_4$ in methanol.

The following facts should be noted when considering the reaction scheme of the reduction in a neutral condition: The reaction proceeded completely stereospecifically with retention of configuration. The reaction with the use of $BF_3(MeOH)_2$ or $B(OCH_3)_3$ instead of $NaBH_4$ gave none of **3** and **4**. Although the hydrogen for replacement of the thallium group came from the solvent, $NaBH_4$ was necessary as a reactant and not as a catalyst. The alkaline $NaBH_4$ reduction of oxymercurials of olefins proceeds *via* formation of an organomercuric hydride (RHgH) which undergoes homolytic dissociation to produce R· and ·HgH radicals, and the hydrogen for replacement of mercury arises from $NaBH_4$ and not from the solvent.[23] If a similar reaction scheme is operative in the reduction of the acetoxythallates of acetylenes and the intermediate organothallium hydride gives the vinyl radicals, they should give a mixture of *cis*- and *trans*-isomers since the vinyl radicals interconvert rapidly and give the isomeric mixtures.[27] For example, the reaction of *trans*-chlorovinylmercury (II) chloride with iodine in DMSO gave completely *trans*-1-chloro-2-iodoethylene by S_E1 mechanism, while a similar reaction gave a mixture of *trans*- and *cis*-isomers (50:50) in CCl_4 or benzene under an irradiation of light by a free-radical

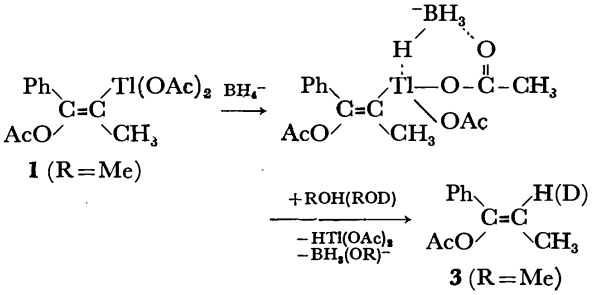

$$HTl(OAc)_2 \longrightarrow HOAc + TlOAc$$

$$1 + BH_3(OR)^- \xrightarrow{-HTl(OAc)_2} 3 + BH_2(OR)_2^-$$

$$\xrightarrow{1} 3 + BH(OR)_3^- \qquad (6)$$

mechanism.[28] Thus the radical reaction scheme may be excluded in our case. Considering the stereochemistry of the product we could assume that the reduction proceeds *via* an electrophilic substitution of thallium in vinylthallium compound by hydrogen or deuterium of the solvent, since the electrophilic substitution of metal in vinylmetal compounds by halogens, proton and metals proceed in almost all cases with retention of configuration, as shown in the scheme (6). This scheme shows why deuterium came from the solvent and not from $NaBD_4$. The borohydride might turn to oxyborohydride such as $B(OR)_4^-$ or $BH(OR)_3^-$. There is a possibility that $BH(OR)_3^-$ species becomes unreactive since the yields of **3** and/or **4** did not exceed 75% (based on $NaBH_4$ charged) in the reactions using a quarter or less mole of $NaBH_4$ and 1 mol of **1** and/or **2**. For example, the reaction of **1** (3 mmol) with $NaBH_4$ (0.75 mmol, 3 mmol equivalent H) gave 2.07 mmol of **3**, and the reaction with **1**+**2** (3.5 mmol) and $NaBH_4$ (0.35 mmol, 1.5 mmol equivalent H) gave 0.91 mmol of a mixture of **3** and **4** (Table 2). The result can be explained by assuming that three out of four hydrogens of BH_4^- were effective for reduction. We have observed similar phenomena in the $NaBH_4$ reduction of the alkoxythallates of styrene.[29]

Reaction of 1(R=Me) with Copper Salts and Halogens. Halogeno-, cyano-, and thiocyanodethallations proceed in the reactions of the arylthallium compounds[10,11] or the alkoxythallates of styrene[8] with copper halides, cyanides, and thiocyanates and in some case with iodine, bromine and potassium salts. In order to investigate whether a similar reaction occurs with the acetoxythallate of acetylene which has vinyl carbon–thallium bond, **1**(R=Me) was treated with copper(II) and (I) salts in various organic solvents. As shown in the following scheme thallium was replaced by iodide, bromide, chloride, cyanide and thiocyanate to give **5**, acetonitrile being chosen as the solvent.

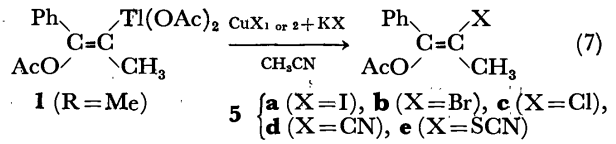

(7)

1 (R=Me) **5** {**a** (X=I), **b** (X=Br), **c** (X=Cl), **d** (X=CN), **e** (X=SCN)

Typical results are summarized in Table 3. Each of the products **5a**—**e** was found by glc and NMR to be uncontaminated with its geometrical isomer. **5a** and **5b** were identical with the products obtained by the reaction of **1** with molecular iodine (in CH_3OH) and bromine (in pyridine), where electrophilic substitution with retention of the configuration is the most plausible reaction scheme if we take into consideration the results of iodination[28] of vinylmercury compound in polar solvent and those of bromination of vinylmercuric bromide in pyridine.[30] We might thus conclude that all the products **5a**—**e** have the same configuration as that of the starting acetoxythallates of alkylphenylacetylenes.

Iododethallation proceeded with copper(I) iodide. Other reactions occurred with copper(II) salts in contrast to the case of the alkoxythallates of styrene having an alkyl carbon–thallium bond, where copper(I) salts were more effective for halogeno- and pseudohalogenodethallations. Although the reaction of **1**(R=Me) with KI afforded **5a** in a good yield, none of **5** was obtained by the use of other potassium salts. Satisfactory results were obtained for bromodethallation by copper salt by the reaction with $CuBr_2$ in the presence of KBr in acetonitrile. Other solvents such as dioxane, DMF, and methanol were also used for bromodethallation, but the yields of **5b** were low. There is a possibility that bromodethallation occurs with free bromine liberated by autodecomposition of $CuBr_2$ into Cu_2Br_2.[31] The result of the separate reaction of **1**(R=Me) with bromine in acetonitrile which gave α,α-dibromopropiophenone (**6**) and none of **5b**, however, excluded the above possibility and showed that $CuBr_2$ itself was

Table 3. Halodethallation of 1 with copper salts

1 (R=Me) (mmol)	Cu salt (mmol)		K salt (mmol)		Solvent (20 ml)	Temp. (°C)	Time (hr)	Products and yields (%) Methylphenylacetylene		**5**
2		0	KI	8	CH_3CN	80	2	trace	**a**	74
2	CuI	4		0	CH_3CN	80	2	4	**a**	40[b]
2	CuI	4	KI	8	CH_3CN	80	2	5	**a**	58
2	$CuBr_2$	4		0	CH_3CN	80	2	3	**b**	20
2	$CuBr_2$	4	KBr	8	CH_3CN	80	2	trace	**b**	50
2	$CuBr_2$	4	KBr	8	CH_3CN	20	24	trace	**b**	19
2	$CuBr_2$	4	KBr	8	Dioxane	100	2	3	**b**	40
2	$CuBr_2$	4	KBr	8	DMF	153	2	2	**b**	21[b]
2	$CuBr_2$	4	KBr	8	CH_3OH	65	2	3	**b**	14
2	$CuBr_2$	4	KBr	8	$CHCl_3$	61	2	0	**b**	2
2	CuBr	4	KBr	8	CH_3CN	80	2	6	**b**	1
2	$CuCl_2$	4	KCl	8	CH_3CN	80	2	trace	**c**	11
2	CuCl	4	KCl	8	CH_3CN	80	2	trace	**c**	1
2	$Cu(CN)_2$	4		0	CH_3CN	80	2	trace	**d**	15
2	CuCN	4		0	CH_3CN	80	2	trace	**d**	3
2	$Cu(NCS)_2$	4	KSCN	8	CH_3CN	80	2	trace	**e**	8
2	CuSCN	4	KSCN	8	CH_3CN	80	2	trace	**e**	trace

a) Based on **1** (R=Me) charged. b) **3** (R=Me) was obtained in 7% yield.

TABLE 4. HALODETHALLATION OF 1 WITH IODINE AND BROMINE

1 (R=Me) (mmol)	X_2 (mmol)	Solvent (20 ml)	Temp. (°C)	Time (hr)	Products and Yields (%)[a]		
					Methylphenylacetylene	5	6
2	I_2 4	CH_3OH	65	3	0	**a** 61	—
10	Br_2 20	Pyridine[b]	20	2	0	**b** 78	0
2	Br_2 4	CH_3CN	20	2	trace	0	82
2	Br_2 4	CH_3OH	20	2	1	**b** 23 **b'** 30	37
2	Br_2 4	CS_2	20	2	1	0	99
2	Br_2 2	CS_2	0	0.5	5	0	41
5b 2	Br_2 2	CH_3CN	20	2	0	**b**<1	>99

a) Based on **1** (R=Me) charged. b) 50 ml.

a reactant in the reaction with **1**. When a mixture of **1**(R=Me) and **2**(R=Me) was treated with $CuBr_2$, a mixture of **5b** and 2-acetoxy-1-bromo-*trans*-1-phenylpropene was obtained as expected. Other reactions such as chloro-, cyano-, and thiocyanodethallations proceeded with the corresponding copper(II) salts, but the yields of the products **5c—e** were low under the reaction conditions shown in Table 3.

In order to prepare an authentic sample of **5**, **1**(R=Me) was treated with iodine and bromine in suitable solvents. **1**(R=Me) reacted with iodine in methanol to give **5a**, while a mixture of **5b**, **6**, and another product (**5b'**, the isomer of **5b**; see Experimental) was obtained by the reaction with bromine. Only **5b** was obtained in pyridine in a good yield, while only **6** was obtained in carbon disulfide just as in the case of acetonitrile. The results of the reaction of **1** with halogens are summarized in Table 4. Since the alkoxythallates of styrene did not react with iodine and bromine,[8] the results show another example of the difference of reactivity between alkyl C–Tl and vinyl C–Tl bonds. The product in the reaction of **1**(R=Me) with bromine depends on the solvent which is in line with the reaction of vinylmercuric bromide.[30] In carbon disulfide, acetonitrile and methanol, the *trans*-addition of bromine to the double bond followed by *trans*-debromothallation may be operative in giving **5b'** which then reacts with another mole of bromine to afford **6**, as shown in the following.

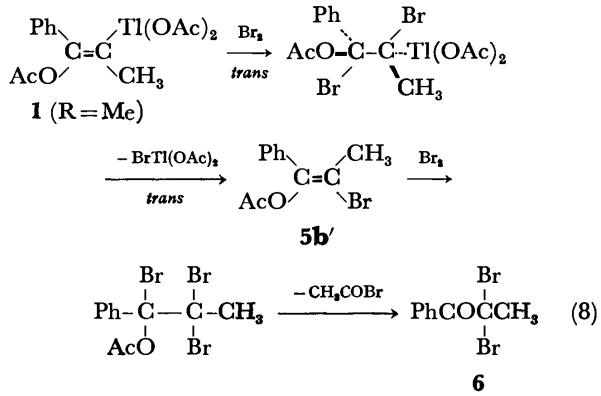

In pyridine, the coordination of pyridine to thallium may activate the C–Tl bond towards the electrophilic attack by bromine. We confirmed that **5b** reacts very easily with bromine in carbon disulfide and acetonitrile to give **6**, while in pyridine the reaction does not proceed under the reaction conditions where halodethallation by halogen was carried out.

Experimental

The IR spectra were taken with Hitachi EPI-S2 and JASCO IR-S spectrometers in paraffin and hexachlorobutadiene mulls. The NMR spectra were recorded with a Varian A-60 spectrometer in $CDCl_3$, CCl_4, or CD_3OD as solvents, using TMS as an internal standard. Glc analyses were carried out on Shimadzu 5APTF and 4BMPF apparatus, using PEG 6000(25%)-Chromosorb W (3m), Apiezon L (30%)-Celite (1m), DEGS(25%)-Shimalite (1m), and EGSS-X(30%)-Chromosorb W (1m) columns (N_2 as carrier gas).

Materials. The following alkylphenylacetylenes were prepared from sodium phenylacetylide and *p*-toluenesulfonic acid alkyl ester:[32] methylphenylacetylene, bp 76—77 °C/18 mmHg (lit,[33] bp 185 °C); ethylphenylacetylene, bp 88—89 °C/16 mmHg (lit,[33] bp 201—203 °C); *n*-propylphenylacetylene, bp 97—104 °C/17 mmHg (lit,[33] bp 102—103 °C/18.5 mmHg); *n*-butylphenylacetylene, bp 82—86 °C/2.5 mmHg (lit,[33] bp 119—121 °C/18 mmHg). *t*-Butylphenylacetylene was prepared from phenylacetylene, ethyl magnesium bromide, and *t*-butyl bromide,[34] bp 92—97 °C/19 mmHg (bp 94—95 °C/18 mmHg). Diphenylacetylene was prepared by the alkaline dehydrobromination of stilbene dibromide;[35] mp 60—61 °C (lit,[35] mp 60—61 °C). Other organic materials were purified before use by distillation. Commercial inorganic materials were used without further purification. $Cu(NCS)_2$ was prepared from $CuSO_4 \cdot 5H_2O$ and KSCN.[36] $Tl(OAc)_3$ was prepared by stirring Tl_2O_3 in acetic acid at 65 °C for 24 hr. All the deuterium compounds, $NaBD_4$ (98%, Merck), CH_3OD (99%, CEA) and D_2O (99.8%, CEA) were used without purification.

Preparation of Acetoxythallates of Acetylenes, 1 and 2. The following preparation of **1**(R=Me) and **2**(R=Me) shows a typical procedure. To a slightly heterogeneous solution of $Tl(OAc)_3$ (3.81 g, 10 mmol) in acetic acid (10 ml) was added methylphenylacetylene (2.3 g, 20 mmol) drop by drop at 65 °C under stirring to give a pale-green solution. When the mixture was kept at 65 °C for 1 hr the color of the solution turned dark green. The solution was cooled down and acetic acid was evaporated off at room temperature with a rotary evaporator. The white solids obtained were purified by dissolution into $CHCl_3$ to remove the insoluble unreacted $Tl(OAc)_3$ (0.63 g), and then by washing with *n*-hexane after evaporation of $CHCl_3$ to remove the unreacted methylphenylacetylene and small amounts of the oxidation products to give a crude mixture of **1**(R=Me) and **2**(R=Me) (3.7 g; 75 and 89% yields based on $Tl(OAc)_3$ charged and consumed respectively); **1**/**2**=2.5 (by NMR), mp 135—

145 °C. The mixture was recrystallized from ethanol-*n*-hexane (1 : 1) mixed solvent and analyzed. **1**(R=Me) (1.0 g) was separated by recrystallization twice from ethanol, several attempts to isolate **2**(R=Me) being unsuccessful. NMR (CD_3OD) of **1**(R=Me) δ 1.85 [s, 6H, $Tl(OCOCH_3)_2$], 2.15 (d, 3H, $\equiv C-CH_3$, $J_{^{205}Tl-H}$=986 Hz, $J_{^{203}Tl-H}$=976 Hz), 2.18 (d, 3H, acetoxy, J_{Tl-H}=13 Hz), 7.40 (s, 5H, phenyl). NMR (CD_3OD) of **2**(R=Me) determined from a mixture of **1** and **2** is as follows: δ 1.83 (d, 3H, acetoxy, J_{Tl-H}=13 Hz), 1.85 [s, 6H, $Tl(OCOCH_3)_2$], 2.30 (d, 3H, J_{Tl-H}=142 Hz), 7.2—7.3 (m, 5H, phenyl, J_{Tl-o-H}=125.5 Hz, J_{Tl-m-H}=64 Hz).

The reaction with ethylphenylacetylene gave an oily product on evaporation of acetic acid. After unreacted $Tl(OAc)_3$ was removed with $CHCl_3$, it was solidified by being left to stand in *n*-hexane for two days or by decantation with *n*-hexane several times to give 3.6 g of a mixture of **1**(R=Et) and **2**(R=Et). This was recrystallized from either CCl_4, benzene, acetone or ethanol-*n*-hexane. Extraction with ether afforded 0.4 g of pure **1**(R=Et). NMR (CD_3OD) of **1**(R=Et) δ 1.15 (m, 3H, $C\underline{H}_3CH_2$-, J_{H-H}=7 Hz, J_{Tl-H}=20 Hz), 1.87 [s, 6H, $Tl(OCOCH_3)_2$], 2.17 (d, 3H, acetoxy, J_{Tl-H}=13 Hz), 2.66 (m, 2H, $CH_3C\underline{H}_2$-, J_{H-H}=7 Hz, J_{Tl-H}=1299 Hz), 7.40 (s, 5H, phenyl). Recrystallization from methanol gave 0.24 g of pure **2**(R=Et) as white needles. NMR (CD_3OD) of **2**(R=Et) δ 1.34 (t, 3H, $C\underline{H}_3CH_2$-, J_{H-H}=7 Hz), 1.85 (d, 3H, acetoxy, J_{Tl-H}=13 Hz), 1.90 [s, 6H, $Tl(OCOCH_3)_2$], 2.68 (m, 2H, $CH_3C\underline{H}_2$-, J_{H-H}=7 Hz, J_{Tl-H}=116 Hz), 7.2—7.3 [m, 5H, phenyl, J_{Tl-o-H}=126 Hz, J_{Tl-m-H}=64 Hz).

3.5 g and 2.9 g of a mixture of **1** and **2** were similarly obtained from *n*-propylphenylacetylene and *n*-butylphenylacetylene, respectively. The products from *n*-butylphenylacetylene, also oily at first, were treated as in the case of ethylphenylacetylene in order to solidify the products. They were recrystallized from either acetone or 1,2-dichloroethane and analyzed. Several attempts to separate each product were unsuccessful. NMR (CD_3OD) spectra of the mixture could be analyzed. $J_{Tl-H(-CH_2-C\equiv)}$ was 1311 and 1316 Hz in **1**(R=*n*-Pr) and **1**(R=*n*-Bu) respectively, couplings of *o*- and *m*-hydrogen of phenyl group with thallium being also observed in **2**(R=*n*-Pr) and **2**(R=*n*-Bu).

All the reactions could be carried out at 50—75 °C without affecting either the ratio or the yield of **1** and **2**. A larger scale reaction (about 10 times) also gave satisfactory results.

Reaction of Methyl- and Ethylphenylacetylenes with $Tl(OAc)_3$. To an acetic acid (10 ml) solution of $Tl(OAc)_3$ (1.9 g, 5 mmol) was added methylphenylacetylene (1.16 g, 10 mmol) at 65 °C and the resulting pale-green solution was kept for 1 hr and then refluxed for 2 hr when the color of the homogeneous solution turned to orange and then to red. After being cooled down to room temperature, aqueous NaCl was added to the solution and the precipitated TlCl was filtered off. The filtrate was extracted with benzene and the extract was washed with aqueous $NaHCO_3$ and dried over Na_2SO_4. The extract was concentrated to *ca.* 5 ml with a rotary evaporator and analyzed by glc with ethyl cinnamate as an internal standard. The products were propiophenone (7%), 1-phenyl-1,2-propanedione (13%), **3**(R=Me) (78%), **4**(R=Me) (29%), α-acetoxypropiophenone (7%), and 1-acetoxy-1-phenylacetone (6%). The last two compounds were not separated by glc, their yields being determined by NMR. The yields were calculated on the basis of $Tl(OAc)_3$ charged. The yields of the above products in another experiment were 5, 12, 67, 25, 7, and 6%, respectively.

A similar treatment of ethylphenylacetylene gave a mixture of the following products; butyrophenone (6%), **3**(R=Et) (44%), **4**(R=Et) (24%), α-acetoxybutyrophenone (4%), 1-acetoxy-1-phenyl-2-butanone (**3**) and an unidentified compound (<3%).

*Reaction of **3**(R=Me) and **4**(R=Me) with $Tl(OAc)_3$.* A mixture of **3**(R=Me) (0.53 g, 3 mmol), $Tl(OAc)_3$ (1.91 g, 5 mmol), and acetic acid (20 ml) was refluxed for 2 hr, 75% of Tl^{3+} salt being consumed (iodometrically). The reaction mixture was treated as described above. Glc analysis showed the presence of unreacted **3**(R=Me) (0.26 mmol), 1-phenyl-1,2-propanedione [0.08 mmol, 3% yield based on **3**(R=Me) charged], propiophenone (0.13 mmol, 4%) and α-acetoxypropiophenone (1.84 mmol, 61%). A similar reaction of a mixture of **3**(R=Me) and **4**(R=Me) (0.53 g, 3 mmol, **3**/**4**=3.0) with $Tl(OAc)_3$ (1.15 g, 3 mmol) in acetic acid (20 ml) gave propiophenone (0.18 mmol, 6%), 1-phenyl-1,2-propanedione (0.21 mmol, 7%), α-acetoxypropiophenone (0.66 mmol, 22%), 1-acetoxy-1-phenylacetone (0.51 mmol, 17%) together with unreacted 1.08 mmol of **3**(R=Me) and 0.09 mmol of **4**(R=Me).

Reaction of Propiophenone, Butyrophenone, and Phenylacetone with $Tl(OAc)_3$. The reaction of propiophenone (1.34 g, 10 mmol) with $Tl(OAc)_3$ (3.81 g, 10 mmol) in acetic acid (30 ml) under reflux for 2 hr gave 1-phenyl-1,2-propanedione (3% yield) and α-acetoxypropiophenone[17] (50% yield, bp 140—145 °C/16 mmHg) as products. A similar reaction using butyrophenone afforded α-acetoxybutyrophenone (23%) and small amounts of unidentified products. Distillation gave pure α-acetoxybutyrophenone; bp 110—115 °C/3 mmHg, IR 1738 and 1695 ($\nu_{C=O}$) cm^{-1}. NMR ($CDCl_3$) δ 1.00 (t, 3H, J_{H-H}=7 Hz, CH_3-), 1.6—2.2 (m, 2H, $-CH_2-$), 2.13 (s, 3H, acetoxy), 5.82 (m, 1H, -CH-), 7.2—7.7 (m, 3H, phenyl), 7.8—8.2 (m, 2H, phenyl). Similarly, 1-acetoxy-1-phenylacetone (74%) and 1-phenyl-1,2-propanedione (4%) were obtained from the reaction of phenylacetone. Distillation gave pure 1-acetoxy-1-phenylacetone; bp 140—147 °C/17 mmHg. IR 1740 ($\nu_{C=O}$), 1228 (ν_{C-O}) cm^{-1}. NMR (CCl_4) δ 2.02 (s, 3H, CH_3-), 2.10 (s, 3H, acetoxy), 5.85 (s, 1H, methine), 7.35 (s, 5H, phenyl). Found: C, 69.28; H, 6.45%. Calcd for $C_{11}H_{12}O_3$: C, 68.73; H, 6.29%.

*Protodethallation of a Mixture of **1** and **2** by Acetic Acid.* A mixture of **1**(R=Me) and **2**(R=Me) (1.5 g, 3 mmol, **1**/**2**=2.6) was dissolved in 20 ml acetic acid and the resulting slightly yellow homogeneous solution was refluxed for 2 hr to give a red solution. After being cooled down to room temperature, the reaction mixture was treated as described above and analyzed by glc. The products were methylphenylacetylene (1% yield), propiophenone (8%), 1-phenyl-1,2-propanedione (7%), **3**(R=Me) (46%), **4**(R=Me) (6%), α-acetoxypropiophenone (13%), and 1-acetoxy-1-phenylacetone (12%). A similar treatment of a mixture of **1**(R=Et) and **2**(R=Et) (**1**/**2**=1.6) gave the following products; ethylphenylacetylene (1%), butyrophenone (12%), **3**(R=Et) (39%), **4**(R=Et) (17%), α-acetoxybutyrophenone (6%), and 1-acetoxy-1-phenyl-2-butanone (5%).

*Reaction of **1** and **2** with $NaBH_4$ in Protic Solvents.* To a methanol (20 ml) solution containing 1.50 g (3.0 mmol) of **1**(R=Me) was added solid $NaBH_4$ (0.06 g, 1.5 mmol) in several portions, the temperature being kept at 0—4 °C. The mixture was then stirred for 1 hr at 0 °C. After the addition of aqueous NaCl and filtration of the resulting TlCl, the filtrate was extracted with benzene, and the extract was treated as described above. Glc analysis showed the presence of 0.09 mmol of methylphenylacetylene and 2.55 mmol (85%) of **3**(R=Me). The retention time of glc and the NMR spectrum of **3**(R=Me) were consistent with those of the sample prepared by the method reported by Fahey and Lee[37] but different from those of its isomer, 1-acetoxy-*cis*-1-phenylpropene.[37] NMR (CCl_4) δ 1.65 (d, 3H, CH_3-C=,

J_{H-H}=7 Hz), 2.16 (s, 3H, acetoxy), 5.75 (q, 1H, =CH, J_{H-H}=7 Hz), 7.0—7.4 (m, 5H, phenyl). A mixture of **1**(R=Me) and **2**(R=Me) (3.7 g, 7.5 mmol) gave a mixture of methylphenylacetylene (0.22 mmol), **3**(R=Me) (4.95 mmol), and **4**(R=Me) (1.80 mmol) by a similar treatment. Distillation gave 0.91 g (5.2 mmol) of a mixture of **3**(R=Me) and **4**(R=Me) (**3**/**4**=3.0), bp 122—130 °C/19.5 mmHg. NMR (CCl_4) of **4**(R=Me) was consistent with that reported by House *et al.*,[38] δ 2.03 (d, 3H, CH_3-C=, J_{H-H}=1 Hz), 2.06 (s, 3H, acetoxy), 5.83 (q, 1H, H-C=, J_{H-H}=1 Hz). 7.0—7.4 (m, 5H, phenyl). Analysis of a mixture of **3** and **4**. Found: C, 75.09; H, 7.02%. Calcd for $C_{11}H_{12}O_2$: C, 74.97; H, 6.86%.

The reaction of **1** (R=Me) with $NaBH_4$ in CH_3OD solvent gave 1-acetoxy-2-deuterio-*trans*-1-phenylpropene; bp 125—129 °C/22 mmHg. NMR (CCl_4) δ 1.64 (s, 3H, CH_3-C=), 2.17 (s, 3H, acetoxy), 7.1—7.4 (m, 5H, phenyl). Found: C, 74.65; H, 6.98%. Calcd for $C_{11}H_{13}O_2$: C, 74.55; H, 7.39%. A mixture of **1** (R=Me) and **2** (R=Me) was reduced by $NaBH_4$ in THF-D_2O (1: 1) solvent at 5 °C for 1 hr to give 1-acetoxy-2-deuterio-*trans*-1-phenylpropene and 2-acetoxy-1-deuterio-*trans*-1-phenylpropene as the products. NMR (CCl_4) of the latter compound, δ 2.04 (s, 3H, CH_3-C=), 2.06 (s, 3H, acetoxy), 7.1—7.4 (m, 5H, phenyl).

The products obtained by a similar treatment in methanol with other oxythallates are as follows. A mixture of **3** (R=Et) and **4** (R=Et) (84% yield by glc, **3**/**4**=1.8); 63% yield by distillation, bp 132—135 °C/19.5 mmHg. **3** (R=Et) was prepared by refluxing butyrophenone in acetic anhydride in the presence of *p*-toluenesulfonic acid, bp 107—108 °C/5 mm Hg. NMR (CCl_4) δ 1.05 (t, 3H, $C\underline{H}_3CH_2$-, J_{H-H}=7 Hz), 1.8—2.3 (m, 2H, $CH_3C\underline{H}_2$-), 2.15 (s, 3H, acetoxy), 5.67 (t, 1H, =CH, J_{H-H}=7 Hz), 7.1—7.4 (m, 5H, phenyl). NMR (CCl_4) of **4** (R=Et) determined from a mixture of **3** (R=Et) and **4** (R=Et) is as follows: δ 1.13 (t, 3H, $C\underline{H}_3CH_2$-, J_{H-H}=7 Hz), 2.07 (s, 3H, acetoxy), 2.27 (q, 2H, $CH_3C\underline{H}_2$-, J_{H-H}=7 Hz), 5.85 (t, 1H, =CH, J_{H-H}=1 Hz), 7.1—7.4 (m, 5H, phenyl). A mixture of **3** (R=*n*-Pr) and **4** (R=*n*-Pr): 67% yield by distillation, bp 142—146 °C/19.5 mmHg. Found: C, 76.28; H, 8.17%. Calcd for $C_{13}H_{16}O_2$: C, 76.44; H, 7.90% A mixture of **3** (R=*n*-Bu) and **4** (R=*n*-Bu): 59% yield by distillation, bp 153—156 °C/17.5 mmHg. Found: C, 77.42; H, 8.67%. Calcd for $C_{14}H_{18}O_2$: C, 77.03; H, 8.31%.

Reaction of 1(R=Me) and 2(R=Me) with NaOH. To a methanol (15 ml) solution of **1** (R=Me) (2 mmol) was added aqueous 3M-NaOH (5 ml) drop by drop, the temperature being kept at 0 °C. After the mixture was stirred for 1 hr at 0 °C, the precipitated Tl_2O_3 was filtered off and the filtrate was treated as usual. Glc analysis showed the formation of a trace amount of methylphenylacetylene and 2 mmol (100% yield) of propiophenone. A similar treatment of a mixture of **1**(R=Me) and **2**(R=Me) (2 mmol, **1**/**2**=0.8) gave methylphenylacetylene (0.05 mmol), propiophenone (0.82 mmol), and phenylacetone (0.23 mmol) as the products.

Reaction of 1(R=Me) with Copper Salts. The following shows a typical procedure. A yellowish green heterogeneous mixture of **1**(R=Me) (1.0 g, 2 mmol), CuI (0.76 g, 4 mmol), and KI (1.3 g, 8 mmol) in acetonitrile (20 ml) was stirred for 2 hr under refluxing temperature. After the reaction mixture had been cooled the dark-yellow precipitates were filtered. The filtrate was added to water and extracted with diethyl ether. Glc analysis of the ether extract using cumene and benzophenone as internal standards showed the presence of 0.1 mmol of methylphenylacetylene and 1.16 mmol (58% yield) of **5a**. Bp 114—116 °C/4 mmHg. NMR (CCl_4) δ 2.04 (s, 3H, acetoxy), 2.47 (s, 3H, CH_3-C=), 7.1—7.6 (m, 5H, phenyl). Found: C, 43.41; H, 3.60%. Calcd for $C_{11}H_{11}O_2I$: C, 43.73; H, 3.67%.

Characterization of other products is as follows. **5b**: bp 97—103 °C/3 mmHg. IR 1768 ($\nu_{C=O}$), 1200 (ν_{C-O}) cm^{-1}. NMR (CCl_4) δ 2.04 (s, 3H, acetoxy), 2.30 (s, 3H, CH_3C=), 7.2—7.6 (m, 5H, phenyl). Found: C, 52.07; H, 4.33%. Calcd for $C_{11}H_{11}O_2Br$: C, 51.79; H, 4.35%. It was revealed by NMR that there was an unidentified compound together with **5b** and **6** in the products obtained by the reaction of **1**(R=Me) with bromine in methanol at 20 °C for 2 hr. We may assign this compound as a geometrical isomer of **5b** [**5b′** (phenyl and methyl groups are on the same side)]; NMR (CCl_4) δ 2.09 (s, 3H, acetoxy), 2.33 (s, 3H, CH_3C=). 2-Acetoxy-1-bromo-*trans*-1-phenylpropene (**5b″**): The reaction of a mixture of **1**(R=Me) and **2**(R=Me) (5.0 g, 10 mmol, **1**/**2**=0.8) with $CuBr_2$ (4.5 g, 20 mmol) and KBr (4.8 g, 40 mmol) in acetonitrile (50 ml) under reflux for 2 hr gave **5b** and **5b″** as products (**5b**/**5b″**=1.13). Distillation gave a mixture of **5b** and **5b″**; 0.91 g (36% yield, **5b**/**5b″**=0.93), bp 95—105 °C/3 mmHg. NMR (CCl_4) of **5b″**, δ 1.81 (s, 3H, CH_3C=), 2.20 (s, 3H, acetoxy), 7.1—7.6 (m, 5H, phenyl). Analysis of a mixture of **5b** and **5b″**. Found: C, 52.22; H, 4.34%. **5c**: IR 1765 ($\nu_{C=O}$), 1200 (ν_{C-O}) cm^{-1}. NMR (CCl_4) δ 2.08 (s, 3H), 2.12 (s, 3H), 7.1—7.6 (m, 5H). Mass spectrum (*m/e*) 210 (M^+). **5d**: IR 2020 (ν_{CN}), 1775 ($\nu_{C=O}$), 1185 (ν_{C-O}) cm^{-1}. Mass spectrum (*m/e*) 201 (M^+). NMR (CCl_4) δ 1.93 (s, 3H, acetoxy), 2.19 (s, 3H, CH_3C=), 7.2—7.8 (m, 5H, phenyl). **5e**: IR 2150 (ν_{SCN}), 1765 ($\nu_{C=O}$), 1192 (ν_{C-O}) cm^{-1}. Mass spectrum (*m/e*) 233 (M^+). NMR (CCl_4) δ 2.11 (s, 3H, acetoxy), 2.22 (s, 3H, CH_3C=), 7.3 (s, 5H, phenyl). **6**: To a solution of **1**(R=Me) (1.0 g, 2 mmol) in CS_2 (15 ml) was added bromine (0.64 g, 4 mmol) in CS_2 (5 ml) drop by drop at 20 °C and the resulting red solution was stirred for 2 hr when the color turned pale orange. Glc analysis revealed the presence of a small amount of methylphenylacetylene and 1.98 mmol (99% yield) of **6**. Distillation gave 0.2 g (34% yield) of pure **6**; bp 100—104 °C/3.5 mmHg. IR 1682 ($\nu_{C=O}$) cm^{-1}. Mass spectrum (*m/e*) 290 (M^+), 292 (M^++2), 294 (M^++4). NMR (CCl_4) δ 2.72 (s, 3H, CH_3-), 7.2—7.6 [m, 3H, phenyl (*m*- and *p*-H)], 8.2—8.5 [m, 2H, phenyl (*o*-H)].

References

1) J. Chatt, *Chem. Rev.*, **48**, 7 (1951).

2) W. Kitching, *Organometal. Chem. Rev.*, **3**, 61 (1968).

3) a) A. E. Borisov, V. D. Vil'chevskaya, and A. N. Nesmeyanov, *Dokl. Akad. Nauk SSSR*, **90**, 383 (1953); *Chem. Abstr.*, **48**, 4434 (1954). b) A. N. Nesmeyanov, A.E. Borisov, I. S. Savel'eva, and M. A. Osipova, *Izv. Akad. Nauk SSSR, Otd. Khim. Nauk*, **1961**, 1249; *Chem. Abstr.*, **56**, 1469 (1962). c) G. Drefahl, G. Heublein, and A. Wintzer, *Angew. Chem.*, **70**, 166 (1958).

4) a) S. Uemura, R. Kitoh, K. Fujita, and K. Ichikawa, This Bulletin, **40**, 1499 (1967). b) K. Ichikawa and S. Uemura, *Yuki Gosei Kagaku Kyokai Shi*, **29**, 400 (1971).

5) A. McKillop, O. H. Oldenziel, B. P. Swann, E. C. Taylor, and R. L. Robey, *J. Amer. Chem. Soc.*, **95**, 1296 (1973).

6) S. Uemura, K. Sohma, H. Tara, and M. Okano, *Chem. Lett.*, **1973**, 545.

7) R. Sharma and N. H. Fellers, *J. Organometal. Chem.*, **49**, C69 (1973).

8) S. Uemura, K. Zushi, A. Tabata, A. Toshimitsu, and M. Okano, This Bulletin, **47**, 920 (1974).

9) S. Uemura, A. Tabata, and M. Okano, *Chem. Commun.*, **1972**, 517.

10) S. Uemura, Y. Ikeda, and K. Ichikawa, *Tetrahedron*, **28**, 5499 (1972).

11) a) S. Uemura, Y. Ikeda, and K. Ichikawa, *ibid.*, **28**, 3025 (1972). b) S. Uemura, S. Uchida, M. Okano, and K. Ichikawa, This Bulletin, **46**, 3254 (1973).
12) a) H. Kurosawa and R. Okawara, *J. Organometal. Chem.*, **10**, 211 (1967). b) H. Kurosawa and R. Okawara, *ibid.*, **19**, 253 (1969). c) A. G. Lee, *ibid.*, **22**, 537 (1970).
13) J. P. Maher and D. F. Evans, *J. Chem. Soc.*, **1965**, 637.
14) A. T. T. Hsieh and G. Wilkinson, *J. Chem. Soc. Dalton*, **1973**, 867.
15) For the reduction of $Tl(OAc)_3$ by acetic acid, see for example; A. South, Jr. and R. J. Ouellete, *J. Amer. Chem. Soc.*, **90**, 7064 (1968). E. C. Taylor, H. W. Altland, G. McGillivray, and A. McKillop, *Tetrahedron Lett.*, **1970**, 5285.
16) Bp 102 °C/27 mmHg. NMR ($CDCl_3$) δ 1.50 (d, 3H, $C\underline{H}_3CH$-), 3.65 (s, 3H, $COOCH_3$), 3.73 (q, 1H, $CH_3C\underline{H}$-), 7.25—7.35 (m, 5H, phenyl). Found: C, 72.85; H, 7.57%.
17) S. Uemura, T. Nakano, and K. Ichikawa, *Nippon Kagaku Zasshi*, **88**, 1111 (1967).
18) See, for example, O. A. Reutov and I. P. Beletskaya, "Reaction Mechanisms of Organometallic Compounds," North-Holland, Amsterdam (1968), Chap. 1—4.
19) J. R. Blackborow, *J. Chem. Soc. Perkin II*, **1973**, 1989. Protonolysis of vinylboron compound by acetic acid has been reported to proceed with retention of configuration by H. C. Brown and G. Zweifel, *J. Amer. Chem. Soc.*, **81**, 1512 (1959).
20) J. Klein and R. Levene, *J. Chem. Soc. Perkin II*, **1973**, 1971.
21) H. C. Brown, "Boranes in Organic Chemistry," Cornell Univ. Press, Ithaca (1972), p. 313—317.
22) For example, a) H. C. Brown and J. H. Kawakami, *J. Amer. Chem. Soc.*, **95**, 8665 (1973) and references therein. b) References cited in Ref. 25.
23) a) F. G. Bordwell and M. L. Douglass, *J. Amer. Chem. Soc.*, **88**, 993 (1966). b) D. J. Pasto and J. Gontarz, *ibid.*, **91**, 719 (1969). c) G. M. Whitesides and J. San Filippo, Jr., *ibid.*, **92**, 6611 (1970). d) G. A. Gray and W. R. Jackson, *ibid.*, **91**, 6205 (1969). e) G. A. Gray, W. R. Jackson, and V. M. A. Chambers, *J. Chem. Soc., C*, **1971**, 200. f) V. M. A. Chambers, W. R. Jackson, and G. W. Young, *Chem. Commun.*, **1970**, 1275; *J. Chem. Soc., C*, **1971**, 2075.
24) G. Chandra, D. Devaprabhakara, and M. S. Muthana, *Curr. Sci.*, **40**, 400 (1971).
25) P. F. Hudrlik and A. M. Hudrlik, *J. Org. Chem.*, **38**, 4254 (1973).
26) R. B. Herbert, *Tetrahedron Lett.*, **1973**, 1375.
27) O. Simamura, "Topics in Stereochemistry," Vol. 4, ed. by E. L. Eliel and N. L. Allinger, Wiley-Interscience, New York, N.Y. (1969), p. 21.
28) I. P. Beletskaya, V. I. Karpov, and O. A. Reutov, *Dokl. Akad. Nauk SSSR*, **161**, 586 (1965); See also Ref. 18, p. 201—206.
29) S. Uemura, A. Tabata, and M. Okano, unpublished data.
30) C. P. Casey, G. M. Whitesides, and J. Kurth, *J. Org. Chem.*, **38**, 3406 (1973).
31) J. C. Barnes and D. N. Hume, *Inorg. Chem.*, **2**, 444 (1963).
32) J. R. Johnson, A. M. Schwartz, and T. L. Jacobs, *J. Amer. Chem. Soc.*, **60**, 1882 (1938).
33) M. T. Bogert and D. Davidson, *ibid.*, **54**, 334 (1932).
34) A. Mortreux and M. Blanchard, *Bull. Soc. Chim. Fr.*, **1970**, 4035.
35) L. I. Smith and M. M. Falkof, "Organic Syntheses," Coll. Vol. III, p. 350 (1955).
36) C. L. Jenkins and J. K. Kochi, *J. Org. Chem.*, **36**, 3095 (1971).
37) R. C. Fahey and D. J. Lee, *J. Amer. Chem. Soc.*, **88**, 5555 (1966).
38) H. O. House, L. J. Czuba, M. Gall, and H. D. Olmstead, *J. Org. Chem.*, **34**, 2324 (1969).

Synthesis of N^{ε}-Hydroxy-L-lysine

Yoshikazu Isowa and Muneki Ohmori

Sagami Chemical Research Center, Nishi-Ohnuma, Sagamihara, Kanagawa 229

(Received April 22, 1974)

Optically active N^{ε}-hydroxy-L-lysine monohydrochloride (L-I·HCl) was synthesized from N^{ε}-tosyl-$N^{\prime}$-benzyloxy-L-lysine (L-II) obtained by the procedure employed for the preparation of N^{δ}-tosyl-N^{δ}-benzyloxy-L-ornithine. Removal of the protecting groups of L-II was carried out by the following two methods: a) treatment of L-II with boron tris(trifluoroacetate) in trifluoroacetic acid gave L-I in one step, which was isolated as 2-nitroindane-1,3-dione salt; b) deprotection of L-II *via* N^{ε}-benzyloxy-L-lysine (L-VIII), detosylation with hydrogen bromide in acetic acid and phenol, followed by debenzylation with hydrogenolysis, gave L-I·HCl having properties identical with those of the natural product obtained from mycobactine.

$N^{\prime}$-Hydroxy-L-lysine (L-I) is an important intermediate in the synthesis of mycobactines, sexadentate chelating agents for ferric iron, which occur naturally and stimulate the growth of mycobacteria.

Snow reviewed the isolation and structual elucidation of L-I.[1] Its synthesis by various methods gave only the racemic form. Rogers and Neilands[2] prepared the $N^{\prime}$-hydroxy-DL-lysine (DL-I) in the form of its 2-nitroindane-1,3-dione salt from the 5-(4-bromobutyl)-hydantoin *via* the corresponding nitro- and hydroxyamino-hydantoin. Lancini, Lazzari, and Diena[3] obtained DL-I by the reaction of hydroxyamine with 5-(4-bromobutyl) hydantoin and the following hydrolysis with hydrochloric acid. Black, Brown, and Wade[4] suggested the preparation of DL-I·2 HCl by reacting diethyl 5-bromo-1-phthalimidopentane-1,1-dicarboxylate with benzaldoxime, followed by the transformation of the nitrone to the corresponding hydroxyamine hydrochloride, the final product being characterized only in solution. It was found that $N^{\prime}$-hydroxy-DL-lysine (DL-I) was obtained from N^{α}-phthalyl-DL-lysine *via* the corresponding nitrone derivative.[5]

L-Isomer of I is a key compound for providing a route to the mycobactine. We wish to report on the synthesis of N^{ε}-hydroxy-L-lysine with the use of N^{ε}-tosyl-$N^{\prime}$-benzyloxy-L-lysine (L-II), obtained by the procedure employed for the preparation of N^{δ}-tosyl-N^{δ}-benzyloxy-L-ornithine.[6] L-II is suitably protected at N^{ε}-position and therefore can be converted into N^{ε}-hydroxy-L-lysine (L-I) by removing the protecting groups under mild conditions without loss of optical purity.

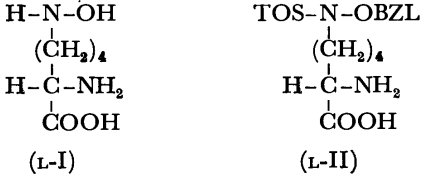

(L-I) (L-II)

The sequence of reactions employed in the preparation of DL-II is given in Fig. 1.

O-Benzyl-*N*-tosylhydroxyamine (III)[6] was first haloalkylated with 1,4-dibromobutane to 4-(*N*-tosyl-*N*-benzyloxy)aminobutyl bromide (IV). This was allowed to react with diethyl sodio-acetamidomalonate, and the product (V) was refluxed with concentrated hydrochloric acid–acetic acid to yield the racemic $N^{\prime}$-tosyl-N^{ε}-benzyloxy-DL-lysine (DL-II).

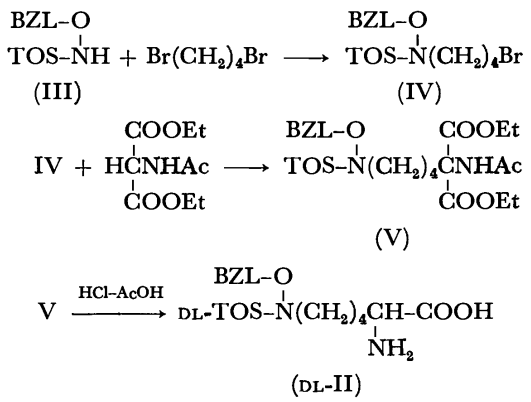

Fig. 1. Synthesis of $N^{\prime}$-tosyl-N^{ε}-benzyloxy-DL-lysine (DL-II): BZL, benzyl; TOS, *p*-toluenesulfonyl; Ac, acetyl.

Optically active N^{ε}-tosyl-$N^{\prime}$-benzyloxy-L-lysine(L-II) was obtained by the enzymatic resolution of N^{α}-acetyl-N^{ε}-tosyl-$N^{\prime}$-benzyloxy-DL-lysine (DL-VI) *via* its anilide (L-VII) with aniline in the presence of papain (Fig. 2).

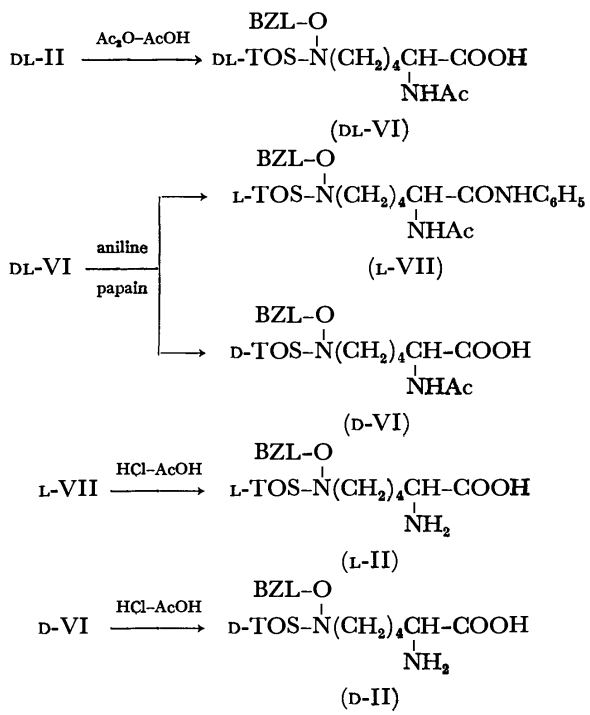

Fig. 2. Optical resolution of N^{α}-acetyl-N^{ε}-tosyl-N^{ε}-benzyloxy-DL-lysine (DL-VI).

The resulting N^{α}-acetyl-N'-tosyl-N'-benzyloxy-L-lysine anilide (L-VII) and N^{α}-acetyl-N^{ϵ}-tosyl-N^{ϵ}-benzyloxy-D-lysine (D-VI) showed optical rotations of $[\alpha]_D^{24}$ −48.6° and $[\alpha]_D^{22}$ −13.3° in chloroform solution. N^{ϵ}-Tosyl-N'-benzyloxy-L-lysine (L-II) and its D-isomer (D-II) prepared by acid hydrolysis of L-VII and D-VI showed optical rotations of $[\alpha]_D^{24}$ +18.4° and $[\alpha]_D^{22}$ −17.9° in acetic acid solution, respectively.

The optically active N^{ϵ}-protected hydroxylysine (L-II) thus obtained was deprotected *via* two different routes, a and b (Fig. 3), to N'-hydroxy-L-lysine (L-I) under mild conditions without racemization.

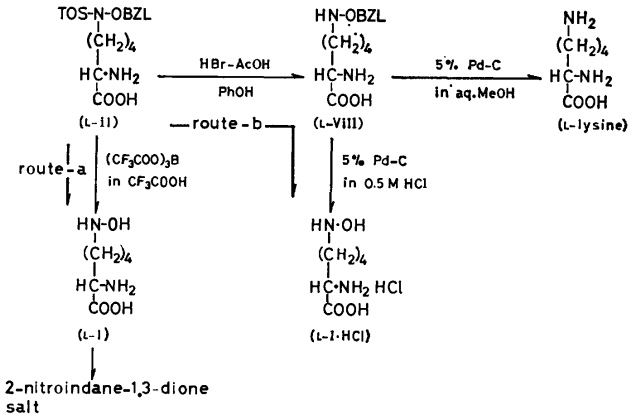

Fig. 3. Deprotection of N^{ϵ}-tosyl-N^{ϵ}-benzyloxy-L-lysine (L-II).

In route-a, the treatment of L-II with boron tris-(trifluoroacetate)[7] followed by neutralization of the product with aqueous ammonia afforded L-I as a colorless solid, mp 223—226 °C (decomp.) and $[\alpha]_D^{24}$ +24.2° (*c* 0.5, M hydrochloric acid) (lit,[8] mp 223—225 °C (decomp.) and $[\alpha]_D^{18}$ +23.9° (*c* 5.1, M hydrochloric acid)), in 58% yield. The N'-hydroxy-L-lysine (L-I) thus obtained was immediately transformed into 2-nitroindane-1,3-dione salt, because of the difficulty of preparing the L-I (HCl-free) in a state of reasonable purity; L-I was relatively unstable in the neutral and alkaline solution. The salt was obtained as pale brown crystals with melting point and the results of elemental analysis agreeing with those of the natural product reported by Snow.[8]

In route-b, the N'-protected hydroxylysine (L-II) was first detosylated with 36% hydrogen bomide in acetic acid in the presence of phenol and the resulting product (L-VIII) was hydrogenolyzed over 5% palladium on carbon in 0.5 M hydrochloric acid to afford the monohydrochloride (L-I·HCl) in 89% yield. In contrast, when the reduction procedure was carried out in a neutral solution *i.e.* in aqueous methanol, L-lysine was obtained in 51% yield. The monohydrochloride (L-I·HCl) could be precipitated from aqueous solution by addition of ethanol, because of the low solubility of L-I·HCl in aqueous ethanolic solution. The hydrochloride (L-I·HCl) thus obtained had mp 192—194 °C (decomp.) and $[\alpha]_D^{24}$ +25.5° in M hydrochloric acid. The hydroxyamine group was detected by the strong red coloration caused by treatment of the product with an alkaline solution of triphenyltetrazolium chloride. The structure of the synthetic L-I·HCl was confirmed by NMR and IR spectroscopy and elemental analysis. In particular, significant NMR-spectral features of L-I·HCl in trifluoroacetic acid corresponded with those of N^{δ}-hydroxy-L-ornithine monohydrochloride.[9]

The optical purity of L-II should be maintained in the reaction sequence, since L-lysine obtained by the hydrogenolysis of L-VIII in a neutral solution showed the same specific rotation as that of an authentic sample[10] and the synthetic specimens of L-I and L-I·HCl exhibited specific rotations identical with the corresponding data for the natural product.[8]

In view of the stability and yield of the desired product, we suggest that route-b (Fig. 3) is preferable for the preparation of N'-hydroxy-L-lysine (L-I).

Experimental

All melting points were determined with a Yanagimoto electric micromelting point apparatus and are uncorrected. Optical rotations were measured with a Yanagimoto automatic polarimeter OR-50. The nuclear magnetic resonance spectra were run on a Varian HA-100 High Resolution NMR spectrometer, using tetramethylsilane as an internal standard. Infrared spectra were recorded on a Hitachi EPI-G3 spectrophotometer as KBr disk.

O-Benzyl-N-tosylhydroxyamine (III). This compound was prepared by the procedure reported.[6]

4-(N-Tosyl-N-benzyloxy)aminobutyl Bromide (IV). To a solution of sodium (20.8 g, 0.902 mol) in ethanol (1.2 l) was added III (250 g, 0.902 mol) with vigorous stirring at 70 °C. After a clear solution was obtained, 1,4-dibromobutane (583 g, 2.70 mol) was added at once. The mixture was refluxed for 6 hr, and evaporated *in vacuo* to give oily material, which was extracted with ethyl acetate (1.4 l), the organic layer being thoroughly washed with water and dried over sodium sulfate. Evaporation of the solvent afforded IV as oily material, which was crystallized from ethyl acetate–*n*-hexane; yield 320 g (86%), mp 56—59 °C.

Found: C, 52.29; H, 5.45; N, 3.21%. Calcd for $C_{18}H_{22}NO_3SBr$: C, 52.43; H, 5.38; N, 3.40%.

Diethyl 5-(N-Tosyl-N-benzyloxy)amino-1-acetamidopentane-1,1-dicarboxylate (V). To a solution of sodium (15.1 g, 0.657 mol) in ethanol (1.0 l) was added diethyl acetamidomalonate (143 g, 0.657 mol) with stirring. After 5 min, IV (271 g, 0.657 mol) was added and refluxed for 8 hr. The solvent was then removed *in vacuo* and the residue was extracted with chloroform (1.2 l). The chloroform layer was successively washed with water, diluted hydrochloric acid and water, dried over sodium sulfate, and evaporated to yield a pale yellow syrup which gave a negative Beilstein test; yield 302 g (84%). Attempts to crystallize the syrup were unsuccessful and it was used for the next step without analysis or purification.

N'-Tosyl-N'-benzyloxy-DL-lysine (DL-II). A solution of V (275 g, 0.502 mol) in a mixture of acetic acid (2.4 l) and concentrated hydrochloric acid (800 ml) was heated under gentle reflux for 8 hr. The solution was evaporated *in vacuo* and 14% aqueous ammonia was added to the residue with ice-cooling. The resulting solid was collected by filtration, washed with water, and recrystallized from aqueous acetic acid; yield 147 g (72%) and mp 178—185 °C (decomp.).

Found: C, 58.87; H, 6.21; N, 6.96%. Calcd for $C_{20}H_{26}N_2O_5S$: C, 59.09; H, 6.45; N, 6.89%.

The product showed blue coloration on heating with an

aqueous solution of ninhydrin.

N^{α}-*Acetyl*-N^{ε}-*tosyl*-N^{ε}-*benzyloxy*-DL-*lysine* (DL-*VI*). Acetic anhydride (40 g, 0.392 mol) was slowly added to a stirred solution of DL-II (121 g, 0.297 mol) in acetic acid (600 ml). After being stirred for 12 hr at room temperature, the solvent was evaporated *in vacuo*. Water was added to decompose excess acetic anhydride and the resulting mixture was extracted with ethyl acetate (600 ml). The organic layer was washed with water and dried over sodium sulfate. The residue obtained on evaporation of the solvent was crystallized from ethyl acetate–petroleum ether to give DL-VI as an amorphous powder; yield 119 g, (89%) and mp 139—141 °C. Recrystallization from ethyl acetate caused no rise in melting point.

Found: C, 58.95; H, 6.47; N, 6.01%. Calcd for $C_{22}H_{28}N_2O_6S$: C, 58.91; H, 6.29; N, 6.25%.

Resolution of N^{α}-*Acetyl*-N^{ε}-*tosyl*-N^{ε}-*benzyloxy*-DL-*lysine* (DL-*VI*); N^{α}-*Acetyl*-N^{ε}-*tosyl*-N^{ε}-*benzyloxy*-L-*lysine Anilide* (L-*VII*). DL-Acetylamino acid (DL-VI) (44.8 g, 0.10 mol) was dissolved in 0.75 M sodium hydroxide (350 ml) and the solution was adjusted to pH 6.20 with 0.5 M citric acid. Papain (15 g) was added to the solution together with freshly distilled aniline (12 ml) and cysteine hydrochloride monohydrate (5.5 g). The mixture was incubated for 36 hr at 38 °C and the anilide deposited was collected by suction and washed with water, 7% aqueous ammonia and water. Recrystallization from methanol–water (3:1) gave clorless crystals; yield 23 g (88%), mp 137—139 °C and $[\alpha]_D^{24}$ −48.6° (*c* 1.0, chloroform).

Found: C, 64.27; H, 6.47; N, 7.84%. Calcd for $C_{28}H_{33}N_3O_5S$: C, 64.22; H, 6.35; N, 8.02%.

N^{α}-*Acetyl*-N^{ε}-*tosyl*-N^{ε}-*benzyloxy*-D-*lysine* (D-*VI*). The above filtrate combined with the washings adjusted to pH 2 with 5 M hydrochloric acid. The precipitate was then collected by suction, washed with water and dried. Recrystallization from ethyl acetate gave colorless crystals; yield 16 g (71%), mp 155—157 °C and $[\alpha]_D^{22}$ −13.3° (*c* 1.0, chloroform).

Found: C, 58.74; H, 6.31; N, 6.10%. Calcd for $C_{22}H_{28}N_2O_6S$: C, 58.91; H, 6.29; N, 6.25%.

N^{ε}-*Tosyl*-N^{ε}-*benzyloxy*-L-*lysine* (L-*II*). L-VII (17.0 g, 32.5 mmol) was dissolved in a mixture of acetic acid (130 ml) and concentrated hydrochloric acid (50 ml). After being refluxed for 6 hr, the solution was evaporated *in vacuo* and aqueous ammonia was added to the residue with ice-cooling. The deposits were collected by suction, washed with water and dried. Recrystallization from dilute acetic acid and treatment with hot methanol gave an amorphous powder; yield 11.4 g (86%), mp 204—207 °C (decomp.) and $[\alpha]_D^{24}$ +18.4° (*c* 1.0, acetic acid).

Found: C, 58.88; H, 6.46; N, 6.66%. Calcd for $C_{20}H_{26}N_2O_5S$: C, 59.09; H, 6.45; N, 6.89%.

N^{ε}-*Tosyl*-N^{ε}-*benzyloxy*-D-*lysine* (D-*II*). This was obtained from D-VI by the method employed for the preparation of L-II; yield 80%, mp 199—204 °C (decomp.) and $[\alpha]_D^{22}$ −17.9° (*c* 1.0, acetic acid).

Found: C, 58.80; H, 6.36; N, 6.87%. Calcd for $C_{20}H_{26}N_2O_5S$: C, 59.09; H, 6.45; N, 6.89%.

N^{ε}-*Hydroxy*-L-*lysine* (L-*I*) (*prepared in route-a*). L-II (10 g, 24.6 mmol) was added at 5 °C to a solution of boron tris(trifluoroacetate) prepared from boron tribromide (66 g, 263 mmol) in trifluoroacetic acid (150 ml). The reaction mixture was then stirred for 48 hr at room temperature and evaporated *in vacuo* below 30 °C. Methanol was added to the residue to decompose excess boron tris(trifluoroacetate) and the mixture was evaporated *in vacuo*. To the oily residue was added 6 M hydrochloric acid (250 ml) and the mixture was refluxed for 1 hr. Insoluble brown material was filtered off and the filtrate was concentrated *in vacuo*. Colorless crystals further precipitated were removed by suction and the filtrate was evaporated to dryness. The semi solid thus obtained was dissolved in ethanol (20 ml) and the solution was adjusted to pH 6—7 with 14% aqueous ammonia to yield a crude solid. The substance was reprecipitated from aqueous solution by adding ethanol and collected by suction. Procedures of neutralization with aqueous ammonia, reprecipitation, and collection by suction should be carried out as quickly as possible to avoid decomposition of hydroxyamine. L-I was obtained as an amorphous solid; yield 2.3 g (58%), mp 223—226 °C (decomp.) and $[\alpha]_D^{24}$ +24.2° (*c* 0.5, M hydrochloric acid).

Found: C, 45.38; H, 8.29; N, 17.19%. Calcd for $C_6H_{14}N_2O_3$: C, 44.43; H, 8.70; N, 17.27%.

The product showed a deep red coloration with alkaline triphenyltetrazolium chloride and an intense blue coloration with ninhydrin, and was negative to the Beilstein test. Successive purification caused the decomposition of hydroxyamine.

Preparation of 2-Nitroindane-1,3-dione Salt of L-*I*. The crystalline 2-nitroindane-1,3-dione salt was prepared by dissolution of L-I (100 mg) in hot water (7 ml) containing 2-nitroindane-1,3-dione (100 mg), followed by slow cooling of the resulting solution. The product (85 mg) was recrystallized twice from water to yield the salt as pale brown crystals; mp 217—218 °C (decomp.) (lit,[8] mp 217.0—217.5 °C (decomp.)).

Found: C, 50.91; H, 5.32; N, 11.75%. Calcd for $C_{15}H_{19}N_3O_7$: C, 50.98; H, 5.42; N, 11.89%.

N^{ε}-*Benzyloxy*-L-*lysine* (L-*VIII*). L-II (4.06 g, 10 mmol) was added at room temperature to a 20 ml solution of 36% hydrogen bromide in acetic acid and phenol (4 g) in a glass-stoppered bottle. After being stirred for 48 hr, the solution was evaporated *in vacuo* at a temperature below 35 °C. The residual syrup was extracted with water and the aqueous layer was washed repeatedly with ether, treated with activated carbon and evaporated *in vacuo* at a temperature below 35 °C. The residue was dissolved in water (5 ml) and adjusted to pH 7—8 with aqueous ammonia to yield a crude solid. Recrystallization from hot water gave L-VIII as a leaflet; yield 1.8 g (73%), mp 238—241 °C (decomp.) and $[\alpha]_D^{23}$ +18.1° (*c* 1.0, M hydrochloric acid).

Found: C, 61.83; H, 7.98; N, 11.21%. Calcd for $C_{13}H_{20}N_2O_3$: C, 61.88; H, 7.99; N, 11.11%.

The NMR spectrum in trifluoroacetic acid showed a multiplet at δ 1.90 (4H; β,γ-CH_2), a multiplet at δ 2.18 (2H; δ-CH_2), a multiplet at δ 3.51 (2H; ε-CH_2), a multiplet at δ 4.36 (1H; α-CH), a singlet at δ 5.19 (2H; BZL-CH_2), a sharp signal at δ 7.46 (8H; α-NH_3^+ and BZL-C_6H_5), and a broad signal at δ 9.57 (2H; ε-NH_2^+).

N^{ε}-*Hydroxy*-L-*lysine Monohydrochloride* (L-*I*·*HCl*) (*prepared in route-b*). A solution of L-VIII (500 mg, 1.98 mmol) in 0.5 M hydrochloric acid (20 ml) was hydrogenolyzed over 5% palladium on carbon (500 mg) at room temperature and atmospheric pressure for 24 hr. After the catalyst was removed by suction, the solution was evaporated to dryness. The residue was dissolved in water and again evaporated to dryness to eliminate excess hydrochloric acid and then dissolved in water (2 ml). The pH of this solution was brought to 4—5 by addition of pyridine. Addition of ethanol (4 ml) to the resulting solution gave a colorless solid, which was reprecipitated from aqueous solution by adding ethanol to afford L-I·HCl as an amorphous powder; yield 350 mg (89%), mp 192—194 °C (decomp.) and $[\alpha]_D^{24}$ +25.5° (*c* 0.22, M hydrochloric acid).

Found: C, 36.41; H, 7.61; N, 14.13%. Calcd for $C_6H_{15}N_2O_3Cl$: C, 36.27; H, 7.61; N, 14.10%.

The product showed a deep red coloration with alkaline triphenyltetrazolium chloride and a blue coloration with ninhydrin, and was positive to the Beilstein test.

Figure 4 shows the NMR spectrum of the synthesized L-I·HCl in trifluoroacetic acid with tetramethylsilane as an internal standard; δ 1.98 (4H; β,γ-CH_2), 2.27 (2H; δ-CH_2), 3.58 (2H; ε-CH_2), 4.44 (1H; α-CH), 7.53 (3H; α-NH_3^+), and 9.95 (2H; ε-NH_2^+).

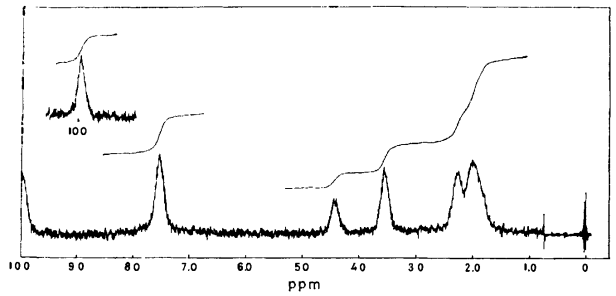

Fig. 4. NMR spectrum of N^{ε}-hydroxy-L-lysine monohydrochloride (L-I·HCl).

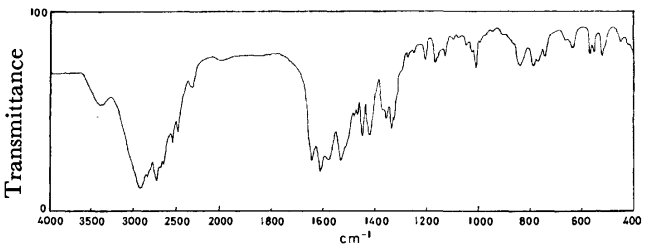

Fig. 5. Infrared spectrum of N^{ε}-hydroxy-L-lysine monohydrochloride (L-I·HCl).

A very close similarity to N^{δ}-hydroxy-L-ornithine monohydrochloride was observed in the IR spectrum (Fig. 5).

Hydrogenation of N^{ε}*-Benzyloxy-L-lysine (L-VIII) in a Neutral Solution.* A solution of L-VIII (200 mg, 0.79 mmol) in a mixture of methanol (10 ml) and water (5 ml) was hydrogenolyzed over 5% palladium on carbon (100 mg) at room temperature under atmospheric pressure for 48 hr. To the mixture was added M hydrochloric acid (5 ml) and the catalyst was filtered off. The filtrate was evaporated, adjusted to pH 5—6 by addition of pyridine and further evaporated. The residue solidified by addition of ethanol was reprecipitated from its aqueous solution by addition of ethanol to yield L-lysine monohydrochloride; yield 74 mg (51%), mp 259—263 °C (decomp., undepressed by admixture with an authentic sample[10]) and $[\alpha]_D^{22}$ +21.4° (*c* 0.38, M hydrochloric acid) (the authentic sample, $[\alpha]_D^{22}$ +20.7° (*c* 0.34, M hydrochloric acid)).

References

1) G. A. Snow, *Bacteriol. Rev.*, **34**, 99 (1970).
2) S. Rogers and J. B. Neilands, *Biochemistry*, **2**, 6 (1963).
3) G. C. Lancini, E. Lazzari, and A. Diena, *Il Farmaco, Ed. Sci.*, **24**, 169 (1969).
4) D. St. C. Black, R. F. C. Brown, and A. M. Wade, *Aust. J. Chem.*, **25**, 2155 (1972).
5) Y. Isowa and M. Sato, Japan 680165 (1973).
6) Y. Isowa, T. Takashima, M. Ohmori, H. Kurita, M. Sato, and K. Mori, This Bulletin, **45**, 1461 (1971).
7) J. Pless and W. Bauer, *Angew. Chem., Int. Edit. Engl.*, **12**, 147 (1973).
8) G. A. Snow, *J. Chem. Soc.*, **1954**, 2588.
9) Y. Isowa, T. Takashima, M. Ohmori, H. Kurita, M. Sato, and K. Mori, This Bulletin, **45**, 1464 (1971).
10) This sample was purchased from Ajinomoto Co., Inc.

Studies of Acyl and Thioacyl Isocyanates. XIV.[1] The Reactions of Benzoyl and Thiobenzoyl Isocyanates with Hydrazones

Otohiko TSUGE* and Shuji KANEMASA

Research Institute of Industrial Science, Kyushu University, Hakozaki, Higashi-ku, Fukuoka 812

(Received April 30, 1974)

Benzoyl (**1**) and thiobenzoyl isocyanates (**2**) reacted with benzaldehyde arylhydrazones and methylhydrazone to give the corresponding semicarbazones as isolated products respectively. In the reactions with acetone arylhydrazones and methylhydrazone, however, the *s*-triazolidin-5-ones whose structures corresponded to the ring tautomers of semicarbazones, were isolated as sole products from the reaction of **1**, and **2** afforded the (4+2) cycloadducts of **2** to the C=N bond of hydrazones and *s*-triazolidin-5-ones. It has been found that in some cases, the semicarbazones isomerize into their ring tautomers, and the isomerization obeys good first-order kinetics taking into account the equilibrium. Although **1** did not react with *p*-tosyl- and benzoylhydrazones, **2** easily added to both hydrazones to yield the corresponding (4+2) cycloadducts.

In a previous paper[2] dealing with the reactions of benzoyl (**1**) and thiobenzoyl isocyanates (**2**) with hydrazines, we reported that **1** reacted with phenylhydrazine to give 1-phenyl-4-benzoylsemicarbazide, while the reaction of **2** with the same hydrazine gave 1,3-diphenyl-Δ^3-triazolin-5-one under the elimination of hydrogen sulfide. It has been also described that the Δ^3-triazolin-5-one was identical with the hydrolytic product of adducts of **1** to benzaldehyde phenylhydrazone (**3a**) and acetone phenylhydrazone (**4a**), and the adducts would be the corresponding 4-benzoyl-2-phenylsemicarbazones, respectively. It has been clarified by Schildknecht and Hatzmann,[3] however, that an adduct[4,5] of cyanic acid to **4a** is not acetone 2-phenylsemicarbazone (**A**) but its ring tautomer, 3,3-dimethyl-1-phenyl-*s*-triazolidin-5-one (**B**), while a product[6] obtained from 2-phenylsemicarbazide and acetone is the semicarbazone (**A**).

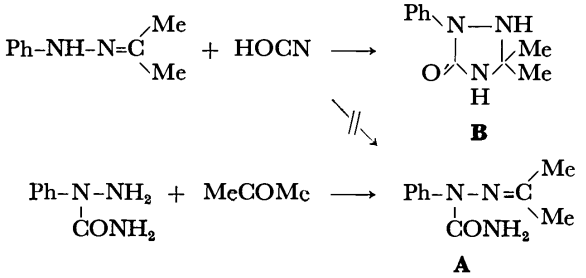

Consequently, we were obliged to reinvestigate whether the products obtained by the reaction of **1** with **3a** and **4a** would be really the corresponding 4-benzoyl-2-phenylsemicarbazones. It has been now proved that the adduct to **4a** is not the semicarbazone but its ring tautomer, although the adduct to **3a** is the semicarbazone. This fact seems to indicate that **1** might react with hydrazone to afford either the semicarbazone or its ring tautomer depending on the nature of carbonyl component of hydrazone. On the other hand, little attention has been paid to the reaction of **2** with hydrazones. Since the reactivity of **2** in 1,4-cycloaddition to C=N bonds is greater than that of **1**,[7-10] the reaction of **2** with hydrazone might be expected to give a (4+2) cycloadduct, besides the semicarbazone and its ring tautomer.

This paper deals with the reactions of **1** and **2** with aryl- and methylhydrazones of benzaldehyde and acetone. In this context, the reactions with *p*-tosyl- and benzoylhydrazones are also described.

Results and Discussion

Reactions with Benzaldehyde and Acetone Arylhydrazones. Benzoyl isocyanate (**1**) reacted with benzaldehyde phenylhydrazone (**3a**) and with acetone phenylhydrazone (**4a**) to give the corresponding 1 : 1 adducts, **5a** and **6a**, in excellent yields, respectively. The IR spectrum of **5a** showed well-defined absorption bands at 3460 (NH), 1760 (C=O), 1510 and 1490 cm^{-1} (Amide II), and the NMR spectrum in deuteriochloroform ($CDCl_3$) exhibited signals at δ 7.1—8.1 (16H, m, aromatic protons and N=C**H**) and 10.55 ppm (1H, broad, N**H**). On the other hand, the IR spectrum of **6a** showed no bands assignable to Amide II absorptions, but displayed characteristic bands at 3190 (NH), 1740, 1640 (C=O), 1330, and 1310 cm^{-1}. In the NMR spectrum in $CDCl_3$ signals appeared at δ 1.70 (6H, s, C**H**$_3$), 4.6 (1H, broad, N**H**), and 6.9—7.8 ppm (10H, m, aromatic protons). These spectral data indicate that **5a** is an adduct of different type from **6a**, although

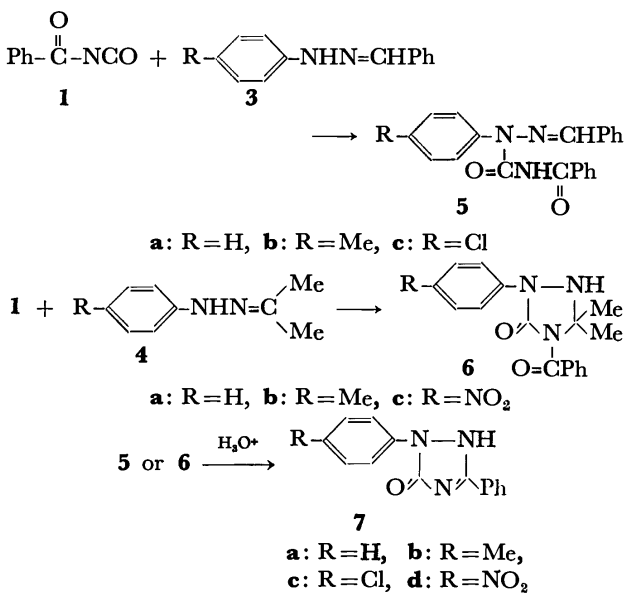

Scheme 1.

* To whom correspondence should be addressed.

hydrolyses of both **5a** and **6a** gave the same product, 1,3-diphenyl-Δ^3-*s*-triazolin-5-one (**7a**), whose structure was established by the identification with an authentic sample.[2]

Schildknecht and Hatzmann[3] reported that in the NMR spectra in $CDCl_3$ acetone 2-phenylsemicarbazone (**A**) showed two singlets (each 3H) assignable to two methyls-protons at δ 1.63 and 2.1 ppm, while two methyls-protons of 3,3-dimethyl-1-phenyl-*s*-triazolidin-5-one (**B**) appeared as a singlet (6H) at δ 1.46 ppm. As mentioned above, **6a** exhibited a singlet (6H) due to two methyls-protons in the spectrum.

On the basis of the spectral data and of the results of hydrolysis, the structures of **5a** and **6a** were deduced as benzaldehyde 4-benzoyl-2-phenylsemicarbazone and 4-benzoyl-3,3-dimethyl-1-phenyl-*s*-triazolidin-5-one, respectively.

Similarly, the reaction of **1** with benzaldehyde *p*-tolyl- (**3b**) and *p*-chlorophenylhydrazones (**3c**) gave the corresponding semicarbazones, **5b** and **5c**, while the *s*-triazolidin-5-ones, **6b** and **6c**, were obtained in the reaction with acetone *p*-tolyl- (**4b**) and *p*-nitrophenylhydrazones (**4c**). On treatment with hydrochloric acid, all **5** and **6** were converted into the corresponding Δ^3-*s*-triazolin-5-ones, **7b**—**7d**, in good yields respectively (Scheme 1).

The reaction of thiobenzoyl isocyanate (**2**) with **3a** afforded benzaldehyde 2-phenyl-4-thiobenzoylsemicarbazone (**8**), whose structure was confirmed on the basis of its spectral data. Hydrolysis of **8** gave Δ^3-*s*-triazolin-5-one **7a**. In the reaction with **4a**, however, two 1:1 adducts, **9a** and **10a**, were obtained in 19 and 60% yields, respectively.

The minor product **9a** was deduced to be 3,3-dimethyl-1-phenyl-4-thiobenzoyl-*s*-triazolidin-5-one on the basis of the following evidence. The IR spectrum of **9a** was quite similar to that of **6a**, and in its NMR spectrum two methyls-protons and NH-proton appeared at δ 1.89 (6H, s) and 4.95 ppm (1H, broad), besides aromatic protons. Treatment of **9a** with hydrochloric acid gave Δ^3-*s*-triazolin-5-one **7a**. On the other hand, the IR spectrum of major product **10a** exhibited characteristic bands at 3310 (NH), 1650 (C=O), and 1530 cm^{-1}, and the NMR spectrum showed signals at

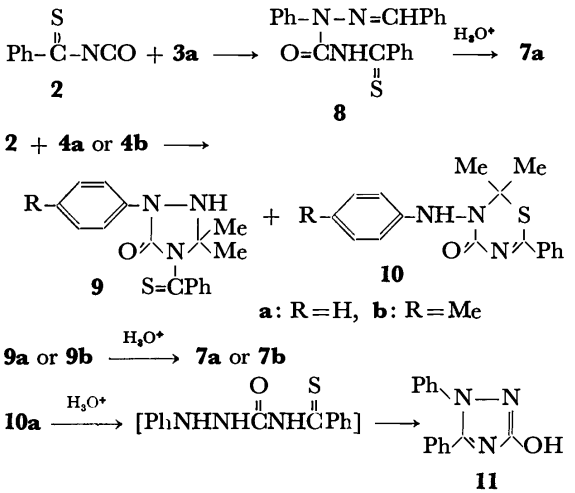

Scheme 2.

δ 1.80 (6H, s, CH_3) and 6.5 ppm (1H, broad, NH), besides aromatic protons. Hydrolysis of **10a** afforded 3-hydroxy-1,5-diphenyltriazole (**11**), whose structure corresponds to that of the compound derived from 1-phenyl-4-thiobenzoylsemicarbazide with the elimination of hydrogen sulfide. The structure of **11** was confirmed by the identification with an authentic sample.[2] On the basis of the above observations, the structure of **10a** was deduced as 3-anilino-2,2-dimethyl-6-phenyl-2,3-dihydro-4H-1,3,5-thiadiazin-4-one, which corresponds to the (4+2) cycloadduct of **2** to the C=N bond of **4a**.

Similarly, **2** reacted with **4b** to give the corresponding *s*-triazolidin-5-one **9b** and 2,3-dihydro-4*H*-1,3,5-thiadiazin-4-one **10b** in 32 and 29% yields, respectively.

Reactions with Benzaldehyde and Acetone Methylhydrazones. The reactions of both isocyanates **1** and **2** with benzaldehyde methylhydrazone (**12a**) afforded the corresponding semicarbazones **13a** and **13b**, whose structures were confirmed on the basis of their spectral data, in good yields respectively.

By the IR and NMR spectroscopic studies it was found that the crystals obtained from the reaction of **1** with acetone methylhydrazone (**12b**) were a mixture of the corresponding semicarbazone **14a** and its ring tautomer **15a**, but no **14a** could be isolated and **15a** was obtained as the sole pure compound from the mixture. Furthermore, the relative amount of **15a** was increased with an increase in the reaction time. Similar phenomena were observed in the reaction of **2** with **12b**, and *s*-triazolidin-5-one **15b**, which on hydrolysis gave 1-methyl-3-phenyl-Δ^3-*s*-triazolin-5-one (**16**), was only isolated (Scheme 3).

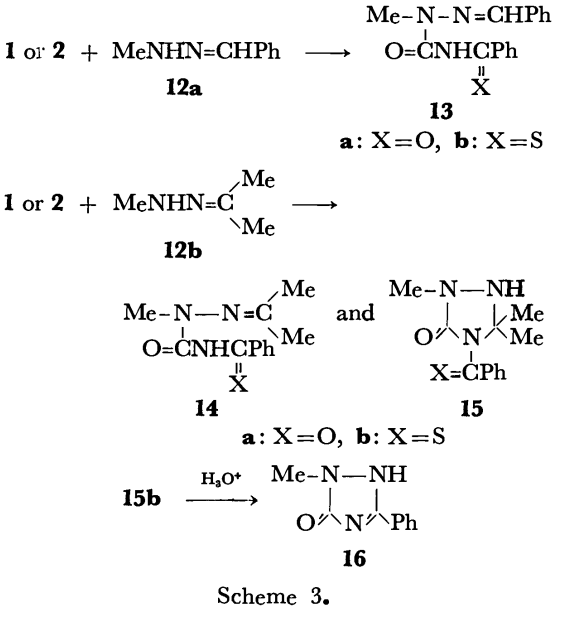

Scheme 3.

The above observations indicate that semicarbazones **14a** and **14b** isomerize into the corresponding ring tautomers **15a** and **15b**, respectively. Consequently, the isomerization was followed by the NMR spectroscopy.

Isocyanate **1** was mixed with **12b** in chloroform at −70 °C, and the NMR spectrum of the reaction mix-

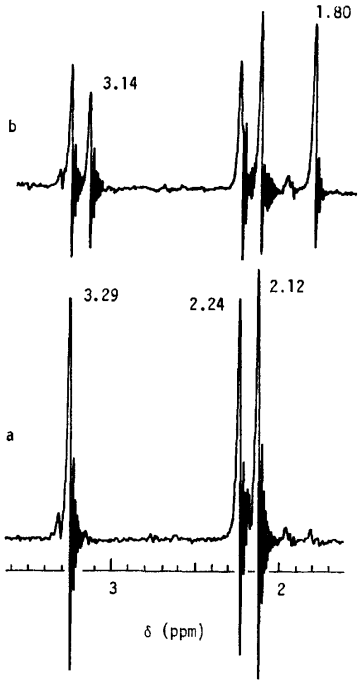

Fig. 1. NMR spectra of the reaction system **1**—**12b** in chloroform at 36.0 °C. a: Pure **14a**. b: A mixture of **14a** and **15a** (44%) after 2.5 hr.

ture was immediately measured at a constant temperature. For example, the NMR spectrum at 36.0 °C is illustrated in Fig. 1-a: three singlets appear at δ 2.12, 2.24, and 3.29 ppm in the same intensity. The singlets at δ 2.12 and 2.24 ppm can be assigned as two methyls-protons of isopropylidene group and that at δ 3.29 is ascribable to the *N*-methyl-protons in the semicarbazone **14a**.[11] The spectrum changes with time. As shown in Fig. 1-b, the initial three singlets decrease in intensity in the same ratio, and new two singlets with the relative intensity of 2: 1 show up at δ 1.80 and 3.14. These new two singlets can be assigned as the 3,3-dimethyls- and *N*-methyl-protons in the *s*-triazolidin-5-one **15a**, respectively. Furthermore, it was found by the IR spectrum that the crude product obtained from the reaction of **1** with **12b** at 0 °C was composed of **14a** and **15a**, and the microanalysis of the product agreed with that of a 1: 1 adduct of **1** to **12b**. These facts indicate clearly that the initial semicarbazone **14a** isomerizes into its ring tautomer **15a**. It was also established that both the isomerizations at 36.0 and 54.0 °C give the equilibrium composition composed of 40% of **14a** and 60% of **15a** after some time.

The first-order rate of the isomerization of **14a** taking into account the equilibrium may be expressed as follows:

$$dx/dt = k(a-x) - k'x \quad (1)$$

where a is the initial concentration of **14a**, x is the concentration of **14a** consumed after t s, and k and k' are the rate constants of the consumption and the formation of **14a** respectively.

If the concentration of **15a** at the equilibrium is x_e,

$$k(a-x_e) - k'x_e = 0 \quad (2)$$

From Eqs. (1) and (2), the rate of the consumption of **14a** may be given by:

$$dx/dt = ka(x_e-x)/x_e \quad (3)$$

Equation (3) then gives:

$$\ln [x_e/(x_e-x)] = kat/x_e$$

As illustrated in Fig. 2, the plots of $\ln[x_e/(x_e-x)]$ *vs.* the reaction times at various temperatures show straight lines. The rate constants k at 30.5, 36.0, 45.5, and 54.0 °C were 4.2×10^{-5}, 9.3×10^{-5}, 2.2×10^{-4}, and 4.0×10^{-4} s^{-1}, respectively. The plots of the logarithm of the rate constants against reciprocal absolute temperatures showed the straight line. The rate of isomerization of **14a** in benzene at 36.0 °C was measured, and the rate constant k was found to be 1.1×10^{-4} s^{-1}: little solvent effect was observed.

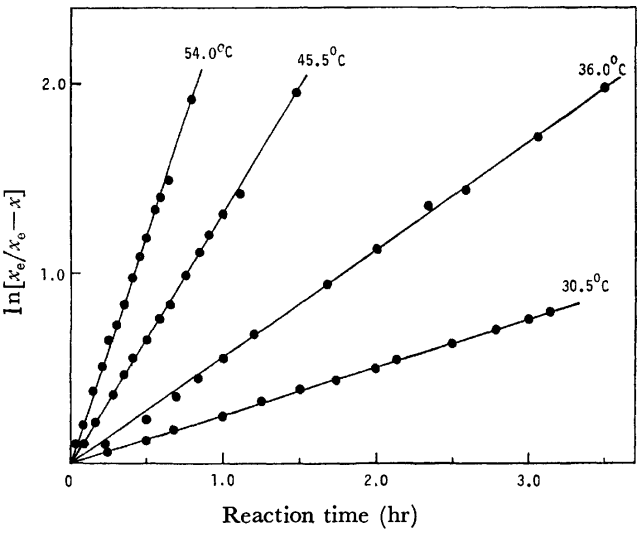

Fig. 2. Plots of the first-order function *vs.* reaction time at various temperatures in the reaction system **1**—**12b**.

The energy parameters calculated on the basis of the above observations are given in Table 1.

It was also clarified by the NMR spectroscopic study that acetone 4-benzoyl-2-phenylsemicarbazone is initially formed in the reaction of **1** with acetone phenylhydrazone (**4a**), and isomerizes into its ring tautomer **6a** with reaction time. The isomerization obeys good first-order kinetics, and the energy parameters and the concentration of **6a** at the equilibrium are also summarized in Table 1.

Table 1. Energy parameters

Parameter[a]	Reaction system	
	1—**12b**	**1**—**4a**
E_a(kcal/mol)	19.2	18.6
A(s^{-1})	3.39×10^9	2.14×10^9
$\Delta H^{\ddagger}_{25}$(kcal/mol)	18.6	18.0
$\Delta S^{\ddagger}_{25}$(cal/mol·deg)	−17.0	−17.7
$\Delta F^{\ddagger}_{25}$(kcal/mol)	23.67	23.27
x_e (%) in $CHCl_3$	60	*ca.* 100

a) E_a: Activation energy; A: Frequency factor; $\Delta H^{\ddagger}_{25}$: Enthalpy of activation at 25 °C; $\Delta S^{\ddagger}_{25}$: Entropy of activation at 25 °C; $\Delta F^{\ddagger}_{25}$: Free energy of activation at 25 °C; x_e: Concentration of *s*-triazolidin-5-one **15a** or **6a** at the equilibrium.

However, semicarbazones **13a** and **13b** did not isomerize into their ring tautomers and were recovered quantitatively even at 80 °C.

Reactions with p-*Tosyl- and Benzoylhydrazones.* On the basis of the results mentioned above, it could be viewed that **1** attacks exclusively the more basic nitrogen atom, and **2** reacts with the more and/or the less basic nitrogen atom of hydrazone. It is then expected that both **1** and **2** would give the (4+2) cycloadducts as predominant products in the reaction with hydrazones having electronwithdrawing groups such as *p*-tosyl and benzoyl.

However, **1** did not react with *p*-tosylhydrazones, **17a** and **17b**, and cyclohexanone benzoylhydrazone (**18**) even when the reaction was carried out under reflux in benzene.

The reaction of **2** with *p*-tosylhydrazones, **17a** and **17b**, afforded the corresponding (4+2) cycloadducts, **19a** and **19b**, whose structures were confirmed on the basis of their spectral data and of the result of hydrolysis.

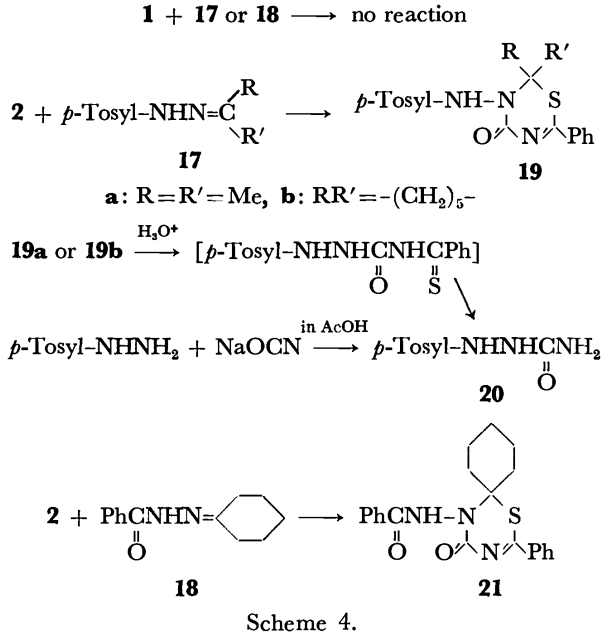

Scheme 4.

Hydrolyses of both **19a** and **19b** afforded 1-*p*-tosylsemicarbazide (**20**), which was identical with an authentic sample prepared from *p*-tosylhydrazine and cyanic acid.

Similarly, **2** reacted with benzoylhydrazone **18** to give the corresponding (4+2) cycloadduct **21** (Scheme 4).

Experimental

All melting and boiling points are uncorrected. The IR spectra were measured as KBr disks, and NMR spectra were determined at 60 MHz with a Hitachi R-20 NMR spectrometer with TMS as an internal reference.

Materials. Benzoyl isocyanate (**1**) was prepared by the reported method.[12] Thiobenzoyl isocyanate (**2**): a solution of 1.0 g of 2-phenylthiazoline-4,5-dione in 10 ml of xylene was heated at 120 °C, giving a reddish violet solution of **2** which was used *in situ*.[13] This solution is referred to as the standard solution of **2**.

Hydrazones were prepared by the reaction of the corresponding hydrazine with carbonyl coumpounds. Benzaldehyde phenyl- (**3a**), mp 152 °C [lit,[14] mp 152.5 °C]; *p*-tolyl- (**3b**), mp 125 °C [lit,[15] mp 125 °C]; *p*-chlorophenylhydrazone (**3c**), mp 129—130 °C [lit,[16] mp 127 °C]; acetone phenyl- (**4a**)- mp 32 °C [lit,[17] mp 21 °C]; *p*-tolyl- (**4b**), mp 51—52 °C [lit,[18] mp 50—52 °C]; *p*-nitrophenylhydrazone (**4c**), mp 149 °C [lit,[19] mp 148—148.5 °C]; benzaldehyde methylhydrazone (**12a**), viscous liquid, NMR ($CDCl_3$) δ: 2.76 (3H, s, N-C**H**$_3$), 5.61 (1H, s, =C**H**), 7.1—7.6 (6H, m, aromatic and N**H**); acetone methylhydrazone (**12b**), bp 115—117 °C, NMR ($CDCl_3$) δ: 1.73, 1.89 (each 3H, s, C**H**$_3$), 2.85 (3H, s, N-C**H**$_3$), 4.32 (1H, broad, N**H**); acetone *p*-tosyl- (**17a**), mp 150 °C [lit,[20] mp 153 °C]; cyclohexanone *p*-tosylhydrazone (**17b**), mp 158 °C [lit,[20] mp 156 °C]; cyclohexanone benzoylhydrazone (**18**), mp 158—159 °C [lit,[21] mp 158—159 °C].

Reaction of 1 with 3a. To a solution of 2.0 g of **3a** in 20 ml of benzene was added 1.5 g of **1** at 0 °C, and then the reaction mixture was stirred at room temperature for 30 min: during which time crystals precipitated. Filtration gave 1.4 g of crystals. The filtrate was evaporated *in vacuo* to leave 2.0 g of crystals. Recrystallization of the combined crystals (3.5 g, 97%) from ethanol afforded 4-benzoyl-2-phenylsemicarbazone (**5a**), mp 164 °C, as colorless needles.

Found: C, 73.32; H, 5.01; N, 12.33%. Calcd for $C_{21}H_{17}N_3O_2$: C, 73.45; H, 4.99; N, 12.24%.

Similarly, **1** reacted with **3b** and **3c** under the same conditions, giving the corresponding semicarbazones quantitatively.

4-Benzoyl-2-*p*-tolylsemicarbazone (**5b**): mp 175—176 °C, colorless needles.

Found: C, 74.21; H, 5.20; N, 11.75%. Calcd for $C_{22}H_{19}N_3O_2$: C, 73.93; H, 5.36; N, 11.75%.

IR: 3380 (NH), 1755 (C=O), 1500 and 1480 cm^{-1} (Amide II).

4-Benzoyl-2-*p*-chlorophenylsemicarbazone (**5c**): mp 177—178 °C, colorless needles.

Found: C, 67.02; H, 4.12; N, 11.14%. Calcd for $C_{21}H_{16}N_3O_2Cl$: C, 66.75; H, 4.24; N, 11.13%.

IR: 3380 (NH), 1750 (C=O), 1500 and 1480 (Amide II).

Reaction of 1 with 4b. To a solution of 4.0 g of **4b** in 20 ml of benzene was added 3.6 g of **1** at 0 °C, and the reaction mixture was stirred at room temperature for 30 min. The mixture was concentrated *in vacuo* to give resinous material, which on trituration with petroleum ether (bp 35—50 °C) crystallized. Recrystallization from ethanol gave 6.8 g (90%) of 4-benzoyl-3,3-dimethyl-1-*p*-tolyl-*s*-triazolidin-5-one (**6b**), mp 161—162 °C (decomp.), as colorless prisms.

Found: C, 70.17; H, 6.22; N, 13.55%. Calcd for $C_{18}H_{19}N_3O_2$: C, 69.88; H, 6.19; N, 13.58%.

IR: 3250 (NH), 1750, 1655 (C=O) and 1320 cm^{-1}. NMR ($CDCl_3$) δ: 1.70 (6H, s, C**H**$_3$), 2.28 (3H, s, -C_6H_4C**H**$_3$), 4.1 (1H, broad, N**H**), 7.0—7.7 (9H, m, aromatic protons).

Similarly, the reaction of **1** with **4a** and **4c** under the same conditions gave the corresponding *s*-triazolidin-5-ones in almost quantitative yields, respectively.

4-Benzoyl-3,3-dimethyl-1-phenyl-*s*-triazolidin-5-one (**6a**): mp 140.5—141 °C (decomp.), colorless prisms.

Found: C, 69.31; H, 6.02; N, 14.12%. Calcd for $C_{17}H_{17}N_3O_2$: C, 69.13; H, 5.80; N, 14.23%.

4-Benzoyl-3,3-dimethyl-1-*p*-nitrophenyl-*s*-triazolidin-5-one (**6c**): mp 203.5 °C (decomp.), pale yellow prisms.

Found: C, 59.95; H, 4.52; N, 16.52%. Calcd for $C_{17}H_{16}N_4O_4$: C, 59.99; H, 4.74; N, 16.46%.

IR: 3230 (NH), 1750, 1660 (C=O) and 1320 cm^{-1}.

Hydrolysis of 5a. A solution of 0.3 g of **5a** in 10 ml of 15% hydrochloric acid was heated at 100 °C for 1 hr. After cooling, filtration gave crystals. Recrystallization from

ethanol afforded 0.24 g (100%) of 1,3-diphenyl-Δ^3-*s*-triazolin-5-one (**7a**), mp 230—231 °C, which was identical with an authentic sample.[2]

Similarly, hydrolysis of **5b**, **5c**, and **6a**—**6c** with hydrochloric acid afforded the corresponding Δ^3-*s*-triazolin-5-ones in good yields, respectively. 1-*p*-Tolyl- (**7b**), mp 232.5 °C [lit,[2] mp 232.5 °C], 1-*p*-chlorophenyl- (**7c**), mp 273 °C [lit,[2] mp 273 °C], and 1-*p*-nitrophenyl-3-phenyl-Δ^3-*s*-triazolin-5-one (**7d**), mp 329—330 °C [lit,[2] mp 329—330 °C], were identified with the respective authentic samples.[2]

Reaction of 2 with 3a. To a standard solution of **2** was added 1.0 g of **3a** at 0 °C: crystals precipitated immediately. Filtration gave pale yellow crystals, which on recrystallization from ethanol afforded 1.5 g (79% yield based on 2-phenylthiazoline-4,5-dione used) of 2-phenyl-4-thiobenzoylsemicarbazone (**8**), mp 163—163.5 °C (decomp.), as pale yellow prisms.

Found: C, 70.38; H, 4.62; N, 11.48%. Calcd for $C_{21}H_{17}N_3OS$: C, 70.18; H, 4.77; N, 11.69%.

IR: 3400 (NH), 1720 (C=O) and 1460 cm^{-1} (Amide II). NMR ($CDCl_3$) δ: 7.1—7.9 (16H, m, aromatic and N=C**H**), 11.5 (1H, broad, N**H**).

Reaction of 2 with 4a. To a standard solution of **2** was added 0.78 g of **4a** at 0 °C, and the reaction mixture was stirred at room temperature for 1 hr: during which time crystals appeared. Filtration gave crystals, which on recrystallization from acetone afforded 0.97 g (60%) of 3-anilino-2,2-dimethyl-6-phenyl-2,3-dihydro-4*H*-1,3,5-thiadiazin-4-one (**10a**), mp 124—125 °C (decomp.), as yellow prisms.

Found: C, 65.54; H, 5.40; N, 13.72%. Calcd for $C_{17}H_{17}N_3OS$: C, 65.58; H, 5.50; N, 13.50%.

The filtrate was concentrated *in vacuo* below 15 °C to leave a residue, which on trituration with diethyl ether gave crystals. Recrystallization from ethanol afforded 0.31 g (19%) of 3,3-dimethyl-1-phenyl-4-thiobenzoyl-*s*-triazolin-5-one (**9a**), mp 141 °C (decomp.), as yellow needles.

Found: C, 65.64; H, 5.26; N, 13.77%. Calcd for $C_{17}H_{17}N_3OS$: C, 65.58; H, 5.50; N, 13.50%.

IR: 3270 (NH), 1720 (C=O) and 1350 cm^{-1}.

Similarly, the reaction of **2** with **4b** afforded the corresponding 1:1 adducts, **9b** and **10b**, in 32 and 29% yields, respectively.

3,3-Dimethyl-4-thiobenzoyl-1-*p*-tolyl-*s*-triazolidin-5-one (**9b**): mp 151.5—152 °C (decomp.), yellow needles.

Found: C, 66.69; H, 5.90; N, 13.00%. Calcd for $C_{18}H_{19}N_3OS$: C, 66.44; H, 5.89; N, 12.92%.

IR: 3260 (NH), 1720 (C=O), 1340 and 1330 cm^{-1}. NMR ($CDCl_3$) δ: 1.90 (6H, s, C**H**$_3$), 2.30 (3H, s, -C_6H_4C**H**$_3$), 5.05 (1H, broad, N**H**), 7.0—7.8 (9H, m, aromatic protons).

2,2-Dimethyl-3-*p*-methylanilino-6-phenyl-2,3-dihydro-4*H*-1,3,5-thiadiazin-4-one (**10b**): mp 115—116 °C (decomp.), yellow prisms.

Found: C, 66.58; H, 5.93; N, 12.89%. Calcd for $C_{18}H_{19}N_3OS$: C, 66.44; H, 5.89; N, 12.92%.

IR: 3310 (NH), 1660 (C=O), 1550 and 1520 cm^{-1}. NMR ($CDCl_3$) δ: 1.80 (6H, s, C**H**$_3$), 2.26 (3H, s, -C_6H_4C**H**$_3$), 6.4 (1H, broad, N**H**), 6.8—7.6 (7H, m, aromatic protons), 8.0—8.3 (2H, m, *o*-protons of 6-phenyl).

Hydrolysis of 10a. A solution of 1.5 g of **10a** in 20 ml of methanol was refluxed with concentrated hydrochloric acid (5 ml) for 30 min. The mixture was concentrated *in vacuo* to leave a residue, which on trituration with aqueous ethanol gave crystals. Recrystallization from ethanol afforded 0.79 g (69%) of 3-hydroxy-1,5-diphenyl-*s*-triazole (**11**), mp 290 °C [lit,[2] mp 290 °C], as colorless needles.

Reaction of 1 with 12a. To a solution of 1.34 g of **12a** in 10 ml of benzene was added 1.47 g of **1** at 0 °C, and then the reaction mixture was stirred at room temperature for 30 min. The mixture was concentrated *in vacuo* to leave a residue, which on trituration with petroleum ether (bp 40—60 °C) gave crystals. Recrystallization from a mixture of benzene and petroleum ether (bp 60—80 °C) afforded 2.4 g (86%) of benzaldehyde 4-benzoyl-2-methylsemicarbazone (**13a**), mp 137—138 °C (decomp.), as colorless needles.

Found: C, 68.54; H, 5.23; N, 14.90%. Calcd for $C_{16}H_{15}N_3O_2$: C, 68.31; H, 5.38; N, 14.94%.

IR: 3450 (NH), 1745 (C=O), 1510 and 1490 cm^{-1} (Amide II). NMR ($CDCl_3$) δ: 3.43 (3H, s, N-C**H**$_3$), 7.3—8.0 (11H, m, aromatic and N=C**H**), 10.45 (1H, broad, N**H**).

Similarly, the reaction of a standard solution of **2** with **12a** gave the 2-methyl-4-thiobenzoylsemicarbazone **13b**, mp 146—147 °C (decomp.), in 74% yield.

Found: C, 64.61; H, 4.95; N, 13.94%. Calcd for $C_{16}H_{15}N_3OS$: C, 64.63; H, 5.09; N, 14.14%.

IR: 3370 (NH), 1735 (C=O) and 1505 cm^{-1} (Amide II). NMR ($CDCl_3$) δ: 3.41 (3H, s, N-C**H**$_3$), 7.3—7.9 (11H, m, aromatic and N=C**H**), 11.4 (1H, broad, N**H**).

Reaction of 1 with 12b. To a solution of 0.86 g of **12b** in 15 ml of benzene was added 1.47 g of **1**, and then the reaction mixture was stirred at room temperature for 10 hr. The mixture was concentrated *in vacuo* to leave a residue, which on trituration with petroleum ether (bp 40—60 °C) gave crystals. The crystals were washed with benzene and then diethyl ether to afford 1.65 g (71%) of 4-benzoyl-1,3,3-trimethyl-*s*-triazolidin-5-one (**15a**), mp 105.5—107 °C (decomp.).

Found: C, 61.78; H, 6.33; N, 18.27%. Calcd for $C_{12}H_{15}N_3O_2$: C, 61.78; H, 6.48; N, 18.02%.

IR: 3230 (NH), 1735 and 1645 cm^{-1} (C=O). NMR ($CDCl_3$) δ: 1.80 (6H, s, C**H**$_3$), 3.14 (3H, s, N-C**H**$_3$), 4.5 (1H, broad, N**H**), 7.3—7.9 (5H, m, aromatic protons).

Similarly, the reaction of a standard solution of **2** with **12b** at 0 °C for 10 min afforded 67% yield of the corresponding *s*-triazolidin-5-one **15b**, mp 106.5—107.5 °C (decomp.), as yellow needles.

Found: C, 57.97; H, 5.89; N, 17.09%. Calcd for $C_{12}H_{15}N_3OS$: C, 57.82; H, 6.07; N, 16.86%.

IR: 3240 (NH) and 1735 cm^{-1} (C=O).

Hydrolysis of 15b. A solution of 0.2 g of **15b** in 10 ml of methanol was stirred with concentrated hydrochloric acid (1 ml) at room temperature for 1 hr: during which time hydrogen sulfide evolved and the mixture turned into a colorless solution. The solution was concentrated *in vacuo* to leave crystals, which on recrystallization from ethanol afforded 0.13 g (93%) of 1-methyl-3-phenyl-Δ^3-*s*-triazolin-5-one (**16**), mp 216.5—217.5 °C, as colorless needles.

Found: C, 61.89; H, 4.96; N, 24.19%. Calcd for $C_9H_9N_3O$: C, 61.70; H, 5.18; N, 23.99%.

IR: 2800—3140 (NH) and 1690 cm^{-1} (C=O). NMR ($CDCl_3$) δ: 3.56 (3H, s, N-C**H**$_3$), 7.4—8.0 (5H, m, aromatic protons), 11.1 (1H, broad, N**H**).

General Kinetic Method. After a solution of **1** in benzene or chloroform was mixed with equimolar amount of **12b** or **4a** at −70 °C, a part of the solution was quickly transferred into a NMR-measurement tube and then the variation in the semicarbazone/*s*-triazolidin-5-one ratio was followed by the NMR spectrum at a constant temperature.

Reaction of 2 with 17a. A standard solution of **2** was heated with 1.09 g of **17a** at 50—70 °C for 5 min, and then the mixture was stirred at room temperature for 1 hr: during which time crystals precipitated. Recrystallization from a mixture of benzene and petroleum ether (bp 60—80 °C) afforded 1.38 g (73%) of 2,2-dimethyl-6-phenyl-3-*p*-tosylamino-2,3-dihydro-4*H*-1,3,5-thiadiazin-4-one (**19a**), mp 149

°C (decomp.), as colorless needles.

Found: C, 55.76; H, 4.91; N, 10.67%. Calcd for $C_{18}H_{19}N_3O_3S_2$: C, 55.52; H, 4.92; N, 10.79%.

IR: 3220 (NH) and 1685 cm^{-1} (C=O). NMR ($CDCl_3$) δ: 1.74, 2.01 (each 3H, s, CH_3), 2.42 (3H, s, $-C_6H_4CH_3$), 7.2—8.1 (10H, m, aromatic and NH).

Similarly, **2** reacted with **17b** to give 63% yield of the corresponding 2,3-dihydro-4*H*-1,3,5-thiadiazin-4-one **19b**, mp 151.5—152 °C (decomp.), as colrless prisms.

Found: C, 59.01; H, 5.36; N, 9.80%. Calcd for $C_{21}H_{23}N_3O_3S_2$: C, 58.73; H, 5.40; N, 9.79%.

IR: 3250 (NH) and 1685 cm^{-1} (C=O). NMR ($CDCl_3$) δ: 2.40 (3H, s, $-C_6H_4CH_3$), 1.5—2.7 (10H, m, CH_2), 7.0—8.1 (10H, m, aromatic and NH).

1-p-Tosylsemicarbazide (20). i) A solution of 0.5 g of **19a** in 10 ml of methanol was refluxed with concentrated hydrochloric acid (5 ml) for 30 min. The mixture was concentrated *in vacuo* to leave crystals, which on recrystallization from ethanol gave 0.21 g (72%) of **20** as colorless prisms, mp 243 °C (decomp.).

Found: C, 41.72; H, 4.73; N, 18.63%. Calcd for $C_8H_{11}N_3O_3S$: C, 41.92; H, 4.84; N, 18.34%.

IR: 3480, 3390, 3060 (NH), 1650 (C=O) and 1170 cm^{-1} (SO_2).

Similarly, hydrolysis of **19b** (0.8 g) with concentrated hydrochloric acid (10 ml) at 100 °C for 5 hr gave 0.43 g (100%) of **20**.

ii) To a suspension of 0.8 g of *p*-tosylhydrazine in 10 ml of acetic acid was slowly added 2.0 g of sodium cyanate at room temperature. The mixture was heated at 70—80 °C for 10 min, and then stirred at room temperature for 1 hr. After it was poured into ice-water, filtration gave crystals, which on recrystallization from ethanol afforded 0.75 g (76.5 %) of **20**, mp 243 °C (decomp.).

Reaction of 2 with 18. To a standard solution of **2** was added 1.13 g of **18** at 0 °C, and the mixture was then stirred at room temperature for 1 hr: during which time crystals precipitated. Recrystallization from benzene afforded 1.5 g (76%) of the 2,3-dihydro-4*H*-1,3,5-thiadiazin-4-one **21**, mp 158.5—159 °C (decomp.), as yellow needles.

Found: C, 66.55; H, 5.75; N, 10.86%. Calcd for $C_{21}H_{21}N_3O_2S$: C, 66.48; H, 5.58; N, 11.08%.

IR: 3320 (NH), 1695 and 1665 cm^{-1} (C=O). NMR ($CDCl_3$) δ: 1.2—1.9 (6H, m, CH_2), 1.9—2.5 (4H, m, CH_2), 7.0—8.2 (10H, m, aromatic protons), 9.91 (1H, s, NH).

This work was supported in part by a Grant-in-Aid of Industrial Scientific Research from the Asahi Glass Co., Ltd. for which the authors' thanks are due.

References

1) Part XIII of this series: O. Tsuge and S. Kanemasa, *J. Org. Chem.*, **38**, 2972 (1973).
2) O. Tsuge, S. Kanemasa, and M. Tashiro, *Tetrahedron*, **24**, 5205 (1968).
3) H. Schildknecht and G. Hatzmann, *Ann. Chem.*, **724**, 226 (1969).
4) A. Arnold, *Ber.*, **30**, 1015 (1897).
5) R. C. Goodwin and J. R. Bailey, *J. Amer. Chem. Soc.*, **46**, 2827 (1924).
6) L. Rolla, *Gazz. chim. ital.*, **38, I**, 327 (1908).
7) O. Tsuge and K. Sakai, This Bulletin, **45**, 1534 (1972).
8) O. Tsuge and S. Kanemasa, *ibid.*, **45**, 2877 (1972).
9) O. Tsuge and S. Kanemasa, *ibid.*, **45**, 3591 (1972).
10) O. Tsuge and S. Kanemasa, *Tetrahedron*, **28**, 4737 (1972).
11) The NMR spectrum of semicarbazone **12b** exhibited three singlets ascribable to two methyls-protons of isopropylidene group and *N*-methyl-protons at δ 1.73, 1.89, and 2.85 ppm, respectively.
12) A. J. Speziale and L. R. Smith, *J. Org. Chem.*, **27**, 4361 (1962); *ibid.*, **28**, 1805 (1963).
13) J. Goerdeler and H. Schenk, *Chem. Ber.*, **98**, 2954 (1965).
14) E. Fischer, *Ann. Chem.*, **190**, 67 (1877).
15) H. von Pechmann and P. Runge, *Ber.*, **27**, 1693 (1894).
16) J. T. Hewitt, *J. Chem. Soc.*, **63**, 868 (1893).
17) W. Theilacker and H. J. Tomuschat, *Ber.*, **88**, 1086 (1955).
18) J. Raschen, *Ann. Chem.*, **239**, 223 (1887).
19) E. Bamberger and H. Sternitzki, *Chem. Ber.*, **26**, 1291 (1893).
20) W. R. Bamford and T. S. Stevens, *J. Chem. Soc.*, **1952**, 4735.
21) O. Tsuge, M. Tashiro, and K. Hokama, *Kogyo Kagaku Zasshi*, **71**, 1203 (1968).

The Crystal and Molecular Structure of Tyramine Hydrochloride

Kyoko TAMURA, Akio WAKAHARA, Takaji FUJIWARA, and Ken-ichi TOMITA
Faculty of Pharmaceutical Sciences, Osaka University, Toneyama, Toyonaka, Osaka 560
(Received May 2, 1974)

The structure of tyramine hydrochloride has been determined by X-ray diffraction method using the data collected by counter diffractometer techniques. Crystals are orthorhombic, with space group *Pbcn*, $Z=8$, $a=19.961$, $b=10.756$, and $c=8.243$ Å. The structure was solved by the direct method with the symbolic addition procedure, and refined by least-squares method. The atoms constituting the tyramine cation lie on the two planes, that is, that of the phenol ring and that of the extended side chain. The dihedral angle between these two planes is 71°. The extended conformation about the C–C bond of aminoethyl group is such that the NH_3^+ group is *trans* with respect to the phenol ring. Half-weighted two independent chlorine ions are found on the two-fold axis with distance of 4.5 Å, having some different modes of hydrogen-bonding system for these two ions.

Tyramine, the decarboxylated amine of tyrosine, is a precursor of *p*-hydroxyphenylacetate in the metabolic pathway of L-tyrosine. It is of particular interest to investigate systematically the structure-activity relationship among tyrosine metabolites, in view of some very important findings about the correlation between the molecular structures and metabolic pathway of tryptophan which were already reported by us.[1-4] This work is undertaken as a part of the programme of studying the crystal structures of the aromatic amino acid metabolites.

Experimental

Commercially obtained tyramine hydrochloride was dissolved in methanol. By slow evaporation, very thin colorless plate-like crystals were grown at room temperature. Oscillation and Weissenberg photographs around the *b*- and *c*-axes showed the crystal to be orthorhombic. From the systematic extinctions, the space group was uniquely determined as *Pbcn*. Unit cell parameters were determined with a Rigaku Denki four circle diffractometer. Density was measured by the flotation method in a mixture of benzene and carbon tetrachloride. The crystal data are listed in Table 1. Three-

Table 1. Crystal data of tyramine hydrochloride

$C_8H_{11}NO\cdot HCl$, M.W. 173.64
colorless and transparent plates, Orthorhombic
$a=19.961(14)$, $b=10.756(7)$, $c=8.243(3)$ Å
$V=1769.8$ Å^3, $Z=8$, $F(000)=736$
μ(for Cu$K\alpha$) $=33.7$ cm^{-1}
$D_m=1.301$ g/cm^3, $D_x=1.303$ g/cm^3
$(0kl)$: $k=2n+1$
Absent spectra; $(h0l)$: $l=2n+1$
$(hk0)$: $h+k=2n+1$
Space group; *Pbcn*

dimensional intensity data were recorded on a computer-controlled four circle diffractometer with Ni-filtered Cu-$K\alpha$ radiation using a crystal mounted about the *b*-axis. The ω-2θ scanning mode was employed at a rate of 2° per minute through the scanning range of $2\theta-0.6°$ for $K\alpha_1$ and $2\theta+0.6°$ for $K\alpha_2$. Background countings were taken for 10 seconds at both sides of each peak. In order to correct the intensities for coincidence loss, the counting rate was kept less than 8000 counts per second with an automatic attenuator mechanism. The intensities of three standard reflections measured for every 25 reflections of the data set showed no decrease in intensity during the run.

The intensities were measured for the 1168 independent reflections with $\sin\theta/\lambda$ less than 0.54. Of these, 576 had the net intensity exceeded three times of its estimated standard deviation; the rest was regarded as unobserved reflections. The data were then adjusted to the absolute scale and normalized structure factor, E, and a list of $\sum_2$ relationships with proper probabilities were calculated.

Determination and Refinement of Structure

The structure of tyramine hydrochloride was solved by direct phase determination using the symbolic addition procedure.[5] Reflections with $|E|>1.2$ were selected, five of them being given a sign or a letter symbol as follows;

h	k	l	phase	$\|E\|$
1	10	1	+	3.035
13	5	2	+	3.185
15	5	1	+	2.567
18	2	2	A	2.989
15	7	2	B	3.140

The phases of 137 reflections were determined in terms of starting signs and letters, and three-dimensional E-maps were computed for the possible four cases. Of these E-maps, one (A=−, B=+) clearly revealed two independent high peaks corresponding to two chlorine atoms, with a distance of 4.5 Å lying on the two-fold axis. Furthermore, the benzene ring plane enables us to distinguish the peaks of tyramine cation from other spurious ones on this map. The positional coordinates of the twelve atoms as selected from the E-map were refined by successive Fourier syntheses.

Further refinement was carried out by the full-matrix least-squares method with unit weight. Four cycles of refinement with the isotropic temperature factor reduced an R index ($R=\sum||F_o|-|F_c||/\sum|F_o|$) to 0.157. More five cycles with anisotropic temperature factors for all non-hydrogen atoms decreased an R value to 0.129. At this stage, a difference Fourier synthesis was calculated to determine the locations of hydrogen atoms. Nine of twelve hydrogen atoms were satisfactorily located with reasonable peak heights. However, three peaks corresponding to ammonium hydrogen atoms were obscure. The positional parameters of these hydrogen atoms were estimated as follows. The amino nitrogen atom has three chlorine neighbors at reasonable

TABLE 2. OBSERVED AND CALCULATED STRUCTURE FACTORS FOR TYRAMINE HYDROCHLORIDE

The columns in each group headed by the values of h and l give k, $2|F_o|$, and $2|F_c|$.

K	FO	FC	K	FO	FC	K	FO	FC	K	FO	FC	K	FO	FC	K	FO	FC	K	FO	FC
H,L= 0 0			2	84	-90	2	27	31	H,L= 13 2			1	32	31	1	25	17	0	39	21
2	75	-71	4	78	84	H,L= 19 1			0	23	-12	2	31	-32	5	33	-43	4	43	45
4	75	66	6	30	-30	1	24	28	1	24	-26	3	69	-81	6	23	-14	5	22	24
8	41	49	8	104	-101	3	35	32	2	35	45	6	30	25	H,L= 16 4			7	62	74
H,L= 1 0			10	40	-33	H,L= 20 1			3	30	30	H,L= 15 3			1	28	24	H,L= 4 6		
1	41	36	H,L= 1 1			2	34	40	4	51	57	1	26	-27	2	32	37	0	75	-64
3	115	-101	1	39	-37	H,L= 0 2			5	116	119	3	26	-25	5	25	1	2	60	-54
5	169	-157	2	296	306	0	156	141	6	25	-20	4	26	33	H,L= 17 4			4	37	-32
7	47	-41	3	41	36	2	375	-411	7	33	-17	H,L= 16 3			3	23	-17	H,L= 5 6		
9	103	-100	4	43	-42	6	65	-61	H,L= 14 2			2	43	-44	H,L= 18 4			3	56	52
11	24	-14	5	108	102	8	34	35	0	91	-95	H,L= 17 3			0	82	73	4	44	-48
H,L= 2 0			7	44	-41	10	22	-23	4	25	-20	2	48	-60	1	24	-14	5	40	46
0	43	53	9	51	-51	H,L= 1 2			H,L= 15 2			3	29	-34	3	31	20	6	29	27
2	68	65	10	65	66	0	209	207	0	29	-29	4	34	32	H,L= 19 4			H,L= 6 6		
6	57	50	H,L= 2 1			1	82	-92	3	30	17	H,L= 19 3			1	23	22	0	66	-65
10	80	73	2	74	77	2	76	80	5	26	19	3	25	-16	H,L= 0 5			2	31	-28
H,L= 3 0			4	160	147	3	147	170	7	47	52	H,L= 0 4			2	101	99	6	29	-23
1	65	-64	6	37	38	5	82	86	H,L= 16 2			0	204	188	4	35	43	H,L= 7 6		
3	144	-124	7	26	26	6	34	33	0	97	-97	2	35	-31	H,L= 1 5			3	30	36
5	249	-218	8	34	-30	7	100	106	3	52	-59	4	65	66	1	78	71	4	28	17
7	54	-52	9	33	29	9	22	33	7	39	22	6	51	-56	3	41	45	5	26	44
9	42	-31	10	23	-23	10	37	-41	H,L= 17 2			8	38	44	8	23	-30	H,L= 8 6		
H,L= 4 0			11	40	-35	11	24	11	0	42	49	10	58	70	H,L= 2 5			0	106	-97
0	174	172	H,L= 3 1			H,L= 2 2			5	34	31	H,L= 1 4			1	29	-17	2	29	-33
2	256	242	1	90	88	0	324	-319	H,L= 18 2			0	59	-49	2	37	39	H,L= 9 6		
4	97	84	2	36	38	1	130	141	2	56	-64	1	71	-67	6	30	-33	0	32	-34
10	58	54	3	185	174	2	99	-118	H,L= 21 2			5	90	-104	8	32	-18	1	25	-21
H,L= 5 0			4	102	-94	3	69	-74	0	25	-17	7	64	-72	9	32	-5	3	28	29
1	24	-27	5	63	57	4	28	16	H,L= 0 3			9	36	-30	H,L= 3 5			4	22	14
3	32	20	H,L= 4 1			7	50	49	2	105	-118	H,L= 2 4			3	33	44	5	38	47
5	60	-58	1	119	-112	8	58	-60	4	42	-50	0	134	128	5	22	-6	6	23	7
7	197	-174	2	123	122	9	32	-33	10	24	21	1	23	-28	6	38	44	H,L= 10 6		
9	29	-22	3	158	152	10	28	-26	H,L= 1 3			2	123	129	7	24	-26	0	82	-85
H,L= 6 0			5	125	-124	H,L= 3 2			1	44	-45	3	27	16	9	25	-25	1	43	-39
0	154	158	8	41	-39	0	93	96	3	102	-110	4	67	83	H,L= 4 5			H,L= 11 6		
2	183	179	10	43	-35	1	79	74	4	56	-60	5	29	-30	3	58	51	0	24	29
4	51	49	H,L= 5 1			2	142	-156	6	27	-19	7	31	14	5	33	-45	1	36	25
6	52	-52	1	85	84	3	109	125	8	68	-70	10	38	32	6	46	45	2	34	9
8	33	31	2	36	31	4	43	-41	10	35	39	H,L= 3 4			8	42	-46	H,L= 12 6		
10	37	40	3	77	75	5	43	46	H,L= 2 3			1	33	42	H,L= 5 5			0	24	-21
H,L= 7 0			4	50	-45	6	38	38	1	126	-127	3	50	-43	2	39	41	H,L= 14 6		
1	40	-38	5	27	-29	7	115	122	2	47	-45	4	45	51	3	56	60	0	40	-36
3	39	-35	6	34	39	9	25	25	3	72	-78	5	113	-124	4	47	-50	2	22	-25
5	126	-119	9	24	-27	H,L= 4 2			5	40	41	7	25	-26	5	41	46	H,L= 1 7		
7	78	-78	H,L= 6 1			0	178	-179	7	38	-35	9	37	-49	H,L= 6 5			3	39	-34
9	30	-24	2	134	133	1	41	-38	8	48	55	H,L= 4 4			2	41	37	H,L= 2 7		
H,L= 8 0			4	26	16	2	112	-126	10	37	34	0	138	125	3	27	29	1	27	11
0	213	207	5	59	49	3	69	-79	H,L= 3 3			2	51	50	4	49	56	2	32	-32
2	109	104	10	26	-34	4	55	-57	2	81	-88	3	53	60	5	23	-15	4	25	-12
4	46	42	H,L= 7 1			7	25	17	4	41	48	4	29	-31	H,L= 7 5			5	23	3
8	23	32	1	66	66	10	28	-38	5	59	-63	7	38	-26	1	22	-24	H,L= 3 7		
10	24	29	3	74	72	H,L= 5 2			6	69	70	8	27	24	2	30	27	3	28	-10
H,L= 9 0			5	25	26	0	25	25	9	41	43	H,L= 5 4			3	29	29	H,L= 4 7		
1	45	-47	8	35	-22	2	56	51	H,L= 4 3			0	23	-29	5	34	34	2	27	-29
3	44	-46	9	47	-30	3	44	43	1	122	-123	1	26	-14	6	35	38	4	25	-17
5	92	-88	H,L= 8 1			4	34	-33	2	46	-46	2	66	65	7	25	-5	5	29	-26
7	87	-81	1	33	-34	5	152	152	3	117	122	3	70	-75	H,L= 8 5			6	41	43
9	26	-14	2	85	84	6	35	30	4	101	-109	5	48	-57	1	24	-6	H,L= 5 7		
H,L= 10 0			4	44	42	7	44	57	5	23	12	7	50	-63	4	47	40	2	24	14
0	120	-108	10	32	-40	9	52	46	9	24	14	9	32	-28	H,L= 9 5			3	32	-22
2	127	128	H,L= 9 1			H,L= 6 2			10	26	33	H,L= 6 4			1	57	54	H,L= 6 7		
4	39	35	1	121	108	0	150	-148	H,L= 5 3			0	152	139	2	25	-4	1	31	-24
10	45	49	2	88	84	2	143	-149	1	33	-32	2	78	76	4	27	-9	2	22	0
H,L= 11 0			3	71	72	3	27	23	3	50	-54	3	31	29	5	27	30	3	28	11
1	38	33	5	35	26	4	52	-52	5	45	-52	4	34	42	7	30	-36	6	31	-35
3	58	-53	8	28	-11	5	23	23	9	33	29	H,L= 7 4			8	31	-37	H,L= 7 7		
5	70	-64	10	39	32	7	28	-22	H,L= 6 3			0	50	-50	H,L= 10 5			1	27	-9
7	90	-80	H,L= 10 1			10	34	-37	1	48	-52	3	50	-48	1	47	-46	2	30	-5
9	27	-15	1	77	-68	H,L= 7 2			8	40	37	5	49	-51	4	26	23	5	24	-27
H,L= 12 0			2	80	78	0	47	-40	10	28	29	7	58	-64	H,L= 11 5			H,L= 9 7		
0	137	134	4	48	45	1	23	21	H,L= 7 3			H,L= 8 4			3	35	35	1	31	34
2	143	136	H,L= 11 1			5	95	99	1	76	-84	0	90	85	5	27	23	5	26	-7
H,L= 13 0			2	75	-68	7	91	90	3	70	-73	1	28	37	6	25	16	H,L= 11 7		
3	80	-77	3	60	58	9	40	28	4	33	-37	2	60	56	H,L= 12 5			1	33	-37
5	39	36	H,L= 12 1			H,L= 8 2			7	32	23	3	48	-45	2	48	53	2	24	-25
7	99	-105	1	50	-44	0	29	-35	H,L= 8 3			H,L= 9 4			3	36	39	H,L= 0 8		
9	24	-17	2	28	22	1	37	29	2	91	-92	0	55	47	H,L= 13 5			0	76	67
H,L= 14 0			3	62	57	2	97	-99	4	36	-39	3	47	-41	1	26	23	2	24	24
0	73	73	4	24	15	3	23	-26	8	24	11	4	27	-18	2	31	17	H,L= 1 8		
2	28	29	6	26	-27	4	45	-51	9	33	22	5	50	-46	3	36	35	0	31	9
4	65	-59	8	30	-40	9	29	14	10	23	14	7	57	-61	H,L= 14 5			3	24	-34
6	22	28	H,L= 13 1			10	41	-47	H,L= 9 3			H,L= 10 4			1	31	28	H,L= 2 8		
8	31	32	3	25	31	H,L= 9 2			1	35	30	0	60	51	2	30	34	0	41	23
H,L= 15 0			4	43	42	1	39	33	2	48	49	1	35	31	5	22	18	H,L= 3 8		
1	30	32	5	41	38	3	36	33	3	72	-72	2	93	104	H,L= 15 5			0	24	11
3	112	-117	6	29	19	5	86	90	4	41	-45	8	25	-8	1	26	23	H,L= 4 8		
5	74	-70	9	31	-25	7	47	55	9	26	28	H,L= 11 4			4	22	19	0	45	51
7	34	22	H,L= 14 1			H,L= 10 2			H,L= 10 3			0	71	62	H,L= 17 5			2	34	32
H,L= 16 0			1	44	41	0	200	-212	8	39	47	1	36	35	1	36	37	H,L= 5 8		
0	66	64	3	86	-83	1	49	-51	H,L= 11 3			2	22	-17	H,L= 0 6			4	37	-39
2	49	54	4	73	75	3	34	27	5	35	-35	3	69	-68	0	31	32	H,L= 6 8		
H,L= 17 0			5	86	86	5	25	-16	7	30	18	5	48	-50	2	94	-84	0	29	27
7	39	-39	6	23	37	8	23	-26	H,L= 12 3			H,L= 12 4			H,L= 1 6			H,L= 7 8		
H,L= 18 0			H,L= 15 1			H,L= 11 2			1	26	27	0	42	38	0	43	-34	1	23	10
0	77	78	3	48	44	0	52	-54	3	32	43	2	23	34	1	26	12	3	34	-36
4	25	33	5	61	68	2	32	-27	4	47	-53	8	26	34	3	32	29	H,L= 8 8		
6	49	-40	6	40	-45	5	58	64	5	57	-60	H,L= 13 4			5	43	46	0	48	49
H,L= 19 0			H,L= 16 1			7	49	56	8	27	16	2	23	-15	7	43	54	2	37	39
5	35	-34	1	45	49	9	34	45	H,L 13 3			7	72	-77	H,L= 2 6			H,L= 9 8		
H,L= 20 0			4	27	33	H,L= 12 2			1	28	-32	H,L= 14 4			0	83	-67	1	26	5
0	22	2	5	47	-45	0	130	-123	3	32	-43	0	39	33	1	27	-12			
2	25	25	H,L= 17 1			1	37	-43	4	44	-45	2	72	78	2	77	-71			
H,L= 21 0			6	26	-17	2	41	-36	5	28	-26	4	27	25	3	28	13			
1	25	-1	7	24	-25	3	46	39	6	34	-48	6	26	-22	8	22	-21			
H,L= 0 1			H,L= 18 1			4	37	-32	H,L= 14 3			H,L= 15 4			H,L= 3 6					

TABLE 3. FINAL POSITIONAL AND THERMAL PARAMETERS WITH THEIR ESTIMATED STANDARD DEVIATIONS IN PARENTHESES ($\times 10^4$)

The anisotropic temperature factors are expressed in the form of $\exp\{-(B_{11}h^2+B_{22}k^2+B_{33}l^2+B_{12}hk+B_{13}hl+B_{23}kl)\}$.

Atom	x/a	y/b	z/c	B_{11}	B_{22}	B_{33}	B_{12}	B_{13}	B_{23}
Cl (1)	0 (0)	807 (6)	7500 (0)	27 (2)	61 (6)	175 (12)	0 (0)	−59 (11)	0 (0)
Cl (2)	0 (0)	4976 (7)	7500 (0)	38 (2)	56 (5)	185 (13)	0 (0)	43 (13)	0 (0)
C (1)	2312 (8)	3715 (15)	9841 (21)	20 (5)	54 (18)	113 (29)	−23 (17)	35 (23)	11 (45)
C (2)	2714 (10)	2768 (19)	10392 (25)	31 (7)	74 (21)	199 (44)	−6 (22)	30 (27)	2 (57)
C (3)	3398 (8)	2669 (15)	9891 (25)	15 (5)	51 (16)	186 (36)	4 (15)	4 (25)	8 (49)
C (4)	3649 (8)	3539 (15)	8868 (22)	11 (4)	49 (16)	154 (33)	−10 (16)	1 (22)	22 (45)
C (5)	3260 (8)	4527 (16)	8362 (23)	15 (4)	63 (18)	163 (35)	−13 (16)	32 (23)	59 (45)
C (6)	2579 (9)	4589 (16)	8798 (21)	20 (5)	59 (18)	138 (30)	6 (15)	−61 (25)	3 (53)
C (7)	1577 (9)	3810 (18)	10348 (25)	16 (5)	88 (20)	189 (41)	−7 (18)	23 (25)	−30 (51)
C (8)	1169 (8)	2808 (20)	9564 (23)	16 (5)	105 (22)	172 (40)	−3 (20)	2 (24)	1 (57)
N	445 (6)	2882 (14)	10022 (20)	16 (4)	71 (14)	148 (25)	−17 (15)	−14 (19)	−70 (41)
O	4292 (5)	3404 (11)	8351 (15)	13 (3)	84 (13)	178 (24)	7 (12)	9 (16)	8 (33)

TABLE 4. FINAL PARAMETERS FOR HYDROGEN ATOMS

Atom	Bound to X	x/a	y/b	z/c	B(Å^2)	X–H(Å)
H (1)	C (2)	0.250	0.210	1.110	4.2	1.01
H (2)	C (3)	0.370	0.192	1.023	4.9	1.04
H (3)	C (5)	0.345	0.518	0.760	3.6	1.01
H (4)	C (6)	0.231	0.535	0.847	5.3	1.02
H (5)	C (7)	0.137	0.459	1.004	3.0	0.97
H (6)	C (7)	0.155	0.368	1.170	2.1	1.13
H (7)	C (8)	0.133	0.184	0.997	2.4	1.14
H (8)	C (8)	0.124	0.285	0.821	3.3	1.13
H (9)	N	0.032	0.215	0.934	5.6	1.00
H (10)	N	0.034	0.353	0.924	6.5	0.97
H (11)	N	0.036	0.352	1.080	9.7	0.96
H (12)	O	0.448	0.410	0.806	4.7	0.88

distances of hydrogen-bonding, and then three hydrogen atoms were placed at proper positions on the N–H···Cl$^-$ line, assuming the N–H distance to be 1.01 Å. The final cycles of refinement, involving the hydrogen atoms with isotropic temperature factors, by the block-diagonal least-squares method dropped R to 0.114. It was thought that unfavorable outer shape of the crystal caused a rather high R factor. Observed and calculated structure factors from the last cycle are given in Table 2, and the final atomic coordinates and thermal parameters with their estimated standard deviations in Table 3 and 4. The atomic scattering factors used throughout the refinement were taken from *International Tables for X-ray Crystallography* (1962). All the numerical calculations were done on an NEAC 2200—700 computer in the computing center of this University using the programs of UNICS system.

Description and Discussion of the Structure

The interatomic distances and valency angles are shown in Fig. 1. In the phenol ring part, the mean C–C distance of 1.388 Å and the C(4)–O distance of 1.361 Å are not significantly different from those values found in L-tyrosine (1.390 and 1.369 Å),[6] L-tyrosine hydrochloride (1.391 and 1.374 Å)[7] and DL-tyrosine (1.393 and 1.371 Å).[8] The small distortions of the

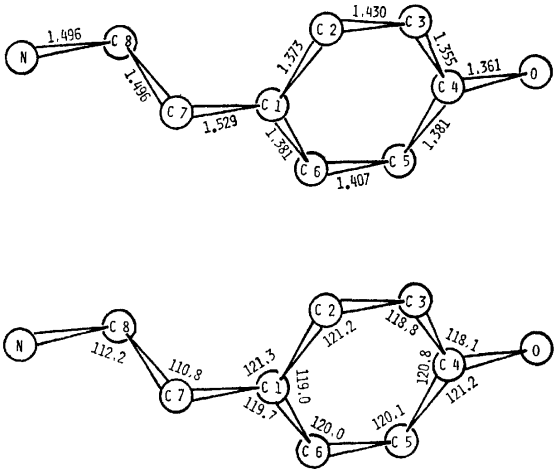

Fig. 1. Bond lengths and angles of tyramine cation. The standard deviations are 0.02 Å in bond lengths and 1.0° in bond angles between non-hydrogen atoms.

external C–C–O angles from 120° at the C(4) atom are frequently observed in phenol derivatives. The larger one always occurs at the angle C–C–O where the C–C bond is *cis* with respect to the O–H bond as suggested by Andersen *et al.*[9] The bond lengths and angles in the ethylamine side chain are very similar to the corresponding values found in other decarboxylated metabolites (amines); phenylethylamine hydrochloride,[10] dopamine hydrochloride,[11] 6-hydroxydopamine hydrochloride,[12] noradrenaline hydrochloride[13] and adrenaline hydrogen tartrate.[14]

Tyramine molecule consists of two planes; phenol ring and the fully extended ethylamine side chain. The dihedral angle between the plane of six-membered ring and the one defined by C(1)–C(7)–C(8)–N is 70.6°. The best plane through the six ring atoms was calculated by the least-squares method. The perpendicular displacements of the non-hydrogen atoms from this plane satisfying the equation: $0.2705X+0.5509Y+0.7895Z=9.8559$, are given in Table 5. The molecular conformation can be described as maximally extended form, *i.e.* the N–C(8) bond is nearly parallel to the C(7)–C(1) bond. The orientation of NH_3^+

Table 5. Deviations of atoms from the least-squares plane through the benzene ring (in Å)

Atom	Distance	Atom[a)]	Distance
C (1)	0.002	C (7)	0.013
C (2)	−0.013	C (8)	1.336
C (3)	0.003	N	1.386
C (4)	0.018	O	0.087
C (5)	−0.029	Cl (1)	4.497
C (6)	0.019	Cl (2)	2.026

a) Excluded from calculation of the plane.

group about the C(7)–C(8) bond is *trans* with respect to the C(1) atom, which is involved in the phenol ring, and the torsion angles as defined by Klyne and Prelog[15] are 179.4° (*anti-periplanar*) and 71.2° (*synclinal*) for C(1)–C(7)–C(8)–N and C(2)–C(1)–C(7)–C(8), respectively. Similar extended conformations were also reported in the crystal structures of phenylethylamine (188.9 and 72.6°),[10] dopamine (174.2 and 79.2°),[11] 6-hydroxydopamine (185.0 and 83.4°)[12] and noradrenaline (176.1 and 81.5°).[13] It is of particular interest to note that the *gauche* conformation about the C(7)–C(8) bond (the folded form) is not yet found in any crystal structure of the decarboxylated metabolite of phenylalanine and tyrosine.

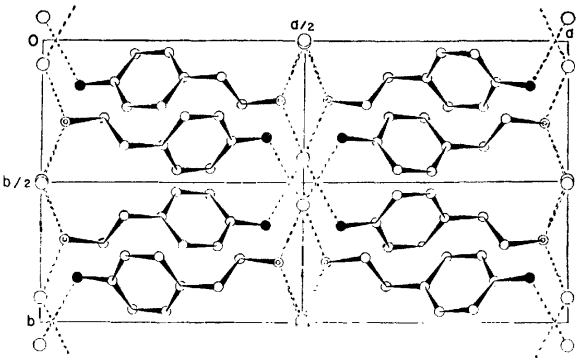

Fig. 2. The crystal structure of tyramine hydrochloride projected along the *c*-axis. The broken lines indicate the hydrogen bonds.

The packing of the molecules in this crystal is illustrated in Fig. 2, which apparently shows the network of hydrogen bonds stabilizing the structure. The crystal structure is describable as consisting of infinite chlorine layers parallel to the *bc*-plane, between which tyramine cations are arranged. The hydroxyl and ammonium hydrogen atoms are all engaged in hydrogen bonds with adjacent chlorine ions. The amino nitrogen atom has three chlorine neighbors at the distances of 3.177, 3.191, and 3.205 Å. The phenol oxygen atom acts as a donor in hydrogen bond to chlorine ion with the length of 3.028 Å. One of the interesting features of this crystal structure is the fact that two independent chlorine ions exist on the two-fold axis with distance of 4.484 Å. There is, therefore, some difference in hydrogen bonding for the two crystallographically independent chlorine ions. The Cl(2) atom is an acceptor in four N–H···Cl⁻ type hydrogen bonds, whereas Cl(1) acts as an acceptor of two N–H···Cl⁻ and two O–H···Cl⁻ hydrogen bonds.

This investigation was partly supported by the research grant from the Ministry of Education, Japan. We wish to express our sincere thanks for this support.

References

1) A. Wakahara, T. Fujiwara, and K. Tomita, *Chem. Lett.*, **1972**, 1139.
2) A. Wakahara, M. Kido, T. Fujiwara, and K. Tomita, This Bulletin, **46**, 2475 (1973).
3) A. Wakahara, T. Fujiwara, and K. Tomita, *ibid.*, **46**, 2481 (1973).
4) A. Wakahara, T. Fujiwara, and K. Tomita, preliminarily reported at the 12th Annual Meeting of Biophysical Society of Japan, Tokyo (1973), Abstract p. 237. A. Wakahara, Dissertation, Faculty of Pharm. Sci., Osaka University (1974).
5) I. L. Karle and J. Karle, *Acta Crystallogr.*, **16**, 969 (1963).
6) A. Mostad, H. M. Nissen, and C. Römming, *Acta Chem. Scand.*, **26**, 3819 (1972).
7) M. N. Frey, T. F. Koetzle, M. S. Lehmann, and W. C. Hamilton, *J. Chem. Phys.*, **58**, 2547 (1973).
8) A. Mostad and C. Römming, *Acta Chem. Scand.*, **27**, 401 (1973).
9) A. M. Andersen, A. Mostad, and C. Römming, *ibid.*, **26**, 2670 (1972).
10) G. Tsoucaris, *Acta Crystallogr.*, **14**, 909 (1961).
11) R. Bergin and D. Carlström, *ibid.*, **B24**, 1506 (1968).
12) M. Kolderup, A. Mostad, and C. Römming, *Acta Chem. Scand.*, **26**, 483 (1972).
13) D. Carlström and R. Bergin, *Acta Crystallogr.*, **23**, 313 (1967).
14) D. Carlström, *ibid.*, **B29**, 161 (1973).
15) W. Klyne and V. Prelog, *Experientia*, **16**, 521 (1960).

An Inversion of Configuration of Threonine and Allothreonine in the *N,O*-Acyl Migration Reaction with Concentrated Sulfuric Acid[1)]

Tateaki WAKAMIYA, Yuzo TARUMI, and Tetsuo SHIBA

Department of Chemistry, Faculty of Science, Osaka University, Toyonaka, Osaka 560

(Received May 2, 1974)

On the *N,O*-acyl migration reaction of β-hydroxy-α-amino acids with concentrated sulfuric acid, a configuration of the carbon atom carrying hydroxyl group was found to be inverted through the reaction. Thus, threonine residue in peptide was converted to allothreonine residue and *vice versa* in the selective chemical cleavage of threonine peptide employing the *N,O*-migration with concentrated sulfuric acid. The reaction mechanism involving S_Ni elimination of *O*-sulfate formed as an intermediate was suggested. The inversion did not occur in the *N,O*-acyl migration reaction with other mineral acids than sulfuric acid.

For the selective chemical cleavage of peptide bonds at β-hydroxy-α-amino acid residue, the *N,O*-acyl migration reaction in strong acids has been studied by many workers.[2)] Although the mechanism of the rearrangement had been discussed by Bergmann *et al.*[3)] and Elliott *et al.*,[2b,4)] a stereochemistry of the reaction has never been clarified yet. In our structural study on the antibiotics tuberactinomycins, we noticed that *threo*-γ-hydroxy-β-lysine was converted to *erythro* form in the *N,O*-migration reaction with concentrated sulfuric acid.[5)] The similar inversion may occur in the chemical cleavage reaction of threonine peptides with concentrated sulfuric acid. In this study, we investigated the *N,O*-acyl migration reaction in threonine peptides with concentrated sulfuric acid from the view point of the configurational change. Consequently, it was found in this reaction that threonine residue was converted to allothreonine residue, and reversely, allothreonine residue changed to threonine residue both in good yields. This fact has been overlooked hitherto in the sequential analysis of peptide using *N,O*-migration reaction with concentrated sulfuric acid. Furthermore, it was proved that this inversion took place certainly at β-carbon atom and not at α-carbon atom of threonine from results of ORD spectra of allothreonines which were obtained from the migration products of several acyl-L-threonine derivatives or L-threonine peptides.

In addition, the migration reaction of acyl derivatives of threonine or allothreonine was also examined, attempting to exploit a novel method for epimerization of threonine or allothreonine. Of the acyl derivatives tested, such as acetyl, benzoyl, benzyloxycarbonyl-threonine and so on, some of them participated to the migration reaction, though the yields were not satisfactory.

Experimental

Materials. The threonine peptides, *i.e.*, DL-alanyl-DL-threonine, benzyloxycarbonylglycyl-DL-threonine, and glycyl-L-threonyl-L-phenylalanine were prepared either by saponification or hydrogenolytic debenzyloxycarbonylation of the corresponding derivatives which had been early synthesized in our laboratory.[6)] The peptides involving DL-amino acids are actually mixtures of diastereoisomers. However, use of such compounds does not disturb the estimation of the epimerization on β-carbon atom of threonine or allothreonine. Benzyloxycarbonylglycyl-L-threonine and benzyloxycarbonyl-L-alanyl-L-threonine were prepared through the active ester method and isolated as dicyclohexylammonium salts. The corresponding allothreonine peptides were also synthesized by the active ester or by the dicyclohexylcarbodiimide method as mentioned below.

Benzyloxycarbonylglycyl-DL-allothreonine. To a solution of DL-allothreonine (1.19 g, 0.01 mol) and sodium hydrogencarbonate (1.85 g, 0.022 mol) in 15 ml of water, a solution of *p*-nitrophenyl benzyloxycarbonylglycinate (3.16 g, 0.01 mol) in 20 ml of dioxane was added. After stirring at room temperature for 50 hr, the reaction mixture was evaporated *in vacuo*. The residue was dissolved in water and insoluble material was filtered off. The filtrate was acidified with 6 M HCl and extracted with ethyl acetate. Ethyl acetate layer was washed with water and dried over anhydrous sodium sulfate. After evaporation of ethyl acetate, the oily residue was crystallized by treatment with petroleum ether. It was recrystallized from ethyl acetate, yield 1.90 g (61.5%), mp 130 °C.

Found: C, 54.35; H, 5.89; N, 8.96%. Calcd for $C_{14}H_{18}O_6N_2$: C, 54.19; H, 5.85; N, 9.03%.

Benzyloxycarbonyl-L-alanyl-DL-allothreonine. This compound was prepared from *p*-nitrophenyl benzyloxycarbonyl-L-alaninate (3.34 g, 0.01 mol) and DL-allothreonine (1.19 g, 0.01 mol) in the same procedure as mentioned above. The product was isolated as a dicyclohexylammonium salt which was recrystallized from ethanol and ether, yield 2.79 g (55.2%).

Found: C, 63.70; H, 8.50; N, 8.35%. Calcd for $C_{27}H_{43}O_6N_3$: C, 64.13; H, 8.57; N, 8.31%.

Benzyloxycarbonyl-DL-allothreonine. DL-Allothreonine (3.00 g, 0.025 mol) was benzyloxycarbonylated according to the synthesis of benzyloxycarbonyl-L-threonine.[7)] The oily product was crystallized as a dicyclohexylammonium salt, yield 9.80 g (89.3%). It was recrystallized from ethanol–ether–petroleum ether, mp 147—149 °C.

Found: C, 66.14; H, 8.83; N, 6.40%. Calcd for $C_{24}H_{33}O_5N_2$: C, 66.33; H, 8.81; N, 6.45%.

Benzyloxycarbonyl-DL-allothreonyl-L-phenylalanine Methyl Ester. Benzyloxycarbonyl-DL-allothreonine dicyclohexylammonium salt (4.50 g, 1.04 mmol) was coupled with methyl L-phenylalaninate hydrochloride (2.24 g, 1.04 mmol) by the dicyclohexylcarbodiimide method in dimethylformamide. The product was recrystallized from ethyl acetate and petroleum ether, yield 4.05 g (94.0%).

Found: C, 63.63; H, 6.38; N, 6.84%. Calcd for $C_{22}H_{26}O_6N_2$: C, 63.75; H, 6.32; N, 6.74%.

DL-Allothreonyl-L-phenylalanine Methyl Ester Hydrobromide. Benzyloxycarbonyl-DL-allothreonyl-L-phenylalanine methyl ester (1.70 g, 0.41 mmol) was dissolved in 5 ml of 30% hydrogen bromide in glacial acetic acid, and anhydrous ether

was added after one hour. The oily product was triturated with anhydrous ether several times and dried over sodium hydroxide *in vacuo*, yield 1.45 g (oil, almost quantitatively).

Benzyloxycarbonyl-L-alanyl-DL-allothreonyl-L-phenylalanine Methyl Ester. Benzyloxycarbonyl-L-alanine (0.60 g, 0.27 mmol) was condensed with DL-allothreonyl-L-phenylalanine methyl ester prepared from its hydrobromide (0.75 g, 0.21 mmol) through the dicyclohexylcarbodiimide method in tetrahydrofuran. The product was recrystallized from ethyl acetate and petroleum ether, yield 0.71 g (73.3%).

Found: C, 61.73; H, 6.71; N, 8.74%. Calcd for $C_{25}H_{31}O_7N_3$: C, 61.84; H, 6.44; N, 8.66%.

Benzyloxycarbonylglycyl-DL-allothreonyl-L-phenylalanine Methyl Ester. Benzyloxycarbonylglycine (0.52 g, 0.25 mmol) was condensed with DL-allothreonyl-L-phenylalanine methyl ester prepared from its hydrobromide (0.70 g, 0.19 mmol) in the similar manner to that mentioned above. The product was recrystallized from ethyl acetate and petroleum ether, yield 0.70 g (76.5%).

Found: C, 59.91; H, 6.29; N, 8.69%. Calcd for $C_{24}H_{29}O_7N_3 \cdot 1/2\,H_2O$: C, 59.99; H, 6.29; N, 8.75%.

Acyl Threonine and Acyl Allothreonine. Acyl derivatives of threonine and allothreonine were synthesized according to the convenient procedure. The melting points of the products are summarized in Table 1.

Table 1. Melting points of acylthreonine and acylallothreonine

Acyl group	Mp (°C)	
	Threonine[a)]	Allothreonine[a)]
CH_3CO	132—133	136—137
	131—132[b)]	
$ClCH_2CO$	121—122	151—152[c)]
CF_3CO	118—120	85—87
C_6H_5CO	145—146	177—178
p-ClC_6H_4CO	185—187	192—193
$C_6H_5OCH_2CO$	142—143	144—145
C_2H_5OCO	157—159[c)]	138—139[c)]
	169—170[b)]	
$C_6H_5CH_2OCO$	103—104[b)]	147—149[c)]

a) DL-Forms were used except b). b) L-Forms were used. c) Isolated as a dicyclohexylammonium salt.

Preparation of O-Sulfate of Threonine and Allothreonine. L-Threonine (1.00 g) was dissolved in 20 ml of concentrated sulfuric acid and allowed to stand for 10 days in a sealed tube. The solution was poured into cold ether. Precipitate was washed with ether several times by decantation and finally filtered off. The crude product was powdered and dissolved in water. The solution was passed through a Dowex 50 W×8 (H^+ form) column. Acidic eluate was concentrated *in vacuo* and the residue was recrystallized from water and acetone to give monohydrate as fine prisms, yield 1.40 g (85%), mp 149—150 °C.

Found: C, 22.00; H, 5.07; N, 6.33; S, 14.71%. Calcd for $C_4H_9O_6NS \cdot H_2O$: C, 22.12; H, 5.10; N, 6.45; S, 14.76%.

DL-Allothreonine (1.00 g) gave fine prisms of *O*-sulfate by the similar procedure, yield 1.35 g (82%), mp 220—230 °C (decomp.).

Found: C, 23.99; H, 4.66; N, 7.03; S, 15.98%. Calcd for $C_4H_9O_6NS$: C, 24.12; H, 4.55; N, 7.03; S, 16.10%.

Ninhydrin Reagent. Ninhydrin reagent was prepared by addition of stannous chloride dihydrate (20 mg) and 0.5 M citrate buffer (5 ml) to a solution of ninhydrin (380 mg) in methylcellosolve (95 ml).

N,O-Migration Reaction. Sample of each 100—200 mg of peptide or acyl derivative of threonine or allothreonine was dissolved in 5—6 ml of concentrated sulfuric acid. The solution was allowed to stand at 20—25 °C for 10—30 days in a sealed tube. The reaction was stopped by pouring the reaction mixture into a plenty of cold ether in the case of peptide or into 25—30 ml of 2 M hydrochloric acid in the case of the acyl derivative.

Paper Chromatographic Separation of Threonine and Allothreonine. Precipitate from the migration product of peptide obtained as mentioned above was hydrolyzed with 6 M hydrochloric acid at 110 °C for 8 hr. Each hydrolyzate was spotted on Toyo Roshi No. 51 filter paper (10×40 cm) on a line of 7 cm length after thorough removal of hydrochloric acid by evaporation. On the other hand, the aqueous acidic solution of the migration product of acyl derivative was heated at 110 °C for 8 hr. Each hydrolyzate was passed through a column of Amberlite IR-45 (OH^- form) and a neutral eluate containing threonine and allothreonine was concentrated *in vacuo*. The residue was dissolved in a small amount of water and spotted on filter paper as mentioned above. Three sheets of the papers for each one sample were developed by use of R-solvent, *i.e.*, supernatant of *n*-butanol–water–acetone–28% ammonium hydroxide (40:30:5:5 v/v). For satisfactory separation of threonine, allothreonine, and alanine, it was necessary to repeat the development a few times.

Estimation of Inversion Rate.[8)] Ninhydrin reagent was sprayed to the developed paper, and then the colored parts of threonine and allothreonine were cut off separately. The combined pieces of paper taken were sufficiently wetted with 0.1 M sodium hydroxide solution in a test tube (13×150 mm) and the tube was placed in a vacuum desiccator overnight on concentrated sulfuric acid. The pH was then brought to 5 with 0.2 M citric acid solution. Ninhydrin reagent (1.0 ml) was added to each tube which was shaken for 5—10 min and kept in a boiling water bath for 25 min. After cooling, distilled water (3 ml) was added, and the extract was poured into volumetric flask of 10 ml. Complete extraction of the colored material from the paper was carried out by treatment with acetone (3 ml). Finally the volume in the flask was adjusted to 10 ml with distilled water. The color strength was estimated using a Hitachi 124 Spectrophotometer at 570 nm. As reference in the colorimetry, a blank part of the same paper of an equal area was treated in the similar manner.

Measurement of ORD Spectra. Each hydrolyzate of migration products of acetyl-L-threonine, ethyloxycarbonyl-L-threonine, benzyloxycarbonylglycyl-L-threonine, benzyloxycarbonyl-L-alanyl-L-threonine, and benzyloxycarbonylglycyl-L-threonyl-L-phenylalanine was chromatographed on Toyo Roshi No. 51 filter paper (40×40 cm, eight sheets). The development was repeated three times each after drying and a part of allothreonine was cut off. Allothreonine was extracted with water from the paper and recrystallized from water and ethanol. ORD spectra were obtained with a JASCO Model ORD/UV-5 in water.

Results and Discussion

The results in the migration reactions of threonine and allothreonine peptides were listed in Table 2, in which the degrees of inversion were summarized as relative ratios of threonine to allothreonine.

As can be seen in Table 2, the configuration on β-carbon atom of both threonine and allothreonine

TABLE 2. RATIOS OF THREONINE AND ALLOTHREONINE RESIDUE IN INVERSION REACTIONS

Peptide[a)]	Reaction days	Ratio (%) Allo-threonine	Threo-nine
Z-Ala-Thr-OH[b)]	30	78	22
H-Ala-Thr-OH[b)]	30	82	18
Z-Gly-Thr-OH[b)]	30	71	29
Z-Gly-Thr-OCH_3[b)]	30	69	31
Z-Gly-Thr-Phe-OH[c)]	30	77	23
H-Gly-Thr-Phe-OH[c)]	30	77	23
Z-Gly-Ath-OH[d)]	10	0	100
Z-Ala-Ath-OH[d)]	10	25	75
	30	0	100
Z-Gly-Ath-Phe-OCH_3[d)]	10	0	100
Z-Ala-Ath-Phe-OCH_3[d)]	10	9	91
	45	0	100

$Z = C_6H_5CH_2OCO-$

a) Amino acids used are of DL-forms in peptides b) and of L-forms in peptides c). In peptides d), alanine and phenylalanine are of L-forms and allothreonine (Ath) is of DL-form.

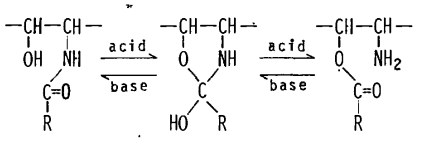

(I)

Fig. 1. Reaction mechanism of rearrangement *via* hydroxyoxazolidine (I).

peptides was inverted in a fairly good yield through the migration reaction in concentrated sulfuric acid. This newly found fact is very important not only stereochemically, but also for a reaction mechanism of *N,O*-acyl migration. Bergmann had first suggested a plausible way *via* hydroxyoxazolidine intermediate (I) for the *N,O*-acyl migration reaction in strong acids (Fig. 1).[3a)] According to this mechanism, the configuration on β-carbon atom carrying hydroxyl group should be retained. There has never been reported that the inversion occurred through the acyl migration reaction of peptides and proteins hitherto investigated and the above mechanism seemed to be accepted in many studies of protein chemistry. On the other hand, there are known some examples in which an inversion of the configuration actually took place in acyl migration reaction. Thus *N*-acyl-(−)-ephedrine was converted to *O*-acyl-(+)-ψ-ephedrine by treatment with hydrochloric acid.[9)] However, this is a special case where the so-called neighboring group effect between methyl and phenyl groups is participated. Such a steric effect cannot be operated at threonine or allothreonine peptides.

In other examples, Elliott pointed out a possibility that an inversion of configuration may occur on an asymmetric carbon atom carrying the hydroxyl group in a reaction of acyl amino alcohol with thionyl chloride through oxazoline ring formation (Fig. 2).[4)] Furthermore, Elliott attempted to reveal a mechanism of acyl migration reaction in concentrated sulfuric acid, however he could not manifest the real reaction mechanism so far.[2b)]

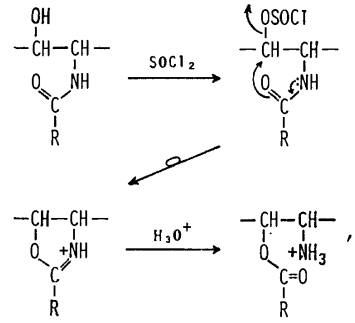

Fig. 2. Reaction mechanism of rearrangement by thionyl chloride accompanied with inversion.

From our experimental results in this study, a configurational change of β-carbon atom of threonine or allothreonine in peptide chain on the acyl migration reaction with concentrated sulfuric acid was demonstrated at the first time. There are suggested two important facts to support the inversion mechanism. First, *O*-sulfate of serine or threonine was readily isolated on simple treatment of these amino acids with concentrated sulfuric acid.[10)] Secondly, Fasman also observed the formation of *O*-sulfate before ester formation in the acyl migration reaction of poly-DL-serine in concentrated sulfuric acid.[11)] Taking these facts into consideration, we now propose the most plausible reaction mechanism as follows (Fig. 3).

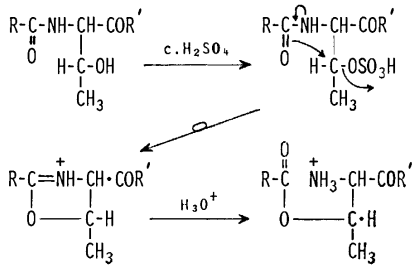

Fig. 3. Proposed mechanism of acyl migration reaction in concentrated sulfuric acid.

According to this mechanism, the *N,O*-acyl migration reaction in concentrated sulfuric acid is initiated by a formation of *O*-sulfate which is known as a strong electron-withdrawing group. A synchronous reaction of S_Ni type by an elimination of *O*-sulfate and an attack of oxygen of carbonyl group resulted in a formation of an oxazoline intermediate which is finally hydrolyzed to *O*-acyl derivative.

We have to examine a possibility that an acyl amino acids may be converted in concentrated sulfuric acid to an oxazolone derivative which causes a racemization at α-carbon atom according to the well-known mechanism. Actually, benzoyl and *p*-chlorobenzoyl derivatives of threonine and allothreonine gave 4-ethylidene-2-phenyloxazolone and 2-*p*-chlorophenyl-4-ethylidene-oxazolone respectively, under the condition employed in the migration reaction, while the formation of such oxazolone compound was never recognized in another

acyl derivatives, *e.g.*, acetyl, ethyloxycarbonyl or benzyloxycarbonylthreonine. If the apparent configurational changes in the latter cases should be due to the racemization at α-carbon atom through the oxazolone formation, allothreonine produced from L-threonine residue must be of D-form. However, measurements of ORD spectra of allothreonine obtained from the migration products of acetyl-L-threonine, ethyloxycarbonyl-L-threonine, benzyloxycarbonylglycyl-L-threonine, benzyloxycarbonyl-L-alanyl-L-threonine, and benzyloxycarbonylglycyl-L-threonyl-L-phenylalanine ascertained the complete retention of the configuration of α-carbon atom in threonine in all cases. The possibility of the inversion through racemization of oxazolone derivatives can also be excluded by the fact that threonine or allothreonine was not obtained by the hydrolysis of the unsaturated oxazolones mentioned above.

Table 3. Inversion rates of acyl derivatives of threonine and allothreonine

Acyl groups	Yields (%) of inversion from	
	Acylthreonine	Acylallothreonine
CH_3CO	16	11
$ClCH_2CO$	22	18
CF_3CO	1	13
$C_6H_5OCH_2CO$	9	18
C_2H_5OCO	39	30
$C_6H_5CH_2OCO$	3	7

Contrary to the peptide migration, an inversion of simple acyl derivatives of threonine and allothreonine occurred only in a low yield (Table 3). The reaction rate of the acyl migration reaction is known to be very slow even in the threonine peptides.[2m,12] Therefore, it may be considered that either the reaction of the acyl derivative proceeded in an extreme slow rate or a simple hydrolysis preceded to the slow migration reaction.

It can be now concluded that the acyl migration reaction with concentrated sulfuric acid leads to a complete inversion of the configuration on β-carbon atom of β-hydroxy-α-amino acids in peptides as far as the migration reaction takes place. In addition, it was confirmed that the inversion occurs only in concentrated sulfuric acid but not in another mineral acids, *e.g.*, hydrochloric acid, hydrobromic acid, and anhydrous hydrogen fluoride.

In view of wide applications of *N,O*-acyl migration reaction of threonine residue with concentrated sulfuric acid for determination of primary structures of peptides or proteins, the stereochemistry of β-carbon atom in threonine must be taken into consideration hereafter based on the new findings in this study.

The authors wish to express their appreciations to Ajinomoto Co. Ltd., for supply of allothreonine.

References and Footnotes

1) Presented at the 28th Annual Meeting of the Chemical Society of Japan, Tokyo, April, 1973; p. 1856. A part was reported in a preliminary form: T. Wakamiya, Y. Tarumi, and T. Shiba, *Chem. Lett.*, **1973**, 236.

2) a) P. Desnuelle and G. Bonjour, *Biochim. Biophys. Acta.* **7**, 451 (1951); b) D. F. Elliott, *Biochem. J.*, **50**, 542 (1952); c) J. C. Crawhall and D. F. Elliott, *ibid.*, **61**, 264 (1955); d) L. Wiseblatt, L. Wilson, and W. B. McConnell, *Can. J. Chem.*, **33**, 1295 (1955); e) L. K. Ramachandran and W. B. McConnell, *ibid.*, **33**, 1638 (1955); f) J. L. Bailey, *Biochem. J.*, **60**, 173 (1955); g) H. Hörmann, W. Grassmann, E. Wünsch, and H. Preller, *Chem. Ber.*, **89**, 933 (1956); h) F. Lucas, J. T. B. Shaw, and S. G. Smith, *Biochem. J.*, **66**, 468 (1957); i) K. Iwai, *Nippon Kagaku Zasshi*, **80**, 1066 (1959); **81**, 1302 (1960), **82**, 1088 (1961); **89**, 1009 (1968); j) L. A. Cohen and B. Witkop, *Angew. Chem.*, **73**, 253 (1961); k) H. Zahn, *Chimia*, **15**, 378 (1961); l) I. Levi, J. W. R. Weed, G. Laflamme, and A. E. Koller, *Can. J. Chem.*, **39**, 2491 (1961); m) S. Sakakibara, K. H. Shin, and G. P. Hess, *J. Amer. Chem. Soc.*, **84**, 4921 (1962).

3) a) M. Bergmann, E. Brand, and F. Weinmann, *Z. Physiol. Chem.*, **131**, 1 (1923); b) A. P. Phillips and R. Baltzly, *J. Amer. Chem. Soc.*, **69**, 200 (1947).

4) D. F. Elliott, *J. Chem. Soc.*, **1949**, 589.

5) T. Wakamiya, T. Shiba, and T. Kaneko, This Bulletin, **46**, 949 (1973). Details of this study will be reported soon elsewhere.

6) T. Kaneko, S. Kusumoto, T. Inui, and T. Shiba, This Bulletin, **41**, 2155 (1968).

7) R. B. Merrifield, *J. Biol. Chem.*, **232**, 43 (1958).

8) L. Fowden, *Biochem. J.*, **48**, 327 (1951).

9) L. H. Welsh, *J. Amer. Chem. Soc.*, **69**, 128 (1947); **71**, 3500 (1949).

10) a) H. C. Reitz, R. E. Ferrel, H. Fraenkel-Conrat, and H. S. Olcott, *ibid.*, **68**, 1024 (1946); b) K. S. Dodgson, A. G. Lloyd, and N. Tudball, *Biochem. J.*, **79**, 111 (1961).

11) G. D. Fasman, *Science*, **131**, 420 (1960).

12) K. Iwai and T. Ando, *Methods in Enzymology*, **11**, 263 (1967).

Synthesis of Streptolidine (Roseonine, Geamine)[1]

Shoichi KUSUMOTO, Shinichi TSUJI, and Tetsuo SHIBA

Department of Chemistry, Faculty of Science, Osaka University, Toyonaka, Osaka 560

(Received August 2, 1974)

Streptolidine (roseonine, geamine) (**1**), a guanidino amino acid component of the streptothricin group antibiotics, was synthesized starting from D-ribose (**8**). The epimino compound (**11b**) was prepared from **8** in five synthetic steps. Azidolysis of **11b** gave the arabino-type compound (**12b**), which in turn was converted to the key intermediate tribenzyloxycarbamido lactone (**23b**) by oxidation of *C*-1. The lactone **23b** was rearranged to the free lactam (**4**) after deprotection, and then guanidinated with cyanogen bromide. The identity of the hydrolysis product of this guanidino lactam with natural streptolidine in all respects certified the proposed structure involving the steric configurations.

Streptolidine is a guanidino amino acid which widely distributes as a constituent of a number of *Streptomyces* antibiotics. It was first isolated from the hydrolyzate of streptothricin and streptolin.[2] The two amino acids thereafter reported, *i.e.*, roseonine from roseothricin[3] and geamine from geomycin,[4] were identified as the same substance. In 1961 Carter *et al.*[5] deduced the chemical structure of this amino acid by means of degradation studies. Its absolute configuration was recently established by X-ray crystallography as **1**.[6] As reported in our preliminary communication,[1] we synthesized streptolidine of the natural configuration from D-ribose.

Results and Discussion

Streptolidine has a unique structure in which a 2-amino-2-imidazoline ring and three asymmetric centers are involved. This peculiar feature in the structure seems to be the reason for delay in the chemical synthesis of the rather small molecule so far. The key intermediate of the synthesis is desired to be (2*S*,3*S*,4*R*)-2,3,5-triamino-4-hydroxypentanoic acid (**2**) or its equivalent, *e.g.*, its lactone (**3**) or lactam form (**4**). In this study, natural pentoses of the corresponding stereochemistry were chosen as the starting materials. Thus, attempts were made to convert three hydroxy groups on *C*-2, 3 and 5 of furanoside molecules stereoselectively into amino groups. In this way, the trouble in separation of stereoisomeric mixture otherwise synthesized can be avoided.

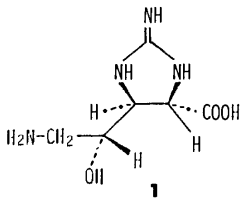

1

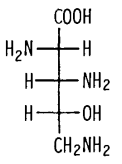

2

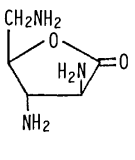

3

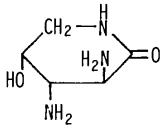

4

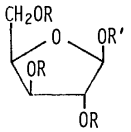

5 R=R'=H

6 R=CH_3SO_2, R'=CH_3

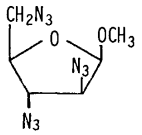

7

Many procedures have been presented to introduce an amino group into a sugar moiety. Among them the S_N2-type displacement of *O*-sulfonate with azide anion seems to be the most promissing one in our case. A synthetic pathway for preparation of **3** from D-xylose (**5**) was first investigated. When methyl 2,3,5-tri-*O*-mesyl-β-D-xylofuranoside (**6**) was treated with sodium azide under various conditions, however, 2,3,5-triazide (**7**) could not be obtained in an appreciable yield. Thus, the approach to **3** by this way was abandoned. The details on this experiment will be presented elsewhere.

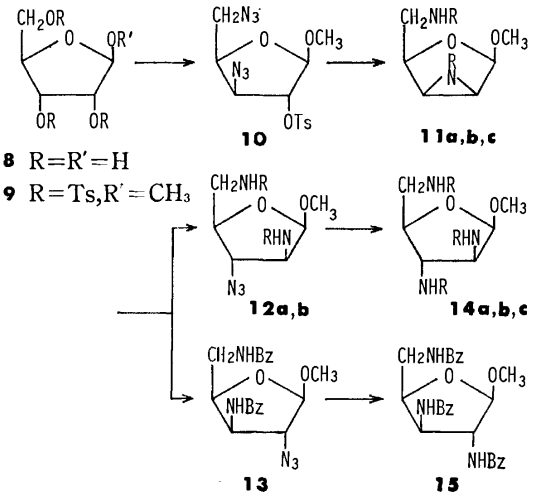

8 R=R'=H

9 R=Ts,R'=CH_3

10

11a,b,c

12a,b

13

14a,b,c

15

a: R=Bz=C_6H_5CO Ts=*p*-$CH_3C_6H_4SO_2$

b: R=$C_6H_5CH_2OCO$

c: R=H

Recently, Hildesheim *et al.*[7] prepared two isomers of monoazido dibenzamido trideoxypentose (**12a** and **13**) through azidolysis of an epimino compound (**11a**) derived from D-ribose (**8**). They assigned tentatively one isomer with a smaller $J_{1,2}$-value of 1 Hz to xylo-type (**13**) and the other with a larger value to arabino-type (**12a**) structure respectively. Each compound could be reduced and benzoylated to give methyl tribenzamido trideoxy xylofuranoside (**15**) and arabinofuranoside (**14a**). Since the compounds **12a** and **14a** have the same steric fashion as in **3**, oxidation of **12a** or **14a** at *C*-1 would be expected to lead to the desired intermediate **3** after several steps of further transformations. Thus, the methyl glycoside of **12a** was hydrolyzed with hydrochloric acid without ap-

preciable cleavage of benzoyl group. However, oxidation of the resulting compound **16** with chromium trioxide in pyridine afforded a mixture of two products. Although the main product showed two carbonyl bands due to amides (1680 and 1645 cm^{-1}) in its IR spectrum, the azide band disappeared, and no signal of an olefin proton in its NMR spectrum was observed. These results together with its molecular formula ($C_{19}H_{16}N_2O_4$) suggest an epimino structure (**17**) for this compound. This assignment was confirmed by the following transformation. Catalytic hydrogenation of **17** afforded a product of a molecular formula $C_{19}H_{18}N_2O_4$, whose NMR spectrum showed signals at δ 2.50 (1H, d, J=10 Hz) and 2.82[8] (1H, q, J=10, 5 Hz). These signals could be attributed to the two hydrogens on *C*-2 of the structure shown in **18**. The epimino ring in **17** obviously resulted from an elimination of the azido group with a participation of the neighboring benzamido group. As a minor product in the oxidation reaction of **16**, a small amount of **19** of the desired azido lactone structure was isolated. This structure was supported from its IR spectrum (2140, 1770 cm^{-1}). Further progress of the synthesis using this azido lactone had to be given up, because of a small amount available.

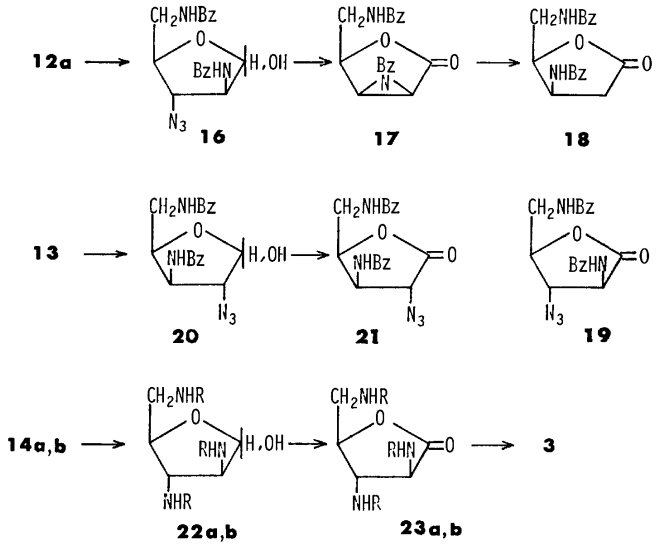

In a parallel experiment, **13** was hydrolyzed to **20**, which was oxidized with chromium trioxide-pyridine to afford an azido lactone (**21**) (ν_{max} 2130, 1790 cm^{-1}) without elimination of the azido group successfully. Decoupling experiments on this lactone (**21**) showed that a doublet signal at δ 4.12 (1H, J=10 Hz) changed to a singlet when the signal at δ 5.25 (1H, quartet-like) coupling further with an NH proton at δ 9.07 (1H, d, J=9 Hz) was irradiated. This result indicates clearly that the signal at δ 4.12 should be due to the proton on *C*-2 and the structure of this lactone must be represented as α-azido structure of xylo-type as shown in **21**. Consequently, it was unequivocally established that both **13** and **20** have the xylo-type configuration in accordance with Hildesheim's assignment. Comparison of the behaviors of **16** and **20** in oxidation reaction indicates that the facile elimination of an azido group occurs particularly at β-position but not α-position to a carbonyl function.

This finding leads to a strategy that the azido group on *C*-3 of **12a** should be reduced prior to the oxidation of *C*-1 in the synthetic approach towards **3**. Thus, the azido glycoside **12a** was first converted to tribenzamido derivative (**14a**) of arabino-type, which was then oxidized to tribenzamido lactone (**23a**) with chromium trioxide in pyridine through a hydrolysis product **22a**. However, the benzoyl groups of **23a** resisted against removal by acid hydrolysis. Thus, on refluxing in 6 M hydrochloric acid, **23a** gave a complex mixture of several products. Methanolysis with dry hydrogen chloride could not give an improved result.

Therefore, the benzoyl group was replaced with benzyloxycarbonyl group for the amino protection. In a simillar manner as in the benzoyl derivative (**11a**), the dibenzyloxycarbonyl epimino compound (**11b**) was prepared from D-ribose. Treatment of **11b** with sodium azide in dimethylformamide (DMF) gave a single product of the arabino-type azido derivative (**12b**). Catalytic hydrogenation of **12b** afforded triamino compound **14c** as trihydrochloride. Both compounds **12b** and **14c** certainly maintain the arabino-type configuration, since benzoylation of **14c** afforded **14a** of the determined structure. After the exhausted benzyloxycarbonylation of **14c** to **14b**, the glycoside linkage was hydrolyzed by refluxing with *p*-toluenesulfonic acid in dioxane to give **22b** in about 35% yield accompanied with 40% of unchanged **14b**. A longer refluxing as far as the starting material disappeared, or use of hydrochloric acid for the hydrolysis gave rather worse results presumably because of the acid-lability of the benzyloxycarbonyl group. The hydrolysis product was isolated through silica gel chromatography and recrystallized from chloroform. Although a compound with a 5-acylaminopentose structure is known to exist often as an equilibrium mixture of the corresponding furanose (**24**) and piperidine (**25**) form,[9] this product seemed to remain mainly in the furanose form (**22b**) during the isolation procedure since a γ-lactone was formed by oxidation of **22b** and no change was observed in the IR spectrum in repeated recrystallization. However, when **22b** was treated with acetic anhydride in pyridine, a diacetate (**26**) was obtained as a sole

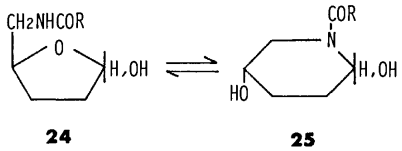

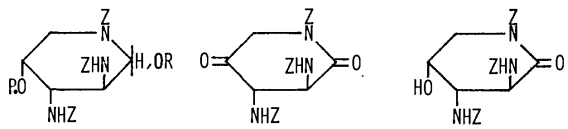

product. This fact might be well elucidated by assuming that the piperidine form (**27**) is preferred in pyridine solution.[10] Similar preferences of piperidine form in *N*-benzyloxycarbonyl derivatives were also reported in some pentoses[11] and in idose series,[12] though it is not a case in the corresponding *N*-acetyl or benzoyl derivatives.[13]

Oxidation of **22b**[14] was effected with chromium trioxide in acetic acid, and the product was isolated by silica gel chromatography. This product could not be obtained in a crystalline state, although its IR spectrum showed, in accordance with the expected γ-lactone structure (**23b**), a carbonyl band at 1800 cm^{-1} together with a broad band at around 1710 cm^{-1} due to benzyloxycarbonyl groups. Removal of the benzyloxycarbonyl groups from this oxidation product with hydrogen bromide in acetic acid afforded an extremely hygroscopic hydrobromide as white powder, whose IR spectrum showed a weak absorption band at 1650 cm^{-1} besides an intensive one at 1800 cm^{-1} due to γ-lactone. The former band should be attributed to an amide carbonyl group of δ-lactam structure (**4**). The elemental analysis of this hydrobromide, in one experimental run, showed the composition of a 7: 3 mixture of lactone (**3**) trihydrobromide and lactam (**4**) dihydrobromide. Since it is improbable that the conversion of **3** into **4** occurred during the deprotection stage or thereafter when no basic condition was employed, the above observation suggests that the oxidation product **23b** might have already contained a small amount of lactam form **29** which arised from **27**. When an aqueous solution of a mixture of the hydrobromide of **3** and **4** was passed through a column of Amberlite IR-45 (OH^- form) and the eluate evaporated *in vacuo*, the residue showed only a carbonyl band due to lactam (**4**) and no other compound was eluted at all. This indicates the easy transformation of **3** trihydrobromide into **4** on neutralization.

The final stage of streptolidine synthesis was carried out as follows. An aqueous solution of a mixture of the hydrobromide of **3** and **4** was brought to pH 11 with 1 M sodium hydroxide. The preferred formation of **4** in this solution was proved by isolation of its bis-4-hydroxyazobenzene-4'-sulfonic acid (HABS) salt. The solution was then treated directly with cyanogen bromide. In this reaction, the amino group on *C*-5 in the lactam form was protected against an action of cyanogen bromide and a selective formation of the 2-amino-2-imidazoline ring between *C*-2 and *C*-3 was expected. The reaction mixture was refluxed with hydrochloric acid to hydrolyze the lactam ring and then subjected to a column of Dowex 50×8 (NH_4^+ form). Elution with 0.2 M ammonia afforded a fraction which showed a single ninhydrin positive spot identical with natural streptolidine on both paper chromatography (PPC) and paper electrophoresis (PEP).

Table 1. Comparison of synthetic and natural streptolidine

	Synthetic	Natural
R_f value on PPC[a]	0.29	0.29
Mobility on PEP[b]	11.0 cm	11.0 cm
Elution time on amino acid analysis	47.0 min	47.0 min
Bis-HABS salt		
mp	250—254°C (dec.)	250—254°C (dec.)
$[\alpha]_D$ in MeOH	+20.5° (*c* 0.29)	+22.1° (*c* 0.29)
Dihydrochloride		
mp	239 °C (dec.)	241 °C (dec.)
$[\alpha]_D^{20}$ in H_2O	+52.2° (*c* 0.16)	+54.2° (*c* 0.15)

a) Isopropanol–HCOOH–H_2O (4:1:1) b) Pyridine–AcOH–H_2O (30:4:966)

This product was isolated as crystalline bis-HABS salt, mp 250—254 °C (decomp.), $[\alpha]_D^{21}$ +20.5° (methanol), which was identical with the same salt of the natural amino acid, mp 250—254 °C (decomp.), $[\alpha]_D^{19}$ +22.1° (methanol). Identity was further confirmed by comparison of mp and IR spectrum of dihydrochloride, mobility on PEP, R_f value on PPC as well as the elution time on amino acid analysis with those of the natural specimen. Consequently, the structure and the stereochemistry of streptolidine were unequivocally established as **1** by the present chemical synthesis.

Experimental

All melting points are uncorrected. The NMR spectra were taken on a Varian T-60 spectrometer in deuteriochloroform unless otherwise stated, using tetramethylsilane as an internal standard. Chemical shifts and coupling constants were recorded in δ values and Hz, and frequencies in cm^{-1}. Optical rotations were measured with Perkin-Elmer polarimeter model 141. Paper electrophoresis (PEP) was carried out in a pyridine–acetic acid–water (30: 4: 966) buffer solution.

*3-Azido-2,5-dibenzamido-2,3,5-trideoxy-*D*-arabinofuranose (**16**).* To a solution of methyl 3-azido-2,5-dibenzamido-2,3,5-trideoxy-β-D-arabinofuranoside (**12a**)[7] (200 mg) in dioxane (60 ml) was added 2 M HCl (40 ml), and the mixture was heated under reflux for 2.5 hr. After cooling, the solution was extracted with CH_2Cl_2. The extract was washed with water, dried over $MgSO_4$ and evaporated to give **16** (155 mg, 80%). Recrystallization was effected from ethyl acetate; mp 187—188 °C.

Found: C, 59.65; H, 5.05; N, 18.53%. Calcd for $C_{19}H_{19}N_5O_4$: C, 59.83; H, 5.02; N, 18.36%.

*Oxidation of **16** with Chromium Trioxide in Pyridine.* To an ice-cooled solution of CrO_3 (240 mg, 2.4 mmol) in dry pyridine (15 ml) was added a solution of **16** (155 mg, 0.41 mmol) in dry pyridine (3 ml). The mixture was stirred at 0 °C for 2 hr, then at room temperature overnight, and extracted with CH_2Cl_2. The extract was treated as usual and evaporated *in vacuo* to leave a brown residue, which was chromatographed on silica gel column. Ethyl acetate–*n*-hexane (2: 1) eluted **17** (100 mg, 73%), which was recrystallized from ethyl acetate–*n*-hexane; mp 196—197 °C; ν_{max} (Nujol) 1680, 1645; $[\alpha]_D^{28}$ +55.6° (*c* 1.87, ethyl acetate).

Found: C, 67.76; H, 4.82; N, 8.48%. Calcd for $C_{19}H_{16}N_2O_4$: C, 67.85; H, 4.80; N, 8.33%.

Further elution with the same solvent afforded a small amount of **19**; mp 167—169 °C; ν_{max} (Nujol) 2140, 1770.

*3,5-Dibenzamido-2,3,5-trideoxy-*D*-xylono-1,4-lactone (**18**).* Hydrogen was passed through a stirred solution of **17** (400 mg, 1.06 mmol) in methanol (20 ml) and concentrated hydrochloric acid (0.13 ml) in the presence of palladium black. After 20 hr, the catalyst was removed by filtration and the solvent evaporated *in vacuo*. The residue was dissolved in

CH_2Cl_2, washed with water, dried over $MgSO_4$ and evaporated to give **18** (216 mg, 52%), which was recrystallized from ethyl acetate–*n*-hexane; mp 212—213 °C; $[\alpha]_D^{28}$ +32.0° (*c* 1.78, ethyl acetate–DMF (3:1)). NMR (in pyridine): 2.50 (1H, d, $J=10$), 2.82 (1H, q, $J=5$, 10).

Found: C, 67.33; H, 5.36; N, 8.28%. Calcd for $C_{19}H_{18}N_2O_4$: C, 67.44; H, 5.36; N, 8.28%.

*2-Azido-3,5-dibenzamido-2,3,5-trideoxy-*D*-xylofuranose (20).* To a solution of methyl 2-azido-3,5-dibenzamido-2,3,5-trideoxy-β-D-xylofuranoside (**13**)[7] (2.75 g, 6.96 mmol) in dioxane (200 ml) was added 1 M HCl (40 ml), and the mixture was heated under reflux for 1.5 hr. After cooling, a reaction mixture was extracted with CH_2Cl_2 and the extract was treated as usual. The residue obtained by evaporation was chromatographed on silica gel column. Elution with CH_2Cl_2–ethyl acetate (4:1) gave unchanged **13** (1.20 g, 44%) and then **20** (0.315 g, 12%). The latter was recrystallized from $CHCl_3$–*n*-hexane; mp 177—179 °C (decomp.).

Found: C, 59.68; H, 5.07; N, 18.48%. Calcd for $C_{19}H_{19}N_5O_4$: C, 59.83; H, 5.02; N, 18.36%.

*2-Azido-3,5-dibenzamido-2,3,5-trideoxy-*D*-xylono-1,4-lactone (21).* To an ice-cooled solution of CrO_3 (420 mg, 4.2 mmol) in dry pyridine (15 ml) was added a solution of **20** (240 mg, 0.63 mmol) in dry pyridine (5 ml). The mixture was stirred at 0° for 20 hr, and extracted with CH_2Cl_2. Working up in the usual manner and evaporation of the solvent *in vacuo* afforded a brown residue, which was chromatographed on silica gel column. Elution with ethyl acetate–*n*-hexane gave **21** (160 mg, 67%), which was recrystallized from ethyl acetate–*n*-hexane; mp 164—166 °C (decomp.); ν_{max} ($CHCl_3$) 2130, 1790. NMR ($CDCl_3$, 100 MHz): around 3.6 and 4.2 (each 1H, m; 2H-5), 4.12 (1H, d, $J=10$; H-2), 4.85 (1H, broad; H-4), 5.25 (1H, q; H-3), 7.3—8.2 (11H; aromatic H and NH-5), 9.07 (1H, d, $J=9$; NH-3).

Found: C, 59.74; H, 4.59; N, 18.03%. Calcd for $C_{19}H_{17}N_5O_4$: C, 60.15; H, 4.52; N, 18.46%.

*2,3,5-Tribenzamido-2,3,5-trideoxy-*D*-arabinofuranose (22a).* A mixture of methyl 2,3,5-tribenzamido-2,3,5-trideoxy-β-D-arabinofuranoside (**14a**)[7] (1.80 g, 3.80 mmol), $CuCl_2 \cdot 2H_2O$ (2.1 g), dioxane (20 ml) and 0.5 M HCl (40 ml) was heated under reflux for 2 hr. After cooling, the mixture was evaporated *in vacuo* to dryness. To the residue was added water (50 ml) and $CHCl_3$ (150 ml), and the mixture was heated under reflux for 30 min. The organic layer was separated, treated as usual and evaporated *in vacuo* to leave a residue, which was recrystallized from $CHCl_3$ to afford **22a** (0.46 g, 26%); ν_{max} (Nujol) 3450, 3340, 1700—1670 (broad).

From the mother liquor was recovered the unchanged **14a** (1.20 g, 67%).

*2,3,5-Tribenzamido-2,3,5-trideoxy-*D*-arabono-1,4-lactone (23a).* To an ice-cooled solution of CrO_3 (0.70 g, 7 mmol) in dry pyridine (30 ml) was added **22a** (600 mg, 1.31 mmol) in dry pyridine (20 ml). The mixture was stirred at 0°C for 4 hr, then at room temperature for 20 hr, and worked up as usual. After evaporation of the solvent *in vacuo*, the residue was chromatographed on silica gel column. Elution with $CHCl_3$–ethyl acetate (1:2) afforded **23a** (470 mg, 78%), which was recrystallized from dioxane–water; mp 217—218 °C; $[\alpha]_D^{28}$ −102.4° (*c* 1.45, DMF).

Found: C, 67.85; H, 5.32; N, 8.87%. Calcd for $C_{26}H_{23}N_3O_5 \cdot 1/5C_4H_8O_2$: C, 67.75; H, 5.22; N, 8.85%.

Attempts for Removal of Benzoyl Groups of **23a**. *1) Hydrolysis with HCl*: Compound **23a** (20 mg) was heated under reflux in 6 M HCl (9 ml) and the progress of the reaction was followed by means of PEP. Even after 5 hr, the reaction was not finished, though there appeared three main spots and the reaction mixture turned into deep brown. Heating for a longer time caused considerable decomposition of the products. Use of acetic acid or dioxane as co-solvent or use of more dilute HCl did not improve the result.

2) Methanolysis: A 15% solution of dry HCl in absolute methanol (10 ml) was added to **23a** (400 mg) and the mixture was heated under reflux for 17 hr. PEP showed the presence of several ninhydrin-positive spots in the mixture, from which **3** could not be isolated.

*Methyl 5-Benzyloxycarbamido-2,3-benzyloxycarbonylepimino-2,3,5-trideoxy-β-*D*-lyxofuranoside (11b).* Benzyloxycarbonyl chloride (18.1 g, 105 mmol) was added portionwise to an ice-cooled solution of methyl 5-amino-2,3-epimino-2,3,5-trideoxy-β-D-lyxofuranoside (**11c**)[7] (5.6 g, 44 mmol) and triethylamine (14.6 ml, 105 mmol) in ethanol (250 ml) during 20 min with stirring. The reaction mixture was stirred at 0 °C for 30 min and at room temperature for 2.5 hr. Then water (400 ml) was added and crystals of **11b** were filtered off (13.5 g, 75%). Recrystallization was effected from ethyl acetate–*n*-hexane; mp 115.5—116.5 °C, $[\alpha]_D^{24}$ −35.7° (*c* 2.02, ethyl acetate).

Found: C, 64.18; H, 5.85; N, 6.79%. Calcd for $C_{22}H_{24}N_2O_6$: C, 64.06; H, 5.87; N, 6.79%.

*Methyl 3-Azido-2,5-dibenzyloxycarbamido-2,3,5-trideoxy-β-*D*-arabinofuranoside (12b).* Sodium azide (10.0 g, 155 mmol) was added to a solution of **11b** (12.8 g, 31.0 mmol) in dry DMF (200 ml), and the mixture was heated at 90 °C for 1 hr with stirring. After cooling, the mixture was filtered through Celite and evaporated to dryness *in vacuo*. Water and CH_2Cl_2 were added to the residue. The organic layer was separated, washed with water, dried over $MgSO_4$ and concentrated *in vacuo*. The remaining syrup was passed through a column of silica gel. Elution with benzene–ethyl acetate (4:1) afforded **12b** (6.5 g, 46%), which was recrystallized from ethyl acetate–*n*-hexane; mp 103.5—105 °C; $[\alpha]_D^{24}$ −27.3° (*c* 2.20, ethyl acetate). NMR: 3.39 (3H, s; CH_3O , 4.77 (1H, d, $J=5$; H-1), 5.16 and 5.19 (each 2H, s; $2C_6H_5C\underline{H}_2O$) and near 7.3 (10H; aromatic).

Found: C, 58.15; H, 5.52; N, 15.30%. Calcd for $C_{22}H_{25}N_5O_6$: C, 58.01; H, 5.53; N, 15.38%.

*Methyl 2,3,5-Triamino-2,3,5-trideoxy-β-*D*-arabinofuranoside (14c) Trihydrochloride.* A solution of **12b** (3.8 g, 8.35 mmol) and concentrated hydrochloric acid (2.5 ml) in methanol (60 ml) was added with 5% palladium on carbon (0.4 g). A slow stream of hydrogen was passed through this mixture with stirring at room temperature overnight. The catalyst was filtered off and ether was added to the filtrate. Trihydrochloride of **14c** was crystallized out as needles; 1.85 g (82%). It was recrystallized from water–methanol–ether; mp 240 °C (decomp.); $[\alpha]_D^{19}$ −57.1° (*c* 1.81, water).

Found: C, 26.71; H, 6.77; N, 15.37; Cl, 39.14%. Calcd for $C_6H_{18}N_3O_2Cl_3$: C, 26.63; H, 6.71; N, 15.53; Cl, 39.31%.

*Methyl 2,3,5-Tribenzyloxycarbamido-2,3,5-trideoxy-β-*D*-arabinofuranoside (14b).* To an ice-cooled solution of **14c** (3.7 g, 14 mmol) and triethylamine (7.5 ml, 54 mmol) in ethanol (120 ml) was added benzyloxycarbonyl chloride (9.1 g, 54 mmol) portionwise during 20 min with stirring. After stirring in an ice-bath for 30 min, triethylamine (5.5 ml, 39 mmol) and benzyloxycarbonyl chloride (3.0 g, 18 mmol) were added and stirring was continued at room temperature for another 1 hr. The product (**14b**) crystallized out was filtered off and recrystallized from $CHCl_3$–*n*-hexane (6.9 g, 90%). An analytical sample was obtained by recrystallization from dioxane–water; mp 202—203 °C, $[\alpha]_D^{19}$ −17.0° (*c* 1.98, $CHCl_3$).

Found: C, 63.43; H, 6.12; N, 7.02%. Calcd for $C_{30}H_{33}N_3O_8 \cdot 1/2C_4H_8O_2$: C, 63.25; H, 6.14; N, 6.92%.

*2,3,5-Tribenzyloxycarbamido-2,3,5-trideoxy-*D*-arabinofuranose*

(22b). To a solution of **14b** (4.28 g) in dioxane (200 ml) was added 2 M aqueous solution of *p*-toluenesulfonic acid (200 ml). The mixture was heated under reflux for 2 hr, then concentrated to half of its volume *in vacuo*, and extracted with $CHCl_3$. The extract was washed with aqueous $NaHCO_3$ and water, dried over $MgSO_4$ and evaporated *in vacuo*. The resulting residue was chromatographed on silica gel column. Elution with $CHCl_3$–ethyl acetate (2: 1) first afforded the unchanged **14b** (1.80 g, 42%) and then **22b** (1.45 g, 35%). The latter was recrystallized from $CHCl_3$; mp 211—212 °C.

Found: C, 63.00; H, 5.71; N, 7.67%. Calcd for $C_{29}H_{31}N_3O_8$: C, 63.38; H, 5.69; N, 7.65%.

*2,3,5-Tribenzyloxycarbamido-2,3,5-trideoxy-*D*-arabono-1,4-lactone (23b).* To a solution of **22b** (2.0 g, 3.6 mmol) in acetic acid (240 ml) was added CrO_3 (0.36 g, 3.6 mmol) in acetic acid–water (4: 1, 3.6 ml). The mixture was stirred at room temperature for 1.5 hr, then added with water, and extracted with $CHCl_3$. The residue obtained by the usual working up was chromatographed on silica gel column. Elution with $CHCl_3$–ethyl acetate (2: 1) afforded unchanged **22b** (0.62 g, 31%) and further elution with the same solvent gave **23b** (0.52 g, 26%) as sticky syrup; ν_{max} ($CHCl_3$) 1800, 1730—1690 (broad).

*1,4-Di-*O*-acetyl-2,3,5-tribenzyloxycarbamido-2,3,5-trideoxy-*D*-arabinopyranose (26).* Acetic anhydride (0.05 ml) was added to a stirred solution of **22b** (29.0 mg) in pyridine (0.3 ml) under ice-cooling. The mixture was set aside at room temperature for 48 hr and then evaporated *in vacuo*. The residue was dissolved in $CHCl_3$ and added with *n*-hexane to afford **26** (23.9 mg, 71%), which was recrystallized from $CHCl_3$–*n*-hexane; mp 186—186.5 °C. NMR: 1.89 and 2.09 (each 3H, s; $2CH_3CO$).

Found: C, 62.40; H, 5.53; N, 6.58%. Calcd for $C_{33}H_{35}N_3O_{10}$: C, 62.55; H, 5.57; N, 6.63%.

*2,3,5-Triamino-2,3,5-trideoxy-*D*-arabono-1,4-lactone (3) Trihydrobromide and 2,3,5-Triamino-2,3,5-trideoxy-*D*-arabono-1,5-lactam (4) Dihydrobromide.* Anisole (0.3 ml) and **23b** (455 mg), containing a small amount of **29** (see text), was dissolved in acetic acid (10 ml) which was previously saturated with dry hydrogen bromide. The mixture was allowed to stand at room temperature for 1.5 hr. Addition of anhydrous ether afforded very hygroscopic white powder (300 mg); ν_{max} (Nujol): 1800, 1650 (weak).

Found: C, 16.62; H, 3.92; N, 11.20; Br, 59.69%. Calcd for a 7: 3-mixture of **3** trihydrobromide ($C_5H_{14}N_3O_2Br_3$) and **4** dihydrobromide ($C_5H_{13}N_3O_2Br_2$): C, 16.51; H, 3.80; N, 11.56; Br, 59.33%.

Transformation of Trihydrobromide of 3 into 4. 1) On Ion Exchange Resin: A mixture of hydrobromide of **3** and **4**, obtained from **23b** (290 mg) was dissolved in water, subjected to a column of Amberlite IR-45 (OH^- form) and eluted with water. The eluate was evaporated *in vacuo* to afford **4** solely as hygroscopic amorphous solid: ν_{max} (Nujol) 1640.

2) With NaOH: The hydrobromide (40 mg) mentioned above was dissolved in water (8 ml). This solution was brought to pH 11 by addition of 1 M NaOH and left stand at room temperature for 2 hr. To this solution was added 4-hydroxyazobenzene-4′-sulfonic acid (HABS) to afford bis-HABS salt of **4**, which was recrystallized from water; mp 190 °C (decomp.); ν_{max} (Nujol) 1640.

Found: C, 46.34; H, 4.92%. Calcd for $C_5H_{11}N_3O_2 \cdot 2(C_{12}H_{10}N_2O_4S) \cdot 3H_2O$: C, 46.08; H, 4.94%.

Streptolidine (1). To an aqueous solution (90 ml) of **4**, prepared from **23b** (0.74 g, 1.35 mmol) using NaOH as mentioned above, was added a solution of BrCN (0.32 g, 3.0 mmol) in water (6.5 ml) portionwise over a period of 2.5 hr with stirring. During this time the pH of the reaction mixture fell to 6.9. The mixture was stirred at room temperature for additional 30 min and then evaporated *in vacuo* to dryness. The residue was heated in 6 M HCl (150 ml) under reflux for 2 hr and then evaporated *in vacuo*. The residue was dissolved in a little water and subjected to a column of Dowex 50×8 (NH_4^+ form, 1.5×36 cm). The column was first washed with water (500 ml) and eluted with 0.2 M NH_4OH. Eluate of each 2 ml was collected and each fraction was tested by means of PEP and PPC (2-propanol–formic acid–water 4:1:1). Fractions 21—31 showed a single ninhydrin-positive spot, which was identical with that of natural streptolidine. Fractions 18—20 and 32—41, containing the same substance overlapped with some other impurities, were combined and again chromatographed as above, affording fractions which showed also a single spot identical with streptolidine. These and the fractions 21—31 in the first chromatography were combined, concentrated *in vacuo* to a small volume, added with 4-hydroxyazobenzene-4′-sulfonic acid (HABS, 150 mg) and heated on a boiling water bath to obtain a clear solution. On cooling, crystals (95 mg) of bis-HABS salt of streptolidine were obtained. From the mother liquor was obtained more amount (37 mg) of them; total 132 mg (12.5% from **23b**). Recrystallization was effected from hot water; mp 250—254 °C (decomp.); $[\alpha]_D^{21}$ +20.5° (*c* 0.29, methanol).

Found: C, 46.23; H, 4.63; N, 14.22; S, 8.08%. Calcd for $C_6H_{12}N_4O_3 \cdot 2(C_{12}H_{10}N_2O_4S) \cdot 2H_2O$; C, 46.15; H, 4.65; N, 14.35; S, 8.21%.

Bis-HABS salt (81 mg) was subjected to PEP using TOYO No. 50 paper (4 pieces of 40 cm length×16 cm width; 1.3 mA/cm, 1.5 hr). The ninhydrin-positive substance was extracted from the paper with 2 M HCl and the extract concentrated *in vacuo* to afford streptolidine dihydrochloride (25.5 mg) as crystalline residue, which was recrystallized from water–ethanol; mp 239 °C (decomp.); $[\alpha]_D^{20}$ +52.2° (*c* 0.115, H_2O).

The IR spectra of bis-HABS salt and dihydrochloride of synthetic streptolidine were fully identical with those of natural specimen. R_f-values on PPC, mobilities on PEP and elution times on amino acid analysis of the synthetic and natural product were all identical (see Table 1).

The authors wish to express their appreciations to Ajinomoto Co., Inc. and Takeda Chemical Industries Ltd., for their kind supplies of the starting materials, and Shionogi Co., Ltd., for gift of the natural specimen.

References

1) This work was preliminarily reported at the 17th Symposium on the Chemistry of Natural Products, Tokyo, Japan, October, 1973; p. 221. S. Kusumoto, S. Tsuji, and T. Shiba, *Tetrahedron Lett.*, **1974**, 1417.

2) H. E. Carter, R. K. Clark, P. Kohn, J. M. Rothrock, W. R. Taylor, C. A. West, G. B. Whitfield, and H. G. Jackson *J. Amer. Chem. Soc.*, **76**, 566 (1954).

3) K. Nakanishi, T. Ito, and Y. Hirata, *ibid.*, **76**, 2845 (1954).

4) H. Brockmann and H. Musso, *Chem. Ber.*, **88**, 648 (1955).

5) H. E. Carter, C. C. Sweeley, E. E. Daniels, J. E. McNary C. P. Schaffner, C. A. West, E. E. van Tamelen, J. R. Dyer, and H. A. Whaley, *J. Amer. Chem. Soc.*, **83**, 4296 (1961).

6) B. W. Bycroft and T. J. King, *Chem. Commum.*, **1972**, 652.

7) J. Hildesheim, J. Cleophax, A. M. Sepulchre, and S. D. Gero, *Carbohyd. Res.*, **9**, 315 (1969).

8) This value was erroneously reported as 2.7 in the preliminary communication.[1]

9) J. S. Brimacombe and A. M. Mofti, *J. Chem. Soc., C*, **1971,** 1634 and references cited therein.

10) In accordance with this assumption, oxidation of **22b** with Collins' reagent in methylene chloride afforded a product, whose IR spectrum suggested the structure **28.** Oxidation of **22b** with chromium trioxide in pyridine gave no γ-lactone (**23b**) as well.

11) H. Paulsen and F. Leupold, *Chem. Ber.*, **102,** 2804 (1969).

12) H. Paulsen and M. Friedmann, *ibid.*, **105,** 731 (1972).

13) Oxidation of **22a** with chromium trioxide in pyridine afforded exclusively the γ-lactone (**23a**), indicating the preference of furanose form even in pyridine in the case of benzoyl derivative.

14) This substance contained a small amount of its piperidine form (**27**), as judged from the formation of lactam derivative (**29**, see text) on oxidation.

Enthalpies of Hydrogen Bond Formation between Diphenylamines and Dimethyl Sulfoxide

Minoru HIROTA, Kazumasa SHINOZUKA, and Yoshiki HAMADA*

Department of Applied Chemistry, Faculty of Engineering, Yokohama National University, Minami-ku, Yokohama 233

**Department of Pharmacy, Meijo University, Showa-ku, Nagoya 468*

(Received May 21, 1974)

Enthalpies of hydrogen bond formation for the diphenylamine–dimethyl sulfoxide systems were determined by infrared spectroscopic method. The ΔH values for 4-methoxy, 4-methyl, unsubstituted, 3-methoxy, 3-chloro, 3-nitro, and 4-nitro-diphenylamines are −9.6, −10.1, −11.1, −11.2, −12.8, −13.9, and −13.9 kJ mol^{-1}, respectively. The substituent effects are discussed in relation with those on N–H stretching frequencies.

N–H stretching absorptions of amines and amides have been investigated extensively, and a large number of reports were published by many authors.[1-10] The substituent effects on the N–H stretching frequencies were also investigated and were correlated with the Hammett's σ-constants. The N–H frequencies of the substituted anilines and *N*-methylanilines increase as the σ-constants increase.[2] However, the trend of the N–H frequency shift in these amines is reversed when the N–H groups are in substituted amides.[6] The reversed gradients of the Hammett plots in the substituted aniline and the amide series could be interpreted by taking into accounts the change in hybridization of the nitrogen atoms in these series of compounds.[10] Anilines were proved to exist as a non-planar conformation from the dipole moment measurement,[11] and this provides an evidence for the sp^3-like hybridization of the nitrogen atom. On the other hand, the planar sp^2 hybridization is evident for the amide nitrogen atom. Thus, it is of interest to investigate whether the nitrogen atom takes a planar (sp^2) or a non-planar (sp^3-like) hybridization in diphenylamines. The recent investigations of the present authors have provided an evidence for the fact that the diphenylamines with electron-donating substituents are still non-planar but those with electron-withdrawing substituents, such as the nitro group, take planar conformations at the nitrogen atoms.[10,12] On the contrary, the proton chemical shifts of the diphenylamines exhibit a normal σ-constant *vs.* chemical shift plot and this means that the electron density on the imino hydrogen atom decreases linearly with the substituent constant. This, in turn, implies that the hydrogen donating power of the imino group increases linearly with the increase in σ-values when the imino group participates in a hydrogen bond. Thus, in spite of the anomalous ν_{N-H} *vs.* σ plot, the hydrogen bond shift ($\Delta\nu$) and the enthalpy of hydrogen bond formation might increase linearly with increasing σ-value.

To examine the above conclusions experimentally, the intermolecular hydrogen bonding between the diphenylamines and dimethyl sulfoxide was investigated by the infrared spectroscopic method. Since diphenylamines are rather weak proton donor, a strong proton acceptor is chosen so as to keep an enough amount of the associated species to determine the formation constant of the hydrogen-bonded complex at an enough low concentration to prevent the effect of the self-association of the amine.

Experimental

The infrared N–H stretching spectra were recorded with a Hitachi Model 225 grating infrared spectrophotometer, and the absorption frequencies were calibrated by the absorption bands of water vapor at 3447.09 and 3442.41 cm^{-1} in order to keep the accuracy of the wavenumber within 0.5 cm^{-1}. The measurements were carried out on the ternary diphenylamine–dimethyl sulfoxide–carbon tetrachloride system at the temperatures ranging from 280 to 330 K. Throughout each measurement, the temperature of the solution was kept sufficiently constant. (The temperature variation was kept within 0.5 K). The enthalpy of hydrogen bond formation was calculated by plotting logarithms of the intensity ratios of the N–H stretching bands arisen from the free and the hydrogen-bonded species of diphenylamine ($\varepsilon_b/\varepsilon_f$) against the reciprocals of the temperatures ($1/T$).

The diphenylamines were prepared by the known methods[13-16] and carefully purified either by distillation or by recrystallization.

Results and Discussion

After several preliminary experiments on the association between diphenylamine and some hydrogen acceptors (namely acetone, dimethylformamide, diethyl ether, and dimethyl sulfoxide), dimethyl sulfoxide was chosen as an appropriate hydrogen acceptor to investigate, the substituent effect on the hydrogen-donating power of diphenylamines. In diphenylamine (0.005 mol l^{-1})–dimethyl sulfoxide (0.1 mol l^{-1})–carbon tetrachloride systems, the N–H stretching absorptions of the

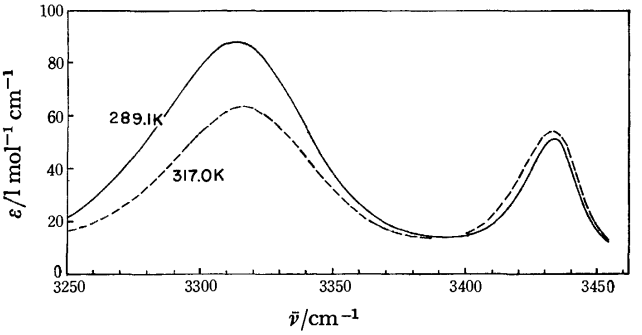

Fig. 1. N–H Stretching absorptions of diphenylamine measured at two temperatures (289.1 K and 317.0 K). The band at 3436 cm^{-1} is assigned to the free species of the amine, and the one at 3314 cm^{-1} to the species associated with dimethyl sulfoxide.

free and the hydrogen-bonded species of diphenylamine are fortunately located separately in the spectra as shown in Fig. 1.

This allows us to use the absorbance to evaluate the amounts of the free and the hydrogen-bonded species without tedious process to separate the two overlapping bands to obtain the integrated intensities. The ratio of the absorbances of the free and the hydrogen-bonded species ($\varepsilon_b/\varepsilon_f$) was determined at various temperatures ranging from 280 to 330 K, and the enthalpy of the hydrogen-bond formation was estimated from the temperature dependence of the equilibrium constant which is assumed to be proportional to $\varepsilon_b/\varepsilon_f$. An example of $\log(\varepsilon_b/\varepsilon_f)$ *vs.* T^{-1} plots is shown in Fig. 2. As the plot can be approximated by a straight line, the enthalpy is estimated from its slope. The results are shown in Table 1 together with the hydrogen bond shifts $\Delta\nu$ which are defined by the equation $\Delta\nu=\nu_f-\nu_b$, where ν_f and ν_b are the NH stretching frequencies of the free and the hydrogen-bonded species of diphenylamines.

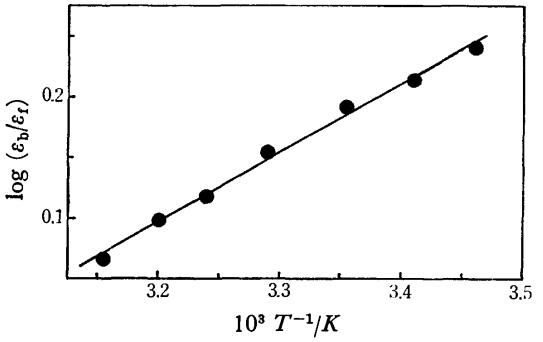

Fig. 2. The temperature dependence of the N-H band intensities of the free and the hydrogen-bonded species of diphenylamine presented as the log ($\varepsilon_b/\varepsilon_f$) *vs.* T^{-1} plot.

Table 1. Hydrogen bond shifts and enthalpies of hydrogen bond formation for diphenylamine–dimethyl sulfoxide–CCl_4 systems

Diphenylamine	ν_{NH}		$\Delta\nu$/cm^{-1}	$-\Delta H$/kJ·mol^{-1}
	ν_f/cm^{-1}	ν_b/cm^{-1}		
4-Methoxy	3432	3320	112	9.6±0.6
4-Methyl	3433	3317	116	10.1±0.6
Unsubstituted	3436	3314	122	11.1±0.6
3-Methoxy	3435	3314	121	11.2±0.8
3-Chloro	3433	3308	125	12.8±1.0
3-Nitro	3433	3301	132	13.9±0.6
4-Nitro	3430	3286	144	13.9±0.6

In order to examine the substituent effect, the enthalpies and the hydrogen bond shifts were plotted against σ values and shown in Figs. 3 and 4, respectively. As expected, the linear relations were observed for both $\Delta\nu$ *vs.* σ and ΔH *vs.* σ plots. This shows that the hydrogen-donating abilities of the diphenylamines increase with the increase in σ values. The result agrees with the substituent effect observed in the series of phenols.

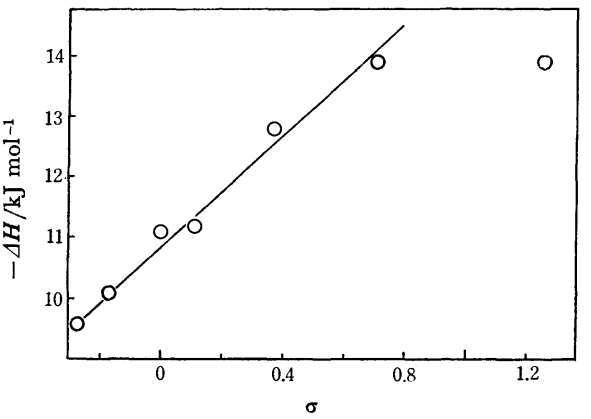

Fig. 3. The ΔH *vs.* σ plot.

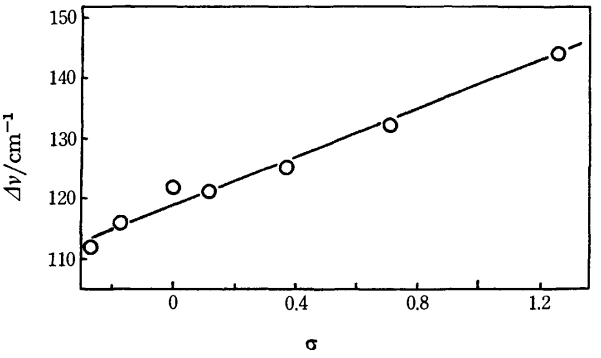

Fig. 4. The $\Delta\nu$ *vs.* σ plot.

The substituent effect on the enthalpies results from the change in acidities of the diphenylamines. In general, a stronger acid forms a stronger hydrogen bond when other conditions are similar. From the electrostatic point of view, this phenomenon is explained that the larger N–H dipole of a diphenylamine carrying an electron-withdrawing substituent attracts more intensely the S–O dipole of dimethyl sulfoxide. By the concept of the charge transfer interaction, the results are interpreted as follows. Lower electron density on the N–H group stablizes its anti-bonding σ*-orbital, and then the unshared electrons of the proton acceptor can interact more easily with the σ*-orbital. Hence, the stronger hydrogen bond is formed when the substituent on the diphenylamine is more electron attracting.[19]

The hybridization of the imino nitrogen atom changes so as to increase the s-character of the nitrogen orbital when the substituent becomes more electronegative. As the s-character of the N atomic orbital increases, the resulting N–H molecular orbitals tend to be lower in energy. This again favors for the hydrogen bond formation. Somewhat convex curvatures of the plots may be caused by the reinforced effect of the electronegativity and the hybridization in the negative σ region. However, further investigation is necessary to estimate their effect separately. A considerable deviation from the line is observed with 4-nitrodiphenylamine, and this may be attributed to the strong conjugation between the nitrophenyl and the imino groups which enforces the both groups planar.

Enthalpies of hydrogen bond formation of the unsubstituted diphenylamine have been measured by several authors employing various hydrogen acceptors. Among the hydrogen acceptors investigated, triethylamine forms the strongest hydrogen bond of which enthalpy is estimated to be $-18.8\,\mathrm{kJ\,mol^{-1}}$. The N–H···O hydrogen bond of diphenylamine is by far weaker. The enthalpies of formation were reported to be -10.0, -10.5, and $-11.7\,\mathrm{kJ\,mol^{-1}}$, respectively, when the acceptors are dioxane, acetone, and methyl acetate.[17,18] Thus, the results of the present authors seem to be consistent with the previous reports. The hydrogen bonding of substituted diphenylamines has never been reported.

The present investigation was partly supported by a Scientific Research Grant from the Ministry of Education of Japan for which the authors are grateful.

References

1) H. C. Flett, *J. Soc. Dye. Colour.*, **68**, 59 (1952).
2) D. Hadzi, "Infrared Spectroscopy and Molecular Structure," ed. by M. Davies (1962), p. 236.
3) T. L. Brown, *J. Phys. Chem.*, **61**, 820 (1957).
4) P. J. Krueger, *Can. J. Chem.*, **40**, 2300 (1962).
5) P. J. Krueger and H. W. Thompson, *Proc. Roy. Soc. Ser. A*, **243**, 143 (1957).
6) H. W. Thompson and D. A. Jameson, *Spectrochim. Acta*, **13**, 236 (1958).
7) J. Itier and A. Casadevall, *Bull. Soc. Chim. Fr.*, **1969**, 2342, 2355, and 3523.
8) M. G. W. Bell, M. Day, and A. T. Peters, *J. Chem. Soc., C*, **1967**, 132.
9) H. Levitsky, G. Norwitz, and D. E. Chasan, *Appl. Spectroscopy*, **22**, 493 (1968).
10) M. Kasai, M. Hirota, Y. Hamada, and H. Matsuoka, *Tetrahedron*, **29**, 267 (1973).
11) R. J. B. Marsden and L. E. Sutton, *J. Chem. Soc.*, **1936**, 599.
12) T. Mizuno, M. Hirota, Y. Hamada, and Y. Ito, *Tetrahedron*, **27**, 6011 (1971).
13) V. Merz and W. Weith, *Ber.*, **13**, 1299 (1880); **14**, 2345 (1881).
14) F. Ullmann and R. Dahrmen, *ibid.*, **41**, 3477 (1908).
15) R. Willstatter and H. Kubli, *ibid.*, **42**, 4138 (1909).
16) A. V. Iogansen, G. A. Kurkchi, and B. V. Rassadin, *Zh. Prikl. Spektrosk.*, **11**, 1054 (1969).
17) A. E. Lutskii, A. A. Axtyrskaya, and V. N. Konel'skaya, *Zh. Obshch. Khim.*, **42**, 1827 (1972).
18) S. F. Bureiko and G. S. Denisov, *Zh. Prikl. Spektrosk.*, **14**, 276 (1971).
19) On the importance of the charge transfer contribution in hydrogen bonding, see a) P. A. Kollman and L. C. Allen, *J. Amer. Chem. Soc.*, **93**, 4991 (1971) and b) S. Bratoz, *Advan. Quantum Chem.*, **3**, 209 (1966).

Superacids and Their Derivatives. V.[1] Kinetics and Mechanism of the Cationic Polymerization of 3,3-Bis(chloromethyl)oxacyclobutane Initiated by Ethyl Trifluoromethanesulfonate. Evidence for Ester Type Propagating Species

Shiro KOBAYASHI, Hidenori DANDA, and Takeo SAEGUSA

Department of Synthetic Chemistry, Faculty of Engineering, Kyoto University, Kyoto 606

(Received April 18, 1974)

Kinetic analysis of the cationic ring-opening polymerization of 3,3-bis(chloromethyl)oxacyclobutane (BCMO) initiated by ethyl trifluoromethanesulfonate ($EtOSO_2CF_3$) was carried out by direct determination of the instantaneous concentrations of monomer, initiator, and propagating species by means of ^1H and ^{19}F NMR spectroscopy. It was established that the polymerization of BCMO proceeds *via* an ester type propagating species (**4**). The propagating species of the first (P_1^*) and subsequent propagations (P_n^*, $n \geqq 2$) were directly observed. The rate constants of initiation (k_i) and propagations of the first (k_{p1}), second (k_{p2}) and subsequent steps (k_{pn}, $n \geqq 3$) were determined. Activation parameters as well as the solvent effect supported the proposed mechanism, in which the rate-determining step is a dipole-dipole reaction between monomer and propagating ester species to form the intermediate cyclic oxonium ions (**7**, **8**, and **10**) as unstable transient species.

In a series of our studies on the reaction of superacid derivatives with cyclic ethers, we have reported kinetic studies on the cationic ring-opening polymerization of tetrahydrofuran (THF) initiated by superacid esters[1,2] and by pyrosulfuryl chloride,[3] and on the oxonium formation from superacid esters and tetrahydropyran.[4] Generally, the cationic ring-opening polymerization of THF by Lewis acid catalysts proceeds *via* cyclic trialkyl oxonium propagating species.[5] In the THF polymerization by superacid ester initiators, however, an equilibrium between cyclic oxonium **1** and ester **2** species of the propagating end is involved during the course of polymerization.[2,6,7]

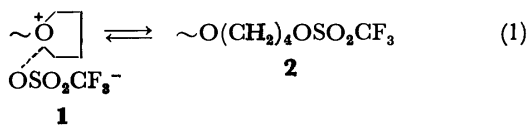

$$\sim\overset{+}{O}\!\square \rightleftharpoons \sim O(CH_2)_4OSO_2CF_3 \quad (1)$$

$OSO_2CF_3^-$ (**1**) (**2**)

It was confirmed by means of ^{19}F NMR spectroscopy that equilibrium (1) takes place in the propagating species of the THF polymerization initiated by ethyl trifluoromethanesulfonate ($EtOSO_2CF_3$).[1]

In the cationic polymerization of four-membered cyclic ethers by acid catalysts, a mechanism involving a cyclic oxonium propagating species **3** is generally accepted.[5,8] As an extension of studies on the cationic polymerization of cyclic ethers initiated by superacid

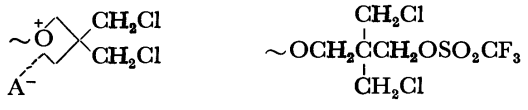

3 **4**

esters, we examined the polymerization of 3,3-bis(chloromethyl)oxacyclobutane (BCMO) by $EtOSO_2CF_3$ initiator. Kinetics of the BCMO polymerization has been carried out by means of ^1H NMR spectroscopy. It was found that an ester type **4** is a propagating species. In the present paper we wish to give clear-out evidence for an ester type propagating species in the polymerization of cyclic ethers.

Results and Discussion

^1H NMR Studies. The polymerization reaction was monitored directly by ^1H NMR spectroscopy. Figure 1 shows examples of ^1H NMR spectra of the reaction system, in which the molar feed ratio of BCMO to $EtOSO_2CF_3$ is 6: 1. In the ^1H NMR spectrum after 5 min at 63 °C (Fig. 1(a)), 55% of the initial $EtOSO_2CF_3$ underwent reaction. A quartet at δ 4.82 (peak H) and a triplet at δ 1.60 (peak I) are due to methylene (2H) and methyl protons (3H) of $EtOSO_2CF_3$, respectively. Peaks H and I diminished with progress of the reaction, peaks A_1, D, E, F, and G increasing. $EtOSO_2CF_3$ was completely consumed at 63 °C within 15 min.

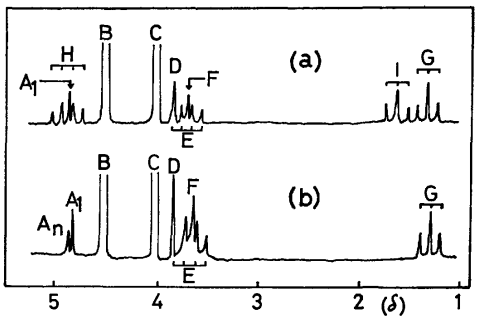

Fig. 1. ^1H NMR spectra of BCMO polymerization mixture by $EtOSO_2CF_3$ in nitrobenzene at 63 °C; (a) after 5 min and (b) after 180 min.

A new peak A_n appears in the ^1H NMR spectrum at a reaction time of 180 min at 63 °C (Fig. 1(b)). Singlet peaks, A_1 at δ 4.80 and A_n at δ 4.83, are assigned respectively to α-methylene protons (2H) of $-OSO_2CF_3$ group in ester type species **5** and **6** (*vide infra*). A signal of the open-chain chloromethyl protons (4H) appears at δ 3.82 (peak D). A peak due to α-methylene protons (2H) of open-chain ether group is observed at δ 3.64 (peak F). A quartet peak E at δ 3.67 and triplet peak G at δ 1.33 are ascribed respectively to methylene protons (2H) and methyl protons (3H) of

TABLE 1. SIGNAL ASSIGNMENTS IN THE POLYMERIZATION MIXTURE OF BCMO BY $EtOSO_2CF_3$ INITIATOR IN NITROBENZENE ((Fig. 1(a) and (b)).

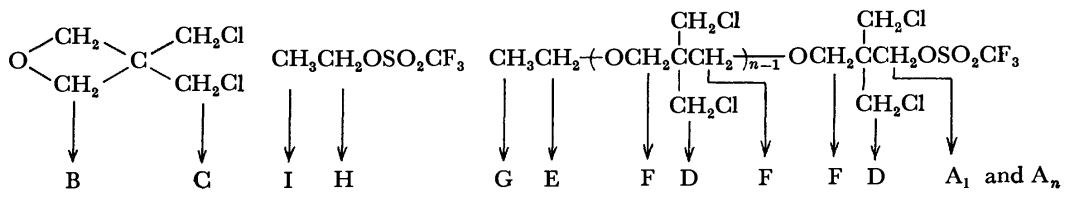

Signal	Chemical shift in ppm[a] (from Me_4Si)
A_1	4.80 (s)
A_n ($n \geqq 2$)	4.83 (s)
B	4.56 (s)
C	4.07 (s)
D	3.82 (—)
E	3.67 (q)
F	3.64 (—)
G	1.33 (t)
H	4.82 (q)
I	1.60 (t)

a) Multiplicity: s=singlet, q=quartet, and t=triplet.

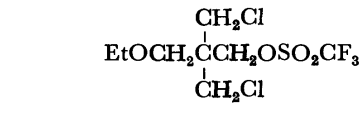

5

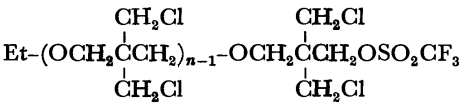

6, $n \geqq 2$

ethoxy group at the polymer end. Large singlets, B and C, are due to α-methylene protons (4H) and chloromethyl protons (4H) of BCMO monomer. Signal assignments given in Fig. 1(a) and (b) are summarized in Table 1.

For the sake of confirmation, a model compound of 3-ethoxy-2,2-bis(chloromethyl)propyl trifluoromethanesulfonate **5** was prepared by the reaction of $EtOSO_2CF_3$ and BCMO (see Experimental). **5** was isolated by distillation *in vacuo*, bp 45—46 °C (0.04mmHg). The NMR spectrum of **5** in nitrobenzene is shown in Fig. 2(a). Chemical shifts of **5** in $CDCl_3$ and in nitrobenzene are given in Table 2. It should be noted that the chemical shift of signal A_1 of **5** in nitrobenzene coincides with that of the polymerization system (Table 1). This provides a strong evidence that signal A_1 of the reaction system is due to α-methylene protons of ester type species ~~~$CH_2OSO_2CF_3$ of **4**. Chemical shifts of other signals in nitrobenzene (Table 2) are almost the same as those of corresponding peaks (Table 1).

An oligomer of **6** was prepared in order to confirm the assignment of peak A_n. The oligomer obtained did not contain **5** at all, and showed no signal at δ 4.80 (peak A_1 region). The average degree of polymerization of **6** was found to be n=2.30 (see Experimental). The signal due to α-methylene protons of ~~~$CH_2OSO_2CF_3$ in **6** appears at δ 4.83 (Fig. 2(b)), which is identical with the chemical shift of peak A_n of the

TABLE 2. SIGNAL ASSIGNMENTS OF THE MODEL COMPOUND **5**

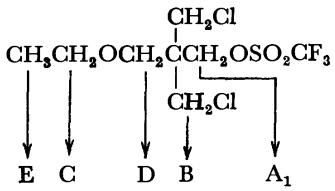

Signal	Chemical shift in ppm[a] (from Me_4Si)	
	in $CDCl_3$	in nitrobenzene
A_1	4.56 (s)	4.80 (s)
B	3.63 (s)	3.84 (s)
C	3.48 (q)	3.67 (q)
D	3.45 (s)	3.65 (s)
E	1.15 (t)	1.34 (t)

a) Multiplicity: s=singlet, q=quartet, and t=triplet.

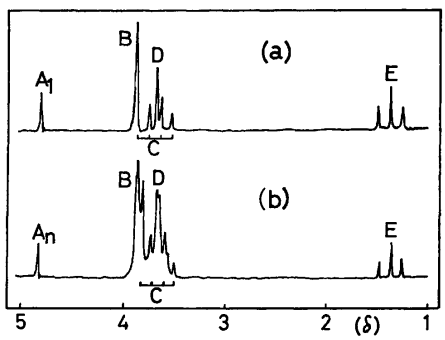

Fig. 2. ^1H NMR spectra in nitrobenzene at 35 °C of (a) **5** and (b) oligomer.

polymerization system. It is reasonable that the methylene proton signal due to ~~~$CH_2OSO_2CF_3$ of **6** appears at a field 0.03 ppm lower than that of **5**, since $Et\{OCH_2C(CH_2Cl)_2CH_2\}_{n-1}$ group in **6** is a little more electron-withdrawing than Et-group in **5**.

In coincidence with the observations of ^1H NMR spectroscopy, a signal due to the CF_3 group of **6** appeared at a lower field than that of **5** in ^{19}F NMR spectroscopy. The fluorine-19 chemical shift of a sharp singlet due to **6** was −3.58 ppm from the external standard of CF_3CO_2H capillary, whereas that due to **5** was −3.44 ppm in nitrobenzene.

Kinetics. The following scheme of reactions explains the course of BCMO polymerization.

Initiation

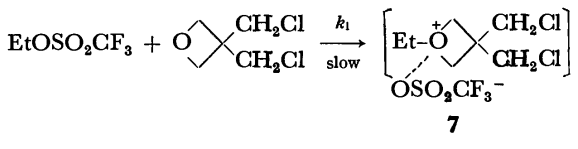

7

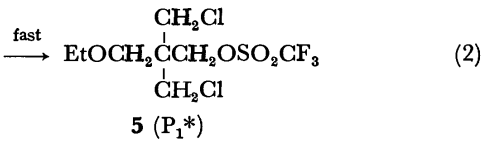

(2)

5 (P_1*)

Propagation

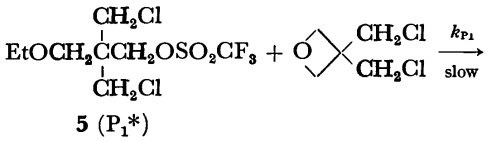

5 (P_1*)

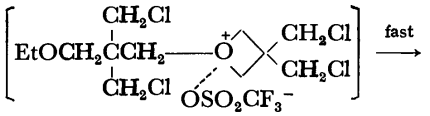

8

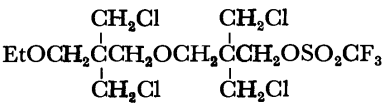

(3)

9 (P_2*)

Generally

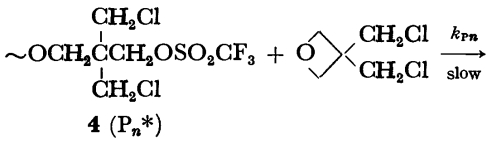

4 (P_n*)

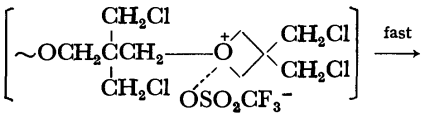

10

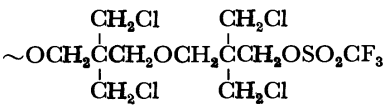

(4)

11 (P^*_{n+1})

Oxonium species **7**, **8**, and **10** might be involved as intermediates. However, these intermediates are not stable under the reaction conditions, undergoing rearrangement quickly to the ester type species **5**, **9**, and **11**, respectively.

The rate of initiation is given by

$$-\frac{d[I]}{dt} = k_i[I][M] \tag{5}$$

where k_i is the rate constant of initiation, and [I] and [M] are the concentrations of $EtOSO_2CF_3$ and BCMO, respectively. Integration of Eq. (5) gives

$$\ln\frac{[I]_0}{[I]_t} = k_i\int_0^t [M]dt \tag{6}$$

where $[I]_0$ is the initial feed concentration of $EtOSO_2CF_3$. The ratio $[I]_0/[I]_t$ was calculated from the integration values of peaks I and G in Fig. 1(a). The integrated value of [M] was obtained by graphical integration on the [M]-time curve. A linear plot of Eq. (6) is shown in Fig. 3, with a slope $k_i=1.4\times10^{-3}$ l/mol·s at 70 °C.

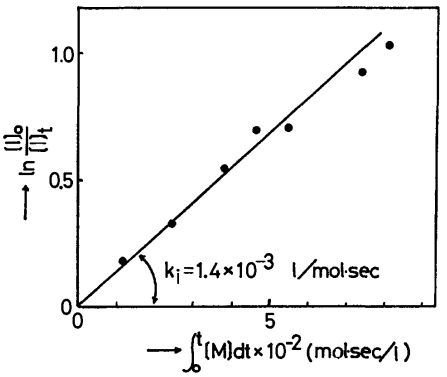

Fig. 3. Plots of Eq. (6) in BCMO polymerization by $EtOSO_2CF_3$ in nitrobenzene at 70 °C: $[I]_0=0.56$ mol/l, $[M]_0=3.90$ mol/l.

After the complete reaction of initiator, the consumption rate of the first propagating species P_1* is given by

$$-\frac{d[P_1^*]}{dt} = k_{p1}[P_1^*][M] \tag{7}$$

where k_{P1} is the rate constant of the first propagation. Integration of Eq. (7) with respect to time gives

$$\ln\frac{[P_1^*]_{t_1}}{[P_1^*]_{t_2}} = k_{p1}\int_{t_1}^{t_2}[M]dt \tag{8}$$

where t_1 and t_2 are reaction times longer than the time required for the complete reaction of initiator. The ratio $[P_1^*]_{t_1}/[P_1^*]_{t_2}$ was obtained by the integration values of peaks A_1 and A_n in Fig. 1(b). Figure 4 shows a linear plot of Eq. (8), with a slope $k_{p1}=1.4\times10^{-5}$ l/mol·s at 70 °C.

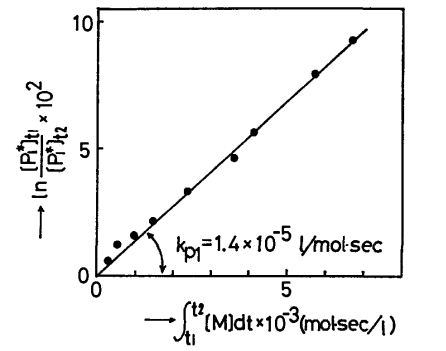

Fig. 4. Plots of Eq. (8) in BCMO polymerization by $EtOSO_2CF_3$ in nitrobenzene at 70 °C: $[I]_0=0.56$ mol/l, $[M]_0=3.90$ mol/l.

Kinetic runs of the BCMO polymerization by $EtOSO_2CF_3$ were similarly carried out at three other temperatures. At lower temperatures between 63—85 °C the reaction rate was small, and the polymerization was followed until P_1^* disappeared. Arrhenius plots of k_i and k_{p1} values were linear, and activation parameters were calculated (Table 3). For higher conversions, the polymerizations were carried out at higher temperatures (*vide infra*).

TABLE 3. RATE CONSTANTS AND ACTIVATION PARAMETERS OF INITIATION (k_i) AND THE FIRST PROPAGATION (k_{p1}) IN THE BCMO POLYMERIZATION BY $EtOSO_2CF_3$ IN NITROBENZENE SOLVENT[a)]

Temp. (°C)	$k_i \times 10^3$ (l/mol·s)	$k_{p1} \times 10^5$ (l/mol·s)
63	0.87	0.90
70	1.4	1.4
78	2.1	1.9
85	3.1	3.1
$\Delta H^{\ddagger}$ (kcal/mol)	12.5	12.5
$\Delta S^{\ddagger}$ (e. u.)	−36	−46

a) Reaction conditions; $[M]_0=3.90$ mol/l, $[I]_0=0.56$ mol/l.

Polymerization by $EtOCH_2C(CH_2Cl)_2CH_2OSO_2CF_3$ (5). According to the scheme of the $EtOSO_2CF_3$-initiated polymerization of BCMO (reaction mechanism (2)—(4)), **5** corresponds to the smallest species of propagation (P_1^*). Thus, the kinetics of polymerization by **5** was studied at higher temperatures. In this case, polymerization starts directly from the first propagating step (reaction mechanism (3)). Figure 5 shows the time-conversion cur e of BCMO monomer at 128 °C.

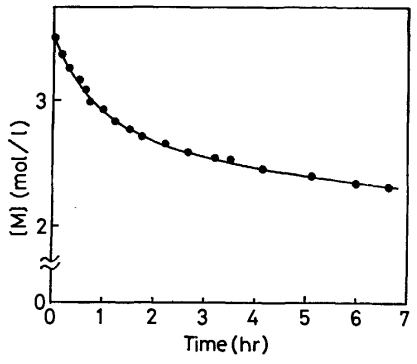

Fig. 5. Relationships between time and monomer conversion in BCMO polymerization initiated with **5** in nitrobenzene at 128 °C: $[5]_0=0.45$ mol/l, $[M]_0=3.50$ mol/l.

The rate of polymerization by **5** is given by

$$-\frac{d[M]}{dt} = k_{p1}[P_1^*][M] + [M]\sum_{n=2} k_{pn}[P_n^*] \qquad (9)$$

The combined value of $[P_1^*]$ and $[P_n^*]$ was found by integration of peaks A_1 and A_n to be constant throughout the kinetic run. This supports the view that the system is of living character under the kinetic reaction conditions. The stoichiometry between the combined value of peaks A_1 and A_n (total 2H) and peak G (3H) was found to hold, *i.e.*, $[P_1^*]+\sum_{n=2}[P_n^*]=[5]_0$. On the assumption that $k_{p2}=k_{p3}=\cdots\cdots=k_{pn}$, integration of Eq. (9) with respect to time from t_1 to t_2 gives

$$\ln\frac{[M]_{t_1}}{[M]_{t_2}} = k_{p1}\int_{t_1}^{t_2}[P_1^*]dt + k_{pn}\int_{t_1}^{t_2}[P_n^*]dt \qquad (10)$$

The $[P_1^*]$-time relationships were obtained by monitoring the reaction with ^1H NMR spectroscopy (peaks A_1 and A_n). Since peaks A_1 and A_n partly overlap with each other, the reaction was also followed by ^{19}F NMR spectroscopy. Signals due to the CF_3 group of **5** and **6** appeared as sharp singlets at −3.91 and −4.08 ppm, respectively, from an external standard of CF_3CO_2H capillary under the polymerization conditions. Results by both methods were in good agreement with each other (Fig. 6). A linear plot of Eq. (8) was made (Fig. 7), whose slope gave $k_{p1}=1.8\times10^{-4}$ l/mol·s at 128 °C.

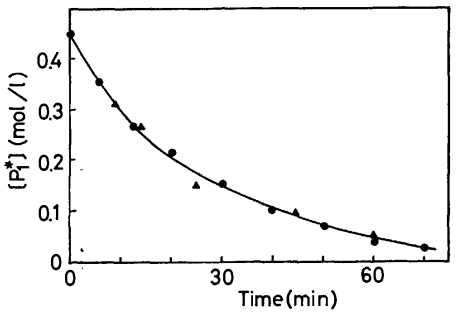

Fig. 6. $[P_1^*]$-time relationships in BCMO polymerization initiated with **5** in nitrobenzene at 128 °C monitored by ^1H NMR (-●-) and ^{19}F NMR (-▲-) spectroscopy: $[5]_0=0.45$ ml/l, $[M]_0=3.50$ mol/l.

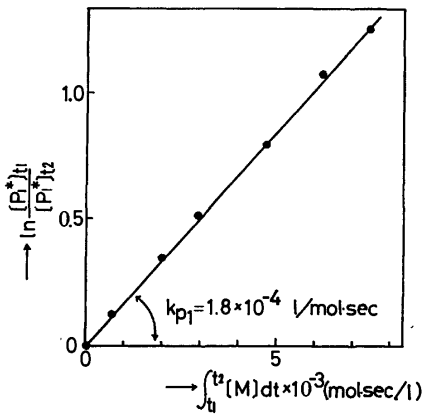

Fig. 7. Plots of Eq. (8) in BCMO polymerization initiated with **5** in nitrobenzene at 128 °C: $[5]_0=0.45$ mol/l, $[M]_0=3.50$ mol/l.

Equation (10) is converted into

$$\ln\frac{[M]_{t_1}}{[M]_{t_2}} - k_{p1}\int_{t_1}^{t_2}[P_1^*]dt = k_{pn}\int_{t_1}^{t_2}[P_n^*]dt \qquad (11)$$

Figure 8 shows a plot of Eq. (11), consisting of two straight lines A and B of different slopes. The plot indicates $k_{p2}>k_{p3}\simeq k_{p4}$. Line A was utilized to calculate k_{p2}, since the monomer consumption in its period corresponded to the stage of the second to third propagation step. Thus, $k_{p2}=5.7\times10^{-5}$ l/mol·s at 128

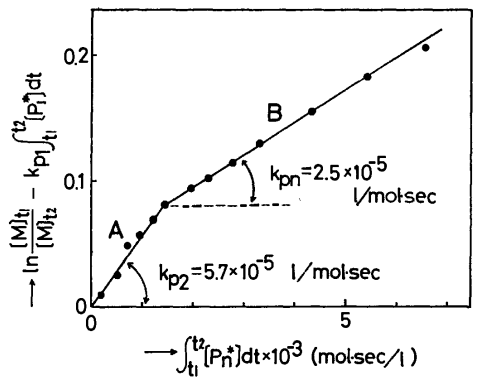

Fig. 8. Plots of Eq. (11) in BCMO polymerization initiated with **5** in nitrobenzene at 128 °C: $[\mathbf{5}]_0=0.45$ mol/l, $[M]_0=3.50$ mol/l.

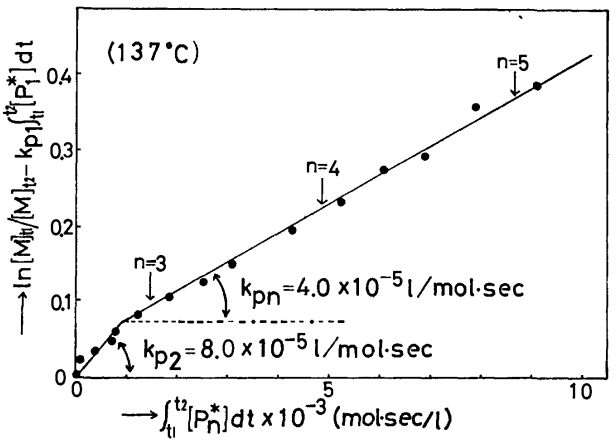

Fig. 9. Plots of Eq. (11) in BCMO polymerization initiated with **5** in nitrobenzene at 137 °C: $[\mathbf{5}]_0=0.37$ mol/l, $[M]_0=3.80$ mol/l.

°C was obtained from the slope of line A. After the reaction stage of line A, the rate constant was calculated to be $k_{p3}=k_{p4}=k_{pn}=2.5\times10^{-5}$ l/mol·s at 128 °C from the slope of line B. It became clear in the polymerization at higher reaction temperature of 137 °C that k_{pn} does not change any more after the third propagation step (Fig. 9), *i.e.*, k_{pn} was constant from $n=3$ to at least $n=5$.

Similar results were obtained with $EtOSO_2CF_3$ initiator instead of **5** initiator at 128 °C. These data along with activation parameters are given in Table 4.

Table 4. Rate constants of propagation and activation parameters in the BCMO polymerization initiated by the compound (**5**) in nitrobenzene solvent

Temp. (°C)	$k_{p1}\times10^5$ (l/mol·s)	$k_{p2}\times10^5$ (l/mol·s)	$k_{pn}\times10^5$ (l/mol·s)
90[a]	3.7	—	—
119[a]	10	3.5	1.5
128[a]	18	5.7	2.5
128[b]	(17)	(6.0)	(2.8)
137[c]	~30	8.0	4.0
ΔH^* (kcal/mol)	13	13	14
ΔS^* (e. u.)	−45	−46	−45

a) Reaction conditions; $[M]_0=3.50$ mol/l, $[\mathbf{5}]_0=0.45$ mol/l. b) $EtOSO_2CF_3$ initiator. c) Reaction conditions; $[M]_0=3.80$ mol/l, $[\mathbf{5}]_0=0.37$ mol/l.

Reaction Mechanism. All the results are in line with the reaction mechanisms (2)—(4). In fact, the propagating species of ester type were observed directly by both ^1H and ^{19}F NMR spectroscopy during the kinetic run. The first propagating species **5** was isolated by vacuum distillation and the **5**-initiated BCMO polymerization commenced directly from the first propagation.

The rate of propagation varied during the course of polymerization *i.e.*, $k_{p1}>k_{p2}>k_{p3}=k_{pn}$ ($n\geqq3$) (Table 4). These values could be determined since P_1^* and P_n^* ($n\geqq2$) were directly observed by both ^1H and ^{19}F NMR spectroscopy. The difference in k_p is due to the difference in electrophilic reactivity of alkyl groups toward BCMO monomer for $n=1$, 2 and $\geqq3$ in **6**. The larger the alkyl chain ($n\geqq3$), the less the reactivity. This might be partly due to the increase of bulkiness of alkyl groups. It could be assumed that **6** is stabilized (deactivated) through an intramolecular coordination as given by **12**, *i.e.*, such cyclization probably becomes more profound for $n\geqq3$ whereas it is not possible for $n=1$.

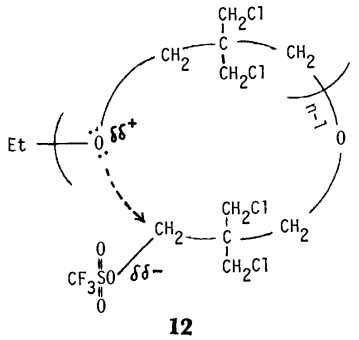

12

Examination of activation parameters (Tables 3 and 4) also supports the mechanisms (2)—(4). They are characterized by a general feature of activation parameters of S_N2 reaction between two neutral molecules producing an ionic species as a final product or a transient intermediate, the combination of low activation enthalpy (favorable for rate) and low activation entropy (unfavorable) taking place in each process.[4] The following reaction is reversible,

$$ROSO_2X + \text{O}\!\!\bigcirc \underset{}{\overset{k_{ox}}{\rightleftharpoons}} R\text{-}\overset{+}{\text{O}}\!\!\bigcirc \qquad (12)$$

R=Me, Et, *n*-Pr; X=CF_3, F, Cl; OSO_2X^-

the process of oxonium formation (k_{ox}) having a relatively low ΔH^* (favorable for k_{ox}) and a low ΔS^* (unfavorable for k_{ox}).[4] A similar phenomenon is often observed in the Menschutkin reaction in which an ammonium ion is formed from alkyl iodide and amine (Eq. (13)).[9]

$$RI + R_3'N \longrightarrow RR_3'\overset{+}{N}I^- \qquad (13)$$

The magnitudes of k_{p1} are about one-hundredth of those of k_i (Table 3). The small k_{p1} value is ascribed to the lower ΔS^* value; ΔH^* values being the same in both cases. The difference in rate of initiation and the first propagation is due to that of the electrophilic reactivity

of alkyl groups attached to OSO_2CF_3 toward the BCMO nucleophile, *e.g.*, CH_3CH_2-group for the former and $EtOCH_2C(CH_2Cl)_2CH_2$-group for the latter. A similar result was reported by Buncel and Millington[10] for the hydrolysis of primary alkyl chlorosulfates (**13**) in 85.3% aqueous dioxane, in which the reactivity of the ethyl group (**13a**) was 4.2×10^2 times as high as that of the

$ROSO_2Cl$

13a $R=CH_3CH_2$-
13b $R=(CH_3)_3CCH_2$-

neopentyl group (**13b**). The alkyl group of propagating species is bulkier (unfavorable) than the neopentyl group of **13b**, whereas α-carbon atom of the former should be more positive due to electron-withdrawing chloromethyl groups (favorable) than that of the latter group. The combination of steric and electronic factors brings forth the reactivity difference of $k_i/k_{p1}\fallingdotseq100$.

TABLE 5. RATE CONSTANTS OF INITIATION (k_i) AND THE FIRST PROPAGATION (k_{p1}) IN THE BCMO POLYMERIZATION BY $EtOSO_2CF_3$ IN THREE DIFFERENT SOLVENTS AT 63 °C[a]

Solvent	$k_i\times10^3$ (l/mol·s)	$k_{p1}\times10^5$ (l/mol·s)
Nitrobenzene	0.87	0.90
Chlorobenzene	0.20	0.17
Methylcyclohexane	——[b]	0.10

a) Reaction conditions; $[M]_0=3.90$ mol/l, $[I]_0=0.56$ mol/l. b) The k_i value could not be determined since the solvent signals overlapped with methyl signals of peaks G and I.

Solvent Effect. In order to obtain information on the mechanistic features, solvent effect was examined. Values of k_i and k_{p1} in the BCMO polymerization by $EtOSO_2CF_3$ initiator in three different solvents at 63 °C are given in Table 5. Both k_i and k_{p1} values increase in polar solvents, *e.g.*, k_{p1} is 5.3 times higher in nitrobenzene than in chlorobenzene. The results also provide evidence for the mechanisms (2)—(4). In the reaction between two neutral molecules of ester type species (electrophile) and BCMO monomer (nucleophile) the ionic transition state **14** will be

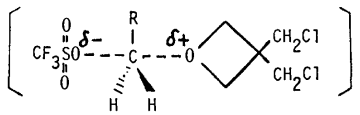

14 R = CH_3- or $\sim CH_2C(CH_2Cl)_2CH_2Cl$

more stabilized by solvation in a polar solvent as compared with the initial state of two neutral molecules. Similarly the oxonium formation (Eq. (12)) was favored in polar solvents, *e.g.*, k_{ox} in nitrobenzene was 2.65 times larger than that in chlorobenzene for R=Et and X=Cl in Eq. (12).[4]

The solvent effect (Table 5) is in sharp contrast to that observed in the cationic polymerization of four-membered cyclic ethers by typical Lewis acids such as BF_3, *i.e.*, k_p values of both unsubstituted and 3-methyloxacyclobutanes by BF_3 initiator were about 9 times higher in a nonpolar solvent of methylcyclohexane than in a polar one of CH_2Cl_2.[8] It is generally accepted that the polymerization of oxacyclobutanes initiated by typical Lewis acids proceeds *via* an S_N2 reaction between the propagating cyclic oxonium **3** (electrophile) and monomer (nucleophile):[5,8]

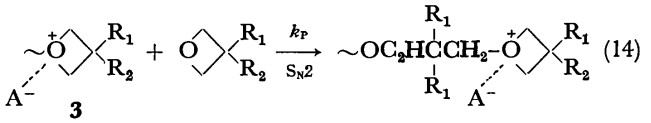

(14)

3

where A^- represents the counter anion derived from initiator. In this case the transition state given by **15** is less solvated than the initial state, since the positive charge is more dispersed in **15** than in the initial state of oxonium. Thus, k_p decreases in a polar solvent with BF_3 catalyst.[8]

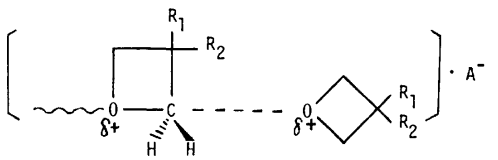

15

In the BCMO polymerization by BF_3, solvent effects were examined by Penczek and Penczek,[11] who found that the polymerization proceed through the oxonium propagating species and that the apparent overall rate of polymerization is greater in more polar solvents. The increase of the overall rate was ascribed to the increase in the rate of initiation, *i.e.*, concentration of the propagating species increased but the propagation rate did not.

In contrast to the present results it has been found that polymerization of oxacyclobutane and of 3-methyloxacyclobutane initiated by $EtOSO_2CF_3$ proceeds *via* oxonium propagating species.[12] The difference is due to two chloromethyl groups of BCMO, which brings about not only a destabilization of intermediate oxonium ions (**7**, **8**, and **10**) but also a decrease in the nucleophilic reactivity of BCMO monomer.

Recently, Pruckmayr and Wu[13] reported on a ^1H NMR study of BCMO polymerization initiated by superacid of fluorosulfuric acid ($HOSO_2F$). However, the rate constants were not determined since the system was complicated owing to the presence of "acidic" proton derived from $HOSO_2F$. Unlike their system the present polymerization with $EtOSO_2CF_3$ was clean, since no such acidic proton is involved. Thus, kinetic analysis was successfully made. Concerning ^1H NMR spectral assignments they ascribed peaks at δ 4.56 and 4.31 in CH_2Cl_2 (peaks A and C in Fig. 7[13]) respectively to the open-chain methylene and the ring methylene protons adjacent to the propagating oxonium **16**. However, it is unlikely that a trialkyl four-membered cyclic

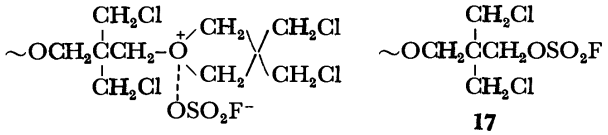

16

17

oxonium such as **16** is observed as a long-lived species under their ^1H NMR measurement conditions. It is also very unlikely that ring methylene protons of **16** appear at higher chemical shift (δ 4.31) than those of BCMO (δ 4.41).[13] We propose here with that a peak at δ 4.56[13] is assigned to α-methylene protons of OSO_2F group of **17**. To support this assignment a signal due to α-methylene protons of OSO_2CF_3 of **5** appears at nearly the same chemical shift of δ 4.60 in CH_2Cl_2,[12] since the chemical shift of α-methylene protons of OSO_2X is not affected by X=F, Cl, and CF_3.[14] Thus, we believe that ester type **17** is involved as a stable propagating species also in the BCMO polymerization by $HOSO_2F$ initiator.

Experimental

Materials. BCMO and all solvents were purified as previously reported.[1,4,15] $EtOSO_2CF_3$ was prepared by the reaction of diethyl sulfate with CF_3SO_3H.[2]

3-Ethoxy-2,2-bis(chloromethyl)propyl trifluoromethanesulfonate **5** was prepared as follows. A mixture of 8.36 mmol of BCMO and 10.0 mmol of $EtOSO_2CF_3$ in 2.0 ml of CH_2Cl_2 was allowed to react for 10 days at 35 °C, in which BCMO was completely consumed. CH_2Cl_2 and excess $EtOSO_2CF_3$ were then removed, and **5** was isolated in 90% yield by vacuum distillation, bp 45—46 °C/0.04 mmHg. The data of the ^1H NMR spectrum are given in Table 2. ^{19}F NMR (nitrobenzene): −3.44 ppm (~~~OSO_2CF_3) (from the external standard of CF_3CO_2H capillary). IR (neat): ν_{max} 1420, 1210, and 1150 cm^{-1} ($-SO_2-$).[16]

Found: C, 28.95; H, 3.94%. Calcd for $C_8H_{13}F_3O_4SCl_2$: C, 28.84; H, 3.90%.

Preparation of Oligomer. A mixture of BCMO (8.30 mmol) and $EtOSO_2CF_3$ (1.20 mmol) in 1.0 ml of nitrobenzene was allowed to react at 100 °C. After 10 hr, signal A_1 disappeared completely, and only signal A_n was observed in the ^1H NMR spectrum. Unchanged BCMO and nitrobenzene were removed *in vacuo*. The residue was an oligomer of oily material (0.60 g). The average degree of oligomerization was determined by ^1H NMR to be n=2.30 from the integration ratio of peaks B, C, and D to peak A_n of the ^1H NMR spectrum (Fig. 2 (b)). ^{19}F NMR (nitrobenzene): −3.58 ppm (~~~OSO_2CF_3) (from the external standard of CF_3CO_2H capillary). IR (neat): ν_{max} 1420, 1210, and 1145 cm^{-1} ($-SO_2-$).[16] The molecular weight of oligomer was determined to be 510 by vapor pressure osmometry, which is close to the calculated value of 535 with n=2.30 in **6**. Thus, the 0.60 g oligomer obtained corresponds to 1.12 mmol, which does not differ much from the concentration of the initiator of $EtOSO_2CF_3$. This indicates that each initiator produces 1 mol of oligomer.

Found: C, 32.56; H, 4.26; F, 10.68; S, 6.45; Cl, 30.60%. Calcd for $C_{14.50}H_{23.40}F_3O_{5.30}SCl_{4.60}$ (n=2.30 in **6**): C, 32.58; H, 4.41; F, 10.66; S, 6.00; Cl, 30.50%.

NMR Measurement. A typical example is as follows. Into an NMR sample tube were introduced 1.67 mmol of BCMO, 0.24 mmol of $EtOSO_2CF_3$ and 0.20 ml of nitrobenzene at −78 °C under nitrogen. The tube was sealed and stirred at the same temperature. The extent of the reaction was negligible at this point. The tube was then inserted into the NMR probe which was kept at a constant temperature. The reaction was then monitored. A Hitachi R-20B NMR spectrometer equipped with radio frequency counters of ^1H (60 MHz) and ^{19}F (56.456 MHz) nuclei was used. The reaction temperature was kept constant within ±1 °C and the experimental error of the NMR analysis was within ±2%.

Molecular Weight Determination. The molecular weight of the oligomer was determined by a vapor pressure osmometer (Hitachi Perkin-Elmer model 115) in dimethylformamide at 55 °C.

References

1) For Part IV. see S. Kobayashi, H. Danda, and T. Saegusa, *Macromolecules*, **7**, 415 (1974).

2) S. Kobayashi, H. Danda, and T. Saegusa, This Bulletin, **46**, 3214 (1973).

3) S. Kobayashi, T. Saegusa, and Y. Tanaka, *ibid*, **46**, 3220 (1973).

4) S. Kobayashi, T. Ashida, and T. Saegusa, *ibid*, **47**, 1233 (1974).

5) a) K. C. Frisch and S. L. Reegen, Ed., "Ring-Opening Polymerizations," Marcel Dekker Inc., New York, N. Y. (1969). b) T. Saegusa and S. Kobayashi, "Progress in Polymer Science Japan," Vol. 6, ed. by S. Onogi and K. Uno, Kodansha Scientific, Tokyo (1973), pp. 107—151.

6) S. Smith and A. J. Hubin, *Polymer Preprints*, **13**, 66 (1972).

7) K. Matyjaszewski, P. Kubisa, and S. Penczek, International Symposium on Cationic Polymerization, Sept. 1973, Rouen, France.

8) T. Saegusa, H. Fujii, S. Kobayashi, H. Ando, and R. Kawase, *Macromolecules*, **6**, 26 (1973).

9) K. B. Wiberg, "Physical Organic Chemistry," John Wiley & Sons, Inc., New York, N. Y. (1963), p. 379.

10) E. Bunsel and J. P. Millington, *Can. J. Chem.*, **43**, 556 (1965).

11) I. Penczek and St. Penczek, *J. Polym. Sci., Part A-1*, **8**, 2465 (1970).

12) S. Kobayashi, H. Danda, and T. Saegusa, unpublished results.

13) G. Pruckmayr and T. K. Wu, *Macromolecules*, **6**, 33 (1973).

14) S. Kobayashi, *Yuki Gosei Kagaku Kyokai Shi*, **31**, 935 (1973).

15) T. Saegusa, S. Matsumoto, and Y. Hashimoto, *Macromolecules*, **3**, 377 (1970).

16) T. Gramstad and R. N. Haszeldine, *J. Chem. Soc.*, **1956**, 173.

Superacids and Their Derivatives. VI.[1] Kinetics of the Cationic Ring-Opening Polymerization of Tetrahydrofuran Initiated by Ethyl 2,4,6-Trinitrobenzenesulfonate

Shiro KOBAYASHI, Tamotsu NAKAGAWA, Hidenori DANDA, and Takeo SAEGUSA

Department of Synthetic Chemistry, Faculty of Engineering, Kyoto University, Kyoto 606

(Received July 11, 1974)

Ethyl 2,4,6-trinitrobenzenesulfonate ("trinitate", EtOTn) was found to induce the ring-opening polymerization of tetrahydrofuran (THF). Kinetic studies of the THF polymerization by EtOTn initiator were carried out in CH_2Cl_2 solution by NMR spectroscopy. The instantaneous concentrations of the counteranion of the propagating oxonium species (**1**) and monomer were directly determined at the same time by the NMR measurement. The rate constants of initiation (k_i) and propagation ($k_{p(i)}$) due to **1** were obtained. Upon the view of $k_{p(i)}$ values with various initiators, it was concluded that the $k_{p(i)}$ values are changed significantly depending on the nature of the counteranion.

In recent several studies on the cationic ring-opening polymerization of tetrahydrofuran (THF) superacids and their ester or anhydride derivatives have been employed as initiator.[2-7] In these studies trifluoromethanesulfonic (TfOH),[2,3,5-7] fluorosulfuric (FSO_3H),[2,7] and chlorosulfuric acids ($ClSO_3H$)[2,4] were used as the superacid component. Primary alkyl esters of these acids are known to form oxonium ions with tetrahydropyran.[8] Generally, initiators are effective for the cationic ring-opening polymerization of THF, when they can form stable trialkyl oxonium ions. 2,4,6-Trinitrobenzenesulfonic acid (TnOH) is well known to be an only acid among organic acids except for TfOH to produce a stable trialkyl oxonium ion in the reaction with ether.[9,10] As an extension of our studies on the superacids and their derivatives, therefore, we examined the THF polymerization initiated by ethyl 2,4,6-trinitrobenzenesulfonate which we wish to abbreviate as "ethyl trinitate" (EtOTn). It was found that EtOTn induced the THF polymerization. Now, we wish to report kinetic results of this system. Kinetic analysis was performed by NMR spestroscopy.

Results and Discussion

NMR Spectroscopy. Figure 1 shows an example of NMR spectrum of the THF polymerization with EtOTn initiator after 60 min at 20 °C in CH_2Cl_2. The initial concentrations of monomer $[M]_0$ and of initiator $[I]_0$ were 6.78 and 0.167 mol/l, respectively. Among the signals in Fig. 1 peaks A at δ 8.84 and B at δ 8.56 should be noted. They are assigned respectively to aromatic protons (2H) of EtOTn (peak A) and of trinitate anion (peak B). The assignment of peak B is supported by the fact that the aromatic protons of triethyloxonium trinitate appears at the same chemical shift of peak B (See Experimental). The pattern of signals C–I is very similar to that of the polymerization mixture by EtOTf initiator, whose signal assignments were already performed.[2] Therefore, only the result of the assignment is shown here as follows;

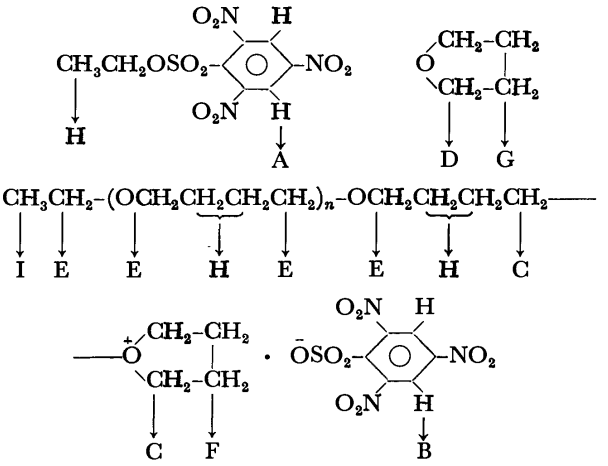

A quartet signal due to methylene protons of EtOTn should appear around at δ 4.8—4.3. However, it is not detected clearly in Fig. 1 because of the low concentration of EtOTn.

Kinetics. The course of the THF polymerization by EtOTn is given by the following reactions (Eqs. (1) and (2)).

Initiation

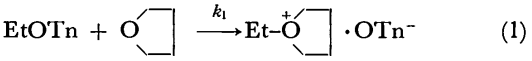

(1)

Propagation

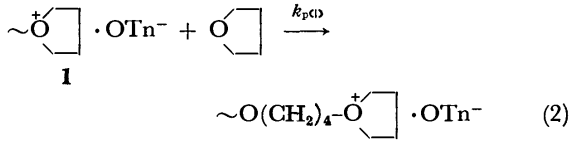

(2)

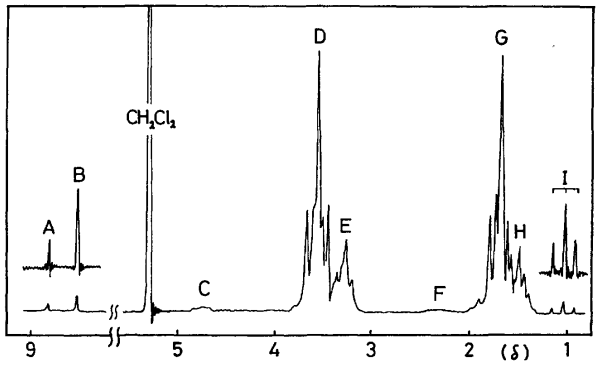

Fig. 1. NMR spectrum of the THF polymerization system initiated by ethyl 2,4,6-trinitrobenzenesulfonate in CH_2Cl_2 after 60 min at 20 °C.

Based on the above reactions of a bimolecular mechanism, the integrated rate equations of initiation and propagation are given by Eqs. (3) and (4), respectively[2,3]

$$\ln \frac{[I]_{t_1}}{[I]_{t_2}} = k_i \int_{t_1}^{t_2} [M]dt \quad (3)$$

and

$$\ln \frac{[M]_{t_1}-[M]_e}{[M]_{t_2}-[M]_e} = k_{p(i)} \int_{t_1}^{t_2} [O^+]dt \quad (4)$$

where k_i and $k_{p(i)}$ denote the rate constants of initiation and of propagation due to the oxonium ion species **1**, $[O^+]$ is the concentration of the oxonium propagating species, and [I], [M], and $[M]_e$ are respectively the initiator, monomer, and equilibrium monomer concentrations.[2]

The peak area of B was equal to two-third of that of triplet peak I throughout the kinetic run, *i.e.*, the molar ratio between the counteranion (OTn^-) of the propagating polymer end **1** and ethyl group at the other polymer end was held unity, *i.e.*, $[O^+]=[I]_0-[I]$. This indicates that the polymerization system was of living character without termination and in addition that the propagating end was mainly the oxonium ion type of **1** in CH_2Cl_2 solution, although the ester type **2** of the propagating end might be involved, as observed in the case of the EtOTf-initiated system.[3] However, the characteristic signal due to α-methylene protons of ~~~CH_2OTn **2** at δ 4.2 region[2] was not detected. It was difficult to determine precisely the concentration of the propagating species **1** directly from the oxonium proton peaks C and F, since both of them were very broad due to the low concentration of **1**.

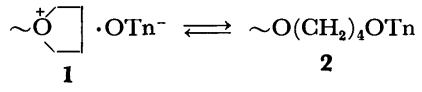

1 **2**

The instantaneous concentrations of EtOTn and **1** were determined by monitoring peaks A and B, respectively. The variation of the monomer concentration was obtained from peaks D and E. It should be noted that both the concentrations of the counteranion of the propagating species **1** and of monomer could directly be determined at the same time by the NMR measurement alone. Figures 2 and 3 show plots of Eqs. (3) and (4), respectively, the slopes of which gave the values of k_i and $k_{p(i)}$. Similarly, the kinetics were carried out also at 0 and 10 °C in CH_2Cl_2. These

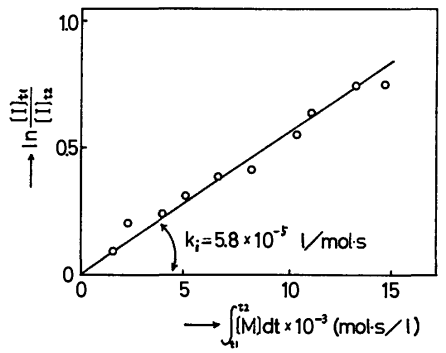

Fig. 2. Plot of Eq. (3) in the THF polymerization at 20 °C in CH_2Cl_2.

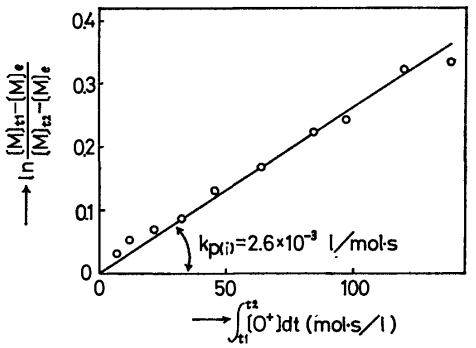

Fig. 3. Plot of Eq. (4) in the THF polymerization at 20 °C in CH_2Cl_2.

results and activation parameters of initiation and propagation are shown in Table 1. The data scattered considerably because $[I]_0$ was low due to the reduced solubility of EtOTn in the system. $[I]_0$ was six times less than that of the previous kinetics of the EtOTf-initiated system.[2,3] The $k_{p(i)}$ value (0.70×10^{-3} l/mol·s at 0 °C) of EtOTn initiator is smaller than that of EtOTf (2.0×10^{-3} l/mol·s at 0 °C).[3] The values of ΔH^* and ΔS^* are also very low in both initiation and propagation. This finding may be related to the bulkiness of OTn group; in both reactions of (1) and (2) the bulky OTn group causing an unfavorable geometry at the transition state (lower ΔS^* value).

Table 1. Rate constants of initiation (k_i) and of propagation ($k_{p(i)}$) and activation parameters in the THF polymerization by EtOTn initiator in CH_2Cl_2 solution[a]

Temp (°C)	$10^3\cdot k_{p(i)}$ (1/mol·s)	$10^5\cdot k_i$ (1/mol·s)
0	0.70	1.6
10	1.5	2.8
20	2.6	5.8
ΔH^*(kcal/mol)	9±1	8±2
ΔS^*(e.u.)	−41±3	−54±5

a) $[M]_0=6.78$ mol/l, $[I]_0=0.167$ mol/l.

Table 2. Rate constants of propagation ($k_{p(i)}$) by various initiators at 0 °C

Initiator	$10^3\cdot k_{p(i)}$ (1/mol·s)	$[M]_0$ (mol/l)	Method[d-f]	Ref.
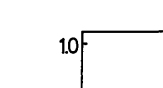	0.70	6.78[b]	d	This work
$EtOSO_2F$	0.8	7.70[b]	d	2
$EtOSO_2Cl$	1.5	7.70[b]	d	2
$EtOSO_2CF_3$	2.0	7.70,[b] 5.30[b]	d,e	2, 3
$Et_3O^+BF_4^-$	3.7	6.3[b]	f	11
BF_3-ECH[a]	4.1	6.3[b]	f	12
BF_3-ECH[a]	4.6	12.6[c]	f	12
$SnCl_4$-ECH[a]	6.7	12.6[c]	f	12
$AlEtCl_2$	7.8	12.6[c]	f	12

a) ECH: epichlorohydrin as a promoter. b) Solution polymerization in CH_2Cl_2. c) Bulk polymerization. d) ^1H NMR spectroscopy. e) ^{19}F NMR spectroscopy. f) Phenoxyl end-capping method.[13]

As to the effect of the counteranion on the rate of the THF polymerization there are several data available. Table 2 lists the rate constants of propagation by various initiators, all of which were determined recently in our laboratory.[11-13] All the rate constants of propagation in Table 2 represent those due to the oxonium ion propagating species ($k_{p(i)}$). It has been presented that the value of $k_{p(i)}$ was not changed depending on the nature of the counteranion.[6,14] However, the $k_{p(i)}$ values in Table 2 vary from 0.70×10^{-3} to 7.8×10^{-3} l/mol·s at 0 °C. Our view is, therefore, that the $k_{p(i)}$ value changes significantly depending on the counteranion derived from the initiator.

Experimental

Reagents. THF and CH_2Cl_2 were purified as previously reported.[2,3] EtOTn was prepared according to Pettitt and Helmkamp[6,10] as follows. A commercial reagent of TnONa·$2H_2O$ was converted by concd HCl solution to the free acid of TnOH, mp 172—174 °C (lit,[10] 174—177 °C). A solution of 2.0 g (6.8 mmol) of TnOH dissolved in hot 15 ml of ethyl acetate was then kept at 5—10 °C. To this solution was added 1.2 g (6.3 mmol) of triethyloxonium tetrafluoroborate[15] in 2 ml of nitromethane and cooled in an ice-bath for 5 min with stirring. The mixture was poured into 25 ml of anhydrous ether. White precipitate was collected by filtration. The precipitate was washed with 5 ml of ether, finally with 3 ml of petroleum ether, and dried *in vacuo* to give 1.6 g of Et_3O^+ OTn^-, mp 88—90 °C (lit,[9] 88—89 °C). NMR (CH_3NO_2); δ 8.55 (sharp s, 2,4,6-$(NO_2)_3C_6H_2$-, 2H), 4.83 (q, $(-CH_2-)_3$ O^+ overlapping partly with CH_3NO_2), and 1.66 (t, $(CH_3-)_3$, 9H). EtOTn was obtained by the thermal decomposition of Et_3O^+ OTn^- at 40—50 °C under the reduced pressure (~0.5 mmHg) for 80 hr, mp 140—141 °C (lit,[9] 142—144 °C). NMR (CH_3NO_2); δ 8.85 (sharp S, 2,4,6-$(NO_2)_3C_6H_2$-, 2H) and 1.46 (t, CH_3-, 3H). The methylene proton signal overlapped with that of CH_3NO_2.

Kinetic Procedures. All operations were carried out under nitrogen. In an NMR sample tube were placed at −78 °C 24.2 mg (0.754 mmol) of EtOTn, 0.250 ml of THF, and 0.200 ml of CH_2Cl_2. The tube was sealed at the same temperature and shaked vigorously at room temperature until EtOTn was completely dissolved to give homogenous solution. The tube was then put into the NMR probe insert which was kept constant at the reaction temperature. Up to this step the reaction proceeded to a small extent. Therefore, this moment was taken to be t_1 when carrying out the kinetic analyses according to Eqs. (3) and (4). Then, the reaction was monitored by recording the spectrum several times on a Hitachi R-20B NMR spectrometer (60 MHz). The reaction temperature was kept constant within ±1 °C and the experimental error of the integration was within ±5%.

References

1) Part V: S. Kobayashi, H. Danda, and T. Saegusa, This Bulletin, **47**, 2699 (1974).
2) S. Kobayashi, H. Danda, and T. Saegusa, *ibid.*, **46**, 3214 (1973).
3) S. Kobayashi, H. Danda, and T. Saegusa, *Macromolecules*, **7**, 415 (1974).
4) S. Kobayashi, T. Saegusa, and Y. Tanaka, This Bulletin, **46**, 3220 (1973).
5) S. Smith and A. J. Hubin, *J. Macromol. Sci.-Chem.*, **A7**, 1399 (1973).
6) K. Matyjaszewski, P. Kubisa, and S. Penczek, Presented at the "International Symposium on Cationic Polymerization" September, 1973, Rouen, France.
7) G. Pruckmayr and T. K. Wu, *Macromolecules*, **6**, 33 (1973).
8) S. Kobayashi, T. Ashida, and T. Saegusa, This Bulletin, **47**, 1233 (1974).
9) D. J. Pettitt and G. K. Helmkamp, *J. Org. Chem.*, **29**, 2702 (1964).
10) G. K. Helmkamp and D. J. Pettitt, "Organic Syntheses," Vol. 46, p. 122 (1966).
11) T. Saegusa and S. Matsumoto, *J. Macromol. Sci.-Chem.*, **A4**, 873 (1970).
12) T. Saegusa and S. Matsumoto, *Macromolecules*, **1**, 442 (1968).
13) a) T. Saegusa, *J. Macromol. Sci.-Chem.*, **A6**, 997 (1972); b) T. Saegusa and S. Kobayashi, *Progr. Polymer Sci. Japan*, **6**, 107 (1973).
14) P. Dreyfuss and M. P. Dreyfuss, *Advan. Chem. Ser.*, **91**, 335 (1969).
15) H. Meerwein, E. Battenberg, H. Gold, E. Pfeil, and G. Willfang, *J. Prakt. Chem.*, **154**, 83 (1939).

Preparation of Diethylaluminium Chelates, $R_2P(S)$-X-$AlEt_2$ (X=NMe, S) and Some Reactions with Carbonyl Compounds

Kouichi URATA, Toshinobu YOGO, Kenji ITOH, and Yoshio ISHII*

Department of Synthetic Chemistry, Faculty of Engineering, Nagoya University, Chikusa-ku, Nagoya 464

(Received July 22, 1974)

New monomeric organoaluminium chelate compounds; *N*-diethylaluminium *N*-methyl dialkylthiophosphinic amide and dialkyldithiophosphinate; $R_2P(S)$-X-$AlEt_2$ (X=NMe, S), were prepared. Spectroscopic results of these compounds indicate an intramolecular coordination of sulfur atom of P=S bond to the organoaluminium moiety. Addition reactions of $Me_2P(S)$-NMe-$AlEt_2$ and $Et_2P(S)$-S-$AlEt_2$ with phenyl isocyanate gave the corresponding 1/1 adducts and only small amount of elimination product was obtained. A reaction of $Me_2P(S)$-NMe-$AlEt_2$ with benzaldehyde gave $Me_2P(S)$-NMe-CH(Et)Ph and PhCH=NMe (by two ways of addition-elimination).

Group III organometallic chelate compounds of dialkyl (or diaryl) dithiophosphinic acid; $R_2P(S)$-S-MR_2' (M=Al, Ga, and In), have been confirmed to exhibit a strong intramolecular interaction between the metal atom and the thiophosphoryl group.[1,2] For instance, Coates prepared two dimethylaluminium derivatives of dimethyl(or diphenyl)dithiophosphinic acid; $R_2P(S)$-S-$AlMe_2$ (R=Me, Ph) and claimed an intramolecular coordination based on their infrared spectra.

The corresponding *N*-alkyl dialkylthiophosphinic organoaluminium amides; $R_2P(S)$-NR'-AlR_2'', have not been reported,[3] and the chemical behavior of these class of organoaluminium chelate compounds; $R_2P(S)$-X-$AlEt_2$ (X=NMe, S), has been unexplored.

In our former paper,[4] diethylaluminium dialkyl *N*-methylphosphoramidates; $(RO)_2P(O)$-NMe-$AlEt_2$ (R=Me, Et), were found to react with carbonyl compounds giving the corresponding imino compounds by way of an addition and subsequent elimination reactions as Eq. (1).

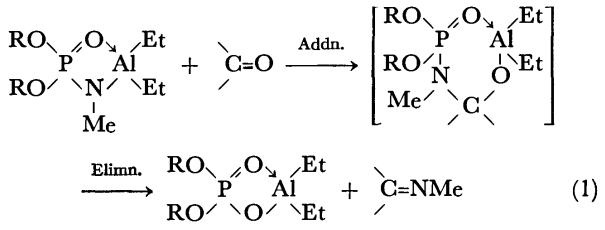

(1)

Therefore, *N*-diethylaluminium *N*-methyl dialkylthiophosphinic amide; $R_2P(S)NMeAlEt_2$, and dialkyldithiophosphinate; $R_2P(S)SAlEt_2$, are expected to react with carbonyl compounds analogously affording the corresponding >C=NMe or >C=S compounds.

We describe here the preparation of chelate compounds of type $R_2P(S)$-X-$AlEt_2$ (X=NMe, S) and their reactions with carbonyl compounds.

Results and Discussion

Preparation of $R_2P(S)$-X-$AlEt_2$ Compounds. *N*-Diethylaluminium *N*-methyl dialkylthiophosphinic amides; $R_2P(S)$-NMe-$AlEt_2$ (Ia—d) were prepared from the reactions between $R_2P(S)NHMe$ (IIIa—d) and Et_3Al in refluxing benzene in 60—80% yields (Eq. (2)).

$$\underset{\text{(IIIa—d)}}{R_2P(S)NHMe} + Et_3Al \xrightarrow[80°C]{\text{benzene}} \underset{\text{(Ia—d)}}{R_2P(S)NMeAlEt_2} + C_2H_6 \quad (2)$$

(R; a=Me, b=Et, c=*i*-Pr, d=*t*-Bu)

The corresponding three dithiophosphinic acid derivatives; $R_2P(S)$-S-$AlEt_2$ (IIa—c) were prepared analogously from the reactions of $R_2P(S)SH$ (IVa—c) with Et_3Al. These new compounds are distillable and their physical, analytical results are summarized in Table 1.

The cryoscopic molecular weight determination in benzene shows that these compounds have monomeric structure in consistent with an intramolecular coordination.

Infrared and NMR Spectra. In Table 2 $\nu_{P=S}$ absorptions of (Ia—d, IIa—c) were compared with those of the parent organophosphorus compounds (IIIa—d, IVa—c) (in the range of 650—550 cm^{-1}).[5] The lower frequency shift of the $\nu_{P=S}$ absorptions in

Table 1. Physical and analytical data of $R_2P(S)$-X-AlE_2 (Ia—d, IIa—c)

Compound			Yield (%)	Bp (°C/mmHg)	Found (%)			Calcd (%)			Mol. wt. Found (Calcd)	Concn (wt%)
	R	X			C	H	Al	C	H	Al		
Ia	Me	NMe	79	87—89 (0.06)	40.26	9.00	12.57	40.57	9.24	13.02	191 (207)	1.80
Ib	Et	NMe	69	94—97 (0.06)	45.44	9.85	11.81	45.94	9.85	11.49	220 (235)	2.52
Ic	*i*-Pr	NMe	66	80—111 (0.33)	50.34	10.18	10.62	50.17	10.33	10.25	239 (264)	2.82
Id	*t*-Bu	NMe	60	116—126 (0.33)	53.50	10.65	10.08	53.58	10.72	9.26	262 (291)	2.62
IIa	Me	S	71	65—68 (0.18)	34.41	7.56	13.10	34.27	7.67	12.83	188 (210)	2.73
IIb	Et	S	67	90—100 (0.25)	40.49	8.29	10.60	40.32	8.46	11.32	246 (238)	2.49
IIc	*i*-Pr	S	85	86—96 (0.20)	44.72	8.85	10.99	45.09	9.08	10.13	232 (266)	2.52

TABLE 2. INFRARED SPECTRA OF $R_2P(S)$-X-$AlEt_2$(Ia—d, IIa—c) AND $R_2P(S)XH$(IIIa—d, IVa—c) (cm^{-1})[a,b]

Compounds	R	X	$\nu^{A}_{P=S}$ of (Ia—d, IIa—c)	$\nu^{B}_{P=S}$ of (IIIa—d, IVa—c)	$\Delta\nu_{P=S}=\nu^{A}_{P=S}-\nu^{B}_{P=S}$	$\nu_{P=N}$ of (Ia—d)
Ia, IIIa	Me	NMe	622 vs, 524 w	652 vs, 588 w	−30, −64	1187 m
Ib, IIIb	Et	NMe	624 vs	651 vs, 569 w	−27	1186 m
Ic, IIIc	*i*-Pr	NMe	622 vs, 543 w	654 vs, 565 w	−32, −22	1186 m
Id, IIId	*t*-Bu	NMe	620 vs	652 vs, 626 w	−32	1192 m
IIa, IVa	Me	S	610 vs, 543 w	650 vs, 602 w	−40, −59	
IIb, IVb	Et	S	570 vs, 548 w	592 vs, 573 w	−22, −25	
IIc, IVc	*i*-Pr	S	623 vs, 543 w	647 vs, 594 w	−24, −51	

a) In 2% benzene solution. b) vs, very strong; m, medium; w, weak.

organoaluminium chelates (−20——60 cm^{-1}) may be explained in terms of the intramolecular coordination of the sulfur atom of thiophosphoryl group to organoaluminium moiety. The appearance of new absorption bands around 1190—1200 cm^{-1} (assignable to $\nu_{P=N}$[6,7]) indicates the contribution of a resonance form (B), in which (p—d)π interaction between phosphorus and nitrogen atom is involved.

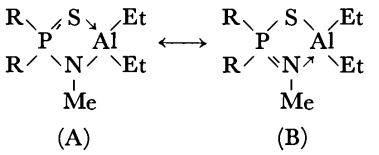

(A) (B)

NMR results are summarized in Table 3. The internal chemical shifts in NMR spectra; $\Delta=\delta AlCH_2-\delta AlCH_2CH_3$ (ppm); are larger ($\Delta=-0.90$——-1.10 ppm) than that of Et_3Al ($\Delta=-0.75$ ppm). Narashimhan[8,9] correlated the electronegativity of the metal (x_M) with internal chemical shifts (Δ) of the ethyl group of ethylmetalloids as $x_M=0.62\Delta+2.07$. The apparent electronegativity values of the aluminium atom (x_{Alapp}) in Ia—d and IIa—c are calculated as 1.39—1.49 (Table 3). This means the aluminium atom in the chelate compounds has more negative charge than that in Et_3Al ($x_{Al}=1.60$, $\Delta=-0.75$ ppm).

The J_{PNCH} values of $R_2P(S)NMeAlEt_2$ (Ia—d) are 17—20 Hz, whereas those of parent compounds $R_2P(S)NHMe$ (IIIa—d) are apparently smaller (11—15 Hz). This indicates the significant contribution of a (p—d)π overlap between phosphorus and nitrogen atoms in (Ia—d) (*cf.* P^{V}=N-CH; J_{PNCH}=20—30 Hz[10,11]). An increase of (p—d)π bonding between phosphorus and nitrogen atoms by diethylaluminium moiety was reported in the case of $Y_2P(O)NMe$-$AlEt_2$ (Y=RO, NR_2).[4]

Reactions of (Ia) and (IIb) with Carbonyl Compounds. The reaction of (Ia) with phenyl isocyanate at 80 °C for 15 hr and subsequent hydrolysis gave only the 1/1 insertion product (V) in 90% yield as Eq. (3). No elimination product (Ph-N=C=N-Me) was obtained.

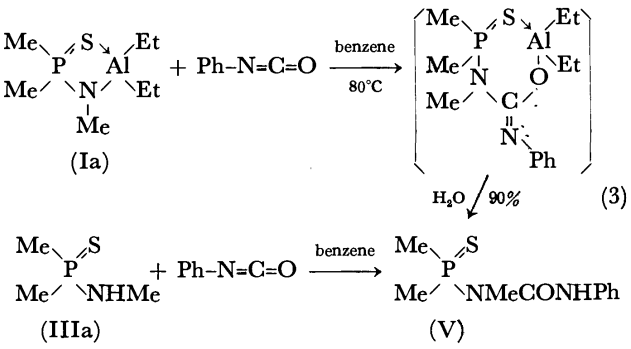

(3)

A reaction of Ia with benzaldehyde gave both *N*-benzylidenemethylamine (30%) and *N*-dimethylthiophosphinyl-*N*-phenylethylcarbinylmethylamine; $(CH_3)_2P(S)$-NCH_3-$CH(C_2H_5)C_6H_5$ (VI) (40%).

TABLE 3. NMR DATA (τ in benzene)

Compound R	X	P-N-CH_3	J_{PNCH}[a]	$AlCH_2$	$AlCH_2CH_3$	J_{HCCH}	χ_{Al}[b]	P-R	J_{PCH}	J_{PCCH}
Ia Me	NMe	7.51	19.1 (14.6)	9.79	8.69	8.3	1.39	8.74d	12.8	
Ib Et	NMe	7.68	18.7 (12.8)	9.64	8.57	8.3	1.41	9.05t, 8.65t 8.05~8.90m		22.5
Ic *i*-Pr	NMe	7.74	17.3 (11.0)	9.71	8.65	8.3	1.41	9.17d, 8.90d 8.20m		18.0
Id *t*-Bu	NMe	7.55	16.5 (11.5)	9.63	8.60	8.3	1.43	8.87d		15.0
IIa Me	S			9.70	8.71	8.3	1.46	8.52d	13.2	
IIb Et	S			9.64	8.67	8.3	1.47	9.23t, 8.86t 8.01—8.88m		22.5
IIc *i*-Pr	S			9.59	8.66	8.0	1.49	9.21d, 8.87d 8.30m		21.0

a) Values in parentheses shows J_{PNCH} of the parent Al-free compound (IIIa—d). b) Apparent electronegativity of aluminium atom calculated by Narashimhan's equation; $\chi_{Alapp}=0.62\Delta+2.07$ ($\Delta=\tau AlCH_2CH_3-\tau AlCH_2$).

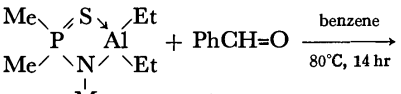

(Ia) PhCH=NMe + $Me_2P(S)NMeCH(Et)Ph$
(30%) (VI) (40%)

Evidence for the structure of (VI) are as follows; (i) the NMR spectrum (Fig. 1) and analyses were consistent with (VI). (ii) The reaction of an analogous dimethylaluminium compound; $Me_2P(S)$–NMe–$AlMe_2$ (VII), affords $Me_2P(S)$–NMe–CH(Me)Ph (VIII, 40%) along with 30% of PhCH=NMe. The NMR spectrum of (VIII) showed a similar spectrum pattern with an analogous known phosphorus compound; Ph_2P–NCH_3–$CH(CH_3)C_6H_5$.[12]

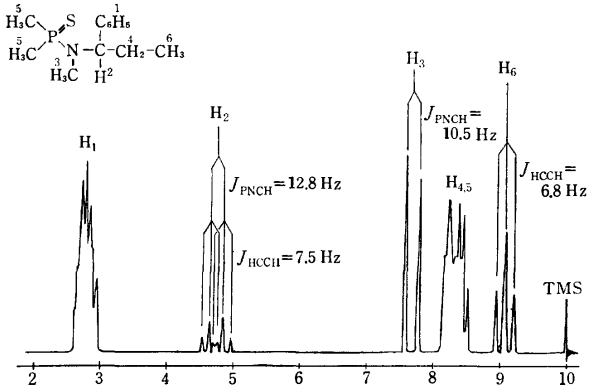

Fig. 1. NMR spectrum of $Me_2P(S)$–NMe–CH(Et)Ph (VI) (in CCl_4).

The formation of $Me_2P(S)$–NMe–CH(R)Ph (VIII for R=Me and VI for R=Et) is explained in terms of an insertion of benzaldehyde into the Al–C bond of (Ia) followed by an elimination of the R–Al–O unit. Plausible mechanism was shown as follows.

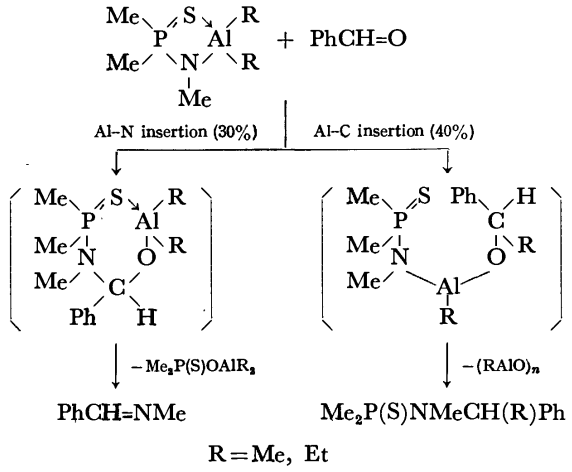

R=Me, Et

The reaction of IIb with Ph–N=C=O at 80 °C for 12 hr and subsequent distillation gave Ph–N=C=S (in only 10% yield). Major product was a 1/1 insertion product, $Et_2P(S)$–S–CONHPh (IX) in 69%, which was obtained by hydrolytic demetallation of the residue.

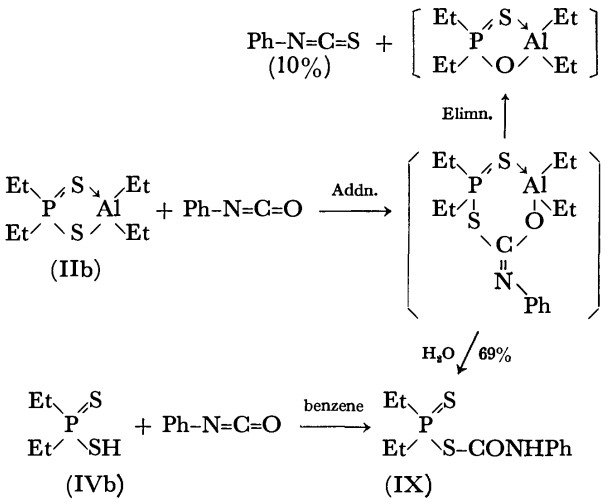

In conclusion, the insertion reactions of carbonyl compounds into an Al–N or an Al–S bond in Ia or IIb take place readily, whereas the subsequent elimination process proceeded to a less extent than the case of $(RO)_2P(O)NMeAlEt_2$ which induced exclusively iminocarbonylation reactions by an addition-elimination process.[4] This difference in reactivity of the elimination process may be due to the acidity of the phosphorus atom.

Experimental

Elemental analyses of organoaluminium compounds were carried out by Alfred Bernhardt Microanal. Lab. in West Germany. Aluminium content was analysed gravimetrically. Molecular weight determination and spectral measurement were carried out under dry nitrogen or argon atomosphere. Molecular weights in benzene solution were determined cryoscopically. Infrared and NMR spectra were recorded with a JASCO IR-S, DG-403G, and JEOL C-60HL spectrometers, respectively.

Commercial Et_3Al and Me_3Al (Ethyl. Corp.) were used without further purification. Organic solvents were thoroughly dried over sodium wire or molecular sieve. Starting phosphorus compounds were redistilled before use. The organophosphorus compounds except *N*-methyl diisopropylthiophosphinic amide (IIIc) and *N*-methyldi-*tert*-butylthiophosphinic amide (IIId), were prepared by the methods of literatures.[13–15]

Preparation of IIIc. A benzene (20 ml) solution of 6.2 g (27.1 mmol) of diisopropylphosphinothioic bromide, prepared from diisopropylphosphinous bromide and sulfur, and Et_3N were added to $MeNH_2$ (10 ml) in 20 ml of benzene at 0 °C. Then the mixture was refluxed for 30 min. After removal of the precipitated ammonium salt, distillation of the filtrate gave liquid product (IIIc) (4.2 g, 23.3 mmol) in 86% yield. Bp 85—88 °C/0.2 mmHg. Found: C, 46.76; H, 9.83; N, 7.97%. Calcd for $C_7H_{18}NPS$: C, 46.90; H, 10.12; N, 7.81%.

Preparation of IIId. A benzene (30 ml) solution of 13.7 g (78.2 mmol) of *N*-methyl amino di-*tert*-butylphosphine[10] was added dropwise to 2.51 g (78.2 mmol) of sulfur suspended in 30 ml of benzene. After refluxing for 6 hr and removal of the solvent, liquid (IIId) (8.5 g, 40.7 mmol) was obtained in 52% yield. Mp 115—117 °C. Found: C, 52.19; H, 10.37; N, 7.07%. Calcd for $C_9H_{22}NPS$: C, 52.14; H, 10.90; N, 6.76%.

Preparation of $R_2P(S)NMeAlEt_2$ (Ia—d). The prepa-

ration of *N*-diethylaluminium *N*-methyl dimethylthiophosphinic amide Ia is shown here as an example. Others (Ib—d) were prepared analogously. 5.62 g (45.6 mmol) of IIIa was added slowly to 3.22 g (45.7 mmol) of Et_3Al in 8 ml of benzene at room temperature. During the addition of IIIa, an evolution of gas was observed. The reaction mixture was heated up to 80 °C and refluxed for 1 hr. After the gas evolution had completely stopped, the solvent was removed. The product Ia was distilled under reduced pressure. Ia: bp 87—89 °C/0.06 mmHg (7.51 g, 36.0 mmol, 79% yield based on used Et_3Al). The data are shown in Tables 1—3.

Preparation of $R_2P(S)$-S-$AlEt_2$ (IIa—c). As an example, preparation of diethylaluminium dimethyldithiophosphinate (IIa) is described. 1.3 g (10.5 mmol) of IVa in 10 ml of benzene was added dropwise to 1.2 g (10.5 mmol) of Et_3Al in 10 ml of benzene at room temperature. Gas evolution was observed. The reaction mixture was heated up to 80 °C and refluxed for 1 hr. The distillation gave the liquid product IIa (bp 67 °C/0.13 mmHg) (1.6 g, 7.67 mmol, 73% yield based on used Et_3Al). The data are shown in Table 1—3.

Preparation of $Me_2P(S)$-NMe-$AlMe_2$ (VII). The reaction between 2.4 g (33.3 mmol) of Me_3Al and 4.1 g (33.3 mmol) of IIIa in 25 ml of benzene afforded VII (4.0 g, 23.3 mmol) as white crystals in 70% yield based on used Me_3Al. Mp 132—136 °C. Found: Al, 15.05%; active methyl groups, 2.08 per mol. Calcd for $C_5H_{15}AlNPS$: Al, 15.81%; active methyl groups, 2.00 per mol. IR (in benzene) 1300 (m), 1290 (m), 940 (s), and 925 (s) cm^{-1}. NMR (in benzene) τ 10.22 ($AlCH_3$, 6H, s), 8.75 (6H, double doublet, J_{PCH}=12.8 Hz), and 7.55 (3H, d, J_{PNCH}=18.8 Hz).

Reaction of Ia with Phenyl Isocyanate. An equimolar mixture of 0.845 g (4.08 mmol) of Ia and 0.486 g (4.08 mmol) of phenyl isocyanate in 20 ml of benzene was held at room temperature for 1 day. An absorption band at 2250 cm^{-1} ($\nu_{N=C=O}$) disappeared completely while instead a new band in the range of 1450—1550 cm^{-1} appeared. Then the reaction mixture was heated to 80 °C and refluxed for 15 hr. Hydrolysis of the mixture with dilute hydrochloric acid solution gave a solid as the 1/1 insertion product (0.886 g, 90%). Mp 117°—119 °C. IR (in CCl_4) 3280 (m), 1680 (s), 1310 (s), 1300 (s), 1235 (s), 945 (s), 923 (s), and 690 (m) cm^{-1}. NMR (in $CDCl_3$) τ 7.86 (6H, d, J_{PCH}=13.5 Hz), 6.45 (3H, d, J_{PNCH}=9.0 Hz), 2.5—3.0 (5H, m), and 2.03 (1H, br. s). An authentic sample of the 1/1 insertion product was prepared by an equimolar reaction of phenyl isocyanate with IIIa in benzene. IR and NMR spectra of the obtained 1/1 insertion product were completely consistent with the authentic sample.

Reaction of Ia with Benzaldehyde. To a solution of 0.8 g (7.2 mmol) of benzaldehyde in 5 ml of benzene was added dropwise 1.5 g (7.2 mmol) of Ia in 5 ml of benzene at room temperature. After 18 hr an absorption band at 1700 cm^{-1} ($\nu_{C=O}$) slightly decreased and a new band at 1650 cm^{-1} ($\nu_{C=N}$) appeared. Then the reaction mixture was heated to reflux. Removal of the solvent and distillation under reduced pressure gave the liquid product, PhCH=NMe (0.54 g, 30%) and $Me_2P(S)NMeCH(Et)Ph$ (VI) (bp 90—100 °C/0.35 mmHg) (0.7 g, 40%). Found: C, 60.14; H, 8.55; N, 5.47%. Calcd for $C_{12}H_{20}NPS$: C, 59.92; H, 8.35; N, 5.80%. IR (in CCl_4) 1298 (s), 1288 (s), 1150 (m), 943 (s), 918 (s), and 710 (s) cm^{-1}. NMR (in CCl_4) τ 9.10 (3H, t, J=6.8 Hz), 8.00—8.55 (8H, m, P-CH_3+CH_2CH_3), 7.71 (3H, d, J_{PNCH}=10.5 Hz), 4.66, 4.88 (1H, double triplet, J_{PNCH}=12.8 Hz, J_{HCCH}=7.5 Hz), and 2.5—2.9 (5H, m).

Reaction of VII with Benzaldehyde. When the mixture of 0.8 g (7.3 mmol) of benzaldehyde and 1.3 g (7.3 mmol) of VII in 15 ml of benzene solution was kept at room temperature for 24 hr, and then heated to refluxing for 12 hr, an absorption band at 1700 cm^{-1} ($\nu_{C=O}$) disappeared completely and a new band at 1650 cm^{-1} ($\nu_{C=N}$) appeared. Removal of the solvent and distillation gave, PhCH=NMe (0.26 g, 30%) and $Me_2P(S)NMeCH(Me)Ph$ (VIII) (bp 95—100 °C/0.3 mmHg) (0.6 g, 40%). IR (in CCl_4) 1290 (s), 1280 (s), 1150 (m), 950 (s), 910 (s), and 705 (m) cm^{-1}. NMR (in CCl_4) τ 8.54 (3H, d, J=6.0 Hz), 8.28 (6H, d, J_{PCH}=12.8 Hz), 7.66 (3H, d, J_{PNCH}=11.3 Hz), 4.71, 4.48 (1H, double quartet, J_{PNCH}=13.5 Hz, J_{HCCH}=6.0 Hz), and 2.5—2.9 (5H, m).

Reaction of IIb with Phenyl Isocyanate. To a benzene solution (10 ml) of 0.61 g (5.12 mmol) of phenyl isocyanate was added a benzene solution (10 ml) of 1.05 g (4.43 mmol) of IIb at room temperature. After leaving the mixture for 18 hr, an absorption band at 2250 cm^{-1} ($\nu_{N=C=O}$) disappeared gradually, along with the appearance of a new band at 2050 cm^{-1} ($\nu_{N=C=S}$). Then the reaction mixture was heated to 80 °C and refluxed for 6 hr, resulting the complete disappearence of $\nu_{N=C=O}$. Removal of the solvent and distillation under reduced pressure gave the liquid product, Ph-N=C=S (bp 70—78 °C/0.5 mmHg) (Ph-N=C=S: bp 95 °C/12 mmHg) (0.16 g, 10%). Hydrolytic demetallation of the residue gave an oil of a derivative of the insertion product (IX) (0.770 g, 69%). IR (in CCl_4) 3260 (m), 1705 (s), 1243 (m), 1154 (m), 1028 (s), and 693 (s) cm^{-1}. NMR (in CCl_4) τ 8.95, 8.58 (6H, double triplet, J_{PCCH}=22.2 Hz, J_{HCCH}=6.8 Hz), 7.50—8.20 (4H, m), 2.33—3.33 (5H, m), and 1.86 (1H, br. s). The authentic sample of the 1/1 insertion product was prepared by an equimolar reaction of Ph-N=C=O with IVb in benzene. The 1/1 insertion product obtained showed the same IR and NMR spectra of the authentic sample.

References

1) G. E. Coates and R. N. Mukherjee, *J. Chem. Soc.*, **1964**, 1295.

2) J. Weidlein, *J. Organometal. Chem.*, **49**, 257 (1973), and references cited therein.

3) Organoboron derivatives of thiophosphinicamides have been reported in recent paper; H. Nöth, D. Reiner, and W. Storch, *Chem. Ber.*, **106**, 1508 (1973).

4) K. Urata, K. Itoh, and Y. Ishii, *J. Organometal. Chem.*, **76**, 203 (1974).

5) J. Boderker, *ibid.*, **56**, 455 (1973).

6) G. Singh and H. Zimmer, *Organometal. Chem. Rev.*, **2**, 279 (1967).

7) W. Wolfsberger and H. Schmidbaur, *J. Organometal. Chem.*, **17**, 41 (1969).

8) J. W. Emsley, J. Feeney, and L. H. Sutcliffe, "High Resolution Nuclear Magnetic Resonance Spectroscopy," Pergamon Press, Oxford, London (1966), p. 675.

9) P. T. Narashimhan and M. I. Rogers, *J. Amer. Chem. Soc.*, **82**, 5983 (1960).

10) O. J. Scherer and G. Scheider, *Chem. Ber.*, **101**, 4184 (1968).

11) O. J. Scherer and P. Klussman, *Z. Anorg. Allgem. Chem.*, **370**, 171 (1969).

12) H. Brunner and W. Rambold, *Angew. Chem.*, **85**, 1118 (1973).

13) K. Sasse, "Methoden der Organischen Chemie, Houben-Weyl," Bd. 12/1, Georg Thieme Verlag, Sttutgart (1963).

14) W. Voskuil and J. F. Arens, *Rec. Trav. Chim. Pays-Bas*, **82**, 302 (1963).

15) W. Kuchen, K. Strolenberg, and J. Metten, *Chem. Ber.*, **96**, 1933 (1963).

Studies of the Reactions of Amines with Sulfur Trioxide. IV.[1] One-step Synthesis of *N*-substituted Imidobissulfates from Amines[2]

Fujio KANETANI and Hachiro YAMAGUCHI

Department of Applied Chemistry, Hiroshima University, 3-8-2 Senda-machi, Hiroshima 730

(Received February 18, 1974)

The scope and limitations of a one-step synthesis of *N*-substituted imidobissulfates, $RN(SO_3K)_2$ (R=Me, Et, *n*-Pr, *iso*-Pr, *n*-Bu, *iso*-Bu, *sec*-Bu, *tert*-Bu, *n*-C_6H_{13}, *cyclo*-C_6H_{11}, $PhCH_2$-, $PhCH_2CH_2$-, $PhCH(CH_3)$-, or Ph), starting from amines and the sulfur trioxide–triethylamine complex are described. The yields are generally good (55—90%). However, with aniline only a poor (13%) yield was obtained. With *tert*-butylamine, *tert*-butylamidosulfate was obtained quantitatively instead of the expected *tert*-butylimidobissulfate. Bis(cyclohexylammonium) salts of the imidobis(sulfuric) acids are prepared, and their properties are briefly recorded.

In a preceding paper[1] we described a new synthesis of *N*-substituted imidobissulfates (III)[3] by the *N*-sulfonation of the corresponding amidosulfates (II)[3] with various sulfonating agents, particularly with the 2-picoline–sulfur trioxide addition compound. In general, *N*-substituted amidosulfates are readily prepared by the interaction of amines (I) with a variety of sulfonating agents,[4] such as chlorosulfuric acid, pyridine–sulfur trioxide, or sulfur trioxide–trimethylamine. Therefore, the reaction of amines with a suitable sulfonating agent appears to provide a more convenient synthetic route to a wide variety of *N*-substituted imidobissulfates (III).

$$\underset{\text{(I)}}{RNH_2} \xrightarrow{B:SO_3} \underset{\text{(II)}}{RNHSO_3^-HB^+} \xrightarrow{B:SO_3} \underset{\text{(III)}}{RN(SO_3^-HB^+)_2}$$

B: Lewis base

However, only a few reports on the formation of *N*-substituted imidobissulfates in the reaction of amines with a sulfonating agent have been recorded. Reitz *et al.*[5] first suggested that benzylimidobissulfate might have been formed in the action of the pyridine–sulfur trioxide complex on benzylamine. Recently, Vrba and Allan[6] have described briefly the preparation of phenylimidobissulfate (aniline-*N*,*N*-disulfonate) by the reaction of a 1 mol equiv. of aniline with a 2 mol equiv. of the 2-picoline–sulfur trioxide complex in chloroform at 0 °C for 1 hr. Very recently, sulfatoethyl- and sulfatopropylimidobissulfates have been prepared[7] in yields of 72.3 and 53.0% respectively by the *N*-sulfonation of 2-hydroxyethyl- and 3-hydroxypropylamines with pyridine–sulfur trioxide in pyridine. We have shown[8] that, under appropriate conditions, methylimidobissulfate can be obtained as the main product in the gas-phase reaction of methylamine with sulfur trioxide.

We wish now to report a one-step synthesis of *N*-substituted imidobissulfates by the *N*-sulfonation of amines with sulfur trioxide–triethylamine. Unlike the complexes of sulfur trioxide with pyridine bases conventionally used in the early work, sulfur trioxide–triethylamine is much more stable and can conveniently be stored in a refrigirator for long periods of time without decomposition.[9] In addition, the latter complex is fairly soluble in the solvents commonly used for the reaction, such as chloroform, 1,2-dichloroethane, and pyridine bases.[9]

Synthesis. The general procedure simply involves adding an amine to a solution of sulfur trioxide–triethylamine in 2-picoline and allowing the reaction mixture to stand at room temperature for 1—3 days. For each reaction, 6—10 mmol of an amine and a 5—10% molar excess of the sulfonating agent were usually used. After the reaction, the solvent was removed.

The product was then converted into the potassium salt by adding aqueous potassium hydroxide. No difficulty was encountered in separating the imidobissulfate from the amidosulfate which was always formed, generally in a small quantity (except for *tert*-butyl-, 1-phenylethyl-, and phenylamidosulfates). Thus, the imidobissulfate was easily separated from the amidosulfate by extracting the latter with methanol. In the case of cyclohexylimidobissulfate, the separation was best achieved by the use of 85 wt% methanol.

First, we examined the effect of changes in the reaction time and the temperature on the product yields. The results are illustrated in Fig. 1 and Table 1. When *n*-butylamine was used as a substrate, the reaction at room temperature was unexpectedly rapid and was virtually complete in 2 hr; a 70% yield of *n*-butylimidobissulfate was obtained. However, increasing the reaction time to 23 hr improved the yield to 80%. On the other hand, the reaction at 80 °C led to considerably lower yields (50—65%). In the

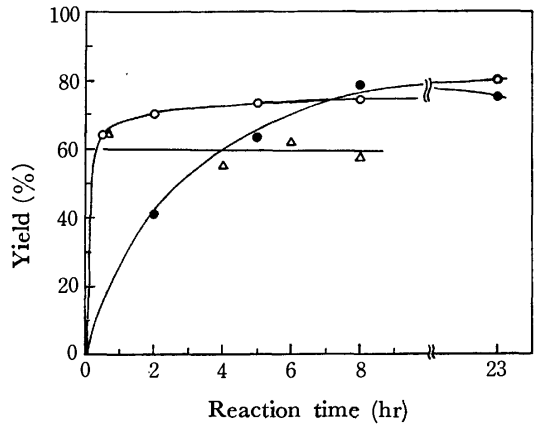

Fig. 1. Effects of reaction time and temperature on the yield of *n*-butylimidobissulfate.
n-Butylamine, 6—10 mmol; *n*-Butylamine: sulfur trioxide–triethylamine molar ratio was ~1:2.1.
● −5 °C; ○ 25—30 °C; △ 75—85 °C.

TABLE 1. EFFECTS OF REACTION TIME AND TEMPERATURE ON THE YIELD OF IMIDOBISSULFATES

RNH$_2$ R	RNH$_2$ pK_a	RNH$_2$ Amount (mmol)	$(C_2H_5)_3$-N-SO_3 (mmol)	Temp (°C)	Time (hr)	Yield[a] (%)
sec-Bu	10.56[b]	7.0	15.2	25—30	23	65
sec-Bu	10.56[b]	7.5	22.3	25—30	46	80
cyclo-C_6H_{11}	10.64[b]	6.4	13.4	28—30	49	60
cyclo-C_6H_{11}	10.64[b]	6.3	13.4	25—30	72	65
$PhCH(CH_3)$		5.6	11.6	26—27	47	35
$PhCH(CH_3)$		7.5	15.9	25—30	82	55
$PhCH(CH_3)$		56.6	113.0	85—95	3	39
$PhCH(CH_3)$		5.9	12.5	85—95	8	4

a) Yields are based on the starting amine and corrected for the purity of the isolated imidobissulfate. b) N. F. Hall and M. R. Sprinkle, *J. Amer. Chem. Soc.*, *54*, 3469 (1932).

case of bulky amines such as *sec*-butylamine, cyclohexylamine, and 2-phenylethylamine, a much longer reaction period (47—82 hr) was required. The yields ranged from 55 to 80% when the reaction was conducted at room temperature. It is noteworthy, however, that the reaction at 90 °C with 1-phenylethylamine as a substrate led to very low yields.

The results with the other amines as substrates are summarized in Table 2.

Benzyl- and 2-phenylethyl- as well as primary alkylimidobissulfates were obtained in yields of 80—93% after a 23-to 48-hr reaction at room temperature. The use of a large excess of sulfur trioxide–triethylamine does not improve the yields, but has a deleterious effect on the product isolation in a pure state. This procedure also works well on a larger (0.1-mol) scale.

TABLE 2. SYNTHESIS OF *N*-SUBSTITUTED IMIDOBISSULFATES BY THE *N*-SULFONATION OF AMINES WITH SULFUR TRIOXIDE–TRIETHYLAMINE[a]

RNH$_2$ R	RNH$_2$ pK_a	RNH$_2$ Amount (mmol)	$(C_2H_5)_3$-N-SO_3 (mmol)	Time (hr)	Yield[b] (%)
CH_3	10.62[f]	98.2	211.6	23	92
C_2H_5	10.63[f]	6.5	13.8	23	89
n-C_3H_7	10.53[f]	8.1	16.5	47	90
iso-C_3H_7	10.63[f]	7.4	15.7	47	75
n-C_4H_9	10.61[g]	12.6	24.9	23	80
n-C_4H_9		6.2	13.8	47	82
iso-C_4H_9	10.43[g]	8.4	17.5	23	85
tert-C_4H_9	10.45[f]	7.4	15.8	46	0[c]
n-C_6H_{13}	10.64[g]	5.8	12.8	48	82
$PhCH_2$	9.34[h]	6.1	12.4	47	83
$PhCH_2CH_2$	9.83[h]	6.5	13.8	23	63
Ph	4.58[i]	6.8	14.9	71	13[d,e]

a) Experiments were carried out at room temperature (25—30 °C). b) Yields are based on the starting amine and corrected for the purity of the isolated products. c) *tert*-Butylamidosulfate was obtained quantitatively. d) Isolated main product was the corresponding amidosulfate. e) Isolated as the sodium salt. Anal. Found: N, 4.70; S, 21.50%. Calcd for $C_6H_5O_6NS_2Na_2$: N, 4.71; S, 21.58%. f) H. K. Hall Jr., *J. Amer. Chem. Soc.*, **79**, 5441 (1957). g) C. W. Hoerr and M. R. McCorkle, *ibid.*, **65**, 328 (1943). h) B. M. Wepster, *Rec. Trav. Chim. PaysBas*, **71**, 1171 (1952). i) N. F. Hall and M. R. Sprinkle, *J. Amer. Chem. Soc.*, **54**, 3469 (1932).

Some attempts to prepare *tert*-butylimidobissulfate by this method were unsuccessful, but *tert*-butylamidosulfate was obtained instead in a nearly quantitative yield. A model shows that the amidosulfate is too sterically hindered to undergo further *N*-sulfonation.

Aniline afforded phenylimidobissulfate in only a poor yield.[11] In this case, the main product was phenylamidosulfate. The low yield of the former compound is most probably due to the low basicity of the amido nitrogen of the latter.

The *N*-sulfonation of primary amines with sulfur trioxide–triethylamine proceeds as is shown in the Scheme. The data described above can best be explained by assuming that an equilibrium exists between amidosulfate (II′) and bis(triethylammonium) imidobissulfate (III′). (1) The temperature, (2) the steric requirement of a substituent on the nitrogen, (3) the basicity of the amido nitrogen, and (4) the basicity of the tertiary amine (triethylamine in this case) forming a sulfur trioxide addition compound are important factors governing the equilibrium and, therefore, the yield of III′.

$$\underset{\text{(I)}}{RNH_2} + (C_2H_5)_3N\text{-}SO_3 \rightleftharpoons \underset{\text{(II′)}}{RNHSO_3^-HN^+(C_2H_5)_3}$$

$$\text{(II′)} + (C_2H_5)_3N\text{-}SO_3 \rightleftharpoons RN\begin{matrix}\diagup SO_3^-HN^+(C_2H_5)_3 \\ \diagdown SO_3^-HN^+(C_2H_5)_3\end{matrix} \quad \text{(III′)}$$

Scheme.

The differences in the product yields as well as in the rate of reaction seem to be ascribable mainly to steric factors. Evidently, a large steric requirement of a substituent on the nitrogen atom, as in cyclohexylamine and 2-phenylethylamine, hinders the attack of the bulky sulfonating agent on the amido nitrogen of II′ by blocking the line of approach. Steric strain due to crowding at the imido nitrogen plays an important role in determining the stabilities of III′ and, hence, the position of the equilibrium between II′ and III′. Thus, at higher temperatures, the equilibrium shifts towards II′.

Preparation and Properties of the Bis(cyclohexylammonium) Salts. Amine salts of unsubstituted imidobis(sulfuric) acid were first prepared by Boatman and Sisler.[12] The procedure involves heating diammonium imidobissulfate with an amine in liquid ammonia, water, or an alcohol solution. Free imidobis(sulfuric) acid readily undergoes the hydrolytic cleavage of the sulfur-nitrogen bond in the aqueous solution; hence, it has not hitherto been isolated.[13] Its salts also undergo ready acid-catalyzed hydrolysis.[14] However, Nakano and Yamaguchi[15] have recently prepared eleven bis(tertiary ammonium) salts of unsubstituted imidobis(sulfuric) acid. Their procedure can successfully be applied to the preparation of the bis(cyclohexylammo-

Table 3. Bis(cyclohexylammonium) imidobissulfates

$RN(SO_3^-H_3N^+-C_6H_{11})_2$

R	Mp (°C)[a]	Recryst. solvent	Analysis (%) N Found (Calcd)	Analysis (%) S Found (Calcd)	Imido-group equiv. Found	Imido-group equiv. (Calcd)
CH_3	195—197.5	*iso*-PrOH	10.80 (10.79)	16.22 (16.46)	399	(389.5)
C_2H_5	181.5—182.5	*iso*-PrOH	10.40 (10.41)	15.98 (15.89)	406	(403.6)
n-C_3H_7	184—184.5	EtOH	10.17 (10.06)	15.38 (15.36)	426	(417.6)
iso-C_3H_7	142—143.5	H_2O	10.16 (10.06)	15.33 (15.36)	432	(417.6)
n-C_4H_9	182.5	EtOH	9.84 (9.74)	14.73 (14.86)	451	(431.6)
iso-C_4H_9	177—178.5	EtOH	9.83 (9.74)	14.66 (14.86)	443	(431.6)
sec-C_4H_9	138.5—140	EtOH[d]	9.71 (9.74)	14.75 (14.86)	450	(431.6)
n-C_6H_{13}	154.5—155.5	EtOH	9.16 (9.14)	13.78 (13.95)	472	(459.7)
Cyclohexyl	b)	H_2O	8.97 (9.18)	13.76 (14.01)	475	(457.7)
$PhCH_2$	212—212.5	H_2O	9.05 (9.03)	13.58 (13.77)	476	(465.6)
$PhCH(CH_3)$	c)	EtOH[d]	8.88 (8.76)	13.35 (13.37)	513	(479.7)

a) In all cases, the melting points depended on the rate of heating, since thermal decomposition (effervescence) occurred on heating. b) Apparent shrinking occurred at 184.5 °C (placed in the bath at 178 °C). However, no definite melting was observed up to 250 °C. c) An indication of melting was observed at 114—126 °C and a meniscus was formed at 140—150 °C. d) Recrystallization was achieved by dissolving the product in ethanol at room temperature, filtering the solution, and setting aside overnight in a refrigirator (−27 °C).

nium) salts of the primary alkyl-substituted imidobis(sulfuric) acid from the potassium salts obtained above, whereas in the case of sterically-strained *sec*-alkyl-, cycloalkyl-, and 1-phenylethylimidobissulfates, considerable hydrolysis occurs. This disadvantage can, however, be overcome by a direct cation-exchange procedure (see the Experimental section). This procedure can be conducted at room temperature, since the ion-exchange process is carried out under neutral conditions.

The bis(cyclohexylammonium) salts so obtained are summarized in Table 3. All the salts are non-hygroscopic, colorless crystals; they are soluble in water, methanol, and ethanol, and practically insoluble in acetone, ether, and ethyl acetate. The stabilities of the *N*-substituted imidobissulfates are dependent on the basicity of the salt-forming bases as well as on the magnitude of the internal strain due to the steric crowding at the imido nitrogen. Thus, primary alkyl- and benzylimidobissulfates can be recrystallized without appreciable degradation from boiling water or ethanol containing a few drops of cyclohexylamine, although prolonged heating (15—30 min) led to a complete decomposition. On the other hand, bis(cyclohexylammonium) 1-phenylethylimidobissulfate decomposed almost instantly in boiling ethanol to afford ethyl sulfate and 1-phenylethylamidosulfate. All the salts also decomposed partially or completely at their melting points, depending on the rate of heating.

$$C_6H_5CH(CH_3)N(SO_3^-H_3N^+C_6H_{11})_2 + C_2H_5OH \longrightarrow C_6H_5CH(CH_3)NHSO_3^-H_3N^+C_6H_{11} + C_2H_5OSO_3^-H_3N^+C_6H_{11}$$

The *trans*-sulfonation and thermal decompositions of the imidobissulfates are currently being studied and will soon be reported.

Experimental

The melting points were measured in sealed capillaries and corrected. The infrared spectra were recorded for potassium bromide discs on a JASCO IR-S spectrometer. The 1,2-dichloroethane was dried over calcium chloride, distilled, and stored over a molecular sieve (type 3A). The triethylamine and 2-picoline were dried by distillation from potassium hydroxide pellets and stored over a molecular sieve (type 3A). The methylamine (anhydrous) was supplied in a cylinder by the Nitto Chemical Industry, Ltd. The other amines were commercially available and were used without further purification.

Preparation of Triethylamine–Sulfur Trioxide Complex. The complex was prepared by adding triethylamine to a solution of sulfur trioxide in 1,2-dichloroethane at from −5 to 10 °C; mp 90.5—93 °C (from water), (lit,[16] 91.5°); ν_{SO_3} 1055 (s), ν_{SO_3} 1290 (s), δ_{CH} 1400 (m), 1447 (m), and 1465 (m) cm^{-1}.

General Procedure for the Sulfonation of Amines with Sulfur Trioxide–Triethylamine. The quantities of the amine and the sulfur trioxide adduct used for each reaction are given in Tables 1 and 2. The appropriate amine in dry 2-picoline (10 ml) was added, drop by drop, to a stirred solution of the sulfur trioxide–triethylamine complex in dry 2-picoline (20 ml). Stirring was continued for five min., and then the mixture was allowed to stand at a given temperature (−5 to 5 °C and 25—30 °C) or heated at 85—95 °C. The solvent was evaporated off under reduced pressure at a bath temperature below 50 °C, and the residue was dissolved cautiously in cold water (25 ml), neutralized with a potassium hydroxide solution, and treated with charcoal. The filtrate was then evaporated to dryness under reduced pressure, and the residue was extracted with methanol[17] (40—60 ml). The residual solid was dissolved in water (20 ml), and a barium acetate solution (5%) was added until no more precipitate was formed. The filtered solution was evaporated to dryness under reduced pressure; the residue was extracted with methanol (30 ml), filtered, and washed with methanol to give the product (92—99% purity, as calculated from the imido-group equivalent[18]).

Conversion into the Bis(cyclohexylammonium) Salts. (a) An ice-cold solution of the potassium salt (0.7 g in 10 ml) was passed through a column of Amberlite IR-120 (H^+ form) which had been externally cooled to −5—0 °C. The eluate was immediately neutralized with an excess of aqueous cyclohexylamine, and the solution was evaporated to dryness at a temperature below 40 °C while kept alkaline. The residue was recrystallized from an appropriate solvent (see Table 3).

(b) A solution of the potassium salt was passed through a column of Amberlite IR-120 (cyclohexylammonium-salt form), and the eluate was evaporated to dryness. The products so obtained were sufficiently pure for practical purposes. Purer products may be obtained by recrystallization from ethanol containing a drop of cyclohexylamine (room temperature→−27 °C).

We wish to thank the Nitro Chemical Industry, Ltd. for its gift of anhydrous methylamine.

References and Footnotes

1) Part III. F. Kanetani and H. Yamaguchi, *Yuki Gosei Kagaku Kyokai Shi*, **32**, 460 (1974).

2) Presented in part at the 29th Annual Meeting of the Chemical Society of Japan, Hiroshima, October 10—14, 1973.

3) Although the names imidodisulfonic acid (also called amine disulfonic acid) or imidodisulfuric acid (used for indexing by the Chemical Abstracts Service), and sulfamic acid have conventionally been used, we prefer the names imidobis(sulfuric) acid and amidosulfuric acid respectively, for they are more consistent with the naming of the imido and amido derivatives of sulfuric acid.

4) A. Dorlars, "Methoden der Organischen Chemie," 4. Aufl., Bd. XI/2, ed. by Eugen Müller, Georg Thieme Verlag, Stuttgart (1958), pp. 645—687.

5) H. C. Reitz, R. E. Ferrel, H. S. Olcott, and H. Fraenkel-Conrat, *J. Amer. Chem. Soc.*, **68**, 1031 (1946).

6) Z. Vrba and Z. J. Allan, *Collection Czech. Chem. Commun.*, **32**, 2035 (1967).

7) Y. Inoue and K. Nagasawa, *J. Org. Chem.*, **38**, 1810 (1973).

8) H. Yamaguchi and F. Kanetani, *Yuki Gosei Kagaku Kyokai Shi*, **31**, 79 (1973).

9) E. E. Gilbert, "Sulfonation and Related Reactions," Interscience Publishers, New York, N. Y. (1965) pp. 7—18.

10) Recently, thermal degradation of di(tertiary ammonium) salts of unsubstituted imidobis(sulfuric) acid into amidosulfate and a tertiary amine-sulfur trioxide adduct has been reported: H. Yamaguchi and T. Fujii, *Nippon Kagaku Kaishi*, **1973**, 2157.

11) It was stated that the pyridine-sulfur trioxide complex is ineffective for the formation of phenylimidobissulfate whereas 2-picoline–sulfur trioxide yields the desired product (see Ref. 6).

12) C. E. Boatman and H. H. Sisler, *J. Amer. Chem. Soc.*, **73**, 559 (1951).

13) L. A. Audrieth, M. Sveda, H. H. Sisler, and M. J. Butler, *Chem. Rev.*, **26**, 49 (1940).

14) a) H. H. Sisler and L. A. Audrieth, *J. Amer. Chem. Soc.*, **60**, 1947 (1938); b) G. J. Doyle and N. Davidson, *ibid.*, **71**, 3491 (1949).

15) K. Nakano and H. Yamaguchi, *Kogyo Kagaku Zasshi*, **67**, 1878 (1964).

16) F. Beilstein and E. Wiegand, *Ber.*, **16**, 1264 (1883).

17) In all cases, the corresponding amidosulfates were isolated from the methanol solution. They were identified by comparing the IR spectra and melting points of their dibutylammonium salts with those of authentic sample (see Ref. 1).

18) F. Kanetani and H. Yamaguchi, *Yuki Gosei Kagaku Kyokai Shi*, **30**, 539 (1972).

The Reactions of β-Hydroxychalcones and 2-Acetoxy-1,3-diarylpropan-1,3-diones with Lead Tetraacetate

Kazu KUROSAWA and Akira MORIYAMA*

Department of Chemistry, Faculty of Science, Kumamoto University, Kurokami, Kumamoto 860

(Received April 13, 1974)

The reaction of β-hydroxychalcone with lead tetraacetate gave benzil. The reaction of 4,4'-dimethoxy-β-hydroxychalcone gave 2-acetoxy-1,3-di(*p*-methoxyphenyl)propan-1,3-dione and 4,4'-dimethoxybenzil. The reactions of 2-acetoxy-1,3-diarylpropan-1,3-diones yielded 2,2-diacetoxy-1,3-diarylpropan-1,3-diones and benzils respectively. The formation of the benzils from β-hydroxychalcones and 2-acetoxy-1,3-diarylpropan-1,3-diones has been shown to involve 1,2-aryl and 1,2-aroyl migration respectively by studies of the oxidations of ^{14}C-labelled compounds.

Carbonyl compounds react with lead tetraacetate to give α-acetoxy derivatives, and β-diketones also react to give mono- and diacetoxy compounds.[1] Our recent results on the reaction of chalcones with lead tetraacetate showed that a chalcone was oxidized to yield 2-acetoxy-1,3-diarylpropan-1,3-dione and 2,3-diacetoxy-1,3-diarylpropan-1-one.[2] This result differs from those of the oxidations of chalcones with thallium(III) acetate and with thallium(III) nitrate, which gave deoxybenzoin derivatives[3] and benzils[4] respectively (Scheme 1).

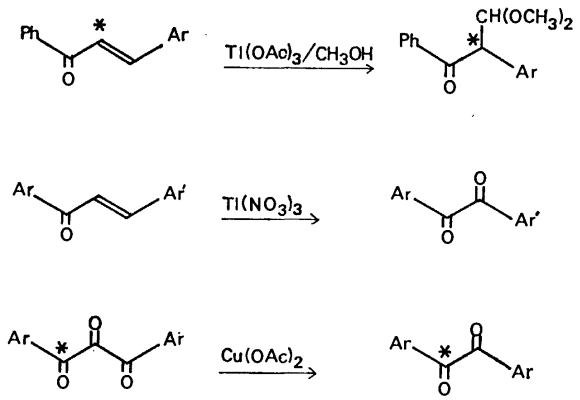

Scheme 1. Ar and Ar' refer to substituted phenyls.

A re-examination of our previous results revealed the presence of a benzil in the reaction mixture together with the acetates, suggesting that the dione could be rearranged and oxidized to the benzil.

Two β-hydroxychalcones (Ia and Ib), which could be the precursors of the dione, and two 2-acetoxy-1,3-diarylpropan-1,3-diones (IIa and IIb) were prepared; the reactions of these compounds with lead tetraacetate were investigated in the hope of substantiating the rearrangement reaction.

When 4,4'-dimethoxy-β-hydroxychalcone (Ib) was oxidized with lead tetraacetate, three compounds (IIb (2%), IIIb (27%), and Vb (20%)) were obtained. The NMR spectrum of IIb ($C_{19}H_{18}O_6$; mp 96 °C) indicated the presence of two methoxy groups [δ 3.80 (s, 6H)], an acetoxy group [δ 2.30 (s, 3H)], a CH unit [δ 6.89 (s, 1H)], and two *para*-substituted phenyl groups [δ 6.91 (d, 4H) and δ 8.40 (d, 4H)]. The spectroscopic evidence suggested that the IIb has the structure of 2-acetoxy-1,3-di(*p*-methoxyphenyl)propan-1,3-dione. The structure of IIb was confirmed by the fact that the identical acetate was obtained from 2-bromo-1,3-di(*p*-methoxyphenyl)propan-1,3-dione by treating it with sodium acetate in boiling acetic acid. The NMR spectrum of IIIb showed the presence of two *p*-methoxyphenyl groups [δ 6.95 (d, 4H), δ 7.89 (d, 4H), and δ 3.85 (s, 6H)], indicating that IIIb has the structure of 4,4'-dimethoxybenzil. This was identified by comparing their IR spectrum with that of an authentic sample. Vb was shown to be anisic acid by a comparison of its melting point and its IR spectrum with those of an authentic specimen.

Similarly, the reaction of β-hydroxychalcone (Ia) with lead tetraacetate gave IIIa (20%) and Va (10%).

When 2-acetoxy-1,3-di(*p*-methoxyphenyl)propan-1,3-dione (IIb) was oxidized with lead tetraacetate, three compounds (IIIb (10%), IVb (4%), and Vb (11%)) were isolated. The NMR spectrum of IVb ($C_{21}H_{20}O_8$; mp 145—146 °C) indicated the presence of two acetoxy groups [δ 2.14 (s, 6H)], two methoxy groups [δ 3.81 (s, 6H)], and two *p*-substituted phenyls [δ 6.38 (d, 4H) and δ 8.12 (d, 4H)], suggesting that IVb has the structure of 2,2-diacetoxy-1,3-di(*p*-methoxyphenyl)propan-1,3-dione. IIIb and Vb were identified with authentic samples. The reaction of 2-acetoxy-1,3-diphenylpropan-1,3-dione (IIa) was also carried out, giving IIIa (19%), IVa (7%), and Va (6%).

In order to establish the nature of the skeletal rearrangement of the β-hydroxychalcones and the 2-acetoxy-1,3-diarylpropan-1,3-diones, the reactions were

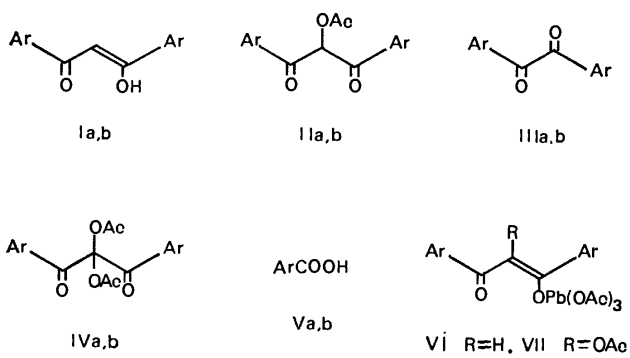

Scheme 2. Ar refers to phenyl in a and *p*-methoxyphenyl in b.

* Present address: Tokushima Factory, Taiho Co., Ltd., Hiraishi, Kawauchi-machi, Tokushima, 77101.

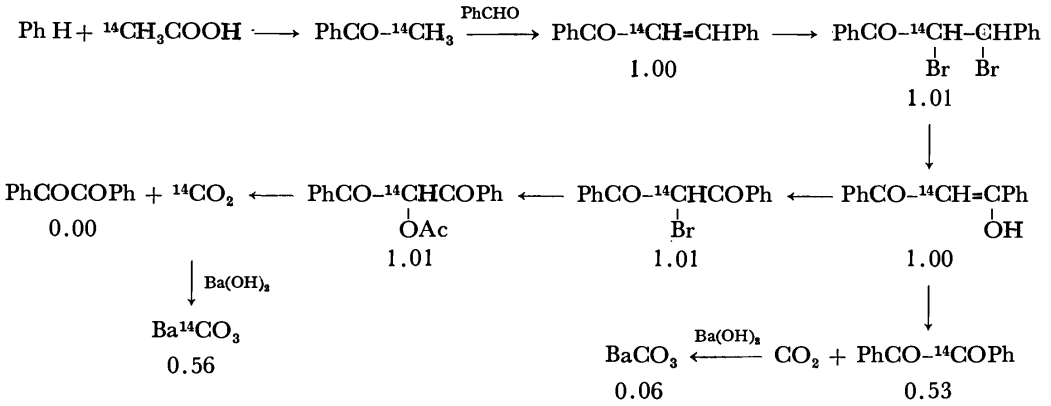

Scheme 3. Syntheses and rearrangement reactions of β-hydroxy[α-^{14}C]chalcone and 2-acetoxy-1,3-diphenyl[2-^{14}C]propan-1,3-dione (the figures under the formulae refer to the specific radioactivities of the compounds relative to chalcone).

repeated using β-hydroxy[α-^{14}C]chalcone and 2-acetoxy-1,3-diphenyl[2-^{14}C]propan-1,3-dione. When 2-acetoxy-1,3-diphenyl[2-^{14}C]propan-1,3-dione was oxidized with lead tetraacetate, inactive benzil (IIIa) and active carbon dioxide as barium carbonate were obtained (Scheme 3). The formation of the inactive IIIa from active IIa has shown clearly that a 1,2-aroyl migration took place and that then the central carbon was lost in the reaction. It has been shown that an aroyl migration is involved in the decarbonylation of 1,3-diarylpropan-1,2,3-trione with cupric acetate[5] (Scheme 1). However, evidence was not available in our case for formulating the reaction intermediate. There may be another pathway yielding carbon dioxide, since an incomplete retention of the radioactivity was observed (the specific radioactivity was 0.56 relative to that of chalcone).

On the other hand, the oxidation of Ia gave radioactive IIIa (the relative specific radioactivity was 0.53) and carbon dioxide (the relative specific radioactivity was 0.06 on barium carbonate). This may indicate that there are at least two pathways which equally lead to benzil: one must involve a 1,2-aryl migration in such a reaction intermediate as VI (Scheme 2), thus yielding the radioactive IIIa, while the other is one *via* IIa, giving the inactive IIIa.

The formation of IIb, IVa, and IVb can be explained by assuming enol intermediates (VI and VII) that are known to be involved in the reaction of ketones with lead tetraacetate.[1] Both IVa and IVb are stable and, therefore, "end products" in the oxidation. This conclusion was confirmed by a separate experiment.

Experimental

All the NMR spectra were recorded for the deuteriochloroform solution with a Hitachi R 24 NMR spectrometer, with tetramethylsilane as the internal reference. The IR spectra were recorded for the chloroform solution with a JASCO IRA-1 grating spectrometer, while the UV spectra were measured for the methanol solution with a Hitachi EPS-3T spectrophotometer. The melting points were determined with a Yanagimoto hot-stage apparatus and were uncorrected. The radioactivity measurements were recorded, for samples crystallized to a constant specific activity, with an Aloka liquid scintillation spectrometer. The scintillator consisted of 0.4% DPO and 0.1% POPOP (Dojindo Chemicals, Kumamoto) dissolved in toluene. Barium carbonate samples were suspended in a gel made up with 4% W/V CAB-O-SIL (Beckmann Instruments Inc,. U.S.A.). Sample counts were repeated twice; the maximum observed error was within ±0.5%.

β-Hydroxychalcone (Ia). β-Hydroxychalcone (Ia) (mp 78 °C) was prepared by the method described in the literature.[6]

4,4'-Dimethoxy-β-hydroxychalcone (Ib). 2-Bromo-1,3-di-(*p*-methoxyphenyl)propan-1,3-dione[7] (1 g) was stirred with zinc powder (3 g) in acetic acid (30 ml) at room temperature for an hour. After the removal of insoluble materials by filtration, water (15 ml) was added to the filtrate. The precipitates were collected and recrystallized from methanol, giving Ib (580 mg, 74%); mp 112—113 °C (lit,[8] mp 114 °C).

2-Acetoxy-1,3-di(p-methoxyphenyl)propan-1,3-dione (IIb). A mixture of 2-bromo-1,3-di(*p*-methoxyphenyl)propan-1,3-dione (2.2 g), anhydrous sodium acetate (4.0 g), and acetic acid (50 ml) was heated under reflux for 5 hr. The reaction mixture was then poured into water and extracted with chloroform. The chloroform was evaporated *in vacuo*, and the residue was allowed to crystallize from ethanol, thus giving colourless prisms (1.3 g, 62%), mp 96 °C, ν_{max}: 1760 and 1690 cm^{-1}; λ_{max} (ε): 291 nm (24700). Found: C, 66.37; H, 5.48%. Calcd for $C_{19}H_{18}O_6$: C, 66.66; H, 5.30%.

2-Acetoxy-1,3-diphenylpropan-1,3-dione (IIa). IIa was obtained in a 65% yield in the manner described above (mp 92—93 °C (lit,[9] mp 90—95 °C)).

Oxidation of β-Hydroxychalcones (Ia and Ib) and 2-Acetoxy-1,3-diarylpropan-1,3-diones (IIa and IIb). A mixture of the substrate (1 mmol), lead tetraacetate (2 mmol for Ia and Ib, and 1 mmol for IIa and IIb), and acetic acid (10 ml) was heated at 100 °C for 3 hr. After the removal of the acetic acid *in vacuo*, the residue was triturated with water and extracted with benzene. The benzene solution was then washed with aqueous sodium carbonate, from which two acids (Va and Vb) were obtained after acidification with concentrated hydrochloric acid. After the removal of the benzene *in vacuo*, the residue was separated on tlc. β-Hydroxychalcone (Ia) yielded IIIa (mp 95 °C (lit,[10] mp 95 °C)) and Va (mp 122 °C). 4,4'-Dimethoxy-β-hydroxychalcone (Ib) gave IIb (mp 96 °C), IIIb (mp 132 °C (lit,[11] mp 133 °C)), and Vb (mp 185 °C). The oxidation of IIa gave IIIa (mp 95 °C), Va (mp 122 °C), and 2,2-diacetoxy-1,3-diphenylpropan-1,3-dione (IVa) (mp 171—172 °C); ν_{max}: 1780 and 1710 cm^{-1}; λ_{max} (ε): 259 nm (22600); δ: 7.2—8.2 (m, 2×

C_6H_5) and 2.14 (s, 2×OAc) (Found: C, 67.13, H, 4.58%. Calcd for $C_{19}H_{16}O_6$: C, 67.06; H, 4.75%). IIb gave IIIb (mp 132 °C), Vb (mp 185 °C), and 2,2-diacetoxy-1,3-di(*p*-methoxyphenyl)propan-1,3-dione (IVb) (mp 145—146 °C); ν_{max}: 1770 and 1700 cm^{-1}; λ_{max} (ε): 299 nm (28100) (Found: C, 63.00; H, 5.07%. Calcd for $C_{21}H_{20}O_8$: C, 62.99; H, 5.04%).

[α-^{14}C]Chalcone. [Me-^{14}C]Acetophenone was prepared by the method described in the literature[3] using sodium [2-^{14}C]acetate (250 μCi, Radiochemical Centre, Amersham, England). [α-^{14}C]Chalcone (mp 55—57 °C) (specific radioactivity: 4.00 μCi/mmol) was prepared by the method described in "Organic Syntheses"[12] in a 76% yield.

[α-^{14}C]Chalcone Dibromide. To a solution of [α-^{14}C]-chalcone (5.0 g) dissolved in benzene (20 ml), we added bromine (3.84 g) at 0 °C. The precipitates (mp 147 °C; 7.25 g; 82%; specific radioactivity, 4.03 μCi/mmol) were used without further purification.

β-Hydroxy[α-^{14}C]chalcone. [α-^{14}C]Chalcone dibromide (7.10 g) was treated with sodium methoxide,[6] thus giving β-hydroxy[α-^{14}C]chalcone (mp 76—77 °C (ethanol); 2.67g; 62%; specific radioactivity, 4.00 μCi/mmol).

2-Bromo-1,3-diphenyl[2-^{14}C]propan-1,3-dione. β-Hydroxy-[α-^{14}C]chalcone (1.48 g) was treated with bromine (1.27 g) in chloroform (10 ml) at 0 °C for an hour to give 2-bromo-1,3-diphenyl[2-^{14}C]propan-1,3-dione (mp 88—89 °C (benzene–light petroleum); 1.56 g; 78%; specific radioactivity, 4.03 μCi/mmol).

2-Acetoxy-1,3-diphenyl[2-^{14}C]propan-1,3-dione. This compound was prepared from 2-bromo-1,3-diphenyl[2-^{14}C]-propan-1,3-dione in the manner described previously (mp 92—93 °C; 51%; specific radioactivity, 4.05 μCi/mmol).

Oxidations of Radioactive Ia and IIa. Radioactive Ia (224 mg) was oxidized with lead tetraacetate (1.33 g) in acetic acid (10 ml) under conditions identical with those described above to give radioactive IIIa (mp 95 °C; 14.2 mg; 7%; specific radioactivity, 2.11 μCi/mmol), Va (mp 122 °C; 6.5 mg; 5%; specific radioactivity, 0.03 μCi/mmol), and carbon dioxide, the latter being later converted to barium carbonate (6.8 mg; specific radioactivity, 0.23 μCi/mmol). The oxidation of the radioactive IIa (282 mg) with lead tetraacetate (444 mg) gave IIIa (mp 95 °C; 32 mg, 14%; specific radioactivity, 0.00 μCi/mmol) and carbon dioxide, which was trapped as barium carbonate (42 mg; 21%; specific radioactivity, 2.25 μCi/mmol).

The authors wish to thank Dr. Emiko Ohoyoshi, of the Radioisotop Centre, and Dr. Kazuta Kitahara and the staff of Faculty of Pharmacology, Kumamoto University, for their kind assistance in the labelling experiments and the measurements.

References

1) R. Criegee "Oxidation in Organic Chemistry," Part A, ed. by K. S. Wiberg, Academic Press, New York and London (1965), p. 277.
2) K. Kurosawa and J. Higuchi, This Bulletin, **45**, 1132 (1972).
3) W. D. Ollis, K. L. Ormand, and I. O. Sutherland, *J. Chem. Soc., C*, **1970**, 119.
4) A. McKillop and B. Swan, *Tetrahedron Lett.*, **1970**, 5281.
5) J. D. Roberts, D. R. Smith, and C. C. Lee, *J. Amer. Chem. Soc.*, **73**, 618 (1951).
6) C. F. H. Allen, R. D. Abell, and J. B. Normington, "Organic Syntheses," Coll. Vol., I, p. 205 (1956).
7) N. V. Saviskaya and M. N. Shchukina, *Zhur. Obshch. Khim.*, **31**, 1015 (1961). *Chem. Abstr.*, **55**, 23496g (1961).
8) Beilsteins "Handbuch der Organischen Chemie," VIII, 2 p. 483.
9) H. Bohme and H. Schneider, *Chem. Ber.*, **91**, 1100 (1958).
10) Beilsteins "Handbuch der Organischen Chemie," VII, p. 747.
11) *ibid.*, VIII, p. 428.
12) E. P. Kohler and H. M. Chadwell, "Organic Syntheses," Coll. Vol., I, p. 78 (1943).

Synthesis of Sequential Polypeptides of L-Leucine and Glycine

Takayoshi Iio and Sho Takahashi*

Department of Physics, Faculty of Science, Nagoya University, Nagoya 464

**Institute for Chemical Research, Kyoto University, Uji, Kyoto 611*

(Received May 7, 1974)

The following sequential polypetides of L-leucine and glycine were synthesized: $(Leu_3Gly)_n$, $(Leu_2Gly)_n$, $(LeuGly)_n$, and $(LeuGly_2)_n$. Polymerization was achieved by self-condensation of the corresponding peptide *p*-nitrophenyl esters. Hydrolysis of the polypeptides were carried out in 90% aqueous trifluoroacetic acid and the time course of liberation of leucine from each polymer was presented. Apparent first-order rate constants ($\times 10^2$), 1.93, 2.86, 2.91, and 4.4 hr^{-1} were obtained for liberation of leucine from $(Leu_3Gly)_n$, $(Leu_2Gly)_n$, $(LeuGly)_n$, and $(LeuGly_2)_n$, respectively.

A number of studies have been made with homo- or random copolypeptides as a model system to understand the secondary structure of protein.[1] Many basic conclusions derived in those works are useful to investigate protein structure including a prediction,[2] their application, however, is surely limited to only qualitative ground. Interactions between side chains of amino acids in proteins are so much complicated that the studies of sequential polypeptides, in which side chains of amino acids are arranged periodically to amplify interactions between them, are desired and will be promising to analyze the interaction quantitatively. With this aspect we previously reported the studies on $(L\text{-}Ala_xGly_y)_n$,[3] it was considered to be necessary to extend the work with sequential polypeptides having much larger side chain. In this paper we will describe the synthesis of $(L\text{-}Leu_xGly_y)_n$ and the behaviors of some leucine polypeptides toward acid hydrolysis, the succeeding paper will deal the conformational studies of the polypeptides in solution.[4]

Results and Discussion

Synthesis. The synthesis of sequential polypeptides having a defined repeating unit of amino acids are usually achieved by a self-condensation of unit peptide active esters, the method has been considered the best general one.[5] Other methods, such as a treatment of peptide free acids with tetraethyl- or bis-*o*-phenylenepyrophosphite,[6] usually required more drastic condition. Among the *p*-nitrophenyl-,[5] pentachlorophenyl-,[7] and *N*-hydroxysuccinimidyl-esters,[8] which are the most widely used active esters, we preferred the *p*-nitrophenyl esters on account of their good crystallinity over *N*-hydroxysuccinimidyl esters. Lorenzi *et al.*[9] compared the polymerization of *N*-hydroxysuccinimidyl- and *p*-nitrophenyl-esters of peptide in the course of their synthesis of $(AlaProGly)_n$, and showed that there were no differences in both products. Our previous experiences on a number of phenyl esters[10] and peptide esters[3] showing *p*-nitrophenyl esters more soluble than pentachlorophenyl esters supported the use of the former: high solubility of the peptide active esters was essential to avoid intramolecular cyclization during the polymerization.

Synthetic steps to the required polymers are shown in Fig. 1. An attempted synthesis of the tripeptide ester (XVIII) *via* azide coupling of (I) and the hydra-

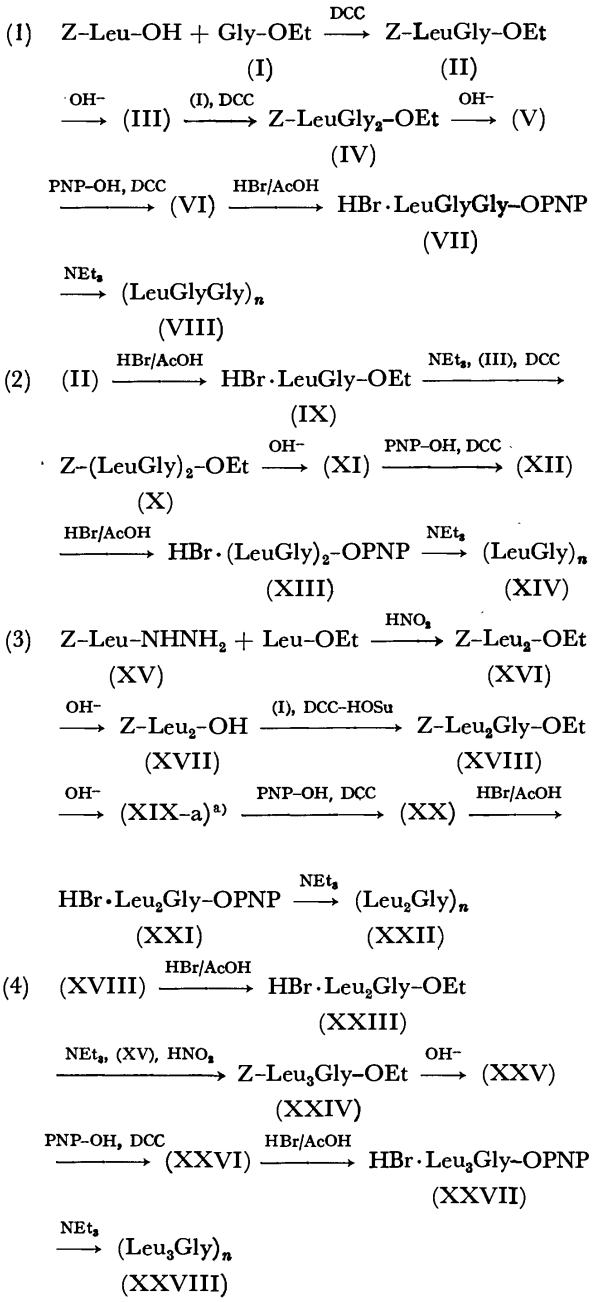

Fig. 1. Steps to the polypeptides, $(Leu_xGly_y)_n$. Abbreviations: Z=benzyloxycarbonyl, PNP=*p*-nitrophenyl. a) Characterized as its dicyclohexylammonium salt, (XIX).

zide of (XVII) in hope to minimize a possibility of racemization of terminal leucine was failed in preparative aspects since the azide derived from XVII was poorly soluble. The use of dicyclohexylcarbodiimide (DCC) in the presence of an equimolar amount of *N*-hydroxysuccinimide (HOSu) was then satisfactorily introduced for a preparative purpose, the resulting XVIII was not distinguished from the product of the azide method in respect of mp; without HOSu, the product had a mp about 10 degrees lower and resisted to further purification.

Concentrated solutions (30—40% in dimethyl sulfoxide) of the polymerizing unit peptide active ester hydrobromides (VII, XIII, XXI, XXVII) were neutralized with triethylamine to afford the polypeptides (VIII, XIV, XXII, XXVIII). The weight average molecular weight was roughly estimated as 30000, 20000, 25000, and 20000 for VIII, XIV, XXII, and XXVIII, respectively, from intrinsic viscosity in dichloroacetic acid.[11]

Hydrolysis of Polypeptides. Estimation of chemical and optical purities of synthetic polypeptides is exclusively achieved by an amino acid analysis and by a measurement of optical rotation on hydrolyzates. The most general condition, hydrolysis in 6 M-hydrochloric acid,[12] was not applicable to the present case by the fact that poor solubilities of leucine polypeptides whose leucine contents were high as in XXII and XXVIII in 6 M or concd hydrochloric acid caused the rate of hydrolysis very slow (after 5 days hydrolysis at 110 °C still precipitates were observed). Among literatures of the synthesis of poly-leucine only two papers reported total hydrolysis: one in 6 M- (40 hr)[13] and the other in 12 M-hydrochloric acid (3—4 days)[14] without comment of results. Other substances used for

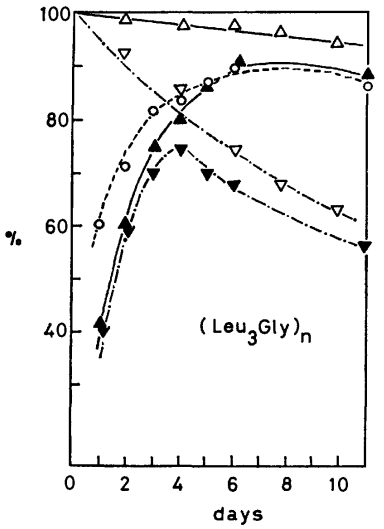

Fig. 2. Hydrolysis of $(Leu_3Gly)_n$ in 90% aq. TFA at 110 °C. Values are given as % of the theoretical values. ○------○: liberation of glycine from the polymer, ▲——▲: liberation of leucine from the polymer, ▼-·-·-▼: optical rotation (at 300 nm) of isolated leucine, △——△: amount of recovered leucine when pure L-leucine was treated in the same condition, and ▽-·-·-▽: optical rotation of L-leucine treated in the same condition.

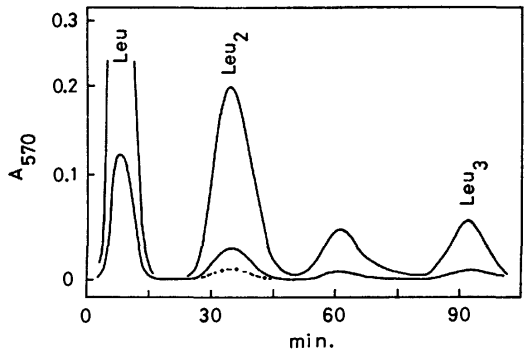

Fig. 3. Amino acid analysis of the hydrolysates of $(Leu_3Gly)_n$. Hydrolysis was carried out in 90% aq. TFA for 3 days (solid line) and 6 days (dotted line). The analyzer column was operated at the standard condition until just berore leucine was eluted, then pH 5.28 buffer was delivered (noted as the time zero on the abscissa). The lower curve was magnified 10 times to yield the upper one.

total hydrolysis, mono-,[15] di-,[16] tri-chloroacetic acid,[15] formic acid,[15] and oxalic acid,[15,17] did not give better results. After looking for another hydrolytic media, especially among perfluoro-acetic, -propionic, and -butyric acid, 90% aqueous trifluoroacetic acid (TFA) was finally adopted as a medium of hydrolysis, and further experiments were carried out with this solvent. The other 90% aqueous perfluoroaliphatic acids or 1:1 mixtures of fluoroacids and concd hydrochloric acid gave approximately similar results in the respect of amino acids liberation upon hydrolysis. Figure 2 illustrated the typical results of the hydrolysis of XXVIII, where liberation of glycine and leucine, values of molecular rotation (at 300 nm) of leucine which was separated on a chromatographic column from the hydrolyzates, and the corresponding results obtained in control experiments were shown. The well-known facts that the rate of hydrolysis of a peptide bond Leu–Leu was about a tenth to a hundredth of those of Leu–Gly, Gly–Leu,[18] and Gly–Gly,[18,19] were clearly reflected in an amino acid analysis of the hydrolyzates (Fig. 3). Figure 3 showed the appreciable amount of Leu_2 and Leu_3 was present in the hydrolyzates. Such fragments also might contribute the molecular rotation in an appreciable manner, this is the reason why optical rotation was measured with isolated leucine itself. Although the molecular rotation of leucine decreased fairly rapidly in this hydrolytic condition (half life 14 days), extrapolation to zero hydrolysis time established that the racemization in XXVIII should be less than 5%. The other polypeptides, VIII, XIV, and XXII, also gave the same result.

Each leucyl peptide bond in the unit (Leu_xGly_y) might have a different rate constant for hydrolysis and thus the appearance of free leucine in the hydrolyzates should be described by a composite of these rate constants.[20] But the actual liberation of leucine from VIII, XIV, XXII, and XXVIII was found to be approximately represented by apparently single first-order kinetics as shown in Fig. 4, at least short period

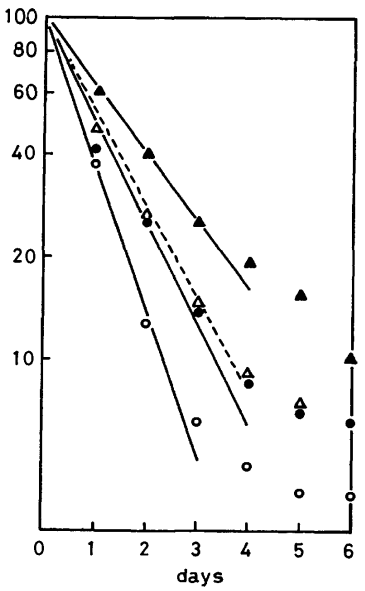

Fig. 4. Semilogarithmic plot of hydrolysis data. The values of 100-x (x is the amount of free leucine yielded from hydrolysis) are plotted against hydrolysis time. ▲——▲: $(Leu_3Gly)_n$, △------△: $(Leu_2Gly)_n$, ●——●: $(LeuGly)_n$, and ○——○: $(LeuGly_2)_n$.

of hydrolysis time was concerned. The estimated apparent-first order rate constants ($\times 10^2$) for appearance of free leucine are 1.93, 2.86, 2.91, and 4.4 hr^{-1} for VIII, XIV, XXII, and XXVIII, respectively, those values would serve as a measure of hydrolysis of leucyl residues from polypeptides.

Experimental

TFA, DCC, and HOSu were purchased from Protein Research Foundation, Osaka. L-Leucine and other reagents were of the purest or reagent grade of commercially available products. All melting points are uncorrected values on a micro hot plate. Viscosities were measured at 25 °C using an Ostwald type viscometer. Optical rotation was measured at 300 nm with a JASCO ORD/UV-5.

Coupling with DCC. DCC reactions were usually carried out at −8 to 0 °C for 4—5 hr, then at 5—8 °C for 12—48 hr with stirring. 1.1 molar equivalent of DCC and 1.2 to 1.5 equivalent of *p*-nitrophenol or an amine component, which was obtained by treating amino acid or peptide ester salts with 1.05 equivalent of NEt_3, were used.[22]

Reaction with HBr/AcOH. Ten mmol of a peptide *p*-nitrophenyl ester was treated with 4 ml of 25% HBr in acetic acid at room temperature for 1—4 hr.

Saponification. NaOH (1.2 equimolar amount) was used.

Hydrolysis. Polypeptide (5 to 10 mg) was suspended in 3 ml of 90% aq. TFA in an ampoule, cooled with liquid nitrogen to solidify, evacuated to 10^{-2} Torr, sealed, and kept at 110 °C. Hydrolyzates were evaporated to dryness *in vacuo*, the residue was dissolved in 0.001 M HCl and analyzed on a JEOL liquid chromatography system according to the method of Spackman *et al.*[21] A JEOL separation system JLC-3 was used to isolate free leucine in hydrolyzates.

Z-Leu-Gly-Gly-OEt (IV). The compound was prepared from (III)[23] and (I) by a DCC reaction in $CHCl_3$ and recrystallized from ethyl acetate–cyclohexane. Yield, 87%, mp 103—105 °C.

Found: C, 59.25; H, 7.25; N, 10.51%. Calcd for $C_{20}H_{29}O_6N_3$: C, 58.95; H, 7.17; N, 10.31%.

Z-Leu-Gly-Gly-OPNP (VI). IV was saponified in methanol with 1.2 M NaOH to afford V, which was esterified by a DCC reaction in tetrahydrofuran. VI was recrystallized from ethyl acetate–ether. Yield, 53%, mp 136—138 °C.

Found: C, 57.73; H, 5.71; N, 11.79%. Calcd for $C_{24}H_{28}O_8N_4$: C, 57.59; H, 5.64; N, 11.20%.

HBr·Leu-Gly-Gly-OPNP (VII). VI was treated with HBr/AcOH to afford VII, which was recrystallized from ethanol–ether. Yield, 48%, mp 191—195 °C (dec.).

Found: C, 43.17; H, 5.19; N, 12.83%. Calcd for $C_{16}H_{23}O_6N_4Br$: C, 42.96; H, 5.18; N, 12.53%.

Z-Leu-Gly-Leu-Gly-OEt (X). II[23] was treated with HBr/AcOH to give IX, which was coupled with III by a DCC reaction in $CHCl_3$. Yield, 85%, mp 157—159 °C (ethanol–ether).

Found: C, 59.72; H, 7.83; N, 11.03%. Calcd for $C_{26}H_{40}O_7N_4$: C, 59.98; H, 7.74; N, 10.76%.

Z-Leu-Gly-Leu-Gly-OPNP (XII). The compound X was saponified in dioxane with 0.43 M NaOH to give XI (obtained as amorphous powder), which was coupled with *p*-nitrophenol by a DCC reaction in tetrahydrofuran. Yield. 67%, mp 168—173 °C (ethanol–ether).

Found: C, 59.80; H, 6.64; N, 12.27%. Calcd for $C_{30}H_{39}O_9N_5$: C, 58.72; H, 6.43; N, 11.41%.

HBr·Leu-Gly-Leu-Gly-OPNP (XIII). XIII, obtained from XII with HBr/AcOH, was recrystallized from ethanol or dioxane. The compound was highly hygroscopic. Yield, 85%, mp 125 °C.

Found: C, 47.05; H, 6.25; N, 12.27%. Calcd for $C_{22}H_{34}O_7N_5Br$: C, 47.15; H, 6.11; N, 12.50%.

Z-Leu-Leu-OEt (XVI). 20 g of Z-Leu-hydrazide (XV) in 150 ml of 1 M HCl and 60 ml of acetic acid was treated with 5.3 g of $NaNO_2$ at −5 °C. The azide was extracted with ether and reacted at the same temperature for 2 hr with ethyl leucinate which was prepared from 19 g of the hydrochloride and 9.9 g of NEt_3. The reaction mixture was kept at 0 °C for 24 hr, then worked up as usual. Yield, 21 g, mp 90—91 °C (ethyl acetate–cyclohexane) (lit, 89—90 °C[25]).

Z-Leu-Leu-Gly-OEt (XVIII). XVI was saponified in acetone with 1 M NaOH to give (XVII) (mp 102—103 °C, lit, 98—101 °C[26]). To a mixture of 14.8 g of I hydrochloride, 10.7 g of NEt_3, and 200 ml of tetrahydrofuran, 36.3 g of XVII and 12.1 g of HOSu were added. The whole mixture was cooled to −15 °C, 22 g of DCC in 70 ml of tetrahydrofuran was added portionwise. After standing at −15 °C for additional 5 hr, then at 0 °C for 2 day, the reaction mixture was worked up as usual. The compound was also obtained from XV and IX or from Z-Leu-Leu-hydrazide[24] and I by the method described in the preparation of XVI. In the last case, treatment of the hydrazide with $NaNO_2$ in HCl–AcOH instantaneously separated the Z-Leu-Leu-azide, part of which was extracted with $CHCl_3$ and was reacted with I. Yield, 29 g, mp 127—128 °C (lit, 111—112 °C[27]) (Found: C, 62.25; H, 8.11; N, 9.26%).

Z-Leu-Leu-Gly-OH, Dicyclohexylammonium Salt (XIX). XVIII was treated in acetone with 1.2 M NaOH to afford the free acid, which was converted into dicyclohexylammonium salt. Yield, 67%, mp 131—133 °C (ethanol).

Found: C, 66.64; H, 9.33; N, 9.47%. Calcd for $C_{34}H_{56}O_6N_4$: C, 66.20; H, 9.15; N, 9.08%.

Z-Leu-Leu-Gly-OPNP (XX). The compound was prepared from XIX and *p*-nitrophenol by a DCC reaction in tetrahydrofuran. Yield, 75%, mp 125 °C (ethanol or ethyl acetate).

Found: C, 60.57; H, 6.60; N, 10.05%. Calcd for $C_{28}H_{36}O_8N_4$: C, 60.42; H, 6.52; N, 10.07%.

HBr·Leu-Leu-Gly-OPNP (XXI). XX was treated with HBr/AcOH to afford XXI, which was recrystallized from ethanol. Yield, 74%, mp 234 °C (dec.).

Found: C, 47.60; H, 6.18; N, 11.10%. Calcd for $C_{20}H_{31}O_6N_4Br$: C, 47.72; H, 6.21; N, 11.13%.

HBr·Leu-Leu-Gly-OEt (XXIII). The compound was prepared from XVIII and HBr/AcOH. Yield, 93%, mp 166—167 °C (ethanol-ether). Found: C, 46.60; H, 7.61; N, 10.08%. Calcd for $C_{16}H_{32}O_4N_3Br$: C, 46.84; H, 7.86; N, 10.24%.

Z-Leu-Leu-Leu-Gly-OEt (XXIV). XXIII (22.4 g) in 100 ml $CHCl_3$ was treated at 0 °C with 5.56 g of NEt_3. The filtrate was added at 0 °C to Z-Leu-azide in 200 ml of ether prepared from 17 g of XV, the solution was kept at 0 °C for 2 day and worked up as usual. Yield, 66%, mp 235—236 °C (ethanol-tetrahydrofuran).

Found: C, 62.36; H, 8.55; N, 9.49%. Calcd for $C_{30}H_{48}O_7N_4$: C, 62.49; H, 8.39; N, 9.72%.

Z-Leu-Leu-Leu-Gly-OH (XXV). XXIV was treated in dioxane with 1 M NaOH to give XXV. Yield, 47%, mp 118—120 °C (tetrahydrofuran-cyclohexane).

Found: C, 61.65; H, 8.00; N, 10.46%. Calcd for $C_{28}H_{44}O_7N_4$: C, 61.27; H, 8.09; N, 10.21%.

Z-Leu-Leu-Leu-Gly-OPNP (XXVI). XXV was coupled with *p*-nitrophenol by a DCC reaction in dimethylformamide-dioxane (1:3). Yield, 50%, mp 208 °C (ethanol).

Found: C, 61.13; H, 7.26; N, 10.51%. Calcd for $C_{34}H_{47}O_9N_5$: C, 60.97; H, 7.07; N, 10.46%.

HBr·Leu-Leu-Leu-Gly-OPNP (XXVII). Prepared from XXVI and HBr/AcOH and recrystallized from dioxane–ether. Yield, 61%, mp 187 °C (dec.).

Found: C, 50.24; H, 6.89; N, 11.08%. Calcd for $C_{26}H_{42}O_7N_5Br$: C, 50.65; H, 6.87; N, 11.36%.

Polymerization of VII, XIII, XXI, and XXVII. 1.1 molar equivalent of NEt_3 was added to a 30—40% solution of VII, XIII, XXI, and XXVII in dimethyl sulfoxide under vigorous stirring. The mixture solidified within several minutes. After standing at room temperature for 2 days, the products were washed with a sufficient volume of ether, dissolved in TFA, and precipitated by adding ether. The procedure of dissolving and precipitation was cycled four times, the precipitates were dried over P_2O_5 and KOH. Yield, 40—60%.

Poly-(Leu-Gly-Gly) (VIII). Viscosity in dichloroacetic acid (DCA): $\eta_{sp}/c=0.267$ ($c=1\%$), $\eta_{int}=0.262$. Amino acid analysis: Leu: Gly=1.0: 1.99 (after 3 day hydrolysis).

Found: C, 52.34; H, 7.61; N, 18.67%. Calcd for $C_{10}H_{17}O_3N_3$: C, 52.85; H, 7.54; N, 18.49%.

Poly-(Leu-Gly) (XIV). Viscosity in DCA: $\eta_{sp}/c=0.151$ ($c=1\%$), $\eta_{int}=0.150$. Amino acid analysis: Leu: Gly=1.0: 0.99 (3 day hydrolysis).

Found: C, 54.13; H, 8.02; N, 15.88%. Calcd for $C_8H_{14}O_2N_2$: C, 56.45; H, 8.29; N, 16.46%.

Poly-(Leu-Leu-Gly) (XXII). Viscosity in DCA: $\eta_{sp}/c=0.221$ ($c=1\%$), $\eta_{int}=0.198$. Amino acid analysis: Leu: Gly=2.0: 0.99 (3 day hydrolysis).

Found: C, 58.89; H, 8.79; N, 15.40%. Calcd for $C_{14}H_{25}O_3N_3$: C, 59.34; H, 8.89; N, 14.83%.

Poly-(Leu-Leu-Leu-Gly) (XXVIII). Viscosity in DCA: $\eta_{sp}/c=0.159$ ($c=1\%$), $\eta_{int}=0.158$. Amino acid analysis: Leu: Gly=3.0: 0.94 (6 day hydrolysis).

Found: C, 58.97; H, 9.00; N, 13.92%. Calcd for $C_{20}H_{36}O_4N_4$: C, 60.58; H, 9.15; N, 14.13%.

We are greatly indebted to Dr. N. Kato at Nagoya University for his kind arrangement of elementary analysis. Thanks are also due to Prof. K. Yamasaki at the same university who kindly made available an ORD spectrometer for the experiment.

References

1) N. Lotan, A. Berger, and E. Katchalski, *Ann. Rev. Biochem.*, **41**, 869 (1972).
2) P. Y. Chou and G. D. Fasman, *Biochemistry*, **13**, 211 (1974).
3) S. Takahashi, This Bulletin, **42**, 521 (1969); T. Iio and S. Takahashi, *ibid.*, **43**, 515 (1970); T. Iio, *Biopolymers*, **10**, 1583 (1971); T. Iio and S. Takahashi, *Bull. Inst. Chem. Res. Kyoto University*, **49**, 80 (1971).
4) T. Iio and S. Takahashi, This Bulletin, in press.
5) D. F. DeTar, W. Honsberg, U. Honsberg, A. Wieland, M. Gouge, H. Bach, A. Tahara, W. S. Briniger, and F. F. Rogers, Jr., *J. Amer. Chem. Soc.*, **85**, 2873 (1963); F. H. C. Stewart, *Aust. J. Chem.*, **18**, 887 (1965).
6) H. Kitaoka, S. Sakakibara, and H. Tani, This Bulletin, **31**, 802 (1958); E. Heidemann and H. W. Bernhardt, *Nature*, **216**, 263 (1967); M. L. Huggins, K. Ohtsuka, and S. Morimoto, *J. Polym. Sci., Part C*, **23**, 343 (1968).
7) J. Kovacs, R. Giannotti, and A. Kapoor, *J. Amer. Chem. Soc.*, **88**, 2282 (1966).
8) B. B. Doyle, W. Traub, G. P. Lorenzi, F. R. Brown, III, and E. R. Blout, *J. Mol. Biol.*, **51**, 47 (1970); G. Ramachandran, A. Berger, and E. Katchalski, *Biopolymers*, **10**, 1829 (1971); R. Katakai, F. Toda, K. Uno, Y. Iwakura, and M. Oya, *Chem. Lett.*, **1973**, 763.
9) G. P. Lorenzi, B. B. Doyle, and E. R. Blout, *Biochemistry*, **10**, 3046 (1971).
10) L. A. Cohen and S. Takahashi, *J. Amer. Chem. Soc.*, **95**, 443 (1973).
11) P. Doty, J. H. Bradbury, and A. M. Holtzer, *ibid.*, **78**, 947 (1956); J. C. Mitchell, A. E. Woodward, and P. Doty, *ibid.*, **79**, 3955 (1957).
12) S. Moore and W. H. Stein, *Meth. Enzymol.*, **6**, 819 (1963).
13) K. D. Kopple and J. J. Katz, *J. Amer. Chem. Soc.*, **78**, 6199 (1956).
14) H. E. Auer and P. Doty, *Biochemistry*, **5**, 1708 (1966).
15) N. Maravalhas, *J. Chromatogr.*, **50**, 413 (1970).
16) R. E. Whitfield, *Science*, **142**, 577 (1963).
17) F. Feigl, *Angew. Chem.*, **70**, 1966 (1958).
18) R. L. Synge, *Biochem. J.*, **39**, 351 (1945); R. Hirohata, Y. Kanda, M. Nakayama, N. Izumiya, A. Nagamatsu, J. Ono, S. Fujii, and M. Kimitsuki, *Z. Physiol. Chem.*, **295**, 368 (1953).
19) K. Heyns, W. Walter, and H. F. Grützmacher, *J. Polym. Sci.*, **30**, 573 (1958).
20) D. A. Long and T. G. Truscott, *Trans. Faraday Soc.*, **59**, 2316 (1963).
21) D. H. Spackman, W. H. Stein, and S. Moore, *Anal. Chem.*, **30**, 1190 (1958).
22) J. P. Greenstein and M. Winitz, "Chemistry of the Amino Acids," Vol. II, John Wiley & Sons, New York, *N. Y.* (1961), p. 763.
23) M. Bergmann, L. Zervas, and J. S. Fruton, *J. Biol. Chem.*, **111**, 225 (1935).
24) CIBA Ltd., Ger. 1112525 (1962).
25) H. Aoyagi, M. Kondo, and N. Izumiya, This Bulletin, **41**, 2772 (1968).
26) E. L. Smith, D. H. Spackman, and W. J. Polgrase, *J. Biol. Chem.*, **199**, 801 (1952).
27) P. M. Hardy, G. W. Kenner, and R. C. Sheppard, *Tetrahedron*, **19**, 95 (1963).

The Synthesis of 1,3,4-Benzotriazepin-5-one Derivatives from Isatoic Anhydrides

Masahiko TAKAHASHI, Saburo ONIZAWA, and Tomonobu SATOH

Department of Industrial Chemistry, Faculty of Engineering, Ibaraki University, Hitachi 316

(Received May 9, 1974)

The reaction of isatoic anhydrides (**1**) with 2-pyridylamidrazone afforded *N*-(2-aminophenyl)-2-pyridylamidrazones (**2**), which were then cyclized with acid to 1,3,4-benzotriazepin-5-one derivatives (**3**). The treatment of isatoic anhydride with 2-pyridylcarbonohydrazide gave 1-(2-aminophenyl)-2-(2-pyridinecarbonyl)-hydrazine (**5**), which was then dehydrated with polyphosphoric acid to 3-(2-aminophenyl)-5-(2-pyridyl)-1,3,4-oxadiazole (**6**), but not to **3**.

There have been several reports on the methods of synthesizing 1,3,4-benzotriazepine derivatives, and these compounds have been synthesized in recent years.

Bush[1] used 1-(2-aminobenzyl)-1-phenylhydrazine as the starting material for the 1,3,4-benzotriazepine system. On the other hand, 5-phenyl-1,3-dihydro-2*H*-1,3,4-benzotriazepin-2-ones[2-4] and 5-phenyl-2,3-dihydro-1*H*-1,3,4-benzotriazepines[5] were prepared from 2-aminobenzophenones. Readily-available isatoic anhydrides were also used as starting materials, and 2,3,4,5-tetrahydro-1*H*-1,3,4-benzotriazepin-2,5-diones,[6-7] -5-ones,[8] and 1,4-dihydro-5*H*-1,3,4-benzotriazepin-5-ones[9] were synthesized. 3,4-Dihydro-1*H*-1,3,4-benzotriazepin-2,5-diones[10] were prepared from *N*-alkyl-*N*-carboxyanthranilate.

We have previously described the synthesis of 1,2,4-triazin-5-ones by the use of amidrazone.[11] In the present paper we wish to report a new method of synthesizing 1,3,4-benzotriazepin-5-ones by the reaction of isatoic anhydride with 2-pyridylamidrazone.

Results and Discussion

The reaction of isatoic anhydride with amines proceeds smoothly, with the evolution of carbon dioxide, to give *o*-aminobenzoylamide derivatives.[12] Thus, the reaction of readily-available 2-pyridylamidrazone[13] and isatoic anhydride (**1a**) in pyridine at room temperature gave *N*-(2-aminobenzoyl)-2-pyridylamidrazones (**2a**). From the substituted isatoic anhydrides (**1b**, **c**), *N*-(substituted-2-aminobenzoyl)-2-pyridylamidrazone (**2b**, **c**) were similarly obtained. The IR spectra of **2a—c** showed NH and CO stretching absorption bands at 3480—3160 and 1630—1618 cm^{-1} respectively. The deamination and cyclization of **2a** were attempted with acid catalysts or an acidic medium, and the treatment of **2a** with 0.05 M H_2SO_4–MeOH gave a yellow product (**3a**) in a moderate yield. **3a** was also formed on the refluxing of **2a** in acetic acid, but in a lower yield. The IR spectra of **3a** showed NH absorption bands at 3300 and 3190 cm^{-1} and CO and C=N absorption bands at 1675 and 1645 cm^{-1} respectively. The results of elemental analysis and the mass spectra supported the molecular formula corresponding to **3a**. The structure of **3a** of 2-(2-pyridyl)-3,4-dihydro-5*H*-1,3,4-benzotriazepin-5-one was further confirmed by the formation of monoacetate (**4**), which was prepared on the heating of **3a** in acetic anhydride. **3b** was similarly obtained from **2b** in a good yield, but the structure of the product (**3c**) from **2c** was obscure from its spectral data.

Langis[9] reported the synthesis of analogous triazepine derivatives, **3**, from isatoic anhydride by a different route; the reaction of isatoic anhydride with acylhydrazines in EtOH afforded 1-aminobenzoyl-2-acylhydrazine (**5**), which were then dehydrated on heating with polyphosphoric acid to form **3**. Thus, we attempted to identify the structure of **3** by this route.

The treatment of **1a** with 2-pyridinecarbonohydrazide in EtOH gave 1-(2-aminobenzoyl)-2-(2-pyridyl)hydrazine (**5a**). The structure of **5a** was confirmed by analysis and by the spectral data. The dehydration of **5a** with polyphosphoric acid was examined under the condition described in the literature,[9] *i.e.*, at 150 °C for 1 hr. The IR and UV spectra of the product (**6a**) were analogous to those of the 4-pyridyl derivative (**6b**) prepared according to the reported procedure,[9] but were different from those of **3a**. However, the analytical data and the molecular weight determined by means of the mass spectrum of **6a** showed the same molecular formula as **3a**. The IR spectrum of **6a** showed two sharp NH absorption bands at 3440 and 3340 cm^{-1}. The absorption bands at 1640 and 1630 cm^{-1} were assigned to C=N stretching and NH deformation vibrations respectively. These data suggested that the structure of the product was not triazepine, **3a**, but 2-(2-aminophenyl)-5-(2-pyridyl)-1,3,4-oxadiazole. The NMR spectrum of **6a** displayed signals at δ 5.35 (NH_2) and at 6.6—8.9 (aromatic protons). Further confirmation of the structures of **3a** and **6a** could be

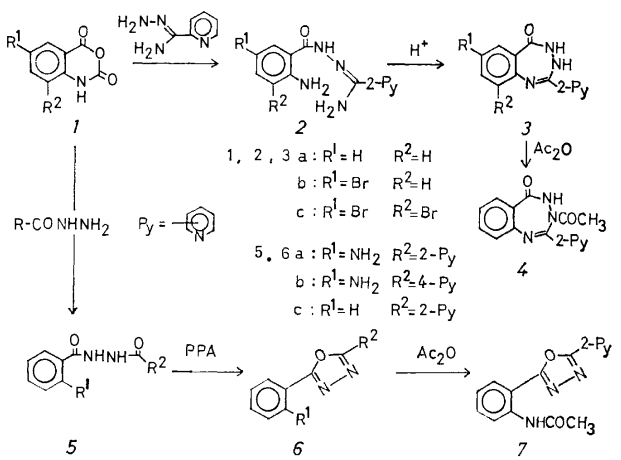

Scheme 1.

obtained by the correlation of the mass spectra; the spectrum of **3a** showed the main peaks at *m/e* 238 (M^+, 100%) and 208 (M^+—NH=NH, 59%), whereas in the case of **6a** the main peaks were at *m/e* 238 (M^+, 100%), 237 (M^+—1, 31%), and 120 (M^+—*o*-aminobenzonitrile, 34%).

The structure assignment of **6a** was further confirmed by a comparison of the analytical and spectral data of the monoacetate (**7**) with those of (**4**); elemental analysis and mass spectra gave an identical molecular formula. The IR spectrum of **4** showed two CO absorptions at 1685 and 1670 cm^{-1}, together with the NH absorption. On the other hand, **7** showed one CO absorption at 1690 cm^{-1}. **4** exhibited a mass spectrum characterized by a M^+ ion at *m/e* 280 (30%) in addition to significant peaks at *m/e* 237 (M^+—$COCH_3$, 93%) and 208 (M^+—$NH{=}NCOCH_3$, 100%). The high intense peaks of the spectrum of **7** at *m/e* 280 (100%), 237 (87%), and 120 (78%) were assigned to the M^+, M^+—$COCH_3$, and M^+—(2-CH_3CONH-C_6H_4-CN) ions respectively.

As the cyclization of diacyl hydrazines on treatment with dehydrating agents has already been reported,[14] we also attempted the cyclization of 1-benzoyl-2-(2-pyridyl)hydrazine (**5c**) as a model compound to 2-phenyl-5-(2-pyridyl)-1,3,4-oxadiazole (**6c**) under the same conditions as in the case of the reaction of **5a** to **6a**; we obtained **6c** in a moderate yield.

The structure of **3** was also supported by the hydrolysis of **3a** with hydrochloric acid to **5a** in a 45% yield.

From the above data, the compounds reported by Langies were not the triazepine derivatives **3** but 1,3,4-oxadiazoles, **6**; our results present a new synthetic route to 1,3,4-benzotriazepin-5-one derivatives.

Experimental

All the melting points are uncorrected. The IR, UV, and NMR spectra were measured with a JASCO Model IRA-2 spectrometer (KBr pellets), a Shimadzu Model MPS-50L spectrometer (in MeOH), and a Hitachi Model R-20 spectrometer respectively. A Shimadzu Model UM-3B apparatus was used for the elemental analysis.

N-(2-Aminobenzoyl)-2-pyridylamidrazone (2a). A mixture of 3.26 g (20 mmol) of **1a** and 3.26 g (24 mmol) of 2-pyridylamidrazone in 50 ml of pyridine was stirred at room temperature for 10 hr. The filtration and washing of the resulting precipitate with MeOH gave 4.26 g (84%) of **2a**. Recrystallization from pyridine afforded white needles; mp 223—225 °C. Found: C, 61.48; H, 5.10; N, 27.36%. Calcd for $C_{13}H_{13}N_5O$: C, 61.20; H, 5.14; N, 27.47%. IR: 3480—3200, 1660, 1630 cm^{-1}. UV λ_{max} nm (log ε): 217 (4.43), 250 (3.99), 317 (4.07), 336 (4.07).

N-(2-Amino-5-bromobenzoyl)-2-pyridylamidrazone (2b). A mixture of 2.42 g (10 mmol) of **1b** and 1.63 g (12 mmol) of 2-pyridylamidrazone in 20 ml of pyridine was refluxed for 1 hr. After cooling, the filtration and washing of the precipitate with MeOH gave 1.84 g (58%) of **2b**. Recrystallization from MeOH afforded yellow needles; mp 220—232 °C. Found: C, 46.60; H, 3.63; N, 20.49%. Calcd for $C_{13}H_{12}N_5OBr$: C, 46.72; H, 3.63; N, 20.96%. IR: 3440—3160, 1625 cm^{-1}. UV λ_{max} nm (log ε): 224 (4.61), 250 (4.43), 290 (4.14), 330 (3.95), 363 (4.04).

N-(2-Amino-3,5-dibromobenzoyl)-2-pyridylamidrazone (2c). **2c** was obtained in a 54% yield in the way which has been described for **2b**. Recrystallization from MeOH afforded yellow needles; mp 232—238 °C. Found: C, 37.39; H, 2.68%. Calcd for $C_{13}H_{11}N_5OBr_2$: C, 37.92; H, 3.01%. IR: 3438—3180, 1618 cm^{-1}. UV λ_{max} nm (log ε): 224 (4.41), 248 (4.21), 355 (4.05).

2-(2-Pyridyl)-3,4-dihydro-5H-1,3,4-benzotriazepin-5-one (3a). A solution of 2.0 g (7.8 mmol) of **2a** in 50 ml of 0.05 M H_2SO_4–MeOH was refluxed for 3 hr. After the subsequent concentration and cooling of the solution, the precipitated crystals were filtered by suction and washed with water to remove the inorganic materials and then with MeOH to give 1.10 g (59%) of **3a**. Recrystallization from $CHCl_3$ afforded yellow needles; mp 247—248 °C. Found: C, 65.17; H, 4.36; H, 23.44%. Calcd for $C_{13}H_{10}N_4O$: C, 65.58; H, 4.24; N, 23.54%. IR: 3300, 3190, 3060, 1675, 1645 cm^{-1}. UV λ_{max} nm (log ε): 233 (4.33), 238 (4.31), 276 (4.17), 303 (3.96), 354 (2.95).

A solution of 200 mg of **2a** in 5.0 ml of acetic acid was refluxed for 3 hr. After cooling, the precipitated crystals were filtered by suction and washed with MeOH to give 59 mg (31%) of yellow products. Subsequent recrystallization from $CHCl_3$ afforded yellow needles, whose IR spectra and mp were identical with those of **3a**.

7-Bromo-2-(2-pyridyl)-3,4-dihydro-5H-1,3,4-benzotriazepin-5-one (3b). **3b** was obtained in a 74% yield in the way described for **3a**. Recrystallization from MeOH afforded yellow needles; mp 249—250 °C. Found: C, 49.69; H, 2.81; N, 17.15%. Calcd for $C_{13}H_9N_4OBr$: C, 49.24; H, 2.86; N, 17.68%. IR: 3260, 3180, 3070, 3040, 2930, 1660, 1645 cm^{-1}. UV λ_{max} nm (log ε): 235 (4.40), 279 (4.26), 307 (3.95), 350 (2.79).

Monoacetate (4) of 3a. A solution of 300 mg of **3a** in 5.0 ml of acetic anhydride was refluxed for 2 hr. After cooling, the precipitated crystals were filtered by suction and washed with a small amount of ethyl acetate to give 145 mg (42%) of **4**. Subsequent recrystallization from benzene afforded yellow plates; mp 193—196 °C. Found: C, 64.17; H, 4.29%. Calcd for $C_{15}H_{12}N_4O_2$: C, 64.27; H, 4.32%. IR: 3270, 1685, 1670, 1650 cm^{-1}. NMR ($CDCl_3$): δ 2.48 (s, 3H), 6.9—8.8 (m, 8H), 9.30 (s, 1H).

1-(2-Aminobenzoyl)-2-(2-pyridyl)hydrazine (5a). A mixture of 2.4 g (15 mmol) of **1a** and 2.0 g (15 mmol) of picolinic acid hydrazide in 50 ml of EtOH was refluxed for 20 hr. After cooling, the precipitates were filtered by suction to give 2.2 g (71%) of **5a**. Recrystallization from MeOH afforded white prisms; mp 210—212 °C. Found: C, 60.93; H, 4.67%. Calcd for $C_{13}H_{12}N_4O_2$: C, 60.93; H, 4.72%. IR: 3500, 3380, 3300, 1685, 1675, 1644 cm^{-1}. UV λ_{max} nm (log ε): 250 (4.08), 338 (3.77).

Hydrolysis of 3a to 5a. A solution of 200 mg of **3a** in the mixing solvent of 5.0 ml of 1 M HCl and 5.0 ml of EtOH was refluxed for 2 hr. After cooling, the solution was neutralized with aqueous Na_2CO_3 and then allowed to stand to give precipitates. After the filtration of the precipitates, one recrystallization from MeOH afforded 97 mg (45%) of white crystals, whose mp and IR spectra were in accord with those of **5a**.

2-(2-Aminophenyl)-5-(2-pyridyl)-1,3,4-oxadiazole (6a). A mixture of 500 mg (2.0 mmol) of **5a** and 2.5 g of polyphosphoric acid was heated at 150 °C with gentle stirring for 1 hr. After cooling, the mixture was stirred into 50 ml of water, and the resulting precipitates were filtered off by suction. The filtrate was made alkaline with aqueous NaOH to give additional precipitates. The combined precipitates were washed with a small amount of MeOH to give 330 mg (61%) of **6a**. Recrystallization from MeOH afforded

needles; mp 170—171 °C. Found: C, 65.60; H, 4.13%. Calcd for $C_{13}H_{10}N_4O$: C, 65.53; H, 4.23%. IR: 3440, 3340, 1640, 1630, 1615 cm^{-1}. UV λ_{max} nm (log ε): 220 (4.38), 249 (4.09), 285 (4.12), 358 (4.08).

2-(2-Aminophenyl)-5-(4-pyridyl)-1,3,4-oxadiazole (6b). **6b** was prepared according to the reported produre. Light yellow prisms; mp 191—192 °C (lit,[9] 180—182 °C). IR: 3440, 3320, 3200, 1635, 1625 cm^{-1}. UV λ_{max} nm (log ε): 221 (4.46), 254 (4.19), 275 (4.24), 366 (4.10).

2-Phenyl-5-(2-pyridyl)-1,3,4-oxadiazole (6c). The crude product of **6c** was obtained in the way described for **6a**. The product was chromatographed on silica gel with the eluent of $CHCl_3$ to give 223 mg (48%) of pure **6c**. Recrystallization from MeOH afforded white needles; mp 131—132 °C. Found: C, 69.62; H, 3.95%. Calcd for $C_{13}H_9N_3O$: C, 69.94; H, 4.06%. IR: 3040, 1608, 1588, 1545 cm^{-1}. UV λ_{max} nm (log ε): 263 (4.19), 289 (4.38).

2-(2-Acetamidophenyl)-5-(2-pyridyl)-1,3,4-oxadiazole (7). A mixture of 250 mg (1.1 mmol) of **6a** and 5.0 ml of acetic anhydride was heated at 130 °C for 2 hr. The subsequent removal of the acetic anhydride *in vacuo* gave a solid residue, which was triturated with a small amount of water, filtered, and washed with MeOH to give 223 mg (72%) of **7**. Recrystallization from MeOH afforded white needles; mp 205—206 °C. Found: C, 64.12; H, 4.34%. Calcd for $C_{15}H_{12}N_4O_2$: C, 64.27; H, 4.32%. IR: 3260, 3200, 3060, 1690, 1616 cm^{-1}. UV λ_{max} nm (log ε): 225 (4.38), 242 (4.22), 287 (4.32), 294 (4.32), 315 (4.15). NMR ($CDCl_3$): δ 2.30 (s, 3H), 7.0—8.9 (m, 8H), 11.03 (s, 1H).

The authors are grateful to Dr. Masatoshi Hirayama for the NMR measurements and to the Sankyo Co., Ltd., for the mass measurements.

References

1) M. Bush, *Ber.*, **27**, 2897 (1894).
2) T. S. Sulkowski and S. J. Childress, *J. Med. Chem.*, **7**, 386 (1964).
3) T. S. Sulkowski and S. J. Childress, U. S. 3176008 (1965); *Chem. Abstr.*, **62**, 16284b (1965).
4) S. Toyoshima, T. Morishita, and T. Nakamura, Japan 7011147 (1970); *Chem. Abstr.*, **73**, 25545b (1970).
5) T. Ishiwaka, M. Sano, K. Isagawa, and Y. Fushizaki, This Bulletin, **43**, 135 (1970).
6) O. Hromatka, F. Krenmüller, and M. Knollmüller, *Monat. Chem.*, **100**, 934 (1969).
7) A. L. Langis and M. P. Charest, *Chim. Ther.*, **2**, 349 (1967).
8) O. Hromatka, M. Knollmüller, and F. Krenmüller, *Monat. Chem.*, **100**, 941 (1969).
9) A. L. Langis, U. S. 3542767 (1970); *Chem. Abstr.*, **74**, 88089x (1971).
10) D. M. Bailey, U. S. 3607866 (1971); *Chem. Abstr.*, **75**, 140910v (1971).
11) M. Takahashi, S. Shirahashi, and N. Sugawara, *Nippon Kagaku Kaishi*, **1973**, 1519.
12) R. P. Staiger and E. C. Wagner, *J. Org. Chem.*, **18**, 1427 (1953).
13) F. H. Case, *ibid.*, **30**, 931 (1965).
14) J. H. Boyer, "Heterocyclic Compound," Vol. 7, ed. by R. C. Elderfield, John Wiley & Sons, Inc., New York (1961), p. 525.

The Synthesis and Oxidation of 4-(*N*-Arylmethylideneamino)-2,6-di-*t*-butylphenols

Eiichiro MANDA

National Chemical Laboratory for Industry, Honmachi, Shibuya-ku, Tokyo 151

(Received May 20, 1974)

4-(*N*-Arylmethylideneamino)-2,6-di-*t*-butylphenols (I) were synthesized through the condensation of 4-amino-2,6-di-*t*-butylphenol hydrochloride and arylaldehydes, and the infrared and electronic spectra of phenols (I) were discussed. The oxidation of phenol (I) with lead dioxide gave a stable phenoxyl radical (II) in solution, and 4,4′-bis[4-(*N*-arylmethylideneamino)-2,6-di-*t*-butyl-2,5-cyclohexadien-1-one] (III) was isolated as a crystalline oxadation product, which was in equilibrium with the radical (II) in solution.

A number of stable 2,6-di-*t*-butylphenoxyl radicals are known to be derived from 2,6-di-*t*-butylphenol derivatives.[1,2] As for 2,6-di-*t*-butylphenoxyl radicals with a double bond at the 4-position of the phenoxyl ring, a few reports have been published on derivatives with –CH=CH–Ar,[3,4] –N=N–Ar,[5] and –CH=N–Ar[6] groups. The synthesis, properties and oxidation of 4-(*N*-arylmethylideneamino)-2,6-di-*t*-butylphenol (I), which is a novel Schiff base in 2,6-di-*t*-butylphenol derivatives, were studied, and the results will be reported in this paper.

Results and Discussion

Schiff bases are generally synthesized through the condensation of amines and aldehydes in ethanol at room temperature,[7] and the maximum yield is attained at the pH range of the reaction mixture of 6—8.[8] Thus, phenols (I) have been prepared through the condensation of arylaldehydes and 4-amino-2,6-di-*t*-butylphenol hydrochloride in the presence of pyridine, since the free aminophenol is quite an unstable compound. Condensation proceeded very easily, and crystals of phenols (I) precipitated from the reaction mixture in a few minutes. The yields of phenols (I) are given in Table 1. Considerable amounts of red-brown, tarry compounds were obtained as by-products, and they might have originated from the oxidation of 4-amino-2,6-di-*t*-butylphenol hydrochloride. In the absence of pyridine, a methoxy derivative of phenol (I) (19%) was obtained after letting the reaction mixture stand for one hour at room temperature, but no other phenols (I) were obtained even after a long period of condensation. This was caused by a decrease in the pH value of the reaction mixture.

TABLE 1. SYNTHESES OF PHENOL (I)

R	Aryl-aldehyde (mol/ EtOH, ml)	4-Amino-2, 6-di-*t*-butyl-phenol·HCl (mol/ EtOH, ml)	Pyri-dine (mol)	Reac-tion time (hr)	Yield (%)
NO_2	0.021/30	0.021/ 5	0.021	1	50
			—	24	—
COOMe	0.012/20	0.012/ 3	0.012	1	53
			—	24	—
Cl	0.021/ 7	0.021/ 5	0.021	1	61
			—	24	—
Unsubst.	0.021/—	0.021/15	0.021	1	43
			—	24	—
MeO	0.021/—	0.021/10	0.021	1	38
			—	1	19

TABLE 2. INFRARED SPECTRA OF PHENOL (I)

R	ν_{OH} (cm^{-1}) free	ν_{OH} (cm^{-1}) assoc.	$\nu_{C=N}$ (cm^{-1})	Medium
NO_2	3630m	3430m	1620w	KBr
	3630s	—	1625w	CCl_4
COOMe	3630m	3410m	1620m	KBr
	3630s	—	1625m	CCl_4
Cl	3630m	3400w	1620m	KBr
	3630s	—	1625m	CCl_4
Unsubst.	3630vw	3150m	1610m	KBr
	3630s	—	1625m	CCl_4
MeO	3630vw	3230m	1615m	KBr
	3630s	—	1625m	CCl_4

ν, stretching; s, strong; m, medium; w, weak; vw, very weak

The infrared spectra of a carbon tetrachloride solution and a KBr disk of phenol (I) were measured, and the results are given in Table 2. The characteristic ν_{OH} bands were observed at 3630—3150 cm^{-1}, and the $\nu_{C=N}$ bands at 1625—1610 cm^{-1}. The strong band of a free OH group was observed at 3630 cm^{-1} for the carbon tetrachloride solution of each phenol (I). In the solid state, however, the intensity of these bands changed to medium for nitro, methoxycarbonyl and chloro derivatives, and to very weak for unsubstituted and methoxy derivative of phenol (I). Correspondingly, broad bands of associating OH groups appeared at 3410—3150 cm^{-1} for phenols (I), and the intensity of the bands of the unsubstituted and methoxy derivative was stronger than the others. The location of $\nu_{C=N}$ bands tended to shift to lower wave numbers in the solid state than in solution. These observations suggest that, in the solid state, phenols (I) are associating as shown below and the bond orders of OH and C=N bonding become lower than in solution. The location of $\nu_{C=N}$ bands of phenols (I) in solution was almost constantly at 1625 cm^{-1}, and no substituent effect was

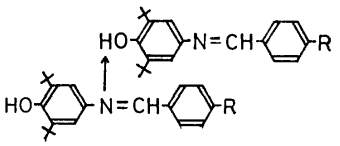

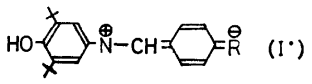

observed. This can be explained by the minor participation of a resonance structure (I') since the electron-attracting power of the sp^2 nitrogen atom compensates that of an electron-attracting substituent. The location of ν_{OH} bands of phenols (I) in solution was at 3630 cm^{-1} and was also independent of the substituents. This may be due to the above resonance effect and to the twisting of the bonding between a nitrogen atom and a phenol ring.[9]

Table 3. Electronic spectra of phenol (I) in *n*-hexane

R	λ_{max}, nm ($\varepsilon \times 10^{-4}$)		
NO_2	262.5(1.73)	303(0.85)	383(1.58)
COOMe	260 (2.02)	282(1.39)	360(1.43)
Cl	253.5(1.83)	274(1.43)	347(1.29)
Unsubst.	252.5(1.04)	271(1.09)	342(1.06)
MeO	251.5(1.04)	281(2.06)	338(1.54)

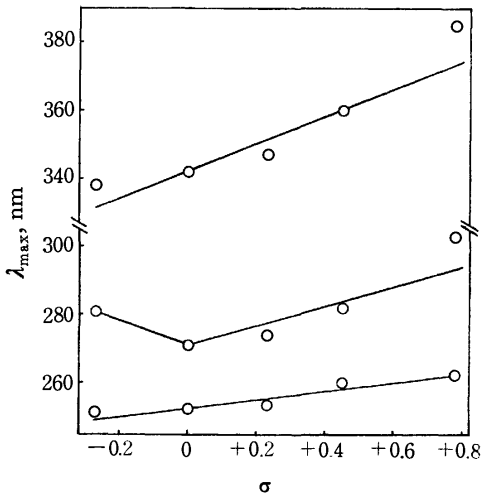

Fig. 1. The correlation of Hammett substitution constants with the wavelength of the absorption maxima of phenols (I)

The electronic spectra of phenols (I) in *n*-hexane were measured and the results are shown in Table 3. Each derivative of phenols (I) has three absorption bands near at 350, 290, and 250 nm, and these bands are similar to those of benzalanilines.[10] Figure 1 gives the correlation of the Hammett substituents (σ)[11] and the wavelength of each absorption maximum. A simple bathochromic effect of the electron-attracting group is observed in the absorption bands at 250 and 350 nm, whereas the same effect is caused by both electron-attracting and electron-releasing group in the bands at 280 nm. These bands may be assigned to result from a charge transfer from the phenol ring to the –N=CH– bonding, from electronic transition throughout the whole π-electron system, and from local excitation without charge transfer.[10]

Phenols (I) in tetrahydrofuran were oxidized with excess amounts of lead dioxide at room temperature

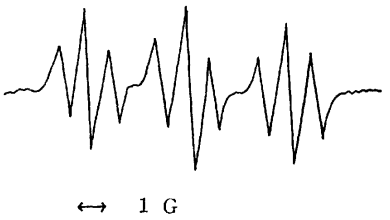

Fig. 2. ESR spectrum of radical (II, R=NO_2)

under nitrogen atmosphere. The color of each reaction mixture turned from yellow to red-brown or yellow-green. The ESR measurement of the reaction mixture of each phenol (I) showed the presence of a stable radical, and the spectrum was considered to be made up of a triplet (with an equal intensity) of triplet (with intensity ratio of 1: 2: 1) (Fig. 2). The observed ESR signals may be assigned to the phenoxyl radical (II), since an odd electron on a nitrogen atom gave a triplet signal (with an equal intensity), and then each peak of this triplet was further split to a triplet (with intensity ratio of 1: 2: 1) by two equivalent *m*-ring protons. The observed ESR hyperfine splitting (Hfs) constants of the radicals (II) are given in Table 4.

Table 4. ESR coupling constants of radicals (II)

R	a_{m-H} (gauss)	a_N
NO_2	1.1	3.4
COOMe	1.2	4.2
Cl	1.0	3.9
Unsubst.	1.0	3.8
MeO	1.1	4.8

The small Hfs value of the nitrogen atom is due to the small spin density on the nitrogen atom, which may be caused by the twisting of the bonding between the nitrogen atom and the phenol ring.[9] The absence of hyperfine splitting by a proton of the methine group may be due to the very small spin density on the methine group. This suggests the very small participation of allylic resonance in the radical (II) which was reported with radical (IV).[3] The Hfs value of the *m*-ring

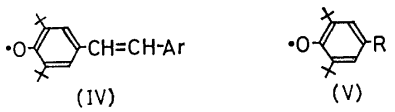

(IV) (V)

proton is independent of the substituents in the radical (II), though a substituent effect was reported with phenoxyl radicals (V).[12] This may be explained by a non-planarity which has been previously been described and by the remoteness of the substituents from the *m*-ring protons.

Yellow crystalline oxidation products were isolated from the reaction mixture of nitro, methoxycarbonyl and chloro derivatives of phenol (I), but unsubstituted and methoxy derivatives gave a tarry material. These crystalline oxidation products of the above three phenol derivatives were not so stable at room temperature and decomposed at their melting points. The results of the isolated crystalline oxidation products are shown in Tables 5 and 6. The results of the elementary analyses

Table 5. Synthesis of cyclohexadienone (III)

R	React. time (min)	Yield (%)	Mp (°C)	Anal. (%) Found (Calcd)				MW.		
				C	H	N	Cl	Found VPO	Found MS	Calcd
N_2O	45	24	152—154	70.69	7.07	7.69	—	692	777	706.9
				(71.36	7.13	7.93	—)			
COOMe	60	16	162—164	74.93	7.73	3.66	—	554	788	732.9
				(75.38	7.70	3.82	—)			
Cl	30	15	119—121	73.10	7.36	4.01	10.52	559	766	685.7
				(73.56	7.35	4.09	10.34)			

Table 6. Spectral data of cyclohexadienone (III)

R	Infrared spectra cm^{-1}, KBr	Electronic spectra λ_{max} nm, ($\varepsilon \times 10^{-4}$)
NO_2	3030, 2950(ν_{CH}), 1650 ($\nu_{C=O}$), 1630 ($\nu_{C=C}$), 1620sh ($\nu_{C=N}$), 1605 (phenyl), 1520, 1345 (ν_{NO_2}), 1245 (*t*-butyl), 820 (δ_{CH})	286 (6.8) 403 (0.2)
COOMe	3030, 2950 (ν_{CH}), 1720, 1650 ($\nu_{C=O}$), 1630 ($\nu_{C=C}$), 1620sh ($\nu_{C=N}$), 1600 (phenyl), 1275 (ν_{C-O}), 1250 (*t*-butyl), 1115 (ν_{C-O}), 820 (δ_{CH})	285 (5.4) 395 (0.8)
Cl	3030, 2950 (ν_{CH}), 1650 ($\nu_{C=O}$), 1630 ($\nu_{C=C}$), 1620sh ($_{C=N}$), 1595 (phenyl), 1245 (*t*-butyl), 820 (δ_{CH})	285 (4.1) 397 (0.6)

ν, stretching; δ, bending; sh, shoulder. Electronic spectra were taken for cyclohexane solution of 2.0×10^{-5} M.

(Table 5) were in good agreement with the calculated values for a dimer of the radical (II). The absence of the ν_{OH} band (3630 cm^{-1}) and the appearance of the $\nu_{C=O}$ band (1650 cm^{-1}) and the $\nu_{C=C}$ band (1630 cm^{-1}) in their infrared spectra (Table 6) suggest that these oxidation products have the 2,5-cyclohexadienone structure.[13] The chemical structure of the dimer of the radical (II) depends on the way of the recombination reaction of the radical (II), *e.g.*, oxygen-carbon coupling, *etc.* The most probable recombination reaction is coupling at the 4-carbon atom of the phenol ring, since oxygen-oxygen coupling is not known with 2,6-di-*t*-butylphenoxyl radicals,[1,2] and since the spin density at the 4-carbon atom is known to be relatively high,[2] whereas ESR measurement showed quite a low spin density on the methine group of the radical (II). Therefore, each isolated oxidation product is 4,4'-bis-[4-(*N*-arylmethylideneamino)-2,6-di-*t*-butyl-2,5-cyclohexadien-1-one] (III). The mass spectrum of each oxidation product showed not only a weak molecular ion peak of cyclohexadienone (III), but also a weak peak of a larger mass number than the above molecular ion peak (Table 5). These unexpected peaks might arise from the formation of some compound in the ion-chamber of a mass spectrometer through the thermolysis and recombination of samples. The mass number of these peaks suggests that the molecular formula of the generating compound is $C_{43}H_{61}N_2O_3Ar$ (Ar=$C_6H_4NO_2$, $C_6H_4COOCH_3$, and C_6H_4Cl, respectively), since the difference in the unexpected mass number of each sample was equal to that in the molecular weight of the corresponding substituents, thus indicating the existence of one aryl group in each generating compound. The molecular weight measurement of oxidation products in benzene by a vapor pressure osmometer gave smaller values than the values calculated for cyclohexadienone (III) (Table 5). The sample solution for molecular weight measurement showed the same ESR spectra as those observed in the

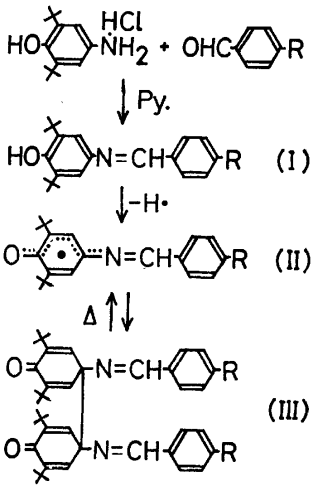

Fig. 3. Reaction path. (I), (II): R=NO_2, COOMe, Cl, H, MeO (III): R=NO_2, COOMe, Cl

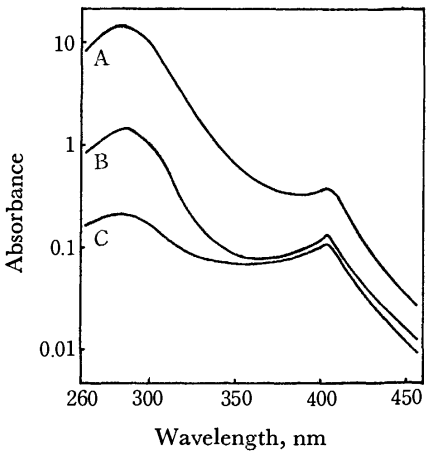

Fig. 4. Electronic spectra of cyclohexadienone (III, R=NO_2) in cyclohexane.
A: 2.0×10^{-5} M, B: 2.0×10^{-6} M, C: 2.0×10^{-7} M

oxidation of phenols (I). The intensity of these ESR signals increased with the rise of temperature, and *vice versa*, and the ESR signals faded gradually at high temperature. These results show the dissociation of cyclohexadienones (III) to radicals (II) in solution, and those radicals then decompose to some other compounds at high temperature. The color of a benzene solution of cyclohexadienone (III) changed from yellow to green with the rise of temperature and returned to yellow upon a lowering of temperature. This color changing can be explained by the above dissociation. The electronic spectra of cyclohexadienones (III) at room temperature showed strong absorption bands near 285 nm and very weak bands near 400 nm (Table 6). The latter bands are due to radicals (II), since the dilution of the sample solution increased the relative intensity of these bands (Fig. 4).

Experimental

4-Amino-2,6-di-t-butylphenol Hydrochloride. 4-Nitroso-2,6-di-*t*-butylphenol[14] (14.1 g, 0.06 mol) and zinc powder (9.8 g, 0.15 mol) were suspended in methanol (180 ml). Hydrochloric acid (35 ml, *ca.* 0.35 mol) was added drop by drop to this suspension over 45 min under refluxing, which was then continued for 30 min after the addition of hydrochloric acid. Then the excess zinc powder was filtered from the reaction mixture, and the solvent (*ca.* 140 ml) was distilled from the filtrate. The concentrate was poured onto cold, degassed water, and the precipitating product was filtered and washed with cold, degassed water and then with cold *n*-hexane. The above isolating process was carried out under a nitrogen atmosphere. The subsequent drying of the product under reduced pressure gave a white powder of crude 4-amino-2,6-di-*t*-butylphenol hydrochloride (13.0 g, 84%, mp 195—203 °C (dec.) (lit,[15] 201—204 °C)), which was used for the preparation of phenols (I) without further purification.

4-(N-Arylmethylideneamino)-2,6-di-t-butylphenols (I). Arylaldehyde in ethanol and pyridine were added to an ethanol solution of 4-amino-2,6-di-*t*-butylphenol hydrochloride, after which the reaction mixture was allowed to stand for 1 hr at room temperature. The precipitating phenol (I) was filtered and washed successively with cold methanol, water and *n*-hexane. Each crude powder of phenol (I) was recrystallized from *n*-hexane. The follwing melting points were observed for each crystal of phenol (I): R=NO_2: yellow-orange needles, 169.0—170.0 °C; R=COOMe: yellow needles, 158.0—160.0 °C; R=Cl: pale yellow needles, 144.0—145.0 °C; Unsubstituted: yellow-orange needles, 151.0—152.0 °C; R=MeO: pale yellow plates, 155.0—157.0 °C. The results of elementary analyses and the molecular weight determination (MS) for prepared phenols (I) were in good agreement with the calculated values.

4,4'-Bis[4-(N-arylmethylideneamino)-2,6-di-t-butyl-2,5-cyclohexadien-1-one] (III). Phenol (I) (2×10^{-4} mol) in dried tetrahydrofuran (20 ml) was put in a Schlenk tube, and lead dioxide (0.09 g, 4×10^{-4} mol) was added to this solution. The reaction mixture was degassed by freezing with liquid nitrogen and brought to room temperature under a nitrogen atmosphere. Oxidation was carried out by shaking the reaction mixture at room temperature for the period shown in Table 5. Then lead oxide was filtered off from the reaction mixture, and the filtrate was evaporated to dryness under reduced pressure. The residual compound was dissolved in degassed cyclohexane (*n*-hexane for the chloro derivative) at room temperature, and the subsequent suitable concentration of this solution under reduced pressure gave yellow crystalline cyclohexadienone (III).

All the melting points were uncorrected. The molecular weight of cyclohexadienone (III) was determined for a benzene solution (0.007 M) at 37 °C with a Mechrolab 302 vapor pressure osmometer. The infrared spectra were recorded with a Shimadzu IR-27G grating spectrophotometer, the electronic spectra, with a Hitachi EPS-2U recording spectrometer, and the ESR spectra, with a Hitachi 771 electron spin resonance spectrometer equipped with a variable temperature accessory.

The author is indebted to Mr. Wasada for measuring the mass spectra.

References

1) E. A. Altwicker, *Chem. Rev.*, **67**, 475 (1967).
2) L. M. Strigun, L. S. Vartanyan, and N. M. Emenuel, *Russ. Chem. Rev.*, **37**, 421 (1968).
3) E. Müller, R. Mayer, H. D. Spanagel, and K. Scheffler, *Ann. Chem.*, **645**, 53 (1961).
4) H. D. Becker, *J. Org. Chem.*, **34**, 121 (1969).
5) E. Manda, This Bulletin, **46**, 2160 (1973).
6) L. G. Blavin, M. S. Postnikova, A. N. Prokof'ev, and V. A. Shabalkin, *Izv. Akad. Nauk SSSR, Ser. Khim.*, **1966**, 408.
7) M. M. Sprung, *Chem. Rev.*, **26**, 297 (1940).
8) C. A. Haley and P. Maitland, *J. Chem. Soc.*, **1951**, 3155.
9) P. Brockhurst, *Tetrahedron*, **18**, 299 (1962).
10) V. I. Minkin, Yu. A. Zhadanov, E. A. Medyantzeva, and Yu. A. Ostroumov, *Tetrahedron*, **23**, 3651 (1967).
11) D. H. McDaniel and H. C. Brown, *J. Org. Chem.*, **23**, 420 (1958).
12) A. L. Buchachenko, "Stable Radicals," Consultants Bureau, New York, N. Y. (1963), p. 66.
13) N. P. Neureiter, *J. Org. Chem.*, **28**, 3486 (1963).
14) M. S. Kharasch and B. S. Joshi, *ibid.*, **27**, 651 (1962).
15) A. Rieker, K. Scheffler, R. Mayer, B. Narr, and E. Müller, *Ann. Chem.*, **693**, 10 (1966).

Fragmentations in Doubly Charged Ion Mass Spectra of Aromatic Carbonyl Compounds

Hiroshi SAKURAI, Akira TATEMATSU, and Hisao NAKATA*

Faculty of Pharmacy, Meijo University, Showa-ku, Nagoya 468

**Department of Chemistry, Aichi Kyoiku University, Kariya, Aichi 448*

(Received June 21, 1974)

2E Doubly charged ion mass spectra of forty-six aromatic carbonyl compounds were determined. The spectra are quite different from those of singly charged ions. Several characteristic fragmentations including a novel [M−CO] peak are discussed. It is suggested that certain isomer pairs can be differentiated by comparing these spectra even when their conventional spectra are almost identical.

In a recent communication,[1] we have reported a novel rearrangement reaction in 2E doubly charged ion mass spectra[2] of acetophenone derivatives. A driving force for the reaction has also been briefly discussed. As an extension of this work, various aromatic carbonyl compounds were examined by the same technique[3] to elucidate any possible structural correlation in fragmentations, and to illustrate the potential usefulness of this spectra for the structural identification purposes.

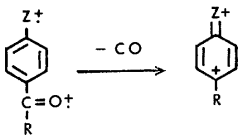

Z = NH_2, OH, OCH_3 or Cl

R = H, CH_3, OH, NH_2 or OCH_3

Scheme 1.

Results and Discussion

The $[M-28]^{2+}$ Peaks. The doubly charged ion mass spectra of forty-six aromatic carbonyl compounds are summarized in Table 1 and Figs. 1 and 2. The characteristic [M−28] peak[1] was observed in most of the *p*-substituted compounds and in some of the *m*-substituted ones.

In order to determine the elemental compositions of the ion, the accurate masses were measured at half mass units of the peak in the conventional spectrum. The results were shown in Table 2. For the six compounds examined, the compositions of the [M−28] peak were unambiguously established as [M−CO]. These results indicate that the [M−28] peak has been produced, as previously suggested,[1] by the fragmentation reaction accompanying a rearrangement that involves a carbonyl side chain.

As is seen from Table 1, the carbonyl compounds whose spectra exhibited the intense [M−CO] peaks have electron-donating substituents such as an amino, a hydroxyl, or a methoxyl group. On the contrary, the spectra of *p*-tolualdehyde (**42**), *p*-methylacetophenone (**43**), and *p*-toluic acid (**44**) did not show the corresponding peak. On the other hand, when an electron-withdrawing, but lone pair electron-containing chlorine atom was introduced, the [M−CO] peak appeared as in the case of *p*-chlorobenzoic acid (**20**) or *p*-chlorobenzamide (**21**). These results suggest that the conjugative stabilization due to the lone pair electrons of the substituents in the product ion plays an important role in this fragmentation reaction [Scheme 1].

The intensity of the [M−CO] peak varies with the substituents. Because the molecular ion peaks were absent in most of the spectra, the height of the commonly observed peak at 62 mass units ($C_5H_2^{2+}$ ion)[3] was taken as an internal standard for intensity correlations. It is evident from Table 3 that the intensities of the [M−CO] peak in *p*-substituted compounds are in the decreasing order of NH_2>OH>OCH_3. This is the same order as Hammett's substituent constants,[4] and these findings confirm the significance of the product ion stabilities in this fragmentation reaction. The methoxyl group seems to be not very effective to stabilize the [M−CO] ion. This is also evidenced from the fact that for *meta* substituted compounds the [M−CO] peak appeared only from benzoic acids and benzamides that have an amino, a hydroxyl, or a chloro substituent.

The nature of the carbonyl group also affects these intensity ratios. For the series of compounds with the same substituent, the ratios are in the following decreasing order: aldehydes>methyl ketones>carboxylic acids>acid amides>methyl esters.

Although the spectra of methyl esters of *p*-amino, *p*-hydroxy, and *p*-methoxybenzoic acids (**12—14**) showed the [M−CO] peak, the corresponding ethyl esters (**15—17**) did not afford this peak. In order to compare the behavior of ester alkyl groups, the conventional mass spectrum of ethyl methyl phthalate was measured. It was found that [M−OC_2H_5] peak was much stronger than [M−OCH_3] peak, and therefore, ethoxyl group appeared to be much better leaving group. If we assume that the elimination reactions of CO and of alkoxyl group from the molecular ion are competitive in the doubly charged ion mass spectrum, the absence of the [M−CO] peak in ethyl benzoates seems to be explicable because a simple cleavage reaction with elimination of the ethoxyl group could be much faster than the elimination of CO, when compared to the case of methyl benzoates. In fact, the [M−OC_2H_5] peak was very prominent in these ethyl esters (**15, 16**).

TABLE 1. 2E DOUBLY CHARGED ION MASS SPECTRA OF AROMATIC CARBONYL COMPOUNDS (RELATIVE INTENSITIES IN PARENTHESES)[a]

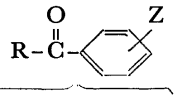

Compd.	R	Z	[M−CO]	[M−R]	[M−R−CO]	[M−R−CO−H]	[M−18]	$[C_nH_2]$ $(n=1,2,\cdots)$	Other fragment ions
(2)	H	*p*-OCH_3	108 (100)					62, 74 (49) (14)	63, 75, 76 (12) (8) (13)
(3)	CH_3	*p*-NH_2	107 (100)	120 (74)	92 (39)	91 (16)	117 (9)		89, 104, 105, 106, 108, 121 (11) (5) (18) (8) (9) (7)
(4)	CH_3	*p*-OH	108 (36)	121 (100)	93 (10)	92 (33)	118 (5)	62, 86 (14) (16)	63, 64, 90, 105, 106, 120, 122 (12) (5) (5) (5) (5) (7) (9)
(5)[b]	CH_3	*p*-OCH_3	122 (74)	135 (22)				62, 74, 86 (100) (29) (29)	63, 64, 75, 76, 77, 78, 87, 92, 123 (38) (16) (17) (48) (5) (13) (5) (7) (7)
(6)	OH	*p*-NH_2	109 (36)		92 (19)	91 (22)		62 (5)	89, 93, 94, 120 (17) (100) (7) (6)
(7)	OH	*p*-OH	110 (100)	121 (24)		92 (18)		62, 74 (63) (19)	63, 64, 75, 94, 111 (20) (7) (7) (41) (8)
(8)	OH	*p*-OCH_3	124 (46)	135 (19)	109 (5)			62, 74 (100) (31)	63, 64, 75, 76, 78, 92, 104 (34) (13) (16) (22) (7) (14) (5)
(9)	NH_2	*p*-NH_2	108 (94)	120 (40)	92 (74)	91 (23)	118 (100)	62, 74 (21) (14)	63, 65, 76, 87, 88, 89, 90, 109, 119 (6) (10) (5) (5) (5) (25) (6) (10) (13)
(10)	NH_2	*p*-OH	109 (17)	121 (10)		92 (6)	119 (100)	62, 74 (13) (5)	63, 89, 91, 94, 120 (9) (8) (7) (8) (10)
(11)	NH_2	*p*-OCH_3	123 (28)	135 (12)		106 (7)		62, 74 (100) (38)	63, 64, 75, 76, 77, 78, 80, 89, 91, 92, 100, 104 (44)(18)(18)(44) (7)(19) (8) (8) (7)(16) (5) (13)
(12)	OCH_3	*p*-NH_2	123 (16)	120 (29)	92 (100)	91 (32)		62 (8)	65, 88, 89, 90, 93 (6) (5) (28) (7) (15)
(13)	OCH_3	*p*-OH	124 (63)	121 (65)	93 (15)	92 (62)	134 (18)	62, 74 (100) (17)	63, 64, 65, 75, 76, 90, 94, 122, 152 (33) (18) (11) (9) (6) (5) (6) (6) (5)
(14)	OCH_3	*p*-OCH_3	138 (43)	135 (7)				62, 74 (100) (23)	63, 64, 75, 76, 77, 78, 92, 104 (37) (20) (12) (38) (6) (24) (10) (8)
(15)	OC_2H_5	*p*-NH_2		120 (100)	92 (68)	91 (19)			89, 93, 121 (9) (7) (10)
(16)	OC_2H_5	*p*-OH		121 (100)	93 (18)	92 (86)		62, 74 (62) (23)	63, 64, 65, 75, 90, 91, 94, 110, 120, 122, 130, 132 (23)(26)(14) (5) (6) (5)(10) (5) (8) (9) (14) (14)
(17)	OC_2H_5	*p*-OCH_3						62, 74 (100) (14)	61, 63, 64, 65, 75, 76, 78, 92 (21) (57) (20) (8) (6) (26) (29) (8)
(19)	CH_3	*p*-Cl	126 (6)	139 (100) 141 (36)	111 (88) 113 (32)	110 (7)		74, 86, 98 (24) (49) (20)	75, 76, 85, 87, 88, 89, 90, 99, 102, 104, 112 (68)(50) (5)(11)(11)(38)(38) (5) (10) (8) (12) 125, 140 (12) (12)
(20)	OH	*p*-Cl	128 (100) 130 (43)	139 (44) 141 (17)	111 (46) 113 (20)	110 (8)		74 (26)	73, 75, 76, 92, 102, 104, 108, 112, 129, 140 (6)(36)(17) (6) (5) (5) (5) (7) (11) (6)
(21)	NH_2	*p*-Cl	127 (100) 129 (35)	139 (12)	111 (26) 113 (9)	110 (6)	137 (6)	74 (31)	75, 76, 91, 100, 101, 128 (48) (32) (22) (6) (6) (9)
(22)	OCH_3	*p*-Cl	142 (9)	139 (14) 141 (6)	111 (42) 113 (11)	110 (9)		62, 74 (5) (68)	75, 76, 112, 134 (100) (50) (6) (28)
(24)	H	*m*-OCH_3						62, 74, 86 (100) (38) (11)	63, 64, 75, 76, 78, 136 (28) (9) (14) (21) (11) (7)
(25)	CH_3	*m*-NH_2		120 (8)	92 (100)	91 (35)		74, 86 (6) (7)	77, 80, 89, 90, 93 (5) (11) (20) (5) (12)

Table 1 (Continued)

Compd.	R	Z	[M−CO]	[M−R]	[M−R−CO]	[M−R−CO−H]	[M−18]	$[C_nH_2]$ $(n=1,2,\cdots)$	Other fragment ions
(**26**)	CH_3	*m*-OH		121 (87)	93 (24)	92 (100)	118 (8)	62, 74, 86 (67) (26) (42)	63, 64, 65, 75, 76, 77, 78, 79, 85, 87, 89, 90 (25)(23)(28)(23) (8) (6) (9)(17) (5)(10) (8)(12) 98, 99, 107, 120, 122 (13) (6) (13) (7) (8)
(**27**)	CH_3	*m*-OCH_3		135 (30)				62, 74, 86 (100) (31) (51)	63, 64, 75, 76, 77, 78, 85, 87, 88, 89, 90, 91, 92, (35)(17)(22)(52)(12)(63) (5)(10) (5) (5)(14) (5)(12) 98, 102, 104 (8) (6) (8)
(**28**)	OH	*m*-NH_2	109 (60)	120 (13)	92 (100)	91 (28)		62, 74 (46) (25)	63, 64, 65, 75, 76, 81, 87, 88, 89, 90, 93 (10) (6) (6) (7) (7) (7) (6)(15)(47)(13)(23)
(**29**)	OH	*m*-OH	110 (25)			92 (12)		62, 74 (100) (12)	63, 64, 65 (30) (16) (9)
(**30**)	OH	*m*-OCH_3		135 (10)				62, 74 (100) (25)	63, 64, 75, 76, 78, 92 (31) (11) (12) (14) (9) (6)
(**31**)	NH_2	*m*-NH_2	108 (8)		92 (14)	91 (11)	118 (100)	62 (6)	89, 119 (10) (12)
(**32**)	NH_2	*m*-OH	109 (9)	121 (7)	93 (6)	92 (16)	119 (100)	62, 74 (85) (17)	63, 64, 65, 87, 88, 89, 91, 100, 110, 120 (39)(19)(14)(10) (8)(13)(26) (6) (6) (7)
(**33**)	NH_2	*m*-OCH_3		135 (24)		106 (6)		62, 74 (100) (44)	63, 64, 73, 75, 76, 77, 78, 79, 80, 88, 89, 91 (41)(12) (5)(15)(42) (9)(25) (5)(11) (5) (9) (5) 92, 100 (13) (7)
(**34**)	OCH_3	*m*-NH_2		120 (40)	92 (100)	91 (29)			88, 89, 93 (5) (15) (15)
(**35**)	OCH_3	*m*-OH				92 (8)		62, 74 (100) (8)	61, 63, 64, 65, 75 (9) (40) (18) (12) (5)
(**36**)	OCH_3	*m*-OCH_3		135 (16)				62, 74 (100) (20)	61, 63, 64, 75, 76, 78, 92 (10) (47) (18) (9) (27) (22) (9)
(**38**)	CH_3	*m*-Cl		139 (75) 141 (14)	111 (100) 113 (27)	110 (5)		74, 86 (22) (51)	75, 76, 87, 88, 89, 90, 98, 102, 104, 112, 125 (100)(59)(14)(14)(47) (6)(24) (13) (5) (6) (6)
(**39**)	OH	*m*-Cl	128 (80) 130 (21)	139 (40) 141 (11)	111 (75) 113 (24)	110 (15)		74 (70)	73, 75, 76, 77, 92, 101, 102, 108, 109, 112 (11)(100)(56) (7)(20) (5) (9) (7) (5) (11) 120, 129 (17) (6)
(**40**)	NH_2	*m*-Cl	127 (78) 129 (25)	139 (24) 141 (7)	111 (78) 113 (25)	110 (11)	137 (9)	74 (70)	73, 75, 76, 77, 89, 91, 92, 100, 101, 102, 103, (7)(100)(70) (5)(11)(57) (6) (20) (15) (6) (7) 104, 108, 112, 119, 120, 128 (6) (6) (10) (5) (5) (5)
(**41**)	OCH_3	*m*-Cl			111 (17)			74 (60)	73, 75, 76, 134 (5)(100) (49) (17)
(**42**)	H	*p*-CH_3		119 (6)	91 (59)	90 (93)		62, 74, 86 (7) (5)(100)	85, 87, 88, 89, 98, 118 (5) (17) (16) (26) (8) (44)
(**43**)	CH_3	*p*-CH_3		119 (8)	91 (100)	90 (18)		86 (19)	87, 89, 92, 102, 104, 118, 132 (5) (11) (6) (22) (7) (9) (6)
(**44**)	OH	*p*-CH_3	108 (6)	119 (16)	91 (92)	90 (100)	118 (62)	62, 86 (6) (88)	85, 87, 88, 89, 92 (5) (30) (35) (41) (12)
(**45**)	CH_3	*m*-CH_3		119 (25)	91 (100)	90 (34)		86 (20)	87, 88, 89, 92, 102, 103, 115, 118 (5) (5) (20) (9) (25) (5) (5) (31)
(**46**)	OH	*m*-CH_3		119 (18)	91 (85)	90 (72)	118 (41)	62, 74, 86 (5) (5)(100)	85, 87, 88, 89, 92 (8) (27) (29) (36) (11)

a) Spectra of compounds **1**, **18**, **23**, and **37** are shown in Figs. 1 and 2. b) Due to the operating conditions of the mass spectrometer, relative intensities of this compound is differeent from those previously reported.[1)]

TABLE 2. OBSERVED AND CALCULATED MASSES OF $[M-28]^{2+}$ PEAKS IN amu.

Compound	Obsd. masses of the peak	Calcd. for $[M-CO]^{2+}$
p-Anisaldehyde (**2**) ($C_8H_8O_2$)	54.0281	54.0288 $[C_7H_8O]^{2+}$
p-Aminoacetophenone (**3**) (C_8H_9NO)	53.5358	53.5367 $[C_7H_9N]^{2+}$
p-Methoxyacetophenone (**5**) ($C_9H_{10}O_2$)	61.0362	61.0366 $[C_8H_{10}O]^{2+}$
p-Aminobenzoic acid (**6**) ($C_7H_7NO_2$)	54.5256	54.5264 $[C_6H_7NO]^{2+}$
Methyl *p*-aminobenzoate (**12**) ($C_8H_9NO_2$)	61.5352	61.5342 $[C_7H_9NO]^{2+}$
Methyl *p*-hydroxybenzoate (**13**) ($C_8H_8O_3$)	62.0260	62.0262 $[C_7H_8O_2]^{2+}$

TABLE 3. THE PEAK INTENSITY RATIOS OF $[M-CO]^{2+}/[62]^{2+}$

	p-NH_2	*p*-OH	*p*-OCH_3
Ar-CHO	—	2.7	2.0
Ar-$COCH_3$	*ca.* 200	2.6	0.7
Ar-COOH	7.3	1.6	0.5
Ar-$CONH_2$	4.5	1.3	0.3
Ar-$COOCH_3$	2.0	0.6	0.4

Other Characteristic Fragment Ion Peaks. Fragment peaks at 62 and 74 mass units were commonly observed. These ions are expected to have the compositions of C_5H_2 and C_6H_2, respectively, and would probably be the same ions as appeared in aromatic hydrocarbons.[3] Particularly for compounds with a hydroxyl or a methoxyl group at *para* or *meta* positions, the 62 peak was very strong and often accompanied by intense peaks at 63 and 64 mass units, whereas these peaks were relatively weak in amino, methyl, or chloro derivatives. On the other hand, a group of intense peaks at 74, 75, and 76 mass units was observed in *p*- or *m*-methoxy and chloro compounds.

A peak at 86 mass units was observed in all acetophenones except for *p*-amino compound, and in methyl substituted benzaldehydes and benzoic acids. This ion would be also a hydrocarbon fragment of C_7H_2.[3] These compounds also exhibited moderately intense peaks at 87, 88, 89, and in some cases at 90 mass units.

The [M—R] peak, resulting from a simple α-cleavage of the carbonyl group, was observed for most of the compounds. Expulsion of carbon monoxide from this ion afforded the [M—R—CO] peak as in ordinary spectra. However, methoxy compounds did not show this [M—R—CO] peak in any appreciable amount. It is of interest that for hydroxy compounds the corresponding peak appeared at 92 mass units rather than at 93. The composition of this 92 ion from methyl *p*-hydroxybenzoate (**13**) was established as C_6H_4O ([M—R—CO—H]), but the structure of the ion is unknown at present. This [M—R—CO—H] peak was also observed in amino and methyl compounds.

Besides these peaks, some other fragmentations are also characteristic of the substituent. For example, amino compounds showed a peak of intermediate intensity at 89 mass units, while methyl compounds afforded a peak at 118 and methoxy derivatives at 78 mass units.

Finally, it is worth noting that the [M—18] peak was the base peak in the spectra of both *p*- and *m*-amino or hydroxybenzamides (**9**, **10**, **31**, **32**), and that the [M—44] peak was significant for *p*-amino or *p*-hydroxybenzoic acid (**6**, **7**).

Discrimination of Isomers. As was discussed in the previous section, the [M—28] peak was characteristic of the compounds that have strong electron-donating substituents. It is, therefore, possible to differentiate the isomer pairs of certain compounds by observing this peak. For example, the conventional spectra of *p*- and *m*-hydroxybenzaldehydes (**1**, **23**) are essentially the same, but in their 2E doubly charged ion spectra only the *p*-compound exhibited a strong [M—28] peak, whereas the peak was negligibly small in the *m*-compound [Fig. 1]. The similar situation was encountered in several other cases, *e.g.*, in *para* and *meta* isomer

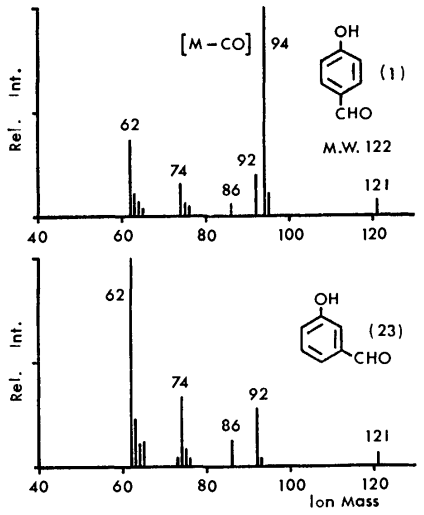

Fig. 1. 2E Doubly charged ion mass spectra of *p*- and *m*-hydroxybenzaldehydes (**1**, **23**).

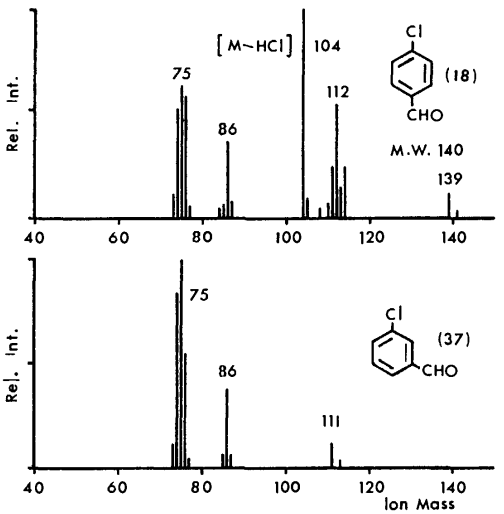

Fig. 2. 2E Doubly charged ion mass spectra of *p*- and *m*-chlorobenzaldehydes (**18**, **37**).

pairs of methoxybenzaldehydes (**2**, **24**), aminoacetophenones (**3**, **25**), and hydroxybenzoic acids (**7**, **29**).

Other characteristic peaks can also be used. Thus, an [M—HCl] peak was very prominent only in *p*-chlorobenzaldehyde (**18**) in doubly charged ion spectra [Fig. 2], while both *p*- and *m*-isomers afforded almost identical spectra in ordinary measurement (singly charged ion spectra).

Conclusion

It is evident from the above results that in doubly charged ion spectra of aromatic carbonyl compounds several different fragmentations were observed from those in conventional spectra. One of the most characteristic peaks of these compounds is the [M—CO] peak. Examination of the substituent effects revealed that the product ion stabilities are the most important factor in this fragmentation reaction.

Although several other structure-spectral pattern-correlations are obtained, the detailed structure of each fragment ion and the precise mechanism of its formation are not elucidated at this stage, and apparently further work is awaited.

On the empirical ground, however, it was found possible to distinguish the isomer pairs of certain compounds by using this spectra. This is of course very limited at present, but it is our hope that after accumulation of many data the 2E doubly charged ion spectrum will be one of the useful diagnostic tools for isomer discrimination and for structural identification of organic compounds.

Experimental

Materials. The most of the compounds were commercial samples of extra pure or guaranteed grade. The following compounds were prepared and characterized by standard procedures: *p*-aminoacetophenone (**3**), *p*-hydroxyacetophenone (**4**), methyl *p*-anisate (**14**), *p*-chloroacetophenone (**19**), *p*-chlorobenzamide (**21**), methyl *p*-chlorobenzoate (**22**), *m*-aminoacetophenone (**25**), *m*-hydroxyacetophenone (**26**), *m*-hydroxybenzoic acid (**29**), *m*-aminobenzamide (**31**), *m*-hydroxybenzamide (**32**), *m*-anisamide (**33**), methyl *m*-aminobenzoate (**34**), methyl *m*-hydroxybenzoate (**35**), methyl *m*-anisate (**36**), *m*-chloroacetophenone (**38**), *m*-chlorobenzamide (**40**), and methyl *m*-chlorobenzoate (**41**).

Doubly Charged Ion Mass Spectra. The spectra were determined with a Hitachi RMU-7 double focusing mass spectrometer by using the previously described method.[3] After the range of mass to charge ratio in ion source was set at *m/e* 600 and the electrostatic sector at 300, the accelerating voltage was adjusted for the desired peak to be observed. Standard operating conditions were as follows: ionizing energy 70 eV, ionizing current 80 μA, source temperature 250 °C, sample pressure $1—5\times10^{-6}$ Torr, and accelerating voltage 1.8 kV.

Accurate Mass Measurements. The accurate mass measurements were carried out on a Hitachi RMH-1 double focusing mass spectrometer. Operating conditions were ionizing energy 70 eV, ionizing current 0.6 mA, source temperature 200 °C, accelerating voltage 6.7 kV and resolution about 30000 (10% valley). Accurate masses of most peaks were determined by using doublets which were made by introducing appropriate reference samples into the spectrometer. In the case of nitrogen containing fragments, the peak appeared between nominal integer masses and, therefore, calculation by using Lagrange's interpolation formula gave reliable results. Data on Table 2 indicate the agreement between the calculated and observed values was satisfactory.

For the peak at 92 mass units from methyl *p*-hydroxybenzoate (**13**), the following result was obtained. Obsd: 46.0133, calcd for $(C_6H_4O)^{2+}$: 46.0131.

References

1) H. Sakurai, A. Tatematsu, and H. Nakata, *Org. Mass Spectrometry*, **7**, 1109 (1973).

2) For recent references on 2E doubly charged ion mass spectra, see, J. H. Beynon, A. Mathias and A. E. Williams, *Org. Mass Spectrometry*, **5**, 303 (1971); T. Ast, J. H. Beynon and R. G. Cooks, *ibid.*, **6**, 749 (1972); T. Blumenthal and J. H. Bowie, *ibid.*, **6**, 1083 (1972).

3) A. Tatematsu, H. Sakurai, H. Nakata and T. Goto, *Shitsuryo Bunseki*, **20**, 331 (1972).

4) O. Exner, "Advances in Linear Free Energy Relationships," ed. by N. B. Chapman and J. Shorter, Plenum Press, London (1972), pp. 28—29.

Reaction of Group IV Organometallic Compounds. XXXI.[1] The Reaction of *N*-Trimethylsilyl- and -stannyl-(diphenylmethylene)amine with Diketene

Hiroharu SUZUKI, Isamu MATSUDA,* Kenji ITOH, and Yoshio ISHII

Department of Synthetic Chemistry, Faculty of Engineering, Nagoya University, Chikusa-ku, Nagoya 464

(Received July 15, 1974)

Linear 1/1 adducts and oxazinone derivative were obtained by the reaction of *N*-trimethylsilyl- and -stannyl-(diphenylmethylene)amine; $Ph_2C{=}N{-}MMe_3$ (M=Si, Sn) with diketene. Consecutive demetallation reaction by ethanethiol for the organostannyl 1/1 adduct, and by methanol for the organosilyl 1/1 adduct gave a piperidine derivative and an oxazinone derivative, respectively.

N-Trimethylsilyl- and -stannyl(diphenylmethylene)-amine; $Ph_2C{=}N{-}MMe_3$ ((I) for M=Si and (II) for M=Sn) have been reported to induce insertion and consecutive cyclization reactions with heterocumulene compounds,[1-4] aldehydes,[3] and acrylonitrile.[3]

Diketene is an attractive component for the preparation of six-membered heterocyclic compounds, because the acyl-oxygen bond cleavage of diketene provides a synthetic equivalence of acetylketene; $CH_3CO{-}CH{=}C{=}O$. For example, the addition of diketene to some carbodiimides and the parent diphenylmethyleneamine gave the corresponding oxazinone derivatives III[5] and IV,[6] respectively.

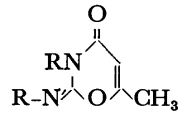

III

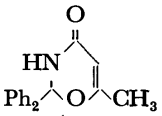

IV

In this paper we describe an insertion of diketene to the metal-nitrogen bond of I and II, and the subsequent cyclization reactions by way of demetallation treatment. The difference of products in both insertion and demetallation steps by changing the metal atom is discussed.

Results and Discussion

The Reaction of N-*Trimethylstannyl(diphenylmethylene)-amine (II).* N-Trimethylstannyl(diphenylmethylene)amine; $Ph_2C{=}N{-}SnMe_3$ (II) reacted exothermically with equimolar amounts of diketene to give the 1/1 adduct (V) as the fairly air-stable crystals in 96% yield. The strong IR absorption band around 1574 cm^{-1} indicates the presence of the carbonyl oxygen atom coordinated to the organotin moiety. Another absorption band at 1673 cm^{-1} was assigned to the C=N stretching frequency. The ^1H NMR spectrum of 1/1 adduct (V) showed resonance peaks at τ 7.05 (2H, m), 5.71 (1H, d, J=1.5 Hz), and 4.43 (1H, m), which were assigned to the methylene and terminal vinylic protons, respectively. The above spectroscopic results are consistent with the depicted structure V in Eq. (1). The participation of the diphenylmethylene group in the 1/1 reaction may be ruled out, since any cyclic product which includes the diphenylmethylene group in the ring skeleton was not obtained at all. Organometallic insertion reactions of diketene have been reported[7,8] to give only one product VII, which involves intramolecular 1,3-shift of a central methylene proton from VI.

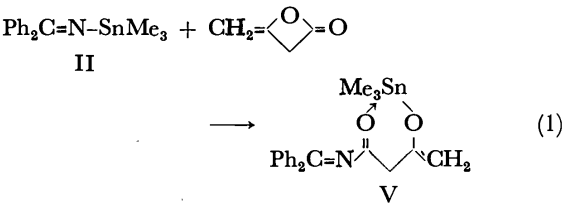

(1)

V

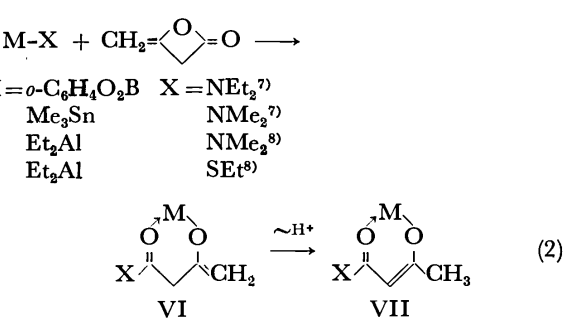

(2)

VI VII

It is noteworthy that the product (V) obtained in the reaction of *N*-trimethylstannyl(diphenylmethylene)-amine with diketene is the first stable organometallic insertion product which does not induce a 1,3-proton shift. The structure of V is also confirmed by the following destannylation reaction. Ethanethiol was added to the 1/1 adduct (V) in order to substitute the trimethylstannyl group with proton. The expected products were the isomers VIIIa—VIIIc; however, the ^1H NMR spectrum of the obtained destannylation product exhibited unexpectedly neither methyl protons nor vinylic protons. Only two pairs of methylene protons (τ 6.95, 2H, s, and τ 6.68, 2H, s) and the one proton attached to the nitrogen atom (τ 2.32, 1H, s, confirmed by D_2O exchange) were observed.

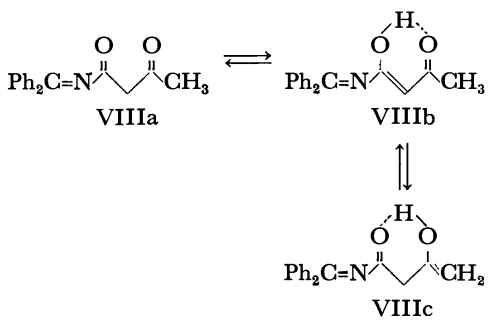

VIIIa VIIIb VIIIc

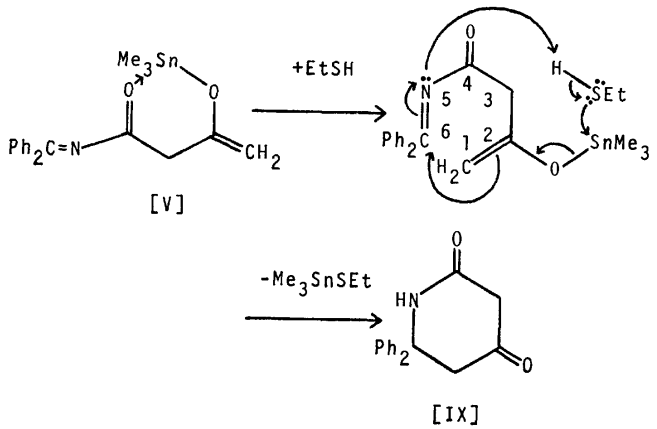

Scheme 1.

Moreover, two strong absorption bands at 1728 and 1661 cm^{-1} are assigned to a ketone and an amide carbonyl stretching frequencies, respectively. The above-mentioned spectroscopic results are consistent with 6,6-diphenylpiperidin-2,4-dione (IX), whose formation may be shown in Scheme 1. The addition of ethanethiol firstly causes the cleavage of the intramolecular coordinated structure because of the difference in the affinity of the tin atom toward oxygen and sulfur atoms. Then the ring closure is induced exclusively by the nucleophilic attack of the terminal carbon atom C(1) to the *exo* double bond at C(6), accompanied by the elimination of trimethylstannyl ethylsulfide. In the present case, diketene behaves as a component $\dot{C}O\text{-}CH_2CO\text{-}\dot{C}H_2$ to [4+2] cycloaddition. This is quite different from the general behavior of diketene which acts as a synthetic equivalence of $CH_3CO\text{-}CH{=}C{=}O$ as described before.

The Reaction of N-*Trimethylsilyl(diphenylmethylene)amine (I).* *N*-Trimethylsilyl(diphenylmethylene)amine (I) reacted with diketene under more vigorous condition than the tin analogue (II) (60 °C, 14 hr). The 1/1 reaction mixture was purified by vacuum distillation (bp 108.0—116.0 °C/0.02 mmHg) and was confirmed as a 1/1 adduct by analysis, whereas the adduct did not show a simple ^1H NMR spectrum (Fig. 1). The detailed measurement of the proton ratio and coupling patterns revealed the presence of three isomers XI, XIII, and XV, structures of which were given in Scheme 2.

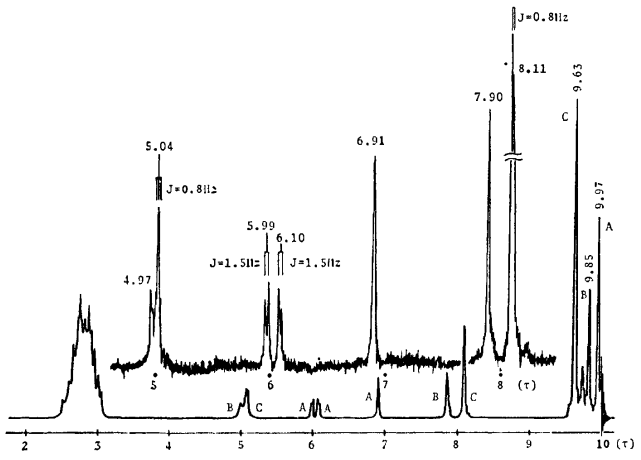

Fig. 1. The ^1H NMR spectrum of distilled mixture (in CCl_4). Resonance peaks A, B, and C were attributed to [XI], [XIII], and [XV], respectively.

There is the possibility of the presence of the structure XII in the 1/1 adduct as reported in the paper[9] that diketene reacted with equimolar amounts of trimethylsilyldiethylamine to give the mixture of XVII and XVIII as shown in Eq. (3).

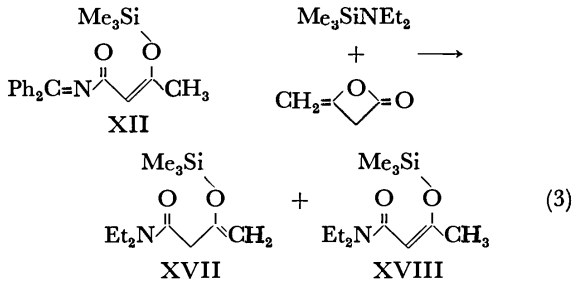

(3)

However, it can be excluded because of the absence of the allyl coupling which is expected in the structure XII.

Table 1.

Reaction temp. (°C)	Total yield of XI, XIII, and XV (%)	Isomer ratio XI : XIII : XV
60	73	3.5 : 1 : 8.0
115	68	0.9 : 1 : 1.3
120	71	0.4 : 1 : 0.8

The observed isomer ratio in the 1/1 adducts was dependent on the reaction temperature as shown in Table 1. The isomer ratio of XI and XV decreased, and that of XIII increased as the elevation of the reaction temperature. This result definitely showed XI and XV were convertible to XIII, which would be thermodynamically the most stable product. Although the 1/1 adduct is composed of three isomers, XI, XIII, and XV, only 2,2-diphenyl-3,4-dihydro-6-methyl-2(1*H*)-1,3-oxazin-4-one (IV) was isolated on desilylation reaction. The yields are quantitative from the methanolysis of the purified 1/1 adduct, and 72% from the methanolysis of the 1/1 reaction mixture. The IV has been prepared by [4+2] cycloaddition reaction of the parent amine; $Ph_2C{=}NH$ with diketene.[6] The above results are summarized in Scheme 2.

The first step is a nucleophilic attack of the nitrogen atom in *N*-trimethylsilyl(diphenylmethylene)amine to the carbonyl carbon of diketene. In the second step, two paths are possible. First possibility is the migration of the trimethylsilyl group from the nitrogen to the oxyanion in X to give XI and XIII. Secondly, a direct ring closure accompanying a 1,3-prototropy gives XV, similar to a reaction of the parent diphenylmethyleneamine with diketene.[6]

It is extremely interesting that two isomeric heterocyclic compounds; IX and IV may be obtained from diketene only by changing the organometallic moiety in another component; *N*-organometallyldiphenylmethyleneamine.

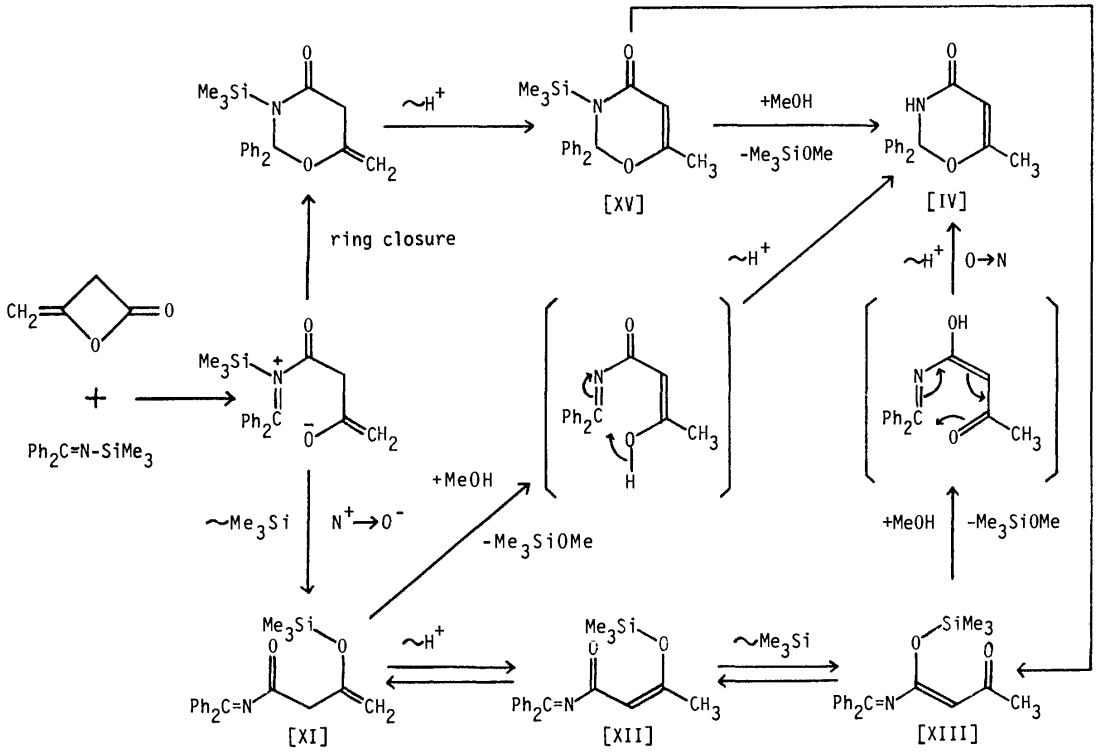

Scheme 2.

Experimental

The mp of V was determined in a sealed capillary filled with argon. Analyses of organometallic compounds were carried out by Alfred Bernhardt Mikroanalytisches Laboratorium, West Germany. IR spectra were recorded on Japan Spectroscopic Co., Ltd., IR-S and DS-403G instruments. Proton NMR spectra were measured with Japan Electron Optics Co., Ltd., C-60HL instrument.

N-Trimethylsilyl(diphenylmethylene)amine[2] and *N*-trimethyltannyl(diphenylmethylene)amine[10] were prepared according to the published procedure. Diketene was distilled before use.

Reaction of N-Trimethylstannyl(diphenylmethylene)amine with Diketene. To a solution of 0.870 g (2.53 mmol) of *N*-trimethylstannyl(diphenylmethylene)amine in *ca.* 3 ml of benzene was added 0.268 g (3.19 mmol) of diketene at 0 °C under nitrogen. The reaction proceeded exothermically. The adduct was precipitated as pale yellow crystals by the addition of *ca.* 4 ml of *n*-hexane after the completion of the reaction. This was identified as 1/1 adduct (V), after the purification by reprecipitation from the mixed solvent of benzene and *n*-hexane (2/4) (1.044 g, 96%). Mp 130.0—133.0 °C. Found: C, 56.29; H, 5.54%. Calcd for $C_{20}H_{23}NO_2Sn$: C, 56.11; H, 5.41%. IR (in $CHCl_3$) 1673 and 1574 cm^{-1}. ^1H NMR (in $CDCl_3$) τ 9.57 (Me_3Sn, $J^{117/119}Sn$–C–H=65.0/68.0 Hz), 7.05 (2H, m), 5.71 (1H, d, J=1.5 Hz) and 4.43 (1H, m).

Destannylation of V. Addition of ethanethiol (2 ml) to a benzene solution (15 ml) of the 1/1 adduct (V) (0.900 g, 2.10 mmol) afforded the destannylated product (IX) (0.513 g, 1.94 mmol) as white prisms in 93% yield. Mp 179.5—181.5 °C. Found: C, 77.17; H, 5.72; N, 5.20%. Calcd for $C_{17}H_{15}NO_2$: C, 76.96; H, 5.69; N, 5.27%. IR (in KBr) 3120, 1728, and 1661 cm^{-1}. ^1H NMR (in $CDCl_3$) τ 6.95 (2H, s), 6.68 (2H, s), 2.72 (10H), and 2.32 (NH, br. s).

Reaction of N-Trimethylsilyl(diphenylmethylene)amine with diketene. The mixture of 1.916 g (7.58 mmol) of *N*-trimethylsilyl(diphenylmethylene)amine and 0.819 g (9.75 mmol) of diketene was heated at 60 °C for 40 hr in a sealed tube. The isomer ratio of [XI]: [XIII]: [XV] was decided by the intensities of proton signals of trimethylsilyl group in ^1H NMR spectrum of the reaction mixture. The reaction mixture was purified by vacuum distillation (bp 108.0—116.0 °C/0.02 mmHg) (1.85 g, 73%). Found: C, 71.22; H, 6.68%. Calcd for $C_{20}H_{23}NO_2Si$: C, 71.18; H, 6.78%. In the ^1H NMR spectrum (in CCl_4), the assignment of proton signals are as follows. XI: τ 9.97 (Me_3Si, 9H, s), 6.91 (2H, s), 6.10 (1H, d, J=1.5 Hz), and 5.99 (1H, d, J=1.5 Hz). XIII: τ 9.85 (Me_3Si, 9H, s), 7.90 (3H, s), and 4.97 (1H, s). XV: τ 9.63 (Me_3Si, 9H, s), 8.11 (3H, d, J=0.8 Hz), and 5.04 (1H, q, J=0.8 Hz).

A mixture of XI, XIII, and XV (2.55 g, 7.57 mmol) was desilylated by the treatment with methanol (5 ml). The desilylated product was isolated in 72% yield (1.45 g) and was identified to IV by the comparison with the authentic sample.[6]

References

1) Part XXX, H. Suzuki, K. Itoh, I. Matsuda, and Y. Ishii, This Bulletin, in press.

2) I. Matsuda, K. Itoh, and Y. Ishii, *J. Chem. Soc., Perkin I*, **1972**, 1678.

3) P. G. Harrison, *ibid.*, **1972**, 130.

4) M. F. Lappert, J. McMeeking, and D. E. Palmer, *J. Chem. Soc., Dalton*, **1973**, 151.

5) R. Lacey, *J. Chem. Soc.*, **1959**, 2134.

6) T. Kato and H. Sakamoto, *Yakugaku Zasshi*, **87**, 1322 (1967).

7) J. R. Horder and M. F. Lappert, *J. Chem. Soc., Ser. A*, **1969**, 173.

8) K. Urata, K. Itoh, and Y. Ishii, *J. Organometal. Chem.*, **63**, 11 (1973).

9) I. F. Lutsenko, Y. I. Baukov, A. S. Kostyuk, N. I. Savelyeva, and V. K. Krysina, *ibid.*, **17**, 241 (1969).

10) L. H. Chan and E. G. Rochow, *ibid.*, **9**, 231 (1967).

Hetera-*p*-carbophanes. IV. The Effect of Rigidity on the Chemical Shifts of Protons in Ansa Chains and Barriers to Rotation of Dioxadioxo[*n*]paracyclophanes[1)]

Kazuhiko SAKAMOTO and Michinori ŌKI*

Department of Chemistry, Faculty of Science, The University of Tokyo, Hongo, Tokyo 113

(Received June 26, 1974)

A series of dioxadioxo[*n*]paracyclophanes with or without methyl groups at the benzene ring were prepared and their PMR spectra compared with those of open-chain analogs as well as with those of paracyclophanes. Rigidity of the ansa chain was found to be an important factor in determining the chemical shifts of the ansa chain protons in addition to the ring current effect. Measurement of the PMR spectra at various temperatures revealed that the chemical shifts of the benzylic protons drifted to a small extent according to temperatures and the phenomenon was attributed to the change of solvation. Barriers to rotation of the aromatic rings in $\mathbf{6}_{15}$ and $\mathbf{6}_{16}$ were obtained as 23.3 and 11.0 kcal/mol, respectively. The barrier was discussed from the stand point of rigidity of the ansa chain.

In previous papers, the conformation of amide groups in and the internal rotation of diazadioxo[*n*]paracyclophane derivatives [$\mathbf{1}_n$ (n=12—16), $\mathbf{2}_n$ (n=11—16), $\mathbf{3}_n$ (n=11—16 and 18), and $\mathbf{4}_{18}$ (n=18)] have been reported.[1,2)] The barriers to rotation in these compounds appeared much higher than those in simple polymethylene paracyclophanes. Since these compounds contain rather rigid sp^2-hybridized structures of amide groups, the higher barrier may be attributed to the rigidity of the ansa chain. The barriers to rotation about a single bond of partial double bond characters are considered to be higher in amide groups than in ester groups because for the former it is necessary to raise the temperature to see the coalescence phenomenon of two signals in PMR spectroscopy[3)] (generally barriers are a little less than 20 kcal/mol) whereas it is necessary to cool the solution fairly deeply to observe signals of *s-cis* and *s-trans* forms by PMR spectroscopy for the latter.[4)] Thus it will be interesting to see the barrier height in heteraparacyclophanes containing two ester groups and compare the results with those of other cyclophanes.

In addition to the above point, the selection of the ester derivatives was hoped to give another advantage in studying the barrier to rotation. The amide compounds tend to crystallize out, when the solution is cooled, to give a difficulty in PMR measurements at the low temperature. Thus, although it was possible to obtain upper limits of the barriers for the amides, the precise value was not measured. Esters are known to be more soluble in ordinary solvents and the better solubility may help to see the change in barrier heights by increasing or decreasing the ansa chain length in a more quantitative fashion.

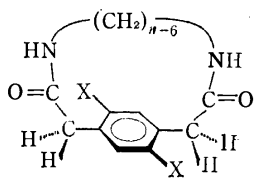

$\mathbf{1}_n$: X=H, n=12—16
$\mathbf{2}_n$: X=CH_3, n=11—16
$\mathbf{3}_n$: X=OCH_3, n=11—16, 18
$\mathbf{4}_n$: X=OC_2H_5, n=18

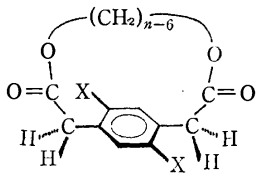

$\mathbf{5}_n$: X=H, n=11—16
$\mathbf{6}_n$: X=CH_3, n=11—16

This paper describes preparations of dioxadioxo[*n*]-paracyclophane derivatives [$\mathbf{5}_n$ (n=11—16) and $\mathbf{6}_n$ (n=11—16)] and discusses the effect of changing the ansa chain on the barrier to rotation. A part of the results on the internal rotation has been reported briefly.[5)]

Experimental

The syntheses of $\mathbf{5}_n$ and $\mathbf{6}_n$ were accomplished by condensation of α,ω-diols with 1,4-phenylenediacetyl dichlorides[2)] with or without methyl groups under high dilution conditions. The former compounds were of commercial origin except 1,10-decanediol.

1,10-Decanediol. Mp 71.5—72.5 °C (lit,[6)] mp 72—74 °C), was prepared by lithium aluminum hydride reduction of diethyl sebacate in ether in an almost quantitative yield.

Syntheses of Dioxadioxo[n]*paracyclophanes ($\mathbf{5}_n$ and $\mathbf{6}_n$).* The condensation between the chlorides and the diols was carried out in essentially the same method as reported previously.[1)] The crude product was chromatographed on silica gel and fractions eluted with hexane-benzene (v/v 9: 1—1: 1) were collected. Recrystallization from hexane gave the desired products. Melting points, analytical data, and yields for the pure compounds are summarized in Table 1.

Syntheses of Polymethylene Bis(2,5-dimethylphenylacetate)s ($\mathbf{7}_n$). A solution of 10 mmol of 2,5-dimethylphenylacetyl chloride in 10 ml of dry ether was slowly added to a stirred solution of 5 mmol of an appropriate α,ω-diol in tetrahydrofuran. After the addition, the reaction mixture was poured into ice–water. Subsequent work-up of the mixture in a usual manner gave a pale yellow oil. Chromatography of this oil on silica gel, using hexane-benzene mixture as eluent gave a pure compound in an almost quantitative yield. Analytical and some other data are tabulated in Table 2.

Measurement of Spectra. The infrared spectra were recorded on either a Hitachi EPI-G2 infra red spectrometer (4000—400 cm^{-1}) or a Perkin-Elmer 112G grating spectrometer (1750—1700 cm^{-1}). The measurements were run with KBr discs or neat liquids for the former instrument and with solutions in either carbon tetrachloride (*ca.* 0.0005 mol/l) or acetonitrile (*ca.* 0.01 mol/l) for the latter. The PMR spectra were measured on a Hitachi R-20B spectrometer operating at 60 MHz at 34 °C. Samples were dissolved in carbon tetrachloride for conventional measurements and the chemical shifts were recorded using TMS as an internal standard. Lanthanide [$Eu(dpm)_3$ and $Eu(fod)_3$-d_{27}] induced shift measurements were performed in deuteriochloroform solutions analogously to the method as reported previously.[7)] For the

TABLE 1. DIOXADIOXO[*n*]PARACYCLOPHANES (5_n and 6_n)

Compound	Molecular formula	Mp (°C)	Analytical data C(%)	Analytical data H(%)	Mol wt (M^+)	Yield (%)	IR (KBr) $\nu_{C=O}$ (cm^{-1})
5_{11}	$C_{15}H_{18}O_4$	147.0—148.0	68.74	6.82	262[a]	14	1730
			68.69	6.92	262[a]		
5_{12}	$C_{16}H_{20}O_4$	135.5—136.5	69.57	7.32	276	13	1725
			69.54	7.30	276		
5_{13}	$C_{17}H_{22}O_4$	110.0—111.0	70.64	7.86	290	18	1730
			70.32	7.64	290		
5_{14}	$C_{18}H_{24}O_4$	94.0—95.0	71.07	7.78	304	14	1730
			71.03	7.95	304		
5_{15}	$C_{19}H_{26}O_4$	45.0—46.0	71.86	7.95	318	16	1730
			71.68	8.23	318		
5_{16}	$C_{20}H_{28}O_4$	38.0—39.0[b]	72.06	8.32	332	30	1730[c]
			72.26	8.50	332		
6_{11}	$C_{17}H_{22}O_4$	80.0—81.0	70.03	7.85	290	12	1735
			70.32	7.64	290		
6_{12}	$C_{18}H_{24}O_4$	92.5—93.5	71.14	8.08	304	26	1735
			71.03	7.95	304		
6_{13}	$C_{19}H_{26}O_4$	51.5—53.0	71.41	7.97	318	32	1730
			71.68	8.23	318		
6_{14}	$C_{20}H_{28}O_4$	78.0—79.0	72.53	8.69	332	35	1725
			72.26	8.50	332		1740
6_{15}	$C_{21}H_{30}O_4$	87.0—88.0	72.75	8.55	346	18	1725
			72.80	8.73	346		
6_{16}	$C_{22}H_{32}O_4$	89.0—90.0	73.05	9.25	360	26	1725
			73.30	8.95	360		

a) The numerical data in the upper column are those found and those in the lower column are the calculated. b) Recrystallized after short path distillation. c) Neat.

TABLE 2. POLYMETHYLENE BIS(2,5-DIMETHYLPHENYLACETATE)S (7_n)

Compound	Molecular formula	Mp (°C)	Analytical data C(%)	Analytical data H(%)	IR (neat) $\nu_{C=O}$ (cm^{-1})
7_{11}	$C_{25}H_{32}O_4$		75.93	7.90[a]	1735
			75.73	8.13[a]	
7_{12}	$C_{26}H_{34}O_4$		76.31	8.12	1735
			76.06	8.35	
7_{13}	$C_{27}H_{36}O_4$		76.49	8.69	1730
			76.38	8.55	
7_{14}	$C_{28}H_{38}O_4$		76.46	8.92	1735
			76.68	8.73	
7_{15}	$C_{29}H_{40}O_4$		77.19	9.10	1740
			76.95	8.91	
7_{16}	$C_{30}H_{42}O_4$	34.5—36.0	77.22	9.12	1740 (1725)[b]
			77.21	9.07	

a) See the footnote of Table 1. b) The numerical datum in parentheses is observed with KBr disc.

DNMR measurements, the solvent system had to be changed in order to meet the requirement of the properties of solvents, as are shown in Table 5. The temperature reading was calibrated by measuring the chemical shift differences between methylene and hydroxy protons of ethylene glycol at the higher temperatures and those between methyl and hydroxy protons of methanol at the lower temperatures. The mass spectra were recorded on a Hitachi RMU-6L spectrometer.

Results and Discussion

PMR Spectra. PMR spectral data of 5_n and 6_n in carbon tetrachloride solutions at 34 °C are summarized in Table 3 together with those of polymethylene bis(2,5-dimethylphenylacetate)s (7_n). Change in signal shapes of the bridge methylene protons in 5_n and 6_n,

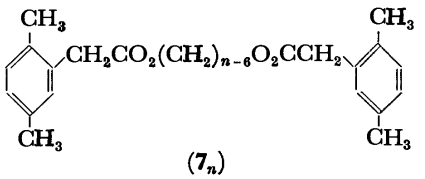

(7_n)

which are remote from the ester moiety, due to the length of the ansa chain is similar with those observed with 2_n and 3_n and reflects rigidity and mobility of the molecules.

The multiplets due to the methylene protons gamma to the oxygen atom of the ester groups in 6_{11} and 6_{12} center at δ 0.45 and 0.80. These chemical shifts are located at the higher magnetic field with respect to those of [*n*]paracyclophanes. Waugh and Fessenden

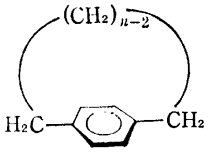

(8_n)

Table 3. NMR data of dioxadioxo[n]paracyclophanes ($\mathbf{5}_n$ and $\mathbf{5}_n$) and polymethylene bis(2,5-dimethylphenylacetate)s ($\mathbf{7}_n$) in carbon tetrachloride at 34 °C (δ from internal TMS)[a]

Compound	Ar-H	CH_2CO	Ar-CH_3	OCH_2	β-CH_2[b]	γ—δ-CH_2[b]
$\mathbf{5}_{11}$	7.16 (s,4H)	3.49 (s,4H)		3.88 (t,4H)	1.18 (m,4H)	0.40 (m,2H)
$\mathbf{5}_{12}$	7.18 (s,4H)	3.48 (s,4H)		3.93 (t,4H)	1.25 (m,4H)	0.72 (m,4H)
$\mathbf{5}_{13}$	7.21 (s,4H)	3.46 (s,4H)		3.98 (t,4H)	1.34 (m,4H)	0.80 (b,6H)
$\mathbf{5}_{14}$	7.19 (s,4H)	3.47 (s,4H)		4.02 (t,4H)	1.45 (m,4H)	1.03 (b,8H)
$\mathbf{5}_{15}$	7.19 (s,4H)	3.47 (s,4H)		4.04 (t,4H)	1.50 (m,4H)	1.05 (b,10H)
$\mathbf{5}_{16}$	7.19 (s,4H)	3.51 (s,4H)		4.07 (t,4H)	1.54 (m,4H)	1.16 (b,12H)
$\mathbf{6}_{11}$	6.90 (s,2H)	3.47(AB-q, J=13.7, $\Delta\delta$=17.6 Hz,4H)	2.27 (s,6H)	3.86 (t,4H)	1.18 (m,4H)	0.45 (m,2H)
$\mathbf{6}_{12}$	6.92 (s,2H)	3.48(AB-q, J=13.8, $\Delta\delta$=16.0 Hz,4H)	2.28 (s,6H)	3.93 (t,4H)	1.26 (m,4H)	0.80 (m,4H)
$\mathbf{6}_{13}$	6.97 (s,2H)	3.45(AB-q, J=13.2, $\Delta\delta$=15.9 Hz,4H)	2.32 (s,6H)	3.98 (t,4H)	1.32 (m,4H)	0.83 (b,6H)
$\mathbf{6}_{14}$	6.93 (s,2H)	3.43(AB-q, J=13.7, $\Delta\delta$=14.7 Hz,4H)	2.27 (s,6H)	4.01 (t,4H)	1.46 (m,4H)	1.05 (b,8H)
$\mathbf{6}_{15}$	6.96 (s,2H)	3.45(AB-q, J=13.6, $\Delta\delta$=14.8 Hz,4H)	2.30 (s,6H)	4.03 (t,4H)	1.50 (m,4H)	1.08 (b,10H)
$\mathbf{6}_{16}$	6.95 (s,2H)	3.43 (s,4H)	2.29 (s,6H)	4.04 (t,4H)	1.50 (m,4H)	1.13 (b,12H)
$\mathbf{7}_{11}$	6.90 (s,6H)	3.44 (s,4H)	2.27, 2.23 (s,s,12H)	3.94 (t,4H)	1.49 (m)[c]	1.37(m)(6H)[c]
$\mathbf{7}_{12}$	6.90 (s,6H)	3.44 (s,4H)	2.26, 2.23 (s,s,12H)	3.95 (t,4H)	1.45 (m)	1.30(m)(8H)
$\mathbf{7}_{13}$	6.90 (s,6H)	3.44 (s,4H)	2.27, 2.23 (s,s,12H)	3.96 (t,4H)	1.50 (m)	1.26(b)(10H)
$\mathbf{7}_{14}$	6.90 (s,6H)	3.45 (s,4H)	2.27, 2.24 (s,s,12H)	3.98 (t,4H)	1.50 (m)	1.23(b)(12H)
$\mathbf{7}_{15}$	6.90 (s,6H)	3.45 (s,4H)	2.27, 2.24 (s,s,12H)	3.99 (t,4H)	1.50 (m)	1.24(b)(14H)
$\mathbf{7}_{16}$	6.90 (s,6H)	3.46 (s,4H)	2.28, 2.26 (s,s,12H)	3.99 (t,4H)	1.50 (m)	1.25(b)(16H)

a) s=singlet, q=quartet, m=multiplet, and b=broad signal b) relative to O-atom c) Since there were so significant overlapping with the integrals of β—δ-methylene protons in $\mathbf{7}_n$ that it was difficult to estimate the intensities of β- and γ—δ-methylene protons respectively, the intensity of β—δ-methylene protons was shown.

have reported that the central bridge methylene protons in [10]- and [12]-paracyclophanes ($\mathbf{8}_n$) give signals at δ 0.80 and 1.0, respectively, and sustain the ring current effect induced by π-electron delocalization.[8] The difference in chemical shifts in these hetera- and homo-cyclophanes could be attributed to the anisotropy effect of atoms or groups in the most-populated conformation.

It has been well known that the shielding of a nucleus can be expressed as the sum of several terms.[9,10] However, in the comparison of the shielding of bridge methylene protons (σ_{CH_2}) in similar molecules such as $\mathbf{6}_n$ and $\mathbf{7}_n$, the difference in the shielding exerted by atoms or groups other than the aromatic ring may be negligible at the first approximation if the conformations of ester groups are the same with each other. The ester group is known to take the *s-trans*[11] conformation in usual cases, but it takes the *s-cis* in some cases.[4,7,12] Lanthanide induced shift in PMR spectra is reported to be a convenient method for diagnosis of the ester conformation. If the ester is the *s-trans*, the ratio of the lanthanide induced shift *versus* [lanthanide]/[substrate] for the ether methylene is almost the same with that of carbonyl methylene, whereas it is about half when the conformation is *s-cis*.[7] Indeed $\mathbf{6}_n$ has been reported to be *s-trans* by this method.[7] Lanthanide induced shifts of $\mathbf{5}_n$ and $\mathbf{7}_n$ were measured and almost the same lanthanide induced shifts were obtained for CH_2O and CH_2CO in all the cases. Infrared spectra of the $\mathbf{5}_n$ and $\mathbf{6}_n$ gave only one band ($\sim$1730 cm^{-1}) for the carbonyl stretching both in carbon tetrachloride and in acetonitrile.[12] It may be concluded from these data that the ester groups in the dioxadioxo[n]paracyclophanes examined here take *s-trans* conformations. Thus an approximation that the difference, $\Delta\sigma_{CH_2}$, in shielding of the bridge methylene is determined by the ring current effect becomes valid. Contribution of the aromatic rings to σ_{CH_2} in $\mathbf{7}_n$ will be much smaller than that in $\mathbf{6}_n$ because the distance (r) between the aromatic ring and the central methylene protons in question in an extended molecule like $\mathbf{7}_n$ is much larger than that in a folded molecule such as $\mathbf{6}_n$ and the effect is propotional to $1/r^3$.

Table 4. High field shift of the central bridge methylene protons induced by diamagnetic ring current in $\mathbf{6}_n$ (ppm)

Number of ansa chain atoms	n=11	12	13	14	15	16
σ_{CH_2} of $\mathbf{7}_n$ $-\sigma_{CH_2}$ of $\mathbf{6}_n$	0.92	0.50	0.43	0.18	0.16	0.12

Increase of the number of ansa chain atoms causes decrease in $\Delta\sigma_{CH_2}$, as is seen in Table 4. The results are close to the values which are expected from the calculation by the Johnson and Bovey method[13] and indicate that the ansa chain conformation of the smaller chain length are fairly fixed to have the bridge-center just above the benzene ring. In such a conformation, the central part of the ansa chain will never come to the shielding cones of the C–O and/or the C=O bonds of the ester group, of which conformation has been deduced to be *s-trans*. Thus, from the stand point of

anisotropy of the ester group, the chemical shift of the bridge-center methylenes of $\mathbf{6}_n$ should be at the lower magnetic field than those of $\mathbf{8}_n$. The fact that, contrary to the simple discussion, the chemical shifts of the central methylene protons of $\mathbf{8}_n$ is at lower magnetic field than those of $\mathbf{6}_n$ may reflect the more flexibility of the methylene chain in $\mathbf{8}_n$ than that in $\mathbf{6}_n$, if the chain lengths are the same, due to the absence of sp^2 hybridized groups and, on an average, the shielding by the ring current effect in $\mathbf{8}_n$ is the less. The barriers to rotation of the aromatic rings reflect this situation also (see the later discussion).

The benzylic protons of $\mathbf{6}_{11}$—$\mathbf{6}_{15}$ give signals of the AB type at δ 3.4—3.5, whereas those of $\mathbf{5}_{11}$—$\mathbf{5}_{16}$ and $\mathbf{6}_{16}$ do signals of the A_2 type at almost the same magnetic field. The AB type signals for $\mathbf{6}_n$ are expected if the aromatic ring rotates slowly on the NMR time scale because, in these cases, the molecules exhibit chirality due to the plane asymmetry. Thus it appears that the rotation of the aromatic ring in $\mathbf{6}_{11}$—$\mathbf{6}_{15}$ is slow whereas that in $\mathbf{6}_{16}$ is fast at room temperature.

Temperature Dependence of the PMR Spectra. The PMR spectra of $\mathbf{6}_n$ were measured at various temperatures to obtain barriers to rotation of the aromatic ring. However, during the course of the study, an unexpected phenomenon appeared. That is, the differences between the chemical shifts of benzylic methylene protons showed small but definite changes within the range of 1.5—3.0 Hz at the temperatures of 34—190 °C, while the coupling constants remained intact. The changes in the chemical shift differences are linearly correlated with temperatures as shown in Fig. 1. The cause for the change cannot be the change in degrees of association of the solute, since the chemical shift differences observed at different concentrations of $\mathbf{6}_{12}$ in dimethyl-d_6 sulfoxide give the same inclinations of straight lines within experimental errors, as are shown in Fig. 2, although the absolute values of the chemical shifts change to some extent.

Such a temperature dependence may be attributed to either the solvation effect or the population effect: the latter concerns with the change in populations of conformers at various temperatures. Ifthe phenomenon were caused by the population effect, the following consideration would apply. Since the principal group which affects the chemical shifts of the benzylic protons is the aromatic ring, conformations made by rotation about the C_{Ar}–C_{CH_2} bonds may be considered: three possible conformations are shown in Fig. 3. The less stable conformers like **9** and **11** should increase in their populations when the temperature is raised. Interestingly, however, the coupling constants of the gem-hydrogens in conformations in **9** and **11** are expected to be larger than that of conformation **10** from the theory by Pople and Bothner-By.[14] This consideration leads to a conclusion that, if it were the population effect that caused the change in chemical shift differences, the coupling constants should have increased as well at higher temperatures. Since the coupling constants were almost the same at various temperatures, the situation discussed above will not apply to the present case. Thus the solvent effect becomes the reason of choice.

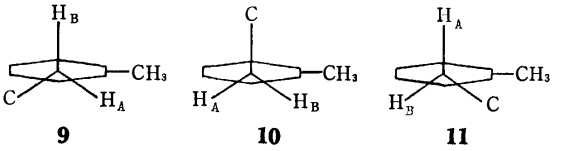

9 **10** **11**

Fig. 3. Rotational isomerism about C_{Ar}–C_{CH_2} bond.

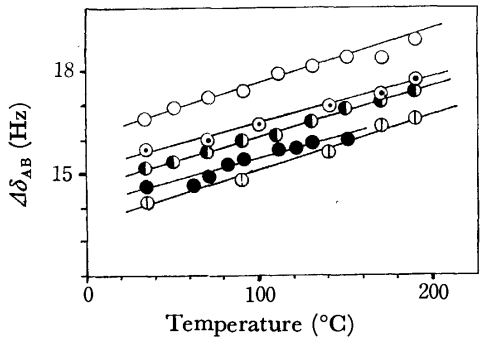

Fig. 1. Temperature dependence of the chemical shift difference between the benzylic methylene protons in $\mathbf{6}_{11}$—$\mathbf{6}_{15}$.
-○-; $\mathbf{6}_{11}$, -⊙-; $\mathbf{6}_{12}$, -◐-; $\mathbf{6}_{13}$, -◑-; $\mathbf{6}_{14}$, -●-; $\mathbf{6}_{15}$.

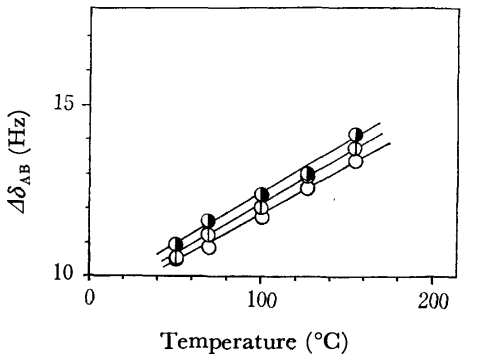

Fig. 2. Temperature dependence of the chemical shift difference between the benzylic methylene protons in $\mathbf{6}_{12}$ in DMSO-d_6.
-○-; 0.052 mol/l, -◑-; 0.25 mol/l, -◑-; 1.0 mol/l.

TABLE 5. FREE ENERGIES OF ACTIVATION FOR INTERNAL ROTATION OF THE AROMATIC RING[a]

Compound	$\Delta\delta_{AB}$ (Hz)	J_{AB} (Hz)	T_c (°C)	$\Delta G_c^{\ddagger}$ (kcal/mol)	Solvent
$\mathbf{2}_{15}$[2]	14.1	15.9	>170	>22.3	$CHCl_2CHCl_2$
$\mathbf{2}_{16}$[2]	(14.1)	(15.9)	<−50	<10.8	$CDCl_3$
$\mathbf{6}_{11}$	18.1	13.9			
$\mathbf{6}_{12}$	17.8	14.3	>190	>23.4	HCB[b]
$\mathbf{6}_{13}$	17.3	13.3			
$\mathbf{6}_{14}$	16.6	14.3			
$\mathbf{6}_{15}$	16.7	13.6	189	23.3	HCB[b]
$\mathbf{6}_{16}$	12.1	14.3	−50	11.0	$CDCl_3$–CS_2 (v/v 1:3)

a) The figures in parentheses are the assumed values.
b) HCB: hexachlorobutadiene.

temperature. Thus the barriers to rotation of the aromatic ring in these compounds must be very high. The minimum free energies of activation (see Table 5) are obtained by putting the NMR parameters into the following Eq. (2),[15] where $\Delta\delta_{AB}$'s were obtained by extrapolation of the straight lines shown in Fig. 1 to the coalescence temperature, when applicable.

$$\Delta G_c^{\ddagger} = 4.57T_c\{9.97+\log_{10}(T_c/\sqrt{\Delta\delta_{AB}^2+6J_{AB}^2})\} \quad (2)$$

As the temperature of a solution of $\mathbf{6}_{15}$ in hexachlorobutadiene was raised, the AB quartet signal gradually broadened accompanied by apparent increase in the chemical shift difference. On further warming, the chemical shift difference decreased and finally merged into a single broad peak. The temperature at which this line shape was attained was regarded as the coalescence temperature (Fig. 4).

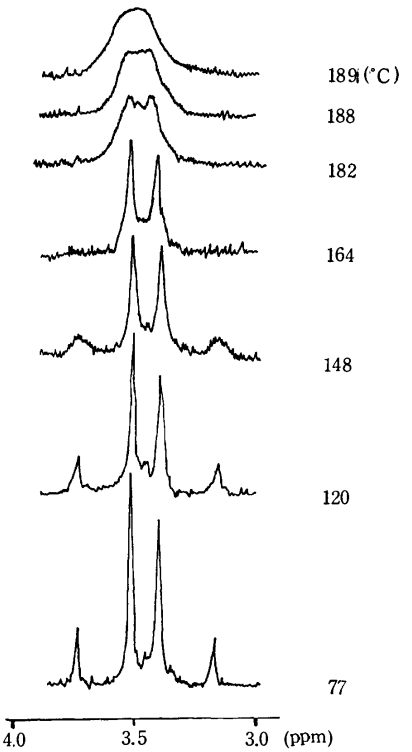

Fig. 4. Temperature dependence of PMR spectrum of $\mathbf{6}_{15}$ in hexachlorobutadiene.

In contrast, a solution of $\mathbf{6}_{16}$ in deuteriochloroform–carbon disulfide had to be cooled to find the coalescence. A chemical shift difference of 12.1 Hz and a coupling constant of 14.3 Hz were obtained at −70 °C. The free energy of activation for rotation in $\mathbf{6}_{16}$ was obtained as 11.0 kcal/mol.

The difference in the free energies of activation for internal rotation between $\mathbf{6}_{15}$ and $\mathbf{6}_{16}$ of the dioxa[*n*]-paracyclophane series is apparently as large as that between $\mathbf{2}_{15}$ and $\mathbf{2}_{16}$ of the diaza[*n*]paracyclophane series. This large difference in the height of barriers is caused by changing the number of methylene groups but one.

Comparison of the barriers and seeking a relation with the rigidity of the ansa chain will be interesting. Unfortunately, however, it is not possible to compare directly the barriers of the $\mathbf{2}_n$ series with those of the $\mathbf{6}_n$ series since the exact values of the former are not known. It might be said that, by and large, the barriers are about the same in both amide chains and ester chains, if the chain lengths are the same (see Table 5).

Rotational barriers for the aromatic rings in 14-substituted [12]paracyclophanes[16] and 1,12-disubstituted [12]paracyclophanes[17] have been reported to be 11—13 kcal/mol and *ca.* 13 kcal/mol, respectively. In contrast, 14,17-disubstituted 1,12-dioxa[12]paracyclophanes have been resolved into optical isomers at room temperature to indicate that the barrier will be more than 25—26 kcal/mol.[18] Apparently, the substitution pattern of the cyclophane must be taken into consideration in discussion of the barrier. Since the compounds discussed here have two methyl groups bonded to aromatic rings, the barrier may best be compared with those compounds resolved by Lüttringhaus and co-workers. Since the compounds of the largest ansa chain which have been resolved into enantiomers are 12 and it has not been possible to resolve a compound with an ansa chain of 14 atoms, it will be natural to assume that the compound of this type having an ansa chain of 14 atoms possesses a barrier lower than 25—26 kcal/mol. Then, since the barrier is lowered by *ca.* 10 kcal/mol by changing the chain length by one at the very critical length, the barrier for a compound having an ansa chain of 15 atoms may be assumed to have *ca.* 15 kcal/mol or less. Now comparison of the estimated barrier with those of the compounds having the ester or the amide groups in the ansa chain clearly indicate that the barrier is heightened by the introduction of these groups. Apparently the flexibility of the ansa chain is reflected to the barrier to rotation of the aromatic ring. Further study is necessary to estimate the effect of the rigidity on the barrier more quantitatively.

We wish to thank Prof. T. Shimanouchi of the University of Tokyo for permission of the use of the Perkin-Elmer 112G spectrometer. Thanks are also due to Dr. H. Nakanishi of National Chemical Laboratory for Industry who gave technical assistance in measurement of the spectra.

References

1) K. Sakamoto and M. Ōki, This Bulletin, submitted for publication.
2) K. Sakamoto and M. Ōki, *ibid.*, **46**, 270 (1973).
3) W. E. Stewart and T. H. Siddall, III, *Chem. Rev.*, **70**, 517 (1970).
4) M. Ōki and H. Nakanishi, This Bulletin, **44**, 3148 (1971).
5) K. Sakamoto and M. Ōki, *Tetrahedron Lett.*, **1973**, 3989.
6) R. H. Manske, "Organic Syntheses," Coll. Vol. II, p. 154 (1950).
7) K. Sakamoto and M. Ōki, This Bulletin, **47**, 2623 (1974).
8) J. S. Waugh and R. W. Fessenden, *J. Amer. Chem. Soc.*, **79**, 846 (1957).

9) O. Yamamoto and K. Hayamizu, "Kakuziki Kyomei Kyusyu," ed. by Y. Yukawa, Maruzen, Tokyo (1967), p. 170.
10) J. A. Pople, *Proc. Roy. Soc., Ser. A*, **239**, 541 (1957).
11) R. J. B. Marsden and L. E. Sutton, *J. Chem. Soc.*, **1936**, 1383; R. J. W. LeFevre and A. Sundaram, Jr., *ibid.*, **1962**, 3904; J. M. O'Gorman, W. Schand, Jr., and V. Schmacker, *J. Amer. Chem. Soc.*, **72**, 4222 (1950); J. K. Wilmshurst, *J. Mol. Spectrosc.*, **1**, 201 (1957).
12) M. Ōki and H. Nakanishi, This Bulletin, **44**, 3419 (1971); **45**, 1552, 1993 (1972).
13) C. E. Johnson, Jr., and F. A. Bovey, *J. Chem. Phys.*, **29**, 1012 (1958).
14) J. A. Pople and A. A. Bothner-By, *ibid.*, **42**, 1339 (1965).
15) J. A. Pople, W. G. Schneider, and H. J. Bernstein, "High Resolution Nuclear Magnetic Resonance," McGraw-Hill Book Co., New York (1958), p. 218; J. W. Emsley, J. Feeney, and C. H. Sutcliffe, "High Resolution Nuclear Magnetic Resonance Spectroscopy," Pergamon Press, Oxford (1965), p. 481.
16) M. Nakazaki, K. Yamamoto, and S. Okamoto, *Tetrahedron Lett.*, **1969**, 4597.
17) M. Nakazaki, K. Yamamoto, and S. Okamoto, This Bulletin, **45**, 1562 (1972).
18) A. Lüttringhaus and G. Eyring, *Ann. Chem.*, **604**, 111 (1957).

The Reaction of Alkyl Halides with Mercuric Thiocyanate

Nanao WATANABE,* Masaya OKANO,** and Sakae UEMURA
Institute for Chemical Research, Kyoto University, Uji, Kyoto 611

(Received July 18, 1974)

The reaction of secondary and tertiary alkyl halides with mercuric thiocyanate in less-polar solvents (*e.g.*, *n*-hexane, di-*n*-butyl ether, and 1,2-dichloroethane) was found to afford predominantly *N*-alkylation products, alkyl isothiocyanates, in contrast to the reaction with potassium salt in DMF. Especially, from *t*-butyl bromide, α-phenethyl bromide and benzhydryl chloride, the corresponding pure isothiocyanates were obtained in good yields. A most probable reaction mechanism is suggested, based on the relative rate data, the stereochemical result of the reaction with optically active α-phenethyl bromide, and the well-known catalytic effect of silver or mercury salt in S_N1 reaction.

The ambident nature of SCN^- has been known for a long time, as illustrated in the following scheme.

$$RX + KSCN \longrightarrow RSCN + KX$$
$$RCOX + KSCN \longrightarrow RCONCS + KX$$

The HASB principle has recently been applied to explain such a mode of attack; that is, alkyl halides react at the soft S atom of SCN^-, while the harder acyl halides react at the harder N atom.[1] In the thiocyanation of certain alkyl halides having a considerable S_N1 reactivity, however, the content of isothiocyanates in the products has been found to reach 35%.[2] This observation is also compatible with the above concept, because the increasing order of hardness of alkyl groups is primary<secondary<tertiary.[1] On the other hand, it has been shown that a change in the reacting site of the nucleophiles is caused by the variation of the counterions in the alkylation of various ambident nucleophiles, such as NO_2^-,[3] CN^-,[4] the anions of 1,3-dicarbonyl compounds,[5] and the anion of formamide.[4] These facts suggest that under appropriate conditions the predominant formation of alkyl isothiocyanates from the corresponding halides might be achieved. In view of the fact that sulfur atom is very powerful nucleophile, it seemed of interest for us to examine whether a preferable attack on the N atom of SCN^- may occur.

Results and Discussion

First of all, we examined the reaction of isopropyl iodide with various metal thiocyanates to know the effect of metal cations on the isomer distribution. The reaction was conducted in less-polar solvent such as *n*-hexane, because the fact is known that in the preparation of alkyl thiocyanates a considerable improvement in yields was achieved by use of polar aprotic solvents.[6] All metal salts used are hardly soluble in *n*-hexane, and the reaction is a heterogeneous process. The results are shown in Table 1. As can be seen from Table 1, $Hg(SCN)_2$ showed the best result for the *N*-alkylation of SCN^-, while other metal salts were less or not satisfactory. Although a predominant attack on the more electronegative (hard) site of the anions has been observed in the alkylation of NO_2^- and CN^- by using silver salts,[4] the attack on the soft S atom was preferred in the alkylation of SCN^- at least in *n*-hexane as solvent by using AgSCN and $Pb(SCN)_2$ as well as KSCN.

Table 1. Reaction of various metal thiocyanates with isopropyl iodide[a]

$M(SCN)_n$	React. temp. (°C)	React. time (hr)	Products Yield[b] (%)	Isomer ratio[c] *i*-PrNCS	*i*-PrSCN
$Hg(SCN)_2$	64—65	6	69	75	25
HgSCN	62—65	7	64	55	45
$Cu(NCS)_2$	63—65	7	12	63	37
CuNCS	61—64	5	0	—	—
$Ni(NCS)_2$	64—65	8	0	—	—
AgSCN	63—65	8	35	20	80
$Pb(SCN)_2$	67—69	10	1	9	91
KSCN	60—65	10	0	—	—
KSCN[d]	65—68	7	4	3	97

a) *i*-PrI and $M(SCN)_n$, each of 38 mmol. *n*-Hexane (30 ml) as solvent. b) Isolated yield. c) Determined by glc. d) 2,5,8,15,18,21-Hexaoxatricyclo[20,4,0,$0^{9,14}$]hexacosane[19] (crown ether) (38 mmol) was added to increase the solubility of KSCN.

Next, the effect of alkyl groups upon the isomer ratio in the products was studied in the reactions of several primary, secondary, and tertiary alkyl or aralkyl bro-

Table 2. Reaction of RBr with $Hg(SCN)_2$[a]

R in RBr	React. temp. (°C)	React. time (hr)	Products Yield[b] (%)	Isomer ratio[c] RNCS	RSCN
n-Bu	80—90	50	23	21	79
$PhCH_2$	70—75	1	74	36	64
i-Pr	70—75	8	44[d]	85	15
c-C_6H_{11}	75—80	11	16	73	27
PhCH(Me)	75—80	0.66	87	99	1[d]
PhCH(Me)	0—1	1	70	99	1[d]
t-Bu	70—72	0.66	68	96	4
Ph_2CH[e]	30—34	2.5	90	100	0[d]

a) RBr and $Hg(SCN)_2$, each of 38 mmol. $(n\text{-Bu})_2O$ (30 ml) as solvent. b) Isolated yield. c) Determined by glc. d) Determined by titration method. e) Chloride.

* Koei Chemical Co., Ltd., Joto-ku, Osaka 536.
** To whom correspondence should be addressed.

mides with $Hg(SCN)_2$ in di-*n*-butyl ether. The reaction mixtures were heterogeneous in all cases. The results are presented in Table 2. As shown in Table 2, isothiocyanates became the predominant isomer when secondary and tertiary bromides were submitted to the reaction, and particularly in cases of the bromides which were capable of forming stable carbonium ions the selectivity was excellent. In addition, a formation of a small amount of the elimination product was observed in the reaction with some bromides. These observations appeared to agree with those expected for S_N1 process.

Since the thermal isomerization of alkyl thiocyanates into isothiocyanates (where alkyl groups are tertiary or aralkyl ones), especially with ease in the presence of $ZnCl_2$, has been known,[7] some controlled experiments on the isomerization were undertaken. For example, when a mixture of *t*-butyl thiocyanate and isothiocyanate (42.6: 57.4) was heated at 70—72 °C for 0.66 hr in di-*n*-butyl ether in the presence of $Hg(SCN)_2$ or $HgBr_2$, the isomer ratio in the resulting mixture was almost unchanged (42.4: 57.6 and 40.9: 59.1, respectively). For a mixture of α-phenethyl thiocyanate and isothiocyanate, a change in the isomer ratio was very little (from 97: 3 to 95.6: 4.4) after heating in di-*n*-butyl ether in the presence of $Hg(SCN)_2$ at 70 °C for 0.75 hr. Similarly, no isomerization was observed in cases of isopropyl and cyclohexyl thiocyanates. Hence, it can be said that the isomer ratios shown in Table 2 are kinetically controlled.

On the other hand, no details on the isomer distribution in the reaction of alkyl halides with alkali metal thiocyanates in polar aprotic solvents have been reported, where the reaction is believed to proceed by S_N2 process. Therefore, we have examined it in DMF solvent using alkyl bromide as alkylating agent. The data are shown in Table 3. Primary and secondary

Table 3. Reaction of RBr with KSCN[a]

R in RBr	React. temp. (°C)	React. time (hr)	Products: Yield[b] (%)	Products: Isomer ratio[c] RNCS	Products: Isomer ratio[c] RSCN
n-Bu	75—80	8	87	1	99
n-Bu	70—75	0.66	89	1	99
$PhCH_2$	75—80	3	95	2	98
i-Pr	75—80	6	81	2	98
c-C_6H_{11}	85—90	6	78	4	96
PhCH(Me)	75—80	0.66	76	3	97[d]
PhCH(Me)	75—80	5	86	52	48[d]
t-Bu	70—75	0.66	37	52	48
Ph_2CH[e]	70—75	0.66	86	100[d]	0[f]
Ph_2CH[e]	30—32	0.66	8[g]	0	100[g]

a) RBr 38 mmol, KSCN 57 mmol. DMF (30 ml) as solvent. b) Isolated yield. c) Determined by glc. d) Determined by titration method. e) Chloride. f) It has been reported that the reaction of benzhydryl bromide with KSCN in boiling benzene or alcohol gives only thermodynamically controlled diphenylmethyl isothiocyanate.[20] g) Determined by NMR. Ph_2CHNCS δ 5.83, Ph_2CHSCN δ 5.63 (in CCl_4).

Table 4. Reaction of *i*-PrX with $Hg(SCN)_2$ in various solvents[a]

X in *i*-PrX	Solvent (30 ml)	React. temp. (°C)	React. time (hr)	Products: Yield[b] (%)	Products: Isomer ratio[c] *i*-PrNCS	Products: Isomer ratio[c] *i*-PrSCN
Br	$(n\text{-Bu})_2O$	70—75	8	44[d]	85	15
I	$(n\text{-Bu})_2O$	70—75	4	72[d]	83	17
Br	*n*-hexane	60—65	22	29	85	15
I	*n*-hexane	60—65	6	69	75	25
Br	$ClCH_2$-CH_2Cl	70—75	18	41	83	17
I	$ClCH_2$-CH_2Cl	65—70	4	66	80	20
Br	CH_3CN	65—70	3.5	5	71	29
I	CH_3CN	60—65	3	16	63	37
I	DMF	75—80	5	11	61	39

a) *i*-PrX and $Hg(SCN)_2$, each of 38 mmol. The reaction was homogeneous only in DMF. b) Isolated yield. c) Determined by glc. d) Determined by titration method.

bromides reacted more readily than tertiary one, as expected, and the obtained alkyl thiocyanates were generally contaminated with few percent of isomeric isothiocyanates, except for some cases. In contrast to the results in di-*n*-butyl ether, the isomerization of α-phenethyl and *t*-butyl thiocyanates to the corresponding isothiocyanates occurred readily in DMF.

The impressive solvent effect on the course of ambident anion alkylations has been mentioned very often.[5] Therefore, the reactions of isopropyl bromide or iodide with $Hg(SCN)_2$ were conducted in various solvents and the effect of solvents on the isomer ratio was studied. The results, which are recorded in Table 4, show that the requirement for the predominant isothiocyanate formation is the use of less-polar solvents such as di-*n*-butyl ether, *n*-hexane, and 1,2-dichloroethane. The isomer ratios were almost constant at least in these solvents. Further, isopropyl iodide reacted more rapidly than the bromide as expected, but the observed isomer ratios for the products obtained from both halides were almost identical. This would be natural if an S_N1 mechanism is operative for this reaction. Of particular interest are the facts that a preference for *N*-alkylation was held even in polar aprotic solvents and that the total yield of two isomers and the product selectivity in a homogeneous system (reaction in DMF) were quite similar to those in a heterogeneous one (reaction in acetonitrile). In addition, the yield of isopropyl thiocyanate formed by the reaction with $Hg(SCN)_2$ in DMF was surprisingly poor (compare the data in Tables 3 and 4), indicating that no considerable amounts of free SCN^- are formed even in a homogeneous system. Significant decreases in the yields of the isomeric mixture for the reaction in DMF and acetonitrile may be ascribed to the strong solvation of the dissolved $Hg(SCN)_2$ species by these solvents, because a strong interaction between metal salts or metal cations with such solvent molecules has been well-known.

In order to obtain further information on the mecha-

nism of the reaction, the studies on the relative reaction rates in alkyl bromides and also on the stereochemistry of the reaction were undertaken. First, by competitive reactions with any two alkyl bromides, the following data were obtained. The observed reactivity

n-BuBr:*i*-PrBr:*t*-BuBr=1:10:10^4 (at 65°C, in *n*-hexane)

$PhCH_2Br$:PhCH(Me)Br=1:7 (at 0—1°C, in *n*-hexane)

order, tertiary≫secondary>primary, appears to confirm that the reaction is essentially pictured as an S_N1 type substitution.[8] Moreover, such an order did not change when the partial rates for each product were compared. Hence, a possibility is considered that both isomeric products are produced *via* a common alkyl cation formed by the attack of $Hg(SCN)_2$ on the halogen atom. That the formation of such a mercury–halogen bond furnishes an important part of the driving force for the ionization is clear from the failure of sulfonates such as isopropyl tosylate to react with $Hg(SCN)_2$ (at 80 °C, for 23 hr, in di-*n*-butyl ether), because sulfonates are known to be generally more reactive than the corresponding bromides toward nucleophiles.[9a] It should be also noted that silver or mercury-salt catalysis of S_N1-like substitution of alkyl halide is quite well-known.[9b]

Second, after treatment of (*R*)-α-phenethyl bromide (optical purity, 62.3%) with $Hg(SCN)_2$ suspended in *n*-hexane (at 0 °C for 1 hr), the isothiocyanate in a mixture of isomeric products (77% yield) was converted into the thiourea derivative by the addition of benzylamine. The isolated *N*-benzyl-*N'*-α-phenethylthiourea after recrystallization from ethanol was almost optically inactive (see Experimental). The same result was obtained by using (*S*)-α-phenethyl bromide (optical purity, 38.7%). Here, there is no possibility that the optically active isothiocyanate was initially formed and then racemized, because no appreciable racemization of (*S*)-α-phenethyl isothiocyanate was observed under reaction conditions (at 0—1 °C, for 1 hr, in *n*-hexane, in the presence of $Hg(SCN)_2$). Further there may be some possibility that in the experiment described above the starting α-phenethyl bromide is racemized catalytically by mercury salt before isothiocyanation. When (*R*)-α-phenethyl bromide was treated with $HgBr_2$ in *n*-hexane (at 0—1 °C, for 1 hr), however, the recovered bromide still retained 22% of optical purity (78% racemization). These results indicate that isothiocyanation proceeds with almost complete racemization. The result that the extent of racemization by $HgBr_2$ agrees well with the total yields of the racemized isomeric mixture of SCN compounds suggest that both reactions proceed through the common ionization step which is rate-determining.

There are some data on the relative reactivity of the S- to the N-end of SCN^- towards carbonium ions. Fava *et al.*[10] found the value $k_S/k_N=5$ toward 4,4'-dimethylbenzhydryl cation in acetonitrile, by estimating the partition of radioactivity. In the solvolysis of 4,4'-dimethylbenzhydryl halides in 65% aqueous acetone containing SCN^-, the same value was obtained.[10] Taft and Cannell[2] obtained the values ranging from 2 to 9, from the product ratio in the reaction of certain carbonium ion precursors. In contrast to these data, much lower values were observed in the reaction of secondary and tertiary alkyl halides with $Hg(SCN)_2$ as described above, regardless of the solvent polarity. For example, the k_S/k_N values calculated from the isomer ratios were 0.41 and 0.18 for isopropyl cation in acetonitrile and di-*n*-butyl ether, respectively, and less than 0.01 for α-phenethyl cation in di-*n*-butyl ether. Such a high selectivity for *N*-alkylation may be correlated with the structure of $Hg(SCN)_2$, which is confirmed to be S-bonded.[11] Since the existence of considerable amounts of free SCN^- in the reaction system is unexpectable as described above, the anion should be present mostly in the form of $XHg(SCN)_2^-$ which is the counter ion at the carbonium ion formation. If this complex ion serves as a source of SCN^-, the reaction with cationic species would occur mainly at the terminal N atom which is the sterically favorable and more electronegative site.

A presumed mechanism for the reaction with secondary and tertiary halides can be summarized in the following scheme.

$$RX + Hg(SCN)_2 \xrightarrow{\text{slow}} R^+ + XHg(SCN)_2^-$$

$$R^+ + XHg(SCN)_2^- \longrightarrow RNCS(\text{major}) + RSCN + HgX(SCN)$$

Finally we must add a short comment on the reaction of primary halides with $Hg(SCN)_2$ in less polar solvents, although no decisive data are available at present. On accounts of considerable instability of primary cations, a push-pull process which involves the push by SCN^-, probably formed in a small amount by the ionization of the dissolved $Hg(SCN)_2$, and the pull by $Hg(SCN)_2$ may be operative in this case together with the mechanism described above. In a similar reaction of alkyl halides with silver nitrate, the contribution of a push-pull mechanism has been already established.[3]

Experimental

All the organic substances, including the solvents, were used after distillation. Commercial metal thiocyanates and $HgBr_2$ (best grade) were used without further purification.

The isomer ratios of alkyl thiocyanates and isothiocyanates were mostly determined by gas chromatography (glc), and in some cases where glc analyses were unapplicable they were determined by titration method or NMR analysis. The glc analyses were carried out with a Shimadzu 5APTF apparatus using Apz-L (1 m) and PEG-6000 (3 m) columns (carrier gas, N_2). The titration method is based on the addition of butylamine to alkyl isothiocyanates.[12] The NMR spectra were obtained on a Varian A-60 spectrometer (solvent, CCl_4; internal standard, TMS). Optical rotations were measured on a JASCO DIP-180 automatic polarimeter.

Reaction of Alkyl Halides with Mercuric Thiocyanate. Several examples of the reaction of isopropyl halides with $Hg(SCN)_2$ are given below.

a) *In* n-*Hexane*: To a stirred suspension of $Hg(SCN)_2$ (12.0 g, 38 mmol) in *n*-hexane (30 ml) isopropyl iodide (6.5 g, 38 mmol) was added slowly at 64—65 °C, and the mixture was kept for 6 hr under stirring. The reaction mixture was cooled and filtered to remove the precipitate of inorganic salts. The solvent in the filtrate was removed, and the

resulting residue was distilled, affording a mixture of isopropyl thiocyanate and isothiocyanate (2.6 g, 69% yield), bp 57—58 °C/45 mmHg. The isomer ratio of S/N by glc was 25/75.

b) *In Di-n-butyl Ether*: In a similar way, isopropyl bromide (9.7 g, 79 mmol) was allowed to react with a suspension of $Hg(SCN)_2$ (24.0 g, 76 mmol) in di-*n*-butyl ether (60 ml) under stirring at 70—75 °C for 8 hr. Since the boiling point of the solvent is close to that of the products in this case, the filtrate was analyzed by glc without the evaporation of the solvent. The observed isomer ratio was 15/85. The amount of isopropyl isothiocyanate in the filtrate was determined by the titration method. Based on this, the total yield was calculated (3.5 g, 44%).

c) *In DMF*: Isopropyl iodide (6.5 g, 38 mmol) was similarly treated with a homogeneous solution of $Hg(SCN)_2$ (12.0 g, 38 mmol) in DMF (30 ml) under stirring at 75—80 °C for 5 hr. The reaction mixture was then cooled, filtered, and poured into a large amount of ether (*ca.* 200 ml), and washed by water (2×100 ml). The ether layer was dried by $MgSO_4$ and evaporated to give an oily residue. Distillation afforded a mixture of the expected thiocyanate and isothiocyanate (0.42 g, 11%), bp 61—64 °C/45 mmHg. By glc, the isomer ratio was found to be 39/61.

Competitive Reactions. To a stirred suspension of $Hg(SCN)_2$ (24.0 g, 76 mmol) in *n*-hexane (60 ml) a mixture of isopropyl bromide (8.5 g, 69.1 mmol) and *t*-butyl bromide (1.05 g, 7.6 mmol) was added slowly at 65 °C. After stirring for 1 hr at that temperature, the mixture was worked up as before. A distillate boiling at 60—62 °C/50 mmHg was collected (0.45 g) and analyzed by glc. The combined yield of isopropyl thiocyanate and isothiocyanate was 0.052% (0.036 mmol) and that *t*-butyl compounds was 50% (3.8 mmol). Then the relative rate for these two bromides was 1:960. In a similar way, the competitive reaction of *n*-butyl and isopropyl bromides (each of 38 mmol) (at 65 °C for 7 hr) afforded the corresponding isomeric mixtures in yields of 1.2 mmol and 12.4 mmol, respectively, indicating a 1:10 relative rate. Similarly, the relative rate of benzyl and α-phenethyl bromides was found to be 1:7 at 0—1 °C. In this case, analysis was carried out by NMR method. The following signals were taken up for analysis: δ values for α-H of benzyl thiocyanate and isothiocyanate was 4.03 and 4.59, and those for α-CH_3 of α-phenethyl thiocyanate and isothiocyanate were 1.78, 1.90(d) and 1.60, 1.70(d).

Stereochemical Data. a) *Reaction of (R)-α-Phenethyl Bromide with $Hg(SCN)_2$ in n-Hexane.* (*R*)-α-Phenethyl bromide, α_D^{20} +105.88° (neat) (optical purity, 62.3%[13]) was prepared from the corresponding optically active alcohol by the procedure of Gerrard.[14] This bromide (3.5 g, 18.9 mmol) was treated with $Hg(SCN)_2$ (9.0 g, 28.4 mmol) in *n*-hexane (30 ml) at 0—1 °C for 1 hr under stirring, and the reaction mixture was worked up as usual. A distillate boiling at 111—112 °C/6.5 mmHg was collected (2.38 g, 77%). This product (1.1 g, 6.74 mmol) was converted into *N*-benzyl-*N'*-α-phenethylthiourea (1.7 g, 94%) by the addition of benzylamine (1.4 g, 13.4 mmol) in ether. Recrystallization from ethanol afforded the pure thiourea, mp 100—101 °C (lit,[11] 100 °C), $[\alpha]_D^{20}$ −0.066 (*c* 5.9, 96% EtOH) (optical purity, 0.26%).[15] Additional crystals obtained from the mother liquor did not show any optical rotation.

Quite similar treatment using (*S*)-α-phenethyl bromide, α_D^{20} −65.74° (neat) (optical purity, 38.7%), gave *N*-benzyl-*N'*-α-phenethylthiourea of $[\alpha]_D^{20}$ −0.020 (*c* 5.9, 96% EtOH), and additional crystals obtained from the mother liquor did not show any optical activity.

b) *Racemization of (R)-α-Phenethyl Bromide with $HgBr_2$ in n-Hexane.* When a solution of the above bromide (1.01 g, 5.47 mmol) in *n*-hexane (10 ml) was treated with $HgBr_2$ (3.0 g, 8.32 mmol) at 0—1 °C for 1 hr, a decrease in the optical rotation from $[\alpha]_D^{20}$ +63.24° to 13.60° (*c* 10.12, *n*-hexane) was observed, which corresponds to 78% of racemization.

c) *Attempted Racemization of (S)-α-Phenethyl Isothiocyanate with $Hg(SCN)_2$ in n-Hexane.* (*S*)-α-Phenethyl isothiocyanate, α_D^{20} +28.76° (neat) was prepared from the corresponding optically active amine by the method of Teventev.[16] This isothiocyanate (7.5 g, 46 mmol) was treated with $Hg(SCN)_2$ (30 g, 95 mmol) in *n*-hexane (100 ml) at 0—1 °C for 1 hr, and it was recovered by distillation after usual work-up procedure. It showed α_D^{20} +28.74° (neat), indicating no loss of the optical activity.

Authentic Samples for Glc Analyses. Alkyl thiocyanates were prepared by the reaction of alkyl bromides with KSCN in DMF,[6] though they were generally contaminated with a small amount of the isomers. Alkyl isothiocyanates were synthesized from the corresponding amines (*via* thiocarbamates) by the method of Martin.[17] Benzhydryl isothiocyanate was isolated from the reaction product by distillation, bp 160—165 °C/4 mmHg, mp 59 °C (from EtOH, lit,[18] 58 °C).

References

1) R. G. Pearson and J. Songstad, *J. Amer. Chem. Soc.*, **89**, 1827 (1967).

2) R. W. Taft, Jr. and L. G. Cannell, National Meeting of the American Chemical Society, Dallas, Tex., April, 1956 (Abstracts of Papers, Organic Division, p. 40-N).

3) N. Kornblum, R. A. Smiley, R. K. Blackwood, and D. C. Iffland, *J. Amer. Chem. Soc.*, **77**, 6269 (1955).

4) For a general survey, see Ref. 3.

5) For example, see a review, W. J. LeNoble, *Synthesis*, **1970**, 1.

6) S. Yoneda, H. Kitano, and K. Fukui, *Kogyo Kagaku Zasshi*, **65**, 1816 (1962), and references cited therein.

7) P. A. S. Smith and D. W. Emerson, *J. Amer. Chem. Soc.*, **82**, 3076 (1960).

8) For typical S_N1 and S_N2 reactions, the following relative rates were found.[9] Solvolysis in formic acid (at 25 °C); EtBr: *i*-PrBr: *t*-BuBr = 1.7: 45: 10^8. Br-Br* exchange in acetone (at 25 °C); *n*-PrBr: *i*-PrBr: *t*-BuBr = 1: 0.02: 0.005.

9) a) C. K. Ingold, "Structure and Mechanism in Organic Chemistry," 2nd Ed., Cornell Univ. Press, Ithaca (1969), pp. 428—457. b) *ibid.*, pp. 479—483.

10) A. Fava, A. Iliceto, A. Ceccon, and P. Koch, *J. Amer. Chem. Soc.*, **87**, 1045 (1965).

11) R. Lasson and A. Miezis, *Acta Chem. Scand.*, **19**, 47 (1965); S. C. Jain and R. Rivest, *Can. J. Chem.*, **47**, 2209 (1969).

12) S. Siggia and J. G. Hanna, *Anal. Chem.*, **20**, 1084 (1948).

13) Based on a specific rotation of the pure compound, α_D^{20} +170° (neat); H. M. R. Hoffman and E. D. Hughes, *J. Chem. Soc.*, **1964**, 1244.

14) W. Gerrard, *ibid.*, **1945**, 848.

15) Ref. 11; Optical purity was calculated on the basis of a specific rotation of the pure compound, $[\alpha]_D^{24}$ −23.4° (*c* 2.3, 96% EtOH).

16) A. P. Terentev, E. G. Rukhadge, and V. V. Dunina, *Dokl. Akad. Nauk SSSR*, **187**, 1328 (1969); *Chem. Abstr.*, **71**, 123767d (1969).

17) D. Martin, E. Beyer, and H. Gross, *Chem. Ber.*, **98**, 2425 (1965).

18) J. V. Brawn, *Ber.*, **45**, 2188 (1912).

19) C. J. Pedersen, *J. Amer. Chem. Soc.*, **89**, 7017 (1967).

20) H. L. Wheeler, *Amer. J. Chem.*, **26**, 345 (1901).

Isotope Effects in the Reactions of ^{80}Br Activated by Isomeric Transition with Various Deuterated Propanes

Enzo Tachikawa and Kenshi Numakura

Division of Chemistry, Japan Atomic Energy Research Institute, Tokai-Mura, Ibaraki 319-11

(Received April 30, 1974)

Product studies of the reactions of recoil ^{80}Br with propanes in binary mixtures with ethane showed that the difference in the energy-loss efficiency of C_3H_8 and C_3D_8 in collision with ^{80}Br was less than 10%. Then, the yields for the substitution of ^{80}Br for atoms or groups have been compared in various deuterated propanes. A reactivity integral-isotope effect has been observed in the yields of products from $CD_3CD_2CD_3$ and $CD_3CH_2CD_3$, except in the case of isopropyl bromide from the latter compound. However, it has been observed only in the yield of iso propyl bromide from $CH_3CD_2CH_3$. These results indicate that the chemical and physical properties of both replaced and residual atoms or groups play a role in the observed isotope effects. With a "complex" formation mechanism, it is suggested that an isotope effect appears mostly when the kinetic energy of the reacting ^{80}Br is at the lower-energy end of the reaction-energy range.

One of the experimental approaches used to obtain valuable information concerning the mechanisms and characteristics of the reactions of energetic atoms is to measure the isotopic variation in the reaction yields from protonated and deuterated reactants. Thus far, the existence of the isotopic preference in the substitution reaction of ^{80}Br for H over D has been demonstrated in CH_4–CD_4[1,2] C_2H_6–C_2D_6[3] and CH_3F–CD_3F[4] systems. However, these observed reactivity integral-isotope effects directly reflect the composite of the primary and secondary isotope effects. The relative importance of the magnitude of these effects can be evaluated through competitive experiments in the intra- and inter-molecular comparisons of various deuterated compounds.

The present paper will deal with the isotopic variation between C_3H_8 and fully- or partially-deuterated propanes in the substitution reaction of the ^{80}Br activated by the isomeric transition. The results obtained cannot be explained solely by the two models so far proposed for the substitution reaction of the recoil tritium atoms; one of them based on the rotational inertia,[6,7] and the other, on the electronegativity[8–10] of the residual group. Instead, the results indicate that a complete explanation must involve an effect combining the physical and chemical properties of the replaced atom or group, and those of the residual group.

Experimental

Sample Preparation and Analysis. The preparation of samples followed the routine procedures used in our previous work for gas-phase bromine hot atom chemistry.[11] The ^{80m}BrBr was formed by irradiating gaseous Br_2 with thermal neutrons for one minute in a JRR-4 reactor at JAERI. The reaction mixture was allowed to stand more than 2 hr to permit a ^{80m}Br^{80}Br parent-daughter equilibium to be established. All the samples contained 65 Torr of oxygen in order to exclude the formation of isopropyl bromide tagged with ^{80}Br by light- or radiation-induced reaction. The total pressure was always kept constant at 710±10 Torr. The reaction products were analyzed by means of a radio-gas chromatograph equipped with a flow-type G-M counter. The results obtained were processed using the BOB 7 series program[12] corrected for the background and for the radioactivity decay of nuclides.

Percentage Yield. The less than 0.1% of propylene present as an impurity in propane significantly interfered with the direct measurement of the total organic yield.[11] Thus, the absolute yield has been measured only from the ^{80}Br–C_2H_6–O_2 (3.2±0.1%) system by a solvent-extraction method. Individual radioactivity yields have been obtained by dividing the activities in the radio-gas chromatogram by the total ^{80}Br activity, as measured with a G-M counter 2 hr after sampling the gases. The relative yields have been normalized to the percentage yields using a conversion factor determined from the sum of the relative yields and from the total organic yield found in the above system. The chief uncertainty involved in this procedure is introduced in the measurement of the total ^{80}Br activity, and the accuracy in the percentage yield obtained is usually limited to ±10%.

Chemicals. Ethane and C_3H_8 of the highest grade were obtained from the Takachiho Chemical Co. The deuterated propanes came from the Merk Sharp and Dohme Co., their listed purities were all 98%. These reagents were used after the freezing-thawing purification had been repeated several times.

Results and Discussion

Bromine-80 activated from the (I.T.) process reacts with hydrocarbons either by an energetic process or by a non-energetic process; the relative importance of the latter depends on the circumstances.

The most common means of identifying energetic reactions is the addition of a chemically-inert moderator to the system. In general, noble gases are used as moderators. Such moderators have no effect on the thermal energy distribution. However, by reducing the excess kinetic energy of an energetic atom in each collision, the moderator will reduce and sometimes eliminate energetic reactions.

Of particular importance is the early recognition that the charge state of the reacting ^{80}Br is primarily controlled by the ionization potential of the constituents of the reaction systems, and that an additional product is formed *via* thermal ionic processes in the presence of an inert gas with a higher ionization potential than that of Br. Thus, the reactions in the binary system have been studied using C_2H_6 as a counterpart as in the previous paper.

Table 1 shows the yield variation in the products in

Table 1. Percent ^{80}Br stabilized in organic combination in C_3D_8–C_2H_6 binary system[a)]

$\frac{C_3D_8}{C_3D_8+C_2H_2}$	Methy bromide (%)	Ethyl bromide (%)	*i*-Propyl bromide (%)	*n*-Propyl bromide (%)	Methylene bromide (%)
1.00	0.77±0.02	0.36±0.02	0.15±0.02	0.49±0.03	0.30±0.03
0.801	0.90±0.02	0.50±0.02	0.13±0.02	0.44±0.02	0.33±0.03
0.545	1.10±0.02	0.69±0.08	0.09±0.01	0.35±0.02	0.39±0.02
0.287	1.25±0.02	0.93±0.02	0.05±0.01	0.20±0.01	0.42±0.01
0.054	1.62±0.02	1.18±0.02	—	0.06±0.01	0.53±0.01
0.00	1.53±0.02	1.23±0.02	—	—	0.40±0.02

a) Average of several measurements

C_3D_8–C_2H_6 mixtures, the m.f. of the latter varying from zero to 1.0. With the addition of C_2H_6, the yields of iso- and *n*-propyl bromides, which are formed only from C_3D_8, decrease from 0.15±0.02 and 0.49±0.03 respectively to zero. However, methyl, ethyl, and methylene bromides are formed from the reactions with either constituent; the observed yields are the sum of those from both constituents. The contribution to the overall observed yield from each constituent can be estimated on the assumption that the relative yield distribution among the products from C_3D_8 remains constant over the entire range of the m.f. of C_3D_8. This permits the calculation of the yields of products at any m.f. of C_3D_8 by simply multiplying the percentage yield of *n*-propyl bromide by the constant determined based on the yields found without the addition of C_2H_6.

The corresponding yields of products originating from C_2H_6 can be obtained as the difference between the calculated yield and the observed yield at any measuring point; the yields are shown in Fig. 1. The results show that the yield decreases to zero with an increase in the m.f. of C_3D_8 and that no significant interference of other possible processes exists in the yield variation. This implies that the thermal ionic process is not important in this binary system as the case in the C_3H_8–C_2H_6 system.[11]

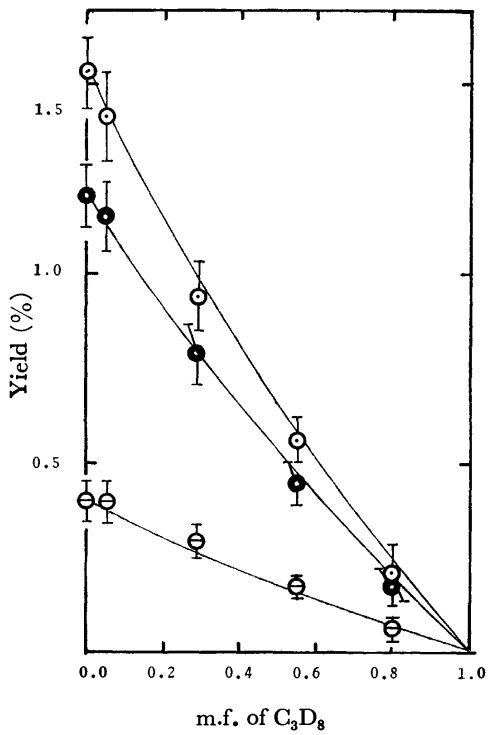

Fig. 1. Estimated and Calculated Yields of Products in Reactions of ^{80}Br with C_2H_6
Estimated yield; ⊙: methyl bromide ●: ethyl bromide, ⊖: methylene bromide, Calculated yield; solid line (equation 1)

The solid lines are the yield curves obtained using this equation;[11]

$$\frac{1}{P}=\frac{\alpha_{(C_3D_8)}}{I}+\frac{\alpha_{(C_2H_6)}}{I}\cdot\frac{f_{(C_3D_8)}+A\cdot f_{(O_2)}}{f_{(C_2H_6)}} \qquad (1)$$

where $A=\alpha_{(O_2)}/\alpha_{(C_3D_8)}$. The f_i is the relative probability of the collision of ^{80}Br with the i component, and where α_i is the average energy loss on collision with the i component. For the calculation, $\alpha_{(C_3D_8)}/\alpha_{(C_2H_6)}$ was equalized to $\alpha_{(C_3D_8)}/\alpha_{(C_2H_6)}$, which had previously been determined as 1.1 with $A=0.65$ in the ^{80}Br–C_3H_8–C_2H_6–O_2 system.[11] The fit of the estimated values on the calculated curve is reasonably good, but at the higher m.f. values of C_3D_8 the deviation becomes large and amounts to roughly 10%. In the present calculation, a little uncertainty in the yield from the major constituent leads to a large uncertainty in the yield from the counterpart; a 10% uncertainty in the former causes roughly 20—30% uncertainty in the latter, which covers the observed deviation in Fig. 1. Thus, the deviation from the solid lines toward the lower yield results mostly from the uncertainty in the yield from C_3D_8, but partly from the moderator-isotope effect[5] between C_3D_8 and C_3H_8. The moderator-isotope effect introduced by replacing H in C_3H_8 by D must be largest between C_3H_8 and C_3D_8, since these are the two extreme compounds. Thus, as for the present analysis, the moderator-isotope effect is considered to be less than 10%. This allows us to compare the yields of products from various deuterated propanes without correction for any difference in the moderating efficiency of these compounds within this limited accuracy.

Reactivity Integral Isotope Effect. Table 2 summarizes the product yields from various deuterated propanes. The *K* values in the table are the yields from fully protomated propane, relative to that from deuterated propane, and are equal to an overall isotope effect in the formation of the products under given conditions.

These results require essentially no correction for the kinetic energy-independent processes of the ^{80}Br atom.

Table 2. Yields of products formed by reactions of ^{80}Br with variously deuterated propanes

Products	Reactant						
	$CH_3CH_2CH_3$ (%)	$CH_3CD_2CH_3$		$CD_3CH_2CD_3$		$CD_3CD_2CD_3$	
		(%)	$(K)^{a)}$	(%)	$(K)^{a)}$	(%)	$(K)^{a)}$
Methyl bromide	1.12±0.11	1.05±0.11	(1.1)	0.82±0.08	(1.4)	0.77±0.08	(1.5)
Ethyl bromide	0.57±0.06	0.54±0.05	(1.1)	0.38±0.04	(1.5)	0.36±0.04	(1.6)
i-Propyl bromide	0.20±0.02	0.15±0.02	(1.3)	0.19±0.02	(1.1)	0.14±0.01	(1.4)
n-Propyl bromide	0.67±0.07	0.60±0.06	(1.1)	0.45±0.05	(1.5)	0.49±0.05	(1.4)
Methylene bromide	0.47±0.05	0.50±0.05	(0.94)	0.35±0.04	(1.3)	0.30±0.03	(1.6)
Total	3.03	2.84		2.19		2.06	

a) $K = \dfrac{\text{Product yield from } CH_3CH_2CH_3}{\text{Product yield from deuterated propane}}$.

In order to make an intermolecular comparison of the product yield, however, the results must be corrected for both the secondary decomposition of the excited primary products[13-15] and the non-equivalence of the ^{80}Br spectrum in each sample.[1,16]

Such unimolecular decomposition processes can be conveniently investigated by pressure-variation experiments, such as were previously carried out with C_3H_8.[11] In the pressure range between 600 to 1600 Torr, the yields of products remained almost constant, and the intermolecular distribution of the ^{80}Br atom among the products was essentially constant. Thus, without further quantitative knowledge concerning the decomposition products, it can only be assumed that a direct comparison of the yields of the individual products requires no significant correction for the secondary decomposition. This is a reasonable assumption since, if such a decomposition occurs, its extent will be as large or greater in protonated than in deuterated compounds. This is the reverse of the isotope effect observed, and any correction for the decomposition tends to further enlarge the isotope effect.

For the second correction for the ^{80}Br atom flux, we need correct knowledge concerning the energy-loss processes of energetic ^{80}Br atoms. However, experimentally, the ^{80}Br atom flux can be controlled by the addition of a large excess of a common molecule as an energy moderator.[16] Table 3 shows the yields of the iso- and *n*-propyl bromides found in the presence of 0.5 m.f. of C_2H_6. The results show a similar trend as in the absence of C_2H_6, a preference for the substitution of H over D atoms.

These results, together with those in Fig. 1 make it reasonably sure that the K values in Table 1 are a good measure of the isotopic variation in the reactivities of various deuterated propanes toward the energetic ^{80}Br atoms.

^{80}Br-for-R Reaction. One of the things shown in Table 1 is that the isotope effect on methyl, ethyl, and methylene bromides appears on both $C_3H_2D_6$ and C_3D_8, but not on $C_3H_6D_2$. These results are not fully predicted either by the rotational inertia effect of the residual group[6] or by the electronegativity[9,10] of the replaced atom or group. The former can predict only an isotope effect on methyl bromide, and the latter essentially no isotope effect.

The absence of the isotope effect on the methyl bromide yield from $C_3H_6D_2$ indicates practically no effect of the D atom in the methylene group on the ^{80}Br-for-ethyl reaction. Thus, the isotope effect on the ^{80}Br-for-ethyl reaction in both $C_3H_2D_6$ and C_3D_8 must originate from the replacement of H by D in the residual methyl group or from that in the methyl in the ethyl group. However, any effect of the D atom separated by C-C bond on the reactivity is generally much less important than that of the D atom attached to the reacting C atom; the observed isotope effect results from the difference in the chemical and physical relaxation of the residual CH_3 and CD_3 groups.

A similar consideration suggests that any consistent explanation for the isotope effect on the ethyl bromide must involve a quick rearrangement of the replaced methyl group for a stable combination between the ^{80}Br atom and the residual ethyl group. These facts indicate that a complete explanation of the isotope effect must be based on the properties of the residual as well as the replaced atom or group.

In the formation of methylene bromide, there are two possible reaction processes; one is the double replacement[17,18] of the H atom and the ethyl group (Reaction 2), while the other is the replacement of two methyl groups (Reaction 3):

$$CH_3CH_2CH_3 + {}^{80}Br \longrightarrow CH_2{}^{80}Br + H + CH_3CH_3 \quad (2)$$

$$CH_3CH_2CH_3 + {}^{80}Br \longrightarrow CH_2{}^{80}Br + 2CH_3 \quad (3)$$

$$CH_2{}^{80}Br + Br_2 \longrightarrow CH_2{}^{80}BrBr + Br \quad (4)$$

Table 3. Yields of *i*- and *n*-propyl bromides in presence of 0.5 m.f. of C_2H_6

Products	Reactant						
	$CH_3CH_2CH_3$ (%)	$CH_3CD_2CH_3$		$CD_3CH_2CD_3$		$CD_3CD_2CD_3$	
		(%)	(K)	(%)	(K)	(%)	(K)
i-Propyl bromide	0.14±0.01	0.10±0.01	(1.4)	0.13±0.01	(1.1)	0.10±0.01	(1.4)
n-Propyl bromide	0.43±0.04	0.40±0.04	(1.1)	0.31±0.03	(1.4)	0.33±0.03	(1.3)

In the former case, the isotopic preference of the substitution of H over D is the origin of the observed isotope effect, while in the latter the rapidity of the adjustment of the two leaving methyl groups to the formation of $CH_2{}^{80}Br$ is the determining factor. At present, no definite conclusion can be drawn. However, the former process seems much more probable than the other, since, in the latter process, both methyl groups can influence the probability of the combination of the resulting methylene with ^{80}Br and an isotope effect nearly twice as large as the observed one can be expected.

^{80}Br-for-H Reaction. Both iso- and *n*-propyl bromides are formed by the ^{80}Br-for-H reaction. In this type of reaction, three kinds of isotope effects resulting from the replacement of H by D in the molecule can be considered. The first kind is the primary isotope effect, an isotopic preference for the substitution of H over D. The second is a secondary isotope effect of D atom attached to the reacting C atom; it is accounted for by the ease of the adjustment for the subsequent stable combination with the ^{80}Br atom with the C-atom. The third is also termed as a secondary isotope effect, but, in this case, the D atom is separated by the C–C bond from the reacting C-atom.

The absence of the isotope effect in the yields of isopropyl bromide from $C_3H_2D_6$ and of *n*-propyl bromide from $C_3H_6D_2$ indicates that the D atom in the methyl group in propane has no measurable effect on the ^{80}Br-for-H reaction in the methylene group, while the D atom in the methylene group has no measurable effect on the reaction in the methyl group. This indicates the absence of the third kind of isotope effect described above.

The first and second kinds of isotope effects cannot be readily distinguished in the present comparison. In principle, an obvious experiment to separate these two possibilities is the measurement of the isopropyl bromide yield from C_3HD_7. However, according to the concept of the inertia model, the second kind of isotope effect is less important when an atom or group larger than a H atom is attached to the same C atom. Thus, the observed isotope effect in the ^{80}Br-for-H reaction may be ascribed principally to the primary isotope effect of the replaced D atom.

When we compare the present isotopic variation in the substitution of H and D with the value of 1.6 ± 0.2 found with the C_2H_6–C_2D_6 pair,[3] a reasonable agreement can be seen.[4] However, those values are much smaller than the value, 2.7 ± 0.3, found with the CH_4–CD_4 pair.[1,2] The only logical explanation of this is that the secondary isotope effect originating from the D atom combined with the reacting C atom is important in methane, but less important in ethane and propane, since in the latter compounds the relaxation of the residual group is essentially controlled by that of the methyl or ethyl group attached to the reacting C atom. This means that the primary isotope effect in the substitution of H(D) can be assigned for a level of 1.4 ± 0.2, and that the large isotope effect in the CH_4–CD_4 pair results from the effect combining the primary and secondary isotope effects.

Origins of Reactivity Integral Isotope Effect. In Table 1 it is obvious that the total organic yield decreases with the number of D atoms in the reactant. A similar trend can also be noticed in the reaction of recoil T with various reactant molecules.[5] These results indicate that the total reactivity integral decreases with the deuteration of the reactant, within an allowance of less than 10% for the moderator isotope effect and with an almost constant extent of unimolecular decomposition of various deuterated products.

When the energetic atom strikes the atoms of a reactant molecule, much of its kinetic energy is transferred into the internal energy of the struck molecule. The atom is, then, imbedded in the electron distribution of the struck molecule and forms a "complex" of a short but still sufficiently long enough lifetime for reasonably normal isotope effects on decomposition to take effect.[5,19] However, it is noticed that the substitution reaction of ^{80}Br for H leaves the resulting products, $R^{80}Br$, with the excitation energy spread over a wide energy range; the average value is estimated to be ~4 eV for RH=cyclopropane.[20]

It is rather unrealistic for a "complex" with such a high excitational energy to show an isotopic preference in its decomposition to the extent observed. One consistent explanation is that the isotope effect in the reaction of ^{80}Br appears mostly when the kinetic energy of the atom is in the lower-energy end of the reaction-energy zone.[21] In these cases, the excess energy of the resulting "complex" is relatively small, and its subsequent decomposition is very sensitive to the properties of the atoms and groups involved. If the formation rates of a "complex" are assumed to be approximately equal for protonated and deuterated molecules, relatively more C–^{80}Br interaction will be ruptured in the latter and the ^{80}Br will emerge very much degraded in energy. This is equivalent to the fact that the reaction probability in a collision of ^{80}Br with C_3D_8 is smaller than in one with C_3H_8 at the lower-energy end of the reaction zone.

Although it has not been confirmed that the same explanation can be applied to the reaction of energetic tritium atoms, this is quantitatively consistent with a trend found in the latter system.[21] The 2.8 eV T atom resulting from the photolysis of TBr shows a much larger isotope effect than does the recoil T atom.[19]

References

1) E. Tachikawa and T. Kahara, This Bulletin, **43**, 1293 (1970).
2) M. Saeki and E. Tachikawa, *ibid.*, **46**, 839 (1973).
3) E. Tachikawa and K. Yanai, *Radiochim. Acta*, **17**, 138 (1972).
4) R. W. Helton, M. Yoong, and E. P. Rack, *J. Phys. Chem.*, **75**, 2072 (1971).
5) E. K. C. Lee and F. S. Rowland, *J. Amer. Chem. Soc.*, **85**, 2907 (1963).
6) R. Wolfgang, *Progr. Reaction Kinetics*, **3**, 97 (1965).
7) E. K. C. Lee, J. W. Root, and F. S. Rowland, "Chemical Effects of Nuclear Transformation," Vol. 1., IAEA, Vienna (1965), p. 55.
8) T. Smail, B. Arezzo, and F. S. Rowland, *J. Phys. Chem.*, **76**, 187 (1972).

9) T.Smail and F.S. Rowland, *ibid.*, **74**, 1859 (1970).
10) S. H. Daniel and Y. N. Tang, *ibid.*, **75**, 301 (1971).
11) K. Numakura and E. Tachikawa, This Bulletin, **46**, 346 (1973).
12) H. Baba, H. Okashita, S. Baba, T. Suzuki, and H. Umezawa, *J. Nucl. Sci. Technol.*, **8**, 703 (1971).
13) C. M. Wai and R. L. Jennings, *J. Phys. Chem.*, **75**, 2698 (1971).
14) K. A. Krohn, N. J. Parks, and J. W. Root, *J. Chem. Phys.*, **55**, 5785 (1971).
15) A. Hosaka and F. S. Rowland, *ibid.*, **75**, 3781 (1971).
16) Y. N. Tang, E. K. C. Lee, E. Tachikawa, and F. S. Rowland, *ibid.*, **75**, 1290 (1971).
17) R. T. K. Baker and R. Wolfang, *ibid.*, **73**, 3478 (1969).
18) M. Saeki, K. Numakura, and E. Tachikawa, This Bulletin, **45**, 1715 (1972).
19) C. C. Chou and F. S. Rowland, *J. Phys. Chem.*, **75**, 1283 (1971).
20) M. Saeki and E. Tachikawa, presented at the 17th Symposium on Radiochemistry in Japan, 1973, Tokyo.
21) F. S. Rowland, "Proceedings of the International School of Physics "Enrico Fermi" Course XLIV-Molecular Beam and Reaction Kinetics," ed. by Ch. Schlier, Academic Press, New York, N. Y. (1970).

Determination of the *Gauche* Dihedral Angle and the Energy Difference between Rotational Isomers of Bromoacetyl Chloride

Kazutoshi TANABE and Shinnosuke SAËKI

National Chemical Laboratory for Industry, Honmachi, Shibuya-ku, Tokyo 151

(Received January 14, 1974)

Infrared absorption intensities of fundamental bands of bromoacetyl chloride were measured in carbon disulfide solution, an absolute intensity method being applied to determine the energy difference between the rotational isomers. In order to determine the dihedral angle of the less stable isomer, normal frequencies and band intensities were calculated for various angles, the results being compared with observed data. The dihedral angle of the *gauche* isomer was found to be 100° which is in good agreement with the angle in chloroacetyl chloride. The energy difference, 0.91 kcal/mol, determined in carbon disulfide solution is in good agreement with the value obtained by the temperature variation method.

The dihedral angle of the *gauche* isomer of chloroacetyl chloride $CH_2ClCOCl$ was determined to be 105°, by calculating normal frequencies and infrared band intensities for both isomers and comparing the results with observed data.[1] The dihedral angle herewith denotes the angle between C–Cl of CH_2Cl and C=O of COCl, the angles of the *trans* and *cis* isomers being 0 and 180°, respectively. However, 105° for the dihedral angle of the less stable form was in some disagreement with results obtained by the other authors.

Nakagawa *et al.*[2-4] obtained 150° by calculating normal frequencies for skeletal vibrations, while Khan and Jonathan[5] obtained 180°. On the other hand, Bellamy and Williams[6] concluded that the *gauche* dihedral angle is 120°, by considering a polar effect on carbonyl frequencies, and Le Fèvre *et al.*[7] obtained 120° by dipole moment analysis.

It is known that, in rotational isomers with a C–C bond as an internal rotational axis, double bonds such as C=C or C=O bonds are apt to take a *cis* position with a single bond on the opposite side. It thus seems reasonable that the *gauche* isomer of haloacetyl halide takes a dihedral angle of 120°, although the dihedral angle of the less stable isomer of CH_2FCOF was determined to be 180° by microwave spectroscopy,[8] the isomer taking a *cis* form. In the case of $CH_2ClCOCl$, owing to repulsive interaction between the two chlorine atoms in a molecule, the dihedral angle of the *gauche* isomer might decrease from 120 to 105°.

In order to support the result for the *gauche* dihedral angle obtained previously, bromoacetyl chloride molecule was treated by the same method as before. The energy difference between the rotational isomers was determined by applying the absolute intensity method.[1,9]

Experimental

The infrared absorption spectrum of $CH_2BrCOCl$ was observed in a carbon disulfide solution with a Perkin-Elmer Model 180 grating spectrophotometer combined with a digital recorder. The spectrum is shown in Fig. 1. Observed frequencies were calibrated by referring to standard gas spectra[10] within an accuracy of 1 cm^{-1}.

Absorption band intensities were evaluated, by means of a FACOM Model 270-30 electronic computer system by processing encoded paper tapes punched out from the digital recorder. Concentration of solutions was 0.05—0.3 (mol/l), thickness of sealed liquid cells with KBr windows being 0.1—1.0 mm. Absorption intensities were evaluated by averaging intensities obtained for at least ten measurements in various concentrations for individual bands. For absorption bands below 400 cm^{-1}, sealed liquid cells with polyethylene windows were used, the absorption intensities being roughly estimated with a planimeter. Other experimental condifions for the intensity measurement were the same as described previously.[1,9,11-15]

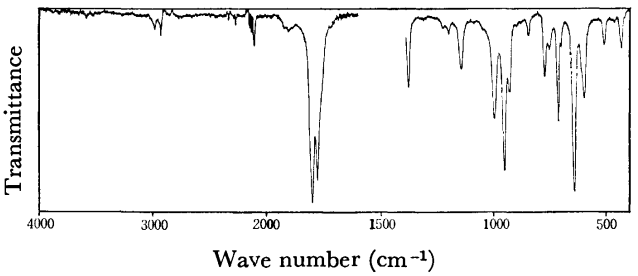

Fig. 1. The infrared absorption spectrum of $CH_2BrCOCl$ observed in carbon disulfide solution.

A Hitachi Model IRH-3 high temperature cell, in combination with a Hitachi Model IRC-2 power regulator, was used for determination of energy difference by the temperature variation method. The temperature of the cell was controlled within 1 °C.

Results and Discussion

In order to determine the dihedral angle of the less stable isomer of $CH_2BrCOCl$, normal frequencies of both isomers were calculated for various angles 60—180°. Force constants based on the local symmetry force field (LSFF) were assumed to take the same values between the rotational isomers. Their values were determined by the least squares method so as to attain the best fit between the calculated and observed frequencies. Since Nakagawa *et al.*[2-4] made assignments for only skeletal vibrations, fundamental frequencies were determined by referring to their assignment and to those of $CH_2ClCOCl$ and $CH_2BrCOBr$.[1]

First the refinement of all the twenty-four force constants was attempted by means of the observed twenty-eight frequency data. Some of the force constants converged showing relatively large standard deviations. Thus three force constants were fixed, and

Table 1. Observed and calculated frequencies of $CH_2BrCOCl$ for various dihedral angles of the less stable isomer (cm^{-1})

Species	i	ν_{obsd}	ν_{calcd} for the dihedral angel of					
			60°	90°	150°	120°	150°	180°
trans A′	1	2946	2947	2947	2947	2947	2946	2946
	2	1812	1798	1800	1803	1804	1799	1797
	3	1388	1399	1399	1399	1398	1397	1394
	4	1237	1227	1226	1226	1227	1233	1235
	5	968	963	967	966	964	969	973
	6	728	724	730	729	726	729	736
	7	658	653	652	652	651	649	647
	8	443	456	438	440	451	469	469
	9	252	263	257	257	258	264	270
	10	181	168	170	169	174	181	189
trans A″	11	2999	2997	2997	2997	2997	2999	2999
	12	1156	1158	1159	1159	1159	1157	1156
	13	944	938	939	939	938	914	898
	14	473	470	472	471	471	473	475
	15	—	97	87	93	90	75	60
gauche A	1	2999	3001	3001	3001	3001	3000	2999
	2	2946	2945	2945	2945	2945	2946	2946
	3	1789	1800	1802	1805	1808	1804	1800
	4	1409	1398	1398	1398	1399	1401	1403
	5	1210	1220	1221	1221	1220	1213	1211
	6	1156	1153	1152	1152	1153	1155	1156
	7	1011	1019	1026	1022	1016	1001	1007
	8	855	858	847	854	865	898	901
	9	713	718	713	711	714	713	711
	10	612	620	617	618	618	615	612
	11	520	526	525	511	500	492	491
	12	473	457	462	469	473	473	470
	13	348	337	353	354	351	333	324
	14	157	169	167	165	163	149	137
	15	—	82	69	74	73	70	63

the other force constants adjusted by the least-squares method. The calculated frequencies and the LSFF force constants with their standard deviations in parentheses are given in Tables 1 and 2, respectively.

The converged values of the force constants show no dependence on the *gauche* dihedral angle, while the calculated normal frequencies show remarkable dependence on the dihedral angle assumed for the less stable isomer. The calculated frequencies for the *trans* ν_{10}, *gauche* ν_{12} bands are in poorer agreement with the observed frequencies, as the dihedral angle of the *gauche* isomer approaches 60°. On the other hand, those for the *trans* ν_8, ν_9, ν_{13}, *gauche* ν_8, ν_{11}, ν_{13}, ν_{14} bands are in poorer agreement as the dihedral angle of the less stable isomer approaches 180° (*cis* form).

In order to examine the agreement more quantitatively, the weighted sum of squared deviations or the residual was computed and plotted against the assumed dihedral angle of the less stable isomer (Fig. 2). The result indicates that the most probable *gauche* dihedral angle is between 90 and 120°. For the angle 150° determined by Nakagawa *et al.*, the residual is much larger than those for angles 90—120°, and their result is not consistent with ours.

For the sake of confirmation, infrared band intensities were computed for various angles assumed for the *gauche* isomer. For intensity parameters, electro-optical parameters based on Gribov's valence-optical theory[16,17] were taken, and their values determined by the least squares method. In order to determine the

Table 2. Converged values and standard deviations of LSFF force constants (Unit: mdyn/Å, mdyn, or mdyn·Å)

LSFF	60°	105°	150°
f(as)	4.78(0.01)	4.78(0.01)	4.79(0.01)
f(ss)	4.86(0.03)	4.86(0.01)	4.86(0.02)
f(CO)	10.70(1.54)	10.71(0.58)	10.69(4.23)
f(sc)	0.47(0.34)	0.47(0.08)	0.47(0.29)
f(wa)	0.53(0.12)	0.53(0.06)	0.49(0.11)
f(tw)	0.61(0.00)	0.61(0.01)	0.61(0.00)
f(CC)	3.50[a)]	3.50[a)]	3.50[a)]
f(ro)	0.78(0.02)	0.79(0.02)	0.75(0.09)
f(CCl)	2.78[a)]	2.78[a)]	2.78[a)]
f(CBr)	2.66[a)]	2.66[a)]	2.66[a)]
f(π)	0.30(0.01)	0.30(0.01)	0.31(0.02)
f(CCO)	1.13(1.16)	1.06(0.54)	1.22(0.52)
f(CCCl)	2.02(0.52)	2.00(0.50)	2.02(3.52)
f(CCBr)	0.86(0.30)	0.88(0.21)	1.03(0.33)
f(to)	0.15(0.03)	0.14(0.36)	0.09(0.06)
f(sc, CC)	0.24(1.54)	0.23(0.37)	0.22(1.19)
f(wa, CC)	0.14(1.04)	0.14(0.36)	−0.02(0.65)
f(CC, CBr)	0.19(1.35)	0.19(0.35)	0.24(1.07)
f(CC, CCO)	0.83(1.06)	0.86(0.52)	0.81(1.50)
f(CC, CCCl)	0.29(1.45)	0.26(0.52)	0.35(1.02)
f(CC, CCBr)	0.16(2.03)	0.16(0.71)	0.13(1.06)
f(CCl, CCO)	0.08(0.73)	0.17(0.25)	0.06(0.77)
f(CCl, CCCl)	−0.30(0.75)	−0.35(0.46)	−0.36(1.31)
f(CBr, CCrB)	0.45(0.69)	0.43(0.33)	0.37(1.99)

ss: CH_2 symmetric stretching, as: CH_2 antisymmetric stretching, sc: CH_2 scissoring, wa: CH_2 wagging, tw: CH_2 twisting, ro: CH_2 rocking, π: out-of-plane beinding, to: torsion. a) Fixed force constants.

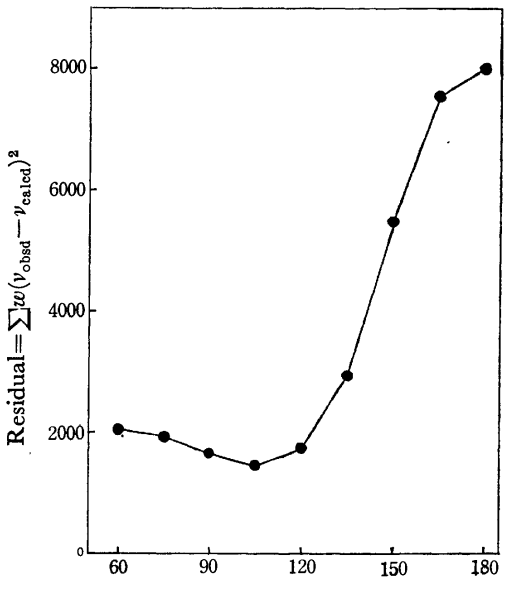

Fig. 2. The plot of residuals against various assumed *gauche* dihedral angles.

TABLE 3. CONVERGD VALUES AND STANDARD DEVIATIONS OF INTENSITY PARAMETERS FOR THE *gauche* DIHEDRAL ANGLES OF 60°, 105°, 150°
(Unit: D/Å, or D)

	60°	105°	150°
μ_{CH}	0.64(0.07)	0.70(0.06)	0.44(0.07)
μ_{CO}	−1.93(0.22)	−1.17(0.21)	−1.04(0.17)
μ_{CCl}	−1.16(0.43)	−1.21(0.32)	−2.14(0.26)
μ_{CBr}	−1.69(0.44)	−1.47(0.27)	−2.15(0.35)
$\delta\mu_{CH}/\delta r_{CH}$	0.59(0.05)	0.58(0.05)	0.60(0.05)
$\delta\mu_{CH}/\delta r_{CH'}$	0.23(0.05)	0.22(0.05)	0.23(0.04)
$\delta\mu_{CH}/\delta\alpha_{HCH}$	0.33(0.08)	0.43(0.07)	0.31(0.07)
$\delta\mu_{CH}/\delta\alpha_{HCBr}$	0.00(0.08)	0.08(0.09)	0.05(0.09)
$\delta\mu_{CH}/\delta\alpha_{HCC}$	−0.71(0.07)	−0.66(0.08)	−0.58(0.07)
$\delta\mu_{CO}/\delta r_{CO}$	−7.11(0.20)	−6.76(0.20)	−6.18(0.19)
$\delta\mu_{CO}/\delta\alpha_{CCO}$	−2.07(0.20)	−1.71(0.17)	−1.71(0.21)
$\delta\mu_{CCl}/\delta r_{CCl}$	−2.52(0.56)	−2.90(0.21)	−3.41(0.47)
$\delta\mu_{CCl}/\delta\alpha_{CCCl}$	−1.86(0.36)	−1.43(0.33)	−0.07(0.44)
$\delta\mu_{CBr}/\delta r_{CBr}$	−3.09(0.39)	−3.19(0.27)	−2.64(0.35)
$\delta\mu_{CBr}/\delta\alpha_{CCBr}$	2.41(0.30)	2.98(0.29)	2.29(0.45)
X	0.68(0.01)	0.70(0.01)	0.67(0.01)

population ratio of the rotational isomers, the absolute intensity method was applied. Converged values and standard deviations of intensity parameters and of the *trans* population ratio parameter are given in Table 3. Calculated band intensities are given in Table 4 together with observed intensities for comparison.

As in the normal frequency calculation, the converged values of the intensity parameters show no dependence on the *gauche* dihedral angle, while the calculated intensities depend remarkably on the *gauche* dihedral angle. The calculated intensities for the 1156, 348 cm^{-1} bands are in poorer agreement with the observed values as the dihedral angle approaches 60°, while those for the 658, 612 cm^{-1} bands are in poorer agreement as the dihedral angle approaches 180°. The plot of residuals against the assumed *gauche* dihedral angles is

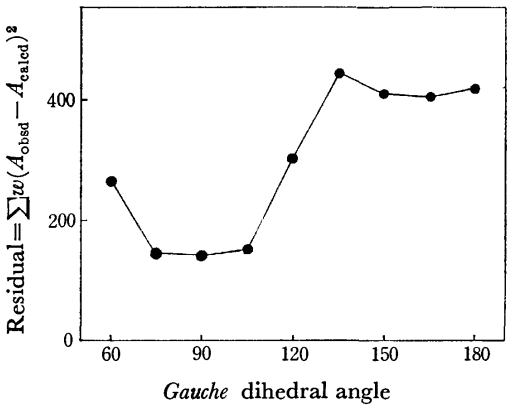

Fig. 3. The plot of residuals against various assumed *gauche* dihedral angles.

TABLE 4. OBSERVED AND CALCULATED INFRARED INTENSITIES FOR VARIOUS DIHEDRAL ANGLES OF THE LESS STABLE ISOMER (Unit: 1 $mol^{-1}\cdot cm^{-2}$)

ν_{trans}	ν_{gauche}	A_{obsd} (Error)	A_{calcd} for the dihedral angle of					
			60°	90°	105°	120°	150°	180°
2999	2999	900 (50)	721	744	725	693	569	539
			192	164	180	198	265	278
2946	2946	950 (50)	656	670	676	694	664	652
			370	343	334	312	381	399
1812		12500 (500)	12310	12076	12213	13073	13567	13792
	1789	7900 (300)	7854	7980	7816	7232	7214	7148
	1409	2600 (100)	598	485	471	440	453	485
1388			1857	2262	2324	2314	2135	2103
1237	1210	980 (50)	921	889	878	861	809	837
			317	243	226	179	342	341
1156	1156	2300 (100)	2005	2031	2017	1983	1551	1414
			625	474	498	517	661	725
	1011		1585	1092	1073	1141	2177	2486
968		10000 (500)	5623	5241	4558	4168	3946	3604
944			2259	2081	1931	1726	996	1064
	855	500 (30)	594	373	430	548	587	559
728	713	2900 (150)	2894	2749	3031	3354	2702	2265
			760	716	1210	1735	1789	1722
658		8700 (400)	8965	9182	9008	7877	3621	2869
	612	3600 (200)	3245	1847	1671	1404	1022	1047
	520	880 (30)	309	871	769	420	570	694
473	473	200 (20)	577	186	176	223	482	555
			686	741	797	719	424	293
443		990 (50)	737	1067	966	924	1483	1398
	348	300 (50)	771	902	779	575	236	93
252		100 (40)	44	78	61	45	22	23
180		300 (100)	344	411	423	411	339	298
	157	—	293	256	261	239	176	63

given in Fig. 3. This also indicates that the most probable dihedral angle of the less stable isomer is between 75 and 105°.

Taking into account the results from normal frequency calculation and intensity computation at the same time it can be concluded that the dihedral angle of the *gauche* isomer of $CH_2BrCOCl$ is $100\pm10°$. This is in line with the angle 105° obtained for $CH_2ClCOCl$.[1]

Nakagawa *et al.*[2] calculated normal frequencies for skeletal vibrations using UBFF force constants derived from related molecules, and concluded that the *gauche* form is considered to have a dihedral angle of 150°. However, the calculated normal frequencies for vibrational modes other than skeletal vibrations are also affected considerably by the assumed *gauche* dihedral angle (Table 1).

The *gauche* isomer of the haloacetyl halide molecule seems to take a dihedral angle of about 120°. However, if we take into account the repulsive force between the halogen atoms in molecule, the dihedral angle might become smaller than 120°. The angle 150° obtained by Nakagawa *et al.* indicates that the two carbon-halogen bonds approach each other from eclipsed configuration between the C–H and C=O bonds. Such an approach does not seem acceptable; the angle 150° is unconvincing.

The angle we obtained is in good accordance with the concept stated above, and might be more reasonable as the *gauche* dihedral angle of $CH_2BrCOCl$.

The energy difference between the *trans* and *gauche* isomers has been evaluated by the same method as before[1] from the converged value of the *trans* population ratio parameter X (Table 3). The entropy term is estimated from principal moments of inertia and fundamental frequencies for both isomers by the equation

$$\exp\left(\frac{\Delta S}{R}\right) = 2\frac{(I_aI_bI_c)_G^{1/2}\prod(1-e^{-h\nu_G/kT})^{-1}}{(I_aI_bI_c)_T^{1/2}\prod(1-e^{-h\nu_T/kT})^{-1}}$$

From the values of this entropy term and of the *trans* population ratio parameter, the energy difference ΔE is evaluated by

$$\frac{1-X}{X} = \exp\left(-\frac{\Delta E}{RT}\right)\cdot\exp\left(\frac{\Delta S}{R}\right)$$

The value 0.91 ± 0.10 (kcal/mol) is thus obtained (Table 5).

In order to confirm the validity of this value, the energy difference was also determined by the temperature variation method. Absorption intensities for the *trans* ν_8 (at 443 cm^{-1}) and *gauche* ν_{11} (at 520 cm^{-1}) bands were measured in a carbon disulfide solution with a high temperature cell in the temperature range 25—100 °C. Although the boiling point of carbon disulfide is 46 °C and its vapor pressure reaches about 5 atm at 100 °C, the experiment could be carried out at 100 °C owing to the air-tightness of the cell.

Table 5. Energy differences of haloacetyl halide molecules (kcal/mol)

Molecule	Vapor	CS_2 solution
$CH_2ClCOCl$	0.97[5]	1.39[1]
$CH_2BrCOCl$	1.0[2]	0.91[a]
$CH_2BrCOBr$	1.9[2]	0.97[1]

a) This study.

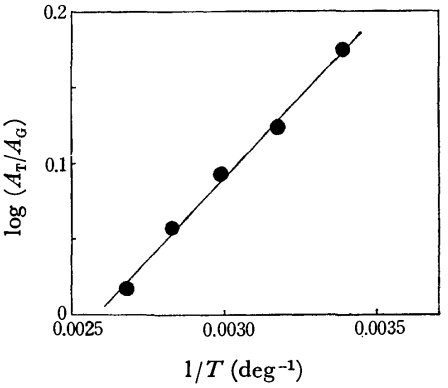

Fig. 4. The van't Hoff plot for determining the energy difference.

The van't Hoff plot for determining the energy difference is given in Fig. 4. From the slope of the least squares fitted straight line, the energy difference of $CH_2BrCOCl$ in carbon disulfide solution was obtained as 0.99 ± 0.10 (kcal/mol). This is in good agreement with the value determined by the absolute intensity method and with the value 1.0 (kcal/mol) obtained by Nakagawa *et al.*

It is of interest to note that in $CH_2ClCOCl$, the energy difference in the vapor phase is smaller than in carbon disulfide solution; in $CH_2BrCOBr$, the former is about twice larger than the latter, and that the situation in $CH_2BrCOCl$ is intermediate between in $CH_2ClCOCl$ and $CH_2BrCOBr$ (Table 5).

References

1) K. Tanabe and S. Saëki, *Spectrochim. Acta*, **28A**, 1083 (1972).
2) I. Nakagawa, I. Ichishima, K. Kuratani, T. Miyazawa, T. Shimanouchi, and S. Mizushima, *J. Chem. Phys.*, **20**, 1720 (1952).
3) S. Mizushima, T. Shimanouchi, I. Nakagawa, and A. Miyake, *ibid.*, **21**, 215 (1953).
4) I. Nakagawa, *Nippon Kagaku Zasshi*, **74**, 243 (1953).
5) A. Y. Khan and N. Jonathan, *J. Chem. Phys.*, **50**, 1801 (1965).
6) L. J. Bellamy and R. L. Williams, *J. Chem. Soc.*, **1958**, 3465.
7) R. J. W. Le Fèvre, M. J. Aroney, and A. N. Singh, *ibid.*, **1965**, 564.
8) E. Saegebarwh and E. B. Wilson, Jr., *J. Chem.Phys.*, **46**, 3088 (1967).
9) K. Tanabe, *Spectrochim. Acta*, **28A**, 407 (1972).
10) I. U. P. A. C., Tables of Wavenumbers for the Calibration of Infrared Spectrometers, Butterworths, London (1961).
11) S. Saëki and K. Tanabe, *Spectrochim. Acta*, **25A**, 1325 (1969).
12) K. Tanabe and S. Saëki, *ibid.*, **26A**, 1469 (1970).
13) K. Tanabe and S. Saëki, This Bulletin, **45**, 32 (1972).
14) K. Tanabe, *Spectrochim. Acta*, **30A**, 1901 (1974).
15) K. Tanabe and S. Saëki, *Spectrochim. Acta*, to be published.
16) L. A. Gribov and E. M. Popov, *Opt. Spectrosc.*, **12**, 304 (1962).
17) L. A. Gribov, "Intensity Theory for Infrared Spectra of Polyatomic Molecules," Consultants Bureau, New York (1964).

The Crystal and Molecular Strucure of Arabinofuranosyladenine Hydrochloride[1]

Tadashi HATA, Sadao SATO, Masakatsu KANEKO, Bunji SHIMIZU, and Chihiro TAMURA

The Central Research Laboratories of Sankyo Co., Ltd., Hiromachi, Shinagawa-ku, Tokyo 140

(Received May 11, 1974)

Crystals of arabinofuranosyladenine hydrochloride are monoclinic, space group $P2_1$, with $a=6.47$, $b=15.56$, $c=6.87$ Å, and $\beta=111.6°$. Intensity data were collected on a four-circle diffractometer with Mo-Kα radiation. The structure was solved by means of Patterson and Fourier methods and refined using block-diagonal least-squares technique. The final *R*-factor for 1681 observed reflections is 4.5%. The sugar conformation is C3′-*endo* and the C(5′)-O(5′) bond is *gauche* to both C(4′)-O(1′) and C(4′)-C(3′). The torsional angle about the glycosidic C–N bond is *anti*, with $\chi_{CN}=29.2°$. The hydrogen-bond scheme is similar to those found in several salts of nucleosides and deoxynucleosides.

9-β-D-Arabinofuranosyladenine (ara-A), first synthesized by Lee *et al.* in 1960,[2] is active against a broad spectrum of DNA virus[3] and inhibits the DNA polymerase.[4] Consequently the conformation of this molecule has been of great interest in comparison with other structurally related nucleosides. In this paper, we describe the molecular and crystal structure of ara-A monohydrochloride (ara-A HCl) with particular attention focussed on conformational aspects and intermolecular interactions of the ara-A cation in the crystalline state.

Experimental

Crystals of ara-A HCl[5] were prepared in our laboratories, and recrystallized from water, in a suitable form for X-ray structure analysis. Crystal dimensions of this salt are; $a=6.47\pm0.02$, $b=15.56\pm0.03$, $c=6.87\pm0.02$ Å, and $\beta=111.6\pm0.3°$ and the space group belongs to $P2_1$. The density was measured by the floatation method in a mixed solution of tetrachloromethane and cyclohexane and found to be 1.544 g/cm³, while the calculated value is 1.558 g/cm³ (if $Z=2$).

A total of 1681 independent reflections were collected on a Rigaku automatic four-circle diffractometer using Zr-filtered Mo-Kα radiation and measured up to $2\theta=60°$ in the θ-2θ scan mode. All data were corrected for the Lorenz and polarization factors but not for absorption.

Determination and Refinement of the Structure

The parameters of the chlorine anion could be obtained from a three-dimensional sharpened Patterson map. After several applications of successive Fourier syntheses a trial structure of the arabinoside emerged except for the hydrogen atoms. The initial refinement for the positional and thermal parameters was carried out by a block-diagonal least-squares technique. Four cycles of this computation dropped the *R*-factor to 8.1%. Then the difference Fourier synthesis was calculated to obtain the hydrogen atoms. These atoms were revealed at reasonable positions. Four more cycles of the least-squares refinement using anisotoropic temperature for the heavy atoms and isotropic factors

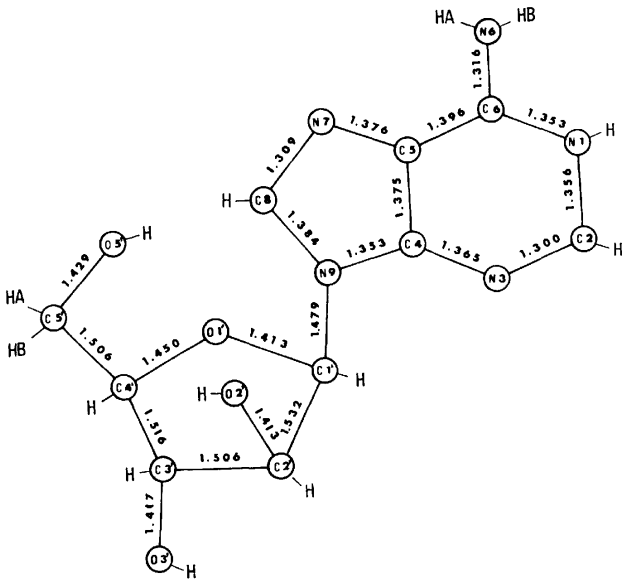

Fig. 2. Bond distances in the arabinofuranosyladenine cation.

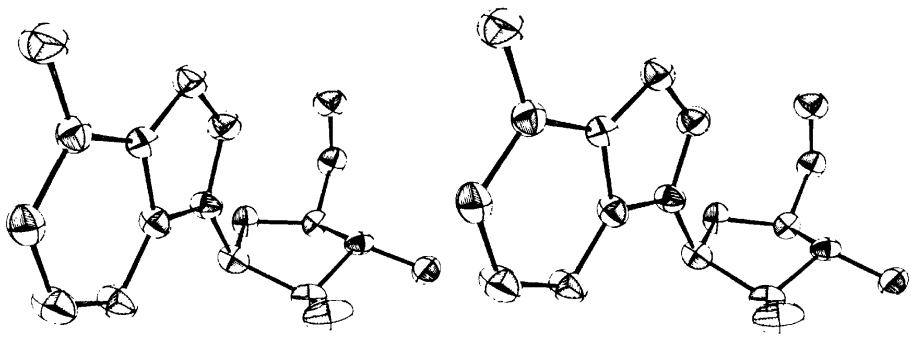

Fig. 1. A stereographic illustration of the arabinofuranosyladenine cation.

for the hydrogen atoms were made. The final R-factor was 4.5% for all observed reflections. Tables 1, 2, and 3 list the positional and thermal parameters, while the observed and calculated structure factors are given in Table 4.[6] A stereographic illustration of the ara-A cation computed by the ORTEP program[7] using these parameters is exhibited in Fig. 1. Bond distances and angles are shown in Figs. 2 and 3 and Table 5.

Table 1. Positional parameters of the non-hydrogen atoms, with their estimated standard deviations in parentheses

All parameters have been multiplied by 10^4.

	x/a	y/b	z/c
Cl	68(2)	−3(1)	−143(2)
N(1)	6441(6)	4092(2)	3824(5)
C(2)	6046(8)	3955(3)	5605(7)
N(3)	4428(7)	3504(3)	5773(6)
C(4)	3115(7)	3167(3)	3889(6)
C(5)	3393(7)	3254(3)	2009(6)
C(6)	5179(7)	3745(3)	1958(6)
N(6)	5670(7)	3889(3)	290(6)
N(7)	1751(6)	2825(2)	439(5)
C(8)	510(7)	2492(3)	1381(6)
N(9)	1266(6)	2684(2)	3495(5)
C(1′)	369(6)	2384(3)	5069(6)
C(2′)	1375(7)	1528(3)	6078(6)
C(3′)	−188(6)	880(3)	4624(6)
C(4′)	−2414(6)	1330(3)	4114(6)
C(5′)	−4244(8)	1061(3)	2112(7)
O(1′)	−1932(5)	2236(2)	4030(5)
O(2′)	3599(5)	1415(3)	6237(5)
O(3′)	−155(5)	50(2)	5444(9)
O(5′)	−3674(6)	1157(2)	301(5)

Table 2. Thermal parameters of the non-hydrogen atoms with their estimated standard deviations

All parameters have been multiplied by 10^4. The thermal parameters are of the form

$T=\exp[-(B_{11}h^2+B_{22}k^2+B_{33}l^2+2B_{12}hk+2B_{13}hl+2B_{23}kl)]$.

	B_{11}	B_{22}	B_{33}	B_{12}	B_{13}	B_{23}
Cl	212(3)	39(0)	140(2)	19(1)	74(2)	5(1)
N(1)	162(10)	23(1)	146(8)	−19(3)	50(8)	−6(3)
C(2)	192(13)	35(2)	127(10)	−20(4)	66(9)	−20(4)
N(3)	177(11)	34(2)	132(8)	−23(4)	73(8)	−14(3)
C(4)	146(11)	22(2)	123(8)	−6(3)	59(8)	−8(3)
C(5)	153(11)	20(2)	110(8)	−3(3)	47(8)	1(3)
C(6)	136(11)	20(2)	123(8)	−6(3)	37(8)	1(3)
N(6)	212(12)	38(2)	137(9)	−35(4)	82(9)	−6(3)
N(7)	175(10)	26(2)	126(8)	−13(3)	47(9)	−2(3)
C(8)	152(11)	27(2)	126(9)	−12(4)	25(8)	2(4)
N(9)	123(9)	26(2)	110(7)	−14(3)	38(6)	−5(3)
C(1′)	132(11)	28(2)	138(8)	−8(4)	69(8)	−8(4)
C(2′)	117(10)	34(2)	112(9)	−1(4)	43(8)	2(3)
C(3′)	107(10)	27(2)	95(8)	11(3)	26(7)	4(3)
C(4′)	102(9)	24(2)	145(9)	4(3)	51(8)	4(3)
C(5′)	138(11)	30(2)	187(11)	0(4)	31(9)	6(4)
O(1′)	111(7)	22(1)	190(8)	3(3)	46(6)	0(3)
O(2′)	104(8)	57(2)	146(7)	12(3)	24(6)	14(3)
O(3′)	215(9)	28(1)	148(7)	21(3)	77(6)	11(3)
O(5′)	179(9)	40(2)	154(8)	18(3)	14(7)	−3(3)

Table 3. Positional and isotropic thermal parameters of the hydrogen atoms, with their estimated standard deviations in parentheses

	x/a	y/b	z/c	B
HN(1)	0.734(9)	0.452(3)	0.357(8)	3.5(1.2)
HC(2)	0.718(8)	0.416(3)	0.681(7)	2.7(1.1)
HAN(6)	0.489(10)	0.357(4)	−0.112(8)	4.2(1.3)
HBN(6)	0.696(9)	0.410(3)	0.038(8)	3.6(1.2)
HC(8)	−0.075(8)	0.220(3)	0.091(7)	3.5(1.2)
HC(1′)	0.041(8)	0.285(3)	0.614(7)	3.2(1.5)
HC(2′)	0.124(9)	0.166(4)	0.752(8)	3.7(1.2)
HC(3′)	0.024(8)	0.088(3)	0.319(7)	3.0(1.1)
HC(4′)	−0.279(8)	0.123(3)	0.534(7)	2.9(1.1)
HAC(5′)	−0.457(8)	0.047(3)	0.233(7)	2.7(1.1)
HBC(5′)	−0.563(9)	0.141(4)	0.168(8)	3.6(1.2)
HO(2′)	0.425(10)	0.160(4)	0.779(8)	4.8(1.4)
HO(3′)	−0.005(9)	0.007(4)	0.668(7)	4.2(1.2)
HO(5′)	−0.298(8)	0.080(3)	0.021(7)	3.0(1.1)

Table 5. Bond lengths and angles, with their estimated standard deviations in parentheses

Atoms	Length, Å	Atoms	Angle, deg.
N(1)-C(2)	1.356(7)	C(2)-N(1)-C(6)	123.0(4)
N(1)-C(6)	1.353(5)	N(1)-C(2)-N(3)	126.2(4)
C(2)-N(3)	1.300(7)	C(2)-N(3)-C(4)	111.3(4)
N(3)-C(4)	1.365(5)	N(3)-C(4)-C(5)	127.0(4)
C(4)-C(5)	1.375(7)	N(3)-C(4)-N(9)	126.8(4)
C(4)-N(9)	1.353(6)	C(5)-C(4)-N(9)	106.2(3)
C(5)-C(6)	1.396(7)	C(4)-C(5)-C(6)	118.2(4)
C(5)-N(7)	1.376(5)	C(4)-C(5)-N(7)	111.0(4)
N(7)-C(8)	1.309(7)	C(6)-C(5)-N(7)	130.8(4)
C(8)-N(9)	1.384(5)	N(1)-C(6)-C(5)	114.3(4)
C(6)-N(6)	1.316(7)	N(1)-C(6)-N(6)	120.1(4)
N(9)-C(1′)	1.479(6)	C(5)-C(6)-N(6)	125.6(4)
		C(5)-N(7)-C(8)	104.0(4)
C(1′)-C(2′)	1.532(7)	N(7)-C(8)-N(9)	112.9(4)
C(1′)-O(1′)	1.413(5)	C(4)-N(9)-C(8)	106.0(4)
C(2′)-C(3′)	1.506(6)	C(4)-N(9)-C(1)′	125.8(3)
C(2′)-O(2′)	1.413(6)	C(8)-N(9)-C(1′)	128.1(4)
C(3′)-C(4′)	1.516(6)		
C(3′)-O(3′)	1.417(6)	N(9)-C(1′)-O(1′)	107.8(3)
C(4′)-C(5′)	1.506(5)	N(9)-C(1′)-C(2′)	113.0(4)
C(4′)-O(1′)	1.450(5)	O(1′)-C(1′)-C(2′)	106.3(4)
C(5′)-O(5′)	1.429(7)	C(1′)-C(2′)-C(3′)	101.8(3)
		C(1′)-C(2′)-O(2′)	113.2(4)
N(1)-H	0.94(6)	C(3′)-C(2′)-O(2′)	112.6(4)
C(2)-H	0.93(4)	C(2′)-C(3′)-C(4′)	101.7(4)
N(6)-HA	1.04(5)	C(2′)-C(3′)-O(3′)	115.9(3)
N(6)-HB	0.87(6)	C(4′)-C(3′)-O(3′)	112.5(4)
C(8)-H	0.88(5)	C(3′)-C(4′)-O(1′)	104.5(3)
C(1′)-H	1.02(5)	C(3′)-C(4′)-C(5′)	116.5(4)
C(2′)-H	1.04(6)	O(1′)-C(4′)-C(5′)	110.0(3)
C(3′)-H	1.12(6)	C(4′)-C(5′)-O(5′)	113.5(4)
C(4′)-H	0.97(6)	C(4′)-O(1′)-C(1′)	109.9(3)
C(5′)-HA	0.96(5)		
C(5′)-HB	1.00(5)		
O(2′)-H	1.03(5)		
O(3′)-H	0.83(6)		
O(5′)-H	0.73(5)		

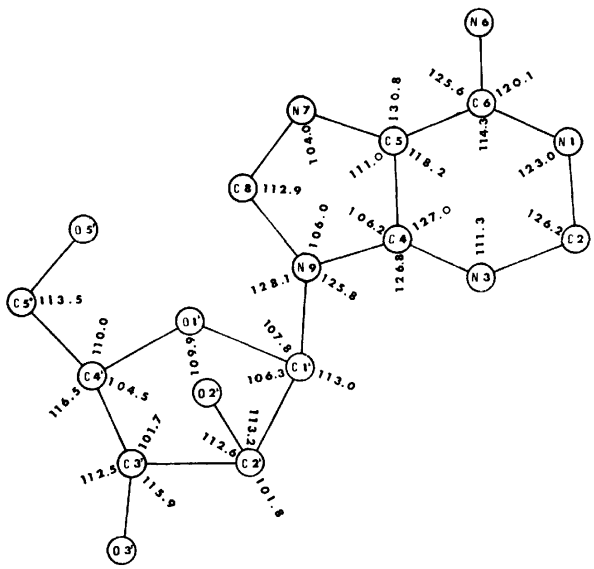

Fig. 3. Bond angles in the arabinofuranosyladenine cation.

Description and Discussion of the Structure

The conformational aspects of the ara-A cation are similar to those usually found in nucleosides and nucleotides. The puckering of this sugar residue is C3'-*endo* in which the atom C(3') is displaced by 0.60 Å from the least-squares plane as constructed in relation to the remaining four atoms in the furanose ring and on the same side as C(5').[8] The torsional angles about the exocyclic C(4')–C(5') bond denoted as ϕ_{OO} and ϕ_{OC} by Shefter and Trueblood[9] are 62.4 and 56.3° respectively, rendering the *gauche-gauche* conformation. The other torsional angle about the glycosidic bond, C(1')–N(9), is *anti* and that of C(8)–N(9)–C(1')–O(1'), χ_{CN},[10] is 29.2°.

The only difference in the molecular features between the ara-A cation and the adenosine cation is the configuration at the carbon atom C(2'); with respect to the furanose ring, the relationship between the OH group and the H atom at C(2') is reversed. The arrangements of atoms around the C(2')–C(1') and C(3')–C(2') bonds are represented in Figs. 4(a) and (b), respectively. The O(2')H group is in the *cis* position N(9) relative to the C(2')–C(1') bond, while oriented *gauche* to O(3') in relation to the C(3')–C(2') bond. Therefore, the torsional angle of O(2')–C(2')–C(1')–N(9), 31.7°, in the ara-A cation becomes smaller than those of 153.7° in adenosine[11] (C3'-*endo*) and 81.5° in the adenosine cation[12] (C2'-*endo*). And there are some short intramolecular non-bonded distances. They are shown in Fig. 5. With respect to the arrangement of atoms around the C(3')–C(2') bond, the O(3')–C(3')–C(2')–O(2') torsional angle of 77.6° in the ara-A cation is larger than those of 45.3° in adenosine and 47.2° in the adenosine cation. In Table 6, these angles are listed.

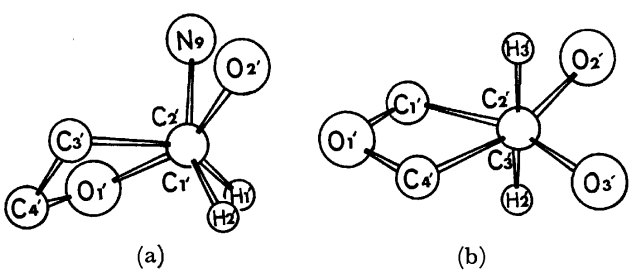

(a) (b)

Fig. 4. Views down (a) the C(2')–C(1') bond and (b) the C(3')–C(2') bond.

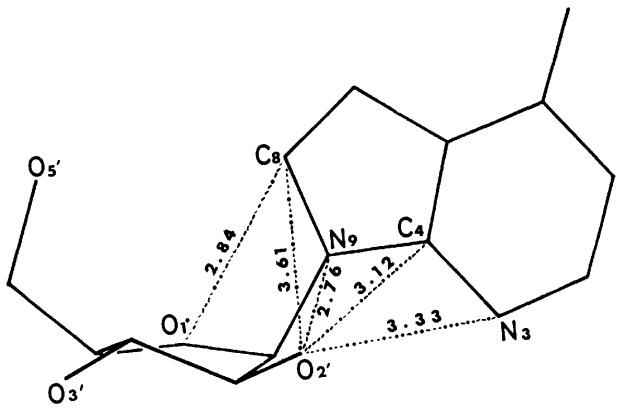

Fig. 5. Intramolecular short nonbonded contacts (Å).

TABLE 6. TORSIONAL ANGLES IN THE ARA-A CATION AND RELATED COMPOUNDS

Puckering of sugar	ara-A cation[a] C3'-*endo*	Adenosine[b] C3'-*endo*	adenosine cation[c] C2'-*endo*
N(9)-C(1')-C(2')-O(2')	31.7°	153.7°	81.5°
N(9)-C(1')-C(2')-C(3')	89.5	92.4	153.7
O(1')-C(1')-C(2')-O(2')	149.7	86.6	161.6
O(1')-C(1')-C(2')-C(3')	28.5	27.3	36.8
O(2')-C(2')-C(3')-O(3')	77.6	45.3	47.2
O(2')-C(2')-C(3')-C(4')	160.1	79.3	162.6
C(1')-C(2')-C(3')-O(3')	160.9	160.4	77.0
C(1')-C(2')-C(3')-C(4')	38.6	35.8	38.4

a) This study b) Ref. 11 c) Ref. 12

The positioning of the O(2') atom seems to affect the bond lengths of C(2')–C(3') and N(9)–C(1') in arabinosyl nucleoside. The C(2')–C(3') bond length of 1.506 Å is shorter than those in adenosine, 1.528 Å, and in the adenosine cation, 1.529 Å, but close to arabinofuranosyl-4-thiouracil[13] (ara-S[4]-U, C3'-*endo*), 1.508 Å. The bond length of N(9)–C(1') in the ara-A cation, 1.479 Å, is slightly longer than those in adenosine, 1.466 Å, and the adenosine cation, 1.460 Å. This tendency is seen in other arabinoside derivatives which are 1.481 Å (ara-S[4]-U), 1.48 Å (ara-T,[14] Cl' *exo*-Ol' *endo*), 1.471 Å (ara-U,[15] C2' *endo*-Cl' *exo*), and 1.475 Å (ara-C HCl,[16] C2'-*endo*).

As in adenosine hydrochloride, the ring of the base residue is protonated at the N(1) atom. No particular differences can be observed in the overall base residue from those found in other salts[17] regardless of the configuration of the arabinofuranosyl residue.

Figure 6 displays the crystal structure of ara-A HCl projected along the a-axis where the hydrogen-bonds

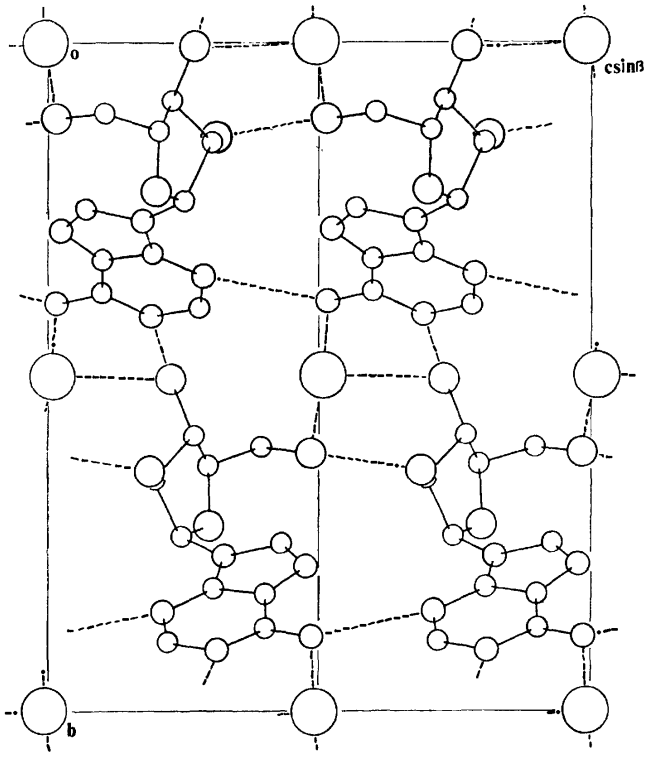

Fig. 6. A projection of the structure viewed down the a-axis. Hydrogen bonds are shown as broken lines.

are indicated by broken lines. Between the cation molecules, there is one hydrogen-bond related by the twofold screw axis and two hydrogen-bonds related by the translational operation. The N(1) atom hydrogen-bonds to O(3′) of the cation at $(1-x, 1/2+y, 1-z)$ in which the N(1) atom acts as a proton-donor, with a N(1)—O(3′) distance of 2.713 Å. The N(6) atom donates one of two hydrogen atoms to N(3) of another cation at $(x, y, -1+z)$ and O(2′) donates its proton to O(5′) at $(1+x, y, 1+z)$ forming usual hydrogen bond distances of 2.966 and 2.728 Å respectively. The chloride anion accepts three hydrogen atoms from O(3′), O(5′), and N(6) with distances of 2.983, 3.124, and 3.284 Å, respectively. Details of the hydrogen-bond distances and angles are given in Table 7.

In order to make a comparison of the hydrogen-bond scheme of ara-A HCl with those of the other HCl salts

Table 7. Hydrogen-bond distances and angles, D–H···A

D–H	A	Distance D–A	Distance H···A	Angle D–H···A
N(1)-H	O(3′)(a)	2.713Å	1.89Å	145°
N(6)-HA	N(3)(b)	2.966	2.05	147
N(6)-HB	Cl^-(c)	3.284	2.43	165
O(2′)-H	O(5′)(d)	2.728	1.88	137
O(3′)-H	Cl^-(e)	2.983	2.16	174
O(5′)-H	Cl^-(f)	3.124	2.42	162

a) at $1-x, 1/2+y, 1-z$. b) at $x, y, -1+z$. c) at $1-x, 1/2+y, -z$. d) at $1+x, y, 1+z$. e) at $x, y, 1+z$. f) at x, y, z.

of nucleoside derivatives, the projections of the crystal structures viewed along the b-axis of ara-A HCl, deoxycytidine hydrochloride (DC HCl),[18] adenosine hydrochloride (A HCl),[12] and arabinofuranosylcytosine hydrochloride (ara-C HCl)[16] are exhibited in Figs. 7(a), (b), (c), and (d). The space group of each crystal is $P2_1$. In these illustrations, the hydrogen-bonds formed between the cations related by a twofold screw axis are drawn by the bold broken lines, and the others are by the normal broken ones. The short intermolecular contacts in the DC HCl assumed to be weak hydrogen-bonds are represented by dotted lines. The noteworthy point in these figures is that some parts in the hydrogen-bond schemes closely resemble each other. In the molecular packings of these crystals, the hydrogen-bonds oriented in a similar manner are listed in the same row of Table 8. Each O(3′)H hydroxy group in all salts donates the hydrogen atom to the chlorine anion in a similar fashion and O(2′)—O(5′) hydrogen-bonds are formed in similar directions except the DC cation, which has no O(2′)H group. On the other hand, in the first three cations in Table 8, the hydrogen-bonds are formed between the cations related by a screw axis. They are N(1)H—O(3′) in the ara-A cation, N(4)H—O(3′) in the DC cation, and N(6)H—O(2′) in the A cation. One of the cations in ara-C HCl does not make hydrogen-bond to the other neighbouring cation related by a screw axis, and no hydrogen-bond forms between O(5′) and Cl^-. The combination of hydrogen-bonds in these molecules distinguishes the molecular arrangement of ara-C HCl from the remain-

Table 8. The hydrogen bonding schemes in various hydrochlorides
Each row shows the hydrogen-bonds oriented in similar directions.

	ara-A HCl[a]	DC HCl[b]	A HCl[c]	ara-C HCl[d]
The hydrogen bond related by screw axis	N(1)H···O(3′)	N(4)HB···O(3′)	N(6)HB···O(2′)	
Hydrogen bonds related by translation	N(6)HA···N(3)	N(4)HA···O(2)		
	O(2′)H···O(5′)		O(2′)H···O(5′)	O(2′)H···O(5′)
				O(5′)H···O(3′)
Other hydrogen bonds	O(3′)H···Cl^-	O(3′)H···Cl^-	O(3′)H···Cl^-	O(3′)H···Cl^-
	O(5′)H···Cl^-	O(5′)H···Cl^-	O(5′)H···Cl^-	
	N(6)HB···Cl^-			
		N(3)H···Cl^-	N(1)H···Cl^-	N(3)H···Cl^-
			N(6)HA···Cl^-	N(4)HA···Cl^-
				N(4)HB···Cl^-

a) arabinofuranosyladenine hydrochloride (This study). b) deoxycytidine hydrochloride (Ref. 18). c) adenosine hydrochloride (Ref. 12). c) arabinofuranosylcytosine hydrochloride (Ref. 16).

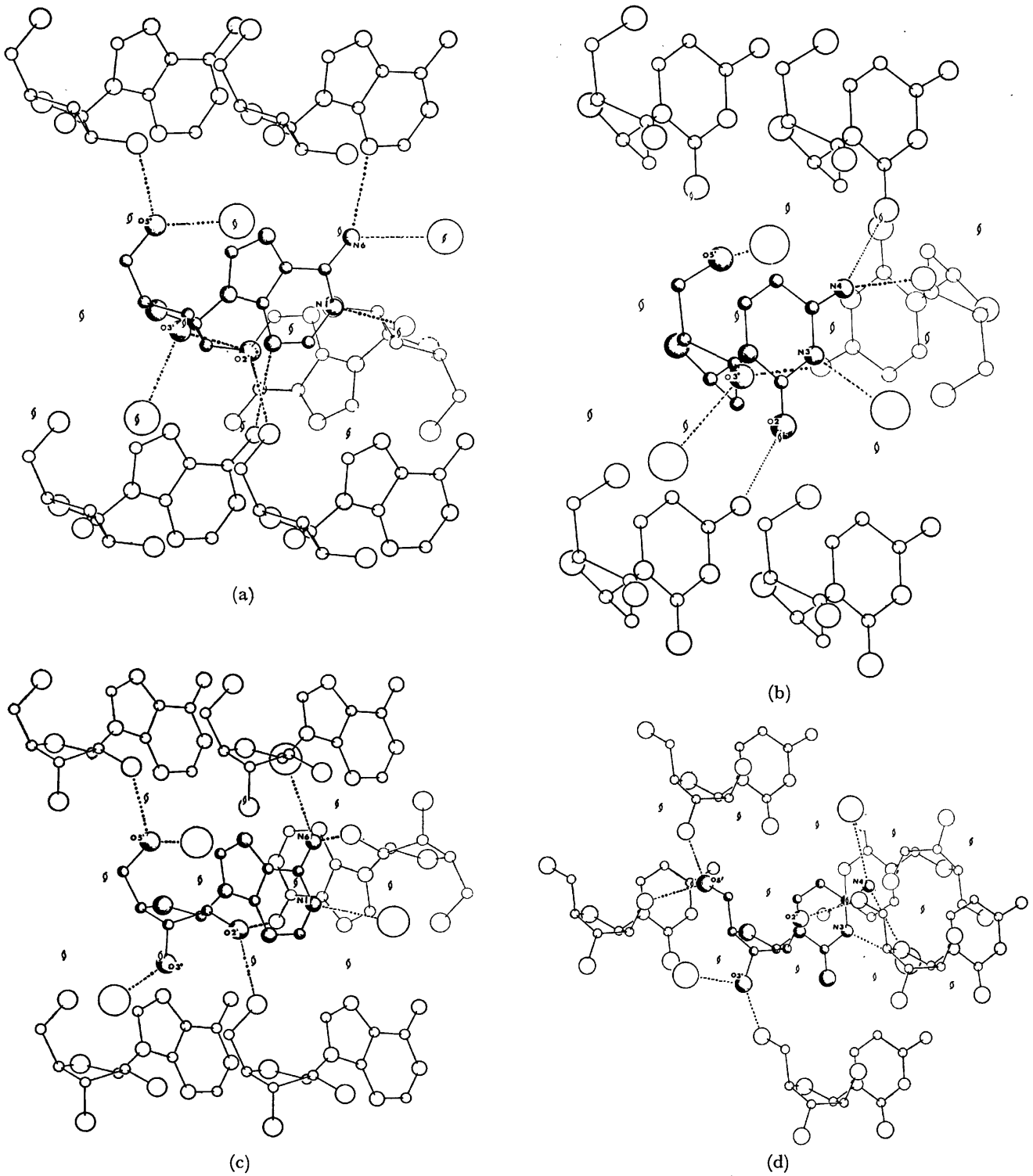

Fig. 7. The crystal structures projected down the b-axis of (a) arabinofuranosyladenine hydrochloride, (b) deoxycytidine hydrochloride, (c) adenosine hydrochloride, and (d) arabinofuranosylcytosine hydrochloride, being drawn from the published parameters. The bold broken lines indicate the hydrogen-bonds related by the acrew axis and the normal broken ones indicate other hydrogen-bonds. The dotted lines indicate weak hydrogen-bonds. Note that the hydrogen-bond schemes in the former three crystals resemble each other.

ing three compounds. The hydrogen-bond net-works of these salts resemble each other in taking an overall view of the crystal structures as shown in Figs. 7(a), (b), and (c). This can be interpreted as indicating that the hydrogen-bond schemes of these nucleoside salts are broadly divided into two categories, one is in ara-C HCl and the other is in the rest of three compounds, thus far.

References

1) Presented in part at the 28th Annual Meeting of the Chemical Society of Japan, Tokyo, April, 1973.
2) W. W. Lee, A. Benitez, L. Goodman, and B. R. Baker, *J. Amer. Chem. Soc.*, **82**, 2648 (1960).
3) F. M. Schabel, Jr., *Chemotherapy*, **13**, 321 (1968).
4) S. S. Cohen, "Progress in Nucleic Acid Research and Molecular Biology," Vol. 5, ed. by J. N. Davidson and W. E. Cohn, New York, N. Y. (1966), p. 1.
5) M. Ikehara, M. Kaneko, and Y. Ogiso, *Tetrahedron Lett.*, **1970**, 4673.
6) Table 4 has been preserved by the office of the Bulletin of the Chemical Society of Japan.
7) C. K. Johnson, Report No. 3794, Oak Ridge National Laboratory, Oak Ridge, Tennessee (1965).
8) C. D. Jardetzky, *J. Amer. Chem. Soc.*, **82**, 229 (1960).
9) E. Shefter and K. N. Trueblood, *Acta Crystallogr.*, **18**, 1067 (1965).
10) M. Sundaralingam, *Biopolymer*, **7**, 821 (1969).
11) T. F. Lai and R. E. Marsh, *Acta Crystallogr.*, **B28**, 1982 (1972).
12) K. Shikata, T. Ueki, and T. Mitsui, *ibid.*, **B29**, 31 (1973).
13) W. Saenger, *J. Amer. Chem. Soc.*, **94**, 621 (1972).
14) P. P. Tougard, *Acta Crystallogr.*, **B29**, 2227 (1973).
15) P. Tollin, H. R. Wilson, and D. W. Young, *ibid.*, **B29**, 1641 (1973).
16) J. S. Sherfinski and R. E. Marsh, *ibid.*, **B29**, 192 (1973).
17) W. Saenger, *J. Amer. Chem. Soc.*, **93**, 3035 (1971).
18) E. Subramanian and D. J. Hunt, *Acta Crystallogr.*, **B26**, 303 (1970).

The Surface Activity of Tetra-*n*-alkylammonium Halides in Aqueous Solutions. The Effect of Hydrophobic Hydration

Kunio TAMAKI

Department of Chemistry, Yokohama City University, Kanazawa-ku, Yokohama 236

(Received May 15, 1974)

Surface tensions are reported for aqueous solutions of a series of homologous tetra-*n*-alkylammonium chlorides, bromides, and iodides (R_4NX) at 25 °C, and the experimental results are discussed with particular reference to the bulk properties of these salts in water. It is found that Me_4NX salts are surface inactive in aqueous solutions and that they may be classified as simple salts. On the other hand, it is found that Et_4NX and higher homologous salts are surface active in aqueous solutions and that the surface activity increases with the number of carbon atoms in the alkyl chains; thus, they are hydrophobic structure-makers in the water phase. The surface tensions for aqueous solutions of Me_4NX salts are only slightly dependent on the kind of counter-ion, such as Cl^-, Br^-, and I^-. In the cases of Et_4NX, Pr_4NX, and Bu_4NX salts, the effectiveness of the anions for the same cation on the surface activity increases progressively in this order: $I^->Br^->Cl^-$.

The physical properties of aqueous solutions of tetra-*n*-alkylammonium salts have been studied by many investigators in terms of the structural changes in liquid water caused by the salts.[1-3] In a previous paper,[4] the surface active properties of tetra-*n*-butylammonium halides in aqueous solutions were discussed with emphasis on the solution behavior of these salts in water. This paper will be concerned with the surface activity of a homologous series of tetra-*n*-alkylammonium chlorides, bromides, and iodides (R_4NX) in aqueous solutions.

Experimental

Pr_4NCl was from Wako Pure Chemical Industries, Ltd., and Pen_4NBr was from Eastman Kodak Co. The other organic chemicals were from Tokyo Kasei Kogyo Co. All the salts were recrystallized from suitable solvents: methanol for Me_4NBr, distilled water for Me_4NI, ethanol for Et_4NI, ethyl acetate for Bu_4NBr and Pen_4NBr, ethanol–diethyl ether mixtures for Pr_4NCl and Bu_4NCl, and ethanol–ethyl acetate mixtures for the other salts. Water was triply distilled.

The surface tensions were measured at 25 ± 0.1 °C by means of the drop-volume method described in a previous paper.[4] Some of the data were checked by the Wilhelmy plate method using a surface tension apparatus, Model ST-1, of Shimadzu Seisakusho Ltd. No surface-ageing phenomenon was observed in this work. With R_4NI salts and Pen_4NBr, measurements were carried out to the solubility limit.

In this work, the solutions were made by weight, and the molar concentration, C, was deduced from the molal concentration, m, and the measured densities. The change in surface tension denoted by $\Delta\sigma$ is defined as; $\sigma_0-\sigma$, where σ_0 and σ are the surface tension of pure water and solution respectively.

Results and Discussion

The Surface Tensions versus *Concentration Curves for R_4NBr.* Figure 1 shows the surface tensions of aqueous solutions of R_4NBr salts as a function of the molal concentration. It may be seen that Me_4NBr slightly raises the surface tension of pure water, whereas Et_4NBr and higher homologous salts reduce the surface tension of pure water, and that the surface activity increases progressively with the number of carbon atoms in the alkyl groups. These facts are reasonably compatible with the results[5] on the surface tensions at 0 °C for the aqueous solutions of Me_4NCl, Et_4NCl, and Pr_4NCl.

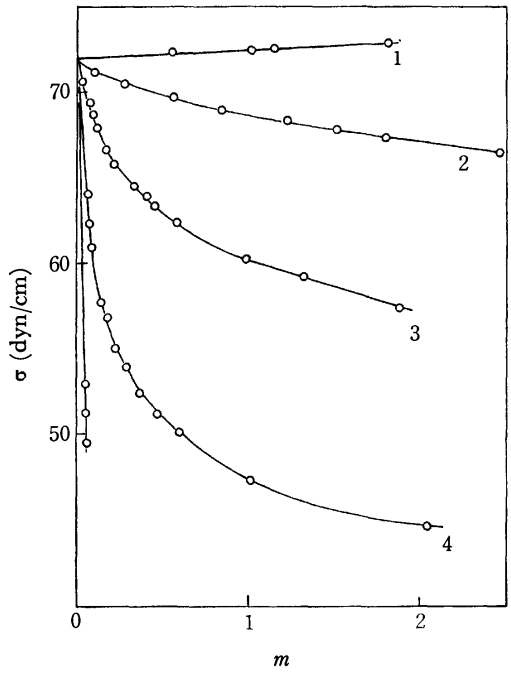

Fig. 1. Surface tension (σ) as a function of molality (m); 1, Me_4NBr; 2, Et_4NBr; 3, Pr_4NBr; 4, Bu_4NBr; 5, Pen_4NBr.

The interaction of simple salts with water may be interpreted in terms of electrostrictive hydration, whereas the interaction of nonpolar organic solutes with water may be interpreted in terms of hydrophobic hydration.[6] The behavior of amphiphilic organic ions in water may be generally discussed in terms of the balance of hydrophobic hydration due to nonpolar groups and electrostrictive hydration due to ionic groups.[7] The phenomenon that the dissolved substance raises the surface tension of pure water has been observed with a variety of simple salts, whether the constituent ions are electrostrictive structure-makers or -breakers.[5] On the other hand, the nonpolar organic solutes, which act as hydrophobic structure-

Table 1. Traube factors (K) for R_4NBr

	$\Delta\sigma=5$ dyn/cm;		$\Delta\sigma=7$ dyn/cm;		$\Delta\sigma=10$ dyn/cm;		$\Delta\sigma=15$ dyn/cm,	
	C (mol/l)	K	C (mol/l)	K	C (mol/l)	K	C (mol/l)	K
Et_4NBr	1.50	10	2.4	8.9	—		—	
Pr_4NBr	0.15	8.3	0.27	8.4	0.55	9.1	1.4	9.3
Bu_4NBr	0.018	9.0	0.032	9.7	0.060	9.0	0.15	9.3
Pen_4NBr	0.0020		0.0033		0.0066		0.016	

makers in water, show the effect of reducing the surface tension of pure water.[8] In view of this relation, the shape of the surface tension-*versus*-concentration curve for an amphiphilic organic salt in aqueous solutions is considered to give a rough criterion of the behavior of the salt in water.[8] In view of the above results, Me_4NBr may be considered to act as a simple salt. With Me_4N^+ ion, the interaction of the ionic part with water will surpass the hydrophobic hydration due to methyl groups. In the cases of Et_4NBr, Pr_4NBr, Bu_4NBr, and Pen_4NBr, conversely, the interaction of alkyl groups with water surpasses the electrostrictive hydration due to the central ionic part; consequently, the transfer of these salts from the bulk phase to the surface phase is a spontaneous process. Thus, they are surface active in aqueous solutions.[4] On the basis of this concept, Et_4NBr, Pr_4NBr, Bu_4NBr, and Pen_4NBr are considered to be classifiable as hydrophobic structure-makers in water. In general, these results of classification by the surface tension method are in fairly good agreement with those by other method.[1-3]

In order to compare the strength of the surface activity for these homologous compounds from Et_4NBr to Pen_4NBr inclusive, the Traube factors are obtained using the $\Delta\sigma$ values *versus* the molar concentration curves (not shown). The Traube factor means, in this case, the ratio of the molar concentration of equal $\Delta\sigma$ values when four alkyl chains of a compound are lengthened by every methylene group—*i.e.*, from Et_4NBr to Pr_4NBr, from Pr_4NBr to Bu_4NBr, and from Bu_4NBr to Pen_4NBr. The results are summarized in Table 1. In the case of a homologous series of strong electrolytes with one alkyl chain, such as sodium alkyl sulfates, the surface activity increases by a ratio of about 2 when the chain of an aliphatic compound is lengthened by one methylene group.[9] If we use this relation, the effect of four alkyl groups on the surface activity may be expected to increase by a factor of about 16 ($=2^4$) with an increase of four methylene groups. Therefore, in the case of the surface activity of spherical amphiphilic salts like R_4NBr salts in water, the effect of nonpolar alkyl groups on the surface activity was diminished by about half as compared with that of straight-chain salts.

Effect of Counter-ions. Figure 2 shows the $\Delta\sigma$ values *versus* the molal concentration curves for Me_4NCl, Me_4NBr, and Me_4NI. Figure 3 also shows the $\Delta\sigma$ values *versus* the logarithms of the molal concentration for Et_4NX and higher homologues. It is found that the surface tensions for R_4NX salts are mainly determined by the chain length; however, there are some specific effects due to the variation in counter-ions.

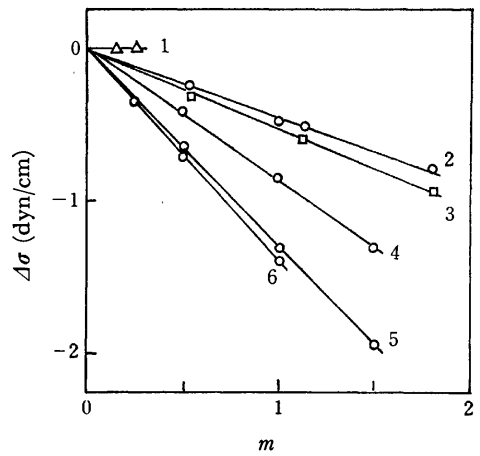

Fig. 2. Change in surface tension ($\Delta\sigma$) as a function of molality (m); 1, Me_4NI; 2, Me_4NBr; 3, Me_4NCl; 4, KI; 5, KBr; 6, KCl.

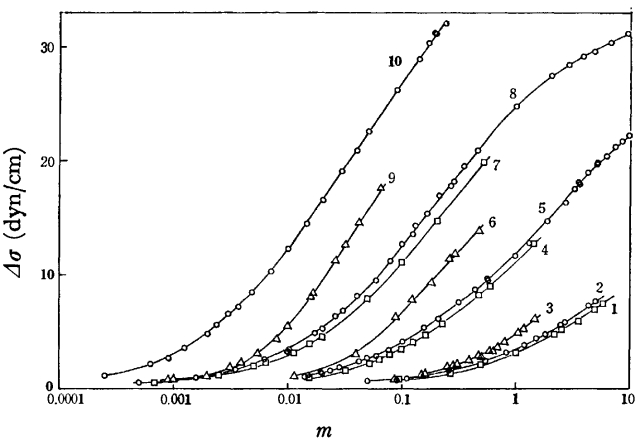

Fig. 3. Change in surface tension ($\Delta\sigma$) as a function of log m; 1, Et_4NCl; 2, Et_4NBr; 3, Et_4NI; 4, Pr_4NCl; 5, Pr_4NBr; 6, Pr_4NI; 7, Bu_4NCl; 8, Bu_4NBr; 9, Bu_4NI; 10, Pen_4NBr.

With Me_4NX salts, the order of raising the surface tension of water is in this order: $Cl^->Br^->I^-$. In the case of alkali halides, the same relation has been reported in the literature[5] as well. For comparison, the results[5] for KCl, KBr, and KI are also plotted in Fig. 2. The overall $\Delta\sigma$ values are slightly larger in the case of Me_4NX salts than in the case of alkali halides; this can probably be interpreted in terms of the effect

of the slightly hydrophobic nature of the methyl groups. The effects of halide ions on the $\Delta\sigma$ values in the case of Me_4NX salts and in the case of alkali halides are comparable with each other. This fact also supports the above conclusion that Me_4NX salts, where $X=Cl^-$, Br^-, and I^-, can be classified as simple salts. As is evident in Fig. 3, the effect of counter-ions on the surface activity for Et_4NX, Pr_4NX, and Bu_4NX salts is quite remarkable; the order of increasing surface activity is $I^->Br^->Cl^-$.

As has been proposed in a previous paper,[8] in the range of low $\Delta\sigma$ values, the $\Delta\sigma$ values are empirically expressed as:

$$\Delta\sigma = AC^{1/2} + BC \quad (1)$$

where A and B are constants. Equation (1) is found to be applicable up to about 7 dyn/cm in the cases of Et_4NX salts and higher homologues. Equation (1) may be converted to:

$$\Delta\sigma/C^{1/2} = A + BC^{1/2} \quad (2)$$

Some examples of the plots of data according to Eq. (2) are shown in Fig. 4. The values of the constants, A and B, are obtained as the intercepts and the slopes respectively of such linear plots; the results are summarized in Table 2. Both A and B values are found to be dependent on the chain length as well as on the kind of counter-ion.

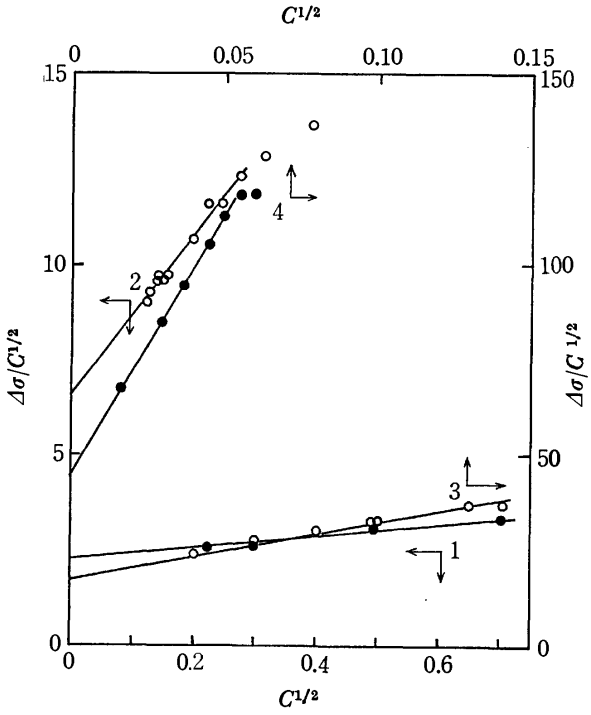

Fig. 4. Plots according to Eq. (2) up to about 7 dyn/cm; 1, Et_4NBr; 2, Pr_4NBr; 3, Bu_4NBr; 4, Pen_4NBr.

TABLE 2. THE CONSTANTS A AND B IN Eq. (2)

	A			B		
	Cl^-	Br^-	I^-	Cl^-	Br^-	I^-
Me_4N^+	0	0	0	−0.5	−0.45	≒0
Et_4N^+	2.4	2.3	1.65	1.1	1.5	3.7
Pr_4N^+	6.6	6.4	4.0	13	19	57
Bu_4N^+	19.5	17	9.0	95	160	440
Pen_4N^+	—	44	—	—	1350	—

The B coefficients are considered to be measures of the surface activity of the salts in water.[8] The value of $-RT \ln B$ is the approximate value of the standard free energy of the transfer of an organic electrolyte from the bulk phase to the surface phase, where R is the gas constant, and T, the absolute temperature. In this case, the standard state for the bulk solution is taken as the state where $C=1$, and the standard state for the surface phase is taken as the state of $\Delta\sigma=1$ dyn/cm. The B value depends on both the chain length and the kind of counter-ion; *i.e.*, it increases with the chain length and with the strength of the electrostrictive structure-breaking action of a counter-ion for a given cation.

From the perfect analogy of Eq. (1) with the equations for other properties such as viscosity, conductivity, and activity coefficient of the aqueous solutions of strong electrolytes, it seems that the A coefficient is related to some type of ion-ion interaction. The A coefficient increases with the chain length, while it decreases with the increase in the size of the counter-ions; *i.e.*, it decreases in the order of $I^-<Br^-<Cl^-$ for each combination of R_4NX salts, as is evident in Table 2. This relation was also found in a previous work[8] for *n*-alkylammonium halides. The less the A values, the more ideal the $\Delta\sigma$ values-*versus*-concentration plots become. From these findings, it may be assumed that the A coefficient is related to the ion-ion interaction of organic salts at the adsorbed layer; *i.e.*, the A coefficient is probably a function which increases with the strength of the adsorbability of organic cations and which decreases in the strength of the interaction of the adsorbed organic ions with their counter-ions at the surface phase.

The Values of Adsorption at the Surface. Lindenbaum and Boyd[10] published the ionic mean activity coefficients for Me_4NX, Et_4NX, Pr_4NX, and Bu_4NX salts in water at 25 °C. From the combination of their results[10] with those shown in Fig. 3, the $\Delta\sigma$ values can be plotted as a function of the activity, as shown in Fig. 5. As the data of the activity coefficient for Bu_4NBr at 25 °C are unavailable, the data for Bu_4NBr

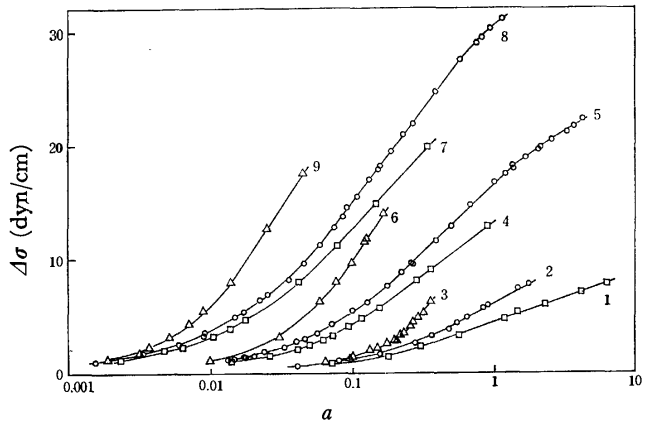

Fig. 5. Change in surface tension ($\Delta\sigma$) as a function of log a; 1, Et_4NCl; 2, Et_4NBr; 3, Et_4NI; 4, Pr_4NCl; 5, Pr_4NBr; 6, Pr_4NI; 7, Bu_4NCl; 8, Bu_4NBr; 9, Bu_4NI.

at 0 °C published by Nomura *et al.*,[11] are used. Because the activity coefficients for Pr_4NBr are independent of the temperature in the range from 0 to 25 °C,[10,11] this procedure is approximately valid. The Gibbs adsorption equation in the form of:

$$\Gamma = (1/2RT)(d\Delta\sigma/d \ln a) \quad (3)$$

will be applied to the data shown in Fig. 5, where Γ is the surface concentration of the solute, and a, the activity. As is shown in Fig. 5, there is fairly wide range of the linear portion on the plots between the $\Delta\sigma$ values and activities for each salt. Using the value of this slope of the linear portion in Fig. 5, the maximum surface concentration for each salt has been calculated; the results are listed in Table 3.

Table 3. The surface concentration at the maximum adsorption (in 10^{-10} mol/cm^2)

	Cl^-	Br^-	I^-
Et_4N^+	0.377	0.622	1.19
Pr_4N^+	0.838	1.05	1.61
Bu_4N^+	1.28	1.43	1.73

The large values of the surface concentration for R_4NI salts are particularly striking, as is evident in Table 3, which may be interpreted in terms of the specific interaction of R_4N^+ ion with I^- ion. The activity coefficients for R_4NI salts in water are very low compared for those of R_4NCl and R_4NBr salts; those for Et_4NI, Pr_4NI, and Bu_4NI salts are especially lower-lying than the Debye-Hückel limiting law.[10,11] These facts imply that R_4NI salts are very stable in water. Many investigators have proposed a specific interaction between R_4N^+ ions and I^- ions in terms of "water structure-enforced ion-pairing,"[12] micelle formation,[10] and structural salting-in.[13] At the surface, the adsorbed R_4N^+ ions will interact to a great extent with I^- ions as counter-ions; therefore, the electrical repulsive potential of the ionized surface will be greatly reduced.[4]

The behavior of R_4NX salts at the surface can probably be deduced if we apply the several surface chemical principles to the results of this work. However, such an attempt is beyond the scope of this paper.

The Behavior of R_4NX Salts in Concentrated Solutions. Some investigators have proposed a micelle formation for R_4NX salts in aqueous solutions. As a critical micelle concentration for Bu_4NBr, Lindenbaum and Boyd[10] reported 0.039 *m* and Rehfeld[14] reported 0.015 *m*. Wirth[15] were of the opinion that the micelle formation occurred above 4.0 *m* in Et_4NBr and above 1.4 *m* in Pr_4NBr solutions. As is evident from the curves for Pr_4NBr and Bu_4NBr in Fig. 3, the $\Delta\sigma$ value increases very rapidly as the concentration is increased, but at higher concentrations this increase is less marked; this situation is somewhat similar to what is seen when the electrolyte forms micelles. It was further observed in this study that the solution of R_4NX salts became highly viscous at higher concentrations, suggesting that the solute-solute interaction plays an important role in such concentrated solutions. However, the behavior of R_4NX salts in concentrated solutions, and especially the possibility of the micelle formation, remain as problems for the future.

References

1) S. Saito, *Hyomen*, **4**, 584 (1968).
2) W-Y. Wen, "Water and Aqueous Solutions, Structure, Thermodynamics, and Transport Prosesses," ed. by R. A. Horne, Wiley-Interscience, New York, N. Y. (1972) p. 613.
3) W-Y. Wen, *J. Solution Chem.*, **2**, 253 (1973).
4) K. Tamaki, This Bulletin, **40**, 38 (1967).
5) "International Critical Tables," Vol. 4, McGraw-Hill Book Co., New York, N. Y. (1929), p. 463.
6) M. J. Blandamer, *Quart. Rev.*, **24**, 169 (1970).
7) K. Tamaki, Y. Ōhara, H. Kurachi, M. Akiyama, and H. Odaki, This Bulletin, **47**, 384 (1974).
8) K. Tamaki, *Kolloid-Z. Z. Polym.*, in press.
9) K. Tamaki, This Bulletin, **38**, 1987 (1965).
10) S. Lindenbaum and G. E. Boyd, *J. Phys. Chem.*, **68**, 911 (1964).
11) H. Nomura, Y. Sakakura, and Y. Miyahara, *Nippon Kagaku Kaishi*, **1973**, 438.
12) R. M. Diamond, *J. Phys. Chem.*, **67**, 2513 (1963).
13) J. E. Desnoyers, M. Arel, G. Perron, and C. Jolicoeur, *ibid.*, **73**, 3346 (1969).
14) S. J. Rehfeld, *J. Amer. Chem. Soc.*, **95**, 4489 (1973).
15) H. E. Wirth, *J. Phys. Chem.*, **71**, 2922 (1967).

Quenching of Excited Mercury Atoms(6^3P_1 and 6^3P_0) in Molecular Collisions

Hiroyuki HORIGUCHI and Soji TSUCHIYA

Department of Pure and Applied Sciences, College of General Education, University of Tokyo, Meguro-ku, Tokyo 153

(Received May 22, 1974)

The lifetime of $Hg(6^3P_0)$ in a gaseous mixture of Ar and N_2 with quenching molecules(Q) was measured by monitoring the decay of the $Hg(6^3P_0)$ concentration following the excitation of Hg by pulsed 253.7 nm radiation. The lifetime in the absence of Q was reduced with the increase in the N_2 pressure, being inversely proportional to the total pressure. This can be attributed to the deactivation by impurities involved in the gas and that by collision on the wall of the reaction cell. Deactivation due to impurities is dominant at a total pressure higher than 50 Torr. With quenchers in the mixture, the lifetime measurement gave the quenching cross-section of $Hg(6^3P_0)$. In addition, the measurement of the stationary concentration of $Hg(6^3P_0)$ made it possible to determine the rate for each of the processes $6^3P_1 \rightarrow 6^3P_0$ and $6^3P_1 \rightarrow 6^1S_0$. Based on the observed ratio, $\alpha = \sigma^2(6^3P_1 \rightarrow 6^1S_0)/\sigma^2(6^3P_0 \rightarrow 6^1S_0)$, quenching molecules are classified into three groups. The first group consists of N_2O, O_2, C_2H_4, C_3H_6, and C_2H_2 with $\alpha = 1.2$. These molecules deactivate $Hg(6^3P)$ to form their triplet states. The second group (CO, NO, H_2, C_3H_8, *i*-,*n*-C_4H_{10}, and $C(CH_3)_4$) in which $\alpha \approx 4$ makes the quenching *via* a short-lived complex $(Hg\text{-}Q)^*$. The last group (CH_4 and C_2H_6) has a value of α larger than 100. This is caused by a weak interaction between potential surfaces of $Hg(6^3P)+Q$ and $Hg(6^1S)+Q$.

In contrast to the $Hg(6^3P_1)$ state, transition from the $Hg(6^3P_0)$ to the ground state (6^1S_0) is weakly allowed by the spin-orbit interaction. The probability calculated by Garstang[1] is $0.18\ s^{-1}$. Thus, the radiative process would be negligible in the deactivation of $Hg(6^3P_0)$ atoms. The lifetime in N_2 has been measured by means of several methods.[2-5] Callear and Norrish[4] suggested that the main quenching process was the collisional deactivation by ground state Hg atoms. However, a very small cross-section (0.03—0.1 Å^2) for the 6^3P_1 quenching by $Hg(6^1S_0)$ was estimated by Waddell and Hurst,[6] and the more recent data of Callear and McGurk[5] indicated that the deactivation was caused mostly by impurities in N_2 gas. The quenching cross-sections of $Hg(6^3P_0)$ by other species were measured by Callear and Williams,[7] who found very small cross-sections and concluded a metastable character of the $Hg(6^3P_0)$ state. However, they later observed a cross-section larger by an order of magnitude than the previous value with use of a new flash device.[5] Their result is consistent with our former measurements.[8]

In this paper we report on the direct measurement of the lifetime of $Hg(6^3P_0)$ in a medium of $Ar+N_2$ mixture together with cross-sections of various molecules for quenching $Hg(6^3P_0)$. The method proposed in the previous paper[9] has been also applied for the measurements of the rates of the processes $6^3P_1 \rightarrow 6^3P_0$ and $6^3P_1 \rightarrow 6^1S_0$. The difference between the collisional processes of $6^3P_1 \rightarrow$ and $6^3P_0 \rightarrow 6^1S_0$ has been discussed.

Experimental

The apparatus and procedure were the same as those described previously,[9] except for the use of pulsed 253.7 nm radiation to excite Hg atoms and to follow a time history of $Hg(6^3P_0)$ concentration. A schematic diagram of the apparatus is shown in Fig. 1. An exciting lamp was a germicidal lamp (Toshiba, 30 W), operated in a pulsed mode. The filament electrodes of the lamp were heated for several minutes by connecting A with B in the switch, which was then moved to the other side. At the final position of the switch, three

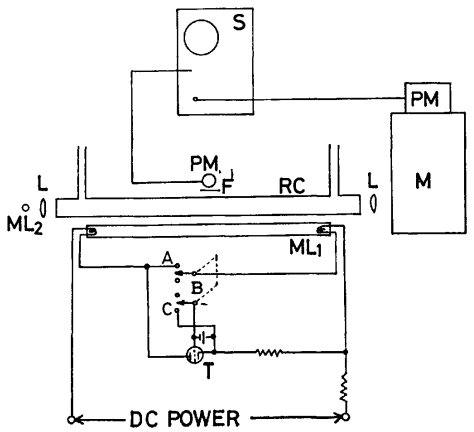

Fig. 1. Schematic diagram of the apparatus.
ML_1: low pressure Hg lamp for 253.7 nm radiation, ML_2: low pressure Hg lamp as a source of 435.8 and 404.7 nm lines, L: quartz lens, RC: reaction cell, M: monochromator, PM: photomultiplier, F: optical filter for 253.7 nm line, S: oscilloscope, T: thyratron.

thyratrons (2D21) made a short circuit between the two electrodes. In this way, the lamp was turned on for a short interval (10—40 ms) during which the connection of B with A changed to that with C, and was turned off in less than 40 μs. The light pulse thus obtained was monitored by a photomultiplier through an interference filter transmitting 253.7 nm radiation, and its out-put was used as a trigger pulse for an oscilloscope (Iwasaki, SS-5004). For the measurement of $Hg(6^3P_0)$ concentration, the 404.7 nm light beam from a low pressure mercury lamp was passed through a reaction cell, whose length and diameter were 100 and 4 cm, respectively. The light beam was fed into a grating monochromator, whose out-put was recorded on the oscilloscope.

Figure 2 shows a typical example of the oscilloscope record. After the exciting lamp is turned on, the intensity of the 404.7 nm line is reduced following an increase of 253.7 nm radiation due to the formation of $Hg(6^3P_0)$ atoms. Turning off of the lamp causes a gradual recovery of the 404.7 nm intensity. The concentration of $Hg(6^3P_0)$ was calculated as described previously. The decay of the $Hg(6^3P_0)$ concentration is exponential against time as seen from Fig. 3,

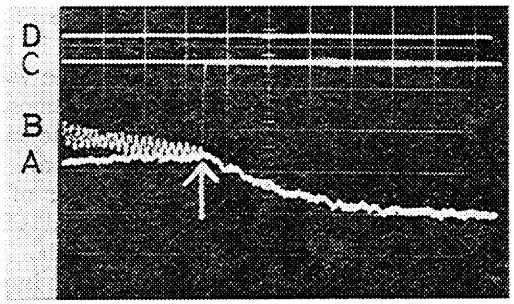

Fig. 2. Oscilloscope trace of the absorption of $Hg(6^3P_0)$ at 404.7 nm after the pulsed irradiation of 253.7 nm radiation into the mixture of $p(NH_3)=1.2\times10^{-2}$, $p(N_2)=0.2$, $p(Ar)=9.8$, and $p(Hg)=1.9\times10^{-4}$ Torr. A: intensity of 404.7 nm line, B: intensity of 253.7 nm radiation (the arrow shows the turning off of the lamp), C: zero for 253.7 nm intensity, D: zero for 404.7 nm intensity, sweep velocity: 5 ms/div.

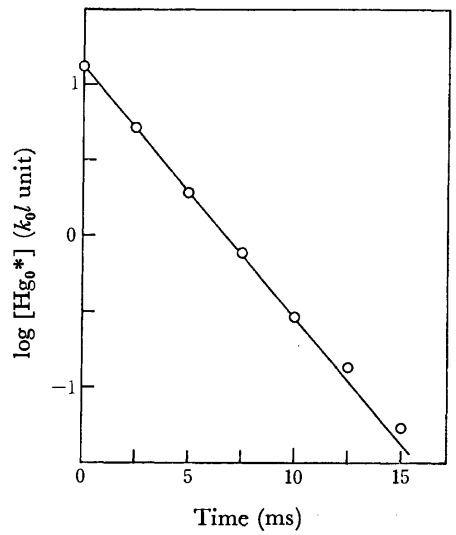

Fig. 3. Decay of the $Hg(6^3P_0)$ concentration obtained from the data given in Fig. 2.

and the lifetime can be defined.

Sample gases employed were commercial. Ar, CO and NO were purified in the same procedure as reported previously. In order to eliminate a trace of O_2, N_2 gas was passed through a U-shaped glass tube packed with small tips of copper at 350 °C. The nominal purity of other gases was: 99.9% for CH_4 and i-C_4H_{10}, 99.7% for C_2H_6, C_3H_8 and n-C_4H_{10}, 99.99% for CO_2, and 99.5% for NH_3. These gases were purified by trap-to-trap distillation in vacuum at liquid nitrogen temperature, their purity being found by gas chromatography to exceed 99.9%. The total pressure of the system was kept constant by adding Ar gas as a diluent to avoid the pressure broadening effect of spectral lines, where Ar could be assumed as a very poor quencher of excited Hg atoms.

Results and Discussion

Lifetime of $Hg(6^3P_0)$ in N_2 and Ar. $Hg(6^3P_0)$ atoms are formed by the reactions:

(i) $Hg + h\nu\,(253.7\,nm) \longrightarrow Hg_1^*$,

(ii) $Hg_1^* \longrightarrow Hg + h\nu\,(253.7\,nm)$,

(iii) $Hg_1^* + N_2 \longrightarrow Hg + N_2$,

(iv) $Hg_1^* + N_2 \longrightarrow Hg_0^* + N_2$,

where Hg, Hg_1^* and Hg_0^* represent Hg atoms of 6^1S_0, 6^3P_1, and 6^3P_0 states, respectively. As reported previously, the rate for Reaction (iii) is negligibly small. Therefore, in a N_2-rich system, all Hg_1^* atoms formed by the 253.7 nm radiation are converted into Hg_0^* atoms. Possible processes for the deactivation of Hg_0^* atoms in a mixture of N_2 and Ar are as follows;

(v) $Hg_0^* + N_2 \longrightarrow Hg + N_2$,

(vi) $Hg_0^* + N_2 \longrightarrow Hg_1^* + N_2$,

(vii) $Hg_0^* + M \longrightarrow Hg + M + h\nu$,

(viii) $Hg_0^* + Hg \longrightarrow 2Hg$,

(ix) $Hg_0^* + Hg \longrightarrow Hg_2^* \longrightarrow 2Hg + h\nu$,

(x)
$$\begin{cases} Hg_0^* + Hg + M \longrightarrow Hg_2^* + M, \\ Hg_2^* \longrightarrow Hg_2 + h\nu\,(335.0\,nm), \\ Hg_2^* + M \longrightarrow Hg_2 + h\nu\,(485.0\,nm), \end{cases}$$

where M stands for N_2 or Ar. Among these processes, Reactions (viii)—(x) cannot be dominant, since the observed lifetime of Hg_0^* is independent of the mercury pressure, as seen from Table 1. Callear and Norrish[4] proposed the cross-section of 18 Å^2 for Reaction (viii). This results in a lifetime shorter than 0.1 ms at $p(Hg)=1.4\times10^{-3}$ Torr, and this is not the case in this experiment. Since their experiment was carried out in a system of atmospheric pressure, there might be a contribution from a termolecular process like Reaction (x). In order to check this possibility, the lifetime was observed under pressures up to 655 Torr. The lifetime is reduced with the increase in the total pressure of the system, and is independent of the mercury pressure in the range of 10^{-4}—10^{-3} Torr. The former fact is due to impurities in the sample gas, and the latter to a small contribution of a termolecular process. The poor efficiency of quenching by Hg_0^*–Hg collisions indicates that potential surfaces of Hg_0^*+Hg and Hg+Hg cross each other at a small internuclear distance where the potential energy is high.[10] Since the radiative transition from the excited state of $Hg_2(^3O_u^-)$ to the ground state is forbidden, Reaction (ix) is impossible. The only possibility is that the excited Hg_2 formed by a collision with a third body makes a spontaneous or a collision-induced transition, *i.e.*, Reaction

Table 1. Lifetime (in ms) of Hg (6^3P_0) in the mixture of Ar+N_2

Total pressure (Torr)	p(Hg) (Torr)		
	1.7×10^{-5}	1.9×10^{-4}	1.4×10^{-3}
1	2.6[a]	2.8[d]	2.6[e]
5	6.6[b]	6.7[d]	7.0[e]
10	10.8[c]	10.0[d]	10.5[e]
50	—	5.0[f]	—
150	—	1.3[g]	1.4[g]
400	—	0.8[h]	0.9[h]
655	—	0.54[i]	0.57[i]

Partial pressure of N_2 (Torr): a) 1.05, b) 1.26, c) 0.52, d) 0.08, e) 0.026, f) 0.05, g) 0.22, h) 4.0, i) 10.0.

(x). However, the spontaneous radiation and the collision-induced radiation rates of $Hg_2(^3O_u^-)$ are 20 s^{-1} and 2.1×10^{-31} $atom^{-2}$ cm^6 s^{-1}, respectively.[11] Thus the rate of Reaction (x) is too small to be measured in the present experiment.

Reaction (vii) for the case of $M=NH_3$ was proposed by Freeman *et al.*,[12] who found that the decay rates of Hg_0 concentration and of luminescence at 347.0 nm were the same. Koskikallio *et al.*[13] found a termolecular mechanism for the deactivation of Hg_0^* by NH_3. This suggests a long-lived complex $Hg–NH_3^*$ emitting the luminescence. However, a luminescence of a similar kind has not been found in N_2, and this suggests that the interaction between N_2 and Hg_0^* may not be strong enough to form a complex with a long lifetime.

The first experimental evidence for Reaction (vi) was reported by Samson.[14] He found a slow decay of 253.7 nm fluorescence after the pulsed irradiation of 253.7 nm light into the N_2–Hg mixture, and attributed the decay to Reaction (vi). More recently, Callear and McGurk[5] also observed a slow decay of fluorescence which they interpreted to be a tracer of Hg_0^* atoms. After the flash excitation of Hg atoms, a quasi-stationary condition for $[Hg_1^*]$ can be assumed since the radiative lifetime of Hg_1^* is very short as compared with the time scale of observation. Then, we get the relation

$$[Hg_1^*]/[Hg_0^*] = k_6[N_2]/(k_2+k_4[N_2]), \quad (1)$$

where Reaction (iii) and the quenching of Hg_1^* by impurities are disregarded. Assuming that this relation holds, the lifetime of Hg_0^* atom can be formulated as

$$1/\tau = [k_2k_6[N_2]/(k_2+k_4[N_2])] + k_5[N_2] + k_Q[Q], \quad (2)$$

where $k_Q[Q]$ represents the contribution of quenching molecules or impurities in a sample gas to the deactivation of Hg_0^*. If we assume a detailed balancing for Reaction (iv) and (vi), the first term in Eq. (2) can be calculated from our previous result for the rate of Reaction (iv). The result is shown in Fig. 4.

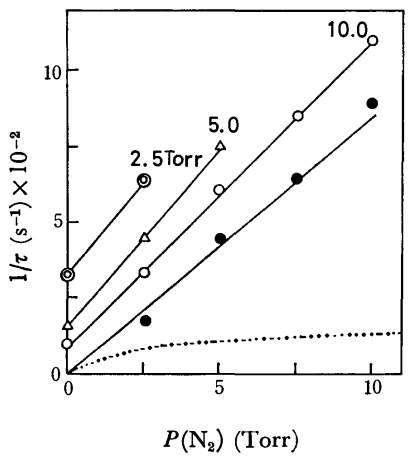

Fig. 4. The reverse of the lifetime of $Hg(6^3P_0)$ in the $Ar+N_2$ mixture against the N_2 pressure.
Total pressure is 10 Torr for ○, 5 for △, 2.5 for ◎ with the Hg pressure of 1.9×10^{-4} Torr, and the dashed line is calculated from Eq. (2). The point ● shows the data at 10 Torr from which the calculated value (dashed line) and the one in the absence of N_2 are subtracted.

The experimental relation of the lifetime of Hg_0^* with the partial pressure of N_2 is shown also in Fig. 4. The reciprocal of the lifetime, from which the value of the first term in Eq. (2) is subtracted, is almost proportional to $[N_2]$, its linear slope giving the rate 85 $Torr^{-1}$ s^{-1} or 1.7×10^{-4} Å^2 of the cross-section. However, this cross-section is larger by an order of magnitude than that observed by Berberet and Clark,[3] who used the N_2 gas made from sodium azide. Since N_2 has a very small quenching cross-section, an impurity in the gas which is less pure than the Ar gas may contribute dominantly to the quenching. If an impurity molecule has a quenching cross-section of 10 Å^2, the purity of N_2 should exceed 99.9999% in order to eliminate the impurity effect. Therefore, the value of 1.7×10^{-4} Å^2 for the cross-section should be assumed as an upper limit.

In Fig. 4 also seen is the increase of the lifetime with the increase in the total pressure. This means that Hg_0^* atoms are deactivated by collisions with the

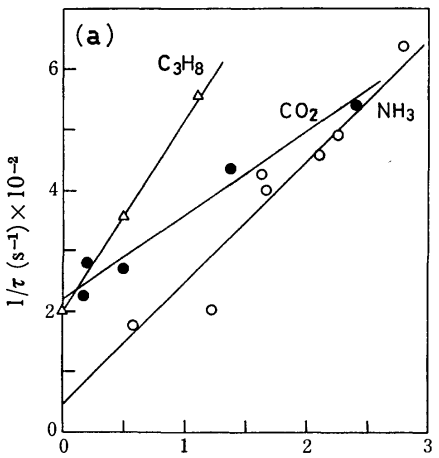

Pressure of NH_3 (Torr$\times2\times10^2$); CO_2, C_3H_8 (Torr$\times10^2$)

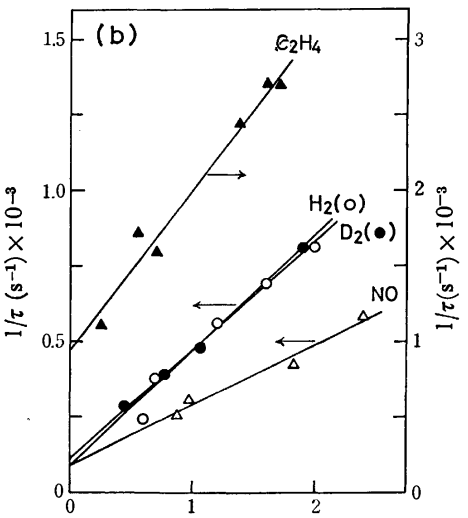

Pressure of H_2, D_2 (Torr$\times10^4$); C_2H_4, NO (Torr$\times5\times10^5$)

Fig. 5. The reverse of the lifetime of $Hg(6^3P_0)$ against a pressure of quencher. The experimental condition except for NH_3, C_2H_4 and NO: $p(N_2)=0.2$, $p(Ar)=9.8$, and $p(Hg)=1.9\times10^{-4}$ Torr; for NH_3: $p(Ar)=10.0$; for C_2H_4: $p(N_2)=4.8$, $p(Ar)=5.8$, for NO: $p(N_2)$ 1.3, $p(Ar)=8.7$ Torr.

Table 2. Quenching cross-sections (σ^2 in Å^2) of $Hg(6^3P_0)$

Quencher	This work	Callear & McGurk[5]	Freeman *et al.*[15]
N_2	$<2\times10^{-4}$	—	—
CH_4	1.4×10^{-4}	2.70×10^{-4}	—
C_2H_6	2.0×10^{-3}	5.73×10^{-3}	2.9×10^{-2}
NH_3	0.016	0.015	0.016
CO_2	0.032	0.033	—
CO	0.69	0.655	2.5
NO	8.0	16.2	13
H_2	2.1	0.956	1.6
D_2	2.9	—	—
C_3H_8	0.073	0.033	—
n-C_4H_{10}	0.93	—	—
i-C_4H_{10}	1.4	—	—
$C(CH_3)_4$	0.11	—	—
N_2O	14	8.48	4.4
O_2	16	12.0	18
C_2H_4	41	26	—
C_3H_6	50	—	—
C_2H_2	36	—	—

wall of the reaction cell, and that diffusion to the wall is the rate-determining step. However, at a total pressure higher than 50 Torr, the reduction of the lifetime is found to be due to the deactivation by impurities.

Quenching Rate of $Hg(6^3P_0)$ with Various Molecules. The lifetime of Hg_0* was measured in a gaseous mixture of N_2 and Ar with a small amount of a quenching gas (Q). The reciprocal of the observed lifetime is plotted as a function of a partial pressure of Q in Fig. 5. The experimental data satisfy the Stern-Volmer relation, and the slope of the line gives the deactivation rate of Hg_0*,

$$\text{(xi)}\quad Hg_0^* + Q \longrightarrow Hg + Q.$$

The results are summarized in Table 2 together with the data of Callear and McGurk[5] and Freeman *et al.*[15] to show the general agreement.

Rates for the Processes of $6^3P_1\rightarrow6^3P_0$ and $6^3P_1\rightarrow6^1S_0$. A method was given to obtain the rate constant for each of the two processes from the 6^3P_1 state,

$$\text{(xii)}\quad Hg_1^* + Q \longrightarrow Hg_0^* + Q,$$

$$\text{(xiii)}\quad Hg_1^* + Q \longrightarrow Hg + Q,$$

based on the measurement of a stationary concentration of Hg_0*.[9] This method was applied to the system of Ar and various quenchers. In the previous work, we also measured the stationary concentration of Hg_1* as a function of a partial pressure of Q, and determined the total quenching rate of Hg_1*. However, a weak absorption of the 435.8 nm line made the observed rate unreliable. In addition, a high pressure of Hg (1.9×10^{-4} Torr) caused an imprisonment of 253.7 nm resonant radiation, so that it is difficult to estimate the effective lifetime of Hg_1* accurately. Hence, we adopted the total quenching rate observed by others in this work. Deech *et al.*[16] measured directly the lifetime of Hg_1* excited by a pulsed radiation. The quenching rate determined through this procedure does not depend on the radiative lifetime. Therefore, their data should be more reliable than those determined by the fluorescence method. For the rates which have not been measured by Deech *et al.*, correction factors are sought by comparing the results of Zemansky,[17] Kang Yang,[18] Darwent,[19] and Campbell *et al.*[20] with those of Deech *et al.*, since it would be reasonable to assume that the relative magnitude of cross-sections determined by the fluorescence method in one laboratory is more reliable.

Table 3. Observed rate (k_{12} in cm^3 molecules^{-1} s^{-1}) for the spin-orbit relaxation of $6^3P_1\rightarrow6^3P_0$.

Colliding molecule	Partial pressure (Torr)	$[Hg_0^*]/[Hg_1^*]_0$[a]	k_{12}	$\sigma^2(6^3P_1\rightarrow 6^3P_0+6^1S_0)$ (Å^2)
CH_4	0.27	10	2.1×10^{-13}	0.08[b]
	0.35	12	2.1	
	0.47	13	1.8	
C_2H_6	0.48	36	2.1×10^{-12}	0.57[b]
	0.68	48	3.1	
NH_3	0.012	36	2.3×10^{-11}	4.05[b]
	0.018	40	2.2	
	0.021	43	2.3	
	0.025	55	2.8	
	0.033	59	3.1	
CO	0.0020	3.8	6.3×10^{-11}	6.91[c]
	0.0031	5.6	8.4	
	0.0049	6.6	9.0	
	0.010	8.0	11.0	
NO	0.00037	0.5	7.6×10^{-11}	35.3[d]
C_3H_8	0.018	12	1.6×10^{-11}	2.23[b]
	0.032	13	1.6	
n-C_4H_{10}	0.0051	3.5	4.3×10^{-11}	5.67[b]
i-C_4H_{10}	0.0046	2.9	5.3×10^{-11}	9.3[e]
$C(CH_3)_4$	0.058	12	1.7×10^{-11}	1.9[f]

a) $[Hg_1^*]_0$ is the $Hg(6^3P_1)$ concentration in the absence of colliding molecules. All the measurements were carried out in the mixture with Ar at 10 Torr, b) the data of Zemansky[17] multiplied by 1.379 as a correction factor, c) the data of Deech *et al.*,[16] d) the value recommended by Cvetanović,[21] e) the value calculated from σ^2 (i-C_4H_{10})/σ^2(n-C_4H_{10}) determined by Darwent,[19] f) the data of Kang Yang.[18]

Based on Eq. (6) of the previous paper, the rate for either of Reaction (xii) and (xiii) can be calculated. The results are summarized in Table 3. In this experiment, Hg_0* was detected faintly in NO, and not in CO_2, H_2, D_2, N_2O, O_2, C_2H_4, C_3H_6, and C_2H_2, for which upper limits of the rates are given from the detection limit of Hg_0*. It is seen that the rate constant k_{12} of CO depends on its partial pressure; a larger CO partial pressure results in a larger value of k_{12}. This is due to disregard of the reverse reaction of (xii). At room temperature, the rate for this reaction is quite small because of its endothermicity. However, it is probable that Reaction (xii) causes the vibrational excitation of a quenching molecule. If the deactivation rate of a vibrationally excited species is not large like that of N_2 or CO, a population in the excited level increases to more than that in the equilibrium state. Thus, the reverse of Reaction (xii) is accelerated since a large endothermicity is covered by

Table 4. Cross-sections (σ^2 in Å^2) of various molecules for quenching Hg(6^3P_1 and 6^3P_0)

Group	Quencher	$6^3P_1 \rightarrow 6^1S_0$	$6^3P_1 \rightarrow 6^3P_0$	$6^3P_0 \rightarrow 6^1S_0$	$\frac{\sigma^2(6^3P_1 \rightarrow 6^1S_0)}{\sigma^2(6^3P_0 \rightarrow 6^1S_0)}$	
					ours	V and M[a]
I	N_2O	22—20	<2	14	1.6—1.3	—
	O_2	19—17	<2	16	1.2—1.1	—
	C_2H_4	48—43	<5	41	1.2—1.0	—
	C_3H_6	57—52	<5	50	1.1—1.0	—
	C_2H_2	43—39	<4	36	1.1—1.0	—
II	CO	3.0	3.9	0.69	4.3	—
	NO	30	5	8.0	3.8	—
	H_2	7.8	<0.1	2.1	3.7	—
	D_2	7.2	<0.1	2.9	2.5	—
	C_3H_8	1.0	1.2	0.073	14	2.6
	n-C_4H_{10}	2.1	3.6	0.93	2.3	3.1
	i-C_4H_{10}	4.8	4.5	1.40	3.4	1.5
	$C(CH_3)_4$	0.3	1.6	0.11	2.8	49
III	CH_4	0.07	0.01	1.4×10^{-4}	500	860
	C_2H_6	0.40	0.17	2.0×10^{-3}	200	6.6
	NH_3	2.75	1.3	0.016	170	—
	CO_2	3.2	<0.02	0.032	100	—

a) calculated by Vikis and Moser[24] based on the RRKM theory.

the vibrational energy of a quenching molecule, and the lifetime of Hg_0* is reduced by the process in which Hg_0* changes to Hg_1* through the reverse of Reaction (xii) and Hg_1* makes a spontaneous transition to the ground state. We therefore adopt a value of k_{12} for CO by the extrapolation to zero pressure of CO. For other gases except N_2, the rate of the vibrational relaxation is so large that an equilibrium state in the system may be assumed.

The final results of the quenching cross-sections are summarized in Table 4 for each of the processes $6^3P_1 \rightarrow 6^1S_0$, $6^3P_1 \rightarrow 6^3P_0$, and $6^3P_0 \rightarrow 6^1S_0$.

Correlation between the Cross-Sections for Processes $6^3P_1 \rightarrow 6^1S_0$ and $6^3P_0 \rightarrow 6^1S_0$. In Fig. 6, the cross-sections of various quenching molecules for the process $6^3P_1 \rightarrow 6^1S_0$ are plotted as a function of the corresponding cross-sections for that of $6^3P_0 \rightarrow 6^1S_0$. It is concluded that quenching molecules can be classified into three groups, each of which has a constant ratio,

$$\sigma^2(6^3P_1 \rightarrow 6^1S_0)/\sigma^2(6^3P_0 \rightarrow 6^1S_0) = \alpha. \quad (3)$$

Though this classification is made empirically, one group with the same α can be characterized by a collision mechanism.

In the first group which consists of C_3H_6, C_2H_4, C_2H_2, O_2, and N_2O, $\alpha \approx 1.2$, and their lowest triplet energy levels are lower than those of the 6^3P_1 and 6^3P_0 states. Thus, in this group of molecules, a mechanism is suggested to be the electronic-to-electronic energy transfer such as

$$\text{(I)}\quad Hg_{1,0}^* + Q \longrightarrow Hg + Q^T.$$

Burton and Hunziker[22] found the formation of the triplet benzene or naphthalene by collisions with excited Hg atoms. This provides a direct evidence for mechanism (I). The collision process occurs through a non-adiabatic crossing from the potential surface of Hg*+Q to that of Hg+Q^T. The crossing is very

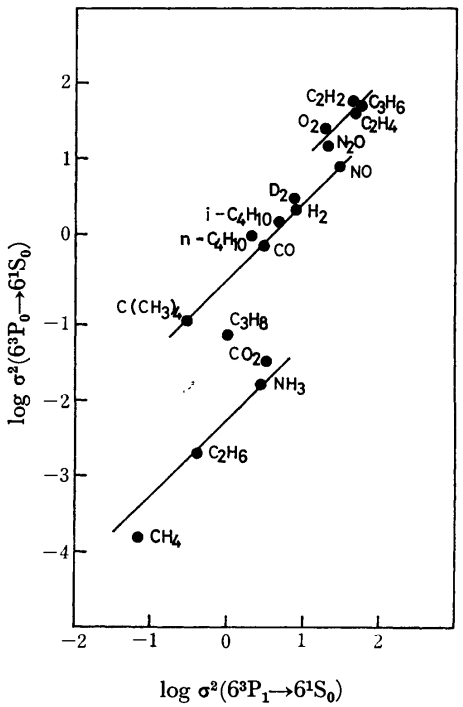

Fig. 6. Correlation of $\sigma^2(6^3P_1 \rightarrow 6^1S_0)$ to $\sigma^2(6^3P_0 \rightarrow 6^1S_0)$ in Å^2.

efficient due to the strong interaction of the 6p electron of Hg with the π^* orbit of quenching molecule. The cross-section is thus close to its gas kinetic one for quenching either of 6^3P_1 and 6^3P_0 states. The potential surface is schematically given in Fig. 7 together with cases for groups II and III.

In the second group which involves H_2, D_2, NO, CO, i-C_4H_{10}, n-C_4H_{10}, $C(CH_3)_4$, and C_3H_8, α is about 4, and their lowest triplet energy levels are higher than or close to that of the 6^3P_1 state. For hydrocarbon

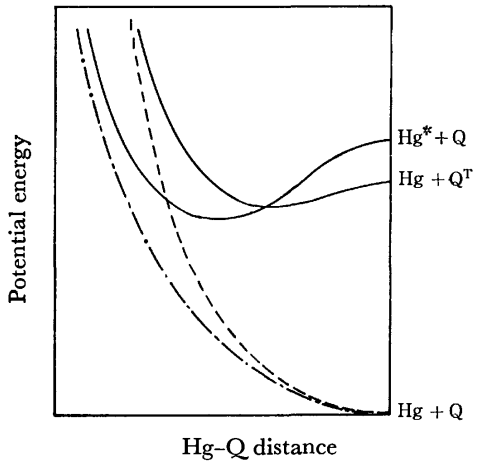

Fig. 7. Schematics of potential surfaces between Hg and Q.

molecules in this group, the quantum yield of H_2 formation is large in the Hg-photosensitized reaction, and the Hg*–CO or –NO collision affords the vibrational excitation of a colliding molecule.[23] This suggests a process *via* a short-lived intermediate:

$$\text{(II)}\quad Hg^* + Q \underset{k_{-a}}{\overset{k_a}{\rightleftharpoons}} (Hg\text{–}Q)^* \begin{cases} \xrightarrow{k_b} \text{decomposition of Q,} \\ \xrightarrow{k_c} \text{vibrational excitation of Q.} \end{cases}$$

Based on this mechanism, the cross-section should be explained as $k_a[(k_b+k_c)/(k_{-a}+k_b+k_c)]$. A large quantum yield of the C–H bond scission of a paraffin hydrocarbon leads to the fact that $k_c \approx 0$ due to a small bond energy of C–H. Assuming the complex (Hg–Q)*, Vikis and Moser[24] applied the RRKM theory to calculate the rate of hydrogen abstraction by excited Hg atoms. The calculated value of the cross-section is larger by an order of magnitude than the present value, but the ratio of α is in agreement for molecules in the second group except neopentane. This means that the difference between the 6^3P_1 and 6^3P_0 quenching is explained simply by the energy content of the complex (Hg–Q)*. In this case, the potential surface between Hg* and Q is weakly attractive, and is crossed by the strongly repulsive surface of Hg+Q as shown in Fig. 7. In the course of sliding down on the latter surface, Q is excited vibrationally or undergoes a decomposition by a mechanism similar to the unimolecular reaction.

The ratio of the quenching cross-section for a hydrocarbon molecule to that of a D-substituted one is of a measurable magnitude. The experimental ratio of $\sigma^2(CH_3CH_2CH_3)$ to $\sigma^2(CH_3CD_2CH_3)$ was determined by Kang Yang[18] as 3.0—8.0, which agreed well with the calculated one by Vikis and Moser based on the RRKM theory. This supports the energy dissipation through the unimolecular decomposition of (Hg–Q)*. However, the situation seems different for H_2 and D_2 because of its small isotope effect. If scheme II is assumed, the rate-controlling step is not the dissociation of (Hg–Q)* for H_2 or D_2, *i.e.*, the rate would be k_a since $k_{-a} \ll k_b$ and $k_c \ll k_b$. The process is a non-adiabatic transition from Hg*+Q to Hg+Q*, and this does not show a large isotope effect. Callear and McGurk[25] proposed two possible mechanisms for quenching Hg* by H_2: an electronically adiabatic route and a non-adiabatic one after H-Hg-H complex was formed by a sideway attack of Hg*.

The third group is characterized by a large ratio of α and by a small cross-section for quenching Hg_1* except NH_3 and CO_2. It is thus probable that there is no crossing between two surfaces of Hg*+Q and Hg+Q, or the crossing point is in an energy region higher than the excitation energy of Hg. Callear and McGurk[5] pointed out a steric hindrance of Hg* inserting into a C–H bond to be the cause of inefficiency of quenching by a simple hydrocarbon such as CH_4 or C_2H_6.

In the quenching of Hg_0* by NH_3, the emission which originated from (Hg-NH_3)* was found by Freeman *et al.*[26] The rate constant for the radiative process

$$Hg(6^3P_0) + NH_3 \longrightarrow (Hg\text{-}NH_3)^* \longrightarrow Hg(6^1S_0) + NH_3 + h\nu$$

was determined to be 3.2×10^{-13} cm^3 molecule^{-1} s^{-1}. This agrees with our result 3.1×10^{-13}. Hence, most of the 6^3P_0 quenching process should be the radiative one. In contrast, $\sigma^2(6^3P_1 \rightarrow 6^3P_0+6^1S_0)$ is of the same order of magnitude as that of a molecule in group II, and the quantum yield of the decomposition of NH_3 at a low pressure is close to 1.[27] Thus, the quenching of Hg_1* by NH_3 should be categorized into group II.

Since the dissociation energy of CO_2 is much larger than the excitation energy of Hg, the reaction scheme for the 6^3P_1 quenching is a triplet formation. The triplet level of CO_2 is uncertain, but the experiment of the thermal decomposition[28] suggests a level near that of the 6^3P state. If this is the case, a small cross-section of the 6^3P_0 quenching may be explained by the fact that the triplet level lies between those of the 6^3P_1 and 6^3P_0 states.

Quantum Yield of Hg(6^3P_0). The quantum yield

Table 5. Quantum yield of Hg (6^3P_0)

Collision partner	This work	Callear and McGurk[5]*	Vikis *et al.*[29]
CH_4	0.13	0.11(0.11)	—
C_2H_6	0.30	1.21(0.67)	0.64
NH_3	0.32	0.64(0.64)	1.05
CO_2	<0.006	~0.02(0.02)	<0.01
CO	0.56	0.57(0.90)	0.88
NO	0.14	<0.10(<0.10)	—
H_2	<0.01	<0.03(<0.03)	—
D_2	<0.01	—	—
C_3H_8	0.54	0.12(0.21)	0.14
n-C_4H_{10}	0.63	—	0.11
i-C_4H_{10}	0.48	—	0.05
$C(CH_3)_4$	0.84	—	0.58
N_2O	<0.09	<0.10(<0.10)	—
O_2	<0.10	<0.10(<0.10)	—
C_2H_4	<0.10	<0.10(<0.10)	—
C_3H_6	<0.09	—	—
C_2H_2	<0.09	—	—

*Uncorrected values in parentheses.

of Hg_0* defined as $\sigma^2(6^3P_1 \rightarrow 6^3P_0)/\sigma^2(6^3P_1 \rightarrow 6^1S_0 + 6^3P_0)$ are given in Table 5. The results are compared with those reported by Callear and McGurk.[5] Their data are corrected by using the total cross-sections of the 6^3P_1 quenching that are adopted in this work. The agreement is within a factor of 2 except C_2H_6. As stated already, the process $6^3P_1 \rightarrow 6^3P_0$ has a possibility to cause the vibrational excitation of a colliding molecule. However, there seems to be no distinct correlation between the cross-section and the resonance energy defect. The quantum yield is large for a molecule in group II and III except H_2, D_2, and CO_2. This suggests that the state mixing between the 6^3P_1 and 6^3P_0 states in the (Hg–Q)* complex may result in the transition to the 6^3P_0 state, and that the production of $Hg(6^3P_0)$ is not efficient if there is a large probability of transition from the Hg*+Q surface to the Hg+Q, *i.e.*, the condition $k_{-a} > k_b + k_c$ in scheme (II) is necessary for a large quantum yield.

References

1) R. H. Garstang, *J. Opt. Soc. Amer.*, **52**, 845 (1962).
2) M. L. Pool, *Phys. Rev.*, **38**, 955 (1931).
3) J. A. Berberet and K. C. Clark, *ibid.*, **100**, 506 (1955).
4) A. B. Callear and R. G. W. Norrish, *Proc. Roy. Soc. Ser. A*, **266**, 299 (1962).
5) A. B. Callear and J. C. McGurk, *J. Chem. Soc. Faraday* II, **69**, 97 (1973).
6) B. V. Waddell and G. S. Hurst, *J. Chem. Phys.*, **53**, 3892 (1970).
7) A. B. Callear and G. J. Williams, *Trans. Faraday Soc.*, **60**, 2158 (1964).
8) H. Horiguchi and S. Tsuchiya, This Bulletin, **44**, 3221 (1971).
9) H. Horiguchi and S. Tsuchiya, *ibid.*, **44**, 1213 (1971).
10) G. Herzberg, "Spectra of Diatomic Molecules," D. Van Nostrand Co., New Jersey (1950) p. 404.
11) A. O. McCoubrey, *Phys. Rev.*, **93**, 1249 (1954).
12) C. G. Freeman, M. J. McEwan, R. F. C. Claridge, and L. F. Phillips, *Chem. Phys. Lett.*, **5**, 555 (1970).
13) J. Koskikallio, A. B. Callear, and J. H. Connor, *ibid.*, **8**, 467 (1971).
14) E. W. Samson, *Phys. Rev.*, **40**, 940 (1932).
15) C. G. Freeman, M. J. McEwan, R. F. C. Claridge, and L. F. Phillips, *Trans. Faraday Soc.*, **67**, 2004 (1971).
16) J. S. Deech, J. Pitre, and L. Krause, *Can. J. Phys.*, **49**, 1976 (1971).
17) M. W. Zemansky, *Phys. Rev.*, **36**, 919 (1930).
18) Kang Yang, *J. Amer. Chem. Soc.*, **89**, 5344 (1967).
19) B. deB. Darwent, *J. Chem. Phys.*, **18**, 1532 (1950).
20) J. M. Campbell, S. Penzes, H. S. Sandhu, and O. P. Strausz, *Int. J. Chem. Kinetics*, **3**, 175 (1971).
21) R. J. Cvetanović, "Progress in Reaction Kinetics," Vol. 2, ed. by G. Porter, Pergamon, New York (1964).
22) C. S. Burton and H. E. Hunziker, *Chem. Phys. Lett.* **6**, 352 (1970).
23) G. Karl, P. Kruus and J. C. Polanyi, *J. Chem. Phys.*, **46**, 224 (1967).
24) A. C. Vikis and H. C. Moser, *ibid.*, **53**, 2333 (1970).
25) A. B. Callear and J. C. McGurk, *J. Chem. Soc. Faraday* II, **68**, 289 (1971).
26) C. G. Freeman, M. J. McEwan, R. F. C. Claridge, and L. F. Phillips, *Chem. Phys. Lett.* **9**, 578 (1971).
27) C. C. McDonald and H. E. Gunning, *J. Chem. Phys.*, **23**, 532 (1955).
28) M. C. Lin and S. H. Bauer, *ibid.*, **50**, 3377 (1969).
29) A. C. Vikis, G. Torrie and D. J. LeRoy, *Can. J. Chem.*, **50**, 176 (1972).

Contribution of d Orbitals in SiH SiH_2, SiH_3, and SiH_4

Jiro HIGUCHI, Shozo KUBOTA,* Toshio KUMAMOTO,** and Ikuo TOKUE***

Department of Chemistry, Faculty of Engineering, Yokohama National University, Minami-ku, Yokohama 233

(Received May 31, 1974)

Semi-empirical calculations have been carried out for SiH_n ($n=1$, 2, 3, and 4) adopting the electron pair bond approximation using hybrid orbitals with d orbitals of Si determined by minimizing the energy of each ground state. The results are satisfactory as a whole for explaining the experimental data of these molecules. The contribution of d orbitals obtained is not very large, but it is important in discussing the energy levels and molecular structures of some low-lying electronic states. It is also shown that the maximum overlap method is not always adequate in determining hybrid orbitals including d orbitals.

Structures of some molecules containing second-row elements differ from those expected in molecules consisting of hydrogen and/or first-row elements. Examples can be found in such molecules as PCl_5 and SF_6, in which participation of the d orbitals of these rather heavy atoms in bonding is appreciable. This is because the d orbitals give a different angular effect from that of the s and p orbitals in bonding.

In the 3d orbital of second-row atoms, the energy is not so high as compared with those of the 3s and 3p valence electrons. Although the 4s and 4p extra-valence shell orbitals are also not high in energy, their mixing with the valence shell orbitals is expected to be very small in the low-lying electronic states.[1] Thus, for a discussion of the electronic properties of a molecule with second-row atoms, inclusion of the 3d orbital should not be completely ignored, although most calculations of these molecules have not always explicitly taken into account the effect of the d-character.

In the present work, a semi-quantitative calculation including the 3d orbitals has been carried out for the electronic structure of ground state for SiH, SiH_2, SiH_3, and SiH_4 which show some different properties from those of the corresponding CH_n molecules,[2-5] together with some excited states of SiH and SiH_2. In this case, the electron pair bond approximation was adopted since the valence bond method is rather useful in discussing the contribution of d orbital in bonding as compared with the molecular orbital method.

Hybrid Orbitals with d-Character

The spatial configurations of SiH, SiH_2, SiH_3, and SiH_4 were assumed to be of symmetry $C_{\infty v}$, C_{2v}, C_{3v}, and T_d, respectively, the coordinate system of these molecules being taken as shown in Fig. 1. For the first-row elements, the orthonormalized set of hybrid orbitals directed to each bond or non-bonding electron can uniquely be constructed from 2s, 2px, 2py, and 2pz orbitals taking the spatial configuration into consideration if a few external conditions such as equivalence of some orbitals are given. However, a similar set of hybrid orbitals including the d orbitals cannot uniquely be determined even if the same number of external conditions is given, and some additional parameters are necessary.

For SiH, SiH_2, SiH_3, and SiH_4 these hybrid orbitals can be expressed as follows:

SiH:

$$\left.\begin{aligned}\chi_1 &= a_0\chi_s - b_0\chi_{p\sigma} + c_0\chi_{d\sigma}\\ \chi_b &= a_1\chi_s + b_1\chi_{p\sigma} + c_1\chi_{d\sigma}\\ \chi_\pi &= \quad b_\pi\chi_{p\pi} + c_\pi\chi_{d\pi}\end{aligned}\right\} \tag{1}$$

SiH_2:

$$\left.\begin{aligned}\chi_1 &= a_0\chi_s + b_0\chi_{pz} + c_0\chi_{dz^2}\\ \left.\begin{matrix}\chi_{b1}\\ \chi_{b2}\end{matrix}\right\} &= a_1\chi_s + b_1\left[\pm\left(\sin\frac{\theta}{2}\right)\chi_{py} - \left(\cos\frac{\theta}{2}\right)\chi_{pz}\right]\\ &\quad + c_1\left[\frac{1}{2}\left(3\cos^2\frac{\theta}{2}-1\right)\chi_{dz^2} - \frac{1}{2}\left(3^{1/2}\sin^2\frac{\theta}{2}\right)\chi_{dx^2-y^2}\right.\\ &\quad \left.\mp\left(3^{1/2}\sin\frac{\theta}{2}\cos\frac{\theta}{2}\right)\chi_{dyz}\right]\end{aligned}\right\} \tag{2}$$

SiH_3:

$$\left.\begin{aligned}\chi_n &= a_0\chi_s + b_0\chi_{pz} + c_0\chi_{dz^2}\\ \chi_{b1} &= a_1\chi_s + b_1[(\sin\beta)\chi_{px} - (\cos\beta)\chi_{pz}]\\ &\quad + c_1\left[\frac{1}{2}(3\cos^2\beta-1)\chi_{dz^2} + \frac{1}{2}(3^{1/2}\sin^2\beta)\chi_{dx^2-y^2}\right.\\ &\quad \left.- (3^{1/2}\sin\beta\cos\beta)\chi_{dxz}\right]\\ \left.\begin{matrix}\chi_{b2}\\ \chi_{b3}\end{matrix}\right\} &= a_1\chi_s + b_1\left[-\frac{1}{2}(\sin\beta)\chi_{px} \pm \frac{1}{2}(3^{1/2}\sin\beta)\chi_{py}\right.\\ &\quad \left.- (\cos\beta)\chi_{pz}\right] + c_1\left[\frac{1}{2}(3\cos^2\beta-1)\chi_{dz^2}\right.\\ &\quad - \frac{1}{4}(3^{1/2}\sin^2\beta)\chi_{dx^2-y^2} \mp (\sin^2\beta)\chi_{dxy}\\ &\quad \left.+ \frac{1}{2}(3^{1/2}\sin\beta\cos\beta)\chi_{dxz} \mp \frac{3}{2}(\sin\beta\cos\beta)\chi_{dyz}\right]\end{aligned}\right\} \tag{3}$$

SiH_4:

$$\left.\begin{aligned}\chi_{b1} &= (1/2)\chi_s + [(3/4)-c^2]^{1/2}\chi_{pz} + c\chi_{dz^2}\\ \chi_{b2} &= (1/2)\chi_s + [(3/4)-c^2]^{1/2}[(8^{1/2}/3)\chi_{px} - (1/3)\chi_{pz}]\\ &\quad + c[-(1/3)\chi_{dz^2} + (4/27^{1/2})\chi_{dx^2-y^2} - (8/27)^{1/2}\chi_{dxz}]\\ \left.\begin{matrix}\chi_{b3}\\ \chi_{b4}\end{matrix}\right\} &= (1/2)\chi_s + [(3/4)-c^2]^{1/2}[-(2^{1/2}/3)\chi_{px}\\ &\quad \pm (2/3)^{1/2}\chi_{py} - (1/3)\chi_{pz}] + c[-(1/3)\chi_{dz^2}\\ &\quad - (2/27^{1/2})\chi_{dx^2-y^2} \mp (2/3)\chi_{dxy} + (2/27)^{1/2}\chi_{dxz}\\ &\quad \pm (2^{1/2}/3)\chi_{dyz}]\end{aligned}\right\} \tag{4}$$

* Present address: Chemical Research Institute of Non-Aqueous Solutions, Tohoku University, Sendai.

** Present address: Fujitsu System Laboratory of Information Processing, Fujitsu Limited, Ota-ku, Tokyo.

*** Present address: Department of Chemistry, Faculty of Science, The University of Tokyo, Bunkyo-ku, Tokyo.

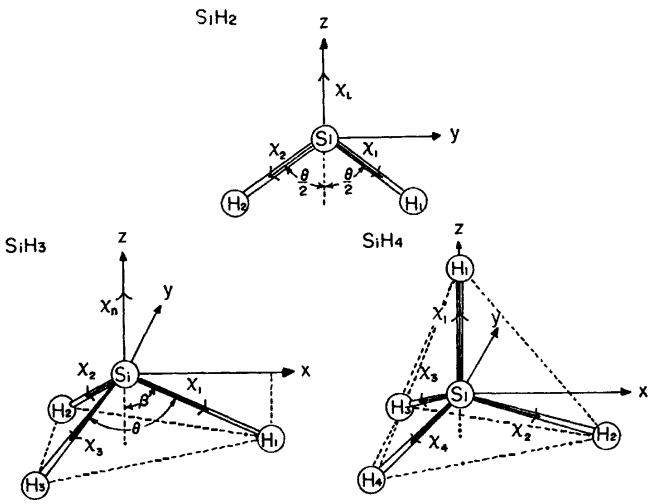

Fig. 1. Coordinate system and hybrid orbitals χ_i's in SiH_n (n=2, 3, and 4).

where l, n, and b denote lone pair, non-bonding and bonding, respectively.

Atomic Orbitals

In the calculation of molecular integrals, the atomic orbitals of Si used are the SCF–AO's (solutions of Hartree-Fock equation in the ^3P state) obtained by Watson and Freeman.[6] Since no 3d orbital is given in their paper, the following orbital was tentatively used:

$$\chi_{3d}^{Si} = 0.1571\chi_{3d}^{STO}(0.25) + 0.7607\chi_{3d}^{STO}(0.50) + 0.1651\chi_{3d}^{STO}(1.00) + 0.0561\chi_{3d}^{STO}(2.00) \quad (5)$$

where $\chi_{3d}^{STO}(\delta)$ is a Slater-type 3d AO with orbital exponent δ. The coefficients of these AO's are chosen so as to give a minimum energy of the ^1D state with electron configuration $3s^23p3d$ by using the above SCF-AO's. The orbital of hydrogen used (χ_H) is the Slater-type 1s AO with orbital exponent 1.00. All the internuclear distances between the silicon and hydrogen are taken to be 1.477 Å, which is the equilibrium distance of SiH_4 molecule.[7]

Method of Calculation

Since the molecular integrals used in semi-empirical valence bond calculations have not always been described with a unified formula, it will be necessary to clarify the definitions used. The procedure is briefly outlined in the following paragraphs. The Hamiltonian of SiH_n (n=1, 2, 3, 4) $\mathcal{H}$ can be expressed in atomic unit as

$$\mathcal{H} = \mathcal{H}_{Si} + \sum_{r=1}^{n}\mathcal{H}_{H(r)} + \sum_{p=1}^{14}\sum_{r=1}^{n}\mathcal{H}_{Si(p)-H(r)} + \sum_{r=s+1}^{n}\sum_{s=1}^{n-1}\mathcal{H}_{H(r)-H(s)} \quad (6)$$

where $\mathcal{H}_{Si}$ and $\mathcal{H}_{H(r)}$ are the atomic term of the Si which includes the 1st to the 14th electrons and that of the r-th hydrogen which includes the $(r+14)$-th electron, respectively, *i.e.*,

$$\mathcal{H}_{Si} = -\frac{1}{2}\sum_{p=1}^{14}\Delta_p - \sum_{p=1}^{14}\frac{14}{r_{Si-p}} + \sum_{p=q+1}^{14}\sum_{q=1}^{13}\frac{1}{r_{p-q}} \quad (p, q = 1\sim14) \quad (7)$$

and

$$\mathcal{H}_{H(r)} = -\frac{1}{2}\Delta_{(r+14)} - \frac{1}{r_{H(r)-(r+14)}} \quad (r = 1\sim n). \quad (8)$$

The $\mathcal{H}_{Si(p)-H(r)}$ and $\mathcal{H}_{H(r)-H(s)}$ are the interatomic interaction terms, *i.e.*,

$$\mathcal{H}_{Si(p)-H(r)} = \frac{1}{R_{Si-H(r)}} + \frac{1}{r_{p-(r+14)}} - \frac{1}{r_{Si-(r+14)}} - \frac{1}{r_{H(r)-p}} \quad (9)$$

and

$$\mathcal{H}_{H(r)-H(s)} = \frac{1}{R_{H(r)-H(s)}} + \frac{1}{r_{(r+14)-(s+14)}} - \frac{1}{r_{H(r)-(s+14)}} - \frac{1}{r_{H(s)-(r+14)}} \quad (10)$$

The treatment is based on the electron pair bond approximation without ionic structure using the hybrid orbitals (1)—(4). Using the Hamiltonian $\mathcal{H}$ (6), the total energy of SiH_n can approximately be expressed as

$$E_{SiH_n} = E_{Si} + \sum_{r=1}^{n}E_{H(r)} + \sum_{r=1}^{n}\sum_{p=1}^{14}(Q_{pr} + c_{p,(r+14)}R_{pr}) + (1-\delta_{1,n})\sum_{r=s+1}^{n}\sum_{s=1}^{n-1}\left(Q'_{rs} - \frac{1}{2}R'_{rs}\right)$$

$$c_{i,j} = \begin{cases} +1 & (i,j\text{: paired orbitals}) \\ -1/2 & (i,j\text{: non-paired orbitals}), \end{cases} \quad (11)$$

where E_{Si} is the energy concerning the Si atom only, $E_{H(r)}$ is the energy of the r-th atom, Q_{ij}'s and R_{ij}'s are the interatomic Coulomb and exchange integrals, respectively,[8] *i.e.*,

$$Q_{pr} = \iint\chi^*_{Si(p)}(p)\chi^*_{H(r)}(r+14)\mathcal{H}_{Si(p)-H(r)} \times\chi_{Si(p)}(p)\chi_{H(r)}(r+14)d\tau_p d\tau_{r+14} \quad (12)$$

$$R_{pr} \simeq \iint\chi^*_{Si(p)}(p)\chi^*_{H(r)}(r+14)\mathcal{H}_{Si(p)-H(r)} \times\chi_{H(r)}(p)\chi_{Si(p)}(r+14)d\tau_p d\tau_{r+14} \quad (13)$$

$$Q'_{rs} = \iint\chi^*_{H(r)}(r+14)\chi^*_{H(s)}(s+14)\mathcal{H}_{H(r)-H(s)} \times\chi_{H(r)}(r+14)\chi_{H(s)}(s+14)d\tau_{r+14}d\tau_{s+14} \quad (14)$$

$$R'_{rs} \simeq \iint\chi^*_{H(r)}(r+14)\chi^*_{H(s)}(s+14)\mathcal{H}_{H(r)-H(s)} \times\chi_{H(s)}(r+14)\chi_{H(r)}(s+14)d\tau_{r+14}d\tau_{s+14}. \quad (15)$$

In Eq. (11), orthogonality among all the orbitals is assumed, except in the evaluation of R_{ij}'s with Eqs. (13) and (15). All the interactions with the inner shells of the Si atom are also included in the same way. The coefficients of the AO's in the hybrid orbitals (1)—(4) are determined so as to minimize the total energy of the corresponding ground state.

In the case of SiH, the treatment is similar to the restricted SCF-LCAO-MO method.[9] For the ground state:

$$^2\Pi\text{: } (\chi_l)^2[(\chi_b)(\chi_H)](\chi_n),^{10} \quad (16)$$

the coefficients of the AO's are determined by solving the following simultaneous equations:

$$\left.\begin{aligned}
&\left[H+Q-\frac{1}{2}R+2J_1-K_1+J_b-\frac{1}{2}K_b+J_{\pi+}-\frac{1}{2}K_{\pi+}\right]\chi_1 \\
&\quad=\varepsilon_{11}\chi_1+\frac{1}{2}\varepsilon_{1b}\chi_b \\
&\left[H+Q+R+2J_1-K_1+J_{\pi+}-\frac{1}{2}K_{\pi+}\right]\chi_b=\varepsilon_{1b}\chi_1+\varepsilon_{bb}\chi_b \\
&\left[H+Q-\frac{1}{2}R+2J_1-K_1+J_b-\frac{1}{2}K_b\right]\chi_{\pi+}=\varepsilon_{\pi\pi}\chi_{\pi+}
\end{aligned}\right\} \quad (17)$$

where

$$H=-\frac{1}{2}\Delta-\frac{14}{r_{Si}}+2J_{1s}-K_{1s}+2J_{2s}-K_{2s}+2J_{2p\sigma}-K_{2p\sigma}+2J_{2p\pi+}-K_{2p\pi+}+2J_{2p\pi-}-K_{2p\pi-} \quad (18)$$

$$J_k\chi_p(p)=\left[\int\chi_k^*(q)(1/r_{p-q})\chi_k(q)d\tau_q\right]\chi_p(p) \quad (19)$$

$$K_k\chi_p(p)=\left[\int\chi_k^*(q)(1/r_{p-q})\chi_p(q)d\tau_q\right]\chi_k(q) \quad (20)$$

$$Q\chi_p(p)=\left[\int\chi_H^*(15)\mathcal{H}_{Si(p)-H(1)}\chi_H(15)d\tau_{15}\right]\chi_p(p) \quad (21)$$

$$R\chi_p(p)=\left[\int\chi_H^*(15)\mathcal{H}_{Si(p)-H(1)}\chi_p(15)d\tau_{15}\right]\chi_H(p). \quad (22)$$

All the calculations were carried out using the two sets of hybrid orbitals with and without d orbitals of Si atom. The most stable structure of the ground state of SiH_2,

$$^1A_1:\ (\chi_1)^2[(\chi_{b1})(\chi_{H(1)})][(\chi_{b2})(\chi_{H(2)})], \quad (23)$$

and that of SiH_3,

$$^2A_1:\ [(\chi_{b1})(\chi_{H(1)})][(\chi_{b2})(\chi_{H(2)})][(\chi_{b3})(\chi_{H(3)})](\chi_n), \quad (24)$$

were determined by changing the bond angle ∠HSiH only. For SiH and SiH_2, the excitation energies to the lower electronic states,

$$\left.\begin{aligned}
&^4\Sigma^-,\ ^2\Delta,\ ^2\Sigma^-,\ ^2\Sigma^+:\ [(\chi_b)(\chi_H)](\chi_\pi)^2(\chi_1) && (25)\\
&^2\Delta:\ (\chi_1)^2[(\chi_b)(\chi_H)](\chi_\delta) && (26)\\
&^2\Sigma^+:\ (\chi_1)^2[(\chi_b)(\chi_H)](\chi_\sigma^*) && (27)
\end{aligned}\right\}\ \text{for SiH}$$

and

$$\left.\begin{aligned}
&^3B_1,\ ^1B_1:\ [(\chi_{b1})(\chi_{H(1)})][(\chi_{b2})(\chi_{H(2)})](\chi_1)(\chi_n) && (28)\\
&^1A_1:\ [(\chi_{b1})(\chi_{H(1)})][(\chi_{b2})(\chi_{H(2)})](\chi_n)^2 && (29)
\end{aligned}\right\}\ \text{for } SiH_2$$

were also calculated using the hybrid orbitals of each ground state. In the vacant orbitals in the ground state, the χ_δ orbital of SiH was taken to be the 3dδ AO of Si, the χ_σ^* was the 3dσ-like orbital which is orthogonal to the χ_1 and χ_b, and the χ_n orbital of SiH_2 which is perpendicular to the molecular plane was assumed to be the 3px AO of Si.[11] In the case of the $^1A_1$ states of SiH_2, only the interaction between configurations (23) and (29) was taken into account so as to give the energies of the $^1\Delta_g$ and the $^1\Sigma_g^+$ states in the linear structure. The other states of SiH_n were calculated in the approximation of single configuration.

Results and Discussion

In the SiH radical, the $D^2\Delta$ and $E^2\Sigma^+$ states are not so high as compared with the lowest $^2\Delta$ and $^2\Sigma^+$ states, while those of the CH are expected to be high-energy excited states. However, no theoretical work has been done for these higher states. Therefore, the excitation energies have been calculated for the low-lying states with configurations (25)—(27). Using the hybrid orbitals determined for the ground state, the lower excited states with configuration (25) obtained are considerably high as compared with the experimental results [$\Delta E_{calc.}(^2\Delta)=5.81$ eV and $\Delta E_{calc.}(^2\Sigma^+)=6.90$ eV, while $\Delta E_{obs.}(^2\Delta)=3.01$ eV and $\Delta E_{obs.}(^2\Sigma^+)=3.84$ eV[12,13]]. This might be due to the fact that the distribution of σ electrons differs a great deal from that of the ground state where the hybridization ratios used in Eq. (1) were determined.[14] On the other hand, the calculated excitation energy of the higher $^2\Delta$ state with configuration (26) is 6.67 eV, in fair agreement with the observed value of the $D^2\Delta$ state [6.02 eV[12,13]]. The agreement might suggest the fact that the distribution of σ electrons in this $^2\Delta$ state does not differ much from that of the ground $^2\Pi$ state. Similarly, the observed higher $^2\Sigma^+$ state ($E^2\Sigma^+$) can be explained to be due to the excitation of one π electron from the ground state $^2\Pi$ into the 3d-like σ orbital (χ_σ^*). The results indicate that the contribution of d orbitals is important in discussing some observed lower electronic states of molecules with second-row atoms.

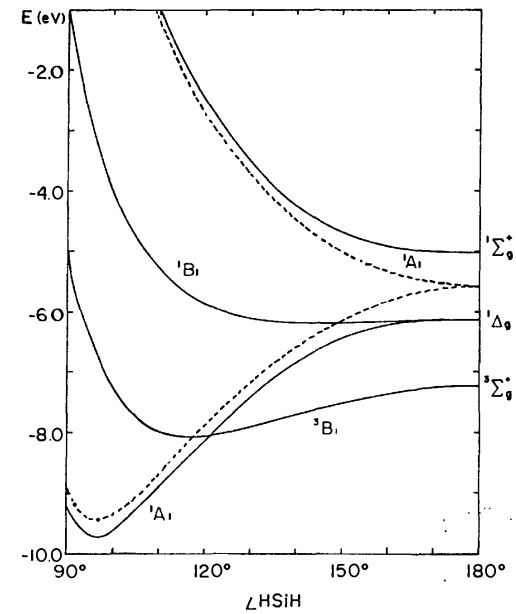

Fig. 2. Lower electronic states of SiH_2 calculated by including d orbitals. The dotted lines indicate the energies of the $^1A_1$ states without interaction between the lowest two configurations. The origin of energy is chosen to be $Si(^3P)+2H(^2S)$.

For the four low-lying states of SiH_2, the potential energy curves were calculated by including the d orbitals of Si as shown in Fig. 2. The dotted lines correspond to the energies without interaction between the lowest two $^1A_1$ configurations. The calculated equilibrium bond angle ∠HSiH in the ground state $^1A_1$ [96°] is in fair agreement with the observed result [92° [2]], while the value of the $^1B_1$ state [145°] is fairly larger than the expeimental [123° [2]]. The calculated energy difference between these states is 3.54 eV while the observed value is 1.93 eV. The disagreement is mainly due to the facts that the electron configuration is apparently different between these states and that

the hybrid orbitals used are determined for the energy of the $^1A_1$ state with configuration (23).

In the case without d orbitals, the bond angle ∠HSiH in each state is generally close to the result with d orbitals and that of the *ab initio* calculation (without d orbitals) by Wirsam.[15] For only the $^1B_1$ state, the bond angle obtained here is fairly large [about 30°] as compared with that of Wirsam, although the energy changes less than 0.5 eV in this vicinity. The difference between the results with and without the d orbitals is not very significant.

In both calculations, the ground state of SiH_2 is obtained as $^1A_1$, in contrast with $^3B_1$ of CH_2. The difference is not essentially due to the effect of the d orbitals, and can be explained by the following electronic properties: If the overalp integral between the valence v orbital (v means s, pσ, *etc.*) and the hydrogen 1s orbital is expressed by S_{vh}, the ratio of $S_{sh}/S_{p\sigma h}$ for SiH_n is fairly smaller than that of CH_n. Accordingly, the stabilization of the Si–H bond due to the inclusion of the s orbital is rather small as compared with that of the C–H bond. The separation between the lowest $^1A_1$ (or $^1B_1$) and $^3B_1$ states of SiH_2 is about three quarters of that of CH_2 near the linear structure.[16] Thus, the $^1A_1$ state of SiH_2 with nearly-rectangular bond angle is located lower than the $^3B_1$ state, in contrast with the case of CH_2.

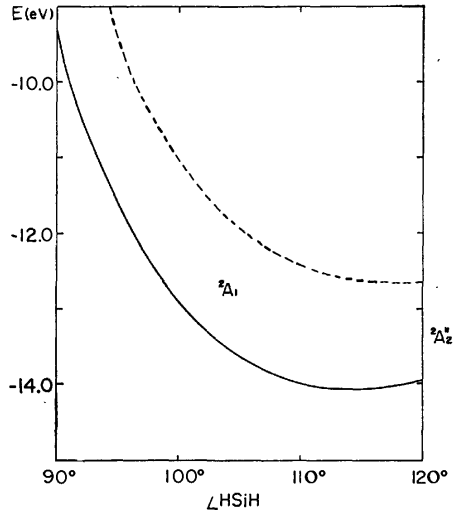

Fig. 3. Electronic energy of $^2A_1$ state of SiH_3 calculated by including d orbitals (full line) and that by disregarding d orbitals (dotted line). The origin of energy is chosen to be $Si(^3P)+3H(^2S)$.

The potential energy curve of the ground state of SiH_3 has been calculated as shown in Fig. 3. The most stable structure obtained is pyramidal (∠HSiH= 114°) by including the contribution of the d orbitals of Si, in consistent with the experimental result,[4] while it is nearly planar (∠HSiH=119°) by disregarding the d-character. The calculated bond angle is in close agreement with the value deduced by Sharp and Symons (113~114°).[17] This might show the facts that the pyramidal structure of SiH_3 is due to an appreciable contribution of the d orbital in the angular effect and that the inclusion of the d orbital is essentially necessary in the calculation of molecules with Si atom.

On the other hand, an *ab initio* calculation by Wirsam[18] and an INDO calculation by Benson and Hudson[19] gave the pyramidal structure for the equilibrium geometry in spite of disregard of the d orbitals. Thus, one may conclude that there are two reasons for the pyramidal structure of SiH_3, in contrast with the nearly-planar structure of CH_3; it is due to the angular contribution of the d orbital of Si and that the stabilization of the Si–H bond due to the inclusion of the s orbital is rather small as compared with the case of the C–H bond.

In general, the energy lowering due to the inclusion of the d orbitals is not very large. The results for the ground states with equilibrium configuration are summarized in Tables 1 and 2. The stabilization energy per Si–H bond differs for the SiH_n molecules each other, this being mainly due to the fact that the contribution of the valence states of the Si atom concerned with each molecule is not quite the same. Actually, the energy lowering increases with decreasing the bond angle ∠HSiH. On the other hand, the contribution

Table 1. Calculated electronic energies in the equilibrium structure of SiH_n relative to the energy of $Si(^3P)+nH(^2S)$.

Hybridization		SiH	SiH_2	SiH_3	SiH_4
s-p-d	E(eV)	−4.64	−9.44	−14.05	−20.20
	∠HSiH	—	96°	114°	(109°28′)[a]
s-p	E(eV)	−3.92	−8.15	−12.66	−18.18
	∠HSiH	—	97°	119°	(109°28′)[a]
	ΔE (eV)	0.73	1.30	1.39	2.03

a) The assumed value.

Table 2. The s-, p-, and d-characters (in per cents) in the equilibrium structures of SiH_n.

		SiH		SiH_2		SiH_3		SiH_4	
	Hybridization	s-p-d	s-p	s-p-d	s-p	s-p-d	s-p	s-p-d	s-p
χ_{bl}	s-character	11.50	9.22	11.21	10.86	28.54	32.65	25.00	25.00
	p-character	83.01	90.78	83.70	89.14	68.03	67.35	71.13	75.00
	d-character	5.49	0.00	5.09	0.00	3.43	0.00	3.87	0.00
χ_l	s-character	88.47	90.78	77.04	78.27	13.51	2.05	—	—
or	p-character	11.09	9.22	22.81	21.73	85.91	97.95	—	—
χ_n	d-character	0.44	0.00	0.15	0.00	0.58	0.00	—	—
χ_π	p-character	99.72	100.00	—	—	—	—	—	—
	d-character	0.28	0.00	—	—	—	—	—	—

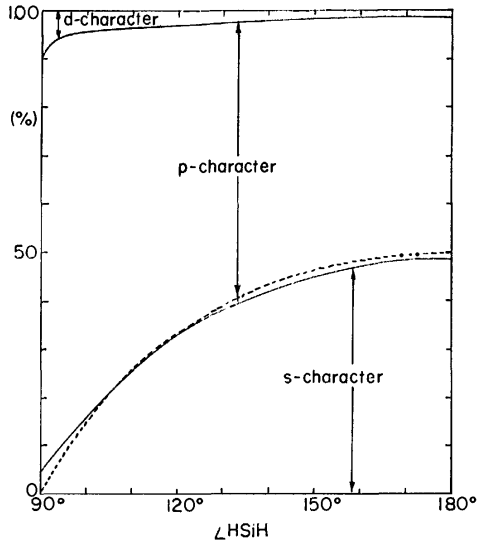

Fig. 4. The s-, p-, and d-characters in the bonding orbital χ_{bi} of SiH_2. The dotted line indicates the s-character calculated by disregarding d orbitals.

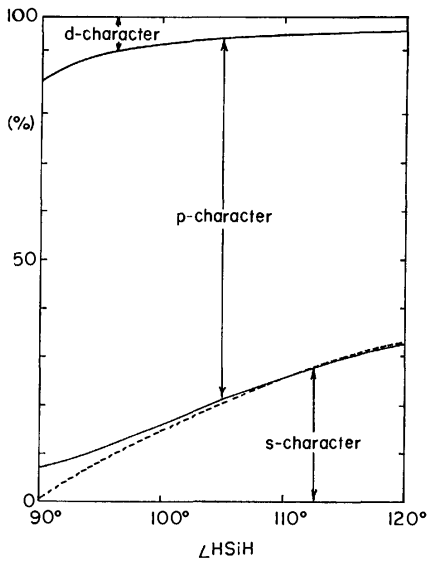

Fig. 5. The s-, p-, and d-characters in the bonding orbital χ_{bi} of SiH_3. The dotted line indicates the s-character calculated by disregarding d orbitals.

the ∠HSiH (Figs. 4 and 5). However, the energy of d-character of Si atom also increases with decreasing lowering is not exactly parallel with the d-character.

In the present calculation, the contribution of d orbital is not very great but should not be completely disregarded. The d-character in the lone pair and the non-bonding orbitals is very small as compared with that of the bonding orbitals (Table 2). This is understandable from the fact that the hybridization of the d orbitals mainly contributes to the bonding energy. For SiH_2 and SiH_3, the maximum value of d-character in the lone pair and the non-bonding orbitals (0.22 and 0.59%, respectively) appeared near bond angles of 110 and 113°, respectively, while the d-character of the bonding orbitals increases with decreasing the bond angle (Figs. 4 and 5). For SiH_4, the relation where

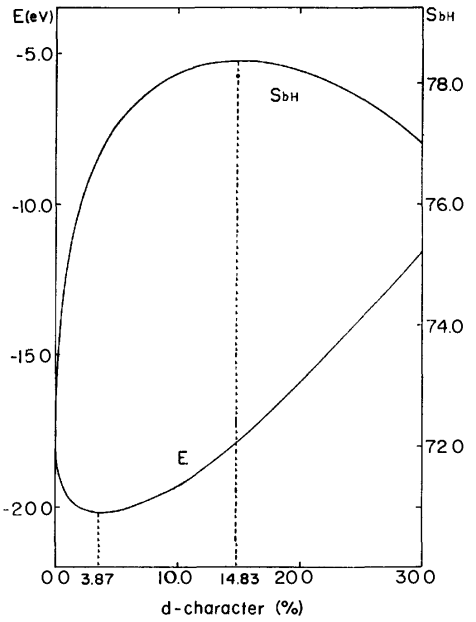

Fig. 6. Effect of d-character for the electronic energy (E) and the overlap integral between χ_{bi} and $\chi_{H(i)}$ [S_{bh}] in SiH_4. The origin of energy is chosen to be $Si(^3P)+4H(^2S)$.

the d-character is equal to the decrease in the p-character due to the inclusion of the d orbitals is exactly satisfied [*cf.* Eq. (4)]. This is also roughly valid for the other SiH_n radicals (Table 2, Figs. 4 and 5).

The maximum value of energy lowering for SiH_4 due to the inclusion of the d orbitals of Si has been obtained to be 2.03 eV at the d-character of 3.87% in the bonding orbital χ_{bi}. On the other hand, the maximum overlapping between the χ_{bi} and the $\chi_{H(i)}$ appeared at the d-character of 14.83% as shown in Fig. 6. This discrepancy may be explained as follows: the stabilization of the Si–H bond due to the exchange energy between the χ_{bi} and the $\chi_{H(i)}$ may increase with increasing the value of the corresponding overlap integral. However, the total energy increases beyond a certain value of the d-character, since the energy of d orbital is rather high as compared with the other valence orbitals of Si. This might suggest the fact that the maximum overlap method[20] is not always adequate in determining the hybrid orbitals with d orbitals.

The present work includes several approximations and assumptions. The atomic orbitals used may not be completely adequate for all the states. Actually, the determination of the 3d orbital is rather tentative but may be allowed for the present purpose. This may be recognized from the fact that the energy levels of Si atom calculated using the present AO's are generally satisfactory in a semi-quantitative sense except that the order of the $^3D(3s^23p3d)$ and $^3P(3s^23p3d)$ states is the reverse of that given in Moore's table.[21] Therefore, the experimental values are not included in the present calculation, although a better result might be obtained by using such values.

The result obtained for the ground state of SiH_n is generally satisfactory as compared with those of other calculations.[15,18,19,22,23] This is partly due to the facts

that the approximation for the exchange integrals (12) and (14) are fairly permissible, as has already been shown by the calculations of CH[9] and CH_2,[24] and that the contribution of ionic structures is not great in the ground states of the molecules. As far as the hybrid orbitals determined for the ground state are used in the approximation of single configuration, the results for the excited states are not so good as in the ground state. However, better results can be expected in a similar treatment if the hybrid orbitals are obtained so as to minimize the energy of the state in question or if the interaction with some other electronic configurations are included.

The authors wish to thank Mr. H. Takahashi for his help in the preliminary calculation of SiH_2.

References

1) J. Higuchi, *J. Chem. Phys.*, **28**, 527 (1958).
2) I. Dubois, G. Herzberg, and R. D. Verma, *ibid.*, **47**, 4262 (1967); I. Dubois, *Can. J. Phys.*, **46**, 2485 (1968).
3) G. Herzberg, "Electronic Spectra of Polyatomic Molecules," D. Van Nostrand Co., Princeton (1966), p. 584.
4) R. L. Morehouse, J. J. Christiansen, and W. Gordy, *J. Chem. Phys.*, **45**, 1751 (1966); G. S. Jackel and W. Gordy, *Phys. Rev.*, **176**, 443 (1968).
5) G. Herzberg, *Proc. Roy. Soc. Ser. A*, **262**, 291 (1961).
6) R. E. Watson and A. J. Freeman, *Phys. Rev.*, **123**, 521 (1961).
7) "Tables of Interatomic Distances and Configuration in Molecules and Ions," Special Publication No. 11, The Chemical Society, London (1958), M. 34.
8) M. Kotani, A. Amemiya, E. Ishiguro, and T. Kimura, "Table of Molecular Integrals," Maruzen Co., Tokyo (1955), p. 54.
9) J. Higuchi, *J. Chem. Phys.*, **22**, 1339 (1954).
10) In the present paper, $[(\chi_A)(\chi_B)]$ means that the χ_A and the χ_B are paired orbitals, except for the quartet state $^4\Sigma^-$ (25).
11) Exactly speaking, the following orbital should be used: $\chi_n = (1-c_n^2)^{1/2}\chi_{px} + c_n\chi_{dxz}$.
12) G. Herzberg, A. Lagerqvist, and B. J. McKenzie, *Can. J. Phys.*, **47**, 1889 (1969).
13) R. D. Verma, *ibid.*, **43**, 2136 (1965).
14) The disagreement is understandable from the energy levels of CH calculated by assuming only the sp^3 configuration of C [corresponding to configuration (25)] as compared with the energy of the ground state $^2\Pi$ with the s^2p^2 of C [corresponding to configuration (16)] [*cf.* Fig. 2 of Ref. 9]. Thus, improved results can be obtained without any change of the present hybrid orbitals if the interaction between configuration (25) and $(\chi_l)^2(\chi_x)^2(\chi_H)$ is included.
15) B. Wirsam, *Chem. Phys. Lett.*, **14**, 214 (1972).
16) Separations for linear SiH_2 and CH_2 are considered to be fairly close to the energy difference between the lowest ^1D and ^3P states of Si and C, respectively. The experimental values for these atoms are given in Moore's table [C. E. Moore, "Atomic Energy Levels," Vol. I, Circular No. 467, National Bureau of Standards, Washington, D. C., (1949), pp. 22 and 144].
17) J. H. Sharp and M. C. R. Symons, *J. Chem. Soc. Ser. A*, **1970**, 3084.
18) B. Wirsam, *Chem. Phys. Lett.*, **18**, 578 (1973).
19) H. G. Benson and A. Hudson, *Theor. Chim. Acta*, **23**, 259 (1971).
20) For example, C. A. Coulson, "Valence," 2nd ed., Oxford University Press, Oxford (1961), p. 76; M. Randic and Z. B. Maksic, *Chem. Rev.*, **72**, 43 (1972).
21) C. E. Moore, "Atomic Energy Levels," Vol. I, Circular No. 467, National Bureau of Standards, Washington, D. C. (1949), p. 144.
22) B. Wirsam, *Chem. Phys. Lett.*, **10**, 180 (1971).
23) P. C. Jordan, *J. Chem. Phys.*, **44**, 3400 (1966).
24) K. Niira and K. Oohata, *J. Phys. Soc. Japan*, **7**, 61 (1952).

Polarographic Investigation of Dissolved Oxygen in Nonaqueous Solvent

Taitiro FUJINAGA and Sachiko SAKURA

Department of Chemistry, Faculty of Science, Kyoto University, Sakyo-ku, Kyoto 606

(Received November 16, 1973)

In a common aprotic solvent, the dissolved oxygen is reduced to superoxide, and then to peroxide with tetraalkylammonium salt as the supporting electrolyte. With alkali metal ion as the supporting electrolyte, it is reduced further to form the third wave. All of these waves are controlled by the successive chemical reaction; namely if the products due to the successive reaction are stable, the reduction potential shifts to more positive direction. When the solvated ion of the supporting electrolyte is small, it forms stable complex with oxygen radicals, hence the reduction waves shift to positive potentials.

The polarographic reduction of oxygen has been investigated in a number of nonaqueous aprotic solvents. In most aprotic solvents such as dimethylformamide, dimethylsulfoxide and acetonitrile, molecular oxygen undergoes two step reduction at the dropping mercury electrode; in the first step, oxygen is reduced to the superoxide anion, and then reduced further to the peroxide anion in the second step. The reaction mechanism of the first wave has been investigated by many authors,[1-4] however, little attention has been drawn to the second wave process. Only a few papers by Johnson *etc*[5] describe that the second reduction wave in 0.1 M Et_4NClO_4–DMSO solution is significantly affected by the addition of alkali metal ions. We found that oxygen was reduced further to form the third wave in the solution of alkali metal ion as the supporting electrolyte.

This paper deals with the results of detailed investigation on the electrolytic reduction of oxygen in aprotic organic solvents, especially with regard to the second and the third waves.

Apparatus and Reagents

Reagents. Dimethylacetamide (DMA) was purified by the double distillation under reduced pressure of nitrogen gas, first over calcium hydride and second over *p*-toluenesulfonic acid. Hexamethylphosphoramide (HMPA) and propylene carbonate (PC) were purified following the method in the previous paper.[6] Tetraalkylammonium perchlorates and alkali metal perchlorates were prepared and purified according to the method described in the previous paper.[6] Dodecyltrimethylammonium chloride was obtained commercially. The polarogram of oxygen was recorded in a solution which was saturated with dried air; air was dried by passing through concentrated H_2SO_4 bubblers before use.

Apparatus. A Yanagimoto polarograph, Type P 8-DP was used to record most current-potential curves. In AC polarography, the PAR (Princeton Applied Research Cooperation, Princeton, N. Y.) polarograph with IR-compensation using three electrodes system was used. The H cell used was the sameas in the previous paper.[6]The silver-silver perchlorate electrode Ag/0.1 M $AgClO_4$ in the solvent was used as the reference electrode. The potential of the reference electrode against the aqueous SCE was +0.439 V, +0.750 V and +0.360 V in DMA, PC, and HMPA, respectively. The DME (A, B) used had *m* values of 1.61_5, 0.80_8 mg/s at an open circiut and $h=62$ cm in DMA. The life times at −2.4 V in 0.05 M Et_4NClO_4–DMA were 3.21_7, 2.64_0 s, respectively. The DME used had *m* values of 0.63_0, and 0.89_0 mg/s at an open circiut and $h=65$ cm, in PC and HMPA, respectively. The drop time at −2.4 V in 0.05 M Et_4NClO_4–PC solution was 1.88_1 s. The drop time at −2.6 V in 0.05 M Et_4NClO–HMPA solution was 1.70_0 s.

Determination of the concentration of oxygen in nonaqueous solution by the iodometric method of Winkler is less satisfactory, especially PC is hardly soluble with water. Assuming that the solvation, if any, of the oxygen molecule should not be radically different in DMA, HMPA, PC, and DMSO, Walden's rule may be applied for the calculation of an approximate diffusion coefficient of oxygen in DMA, HMPA and PC as solvent. At 25 °C the viscosity of DMSO[2] is 1.95 cp, while those of DMA,[7] HMPA[9] and PC[10] are 0.92, 3.23 and 2.53 cp. The diffusion coefficient of oxygen in DMSO[2] is *ca.* 2.76×10^{-5} cm^2 s^{-1}. Hence from Walden's rule the diffusion coefficients of oxygen in DMA, HMPA and PC should be 5.85, 1.67, 2.13×10^{-5} cm^2 s^{-1}. Substituting into the Ilkovič equation, the concentrations of oxygen are *ca.* 0.923, 1.29, and 1.03 mM in DMA, HMPA and PC solution, respectively.

Results

Reduction of the Dissolved Oxygen in DMA. The dissolved oxygen gave three waves in DMA in the presence of 0.05 M alkali metal ion as the supporting

TABLE 1. POLAROGRAPHIC DATA OF OXYGEN IN DMA AT 25 °C

	r_s[a]	$(E_{1/2})_1$	$(E_{1/2})_2$	$(E_{1/2})_3$
Me_4N^+	2.56	−1.35(1.18)	−1.75(0.78)	−2.52(0.01)
Et_4N^+	2.69	−1.40(1.13)	−2.15(0.38)	
Pr_4N^+	3.41	−1.40(1.13)	−2.70(−0.17)	
Bu_4N^+	3.90	−1.40(1.13)	−2.96(−0.43)	
Hex_4N^+	4.74	−1.40(1.13)		
TDDMB ion	4.80	−1.40(1.13)	−2.00(0.53)	
Dodecyltrimethylammonium ion		−1.41(1.12)	−1.91(0.62)	−2.63(−0.10)
Li^+	4.18	Max.		
Na^+	3.5	−1.31(1.22)	−1.71(0.82)	Max.
K^+	3.5	−1.31(1.22)	−1.82(0.71)	−2.37(0.16)
Rb^+	3.55	−1.31(1.22)	−1.81(0.72)	−2.22(0.31)
Cs^+	3.38	−1.31(1.22)	−1.57(0.96)	−2.04(0.49)

Underscripts of 1, 2, and 3 mean the first, the second and the third wave, respectively. Half-wave potentials in parentheses are referred to the reduction potential of rubidium ion. Concentration of the supporting electrolyte is 0.05 M. a); Ref. 7), 8).

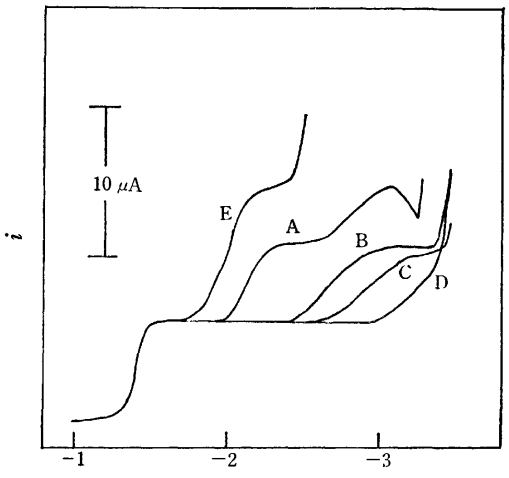

Fig. 1. Polarograms of dissolved oxygen in R_4NClO_4–DMA solutions.
Supporting electrolyte: A) Et_4NClO_4, B) Pr_4NClO_4, C) Bu_4NClO_4, D) HeX_4NClO_4 and E) TDDMB ion. Each in 0.05 M. With the DME (A).

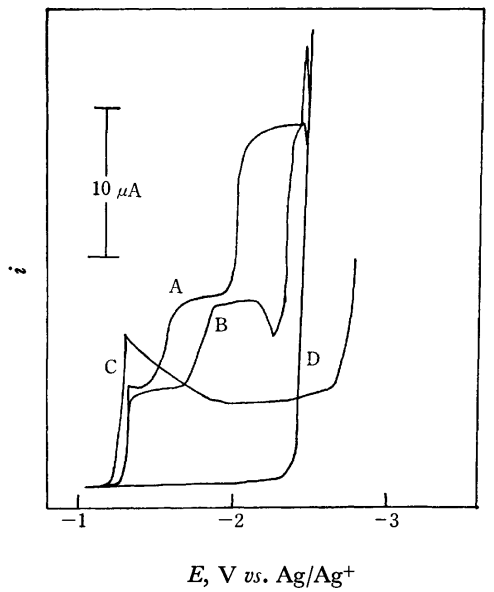

Fig. 2. Polarograms of dissolved oxygen in alkali metal ion–DMA solution.
Supporting electrolyte: A) $CsClO_4$, B) $KClO_4$ and C) $LiClO_4$. Each in 0.05 M.
D) Residual current in $CsClO_4$–DMA solution. With the DME (A).

electrolyte, corresponding to one-electron, one-electron, and two-electrons process respectively; a maximum appeared at the third wave when sodium ion was used as the supporting electrolyte. When lithium ion was used as the supporting electrolyte, only the first wave was observed. When 0.05 M tetraalkylammonium ion was used as the supporting electrolyte, the dissolved oxygen gave two waves, each corresponding to one-electron process. Their half-wave potentials are summarized in Table 1. Some typical polarograms are shown in Figs. 1 and 2.

The half-wave potential shifted to negative side with the increase of the radius of the solvated ion. The extent of the shift was the least pronounced with the first wave and more pronounced with the second wave. The third wave was most influenced by the radius of the supporting electrolyte cation, although in many cases except with cesium, rubidium, potassium, tetramethylammonium, and dodecyltrimethylammonium ion, the third wave shifted too negative to be observable before the final rise. In the case of alkali metal ion used as the supporting electrolyte, oxygen is reduced most easily in the presence of cesium ion and least in the presence of lithium ion. With tetraalkylammonium ion as the supporting electrolyte, oxygen is reduced most easily in the presence of tetramethylammonium ion. With the increase of the size of the solvated ion, the shift of the half wave potential to negative becomes pronounced. With 0.05 M tetrahexylammonium ion as the supporting electrolyte, the second wave shifts too negative to appear before the final rise. However, with 0.05 M tetradecyl-dimethyl-benzylammonium (TDDMB) ion, oxygen gave a well-defined second wave, although the size of the cation is larger than tetrahexylammonium ion.

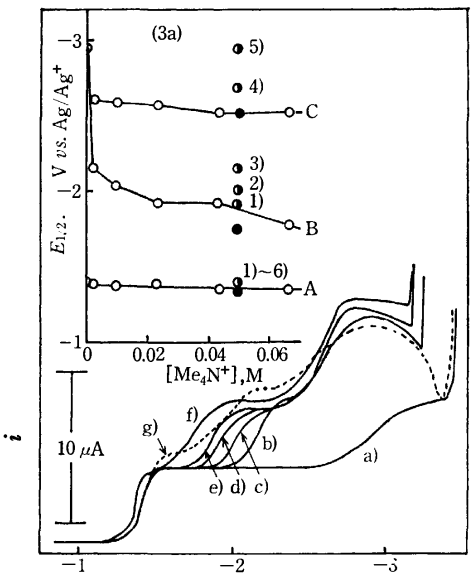

Fig. 3. Effect of methyl groups on the reduction of oxygen in 0.05 M Bu_4NClO_4 solution. With the DME (B).
Me_4NClO_4 concentration; a) 0, b) 2.5, c) 10.0, d) 24.0 and e) 43.6 mM.
f) 0.05 M Me_4NClO_4 solution, g) 0.05 M dodecyltrimethylammonium chloride solution.

Fig. 3a. Half wave potential of oxygen's reduction and concentration of tetramethylammonium ion.
○ A: the first wave, B: the second wave, C: the third wave in mixed with Me_4N^+ and Bu_4N^+ supporting electrolyte solution, ● 0.05 M Me_4NClO_4 solution, ◑ 0.05 M other tetraalkylammonium ion solution; 1) dodecyltrimethylammonium ion, 2) TDDMB ion, 3) tetraethylammonium ion, 4) tetrapropylammonium ion, 5) tetrabutylammonium ion, 6) tetrahexylammonium ion. 1)~5) the first and the second waves, 6) only the first wave.

The presence of methyl groups may be responsible for the oxygen reduction at a relatively positive potential. Figures 3 and 3a show that the half wave potentials of the second wave of oxygen shift to the positive potential with the increase of the concentration of tetramethylammonium ion and that the numbers of methyl groups in the large cation are also responsible for the positive shift (See the cases of TDDMB ion and dodecyltrimethylammonium ion used as the supporting electrolyte).

The effect of the supporting electrolyte cation on AC polarograms was also examined. The first peak is relatively sharp and high showing that the process is reversible. The peak height of the second wave is about one tenth of that of the first wave, and its shape is distorted. This fact suggests that the process is irreversible. The third peak is not appearing in AC polarogram.

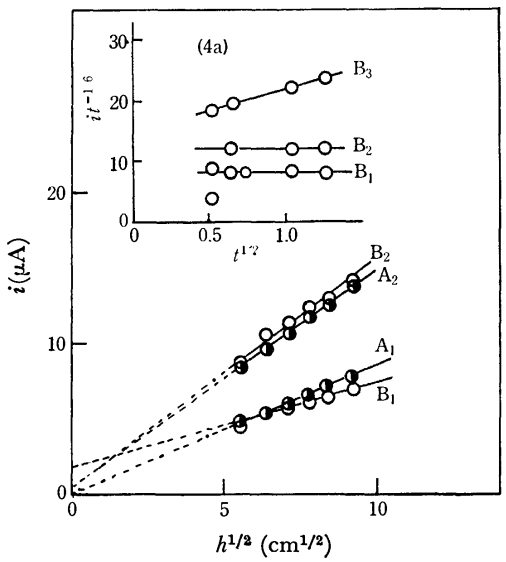

Fig. 4. Change of the limiting currents with the height of the mercury column in DMA solution.
Supporting electrolyte: A) Et_4NClO_4 and B) $CsClO_4$. Each in 0.05 M. Underscript 1, 2, and 3 mean the first, the second and the third wave. With the DME (A).

Fig. 4a. The relationship between $it^{-1/6}$ and $t^{1/2}$ in 0.05 M $CsClO_4$–DMA solution.

Figure 4 shows the relationship between the square root of mercury height and the limiting current of oxygen in tetraethylammonium perchlorate and cesium perchlorate as the supporting electrolyte. With tetraethylammonium ion, the first wave is diffusion-controlled, and the second wave may include a little kinetic current. With cesium ion as the supporting electrolyte, both the first and the second waves may include a little kinetic current. At the potential of the third wave, the drop time increased extraordinary, therefore in Fig. 4a, the values of $it^{-1/6}$ are plotted against $t^{1/2}$ using the mechanical drop time controller. Here, i is the limiting current in μA; t is the controlled drop time. For the first and the second waves, the values of $it^{-1/6}$ are almost independent of $t^{1/2}$, as is to be expected almost for the diffusion-controlled current, but a little kinetic current. For the third wave, however, the values of $it^{-1/6}$ increase with an increase of $t^{1/2}$, showing that a kinetic factor is involved. This conclusion agrees well with the results of AC polarograms and Cyclic voltammograms as the following mention.

With the addition of water in the solution of 0.05 M tetrahexylammonium perchlorate in DMA, the second wave of oxygen begins to appear. With the increase of the concentration of tetrahexylammonium perchlorate over 0.075 M, the second wave also begins to appear.

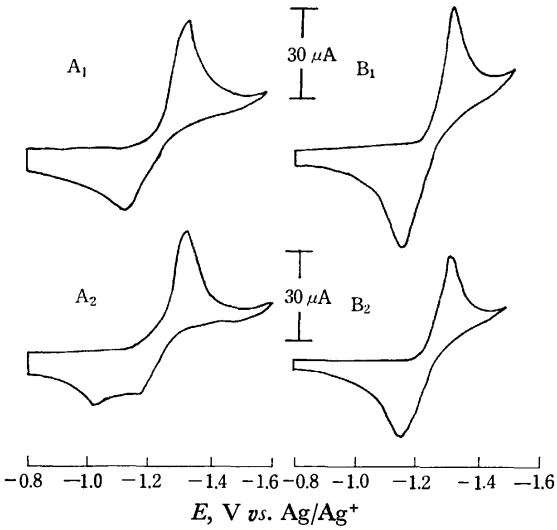

Fig. 5. Cyclic Voltammetry of oxygen in DMA solution.
Supporting electrolyte: A) $KClO_4$ and B) $CsClO_4$. Each in 0.05 M. Scan rate: 1, 100 mV/s and 2, 50 mV/s. Mercury drop is 0.1 μl.

Figure 5 demonstrates the cyclic polarograms of oxygen in the solutions of cesium perchlorate and potassium perchlorate.

When tetraethyl or tetrabuthylammonium perchlorate is used as the supporting electrolyte, electrode process of the first wave of oxygen is reversible, as has been studied already.[11] With alkali metal perchlorate as the supporting electrolyte, the process, however, is not fully reversible: Figure 5 shows that the anodic peak appears at fairly more positive potential than the cathodic peak.

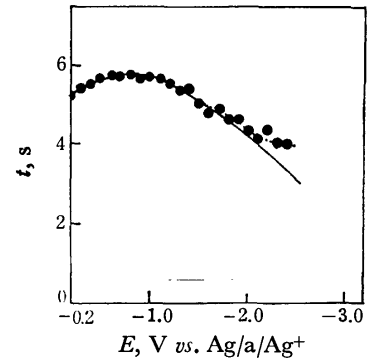

Fig. 6. Electrocapillary curve in 0.05 M $CsClO_4$–DMA solution.
—●— With O_2.
——— Without O_2. With the DME (A).

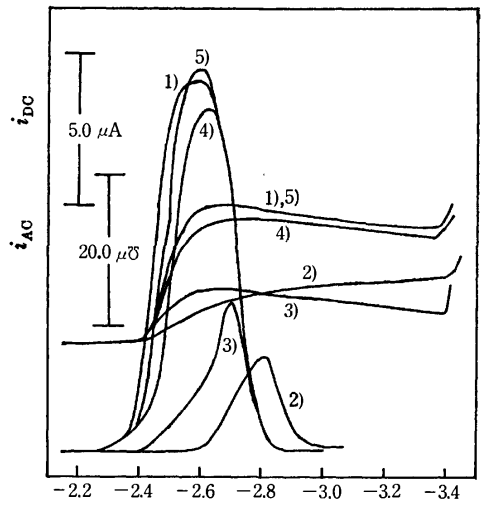

Fig. 7. Effect of oxygen on the reduction of 2.85 mM potassium ion in 0.05 M Bu_4NClO_4-DMA solution. 1) nitrogen gas bubbled to remove oxygen throughly 2) air-O_2 saturated, 3), 4), and 5) nitrogen gas bubbled for 5, 10, 30 s in 2) solution, respectively. Gas flow rate: 12.10 ml/s. With the DME (B).

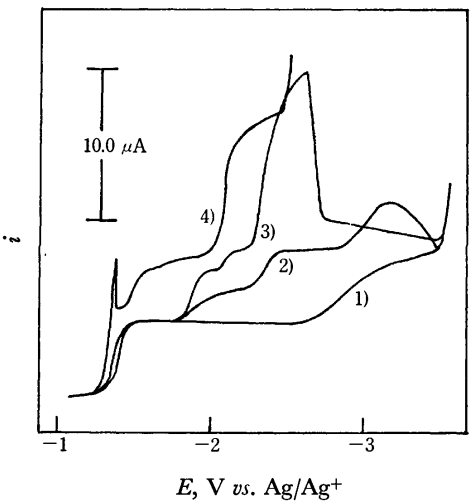

Fig. 8. Effect of the cesium ion on the reduction of oxygen in 0.05 M Bu_4NClO_4-DMA solution. Cesium perchlorate concentrations are; 1) 0, 2) 2.5 and 3) 5.0 mM. 4) is 0.05 M $CsClO_4$ solution. With the DME (B).

In the second and the third waves, no anodic peak appears probably because the seccessive chemical reactions will make the process irreversible.

Figure 6 shows the electrocapillary curves, in the presence and absence of oxygen in 0.05 M cesium perchlorate-DMA solution. In the figure, at a more negative potential than −2.0 V, the drop time is larger in the presence of oxygen than that in the absence. However, the difference can not be seen with the tetraalkylammonium ion as the supporting electrolyte.

Figure 7 shows that the reduction of alkali metal ion is disturbed by the presence of oxygen.

The third wave of oxygen appeared in the presence of alkali metal ion in the tetraalkylammonium ion solution (Fig. 8).

Reduction of the Dissolved Oxygen in HMPA or PC. The values of the half-wave potentials of oxygen in HMPA and in PC are tabulated in Table 2.

In HMPA, similar results to those in DMA are obtained. However, with 0.05 M sodium perchlorate, the second wave overlaps with the third wave which is accompanied by a maximum. With 0.05 M lithium perchlorate, the second wave can be seen. The dependence of negative shift of each waves upon the size

Table 2. Polarographic data of oxygen in HMPA and PC at 25 °C

		r_s[a]	$(E_{1/2})_1$	$(E_{1/2})_2$	$(E_{1/2})_3$
HMPA	Me_4N^+	3.22	−1.35[b] (1.00)	−1.67[b] (0.68)	
	Et_4N^+	2.73	−1.32 (1.03)	−1.89 (0.46)	
	Pr_4N^+	3.73	−1.32 (1.03)	−2.08 (0.27)	
	Bu_4N^+	4.33	−1.32 (1.03)	−2.35 (0.00)	
	Hex_4N^+	5.68	−1.33 (1.02)		
	TDDMB ion		−1.27 (1.08)	−1.75 (0.60)	
	Li^+	4.88	$(-1.36)_{Max}$	−1.92 (0.43)	
	Na^+	4.38	−1.32 (1.03)	$(-2.0)_{Max}$	
	K^+	4.20	−1.24 (1.11)	−1.71 (0.64)	−2.13 (0.22)
	Rb^+	4.20	−1.22 (1.13)	−1.66 (0.69)	−2.05 (0.30)
	Cs^+	3.98	−1.17 (1.18)	−1.52 (0.83)	−1.86 (0.49)
PC	Me_4N^+	2.18	$(-1.61)_{Max}$	−2.31[b] (0.46)	
	Et_4N^+	2.34	−1.64 (1.13)	−2.45 (0.32)	
	Bu_4N^+	3.47	−1.62 (1.15)	−2.92(−0.15)	
	Hex_4N^+		−1.62 (1.15)	−3.31(−0.54)	
	TDDMB ion		$(-1.54)_{Max}$	b)	
	Li^+	3.37	$(-1.24)_{Max}$		
	Rb^+	2.31	(−1.58)[c] (1.19)	(−2.26)[c] (0.51)	
	Cs^+		$(-1.47)_{Max}$		

Subscripts of 1, 2, and 3 mean the first, the second and the third wave, respectively. Concentration of the supporting electrolyte is 0.05 M. a); Ref. 9) and 12). b); Measurements are difficult. c); With the controlled drop time 0.40 s used in Fig. 10.

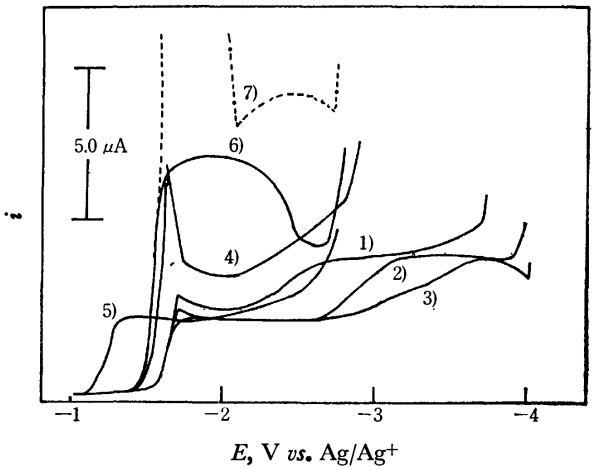

Fig. 9. Polarograms of dissolved oxygen in PC solution. Supporting electrolyte; 1) Et_4NClO_4, 2) Bu_4NClO_4, 3) Hex_4NClO_4, 4) TDDMB-perchlorate, 5) $LiClO_4$, 6) $RbClO_4$ and 7) $CsClO_4$. Each in 0.05 M.

of the cation is more remarkable in HMPA than that in DMA.

In PC, generally oxygen is more easily reduced than in DMA or HMPA. (See the values of half-wave potentials referred to the reduction potential of rubidium ion in Tables 1 and 2). The typical results are shown in Fig. 9. Even in 0.05 M tetrahexylammonium ion as the supporting electrolyte, oxygen gave two waves. With alkali metal ion such as cesium or rubidium ion as the supporting electrolyte, the reduction products of oxygen react with them more strongly in PC than in DMA or HMPA. At the potential of the first wave, the strong adsorption of the reaction product occurrs and the drop time becomes 1.3 times larger than that with tetraalkylammonium ion. If polarograms are measured by controlling the drop time of the DME to be very short (0.40 s) using a mechanical drop time controller, well-defined two waves appear. (Fig. 10)

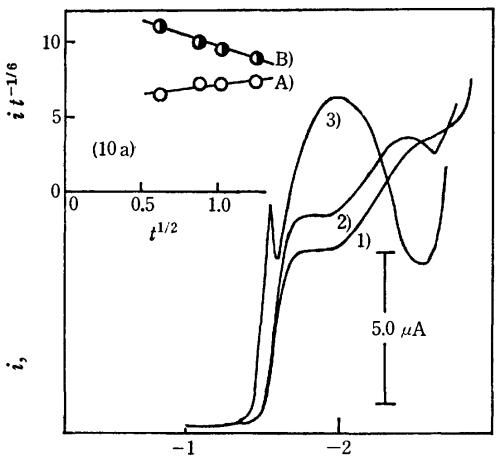

Fig. 10. Polarograms of dissolved oxygen in 0.05 M $RbClO_4$-PC solution. Using the controlled drop time: 1) $t=0.40$, 2) $t=0.80$ s and 3) natural drop time.

Fig. 10a. The relationship between $it^{-1/6}$ and $t^{1/2}$ of Fig. 10.
A) the first wave, B) the second wave

From Fig. 10a which shows the relationship between $it^{-1/6}$ and $t^{1/2}$, both the first and the second waves may be concluded to be kinetic in nature.

The most important determing factor influencing these waves is the degree of solvation of the supporting electrolyte cations in the solvents. The solvation is known to become stronger in the order: PC≪DMA< HMPA.

Discussion

When tetraalkylammonium perchlorate is used as the supporting electrolyte, molecular oxygen is carried to the electrode surface by diffusion and is reduced to the superoxide ion by one-electron process, followed by further one-electron reduction process to the peroxide ion. Complex formation between the anion radical and tetraalkylammonium cation influences the reduction potential of oxygen and the reversibility of the process. In the first wave, the process is reversible and diffusion-controlled and in the second wave, process is irreversible because of the presence of successive chemical reaction.

When alkali metal perchlorate is used instead as the supporting electrolyte, oxygen is reduced similarly as in the case of tetraalkylammonium perchlorate, but the superoxide, the reaction product of the first wave and the peroxide, that of the second wave, both react consecutively with alkali metal ions. Therefore, the first and the second waves appear as kinetic current. The fact that the reduction of alkali metal ion is disturbed by the presence of trace of oxygen (Fig. 7) also indicates the presence of the consecutive reaction between the oxygen anion radicals and the alkali metal ions.

Moreover, when sodium, potassium, rubidium and cesium perchlorates are used as the supporting electrolyte, a third new wave appears at the potential a little in advance to their final rise (the metal reduction); the reduction seemed to proceed by two electron process. (Fig. 2) The reduction process for the third wave may therefore be written as;

$$O_2^{2-} + 2e \rightleftarrows 2O^{2-}$$

From the behaviors of the third wave, which is extremely irreversible and kinetically controlled and from the facts that the third wave appears in the presence of alkali metal ions, it may be concluded that the following consecutive reaction may be taking place at the electrode solution interface;

$$O^{2-} + 2M^+ \longrightarrow M_2O$$

In the solution containing alkali metal ions, the drop time is remarkably increased by the presence of air. It is also due to the fact that chemical reaction between oxygen anion radical and alkali metal ion occurred in the electrical double layer or on the electrode surface strongly.

The chemical reactions mentioned above seem to correlate closely with the size of the solvated ions of the supporting electrolyte. In spite of a large radius

of TDDMB ion, however, the half-wave potential of oxygen is relatively positive in both HMPA and DMA. The presence of methyl groups may be responsible for the oxygen reduction at a relatively positive potential. (Figs. 3 and 3a).

Authors wish to thank Professors R. Takahashi at the Ritsumeikan University and A. Saito at the Kobe University for their kind offer of their polarographic instruments. Authors also appreciate the financial grant by the Ministry of Education in persuing the present research.

References

1) C. K. Mann and K. K. Barnes, "Electrochemical Reactions in Non-aqueous Systems," Marcel Dekker, INC., N. Y. (1970), p. 497 and references in it; D. Bauer and J-P. Beck, *J. Electroanal. Chem.*, **40**, 233 (1972).

2) T. Fujinaga, K. Izutsu, and T. Adachi, This Bulletin, **42**, 140 (1969); A. Iwase and T. Ito, *ibid.*, **42**, 2064 (1969).

3) D. C. Luehrs and D. G. Leddy, *J. Electoanal. Chem.*, **41**, 113 (1973).

4) D. L. Maricle and W. G. Hodgson, *Anal. Chem.*, **37**, 1562 (1965).

5) L. Johnson, K. H. Pool and R. E. Hamm, *ibid.*, **38**, 183 (1966); **39**, 888 (1967).

6) K. Izutsu, S. Sakura and T. Fujinaga, This Bulletin, **45**, 445 (1972); **46**, 493 (1973); **46**, 2148 (1973).

7) T. Fujinaga and S. Sakura, *Nippon Kagaku Kaishi*, **1973**, 2227. 11, 1 (1973).

8) J. E. Prue, P. J. Sherrington, *Trans. Faraday Soc.*, **57**, 1806 (1961); G. R. Lester, T. A. Gover and P. G. Sears, *J. Phy. Chem.*, **60**, 1076 (1956); W. A. Miller and D. W. Watts, *J. Amer. Chem. Soc.*, **89**, 6858 (1967).

9) T. Fujinaga, K. Izutsu and S. Sakura, *Nippon Kagaku-kaishi*, **1973**, 191.

10) T. Fujinaga and K. Izutsu, *Pure Appl. Chem.*, **27**, 275 (1971).

11) M. E. Peover and B. S. White, *Electrochimica Acta*, **11**, 1061 (1966).

12) N. Matsuura, K. Umemoto, and H. Takeda, the 28th National Meeting of the Chemical Society of Japan, (Spring), 4E08 (1973).

Characterization of the Oxalato Complex of Manganese(IV)[1]

Yukichi YOSHINO, Iwao TAMINAGA, Masakazu KOKISO, and Takashi UEHIRO

Department of Chemistry, College of General Education, The University of Tokyo, Meguro-ku, Tokyo 153

(Received November 30, 1973)

The preparation and analysis of the oxalato complex of manganese(IV), referred to as $K_2[Mn(OH)_2(C_2O_4)_2]\cdot 2H_2O$ by Cartledge and Ericks, were reexamined. Measurements of magnetic moment confirmed the unusually low value, 2.48 B.M. at room temperature. The infrared spectra of the complex suggest the presence of oxide bridges between manganese atoms. The electrical conductance of aqueous solution of the complex salt at 0 °C has been measured in various concentrations. The results indicate that the complex anion is dimeric both in solid and in solution. The electronic spectra of the complex in powder and solution states were measured, and some decomposition processes discussed. It was proposed that the complex should be formulated as a dimer with two oxide bridges, $[Mn_2O_2(C_2O_4)_4]^{4-}$.

The preparation and properties of oxalato complex of quadrivalent manganese were first reported by Cartledge and Ericks.[2] Grey measured the magnetic moment of the complex and obtained the value 2.79 B.M. at room temperature.[3] This is much smaller than the spin-only value 3.87 B.M. for an ion of d^3 configuration. However, no detailed explanation has been given so far.

The present paper describes some physico-chemical measurements involving magnetic susceptibility, infrared and diffuse reflectance spectra of the solid complex as well as the electrical conductivity and electronic spectra of aqueous solutions. The results obtained are consistent with formulation of the complex anion as a dimer with two oxide bridges.

Experimental

Preparation of the Complex. The original method of preparation by Cartledge and Ericks[2] was followed with a slight modification. To 0.14 mol of oxalic acid dihydrate dissolved in 250 ml of redistilled water at 0 °C was added 0.04 mol of powdered potassium permanganate and 0.026 mol of patassium oxalate. Under vigorous agitation, the reaction began to take place at 7 °C evolving carbon dioxide, when the reaction mixture was cooled quickly to 0 °C. When the reaction was complete, the solution was filtered through a cold glass filter, the filtrate being collected in a beaker placed in a freezing mixture. To the filtrate was added 70 ml of cold ethanol in portions, the temperature being kept at 0 °C. The precipitated crystals were filtered off rapidly and washed successively with ice-cold 50% ethanol, 99% ethanol and absolute ether. The green crystals thus obtained were dried *in vacuo* over silica gel in a dark refrigerator (−5 °C). Although Cartledge and Ericks reported that under a microscope the solid was a mixture of green and golden yellow crystals, we obtained only green crystals in all runs. Found: K, 21.72; Mn, 15.17; $C_2O_4^{2-}$, 49.10%; Oxid. equiv., 181.2. Calcd for $K_4[Mn_2O_2(C_2O_4)_4]\cdot 4H_2O$: K, 21.65; Mn, 15.21; $C_2O_4^{2-}$, 48.74%; Oxid. equiv., 180.5.

Potassium trioxalatomanganate (III) was prepared by the method of Cartledge and Ericks.[4] Potassium dioxalatomanganate(II) was obtained by the reaction of manganese(II) oxalate and potassium oxalate.

Magnetic Measurements. Magnetic measurements were carried out at room temperature with the usual Gouy apparatus. Temperature dependence of the magnetic susceptibility was measured by the Fonor method[5] with an apparatus constructed at the Cryogenic Center of the University of Tokyo. Magnetic measurement of the aqueous solution of the complex was carried out by the method of Russel *et al.*[6]

Electrical Conductances. These were measured with a Yokogawa model BV-Z-103B conductivity bridge and platinized platinum electrodes. Sample solutions were prepared with CO_2-free water of 0 °C just before each measurement. The cell was thermostated at 0 °C. The temperature equilibrium was attained after 10 min. No significant decomposition took place during the course of measurements.

Spectral Measurements. The infrared spectra were measured by Nujol and hexachloro-1,3-butadiene mull methods with a model 403G infrared spectrophotometer (Japan Spectroscopic Co.). The electronic spectra of the complex in both solution and powder states were measured with Hitachi EPS-2 and 124 spectrophotometers. Temperature was controlled by circulating ice-water through a cell compartment. In order to remove cloudiness from the cell walls, a nitrogen gas stream was passed to the surface of the cell.

Potentiometric Titration. A Toa Electronics Ltd. model HM-5A pH meter with an HP-105 bright platinum electrode and an HC-907 calomel reference electrode was employed.

X-ray Measurements. The X-ray powder patterns were taken with a Rigaku Denki Geigerflex diffractometer using Ni-filtered Cu-$K\alpha$ radiation. Relatively strong peaks were observed at lattice spacings d's(A): 8.58, 7.96, 7.19, 3.63 and 3.30, indicating that the solid sample is crystalline.

Results and Discussion

Magnetic Properties. The magnetic susceptibility of the oxalato complex of manganese(IV) at room temperature increases with the elapse of time. This change is accompanied by the decrease in mass and increase in oxidation equivalent. Thus magnetic measurements were carried out as soon as the samples were prepared. Although somewhat higher values were obtained in earlier runs, repeated preparation and measurement of the susceptibility gave the magnetic moment, $\mu_{eff}=2.48$ B.M. (15.5—18.0 °C), which is definitely much below the spin-only value (*i.e.*, 3.87 B.M.).

The dried complex salt is soluble to some extent in water at room temperature but rapidly decomposes to give a colloidal solution. In the presence of oxalate ions, however, the complex is fairly stable in a cold solution. Thus the magnetic susceptibilities of the complex in oxalate solutions were measured at 3 °C. Results: 2.8 B.M. for 4.94×10^{-3} M solution and 2.7 B.M. for 15.05×10^{-3} M solution.

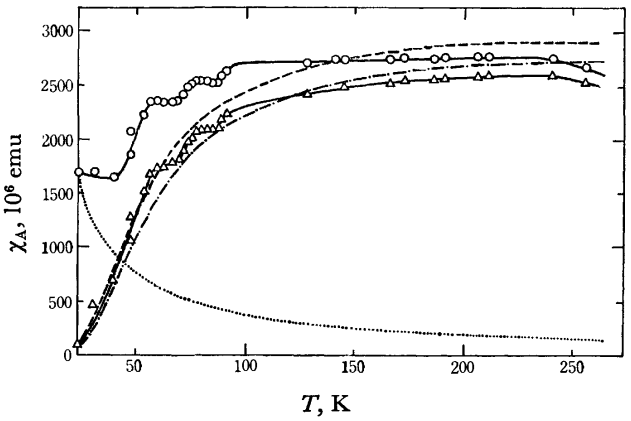

Fig. 1. Temperature dependence of magnetic susceptibility of the oxalato complex of manganese (IV).
—○—: experimental, —△—: experimental corrected for 1.9% Mn(III), ----; ·····: calculated for a binuclear cluster, $S_1=S_2=3/2$, $J=75$ "degrees" (-----) and $J=80$ "degrees" (-·-·-), $g=2.00$ and $N\alpha=0$, ····: 1.9% Mn(III) with $\mu=3.87$ B.M.

In order to clarify the nature of the sub-normal moment, the temperature dependence of the susceptibility was examined in the range 300—23 K. The results are given in Fig. 1. It should be noted that the magnetic behavior of the complex deviates significantly from the Curie-Weiss law; the susceptibility remains nearly constant over the temperature range 240—90 K, but decreases abruptly and stepwise below 90 K. This suggests that there exists a large antiferromagnetic interaction between manganese atoms. Curves calculated by assuming binuclear cluster with $S_1=S_2=3/2$, $g=2.00$, $J=80$ or 75 "degrees" and $N\alpha=0$ are shown in Fig. 1.[7] They might account qualitatively for the temperature independent susceptibility in the higher temperature range, the deviation becoming significant in the lower temperature range. It was found during the course of study on the decomposition of the complex that the reaction is initiated by a trace of manganese(III) and proceeds autocatalytically. Thus, it was assumed that the complex contains some paramagnetic manganese(III) impurities formed during the course of measurement. The experimental values corrected for 1.9% of manganese(III) are plotted in Fig. 1. The curve so obtained fits fairly well the calculated one with $J=75$ "degrees" in the lower temperature range (below 60 K). However, the reason for the stepwise decrease in the susceptibility in the range 90—60 K is not clear.

Infrared Spectra. Main absorption peaks of the IR spectrum of the manganese(IV) oxalato complex are given in Table 1. For the sake of comparison, the IR data for both Mn(III) and Mn(II) oxalato complexes are also given. Tentative assignments of the bands are based on the works of Fujita *et al.*[8,9]

The bands at 3000—3600 cm^{-1} are much broader than expected for hydroxide ion in a complex.[10] They were assigned to the stretching vibrations of O–H of the water molecule.

Only the manganese(IV) complex gives two characteristic bands in the region 600—700 cm^{-1} (Fig. 2).

Table 1. Infrared spectra of oxalato complexes of manganese (cm^{-1})

$K_4[Mn_2O_2(ox)_4]\cdot 4H_2O$	$K_3[Mn(ox)_3]\cdot 3H_2O$	$K_2[Mn(ox)_2]\cdot 2H_2O$	Tentative assignments
3540(s) br	3550(s) br		ν(O–H)
3450(s)	3440(s)	3430(s) br	of H_2O
1712(s)	1711(sh)	1663(s)	
1673(s)	1682(s) br	1615(s) br	ν_{as}(C=O)
	1632(s)	1570(s)	
1377(s)	1378(s)	1453(s)	ν_s(C–O)
1230(s)	1256(s)	1315(s)	
895(m)	893(m)		
		855(m)	
812(m)	807(m)		
791(m)	788(m)	766(m)	
642(m) br			$\nu(Mn_2O_2)$
618(m)			
	585(w)		
545(m)	522(m)br	494(w)	ν(Mn–O)
472(m)	485(m)	473(w)(sh)	
422(m)	396(m)	370(w)	ν(Mn–O)
338(m)			
306(w)br	282(w)br	256(m)	

s: strong, m: medium, w: weak, br: broad, sh: shoulder.
ox: $C_2O_4^{2-}$.

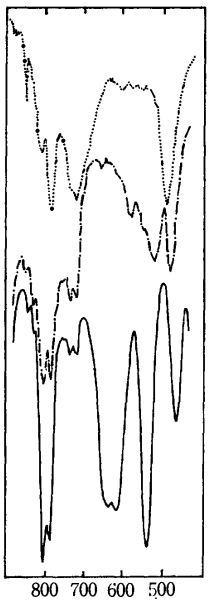

Fig. 2. IR spectra of oxalato complexes of manganese (in Nujol mulls).
——: $K_4[Mn_2O_2(C_2O_4)_4]\cdot 4H_2O$,
-·-·-: $K_3[Mn(C_2O_4)_3]\cdot 3H_2O$
····: $K_2[Mn(C_2O_4)_2]\cdot 2H_2O$

They might be assigned to the stretching modes of Mn_2O_2 bridges expected for binuclear complexes with two oxygen bridges.[11] It is noteworthy in this connection that the bands due to the bridging Mn–O bonds of poly, *catena*-oxo-*N*,*N*′-ethylenebis(salicylideneiminato)manganese(IV) appeared in the same region.[12]

The bond between manganese and oxygen of oxalato

ligand (ν(Mn-O)) becomes stronger as the oxidation state of manganese atom increases. Fujita *et al.* pointed out that, in oxalato complexes of divalent metals, a shift of the M–O stretching band to a higher frequency is accompanied by a shift of the antisymmetric C–O stretching frequency to a higher frequency together with a shift of symmetric C–O stretching band to a lower frequency.[8,9] An analogous relationship exists in the three oxalato complexes of manganese of different oxidation states (Fig. 3).

Electrical Conductance. The electrical conductance of the complex in aqueous solution at 0 °C was measured in the concentration range 10^{-3}—10^{-2} equivalent/l.

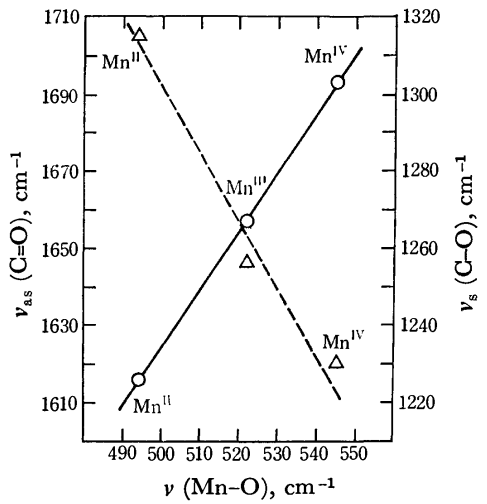

Fig. 3. Relationship between Mn–O stretching frequencies and C=O or C–O stretching frequencies of the oxalato complexes of manganese.
○: ν(C=O), △: ν(C–O).

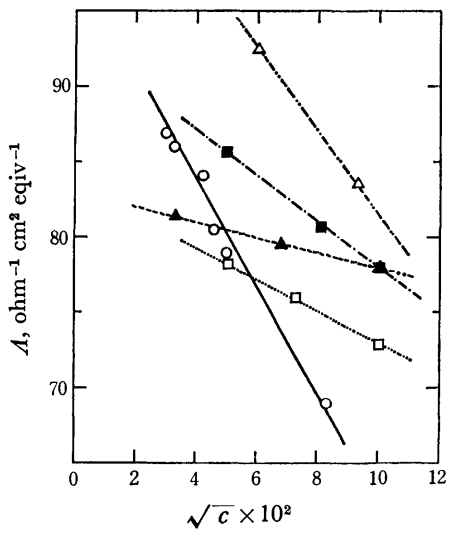

Fig. 4. Equivalent conductance (Λ, ohm^{-1} cm^2 equiv^{-1}) at 0 °C plotted against square root of concentrations (c, equiv/l) for the complex $K_4[Mn_2O_2(C_2O_4)_4]\cdot 4H_2O$ and for typical 1:1, 1:2, 1:3, and 1:4 electrolytes.
○: $K_4[Mn_2O_2(C_2O_4)_4]\cdot 4H_2O$, △: $K_4[Fe(CN)_6]$, ■: $K_3[Fe(CN)_6]$, □: K_2SO_4, ▲: KCl.

The equivalent conductance was plotted against the square root of the concentration (Fig. 4). For comparison, similar plots for salts of different valence types are also shown. The slope of the straight line for the oxalato complex resembles that for 4:1 electrolyte rather than for the 2:1 one.

Table 2. Electronic spectra of the oxalato complex of manganese(IV) and some other complexes of d^3 configuration (cm^{-1})

$K_4[Mn_2O_2(C_2O_4)_4]\cdot 4H_2O$	$[MnF_6]^{2-}$ [b]	$[Cr(C_2O_4)_3]^{3-}$ [b]	$[CrF_6]^{3-}$ [b]	Transitions[c]
26000(3.46)[a]	21750	17500	14900	$^4A_{2g}\rightarrow {}^4T_{2g}(F)$
	28200	23900	22700	$^4A_{2g}\rightarrow {}^4T_{1g}$
			34400	$^4A_{2g}\rightarrow {}^4T_{2g}(P)$
13700(2.15)[a] 15000(2.40)[a]	16300	14300	15700 (16400)	$^4A_{2g}\rightarrow \{{}^2T_{1g}, {}^2E_g\}$
19600(2.34)[a]			(22000)	$^4A_{2g}\rightarrow {}^2T_{2g}$
33600(3.96)[a]				charge transfer
36000(3.99)[a]				inner ligand

a) Values in parentheses relate to logarithms of molar extinction coefficients. b) cited from Ref. 13. c) tentative assignments for $K_4[Mn_2O_2(C_2O_4)_4]\cdot 4H_2O$.

Electronic Spectra. Cartledge and Ericks reported on the visible absorption spectrum of the complex in oxalic acid solution.[2] We measured the spectra in a wider range involving the ultraviolet region in cold oxalate solutions. The absorption bands tentatively assigned, assuming d^3 configuration in an octahedral ligand field, are listed in Table 2 together with those of the mononuclear complexes of the iso-electronic configuration. As is predicted from the spectrochemical series, the 10Dq ($^4A_{2g}\rightarrow {}^4T_{2g}(F)$) of the oxalato complex of manganese(IV) is larger than that of $[MnF_6]^{2-}$ or $[Cr(C_2O_4)_3]^{3-}$.[13] The second d-d transition peak ($^4A_{2g}\rightarrow {}^4T_{1g}$) may be concealed by a broad charge transfer or inner ligand transition band. The intensities of the spin-forbidden transitions are considerably higher than expected. This might be due to metal-metal antiferromagnetic coupling.[14]

Figure 5 shows a diffuse reflectance spectrum of the solid complex (a) and a spectrum of the complex in a cold oxalate solution in the region 8000—22000 cm^{-1} ((b), Curve I). They are similar in shape and their peak positions are almost the same. We might say that no significant decomposition of the complex takes place in a cold oxalate solution.

When a sample solution containing oxalate was brought to room temperature, the deep green solution turned brown and later changed into pink forming trioxalatomanganate(III) ion. The latter eventually decomposed to give manganese(II) complexes. These changes are clearly seen in the spectral features shown in Fig. 5. As the absorption maximum at 15000 cm^{-1}

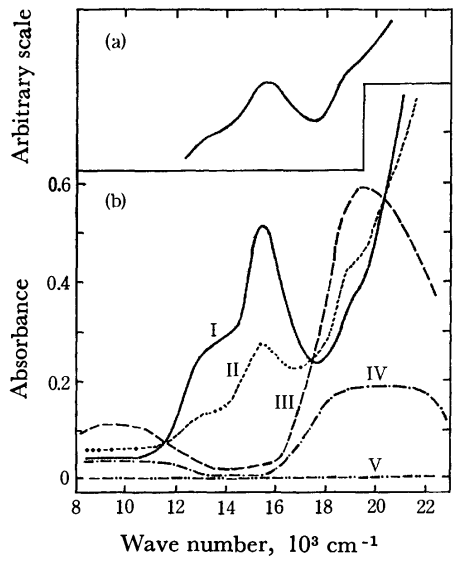

Fig. 5. Decomposition of the oxalato complex of manganese(IV) followed by spectral measurements.
(a) Diffuse reflectance spectrum of the solid complex.
(b) Time and temperature dependence of electronic spectra of the complex: 2.06×10^{-3} M in 0.1 M $Na_2C_2O_4$-$H_2C_2O_4$ solution (pH 4.9).
I: after 12 min, 4 °C, II: after 175 min, 5 °C, III: after 222 min, 18 °C, IV: after 239 min, 18 °C, V: after 12 hr, room temp.

decreases, the peak of trioxalatomanganate(III) at 19200 cm^{-1} increases in the initial stage. There appear three isosbestic points at 11800, 17300, and 20400 cm^{-1}. In connection with these changes, an attempt was made to follow the change in the magnetic susceptibility of manganese in 0.1 M oxalate solution (pH 4.9). Approximate values of the magnetic moment in 1.51×10^{-2} M (Mn) solution at 4—5 °C are as follows:

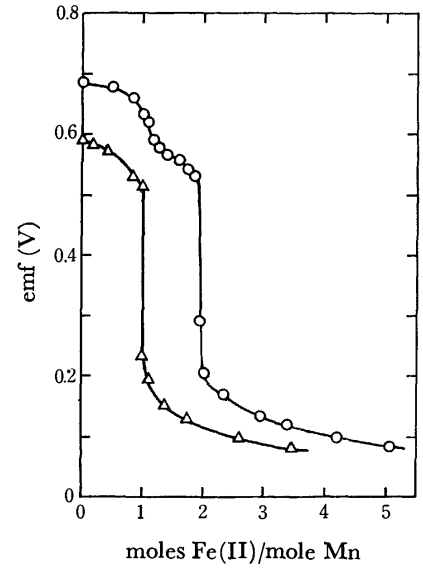

Fig. 6. Potentiometric titration of oxalato complexes of manganese (IV) and manganese (III) at 0 °C.
○: $K_4[Mn_2O_2(C_2O_4)_4]\cdot4H_2O$,
△: $K_3[Mn(C_2O_4)_3]\cdot3H_2O$.

color	: green	brown	red	colorless
μ_{eff} (B.M.):	2.7	3.6	4.6	5.7

These results also confirm the view that the manganese(IV) complex is reduced finally to manganese(II) *via* manganese(III).

Potentiometric Titration. A solution of the complex was titrated with iron(II) solution at low temperature. The result is illustrated in Fig. 6. For the sake of comparison, a titration curve of trioxalatomanganate(III) is also shown. The manganese(IV) complex gives two inflexion points corresponding to the steps, Mn(IV) to Mn(III) and Mn(III) to Mn(II). The standard redox potential, $E°$ for a couple, Mn(IV)-oxalato complex/$[Mn(C_2O_4)_4]^{3-}$ was evaluated as *ca.* 0.95 V (NHE) at 0 °C. This value agrees with that calculated from the literature.[15]

Plausible Formula of the Complex. For the oxalato complex of manganese(IV), Cartledge and Ericks presented a formula $K_2[Mn(OH)_2(C_2O_4)_2]\cdot2H_2O$ on the basis of chemical analysis. However, it seems difficult to explain all the above-mentioned behavior of the complex with this formula.

Although the exact nature of the sub-normal magnetic moment has not been clarified yet, there is hardly any doubt that an exchange interaction between manganese atoms bridged by oxygen atoms exists in the complex anion. The electrical conductance behavior and infrared spectra support a dimeric structure. In this connection, di-μ-oxo structure of tetrakis(bipyridine)-dimanganese(III, IV) complex determined by X-ray diffraction could be compared.[16] Taking into account the above results, we propose as a plausible formula of the oxalato complex of manganese(IV) the following:

$$K_4[(C_2O_4)_2Mn\begin{matrix}O\\O\end{matrix}Mn(C_2O_4)_2]\cdot4H_2O$$

The authors thank Messrs. Suguru Takayama and Kichizo Asai for magnetic measurements at low temperatures. They are also grateful to Dr. Akira Ouchi for a number of helpful discussions. A part of the expense of this study was defrayed by a Grant for Scientific Research of the Ministry of Education.

References

1) Presented at the 23rd Symposium on Coordination Chemistry, Fukuoka, October, 1973.
2) G. H. Cartledge and W. P. Ericks, *J. Amer. Chem. Soc.*, **58**, 2069 (1936).
3) J. T. Grey, Jr., *ibid.*, **68**, 605 (1964).
4) G. H. Cartledge and W. P. Ericks, *ibid.*, **58**, 2061 (1936).
5) S. Fonor, *Rev. Sci. Instr.*, **27**, 548 (1956).
6) C. D. Russel, G. R. Cooper, and W. C. Vosburgh, *J. Amer. Chem. Soc.*, **65**, 1301 (1943).
7) A. Earnshaw, "Introduction to Magnetochemistry," Academic Press, London and New York (1968), p. 76.
8) J. Fujita, K. Nakamoto, and M. Kobayashi, *J. Phys. Chem.*, **61**, 1014 (1957).
9) J. Fujita, A. E. Martell, and K. Nakamoto, *J. Chem. Phys.*, **36**, 324 (1962).
10) K. Nakamoto, "Infrared Spectra of Inorganic and Coordination Compounds," 2nd ed., Wiley-Interscience, New

York (1970), p. 82.
11) W. P. Griffith, *J. Chem. Soc.*, *A*, **1969**, 211.
12) T. Matsushita, T. Yarino, T. Shono, and K. Shinra, This Bulletin, **46**, 1712 (1973).
13) C. K. Jørgensen, "Absorption Spectra and Chemical Bonding in Complexes," Pergamon Press, Oxford (1962), p. 290.
14) C. K. Jørgensen, "Modern Aspects of Ligand Field Theory," North-Holland Publishing Co., Amsterdam (1971), p. 321.
15) W. M. Latimer, "Oxidation Potentials," 2nd ed., Prentice-Hall, Inc., Englewood Cliffs, N. J. (1952), p. 234.
16) P. M. Plaskin, R. C. Stoufer, M. Mathew, and G. T. Palnik, *J. Amer. Chem. Soc.*, **94**, 2121 (1971).

Reactions of π-Allylic Palladium(II) Complexes of Acetoacetate Esters with Pyridine and Its Derivatives

Shigeru BABA, Tamotsu SOBATA, Tetsuya OGURA, and Shinichi KAWAGUCHI*

Department of Chemistry, Faculty of Science, Osaka City University, Sumiyoshi-ku, Osaka 558

(Received January 18, 1974)

The π-allylic palladium(II) complexes of ethyl and benzyl acetoacetate esters react with pyridine and its derivatives to afford the terminal-carbon-bonded complexes $PdCl(CH_2COCH_2COOCH_2R)L_2$, where $R=CH_3$ or C_6H_5, and L=pyridine or its derivative. The NMR spectra unequivocally establish the bonding type in these complexes. The pyridine and 4-methylpyridine complexes are a mixture of *cis* and *trans* isomers in a ratio of 1:5, while 2-methyl- and 2,6-dimethyl-pyridine complexes are *trans* exclusively. The relative stabilities of these complexes are compared.

In a previous paper[1] we reported on the central-carbon-bonded palladium(II) complexes of acetylacetone obtained by the reactions of bis(acetylacetonato)-palladium(II) with triphenylphosphine or nitrogen bases such as pyridine, diethylamine and *N*-methylbenzylamine. This paper describes the preparation and characterization of the terminal-carbon-bonded palladium(II) complexes of acetoacetate esters.[2]

Results and Discussion

The π-allylic palladium(II) complex of ethyl acetoacetate, di-μ-chlorobis(π-1-ethoxycarbonyl-2-hydroxyallyl)dipalladium(II) [**1**] was prepared by the reaction of diketene with the tetrachloropalladate(II) in ethanol.[3] The corresponding complex of benzyl acetoacetate [**2**] was obtained by the reaction of diketene with dichlorobis(benzonitrile)palladium(II)in dichloromethane containing benzyl alcohol.

π-Allylic palladium(II) complexes of acetoacetate esters reacted with excess pyridine or its derivatives in benzene at room temperature to yield stable terminal-carbon-bonded complexes in high yields (82—95%).

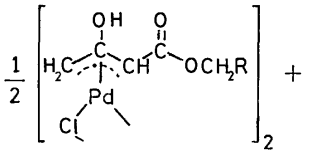

$R=CH_3$ [**1**] or C_6H_5 [**2**]

$\longrightarrow PdCl(CH_2COCH_2COOCH_2R)L_2$ (i)

$R=CH_3$, L=py [**3a**] or 1/2(2,2′-bipy) [**3b**]
$R=C_6H_5$, L=py [**4a**], 2-Me-py [**4b**], 4-Me-py [**4c**], 2,6-Me_2-py [**4d**], or 1/2(2,2′-bipy) [**4e**]

Analytical data of the products are summarized in Table 1. The conversion of the π-allylic linkage of the acetoacetate ligand into the σ-bonding seems to be preceded by the bridge splitting reaction of the dimeric complex. A monomeric π-allylic complex [**5**] was isolated as yellow-green crystals in the reaction of the benzyl ester complex with an equivalent amount of pyridine.

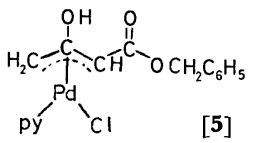

[**5**]

* To whom correspondence should be addressed.

TABLE 1. TERMINAL-CARBON-BONDED PALLADIUM(II) COMPLEXES OF ACETOACETATE ESTERS

Complex[a]	Color	Anal, found (calcd) % C	H	N	Mol wt[b] found (calcd)	Dec. temp °C
PdClY-$(py)_2$	pale yellow	44.47 (44.75)	4.44 (4.44)	6.55 (6.53)	430 (429)	110
PdClY-(bipy)	yellow	44.42 (44.99)	3.92 (4.01)	6.75 (6.56)	410 (427)	166
PdClY′-$(py)_2$	pale yellow	50.79 (51.34)	4.36 (4.30)	6.01 (5.70)	480 (491)	107
PdClY′-(2-Me-py)$_2$	yellow	52.82 (53.19)	4.89 (4.85)	5.65 (5.40)	512 (519)	104
PdClY′-(4-Me-py)$_2$	pale yellow	52.61 (53.19)	4.98 (4.85)	5.65 (5.40)	500 (519)	105
PdClY′(2,6-Me_2-py)$_2$	yellow	53.86 (53.97)	5.31 (5.43)	5.36 (5.03)	540 (556)	136
PdClY′-(bipy)	yellow	51.44 (51.55)	4.02 (3.91)	5.82 (5.73)	483 (489)	145

a) $Y=CH_2COCH_2COOCH_2CH_3$, $Y'=CH_2COCH_2COOCH_2C_6H_5$. b) Determined in dichloromethane at 25 °C.

IR Spectra. The IR spectra of the parent π-allylic complexes **1** and **2** have the ν(OH) and ν(C=O) bands at around 3200 and 1670 cm^{-1}, respectively. On the other hand, the product complexes **3** and **4** show no absorption band around 3200 cm^{-1}, but exhibit two strong ν(C=O) vibrations at around 1730 and 1640 cm^{-1} (Table 2). This demonstrates that the π-allylic linkage of the enolate anion of acetoacetate esters was converted into the σ-carbon-bonding of the ketonic tautomer.

Two modes of linkage can be considered for the unidentate carbon-bonding of the acetoacetate ester to palladium(II), terminal-carbon-bonding (**A**) and central-carbon-bonding (**B**).

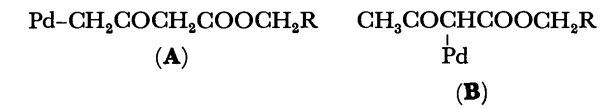

Structure **B** was realized in the case of acetylacetone, and the ν(C=O) vibrations of the central-carbon-bonded ligand causes absorption at 1665 and 1632 cm^{-1}.[1] If this were also the case for the acetoacetate-ester ligand, the ν(C=O) bands should appear in the 1600—

Table 2. Characteristic IR bands (cm^{-1}) in Nujol[a)]

Complex[b)]	ν(OH)	ν(C=O) ketone	ν(C=O) ester	ν(Pd-C)	ν(Pd-Cl)	ν(Pd-N)
Starting complex[1]	3200m		1675vs	548s[c)]	270s	
PdClY $(py)_2$ [3a]		1650vs	1740vs	540s	283s, 355m	250m
PdClY (bipy) [3b]		1640vs	1730vs	543s	335s	243m
Starting complex[2]	3220m		1670vs	498s[c)]	265m	
PdClY′ $(py)_2$ [4a]		1645vs	1735vs	508s	321s, 357w	240m
PdClY′(2-Me-py)[4b]		1640s	1730vs	498s	288s	250m
PdClY′(4-Me-py)$_2$[4c]		1655vs	1740vs	507s	260s	255sh
PdClY′(2,6-Me_2-py)$_2$ [4d]		1660vs	1745vs	498s	305s	258s
PdClY′ (bipy) [4e]		1635vs	1730vs	504s	328s	240m
π-Allylic monomer[5]	3200w		1675vs			

a) vs: very strong, s: strong, m: medium, w: weak, sh: shoulder. b) Y=$CH_2COCH_2COOCH_2CH_3$, Y′=CH_2-$COCH_2COOCH_2C_6H_5$ c) π-allylic skeletal deformation

1700 cm^{-1} region. Contrary to expectation, the IR spectra of compounds **3** and **4** showed a ν(C=O) band in the 1600—1700 cm^{-1} region and another one in the frequency region higher than 1700 cm^{-1}. The spectra can be interpreted satisfactorily on the basis of structure **A**.

The ν(C=O) vibrations of the keto tautomer of free acetylacetone cause absorption at 1727 and 1707 cm^{-1},[4)] but shift towards the lower frequency region (1665 and 1632 cm^{-1}) by ligation to the palladium atom *via* the central carbon atom.[1)] When the acetoacetate-ester ligand coordinates to the palladium atom *via* the terminal carbon atom, the ν(C=O) band due to the ketonic carbonyl group should shift towards the lower frequency side to an extent similar to that in the case of central-carbon ligation. On the other hand, the ester carbonyl group is situated far from the metal atom and is far less influenced by coordination. Thus, of the two observed ν(C=O) bands of compounds **3** and **4**, the lower frequency band is assigned to the ketonic carbonyl group and the higher frequency one to the ester carbonyl group.

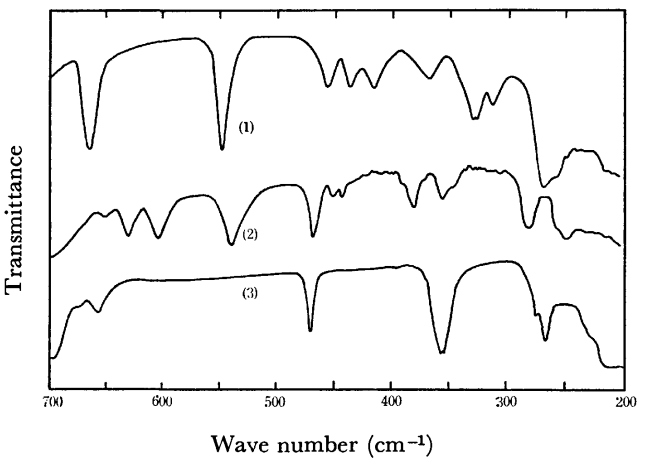

Fig. 1. The IR spectra in the 700—200 cm^{-1} region of the π-allylic palladium(II) complex dimer of ethyl acetoacetate (curve 1), PdCl($CH_2COCH_2COOC_2H_5$)-$(py)_2$ (curve 2) and *trans*-$PdCl_2(py)_2$ (curve 3) in Nujol mull.

For the sake of comparison the IR spectrum of the carbon-bonded bis(pyridine) complex **3a** in the 700—200 cm^{-1} region is shown together with spectra of the parent π-allylic complex **1** and *trans*-$PdCl_2(py)_2$ in Fig. 1. The spectrum of complex **1** is readily interpreted by reference to the metal isotope effect reported by Shobatake and Nakamoto[5)] on the metal-ligand vibrations in π-allyl complexes of palladium(II). Thus the strong band at 548 cm^{-1} (curve 1) corresponds to the 512 cm^{-1} peak in $[PdCl(C_3H_5)]_2$ and is assigned to the CCC bending mode. The three-peaks pattern in the 460—410 cm^{-1} region resembles that of the latter compound in the 410—350 cm^{-1} region, and is ascribed to ν(Pd-allyl) vibrations. The strongest peak at 270 cm^{-1} accompanied by a shoulder at 255 cm^{-1} is similarly attributed to the bridging Pd-Cl stretching vibrations. These assignments are also consistent with those of Adams and Squire[6)] for $[PdCl(C_3H_5)]_2$. Neither a strong peak at 665 cm^{-1} nor bands in the 370—310 cm^{-1} region are observed for $[PdCl(C_3H_5)]_2$. These are considered to be due to the ligand vibrations.

The spectrum of *trans*-$PdCl_2(py)_2$ is very simple (curve 3, Fig. 1). The bands observed at 357 and 268 cm^{-1} are assigned to the ν(Pd–Cl) and ν(Pd–N) vibrations, respectively. Pfeffer *et al.*[7)] observed the ν(Pd–Cl) bands at 358, 356, and 373 cm^{-1}, and the ν(Pd–N) bands at 278, 302, and 306 cm^{-1} for *trans*-$PdCl_2L_2$ with pyridine, 4-methylpyridine and 4-ethylpyridine as L, respectively. Norbury and Sinha also observed the ν(Pd–Cl) bands at 360 and 359 cm^{-1} for *trans*-$PdCl_2(AsPh_3)_2$ and *trans*-$PdCl_2(PPh_3)_2$, respectively.[8)]

The spectrum of PdCl($CH_2COCH_2COOC_2H_5$)$(py)_2$ [**3**] (curve 2, Fig. 1) is much more complicated than that for *trans*-$PdCl_2(py)_2$ (curve 3). As is revealed by the NMR spectra, the compound is a mixture of *cis* and *trans* isomers in a ratio *ca.* 1 : 5. The strong band at 283 cm^{-1} is assigned to the stretching vibration of the Pd–Cl bond *trans* to the alkyl ligand, since the possibility of chloride bridging is excluded by analytical and molecular-weight data (Table 1). The strong *trans*-influence of the alkyl ligand is well-known[9)]. Another band (355 cm^{-1}) and a shoulder (347 cm^{-1}) in the terminal ν(Pd–Cl) region might be ascribed to the ν(Pd–Cl) vibration in the *cis* isomer. The broad band of medium intensity at 250 cm^{-1} is assigned to the ν(Pd–N) vibration. The frequency is a little lower than 268 cm^{-1} in *trans*-$PdCl_2(py)_2$.

Three bands are observed in the 640—500 region where *trans*-$PdCl_2(py)_2$ has no absorption. The strong peak at 540 cm^{-1} is assigned to the ν(Pd–C) vibration. In recent years an increasing number of palladium(II) complexes containing the Pd–C linkage have been reported, but data of the ν(Pd–C) vibration are rather

Table 3. NMR data for methylene protons in the terminal-carbon-bonded palladium(II) complexes of acetoacetate esters[a]

Complex[b]	$CH_2^{(a)}$		$CH_2^{(b)}$		$CH_2^{(c)}$	
$PdClY(py)_2$ [**3a**]	7.33	7.16	7.03	6.16	5.87[c]	5.80[c]
PdClY(bipy) [**3b**]		7.13		6.00		5.86[c]
$PdClY'(py)_2$ [**4a**]	7.27	7.03	6.90	6.03	4.80	4.76
$PdClY'(2\text{-Me-py})_2$ [**4b**]	7.48		6.93		4.93	4.88
$PdClY'(4\text{-Me-py})_2$ [**4c**]	7.37	7.20	6.90	6.10	4.83	4.80
$PdClY'(2,6\text{-Me}_2\text{-py})_2$ [**4d**]	7.70		7.33		5.00	
PdClY'(bipy) [**4e**]		7.13		5.96		4.83

a) Chemical shift (τ) recorded at 60 MHz in $CDCl_3$ with Me_4Si as the internal reference. Signals are singlet unless otherwise stated. b) $Y=CH_2^{(a)}COCH_2^{(b)}COOCH_2^{(c)}CH_3$, $Y'=CH_2^{(a)}COCH_2^{(b)}COOCH_2^{(c)}C_6H_5$. c) Quartet, $J=7$ Hz.

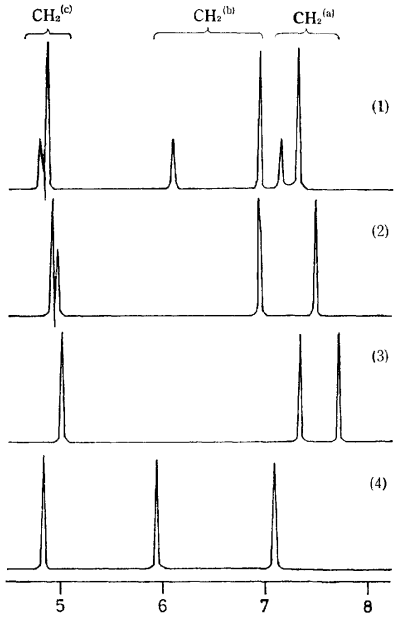

Fig. 2. The NMR spectra of $PdCl(CH_2^{(a)}COCH_2^{(b)}COOCH_2^{(c)}C_6H_5)L_2$ in the methylene signal region recorded at 60 MHz with TMS as an internal reference in $CDCl_3$: L=py (curve 1), 2-Me-py (curve 2), 2,6-Me_2-py (curve 3), or 1/2 (2,2'-bipy) (curve 4).

scarce. The ν(Pd-C) bands in the Pd(2,4-pentanedionato-O,O')(2,4-pentanedionato-C^3)L complexes were observed at 540, 524, 519, and 518 cm^{-1} for L= PPh_3, py, $NHEt_2$, and $NH(Me)CH_2Ph$, respectively.[1] Dietl *et al.* reported that the peak at 487 or 530 cm^{-1} is assigned to the ν(Pd-C) vibration in $[PdCl_2(C_2Me_2)_3]_2$.[10] Other bands appearing in the 700—600 and 500—370 cm^{-1} regions seem to be due to ligand vibrations (curve 2, Fig. 1).

Characteristic IR bands of each of the terminal-carbon-bonded palladium(II) complexes of acetoacetate esters were assigned in a similar way and are given in Table 2.

NMR Spectra. The NMR spectra of products **3** and **4**, summarized in Table 3, unequivocally establish structure **A**. A spectrum of the benzyl ester complex **4e** involving 2,2'-bipyridine as a base exhibits three singlet peaks of equal intensity at 7.13, 5.96, and 4.83 τ (Fig. 2). These are assigned to the three methylene groups; the nearest to palladium, the central and the benzyl methylenes, respectively.

Geometrical isomerism is possible in the case of complexes containing unidentate ligands, both *cis* and *trans* isomers being formed, but not in the case of 2,2'-bipyridine complexes. The spectrum of the pyridine complex **4a** involves two sets of methylene signals. Chemical shifts of the three minor peaks are close to those of the methylene signals of the 2,2'-bipyridine complex **4e**, suggesting that they are attributable to the *cis* isomer of **4a**. The other set of stronger peaks are thus assigned to the *trans* isomer. The intensity ratio of the *trans* and *cis* peaks is nearly equal for each of the three methylene signal pairs amounting to *ca.* 5:1. Isomerization of palladium(II) complexes is usually slow in the absence of free ligands,[11] and the observed figure reflects the relative yield of the two isomers in reaction (i). A single crystal of compound **4a** submitted for X-ray analysis was composed of *cis* molecules.[12]

The same situation was also observed for the 4-methylpyridine complex **4c**. Only three methylene signals, however, were observed for the 2,6-dimethylpyridine complex **4d**. Their chemical shifts are higher than those for the *trans* isomer of the pyridine complex **4a**. Thus it seems reasonable to consider that the *trans* isomer was yielded exclusively in the case of the bis-(2,6-dimethylpyridine) complex, since the *cis* isomer is quite unfavorable because of the steric hindrance of the methyl substituents. The methyl proton signal of the coordinated 2,6-dimethylpyridine is observed as a sharp singlet at 6.62 τ, shifting towards the down-field side by *ca.* 1 τ on ligation. The free ligand added to this solution causes absorption at 7.48 τ, indicating no sign of the ligand exchange.

The spectrum of the 2-methylpyridine complex **4b** exhibits a different pattern. The two peaks observed at 7.48 and 6.93 τ are assigned to the $CH_2^{(a)}$ and $CH_2^{(b)}$ protons, indicating that the complex has the *trans* configuration just as in the case of the 2,6-dimethylpyridine complex. The benzyl methylene protons are observed as two separate peaks at 4.93 and 4.88 τ in the area ratio 3:7. A slight splitting of the $CH_2^{(b)}$ signal can be seen in the 100 MHz spectrum. In the case of the corresponding 2-ethylpyridine complex, the $CH_2^{(b)}$ protons afford two distinct peaks; the area ratio for $CH_2^{(b)}$ signals at 7.00 and 6.95 τ and that for $CH_2^{(c)}$ signals at 4.96 and 4.88 τ are both 3:7. Since the $CH_2^{(a)}$ signal shows no splitting in either case, these features do not suggest the coexistence of *cis* isomers, but seem to indicate that the $CH_2^{(c)}$ and even $CH_2^{(b)}$ protons can occupy two non-equivalent positions.

Splitting of the $CH_2^{(c)}$ and $CH_2^{(b)}$ proton signals is not observed for complexes of symmetric bases such as pyridine, 4-methyl- and 2,6-dimethyl-pyridines, but appears only in the spectra of unsymmetrically 2-substituted pyridine complexes. Steric hindrance for the free rotation of 2-substituted pyridine ligands about the M–N bond in palladium(II)[13] and platinum(II)[14]

complexes has been well documented by studies of variable-temperature NMR spectra. For the present 2-methylpyridine complex **4b** also locked structures might be assumed in which the pyridine rings are fixed perpendicular to the coordination plane of palladium(II). Two conformations are considered; (a) methyl groups of the two 2-methylpyridine ligands exist on the same side of the coordination plane (syn), and (b) they lie on the opposite sides of the square plane (anti). The spectrum of $PdCl(CH_2COCH_2COOCH_2Ph)(2\text{-Et-py})_2$ exhibits a multiplet centered at 8.5 τ which is slightly more complicated than a double-triplet, and another multiplet (nearly double-quartet) at 6.34 τ. These resonances are assigned to the methyl and methylene protons of the ethyl group attached to pyridine, respectively, and seem to disclose the coexistence of the locked syn and anti structures.

Splitting of the $CH_2^{(c)}$ and $CH_2^{(b)}$ proton signals of the 2-alkylpyridine complexes might be related to such a relative conformation of the two pyridine ligands, although the exact locked structure of the dangling benzyl ester ligand is not certain. The reason why the $CH_2^{(a)}$ protons give a single resonance is not clear either, but the rotation of the ester ligand about the Pd–C bond might equal the averaged magnetic circumstances of $CH_2^{(a)}$ protons in the syn and anti configurations.

Substitution of Pyridine Ligands with Other Pyridines. In order to find the relative stability of the complexes containing various pyridine derivatives, substitution of the pyridine ligands with other pyridines was examined. Qualitative results were obtained by substitution reactions for several hours at room temperature, and reveal some interesting features (Table 4).

Table 4. Substitution of pyridine ligands L in $PdCl(CH_2COCH_2COOCH_2C_6H_5)L_2$ with other pyridine derivatives L′ in dichloromethane at room temperature[a)]

L′ \ L =	py	2-Me-py	4-Me-py	2,6-Me_2-py	bipy
py	—	○	○	×	×
2-Me-py	○	—	○	×	×
4-Me-py	○	○	—	×	×
2,6-Me_2-py	×	×	×	—	×
bipy	○	○	○	○	—

a) ○ indicates the replacement of the ligand L by L′. × indicates no reaction, the starting complex being recovered.

Unsubstituted, 2-methyl-, and 4-methyl-pyridines show similar behavior, being interchangable with each other. The bis(2,6-dimethylpyridine)-complex is very stable, the ligand not being displaced by the other unidentate pyridines. The inertness for substitution reactions can be ascribed to steric shielding of the metal atom by the *ortho*-substituents in the pyridine ligand. On the other hand 2,6-dimethylpyridine is very weak as an attacking nucleophile. It can not substitute any pyridine ligand coordinated to palladium(II). The *ortho*-substituents might retard the nitrogen atom to approach the metal atom. 2,2′-Bipyridine is the most powerful ligand. It can displace any unidentate pyridines in the coordination sphere; once it is bonded to palladium(II), it is not replaced by any unidentate pyridines. Such extraordinary stability must be due to the chelate effect.

Supplementary Discussion. The currently favored mechanism for the syn-anti isomerization in π-allyl complexes involves a σ-bonded intermediate.[15)] π-Allylpalladium(II) complexes have also been widely suggested as intermediates in various catalytic reactions.[16)] The conversion of π-allyl into σ-allyl can usually be detected by NMR-spectral observations. Only a few reports have appeared on the isolated σ-allyl palladium(II) compounds.[17)]

In the present reactions the starting π-allylic complexes gave stable σ-alkyl palladium(II) compounds. However, the σ-2-hydroxyallyl moiety was not retained, but the accompanying tautomeric transformation caused the terminal-carbon-bonded acetoacetate-ester complexes. Similar π-allyl complexes **6**[18,19)] and **7**[20)] react with bases such as pyridine and triphenylphosphine to afford monomeric complexes, but the σ-allylic complexes are not stable enough to be isolated. These results suggest that the neighboring carbonyl group plays some role of stabilizing the σ-carbon bonding.

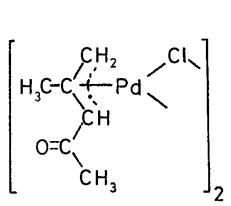

[6]

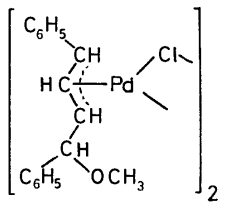

[7]

Both the chelating acetylacetonate ligand and π-allylic acetoacetate-ester ligand can be converted into the σ-carbon bonding to palladium(II). However, the former prefers central carbon bonding, and the latter terminal-carbon bonding. This might be due to certain electronic and/or steric factors. The terminal-carbon bonding of a β-dicarbonyl compound to a transition metal has not yet been reported, but $TeCl_2(acac)_2$, obtained as a by-product in the reaction of tellurium(IV) chloride with acetylacetone, was found to be of such a bonding type.[21)] In contrast to the present palladium(II) complex, the acetylacetonate ligand in this tellurium(IV) complex has the enol (hydrogen chelate) form.

Experimental

π-Allylic Palladium(II) Complexes of Acetoacetate Esters. The ethyl acetoacetate complex, di-μ-chlorobis(π-1-ethoxycarbonyl-2-hydroxyallyl)dipalladium(II) [**1**] was synthesized according to Tezuka *et al.*[3)] The corresponding benzyl acetoacetate complex, di-μ-chlorobis(π-1-benzyloxycarbonyl-2-hydroxyallyl)dipalladium(II) [**2**] was prepared by adding diketene dropwise to a dichloromethane solution (12 ml) of dichlorobis(benzonitrile)palladium(II) containing 2 ml of benzyl alcohol at 0 °C. Dark red color of the solution faded gradually and a yellow precipitate appeared in 10—20 min. The product was filtered and washed repeatedly with petroleum ether. Yield: 0.67 g, 81%. Found: C, 39.55; H, 3.40%. Calcd for $C_{11}H_{11}O_3ClPd$: C, 39.66; H, 3.32%.

Tetrahydrofuran and dichloromethane are suitable solvents for recrystallization. Crude products were used without recrystallization in the following reactions.

Reaction of π-Allylic Palladium(II) Complexes of Acetoacetate Ester **1** *and* **2** *with Pyridine or Its Derivatives.* Pyridine (2—3 ml) was added with stirring to a suspension of the ethyl ester compex (0.7 g) in benzene (10 ml). The mixture turned immediately to a clear yellow-green solution. Petroleum ether was added to this solution to separate the precipitate. Yield: 1.0 g, 91%. The product was dissolved in dichloromethane and recrystallized by addition of petroleum ether. The other reaction of π-allylic palladium(II) complexes of acetoacetate esters with pyridine derivative were performed in a similar way, affording the following yields: **3b**, 82%; **4a**, 82%; **4b**, 84%; **4c**, 96%; **4d**, 94%; **4e**, 95%.

The monomeric intermediate chloro(pyridine) (π-1-benzyloxycarbonyl-2-hydroxyallyl)palladium(II) [**5**] was isolated in the following way. Pyridine (0.043 g, 0.54 mmol) was added to a suspension of the starting benzyl-ester complex **2** (0.177 g, 0.53 mmol) in dichloromethane. The resulting clear solution was evaporated to dryness, and the residue was extracted with benzene to remove the final carbon-bonded product **4a**. The remaining residue was then extracted with dichloromethane to obtain the π-allylic monomer **5** in a 45% yield. Found: C, 46.21; H, 3.50; N, 3.30%. Calcd for $C_{16}H_{16}NO_3ClPd$: C, 46.62; H, 3.91; N, 3.39%. Molecular weight could not be determined, since **5** was unstable in solution and readily disproportionated into the dimeric parent complex **2** and the final carbon-bonded bis(pyridine) complex **4a**.

Substitution of Pyridine Ligands with Other Pyridines. To a solution of each complex in dichloromethane, an excess amount of another free ligand was added and allowed to react for 3—4 hr. Petroleum ether was then added to this solution to separate the palladium(II) complex, which was identified by the IR assay.

Measurements. Infrared spectra were measured with JASCO IR-E (4000—600 cm^{-1}) and Hitachi grating EPI-L spectrophotometers. The NMR spectra were recorded at 60 MHz with tetramethylsilane as an internal reference on JEOL C60-HL and PS-100 spectrometers. The molecular weight was determined in dichloromethane at 25 °C by means of vapor pressure osmometry with an apparatus manufactured by Knauer, Germany.

The authors are grateful to Mr. J. Gohda and Miss M. Iwao for the elemental analyses and NMR measurements. Financial aid by the Ministry of Education and supply of diketene by Daicel Co., Ltd. are gratefully acknowledged.

References

1) S. Baba, T. Ogura, and S. Kawaguchi, This Bulletin, **47**, 665 (1974).
2) A short communication appeared in *Inorg. Nucl. Chem. Lett.*, **8**, 605 (1972).
3) Y. Tezuka, T. Ogura, and S. Kawaguchi, This Bulletin, **42**, 443 (1969).
4) R. Mecke and E. Funck, *Z. Elektrochem.*, **60**, 1124 (1956); E. E. Ernstbrunner, *J. Chem. Soc. A*, **1970**, 1558.
5) K. Shobatake and K. Nakamoto, *J. Amer. Chem. Soc.*, **92**, 3339 (1970).
6) D. M. Adams and A. Squire, *J. Chem. Soc. A*, **1970**, 1808.
7) M. Pfeffer, P. Braunstein, and J. Dehand, *Inorg. Nucl. Chem. Lett.*, **8**, 497 (1972).
8) A. H. Norbury and A. I. P. Sinha, *J. Inorg. Nucl. Chem.*, **35**, 1211 (1973).
9) For example, B. Crociani, T. Boschi, R. Pietropaolo, and U. Belluco, *J. Chem. Soc. A*, **1970**, 531.
10) H. Dietl, H. Reinheimer, J. Moffat, and P. M. Maitlis, *J. Amer. Chem. Soc.*, **92**, 2276 (1970).
11) F. Basolo and R. G. Pearson, "Mechanisms of Inorganic Reactions," 2nd ed. Wiley, New York, N. Y. (1967), p. 423.
12) N. Kasai, *et al.*, to be published.
13) J. W. Faller and M. J. Mattina, *Inorg. Chem.*, **11**, 1296 (1972).
14) F. Coletta, R. Ettorre, and A. Gambaro, *J. Chem. Soc. Dalton*, **1973**, 684.
15) *Cf. e. g.*, J. W. Faller and M. T. Tully, *J. Amer. Chem. Soc.*, **94**, 2676 (1972).
16) P. M. Maitlis, "The Organic Chemistry of Palladium," Vol. 2, Academic Press, New York, N. Y. (1971).
17) M. Hancock, M. N. Levy, and M. Tsutsui, "Organometallic Reactions," Vol. 4, Wiley-Interscience, New York, N. Y. (1972), p. 1.
18) G. W. Parshall and G. Wilkinson, *Inorg. Chem.*, **1**, 896 (1962).
19) J. W. Faller, M. T. Tully, and K. J. Laffey, *J. Organometal. Chem.*, **37**, 193 (1972).
20) B. F. G. Johnson, J. Lewis, and D. A. White, *J. Chem. Soc. A*, **1970**, 1738.
21) D. H. Dewar, J. E. Fergusson, P. R. Hentschel, C. J. Wilkins, and P. P. Williams, *J. Chem. Soc.*, **1964**, 688.

Stereoselectivity in the Formation of Oxalato-L-aspartato-ethylenediaminecobalt(III) Complex[1]

Mitsuaki TAKEUCHI and Muraji SHIBATA

Department of Chemistry, Faculty of Science, Kanazawa University, Kanazawa 920

(Received March 25, 1974)

The complex [Co(ox)(L-aspH)(en)] has been prepared by the reaction of the dioxalatoethylenediaminecobalt-(III) complex with L-aspartic acid and separated into four diastereoisomers by means of ion-exchange chromatography: *mer*-Δ-, *mer*-Λ- and *fac*-Δ-[Coox(L-aspH)en]·H_2O, and *fac*-Λ-[Coox(L-aspH)en]·$2.5H_2O$. They were characterized by their absorption, CD and PMR spectra. Stereoselectivity has been found in the *mer*-Δ and *fac*-Λ isomers with degrees exceeding 80%. Related isomeric complexes containing L-glutamate or L-leucinate ion in place of L-aspartate have also been investigated, much less selectivity (~60%) being observed.

In order to study stereoselectivity we examined the mixed L-aspartato complexes with glycine,[2] L-alanine,[3] and L-proline.[4] It was found that the stereoselectivity observed can be explained in terms of the interaction between the uncoordinated β-carboxylate group in the chelated aspartate ion and the adjacent ligand.

In the present work, a mixed complex consisting of L-aspartate ion (L-asp), oxalate ion and ethylenediamine was chosen in order to obtain proof for the selectivity. The *mer* isomers of the mixed aminoacidato complexes used in the previous works consisted of three geometrical isomers. The present complex gives only one form for either *mer* or *fac* arrangement with respect to donor N (or O) atoms. Thus, the study on stereoselectivity could be simplified. For the sake of comparison the corresponding L-glutamato and L-leucinato complexes were also studied.

Experimental

Preparation. Preparation and chromatographic separation of the [Coox(L-asp)en]$^-$ complex were carried out as follows: The complex Na[Co(ox)$_2$en]·H_2O[5] (6.7 g, 0.02 mol), L-aspartic acid (2.7 g, 0.02 mol) and NaOH (0.8 g, 0.02 mol) were dissolved in water (250 ml). After the pH of the solution had been adjusted to *ca.* 9.0 with a NaOH solution, activated charcoal (1.0 g) was added and the mixture was allowed to stand for a week at room temperature (~15 °C) with occasional stirring, whereupon the solution turned red-violet. After the removal of a small amount of the precipitate and charcoal by filtration, a portion (50 ml) of the filtrate was charged on a cation-exchange column containing 100—200 mesh Dowex 50 W×8 resin in H-form (7.0×27 cm). Chromatographic separation was carried out by passing water at a rate of *ca.* 0.5 ml/min. The foremost band was of unreacted [Co(ox)$_2$en]$^-$ species. After a while two closely spaced but completely separated violet bands descended the column, followed by other two red bands with a narrow distance. These were collected in fractions and labeled from A-1 to A-4. This separation procedure was repeated several times in order to store up the same fractions. Each stored fraction was concentrated to a small volume with a rotary evaporator at 30 °C. The concentrated solution thus obtained was kept in a refrigerator for a few days in order to precipitate the desired isomer as its hydrogen compound. Each recrystallization was performed from water.

Such complexes as [Coox(en)$_2$]$^+$, [Co(L-asp)(en)$_2$]$^+$[6,7] and [Co(L-asp)$_2$(en)]$^-$[7] were also produced, but they remained at the top of the column during the separation of the desired isomers.

Preparation and chromatographic separation of the [Coox-(L-glu)en]$^-$ complex were carried out as in the case of the aspartato complex; L-glutamic acid (2.9 g, 0.02 mol) was used.

Chromatographic separation gave two bands, violet and red. They were collected in fractions and labeled G-1 and G-2. A pair of diastereoisomers could be isolated by fractional crystallization from G-1. Another pair of diastereoisomers was obtained from G-2 by the following procedure. The solid material (100 mg) obtained by evaporating the fraction was dissolved in a minimum amount of water slightly alkalinized with aqueous NaOH, the pH of the solution being made *ca.* 7.0. The solution was poured into a column containing G-15 Sephadex (2×100 cm), and washing with water was continued at a rate of *ca.* 0.07 ml/min. The red band spread with the elapse of time. After several hours, there appeared a broadened band having different tones of color in the first and second halves. The band was collected in a number of fractions and subjected to CD measurement. The first half showed a (−) sign and the second a (+) sign at the main CD peak. The chromatographic separation was repeated several times in order to store up the fractions with the same sign. The same fractions collected were concentrated and rechromatographed. From the final two fractions thus obtained a pair of diastereoisomers was obtained by evaporating and acidifying with 6 M HCl.

For preparation and separation of the [Coox(L-leu)en] complex, L-leucine (2.6 g, 0.02 mol) and Dowex 50 W×8 resin in Na-form were used. The procedure was the same as in the case of the L-aspartato complex. The chromatographic separation gave three bands violet, red and red in turn. They were collected in fractions labeled L-1, L-2 and L-3. From L-1 a pair of diastereoisomers was obtained by fractional crystallization. Each of the other diastereoisomers was obtained from L-2 and L-3 each.

For all diastereoisomeric complexes, recrystallization was carried out until their main CD peaks became constant.

Formation Ratios. The formation ratios between the bands separated chromatographically were evaluated from the spectral data of the isolated complexes.

Measurements. The absorption spectra were measured with a Hitachi Model 323 Recording Spectrophotometer. The circular dichroism spectra were recorded on a JASCO Model ORD/UV-5 spectropolarimeter. The proton magnetic resonance spectra were recorded on a JEOL JNM-PS-100 NMR spectrometer at *ca.* 22 °C, with deuterium oxide as a solvent. Sodium carbonate and 20% deuterium chloride in D_2O were used for pD adjustment. The values of the chemical shifts were referred to internal sodium 2,2-dimethyl-2-silapentane-5-sulfonate (DSS) or sodium D_4-trimethylsilylpropionate (TMSP). The pD of the PMR sample was measured with a Beckman Model G pH meter.

Results and Discussion

Characterization of Isomers. Elemental analyses, absorption spectra and CD spectra are summarized in Table 1. The geometrical form (*mer* or *fac*) of each isolated compound could easily be identified by its absorption spectrum. The absolute configuration (*Δ* or *Λ*) of a given geometrical isomer was determined from the sign of main CD peak. The CD spectra of the isolated compounds are shown in Figs. 1 and 2. The four possible isomers of the [Coox(L-aminoacidate)-en]-type complex are given in Fig. 3.

The chromatographic separation of the L-aspartato complex into the four isomers was carried out with the cation-exchange resin in H-form. In the beginning, an anion-exchange resin in Cl-form was used for the separation of anionic species $[Coox(L\text{-}asp)en]^-$. An extremely long column was necessary since washing procedure gave a diffuse band on the column and successive elution with an aqueous solution of electrolyte made each band spread considerably. In contrast, complete separation of the four isomers was achieved by the use of the cation-exchanger in a short period of elution. For example, elution for two weeks on an anion-exchanger column could be reduced to two days on a cation-exchange column. This improved procedure was used for the separation of the L-glutamato complex species.

In the case of the L-aspartato complex, four isomers were completely separated in the order *mer-Δ-mer-Λ-*

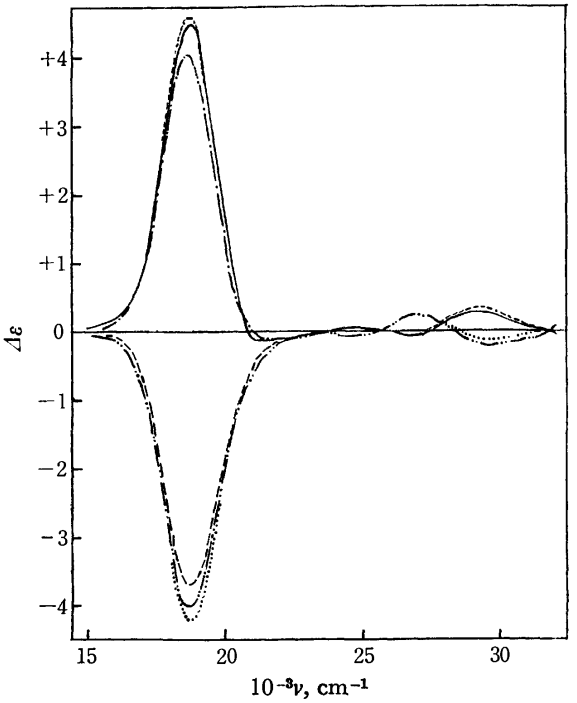

Fig. 1. CD spectra of *fac*-[Coox(L-am)en]-type complexes.
—— *fac-Λ* (L-am=L-aspH)
—·— *fac-Λ* (L-gluH) ------ *fac-Λ* (L-leu)
-··- *fac-Δ* (L-aspH) —— *fac-Δ* (L-gluH)
···· *fac-Δ* (L-leu)

Table 1. Elemental analyses, absorption and CD spectral data

Label	Complex	Elemental anal., %[a] C	H	N	Band I $10^{-3}\bar{\nu}_{max}$ cm^{-1}	ε_{max}	Band II $10^{-3}\bar{\nu}_{max}$ cm^{-1}	ε_{max}	CD $10^{-3}\bar{\nu}_{max}$ cm^{-1}	$\Delta\varepsilon_{max}$
A-1	*mer-Δ*-[Coox(L-aspH)en]·H_2O	26.73	4.34	11.79	*ca.* 19.3	96	26.95	175	17.7	−2.03
		(26.90)	(4.52)	(11.77)					20.9	−1.43
A-2	*mer-Λ*-[Coox(L-aspH)en]·H_2O	26.91	4.71	11.91	*ca.* 19.3	96	26.95	180	17.8	+1.95
		(26.90)	(4.52)	(11.77)					20.4sh	+1.24
A-3	*fac-Λ*-[Coox(L-aspH)en]·2.5H_2O	25.02	5.28	10.98	19.2	173	27.25	193	18.7	+4.51
		(25.01)	(4.99)	(10.94)					21.4	−0.14
A-4	*fac-Δ*-[Coox(L-aspH)en·]H_2O	27.18	4.80	11.65	19.2	157	27.25	170	18.8	−4.03
		(26.90)	(4.52)	(11.77)						
G-1	*mer-Δ*-[Coox(L-gluH)en]·0.5H_2O	29.47	5.10	11.33	*ca.* 19.3	95	26.95	180	17.5	−2.42
		(29.74)	(5.07)	(11.56)					20.7	−1.52
	mer-Λ-[Coox(L-gluH)en]·1.5H_2O	28.52	5.36	11.07	*ca.* 19.3	104	26.95	197	17.8	+2.07
		(28.34)	(5.36)	(11.02)					20.5	+1.41
G-2	*fac-Λ*-[Coox(L-gluH)en]·H_2O	29.06	5.02	11.17	19.2	149	27.25	170	18.6	+4.06
		(29.02)	(5.21)	(11.28)					21.4	−0.11
	fac-Δ-[Coox(L-gluH)en]·H_2O	29.33	5.30	11.29	19.2	140	27.25	155	18.7	−3.70
		(29.02)	(5.21)	(11.28)						
L-1	*mer-Δ*-[Coox(L-leu)en]·1.5H_2O	33.24	6.78	11.31	*ca.* 19.3	98	26.95	184	17.5	−2.46
		(32.98)	(6.37)	(11.54)					20.8	−1.45
	mer-Λ-[Coox(L-leu)en]·1.5H_2O	32.68	6.63	11.67	*ca.* 19.3	101	26.95	195	17.8	+1.81
		(32.98)	(6.37)	(11.54)					20.5	+1.27
L-2	*fac-Δ*-[Coox(L-leu)en]·2.5H_2O	31.76	6.76	11.14	19.2	155	27.25	173	18.7	−4.20
		(31.42)	(6.59)	(10.99)						
L-3	*fac-Λ*-[Coox(L-leu)en]·2.5H_2O	31.41	6.32	11.14	19.2	161	27.25	187	18.6	+4.60
		(31.42)	(6.59)	(10.99)					21.4	−0.08

a) ( ): calcd.

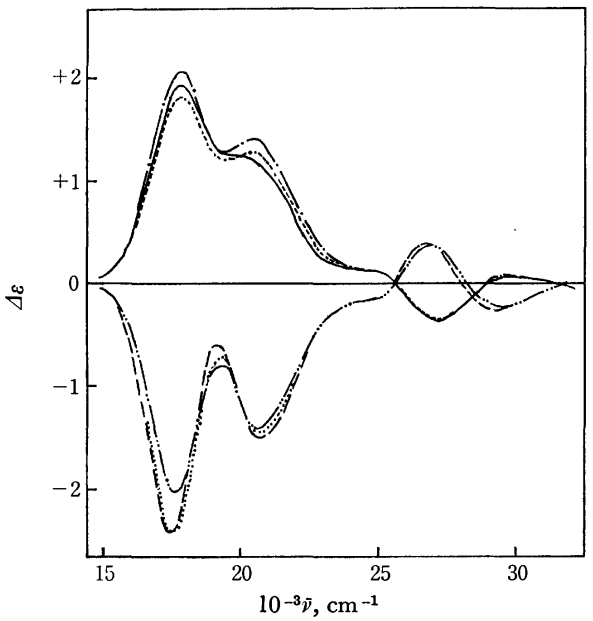

Fig. 2. CD spectra of *mer*-[Coox(L-am)en]-type complexes.

—— *mer*-Λ (L-am=L-aspH)
—·— *mer*-Λ (L-gluH) ------ *mer*-Δ (L-leu)
—··— *mer*-Δ (L-aspH) ----- *mer*-Δ (L-gluH)
···· *mer*-Δ (L-leu)

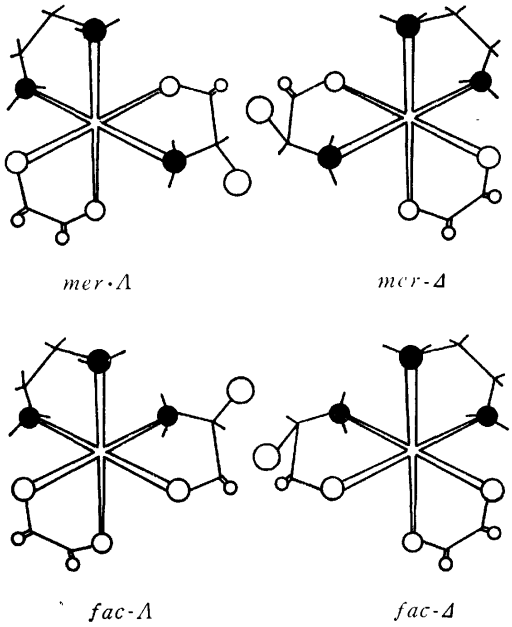

Fig. 3. Possible four isomers of [Coox(L-am)en]-type complex.

fac-Λ-*fac*-Δ, while for the L-glutamato complex only two fractions corresponding to *mer*- and *fac*-forms were obtained. This might be due to the different uncoordinated carboxylate groups (β- and γ-COO^-).

The CD spectra of the Δ and Λ diastereoisomers of *fac*-form exhibit a sharp peak in the first absorption band region (Fig. 1), similar to those of the tris-type complexes of L-amino acids.[4,8,9] On the other hand, the spectra of the Δ and Λ diastereoisomers of *mer*-form exhibit two peaks with the same signs in the first

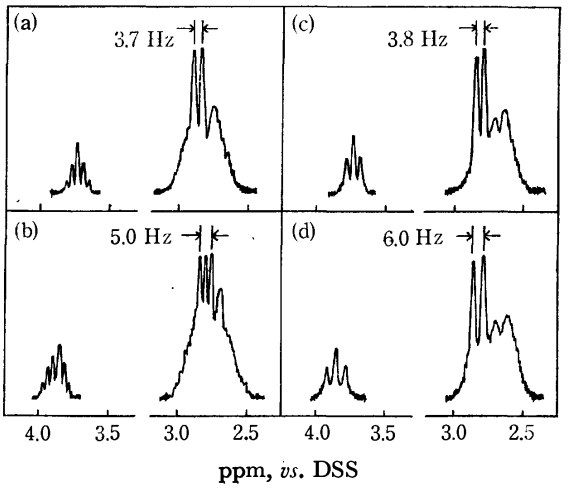

Fig. 4. PMR spectra of [Coox(L-aspH)en] in D_2O (pD 4.3—5.3).
(a) *mer*-Δ isomer (b) *mer*-Λ isomer
(c) *fac*-Λ isomer (d) *fac*-Δ isomer

absorption band region (Fig. 2). The *mer*-Δ isomers of the [Co(L-pro)$_3$][8] and [Co(L-pro)$_2$(L-asp)]$^-$[4] complexes reveal a small shoulder at shorter-wave-length-side in the first absorption band region.

Figure 4 shows the PMR spectra of the four isomers of the L-aspartato complex. It can be seen that the two sharp lines appearing in the vicinity of 2.8 ppm and multiple lines in the vicinity of 3.8 ppm are due to the CH_2 and CH groups, respectively, of the coordinated aspartate ion.[6] The isomers can be classified into those of narrow width (*mer*-Δ and *fac*-Δ) and those of broad width (*mer*-Λ and *fac*-Λ). The difference in line-width may be related to the different orientation of aspartate side-chains in the two types. A similar discussion was given previously.[4]

The isomers of the L-glutamato complex exhibited too complicated spectra for obtaining any information.

The PMR spectra, partly of CH_3 proton resonance, of the four isomers of L-leucinato complex were measured. The results show two well-separated doublets indicating different chemical environments of two CH_3 groups of the isobutyl group for the isomers.

Table 2. Percentage compositions of reaction mixtures

	mer-Λ	*mer*-Δ	*fac*-Λ	*fac*-Δ
[Coox(L-aspH)en]	72	11	14	3
[Coox(L-gluH)en]	48	32	11	9
[Coox(L-leu)en]	49	35	8	8
[Coox(gly)en][a]	84		16	

a) Percentage composition was evaluated from spectral data.[10]

Stereoselectivity. The percentage compositions of all isomers in the reaction mixture are given in Table 2. For comparison, the values for the [Coox(gly)en] are also included. The formation of the *mer* isomer (Λ+Δ) in each complex is more abundant than that of the *fac* isomer (Λ+Δ). The amount of formation of the isomers for the L-glutamato and L-leucinato complexes increases in the order *fac*-Δ≃*fac*-Λ<*mer*-Λ<

TABLE 3. PERCENTAGE COMPOSITIONS OF DIASTEREOISOMERS

	[Coox(L-aspH)en]	[Coox(L-gluH)en]	[Coox(L-leu)en]	$[Co(gly)_2(L\text{-asp})]^{-}$ [2]	$[Co(gly)_2(L\text{-glu})]^{-}$ [9]
mer-Δ	87	60	58	39	50
fac-Δ	82	55	51	11	40

mer-Δ, and that for the L-aspartato complex in the order *fac-Δ*<*mer-Λ*≃*fac-Λ*<*mer-Δ*. The increase of *fac-Λ* can be understood in terms of favorable interaction.

The stereoselectivity in a given complex is expressed in percentage composition of a diastereoisomeric pair. The results are given in Table 3, together with the data of the L-aspartato[2] and L-glutamato[9] complexes. As was expected, a marked stereoselectivity of over 80% was found in both the *mer-Δ* and *fac-Λ* isomers for the L-aspartato complex. This can be understood on the basis of stereo models; a favorable interaction through a hydrogen bond between the β-carboxylate group of the coordinated L-aspartate ion and an amino group of the chelated ethylenediamine is possible for the *mer-Δ* and *fac-Λ* isomers; on the other hand, an electrostatic repulsive interaction between the β-carboxylate group and an oxygen atom of the chelated oxalate ion is possible for the *mer-Λ* and *fac-Δ* isomers.

The stereoselectivity in the $[Co(gly)_2(L\text{-glu})]^{-}$ complex is much less than that in the corresponding L-aspartato complex.[9] This may be due to the lower ability of the γ-carboxylate group to interact with the adjacent group. The *mer-Δ* and *fac-Λ* isomers for the present L-glutamato complex also showed ~60% selectivity. The L-leucinato complex having an isobutyl group as the side-chain of the amino-acidate ion also showed a comparable stereoselectivity. This suggests that such a low selectivity can not be discussed in a similar way to that for the L-aspartato complex.

In the $[Co(gly)_2(L\text{-asp})]^{-}$ complex, the percentage compositions of the *fac-Δ* and *mer-Λ* isomers were reported to be 89 and 61%, respectively.[2] The lower selectivity of the *mer-Λ* isomer is due to the fact that a geometrical isomer for the *mer-Δ* diastereoisomer, *trans*-(N)*cis*(O), is favorable for the interaction of the β-carboxylate group. The present work showed selectivity in the same order as between the *mer-Δ* and *fac-Λ* isomers of the L-aspartato complex. It has been confirmed that the stereoselectivity in a complex containing L-aspartate ion as a bidentate ligand is closely related to a favorable interaction of the β-carboxylate group of the aspartate ion with the adjacent ligand.

References

1) Presented at the 23rd Symposium on Coordination Chemistry, Fukuoka, 17 October, 1973.
2) K. Kawasaki, J. Yoshii, and M. Shibata, This Bulletin, **43**, 3819 (1970).
3) T. Matsuda, T. Okumoto, and M. Shibata, *ibid.*, **45**, 802 (1972).
4) T. Matsuda and M. Shibata, *ibid.*, **46**, 3104 (1973).
5) F. P. Dwyer, I. K. Reid, and F. L. Garvan, *J. Amer. Chem. Soc.*, **83**, 1285 (1961).
6) J. I. Legg and J. Steele, *Inorg. Chem.*, **10**, 2177 (1971).
7) Y. Kojima and M. Shibata, *ibid.*, **12**, 1009 (1973).
8) R. G. Denning and T. S. Piper, *ibid.*, **5**, 1056 (1966).
9) K. Kawasaki and M. Shibata, This Bulletin, **45**, 3100 (1972).
10) N. Matsuoka, J. Hidaka, and Y. Shimura, *ibid.*, **39**, 1257 (1966).

Metal Complexes of Amino Acids. V.[1] μ-Aminocarboxylato Bi- and Tri-nuclear Complexes of Cobalt(III)

Takaji YASUI, Tomoharu AMA, Hideki MORIO, Minahiro OKABAYASHI, and Yoichi SHIMURA*

Faculty of Arts and Science, Kochi University, Asakura, Kochi 780

**Department of Chemistry, Faculty of Science, Osaka University, Toyonaka, Osaka 560*

(Received May 4, 1974)

Some new binuclear and trinuclear complexes containing μ-aminocarboxylato ligands, $[(NH_3)_5Co(OCORNH_2)Co\,NO_2(acac)_2](ClO_4)_2$ (R = CH_2, $(CH_2)_2$, and $CH(CH_3)$ for glycinato, β- and DL-alaninato ligands) and $[en_2Co\{(OCORNH_2)Co\,NO_2(acac)_2\}_2]ClO_4$ (R = CH_2 and $(CH_2)_2$), have been prepared and characterized on the basis of their elemental analyses, visible and ultraviolet absorption, infrared, and PMR spectra. It was concluded that the NH_2 end of the μ-aminocarboxylato bridge occupies a coordination position *trans* to the NO_2 ligand, and the COO ends of two μ-aminocarboxylato bridges in the trinuclear complex occupy positions *trans* to each other.

It is well-known that an aminocarboxylate anion or its parent acid coordinates to a cobalt(III) ion as a unidentate,[1-7] or a bidentate[8-12] ligand, and in some cases also as a tridentate ligand such as aspartate[13,14] and histidinate.[15] Previously we reported the $[Co(NH_3)_5(aaH)]X_3$,[2] *trans*-$[Coen_2(aaH)_2]X_3$,[3] and *cis*-$[Co(NH_3)_4(aaH)_2]X_3$[1] complexes containing various amino acids (abbreviated as aaH). The amino acid binds to a cobalt(III) ion as a unidentate ligand through its carboxylate group, the $-NH_3^+$ group being free. Recently the complexes of *N*-bonded unidentate amino acids, aminocarboxylates or amino acid esters were also prepared.[5-7] Pellizer *et al.*[16] suggested the occurrence of some μ-aminocarboxylato binuclear complexes in solution in the course of studies on the substitution reaction of a Vitamin B_{12} model complex.

In the present paper, formation and preparation of some μ-aminocarboxylato complexes by the reaction between the $[Co(aa)(NH_3)_5]^{2+}$ or *trans*-$[Co(aa)_2en_2]^{1+}$ ion and the $[Co(NO_2)_2(acac)_2]^-$ ion are reported. The complexes isolated are characterized on the basis of their elemental analyses, visible and ultraviolet absorption, infrared, and PMR spectra. The amino acids and their abbreviations (in parentheses) are as follows: glycine NH_2CH_2COOH (glyH), β-alanine $NH_2CH_2CH_2COOH$ (β-alaH), L- and DL-alanine $NH_2CH(CH_3)COOH$ (L- and DL-alaH), and γ-aminobutyric acid $NH_2CH_2CH_2CH_2COOH$ (γ-ambutH).

Experimental

Preparation of Starting Materials. Pentaammine(amino acid)cobalt(III) Complexes: $[Co(NH_3)_5(glyH)](ClO_4)_3\cdot H_2O$, $[Co(NH_3)_5(\beta\text{-alaH})](ClO_4)_3$, $[Co(NH_3)_5(L\text{-alaH})](ClO_4)_3\cdot 2H_2O$, $[Co(NH_3)_5(DL\text{-alaH})](ClO_4)_3\cdot H_2O$, and $[Co(NH_3)_5(\gamma\text{-ambutH})](ClO_4)_3$, and the pentaammine(aminocarboxylato) complex, $[Co(gly)(NH_3)_5](ClO_4)_2$, were prepared by the method reported.[2] The *trans*-$[Co\,en_2(aaH)_2](ClO_4)_3$ (aaH = glyH, β-alaH, L-alaH and γ-ambutH) complexes were prepared by using the same method as that described.[3] These complexes were recrystallized from aqueous solution by addition of a small amount of ethanol and saturated sodium perchlorate solution. The glycine, β-alanine and γ-aminobutyric acid complexes are new ones.

Found: C, 15.44; H, 4.14; N, 13.42%. Calcd for $[Co\,en_2(glyH)_2](ClO_4)_3 = C_8H_{26}N_6O_{16}Cl_3Co$: C, 15.31; H, 4.18; N, 13.39%.

Found: C, 18.12; H, 4.63; N, 13.11%. Calcd for $[Co\,en_2(\beta\text{-alaH})_2](ClO_4)_3 = C_{10}H_{30}N_6O_{16}Cl_3Co$: C, 18.32; H, 4.62; N, 12.82%.

Found: C, 20.78; H, 4.94; N, 12.26%. Calcd for $[Co\,en_2(\gamma\text{-ambutH})_2](ClO_4)_3 = C_{12}H_{34}N_6O_{16}Cl_3Co$: C, 21.08; H, 5.02; N, 12.29%.

Preparation of $Na[Co(NO_2)_2(acac)_2]$ complex was carried out by the method of Rosenheim and Garfunkel.[17]

Preparation of μ-Aminocarboxylato Binuclear Complexes. $[(NH_3)_5Co(gly)Co\,NO_2(acac)_2](ClO_4)_2\cdot 3H_2O$: The pH of an aqueous solution containing 2.5 g of $[Co(NH_3)_5(glyH)](ClO_4)_3\cdot H_2O$ in 25 ml of water was adjusted to 9.0 with sodium hydroxide (1 M). To this solution was added 1.8 g of $Na[Co(NO_2)_2(acac)_2]$. The resulting solution was kept in a water-bath at 30 °C for two hr and then kept in a refrigerator overnight. The brownish-red needle crystals formed were filtered and washed with a water–ethanol (1: 1) mixture and then with 95% ethanol. From the filtrate another crop of the complex was obtained by adding a saturated solution of sodium perchlorate. Recrystallization was carried out by adding a small amount of saturated sodium perchlorate solution to a concentrated solution and by keeping the mixture in a refrigerator. The separated complex was dried over $CaCl_2$ in a vacuum desiccator. The yield was *ca.* 2.3 g. The complex was readily soluble in water and acetone, but insoluble in absolute ethanol and ether.

Found: C, 18.74; H, 5.16; N, 12.62%. Calcd for $C_{12}H_{39}N_7O_{16}Cl_2Co_2$: C, 18.61; H, 5.09; N, 12.62%.

The same binuclear complex was also obtained from $[Co\,gly(NH_3)_5](ClO_4)_2$ (2.0 g) and $Na[Co(NO_2)_2(acac)_2]$, the yield being *ca.* 2.3 g.

$[(NH_3)_5Co(\beta\text{-ala})Co\,NO_2(acac)_2](ClO_4)_2$. Brown needle crystals were obtained by a similar procedure to that for the μ-gly binuclear complex except for the use of $[Co(NH_3)_5(\beta\text{-alaH})](ClO_4)_3$ (2.6 g) instead of $[Co(NH_3)_5(glyH)](ClO_4)_3\cdot H_2O$. This complex was more soluble in water than the μ-gly complex. The crystals obtained were dried over P_4O_{10} in a vacuum desiccator. The yield was *ca.* 1.5 g.

Found: C, 21.30; H, 5.00; N, 12.93%. Calcd for $C_{14}H_{37}N_7O_{16}Cl_2Co_2$: C, 21.26; H, 4.81; N, 13.36%.

$[(NH_3)_5Co(DL\text{-ala})CoNO_2(acac)_2](ClO_4)_3\cdot 2H_2O$. This complex was prepared by the same method as that employed for the μ-gly binuclear complex except for the use of $[Co(NH_3)_5(DL\text{-alaH})](ClO_4)_3\cdot H_2O$ (2.6 g). The yield was 1.5 g.

Found: C, 20.24; H, 5.18; N, 12.89%. Calcd for $C_{13}H_{39}N_7O_{18}Cl_2Co_2$: C, 20.27; H, 5.11; N, 12.73%.

Preparation of the μ-L-ala binuclear complex was repeatedly attempted in the same way as for the DL-ala complex, but no

pure complex was obtained. Preparation of the binuclear complex of γ-ambut was also unsuccessful, some dark brown crystals of an undesired composition being separated instead.

Preparation of μ-Aminocarboxylato Trinuclear Complexes. $[en_2Co\{(gly)CoNO_2(acac)_2\}_2]ClO_4 \cdot 1.5NaClO_4 \cdot 6H_2O$: The pH of an aqueous solution containing 2.5 g of *trans*-$[Co\text{-}en_2(glyH)_2](ClO_4)_3$ in 40 ml of water was adjusted to pH 9.0 with sodium hydroxide (1 M). To this solution was added 3.0 g of $Na[Co(NO_2)_2(acac)_2]$. The resulting solution was kept in a water-bath at 30 °C for two hours and cooled in an ice-bath. Crystals of the trinuclear complex deposited as brown flakes with addition of a saturated aqueous solution of sodium perchlorate. The crystals were filtered and washed with a saturated aqueous solution of sodium perchlorate, a small amount of ethanol and then with ether.

Recrystallization was performed from cold aqueous solution by addition of a saturated solution of sodium perchlorate, the resulting solution being kept in a refrigerator. The yield was *ca.* 1.3 g. The complex was soluble in water and acetone, but insoluble in absolute ethanol and ether.

Found: C, 25.52; H, 5.04; N, 8.55%. Calcd for $C_{28}H_{64}N_8O_{32}Cl_{2.5}Co_3$: C, 25.38; H, 4.87; N, 8.45%.

$[en_2Co\{(\beta\text{-}ala)CoNO_2(acac)_2\}_2]ClO_4 \cdot 3NaClO_4 \cdot 5H_2O$. A brown complex was obtained as flake crystals by a similar method to that for the μ-gly trinuclear complex. The yield was *ca.* 1.0 g.

Found: C, 23.14; H, 4.52; N, 7.61%. Calcd for $C_{30}H_{66}N_5O_{37}Cl_4Na_3Co_3$: C, 23.72; H, 4.39; N, 7.37%.

Repeated attempts were made to prepare trinuclear complexes containing DL-ala, L-ala and γ-ambut, but were unsuccessful.

Estimation for the Formation of μ-Aminocarboxylato Complex in Solution. The % formation of the μ-gly binuclear complex was estimated as follows. $[Co(NH_3)_5(glyH)](ClO_4)_3 \cdot H_2O$ (2.50 g, 4.67×10^{-3} mol) was dissolved in 25 ml of water (an almost saturated solution was obtained), the pH being adjusted to 9.0 with 1 M-NaOH. The solution was made 50 ml in volume with water and then kept in a water-bath with a thermostat. It was then mixed with an aqueous solution containing 1.78 g (4.67×10^{-3} mol) of $Na[Co(NO_2)_2(acac)_2]$ in 50 ml of water. The mixed solution was transferred to a 100 ml Erlenmeyer flask with a stopper and kept at an appropriate temperature (20.0, 30.0, 40.0 or 50.0±0.1 °C). A 10 ml portion of the reactant solution, picked up at intervals several minutes to several hours after mixing, was quickly poured into a short column (4.5 cm × 5.5 cm) containing 60 ml (syrup state) of cation-exchange SP-Sephadex (C-25). The unreacted complex anion, $[Co(NO_2)_2(acac)_2]^-$, was removed by washing with water. The adsorbed μ-gly binuclear complex was carefully eluted out with 2 M-$NaClO_4$. The unreacted complex cation ($[Co(gly)(NH_3)_5]^{2+}$ or $[Co(NH_3)_5(glyH)]^{3+}$) remained as a red band. The eluted solution was made 100 ml in volume with 2 M-$NaClO_4$ solution. The concentration of the binuclear complex was estimated by comparing the absorbance measured at 405 nm with that of the prepared complex. The absorbance at 405 nm of the unreacted gly complex, $[Co(gly)(NH_3)_5](ClO_4)_2$ or $[Co(NH_3)_5(glyH)](ClO_4)_3$, is negligible in comparison with that of the μ-gly binuclear complex (Fig. 5). Similar tests (at only 30 °C) were also performed for the L-ala, β-ala and γ-ambut complexes.

Tests of the di-μ-aminocarboxylato trinuclear complexes of gly, β-ala and γ-ambut at 30 °C were carried out in the same way as for the μ-gly binuclear complex except for the use of *trans*-$[Co\ en_2(aaH)_2]^{3+}$ (3.98×10^{-3} mol) and $[Co(NO_2)_2(acac)_2]^-$ (7.96×10^{-3} mol).

Measurements. The absorption spectra were measured in aqueous solutions with a Hitachi Model EDS-3T spectrophotometer. The infrared spectra were obtained with a JASCO IR-S infrared spectrophotometer. The PMR spectra were recorded on a JEOL Model MH-100 high-resolution spectrometer with DSS as an internal standard.

Results and Discussion

Formation of μ-Aminocarboxylato Complex. The % formation and pH value *versus* reaction time for the μ-gly binuclear complex at 20, 30, 40, and 50 °C are shown in Fig. 1. Formation of the μ-gly binuclear complex began instantly after mixing two aqueous solutions containing $[Co(gly)(NH_3)_5]^{2+}$ and $[Co(NO_2)_2(acac)_2]^-$, respectively. The maximum formation (*ca.* 72.5%) was observed after 2—3 hr at 30 °C. At higher temperatures (40 and 50 °C) the formation curve reached its maximum a few minutes after mixing and then began to decrease sharply. This indicates that rapid decomposition of the formed μ-gly binuclear complex occurs at higher temperatures. At lower temperature (20 °C) the formation curve indicated lower values than at 30 °C within 5 hr of reaction time, but higher values after 5 hr.

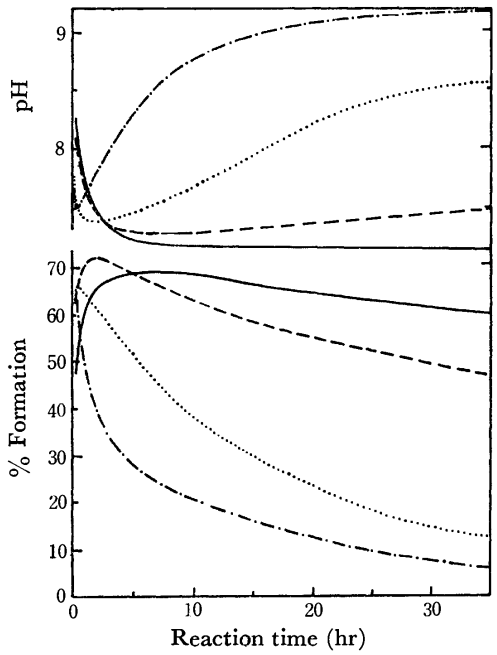

Fig. 1. % Formation and pH *vs.* reaction time for μ-gly binuclear complex at various temperatures, 20 °C (——), 30 °C (----), 40 °C (····), and 50 °C (-·-·-).

In order to coordinate the amino end of the pentaammine(O-glycine)cobalt(III) complex ion to another cobalt(III) ion, the amino end ($-NH_3^+$) should be deprotonated producing free amino group ($-NH_2$). It could be assumed that the pK value of the $[Co(NH_3)_5(glyH)]^{3+}$ is located at around 9. Formation tests and preparation of the μ-aminocarboxylato binuclear complexes were performed with use of pH-adjusted (*ca.* pH 9) solutions of the protonated complexes, $[Co(NH_3)_5(aaH)](ClO_4)_3$. A sharp decrease in the pH at the beginning of the reaction (Fig. 1) indicates the coordination of the amino group, and the increment

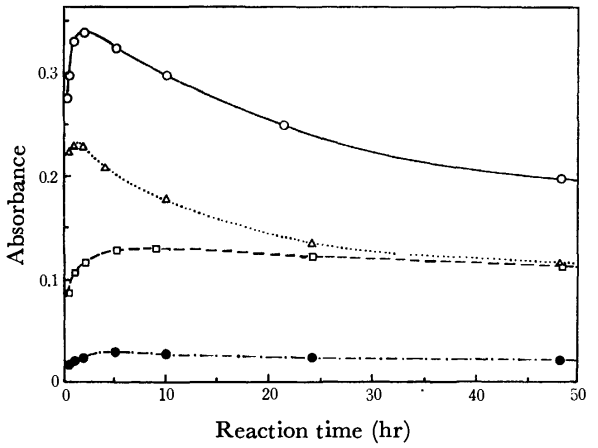

Fig. 2. The plots of absorbance *vs.* reaction time for binuclear complexes. μ-gly (—○—), μ-L-ala (··△··), μ-β-ala (--□--), and μ-γ-ambut (-·●·-).

of the pH with the progress of reaction at higher temperatures (40 and 50 °C) can be attributed to the detachment of the amino group or of ammonia molecule during the course of decomposition of the μ-gly binuclear complex.

The formation cruves of binuclear complexes are compared for gly, L-ala, β-ala, and γ-ambut (Fig. 2). The relative degree of formation is in the order

$$\text{gly} > \text{L-ala} > \beta\text{-ala} > \gamma\text{-ambut.}$$

Formation curves of the di-μ-aminocarboxylato trinuclear complexes for gly, β-ala and γ-ambut at 30 °C are compared in Fig. 3. The formation and decomposition of the μ-gly trinuclear complex proceeds rapidly as compared with those of β-ala and γ-ambut complexes. This phenomenon coincides with the case of the binuclear complexes. The maximum % formation which was estimated experimentally for the μ-gly trinuclear complex (*ca.* 24%) was considerably low as compared with that for μ-gly binuclear complex (72.5%).

The μ-aminocarboxylato binuclear and trinuclear complexes are relatively stable in aqueous solution in the pH region 3—8, but less stable for pH>9. Only one band appeared when these complexes were developed in a cation-exchange resin column, showing that they consist of one species each.

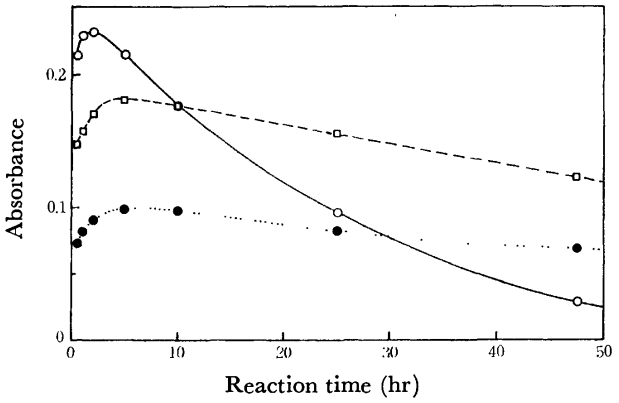

Fig. 3. The plots of absorbance *vs.* reaction time for trinuclear complexes. di-μ-gly (—○—), di-μ-β-ala (--□--), and di-μ-γ-ambut (··●··).

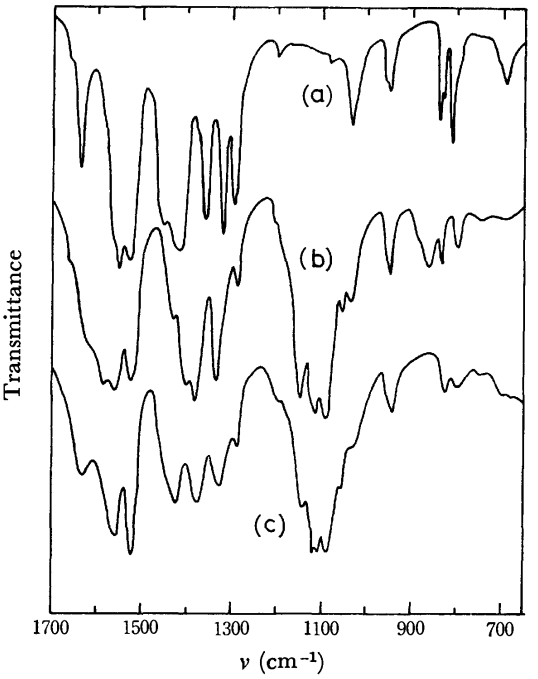

Fig. 4. Infrared spectra of (a) $Na[Co(NO_2)_2(acac)_2]$, (b) μ-gly binuclear, and (c) di-μ-gly trinuclear complexes.

In the preparation of binuclear complexes for L- and β-ala, and γ-ambut, in some cases complexes such as $[Co(NH_3)_5(aaH)][Co(NO_2)_2(acac)_2]_3$ were also separated. These complex-to-complex salts split into two bands brown and orange in color on the column, easily distinguishable from the μ-aa binuclear complexes.

Infrared Spectra. The infrared spectra of μ-gly binuclear and di-μ-gly trinuclear complexes are shown in Fig. 4 together with the spectrum of the starting acetylacetonato complex, $Na[Co(NO_2)_2(acac)_2]$.

These complexes show intense absorption bands in the 1520—1560 cm^{-1} region, which are assigned to the C=O and C=C stretching vibrations of the coordinated acetylacetonate.[18-20] The bands of 825 and 1325 cm^{-1} are assigned to the NO_2^- bending and asymmetric stretching modes,[19] respectively. The medium bands which appear near 1630 cm^{-1} are attributed to the coordinated carboxyl group. They are generally recognized in several aminocarboxylato cobalt(III) complexes. The present μ-aminocarboxylato complexes show intense bands characteristic of ClO_4^- in the 1060—1140 cm^{-1} region. This confirms that the complex ions are electro-positive.

Absorption Spectra. The absorption spectra of the μ-aminocarboxylato binuclear and trinuclear complexes show a similar behavior to that of the starting $Na[Co(NO_2)_2(acac)_2]$ complex (Fig. 5). The absorption spectra of acetylacetonato metal complexes in general have been studied.[18,20,21] Referring to these studies the band peaks observed at 515 and 535 nm for the bi- and tri-nuclear complexes, respectively, are attributed to the d—d transition ($^1A_{1g} \rightarrow {}^1T_{1g}$ in O_h per-

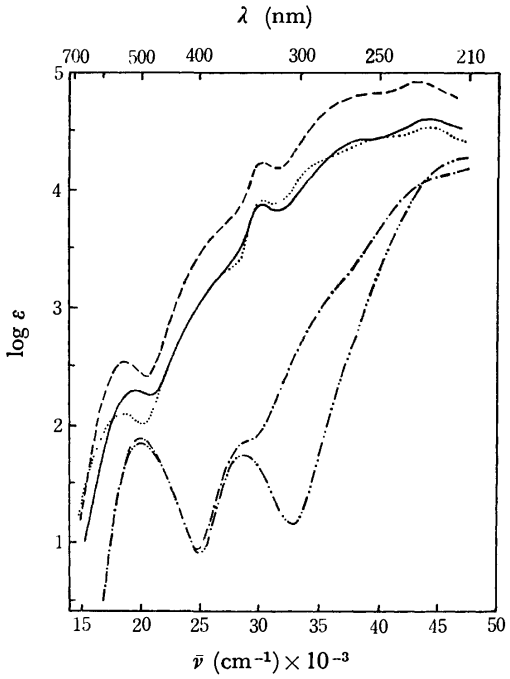

Fig. 5. Absorption spectra of μ-gly binuclear (——), di-μ-gly trinuclear (----), $[Co(NO_2)_2(acac)_2]^-$ (····), $[Co(gly)(NH_3)_5]^{2+}$ (-·-·-), and $[Co(NH_3)_5(glyH)]^{3+}$ (-··-) complex ions in aqueous solutions.

centage).[18] A metal-enolate charge transfer band ($d_\pi \rightarrow \pi^*$) appears in the 330—350 nm region. The broad and shoulder bands near 225 and 260 nm are attributed to the enolate $\pi \rightarrow \pi^*$ transitions. The absorption curves of the μ-gly binuclear and di-μ-gly trinuclear complexes coincided with the summation curves of $[Co(aaH)(NH_3)_5]^{3+}$ and $[Co(NO_2)(NH_3)(acac)_2]$[18] (1 : 1 mixture), and of *trans*-$[Co\ en_2(aaH)_2]^{3+}$ and $[Co(NO_2)(NH_3)(acac)_2]$ (1 : 2 mixture), respectively. These results support the view that the complexes obtained consist of the binuclear and trinuclear compositions. Proposed structures for these bi- and trinuclear complex ions are shown in Figs. 6 and 7.

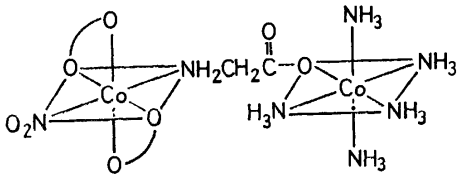

Fig. 6. The structure of μ-gly binuclear complex.

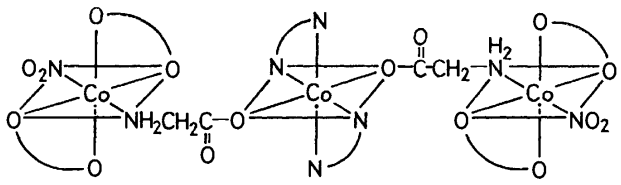

Fig. 7. The structure of di-μ-gly trinuclear complex.

Proton Magnetic Resonance Spectra. The PMR data of the μ-gly binuclear and trinuclear complexes are given in Table 1. These μ-gly complexes show a pair of singlet resonances in the 2.15—2.22 and 5.84—5.88 ppm regions corresponding to the methyl and methin protons, respectively, of acetylacetonato ligands. The singlet resonances suggest that four methyl groups and two methin groups in the μ-gly binuclear complex and eight methyl groups and four methin groups in the di-μ-gly trinuclear complex lie in the same chemical environment. Thus it is reasonable to conclude that the bi- and tri-nuclear complexes take the *trans* structure with respect to the NH_2 group of the μ-glycinato ligand and NO_2^- (Figs. 6 and 7). If these complexes take the *cis* structure, they would show a more complicated pattern of proton resonances.

Table 1. PMR[a] data of gly complexes

Complexes	Chemical shift (ppm)		
	CH_3(acac)	CH_2(gly)	CH(acac)
$Na[Co(NO_2)_2(acac)_2]$	2.14		5.67
$[Co(gly)(NH_3)_5](ClO_4)_2$		3.40	
$[Co(NH_3)_5(glyH)](ClO_4)_3$		3.79	
μ-Gly binuclear	2.15	3.03	5.88
Di-μ-gly trinuclear	2.22	2.85[b]	5.84

a) Internal standard is DSS in D_2O. b) Overlaps with CH_2 of ethylenediamine.

The center cobalt(III) of the di-μ-gly trinuclear complex is also expected to have the *trans* structure with respect to the carboxyl groups of the two μ-glycinato ligands from the appearance of a strong singlet resonance for methylene protons of ethylenediamine at 2.85 ppm.

Boucher and Bailar[18] reported the replacement of one NO_2^- ligand of $[Co(NO_2)_2(acac)_2]^-$ by several amine ligands, and suggested the *trans* structure of the starting dinitro complex and the product nitroamine complexes from the view point of *trans* effect of the NO_2^- ligand. In our case the replacement of one NO_2^- ligand in $[Co(NO_2)_2(acac)_2]^-$ by the amino end of $[Co(aa)(NH_3)_5]^{2+}$ also produces a complex having *trans* structure with respect to the NO_2^- and the amino end. In conclusion it is proposed that the present bi- and tri-nuclear complexes have structures such as shown in Figs. 6 and 7.

References

1) Part IV of this series: T. Yasui, J. Fujita, and Y. Shimura, This Bulletin, **42**, 2081 (1969).
2) J. Fujita, T. Yasui, and Y. Shimura, *ibid.*, **38**, 654 (1965).
3) T. Yasui, J. Hidaka, and Y. Shimura, *ibid.*, **39**, 2417 (1966).
4) C. J. Hawkins and P. J. Lawson, *Inorg. Chem.*, **9**, 6 (1970).
5) M. D. Alexander and D. H. Busch, *ibid.*, **5**, 1590 (1966).
6) Y. Fujii, This Bulletin, **45**, 3084 (1972).
7) G. G. Dellenbaugh and B. E. Douglas, *Inorg. Nucl. Chem. Lett.*, **9**, 1255 (1973).
8) Y. Shimura, This Bulletin, **31**, 173; 315 (1958).
9) a) C. T. Liu and B. E. Douglas, *Inorg. Chem.*, **3**, 1356 (1964); b) S. K. Hall and B. E. Douglas, *ibid.*, **8**, 372 (1969).
10) T. Yasui and B. E. Douglas, *ibid.*, **10**, 97 (1971).
11) N. Matsuoka, J. Hidaka, and Y. Shimura, This Bulletin, **40**, 1868 (1967); **45**, 2491 (1972), *Inorg. Chem.*, **9**, 719 (1970).
12) a) K. Nakai, S. Kanazawa, and M. Shibata, This

Bulletin, **45**, 3544 (1972); b) Y. Kojima and M. Shibata, *Inorg. Chem.*, **12**, 1009 (1973).
13) S. Yamada, J. Hidaka, and B. E. Douglas, *ibid.*, **10**, 2187 (1971).
14) I. Oonishi, M. Shibata, F. Marumo, and Y. Saito, *Acta Crystallogr. (B)* **29**, 2448 (1973).
15) S. Bagger, K. Gibson, and C. S. Sørensen, *Acta Chem. Scand.*, **26**, 2503 (1972).
16) G. Pellizer, G. R. Tauszik, and G. Costa, *J. Chem. Soc. Dalton*, **1973**, 317.
17) A. Rosenheim and A. Garfunkel, *Ber.*, **44**, 1865 (1911).
18) L. J. Boucher and J. C. Bailar, Jr., *J. Inorg. Nucl. Chem.*, **27**, 1093 (1965).
19) K. Nakamoto, "Infrared Spectra of Inorganic and Coordination Compounds," 2nd ed., Wiley-Interscience, New York, 1970.
20) D. W. Barnum, *J. Inorg. Nucl. Chem.*, **21**, 221 (1961); *ibid.*, **22**, 183 (1961).
21) I. Hanazaki, F. Hanazaki, and S. Nagakura, *J. Chem. Phys.*, **50**, 276 (1969).

Synthesis of Chelating Agents. XI. Synthesis and Chelating Behavior of Diaxial *trans*-Decahydronaphthylene-*trans*-2,3-dinitrilotetraacetic Acid*

Tairoku YANO, Hiroshi KOBAYASHI, and Keihei UENO

Department of Organic Synthesis, Faculty of Engineering, Kyushu University, Hakozaki, Higashi-ku, Fukuoka 812

(Received May 14, 1974)

Diaxial *trans*-decahydronaphthylene-*trans*-2,3-dinitrilotetraacetic acid (D[A.A]TA) was synthesized by carboxymethylation of diaxial *trans*-decalin-*trans*-2,3-diamine. The acid dissociation constants as well as chelate stability constants for alkaline earth metal ions were determined by potentiometric titration. The probable structure and chelating behavior of D[A.A]TA in aqueous solutions were discussed in reference to some related complexane ligands.

With hoping to elucidate steric effect on chelate formation with complexane-type ligands, we have synthesized several 1,2-dinitrilotetraacetic acids and precursory diamines of specific configurations.

In continuation of the previous works,[1] this paper deals with synthesis and chelating behaviors of diaxial *trans*-decahydronaphthylene-*trans*-2,3-dinitrilotetraacetic acid (D[A.A]TA), which was derived from diaxial *trans*-decalin-*trans*-2,3-diamine.[2] Two six-membered rings in *trans*-decalin framework are well known to be incapable of inversion from one chair form to another on account of the rigid structure at the ring junctions.

Consequently, two nitrilodiacetic acid substituents in D[A.A]TA are in an antiperiplanar conformation, both pointing along the axial direction, providing configurations in respect to the amino groups are retained intact through the derivation and the cyclohexane ring under consideration takes a chair form.

Although this work had started with an aim of verifying the above anticipation, the presented results indicated that such a conformation was unlikely, in conclusion.

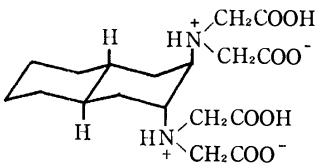

Structure 1

Experimental

Infrared and NMR spectra were measured on a JASCO DS-403G and Varian A-60 instruments, respectively, the latter with an internal reference of TMS or proton in heavy water, which was set at 5.0 ppm downfield from TMS.

Synthesis of Ligand. Diaxial trans-*Decahydronaphthylene*-trans-*2,3-dinitrilotetraacetic Acid* (D[A.A]TA, structure 1). The tetraacetic acid was synthesized by the alkaline condensation of bromoacetic acid with diaxial *trans*-decalin-*trans*-2,3-diamine (D[A.A]). Conditions of typical run was as follows.

A solution of 0.5 g (2.1 mmol) of D[A.A]·2HCl in 20 ml of water was placed in a 100 ml reaction vessel. The solution was made neutral to phenolphthalein with 5 M aqueous sodium hydroxide. Into this solution, a solution of 2 g (14.4 mmol) of bromoacetic acid in 10 ml of water, which had been neutralized in advance with sodium hydroxide solution below 10 °C, was added under stirring and the temperature of the solution was raised to 80 °C. The pH of the reaction mixture was maintained in the range of 9—10 (red to phenolphthalein) with an occasional addition of 5 M aqueous sodium hydroxide. After adding 12.5 mmol of sodium hydroxide, the resulting solution was acidified with conc. hydrochloric acid and was evaporated under reduced pressure. The residue was dissolved in water, followed by adjusting pH of the aqueous solution to 1.8 and stored in a refrigerator for a week to complete the precipitation of free D[A.A]TA. The crude product was then collected by filtration and recrystallized from water. Yield: 420 mg (51%). It decomposed at 186—188 °C. NMR (in D_2O): δ; 1—2.4 ppm (broad band with an appreciable quartet, 14H), 4.13, 3.86, 3.79, and 3.52 (double doublets, $J_{AB}=16.2$ Hz, 8H, two protons were concealed behind the double doublets). IR: ν_{COOH} 1753 cm^{-1}. Found: C, 51.99; H, 7.15; N, 6.59%. Calcd for $C_{18}H_{28}N_2O_8\cdot H_2O$: C, 51.68; H, 7.18; N, 6.70%.

1,3-Bis(cyanomethyl)-trans-*cisoid*-trans-*perhydronaphtho[2,3-d]imidazole.* To a cold solution of diequatorial *trans*-decalin-*trans*-2,3-diamine dihydrochloride (0.12 g, 0.5 mmol) in 0.4 M hydrochloric acid (3 ml), an aqueous 36% formaldehyde (0.16 g, 2 mmol) and sodium cyanide (98 mg, 2 mmol) was successively added and a resulting mixture was kept in a pressure bottle. The mixture was allowed to stand for 3 hr at room temperature with occasional shaking. The precipitate obtained was recrystallized from ethanol. IR: ν_{CN} 2240 cm^{-1}. Mp: 131—132 °C. Yield: 76 mg (59%). NMR (in $CDCl_3$): δ; 0.9—2 ppm (14H), 2.2—2.6 (2H), 3.62 (4H), 3.83 (2H). MS: *m/e***, 258 (M^+), 257 (M^+-1), 231 (M^+-27), 218 (M^+-40). Found: C, 69.91; H, 8.58; N, 21.54%. Calcd for $C_{15}H_{22}N_4$: C, 69.73; H, 8.58; N, 21.84%.

Diaxial trans-*decahydronaphthylene*-trans-*2,3-dinitrilotetraacetonitrile* was synthesized in a similar manner to that described above, except the reaction temperature being 40 °C. IR: ν_{CN} 2235 cm^{-1}. Mp: 167—171 °C. Yield: 49 mg (30%). NMR (in $CDCl_3$): δ; 0.8—1.9 ppm (14H), 2.8—3.1 (2H), 3.77 (8H). MS: *m/e***, 324 (M^+), 286 (M^+-38), 284 (M^+-40), 257 (M^+-67). Found: C, 66.23; H, 7.54; N, 25.34%. Calcd for $C_{18}H_{24}N_6$: C, 66.67; H, 7.41; N, 25.93%.

Determination of Chelate Stability Constants. The details of an apparatus were described previously.[1] A pH measurement was carried out at 25.0 °C in an aqueous solution of ionic

* Contribution No. 335 from the Department of Organic Synthesis, Kyushu University.

** Measured with a JEOL JMS-01SG by courtesy of Prof. Kawasaki and Miss Kawamura in Faculty of Pharmacy, Kyushu University, to whom the authors are grateful.

strength of 0.10 with potassium nitrate. Calibration of a pH-meter was also described previously.[1] Determination of a chelate stability constant with an alkaline earth metal ion involves direct pH titrations of 100 ml of a ligand solution in which concentration of the ligand was 1×10^{-3} M and a metal ion was present in 1: 1 and 10: 1 mole ratios of a metal nitrate to a ligand.

Calculation of Equilibrium Constants. Acid Dissociation Constants. The titration curve of D[A.A]TA is shown in Fig. 1. The definition of equilibrium constants discussed in this paper, are listed in Table 1. It can be seen from Fig. 1 that the acid dissociations of first two steps, third step and fourth step are clearly separated from each other. Therefore, the acid dissociation constants of the free ligand were calculated by the standard procedure.[3]

Table 1. Definition of equilibrium constants

1) Acid dissociation constnts of D[A.A] TA
$K_1=[H_3A^{1-}][H^+]/[H_4A]$
$K_2=[H_2A^{2-}][H^+]/[H_3A^{1-}]$
$K_3=[HA^{3-}][H^+]/[H_2A^{2-}]$
$K_4=[A^{4-}][H^+]/[HA^{3-}]$
2) Composite acid dissociation constants[4]
$K_3'=[H^+]([HA^{3-}]+[MHA^{1-}])/[H_2A^{2-}]$
$K_4'=[H^+]([A^{4-}]+[MA^{2-}]+[M_2A])/([HA^{3-}]+[MHA^{1-}])$
3) Chelate stability constants of D[A.A]TA
$K_{MHA}=[MHA^-]/[M^{2+}][HA^{3-}]$
$K_{MA}=[MA^{2-}]/[M^{2+}][A^{4-}]$
$K^H_{MHA}=[H^+][MA^{2-}]/[MHA^{1-}]$
$K_{M_2A}=[M_2A]/[M^{2+}][MA^{2-}]$

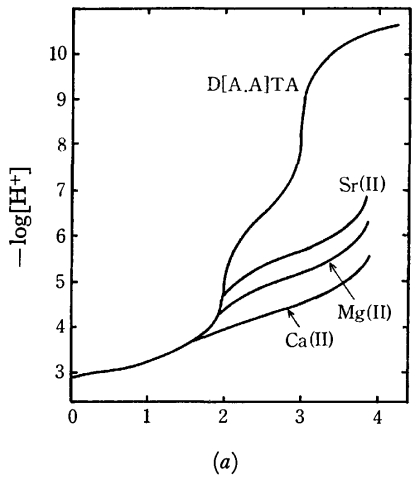

(*a*)

Fig. 1. Potentiometric titration curves of alkaline earth metal-chelates at 25.0 °C in 0.10 M KNO_3 with molar ratio of metal ion to ligand; 1: 1. Concentration of D[A.A]TA: 1×10^{-3} M.

Chelate Stability Constants. As the two nitrilodiacetic acid groups of the ligand are situated on the opposite sides of the rigid cyclohexane ring, the ligand may form MA type as well as M_2A type chelates. Accordingly, the chelate stability constants for alkaline earth metal ions were calculated by the Schwarzenbach's procedure,[4] assuming the formation of MA, MHA and M_2A type chelates. The procedure of calculation was a standard one, using the composite acid dissociation constants K_3' and K_4' on the titration data of 10: 1 solution.

Computations were carried out by use of a FACOM 230-60 of the Computor Center in Kyushu University.

Results and Discussion

Synthesis. D[A.A]TA was obtained by carboxymethylation of diaxial *trans*-decalin-*trans*-2,3-diamine. Although no direct evidence was provided, it is reasonable on the basis of the employed reaction conditions that configurations in respect to the substituents are regarded to be retained intact.

Cyanomethylation and carboxymethylation were also applied to 2,3-*cis*- and diequatorial 2,3-*trans*-diamine derivatives of *trans*-decalin under various conditions. Both isomeric diamines afforded no definite product except an imidazolidine derivative by cyanomethylation of the diequatorial *trans*-diamine. It is likely that, upon the cyanomethylation of the 1,2-diamino groups in the close vicinity to each other such as the above diamines, an imidazolidine ring closure proceeds prior to the fourth cyanomethylation reaction, giving no tetracyanomethyl derivative.[5,6]

The fact that the expected tetracyanomethyl- and tetracarboxymethyl derivatives were afforded only from the diaxial 2,3-*trans*-diamine in which two amino groups were separated apart from each other, is regarded as an indication of little steric interaction between the two amino groups on the reaction processes, as well as another support for the configuration of D[A.A]TA.

Table 2. Acid dissociation constants and ΔpK (2−1) and ΔpK (4−3) values of D[A.A]TA and related compounds

Compound	pK_1	pK_2	pK_3	pK_4	ΔpK (2−1)	ΔpK (4−3)	Favorable configuration of two NDA groups
D[A.A]TA	2.26	3.04	6.47	10.61	0.78	4.14	skew
t-THDTA[5]	1.9	3.54	5.99	10.30	1.64	4.31	skew
t-1,2-CYDTA[7]	2.40	3.55	6.14	11.70	1.15	5.56	skew
t-1,2-CPDTA[8]	2.41	2.92	7.42	10.31	0.51	2.89	*trans*
EDTA[9]	1.99	2.67	6.16	10.23	0.68	4.07	*trans*
1,3-CYDTA[10]	1.77	2.57	8.55	10.91	0.80	2.36	—
1,4-CYDTA[10]	2.07	2.52	9.04	10.86	0.45	1.82	—

t-THDTA: 1,2,3,4-Tetrahydronaphthylene-*trans*-2,3-dinitrilotetraacetic acid. CYDA: Cyclohexylenedinitrilotetraacetic acid. *t*-1,2-CPDTA: *trans*-1,2-Cyclopentylenedinitrilotetraacetic acid.

Acid Dissociation. Table 2 summarizes the acid dissociation constants of D[A.A]TA, along with those of some related complexane ligands. In the deprotonation process of a tetrabasic complexane, the first two steps and the last two correspond to the dissociation of carboxylic protons and ammonium protons, respectively.

In respect to the magnitude of difference between the pK-values of the first two, ΔpK(2−1), and that between the last two, ΔpK(4−3), the tetrabasic complexanes can be classified into two groups. As discussed previously,[2] a complexane ligand, in which two nitrilodiacetic acid (NDA) groups are far remote from each other, gives a relatively smaller ΔpK values, in comparison with those with two NDA groups in

close proximity to each other. And as far as concerned with acid dissociation process, D[A.A]TA behaves in a quite similar manner to those of the latter group.

If the above presumption is true regarding the spatial relationship between the two NDA groups in this compound, a cyclohexane ring bearing the substituents must take a skew-boat form, in which the vicinal NDA groups can be in a synclinal conformation.

TABLE 3. CHELATE STABILITY CONSTANTS OF D[A.A]TA AND RELATED COMPLEXANES 25.0 °C, μ=0.10 (KNO_3)

Compound	log K_{MA}		
	Mg(II)	Ca(II)	Sr(II)
D[A.A]TA	10.36	11.54	9.34
t-THDTA[5]	10.28	11.63	9.56
t-1,2-CYDTA[11]	10.3	12.2	9.97
t-1,2-CPDTA[8]	9.05	11.08	9.45
EDTA[12]	8.69	10.70	8.63
1,3-CYDTA[10]	4.64	4.77	—
1,4-CYDTA[10]	4.30	4.19	—
N-Me-IDA[13]	3.44	3.75	2.85

N-Me-IDA: *N*-Methyliminodiacetic acid

Chelate Stability. Stability constants of the alkaline earth metal chelates of D[A.A]TA are listed in Table 3 along with those of some related complexane-type ligands. The value of log K_{M_2A} of D[A.A]TA, being negative, indicated that this ligand formed predominantly a 1:1 chelate with alkaline earth metal ions. The values of K_{MA} also agreed well with those obtained by the Bjerrum's method, where the formation of an M_2A type chelate was neglected.

Tetrabasic complexanes in Table 3 may be classified in respect to the capability of two NDA groups coordinating to a same metal ion. Those with NDA groups which are spatially separated apart from each other, show much lower chelate stabilities than those with the ligand substituents in the vicinity to each other. Each NDA group in the former class, at the extremity, would coordinate independently to a separate metal ion. The log K_{MA} value of such a tetrabasic complexane could be estimated to fall in the range of 3—4, if a statistical correction of 0.3 was applied to those of *N*-methyliminodiacetic acid.

As one can seen in Table 3, D[A.A]TA belongs to the class of the high chelate stability, the value being comparable to that of *t*-1,2-CYDTA, in which two NDA groups are in a synclinal form. Combined with the value of K_{M_2A} of D[A.A]TA, these results provide strong evidences for the conclusion that six donor atom on the D[A.A]TA are in a conformation favorable for coordinating simultaneously to a single metal ion. A molecular model study indicates that D[A.A]TA can work as a hexadentate ligand only in the case where the dihedral angle between the two NDA groups falls in the *syn*-region, and that, in turn, the cyclohexane ring bearing the NDA groups must be in a skew-boat

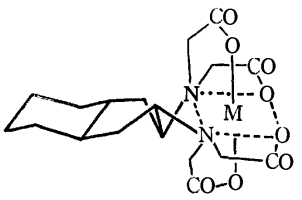

Structure 2

form, as shown in structure 2.

The enthalpy difference between the chair and skew-boat form in *trans*-decalin is calculated to be 5.5 kcal/mol.[14] The steric instability of the skew-boat form in D[A.A]TA, however, can be compensated enough by the relatively large free energy gain with the formation of coordination bonds.

One might notice that *t*-1,2-CPDTA behaves in similar manner to 1,3- and 1,4-CYDTA rather than to *t*-1,2-CYDTA upon a reaction with proton, while in the reverse manner with divalent metal ions. This would be most probable on account of sizes of cations. When *t*-1,2-CPDTA takes a half-chair form, two NDA groups are in synclinal conformation, possibly coordinating to a metal ion which has much larger radius than proton.

The authors are grateful to the Ministry of Education, Japanese Government, for financial support to this work.

References

1) Part X: T. Yano, H. Kobayashi, and K. Ueno, This Bulletin, in press.
2) T. Yano, H. Kobayashi, and K. Ueno, *ibid.*, **46**, 985 (1973).
3) G. Schwarzenbach, A. Willi, and R. O. Bach, *Helv. Chim. Acta*, **30**, 1303 (1947).
4) G. Schwarzenbach and H. Ackermann, *ibid.*, **31**, 1029 (1948).
5) T. Yano, H. Kobayashi, and K. Ueno, This Bulletin, **43**, 3167 (1970).
6) T. Yano, H. Kobayashi, and K. Ueno, *ibid.*, **45**, 1249 (1972).
7) T. Moeller and T. M. Hseu, *J. Inorg. Nucl. Chem.*, **23**, 1635 (1962).
8) H. Kroll and M. Gordon, *Ann. N. Y. Acad. Sci.*, **88**, 341 (1960).
9) G. Schwarzenbach and G. Anderegg, *Helv. Chim. Acta*, **40**, 1773 (1957).
10) G. Schwarzenbach and G. Anderegg, *ibid.*, **32**, 1682 (1949).
11) D. L. Wright, J. H. Holloway, and C. N. Reilley, *Anal. Chem.*, **37**, 884 (1965).
12) G. Schwarzenbach, G. Gat, and G. Anderegg, *Helv. Chim. Acta*, **37**, 937 (1954).
13) G. Schwarzenbach, G. Anderegg, W. Schneider, and M. Sen, *ibid.*, **38**, 1147 (1955).
14) W. S. Johnson, V. J. Bauer, J. L. Margrave, M. A. Frisch, L. H. Dreger, and W. N. Hubard, *J. Amer. Chem. Soc.*, **83**, 606 (1961).

Kinetics of Ligand Isotopic Exchange of Tris(acetylacetonato)gallium(III) and Related β-Diketonato Complexes in Tetrahydrofuran

Chinmoy CHATTERJEE,* Kazuyo MATSUZAWA, Hiroaki KIDO, and Kazuo SAITO**

Department, of Chemistry, Faculty of Science, Tohoku University, Aoba, Aramaki, Sendai 980

(Received July 29, 1974)

The rate of isotopic exchange of tris(acetylacetonato)gallium(III)[Ga(acac)$_3$] and acetylacetone-^{14}C(Hacac) in tetrahydrofuran (THF) is expressed by the formula $R=[\text{complex}](k_1+k_2[H_2O]+k_3[\text{Hacac}])$ and the k_1, k_2, and k_3 are $\leq 2\times10^{-6}$ s^{-1}, 0.31×10^{-3} M^{-1} s^{-1} and 0.71×10^{-4} M^{-1} s^{-1}, at 0 °C, respectively. The activation enthalpies and entropies are 18 ± 2 and 19 ± 2 kcal·mol^{-1}, and -13 ± 6 and -20 ± 6 cal·K^{-1} mol^{-1}, for k_2 and k_3, respectively. Trichloroacetic acid gives acid catalysis. A dissociative mechanism through an intermediate containing a unidentate ligand is suggested. The isotopic exchange rate decreases in the sequence In>Ga>Al for a given β-diketonato complex, and with increase in pK_a of the β-diketone for given central metal ions.

Little information is available concerning the kinetics and mechanism of complex formation reactions of gallium(III) ions. Eigen gave the half-life of coordinated water molecules in gallium(III) perchlorate in water to be of the order of 10^{-3} s.[1] Fiat and Connick, and Movius and Matwiyoff studied the exchange of solvent molecules coordinated to Ga(III) in water[2] and dimethylformamide,[3] respectively, and compared the activation parameters with those for aluminium(III). On the basis of small ΔH^* and big minus ΔS^* values, they suggested an S_N2 mechanism for the gallium(III) ions.

We found that the ligand isotopic exchange of tris-type complexes of octahedral aluminium(III) with acetylacetone[4] and dibenzoylmethane[5] in various organic solvents is much slower than that of coordinated solvent molecules in $[Al(H_2O)_6]^{3+}$ in water,[1,2,6] and discussed the mechanism. We have now examined the rate of isotopic exchange of some β-diketonato complexes of aluminium(III), gallium(III), and indium(III), and found that the rate of exchange of tris(acetylacetonato)-gallium [Ga(acac)$_3$] with acetylacetone-^{14}C(Hacac) is measurable in some organic solvents including tetrahydrofuran (THF). Detailed kinetic studies are given and the results compared with those of related complexes.

Experimental

Materials. *The Labelled Ligands*: Acetylacetone-^{14}C (Hacac) was prepared similarly to the method given in Ref. 4, and the specific activity was adjusted to *ca.* 0.02 μCi per mg, the water content being *ca.* 10^{-1} M. Dibenzoylmethane-^{14}C (Hdbm) was synthesized from acetic acid (12 g, 0.2 mol) containing 1 mCi ^{14}C *via* acetophenone by the usual method. On recrystallization from ethanol for three times, the yield was 29% on the basis of acetic acid, the specific activity being *ca.* 0.03 μCi per mg. Benzoylacetone-^{14}C (Hbzac) was similarly prepared by use of ethylacetate in place of ethyl benzoate. The yield was 34%, the specific activity being 0.01 μCi per mg.

The Complexes. Tris(acetylacetonato)gallium(III)was synthesized by a similar method to Moeller and Gulyas's[7] by use of ethanol and gallium(III) chloride in place of dioxane and gallium(III) sulfate respectively. The yield was *ca.* 73%. The product was sublimed at 1 mmHg at 180 to 185 °C to give colorless crystals with mp 190 to 192 °C. Tris-(benzoylacetonato)gallium(III) was prepared from gallium-(III) chloride solution (0.003 mol in 3 ml of water) by adding Hbzac (0.013 mol) in ethanol (30 ml) and adjusting the pH with sodium acetate (1.2 g in 3 ml of water). The product was recrystallized from a mixture of THF and petroleum ether containing Hbzac, and washed with diethylether. The yield was *ca.* 90%. This is a mixture of *mer* and *fac* isomer, but was used without separation for the isotopic exchange studies.

Tris(1-oxo-1,3-diphenyl-2-prope-3-olato)gallium(III) [Ga-(dbm)$_3$] was synthesized from gallium(III) chloride solution (0.002 mol in 2 ml of water) by treating with Hdbm (0.0089 mol in 90 ml ethanol) and sodium acetate solution (0.8 g in 3 ml of water). The crude product was dissolved in THF (11 ml) containing a small amount of Hdbm, filtered and treated with petroleum ether to give colorless crystals, which were washed with chilled diethylether and dried *in vacuo*. mp 284.5~286.5 °C (literature value 284 °C; prepared in dioxane by use of metallic sodium in place of sodium acetate).[8] The yield was *ca.* 80%.

Tris(benzoylacetonato)aluminium(III) [Al(bzac)$_3$] was similarly prepared according to Baly and Desch's method[6] the yield being *ca.* 93%. Bis(1-oxo-1,3-diphenyl-2-prope-3-olato) beryllium [Be(dbm)$_2$] was prepared similarly to [Ga(dbm)$_3$] in aqueous ethanol, and crystallized from THF by adding petroleum ether. The yield was 39%. The corresponding indium (III) complexes were also synthesized similarly to those of the aluminium(III) complexes.[9] They are sensitive towards atomospheric moisture and the organic solvents should be carefully dehydrated.

Trichloroacetic acid, THF, and the reagents for scintillation spectrometry were purified as in the literature.[4]

Kinetic Runs. The essential scheme of the experimental procedure is the same as that in Ref. 4. The gallium(III) complexes are, however, more soluble in various organic solvents, and the rate is much larger than that of the aluminium(III) complexes. Hence the procedure was slightly modified as follows. The complex (0.05 to 0.2 M) and the labelled ligand solution in THF (0.05 to 0.2 M) were kept in a thermostat, mixed swiftly and dispensed into five small glass-stoppered tubes, so that each tube contains *ca.* 2 ml of the reaction mixture. They were kept in the thermostat and taken out one by one at appropriate time intervals. The content was added into chilled petroleum ether (−20 °C) to arrest the exchange reaction. Crystalline complexes precipitated immediately or after certain lapse of time, which were filtered off or decanted, washed with cold diethyl or

* On leave from Indian Association for the Cultivation of Science, Calcutta, India.

** Correspondences should be addressed.

petroleum ether and dried at 60 °C for 2 hr. A weighed amount of the complex (3 to 7 mg) was dissolved in anisole (15 ml) containing 0.4% *p*-terphenyl and 0.01% POPOP [*p*-di(5-phenyl-2-oxazolyl)-benzene] and submitted to scintillation counting.

Measurements. The counting rate was recorded with the automatic counter Unilux IIA from Nuclear Chicago. The absorption spectra were recorded with a Hitachi 124 spectrometer. Water content was measured by Karl-Fischer titration.

Results and Discussion

The absorption spectra of the reaction mixtures remained unchanged throughout the kinetic runs for all the systems, and the recovered complexes were pure. McKay plots gave always linear plots. Hence no other reaction than the isotopic exchange took place under the given experimental conditions.

The rate of exchange, R is expressed by Eq. (1)

$$R = -2.3[3ab/(3a+b)][\log(1-F)]/t \quad (1)$$

where a, b, t, and F stand for the concentrations of the complex and of the free ligand, the lapse of time and the fraction of reaction, respectively.

TABLE 1. INFLUENCE OF THE CONCENTRATION OF COMPLEX AND OF TRICHLOROACETIC ACID ON THE EXCHANGE RATE

[complex]/M	[acid]/M	$[H_2O]$/M	R/M·s	k_0/s^{-1}
0.050	0	0.036	1.1×10^{-6}	2.2×10^{-5}
0.10	0	0.036	2.2×10^{-6}	2.2×10^{-5}
0.13	0	0.036	2.9×10^{-6}	2.2×10^{-5}
0.070	0	0.025		1.4×10^{-5}
0.070	0.0029	0.025		2.2×10^{-5}
0.070	0.0053	0.025		3.0×10^{-5}
0.070	0.0074	0.025		3.6×10^{-5}

at 0 °C; [Hacac]=0.070 M

Tris(acetylacetonato)gallium(III). Kinetic Formula: The R values are proportional to the initial concentration of the complex as shown in Table 1. The variation of k_0 with water concentration under otherwise identical conditions is shown in Fig. 1, indicating the operation of two concurrent paths given in Eq. (2)

$$R = k_0 a = a(k_1 + k_2[H_2O]) \quad (2)$$

Arrhenius plots of k_1 and k_2 at 0, 10, and 20 °C gave almost parallel lines and the ΔH^* are 19±2 and 18±2 kcal/mol, respectively. The dependence of k_0 upon the concentration of free ligand in the presence of differing amounts of water is illustrated in Fig. 2. The gradient indicates the ligand-catalysed rate constants, which are not affected by the water concentration. These results infer the presence of three independent paths as shown in Eq. (3)

$$R = a(k_1 + k_2[H_2O] + k_3 b) \quad (3)$$

The rate constants obtained from the diagrams, and the activation parameters are listed in Table 2. Because of experimental difficulty the error for k's are *ca.* ±10%. Since the contribution of k_1 term is very small, the activation parameters for k_i can be reckoned as those for the k_3 path.

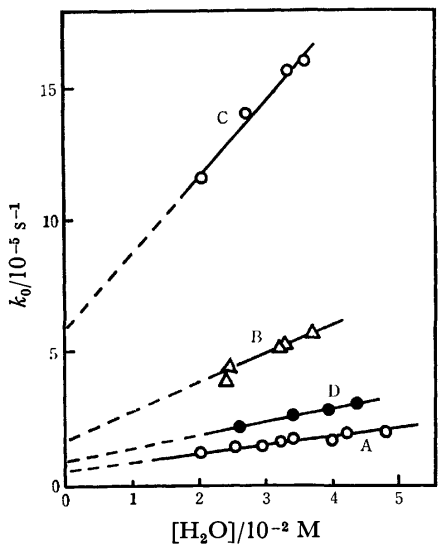

Fig. 1. Relationship between k_0 and water concentration.
A, 0 °C; B, 10 °C; C, 20 °C; D, 0 °C, [trichloroacetic acid]=0.0029 M; [Hacac]=0.070 M (for all).

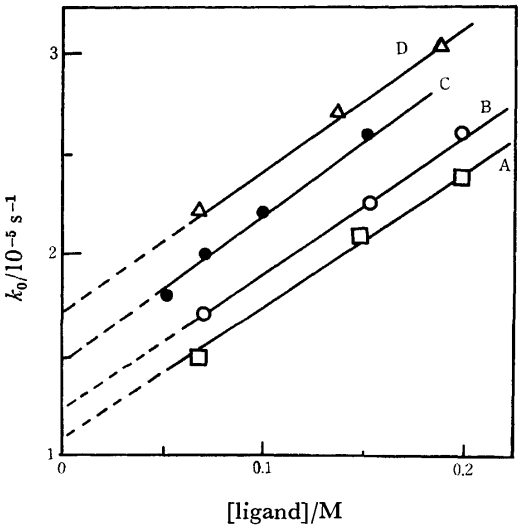

Fig. 2. Influence of ligand concentration upon k_0 in the presence of varying amounts of water for [Ga(acac)$_3$]. 0 °C; $[H_2O]$=A, 0.029, B, 0.036, C, 0.043, and D, 0.050 M.

Trichloroacetic acid catalyses the exchange reaction as shown in Table 1. The extent depends on the water concentration as seen in Fig. 1, and the overall rate in the presence of this acid is given by Eq. (4). Weaker

TABLE 2. KINETIC DATA AND ACTIVATION PARAMETERS FOR THE ISOTOPIC EXCHANGE BETWEEN [Ga(acac)$_3$] AND Hacac-^{14}C IN THF

Temp/°C	k_1 / 10^{-6} s^{-1}	k_2 / 10^{-3} M^{-1} s^{-1}	k_3 / 10^{-4} M^{-1} s^{-1}
0	≤2	0.31	0.71
10	≤4	1.1	2.2
20	≤6	2.8	8.3
ΔH^*/kcal·mol^{-1}		18±2	19±2
ΔS^*/cal·K^{-1}mol^{-1}		−13±6	−20±6

Table 3. Comparison of the kinetic data between [Al(acac)$_3$] and [Ga(acac)$_3$] in THF at 25 °C

	Al(III)	Ga(III)[b]
$k_1/M^{-1}s^{-1}$[a]	8.3×10^{-8}	$\leq4\times10^{-6}$
$k_2/M^{-1}s^{-1}$	3.3×10^{-4}	4.2×10^{-3}
$k_3/M^{-1}s^{-1}$	0	1.1×10^{-3}
$k_1'/M^{-1}s^{-1}$	1.6×10^{-4}	(1.5×10^{-3})[c]
$k_2'/M^{-2}s^{-1}$	2.0×10^{-2}	(4.1×10^{-2})[c]
$\Delta H^{\neq}$/kcal·mol^{-1} for k_1	21	—
$\Delta H^{\neq}$/kcal·mol^{-1} for k_2	21	18
$\Delta H^{\neq}$/kcal·mol^{-1} for k_3	—	19
$\Delta S^{\neq}$/cal·mol^{-1}K^{-1} for k_2	−7.8	−13

a) observed k_1 devided by 12, molar concentration of solvent THF. b) k's converted into the values with the aid of the activation enthalpies. c) at 0 °C.

organic acids failed to give such an acid catalysis.

$$R = a\{k_1'[\text{acid}] + [H_2O](k_2 + k_2'[\text{acid}]) + k_3 b\} \quad (4)$$

The k_1' and k_2' are given in Table 3.

Exchange Mechanism for [Ga(acac)$_3$]: The gallium(III) complex gives much faster isotopic exchange than the aluminium(III) does. The kinetic formulae (3) and (4) are similar to those of the corresponding aluminium(III) complex.[4] We discussed that [Al(acac)$_3$] was in a rapid equilibrium with an intermediate which had one of the ligands as unidentate, and the break of the remaining bond should be the rate-determining step, on the basis of the similarity of $\Delta H^{\neq}$ values for the kinetic terms. Water and acid protons were reckoned to occupy the vacant coordination site and the free end of the unidentate ligand, respectively, and to retard the recombination of the unidentate ligand. Such occupations were considered to affect the $\Delta H^{\neq}$ values little.

The fact that k_2 and k_3 paths for the gallium(III) complex have almost equal activation enthalpies suggests that both paths would have a common rate-determining step. If water and Hacac gave nucleophilic attack towards [Ga(acac)$_3$] itself in the rate-determining step, the $\Delta H^{\neq}$ values should differ significantly, because they must have different affinities towards the substrate. We consider that the common rate-determining step would be the break of the second Ga–O bond of the unidentate ligand as shown in Fig. 3. Both water and Hacac molecule occupy the vacant coordination site of the intermediate to retard the recombination and to facilitate the break of the Ga–O bond of the unidentate ligand to some extent.

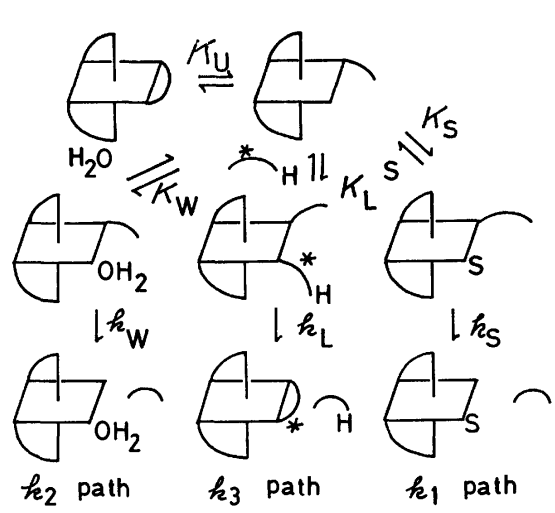

Fig. 3. Plausible reaction mechanism for the isotopic exchange between [Ga(acac)$_3$] and Hacac-^{14}C in THF. S, solvent molecule.

Pinnavaia *et al.* studied site exchange of the mixed ligand complex [Ga(acac)$_2$(dbm)] in benzene by PMR spectroscopy and obtained first-order rate constant 8.8×10^{-2} s^{-1} at 25 °C, the Arrhenius activation enthalpy and $\Delta S^{\neq}$ being 20.6±2.7 kcal/mol and 3.5±8.0 e.u., respectively.[10] They considered that a five-coordinated intermediate mechanism[11] would operate in the site exchange. This result supports our consideration that the nucleophilic interaction of the free ligand operates not on the complex itself but on the intermediate with one unidentate ligand.

When the rate and the equilibrium constants are defined as shown in Fig. 3, the k_1, k_2, and k_3 are written as follows:

$$k_1 = k_s K_s K_u \quad k_2 = k_w K_w K_u \quad k_3 = k_L K_L K_u \quad (5)$$
$$[K_u(K_s + K_w[H_2O] + K_L[L]) \ll 1]$$

The acid-catalyzed term would be interpreted similarly as for [Al(acac)$_3$], k_1' and k_2' terms being related to different proton carriers. The basicity of the unidentate ligand must be small and only a strong acid like trichloroacetic can give acid catalysis.

Comparison with the Mechanism for [Al(acac)$_3$]: There are two differences between the kinetic formulae for [Ga(acac)$_3$] and [Al(acac)$_3$]. The latter has a significant contribution of the k_1 path in THF, whilst the former not. The other difference is the participation of free Hacac in the rate-determining step for [Ga(acac)$_3$]. In the absence of water, (although experimentally impracticable) [Ga(acac)$_3$] and [Al(acac)$_3$] would undergo isotopic exchange *via* the ligand (k_3) and the solvent assisted path (k_1), respectively.

Tervalent gallium has a larger octahedral ionic radius (0.62 Å), than tervalent aluminium (0.51 Å), and the approach of free Hacac to the vacant cooridnation site would be easier to result in larger K_L, and hence larger k_3. Fiat and Connick[2] compared the activation parameters for the water exchange of gallium(III) and aluminium(III) perchlorate solution and suggested S_N2 and S_N1 mechanism for them, respectively. A similar trend is seen here, although the substrate should not be the complex itself but the intermediate with a unidentate ligand.

The affinities between the tervalent ion of gallium and aluminium with water, which are represented by their hydration energies, are almost equal (*ca.* 1% difference for *ca.* 1000 kcal/mol). Hence K_w values for both complexes would not differ much. Larger k_w for [Ga(acac)$_3$] than for [Al(acac)$_3$] should be responsible for larger k_2 for [Ga(acac)$_3$] than for [Al(acac)$_3$]. The difference in $\Delta H^{\neq}$ values of site exchange of gallium(III) and aluminium(III) complexes with given β-diketonato ligands is *ca.* 3 kcal/mol.[10,11] The difference in $\Delta H^{\neq}$ values for the k_2 path in Table 3 is almost

equal to those for the site exchange. The ease of break of the first M–O bond of a given β-diketonato chelate would be paralleled by that of the second M–O bond. The rate-determining step for the site exchange should be either the break of the first M–O bond or the internal rearrangement of the five-coordinated intermediate. No explicit information is given as to the rate-determining step in the literatures,[10,11] but it is very likely that the break of the first M–O bond is the rate-determining step.

TABLE 4. RATE OF ISOTOPIC EXCHANGE OF SOME β-DIKETONATO COMPLEXES OF TYPICAL ELEMENT IONS IN THF

Complex	Temp./°C	b[b)]	$[H_2O]$	k_0/s^{-1}
$[Al(acac)_3]$	25	0.050	0.015	4.2×10^{-6}
$[Al(bzac)_3]$	0	0.050	0.16	3.3×10^{-7}
$[Al(bdm)_3]$	0	0.050	0.015	1.0×10^{-8}
$[Ga(acac)_3]$	0	0.050	0.050	1.9×10^{-5}
$[Ga(bzac)_3]$	0	0.050	0.050	5.0×10^{-6}
$[Ga(dbm)_3]$	0	0.050	0.050	3×10^{-6}
$[In(dbm)_3]$	0	0.050	0.098	$>1\times10^{-3}$
$[Be(acac)_2]$[a)]	30	1.0	—	2.1×10^{-5}
$[Be(bzac)_2]$	50	0.070	0.027	1.4×10^{-6}
$[Be(dbm)_2]$	50	0.070	0.041	1.1×10^{-6}

a) Ref. 13 b) concentration of free β-diketone.

Kinetics of Isotopic Exchange of Related Complexes. The rates are summerized in Table 4. The benzoylacetonato complexes give geometrical isomers, *mer* and *fac*. Their inter-conversion was studied by many authors by NMR spectroscopy and found to be very fast under the given experimental conditions.[10] Hence they were used without separation. Indium(III) complexes were very sensitive towards water in THF and only $[In(dbm)_3]$ allowed kinetic measurements. All the systems listed in Table 4 gave no net chemical change during the kinetic runs under the given conditions and the McKay plots were all linear. The R values were found to be proportional to the complex concentration, and k_0 values are listed. Although detailed kinetic studies were not made, we can compare the overall lability of these complexes with reference to the nature of the metal ions and of the ligands.

The following sequence shows the order of lability of acetylacetonato complexes towards isotopic exchange in organic solvents. The reaction mechanism differs from one another, and was discussed or will be discussed elsewhere.

Ti(IV)[12]>In(III)>Ga(III)>Al(III)[4]>Be(II)[13]>
Pd(II)[14]>Co(III)[15]>Si(IV)[16]>Ge(IV)[17]>Cr(III)[12]

However, so far as the gallium family elements concern, the order of lability is equal to that of water exchange. The order of lability between gallium(III) and aluminium(III) seems to be reversed, when ligands with nitrogen donors are involved (*e.g.* 8-quinolinolato[18] and EDTA[19] complexes). For ligands with oxygen donors only, the order for these two elements seems to be common, although different rate-determining steps may be involved.

Table 4 shows that the lability for a given metal ion decreases in the sequence, Hacac>Hbzac>Hdbm. The pK_a values increase in this order and the metal-ligand bond is expected to increase in this sequence. Although the metal complexes have various reaction paths for isotopic exchange, the basicity of ligands seems to give predominant influence.

The authors thank the Ministry of Education for Grant-in-Aid, and to the Japan Society for the Promotion of Science for Post-doctoral Fellowship to one of us (C.C.).

References

1) H. H. Diebler, M. Eigen, G. Ilgenfritz, G. Maass, and R. Winkler, *Pure and Applied Chem.*, **20**, 93 (1969); **6**, 105 (1963).
2) D. Fiat and R. E. Connick, *J. Amer. Chem. Soc.*, **90**, 608 (1968).
3) W. G. Movius and N. A. Matwiyoff, *Inorg. Chem.*, **8**, 925, 847 (1969).
4) K. Saito and K. Masuda, This Bulletin, **41**, 384 (1968); **43**, 119 (1970).
5) K. Matsuzawa and K. Saito, *ibid.*, **46**, 2777 (1973).
6) H. W. Baldwin and H. Taube, *J. Chem. Phys.*, **33**, 206 (1958).
7) T. Moeller and E. Gulyas, *J. Inorg. Nucl. Chem.*, **5**, 246 (1958).
8) H. Funk and A. Paul, *Z. Anorg. Allg. Chem.*, **330**, 70 (1964).
9) E. C. C. Baly and C. H. Desch, *J. Chem. Soc.*, **87**, 773 (1905).
10) T. J. Pinnavaia, J. M. Sebeson, II, and D. A. Case, *Inorg. Chem.*, **8**, 644 (1969).
11) R. C. Fay and T. S. Piper, *ibid.*, **3**, 348 (1964).
12) H. Kido and K. Saito, unpublished.
13) A. Barabas, *Inorg. Nucl. Chem. Lett.* **6**, 775 (1971).
14) K. Saito and M. Takahashi, This Bulletin, **42**, 3462 (1969).
15) K. Saito and M. Murakami, *ibid.*, **45**, 2472 (1972).
16) T. Inoue and K. Saito, *ibid.*, **46**, 2417 (1973).
17) A. Nagasawa and K. Saito, *ibid.*, **47**, 131 (1974).
18) K. Saito, M. Takahashi, Y. Miyakawa, and K. Masuda, *ibid.*, **41**, 1139 (1968).
19) M. Tsuchimoto, *ibid.*, in press.

Ringspaltungsreaktion von Thiadiazolo- und Triazolopyrimidin-Derivaten

Takayuki OKABE, Eiji TANIGUCHI und Kazuyuki MAEKAWA
Landwirtschaftliche Fakultät, Kyushu Universität, Fukuoka 812

(Eingegangen am 14, Mai 1974)

The ring-opening and rearrangement reaction of 7-methyl-5*H*-1,3,4-thiadiazolo[3,2-*a*]pyrimidin-5-ones (I) and the alternative isomeric 7-ones (XI) has been studied. I (R=H) and XI (R=H) gave quantitatively through N-N bond cleavage methylthiouracil (III) by treating with 5% NaOH, while they yielded 4-methyl-2-thiocyanato-6(1*H*)pyrimidone (II) by treating with liquid ammonia. By treating I and XI (R=alkyl) with 5% NaOH, the S-C bond cleaved to produce the corresponding acylaminopyrimidine derivatives (IV and IV') and 3-amino-pyrimidinethione (V and V'). The treatment of 2-hydrazino derivative (I; R=NHNH$_2$) with 5% NaOH gave 1-amino-2-mercapto-7-methyl-5*H*-*s*-triazolo[1,5-*a*]pyrimidin-5-one (VIII) through ring-opening and recyclization. On the other hand, the pyrimidine moiety of I (R=Et and *i*-Pr) cleaved by the action of chlorine to afford 2-amino-1,3,4-thiadiazole (X; R=Et and *t*-Pr).

Indem man Amino-triazol bzw. 2-Amino-1,3,4-thiadiazol oder seine Derivate mit verschiedene β-Ketosäuren oder ihren Derivaten in Gegenwart von Polyphosphorsäure erhitzte, erhielt man Triazolo[1,5-*a*]-pyrimidin, Triazolo[4,3-*a*]pyrimidin. bzw. Thiadiazolo[3,2-*a*]pyrimidine.[1-4]

Diese kondensierten heterocyclischen Verbindungen wurden nicht nur durch Nukleophile substituiert, sondern auch an ihren Triazol- bzw. Thiadiazol-ringen unter Spaltung von den Ringen angegriffen.

Hinsichtlich des Oxadiazolo[3,2-*a*]pyrimidin berichteten Gehlen *et al.*, daß die Ringöffnung am O-Brücke vom Oxadiazolring stattfand.[5] Andererseits, über Thiadiazolo[3,2-*a*]pyrimidin beschrieben Tsuji *et al.*, daß unter gleichen Bedingungen wie die von Gehlen *et al.*, die Spaltung an der N-N-Bindung vom Thiadiazolring vielmehr sich eintrat.[6]

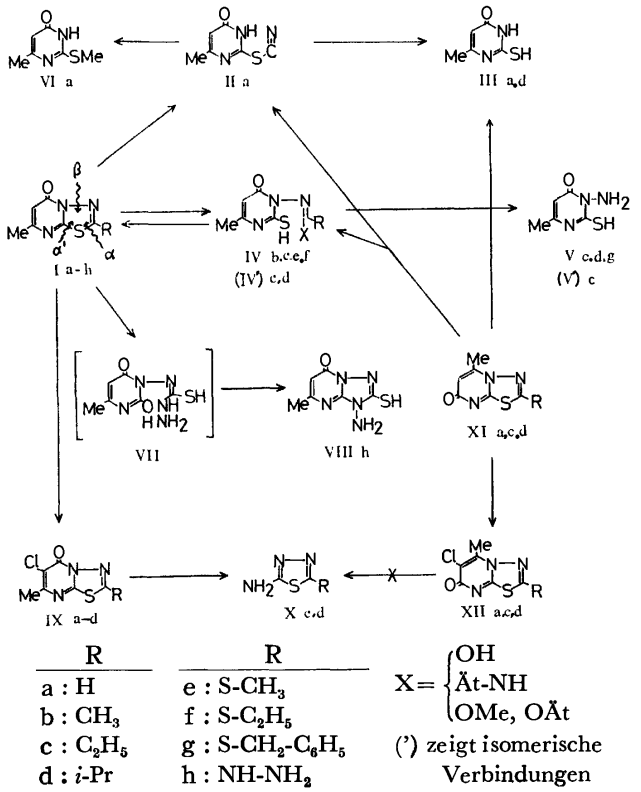

Fig. 1. Spaltung von Thiadiazolo[3,2-*a*]pyrimidin durch Alkali bzw. Chlor

Beide Verfasser isolierten ein Säureamid bzw. Isothiocyanat als Übergangsstoffe jede für sich. Diese Übergangsprodukte gaben demnach durch Hydrolyse mittels Säure 3-Amino-6-methylthiouracil bzw. 6-Methylthiouracil. Nämlich, ist es noch nicht sicher erklärt worden, ob die erste Öffnung des fünfgliedrigen Rings nach Weg α (einschließlich α') oder nach β (Fig. 1) stattfand. Ferner, ob diese Tatsache auf Unterschiede vom Heteroatom (O bzw. S) oder auf Verschiedenheit vom Rest R beruht, läßt es sich noch nicht erläutern.

Um Ringöffnung von der obengenannten heterocyclischen Verbindung mittels Nukleophils zu erklären, wurde dieser Versuch vorgenommen.

Als Folge wurde es gefunden, daß die Öffnung durch Alkali zwar nach Art der Substituenten verschieden war, aber sie vorwiegend nach Weg α (einschließlich α') verläuft. Falls flüssiges Ammoniak oder NaOMe angewendet wurde, so brachte die Öffnungsreaktion mit sich nach Weg β.

Der Weg α übertraf zudem überhaupt α'. Lediglich im Fall, das der Rest R NH–NH$_2$ ist, fand wieder ein Ringschluß nach der Ringöffnung statt, um die Verbindung (VIII h in Fig. 1) zu ergeben.

Andererseits, in Hinsicht auf Öffnung von Pyrimidinring berichteten Bredereck *et al.* schon ein Verfahren, in welchem Triazolopyrimidin mit primärem Amin oder Hydrazin erwärmt wurde.[7] Dunwell und Evans beschrieben, dass 7*H*-Thiazolo[3,2-*a*]pyrimidin-7-on als Spaltungsprodukt mittels Amins im Gegenwart von Tetramethylammoniumhydroxyd Thiazolin-Derivat lieferte.[8] Da Amin jedoch, wie obengennanten, Triazolo- bzw. Thiadiazol-Hälfte zersetzt, wurde die Ringspaltung von Pyrimidin-Hälfte unter Anwendung von Chlor vorgenommen.

Infolgedessen wurde es gefunden, daß Chlor in $CHCl_3$ Lösung bei 0 °C an der höchste Elektronendichte besitzenden C_6-Stelle[9,10] von Thiadiazolo[3,2-*a*]pyrimidin umsetzte. Überflüssiges Chlor verursachte gerade bei 0 °C die Ringöffnung von Pyrimidin-Hälfte, um 2-Amino-5-substituierte-1,3,4-Thiadiazolo-Derivate zu erzeugen.

Andere *s*-Triazolo[4,3-*a*]pyrimidin und Triazolo-[1.5-a] pyrimidin als diese waren beständig unter diesen Reaktionsbedingungen.

Beschreibung der Versuche

1) Darstellung von 3-Acylamino-6-methyl-(bzw. 4-methyl)-thiouracil (IV bzw. IV'), und 3-Amino-6-methyl(bzw. 4-methyl)-thiouracil (V bzw. V') aus I (bzw. XI). Indem man I (R=Me) mit warmer 5% NaOH Lösung einige Stunden lang bewahrte, erhielt man IV (R=Me) mit befriedigender Ausbeute. I (R=Ät) gab aber unter ziemlich milder Bedingung (5% NaOH, Raumtemperatur, 1 stündiges Stehen; oder mit verd. Hydrazin-hydrat) IV (R=Ät). I (R=*i*-Pr) lieferte in gleichen Umständen 3-Amino-6-methyl-4(3*H*)-oxo-2(1*H*)-pyrimidinthion V anstatt IV (R=*i*-Pr), während XI (R=Ät, *i*-Pr) entsprechende isomerische 3-Acylamino-4-methyl-6(5*H*)-oxo-2(1*H*)-pyrimidinthion IV' (R=Et, *i*-Pr) gab.

(a) 3-Acetylamino-6-methyl-4(3H)-oxo-2(1H)-pyrimidinthion (IV, R=CH_3). *Methode A)*: Eine Suspension von 2 g I (R=Me) in 30 ml von 5% NaOH wurde 6 Stunden lang bei Raumtemperatur umgerührt, um aufzulösen. Die Lösung wurde dann mit verd. HCl neutraliziert und i. Vak. eingeengt. Nach Abkühlung wurde der ausgeschiedene Niederschlag gesammelt und mit Eis-Wasser gewaschen. Durch Umkristallisierung aus MeOH erhielt man farblose Nadeln von Schmelzpt. 255—257 °C. Ausbeute 1.4 g (72%).

$\lambda_{max\,(H_2O)}$ 210, 275, 291 nm (ε 10000, 8500, 9200).

Anal. $C_7H_9O_2SN_3$

Ber.	C 42.21	H 4.55	N 21.10
Gef.	C 42.30	H 4.48	N 21.13

Diese Verbindung wurde auch durch nachstehende unabhängige Route aufgebaut. Ein Gemisch von 4 g Acetylthiosemicarbazid und 2.7 g Diketen in 10 ml AcOH wurde unter Rückfluß 2 Stunden lang erhitzt. Nachdem AcOH abgedampft wurde, wurde der Rückstand von MeOH umkristallisiert. Schmelzpt. 256—257 °C $\lambda_{max\,(H_2O)}$ 209, 275, 290 nm(ε 11000, 8600, 9200).

Anal. $C_7H_9O_2SN_3$

Ber.	C 42.21	H 4.55	N 21.10
Gef.	C 41.97	H 4.61	N 21.00

Die von beidem Verfahren erhältlichen Verbindungen wurden durch die Mischprobe und durch die Vergleichung von IR-Spektren identifiziert.

(b) 3-(S-Äthyl-O-methylformamido)-6-methyl-4(3H)-oxo-2(1H)-pyrimidinthion (IV, R=Et). If (1.5 g) wurde in 45 ml MeOH aufgelöst und mit 5 ml 5% NaOH versetzt, und dann bei Raumtemperatur 50 Minuten lang umgerührt. Danach wurde das Reaktionsgemisch mit HCl angesäuert und i. Vak. verdampft. Der erhaltene ölige Rückstand erhartete nach übernächtlichem Stehen in der wäßrigen Suspension. Das rohe Produkt wurde aus MeOH umkristallisiert. Ausbeute 0.5 g, Schmelzpt. 162—163 °C. λ_{max} 276, 246, 208 nm.

Anal. $C_9H_{13}O_2S_2N_3$

Ber.	C 41.70	H 5.06	N 16.21
Gef.	C 41.51	H 5.02	N 16.22

Aus der nachfolgenden Tatsache läßt sich folgern, daß die Verbindung die durch Spaltung von der S–C Bindung entstandene IVf (X=OÄt), 3-(*S*-Äthyl-*O*-methylformamido)-Verbindung ist. Nämlich ist das IR-Spektrum ganz ähnlich mit dem von IVc (Fig. 2), und ferner verwandelt sich diese Verbindung durch Behandlung mit ÄtONa in seiner äthanolischen Lösung zu If wieder. (Es wurde mittels der Mischprobe und Vergleichung von Massenspektren festgestellt.)

Aus If (R=S–Me) gewann man ebenso $C_8H_{11}OS_2N_3$ (Schmelzpt. 204—205 °C) und diese Verbindung wurde als IVe geschlossen.

IR-Spektren von 3-Acylamino-6-methyl-2-thiouracil (abgeleitet von I) und 3-Acylamino-4-methyl-2-thiouracil (abgeleitet von XI) wurden in Fig. 2 gezeigt.

(c) 3-Amino-6-methyl-4(3H)-oxo-2(1H)-pyrimidinthion (V). *Methode B)*: Eine Suspension von 1.8 g Ic(R=Ät) in 20 ml von 5% NaOH wurde unter Umrührung bei 70—80 °C 7. Stunden lang erhitzt. Nach Abkühlung wurde das Gemisch mit konz. HCl neutralisiert. Der dabei ausgeschiedene Niederschlag wurde gesammelt, mit Wasser gewaschen, und dann aus MeOH umkristallisiert. Ausbeute, 1.1 g (61%).

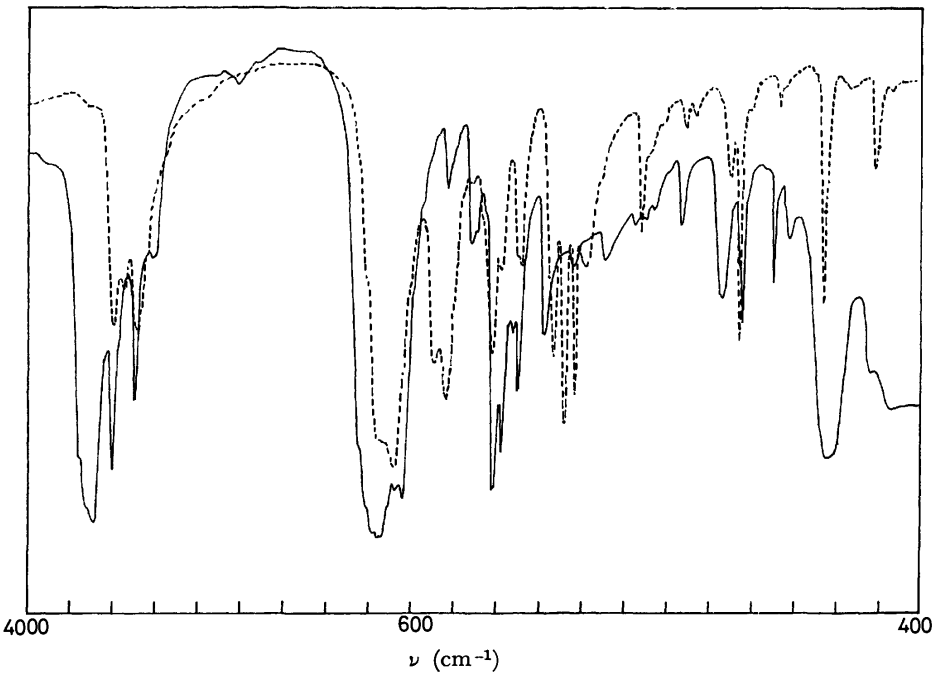

Fig. 2. IR-Spektren von 3-Acylamino-6-methyl(bzw. 4-methyl)-2-thiouracil
····: 3-Acylamino-6-methyl-2-thiouracil (aus I)
——: 3-Acylamino-4-methyl-2-thiouracil (aus XI)

Schmelzpt. 247—248 °C. $\lambda_{max(H_2O)}$ 234, 275 nm (ε 8600 11000). $\nu_{max(KBr)}$ 1640, 1600, 1540 cm^{-1}.

Anal. $C_5H_7OSN_3$

Ber.	C 38.22	H 4.49	N 26.74
Gef.	C 38.49	H 4.46	N 26.83

Methode C): Das Gemisch von 2 g Ic (R=Et) und 5 g Hydrazin-hydrat in 15 ml MeOH ließ bei Raumtemperatur über Nacht stehen. Der entstandene Niederschlag wurde nach Waschen mit Wasser aus MeOH umkristallisiert. Ausbeute, 0.3 g (22%). Die Mischprobe und IR-Spektra wiesen darauf hin, dass beide Produkten mit authentischer Probe identisch waren.[11,12]

2) Darstellung von 4-Methyl-2-thiocyano-6(1H)-pyrimidon (II) aus I und XI. Methode D): *(i)* Zur Suspension von 1.5 g Ia (R=H) in 40 ml MeOH, das im voraus mit festem Kohlendioxid und Aceton abgekühlt, wurde Ammoniak durchgeleitet, bis das Flüssigkeitsmaß ans beinahe 80 ml erreichte. Nachdem das Reaktionsgemisch bei derselben Bedingung 2 Stunden lang stehen gelassen wurde, wurde es in der Dauer einer Nacht langsam auf Raumtemperatur gebracht. Das Gemisch wurde i. Vak. verdampft und der Rückstand wurde aus MeOH–AcOÄt umkristallisiert. Schließlich erhält man in befriedigender Ausbeute (86%) eine Verbindung, deren Zusammensetzung $C_6H_8OSN_4$ ist, und die IR-Absorption von SCN-Gruppe an 2170 cm^{-1} zeigt. Schmelzpt. 100—101 °C, $\lambda_{max(H_2O)}$ 211, 235, 270 nm (ε 10000, 6000, 3200). $\nu_{max(KBr)}$ 2170 cm^{-1} (SCN).

Anal. $C_6H_5OSN_3 \cdot NH_3$

Ber.	C 39.13	H 4.38	N 30.43
Gef.	C 39.11	H 4.40	N 30.20

Das Massenspektrum dieser Verbindung zeigte Molekülarion bei *m/e* 167, übereinstimmend mit $C_6H_5OSN_3$, das durch Abspaltung von SCN-Radikal Ion *m/e* 109 zeugte. Auf Grund dieser Tatsache ist es wahrscheinlich, die Thiocyanat enthaltende Struktur für diese Verbindung anzuwenden. Diese Struktur wurde weiter dadurch festgestellt, daß man durch basische Hydrolyse daraus Methylthiouracil (III) erhielt.

(ii) Aus XI: 7-Oxo-Verbindung XI (R=H) wurde mit flüssigem Ammoniak in ähnlicher Weise wie oben genannten behandelt, infolgedessen war das erhaltene Zersetzungsprodukt ganz identisch mit der von I (R=H)abgeleiteten Verbindung. Ausbeute 70%. Schmelzpt. 100—101 °C.

Anal. $C_6H_8OSN_4$

Ber.	C 39.13	H 4.38	N 30.43
Grf.	C 39.05	H 4.24	N 30.24

3) Darstellung von 2-Methylthio-pyrimidin-Derivaten (VI) aus I. Methode E): Die Spaltung der N-N-Bindung von I fand methanolischer Natrium-Methoxyd Lösung und auch in verd. NaOH Lösung mit unbefriedigender Ausbeute statt. Die Behandlung von I (R=H) mit methanolischer NaOMe Lösung zeugte 4-Methyl-2-methylthio-6(1*H*)-pyrimidon VI neben II.

Eine Suspension von 3.9 g I (R=H) in 50 ml absolutem MeOH wurde biszu 0 °C abgekühlt und hierzu 0.6 g Natrium zugesetzt. Nach Verschwinden von Natrium wurde das Gemisch weiter 50 Minuten lang umgerührt, dann mit AcOH neutralisiert. Das aus AcONa freigesetzte Filtrat wurde i. Vak. verdampft und der Rückstand wurde aus MeOH umkristallisiert. Ausbeute, 0.9 g (23%). Schmelzpt. 100—101 °C. Diese Verbindung war identisch mit der nach Methode D dargestellten.

Das Filtrat, das oben erwähnte Verbindung entfernt wurde, wurde i. Vak. verdampft, um farblose Kristalle niederzuschlagen. Umkristallisation wurde aus AcOEt durchgeführt. Ausbeute, 450 mg. Schmelzpt. 212—215 °C. $\lambda_{max(H_2O)}$ 230, 260^{sch}, 282^{sch} nm (ε 17800, 7800, 4500).

Anal. $C_6H_8OSN_2$

Ber.	C 46.15	H 5.16	N 17.94
Gef.	C 46.06	H 5.16	N 18.03

Massenspektren von dieser Verbindung zeigten Molekülarion bei *m/e* 156, übereinstimmend mit Molekül $C_6H_8OSN_2$, das dann nach Spaltung von SCH_3 Radikal Ion *m/e* 109 gab. Diese Verbindung wurde mittels der Mischprobe und IR-Spektren als VI festgestellt.[13]

4) Entstehung von 4-Methyl-2-thiouracil (III) aus I bzw. XI. Methode A): *(a)* Eine Suspension von 1 g I (R=H) in 20 ml 5% NaOH wurde bei Raumtemperatur eine Stunde lang umgerührt. Die erhaltene klare Lösung wurde mit konz. HCl (unter Entwicklung von Gas) angesäuert, dann abgekühlt. Der Niederschlag wurde gesammelt, mit Eis-Wasser gewaschen und aus wäßr. ÄtOH umkristallisiert. Ausbeute, 0.6 g (72%). Schmelzpt. 320—324 °C. $\lambda_{max(H_2O)}$ 215, 275 nm (ε 10000, 10000).

Anal. $C_5H_6OSN_2$

Ber.	C 42.25	H 4.26	N 19.71
Gef.	C 42.25	H 4.22	N 19.86

(b) Aus XI: XI (R=H) wurde mit 5% NaOH nach gleichem Verfahren wie obengenanntem behandelt und dadurch zur III zersetzt. Ausbeute, 70%.

Methode F): Ein Gemisch von 3 g XI (R=H), 20 ml Isobutylamin und 7 Tropfen von Tetramethylammonium hydroxyd wurde unter Rückfluss 4 Stunden lang erhitzt. Dann wurde das Gemisch i. Vak. verdampft und der erhaltene Niederschlag wurde aus MeOH umkristallisiert. Ausbeute, 0.9 g (35%).

Schließlich wurde diese Verbindung von Vergleichung mit authentischem Präparate identifiziert.[14]

Die Ringspaltung von 7-Oxo- bzw. 5-Oxo-thiadiazolopyrimidin durch Alkali wurde in Tafel 1 und 2 zusammengefaßt.

5) Darstellung von 1-Amino-2-mercapto-5-oxo-7-methyl-s-triazolo-[1,5-a]pyrimidin (VIII) durch Umlagerung von I (R=NHNH$_2$). Eine Suspension von 1 g Ih (R=$NHNH_2$) in 10 ml 5% NaOH Lösung liess bei Raumtemperatur unter ganz nächtlichem Umrühren stehen. Nach Entfernung des unlöslichen Restes, wurde das Filtrat mit HCl angesäuert, und dann i. Vak. verdampft. Der Rückstand wurde aus wäßr. MeOH umkristallisiert. Ausbeute, 750 mg (63%). Schmelzpt. über 300 °C. $\lambda_{max(H_2O)}$ 236, 280 nm (ε 21100, 10600), *m/e*: 197 (M^+), $\nu_{max(KBr)}$ 3470 cm^{-1} (NH), 2625 cm^{-1} (SH).

Anal. $C_6H_7OSN_5$

Ber.	C 36.55	H 3.58	N 35.52
Gef.	C 36.81	H 3.60	N 35.65

Das IR-Spektrum zeigte ein scharfes Band an 3475 und 3280 cm^{-1} und ein breites Band an 2625 cm^{-1}, das jedes für sich die Anwesenheit von NH_2- und SH-Substituenten andeutete. Die Massenspektren diesser Verbindung zeigten Molekülarion an *m/e* 197, übereinstimmend mit der Formel $C_6H_7OSN_5$. Aus dem Molekülarion wurde S eliminiert, folglich Ion von *m/e* 165 hervorgebracht, dann daraus NH_2-Radikal ausgeschlossen wurde.

1-Amino-2-benzylthio-7-methyl-5H-s-triazolo[1, 5-a]pyrimidin-5-on: Die oben genannte Verbindung wurde in alkalischem Milieu mit Benzylchlorid umgesetzt, um S-Benzyl-Derivat zu liefern. Schemelzpt. 273—274 °C.

Anal. $C_{13}H_{13}OSN_5$

Ber.	C 54.35	H 4.56	N 24.38
Gef.	C 54.34	H 4.55	N 24.33

Das IR-Spektrum zeigte ein scharfes Band an 3270 und 3175 cm^{-1}, das auf Anwesenheit von Amino-Substituent und Verschwinden von SH hinwies. Die Massenspektren von Benzylthio-Derivate darlegten Molekülarion an *m/e* 287, daraus Radikal NH_2 eliminiert wurde, und Ion *m/e* 271 lieferte, das

Tafel 1. Ringspaltung von 7-Methyl-2-substituierte-5*H*-Thiadiazolo[3,2-*a*]pyrimidin-5-on

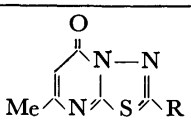

R=	Reaktionsbedingungen: Mittel	Temp.	Dauer	Produkt	Schmelzpt. (°C)	Ausbeute (%)	UV-Spektren λ_{max} (H_2O) $\varepsilon \times 10^{-3}$
H	5% NaOH	Rt	1	4-Me-2-thiouracil	320—324	72	215, 275 (10, 10)
	70% $ÄtNH_2$	Rt	2/3	4-Me-2-thiouracil		65	
	MeONa	Rt	2/3	2-MeS-6-OH-4-Me-pyrimidin	212—215	11	
	Flüss. NH_3	−20 °C	2	und 2-SCN-6-OH-4-Me-pyrimidin	100—101	23	
Me	5% NaOH		6	3-AcNH-2-SH-4-OH-6-Me-pyrimidin	256—257	72	210, 275, 291 (10, 8.5, 9.2)
Ät	5% NaOH	70—80 °C	7	3-NH_2-6-Me-2-thiouracil	247—248	61	
	NH_2-NH_2	Rt	24	3-NH_2-6-Me-2-thiouracil		22	
	5% NaOH	Rt	7/4	3-Propionyl-NH-6-Me-2-thiouracil	260—261	70	
i-Pr	5% NaOH	Rt	2	4-Me-2-thiouracil	320—324	57	
S-Me	5% NaOH MeOH	Rt	2	$C_8H_{11}OS_2N_3$	204—205	43	
S-Ät	5% NaOH MeOH	Rt	2	$C_9H_{13}O_2S_2N_3$	162—163	21	208, 246, 276
S-CH_2-C_6H_5	5% NaOH	Rt	3/2	3-NH_2-6-Me-2-thiouracil	247—248	53	
NH_2-NH_2	5% NaOH	Rt	12	1-NH_2-2-SH-7-Me-5H-triazolo-[1,5-*a*]pyrimidin	über 300	45	236, 280, (21.1, 10.6)
Ät	Cl_2 in $CHCl_3$	0—10 °C	2	2-NH_2-5-Ät-1,3,4-thiadiazol	91—93	87	
i-Pr	Cl_2 in $CHCl_3$	0—10 °C	2	2-NH_2-5-*i*-Pr-1,3,4-thiadiazol	121—122	74	

Rt: Raumtemperatur, Rl: Rücklauf

Tafel 2. Ringspaltung von 5-Methyl-2-substituierte-7*H*-thiadiazolo[3,2-*a*]pyrimidin-7-on

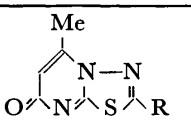

R=	Reaktionsbedingungen: Alkali	Temp.	Dauer	Produkt	Schmelzpt. (°C)	Ausbeute	UV-Spektren $\lambda_{max(H_2O)}$ $\varepsilon \times 10^{-3}$
H	5% NaOH	Rt	1	4-Me-2-thiouracil	320—324	35	
	70% $EtNH_2$	Rt	3/4	4-Me-2-thiouracil		47	
	i-$BuNH_2$	Rl	4	4-Me-2-thiouracil		35	
	MeONa	Rt	1	4-Me-2-thiouracil		27	
	Flüss. NH_3	−20 °C	2	2-SCN-6-OH-4-Me-pyrimidin	100—101	75	
Ät	5% NaOH	Rt	1	3-Propionyl-NH-2-SH-4-Me-6-OH-pyrimidin	199—200	50	256, 261 (11.2, 9.5)
i-Pr	5% NaOH	Rt	2	3-*i*-Bu-NH-2-SH-4-Me-6-OH-pyrimidin	240—241	50	256, 260 (11.8, 11.7)

weiter nach Verlierung von Benzylthioradikal Ion *m/e* 148 ergab.

Auf diesen Befunde wurde oben erwähnte Verbindung als 1-Amino-2-mercapto-7-methyl-5*H*-*s*-triazolo[1,5-*a*] pyrimidin-5-on geschlossen.

6) Einwirkung von Chlor auf I und XI. Die Umsetzung von I bzw. XI (R=H, Et, *i*-Pr) mit äquivalenter Menge von Chlor in $CHCl_3$ Lösung bei 0—10 °C erzeugte jede für sich entsprechende 6-Chloro-2-alkyl-7-methyl-5*H*-thiadiazolo-[3,2-*a*]pyrimidin-5-on bzw. 6-Chloro-2-äthyl(od. *i*-Pr)-5-methyl-7*H*-thiadiazolo[3,2-*a*]pyrimidin-7-on.

Die Monochlor-Derivate (IX, R=Ät, *i*-Pr) reagierten

dennoch weiter mit überschüssigem Chlor und lieferten jede für sich 2-Amino-5-äthyl, bzw. 2-Amino-5-isopropyl-1,3,4-thiadiazol. Folglich entstanden diese Thiadiazol-Derivate wahrscheinlich durch 6-Chlor-Derivate und nachfolgende Spaltung von Pyrimidinring.

Es ist nennenswert, daß 7-Oxo-Derivat in gleicher Bedingung keine Thiadiazol-Derivat gab.

(a) Umsetzung von Chlor in der Stelle 6 von I: Wenn man in $CHCl_3$ (oder AcOH) Lösung von I (R=H od. Me) unter Kühlung mit Eis-Wasser Chlorgas durchleitet, so kann man Monochlor-Verbindung mit befriedigender Ausbeute erhalten. Sie ist identisch mit 6-Chlor-5*H*-thiadiazolo[3,2-*a*]pyrimidin-5-on, das aus 2-Amino-1,3,4-thiadiazol und 2-Chlor-acetessigsäureäthylester in Gegenwart von Polyphosphorsäure unabhängig synthetisiert wurde.[4]

Aus XI (R=H) wurde man in ähnlicher weise 6-Chlor-Verbindung erhalten. Ausbeute 85%. Schmelzpt. 195—196 °C.

Anal. $C_6H_4OSN_3Cl$

Ber.	C 35.75	H 2.00	N 20.85
Gef.	C 35.55	H 2.20	N 21.22

Falls R S-Alkyl war, fand die Oxydation von Seitenkette auch statt.

(b) Darstellung von Thiadiazol-Derivaten (X) aus I: (i), Zu einer Lösung von 5 g I (R=Et) in 30 ml $CHCl_3$ wurde Chlorgas bei 0—10 °C durchgeleitet. Der vorläufig entstandene Niederschlag war nach weiter Durchleitung von Chlorgas entschwunden. Nachdem die Reaktionslösung bei Raumtemperatur über Nacht stehen gelassen wurde, wurde das Lösungsmittel *in vacuo* entfernt, um Zersetzungsprodukt zu erhalten. Das erhaltene Produkt wurde mit Äther gewaschen und aus AcOÄt-MeOH-Äther umkristallisiert. Ausbeute, 3.7 g (87%), Schmelzpt. 91—93 °C, $\lambda_{max(H_2O)}$ 251 nm (ε 7100).

Anal. $C_4H_7SN_3 \cdot HCl$

Ber.	C 29.01	H 4.71	N 25.38
Gef.	C 28.97	H 4.71	N 25.35

Durch die Mischprobe und Vergleichung von IR-Spektren wurde diese Verbindung mit 2-Amino-5-äthyl-1,3,4-thiadiazol identifiziert.[15]

(ii) Eine Lösung von 4 g I (R=*i*-Pr) wurde mit überschüssigem Chlor nach oben beschriebenem Verfahren behandelt. Das erhältliche Zersetzungsprodukt wurde aus MeOH-AcOÄt umkristallisiert. Ausbeute, 2.8 g (74%). Schmelzpt. 121—122 °C. $\lambda_{max(H_2O)}$ 251 nm (ε 5500).

Anal. $C_5H_9SN_3 \cdot HCl$

Ber.	C 33.43	H 5.56	N 23.40
Gef.	C 33.36	H 5.63	N 23.39

Diese Verbindung wurde nach Vergleichung mit authentischem Präparat[15] als 2-Amino-5-isopropyl-1,3,4-thiadiazol festgestellt.

Literaturen

1) T. Okabe, E. Taniguchi, und K. Maekawa, *Sci. Bull. Fac. Agr. Kyushu Univ.*, **26**, 105 (1972).

2) T. Okabe, E. Taniguchi, und K. Maekawa, *J. Fac. Agr. Kyushu Univ.*, **17**, 195 (1973).

3) T. Okabe, E. Taniguchi, und K. Maekawa, *Agr. Biol. Chem.*, **37**, 441 (1973).

4) T. Okabe, K. Maekawa, und E. Taniguchi, *ibid.*, **37**, 1197 (1973).

5) H. Gehlen und B. Simon, *Archiv Pharm.*, **303**, 501 (1970).

6) T. Tsuji und Y. Kamo, *Chem. Lett.*, **1972**, 641.

7) H. Bredereck, F. Effenberger, und W. Resemann, *Angew. Chem. Intern. Ed.*, **1**, 219 (1962).

8) D. W. Dunwell und D. Evans, *J. Chem. Soc., C*, **1971**, 2094.

9) E. Kleinpeter, R. Borsdorf, G. Fischer, und H. J. Hofmann, *J. Prakt. Chem.*, **314**, 515 (1972).

10) C. Glier, F. Dietz, M. Scholz, und G. Fischer, *Tetrahedron*, **28**, 5789 (1972).

11) L. Francis, *Can. J. Chem.*, **37**, 1221 (1959).

12) T. Tsuji und T. Ueda, *Chem. Pharm. Bull.*, **12**, 2530 (1971).

13) J. Stanek, *Chem. Listy*, **52**, 375 (1958).

14) R. N. Lacey, *J. Chem. Soc.*, **1954**, 839.

15) F. L. Chubb und J. Nissenbaum, *Can. J. Chem.*, **37**, 1221 (1959).

Alkoxythiocyanation and Alkoxyiodination of Olefins with Copper(II) Salts

Akira Onoe, Sakae Uemura,* and Masaya Okano
Institute for Chemical Research, Kyoto University, Uji, Kyoto 611
(Received February 15, 1974)

A simple and convenient method for the preparation of vicinal alkoxythiocyano- and alkoxyiodoalkanes is described. The reaction of olefins with copper(II) salts, such as chloride, bromide and sulfate, and potassium thiocyanate or iodide in alcohols readily affords the compounds in good yields. From vinyl acetates, alkyl vinyl ethers and α,β-unsaturated aldehydes, the products are obtained in the form of dialkyl acetals. The reaction mechanism is discussed.

Baird *et al.*[1] reported the preparation of chloroiodoalkanes with the use of copper(II) chloride, metal iodide and olefins in acetonitrile. We found that when the reaction was carried out in alcohol, the main products were alkoxyiodoalkanes instead of chloroiodoalkanes, and that when KSCN was used, alkoxythiocyanoalkanes were obtained. Since the preparation of alkoxyiodo- and alkoxythiocyanoalkanes has so far been restricted to the reaction of olefin with iodine in alcohol in the presence of catalysts such as HgO[2] and $AgClO_4$[3] for the former, and to that with $Tl(OAc)_3$ and KSCN in alcohol for the latter,[4] we wish to report a simple and efficient synthetic method for these compounds using copper(II) salts.

Results and Discussion

The reaction was carried out by adding olefinic hydrocarbons to a homogeneous alcoholic solution of copper(II) chloride and KSCN or KI at an appropriate temperature, the mixture being kept for 0.3—5 hr. Styrene, cyclohexene, vinyl esters, vinyl ethers and α,β-unsaturated aldehydes were chosen as the olefinic substrates. The products were vicinal alkoxythiocyano- (**1a**—**5a**) or alkoxyiodoalkanes (**1b**—**5b**). The general reaction is illustrated by the following scheme.

$$\text{>C=C<} + 2CuCl_2 + KY + ROH \longrightarrow \text{>C(OR)—C(Y)<} + 2CuCl + KCl + HCl \quad (1)$$

(Y=SCN, I)

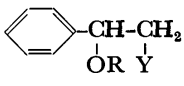

1 (**a**, Y=SCN; **b**, Y=I)

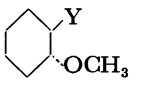

2 (**a**, Y=SCN; **b**, Y=I)

Some typical results with the former two and last three olefins are summarized in Tables 1 and 2, respectively. Copper(II) bromide, sulfate, nitrate and iron(III) chloride could also be used in the reaction, although these salts were less effective than copper(II) chloride. All the products obtained from the reaction of cyclohexene were found to be *trans*.

In the reactions of vinyl and isopropenyl acetates, the products (**3a** and **3b**) were isolated in the form of dialkyl acetals, no compounds containing acetoxy group being obtained.

$$CH_2{=}C(R)(OAc) \xrightarrow[R'OH]{CuCl_2,\ KY} YCH_2C(OR')_2\text{-}R \quad (2)$$

3 (**a**, Y=SCN; **b**, Y=I)

The products of the reaction of alkyl vinyl ethers were

Table 1. Alkoxythiocyanation and alkoxyiodination of styrene and cyclohexene

Olefin (100 mmol)	Cu(II) salt (100 mmol)	K salt (100 mmol)	Solvent (100 ml)	Temp. (°C)	Time (hr)	Products and Yield (%)[a]	
Styrene	$CuCl_2$	KSCN	CH_3OH	65	5	**1a**(R=CH_3)	31
Styrene	$CuSO_4\cdot5H_2O$	KSCN	CH_3OH	65	2	**1a**(R=CH_3)	12
Styrene	$CuCl_2$	KI[b]	CH_3OH	65	2	**1b**(R=CH_3)	91
Styrene	$CuBr_2$	KI	CH_3OH	65	2	**1b**(R=CH_3)	94
Styrene	$CuSO_4\cdot5H_2O$	KI	CH_3OH	65	2	**1b**(R=CH_3)	61
Styrene	$CuCl_2$	KI	C_2H_5OH	78	2	**1b**(R=C_2H_5)	81
Styrene	$CuCl_2$	KI	*n*-C_3H_7OH	97	3	**1b**(R=*n*-C_3H_7)	90
Styrene	$CuCl_2$	KI	*n*-C_4H_9OH	118	3	**1b**(R=*n*-C_4H_9)	91
Styrene	CuCl[c]	I_2[d]	CH_3OH	65	2	**1b**(R=CH_3)	86[e]
Cyclohexene	$CuCl_2$	KSCN	CH_3OH	65	2	**2a**	30[f]
Cyclohexene	$CuSO_4\cdot5H_2O$	KSCN	CH_3OH	65	2	**2a**	10
Cyclohexene	$CuCl_2$	KI	CH_3OH	65	2	**2b**	13[g]
Cyclohexene	$CuSO_4\cdot5H_2O$	KI	CH_3OH	65	2	**2b**	53
Cyclohexene	CuCl[c]	I_2[d]	CH_3OH	65	2	**2b**	64[e]

a) Based on Cu(II) salt charged and scheme 1. b) KI, 50 mmol. When 100 mmol of KI was used, **1b** (R=CH_3) was obtained in 97% yield. c) 10 mmol. d) 50 mmol. e) Based on I_2 charged. f) By-product: *trans*-1-chloro-2-thiocyanocyclohexane, 12%. g) By-product: *trans*-1-chloro-2-iodocyclohexane, 29%.

Table 2. Alkoxythiocyanation and alkoxyiodination of vinyl ester, alkyl vinyl ether, and α,β-unsaturated aldehyde[a)]

Olefin (100 mmol)	K salt (100 mmol)	Solvent (100 ml)	Temp. (°C)	Time (hr)	Products and Yield[b)] (%)	
CH_2=CHOAc	KSCN	CH_3OH	62	3	**3a**(R=H, R′=CH_3)	86
CH_2=CHOAc	KSCN	C_2H_5OH	60	1	**3a**(R=H, R′=C_2H_5)	63
CH_2=CHOAc	KSCN	$HOCH_2CH_2OH$	70	3	**3a**[R=H, (OR′)$_2$=O(CH_2)$_2$O]	77
CH_2=CHOAc	KI	CH_3OH	62	1	**3b**(R=H, R′=CH_3)	86
CH_2=C(CH_3)OAc	KSCN	$HOCH_2CH_2OH$	65	3	**3a**[R=CH_3, (OR′)$_2$=O(CH_2)$_2$O]	93
CH_2=CHOC_2H_5[c)]	KSCN	CH_3OH	30	0.25	**4a**(R=C_2H_5, R′=CH_3)	59
CH_2=CHOC_2H_5[c)]	KSCN	CH_3OH	50	3	**4a**(R=C_2H_5, R′=CH_3) **3a**(R=H, R′=CH_3)	18 47
CH_2=CHOC_2H_5[c)]	KSCN	t-C_4H_9OH	55	3	**4a**(R=C_2H_5, R′=t-C_4H_9)	52
CH_2=CHOC_2H_5[c)]	KSCN	$HOCH_2CH_2OH$	35	1	**4a**(R=C_2H_5, R′=CH_2CH_2OH) **3a**[R=H, (OR′)$_2$=O(CH_2)$_2$O]	54 2
CH_2=CHOC_2H_5[c)]	KSCN	$HOCH_2CH_2OH$	60	5	**3a**[R=H, (OR′)$_2$=O(CH_2)$_2$O]	77
CH_2=CHOC_2H_5[c)]	KI	CH_3OH	35	0.25	**4b**(R=C_2H_5, R′=CH_3) **3b**(R=H, R′=CH_3)	58 19
CH_2=CHO-n-C_4H_9	KSCN	t-C_4H_9OH	70	3	**4a**(R=n-C_4H_9, R′=t-C_4H_9)	69
CH_2=CHO-n-C_4H_9	KI	i-C_3H_7OH	62	3	**3b**(R=H, R′=i-C_3H_7)	54
CH_2=CHCHO	KSCN	CH_3OH	63	1	**5a**(R=H, R′=CH_3)	72
CH_2=CHCHO	KI	CH_3OH	62	1	**5b**(R=H, R′=CH_3)	83
CH_3CH=CHCHO	KSCN	CH_3OH	35	1	**5a**(R=R′=CH_3)	89
CH_3CH=CHCHO	KI	CH_3OH	30	1	**5b**(R=R′=CH_3)	97

a) $CuCl_2$, 100 mmol. b) Based on $CuCl_2$ charged. c) 200 mmol.

4 and/or **3**, the amounts of both products depending on the reaction conditions. Higher temperature and longer time favored the exchange of alkoxy group, giving **3** as the main product.

$$CH_2{=}C(H)(OR) \xrightarrow[R'OH]{CuCl_2,\ KY} YCH_2C(OR')(H) \xrightarrow{R'OH} \textbf{3a or 3b}\ (R{=}H) \quad (3)$$

4 (**a**, Y=SCN; **b**, Y=I)

Under the same or even more drastic conditions, the reaction of diethyl or di-*n*-butyl acetal of acetaldehyde with copper(II) chloride and KSCN or KI gave none or only trace amounts of **3** and/or **4**. The result excludes such reaction schemes as one in which alcohol adds to the double bond at first, followed by the attack of Y. The reaction of acrolein and crotonaldehyde under similar conditions gave the products also in the form of dialkyl acetal. According to Castro *et al.*[5)]

$$RCH{=}CHCHO \xrightarrow[R'OH]{CuCl_2,\ KY} RCH(OR')CH(Y)CH(OR')_2 \quad (4)$$

5 (**a**, Y=SCN; **b**, Y=I)

the reaction of acrolein with copper(II) chloride or bromide in methanol gave **5** (R=H, R′=CH_3, Y=Cl, or Br) in 12—39% yield. They proposed that the reaction proceeds through the addition of methanol to acrolein affording β-methoxypropionaldehyde followed by the attack of chlorine or bromine of copper(II) salt on the α-position of the saturated aldehyde thus formed. In order to see whether the same reaction scheme is operative in our case, the reaction of butyraldehyde with copper(II) chloride was carried out in the presence of KSCN in refluxing methanol for 1 hr. The yield of 1,1-dimethoxy-2-thiocyanobutane,[6)] however, was quite low (19%) as compared with the 89% yield for **5** obtained from crotonaldehyde. This indicates that the reaction scheme proposed by Castro *et al.*[5)] is partly operative, but not important in our case. Thus the main route for the formation of **5** would be the attack of Y on double bond followed by addition of the alkoxy group.

The reaction scheme for the formation of **1**—**5** can be described as follows.

$$2CuX_2 + 2Y^- \longrightarrow 2CuX + Y_2 + 2X^- \quad (5a)$$

$$CuX + Y_2 \rightleftharpoons [CuXY]^-Y^+ \quad (5b)$$

$$\text{>C=C<} + [CuXY]^-Y^+ \longrightarrow \left[\text{>C(Y)—C<}\right][CuXY]^- \xrightarrow{ROH} \text{>C(OR)—C(Y)<} \quad (5c)$$

The first step is the oxidation of thiocyanate or iodide anion by copper(II) salt to form a molecular thiocyanogen or iodine (Scheme 5a, Y=SCN or I). These molecules are activated by complexation with copper(I) salt (Scheme 5b), the electrophilic attack to olefin being followed by addition of the alkoxy group (Scheme 5c). The fact that **1**—**5** are all Markownikov addition products and that the products obtained in the reaction of cyclohexene are *trans*, supports the reaction shceme. In connection with this, the following observations are worth noting. **1** (R=CH_3, Y=I) was obtained in a good yield by refluxing styrene and iodine in methanol in the presence of copper(I) chloride (Table 1). In the absence of copper(I) salt, however, the reaction did not give **1** under similar conditions. Similar phenomena were observed with cyclohexene as a substrate. The reaction of cyclohexene with a mixture of silver(I) thiocyanate and bromine in methanol, which has been known to evolve thiocyanogen,[7)] at 20 °C for 2 hr afforded 19% yield or a trace amount of *trans*-1-

methoxy-2-thiocyanocyclohexane, **2a**, in the presence or absence of copper(I) chloride, respectively.

Nuclear thiocyanation at a *para* position occurred with reactive aromatic compounds such as phenol or *N,N*-dimethylaniline by this reaction system. Thus, *p*-thiocyanophenol [mp 52 °C (recrystallized from H_2O), lit,[8] mp 52—53 °C] was obtained in 51% yield by refluxing phenol, copper(II) chloride and potassium thiocyanate in methanol for 2 hr.

Experimental

The NMR spectra were measured with a Varian A-60 spectrometer in $CDCl_3$, using TMS as an internal standard. The IR and mass spectra were measured with Hitachi EPI-S2 and JEOL JMS-01SG spectrometers, respectively. Glc analysis was carried out on Shimadzu 5APTF and 4BMPF apparatus, using PEG 6000(25%)-Chromosorb W(3 m) and Apiezon L(30%)-Celite(1 m) columns(carrier gas, N_2).

Materials. All the organic materials were distilled before use. Commercial anhydrous $CuCl_2$ and $CuBr_2$ and other inorganic salts were used without further purification.

Preparation of 3a(R=H, R'=CH_3) from Vinyl Acetate. The following is a typical experimental procedure for alkoxythiocyanation, alkoxyiodination being similarly carried out. Vinyl acetate(8.6 g, 0.1 mol) was added at 62 °C under stirring to a greenish-black homogeneous solution of anhydrous $CuCl_2$ (13.4 g, 0.1 mol) and KSCN(9.7 g, 0.1 mol) in methanol(100 ml). In 20 min the color of the reaction mixture turned to pale yellow and a large amount of white precipitate of CuCl was formed. After 3 hr, 400 ml of water was added and then CuCl(8.9 g, 0.09 mol) was filtered. The filtrate was extracted with diethyl ether and the extract was evaporated by a rotary evaporator to *ca.* 20 ml which contained 0.043mol (86% yield) of 1,1-dimethoxy-2-thiocyanoethane **3a**(R=H, R'=CH_3). Distillation gave 4.41 g (0.03 pure compound; bp 106—107 °C/19 mmHg. IR, 2160 (s) mol) of (ν_{SCN}), 1120 (s) (ν_{C-O}) and 1070 (s) (ν_{C-O}) cm^{-1}. NMR, δ 3.12 (d 2H, J=5 Hz), 3.42 (s. 6H), 4.60 (t 1H, J=5 Hz). Found: C, 40.40; H, 6.40; N, 9.47%. Calcd for $C_5H_9NO_2S$: C, 40.80; H, 6.16; N, 9.52%. 2,4-Dinitrophenylhydrazone (2,4-DNP) of **3a**, mp 173—175 °C(yellow crystals, from EtOH).

Identification of the Products. Data on alkoxythiocyanation and alkoxyiodination are given in Tables 1 and 2. **1a**-(R=CH_3), bp 129—130 °C/6 mmHg(lit,[9] 146—147 °C/9 mmHg). **1b**(R=CH_3), bp 94.5 °C/3 mmHg(lit,[2b] 107—108 °C/5 mmHg). **1b**(R=C_2H_5), bp 95.5—96 °C/3 mmHg(lit,[2b] 142—144 °C/14 mmHg). **1b**(R=*n*-C_3H_7), bp 102.5—103 °C/3 mmHg, Found: C, 45.60; H, 5.47%. Calcd for $C_{11}H_{15}IO$: C, 45.53; H, 5.21%. **1b**(R=*n*-C_4H_9), bp 105.5 °C/4 mmHg. Found: C, 47.80; H, 5.87%. Calcd for $C_{12}H_{17}IO$: C, 47.38; H, 5.64%.

2a, bp 108—109.5 °C/18 mmHg. NMR, δ 1.2—2.0(m. 6H), 2.9—3.2 (m. 2H, >CHSCN and >CHOCH$_3$), 3.40(s 3H, OCH$_3$). IR, 2150(s) (ν_{SCN}). **2b**(bp 99.5—101 °C/20 mmHg); identical in glc and NMR with the compounds prepared by the reported method using HgO (red)[2a] or $AgClO_4$[3] as a catalyst, and assigned to *trans*[10] (lit,[2a] bp 114 °C/49 mmHg). *trans*-1-Chloro-2-thiocyanocyclohexane; identical with the compound prepared by the method using $Pb(SCN)_2$ and Cl_2.[8] It was also prepared by the reaction of cyclohexene with $Pb(SCN)_2$ and $SbCl_5$; bp 110—112 °C/4 mmHg(lit,[8] bp 154—156 °C/21 mmHg). *trans*-1-Chloro-2-iodocyclohexane; identical with the compound prepared by the method[1a] from cyclohexene, $CuCl_2$ and I_2 in pentane, bp 66—66.5 °C/4 mmHg (lit,[1a] bp 37 °C/0.2 mmHg).

3a(R=H, R'=C_2H_5), bp 85 °C/5 mmHg. Found: C, 47.62; H, 7.71; N, 7.86%. Calcd for $C_7H_{13}NO_2S$: C, 47.97; H, 7.47; N, 7.99%. **3a**[R=H, (OR')$_2$=O(CH_2)$_2$O], bp 97.5—98 °C/5 mmHg, NMR, δ 3.20 (d 2H, J=3 Hz), 4.00 (m 4H), 5.22 (t 1H, J=3 Hz). Found: C, 48.25; H, 7.88; N, 7.66%. Calcd for $C_5H_7NO_2S$: C, 47.97; H, 7.48; N, 7.99%. **3a**[R=CH_3, (OR')$_2$=O(CH_2)$_2$O], bp 84 °C/3.5 mmHg. NMR(CCl_4), δ 1.45 (s 3H), 3.17 (s 2H), 4.02 (s 4H). **3b** (R=H, R'=CH_3), bp 37 °C/5 mmHg. Found: C, 22.20; H, 4.37%. Calcd for $C_4H_9IO_2$: C, 22.23; H, 4.20%. 2,4-DNP, mp 145—148 °C (yellow crystals, from EtOH). **3b** (R=H, R'=*i*-C_3H_7), bp 55.5 °C/3 mmHg. Found: C, 35.65; H, 6.63%. Calcd for $C_8H_{17}IO_2$: C, 35.30; H, 6.30%.

4a (R=C_2H_5, R'=CH_3), bp 85 °C/5 mmHg. Found: C, 44.46; H, 7.32; N, 8.64%. Calcd for $C_6H_{11}NO_2S$: C, 44.70; H, 6.88; N, 8.69%. **4a** (R=C_2H_5, R'=*t*-C_4H_9), bp 97.5—98 °C/6 mmHg. Found: C, 52.60; H, 8.80; N, 7.08%. Calcd for $C_9H_{17}NO_2S$: C, 53.17; H, 8.43; N, 6.89%. **4a** (R=C_2H_5, R'=CH_2CH_2OH), bp 135—136 °C/8 mmHg. Found: C, 44.35; H, 7.18; N, 7.25%. Calcd for $C_7H_{13}NO_3S$: C, 43.96; H, 6.85; N, 7.32%. **4a** (R=*n*-C_4H_9, R'=*t*-C_4H_9), bp 105.5—106 °C/4 mmHg. Found: C, 56.20; H, 9.24; N, 6.39%. Calcd for $C_{11}H_{21}NO_2S$: C, 57.10; H, 9.15; N, 6.05%. **4b** (R=C_2H_5, R'=CH_3), bp 38 °C/4 mmHg. Found: C, 26.56; H, 5.08%. Calcd for $C_5H_{11}IO_2$: C, 26.10; H, 4.82%.

5a (R=H, R'=CH_3), bp 98—99 °C/5 mmHg. Found: C, 43.43; H, 7.05; N, 7.08%. Calcd for $C_{17}H_{13}NO_3S$: C, 43.96; H, 6.86; N, 7.33%. **5a** (R=R'=CH_3), bp 91.5—93 °C/5 mmHg. Found: C, 46.55; H, 7.65; N, 6.80%. Calcd for $C_8H_{15}NO_3S$: C, 46.80, H, 7.37; N, 6.82%. **5b** (R=H, R'=CH_3), bp 80.5 °C/5 mmHg. Found: C, 27.87; H, 5.43%. Calcd for $C_6H_{13}IO_3$: C, 27.60; H, 5.40%. **5b** (R=R'=CH_3), bp 83.5—84 °C/5 mmHg. Found: C, 30.69; H, 5.76%. Calcd for $C_7H_{15}IO_3$: C, 30.67; H, 5.51%.

Reaction Conditions, Yields and Identification of Products Other than Those Shown in Tables 1 and 2. From styrene: 82 °C, 3 hr, **1b** (R=*i*-C_3H_7) 35%, bp 95.5—96 °C/3 mmHg. Found: C, 46.20; H, 5.39%. Calcd for $C_{11}H_{15}IO$: C, 45.53; H, 5.21%. 82 °C, 2 hr, **1b** (R=*t*=C_4H_9) 32%, bp 100—101.5 °C/3 mmHg, NMR, δ 1.16 (s 9H), 3.24 (d 2H, J=6.5 Hz), 4.62 (t 1H, J=6.5 Hz), 7.27—7.36 (m 5H). From vinyl acetate: 60 °C, 5 hr, **3a** (R=H, R'=*n*-C_3H_7) 36%, bp 105—106.5 °C/5 mmHg. Found: C, 53.16; H, 9.15; N, 6.35%. Calcd for $C_9H_{17}NO_2S$: C, 53.17; H, 8.43; N, 6.89%. 60 °C, 5 hr, **3a** (R=H, R'=*n*-C_4H_9) 52%, bp 124.5—125 °C/5 mmHg. Found: C, 56.50; H, 9.72; N, 6.00%. Calcd for $C_{11}H_{21}NO_2S$: C, 57.10; H, 9.15; N, 6.06%. 60 °C, 1 hr, **3b** (R=H, R'=C_2H_5) 84%, bp 57.5—59 °C/5 mmHg (lit,[11] 100 °C/10 mmHg). 25 °C, 2 hr, **3b** (R=H, R'=*n*-C_3H_7) 39%, bp 74 °C/5 mmHg. Found: C, 34.93; H, 6.42%. Calcd for $C_8H_{17}IO_2$: C, 35.31; H, 6.30%. 60° C, 1 hr, **3b** (R=H, R'=*n*-C_4H_9) 37%, bp 103.5—104 °C/5 mmHg. Found: C, 39.78; H, 7.33%. Calcd for $C_{10}H_{21}IO_2$: C, 40.01; H, 7.05%. 25 °C, 1 hr, **3b** (R=H, R'=*i*-C_4H_9) 38%, bp 89—89.5 °C/5 mmHg. Found: C, 39.06; H, 7.35%. Calcd for $C_{10}H_{21}IO_2$: C, 40.01; H, 7.05%.

cis-1-Methoxy-2-thiocyanocyclohexane. **2b** (5.0 g, 20 mmol) was added at 110 °C to a stirred solution of KSCN (3.7 g, 40 mmol) in DMF (50 ml). After 12 hr water was added and extracted with diethyl ether. Distillation of the product gave 1.6 g of pure compound (9.4 mmol, 47% yield); bp 95—97 °C/5 mmHg. The retention time of the compound (t_R=7.7 min) was longer than that of **2a** (t_R=7.1 min) in the glc using Apiezon-L column (1 m) (column temp. 150 °C; N_2 100 ml/min). NMR, δ 1.4—2.1 (m 8H), 3.37 (s 3H, OCH$_3$), 3.4—3.8 (m 2H, >CHSCN and >CHOCH$_3$). IR

2150 (s) (ν_{SCN}). Mass spectrum (*m/e*) 171 (M^+). Attempts to prepare *cis*-1-chloro-2-thiocyanocyclohexane from the reaction of *trans*-1-chloro-2-iodocyclohexane with KSCN were unsuccessful.

References

1) a) W. C. Baird, Jr., J. H. Surridge, and M. Buza, *J. Org. Chem.*, **36**, 2088 (1971). b) W. C. Baird, Jr., J. H. Surridge, and M. Buza, *ibid.*, **36**, 3324 (1971).

2) a) L. Brunel, *C. R. Acad. Sci. Paris*, **135**, 1056 (1902). b) M. Tiffeneau, *ibid.*, **145**, 813 (1907).

3) L. Birckenbach and J. Goubeau, *Ber.*, **65B**, 395 (1932).

4) H. Mitani, T. Ando, and Y. Yukawa, *Chem. Lett.*, **1972**, 455.

5) C. E. Castro, E. J. Gaughan, and D. C. Owsley, *J. Org. Chem.*, **30**, 587 (1965).

6) Bp 102—102.5 °C/5 mmHg. Found: C, 48.25; H, 7.85; N, 7.66%. Calcd for $C_7H_{13}NO_2S$: C, 47.97; H, 7.48; N, 7.99%.

7) E. Söderbäck, *Ann. Chem.*, **419**, 238 (1919).

8) A. B. Angus and R. G. R. Bacon, *J. Chem. Soc.*, **1958**, 774.

9) S. Uemura, K. Zushi, A. Tabata, A. Toshimitsu, and M. Okano, This Bulletin, **47**, 920 (1974).

10) M. Mousseron and M. Canet, *C. R. Acad. Sci. Paris*, **233**, 484 (1951).

11) J. Hesse, *Ber.*, **30**, 1442 (1897).

Reactions of Methylcalcium Iodide. II. Carboxylation, Metalation, and Metal-Halogen Exchange Reactions

Nariyoshi KAWABATA,* Hirotsugu YOSHIMURA, and Shinzo YAMASHITA
Department of Chemistry, Faculty of Polytechnic Science, Kyoto Institute of Technology, Matsugasaki, Sakyo-ku, Kyoto 606
(Received March 22, 1974)

Utility of methylcalcium iodide in several organic reactions in tetrahydrofuran was shown. Carboxylation of methylcalcium iodide at −70 °C gave acetic acid in 57—63% yield. Metallation of indene and fluorene by methylcalcium iodide at −30 °C gave 3-indenyl- and 9-fluorenylcalcium iodides in 99 and 93% yields, respectively. Metal-halogen exchange reactions of methylcalcium iodide with halobenzenes were rather slow.

Although reactions of organocalcium halides have been studied, available data are limited. Yields of products are generally low, particularly in the reactions of aliphatic organocalcium halides. We demonstrated that methylcalcium iodide is a useful organometallic reagent in several organic reactions in tetrahydrofuran.[1] Reactions with ketones, aldehydes and esters gave the corresponding addition products in good yields. Both coupling and addition reactions were observed in the reactions with acid halides. They gave the corresponding ketones in low yields by the reaction with nitriles, reacting slowly with benzyl chloride and 1,1-diphenylethylene, but not reacting with cyclohexene. We have examined the utility of methylcalcium iodide in carboxylation, metalation, and metal-halogen exchange reactions.

Results and Discussion

Bryce-Smith and Skinner[2] reported that carboxylation of phenylcalcium iodide at −50 to −30 °C in tetrahydrofuran afforded benzoic acid in a high yield, whereas that of *n*-butyl- and *n*-pentylcalcium iodides at 20—25 °C in diethyl ether gave the corresponding carboxylic acids in only 10 and 9% yields, respectively. They observed the formation of the corresponding ketones and carbinols besides the carboxylic acids. However, we found that carboxylation of methylcalcium iodide at −70 °C in tetrahydrofuran gave acetic acid in 53—57% yield based on methyl iodide used in the preparation of methylcalcium iodide. Since the yield of methylcalcium iodide was in the range 91—93% based on methyl iodide, the yield of acetic acid based on methylcalcium iodide would be 57—63%. Gas chromatographic analyses also showed the presence of acetone and *tert*-butyl alcohol in 17 and 11% yields based on methyl iodide (18 and 12% yields based on methylcalcium iodide), respectively. The discrepancy of our results with those of Bryce-Smith and Skinner[2] could be partly attributed to the difference in the reaction temperature. The addition of alkylcalcium iodide to calcium carboxylate formed by the reaction of alkylcalcium iodide with carbon dioxide might be more significant at higher temperature.

Kocheshkov and co-workers[3,4] reported that metallation of indene and fluorene by phenylcalcium iodide followed by carboxylation gave the corresponding carboxylic acids in good yields. They stated that metallation of indene, fluorene and related hydrocarbons by alkylcalcium iodides followed by carboxylation afforded the corresponding carboxylic acids in very low yields.[3] However, we found that metalation of indene by methylcalcium iodide at −30 °C followed by carboxylation gave indene-3-carboxylic acid in 99% yield, mp 161 °C.

We used an excess amount of calcium metal in the preparation of methylcalcium iodide. Indene-3-carboxylic acid could be partly derived from the direct metalation of indene by the excess calcium metal. We found that direct metallation of indene by metallic calcium in tetrahydrofuran under similar reaction conditions gave only a trace of indene-3-carboxylic acid after carboxylation. Direct metallation seems to be a rather slow reaction, *e.g.*, Fischer and Stölzle[5] obtained bis(cyclopentadienyl)calcium in 27% yield from calcium metal and cyclopentadiene in 3—4 hr in refluxing tetrahydrofuran.

Kocheshkov and co-workers[3,4] described the formation of indene-1-carboxylic acid. However, the melting point 154 °C shows that the product was indene-3-carboxylic acid. The melting points of indene-1- and indene-3-carboxylic acids were reported to be 73.5—74 °C[6] and 159.5—161 °C,[7] respectively.

We also found that fluorene-9-carboxylic acid was formed in 93% yield by the metallation of fluorene with methylcalcium iodide at −30 °C followed by carboxylation.

Thus the metalation of indene and fluorene by methylcalcium iodide provides an excellent method for preparation of 3-indenyl- and 9-fluorenylcalcium iodides, which is in contrast to that described.[3,4] The discrepancy could be ascribed to low purity of alkylcalcium iodides.

Bryce-Smith and Skinner[2] reported that the reaction of α-bromonaphthalene with phenylcalcium iodide gave α-naphthylcalcium iodide in an excellent yield. However, no information can be found in literature on the metal-halogen exchange reaction of alkylcalcium halides. We found that the reactions of methylcalcium iodide with halobenzenes were rather slow. Reactions of methylcalcium iodide with bromobenzene in tetrahydrofuran at −30 °C gave a trace of benzoic acid after carboxylation. Gas chromatographic analysis also indicated the presence of a nearly quantitative amount of unchanged bromobenzene in the reaction products.

* To whom correspondence should be addressed.

Neither toluene nor biphenyl was detected.

On the other hand, longer reaction time and higher reaction temperature improved the yield to some extent. The reaction at 20 °C for 24 and 45 hr gave benzoic acid in 11 and 36% yields, respectively, after carboxylation. The reactions of methylcalcium iodide with chlorobenzene, bromobenzene and iodobenzene at 23 °C for about 50 hr gave benzoic acid in 21, 42, and 38% yields, respectively. The reaction of *n*-propylcalcium iodide with bromobenzene at 20 °C for 40 hr gave benzoic acid in 80% yield. We used excess calcium metal in the preparation of methyl- and *n*-propylcalcium iodide. The reaction of unchanged calcium metal with halobenzenes to give phenylcalcium halides was significant under these reaction conditions. Still longer reaction time and higher reaction temperature would not markedly improve the yield, since the loss of organocalcium halides by the reaction with the solvent, tetrahydrofuran, becomes significant under the conditions.[1,2]

Experimental

Gas chromatographic analyses were carried out on a Shimadzu GC-4A or GC-4B gas chromatograph using columns of Chromosorb 101 (80—100 mesh) and 20% polyethylene glycol 6000 on Celite 545 (60—80 mesh) for carboxylic acids and other products, respectively. Proton magnetic resonance spectra were obtained with a Varian T-60-A spectrometer using dimethyl-d_6 sulfoxide or carbon tetrachloride as the solvent and tetramethylsilane as an internal standard.

Materials. Methylcalcium iodide and *n*-propylcalcium iodide were prepared in tetrahydrofuran.[8] Tetrahydrofuran was purified by distillation in the presence of benzophenone sodium ketyl under a nitrogen atmosphere. Nitrogen was purified by being passed through a tube containing copper turnings in a furnace at 170 °C followed by drying with phosphorus pentoxide. Methyl iodide, *n*-propyl iodide, chlorobenzene, bromobenzene, iodobenzene, and indene were dried over calcium hydride and distilled. Fluorene was dried by being kept over phosphorus pentoxide in a desiccator. Carbon dioxide was dried by being passed through calcium chloride, silica gel, and concentrated sulfuric acid. Commercial authentic samples and other chemicals were used without further purification.

Procedure. The reaction vessel was a two- or one-necked flask equipped with three-way cocks. Each cock was connected with a nitrogen inlet and a rubber serum cap. Methylcalcium iodide and *n*-propylcalcium iodide were prepared in the flask under nitrogen atmosphere. Various reactants were added to this organocalcium compound with a hypodermic syringe under nitrogen atmosphere. Carboxylation was carried out by passing carbon dioxide through a stainless steel needle.

Reaction of Methylcalcium Iodide with Carbon Dioxide. Carbon dioxide was passed through a suspension of methylcalcium iodide in tetrahydrofuran at −70 °C for 2 hr, after which water was added. The precipitate was washed with diethyl ether, and 20% hydrochloric acid was added to the precipitate. Extraction with diethyl ether and elimination of the solvents and other materials of lower boiling points under a reduced pressure gave a mixture of acetic acid and water. Its NMR spectrum indicated the absence of impurity other than water, and showed the yield of acetic acid to be 57% based on the methyl iodide used in the preparation of methylcalcium iodide.

In another run, carbon dioxide was passed through a suspension of methylcalcium iodide in tetrahydrofuran at −70 °C for 1 hr, and then water and 20% hydrochloric acid were added. The reaction mixture was subjected to gas chromatographic analyses. The yield of acetic acid was 53% based on methyl iodide. Gas chromatographic analyses also showed the presence of acetone and *tert*-butyl alcohol in 17 and 11% yields, respectively, based on methyl iodide in the reaction mixture.

Metallation of Indene by Methylcalcium Iodide. To methylcalcium iodide prepared from 0.35 g (8.8 mmol) of calcium and 0.98 g (6.9 mmol) of methyl iodide was added 0.57 g (4.9 mmol) of indene in 2.0 ml of tetrahydrofuran. The reaction mixture was allowed to stand at −30 °C for 2.5 hr under stirring, and carbon dioxide was passed through the reaction mixture at −70 °C for 1 hr, and then 10.0 ml of 20% hydrochloric acid was added. Extraction with diethyl ether and evaporation of the solvent under reduced pressure left a solid, which was washed with carbon tetrachloride and dried over phosphorus pentoxide under reduced pressure in a desiccator. Purity of the product was checked by its NMR spectrum. Yield of indene-3-carboxylic acid was 0.78 g (99% based on indene), mp 161 °C (lit,[7] 159.5—161 °C). The reaction of 0.12 g (3.0 mmol) of calcium metal with 0.69 g (5.9 mmol) of indene in 15.0 ml of tetrahydrofuran under similar conditions gave a trace of indene-3-carboxylic acid after carboxylation. The result shows that direct metalation of indene by the excess calcium metal, used in the preparation of methylcalcium iodide, was not significant under the above reaction conditions.

Metallation of Fluorene by Methylcalcium Iodide. To methylcalcium iodide prepared from 0.30 g (7.4 mmol) of calcium and 0.82 g (5.8 mmol) of methyl iodide was added, 0.77 g (4.6 mmol) of fluorene in 3.0 ml of tetrahydrofuran, and the mixture was kept at −30 °C for 3 hr under stirring. Carbon dioxide was passed through the mixture at −70 °C for 1 hr, and the reaction mixture was treated in a similar manner to that in the metalation of indene. Yield of fluorene-9-carboxylic acid was 0.91 g (93% based on fluorene), mp 225 °C. Melting points were reported to be in the range 225—232 °C.[9-12]

Reaction of Methylcalcium Iodide with Halobenzenes. To methylcalcium iodide prepared from 0.31 g (7.7 mmol) of calcium and 0.89 g (6.2 mmol) of methyl iodide was added, 0.56 g (5.0 mmol) of chlorobenzene in 2.0 ml of tetrahydrofuran and the mixture was allowed to react at 23 °C for 49 hr under stirring. Passage of carbon dioxide at −70 °C for 1 hr led to the formation of benzoic acid. Gas chromatographic analyses indicated the yield of benzoic acid to be 21% based on chlorobenzene, and the presence of trace of benzene in the reaction products. The reaction of 0.054 g (1.3 mmol) of calcium metal with 0.32 g (2.9 mmol) of chlorobenzene in 6.8 ml of tetrahydrofuran under similar conditions gave a trace of benzoic acid after carboxylation.

To methylcalcium iodide prepared from 0.30 g (7.4 mmol) of calcium metal and 0.85 g (6.0 mmol) of methyl iodide was added 0.75 g (4.8 mmol) of bromobenzene in 2.0 ml of tetrahydrofuran, and the mixture was allowed to react at 23 °C for 49.5 hr under stirring. The reaction mixture was treated in a similar manner. The yield of benzoic acid determined by gas chromatography was 42% based on bromobenzene. Gas chromatographic analysis showed the presence of benzene in 0.4% yield based on bromobenzene. The reaction of 0.12 g (3.0 mmol) of calcium metal with 1.04 g (6.6 mmol) of bromobenzene in 15.0 ml of tetrahydrofuran under similar conditions gave a trace of benzoic acid after carboxylation.

To methylcalcium iodide prepared from 0.27 g (6.7 mmol)

of calcium and 0.83 g (5.8 mmol) of methyl iodide was added 0.89 g (4.4 mmol) of iodobenzene in 2.0 ml of tetrahydrofuran. The mixture was allowed to react at 23 °C for 49.5 hr under stirring, and treated in a similar manner. Gas chromatographic analyses showed the formation of benzoic acid in 38% yield based on iodobenzene, as well as a trace of benzene. The reaction of 0.056 g (1.4 mmol) of calcium metal with 0.59 g (2.9 mmol) of iodobenzene in 7.0 ml of tetrahydrofuran under similar conditions gave 0.64 mmol of benzoic acid (22% based on iodobenzene and 46% based on metallic calcium) after carboxylation. The result indicates the formation of phenylcalcium iodide under the above reaction conditions by the direct reaction of iodobenzene with excess calcium metal.

Reaction of n-*Propylcalcium Iodide with Bromobenzene.* To *n*-propylcalcium iodide prepared from 0.11 g (2.7 mmol) of calcium and 0.36 g (2.1 mmol) of *n*-propyl iodide was added 0.16 g (1.0 mmol) of bromobenzene and the mixture was allowed to react at 20 °C for 40 hr under stirring. A similar treatment of the mixture led to the formation of benzoic acid in 80% yield based on bromobenzene. The yield was determined by gas chromatography.

The authors are grateful to Mr. Akira Matsumura for his assistance in the preliminary experiments of this work.

References

1) N. Kawabata, H. Nakamura, and S. Yamashita, *J. Org. Chem.*, **38**, 3403 (1973).
2) D. Bryce-Smith and A. C. Skinner, *J. Chem. Soc.*, **1963**, 577.
3) K. A. Kocheshkov, M. A. Zemlyanichenko, and N. I. Sheverdina, *Izv. Akad. Nauk SSSR, Ser. Khim.*, **1971**, 2617.
4) M. A. Zemlyanichenko, N. I. Sheverdina, and K. A. Kocheshkov, *Dokl. Akad. Nauk SSSR*, **202**, 595 (1972).
5) E. O. Fischer and G. Stölzle, *Chem. Ber.*, **94**, 2187 (1961).
6) O. Meth-Cohn and S. Gronowitz, *Chem. Commun.*, **1966**, 81.
7) W. S. Knowles, J. A. Kuck, and R. C. Elderfield, *J. Org. Chem.*, **7**, 374 (1942).
8) N. Kawabata, A. Matsumura, and S. Yamashita, *Tetrahedron*, **29**, 1069 (1973).
9) A. Jeanes and R. Adams, *J. Amer. Chem. Soc.*, **59**, 2608 (1937).
10) R. T. Burtner and J. W. Cusic, *ibid.*, **65**, 262 (1943).
11) R. S. Yost and C. R. Hauser, *ibid.*, **69**, 2325 (1947).
12) R. T. Arnold, W. P. Parham, and R. M. Dodson, *ibid.*, **71**, 2439 (1949).

The Thermal Reactions of Azido-1,3,5-triazines

Ryuichi KAYAMA, Shigeru HASUNUMA, Shizen SEKIGUCHI, and Kohji MATSUI
Department of Chemistry, Faculty of Engineering, Gunma University, Kiryu, Gunma 376
(Received April 20, 1974)

Azido-*s*-triazines containing -Cl, $-OCH_3$, and $-N(CH_3)_2$ groups were synthesized, and their thermal reactions with some hydrocarbons were investigated with respect to the reaction products and the reaction kinetics. With non-olefinic hydrocarbons the reactions were found to proceed *via* a nitrene intermediate; in the reactions with cyclohexane, cyclohexylamino-*s*-triazines and amino-*s*-triazines were obtained. On the other hand, with olefinic hydrocarbons the reactions took place *via* a bimolecular mechanism involving a formation of an intermediate of the triazoline type; in the reactions with cyclohexene, cyclohexenylamino-*s*-triazines were obtained along with amino-*s*-triazines. In both cases, the yields of alkylamino and alkenylamino-*s*-triazines increased with the electron-withdrawing power of the substituents in the *s*-triazine nucleus.

There have been a number of studies of the thermal and photochemical reactions of azido compounds;[1] in recent years the reactions and structures of azido derivatives of nitrogen heteroaromatics such as pyridine,[2,3] pyridazine,[4] pyrimidine,[5-8] pyrazine,[9,10] quinoline,[11] and acridine[12] have been investigated.

Azido-*s*-triazines have been known for a long time; however, little is known about their reactions. In the reactions of azido-*s*-triazines with such nucleophiles as sodium hydroxide[13] and ammonia,[14] the azido group is replaced by hydroxy and amino groups, while some azido-*s*-triazines are known to decompose violently on heating.[13,15] Recently, the presence of a nitrene intermediate was confirmed in the photolysis of azido-*s*-triazine,[16] and amino-*s*-triazines were obtained from azido-*s*-triazines upon irradiation in methanol.[17] However, the details of the thermal and photochemical reactions of azido-*s*-triazines have not yet been revealed. On the other hand, the thermolysis and photolysis of azido-*s*-triazines may provide useful and convenient routes for the preparation of a number of *s*-triazine derivatives which would otherwise be difficult to synthesize. This paper will report on the thermal reactions of azido-*s*-triazines with several hydrocarbons.

Results and Discussion

Syntheses of Azido-s-triazines. Azido-*s*-triazines containing -Cl, $-OCH_3$, and $-N(CH_3)_2$ groups in the *s*-triazine nucleus were prepared by the condensation of the corresponding chloro-*s*-triazines with sodium azide. Table 1 lists the compounds thus obtained. These monoazido-*s*-triazines are thermally-stable compounds. Compound **1** is distillable, while Compound **2** can be sublimed under reduced pressure; all of them decomposed at about 200 °C, showing no significant substituent effect upon their thermal stabilities.

Structure of Azido-s-triazines. It is well known that an azidoazomethine-tetrazole equilibrium exists in 2-azido-nitrogen heteroaromatics; the position of the equilibrium is known to depend upon the solvent, the temperature, and the electronegativity of the heterocyclic ring. Generally, the electron-withdrawing ability of the heterocyclic ring is considered to stabilize the azido form;[18] azido-pyridines exist in equilibrium with the tetrazole form, but the equilibrium lies strongly on the side of the tetrazole,[19] and azido-pyrimidines exist in both the azido and tetrazole forms, while 2-amino-4,6-diazido-*s*-triazine is known to exist in the diazido form.[20]

The IR spectra of these azido-*s*-triazines in KBr discs have a strong and sharp characteristic band near 2100 cm^{-1} assignable to the azido group, suggesting that these compounds exist in the azido form in a solid state. In addition, the PMR spectra of Compounds **2** and **3** in CCl_4, $CDCl_3$, DMSO-d_6, and CF_3COOH at 40 and 60 °C showed a signal assignable to $-OCH_3$ or $-N(CH_3)_2$ as a singlet in every case in spite of the wide diversity in the nature of the solvent (see Table 2), indicating the absence of tautomeric tetrazole, which should possess two kinds of methoxy or dimethylamino groups respectively; azido-*s*-triazines containing ordinary substituents in the *s*-triazine nucleus exist in the azido form not only in a solid state, but also in a solution, regardless of the solvent employed. The fact that the azido form is the sole species in Compound **3**

TABLE 1. 4,6-DISUBSTITUTED 2-AZIDO-*s*-TRIAZINES

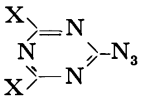

No.	Substituent	Mp (°C)	Decomp. (°C)	Solvent for recrystallization	Anal. (%) Found C	Found H	Found Cl	Cacld C	Cacld H	Cacld Cl
1	Cl	60—61 (85) [a]	205	Ligroin	—	—	37.41	—	—	37.12
2	OCH_3	85—85.5	195	Benzene-Ligroin	32.62	3.64	—	32.97	3.32	—
3	$N(CH_3)_2$	106—107	205	Methanol	39.99	6.10	—	40.37	5.81	—

a) C. Hart, *J. Amer. Chem. Soc.*, 1922 (1928).

TABLE 2. PMR DATA OF 2-AZIDO-4,6-DIMETHOXY-*s*-TRIAZINE (**2**) AND 2-AZIDO-4,6-BIS(DIMETHYLAMINO)-*s*-TRIAZINE (**3**)

Solvent	Chemical shifts (δ)[a]	
	2	**3**
CCl_4	4.00	3.11
$CDCl_3$	4.05	3.13
DMSO-d_6	3.98	3.07
CF_3COOH	4.40	3.37

a) TMS was used as the internal standard.

[the bis(dimethylamino)-*s*-triazinyl group is known to be the least electron-attracting group among the common *s*-triazinyl groups][21] suggests that the presence of

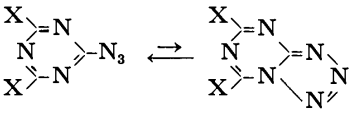

X=-Cl, $-OCH_3$, $-N(CH_3)_2$

three ring nitrogen atoms in the heterocyclic nucleus is sufficient for the electron-withdrawing power of the heterocycle to shift the azidoazomethine-tetrazole equilibrium far to the left, regardless of the substituents in the heterocycle.

Reactions of Azido-s-triazines with Hydrocarbons. It is known that acyl azides, such as azido formates and sulfonyl azides, decompose thermally or photochemically to give the corresponding nitrenes, which then react with aliphatic hydrocarbons to give alkylamino derivatives as the insertion products. On the other hand, it is known that, in the thermal reactions with aliphatic hydrocarbons, ordinary aryl azides do not afford the corresponding nitrene insertion products as the major products. Recently, it was reported that, in the reaction of phenyl azide with cyclohexane, *N*-cyclohexylaniline was obtained with aniline.[22] The situation of the *s*-triazinyl group as a aromatic group is of interest because of its strong electron-attracting character.

When the azido-*s*-triazines were heated in cyclohexane at 180—190 °C under pressure, the corresponding amino-*s*-triazines and cyclohexylamino-*s*-triazines were obtained as the major products in every case.

TABLE 3. YIELDS OF AMINO- AND CYCLOHEXYLAMINO-*s*-TRIAZINES IN THE REACTIONS OF AZIDO-*s*-TRIAZINES WITH CYCLOHEXANE AT 190 °C

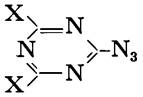

Azido-*s*-triazine	Substituent X	Yields (%)	
		Amino-*s*-triazine	Cyclohexylamino-*s*-triazine
1	Cl	—	23<[a]
2	OCH_3	15	22
3	$N(CH_3)_2$	17	trace

a) Isolated after methoxydechlorination.

Table 3 lists the yields of these *s*-triazine derivatives.

In the case of Compound **1**, because of the presence of active chlorine atoms in the *s*-triazine nucleus, the formation of a large quantity of a metal-containing decomposition product (the metallic constituents of the by-products are considered to result from the autoclave used) was observed. Therefore, the yields of the major reaction products should increase in the reactions in inert reactors.

From Table 3 it is obvious that the substituents in the *s*-triazine nucleus considerably affect the yields of the products; it can be said that the electron-withdrawing substituents in the *s*-triazine nucleus favor the formation of cyclohexylamino-*s*-triazine and that, in the thermal reactions of aryl azides with aliphatic hydrocarbons, the yields of the alkylamino derivatives become higher with an increase in the acidic character of the aryl group.

On the other hand, when azido-*s*-triazines were heated in cyclohexene under pressure at 180—190 °C, the corresponding amino-*s*-triazines and cyclohexenylamino-*s*-triazines were obtained in every case, as is shown below.

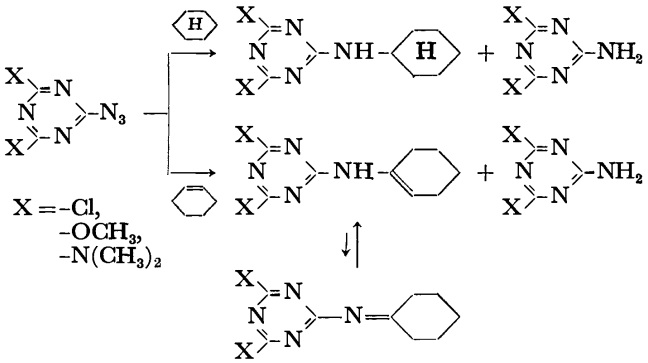

Table 4 lists the yields of the amino- and cyclohexenylamino-*s*-triazines thus obtained. In the reaction of Compound **1** with cyclohexene, the formation of a large quantity of metal containing decomposition product was also observed.

From the concept[23] generally accepted for the structure of ordinary enamines possessing a secondary nitrogen atom, the tautomeric equilibrium between enamine and imino forms in *s*-triazinyl enamines can be expected

TABLE 4. YIELDS OF AMINO- AND CYCLOHEXENEYLAMINO-*s*-TRIAZINES IN THE REACTIONS OF AZIDO-*s*-TRIAZINES WITH CYCLOHEXENE AT 190 °C

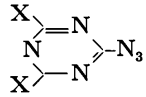

Azido-*s*-triazine	Substituent X	Yields (%)	
		Amino-*s*-triazine	Cyclohexenylamino-*s*-triazine
1	Cl	—	22<[a]
2	OCH_3	16	44
3	$N(CH_3)_2$	17	—

a) Isolated after methoxydechlorination.

Table 5. PMR data of 2-(cyclohexene-1-ylamino)-4,6-dimethoxy-*s*-triazine

Solvent	Chemical shifts (δ)[a]			
	$-(CH_2)_4-$(m)[b]	CH_3O-(s)[b]	=CH–(m)[b]	–NH–(b)[b]
CCl_4	1.50—2.50 (8)[c]	3.88 (6)[c]	5.93 (1)[c]	7.40 (1)[c]
$CDCl_3$	1.30—2.50 (8)	3.91 (6)	6.05 (1)	6.95 (1)
DMSO-d_6	1.43—2.43 (8)	3.87 (6)	5.96 (1)	8.91 (1)

a) TMS was used as the internal standard. b) m: multiplet, s: singlet, b: broad. c) Indicates the number of protons.

to lie far to the side of the imino form. However, in the PMR spectra of cyclohexenylamino-*s*-triazines, the presence of NH and olefinic protons was observed in a ratio of 1 : 1, as is shown in the case of the dimethoxy-*s*-triazine derivative (see Table 5). This fact indicates that the cyclohexenylamino-*s*-triazine exists as the enamine form, suggesting that the strong electron-attracting character of the *s*-triazinyl group prevents the overlap of the lone pair of electrons on the -NH- nitrogen with the π electrons of the enaminic double bond, and that the N→C migration of the NH proton to form the imino form becomes difficult; in ordinary *s*-triazine derivatives the enamine form may be the stable one, as in the cases of *N*-acyl vinylamines[24] and *N*-ethoxycarbonylcyclohexenylamine.[25]

Kinetics of the Reactions of Azido-s-triazines with Hydrocarbons. As has been described above, azido-*s*-triazines react thermally with cyclohexane and cyclohexene to give the insertion and abstraction products of the nitrenes corresponding in appearance. Thus, in order to make clear the progress of the reactions of azido-*s*-triazines with these hydrocarbons, kinetic measurements of the reactions were carried out.

When azido-*s*-triazines were heated in hydrocarbons, an evolution of nitrogen was observed in every case. Therefore, for the kinetic measurements, an increase in the volume of nitrogen evolved was followed with the lapse of time in various substrates. Since a plot of

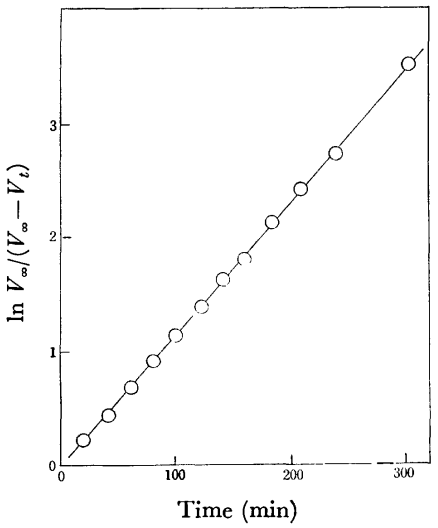

Fig. 1. Decomposition of 2-azido-4,6-dimethoxy-*s*-triazine in acetophenone at 184.3 °C.

ln $V_\infty/V_\infty - V_t$ (where V_t and V_∞ are the volumes of nitrogen evolved at time t and at an infinite time respectively) against the reaction time, t, was found to give a straight line up to about a 90% conversion of the azido-*s*-triazines, as is shown in Fig. 1, the first-order rate constants for the decomposition of azido-*s*-triazines were calculated from the slopes of the straight lines; they are listed in Table 6.

From Table 6 it is obvious that, in the reactions with cyclohexane, decalin, tetralin, diphenyl ether, and dimethyl terephthalate, there was little variation in the rate in spite of the wide diversity in the nature of the substrates, suggesting that the rate-determining step of these reactions is the loss of nitrogen and the formation of an electron-deficient nitrene species. The substrates were assumed to participate merely as solvents. For a detailed discussion of the reactions of azido-*s*-

Table 6. Rate constants for the decomposition of azido-*s*-triazines in various substrates at 184.3 °C

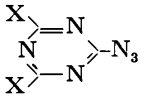

Substrate	$k_1 \times 10_1$ (s^{-1})		
X=	-Cl	$-OCH_3$	$-N(CH_3)_2$
Cyclohexane	—	2.88	—
Decalin	3.07	2.36	3.38
Tetralin	2.30	2.21	3.04
Diphenyl ether	—	1.83	3.42
Acetophenone	—	2.06	4.39
Dimethyl terephthalate[a]	—	1.94	—
Cyclohexene	b)	66.9	20.9
1-Tetradecene	b)	61.0	33.7
Methyl oleate	31.9	26.1	12.0
Diethyl maleate	70.2	59.4	82.0

a) measured with 43.5% Decalin solution b) Rate constant was too fast to measure.

Table 7. Rate constants for the decomposition of 2-azido-4,6-dimethoxy-*s*-triazine at various temperatures

Temp. (°C)	$k_1 \times 10_4$ (s^{-1})		
	Decalin	Cyclohexene	Methyl oleate
154.0	—	—	6.48
164.2	—	22.7	11.0
174.2	0.96	39.7	15.6
184.3	2.36	66.9	26.1
194.0	5.45	—	—

Table 8. Activation parameters for the decomposition of 2-azido-4,6-dimethoxy-*s*-triazine

Substrate	$\Delta H^{\ddagger}$ (kcal·mol^{-1})	$\Delta S^{\ddagger}$ (184.3 °C) (cal·deg^{-1}·mol^{-1})
Decalin	36.7	+4
Cyclohexene	21.0	−23
Methyl oleate	16.8	−34

triazines with these substrates, the temperature dependence of the reaction constant for the decomposition of Compound **2** was measured in decalin; the results are listed in Table 7. From these values, the activation parameters for the reaction were calculated; they are shown in Table 8.

The entropy of activation of +4.0, which is comparable in magnitude to those of the reactions of sulfonyl azides with similar substrates, suggests that the reaction is of the first order involving the nitrene intermediate;[26] it can be generally said that the thermal reactions of azido-*s*-triazines with non-olefinic hydrocarbons proceed *via* a nitrene intermediate.

On the other hand, in the reactions of azido-*s*-triazines with olefinic hydrocarbons, the situation was different from that described above. For example, the rate constants for the reactions of Compound 2 with cyclohexene, 1-tetradecene, methyl oleate, and dimethyl maleate were larger than those for the reactions with non-olefinic substrates and (see Table 5) differed significantly from each other, suggesting that the rate-determining step of these reactions is not the loss of nitrogen from azido-*s*-triazines. Moreover, the entropies of activation were of a large negative value, as is shown in Table 8. Therefore, it is unlikely that the decomposition of azido-*s*-triazines in olefinic hydrocarbons proceeds *via* a nitrene intermediate; it may be reasonable to consider that the reactions of azido-*s*-triazines with olefins take place *via* a bimolecular mechanism involving an intermediate of the triazoline type which decomposes rapidly under the cleavage of the nitrogen to give the final products.[27]

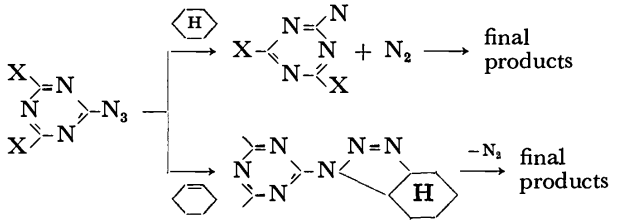

If this reaction process is correct, the amino-*s*-triazines in the reactions with olefins should result from the triazoline intermediates or cyclohexenylamino-*s*-triazines.

When Compound 2 was heated at 120 °C in cyclohexane for 40 hr, merely 5% of the azide was decomposed, forming amino-*s*-triazine in a yield of 6% of the decomposed azide. However, when Compound 2 was heated in cyclohexene at 120 °C for 30 hr, all of the azide was decomposed to yield cyclohexenylamino-*s*-triazines in a yield of 34% and amino-*s*-triazine in a yield of 26%. In addition, the cyclohexenylamino-*s*-triazines gave the corresponding amino-*s*-triazines in good yields upon heating in olefinic substrates under similar reaction conditions, suggesting that the amino-*s*-triazines in the reactions of azido-*s*-triazines with olefins did not result from the nitrene intermediates, but, rather, from the cyclohexenylamino-*s*-triazines. Details of the decomposition of cyclohexenylamino-*s*-triazines are now being studied and will be reported elsewhere.

Experimental

All the melting points are uncorrected.

The infrared spectra were measured in potassium bromide discs on a Jasco D-301 spectrometer. The NMR spectra were recorded on a Varian A-60D spectrometer. The ultraviolet spectra were recorded on a Hitachi-124 UV-VIS spectrometer. The elemental analyses were performed in the Micro-analytical Center of Gunma University.

The identification of the reaction products was performed by means of studying their NMR and infrared spectra, by elemental analyses, by a molecular-weight determination, and by a mixed-melting-point test with an authentic sample.

Materials. A typical preparation is shown in the case of Compound **2**. A solution of 7.5 g (0.115 mol) of sodium azide in 80 ml of water was stirred, drop by drop, into a solution of 13.5 g (0.075 mol) of 2-chloro-4,6-dimethoxy-*s*-triazine in 100 ml of acetone at 40 °C. After stirring for 4 hr at 40 °C, the reaction mixture was poured into 300 ml of ice-water. The precipitate was then filtered and dried to give 9.5 g (84%) of a crude product. The recrystallization of the product from benzene–ligroin gave an analytical sample of Compound **2**. Mp 85—85.5 °C. IR (KBr) cm^{-1}: (N_3) 2140 and (*s*-triazine) 810. DTA: 85 °C (endothermic) and 195 °C (exothermic).

Reactions of Azido-s-triazines with Cyclohexane. Typical examples will be shown in the cases of Compounds **1** and **2**.

1) A solution of 7.0 g (0.037 mol) of Compound 1 in 50 ml of cyclohexane was heated for 7 hr at 180—190 °C in an autoclave. After the solvent had then been evaporated *in vacuo*, the residue was treated with a solution of 5.4 g (0.1 mol) of sodium methoxide in 50 ml of methanol for 12 hr at room temperature. After the insoluble matter had been filtered off, the solution was evaporated *in vacuo*. From the benzene extract of the residue, 2-cyclohexylamino-4,6-dimethoxy-*s*-triazine was obtained in a yield of 23%; mp 123.5—125.5 °C (methanol–water).

2) A solution of 5.0 g (0.026 mol) of Compound **2** in 50 ml of cyclohexane was heated for 7 hr at 180—190 °C in an autoclave. After the reaction mixture had then been cooled to room temperature, the crystal was filtered to give 0.7 g (yield, 16%) of 2-amino-4,6-dimethoxy-*s*-triazine; mp 214—216 °C (lit,[28] 219 °C). The filtrate was evaporated in vacuo; then the residue was purified by silica gel column chromatography [developing solvent, benzene: acetone = 100: 5 by volume] to give 1.5 g (yield 22%) of 2-cyclohexylamino-4,6-dimethoxy-*s*-triazine; mp 127—128 °C (lit,[28] 127—129 °C).

In the reaction of Compound **3** with cyclohexane 2-amino-4,6-bis(dimethylamino)-*s*-triazine (yield, 17%) dioxane (mp 221—222 °C) (lit,[29] 222 °C) was obtained along with a small amount of 2-cyclohexylamino-4,6-bis(dimethylamino)-*s*-triazine.

Cyclohexylamino-s-triazines. A typical preparation of an authentic sample of cyclohexylamino-*s*-triazine is shown below in the case of 2-cyclohexylamino-4,6-bis(dimethylamino)-*s*-triazine. A solution of 2.0 g (0.01 mol) of 2-chloro-4,6-bis(dimethylamino)-*s*-triazine in 30 mol of cyclohexylamine was refluxed for 8 hr, and then the mixture was poured into 300 ml of ice-water. After the mixture had then been

neutralized with hydrochloric acid, the crystal was filtered and dried. Recrystallization from petroleum ether gave 1.3 g of an analytical sample of 2-cyclohexylamino-4,6-bis(dimethylamino)-*s*-triazine. Mp 68—69 °C. Found: C, 58.79; H, 9.40%. Calcd for $C_{13}H_{24}N_6$: C, 59.06; H, 9.15%.

Reaction of Azido-s-triazines with Cyclohexene. A typical example is shown in the case of Compound 2.

A solution of 20.0 g (0.11 mol) of Compound 2 in 200 ml of cyclohexene was heated for 7 hr at 180—190 °C in an autoclave. After the reaction mixture had then been cooled to room temperature, the crystals were filtered off to give 2.0 g (yield, 12%) of 2-amino-4,6-dimethoxy-*s*-triazine; mp 215—216 °C (lit,[28] 219 °C). From the filtrate, 13.0 g of 2-(cyclohexene-1-ylamino)-4,6-dimethoxy-*s*-triazine were obtained as a crystalline precipitate after cooling for 1 night at 0 °C. Mp 92—93 °C (Ligroin). Found: C, 56.14; H, 7.03; N, 23.47%. Calcd for $C_{11}H_{16}N_4O_2$: C, 55.91; H, 6.83; N, 23.72%. Mass: m/e=236. IR, cm^{-1}: (NH) 3150, (C=C) 1670, and (*s*-triazine) 815.

The compound absorbed 1 mol of bromine in chloroform and was oxidized by potassium permanganate in pyridine at room temperature.

Kinetic Measurements. The kinetic measurements were carried out by following the increase in the volume of nitrogen evolved or the decrease in the intensity of the N_3 band of azido-*s*-triazine [Compound **1**=2140 cm^{-1}: Compound **2**=2160 cm^{-1}; Compound **3**=2125 cm^{-1}].

The nitrogen evolation rates were measured by the methods of Overberger[30] and Leffler.[31] 40 ml of a substrate in a 100 ml long-necked flask was immersed in a constant-temperature bath controlled to±0.1 °C using polyethylene glycol and then allowed to reach the equilibrium temperature and pressure.

A weighed amount of the azide, 0.002—0.003 mol in 10 ml of the substrate, was poured into the flask. The flask was connected to the azotometer through a small condenser and a stopcock, and the reading of the volume was adjusted to zero. The stopcock was then closed, the solution was shaken well, and the measurement was started. The volume change in the nitrogen was followed for 90% of the reaction. The infinity volume of gas was determined by the reading after no increase in gas volume was observed (after about 6—7 hr).

In the reactions with cyclohexane, cyclohexene, and diethyl maleate, the kinetic runs were carried out by measuring the decrease in the intensity of the N_3 band.[32] A typical run is shown below in the reaction of Compound **2** with cyclohexane. A solution of Compound **2** in cyclohexane (0.14 mol/l) was heated in a constant-temperature bath in about 20 small glass sealed tubes 12 cm in length and 8 mm in diameter. At intervals of about 10 min the tubes were poured into cold water to stop the reaction, and the IR spectra of the solutions were measured. The first-order rate constant for the decomposition of the azido-*s*-triazine was calculated using Eq. (1):

$$k_1 t = -\ln [\log (T_\infty/T_0)/\log (T_\infty/T_t)] \quad (1)$$

where T_∞, T_t, and T_0 represent the transmittances at an infinite time, at time t, and at time zero respectively.

References

1) For example, "The Chemistry of the Azido Group," ed, by S. Patai (1971), Interscience Publishers.
2) W. D. Crow and C. Wentrup, *Chem. Commun.*, **1969**, 1387.
3) T. Sasaki, K. Kanematsu, and M. Murata, *Tetrahedron*, **27**, 5359 (1971).
4) B. Stanovnik, *Tetrahedron Lett.*, **1971**, 3211.
5) C. Wentrup and W. D. Crow, *Tetrahedron*, **26**, 4915 (1970).
6) C. Wentrup and W. D. Crow, *ibid.*, **26**, 4969 (1970).
7) C. Wentrup and W. D. Crow, *ibid*,. **27**, 361 (1971).
8) J. A. Hyatt and J. S. Swenton, *J. Heterocycl. Chem.*, **9**, 409 (1972).
9) C. Wentrup, *Helv. Chim. Acta*, **55**, 565 (1972).
10) T. Sasaki, K. Kanematsu, and M. Murata, *Tetrahedron*, **28**, 2383 (1972).
11) C. Wentrup, *ibid.*, **27**, 367 (1971).
12) A. C. Mair and M. F. G. Stevens, *J. Chem. Soc., Perkin Trans. I*, **1972**, 161.
13) E. Ott and E. Ohse, *Ber.*, **54**, 179 (1921).
14) C. V. Hart, *J. Amer. Chem. Soc.*, **50**, 1922 (1928).
15) H. Kast and A. Haid, *Z. Angew. Chem.*, **38**, 43 (1924).
16) R. M. Moriarty and M. Rahman, *J. Amer. Chem. Soc.*, **88**, 842 (1966).
17) B. E. Pape and M. J. Zabik, *J. Agr. Food Chem.*, **20**, 316 (1972).
18) R. N. Bulter, *Chem. Ind.*, **1973**, 371; H. Reimlinger, *Chem. Ber.*, **103**, 1900 (1970).
19) R. Huisgen and K. F. Fraunberg, *Tetrahedron Lett.*, **1969**, 2595.
20) R. A. Henry, *J. Org. Chem.*, **31**, 1973 (1966).
21) Y. Ohto, Y. Hashida, S. Sekiguchi, and K. Matsui, This Bulletin, **47**, 1301 (1974).
22) J. H. Hall, J. W. Hill, and J. Fargher, *J. Amer. Chem. Soc.*, **90**, 5315 (1968); J. H. Hall, J. W. Hill, and H. C. Tsai, *Tetrahedron Lett.*, **1965**, 2211.
23) S. K. Malhotra, "Structure and Physical Properties of Enamines," in "Enamines," ed. by A. G. Cook, Marcel Dekker (1969), p. 2; G. Optiz, H. Hellmann, and H. W. Schubert, *Ann. Chem.*, **623**, 117 (1959).
24) D. B. Ishai and R. Giber, *Tetrahedron Lett.*, **1965**, 4523.
25) W. Lowski and T. W. Mattingly, Jr., *J. Amer. Chem. Soc.*, **87**, 1947 (1965).
26) D. S. Breslow, T. J. Prosser, A. F. Marcantonio, and C. A. Genge, *ibid.*, **89**, 2384 (1967); D. S. Breslow, M. F. Sloan, N. R. Newburg, and W. B. Renfrow, *ibid.*, **91**, 2273 (1969).
27) G. L'abbe, *Chem. Rev.*, **69**, 355 (1969).
28) J. Thurston, J. Dudley, D. Kaiser, I. Hechenbleickner, F. Schaefer, and D. Holm-Hansen, *J. Amer. Chem. Soc.*, **73**, 2981 (1951).
29) W. Zerweck and K. Keller, U. S. P., 2228161 (1941).
30) C. G. Overberger, M. T. O'shanghnessy, and H. Shalit, *J. Amer. Chem. Soc.*, **71**, 2661 (1949).
31) J. E. Leffler and Y. Tsuno, *J. Org. Chem.*, **28**, 902 (1963).
32) P. Walker and W. A. Waters, *J. Chem. Soc.*, **1962**, 1632.

The Synthesis of 2,4-Dehydrohomoadamantane[1)]

Ryohei YAMAGUCHI, Takeo KATSUSHIMA, and Mituyosi KAWANISI

Department of Industrial Chemistry, Faculty of Engineering, Kyoto University, Yoshida, Sakyo-ku, Kyoto 606

(Received April 26, 1974)

A synthesis of 2,4-dehydrohomoadamantane (I) is described. a) The UV irradiation of a solution of 4-homoadamantene (IV) in xylene containing a small amount of methanesulfonic acid under nitrogen gave a 2: 1 mixture of I and IV after 7 day; this mixture afforded pure I in a 40% isolation yield. b) The oxidation of 4-homoadamantyl hydrazone (XI) by $Pb(OAc)_4$, NiPO, and MnO_2 (active) gave a 7—11: 1 mixture of I and IV respectively. It was observed that the ratio of I to IV depends on the reaction temperature, and that the oxidation of XI by $Pb(OAc)_4$ at −78 °C gave thirty times as much I as IV. The addition of MeOH as a proton source reduced the ratio of I to IV in the cases of NiPO and MnO_2. The Bamford-Stevens reactions of 4-homoadamatyl tosylhydrazone (II) were effected in aprotic as well as in protic solvents. The ratio of I to IV was inverted under aprotic and protic conditions. The selectivities in the oxidation of XI and the Bamford-Stevens reactions of II were explained by considering the conformations of 4-homoadamantylidene (XII) and the 4-homoadamantyl cation (VIII).

When cage compounds include a cyclopropane ring in their framework, their chemistry is intriguing in view of recent advances in the field of cyclopropane chemistry;[2)] such compounds can be adequate precursors of further substituted cage compounds. For example, 2,4-dehydroadamantane has been used in the stereochemical studies of photobromination of cyclopropanes;[3)] it is also effective as the precursor of a variety of 2- and 2,4-substituted adamantane derivatives.[4)]

Consequently, it is likely that 2,4-dehydrohomoadamantane (I) is a potential precursor of yet-unknown 2- and 2,4-substituted homoadamantane derivatives (Scheme 1, Eq. (1)). As for the synthesis of I, Schleyer *et al.* reported that the Bamford-Stevens reaction of 4-homoadamantyl tosylhydrazone (II) gave I (25.7%) and 4-homoadamantene (IV) (33.6%), along with a small amount of 4-homoadamantyl azine (V)[5)] (Scheme 1, Eq. (2)). According to their procedure, however, not only was the yield of I unsatisfactory, but also a rather larger amount of IV was produced. In this report we wish to describe a synthesis of I *via* a) a "hot" 4-homoadamantyl cation (VIII) generated photochemically and b) 4-homoadamantylidene (XII) generated by the oxidation of 4-homoadamantyl hydrazone (XI).

Results and Discussions

Photochemical Synthesis of I via *"Hot" (Vibrationally-excited) 4-Homoadamantyl Cation.* In a previous communication,[6)] we reported that the BTX-sensitized photochemical reaction of IV in acetic acid afforded I, along with 4- and 3-homoadamantyl acetates (VI and VII) (Scheme 1, Eq. (3)). On the other hand, there have been two reports on the acetolysis of 4-homoadamantyl tosylate giving IV and VI.[7a)] These differences can be explained by assuming a vibrationally-excited nature of the VIII formed photochemically.[7b,8)] In order to obtain I effectively, we investigated the reaction conditions under which no adducts, namely, VI and VII, were produced. Since the formation of adducts is caused by a nucleophilic attack of the protic solvent (in this case, acetic acid) on the cation before the completion of the deprotonation to produce I as well as IV, it is hoped that the use of the proton source with a poor nucleophilicity will increase the yield of I. This was to be the case when use was made of methanesulfonic acid, which has almost no nucleophilicity, as the proton source.

The UV irradiation of a solution of IV in xylene (commercial mixture) containing methanesulfonic acid under nitrogen gave a 2: 1 mixture of I and IV after 7 day; this mixture was chromatographed on a 15% $AgNO_3$-alumina column eluted by petroleum ether, giving pure I in a 40% isolation yield (Scheme 1, Eq. (4)).

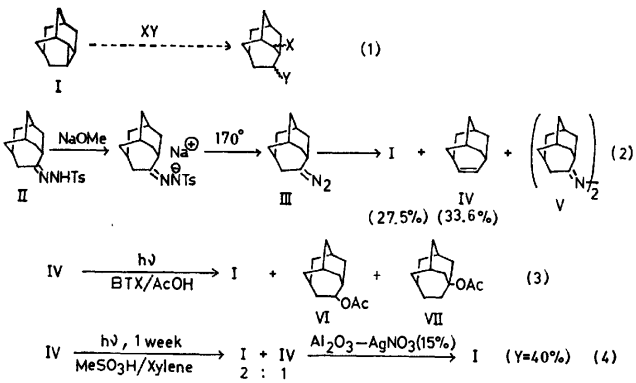

Scheme 1.

Upon the replacement of methanesulfonic acid by sulfuric or hydrochloric acid as a proton source, I was not produced, presumably because of the sensitivity of the resulting I toward these acids. The addition of

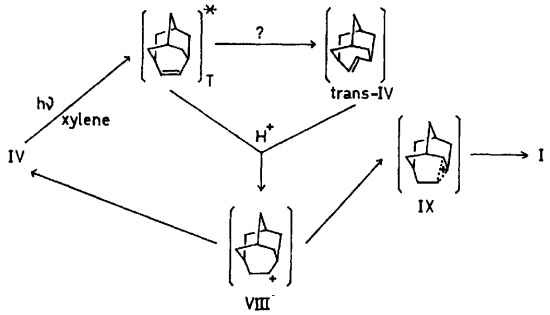

Scheme 2.

tert-butyl alcohol to increase the solubility of methanesulfonic acid (methanesulfonic acid dissolves poorly in xylene) caused only a slight isomerization to I.

The possible mechanism of the photoisomerization of IV to I is depicted in Scheme 2. Since the 4-homoadamantyl cation (VIII), produced according to the general pattern of the polar photochemistry of cycloalkenes,[8] can be expected to be in a vibrationally-excited state, VIII must have the enhanced nature of the nonclassical cation (IX), which can be nicely deprotonated to give I.

Selective Synthesis of I by the Oxidation of 4-Homoadamantyl Hydrazone (XI). The intramolecular γ-C–H insertion of carbene intermediates is one of the most general methods of cyclopropane formation in the skeleton of cage compounds. The Bamford-Stevens reaction, the alkaline-thermolysis of tosylhydrazone, has been repeatedly used to synthesize numerous cage compounds involving cyclopropane rings.[9] The distribution of a cyclopropane and an olefin in the resulting mixture varies according to the structure of the reactants (Scheme 3). For example, Bamford-Stevens reactions of tosylhydrazones of norcamphor and camphor gave exclusively nortricyclene and tricyclene respectively[10,11] (Scheme 3, Eqs. (1) and (2)), but the tosylhydrazone of bicyclo[2.2.2]octan-2-one afforded tricyclo[3.2.1.$0^{2,7}$]-octane (70%) and bicyclo[2.2.2]oct-2-ene (30%)[12] (Scheme 3, Eq. (3)). When the resulting olefin violates Bredt's Rule,[13] only the cyclopropane compound was produced. For example, adamantyl tosylhydrazone gave 2,4-dehydroadamantane (65%) along with a slight amount of adamantane[14] (Scheme 3, Eq. (4)). As mentioned above, in the homoadamantane derivative the Bamford-Stevens reaction of II gave I (27.5%) and IV (33.6%).[5]

Friedman and Shechter successfully explained the distributions of olefins, cyclopropanes, and other transannular insertion products in Bamford-Stevens reactions of tosylhydrazones of 5- to 10-membered ring ketones by a consideration of the conformation of each carbene intermediate; they found that the distribution of the products depended on the conformations of the carbene intermediates.[15] While in a Bamford-Stevens reaction a higher temperature (100—200 °C) is generally required to complete the decomposition of the salt of the tosylhydrazone, the conformation of the carbene intermediate generated at the higher temperature would be different from that of one generated at lower temperature. Therefore, if the corresponding carbene can be produced at a lower temperature, we can expect that the product distribution will be varied. One of the well-known methods of producing a diazoalkane, a precursor of a carbene, at a low temperature is the oxidation of the appropriate hydrazone. As an example of cyclopropane formation by the oxidation of hydrazone, the oxidation of the hydrazone of camphor by mercuric oxide is typical in giving tricyclene exclusively;[16] this result is in good agreement with that of the Bamford-Stevens reaction, and no effect of lowering the reaction temperature was observed upon the distribution of the products in the bicyclo[2.2.1]heptane system, which is highly rigid (Scheme 3, Eq. (5)).

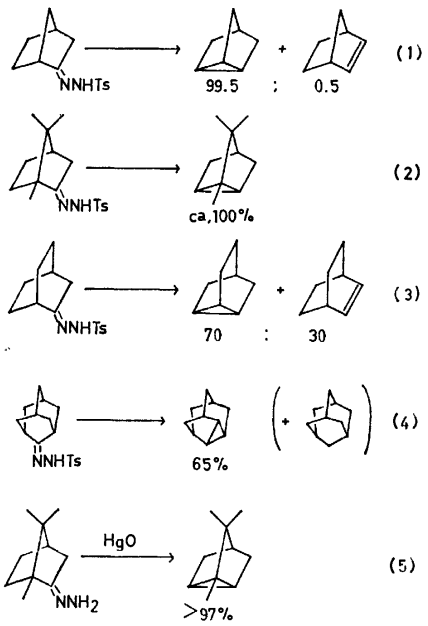

Scheme 3.

In the homoadamantane system, however, we found that the oxidation of 4-homoadamantyl hydrazone (XI) by $Pb(OAc)_4$ at room temperature gave 8 times more I than IV; this result is greatly different from that of the Bamford-Stevens reaction.[17] In order to obtain I exclusively we studied in detail the oxidation of XI, taking the kind of oxidant and the reaction temperature as well as the catalytic effects into consideration. Finally, we will discuss the cause of the selectivity observed in the oxidation of XI in comparison with the Bamford-Stevens reactions under aprotic and protic conditions.

The hydrazone (XI) was prepared by treating 4-homoadamantanone (X) with an excess of hydrazine hydrate, along with V (20—25%) (Scheme 4). This hydrazone is considerably labile and is easily converted into V even at room temperature. Therefore, in the actual process we used the crude XI for the following oxidation immediately after it has been prepared containing an unspecified amount of V; the yields of the products were estimated on the basis of X, the starting material for XI.

Oxidants: Several oxidants were examined for the oxidation of XI (Scheme 4, Eq. (2); the results are summarized in Table 1. While mercuric oxide did not

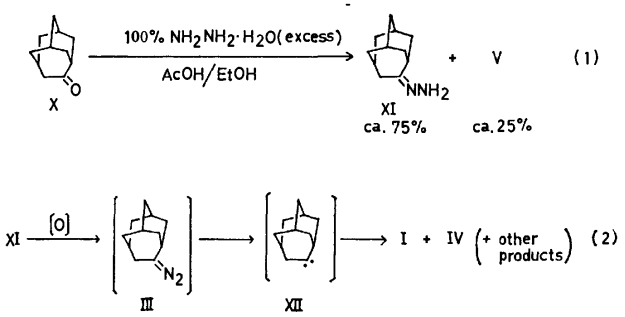

Scheme 4.

oxidize XI, probably because of its low oxidizing ability, lead tetraacetate ($Pb(OAc)_4$), nickel peroxide (NiPO),[18] and active manganese dioxide (MnO_2)[19] all did oxidize XI. In the case of $Pb(OAc)_4$, 4-homoadamantyl acetate (VI) was produced, while in the case of NiPO as well as MnO_2, 4-homoadamantanol (XIII) and X were produced.

As is shown in Table 1, 7—11 times more I is produced than IV. Since it is thought that both reactions, the oxidation of XI and the Bamford-Stevens reaction of II, must have the same intermediate, 4-homoadamantylidene (XII) generated *via* 4-diazohomoadamantane (III), such a selectivity must result from changing the reaction conditions, especially the reaction temperature.[20] Therefore, we next studied the temperature effect.

Table 1. Oxidation of XI[a]

Oxidant	I+IV (%)[b]	I/IV[c]
HgO	—	—
$Pb(OAc)_4$	37.6	8.7
NiPO	36.8	11.5
MnO_2(active)	43.5	7.2

a) One equivalent of oxidant was used in CH_2Cl_2 solution at room temp. b) Isolated yield. c) Determined by glc (PEG 20M, 180 °C).

Temperature Effect: The oxidation of XI by $Pb(OAc)_4$ was effected at a variety of temperatures. The results are summarized in Table 2.[21] Clearly, a temperature effect was observed; at −78 °C thirty times as much I was produced as IV. These temperature effects imply that some conformational contributions must operate in the transition state (*vide infra*).

Table 2. Temperature effect in the oxidation of XI[a]

Temp.	I+IV (%)[b]	I/IV[c]	VI (%)[b]
Room temp.	37.6	8.7	24
−15 °C	42.6	15.4	23
−30	44.8	23.9	21
−78	63.9	32.4	14

a) One equivalent of $Pb(OAc)_4$ was used in CH_2Cl_2 solution. b) Isolated yield. c) Determined by glc (PEG 20M, 180 °C).

Catalytic Effect: In general, a catalytic effect is regarded as another important factor which may govern a carbene reaction. It is well known that, in the presence of a catalyst, such as copper salt, some selectivity has been observed in carbene reactions.[22] We have tried copper(II) acetylacetonate ($Cu(acac)_2$) and cuprous chloride (CuCl) as catalysts. The former is soluble in organic solvents, and the latter, insoluble. The results were rather disappointing; they are summarized in Table 3. It can safely be said that a catalytic effect hardly works in these cases; under these conditions it is doubtful that the resulting carbene is actually modified by the copper ion.

The Effect of a Protic Solvent: It is well known that, in the presence of an appropriate proton source, a diazo compound is converted to a corresponding carbocation *via* a diazonium ion, the behavior of which is generally very different from that of a corresponding carbene.[11] Since the oxidation of XI by $Pb(OAc)_4$, NiPO, and active MnO_2 is accompanied by the production of acetic acid in the former case, and by that of water in the latter two cases, and since both acetic acid and water are able to become appropriate proton sources, we examined the selectivity of the oxidation reactions in the presence of a larger amount of the proton source. The results are summarized in Table 4. In the cases of NiPO and MnO_2 the addition of methanol diminished the ratio of I to IV; this implies that the selectivity is reduced in the carbocation process. In the case of $Pb(OAc)_4$ the addition of methanol or acetic acid did not cause any marked change in the ratio of I to IV; the reason for this is not clear, but if a carbene formation and a diazonium ion formation would compete each other, in the case of $Pb(OAc)_4$ I and IV would be produced predominantly *via* a carbene, and therefore the ratio of I to IV would not be affected.

Table 3. The oxidation of XI in the presence of copper ion[a]

Copper ion	Temp.	I/IV[b]
$Cu(acac)_2$	Room temp.	11
$Cu(acac)_2$	−15 °C	16
CuCl	Room temp.	8

a) $Pb(OAc)_4$ in CH_2Cl_2 was added to the solution of XI and $Cu(acac)_2$ or CuCl in CH_2Cl_2. b) Determined by glc (PEG 20M, 180 °C).

Table 4. The oxidation of XI in the presence of proton source

Run	Oxidant	H^+-Source	Additive	I/IV[a]
1	$Pb(OAc)_4$	—	K_2CO_3	10.4
2	$Pb(OAc)_4$	AcOH	—	11.6
3	$Pb(OAc)_4$	MeOH	—	9.9
4	NiPO	—	$MgSO_4$	9.5
5	NiPO	MeOH	$MgSO_4$	5.9
6	MnO_2	—	$MgSO_4$	9.5
7	MnO_2	MeOH	$MgSO_4$	4.9

a) Determined by glc (PEG 20M, 180 °C).

Bamford-Stevens Reactions of II in Aprotic and Protic Solvents: In order to compare the results of the oxidation of XI, we effected the Bamford-Stevens reactions of II in aprotic as well as in protic solvents. It has been established that, in an aprotic solvent such as diglyme, the reaction proceeds *via* a carbene, whereas in a protic solvent such as ethylene glycol the reaction proceeds *via* a carbocation (diazonium ion).[11] The results obtained here are summarized in Table 5. In diglyme, more than 2.7 times as much of the IV olefin was produced as of the I cyclopropane, whereas in ethylene glycol more than 1.9—2.5 times as much of I was produced as of IV. It is of interest that the ratio of I to IV under aprotic conditions is inverted in comparison with that under protic conditions. These results are very informative in elucidating the cause of the selectivity.

Table 5. Bamford-Stevens reaction of II

$$\text{II} \xrightarrow[\text{Base, Solvent}]{140\ ^\circ\text{C}} \text{I} + \text{IV}$$

Solvent	Base (equiv.)	I : IV[a)]
Diglyme	NaOMe (3.4)	1 : 2.7
Diglyme	NaH (1.9)	1 : 2.8
Ethylene glycol	Na (1.7)	1.9 : 1
Ethylene glycol	Na (3.4)	2.3 : 1
Ethylene glycol	Na (10)	2.5 : 1

a) Determined by glc (PEG 20M, 180 °C).

Mechanistic Considerations: As has been mentioned above, for an intramolecular carbene insertion reaction the distribution of the products seems to depend on the conformation of the corresponding carbene intermediate. In other words, the choice of the formation of cyclopropane and/or olefin is thought to depend on the degree of overlap of the γ-C–H bond and the β-C–H bond with the vacant sp^2-orbital of (singlet) carbene.

As to the conformation of the homoadamantane system, Schleyer *et al.* have argued on the basis of the obtained results in their studies of the infrared intramolecular hydrogen-bonding-shift of *cis*-4,5-homoadamantanediol and quantitative conformational analysis calculations.[23] According to them, the preferred conformation in the XIV homoadamantane system is essentially untwisted, but this system is so flexible that the dihedral angle varies from 0 to *ca.* 30° (see XIVa and XIVb in Fig. 1). In the XII carbene, the XIIa conformer might be very favorable for γ-C–H insertion producing I, while the XIIb conformer might be very favorable for producing IV. A model investigation[24] tells us that the 2-C–H_a or 9-C–H_a (γ-C–H) bond occupies a more favorable position to overlap with the sp^2-vacant orbital at C-4 (note that the 2-C–H_a or 9-C–H_a bond and the sp^2-vacant orbital at C-4 are coplanar) than 5-C–H_b (β-C–H), while the dihedral angle between the 5-C–H_b (β-C–H) bond and the sp^2-vacant orbital at C-4 is about 30°. For XIIb, the dihedral angle is about 0°, while the 2-C–H_a or 9-C–H_a bond and the sp^2-vacant orbital at C-4 are out-of-plane. At lower temperatures (oxidation conditions), the contribution of the XIIa conformer might be larger than that of XIIb because there is no strain due to the eclipsed form of C-4-H and C-5-H for XIIa, but XIIb might have some torsional strain. At higher temperatures (Bamford-Stevens conditions), the energy difference between XIIa and XIIb might be overcome by the temperature factor and the entropy factor might play an important role, so that the contribution of XIIb might be larger than that of XIIa.

In the VIII carbocation, at lower temperatures the contribution of the VIIIa conformer might be larger than that of VIIIb for the same reasons as in the case of XII. The reduced ratio of I to IV in the carbocation process is caused by the lower γ-C–H insertion ability of VIII than that of XII. At higher temperatures, however, VIIIa might also be more stable than VIIIb, since the VIIIb conformer might have some strain due to the eclipsed form of C-4-H and C-5-H.

We think that the selectivity in the oxidation of XI and the Bamford-Stevens reaction can be well explained by considering the conformations of the XII carbene and the VIII carbocation.

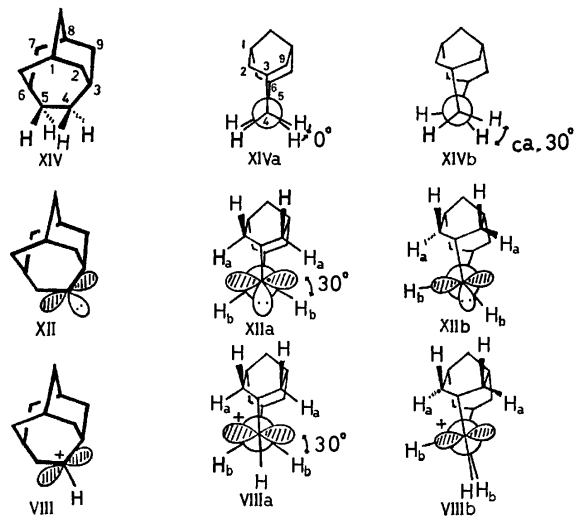

Fig. 1. Conformations of XIV, XII, and VIII.

In conclusion, lowering the reaction temperature in the intramolecular insertion reaction of XII promotes the γ-C–H insertion, thus producing I at the expense of the β-C–H insertion. At −78 °C, the oxidation of XI by $Pb(OAc)_4$ gives I exclusively. To date, this is the most efficient method of obtaining I.

Experimental

All the temperatures are uncorrected. The IR spectra were obtained on a Shimazu IR-27 spectrometer. The MS spectra were taken by using a Hitachi RMS-4 mass spectrometer. The PMR spectra were obtained on an EM-360 spectrometer, TMS being chosen as the internal standard.

Photochemical Synthesis of I. A mixture of IV (500 mg; 3.4 mmol) in 50 ml of xylene (a commercial mixture) containing methanesulfonic acid (0.5 ml) was irradiated by means of a 300 W medium-pressure mercury lamp under nitrogen for 7 day. The glc analysis (PEG 20 M, 180 °C) showed a 2: 1 mixture of I and IV. The reaction mixture was poured into water and neutralized by sodium hydrogen carbonate, and then the organic layer was collected and dried (Na_2SO_4). After the xylene solution has been passed through an alumina column to remove the acid throughly, the xylene was quickly removed under reduced pressure. The residue was chromatographed on a silver nitrate-alumina (15% silver nitrate) column. Elution by petroleum ether (40—50 °C) gave pure I (200 mg, 40%), while elution by petroleum ether-ether (8: 2) gave IV (90 mg). Compound I has the following properties: mp 226—229 °C (sealed tube) (lit,[5] mp 209—210 °C); MS: *m/e* 148 (M^+, 100%); PMR $\delta(CCl_4)$ 0.53—2.33 (broad complex multiplet); ^{13}C-NMR $\delta(CDCl_3$, downfield from TMS, proton-decoupled) 38.80 (CH_2), 32.42 ($2CH_2$), 28.61 ($2CH_2$), 26.79 (2CH), 21.59 (CH), 12.78 (CH), 10.26 (2CH), measured by JEOL PS 100/PFT 100 (25.1 MHz).

Oxidation of XI by $Pb(OAc)_4$. A mixture of X (4.0 g; 24.4 mmol), 100% hydrazine hydrate (4.9 g; 97.6 mmol), and glacial acetic acid (1.7 g; 24.4 mmol) in 80 ml of anhydrous ethanol was refluxed for 4 hr under nitrogen. The reaction mixture was then cooled to room temperature, and

the ethanol was removed under reduced pressure. Methylene chloride (CH_2Cl_2, 100 ml) was added to the residue, and the aqueous layer was separated. The organic layer was washed succesively with a 10% NaOH solution saturated with NaCl and with brine, and then dried ($CaCl_2$). Glc analysis showed that the CH_2Cl_2 solution contained XI (*ca.* 75%; mp 32—34 °C; MS: *m/e* 178 (M^+, 100%), 134 (72%). 93 (69%), 79 (49%); IR (Nujol) 3200, 2840, 1620, 1440, 1345, 1080 cm^{-1}; NMR $\delta(CCl_4)$ 1.15—1.04 (m, 16H), 4.50 (broad s, 2H, NH_2)) and V (*ca.* 25%; mp>290 °C; MS: *m/e* 149 (100%), IR (nujol) 2850, 1615, 1445, 1375, 1085, 940 cm^{-1}; NMR $\delta(CDCl_3)$ 1.25—3.21 (m)).[5] The $CaCl_2$ was filtered off, and $Pb(OAc)_4$ (12 g) free from AcOH in CH_2Cl_2 (120 ml) was added drop by drop to the above filtrate at −78 °C. The reaction mixture was stirred for 1.5 hr at −78 °C and then warmed to room temperature. After 40 ml of water has been added to the reaction mixture to quench the unreacted $Pb(OAc)_4$, the mixture was stirred overnight, filtered, washed succesively with a saturated $NaHCO_3$ solution and with brine, and dried ($CaCl_2$). After the removal of the CH_2Cl_2, the residue was chromatographed on alumina. Elution by *n*-hexane gave 2.29 g of hydrocarbon, which was shown by glc analysis to contain I (2.22 g, 61.5%) and IV (0.07 g, 1.9%). Elution by *n*-hexane–CH_2Cl_2 (1: 1) gave the VI acetate (0.69 g, 13.6%).

When other oxidants were employed, the procedures were essentially the same as that in the case of $Pb(OAc)_4$ except that the hydrazone solution was added to the CH_2Cl_2 solution containing the dispersed oxidant.

The azine (V) was recovered in the cases of NiPO and MnO_2, but not in the case of $Pb(OAc)_4$.

The Oxidation of XI in the Presence of a Protic Solvent. The procedures were essentially the same as that described above. The ratios of I to IV were determined by glc (PEG 20 M, 180 °C) (Table 4). In Run 1, K_2CO_3 was added as a neutralizing agent, but VI was still produced. In Run 2, $Pb(OAc)_4$ in CH_2Cl_2 was added to the solution of XI in CH_2Cl_2–AcOH (1: 1); a larger amount of VI was produced than in Run 1. In Run 3, $Pb(OAc)_4$ in CH_2Cl_2 was added to the solution of XI in CH_2Cl_2–MeOH (1: 1), and VI and 4-methoxyhomoadamantane (XIV) (MS: *m/e* 180 (M^+); NMR $\delta(CCl_4)$ 1.95—2.40 (broad m, 16H), 3.20 (s, 3H, OCH_3), 3.20—3.43 (m, 1H, $CHOCH_3$)[25] were produced. In Runs 4 and 6, $MgSO_4$ was added as a dehydrating agent, but XIII as well as X were produced in both cases. In Runs 5 and 7, the solution of XI in CH_2Cl_2 was added to a solution of CH_2Cl_2–MeOH (1: 1) containing an oxidant (NiPO or MnO_2) and $MgSO_4$; in both cases XIII, XIV, and X were produced.

Bamford-Stevens Reactions in Aprotic and Protic Solvents. 4-Homoadamantyl tosylhydrazone (II) was obtained by the standard procedure.[5,26] A mixture of II (332 mg, 1.0 mmol) and the base (NaOMe, 185 mg, 3.4 mmol; NaH, 100 mg, 1.9 mmol) in diglyme (5 ml, distilled over NaH) was heated at 140 °C for 1 hr. The reaction mixture was then cooled to room temperature and poured into water. The organic material were extracted with petroleum ether, washed with brine, and dried (Na_2SO_4). The solvent was then evaporated, and the residue was chromatographed on alumina. Elution by *n*-hexane gave the mixture of two hydrocarbons, I and IV (67.2 mg, 45%; 90.8 mg, 61%), the ratio of which was determined by glc. Elution by CH_2Cl_2 gave a small amount of V and an unidentified material.

Three kinds of mixtures of II (232 mg, 1.0 mmol) and Na (39 mg, 1.7 mmol; 78 mg, 3.4 mmol; 232 mg, 10 mmol) in 5 ml of ethylene glycol (distilled over Na) were heated at 140 °C for 1 hr. Each reaction mixture was cooled to room temperature and poured into water. The organic materials were extracted with petroleum ether, washed with brine, and dried (Na_2SO_4). The solvent was evaporated, and the residue was chromatographed on alumina. Elution by *n*-hexane gave two hydrocarbons, I and IV (53 mg, 36%; 34 mg, 23%; and 72 mg, 49%, respectively), the ratio of which was determined by glc. Elution by CH_2Cl_2 gave a trace amount of another material, which was presumably β-hydroxyethyl-4-homoadamantyl ether (XV) (MS: *m/e* 210 (M^+), 148 (100%); IR (neat) 3350, 2900, 1450, 1080 cm^{-1}; NMR δ, (CCl_4) 1.10—2.60 (broad m, 17H), 3.31—3.69 (broad m, 5H)), but its exact structure was not investigated further because the specimen was too small.

It was confirmed that I and VI were stable under the reaction conditions (excess base and excess sodium salt of *p*-toluenesulfinic acid in diglyme or ethylene glycol at 140 °C for 1 hr) of the control experiments.

References and Footnotes

1) Trivial nomenclature based on homoadamatane numbering; see reference 5.

2) D. Wendisch, Houben-Weyl. "Methoden der organischen Chemie," Georg Thieme Verlag, Stuttgart, Bd. 4/3, (1971).

3) K. J. Shea and P. S. Skell, *J. Amer. Chem. Soc.*, **95**, 6728 (1973).

4) A.C. Udding, J. Strating, and H. Wynberg, *Tetrahedron Lett.*, 1345 (1968).

5) Z. Majerski, S. H. Liggero, and P. v. R. Schleyer, *Chem. Commun.*, **1970**, 949.

6) R. Yamaguchi, S. Arimatsu, and M. Kawanisi, *Chem. Lett.*, **1973**, 121.

7) a) J.E. Nordlander, F. Y.-H. Wu, S. P. Jindal, and J. B. Hamilton, *J. Amer. Chem. Soc.*, **91**, 3962 (1969); P. v. R. Schleyer, E. Funke, and S. H. Liggero, *ibid.*, **91**, 3965 (1969). b) Recent report by the Majerskis described the unusual rearrangement of 4-homoadamantyl cation (**VIII**) forming 2-methyladamantane, homoadamantane and 4-homoisotwistane when **IV** or **XIII** was treated with sulfuric acid in the presence of pentane. In spite of all efforts these compounds could not be detected in the photolysate in our hand. K. M. Majerski and Z. Majerski, *Tetrahedron Lett.*, **1973**, 4915.

8) P. J. Kropp, *J. Amer. Chem. Soc.*, **91**, 5783 (1969) and references cited therein; *Idem*, *Pure Appl. Chem.*, **24**, 585 (1970); J. A. Marshall, *Accounts Chem. Res.*, **2**, 33 (1969); *Idem*, *Science*, **170**, 130 (1970).

9) a) See ref. 1, p. 347; b) W. Kirmse, "Carbene Chemistry," 2nd Ed., Academic Press, London, p. 236 (1971).

10) P. K. Freeman, D. E. George, and V. N. M. Rao, *J. Org. Chem.*, **29**, 1683 (1964).

11) J. W. Powell and M. C. Whiting, *Tetrahedron*, **7**, 305 (1959); R. H. Shapiro, J. H. Duncan, and J. C. Clopton, *J. Amer. Chem. Soc.*, **89**, 1442 (1967).

12) C. A. Grob and J. Hostynek, *Helv. Chim. Acta*, **46**, 1676 (1963).

13) The word "Bredt's Rule" is used in a context of strained bridgehead olefin: For detailed discussion, see G. Köbrich, *Angew. Chem.*, **85**, 494 (1973).

14) A. C. Udding, *Chem. Commun.*, **1966**, 657.

15) L. Freedman and H. Shechter, *J. Amer. Chem. Soc.*, **83**, 3159 (1961).

16) H. Meerwein and K. v. Emster, *Ber.*, **53**, 1915. (1920); W. Reusch, M. W. Dicarlo, and L. Traynor, *J. Org. Chem.*, **26**, 1711 (1961).

17) Preliminary report: R. Yamaguchi, K. Katsushima, T. Imagawa, and M. Kawanisi, *Synth. Commun.*, **1974**, 83.

18) K. Nakagawa, H. Onoue, and K. Minami, *Chem. Commun.*, **1966**, 730.

19) J. Attenburrow, A. F. B. Cameron, J. H. Chapman, R. M. Evans, B. A. Hams, A. B. A. Jansen, and T. Walker, *J. Chem. Soc.*, **1952**, 1094.

20) Schleyer *et al.* employed a vaccum pyrolysis method and described that III was isolated and at room temperature slowly decomposed to I and IV (45: 55). The ratio of I to IV are very different from that obtained in the oxidaiton of XI at room temperature. A possible explanation of such a difference is that III might partially decompose at 170° (pyrolysis temperature) or the selectivity of the decomposition in solid state might be different from that in solution. But we think that the selectivity depends on the reaction temperature as mentioned in the text. (see ref. 5)

21) With NiPO and MnO_2, it was concluded that the lowest limit of the temperature at which the oxidation took place was 0—5 °C by observation of nitrogen evolved, but the yield was reduced and the ratio of I to IV was almost the same as that in the case of room temperature.

22) See ref. 8b, p. 85.

23) P. v. R. Schleyer, E. Funke, and S. H. Liggero, *J. Amer. Chem. Soc.*, **91**, 3965 (1969); T. M. Corrie, E. M. Engler, R. C. Bingham, and P. v. R. Schleyer, *Tetrahedron Lett.*, **1972**, 3039; E. M. Engler, L. Chang, and P. v. R. Schleyer, *ibid.*, **1972**, 2525.

24) FMM-Model: Prentice-Hall, Inc. Englewood Chiffs, N. J.

25) J. A. v. Zorge, J. Strating, and H. Wynberg, *Rec. Trav. Chim.*, **89**, 781 (1970).

26) M. Jones, Jr., A. M. Harrison, and K. R. Rittig, *J. Amer. Chem. Soc.*, **91**, 7462 (1969).

Photochemistry in Micellar System. I. Stabilization of the Radical Anions of Anthraquinonesulfonates[1]

Koji KANO and Taku MATSUO*

Department of Organic Synthesis, Faculty of Engineering, Kyushu University, Hakozaki, Higashi-ku, Fukuoka 812

(Received March 15, 1974)

Micellar effects on the photochemical reactions of sodium 9,10-anthraquinone-2-sulfonate and disodium 9,10-anthraquinone-2,6-disulfonate were studied by means of ESR and electronic spectroscopy. In the presence of anionic and non-ionic surfactants, irradiation of the quinones in aerobic phosphate buffer (pH 8.0) gave the corresponding radical anions, which were incredibly long-living (over several weeks) as compared with irradiation without surfactant. Plausible mechanisms of the micellar effects on the stabilization of the radical anions are discussed.

Micellar effects have been observed for many thermal reactions which indicate a close resemblance between micelle- and enzyme-catalyzed reactions.[2-4] In the case of photochemical reactions, however, only a few investigations have been carried out. Photoinduced substitution of some nitroaromatics was found to be affected by the addition of surfactants in a manner indicative of typical micellar effects.[5] Both anionic and nonionic surfactants have been reported to accelerate the photoreduction of riboflavin and flavin mononucleotide.[6-9] The photodecomposition of *p*-benzoquinone was also found to be accelerated in the presence of anionic surfactants.[10]

In the present paper, micellar effects on the photochemistry of anthraquinone sulfonates are described. In addition to the extensively investigated photofading and phototendering of anthraquinoid vat dyes,[11,12] anthraquinones have been known to be good sensitizers in photooxidation of organic substrates, where a cyclic process involving the semiquinone radical was suggested to play an important role.[13] Reduction-oxidation cycle of quinones is also very important for electron transport in biological membranes. We have studied the photochemistry of sodium 9,10-anthraquinone-2-sulfonate (AQS) in micellar systems, and found that the radical anion ($AQS^{\cdot}$) is extremely stabilized in the presence of surfactants.[14] The behavior of the stabilized radical anions in micellar systems is discussed in detail.

Experimental

Materials. Sodium 9,10-anthraquinone sulfonates and sodium laurate, NaL (Tokyo Kasei Kogyo Co. Ltd.) were recrystallized from water and 50% aqueous methanol, respectively. Sodium lauryl sulfate (NaLS) of three different grades was used; extra pure grade (Tokyo Kasei), that used for biochemistry (Wako Pure Chem.), and NaLS (Tokyo Kasei) recrystallized from 50% aqueous methanol. The results were all the same. Polysorbate-80 (P-80) (Ishizu Pharm. Co.) was used without further purification. Water was distilled and deionized with a column of ion-exchange resin.

The critical micelle concentrations (CMC) of NaLS and NaL were determined by the fluorescent probe method at room temperature. Magnesium 1-anilinonaphthalene-8-sulfonate (ANS) was chosen as a model probe suitable for examining the binding of sodium 9,10-anthraquinone sulfonates. An abrupt increase in fluorescence yields of ANS (1.0×10^{-4} M) in water was observed on the addition of NaLS above 8.5×10^{-3} M and also of NaL above 2.8×10^{-2} M. The values are in good agreement with the CMC of NaLS and NaL in the literature.[2] It is well-known that the CMC of anionic and cationic surfactants are lowered by addition of inorganic salts.[3] Most experiments were carried out in phosphate buffer solutions; the CMC of the anionic surfactants in our systems is expected to be lower than those in pure water.

Irradiation. *Method A*: The solution in a Pyrex tube (ϕ 15 mm) was irradiated with a Riko 100 W high-pressure mercury lamp using a Riko rotary photolysis apparatus RH 400—10 W at room temperature.

Method B: The solution in a quartz cell (10 mm width) placed 5 cm from the center of the lamp, was irradiated with a Riko 100 W high-pressure mercury lamp at room temperature.

ESR Measurement. The ESR spectra of the photolyzed solution in a Pyrex capillary tube (ϕ *ca.* 1 mm) were measured with a JEOL Model JES-ME-3X spectrometer (X-band), using 100 kHz field modulation. Peroxylamine sulfonate was used as standard material for determining the *g*-value.

Results

Spectral Change during Photolysis. Irradiation of AQS and/or disodium 9,10-anthraquinone-2,6-disulfonate (AQDS) in aqueous media without surfactants gives colored stable products, whose major components are hydroxylated anthraquinones.[15,16] Progressive spectral changes during the photolysis (method B) of AQS and AQDS in the aerobic phosphate buffer (pH 8.0) are shown in Fig. 1.

In the presence of NaLS above the CMC,[17] the spectral changes under irradiation (method B) of the aerobic solutions (pH 8.0) of both anthraquinone sulfonates (AQS and AQDS) differ drastically from those shown in Fig. 1. The absorption maxima of the photoproducts from AQS were observed at 378.5, 394.5, ~420, and ~470 nm (Fig. 2). In the case of AQDS, the absorption maxima were found at 382, 401, and 473 nm. These absorption bands gradually disappeared on mixing the solution with air. The bands at 378.5 (AQS) and 382 nm (AQDS) were assigned to the corresponding diol derivatives ($AQSH_2$ and $AQDSH_2$) by comparing the spectra with those of

* To whom inquiries should be addressed.

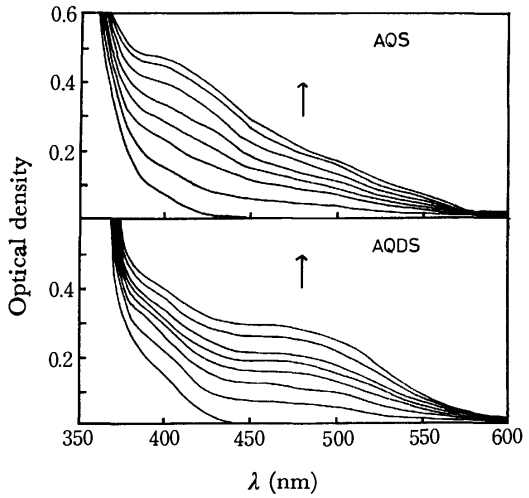

Fig. 1. Progressive spectral changes during photolysis of AQS and AQDS in non-micellar systems: $[AQS]_0 = 5.0 \times 10^{-4}$ M, $[AQDS]_0 = 1.0 \times 10^{-3}$ M, in 0.033 M phosphate buffer (pH 8.0). The spectra were measured at intervals of 20 s.

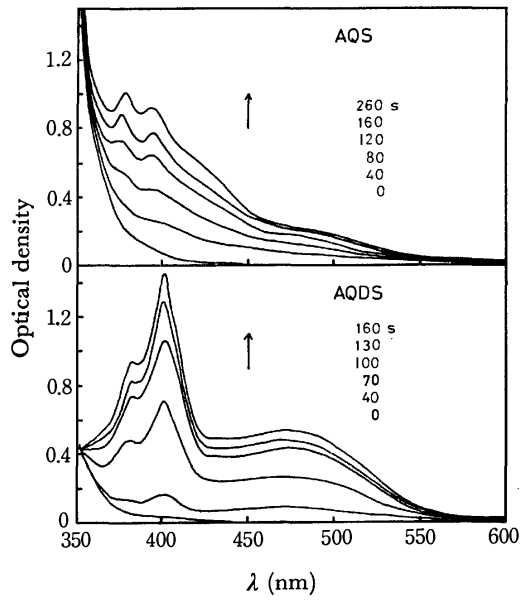

Fig. 2. Progressive spectral changes during photolysis of AQS and AQDS in micellar system: $[AQS]_0 = 5.0 \times 10^{-4}$ M, $[AQDS]_0 = 2.0 \times 10^{-4}$ M, $[NaLS] = 2.0 \times 10^{-2}$ M, in 0.033 M phosphate buffer (pH 8.0).

authentic samples. Essentially, the same absorption bands were observed when NaL and P-80 were used in place of NaLS except for the fact that the absorption at ~470 nm in AQS–NaLS system shifted towards 460 nm in the case of NaL and P-80. The absorption maxima at 394.5 (AQS) and 401 nm (AQDS) coincide with those of the radical anions of AQS ($AQS^{\cdot-}$) and AQDS ($AQDS^{\cdot-}$) obtained by flash technique.[18,19] The absorption bands at 505 nm of $AQS^{\cdot-}$ [18] and at 520 nm of $AQDS^{\cdot-}$,[19] however, could not be detected in the presence of surfactants. These bands were presumably shifted towards shorter wavelengths (~470 and 473 nm) by the influence of surfactants.

ESR Spectra Measurement. An aerobic solution (pH 8.0) of AQS containing NaL near the CMC[20] in a pyrex tube (ϕ 1 mm) was irradiated with a 100 W high-pressure mercury lamp for 20 min, and the yellow solution obtained was examined by means of ESR spectroscopy at room temperature (Fig. 3). The splitting constant (ΔH), number of lines, and g-value were 0.25 gauss, 21, and 2.0042, respectively. No ESR signal was obtained when the aerobic solution (pH 8.0) was irradiated in the absence of surfactants. In the case of AQDS, long-living ESR signals were obtained upon irradiation of the aerobic aqueous solution (pH 8.0) in the presence of NaLS (Fig. 4). The same ESR signals were also observed even in the absence of surfactants, but the spectra disappeared in a few hours after irradiation. The splitting constant, number of lines, and g-value were 0.45 gauss, 11, and 2.0044, re-spectively.

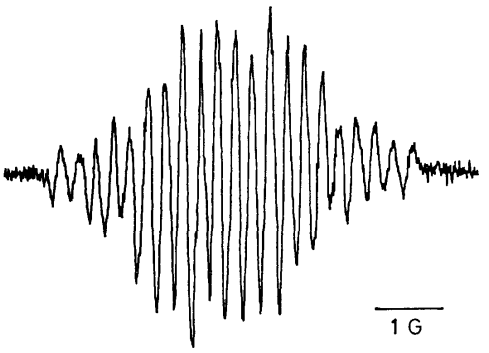

Fig. 3. ESR spectrum of $AQS^{\cdot-}$ generated by the photolysis of aerobic aqueous buffered solution (pH 8.0) of AQS (3.0×10^{-3} M) containing NaL (2.0×10^{-2} M).

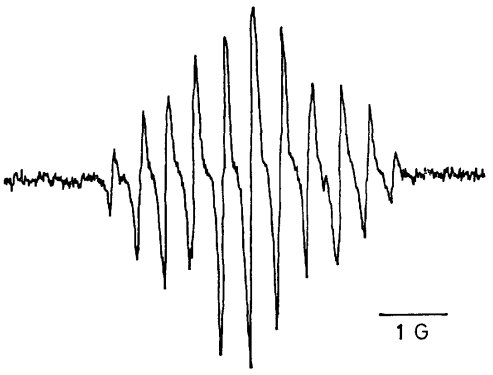

Fig. 4. ESR spectrum of $AQDS^{\cdot-}$ generated during the photolysis of aerobic aqueous buffered solution (pH 8.0) of AQDS (5.0×10^{-3} M) containing NaLS (4.0×10^{-2} M).

As regards the analysis of the hyperfine structure, the above ESR spectra were identified with those of the radical anions of AQS and AQDS.[21]

Phillips *et al.* obtained the ESR spectra of $AQS^{\cdot-}$ during the photolysis of anaerobic alkaline solutions (>pH 11) of AQS.[18,21] They reported that no ESR signal was obtained below pH 11.[18] By the use of flash technique, they also found that $AQS^{\cdot-}$ has a relatively long lifetime in an anaerobic solution (several ms), and rapidly decays in the aqueous solution by

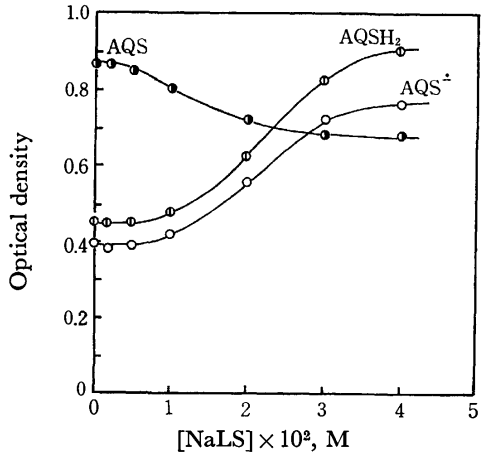

Fig. 5. Effect of NaLS concentration on $AQS^{\cdot-}$ and $AQSH_2$ formation: $[AQS]_0=5.0\times10^{-4}$ M, in 0.033 M phosphate buffer (pH 8.0). The solutions were irradiated for 5 min at room temperature, and the optical density at 256 nm was measured after the photolyzed solutions were diluted by 25-fold with water.

the addition of oxygen.[18] $AQS^{\cdot-}$ we obtained in the presence of NaL lived over two months in a sealed tube even in the case of aerobic solution. Although, $AQDS^{\cdot-}$ has a considerably long lifetime (a few hours) even in the absence of surfactant, it lived over several weeks in the aerobic solution in the presence of NaLS. These observations suggest that both $AQS^{\cdot-}$ and $AQDS^{\cdot-}$ are markedly stabilized in the presence of surfactants.

Effect of Surfactant Concentration on $AQS^{\cdot-}$ Formation. An aerobic aqueous solution (pH 8.0) of AQS containing appropriate amounts of NaLS was irradiated for 5 min (method A). The optical density at the absorption maxima of $AQS^{\cdot-}$ (394 nm), diol derivative ($AQSH_2$, 378.5 nm), and AQS (256 nm) is plotted against the concentration of NaLS in Fig. 5. The

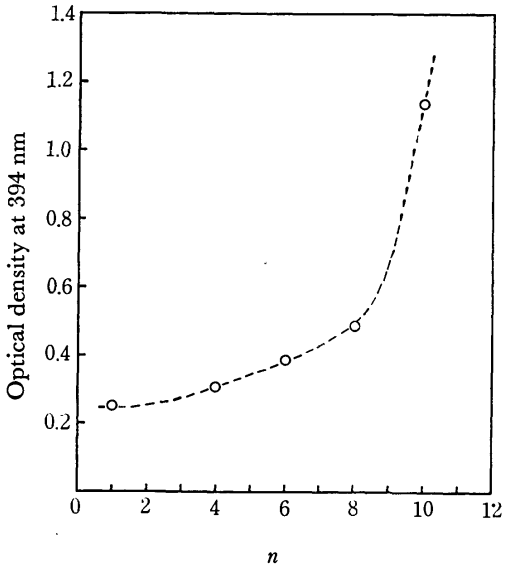

Fig. 6. Effect of alkyl chain length of sodium carboxylate on $AQS^{\cdot-}$ formation: $[AQS]_0=1.0\times10^{-3}$ M, $[CH_3(CH_2)_nCOONa]=2.0\times10^{-2}$ M, in 0.033 M phosphate buffer (pH 8.0). The solutions were irradiated for 20 s at room temperature.

formation of $AQS^{\cdot-}$ and $AQSH_2$ and the disappearance of AQS markedly increased at NaLS concentrations above *ca.* 1.0×10^{-3} M, plateau regions being observed at higher NaLS concentrations. This surfactant concentration profile suggests that the micelles formed by aggregation of the surfactant in aqueous solution contribute to the stabilization of $AQS^{\cdot-}$.

Effect of Alkyl Chain Length of Surfactant on Stabilization of $AQS^{\cdot-}$. An aerobic aqueous solution (pH 8.0) of AQS containing sodium carboxylates ($CH_3(CH_2)_n$-COONa) was irradiated for 20 s (method B). The optical density at 394 nm ($AQS^{\cdot-}$ formation) is plotted against the number of methylene groups (n) in the alkyl chain in Fig. 6. Since the formation of $AQS^{\cdot-}$ becomes significant for $n>8$, it is evident that $AQS^{\cdot-}$ is greatly stabilized by binding with an aggregate of carboxylates capable of forming micelles.

Table 1. Effect of acetone content on stabilization of $AQDS^{\cdot-}$[a]

Aceton, % (v/v)	Φ/Φ_0[b]
0	1
5	0.87
10	0.82
15	0.64
20	0.55

a) Aerobic phosphate buffer solutions (0.033 M, pH 8.0) of AQDS (2.0×10^{-4} M) containing NaLS (2.0×10^{-2} M) and acetone were irradiated at room temperature for 1 min. b) Relative quantum yields were determined by measurement of optical density at 475 nm, absorption maximum of $AQDS^{\cdot-}$.

Effect of Acetone on Stabilization of $AQDS^{\cdot-}$. The effects of acetone were studied in the AQDS-NaLS system. The relative quantum yields for the formation of $AQDS^{\cdot-}$ in solutions containing various amounts of acetone are given in Table 1. The generation of $AQDS^{\cdot-}$ was suppressed with increasing acetone content, as was also the formation of $AQDSH_2$. Not only acetone but *tert*-butanol also greatly reduced the formation of $AQDS^{\cdot-}$ and $AQDSH_2$. The relative quantum yield for the formation of $AQDS^{\cdot-}$ was 0.58 when the aerobic 10% (v/v) aqueous *tert*-butanol solution (pH 8.0) of AQDS (2.0×10^{-4} M) containing NaLS (2.0×10^{-2} M) was irradiated.

Salt Effect on $AQDS^{\cdot-}$ Formation. It is known that ionic-micellar catalysis tends to be significantly affected by addition of electrolyte.[22] We have studied the salt effects on the radical anion formation in the AQDS-NaLS system.

Aqueous solutions (pH 8.1) of AQDS containing

Table 2. Salt effect on $AQDS^{\cdot-}$ formation[a]

Electrolyte	Φ/Φ_0
—	1
$MgSO_4$(2.0×10^{-2}M)	0.48
Na_2SO_4(2.0×10^{-2}M)	0.84

a) $[AQDS]_0=2.0^{-4}\times10^{-2}$M, $[NaLS]=2.0\times10^{-2}$ M in 0.033 M phosphate buffer (pH 8.1).

NaLS and appropriate amounts of salts were irradiated with filtered light (>350 nm). The optical density at 470 nm ($AQDS^{\cdot-}$ formation) was monitored and the relative quantum yields for $AQDS^{\cdot-}$ formation were determined. The results obtained are summarized in Table 2. The formation of $AQDS^{\cdot-}$ was significantly supressed by the addition of Mg^{2+}.

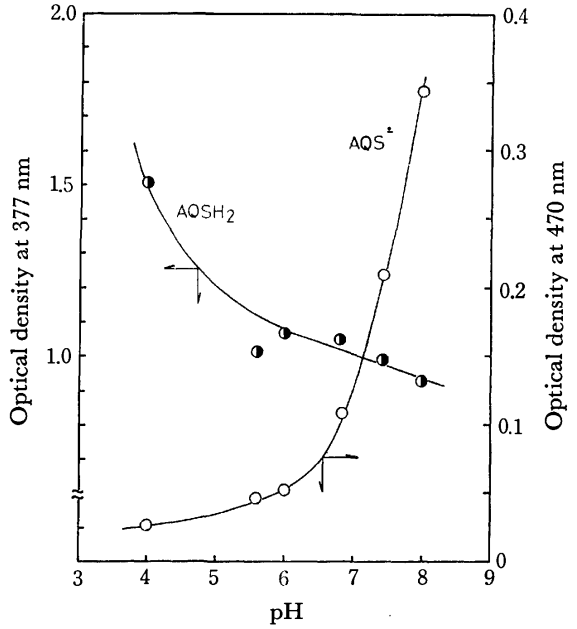

Fig. 7. pH dependence on $AQS^{\cdot-}$ and $AQSH_2$ formation: $[AQS]_0 = 5.0 \times 10^{-4}$ M, [P-80] = 0.2116 g/dl. The phthalate (pH 4.0, 0.1 M) and phosphate buffers (pH 5.6—8.0, 0.033 M) were used. The solutions were irradiated for 10 min under a nitrogen atmosphere at room temperature.

pH Dependence on $AQS^{\cdot-}$ and $AQSH_2$ Formation. The pH dependence on the formation of $AQS^{\cdot-}$ and $AQSH_2$ in the presence of P-80 was examined by the use of phthalate and phosphate buffers (pH 4.0—8.0). Anaerobic solutions of AQS containing P-80 (0.2116 g/dl)[23] were irradiated for 10 min (method A). The formation of $AQSH_2$ and $AQS^{\cdot-}$ was monitored by optical density at 377 and 470 nm, respectively. The pH profile is shown in Fig. 7. The yield of $AQSH_2$ decreased with increasing pH, the formation of $AQS^{\cdot-}$ being apparently enhanced above pH 6.8. Exactly the same pH dependence of the $AQS^{\cdot-}$ formation was reported in the flash photolysis of AQS in the absence of surfactant.[18]

Reaction of Radical Anions with H^+. Since the radical anions of AQS and AQDS are greatly stabilized in micellar systems, the reactivity of $AQS^{\cdot-}$ and/or $AQDS^{\cdot-}$ can be easily investigated. We first studied the reaction of radical anions with H^+.

An aerobic solution of AQDS (2.0×10^{-4} M) in 0.033 M phosphate buffer (pH 8.0) containing 2.0×10^{-2} M of NaLS was irradiated for 3 min (method B). After the photolyzed solution was carefully diluted 20-fold either with water or with 0.75 N sulfuric acid, the UV spectra were measured (Fig. 8). The absorption maxima in water were observed at 262, 273, and 284 nm. The spectra were compared with those of

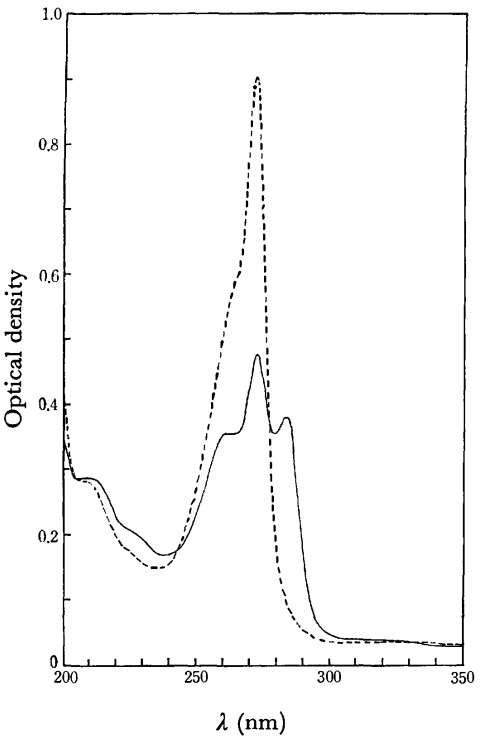

Fig. 8. UV spectra of photolyzed solution of AQDS which were diluted with water (solid line) and with 0.75 N sulfuric acid (dotted line).

authentic samples, and the absorption bands at 262 and 273 nm were assigned to AQDS and $AQDSH_2$, respectively. In the sulfuric acid solution, the absorption band at 284 nm completely disappeared and the intensity of the absorption band at 273 nm ($AQDSH_2$) increased. These spectral data suggest that the absorption band at 284 nm is attributed to $AQDS^{\cdot-}$ and that

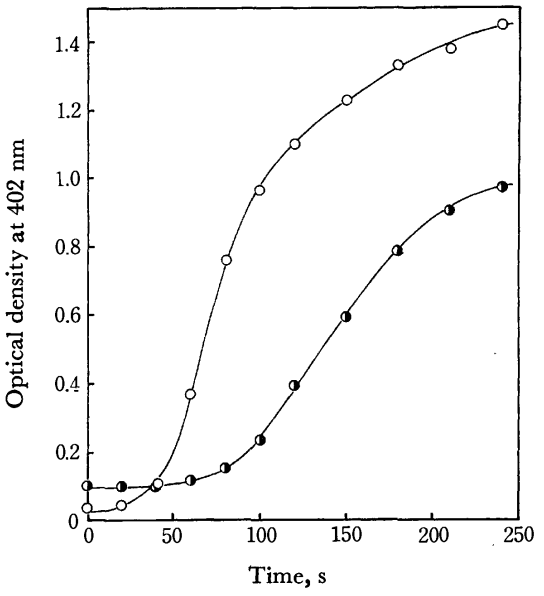

Fig. 9. Effect of Fe^{3+} on $AQDS^{\cdot-}$ formation: the aerobic phosphate buffer solutions (0.033 M, pH 8.0) of AQDS (2.0×10^{-4} M) containing NaLS (2.0×10^{-2} M) were irradiated in the absence (—○—) and in the presence of Fe^{3+} (—◑—, $[FeCl_3] = 5.2 \times 10^{-4}$ M) at room temperature.

$AQDS^{\cdot-}$ reacts with H^+ to produce the anthrahydroquinone.

The same results were obtained in the reaction of $AQS^{\cdot-}$. The absorption maxima of AQS, $AQSH_2$, and $AQS^{\cdot-}$ were observed at 259, 269, and 277 nm, respectively.

Reaction of $AQDS^{\cdot-}$ with Fe^{3+}. We next examined the electron transfer reaction from $AQDS^{\cdot-}$ to ferric ion.

An aerobic aqueous solution (pH 8.0) of AQDS containing NaLS was irradiated in the presence of Fe^{3+} (method B). The formation of $AQDS^{\cdot-}$ monitored at 402 nm is plotted against irradiation time in Fig. 9.

In the absence of Fe^{3+}, the formation of $AQDS^{\cdot-}$ was observed after a short induction period (*ca.* 20 s). In the presence of Fe^{3+}, however, the induction period for the formation of the radical anion was considerably prolonged (*ca.* 60 s), the yield of $AQDS^{\cdot-}$ being reduced. After irradiation, *o*-phenanthroline, 0.1 N sulfuric acid, and sodium acetate–sulfuric acid buffer (pH 4.4) were added to the photolyzed solution. A red solution was obtained and the spectra clearly indicated the formation of *o*-phenanthroline–Fe^{2+} complex (λ_{max} 500 nm). Thus it could be concluded that $AQDS^{\cdot-}$, the primary photoproduct, transfers an electron to Fe^{3+} which affords AQDS and Fe^{2+} as the final products.

Discussion

Phillips *et al.* found that flash photolysis of AQS in air-saturated aqueous solution (pH 3.07) gives two transient species with absorption maxima at 455 and 505 nm.[18] They assigned the transient bands at 455 and 505 nm to the cation and anion radicals of AQS, respectively. From the results the formation of $AQS^{\cdot-}$ was explained by the following reaction:

$$AQS^* + AQS \longrightarrow AQS^{\cdot+} + AQS^{\cdot-} \quad (1)$$

This scheme involving triplet excimer, however, was not supported by the kinetic data obtained by means of ns laser photolysis.[12]

Kuzmin and Chibisov studied the flash photolysis of aqueous AQDS solutions in the presence of inorganic anions (0.1 M) and found that an electron is transferred from inorganic anions (CO_3^{2-}, Cl^-, SO_4^{2-}, NO_3^-, PO_4^{3-}, SO_3^{2-}, SeO_3^{2-}, and SCN^-) to AQDS in the triplet state yielding $AQDS^{\cdot-}$ (two strong bands at 400 and 520 nm) and one-electron oxidized inorganic anions:[19]

$$AQDS^* + X^{n-} \longrightarrow AQDS^{\cdot-} + X^{(n-1)\cdot} \quad (2)$$

In our system also anions such as $CO_2^{\cdot-}$, $OSO_3^{\cdot-}$, HPO_4^{2-}, and $H_2PO_4^-$ coexisted with AQS or AQDS. The radical anions, however, could not be detected by means of ESR and electronic spectroscopy in the case of AQS with no surfactants, the quantum yield for the formation of $AQDS^{\cdot-}$ in the presence of micelles not increasing with addition of SO_4^{2-} (Table 2). $AQS^{\cdot-}$ and $AQDS^{\cdot-}$ were also stabilized in the presence of P-80, non-ionic surfactant, as in the case of NaL and/or NaLS system. The results suggest that the electron-transfer reactions from the above anions to photoexcited quinones are not significant to account for the formation of stabilized anion radicals in our systems.

By the use of pulse radiolysis and flash photolysis techniques, the pK values for the semiquinone radical-anions of AQS and AQDS have been determined to be 3.25[24] and 2.30[19] respectively. However, the pH effects on the $AQS^{\cdot-}$ formation in micellar system

$$A^{\cdot-} + H^+ \overset{K}{\rightleftharpoons} AH\cdot \quad (3)$$

we observed cannot be simply explained by the pK value. Below pH 6.0, only anthrahydroquinone ($AQSH_2$) was formed and the formation of $AQS^{\cdot-}$ became significant above pH 6.8 (Fig. 7). This is similar to the pH effects on the $AQS^{\cdot-}$ transient absorption 800 μs after flash photolysis in non-micellar system.[18] At low pH region, both radical anion and semiquinone radical seem to decay rapidly by the disproportionation:[25,26]

$$2A^{\cdot-} \longrightarrow A + A^{2-} \quad (4)$$

$$A^{2-} + 2H^+ \longrightarrow AH_2 \quad (5)$$

$$2AH\cdot \longrightarrow AH_2 + A \quad (6)$$

At higher pH (6.8—8.0), the photolyzed micellar solutions of AQS and/or AQDS contained A, $A^{\cdot-}$, and AH_2. In addition to $A^{\cdot-}$ (λ_{max} 396 and 472 nm) and AH_2 (λ_{max} *ca.* 380 nm), dianion of A (A^{2-}) was detected by means of electronic spectroscopy (λ_{max} 436 nm)[27] when AQS in 0.1 M NaOH was irradiated in the presence of NaLS. The following two equilibria involving A^{2-} should also be taken into consideration to account for the data obtained at higher pH region:

$$AH_2 + 2OH^- \rightleftharpoons A^{2-} + 2H_2O \quad (7)$$

$$A^{2-} + A \rightleftharpoons 2A^{\cdot-} \quad (8)$$

The anthrahydroquinones ($AQSH_2$ and $AQDSH_2$) are stable only in acidic media. They are very easily oxidized to original quinones in aerobic neutral and alkaline solutions without surfactants. In the presence of the anionic and non-ionic surfactants, however, these diol derivatives were scarcely oxidized even in 0.1 M NaOH. It is evident that the surfactants play an important role to stabilize the diol derivatives.

The surfactant concentration profile indicates that both $AQS^{\cdot-}$ and $AQSH_2$ are stabilized by binding with micelles (Fig. 5). Existence of typical micellar effects is also manifested by the fact that only micelle-forming carboxylates can stabilize $AQS^{\cdot-}$ (Fig. 6). It seems rather odd, however, that the anionic species such as $A^{\cdot-}$ bind with anionic micelles. In general, negatively charged substrates, such as 1-anilinonaphthalene-8-sulfonate (ANS) and *N,N*-dimethyl-1-anilinonaphthalene-5-sulfonate, are adsorbed by cationic and non-ionic micelles, but not anionic ones.[28] The binding constant for anthraquinone sulfonate ion-anion micelle system is thus expected to be quite small.[29] No matter how small the binding constant is, some of the anthraquinone sulfonate will be bound to the micelles. These bound species may give the radical anion on photoexcitation. The long lifetimes of the radical anions suggest that the rate of exchange between the micelles and bulk water is extremely small.

The absorption maxima of $AQS^{\cdot-}$ and $AQDS^{\cdot-}$ in non-micellar systems have been found at 395 and

505 nm[18] and 400 and 520 nm[19] respectively. In the presence of micelles, the longer wavelength absorption bands of the anion radicals exhibit a remarkable blue shift (~35 and 47 nm, respectively). When the charged substrates such as $AQS^{\cdot-}$ and $AQDS^{\cdot-}$ bind with anionic micelles, the substrates are incorporated to the Stern layer surrounded by highly concentrated counter cations. The radical anions within the Stern layer, therefore, might form a contact ion pair with cations in the charged double layer. The pair is expected to absorb at shorter wavelengths than the solvent separated ion pair in non-micellar system. In the case of non-ionic micelles, the contact ion pair may be stabilized at the micelle-water interface.

Organic solvents, such as dioxane and alcohols, influence the reactions in micellar systems.[2,3] Since dioxane and alcohols are not adequate because of their hydrogen donative properties, we examined the effects of organic additives with the use of acetone and *tert*-butanol, both of which markedly inhibit the formation of $AQDS^{\cdot-}$ and $AQDSH_2$ in micellar systems. A possible explanation may be that the CMC of the surfactant increases on the addition of organic additives. An alternative may be that $AQDS^{\cdot-}$ and $AQDSH_2$ are displaced from the micellar phase by the additives.[3] No matter which the case is, it is clear that the binding of $AQDS^{\cdot-}$ and $AQDSH_2$ with micelles is essential for the stabilization of these substrates.

It has been reported that the microviscosity of the NaLS micelle interior increases about 3- to 6-fold with the addition of Mg^{2+}.[30] We have also studied the effects of Mg^{2+} on the photochemistry of AQDS-NaLS system. Addition of Mg^{2+} reduced the formation of both $AQDS^{\cdot-}$ ($\Phi/\Phi_0=0.48$) and $AQDSH_2$ (Table 2). Contribution of the coexisting sulfate ion (SO_4^{2-}) is considered to be small as verified by the addition of Na_2SO_4 ($\Phi/\Phi_0=0.84$). The permeation of $AQDS^{\cdot-}$ and/or $AQDSH_2$ into the micelles might change due to the contraction of charged heads and the increased rigidity of micelle interior as caused by the addition of Mg^{2+}.

All the results indicate that the anthraquinone radical anions and anthrahydroquinones are extremely stabilized by binding with micelles.

It is surprising that neither $A^{\cdot-}$ nor AH_2 is oxidized in the micellar systems in spite of its aerobic alkaline conditions. One reason might be that the hydroxide ion concentration in the microenvironment of anionic micelles is lower than that in the bulk since the electrostatic repulsion keeps hydroxide anions away from the negatively charged micelle surface. Thus the micelle interior would afford a favorable environment for AH_2, which exists as a stable species only at low pH region. In contrast, rapid and complex reactions were observed for AQS and/or AQDS when they were irradiated in the presence of hexadecyltrimethylammonium bromide (cationic surfactant) whose micelle surface is covered with locally concentrated hydroxide ions.

In non-micellar system, $AQS^{\cdot-}$ has been reported to react with oxygen very easily:[31]

$$AQS^{\cdot-} + O_2 \xrightarrow{k} A + O_2^{\cdot-} \quad k\ ca.\ 5\times10^8 M^{-1}\cdot s^{-1} \qquad (9)$$

Recently, the oxygen concentration and/or oxygen mobility in micelle interior were found to decrease appreciably with aging of the micellar system.[30,32,33] We found, however, that $A^{\cdot-}$ and AH_2 were easily stabilized in fresh micellar solutions as well as in old ones. Since many problems remain unsolved as regards the oxygen concentration within micelles,[30,32-34] no detailed discussion could be given. However, it is clear at least that the scavenging of $A^{\cdot-}$ by oxygen is markedly reduced in the presence of anionic and non-ionic micelles.

If the above micellar effects are simply ascribed to the protection of $A^{\cdot-}$ and AH_2 from the attack of oxygen, $A^{\cdot-}$ should also be stabilized in a well-degassed non-micellar system. In the absence of micelles, however, the photolysis of AQS in anaerobic aqueous media afforded only hydroxylated anthraquinones.[15,16] Studies of radiolysis in the micellar system revealed that the reaction of benzene with a hydroxyl radical is considerably inhibited in the presence of anionic, cationic, and non-ionic micelles,[34] and that the hydroxyl radical is rapidly scavenged by the surfactant to produce relatively inert radicals ($k\simeq10^9\ M^{-1}\cdot s^{-1}$).[35] The same type of protection against the hydroxyl radical would operate in the case of anthraquinones in a micellar system, since the hydroxylated anthraquinones have been reported to be formed by the attack of hydroxyl radicals.[12,15,16,24,27]

The radical anions of anthraquinone sulfonates are so stable in the presence of micelles that the reactivity of these radical anions was easily investigated.

The reactions of $AQS^{\cdot-}$ and $AQDS^{\cdot-}$ with H^+ yielded the corresponding anthrahydroquinones. Since pK of AQSH· and AQDSH· are 3.25[24] and 2.90[19] respectively, $AQS^{\cdot-}$ and $AQDS^{\cdot-}$ are protonated in 0.75 N H_2SO_4 to give semiquinone radicals, followed by disproportionation to produce anthrahydroquinones and original quinones:[26]

$$A^{\cdot-} + H^+ \longrightarrow AH\cdot \qquad (10)$$

$$2AH\cdot \longrightarrow AH_2 + A \qquad (11)$$

It is well-known that some quinones and ferric ion play an important role as electron carriers in biological systems. Since micelles are known to be good models of biological membrane, we used a micellar solution to construct a model system of the electron transport across membrane: $AQDS^{\cdot-}$ in NaLS micelles *vs.* ferric chloride in the aqueous phase. An electron was successfully transferred from $AQDS^{\cdot-}$ to Fe^{3+} in this system:

$$AQDS^{\cdot-} + Fe^{3+} \longrightarrow AQDS + Fe^{2+} \qquad (12)$$

Further improvement of the model system is expected to clarify the role of biological membranes in electron transport phenomena.

Conclusion

Remarkably long-living radical anions of 9,10-anthraquinone sulfonates are formed in the presence of micelles of anionic and non-ionic surfactants. All of the experimental data suggest that the stabilization of these radical anions is attributed to micellar effects, which are somewhat novel because the anionic species are

considered to be bound with anionic micelles. The relevant micellar effects can be summarized as follows:

a. Since hydroxyl radicals are efficiently scavenged by the surfactants, hydroxylation of the quinones does not take place in micellar systems.

b. The pH in a micellar system might favor the formation of the radical ions, which are involved in the following equilibria:

$$A^{\cdot-} + H_2O \rightleftarrows AH\cdot + OH^-$$
$$2AH\cdot \rightleftarrows AH_2 + A$$
$$AH_2 + 2OH^- \rightleftarrows A^{2-} + 2H_2O$$
$$A^{2-} + A \rightleftarrows 2A^{\cdot-}$$

c. The decay of the radical ion is extremely retarded because of low reactivities of quenchers such as oxygen in micellar interior.

The fact that the radical anions are stabilized by binding with micelles is interesting in relation to the electron transport in biological membranes.

References

1) Contribution No. 332 from the Department of Organic Synthesis, Faculty of Engineering, KyushuUniversity.

2) E. J. Fendler and J. H. Fendler, "Advances in Physical Organic Chemistry," Vol. 8, ed. by V. Gold, Academic Press, New York, N. Y., (1970), p. 271.

3) E. H. Cordes and C. Gitler, "Progress in Bioorganic Chemistry," Vol. 2, ed. by E. T. Kaiser and F. J. Kézdy, John Wiley and Sons, New York, N. Y., (1973), p. 1.

4) Ed. by E. H. Cordes, "Reaction Kinetics in Micelles," Plenum Publishing Co., New York, N. Y., (1973).

5) R. R. Hautala and R. L. Letsinger, *J. Org. Chem.*, **36**, 3762 (1971).

6) H. B. Kostenbauder and P. P. DeLuca, *J. Phys. Chem.*, **67**, 1395 (1963).

7) H. B. Kostenbauder and P. P. DeLuca, *Nature*, **199**, 999 (1963).

8) H. B. Kostenbauder, P. P. DeLuca, and C. R. Kowarski, *J. Pharm. Sci.*, **54**, 1243 (1965).

9) C. R. Kowarski, *ibid.*, **58**, 360 (1969).

10) K. Kano and T. Matsuo, *Chem. Lett.*, **1973**, 1127.

11) N. K. Bridge, *J. Soc. Dyers Colourist*, **76**, 484 (1960).

12) K. P. Clark and H. I. Stonehill, *J. Chem. Soc. Faraday I*, **68**, 577 (1972).

13) J. L. Bolland and H. R. Cooper, *Proc. Roy. Soc. Ser. A*, **225**, 405 (1954).

14) K. Kano and T. Matsuo, *Chem. Lett.*, **1974**, 11.

15) B. Mooney and H. I. Stonehill, *Chem. Ind.*, **1961**, 1309.

16) A. D. Broadbent, *Chem. Commun.*, **1967**, 382; A. D. Broadbent and R. P. Newton, *Can. J. Chem.*, **50**, 381 (1972).

17) The CMC of NaLS is 8.1×10^{-3} M (25 °C).[2)]

18) G. O. Phillips, N. W. Worthington, J. F. McKellar, and R. R. Sharpe, *J. Chem. Soc. A*, **1969**, 767.

19) V. A. Kuzmin and A. K. Chibisov, *Chem. Commun.*, **1971**, 1559.

20) The CMC of NaL is 2.4×10^{-2} M (25 °C).[2)]

21) P. J. Baugh, G. O. Phillips, and J. C. Arthur, Jr., *J. Phys. Chem.*, **70**, 3061 (1966).

22) C. A. Bunton, "Reaction Kinetics in Micelles," ed. by E. H. Cordes, Plenum Publishing Co., New York, N. Y., (1973), p. 73.

23) The CMC of P-80 is 1.3×10^{-3} g/dl (25 °C).[2)]

24) B. E. Hulme, E. J. Land, and G. O. Phillips, *J. Chem. Soc. Faraday I*, **68**, 1992 (1972).

25) N. K. Bridge and G. Porter, *Proc. Roy. Soc. Ser. A*, **244**, 259 (1958).

26) N. K. Bridge and G. Porter, *ibid.*, **244**, 276 (1958).

27) K. P. Clark and H. I. Stonehill, *J. Chem. Soc. Faraday I*, **68**, 1676 (1972).

28) M. T. Flanagan and S. Ainsworth, *Biochim. Biopys. Acta*, **168**, 16 (1968).

29) Although Flanagan and Ainsworth[28)] have reported that ANS does not bound with anionic micelles, we have observed that the fluorescence intensity of ANS is markedly increased above the CMC of NaLS and NaL (see experimental section).

30) M. Gratzel and J. K. Thomas, *J. Amer. Chem. Soc.*, **95**, 6885 (1973).

31) R. L. Willson, *Trans. Faraday Soc.*, **67**, 3020 (1971).

32) R. C. Dorrance and T. F. Hunter, *J. Chem. Soc. Faraday I*, **68**, 1312 (1972).

33) S. C. Wallace and J. K. Thomas, *Radiat. Res.*, **54**, 49 (1973).

34) J. H. Fendler, G. W. Bogan, E. J. Fendler, G. A. Infante, and P. Jirathana, "Reaction Kinetics in Micelles," ed. by E. H. Cordes, Plenum Publishing Co., New York, N. Y., (1973), p. 53.

35) K. N. Bansal, L. K. Patterson, E. J. Fendler, and J. H. Fendler, *Int. J. Radiat. Phys. Chem.*, **3**, 321 (1971).

Nuclear Magnetic Resonance Study of the Kinetics of Ligand Exchange on the Oxovanadium(IV)-malonato Complex

Hiroshi TOMIYASU,* Satoshi ITO,** and Shiro TAGAMI

Department of Chemistry, Faculty of Science, Shinshu University, Asahi, Matsumoto 390

(Received April 26, 1974)

The kinetics of malonate exchange on $VO(mal)_2^{2-}$ has been studied by the NMR line-broadening method. The reaction was found to be dependent on the Hmal and hydrogen-ion concentrations, and the mechanism producing the intermediate complexes, where malonic acid was coordinated partly as an unidentate ligand, was estimated from the rate law. The activation parameters were determined for the acid-independent and acid-catalyzed paths as: $\Delta H^* = 8.6$ kcal/mol, $\Delta S^* = -16.2$ e.u., and $\Delta H^* = 8.9$ kcal/mol, $\Delta S^* = -13.5$ e.u.

A number of kinetic studies of the ligand substitution of various oxovanadium(IV) complexes have been reported. These include H_2O exchange by ^{17}O NMR,[1-3] CH_3CN, glycine and other ligand exchanges by proton NMR,[4,5] the formation of $VOHGly^{2+}$ and $VO(Tart)_2^{2-}$ by the stopped-flow and Temp.-Jump methods,[5-7] and the rapid interaction of axial- or second-sphere water by NMR and ESR.[3,8,9,14]

We found in a previous work that, in the formation of the chelate complex, $VO(Gly)^+$, the rate-determining step was the path from $VOGly^+$, which represents the deprotonated form of $VOHGly^{2+}$, to $VO(Gly)^+$ instead of the formation of $VOHGly^{2+}$, where glycine is coordinated on the equatorial position as a unidentate ligand.[5,7]

This led to the problem of the unusual reactivity of bidentate ligands which are coordinated on VO^{2+} as unidentate ligands. In this work we wish to report the kinetics of malonate exchange on $VO(mal)_2^{2-}$ † in order to discuss the problems which arose from the previous work.

Experimental

The preparation and analysis of the VO^{2+} stock solution were described in a previous paper.[5] Reagent-grade malonic acid (Wako Pure Chemicals, Co. Ltd.) was recrystallized twice from distilled water and dried under reduced pressure. The sodium perchlorate was prepared from stoichiometric amounts of Na_2CO_3 and $HClO_4$ and was purified by recrystallization from an aqueous solution. A JEOL Co. Ltd. JNM-4H-100 NMR spectrometer was used to record the NMR spectra. The peak observed was that of the methylene protons of malonic acid in the bulk phase. The spectrophotometric measurements were made at 25 °C on a Shimadzu MPS-50L spectrometer. The pH of each solution was measured with a Hitachi-Horiba pH meter F-7ss equipped with a glass electrode, Horiba 1026-05T.

Results and Discussion

Absorption Spectrum of the Oxovanadium(IV)-malonate Complex. The absorption spectrum and the electronic structure of the VO^{2+} complexes have been studied elsewhere.[12] The two absorption bands at about 760 and 630 nm which are characteristic of the VO^{2+} ion were observed at slightly shifted wavelengths of 780 and 600 nm in the presence of malonic acid, according to the complex formation. The optical densities of the malonato-complex were much larger than those of the aquo-complex in both bands; therefore, the observed absorbances increased as the concentration of malonic acid or the pH of solution was increased. Under the conditions of malonic acid$>$1.0 M and pH$>$2.8, the complex formation was saturated and no further increase in absorbance was observed. In such conditions, all the VO^{2+} ions were present as dimalonatooxovanadium(IV) ions, $VO(mal)_2^{2-}$, which may be analogous to diglycinatooxovandium(IV), $VO(Gly)_2$, which was studied in earlier works.[5,10] The $VO(mal)_2^{2-}$ thus prepared was very stable, and the absorption spectrum did not change for several days at the pH of 4.5.

NMR Measurements. Swift and Connick derived the relaxation time in a paramagnetic solution from a rigorous solution of the Bloch equation.[11] If the chemical exchange between the metal ion and the ligand controls the relaxation process, the observed relaxation time T_2, is related to the life-time of a ligand staying in the environment of the coordination sphere by;

$$1/T_2 - 1/T_{2a} = P_m/\tau_m \quad (1)$$

where T_{2a} is the relaxation time in the absence of metal ions and where P_m is approximated in a dilute solution as;

$$P_m = n[\text{complex}]/[\text{total ligand}] \quad (2)$$

wher n is the number of coordinated ligands. In this work, [ligand] corresponds to the total concentration of malonic acid, and n is assumed to be 2. Thus, the rate constant for the dissociation of a ligand from the coordination sphere is given by;

$$k' = \tau_m^{-1} \quad (3)$$

Whether or not a chemical exchange controls the relaxation process can be tested by plotting $\log(1/T_2 - 1/T_{2a})$ as a function of the reciprocal temperature. Equation (1) is applicable if the graph of $\log(1/T_2 - 1/T_{2a})$ *vs.* $1/T$ is linear, with a negative slope. The full line-width at the half height of malonate methylene protons is listed in Table 1 for various malonic acid concentrations. The line-width in the absence of VO^{2+}

* To whom correspondence should be addressed.

** Present address: Department of Chemistry, Faculty of Science, Osaka University.

† For the purpose of convenience, the oxovanadium(IV) ion will be written as VO^{2+} and the malonate and bimalonate ions will be abbreviated as "mal" and "Hmal" respectively.

Table 1. Line-width of malonate methylene protons for various temperatures at ionic strength=1.4, $[VO^{2+}]=0.00719$M and [Malonic acid]=1.5M

Temp. (°C)	Line-width (Hz)	$(1/T_2-1/T_{2a})/P_m$ $(10^3\times s^{-1})$
0	$5.0_6\pm0.7_1$	$1.19\pm0.2_3$
5	$4.5_8\pm0.4_0$	$1.03\pm0.1_3$
10	$4.6_2\pm0.5_4$	$1.06\pm0.1_8$
15	$3.6_9\pm0.1_4$	$0.74\pm0.0_5$
20	$4.8_6\pm0.4_0$	$1.12\pm0.1_3$
25	$6.0_3\pm0.6_9$	$1.51\pm0.2_3$
29	$6.0_9\pm0.6_5$	$1.53\pm0.2_1$
35	$9.2_7\pm0.7_5$	$2.57\pm0.2_5$
38	$10.6_2\pm0.4_9$	$3.01\pm0.1_6$
45	$13.2_7\pm0.4_9$	$3.88\pm0.1_6$
50	$17.2_9\pm1.1$	$5.20\pm0.3_7$
55	$21.6_7\pm1.3$	$6.63\pm0.4_4$
60	$23.2_1\pm1.6$	$7.14\pm0.5_2$
65	$28.5_6\pm1.0$	$8.89\pm0.3_0$
70	$29.2_7\pm1.0$	$9.12\pm0.3_0$
76	$32.0_7\pm1.5$	$10.04\pm0.4_9$

Table 2. Line-width of malonate methylene protons in the absence of VO^{2+}

[Malonic acid] (M)	Ionic strength	Temp. (°C)	Line-width (Hz)
0.70	1.4	25	$1.4_1\pm0.1_8$
1.25	1.4	25	$1.2_2\pm0.2_6$
1.50	1.4	25	$1.2_0\pm0.2_6$
1.75	1.4	25	$1.1_7\pm0.1_2$
1.50	1.4	38	$1.4_3\pm0.1_8$
1.50	3.0	25	$1.4_6\pm0.0_9$
1.50	3.0	70	$1.2_3\pm0.1_4$

was very sharp, and, as is shown in Table 2, no broadening was observed within the limits of experimental error in solutions of high malonic acid concentrations, where a relatively high viscosity would be expected compared with that of pure water. Therefore, the effect of the viscosity on the line-width of the malonate methylene proton may be ignored in the solutions studied. From Tables 1 and 2, $\log(1/T_2-1/T_{2a})/P_m$ can be calculated; the plot *vs.* $1/T$ is shown in Fig. 1. It can be seen in Fig. 1 that a linear relationship is obtained over most of the temperature range studied; hence, Eq. (1) is applicable.

The rate constants, k', thus obtained in the low pH range are listed in Tables 3 and 4 at 25 °C. In higher pH values (above 4), the reaction is too slow at 25 °C

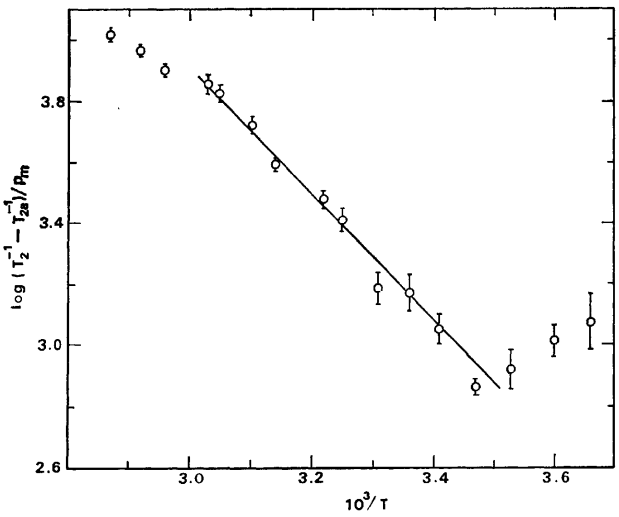

Fig. 1. Plot of line-width of methylene proton of malonic acid as a function of reciprocal temperature.

for us to be able to determine the accurate value of k' from the line-width measurements; therefore, the data listed in Tables 5 and 6 represent the values at 40 °C.

It can be seen in Tables 3 and 4 that k' increases with the concentrations of malonic acid. This suggests that the reaction is first order in relation to both $VO(mal)_2^{2-}$ and malonic acid. Since H_2mal seems unlikely to react with $VO(mal)_2^{2-}$, Hmal or mal must be important for the substitution reaction. However, in the high pH region (pH>4.6), it can be seen in Table 6 that k' becomes smaller as the pH of the solution increases, where [mal] increases, while [Hmal] decreases in this pH region. From these facts, we may

Table 4. Hydrogen ion dependence on the rate of malonate exchange at 25 °C and ionic strength=1.4 in low pH solutions $[VO^{2+}]=0.00719$ M, [Malonic acid]=1.50 M

pH	[Hmal] (M)	k' $(s^{-1}\times10^{-3})$	k $(M^{-1}$ $s^{-1}\times10^{-3})$
2.30	0.348	1.9	5.5
2.37	0.393	1.9	4.8
2.45	0.449	1.9	4.2
2.60	0.564	1.8	3.2
2.77	0.707	1.9	2.7
2.95	0.861	1.6	1.9
3.60	1.29	1.5	1.1_7
4.05	1.42	1.5	1.0_1[a]

a) Ionic strength=1.6

Table 3. Rate constants for various malonic acid concentrations at 25 °C and ionic strength= 1.4

$[VO^{2+}]$ $(M\times10^3)$	[Malonic acid] (M)	pH	[Hmal] (M)	k'[a] $(s^{-1}\times10^{-3})$	$k(M^{-1}s^{-1}$ $\times10^{-3})$	k_{cal} $(s^{-1}\times10^{-3})$
7.19	0.700	3.73	0.623	0.74	1.2	0.76
7.19	1.00	3.30	0.751	1.2	1.6	1.1_2
7.19	1.25	3.40	0.990	1.5	1.5	1.3_9
7.19	1.50	3.40	1.19	1.7	1.4	1.6_7
7.19	1.75	3.57	1.49	2.1	1.4	1.9_2[b]

a) k' represents the first-order rate constant for VO^{2+} and is related to k by $k'=k$[Hmal]. b) Because of high malonic acid concentration, an ionic strength was held at 1.6.

Table 5. Rate constants for various malonic acid concentrations at 40 °C and ionic strength = 3.0

$[VO^{2+}]$ ($M\times10^{3}$)	[Malonic acid] (M)	pH	[Hmal] (M)	k' ($s^{-1}\times10^{-3}$)	k ($M^{-1}s^{-5}\times10^{-3}$)
7.23	1.00	4.49	0.952	2.13	2.24
7.23	1.25	4.50	1.19	2.53	2.13
7.23	1.50	4.61	1.40	3.11	2.22
7.23	1.75	4.61	1.64	3.35	2.04
7.23	2.00	4.60	1.88	3.56	1.86
					—
				Average =	2.10

Table 6. pH dependence on the rate of malonate exchange at 40 °C and ionic strength = 3.0 in high pH solutions

$[VO^{2+}]=0.00723$ M, [Malonic acid] = 1.50 M

pH	[Hmal] (M)	k' ($s^{-1}\times10^{-3}$)	k ($M^{-1}s^{-1}\times10^{-3}$)
4.31	1.45	2.85	1.96
4.56	1.42	3.11	2.19
4.62	1.40	3.11	2.22
4.73	1.38	2.58	1.87
4.91	1.32	2.53	1.92
5.00	1.29	2.50	1.93
5.50	0.962	1.82	1.89
			—
		Average =	2.00

conclude that mal is also inactive and that Hmal is the only species which interacts directry with $VO(mal)_2^{2-}$. The second-order rate constant, k, where $k=k'/[\text{Hmal}]$, is constant within the limits of experimental error, as is shown in Tables 3, 5, and 6 for various malonic acid concentrations.

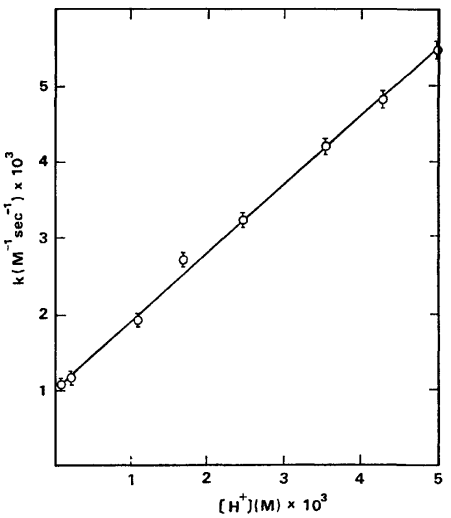

Fig. 2. Plot of rate constant, k, *vs.* hydrogen ion concentration.

The hydrogen-ion dependence for k is shown in Table 4. As can be seen in Fig. 2, the plot of k *vs.* $[H^+]$ is linear; k is given by the following equation:

$$k = k_1 + k_2[H^+] \quad (4)$$

The values of k_1 and k_2 are obtained from the intercept and the slope of Fig. 2 as 1.1×10^3 $M^{-1}s^{-1}$ and 8.4×10^5 $M^{-2}s^{-1}$ respectively. The first term gives the estimated value for k in the high pH region; it agrees very closely with that of 0.91×10^3 $M^{-1}s^{-1}$ which was obtained experimentally from the measurement at pH = 5.5 and 25 °C. The second term corresponds the acid-catalyzed path, which is predominant in the low pH region. In Table 3 the values calculated for k using Eq. (4), k_{cal}, are listed. These values are in satisfactory agreement with the observed values. The activation parameters for both paths were determined from the measurements at pH = 5.50 and pH = 2.45. They are $\Delta H^{\ddagger}=8.6$ kcal/mol, $\Delta S^{\ddagger}=-16.2$ e.u. for the acid-independent path and $\Delta H^{\ddagger}=8.9$ kcal/mol, $\Delta S^{\ddagger}=-13.5$ e.u. for the acid-catalyzed path.

From the potentiometric and spectrophotometric studies,[13] we found that VO^{2+} formed such complexes that bidentate ligands, malonic acid and glycine, are coordinated on the equatorial position as unidentate ligands. Furthermore, in a kinetic study of the formation of the chelate complex, $VO(Gly)^+$,[7] it was found that the rate of chelation from the unidentate complex, $VOGly^+$, was surprisingly slow (35 s^{-1}) compared with that of the formation of $VOHGly^{2+}$ (1.3×10^3 $M^{-1}s^{-1}$)[5] or water exchange on the equatorial positions of the VO^{2+} aquo complex (500 s^{-1}).[1,2] This reaction, which we called the "slow chelation process", was estimated to proceed through the intermediate complex, where the $-COO^-$ and $-NH_2$ of the glycinate ion may be coordinated on the equatorial position and the position above the triangular face of the tetragonal pyramid structure.

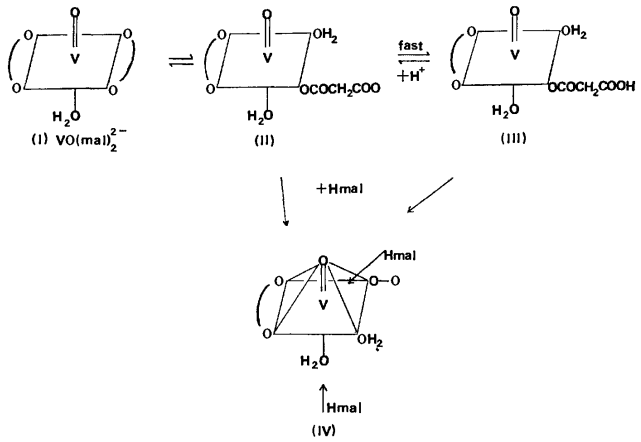

Fig. 3. Reaction scheme of malonate exchange on VO $(mal)_2^{2-}$.

These findings suggest that the first step of malonate exchange on $VO(mal)_2^{2-}$ is the dissociation of one of the chelate rings forming an intermediate complex (II) in Fig. 3, where one of the two malonate ions on equatorial positions is coordinated as a unidentate ligand. In an acidic solution, the (II) complex may be protonated to form a (III) complex. Then, these complexes, (II) and (III), which are analogous in structure to the $VOGly^+$ and $VOHGly^{2+}$ respectively,

could accept the attack of Hmal from the axial position or the position above the triangular face of the tetragonal pyramid structure, as is estimated in the chelation process of $VO(Gly)^+$.

Since the equilibrium between (II) and (III) should be very fast, the rate Eq. (4) can be explained by the following processes: (I)→(II)→(IV) for the acid-independent path and (I)→(II)⇄(III)→(IV) for the acid-catalyzed path. The approximately identical values of ΔH^* for the two paths may support substitution mechanisms similar to those described above.

The authors would like to thank Professor Hiroshi Fukutomi of Tokyo Institute of Technology for his helpful discussions.

References

1) K. Wüthrich and R. E. Connick, *Inorg. Chem.*, **6**, 583 (1967).
2) J. Reuben and D. Fiat, *ibid.*, **6**, 579 (1967).
3) K. Wüthrich and R. E. Connick, *ibid.*, **7**, 1377 (1968).
4) N. S. Angerman and R. E. Jordan, a) *ibid.*, **8**, 65 (1969); b) *ibid.*, **8**, 1824 (1969).
5) H. Tomiyasu, K. Dreyer, and G. Gordon, *ibid.*, **11**, 2409 (1972).
6) K. Kustin and R. Pizer, *ibid.*, **9**, 1536 (1970).
7) H. Tomiyasu and G. Gordon, Proceedings of 15th International Conference on Coordination Chemistry, 423 (1973).
8) F. A. Walker, R. L. Carlin, and P. H. Rieger, *J. Chem. Phys.*, **45**, 4181 (1966).
9) N. S. Angerman and R. E. Jordan, *ibid.*, **54**, 837 (1971).
10) H. Tomiyasu and G. Gordon, *J. Coord. Chem.*, **3**, 47 (1973).
11) T. J. Swift and R. E. Connick, *J. Chem. Phys.*, **37**, 307 (1962).
12) C. J. Ballhausen and H. B. Gray, *Inorg. Chem.*, **1**, 111 (1962).
13) S. Ito, H. Tomiyasu, and H. Ohtaki, This Bulletin, **46**, 2238 (1973).
14) G. A. Miller and R. E. D. McClung, *Inorg. Chem.*, **12**, 2522 (1973).

Hydrogen Redistribution of Acetone on ZnO Catalysts

Ken-ichi NAGAI, Ken-ichi TANAKA, and Koshiro MIYAHARA
Research Institute for Catalysis, Hokkaido University, Sapporo 060
(Received February 12, 1974)

The hydrogen redistribution reaction between d_0-acetone and d_6-acetone was carried out at −10—60 °C over ZnO catalysts subjected to various modes of pretreatment. The activity of ZnO was several times larger than that of Zn metal, being hardly affected by the conditions of pretreatment below 350 °C and illumination with a mercury lamp. The rate of hydrogen redistribution was proportional to the amount of chemisorbed acetone which obeys the Langmuir adsorption isotherm. The activation heat of redistribution and the heat of acetone chemisorption were estimated to be 14 ± 2 and 10 ± 1 kcal/mol, respectively. The time course of the relative amounts of d_n-acetones, independent of the catalyst or its activity, was reproducible by a calculation based on the stepwise exchange model for the hydrogen exchange of acetone. About half of the chemisorbed acetone was found to be active for the redistribution or exchange of hydrogen. From the results and IR spectrometric study of acetone adsorbed on ZnO, the hydrogen redistribution of acetone was concluded to proceed *via* a chemisorbed acetone with an enol type configuration on a pair of sites, Zn^{2+}–O^{2-}, of ZnO surface.

It is well-known that ZnO catalyzes the dehydrogenation of isopropyl alcohol selectively. The hydrogenation of acetone has been found[1] to proceed on ZnO catalyst in the presence of a large excess of hydrogen at temperatures above *ca.* 100 °C, accompanied by a rapid redistribution of hydrogen in methyl groups of acetone. With regard to this hydrogen redistribution reaction, Hine *et al.*[2] reported that d_6-acetone was dedeuterated in acidic or alkaline aqueous solution, being catalyzed by hydrogen or hydroxyl ion, respectively. It is thus of interest to study the mechanism and nature of the active sites on ZnO surface of the present reaction. The reaction was investigated with a mixture of 85% of d_0-acetone ($(CH_3)_2CO$) and 15% of d_6-acetone ($(CD_3)_2CO$), ZnO and Zn metal subjected to various modes of pretreatment being used as catalyst.

Experimental

Powdered ZnO (Kadox-25 from New Jersey Zinc Co.) or Zn metal, first pressed into a wafer *ca.* 0.2 mm thick, was crushed into few mm wide. A known amount of catalyst was mounted in the bottom of a U-tube reactor of a conventional, closed circulating system, volume *ca.* 250 ml, and was activated by varied pretreatment (Table 1). In order to minimize contamination of the catalyst without cold traps, Apiezon grease of the stop cocks was well degassed prior to the experiment.

Chemically pure d_0-acetone from Wako Chem. Co. and d_6-acetone of 99D% from Merck Co. were dried by passing through a $CaCl_2$-tube and then repeatedly distilled in a vacuum. The sample of d_6-acetone contained d_5- and d_4-acetone in a few percent. Reactions were carried out at −10—60 °C under pressures of 0.5—80 mmHg of acetone. In order to estimate the ratio of the amount of adsorbed acetone active for redistribution to the total acetone adsorbed on ZnO, measurements were made of the adsorption isotherm of acetone, the hydrogen exchange between gaseous d_0-acetone and preadsorbed d_6-acetone and the hydrogen redistribution between d_0- and d_6-acetone over ZnO preliminarily saturated with adsorbed d_6-acetone. During some runs of the reaction of the d_0- and d_6-acetone mixture, the catalyst was illuminated with a mercury lamp of medium pressure (Toshiba H-400-P).

TABLE 1. PRETREATMENT OF THE CATALYSTS

Original form	No. of catalysts	Pretreatment	Visible change
ZnO powder,[a] 0.334 g	I	Evacuated at 300 °C for 1 hr	None
	II	Evacuated at 350 °C for 3 hr	Colored with dark green
	III	Evacuated at 450 °C for 3 hr	Zn deposited on the upper part of the reactor
	IV	Heated at 450 °C for 3 hr in 200 mmHg H_2 and then evacuated at 300 °C for 1 hr	Similar as above
Zn powder,[b] 0.380 g	V	None	None
	VI	Heated at 200 °C for 0.5 hr in 5 mmHg O_2 and then evacuated at 200 °C for 1 hr	None
	VII	Heated at 350 °C for 0.5 hr in 5 mmHg O_2 and then evacuated at 300 °C for 1 hr	None
	VIII	Heated at 400 °C for 0.5 hr in 5 mmHg O_2 and then evacuated at 300 °C for 1 hr	ZnO deposited on the upper part of the reactor

a) Prior to pretreatment, pressed Kadox-25 was heated at 450 °C in few cmHg O_2 for 14 hr, evacuated for 3 hr at 350 °C, heated again in O_2 for 0.5 hr and then cooled to the temperature of pretreatment. b) Prior to pretreatment, pressed Zn powder was heated at 350 °C for 14 hr and then evacuated for 1 hr at 350 °C.

Sampled gases were analyzed with a mass spectrometer (Hitachi RMU-6); ionization voltage 70 V. Relative peak heights of *m/e* 58—65 give relative amounts of d_n-acetones $n=0, 1, —, 6$ since no fragments of acetone were present in this region of the spectra.

Results and Discussion

The initial activity of ZnO catalysts was fairly high but decreased to a steady value after several runs of reaction were repeated followed by evacuation at room temperature (Table 1). Figure 1 shows a typical time course of the reaction with a mixture of 85% d_0- and 15% d_6-acetone carried out on the stabilized catalyst II, with surface area *ca.* 4 m²/g Cat.

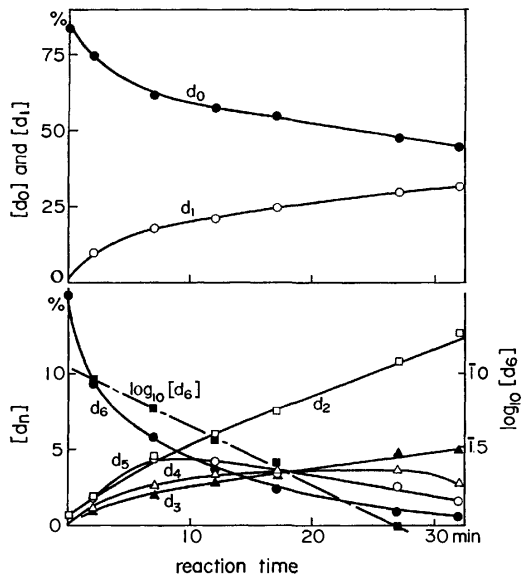

Fig. 1. Time courses of the relative amounts of d_n-acetones formed by the hydrogen redistribution with a 20 mmHg mixture of 85% d_0- and 15% d_6-acetone on ZnO (the catalyst II) at 0 °C.

The relative amounts of respective d_n-acetones depend solely upon the relative amount of d_6-acetone (Fig. 2). This suggests that the hydrogen redistribution reaction obeys the same rate equation, irrespective of the pretreatment of the catalyst. The presence of maxima of d_4- and d_5-acetone in the time courses (Fig. 1) suggests a stepwise hydrogen exchange mechanism, *i.e.*, not more than one hydrogen atom undergoes exchange before desorption of adsorbed acetone molecule. The full curves in Fig. 2 represent the results of simulation by the stepwise mechanism,

$$d_n\text{-acetone} \rightleftarrows a_m + h, \qquad (1)$$

where h is an adsorbed H or D atom and a_m ($m=n$ or $n-1$) is the adsorbed species of acetone loosing h. Provided that the kinetic hydrogen isotope effect on the rate of reaction (1) is negligible and the steady state condition is established for respective a_m's, we can derive the following equations which give the relative amounts of d_n-acetones, $[d_n]$, as a function of $[d_6]$.

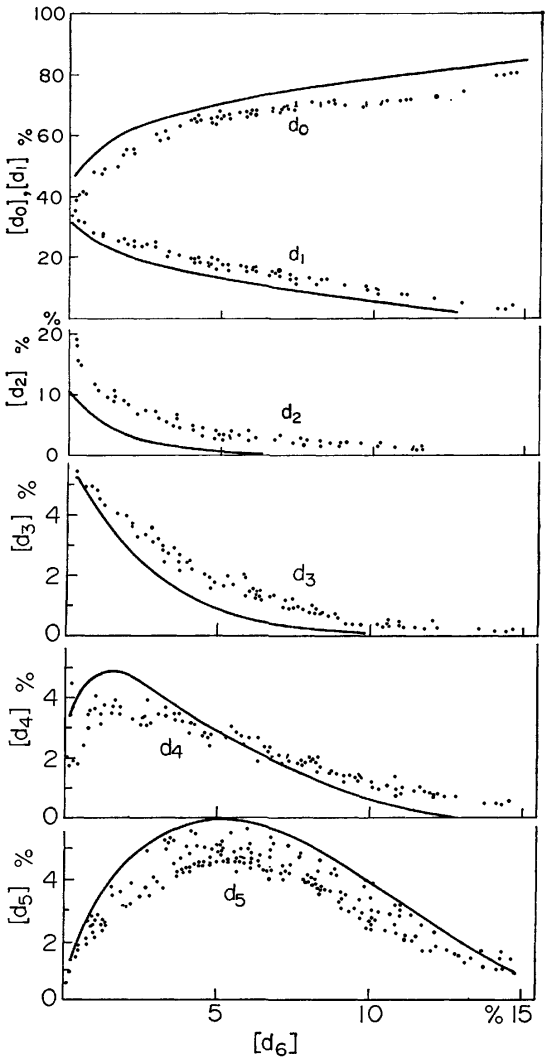

Fig. 2. The relations among the relative amounts of d_n-acetones formed by the hydrogen redistribution with a mixture of 85% d_0- and 15% d_6-acetone. Plots are the experimental results obtained by the use of all the catalysts listed on Table 1 and the full curves are those calculated by Eqs. (2).

$$\left.\begin{aligned} \frac{d[d_n]}{d[d_6]} &= \frac{[a_n](1-x)+[a_{n-1}]x-[d_n]}{[a_6](1-x)-[d_6]} \\ \frac{d[a_n]}{dt} &= \frac{(6-n)[d_n]}{6} + \frac{n[d_{n+1}]}{6} - [a_n] = 0, \end{aligned}\right\} \qquad (2)$$

where x is the D atomic fraction of h, being equal to 0.15 in the present reaction. In spite of the crude approximation in the simulation and no correction being made as regards ^{13}C and H contained in the d_6-acetone sample, observations for all the catalysts were well reproduced.

A linear relation of $\log_{10}[d_6]$ *vs.* time indicates that the rate of $[d_6]$ decrease obeys the first-order rate equation (Fig. 1(b)).

$$-d[d_6]/dt = (v_{ex}M/P_AV)[d_6], \qquad (3)$$

where P_A is the total pressure of acetone, V the volume of reaction system and M the weight of catalyst used. Constant v_{ex} is the exchange rate (ml·mmHg/min·g Cat.) and a measure of catalytic activity. The values

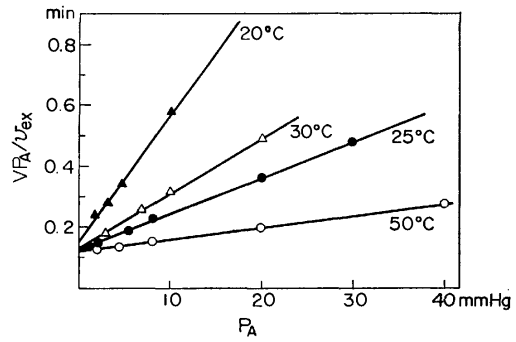

Fig. 3. Dependence of the exchange rate, v_{ex}, on acetone pressure. The experimental condition is similar to the case of Fig. 1.

of v_{ex} obtained for the catalyst II at various acetone pressure and temperatures establish the following relation (Fig. 3).

$$v_{ex} = k_{ex}K_A P_A/(1+K_A P_A), \quad (4)$$

where k_{ex} and K_A are the apparent rate constant of the exchange and the apparent equilibrium constant of acetone adsorption on ZnO catalyst, respectively. The activation heat of the exchange and the heat of acetone adsorption were evaluated to be 14 ± 2 and 10 ± 1 kcal/mol, respectively, from the results given in Fig. 4. The activation heats are nearly the same for all the catalysts. This indicates the same mechanism for all the reactions.

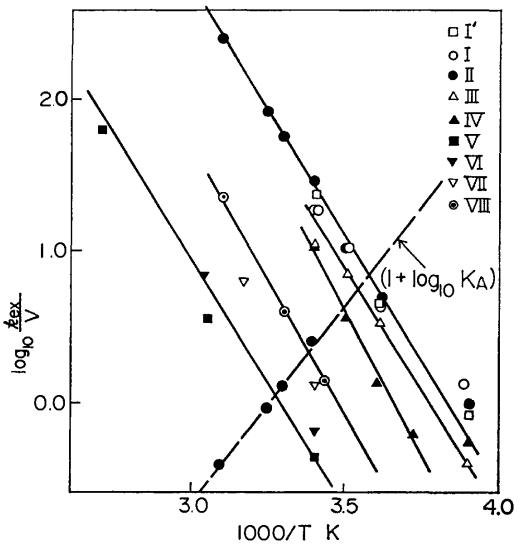

Fig. 4. Temperature dependences of the exchange rate constant, k_{ex}, and the adsorption constant, K_A (mmHg). Annexed figures are the number of the catalyst used.

The ZnO catalyst evacuated at a temperature below 350 °C gives a catalytic activity (Fig. 4), several tens times larger than that of the Zn metal. The activity of ZnO which decreased with evacuation at 450 °C is probably due to the deposition of Zn metal on ZnO surface (Table 1). In contrast, Zn metal became active with preliminary heating in oxygen. The high activity of ZnO as compared with Zn was further proved by use of catalyst VIII consisting of ZnO deposition on the upper part of the U-tube reactor and Zn metal at the bottom. The exchange reaction rate did not change by cooling the bottom of the reactor to −10 °C, where Zn metal was mounted, indicating that the reaction mainly takes place on ZnO deposited on upper part of the reactor wall.

Adsorption isotherms of acetone on the catalyst II were determined at temperatures 0—100 °C and at P_A up to a few mmHg. Saturated adsorption was observed at 0 °C, its amount being estimated to be 1.5 ml/g Cat. The adsorbed amount at 0 °C and 1 mmHg of P_A was 0.93 times this saturated adsorption, whereas it was 0.5 during the course of redistribution reaction according to the value of K_A (Fig. 4) and the adsorption isotherm

$$n = n_\infty K_A P_A/(1+K_A P_A) \quad (5)$$

derived from Eq. (4), where n is the amount of adsorbed acetone active for hydrogen redistribution and n_∞ its saturated value. The difference in the fractions of adsorbed acetone suggests that only a part of adsorbed acetone contributes to the hydrogen redistribution. This result was further supported by the hydrogen exchange reaction between gaseous d_0-acetone and preadsorbed d_6-acetone as follows. The reaction vessel was divided into A and B, the former containing catalyst II. A known amount of d_6-acetone was introduced into A and brought into adsorption equilibrium with the catalyst. d_0-Acetone was then introduced into B at an equal pressure to the residual pressure in A and was mixed with d_6 acetone in A by circulating over the catalyst causing hydrogen redistribution. The deuterium atomic fraction y_∞ in gaseous acetone at exchange equilibrium is given by

$$y_\infty = (N_6+n)/(N_0+N_6+n),$$

where N_0 and N_6 are amounts of gaseous d_0- and d_6-acetone, respectively, and n is the amount of preadsorbed d_6-acetone active for the hydrogen exchange. y_∞ is given by the steady value of y_A (Fig. 5). n was evaluated at 0.62 or 0.56 ml/g Cat. By introducing this value into Eq. (5), n_∞ was evaluated at 0.68 or 0.66 ml/g Cat., which is also *ca.* a half of the amount of saturated adsorption of acetone (1.5 ml/g Cat.). Thus, k_{ex} and K_A are proved to be the rate constant of the hydrogen redistribution and the equilibrium constant of the chemisorption of active acetone for the exchange, respectively.

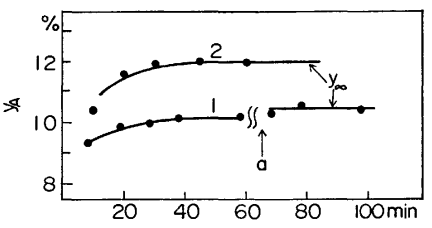

Fig. 5. Hydrogen exchange between d_6-acetone preadsorbed on the catalyst II and gaseous d_0-acetone at 0 °C.
Curve 1: 0.19 g ZnO and 6 mmHg at the adsorption equilibrium, curve 2: 0.5 g ZnO and 10 mmHg. At the time, *a*, of curve 1 the temperature was raised to 40 °C to accelerate the exchange.

The value of n_∞, being *ca.* a half of the monolayer on ZnO surface, indicates that the active sites for the hydrogen redistribution is the normal crystal plane but not the interstitial zinc[3] and/or the anion vacancies,[4] which might be far rarer than the normal lattice points of ZnO surface and have been reported to be active for the oxidation of CO, decomposition of N_2O[5] and so on. For the sake of confirmation catalyst II was illuminated with a mercury lamp of medium pressure in the course of the redistribution reaction. The rate did not change with illumination, indicating that the conduction electrons and/or the interstitial zinc is not responsible for the reaction.

From the above conclusions on the mechanism and the active sites of the exchange reactions and the results of the IR spectrometric study,[1] which established the presence of acetone chemisorbed on ZnO surface dissociatively with an enol-type configuration, the hydrogen redistribution reaction of acetone is supposed to be caused *via* acetone chemisorbed on a pair of sites, Zn^{2+}–O^{2-}, of ZnO surface such as

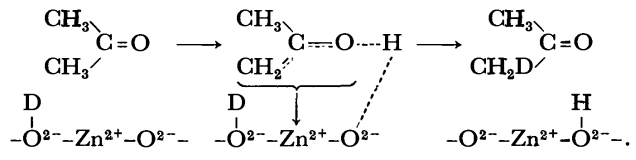

References

1) K. Nagai, to be published.
2) J. Hine, J. C. Kaufmann, and M. S. Cholod, *J. Amer. Chem. Soc.*, **94**, 4590 (1972).
3) M. N. Danchevskaya, G. P. Panasyuk, and N. I. Kobozev, *Zh. Fiz. Khim.*, **43**, 671 (1961).
4) O. V. Krylov and E. A. Fokina, Proc. IV International Congress on Catalysis, Moscow, 1968, Vol. 2, p. 229, Publ. 1971.
5) K. Tanaka and G. Blyholder, *J. Phys. Chem.*, **76**, 1807 (1972).

Kinetic Studies on the Selenization of Silver

Jun-ichiro MIZUSAKI, Kazuo FUEKI, and Takashi MUKAIBO
Department of Industrial Chemistry, Faculty of Engineering, The University of Tokyo, Hongo, Bunkyo-ku, Tokyo 113

(Received May 2, 1974)

In order to elucidate the kinetics of selenization of silver by liquid selenium, the Ag/Ag_2Se interface reaction rate, the ionic conductivity of Ag^+ in Ag_2Se layer, the $Ag_2Se/Se(l)$ interface reaction rate, and the over-all reaction rate were determined. The Ag/Ag_2Se interface reaction rate was found to be given by

$$v = 1.6 \times 10^9 \{\exp(-32300/RT)\}(a_{Se}) \quad \text{eqv cm}^{-2}\cdot\text{s}^{-1}$$

The following mechanism was proposed for the interface reaction.

$$2Ag(Ag) + Se(Ag_2Se) \longrightarrow 2Ag^+(Ag_2Se) + Se^{2-}(Ag_2Se)$$

It was found that the driving force of the $Ag_2Se/Se(l)$ interface reaction is very small and Ag_2Se is in equilibrium with Se(l). On an assumption that the over-all reaction is controlled by both the Ag/Ag_2Se interface reaction and the diffusion of Ag^+ in Ag_2Se, the over-all reaction rates were calculated. The results agree with the observed ones.

Tarnishing reaction of metals proceeds in three steps; (i) reaction at the metal/scale interface, (ii) diffusion of electrons and ions through the growing scale and (iii) reaction at the gas (or liquid)/scale interface. Most kinetic studies on dry corrosion are concerned with the measurement and analysis of over-all reaction. If diffusion is rate controlling, the parabolic law holds, and if the interface reactions are rate controlling, the linear law holds. However, neither law holds if the reaction is controlled by both diffusion and interface reactions.

In order to determine the rate-controlling step more precisely, it is desirable to measure the reaction rate of each step separately and to compare the observed over-all reaction rate with the one calculated from the rates of three steps. For example, if step (ii) is rate controlling, the parabolic rate constant is related to the diffusion constant of the slowest diffusion species, as given by Wagner's equation.[1] If step (i) or (iii) is rate controlling, the linear rate constant should be equal to the rate of reaction at either one of two interfaces. Rickert and Tostmann studied the sulfurization of silver by sulfur vapor from this viewpoint.[2] Wagner, Rickert and their co-workers explained the sulfurization of silver and copper by liquid sulfur as controlled by steps (i) and (ii).[3,4] However, no work has been carried out on the reaction controlled by more than one step, with separate measurement of the reaction rate of each step and a comparison of the over-all reaction rate with the calculated one.

The purpose of the present study is to measure the Ag/Ag_2Se interface reaction rate, the ionic conductivity of Ag^+ in Ag_2Se, the $Ag_2Se/Se(l)$ interface reaction rate and the over-all reaction rate of selenization of silver by liquid selenium, and to compare the observed over-all reaction rate with the one calculated from the results of separate measurements.

Tubandt and his co-workers investigated the selenization of silver by solid selenium,[5,6] but that by liquid selenium has not been studied yet. Rickert, in a study on the Ag/Ag_2Se interface reaction,[7] recently found that the reaction rate was proportional to the -1.5—-3.0 power of activity of silver in Ag_2Se. However, we found it to be proportional to the -2 power.[8] This led us to reinvestigate kinetically the Ag/Ag_2Se interface reaction. So far no work on liquid/scale interface reaction seems to have been carried out yet.

Experimental

Materials. Silver (99.9%) and selenium (99.99%) were used. Cylindrical silver selenide was Prepared by the reaction of silver with selenium in a Pyrex tube. The product was sliced into pellets. AgI pellets, 3—7 mm thick, were prepared by pressing AgI powder under a pressure of 7 t/cm^2. Sometimes, $AgI-Al_2O_3$ pellets, 1 mm thick, were employed as an electrolyte. They were prepared by mixing nearly the same amounts of powdery AgI and Al_2O_3 and pressing the mixture.

Measurement of the Rate of Ag/Ag_2Se Interface Reaction. The coulometric titration method was employed. The apparatus is shown in Fig. 1. A pressure of 4 kg/cm^2 was applied to the Ag/Ag_2Se interface with a Pyrex tube to secure contact between the pellets. Since Ag_2Se and AgI tend to deform plastically, Ag/Ag_2Se interface often underwent bending in a cell $Ag/Ag_2Se/AgI/Ag$, and the interface reaction did not proceed uniformly. However, an $AgI-Al_2O_3$ pellet

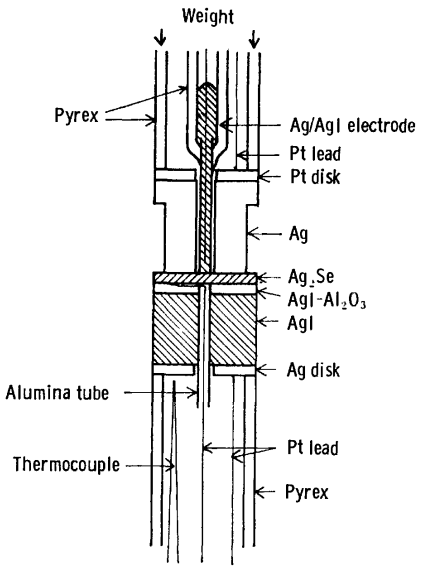

Fig. 1. Apparatus for the coulometric titration method.

unterwent no plastic deformation. Thus a thin AgI-Al_2O_3 pellet was inserted between AgI and Ag_2Se pellets. The detail of this method was described elsewhere.[9,10]

Measurement of the Rate of $Ag_2Se/Se(l)$ Interface Reaction. The apparatus is shown in Fig. 2. Three pellets of Ag, AgI, and Ag_2Se(I), 10 mm in diameter, were assembled in series and pressed with a Pyrex tube, 10 mm in outer and 6 mm in inner diameter. The lower end of the Pyrex tube was finished as flat as possible so that liquid selenium might be kept in the tube without leaking. An Ag/AgI electrode in a small alumina tube, 1.2 mm in outer diameter, was placed in the pyrex tube and the tip was brought to contact with the Ag_2Se(I) pellet.

The reaction rate was measured as an electric current with an ammeter and the potential difference between Ag_2Se-(I) pellet and Ag with a potentiometer. The thickness of the Ag_2Se(II) layer formed, Δx, was calculated by integrating the reaction rate with respect to time.

Measurement of the Selenization of Silver by Liquid Selenium. Wagner's pellet method[1,4,9,11] was used. A silver cylinder, 8 mm in diameter, and an Ag_2Se(I) pellet, 10 mm in diameter,

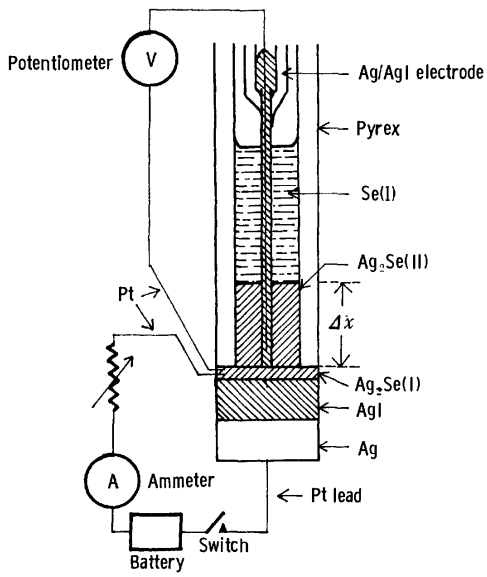

Fig. 2. Apparatus for the measurement of the rate of $Ag_2Se/Se(l)$ interface reaction.

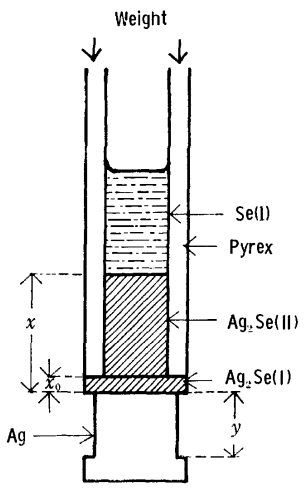

Fig. 3. Apparatus for the measurement of over-all reaction rate.

were assembled and pressed with a Pyrex tube, 10 mm in outer diameter and 6 mm in inner diameter (Fig. 3). A pressure of 4 kg/cm^2 was applied to the Ag/Ag_2Se interface by means of a spring. The lower end of the Pyrex tube was made flat so that the liquid selenium could be kept in the tube without leaking. It was difficult to observe the position of $Ag_2Se/Se(l)$ interface from outside, so the reaction was followed by observing the length of the silver cylinder y by means of a cathetometer. The increased length of selenide scale, $x-x_0$, was calculated from the decreased length of the silver cylinder, y_0-y, where x_0 and y_0 are the thickness of the silver selenide pellet and the length of the silver cylinder at the beginning of the reaction, respectively. Values of x_0 were 0.153 cm (250 °C), 0.070 cm (300 °C), and 0.114 cm (350 °C), and y_0 was 0.3 to 0.8 cm. After the reaction was completed, the thickness of the formed scale was measured and compared with the calculated thickness.

Results and Discussion

Ag/Ag_2Se Interface Reaction. a_{Ag}'', the silver activity of Ag_2Se at the Ag/Ag_2Se interface is calculated from E'', the potential difference between Ag_2Se and Ag by

$$E'' = -\frac{2.303RT}{F}\log a_{Ag}'' \qquad (1)$$

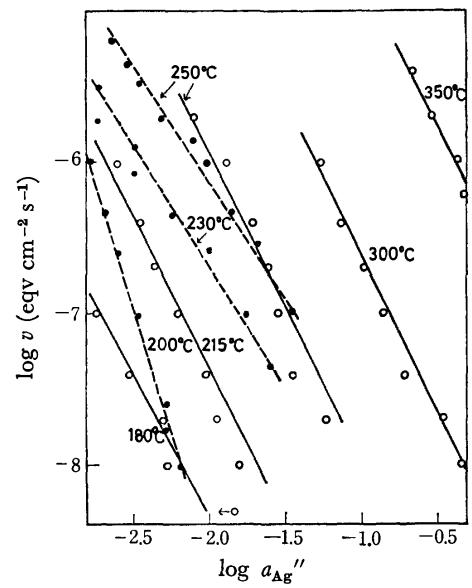

Fig. 4. Plot of log v *vs.* log a_{Ag}''
○: This work. ●: Rickert.

A plot of the logarithm of reaction rate v(eqv cm^{-2} s^{-1}) against log a_{Ag}'' is given in Fig. 4. Solid lines show our results and broken lines the ones by Rickert.[7] The values of n by Rickert vary from −1.5 to −3.0, while ours are close to −2.0, irrespective of the temperature, being essentially the same as $n=-1.9$ to −2.3

Table 1. Values of n

Temperature (°C)	n
180	−2.0±0.5
215	−2.2±0.6
250	−1.9±0.5
300	−1.9±0.4
350	−1.8±0.4

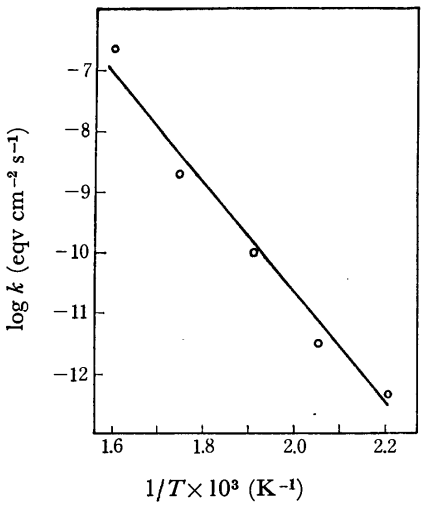

Fig. 5. Arrhenius plot of k.

for the Ag/Ag_2S interface reaction.[9]

The rate constants at $\log a_{Ag}''=0$, k, can be obtained from the intercept of the extrapolated lines with the ordinate. Figure 5 shows the Arrhenius plot of k. We see that linearity holds. Thus, the rate equation is expressed in the forms:

$$v = 4.0\times10^{7}\{\exp(-42000/RT)\}(a_{Ag}'')^{-2} \quad \text{eqv cm}^{-2}\cdot\text{s}^{-1} \tag{2}$$

$$v = 4.0\times10^{7}\{\exp(-42000/RT)\}(a_{Se}''/a_{Se}^{*}) \quad \text{eqv cm}^{-2}\cdot\text{s}^{-1} \tag{3}$$

where a_{Se}'' and a_{Se}^{*} denote the selenium activity in Ag_2Se at the Ag/Ag_2Se interface during the course of reaction and that in equilibrium, respectively. According to Kiukkola and Wagner,[12] ΔG°, the standard free energy of formation of Ag_2Se in a temperature range 167—400 °C is given by

$$\Delta G^\circ = -9.76 - 0.0074T = RT\ln a_{Se}^{*} \quad \text{kcal}\cdot\text{mol}^{-1} \tag{4}$$

by means of which, Eq. (3) can be rewritten as

$$v = 1.6\times10^{9}\{\exp(-32300/RT)\}(a_{Se}'') \quad \text{eqv cm}^{-2}\cdot\text{s}^{-1} \tag{5}$$

Ag_2Se and Ag_2S have the same crystal structure,[13] and the high ionic conductivity of silver ions. Moreover, n is nearly the same. Thus, the same mechanism as in the Ag/Ag_2S interface reaction[9] is proposed for the Ag/Ag_2Se interface reaction:

$$2Ag(Ag) + Se(Ag_2Se) \longrightarrow 2Ag^{+}(Ag_2Se) + Se^{2-}(Ag_2Se) \tag{6}$$

where, (Ag) denote the metal phase and (Ag_2Se) the silver selenide phase.

$Ag_2Se/Se(l)$ Interface Reaction and Ionic Conductivity of Ag^+ in Ag_2Se. When the switch is turned off, $Ag_2Se(I)$ is in equilibrium with liquid selenium (Fig. 2) and the potential difference E° between Ag_2Se and Ag is given by

$$E^\circ = -\Delta G^\circ/2F \tag{7}$$

where ΔG° is the free energy of formation of Ag_2Se. If the silver activity in Ag_2Se in equilibrium with liquid selenium is represented by a_{Ag}^{*}, we have

$$E^\circ = -\frac{2.303RT}{F}\log a_{Ag}^{*} \tag{8}$$

When the switch is turned on, Ag^+ ions are transported from Ag to the $Ag_2Se(I)/Se(l)$ interface through AgI and $Ag_2Se(I)$, while electrons flow from Ag to the $Ag_2Se(I)/Se(l)$ interface through the outer circuit and $Ag_2Se(I)$. Ag^+ ions and electrons arriving at the $Ag_2Se(I)/Se(l)$ interface react with liquid selenium to form $Ag_2Se(II)$. As a result, the $Ag_2Se(II)$ layer grows in the pyrex tube and the Ag/AgI electrode is buried in the $Ag_2Se(II)$ layer. When a constant current I_0 is let to flow constantly, the reaction at the $Ag_2Se(II)/Se(l)$ interface proceeds at a rate $I_0/2F$ and the difference in silver activity takes place at the interface between $Ag_2Se(II)$ and Se(l). If silver activities in $Ag_2Se(II)$ at the $Ag_2Se(II)/Se(l)$ interface and in $Ag_2Se(I)$ are a_{Ag}' and $a_{Ag}(\Delta x)$, respectively, and the thickness of $Ag_2Se(II)$ layer is Δx, the following relations are obtained.

$$E' - E(\Delta x) = \frac{I_0\cdot\Delta x}{\sigma_{Ag^+}\cdot S} \tag{9}$$

$$E' = -\frac{2.303RT}{F}\log a_{Ag}' \tag{10}$$

$$E(\Delta x) = -\frac{2.303RT}{F}\log a_{Ag}(\Delta x) \tag{11}$$

where S is the cross-sectional area of $Ag_2Se(II)$ layer, and σ_{Ag^+} is the ionic conductivity of Ag^+ in Ag_2Se. In Eq. (9), σ_{Ag^+} is assumed to be independent of the silver activity in Ag_2Se.[14,15]

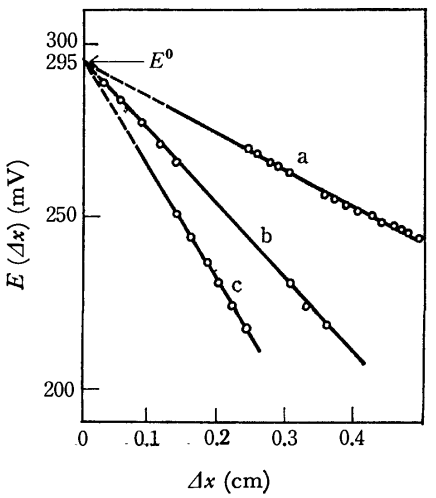

Fig. 6. Plot of $E(\Delta x)$ *vs.* Δx; reaction rate at $Ag_2Se/Se(l)$ interface at 250°C.
a: $I_0\cdot S^{-1}=385$ mA·cm^{-2} b: $I_0\cdot S^{-1}=770$ mA·cm^{-2}
c: $I_0\cdot S^{-1}=1155$ mA·cm^{-2}

Figure 6 shows the plots of $E(\Delta x)$ *vs.* Δx at 250 °C. E' is determined from the intercepts of the extrapolated lines with the ordinate, $\Delta x=0$. E° is shown by an arrow. E' is independent of the current and coincides with E°. It is thus concluded that the interface reaction proceeds with very small driving force, Ag_2Se being actually in equilibrium with Se(l). Equation (9) indicates that σ_{Ag^+} can be obtained from the slope of the plots in Fig. 6. The value 3.6 ohm^{-1} cm^{-1} obtained is in good agreement with the result obtained

by the four probe conductivity measurement by Okazaki.[16]

Contribution of Three Steps to the Over-all Reaction. Wagner and Rickert,[3] and Donner and Rickert[4] treated the sulfurization of silver and copper by liquid sulfur as controlled by both diffusion and metal/scale interface reaction. Ag_2Se and Se(l) are actually in chemical equilibrium during the reaction. The over-all reaction of selenization is considered to be controlled by both the diffusion in Ag_2Se and the Ag/Ag_2Se interface reaction, and Rickert-Wagner's method can be used for the analysis.

For the diffusion step, we have

$$\frac{dx}{dt} = \frac{\sigma_{Ag^+} \cdot V \cdot RT}{2x} \log \frac{a_{Ag}''}{a_{Ag}^*} = -\frac{\sigma_{Ag^+} \cdot V}{2F \cdot x}(E^\circ - E'') \quad (12)$$

and for the reaction at Ag/Ag_2Se interface,

$$\frac{dx}{dt} = \frac{V \cdot S_i \cdot k}{2S_l \cdot F}(a_{Ag}'')^{-2} = \frac{V \cdot S_i \cdot k}{2S_l \cdot F} \exp\left(\frac{2E''F}{RT}\right) \quad (13)$$

where V is the molar volume of Ag_2Se, x the thickness of Ag_2Se layer, S_i the area of Ag/Ag_2Se interface, and S_l the cross-sectional area of the grown Ag_2Se layer. From Eqs. (12) and (13) we obtain the following expressions for x and t.

$$\log x = \log \frac{\sigma_{Ag^+} \cdot S_l}{k \cdot S_i} + \log (E^\circ - E'') - \frac{2E''F}{2.303RT} \quad (14)$$

$$\log (t+t^0) = \log \frac{S_l^2 \cdot \sigma_{Ag^+} \cdot F}{4k^2 \cdot S_i^2 \cdot V} + \log \left\{\frac{RT}{F} - 4(E^\circ - E'')\right\} - \frac{4E''F}{2.303RT} \quad (15)$$

where t^0 is a constant determined by the initial condition $x=x_0$ for $t=0$. Eliminating E'' from Eqs. (14) and (15), and inserting the σ_{Ag^+} value and k value we obtained, we obtain x as a function of t. In Fig. 7, solid lines show the calculated values and open circles the observed values. Agreement between the calculated and observed results is good.

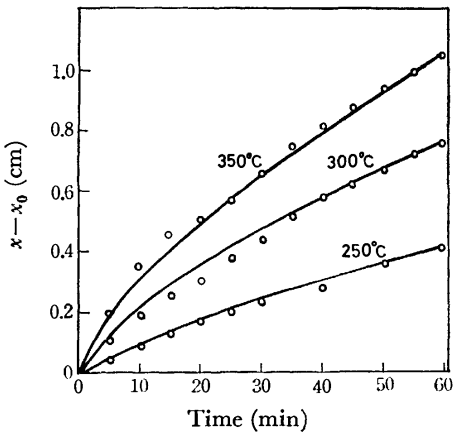

Fig. 7. Plot of $x-x_0$ *vs.* time.
○: observed values ——: calculated values

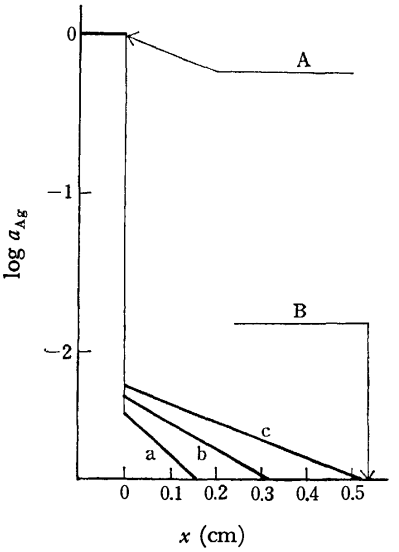

Fig. 8. Distribution of a_{Ag} in Ag_2Se layer under reaction at 250 °C.
a: $t=0$ min b: $t=25$ min c: $t=50$ min
A: Ag_2Se is in equilibrium with metallic silver
B: Ag_2Se is in equilibrium with liquid selenium

The distribution of silver activity during the reaction can be obtained by combining Eqs. (14) and (15). Figure 8 shows the plots of $\log a_{Ag}$ against x. We see that the Ag/Ag_2Se interface reaction is the slowest.

Summary

(1) The Ag/Ag_2Se interface reaction was investigated kinetically. The rate equation is found to be

$$v = 1.6 \times 10^9 \{\exp(-32300/RT)\}(a_{Se}) \text{ eqv cm}^{-2} \cdot \text{s}^{-1}.$$

The following mechanism was proposed.

$$2Ag(Ag) + Se(Ag_2Se) \longrightarrow 2Ag^+(Ag_2Se) + Se^{2-}(Ag_2Se)$$

(2) The rate of $Ag_2/Se(l)$ interface reaction and the ionic conductivity of Ag^+ in Ag_2Se were measured. It was found that Ag_2Se and Se(l) are actually in chemical equilibrium during the course of reaction.

(3) The over-all reaction rate of silver selenization was determined kinetically. Assuming that the selenization is controlled by both the diffusion of Ag^+ ions and the Ag/Ag_2Se interface reaction, the over-all reaction rates were calculated. The calculated values agreed with observed ones.

References

1) C. Wagner, *Z. Phys. Chem.*, **B21**, 25 (1933).
2) H. Rickert and K. H. Tostmann, *Werkstoffe Korrosion*, **21**, 965 (1970).
3) C. Wagner and H. Rickert, *Z. Phys. Chem., N. F.*, **31**, 32 (1962).
4) D. Donner and H. Rickert, *ibid.*, **60**, 11 (1968).
5) C. Tubandt and H. Reinhold, *Z. Phys. Chem.*, **B24**, 22 (1934).
6) C. Tubandt, H. Reinhold, and A. Neumann, *Z. Electrochem.*, **39**, 227 (1933).
7) H. Rickert, "Fast Ion Transport in Solids," ed. by

W. van Gool, p. 523, North-Holland Publishing Co., Amsterdam/American Elsevier Publishing Co., New York, (1973).
8) J. Mizusaki, K. Fueki, and T. Mukaibo, The 39th Annual Meeting of the Electrochemical Society of Japan (March 29—31, 1972 in Tokyo), Preprint pp. C-310.
9) J. Mizusaki, K. Fueki, and T. Mukaibo, This Bulletin, **46**, 1663 (1973).
10) H. Rickert and C. D. O'Briain, *Z. Phys. Chem., N. F.*, **31**, 71 (1962).
11) H. Rickert, *ibid., N. F.*, **23**, 355 (1960).
12) K. Kiukkola and C. Wagner, *J. Electrochem. Soc.*, **104**, 308 (1958).
13) P. Rahlfs, *Z. Phys. Chem.*, **B31**, 157 (1936).
14) S. Miyatani, *J. Phys. Soc. Japan*, **13**, 317 (1958).
15) N. Valverde, *Z. Phys. Chem., N. F.*, **70**, 128 (1970).
16) H. Okazaki, *J. Phys. Soc. Japan*, **23**, 355 (1967).

Determination of the Optical Purity of Amino Acids by Complex Formation.* Determination of Optimum Condition for Rotational Measurement

Yuki FUJII**

Department of Chemistry, Faculty of Science, Hiroshima University, Hiroshima 730

(Received February 22, 1974)

A new method has been established for the determination of the optical purity of a small amount of amino acids (alanine, valine, leucine, and glutamic acid). The method utilizes the fact that when an optically active amino acid is dissolved in an alkaline solution of $K[Co(acac_2en)(gly)_2]$, the solution shows much larger optical rotation than the free amino acid in the visible region. 1/50 to 1/100th the amount of an amino acid (about 0.1—0.05 grams) suffices for the determination of optical purity as compared with that needed in the usual method. The optimum conditions for measurement are: wavelength, 500 nm; pH, 10.00; time required to establish the substitution equilibrium, 6—8 hours; concentration of the complex, $(4—5)\times10^{-3}$ mol l^{-1}; concentration of amino acid, $(2—1)\times10^{-2}$ mol l^{-1}.

The optical purity of amino acids is usually determined by their optical rotations at the Na-D line.[1-4] These are generally so small that concentrated solutions (about 0.1—1.0 mol l^{-1}) are needed. For example, a 1.12 mol l^{-1} solution (6M-HCl) of optically pure L-alanine shows α_D-value only $+0.14°$ with a 1 cm cell. Thus, several grams of sample is required for the usual method. The quantity of amino acids handled in biochemical research is so small that it is difficult to measure the optical rotation in such cases. Great improvements have been made in polarimeters and it has become possible to measure the optical rotation of active compounds with an accuracy of 10^{-3} °, but further improvement cannot be expected. Badr *et al.*[5] reported that when an amino acid in anhydrous methanol containing a base is treated with excess carbonyl compound, a considerably large optical rotation is observed in the 250 nm region. The reaction is useful for the assignment of the configuration of a small amount of amino acid, but as it is not quantitative, the method has not been used to determine the optical purity of amino acids.

It was found that cobalt(III)–acac$_2$en-complex, $[Co(acac_2en)(X)_2]^-$ ($acac_2en^{2-}$ = *N,N'*-ethylenebis(acetylacetonimine) dianion, X^-=amino acid anion) has the following characteristics:[6] 1) The amino acidato ligand X^-, coordinated as a unidentate ligand at the axial site of the complex, is labile and easily replaced by an other amino acidato ligand Y^- under alkaline conditions. The reaction between the complex $[Co(acac_2en)(X)_2]^-$ and Y^- can be described by

$$[Co(acac_2en)(X)_2]^- + Y^- \rightleftharpoons [Co(acac_2en)(X)(Y)]^- + X^- \quad (1)$$

$$[Co(acac_2en)(X)(Y)]^- + Y^- \rightleftharpoons [Co(acac_2en)(Y)_2]^- + X^- \quad (2)$$

2) When the amino acidato ligand at the axial site is optically active, the complex shows a much larger optical rotation than the free amino acid in the visible region. These results suggest that if an optically active amino acid is mixed with optically inactive $[Co(acac_2en)(X)_2]^-$ under alkaline conditions, rapid exchange reactions such as (1) and (2) occur, and the mixed solution shows a much larger optical rotation than the solution containing the amino acid only. On this basis, we established a new method to determine the optical purity of a small amount of amino acid. Determination of the optimum condition for rotational measurements is discussed herewith.

Experimental

Preparation of Complexes. $K[Co(acac_2en)(gly)_2]\cdot2H_2O$ was prepared by the method reported.[6] The other complexes were prepared by a method similar to that used for $[Co(acac_2en)(NH_3)_2]Cl\cdot2H_2O$.[7,8] The elemental analysis data of new complexes are as follows: *N,N'*-ethylenebis(benzoylacetoniminato)diamminecobalt(III) chloride dihydrate, $[Co(bzac_2en)(NH_3)_2]Cl\cdot2H_2O$, Found: C, 51.89; H, 5.99; N, 10.26%. Calcd for $C_{22}H_{28}N_4O_2CoCl\cdot2H_2O$: C, 51.72; H, 6.33; N, 10.97%. *N,N'*-Ethylenebis(trifluoroacetylacetoniminato)diamminecobalt(III) chloride monohydrate, $[Co(tfac_2en)(NH_3)_2]Cl\cdot H_2O$, Found: C, 29.83; H, 4.16; N, 11.93%. Calcd for $C_{12}H_{18}N_4O_2CoF_6Cl\cdot H_2O$: C, 30.23; H, 4.24; N, 11.76%.

Reagents. All chemicals were of analytical grade and used without further purification. Specific rotations measured by the usual method are as follows (% given in ( ) is the optical purity of amino acid). L-alanine (100%), $[\alpha]_D^{25}=+15.0°$, D-alanine (100%), $[\alpha]_D^{25}=-14.9°$ (5 g/50 ml of 6M-HCl); L-valine (100%), $[\alpha]_D^{25}=+28.5°$, D-valine (100%), $[\alpha]_D^{25}=-28.5°$ (4 g/50 ml of 6M-HCl); L-leucine (100%), $[\alpha]_D^{25}=+16.3°$, D-leucine (100%), $[\alpha]_D^{25}=-16.3°$ (2 g/50 ml of 6M-HCl); L-glutamic acid (100%), $[\alpha]_D^{25}=+32.4°$, D-glutamic acid (100%), $[\alpha]_D^{25}=-32.3°$ (5 g/50 ml of 2M-HCl). Amino acids of different optical purity were prepared by mixing optically pure amino acid with racemic amino acid (for example, L-alanine (50%) was prepared by mixing L-alanine (100%) with racemic alanine (0%) in a ratio of 1:1).

Measurements. The ORD and CD spectra were recorded at 25 °C on a JASCO Model ORD/UV-5 spectrophotometer with a CD attachment. The absorption spectra were measured at 25 °C with a Shimadzu UV-200 double beam spectro-

* A part of this work was reported in *Chem. Lett.*, **1974**, 43.

** On leave from the Department of Chemistry, Ibaraki University, 2-1-1, Bunkyo-cho, Mito, Ibaraki 310.

photometer. The pH was measured with a Hitachi-Horiba Model F-7 pH-meter at 25 °C.

Results and Discussion

Determination of the Optimum Condition for Rotational Measurement. The molar rotations of L-alanine (100%) and its metal complexes are given in Table 1. The [M]-values of metal complexes containing amino acids are greater than those of free amino acids at special wavelengths, the [M]-values of Co(acac$_2$en)-complex being remarkably large. From a comparison of the [M]-values per one mole of amino acid, we see that the amino acid coordinated to the Co(acac$_2$en)-complex has 100—200 times as large an optical rotation as the free amino acid. The AB, CD, and ORD spectra of solutions prepared by mixing optically inactive K[Co(acac$_2$en)(gly)$_2$] with a large excess (100 times) of alanine under alkaline conditions are shown in Fig. 1. We see that ORD- and CD-intensities of the mixed solutions are in line with the optical purities of the alanine. The results suggest that the optical purity of amino acids can be determined by comparing the rotational (and also CD) value of a solution containing K[Co(acac$_2$en)(gly)$_2$] and optically pure amino acid with that of a solution containing the complex and the amino acid whose optical purity is to be determined. In this case a large excess of amino acid is used. However, when a small excess of amino acid (100%) is mixed with the glycinato complex solution, the resulting solution shows a small optical rotation as compared with that of the complex solution containing a large excess of amino acid (100%). This is due to the incomplete replacement reaction. Thus, the determination of optimum concentrations of the complex and amino acid is very important.

K[Co(acac$_2$en)(gly)$_2$] was used as an optically inactive Co(acac$_2$en)-complex, and alanine, valine, leucine and glutamic acid were examined. Since the chemical and spectral behavior of L- and D-form amino acids is the same except for the inversion of the CD- and ORD-signs, and the four amino acids behave similarly, L-alanine is given here with as an example. Although free amino acid is CD-inactive in the visible region, it becomes CD-active upon complex formation. Both CD- and ORD-intensities were therefore used to investigate optimum conditions.

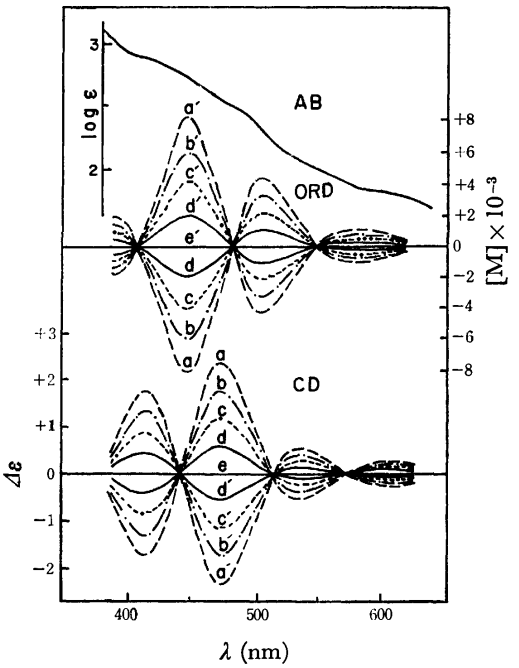

Fig. 1. AB, CD, and ORD spectra of the aqueous solution containing K[Co(acac$_2$en)(gly)$_2$] and a large excess (100 times) of alanine. The solution pH is 10.00. a and a′, L-alanine (100%) and D-alanine (100%); b and b′, L- and D-alanine (75%); c and c′, L- and D-alanine (50%); d and d′, L- and D-alanine (25%); e, racemic alanine.

Wavelength: The mixed solutions show ORD peaks at 380, 450, 500, and 580 nm, and CD peaks at 425, 475, 540, and 600 nm (Fig. 1). Peaks near 600 nm have low intensities, and those near 400 nm are accom-

Table 1. Molar rotation of L-alanine (100%) and its metal complexes

Compound	Molar rotation per one mole of complex* (°m^{-1} mol^{-1} l)	Molar rotation per one mole of amino acid (°m^{-1} mol^{-1} l)	Wavelength (nm)	Solvent
L-Alanine[1]		+2.41	500	Water
		+1.75	589	Water
		+20.76	500	2M-HCl
		+12.74	589	2M-HCl
		+7.06	500	2M-NaOH
		+4.14	589	2M-NaOH
K[Co(acac$_2$en) (L-ala)$_2$][6]	+4513	+2257	500	Water
	−9595	−4798	450	Water
[Co(NH$_3$)$_5$(L-alaH)](ClO$_4$)$_3$[8]	*ca.* −100	*ca.* −100	500	Water
trans-[Co(en)$_2$(L-alaH)$_2$]Cl$_3$[9]	+635	+318	500	Water
	−615	−308	*ca.* 590	Water
[Co(NH$_3$)$_4$(L-ala)]SO$_4$[8]	*ca.* −900	*ca.* −900	500	Water
[Cu(L-ala)$_2$][1]	+155	+78	522	Water
	−265	−133	654	Water

* Maximum values in the visible region.

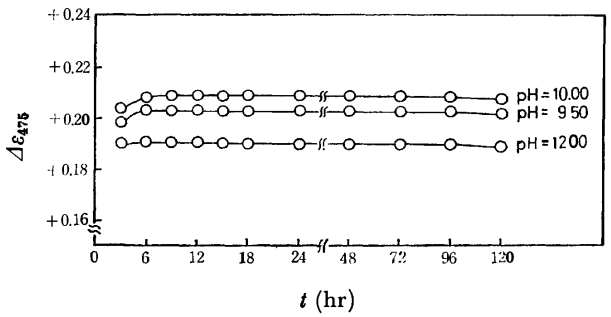

Fig. 2. The time dependence on the substitution equilibrium between K[Co(acac$_2$en)(gly)$_2$] and L-alanine (100%) at various pH. $C_{complex}=2.0\times10^{-3}$ mol l^{-1}, $C_{L-alanine}=2.0\times10^{-2}$ mol l^{-1}, $\mu=0.1$ (Na_2CO_3+$NaHCO_3$), T=25 °C.
$\Delta\varepsilon$ is given by the values for one mole of L-alanine at 475 nm.

panied by strong absorptions, and are therefore not suitable for measurements of CD- and ORD-intensities. The wavelengths of peaks at 475 nm (CD) and 500 nm (ORD) were chosen as their intensities are strong, and their CD- and ORD-signs coincide with the ORD-sign of free amino acids.

Time Dependence: In order to employ complex formation reactions such as (1) and (2) for determination of the optical purity of amino acids, it is necessary for the substitution reaction in solution to be in equilibrium. Thus the time needed to reach equilibrium was examined (Fig. 2). It is seen that 6—8 hr was required and that is less dependent on the pH of the solution. The solutions show constant CD-intensities for 3—4 days, which gradually decrease owing to the racemization of the optically active amino acid in a basic condition. The CD- and ORD-intensities of the mixed solutions were thus measured 10—24 hr after preparation of the solution.

pH-Dependence: The CD-intensity (and also ORD-intensity) depends upon the pH of the solution. The pH-dependence is shown in detail in Fig. 3. The solution shows maximum intensity at pH *ca.* 10. The intensity decreases in low pH region and in an alkaline

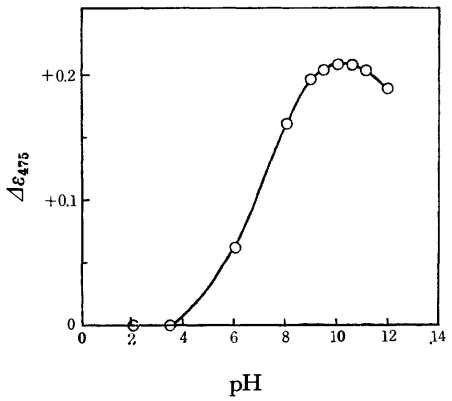

Fig. 3. The pH dependence on the CD-intensities of the mixed solutions containing L-alanine (100%). $\Delta\varepsilon$ is given by the values for one mole of L-alanine at 475 nm. $C_{complex}=2.0\times10^{-3}$ mol l^{-1}, $C_{L-alanine}=2.0\times10^{-2}$ mol l^{-1}, $\mu=0.1$ (Na_2CO_3+$NaHCO_3$), $T=25$ °C.

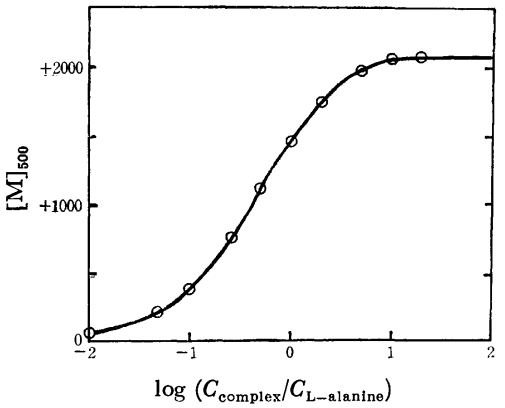

Fig. 4. Molar rotations of the mixed solutions containing K[Co(acac$_2$en)(gly)$_2$] and L-alanine (100%) in various mixing ratio. The pH of the solutions is 10.00. $[M]_{500}$ is given by the values for one mole of L-alanine. $\mu=0.1$ (Na_2CO_3+$NaHCO_3$), $T=25$ °C.

region above pH=10. This decrease seems to be due to the formation of aquo- and hydroxo-complexes in acidic and strongly basic conditions, respectively.

In order to adjust both the ionic strength μ and pH, a 1:1 mixture of Na_2CO_3 and $NaHCO_3$ was added to the solution. The coordination of CO_3^{2-} and HCO_3^- to the complex could be neglected for $\mu=(0.05—0.2)$.

Concentrational Dependence: The ORD-intensities of solutions containing K[Co(acac$_2$en)(gly)$_2$] and L-alanine (100%) in various concentrations are shown in Fig. 4. The results for CD-intensities are given in Table 2. It is observed that the larger the mixing ratio $C_{complex}/C_{L-alanine(100\%)}$, the greater the CD- and ORD-intensities per one mole of L-alanine (100%). Thus, in order to measure the CD- and ORD-intensities in high sensitivity for amino acid, a high concentration of complex and a low concentration of amino acid should be used. However, since the solution shows strong absorption in the visible region, the complex

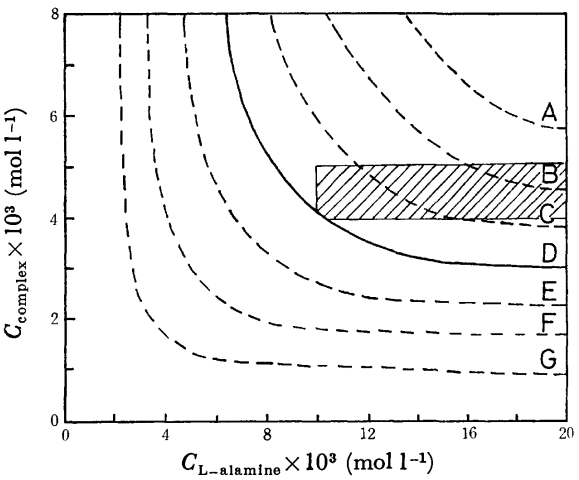

Fig. 5. The estimated rotations at 500 nm of the mixed solutions containing K[Co(acac$_2$en)(gly)$_2$] and L-alanine (100%) under various concentrational conditions. α_{500}-values are given by the contours (° cm^{-1}): A, $\alpha_{500}=1.6\times10^{-1}$; B, $\alpha_{500}=1.4\times10^{-1}$: C, $\alpha_{500}=1.2\times10^{-1}$; D, $\alpha_{500}=1.0\times10^{-1}$; E, $\alpha_{500}=0.8\times10^{-1}$; F, $\alpha_{500}=0.6\times10^{-1}$; G, $\alpha_{500}=0.4\times10^{-1}$.

Table 2. CD intensities of solutions containing K[Co(acac$_2$en)(gly)$_2$] and L-alanine (100%) in various mixing ratio

pH=10.00, μ=0.1 (Na_2CO_3+$NaHCO_3$), T=25 °C, λ=475 nm.

Mixing ratio ($C_{complex}/C_{alanine}$)	Concentration (mol l^{-1})	$(\Delta\varepsilon)_{obs}$ ($cm^{-1}\times10^2$)	$\Delta\varepsilon_{obs}$ for one mole of alanine (cm^{-1} mol^{-1} l)	$\Delta\varepsilon_{calcd}$ for one mole of alanine (cm^{-1} mol^{-1} l)
10	$C_{complex}=5.0\times10^{-3}$	+0.056	+1.12	1.11
	$C_{alanine}=5.0\times10^{-4}$	+0.056	+1.12	
5	$C_{complex}=4.0\times10^{-3}$	+0.169	+1.06	1.07
	$C_{alanine}=8.0\times10^{-4}$	+0.170	+1.06	
2	$C_{complex}=4.0\times10^{-3}$	+0.378	+0.945	0.942
	$C_{alanine}=2.0\times10^{-3}$	+0.380	+0.950	
1	$C_{complex}=5.0\times10^{-3}$	+0.399	+0.798	0.795
	$C_{alanine}=5.0\times10^{-3}$	+0.398	+0.796	
1/2	$C_{complex}=5.0\times10^{-3}$	+0.593	+0.593	0.606
	$C_{alanine}=1.0\times10^{-2}$	+0.598	+0.598	
1/4	$C_{complex}=4.0\times10^{-3}$	+0.656	+0.410	0.411
	$C_{alanine}=1.6\times10^{-2}$	+0.657	+0.411	
1/5	$C_{complex}=2.0\times10^{-3}$	+0.354	+0.354	0.354
	$C_{alanine}=1.0\times10^{-2}$	+0.354	+0.354	
1/10	$C_{complex}=2.0\times10^{-3}$	+0.416	+0.208	0.209
	$C_{alanine}=2.0\times10^{-2}$	+0.414	+0.207	
1/20	$C_{complex}=2.0\times10^{-3}$	+0.458	+0.115	0.115
	$C_{alanine}=4.0\times10^{-2}$	+0.462	+0.116	
1/100	$C_{complex}=2.0\times10^{-3}$	+0.510	+2.55 ($\Delta\varepsilon_{obs}$ for one mole of complex)	
	$C_{alanine}=2.0\times10^{-1}$			

concentration cannot be made higher than *ca.* 5.0×10^{-3} mol l^{-1}. If a very low concentration of amino acid is used, the solution shows negligibly small CD- and ORD- intensities. Under these circumstances, it is difficult to determine the optimum concentrations. The solution equilibrium was therefore treated theoretically and an estimation of rotational values of the mixed solutions was examined. Results of calculation for the rotational values of the mixed solutions are shown in Fig. 5, where the estimated rotations are indicated by contours. The solid line indicates the α_{500}-value of 0.1° cm^{-1}, which is the minimum limit to obtain a rotational value to three significant figures. The optimum concentrations for rotational measurement are determined to be $C_{complex}=(5-4)\times10^{-3}$ mol l^{-1}, $C_{alanine}=(1-2)\times10^{-2}$ mol l^{-1} (shaded area, Fig. 5).

Theoretical Approach to Solution Equilibrium and Rotational Values of the Mixed Solution. When we mix K[Co(acac$_2$en)(gly)$_2$] with optically active amino acid YH in the initial concentrations of x mol l^{-1} and y mol l^{-1}, respectively, the concentrations of the complexes under equilibrium conditions can be written as follows:

$$C_{[Co(acac_2en)(gly)_2]^-} = [4x^2/(\alpha H_{gly})^2 Z]x \quad mol\cdot l^{-1},$$

$$C_{[Co(acac_2en)(gly)(Y)]^-} = [4xyD/(\alpha H_{gly})(\alpha H_Y)Z]x \quad mol\cdot l^{-1},$$

$$C_{[Co(acac_2en)(Y)_2]^-} = [y^2D^2/(\alpha H_Y)^2 Z]x \quad mol\cdot l^{-1},$$

where $Z=[4x^2/(\alpha H_{gly})^2+4xyD/(\alpha H_{gly})(\alpha H_Y)+y^2D^2/(\alpha H_Y)^2]$, αH_{gly} and αH_Y are αH-values of glycine and YH, respectively. D is a parameter which represents the relative coordinating ability of amino acids, taking the coordinating ability of gly^- as 1.00. Amino acids including glycine were thought to coordinate to Co(acac$_2$en)-complex in their anionic forms, and were assumed to distribute to Co(acac$_2$en)-complex statistically.[6] In the above expression, aquo- and hydroxo-complexes were neglected. The compounds which contribute to the rotation (and CD-intensity) are [Co(acac$_2$en)(gly)(Y)]$^-$, [Co(acac$_2$en)(Y)$_2$]$^-$, free Y^- and YH. Thus, the rotational value (or CD-intensity) at wavelength λ of the mixed solution is given by

$$A_\lambda = F\{B_\lambda x[2xyD/(\alpha H_{gly})(\alpha H_Y)+y^2D^2/(\alpha H_Y)^2]/Z+E_\lambda\} \quad (3)$$

where A_λ is the rotational value (or CD-intensity) at λ of the solution, B_λ the molar rotation (or molar CD-intensity) at λ of [Co(acac$_2$en)(Y)$_2$]$^-$ in which Y^- is an optically pure amino acid anion, E_λ the total rotational value (or CD-intensity) of free Y^- and YH, and F the optical purity of the amino acid YH, given by F=[concentration of optically active amino acid]/[total concentration of amino acid]. The molar rotation (or CD-intensity) of [Co(acac$_2$en)(gly)(Y)]$^-$ was assumed to be $1/2\times B_\lambda$, because the vicinal effect is generally additive.[11,12] If we mix K[Co(acac$_2$en)-(gly)$_2$] with optically pure amino acid, the rotational value (or CD-intensity) of the solution can be calculated by putting F=1. B_λ-values were estimated from the ORD- and CD-intensities of the solution containing K[Co(acac$_2$en)(gly)$_2$] and a large excess of optically pure amino acids. E_λ-values were estimated to be zero because free amino acids show negligibly small optical rotations in low concentrations and they are CD-inactive in the visible region. D-values of the solutions were estimated from the observed CD-intensities of the solutions having various mixing ratio, $C_{complex}/C_{aminoacid(100\%)}$. The values of B_λ and D thus determined are listed in Table 3.

By using these values, the CD- and ORD-intensities of the mixed solutions were calculated by Eq. (3). The results are given in Table 2 and Fig. 4. The

Table 3. Parameters B_i and D

Amino acid	pK_1	pK_2	B_{475} (CD) (cm^{-1} mol^{-1} l)	B_{500} (ORD) ($°m^{-1}$ mol^{-1} l)	D
Glycine	2.350	9.780	0.00	0	1.00
L-Alanine (100%)	2.348	9.866	+2.55	+4735	0.98
L-Valine (100%)	2.286	9.744	+4.95	+6625	0.90
L-Leucine (100%)	2.328	9.744	+4.70	+9220	0.77
L-Glutamic acid (100%)	2.10	4.07	+2.50	+6140	0.76
		9.47 (pK_3)			

Table 4. pH dependence of a mixed solution of L-alanine (100%)
$C_{K[Co(acac_2en)(gly)_2]}=5.0\times10^{-3}$ mol l^{-1}, $C_{L\text{-alanine}}=5.0\times10^{-2}$mol l^{-1}, $\mu=0.1$ (Na_2CO_3+$NaHCO_3$), T=25°C, λ =475 nm.

pH	$(\Delta\varepsilon)$ ($cm^{-1}\times10^2$)	$\Delta\varepsilon_{obs}$ for one mol of alanine (cm^{-1}. mol^{-1}.l)	$\Delta\varepsilon_{calcd}$ for one mol of alanine (cm^{-1}. mol^{-1}.l)
8.00	+0.750	+0.150	0.204
9.00	+0.976	+0.195	0.191
9.50	+1.008	+0.202	0.203
10.00	+1.030	+0.206	0.209
10.50	+1.036	+0.207	0.211
11.00	+1.020	+0.204	0.211
12.00	+0.944	+0.189	0.212

calculated values agree with the observed ones. The pH-dependence of Eq. (3) is given in Table 4. Agreement between the calculated and observed values is good in the pH region 9—10.5, but not in the others. The discrepancy might be due to the formation of aquo- and hydroxo-complexes. It is thus concluded that Eq. (3) holds in the pH region where the formation of aquo- and hydroxo-complexes is negligble.

The coordinating abilities (D-value) of the amino acids depend upon their basicity and steric factor. For the above system, the linear relation between the D-values and pK_2-values (pK_3 for L-glutamic acid) of the amino acids can not be found, since all the amino acids cited have nearly the same pK_2-values (pK_3 for L-glutamic acid) (the amino acid anion coordinates to Co(acac$_2$en)-complex with its amino group,[6] and therefore its pK_2-value was considered). Since the decreasing order of the D-values coincides with the increasing order of the steric crowding of the amino acids, it is assumed that the difference in coordinating ability of the amino acids to Co(acac$_2$en)-complex is mainly dependent on the steric factor.

Calibration Curve. The CD- (475 nm) and ORD- (500 nm) intensities were thus measured with solutions containing K[Co(acac$_2$en)(gly)$_2$] and amino acids of various optical purities. Experimental conditions were as follows: $C_{complex}=4.0\times10^{-3}$mol l^{-1}, $C_{aminoacid}=1.6\times10^{-2}$ mol l^{-1}, pH of the solution=10.00, $\mu=0.1$ (Na_2CO_3+$NaHCO_3$), cell length=1.0 cm, time=10—24 hr. From the results of measurements, calibration curves were obtained for four amino acids. All showed a linear relation between the ORD- (CD) intensities of the mixed solutions and the optical purities of the amino acids, the error being within 1%. It is concluded that we can determine the optical purity of a small amount of amino acid by comparing the ORD- (CD) intensity of a mixed solution containing optically pure amino acid with that of a mixed solution containing the amino acid whose optical purity is to be determined. The ORD- and CD-intensities of solutions prepared by mixing K[Co(acac$_2$en)(gly)$_2$] and optically pure amino acids are given in Table 5.

Table 5. CD- and ORD-intensities of a mixed solution containing K[Co(acac$_2$en)(gly)$_2$] and optically pure amino acid
$C_{complex}=4.0\times10^{-3}$ mol l^{-1}, $C_{amino\ acid}=1.6\times10^{-2}$ mol l^{-1}, pH of the solution=10.00, μ =0.1 (Na_2CO_3+$NaHCO_3$), T=25 °C, Time=(10—24) hr.

Amino acid	α_{500} ($°cm^{-1}$)	$\Delta\varepsilon_{475}$ (cm^{-1})
L-Alanine (100%)	+0.122	$+6.56\times10^{-3}$
D-Alanine (100%)	−0.122	-6.56×10^{-3}
L-Valine (100%)	+0.171	$+12.85\times10^{-3}$
D-Valine (100%)	−0.171	-12.85×10^{-3}
L-Leucine (100%)	+0.225	$+11.41\times10^{-3}$
D-Leucine (100%)	−0.225	-11.41×10^{-3}
L-Glutamic acid (100%)	+0.151	$+6.13\times10^{-3}$
D-Glutamic acid (100%)	−0.151	-6.13×10^{-3}

The solution for rotational measurement is prepared as follows: 20 ml of a 1.0×10^{-2} mol l^{-1} solution of K[Co(acac$_2$en)(gly)$_2$]·2H$_2$O (M.W.=504.48) and 5 ml of a buffer solution (0.2 mol l^{-1} Na_2CO_3+0.2 mol l^{-1} $NaHCO_3$) are mixed together. Then an amino acid (8.0×10^{-4} mol) is dissolved in this solution. The pH of the solution is adjusted to 10.00 by 0.1N-NaOH, the solution being made up to 50 ml with water. The rotational measurement is carried out after the solution is allowed to stand for about 10 hr at 25 °C.

Comparison with the Usual Method. The usual method requires 5—10 grams of amino acids to determine the optical purity. The method established herewith requires only *ca.* 0.1 g (8.0×10^{-4} mol). As small a quantity as 1/50 to 1/100 th of the sample suffices for the determination of the optical purity as compared with that needed in the usual method.

Other Schiff-Base Complexes. Several other cobalt(III)-Schiff-base complexes were examined in order to find other complexes which show larger a optical rotation than K[Co(acac$_2$en)(gly)$_2$] when they react with optically active amino acids, and which cause a more rapid substitution reaction of the axial ligand. The results are shown in Fig. 6. The Co(acac$_2$en)-

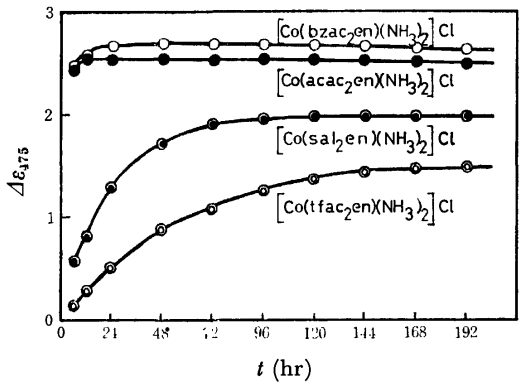

Fig. 6. The time dependence on the CD-intensity (475 nm) of the mixed solution containing Co(III)-Schiff-base complex and L-alanine (100%). $\Delta\varepsilon$ is given by the values for one mole of complex.
$C_{complex}=4.0\times10^{-3}$ mol l^{-1}, $C_{L\text{-alanine}}=8.0\times10^{-2}$ mol l^{-1}, the pH of the solution=9.50, $\mu=0.2$ (Na_2CO_3+$NaHCO_3$), $T=25$ °C.

complex is the most suitable for rotational measurement. All the complexes investigated, [Co(acac$_2$en)(NH$_3$)$_2$]Cl, [Co(bzac$_2$en)(NH$_3$)$_2$]Cl, [Co(tfac$_2$en)(NH$_3$)$_2$]Cl, and [Co(sal$_2$en)(NH$_3$)$_2$]Cl, show AB, CD, and ORD spectra similar to those for K[Co(acac$_2$en)(gly)$_2$] when mixed with L-alanine (100%). A long time is needed to establish the substitution equilibrium except for the Co(acac$_2$en)-complex. Since the chemical and spectral behavior of [Co(acac$_2$en)(NH$_3$)$_2$]Cl is very similar to that of K[Co(acac$_2$en)(gly)$_2$] and the preparation of the amine-complex is easier than that of the glycinato-complex, [Co(acac$_2$en)(NH$_3$)$_2$]Cl might be substituted for K[Co(acac$_2$en)(gly)$_2$].

The author wishes to express his deep thanks to Professor Hayami Yoneda and Associate Professor Yoshihiko Kushi, Hiroshima University, for their guidance and encouragement during the course of the work, and also to Dr. Ushio Sakaguchi and Dr. Katsuhiko Miyoshi for their stimulating discussion and helpful suggestions.

References

1) J. P. Greenstein and M. Winitz, "Chemistry of the Amino Acids," Wiley, New York, 1961, p. 1724.
2) S. Akabori and S. Mizushima, "Tampakushitsu Kagaku," (Protein Chemistry), Kyoritsu-shuppan, Tokyo, 1954, Vol. 1, p. 551.
3) K. Hayashi, Y. Fujii, R. Saito, H. Kanao, and T. Hino, *Agr. Biol. Chem.*, **30**, 1221 (1966).
4) T. Kaneko, Y. Izumi, I. Chibata, and T. Ito, "Aminosan Kogyo" (Industry of Amino Acids), Kodansha, Tokyo, 1973, p. 241.
5) Z. Badr, R. Bonnett, W. Klyne, R. J. Swan, and J. Wood, *J. Chem. Soc., C* **1966**, 2047.
6) Y. Fujii, This Bulletin, **45**, 3084 (1972).
7) G. T. Morgan and J. D. Smith, *J. Chem. Soc.*, **127**, 2030 (1925).
8) S. Yamada, H. Nishikawa, and E. Yoshida, *Proc. Japan Acad.*, **40**, 211 (1964).
9) J. Fujita, T. Yasui, and Y. Shimura, This Bulletin, **38**, 654 (1965).
10) T. Yasui, J. Hidaka, and Y. Shimura, *ibid.*, **39**, 2417 (1966).
11) N. Koine, N. Sakota, J. Hidaka, and Y. Shimura, *ibid.*, **43**, 1737 (1970).
12) N. Koine, N. Sakota, J. Hidaka, and Y. Shimura, *Chem. Lett.*, **1972**, 543.

The Selectivity Evaluation of an Ion-selective Electrode with a Liquid Membrane by Electrode Response to a Foreign Ion

Akinori Jyo, Masanori Torikai, and Nobuhiko Ishibashi*

Department of Applied Analytical Chemistry, Faculty of Engineering, Kyushu University, Fukuoka 812

(Received July 13, 1974)

The potential responses of liquid-membrane electrodes to foreign ions were examined. The electrode response obeyed the Nikolsky equation when the selectivity for the foreign ion was nearly equal to or higher than that for the objective ion and when the concentration of the foreign ion in the sample solution was sufficiently higher than that of the ion-exchanger in the liquid membrane. The Nikolsky equation, however, did not hold for the response when the selectivity for the foreign ion over the objective ion was extremely low or when the concentration of the sample was not so high. Such a non-ideal response was ascribed to the variation in the ionic composition at the membrane-solution interface caused by the ion-exchange. From the measurement of the electrode potential under conditions when the response obeyed the Nikolsky equation, the selectivity coefficient for the foreign ion over the objective ion could be obtained successfully as an intrinsic value of the electrode membrane. The selectivity value thus obtained was in good agreement with the value estimated from the Sandblom-Eisenman-Walker theory on the electrode selectivity. The additivity of the membrane potential was also described.

In recent years, many liquid membrane electrodes have been developed for the activity measurements of various inorganic and organic ions in aqueous solutions.[1-4] The selectivities of these electrodes have been evaluated by using several methods, such as the mixed-solution method and the separate-solution method.[5-7] It has been observed, however, that the selectivity values thus obtained are not always constant but vary with the method employed and the conditions of measurement.[5,8,9]

In a previous communication, Yoshida and one of the present authors (N.I.) have briefly reported on one way to evaluate an intrinsic selectivity value for a given electrode.[10] This paper will describe the details of this approach and will present the selectivity values of several liquid membrane electrodes obtained through the approach. The relationship between the selectivity values and ionic parameters, such as the mobility and the ion-partition coefficient, will also be mentioned.

Experimental

Reagents and Sensitive Liquid Membranes. All the chemicals used were of a reagent-grade quality. Aqueous solutions of sodium salts of various inorganic and organic anions were used as sample and reference solutions. In the case of cation-selectivity evaluation, aqueous solutions of alkali metal chlorides and quaternary ammonium chlorides were used. A liquid ion-exchanger membrane consisted of an organic solution of an ion-pair of an objective ion with an ion-exchange-site ion, such as the crystal violet, tris-(bathophenanthroline)iron(II), methyltricaprylylammonium, and dipicrylaminate ions. Nitrobenzene, nitromethane, 1,2-dichloroethane, chloroform, and 1-decanol were used as solvents of the membranes. The liquid membrane solutions were prepared by the same procedures as in previous papers.[11,12]

Potential Measurement. A glass U-tube cell reported on in a previous paper was used for the set-up of the cell (1) in order to evaluate the selectivity of the i-ion-sensitive membrane to the foreign j-ion:[13]

+SCE or Ag–AgCl/Reference Solution (i)/
Liquid Membrane (S–i)/Sample Solution (j)/
SCE or Ag–AgCl− (1)

where S denotes the ion-exchange site in the membrane. The electromotive force of Cell (1) was measured by using a Takeda Riken Electrometer TR-8651. A silver/silver chloride electrode was used as the reference electrode for the study of the cation selectivity. A saturated calomel electrode (SCE) was used in evaluations of the anion selectivities. A sample or reference solution was connected to the reference electrode by means of an agar salt bridge saturated with potassium chloride or ammonium chloride.

Alternatively, the electromotive force of Cell (2) was measured according to Shean's method.[14]

+SCE/Solution (i)/Membrane (i)/Membrane (j)/
Solution (j)/SCE− (2)

Results and Discussion

Electrode Responses for Solutions of Foreign Ions. In the determination of the selectivity coefficient of an ion-selective electrode with a liquid membrane, it is usually assumed that the electrode response for a sample solution containing a monovalent objective ion, i, as well as a foreign ion, j, obeys the following Nikolsky equation (3):

$$E_M = \pm 2.303RT/F \log ((a_i'' + K_{i,j}^{Pot} a_j'')/a_i') \quad (3)$$

where a_i and a_j are the activities of the corresponding ions, i and j. Prime and double prime refer to the reference and sample solutions respectively. The $K_{i,j}^{pot}$ symbol represents the potentiometric selectivity coefficient for the j ion over the i ion. The plus and minus signs at the top in Eq. (3) stand for the responses of cation- and anion-selective electrodes respectively. For a sample solution containing the j ion alone, Eq. (3) reduces to:

$$E_M = \pm 2.303RT/F \log (K_{i,j}^{Pot} a_j''/a_i') \quad (4)$$

From Eq. (4), a plot of E_M against $\log a_j''$ may be expected to be on a straight line with a Nernstian slope under a constant activity of a_i'.

* To whom any correspondence should be addressed.

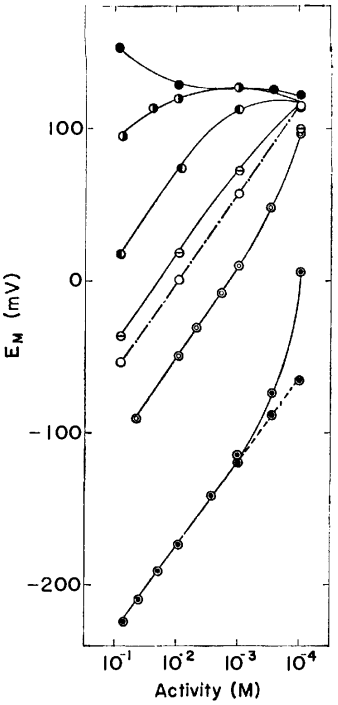

Fig. 1. Potential responses of the hydrogenmaleate ion-selective electrode for the solutions of foreign anions.
Membrane: 10^{-4} M nitrobenzene solution of crystal violet salt of hydrogenmaleate.
Temp. 20 °C.
○: hydrogenmaleate (— - —), ●: acetate, ◑: chloride, ◐: anthranilate, ⊖: trifluoroacetate, ◎: hydrogenphthalate, ⊙: perchlorate (Broken line shows the membrane potential of the cell (2)).

Figure 1 shows the observed potentials of the hydrogenmaleate ion-selective electrode for the sample solutions, each solution containing only a single anion species. The conversions of the concentrations of the ions to ionic activities were made by means of the Debye-Hückel equation, using Kielland's ion-size parameters,[15] except for the activities of hydrogenmaleate, hydrogenphthalate, and trifluoroacetate ions, which were calculated by using the values of the parameters assumed in previous papers.[16,17] The parameter for the anthranilate ion was assumed to be equal to that of the chlorobenzoate ion. For the solution of the objective hydrogenmaleate ion, a Nernstian response was obtained over a wide concentration range.[17] The electrode responses for the solutions of foreign ions, however, were not always Nernstian. Foreign ions (acetate, chloride, trifluoroacetate and anthranilate ions) giving higher potentials than hydrogenmaleate ion do not so seriously interfere with the activity measurement of the hydrogenmaleate ion, as may be understood from their low selectivities as estimated by means of Eq. (4). Potential-activity curves on these kinds of ions have lower slopes at low activity levels than does a Nernstian one, as is shown in Fig. 1. In the cases of acetate and chloride ions, the potentials were unstable in the initial stage of measurement and it took several hours to attain stationary values of potentials. The reproducibility was also relatively poor, especially at low activity levels. For trifluoroacetate and anthranilate ions, the electrode shows stable and reproducible potentials which obey Eq. (4) down to 10^{-3} M, although the potential drifts were observed initially and a period of more than 60 min was required to obtain constant values of the potentials at 10^{-4} M. Foreign ions (hydrogenphthalate and perchlorate ions) giving lower potentials than the hydrogenmaleate ion seriously interfere with the activity measurement of the hydrogenmaleate ion, even if trace amounts of these kinds of ions coexist in the sample solutions. In the activity levels higher than $10^{-2.5}$ M, the electrode potentials were stable and reproducible; they obeyed Eq. (4). On the other hand, remarkable potential drifts were observed initially, and it took several hours to attain constant potentials at activity levels lower than 10^{-3} M. The slopes of the activity-potential curves in such a stationary state were higher than a Nernstian slope.

Thus, the slopes of the potential-activity curves for foreign ions at low activity levels are different from a theoretical Nernstian value. The slope of the potential-activity curve for the foreign ion with a selectivity lower than that of the objective ion is lower than a Nernstian slope, while that for the foreign ion with a higher selectivity is higher. Response patterns similar to those of foreign ions were observed on the responses of the chloride, nitrate, hydrogenphthalate, and perchlorate ion-selective electrodes prepared in this laboratory. As may be seen in Fig. 2, the commercial nitrate ion-selective electrode of Orion 92-07 also showed a similar response pattern.

When the i-ion-selective electrode is immersed in a sample solution containing the j ion alone, the following ion-exchange reaction (5) occurs between the membrane and the sample solution, resulting in the forma-

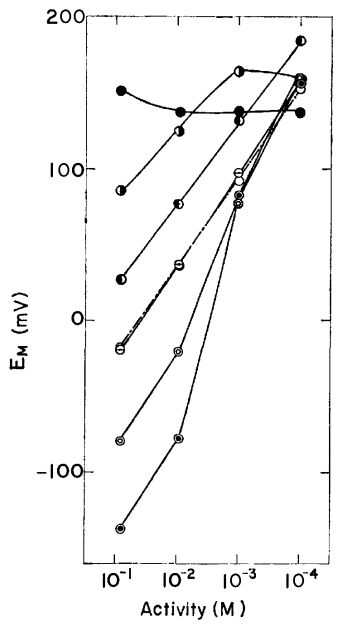

Fig. 2. Potential responses of the nitrate ion-selective electrode (Orion 92-07) for the solutions of foreign anions.
Temp. 20 °C.
○: nitrate (— - —), ●: acetate, ◑: chloride, ◐: bromide, ⊖: chlorate, ⊙: perchlorate, ◎: iodide.

tion of a diffusion layer containing the j ion as well as the i ion:

$$\text{i (Membrane)} + \text{j (Solution)} \rightleftarrows \text{j (Membrane)} + \text{i (Solution)} \quad (5)$$

Hence, it is more realistic to describe the electrode potential or membrane potential by means of Eq. (3), with the activities of the i and j ions on the aqueous side of the interface, $a_i''(0)$ and $a_j''(0)$. Since the ion-exchange process (5) proceeds stoichiometrically in most cases, it may reasonably be assumed that $a_j''(0)$ is approximately equal to $a_j''-a_i''(0)$. Accordingly, the electode response to a foreign anion, j, may be expressed as follows:

$$E_M = -2.303RT/F \log ((a_i''(0)+K_{i,j}^{pot}(a_j''-a_i''(0)))/a_i') \quad (6)$$

If the value of $K_{i,j}^{pot}$ is smaller than unity, the value of $(a_i''(0)+K_{i,j}^{pot}(a_j''-a_i''(0))$ is greater than the value of $K_{i,j}^{pot}\ a_j''$. Therefore, the electrode potential, E_M, is lower than that which would be expected from Eq. (4). If the activity of the j ion in the sample solution, a_j'', is very high, and if $K_{i,j}^{pot}$ is moderately small, the potential will be governed by the $K_{i,j}^{pot}\ a_j''$ quantity. Accordingly, the slope of the potential-activity curve is lower at low concentrations of the j ion and tends to approach a Nernstian slope at higher concentrations. In the cases of the acetate and chloride ions, however, $K_{i,j}^{pot}$ is much smaller than unity and the observed slope is quite different from the theoretical one. This means that the evaluation of $K_{i,j}^{pot}$ by means of Eq. (4) by using the activity of the foreign ion, j, in the bulk of the sample solution and the observed potential is practically difficult. On the other hand, $K_{i,j}^{pot}$ is nearly equal to unity in the cases of the anthranilate and trifluoroacetate ions. Hence, the observed potentials obey Eq. (4) at higher concentrations. Thus, the $K_{i,j}^{pot}$ can be determined by means of Eq. (4).

If a value of $K_{i,j}^{pot}$ is greater than unity, the value of $(a_i''(0)+K_{i,j}^{pot}(a_j''-a_i''(0))$ may be smaller than that of $K_{i,j}^{pot}a_j''$. Consequently, the electrode potential, E_M, becomes higher than that calculated from Eq. (4). The value of $(a_i''(0)+K_{i,j}^{pot}(a_j''-a_i''(0))$ is approximately equal to the value of $K_{i,j}^{pot}\ a_j''$ if the concentration of the j ion in the sample solution is sufficiently higher than that of the ion-exchanger or the objective counter ion in the membrane. At such high activity levels of the j ion, the electrode response, again, would obey Eq. (4); it is also possible to evaluate $K_{i,j}^{pot}$ from the observed potential and the a_j'' activity in the bulk of the sample solution. The responses of the hydrogenmaleate electrode to the perchlorate and hydrogenphthalate ions are examples of this kind of response.

Thus, the observed potential does not always correspond to a true activity of the j ion in the bulk of the sample solution, when the value of $K_{i,j}^{pot}$ differs too greatly from unity.

Additivity of the Electrode Potential or Membrane Potential. When the $K_{i,j}^{pot}$ is nearly equal to or greater than unity, and when the concentration of the foreign ion, j, in the sample solution is sufficiently higher than that of the ion-exchanger in the liquid membrane, the counter ion within the membrane in the neighborhood of the solution-membrane interface is exchanged almost completely by the foreign j ion. That is, Cell (1) is essentially converted into Cell (2). The electrode potential or membrane potential measured under such conditions can be regarded as substantially a kind of bi-ionic potential (B.I.P.) in the liquid ion-exchanger system; it obeys Eq. (4), as was mentioned in the previous section. As is illustrated in Fig. 1, this expectation can be experimentally confirmed by measuring the membrane potential of Cell (2), which consists of two component membranes responsive to hydrogenmaleate and perchlorate respectively. Shean *et al.* have found the additivity of the B.I.P.s arising across the liquid ion-exchanger membranes which consist of a given ion-exchanger in a given solvent of the membrane.[14] An analogous additivity of the potential has been observed on the electrode potential or membrane potential of Cell (1) as follows:

$$E_{M(1,n)} = E_{M(1,2)} + E_{M(2,3)} + \cdots + E_{M(i,i+1)} + \cdots + E_{M(n-1,n)} \quad (7)$$

where $E_{M(1,n)}$ and $E_{M(i,i+1)}$ are the membrane potentials of Cells (8) and (9) respectively.

Reference Solution | Liquid Membrane | Sample Solution (8)

Counter Ion, 1 (a_1') | (S-1) | Counter Ion, n (a_n'')

Reference Solution | Liquid Membrane | Sample Solution

Counter Ion, i (a_i') | (S-i) | Counter Ion, $i+1$ (a_{i+1}'') (9)

(i: 1, 2, ···, $n-1$)

Table 1. Additivity of membrane potential (I) at 20 °C Alkali Metal Ion-selective Electrodes

Counter ion in membrane[a]	Reference solution (1.00×10^{-1}M)	Membrane potential $E_{M(i,j)}$ in mV				
		Sample solution (1.00×10^{-1}M)				
		NaCl	KCl	RbCl	CsCl	$(Pr)_4NCl$
Na^+	NaCl	0	116	156	203	473
		(116)[b]	(40)	(47)	(270)	
K^+	KCl	−100	0	41	90	355
		(100)	(41)	(49)	(265)	
Rb^+	RbCl	−122	−38	0	46	315
		(84)	(38)	(46)	(269)	
Cs^+	CsCl	−155	−82	−45	0	269
		(73)	(37)	(45)	(269)	

a) Membranes are 1.0×10^{-4} M nitrobenzene solutions of alkali metal dipicrylaminates. b) Figures in parentheses denote differences between adjacent potential values.

TABLE 2. ADDITIVITY OF MEMBRANE POTENTIAL (II), AT 20 °C
Anion-selective Electrodes

Solvent of membrane	Counter ion in membrane	Reference solution (1.00×10^{-2}M)	Membrane potential in mV
			Sample solution, as sodium salt (1.00×10^{-2}M)
			Cl^- HMA^- Saicylate HPA^- ClO_4^-
Nitrobenzene[a]	Cl^-	NaCl	0 −155 −198 −204 −329 (−155) (−43) (−6) (−125)
	HMA^- [b]	NaHMA	0 −43 −50 −177 (−43) (−7) (−127)
	HPA^- [c]	NaHPA	0 −125 (−125)
1,2-Dichloroethane[a]	Cl^-	NaCl	0 −138 −172 −180 −300 (−138) (−34) (−8) (−120)
	HMA^-	NaHMA	0 −34 −43 −160 (−34) (−9) (−117)
	HPA^-	NaHPA	0 −116 (−116)
Chloroform[a]	Cl^-	NaCl	0 −129 −139 −165 −198 (−129) (−10) (−26) (−33)
	HMA^-	NaHMA	0 −10 −35 −70 (−10) (−25) (−35)
	HPA^-	NaHPA	0 −33 (−33)
		(1.00×10^{-1}M)	(1.00×10^{-1}M)
			Cl^- Br^- NO_3^- I^- ClO_4^- SCN^-
1-Decanol[d]	Cl^-	NaCl	0 −25 −31 −67 −75 −94 (−25) (−6) (−36) (−8) (−19)
	NO_3^-	$NaNO_3$	31 6 0 −36 −45 −64 (−25) (−6) (−36) (−9) (−19)

a) Crystal violet was used as the ion-exchange site in the membrane (1.00×10^{-4} M). b) HMA^- denotes hydrogenmaleate ion. c) HPA^- denotes hydrogenphthalate ion. d) Methyltricaprylylammonium ion was used as the ion-exchange site in the membrane (1.00×10^{-3} M).

Here, 1, 2, —, n-1, and n are monovalent counter ions with the same sign of charge. In order for Eq. (7) to be valid, the following requirements (10) should be satisfied in addition to the conditions of the concentrations of the sample solution and liquid membrane solution mentioned at the beginning of this section:

$$\left.\begin{aligned} &a_i' = a_{i+1}' \quad (i\text{: } 1, 2, \cdots, n-2)\\ &a_i'' = a_{i+1}'' \quad (i\text{: } 2, 3, \cdots, n-1)\\ &K_{i,j}^{Pot} \gtrsim \text{unity} \quad (i\text{: } 1, 2, \cdots, n-1) \end{aligned}\right\} \qquad (10)$$

In Table 1, the membrane potentials of alkali metal ion-selective electrode membranes, which consist of 10^{-4} M nitrobenzene solutions of dipicrylaminates of alkali metals, are summarized. The membrane containing sodium dipicrylaminate gives a potential difference of 473 mV between the solutions of sodium chloride and tetrapropylammonium chloride $(Pr)_4NCl$. This is almost entirely consistent with the algebraic sum of $E_{M(Na,K)}$, $E_{M(K,Rb)}$, $E_{M(Rb,Cs)}$, and $E_{M(Cs,(Pr),N)}$, which is 472 mV. On the other hand, the membrane containing cesium dipicrylaminate yields a potential difference of −155 mV between the solutions of cesium chloride and sodium chloride. This is not equal to the sum of $E_{M(Cs,Rb)}$, $E_{M(Rb,K)}$, and $E_{M(K,Na)}$, which is −183 mV. Thus, the additivity of the potential does not hold when the $K_{i,j}^{pot}$ is considerably smaller than unity. The additivity relation was also observed on the potentials of the liquid membranes responsive to monovalent anions, as is illustrated in Table 2.

When the $K_{i,j}^{pot}$ is sufficiently less than unity or when the concentration of the foreign ion in the sample solution is not sufficiently higher than that of the ion-exchanger in the liquid membrane, Cell (1) is not converted into Cell (2), but into the two ionic cells on the foreign ion and the objective ion. Therefore, the additivity of the potential does not hold under such conditions.

Inter-ionic Selectivity of the Liquid Membrane. From the additivity of the membrane potential, one can obtain the following Eq. (11):

$$K_{i,n}^{Pot} = K_{1,2}^{Pot} K_{2,3}^{Pot} \cdots K_{i,i+1}^{Pot} \cdots K_{n-1,n}^{Pot} \qquad (11)$$

where $K_{i,i+1}^{pot}$ is the selectivity coefficient of the i-ion selective electrode for the $i+1$ ion over the i ion. Judging from the conditions on the additivity of the membrane potential, the selectivity for the 1, 2, —, n ions should increase in the sequence of the numbers. Equation (11) implies that the inter-ionic selectivity of a liquid membrane consisting of a given ion-exchange site and a given solvent of the membrane can be evaluated from the potential measurements of the l-ion selective electrode for the solutions of foreigh ions, 2, 3, —, n. The 1 ion as a reference on selectivity evaluation should have such a degree of extractability

Table 3. Membrane potentials ($E_{M(Cl,j)}$ or B.I.P.$_{Cl,j}$) and selectivity coefficients (log $K_{Cl,j}^{pot}$), Temp. 20 °C

Ion (j)	Solvent of membrane: Nitrobenzene[a]		1,2-Dichloroethane[a]		Chloroform[a]		1-Decanol[b]	
	$E_{M(Cl,j)}$[c] (mV)	log $K_{Cl,j}^{pot}$	$E_{M(Cl,j)}$[c] (mV)	log $K_{Cl,j}^{pot}$	$E_{M(Cl,j)}$[c] (mV)	log $K_{Cl,j}^{pot}$	$E_{M(Cl,j)}$[c] (mV)	log $K_{Cl,j}^{pot}$
Cl^-	0	0.00	0	0.00	0	0.00	0	0.00
Br^-	−88	1.51	−78	1.34	−79	1.36	−25	0.43
NO_3^-	−145	2.49	−124	2.13	−81	1.39	−31	0.53
ClO_3^-	−160	2.75	−142	2.44	−96	1.65	−29	0.50
I^-	−224	3.85	−204	3.51	−178	3.06	−67	1.15
SCN^-	−242	4.16	−223	3.83	−168	2.89	−94	1.61
BF_4^-[e]	−270	4.64	−241	4.14	−126	2.17	−24	0.41
ClO_4^-	−329	5.66	−300	5.16	−198	3.40	−75	1.29
Benzoate	−57	0.97	−46	0.79	−17	0.28	−75	1.26
p-Aminosalicylate[e]	−101	1.74	—	—	−22	0.38	—	—
Trifluoroacetate[e]	−130	2.24	—	—	−67	1.15	—	—
Benzenesulfonate[e]	−135	2.32	−87	1.50	—	—	−58	1.00
Hydrogenmaleate[e]	−155	2.67	−138	2.37	−129	2.22	−56	0.96
Salicylate[e]	−198	3.40	−172	2.96	−139	2.39	−122	2.10
Hydrogenphthalate[e]	−204	3.51	−180	3.09	−165	2.84	−91	1.56
Benzylate[e]	−214	3.68	−197	3.39	−162	2.79	—	—
1-Naphthalenesulfonate[e]	−215	3.70	−205	3.51	—	—	−99	1.70

a) Membranes consisted of an organic solution of chloride salt of crystal violet (1.0×10^{-4}M). b) The membrane consisted of 1-decanol solution of methyltricaprylylammonium chloride (1.0×10^{-3}M). c) Concentrations of reference and sample solutions were 1.00×10^{-2}M. d) Concentrations of reference and sample solutions were 1.00×10^{-1} M. e) Selectivity coefficients were calculated by using concentrations instead of activities.

Table 4. Membrane potentials ($E_{M(Na,j)}$ or B.I.P.$_{Na,j}$) and selectivity coefficients (log $K_{Na,j}^{pot}$), at 20 °C

Ion (j)	Solvent of membrane: Nitrobenzene[a]		Nitromethane[a]	
	$E_{M(Na,j)}$[b] (mV)	log $K_{Na,j}^{pot}$	$E_{M(Na,j)}$[b] (mV)	log $K_{Na,j}^{pot}$
Na^+	0	0.00	0	0.00
K^+	116	2.00	79	1.37
Rb^+	156	2.70	112	1.94
Cs^+	203	3.50	144	2.49
Tetramethylammonium	297	5.12	—	—
Tetraethylammonium	380	6.52	—	—
Tetrapropylammonium	473	8.11	—	—

a) Membranes consisted of an organic solution of sodium dipicrylaminate (1.0×10^{-4}M). b) Concentrations of reference and sample solutions were 1.00×10^{-1}M.

that the ion is sufficiently confined to the membrane for us to obtain the stable potential. Therefore, chloride and sodium ions were selected as our references. In Table 3, the membrane potentials of the chloride ion-selective electrodes for solutions of various anions are listed. The selectivity coefficients in the table are values relative to the reference chloride ion. The selectivity values for monovalent cations are summarized in Table 4, along with the membrane potentials of the sodium ion-selective electrodes. With respect to anion selectivity, nitrobenzene and 1,2-dichloroethane give membranes with a higher inter-ionic selectivity than chloroform. The 1-decanol membrane has a low inter-ionic selectivity. For cations, the nitrobenzene mem-

Table 5. Selectivity coefficients of carboxylate ion-selective electrodes, Temp. 20 °C

Electrode[a] (i)	Interferant (j)	Selectivity coefficient (log $K_{i,j}^{pot}$): Obtained by the mixed solution methods	Calculated value
Hydrogenmaleate[b]	Cl^-	−2.5	−2.67
	Br^-	−1.0	−1.16
	NO_3^-	−0.2	−0.18
	I^-	0.9	1.19
	ClO_4^-	2.9	2.99
Hydrogenphthalate[b]	Cl^-	−3.1	−3.51
	Br^-	−2.1	−2.00
	NO_3^-	−1.2	−1.02
	I^-	0.0	0.34
	ClO_4^-	1.8	2.15
Trifluoroacetate[c]	Cl^-	−2.1	−2.24
	Br^-	−0.9	−0.73
	NO_3^-	0.0	0.25
	I^-	1.3	1.61
	ClO_4^-	3.2	3.42

a) Liquid membranes were nitrobenzene solutions of crystal violet salts of objective anions (1.0×10^{-4}). b) Selectivity values in first column were determined based on the mixed solution method II A in Ref. 5. c) Selectivity values in first column were determined by the mixed solution method II C in Ref. 5.

Table 6. Selectivity coefficients of nitrobenzene membranes containing tris(bathophenanthroline)-iron(II) ion as an ion-exchange site (Temp. 20 °C).

Counter ion in membrane	Reference solution	Sample solution (as sodium salt)		Membrane potential in mV	Selectivity coefficient	
HMA^- [a]	NaHMA (1.00×10^{-2}M)	Salicylate	(1.00×10^{-2}M)	− 44		0.76 (0.74)[c]
		HPA^-	(1.00×10^{-2}M)	− 49	$\log K_{HMA,j}^{pot}$	0.84 (0.87)
		ClO_4^-	(1.00×10^{-2}M)	−177		3.04 (3.04)
HPA^- [a]	NaHPA (1.00×10^{-2}M)	ClO_4^-	(1.00×10^{-2}M)	−125	$\log K_{HPA,j}^{pot}$	2.15 (2.15)
NO_3^- [b]	$NaNO_3$ (1.00×10^{-1}M)	BF_4^-	(1.00×10^{-2}M)	−128	$\log K_{NO_3,j}^{pot}$	2.20 (2.15)

a) Concentrations of ion-exchangers were 1.0×10^{-4}M. HMA: hydrogenmaleate, HPA: hydrogenphthalate. b) The concentration of the ion-exchanger was 5.0×10^{-4}M. c) Figures on parentheses are values of the nitrobenzene membrane containing crystal violet as an ion-exchange site.

brane exhibits a slightly higher inter-ionic selectivity than the nitromethane membrane. The selectivity sequence of anions is approximately consistent with the Hofmeister anion series on the nitrobenzene and 1,2-dichloroethane membranes. The chloroform and 1-decanol membranes show a somewhat different order of anion selectivity from the nitrobenzene and 1,2-dichloroethane membranes. Relatively high selectivities for halide ions are observed on the chloroform membrane. On the 1-decanol membrane, the selectivities for perchlorate and borofluoride ions are lowered, while organic anions show a relatively higher selectivity than do inorganic anions.

From the selectivity values in Tables 3 and 4, one can obtain the selectivity coefficient of a given ion-selective electrode for any ion by using Relation (11). The selectivity coefficients of the hydrogenmaleate ion-selective electrode with the nitrobenzene membrane, for example, are thus calculated: the value for perchlorate over hydrogenmaleate (HMA), $\log K_{HMA,ClO_4}^{pot}$, is $\log K_{Cl,ClO_4}^{pot}$ minus $\log K_{Cl,HMA}^{pot}$, which is 2.29, while that for bromide, $\log K_{HMA,Br}^{pot}$, is $\log K_{Cl,Br}^{pot}$ minus $\log K_{Cl,HMA}^{pot}$, which is −1.16, and so on. In Table 5, the calculated selectivity values are compared with the values determined by the usual mixed-solution methods.[5] The values are consistent with each other in order of magnitude.

Relationship between the Selectivity Coefficient and Ionic Parameters. Sandblom and his co-workers have proposed theoretical expressions of the potentials arising across the liquid ion-exchanger membranes.[18,19] According to their theory, the membrane potential in the electrochemical system (1) is given by Eq. (12), when the site and counter ions dissociate completely in the liquid membrane:

$$E_M = \pm 2.303RT/F \log (u_j k_j a_j''/u_i k_i a_i') \qquad (12)$$

Table 7. Comparison of selectivity coefficients obtained with theoretical values

Ion (j)	$\log (k_i/k_j)$	λ° ($cm^2\Omega^{-1}$)[c]	Theoretical value $\log (k_i\lambda_j^\circ/k_i\lambda_j^\circ)$	Experimental value $\log K_{i,j}^{pot}$
Na^+ (i)	0.0[a]	16.02	0.0	0.00
K^+	1.9[a]	17.53	1.9	2.00
$(CH_3)_4N^+$	5.4[a]	17.0	5.4	5.12
$(C_2H_5)_4N^+$	7.0[a]	16.1	7.0	6.52
Cl^- (i)	0.0[b]	22.68	0.0	0.00
Br^-	1.6[b]	21.93	1.6	1.51
I^-	3.7[b]	21.25	3.7	3.85
ClO_4^-	5.4[b]	17.7	5.3	5.77

a) Taken from Ref. 22. b) Ref. 23. c) Ref. 24.

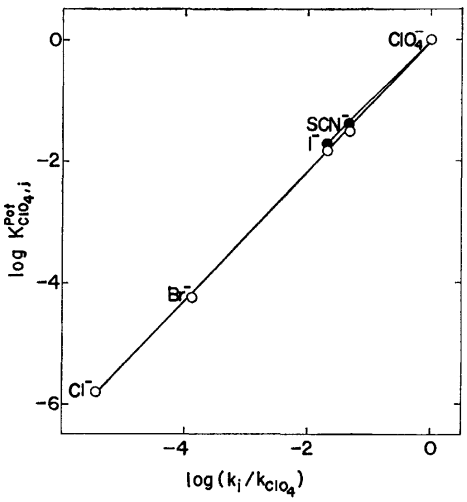

Fig. 3. Relationship between the selectivity coefficent and the ion partition coefficient.
○: nitrobenzene membrane,
●: 1,2-dichlorothane membrane.

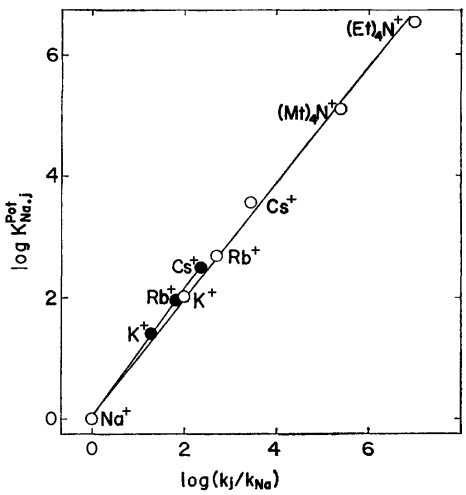

Fig. 4. Relationship between the selectivity coefficient and the ion partition coefficient.
○: nitrobenzene membrane,
●: nitromethane membrane.

Table 8. Selectivity coefficients of 1,2-dichloroethane membranes containing tris(bathophenanthroline)iron(II) as an ion-exchange site Temp. 20 °C

Counter ion in membrane	Reference solution	Sample solution (as sodium salt)	Membrane potential in mV	Selectivity coefficient	
HMA^- a)	NaHMA (1.00×10^{-2}M)	Salicylate (1.00×10^{-2}M)	− 33		0.57 (0.58)c)
		HPA^- (1.00×10^{-2}M)	− 42	$\log K_{HMA,j}^{pot}$	0.72 (0.74)
		ClO_4^- (1.00×10^{-2}M)	−158		2.72 (2.75)
HPA^- a)	NaHPA (1.00×10^{-3}M)	ClO_4^- (1.00×10^{-2}M)	−117	$\log K_{HPA,j}^{pot}$	2.02 (1.99)
NO_3^- b)	$NaNO_3$ (1.00×10^{-2}M)	BF_4^- (1.00×10^{-1}M)	−117	$\log K_{NO_3,j}^{pot}$	2.02 (2.01)

a) Concentrations of ion-exchangers in membranes were 1.0×10^{-4}M. b) The concentration of the ion-exchanger was 5.0×10^{-4}M. c) Figures in parentheses are values of the 1,2-dichloroethane membranes containing crystal violet as an ion-exchange site.

where u_i and u_j are the mobilities of the i and j ions, respectively and where k_i and k_j are the partiton coefficients of the corresponding ions between water and the solvent of the membrane. From Eqs. (4) and (12), the selectivity coefficient for the membrane of the complete-dissociation type may be represented by ionic parameters as follows:

$$K_{i,j}^{pot} = u_j k_j / u_i k_i = \lambda_j^\circ k_j / \lambda_i^\circ k_i \qquad (13)$$

where λ_i° and λ_j° are the limiting single-ion conductivities of the i and j ions respectively. Equation (13) implies that the selectivity coefficient of the ion-selective electrode with the liquid membrane of the complete-dissociation type is not dependent on the ion-exchange site species. The counter ion and site ion dissociate almost completely in the nitrobenzene membrane at such low concentrations of the ion-exchanger as 10^{-4} M, as judged from the dissociation constants in the literature.[11,20,21] In Table 6, the selectivity values of the nitrobenzene membranes containing the tris (bathophenanthroline)iron(II) ion as the ion-exchange site are compared with those of the membranes containing the crystal violet site. A good agreement is observed between the values of the two membranes. In Table 7, the selectivity values obtained are also compared with the theoretical values computed from Eq. (13) by employing ionic parameters quoted from the literature.[22-24] The experimental values are in good agreement with the theoretical ones. Since limiting single-ion conductivities are not so different among the ions, the selectivity coefficients may be said to be predominantly governed by the ion-partition coefficients. As is shown in Figs. 3 and 4, a good mutuality between the selectivity values and the reported ion-partition coefficients was also observed on the 1,2-dichloroethane and nitromethane membranes.[20,25] Table 8 shows a comparison of the selectivity values between the 1,2-dichloroethane membranes containing the tris(bathophenanthroline)iron(II) ion and the crystal violet ion as the ion-exchange sites. In these membranes, the selectivity values are also scarcely dependent on the site species.

The authors would like to express their thanks to Mr. Nobuo Yoshida for his helpful discussions. They also greatly acknowledge the financial support of the Ministry of Education (General Research B, Grant No. 847042, 1973).

References

1) W. Simon, H. Wuhrmann, M. Vašák, L. A. R. Pioda, R. Dohner, and Z. Štefanac, *Angew. Chem. Intern. Edit.*, **9**, 445 (1970).
2) R. P. Buck, *Anal. Chem.*, **44**, 270 R (1972).
3) N. Ishibashi, *Denki Kagaku*, **42**, 112 (1974).
4) J. Koryta, *Anal. Chim. Acta*, **61**, 329 (1972).
5) G. J. Moody and J. D. R. Thomas, "Selective Ion Sensitive Electrodes," Merrow Pub. Co. Watford, England (1972).
6) S. Back, *Anal. Chem.*, **44**, 1696 (1972).
7) R. E. Reinsfelder, and F. A. Schultz, *Anal. Chim. Acta*, **65**, 425 (1973).
8) K. Srinivasan, and G. A. Rechnitz, *Anal. Chem.*, **41**, 1203 (1969).
9) G. J. Moody, R. B. Oke, and J. D. R. Thomas, *Analyst*, **95**, 910 (1970).
10) N. Yoshida and N. Ishibashi, *Chem. Lett.*, **1974**, 493.
11) N. Ishibashi, H. Kohara, and N. Uemura, *Bunseki Kagaku*, **21**, 1072 (1972).
12) N. Ishibashi, H. Kohara, and K. Horinouchi, *Talanta*, **20**, 867 (1973).
13) N. Ishibashi and H. Kohara, *Anal. Lett.*, **4**, 785 (1971).
14) G. Shean and K. Sollner, *J. Membrane Biology*, **9**, 297 (1972).
15) J. Kielland, *J. Amer. Chem. Soc.*, **59**, 1675 (1937).
16) N. Ishibashi and A. Jyo, *Microchem. J.*, **18**, 220 (1973).
17) A. Jyo, M. Yonemitsu, and N. Ishibashi, This Bulletin, **46**, 3734 (1973).
18) J. Sandblom, G. Eisenman, and J. L. Walker, Jr., *J. Phys. Chem.*, **71**, 3862 (1967).
19) G. Eisenman, *Anal. Chem.*, **40**, 310 (1968).
20) Y. Yamamoto, E. Sumimura, K. Miyoshi, and A. Tominaga, *Anal. Chim. Acta*, **64**, 225 (1973).
21) S. Motomizu, K. Toei, and T. Iwachido, This Bulletin, **42**, 1006 (1969).
22) J. Rais, *Collection Czechoslov. Chem. Commun.*, **36**, 3253 (1971).
23) Y. Yamamoto, T. Tarumoto, and F. Iwamoto, *Anal. Chim. Acta*, **64**, 1 (1973).
24) J. F. Coetzee and G. P. Cunningham, *J. Amer. Chem. Soc.*, **87**, 2529 (1965).
25) G. R. Haugen and H. L. Friedman, *J. Phys. Chem.*, **72**, 4549 (1968).

NOTES

BULLETIN OF THE CHEMICAL SOCIETY OF JAPAN, VOL. 47 (11), 2869—2870 (1974)

A Solvated Electron Formed from the Water by the Irradiation of the Recoil Particles of $^{10}B(n,\alpha)^{7}Li$ and $^{6}Li(n,\alpha)T$

Akira YOKOHATA and Satoru TSUDA

Department of Chemistry, Faculty of Engineering, Hiroshima University, Senda-machi, Hiroshima 730

(Received January 23, 1974)

Synopsis. The G values of a solvated electron produced by ionizing radiation from the (n,α) activation of boron and lithium were estimated to be 0.36 ($\pm$0.06) and 0.50 ($\pm$0.05) in neutral aqueous solutions ($ClCH_2COOH$–N_2O), and 0.24 ($\pm$0.05) and 0.46 ($\pm$0.05) in alkaline aqueous solutions ($K_3Fe(CN)_6$–NaOH), respectively.

The dependence of the radical yield in irradiated aqueous solutions on the LET (linear energy transfer) of the radiation has been actively investigated.[1-2] In water radiolysis, the free radical yields decrease and the molecular yields increase with an increase in the LET of the radiation. This effect is believed to be due to an increasing combination of radicals in the spurs and tracks as the density of radicals along the tracks increases.

However, only a few data have been reported[2] regarding the yield of solvated electrons in water irradiated by the radiations of high LET. In this paper, we will report some data obtained with high LET radiations from the $^{10}B(n,\alpha)^{7}Li$ and $^{6}Li(n,\alpha)T$ reactions. Neutral aqueous monochloroacetic acid–nitrous oxide and alkaline aqueous potassium ferricyanide solutions were selected as reaction systems suitable for this purpose.

Experimental

The experiments were carried out in the thermal neutron facility (E-2) of the nuclear reactor at Kyoto University.

The thermal neutron flux, as measured by an Al–Au wire, was in the range from 1.8×10^{10} to 8.6×10^{10} n cm^{-2} s^{-1}, depending upon the exact position of the sample. The flux of the fast neutrons was relatively small. The dose rate of the γ-ray background was measured with a Fricke dosimeter. Each experiment was repeated at least 6 times; the coefficient of variation was less than $\pm$10%.

To determine, in the first instance, whether the presence of boric acid, sodium borate, or lithium sulfate affected the reactions of the solvated electron in irradiated $ClCH_2COOH$–N_2O and alkaline $K_3Fe(CN)_6$ solutions, some experiments using ^{60}Co γ-rays were carried out; these experiments confirmed that they cannot compete significantly with the other solutes for solvated electrons in the range of concentrations using here.

The pH of the $ClCH_2COOH$–N_2O system was adjusted with NaOH. All the chemicals used were of a reagent grade. The N_2O was purified by several distillations on a vacuum line, prior to introduction into the irradiation vessel containing the degassed solution. The amount of N_2O in the solution was determined by the measurement of the pressure drop after the solution had stood for about 24 hr at room temperature.

The irradiation vessels were cleaned with boiling nitric acid and then triply rinsed with distilled water. Eight-ml portions of solutions containing ^{10}B or ^{6}Li were sealed in a silica tube.

The aquopentacyanide ions were spectrophotometrically determined by the method using NaN_3.[3] The presence of boric acid or sodium borate and lithium sulfate did not interfere with those measurements.

Results and Discussion

Neutral Aqueous Monochloroacetic Acid–Nitrous Oxide Solutions. The yield of solvated electrons can be estimated in neutral aqueous monochloroacetic acid–nitrous oxide solutions. The pertinent reactions to be considered are:

$$e^-_{aq} + ClCH_2COO^- \longrightarrow Cl^- + CH_2COO^- \quad (1)$$

$$e^-_{aq} + N_2O \longrightarrow N_2 + O^- \quad (2)$$

$$H + ClCH_2COO^- \longrightarrow H_2 + ClCHCOO^- \quad (3)$$

$$\searrow\ Cl^- + CH_2COO^- + H^+ \quad (4)$$

$$OH + ClCH_2COO^- \longrightarrow H_2O + ClCHCOO^- \quad (5)$$

$$\searrow\ Cl^- + R\ (R;\ \text{radical}) \quad (6)$$

Dainton and Peterson[4] have investigated the γ-radiolysis of aqueous N_2O solutions and shown that this solute has a relatively high reactivity to the solvated electrons, leading to the formation of nitrogen (Reaction 2). Hydrogen atoms, on the other hand, react very slowly with N_2O. This system, therefore, is a useful one for the determination of the yield of solvated electrons. In fact, Eq. (7) has been confirmed by the present authors in their γ-ray experiment with 1×10^{-3} M $ClCH_2COOH$–8×10^{-3} M (or higher concentrations) N_2O at pH=6.5.[5] In the system studied here, the value of $G(N_2)$ calculated from the dose of the γ-ray background in the nuclear reactor was 2.8, consistent with that obtained from the γ-ray irradiation.

$$G_{e^-_{aq}} = G(N_2) \quad (7)$$

Figures 1 and 2 show the relationship between the amounts of N_2 of [B] or [Li], where [B] and [Li] denote the concentrations of $Na_2B_4O_7$ and Li_2SO_4, respectively.

The G values of the solvated electrons were calculated from Eqs. (8) and (9):

$$^{B}G_{e^-_{aq}} = \frac{(N_2)}{[B]\sigma_B\phi t E_0(B)\gamma}\times 100 \quad (8)$$

$$^{Li}G_{e^-_{aq}} = \frac{(N_2)}{[Li]\sigma_{Li}\phi t E_0(Li)}\times 100 \quad (9)$$

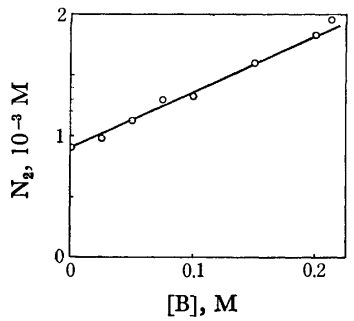

Fig. 1. Relationship between amount of nitrogen formed and concentration of boron.
Thermal neutron flux: 8.6×10^{10} n cm^{-2} s^{-1}
Irradiation time: 135 min
Initial concentration:
1.0×10^{-3} M $ClCH_2COOH-2.6\times10^{-2}$ M N_2O
pH: 6.0 B: $Na_2B_4O_7$

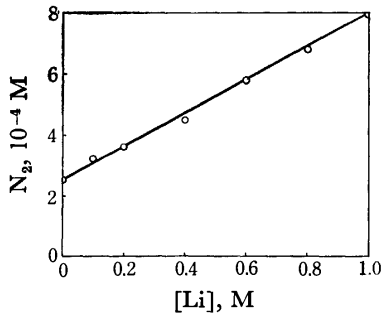

Fig. 2. Relationship between amount of nitrogen formed and concentration of lithium.
Thermal neutron flux: 1.8×10^{10} n cm^{-2} s^{-1}
Irradiation time: 300 min
Initial concentration:
1.0×10^{-3} M $ClCH_2COOH-2.4\times10^{-2}$ M N_2O
pH: 6.0 Li: Li_2SO_4

The boron absorption cross-section, σ_B, is taken as 755×10^{-24} cm^2.[6] The average energy absorbed by the solution from the heavy-particle recoils, E_0(B), is taken as 2.35×10^6 eV per nuclear event. The lithium absorption cross-section, σ_{Li}, is taken as 71×10^{-24} cm^2, and E_0(Li), as 4.78×10^6 eV.[7] Thus, from the slope of the curve, $^{B}G_{e_{aq}^-}$ and $^{Li}G_{e_{aq}^-}$ were estimated to be 0.36 ($\pm$0.06) and 0.50 ($\pm$0.05) respectively.

Alkaline Aqueous Solution of Potassium Ferricyanide. In order to secure further evidence of the yield of solvated electrons, the study was extended to another system, the $K_3Fe(CN)_6$-0.1 M NaOH solution. In this system, attention was directed toward the reaction of e_{aq}^- with $Fe(CN)_6^{3-}$.

It has been reported that aquopentacyanide is formed *via* the following competitive reaction:

$$e_{aq}^- + Fe(CN)_6^{3-} \longrightarrow Fe(CN)_6^{4-} \quad (10)$$

$$\searrow\ Fe(CN)_5OH_2^{3-} + CN^- \quad (11)$$

Then, in the range from 5×10^{-3} M to 1×10^{-2} M $Fe(CN)_6^{3-}$, Eq. (12) was confirmed:[8]

$$G_{e_{aq}^-} \simeq 2G(Fe(CN)_5OH_2^{3-}) \quad (12)$$

where the yield of aquopentacyanide was determined by using the NaN_3 method.[3]

Figures 3 and 4 show that the relation of the yield

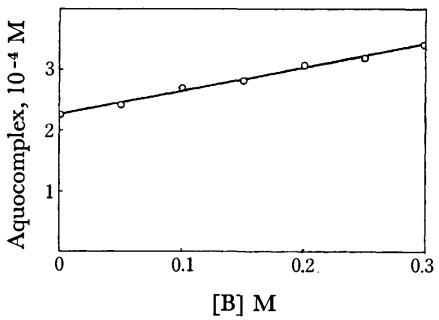

Fig. 3. Relationship between amount of aquocomplex formed and concentration of boron.
Thermal neutron flux: 5.1×10^{10} n cm^{-2} s^{-1}
Irradiation time: 52 min
Initial concentration:
5.0×10^{-3} M $Fe(CN)_6^{3-}$—0.1 M NaOH
B: $Na_2B_4O_7$

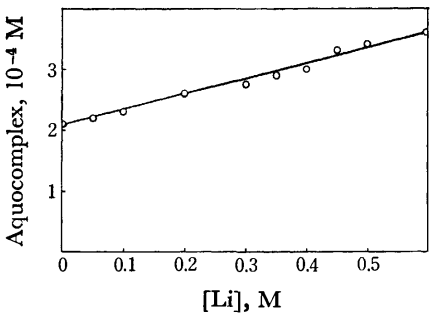

Fig. 4. Relationship between amount of aquocomplex formed and concentration of lithium
Thermal neutron flux: 5.6×10^{10} n cm^{-2} s^{-1}
Irradiation time: 64 min
Initial concentration:
5.0×10^{-3} M $Fe(CN)_6^{3-}$—0.1M NaOH
Li: Li_2SO_4

of the aquocomplex to [B] or [Li] is linear. Thus, the radiolytic yield of the aquocomplex formed by the recoil particles was obtained from the slopes.

By applying the yield of the product to Eq. (12), $^{B}G_{e_{aq}}$ and $^{Li}G_{e_{aq}}$ can be estimated to be about 0.24 ($\pm$0.05) and 0.46 ($\pm$0.05), respectively.

The difference in the yields between the systems of the neutral aqueous potassium ferricyanide solutions, though small, might be caused by the difference in pH.

References

1) N. F. Barr and R. H. Schuler, *J. Phys. Chem.*, **63**, 808 (1959).
2) A. Henglein, K.-D. Asmus, F. Scholes, and M. Simic, *Z. Phys. Chem. N. F.*, **45**, 39 (1965).
3) S. Ohno, This Bulletin, **40**, 1765 (1967).
4) F. S. Dainton and D. B. Peterson, *Proc. Roy. Soc. Ser., A*, **267**, 443 (1962).
5) A. Yokohata, T. Ohmura, and S. Tsuda, *J. Phys. Chem.*, **73**, 4013 (1969).
6) S. J. Hughes and J. A. Harvey, A. E. C. Document BNL 325 (1955).
7) R. H. Schuler and N. F. Barr, *J. Amer. Chem. Soc.*, **78**, 5756 (1956).
8) A. Yokohata, This Bulletin, **42**, 658 (1969).

BULLETIN OF THE CHEMICAL SOCIETY OF JAPAN, VOL. 47 (11), 2871—2872 (1974)

MCNDO/2 Calculation of the Radiative Lifetimes of the Triplet States of the Nucleic Acid Bases

Mamoru KAMIYA and YUKIO AKAHORI
Shizuoka College of Pharmacy, Oshika, Shizuoka-shi 421

(Received March 22, 1974)

Synopsis. The radiative lifetimes of the lowest excited triplet states of the nucleic acid bases were calculated using a first-order perturbation treatment of the spin-orbit coupling. The calculated lifetimes were in the sequence of pyrimidines> purines; that of thymine was found to be largest. The relation between the radiative lifetimes and biological photodeactivation was discussed.

The electronic properties of the triplet states of the nucleic acid bases are of biological interest. A few experiments have suggested that the excited triplet states, in particular those of the pyrimidine bases, are responsible for the biological photodeactivation of the nucleic acids,[1-4] though the excited singlet states are also assumed to work as precursors in the energy-transfer process.[5] Taking notice of such characteristics of the triplet states, SCFCI and UHF calculations have been carried out for the energy states and electronic populations of the lowest triplets of the nucleic acid bases.[6]

Here, an attempt was made to estimate the radiative lifetimes of the lowest excited tri let states of the nucleic acid bases. That is, the singlet-triplet transition probability induced by spin-orbit coupling was calculated by a first-order perturbation method. The calculation was done according to the all-valence-electron SCF method of Jaffe *et al.*[7] The electric-dipole transition moment between the ground and lowest triplet states is given as:

$$\mathbf{M}(0, \Gamma_r) = \sum_k \{[\langle {}^1\Phi_k|H_{so}|{}^3\Phi_1^{\Gamma_r}\rangle^*/({}^3E_1 - {}^1E_k)]\mathbf{M}({}^1\Phi_0, {}^1\Phi_k)\} + \sum_m \{[\langle {}^3\Phi_m^{\Gamma_r}|H_{so}|{}^1\Phi_0\rangle/({}^1E_0 - {}^3E_m)]\mathbf{M}({}^3\Phi_1^{\Gamma_r}, {}^3\Phi_m^{\Gamma_r})\}$$

where Γ_r is the component of the triplet spin functions. It is chosen as:

$$\Gamma_-: [\alpha(p)\alpha(q) - \beta(p)\beta(q)]$$
$$\Gamma_z: [\alpha(p)\beta(q) + \alpha(q)\beta(p)]$$
$$\Gamma_+: i[\alpha(p)\alpha(q) + \beta(p)\beta(q)]$$

The unperturbed wave function was calculated by the modified CNDO/2 method; the parameters used (in eV units) were as follows:

$-1/2(I_s + A_s)$: 7.176(H), 14.051(C), 19.316(N), 25.390(O)
$-1/2(I_p + A_p)$: 5.572(C), 7.275(N), 9.111(O)
γ_{AA} : 12.845(H), 11.089(C), 12.016(N), 13.599(O)
$\beta_A{}^0$: −12(H), −17(C), −26(N), −45(O)

The two-center Coulomb integral was calculated by the Ohno approximation.[8] The geometries of the heterocyclic rings were assumed as regular hexagon and pentagon, both with the ring-distance of 1.39 Å. The other bond-lengths were chosen as $R_{>C-H}$=1.08 Å, $R_{>C-NH_2}$=1.34 Å, $R_{>N-H}$=1.03 Å, $R_{>C=O}$=1.20 Å, $R_{>C-CH_3}$=1.51 Å, and $R_{>C-H}$=1.12 Å. The atomic

TABLE 1. CALCULATED RESULTS OF THE RADIATIVE LIFETIME OF THE LOWEST EXCITED TRIPLET OF THE NUCLEIC ACID BASES

	pyrimidine		cytosine 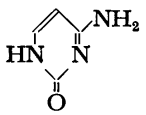		uracil 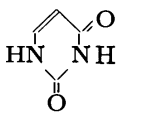		thymine 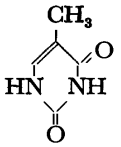	
spin state	$f_{T_1\to G}$	τ_{T_1} (s)	$f_{T_1\to G}$	τ_{T_1} (s)	$f_{T_1\to G}$	τ_{T_1} (s)	$f_{T_1\to G}$	τ_{T_1} (s)
Γ_-	0.19×10^{-9}	4.37	0.32×10^{-9}	2.72	0.70×10^{-9}	1.22	0.31×10^{-9}	3.32
Γ_z	0.13×10^{-9}	6.42	0.17×10^{-10}	52.75	0.20×10^{-10}	44.18	0.16×10^{-10}	62.23
Γ_+	0.59×10^{-9}	1.46	0.22×10^{-7}	0.04	0.11×10^{-8}	0.80	0.26×10^{-9}	3.95
		Av. 4.08		Av. 18.50		Av. 15.40		Av. 23.16

	9H-purine 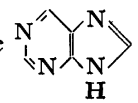		adenine 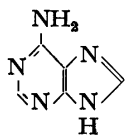		guanine 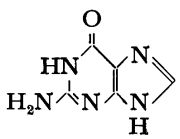	
spin state	$f_{T_1\to G}$	τ_{T_1} (s)	$f_{T_1\to G}$	τ_{T_1} (s)	$f_{T_1\to G}$	τ_{T_1} (s)
Γ_-	0.35×10^{-8}	0.27	0.24×10^{-8}	0.36	0.33×10^{-8}	0.25
Γ_z	0.25×10^{-8}	0.38	0.38×10^{-9}	2.28	0.10×10^{-8}	0.83
Γ_+	0.62×10^{-9}	1.53	0.11×10^{-8}	0.81	0.62×10^{-8}	0.14
		Av. 0.73		Av. 1.15		Av. 0.40

parameters in the spin-orbit Hamiltonian (H_{SO}), which represent the effective electric field acting on the electron, were adopted from the atomic data;[9] 28 cm^{-1} for C, 70 cm^{-1} for N, and 152 cm^{-1} for O. The perturbation calculations were done by mixing the lowest 25 excited states.

The calculated results on the oscillator strength of the S–T transition and radiative lifetime of the lowest triplets are given in Table 1. The average value of the calculated lifetimes of the triplet components is largest in thymine. Admitting that the radiative lifetime does not necessarily play an important role in the photodimerization reaction, which proceeds under severe steric restrictions, this finding is of interest because thymine in irradiated nucleic acids undergoes an efficient dimerization. A low-temperature experiment at 77 K indicates that the lifetimes of the phosphorescence of adenine and guanine residues are 2.5 and 1.25 s respectively.[10] In this case, the agreement between the predicted and experimental data is considerably good. On the whole, this calculation shows that the radiative lifetimes of the triplet pyrimidine bases are rather longer than those of the triplet purine bases.

The numerical calculation was performed using a HITAC 5020–E and 8800/8700 Computers at the University of Tokyo. The authors wish to thank Dr. Fumihiko Hirota of Shizuoka University for his useful discussion and advice.

References

1) A. A. Lamola and J. P. Mittal, *Science*, **154**, 1560 (1966).
2) J. G. Burr, *Advan. Photochem.*, **6**, 193 (1968).
3) I. H. Brown and H. E. Johns, *Photochem. Photobiol.*, **8**, 273 (1970).
4) J. Eisinger and R. G. Shulman, *Science*, **161**, 1311 (1968).
5) G. J. Fisher and H. E. Johns, *Photochem. Photobiol.*, **11**, 429 (1970).
6) C. Nagata, A. Imamura, Y. Tagashira, M. Kodama, and F. Fukuda, *J. Theoret. Biol.*, **9**, 357 (1965); A. Pullman, "Proceedings of the International Symposium on the Triplet State, Beirut," ed. by A. B. Zahlan, Cambridge University Press (1967), p. 515.
7) R. L. Ellis, R. Squire, and H. H. Jaffe, *J. Chem. Phys.*, **55**, 3499 (1971).
8) K. Ohno, *Theoret. Chim. Acta*, **2**, 219 (1964).
9) E. U. Condon and G. H. Shortley, "Theory of Atomic Specta," Cambridge University Press (1935).
10) M. Gueron, R. G. Shulman, and J. Eisinger, "Proceedings of the International Symposium on the Triplet State, Beirut," ed. by A. B. Zahlan, Cambridge University Press (1967), p. 505.

BULLETIN OF THE CHEMICAL SOCIETY OF JAPAN, VOL. 47 (11), 2873—2874 (1974)

Charge-transfer and Proton-transfer in the Formation of Molecular Complexes. X.[1] Picric Acid Complexes with 2,5-Dichloroaniline

Yoshio MATSUNAGA, Gunzi SAITO,* and Naoto SAKAI

Department of Chemistry, Faculty of Science, Hokkaido University, Sapporo 060

(Received April 13, 1974)

Synopsis. Yellow 2,5-dichloroanilinium picrate was found to isomerize into a red complex of the charge-transfer type at 74 °C with a heat of transition of 4.2 kcal/mol. In addition, a charge-transfer complex with a 1: 3 mole ratio was isolated.

Previously we demonstrated that the picrates of all the anilines with pK_a values of less than 3 isomerize into charge-transfer complexes upon melting if not by an enantiotropic transition.[2] Moreover, the chance of finding complex isomers was recognized to be high in the salts derived from *o*-haloanilines.[1,3] The combinations reported to date include picric acid with *o*-bromo- and *o*-iodo-anilines found by Hertel,[4] and methylpicric acid with *o*-chloro- and *o*-bromo-anilines and trinitrobenzoic acid with *o*-chloroaniline, both found by us.[1,3] As 2,5-dichloroaniline has a pK_a value in the above-mentioned range (that is, 1.57),[5] and as its structure fits into the group of *o*-haloanilines, there is a possibility that its picrate exhibits the phenomenon of complex isomerism. However, it must be added that an isomeric amine, 2,4-dichloroaniline, has been known to form only a salt with picric acid.[4]

When equimolar amounts of the component compounds separately dissolved in hot methanol were mixed, yellow fine crystals were precipitated. The composition appeared to be 1: 1. Calcd for $C_6H_5NCl_2 \cdot C_6H_3N_3O_7$: C, 36.85; H, 2.06; N, 14.32; Cl, 18.13%. Found: C, 36.68; H, 1.99; N, 14.38; Cl, 17.40%. The product is a true phenolate, as is indicated by the presence of the vibrational pattern characteristic of the anilinium ion extending from 2400 to 3000 cm^{-1}. A color change to red was observed at 74 °C. The isomerization into a complex of the charge-transfer type was confirmed by the replacement of the above-mentioned NH_3^+ pattern by the NH_2 bands appearing at 3375 and 3475 cm^{-1}, and also by the change in the electronic spectrum (see Fig. 1). The maximum of the newly-appeared absorption is located close to that of the charge-transfer absorption in the corresponding *s*-trinitrobenzene complex. Nevertheless, the picric acid complex is more deeply colored than the *s*-trinitrobenzene complex, mainly because of the difference in breadth. The heat of transition was estimated to be about 4.2 kcal/mol by use of a differential scanning calorimeter.

When chloroform was employed as the solvent and the mixture was kept in a refrigerator for a few days, the initially-appearing yellow crystals were replaced by red ones. This complex is of a 1: 3 mole ratio and can be kept at room temperature without any noticeable change. Calcd for $C_6H_5NCl_2 \cdot 3C_6H_3N_3O_7$: C, 33.94; H, 1.66; N, 16.49; Cl, 8.35%. Found: C, 33.34; H, 1.50; N, 16.62; Cl, 7.79%. The NH_2 pattern in the vibrational spectrum demonstrates the absence of proton-transfer. As is shown in Fig. 1, the electronic absorption in the visible region is relatively weak if compared with that in the red 1: 1 complex, but the location is essentially the same as that in the latter. Therefore, this 1: 3 complex is undoubtedly

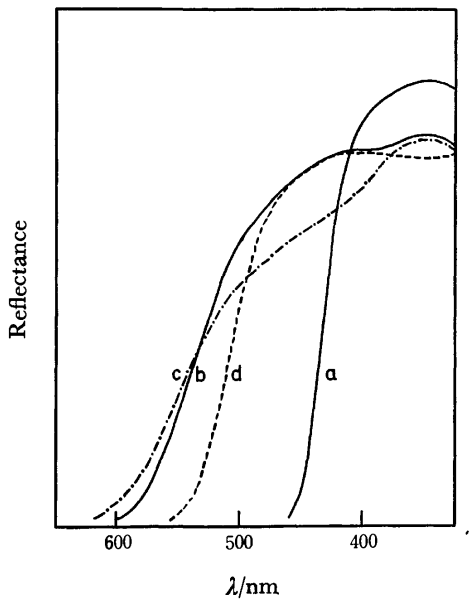

Fig. 1. Reflectance spectra of 2,5-dichloroaniline–picric acid; (a) the yellow 1: 1 salt, (b) the red 1: 1 complex, and (c) the red 1: 3 complex, and (d) the spectrum of the corresponding *s*-trinitrobenzene complex.

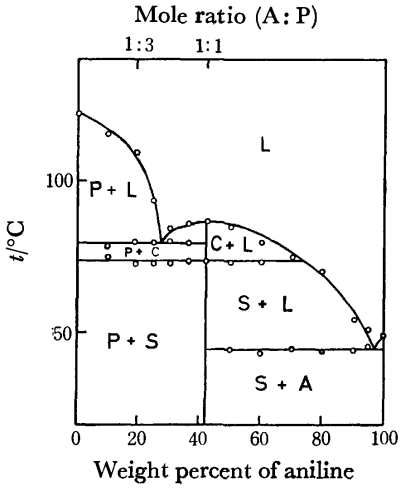

Fig. 2. The 2,5-dichloroaniline–picric acid phase diagram.

* Present address: Department of Chemistry, Emory University, Atlanta, Georgia 30322, U.S.A.

of the charge-transfer type. An endothermic peak of about 4.8 kcal/mol was recorded at 69 °C in the thermogram. Once heated above this temperature, the color turns yellow after storage at room temperature for a few days.

The phase diagram of the 2,5-dichloroaniline–picric acid system was prepared by the calorimetric method in an effort to find out whether or not there is salt with a 1:3 composition. The results presented in Fig. 2 clearly indicate that the 1:1 salt and its isomeric complex of the charge-transfer type are the only compounds formed between picric acid and 2,5-dichloroaniline by direct fusion. At the composition of the red 1:3 complex, the room-temperature phase was a mixture of the 1:1 salt and picric acid. The eutectic point at which the 1:1 complex (C in Fig. 2) and picric acid (P) coexist with liquid (L) was found at 80 °C and at about a 27 weight percentage of aniline, and that at which the 1:1 salt (S) and aniline (A) coexist with liquid, at 45 °C and at a small weight percentage of the acid.

References

1) Part IX: Y. Matsunaga and R. Osawa, This Bulletin, **47**, 1589 (1974).
2) G. Saito and Y. Matsunaga, *ibid.*, **44**, 3328 (1971).
3) N. Inoue and Y. Matsunaga, *ibid.*, **46**, 3345 (1973).
4) E. Hertel, *Ann.*, **451**, 179 (1926).
5) M. Gillois and P. Rumpf, *Bull. Soc. Chim. France*, **1954**, 112.

BULLETIN OF THE CHEMICAL SOCIETY OF JAPAN, VOL. 47 (11), 2875—2876 (1974)

A Mössbauer Study of the Valence States of ^{119}Sn after the EC Decay of ^{119}Sb in Antimony and Tellurium Iodides

Fumitoshi AMBE and Shizuko AMBE

The Institute of Physical and Chemical Research, Wako-shi, Saitama 351

(Received May 2, 1974)

Synopsis. The ^{119}Sn-Mössbauer emission spectra of $^{119}SbI_3$ and $^{119m}TeI_4$ sources showed the formation of Sn(II) and Sn(IV) species after the EC decay of ^{119}Sb in the matrices.

The measurement of the Mössbauer emission spectra enables one to estimate the chemical species produced by nuclear decay in solids.[1] In previous papers,[2-4] we reported a series of studies of ^{119}Sn after the EC decay of ^{119}Sb in metals, oxides, and chalcogenides of antimony and tellurium. This paper will describe an extension of these studies to iodides.

The 38.0 hr ^{119}Sb populates the 23.8 keV Mössbauer level of ^{119}Sn by 100% EC decay. The resonant γ-rays emitted from the level provide useful information on the electronic state of the ^{119}Sn atoms in the solid after the decay. We measured the Mössbauer emission spectra of ^{119}Sn arising in antimony iodide labeled with ^{119}Sb and also those of ^{119}Sn produced by the successive EC decays of 4.7 day ^{119m}Te *via* ^{119}Sb in tellurium iodide.[5]

The procedures for producing the source nuclides and for preparing the ^{119}Sb metal and $^{119m}TeO_2$ were reported elsewhere.[4,6,7] The $^{119}SbI_3$ sources were prepared by reacting the ^{119}Sb metal powder with iodine in refluxing toluene. The product was purified by repeated sublimation in a vacuum at 145 °C, yielding the iodide in the orange modification. The $^{119m}TeI_4$ samples were obtained by evaporating a solution of $^{119m}TeO_2$ in concd hydriodic acid over P_2O_5, SiO_2, and CaO under reduced pressure. The residue was thoroughly ground and then dried over fresh P_2O_5, SiO_2, and CaO in a vacuum until a constant weight ($\pm$0.1%) was attained. The source materials were identified by the Debye-Scherrer patterns, while their purity was checked by the titrimetrical determination of the component elements.

The ^{119}Sn-Mössbauer emission spectra of the iodides were measured against a $BaSnO_3$ absorber (0.9 mg ^{119}Sn/cm^2) by means of a conventional spectrometer with a transducer operated in the constant acceleration mode. Both the source and absorber were maintained at the temperature of liquid nitrogen in a cryostat. The 23.8 keV γ-rays were detected with a 2 mm NaI scintillator through an 80 μm Pd critical absorber for Sn KX-rays. In the case of the $^{119m}TeI_4$ samples, the change in the spectra with the time was followed until a constant value was obtained for the Sn(II)-to-Sn(IV) line-intensity ratio, so that the contribution of the ^{119}Sb arising from ^{119m}Te during the preparation of the samples was eliminated. The data were processed on the FACOM 230—60 and 75 computers of the Institute.

Typical spectra obtained are given in Fig. 1. The Mössbauer parameters of the emission lines, as determined by least-squares fitting, are summarized in Table

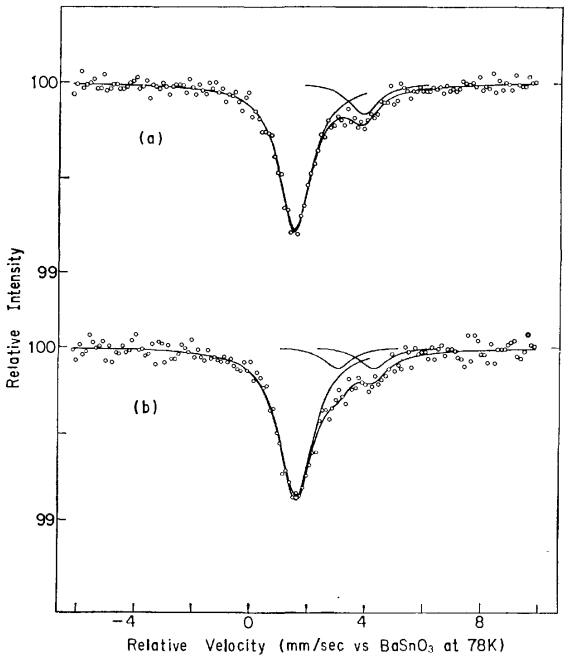

Fig. 1. ^{119}Sn-Mössbauer emission spectra of (a) $^{119}SbI_3$ and (b) $^{119m}TeI_4$ at 78 K against $BaSnO_3$ at 78 K. (In the abscissa a velocity of approach is taken negative.)

TABLE 1. MÖSSBAUER PARAMETERS OF THE EMISSION SPECTRA OF ^{119}Sn IN $^{119}SbI_3$ AND $^{119m}TeI_4$ AND OF THE ABSORPTION SPECTRA OF THE CORRESPONDING TIN IODIDES AT LIQUID NITROGEN TEMPERATURE

Source materials	Emission lines (this work)			Absorption lines (from the literature)			
	Isomer shift[a] (mm/s)	Quadrupole splitting (mm/s)	Assigned valence	Corresponding tin compounds	Isomer shift[b] (mm/s)	Quadrupole splitting (mm/s)	Ref.
$^{119}SbI_3$	1.50±0.05	—	Sn(IV)	SnI_4	1.55	—	8
	3.9 ±0.2	—	Sn(II)	SnI_2	3.88	—	9
$^{119m}TeI_4$	1.56±0.05	—	Sn(IV)	(see above)			
	3.5 ±0.3	1.4±0.3	Sn(II)	(see above)			

a) Relative to $BaSnO_3$ at 78 K. b) Relative to $BaSnO_3$.

1, together with the corresponding values of the absorption lines of tin iodides reported in the literature.[8,9]

As can be seen in Fig. 1(a), the emission spectra of ^{119}Sn arising in $^{119}SbI_3$ consisted of two lines, which can be attributed to the Sn(IV) and Sn(II) states by comparing their isomer shifts with those of tin iodides (Table 1). Similarly, the $^{119m}TeI_4$ sources gave emission lines in the Sn(IV) and Sn(II) regions. The computer fitting of the spectra with two Lorentzians resulted in a broad Sn(II) line accompanying the dominant Sn(IV) line. The further decomposition of the Sn(II) line into a symmetric doublet gave a quadrupole splitting value of 1.4 mm/s, as is shown in Fig. 1(b) and Table 1, giving rise to an improvement in the χ^2 value by 1.6%.

Since the EC decay is accompanied by a change in the atomic number, the ^{119}Sn atoms arising in the source materials must inevitably be in defect states associated with the local disturbance of the crystal lattice. The recoil energy accompanying the decay of ^{119}Sb is estimated to be much smaller than the threshold energy required to displace an atom from its normal lattice site, while the recoil energy of the EC decay of ^{119m}Te to ^{119}Sb is of the same order of magnitude as the displacement energy.

In SbI_3, each Sb is at the center of a nearly perfect octahedron of iodine atoms.[10] Therefore, the ^{119}Sn-(IV) atoms arising in $^{119}SbI_3$ may be expected to be in an electronic configuration different from that of SnI_4, in which tin atoms are surrounded by a practically regular tetrahedron of iodine atoms.[10] However, no significant difference was found between the isomer shift of the Sn(IV) emission line of $^{119}SbI_3$ and that of the absorption line of SnI_4. Similarly, the isomer shift of the Sn(II) emission line is essentially identical with that of SnI_2. The crystal structure of TeI_4 seems not to have been determined yet. The powder X-ray diffraction pattern and the ^{125}Te-Mössbauer absorption spectrum of TeI_4[11] show that its structure is different from that of SnI_4, the site symmetry of the Te atom not being cubic. However, no significant difference was found between the isomer shift of the Sn(IV) emission line of $^{119m}TeI_4$ and that of SnI_4. The quadrupole splitting observed for the Sn(II) line of the $^{119m}TeI_4$ source is the only parameter found for the emission lines that is different from the corresponding value of the absorption line. SnI_2 has a monoclinic structure consisting of infinite $(SnI_3)_\infty^{n-}$ trigonal prisms, the coordination number of the tin atoms being seven.[12] The Mössbauer absorption spectrum of SnI_2, however, shows no resolvable quadrupole splitting.[9] The large quadrupole splitting of the Sn(II) emission line of $^{119m}TeI_4$ suggests a much more distorted configuration of iodine ligands around the defect ^{119}Sn atom in the TeI_4 matrix.

It is interesting to compare the present results on iodides with those on oxides and chalcogenides reported previously.[4] In the series of antimony chalcogenides, the fraction of Sn(II) increased with the decrease in the electronegativity of the chalcogen ligand. The distribution ratio of ^{119}Sn between the Sn(II) and Sn(IV) states in $^{119}SbI_3$ is closer to that of $^{119}Sb_2S_3$ than to that of $^{119}Sb_2Te_3$. This corresponds to the fact that the electronegativity of iodine is close to that of sulfur. The finding that the ^{119}Sn atoms were distributed between the Sn(II) and Sn(IV) states in $^{119m}TeI_4$ presents an interesting contrast with the result for $^{119m}TeO_2$, for which no Sn(II) species was observed. In $^{119m}TeO_2$, the similarity of the crystal structures of TeO_2 and SnO_2 is considered to exclude the stabilization of ^{119}Sn as Sn(II). The absence of such an effect in TeI_4 as well as the lower electronegativity of iodine may have allowed the stabilization of a part of ^{119}Sn as Sn(II).

We thank Prof. N. Saito for his interest and continual encouragement. We are grateful to the staff of IPCR cyclotron for irradiations and to Mr. Y. Iimura for powder X-ray pattern measurements.

References

1) G. K. Wertheim, "The Electronic Structure of Point Defects," ed. by S. Amelinckx, R. Gevers, and J. Nihoul, North-Holland Publishers, Amsterdam (1971), p. 1.

2) F. Ambe, H. Shoji, S. Ambe, M. Takeda, and N. Saito, *Chem. Phys. Lett.*, **14**, 522 (1972).

3) F. Ambe and S. Ambe, *Phys. Lett.*, **43A**, 399 (1973).

4) F. Ambe, S. Ambe, H. Shoji, and N. Saito, *J. Chem. Phys.*, **60**, 3773 (1974).

5) Similar experiments on $^{119}SbI_3$ have recently been carried out by Y. Llabador (Private communication from Prof. J. P. Adloff to Prof. N. Saito).

6) F. Ambe, S. Ambe, and H. Shoji, *Radiochem. Radioanal. Lett.*, **15**, 349 (1973).

7) S. Ambe, F. Ambe, and N. Saito, *Radiochim. Acta*, **19**, 121 (1973).

8) S. Bukshpan and R. H. Herber, *J. Chem. Phys.*, **46**, 3375 (1967).

9) N. N. Greenwood and A. Timnick, *J. Chem. Soc. A*, **1971**, 676.

10) R. W. G. Wyckoff, "Crystal Structures," Vol. 2, Interscience Publishers, New York (1965), pp. 45, 131.

11) P. Jung and W. Triftshäuser, *Phys. Rev.*, **175**, 512 (1968).

12) W. Moser and I. C. Trevena, *Chem. Commun.*, **1969**, 25.

BULLETIN OF THE CHEMICAL SOCIETY OF JAPAN, VOL. 47 (11), 2877—2878 (1974)

Heat of Evaporation of Polyoxyethylene Dodecyl Ethers

Masao NAKAMURA, Kazuo EDA, and Kiiti KOSIYAMA

Department of Chemistry, Faculty of Science, Tokai University, Hiratsuka, Kanagawa 259-12

(Received May 15, 1974)

Synopsis. The heat of evaporation has been measured by the vapor pressure method for polyoxyethylene dodecyl ethers, $C_{12}H_{25}(OC_2H_4)_nOH$ (n=0, 1, 2, 3, and 4). It has been deduced that the polyoxyethylene chain is in a cyclic state in the vapor phase due to the intramolecular hydrogen bonding of the terminal OH group with an oxygen atom in the chain.

Measurements of heat of solution have been carried out for the study of the dissolved state of surfactant in solution.[1-4] In order to deduce the dissolved state energetically from the heat of solution, we should know the intermolecular cohesive energy of the solute in a pure liquid or solid state. The measurement of heat of evaporation is useful for obtaining the cohesive energy of a pure liquid, since cohesion in the vapor phase is negligible below the normal pressure. We have tried to obtain the relation between the heat of evaporation and degree of polymerization of the polyoxyethylene chain in polyoxyethylene dodecyl ethers, typical nonionic surfactants.

Polyoxyethylene dodecyl ethers, $C_{12}H_{25}(OC_2H_4)_nOH$ (n=0, 1, 2, 3, and 4), were obtained from Nippon Surfactant Industry Co., dodecanol corresponding to n=0. Each sample has a purity above 99% and no distribution of polymerization in the hydrophilic part as verified by gas chromatography.

The heat of evaporation was obtained by the vapor pressure method. The apparatus used was a glass semimicrodistiller (Shibata Glass Co.) with a large gas tank inserted in the vacuum line between the distiller and the pump to eliminate the fluctuation of pressure in the apparatus. The pressure was kept constant, the liquid in the bottle was heated gently with an electric heater, and the temperature was recorded in both vapor and liquid phases. The temperature of liquid phase had slowly risen, several hours after which that of vapor phase rose steeply and remained at a certain temperature. The constant temperature of vapor phase was regarded to be the boiling point corresponding to the pressure.

The results obtained in the pressure range 2—30 Torr are shown in Fig. 1 for polyoxyethylene dodecyl ethers of the degree of polymerization n up to 4 and dodecane. For dodecanol (n=0) and dodecane, the observed values (open circle) agree well with the values in the literature (filled circle).[5] If the molar volume of the liquid phase is neglected in comparison with that of the vapor, and if the vapor phase is assumed to behave as a perfect gas and the molar heat of evaporation $\Delta_e h$ is independent of temperature, then the equation of Clausius-Clapeyron can be written as[6]

$$\ln p = -\frac{\Delta_e h}{RT} + C \qquad (1)$$

where p is the vapor pressure at the absolute temperature T, R the gas constant, and C a constant independent of temperature. The fact that the plots of $\log p$ *vs.* $1/T$ (Fig. 1) lie in a straight line for every sample indicates that the molar heat of evaporation is independent of temperature in the range of measure-

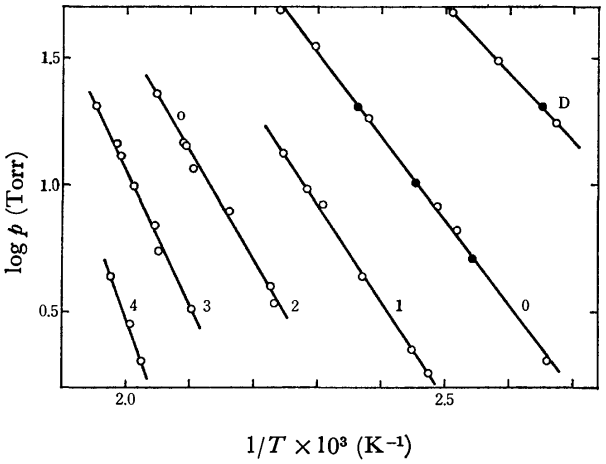

Fig. 1. The variation of vapor pressure with temperature for $C_{12}H_{25}(OC_2H_4)_nOH$ (n=0—4) and dodecane (D).

TABLE 1. MOLAR HEATS OF EVAPORATION ($\Delta_e h$) OF $C_{12}H_{25}(OC_2H_4)_nOH$ (n=0—4) AND DODECANE (D)

n	$\Delta_e h$ (kcal/mol)
0	15.1
1	17.7
2	19.7
3	25.3
4	31.0
D	12.7

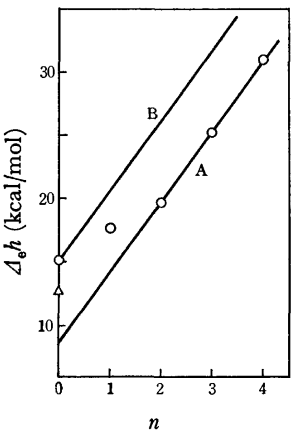

Fig. 2. The relationship between molar heat of evaporation ($\Delta_e h$) and degree of polymerization of $C_{12}H_{25}(OC_2H_4)_nOH$.
△: the value of dodecane

ments.

The molar heats of evaporation obtained from the inclinations of the straight lines are listed in Table 1. The relationship between the molar heat of evaporation $\Delta_e h$ and the degree of polymerization n of the polyoxyethylene chain is shown in Fig. 2. $\Delta_e h$ increases linearly with n in the range 2—4, as shown by the straight line A. Its inclination gives 5.6 kcal/mol of an oxyethylene unit, which corresponds roughly to the molar heat of evaporation of dimethyl ether, 5.1 kcal/mol.[7] This means that the situation does not differ among the molecules in the range, except in the number of oxyethylene units. The extrapolated value of line A to $n=0$, however, is less than the molar heat of evaporation of the dodecanol, which corresponds to $n=0$, by *ca.* 6.6 kcal/mol. This means that the terminal OH groups of polyoxyethylene chain is not in the same state as in the alcoholic OH group. The terminal OH group may be considered to be intramolecular hydrogen bonded with an oxygen atom in the polyoxyethylene chain in the vapor phase, because the exothermic 6.6 kcal/mol corresponds to the energy of a hydrogen bond.[8] It may be reasonable to consider that the polyoxyethylene chain in the liquid state is in a linearly extended state, because it is more probable for the terminal OH group to interact with the neighboring molecule, and the extrapolated value is less than the molar heat of evaporation of dodecane (triangle in Fig. 2).

The molar heat of evaporation of $n=1$ is higher than line A by *ca.* 3.5 kcal/mol, which can be interpreted by the loss of energy of the intramolecular hydrogen bond since the molecule can form a 5-membered ring only. The fact also confirms the concept that the polyoxyethylene chain is cyclic in the vapor phase owing to the intramolecular hydrogen bonding.

If a molecule were to be linearly extended with no intramolecular hydrogen bond as in the liquid phase, the value of $\Delta_e h$ would fall on a straight line B parallel to line A and pass through the value of dodecanol. Thus, the molar cohesive energies of these liquids are equal to the values corresponding to line B minus RT, which is the work of volume expansion at the evaporation of 1 mol of liquid.

References

1) E. Hutchinson, K. E. Manchester, and L. Winslow, *J. Phys. Chem.*, **58**, 1124 (1954).

2) E. D. Goddard, C. A. Hoeve, and G. C. Benson, *ibid.*, **61**, 593 (1957).

3) L. Benjamin, *ibid.*, **68**, 3575 (1964).

4) K. Shinoda, S. Hiruta, and K. Amaya, *J. Colloid Sci.*, **21**, 102 (1966).

5) Nipponkagakukai, "Kagakubenran (Kisohen II)," Maruzen, Tokyo (1966), p. 581.

6) I. Prigogine, R. Defay, and D. H. Everett, "Chemical Thermodynamics," Longmans Green, London (1952), p. 193.

7) Ref. 5, p. 758.

8) G. C. Pimentel and A. L. McClellen, "The Hydrogen Bond," Freeman, San Francisco (1960).

BULLETIN OF THE CHEMICAL SOCIETY OF JAPAN, VOL. 47 (11), 2879—2880 (1974)

The Dipole Moment of Benzaldehyde

Yoshiyuki KAWASHIMA* and Kunio KOZIMA**

Laboratory of Molecular Spectroscopy, Tokyo Institute of Technology, O-okayama, Meguro-ku, Tokyo 152

(Received May 17, 1974)

Synopsis. The dipole moment and its components along the principal axes were determined by measuring the Stark effects of the rotational transitions. The most probable direction of the moment was discussed.

The microwave spectra of benzaldehyde in the ground and in the excited torsional states have been studied in detail by Kakar *et al.*,[1] especially with regard to the barrier to internal rotation of the aldehyde group. However, its electric dipole moment has not yet been determined by using the spectrum. By the dielectric constant measurements, various values of the moment, ranging from 2.72[2] to 3.03 D,[3] have been obtained in various nonpolar solvents. Therefore, it seemed that it would be interesting to determine the value by means of the Stark effect of the spectrum and to ascertain the orientations of the components of the moment.

Experimental

The microwave spectrum and its Stark effect were measured by using a conventional 100-kHz square-wave Stark modulation spectrometer. The measurements were made at room temperature by using a 3-m absorption cell.

The sample of benzaldehyde, obtained from a commercial source, was purified by distillation *in vacuo* (bp 66—67 °C/12 mmHg).

Results and Discussion

Kakar *et al.*[1] have reported the frequencies of the high J R- and Q-branch transitions, from which they determined the rotational constants. Since lower J transitions are adequate for determining the value of the dipole moment, we searched for the rotational lines of the transitions of $J=4\leftarrow3$. As are shown in Table 1, the transition frequencies for the ground vibrational state could be observed at almost the same values as these calculated from the known rotational constants.[1] These assignments were ascertained by means of their Stark displacements. It is certain that the rotational constants are not affected by the centrifugal distortion.

TABLE 1. OBSERVED AND CALCULATED FREQUENCIES OF THE $J=4\leftarrow3$ TRANSITIONS IN THE GROUND VIBRATIONAL STATE[a)]

Transition	ν_{obsd}(MHz)	ν_{calcd}(MHz)
$4_{04}\leftarrow3_{03}$	10831.41	10831.42
$4_{13}\leftarrow3_{12}$	11741.06	11741.11
$4_{13}\leftarrow3_{13}$	10309.46	10309.54

a) Maximum uncertainty of the observed values is ±0.10 MHz.

TABLE 2. STARK EFFECT AND DIPOLE MOMENT OF BENZALDEHYDE[a)]

Transition		Shift MHz (kV/cm)$^{-2}$ Obsd	Calcd
$4_{04}\leftarrow3_{03}$	$M=1$	−4.37±0.11	−4.32
	$M=2$	9.96±0.10	10.28
$4_{13}\leftarrow3_{12}$	$M=1$	3.02±0.08	2.83
$4_{14}\leftarrow3_{13}$	$M=0$	−6.14±0.11	−6.17
	$M=2$	28.26±0.47	28.17

$\mu_a=2.96_6\pm0.02_7$ D; $\mu_b=1.23_9\pm0.02_8$ D

$\mu_{total}=3.21_4\pm0.03_7$ D

$\theta=\tan^{-1}(\mu_b/\mu_a)=22.67\pm0.72°$

a) Electric-field calibration was made with OCS for which $\mu=0.7152$ D.

By using the transitions shown above, the components of the dipole moment for the ground vibrational state were determined from the second-order Stark effect. The values thus obtained are shown in Table 2, together with the observed and calculated Stark coefficients. The symbols used have their usual meanings. The obtained value of the total dipole moment is higher than those obtained by dielectric constant measurements in various solutions. Of the various values obtained in solutions, the value of 3.03 D in cyclohexane and that of 3.02 D in benzene obtained by Jones *et al.*[3] may be considered to be most plausible.

The principal axes, the a- and b-axes, for this planar molecule, as determined from the molecular parameters reported,[1] are shown in Fig. 1. It is reasonable to consider that the negative end of the C=O bond moment points toward the oxygen atom and that the total dipole moment is mainly due to the C=O bond moment.

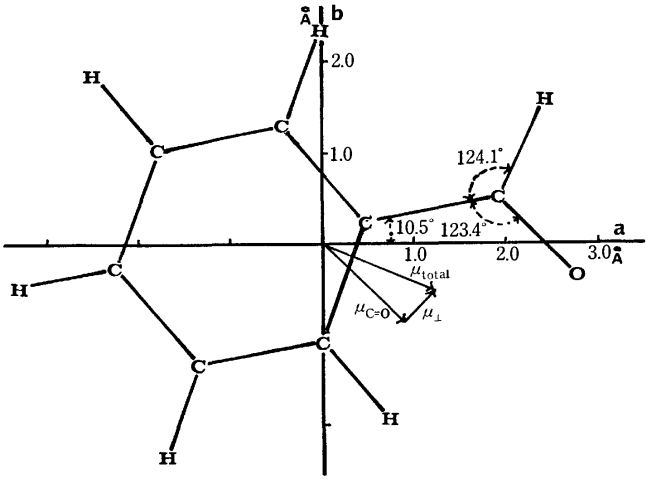

Fig. 1. The principal axes and the direction of the dipole moment of benzaldehyde.

* Present address: Faculty of Science and Engineering, Chuo University, Kasuga 1-chome, Bunkyo-ku, Tokyo 112.

** To whom correspondence should be addressed.

Therefore, of the four possible directions of the total dipole moment, the direction of μ_{total} indicated in Fig. 1 by an arrow is the most probable, for this direction makes the smallest angle of 23.4° with the direction of the C=O bond moment. The direction of μ_{total} makes an angle of 33.2° with the bond joining the carbon atom of the aldehyde group with the carbon atom of the benzene ring. This value is very close to that of 34.6° estimated for the same angle from the value of the dipole moment of the dichloro-derivative.[3] Therefore, the $\mu_{C=O}$ component of the dipole moment parallel to the C=O bond is calculated to be 2.95 D and the $\mu_{\perp}$ component of the dipole moment perpendicular to $\mu_{C=O}$ is 1.28 D. The value of $\mu_{\perp}$ may be due to the inductive effect of the moment of $\mu_{C=O}$ and to the partial migration of the π-electrons of the benzene ring to the C=O bond.

References

1) R. K. Kakar, E. A. Rinehart, C. R. Quade, and T. Kojima, *J. Chem. Phys.*, **52**, 3803 (1970).
2) J. W. Williams, *J. Amer. Chem. Soc.*, **50**, 2350 (1928).
3) R. A. Y. Jones, A. R. Katritzky, and A. V. Ochkin, *J. Chem. Soc., B*, **1971**, 1795.

BULLETIN OF THE CHEMICAL SOCIETY OF JAPAN, VOL. 47 (11), 2881—2882 (1974)

The ESR of Alkyl Phenyl Nitroxide Radicals Studied as Hindered Rotation

Toshio NISHIKAWA and Kazuo SOMENO

National Chemical Laboratory for Industry, Honmachi, Shibuya-ku, Tokyo 151

(Received May 24, 1974)

Synopsis. The ESR spectra were obtained in the series of *N*-methyl, *N*-ethyl, *N*-*n*-propyl, *N*-isopropyl, *N*-*n*-butyl, and *N*-*tert*-butyl phenyl nitroxide radicals. Two tendencies were found in the hyperfine splitting constants and were explained as hindered rotation.

In *N*-alkyl phenyl nitroxide (*N*-alkyl PNO-) radicals, the ESR spectra would be affected because of the hindered motion with respect to the substituted alkyl group. In these radicals, there may exist the two kinds of hindered rotation, about the σ bond between nitrogen and alkyl carbon and about the π bond between nitrogen and phenyl carbon. It is an interesting question whether the hindered-rotation model is applicable to these rather large molecules.

The hyperfine splitting constants were obtained in the series of *N*-methyl, *N*-ethyl, *N*-*n*-propyl, *N*-isopropyl, *N*-*n*-butyl, and *N*-*tert*-butyl PNO radicals. From these data, two tendencies were apparent for a change of the hyperfine splitting constants; we discussed them as hindered rotation and compared our results with Stone and Maki's calculations.[2]

Experimental

N-Alkyl PNO radicals were prepared by the oxidation of the corresponding *N*-alkyl-substituted aniline or *N*,*N*-di-alkyl-substituted aniline by perbenzoic acid. For obtaining *N*-alkyl-substituted PNO, care should be taken with regard to the quantity of oxidizing agent, since an excess of perbenzoic acid produces unsubstituted PNO, which is more stable. The ESR measurements were done in an about 10^{-3} mol/l toluene solution.

Results and Discussion

The observed hyperfine splitting constants are shown in Table 1. Two tendencies can be seen from Table 1:

(A) The hyperfine splitting constants of nitrogen (a_N), the *o*- and *p*-protons ($a_{H(o,p)}$) and the *m*-proton ($a_{H(m)}$) are almost all equal except that of *N*-*tert*-butyl PNO, in which a_N is larger and $a_{H(o,p)}$ is smaller.

(B) The hyperfine splitting constants of alkylprotons ($a_{H(CH_3)}$, $a_{H(CH_2)}$, and $a_{H(CH)}$) may be classified into three groups, according to the number of protons.

Table 1. Observed hyperfine splitting constants for *N*-alkyl PNO (in G)

Alkyl	Methyl	Ethyl	*n*-Propyl	*i*-Propyl	*n*-Butyl	*t*-Butyl
a_N	10.65	10.42	10.31	10.65	10.36	12.44
$a_{H(CH_3)}$	9.69					
$a_{H(CH_2)}$		7.84	7.34		7.28	
$a_{H(CH)}$				3.47		
$a_{H(o,p)}$	2.75	2.80	2.58	2.69	2.74	1.90
$a_{H(m)}$	1.01	1.01	0.90	0.90	1.00	0.90

Table 2. Calculated spin densities for PNO and *N*-alkyl PNO

Position	PNO	*N*-Alkyl PNO
N	0.4425	0.4770
O	0.3272	0.3074
1	−0.0353	−0.0474
2	0.1298	0.1313
3	−0.0592	−0.0603
4	0.1246	0.1210

In MO Parameters, such as

$\alpha_N=\alpha_C+h_N\beta_{CC}$

$\beta_{NO}=k_{NO}\beta_{CC}$

and so on, the following values are used,

$h_N=1.5$ for PNO

$h_N=1.4$ for *N*-alkyl PNO

$h_O=1.3$, $k_{NO}=0.7$

$h_1=1.0$, $k_{N1}=1.0$

The data might be considered to reflect the unpaired spin distribution, arising from two types of hindered rotation.

The tendency (A) seems to suggest that the spin densities on the aromatic-ring carbons are constant independent of the kind of substituted alkyl group, except in the case of *N*-*tert*-butyl PNO.

For the purpose of further discussion, McLachlan's spin-density calculation was carried out with substituted and unsubstituted PNO radicals, as is shown in Table 2.

According to our previous calculations on unsubstituted PNO,[1] an alkyl substitution was treated as the inductive effect on the nitrogen atom as follows:

$$\alpha_{N'} = \alpha_N + h\beta_{CC} \quad (1)$$

while the other MO parameters were taken as having the same values.

On the assumptions that $h=-0.1$, which may be considered acceptable in these cases, and that the same relationship held:

$$\left.\begin{aligned} &a_N = Q_1\rho_N + Q_2\rho_O \\ &a_{H(o)} = Q\rho_2, \quad a_{H(p)} = Q\rho_4 \\ &\text{where } Q_1 = 30.5, \quad Q_2 = -13.6 \\ &\qquad Q = -22.5 \end{aligned}\right\} \quad (2)$$

the splitting constants, a_N, $a_{H(o)}$, and $a_{H(p)}$, were calculated to be 10.37, 2.95, and 2.72 G, respectively.

Thus, the planar structure for *N*-alkyl substitution, except in the case of the *N*-*tert*-butyl group, may be plausible, since the observed splitting constants can be explained by using the same parameters as in *N*-unsubstituted PNO. When the resonance integral between nitrogen and alkyl carbon is decreased, corre-

sponding to the twisting about the bond, the spin densities, ρ_N and ρ_O, are increased, and ρ_2, ρ_4, and ρ_6 are decreased; then the splitting constant, a_N becomes increased and $a_{H(\omega)}$ and $a_{H(o)}$ are decreased. This seems to imply non-planarity for *N-tert*-butyl PNO.

The (B) tendency was interpreted according to Stone and Maki's treatment[2] on the basis that the hindered rotation about the single bond may be assumed in these cases.

When the alkyl proton internally rotates about the equilibrium angle, θ_0, under the potential function:

$$V = \frac{1}{2}V_0(1-\cos 2\alpha) \tag{3}$$

the hyperfine splitting constants for the alkyl proton can be given as the function of the average value of the overlapping angle and the π-spin density of the adjacent nitrogen atom:

$$a_H = B\langle\cos^2\theta\rangle\rho_N \tag{4}$$

where:

$$\langle\cos^2\theta\rangle = \frac{\sum_i g_i\langle\cos^2\theta\rangle_i \exp(-E_i/kT)}{\sum_i g_i \exp(-E_i/kT)}$$

$$\langle\cos^2\theta\rangle_i = \langle\psi_i(\alpha)|\cos^2(\theta_0+\alpha)|\psi_i(\alpha)\rangle$$

The energy value, E_i, and the corresponding wave function, ψ_i, are calculated in the numerical solution of the Mathieu function for the given potential barrier and the moment of inertia.[3]

The above approximation may be considered to be possible, since the spin density on the nitrogen atom, ρ_N, may be regarded as constant independent of the kind of alkyl group, except in the case of *N-tert*-butyl PNO.

For *N*-methyl PNO, it may be considered that the methyl group freely rotates at room temperature. When $\langle\cos^2\theta\rangle$ is one half for free rotation and when $a_{H(CH_3)}$ is replaced by 9.69 G from Table 1, $B\rho_N$ is given as 19.38. When ρ_N is taken as 0.477 from Table 2, B is obtained as 40.8 G, which is close to the value of 41 ± 6 G in Stone and Maki's calculation. This may show that their method is well applicable to *N*-alkyl PNO radicals.

For *N*-ethyl, *N-n*-propyl, and *N-n*-butyl PNO, which have CH_2 protons, it is evident that the rotation may be restricted, since the observed splitting constants become smaller than that for *N*-methyl PNO. In the case of *N*-ethyl PNO, the splitting constant, $a_{H(CH_2)}$, was calculated as 7.82 G when the potential barrier V_0=0.78 kcal/mol, in contrast with the observed value of 7.84 G. Similarly, for *N-n*-propyl PNO, 7.40 G was obtained when V_0=1.40 kcal/mol.

For *N*-isopropyl PNO, which has a CH proton, 3.31 G was obtained as $a_{H(CH)}$ when V_0=2.30 kcal/mol.

Stone and Maki reported in their paper that the potential barriers are 0.34 and 1.11 kcal/mol for CH_2 and CH protons of nitroalkane radicals respectively. The fact that the ratios of the potential barrier with CH to CH_2 are similar between the present data and theirs (3 and 3.3) suggests a resemblance of the hindered rotational models. The larger values in the present case may result from the increase in steric hindrance and the stabilization of π-conjugation due to the aromatic ring.

For a more detailed discussion, it will be necessary to consider the validity of the 2-fold symmetry or to evaluate the non-bonded interaction; those may be difficult problems.

References

1) O. Kikuchi and K. Someno, This Bulletin, **40**, 2549 (1967).

2) E. Stone and A. Maki, *J. Chem. Phys.*, **37**, 1326 (1962).

3) T. Nishikawa, K. Someno, and M. Kaise, Abstract of the 10th ESR Symposium, the Chemical Society of Japan, (1971), p. 6.

BULLETIN OF THE CHEMICAL SOCIETY OF JAPAN, VOL. 47 (11), 2883—2884 (1974)

Field Ionization of Highly-excited Helium and Hydrogen Atoms Produced by Electron Impact

Takemasa SHIBATA, Tsutomu FUKUYAMA, and Kozo KUCHITSU

Department of Chemistry, Faculty of Science, The University of Tokyo, Hongo, Bunkyo-ku, Tokyo 113

(Received June 26, 1974)

Synopsis. The ionization of long-lived highly-excited helium atoms produced by electron impact was observed using an electrostatic field up to 8.3 kV/cm; the decrease of the He^+ intensity produced by collisions of He** with H_2O was measured as a function of the field strength using a mass filter. By use of the theory of Bailey *et al.*, the principal quantum numbers of the highly excited He were estimated to range from 16 to 40. A similar but slower decrease of H^+ due to H** atoms produced by electron impact on H_2O was also observed.

In previous papers[1,2] by the authors long-lived excited states of helium, He* (2^1S and 2^3S) and He** (in the highly-excited states) were produced by electron impact, and the ions formed by collisions with H_2O were detected by a mass filter. The observed ions, H^+, HeH^+, OH^+, and H_2O^+, which exhibited similar dependences on the target pressure and the electron accelerating voltage (with appearance potentials of about 20 eV), were assigned to be those produced by impact of He* on H_2O. On the other hand, another observed species, He^+, varied differently with the target pressure and the accelerating voltage (with an appearance potential of about 25 eV). It was then concluded that the He^+ ions were produced by collisions of He** with H_2O. In parallel with this observation, H^+ ions were observed when H_2O vapor was used in place of He, and their origin was interpreted to be due to highly-excited hydrogen atoms, H**, produced by electron impact dissociation of H_2O.

Various experiments[3-8] and theories[9,10] have shown that highly-excited atoms are ionized by a moderate electric field. For example, field ionization of highly-excited hydrogen atoms were observed by Riviere and Sweetman.[4] They derived an empirical relation for the smallest principal quantum number n of the states which can be ionized by a field of given strength, E_n. In their work, highly-excited hydrogen atoms with n=9—23 and with kinetic energies of 50 keV were produced by charge transfer collisions of protons with gas molecules. According to the calculations of Bailey *et al.*[10] on the ionization probability for hydrogen with n=1—25, E_n is a very slowly-varying function of the time spent by the atom in the field.[5]

The purpose of the present study is two-fold: (1) to confirm by means of field ionization that highly-excited states are in fact produced by electron impact and are involved in the above-mentioned processes, and (2) to estimate, even roughly, the range of their principal quantum numbers using the relationship between the field strength and the fraction of excited states ionized by the field.[8]

Experimental

The apparatus used in the present study was described in the previous paper.[1] A parallel-plate condenser (9 mm × 25 mm with a 3 mm spacing) was placed between the excitation region and collision chamber, as shown in Fig. 1. One of the plates was grounded, and the potential of the other plate was varied from 0 to −2.5 kV. The field strength was calculated from the potential applied to the electrodes divided by the spacing and was estimated to have an uncertainty of about 10%.

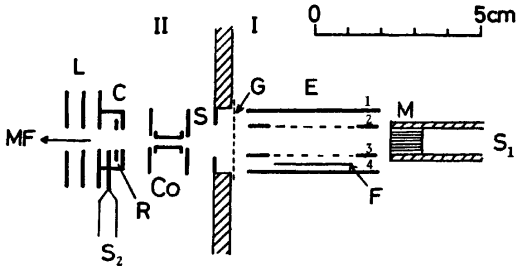

Fig. 1. Apparatus composed of section I for producing long-lived excited atoms by electron impact and section II, in which a parallel-plate condenser Co, a collision chamber C, and a mass filter MF are installed.

The helium gas was introduced into the excitation region through a multichannel orifice M and was subjected to electron impact. The He pressure at source S_1 was about 0.4 Torr. The accelerating voltage of the exciting electrons was about 100 V, and the trap current measured at electrode 1 was about 400 μA. The excited neutral species were separated from accompanying ions by electrostatic potentials and were allowed to collide with the H_2O target in the collision chamber C. The pressure of the target H_2O measured at source S_2 was about 0.3 Torr. The sample pressures were measured using oil manometers. The background pressure outside the collision chamber was about 2×10^{-6} Torr. Ions produced in the collision chamber were measured by a quadrupole mass filter.

Results and Discussion

In Fig. 2, the mass spectra observed with zero electric field (A) and with 0.75 kV applied to the condenser (B) are shown. The variations of the intensities of He^+ and H_2O^+ ions with electric field strength are shown in Fig. 3. The He^+ intensity was found to decrease monotonically with increasing field strength. This behavior can be interpreted as follows: A fraction of the highly-excited states He** are ionized by the field and do not enter the collision chamber. On the other hand, the H_2O^+ intensity did not depend on the electric field; this is because the He* metastable

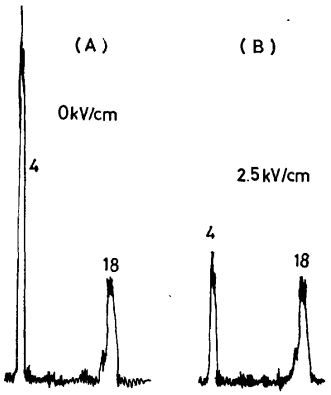

Fig. 2. Mass spectra of the ions produced by collisions of long-lived excited species of He with H_2O.

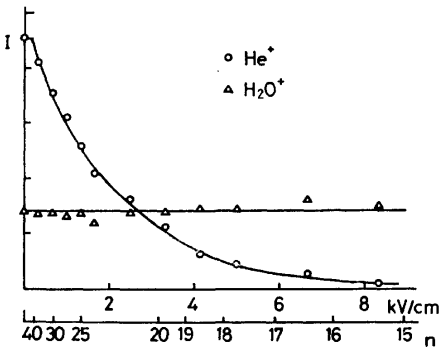

Fig. 3. Ion intensities (in arbitrary units) plotted as a function of electric field strength. The He^+ and H_2O^+ ions are produced by collisions of He** and He* respectively, with H_2O. The principal quantum numbers n which can be ionized by a given field strength are estimated and indicated on the abscissa.

states are not quenched in the range of field strengths applied here.[11] The latter observation also shows that the voltage applied to the condenser plates did not significantly disturb the field in the vicinity of the collision chamber so as to affect the efficiency of the detector.

The principal quantum numbers n which can be ionized by a given field strength E_n were estimated using the theoretical relationship between the lifetime and the electric field strength given by Bailey *et al.*[10] The estimates are indicated along the abscissa of Fig. 3. The correspondence between n and E_n is not unique, however, since the various different states with the same n have different threshold field strengths for ionization. The present estimate shown in Fig. 3 corresponds to the component of the lowest energy given by Bailey *et al.*[12] This choice is given support by the results of Il'in *et al.*;[5] the $n-E_n$ relation they observed in the range $17 \geq n \geq 14$ coincides with that for the lowest components calculated by Bailey *et al.*[10] Figure 3 provides an approximate range of the n values of He** present in the region between the condenser plates, $40 \gtrsim n \gtrsim 16$. Excited states with smaller n probably have lifetimes shorter than the time of flight (about 50 μs) from the excitation region to the electric field, while those with larger n are probably ionized in the excitation region or in its vicinity by a weak electric field.

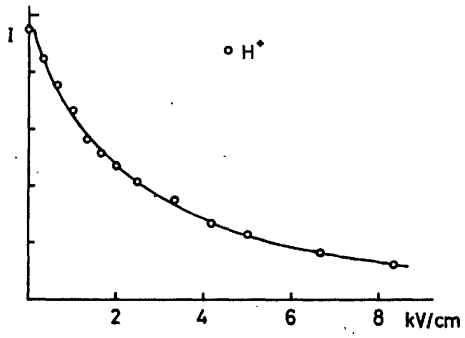

Fig. 4. Ion intensities (in arbitrary units) plotted as a function of electric field strength. The H^+ ion is produced by collision of H** with H_2O.

The corresponding field ionization of the H** species produced from H_2O by electron impact was also observed. The H^+ intensity is plotted as a function of the field strength in Fig. 4. In contrast to the He** case, about 20% of the H^+ intensity observed at zero field was detected even at 8.3 kV/cm. One of the possible explanations for this observation is the following: The highly-excited hydrogen atoms gain kinetic energies as a result of the dissociation of H_2O that are higher than that of the He** atoms (thermal), and hence, the time of flight of H** from the excitation region to the collision chamber is shorter than that of the He**. Therefore, larger fractions of the highly-excited states of hydrogen with shorter lifetimes, *i.e.*, smaller n values, than those of helium can reach the electric field and pass through it without being ionized.

The authors wish to thank Drs. W. Shearer-Izumi and M. Matsuzawa for their critical reading of the manuscript.

References

1) T. Shibata, T. Fukuyama, and K. Kuchitsu, *Shitsuryo Bunseki (Mass Spectrosc.)*, **21**, 217 (1973).
2) T. Shibata, T. Fukuyama, and K. Kuchitsu, *Chem. Lett.*, **1974**, 75.
3) H. R. von Traubenberg, R. Gebaier, and G. Lewin, *Naturwiss.*, **18**, 417 (1930).
4) A. C. Riviere and D. R. Sweetman, Proc. of 6th Int. Conf. on Ionization Phenomena in Gases, Paris 1963, Vol. 1, p. 105.
5) R. N. Il'in, V. A. Oparin, I. T. Serenkov, E. S. Solov'ev, and N. V. Fedorenko, *Zh. Eksp. Teor. Fiz.*, **59**, 103 (1970).
6) S. A. Kupriyanov, *Zh. Eksp. Teor. Fiz. Pisma*, **5**, 245 (1967).
7) M. Tsuchiya, T. Sakurai, S. Maruyama, and H. J. Svec, *Shitsuryo Bunseki*, **19**, 217 (1971).
8) A similar experiment on the field ionization of He** has been carried out in the laboratory of Dr. A. Niehaus at the University of Freiburg, Germany. H. Schäfer, thesis, 1970, private communication from Dr. M. Matsuzawa.
9) C. Lanczos, *Z. Physik*, **68**, 204 (1931).
10) D. S. Bailey, J. R. Hiskes, and A. C. Riviere, *Nuclear Fusion*, **5**, 41 (1965).
11) C. E. Johnson, *Phys. Rev.*, **A7**, 872 (1973).
12) The original calculation given in Ref. 10 extends from $n=1$ to $n=25$. The relation for larger n values has been estimated by extrapolation.

BULLETIN OF THE CHEMICAL SOCIETY OF JAPAN, VOL. 47 (11), 2885—2886 (1974)

The Properties of the Liquid Nitron Nitrate Membrane Electrode

Akira TATEDA and Hiroko MURAKAMI

College of General Education, Kyushu University, Ropponmatsu, Fukuoka 810

(Received February 18, 1974)

Synopsis. The preparation and properties of the nitron nitrate nitrobenzene liquid membrane electrode, which is responsive to nitrate ions, are described. Special attention is given to the selectivity characteristics. High selectivities for NO_3^- over NO_2^-, $C_2H_3O_2^-$, Cl^-, CrO_4^{2-}, and SO_4^{2-} were observed.

Nitron(1,4-diphenyl-3,5-endanilo-4,5-dihydro-1,2,4-triazole) is a gravimetric analytical reagent specific for nitrate.[1] An electrode using nitron as an ion exchange site in a liquid membrane was prepared, but it showed poor selectivity characteristics.[2] This experiment was undertaken in order to investigate further the properties of the nitron nitrate membrane electrodes responsive to nitrate ions, using nitron nitrate dissolved in nitrobenzene.

Experimental

Reagents. Nitron nitrate was prepared by the usual method.[3] Several recrystallizations from hot dilute surfuric acid were performed until a silky white nitron nitrate precipitate was obtained. The other reagents were of an analytical reagent grade and were used without further purification.

Construction of Nitron Nitrate Membrane Electrodes. Nitron liquid membrane electrodes were constructed by using an Orion calcium electrode barrel (92–20) in which a nitron nitrobenzene solution as a liquid ion exchanger and a reference phase were placed, using an Orion membrane (92–20–04) as a separator. The nitron nitrobenzene solution was prepared by shaking a suspension of excess nitron nitrate in a 10^{-2} M $NaNO_3$ solution with the same volume of nitrobenzene. The nitrobenzene phase was separated and filtered to remove any turbidity from the insoluble nitron nitrate. To determine the concentration of nitron in nitrobenzene, a 50 ml portion of the nitrobenzene solution was evaporated to dryness in a platinum crucible at 180 °C; the weight of the residue was 0.456 g/l. The inner-reference phase comprised an Ag–AgCl electrode immersed in an aqueous solution containing 5×10^{-3} M $NaNO_3$ and 5×10^{-3} M NaCl saturated with AgCl.

The cell assembly for the measurement of the potential was:

$$-\text{SCE}|\text{Test soln.}|\text{Membrane}|\text{Ref. soln.}|\text{Ag–AgCl}+$$

The potential measurements were made relative to a Corning 476109 calomel reference electrode with a ceramic junction using an Orion Model 801 digital pH meter at room temperature (16—18 °C). The individual ion activities were calculated from the extended Debye-Hückel equation.

Results and Discussion

Figure 1 shows typical response curves for the nitron liquid membrane electrode in the $NaNO_3$, $Mg(NO_3)_2$, and $Ce(NO_3)_3$ solutions, respectively. It is clear that the nature and type of charge of the cation present do not substantially influence the potentiometric response of the membrane electrodes to nitrate ions with respect to either the linear response or the slope of the calibration curves. Linear responses to the nitrate ion concentrations are obtained over the range from 10^0 to 10^{-3} M; the slope of the linear plot against $-\log a_{NO_3^-}$ is 53—54 mV per decade for the membrane electrode.

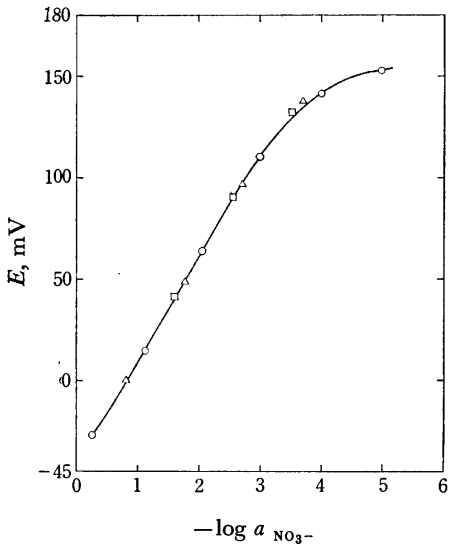

Fig. 1. Response curves for nitron membrane electrode in pure nitrate solutions.
○: $NaNO_3$, △: $Mg(NO_3)_2$, □: $Ce(NO_3)_3$.

Equilibrium potantials (±0.5 mV) are attained within 1—3 min for the membrane electrode.

Figure 2 shows the electrode response to nitrate ions in solutions of various pH values. The pH values of the solutions were adjusted from 2 to 12 by the addition of small amounts of a HCl or NaOH solution. The results show that the electrodes are insensitive to the pH change from 2 to 9 and that, at low concentrations, the pH ranges are somewhat reduced. In alkaline solutions, a sharp potential change in the negative direction is observed because the electrode responds

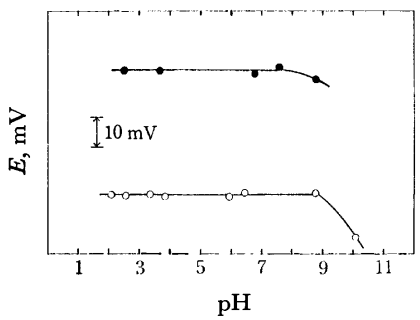

Fig. 2. Electrode response as a function of pH.
○: 0.1 M $NaNO_3$, ●: 1×10^{-3} M $NaNO_3$.

Table 1. Selectivity constants, K_j of nitron liquid membrane electrode

Anion	K_j	
	Method I[a)]	Method III[a)]
ClO_4^-	1.6×10^{2}	1.9×10^{2}
I^-	14	13
ClO_3^-	1.7	2.4
Br^-	0.13	6.8×10^{-2}
NO_2^-	6.4×10^{-2}	3.3×10^{-2}
$C_2H_3O_2^-$	4.8×10^{-2}	6.0×10^{-3}
Cl^-	6.0×10^{-3}	3.3×10^{-3}
CrO_4^{2-}	2.2×10^{-2}	—
SO_4^{2-}	1.4×10^{-3}	—

a) The same method number in Ref. 4.

preferentially to hydroxide ions.

The selectivity constants, K_j were calculated from the electrode potentials measured in 10^{-1} M solutions of pure $NaNO_3$ and a pure interferant (Method I) and from the graphical method (Method III) in the literature[4]; the results are shown in Table 1.

The performance of the nitron nitrobenzene membrane electrode was compared with essentially the same type of electrode in which nitron had been dissolved in benzylalcohol.[2] Both electrodes show a linear response from 10^0 to 10^{-3} M $NaNO_3$ solutions, but the slope of the linear plot of the nitron nitrobenzene membrane (53—54 mV) is larger than that of the nitron benzylalcohol membrane (40 mV). For the anions tested, the nitron nitrobenzene membrane shows considerably less interference than the nitron benzylalcohol membrane ($K_{Cl^-}=0.294$, $K_{C_2H_3O_2^-}=0.095$, $K_{SO_4^{2-}}=0.102$). There is also a significant difference in the numerical values of the selectivity constants for Cl^-. Therefore, the response curve for the present membrane electrode was also constructed in NO_3^- solutions containing 10^{-2} M NaCl; it is shown in Fig. 3. The results support the idea that the selectivity constant for Cl^- is of the order of 10^{-3}. The selectivity constants depend on the concentrations of both the sample solution and the ion exchanger in the membrane, and deteriorate with an increase in the concentration of the ion exchanger in the membrane.[5] In the case of a hydroxylic solvent like alcohol, nearly equal selectivity

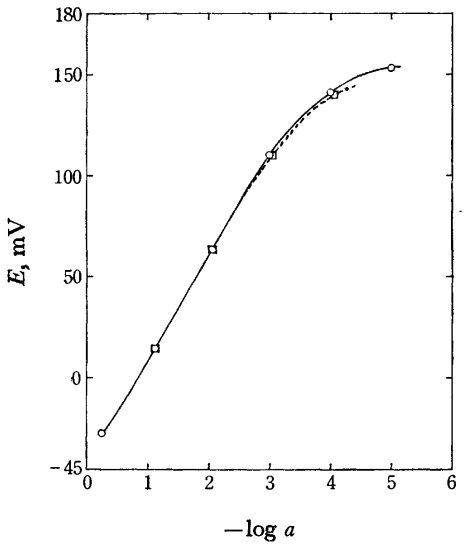

Fig. 3. Response of nitron membrane electrode to NO_3^- and to NO_3^- in 10^{-2} M NaCl.
○: NO_3^-, □: NO_3^- in 10^{-2} M NaCl.

constants are observed because of the solvation of the anions in the organic phase to a degree nearly equal to that of water.[6] From these considerations, the difference of the selectivity constants between the membranes of nitron nitrate in nitrobenzene and in benzylalcohol may be ascribed to the difference in the properties of the solvents, *e.g.* the solubilities of nitron nitrate in the organic phases (0.456 g/l nitrobenzene, 11.5 g/l benzylalcohol[2]).

References

1) A. J. Clear and M. Roth, "Treatise on Analytical Chemistry," Part II, Vol. 5, ed. by I. M. Kolthoff and P. J. Elving, Interscience Publishers, New York (1961), p. 273.
2) A. V. Gordievskii, V. S. Shterman, A. Y. Syrclenkov, N. I. Savvin, and A. F. Zhukov, *Zh. Anal. Khim.*, **27**, 772 (1972).
3) S. W. Dollons, *Analyst*, **32**, 349 (1907).
4) K. Srinivasan and G. A. Rechnitz, *Anal. Chem.*, **41**, 1203 (1969).
5) N. Yoshida and N. Ishibashi, *Chem. Lett.*, **1974**, 493.
6) R. E. Reinsfelder and F. A. Schultz, *Anal. Chem. Acta*, **65**, 425 (1973).

BULLETIN OF THE CHEMICAL SOCIETY OF JAPAN, VOL. 47 (11), 2887—2888 (1974)

Binuclear Copper(II) Propionate Complexes with *N*-Arylsalicylideneamines

Tadashi Tokii, Shuji Emori, and Yoneichiro Muto

Department of Chemistry, Faculty of Science and Engineering, Saga University, Saga 840

(Received March 29, 1974)

Synopsis. Two copper(II) propionate complexes with *N*-arylsalicylideneamines have been prepared. The magnetic and spectral properties of these complexes indicate that they have a carboxylate-bridged binuclear structure.

As a part of a program of magnetochemical studies of polynuclear copper(II) complexes, we have been studying a variety of copper(II) alkanoate complexes with salicylideneamines. In this paper we will report the preparative, magnetic, and spectral properties of newly-prepared copper(II) propionate complexes with the compositions of Cu(Sal·N·ph)$C_2H_5CO_2$ and Cu(Sal·N·*p*-tol)$C_2H_5CO_2$, where Sal·N=·O·C_6H_4·CH=N, ph=phenyl, and *p*-tol=*p*-tolyl. For comparison with the corresponding chloride complexes, cryomagnetic and IR spectral measurements have also been made of the Cu(Sal·N·*p*-tol)Cl complex, the preparation and some characterization of which were previously reported.[1]

Results and Discussion

The Cu(Sal·N·*p*-tol)$C_2H_5CO_2$ complex was readily prepared by the reaction of the parent complex, Cu(Sal·N·*p*-tol)$_2$, with copper(II) propionate in hot ethanol. On the other hand, the preparation of Cu(Sal·N·ph)$C_2H_5CO_2$ was found to be much more difficult. We also found that, in the reaction of copper(II) propionate with the salicylideneamine complex, Cu(Sal·N·ph–X)$_2$, where ph–X represents the monosubstituted phenyl group with the X substituent, the preparation of no propionate complexes was accomplished under reaction conditions similar to those above when X=*o*-Cl, *m*-Cl, *p*-Cl, *p*-NO_2, *o*-CH_3, and *m*-CH_3 in Cu(Sal·N·ph–X)$_2$. This fact seems to indicate that both the polar and steric natures of the substituents play an important role in the formation of Cu(Sal·N·ph–X)$C_2H_5CO_2$.

The magnetic susceptibility data in the temperature range of 80—300 K for the propionate complexes are well represented by the Bleaney-Bowers equation:[2]

$$\chi_A = \frac{g^2N\beta^2}{3kT}\left(1+\frac{1}{3}\exp\frac{-2J}{kT}\right)^{-1} + N\alpha \qquad (1)$$

where $-2J$ is equal to the energy separation between the singlet and triplet states, which gives the degree of the strength of the magnetic interaction, and where the other symbols have their usual meanings. By the best fit of the observed cryomagnetic data to Eq. (1), assuming $N\alpha=60\times10^{-6}$ emu/mol, the values of $-2J=101$ cm^{-1} and $g=2.14$ were evaluated for both the propionates (Fig. 1). The close agreement between the observed and calculated temperature dependences indicates that the propionate complexes have a binuclear structure in crystals. The antiferromagnetic interaction ($J<0$) was also reflected in the X-band ESR spectra of these complexes; *i.e.*, the spectra showed a weak signal at about 1500 G which may be assigned to the $\Delta M_s=2$ transition characteristic of magnetically-coupled copper(II) ions.[2]

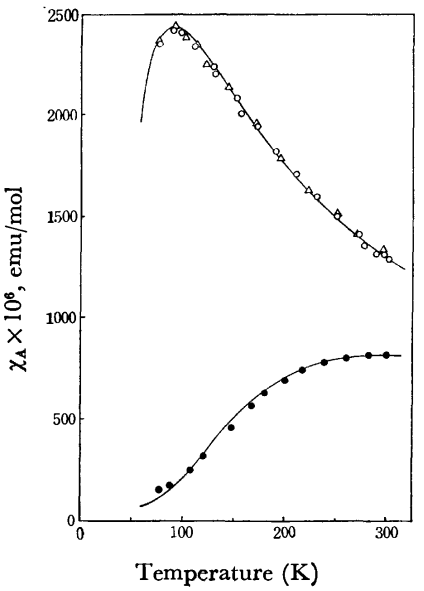

Fig. 1. Variation of magnetic susceptibilities with temperature.
○: Cu(Sal·N·ph)$C_2H_5CO_2$ (μ_{eff}=1.73 B.M. at 26 °C)
△: Cu(Sal·N·*p*-tol)$C_2H_5CO_2$ (μ_{eff}=1.74 B.M. at 23 °C)
●: Cu(Sal·N·*p*-tol)Cl (μ_{eff}=1.35 B.M. at 27 °C)
The solid curves represent the Bleaney-Bowers equation.

The χ_A *vs.* T data of the chloride complex, Cu(Sal·N·*p*-tol)Cl, were also fitted to the theoretical curve calculated from Eq. (1) with the values of $-2J=330$ cm^{-1}, $g=2.15$, and $N\alpha=60\times10^{-6}$ emu/mol (Fig. 1). The $-2J$ value is large and practically the same as the value of 360 cm^{-1} determined by Harris *et al.*[3] for the phenyl complex, Cu(Sal·N·ph)Cl. This indicates the presence of a very much stronger antiferromagnetic interaction in these chloride complexes than in the corresponding propionate complexes.

The reflectance spectral pattern of the propionates, which indicates a square planar configuration around the copper(II) ion, is different from those of the chlorides to which a pseudo-tetrahedral configuration was previously assigned[1,4] (Fig. 2). Furthermore, these spectral and magnetic properties are contrary to the expectation from the linear relation, "higher energy of

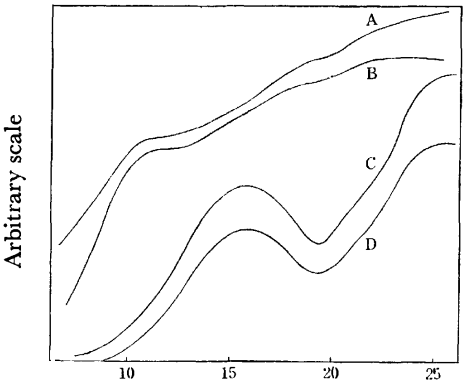

Fig. 2. Reflectance spectra.
A: Cu(Sal·N·ph)Cl B: Cu(Sal·N·*p*-tol)Cl
C: Cu(Sal·N·ph)$C_2H_5CO_2$
D: Cu(Sal·N·*p*-tol)$C_2H_5CO_2$

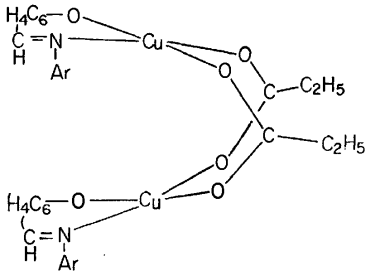

Fig. 3. Proposed binuclear structure of Cu(Sal·N·Ar)-$C_2H_5CO_2$.
(Ar=phenyl or *p*-tolyl group)

d-d bands—lower magnetic moment," established for a series of binuclear copper(II) halide complexes with pyridine *N*-oxides[5] and salicylideneamines.[1,4]

The chloride complexes showed a strong band at *ca.* 1550 cm^{-1}, while the band appears at *ca.* 1530 cm^{-1} for the parent bis-salicylideneamine complexes.[3] This band shift to higher energies indicates that, in these chlorides, the binuclear molecule is formed by phenolic oxygen atoms.[6] On the other hand, no significant band shift was observed for the propionate complexes, suggesting that, in these complexes, no phenolic oxygen-bridged structure exists.

These magnetic and spectral data suggest that the propionates possess a carboxylate-bridged binuclear structure analogous to that of copper(II) propionate *p*-toluidine, $[Cu_2(C_2H_5CO_2)_4 \cdot p\text{-toluidine}_2]_n$, the structure of which was recently determined by X-ray analysis.[7] One of the probable binuclear structures is given in Fig. 3.

The difference in magnetic interaction between the propionate and chloride complexes is attributable to change in structure from carboxylate-bridged to phenolic oxygen-bridged entities. In support of this conclusion, it should be noted that the $-2J$ value determined for the propionate complexes in this study is in good agreement with the value of 105 cm^{-1} reported by Yawney *et al.*[7] for copper(II) propionate *p*-toluidine, for which a pair-by-pair spin-spin coupling between copper(II) ions through the carboxylate groups was suggested to account for the demagnetization.[7]

Experimental

Preparation of the Propionates. A mixture of copper(II) propionate monohydrate and bis-(*N*-arylsalicylideneaminato)-copper(II) in ethanol was stirred on a hot plate for an hour. The mole ratio of $Cu(C_2H_5CO_2)_2H_2O$ to $Cu(Sal \cdot N \cdot Ar)_2$ was 3:1 for the phenyl complex and 1.2:1 for the tolyl complex. The alcoholic solution was then filtered, and the filtrate was concentrated by warming it gently to produce green crystals. The product was filtered off, washed twice with ethanol and once with ether, and dried at *ca.* 70 °C. Anal. Phenyl complex. Found: C, 57.67; H, 4.56; N, 4.11; Cu, 19.18%; Calcd. for $C_{16}H_{15}NO_3Cu$: C, 57.74; H, 4.54; N, 4.20; Cu, 19.09%. Tolyl complex. Found: C, 58.79; H, 4.91; N, 4.03; Cu, 18.33%; Calcd for $C_{17}H_{17}NO_3Cu$: C, 58.86; H, 4.94; N, 4.04; Cu, 18.32%.

Physical Measurements. The magnetic susceptibilities were determined over the temperature range of 80—300 K by the Gouy method using an apparatus which was described previously.[4] The ESR (X-band) spectra were measured on powder samples using a JES-ME-1X spectrometer. The reflectance spectra were obtained on a Hitachi EPR-3T recording spectrophotometer. The IR absorption spectra were recorded on a Hitachi EPI-G2 IR spectrophotometer.

References

1) M. Kato, Y. Muto, H. B. Jonassen, K. Imai, K. Katsuki, and S. Ikegami, This Bulletin, **42**, 2555 (1969).
2) B. Bleaney and K. D. Bowers, *Proc. Roy. Soc., Ser. A*, **214**, 451 (1952).
3) C. M. Harris and E. Sinn, *J. Inorg. Nucl. Chem.*, **30**, 2723 (1968).
4) M. Kato, K. Imai, Y. Muto, T. Tokii, and H. B. Jonassen, *ibid.*, **35**, 109 (1973).
5) Y. Muto, M. Kato, H. B. Jonassen, and L. C. Cusachs, This Bulletin, **42**, 417 (1969).
6) E. Sinn and C. M. Harris, *Coord. Chem. Rev.*, **4**, 391 (1969).
7) D. B. W. Yawney, J. A. Moreland, and R. J. Doedens, *J. Amer. Chem. Soc.*, **95**, 1164 (1973).

BULLETIN OF THE CHEMICAL SOCIETY OF JAPAN, VOL. 47 (11), 2889—2890 (1974)

Synthesis of Chelating Agents. XII.[1] Chelating Behavior of 3,3-Dimethylbutane-1,2-diamine-*N,N,N',N'*-tetraacetic Acid with Some Alkaline Earth Metals*

Tairoku YANO, Yuzo YANAGIHARA, Hiroshi KOBAYASHI, and Keihei UENO

Department of Organic Synthesis, Faculty of Engineering, Kyushu University, Hakozaki, Higashi-ku, Fukuoka 812

(Received May 14, 1974)

Synopsis. The chelate stability constants of 3,3-dimethylbutane-1,2-diamine-*N,N,N',N'*-tetraacetic acid with some alkaline earth metal ions were determined at 25.0 °C and at an ionic strength of 0.10 with KNO_3 as supporting electrolyte by a potentiometric method.

Synthesis and acid dissociation study of 3,3-dimethylbutane-1,2-diamine-*N,N,N',N'*-tetraacetic acid (BEDTA) was previously reported.[2] This note is to report on the chelating behavior of the above ligand with alkaline earth metal ions.

Experimental and Calculation

Potentiometric measurements were carried out at 25.0± 0.1 °C in aqueous solutions and at an ionic strength of 0.10 with KNO_3 as supporting electrolyte. Apparatus and procedures were the same as described previously.[1] A solution of the ligand (10^{-3} M, 100 ml) was titrated with 0.1 N KOH solution free from carbonate ion in the presence of an equimolar amount of an alkaline earth metal ion. The titration curves obtained were shown in Fig. 1. Since BEDTA forms exclusively a 1:1 chelate with a multivalent metal ion,

$$M^{m+} + A^{4-} \rightleftarrows MA^{m-4}$$

the stability constant $K_{MA}(=[MA^{m-4}]/[M^{m+}][A^{4-}])$ was calculated according to the Bjerrum's standard method.[3]

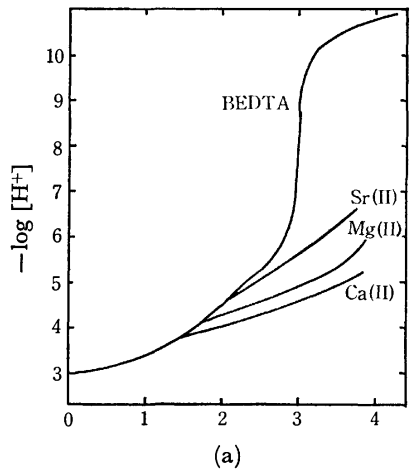

(a)

Fig. 1. Potentiometric titration curves of the alkaline earth metal chelates at 25.0 °C in 0.10 M KNO_3 solution, where the mole ratio of a metal ion to the ligand is 1:1 and the concentration of BEDTA 10^{-3} M.

TABLE 1. STABILITY CONSTANTS OF BEDTA AND RELATED LIGANDS WITH SOME ALKALINE EARTH METALS

Compound	log K_{MA}		
	Mg(II)	Ca(II)	Sr(II)
BEDTA	11.0	11.8	9.4
EDTA[7]	8.69	10.70	8.63
PDTA[8a]	10.29	11.47	9.61
dl-BDTA[8b]	11.33	11.49	10.10

a) PDTA: Propane-1,2-diaminetetraacetic acid
b) *dl*-BDTA: *dl*-Butane-2,3-diaminetetraacetic acid

* Contribution No. 336 from the Department of Organic Synthesis, Kyushu University.

Results and Discussion

Stability constants of BEDTA chelates with alkaline earth metal ions are summarized in Table 1 along with those of some methylated homologues of EDTA. One can readily notice that BEDTA is one of the complexane ligands that give the most stable chelates with alkaline earth metal ions. Among them, calcium(II) ion forms the most stable chelate, and magnesium(II) and strontium(II) afford decreasingly less stable ones. Though this stability order is the same as generally observed in complexane ligands, it is noted that the difference between the stabilities of the calcium(II) and magnesium(II) chelates is relatively small as compared with those of the other EDTA homologues.

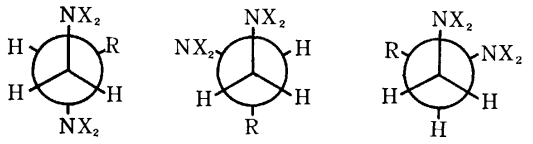

(I) (II) (III)

PDTA: X=CH_2COO^-, R=methyl
BEDTA: X=CH_2COO^-, R=*t*-butyl
BEDA: X=H, R=*t*-butyl

Upon chelate formation with a metal ion, the BEDTA tetraanion moiety would take the *syn*-conformation of II preferably to III since the latter, though being also of a *syn*-conformation, would be subject to considerable steric hindrance between *t*-butyl group and the resulting out-of-plane (R) glycinate ring.[4] A study on the rotational isomerism of propane-1,2-diaminotetraacetic acid (PDTA) in a solution showed that among the conformations of the free tetraanion, I, II, and III, the latter two were present to an equal extent.[5] Increased size of the alkyl substituent in BEDTA, however, would favor to the less congested conformation II and, therefore, presumabley causes the increase in the fraction of II, while decreases that of III.

The precursory diamine, 3,3-dimethyl-1,2-diaminobutane (BEDA), was found to form also very stable

complexes as compared with those of homologous 1,2-diamines. This behavior upon chelate formation was also ascribed to the bulkiness of *t*-butyl group which restricted the internal rotation in the free ligand molecule to fix the two amino group in a *syn-clinal* position II favorable to chelate ring formation.[6] Although no direct evidence was obtained, the behavior of the precursory diamine and the molecular model study of BEDTA indicated the predominance of the conformer II in the free tetraanion of BEDTA.

Thus an entropy contribution due to the steric effect, as well as an enthalpy contribution due to the electron-releasing effect of *t*-butyl group, would be responsible for the high stability of the present complexane ligand.

References

1) Part XI: T. Yano, H. Kobayashi, and K. Ueno, This Bulletin, **47**, 2806 (1974).
2) Y. Yanagihara, T. Yano, H. Kobayashi, and K. Ueno, *ibid.*, **45**, 554 (1972).
3) T. Yano, H. Kobayashi, and K. Ueno, *ibid.*, **43**, 3167 (1970).
4) R. J. Day and C. N. Reilley, *Anal. Chem.*, **37**, 1326 (1965).
5) J. L. Sundmeier and A. J. Senzel, *ibid.*, **40**, 1693 (1968).
6) Part X: T. Yano, H. Kobayashi, and K. Ueno, This Bulletin, in press.
7) G. Schwarzenbach, G. Gut, and G. Anderegg, *Helv. Chim. Acta*, **37**, 937 (1954).
8) J. H. Grimes, A. J. Huggard, and S. P. Wilford, *J. Inorg. Nucl. Chem.*, **25**, 1225 (1963).
9) H. M. N. H. Irving and R. Parkins, *ibid.*, **28**, 1629 (1966).

BULLETIN OF THE CHEMICAL SOCIETY OF JAPAN, VOL. 47 (11), 2891—2892 (1974)

The Spectrophotometric Determination of Boron in Condensed Water from Fumaroles*

Akinori Isozaki and Satori Utsumi

College of Science and Technology, Nihon University, Chiyoda-ku, Tokyo 101

(Received May 29, 1974)

Synopsis. A simple and accurate spectrophotometric method for determining boron in condensed water from fumaroles has been developed. The proposed method is based on the methylene blue-tetrafluoroborate ion pair. It was possible to determine micro amounts of boron with satisfactory results without any interference of foreign ions.

The tetrafluoroborate ion (BF_4^-) forms an ion pair with methylene blue, which may be easily extracted by 1,2-dichloroethane. The present authors have investigated this method in greater detail[1] and applied it to the determination of micro amounts of boron in natural waters[2] and rocks.[3] The determination of boron in condensed water from fumaroles[4-6] has been almost always performed by a titration method using a sodium hydroxide solution and mannitol. However, it seems difficult to determine boron at lower concentrations such as 0.1 ppm. Onishi[7] has determined the BF_4^- in natural waters by a spectrophotometric method on the basis of the methylene blue ion-pair. However, he has not reported in detail about the total boron. There are also some problems regarding the pretreatment of the sample. In the present work, the authors investigated a simple and accurate method for the determination of total boron in condensed water.

Results and Discussion

Reagents and Apparatus. *Standard Boric Acid Solution* (0.25 and 2.5 ppm as boron). *Standard Tetrafluoroboric Acid Solution* (0.25 ppm as boron): Add 50 ml of a standard boric acid solution (2.5 ppm as boron) and 5 ml of 5% hydrofluoric acid to a 500 ml polyethylene measuring flask. After the mixture has been allowed to stand for 24 hr, dilute to exactly 500 ml with water. *Silver Sulfate Solution* (0.01 M): Dissolve 1.5 g of silver sulfate in water and dilute to 500 ml. This solution contains 10 mg of silver ions per 5 ml. A Hitachi double-beam spectrophotometer (Model 124) and 10 mm cells were used to measure the absorbance. The other reagents and apparatus used in this investigation were the same as those described in a previous paper.[1]

Sampling. Fumarolic gas is collected by means of a quartz tube inserted into a fumarole. The cooling parts and sampling flask were also made of quartz.

Procedure. In a 100 ml platinum dish, place the condensed water so that it contains below 1.0 μg of boron, add 1.0 ml of a 0.5 M potassium hydroxide solution and 0.5 ml of a 30% hydrogen peroxide solution, and then dilute to 10 ml with water. Place the platinum dish in a water bath at boiling. After evaporation to dryness, dissolve the cake with 4 ml of a 0.5 M sulfuric acid solution. Transfer the solution to a polyethylene separatory funnel and wash the platinum dish with 13 ml of water. Into the separatory funnel, add 3 ml of a 5% hydrofluoric acid and allow the mixture to stand for 30 min at room temperature. Then add 3 ml of a 0.001 M methylene blue solution and 10 ml of 1,2-dichloroethane, and shake the separatory funnel for 1 min. Transfer the organic layer into another separatory funnel containing 5 ml of a 0.01 M silver sulfate solution and shake it for 1 min. After it has stood for about 20 min, measure the absorbance of the dichloroethane phase at 660 nm, using dichloroethane as the reference. The calibration curve was prepared by taking 0.0, 1.0, 2.0, 3.0, and 4.0 ml of a 0.25 ppm standard boric acid solution. It was reproducible within an error of ±0.02 μg of boron.

Effect of Foreign Ions. In order to confirm the effect of foreign ions, which are usually present in condensed water from fumaroles, and eliminate the interfering ions, the experiments were made both in the presence of 0.5 μg of boron and in its absence. The experimental results are given in Table 1. Sulfide and sulfite ions interfered with the determination of boron under masking with 10 mg of silver ions. However, by this procedure these ions could be decomposed by oxidation with hydrogen peroxide in an alkaline solution. It was found suitable from several experiments to use 0.5 ml of 30% hydrogen peroxide for the oxidation.

Effect of the Volatilization of Boron. When a solution containing borate ions is concentrated or evaporated to dryness, an alkaline solution has been used. On the other hand, BF_4^- exists in a strongly acid-condensed water containing a larger amount of fluo-

Table 1. Effect of foreign ions

Ions added (mg)	Absorbance: Masking with 10 mg Ag^+		Absorbance: This procedure	
	Blank	0.5 μg B	Blank	0.5 μg B
None	0.109	0.493	0.123	0.498
S^{2-} 1, Cl^- 1	0.206	0.546	0.134	0.507
SO_3^{2-} 1, Cl^- 1	0.150	0.488	0.122	0.490
$S_2O_3^{2-}$ 0.1	0.138	0.519	0.119	0.484
$S_2O_6^{2-}$ 0.1	0.095	0.488		
$S_4O_6^{2-}$ 0.1	0.124	0.529		
CO_3^{2-} 1	0.101	0.495		
Cl^- 10	0.112	0.503		

* Presented at The 22th Annual Meeting of The Japan Society for Analytical Chemistry, Fukuoka, Nov., 1973.

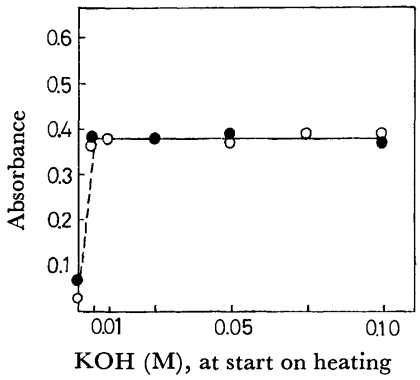

Fig. 1. Effect of volatilization of boron.
○: H_3BO_3 (0.5 μg as B), ●: HBF_4 (0.5 μg as B); against reagent blank

TABLE 2. DETERMINATION OF BORON IN CONDENSED WATER FROM FUMAROLES

Sample	Boron found ppm	Relative std. devn. %	Titration ppm
Hakone Ōwaku-dani, 122.5 °C (December 26, 1972)	3.9 3.8 4.0 / 4.0 4.0 3.7	3.3	3.9 3.8
Iwate-san, 402 °C (July 20, 1972)	1.2 1.2 1.2 / 1.3 1.2 1.1	5.2	1.1 0.6
Kagoshima Iō-Jima, 97°C (August 25, 1973)	0.21 0.18 0.20 / 0.20 0.22	7.5	

ride;** therefore, it is necessary to examine the volatilization of BF_4^-. Several experiments were made in order to examine the volatilization of boron by using a standard boric acid solution or tetrafluoroboric acid solution and by changing the amount of potassium hydroxide, according to the above procedure. As can be seen in Fig. 1, the loss of boron in both cases was insignificant except in the absence of alkali. Therefore, 1 ml of 0.5 M potassium hydroxide was added in the present work.

The Determination of Boron in Condensed Water from Fumaroles. The boron in some condensed waters was determined by the present method. The results listed in Table 2 show good agreement within the limits of experimental error. A colloidal sulfur sometimes exists in condensed water. It was found that the amount of boron adsorbed on sulfur was negligible. The analytical results obtained by a titration method[8] are also shown in Table 2. It was difficult to determine less than 1 ppm of boron by the titration method. Further, it was found that when a sample is rich in BF_4^-, the titration method gives a considerable error in the results because of trouble at pH adjustment from the fundamental experiment. The present method may be applied not only to condensed water from fumaroles, but also to hot spring water and thermal water in active volcanic areas.

The authors are much obliged to Dr. T. Ozawa and Dr. M. Yoshida of the Tokyo Institute of Technology for kindly supplying the samples of condensed water and for their many helpful discussions during this work.

** Onishi[7] reported that in some cases the ratio of the BF_4^--type boron against the total boron is 90%.

References

1) S. Utsumi, S. Ito, and A. Isozaki, *Nippon Kagaku Zasshi*, **86**, 921 (1965).
2) S. Utsumi and A. Isozaki, *ibid.*, **88**, 545 (1967).
3) A. Isozaki and S. Utsumi, *ibid.*, **88**, 741 (1967).
4) S. Matsuo, *J. Earth Sci.*, **9**, 80 (1961).
5) H. Wada and T. Suzuoki, read at the Symposium on Geochemistry of the Geochemical Society of Japan and the Chemical Society of Japan, October, 1967.
6) S. Ueno, *ibid.*, October, 1969.
7) T. Onishi, This Bulletin, **42**, 127 (1969).
8) William Horwitz, "Official Methods of Analysis of the Association of Official Agricultural Chemists," 8th ed., p. 586 (1955).

BULLETIN OF THE CHEMICAL SOCIETY OF JAPAN, VOL. 47 (11), 2893—2894 (1974)

The Reaction of Biguanides and Related Compounds. XI.[1] The Interaction of Ethylene Carbonates with Arylbiguanides and Related Compounds.

Mitsuru FURUKAWA, Takatoshi YOSHIDA, and Seigoro HAYASHI

Faculty of Pharmaceutical Sciences, Kumamoto University, Oe-hon Machi, Kumamoto 862

(Received February 12, 1974)

Synopsis. The treatment of arylbiguanides with ethylene carbonates afforded 1-aryl-4,6-diimino-2-oxo-hexahydro-*s*-triazines, which were then readily converted into 1-arylisocyanuric acid by hydrolysis with concentrated hydrochloric acid.

A number of previous workers have shown that the addition of carboxylic esters, ketones, and aldehydes to biguanides is followed by the immediate cyclization of the intermediates to amino-*s*-triazines.[2] In continuation of our investigation on the cyclization of systems containing carbonyl groups to biguanides and its homologues, we examined the behavior of ethylene carbonates (**1**) toward arylbiguanides (**2**) and *N*-amidino-*O*-alkylisoureas (**3**).

When **1a** and **2** were heated in ethanol or, preferably, allowed to stand in dimethylformamide (DMF), a product was yielded in a comparatively good yield. The same product was also obtained by treating **1b** with **2** under similar conditions. This result obviously indicates that the ethylene moiety originating from **1a** is not retained in the molecule of the product. The mass spectrum of the product exhibited a strong molecular ion peak corresponding to that of the condensation product of molecular equivalents of **1a** and **2**, with the elimination of ethylene glycol. The infrared (IR) spectrum showed the absorptions assignable to amino and imino groups in the regions of 3450 and 3260 cm^{-1} and that due to a carbonyl group near 1680 cm^{-1}. These results suggest that the products are 2-oxo-hexahydro-*s*-triazines, though two isomeric structures, 1-aryl-4,6-diimino-2-oxo-hexahydro-*s*-triazine (**4**) and 2-arylimino-4-imino-6-oxo-hexahydro-*s*-triazine (**5**), due to the orientation of the cyclization are possible. Although support for **4** was provided by observing the fragment-ion peak probably arising from the arylisocyanate ion formed by the decomposition of the molecular ion in the mass spectrum, a distinction between **4** and **5** on the basis of the results of elemental analyses and the spectral data alone is impossible. In order to elucidate the structure, the product was hydrolyzed with hydrochloric acid to give 1-arylisocyanuric acid

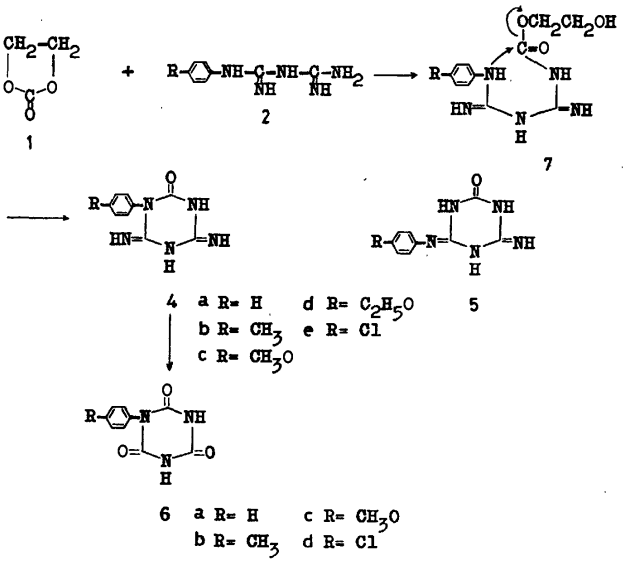

Scheme 1.

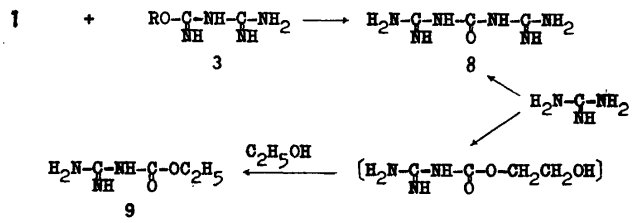

Scheme 2.

TABLE 1. 1-ARYL-4,6-DIIMINO-2-OXO-HEXAHYDRO-*s*-TRIAZINE (**4**)

Compd.	Yield (%) in EtOH	Yield (%) in DMF	Mp (°C)	Formula	Analysis % Found (Calcd) C	H	N
4a	70	74	>360	$C_9H_9ON_5$	52.86 (53.19)	4.61 (4.46)	34.43 (34.47)
4b	84	91	349—350	$C_{10}H_{11}ON_5$	55.06 (55.29)	5.45 (5.10)	31.98 (32.24)
4c	74	89	348—349	$C_{10}H_{11}O_2N_5$	51.82 (51.49)	5.08 (4.75)	29.79 (30.03)
4d	58	63	350—351	$C_{11}H_{13}O_2N_5$	53.02 (53.43)	5.40 (5.30)	28.23 (28.33)
4e	38	39	>360	$C_9H_8ON_5Cl$	45.85 (45.48)	3.54 (3.39)	29.44 (29.47)

Table 2. 1-Arylisocyanuric acid (6)

Compd.	Yield (%)	Mp (°C)	Formula	Analysis % Found (Calcd) C	H	N
6a	35	307—308	$C_9H_7O_3N_3$	52.43 (52.68)	3.21 (3.44)	20.52 (20.48)
6b	71	300—301	$C_{10}H_9O_3N_3$	54.86 (54.79)	4.36 (4.14)	18.59 (19.17)
6c	30	269—270	$C_{10}H_9O_4N_3$	51.04 (51.06)	4.13 (3.86)	17.35 (17.85)
6d	60	301—302	$C_9H_6O_3N_3Cl$	44.63 (45.11)	2.70 (2.52)	17.49 (17.53)

(**6**).[3] The IR spectrum of **6** exhibited the characteristic three absorption bands assignable to the carbonyl groups in the region of 1700—1800 cm^{-1}, and the mass spectrum showed the molecular ion as the most abundant peak. Detailed data on **4** and **6** are summarized in Tables 1 and 2.

The formation of **4** probably proceeds step by step as follows: the initial addition of **2** to **1a** may occur theoretically at the central (N^3) or at the equivalent terminal nitrogen atom (N^5), of which only the latter case is capable of yielding *s*-triazine on cyclization. The N^3 atom is inactive, and the nucleophilic attack of this nitrogen is unknown. The interaction of the ester carbonyl group in the intermediate (**7**) would occur rapidly with the N^1 atom rather than with the N^2 atom or more **2**, giving **4**, but not **5** or a bis-compound. The formation of the acyl intermediate, **7**, in the reaction of **2** with carboxylic esters was suggested by Overberger[4] and Shapiro,[5] and elucidated by us.[6]

The reaction of **1a** with **3** is also expected to undergo cyclization to *s*-triazines. However, no formation of any of the *s*-triazines anticipated was observed. The heating of equimolar quantities of **1a** and **3** in ethanol unexpectedly gave *N,N'*-carbonyl-*bis*-guanidine (**8**), whose structure was established by a comparison of it with an authentic sample prepared from **1a** and guanidine.

The IR spectrum of **8** showed the strong absorption assignable to a carbonyl group at 1660 cm^{-1}, and the absorption pattern was quite similar to that of guanidine. Compound **8** would be formed by the reaction of **1a** with the guanidine formed by the decomposition of **3**. The facile decomposition of **3** to guanidine was practically observed. The heating of equimolar quantities of **1a** and guanidine in ethanol also gave a low yield of **8**, as had been expected. On the other hand, when **1a** was treated with one-half equivalent amount of guanidine, a mixture of **8** and ethyl guanidinocarboxylate (**9**)[7] was obtained in a low yield. Compound **9** would be formed by the ester exchange of an intermediate β-hydroxyethyl guanidinocarboxylate with the ethanol used as the solvent. The conversion of **9** to **8** was also observed upon heating with guanidine in ethanol.

Experimental

1-Aryl-4,6-diimino-2-oxo-hexahydro-s-triazine (4). General Procedure: 1) A mixture of arylbiguanide (4 mmol) and ethylene carbonate (4 mmol) in ethanol (20 ml) or in DMF (1 ml) was refluxed for 2 hr or allowed to stand for a few days at room temperature respectively. The precipitates thus deposited were collected by filtration upon cooling. Purification was carried out by neutralizing a solution of the precipitates in an aqueous sodium hydroxide solution with dilute hydrochloric acid. The detailed data are summarized in Table 1. 2) A solution of arylbiguanide (4 mmol) and propylene carbonate (4 mmol) in ethanol (20 ml) was heated for 2 hr under reflux. The precipitates thus deposited were collected by filtration while hot. The precipitates were identified with an authentic sample prepared by Procedure 1 by means of a mixed-melting-point determination and by a comparison of the IR spectra.

1-Arylisocyanuric Acid (6). General Procedure: A suspension of 1-aryl-4,6-diimino-2-oxo-hexahydro-*s*-triazine (2 mmol) in concentrated hydrochloric acid (10 ml) was heated for 12 hr under reflux. The suspended solid was gradually dissolved, and the precipitates were newly separated. The precipitates were collected by filtration while hot and washed with dilute hydrochloric acid. The detailed data are summarized in Table 2.

N,N'-Carbonyl-bis-guanidine (8). Into a solution of sodium ethoxide (0.34 g, 5 mmol) in ethanol (20 ml), we stirred *N*-amidino-*O*-alkylisourea hydrochloride (5 mmol). The precipitates were then filtered off, and ethylene carbonate (0.44 g, 5 mmol) was added to the filtrate. The mixture was heated for 2 hr, and the precipitates thus deposited were collected by filtration. Recrystallization from dilute ethanol gave a 40% yield of colorless prisms; mp>360 °C. Found: C, 21.99; H, 6.67; N, 50.69. Calcd for $C_3H_8ON_6H_2O$: C, 22.22; H, 6.22; N, 51.21. The same compound was also obtained in a 50% yield by the reaction of ethylene carbonate with an excess of guanidine and in a 70% yield by the treatment of guanidine with ethyl guanidinocarboxylate.

Ethyl Guanidinocarboxylate (9). A solution of guanidine (0.30 g, 5 mmol) and ethylene carbonate (0.88 g, 10 mmol) in ethanol (10 ml) was refluxed for 4 hr and then concentrated. The precipitates (0.02 g, 5.8%) of *N,N'*-carbonyl-bis-guanidine were filtered off, and the filtrate was evaporated by distillation and then allowed to stand overnight to give colorless prisms (0.05 g, 6.7%) melting at 93—95 °C.

References

1) Part X: M. Furukawa, M. Goto, and S. Hayashi, This Bulletin, **47**, 1977 (1974).

2) a) E. J. Modest, "Heterocyclic Compounds," ed. by R. C. Elderfield, ed., Wiley, New York and London, 1961, Vol. 7, pp. 627, 663. b) E. M. Smolin and L. Rapoport, "*s*-Triazines and Derivatives," Interscience, New York (1959), pp. 225, 239, 242, 258, 283.

3) W. J. Close, *J. Amer. Chem. Soc.*, **75**, 3617 (1953).

4) C. G. Overberger and S. L. Shapiro, *ibid.*, **76**, 93 (1954).

5) S. L. Shapiro, V. A. Parrino, and L. Freedman, *J. Org. Chem.*, **25**, 379 (1960).

6) a) M. Furukawa and S. Hayashi, *Synthesis*, **1973**, 536. b) M. Furukawa, T. Yoshida, M. Goto, and S. Hayashi, *Chem. Pharm. Bull.* (Tokyo), **21**, 2594 (1973).

7) L. A. Pinck and J. S. Blair, *J. Amer. Chem. Soc.*, **49**, 509 (1929).

BULLETIN OF THE CHEMICAL SOCIETY OF JAPAN, VOL. 47 (11), 2895—2896 (1974)

The Syntheses of Acronycidine and 4,5,8-Trimethoxyfuro[2,3-*b*]quinoline

Tetsuya SEKIBA

Faculty of Chemical Engineering, Toyama Technical College, Hongo, Toyama 930

(Received March 13, 1974)

Synopsis. 2,3-Dihydroacronycidine (VIa) was obtained from 2,3,5-trimethoxyaniline by condensation with diethyl β-benzyloxyethylmalonate, methylation, debenzylation, and then cyclodehydration. The dehydrogenation of VIa gave acronycidine in relatively high yields.

Acronycidine was isolated from the bark of both *Acronychia baueri*[1] and *Melicope fareana*.[2] Its structure was proposed to be 4,5,7,8-tetramethoxyfuro[2,3-*b*]-quinoline (Ia) on the basis of spectral and degradative studies.[3] 4,5,8-Trimethoxyfuro[2,3-*b*]quinoline (Ib) has not yet been found in any natural source, but it is considered useful to synthesize this substance, which may be expected to occur in nature. Govindachari and his co-workers[4] attempted, without success, to synthesize the 2,3-dihydro-derivative of Ia according to the method of Ohta and Mori.[5] They obtained it, therefore, by another route,[6] but never attempted to synthesize Ia. A previous paper[7] reported the successful dehydrogenation of 2,3-dihydrofuroquinoline in dry benzene into furoquinoline with DDQ (2,3-dichloro-5,6-dicyanobenzoquinone).

The present paper will describe convenient syntheses of Ia and Ib from 2,3,5-trimethoxyaniline (IIa)[8] and 2,5-dimethoxyaniline (IIb) by a modification of a method previously reported[7] according to Ohta and Mori's method. By careful heating under reduced pressure, the condensation of IIa and IIb and diethyl β-benzyloxyethylmalonate without any solvent gave the 4-hydroxy-2-quinolone derivatives (IIIa, b), which were then easily methylated with diazomethane into 4-methoxy compounds (IVa, b). Although the attempted cyclodebenzylation of IVa and IVb with PPA was unsuccessful, the debenzylation of IVa and IVb with hydrogen in the presence of 5% Pd–C gave 3-(β-hydroxyethyl)-4-methoxy-2-quinolone derivatives (Va, b). The IR spectra of Va and Vb indicated the presence of a hydroxyl group (*ca.* 3440 cm^{-1}), while the NMR spectra of Va and Vb indicated the absence of the methylene protons and the phenyl protons of the benzyl group, which were present in the spectra of IVa and IVb, and exhibited a signal for one proton (δ *ca.* 3.63 bs ppm) of the hydroxyl group which easily disappeared upon deuterium exchange. The cyclodehydration of Va and Vb with PPE (polyphosphate ester) yielded 2,3-dihydrofuro[2,3-*b*]quinoline derivatives (VIa, b). The structures of VIa and VIb were assigned on the basis of the NMR spectra, which showed signals at δ *ca.* 3.42 t and 4.58 t attributable to two methylene protons of a dihydrofuran-ring system. The dehydrogenation of VIa and VIb by the DDQ method gave furo[2,3-*b*]quinoline derivatives (Ia; acronycidine[1] and Ib; 4,5,8-trimethoxyfuro[2,3-*b*]quinoline). The synthetic acronycidine (Ia) was shown to be identical with a natural specimen by a mixed-melting-point determination and by a comparison of their IR, UV, and NMR spectra* (Table 1).

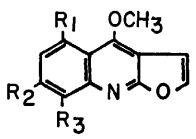

I

II

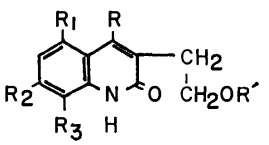

III, R = OH, R′ = $CH_2C_6H_5$

IV, R = OCH_3, R′ = $CH_2C_6H_5$

V, R = OCH_3, R′ = H

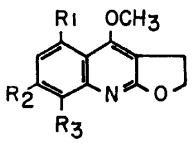

VI

a), $R_1 = R_2 = R_3 = OCH_3$ b), $R_1 = R_3 = OCH_3$, $R_2 = H$

Experimental

3-(2-Benzyloxyethyl)-4-hydroxy-2-quinolones (IIIa,b). A mixture of IIa (4.5 g) or IIb (3.7 g) and diethyl β-benzyloxyethylmalonate (7.4 g) was heated under reduced pressure (*ca.* 70 mmHg). The temperature was then raised to 180 °C over a period of 30 min, maintained at that temperature for further 30 min, and then raised and kept at 250 °C for 30 min. The cooled reaction mixture was then dissolved in chloroform. The chloroform solution was treated in a way similar to that used in a previous paper.[7] IIIa: Mp 160—161 °C (colorless needles from ethanol) (yield, 65%). IR (cm^{-1}, Nujol): 3360, 1655. UV: λ_{max}^{EtOH} nm(log ε); 220 (4.80), 238(sh) (4.63), 256 (4.50), 265 (4.50), 311.5 (4.34), 326.5 (4.24). NMR ($CDCl_3$): δ 3.97, 4.01, 4.03 (each 3H, s, $-OC\underline{H}_3$), 3.01, 3.78 (each 2H, t, J=7.0 Hz, $-C\underline{H}_2$), 4.36 (2H, s, Ph-$C\underline{H}_2$), 6.93 (1H, s, Ar-$\underline{H}$), 9.04 (1H, s, $-O\underline{H}$), 9.48 (1H, s, $-N\underline{H}$). Found: C, 65.55; H, 5.97; N, 3.64%. Calcd for $C_{21}H_{23}O_6N$: C, 65.44; H, 6.02; N, 3.63%. IIIb: Mp 138.5—140.5 °C (pale yellow cubes from ethyl acetate) (yield, 40%). IR (cm^{-1}, Nujol): 3220, 1635. UV: λ_{max}^{EtOH} nm(log ε); 210 (4.50), 224 (sh) (4.26), 244 (4.25), 253 (4.31), 262 (4.34), 292 (3.99), 304 (3.94). NMR ($CDCl_3$): δ 3.88, 3.96 (each 3H, s, $-OC\underline{H}_3$), 3.00, 3.71 (each 2H, t, J=7.2 Hz, $-C\underline{H}_2$), 4.56 (2H, s, Ph-$C\underline{H}_2$), 6.25, 6.79 (2H, ABq, J=8.4 Hz, Ar-$\underline{H}$), 9.00 (1H, bs, $-O\underline{H}$), 9.55 (1H, bs, $-N\underline{H}$). Found: C, 67.58; H, 5.94; N, 3.86%. Calcd for $C_{20}H_{21}O_5N$: C, 67.59; H, 5.96; N, 3.94%.

3-(2-Benzyloxyethyl)-4-methoxy-2-quinolones (IVa,b). Diazomethane method: IVa: Mp 135—137 °C (pale yellow plates from ethanol) (yield, 96%). IR (cm^{-1}, Nujol): 1635. UV: λ_{max}^{EtOH} nm(log ε); 212.5 (4.62), 236.5 (4.29), 257.5 (4.34), 265.5 (4.42), 316 (4.19), 325(sh) (4.08). NMR ($CDCl_3$):

* The UV, IR, NMR spectra, and mp of natural acronycidine were measured in this laboratory.

Table 1. Furo[2,3-*b*]quinolines (Ia,b)

Compound	Mp (°C)	Cryst. form	IR (cm^{-1}) Nujol	Yield (%)	Formula	Analysis (%) Found C H N	Analysis (%) Calcd C H N	UV λ_{max}^{EtOH}	UV nm(log ε)
Ia	136.5—	Colorless[a]	1620	55	$C_{15}H_{15}O_5N$	62.23	62.28	256	(4.88) 346 (3.96)
(Synthetic)	138.5	prisms	1505			5.18	5.23		
						4.89	4.84		
Ia	136—		1620					256	(4.88) 346 (3.96)
(Natural)	137.5		1505						
Ib	110—	Colorless[b]	1615	65	$C_{14}H_{13}O_4N$	64.61	64.86	231	(4.43) 311.5_{sh} (3.57)
	111.5	plates	1505			4.89	5.05	254	(4.61) 325_{sh} (3.72)
						5.46	5.40	277_{sh}	(3.81) 350 (3.83)

a) from ethanol b) from petroleum benzine.

δ 3.84 (3H, s, -OC<u>H</u>$_3$). Found: C, 66.35; H, 6.41; N, 3.45%. Calcd for $C_{22}H_{25}O_6N$: C, 66.15; H, 6.31; N, 3.51%. IVb: Mp 156.5—158.5 °C (colorless plates from ethanol) (yield, 50% (IIIb; 50% recover)). IR (cm^{-1}, Nujol): 1640. UV: λ_{max}^{EtOH} nm(log ε); 209 (4.70), 244 (4.20), 262(sh) (4.39), 269 (4.40), 300 (4.09), 310 (3.98). NMR ($CDCl_3$): δ 3.78 (3H, s, -OC<u>H</u>$_3$). Found: C, 68.06; H, 6.20; N, 3.73%. Calcd for $C_{21}H_{23}O_5N$: C, 68.28; H, 6.28; N, 3.79%.

3-(2-Hydroxyethyl)-4-methoxy-2-quinolones (Va,b). To a hydrogen-saturated solution of Pd-C (5%, 2.0 g) in absolute ethanol, IVa or IVb (5.0 g) was added; the mixture was then stirred for 4 hr at *ca.* 70 °C in an atmosphere of hydrogen. After the catalyst had been filtered off, the filtrate was evaporated under a vacuum. The residue was recrystallized to give Va or Vb. Va: Mp 153—155 °C (colorless prisms from benzene) (yield, 98%). IR (cm^{-1}): 3440, 1610. UV: λ_{max}^{EtOH} nm(log ε); 217 (4.73), 238(sh) (4.50), 257.5(sh) (4.54), 265.5 (4.60), 316 (4.38), 329.5 (4.29). NMR ($CDCl_3$): δ 3.63 (1H, bs, -O<u>H</u>). Found: C, 57.98; H, 5.99; N, 4.55%. Calcd for $C_{15}H_{19}O_6N$: C, 58.24; H, 6.19; N, 4.53%. Vb: Mp 157—158.5 °C (colorless needles from ethanol) (yield, 77%). IR (cm^{-1}, Nujol): 3320, 1620. UV: λ_{max}^{EtOH} nm(log ε); 209 (4.44), 242 (4.12), 265 (4.32), 299 (3.97), 310(sh) (3.89), 338(sh) (3.24). NMR ($CDCl_3$): δ 3.30 (1H, bs, -O<u>H</u>). Found: C, 58.98; H, 6.20; N, 4.92%. Calcd for $C_{14}H_{17}O_5N$: C, 60.20; H, 6.14; N, 5.02%.

2,3-Dihydrofuro[2,3-b]quinolines (VIa,b). A mixture of Va or Vb (1.0 g) and PPE (15 g) was heated at 120—130 °C for 2 hr. The cooled mixture was then poured into water, and the insoluble materials were filtered off. The aqueous solution was neutralized with diluted aqueous ammonia. The precipitate was collected, washed with water, and recrystallized to give VIa or VIb. VIa: Mp 191—192 °C (lit,[3] 188.5—190.5 °C) (colorless plates from ethanol) (yield, 70%). IR (cm^{-1}, Nujol): 1620, 1505. UV: λ_{max}^{EtOH} nm(log ε); 218.5 (4.56), 258.5 (4.70), 308.5 (3.84), 325(sh) (3.74). NMR ($CDCl_3$): δ 3.88, 3.90, 3.93, 3.96 (each 3H, s, -OC<u>H</u>$_3$), 4.58, 3.42 (each 2H, t, J=7.8 Hz, α,β-C<u>H</u>$_2$), 6.47 (1H, s, Ar-<u>H</u>). Found: C, 61.79; H, 5.83; N, 4.89%. Calcd for $C_{15}H_{17}O_5N$: C, 61.85; H, 5.88; N, 4.81%. VIb: Mp 149.5—151.5 °C (colorless needles from ethanol) (yield, 78%). IR (cm^{-1}, Nujol): 1620, 1505. UV: λ_{max}^{EtOH} nm(log ε); 213 (4.46), 259 (4.46), 295 (3.66), 337(sh) (3.50). NMR ($CDCl_3$): δ 3.86, 3.94, 3.98 (each 3H, s, -OC<u>H</u>$_3$), 4.63, 3.47 (each 2H, t, J=7.8 Hz, α,β-C<u>H</u>$_2$), 6.65, 6.85 (each 1H, ABq, J=7.8 Hz, Ar-<u>H</u>). Found: C, 64.62; H, 5.81; N, 5.34%. Calcd for $C_{14}H_{15}O_4N$: C, 64.36; H, 5.79; N, 5.36%.

Furo[2,3-b]quinolines (Ia,b). A mixture of VIa or VIb (1.0 g) and DDQ (1.0 g) in dry benzene (150 ml) was treated by a method similar to that used in a previous paper.[7] The resulting precipitate was collected and recrystallized to give Ia or Ib (Table 1). The mixed melting point of synthetic Ia with a natural specimen was not depressed. Ia: NMR ($CDCl_3$): δ 3.96, 4.02, 4.31 (3H×4, s, -OC<u>H</u>$_3$), 6.60 (1H, s, Ar-<u>H</u>), 7.00, 7.53 (each 1H, d, J=3.0 Hz, Furan-<u>H</u>). Ib: NMR ($CDCl_3$): δ 3.88, 4.00, 4.28 (each 3H, s, -OC<u>H</u>$_3$), 6.70, 6.92 (each 1H, ABq, J=8.4 Hz, Ar-<u>H</u>), 7.02, 7.60 (each 1H, d, J=2.4 Hz, Furan-<u>H</u>).

The author wishes to express his deep gratitude to Professor Kenji Fukui, Hiroshima University, for his encouragement through the course of this work, and also to Dr. J. A. Lamberton, C S I R O, Australia, for his gift of a natural specimen.

References

1) F. N. Lahey and W. C. Thomas, *Aust. J. Sci. Res.*, **A2**, 423 (1949).
2) J. R. Price, *ibid.*, **A2**, 249 (1949).
3) F. N. Lahey, J. A. Lamberton, and J. R. Price, *ibid.*, **3A**, 155 (1950).
4) T. R. Govindachari, B. R. Pay, S. Prabhakar, P. S. Santhanam, and V. Sudarsanam, *Indian J. Chem.*, **3**, 71 (1965).
5) T. Ohta and Y. Mori, *Tokyo Yakka Daigaku Kenkyu Nempo*, **10**, 100 (1960); *Chem. Abstr.*, **56**, 4806 (1962).
6) M. F. Grundon and N. J. McCorkindale, *J. Chem. Soc.*, **1957**, 2177.
7) T. Sekiba, This Bulletin, **46**, 577 (1973).
8) H. Richtzenhain and R. Nippus, *Chem. Ber.* **82**, 408 (1949).

BULLETIN OF THE CHEMICAL SOCIETY OF JAPAN, VOL. 47 (11), 2897—2898 (1974)

The Alkylation of *m*-Cresol with Propylene by Supported Metal Sulfates

Masahiro NITTA, Katsumi YAMAGUCHI, and Kazuo AOMURA
Faculty of Engineering, Hokkaido University, Sapporo 060

(Received February 4, 1974)

Synopsis. The alkylation of *m*-cresol with propylene over supported metal sulfate catalysts was studied at 250 °C under atmospheric pressure. The activity of the catalyst varied with the kind of sulfate and the calcination temperature, whereas the selectivity to thymol was independent of those factors and depended on the type of carrier instead.

The alkylates of phenols are quite often useful for the processing of raw materials related to perfumery, antiseptics, dyes, and synthetic resins.[1] Thymol (2-isopropyl-5-methylphenol), an important raw material in perfumery, is usually obtained by the liquid-phase reaction of *m*-cresol and propylene in the presence of an acidic catalyst; alkylation in the vapor phase is rare,[2] except for one patent.[1a] Moreover, the details of the catalysis in that patent are unclear.

In this paper, the vapor-phase alkylation of *m*-cresol with propylene over supported sulfate catalysts will be reported in order to clarify the factors governing the activity and the selectivity for thymol formation.

The propylene was obtained from the Mitsubishi Petrochemical Co., Ltd. Commercial *m*-cresol was purified by distillation under reduced pressure; its purity was estimated to be over 99.5% by means of gas chromatography. Porous silica-gel (Davison RD gel) and activated alumina (Nishio Industies Co., Ltd., KHD-24) were used as the catalyst carriers. The sulfates were guaranteed reagents purchased from the Kanto Chemical Co., Inc. Each sulfate was 1.0 mmol per unit of weight of the carrier. All the catalysts were prepared by impregnating the carrier with an aqueous solution of a sulfate for a day and then by drying it at 120 °C in the air. It was assumed that all of the sulfate was supported on the carrier.

The activity test was carried out in a flow system under atmospheric pressure. A catalyst (10—20 mesh) packed in a glass tube reactor was activated at a given temperature for 3 hr in a nitrogen stream before the reaction. The liquid products, which were collected every 20 min, was analyzed by gas chromatography with a column containing lanolin (5 wt%) and LAC (0.5 wt%) supported on Chromosorb AW (2 m, 145 °C).

The acidic properties of the catalysts were measured by the usual *n*-butylamine titration using the Hammett indicators. The surface areas of the catalysts were measured by the BET method.

In this alkylation, the liquid products obtained were thymol and its three isomers, *iso*-thymol, and a small quantity (3 mol%) of an unknown component.* Among those products, the thymol (obtained in a *ca.* 70% yield) is the most desirable, as has been mentioned above. The initial conversion of *m*-cresol by extrapolation to zero time was taken as the catalytic activity, for the conversion decreased gradually with the time. The selectivity of the catalyst was expressed by the ratio of the thymol to all of the thymol isomers, and it was held constant throughout the time on stream. The activities and the selectivities of the various catalysts are shown in Table 1. The activities of the carriers were poor, though they were measurable. It is clear that the addition of the sulfates, with the exception of the Li and Na salts, increases the activity of the carrier. The activity varied with the kind of sulfate. These catalysts gave a high selectivity for thymol formation, though it was difficult to ascertain the equilibrium composition of thymol isomers. The activities seem to have no direct relation to the surface areas. The silica-carrier catalysts showed a selectivity of *ca.* 70%, while the alumina-carrier catalysts showed one of *ca.* 60%. From these facts it can be considered that the activity depends upon the property of the sulfate and that the selectivity depends upon the property of the carrier.

Metal sulfate is a well-known solid acid and catalyzes various reactions.[3] Fukui *et al.* have reported that the sulfates supported on silica-alumina are effective for the ethylation of benzene.[4] They supposed that the modified acid sites of the sulfate produced on the carrier are responsible for the activity. Therefore, the acidities of the present catalysts were measured (Tables 1 and 2). A rough correlation between the acidities (the amount of acid sites having the strength with $H_0 \leqq +3.3$) and the activities was found for a series of catalysts of a given carrier. In spite of its higher acidity, the acid sites of both carriers seem to be ineffective for the alkylation. These facts support Fukui's

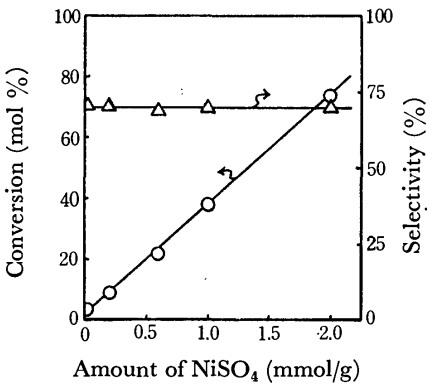

Fig. 1. Effect of supported amount of $NiSO_4$ on SiO_2.
Conditions: W/F = 19.5 g·hr/mol, reaction temp. = 250 °C, calcination temp. = 300 °C, propylene/*m*-cresol = 1.0 mol/mol.
○: *m*-cresol conversion, △: thymol selectivity.

* We assumed the relative mole sensitivity of the unknown to be the same as those (0.78) of the thymol isomers to *m*-cresol.

Table 1. Activities and acidities of supported metal sulfate catalysts

Catalyst[a]	Conversion[b] (mol %)	Selectivity (%)	Acidity, (mmol/g) $H_0 \leqq -3.0$	Acidity, (mmol/g) $H_0 \leqq +3.3$	Surface area (m^2/g)
SiO_2 (small pore)	4.0	67	0.20	0.61	817
Li_2SO_4–SiO_2	5.0	69	0.20	0.32	—
Na_2SO_4–SiO_2	0	—	0	0.26	744
$BeSO_4$–SiO_2	30	69	0.06	0.56	—
$MgSO_4$–SiO_2	27	69	0.09	0.48	—
$NiSO_4$–SiO_2	37	70	0.03	0.69	731
$Al_2(SO_4)_3$–SiO_2	47	69	0.60	0.69	—
Al_2O_3	0.1	57	0	0.34	326
Li_2SO_4–Al_2O_3	0	—	0	0	—
Na_2SO_4–Al_2O_3	0	—	0	0	312
$BeSO_4$–Al_2O_3	37	60	0	0.14	—
$MgSO_4$–Al_2O_3	1.2	60	0	0.05	—
$NiSO_4$–Al_2O_3	2.8	56	0	0.12	302
$Al_2(SO_4)_3$–Al_2O_3	42	56	0	0.35	—

a) Supported amount = 1.0 mmol/g, Calcination temp. = 300 °C. b) Reaction conditions: Temp. = 250 °C, W/F = 19.5 g·hr/mol, propylene/*m*-cresol = 1.0 (mol/mol).

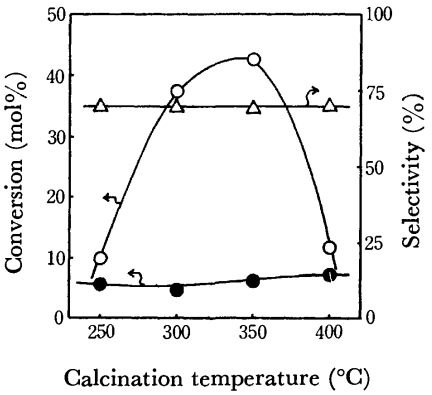

Fig. 2. Effect of calcination temperature of catalyst. Catalyst: $NiSO_4$–SiO_2, Conditions are the same as those in Fig. 1.
○: *m*-cresol conversion of $NiSO_4$–SiO_2, ●: *m*-cresol conversion of SiO_2, △: thymol selectivities of SiO_2 and $NiSO_4$–SiO_2.

proposal. Furthermore, the fact that the activity per unit of weight of the catalyst increased with the $NiSO_4$ content, as is shown in Fig. 1, supports the idea that the effective active sites arise essentially from the sulfate. This has also been domonstrated by the effect of the calcination temperature on the activity, as is shown in Fig. 2. That is to say, the activity of $NiSO_4$–SiO_2 varied with the calcination temperature, though the activity of the carrier itself did not vary. This curve, having its maximum at 350 °C, agrees well with the variation in the acidity of heat-treated $NiSO_4$ which was previously determined by one of present authors and others.[5,6]

The selectivity was held constant in Figs. 1 and 2, independent of the supported amount of sulfate and of the calcination temperature, as would be expected when the carrier was the same. Further, in order to elucidate the selectivity, a few typical solid acid catalysts were tested. The results, shown in Table 2, reveal that the selectivity is not governed by the acid strength of the catalyst. The selectivity of large-pore SiO_2 (80—100 Å) in Table 2 is lower than that of small-pore SiO_2 (22 Å) in Table 1. This suggests that, on the small-pore catalysts, the reactant molecules take a particular adsorbed state favorable to thymol formation. Details of the selectivity will be reported, along with data on other catalysts, at a later date.

Table 2. Acidity and selectivity of various acid catalysts

Catalyst	Acidity (mmol/g) $H_0 \leqq -3.0$	Acidity (mmol/g) $H_0 \leqq +3.3$	Conversion[d] (mol%)	Selectivity (%)
SiO_2(large pore)	0.10	0.14	2	62
SiO_2–Al_2O_3[a]	0.20	0.29	14	48
H_2SO_4–Al_2O_3[b]	0.37	0.50	25	63
H_3PO_4–celite[c]	0.48	0.58	30	45

a) Commercial catalyst obtained from the Japan Gasoline Co., Ltd. b) Supported amount of H_2SO_4 = 1.0 mmol/g. c) Commercial solid phosphoric acid obtained from the Japan Gasoline Co., Ltd. d) Reaction conditions are the same as Table 1.

We are grateful to Dr. Fujio Fujiwara of the Osaka Munucipal Technical Research Institute for providing the samples used for the analysis of thymol isomers.

References

1) a) Japan patent, SHO 46-3053; b) U.S. 3479410 (1967).
2) S. H. Patinkin and B. S. Friedman, "Friedel-Crafts and Related Reactions," Vol. II, ed. by G. A. Olah, Interscience Publishers, N. Y. (1964), p. 1.
3) K. Tanabe and T. Takeshita, "Advances in Catalysis," Vol. 17, Academic Press, N. Y. (1967), p. 315.
4) Y. Fukui, H. Takaoka, J. Ishii, K. Hirai, and T. Takahashi, This Bulletin, **40**, 446 (1967).
5) K. Tanabe and R. Ohnishi, *J. Res. Inst. Catalysis, Hokkaido Univ.*, **10**, 229 (1962).
6) K. Tanabe and M. Nitta, *Bull. Japan Petrol. Inst.*, **14**, 47 (1972).

BULLETIN OF THE CHEMICAL SOCIETY OF JAPAN, VOL. 47 (11), 2899—2900 (1974)

The Solid-State Spectra of Several Rhodizonates[1)]

Jun-ichi AIHARA

Department of Chemistry, Faculty of Science, Hokkaido University, Sapporo 060

(Received February 26, 1974)

Synopsis. The charge-transfer transitions between the anions were observed in the absorption spectra of alkali-metal rhodizonates in the solid state. Ammonium ions enhanced the electronic transition of this kind, whereas the solid-state spectrum of the barium salt was similar to the solution spectrum of the rhodizonate ion.

More than a decade ago, West *et al.* pointed out that the oxocarbons with a general formula of $C_nO_n^{2-}$ may be considered as a new class of aromatic compounds.[2)] The assignment of the vibrational spectra confirmed the presence of aromaticity in the dianion of rhodizonic acid ($C_6O_6^{2-}$).[3)] The electronic spectra of the rhodizonates have often been observed in aqueous solutions.[4)] Though the absorption spectra for the crystals are lacking, some salts are strikingly characterized by deep coloration in the solid state. In order to clarify the electronic structure of these rhodizonates, we attempted to obtain the absorption spectra of the salts in the solid state.

Experimental

The lithium, sodium, potassium, and ammonium rhodizonates were prepared from inositol and the corresponding acetates by the method developed by Preisler and Berger.[5)] The rubidium, cesium, and strontium salts were prepared by the metathesis reaction of the lithium salt. Commercial barium salt was used without further treatment. The absorption spectra of the solid rhodizonates were obtained by applying the Kubelka-Munk function to the diffuse reflection spectra of the samples dispersed in sodium chloride. The gross spectral shapes were in good accordance with those derived from the transmission spectra of the Nujol mulls.

Results and Discussion

Figure 1 shows the absorption spectra of three typical rhodizonates in the solid state. The solution spectrum of rubidium rhodizonate is therein compared to them. As may easily be seen, the solid-state spectrum of the brown barium salt has a close resemblance to that of the aqueous solution. In both absorption spectra, there is a distinct and isolated band in the visible region. The absorption maximum of this principal band is located at 20800 cm^{-1} in the solution spectrum and is followed by an accompanying shoulder near 22700 cm^{-1}. It has been suggested that such a doublet structure is due to the Jahn-Teller distortion in the excited state.[2)] On the basis of the similarity to the solution spectrum, the first absorption band of the barium salt is attributable to the intramolecular transition of the rhodizonate ion except for the perceptible absorption tail on the low-energy side. The corresponding peak and shoulder are present at 19800 and 22500 cm^{-1} respectively in the spectrum of the solid barium salt. The absorption spectrum of the red-brown strontium salt is of the same type as that of the barium salt.

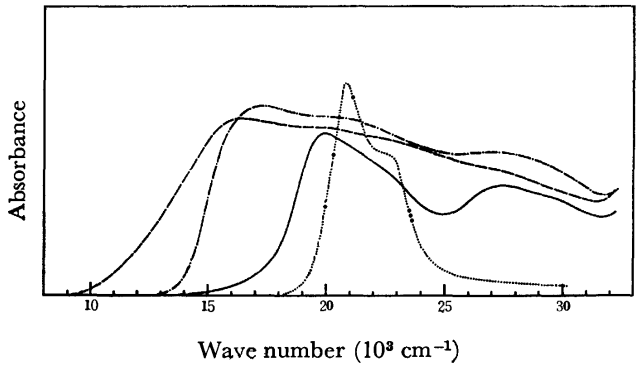

Fig. 1. The absorption spectra of the solid barium (——), rubidium (-·-·-), and ammonium (– – –) rhodizonates, and the aqueous solution of rubidium rhodizonate (····).

On the contrary, the solid rubidium rhodizonate appears almost black; indeed, it exhibits quite a different spectrum, one in which the principal band is considerably diffused around 20000 cm^{-1}. Here, it must be noted that the principal band is noticeably preceded by an intense new absorption band probably centered at about 17000 cm^{-1}. This additional band was found neither in the spectrum of the solid barium salt nor in the solution spectrum. The low-energy portion of the spectrum was found by diffuse reflection spectroscopy to diminish gradually when the sample was ground with sodium chloride. That is, the intensity ratio of the principal band to the additional one increases by this treatment. From this viewpoint, the interionic character of the latter band is strongly supported for this salt. Such a peculiar feature is substantially common to all alkali-metal salts except for the lithium salt, though the colors of the salts vary from the dark green of sodium salt to the dark violet of potassium and cesium salts.

Another clue to this effect is given by the crystal structure of rubidium rhodizonate as determined by X-ray diffraction.[2)] This salt forms a layer-type structure with the planar anions arranged in stacks. A more interesting finding was that the carbon atoms of anions in the adjacent layers approach each other quite closely. The separation distance is 3.30 Å, which is closer than the van der Waals distance. Such a crystal structure is a replica of the crystalline TCNQ (Tetracyanoquinodimethane) anion-radical salt, where the TCNQ anions are stacked face-to-face in the same columns.[6)]

If one remembers that the charge-transfer occurs between the TCNQ anions in the crystal and induces the absorption band in the near infrared region,[7)] the

same effect can be expected in the rubidium rhodizonate crystal. In other words, it may be reasoned by analogy with the columnar structure and the related electronic spectrum of the solid TCNQ salt that the additional absorption band found in the solid-state spectrum of rubidium rhodizonate can be assigned with little difficulty to the charge-transfer transition between the adjacent rhodizonate anions. It must have been this kind of absorption band that MacIntyre and Werkema predicted for the solid potassium squarate ($K_2C_4O_4$).[8] They concluded that the formation of the charge-transfer self-complex can be nicely represented by a crystal structure similar to that of the TCNQ salt.

The black ammonium rhodizonate crystal has similar spectral features, with the additional charge-transfer band further broadened to the lower-energy side. This fact is suggestive of the closer stacking of the rhodizonate anions in the solid. As in the ammonium croconate crystal ($(NH_4)_2C_5O_5$),[9] each ammonium ion is supposedly bonded to two oxygen atoms in the molecular plane below the nitrogen atom, and to two more oxygen atoms in the plane above, so as to enhance the charge-transfer interaction between anions. The charge-transfer band of the dark green lithium salt is similarly broadened.

On the other hand, the proposed structure of the barium salt is a chain polymer,[10] in which each rhodizonate ion is chelated to two different barium ions, giving a square planar arrangement of oxygen atoms about the barium ion. Since such a structure does not always coincide with the most favorable arrangement for the interaction between the anions in the different chains, the long absorption tail of the barium salt may be a result of the weakened interionic charge-transfer interaction. In all cases, the principal band is preserved around 20000 cm^{-1}.

So far, the appearance of the charge-transfer band between the same kind of ions in the crystal has been considered as one of the most distinguished characteristics of the organic ion-radical salt. In conclusion, it should be emphasized that such diamagnetic compounds as alkali-metal rhodizonates also exhibit pronounced charge-transfer bands between anions in the solid state.

References

1) Part IV of "Organic Charge-Transfer Self-Complexes"; Part III: A. Sasaki, J. Aihara, and Y. Matsunaga, This Bulletin, to be published. This work was financially supported by the Fuji Photo Film Co., Ltd.

2) R. West and J. Niu, "Nonbenzenoid Aromatics," Vol. I, ed. by J. P. Snyder, Academic Press, New York, N. Y. (1969), Chap. 6.

3) R. T. Bailey, *J. Chem. Soc. Ser. B*, **1971**, 627.

4) See, *e.g.*, B. Eistert and G. Bock, *Angew. Chem.*, **70**, 595 (1958).

5) P. W. Preisler and L. Berger, *J. Amer. Chem. Soc.*, **64**, 67 (1942).

6) C. J. Fritchie, Jr. and P. Arther, Jr., *Acta Crystallogr.*, **20**, 892 (1966); A. Hoekstra, T. Spoelder, and A. Vos, *ibid.*, **B28**, 14 (1972).

7) H. Kuroda, S. Hiroma, and H. Akamatu, This Bulletin, **41**, 2855 (1968); S. Hiroma, H. Kuroda, and H. Akamatu, *ibid.*, **44**, 9 (1971).

8) W. M. MacIntyre and M. S. Werkema, *J. Chem. Phys.*, **40**, 3563 (1964).

9) N. C. Baenziger and J. J. Hegenbarth, *J. Amer. Chem. Soc.*, **86**, 3250 (1964).

10) R. West and H. Y. Niu, *ibid.*, **85**, 2586, 2589 (1963).

BULLETIN OF THE CHEMICAL SOCIETY OF JAPAN, VOL. 47 (11), 2901—2902 (1974)

Synthetic Photochemistry. V.[1] Azulene Derivatives from the Photoadducts of Methyl Acetopyruvate with Cycloheptatriene

Hitoshi TAKESHITA and Akira MORI

Research Institute of Industrial Science, Kyushu University, Hakozaki, Fukuoka 812

(Received March 14, 1974)

Synopsis. Two azulene derivatives, 1-methoxycarbonyl-3-methylazulene (III) and 1-methoxycarbonyl-2-methylazulene (IV), were obtained by the pyrolysis of the photoproducts of methyl acetopyruvate–cycloheptatriene. IV was understood to be derived from a subsequent photopinacolization of an unisolable $[2+2]\pi$ photoadduct (VIII).

In the course of our studies of the photocycloaddition reaction of methyl acetopyruvate (I) with cycloheptatriene (II),[2] we noticed a characteristic coloration which should indicate a formation of azulene derivatives during the work-up. This paper will discuss the structures and mechanism of the formation of the azulene derivatives.

When the reaction mixture was heated *in vacuo*, a dark colored fraction was obtained after the distillation of most of the volatile fraction. The subsequent silica gel chromatographic separation of this afforded two azulene derivatives, III (blue needles) and IV (blue violet solids).[3] Both III and IV were analyzed to be $C_{13}H_{12}O_2$ arising from 1 : 1 adducts of I and II. Since III and IV both have the aromatic methyl group [δ: 2.61 (III), and 2.85 (IV)] and the methoxycarbonyl group [δ: 3.87 (III), and 4.01 (IV), $\nu_{C=O}$: 1675 (III), and 1677 cm^{-1} (IV)] on the five-membered ring [1H singlet at δ: 8.09 (C_2–H of III), and 7.17 (C_8–H of IV)], the determination of the position of either of the substituents should clarify their structures. In the NMR spectra, III [δ: 9.52 (dd, J=9.5, 2.0 Hz)] and IV [δ: 9.63 (dd, J=10.0, 2.0 Hz)] both have C_5–H signals at a very low field, disclosing the presence of a methoxycarbonyl group at the C_1-position for these compounds. Therefore, by the use of Plattner's well-known rule on the UV- and visible absorption maxima of azulenes[4] [λ_{max}^{MeOH}: 564 (III), and 530 nm (IV). $\lambda^{predict}$: 557 (III), and 519 nm (IV)], their structures have been deduced to be as shown.

Chart 1.

Since the absence of the azulenes in the original reaction mixture has been ascertained by a careful inspection of the NMR spectra of the fractions obtained by silica gel chromatography prior to the distillation, the azulenes must be formed during the distillation.

When the photoadducts of I and II[2] were pyrolyzed, only the ene-reaction product (V) was shown to develop a coloration due to the azulenoid compound, which consisted solely of a blue isomer (III). On the other hand, the most polar fraction of the photoproducts of I and II was also shown to give a coloration due to azulene derivatives by pyrolyzing under a nitrogen atmosphere; indeed, the presence of III and IV in the product mixture was proved by direct comparisons. We failed to isolate azulene-precursors due to the extreme instability and the limited quantity available,[5] but it seems reasonable to consider the precursors of the azulenes as glycol derivatives (VI and VII), which may be supposed to come from a further photochemical reaction of their primary products (V and VIII). Therefore, the following scheme may be proposed:

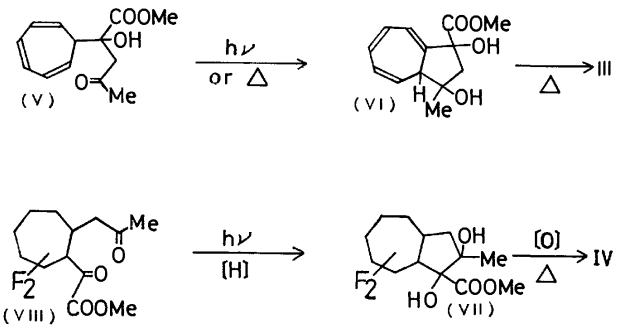

Chart 2.

VI (a 1,3-glycol) can be formed by an intramolecular hydrogen abstraction with the excited carbonyl group of V, and its aromatization needs the elimination of only two moles of water. On the other hand, VII (a 1,2-glycol) corresponds to a photo-reductive pinacolization product of VIII, being a $(2+2)\pi$ cycloadduct. Although VIII has not been detected in the products of I and II, an analogous reaction was reported in the literature;[6] furthermore, the presence of excess II may facilitate the reduction process. The dehydration of VII should give a dihydroazulene derivative, whose type of compounds undergoes a spontaneous aromatization.

It is worthwhile to note that it seems superficially that the formation of III and IV could be interpreted in terms of an "oxabicyclobutane" intermediate.[7] The concept has been frequently mentioned, but never verified.[8] The present results, either, since no product directly linked to compound (IX) has been detected, and since it would be improbable to assume that all the photo-products of IX with II are too unstable to be characterized, do not seem to favor the concept.

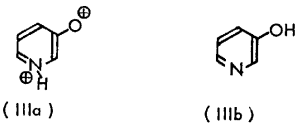

Chart 3.

To date, there have been considerable interests in the non-dehydrogenative preparation of the azulene skeleton by various cyclizations of propenyl-substituted seven-membered derivatives. Indeed, two successful experiments have been reported; Tsuruta *et al.*[9] have obtained 1,2-dicyanoazulene by a thermal rearrangement of 8-(2,2-dicyanovinyl)-heptafulvene, and Watanabe *et al.*[10] have used an acid-induced cyclization of 2-(7-tropyl)-benzaldehyde to afford benz[a]azulene, although uncondensed azulene was not obtained by this method. The formation of III from V thus constitutes a facile synthesis of azulene derivatives; according to one view of the initial photochemical step, this could be a rather general method for the preparation of 1-carboxy-2-, and/or -3-alkyl azulenes.[11] Although the yields, in the present stage, are insufficient, an improvement for the aromatization of V may not be difficult.

Experimental

Pyrolysis of the Whole Photoproduct Mixture of I and II. I (6.00 g) was dissolved in II (100 ml) and dioxane (200 ml), and the mixture was irradiated by means of a 450 W high pressure mercury lamp for 95 hr until it showed a negative ferric chloride test. Then the mixture was distilled under reduced pressure to remove a polymeric material. The higher boiling fraction (bp 172—184 °C/4 mmHg, 3.67 g) developed a dark-coloration by cooling. Silica gel column chromatography of the above afforded blue needles (III, mp 61—62 °C, 85 mg) (Found: C, 78.29; H, 6.13%. Calcd for $C_{13}H_{12}O_2$: C, 77.98; H, 6.04%) and a blue-violet solid (IV, 115 mg) (Found: C, 77.86; H, 6.11%) in addition to the previously-reported products,[2] methyl tropylglyoxalates (140 mg), ene-product (V, 105 mg), (4+2)π-cycloadduct (102 mg), and (6+2)π-cycloadduct (34 mg). The most polar fraction (75 mg) eluted with methanol–ether showed a strong ν_{OH} in the IR spectrum.

Pyrolysis of V; Formation of III. V (300 mg) was sealed in a glass tube and heated at 190 °C for 3 hr. The subsequent fractionation of the mixture afforded III (~3 mg) and methy ltropylglyoxalate (20 mg), together with recovered V (80 mg).

Pyrolysis of the Polar Fractions of Photoproducts; Formation of III and IV. The most polar portion of eluate (0.3 g) of the chromatography was heated in a sealed tube at 190 °C for 30 min. The mixture was then chromatographed through silica gel, and the blue fractions were collected to give III (~1 mg) and IV (~1 mg).

We wish to thank The Ministry of Education for its financial support, and Mr. I. Ohmori, Tohoku University, for his taking part in the experiments.

References

1) Part IV: H. Takeshita, A. Mori, and S. Ohta, This Bulletin, **47**, 2437 (1974).

2) H. Takeshita, A. Mori, and S. Itô, *ibid.*, **47**, 1767 (1974).

3) Spectral (NMR, UV) properties of this compound are in well accord with the reported data of 1-ethoxycarbonyl-2-methylazulene. *cf.* T. Nozoe, K. Takase, T. Nakazawa, and S. Fukuda, *Tetrahedron.*, **27**, 3357 (1971).

4) Pl. A. Plattner, A. Fürst, A. Müller, and A. R. Somerville, *Helv. Chim. Acta*, **34**, 971 (1951).

5) Unless the freshly prepared fraction was used, no IV was obtained from the pyrolyzate, thus the precursor of IV is much unstable than that of III.

6) H. Hikino and P. de Mayo, *J. Amer. Chem. Soc.*, **86**, 3582 (1964).

7) *e.g.*, a) E. J. Corey, J. D. Bass, R. LaMahien, and R. B. Mitra, *ibid.*, **86**, 5574 (1964); b) N. Furutachi, Y. Nakadaira, and K. Nakanishi, *ibid.*, **91**, 1028 (1969).

8) L. E. Friedlich and G. B. Schuster, *ibid.*, **94**, 1193 (1972).

9) H. Tsuruta, T. Sugiyama, and T. Mukai, *Chem. Lett.*, **1972**, 185.

10) T. Watanabe and N. Soma, *Chem. Pharm. Bull.*, **20**, 2215 (1971).

11) An extention of the reaction is presently undergoing. Homologs of I have shown the formation of azulenes, but acetylacetone or other simple β-diketones gave no azulene derivatives.

BULLETIN OF THE CHEMICAL SOCIETY OF JAPAN, VOL. 47 (11), 2903—2904 (1974)

Pyrolysis of Dialkyl 2-Acyloxyalkylphosphonates

Yoshiki OKAMOTO, Toshikazu KAWAI, and Hiroshi SAKURAI

The Institute of Scientific and Industrial Research, Osaka University, Yamada-kami, Suita-shi, Osaka 565

(Received March 28, 1974)

Synopsis. The pyrolysis of dialkyl 2-acyloxyalkylphosphonates at 220—240 °C gave the corresponding alkyl carboxylates and olefins by the elimination of metaphosphoric acid $(HPO_3)_n$.

Tsurugi and his co-workers[1] reported that the pyrolysis of dimethyl 2-acetoxyethyl- or dimethyl 3-acetoxypropylphosphonate at 550—600 °C gave dimethyl vinyl- or dimethyl 3-propenylphosphonate in 51—58% yields respectively, but in the case of diethyl and dipropyl 2-acetoxyethylphosphonates, the corresponding unsaturated phosphonates could not be obtained.

We have found that dialkyl 2-acetoxyethylphosphonates (I), except in the case of the dimethyl derivative, gave alkyl carboxylates and olefins at 220—240 °C, along with the formation of metaphosphoric acids, $(HPO_3)_n$.

The I compounds were prepared by the reaction of acyl chlorides with the corresponding hydroxy derivatives, derived from dialkyl 2-oxoethylphosphonates by treating them with sodium borohydride.[2]

$$RCOOR'CHCR''HPO(OR''')_2 \quad (I)$$

	R	R′	R″	R‴
I-a	CH_3	C_6H_5	H	C_2H_5
I-b	CH_3	C_6H_5	H	C_3H_7
I-c	CH_3	C_6H_5	H	CH_3
I-d	CH_3	C_6H_5	H	*iso*-C_3H_7
I-e	CH_3	CH_3	H	C_2H_5
I-f	CH_3	H	C_6H_5	C_2H_5
I-g	CH_3	C_6H_5	CH_3	C_2H_5
I-h	C_2H_5	C_6H_5	H	C_2H_5

Diethyl styrylphosphonate (II-a) was prepared from styrene and phosphorus pentachloride by the method of Anisimov.[2] Ethyl hydrogen styrylphosphonate (II-b) was prepared by the hydrolysis of II-a, using sodium hydroxide in ethanol. Styrylphosphonic acid (II-c) was prepared by the hydrolysis of II-a with 6-M hydrochloric acid. Acetyl diethyl phosphate was prepared by the phosphorylation of acetic acid with tetraethyl phosphorous-phosphoric anhydride.[3]

In each run of the pyrolysis of the phosphonate, 0.1 mol of the phosphonate was decomposed in a 10 ml distilling flask heated at the rate of 5 °C/min in a metal bath. The decomposition of the phosphonate began in the range from 220—240 °C and was finished in a few minutes. The pyrolysis products were trapped in a tube cooled with ice water. They were analyzed by means of glc on a 3 m×3 mmϕ column, packed with NDP (20%) on Celite (60—80 mesh), at the column temperature of 90 or 120 °C, using nitrogen gas as the carrier. The glc peaks were identified by comparing their retention times with those of authentic samples. The distillable products from I are given in Table 1.

Table 1. The products obtained by the pyrolysis of I

Phosphonate	Beginning temp. of decomp. °C	Product (Yield %)
I-a	198—100	$C_6H_5CH=CH_2$ (90.7), CH_3COOEt (80.0)
I-b	195—200	$C_6H_5CH=CH_2$ (92.3), CH_3COOPr (84.3)
I-c	340[a]	
I-d	168—170	$C_6H_5CH=CH_2$ (80.9), CH_3COO-IsoPr(68.7)
I-e	195—198	$CH_3CH=CH_2$[b], CH_3COOEt (80.1)
I-f	195—197	$C_6H_5CH=CH_2$ (31.4), CH_3COOEt (46.3)
I-g	198—200	*t*-$C_6H_5CH=CHCH_3$ (42.5), CH_3COOEt (59.0)
I-h	195—197	$C_6H_5CH=CH_2$ (90.0), C_2H_5COOEt (80.9)

a) boiling point. b) undetermined.

The temperature of the beginning of the decomposition were determined from the TGA curves. In the pyrolysis of those compounds, acetic acid or diethyl α,β-unsaturated phosphonate could not be detected. Ethylene was detected in all cases except I-b, -c, and -d. The analytical values of the pyrolyzed residues of I-a, -b, and -h were approximately in agreement with the $(HPO_3)_n$ formula. The decomposition temperature was affected by the structure of the alkoxy group (R‴O). I-c did not decompose even at 340 °C, its boiling point. I-d began to decompose at 168 °C. When small amounts of phosphoric acid were added, the temperature of the decomposition of I-a fell to 162 °C. The acid effectively catalyzed the initiation of the decomposition. The activation energy of the thermal decomposition of I-a was 33.1±3 kcal/mol, estimated from a TGA curve, on the assumption that the reaction obeyed first-order kinetics;[4] its value hardly changed upon the addition of the acid. The results of the thermal decompositions of II-a, -b, and -c are given in Table 2.

Table 2. The products obtained by the pyrolysis of II

Phosphonate	Beginning temp. of decomp. °C	Products (%)
II-a	260—265	$C_6H_5CH=CH_2$ (65)
II-a[a]	235—240	$C_6H_5CH=CH_2$ (91)
II-b	200—205	$C_6H_5CH=CH_2$ (48)
II-c	265—270	$C_6H_5CH_2CH_3$(22.4), C_6H_5 (25.5)

a) H_3PO_4 (5%) was added.

The pyrolysis behavior of II-a, which decomposed at a higher temperature than did I-a or -h, implied that the former is not involved as an intermediate in the thermal decomposition of the latter two. The temperature of the decomposition of II-c was the same as that of I-a, but the yield of styrene from the former was lower than that from the latter. This finding presumably eliminates the possibility of II-c being an intermediate in the pyrolysis of I-a. It was also supported experimentally by the DTA and TGA curves that the pyrolysis did not proceed step by step with the rise in the temperature. The pyrolysis of an equimolar mixture of I-b and -h began at 220 °C to give propyl acetate, ethyl acetate, ethyl propionate, and propyl propionate in the mole ratio of 1.1: 1.0: 1.3: 1.2. When the same mixture was pyrolyzed at 220—230 °C in a 10% solution of paraffinic hydrocarbon (mp 68—70 °C), the alkyl carboxylates mentioned above were given in the mole ratio of 0.9: 1.0: 1.3: 1.0. In the analysis of the phosphonate mixture immediately after the beginning of the decomposition, the ester-exchange between the phosphonates could not be observed. These facts implied that the formation of alkyl carboxylates might involve an intermolecular process. The pyrolysis of I may proceed by means of Scheme 1.

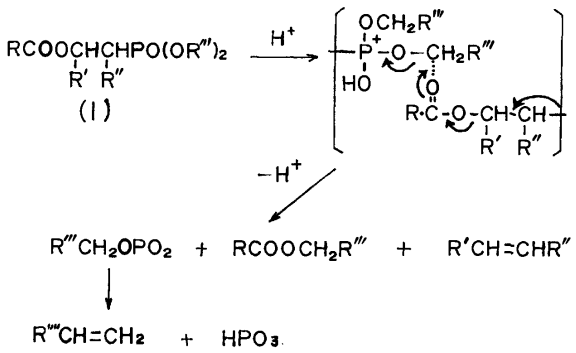

Scheme 1.

The nucleophilic attack of the carbonyl oxygen of the acetoxy group on the methylene carbon of the alkoxy group, followed by the migration of electrons as described in Scheme 1, resulted in the formation of alkyl carboxylate and olefin.

Another possible mechanism (Scheme 2) to account for the formation of those products can be proposed: At first, the nucleophilic attack of carbonyl oxygen occurred on the phosphorus atom and resulted in the formation of acyl dialkyl phosphate, followed by further decomposition in which alkyl carboxylate was given in the manner described above.

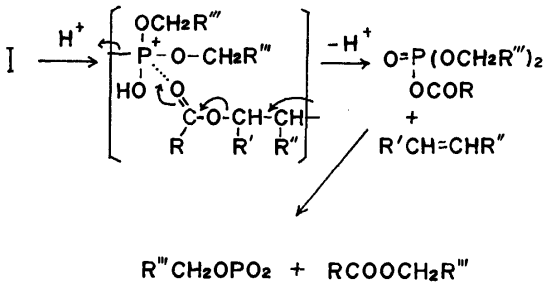

Scheme 2.

We found that acetyl diethyl phosphate decomposed to give ethyl acetate in a 70% yield at 170—190 °C.

It was reported that 2-hydroxyphosphonic acid bis-(dimethylamide) underwent thermal decomposition to olefin and phosphoric acid bis-amide at reflux in a toluene solution.[5] In this reaction, it was assumed that the nucleophilic attack of the alkoxy anion on the phosphorus atom and the formation of a four-membered ring transition state were involved.

However, in our experiments, under the same conditions, the analogous transformation of diethyl 2-hydroxy-2-phenylethylphosphonate to olefin and the phosphoric acid diester did not occur, even though trace amounts of phosphoric acid were present, but diethyl α,β-unsaturated phosphonate was obtained in a 60% yield. The difference in behavior may arise from the difference in the electrophilicity of the phosphorus atom. The nucleophilic attack of the carbonyl oxygen of I may preferably occur at the methylene carbon (Scheme 1) rather than at phosphorus (Scheme 2). Scheme 1 resembles that of the pyrolysis of halogenated alkyl phosphates, in which the nucleophilic attack of halogen occurred preferentially at the methylene or methine carbon of an alkoxy group to give alkyl halide in an appreciable yield.[7]

References

1) M. Yamagami, R. Nakao, T. Fukumoto, and J. Tsurugi, *Nippon Kagaku Kaishi*, **1972**, 1991.

2) K. Sasse, "Methoden der Organischen Chemie, XII/1, Organisch Phosphoverbindungen" ed. by E. Müller, Georg Thieme Verlag. Stuttgart (1963), p. 393.

3) J. Michalski and T. Modro, *Chem. Ber.*, **95**, 1629 (1962).

4) E. S. Freeman and B. Carrol, *J. Phys. Chem.*, **62**, 394 (1958).

5) E. J. Corey and G. T. Kwiathowski, *J. Amer. Chem. Soc.*, **90**, 6816 (1968).

6) Y. Okamoto, N. Kimura, and H. Sakurai, This Bulletin, **47**, 1294 (1974).

BULLETIN OF THE CHEMICAL SOCIETY OF JAPAN, VOL. 47 (11), 2905—2906 (1974)

Metal Phosphinylides and Phosphinothioylides. III.[1] Reactions of Lithium Diphenylphosphinylide and Diphenylphosphinothioylide with Acetone and Bromoacetone

Masaaki YOSHIFUJI, Hideyuki GOMI, and Naoki INAMOTO

Department of Chemistry, Faculty of Science, The University of Tokyo, Hongo, Tokyo 113

(Received May 14, 1974)

Synopsis. Reaction of acetone with $[Ph_2PO]Li$ gave 1-hydroxy-1-methylethyl- (**2a**), 1,1-dimethyl-3-oxobutyldiphenylphosphine oxides (**3a**) and 2,6-bis(diphenylphosphinyl)-2,6-dimethylheptan-4-one (**4a**). The corresponding sulfide **2b** was obtained in the case of $Ph_2P(S)H$, and **3b** and **4b** in the case of $[Ph_2PS]Li$ (**5b**). Bromoacetone reacted with **5b** through substitution reaction.

It has been reported that the reaction of acetone with diphenylphosphinylmagnesium bromide (**1a**), prepared from three molar amounts of phenylmagnesium bromide and diethyl phosphite, gave phosphine oxides **2a** and **4a**, the latter being considered to be formed by addition of **1a** to phorone formed from acetone and ethoxide ion.[2]

$$[Ph_2PX]M + Me_2CO \longrightarrow Ph_2P(X)CMe_2OH$$

1, M=MgBr; a, X=O — **2**
5, M=Li; b, X=S

$$+ Ph_2P(X)CMe_2CH_2COMe$$

3

$$+ (Ph_2P(X)CMe_2CH_2)_2CO$$

4

If **4a** is formed by the suggested mechanism, **3a** should be formed by addition of **1a** to mesityl oxide produced during the course of reaction.

This paper describes reactions of acetone and some ketones with lithium diphenylphosphinylide (**5a**) or diphenylphosphinothioylide (**5b**).

Reaction of **5a** with acetone afforded three phosphine oxides **2a**, expected **3a** and **4a**. The separation of these compounds was difficult, and **2a** and **3a** were isolated only in 7.4 and 20% yields, respectively. **4a** was identified by NMR, which exhibited signals at δ 1.37 (d, J_{PCCH} 16.8 Hz, Me), 2.67 (d, J_{PCCH} 7.8 Hz, CH_2), and 7.3—8.2 (m, Ph), from the crude mixture. The data were in agreement with the reported one.[2]

Reaction of **5b** with acetone did not give **2b**, but gave **3b** (43%), **4b** (23%) and 2-diphenylphosphinothioyl-6-diphenylphosphinyl-2,6-dimethylheptan-4-one (**6**) (4%).

$$Ph_2P(S)CMe_2CH_2COCH_2CMe_2P(O)Ph_2 \quad \mathbf{6}$$

By the reaction of **5b** with mesityl oxide, **3b** was also obtained in 40% yield. No **4b** could be isolated from **5b** and phorone. The following stepwise mechanism would be more reasonable. Slightly excess amount of *n*-butyllithium acts as a base for the condensation of acetone.

$$2Me_2CO \xrightarrow{n\text{-BuLi}} Me_2C{=}CHCOMe \xrightarrow{5} \mathbf{3} \xrightarrow[Me_2CO]{n\text{-BuLi}}$$

$$Ph_2P(X)CMe_2CH_2COCH{=}CMe_2 \xrightarrow{5} \mathbf{4}$$

Formation of **6** indicates desulfurization of **5b** during the course of preparation or reaction,[3] and then oxidation of the phosphorus atom in the intermediate product during the treatment.

Reaction of diphenylphosphine sulfide (**7**) with acetone gave **2b** in 23 and 86% yields in tetrahydrofuran (THF) and in acetone, respectively. The yields were determined by means of NMR, since **2b** decomposed with recrystallization from benzene–ethanol and on silica gel column.

Acetophenone and benzophenone did not react with **5b**.

Reaction of **5b** with bromoacetone gave 2-oxopropyldiphenylphosphine sulfide (**8**) in 65% yield. The result is in contrast to the reaction with chloroacetone,[4] which gives phosphinyl-substituted epoxide.

$$Ph_2P(S)CH_2COMe \quad \mathbf{8}$$

Experimental

All boiling and melting points are uncorrected. ^{1}H-NMR spectra were measured with a Hitachi R-24 spectrometer using TMS as an internal standard. ^{31}P-NMR spectra were measured with a Hitachi R-20B-R-204-PB spectrometer using 85% H_3PO_4 as an external standard. All the reactions were carried out under nitrogen atmosphere.

Reaction of Acetone with 5a. Acetone (5.15 g, 89 mmol) was added to a solution of **5a** prepared from diphenylphosphine oxide[5] (4.07 g, 20 mmol) and *n*-BuLi (21 mmol) in THF (80 ml), and the mixture was stirred for 19 hr at 30 °C and refluxed for 18 hr. After evaporation, the residue was treated with water and extracted with chloroform. Removal of the solvent from the dried extract gave a tarry mixture of **2a**, **3a**, and **4a** (by NMR), which was chromatographed on silica gel with ethyl acetate and methanol to afford **3a** (1.23 g, 20%), mp *ca.* 75 °C (lit,[6] 76.5—77.5 °C), and **2a** (0.39 g, 7.4%), mp 140—142 °C (from acetone) (lit,[2] 144—145 °C), δ_P ($CHCl_3$): −34.2 ppm. Acidification of the aqueous layer gave diphenylphosphinic acid (1.88 g, 43%).

Reaction of Acetone with 5b. A mixture of **5b**, prepared from **7**[7] (4.54 g, 21 mmol) and *n*-BuLi (23 mmol) in THF (60 ml), and acetone (4.57 g, 79 mmol) was stirred for 5 hr and refluxed for 15 hr. After a similar work-up to that with **5a**, ether was added to the residue to precipitate **4b**. The filtrate was chromatographed on silica gel with benzene and chloroform to afford **6**, oily **3b** and tarry products. On adding ether to the tarry products, **4b** precipitated, and **3b** was obtained from the filtrate.

3b: yield 2.82 g (43%). The IR and NMR spectra were in agreement with those of a sample obtained from **5b** and mesityl oxide.

4b: mp 178—179 °C (from EtOH), yield 1.36 g (23%). IR (KBr): 1705 cm^{-1} (C=O); NMR ($CDCl_3$): δ 1.45 (d, J_{PCCH} 18 Hz, 12H, 4Me), 2.81 (d, J_{PCCH} 9.2 Hz, 4H, $2CH_2$),

and 7.4—8.2 (m, 20H, 4Ph); δ_P ($CHCl_3$): −60.3 ppm.

Found: C, 68.96; H, 6.01; S, 11.43%. Calcd for $C_{33}H_{36}OP_2S_2$: C, 68.97; H, 6.31; S, 11.43%.

6: mp 151—152 °C (from EtOH), yield 0.24 g (4%). IR (KBr): 1710 (C=O), 1180 (P=O), and 540 cm^{-1} (P=S); NMR ($CDCl_3$): δ 1.35 (d, J_{PCCH} 16.2 Hz, 6H, P(O)CMe_2), 1.55 (d, J_{PCCH} 17.6 Hz, 6H, P(S)CMe_2), 2.64 (d, J_{PCCH} 8.4 Hz, 2H, CH_2 (P(O) side)), 2.83 (d, J_{PCCH} 9 Hz, 2H, CH_2 (P(S) side)), and 7.3—8.2 (m, 20H, 4Ph); δ_P ($CHCl_3$): −37.0 (P=O) and −62.0 ppm (P=S).

Found: C, 70.75; H, 6.43; S, 5.58%. Calcd for $C_{33}H_{36}O_2P_2S$: C, 70.95; H, 6.50; S, 5.74%.

Reaction of Acetone with **7**. 1) A mixture of **7** (1.49 g, 6.8 mmol) and acetone (12.76 g, 220 mmol) in THF (45 ml) was stirred for 17 hr at room temperature and then refluxed for 16 hr. Removal of THF gave white crystals (1.60 g). The NMR spectrum showed them to be a mixture of **7** and **2b**. The yield of **2b** was estimated to be 23% by means of NMR.

2) A solution of **7** (1.27 g, 5.8 mmol) in acetone (100 ml) was stirred for 19 hr at room temperature and then refluxed for 22 hr. The yield of **2b** was estimated to be 86%; δ_P ($CHCl_3$): −55.6 ppm. The melting point of the mixture was 110—117 °C (lit,[8] **2b**: 118—120 °C).

Reaction of **5b** *with Mesityl Oxide*. To a solution of **5b** prepared from **7** (4.00 g, 18 mmol) and *n*-BuLi (20 mmol) in THF (40 ml) was added mesityl oxide (2.54 g, 26 mmol) in THF (10 ml). The mixture was stirred for 35 hr at room temperature and then for 4 hr at 40 °C. Similar treatment gave a tarry product, which was chromatographed on silica gel with benzene and distilled under reduced pressure to give oily **3b** (2.30 g, 40%), bp 222 °C/1.5 mmHg. IR (neat): 1720 (C=O) and 645 cm^{-1} (P=S); NMR ($CDCl_3$): δ 1.51 (d, J_{PCCH} 18 Hz, 6H, CMe_2), 2.07 (s, 3H, COMe), 2.93 (d, J_{PCCH} 9 Hz, 2H, CH_2), and 7.3—8.3 (m, 10H, 2Ph); δ_P ($CHCl_3$): −60.7 ppm.

Found: C, 68.53; H, 6.41; S, 10.27%. Calcd for $C_{18}H_{21}OPS$: C, 68.33; H, 6.69; S, 10.13%.

Reaction of **5b** *with Bromoacetone*. To a solution of **5b** prepared from **7** (2.22 g, 10 mmol) and *n*-BuLi (13 mmol) in THF (30 ml) was added dropwise bromoacetone[9] (2.19 g, 16 mmol) in THF (20 ml) under ice-cooling, and the mixture was stirred for 16 hr at room temperature. After a similar work-up, the tarry residue was subjected to alumina dry column chromatography with chloroform. No crystals were obtained, but the following NMR spectrum showed that the main product was **8**, 1.82 g (65%). IR (neat): 1720 (C=O) and 620 cm^{-1} (P=S); NMR ($CDCl_3$): δ 2.31 (s, 3H, Me), 3.75 (d, J_{PCH} 15 Hz, 2H, CH_2), and 7.4—8.2 (m, 10H, 2Ph).

One of the authors (N. I.) thanks the Ministry of Education for financial support.

References

1) For Part II see K. Goda, H. Gomi, M. Yoshifuji, and N. Inamoto, This Bulletin, **47**, 2453 (1974).

2) P. F. Cann, S. Warren, and M. R. Williams, *J. Chem. Soc., Perkin I*, **1972**, 2377.

3) T. Emoto, H. Gomi, M. Yoshifuji, R. Okazaki, and N. Inamoto, This Bulletin, **47**, 2449 (1974).

4) G. Sturtz, *Bull. Soc. Chim. France*, **1964**, 2333.

5) G. I. Derkach and A. V. Kirsanov, *Zh. Obshch. Khim.*, **29**, 1815 (1959); *Chem. Abstr.*, **54**, 8682a (1960).

6) P. F. Cann, D. Howells, and S. Warren, *J. Chem. Soc., Perkin II*, **1972**, 304.

7) G. Peters, *J. Amer. Chem. Soc.*, **82**, 4751 (1960).

8) G. Peters, *J. Org. Chem.*, **27**, 2198 (1961).

9) P. A. Levene, "Organic Syntheses," Coll. Vol. II, p. 88 (1943).

BULLETIN OF THE CHEMICAL SOCIETY OF JAPAN, VOL. 47 (11), 2907—2908 (1974)

The Reaction of Several *o*-Methoxy Aromatic Aldehydes with Ethylthioxide. Novel Substitution and Condensation

Masaaki IWATA and Sakae EMOTO

The Institute of Physical and Chemical Research, Wako-shi, Saitama 351

(Received June 13, 1974)

Synopsis. The reaction of *o*- and *p*-anisaldehyde with potassium ethylthioxide in diglyme at 90—120 °C gave the corresponding demethylated products, while 2,6-dimethoxybenzaldehyde and 9-(2-*p*-cymenyl)-2-methoxy-1-anthraldehyde afforded two novel condensation and substitution products, VII and VI respectively.

Although many demethylation methods of methyl aryl ethers have been reported, few have referred to the direct demethylation of *o*-methoxy aromatic aldehydes except when Lewis acids have been used. For the establishment of "asymmetric inversion catalysts,"[1] the demethylation of a key intermediate, 9-(2-*p*-cymenyl)-2-methoxy-1-anthraldehyde (IV), was required. IV was not satisfactorily demethylated by Lewis acids, *e.g.*, $AlCl_3$, BBr_3, or BCl_3. Therefore, we attempted the indirect demethylation of methoxy-aromatic aldehydes with the ethylthioxide anion,[2] where the aldehyde group may be first blocked by ethylthioxide to form thioacetal and then regenerated by the use of cupric chloride and cupric oxide.[3] The treatment of *o*- or *p*-anisaldehyde, I or II, by this process gave a satisfactory product; however, the application of the method to some other methoxyaldehydes afforded novel results. The present paper will describe these reactions of ethylthioxide with methoxy-aromatic aldehydes.

For the treatment of methoxy-aromatic aldehydes with ethylthioxide (Process **A**), potassium ethylthioxide, prepared *in situ* by the reaction of potassium metal with ethanethiol in diglyme, was stirred with the compounds from I to V at 95—120 °C. During the reaction, the anisaldehydes, I and II, were changed to the corresponding 2- and 4-bis(ethylthio)methylphenols, which were detected on tlc spots. However, the corresponding bis(ethylthio)methyl-derivatives of 2,6-dimethoxybenzaldehyde (III) or 9-(2-*p*-cymenyl)-2-methoxy-3-anthraldehyde (V) did not give rise to any further demethylation. On the other hand, IV gave only a novel substitution product in which the methoxy group was replaced by the ethylthio group, while the aldehyde group remained. On the basis of the spectral analyses, this was shown to be 9-(2-*p*-cymenyl)-2-ethylthio-1-anthraldehyde (VI).

After the reaction had been accomplished, the mixture was acidified with 6M HCl and extracted with ethyl acetate. The organic layer was dried, and the solvents were evaporated under reduced pressure. The residue was then used in the next reaction.

To regenerate the aldehyde group, (Process **B**), the ethylthio compound described above was refluxed in aqueous acetone in the presence of cupric chloride and cupric oxide.[3] By this process, the bis(ethylthio)-methyl group was converted quantitatively to the aldehyde group in the cases of I, II, and V. However, the bis(ethylthio)methyl derivative of III was condensed with acetone to form (*E*)-2,6-dimethoxybenzalacetone (VII). VI was stable under Process **B**. The results obtained after Processes **A** and **B** are collected in Table 1.

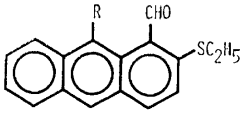

R=2-*p*-cymenyl

VI

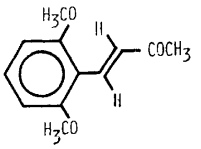

VII

TABLE 1. RESULTS OF THE REACTION OF METHOXY-AROMATIC ALDEHYDES WITH ETHYLTHIOXIDE FOLLOWED BY THEIR TREATMENTS WITH CUPRIC CHLORIDE AND CUPRIC OXIDE IN ACETONE

Starting material	Product	Fate of methoxy[a]	Yield (%)
I	Salicylaldehyde	A	52[b]
II	4-Hydroxybenzaldehyde	A	43[b]
III	(VII)	B	32[b]
IV	(VI)	C	71[b]
V	9-(2-*p*-Cymenyl)-2-methoxy-3-bis(ethylthio)methylanthracene	B	81[c]

a) A. demethylation B. survival C. substitution b) total yield after the processes **A** and **B**. c) yield after the process **A**. The product was converted to the starting material by the process **B**.

In order to establish which, the formation of thioacetal or its demethylation, is first, several methoxy-aromatics were treated with the same reagents as in Process **A**. None of the substances, anisole, *m*-dimethoxybenzene, and 9-(2-*p*-cymenyl)-2-methoxyanthracene, was demethylated or substituted by the ethylthio group, and the starting materials were recovered. Therefore, it may be deduced that the formation of thioacetal precedes demethylation in I, II, III, and V. The abnormal reactivity of the thioacetals of III and V can be explained by the steric requirement and by the potential reactivity of the anthracene derivative to ethylthioxide, respectively. Since VII was prepared directly by the reaction of III with acetone in the presence of cupric chloride, VII is assumed to be formed after the regeneration of the aldehyde group from the bis(ethylthio)methyl group. As regards the condensation mechanism and the general reaction, subsequent works are undertaken.

The novel direct substitution of a methoxy group by

an ethylthio group in IV may be caused by the non-coplanarity between the aldehyde group and the aromatic ring;[1] it is supported by the concept of symbiosis. According to the HSAB principle,[4] the ethylthioxide anion is a soft base and the aryl cation is a soft acid. Therefore, the formation of VI is symbiotically more favored than the demethylation of IV. The problem remained to discover why demethylation occurs with the aid of ethylthioxide, as may be seen in the cases of I, II, and the compounds cited in Ref. 2.

Experimental

The melting points are uncorrected. The IR spectra were recorded on a Shimadzu IR-27 instrument. The NMR spectra were obtained using a Varian HA-100D spectrometer, with TMS as an internal standard. The mass spectra and the exact mass measurements were performed with a Model JMS-O1SG instrument (Japan Electron Optics Laboratory Co.). Merck Art. 7734 was used for the preparative separation of products on a silica gel column by elution chromatography, and Wakogel B-5 UA, for the thin-layer chromatography.

The starting materials, *o*- and *p*-anisaldehydes, (I) and (II), were commercially available. The compounds from III to V were prepared by a previously-reproted method.[1]

The Protection of the Aldehyde Group and Demethylation or Substitution (Process A). General Procedure. Potassium (0.03 mol) was added to a cooled solution of excess amounts of ethanethiol (10—15 ml) and 20 ml of diglyme to form, *in situ*, ethylthioxide. After the complete dissolution of the potassium metal, 0.01 mol of methoxy-aldehyde was added to the solution, after which the mixture was heated with gentle stirring at 95—110 °C for 20—24 hr. The mixture was then acidified with 50 ml of water containing a suitable amount of 6M HCl and extracted twice with 50 ml portions of ethyl acetate. The organic layer was then dried over anhydrous Na_2SO_4, and the solvents were evaporated under reduced pressure. The residue was used in the next reaction.

The Regeneration of the Aldehyde Group by the Deprotection of the Ethylthio Group (Process B). General Procedure. The crude residue was refluxed with cupric chloride (2 mol equiv.) and cupric oxide (4 mol equiv.) in 50 ml of aq. 99% acetone for 1—1.5 hr.[3] After the usual work-up, the residue was chromatographed on a silica gel column to give the products.

The products after the successive treatment of *o*- and *p*-anisaldehydes by Processes **A** and **B** were identified as salicyladehyde and 4-hydroxybenzaldehyde respectively; their structures were determined by a comparison of their spectral data, their behavior on tlc, and their melting points with those of authentic samples.

The successive treatments of 2,6-dimethoxybenzaldehyde (III) with Processes **A** and **B** resulted in the formation of (*E*)-2,6-dimethoxybenzalacetone (VII).[5] Mp 89—91 °C. NMR (CCl_4): δ 2.26 (3H, s, $-COCH_3$), 3.88 (6H, s, $-OCH_3$), 6.49 (2H, d, $J_{3,4}=8.4$ Hz, $C_{3,5}$–H), 6.97 (1H, d, $J_{\alpha,\beta}=16.6$ Hz, C_α–H), 7.18 (1H, d, $J_{3,4}=8.4$ Hz, C_4–H), and 7.77 (1H, d, $J_{\alpha,\beta}=16.6$ Hz, C_β–H) ppm.

The successive treatments of 9-(2-*p*-cymenyl)-2-methoxy-1-anthraldehyde (IV) by Processes **A** and **B** gave 9-(2-*p*-cymenyl)-2-ethylthio-1-anthraldehyde (VI) in a 71% yield; it was a yellow viscous liquid. VI was unstable on exposure to air, and it was difficult to make the elemental analyses coincide. The exact mass measurement: Found (for a parent peak at *m/e* 398) 398.16724. Calcd for $C_{27}H_{26}OS$: 398.17048. IR (neat): $\nu_{C=O}$ 1668 cm^{-1}. NMR (CCl_4): δ 1.27 (6H, d, $J=7.0$ Hz, $-CH(\underline{CH_3})_2$), 1.28 (3H, t, $J=7.0$ Hz, $-CH_2-\underline{CH_3}$), 1.89 (3H, s, Ar–$\underline{CH_3}$), 2.88 (2H, quar, $J=7.0$ Hz, $-\underline{CH_2}-CH_3$), 2.90 (1H, quin, $J=7.0$ Hz, $-\underline{CH}(CH_3)_2$), 7.01 (1H, broad s, C_2'–H), 7.42 (1H, d, $J=9.0$ Hz, C_3–H), 7.93 (1H, d, $J=9.0$ Hz, C_4–H), 8.36 (1H, s, C_{10}–H), and 9.39 (1H, s, –CHO) ppm.

The treatment of 9-(2-*p*-cymenyl)-2-methoxy-3-anthraldehyde (V) by Process **A** produced 9-(2-*p*-cymenyl)-2-methoxy-3-bis(ethylthio)methylanthracene in an 81% yield; it was a fluorescent viscous pale green liquid. It was unstable on exposure to air and it was difficult to make the elemental analyses coincide. However, the structure was confirmed by spectral measurements of the crude sample. NMR (CCl_4): δ 1.24 (6H, t, $J=6.6$ Hz, $-CH_2-\underline{CH_3}$), 1.30 (6H, d, $J=7.8$ Hz, $-CH(\underline{CH_3})_2$), 1.85 (3H, s, Ar–$\underline{CH_3}$), 3.68 (3H, s, $-OCH_3$), 5.44 (1H, s, S–$\underline{CH}$–S), 6.58 (1H, s, C_1–H), 7.06 (1H, broad s, C_2'–H), 8.13 (1H, s, C_4–H), and 8.34 (1H, s, C_{10}–H) ppm. In addition, when this product was treated with the reagents of Process **B**, V was recovered in a quantitative yield.

The author wishes to thank Mr. Jun Uzawa and Mrs. Tamiko Chijimatsu for their NMR spectral measurements, and the staff of the Organic Microanalysis Laboratory in this Institute for their elemental analyses. This study was supported in part by a Grant for Life Science from this Institute.

References

1) M. Iwata and S. Emoto, This Bulletin, **47**, 1687 (1974).

2) G. I. Feutrill and R. N. Mirrington, *Tetrahedron Lett.*, **1970**, 1327.

3) K. Narasaka, T. Sakashita, and T. Mukaiyama, This Bulletin, **45**, 3724 (1972).

4) R. G. Pearson, *J. Amer. Chem. Soc.*, **85**, 3533 (1963); *ibid.*, **89**, 1827 (1967); *Science*, **151**, 172 (1966); *J. Chem. Educ.*, **45**, 581 (1968).

5) M. Miyano, S. Muraki, T. Kusunoki, T. Morita, and M. Matsui, *Nippon Nogeikagaku Kaishi*, **34**, 683 (1960).

BULLETIN OF THE CHEMICAL SOCIETY OF JAPAN, VOL. 47 (11), 2909—2910 (1974)

The Reaction of Ethyl Azidoformate with Electron Deficient Olefins and the Thermal Ring Opening of the Resulting Aziridines.

Tamejiro HIYAMA, Hiroaki TAGUCHI, and Hitosi NOZAKI
Department of Industrial Chemistry, Kyoto University, Yoshida, Kyoto 606

(Received July 10, 1974)

Synopsis. Thermal or photochemical decomposition of ethyl azidoformate in mesityl oxide or in methyl crotonate afforded the corresponding aziridines. Thermal C–C bond cleavage of aziridine-1-carboxylates thus obtained is described.

In continuation of the investigation on the reaction of ethyl azidoformate (I) with carbonyl compounds[1] we have examined the thermal and photochemical decomposition of I in mesityl oxide (IIa) or methyl crotonate (IIb) as a solvent.

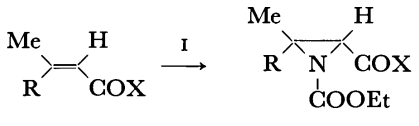

IIa R=X=Me IIIa R=X=Me
b R=H, M=OMe b R=H, X=OMe

The azide I solutions in IIa or IIb were irradiated with a mercury lamp. When nitrogen evolution had ceased, the solvent was evaporated *in vacuo* and the residue was distilled to afford the adduct IIIa or IIIb. Thermal decomposition of I in IIa or IIb resulted in the improvement of the yields. Both photolysis and thermolysis gave the *trans* isomer of IIIb exclusively.[2,3] In these reactions none of the products arising from carbonyl attack of I on II has been obtained. The reaction discloses a new route to aziridine-2-carboxylic acids, which are useful intermediates in the preparation of β-hydroxyvaline[4] and β-lactams.[5] Photolytic or thermal decomposition of I in methyl acrylate yielded no nitrene adducts but acrylate polymer only.

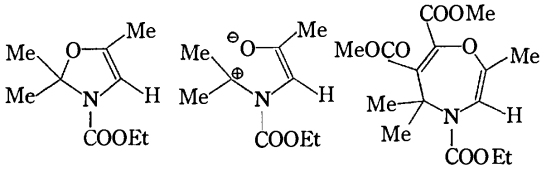

IV V VI

Upon heating in refluxing *p*-xylene aziridine IIIa was isomerized to IV.[6] The intermediary azomethine ylide V[7] was characterized by successful trapping with dimethyl acetylenedicarboxylate, which afforded the cycloadduct VI. The structure VI was confirmed spectrometrically (Experimental). The well-established mode of azomethine ylide cycloaddition[8] should give rise to 2,5-dihydropyrroles, which were absent among products of the present thermolysis. The apparently unusual behavior of V is ascribed to the presence of ethoxycarbonyl group on the nitrogen atom instead of the alkyl or aryl group of the recorded cases.[8,9]

The carbon-carbon double bond in II is thus cleft smoothly in the sequence of reactions.

Experimental[10]

Thermolysis of Ethyl Azidoformate in Mesityl Oxide. Ethyl azidoformate (3.0 g, 26 mmol) in mesityl oxide (15 ml) was added drop by drop to mesityl oxide (45 ml) at 130 °C under a nitrogen atmosphere. After the nitrogen evolution having ceased the excess of mesityl oxide was recovered *in vacuo*. Distillation of the residue afforded ethyl 2-acetyl-3,3-dimethylaziridine-1-carboxylate (IIIa) (2.7 g, 56% yield). Bp 73 °C/3 mmHg; IR (neat): 1725, 1365, 1305, 1260, 1240, 1176, 1096, 800 cm^{-1}; NMR (CCl_4): δ 1.24 (s, 3H), 1.27 (t, J=7 Hz, 3H), 1.34 (s, 3H), 2.14 (s, 3H), 2.75 (s, 1H), 4.07 (q, J=7 Hz, 2H); MS: *m/e* (relative abundance) 185 (M^+, 7), 170 (23), 112 (35), 98 (61), 70 (60), 43 (100); Found: C, 58.5; H, 8.3; N, 7.3%. Calcd for $C_9H_{15}NO_3$: C, 58.4; H, 8.2; N, 7.6%.

Photolysis of I in IIa. The azide I (1.00 g) was dissolved in IIa (10 ml) in a quartz tube. The solution was degassed by bubbling nitrogen gas for *ca.* 2 hr and irradiated with a 200 W high-pressure mercury lamp until nitrogen evolution ceased (2 days). Work-up yielded IIIa (0.64 g, 39% yield).

Thermolysis of I in Methyl Crotonate (IIb). Ethyl azidoformate (0.45 g, 3.9 mmol) was decomposed in methyl crotonate (9 ml) at 120 °C. Distillatory work-up gave ethyl 2-methoxycarbonyl-3-methylaziridine-1-carboxylate (IIIb) (0.53 g, 72% yield). Bp 71 °C/3 mmHg; IR (neat): 1752, 1732, 1445, 1332, 1300, 1217, 1194, 795 cm^{-1}; NMR (CCl_4): δ 1.23 (t, 3H), 1.32 (d, J=3 Hz, 3H), 2.70 (s, 1H), 2.73 (q, J=3 Hz, 1H), 3.74 (s, 3H), 4.11 (q, 2H); MS: *m/e* (relative abundance) 187 (M^+, 13), 155 (20), 114 (38), 83 (55), 59 (100); Found: C, 51.1; H, 7.1; N, 7.5%. Calcd for $C_8H_{13}NO_4$: C, 51.3; H, 7.0; N, 7.5%.

Photochemical procedure performed similarly as described for IIIa gave IIIb in 70% yield.

Thermal Isomerization of IIIa. The aziridine IIIa (198 mg, 1.1 mmol) was dissolved in *p*-xylene (10 ml) and the solution heated to reflux for 2 hr under a nitrogen atmosphere. Concentration *in vacuo*, followed by preparative tlc of the residue (silica gel, benzene, R_f 0.6), gave 3-ethoxycarbonyl-2,2,5-trimethyl-4-oxazoline (IV) (86 mg, 43% yield). Bp 90 °C (bath temp.)/3 mmHg; IR (neat): 1700, 1635, 1420, 1215, 1070, 844, 750, 672 cm^{-1}; NMR (CCl_4): δ 1.25 (t, 3H), 1.63 (s, 6H), 1.76 (d, J=1.2 Hz, 3H), 4.07 (q, 2H), 5.80 (q, J=1.2 Hz, 1H); MS: *m/e* (relative abundance) 185 (M^+, 15), 174 (16), 112 (20), 73 (100), 70 (57); Found: C, 58.1; H, 8.1; N, 7.4%. Calcd for $C_9H_{15}NO_3$: C, 58.4; H, 8.2; N, 7.6%.

Reaction of IIIa with Dimethyl Acetylenedicarboxylate. A mixture of IIIa (525 mg, 2.84 mmol) and dimethyl acetylenedicarboxylate (412 mg, 2.90 mmol) was dissolved in *p*-xylene (2 ml) and the solution heated to reflux for 15 hr. Work-up and the subsequent preparative tlc (silica gel, benzene, R_f 0.2) gave 4-ethoxycarbonyl-6,7-dimethoxycarbonyl-2,5,5-trimethyl-4,5-dihydro-1,4-oxazepine (VI) (832 mg, 89% yield). Bp 150 °C (bath temp.)/0.1 mmHg; IR (neat): 1720, 1649, 1436, 1378, 1336, 1237, 1112 cm^{-1}; NMR (CCl_4): δ 1.25 (t, 3H), 1.52 (s, 3H), 1.58 (d, J=1.2 Hz, 3H), 1.60 (s, 3H),

3.74 (s, 3H), 3.75 (s, 3H), 4.04 (q, 2H), 4.70 (q, $J=1.2$ Hz, 1H); MS: *m/e* (relative abundance) 327 (M^+, 5), 312 (13), 270 (4), 238 (14), 198 (21), 166 (100), 119 (12), 116 (3), 98 (13); Found: C, 54.8; H, 6.5; N, 4.2%. Calcd for $C_{15}H_{21}NO_7$: C, 55.0; H, 6.5; N, 4.3%.

The authors are indebted to Dr. Shinsaku Fujita for his valuable discussion. Financial support from the Ministry of Education, the Japanese Government, is acknowledged with pleasure.

References

1) T. Hiyama, H. Taguchi, S. Fujita, and H. Nozaki, This Bulletin, **45**, 1863 (1972).

2) H. Nozaki, Y. Okuyama, and S. Fujita, *Can. J. Chem.*, **46**, 3333 (1968).

3) W. Lwowski, "The Chemistry of the Azido Group," ed. by S. Patai, John Wiley and Sons, New York (1971), p. 529; W. Lwowski, "Nitrenes," ed. by W. Lwowski, John Wiley and Sons, New York, p. 185 (1970).

4) C. Berse and P. Bessette, *Can. J. Chem.*, **49**, 2610 (1971).

5) J. A. Deyrup and S. C. Clough, *J. Amer. Chem. Soc.*, **91**, 4590 (1969); *J. Org. Chem.*, **35**, 3424 (1970); **39**, 902 (1974).

6) J. E. Baldwin, R. G. Pudussey, A. K. Qureshi, and B. Sklarz, *J. Amer. Chem. Soc.*, **90**, 5325 (1968); F. Texier and R. Carrié, *C. R. Acad. Sci. Paris, Ser. C*, **271**, 958 (1970); A. Foucaud and M. Baudan, *ibid.*, **271**, 1613 (1970); A. Padwa and W. Eisenhardt, *Chem. Commun.*, **1968**, 380.

7) S. R. Tanny and F. W. Fowler, *J. Amer. Chem. Soc.*, **95**, 7530 (1973); P. Dowd and K. Kang, *Chem. Commun.*, **1974**, 258; J. Bastide, J. Hamelin, F. Texier, and Y. V. Quang, *Bull. Soc. Chim. Fr.*, 2871 (1973); G. Stuckwisch, *Synthesis*, **1973**, 469.

8) T. Dominh and A. M. Trozzolo, *J. Amer. Chem. Soc.*, **94**, 4046 (1972); A. Robert, J. J. Pommeret, and A. Foucaud, *Tetrahedron Lett.*, **1971**, 231; F. Texier and R. Carrié, *ibid.*, **1969**, 823; J. H. Hall and R. Huisgen, *Chem. Commun.*, **1967**, 1187; J. H. Hall, R. Huisgen, C. H. Ross, and W. Scheer, *ibid.*, 1188 (1971); J. W. Lown and K. Matsumoto, *Yuki Gosei Kagaku*, **29**, 760 (1971).

9) The aziridine IIIb was recovered unchanged when it was heated in *p*-xylene, but upon heating with dimethyl fumarate, dimethyl maleate, or dimethyl acetylenedicarboxylate, the respective adduct was obtained albeit in low yields. Structural analysis of the adduct could not be attained.

10) IR spectra were taken on a Shimadzu spectrometer IR-27G, MS spectra on a Hitachi RMU-6L spectrometer, NMR spectra on a JEOL C-60H spectrometer. All temperatures are uncorrected.

BULLETIN OF THE CHEMICAL SOCIETY OF JAPAN, VOL. 47 (11), 2911—2912 (1974)

Optical Resolution and Configuration of *cis*-β-Phenylglycidic Acid[1)]

Kaoru HARADA and Yousuke NAKAJIMA

Institute for Molecular and Cellular Evolution, Department of Chemistry, University of Miami, Coral Gables, Florida 33134 U.S.A.

(Received March 18, 1974)

Synopsis. DL-*cis*-β-phenylglycidic acid was resolved using (−)-ephedrine. The configurations of α- and β-carbons of the resolved *cis*-(+)-glycidic acid were determined by oxydative and hydrogenolytic reactions.

The chemistry of epoxide has been studied extensively. Reviews have been presented in several articles.[2,3)] Darzens' reaction in the synthesis of glycidic acids has been reviewed.[4)] Several ammonolysis and aminolysis reactions of glycidic acids have been reported.[5-14)]

In previous studies from this laboratory, racemic *trans*-2,3-epoxy-β-phenylpropionic acid,[15)] *trans*-2,3-epoxybutyric acid,[16)] and *trans*-2,3-epoxysuccinic acid[17)] were optically resolved and their absolute configurations were determined.

In the present study, *cis*-β-phenylglycidic acid (II) was prepared from the corresponding *trans*-β-phenylglycidic acid (I) [18)] and the *cis*-glycidic acid was subjected to optical resolution. The phenylglycidic acid is an unstable compound in the free state and it decarboxylates easily to form phenylacetaldehyde at room temperature. However, by the use of rapid procedures under cold conditions, the resolution of the *cis*-glycidic acid was carried out without difficulty. The racemic *cis*-glycidic acid (III′) was resolved using (−)-ephedrine. The crystallized glycidic acid-(−)-ephedrine salt (IV) shows levorotatory $[\alpha]_D^{25}$ −27°. From this salt, optically active *cis*-phenylglycidic acid was precipitated as a potassium salt (V). The potassium salt of the *cis*-phenylglycidic acid (V) showed dextrotatory $[\alpha]_D^{25}$ +4.4°. The diastereomeric *cis*-(−)-glycidic acid-(−)-ephedrine salt was syrupy and could not be crystallized. The resolved *cis*-(+)-glycidic acid was treated with aqueous ammonia. Paper chromatography of the ammonolysis products using Shaw-Fox' solvent[19)] and the results obtained by automatic amino acid analysis (Phoenix K-5000), indicated that the product was predominantly phenylisoserine (VI). The presence of a small amount of *threo*-phenylserine was confirmed in the reaction mixture by paper chromatography[19)] and by amino acid analysis.

The phenylisoserine (VI) was benzoylated and the resulting *N*-benzoyl phenylisoserine (VII) was oxidized with potassium permanganate.[15)] (*R*)-(−)-*N*-Benzoylphenylglycine (VIII) ($[\alpha]_D^{25}$ −119.3°) was obtained. Therefore, the configuration of the β-carbon of the phenylisoserine (VI) is (*R*). On the other hand, resolved *cis*-(+)-glycidic acid (IV) was hydrogenolyzed to convert it to (*S*)-(−)-α-hydroxy-β-phenylpropionic acid (IX). The results indicate that the configuration of the α-carbon of the *cis*-(+)-glycidic (V) is (*S*). These results obtained by the use of *cis*-(+)-glycidic acid, together with the consideration of the S_N2-type nucleophilic substitution of the β-carbon of the glycidic acid with ammonia, indicate that the configuration of the resolved (+)-glycidic acid (V) would be 2(*S*), 3(*S*), respectively. The reaction processes are summarized in Scheme 1.

Experimental

Ethyl (±)-cis-β-Phenylglycidate (II). The *cis*-glycidic acid ester (II) was prepared from ethyl *trans*-β-phenylglycidate (I) by the method described in the literature.[18)] The compound (II) was gas chromatographically pure and the retention time was earlier than that of *trans*-β-phenylglycidate. bp 122—125 °C/4.2 mmHg.

Potassium cis-β-Phenylglycidate (III). The compound (II) (10.0 g) in 20 ml of absolute ethanol was added slowly to a solution of potassium hydroxide (5.0 g) in 30 ml of absolute ethanol under cooling. The agitation was continued

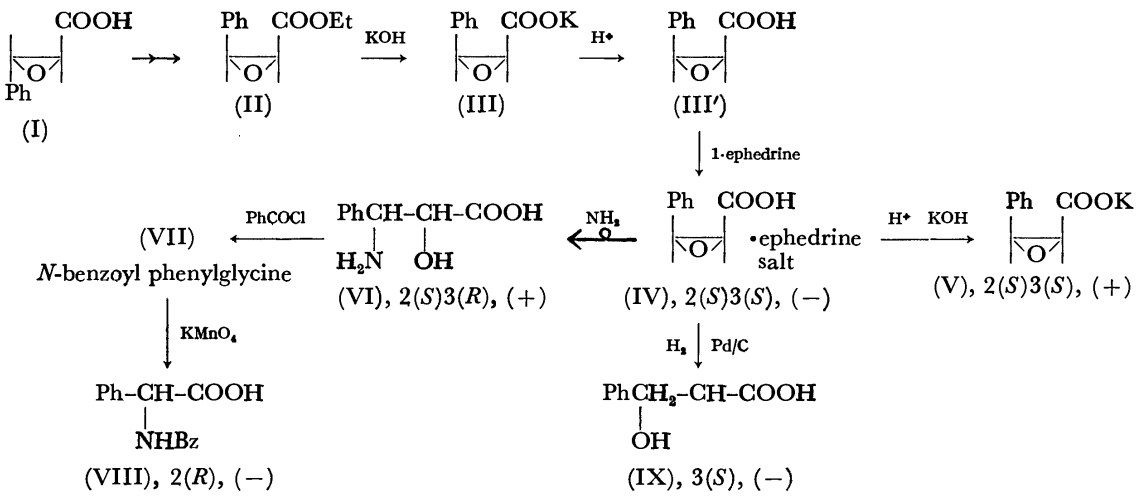

Scheme 1

for 3 hr. The precipitated potassium salt was filtered and washed with ethanol repeatedly. Yield, 9.4 g, mp 191—193 °C (decomp.).

Optical Resolution of cis-*β-Phenylglycidic Acid (III')*. Potassium β-phenylglycidate (III) (8.3 g) was dissolved in 60 ml of water. Crushed ice and 40 ml of ether were added to the solution. To this mixture, 40 ml of 1 M hydrochloric acid was added and the liberated free glycidic acid was extracted with ether. Two additional ether extractions (40 ml×2) were carried out. The combined ether solution was dried with anhydrous sodium sulfate. To the dried ether solution, 6.78 g of (−)-ephedrine in 20 ml of ether was added. The mixture was kept at room temperature overnight. The resulting salt seemed to be amorphous; however, crystallization took place. After evaporation of ether, the syrupy residue which contained crystalline salt was digested with 30 ml of acetone and filtered. White crystals (IV) were obtained, yield 3.45 g; mp 138—140 °C. This was recrystallized from ethanol. Yield, 3.0 g; mp 145–146 °C, $[\alpha]_D^{25}$ −27.2° (*c* 2.77, ethanol). Additional crystals (1.18 g) were obtained from the salt mixture.

The resolved (−)-salt (1.0 g) in 15 ml of water was acidified to pH 2 with 6 M hydrochloric acid under ice cooling. The liberated free glycidic acid was extracted with ether. The ether solution was dried with anhydrous sodium sulfate and the solvent was evaporated. The residual oil was dissolved in 5 ml of ethanol. To this, potassium hydroxide (0.17 g) in 1 ml of ethanol was added. The precipitated potassium salt of optically active *cis*-phenylglycidic acid (V) was collected by filtration. Yield, 150 mg; mp 203—204 °C (decomp.), $[\alpha]_D^{25}$ +4.4° (*c* 0.98, H_2O).

Ammonolysis of (+)-β-Phenylglycidic Acid. The crystallized (+)-β-phenylglycidic acid-(−)-ephedrine salt (IV, 3.0 g) was dissolved in 70 ml of concentrated aqueous ammonia. The solution was kept at room temperature for 6 days. The reaction mixture was evaporated to dryness under reduced pressure. Paper chromatography using Shaw-Fox solvent[19] indicates that the major product is *threo*-β-phenylisoserine (R_f 0.33). A small amount of *threo*-β-phenylserine (R_f 0.53) was identified. Amino acid analysis showed that the ratio of phenylisoserine and phenylserine is 29.2: 1. The evaporated reaction mixture was dissolved in a minimum amount of water and the pH was adjusted to 6 using 6 M hydrochloric acid. The precipitated (+)-*threo*-β-phenylisoserine (VI) was recrystallized from water. The VI was paper chromatographically pure. Yield, 1.1 g; mp 256—257 °C (decomp.); $[\alpha]_D^{25}$ +14.9° (*c* 0.737, 6 M HCl).

Found: C, 59.41; H, 6.17; N, 7.65%. Calcd for $C_9H_{11}NO_3$: C, 59.66; H, 6.12; N, 7.73%.

It has been known that Shaw-Fox paper chromatographic solvent[19] resolves diastereomers of threonine and phenylserine. This study indicates that the solvent also resolve diastereomers of phenylisoserine (*threo*-phenylisoserine, R_f 0.33; *erythro*-phenylisoserine, R_f 0.26).

threo-(+)-N-*Benzoylphenylisoserine (VII).* *threo*-(+)-Phenylisoserine (VI) was benzoylated by the usual Schotten-Baumann procedure. The yield was 65% after recrystallization from ethanol-water (3: 7). mp 168—169 °C, $[\alpha]_D^{25}$ +36.5° (*c* 1.45 EtOH).

Found: C, 67.35; H, 5.26; N, 4.79%. Calcd for $C_{16}H_{15}NO_4$: C, 67.36; H, 5.30; N, 4.91%.

Oxidation of N-*Benzoyl*-threo-(+)-*phenylisoserine (VII).* A weight of 0.85 g of VII was dissolved in a mixture of 3 ml of 1 M sodium hydroxide and 5 ml of water. To this, 0.948 g of powdered potassium permanganate was added slowly in a period of 35 min with stirring and cooling. After an additional 15 min of stirring, 0.8 g of sodium sulfite was added and the reaction mixture was stirred for 10 min. The reaction product was treated in a similar way as described in an earlier study.[15] Crude *N*-benzoylphenylglycine (VIII) (200 mg) was obtained. mp 178—182 °C. This was recrystallized from a mixed solvent of water and ethanol (4: 6). Yield, 120 mg; mp 196.5—198 °C; $[\alpha]_D^{25}$ −119.3° (*c* 0.845, ethanol).

Found: C, 70.62; H, 5.15; N, 5.43%. Calcd for $C_{15}H_{13}O_3N$: C, 70.58; H, 5.13; N, 5.49%.

(S)-(−)-α-*Hydroxyphenylpropionic Acid (IX).* The crystallized optically active phenylglycidic acid (−)-ephedrine salt (IV, 1.0 g) in 25 ml of water was hydrogenated with 1.0 g of 5% palladium on charcoal for 2 hr at room temperature. From the reaction mixture, 380 mg of crude (*S*)-(−)-α-hydroxy-β-phenylpropionic acid (IX) was obtained. mp 120—122 °C. This was recrystallized from benzene. Yield, 340 g, mp 123—124 °C; $[\alpha]_D^{25}$ −20.7° (*c* 2.11, H_2O).

Found: C, 65.26; H, 6.17%. Calcd for $C_9H_{10}O_3$: C, 65.05; H, 6.07%.

This work was supported by grant No. NGR 10-007-052 from the National Aeronautics and Space Administration, U.S.A.

References

1) Stereochemistry of Glycidic Acid IV, Part III; see Ref. 17. Contribution no. 273 of the Institute for Molecular and Cellular Evolution, University of Miami.

2) S. Winstein and R. B. Henderson, "Heterocyclic Compounds," Vol. 1, R. E. Elderfield, ed., John Wiley and Sons, Inc., New York, (1950), p. 22.

3) R. E. Parker and N. S. Isaacs, *Chem. Rev.*, **59**, 737 (1959).

4) M. S. Newman and B. J. Magerlein, *Org. Reactions*, **5**, 413 (1949).

5) P. Melikow, *Ber.*, **13**, 956 (1880).

6) E. Erlenmeyer, *ibid.*, **13**, 1077 (1880).

7) M. O. Forster and K. A. N. Rao, *J. Chem. Soc.*, **1926**, 1943.

8) O. von Schickh, German Patent 583243 (1933); *Chem. Abstr.*, **28**, 260 (1934).

9) E. Fourneau and J. R. Billeter, *Bull. Soc. Chim. France*, (5) **6**, 1616 (1939); (5) **7**, 593 (1940).

10) S. N. Danilov and V. F. Martynow, *Zh. Obsch. Khim.*, **22**, 1572 (1952).

11) V. F. Martynov, *Dokl. Akad. Nauk SSSR*, **89**, 869 (1953).

12) T. Kaneko and T. Inui, *Nippon Kagaku Zasshi*, **82**, 743 (1961).

13) T. Inui and T. Kaneko, *ibid.*, **82**, 747 (1961).

14) Y. Liwchitz, Y. Rabinsohn, and D. Peerera, *J. Chem. Soc.*, **1962**, 1116.

15) K. Harada, *J. Org. Chem.*, **31**, 1407 (1966).

16) K. Harada and J. Oh-hashi, This Bulletin, **39**, 2311 (1966).

17) J. Oh-hashi and K. Harada, *ibid.*, **40**, 2977 (1967).

18) C. C. Tung and A. J. Speziale, *Chem. Ind.*, 1985 (1963); C. C. Tung and A. J. Speziale, *J. Amer. Chem. Soc.*, **87**, 2683 (1965).

19) K. N. F. Shaw and S. W. Fox, *ibid.*, **75**, 3421 (1953).

BULLETIN OF THE CHEMICAL SOCIETY OF JAPAN, VOL. 47 (11), 2913 (1974)

The Tautomerism of 2-Amino-5-nitrosotropone

Kimiaki IMAFUKU, Yasuyoshi TAKATA,* and Hisashi MATSUMURA

Department of Chemistry, Faculty of Science, Kumamoto University, Kurokami, Kumamoto 860

(Received May 13, 1974)

Synopsis. It was confirmed that 2-amino-5-nitrosotropone (II) exists in its tautomeric form (IIb) by the measurement of its dissociation constant and UV spectra.

Previously, it was established[1] that the methylation of 5-nitrosotropolone (I) with diazomethane does not give its methyl ether, while its acetylation and benzoylation afforded, respectively, the corresponding acetate and benzoate of tropoquinonemonoxime (Ib).

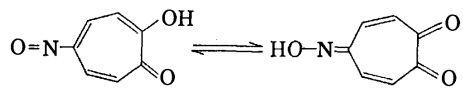

Ia Ib

In the course of measurements[2] of the dissociation constants of several 4-, 5-, and 6-substituted 2-aminotropones, 2-amino-5-nitrosotropone (II) was found to show an extremely larger pK_a value (5.68) than those of other 2-aminotropones.

In order to reveal these differences between 2-amino-5-nitrosotropone (II) and other 2-aminotropones, we assumed its tautomeric form (IIb), which is similar to Ib, and compared II with 5-nitrosotropolone (I).

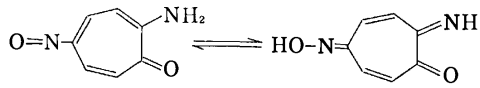

IIa IIb

Experimental

Materials. 5-Nitrosotropolone (I) was prepared by the nitrosation of tropolone,[1,3] while 2-amino-5-nitrosotropone (II) was obtained by its ammonolysis.[1]

Measurement of Dissociation Constants. The dissociation constants were measured spectrophotometrically in 50% aqueous methanol at 20 °C using the method of Albert and Serjeant.[4]

The absorption spectra were taken on a Hitachi spectrophotometer (EPS-3T), and the pH values were measured by means of a Hitachi-Horiba pH meter (F-5).

Results and Discussion

The dissociation constants are listed in Table 1. In spite of the strong electron-withdrawing effect of the nitroso group, the pK_a value of 2-amino-5-nitrosotropone (II) is remarkably larger than those of other 2-aminotropones [pK_a=2.63 (5-methyl) to 1.34 (5-chloro)][2] and is close to the pK_a value of 5-nitrosotropolone (I).

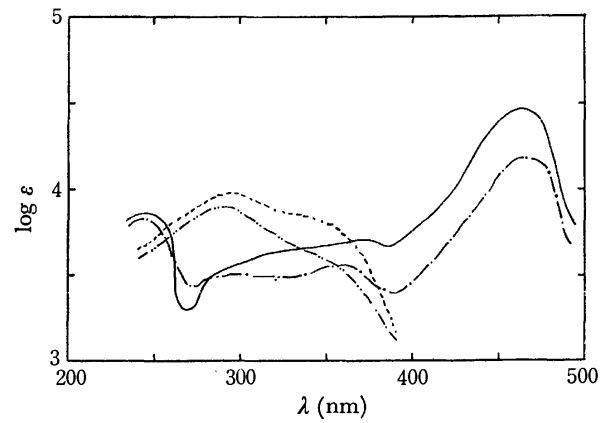

Fig. 1. The UV spectra of 5-nitroso compounds
I: —— pH 7.30, ------ pH 1.31
II: ····· pH 7.52, -·-· pH 1.89

Table 1. Dissociation constants

Compound	pK_a
I	5.63
II	5.68

Furthermore, the two 5-nitroso-substituted compounds (I and II) show very similar spectral patterns in both acidic and basic media, as is shown in Fig. 1.

Consequently, it was revealed that 2-amino-5-nitrosotropone (II) exists also in the tautomeric structure (IIb). It is thought that the pK_a values of I and II are due to the dissociation of the OH group in the oxime form.

In addition, it is known[5] that *p*-nitrosophenol, which exists in similar tautomers, shows a lower pK_a value (6.36) than do other phenols [pK_a=10.26 (*p*-methyl) to 7.15 (*p*-chloro)].

The authors wish to thank Professor Tetsuo Nozoe and the Sankyo Co., Ltd., for the supply of tropolone.

References

1) T. Nozoe, M. Sato, and T. Matsuda, *Sci. Repts. Tohoku Univ., I*, **37**, 407 (1953).

2) K. Imafuku, Y. Takata, and H. Matsumura, This Bulletin, **47**, 1809 (1974).

3) W. von E. Doering and L. H. Knox, *J. Amer. Chem. Soc.*, **73**, 828 (1951).

4) E. Albert and E. P. Serjeant, "Ionization Constants of Acids and Bases," Methuen, London (1962), Chap. 4.

5) L. A. Cohen and W. M. Jones, *J. Amer. Chem. Soc.*, **85**, 3397 (1963).

* Present address: Dainichi-seika Color & Chemicals Mfg. Co., Ltd., Iwata-shi, Shizuoka 438.

The Application of an MC-SCF Theory to Organic Chemical Reactions

Osamu KIKUCHI and Katsutoshi AOKI

Department of Chemistry, Tokyo Kyoiku University, Otsuka, Tokyo 112

(Received November 24, 1973)

MC-SCF equations have been derived with the help of Segal's partition-basis-set technique; these equations can be used for the calculation of the potential curves of many organic reactions. They were applied to two typical organic reactions, and the results were compared with those obtained by CI methods. The corrections of the SCF-CI energies by the MC-SCF procedure were small for the present system.

The Hartree-Fock(HF) wavefunction describes the ground state of a normal molecule passably well, and its mixing with the excited configurations is generally small. However, the HF wavefunction is unreliable for a molecular system in which the interaction between the HF wavefunction and some excited configuration functions is very large. Such a breakdown of the HF method[1] occurs in the study of a thermally-"forbidden" reaction, during which an occupied MO crosses a vacant MO. The part of a potential curve in this region is much more unreliable than the other parts of the potential curve. Multi-configuration(MC) wavefunctions, thus, should be used so as to obtain reliable potential curves for these types of reactions. Here, the criterion of a reliable potential curve is that the potential curve has an equal reliability at all of its points.

Configuration interaction(CI) methods are easy to use, and many potential curves of these types of reactions have been obtained by CI methods.[2] MC-SCF methods have also been applied to some reactions by Basch.[3] In MC-SCF methods, the configurations to be included vary with the type of reaction and with the electronic state under consideration. The SCF equations, thus, must be derived separately for each state of each reaction. As a matter of practical convenience, it would be desirable to have MC-SCF equations which could be used for many types of reactions and many types of states. In this paper, we will consider the configurations which give the most reliable potential curves of many types of reactions, and an MC-wavefunction will be set up. Using Segal's "partition-basis-set" technique,[4] Fock-type equations will be derived for the wavefunction. These equations will then be applied to two reactions, and the results will be compared with those obtained by the CI method.

Theory

First, let us consider the configurations which give the lowest singlet potential curve whose reliability is the same at all of its points. The configurations to be included are determined from the MO correlation diagram of the reaction under consideration. Figure 1 shows two typical features of MO correlation diagrams: in the first case, (a), the crossing of an occupied MO and a vacant MO occurs during the reaction process, while in the second case, (b), the difference between their MO energies becomes small (or two MO's are degenerate) on one side of the diagram. Examples of these cases are: (a) the disrotatory process of the cycloaddition reaction of *cis*-butadiene and (b) the dimerization of the methyl radical to form ethane. In the case of (a), the lowest closed-shell configuration changes near the crossing region. In this region, the mixing of the lower configurations, $(\cdots\phi_i^2\phi_k^0)$ and $(\cdots\phi_k^2\phi_i^0)$, is very large, and neither one of them separately, but a linear combination of them, can be a good approximation to the wavefunction of the lowest state. For the reaction whose MO correlation diagram has the feature (a) or (b) of Fig. 1, the lowest singlet potential curve should be described by the MC-wavefunction including the $\psi=(\cdots\phi_i^2\phi_k^0)$ and $\psi=(\cdots\phi_k^2\phi_i^0)$ configurations, and $\psi=(\cdots\phi_i^1\phi_k^1)$ one, if nescessary.

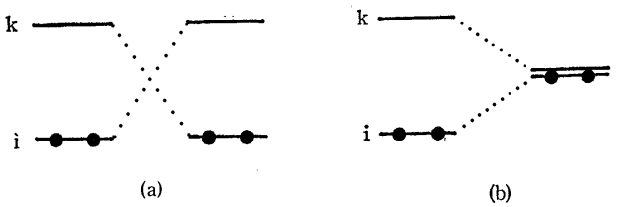

Fig. 1. Typical features appearing in MO correlation diagrams.
(a): Reaction process during which the crossing of an occupied MO and a vacant MO occurs.
(b): Reaction process at one side of which the difference between an occupied MO energy and a vacant MO energy becomes small.

There are actually many chemical processes whose MO correlation diagrams are more complex. In order to obtain MC-SCF equations which can be used for many reactions, two occupied MO's (i and j) and two vacant MO's (k and l) were selected, and all the singly- and doubly-excited singlet configurations derived from these four orbitals were taken into account. The lowest and some excited singlet potential curves of many chemical reactions can be described by this wavefunction. Thus, the MC-wavefunction was written as:

$$\begin{aligned}{}^1\Phi = {} & C_0\Psi_0 + C_1\Psi_i^k + C_2\Psi_i^l + C_3\Psi_j^k + C_4\Psi_j^l + C_5\Psi_{ii}^{kk} \\ & + C_6\Psi_{ii}^{ll} + C_7\Psi_{jj}^{kk} + C_8\Psi_{jj}^{ll} + C_9\Psi_{ii}^{kl} + C_{10}\Psi_{jj}^{kl} \\ & + C_{11}\Psi_{ij}^{kk} + C_{12}\Psi_{ij}^{ll} + C_{13}\Psi_{ij}^{kl}(1) + C_{14}\Psi_{ij}^{kl}(2) \end{aligned} \quad [1]$$

with

$$\sum_i C_i^2 = 1$$

where the configuration functions are:

$$\Psi_0 = |\ldots i\bar{i}j\bar{j}|$$

$$\Psi_i^k = \frac{1}{\sqrt{2}}\{|\ldots i\bar{k}j\bar{j}| + |\ldots k\bar{i}j\bar{j}|\}$$

$$\Psi_{tt}^{kk} = |\ldots k\bar{k}j\bar{j}|$$

$$\Psi_{tt}^{kl} = \frac{1}{\sqrt{2}}\{|\ldots k\bar{l}j\bar{j}| + |\ldots l\bar{k}j\bar{j}|\}$$

$$\Psi_{tj}^{kk} = \frac{1}{\sqrt{2}}\{|\ldots i\bar{k}k\bar{j}| + |\ldots k\bar{i}j\bar{k}|\}$$

$$\Psi_{tj}^{kl}(1) = \frac{1}{2}\{|\ldots i\bar{k}l\bar{j}| + |\ldots k\bar{i}j\bar{l}| + |\ldots\bar{i}\bar{k}jl| + |\ldots ik\bar{j}\bar{l}|\}$$

$$\Psi_{tj}^{kl}(2) = \frac{1}{2\sqrt{3}}\{2|\ldots i\bar{k}j\bar{l}| + |i\bar{k}l\bar{j}| + |\ldots k\bar{i}j\bar{l}| + 2|\ldots k\bar{i}l\bar{j}| - |\ldots\bar{i}\bar{k}jl| - |\ldots ik\bar{j}\bar{l}|\}$$

and where the others are obtained by changing the indices, i and j or/and k and l, in these configuration functions. The electronic energy of [1] is written as:

$$E_{\text{elec}} = E_g + \sum_{p,q} A_{pq}L_{pq} + \sum_{p,q,r,s} B_{pqrs}\langle pq|rs\rangle$$

where p, q, r, and s run over four orbitals, i, j, k, and l; where A_{pq} and B_{pqrs} are expressed by the configuration expansion coefficients (they are given in the Appendix). Also,

$$E_g = \sum_{t}^{\text{occ}} 2I_{tt} + \sum_{t,u}^{\text{occ}} \{2\langle tt|uu\rangle - \langle tu|ut\rangle\}$$

$$L_{rs} = I_{rs} + \sum_{t}^{\text{occ}} \{2\langle tt|rs\rangle - \langle ts|rt\rangle\}$$

$$I_{rs} = \int \phi_r^*(1)H_{\text{core}}(1)\phi_s(1)d\tau$$

$$\langle rs|tu\rangle = \int \phi_r^*(1)\phi_s(1)\frac{e^2}{r_{12}}\phi_t^*(2)\phi_u(2)d\tau$$

where t and u in the first two equations run over the doubly-occupied and i and j orbitals.

A troublesome aspect of implementing the MC-SCF formalism involves the handling of the off-diagonal Lagrangian multipliers, which insure orthonormality between open- and closed-shell orbitals of the same symmetry.[5] Segal has put forward the "partition-basis-set" technique, which simplifies the calculation of the wavefunctions of the excited states of molecules.[4] His method corresponds to a partial variational method, in which the variations of open-shell orbitals are expanded by virtual orbitals. Thus, the MO's obtained by this method are not the optimum ones.[6] However, its simplicity makes it possible to obtain many types of MC-SCF wavefunctions easily. This technique, which has been applied to the calculation of MC-SCF wavefunctions by Basch,[3] was used in the present study. The Fock-type equations obtained are:

$$F_\lambda|\phi_\lambda\rangle = \varepsilon_\lambda|\phi_\lambda\rangle \qquad (\lambda=1, 2, \ldots\ldots, i-1)$$

$$F_p|\phi_p\rangle + \sum_{q\neq p} F_{pq}|\phi_q\rangle = \varepsilon_p|\phi_p\rangle \qquad (p=i, j, k, l)$$

The second equations were converted to eigenvalue forms by rewriting the equations using the operators defined by:

$$F'_{pq} = F_{pq}|\phi_q\rangle\langle\phi_p|$$

and by adding the following quantity to both sides of the equation:

$$\sum_{q\neq p} F'^{\dagger}_{pq}|\phi_p\rangle = \sum_{q\neq p}|\phi_p\rangle\langle\phi_q|F_{qp}|\phi_p\rangle$$

The final eigenvalue forms are:

$$F_\lambda|\phi_\lambda\rangle = \varepsilon_\lambda|\phi_\lambda\rangle \qquad (\lambda=1, 2, \ldots\ldots, i-1) \qquad [3\text{-}1]$$

$$F_p|\phi_p\rangle = \varepsilon_{p'}|\phi_p\rangle \qquad (p=i, j, k, l) \qquad [3\text{-}2]$$

The operators F_λ and F_p are given by:

$$F_\lambda = H_{\text{core}} + \sum_t (2J_t - K_t) + \sum_{r,s}\frac{1}{2}A_{rs}(2f_{rs} - g_{rs})$$

$$F_p = F_{pp} + \sum_{r(\neq p)}\{F_{pr}|\phi_r\rangle\langle\phi_p| + |\phi_p\rangle\langle\phi_r|F_{rp}\}$$

$$F_{pp} = (\delta_{pi}+\delta_{pj})F_\lambda + \frac{1}{2}A_{pp}\{H_{\text{core}} + \sum_t(2J_t - K_t)\} + \sum_{r,s}(B_{pprs}f_{rs} + B_{psrp}g_{rs}) - \sum_r B_{pprp}f_{rp}$$

$$F_{pq} = \frac{1}{2}A_{pq}\{H_{\text{core}} + \sum_t(2J_t - K_t)\} + \sum_{\substack{r(\neq p,q)\\ s(\neq p,q)}} B_{pqrs}f_{rs} + \sum_{r(\neq p,q)}\{B_{pqpr}f_{pr} + B_{pqrq}f_{rq} + B_{prrq}g_{rr}\} + B_{pqqq}f_{qq} + B_{pqpq}f_{pq} \qquad (p\neq q)$$

where t runs over orbitals which are doubly occupied in the Ψ_0 configuration, and where r and s run over four orbitals, i, j, k, and l. The J_t, K_t, and H_{core} operators have their usual meanings, and the f and g operators are defined by:

$$f_{rs}(1)\phi_t(1) = \left(\int\frac{e^2}{r_{12}}\phi_r^*(2)\phi_s(2)d\tau_2\right)\phi_t(1)$$

$$g_{rs}(1)\phi_t(1) = \left(\int\frac{e^2}{r_{12}}\phi_r^*(2)\phi_t(2)d\tau_2\right)\phi_s(1)$$

$_{p}'$ is connected with the Lagrangian multiplier, ε_p, by:

$$\varepsilon_{p'} = \varepsilon_p + \sum_{r(\neq p)}\langle r|F_{rp}|p\rangle.$$

If the variation method is applied so as to minimize the E_{elec} with respect to the LCAO coefficients, $\mathbf{c}$, of

$$\phi_r = \boldsymbol{\chi}\mathbf{c}_r$$

equations equivalent to [3-1] and [3-2] are obtained.

$$\mathbf{F}_\lambda\mathbf{c}_\lambda = \mathbf{c}_\lambda\varepsilon_\lambda \qquad (\lambda=\text{inner MO's}) \qquad [4\text{-}1]$$

$$\mathbf{F}_p\mathbf{c}_p = \mathbf{c}_p\varepsilon_{p'} \qquad (p=i, j, k, l) \qquad [4\text{-}2]$$

where the matrices, $\mathbf{F}_\lambda$ and $\mathbf{F}_p$, are evaluated with the corresponding operator and the set of AO's.

The configuration expansion coefficients and the orbital expansion coefficients are determined by the following process.[3a]

(1) From an initial LCAO-MO set, the CI matrix elements, H_{ab}, are calculated, while the configuration expansion coefficients are determined from the lowest-energy solution of the secular determinant:

$$|H_{ab} - E\delta_{ab}| = 0$$

(2) From the above set of orbitals and the newly-obtained configuration expansion coefficients, the Hermitian matrices, $\mathbf{F}_\lambda$ and $\mathbf{F}_p$, of Eqs. [4] are calculated.

(3) Eq. [4-1] is solved in the usual manner to obtain the set of occupied MO's, ϕ_λ, and the set of orthogonal virtual MO's.

(4) The MO's ϕ_i, ϕ_j, ϕ_k, and ϕ_l, are successively determined by Segal's technique[4] from the virtual MO's obtained in (3).

(5) The procedure reverts to (1), and the process

is continued until the convergency of the total energy and AO bond populations is achieved.

While the excited states, as well as the ground state, can be evaluated by means of this procedure, the wavefunctions obtained by this procedure are not the optimum ones and are not correct to the first-order; that is, Brillouin's theorem does not hold for these wavefunctions.[4,6] First-order accuracy may be achieved by a CI calculation in which all the wave-functions formed by single excitations from the present MC-SCF function are included. This problem was not, however, examined in this paper.

Examples

The present MC-SCF method can be used for the calculations of the potential curves which are described by the wavefunction [1]. It was applied here to two reactions, the cycloaddition of *cis*-butadiene to form cyclobutene, and the dimerization of methylene to form ethylene. The lowest (ground-state) potential curves obtained were compared with those obtained by the CI method, in which the same approximation as in the MC-SCF method was used. The CI method is easy to use for the calculation of the potential curves of forbidden reactions. It is, thus, worth comparing the results obtained by the MC-SCF and CI methods. Semi-empirical method were used in the present applications because they are easily applicable to organic chemical reactions including rather large molecules. The INDO approximation,[7] which is one of the most widely accepted semi-empirical approximations, was used in the second example. In the first example, the MINDO/2 approximation[8] was used, since the MINDO /2-CI calculation for this reaction has already been performed.[9]

The Disrotatory Process of Cycloaddition of cis-*Butadiene to Form Cyclobutene.* The lowest singlet potential curve of this process was calculated for the ideal path, in which the molecule has C_s symmetry. The wavefunction can be described by two configurations, as was pointed out in the previous section:

$$^1\Phi = C|\ldots(5a'')^2| + C'|\ldots(7a')^2|$$

where $5a''$ and $7a'$, which correspond to the i and k orbitals in Fig. 1-(a) respectively, are anti-symmetric and symmetric with respect to the symmetry plane, which bisects the C_2-C_3 bond and is perpendicular to the carbon skeleton. The rotation angle of the CH_2 group was varied from 0°(*cis*-butadiene) to 90°(cyclobutene) in steps of 15°. The other geometrical parameters were gradually varied from those of *cis*-butadiene to those of cyclobutene. At each rotation angle, the SCF MO's of the all-valence electrons were obtained by means of the MINDO/2 method; these values were then used as the initial MO's of the MC-SCF procedure and as the basic MO's in the CI calculation. The total energy is the sum of the electronic energy and the core-repulsion energy, as calculated by means of the MINDO/2 approximation.[8]

The orbital expansion coefficients of $7a'$ and $5a''$ orbitals at $\theta=45°$ are shown in Table 1. The differences between the orbital expansion coefficients obtained by the MC-SCF method and the CI method are small. This was also observed for the orbitals at other points in the reaction process. The differences in configuration expansion coefficients between the two methods are also small (Table 2). Thus, no remarkable difference in the total energy between the two methods was observed during the process (<0.2 eV, Table 3). The overall shapes of both potential curves were similar to that obtained by a larger CI calculation in which 20 configuration functions were included.[9] Thus, a small MC-wavefunction is passable in the semi-empirical study of the present process.

The deviation of the energy obtained by the single-configuration wavefunction from that obtained by two configuration wavefunction largely depends on the rotation angle of the CH_2 group. At $\theta=45°$, the difference is 1.36 eV, which is much larger than those of normal molecules: 0.19 eV for *cis*-butadiene and 0.42 eV for cyclobutene. Thus, MC-wavefunctions should be used in the study of the forbidden reaction so as to obtain a reliable potential curve.

Dimerization of Triplet Methylene to Form Ethylene. The least-motion approach of two triplet ($^3B_1$) methylenes, or the least-motion dissociation of ethylene, was considered. It may be seen in Fig. 2 that the lowest closed-shell configuration changes from (core)$^8\sigma^2\pi^2$ to (core)$^8\sigma^2\sigma^{*2}$ during the dissociation of ethylene to methylenes. The lowest state(ground state) of methylene dimer is sufficiently described by the following configurations:[10]

(core)$^8\sigma^2\pi^2$ at $R_{cc}\sim R_0$, the value of normal ethylene,
(core)$^8\sigma^2\pi^2$ and (core)$^8\sigma^2\pi^{*2}$ at $R_{cc}\sim 2.0$ Å,
(core)$^8\sigma^2\pi^2$, (core)$^8\sigma^2\pi^{*2}$, (core)$^8\sigma^{*2}\pi^2$, (core)$^8\sigma^{*2}\pi^{*2}$, and (core)$^8\sigma\sigma^*\pi\pi^*$ at $R_{cc}>3.0$ Å,

where σ, σ^*, π, and π^* are the MO's of the D_{2h} methylene dimer. The wavefunction of the lowest state of the methylene dimer, whose C–C separation varies from R_0 to ∞, was written as:

$$^1\Phi = C_0\Psi_0 + C_5\Psi_{ii}^{kk} + C_6\Psi_{ii}^{ll} + C_7\Psi_{jj}^{kk} + C_8\Psi_{jj}^{ll} + C_{13}\Psi_{ij}^{kl}(1) + C_{14}\Psi_{ij}^{kl}(2)$$

so that the wavefunction always involves the above configurations whether the lowest closed-shell configuration is (core)$^8\sigma^2\pi^2$ or (core)$^8\sigma^2\sigma^{*2}$. The dissociation of ethylene has been studied by Basch.[3a] In his MC-SCF treatment, the first five configurations in the above wavefunction were taken into account. Thus, his wavefunction does not correctly represent the two $^3B_1$ methylenes at $R_{cc}\rightarrow\infty$.[10]

Calculations were also carried out for several C–C separations with a fixed CH_2 unit in an ideal geometry: CH=1.10 Å and ∠HCH=120°. The INDO approximation[7] was used for this process. The total energy of the lowest singlet state of the methylene dimer is shown in Table 3. The overall shape of the lowest potential curve was similar to that obtained by Basch.[3a] It may be seen from Table 3 that the difference between the single-configuration energy and the MC-SCF energy depends largely on the C-C separation. This was observed between the single-configuration energy and the CI energy calculated with 40 configuration

TABLE 1. ORBITAL EXPANSION COEFFICIENTS OF $5a''$ AND $7a'$ MO'S AT THREE TYPICAL ROTATION ANGLES OF CH_2 GROUPS[a]

AO[d]		$5a''$ MO[b]			$7a'$ MO[c]		
		0°	45°	90°	0°	45°	90°
C_1	2s	0.0000	0.1857	0.0000	0.0000	0.1602	0.0000
		(0.0000)	(0.1936)	(0.0000)	(0.0000)	(0.1455)	(0.0000)
	$2p_x$	0.0000	−0.4586	0.0000	0.0000	−0.3598	0.0000
		(0.0000)	(−0.4309)	(0.0000)	(0.0000)	(−0.3900)	(0.0000)
	$2p_y$	0.0000	−0.2382	0.0000	0.0000	−0.1888	0.0000
		(0.0000)	(−0.2298)	(0.0000)	(0.0000)	(−0.1800)	(0.0000)
	$2p_z$	0.5712	0.3487	−0.0418	0.5592	0.3455	0.1401
		(0.5616)	(0.3509)	(0.0404)	(0.5574)	(0.3455)	(0.1407)
C_2	2s	0.0000	0.0239	0.0000	0.0000	−0.0765	0.0000
		(0.0000)	(−0.0005)	(0.0000)	(0.0000)	(−0.0922)	(0.0000)
	$2p_x$	0.0000	−0.0478	0.0000	0.0000	0.0629	0.0000
		(0.0000)	(−0.0447)	(0.0000)	(0.0000)	(0·0665)	(0.0000)
	$2p_y$	0.0000	0.0402	0.0000	0.0000	0.0737	0.0000
		(0.0000)	(0.0314)	(0.0000)	(0.0000)	(0.0665)	(0.0000)
	$2p_z$	0.4169	0.2070	0.6987	−0.4327	−0.3527	−0.6553
		(0.4297)	(0.2363)	(0.6851)	(−0.4351)	(−0.3216)	(−0.6530)
H_1	1s	0.0000	0.0424	0.0709	0.0000	−0.1827	−0.1596
		(0.0000)	(0.0518)	(0.1204)	(0.0000)	(−0.1640)	(−0.1640)
H_2	1s	0.0000	−0.1507	−0.0709	0.0000	−0.0430	0.1596
		(0.0000)	(−0.1747)	(−0.1204)	(0.0000)	(−0.0428)	(0.1640)
H_3	1s	0.0000	0.0704	0.0000	0.0000	0.1226	0.0000
		(0.0000)	(0.0944)	(0.0000)	(0.0000)	(0.1596)	(0.0000)

a) SCF-MO's are also shown in parentheses. b) Add the other half part which is asymmetric with respect to the symmetry plane. c) Add the other half part which is symmetric with respect to the symmetry plane. d) C_1, terminal carbon; H_1 and H_2 methylene protons; x axis, parallel to C_2-C_3 bond; z axis, parpendicular to the carbon skeleton.

TABLE 2. TOTAL ENERGY AND CONFIGURATION EXPANSION COEFFICIENTS OF THE LOWEST SINGLET STATE ALONG THE CYCLOADDITION OF *cis*-BUTADIENE TO CYCLOBUTENE

θ[b]	MC-SCF			SCF-CI			SD[a]
	E (eV)	C	C'	E (eV)	C	C'	E (eV)
0°	−607.14	0.9859	−0.1672	−607.14	0.9869	−0.1612	−606.95
15°	−606.69	0.9796	−0.2011	−606.67	0.9820	−0.1887	−606.47
30°	−605.76	0.9463	−0.3233	−605.70	0.9581	−0.2864	−605.39
45°	−605.14	0.6546	−0.7559	−605.14	0.6410	−0.7676	−603.78
60°	−605.95	0.2658	−0.9640	−605.77	0.2635	−0.9646	−605.44
75°	−607.28	0.1748	−0.9846	−607.07	0.0875	−0.9962	−607.01
90°	−608.29	0.2302	−0.9731	−608.26	0.2218	−0.9751	−607.87

a) Obtained by single-configuration SCF method. b) $\theta=0°$ corresponds to *cis*-butadiene and $\theta=90°$ to cyclobutene.

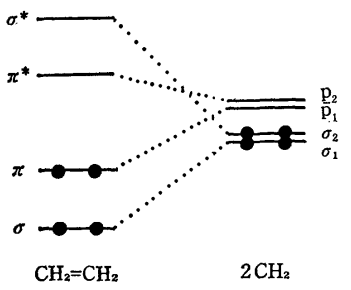

Fig. 2. MO correlation diagram connecting four MO's of ethylene and two methylenes.

TABLE 3. THE LOWEST SINGLET ENERGY (eV) OF D_{2h} METHYLENE DIMER

R_{cc}(Å)	MC-SCF	SCF-CI	SD[a]
1.30	−451.35	−451.12	−450.62
1.50	−449.93	−449.59	−448.66
2.00	−438.91	−438.68	−435.36
2.50	−431.42	−431.32	−427.42
3.00	−429.02	−429.00	−427.32

a) Energies obtained by single-configuration SCF method. The lowest closed-shell configuration at large C-C separation is $(\cdots\sigma^2\sigma^{*2})$ which does not contribute to the lowest singlet state of D_{2h} methylene dimer.

functions. Thus, the breakdown of the HF method in the intermediate region of the process gives a largely unreliable potential curve. The correction of the SCF-CI energy by the MC-SCF procedure was small (Table 3) in the present case, as in the previous example. This may be a result of the limited AO basis in the semi-empirical methods.

As a result, in semi-empirical all-valence electron calculations, the MC-SCF method or a rather large CI method may be sufficient to produce potential curves which remove the error originating from the HF method and which have a reliability comparable to that of the HF molecular ground state of a usual molecule.

The authors wish to express their thanks to Professor Keizo Suzuki for his helpful suggestions. The calculations were carried out by a HITAC 8800 computer at The University of Tokyo.

Appendix

A_{pq} and B_{pqrs} in Eq. (2) are expressed by the configuration expansion coefficients as follows. The others are obtained from the relations, $A_{pq}=A_{qp}$ and $B_{pqrs}=B_{qpsr}=B_{srqp}=B_{rspq}$.

$$A_{ii} = -(C_1^2 + C_2^2 + 2C_5^2 + 2C_6^2 + 2C_9^2 + C_{11}^2 + C_{12}^2 + C_{13}^2 + C_{14}^2)$$

$$A_{jj} = -(C_3^2 + C_4^2 + 2C_7^2 + 2C_8^2 + 2C_{10}^2 + C_{11}^2 + C_{12}^2 + C_{13}^2 + C_{14}^2)$$

$$A_{kk} = C_1^2 + C_3^2 + 2C_5^2 + 2C_7^2 + C_9^2 + C_{10}^2 + 2C_{11}^2 + C_{13}^2 + C_{14}^2$$

$$A_{ll} = C_2^2 + C_4^2 + 2C_6^2 + 2C_8^2 + C_9^2 + C_{10}^2 + 2C_{12}^2 + C_{13}^2 + C_{14}^2$$

$$A_{ij} = -(C_1C_3+C_2C_4+\sqrt{2}\{C_5C_{11}+C_6C_{12}+C_7C_{11}+C_8C_{12}+C_9C_{13}+C_{10}C_{13}\})$$

$$A_{kl} = C_1C_2 + C_3C_4 + \sqrt{2}\{C_5C_9+C_6C_9+C_7C_{10}+C_8C_{10}+C_{11}C_{13}+C_{12}C_{13}\}$$

$$A_{ik} = \sqrt{2}C_0C_1 + \sqrt{2}C_1C_5 + C_2C_9 + C_3C_{11} + \frac{\sqrt{2}}{2}C_4C_{13} + \frac{\sqrt{6}}{2}C_4C_{14}$$

$$A_{il} = \sqrt{2}C_0C_2 + \sqrt{2}C_2C_6 + C_1C_9 + C_4C_{12} + \frac{\sqrt{2}}{2}C_3C_{13} - \frac{\sqrt{6}}{2}C_3C_{14}$$

$$A_{jk} = \sqrt{2}C_0C_3 + \sqrt{2}C_3C_7 + C_1C_{11} + C_4C_{10} + \frac{\sqrt{2}}{2}C_2C_{13} - \frac{\sqrt{6}}{2}C_2C_{14}$$

$$A_{jl} = \sqrt{2}C_0C_4 + \sqrt{2}C_4C_8 + C_2C_{12} + C_3C_{10} + \frac{\sqrt{2}}{2}C_1C_{13} + \frac{\sqrt{6}}{2}C_1C_{14}$$

$$B_{iiii} = C_5^2 + C_6^2 + C_9^2$$

$$B_{jjjj} = C_7^2 + C_8^2 + C_{10}^2$$

$$B_{kkkk} = C_5^2 + C_7^2 + C_{11}^2$$

$$B_{llll} = C_6^2 + C_8^2 + C_{12}^2$$

$$B_{iikk} = -\frac{1}{2}(C_1^2+4C_5^2+2C_9^2+2C_{11}^2+C_{13}^2+C_{14}^2)$$

$$B_{iill} = -\frac{1}{2}(C_2^2+4C_6^2+2C_9^2+2C_{12}^2+C_{13}^2+C_{14}^2)$$

$$B_{jjkk} = -\frac{1}{2}(C_3^2+4C_7^2+2C_{10}^2+2C_{11}^2+C_{13}^2+C_{14}^2)$$

$$B_{jjll} = -\frac{1}{2}(C_4^2+4C_8^2+2C_{10}^2+2C_{12}^2+C_{13}^2+C_{14}^2)$$

$$B_{ikki} = C_1^2 + C_5^2 + \frac{1}{2}(C_9^2+C_{11}^2) + \frac{1}{4}(C_{13}^2+3C_{14}^2+2\sqrt{3}C_{13}C_{14})$$

$$B_{illi} = C_2^2 + C_6^2 + \frac{1}{2}(C_9^2+C_{12}^2) + \frac{1}{4}(C_{13}^2+3C_{14}^2-2\sqrt{3}C_{13}C_{14})$$

$$B_{jkkj} = C_3^2 + C_7^2 + \frac{1}{2}(C_{10}^2+C_{11}) + \frac{1}{4}(C_{13}^2+3C_{14}^2-2\sqrt{3}C_{13}C_{14})$$

$$B_{jllj} = C_4^2 + C_8^2 + \frac{1}{2}(C_{10}^2+C_{12}^2) + \frac{1}{4}(C_{13}^2+3C_{14}^2+2\sqrt{3}C_{13}C_{14})$$

$$B_{iijj} = \frac{1}{2}(C_{11}^2+C_{12}^2+C_{13}^2+C_{14}^2)$$

$$B_{kkll} = \frac{1}{2}(C_9^2+C_{10}^2+C_{13}^2+C_{14}^2)$$

$$B_{ijji} = \frac{1}{2}(C_{11}^2+C_{12}^2+C_{13}^2-C_{14}^2)$$

$$B_{klik} = \frac{1}{2}(C_9^2+C_{10}^2+C_{13}^2-C_{14}^2)$$

$$B_{iiij} = \frac{\sqrt{2}}{2}(C_5C_{11}+C_6C_{12}+C_9C_{13})$$

$$B_{ijjj} = \frac{\sqrt{2}}{2}(C_7C_{11}+C_8C_{12}+C_{10}C_{13})$$

$$B_{kkkl} = \frac{\sqrt{2}}{2}(C_5C_9+C_7C_{10}+C_{11}C_{13})$$

$$B_{klll} = \frac{\sqrt{2}}{2}(C_6C_9+C_8C_{10}+C_{12}C_{13})$$

$$B_{iiik} = -\frac{1}{2}(\sqrt{2}C_1C_5+C_2C_9)$$

$$B_{iiil} = -\frac{1}{2}(\sqrt{2}C_2C_6+C_1C_9)$$

$$B_{jjjk} = -\frac{1}{2}(\sqrt{2}C_3C_7+C_4C_{10})$$

$$B_{jjjl} = -\frac{1}{2}(\sqrt{2}C_4C_8+C_3C_{10})$$

$$B_{ikkk} = \frac{1}{2}(\sqrt{2}C_1C_5+C_3C_{11})$$

$$B_{illl} = \frac{1}{2}(\sqrt{2}C_2C_6+C_4C_{12})$$

$$B_{jkkk} = \frac{1}{2}(\sqrt{2}C_3C_7+C_1C_{11})$$

$$B_{jlll} = \frac{1}{2}(\sqrt{2}C_4C_8+C_2C_{12})$$

$$B_{ijij} = C_5C_7 + C_6C_8 + C_9C_{10}$$
$$B_{klkl} = C_5C_6 + C_7C_8 + C_{11}C_{12}$$
$$B_{ikik} = C_0C_5$$
$$B_{ilil} = C_0C_6$$
$$B_{jkjk} = C_0C_7$$
$$B_{jljl} = C_0C_8$$
$$B_{iijk} = -\frac{1}{2}C_1C_{11} - \frac{\sqrt{2}}{4}C_2C_{13} + \frac{\sqrt{6}}{4}C_2C_{14}$$
$$B_{iijl} = -\frac{1}{2}C_2C_{12} - \frac{\sqrt{2}}{4}C_1C_{13} - \frac{\sqrt{6}}{4}C_1C_{14}$$
$$B_{jjik} = -\frac{1}{2}C_3C_{11} - \frac{\sqrt{2}}{4}C_4C_{13} - \frac{\sqrt{6}}{4}C_4C_{14}$$
$$B_{jjil} = -\frac{1}{2}C_4C_{12} - \frac{\sqrt{2}}{4}C_3C_{13} + \frac{\sqrt{6}}{4}C_3C_{14}$$
$$B_{kkil} = \frac{1}{2}C_1C_9 + \frac{\sqrt{2}}{4}C_3C_{14} - \frac{\sqrt{6}}{4}C_3C_{14}$$
$$B_{kkjl} = \frac{1}{2}C_3C_{10} + \frac{\sqrt{2}}{4}C_1C_{13} + \frac{\sqrt{6}}{4}C_1C_{14}$$
$$B_{llik} = \frac{1}{2}C_2C_9 + \frac{\sqrt{2}}{4}C_4C_{13} + \frac{\sqrt{6}}{4}C_4C_{14}$$
$$B_{lljk} = \frac{1}{2}C_4C_{10} + \frac{\sqrt{2}}{4}C_2C_{13} - \frac{\sqrt{6}}{4}C_2C_{14}$$
$$B_{ijkl} = -\frac{\sqrt{2}}{4}C_2C_{13} - \frac{\sqrt{6}}{4}C_2C_{14} - \frac{1}{2}C_1C_{11}$$
$$B_{ijlk} = -\frac{\sqrt{2}}{4}C_1C_{13} + \frac{\sqrt{6}}{4}C_1C_{14} - \frac{1}{2}C_2C_{12}$$
$$B_{jikj} = -\frac{\sqrt{2}}{4}C_4C_{13} + \frac{\sqrt{6}}{4}C_4C_{14} - \frac{1}{2}C_3C_{11}$$
$$B_{jilj} = -\frac{\sqrt{2}}{4}C_3C_{13} - \frac{\sqrt{6}}{4}C_3C_{14} - \frac{1}{2}C_4C_{12}$$
$$B_{klik} = \frac{\sqrt{2}}{4}C_3C_{13} + \frac{\sqrt{6}}{4}C_3C_{14} + \frac{1}{2}C_1C_9$$
$$B_{kljk} = \frac{\sqrt{2}}{4}C_1C_{13} - \frac{\sqrt{6}}{4}C_1C_{14} + \frac{1}{2}C_3C_{10}$$
$$B_{likl} = \frac{\sqrt{2}}{4}C_4C_{13} - \frac{\sqrt{6}}{4}C_4C_{14} + \frac{1}{2}C_2C_9$$
$$B_{lkjl} = \frac{\sqrt{2}}{4}C_2C_{13} + \frac{\sqrt{6}}{4}C_2C_{14} + \frac{1}{2}C_4C_{10}$$
$$B_{ikkl} = -\sqrt{2}(C_5C_9 + C_6C_9) - \frac{\sqrt{2}}{2}(C_{11}C_{13} + C_{12}C_{13}) - \frac{1}{2}C_1C_2$$
$$B_{jjkl} = -\sqrt{2}(C_7C_{10} + C_8C_{10}) - \frac{\sqrt{2}}{2}(C_{11}C_{13} + C_{12}C_{13}) - \frac{1}{2}C_3C_4$$
$$B_{kkij} = -\sqrt{2}(C_5C_{11} + C_7C_{11}) - \frac{\sqrt{2}}{2}(C_9C_{13} + C_{10}C_{13}) - \frac{1}{2}C_1C_3$$
$$B_{llij} = -\sqrt{2}(C_6C_{12} + C_8C_{12}) - \frac{\sqrt{2}}{2}(C_9C_{13} + C_{10}C_{13}) - \frac{1}{2}C_2C_4$$
$$B_{ikli} = C_1C_2 + \frac{\sqrt{2}}{2}(C_5C_9 + C_6C_9) + \frac{\sqrt{2}}{4}(C_{11}C_{13} + C_{12}C_{13}) - \frac{\sqrt{6}}{4}(C_{11}C_{14} - C_{12}C_{14})$$
$$B_{jklj} = C_3C_4 + \frac{\sqrt{2}}{2}(C_7C_{10} + C_8C_{10}) + \frac{\sqrt{2}}{4}(C_{11}C_{13} + C_{12}C_{13}) + \frac{\sqrt{6}}{4}(C_{11}C_{14} - C_{12}C_{14})$$
$$B_{kijk} = C_1C_3 + \frac{\sqrt{2}}{2}(C_5C_{11} + C_7C_{11}) + \frac{\sqrt{2}}{4}(C_9C_{13} + C_{10}C_{13}) - \frac{\sqrt{6}}{4}(C_9C_{14} - C_{10}C_{14})$$
$$B_{lijl} = C_2C_4 + \frac{\sqrt{2}}{2}(C_6C_{12} + C_8C_{12}) + \frac{\sqrt{2}}{4}(C_9C_{13} + C_{10}C_{13}) + \frac{\sqrt{6}}{4}(C_9C_{14} - C_{10}C_{14})$$
$$B_{ijik} = -\frac{1}{2}(\sqrt{2}C_3C_5 + C_4C_9)$$
$$B_{ijil} = -\frac{1}{2}(\sqrt{2}C_4C_6 + C_3C_9)$$
$$B_{jijk} = -\frac{1}{2}(\sqrt{2}C_1C_7 + C_2C_{10})$$
$$B_{jijl} = -\frac{1}{2}(\sqrt{2}C_2C_8 + C_1C_{10})$$
$$B_{kikl} = \frac{1}{2}(\sqrt{2}C_2C_5 + C_4C_{11})$$
$$B_{kjkl} = \frac{1}{2}(\sqrt{2}C_4C_7 + C_2C_{11})$$
$$B_{likk} = \frac{1}{2}(\sqrt{2}C_1C_6 + C_3C_{12})$$
$$B_{ljlk} = \frac{1}{2}(\sqrt{2}C_3C_8 + C_1C_{12})$$
$$B_{ikil} = \frac{\sqrt{2}}{2}C_0C_9$$
$$B_{jkjl} = \frac{\sqrt{2}}{2}C_0C_{10}$$
$$B_{kikj} = \frac{\sqrt{2}}{2}C_0C_{11}$$
$$B_{likj} = \frac{\sqrt{2}}{2}C_0C_{12}$$
$$B_{ikjl} = \frac{1}{2}(C_0C_{13} + \sqrt{3}C_0C_{14})$$
$$B_{iljk} = \frac{1}{2}(C_0C_{13} - \sqrt{3}C_0C_{14})$$
$$B_{ikij} = C_1C_4 + \frac{1}{2}(C_5C_{13} + C_8C_{13} + C_9C_{12} + C_{10}C_{11}) + \frac{\sqrt{3}}{2}(C_5C_{14} + C_8C_{14})$$
$$B_{ilkj} = C_2C_3 + \frac{1}{2}(C_6C_{13} + C_7C_{13} + C_9C_{11} + C_{10}C_{12}) - \frac{\sqrt{3}}{2}(C_6C_{14} + C_7C_{14})$$
$$B_{ijkl} = -(C_6C_{13} + C_7C_{13} + C_9C_{11} + C_{10}C_{12}) - \frac{1}{2}C_2C_3$$

$$B_{ijlk} = -(C_5C_{13}+C_8C_{13}+C_9C_{12}+C_{10}C_{11}) - \frac{1}{2}C_1C_4$$

References

1) T. E. H. Walker, *Chem. Phys. Lett.*, **9**, 174 (1971); A. R. Gregory, *ibid.*, **11**, 271 (1971).

2) K. Hsu, R. J. Buenker, and S. D. Peyerimhoff, *J. Amer. Chem. Soc.*, **93**, 2117 (1971); J. E. Del Bene, *ibid.*, **94**, 3713 (1972); J. S. Wright and L. Salem, *ibid.*, **94**, 322 (1972); W. H. Fink, *ibid.*, **94**, 1073, 1078 (1972); O. Kikuchi, "Chemical and Biochemical Reactivity," ed. by E. D. Bergmann and B. Pullmann, Academic Press, London & New York, in press.

3) (a) H. Basch, *J. Chem. Phys.*, **55**, 1700 (1971); (b) H. Basch, *Theor. Chim. Acta*, **28**, 151 (1973).

4) G. A. Segal, *J. Chem. Phys.*, **53**, 360 (1970).

5) G. Das and A. C. Wahl, *ibid.*, **56**, 1769 (1972).

6) For the correct variational equations for the general SCF orbitals, see K. Hirao and K. Nakatsuji, *ibid.*, **59**, 1457 (1973).

7) J. A. Pople, D. Beveridge, and P. Dobosh, *ibid.*, **47**, 2026 (1967).

8) M. J. S. Dewar and E. Haselbach, *J. Amer. Chem. Soc.*, **92**, 590 (1970); N. Boder, M. J. S. Dewar, A. Harget, and E. Haselbach, *ibid.*, **92**, 3854 (1970).

9) O. Kikuchi, This Bulletin, **47**, 1551 (1974).

10) O. Kikuchi, *Chem. Lett.*, **1972**, 1121.

Synthesis of Methyl Isobutyl Ketone from Acetone and Hydrogen Catalyzed by Palladium Supported on Zirconium Phosphate

Yoshiaki WATANABE, Yoshito MATSUMURA, Yusuke IZUMI, and Yukio MIZUTANI
Tokuyama Soda Co., Ltd., Mikage-cho, Tokuyama, Yamaguchi 745
(Received December 17, 1973)

The one-step synthesis of methylisobutyl ketone from acetone and hydrogen was investigated by using palladium supported on zirconium phosphate, a bifunctional catalyst. Effects of reaction variables on both the conversion of acetone and the selectivity of methylisobutyl ketone were examined. The experiments were carried out with a continuous flow unit at 110—140 °C and 7—25 kg/cm² over a range of liquid hourly space velocity of acetone for 2—15 hr^{-1} with a mole ratio of hydrogen to acetone in the range 0.2—1.45. Under these conditions, the conversion of acetone was 20—40%, the selectivity of methylisobutyl ketone being as much 90—97 mol%. It is suggested that the one-step reaction proceeds *via* a consecutive mechanism.

Interest has been shown in the one-step direct synthesis of methylisobutyl ketone from acetone and hydrogen.

$$2CH_3COCH_3 + H_2 \rightarrow (CH_3)_2CHCH_2COCH_3 + H_2O \quad (1)$$

A number of bifunctional catalysts effective for both condensation and hydrogenation have been proposed for direct synthesis.[1,2] However, such catalysts containing basic substances for aldolization of acetone as KOH–Al_2O_3–Pd and SiO_2–MgO–Pd were found to be impractical because of low yield of methylisobutyl ketone.

Most commercial methods for producing methylisobutyl ketone are based on the conventional three-stage process; the aldol condensation of acetone to form diacetone alcohol catalyzed by a base, the dehydration of the alcohol to mesityl oxide with an acid, and the hydrogenation of the unsaturated ketone to methylisobutylketone with nickel or copper chromite catalyst.

Recently, some bifunctional catalysts containing palladium and cation-exchange resins have been reported for the selective one-step synthesis of methylisobutyl ketone.[3-8]

It was found that zirconium phosphate, an inorganic cation-exchanger, shows an excellent catalytic activity for the selective condensation of acetone to mesityl oxide.[9]

Attempts were made to prepare a bifunctional catalyst suitable for the selective one-step conversion of acetone and hydrogen into methylisobutyl ketone by finely dispersing palladium metal onto zirconium phosphate by means of ion-exchange technique.

The present paper is concerned with the general characteristic of the one-step synthesis of methylisobutyl ketone with the new catalyst.

Experimental

Catalyst Preparation. Palladium chloride (0.5 g) was added to an aqueous solution of zirconium oxychloride ($ZrOCl_2 \cdot 8H_2O$ 97 g/H_2O 3 l) and dissolved by heating. 33 g of phosphoric acid (85 vol%) was diluted with 3 litres of water. The former solution was added to the latter under stirring at room temperature for half an hour. After the reaction, the pH of the reaction mixture was adjusted to 5.0 with ammonia (14%). Stirring was continued for 4 hr, and the reaction mixture was allowed to stand for 24 hr. The resulting precipitate was then filtered, washed with water and dried at 110 °C. The dried gel obtained was crushed into 16—24 mesh particles and calcined at 400 °C for 8 hr in a stream of hydrogen. The palladium content of the resulting catalyst was 0.5 wt.%.

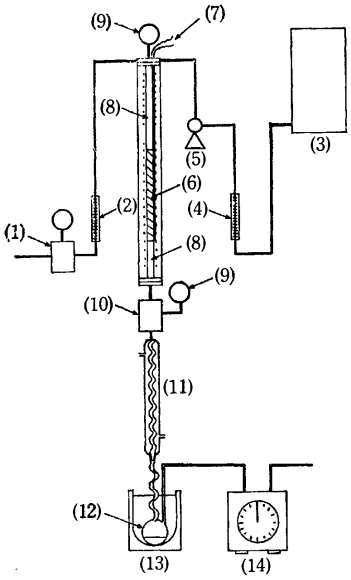

Fig. 1. Reaction apparatus.
(1): Pressure controller, (2): rotor meter, (3): acetone storage tank, (4): rotor meter, (5): plunger pump, (6): catalyst, (7): thermocouple, (8): porcelain chips, (9): pressure gauge, (10): pressure control valve, (11): water condenser, (12): receiver, (13): methanol-dry ice bath, (14): gas meter.

Apparatus and Procedure. Experiments were carried out with a continuous flow unit (Fig. 1). A stainless steel tube, 500 mm in length and 10 mm in inside diameter, was used as a reactor. The reactor was heated electrically with heaters separately controlled. Temperatures at the reaction zone were measured with thermocouples inserted in a thermowell extending longitudinally through the center of the reactor.

The catalyst in the form of 16—24 mesh particles (15 ml) was packed in the middle of the reactor. The remainder of the reactor was filled with porcelain chips and served as a preheating section. The chips were previously confirmed to have no appreciable catalytic activity.

After temperature and pressure had reached difinite levels (usually after 2 hr), the liquid products were collected in a receiver held in a methanol-dry ice bath and analyzed by

means of gas chromatography.

The operating conditions were so chosen that acetone was always kept in the liquid state in the reactor. The major by-products were isopropyl alcohol, mesityl oxide and diisobutyl ketone. Other by-products such as hexanes and higher ketones were found in trace amount.

The conversion of acetone and the selectivity of each component were defined by the following equations:

$$\% \text{ conversion} = \frac{y_{IPA} + 2(y_{MIBK} + y_{MO}) + 3y_{DIBK}}{y_A + y_{IPA} + 2(y_{MIBK} + y_{MO}) + 3y_{DIBK}}$$

$$\% \text{ selectivity} = \frac{y_{IPA},\ 2y_{MIBK},\ 2y_{MO} \text{ or } 3y_{DIBK}}{y_{IPA} + 2(y_{MIBK} + y_{MO}) + 3y_{DIBK}}$$

where y_{IPA}, y_{MIBK}, y_{MO}, y_{DIBK} and y_A denote mole fractions of isopropyl alcohol, methylisobutyl ketone, mesityl oxide, diisobutyl ketone and unconverted acetone, respectively.

Analysis. The product was determined by use of Shimadzu GC-2B gas chromatographic apparatus with the column (3 m in length, 4 mm in diameter) containing 30—60 mesh Shimalite coated with 15% PEG-1,000. Both the column and detector were kept at 95 °C. The flow rate of carrier gas (H_2) was adjusted to 60 ml/min.

Results

Effect of Mass Transfer. Acetone conversion changes with the acetone flow rate at a fixed liquid hourly space velocity (LHSV) and with catalyst particle size (Table 1). The data indicate that the effect of linear velocity on the acetone conversion is insignificant so long as the size of particles remains below 0.5 mm.

Table 1. Effect of mass transfer

Catalyst		Acetone Charge Rate (mol/hr.)	Acetone Conversion (%)
Mesh	Mean Particle Diameter (mm)		
8—12	1.880	0.275	18.3
		0.550	17.9
		0.825	18.1
16—24	0.846	0.550	19.4
		0.825	19.5
24—48	0.491	0.275	20.8
		0.550	20.7
		0.825	20.8
48—100	0.221	0.550	20.7
		0.825	20.5

Data obtained at 122 °C, 19.5 kg/cm², 4 hr⁻¹.
Acetone LHSV and 0.4 hydrogen/acetone mole ratio.

Effect of Temperature. The conversion of acetone and the selectivity of each component in the temperature range 110—140 °C are shown in Fig. 2. The conversion of acetone increased monotonously with temperature throughout the range. Although the selectivity gradually decreased with an increase in conversion, it still remained above 90 mol%. The major by-product was diisobutyl ketone, a trimeric condensate of acetone, formation of which being accelerated with a rise in temperature. The amount of another by-product, isopropyl alcohol, was almost unchanged with temperature remaining as low as 2 mol%.

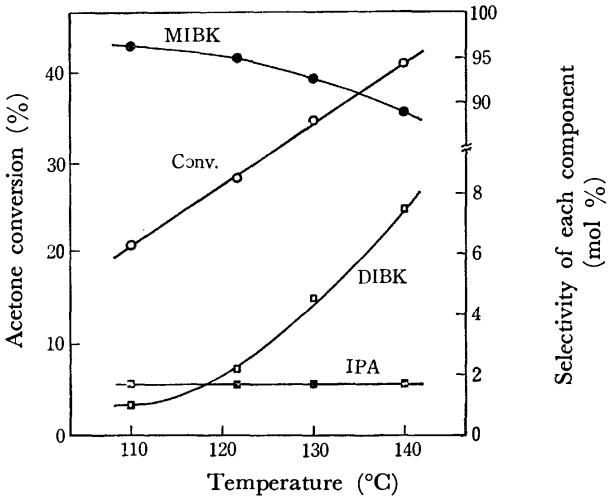

Fig. 2. Effect of temperature.
Data obtained at 20 kg/cm², 4 hr⁻¹ acetone LHSV, 0.4 hydrogen/acetone mole ratio.

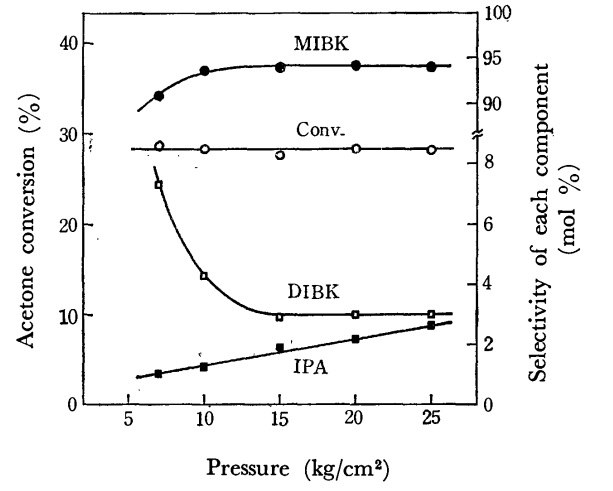

Fig. 3. Effect of pressure.
Data obtained at 120 °C, 4 hr⁻¹ acetone LHSV, 0.3 hydrogen/acetone mole ratio.

No mesityl oxide was detected.

Effect of Pressure. Figure 3 shows the effect of total pressure on the conversion of acetone and the selectivity to each component in the range 7—25 kg/cm². No appreciable change in acetone conversion with pressure was observed. However, the amount of isopropyl alcohol increased gradually with increase in pressure, the change being approximately linear. In contrast, the selectivity to diisobutyl ketone decreased with increase in pressure. The increase in the formation of diisobutyl ketone at a lower pressure or higher temperature suggests that the formation of diisobutyl ketone became dominant in vapour-phase reaction.

Thus, it is always necessary to keep acetone at the liquid phase by high pressure operation in order to obtain a good yield of methylisobutyl ketone.

Effect of Acetone Space Velocity. Figure 4 shows the effect of acetone space velocity on its conversion at 120 °C. Although the conversion decreased with increase in the space velocity, the change was less pro-

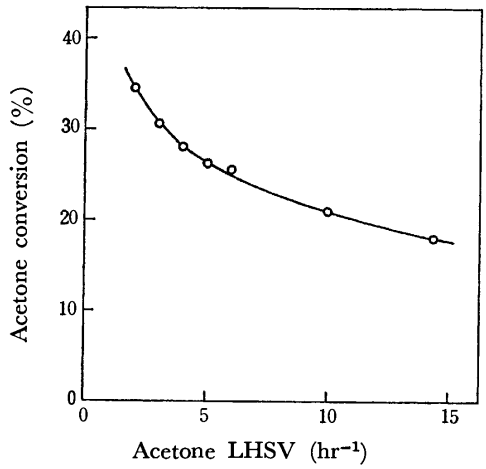

Fig. 4. Effect of acetone LHSV on acetone conversion.
Data obtained at 20 kg/cm², 0.3—0.4 hydrogen/acetone mole ratio.

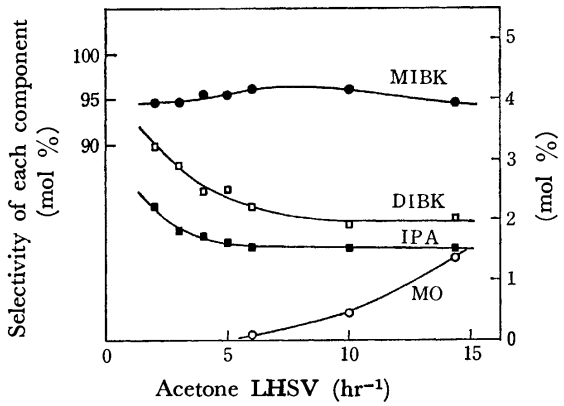

Fig. 5. Effect of acetone LHSV on selectivities.
Data obtained at 20 kg/cm², 120 °C, 0.3—0.4 hydrogen/acetone mole ratio.

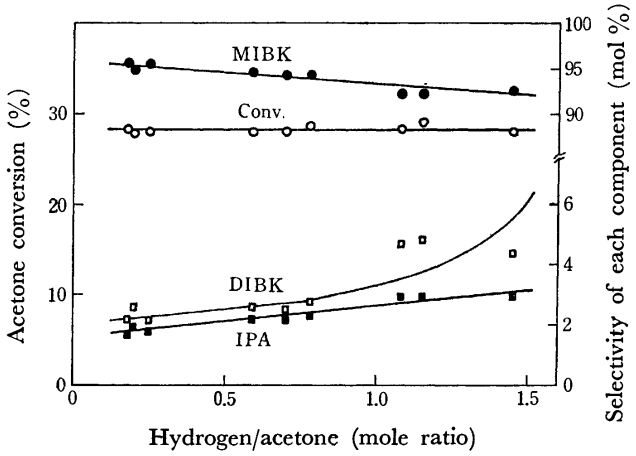

Fig. 6. Effect of mole ratio of hydrogen/acetone.
Data obtained at 120 °C, 20 kg/cm², 4 hr⁻¹ acetone LHSV.

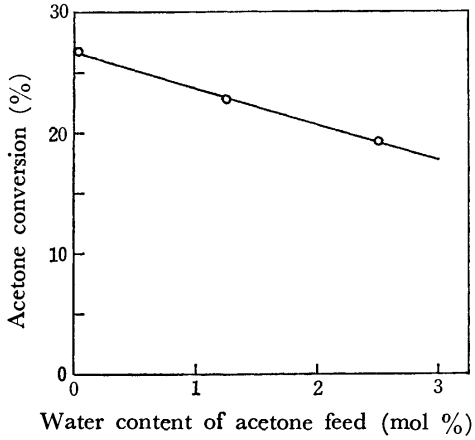

Fig. 7. Effect of water content of acetone feed on acetone conversion.
Data obtained at 120 °C, 20 kg/cm², 4 hr⁻¹ acetone LHSV, 0.3—0.4 hydrogen acetone mole ratio.

nounced in the LHSV range 5.0—15.0.

The formation of both isopropyl alcohol and diisobutyl ketone decreased with increase in space velocity (Fig. 5). These changes became slight for LHSV above 6. Mesityl oxide was detectable in the reaction products at an LHSV higher than 5.0. The change in the selectivity of methylisobutyl ketone was small under the conditions given.

Effect of Mole Ratio of Hydrogen/Acetone. The conversion of acetone remained almost unchanged, whereas the selectivity to isopropyl alcohol and diisobutyl ketone increased with an increase in mole ratio (Fig. 6). The change of selectivity to diisobutyl ketone was noticeable as compared with a slight linear change of isopropyl alcohol. No mesityl oxide was detected under these reaction conditions.

The preferable range of the mole ratio of hydrogen/acetone was deduced to be 0.2—0.4.

Effect of Water in Acetone Feed. The conversion of acetone decreased rapidly with an increase in the water content, the change being approximately linear (Fig. 7).

Since the water content of commercial acetone is usually as low as under 500 ppm, the commercial grade of acetone has no adverse effect upon the conversion of acetone to methylisobutyl ketone.

Discussion

Formation of mesityl oxide as an intermediate product under higher LHSV conditions suggests that the one-step reaction probably proceeds *via* a consecutive reaction mechanism:

$$2CH_3COCH_3 \rightleftharpoons (CH_3)_2C{=}CHCOCH_3 + H_2O \quad (2)$$

$$(CH_3)_2C{=}CHCOCH_3 + H_2 \rightarrow (CH_3)_2CHCH_2COCH_3 \quad (3)$$

The retardation of the acetone conversion into methylisobutyl ketone by the presence of water in the acetone feed is explained in terms of the reversibility of (2).

The conversion of acetone is much higher in the one-step synthesis of methylisobutyl ketone than in the synthesis of mesityl oxide under similar reaction conditions. This can be confirmed by direct comparison with the data.[9] This indicates that, in the direct conversion of acetone and hydrogen into methylisobutyl ketone, the conversion of acetone in (2) is enhanced by a rapid change of mesityl oxide into methylisobutyl ketone by (3).

Formation of isopropyl alcohol is due to the hydro-

Table 2. Results of vapor-phase reaction

Pressure (kg/cm²)	Conversion (%)	Selectivity (mol %)			
		MIBK	IPA	DIBK	Higher ketone[a)]
2.1	40.7	66.6	3.8	26.3	3.3
1.2	38.7	65.6	2.9	28.5	3.0
0.5	38.9	62.4	3.0	31.8	2.8
0.2	34.3	64.0	1.6	31.7	2.7

a) 4,6-Dimethyl heptanone-2
Data obtained at 130 °C, 4 hr^{-1} acetone LHSV and 0.8—1.1 hydrogen/acetone mole ratio.

genation of acetone, and another by-product, diisobutyl ketone, is probably formed by further condensation of methylisobutyl ketone with acetone. Formation of diisobutyl ketone is considered to be dominant in vapour-phase reaction. For the sake of confirmation, one-step reaction in vapor-phase was examined. The results indicate that the presumption is reasonable (Table 2).

The authors wish to thank Prof. Yoshinobu Takegami, Kyoto University and Dr. Yasuharu Onoue, Director of Tokuyama Soda Co. for their valuable discussions and advice.

References

1) Commercial Solvents Corp., U.S. 2499172 (1950).
2) Distillers Co., Brit. 656405 (1951).
3) Rheinpreussen A. G., Ger. 1193931 (1965); Ger. 1238453 (1967); Ger. 1260454 ((1968).
4) Scholven-Chemie A. G., Neth. 6812327 (1969).
5) Showa Denko Co., Japan 46-2009 (1971); Japan 46-2643 (1971).
6) Sumitomo Chemical Ind., Japan 47-15809 (1972; Japan 47-15810 (1972); U.S. 3,666,816 (1972).
7) H. Giehring, *Brennstoff Chem.*, **49** (8) 229 (1968).
8) Y. Mita, *J. Japan Petrol. Inst.*, **15** (2) 130 (1972).
9) Y. Watanabe, Y. Matsumura, Y. Izumi, and Y. Mizutani (unpublished).

Charge-Transfer Transitions Associated with Tricyanovinyl Aromatics[1)]

Akira SASAKI, Jun-ichi AIHARA, and Yoshio MATSUNAGA[2)]
Department of Chemistry, Faculty of Science, Hokkaido University, Sapporo 060
(Received January 26, 1974)

Four tricyanovinyl aromatic compounds were spectroscopically investigated in various phases. The solid-state spectra distinctly display both intra- and inter-molecular charge-transfer bands in the visible region. The formation of the charge-transfer self-complex is, however, markedly hindered in the fluid phases. The dual charge-transfer properties were also examined for these compounds.

When an electron-accepting moiety is directly bonded to an electron-donor molecule within a single electronic conjugate system, the uppermost filled valence orbital will be akin to that of the unsubstituted electron donor, the lowest vacant orbital being localized in the electron-accepting group.[3,4)] As can easily be predicted from such an electronic structure, the first absorption band originates from the so-called intramolecular charge-transfer transition, *i.e.*, the transition between the two orbitals denoted above.

In some cases, specific intermolecular interactions are additionally observed for such a compound. The simultaneous presence of the intra- and inter-molecular charge-transfer transitions was first observed for 2,4,6-trinitro-*p*-terphenyl.[5)] In a previous paper, we ourselves reported that two anisyl-*p*-benzoquinones form charge-transfer self-complexes in the solid state.[6)] In this article, we would like to present other typical examples of intramolecular charge-transfer compounds, tricyanovinyl aromatics.

Experimental

Tetracyanoethylene (TCNE) often reacts with aromatic compounds to give the corresponding tricyanovinyl aromatics. Four tricyanovinyl aromatic compounds were prepared according to the method developed by Sausen *et al.*[7)] The reaction products of *N,N*-dimethylaniline (DMA), pyrrole, indole, and 2,6-xylenol (xylenol) were *p*-(tricyanovinyl)-*N,N*-dimethylaniline (TCV-DMA), 2-(tricyanovinyl)-pyrrole (TCV-pyrrole), 2-(tricyanovinyl)-indole (TCV-indole), and 4-(tricyanovinyl)-2,6-xylenol (TCV-xylenol), respectively. All the absorption spectra were taken by using a Beckman DK-2A spectrophotometer.

Results and Discussion

Figures 1—4 show the absorption spectra of TCV-DMA, TCV-pyrrole, TCV-indole, and TCV-xylenol respectively in two phases. Every solution spectrum is composed of a single absorption band in the visible region. The absorption peaks are located at 19500 cm^{-1} ($\varepsilon_{max}=5.78\times10^4$), 23800 cm^{-1} ($\varepsilon_{max}=2.59\times10^4$), 21900 cm^{-1} ($\varepsilon_{max}=2.13\times10^4$), and 23900 cm^{-1} ($\varepsilon_{max}=2.88\times10^4$) for TCV-DMA, TCV-pyrrole, TCV-indole, and TCV-xylenol respectively in chloroform.

A similar tendency in transition energies is found among the charge-transfer bands of the TCNE complexes with parent aromatic compounds. The combinations of TCNE with DMA, pyrrole, indole, and xylenol induce the characteristic charge-transfer bands with maxima at 14300, 18800, 18600, and 19100 cm^{-1} respectively in chloroform. These values could not be observed accurately enough, since these donor-acceptor systems are quite reactive in solution. However, these charge-transfer bands are consistent with the first bands of the tricyanovinyl compounds in that a similar orderliness in transition energies is found in both cases. Such parallelism enables one to assign the latter bands to the intramolecular charge-transfer transitions. It is strongly suggested that the ionization potentials of the parent compounds increase in this order: DMA≪indole≤pyrrole<xylenol. Actually, the vertical ionization potential of DMA (7.51 eV)[8)] is much

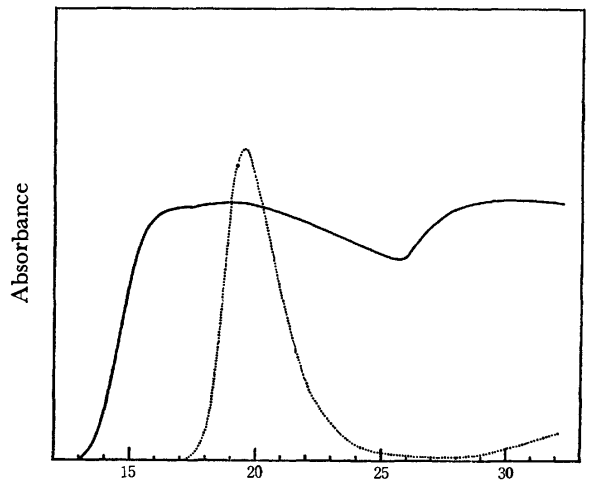

Fig. 1. Absorption spectra of TCV-DMA in chloroform solution (·····), and in the solid state (——).

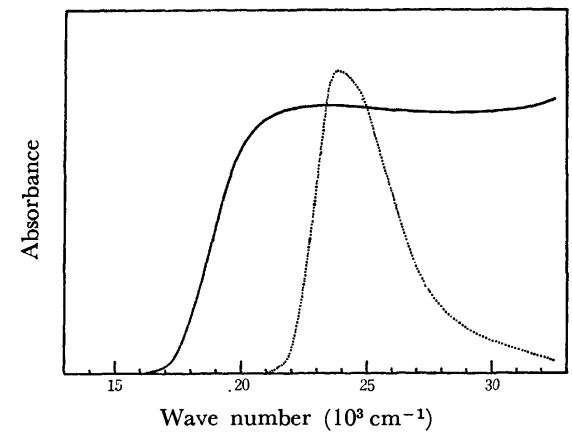

Fig. 2. Absorption spectra of TCV-pyrrole in chloroform solution (·····), and in the solid state (——).

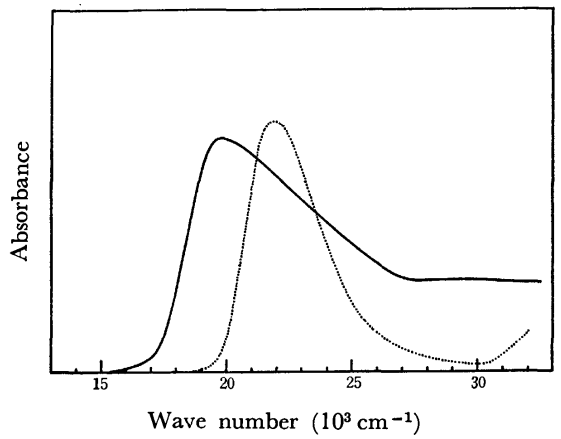

Fig. 3. Absorption spectra of TCV-indole in chloroform solution (·····), and in the solid state (——).

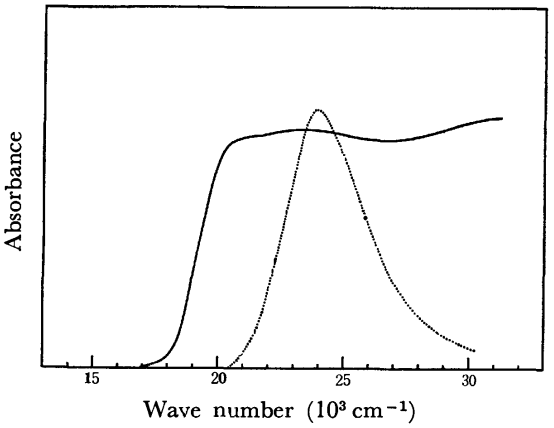

Fig. 4. Absorption spectra of TCV-xylenol in chloroform solution (·····), and in the solid state (——).

lower than that of pyrrole (8.21 eV),[9] though the other ionization potentials have not yet been determined. The smooth and isolated contour of the absorption band also characterizes the intramolecular charge-transfer transition. These absorption bands are very asymmetric, indicating that the 0–0 transitions are the strongest.

In view of the above discussion, the electron-donating orbital is supposedly located in the aromatic portion, whereas the tricyanovinyl group acts as an electron acceptor. Therefore, we can fully expect, in solution, the formation of the self-complex, where there would be a finite overlap between the donor orbital of one molecule and the acceptor orbital of a second molecule. However, the absorption spectra obtained over a 10^2-fold range of concentrations did not show any failure to obey Beer's law. No new bands were detected in the solution spectra.

If one takes into consideration the fact that 2,4,6-trinitro-*p*-terphenyl (TNTP) forms a self-complex in solution,[5] the behavior of tricyanovinyl compounds appears somewhat unusual. For example, the donor portion of TCV-DMA has more electron-donating ability than that of TNTP (diphenyl). The vertical ionization potential of diphenyl is 8.41 eV,[10] which is higher by 0.9 eV than that of DMA. On the other hand, the electron affinity of the trinitrophenyl moiety is considered to be similar to, or, more probably, less than that of the tricyanovinyl group, as will be discussed later. Since the contrast between the donor and acceptor orbitals is more striking for the tricyanovinyl compound, the dimerization in solution must have been hindered by some other effects, such as the unfavorable shapes of the molecular orbitals concerned.

On the other hand, the TCV-DMA crystal is deep blue and is in marked contrast with the deep red solution of the same compound. As is shown in Fig. 1, the gross absorption spectrum of the solid TCV-DMA is quite different from the solution spectrum in that the lower-energy part near 16000 cm^{-1} is much intensified in the former spectrum. The absorption peak around 19000 cm^{-1} in the solid-state spectrum corresponds well to the 19500 cm^{-1} band in the solution spectrum; it is assigned to the intramolecular charge-transfer transition.

Here, it must be noted that the intensified component near 16000 cm^{-1} is considered to be another absorption band. The presence of the two different bands is supported by the shape consideration of the spectrum. There is a distinct break, *i.e.*, an inflection point, around 17500 cm^{-1} in the solid-state spectrum. As may easily be seen, the intensity of the additional band on the low-energy side is comparable to that of the main band arising from the intramolecular transition. The first band can be attributed with little difficulty to the intermolecular transition. The spectral shape of TCV-xylenol also suggests that the solid-state spectrum consists of two different absorption bands in the visible region. By analogy with the case of TCV-DMA, the low-energy portion of the spectrum is considered to be due to the intermolecular interactions.

However, it is not clear whether or not the solid TCV-indole has the same spectral features. The whole spectrum appears to be composed of a single absorption band. The intramolecular absorption is supposedly covered by the predominant intermolecular charge-transfer band.

In connection with the above spectral behavior, one should remember the crystal structure of (2,2-dicyanovinyl)-ferrocene.[11] In the structure, the short distance between the dicyanovinyl moiety and the cyclopentadienyl ring of the adjacent molecule suggests, though not decisively, a donor-acceptor interaction analogous to that found in the molecular complex of ferrocene with TCNE. For another dicyanomethylene compound, 9-(dicyanomethylene)-2,7-dinitrofluorene, such self-complexing is postulated as giving rise to enhanced photoconductivity.[12] Therefore, the intermolecular interactions associated with tricyanovinyl compounds can similarly be considered to be of the charge-transfer type.

Various properties of tricyanovinyl compounds were first systematically studied by Sausen *et al.*[7] They compared these compounds with the corresponding dicyanovinyl compounds. It was then found that the investigated tricyanovinyl compounds show transition energies in ethanol about 0.4 eV lower than those of the dicyanovinyl counterparts. The extinction coefficients are smaller for the former group of compounds.

These facts imply that the tricyanovinyl group is considerably stronger as an electron acceptor than the dicyanovinyl group, and is probably stronger than the dicyanomethylene moiety. The larger electron affinity would more stabilize the charge-transfer self-complex, at least, in the crystal.

One might safely say that the self-complex formation is attained to 100 per cent in the crystal, if it is formed at all. Accordingly, the intensity of the additional band, *i.e.*, the intermolecular charge-transfer band, is comparable to that of the intramolecular charge-transfer band, as was suggested before.

However, the deep blue TCV-DMA crystal easily turns red upon being ground softly with sodium chloride. The dispersed material clearly shows the monomeric spectrum. The low-energy portion of the absorption spectrum diminishes rapidly on grinding. The evaporated film also shows a substantial decrease in the contribution of the intermolecular charge-transfer interactions to the spectrum. Such effects are also encountered among the other three tricyanovinyl compounds, though the change in color is rather modest. This aspect of the compounds in turn emphasizes the fragility of the charge-transfer interactions in the crystal as in solution.

The colors of the molten tricyanovinyl compounds are all similar to those of the corresponding solutions. The monomeric behavior of these compounds even in the pure melts would explain the behavior in solution, where the molecular association constants are obviously negligible. A free molecular motion seems easily to liberate these compounds from the dimerization in fluid phases. Such a situation is quite the same as for *o*-anisyl-*p*-benzoquinone.[6]

In order to estimate further the dual charge-transfer properties, *i.e.*, the electron-donating and -accepting abilities, of tricyanovinyl compounds, we examined the absorption spectra of the mixtures of these compounds with other typical electron donors and acceptors. Figure 5 shows the absorption spectra of TCV-pyrrole in the liquid DMA. The gross absorption spectra are very similar to the other solution spectra of this compound. However, a long absorption tail is noticeably preceded by the main band. For the four tricyanovinyl compounds, an absorption tail always begins at about 15000 cm^{-1}. Accordingly, the absorption tail of TCV-DMA is almost degenerate with the main band in DMA.

Such an absorption tail can be considered as a part of the charge-transfer band arising from the intermolecular interactions. In other words, it is related to the transition from the highest filled orbital of DMA to the lowest vacant orbital of the tricyanovinyl compound. The absorption tail is dependent on the ionization potential of the electron donor. When aniline is employed as a solvent, the edge of the absorption tail advances to about 16500 cm^{-1}. The absorption spectra taken in α-methylnaphthalene do not show any absorption tails. Instead, the absorbance in the higher-energy region around 25000 cm^{-1} increases to some extent. Considering that the absorption tails are preserved at almost the same photon energies in a given solvent for the four tricyanovinyl compounds, the electron-accepting ability should be similar among them. This fact further supports the previously-mentioned idea that the acceptor orbital is mainly localized in the tricyanovinyl moiety of the compound.

Since the absorption peak of the charge-transfer band could not be detected in these systems, the accurate estimate of the electron affinity was made difficult for the tricyanovinyl compound. However, by comparing the absorption edge of any compound to those of many other electron acceptors in the same donor solvent, it is not impossible to determine roughly the electron affinity of the compound. In the present case, the absorption edge of 1,3,5-trinitrobenzene (TNB) is found to fit well that of TCV-pyrrole in DMA, as is shown in Fig. 5. Therefore, the electron affinity of the tricyanovinyl compound is estimated to be similar to that of TNB, which is approximately 1.9 eV.[13]

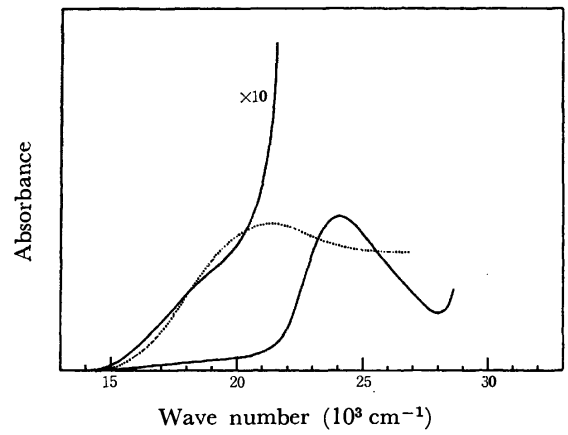

Fig. 5. Absorption spectra of TCV-pyrrole (——), and TNB (·····) in DMA solution.

On the other hand, no combinations of such tricyanovinyl compounds with typical electron acceptors, such as TCNE and chloranil, exhibited any intermolecular interactions supported by the absorption bands. The ordinarily-prepared solution is seemingly too deficient in concentration for the intermolecular charge-transfer to be observed. The small association constants between them are easily inferrable from the case mentioned above, where the additional absorption band of the tricyanovinyl compound is still weak in a pure donor solvent, such as DMA. If any strong acceptor were employed as a solvent, the charge-transfer band could be appreciably detected. At present there are no solvents suitable for this purpose. However, the absorption band of the self-complexed TCV-DMA in the solid suggests that the ionization potential of the isolated TCV-DMA is not very different from that of DMA and is possibly somewhat smaller than that.

In summary, tricyanovinyl aromatics are typical intramolecular charge-transfer compounds. Though they are considered to be at once good electron acceptors and good electron donors, every aspect of the absorption spectra is consistent with quite small association constants of these compounds, either with any other partner molecules or with themselves.

References

1) Part III of "Organic Charge-Transfer Self-Complexes"; Part II: This Bulletin, to be published. This work was financially supported by the Fuji Photo Film Co., Ltd.
2) All correspondences should be made either to JA or YM.
3) S. Nagakura and J. Tanaka, *J. Chem. Phys.*, **22**, 236 (1954).
4) R. L. Hansen, *J. Phys. Chem.*, **70**, 1646 (1966).
5) R. L. Hansen and J. J. Neumayer, *ibid.*, **71**, 3047 (1967).
6) J. Aihara, G. Kushibiki, and Y. Matsunaga, This Bulletin, **46**, 3584 (1973).
7) G. N. Sausen, V. A. Engelhardt, and W. J. Middleton, *J. Amer. Chem. Soc.*, **80**, 2815 (1958).
8) A. D. Baker, D. P. May, and D. W. Turner, *J. Chem. Soc. B*, 22 (1968).
9) P. J. Derrick, L. Åsbrink, O. Edqvist, and E. Lindholm, *Spectrochim. Acta*, **A27**, 2525 (1971).
10) J. H. D. Eland, *Int. J. Mass Spectrum. Ion Phys.*, **4**, 37 (1970).
11) A. P. Krukonis, J. Silverman, and N. F. Yannoni, *Acta Crystallogr.*, **B28**, 987 (1972).
12) J. Silverman, A. P. Krukonis, and N. F. Yannoni, *ibid.*, **B24**, 1481 (1968).
13) M. Batley and L. E. Lyons, *Nature*, **196**, 573 (1962).

The Infrared Intensities of Stretching Fundamentals in Gaseous and Crystalline Cyanoacetylene

Masakatsu UYEMURA* and Shiro MAEDA

Research Laboratory of Resources Utilization, Tokyo Institute of Technology, Meguro-ku, Tokyo 152

(Received February 19, 1974)

The absolute intensities of the stretching fundamentals of cyanoacetylene and cyanoacetylene-d were measured in gaseous and crystalline (77 K) states. As had been expected from the previous result for hydrogen cyanide, a striking intensity increase upon crystallization was observed not only for $\nu_{CH(CD)}$ but also for the other fundamentals. The observed intensities were reduced to dipole-moment derivative with respect to the internal coordinates, $\partial\mu/\partial r$. Then, by taking advantage of the strictly linear geometry of hydrogen-bonded chains in the crystals, it was demonstrated that the derivative with respect to the hydrogen-bonded distance, $[\partial\mu/\partial r_{N\cdots H}]$, was primarily responsible for the remarkable change in $\partial\mu/\partial r$; this was in accordance with the previous conclusion for hydrogen cyanide. A discrepancy from this view which appeared for $\partial\mu/\partial r_3$ was interpreted as being mainly caused by the vibronic behavior of π-electrons.

The infrared intensity characteristics of hydrogen-bonded systems are well known and have generally been interpreted in terms of a charge-transfer mechanism.[1-4] However, since there have been rather few quantitative intensity studies of those systems so far, there still seems to be need for such detailed investigations as will give positive evidence for the importance of the charge-transfer contribution. In a previous study of crystalline HCN and DCN, particular attention was given to the fact that not only the C–H (C–D) stretching but also the C≡N stretching absorption was remarkably intensified compared with gaseous ones; the analysis of those changes was then able to deduce a very large dipole-moment derivative properly attributable to the intermolecular charge transfer.[5] In that case, a strictly linear structure of hydrogen-bonded chains in the crystal furnished a very favourable condition for interpreting the results. In order to confirm the above conclusion for the N···H–C hydrogen-bonded system, cyanoacetylene and its deuterated derivative were studied from the same point of view, as these linear molecules are known to form linear hydrogen-bonded chains in a crystal just like hydrogen cyanide.[6]

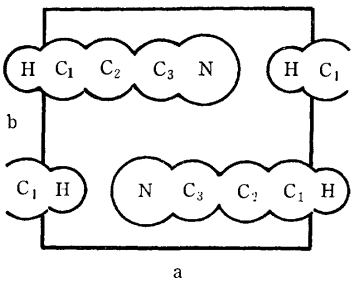

Fig. 1. Crystal structure of cyanoacetylene.

The crystal structure of cyanoacetylene determined by X-ray diffraction at 248 K is shown in Fig. 1, which belongs to the space group C_{2h}^2—$P2_1/m$ and which has two molecules per unit cell. In this structure, a linear hydrogen-bonded chain is surrounded by four parallel and two anti-parallel identical chains at intervals of 3.6 Å, and the $R_{N\cdots H-C}$ distance, 3.27 Å, is slightly longer than that of hydrogen cyanide ($R_{N\cdots H-C}$=3.18 Å).[6]

TABLE 1. CORRELATION DIAGRAM FOR CRYSTALLINE CYANOACETYLENE

	Molecule $C_{\infty v}$	Site C_s	Factor C_{2h}	Activity
ν_1, ν_2	Σ^+	A′	A_g	(*R*)
ν_3, ν_4			B_g	(*R*)
ν_5, ν_6	*II*	A″	A_u	(*IR*)
ν_7			B_u	(*IR*)

According to the correlation diagram, Table 1, each stretching fundamental is predicted to give only one infrared active crystal component, while each degenerate bending has two active components caused by the site-group splitting. The present work deals with the intensities of only stretching fundamentals, because our instrument was not able to cover the whole bending region. As we are primarily interested in the vibrations accompanying hydrogen-bonded stretching, the present result is not affected by the lack of intensity data on bending fundamentals.

Experimental

The HCCCN was kindly offered by Takeda Chemical Industries, Ltd., from their stock. The DCCCN was obtained by mixing the HCCCN with weakly alkaline D_2O, and both samples were distilled within a vacuum line just before the spectroscopic measurements, in order to remove any residual water and colored impurities. Their infrared spectra showed no indication of impurities except for a minute amount of HCCCN in the DCCCN sample, whose deuterium concentration was determined to be 98 mole% in both gas and crystal by measuring the intensity of the residual C–H stretching band.

The gaseous intensities were determined by the Wilson-Wells method.[7] The area of absorption

$$B' = \int \ln(T_0/T)d\nu$$

was measured using a 10 cm-length cell, with helium gas for pressure broadening. Sufficient broadening was achieved at a pressure of less than 170 Torr for every stretching band with a spectral slit width of 1 cm^{-1} or somewhat less. It was confirmed by observing the intensity by varying the total

* Present address: Faculty of Engineering, Tokyo College of Photography, Atsugi, Kanagawa, 243-02.

pressure; the intensity increase from 9 Torr to 170 Torr was a little less than 5%. The good linearity of Beer's law plots obtained to very low concentration seems to support it also. The ν_1, ν_2, and ν_3 frequencies of gaseous HCCCN were essentially identical with those reported by Turrell *et al.*[8] A weak absorption was observed in the ν_4 fundamental region of gaseous HCCCN, whereas no well-defined absorption band was observed in the ν_4 region (750~900 cm^{-1}) of gaseous DCCCN, even under its saturated vapor pressure.

The crystalline spectra were obtained at 77 K by an experimental procedure similar to that used for hydrogen cyanide.[5] In the process of evaluating intensities, the density at 248 K from the X-ray experiment[6] was used temporarily because no value was available for 77 K. The refractive index of the crystal at the wavelength of one micron, where the interference fringes were recorded for measuring the film thicknesses, was tentatively calculated based on the Lorentz-Lorenz formula using the atomic refraction data for the Na-D line.[9]

Results

The observed frequencies are shown in Table 2, together with those reported earlier.[8] In the ν_4 fundamental region of gaseous HCCCN, a broad and weak absorption attributable to the overlap of two parallel bands was observed. We provisionally assigned the 863 cm^{-1} band to ν_4 and the 887 cm^{-1} to $\nu_5+\nu_7$, following Job and King for the latter assignment[8] (Fig.

Table 2a. Observed and calculated frequencies of gaseous cyanoacetylene (cm^{-1})

HCCCN	Observed			Calculated
	Turrell *et al.*[a]	Job *et al.*[a]	This work	
ν_1(C-H)	3328.5±3	3328	3327	3329
ν_2(C≡C)	2271.0±0.8	2271	2272	2275
ν_3(C≡N)	2078.0±4	2078	2077	2081
ν_4(C-C)	—	—	863	868
DCCCN				
ν_1(C-D)		2608	2607	2604
ν_2(C≡C)		2250	2251	2248
ν_3(C≡N)		1968	1956	1953
ν_4(C-C)		—	—	855

Table 2b. Observed and calculated frequencies of crystalline cyanoacetylene (cm^{-1})

HCCCN	Observed		Calculated
	Turrell *et al.*[a]	This work	
ν_1(C-H)	3204±5	3204	3208
ν_2(C≡C)	2271.3±1	2271	2277
ν_3(C≡N)	2066±1	2066	2072
ν_4(C-C)	879.5±4	882	881
DCCCN			
ν_1(C-D)		2544	2538
ν_2(C≡C)		2246	2240
ν_3(C≡N)		1932	1927
ν_4(C-C)		868	869

a) Ref. 8.

Table 2c. Force constants of cyanoacetylene (md/Å)

	Gas[b]	Crystal[c]
K_1	5.904	5.338
K_2	16.92	17.17
K_3	6.866	7.006
K_4	16.05	15.39
K_{23}	1.55	1.74
K_{34}	−0.208	−0.501
K_5	—	0.149 (assumed)[c]

b) Potential function was assumed as follows;
$2V=K_1r_1^2+K_2r_2^2+K_3r_3^2+K_4r_4^2+2K_{23}r_2r_3+2K_{34}r_3r_4$.
For the definition of internal coordinates, see Ref. 15.
c) Potential function for the optically-active normal mode in crystal was assumed as follows, where r_t signifies the translationally invariant sum of internal coordinates as defined by Eq. (3). Hydrogen bond stretching force constant K_5 was estimated from Lippincott-Schroeder's potential.[14]
$2V=(K_1+K_5)r_1^2+(K_2+K_5)r_2^2+(K_3+K_5)r_3^2+(K_4+K_5)r_4^2+2(K_{23}+K_5)r_2r_3+2(K_{34}+K_5)r_3r_4$.

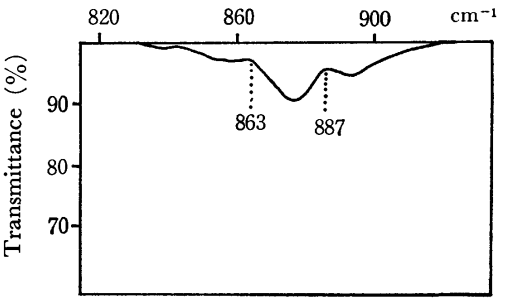

Fig. 2. Spectrum of ν_4 in gaseous HCCCN.

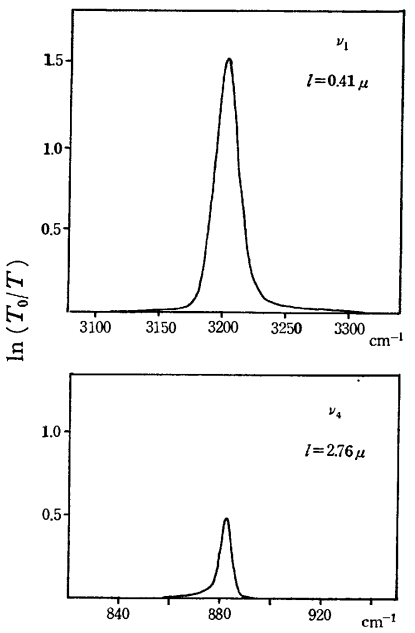

Fig. 3. Spectra of ν_1 and ν_4 in crystalline HCCCN.

2). Although Turrell *et al.* reported two additional broad absorptions at about 3200 cm^{-1} and 800 cm^{-1} in an HCCCN crystal, neither of these nor any of the corresponding bands in DCCCN was found in the present study (Fig. 3). The frequencies and breadth of these bands seem to suggest that they originate from the H_2O in HCCCN.[4]

The integrated absorption coefficient, A, was determined from Beer's law plots shown in Figs. 4 and 5, except for the gaseous ν_4 bands, which were so weak under the present observing conditions that no significant plots were obtainable. The $A(\nu_4)$ value of gaseous HCCCN was roughly estimated by comparing the peak height of the P-branch with that of ν_3, while no appreciable intensity was detected for ν_4 of DCCCN, as has been stated before. The values of the intensities thus determined are given in Table 3, in which the effective field correction by means of Polo-Wilson's equation[10] has already been incorporated in the crystalline values.

It should be noticed that the above intensities include errors from various sources; the accuracy of crystalline values can be especially seriously influenced by the slit width used and by the finite range of the frequency in integration. In the present observation, the slit width was normally much less than, or, at most,

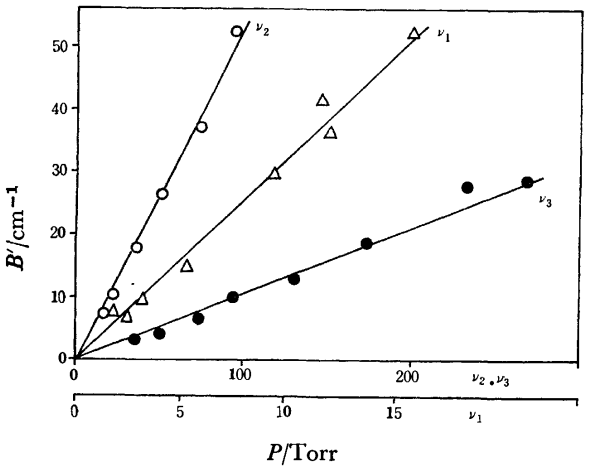

Fig. 4a. Beer's law plots of gaseous HCCCN.

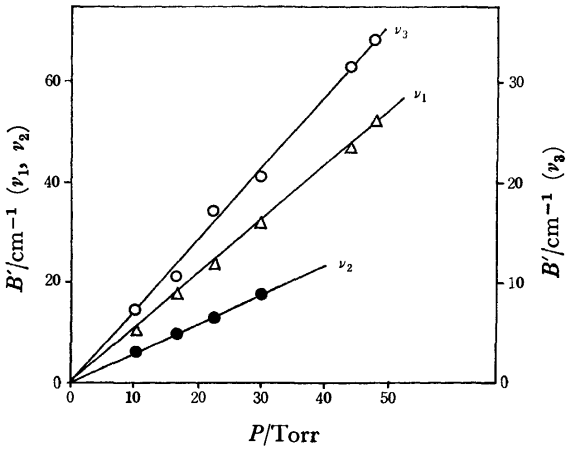

Fig. 4b. Beer's law plots of gaseous DCCCN.

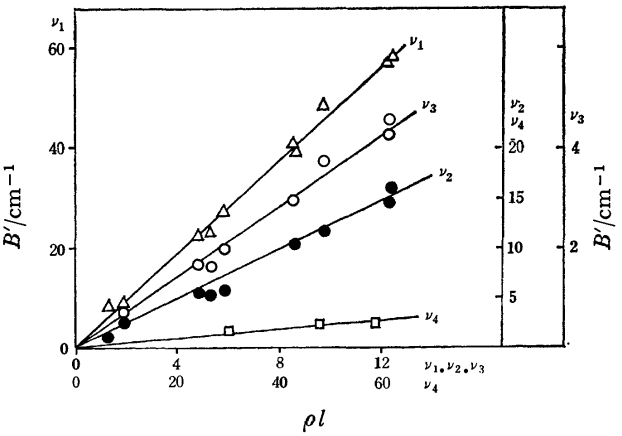

Fig. 5a. Beer's law plots of crystalline HCCCN (ρl in 10^{-4} mM cm^{-2}).

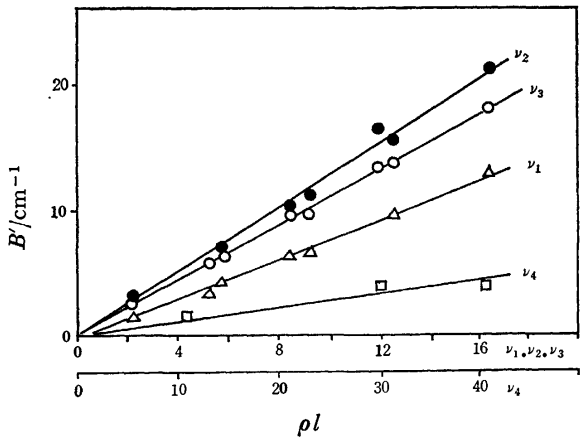

Fig. 5b. Beer's law plots of crystalline DCCCN (ρl in 10^{-4} mM cm^{-2}).

equal to, one-half of the band-width, and the integration was carried out over ten times the band width or more. Assuming a Lorentzian shape of the band, the maximum errors due to these sources are estimated at 6% and 7% respectively.[11] Taking other factors into consideration, the composite error is estimated at about 20% for crystals and about 15% for gases, considering some additional sources of error (for example, the uncertainty of the density at 77 K, the inhomogeneity of the film thicknesses, *etc*) in the former case. A criterion of the accuracy may be obtained by examining the validity of the intensity F-sum rule;[12] then, it is seen that the sums:

$$\sum_i (1/\lambda_i)\,|\partial\mu/\partial Q_i|^2$$

for H and D species agree within an error of 9% for the gas and 4% for the crystal, where λ_i is an eigenvalue ($\lambda_i=4\pi^2\nu_i^2$); $\partial\mu/\partial Q_i$ is given immediately below.

The integrated intensity, A, is related to the derivative of the dipole moment with respect to a normal coordinate, Q_i, by:[13]

$$A(\nu_i) = (N\pi/3c^2)\,|\partial\mu/\partial Q_i|^2 \qquad (1)$$

For crystalline intensities, Q_i should be an optically-active (wave vector $K=0$) normal coordinate of the crystal. The transformation to the derivatives with respect to the internal coordinates, r_i, is expressed as;[13]

Table 3. Observed intensities $A(r_i)$ of cyanoacetylene (10^4 darks)

		r_1	r_2	r_3	r_4
Gas	HCCCN	0.604±0.091	0.0992±0.0149	0.0193±0.0029	~0.0006
	DCCCN	0.202±0.030	0.110 ±0.016	0.133 ±0.020	<0.0002
Cryst.	HCCCN	3.53 ±0.71	0.933 ±0.187	0.271 ±0.054	0.035±0.007
	DCCCN	0.577±0.115	0.963 ±0.193	0.824 ±0.165	0.076±0.015

Table 4. Possible combinations of relative signs in $(\partial\mu/\partial Q_1, \partial\mu/\partial Q_2, \partial\mu/\partial Q_3, \partial\mu/\partial Q_4)$ (D/Å)

Gas		++++	+−++	++−+	+++−	+−−+	++−−	+−+−	+−−−[a]
$\partial\mu/\partial r_1$	HCCCN	0.989	1.137	1.100	0.976	1.249	1.088	1.124	1.236
	DCCCN	0.048	0.392	0.980	0.032	1.324	0.964	0.964	1.310
$\partial\mu/\partial r_2$	HCCCN	−1.250	−0.245	−0.383	−1.401	0.614	−0.535	−0.405	0.461
	DCCCN	−1.985	−1.664	0.215	−2.078	0.538	0.124	−1.756	0.446
$\partial\mu/\partial r_3$	HCCCN	0.463	−0.173	0.447	0.210	−0.188	0.193	−0.427	−0.442
	DCCCN	0.629	−0.006	0.345	0.483	−0.290	0.199	−0.152	−0.437
$\partial\mu/\partial r_4$	HCCCN	−0.438	1.222	−1.061	−0.602	0.599	−1.225	1.058	0.436
	DCCCN	−0.527	1.504	−1.564	−0.620	0.465	−1.658	1.409	0.373
Cryst.		++++	+−++	++−+	+++−	+−−+[a]	++−−	+−+−	+−−−
$\partial\mu/\partial r_1$	HCCCN	2.255	2.721	2.709	2.155	3.176	2.610	2.622	3.077
	DCCCN	−0.588	0.492	1.962	−0.897	3.042	1.652	0.183	2.733
$\partial\mu/\partial r_2$	HCCCN	−3.630	−0.733	−0.284	−4.811	2.612	−1.466	−1.915	1.430
	DCCCN	−3.546	−3.052	1.932	−5.400	2.426	0.079	−4.906	0.572
$\partial\mu/\partial r_3$	HCCCN	2.012	−0.080	2.110	0.000	0.018	0.098	−2.092	−1.994
	DCCCN	2.994	0.897	2.470	−0.003	0.367	−0.532	−2.106	−2.636
$\partial\mu/\partial r_4$	HCCCN	−0.748	4.269	−2.944	−2.086	2.073	−4.281	2.931	0.735
	DCCCN	−0.870	5.084	−3.497	−2.853	2.458	−5.480	3.101	0.476

a) Best combination.

$$\partial\mu/\partial r_i = \sum_j L_{ji}^{-1}\partial\mu/\partial Q_j, \quad (2)$$

where r_i for the crystalline case stands for a translationally-invariant linear combination of molecular r_i's. According to the crystal structure given before, the interaction between different chains of molecules may be much smaller than that due to hydrogen bonding, so that the crystal may be approximated by a one-dimensional chain in the following considerations. Then, the r_i in Eq. (2) for the crystal may be:

$$r_i = (1/\sqrt{n})\sum_j r_i^j \quad (3)$$

where r_i^j is the i-th coordinate of the j-th molecule of a chain and where n represents the number of molecules conforming to the periodic boundary condition.

The L_{ji}^{-1} in Eq. (2) was calculated based on the force constants given in Table 2, which reproduce the observed frequencies with deviations less than 0.5%. The force constant of a hydrogen-bond K(N···H), was obtained assuming a Lippincott-Schroeder potential.[14] Since the sign of $\partial\mu/\partial Q_i$ is not determinable experimentally, eight different sets of values are possible for $\partial\mu/\partial r_i$'s, corresponding to eight different combinations of relative signs among the four $\partial\mu/\partial Q_i$'s. It may be seen in Table 4 that the best consistencies between HCCCN and DCCCN are obtained in the (+−−−) combination for the gas and in the (+−−+) combination for the crystal. The final values of $\partial\mu/\partial r_i$ are given in Table 5, where two alternative sets of the signs are still present. Hereafter, the absolute sign of the derivatives will be defined so that a positive $\partial\mu/\partial r_{s_1}$ represents the increase in the dipole moment in the $^+$HCCCN$^-$ or $^+$HCN$^-$ direction caused by the s-t stretching.

Table 5. $\partial\mu/\partial r_i$ in gaseous and crystalline cyanoacetylene and change of $\partial\mu/\partial r_i$ (D/Å)

	Gas	Cryst.	Change of $\partial\mu/\partial r_i$
$\partial\mu/\partial r_1$	1.28	3.11	1.83
$\partial\mu/\partial r_2$	0.45	2.52	2.07
$\partial\mu/\partial r_3$	−0.44	0.19	0.63
$\partial\mu/\partial r_4$	0.41	2.27	1.86

Finally, it must be pointed out that the observed $\partial\mu/\partial r_3$ value of cyanoacetylene may contain a larger error than the others. That is, the intensity of ν_4, to which C–C stretching is mainly responsible, is extremely weak, so that the major contribution to $\partial\mu/\partial r_3$ comes from the other fundamental intensities through $\boldsymbol{L}^{-1}$ matrix elements, *i.e.* $L_{i,3}^{-1}$ $(i=1,2,3)$.

Discussion

Since the criterion of Table 4 does not disclose the absolute sign of $\partial\mu/\partial r$, it has to be determined on other bases. In the case of hydrogen cyanide, the sign of the gaseous derivatives was already known through the analysis of the vibration-rotation bands;[16] the crystalline one was chosen so that the observed differences, $\Delta(\partial\mu/\partial r)=(\partial\mu/\partial r)_{\text{crystal}}-(\partial\mu/\partial r)_{\text{gas}}$, which were remarkable not only in $\partial\mu/\partial r_{CH}$ but also in $\partial\mu/\mu r_{C\equiv N}$,

could be interpreted consistently in terms of an intermolecular contribution $[\partial\mu/\partial r_{N\cdots H}]$, given below. In fact, only such a choice of the sign made possible a reasonable interpretation; the resulting large negative $[\partial\mu/\partial r_{N\cdots H}]$ value was attributed to the vibrational contribution of the charge-transfer effect in hydrogen bonding.[5]

As for the absolute signs of $\partial\mu/\partial r_1$ in cyanoacetylene,[15] it seems most reasonable to assume that they are positive both in gas and in the crystal, so as to give similar values to those of hydrogen cyanide, because the C-H bond properties cannot be much different between these molecules and the effects of hydrogen bonding may also be alike in view of their similar crystal structures. In fact, any other sign combination proves to give quite an unintelligible situation regarding the interpretation of $\partial\mu/\partial r_1$ and $\partial\mu/\partial r$'s. Table 5 shows the results obtained assuming the absolute sign proposed above.

According to considerations similar to those made before,[5] the observed crystalline derivatives may be expressed as:

$$\partial\mu/\partial r_i = [\partial\mu/\partial r_i] - [\partial\mu/\partial r_{N\cdots H}], \tag{4}$$

where the brackets signify that the derivative is unconstrained by the condition for the optically-active coordinates:[17]

$$r_1 + r_2 + r_3 + r_4 + r_{N\cdots H} = 0. \tag{5}$$

Then, we obtain

$$\begin{aligned}\Delta(\partial\mu/\partial r_i) &= (\partial\mu/\partial r_i)_{\text{crystal}} - (\partial\mu/\partial r_i)_{\text{gas}} \\ &= \Delta[\partial\mu/\partial r_i] - [\partial\mu/\partial r_{N\cdots H}],\end{aligned} \tag{6}$$

where the change of a derivative is resolved into a purely intramolecular part ($\Delta[\partial\mu/\partial r_i]$) and a concurrent intermolecular term ($[\partial\mu/\partial r_{N\cdots H}]$).

Now, it may be noted in Table 5 that the three $\Delta(\partial\mu/\partial r_i)$ values are fairly close each other and comparable to the corresponding values in hydrogen cyanide with the exception of $\Delta(\partial\mu/\partial r_3)$. Therefore, if the previous conclusion that $[\partial\mu/\partial r_{N\cdots H}]$ is primarily responsible for $\Delta(\partial\mu/\partial r_i)$ is essentially valid here, there must be adequate reasons for the abnormally small value of $\Delta(\partial\mu/\partial r_3)$. Therefore, it may be proper to investigate such reasons in (a) the behavior of conjugated π-electrons during vibration, (b) the polarization of σ-electron due to the electrostatic field by neighboring molecules, and (c) the polarization of σ-electrons due to the intermolecular charge transfer through the hydrogen bond. In these effects, the behavior of conjugated π-electrons seems to be most significant, as will be shown below.

Assuming that the dipole moment is simply given by:

$$\mu = \Sigma_i q_i x_i, \tag{7}$$

where q_i and x_i are the charge density and the coordinate of the i-th atom, its derivative with respect to s-t stretching is:

$$\partial\mu/\partial r_{st} = \Sigma_i\{(\partial q_i/\partial r_{st})x_i + q_i(\partial x_i/\partial r_{st})\}, \tag{8}$$

In a simple MO consideration for π-electrons, it may be appropriate to represent the effect of s-t stretching by a change in the resonance integral, β_{st}. Thus, confining ourselves to π-electrons, we may obtain

$$\partial q_i/\partial r_{st} = (\partial q_i/\partial\beta_{st})(\partial\beta_{st}/\partial r_{st}) = \pi_{i,st}(d\beta_{st}/dr_{st}), \tag{9}$$

where $\pi_{i,st}$ is the atom-bond polarizability.[18] It may be noticed here that always $d\beta_{st}/dr_{st} > 0$. In the present approximate consideration, the hydrogen-bonding perturbation to π-electrons may be represented by the change in the Coulomb integrals of C_1 and N; $\Delta\alpha_1$ and $\Delta\alpha_4$. Then, we obtain:

$$\begin{aligned}\Delta\left(\frac{\partial\mu}{\partial r_{st}}\right)_\pi &= \Sigma_i\left(\frac{\partial\pi_{i,st}}{\partial\alpha_1}\Delta\alpha_1 + \frac{\partial\pi_{i,st}}{\partial\alpha_4}\Delta\alpha_4\right)\frac{\partial\beta_{st}}{\partial r_{st}}x_i \\ &\quad + \Sigma_i(\pi_{i,1}\Delta\alpha_1 + \pi_{i,4}\Delta\alpha_4)\frac{\partial x_i}{\partial r_{st}},\end{aligned} \tag{10}$$

where $\pi_{i,j}$ is the atom-atom polarizability;[18] an explicit form of $(\partial\pi_{i,st}/\partial\alpha_j)$ is given in the Appendix. The use of the π-wave function based on a CNDO calculation gives the numerical expression in Table 6.

In Table 6, it is notable that the first term of $\Delta(\partial\mu/\partial r_3)_\pi$ is of a sign opposite to those of the other two. Since the perturbation may be taken such that $\Delta\alpha_1 > 0$ and $\Delta\alpha_4 < 0$, because of either electrostatic and charge-transfer interactions, the first term above may certainly serve to lower the value of $\Delta[\partial\mu/\partial r_3]$, while it raises the other two.

TABLE 6. π-ELECTRON CONTRIBUTION TO $\Delta[\partial\mu/\partial r]$ CALCULATED BY USING CNDO WAVE FUNCTIONS (in atomic units)[a]

r_{st}	$\Delta[\partial\mu/\partial r_{st}]$
r_2	$(18.1\Delta\alpha_1 - 6.1\Delta\alpha_4)(\partial\beta_2/\partial r_2) + (2.4\Delta\alpha_1 - 0.4\Delta\alpha_4)$
r_3	$-(15.5\Delta\alpha_1 - 15.6\Delta\alpha_4)(\partial\beta_3/\partial r_3) + (0.3\Delta\alpha_1 - 0.3\Delta\alpha_4)$
r_4	$(6.0\Delta\alpha_1 - 17.3\Delta\alpha_4)(\partial\beta_4/\partial r_4) + (0.4\Delta\alpha_1 - 2.3\Delta\alpha_4)$

a) The resonance integrals are numbered in the same way as r_i. See Ref. 15.

Besides the π-electron contribution (a) mentioned above, $\Delta[\partial\mu/\partial r_i]$ should be influenced by the σ-electron polarization, which is caused by the electrostatic field (b) and also by the intermolecular charge transfer (c) as described by such resonance structures:

$$\equiv N\ \dot{H}—C\equiv C—C\equiv\overset{+}{N}—H\ \bar{C}$$

$$\equiv\overset{+}{N}—H\ \bar{C}\equiv C—C\equiv N\ H—C$$

However, in view of the fact that C–H bending intensity was almost unchanged in hydrogen cyanide,[5] as is generally observed in hydrogen-bonded systems, the (b) effect does not seem very important. On the other hand, the (c) effect may reduce $\Delta[\partial\mu/\partial r_i]$ more or less except in the case of C–H, resulting in a rather large negative $\Delta[\partial\mu/\partial r_3]$ value in cooperation with the (a) effect. On the other hand, $\Delta[\partial\mu/\partial r_2]$ and $\Delta[\partial\mu/\partial r_4]$ may become less important because the (c) and (a) effects tend to cancel each other out.

The consideration given above, though it is only qualitative, seems to explain the discrepancy in $\Delta(\partial\mu/\partial r_3)$ rather convincingly. We may, then, consider that, in all probability, the present result further demonstrates the importance of the intermolecular dipole-moment derivative $[\partial\mu/\partial r_{N\cdots H}]$. As a rough estimate,

the value of $[\partial\mu/\partial r_{N\cdots H}]$ may be comparable to the observed $\Delta(\partial\mu/\partial r_1)$ value with a negative sign, because the previous estimate, -1.4 D/Å, for hydrogen cyanide seems to be too low because the effect of $\Delta[\partial\mu/\partial r_{C\equiv N}]$ was ignored then.

The authors wish to thank the Takeda Chemical Industries, Ltd., for giving them the cyanoacetylene sample.

Appendix

The atom-bond polarizability, $\pi_{r,st}$, is given in terms of the LCAO MO coefficients as:[18]

$$\pi_{r,st} = \partial q_r/\partial\beta_{st}$$

$$= 4\sum_{j=1}^{m}\sum_{k=m+1}^{n} C_{rj}C_{rk}(C_{sj}C_{tk}+C_{tj}C_{sk})/(\varepsilon_j-\varepsilon_k)$$

($1\sim m$: occuppied MO, $m+1\sim n$: vacant MO) (A1)

Now, for a small perturbation, $\boldsymbol{J}$, in the Hamiltonian matrix, the perturbed orbital energy and LCAO MO coefficients are given by:

$$\varepsilon_j = \varepsilon_j^\circ + \tilde{\boldsymbol{C}}_j^\circ \boldsymbol{J}\boldsymbol{C}_j^\circ,$$

$$\boldsymbol{C}_j = \boldsymbol{C}_j^\circ + \sum_{k\neq j}\{\tilde{\boldsymbol{C}}_k^\circ \boldsymbol{J}\boldsymbol{C}_j^\circ/(\varepsilon_j^\circ-\varepsilon_k^\circ)\}\boldsymbol{C}_k^\circ \quad \text{(A2)}$$

where $\boldsymbol{C}_j$ is a column vector of coefficients for the j-th MO and where the superscript $^\circ$ denotes unperturbed values. On the basis of these equations, the following expressions are obtained straightforwardly for a diagonal term, $J_{u,u}=\Delta\alpha_u$:

$$\partial\pi_{r,st}/\partial\alpha_u = 4\sum_{j=1}^{m}\sum_{k=m+1}^{n}\frac{C_{rj}C_{rk}}{\varepsilon_j-\varepsilon_k}\Bigg\{(C_{sj}C_{tk}+C_{tj}C_{sk}) \times\left[\frac{C_{rj}^{(u)}}{C_{rj}}+\frac{C_{rk}^{(u)}}{C_{rk}}-\frac{C_{uj}^2-C_{uk}^2}{\varepsilon_j-\varepsilon_k}\right]+C_{sj}^{(u)}C_{tk} +C_{sj}C_{ik}^{(u)}+C_{ij}^{(u)}C_{sk}+C_{tj}C_{sk}^{(u)}\Bigg\}, \quad \text{(A3)}$$

$$C_{rj}^{(u)} = \sum_{\substack{l=1\\ l\neq j}}^{n}\{C_{rl}C_{ul}C_{uj}/(\varepsilon_j-\varepsilon_l)\} \quad \text{(A4)}$$

where the superscript $^\circ$ is omitted from every symbol for the sake of brevity.

References

1) H. Tsubomura, *J. Chem. Phys.*, **24**, 927 (1956).
2) P. G. Puranik and V. Kumar, *Proc. Ind. Acad. Sci.*, **58**, 29 (1963); *ibid.*, **58**, 327 (1963).
3) K. Szczepaniak and A. Tramer, *J. Phys. Chem.*, **71**, 3035 (1967).
4) S. Ikawa and S. Maeda, *Spectrochim. Acta*, **24A**, 655 (1968).
5) M. Uyemura and S. Maeda, This Bulletin, **45**, 1081 (1972).
6) F. V. Shallcross and G. B. Carpenter, *Acta Crystallogr.*, **11**, 490 (1958); W. J. Dulmage and W. N. Lipscomb, *ibid.*, **4**, 330 (1951).
7) E. B. Wilson. Jr. and J. A. Wells, *J. Chem. Phys.*, **14**, 578 (1946).
8) V. A. Job and G. W. King, *Can. J. Chem.*, **41**, 3132 (1963); G. C. Turrell, W. Johns and A. Maki, *J. Chem. Phys.*, **26**, 1544 (1957).
9) Landort-Börnstein, Zahlenwerte und Function, II Band, 8 Teil (Optische Konstante), Springer (1962).
10) S. R. Polo and M. K. Wilson, *J. Chem. Phys.*, **23**, 2376 (1955).
11) D. A. Ramsay, *J. Amer. Chem. Soc.*, **74**, 72 (1952).
12) B. L. Crawford Jr., *J. Chem. Phys.*, **20**, 977 (1952).
13) J. Overend, "Infrared Spectrsocopy and Molecular Structure," ed. by M. Davis, Elsevier Pub. Co., Amsterdam (1963), p. 374.
14) E. R. Lippincott and R. Schröder, *J. Chem. Phys.*, **23**, 1099 (1955).
15) The stretching coordinates of C–H, C≡C, C–C and C≡N of cyanoacetylene are defined as r_1, r_2, r_3 and r_4 respectively.
16) D. R. Eaton, *Proc. Roy. Soc.* (London), *Ser. A*, **251**, 486 (1959).
17) The $r_{N\cdots N}$ in Eq. (6) stands for the optically active coordinate arising from hydrogen bond stretching as r_t in Eq. (3).
18) M. J. S. Dewar, "The Molecular Orbital Theory of Organic Chemistry," McGraw-Hill Book Company, New York (1969), p. 198.

Group Interactions in Polyelectrolytes. VIII.[1] The Amination of Chloromethylated Polystyrene with Secondary Amines and the Quaternization of the Aminated Polymer

Hiroshi KAWABE

The Institute of Physical and Chemical Research, Wako-shi, Saitama 351

(Received March 8, 1974)

The amination of chloromethylated polystyrene (CMPS) and benzyl chloride with diethyl amine, diethanolamine, and di-*n*-butylamine was investigated kinetically in *N,N*-dimethylformamide (DMF), dimethyl sulfoxide (DMSO), or dioxane. The apparent second-order rate constant decreased as the amination proceeded in the amination of CMPS with diethylamine and di-*n*-butylamine in DMF as well as in dioxane. Although a similar deceleration was also observed in the amination of CMPS with diethanolamine in DMF and DMSO, acceleration was observed during the course of the amination in dioxane. It is assumed that the deceleration and the acceleration are due to the steric obstruction and to the formation of a hydrogen bond by the neighboring groups in the transition state respectively. The intrinsic rate constants of the amination of CMPS were almost the same as those of benzyl chloride. The rate of the amination with diethanolamine was lower than that of the amination with diethylamine because of the inductive effect of the hydroxyl group. The rate constants in different solvents were in this order; DMSO > DMF ≫ dioxane. The aminated CMPS with diethanolamine ($pK_0 = 7.37$) was quaternized with methyl iodide or bromoacetic acid in 50% aq. DMF. The deceleration due to the electrostatic effect of the neighboring groups was observed in the quaternization.

The effect of the species of amines and solvents on the kinetics in the amination of chloromethylated polystyrene (CMPS) was previously investigated by Kawabe and Yanagita.[1-4] Although most of the amination with primary amines such as butylamine isomers conformed to the ordinary second-order rate equation, deceleration was observed during amination with such secondary amines as diethylamine and di-*n*-butylamine. On the other hand, acceleration was observed during amination with 2-aminobutanol in dioxane, though the amination with the amine in *N,N*-dimethylformamide (DMF) and dimethyl sulfoxide (DMSO) obeyed the ordinary second-order kinetics.

In the above reactions, charged groups were not formed on the polymer molecules, because CMPS was aminated with a large excess of primary or secondary amine. On the other hand, in the Menschutkin reaction of polymers, during which quaternary ammonium groups are formed on polymer molecules, the following two different kinetic behaviors were reported; one was an ordinary second-order kinetics, while the other was modified by the deceleration because of the electrostatic repulsion among the charged groups. Noda and Kagawa[5] found that the amination of CMPS with triethylamine in DMF conformed to the second-order kinetics. Fouss *et al.*[6] observed that the rate of the quaternization of poly-4-vinyl-pyridine with *n*-butylbromide in tetramethylene sulfon or propylene carbonate decreased rapidly beyond half-quaternization.

In the present study, the kinetics of the aminations of CMPS and benzyl chloride with diethanolamine has been compared with that of the aminations with diethylamine, and also the quaternization of the CMPS aminated with diethanolamine has been investigated kineticcally.

Experimental

Chloromethylated polystyrene (CMPS). The CMPS was prepared and purified by the procedures described in previous papers.[2-4] The chlorine contents and the molecular weights of the CMPS used in the present study are tabulated in Table 1.

Table 1. Chlorine content and molecular weight of CMPS

Code	Content of Cl %	Degree of chloromethylation	Molecular weight
SC-5	21.15	0.874	10.3×10^4
SC-7	19.53	0.782	
SC-8	22.11	0.931	9.2×10^4
SC-11	21.75	0.909	12.4×10^4

Aminated Chloromethylated Polystyrene (AMPS). Five grams of CMPS (SC-5) were dissolved in 200 ml of DMF, and to the solution we then added 300 ml of a DMF solution containing 60 g of diethanolamine. The reaction mixture thus obtained was kept at 50 °C for 2 days. After it was ascertained that the reaction had proceeded quantitatively, the reaction mixture was cooled to room temperature and was poured into water to precipitate the aminated polymer. The polymer, which was dried *in vacuo*, was easily soluble in DMF, but less soluble in dioxane, methyl ethyl ketone, and benzene. The polymer was dissolved in 25 ml of DMF, and a 45-ml portion of benzene was added to the solution. This solution was poured into 350 ml of ligroin to precipitate the polymer. After two reprecipitations, the polymer was dried *in vacuo* to give a yield of 4.6 g. Elementary analysis and acid-base titration were carried out with this dried sample. The nitrogen content of the sample was found to be 6.10%, and no chlorine was found. The content of amine combined with CMPS was found, by titration, to be 4.23 mmol/g. The value of the nitrogen content calculated from the degree of the amination on the basis of Eq. (1) and the value calculated from the titration data both agreed with that of elementary analysis, as is shown in Table 2.

Table 2. Nitrogen contents of AMPS

Elementary analysis %	Calculated from titration %	Calculated from conversion %
6.10	5.96	5.93

$$[N\%] = \frac{14.01xy \times 100}{221.99xy + 152.61x(1-y) + 104.14(1-x)} \quad (1)$$

In Eq. (1), x is the degree of the chloromethylation of polystyrene, and y is the degree of the amination of the chloromethyl group; $x=0.874$ and $y=1.00$ in this experiment. The figures in the denominators are molecular weights of *N,N*-bis(2-hydroxyethyl)-aminomethyl styrene, chloromethyl styrene, and styrene respectively.

Other Chemicals. The amines, the solvents, and the other liquid chemicals, all of a reagent grade, were distilled before use; they were proved to be pure by their refractive indices. All the other chemicals were of a reagent grade and deionized, decarbonized water was used.

Kinetic Measurements. Amination of CMPS and Benzyl Chloride: The rate of the amination was measured as has been described in a previous paper.[4] The experimental conditions in the amination of CMPS are listed in Table 3. In Run 7, since the reaction mixture was emulsified during the reaction, it was distributed in test tubes dipped in a thermostat to avoid uneven sampling, as has been described in another previous paper.[1]

Quaternization of AMPS: AMPS (N content: 6.10%) was quaternized with mthyl iodide and bromoacetic acid in 50% aq. DMF in a vessel protected from light. The rates of the reactions were measured by the same procedures as those used for the amination. The experimental conditions are shown in Table 4.

Viscometric Measurements. In the amination of CMPS, the viscosity change in the reaction mixture was also checked for Runs 4, 6, 11, and 13 by the procedure described in a previous paper.[4]

Acid-base Titration of AMPS. A portion of AMPS (0.1185 g) was dissolved in 18 ml of DMF, and the solution was diluted to 50 ml by adding water. This solution was titrated first with 8 ml of 0.0989 M HCl; after the addition of 5g of sodium chloride (about a 1.5 M concentration), the solution was back-titrated with 0.1008 M NaOH. The pH of the solution was measured with glass and calomel electrodes by means of a Beckman Model G pH meter. In the back-titration, 15.6 ml of DMF in all was added to avoid the precipitation of the polymer.

Results

Amination with Diethylamine in DMF. As has been described in a previous paper,[1] the amination of benzyl chloride could be expressed by Eq. (2), and the over-all kinetics of the amination of chloromethylated polystyrene (CMPS) in the presence of a large excess of diethylamine ($a \gg b$) could be expressed by Eq. (3):

$$kt = \frac{1}{(a-b)t} \ln \frac{b(a-x)}{a(a-b)} \equiv \bar{k}t \quad (2)$$

$$\beta = x/b = 1 - \frac{k_1-k_2}{2k_1-k_2} e^{-2k_1at} - \frac{k_1}{2k_1-k_2} e^{-k_2at} \quad (3)$$

$$k_1 = \frac{1}{[(2-k_2/k_1)a-b]t} \ln \frac{1-\alpha}{1-(2-k_2/k_1)\beta} \quad (4)$$

$$\bar{k}t = k_2t + C \quad (5)$$

where a and b are the initial concentrations of an amine and the chloromethylgroup respectively, and where x is the concentration of chloride ions after time t; k_1 and k_2 are the rate constants of the elementary reactions which are independent of the neighboring groups and which are dependent on their steric effect respectively. C in Eq. (5) is a constant in a given system: $C=\ln[(1-$

Table 3. Conditions of amination of CMPS

Run	Amine[a]	Solvent	Temp.[b] °C	CMPS	a,[c] mol/l	b,[d] mol/l	a/b
1	A	DMF	10	SC-8	0.8315	0.0416	20.0
2	A	DMF	15	SC-8	0.8353	0.0417	20.0
3	A	DMF	20	SC-8	0.8289	0.0413	20.0
4	A	DMF	25	SC-8	0.8321	0.0416	20.0
5	A	DMF	30	SC-8	0.8319	0.0416	20.0
6	B	DMF	25	SC-8	0.8312	0.0416	20.0
7	C	dioxane	40	SC-11	0.8648	0.0439	19.7
8	C	DMF	10	SC-11	0.8628	0.0401	21.5
9	C	DMF	20	SC-11	0.8667	0.0411	21.1
10	C	DMF	30	SC-11	0.8671	0.0536	19.9
11	C	DMF	40	SC-11	0.8625	0.0413	20.9
12	C	DMSO	20	SC-7	0.7667	0.0382	20.1
13	C	DMSO	25	SC-7	0.7395	0.0367	20.1
14	C	DMSO	30	SC-7	0.7339	0.0367	20.0

a) A: diethylamine, B: di-*n*-butylamine, C: diethanolamine. b) Temp. was maintained constant within ±0.1°. c) a: Initial concentration of amine. d) b: Initial concentration of CMPS expressed in moles of chloromethyl group per liter of the solution.

Table 4. Conditions of quaternization of AMPS

Halide	Solvent	Temp.,[a] °C	a,[b] mol/l	b,[c] mol/l	a/b
Methyl iodide	50% aq. DMF	30	0.3797	0.0362	10.5
Bromoacetic acid	50% aq. DMF	30	0.2877	0.0228	12.6

a) Temp. was maintained constant within ±0.1 °C. b) a: Initial concentration of halide. c) b: Initial concentration of AMPS expressed in moles of amino group per liter of the solution.

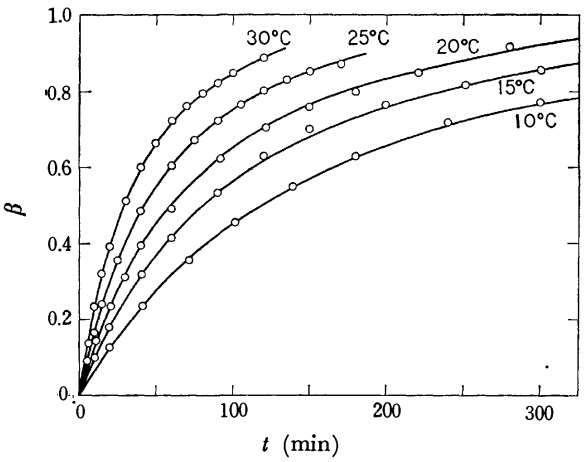

Fig. 1. Amination of CMPS with diethylamine in DMF.
——: calculated on the basis of Eq. (3).

$\chi/a)/(1-\chi/b)]-k_2(a-b)\tau$.[1]

The results of the amination of CMPS with diethylamine at different temperatures are shown in Fig. 1, where the solid lines are these calculated on the basis of Eq. (3). The observed values, represented by the white circles, substantially fall on the calculated lines. The rate constants of the amination of benzyl chloride and CMPS, as computed by Eqs. (2), (4), and (5), are listed in Table 5. The values of E_a, the activation energy, and A, the frequency factors, computed by the mean-squares method are also listed in Table 5.

It was shown in a previous paper[4] that deceleration was observed during the amination of CMPS with di-*n*-butylamine in DMF and that the kinetics could be described by Eq. (3). In the present study, the rate of CMPS at 25 °C has been compared with that of benzyl chloride. The results were:

(Benzyl Chloride) $k_B=1.19\times10^{-2}$ l/mol min
(CMPS $k_1=1.26\times10^{-2}$, $k_2=3.98\times10^{-3}$ l/mol min
$k_2/k_1=0.31$, $k_1/k_B=1.06$

Amination with Diethanolamine in DMF and DMSO. Deceleration such as that described in the preceding section was also observed in the amination of CMPS with diethanolamine. The courses of the aminations in DMF and DMSO could be fully expressed on the basis of Eq. (3). The rate constants of CMPS are listed in Tables 6 and 7, along with the rate constants of benzyl chloride, k_B. In the table are also listed the values of E_a and A, which were computed by the least-squares method.

Amination of CMPS with Diethanolamine in Dioxane. The results of kinetic measurements in the amination of CMPS with diethanolamine in dioxane at 40 °C are shown in Fig. 2. The plot of β against t is represented by a sigmoid curve, which indicates the acceleration during the reaction. The plot of kt against t is nearly represented by two straight lines which intersect at

Table 5. The amination of CMPS and benzyl chloride with diethylamine in DMF

Temp. °C	Rate const. $\times10^2$ l/mol·min				E_a kcal/mol	log A[c]
	k_1[a]	k_2[a]	k_B[b]			
5			0.457			
10	0.861	0.430	0.645	(k_1)	11.7±0.2	6.93±0.16
15	1.29	0.612	0.950			
20	1.75	0.861	1.36	(k_2)	12.2±0.2	7.05±0.12
25	2.38	1.24	1.93			
30	3.48	1.81	2.82	(k_B)	12.1±0.1	7.18±0.06
35			3.71			

a) k_1 and k_2: Rate constants of CMPS. b) k_B: Rate constants of benzyl chloride. c) A is expressed in l/mol·min.

Table 6. The amination of CMPS and benzyl chloride with diethanolamine in DMF

Temp. °C	Rate const. $\times10^2$, l/mol·min				E_a kcal/mol	log A[c]
	k_1[a]	k_2[a]	k_B[b]			
10	0.285	0.210	0.331			
20	0.659	0.429	0.724	(k_1)	12.8±0.3	7.33±0.18
30	1.36	0.900	1.52	(k_2)	12.8±0.1	7.15±0.13
40	2.50	1.83	2.90	(k_B)	12.8±0.1	7.38±0.04

a) k_1 and k_2: Rate constants of CMPS. b) k_B: Rate constants of benzyl chloride. c) A is expressed by l/mol·min.

Table 7. The amination of CMPS and benzyl chloride with diethanolamine in DMSO

Temp. °C	Rate const. $\times10^2$, l/mol·min				E_a kcal/mol	log A[c]
	k_1[a]	k_2[a]	k_B[b]			
20	3.25	2.58	3.92	(k_1)	11.7±0.1	7.27±0.09
25	4.58	3.67	5.46	(k_2)	12.0±0.1	7.35±0.06
30	6.33	5.10	7.66	(k_B)	11.7±0.1	7.35±0.08

a) k_1 and k_2: Rate constants of CMPS. b) k_B: Rate constants of benzyl chloride. c) A is expressed in l/mol·min.

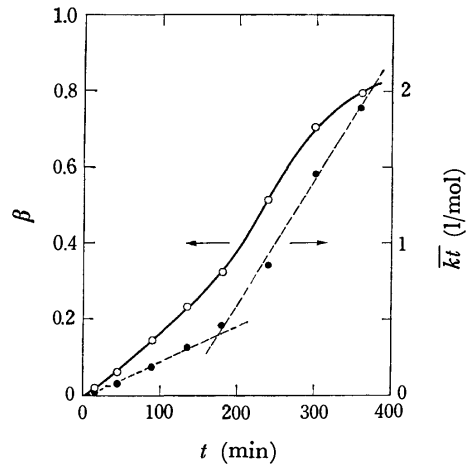

Fig. 2. Amination of CMPS with diethanolamine in dioxane at 40 °C.

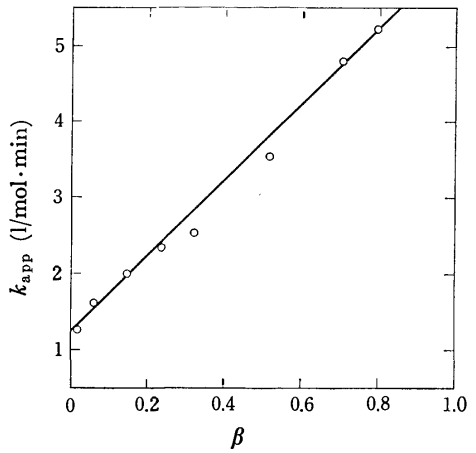

Fig. 3. Plot of k_{app} *vs.* β in the amination of CMPS with diethanolamine in dioxane at 40 °C.

$\beta \approx 1/3$. The rate constant calculated on the basis of Eq. (2) is not constant, but increases with β. The plot of this apparent rate constant, k_{app}, against the β shown in Fig. 3 is represented by a straight line. Such kinetic behavior is analogous to that exhibited in the amination of CMPS with 2-aminobutanol in dioxane, and the line in Fig. 3 may be expressed by this equation:[3]

$$k_{app} = k_0(1+m\beta) \qquad (6)$$
$$k_0 = 1.25\times10^{-3}$$
$$m = 4.0$$

Viscosity Change During the Amination of CMPS. The viscosity ratios $(H\equiv(\eta_{sp}/C_p)/(\eta_{sp}/C_p)_{\beta\to0})$[4] in the amination of CMPS in DMF and DMSO are plotted against β in Fig. 4. The H value decreases with β in the amination with alkyl amines, while it increases with β in the amination with aminoalcohols.

Acid-base Titration of Aminated Chloromethylated Polystyrene (AMPS). AMPS (N%=6.10), which was obtained by the amination of CMPS with diethanolamine, is analogous in its chemical structure to poly[bis-(2-hydroxyethyl)aminomethyl styrene] (N%=6.33). An aq. DMF solution of AMPS was titrated first with hydrochloric acid and then with a sodium hydroxide

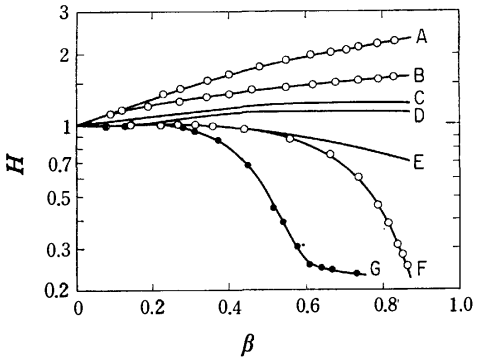

Fig. 4. Viscosity change of a reaction mixture in the amination of CMPS.
A: with diethanolamine in DMSO at 25 °C. B: with diethanolamine in DMF at 40 °C. C: with 2-aminobutanol in DMSO at 30 °C.[4] D: with 2-aminobutanol in DMF at 40 °C.[4] E: with *s*-butylamine in DMF at 50 °C.[1] F: with diethylamine in DMF at 25 °C. G: with di-*n*-butylamine in DMF at 25 °C.

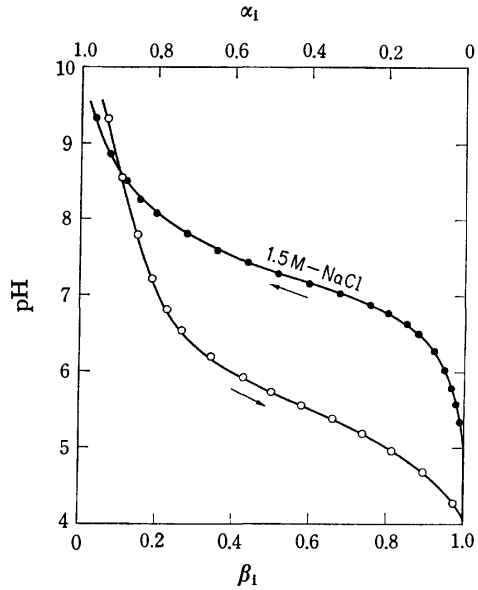

Fig. 5. Titration curve of AMPS.

solution in the presence of 1.5 M NaCl. The titration curves are shown in Fig. 5, where β_1 is the degree of ionization of the base and where α_1 $(=1-\beta_1)$ is the degree of dissociation of the conjugated acid.

It has been established that the titration data of some polyelectrolytes can be expressed by a modification of the Henderson-Hasselbach equation:[7]

$$pH = pK_a - n'[(1-\alpha_1)/\alpha_1] \qquad (7)$$

where pK_a and n' are empirical constants. This relation is, in general, hard to apply to polymeric bases such as polyethyleneimine and polyvinylamine.[8] However, the titration data of AMPS fit Eq. (7); $pK_a=5.76$ and $n'=1.25$ in the absence of salt, and $pK_a=7.37$ and $n'=1.0$ in the presence of added salt. Accordingly, the pK_a value of 7.37 is considered to represent the intrinsic dissociation constant of AMPS (pK_0), and this value is close to the dissociation constant of bis(2-hydroxypropyl)benzylamine ($pK=7.5$) reported by Boivin.[9]

Quaterinization of AMPS. AMPS could be *N*-methylated easily and completely with methyl iodide in 50% aq. DMF. AMPS was unreactive to chloroacetic acid, while it was quantitatively *N*-carboxymethylated with bromoacetic acid. In both the quaternizations, the deceleration was marked beyond the half-quaternization point. The kinetics of the two reactions can be described by Eqs. (3), (4), and (5), where a is the initial concentration of methyl iodide or bromoacetic acid, b is that of the amine groups of AMPS, and x is the concentration of halogen ions after time t. The courses of these reactions are shown in Fig. 6, where the white circles indicate the observed values and where the solid lines indicate those calculated on the basis of Eq. (3). The course of the latter reaction could also be expressed by Eq. (3). The rate constants of these reactions are tabulated in Table 8.

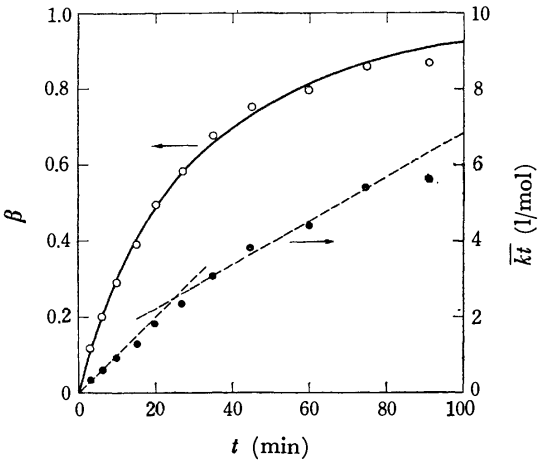

Fig. 6. Quaternization of AMPS with methyl iodide in 50% aq. DMF at 30 °C.
——: calculated on the basis of Eq. (3).

TABLE 8. THE QUATERNIZATION OF AMPS

Halide	Temp. °C	Rate const. $\times 10^2$ l/mol·min		k_2/k_1
		k_1	k_2	
Methyl iodide	30	10.4	5.89	0.57
Bromoacetic acid	30	3.54	2.05	0.58

Discussion

Acceleration and Deceleration during the Amination of CMPS. We observed a stronger acceleration during the amination of CMPS with diethanolamine in dioxane than in amination with 2-aminobutanol.[3] On the other hand, deceleration was observed during the amination of CMPS with diethanolamine in DMF and DMSO, while the kinetics of the amination with 2-aminobutanol obeyed the ordinary second-order kinetics in both the solvents.[4] Comparing this kinetic behavior in the amination with aminoalcohols with that in the amination with the corresponding alkylamines, it was found that the amination with *s*-butylamine (2-aminobutane) conformed to the second-order rate equation in dioxane and DMF and that the amination with diethylamine was decelerated in both dioxane and DMF.[1] Therefore, the hydroxyl groups of the aminoalcohols are obviously involved in the acceleration phenomena in dioxane. It is reasonable to presume that the hydroxyl groups of the already-aminated neighbors form the hydrogen bond with the chlorine of the chloromethyl groups in the transition state of the amination and that the formation of this hydrogen bond is obstructed in dipolar aprotic solvents, such as DMF and DMSO.

The slope of the $\overline{kt}$ *vs.* t plot beyond $\beta \approx 1/3$, which is shown in Fig. 2, is considered to be a rate constant of the chloromethyl group under the accelerating effect of the neighboring groups (k_2);[3] it will be given by $\Delta\overline{kt}/\Delta t$ on the basis of Eq. (5); $k_2 = 8.25 \times 10^{-3}$ l/mol min, $k_2/k_0 = 6.6$ (40 °C).

Comparison between the Rates of CMPS and Benzyl Chloride. In the present study, a comparison of the intrinsic amination rate constant of CMPS (k_p) and the corresponding rate constant of benzyl chloride (k_B), showed that $k_p < k_B$ with diethanolamine ($k_1/k_B = 0.88$ (DMF), $k_1/k_B = 0.83$ (DMSO)), while $k_p > k_B$ with diethylamine ($k_1/k_B = 1.23$ (DMF)) and with di-*n*-butylamine ($k_1/k_B = 1.06$ (DMF)). Table 9 shows the activation parameters in the amination of CMPS and benzyl chloride with diethylamine and diethanolamine; $\Delta H^{\ddagger}$, the enthalpy of activation, $\Delta S^{\ddagger}$, the entropy of activation, and $\Delta G^{\ddagger}$, the free energy of activation, all of which have been calculated for 25 °C by means of

TABLE 9. THERMODYNAMIC QUANTITIES AT 25 °C IN THE AMINATION OF CMPS AND BENZYL CHLORIDE

Amine	Solvent	Chloride	$\Delta H^{\ddagger}$ kcal/mol	$\Delta S^{\ddagger}$ e. u.	$\Delta G^{\ddagger}$ kcal/mol
Diethyl	DMF	CMPS, k_1	11.2±0.2	−36.9±0.7	22.1
		k_2	11.6±0.2	−36.4±0.6	22.5
		Benzyl	11.5±0.1	−35.8±0.3	22.2
Diethanol	DMF	CMPS, k_1	12.2±0.3	−35.1±0.8	22.7
		k_2	12.2±0.1	−35.9±0.6	22.9
		Benzyl	12.2±0.1	−34.9±0.2	22.6
Diethanol	DMSO	CMPS, k_1	11.2±0.1	−35.4±0.4	21.7
		k_2	11.4±0.1	−35.0±0.4	21.8
		Benzyl	11.2±0.1	−35.0±0.4	21.6

the equations described in a previous paper.[4]

Although k_p is generally almost the same as k_B, and although there are not many differences in $\Delta H^{\ddagger}$ and $\Delta S^{\ddagger}$ between CMPS and benzyl chloride, some features in regard to these parameters may be deduced from the data obtained thus far. It was previously shown, in the amination with butylamine isomers and 2-aminobutanol in a dipolar aprotic solvent, that $k_p<k_B$; this was attributed to the $\Delta S^{\ddagger}$ value of CMPS being lower than that of benzyl chloride.[1] In addition, it was shown that, in most cases, the $\Delta H^{\ddagger}$ value of CMPS was lower than that of benzyl chloride.[1,4,10] In a dipolar aprotic solvent, the solvation of the transition state plays an important role in the determination of the amination rate, and it may be sterically obstructed by the neighboring groups of the polymer, resulting in the $\Delta S^{\ddagger}$ value for CMPS being lower than that for benzyl chloride. On the other hand, if such an energetic interaction as that due to the London dispersion force is operative between alkyl groups of the amine molecule and non-polar polymer segments at the transition state, it will lower the $\Delta H^{\ddagger}$ value for CMPS as compared with that for benzyl chloride.

In the amination with diethylamine, the fact shown in Table 9 that the $\Delta G^{\ddagger}$ of CMPS is a little lower than that of benzyl chloride ($k_p>k_B$) may be explained by the fact that the lower $\Delta H^{\ddagger}$ value surpasses the lower value of $\Delta S^{\ddagger}$. In the amination with diethanolamine with two hydroxyl groups, however, since the $\Delta H^{\ddagger}$ and $\Delta S^{\ddagger}$ values are almost the same for CMPS and benzyl chloride, it is difficult to explain value of the $\Delta G^{\ddagger}$ of CMPS being little higher than that of benzylchloride ($k_p<k_B$) in terms of the differences in the $\Delta H^{\ddagger}$ and $\Delta S^{\ddagger}$ values.

Effect of Amine on the Amination Rate. The $\Delta G^{\ddagger}$ values in the amination with diethylamine are comparable to those with *n*-butylamine or isobutylamine,[1] and there is little difference in the $\Delta H^{\ddagger}$ and $\Delta S^{\ddagger}$ values. These results may be explained by the face that the steric hindrance by the benzene ring to the alkyl group of the secondary amine in the transition state is not so large as the hindrance to that of *n*-butylamine or isobutylamine, and also by the fact that the basicity of the secondary amine is higher than that of the primary amines. On the other hand, the higher $\Delta G^{\ddagger}$ value with diethanolamine than that with diethylamine is due to the higher $\Delta H^{\ddagger}$ value; this may be ascribed to the inductive effect of the hydroxyl groups, as in the case of 2-aminobutanol.[1]

Effect of the Solvent on the Amination Rate. The $\Delta G^{\ddagger}$ values in the amination with diethanolamine in DMSO are about 1 kcal/mol lower than the corresponding values in DMF. This is due merely to the difference in $\Delta H^{\ddagger}$, as was the case of the amination with 2-aminobutanol.[4] Since both DMF and DMSO are dipolar aprotic solvents, the lower $\Delta H^{\ddagger}$ in DMSO is considered to be caused by the stronger solvation of the transition state in DMSO resulting from its stronger polarity.

Quaternization of AMPS. Charged groups are not formed on polymer molecules in the amination of DMPS with primary and secondary amines, because the hydrochloric acid produced by the reaction is transformed to amine, which is present in a large excess. The deceleration observed in the amination of CMPS is due to the steric hindrance of the neighboring groups. In the reaction of AMPS with methyl iodide and bromoacetic acid in 50% aq. DMF, however, the observed deceleration may be ascribed to the electrostatic interactions, because charged groups (quaternary ammonium groups) are formed on the polymer in these reactions. The assumption of the electrostatic effect is supported, by the acid-base titration data of AMPS, and also by the facts shown in Table 8, which indicates that the k_2/k_1 ratio is almost the same for two reactions with different quaternizing reagents. The facts that the deceleration is marked beyond $\beta\approx 1/2$ and that the over-all kinetics can be followed by Eq. (3) suggest that k_1 represents the intrinsic rate constant and k_2, the rate constant under the influence of two nearest-neighboring charged groups.

The author wishes to express his thanks to Dr. Masaya Yanagita for his valuable discussions. He is also grateful to Mr. Kazuaki Kawamura, Mr. Masayuki Takahashi, and Mr. Jun-ichi Nagase for their helpful assistance in preparing the polymer and in carrying out the measurements.

References

1) VII. H. Kawabe and M. Yanagita, This Bulletin, **46**, 3627 (1973).
2) H. Kawabe and M. Yanagita, *ibid.*, **41**, 1518 (1968).
3) H. Kawabe and M. Yanagita, *ibid.*, **44**, 896 (1971).
4) H. Kawabe and M. Yanagita, *ibid.*, **46**, 38 (1973).
5) I. Noda and I. Kagawa, *Kogyo Kagaku Zasshi*, **66**, 857 (1963).
6) R. M. Fouss, M. Watanabe, and R. D. Coleman, *J. Polymer Sci.*, **48**, 5 (1960).
7) A. Katchalsky, N. Shavit, and H. Eisenberg, *ibid.*, **13**, 69 (1954).
8) H. Kawabe and M. Yanagita, This Bulletin, **43**, 2706 (1970).
9) J. L. Boivin, *Can. J. Chem.*, **36**, 1405 (1958).
10) It has been found in the amination with *i*- and *s*-butylamine in dioxane that $k_p>k_B$ and the $\Delta H^{\ddagger}$ values of CMPS are lower than the corresponding values of benzyl chloride. (The present author's data to be published in this Bulletin).

Effects of Pressure on Organic Reactions. VI.* The Acid-catalyzed Rearrangement of Benzopinacol in Acetic Acid

Katsuhiro TAMURA** and Takashi MORIYOSHI

Department of Chemical Engineering, Faculty of Engineering, Tokushima University, Minamijosanjima-cho, Tokushima 770

(Received April 8, 1974)

The rates of the acid-catalyzed rearrangements of benzopinacol and of tetraphenylethylene oxide in acetic acid have been measured in the range of 35—45 °C at pressures up to 983 kg/cm². It was proved under pressures that the rearrangement of pinacol proceeds through two routes, with three processes. The probable mechanism for each process has been discussed in the light of the activation parameters, particularly the volume parameters ($\Delta V^{\neq}$ and ΔV). Consequently, it may be probably inferred that the classical carbonium ion is an intermediate in the rearrangement of oxide, but not in the other two processes, *i.e.*, the conversion of pinacol to oxide and the direct rearrangement to pinacolone, and that the transition states in the two processes of rearrangement must be clearly distinguished.

The acid-catalyzed rearrangement of benzopinacol (P) to β-benzopinacolone (K) has already been studied kinetically by Gebhart and Adams[1] in acetic acid under atmospheric pressure. Their results indicate that P undergoes two concurrent reactions, consisting of three processes (I, II and III), as is shown in Scheme 1; one reaction is an indirect conversion to K through the intermediate formation of tetraphenylethylene oxide (E), and the other, a direct conversion. On the basis of the facts that correlations existed between the acidity function of the medium and the rate constant of each of the reactions involved, and that the entropies of activation ($\Delta S^{\neq}$) were found to be greatly positive, the authors suggested that any process of interest probably takes place by means of the A-1 mechanism, involving the formation of the classical carbonium ion.

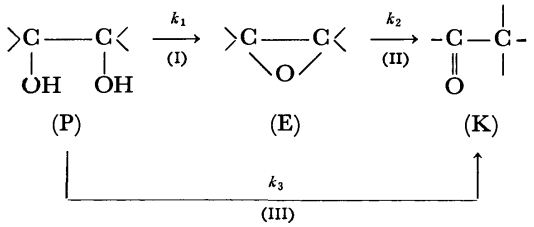

Scheme 1

However, their reasoning seems not to be natural in giving the same transition state for different processes; further, the grounds stated by them are not necessarily helpful and decisive for determining the mechanism, as was pointed out by Whalley.[2] In order to find a more plausible explanation for the reaction mechanism, it is a useful tool to measure the volume changes of the reacting species attending the progress of the reaction.

In this paper, we will describe the effects of temperature and pressure on the acid-catalyzed rearrangements of P and E in acetic acid. Both the volume of activation ($\Delta V^{\neq}$) and the volume change of the complete reaction (ΔV) will be discussed together with the other parameters in order to understand the structures of the transition states for the processes under consideration.

Experimental

Materials. P prepared[3] was recrystallized from benzene and ligroin. E prepared[4,5] was recrystallized three times from a mixture of anhydrous ethanol and chloroform (10 : 1). K was prepared from P by boiling it with iodine in glacial acetic acid;[6] it was then recrystallized from benzene and ligroin. All the materials were identified by checking the mp and by elemental analyses. Commercial glacial acetic acid was distilled from potassium permanganate; the distillate was then dried over phosphorus pentoxide and redistilled. The stock solution of perchloric acid used as a catalyst was prepared by diluting commercial, analytical-grade 70% aqueous acid with the purified glacial acetic acid; it was titrated against a standard solution of sodium acetate in acetic acid by means of the potentiometric method. The other chemicals were of a reagent grade and were used without further purification.

Analytical Methods. Both P and K were analyzed by a small modification of the methods described by Gebhart and Adams.[1] The optical densities for the determination of K were measured with a Hitachi Model 139 UV-VIS spectrophotometer.

Kinetic Measurements. All the runs under atmospheric pressure and high pressures were carried out with a pressure apparatus described previously.[7] The reaction mixture was made up by adding the required amount of perchloric acid solution to a preheated acetic acid solution of P. The concentration of the reaction mixture was initially about 0.014 M in P and was 5.74×10^{-4} M in perchloric acid. The first sampling in the kinetic run was made after allowing one hour for thermal equilibrium to be attained; the sample removed was then analyzed for P and K. The same operation was repeated five times at intervals of one or two hours for each run. A similar procedure was also employed in the rearrangement of E at the same concentration of the catalyst as in the case of P. Six samples were taken during a kinetic run and were analyzed only for K. The initial concentration of E was determined from the amount of K produced at the completion of reaction after at least ten half-lives; it was approximately 5.6×10^{-3} M in all the runs.

Measurements of the Partial Molar Volumes. The partial molar volumes of the concerned substances in acetic acid were determined from density measurements according to the usual method. The pycnometers used were of the Ostwald-Sprengel type, with a capacity of about 20 ml.

* Part V of this series: T. Moriyoshi, *Rev. Phys. Chem. Japan*, **41**, 22 (1971).

** Present address: Department of Applied Chemistry, Faculty of Engineering, Osaka City University, Sumiyoshi-ku, Osaka 558.

Results

The reaction manner shown in Scheme 1 can be expected to be true also at high pressures, as is illustrated in Fig. 1, which shows a typical plot of the concentration against the time for a run at 40 °C and 232 kg/cm².

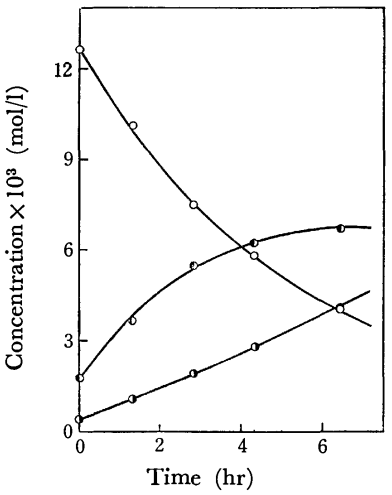

Fig. 1. Variation with time of the concentration at 40 °C and 232 kg/cm².
○: Benzopinacol, ◐: Tetraphenylethylene oxide, ◑: β-Benzopinacolone

Assuming that, in each of the three processes, the first-order rate law is obeyed exactly and that the reverse reaction from E to P does not occur, the concentration ratio, [E]/[P], at an arbitrary time, t, can be represented by the equation:

$$\frac{[E]}{[P]} = \left\{\frac{k_1}{k_p-k_2}+\frac{[E]_0}{[P]_0}\right\}\exp(k_p-k_2)t - \frac{k_1}{k_p-k_2}, \qquad (1)$$

where the k's are the rate constants for the processes shown in Scheme 1, k_p is the sum of k_1 and k_3, and $[E]_0$ and $[P]_0$ are the concentrations of E and P respectively at zero time in kinetics. Since k_p can be determined from the rate of the disappearance of P and k_2, from a separate run for the rearrangement of E to K under the same conditions, it is possible to evaluate k_1 from the slope or the intercept of a straight line obtained from a plot of [E]/[P] against $\exp(k_p-k_2)t$. Finally, k_3 can be calculated from this relation: $k_p = k_1+k_3$. As an example, the plot obtained from the results in Fig. 1 is illustrated in Fig. 2. From the fact that there is a satisfactory linear relationship between [E]/[P] and $\exp(k_p-k_2)t$, the validity of the above assumption is supported for the kinetics at high pressures; this is in agreement with the observations to be described below. The separation of k_p into two components, k_1 and k_3, was thus made from similar plots obtained under various conditions. The rate constants measured for the three processes are listed in Table 1. The mean error is within about a few per cent for k_p and k_2, and somewhat greater for k_1. However, it is apparent from the large difference in numerical value between k_1 and k_3 that the error for k_3 extracted from k_p is over ten times that for k_1. The second-order rate constants were obtained by dividing

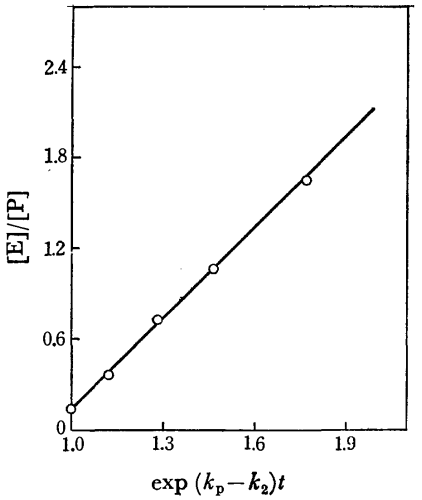

Fig. 2. A plot of [E]/[P] *vs.* $\exp(k_p-k_2)t$ at 40 °C and 232 kg/cm².

Table 1. Rate constants for each process, $k\times10^2$ ($l\cdot mol^{-1}\,s^{-1}$)

Temp. (°C)		Pressure (kg/cm²) 1	232	489	735	983
35	k_p	4.23	4.25	4.38		
	k_1	4.02	3.93	3.92		
	k_2	2.11	2.41	2.70		
	k_3	0.21	0.32	0.46		
40	k_p	8.60	8.69	8.80		8.82
	k_1	8.02	7.90	7.71		6.76
	k_2	3.81	4.40	5.37	6.23	7.32
	k_3	0.58	0.79	1.09		2.06
45	k_p	17.5	17.7	18.0		18.1
	k_1	16.1	15.9	15.7		14.3
	k_2	6.92	8.11	9.71	11.5	13.6
	k_3	1.4	1.8	2.3		3.8

the first-order constants by the concentration of the catalyst, as corrected for the thermal expansion and compression of the solvent, taken by extrapolating the data in the literature.[8]

It may be also verified that, at high pressures, the rate observed cannot be explained in terms of a simplified reaction scheme neglecting the direct rearrangement of P. The concentration values at time t can be calculated from Eq. (1) and the over-all rate equation of P ($[P]=[P]_0e^{-k_pt}$), with the initial concentrations ($[P]_0$, $[E]_0$ and $[K]_0$) in kinetics. For example, in the reaction shown in Fig. 1, the values calculated by assuming that $k_3=0$ and $k_1=k_p$ in Eq. (1) are $[P]=5.83\times10^{-3}$ M, $[E]=6.67\times10^{-3}$ M, and $[K]=2.30\times10^{-3}$ M at $t=259$ min, while the corresponding values obtained from the values of the rate constants ($k_3\neq0$) given in Table 1 are $[P]=5.83\times10^{-3}$ M, $[E]=6.18\times10^{-3}$ M, and $[K]=2.79\times10^{-3}$ M. The experimental values are $[P]=5.81\times10^{-3}$ M, $[E]=6.19\times10^{-3}$ M, and $[K]=2.80\times10^{-3}$ M, in good agreement with the latter. The activation parameters evaluated in the usual way are summarized in Table 2. Our values of

TABLE 2. ACTIVATION PARAMETERS

Parameter	Condition	Process I	Process II	Process III
$\Delta V^{\neq}$ (cm³/mol)	35 °C	2.3	−15.5	−44
	40	2.1	−17.6	−34
	45	1.9	−18.6	−28
E_a (kcal/mol)	1 kg/cm²	27.0	23.2	35
	232	27.1	23.8	32
	489	27.1	24.1	29
	735		24.1	
	983	27.5	24.4	24
$\Delta S^{\neq}$[a] (cal/deg·mol)	1 kg/cm²	20.6	7.0	41
	232	20.9	9.2	32
	489	20.9	10.5	23
	735		10.8	
	983	21.8	12.1	8

a) at 45 °C.

E_a and $\Delta S^{\neq}$ at 1 kg/cm² are somewhat different from those of Gebhart and Adams, but the difference seems to be due to the difference in reaction conditions, mainly in the temperature.

Discussion

Volume of Activation and Volume Change of the Reaction. Process I: Two mechanisms can be proposed for this process; they are shown in Scheme 2:

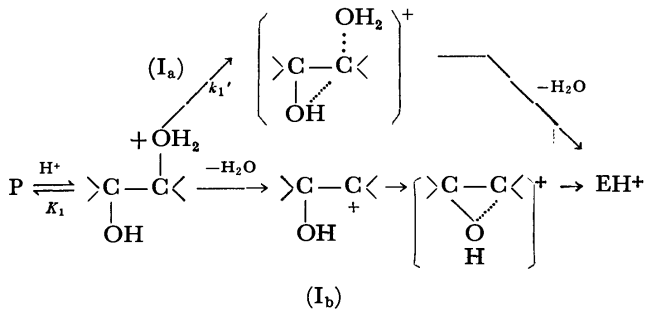

(I$_b$)

Scheme 2

where the molecules in square brackets denote the transition states. It is generally accepted that the volume of activation is negative in a simultaneous bond-forming and bond-breaking process. The $\Delta V^{\neq}$ in Mechanism (I$_a$) must be a small value near to zero, because the volume contraction described above offsets the increase in volume by the desolvation of solvent around an attacking hydroxyl group and by the dispersion of the electric charge arising from a ring structure formed partly in the transition state. Two possible rate-determining steps postulated in Mechanism (I$_b$), *i.e.*, the elimination of a water molecule and the formation of an oxide ring from a carbonium ion, will lead to a larger positive value of $\Delta V^{\neq}$ than the values observed, judging from the structural and electrostrictive contributions to the volume. The results for the hydrolysis of aliphatic epoxides reported by Koskikallio and Whalley,[9] although different from the present case in the solvent used, give useful information which helps us to choose Mechanism (I$_a$). They concluded that the hydrolysis proceeds by the A-2 mechanism, in which a water molecule attacks the C_α atom from the back and synchronously the C_α–O bond of the oxide ring stretches. The $\Delta V^{\neq}$ value for the reactions of the glycol to oxide becomes 2—3 cm³/mol, calculating from the values of $\Delta V^{\neq}$ and of ΔV for the hydrolyses of ethylene and propylene oxides. The estimated values agree well with those for the present reaction, given in Table 2. This implies that Process I is similar to the reverse hydrolysis of epoxide and that it probably proceeds through Mechanism (I$_a$). The same conclusion may also be expected from the results for trimethylene oxide[10] and epichlorohydrin.[10,11]

P probably consists of two conformers, the *trans*- and *gauche*-types being in equilibrium. The steric factor must largely participate in the reaction, so that in I$_a$ the *trans*-type is more favorable than the *gauche*-one. The results for the hydrolysis of 1,2-epoxy-1,2-dimethylcyclopentane[12] support this theory.

Process III: This process is formally analogous to Process I except for the difference between the two attacking groups, hydroxyl and phenyl. As has been mentioned above, the precision of k_3 is very poor in comparison with that of the other constants, so that the activation parameters evaluated are not correct enough to permit an exact discussion. However, it is noteworthy that the values of $\Delta V^{\neq}$ are large and negative, while those of $\Delta S^{\neq}$ large and positive, as is shown in Table 2, in contrast to the results for aliphatic pinacol reported previously.[13] Such anomalous findings, which have been also obtained for Process II with the same phenyl shift, suggest the participation of π-electrons of the shifting phenyl group besides the usual structural and electrostrictive contributions. This participation can be expected to result in much volume contraction despite the volume decrease being reduced by the charge delocalization, judging from the phenomena pointed out by le Noble *et al.*[14] in solvolysis reactions. If it is permissible to make a further deduction, a random packing may be presumed to occur in the reorganization of the solvent environment due to the changing interaction between the reacting species and the solvent, accompanied by π-participation. These considerations, while leaving some logical doubt, suggest that a synchronous mechanism with a phenyl shift as the slow step, similar to I$_a$, is also probable in this process. Generally, the ring structure with an electric charge dispersed is stable in such a lower dielectric medium as acetic acid. In this mechanism, a *gauche*-conformer is suitable. The results of the rearrangements of 1,2-dimethylcyclopentane-1,2-diol[12] and of *cis*- and *trans*-1,2-diphenylacenaphthene-1,2-diol[15] support the above mechanism.

Process II: In the mechanism (II$_a$) shown in Scheme 3, in which the rate-determining cleavage of the C–O bond in the protonated oxide occurs simultaneously with the phenyl shift, there is necessarily a serious steric retardation and an additional energy is required for forming a bicyclic structure. A comparison of the activation parameters for this process with those for

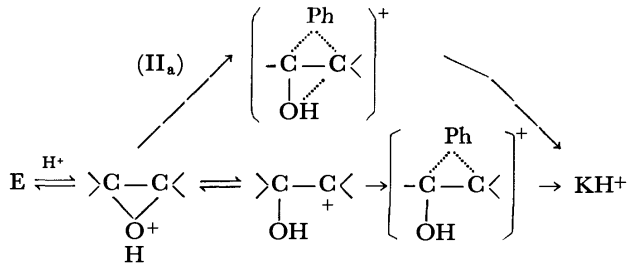

Scheme 3

the others in Table 2 leads us to reject the mechanism as unacceptable. In an alternate mechanism (II_b), two slow steps, *i.e.*, the cleavage of the protonated oxide to the classical carbonium ion and the shift of the phenyl group in the resulting ion, may be postulated. In the mechanism with the former slow step, $\Delta V^{\neq}$ can be expected to be positive because of the stretching of the C–O bond in the oxide ring, accompanied by the dispersion of the ionic charge; this is evidently incompatible with the observed values, even if the volume change for the protonation step is permitted to be somewhat negative. The latter mechanism involves the formation of the carbonium ion besides the protonation in the pre-equilibrium step. The increase in volume by a cleavage of oxide ring is usually in the range from few to several cm^3/mol,[16] but it is somewhat reduced if serious steric hindrance does not occur in the solvation of the resulting carbonium ion. The subsequent slow step can be thought to cause the fairly large contraction of the volume as a result of a ring closure, which is probably subject to such phenyl participation as has been described for Process III, although differing from that only in the absence of a leaving water molecule in the transition state. These considerations lead to the conclusion that this mechanism seems to explain the findings for $\Delta V^{\neq}$ more satisfactorily than the others discussed.

The schematic diagram in Fig. 3, which shows the volume changes along the reaction co-ordinate, provides strong evidence for the suggested structure of the transition state in Process II. In the curve illustrated for this process, the first small peak denotes the position of the carbonium ion as an intermediate. For simplification, there is no indication of any volume change for the proton-transfer step involved in each process. The volume change for that from H_3O^+ in an aqueous solution is usually small and negative,[17] but in such a lower dielectric medium as acetic acid it becomes very negative as a result of the combination of ion-pair formation from dissolved acid and the action of $CH_3COOH_2^+$ as a proton-donor. The partial molar volumes of the concerned substances were determined in order to evaluate the volume change for the complete reaction for each process. The results are given in Tables 3 and 4. From this diagram, along with the values shown in Table 4, it is clear that there is an apparent difference in the volume of the transition state between Processes II and III. If Process II proceeds by way of II_b, as deduced, Process III cannot proceed by way of a mechanism forming a classical carbonium ion in agreement with the reasoning discussed above, because its transition state differs from that of II_b.

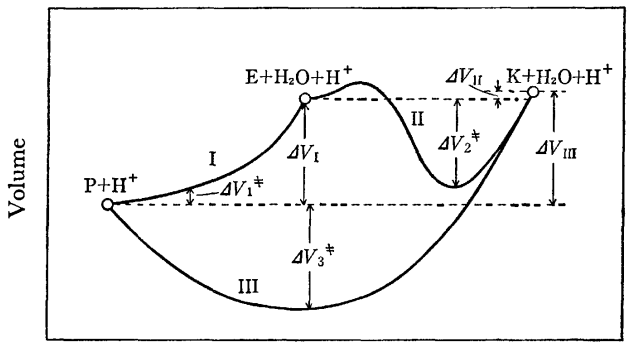

Reaction co-ordinate

Fig. 3. Schematic diagram of the volume change along reaction co-ordinate at 40 °C.

Observed Volume of Activation and Its Constituent Terms. If one assumes that there is an equilibrium between the two conformers in P, of which the *trans*-type converts to E, and the *gauche*-one, to K, the over-all reaction rate for P can be expressed by the equation:

$$R = \frac{K_1 k_1' h_0}{1+K'}[\mathrm{P}] + \frac{K' K_3 k_3' h_0}{1+K'}[\mathrm{P}], \tag{2}$$

where K is the pre-equilibrium constant, and k', the rate constant for the slow step, and where the subscripts refer to the corresponding processes. K' is an equilibrium constant between the two conformers, and h_0, Hammett's acidity function ($H_0 = -\log h_0$). Therefore, the apparent second-order rate constants measured for the two processes may be given as follows:

$$k_1 = \frac{K_1 k_1'}{1+K'} \cdot \frac{h_0}{[\mathrm{HClO_4}]} \tag{3a}$$

and

$$k_3 = \frac{K' K_3 k_3'}{1+K'} \cdot \frac{h_0}{[\mathrm{HClO_4}]}, \tag{3b}$$

where $[HClO_4]$ is the concentration of the catalyst. From Eq. (3a), the observed volume of activation for Process I, $\Delta V_1^{\neq}$, is given as a composite quantity:

$$\Delta V_1^{\neq} = \Delta V_1 + \Delta V_1^{\neq'} + \frac{RT\partial \ln\{[\mathrm{HClO_4}]/h_0\}}{\partial P} + \frac{RT\partial \ln(1+K')}{\partial P}, \tag{4}$$

where ΔV_1 is the volume change for the pre-equilibrium step, and $\Delta V_1^{\neq'}$, the volume of activation for the step in which a hydroxyl group attacks the adjacent carbon atom, as is shown in Scheme 2. A similar equation can be also derived from Eq. (3b) for Process III. The fourth term on the right-hand side in Eq. (4) is likely to be negligible because the pressure dependence of K' is probably small; *i.e.*, there is no substantial difference in volume between the two conformers of P. The third term may be estimated approximately in the following way:[13,18] if the change in h_0 with pressure can be assumed to be due to only the change in the concentration of the acid, then:

TABLE 3. PARTIAL MOLAR VOLUMES AT 40 °C

Substance	$\overline{V}$ (cm³/mol)
P	310
E	317
K	318
H_2O	12.2

TABLE 4. VOLUME CHANGES OF COMPLETE REACTION AT 40 °C AND 1 kg/cm²

Process	ΔV (cm³/mol)
I	19
II	1
III	20

$$\frac{RT\mathrm{d}\ln\{[HClO_4]/h_0\}}{dP} = RT\beta\left[1-\frac{\mathrm{d}\ln h_0}{\mathrm{d}\ln[HClO_4]}\right], \quad (5)$$

where β is the compressibility of the reaction mixture, assumed to be approximately that of the solvent. From the results of Ludwig and Adams,[19] $\mathrm{d}\ln h_0/\mathrm{d}\ln[HClO_4]=1.05$ and so:

$$\frac{RT\mathrm{d}\ln\{[HClO_4]/h_0\}}{dP} = -0.12\ \mathrm{cm^3/mol}.$$

This value leads the third term apparently being insignificant under the present conditions, if the assumption for h_0 is actually valid. The dielectric constant of acetic acid increases with an increase in pressure, so the dissociation constant of perchloric acid in acetic acid will increase; this results in an increase in h_0. Hence, the assumption described above would not strictly hold for the present case. Since h_0 under high pressure has not yet, unfortunately, been measured, it is impossible to discuss this subject in detail. The value of $[HClO_4]/h_0$ corrected for the compression and thermal expansion of the reaction mixture will decrease with an increase in pressure, judging from the fact that the concentration of the catalyst at 40 °C increases only 1.074 times[20] at 1000 kg/cm² compared with 1 kg/cm². This consideration brings about a larger negative value for the third term in Eq. (4) than -0.12 cm³/mol; consequently, the net value of $(\Delta V_1+\Delta V_1^{*\prime})$ may be expected to have a larger value than that observed. Similar considerations must also be made for the volume of activation of Process III. Furthermore, since the acidity function term, Eq. (5), is present also in ΔV_2^* derived as a composite quantity for Process II, this term does not need to be considered when comparing the ΔV^* values of the processes.

Entropy of Activation. The results listed in Table 2 can be seen to satisfy roughly the pseudo-thermodynamic relationship:

$$(\partial\Delta V^*/\partial T)_P = -(\partial\Delta S^*/\partial P)_T. \quad (6)$$

The partial derivatives of ΔV^* and ΔS^* for Process III are opposite in direction to those for the rearrangement of aliphatic pinacol.[13] The findings support the reasoning that the former proceeds through a mechanism different from that for the latter, described above. On the basis of the large positive values of ΔS^*, Gebhart and Adams suggested that the classical carbonium ion is an intermediate in the processes under consideration. However, the problem concerning ΔS^* does not seem to be so simple because of the desolvation caused by the shift of the phenyl group.[21] It seems that the most significant part of the positive contribution to ΔS^* for Processes I and III is due to the desolvation in the step of the ring closure of the hydroxyl group or in that of the shift of the phenyl group, with the elimination of water. In addition, the phenyl participation proposed above seems likely to exert a more positive effect on ΔS^* for both processes, II and III. However, in the former the extent of the contribution must certainly be reduced because of the possible solvation of the carbonium ion; this is in qualitative agreement with the findings. Since the entropy change for the proton-transfer step is generally positive, but tends to have values over a relatively wide range dependent on the substrate,[17] those in the present cases are difficult to estimate.

From the results in Table 1, the proportion of the formation of K by the direct rearrangement (III) can be found to increase with the pressure, from 8 to 21% at 45°C between 1 and 983 kg/cm². Evidently, this increase results from the decrease in E_a with the pressure, as is shown in Table 2. Furthermore, a consideration according to the relationship given thermodynamically:

$$\Delta V^* = \left(\frac{\partial\Delta H^*}{\partial P}\right)_T - T\left(\frac{\partial\Delta S^*}{\partial P}\right)_T \quad (7)$$

reveals that the effect of pressure on this process is not entropy-controlling, but enthalpy-controlling.

References

1) H. J. Gebhart, Jr. and K. H. Adams, *J. Amer. Chem. Soc.*, **76**, 3925 (1954).
2) E. Whalley, "Advances in Physical Organic Chemistry," Vol. 2, ed. by V. Gold, Academic Press Inc., New York, N. Y. (1964), p. 93.
3) W. E. Bachmann, "Organic Syntheses," Coll. Vol. II, p. 71 (1943).
4) H. Staudinger and H. Freudenberger, "Organic Syntheses," Coll. Vol. II, p. 573 (1943).
5) J. Schmidlin und R. von Escher, *Ber.*, **43**, 1153 (1910).
6) W. E. Bachmann, "Organic Syntheses," Coll. Vol. II, p. 73 (1943).
7) T. Moriyoshi, *Rev. Phys. Chem. Japan*, **40**, 102 (1971).
8) J. Timmermans, "The Physico-chemical Constants of Binary Systems in Concentrated Solutions," Vol. 4, Interscience Publishers, Inc., New York (1960), p. 368.
9) J. Koskikallio and E. Whalley, *Trans. Faraday Soc.*, **55**, 815 (1959).
10) W. J. le Noble and M. Duffy, *J. Phys. Chem.*, **68**, 619 (1964).
11) J. G. Pritchard and I. A. Siddiqui, *J. Chem. Soc. Perkin II*, **1973**, 452.
12) C. A. Bunton and M. D. Carr, *J. Chem. Soc.*, **1963**, 5861.
13) T. Moriyoshi and K. Tamura, *Rev. Phys. Chem. Japan*, **40**, 48 (1970).
14) W. J. le Noble, B. L. Yates, and A. W. Scaplehorn, *J. Amer. Chem. Soc.*, **89**, 3751 (1967).

15) P. D. Bartlett and R. F. Brown, *ibid.*, **62**, 3927 (1940).
16) The value is estimated from the differences in molar volume between aliphatic epoxides and the corresponding alcohols.
17) E. Whalley, *Trans. Faraday Soc.*, **55**, 798 (1959).
18) R. J. Withey and E. Whalley, *ibid.*, **59**, 901 (1963).
19) F. J. Ludwig and K. H. Adams, *J. Amer. Chem. Soc.*, **76**, 3853 (1954).
20) The compression of acetic acid at 40 °C and 1000 kg/cm^2 was calculated from Gibson's value (*J. Amer. Chem. Soc.*, **57**, 284 (1935)) of compression at 25 °C with Tyrer's values (*J. Chem. Soc.*, **105**, 2534 (1914)) of compressibility, by assuming that there is a linear relationship between them.
21) R. Goto, T. Asano, K. Matsumoto, and A. Sera, *Rev. Phys. Chem. Japan*, **37**, 16 (1967).

Deuterium Isotope Effects on the Redox Decomposition of Hydroxymercurated Propene and 2-Butenes in an Aqueous Solution

Sumio SHINODA and Yasukazu SAITO

Department of Synthetic Chemistry, Faculty of Engineering, University of Tokyo, Hongo, Bunkyo-ku, Tokyo 113

(Received May 20, 1974)

Kinetic deuterium isotope effects on the redox decomposition of hydroxymercurated propene, *cis*-, and *trans*-2-butenes in an aqueous solution ($CH_3CH(OH)CHRHg^+ \rightarrow CH_3COCH_2R + Hg(0) + H^+$; R=H, CH_3) were determined by following the reaction *in situ* by means of PMR spectroscopy. Taking advantage of the PMR characteristics, the identity of the reaction conditions was confirmed by comparing the rates for the reactant mixtures (*e.g.*, $CH_3CH(OH)CH_2Hg^+ + CH_3CD(OH)CH_2Hg^+$). The mercurials, deuterated on either β-carbon ($CH_3CD(OH)CH_2Hg^+$, $CH_3CD(OH)CHCH_3Hg^+$) or α-carbon ($CH_3CH(OH)CDHHg^+$, $CH_3CH(OH)CDCH_3Hg^+$), gave primary and secondary deuterium isotope effects of 1.35—1.40 and 1.17—1.19 respectively. A possible structure of the activated complex was proposed in accord with the observed nature of the intramolecular hydrogen shift.

The oxidation of olefins by aqueous mercuric salts[1] is known to produce unsaturated aldehydes,[2-5] saturated aldehydes,[3,4] allylic alcohols,[5] or saturated ketones[6] under various reaction conditions. In the case of milder conditions, it has been found[6,7] that propene and 2-butenes are oxidized stoichiometrically to acetone and methyl ethyl ketone respectively. The overall reaction consists of a fast[8] hydroxymercuration of the olefins[9] (Eq. (1)), followed by a rate-limiting redox decomposition of the mercurials thus formed into corresponding ketones (Eq. (2)):

$$CH_3CH{=}CHR + Hg^{2+} + H_2O \longrightarrow CH_3-\underset{OH}{\overset{H}{C}}-\underset{Hg^+}{\overset{H}{C}}-R + H^+ \quad (1)$$

$$CH_3-\underset{OH}{\overset{H}{C}}-\underset{Hg^+}{\overset{H}{C}}-R \longrightarrow CH_3-\overset{O}{\overset{\|}{C}}-\overset{H}{C}-R + Hg(0) + H^+ \quad (2)$$

where R=H, CH_3

The intermediate mercurials are so stable that the second process can be pursued by PMR spectroscopy *in situ*[6] at appropriate temperatures. Prior articles reported data concerning the stoichiometry,[6] the rate equation,[6,7] the rate dependence on the added electrolytes,[7] product analysis from the D_2O solution,[10] and the alkyl-substituent effect on the rate.[11] In the present paper, we wish to report on deuterium isotope effects in the redox decomposition of hydroxymercurated propene and 2-butenes.

In order to measure the kinetic isotope effect accurately, it is desirable to determine the rates for both the labeled and unlabeled reactants in mixed solutions, because the identity of the reaction conditions is thus best assured. As far as the deuterium isotope effect is concerned, PMR spectroscopy appears especially suited for the analysis of reactions on account of its reasonable facility in differentiation between deuterated and undeuterated reactants *in situ*.[12]

With regard to olefin oxidation by other metal ions in an aqueous solution, similar reaction schemes have also been postulated for Pd(II),[13] Tl(III),[13] and Rh(III),[14] for which, in contrast to Hg(II), the redox decomposition of hydroxymetallation adducts has been claimed to occur after the rate-limiting (*e.g.*, hydroxymetallation) process. In view of the established usefulness of isotope effects in the elucidation of reaction mechanisms,[15] it seemed of particular interest to determine directly the isotope effects on the redox-decomposition process, which is possible only in the case of Hg(II) oxidation.

Results

Primary Deuterium Isotope Effect on the Decomposition of Hydroxymercurated Propene-2-d_1. It was previously confirmed that the redox decomposition of hydroxymercurated olefins involves an intramolecular shift of β-hydrogen to α-carbon (Eq. (2)),[1,11] and that the decomposition rate is first order with respect to the mercurial.[6,7] Therefore, if the first-order rate constants for hydroxymercurated propene, $CH_3CH(OH)CH_2Hg^+$ (**1**), and hydroxymercurated propene-2-d_1, $CH_3CD(OH)CH_2Hg^+$ (**2**), are designated by k_H and k_D^{prim} respectively, k_H/k_D^{prim} represents the primary deuterium isotope effect for the intramolecular 1,2-hydrogen shift in the redox decomposition of **1**:

$$CH_3CH(OH)CH_2Hg^+ \xrightarrow{k_H} CH_3COCH_3 + Hg(0) + H^+ \quad (3)$$

$$CH_3CD(OH)CH_2Hg^+ \xrightarrow{k_D^{prim}} CH_3COCDH_2 + Hg(0) + H^+ \quad (4)$$

Figure 1 shows the time-sequential PMR spectra for the decomposition of **1** and **2** in a mixed solution (1.5 m, $[\mathbf{2}]_0/[\mathbf{1}]_0$: 0.20). It is obvious from Fig. 1 that the difference in the rate of decomposition is not very large between **1** and **2**. The concentrations of the reactants during the reaction were determined from the doublet peak for **1** ($CHC\underline{H}_3$; δ 1.21) and the singlet peak for **2** ($CDC\underline{H}_3$; δ 1.20) by planimetry on an expanded scale. The absence of H-D exchange between **2** and the H_2O solvent was confirmed by following the decomposition of **2** alone under identical conditions; no doublet peak appeared at δ 1.21.

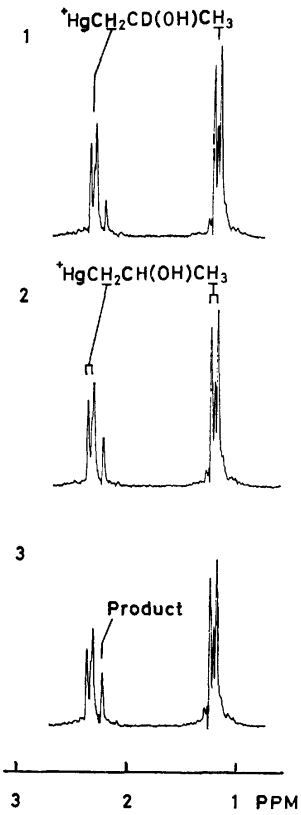

Fig. 1. The time-sequential PMR spectra obtained *in situ* for the redox decomposition of $CH_3CD(OH)CH_2Hg^+$ and $CH_3CH(OH)CH_2Hg^+$ at 38.0 °C in the mixed solution. These spectra were taken with deuterium irradiation at 15.349390 MHz after (1) 9.4 min, (2) 20.5 min, (3) 31.3 min from the moment of raising the solution temperature.

From the time-dependence of the concentrations of **1** and **2**, based on the first-order rate equations (Eqs. (5) and (6)), Eq. (7) is obtained as a formula to give the value of k_H/k_D^{prim}:

$$\log([\mathbf{1}]/[\mathbf{1}]_0) = -k_H t \quad (5)$$

$$\log([\mathbf{2}]/[\mathbf{2}]_0) = -k_D^{prim} t \quad (6)$$

$$\frac{k_H}{k_D^{prim}} = \frac{\log([\mathbf{1}]/[\mathbf{1}]_0)}{\log([\mathbf{2}]/[\mathbf{2}]_0)} \quad (7)$$

Figure 2 is a plot of the right-hand side of Eq. (7) *vs.* the time for solutions of the reactant mixture (1.5 m, $[\mathbf{2}]_0/[\mathbf{1}]_0$: 0.20 and 0.32); from the figure k_H/k_D^{prim} was determined to be 1.40 (±0.05; standard deviation).

Secondary Deuterium Isotope Effect on the Decomposition of Hydroxymercurated Propene-1-d_1. As it is bonded directly to mercury, the α-carbon of the mercurial may undergo a very drastic change during the course of redox decomposition; through this change a secondary kinetic isotope effect can be expected if a deuterium substituent is introduced at that carbon:

$$CH_3CH(OH)CDHHg^+ \xrightarrow{k_D^{sec}} CH_3COCDH_2 + Hg(0) + H^+ \quad (8)$$

In order to determine the isotope effect accurately, the decomposition rates were measured for the mixture

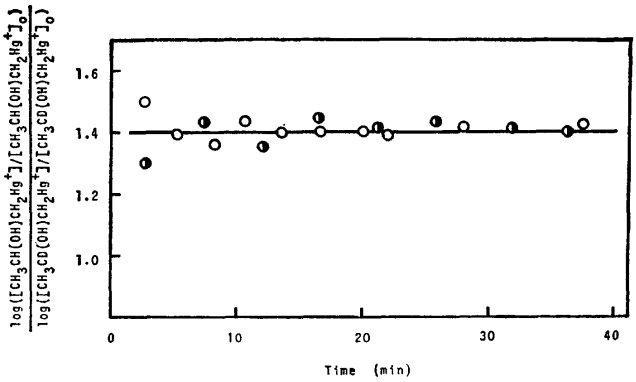

Fig. 2. Plot of $(\log([CH_3CH(OH)CH_2Hg^+]/[CH_3CH(OH)CH_2Hg^+]_0))/(\log([CH_3CD(OH)CH_2Hg^+]/[CH_3CD(OH)CH_2Hg^+]_0))$ *vs.* the time for the redox decomposition of $CH_3CH(OH)CH_2Hg^+$ and $CH_3CD(OH)CH_2Hg^+$ at 38.0 °C in the mixed solution. ○ and ◑ correspond to the ratio of initial concentrations $([CH_3CD(OH)CH_2Hg^+]_0/[CH_3CH(OH)CH_2Hg^+]_0)$ of 0.20 and 0.32 respectively.

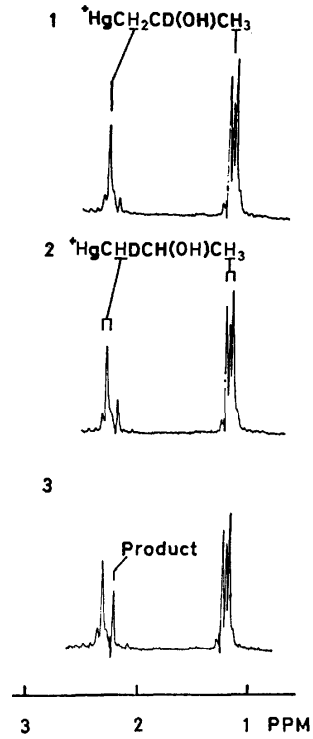

Fig. 3. The time-sequential PMR spectra obtained *in situ* for the redox decomposition of $CH_3CD(OH)CH_2Hg^+$ and $CH_3CH(OH)CDHHg^+$ at 38.0 °C in the mixed solution. These spectra were taken with deuterium irradiation at 15.349390 MHz after (1) 3.0 min, (2) 10.6 min, (3) 32.1 min from the moment of raising the solution temperature.

of **2** and $CH_3CH(OH)CDHHg^+$ (**3**) which was obtained by the hydroxymercuration of a mixed gas of propene-2-d_1 and propene-1-d_1. Figure 3 shows the time-sequential PMR spectra for the conversion of **2** and **3** into the product, acetone-d_1, in a mixed solution (1.5 m, $[\mathbf{2}]_0/[\mathbf{3}]_0$: 0.34). The concentration of **3** during the reaction was determined in the same manner

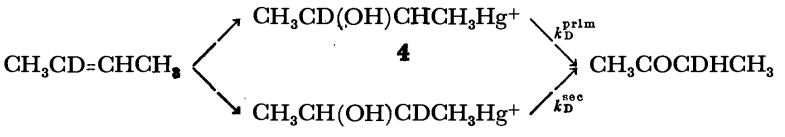

Scheme I.

as before by using the doublet peak at δ 1.21. From a plot of the right-hand side of Eq. (9) *vs.* the time, k_D^{sec}/k_D^{prim} was determined to be 1.20 (±0.05). Accordingly, the value of the secondary deuterium isotope effect is 1.17 (1.40/1.20).

$$\frac{k_D^{sec}}{k_D^{prim}} = \frac{\log([\mathbf{3}]/[\mathbf{3}]_0)}{\log([\mathbf{2}]/[\mathbf{2}]_0)} \quad (9)$$

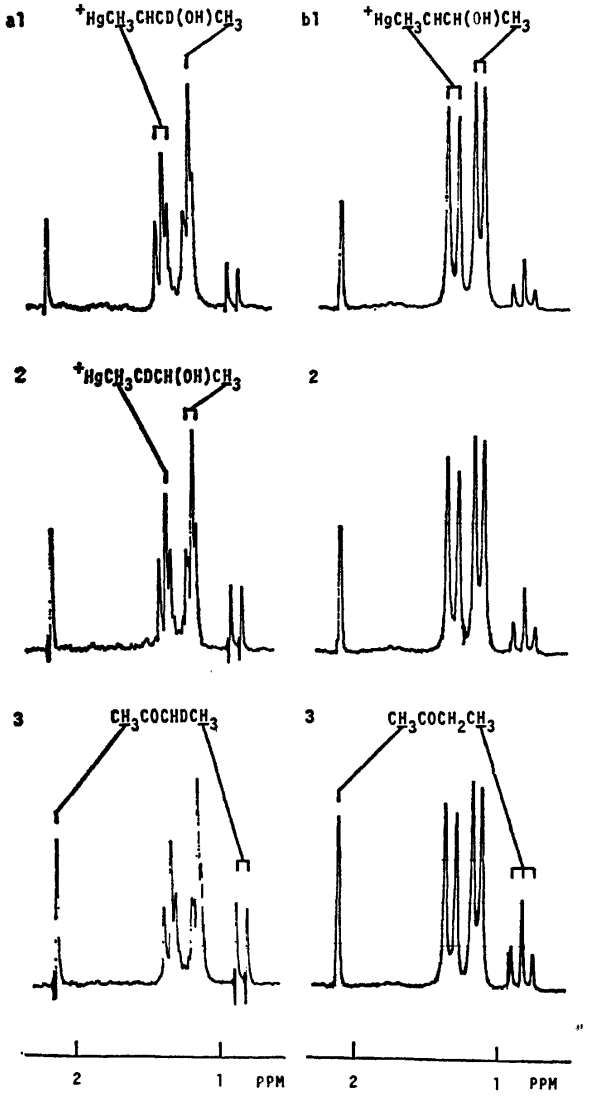

Fig. 4. The time-sequential PMR spectra obtained *in situ* for the redox decomposition of hydroxymercurated *cis*-2-butene-2-d_1 (**a**) and *cis*-2-butene (**b**) at 0.2 °C. These spectra were taken after (**a**) (1) 7.4 min, (2) 20.0 min, (3) 35.8 min with deuterium irradiation at 15.349390 MHz, and after (**b**) (1) 3.0 min, (2) 8.0 min, (3) 21.5 min from the moment of raising the solution temperature.

Deuterium Isotope Effects on the Decomposition of Hydroxymercurated 2-*Butene*-2-d_1. By the hydroxymercuration of 2-butene-2-d_1, two kinds of deuterated mercurials, $CH_3CD(OH)CHCH_3Hg^+$ (**4**) and $CH_3CH(OH)CDCH_3Hg^+$ (**5**), were obtained as an isomeric mixture. By comparing the decomposition rates of **4** and **5** for the mixture (Scheme I), the value of k_D^{sec}/k_D^{prim} was determined with sufficient accuracy.

Figure 4 shows the time-sequential PMR spectra for the redox decomposition of hydroxymercurated *cis*-2-

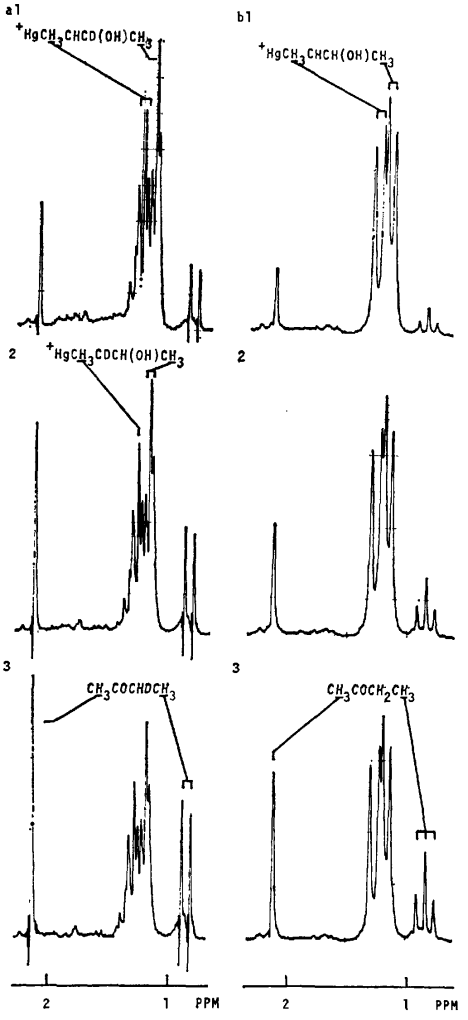

Fig. 5. The time-sequential PMR spectra obtained *in situ* for the redox decomposition of hydroxymercurated *trans*-2-butene-2-d_1 (**a**) and *trans*-2-butene (**b**) at 0.7 °C. These spectra were taken after (**a**) (1) 10.9 min, (2) 31.9 min, (3) 53.7 min with deuterium irradiation at 15.349390 MHz, and after (**b**) (1) 2.8 min, (2) 19.6 min, (3) 33.4 min from the moment of raising the solution temperature.

butene-2-d_1 (**a**) and *cis*-2-butene (**b**). Similar spectral sequences for the *trans*-isomers are shown in Fig. 5. Obviously, a marked contrast in the spectral pattern at δ 0.85 can be seen between the two sequences; this unequivocally indicates that methyl ethyl ketone-3-d_1 ($CH_3COCDHC\underline{H}_3$; doublet) is produced by the decomposition of the deuterated mercurials. This was confirmed by a mass-spectrometric analysis of the product (d_1: 99.2%, d_0: 0.8%) and was consistent with the prior finding that no deuterium incorporation into the product was observed when D_2O was used as the solvent.[11] These facts are decisive evidence for the mechanism of the intramolecular 1,2-hydrogen shift in the redox decomposition.

From a plot of the right-hand side of Eq. (10) *vs.* the time, k_D^{sec}/k_D^{prim} was determined to be 1.15 ($\pm$0.05) for both isomers:

$$\frac{k_D^{sec}}{k_D^{prim}} = \frac{\log ([\mathbf{5}]/[\mathbf{5}]_0)}{\log ([\mathbf{4}]/[\mathbf{4}]_0)} \qquad (10)$$

Experimental difficulties were encountered in following the reaction for mixtures of **4** or **5** with the corresponding undeuterated mercurial because of their inadequate PMR characteristics. Nevertheless, a comparison of the rate constants for deuterated and undeuterated mercurials was possible by pursuing each of the reactions in separated runs under identical reaction conditions (three determinations); a magnitude of isotope effects similar to that for propene was obtained (Table 1).

Table 1. Kinetic deuterium isotope effects on the redox decomposition of hydroxymercurated propene, *cis*- and *trans*-2-butenes

Olefin	Isotope effect $\left(\frac{k_H}{k_D}\right)_{prim}$	Isotope effect $\left(\frac{k_H}{k_D}\right)_{sec}$
propene[a]	1.40	1.17
cis-2-butene[b]	1.35	1.17
trans-2-butene[c]	1.37	1.19

Reaction temperatures are (a) 38.0 °C, (b) 0.2 °C, and (c) 0.7 °C, respectively.

Discussion

The mechanism of the intramolecular 1,2-hydrogen shift in the redox decomposition of β-hydroxyalkylmetal complexes has been proposed for the case of Pd(II)[13] and Rh(III)[14] as well as for the case of Hg(II).[1,10] Further, the lack of glycols in the product has commonly been interpreted as strong evidence against a simple carbonium-ion mechanism through the heterolysis of the carbon-metal σ-bond.[10,13,14] For the redox processes, some such assistance of the metals seems to be required for the hydrogen shift to occur concertedly with the two-electron transfer along the carbon-metal bond.

For the elucidation of transition-state structures, the kinetic isotope effect is considered to be one of the most important methods, since it has definitely been understood on the basis of the partition functions of the reactant and the transition state.[16] Usually, the values of the primary deuterium isotope effect for intramolecular hydrogen migration are small, along with a small angle (60°—90°) between the bonds to the migrating hydrogen in the transition state; according to the detailed calculations of O'Ferrall,[17] the values observed for the present case (1.35—1.40) can reasonably be associated with the three-membered cyclic transition state of the 1,2-hydride rearrangement. In practice, the observed values are close to those of the pinacol rearrangement (~1.6), in which the hydride rearrangement was presumed to be concerted with the breaking of a bond between carbon and a leaving group at the migration terminus; its transition-state structure has been claimed to resemble a non-classical carbonium ion.[18,19]

Secondary isotope effects are understandable in terms of force-constant changes at the position of the isotopic substitution between the reactant and the transition state;[20] substantial force-constant changes are, more or less, incident to the hybridization changes. As is typically observed in S_N1 solvolysis,[21] the secondary deuterium isotope effect of 1.1—1.3 corresponds to the hybridization change of deuterated carbon from sp^3 to sp^2.[22] Therefore, the observed magnitude of secondary deuterium isotope effects in the present case seems to be explained satisfactorily by the sp^2 character of α-carbon in the transition state; this is consistent with the previous suggestion to account for the pattern of the alkyl-substituent effect on the decomposition rate.[11]

As to the stereochemistry of the hydrogen shift in the redox decomposition of hydroxymercurials, an antimode with respect to the leaving mercury was strongly suggested by the product distribution (ketone or epoxide) for hydroxymercurated cyclic olefins.[23] Taking into consideration the foregoing results on deuterium isotope effects, together with the suggested stereochemistry, a structure such as is depicted below may be proposed for the transition state of the redox decomposition of hydroxymercurials. In view of the well-known affinity of mercuric ions for olefinic π-electrons,[24,26] it seems likely that mercury facilitates the *anti*-wise hydrogen shift by anchimeric assistance; this is in contrast to the case of Pd(II), for which *syn*-wise assistance through Pd(II)-hydrogen interaction has been postulated.[27]

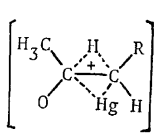

(R = H, CH_3)

Experimental

The FMR spectra were recorded on a JEOL PS-100 spectrometer. The deuterium decoupling was carried out with a JEOL OA-1 synthesizer. The mass spectra were obtained using a Hitachi RMU-6 spectrometer.

All the reagents and solvents were of a G. R. grade. The diethyl ether and tetrahydrofuran were dried over calcium chloride, refluxed with metallic sodium, and distilled im-

mediately before use.

Preparation of cis- *and* trans-*2-Butene-2*-d_1. The *cis*- and *trans*-2-bromo-2-butenes were prepared by the procedure of Caldwell[28] (bromination followed by the dehydrobromination of *trans*- and *cis*-2-butenes respectively). The lithiation of each 2-bromo-2-butene by metallic lithium in dry diethyl ether was effected at room temperature by standard procedures.[29] The reaction mixture was quenched at 0 °C with deuterium oxide (Merck, 99.75 atom% deuterated) under a dry-nitrogen-gas stream, with the gas-phase components trapped by a Dewar condenser of liquid nitrogen. The solvent ether was removed by condensation with a Dry Ice–ethanol trap fitted before the liquid-nitrogen trap. The isomeric purities of the products were determined by glpc (20% dimethylsulfolane on Celite) to be 97% and 96% for *cis*- and *trans*-2-butene-2-d_1 respectively. Mass spectral analysis at 58—68 gave 99.5% d_1 and 0.5% d_0 components for each of them.

Preparation of the Mixed Gas of Propene-1-d_1 and Propene-2-d_1. The mixture of 1- and 2-bromopropene was prepared by a similar procedure, but using propene instead of 2-butene as the starting material. The Grignard reagents formed from the mixture of bromopropenes in dry tetrahydrofuran[30] were decomposed at 0 °C with deuterium oxide. The product, a propene-1-d_1 and propene-2-d_1 mixture, was isolated in the manner described above. The isotopic purity of the product was confirmed by mass spectrometry as 99.5% d_1 and 0.5% d_0.

Preparation of Propene-2-d_1. 2-Bromopropene was obtained by the fractional distillation of the bromopropene mixture (isomeric purity of 99.7% by glpc); it was then converted into propene-2-d_1 in the same manner as in the case of the mixture. The isotopic purity of the product (99.5% d_1 and 0.5% d_0) was unchanged from the case of the mixture.

Kinetic Studies in the Redox Decomposition of the Hydroxymercurials. Olefins were transferred *via* a vacuum line into an aqueous solution consisting of 3.00 M of mercuric perchlorate at 0 °C until all the mercuric ions had been consumed by hydroxymercuration. The solutions of hydroxymercurated olefins were diluted with identical amounts of a 3.00 M aqueous mercuric perchlorate solution. A part of the solution was transferred into a PMR sample tube and kept in a Dry Ice-ethanol trap. The reaction was started by inserting the tube into the probe of the PMR spectrometer; by this means the solution temperature was raised up to the probe temperature (calibrated by the relative chemical shifts of ethyleneglycol), and the reaction was pursued by taking the spectra in sequence. For the mixed-reactant systems, the overlapped portions of their peaks were reasonably resolved, as was confirmed by the agreement of the resolved and synthesized line shapes, since each of the spectra was separately obtainable under identical measuring conditions.

During the reaction, no evolution of gas due to olefin formation by deoxymercuration[9] was observed. The PMR-spectral parameters of the hydroxymercurated propene and 2-butenes were tabulated in a prior paper.[6]

The authors wish to express their gratitude to Professor Yukio Yoneda for his helpful discussions and encouragement, and to Professor Richard L. Schowen for his valuable suggestions.

References

1) For a recent review of oxidation of olefins with mercuric salts, see H. Arzoumanian and J. Metzger, *Synth.* 527 (1971).
2) B. C. Fielding and H. L. Roberts, *J. Chem. Soc., A*, **1966**, 1627.
3) J. C. Strini and J. Metzger, *Bull. Soc. Chim. Fr.*, **1966**, 3145, 3150.
4) B. Charavel and J. Metzger, *ibid.*, 4865 (1968).
5) H. B. Tinker, *J. Organometal. Chem.*, **32**, C25 (1971).
6) Y. Saito and M. Matsuo, *ibid.*, **10**, 524 (1967).
7) M. Matsuo and Y. Saito, This Bulletin, **44**, 2889 (1971).
8) J. Halpern and H. B. Tinker, *J. Amer. Chem. Soc.*, **89**, 6427 (1967).
9) W. Kitching, *Organometal. Chem. Rev.*, **3**, 61 (1968).
10) M. Matsuo and Y. Saito, *J. Org. Chem.*, **37**, 3350 (1972).
11) Y. Saito, "Some Theoretical Problems of Catalysis," ed. by T. Kwan, G. K. Boreskov, and K. Tamaru, University of Tokyo Press, Tokyo (1973), p. 241.
12) D. D. Maness and L. D. Turrentine, *Tetrahedron Lett.*, 755 (1973).
13) P. M. Henry, *Advan. Chem. Ser.*, **70**, 126 (1968).
14) B. R. James and M. Kastner, *Can. J. Chem.*, **50**, 1698 (1972).
15) For a recent review of kinetic isotope effects, see "Isotope Effects in Chemical Reactions," ed. by C. J. Collins and N. S. Bowman, Van Nostrand Reinhold, New York, N. Y. (1970).
16) J. Bigeleisen and M. Wolfsberg, *Advan. Chem. Phys.*, **1**, 15 (1958).
17) R. A. M. O'Ferrall, *J. Chem. Soc. B*, **1970**, 785.
18) W. B. Smith, R. E. Bowman, and T. J. Kmet, *J. Amer. Chem. Soc.*, **81**, 997 (1959).
19) W. B. Smith, T. J. Kmet, and P. S. Rao, *ibid.*, **83**, 2190 (1961).
20) M. Wolfsberg, *Ann. Rev. Phys. Chem.*, **20**, 449 (1969).
21) R. E. Weston, Jr., *Ann. Rev. Nucl. Sci.*, **11**, 439 (1961).
22) A. Steritwieser, Jr., R. H. Jagow, R. C. Fahey, and S. Suzuki, *J. Amer. Chem. Soc.*, **80**, 2326 (1958).
23) R. A. Kretchmer, R. A. Conrad, and E. D. Mihelich, *J. Org. Chem.*, **38**, 1251 (1973).
24) R. D. Bach and H. F. Henneike, *J. Amer. Chem. Soc.*, **92**, 5589 (1970).
25) M. Matsuo and Y. Saito, *J. Organometal. Chem.*, **27**, C41 (1971).
26) K. Ichikawa, S. Fukushima, H. Ouchi, and M. Tsuchida, *J. Amer. Chem. Soc.*, **80**, 6005 (1958).
27) P. M. Henry, *ibid.*, **86**, 3246 (1964).
28) R. A. Caldwall, *J. Org. Chem.*, **35**, 1193 (1970).
29) R. G. Jones and H. Gilman, "Organic Reactions," Vol. 6, ed. by R. Adams, John Wiley & Sons, Inc., New York, N. Y. (1951), p. 339.
30) D. Seyferth, *Progr. Inorg. Chem.*, **3**, 129 (1962).

Ligand-Ligand Interaction in $[Zn(1,10\text{-phenanthroline})_2(H_2O)_2](NO_3)_2$ and $[Zn(2,2'\text{-bipyridyl})_3](NO_3)_2$

Takeshi OHNO and Shunji KATO

Institute of Chemistry, College of General Education, Osaka University, Toyonaka, Osaka 560

(Received May 28, 1974)

The interaction between ligands in the excited state and in the ground state was examined by exploring the photophysical behaviors of ligands in the bis- and the tris-bidentate complexes. Although no exciton splitting was observed in the absorption spectra of $[Zn(bipy)_3](NO_3)_2$ and $[Zn(phen)_2(H_2O)_2](NO_3)_2$ at 77 K, the fluorescence yields of both complexes increased in comparison with those of the corresponding mono-bidentate complexes. It is probable that this change is caused by a delocalization of the excited singlet state, because a variation in Franck-Condon factors and a depolarization of the fluorescence accompanied it. In addition to the ligand-ligand interaction 1,10-phenanthroline and 2,2'-bipyridyl suffered from coordination effects. They have larger fluorescence yields and smaller phosphorescence yields than the free molecules. The decrease on the transition rate of the intersystem crossing is probably due to the changes in the energy levels of $^1(n\text{-}\pi^*)$ and $^3(n\text{-}\pi^*)$, caused by the metal-ligand bond using a "non-bonding" orbital in the free ligands.

The photochemistry of ligands in coordination compounds is affected not only by the metal-ligand bond, but also by ligand-ligand interaction. Some kinds of interaction between a ligand in its electronic excited state and ligand(s) in its ground state have been investigated in the case of β-diketonato complexes.[1] While a doubly- or a triply-degenerated state of the bis- or the tris-β-diketonato complexes was not split greatly by ligand-ligand interaction, three phenomena suggesting some weak interaction were observed: (i) an enhancement of spin-orbital interaction, (ii) a depolarization of the fluorescence, and (iii) a variation in the Franck-Condon factors of the radiative transition processes.

These interactions were examined in the cases of bis-1,10-phenanthroline* and tris-2,2'-bipyridyl** complexes of the zinc ion, which have more resolved spectra than the β-diketonato complexes of aluminium. These complexes were also examined with regard to the effects of the zinc-ligand bond on the excited states of the ligands. We will discuss the fact that ligands coordinating to Zn^{2+} have larger fluorescence yields than the free ligands, unlike the expectation based on the "heavy atom effect".[2]

Experimental

Materials. $[Zn(phen)_2(H_2O)_2](NO_3)_2$ and $[Zn(bipy)_3](NO_3)_2$ were prepared by heating a 50% ethanol solution of $Zn(NO_3)_2$ and the corresponding ligand. The prepared complexes were recrystallized from water two times. The free ligands, 1,10-phenanthroline·$2H_2O$ and 2,2'-bipyridyl were recrystallized from ethanol. The water was distilled twice, while Wako G. R. methanol was used without further purification.

Procedure. All the materials were dissolved in a mixture of methanol and water (4 : 1 by volume). Solutions of the mono-bidentate complexes were prepared by the addition of $Zn(NO_3)_2$ (5×10^{-4} M) and free ligand (5×10^{-5} M) to the mixed solvent. The absence of the free ligand is practically supported by the large stability constants ($\log K=6.4$ for $[Zn(phen)]^{2+}$ [3] and $\log K=5.4$ for $[Zn(bipy)]^{2+}$ [4] in an aqueous solution) and the disappearance of the absorption spectrum due to the free bipy.

Measurements. The measurements of the absorption and emission spectra, the emission yields, the emission lifetimes and the emission polarizations at 77 K were carried out in the way reported in the previous paper.[1] The emission spectra were calibrated against the fluorescence spectra of phenol, benzene, naphthalene,[5] and β-naphthole.[6] The corrected spectra agreed with those obtained by Chen's method using rhodamin B.[7]

Results and Discussion

Effect of Coordination on the Excited States of Ligand Absorption and Emission Spectra: As Fig. 1 shows, at the temperature of boiling nitrogen, free bipy in a mixed solvent of metanol and water (4 : 1) has a broad absorption band in the near ultra violet region whereas the absorption band of bipy coordinating to Zn^{2+} was a well-resolved structure and is shifted to a lower frequency (0—0': 32400 cm^{-1}). Such a shifted spectrum has also been found by Schläfer in the case of the mono-bipy complexes of Zn^{2+}, Cd^{2+}, Mn^{2+}, Co^{2+}, Ni^{2+}, and Fe^{2+} in water at room temperature; Schläfer considered these changes to be caused by the Stark effect of central ions on the ligand.[8] This consideration has been proven by Hanazaki and Nagakura on the basis of their P-P-P SCF-CI calculation of π-π^* transitions.[9] However, the lack of any determination of the n-π^* level, a result of the strong π-π^* band, leaves the question open whether the lowest level in n–π^* or π-π^*.***

Moreover, the coordinating bipy emitted a well-resolved fluorescence (see Fig. 2), which took a good mirror image with the absorption spectrum. Consequently, the fine structure of the absorption may safely be attributed not to another electronic transition, but to the vibrational structure of a single electronic transition, because sub-bands of fluorescence other than 0'-0 band are usually assigned to the vibrational structure with no doubt. This is supported by the fact that the fluorescence has a high polarization value (0.40),

* 1,10-phenanthroline will be abbreviated to "phen" heareafter.

** 2,2'-bipyridyl will be abbreated to "bipy" hereafter.

*** For pyridine, n-π is considerably lower (34769 cm^{-1}) than π-π^* (38350 cm^{-1}).[10]

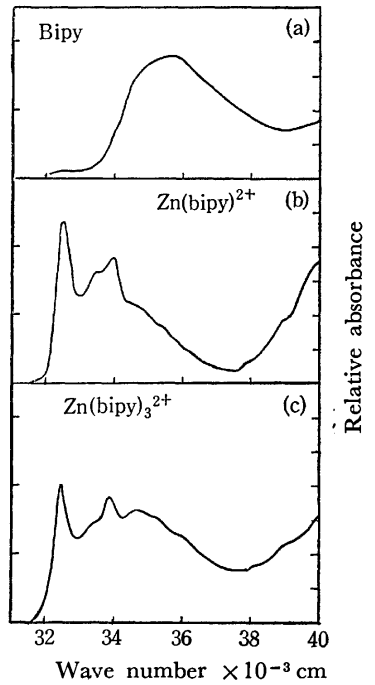

Fig. 1. Absorption spectra of bipy and its complexes of zinc ion in methanol and water (4 : 1 by volume) at 77 K.
(a) bipy: 4×10^{-5} M, (b) bipy: 4×10^{-5} M and $Zn(NO_3)_2$: 2×10^{-4} M, (c) $[Zn(bipy)_3](NO_3)_2$: 2×10^{-5} M and bipy: 4×10^{-5} M

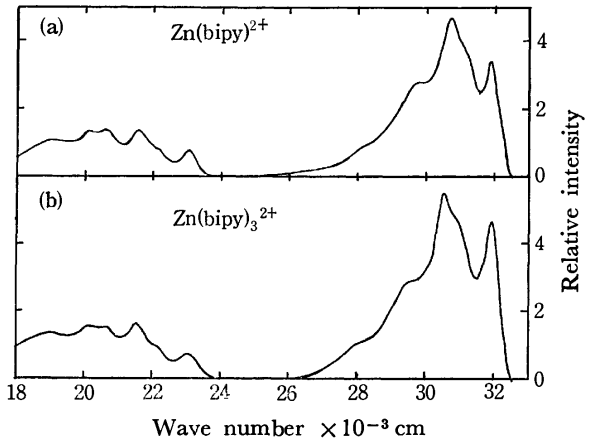

Fig. 2. Emission spectra of mono-bipy complex and $[Zn(bipy)_3](NO_3)_2$ in methanol and water (4 : 1 by volume) at 77 K.
(a) bipy: 5×10^{-5} M and $Zn(NO_3)_2$: 2×10^{-4} M
(b) $[Zn(bipy)_3](NO_3)_2$: 2.4×10^{-5} M

independent of the excitation ligand through $32\sim36\times10^3$ cm^{-1}. According to SCF-CI calculations of the free *cis*-bipy,[9,11] the transition moment to the first excited state of the B_1 symmetry is several tens of times as large as that to the second one of the A_1 symmetry lying 1×10^3 cm^{-1} above. Therefore, the assignments of the sub-bands are most probable.

It has been reported that the free form of phen has three kinds of transitions through $29\sim40\times10^3$ cm^{-1}. They have been assigned to ^1L_b, ^1L_a, and ^1B_a in the order of transition energy by measureing the fluorescence polarization with the excitation wavelength at 77 K[12] and by P-P-P SCF-CI calculations.[13] The coordination of phen to Zn^{2+} brought no essential change in the absorption spectrum, as Fig. 3 shows. However, one can recognize the following three changes; (i) the shoulders of the free form at 30000 and 31560 cm^{-1} disappear, (ii) the 0-0′ bands of the three transitions become more distinct (^1L_b: 29300, ^1L_a; 34200, and ^1B_a: 36900 cm^{-1}), and (iii) they shift to lower frequency by $250\sim600$ cm^{-1} than those of the free form.

The fluorescence of the coordinating phen due to the transition from ^1L_b to the ground state has a structure similar to that of the free form (see Fig. 4). As for the fluorescence polarization, while the free phen has a constant polarization (0.19) on excitation with $29\sim36\times10^3$ cm^{-1}, the coordinating form has a different value (0.15) when observed on excitation to ^1L_b from that (0.11) when observed on excitation to ^1L_a.

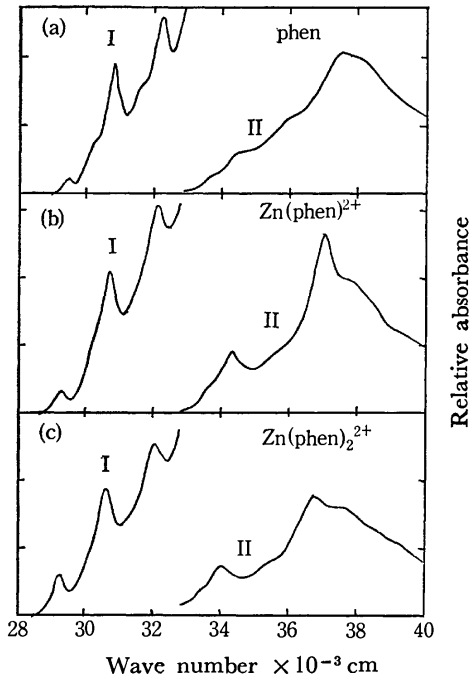

Fig. 3. Absorption spectra of phen and its complexes of zinc ion in methanol and water (4 : 1 by volume) at 77 K.
(a) I···phen: 8×10^{-4} M, II···phen: 2×10^{-5} M
(b) I···phen: 8×10^{-4} M, and $Zn(NO_3)_2$: 5×10^{-3} M, II···phen: 2×10^{-5} M and $Zn(NO_3)_2$: 1×10^{-3} M
(c) I···$[Zn(phen)_2(H_2O)_2](NO_3)_2$: 4×10^{-4} M, II··· $[Zn(phen)_2(H_2O)_2](NO_3)_2$: 1×10^{-5} M

TABLE 1. QUANTUM YIELDS OF EMISSIONS IN METHANOL AND WATER (4 : 1) AT THE TEMPERATURE OF BOILING NITROGEN

	F	P	F/P	τ_p s
$[Zn(bipy)]^{2+}$	0.30	0.015	20	1.75
$[Zn(bipy)_3]^{2+}$	0.39	0.019	20	1.75
phen	0.014	0.07	0.2	1.49
H^+ phen	0.03	0.04	1.75	—
$[Zn(phen)]^{2+}$	0.050	0.040	1.25	2.81
$[Zn(phen)_2(H_2O)_2]^{2+}$	0.070	0.040	1.75	2.59
H_2^{2+} phen	—	—	2	—

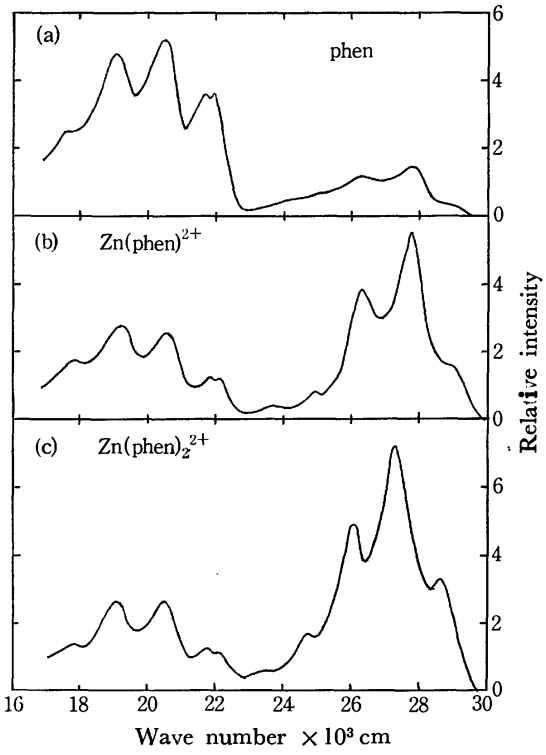

Fig. 4. Emission spectra of phen and its complexes of zinc ion in methanol and water (4 : 1 by volume) at 77 K.
(a) phen: 5×10^{-4} M, (b) phen: 5×10^{5} M and $Zn(NO_3)_2$: 2×10^{-4} M, (c) $[Zn(phen)_2(H_2O)_2](NO_3)_2$: 2×10^{-5} M

Yields of Emissions: While the free bipy emits only a weak phosphorescence at 77 K, the coordinating form emits a very strong fluorescence not only at the low temperature but also at room temperature. The yields of the fluorescence, listed up in Table 1, reach 0.30. The following considerations make it probable that such an appearance of the strong fluorescence originates from changing the lowest singlet excited state from the n-π^* state to the π-π^* state because of its coordination; (i) Coordination through nitrogen atoms of bipy to metal ions, not only Zn^{2+} but also Cd^{2+}, gives rise to a fall in the π-π^* level due to pyridyl-pyridyl interaction in the pseudo planar forms of *cis*-bipy and a rise of n-π^* level due to the coordination using "non-bonding" orbitals on nitrogen atoms. Therefore, the appearance of the strong fluorescence may be attributable to either a fall in the π-π^* level or a rise in the n-π^* level, or to both. (ii) Although no fluorescence was observed in 0.1 M HCl, in which mono-protonated bipy with the planar forms of *cis*-bipy is predominant, fluorescence was observed in an 80% sulfuric acid solution, in which bipy is changed into the di-protonated form of *trans* bipy. Therefore, a fall of π-π^* due to the pseudo planar forms of *cis*-bipy is not always needed for a strong fluorescence. (iii) It is generally believed that because n-π^* has a long radiative lifetime (10^{-7} s) because of a partly-allowed transition, other processes—intersystem crossing and internal conversion—take place much more easily, resulting in the absence of fluorescence. This is the case for pyridine. (iv) Because the coordination of bipy to metal ions raises the n-π^* states as hydrogen bonding and protonation do, the lowest singlet state of the coordinating bipy may be changed from n-π^* to π-π^*, of which, in the free form, the latter seems to be nearer to the former on account of pyridyl-pyridyl interation than in pyridine.

As for phen, the free form of which emits a fluorescence of a medium intensity in addition to a phosphorescence, its coordination to the zinc ion gave rise to an enhancement of the fluorescence and diminution of the phosphorescence (see Table 1). Because such a change in the emission yields was observed a little in 0.1 M HCl and moderately in a 90% sulfuric acid solution, as Table 1 shows, it is probable that a change in the energy level of n-π^* excited states with coordination or protonation results in the variation in the emission yields. However, since the weak lowest band may safely be regarded as a transition to the π-π^* state in all the forms and does not vary in intensity with coordination and protonation, the enhancement of the fluorescence is not caused by a change in the radiative transition rate, but by a change in the non-radiative transition rate. It has been reported that the yield of the phosphorescence of phen is the largest of the nine phenanthrolines.[14] Perkampus *et al.* assumed that the largest intersystem crossing rate was attributable to the small separation between ^1L_b and unknown higher triplet state(s). If the higher triplet state(s) is the n-π^* state, whose level is dependent on the positions of the nitrogen atoms in the free form, the coordination of phen will considerably raise ^{3}(n-π^*) as well as ^{1}(n-π^*) and make the rate of the ^{3}(π-π^*) formation ($^1L_b\rightarrow{}^3$(n-π^*)$\rightarrow{}^3$(π-π^*) or $^1L_b\rightarrow{}^1$(n-π^*)$\rightarrow{}^3$(n-π^*)) slower. This change will give rise to a larger yield of fluorescence, which must be similar to those of other phenanthrolines (0.1$\sim$0.5 in a mixed solvent of ether and ethanol (1 : 1)) and phenanthrene (0.17 in EPA[15]). As Table 1 shows, this is indeed the case.

After all, the variation in the n-π^* levels with their coordination results in a large fluorescence yield in the cases of both bipy and phen. Moreover, the enhancement mechanism is different from that in the case of β-diketonates, in which the metal-ligand bond prevents their excited states from making a radiationless transition to the ground state.[1] It is worthwhile noticing that the fluorescence of ligands is enhanced by coordination to Zn^{2+}, contrary to the expectation deduced from the heavy-atom effect. In the case of porphyrin complexes, in fact, the enhancement of the phosphorescence yield with the complex formation has been accounted for in terms of the heavy-atom effect.[2]

Interaction between Ligands in the Excited State and in the Ground State. Absorption and Emission Spectra: Since the tris-bipy complex of Zn^{2+} has three large ligands with an allowed transition along their longer axes, it may be expected that an exciton interaction among the three ligands removes the three fold degeneracy of the excited state associated with the transition, resulting in some splitting between the states with E and A_2 symmetries as well as in the case of $[Fe(bipy)_3]^{2+}$. However, a comparison of the absorption spectra between the tris- and the mono-bipy com-

plexes showed no difference not even at 77 K. As Fig. 1 shows, the tris-bipy complex has an absorption spectrum very similar to that of the mono-bipy complex. The broad band at the higher-frequency regions in the spectra for the tris-bipy complex is due to the free bipy, which is added to suppress the dissociation of the tris-bipy complex. Further, the band widths of the tris-bipy complex are seen to be the same as those of the mono-bipy complex for the sharpest 0-0′ band (its width: 460 cm^{-1}); therefore, the splitting of the vibronic bands should be very small if any. Such a weak interaction in $[Zn(bipy)_3]^{2+}$ has been suggested in view of the mirror-image relationship.[16] However, these results do not necessarily preclude any ligand-ligand interaction, because the change in the fluorescence yield and the fluorescence polarization may suggest a weak interligand interaction in addition to the circular dichroism of the tris-bipy complexes of Fe^{2+},[17] as will be discussed later.

For $[Zn(phen)_2(H_2O)_2](NO_3)_2$, which easily forms a tris-phen complex in the presence of excess phen, the coordinating nitrogen atoms of two phen are considered to locate at the apices of an octahedron and two H_2O at the vicinal apices. This is supported by the fact that two phen of some bis-phen complexes do not lie coplanar as a result of the repulsion between α-hydrogen atoms of two phen.[18] Therefore, the bis-phen complexes of zinc may also be expected to have such a ligand-ligand interaction, as was proposed in the tris-phen complex of Fe^{2+}.[17]

For the strongest band at 37,050 cm^{-1} (^1B_a in the free phen), which has been expected to have a large exciton interaction,[17] the absorption band of $[Zn(phen)_2(H_2O)_2]^{2+}$ has a similar structure, consisting of a strong peak (0-0′) and a shoulder (0-1′) on 700 cm^{-1} side higher than that of the mono-phen complex, as Fig. 3 shows. Since no splitting of the electronic transition is distinctly recognized, the exciton interaction can not be regarded as a "strong coupling" as defined by Simpson and Peterson.[19] And it is not possible to estimate the weak exciton interaction quantitatively on any vibronic coupling theory, because not all the electronic bands are distinctly resolved into sub-bands.

The difference in the relative intensities of the sub-bands, the Franck-Condon factors, are observed between the absorption spectra of $[Zn(phen)_2(H_2O)_2]^{2+}$ and the mono-phen complex (see Table 2). Generally speaking, the Franck-Condon factors of an intra-ligand transition may be expected to be varied by both the metal-ligand interaction and the ligand-ligand interaction, as are the energy and the total intensity of the transition. It is assumed that the ligand-ligand interaction, which gives rise to a delocalization of the excited state through two ligands and to a smaller distortion and displacement of the excited state, is reflected in the Franck-Condon factors of the lowest band of $[Zn(phen)_2(H_2O)_2]^{2+}$, which is larger than that of the mono-phen complex, and that the metal-ligand interaction is not so large as to change the Franck-Condon factors of the transition in the latter complex. Further, it is noticed that the Franck-Condon factors obtained by the analyses of the fluorescence spectra have a distribution similar to those obtained from the absorption spectra. These considerations show the existence of a weak interaction between a phen in the ground state and a phen in the excited state. On the other hand, it is assumed that, for the strong band (^1B in the free phen), the metal-ligand interaction has an effect on the relative intensities of the sub-bands, which are seen at 37,050 cm^{-1} (0-0′) and 37,800 cm^{-1} for the mono-phen complex, and at 36,800 cm^{-1} (0-0′) and 37,500 cm^{-1} for the bis-phen complex. This assumption is supported by the fact that the intensity of the 0-0′ band is stronger for the mono-phen complex than for the bis-phen complex, in which Zn^{2+} is shared by two phens. Though the variations in the Franck-Condon factors are not clear in the cases of the bipy complexes, a weak interaction between three bipys is probable.

Table 2. Relative intensities of vibronic lines normalized to the intensity of 0′-0

	Fluorescence		
	0′-0	0′-1	0′-2
$[Zn(bipy)]^{2+}$		1.00[a]	0.55
$[Zn(bipy)_3]^{2+}$		1.00[a]	0.52
phen	1.0	3.6	3.4
$[Zn(phen)]^{2+}$	1.0	3.51	2.51
$[Zn(phen)_2(H_2O)_2]^{2+}$	1.0	2.43	1.52

a) It is compared to the intensity of 0′-1 because 0′-0 is reduced by reabsorption.

Yields of Emission: As Table 1 shows, the fluorescence yields of the bis- and the tris-bidentate complexes were significantly greater than that of the corresponding mono-bidentate one; however, the absorption coefficient per ligand is not different. Therefore, it is likely that the fluorescence enhancement is due to a decrease in the rates of the non-radiative processes. Especially, the rate of internal conversion ($S_1 \rightarrow S_0$), which is affected by the Franck-Condon factors ($<0'|v>^2$) with very large v-values, according to Siebrand,[20] can be expected to be less than that of the mono-bidentate complex by taking account of the less distortion and displacement of the lowest excited state of $[Zn(phen)_2(H_2O)_2]^{2+}$. Therefore, it is reasonable to say that the fluorescence enhancement originates from the weak ligand-ligand interaction, as has been proposed in the preceding section.

Polarizations of Emission: Fluorescence in a rigid solvent depolarizes on the excitation of polarized light, when (a) an upper excited state with a moment in a different direction is directly excited, (b) an energy transfer takes place from an excited ligand to another ligand(s) in a complex ion, or (c) a new state with a transition moment along two or three axes is produced by interaction between ligands which individually have a transition moment along one axis. Therefore, the fluorescence polarization of the tris-bidentate complexes gives information about an energy transfer on excitation to the lowest excited state (S_1) or on the appearance of a new excited state. As Table 3 shows,

Table 3. Fluorescence polarization measured in methanol and water (4 : 1) at the temperature of boiling nitrogen on excitation to S_1

	P_F	P_P
$[Zn(bipy)]^{2+}$	0.40	
$[Zn(bipy)]_3^{2+}$	0.05	
phen	0.19, 0.19[a]	−0.25, −0.25[a]
$[Zn(phen)]^{2+}$	0.15, 0.11[a]	−0.12, −0.18[a]
$[Zn(phen)_2(H_2O)_2]^{2+}$	−0.014, 0.05[a]	−0.038, −0.070[a]

a) The value was observed on excitation to S_2 (^1L_a).

the fluorescence of the tris-bipy complex was considerably depolarized as compared with that of the monobidentate complex, on excitation to S_1. Therefore, it is certain that some interactions are operative between ligands in the excited state and the ground state. An energy transfer between ligands is unlikely, because neither excitation nor emission is localized in one ligand; both are delocalized through ligands, as was mentioned in the preceding sections. The next problem is in the estimation of the energy splitting between the two states of E and A_2 symmetry by means of the analysis of the fluorescence polarization. Although the states of E and A_2 symmetry participate in the absorption process because of the splitting between them, it depends on the energy splitting whether or not the upper state of A_2 symmetry participates in the fluorescence process. When the splitting is below 70 cm^{-1}, both E and A_2 are emissive at 77 K, while when it is over 100 cm^{-1}, only the state of E fluoresces practically. As Table 4 shows, the fluorescence polarization is determined by the direction of the transition moment of the emitting state(s). The observed value (0.05) for the tris-bipy complex is the nearest to the ideal value (0.09), which is calculated by assuming both states to be emissive.

The energy splitting (70 cm^{-1}) in $[Zn(bipy)_3]^{2+}$ is similar to that[17] in $[Ni(bipy)_3]^{2+}$, which has been obtained by fitting the measured shape of the circular dichroism to the theoretical one based on the vibronic coupling theory of Perrin and Gouterman.[21] Recently, Mason *et al.*[22] reconstituted the observed intensity of circular dichroism by assuming the interaction to be 350 cm^{-1}, based on the vibronic coupling theory. However, since both the reconstituted spectra of circular dichroism were much more complex than the observed ones, the inter-ligand interaction of 350 cm^{-1} seems to be overestimated. Therefore, it is not improbable that the energy splitting in $[Zn(bipy)_3]^{2+}$ is smaller than 70 cm^{-1}.

Table 4. Ideal polarization of fluorescence on excitation to both states having E and A_2 symmetry

Emissive state	P
E	−0.174
A_2	0.222
E and A_2	0.090

The tris-phen complex is complicated, because the mono-phen complex had a considerable depolarization even, upon excitation to S_1 (^1L_b of the free phen).

References

1) T. Ohno and S. Kato, This Bulletin, **47**, 1901 (1974).
2) R. S. Becker and J. E. Allison, *J. Phys. Chem.*, **67**, 2669 (1963).
3) I. M. Kolthoff, D. L. Leussing, and T. S. Lee, *J. Amer. Chem. Soc.*, **73**, 390 (1951).
4) M. Yasuda and K. Yamazaki, *ibid.*, **78**, 1324 (1956).
5) E. Lippert, W. Nigele, I. Seibold-Blankenstein, and U. Straiger, *Z. Anal. Chem.*, **170**, 1 (1960).
6) C. A. Parker, *Anal. Chem.*, **34**, 502 (1962).
7) R. F. Chen, *Anal. Biochem.*, **20**, 339 (1967).
8) H. L. Schläfer, *Z. physik. Chem. (N. F.)* **8**, 373 (1956).
9) I. Hanazaki and S. Nagakura, *Inorg. Chem.*, **8**, 648 (1969).
11) Y. Kondo, *J. Chem. Phys.*, **41**, 3928 (1964).
10) J. H. Rush and H. Sponer, *ibid.*, **20**, 1847 (1952).
12) H. Grpper and F. Dorr, *Z. Electrochem.*, **67**, 46 (1963).
13) T. Ito, N. Tanaka, I. Hanazaki, and S. Nagakura, *Sci. Repts. Tohoku Univ., First Ser.*, **50**, 168 (1967).
14) H. -H. Perkampus and A. Knop, *Z. Naturforsh*, **23a**, 849 (1968).
15) V. L. Ermolaev and E. B. Svensnikova, *Opt. Spectry.*, **16**, 320 (1964).
17) S. F. Mason, *J. Chem. Soc. (A)*, **1969**, 1428.
16) R. G. Bray, J. Ferguson, and C. J. Hawkins, *Aust. J. Chem.*, **22**, 2091 (1969).
18) E. D. Mckenzie, *Cood. Chem. Rev.*, **6**, 187 (1971).
19) W. T. Simpson and D. L. Peterson, *J. Chem. Phys.*, **26**, 588 (1957).
20) W. Siebrand, *ibid.*, **46**, 440 (1967).
21) M. H. Perrin and M. Gouterman, *J. Chem. Phys.*, **46**, 1019 (1967).
22) S. F. Mason, B. J. Peart, and R. E. Waddell, *J. Chem. Soc. Dalton*, **1973**, 944.

Kinetic Studies on Olefin Epoxidation by Peroxo Molybdenum Complex ($MoO(O_2)_2HMPT$)

Hironori ARAKAWA, Yoshihiko MORO-OKA, and Atsumu OZAKI

Research Laboratories of Resources Utilization, Tokyo Institute of Technology, Ohokayama, Meguro-ku, Tokyo 152

(Received December 14, 1973)

Oxidation of olefin by peroxo molybdenum complex selectively yields epoxide at room temperature. The nature of the interaction of olefin with molybdenum and that of the peroxo molybdenum complex has been investigated in terms of coordination constant K of olefin and rate constant k_2 of decomposition of the peroxo molybdenum-olefin complex, attention being paid to the substituent effect of olefin. The coordination constant increases with the extent of alkyl substitution on double bonded carbon, a tendency opposite to that on Pd(II), or Rh(I). The coordination state of olefin on molybdenum seems to differ from that on Pd(II) or Rh(I), for which π-back donation of metal d-electron is accepted to play an important role. The coordination complex on molybdenum is accordingly assigned to a π-complex with some electron donated to molybdenum. A remarkable steric effect of alkyl substituent is observed, disclosing a difference from the oxidation of uncoordinated olefin. Since k_2 increases with K, revealing a similar substituent effect of olefin, the peroxo oxygen seems to be electrophilic, and the peroxo oxygen-molybdenum bond seems to be rather covalent than ionic, thus giving rise to epoxidation.

The selective epoxidation of olefin by new peroxo complexes of molybdenum(VI) such as $MoO(O_2)_2L$[1] was found by Mimoun *et al.*,[2] followed by the demonstration by Sharpless *et al.*[3] by means of ^{18}O tracer that the peroxo oxygen of complex I is exclusively transferred to the olefin, the oxo oxygen not being involved in the oxidation:

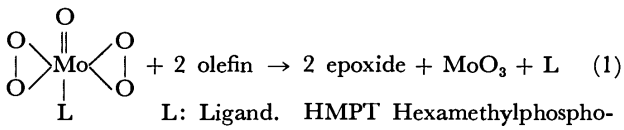

$$+ 2 \text{ olefin} \rightarrow 2 \text{ epoxide} + MoO_3 + L \quad (1)$$

L: Ligand. HMPT Hexamethylphosphotriamide

I

Some molybdenum salts act as an effective catalyst for the epoxidation of olefin with organic hydroperoxides.[4] The peroxo species of molybdenum such as I seems to be important as a key intermediate in the oxidation of olefins by organic peroxides. Thus the nature of interaction between molybdenum and olefin calls for further investigation. This has been done in terms of kinetic constants associated with Reaction (1).

According to Mimoun *et al.*,[2] the epoxidation of olefin by I consists of two steps; A reversible coordination of olefin to I to form a one to one adduct (complex II) and an irreversible decomposition of complex II to form epoxide.

$$\underset{\text{I}}{MoO(O_2)_2L} + \text{olefin} \underset{k_{-1}}{\overset{k_1}{\rightleftharpoons}} \underset{\text{II}}{MoO(O_2)_2L(\text{olefin})} \quad (2)$$

$$k_1/k_{-1} = K$$

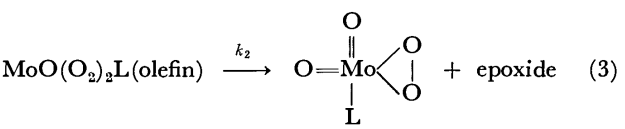

$$\text{epoxide} \quad (3)$$

II III

We determined coordination constants K of olefin to a peroxo molybdenum complex $MoO(O_2)_2HMPT$, and rate constants k_2, for the decomposition of II to epoxides for 22 mono-olefins by kinetic measurements. From the results the nature of active oxygen of peroxo molybdenum complex and that of the interaction between olefin and molybdenum are discussed.

Experimental

Preparation of Peroxo Complex. $MoO(O_2)_2HMPT$ was prepared by the method of Mimoun *et al.*[1] 50 g (0.348 mol) of molybdenum trioxide was suspended in 250 ml of 30% hydrogen peroxide with stirring at 40 °C for 2 hr. 62.3 g of HMPT(0.348 mol) was added dropwise to the suspension and the mixture was stirred for 2 hr at 10 °C. A yellow crystalline precipitate was obtained ($MoO(O_2)_2HMPT\text{-}(H_2O)$). The precipitate was filtered off, washed three times with ethyl ether, and recrystallized from methanol solution at 40 °C; yield 76.2 g (80%). This was allowed to stand for 1 week in a cool and dark place *in vacuo* on phosphoric anhydride to remove water. Removal of water was confirmed by IR spectroscopy.

IR;

ν_{O-O} 865 cm^{-1}, 875 cm^{-1}; $\nu_{MO<}$ *sym* 540 cm^{-1}, *asym* 595 cm^{-1}; $\nu_{Mo=O}$ 965 cm^{-1}; ν_{P-O} 1188 cm^{-1}; ν_{N-P-O} 755 cm^{-1}, 765 cm^{-1}.

Found: C, 20.34; H, 5.25; N, 11.80%. Calcd for $C_6H_{18}N_3O_4PMo$: C, 20.34; H, 5.25; N, 11.92%.

Procedure. All the runs for liquid olefin were carried out under ambient pressure with dry nitrogen in a 30 ml glass flask. The solvent used was dry ethylene dichloride. The reaction was started by addition of olefin to the ethylene dichloride solution of I. All kinetic measurements were made in the solution of a fixed concentration of I with excess olefin. When the initial concentration of olefin was changed, the corresponding amount of parafin was added to keep the total amount of hydrocarbon constant, thus avoiding a change in the solvent effect. The standard composition of the reaction mixture was as follows; $MoO(O_2)_2$ HMPT 0.05 mol/l, ethylene dichloride 9.6 mol/l, olefin 0.5—2.5 mol/l, and paraffin balance. The selectivity to epoxide being higher than 95% with respect to the active oxygen consumed, the reaction rates were measured by increase in the concentration of epoxide which was determined by gas chromatography. The runs for gaseous olefins were carried out with a conventional apparatus for gas absorption under constant pressure. The reaction rates were determined by the rates of absorption of gaseous olefins after the dissolution equilibrium had been attained. It was confirmed that epoxide formation can be followed by the absorption.

Analysis of Kinetic Result. The kinetic constants were determined according to the mechanism and rate equation

given by Mimoun *et al.*[2] If the reaction of Eq. (2) is fast and the reaction of Eq. (3) is rate-determining, the rate of disappearance of the complex I is given by

$$V = -\frac{d[I]}{dt} = \frac{k_2K[\text{olefin}][I]}{1 + K[\text{olefin}]} = k'[I] \quad (4)$$

under the present conditions of excess olefin, where k' is a constant under a fixed excess concentration of olefin, and represents the specific rate of epoxidation. The values of k' were obtained from the first-order plots with respect to I under different concentrations of olefin and plotted against the olefin concentration according to the equation

$$\frac{1}{k'} = \frac{1}{k_2} + \frac{1}{k_2K[\text{olefin}]} \quad (5)$$

Straight lines were obtained for different olefins. k_2 and K were determined from the intercept and slope of the straight line.

For the sake of confirmation, temperature dependence of k_2 and K was examined with cyclohexene in the range 0—30 °C. The Arrhenius plots are shown in Fig. 1. Straight lines were obtained as expected. The activation energy and the heat of coordination are 17.2 kcal/mol and 5.7 kcal/mol respectively.

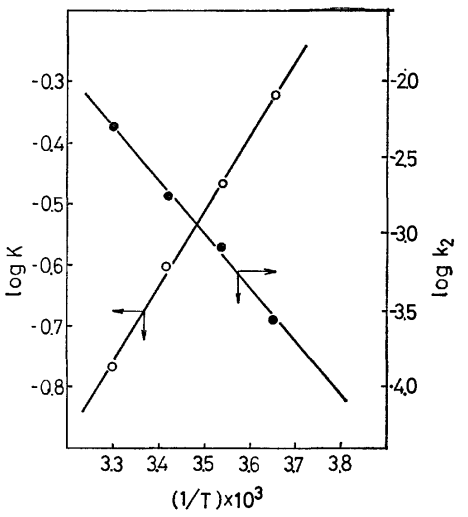

Fig. 1. The Arrhenius plots of k_2 and K with cyclohexene. Condition; olefin concentration: 1.0 mol/l, temperature: 0°C—30°C, solvent: ethylene dichloride.

Results and Discussion

The Effect of Olefin Structure on the Kinetic Constant. The epoxidation of olefins tested were selective and stereo-specific as reported by Mimoun *et al.* The kinetic constants were determined at 20 °C with 22 olefins. Values of k_2 and K are summarized in Table 1, together with the rate of epoxidation k' at 1.0 mol/l of olefin concentration.

The following general trends are indicated.

(1) The larger the reaction rate k', the larger both k_2 and K. There is a parallelism between k_2 and K.

(2) Steric effect is observed in both k_2 and K. The alkyl substitution on the double-bonded carbon

Table 1. Kinetic data of various olefins at 20 °C in ethylene dichloride

Type of substitution	Olefin	Rate constant $k_2\times10^3$ (s^{-1})	Coordination constant K (l/mol)	Specific rate at 1.0 mol/l-olefin $k\times10^5$ (s^{-1})
	C_4			
α	1-Butene	0.25	0.16	3.4
αβ	*cis*-2-Butene	0.87	0.27	21.5
αβ	*trans*-2-Butene	0.44	0.18	5.3
αα	Methyl propene	0.72	0.34	21.0
	C_5			
α	1-Pentene	0.20	0.14	2.5
α	3-Methyl 1-butene	0.17	0.15	2.2
αβ	*cis*-2-Pentene	1.11	0.23	16.0
αβ	*trans*-2-Pentene	0.43	0.17	4.9
αα	2-Methyl 1-butene	0.53	0.24	11.5
ααβ	2-Methyl 2-butene	1.65	0.39	42.8
αβ	Cyclopentene	0.81	0.23	16.4
	C_6			
α	1-Hexene	0.19	0.13	2.0
α	3,3-Dimethyl 1-butene	0.16	0.15	1.8
αα	2-Methyl 1-pentene	0.50	0.32	12.1
ααβ	2-Methyl 2-pentene	1.69	0.51	57.8
ααββ	2,3-Dimethyl 2-butene	1.96	0.80	86.2
αβ	Cyclohexene	0.89	0.25	17.8
	Others			
αβ	4-Methyl cyclohexene	0.86	0.25	17.7
ααβ	1-Methyl cyclohexene	1.22	0.33	30.4
ααβ	2,4-Dimethyl 2-pentene	1.00	0.16	10.2
ααβ	2,4,4-Trimethyl 2-pentene	0.50	0.10	4.8
ααββ	2,3-Dimethyl 2-pentene	2.08	0.77	94.7

atoms by secondary or tertiary alkyl group instead of primary alkyl group reduces both k_2 and K. For example,

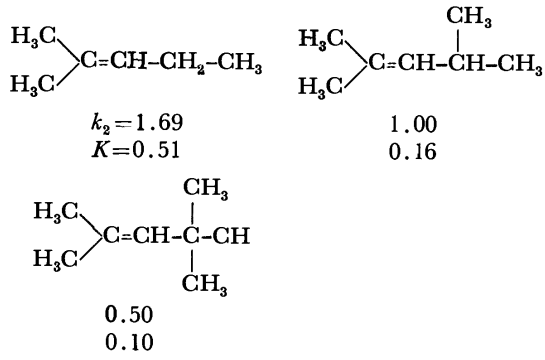

The values for *cis*-olefin are larger than those for the corresponding *trans*-olefin.

(3) In the absence of the steric effect, the values of k_2 and K increase with the number of alkyl substituents;

$$\alpha\alpha\beta\beta > \alpha\alpha\beta > \alpha\alpha,\ \alpha\beta > \alpha$$

where α and β denote the number and position respectively, of the alkyl substitution.

Interaction of Olefin with Peroxo Molybdenum Complex. The nature of metal ion-olefin complex has been extensively investigated in terms of coordination constant or stability constant.[5,6] According to Hartely,[7] metal ions can be classified into two groups by the electronic effect of olefin substituents on the stability of metal ion-olefin complex. The first group (type A), comprising Ag(I) and Cu(I), shows a decrease in stability, while the second group (type B), Ni(0), Pt(0), Pt(II), Rh(I), shows an increase in stability as the electron-withdrawing ability of the olefin substituents increases.

In order to clarify the interaction between olefin and peroxo molybdenum complex, the values of K we obtained are compared with the stability constants of acacRh(C_2H_4)-olefin determined by Cramer.[6] Both constants are plotted in Fig. 2. In order to eliminate the steric effect, comparison is made only for those olefins having primary alkyl substituents. The electronic effect of alkyl substituent is exactly the opposite in the two systems, *viz.*, K_{Mo} increases, while K_{Rh} decreases, with the extent of substitution at the double-bonded carbon. Since the alkyl substituent is electron donating, the above result indicates that Mo(VI) belongs to type A.

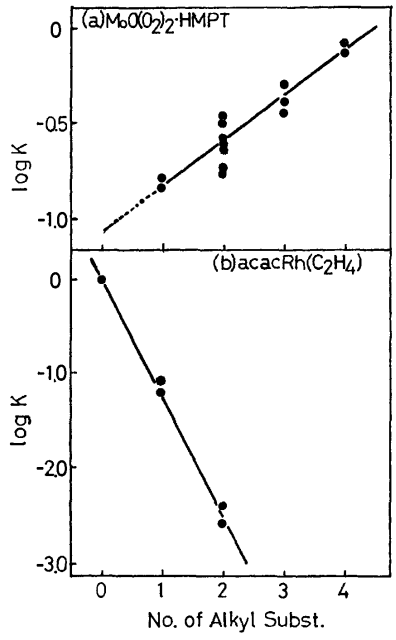

Fig. 2. Variation of coordination constant, K_{Rh} and K_{Mo}, with extent of alkyl substitution.
(a): this work, (b): taken from the data in Ref. 6.

The metal ion-olefin interaction has been interpreted in terms of the molecular orbital description of metal-olefin bond. In case of type A ion, the σ (olefin to metal) bond is important. An increase in the availability of the olefinic π-electrons increases the stability of the metal-olefin complex, while in the case of type B ion, the π(metal to olefin) bond is important and the effect of the olefinic π-electrons is opposite. This is demonstrated by the result shown in Fig. 2.

Since the formal charge of molybdenum is Mo(VI), the back-donation of olefin seems unlikely. This was suggested by Mimoun *et al.*, and confirmed by us. The steric effect and the larger coordination constant of *cis*-olefin than of corresponding *trans*-isomer are reported in π-complex.[5-7]

Effect of Alkyl Substitution on k_2. All the data of of k_2 are plotted against K in Fig. 3., where an open circle denotes secondary or tertiary alkyl-substituted olefin. k_2 appears to increase linearly with K. However there are some deviations. i) The k_2 of $\alpha\alpha$ type olefin is substantially less than that of the corresponding $\alpha\alpha\beta$ and even $\alpha\beta$, although K is of the same magnitude. It appears that $\alpha\beta$ disubstitution preferentially increases k_2. The relatively large k_2 of 2,4-dimethyl- and 2,4,4-trimethyl-2-pentene is in conformity with this tendency, while their low values of K may be due to the steric effect. ii) The k_2 of $\alpha\alpha\beta\beta$ type olefins (2,3-dimethyl-2-butene and 2,3-dimethyl-2-pentene) are not so large as expected from its K value. It is obvious that the alkyl substitution favorable for the coordination is not always favorable for the reaction of coordinated olefin, suggesting a steric effect in the reaction.

The general trend of k_2 increasing with K might be understood as a linear free energy relationship. It is also explainable in terms of reaction scheme as suggested by Mimoun *et al.*:

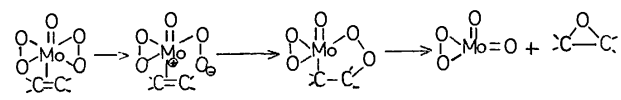

Since the charge transfer from olefin to molybdenum would be increased by the alkyl substitution, resulting in a more positively charged olefin molecule, the nucleophilic attack of peroxo oxygen on the coordinated olefin might be enhanced by the alkyl substitution at the double bonded carbon.

Nature of Peroxo Oxygen in the Molybdenum Complex. The nature of peroxo oxygen is examined by comparing k_2 with rates or rate constants of various addition reactions of oxygen to olefin. Rates or rate constants are plotted against the number of primary alkyl substituents

on double bonded carbon of olefins (Fig. 4). The quoted values are the average of olefins of the same alkyl substituent number, the reactants being peracetic acid,[8] atomic oxygen[8] and singlet oxygen $O_2(^1\Delta_g)$.[9] The last one is accepted to be the active species of dye-sensitized photo-oxidation to form allylic peroxide. These three reactants are admittedly electrophilic and directly attack the unsaturated carbon atom.[10,11]

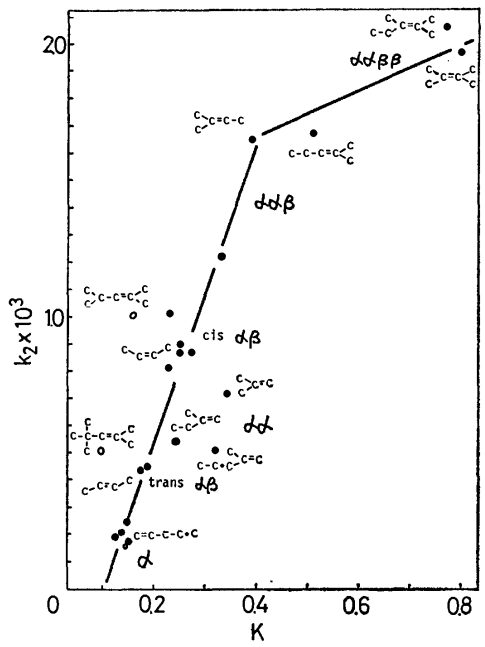

Fig. 3. Correlation between k_2 and K for olefins.

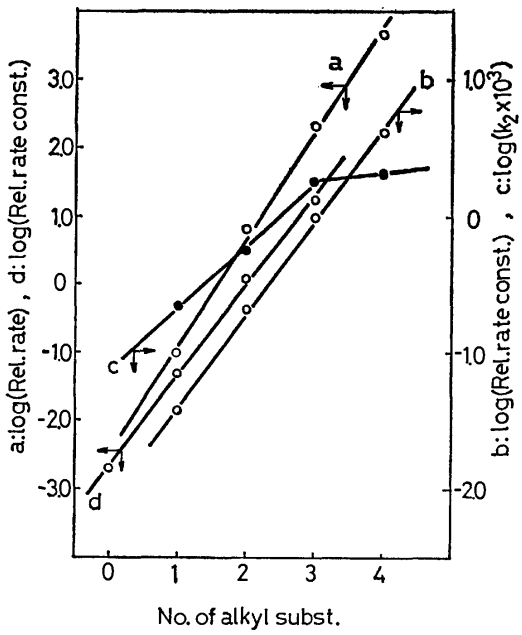

Fig. 4. Relative rate or rate constant of electrophilic oxygen as functions of number of alkyl substituents on double bonded carbon atom.
a: $O_2(^1\Delta g)$ Relative rate. Taken from the data in Ref. 10. b; O(3P) Relative rate constant. Taken from the data in in Ref. 8. c: k_2x10^3 of this work. d: Peracetic acid Relative rate constant. Taken from the data in Ref. 8.

Since k_2 increases with the extent of alkyl substitution as other rate or rate constants (Fig. 4), the peroxo oxygen in $MoO(O_2)_2HMPT$ can be accepted as electrophilic.

The results are in line with the suggestion made by Mimoun *et al.* on the basis of k' instead of k_2 we have examined. This would be expected if k' runs parallel with k_2. However, since k' is a function of k_2, K and olefin concentration, there should be difference between k' and k_2. In fact, k_2 remarkably deviates from the linear relationship with K (Fig. 3), whereas k' is approximately linear with respect to K. A similar feature is obvious in Fig. 4. The k_2 of $\alpha\alpha\beta\beta$ olefin is substantially less than expected from linearity, whereas the linearity is extended to include $\alpha\alpha\beta\beta$ olefin for the other three, non-coordinated oxygen species. Another feature characteristic of k_2 would be the steric effect of olefin, which is not observed with the other three compounds. Such characteristic features observed with k_2 are assumed to be caused by the required coordination of olefin to molybdenum.

The selective epoxidation of olefin by $MoO(O_2)_2$-HMPT complex should be explained in terms of the electrophilic nature of peroxo oxygen. In fact, oxygen anion O^- and superoxide O_2^- having negative values of electron affinity do not give epoxide, whereas the atomic oxygen and $O_2(^1\Delta_g)$ have positive values and give epoxide. Oxygen complexes of group VIII metals are also known to be ineffective for epoxidation. Cook *et al.* estimated the effective charge of coordinated oxygen in $PtO_2(P\phi_3)_2$ as $O_2^{1.8-}$ by means of ESCA.[12] Since the electrophilicity of oxygen depends on its effective charge, the electrophilic nature of peroxo oxygen suggests that the peroxo oxygen has a much lower effective charge than its formal one O_2^{2-}. The higher selectivity of epoxidation by molybdenum complex, in constrast to group VIII metal complexes, may be understood on the basis of different effective charges of O_2 in the complexes.

References

1) H. Mimoun, I. Seree de Roch, and L. Sajus, *Bull. Soc. Chim. France*, **1969**, 1481.
2) H. Mimoun, I. Seree de Roch, and L. Sajus, *Tetrahedron*, **26**, 37 (1970).
3) K. Sharpless, J. Townsend, and D. R. Williams, *J. Amer. Chem. Soc.*, **94**, 295 (1972).
4) a) J. Kollar, Belgian Patent 641452 (1964). b) G. B. Payne and P. H. Williams, *J. Org. Chem.*, **24**, 54 (1959). c) K. A. Saegebarth, *ibid.*, **24**, 1212 (1959). d) N. Indictor and W. F. Brill, *ibid.*, **30**, 2074 (1965).
5) P. M. Henry, *J. Amer. Chem. Soc.*, **88**, 1595 (1966).
6) R. Cramer, *ibid.*, **89**, 4621 (1967).
7) F. R. Hartley, *Chem. Rev.*, **73**, 163 (1973).
8) S. Sato and R. J. Cvetanovic, *J. Amer. Chem. Soc.*, **81**, 3223 (1959).
9) C. S. Foote and S. Wexler, *ibid.*, **86**, 3380 (1964).
10) K. R. Copecky and H. J. Reich, *Can. J. Chem.*, **43**, 2265 (1965).
11) D. R. Kearns, *Chem. Rev.*, **71**, 395 (1971).
12) C. D. Cook, K. Y. Wan., U. Gelius, K. Hamrin, G. Johansson, E. Olsson, H. Siegbahn, C. Nording, and K. Siegbahn, *J. Amer. Chem. Soc.*, **93**, 1094 (1971).

Vibrational Assignments and Rotational Isomerism of Dichloroethylmethylsilane and 2,2-Dichlorobutane

Keiichi OHNO, Yuji SHIRO,* and Hiromu MURATA

Department of Chemistry, Faculty of Science, Hiroshima University, Higashisenda-machi, Hiroshima 730

**Shinonome Branch, Faculty of Education, Hiroshima University, Shinonome-3-chome, Hiroshima 734*

(Received December 28, 1973)

The vibrational spectra of dichloroethylmethylsilane and 2,2-dichlorobutane have been measured. The vibrational assignments of these molecules have been made in relation to the rotational isomerism. The normal vibration calculations based on the modified Urey-Bradley force field have been carried out and have confirmed for both molecules that, in the liquid state, the *trans* and *gauche* isomers coexist, while the *trans* isomer alone persists in the crystalline state.

A number of studies concerning rotational isomerism around a C–C bond as an axis have been reported.[1] Recently, the existence of the rotational isomers around a C–Si bond in the homologous series of alkylsilanes has become apparent.[2] We have taken an interest in studying the rotational isomerism in the homologous series of alkylsilanes. In this paper, we will deal with the vibrational assignments and the rotational isomerism of dichloroethylmethylsilane and its analogues, *viz.*, 2,2-dichlorobutane.

Experimental

Dichloroethylmethylsilane was prepared from methyltrichlorosilane by adding C_2H_5MgBr.[3] 2,2-Dichlorobutane was prepared by the reaction of ethyl methyl ketone with PCl_5.[4]

The infrared spectra in the 250—4000 cm^{-1} region were recorded on a Perkin-Elmer instrument(Model 621). For the measurements in the crystalline state in this region, the vapor was condensed on a CsI window cooled with liquid nitrogen; the sample was then annealed near the melting point. For the spectra of dichloroethylmethylsilane in the 30—400 cm^{-1} region, a Hitachi Fis-3 far-infrared spectrometer equipped with a cell of polyethylene windows was used. The Raman spectra of dichloroethylmethylsilane in the liquid state were recorded on a JEOL Raman spectrometer (Model JRS-02AS), using an argon-ion laser(488.0 nm) for excitation.

Rotational Isomerism

Figure 1 shows the infrared and Raman spectra of $C_2H_5SiCl_2CH_3$ in the region below 900 cm^{-1}. The $SiCl_2$ stretching vibrations can be expected in the 400—600 cm^{-1} region from a comparison of the spectra with those of $(CH_3)_2SiCl_2$.[5] In the infrared spectra, the very-strong pair band at 546 and 530 cm^{-1} and the strong pair band at 471 and 467 cm^{-1} are observed in the liquid state. In the supercooled liquid state before annealing, the absorption intensities of both the higher-frequency bands of the pairs are weaker than the lower-frequency bands, while the reverse is true in the liquid state. In the crystalline state, both the lower-frequency bands of the two pairs persist, while the disappeared bands again appear with a rise in the temperature. These results indicate that rotational isomers exist in the liquid state, while one isomer persists in the crystalline state. On the other hand, in the Raman spectra, the very-strong pair counterpart at 460 and 470 cm^{-1} and the very-weak pair counterpart at 531 and 540 cm^{-1}, corresponding to the pair bands around 470 and 540 cm^{-1} respectively in the infrared spectra, are observed in the liquid state; they are, therefore, assigned to the $SiCl_2$ symmetric and antisymmetric stretching vibrations respectively.

On the other hand, Fig. 2 shows the infrared

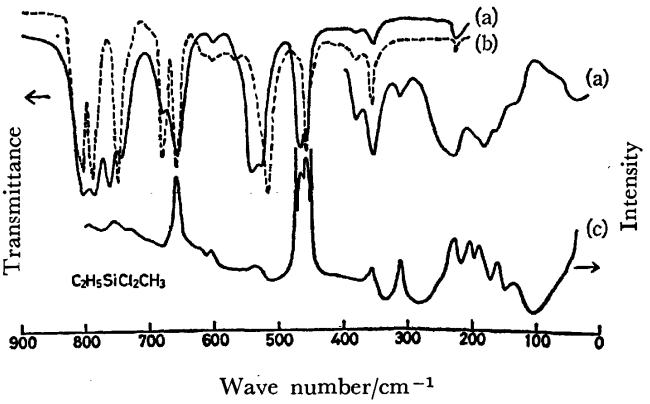

Fig. 1. The vibrational spectra of dichloroethylmethylsilane.
(a): the infrared spectra in the liquid state, (b): the infrared spectra in the crystalline state, (c): the Raman spectra in the liquid state.

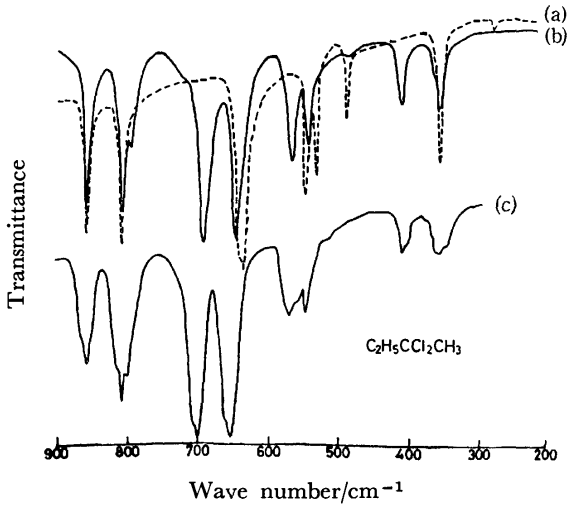

Fig. 2. The infrared spectra of 2, 2-dichlorobutane.
(a): in the crystalline state, (b): in the liquid state, (c): in the gaseous state at room temperature.

spectra of 2,2-dichlorobutane in the 250—900 cm^{-1} region. For alkyl chlorides, useful information about the rotational isomerism has been obtained from the C-Cl stretching and skeletal deformation vibrations.[1] In this molecule, the very-strong pair band at 692 and 645 cm^{-1} and the strong pair band at 567 and 544 cm^{-1} in the liquid state, clearly separated from each other, are observed; they are easily assigned to the CCl_2 antisymmetric and symmetric stretching vibrations respectively by reference to the spectra of 2,2-dichloropropane,[6] while both the higher-frequency bands of the pairs disappear in the crystalline state. In Fig. 2, the split pattern of the band at 544 cm^{-1} in the crystalline state may be due to the influence of the crystalline field because, in the supercooled liquid state before annealing, this pattern is not observed. The tendency of the CCl_2 stretching vibrations is the same as that of the $SiCl_2$ stretching vibrations. Therefore, it may be expected that, for both molecules, only one isomer with the same molecular form persists in the crystalline state, while two isomers coexist in the liquid state.

The results of the normal vibration calculations, which will be given in Tables 4 and 5, indicate that the antisymmetric and symmetric YCl_2 stretching vibrations (Y=C, Si) for the *gauche* isomer are higher in frequency than those for the *trans* isomer and that, among the skeletal deformation vibrations, the highest-frequency vibration for the *trans* isomer is higher in frequency than that for the *gauche* isomer. The conclusion regarding the molecular form obtained from the skeletal deformation vibration is consistent with that obtained from the YCl_2 stretching vibrations.

Energy Difference between Isomers. For 2,2-dichlorobutane, the relative intensities of the bands at 692 and 645 cm^{-1} assigned to the CCl_2 antisymmetric stretching vibration for the *gauche* and *trans* isomers respectively are measured in the gaseous state at ten different temperatures; in the crystalline state the former disappears, while the latter persists. Figure 3 shows some typical examples of the infrared bands at 301, 320, 343, 368, and 399 K. From the observed optical densities, the energy difference between the isomers

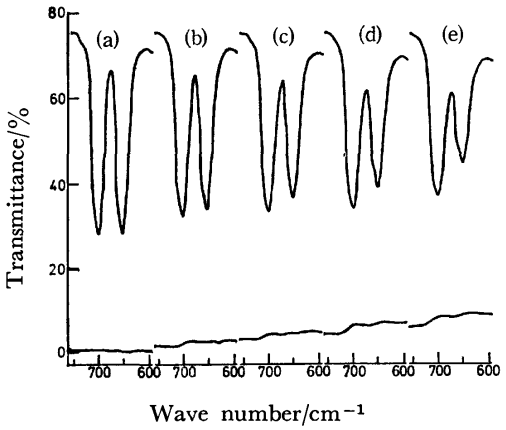

Fig. 3. The relative intensities of the infrared bands at 692 and 645 cm^{-1} in the gaseous state.
Upper: absorption spectra, Lower: base line; (a): at 301 K, (b): at 320 K, (c): at 343 K, (d): at 368 K, (e): at 399 K.

is found to be *ca.* 0.5 kcal/mol, where the *trans* isomer is more stable than the *gauche* isomer. This value is in good agreement with the value estimated by means of the interactions of the atoms in the 1,3 positions lying on parallel bonds which has been presented by Štokr *et al.*[8] However, for dichloroethylmethylsilane, measurements of the relative intensities of the bands cannot

Table 1. Vibrational frequencies of dichloroethylmethylsilane[a] (cm^{-1})

Infrared Liquid Int.	Infrared Crystal Int.	Raman Liquid Int.	Assignment
2970 s	2970 s	2975 s	C-H str.
2944 m	2944 m	2943 s	
2917 m	2917 w	2911 vvs	
2885 m	2888 s	2884 vs	
1468 sh m	1466 m		CCH_3 asym. def.
1461 m	1455 m	1462 w	
1410 m	1408 m	1406 w	$SiCH_3$ asym. def.
1401 sh m	1399 w		CH_2 sci.
1384 w	1376 w	1381 vw	CCH_3 sym. def.
	1366 vw		
1262 vs	1264 s	1261 vw	$SiCH_3$ sym. def.
1242 m	1246 m	1241 w	CH_2 wag.
1232 w	1232 w	1230 vw	CH_2 twist.
1087 b w			
1021 m	1025 m	1019 w	C-C str.
1011 s	1015 vw	1011 mw	
974 sh w	974 vw	973 w	CCH_3 rock.
965 m	959 m		
806 vs	807 vs	807 vw	$SiCH_3$ rock.
788 vs	792 vs		
767 vs	—	766 w	C-Si antisym. str.
748 s	754 vs	746 w	
	705 vw		
685 m	684 s		CH_2 rock.
662 s	663 vs	662 m	C-Si sym. str.
606 w	609 w	604 w	
	574 w		
	565 w	557 w	
543 vs	—	540 w	$SiCl_2$ antisym. str.
531 vs	518 vs	531 w	
	477 w		
470 s	—	470 vvs	$SiCl_2$ sym. str.
461 s	459 s	460 vvs	
427 vw		426 vw	
383 w	384 w	383 w	
356 m	356 m	357 mw	Skeletal def. or torsion
315 vw	—	314 m	
231 m	228 w	231 s	
		199 ms	
184 m		183 s	
167 sh w		164 ms	
138 w		134 m	
		79 mw	

a) Int.=intensity; s, m, w=strong, medium, weak; v=very; sh=shoulder; and b=broad.

Table 2. Vibrational frequencies of 2,2-dichlorobutane[a] (cm^{-1})

Infrared				Raman[b]		Assignment
Gas	Int.	Liquid	Int.	Crystal	Int.	Liquid Int.	
2996				3001	w		
2990	vs	2980	vs	2973	s	2986 4b	
2987							
2951							
2941	vs	2944	s	2936		2936 6b	C-H str.
					m		
2930		2930 sh	ms	2921			
2897 sh	w	2892	ms				
		2866	vw	2875	m		
2850 sh	w	2848	vw				
1465		1463	s	1465	s		
1460		1454	s	1453			
	s				s	1441 4b	CH_3 asym. def.
1452				1447			
1446		1443	s	1443	w		
1438				1436			
	m	1427	mw		s		CH_2 sci.
1432				1432			
1394 sh							
1389	s			1379			
					s		
1382	vs	1382	s	1376		1380 1	CH_3 sym. def.
1343	w	1342	w	1348	w		
1335	w	1332	w	1343	m	1329 0	
1287							
1280	m	1283 sh		1284			
			m		s		
1275		1279		1277		1272 1	CH_2 wag.
						1224 0	CH_2 twist.
		1185	w				
1172	m	1170	m	1174	s	1167 1	
1148 b	s	1146	s	—			
1128				1136	m		
	vs						
1123		1120	s	1122		1113 1	
					s		
				1111			
1102							
1097	vs	1091	s	—		1088 1	
1092				1087	vw		
				1075	vw		C-C str. or CH_3 rock.
1042		1042 sh					
			ms				
1037	s	1037		1034			
					s		
1030				1033		1020 1/2	
1007		1008	w	—			
998	m	999	w	998	s		
991							
982	m	982	m	—		977 1	
859							
	s	859	s	856	s	853 2	
854							
815							
809	s	808	s	808	s		CH_2 rock.
803		796	m	—		793 0	
708							
701	vs	692	vs	—		688 3	
696							CCl_2 antisym. str.
662							
656	vs	645	vs	635	vs	642 3	

Table 2. Continued

Infrared Gas Int.	Infrared Liquid Int.	Infrared Crystal Int.	Raman[b] Liquid Int.	Assignment
572, 560 m	567 m	—	566 4	CCl_2 sym. str.
548 m	544 m	545, 529 s	544 4	
	490 vw	488 m	486 0	
418, 413, 406 m	413 m	—	410 2	
375, 368, 365 m	367 sh m	—		Skeletal def. or torsion
357, 353 m	358 m	356 s	362 4	
		281 vw	276 2	
			252 2	
			202 2	

a) See a) of Table 1. b) See Ref. 18.

be made because of the overlapping of the bands assigned to the $SiCl_2$ stretching vibrations in the gaseous state.

Vibrational Assignments

The *trans* form of dichloroethylmethylsilane and 2,2-dichlorobutane may have C_s symmetry. The 36 normal modes are reduced by group theory to 21 modes of the A′ species and 15 of A″. The *gauche* form belongs to the trivial point group C_1. All of the 36 modes are of the same symmetry species. All of the fundamental vibrations of the *trans* and *gauche* forms are infrared and Raman-active. The observed frequencies are given in Tables 1 and 2, together with the brief vibrational assignments.

Dichloroethylmethylsilane. It is expected that the vibrations of the $SiCH_3$ group are considerably lower in frequency than the corresponding vibrations of the CCH_3 group because of the difference in the electronegativity of the adjacent atom. Actually, these vibrations of the CCH_3 and $SiCH_3$ groups are observed at different frequencies clearly separated from each other. The infrared spectra of dichloroethylmethylsilane in the 800—1500 cm^{-1} region are not so different in the liquid and crystalline states, and they are close to the superposition of the spectra of ethyltrichlorosilane[9] and methyltrichlorosilane.[10] The infrared spectra in the 400—800 cm^{-1} region are also similar to those of dimethyldichlorosilane.[5] Therefore, the vibrational assignments in the 400—1500 cm^{-1} region can easily be made by a comparison of the spectra with those of analogues. The bands in the region below 400 cm^{-1} may be assigned to the skeletal deformation or torsional vibrations. However, the vibrational assignments in this region cannot be made easily, for a large mode mixing among the several skeletal deformation vibrations must be expected; they are tentatively assigned in Table 4 on the basis of the results of the normal vibration calculations.

2,2-Dichlorobutane. In the infrared spectra in the 300—1500 cm^{-1} region, as too many bands for a unique molecular form are observed in the liquid state and as several bands vanish in the crystalline state, it may be concluded that rotational isomers coexist in the liquid state, while only one isomer persists in the crystalline state. The infrared spectra show that most of the vibrations of the two CH_3 groups may be coincident with each other, because the presence of one CH_3 group is sufficient to account for the number of observed bands. Therefore, the infrared spectra in the 1200—1500 cm^{-1} region can easily be assigned on the basis of a comparison of the spectra with those of analogues, such as CH_3CCl_3[11] and CH_3CH_2X.[12] The bands in the 800—1200 cm^{-1} region may be assigned to the C–C stretching or CH_3 rocking vibrations, but three C–C stretching and four CH_3 rocking vibrations are expected for a unique molecular form and may mix with each other in the same symmetry species. Therefore, the vibrational assignments in this region are made from the results of the normal vibration calculations. On the other hand, the strong infrared bands at 796 and 808 cm^{-1} and the weak Raman counterpart at 793 cm^{-1} are assigned to the CH_2 rocking vibrations. The very-strong pair band around 670 cm^{-1} and the strong pair band around 550 cm^{-1} are easily assigned to the CCl_2 stretching vibrations, as has already been mentioned. The infrared bands in the region below 500 cm^{-1} may be assigned to the skeletal deformation or torsional vibrations. These bands are assigned on the basis of the results of the normal vibration calculations, because large mixings of the modes are expected.

Normal Vibration Calculation

The normal vibrations were calculated on the basis of the modified Urey-Bradley force field in order to determine the molecular forms and the vibrational assignments. The force constants were transferred from those of $CH_3CH_2SiH_3$[13] and $(CH_3)_2SiCl_2$[5] for $C_2H_5SiCl_2CH_3$ and from those of $CH_3CHClCHClCH_3$[14]

Table 3. Force constants for dichloroethylmethylsilane and 2,2-dichlorobutane[a)]

	$C_2H_5SiCl_2CH_3$		
K(C-H)	4.297	Y(C-C)	0.109
K(C-C)	2.400	Y(C-Si)	0.052
K(C-Si)	1.991	p(C-H)	−0.070
K(Si-Cl)	2.590 (2.226)	p(Si-Cl)	(0.174)
H(C-C-H), CH_3	0.164	F(C·C·H), CH_3	0.470
H(H-C-H), CH_3	0.370	F(H·C·H), CH_3	0.200
H(C-C-Si)	0.087	F(C·C·Si)	0.540
H(Si-C-H)	0.123	F(Si·C·H)	0.271
H(C-C-H), CH_2	0.278	F(C·C·H), CH_2	0.540
H(H-C-H), CH_2	0.331	F(H·C·H), CH_2	0.200
H(C-Si-C)	0.110	F(C·Si·C)	0.040
H(C-Si-Cl)	0.085	F(C·Si·Cl)	0.162
H(Cl-Si-Cl)	0.059	F(Cl·Si·Cl)	0.290
κ(CCH_3)	0.008	κ($SiCl_2$)	0.130
κ(CH_2)	−0.040	κ($SiCH_3$)	−0.050
	$C_2H_5CCl_2CH_3$		
K(C-H)	4.350	Y(C-C)	0.109
K(C-C)	2.750	p(C-H)	−0.086
K(C-Cl)	1.697 (1.353)	p(C-Cl)	(−0.090)
H(C-C-H), CH_3	0.186	F(C·C·H), CH_3	0.470
H(H-C-H), CH_3	0.370	F(H·C·H), CH_3	0.200
H(C-C-C)	0.275	F(C·C·C)	0.335
H(C-C-H), CH_2	0.186	F(C·C·H), CH_2	0.470
H(H-C-H), CH_2	0.343	F(H·C·H), CH_2	0.200
H(C-C-Cl)	0.087	F(C·C·Cl)	0.747
H(Cl-C-Cl)	0.062	F(Cl·C·Cl)	0.697
κ(CH_2)	0.100	κ(CH_3)	0.008

a) All the force constants are transferred from ethylsilane[13)] and dimethyldichlorosilane[5)] for dichloroethylmethylsilane and from 2,3-dichlorobutane[14)] and dichloromethane[15)] for 2,2-dichlorobutane. The adjusted force constants are given in brackets. The units of the force constants are in mdyn/Å for stretching, K; bending, H; repulsion, F; and bond-interaction, p; and in mdyn·Å for intramolecular tension, k; and internal rotation, Y.

and CH_2Cl_2[15)] for $C_2H_5CCl_2CH_3$. The following assumptions were made for the force field: 1) the bond-interaction constant, p(C–H), was added in order to reproduce the observed C–H stretching frequencies, 2) the torsional force constant, Y(C–C), was assumed to be the value (3.49 kcal/mol) obtained from the reported far-infrared band for the CH_3 torsion of ethyl chloride[16)] and the Y(C–Si) constant was assumed to be the value(1.65 kcal/mol) of dimethylsilane determined by microwave study,[17)] and 3) for $C_2H_5SiCl_2CH_3$, the force constants, H(H–C–H) and F(H·C·H), were assumed to be the same values for the CCH_3 and $SiCH_3$ groups, while for $C_2H_5CCl_2CH_3$, the force constants, H(H–C–H), H(C–C–H), F(H·C·H) and F(C·C·H), were assumed to be the same values for both the CH_3 groups.

The force constants used in the calculation are given in Table 3. The vibrational frequencies in the region below 1200 cm^{-1} depend more conspicuously upon the azimuthal angle of internal rotation. Therefore, the observed and calculated frequencies in this region are given in Tables 4 and 5, together with the predominant symmetry coordinates in the potential energy distributions. Set I of the calculation in Tables 4 and 5 shows the calculations using all the transferred force constants given in Table 3. A fair agreement is obtained between the observed and calculated frequencies, except for a few vibrations. Especially, the calculated frequencies of the YCl_2 stretching (Y=C, Si) and the highest-frequency skeletal deformation vibrations indicate that, for both dichloroethylmethylsilane and 2,2-dichlorobutane, the bands persisting in the crystalline state are attributable to the *trans* form, while the bands disappearing in the crystalline state are attributable to the *gauche* form. However, as the calculated YCl_2 stretching frequencies indicate that the values of both the force constants, K(C–Cl) and K(Si–Cl), have to be smaller than the transferred values, only these constants, K(C–Cl) and K(Si–Cl), are adjusted in order to reproduce the observed frequencies. We still cannot reproduce the separations between the YCl_2 antisymmetric and symmetric stretching frequencies satisfactorily. Therefore, the bond-interaction constants, p(C–Cl) and p(Si–Cl), are introduced.

The results of the calculations obtained in this modification are given in Set II of the calculation in Tables 4 and 5. The values of the adjusted force constants are K(C–Cl)=1.353, p(C–Cl)=−0.090, K(Si–Cl)=2.226, and p(Si–Cl)=0.174 mdyn/Å. It is inter-

TABLE 4. OBSERVED AND CALCULATED FREQUENCIES OF DICHLOROETHYLMETHYLSILANE (cm^{-1})[a]

	Trans form				*Gauche* form			
	Obsd	Calcd			Obsd	Calcd		PED
		Set I	Set II			Set I	Set II	
A′	1021	1020	1020	A	1011*	1022	1022	ν(C–C)
	974	968	968		974	968	968	$r(CCH_3)$
	806	798	797		806	798	797	$r(SiCH_3)$
					767*	749	748	ν_a(C–Si), $r(CH_2)$
	748	729	729					ν_a(C–Si)
	662	682	679		662	667	663	ν_s(C–Si)
	461	471	460		470*	481	469	$\nu_s(SiCl_2)$
	356	342	342					δ(CCSi), $w(SiCl_2)$
					315*	319	316	δ(CCSi)
	231	220	220		231	234	234	δ(CCSi), $w(SiCl_2)$
					231	223	223	$w(SiCl_2)$, $r(SiCl_2)$
	184	184	184					$s(SiCl_2)$, $w(SiCl_2)$
					167	176	176	$s(SiCl_2)$, $\tau(SiCH_3)$
	138	134	134					$w(SiCl_2)$, $s(SiCl_2)$, δ(CSiC)
A″	965	967	967		965	967	967	$r(CCH_3)$
	788	796	793		788	795	792	$r(SiCH_3)$
	685	727	725					$r(CH_2)$
					685	708	707	$r(CH_2)$, ν_a(C–Si)
	531	585	531		543*	602	549	$\nu_a(SiCl_2)$
	—	241	241		—	240	240	$\tau(CCH_3)$
	231	233	232					$r(SiCl_2)$
					199	196	196	$r(SiCl_2)$, $t(SiCl_2)$
	184	188	188					$t(SiCl_2)$
					—	154	154	$\tau(SiCH_3)$, δ(CSiC), $s(SiCl_2)$
	—	152	152					$\tau(SiCH_3)$, $t(SiCl_2)$
					138	134	134	$t(SiCl_2)$
	—	56	56		79	58	58	τ(skel)

a) The observed infrared frequencies in the liquid state are listed, where asterisks indicate the bands disappearing in the crystalline state. The vibrational frequencies below 1200 cm^{-1} are included. Potential energy distributions are shown for the internal symmetry coordinates, where only contributions greater than 20% are included. ν, δ, s, w, t, r, and τ denote the stretching, deformation, scissoring, wagging, twisting, rocking, and torsional modes and a and s denote the antisymmetric and symmetric modes, respectively.

esting to note that the value of p(C–Cl) is negative, while that of p(Si–Cl) is positive. It is also noticeable that the frequency differences of the YCl_2 stretching vibrations between the antisymmetric and symmetric modes and between the *trans* and *gauche* forms for $C_2H_5SiCl_2CH_3$ are smaller than those for $C_2H_5CCl_2CH_3$. This may be because, for the nonlinear YX_2-type molecule, the off-diagonal element of the **G**-matrix between the stretching modes is $\cos\alpha\mu_y$ (μ_y is the reciprocal of the mass of the atom, Y).[7] Therefore, the separation frequency between the antisymmetric and symmetric modes of the YCl_2 stretching may be mainly affected by the mass of the atom, Y, though the quite reverse influence of the corresponding off-diagonal element of the **F**-matrix containing only the repulsive force constant, F(Cl·Y·Cl), in the simple Urey-Bradley force field($F'=-0.1F$) can be expected, and though the couplings of the YCl_2 stretching modes with the other modes are not taken into account. In order to predict well the observed YCl_2 stretching frequencies, the bond-interaction constant, p(Y–Cl), is necessary.

On the other hand, the frequency separation of the YCl_2 stretching modes between the different molecular forms may be mainly influenced by the vibrations of the adjacent groups, which, in combination with the YCl_2 stretching modes, give the off-diagonal **G**-matrix elements containing the azimuthal angle, such as the Y–C–C bending and CH_2 rocking modes for $C_2H_5YCl_2CH_3$ (Y=C, Si). The larger couplings are expected from the perturbation theory[7] when the vibrational frequencies come close to one another. The separations of the YCl_2 stretching modes with both the CH_2 rocking and Y–C–C bending modes for $C_2H_5CCl_2CH_3$ are smaller than those of $C_2H_5SiCl_2CH_3$. Therefore, it can be expected that the separations of the YCl_2 stretching vibrations between the different molecular forms for $C_2H_5CCl_2CH_3$ are larger than those for $C_2H_5SiCl_2CH_3$. This is supported by the results of the potential energy distributions of the modes, given in Tables 4 and 5.

Table 5. Observed and calculated frequencies of 2,2-dichlorobutane (cm^{-1})[a)]

	Trans form				*Gauche* form			
	Obsd	Calcd			Obsd	Calcd		PED
		Set I	Set II			Set I	Set II	
A′	1170	1156	1153	A				ν(C–C)
					1146*	1154	1150	ν(C–C), $t(CH_2)$
	1120	1112	1108					ν(C–C)
					1091*	1103	1100	ν(C–C), $r(CH_3)$, $r(CH_2)$
	1037	1048	1047		1042*	1074	1072	ν(C–C)
	999	989	989		982*	985	985	$r(CH_3)$
	859	876	874		859	873	871	$r(CH_3)$, ν(C–C)
					567*	597	568	$\nu_s(CCl_2)$, δ(CCC)
	544	576	547					$\nu_s(CCl_2)$
	490	481	479					$w(CCl_2)$, δ(CCC)
					413*	416	409	$w(CCl_2)$
					367*	377	374	δ(CCC), $w(CCl_2)$
	358	347	345					δ(CCC)
	276	265	265		252	257	257	$s(CCl_2)$
	202	190	190		202	190	190	δ(CCC), $t(CCl_2)$, $r(CCl_2)$
A″	1037	1076	1075					$r(CH_3)$, $r(CH_2)$
					1008*	1026	1021	$r(CH_3)$, ν(C–C)
	999	997	996		982*	996	995	$r(CH_3)$
	808	860	859					$r(CH_2)$, $r(CH_3)$
					796*	839	837	$r(CH_2)$, $r(CH_3)$, ν(C–C)
					692*	719	691	$\nu_a(CCl_2)$, $r(CCl_2)$, δ(CCC)
	645	665	632					$\nu_a(CCl_2)$, $r(CCl_2)$
	358	366	364					$r(CCl_2)$
					358	359	357	$r(CCl_2)$, $w(CCl_2)$
	276	302	301		276	302	302	$t(CCl_2)$
	—	240	240		—	240	240	$\tau(CH_3)$
	—	222	222		—	228	228	$\tau(CH_3)$
	—	81	81		—	86	87	τ(skel)

a) See a) of Table 4.

The authors wish to express their thanks to Professor Tatsuo Miyazawa and to the staff of his research group of Osaka University for allowing us to use their instruments and for their technical assistance. One of the authors(K. O) especially is grateful to Professor Michiro Hayashi of Hiroshima University for his helpful discussions.

References

1) For examples, S. Mizushima, "Structure of Molecules and Internal Rotation", (Academic Press Inc., New York, 1954); I. Nakagawa, C. Tanaka, and M. Tasumi, *Kagaku no Ryōiki*, **18**, 623 (1964); J. J. Shipman, V. L. Folt, and S. Krimm, *Spectrochim. Acta*, **18**, 1603 (1962).

2) S. E. Rudakova and Yu. A. Pentin, *Opt. Spectry.*, **21**, 240 (1967); M. Hayashi, K. Ohno, and H. Murata, This Bulletin, **46**, 2044 (1973).

3) R. N. Lewis, *J. Amer. Chem. Soc.*, **69**, 717 (1947).

4) A. L. Henne, M. W. Renoll, and H. M. Leicester, *ibid.*, **61**, 938 (1939).

5) K. Shimizu and H. Murata, *J. Mol. Spectrosc.*, **4**, 214 (1960).

6) P. Klaboe, *Spectrochim. Acta*, **26A**, 977 (1970).

7) E. B. Wilson, J. C. Decius, and P. C. Cross, "Molecular Vibrations," McGraw-Hill Book Company, Inc., New York, (1955).

8) J. Štokr, S. Dirlikov, B. Obereigner, and B. Schneider, *J. Mol. Structure*, **8**, 449 (1971).

9) S. E. Rudakova and Yu. A. Pentin, *Opt. Spectry.*, **18**, 339 (1957).

10) K. Shimizu and H. Murata, This Bulletin, **32**, 46 (1959).

11) K. Tanabe, S. Saëki, and M. Mizuno, Symposium on Molecular Structure, Fukuoka (1969), paper 3A2.

12) T. Shimanouchi, Tables of Molecular Vibrational Frequencies, Part I, Bulletin NSRDSNBS 6, p. 40 NBS 6, Washington, D. C. (1967).

13) K. Ohno, M. Hayashi, and H. Murata, *J. Soc. Hiroshima Univ.*, **36**, Ser A 121 (1972).

14) Y. Shiro, H. Enokido, K. Murakami, and H. Murata, *Nippon Kagaku Zasshi*, **90**, 743 (1969).

15) T. Shimanouchi and I. Suzuki, *J. Mol. Spectrosc.*, **8**, 222 (1962).

16) F. A. Miller and F. E. Kiviat, *Spectrochim. Acta*, **25A**, 1363 (1969).

17) L. Piercé, *J. Chem. Phys.*, **34**, 498 (1961).

18) L. Kahovec and K. W. F. Kaholrausch, *Z. Phys. Chem.*, **48B**, 10 (1940).

The Crystal Structure of Dichlorobis(acetoxime)palladium

Yukishige KITANO,* Kiyotomi KOBORI,* Masamitsu TANIMURA,* and Yukio KINOSHITA**

Basic Research Laboratories, Toray Industries, Inc., 1,111 Tebiro, Kamakura 248

(Received January 8, 1974)

The crystal structure of dichlorobis(acetoxime)palladium, $PdCl_2(C_3H_6NOH)_2$, has been determined from three-dimensional single-crystal X-ray photographic data. The crystals belong to the monoclinic system (space group $P2_1/a$), with two formula units in a cell with dimensions: $a=8.709\pm0.007$, $b=13.996\pm0.005$, $c=4.756\pm0.006$ Å, and $\beta=95.60\pm0.05°$. The structure was established by the heavy-atom method and was refined by the block-diagonal least-squares procedure. The Pd atoms are spaced at intervals of 4.76 Å along the c-axis and have a *trans* planar coordination, with two Cl atoms at 2.30 Å and two N atoms of the oxime groups at 2.03 Å. The oxime plane is twisted about the Pd–N bond by 72.7° from the coordination plane defined by the Pd, Cl, and N atoms. The complex molecules are hydrogen-bonded with each other in strings of an indefinite length along the c-axis, and the hydrogen-bond distance between the O atom of the oxime and the Cl atom is 3.07 Å.

As part of a systematic study of the crystal structures of the palladium-complexes, the crystal structures of the stable monoxime-palladium complexes have been investigated in order to ascertain the conformational features around the metals. In the previous papers of this series, the crystal structures of $PdCl_2(C_6H_{10}NOH)_2$[1] and $[Pd(\pi\text{-}C_3H_5)Cl]_2C_6H_{10}NOH$[2] were descrived. In this investigation the crystal of dichlorobis(acetoxime)-palladium was subjected to X-ray crystal-structure analysis in order to obtain structural information.

Experimental

Dichlorobis(acetoxime)palladium, $PdCl_2(C_3H_6NOH)_2$, was prepared by mixing palladium chloride and acetoxime[3] and was recrystallized from a tetrahydrofuran solution as a reddish yellow crystal elongated in the c direction. The unit-cell dimensions were determined from Weissenberg and precession photographs, taken about the three axes. The density was measured by flotation in an ethyl iodide-toluene mixture at 25 °C. The crystal data are summarized in Table 1.

The three-dimensional intensity data were collected from equi-inclination Weissenberg photographs taken with Ni-filtered CuKα radiation. The multiple-film technique was used, and the layers from zero to first about the a-axis and those from zero to third about the c-axis were recorded. The relative intensities, estimated visually by comparison with a calibrated intensity scale, were corrected for the usual Lorentz and polarization factors. No corrections were made for the small absorption errors. A total of 841 independent reflections was used for the structure determination.

TABLE 1. CRYSTAL DATA

Dichlorobis(acetoxime)palladium, $C_6H_{14}N_2O_2Cl_2Pd$
Molecular weight: 323.5
Monoclinic
$a=8.709\pm0.007$Å
$b=13.996\pm0.005$
$c=4.756\pm0.006$
$\beta=95.60\pm0.05°$
$V=576.8$ Å^3
$D_m=1.83$ g·cm^{-3}, $D_x=1.862$ g·cm^{-3} for $Z=2$
Systematic absences, $h0l$ with $h=2n+1$
$0k0$ with $k=2n+1$
Space group $C_{2h}^5-P2_1/a$ (No. 14)

Structure Determination

The structure was established by the heavy-atom method. Since there are two molecules in the cell of the $P2_1/a$ space group, the palladium atoms must be at the centers of symmetry. The position of the chlorine atom was readily deduced from a three-dimensional sharpened Patterson synthesis. The successive Fourier syntheses phased initially by the palladium and chlorine atoms enabled the positions of the carbon, nitrogen, and oxygen atoms of the oxime to be determined and resulted in a reduction of R to 0.258. R is defined throughout as $\Sigma||F_o|-|F_c||/\Sigma|F_o|$, where the sums are over the unique, observed non-zero reflections only. The structure thus obtained was refined by the least-squares method. Four cycles of least-squares refinement using individual isotropic temperature factors, followed by one cycle using individual anisotropic temperature factors, reduced R to 0.132. Three more cycles of refinement of the non-hydrogen atoms with anisotropic temperature factors led to a final R-index of 0.083. Throughout the refinement of the structure, equal weights were employed for all the reflections and the atomic scattering factors were adopted from the International Tables for X-ray Crystallography.[4] The main part of the calculations was performed

TABLE 2. THE ATOMIC COORDINATES OF DICHLOROBIS-(ACETOXIME)PALLADIUM, ALONG WITH ESTIMATED STANDARD DEVIATIONS IN PARENTHESES

Atom	x/a	y/b	z/c
Pd	0	0	0
Cl	0.0960(4)	0.1176(4)	−0.2705(5)
O	0.2997(11)	0.0165(12)	0.3287(13)
N	0.2201(11)	−0.0410(11)	0.1174(13)
C(1)	0.2278(17)	−0.1722(18)	−0.1906(20)
C(2)	0.2982(14)	−0.1099(16)	0.0257(16)
C(3)	0.4663(15)	−0.1263(18)	0.1463(19)

* Present address: Pioneering Research and Development Laboratories, Toray Industries, Inc., Sonoyama, Otsu, 520.

** Present address: Ehime Laboratories, Toray Industries, Inc., Masaki, Ehime.

TABLE 3. ANISOTROPIC THERMAL PARAMETERS IN THE FORM OF
$\exp[-(B_{11}h^2+B_{22}k^2+B_{33}l^2+B_{12}hk+B_{13}hl+B_{23}kl)]$
Each value is multiplied by 10^4 and the estimated standard deviations are shown in parentheses.

Atom	B_{11}	B_{22}	B_{33}	B_{12}	B_{13}	B_{23}
Pd	69(2)	43(0)	420(9)	6(2)	15(6)	−23(5)
Cl	106(5)	48(2)	542(26)	−6(6)	54(17)	−2(12)
O	125(17)	60(7)	732(85)	−2(18)	12(59)	−84(39)
N	87(16)	44(6)	421(76)	−2(17)	−32(55)	19(35)
C(1)	140(27)	62(11)	660(86)	76(28)	−109(89)	−90(59)
C(2)	94(20)	60(10)	396(94)	18(23)	141(67)	66(47)
C(3)	86(22)	71(11)	688(86)	26(25)	12(80)	25(60)

on IBM 7090 and 360 computers using the ERFR 2 program for Fourier synthesis[5] and the HBLS IV program for the structure-factor and least-squares-refinement calculations.[6] The positional and anisotropic thermal parameters, along with their estimated standard deviations, are listed in Tables 2 and 3 respectively. The tables of the final observed and calculated structure factors are preserved by the Chemical Society of Japan (Document No. 7424).

Results and Discussion

The principal interatomic bond lengths and angles, along with their estimated standard deviations, are listed in Table 4. A perspective view of the molecule,

TABLE 4. INTERATOMIC DISTANCES AND ANGLES ALONG WITH THEIR ESTIMATED STANDARD DEVIATIONS IN PARENTHESES

Atoms	Distance	Atoms	Angle
Pd-Cl	2.30(2) Å	Cl-Pd-N	88.3(0.5)°
Pd-N	2.03(2)	Pd-N-O	114.8(0.5)
N-O	1.41(3)	Pd-N-C(2)	129.8(0.5)
N-C(2)	1.28(3)	O-N-C(2)	115.5(0.5)
C(1)-C(2)	1.44(3)	N-C(2)-C(1)	119.8(0.5)
C(2)-C(3)	1.53(3)	N-C(2)-C(3)	120.3(0.5)
		C(1)-C(2)-C(3)	120.1(0.5)

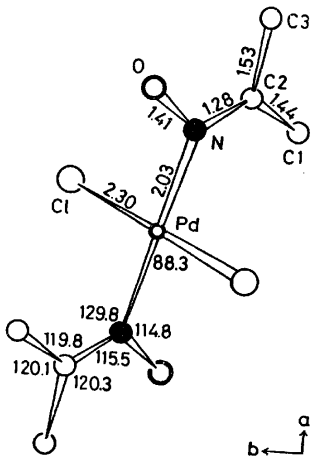

Fig. 1. A perspective view of the molecule along the c-axis.

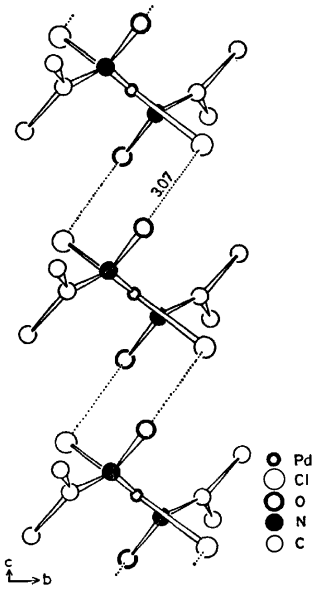

Fig. 2. The molecular arrangement viewed down the a-axis. The hydrogen bonds are shown by dotted lines.

with the numbering of atoms, as viewed along the c-axis is shown in Fig. 1. Figure 2 represents the mode of hydrogen bonding and the molecular arrangement viewed down the a-axis.

The crystal structure of dichlorobis(acetoxime)palladium closely resembles that of dichlorobis(cyclohexanone oxime) palladium.[1] The palladium atoms at the centers of symmetry are spaced at intervals of 4.75 Å along the c-axis and are coordinated in a square-planar configuration by two chlorine atoms and two nitrogen atoms of the oximes, the Pd–Cl and Pd–N distances being 2.30 and 2.03 Å respectively. As Fig. 2 shows, the complexes are hydrogen-bonded with each other in strings of an indefinite length along the *c*-axis; the distance between the oxygen atoms of the oxime groups and the chlorine atoms is 3.07 Å. The bond distances and angles in this complex are compared with the corresponding ones in $PdCl_2$-$(C_6H_{10}NOH)_2$[1] and $[Pd(\pi\text{-}C_3H_5)Cl]_2C_6H_{10}NOH$[2] in Table 5. The Pd-Cl bond length of 2.30 Å is longer than the value of 2.24 Å in $PdCl_2(C_6H_{10}NOH)_2$, but is in good agreement with those found in $(PdCl_2)_n$ (2.31 Å),[7] $C_7H_8PdCl_2$ (2.31 Å),[8] and $[(C_6H_5CN)$-$PdCl_2]_2$ (2.35 Å).[9] The Pd–N bond length of 2.03 Å

Table 5. Comparison of the selected interatomic bond distances and angle in some palladium-oxime complexes

Atom	$PdCl_2(C_3H_6NOH)_2$[a]	$PdCl_2(C_6H_{10}NOH)_2$[1]	$[Pd(\pi\text{-}C_3H_5)Cl]_2\cdot C_6H_{10}NOH$[2]
Pd-Cl	2.30 Å	2.24 Å	2.41—2.45 Å
Pd-N	2.03	2.08	2.10
N-O	1.41	1.42	1.39
N-C	1.28	1.29	1.28
Cl-O	3.07[b]	2.93[b]	3.03[c]
Cl-Pd-N	88.3°	86°	92.1°

a) Present work. b) Intermolecular hydrogen bond. c) Intramolecular hydrogen bond.

is a little shorter than the lengths in $PdCl_2(C_6H_{10}NOH)_2$ and $[Pd(\pi\text{-}C_3H_5)Cl]_2C_6H_{10}NOH$. It, however, agrees well with the values of 2.031 Å in bis-(*N*-isopropyl-3-ethylsalicylaldiminato) palladium,[10] 2.032 Å in the tetragonal form of bis-(*N*-isopropyl-3-methylsalicylaldiminato)palladium,[11] and 2.032 and 2.043 Å in bis(ethylenediamine)palladium(II) chloride.[12]

The C-C bond lengths in the oxime group of 1.44 and 1.53 Å found here are not greatly different from the corresponding values for the other oximes[13] which lie between 1.44 and 1.56 Å. The C–N bond distance of 1.28 Å suggests its double-bond character and is comparable to similar distances in acetoxime and other oximes.[14] Although the present value of 1.41 Å for the N-O bond length appears to be somewhat shorter than the values obtained for acetoxime, it is probably not unwarranted when it is compared with the values of 1.41 Å in formamidoxime,[15] 1.42 Å in $PdCl_2(C_6H_{10}NOH)_2$, and 1.39 Å in $[Pd(\pi\text{-}C_3H_5)Cl]_2C_6H_{10}NOH$.

The palladium coordination plane, as defined by the Pd, Cl, and N atoms, is expressed by the equation:[16]

$$0.048\,X + 0.805\,Y + 0.998\,Z = 0$$

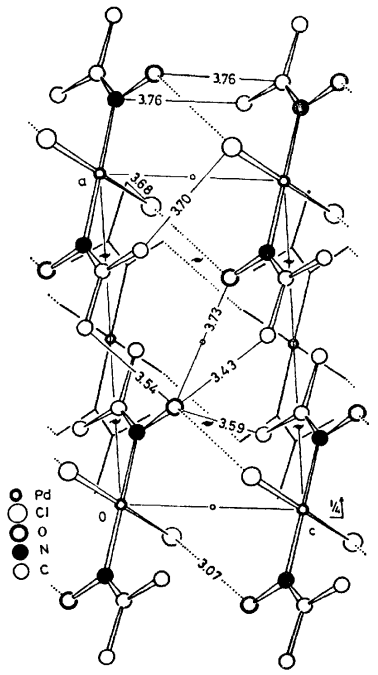

Fig. 3. The crystal structure projected along the b-axis. The intermolecular atomic contacts less than 3.8 Å are shown by solid lines and the hydrogen bonds are shown by dotted lines.

The equation for the best-plane containing O, N, C(1), C(2), and C(3) atoms is:

$$-0.389\,X - 0.748\,Y + 0.920\,Z = 0.024.$$

The deviations of the five atoms from this plane are within 0.01 Å. The chlorine atom at the $(x, y, c+z)$ position, which is connected by a hydrogen bond with the oxygen atom of the oxime, is separated from this plane by 1.54 Å. The dihedral angle between the oxime plane and the palladium coordination plane is 72.7°, which is comparable to the corresponding value of 81.0° between the palladium square-planar plane and the best-plane of the O–N–C$\langle^{C}_{C}$ fragment of the cyclohexanone oxime in $PdCl_2(C_6H_{10}NOH)_2$.

Figure 3 shows the molecular packing projected along the b-axis. The intermolecular atomic contacts less than 3.8 Å are shown by solid lines. The hydrogen bonds are also shown by dotted lines. None of the atoms is significantly shorter than the normal van der Waals contact.

The authors are grateful to Dr. Masaji Ohno for his kindness of supplying the compound.

References

1) M. Tanimura, T. Mizushima, and Y. Kinoshita, This Bulletin, **40**, 2777 (1967).
2) Y. Kitano, T. Kajimoto, M. Kashiwagi, and Y. Kinoshita, *J. Organometal. Chem.*, **33**, 123 (1971).
3) Toray Industries, Inc., Japanese Pat. 41–5445 (1966).
4) "International Tables for X-ray Crystallography," Vol. III, Kynoch Press, Birmingham, (1962).
5) W. G. Sly, D. P. Shoemaker, and J. H. Van den Hende, "ERFR 2, Two and Three-Dimensional Crystallographic Fourie Summation Program," 1962.
6) Y. Okaya and T. Ashida, "HBLS IV, The Universal Crystallographic Computation Program System (I)," The Crystallographic Society of Japan, Tokyo (1967), p. 65.
7) A. F. Wells, *Z. Krist.*, **100**, 189 (1939).
8) N. C. Baezinger, J. R. Doyle, and C. Carpenter, *Acta Crystallogr.*, **14**, 304 (1961).
9) J. R. Holden and N. C. Baezinger, *ibid.*, **9**, 194 (1956).
10) R. L. Braun and E. C. Lingafelter, *ibid.*, **22**, 787 (1967).
11) P. C. Jain and E. C. Lingafelter, *ibid.*, **23**, 127 (1967).
12) J. R. Wiesner and E. C. Lingafelter, *Inorg. Chem.*, **5**, 1770 (1966).
13) W. C. Hamilton, *Acta Crystallogr.*, **14**, 95 (1961).
14) T. K. Bierlein and E. C. Lingafelter, *ibid.*, **4**, 450 (1951).
15) D. Hall and F. J. Llewellyn, *ibid.*, **9**, 108 (1956).
16) The equation of the best-plane refers to an orthogonal coordinate system in which *X*, *Y*, and *Z* in Å are parallel to a, b, and c*, respectively.

The Effect of Organic Additives on the Micelle Formation of Dodecylammonium Halides in Aqueous Solutions

Shigeyoshi MIYAGISHI

Department of Industrial Chemistry, Faculty of Technology, Kanazawa University, Kodatsuno, Kanazawa 920

(Received January 14, 1974)

The critical micelle concentration (CMC) of dodecyl ammonium halides and the degree of dissociation of the micelle (α) of dodecylammonium chloride were determined as functions of the concentrations of the organic additives by measuring the conductivity and the emf of the following cell: calomel/1 M-KCl/sample solution/AgCl, Ag. The CMC was raised more in the presence of acetone and dioxane than in that of acetamide, formamide, urea, and methanol, and was diminished by adding alcohols (C_2—C_4). The effect of the alcohols on CMC decreased in the order of the diminished hydration of the counterion, acetone and dioxane were considered to affect the dodecylammonium iodide solution specifically. The dissociation of the micelle was enhanced in the presence of organic additives. Further, we estimated the solubilized amount of the additives from the degree of dissociation of the micelle and attempted to make quantitative estimation of the increment of CMC produced by organic additives.

The micelle formation in an aqueous solution is known to be affected by organic additives, and there have been many investigations concerning the effects of organic additives on the CMC of anionic[1-4] and cationic[1,5,6] surfactants. Shinoda[7] and Shirahama and Kashiwabe[8] explained the decrease in the CMC in the micellar solutions containing alcohols in terms of the solubilization of alcohol into the micelle. On the other hand, some organic additives gave an increment in CMC, and this cannot be explained by their theories. Emerson and Holtzer[1] found qualitative correlations between the hydrophobic nature of an additive and its micellar breaking-up power, but the correlations are limited.

It is well known that the micellar solutions are influenced by changing the counterion. Schick[2] studied the effect of counterion hydration on the CMC and found that the increment in CMC on urea addition increased in the following order: lithium-, sodium- and tetramethyl ammonium dodecylsulfate. He interpreted this order in terms of the structural concept of water.

At present, however, we have not yet obtained enough knowledge to understand the effects of organic additives on the CMC. Therefore, we attempted to study the effects of aprotic and protonic additives on the micellar solutions of dodecylammonium halides by determining their CMC and the degree of dissociation of their micelles, and tried to estimate the solubilized amount from the degree of dissociation.

Experimental

The dodecylammonium chloride (DACl), -bromide (DABr), and -iodide (DAI) were prepared by the neutralization of dodecylamine (bp 100 °C/5 mmHg) with the corresponding hydrohalic acid and were recrystallized five times from ethanol–ether. The organic additives were distilled before use, but urea and acetamide were of a reagent grade and were used without further purification.

The CMC (C) was determined by the electric-conductivity method. The determination of the activity (a) of the counterion was carried out by using the following cell:

$$\mathrm{Hg,\ Hg_2Cl_2\,|\,1\ M\text{-}KCl\,|\,DACl\ soln.\,|\,AgCl,\ Ag}$$

The degree of dissociation of the micelle (α) was then calculated by using Botré *et al.*'s equation:[9]

$$a = \gamma\{C+\alpha(C_t-C)\} \tag{1}$$

where C_t is the concentration of the surfactant. The Silver-silver chloride electrode prepared by the dry method[10] was calibrated by potassium-chloride solution; its activity coefficient, γ, was estimated by means of this equation:[11]

$$\log\gamma = -\frac{A_0\sqrt{C_1}}{1+B_0\sqrt{C_1}} - D_0C_1 \tag{2}$$

where C_1 is the concentration of potassium chloride, and where A_0, B_0, and D_0 are constants.

These experiments were carried out at 35.0 °C because of the low solubility of DABr at 25.0 °C.

Results and Discussion

The Effect of Alcohol on Micelle Formation. The addition of alcohols to the micellar solution is well known to depress the CMC; however, little attention has been paid to the importance of the counterion with respect to the effects of organic additives. The effects of changing the counterion was studied as one of the primary subjects of this investigation. As illustrated in Figs. 1 and 2, the CMC of dodecylammonium halides

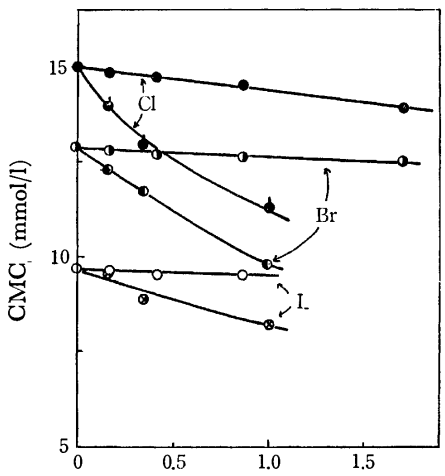

Fig. 1. Effect of ethanol and *n*-propanol on CMC.
●, ◑, ○: ethanol, ⬮, ◐, ⊗: *n*-propanol

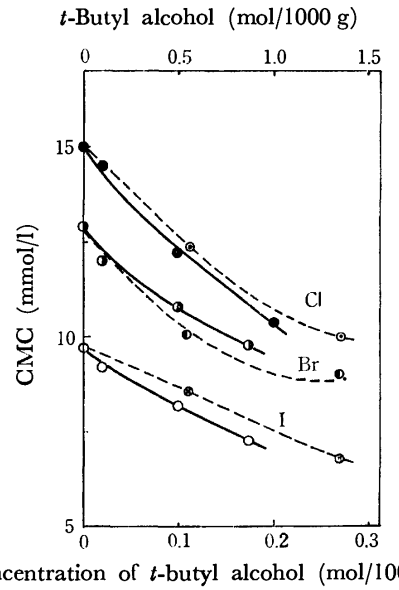

Fig. 2. Effect of butanols on CMC.
——; *t*-butyl alcohol, - - - -: *n*-butanol.

and the effects of alcohols on it decreased in the order of the diminished hydration of the counterion. This order is in line with that of the degree of dissociation of the halide micelles and the salting-out power of the halide anions.[12,13] On the other hand, the depression of the CMC is related to the free energy of the transfer of an alcohol molecule from the water to the micelle phase.[8]

Therefore, the above results suggest that the counterion affects its free energy through the destruction of the water structure around the alcohol molecule and the looseness of the surface charge on a micelle, although the main factor in the depression of the CMC is the carbon number in the alcohol molecule.

The organic additive, in addition to its solubilization effect, modifies the properties of the medium. Figure 3 indicates that the latter effect predominated in the presence of methanol and was influenced almost not at all by changing the counterion.

The Effects of Urea, Formamide, and Acetamide on Micelle Formation. The effect of amide on the CMC has been determined as a function of the amide concentration. The CMC increased with an increase in the

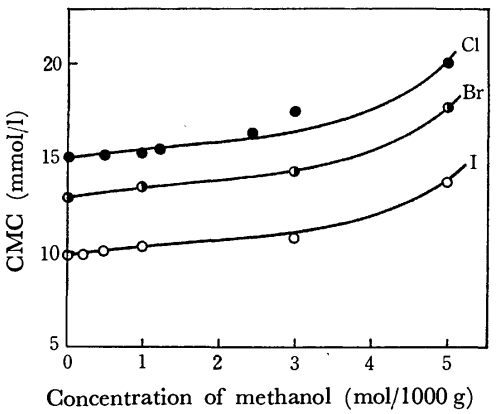

Fig. 3. Effect of methanol on CMC.

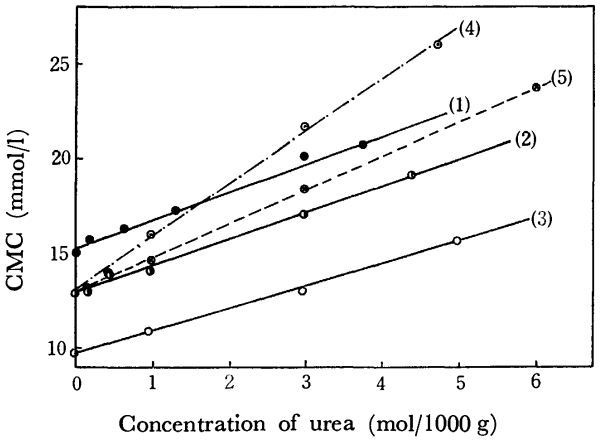

Fig. 4. Effect of amides on CMC.
(1): DACl——urea, (2): DABr——urca, (3): DAI ——urea, (4): DABr——acetamide, (5): DABr—— formamide.

urea concentration, and no significant difference in susceptibility to change in the CMC on urea addition was observed at 35.0 °C among the dodecylammonium halides (Fig. 4). It has been reported by Schick, however, that the increment in the CMC of dodecylsulfates at 10—45 °C on urea addition increased in the order of the diminished hydration of the counterion.[2] This may be attributable to the weaker hydration of halide anions compared with that of alkali cations.

On the other hand, the order of effectiveness in breaking up the micelle was: acetamide>formamide> urea. Urea raises the dielectric constant of water,[14] acetamide lowers it,[14] and formamide may raise it because of its high dielectric constant. Acetamide, furthermore, has a stronger hydrophobic character. The lowering of the dielectric constant and the hydrophobic character are considered to break up the micelle through an increment in the electrostatic repulsion on the micelle surface and a reduction of the interfacial energy between the hydrocarbon chain of single ions and water. Therefore, the above result may be attributable to these two effects. In all the micellar solutions containing alcohols except for methanol, however, the solubilization effect is more significant than these effects.

The Effect of Acetone and Dioxane on Micelle Formation. The alcohols and amides described above were protonic additives; the effects of aprotic solvent—acetone and dioxane—were also studied.

As is shown in Figs. 5 and 6, the addition of acetone or dioxane into the dodecylammonium halide solutions resulted in the increment of CMC, the effect of this on the DAI solution was different, however. In the presence of dioxane, the DAI solution became yellowish and precipitation resulted from the addition of many dioxane. It is known that a complex results from the interaction between acetone and the iodine ion.[15] Accordingly, the addition of the aprotic solvents is considered to affect the DAI solution specifically.

In summary, the CMC of dodecylammonium halide was raised more in the presence of aprotic solvents

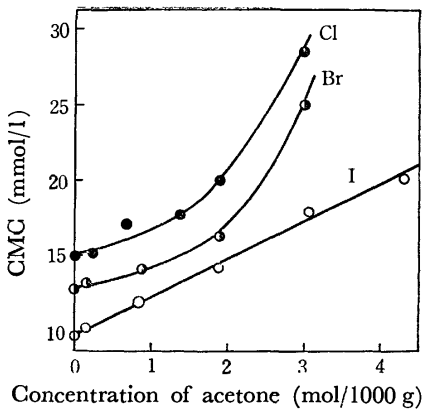

Fig. 5. Effect of acetone on CMC.

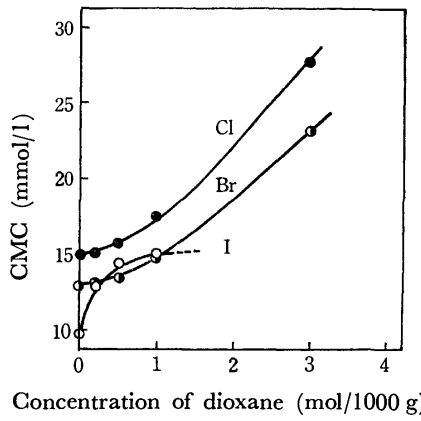

Fig. 6. Effect of dioxane on CMC.

than in that of amides and was depressed by the addition of alcohols; a change in the counterion was more effective on the reduction of the CMC than on its increment.

The Influence of Organic Additives on the Degree of Dissociation of Micelle. The dissociation of an electrolyte is depressed by adding salts or by lowering the dielectric constant of the medium; that of a micelle is also depressed by added salts. Therefore, a micelle may be expected to be less dissociative in the presence of an organic additive with a low dielectric constant. Figure 7, however, shows the opposite results. A sodium tetradecyl sulfate (STS) solution containing dioxane[16] and sodium dodecylsulfate (SDS) and dodecyltrimethylammonium bromide in a 3 M urea solution[17] also gave the same results.

Stern[18] derived the following equation concerning adsorption on the double layer;

$$\frac{n}{N-n} = \frac{AM}{1000} C_i \exp(-\Delta G/kT) \tag{3}$$

where n and N are number of adsorbed molecules on the surface and its maximum number, A is a constant, M is the molecular weight of the solvent, C_i is the concentration of the adsorbate, and ΔG is the free energy of transfer from a bulk solution to the surface.

If a micelle consists of N monomers and N' organic additives and n counterions, n/N may be equal to $1-\alpha$, and when the micelle is large, Stern's equation can be applied to its surface. Thus, we obtain:

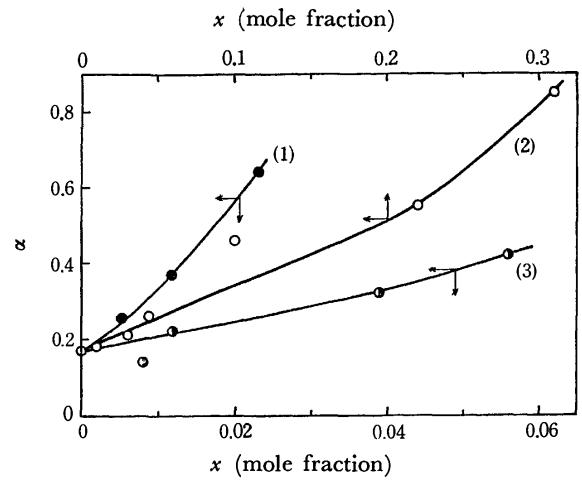

Fig. 7. Effect of organic additives on α in DACl solutions.
1): n-propanol, 2): methanol, 3): acetone.

$$\frac{1-\alpha}{\alpha} = \frac{AM}{1000} C_i \exp(-\Delta G/kT) \tag{4}$$

As ΔG consists of the electrostatic energy, $\Delta G_{\text{elec.}}$, and the chemical energy, $\Delta G_{\text{chem.}}$, Equation (4) becomes:

$$\frac{\alpha}{1-\alpha} = \frac{1000}{AMC_i} \exp(\Delta G_{\text{elec.}} + \Delta G_{\text{chem.}}) \tag{5}$$

The electrostatic energy is given by:

$$\Delta G_{\text{elec.}} = -kT \ln \frac{2000\pi\sigma^2}{DNkTC_i} \tag{6}$$

$$\sigma = x_s \sigma_1 \tag{7}$$

where σ_1 and σ are the charge densities of the micelle containing no and $1-x_s$ organic additives, x_s is the mole fraction of the surfactant in the micelle, and D is the dielectric constant of the solvent. Further, we assume the following two equations;

$$M = M_1(1-x) + xM_2 \tag{8}$$

$$\Delta G_{\text{chem.}} \approx \Delta G_{\text{sol.}} = -\Delta G_2 x - \Delta G_1(1-x) \tag{9}$$

where $\Delta G_{\text{sol.}}$ is the desolvation energy, ΔG_1 and ΔG_2 are solvation energies of water and the organic additive respectively, and x is the mole fraction of the organic additive. Equation (5) can then be rewritten as:

$$\ln \frac{\alpha}{1-\alpha} = \ln \frac{1000}{AM_1C_i} - \ln\left\{1+\left(\frac{M_2}{M_1}-1\right)x\right\} - \ln \frac{2000\pi\sigma_1^2}{D_1NkTC_i} - 2\ln x_s + \ln \frac{D}{D_1} - \frac{\Delta G_1}{kT} + \frac{\Delta G_1 - \Delta G_2}{kT} x \tag{10-a}$$

When the micellar solution does not contain the organic additive, (10-a) becomes (10-b):

$$\ln \frac{\alpha_1}{1-\alpha_1} = \ln \frac{1000}{AM_1C_i} - \ln \frac{2000\pi\sigma_1^2}{D_1NkTC_i} - \frac{\Delta G_1}{kT} \tag{10-b}$$

From (10-a) and (10-b), we obtain:

$$\ln \frac{\alpha}{1-\alpha} = \ln \frac{\alpha_1}{1-\alpha_1} - \ln\left\{1+\left(\frac{M_2}{M_1}-1\right)x\right\} - 2\ln x_s + \ln \frac{D}{D_1} + \frac{\Delta G_1 - \Delta G_2}{kT} x \tag{10}$$

Accordingly, by measuring α and α_1, we can calculate the solubilized amount of the organic additive, x_m

$(=1-x_s)$. The amount of the organic additive in the micelle phase was less than 5% of its amount in the bulk phase; therefore, the value of x was regarded as the total of the added amount. For the values of $(\Delta G_1-\Delta G_2)/kT$, those of hydrochloric acid or sodium hydroxide[19] were used as an expedient; that is, 4.65, 6.28, 7.19, and 14.8 were used for the systems of DACl-methanol, -propanol, -acetone, and STS-dioxane respectively.

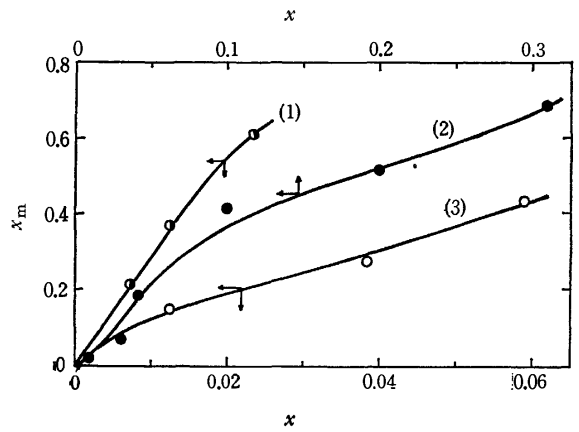

Fig. 8. Solubilization of organic additives in DACl solutions.
1): *n*-propanol 2): methanol, 3): acetone.

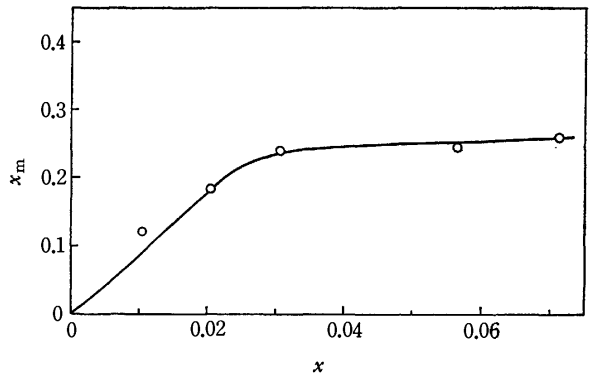

Fig. 9. Solubilization of dioxane in sodium tetradecyl-sulfate solution*.
*; x_m was calculated from α in Ref 14.

As is shown in Figs. 8 and 9, x_m increases with the concentration of the additives and attains a large value in high concentrations. The large value of the solubilized amount can be explained by considering that the large micelle to which Equation (1) can be applied does not exist in high concentrations of the additive. The aggregate, however, changes continuously from the micelle to the oligomer with the concentration of the additive; therefore, it is difficult to divide the micelles into two regions, so we call them all "micelles". According to Uehara *et al.*, however, the CMC and the aggregation number of SDS could be determined in high methanol concentrations.[4]

The Dependence of the CMC on the Concentration of Organic Additives. We attempted to estimate the dependence of the CMC on the additive concentration from the degree of dissociation of a micelle.

In a micellar solution the chemical potential of the surfactant ion in the bulk solution is equal to that in the micelle phase. Therefore,

$$\mu_b^\circ + kT\ln Cf = \mu_m^\circ + kT\ln x_s f_s + e\phi \tag{11}$$

$$e\phi = kT\ln\frac{2000\pi\sigma^2}{DNkTC_1} \tag{12}$$

where μ_b° and μ_m° are the standard chemical potentials of the surfactant ion in the bulk solution and in the micelle phase respectively, f and f_s are the activity coefficients of the surfactant ions in the bulk solution and in the micelle phase respectively, and $e\phi$ is the electrostatic work. In the absence of added salt, C_1 is equal to C; therefore, from Eqs. (7), (11), and (12) we obtain

$$2\ln Cf = \frac{\mu_m^\circ-\mu_b^\circ}{kT} + \ln\frac{2000\pi\sigma_1^2x_s^2}{DNkT} + \ln x_s + \ln f_s \tag{13-a}$$

When the micellar solutions do not contain organic additives, (13-a) becomes:

$$2\ln C_1f_1 = \frac{\mu_m^\circ-\mu_b^\circ}{kT} + \ln\frac{2000\pi\sigma_1^2}{D_1NkT} \tag{13-b}$$

Therefore, we obtain:

$$2\ln C/C_1 + 2\ln f/f_1 = 3\ln x_s - \ln D/D_1 + \ln f_s \tag{13}$$

If the following equation is assumed as a first approximation:

$$\ln f_s - 2\ln f/f_1 = k_1x \tag{14}$$

where k_1 is a constant, we obtain:

$$2\ln C/C_1 = 3\ln x_s - \ln D/D_1 + k_1x \tag{15}$$

As the x_s value is obtained from Eq. (10), Equation (15) finally becomes:

$$\ln\frac{C}{C_1} = \frac{3}{4}\left[\ln\frac{\alpha_1}{1-\alpha_1} - \ln\frac{\alpha}{1-\alpha} - \ln\left\{1+\left(\frac{M_2}{M_1}-1\right)x\right\} + \frac{\Delta G_1-\Delta G_2}{kT}x\right] + \frac{1}{4}\ln\frac{D}{D_1} + \frac{1}{2}k_1x \tag{16}$$

Here, k_1 was taken as fitting with the experimental values. Figures 10 and 11 show the comparison between the theoretical and the experimental values. It is seen that the agreement between the experimental

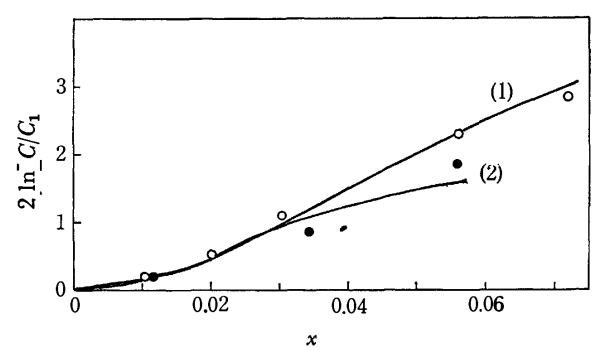

Fig. 10. Comparison of $2\ln(C/C_1)$ values with the calculated values.
(1) Sodium tetradecyl sulfate—dioxane, $k_1=52.3$, (2): DACl—acetone, $k_1=54$. The solid lines are the calculated values.

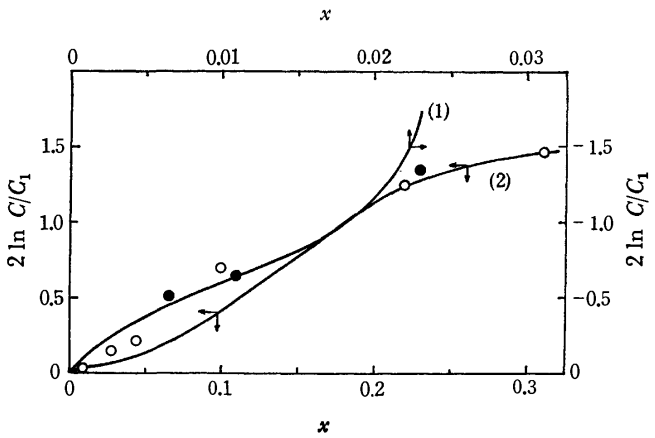

Fig. 11. Comparison of $2 \ln (C/C_1)$ values with the calculated values in DACl solutions.
1) *n*-propanol, k_1=59, 2) methanol, k_1=15.2 The solid lines are the calculated values.

and theoretical curves is rather good in spite of some approximations.

The author wishes to thank Professor Ryohei Matuura of Kyushu University and Assistant Professor Moire Nishida of Kanazawa University for their helpful discussions and advice.

References

1) M. F. Emerson and A. Holtzer, *J. Phys. Chem.*, **71**, 3320 (1967).
2) M. J. Schick, *ibid.*, **68**, 3585 (1964).
3) K. Shirahama and R. Matuura, This Bulletin, **38**, 373 (1965).
4) H. Uehara, M. Manabe, and R. Matuura, *Mem. Fac. Sci., Kyushu Univ.*, **C**, **8**, 55 (1972).
5) S. H. Herzfeld, M. L. Corrin, and W. D. Harkins, *J. Phys. Colloid Chem.*, **54**, 271 (1950).
6) P. Mukerjee and A. Ray, *J. Phys. Chem.*, **67**, 190 (1963).
7) K. Shinoda, This Bulletin, **26**, 101 (1953).
8) K. Shirahama and T. Kashiwabara, *J. Colloid Interface Sci.*, **36**, 65 (1971).
9) C. Botré, V. L. Crescenz, and A. Mele, *J. Phys. Chem.*, **63**, 650 (1959).
10) I. Oiwa, *Sci. Rep. Tohoku Univ.*, **37**, 34 (1953).
11) R. A. Robinson and R. H. Stokes, "Electrolyte Solutions," 2nd Ed. Revised, Butterworths, London (1971), p. 231.
12) T. Ingram and M. N. Johns, *Trans. Faraday Soc.*, **65**, 297 (1969).
13) M. Shirai and B. Tamamushi, This Bulletin, **30**, 411 (1957).
14) J. Wyman, *Chem. Rev.*, **19**, 213 (1936).
15) S. Asahara, M. Seno, and K. Arai, "Yobai Koka," Sangyo Tosho, Tokyo (1970), p. 68.
16) I. Satake and G. Sugihara, *Mem. Fac. Sci., Kyushu Univ., C*, **7**, 27 (1970).
17) J. Piercy, M. N. Jones, and G. Ibbotson, *J. Colloid Interface Sci.*, **37**, 165 (1971).
18) O. Stern, *Z. Electrochem.*, **30**, 508 (1924).
19) J. Padova, *J. Phys. Chem.*, **72**, 796 (1968).

A Study of the Inosine–Hydrochloric Acid–Water and Inosine–Sulfuric Acid–Water Systems

Yoshihisa SUZUKI and Tadao TOKI

Central Research Laboratories, Ajinomoto Co., Inc., Suzuki-cho, Kawasaki 210

(Received April 1, 1974)

Solubility data have been obtained for the inosine-HCl-H_2O and inosine-H_2SO_4-H_2O systems at 5 °C. The acid hydrolysis of inosine was satisfactorily prevented under the present conditions. Three new acid salts of inosine have been obtained: (1) $C_{10}H_{12}N_4O_5 \cdot HCl \cdot (1/2)H_2O$ in the A-form, (2) $C_{10}H_{12}N_4O_5 \cdot HCl \cdot (1/2)H_2O$ in the B-form, and (3) $C_{10}H_{12}N_4O_5 \cdot H_2SO_4 \cdot 2H_2O$. Their X-ray powder diffraction data are given. All of them are incongruent and decomposed by pure water; however, they are stable in air during storage at room temperature.

In order to contribute to the process design of the separation or purification of inosine, its solubility in several mineral acid solutions was studied. Inosine is known to be susceptible to acid hydrolysis, giving hypoxanthine and D-ribose. However, the hydrolysis was practically negligible at 5 °C within certain periods. The equilibria for the inosine-HCl–H_2O and inosine–H_2SO_4-H_2O systems were satisfactorily determined. No data have been found in the literature concerning the subject of the present study.

Results and Discussion

Table 1 shows the composition data for the inosine–hydrochloric acid-water system at 5 °C. The equilibrium was achieved by the dissolution of the crystals to acid solutions. The mixture was usually shaken overnight at 5 °C. These conditions were generally sufficient to achieve the equilibrium. However, there was a fear of the hydrolysis of inosine in high concentrations of hydrochloric acid, so the shaking period for the equilibrium was shortened to 5 hr when the concentration of hydrochloric acid was higher than 16% (Runs No. 9—11). In spite of the above treatment, we could not completely prevent the hydrolysis in high concentrations of hydrochloric acid. The data obtained in these runs had some deviations (within 10%). On the other hand, there was no significant hydrolysis when the concentration of hydrochloric acid was less than about 10%.

TABLE 1. COMPOSITION DATA FOR THE INOSINE–HYDROCHLORIC ACID–WATER SYSTEM AT 5 °C

Run No.	Solution (Weight %)			Wet residue (Weight %)		Solid phase[a]
	Inosine	HCl	Hx[b]	Inosine	HCl	
lit.[c]	0.76	0	–	—	—	I2
1	4.50	1.77	–	63.18	0.54	I2
2	6.82	2.67	–	62.50	0.82	I2
3	13.76	4.06	–	72.80	6.44	I2+A
4	13.35	4.11	–	70.61	4.77	I2+A
5	13.86	4.03	–	44.73	4.74	I2+A
6	6.40	7.72	–	58.39	10.51	A
7	4.44	13.15	+	55.68	11.72	A
8	4.24	15.28	+	56.26	11.07	A
9	4.03	16.42	0.2	59.80	12.79	A+B
10	4.03	17.48	0.2	53.60	11.40	A+B
11	4.65	19.71	0.3	56.66	13.01	B

a) I2: Inosine di-hydrate, $C_{10}H_{12}N_4O_5 \cdot 2H_2O$. A: Inosine hydrochloride in the A-form, $C_{10}H_{12}N_4O_5 \cdot HCl \cdot (1/2)H_2O$. B: Inosine hydrochloride in the B-form, $C_{10}H_{12}N_4O_5 \cdot HCl \cdot (1/2)H_2O$. b) Hx.: Hypoxanthine. c) Y. Suzuki, This Bulletin, **47**, 2549 (1974).

The system shows the formation of two new solid phases which possess the same molecular formula, but different crystal structures. They are both inosine monohydrochloride hemihydrate. The one stable in lower concentrations of hydrochloric acid was named the A-form, and the other, stable in higher concentrations, the B-form. Their X-ray powder diffraction data are shown in Table 2.

TABLE 2. X-RAY POWDER DIFFRACTION DATA OF SOME MINERAL ACID SALTS OF INOSINE

$C_{10}H_{12}N_4O_5 \cdot HCl \cdot (1/2)H_2O$ A-Form		$C_{10}H_{12}N_4O_5 \cdot HCl \cdot (1/2)H_2O$ B-Form		$C_{10}H_{12}N_4O_5 \cdot H_2SO_4 \cdot 2H_2O$	
d(Å)	I/I_0[a]	d(Å)	I/I_0[a]	d(Å)	I/I_0[a]
8.30	40	8.01	100	8.54	100
6.19	15	6.11	5	6.11	10
5.40	20	5.64	5	5.13	25
4.84	5	5.25	10	4.87	5
4.60	5	4.80	5	4.48	5
4.13	10	4.33	5	4.29	25
3.67	100	4.13	5	4.06	5
3.28	10	4.00	10	3.72	60
3.22	15	3.85	5	3.62	10
3.18	10	3.53	90	3.43	10
3.05	10	3.28	10	3.33	15

a) The scale of the intensity (I/I_0) is so chosen as to make the most intense line have the value 100.

The crystals in the A-form appeared in the region where the concentration of hydrochloric acid is between about 4% (Runs No. 3—5 in Table 1) and about 17% (Runs No. 9—10 in Table 1), while the B-form appears above about 17%. Neither of these two salts could be crystallized from an equimolar solution of inosine and hydrochloric acid. They could be obtained from a solution containing a large excess of hydrochloric acid. Therefore, the salts were concluded to be incongruent and decomposed by pure water. An excess amount of the salts added to pure water could not remain in the salt-form in the residue, but changed into the inosine-dihydrate-form.

On the other hand, they were stable in air during storage for at least one month at room temperature when the mother liquor was completely removed from the crystal surface by washing with an organic solvent such as ethanol. When the removal of the mother liquor was insufficient, the crystals of the salts gradually became dark, probably because the acid in the mother liquor reacted with the ribose moiety of the inosine in the crystal. The solubility of inosine increased with an increase in the concentration of hydrochloric acid up to about 4%, and then gradually decreased with a further increase in the acid concentrations; it became constant beyond a 14% concentration of the acid. It is of interest that the solid phase changes from inosine dihydrate to inosine hydrochloride hemihydrate at a point where a sharp change in the solubility is observed, while inosine hydrochloride in the solid phase changes from the A-form to the B-form at a point where an almost constant solubility is observed.

Table 3. Composition data for the inosine–sulfuric acid–water system at 5 °C

Run No.	Solution (Weight %)			Wet Residue (Weight %)		Solid Phase[a]
	Inosine	H_2SO_4	Hx.[b]	Inosine	H_2SO_4	
lit.[c]	0.76	0	–	—	—	I2
1	2.31	1.37	–	54.24	—	I2
2	9.11	5.31	–	74.51	1.35	I2
3	11.03	8.02	–	75.68	1.91	I2
4	15.88	10.12	–	—	—	I2+ S
5	17.44	9.50	–	55.33	20.56	S (m)
6	13.28	10.87	–	54.77	21.73	S
7	7.29	14.00	–	56.89	22.08	S
8	2.90	23.39	0.03	54.83	24.43	S
9	2.00	30.00	+	53.83	24.71	S

a) I2: Inosine di-hydrate, $C_{10}H_{12}N_4O_5 \cdot 2H_2O$. S: Inosine sulfate, $C_{10}H_{12}N_4O_5 \cdot H_2SO_4 \cdot 2H_2O$. m: metastable.
b) Hx.: Hypoxanthine. c) See Table 1.

Table 3 shows the composition data for the inosine–sulfuric acid–water system at 5 °C. The hydrolysis of inosine in this system was much less than that in the hydrochloric acid system, so, practically, it could be disregarded. This system gave a new solid phase, the monosulfuric acid salt of inosine dihydrate. This acid salt of inosine could be obtained when the concentration of sulfuric acid was higher than 10% (Runs No. 4 in Table 3). These crystals had a plate-like appearance. Although they are incongruent and are decomposed by pure water, they are stable in air during storage for at least one month at room temperature, as in the case of the hydrochloric acid salt of inosine.

The solubility of inosine increased with an increase in the concentration of sulfuric acid until the concentration of sulfuric acid reached about 10%; it gradually decreased beyond that point.

It is interesting that both hydrochloric acid and sulfuric acid form salts with inosine, keeping an equivalent mole ratio in spite of the different valences of the acids.

Experimental

Materials. The inosine used was of a commercial A-grade of the Ajinomoto Co., Inc.; the other materials were of a reagent grade.

Analysis. The inosine was determined by means of the UV absorbance at 250 nm in 0.1 M HCl using the molar extinction coefficient of 11,800. The acids were determined by titration with standard NaOH, using a methyl red-bromocresol green indicator. The chlorine was determined by the Volhard method. The X-ray (Cu$K\alpha$) powder diffraction patterns were used for the identification of the solid phase in equilibrium. The degree of hydration of the crystals was determined by Karl Fischer titration. One-dimensional ascending paper chromatography (PC) was carried out on Toyo-Filterpaper No. 51A, the following solvent system being used: *n*-butanol-acetic acid-water (4 : 1 : 1). The hydrolysis of inosine into hypoxanthine was checked by PC (R_f, inosine, 0.25; hypoxanthine, 0.42), using UV-light.

Preparation of the Crystals. *Inosine Monohydrochloride Hemihydrate in the A-Form:* Inosine (6.0 g) was dissolved in aqueous 13% (w/w) HCl (50 ml), and the resultant solution was cooled in an ice-box for a week. The large prism crystals thus precipitated were filtered out and then dried in air. Yield, 2.1 g; mp 112 °C (colored)-130 °C (decomp. with darkening). One UV-absorbing spot was observed on PC (R_f, 0.25). Found: H_2O, 3.44; Cl, 11.1; Acid for HCl, 11.6%; $\varepsilon_{250\,nm}$ in 0.1 M HCl, 9,940. Calcd for $C_{10}H_{12}N_4O_5 \cdot HCl \cdot (1/2)H_2O$: H_2O, 2.87; Cl, 11.32; Acid for HCl, 11.65%; ε, 10090.

Inosine Monohydrochloride Hemihydrate in the B-Form: Inosine (8.6 g) was dissolved in aqueous 21% (w/w) HCl (50 ml), and the resultant solution was cooled in an ice-box overnight. The precipitated fine prism crystals were filtered out, washed with ethanol and ether, and then dried in air. Yield, 5.9 g; mp 122 °C (colored)-130 °C(decomp. with darkening). One UV-absorbing spot was observed on PC (R_f, 0.25). Found: H_2O, 2.44; Cl, 11.2; Acid for HCl, 11.7%; $\varepsilon_{250\,nm}$ in 0.1 M HCl, 9,940. Calcd for $C_{10}H_{12}N_4O_5 \cdot HCl \cdot (1/2)H_2O$: H_2O, 2.87; Cl, 11.32; Acid for HCl, 11.65%; ε, 10090.

Inosine Monosulfate Dihydrate: Inosine (6.2 g) was dissolved in aqueous 31% (w/w) H_2SO_4 (45 ml), and the resultant solution was cooled in an ice-box overnight. The precipitated plate crystals were filtered out and dried in air. Yield, 7 g; mp 108—112 °C. One UV-absorbing spot on PC was observed (R_f, 0.25). Found: H_2O, 7.47; Acid for H_2SO_4, 25.1%; $\varepsilon_{250\,nm}$ in 0.1 M HCl, 7,890. Calcd for $C_{10}H_{12}N_4O_5 \cdot H_2SO_4 \cdot 2H_2O$: H_2O, 8.96; Acid for H_2SO_4, 24.38%; ε, 7,870.

Solubility Measurement. A sufficient amount of the crystals, usually inosine was added to aqueous HCl (0—20%) or aqueous H_2SO_4 (1—20%) to make a slurry in tightly-capped glass bottles at 5 °C. Inosine hydrochloride in the A-form was used for Runs No. 3, 8 and 10 in Table 1, and the B-form, for Run No. 9. Inosine sulfate was used for Runs No. 5—8 in Table 2. The mixtures were shaken at 5 °C for 16 hr except for Runs No. 9—11 (for 5 hr) in Table 1. Then, the mixtures were quickly filtered with a glass filter. The clear solutions and the wet residues were sampled, diluted to appropriate volumes, and submitted to analysis. The residues were examined by means of the X-ray method.

The authors wish to thank Miss Yoshie Arai for her technical assistance.

The Thermal Reaction of Hydrogen and Nitric Oxide

Kohji TADASA,* Naomi IMAI, and Tetsuo INABA

Faculty of Liberal Arts and Sciences, University of Osaka Prefecture, Sakai, Osaka 591

(Received May 1, 1974)

The kinetics of the H_2–NO pyrolysis was studied at 400 °C; the reaction was found to be first-order in H_2 and to be independent of NO. It is suggested that the reaction proceeds by means of a free-radical chain mechanism: $H_2+NO(surface)\rightarrow HNO+H(1)$, $H+NO\rightleftharpoons HNO$ (2), $2HNO\rightarrow 2OH+N_2$ (3), $OH+H_2\rightarrow H_2O+H(4)$ and $2HNO\rightarrow H_2O+N_2O(5)$. This reaction scheme resembles that proposed for the CH_2O–NO pyrolysis at 500 °C except for the initiating step (1), which takes place on the wall of the vessel in the H_2–NO pyrolysis.

In this laboratory, the effect of nitric oxide on formaldehyde pyrolysis has been studied at 500°C.[1] As the H atom, in the chain decomposition of formaldehyde, is a chain carrier, it is desirable to know the reaction of a system containing H and NO in order to elucidate the above reaction. In order to follow the H_2–NO reaction, the H–NO reaction has been investigated by several workers; Hinshelwood and Mitchell in the range of 700°—805 °C,[2] Graven at 850°—1060 °C,[3] Kaufman and Decker at 900°—1152 °C,[4] and recently Wilde at 800°—1060 °C.[5] Wilde presented the following scheme:

$$H_2 + NO \rightleftharpoons HNO + H$$
$$HNO + NO \longrightarrow N_2O + OH$$
$$OH + H_2 \longrightarrow H_2O + H$$
$$H + NO + M \rightleftharpoons HNO + M$$
$$(2HNO \longrightarrow N_2O + H_2O)$$

No work, however, has been reported on the H_2–NO reaction below 500 °C. In this work, the kinetics of the H_2–NO pyrolysis has been studied mainly at 400 °C, and a reaction scheme has been derived.

Experimental

Materials. The nitric oxide and hydrogen used were obtained from the Takachiho Kagaku Co., Ltd., in research-grade purities of 99.6% and 99.95% respectively. They were used without further purification.

Apparatus. The apparatus used in the present work was similar to that described previously.[1] Two cylindrical vessels were used: an unpacked quartz one of 262 cm^3, with a S/V ratio of 0.83 cm^{-1}, and a packed Pyrex one of 124 cm^3, with a S/V ratio of 11.3 cm^{-1}.

Procedure. The required quantities of hydrogen and nitric oxide were introduced into the vessel, which had been kept at the experimental temperature. The products of decomposition were then separated and collected by means of cold traps and a Toepler gauge, and analysed quantitatively by means of a gas chromatograph.

Water, one of the product, was converted to hydrogen by treating it with the sodium evaporated onto the surface of a glass trap as a thin layer; then its amount was determined, though the measurement was not very accurate. Except for the case of water, the analytical technique used was similar to that described previously.[1]

Results

The products detected in the thermal reaction of the H_2–NO system are nitrogen, nitrous oxide, and water. Figure 1 shows the temperature dependence of each product after a pyrolysis of two hours at temperatures ranging from 20° to 500 °C.

Figures 2 and 3 show the effects of the nitric oxide and hydrogen pressures respectively on each product formation in the thermal reaction at 400 °C. Figures 4 and 5 show the dependences of the nitrogen and nitrous oxide formations in the packed vessel at 400 °C on the nitric oxide and hydrogen pressures respectively. Figures 2—5 demonstrate that the formation of nitrogen is first-order in relation to hydrogen and zero-order in relation to nitric oxide in both the unpacked and packed vessels, while that of nitrous oxide obeys a

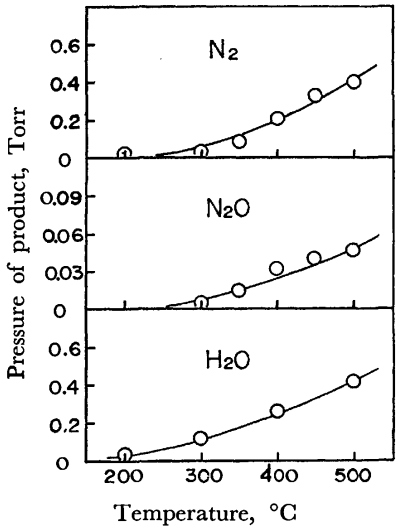

Fig. 1. Temperature dependences of product amounts for the pyrolyses of 50 Torr H_2 and 50 Torr NO in the unpacked vessel for 2 hr.

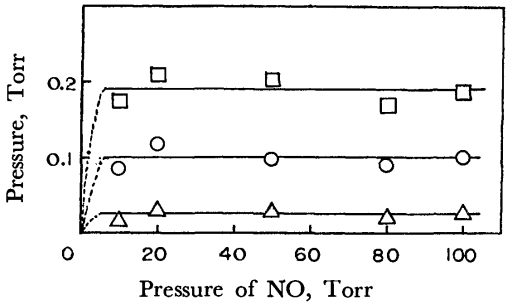

Fig. 2. Plot of amount of product *vs.* NO pressure for the pyrolysis of 20 Torr (fixed) H_2 and NO in the unpacked vessel at 400°C for 2 hr.
□: H_2O, ○: N_2, △: N_2O

* Present address: Department of Agricultural Chemistry, College of Agriculture, University of Shinshu, Ina, Nagano 396.

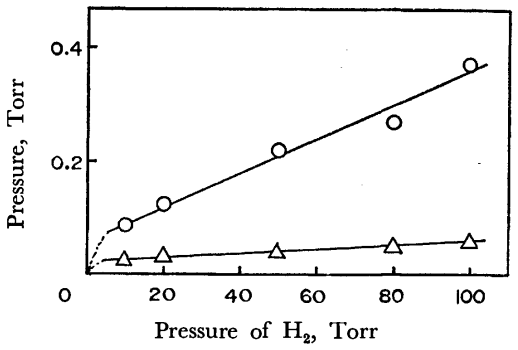

Fig. 3. Plot of amount of product *vs.* H_2 pressure for the pyrolysis of 20 Torr (fixed) NO and H_2 in the unpacked vessel at 400°C for 2 hr.
○: N_2, △: N_2O

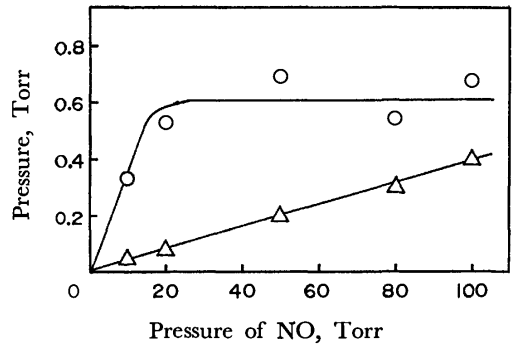

Fig. 4. Plot of amount of product *vs.* NO pressure for the pyrolysis of 20 Torr (fixed) H_2 and NO in the packed vessel at 400°C for 2 hr.
○: N_2, △: N_2O

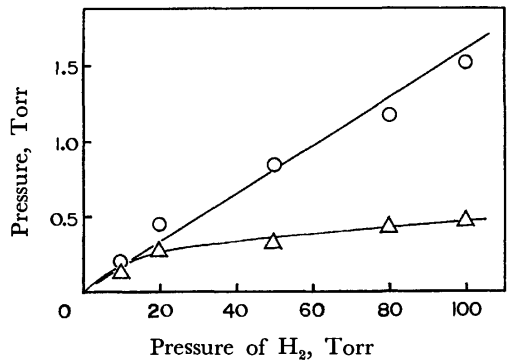

Fig. 5. Plot of amount of product *vs.* H_2 pressure for the pyrolysis of 80 Torr (fixed) NO and H_2 in the packed vessel at 400°C for 2 hr.
○: N_2, △: N_2O

different rate low in each vessel. (The amount of water was not determined in the packed vessel.)

Discussion

As is indicated in Fig. 1, the H_2–NO reaction begins to occur at about 300 °C and is accelerated as the temperature increases within the range employed. The facts that the H_2–NO reaction begins to occur at a relatively low temperature and that the main reactions, by which water and nitrogen are formed, are not dependent on the nitric oxide pressure (Fig. 2) predict that an initiation reaction is the surface reaction. This suggestion is confirmed by the results in the packed vessel (Figs. 4 and 5), *i.e.*, the rate of the formation of nitrogen, one of the main products, is increased by the increase in the S/V ratio compared with that in the unpacked vessel (Figs. 2 and 3), even though the rate law is not changed.

In the present laboratory, the pyrolysis of formaldehyde with nitric oxide has been studied at 500 °C; we obtained this stoichiometric relation:[1)]

$$CH_2O + NO \longrightarrow CO + H_2O + (1/2)N_2$$

though it is very rough. In the present work, a similar rough stoichiometry seems to hold:

$$H_2 + NO \longrightarrow H_2O + (1/2)N_2$$

On the other hand, different rate laws are observed in each pyrolysis: *i.e.*, in the CH_2O pyrolysis, it is:

$$-d[CH_2O]/dt = k[CH_2O][NO]$$

while in the H_2 pyrolysis it is:

$$-d[H_2]/dt = k[H_2]$$

with a sufficient amount of NO being present in each case.

The facts hitherto presented suggest a chain mechanism of the H_2–NO pyrolysis, which consists of a different initiating step and of consequent steps analogous to those proposed in the CH_2O–NO pyrolysis:[1)]

$$H_2 + NO(\text{surface}) \longrightarrow HNO + H \quad (1)$$

$$H + NO + M \rightleftharpoons HNO + M \quad (2)$$

$$2HNO \longrightarrow 2OH + N_2 \quad (3)$$

$$OH + H_2 \longrightarrow H_2O + H \quad (4)$$

$$2HNO \longrightarrow H_2O + N_2O \quad (5)$$

In this scheme, Reaction (1) is the chain-initiating step, (2), (3), and (4) are the chain-carrying steps, and (5) the chain-ending step. Reaction (1) is proposed because of the surface effect on this reaction and the independency of the rate in relation to the NO pressure. Reaction (3) has been proposed in the study of the CH_2O–NO pyrolysis[1)] and suggested to be faster than (5) at 500 °C.

Making the usual steady-state assumption of transient species (H, OH, and HNO), the above reaction scheme yields the following rate equation:

$$R_{N_2} = R_3 = (k_3/k_5)R_5 = (k_3/k_5)R_1$$

where R refers to the rate of the reaction shown by a suffix or that of the formation of the product shown by a suffix. If Reaction (1) is first-order in relation to H_2 and zero-order in relation to NO,

$$R_{N_2} = (k_1k_3/k_5)[H_2]$$

The value of k_1 should depend on the amount of the surface area. A similar treatment of the reaction scheme also yields this rate equation:

$$R_{H_2O} = R_4 + R_5 = 2R_3 + R_5$$

If the reaction chain is sufficiently long, R_5 may be neglected compared with R_3. Then

$$R_{H_2O} \simeq 2R_3 = 2R_{N_2}$$

These rate equations satisfy both the kinetics and the

stoichiometry described above. The possibilities of the occurences of the other reactions were examined in a manner described in a previous work and so are omitted here; *cf* Table 1 in Ref. 1.

The above scheme also leads to this equation:

$$R_{N_2O} = k_1[H_2]$$

which is consistent with the results obtained in the unpacked vessel (Figs. 2 and 3). In the packed vessel, however, the rate of the N_2O formation does not follow this equation (Figs. 4 and 5). As another source of nitrous oxide, Reaction (6) may be presumed:

$$HNO + NO \longrightarrow N_2O + OH \quad (6)$$

This reaction has been proposed in the temperature range of 800°—1060 °C[3] and has presumed to take place simultaneously with (5) in the CH_2O–NO pyrolysis at 500 °C.[1]

The rate of the N_2O formation due to (6) may be expressed as:

$$R_{N_2O(6)} = (k_1^{1/2}k_6/k_5^{1/2})[H_2]^{1/2}[NO]$$

This equation appears to agree with the results in the packed vessel (Figs. 4 and 5). Reaction (6) should have a heterogeneous nature at 400 °C, since N_2O seems to be formed predominantly by Reaction (6) in the packed vessel and by Reaction (4) in the unpacked vessel.

The occurrence of (6), in addition to (1)—(5), does not affect the rate equations of the N_2 and H_2O formations.

Reactions (7)[6] and (8)[7] have been proposed between nitroxyl and nitric oxide at lower temperatures:

$$HNO + 2NO \longrightarrow N_2 + H + NO_3 \quad (7)$$

$$HNO + 2NO \longrightarrow HNO_3 + N_2 \quad (8)$$

Reaction (7), followed by (2), causes the chain disproportionation of nitric oxide, which may be represented stoichiometrically as:

$$3NO \longrightarrow N_2 + NO_3$$

(Reaction (7) does not affect the rate of the formation of another product.) Reaction (7) has also been suggested, in the studies of CH_2O–NO photolysis[8] and H_2–NO photosensitization reaction[9] carried out in this laboratory, as taking place in the system containing hydrogen atoms and nitric oxide at lower temperatures. At 500 °C, however, the disproportionation of nitric oxide was indicated not to occur by the study of the CH_2O–NO pyrolysis.[1]

The rate of N_2 formation due to (7) may be represented as:

$$R_{N_2(7)} = (k_1^{1/2}k_7/k_5^{1/2})[NO]^2[H_2]^{1/2}$$

Reaction (7) does not seem to be as important as (3) as the N_2 source in the present conditions because of the disaccordance between the above rate equation and the rate law of N_2 formation observed, and also because of the failure to detect any NO_3 in the products.

Reaction (8) is also omitted, since (8) terminates the reaction chain; thus, the occurrence of this reaction alters the rate law of the main reaction. This has already been examined in a manner described previously.

References

1) K. Tadasa, N. Imai, and T. Inaba, This Bulletin, 47, 548 (1974).
2) C. N. Hinshelwood and J. W. Mitchell, *J. Chem. Soc. A*, **1936**, 378.
3) Wendell M. Graven, *J. Amer. Chem. Soc.*, **79**, 3697 (1957).
4) F. Kaufman and L. J. Decker, Eigth Sympoisum(International) on Combustion, p. 139, Williams and Wilkins: Baltimore (1959).
5) Kenneth A. Wilde, *Combust. and Flame*, **13**, 173 (1969).
6) E. A. Arden and L. Phillips, *J. Chem. Soc. A*, **1964**, 5118.
7) O. P. Strausz and H. E. Gunning, *Trans. Faraday Soc.*, **60**, 347 (1964).
8) K. Tadasa, N. Imai, and T. Inaba, unpublished work.
9) K. Tadasa, N. Imai, and T. Inaba, unpublished work.

The Singlet-Triplet Absorption Spectra of Heterocyclic Amine *N*-Oxides. II. Pyridine *N*-Oxide Derivatives

Masumi YAMAKAWA, Kiyoshi EZUMI, Yoshiko MIZUNO, and Tanekazu KUBOTA

Shionogi Research Laboratory, Shionogi & Co., Ltd., Fukushima-ku, Osaka 553

(Received July 4, 1974)

The singlet-triplet absorption spectra of various pyridine *N*-oxide derivatives with an electron-donating substituent have been observed by applying the oxygen-intensification technique. The nature of the lowest triplet (T_1) states of these *N*-oxides and the substituent effect on the T_1 state of pyridine *N*-oxide have been discussed experimentally and theoretically. The T_1 states of the above substituted pyridine *N*-oxides were assigned to a π-π^* transition of a ^3L_a (CT) nature; $^3A_1$ for the *p*-substituted pyridine *N*-oxides. All the singlet-triplet absorption bands as well as the singlet π-π^* bands recorded here show a blue shift in polar solvents; this phenomenon is also discussed. Last, the mutual relation between the contact charge-transfer bands and the singlet-triplet absorption bands, both enhanced by compressed oxygen, has been discussed, since, for pyridine *N*-oxides with *p*-$N(CH_3)_2$, *p*-OCH_3, and *m*-NH_2, we could not record the singlet-triplet absorption band clearly.

In our foregoing papers[1,2] we discussed the characteristics of the lowest triplet state (T_1) of such basic heterocyclic amine *N*-oxides as pyridine *N*-oxide and quinoline *N*-oxide, and of nitro-substituted pyridine and quinoline *N*-oxides. The former was obtained by measuring the singlet-triplet (T_1←S) absorption spectra using the technique of high-pressure oxygen perturbation, and the latter, by recording the phosphorescence spectra as well as the T_1←S absorption spectra. As one of the most remarkable conclusions obtained from those studies, the T_1 state of pyridine *N*-oxide (PNO) and 4-nitropyridine *N*-oxide (4NPO) was identified as $^3A_1$ (π-π^*), which corresponds to the $^1A_1$ strong absorption band appearing in a longer-wavelength region;[1,2] this information is valuable for interpreting the primary process of the photochemical reaction of these compounds.[3] As an extension of these investigations, we would like to report, in this paper, on the T_1←S absorption spectra and the contact charge-transfer (CCT) spectra of PNO derivatives with an electron-donating substituent, these spectra being obtained under compressed-oxygen perturbation. The substituent effect on the T_1←S band of PNO as well as the solvent effect on it has also been discussed on the basis of the experimental results and also by applying the PPP SCF–MO–CI calculation.

Experimental

The high-pressure absorption cell employed for recording the T_1←S absorption spectrum under compressed-oxygen perturbation is the same as was described in our previous paper.[1]

The samples used in this paper are listed in Table 1. These, except for 3-aminopyridine *N*-oxide (3APNO), were synthesized and carefully purified by methods previously reported.[4] The 3APNO free base has been obtained by neutralizing its HCl salt with Na_2CO_3 in CH_3OH, and purified by repeated sublimations:[5] mp 124.5—125.0 °C. The above 3APNO HCl salt was crystallized from a reflux solution of a 3M HCl aqueous solution of 3-acethylaminopyridine *N*-oxide, which had been synthesized by the oxidation of the corresponding pyridine base with *m*-chloroperbenzoic acid.[5,6] The solvent used were CH_2Cl_2, CH_3CN, and CH_3OH, all of which were spectrograde in purity; they were dried sufficiently with a Mg ribbon (for CH_3OH alone) or $CaCl_2$, and then rectified carefully.

Results and Discussion

T_1←S Absorption Spectra of PNO Derivatives. The effects of the compressed-oxygen perturbation on the electronic spectra of PNO derivatives with an electron-donating substituent may be experimentally classified

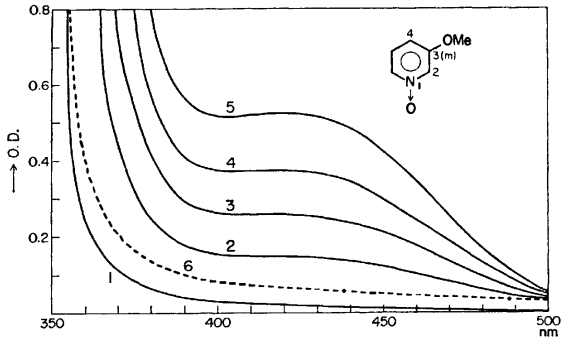

Fig. 1. Singlet-triplet absorption spectra of *m*-methoxy pyridine *N*-oxide (0.925 mol/l in CH_3CN) caused by applied oxygen pressure. The oxygen pressure is 0, 30, 60, 92, and 140 kg/cm² for curves 1, 2, 3, 4, and 5, respectively. Curve 6 is for the spectrum after removal of the oxygen.

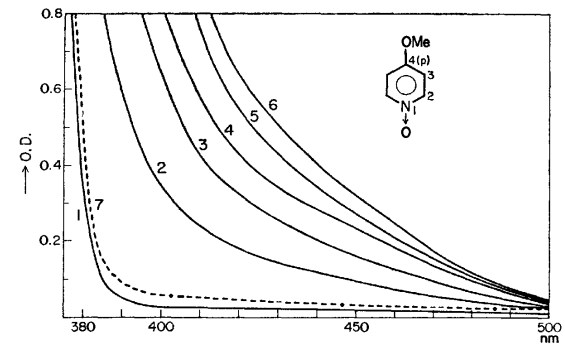

Fig. 2. The spectral change of *p*-methoxy pyridine *N*-oxide (0.290 mol/l in CH_3CN) in visible region with the applied oxygen pressure, which is 0, 37, 65, 93, 120, and 140 kg/cm² for the curves 1, 2, 3, 4, 5, and 6, respectively. Curve 7 is for the spectrum after removal of the oxygen.

Table 1. Observed and calculated transition energies to the lowest triplet state (T_1), observed ^1L_a energy, and observed ^1L_a-T_1 energy separation (in kK unit) for substituted pyridine *N*-oxides

Substituent	T_1←S band			^1L_a band	^1L_a-T_1	T_1 (calcd)	ΔT_1 [b]	T_1* [c]	T_1** [d]
	CH_2Cl_2	CH_3CN	CH_3OH	CH_2Cl_2	Separation[a]				
H	23.46	23.87	25.51	36.18	12.72	15.63	7.83	23.55	23.28
p-CH_3	23.55	22.8	24.9	35.86	12.04	16.04	7.51	23.23	23.69
p-Cl	22.46	22.75	24.36	35.15	12.69	15.71	6.75	22.52	23.36
p-CH_3O	CCT	CCT	CCT	35.46	—	14.51	—	22.83	22.16
p-$(CH_3)_2N$	CCT	CCT	CCT	32.87	—	11.99	—	20.24	19.64
m-CH_3	23.61	23.87	25.71	36.06	12.45	15.68	7.93	23.43	23.33
m-Cl	22.68	22.76	24.58	35.80	13.12	15.66	7.02	23.17	23.31
m-CH_3O	23.80	23.95	25.64	36.28	12.48	14.97	8.83	23.65	22.62
m-NH_2	—[e]	CCT	CCT	36.06	—	15.04	—	23.41	22.69

a) The values in CH_2Cl_2. b) Differences between the observed and the calculated T_1 energies. c) The estimated T_1 energies using the equation 1 in Text. d) The estimated T_1 energies using the equation 2 in Text. e) The T_1←S spectrum could not be recorded in CH_2Cl_2 because of its low solubility.

into two groups. In the first group, the T_1←S absorption band appears clearly in a visible region. The substituents belonging to this group are *m*- and *p*-CH_3, *m*- and *p*-Cl, and *m*-OCH_3; all are in a relatively weak interaction between the substituent and the N→O group. A typical example is given in Fig. 1 for *m*-methoxy-PNO. The substituents belonging to the other group are *p*-$N(CH_3)_2$, *m*-NH_2, and *p*-OCH_3; in this group, the T_1←S absorption band is not clearly observed, as Fig. 2 shows for the case of *p*-methoxy-PNO. In this case, however, the oxygen-sensitive end absorption appears in a visible region with quite a strong intensity; the nature of this band will be discussed below. The observed values of the T_1←S absorption spectra are listed in Table 1, along with the other relevant spectroscopic and theoretical data.

The characteristics of the ^1L_a band given in Table 1 have already been discussed in detail;[7] it has the nature of an intramolecular CT band from the *N*-oxide-group oxygen atom to the conjugated residue. In the first paper[1] in this series, we also identified the lowest triplet state (T_1) of PNO as ^3L_a (*i.e.*, $^3A_1$) on the basis of a detailed discussion of the T_1 state of basic heterocyclic amine *N*-oxides. Thus, only the substituent effect on the T_1 state of PNO will be discussed here. Checking the data in Table 1, we can see that the T_1←S band and the ^1L_a band both shift parallel with the electron-donating substituent introduced into PNO. A *p*-substituent with a strong electron-donating ability may be especially effective for the red shift of the T_1←S band, as may be inferred from the values of T_1*, T_1**, and the ^1L_a band listed in Table 1. In Fig. 3 the above relation is illustrated using the observed values, where a linear relation holds qualitatively between the ^1L_a and the T_1←S bands. Conversely, this experimental fact seems to support the idea that the T_1 state of these compounds is of a ^3L_a π-π^* nature.[1,8] Next, let us examine the value of the singlet-triplet separation—in the present case, the ^1L_a—T_1 separation. This value is larger than 12000 cm^{-1} throughout all the compounds, as Table 1 shows. This also supports the idea that the T_1 state is of a π-π^* nature.[9] Moreover, the above ^1L_a—T_1 separation value is in the 12.5—13 kK (1 kK=1000 cm^{-1}) range and is almost constant—*i.e.*, 12.63 kK on the average. The T_1-state energy of the compounds used here may then be calculated from Equation 1:

$$T_1^* = {}^1L_a\,(\text{obsd}) - 12.63 \qquad (1)$$

The values thus obtained are indicated by T_1* and are included in Table 1, in which the T_1* values for the PNO derivatives with *p*-OCH_3, *p*-$N(CH_3)_2$, and *m*-NH_2 substituents are also shown, although attempts to measure these were unsuccessful. The agreement between T_1 (obsd) and T_1* is quite good.

The characters of the T_1 states experimentally discussed hitherto were also supported by the PPP-type SCF-MO-CI calculation, the method of which was the same as was employed for the singlet- and triplet-energy calculation of PNO, *etc.*;[1] *i.e.*, the two-electron repulsion integral, $\gamma_{\mu\nu}$, is estimated by means of the Beveridge and Hinze equation.[10] The parameterization for the atoms pertinent to the pyridine *N*-oxide part

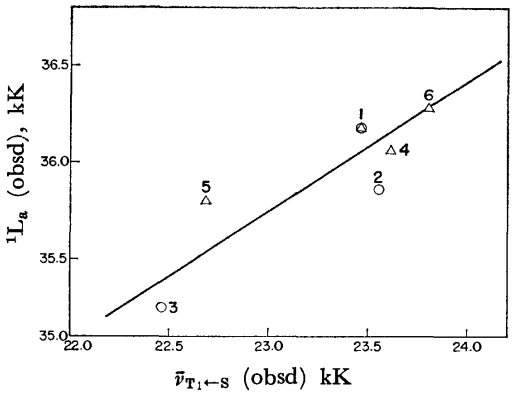

Fig. 3. Mutual correlation between the observed T_1←S absorption band and the observed ^1L_a band for substituted pyridine *N*-oxides. The substituent is *p*-CH_3, *p*-Cl, *m*-CH_3, *m*-Cl, and *m*-OCH_3 for the number 2 to 6, respectively. The number 1 is for pyridine *N*-oxide itself.

is the same as that given in a previous paper.[1] For substituents, the valence-state ionization potential (I_p) and the electron affinity (E_A) were determined by referring to the papers by Zahradnik *et al.*[11] The values of β_{XY}^{core} pertaining to the substituents were also estimated according to Zahradnik *et al.*[11] The values (eV) of I_p and E_A for the substituents are in this order: 25.07 and 13.80 for Cl; 32.90 and 10.00 for -Ö-; 27.30 and 9.30 for -N̈H$_2$; and 25.46 and 8.11 for -N̈(CH$_3$)$_2$. For the CH$_3$ group of the type, >-CH$_3$, the inductive model was adopted; *i.e.*, the I_p of the carbon atom bonded to the CH$_3$ group is reduced by 1 eV.[12] The $-\beta_{XY}^{core}$ (eV)[13] and the bond-length (Å) values pertaining to the substituents are in this order: 0.948 and 1.730 for >C–Cl; 1.000 and 1.356 for >C–Ö- and 1.896 and 1.431 for >C–N̈-. The calculation showed that the nature of the lowest T_1 state is always ^3L_a; $^3A_1$ for *p*-substituted PNO derivatives and that the T_1 energy level is quite a bit lower (12—8 kK for *p*-substituents and 13—5 kK for *m*-substituents) than that of the T_2-energy level. These facts support the discussions about the assignment of the T_1 state on the basis of the experimental results presented above. The calculated T_1 energies are listed in Table 1. The fact that the calculated values are always lower than the observed values is a well-known general tendency in the PPP semi-empirical calculation of T_1-state energy unless a special refinement is used in the estimation of the electron-repulsion terms.[14] However, note that the difference, ΔT_1, between the observed and the calculated T_1 energies is in the range of 7—8 kK, except for the *m*-OCH$_3$ derivative, and almost constant; average $\Delta T_1 = 7.65$ kK. Thus, the observed T_1 energies can also be expressed by Equation 2, the values of T_1** being listed in Table 1:

$$T_1^{**} = T_1(\text{calcd}) + 7.65 \qquad (2)$$

It is noticeable that the T_1** values are quite close to the T_1* values obtained from Equation 1. This may also support the assignment of the present T_1 states. The T_1 energy of the compounds with *p*-OCH$_3$, *p*-N(CH$_3$)$_2$, and *m*-NH$_2$ substituents, whose triplet energies were not obtained here experimentally (*vide infra*), seems to be between T_1* and T_1** values in magnitude (see Table 1).

Solvent effect on the T_1←S Absorption Spectra of PNO Derivatives. It was reported in the foregoing papers[1,2] that the blue-shift phenomenon on the T_1←S absorption band of PNO, *etc.* is observed in polar solvents, especially in protic solvents such as alcohols; this is just like the π-π^* singlet bands of those *N*-oxides behave in solvents.[7] The mechanism was then discussed in detail. We have now examined whether or not this kind of solvent effect is also observed in the T_1←S band of PNO derivatives. As a result, it can safely be said that all of the T_1←S bands recorded on PNO derivatives (see Table 1) show a blue shift due to the solvent change from CH_2Cl_2 to CH_3CN and CH_3OH; methanol particularly brings about a larger blue shift than acetonitrile. Of course, this is attributable to the hydrogen-bonding interaction of methanol with *N*-oxides, as has well been verified.[15,16] These phenomena indicate a smaller solute-solvent interaction at the T_1 excited state than in the ground state;[1] this can reasonably be explained by taking into account the intramolecular charge transfer from the oxygen atom of the *N*-oxide group, or from the substituent, to the conjugated ring residue. In turn, by comparing the magnitude of the above blue-shift ability between the T_1←S and ^1L_a←S (a strong singlet band appearing in the near-ultraviolet region) absorption bands, we have found that the former band shows almost the same magnitude as, or is a little smaller than, that of the latter.[17] However, taking account of the difference in the solute-solvent interaction potential curves among the ground, T_1, and ^1L_a states,[18] and also referring to the light-absorption mechanism according to the Franck-Condon principle,[18] the above fact may suggest that the ability of solute-solvent interaction, especially of hydrogen-bonding interaction, may be larger at the T_1 state than at the ^1L_a state, since the above-mentioned intramolecular charge-transfer effect would be smaller in the T_1 state than in the ^1L_a state.

Contact Charge-transfer Spectra with Oxygen. As has been described above, the compounds with the substituents of *p*-N(CH$_3$)$_2$, *p*-OCH$_3$, and *m*-NH$_2$, where quite a strong resonance of the substituent with the PNO ring is to be expected, do not exhibit a well-defined T_1←S absorption band, but the oxygen-sensitive end absorption appears in the visible region with quite a strong intensity. Keeping these facts in mind, it should also be remembered that many organic compounds bring about contact charge-transfer spectra in the visible-to-near-ultraviolet region by means of interaction with oxygen,[19] and that the smaller the ionization potential of the compounds is, the larger is the red shift of the contact charge-transfer spectra.[20] Our molecular orbital calculation described above led us to the conclusion that the highest MO energies of *p*-N-

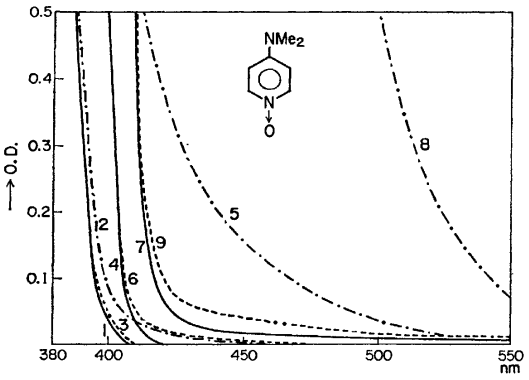

Fig. 4. The effect of oxygen pressure on the absorption spectra in a visible region of *p*-dimethylaminopyridine *N*-oxide at several concentrations in CH_3CN. The sample concentrations for curves 1, 2, and 3 are 6.61×10^{-4} mol/l; for 4, 5, and 6 7.81×10^{-3} mol/l; and for 7,8, and 9 saturated solution. The oxygen pressure is zero for curves 1, 4, and 7; 130 kg/cm^2 for 2, 5, and 8. Curves 3, 6, and 9 are for the spectra after removal of the oxygen.

$(CH_3)_2$, *p*-OCH_3, and *m*-NH_2 substituted PNO's are considerably higher, particularly for the *p*-$N(CH_3)_2$ substituent, than those of the others, so that there is a possibility that the CCT spectra of these compounds occur in quite a longer-wavelength region. In addition, this possibility may be much greater in our case, since those experiments have been done under a high oxygen pressure. For these reasons, the end absorption in the visible region of the CCT spectra observed for the above three substances may cover the $T_1 \leftarrow S$ absorption band enhanced by compressed-oxygen perturbation, so we could not record the $T_1 \leftarrow S$ absorption band clearly in these cases. To check the effect of the oxygen pressure on the visible-end absorption of *p*-dimethylamino-PNO, a typical example, dissolved (in several concentrations) in CH_3CN, the experiments illustrated in Fig. 4 were carried out. The change in the spectra upon introducing compressed oxygen gas or on removing it is reversible. However, a careful check of many experiments of this kind indicates that, although the end absorption is intensified strongly and monotonously with an increase in the oxygen pressure, no absorption maximum appears there (see Fig. 4). One may, then, conjecture that the band maxima of the CCT spectra may exist in a much shorter wavelength region than that shown in Fig. 4.

References and Notes

1) T. Kubota, M. Yamakawa, and Y. Mizuno, This Bulletin, **45**, 3282 (1972).

2) M. Yamakawa, T. Kubota, K. Ezumi, and Y. Mizuno, *Spectrochim. Acta*, **30A**, 2103 (1974).

3) a) G. G. Spence, E. C. Taylor, and O. Buchardt, *Chem. Rev.*, **70**, 231 (1970); b) I. Ono and N. Hata, This Bulletin, **46**, 3658 (1973); c) N. Hata, I. Ono, and K. Osaka, *ibid.*, **46**, 3363 (1973); d) C. Kaneko, Chemistry Review (in Japanese), No. 1, 131 (1973), The University of Tokyo Press.

4) T. Kubota, K. Nishikida, H. Miyazaki, K. Iwatani, and Y. Ōishi, *J. Amer. Chem. Soc.*, **90**, 5080 (1968); T. Kubota and H. Miyazaki, This Bulletin, **39**, 2057 (1966), *etc.*

5) F. Leonard and A. Wajngurt, *J. Org. Chem.*, **21**, 1077 (1956).

6) E. Ochiai, "Aromatic Amine Oxides," Elsevier, Amsterdam (1967).

7) a) T. Kubota, *Nippon Kagaku Zasshi*, **80**, 578 (1959); This Bulletin, **35**, 946 (1962); b) M. Yamakawa, T. Kubota, and H. Akazawa, *Theor. Chim. Acta*, **15**, 244 (1969); c) H. Miyazaki, T. Kubota, and M. Yamakawa, This Bulletin, **45**, 780 (1972); d) G. Gottarelli and B. Samori, *Spectrochim. Acta*, **30A**, 417 (1974); e) See also footnote 2 in the reference 1 of this paper.

8) If the T_1 state is of triplet n-π^* nature, the substituent such as *p*-$N(CH_3)_2$, *p*-OCH_3, *etc.* would bring about the blue shift of the $T_1 \leftarrow S$ band.

9) Detailed discussions on this point were given in the references 1 and 2.

10) D. L. Beveridge and J. Hinze, *J. Amer. Chem. Soc.*, **93**, 3107 (1971).

11) R. Zahradnik, I. Tesařova, and J. Pancíř, *Collet. Czech. Chem. Commun.*, **36**, 2867 (1971); J. Pancíř and R. Zahradnik, *Theor. Chim. Acta*, **14**, 426 (1969); See also K. Nishimoto, *ibid.*, **7**, 207 (1967), the treatment of this reference being applied for determining the I_P and E_A of $\ddot{N}(CH_3)_2$ by connecting with those of $\ddot{N}H_2$ given in Zahradnik *et al.* (*vide supra*).

12) P. Lazzeretti and F. Taddei, *Mol. Phys.*, **22**, 941 (1971).

13) These values were obtained by multiplying the ratio of (β_{cx}/β_{cc}) given by Zahradnik *et al.*[11] to the present β_{cc}^{core} value (−2.370 eV). For $\beta_{C-O;}^{core}$, however, we estimated it so as to reproduce the UV spectrum of azoxyanisole. Detail was presented at the Symposium of Structure Chemistry and the Electronic State of Molecules (Sendai, October 1972, Abstract p. 65) by Ezumi *et al.*

14) K. Nishimoto, *Theor. Chim. Acta*, **5**, 74 (1966); *ibid.*, **7**, 207 (1967).

15) N. Mataga and T. Kubota, "Molecular Interactions and Electronic Spectra," Chapters 6 and 7, Dekker, New York (1970).

16) Here note that the dielectric constant, which plays an important role for the solvent shift due to long range electrostatic terms, of acetonitrile and methanol is 37.5 and 32.63, respectively, and almost the same in magnitude.

17) See also reference 1.

18) For detailed description on these points, see footnote 18 in our previous paper.[1] This is attributed to the problem of Franck-Condon stabilization energy.[15]

19) H. Tsubomura and R. S. Mulliken, *J. Amer. Chem. Soc.*, **82**, 5966 (1960); H. Ishida, H. Takahashi, H. Sato, and H. Tsubomura, *ibid.*, **92**, 275 (1970); This Bulletin, **43**, 3130 (1970).

20) This kind of CCT spectra may be thought to take place by the charge transfer from the highest occupied molecular orbital of electron donors to thee lectron accepting orbitals (degenerated π and $\bar{\pi}$ orbitals) of oxygen (electron acceptor), and to borrow the intensity from strong π-π^* transition of the donor in CCT complexes.[19] In several amines *etc.* the CCT full spectra with maxima were observed by oxygen perturbation.[19]

Radiotracer Studies of the Adsorption of an Ampholytic Surfactant, *N*-dodecyl-β-alanine, at the Aqueous Surface

Takeo Okumura,* Akio Nakamura, Kazuo Tajima, and Tsunetaka Sasaki

Department of Chemistry, Faculty of Science, Tokyo Metropolitan University, Tokyo 158

(Received July 19, 1974)

A tritiated ampholytic surfactant, *N*-dodecyl-β-alanine, $C_{10}H_{21}$-$(CHT)_2$-NH_2^+-$(CH_2)_2$-COO^-, was synthesized, and the amount of adsorption on an aqueous surface was measured directly by the radiotracer method. The adsorption isotherm near the neutral pH region showed a saturation value of 3.73×10^{-10} mol/cm^2 above the concentration of about 1/5 of the critical micelle concentration in the absence of added salt, and a value of 4.74×10^{-10} mol/cm^2 above the critical micelle concentration in the presence of 1 mol/l NaCl. In the presence of 1 mol/l NaCl, no effect of pH on the adsorption was found. The Gibbs adsorption isotherm applicable to the aqueous ampholytic surfactant was derived. The observed amounts of adsorption in the presence and absence of NaCl were in good agreement with the values calculated from the Gibbs adsorption isotherm, using the surface tension data measured by the Wilhelmy plate method.

Although the bulk properties of aqueous solutions of ampholytic surfactants have been studied by many investigators,[1-4] the studies of such surface properties of aqueous ampholytic surfactant solutions as surface tension and adsorption are rather rare.[3-4] Especially, no direct measurement of the adsorption of an ampholytic surfactant on an aqueous surface has yet been reported as far as the present authors are aware. Such a measurement of adsorption is important, however, from both theoretical and practical points of view, as in the cases of aqueous anionic and nonionic surfactant solutions previously reported.[5-6]

In the present study, a tritiated ampholytic surfactant, *N*-dodecyl-β-alanine(NDA), was synthesized in order to measure the amount of adsorption directly by the radiotracer method, and in order to confirm the applicability of the Gibbs adsorption isotherm derived for an aqueous ampholytic surfactant solution.

Experimental

Materials. Tritiated *N*-dodecyl-β-alanine(TNDA) was synthesized according to the following process, the details of which will be reported elsewhere.[7] Tritiated dodecanoic acid(I), obtained by tritiating dodecenoic acid, was allowed to react with urea for five hours at 170—180 °C to form dodecanoic acid amide(II). By the subsequent reduction of (II) using lithium aluminium hydride in ethyl ether, tritiated dodecylamine(III) was obtained. TNDA was obtained by the reaction of (III) with β-propiolactone in acetonitrile for an hour at 30 °C.[8] A crude product was purified by repeated recrystallizations from a mixture of acetone and ethyl alcohol (1 : 1), followed by drying in a vacuum. Thin-layer chromatography confirmed the absence of unreacted materials in the final product. The infrared spectra of the product, as well as the nonradioactive one used, confirmed the zwitterionic structure.[2] The specific activity of the sample was about 16 Ci/mol.

Sodium chloride was purified by fusing a comercial extra-pure-grade reagent for five hours in a platinum crucible to remove any surface-active contaminants. The water used for preparing the solutions was obtained by first refluxing ordinarily distilled water with acid permanganate, then distilling it from an alkaline permanganate solution, and finally distilling it twice using a Hysil flask. The hydrochloric acid used for controlling the pH of solutions in the acid region was purified by the distillation of a dilute extra-pure-grade reagent. The sodium hydroxide used for controlling the pH in the alkaline region was purified by the recrystallization of extra-pure-grade reagent from triple-distilled water.

Methods and Procedures. The method and apparatus for the measurements of the adsorption by the radiotracer method were similar to those described previously.[5] The total radioactivity over the surface, R_1, and the radioactivity from the bulk solution, R_2, of an aqueous TNDA solution which had attained an adsorption equilibrium were measured by means of a sheet scintillation counter at 30 °C. The radioactivity corresponding to the adsorbed molecules, R_1-R_2, was calculated and multiplied by a conversion factor to obtain the amount of adsorption.[5,6] To eliminate the effects of atmospheric carbon dioxide and the evaporation of the solution, the measurements were made in a humidified nitrogen atmosphere.

The surface tension was measured by the Wilhelmy plate method.[9] To obtain the equilibrium values, the time dependence of the surface tension was self-recorded, and extrapolated to infinite time.[10] The drop weight method was also used for the sake of comparison.

Results and Discussion

Adsorption of NDA. Figure 1 shows the time dependence of the total radioactivity over the surface of TNDA solutions of various concentrations. The time required for attaining a steady value was about 60 minutes for the solutions studied; this is longer than the time observed for the adsorption of sodium dodecylsulfate(SDS),[5] probably because of the adsorption from a relatively dilute solution in the case of NDA as compared with that of SDS. The steady count rate obtained from Fig. 1 was taken as the equilibrium value, R_1, which is plotted against the NDA concentration in Fig. 2. The concentration dependence of the radioactivity due to the bulk of a solution, R_2, was estimated as a straight line passing through the point of origin with the same inclination as that of the linear part of the R_1 *vs.* concentration curve in Fig. 2, as has been confirmed in the case of the direct measurement of R_2.[5,6] The amount of adsorption, Γ^A, at an aqueous surface is obtained as:

$$\Gamma^A = k(R_1-R_2)$$

* Household Goods Research Laboratories, Kao Soap Co., Ltd., Sumida-ku, Tokyo 131

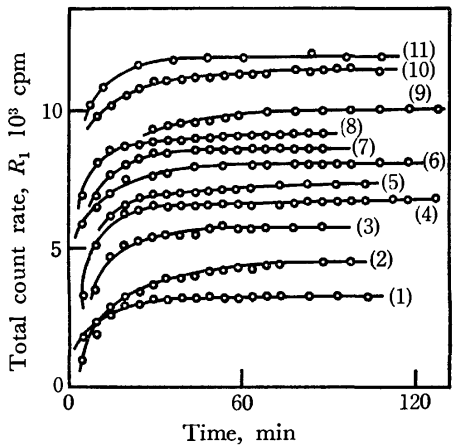

Fig. 1. Time dependence of total radioactivity, R_1, over solution surface.
Concentration of NDA (10^{-5} mol/l)
(1) 0.451 (2) 0.756 (3) 1.06 (4) 1.71
(5) 4.12 (6) 10.7 (7) 17.1 (8) 22.7
(9) 43.0 (10) 85.6 (11) 120.0

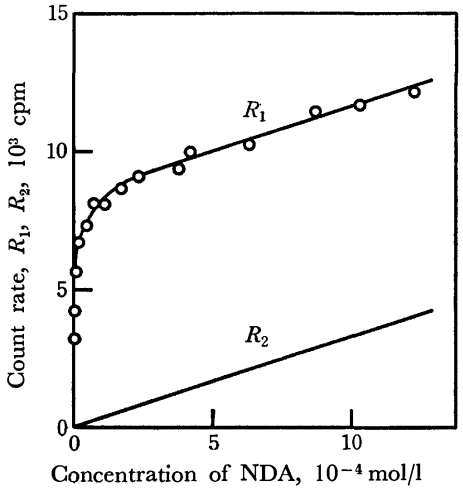

Fig. 2. Total and bulk radioactivities *vs.* concentration.

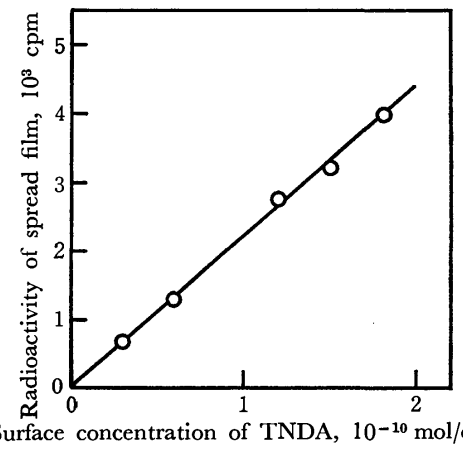

Fig. 3. Surface radioactivity *vs.* surface concentration.

where k is the conversion factor. Figure 3 shows the relation between the surface concentration of TNDA spread on the surface of a saturated ammonium nitrate solution and the radioactivity due to the spread film. The k value was calculated from the slope as 4.55×10^{-14} mol/cm²/cpm.

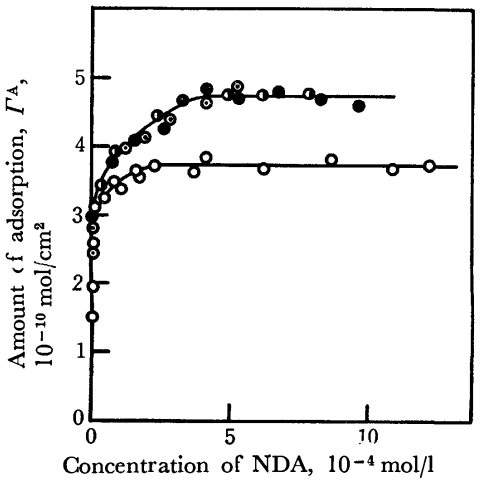

Fig. 4. Adsorption of NDA at aqueous surface.
Addition of ○: 0 mol/l NaCl, near neutral pH, ●: 1 mol/l NaCl, near neutral pH ⊙: 1 mol/l NaCl, pH 2.0 ◑: 1 mol/l NaCl, pH 12.0

The amounts of adsorption, Γ^A, with and without added salt plotted against the concentration of NDA near a neutral pH are shown in Fig. 4. The amounts of adsorption increase with the concentration and attain saturated value of 3.73×10^{-10} mol/cm² above a concentration of about 2×10^{-4} mol/l in the absence of added salt, and value of 4.74×10^{-10} mol/cm² above a concentration of about 4×10^{-4} mol/l in the presence of 1 mol/l NaCl.

The effect of the pH on the adsorption was studied further, since an ampholytic surfactant was expected to be sensitive to changes in the pH. However, the adsorption isotherm for the NDA systems of pH 2 and 12 in the presence of 1 mol/l NaCl showed no detectable change in the amount of adsorption, as is shown in Fig. 4. This may be explained as being due to the contraction of the ionic atmosphere around the polar head caused by the addition of concentrated NaCl, which makes NDA less ionic in nature.

In Table 1, the saturated amount of adsorption of NDA near the neutral pH obtained in the present study is compared with that of sodium dodecylsulfate(SDS),[5] an anionic surfactant, or hexaoxyethylenedodecylmonoether($D(EO)_6$),[6] a nonionic surfactant, with equal lengths of the hydrocarbon chain. The amount is larger for NDA than for the other two substances, perhaps because of the neutralization of the charges of the NDA polar head groups by intra- and/or inter-

Table 1. Saturated amount of adsorption near neutral pH

Surfactants	Amount of adsorption (10^{-10} mol/cm²)
NDA	3.73 (30 °C)
SDS	3.19 (25 °C)[5]
$D(EO)_6$	2.73 (30 °C)[6]

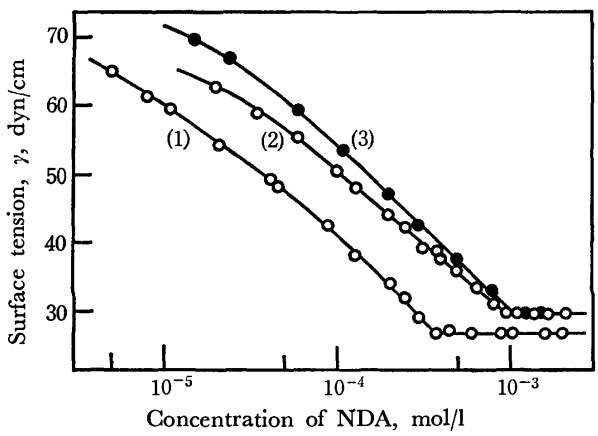

Fig. 5. Surface tension *vs.* concentration of NDA curve.
(1) presence of 1 mol/l NaCl (Wilhelmy plate method)
(2) absence of added salt (Wilhelmy plate method)
(3) absence of added salt (drop weight method)

molecular salt formation in the isoelectric region.

Surface Tension. Figure 5 shows the curves of the surface tension *vs.* the concentration of NDA with and without 1 mol/l NaCl. It may be seen in Fig. 5 that, in the absence of added salt, the slope is constant in the region of NDA concentrations from about 2×10^{-4} mol/l to the CMC, while in the presence of added salt the slope gradually increases up to the CMC. The data obtained by the drop weight method in the former case are also plotted in Fig. 5 as filled circles. It may be seen that the values obtained by the drop weight method are higher than those obtained by the Wilhelmy method; the former values cannot be used for further calculation, as will be discussed later.

The Gibbs Adsorption Isotherm. The Gibbs adsorption isotherm is written, in a general form, as[11]

$$-\mathrm{d}\gamma/RT = \sum_i \Gamma_i \,\mathrm{d}\ln a_i \qquad (1)$$

where γ denotes the surface tension, and Γ_i and a_i, the surface excess and the activity of the i'th solute respectively.

1. *The Case of the Absence of Added Salt*: Equation (1) may be rewritten for an ampholytic surfactant solution as:

$$-\mathrm{d}\gamma/RT = \Gamma_{A^\pm}\,\mathrm{d}\ln C_{A^\pm} + \Gamma_{A^+}\,\mathrm{d}\ln C_{A^+} + \Gamma_{A^-}\,\mathrm{d}\ln C_{A^-} + \Gamma_{H^+}\,\mathrm{d}\ln C_{H^+} + \Gamma_{OH^-}\,\mathrm{d}\ln C_{OH^-} \qquad (2)$$

where the subscripts $A^\pm$, A^+, A^-, H^+ and OH^- refer to the zwitterion, the cation, the anion of the ampholyte NDA, the hydrogen ion, and the hydroxide ion respectively. Since the concentration of the surfactant used is of the order of magnitude of 10^{-4} mol/l, the acitivity terms in Eq. (2) may safely be replaced by the concentration.

Further, we obtain the following relations:

$$K_1 = C_{A^\pm}C_{H^+}/C_{A^+} \qquad (3)$$

$$K_2 = C_{A^-}C_{H^+}/C_{A^\pm} \qquad (4)$$

$$K_w = C_{H^+}C_{OH^-} \qquad (5)$$

$$\Gamma_{A^+} + \Gamma_{H^+} = \Gamma_{A^-} + \Gamma_{OH^-} \qquad (6)$$

where K_1 and K_2 express the first and second dissociation constants of NDA, considered as a dibasic acid, and K_w, the dissociation constant of the water. Equation (6) represents the electrical neutrality of the adsorbed ionic species. By substituting the logarithmic forms of Eqs. (3) and (4) into Eq. (2), we obtain:

$$-\mathrm{d}\gamma/RT = (\Gamma_{A^\pm}+\Gamma_{A^+}+\Gamma_{A^-})\,\mathrm{d}\ln C_{A^\pm} + (\Gamma_{A^+}-\Gamma_{A^-}+\Gamma_{H^+})\,\mathrm{d}\ln C_{H^+} + \Gamma_{OH^-}\,\mathrm{d}\ln C_{OH^-} \qquad (7)$$

Here, we used these notations:

$$\Gamma^A = \Gamma_{A^\pm} + \Gamma_{A^+} + \Gamma_{A^-} \qquad (8)$$

as the total adsorption amount of NDA, and

$$C^A = C_{A^\pm} + C_{A^+} + C_{A^-} \qquad (9)$$

as the total bulk concentration of NDA. By substituting Eqs. (5), (6) and (8) into Eq. (7) we obtain:

$$-\mathrm{d}\gamma/RT = \Gamma^A\,\mathrm{d}\ln C_{A^\pm} \qquad (10)$$

Further, from Eqs. (3), (4) and (9) we obtain this relation:

$$\mathrm{d}\ln C_{A^\pm} = \mathrm{d}\ln C^A + [(C_{A^-}-C_{A^+})/C^A]\,\mathrm{d}\ln C_{H^+}$$

which, together with Eq. (10), gives:

$$-\mathrm{d}\gamma/RT\,\mathrm{d}\ln C^A = \Gamma^A[1+K(\mathrm{d}\ln C_{H^+}/\mathrm{d}\ln C^A)] \qquad (11)$$

where:

$$K = (C_{A^-}-C_{A^+})/C^A$$

On the other hand, using Eqs. (3), (4), and (9), we obtain:

$$K = (K_1K_2-C_{H^+}^2)/(C_{H^+}^2+K_1C_{H^+}+K_1K_2) \qquad (12)$$

In the pH region near the isoelectric point, the second term in the brackets of Eq. (11) is calculated using these experimental data: $K_1=3.1\times10^{-4}$, $K_2=1.3\times10^{-10}$ mol/l, $C_{H^+}=10^{-6}$ mol/l and $(\mathrm{d}\ln C_{H^+}\ \mathrm{d}\ln C^A)<0.1$ for the present experimental conditions of $C^A=10^{-4}$ to 10^{-3} mol/l. The order of magnitude is about 10^{-4}, which is negligible compared with unity. Thus, Eq. (11) can eventually be reduced for the NDA solution to a simple form,

$$\Gamma^A = -\mathrm{d}\gamma/RT\,\mathrm{d}\ln C^A \qquad (13)$$

2. *The Case of the Presence of Excess Added Salt*: In the presence of excess NaCl (1 mol/l in the present study) Eq. (1) still holds, since $\mathrm{d}\ln C_{Na^+}=0$, and $\mathrm{d}\ln C_{Cl^-}=0$. Therefore, the calculations are the same as in the case of Eqs. (1) to (5). The electrical neutrality of the adsorbed ionic species is expressed, instead of Eq. (6), as:

$$\Gamma_{Na^+} + \Gamma_{A^+} + \Gamma_{H^+} = \Gamma_{Cl^-} + \Gamma_{A^-} + \Gamma_{OH^-}$$

Therefore, the equation corresponding to Eq. (10) may be written as:

$$-\mathrm{d}\gamma/RT = \Gamma^A\,\mathrm{d}\ln C_{A^\pm} + (\Gamma_{Cl^-}-\Gamma_{Na^+})\,\mathrm{d}\ln C_{H^+}$$

and Equation:

$$-\mathrm{d}\gamma/RT\,\mathrm{d}\ln C^A = \Gamma^A + (K\Gamma^A+\Gamma_{Cl^-}-\Gamma_{Na^+}) \times (\mathrm{d}\ln C_{H^+}/\mathrm{d}\ln C^A) \qquad (14)$$

is obtained instead of Eq. (11).

It should be noted that Eq. (14) holds also for the system in the presence of HCl or NaOH so long as NaCl is present in a larger amount than the other solute. Therefore, if the pH is also kept, or happens to be constant, the second term of Eq. (14) may drop and a

simple equation may result:

$$\Gamma^{A} = -(d\gamma/RT\, d\ln C^{A})_{pH,\ excess\ NaCl} \quad (15)$$

The condition of Eq. (15) was actually satisfied for the ampholyte NDA containing excess NaCl without added acid or alkali.

Calculation of the Adsorption Amount by Means of the Gibbs Adsorption Isotherm. The amount of adsorption, calculated from the data of Fig. 5 by applying Eqs. (13) and (15), is shown by Curves A, B and C in Fig. 6. The figure also contains, for the sake of comparison, the results by Durham[4] by the use of the drop weight method (Curve D). It may be seen that the values obtained by the radiotracer method for the systems both with and without added salt are in good agreement with those calculated from the data obtained by the Wilhelmy plate method (A and C). The values calculated from the data obtained by the drop weight method (B and D) are, however, distinctly higher than the observed ones. The disagreement of the values obtained by the drop-weight method may be ascribed to the application of the Gibbs adsorption isotherm to the nonequilibrium surface tension data.

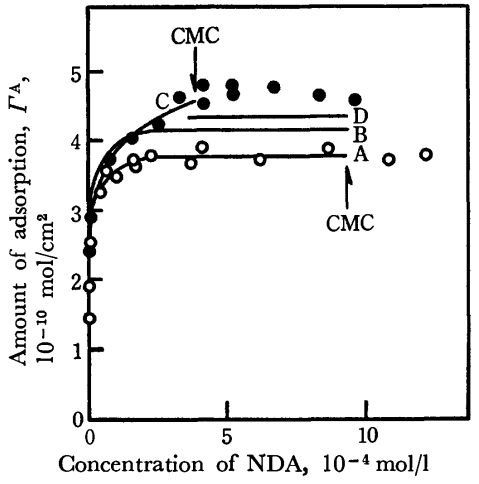

Fig. 6. Observed and calculated values.
Observed values: ○; in the absence of added salt
●; in the presence of 1 mol/l NaCl
Calculated values: in the absence of NaCl; (A) Wilhelmy plate method, (B), (D)[4] drop weight method, in the presence of 1 mol/l NaCl; (C) Wilhelmy plate method.

Thus, the agreement between the calculated and observed values indicates the validity of the Gibbs adsorption isotherm derived in the present study. It is confirmed experimentally that, for aqueous ampholytic surfactant solutions in an isoelectric region, where $K_1K_2 \fallingdotseq C_{H^+}^2$ and where, therefore, $K \fallingdotseq 0$, the Gibbs adsorption isotherm is applicable in a form similar to that used for a nonionic surfactant.[6] This can be also explained by the quasi-nonionic nature of the ampholytic surfactant NDA due to the intra- and/or intermolecular neutralization of the charges of polar heads in the solution of its isoelectric region, as has been pointed out with regard to the dependence of the critical micelle concentration on the temperature and added salt,[2] and with regard to a relatively large amount of the saturated adsorption of NDA mentioned above.

References

1) K. Tori and T. Nakagawa, *Kolloid-Z.*, **187**, 44 (1963); *ibid.*, **188**, 47 (1963); *ibid.*, **191**, 42 (1963); A. H. Beckett and R. J. Woodward, *J. Pharm. Pharmcol.*, **15**, 422 (1963); P. Molyneux, C. T. Phodes, and J. Swarbrick, *Trans. Faraday Soc.*, **61**, 1043 (1965); J. Swarbrick and J. Daruwala, *J. Phys. Chem.*, **74**, 2627 (1969); *ibid.*, **74**, 1293 (1970); K. W. Herrmann, *J. Colloid Sci.*, **22**, 352 (1966); F. Tokiwa and Ohki, *J. Phys. Chem.*, **71**, 1824 (1967).
2) T. Okumura, K. Tajima, and T. Sasaki, This Bulletin, **47**, 1067 (1974).
3) Tori and T. Nakagawa, *Kolloid-Z.*, **189**, 50 (1963); *ibid.*, **191**, 48 (1963).
4) K. Durham, 3rd Int. Congr. Surface Active Substances, **2**, 130 (1960).
5) K. Tajima, M. Muramatsu, and T. Sasaki, This Bulletin, **43**, 1991 (1970); K. Tajima, *ibid.*, **43**, 3063 (1970).
6) K. Tajima, M. Iwahashi, and T. Sasaki, *ibid.*, **44**, 3251 (1971).
7) to be published.
8) T. L. Gresham, J. E. Jansen, F. W. Shaver, R. A. Bankert, and F. T. Friedorek, *J. Amer. Chem. Soc.*, **73**, 3161 (1951).
9) M. Koshinuma, A. Nakamura, T. Seimiya, and T. Sasaki, This Bulletin, 45, 344 (1972).
10) M. Nakamura, and T. Sasaki, *ibid.*, **43**, 3367 (1970).
11) E. A. Guggenheim, "Thermodynamics," North Holland Publishing Co., Amsterdam (1957), p. 50.

The Adsorption of the Aminoethyl Derivatives of Poly(vinyl alcohol) onto Bemberg Rayon Fibers[1)]

Mitsuo HIGUCHI, Takatoshi KOYAKUMARU,* and Ryoichi SENJU

Department of Forest Products, Faculty of Agriculture, Kyushu University, Hakozaki, Higashi-ku, Fukuoka 812

(Received July 24, 1974)

A series of aminoethyl derivatives of poly(vinyl alcohol) was synthesized, and their adsorption behavior onto a cellulosic fiber was investigated. The results indicate that the primary factor causing adsorption is the charge interaction at the solid-liquid interface; the adsorption was suppressed as the concentration of a foreign salt (NaCl) exceeded 0.02 M, and polymers bearing no cationic group poly(vinyl alcohol) and its aminoethyl derivatives in the un-ionized state) exhibited no appreciable adsorption. The results also demonstrate that the primary variable controlling the amount of adsorption is the charge density on the polymer; the amount of adsorption increases steeply with an increase in the charge density up to a maximum, and then decreases with the increase in the charge density.

Although numerous papers have been published and a considerable amount of information has been accumulated on the adsorption of macromolecules from solution onto solid surfaces, those concerned with polyelectrolytes are comparatively few and insufficient;[2)] therefore, it seems desirable to accumulate additional experimental data. This paper will present our findings on the adsorption of a polyamine of a hydrophilic nature from aqueous solutions onto a solid of a hydrophilic nature. Incidentally, though more than 50 kinds of cationic polymers have appeared up to the present time in the literature, there are few polymers which have only primary amino groups as ionizable groups and which are, besides, soluble in water over a wide pH range. The present authors synthesized a series of aminoethyl derivatives of poly(vinyl alcohol). These polymers are unique in bearing primary amino groups together with hydroxyl groups and in their hydrophilic nature.

Experimental

Materials. A Bemberg rayon fiber, considered to have the smoothest surface among cellulosic fibers, was used as the adsorbent. The fibers were 1.31 den and 2 mm in length, with round sections 12 μ in diameter. The adsorbent was subjected to five 24 hr soaks in ethanol and four 24 hr soaks in distilled water to remove the scouring agents and any other impurities. The geometrically-calculated surface area of the fibers was 3500 cm^2/g in the wet state.

Aminoethyl derivatives of poly(vinyl alcohol) and cellulose, (henceforth referred to as AEPVA and AEC respectively) were prepared through the Hofmann degradation of the corresponding carbamoylethyl derivatives. The carbamoylethyl derivatives were prepared by means of a Michael reaction of acrylamide, with care taken to avoid the formation of carboxyl groups by using a large excess of acrylamide at low temperatures (10~15 °C). A water-soluble derivative of cellulose was prepared by dissolving cotton linters in a 40% benzyltrimethylammonium hydroxide solution and by then adding a large amount of a 35% acrylamide aqueous solution. Polymers of above 99% conversion of the carbamoylethyl group into the aminoethyl group were used as the adsorbates. The variation in the amino-group content of the polymers was accomplished by the control of the degree of carbamoyl-

* Present address: Technical Research Institute, Rengo Co., Ltd., Oohiraki-cho, Fukushima-ku, Osaka 553.

TABLE 1. POLYMERS STUDIED

Polymer	Code	DS[a)]	E.W.[b)]	$[\eta]$[c)]
Poly(vinyl alcohol)	PVA	0		0.645[d)]
Hydroxyethylated poly(vinyl alcohol)	HEPVA	0.05		0.623
Aminoethylated poly(vinyl alcohol) (AEPVA)	1	0.043	1066.3	0.641
	2	0.095	506.2	0.502
	3	0.150	336.3	0.630
	4	0.204	258.7	0.714
	5	0.260	212.2	0.345
	6	0.260	212.2	0.725
	7	0.260	212.2	0.903
	8	0.278	201.3	0.802
Aminoethylated cellulose	AEC	1.01	203.4	3.23

a) Degree of substitution: per monomer unit for HEPVA and AEPVA, per AGU for AEC. b) Equivalent molecular weight per amino group. c) Intrinsic viscosity in a 1M-$NaNO_3$ solution at 30 °C. d) Number-averaged molecular weight: *ca.* 6×10^4

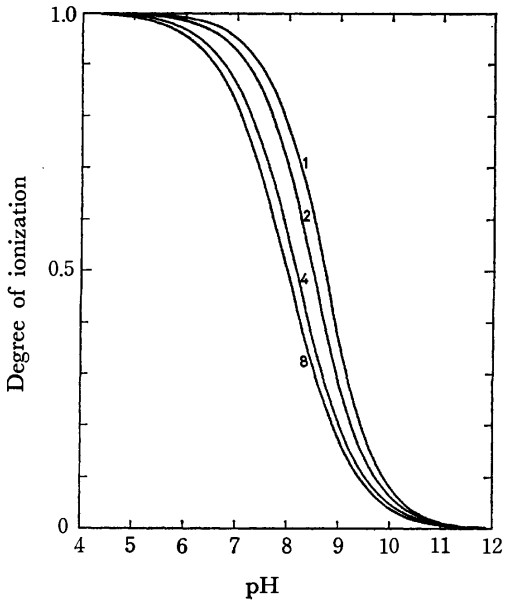

Fig. 1. Relationships between pH and degree of ionization for AEPVA.
The numbers 1, 2, 4, and 8 denote the code numbers for the polymers in Table 1.

ethylation. The aminoethyl derivatives were subjected to fractional precipitation in a 0.5 M sodium acetate aqueous solution, with acetone as the precipitant. All the adsorbates were purified from about 0.1 M NaOH solutions by dialysis in deionized water. The properties of the polymers used are shown in Table 1, while the relationships between the pH and the degree of ionization of the aminoethyl derivatives are shown in Fig. 1.

Adsorption Procedure. A weighed quantity of wet fibers (net 2 g) and 100 ml of a polymer solution of a known concentration were enclosed in a 150-ml polystyrene vessel and shaken for 24 hr at 20 °C. After this process, the pH of the mixture was measured using a Hitachi-Horiba F5 pH meter; then the fibers were filtered off, and the solution was analyzed. The amount of adsorption was calculated from the difference in the polymer concentration measured before and after the adsorption process. The pH of the adsorption system was set by the use of acetic acid, ammonia, HCl, or NaOH.

Analytical Methods. Colloid titration[3] was used to determine the concentration of the aminoethyl derivatives before and after each adsorption run. An aliquot portion of the polymer solution was taken, buffered to pH 4 with acetic acid, and then titrated with a N/500 potassium poly(vinyl sulfate) solution, using toluidine blue as the indicator.

A spectrophotometric method[4] was used for the determination of the concentrations of poly(vinyl alcohol) (PVA) and its hydroxyethyl derivative (HEPVA). The absorbance of the colored PVA-iodine complex formed in the presence of boric acid was measured at 660 mμ.

The degree of ionization of the aminoethyl derivatives was calculated from the results of pH titration. A 200-ml portion of a N/200 AEPVA solution was titrated with M/10 HCl at 20 °C under a N_2 atmosphere by the use of a Hitachi-Horiba F5 pH meter.

Results

Adsorption of PVA and HEPVA. No appreciable adsorption took place in the 3∼12 pH range, in contrast with the cases of the adsorption of PVA from aqueous solutions by titanium dioxide[5] or by sodium montmorillonite.[6] This result demonstrates that neither hydrogen bonding nor hydrophobic interactions come into play to cause adsorption in this cellulose–PVA–water system.

Effect of the pH on the Adsorption of AEPVA. As the example (Fig. 2) shows, the saturation adsorption capacity is greatly dependent on the pH of the system. The amount of adsorption increased as the pH increased, but to only a small extent in the 3∼7 pH range, steeply above pH 8, and attained to a maximum at a pH of about 10.3. Above this point, the adsorption capacity decreased steeply with the increase in pH; no appreciable adsorption took place above pH 12.

Effect of the Amino-group Content. Table 2 shows the amounts of the maximum adsorptions of AEPVA of various amino-group contents at pH 4.5 and 10.9. At pH 4.5, the amount of adsorption decreased with the increase in the amino-group content; this is consistent with the earlier finding that the increase in the charge density on the macromolecule causes a decrease in the adsorption.[2] At pH 10.9, however, the amount of adsorption increased with the increase in the amino-group content. The amount of the ionized amino group in the polymer adsorbed also varied with the amino-group content; this fact indicates that the stoichiometric interaction between the surface charge and the polymer charge does not alays determine the amount of adsorption.

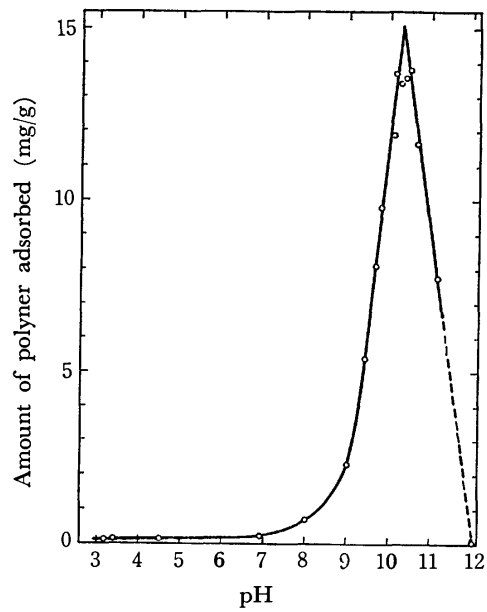

Fig. 2. Variation of the adsorption capacity with pH. Adsorbate: AEPVA-8. Concentration of foreign electrolytes added: 0.001 N.

Table 2. Amounts of maximum adsorption of AEPVA of various amino-group contents at pH 4.5 and 10.9

AEPVA	Amino-group content[a]	Amount adsorbed: Polymer weight (mg/g)		Amount adsorbed: Ionized amino group[b] (eq/g) × 10^6	
		pH 4.5	pH 10.9	pH 4.5	pH 10.9
1	0.043	5.6		5.2	
2	0.095	2.0	3.7	4.0	0.06
3	0.150	0.6	4.5	1.8	0.10
4	0.204	0.3	5.3	1.2	0.14
6	0.260	0.2	6.7	0.8	0.20
8	0.278	0.1	8.9	0.5	0.26

a) Number of the amino group per vinyl monomer unit. b) Calculated from the amount adsorbed, the amino-group content, and the degree of ionization of the corresponding polymer.

Effect of Molecular Size. Figure 3 shows that the dependence of the amount of adsorption on the molecular size of the polymer is very small in comparison with that on the amino-group content at both pH 4.5 and pH 10.9. This result may confirm that the fiber surface is nonporous with regard to the adsorption of the polymers used.

Effect of Electrolyte Added. Figure 4 shows the effects of the NaCl concentration on the adsorption of AEPVA at pH 4.5 and 10.9. At pH 4.5, the addition of NaCl increased the amount of adsorption until its concentration reached about 5×10^{-3} mol/l; above this point, however, it had an inverse effect, and no ap-

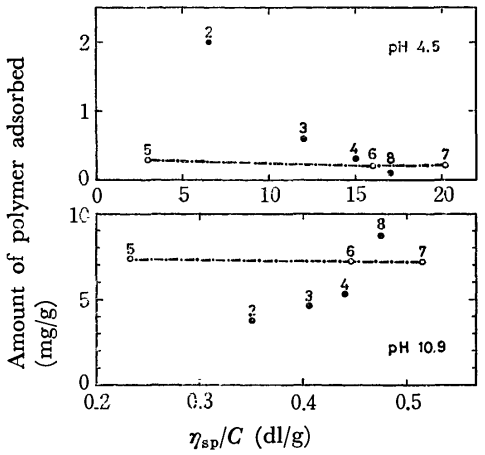

Fig. 3. Plots of the adsorption capacity against a parameter for polymer coil dimension. The numbers, 2~8, denote the code numbers for AEPVA. AEPVA-5, -6, and -7 have the same amino-group content. The variation of the adsorption capacity can be ascribed to the effect of the amino-group content; the dotted lines show very little effect of the size of polymer moleculcs.

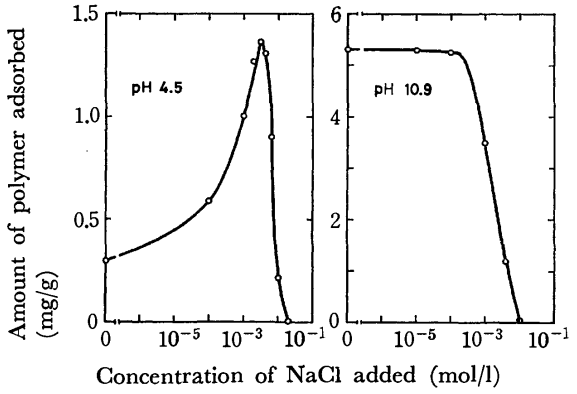

Fig. 4. Variation of the adsorption capacity with the concentration of NaCl added. Adsorbate: AEPVA-4.

preciable adsorption took place when the concentration of NaCl exceeded 2×10^{-2} mol/l. At pH 10.9, the amount of adsorption always decreased as the concentration of NaCl increased. These phenomena suggest that the primary driving force of adsorption is the electrostatic force of attraction between the solid surface and the solute polymer.

Comparison of the Adsorption Behavior of AEPVA with That of AEC. Figure 5 shows the adsorption isotherms for the AEPVA of a flexible chain and for the AEC of a rigid chain. The two polymers used are alike in amino-group content and in molecular weight. At pH 4.5, the adsorption behavior of AEPVA is almost identical with that of AEC; this result suggests that the AEPVA molecules as well as AEC molecules are adsorbed in a stretched (and flat) conformation at the surface. On the other hand, at pH 10.9, there is a remarkable difference between the adsorption isotherm for AEPVA and that for AEC. This may be due to the difference in molecular shape at the surface.

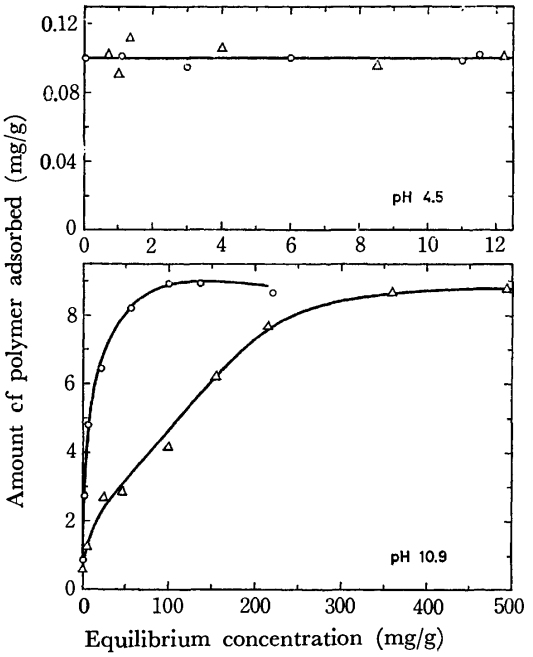

Fig. 5. Comparison of the adsorption behavior of AEPVA with that of AEC.
(○): AEPVA-8, (△): AEC.

Discussion

The results of the adsorption of PVA and the effect of the pH on the adsorption of AEPVA indicate that the aminoethyl group is essential for the adsorption of AEPVA and that the un-ionized amino group plays no important role in the adsorption. Considering these

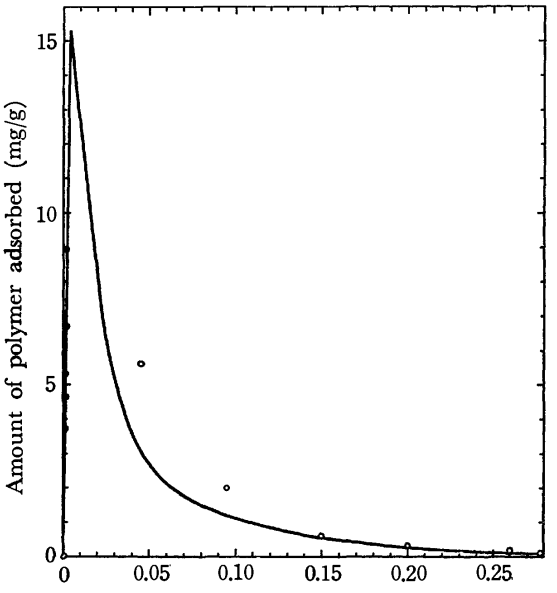

Fig. 6. Dependence of the adsorption capacity on the polymer charge-density.
Solid curve: calculated from the data on the pH-dependence of the adsorption of AEPVA-8 (Fig. 2).
Points: calculated from the data on the absorption of AEPVA of various amino-group contents at fixed pH (○: pH 4.5, ●: pH 10.9).

facts in connection with the fact that the adsorption is suppressed when the NaCl concentration is increased above 0.02 mol/l, we can conclude that the primary factor causing adsorption in this cellulose-AEPVA–water system is the charge interaction at the solid-liquid interface.

It can also readily be noticed that the positive charge on AEPVA is the primary variable controlling the amount of adsorption. The dependence of the maximum amount of adsorption on the charge density of AEPVA is illustrated in Fig. 6. It is clear that the amount of adsorption is a function of the charge density on the polymer, though the variation in the charge density on the fiber surface with the pH is not taken into account in this figure. The adsorption increases steeply in approximate proportion to the charge density up to a maximum, at which the solute polymers bear the ionized amino groups in a ratio of 1 to 200~300 of vinyl monomer units, and then decreases with the increase in the charge density. Incidentally, at the point of maximum adsorption about 500 vinyl monomer units, in a rough estimation, are found per 100 Å^2 of fiber surface; if it were assumed that the polymer molecules are adsorbed in a spherical conformation at the surface, this signifies multilayer surface coverage, while if monolayer adsorption were assumed, it indicates that polymers are attached to the surface by a few segments in long loops extending out into the liquid phase. On the other hand, at the point of the ionized-amino-group content (0.278), only 3 vinyl monomer units are found per 100 Å^2 of fiber surface; this corresponds to only a one-third surface coverage even if a completely flat accommodation at the surface were assumed.

The steep rise in the adsorption capacity in the region of low-charge densities may be ascribed to the increase in the electrostatic force of attraction between the polymer and the fiber surface.

With regard to the decrease in the adsorption capacity with the increase in the charge density in the region of the ionized-amino-group content above 0.004, either of the following two explanations appears to be possible. First, it may be considered that the number of polymer molecules required to fill up the binding sites (anionic sites) of the fiber surface decreases as the positive charge on the polymer increases, thus leading to a reduction in the amount of polymer adsorbed. Another explanation is that the spatial requirement per molecule at the surface increases as the charge density of the polymer increases because of the expansion of the polymer coil by the intramolecular repulsion of the ionic groups, thus causing the reduction of the adsorption. However, in the region of higher charge densities these two explanations may be inadequate, because it is considered that, at some point (with regard to the charge density), polymers start to adsorb in a flat conformation at the surface and that, from some point, the saturation of adsorption takes place, leaving a considerable amount of surface area uncovered. In this region, the reduction of adsorption may be ascribed to the increase in the electrostatic force of repulsion between the adsorbed polymer and the solute polymer.

The authors wish to express their appreciation to Professor Isao Sakata, Faculty of Agriculture, Kyushu University, for his valuable suggestions.

References and Footnotes

1) Derivatives of Natural Polymers and Their Applications. XI. Part X of this series: M. Higuchi, K. Takeshita, and R. Senju, This Bulletin, **47**, 1451 (1974).
2) This subject has recently been reviewed by B. J. Fontana, "The Chemistry of Biosurfaces," ed. by M. L. Hair, Dekker, New York (1971), p. 114.
3) R. Senju, *Kobunshi*, **22**, (256), 407 (1973).
4) J. H. Finley, *Anal. Chem.*, **33**, 1925 (1961).
5) K. Nakanishi, *Rep. Progr. Polym. Phys. (Japan)*, **5**, 52 (1962).
6) D. J. Greenland, *J. Colloid Sci.*, **18**, 647 (1963).

Interaction between Water and Hydroxylated Surface of Silica-Alumina

Tetsuo MORIMOTO, Mahiko NAGAO, and Junichiro IMAI

Department of Chemistry, Faculty of Science, Okayama University, Tsushima, Okayama 700

(Received May 13, 1974)

The interaction between water and the fully-hydroxylated surfaces of silica,alumina and silica-alumina has been investigated by measuring the physisorption isotherms of water at three temperatures and by computing the isosteric heat of adsorption and the site energy distribution therefrom. The number of adsorption site evaluated on the surfaces of each of the two component oxides decreases exponentially with the increase in the site energy, whereas that of the silica-alumina samples gives a peak at a relatively high energy region, suggesting the presence of strong water-physisorption sites characteristic to silica-alumina. These results can be elucidated on the basis exponentially of the postulation that new sites having protonic acid character appear when the two component oxides contact with each other, as described previously. Furthermore, it is found that the strength of such new sites for physisorption of water increases with decreasing content of alumina in silica-alumina.

Silica-alumina is one of the solid-acid catalysts; its interactions with basic molecules such as ammonia[1-6] and amines[7,8] are widely studied, while the quantitative investigations on the interactions with water are very few, though the fact that the Lewis acid sites on silica-alumina can transfer to the Brönsted acid sites by adsorbing water molecules is well known.[1,9]

In the preceding paper,[10] the present authors described a finding that the number of sites for the physisorption of water on silica-alumina is more than the number calculated from the simple addition of the values obtained on each component oxide. This result was explained by postulating the appearance of new sites for water physisorption in the vicinity of the contact region of the two component oxides. The postulation predicts the new sites thus formed to have the character of protonic acid sites. The measurements of the infrared spectrum of *n*-butylamine adsorbed on the same samples of silica-alumina substantiated the appearance of strong protonic acid sites which are absent on the surfaces of the individual oxides, the strength of which increases with decreasing amount of alumina in silica-alumina.[11] Here, it must be interesting to study the energetic aspect of the interaction between water molecules and the new sites produced on silica-alumina.

On working the thermodynamics of water physisorption on the surfaces of a metal oxide, however, difficulties arise in the preparation of the surface. The present authors have intended to study the surface properties of metal oxides in relation to the amount of chemisorbed species such as CO_2 and hydroxyl groups.[12-14] During the course of this study, it has become clear that the surface of metal oxides usually adsorbs water at a time physically and chemically at room temperature, the desorbability of the chemisorbed water being dependent upon the nature of the oxides.[12] Furthermore, the rate of chemisorption of water on silica was found to be considerably smaller than that on the other oxides.[10]

The purpose of this work is therefore to prepare with special precautions the fully hydroxylated surfaces of silica-alumina, and then to study the energetics of the interaction of water with them by measuring the physisorption isotherms of water and by evaluating the differential heat of adsorption and the site energy distribution.

Experimental

Materials. The samples used in this study were the same as those used in the previous works.[10,11] Pure silica (S) was prepared by the hydrolysis of ethylsilicate in water. Pure alumina (A) was produced by hydrolysing aluminum isopropoxide in 2-propanol-water mixture. By mixing the two kinds of pure samples in aqueous gel state in an agate ball mill for 30 min, three kinds of silica-alumina samples containing 25, 50, and 75 wt% of alumina (SA-25, SA-50, and SA-75) were prepared. These gels were all washed with distilled water, dried at 100 °C for 20 hr, and calcined at 500 °C for 10 hr in air.

The specific surface area of the samples was determined by means of the BET method using the nitrogen adsorption at the temperature of liquid nitrogen, where the cross-sectional area of a nitrogen molecule was assumed to be 16.2 Å^2. The surface areas of the samples treated at 600 °C for 4 hr in a vacuum of 10^{-5} Torr were found to be 640, 189, 423, 427, 317 m^2/g for samples S, A, SA-25, SA-50, and SA-75, respectively.

Water Adsorption Isotherm. Water adsorption isotherms were measured volumetrically by using a conventional apparatus equipped with an oil manometer which serves to read sensitively the equilibrium pressure. In order to study the thermodynamics of water physisorption, it is necessary to prepare the completely-hydrated surfaces of the samples. For this purpose, the water adsorption procedure was performed in the following way. After degassing a sample at 600 °C for 4 hr, the first adsorption isotherm of water was measured at 25 °C. Next, the sample was exposed to the saturated water vapor at 25 °C for 12 hr in order to prepare the fully-hydroxylated surface, because the rate of surface hydroxylation of silica has been found to be considerably slow in a relatively low pressure of water.[10] Since the temperature at which surface hydroxyl groups start to be removed depends on the nature of oxides,[10,12] it will be delicate to establish the exact condition under which the physisorbed water is removed completely and all the surface hydroxyl groups are left. Here, in order to obtain a surface state reproducible and approximate to that described just above, the sample was subjected to the following treatment. The fully-hydroxylated surface was degassed at 30 °C for 4 hr in a vacuum of 10^{-5} Torr in order to remove physisorbed water, and then the second adsorption isotherm was measured at the same temperature as before. The degassing of the sample under the above condition and the measurement of adsorption isotherm at different temperatures (10, 18, and 25 °C) were further repeated on the same sample taken. The equilibrium

for the second adsorption was attained 30 min after each dose of water vapor. When the second adsorption measurement was carried out repeatedly at the same temperature after degassing the sample, the isotherms obtained were in good agreement with each other, which substantiates the reproducibility of the fully-hydroxylated surfaces of the samples and consequently the reliability of the thermodynamical data of physisorbed water calculated therefrom.

Results and Discussion

The first and second adsorption isotherms obtained on pure alumina are given in Fig. 1. The first adsorption isotherm involves the amounts of both physisorbed and chemisorbed water, while the second adsorption isotherm involves only physisorbed water; the difference between them should consequently be the amount of chemisorbed water.[12,14] Figure 2 shows the adsorption isotherms of water on silica. It can be seen from Fig. 2 that the shape of the adsorption isotherms on silica is quite different from that on alumina; the amount of adsorbed water in the second adsorption on silica is greater than that in the first one, contrary to the case of alumina. This queer phenomenon is considered to be due to a slow rate of rehydroxylation of the silica surfaces, as discussed in the previous paper.[10]

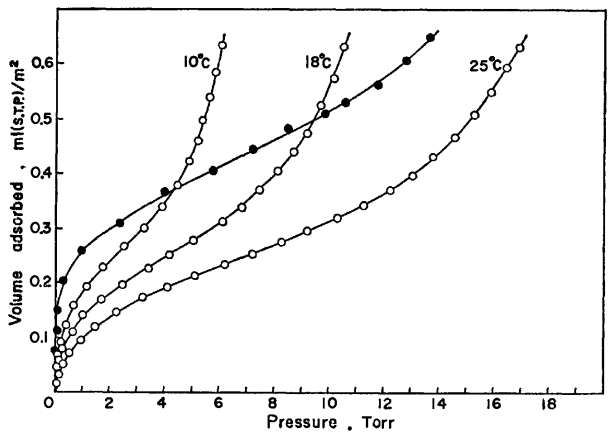

Fig. 1. Adsorption isotherms of water on alumina: ●, first adsorption at 25°C; ○, second adsorption on hydroxylated surface at 10, 18, and 25°C.

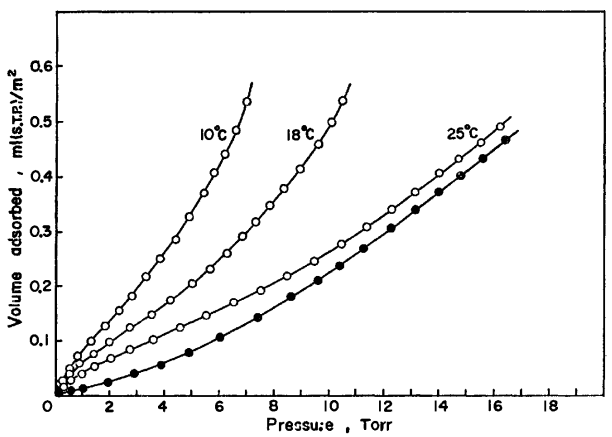

Fig. 2. Adsorption isotherms of water on silica: ●, first adsorption at 25°C; ○, second adsorption on hydroxylated surface at 10, 18, and 25°C.

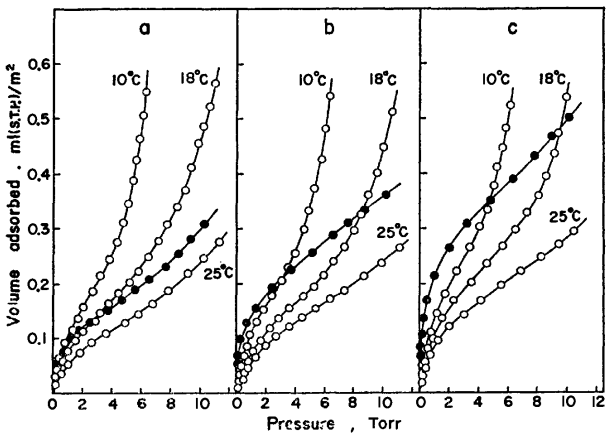

Fig. 3. Adsorption isotherms of water on silica-alumina: (a) SA-25, (b) SA-50, (c) SA-75; ●, first adsorption at 25°C; ○, second adsorption on hydroxylated surface at 10, 18, and 25°C.

The adsorption isotherms of water on the silica-alumina samples (SA-25, SA-50, and SA-75) are illustrated in Fig. 3. The sample SA-25 containing the least amount of alumina gives apparently the same type of isotherms as that of pure alumina, while the isotherms on the other samples are slightly modified from those of the sample SA-25. In addition, the difference between the first and the second adsorption isotherms seems to increase with the increase in alumina content.

From the physisorption isotherms obtained at different temperatures, the isosteric heat of adsorption, q_{st}, can be computed by using the Clausius-Clapeyron equation:

$$\frac{d\ln P}{dT} = \frac{q_{st}}{RT^2} \tag{1}$$

The isosteric heat q_{st} is the heat of adsorption at a constant amount of adsorption, being greater by RT than the differential heat of adsorption. Integrating the Eq. (1), we can obtain the equation (2):

$$\ln P = -\frac{q_{st}}{RT} + C \tag{2}$$

The value q_{st} can be determined from the slope of the linear plot of $\ln P$ *vs.* $1/T$. The value q_{st} thus obtained is represented in Fig. 4 as a function of the surface coverage θ, the latter being referred to the monolayer capacity of water calculated by applying the BET method to the second adsorption isotherm. Figure 4 shows that the q_{st} values obtained on all the samples tested decrease almost exponentially with coverage, which gives an evidence for the surface heterogeneity of hydroxylated surfaces for water physisorption, and that the strength of the sites depends on the nature of the substrates, being greater on aluminol than on silanol. On the surfaces of the silica-alumina samples, the interaction energies lie between those of the two pure oxides, but not additive. The isosteric heats on the surface of SA-25 are relatively larger than the others.

The differential entropy, $\bar{S}_s$, of adsorbed water can

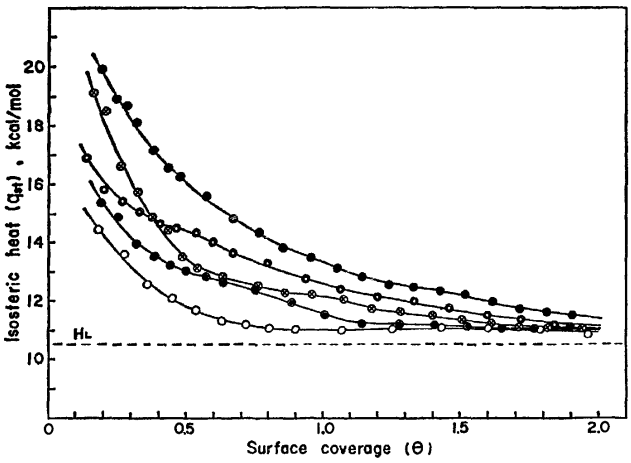

Fig. 4. Isosteric heat of adsorption of water physisorbed on silica, alumina, and silica-alumina: ○, S; ●, A; ◎, SA-25; ⊙, SA-50; ⊗, SA-75. Broken line indicates the heat of liquefaction of water at 25°C.

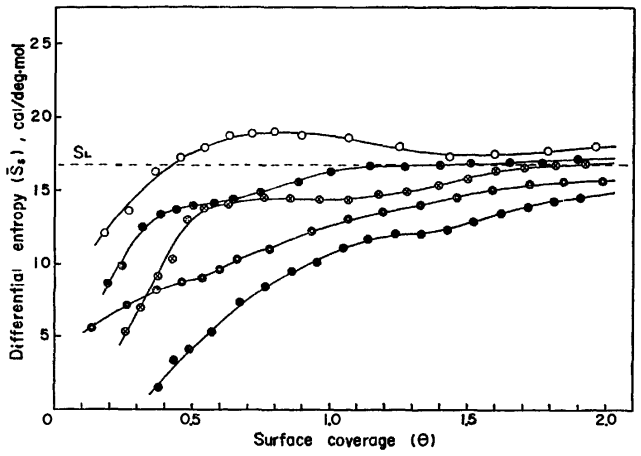

Fig. 5. Differential entropy of physisorbed water on silica, alumina, and silica-alumina: ○, S; ●, A; ◎, SA-25; ⊙, SA-50; ⊗, SA-75. Broken line indicates the entropy of liquid water at 25°C and 1 atm.

be calculated by the following equation:[15,16]

$$\bar{S}_s = -\frac{q_{st}}{T} + R \ln P_0/P + S_g^\circ \qquad (3)$$

Here, P_0 is the standard pressure, P the equilibrium pressure, and S_g° the standard entropy of water vapor (45.11 cal/deg·mol at 25 °C and 1 atm). Figure 5 shows the plots of the differential entropy against the coverage. It can be seen from Fig. 5 that water molecules are adsorbed more strongly on surface hydroxyl groups of alumina with less mobility than on those of silica. The entropy of water adsorbed on the surfaces of silica-alumina lies between those on the two single oxides.

Assuming that the number of adsorbed molecules expresses the number of sites, the site energy distribution can be estimated from the relation:[17]

$$g(\varepsilon) = \frac{dN}{d(H_d)} \qquad (4)$$

Here, N is the number of adsorption sites, and H_d the differential heat of adsorption. Practically, the

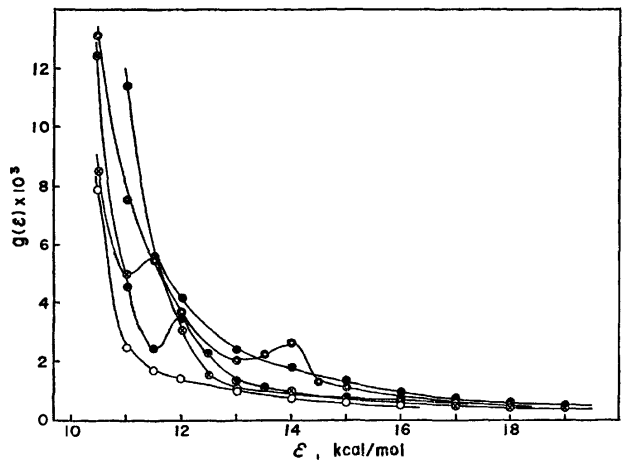

Fig. 6. Site energy distribution for the physisorption of water on silica, alumina, and silica-alumina: ○, S; ●, A; ◎, SA-25; ⊙, SA-50; ⊗, SA-75.

distribution can be calculated by the graphical differentiation of the plot of q_{st} *vs.* adsorbed amount. The site energy distribution curve thus obtained is represented in Fig. 6. Figure 6 shows that the number of adsorption sites with higher energies is much more on alumina than on silica, and that both curves decrease monotonously. On the other hand, the distribution curves on the silica-alumina samples reveal a marked peak at a higher energy region, which is not observed on the surfaces of each of the individual oxides. Furthermore, it is to be noted that the peak appears at the higher energy of adsorption on the silica-alumina samples containing the less amount of alumina: at 14, 12, and 11.5 kcal/mol for SA-25, SA-50, and SA-75, respectively. The appearance of these peaks may probably be associated with the new adsorption sites characteristic of the silica-alumina samples.

It has been known that there exist aprotonic acid sites on the surfaces of silica-alumina degassed at relatively higher temperatures, which can convert to protonic acid sites when exposed to water vapor.[1,9] In the preceding work,[11] it has been found that the infrared spectra of *n*-butylamine adsorbed on the present samples of silica-alumina have the band at 1540—1520 cm^{-1}, which is assigned to the symmetrical NH_3^+ bending vibration, and that the strength of this band decreases and at the same time the frequencies of the band shift to 1520—1503 cm^{-1} by pumping off the sample disk at elevated temperatures; these findings have never been observed on pure silica or alumina. The infrared studies have also led to another conclusion that the strength of the protonic acid sites increases with the decrease in the amount of alumina in silica-alumina. Similar conclusions obtained on the adsorption sites for *n*-butylamine as found by the infrared studies and for water as found by the present investigation seem to be explainable from the same stand point in the following way.

In the previous paper,[10] the formation of the additional physisorption sites for water on silica-alumina, which are absent on the surfaces of each of the component oxides, has been expressed schematically as

follows:

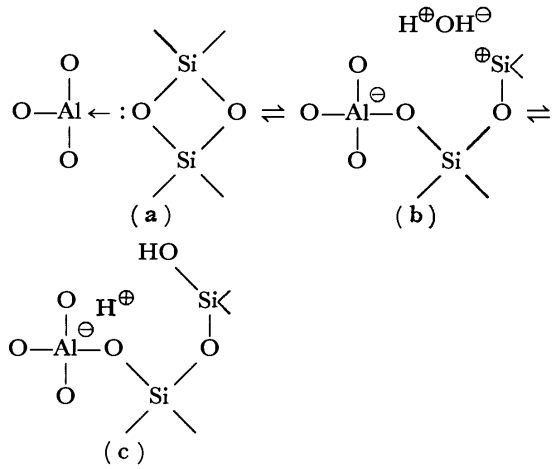

When the surfaces of both alumina and silica contact with each other, aluminum atom will attract the lone pair electrons on the oxygen atoms of silica owing to a strong electron-accepting ability of aluminum atoms (a); this will result in the splitting of Si–O–Si bonds and the formation of Al–O–Si bonds (b). When such surfaces are exposed to water vapor, a water molecule will be chemisorbed through the dissociation (c) to form a proton attached to an aluminum atom and a hydroxyl group bonded to a silicon atom. According to this proposition, a new type of sites formed should have the character of the Brönsted acid. It may be valid to consider that such an acidic site formed on silica-alumina acts as a stronger adsorption site for water compared to surface hydroxyl groups on each component oxide. Thus, the distribution curves on silica-alumina in Fig. 6 can be interpreted to reveal the overlapped effects of both the water adsorption to hydroxyl groups on heterogeneous surfaces through hydrogen bonding and that onto protonic sites, which appear to be relatively uniform in energy, through hydration.

In conclusion, three kinds of adsorbed water may thus be present in the first physisorption layer of water on silica-alumina:

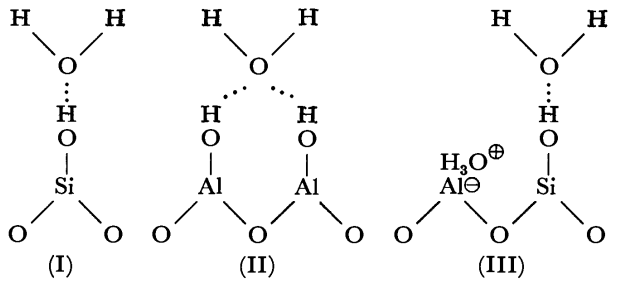

The physisorption mode on silica (I) is possibly due to the fact that the population of surface hydroxyl groups is fairly small (less than 5 OH's/100 Å^2),[18,19] the ratio of H_2O : OH being nearly equal to 1 : 1 as indicated in the previous work,[10] and that the interaction energy is rather smaller and moreover the mobility of the physisorbed water is higher as indicated in the present work.

On the surface of alumina, however, the situation may be different from the case of silica: a water molecule will be physisorbed on two hydroxyl groups (II). This can be led from the fact that the hydroxyl groups of about 14 OH's/100 Å^2 are present on the surface of alumina, the ratio of H_2O : OH being about 1 : 2;[10] this physisorption mode may also be supported by larger adsorption energies (Fig. 4) and smaller entropies of adsorbed water (Fig. 5), compared to those on silica or silica-alumina.

The additional physisorption mode of water (III) will appear on the new sites, which should be produced in the vicinity of the contact region of the two component oxides according to the present preparation method of the samples. The physisorption of water on such new sites, indeed, implies the hydration of proton on the surfaces. The heat of hydration of proton in solution is well known to be very large (258 kcal/g·ion).[20] Abnormally large heats of adsorption of water observed on the surfaces of silica-alumina can thus be interpreted by the hydration of proton sites which also act as the strong Brönsted acid sites. However, the fact that the strength of the site energy is greater on silica-alumina samples containing smaller amount of alumina remains to be solved.

References

1) J. E. Mapes and R. R. Eischens, *J. Phys. Chem.*, **58**, 1059 (1954).
2) A. Clark, V. C. F. Holm, and D. M. Blackburn, *J. Catal.*, **1**, 244 (1962).
3) P. Y. Hsieh, *ibid.*, **2**, 211 (1963).
4) A. E. Hirschler, *ibid.*, **6**, 1 (1966).
5) F. S. Stone and L. Whalley, *ibid.*, **8**, 173 (1967).
6) M. R. Basila and T. R. Kantner, *J. Phys. Chem.*, **71**, 467 (1967).
7) A. C. Zettlemoyer and J. J. Chessick, *ibid.*, **64**, 1131 (1960).
8) M. R. Basila, T. R. Kantner, and K. H. Rhee, *ibid.*, **68**, 3197 (1964).
9) E. P. Parry, *J. Catal.*, **2**, 371 (1963).
10) T. Morimoto, M. Nagao, and J. Imai, This Bulletin, **44**, 1282 (1971).
11) T. Morimoto, J. Imai, and M. Nagao, *J. Phys. Chem.*, **78**, 704 (1974).
12) T. Morimoto, M. Nagao, and F. Tokuda, This Bulletin, **41**, 1533 (1968).
13) T. Morimoto and K. Morishige, *ibid.*, **47**, 92 (1974).
14) T. Morimoto, M. Nagao, and F. Tokuda, *J. Phys. Chem.*, **73**, 243 (1969).
15) R. M. Barrer, *J. Colloid Interface Sci.*, **21**, 415 (1966).
16) J. E. Benson, K. Ushiba, and M. Boudart, *J. Catal.*, **9**, 91 (1967).
17) J. J. Chessick and A. C. Zettlemoyer, *J. Phys. Chem.*, **62**, 1217 (1958).
18) H. P. Boehm, *Advan. Catal.*, **16**, 179 (1966).
19) T. Morimoto and H. Naono, This Bulletin, **46**, 2000 (1973).
20) E. A. Moelwyn-Hughes, "Physical Chemistry," Pergamon, London (1957).

Phase Transition of Solid Hexabromoethane

Tsutomu KOIDE, Masami TSUJINO, Kazuhiro SAWADA, and Tsutomu ODA
Laboratory of Physical Chemistry, The Kyoiku University, Tennoji, Osaka 543
(Received June 12, 1974)

The phase transition point of solid hexabromoethane was found at 177 °C, above which the crystal is a body centered cubic lattice with two molecules in a unit cell, having a cell length of 7.80 Å at 185 °C. From an analysis of entropy change, it seems that random orientations of the molecular axis would occur at the transition point. The influence of halogen substitution is discussed. It was concluded that the phase transition will be dominated mainly by the geometrical properties of the molecules.

Many attempts were made to investigate the molecular behavior in the solid state of a series of hexasubstituted ethane derivatives. Consequently, it was revealed that the molecules easily obtain the freedom of rotational motion in the solid phase below the melting point because they have almost globular molecular shape and lose the freedom at the transition point on cooling.

From X-ray studies,[1] the molecules in the cubic phase (above 71 °C) of hexachloroethane, C_2Cl_6, assume statistically random orientation with their center of gravity at the lattice point.[2] This situation is supported by a small entropy of melting.[3] The orientational freedom of the molecule becomes frozen at the transition points, 45 and 71 °C, below which the crystal is no longer cubic and shows optical anisotropy.[4]

The small entropy of melting was also obtained for hexafluoroethane,[5] C_2F_6. Unfortunately, there is no crystal data of the solid state below the melting point. However, Lewis *et al.*[6] recently investigated the crystal structure below the transition point −169.18 °C[5] by the X-ray and the spectroscopic methods, and they indicated that there remained disorder concerning molecular orientation in the crystal lattice of the low temperature phase. The small entropy of melting and the result of Lewis *et al.* suggest that the molecule of the high temperature phase of C_2F_6 is in a state similar to the case of the highest temperature phase of C_2Cl_6.

The structure of hexabromoethane, C_2Br_6, at room temperature was investigated by Yardley[7] and analyzed in detail by Snaauw and Wiebenga.[8] Snaauw *et al.* also reported existence of two transition points in the solid state at 140—147 °C and about 210 °C from observation under a polarized microscope, and they suggested the highest temperature phase is probably cubic. However, there has been no crystal data on the highest temperature phase of C_2Br_6.

The object of this paper is in the first place to determine the temperature of the phase transition of solid C_2Br_6 by the thermal method and in the second place to discuss on the mechanism of phase transition in the solid state of C_2X_6 type molecules, where X denotes a halogen atom.

Experimental

The apparatus of differential thermal analysis (DTA) was reported in a previous paper.[9] The sample was sealed in a glass cell in order to prevent sublimation of sample.

For X-ray studies, a powder diffractometer (ADG-102 Toshiba Electric Co.) was used for room temperature investigations and a high-temperature X-ray camera was used for high temperature investigations. The powder sample was sealed in a thin walled Pyrex capillary tube. The temperature of the sample was measured by a copper-constantan thermocouple placed near the sample tube. The difference in temperature between the position of the thermocouple and the sample tube was calibrated beforehand.

The sample was prepared by bromination of hexachloroethane with bromine, following Korshak and Matveeva.[10] Aluminum powder, about 0.1 g, was added to a mixture of hexachloroethane (40 g) and bromine (160 g) in a flask at five-minute intervals over about six hours. The total aluminum added was 9.2 g. After the reaction, a solid mixture was treated with ethanol and recrystallized twice from benzene. The sample was further purified by sublimation at 50~55 °C in a vacuum of 10^{-1} Torr. Anal: C 4.8% (found), 4.77% (calcd.). By DTA measurement, the melting point was found to be 200 °C, accompanied by partial decomposition; literature values, 200~210,[10] above 210,[8] 198—199[11] and below 205 °C.[12]

Results

DTA measurement was carried out over a temperature range from −160 to 210 °C with a heating rate 1 °C min^{-1}. Two endothermic peaks appeared on the thermogram at 177 and 200 °C. The peak at 177 °C corresponds to the transition point of the solid phase. On cooling, the transition occurred at 168 °C. The heat of transition was estimated as 1.3±0.1 kcal mol^{-1} from the peak area referring the calibration curve, which corrected by comparison of peak areas of hexachloroethane (transition), naphthalene (melting), benzoic acid (melting) and potassium fluoride (melting). By slow heating under a polarized microscope the crystal, which shows birefrigence, became isotropic at 177 °C.

From X-ray diffracto-diagram of the powder sample, using CuK_α radiation, the following cell dimensions were obtained at room temperature; a=11.95, b=10.72 and c=6.72 Å. They are in good agreement with the results of Snaauw *et al.*,[8] a=12.00, b=10.64, c=6.67 Å, space group D_{2h}^{15} and also Yardley's data. Up to transition point, observed X-ray diagrams were almost the same as that obtained at room temperature.

At 185 °C, we obtained X-ray powder photographs, on which only three lines appeared. Referring to the optical isotropy of the high temperature phase, we could index the reflections with a body-centered cubic lattice containing two molecules in a unit cell. The edge length is 7.80 Å, the calculated density being 3.52 g cm^{-3}.

Discussion

Snaauw *et al.* reported two transition points in solid C_2Br_6 at 140~147 °C and 210 °C by optical observation. Their data are different from present result, 177 °C. We repeated DTA measurement and optical observation several times, but could not find any change at temperatures Snaauw reported. The reason for this discrepancy is not evident. Concerning the transition temperature, the other sample (sample II), prepared by short-time bromination of hexachloroethane (about 2.5 hr), showed two transition points at 162 and 178 °C, and it melted at 211 °C. The values of carbon content 5.06% in this sample II is quite different from the calculated one, 4.77%. A fluorescent X-ray analysis of sample II gives a content ratio as Br : Cl=8 : 1. The molecular formula $C_2Br_{5.33}Cl_{0.67}$ corresponds to 5.06% of carbon content. These results suggest that sample II should contain residual chlorine of hexachloroethane.

Since there are two molecules in the unit cell with a body-centered structure, it is reasonable to place the center of the molecules at the positions, *0,0,0* and *1/2, 1/2, 1/2*, of which the symmetry should be at least *T*-23. On the other hand, if we assume the molecule has a *trans*-configuration, the molecular point symmetry should be D_{3d}. In order that the molecule attains the cubic symmetry, it is necessary to take into account some statistical arrangements for explaining the structure of the crystal, as was done in the X-ray studies of other plastic crystals.[1,2] One of the statistical arrangements of the molecule is that the molecular axis (the central C–C bond) runs parallel to the four body-diagonals of the unit cell with equal probability.

Figure 1 shows the unit cell lengths of the cubic phases of hexasubstituted ethane derivatives as a function of the number of halogen atoms in a molecule. The unit cell length expanded slightly from 7.69 Å in $C_2(CH_3)_6$ to 7.80 Å in C_2Br_6 increasing with an increase in number of bromine atoms in a molecule, except for $C_2(CH_3)_5Br$, as shown by the solid line in Fig. 1. On the other hand, the unit cell length diminished with increasing number of chlorine atoms as shown by the dashed line. On view of carbon–halogen bond distances and van der Waals radii, these relations seem to be rational. As shown in Fig. 2, melting and transition points show gradual change with the molecular weight. The difference between the melting and the transition points reduces from 232 °C in $C_2(CH_3)_6$ to 37 °C in C_2Br_6. C_2F_6 shows especially low melting and transition points. It is probably because the covalent radius and also the van der Waals radius of fluorine are smaller than that of carbon atom or methyl group.

Now we shall infer from the entropy consideration what sorts of molecular motions would be excited on passing through the transition point. Referring to the results of X-ray studies of C_2Cl_6, the following structural model for compounds of general fromula C_2X_6 may be assumed to estimate the contribution of the molecular motion to the entropy. In the highest temperature phase of each substance, the molecular

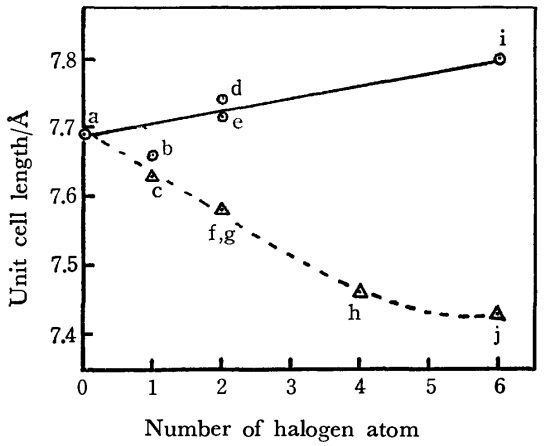

Fig. 1. The unit cell length of the cubic phase of C_2X_6 type molecule and the number of halogen atom. a: $C_2(CH_3)_6$ b: $C_2(CH_3)_5Br$ c: $C_2(CH_3)_5Cl$ d: $Br(CH_3)_2C$-$C(CH_3)_2Br$ e: $Br_2(CH_3)C$-$C(CH_3)_3$ f: $Cl(CH_3)_2C$-$C(CH_3)_2Cl$ g: $Cl_2(CH_3)C$-$C(CH_3)_3$ h: Cl_3C-$C(CH_3)_2Cl$ i: C_2Br_6 j: C_2Cl_6

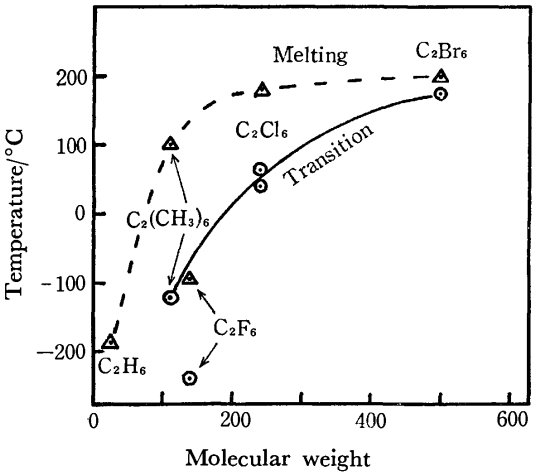

Fig. 2. Melting and transition points of C_2X_6 type crystal as a function of molecular weight.

axis (the central C–C axis) runs parallel to the four body-diagonals in a random fashion. The internal rotation about molecular axis and overall molecular rotation around molecular axis begin to be fully excited. These motions are essentially frozen-in in the lowest phase.

The contribution from the increase of orientational freedom is given by $R \cdot \ln 4$. The increase in entropy by internal rotation is calculable by use of Pitzer's table[13] assuming the potential barrier hindering the internal rotation as shown in Table 1. The contribution from overall axial rotation can be calculated from the following equation

$$\Delta S = R\left[\ln \frac{1}{\pi\sigma}\left\{\frac{8\pi^3 I_m RT}{h^2}\right\}^{1/2} + \frac{1}{2}\right]$$

where I_m is the moment of inertia about the rotational axis and σ is the symmetry number. In this case, $\sigma=3$ was used. The calculated entropy for each type of motion is given in Table 1.

In the case of C_2F_6, the sum of contributions from these motions 9.21 cal mol^{-1} K^{-1} is slightly larger

TABLE 1. CALCULATED AND OBSERVED ENTROPIES

	$C_2(CH_3)_6$	C_2F_6	C_2Cl_6	C_2Br_6
V, kcal mol^{-1}	4.7[16]	4.35[5]	10.8	—
I_m	366.9	307.2	960.58	—
S_{ir}, cal mol^{-1} deg^{-1}	3.27	2.15	4.79	—
S_{rot}, cal mol^{-1} deg^{-1}	—	4.30	6.63	7.89
S_{ori}, cal mol^{-1} deg^{-1}	2.76	2.17	2.76	2.76
S_{obsd}	3.134[16]	8.59[5]	1.93 (45 °C)[14] 5.66 (71 °C)	2.9±0.2*

V; Hindering potential barrier to internal rotation, S_{ir}; Entropy of internal rotational freedom, S_{rot}; Entropy of overall rotational freedom, I_m; Moment of inertia, S_{ori}; Entropy of orientational freedom, S_{obsd}; Observed entropy, *; Present work

than the observed entropy of transition 8.59 cal mol^{-1} deg^{-1}.[5] Assuming the contribution of reorientational disorder is to be $R\cdot\ln 3$, one obtains calculated total entropy as 8.62 cal mol^{-1} deg^{-1}, showing good agreement with the observed one. Therefore, it may be inferred that the molecule of C_2F_6 obtains at the transition point −169.18 °C the freedoms of internal and overall rotational motions and the degrees of freedom concerning molecular orientation satisfying $R\cdot\ln 3$, which is consistent with the conclusion of Lewis *et al.*,[7] *i.e.* there remains disorder concerning molecular orientation in the low temperature phase.

For the case of C_2Cl_6, any calculated value does not agree with the observed values of transition entropy, 1.93 cal mol^{-1} deg^{-1} at 45 °C or 5.66 cal mol^{-1} deg^{-1} at 71 °C. However, the sum of contributions of the orientational disorder and the internal rotation 7.84 cal mol^{-1} deg^{-1} is almost in agreement with the total observed value 7.59 cal mol^{-1} deg^{-1}. This agreement suggests that the reorientational and internal rotational freedoms should be acquired accompanying phase changes from the lowest to the highest solid phase through the intermediate phase. As no crystal data are found in the literature for the crystal between 45 °C and 71 °C, it is impossible to conclude what sorts of the two motions are activated at each transition point.

By comparison of calculated and observed entropies in the case of C_2Br_6, mechanism of the transition seems to be the occurrence of orientational randomness of the molecular axis.

The observed entropy 3.134 cal mol^{-1} deg^{-1} of $C_2(CH_3)_6$ is larger than the calculated value 2.76 cal mol^{-1} deg^{-1} for a model of molecular orientational disorder. An investigation of the molecular motion of solid $C_2(CH_3)_6$ by nuclear magnetic resonance method[15] revealed that the internal and overall axial rotations are excited, if not fully, even in the low temperature phase. Therefore, the main contribution to the phase transition is considered as the excitation of orientational motion of the molecular axis.

Now, it seems that there exists a general tendency concerning the transition mechanism for C_2X_6 type molecules, where X denotes halogen atoms. Three motions are excited at transition point of C_2F_6, *i.e.* internal, overall axial rotations and orientational disorder. For C_2Cl_6, overall axial rotation is ruled out from these three motions. In the case of C_2Br_6, only orientational disorder is allowed.

The hindering potential barrier against the internal rotation increases from 4.35 kcal mol^{-1} of C_2F_6 to 10.8 kcal mol^{-1} of C_2Cl_6 as shown in Table 1. The hindering potential barrier of C_2Br_6 is not available in the literature, however it seems to be larger than that of C_2Cl_6. The increase of hindering potential barriers is consistent with the enlargement of the geometrical extension of the molecule, *i.e.* van der Waals radii, bond lengths of C–X bond and atomic radii. From these discussions, the influence on the mechanism of phase transition of replacement of X by halogen atoms in C_2X_6 type molecule seems to depend on mainly the variance of geometrical factor of the molecules, which governs the capability of rotational motions.

The authors gratefully acknowledge Professor H. Chihara of Osaka University for reading the manuscript.

References

1) C. D. West, *Z. Krist.*, **88**, 195 (1934); C. Finbak, *This. Kjem. Bergv.*, **17**, 2 (1937), *Chem. Zentr.*, **1938**, 1077.
2) M. Atoji, T. Oda, and T. Watanabe, *Acta Crystallogr.*, **6**, 868 (1953).
3) S. Seki, M. Momotani, This Bulletin, **23**, 30 (1950).
4) W. Schwartz, *Z. Krist.*, **25**, 614 (1896); Y. Sasada and M. Atoji, *J. Chem. Phys.*, **21**, 145 (1953).
5) E. L. Pace and J. G. Aston, *J. Amer. Chem. Soc.*, **70**, 566 (1948).
6) A. Lewis and E. L. Pace, *J. Chem. Phys.*, **58**, 3661 (1973).
7) K. Yardley, *Proc. Roy. Soc., Ser. A*, **118**, 449 (1928).
8) G. J. Snaauw and E. H. Wiebenga, *Rec. Trav. Chim., Pays-Bas*, **61**, 253 (1942).
9) T. Koide, T. Oda and I. Nitta, This Bulletin, **29**, 738 (1956).
10) V. V. Korschak and N. G. Matveeva, *Izvest. Akad. Nauk. S. S. R. Otdel. Khim.*, **1958**, 344 (1958).
11) W. Taylor and A. M. Ward, *J. Chem. Soc.*, **1934**, 2003.
12) A. Mouneyrat, *Bull. Soc. Chim.*, [3] **19**, 177 (1898).
13) K. S. Pitzer, *J. Chem. Phys.*, **5**, 469 (1937) and K. S. Pitzer and W. D. Gwinn, *ibid.*, **10**, 428 (1942).
14) Y. Morino and E. Hirota, *J. Chem. Phys.*, **28**, 185 (1958).
15) T. Koide, This Bulletin, **40**, 2026 (1967).
16) D. W. Scott, D. R. Douslin, M. S. Gross, G. D. Oliver, and H. M. Huffman, *J. Amer. Chem. Soc.*, **74**, 883 (1952).

Experimental Determination of Ionization Potentials of Organic Amines, β-Carotene and Chlorophyll a

Yoshihiro NAKATO, Takeshi CHIYODA,* and Hiroshi TSUBOMURA

Department of Chemistry, Faculty of Engineering Science, Osaka University, Toyonaka, Osaka 560

(Received June 7, 1974)

Ionization potentials(I_p's) of several organic compounds have been determined by the method of photo-current measurements in gas and organic solvents. It has been found that the vapor-phase I_p's, calculated from those determined from the onsets of the photo-currents in solutions by using Born equation for the solvation energies of the cations and a common term for the energy of the electron in solution, agree well with those measured in the vapor phase. Based on this result, the I_p's of molecules in the gas phase can be derived from those measured in the solution. This method is useful for the determination of I_p's of large molecules which cannot be obtained in the gas phase. Some of the I_p's obtained are: 5.6 for 1,1,4,4-tetrakis(dimethylamino)butadiene, 5.7 for 3,3′-dimethyl-2,2′-bibenzothiazolinylidene, 6.4 for β-carotene, 6.1 for chlorophyll a, 6.3 for dihydridobis(π-cyclopentadienyl)tungsten (eV unit). The conditions of lowering the I_p's of organic molecules are discussed.

Recently, we found that tetraaminoethylenes have ionization potentials (I_p's) of *ca.* 5.4 eV,[1] which are, to our knowledge, the lowest I_p's of organic compounds reported so far, even comparable with that of the lithium atom. These interesting results stimulated us to search for other organic compounds with still lower I_p's. In this paper, some of the results of our trials along this direction are reported.

All previous methods to obtain the I_p's of molecules are applicable only to compounds with enough vapor pressures.[2,3] For example, no measurements of the I_p's of large molecules, such as chlorophylls, and carotenes, have yet been made. For such molecules, only the photo-electric work functions in the solid phase were reported.[4]

We have studied the photo-ionization of molecules not only in the gas phase but also in solutions, and found a simple relation between the gas phase I_p's and the photo-current threshold in the solution.[5] Based on this relation, it is possible to calculate the gas phase I_p's of large molecules from the photo-current thresholds in the solutions. This new method has been applied in this work to the determinations of the I_p's of some large molecules.

Experimental

The preparation and handling of tetrakis(dimethylamino)-ethylene, (TMAE), and 1,1′,3,3′-tetramethyl-2,2′-biimidazolidinylidene, (TMBI), were described previously.[1,5] 1,1,4,4-tetrakis(dimethylamino)butadiene, (TMAB),[6] and 3,3′-dimethyl-2,2′-bibenzothiazolinylidene, (DMBT),[7] were prepared according to the literature. Dihydridobis(π-cyclopentadienyl)tungsten, $(C^p)_2WH_2$, and dispiro[2.2.2.2]deca-4,9-diene were offered from Nakamura and Otsuka,[8] and Tsuji and Nishida,[9] respectively. A Merck reagent dimethylphenylphosphine was used. All these compounds except dispiro[2.2.2.2]deca-4,9-diene are highly reactive with atmospheric oxygen and were treated in the similar way as TMAE and TMBI.[1,5] Chlorophyll a was prepared from fresh spinach and purified by column chromatography according to the literature.[10] β-Carotene, a Wako GR grade reagent, was used without further purification. A Merck NMR grade tetramethylsilane (TMS) and a Wako spectroquality isooctane were dried with Na–K mirrors in ampoules connected to a vacuum line just before use.

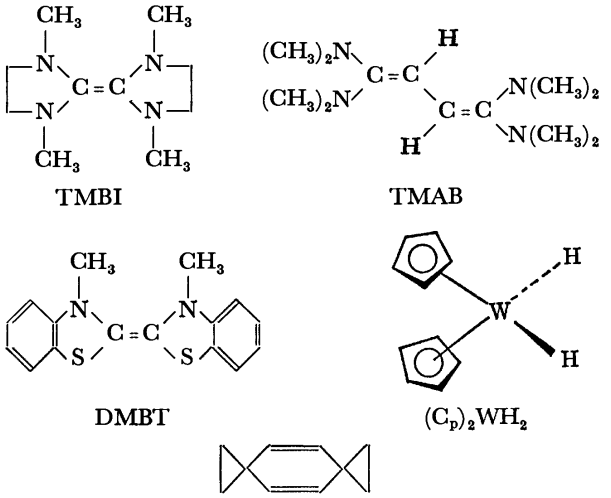

Absorption spectra and photo-ionization curves in the vacuum ultraviolet region were measured with a Nalumi vacuum monochromator. Photo-currents in solutions were measured by using a quartz cell equipped with two parallel platinum plate electrodes. The details of the experimental apparatus and procedure were described elsewhere.[1,5]

Results

The Photo-ionization in the Gas-phase. Figure 1 shows the photo-ionization curve for 1,1,4,4-tetrakis(dimethylamino)butadiene, (TMAB). σ_i^{rel} is the relative photo-ionization cross section, which is calculated by using the equation, $\sigma_i^{rel}=\sigma\cdot i/(I_0-I)$, where σ, i and I_0-I are the relative absorption cross section, the photo-current and the relative light intensity absorbed by the sample vapor, respectively. As in the previous work,[1] the point of appearance of σ_i^{rel} is taken as an upper limit for the first adiabatic ionization potential (I_p), and the maximum of $d\sigma_i^{rel}/dE$, the first derivative of σ_i^{rel}, as the vertical I_p. Because of the relatively low vapor pressure of TMAB, the slit-width of the monochromator had to be broadened, resulting in a somewhat large error.

The photo-ionization curves for dimethylphenylphosphine and dispiro[2.2.2.2]deca-4,9-diene were also measured. In these cases, however, only the adiabatic

* Present address: Mitsubishi Petrochemical Co. Ltd., Chiyoda-ku, Tokyo.

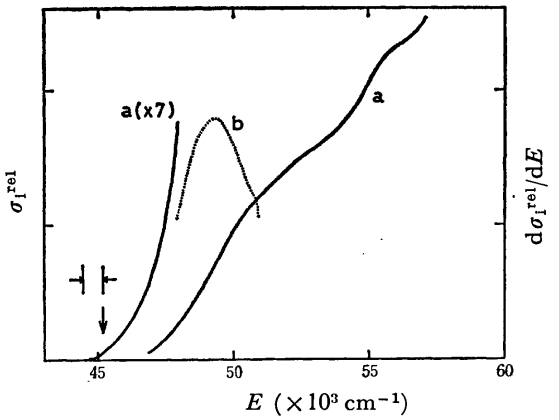

Fig. 1. Gas-phase photo-ionization of TMAB; curve a shows σ_i^{rel} *vs* E and curve b $d\sigma_i^{rel}/dE$ *vs* E. The photoionization threshold is shown by an arrow. The energy spread of the photon beam at the threshold is also indicated.

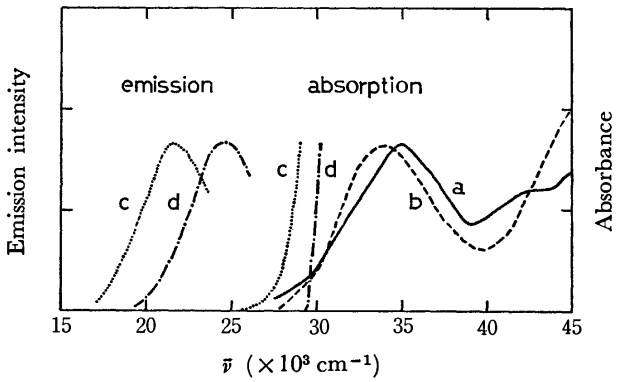

Fig. 2. Absorption and emission spectra of TMAB; curve a for the vapor, curve b for the tetramethylsilane solution at 25°C, curve c for the concentrated 3-methylpentane solution at 25°C, and curve d for the same one at 77 K.

TABLE 1. GAS-PHASE IONIZATION POTENTIALS (eV)

Compounds	Adiabatic ionization potential	Vertical ionization potential
TMAB	5.6±0.10	6.14±0.10
Dimethylphenyl-phosphine	7.58±0.05	——
Dispiro[2.2.2.2]-deca-4,9-diene	7.33±0.05	——

I_p's could be determined since these compounds had relatively high I_p's, near the limit of our experimental apparatus. The observed I_p's are summarized in Table 1.

Figure 2 shows the absorption and emission spectra of TMAB. Both the absorption spectra in the range of 25000—30000 cm^{-1} and the emission spectra are blue-shifted by change from the vapor phase to the liquid solution, and further to the solid solution. These behaviors are quite the same as those of the first absorption band and the emission band of TMAE, which were assigned to the transition between the first Rydberg state and the ground state.[1,5] It can, therefore, be concluded that the first excited singlet state of TMAB is of Rydberg character.

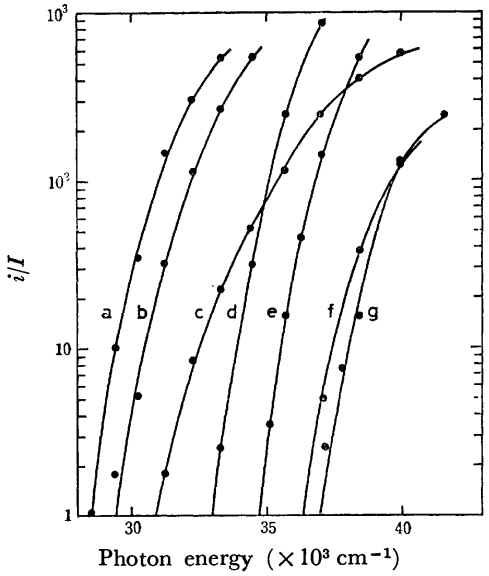

Fig. 3. Photo-ionization curves of various organic compounds in tetramethylsilane; a: TMAE, b: TMBI, c: TMAB, d: DMBT, e: $(C_p)_2WH_2$, f: chlorophyll a. g: β-carotene. All solutions are deaerated. Applied field is 400 V/cm. The half-width of the light of illumination is 10 nm.

The Photo-ionization in Organic Solutions. The photo-currents measured for several organic compounds in tetramethylsilane (TMS) are shown as functions of photon energy in Fig. 3, where the ordinate shows the photo-current (i) divided by the intensity of illumination (I). It should be noted that even the photo-currents of large molecules, such as chlorophyll a and β-carotene, can be measured easily in the solutions. The photo-currents in isooctane show similar behavior.

The photo-current threshold in a solution of a molecule, M, $E_{th}(M)$, is related with the gas-phase I_p, $I_g(M)$, as follows.[5]

$$E_{th}(M) = I_g(M) + S(M) - S(M^+) + E(e) \quad (1)$$

where $S(M)$ is the solvation energy for M and $S(M^+)$ that for the cation, M^+, and $E(e)$ the energy of the electron photoejected into the solvent. $E(e)$ can be taken as the energy of an electron at the bottom of the conduction band of the solvent relative to the vacuum level, which is expressed by $E_s^0(e)$ in Ref. 5 or by V_0 in Ref's. 11 and 12.

$S(M^+)$ can be divided into two parts,

$$S(M^+) = S_B(M^+) + S'(M^+) \quad (2)$$

where $S_B(M^+)$ is the part of the solvation energy relevant only to the mono-positive charge on the cation, M^+, approximated by the Born equation,[13] and $S'(M^+)$ the remaining part of the solvation energy.

$$S_B(M^+) = (e^2/2a)(1-1/\varepsilon_{op}) \quad (3)$$

where a is the radius of the sphere for the cation, M^+, and ε_{op} the optical dielectric constant of the solvent ($\varepsilon_{op}=n^2$, n is the refractive index). The method of calculation of the radius a for the cation, M^+, is given in the Appendix.

Table 2. The values of E(e) calculated from observed ionization energies in the vapor and solutions (eV unit)

Compound	I_g	E_{th}		a(Å)	E(e)	
		in TMS	in *iso*-octane		in TMS	in *iso*-octane
TMAE	5.36±0.02[b]	3.54±0.11	——	3.21	−0.79	——
TMBI	5.41±0.02[b]	3.65±0.11	4.02±0.13	3.25	−0.74	−0.32
TMAB	5.60±0.10	3.83±0.13	4.28±0.15	3.23	−0.75	−0.24
TMPD[a]	6.20±0.02[c]	4.40[d]	——	3.24	−0.78	——

a) *N,N,N',N'*-Tetramethyl-*p*-phenylenediamine. b) See Ref. 1. c) See Ref. 14. d) S. S. Takeda, N. E. Houser, and R. C. Jarnagin, *J. Chem. Phys.*, **54**, 3195 (1971); R. A. Holroyd, *ibid.*, **57**, 3007 (1972).

Table 3. Gas-phase ionization potentials calculated from observed photo-current thresholds in solutions (eV unit)

Compound	E_{th}		a(Å)	I_g[a] calcd from E_{th}	
	in TMS	in isooctane		in TMS	in isooctane
DMBT	4.09±0.14	4.43±0.16	3.70	5.8	5.7
$(C_p)_2WH_2$	4.30±0.15	4.64±0.18	2.50	6.4[b]	6.3[b]
Chlorophyll a	4.50±0.17	——	3.82	6.1	—
β-carotene	4.59±0.18	5.02±0.22	3.30	6.4	6.4

a) The error estimated will be 0.2 eV at most. b) The value obtained from the CT absorption bands is 6.3 eV; Ref. 8.

Under the approximation that $S'(M^+)$ is nearly equal to $S(M)$, Eq. (1) is expressed as

$$E_{th}(M) = I_g(M) - S_B(M^+) + E(e) \quad (4)$$

From the data for the four compounds shown in Table 2, where the ionization potentials both in the gas phase and in the solutions are determined experimentally, E(e) can be calculated by using Eq's. (3) and (4). The results are shown in Table 2, together with the radius a used. It is found that the values of E(e) are nearly constant for each solvent, as expected from the definition. This shows that the Eq's (3) and (4) are fairly good approximations.

Now, based on the values of E(e) obtained above and the Eq's (3) and (4), it is possible to calculate I_g(M) from E_{th}(M). The results are given in Table 3. As expected, the values of I_g(M) calculated from E_{th}(M) in tetramethylsilane (TMS) are in good agreement with those from E_{th}(M) in isooctane.

Discussion

As TMAE and TMBI have very interesting properties, both chemically and physically, it seemed to be a challenging problem to seek for organic molecules having still lower ionization potentials. As the results show, this trial has failed so far: All molecules dealt with in this paper have I_p's higher than that of TMAE. Here, we wish to give some criteria for the conditions which can lower the I_p of a molecule based on the present results, as well as those already obtained.

It is well known that, for aromatics and conjugated polyenes, the I_p's become lower with the length of conjugated chain. It is also known that the I_p gets lower, the more amino groups, or preferably dimethylamino groups, are substituted in the conjugated molecules. Thus, the I_p's of benzene, aniline, dimethylaniline, and *N,N,N',N'*-tetramethyl-*p*-phenylenediamine are 9.24, 7.70, 7.14 and 6.20 eV, respectively.[1,14] The lowering of I_p by conjugation is attributed to an increased stabilization of the cations. The effect of amino group is of course due to the non-bonding electrons in the nitrogen atom having itself a low I_p. The effect of methyl substitution, more generally speaking, alkyl substitution, has been attributed to the inductive, or hyperconjugative effect of the substituent. However, we propose another view that the steric repulsion of an alkyl group toward the nitrogen non-bonding electrons might be a reason.

In the case of TMAE, as an example, the four dimethylamino groups are believed to lie nearly perpendicular to the $N_2C{=}CN_2$ plane of the molecule.[1] In this molecule, therefore, the nitrogen lone pairs can hardly conjugate with the π-electrons of the ethylene bond. In TMBI, on the other hand, the nitrogen lone pair orbitals are thought to be nearly parallel to the latter. From these facts, it can be asserted that the conjugational effect will lower the I_p of TMBI compared to TMAE. The fact that the I_p of TMAE is quite low, even lower than that of TMBI seems to be attributable to the large steric repulsion of methyl electrons toward the nitrogen lone pair; in other words, due to the extremely large crowding of the methyl groups aronnd each N atom as is seen clearly from the structure model of TMAE (Fig. 4). These steric repulsions certainly destabilize the nitrogen lone pair electrons in the molecule, leading to the lowering of I_p. On the other hand, the less steric repulsion and the more conjugational effect cansel each other in TMBI, leading to an I_p accidentally almost equal to that of TMAE.

In the present results, the I_p of TMAB (tetrakis-(dimethylamino)butadiene) is found to be slightly

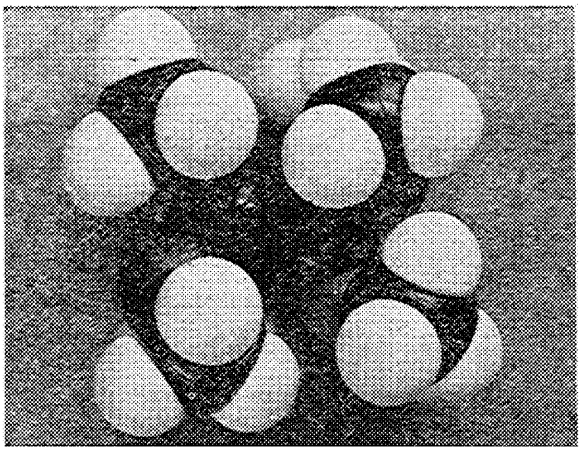

(A)

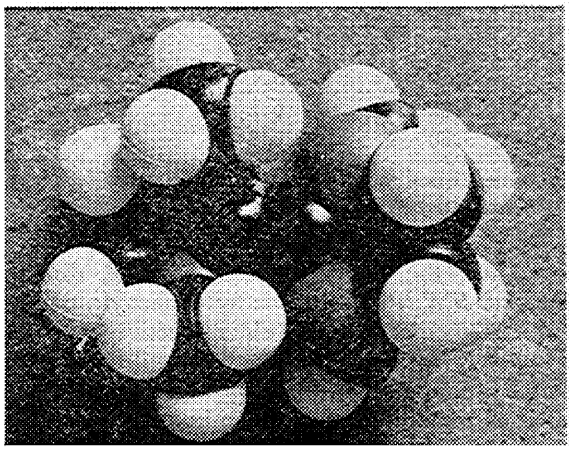

(B)

Fig. 4. The molecular models of TMAE (A) and TMBI (B).

higher than that of TMAE ($I_p^{adiabatic}$ 5.36, $I_p^{vertical}$ 6.11 eV). This can also be explained in a similar way: Increased conjugated chain length and less crowding around N atoms. In TMAE, the direct repulsion between the N lone pairs might also be responsible for lowering the I_p.[1)]

The sulfur atom included in a conjugated system is also regarded to be a factor to lower the I_p, because of its non-bonding pair with a relatively low I_p. It is significant that DMBT has an I_p comparable to that of TMAE.

Unexpectedly low I_p's for both dispiro[2.2.2.2]deca-4,9-diene and $(C_p)_2WH_2$ are obtained. The I_p of $(C_p)_2WH_2$ was reported to be $\sim$7000 cm^{-1} lower than that of dimethylaniline from their charge transfer absorption bands with several olefins as the common acceptors, being $\sim$6.3 eV, which is in good agreement with the value obtained in this work.

The I_p of dimethylphenylphosphine is higher than that of dimethylaniline(7.14 eV). It was also reported that the I_p of triphenylphosphine was higher than that of triphenylamine.[14)] From these results, it seems that the substitution of the N atom of amino compounds by the P atom is generally ineffective to lower the I_p's.

The I_p's of chlorophyll a and β-carotene obtained here are probably the first reliable ones ever observed. The present method can be applied to other biologically important compounds. The main error seems to originate from the calculation of $S_B(M^+)$ by the use of the Born equation. It seems likely that the Born equation is a good approximation in non-polar solvents, but the calculation of radius a for the solute molecule is somewhat erroneous because of its non-spherical shape(see Appendix). It should, however, be noted that as the radius becomes larger, $S_B(M^+)$ becomes smaller and so does the error. For example, the values of $S_B(M^+)$ are 1.2, 1.0 and 0.9 eV at a=3, 3.5 and 4 Å, respectively. Therefore, the error estimated seems to be 0.2 eV at most.

Appendix

To apply Born equation to a non-spherical molecular ion, an appropriate average radius must be given from the molecular geometry. Let us consider tetramethyl-*p*-phenylenediamine (TMPD) as an example. The molecular shape is approximated as illustrated in Fig. 5. The average radius a was calculated by using the following equation,

$$1/a = \sum_i (1/r_i) \cdot (\Delta S_i \cdot \cos\theta_i / 4\pi r_i^2) \quad (5)$$

where ΔS_i is, as shown in Fig. 5, a fraction of the surface of the molecule, taken appropriately so that the distance between the center of the molecule, 0, and any point on that fraction of the surface does not change largely from an average distance r_i set up for each of the fractions ΔS_i, and θ_i is the angle between r_i and the normal to the plane of ΔS_i. The summation is made over all the surface area. The calculations of a for other compounds have been made in a similar way.

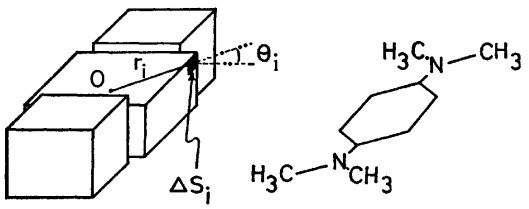

Fig. 5. The molecular shape of TMPD used to calculate the radius a.

The above method can be rationalized by the following argument: Let us consider a non-spherical molecular ion with a center of symmetry, existing in a dielectric medium. By taking dS a planar element of molecular surface, r the distance between the surface element and the center of the molecule and θ the angle between r and the normal to the plane of dS, the element of solid angle, dΩ, is given as follows.

$$d\Omega = dS \cdot \cos\theta / r^2 \quad (6)$$

Under the assumption that the electric charge of the molecular ion, e, is located at its center, the ion-medium electrostatic interaction energy within the region of this elemental solid angle can be expressed as

$$(e^2/2r) \cdot (1 - 1/\varepsilon) \cdot (d\Omega/4\pi)$$

where ε is the dielectric constant of the medium. The total interaction energy is obtained by integrating the above expression,

$$(e^2/2) \cdot (1 - 1/\varepsilon) \cdot \int (1/r)(d\Omega/4\pi) \quad (7)$$

Equation 5 can be regarded as approximating the integral part of Eq. 7 by a summation, and taking it to be $1/a$ so as to make the energy expressed by the Born equation.

The authors wish to thank Professors A. Nakamura and S. Otsuka, and Professors T. Tsuji and S. Nishida for providing $(C_p)_2WH_2$ and dispiro[2.2.2.2]deca-4,9-diene, respectively. We wish also to thank Mr. T. Ohnishi for his assistance in experiment.

References

1) Y. Nakato, M. Ozaki, and H. Tsubomura, This Bulletin, **45**, 1299 (1972).
2) K. Watanabe, T. Nakayama, and J. Mottle, *J. Quant. Spectry. Radiative Transfer*, **2**, 369 (1962); F. I. Vilesov, *Soviet Physics Uspekhi*, **6**, 888 (1964).
3) D. W. Turner, "Molecular Photoelectron Spectroscopy," Wiley-Interscience, London (1970).
4) F. I. Vilesov and M. E. Akopyan, "Elementary Photoprocesses in Molecules," ed by B. S. Neporent, translated from Russian, Consultant Bureau, New York (1968), p. 32.
5) Y. Nakato, M. Ozaki, and H. Tsubomura, *J. Phys. Chem.*, **76**, 2105 (1972).
6) H. Weingartenten and W. A. White, *J. Org. Chem.*, **31**, 2874 (1966).
7) H. -W. Wanzlick, H. -J. Kleiner, I. Lasch, H. U. Füldner, and H. Steinmaus, *Liebigs Ann. Chem.*, **708**, 155 (1967).
8) A. Nakamura and S. Otsuka, *J. Amer. Chem. Soc.*, **95**, 5091, 7262 (1973).
9) T. Tsuji, S. Nishida, and H. Tsubomura, *Chem. Commun.*, **1972**, 284; T. Tsuji and S. Nishida, *J. Amer. Chem. Soc.*, **95**, 7519 (1973).
10) L. P. Vernon and G. R. Seely, "The Chlorophylls," Academic Press, New York and London (1966), p. 53.
11) B. E. Springett, M. H. Cohen, and J. Jortner, *J. Chem. Phys.*, **48**, 2720 (1968).
12) R. A. Holroyd and M. Allen, *ibid.*, **54**, 5014 (1971).
13) M. Born, *Z. Physik.*, **1**, 45 (1920).
14) Y. Nakato, M. Ozaki, A. Egawa, and H. Tsubomura, *Chem. Phys. Lett.*, **9**, 615 (1971).
15) A. Terenin and F. Vilessov, *Advan. Photochem.*, **2**, 385 (1964).

The Microwave Spectrum, the r_s Structure and the Dipole Moment of the *TT* Isomer of Diethyl Ether

Michiro HAYASHI and Kazunori KUWADA

Department of Chemistry, Faculty of Science, Hiroshima University, Higashi-sendamachi, Hiroshima 730

(Received June 27, 1974)

The microwave spectra of six isotopic species of diethyl ether were measured in relation to the molecular form and dipole moment. Transitions of the *TT* (*trans-trans*) isomer could be assigned and the r_s structure of this isomer was obtained by the substitution method. The structural parameters of the *TT* isomer of diethyl ether are; r(CO) 1.408 Å, r(CC) 1.516 Å; α(COC) 112°25′, α(OCC) 108°37′ for the skeleton; r(CH) 1.093 Å, α(CCH) 110°11′, α(OCH) 110°10′, α(HCH) 107°29′ for the CH_2 group and r(CH) 1.090 Å, α(CCH_s) 110°35′, α(CCH_a) 110°15′, α(H_sCH_a) 108°48′, α(H_aCH_a) 108°4′ for the CH_3 group. The dipole moment was determined to be 1.061±0.018 D from the Stark effect measurement for the *TT* isomer. A discussion was made on the structure and the dipole moment of the *TT* isomer of diethyl ether in comparison with those of the similar molecules.

Infrared and Raman spectra of diethyl ether were extensively studied by several authors.[1] They reported that at least two rotational isomers existed in the gaseous and liquid states, one of which was presumably in th *trans-trans* form (the *TT* form).

We measured the microwave spectra of diethyl ether in order to confirm the molecular forms of the isomers. As was already reported in a previous note,[2] the microwave spectra of the *TT* isomer of the normal species of diethyl ether were easily assigned, though the spectra were not so strong and their Stark patterns were not clearly resolved. The measurements were extended to its five isotopic species and the r_s structure of the *TT* isomer could be determined by the substitution method.

The dipole moment of this isomer was determined by the Stark effect measurements of the spectra.

We found very many weak spectra all over the frequency region, which may belong to other isomers. However, they are so complicated that the analysis was abandoned for them.

In the present paper, the r_s structure and the dipole moment of the *TT* isomer of diethyl ether will be given and discussed in comparison with those of the similar molecules such as dimethyl ether and ethyl halides.

Experimental

A commercial product was used for the normal species of diethyl ether. One of the deuterated species ($CH_3CHDOEt$) was prepared by the reaction of a mixture of acetaldehyde and ethanol with hydrogen chloride followed by the reduction of the resultant $CH_3CHClOEt$ with $LiAlD_4$ in *n*-butyl ether.[3] The other deuterated species (CH_2DCH_2OEt) was prepared by the Williamson method, *i.e.*, by treating sodium ethoxide with CH_2DCH_2Br which was prepared by the reaction of ethylene and DBr with $AlBr_3$ as a catalyst.[4] The ^{13}C species were prepared by the Williamson method using $^{13}CH_3CH_2I$ and $CH_3{}^{13}CH_2I$ (90 atom% ^{13}C, Merck Sharp & Dohme, Canada), respectively.

The microwave spectra were measured in the region from 8500 to 34000 MHz with conventional sinusoidal- and square-wave Stark modulation spectrometers at the temperature of dry ice.

The r_s Structure

The *b*-type transition are expected for the *TT* isomer of diethyl ether. The observed transition frequencies with $J \leqq 10$ are shown in Table 1.

The rotational constants were determined by the least-squares technique from all the observed frequencies in the table so as to fit in with a modified rigid rotor expression which was including only the $D_J(J(J+1))^2$ term of the centrifugal distortion contributions. The rotational constants and the moments of inertia are in Table 2. The quantities $P_c(=(I_a+I_b-I_c)/2)$ and and $\Delta P_c(=P_c(\text{isotopic})-P_c(\text{parent}))$ in the table are quite reasonable when comparing with the reported values of other molecules.[5]

Since the moments of inertia in the ground state are available for the normal and each of its singly substituted isotopic species, it is possible to calculate the coordinates of each atom directly from Kraitchman's equations[6] except the x_b coordinate of the oxygen atom which can be solved by the use of the first moment equation. However, the x_b coordinate of the in-plane hydrogen (H_s) is small so that zero-point energy contributions of the vibrations to $\Delta I_a(=I_a(\text{isotopic})-I_a(\text{parent}))$ reduce the reliability of the calculated value from Kraitchman's equation for the x_b coordinate. On the other hand, all the coordinates for the out-of-plane hydrogen (H_a) and the x_a coordinate for the H_s atom are large and Karitchman's equations reliably fix their values. Thus one assumption is required to completely determine the structure of the *TT* isomer from the present data. We chose to assume the CH_a and CH_s bond distances to be equal.

Table 3 lists the coordinates of each atom of the *TT* isomer of diethyl ether. The moments of inertia as calculated from the coordinates are compared with the experimental moments of inertia as shown in Table 2. The deviations $\delta I_g(=I_g(\text{obsd})-I_g(\text{calcd}))$ are sizable and always positive, but this is to be expected for the r_s structure.

The structural parameters as derived from the coordinates are shown in Table 3. The assumption imposed on the CH bond distances of the methyl group has little influence on the structural parameters except $r(CH_s)$ and $\alpha(H_sCC)$. That is, the x_b coordinate of the H_s atom calculated directly from Kraitchman's equation is 0.2020±0.0053 Å which gives the value of −0.2576±0.0023 Å for the x_b coordinate of the oxygen atom. These values give the parameters of 1.409±0.003 Å, 112°13′±16′, 108°31′±10′, 110°13′± 20′ and 109°20′±30′ for r(CO), α(COC), α(OCC),

Table 1. Observed frequencies[a] for the *TT* isomer of diethyl ether (MHz)

Transition	$(CH_3CH_2)_2O$	$CH_3CHDOEt$	*s*-CH_2DCH_2OEt[b]	*a*-CH_2DCH_2OEt[b]	$^{13}CH_3CH_2OEt$	$CH_3{}^{13}CH_2OEt$
$1_{10} \leftarrow 1_{01}$	15854.38(0.00)	14607.30(0.01)	15920.33(−0.04)	14835.95(−0.14)	15806.98(−0.12)	15695.17(0.00)
$2_{11} \leftarrow 2_{02}$	15997.67(−0.09)	14754.45(0.01)	16051.41(0.06)	14974.92(−0.38)	15945.01(−0.10)	15839.27(−0.03)
$3_{12} \leftarrow 3_{03}$	16214.55(−0.08)	14976.75(−0.48)	16249.21(−0.10)	15186.02(0.10)	16153.72(−0.07)	16057.43(0.09)
$4_{13} \leftarrow 4_{04}$	16507.16(0.00)	15278.10(−0.01)	16516.13(0.07)	15470.17(0.02)	16435.21(0.05)	16351.54(0.05)
$5_{14} \leftarrow 5_{05}$	16878.22(0.02)	15660.35(−0.00)	16853.90(−0.07)	15830.77(−0.08)	16791.97(0.09)	16724.68(0.01)
$6_{15} \leftarrow 6_{06}$	17331.21(−0.10)	16128.08(0.08)	17266.02(0.01)	16271.66(0.07)	17227.27(0.02)	17180.50(−0.01)
$7_{16} \leftarrow 7_{07}$	17870.70(0.02)	16685.85(0.03)	17755.61(−0.08)	16796.68(0.07)	17745.09(−0.09)	17723.26(−0.02)
$8_{17} \leftarrow 8_{08}$	18501.18(0.05)	17339.28(0.00)	18327.16(0.13)	17410.73(0.00)	18350.17(0.01)	18357.87(−0.03)
$9_{18} \leftarrow 9_{09}$	19228.15(0.11)	18094.42(0.03)	18984.71(0.16)	18119.31(−0.03)	—[c]	19089.85(0.07)
$10_{19} \leftarrow 10_{010}$	20057.13(−0.08)	18957.72(0.05)	19733.05(−0.12)	18928.29(0.04)	19841.74(0.00)	19924.96(−0.04)
$1_{11} \leftarrow 0_{00}$	—[c]	18761.60(0.00)	19942.70(−0.26)	—[c]	19913.20(0.32)	19870.49(0.13)
$2_{12} \leftarrow 1_{01}$	24261.37(−0.09)	22915.80(−0.09)	23965.40(−0.15)	23017.06(−0.05)	24018.80(0.15)	24045.58(0.05)
$3_{13} \leftarrow 2_{02}$	28394.31(0.17)	26997.64(0.08)	27923.55(0.22)	27039.03(0.20)	28056.05(−0.13)	28149.45(−0.04)
$4_{14} \leftarrow 3_{03}$	32457.18(−0.01)	31008.02(0.04)	31817.42(0.10)	30993.05(0.05)	32026.50(−0.09)	32183.32(−0.13)
$5_{15} \leftarrow 4_{04}$		34949.48(0.12)				
$6_{06} \leftarrow 5_{15}$	11299.54(−0.30)	12293.53(−0.05)		11580.72(−0.09)	10690.37(0.06)	11297.72(0.00)
$7_{07} \leftarrow 6_{16}$	16027.00(0.27)	16979.00(−0.12)	14491.73(0.21)	16177.47(−0.03)	15301.35(0.01)	15998.12(−0.01)
$8_{08} \leftarrow 7_{17}$	20802.82(−0.02)	21712.56(−0.03)	19042.47(−0.47)	20821.05(−0.07)	19960.39(−0.05)	20747.73(0.10)
$9_{09} \leftarrow 8_{18}$	25622.27(−0.01)	26487.32(0.03)	23636.31(0.13)	25505.78(0.03)	24662.06(−0.04)	25540.24(0.03)
$10_{010} \leftarrow 9_{19}$	30478.54(−0.02)	31295.96(0.03)	28265.85(0.06)	30224.93(0.04)	29400.31(0.04)	30369.21(−0.06)

a) Figures in parentheses indicate the differences of the observed and calculated frequencies. $\delta\nu = \nu(\text{obsd}) - \nu(\text{calcd})$. b) "*s*-" and "*a*-" refer to the symmetric and asymmetric forms, respectively, with respect to the molecular plane. c) Overlapped with the other transition.

Table 2. Observed rotational constants (MHz) and moments of inertia (amu·Å^2)[a]

	$(CH_3CH_2)_2O$	$CH_3CHDOEt$	*s*-CH_2DCH_2OEt	*a*-CH_2DCH_2OEt	$^{13}CH_3CH_2OEt$	$CH_3{}^{13}CH_2OEt$
A	17956.15 (29)	16684.45 (30)	17931.67 (43)	16881.35 (30)	17859.99 (27)	17782.77 (15)
B	2244.19 (2)	2223.20 (2)	2141.47 (3)	2183.50 (2)	2190.00 (2)	2230.74 (1)
C	2101.77 (2)	2077.15 (2)	2011.30 (3)	2045.26 (2)	2052.89 (2)	2087.59 (1)
D_J[b]	−1.58	−3.56	−3.00	−4.55	−4.06	−3.82
δ[c]	0.12	0.12	0.17	0.12	0.11	0.06
I_a	28.1450(5)	30.2721(5)	28.1834(7)	29.9370(5)	28.2965(4)	28.4194(2)
δI_a[d]	0.3943	0.3944	0.4029	0.3945	0.3943	0.3943
I_b	225.1935(18)	227.3192(20)	235.9950(30)	231.4527(19)	230.7655(19)	226.5507
δI_b[d]	1.0653	1.0655	1.0657	1.0654	1.0653	1.0653
I_c	240.4525(26)	243.3024(28)	251.2688(42)	247.0965(28)	246.1778(29)	242.0855(14)
δI_c[d]	1.1258	1.1256	1.1112	1.1256	1.1276	1.1272
P_c[e]	6.4430(16)	7.1445(18)	6.4548(26)	7.1466(17)	6.4421(17)	6.4423(8)
ΔP_c[f]	—	0.7015(24)	0.0118(31)	0.7036(23)	−0.0009(24)	−0.0007(18)

a) Figures in parentheses indicate the uncertainties attached to the last significant figures calculated from 2.5 times the standard deviation. b) 10^4 times the coefficient of $[J(J+1)]^2$ term of the centrifugal distortion contribution. c) Standard deviation of the observed frequencies from the calculated frequencies. d) $\delta I_g = I_g(\text{obsd}) - I_g(\text{calcd})$, (g=a, b and c). I_g(calcd) was calculated from the r_s structural parameters listed in Table 3. Since the x_b coordinate of the H_s atom was calculated by assuming $r(CH_a) = r(CH_s)$, δI_a and δI_c of *s*-CH_2DCH_2OEt species which are related to this coordinate, make slight differences from those of the other species. e) $P_c = (I_a + I_b - I_c)/2$. f) $\Delta P_c = P_c(\text{isotopic}) - P_c(\text{parent})$.

Table 3. Atom coordinates (Å) and structural parameters[a]

Atom	x_a	x_b	x_c
O	0	−0.2546 (21)[b]	0
C (CH_2)	±1.1699 (22)	0.5282 (12)	0
C (CH_3)	±2.3712 (14)	−0.3967 (20)	0
H (CH_2)	±1.1913 (25)	1.1745 (25)	±0.8818 (38)
H_s (CH_3)	±3.2977 (13)	0.1782 (75)[c]	0
H_a (CH_3)	±2.3548 (12)	−1.0368 (28)	±0.8825 (37)

CH_3 group		CH_2 group		Skeleton	
$r(CH_s)$	1.090 Å (0.004)	r(CH)	1.093 Å (0.003)	r(CO)	1.408 Å (0.002)
$r(CH_a)$	1.090 Å (0.004)	α(CCH)	110°11′ (19′)	r(CC)	1.516 Å (0.003)
$\alpha(CCH_s)$	110°35′ (19′)	α(OCH)	110°10′ (19′)	α(COC)	112°25′ (16′)
$\alpha(CCH_a)$	110°15′ (19′)	α(HCH)	107°29′ (32′)	α(OCC)	108°37′ (10′)
$\alpha(H_sCH_a)$	108°48′ (37′)				
$\alpha(H_aCH_a)$	108° 4′ (33′)				

a) The figures in parentheses indicate the 99% reliability intervals. b) Calculated by the use of the first moment equation from the x_b coordinaties of the other atoms. c) Calculated from the x_a coordinate of the H_s atom and the coordinates of the C and H_a atoms, assuming that $r(CH_s)=r(CH_a)$.

Table 4. The Stark coefficients of the *TT* isomer of diethyl ether

Transition	$\Delta\nu/E^2$ [$\times 10^{-4}$ MHz/(V/cm)^2]	
	Obsd	Calcd
$1_{10} \leftarrow 1_{11}$ $M=1$	0.399±0.006	0.395
$2_{11} \leftarrow 2_{02}$ $M=2$	0.469±0.007	0.463
$3_{12} \leftarrow 3_{03}$ $M=3$	0.498±0.010	0.492
$2_{12} \leftarrow 1_{01}$ $M=1$	0.626±0.020	0.633
$3_{13} \leftarrow 2_{01}$ $M=0$	−0.308±0.010	−0.329
	$\mu=1.061\pm0.018$D	

α(OCH) and $\alpha(H_sCH_a)$, respectively. They are essentially equal to those given in Table 3 within the experimental error limit. On the other hand, the values of 1.103±0.004 Å and 109°32′±17′ are obtained for $r(CH_s)$ and $\alpha(H_sCC)$. However, an asymmetric CH_3 structure derived from these values is less believable than the nearly symmetric CH_3 structure given in Table 3.

Dipole Moment

The dipole moment of the *TT* isomer of diethyl ether was quantitatively determined by Stark-effect measurements of five transitions for the normal species. The spectrometer was calibrated with OCS[7] before and after measurements on diethyl ether.

For the *TT* isomer, the dipole moment has to be parallel to the b-inertial axis from the symmetry. The observed and calculated Stark coefficients[8] are shown in Table 4. By the least-squares technique, the dipole moment was determined to be $\mu=1.061\pm0.018$ D. A value of 1.16 D based on dielectric constant measurements was reported in the literature.[9]

Discussion

A comparison of the r_s structure of the *TT* isomer of diethyl ether with that of *trans*-ethyl alcohol is of primary interest. Unfortunately, this is impossible at present, since the reported structure of *trans*-ethyl alcohol is not the r_s structure but the r_0 structure obtained with several assumptions.[10]

However, a comparison is possible with those of the molecules, of which the r_s structures were reported in the literatures. First, the CO bond distance of the *TT* isomer is essentially equal to that of dimethyl ether[11] while the COC angle is slightly larger than that of dimethyl ether. Second, the CC bond distance is about 0.01 Å shorter than that of propane,[12] slightly shorter than those of ethyl chloride[13] and bromide[14] and about 0.01 Å longer than that of ethyl fluoride,[15] though it is difficult to interprete the significance of this fact.

Third, and most noticeable, both the CCO and HCH angles of the CH_2 group for the *TT* isomer are abnormally smaller than tetrahedral. This anomalous feature of the angles of the CH_2 group may be explained by the tilted ethyl group towards the lone pair electrons of the oxygen atom in the similar manner as the tilted methyl group in dimethyl ether.[11,16]

The dipole moment of the *TT* isomer of diethyl ether is 1.061 D which is smaller than that of dimethyl ether (1.310 D).[11] From the observed dipole moments, the apparent bond moment on the CO bond can be calculated to be 1.167 and 0.952 D for dimethyl ether and diethyl ether, respectively. The decrease of the apparent bond moment for diethyl ether may be interpreted as due to the induction effect[17] of the CO bond moment on the CC bond.

References

1) R. G. Synder and G. Zerbi, *Spectrochim. Acta*, **23A**, 291 (1967); H. Wieser, W. G. Laidlaw, P. J. Krueger, and H. Fuhrer, *ibid.*, **24A**, 1055 (1968); A. D. H. Clague and A. Danti, *ibid.*, **24A**, 439 (1968).

2) M. Hayashi, H. Iamishi, K. Ohno, and H. Murata, This Bulletin, **44**, 299 (1971).

3) C. S. Marvel and P. K. Porter, "*Organic Syntheses*," Coll. Vol I, p. 377 (1941).

4) A. Murrey, III and D. L. Williams, "Organic Syntheses with Isotopes," Part II, Interscience, New York (1958), p. 1471.
5) D. R. Herschbach and V. W. Laurie, *J. Chem. Phys.*, **40**, 3142 (1964).
6) J. Kraitchman, *Amer. J. Phys.*, **21**, 117 (1953).
7) J. S. Muenter, *J. Chem. Phys.*, **48**, 4544 (1968).
8) S. Golden and E. B. Wilson, Jr., *ibid.*, **16**, 669 (1948).
9) C. P. Smyth, "Dielectric Behavior and Structure," McGraw-Hill, New York (1955), p. 298.
10) Y. Sasada, M. Takano, and T. Satoh, *J. Mol. Spectrosc.*, **38**, 33 (1971).
11) U. Blukis, P. H. Kasai, and R. J. Myers, *J. Chem. Phys.*, **38**, 2753 (1963).
12) D. R. Lide, Jr., *ibid.*, **33**, 1514 (1960).
13) R. H. Schwendeman and G. D. Jacobs, *ibid.*, **36**, 1245 (1962).
14) C. Flanagan and L. Pierce, *ibid.*, **38**, 2963 (1963).
15) L. Nygaard, *Spectrochim. Acta*, **22A**, 1261 (1966).
16) L. Pierce and M. Hayashi, *J. Chem. Phys.*, **35**, 479 (1961).
17) I. Miyagawa, *Nippon Kagaku Kaishi*, **75**, 1061 (1954).

Apparent Dipole Moments and Dielectric Relaxation Times of 1,4-Benzoquinone and Its Derivatives in Solutions

Tohru NAGAI, Hiroaki TAKAHASHI, and Keniti HIGASI*
Department of Chemistry, Waseda University, Shinjuku, Tokyo 160
Leslie E. SUTTON and David WADDINGTON
Physical Chemistry Laboratory, South Parks Road, Oxford, England
(Received August 27, 1974)

Atom polarisations, apparent dipole moments and dielectric relaxation times of 1,4-benzoquinone in various solvents were determined together with those of some of its derivatives in benzene solution. Solvent effects on the apparent dipole moments of 1,4-benzoquinone and its derivatives were examined in comparison with the absorption spectra in the submillimetre region.

In spite of the observation that 1,4-benzoquinone has a centre of symmetry[1] it has been shown to exhibit an apparent permanent dipole moment of appreciable magnitude, 0.67 D, in solution.[2] The observed large dipole moment could be due solely to an exceptionally large atom polarisation[3] if there were no solute-solvent interaction.[4] The observations of polarisation in the vapour phase[3] show that the latter is not a major cause of the apparent moment.

First, in the present work a new determination of the atom polarisation was made for 1,4-benzoquinone by dielectric measurements at an extremely high frequency (96.52 GHz, 3.219 cm^{-1}). The experimental atom polarisation thus obtained was compared with the values calculated by Waddington *et al.*[5] from its absorption spectrum over the whole infrared range.

Secondly, the nature of solute-solvent interaction was investigated by measuring apparent dipole moments and relaxation times of 1,4-benzoquinone in a variety of solvents.

Thirdly, not only 1,4-benzoquinone (A), but also its derivatives, 2,5-dimethyl-1,4-benzoquinone (B), 2,5-dichloro-1,4-benzoquinone (C) and 2,5-di-*tert*-butyl-1,4-benzoquinone (D) were studied using the same procedure.

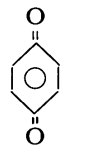
(A)

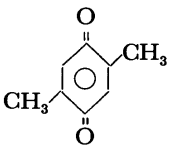
(B)

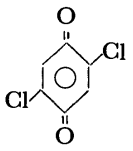
(C)

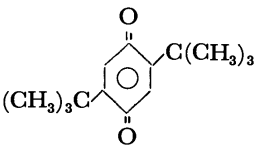
(D)

Experimental

By use of the apparatus and techniques described previously[6] dielectric and optical measurements were carried out at the frequencies 1 MHz, 96.52 GHz and that the Na–D line. The real and unreal dielectric constants ε' and ε'' of the dilute solutions measured at 96.52 GHz are assumed to be linear with the concentration (weight fraction w_2) of the solute.

$$\varepsilon' = \varepsilon_1' + a'w_2 \qquad \varepsilon'' = \varepsilon_1'' + a''w_2 \tag{1}$$

in which subscripts 1 and 2 refer to the pure solvent and to the solute, respectively. Similarly the dielectric constant at any frequency (including the static one, ε_0, and the high frequency limiting value, ε_∞), the squares of refractive indices n_D^2 and the specific volumes v are also assumed to be linear with the concentration.†

$$\varepsilon_0 = \varepsilon_{10} + a_0w_2, \quad \varepsilon_\infty = \varepsilon_{1\infty} + a_\infty w_2 \qquad n_D^2 = n_{1D}^2 + a_D w_2, \quad v = v_1 + bw_2 \tag{2}$$

The total, *i.e.*, low frequency molecular polarisation of the solute at infinite dilution was obtained from the Halverstadt-Kumler equation.[7]

$$P_2 = M_2\left\{\frac{3a_0v_1}{(\varepsilon_{10}+2)^2} + (v_1+b)\frac{\varepsilon_{10}-1}{\varepsilon_{10}+2}\right\} \tag{3}$$

in which M_2 is the molecular weight of the solute. The distortion polarisation P_E+P_A is, in principle, obtainable using a_∞ and $\varepsilon_{1\infty}$ instead of a_0 and ε_{10} in Eq. (3), respectively.[8] The difference $\varepsilon_1'-\varepsilon_{1\infty}$ expresses the effect of dispersion in the microwave region.

$$P_A + P_E = M_2\left\{\frac{3a_\infty v_1}{(\varepsilon_{1\infty}+2)^2} + (v_1+b)\frac{\varepsilon_{1\infty}-1}{\varepsilon_{1\infty}+2}\right\} \tag{4}$$

Similarly, by use of n_{1D}^2 and a_D the molar refraction for the D-line is given by

$$R_D = M_2\left\{\frac{3a_Dv_1}{(n_{1D}^2+2)^2} + (v_1+b)\frac{n_{1D}^2-1}{n_{1D}^2+2}\right\} \tag{5}$$

If the system under consideration is characterized by a single Debye dispersion, then the relaxation time will be obtained from either of the following two equations[9]

$$\tau = \frac{1}{\omega}\frac{a''}{a'-a_\infty} \equiv \tau(1) \tag{6}$$

$$\tau = \frac{1}{\omega}\frac{a_0-a'}{a''} \equiv \tau(2) \tag{7}$$

where ω is the frequency of observation. The limiting value a_∞ is obtainable from Eqs. (6) and (7).

$$a_\infty = a' - \frac{(a'')^2}{a_0-a'} \equiv a_G \tag{8}$$

It is impossible to determine a_∞ experimentally on the basis of Eq. (8) because of other extra dispersions; however, we shall assume tentatively that a_G evaluated from the a' and a'' at a very high frequency (96.52 GHz) would approximate to a_∞. On the basis of the above assumption Eq. (4) can be

* Visiting scientist at the University of Oxford from July to September, 1972, by agreement with the Royal Society, London, the Japan Academy, the Science Council of Japan and the Japan Society for the Promotion of Science.

† The parameter a_∞ in Eq. (2) will be discussed later (see Eq. (8)).

Table 1. Experimental results at 25 °C

Solute	Solvent	a_0	a'	a''	a_D	a_G	b	P_2[a] (cm^3)	$(P_E+P_A)_G$ (cm^3)	R_D[a] (cm^3)
(A)	[Bz]	0.523	0.490	0.031	0.081	0.462	−0.302	37.8	36.6	28.4
(A)	[Xy]	0.546	0.493	0.036	0.101	0.468	−0.331	38.1	36.5	28.4
(A)	[M]	0.563	0.512	0.033	0.103	0.490	−0.336	38.4	36.8	28.3
(A)	[Dx]	0.691	0.661	0.035	0.296	0.620	−0.131	38.4	37.2	28.8
(A)	[CCl_4]	1.052	0.962	0.064	0.331	0.917	0.214	38.6	37.1	28.9
(A)	[Hx]	0.450	—	—	0.208	—	−0.631	36.0	—	28.3
(A)	[Hp]	0.469	—	—	0.194	—	−0.602	36.5	—	28.0
(A)	[CHx]	0.462	—	—	0.143	—	−0.384	36.8	—	28.7
(B)	[Bz]	0.453	0.347	0.021	0.054	0.342	−0.230	48.7	46.0	37.9
(C)	[Bz]	0.460	0.386	0.023	0.162	0.379	−0.509	48.8	46.2	38.4
(D)	[Bz]	0.261	0.183	0.037	−0.016	0.166	−0.115	78.4	74.6	66.9

Solute: (A) 1,4-benzoquinone, (B) 2,5-dimethyl-1,4-benzoquinone, (C) 2,5-dichloro-1,4-benzoquinone and (D) 2,5-di-*tert*-butyl-1,4-benzoquinone.

Solvent: [Bz] benzene, [Xy] *p*-xylene, [M] mesitylene, [Dx] dioxan, [CCl_4] carbon tetrachloride, [Hx] *n*-hexane, [Hp] *n*-heptane and [CHx] cyclohexane.

a) The errors in P_2 and R_D are all about ± 0.2 cm^3.

rewritten by using a_G and ε_1' instead of a_∞ and $\varepsilon_{1\infty}$, respectively.[8]

$$(P_E+P_A)_G = M_2\left\{\frac{3a_G v_1}{(\varepsilon_1'+2)^2} + (v_1+b)\frac{\varepsilon_1'-1}{\varepsilon_1'+2}\right\} \quad (9)$$

All the compounds used in this study were obtained from commercial sources. Purchased materials of the best grade were purified by repeated recrystallization from benzene. The melting points of the purified samples were: 1,4-benzoquinone 113 °C, 2,5-dimethyl-1,4-benzoquinone 123 °C 2,5-dichloro-1,4-benzoquinone 160 °C, and 2,5-di-*tert*-butyl-1,4-benzoquinone 150 °C. Solvents: benzene, *p*-xylene, mesitylene, dioxan, carbon tetrachloride, *n*-hexane, *n*-heptane, and cyclohexane of the best grade were carefully purified by distillation before the dielectric measurements.

Results and Discussion

Atom Polarisation. In Table 1 are given several observed basic parameters and the polarisations derived therefrom. Five parameters are slopes a_0(static), a', a'' (96.52 GHz), a_D(optical) and b(volume) obtained from three to four dilute solutions for each solute by use of Eqs. (1) and (2) and the remaining a_G is evaluated from a', a'' and a_0 using Eq. (8). Three polarisations P_2, $(P_E+P_A)_G$ and R_D are calculated from a_0 and Eq. (3), from a_G and Eq. (9) and from a_D and Eq. (5), respectively.

In Table 2 are given three atom polarisations. P_A(exp) is obtained as $(P_E+P_A)_G-R_D$. This procedure for evaluating P_A(exp) has two sources of error. One is that $(P_E+P_A)_G$ is not necessarily equal to P_E+P_A. This is because a_G and ε_1' would differ from a_∞ and $\varepsilon_{1\infty}$, respectively. We may safely assume $\varepsilon_1' \simeq \varepsilon_{1\infty}$ for non-polar solvents; but sometimes a_G appears to be slightly larger than the probable a_∞ values. For instance, $(P_E+P_A)_G$ would be larger than the true distortion polarisation, if it included some of the effects of dipole relaxation, *e.g.*, alkyl acetates.[10]

The other source of error is that R_D is not equal to the electron polarisation P_E at 96.52 GHz which we really want to have. Again R_D is usually slightly larger than P_E at zero frequency, *e.g.*, 1.1—1.4 cm^3 for halobenzenes.[11] However, $(P_E+P_A)_G-R_D$ is probably a good estimate of P_A. P_A(exp) compares well with P_A(calc) calculated from the absorption spectra by Waddington *et al.*[5]

The radio-visible polarisation difference P_2-R_D is found to be larger than P_A(exp) since P_2 represents a total polarisation, *i.e.*, the sum of any orientation polarisation plus the distortion polarisation.

Molar Polarisation P_2 in Various Media. The $(P_E+P_A)_G$ values recorded in Table 1 for 1,4-benzoquinone are almost equal to the P_2 value observed in the vapour phase by Coop and Sutton.[3] This indicates that the $(P_E+P_A)_G$ values are not appreciably affected by solute-solvent interactions.

$(P_E+P_A)_G$ values could not be observed for the relatively dilute solutions which were all that could be obtained in *n*-hexane, *n*-heptane and cyclohexane; but for these the P_2 values (36.0 to 36.8 cm^3) observed at radio frequencies are also equal to the vapour phase value of P_2 (36.55 cm^3) within the limit of experimental error.†† Consequently the dipole moments of 1,4-benzoquinone in these solvents may be taken to be zero.

In solutions of 1,4-benzoquinone in the aromatic solvents, in carbon tetrachloride and in 1,4-dioxan, P_2 is 1—2 cm^3 greater than $(P_E+P_A)_G$. Moreover, a_0 is greater than a_G and a Cole-Cole dispersion seems to exist (Fig. 1). These facts suggest that 1,4-benzoquinone becomes slightly polar in benzene and possibly

†† Recently John Haigh[12] obtained $P_2=36.99\pm0.5$ cm^3 at 29.7 cm^{-1} in benzene which is slightly larger than $(P_E+P_A)_G=36.6\pm0.5$ cm^3 deduced at 3.22 cm^{-1} (96.52 Hz). From the observed absorption peak at 110 cm^{-1} of 1,4-benzoquinone in CCl_4 the fall of polarisation from its maximum situated at about 96 cm^{-1} is expected to occur on both sides of the frequency. Using the Kramers-Kronig relation we calculated the polarisation for the submillimetre region. The results corrected to Haigh's value at 29.7 cm^{-1} are the following: $P(cm^3)/\bar{\nu}(cm^{-1})$ 36.5/0; 36.99/29.7; 37.2/50; 40.8/90; 41.8/96; 41.1/100; 25.4/112; 14.2/120; 21.1/150; 25.2/200.

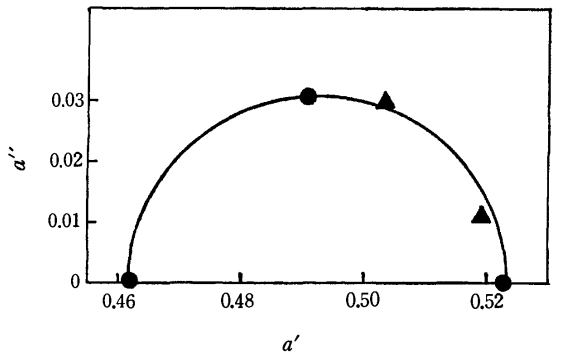

Fig. 1. Cole-Cole plot of 1,4-benzoquinone in benzene solution at 25°C.
●: Present work. ▲: C, W, N. Cumper and R. F. Rossiter, *J. Phys. Chem.*, **76**, 525 (1972).

TABLE 2. ATOM POLARISATIONS

Compound	P_A(exp) (cm³)	P_A(calc) (cm³)	P_2-R_D (cm³)
(A) in [Bz]	8.2±1.0	8.1±2.1	9.4±0.2
[Xy]	8.1±1.0	—	9.7±0.2
[M]	8.5±1.0	8.2±2.2	10.1±0.2
[Dx]	8.4±1.3	8.5±2.6	9.6±0.3
[CCl_4]	8.2±1.5	9.6±2.2	9.7±0.3
(B) in Bz	8.1±1.5	8.4±2.1	10.8±0.2
(C) in Bz	7.8±1.8	—	10.4±0.2
(D) in Bz	7.7±2.0	—	11.5±0.2

See Table 1 regarding the codes (A), (B), (C), (D) for the solutes and [Bz], *etc.*, for the solvents.

in other solvents of this group.

Dipole Moments and Relaxation Times. In Table 3 dipole moments and relaxation times for 1,4-benzoquinone and its derivatives in solutions are collected. In this table dipole moments μ were obtained from the following equation,

$$\mu(\mathrm{D}) = 0.0128\sqrt{\{P_2-(P_E+P_A)_G\}T} \qquad (10)$$

where T is the absolute temperature; and the relaxation time $\tau(2)$ is obtained from a' and a'' for $\omega=2\pi(9.652)\times 10^{10}$ and a_0(static) on the basis of Eq. (7). All the $\tau(2)$ values are much smaller than would be expected for the rotation of a dipolar molecule the size of 1,4-benzoquinone. According to Crump and Price,[4] following Anderson and Smyth,[13] the polarity arises from complex formation between molecules of 1,4-benzoquinone (electron acceptor) and solvent (electron donor); and $\tau(2)$ is controlled by the lifetime of the complex, not by the time of rotation of a long-lived dipole. The accuracy of measurement of the moments of the complexes hardly warrants any attempt to correlate them with the base strengths of the solvents; and much the same applies to the relaxation times $\tau(2)$.

Far Infrared Absorption. The effects of solvents upon the submillimetre wave absorption of 1,4-benzoquinone, previously shown by Waddington *et al.*[5] to be a bending mode, are very striking. Two features are immediately apparent. Shifts occur to higher frequencies (so-called blue shifts) and are large. An attempt was made to study the dependence of absorption

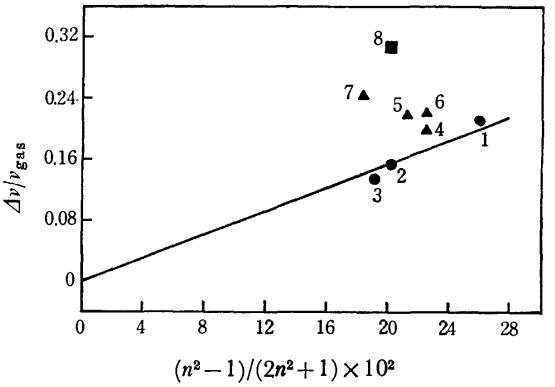

Fig. 2. Solvent dependence of the far-infrared absorption band of 1,4-benzoquinone.
Solvents: 1 carbon disulphide, 2 cyclohexane, 3 *n*-heptane, 4 benzene, 5 carbon tetrachloride, 6 mesitylene, 7 hexafluorobenzene and 8 dioxan.

frequencies upon solvents on the basis of the simple electrostatic treatment given by Kirkwood[14] and by Bauer and Magat.[15] Their model imagines a polar oscillating molecule placed at the centre of a spherical cavity in a continuous dielectric medium of refractive index n. Charges are set up on the walls of the cavity and produce an electric field which reduces the effective force constant of the molecule. The model leads to the equation;

$$\frac{\bar{\nu}_{vap}-\bar{\nu}}{\bar{\nu}_{vap}} = C\frac{(n^2-1)}{(2n^2+1)} \qquad (11)$$

in which C is a positive constant and so allows only the prediction of "red" shifts and cannot explain the observations reported here. If, however, the above equation can be used even when C is negative then a plot of $(\bar{\nu}_{vap}-\bar{\nu})/\bar{\nu}_{vap}$ against $(n^2-1)/(2n^2+1)$ allows us to classify the observations into three groups(Fig. 2). The explanation of the observed frequency increases probably is that the solvent molecules enclathrate and hem in the vibrating solute molecules thus making it more difficult for the quinone molecule to bend. The effectiveness of this process would be expected to increase with increasing solvent-solute attraction. It is hence not unreasonable to suppose that deviation from a linear relationship between the relative shift in the bending frequency $(\bar{\nu}_{vap}-\bar{\nu})/\bar{\nu}_{vap}$ and a function of the dielectric constant of the solvent such as $(n^2-1)/(2n^2+1)$ would indicate the presence of special solvent-solute attractions. These attractions are likely to be due to the solvents behaving as weak electron donors to the 1,4-benzoquinone. The results may be classified into three groups. The *first* group consists of carbon disulphide, cyclohexane, and *n*-heptane the points for which lie on a straight line passing through the gas phase point. This may indicate an interaction due to polarisation of the solvent by the double dipole field of the solute. Deviations from this straight line are observed in the *second* group; benzene, carbon tetrachloride, mesitylene and hexafluorobenzene; and especially in the *third* group; dioxan. These may indicate specific hyperpolarisation which is much the same as donor-acceptor interaction. Hexafluoroben-

Table 3. Dipole moments and relaxation times at 25° C

Solute	Solvent	μ(D)	τ(2)(ps)
(A)	Benzene	0.24	1.76
	p-Xylene	0.28	2.37
	Mesitylene	0.29	2.50
	Dioxan	0.25	1.39
	CCl_4	0.27	2.33
(B)	Benzene	0.36	8.26
(C)	Benzene	0.36	5.25
(D)	Benzene	0.43	3.49

zene is not normally regarded as an electron donor but rather as an electron acceptor. However, it seems possible that the carbonyl groups in 1,4-benzoquinone can act as electron donors to strong electron acceptors.

From an examination of the dielectric data no significant difference was noticed between the *second* and *third* groups and small but finite dipole moments of 0.24—0.29D are observed in these cases (Table 3) whilst the molecules belonging to the *first* group have no dipole moment. This would imply that no interaction of the donor-acceptor type occurs with the molecules of the *first* group.

Concluding Remarks

The following conclusions are reached from the present investigation.

1) 1,4-Benzoquinone is non-polar in the free state.

2) Polarity is produced when 1,4-benzoquinone is transferred from the gaseous phase into solutions in certain solvents such as benzene, dioxan, and carbon tetrachloride.

3) From dipole moments and dielectric relaxation times the above polarity is considered as due not to a conventional permanent dipole moment, but rather as due to some other cause such as the production of short-lived donor-acceptor complexes.

Two of us D. W. and L.E.S. wish to thank the Science Research Council of Great Britain for financial assistance.

References

1) J. Trotter, *Acta Crystallogr.*, **13**, 86 (1960).
2) D. L. Hammick, G. C. Hampson, and G. I. Jenkins, *J. Chem. Soc.*, **1938**, 1263.
3) I. E. Coop and L. E. Sutton, *ibid.*, **1938**, 1269.
4) R. A. Crump and A. H. Price, *Trans. Faraday Soc.*, **66**, 92 (1970).
5) J. Haigh, K. M. Jinks, A. G. Leach, B. D. Milligan, L. E. Sutton, and D. Waddington, *J. Chem. Soc. Faraday II*, **70**, 779 (1974).
6) K. Chitoku, K. Higasi, M. Nakamura, Y. Koga, and H. Takahashi, This Bulletin, **44**, 992 (1971).
7) I. F. Halverstadt and W. D. Kumler, *J. Amer. Chem. Soc.*, **64**, 2988 (1942).
8) Y. Koga, H. Takahashi, and K. Higasi, This Bulletin, **46**, 3359 (1973).
9) K. Higasi, *ibid.*, **39**, 2157 (1966).
10) Y. Koga, H. Takahashi, and K. Higasi, *ibid.*, **47**, 84 (1974).
11) S. K. Garg and C. P. Smyth, *J. Chem. Phys.*, **43**, 1397 (1965).
12) J. Haigh, personal communication.
13) J. E. Anderson and C. P. Smyth, *J. Amer. Chem. Soc.*, **85**, 2904 (1963).
14) J. G. Kirkwood, cited in W. West and R. T. Edwards, *J. Chem. Phys.*, **5**, 14 (1937).
15) E. Bauer and M. Magat, *J. Phys. Radium*, **9**, 319 (1938).

Hydrate Crystals of Alkali Metal-Chloranil and -Bromanil Salts and Their Optical and Magnetic Properties

Shoji HIROMA and Haruo KURODA

Department of Chemistry, Faculty of Science, The University of Tokyo, Hongo, Bunkyo-ku, Tokyo 113

(Received August 28, 1974)

The potassium-chloranil ($K^+ \cdot CA^-$), sodium-chloranil ($Na^+ \cdot CA^-$) and sodium-bromanil ($Na^+ \cdot BA^-$) salts were found to form hydrates when their crystalline powders are exposed to a humid air. In the single crystal spectrum of $K^+ \cdot CA^-$, the charge-transfer band significantly increased its intensity on hydration, exhibiting the same polarization as in the spectrum of the water-free state. It was concluded that CA^- ions in the hydrate crystal are closely stacked on each other to form columns as in the water-free crystal and the charge transfer interaction between CA^- ions is stronger in the hydrate crystal than in the water-free crystal. The spin concentration of $K^+ \cdot CA^-$ markedly decreased on hydration, it being 2.2×10^{22} spins per mol in the state of hydrate while 5.5×10^{23} spins per mol in the water-free state. The hydration resulted in an increase of the intensity of charge-transfer band and a decrease of the spin concentration also in the cases of $Na^+ \cdot CA^-$ and $Na^+ \cdot BA^-$. It is also shown that organic solvents such as acetone, methy ethyl ketone and dichloromethane can enter into the crystal lattice of $K^+ \cdot CA^-$ to form the solvent-containing crystals.

The potassium-chloranil salt, $K^+ \cdot CA^-$, has been reported[1] to exhibit a phase transition in the temperature range, 210—270 K, where it changes from the low spin state to the high spin state. Since this type of phase transition is of general interest in connection with the electronic behaviors of organic radical salts, we investigated the changes of the electronic spectrum of the $K^+ \cdot CA^-$ crystal below and above the transition point by means of a microspectrophotometer equipped with a cryostat at the sample stage.[2] In the course of this investigation, we found that, at the room temperature, the crystal spectrum appreciably changed on pumping out the air from the cryostat, but the original spectrum was recovered when the atmospheric air was introduced. We have concluded that the above spectral change takes place because the $K^+ \cdot CA^-$ crystal absorbs water to be a hydrate when kept in the atmospheric air, but this hydrate easily loses water molecules when kept in vacuum.

In the solution, the chloranil anion is known to be quite unstable in the presence of water. In effect, we need to exclude water thoroughly from the solvent which is used in synthesizing the $K^+ \cdot CA^-$ salt. Therefore it has been generally believed that the $K^+ \cdot CA^-$ salt decomposes when exposed to a humid air. However, we found that this is not necessarily the case. The $K^+ \cdot CA^-$ salt does not decompose, but forms a hydrate in a humid air. We found also that the sodium-chloranil, $Na^+ \cdot CA^-$, and sodium-bromanil, $Na^+ \cdot BA^-$, have a much strong tendency to form hydrates when exposed to the atmospheric air, which are again not very much unstable. It was recently reported also by Tsuda *et al.* that the powder of $Na^+ \cdot CA^-$, obtained by the ordinary procedures of preparation, was in the state of hydrate.[3]

In the present paper, we will report the experimental evidences for the formation of the hydrates of $K^+ \cdot CA^-$, $Na^+ \cdot CA^-$ and $Na^+ \cdot BA^-$, and discuss some of the electronic properties of these hydrates.

Experimental

The crystalline powders of $K^+ \cdot CA^-$, $K^+ \cdot BA^-$, $Na^+ \cdot CA^-$ and $Na^+ \cdot BA^-$ were prepared according to the procedures reported by Torrey and Hunter,[4] by using acetone as the solvent. The water-free powders of these salts were obtained by drying the salt powders over phosphorus pentoxide in a vacuum desiccator (at about 10^{-3} Torr). The powder specimens of various water contents were obtained by exposing the synthesized powders of the salts to the air, with or without controlling the humidity, for different lengths of time.

The X-ray powder diffraction patters were obtained with an automatic recording X-ray diffractometer, Geigerflex (Rigaku Denki), employing CuK_α radiation.

We carried out the differential thermal analysis (DTA) or differential scanning calorimetry (DSC) simultaneously with the thermogravimetric analysis (TGA) by means of a Rigaku TG-DTA (DSC) apparatus with the heating rate, 2.5 °C/min. The powders of KNO_3 and NH_4NO_3 were used as the reference for determining the enthalpy change corresponding to an endothermic peak of a DTA (or DSC) curve.

The polarized absorption spectra of single crystals, in the wave number region from 8000 cm^{-1} to 38000 cm^{-1}, were measured with a microspectrophotometer, a modification of Olympus MSP-IV equipped with a cryostat at the sample stage.[5] The sample crystals of microscopic size were mounted on a thin quartz plate, and placed in the cryostat.

The ESR absorptions of the powder samples were measured at the room temperature with a JEOL-ME spectrometer (at 9.4 GHz). The spin concentration was determined from the integrated intensity by using DPPH as the reference.

The infrared spectra of the powder samples were measured by means of the Nujol mull method.

Results and Discussion

Characterization of the Hydrates. The infrared spectrum of the powder of $K^+ \cdot CA^-$ was found to vary depending on the treatment after the synthesis. The infrared spectra of the two typical cases are compared in Fig. 1(a): the spectrum I was obtained when the salt powder had been kept in the atmospheric air for a few hours after the synthesis, and the spectrum II was obtained when it had been dried in a vacuum desiccator containing silica gel as the desiccating agent. The spectrum I shows absorption bands at 3400, 1630 1000 cm^{-1} whereas these bands are missing in the spectrum II, and, at the same time, other bands of the former spectrum are a little shifted as compared with

the corresponding bands of the latter spectrum.

The infrared spectrum of $K^+ \cdot CA^-$ was previously studied by Iida[6] and by Girlando *et al.*[7] The spectrum II of Fig. 1(a) coincides with the results reported by these authors, and all absorption bands in this spectrum are assignable to the vibrational modes due to the CA^- ion. On the other hand, the 3400, 1630 and 1000 cm^{-1} bands of the spectrum I can be attributed neither to the CA^- ion nor to the neutral molecule of chloranil. It is also hard to find any chemical species that could be responsible for these bands among the possible decomposition products of the CA^- ion. The above bands disappeared when the powder that had given the spectrum I, was dried in a vacuum desiccator. Conversely, the corresponding bands appeared when we exposed the powder that had given the spectrum II, to the atmospheric air for a few hours. The processes described above were comfirmed to be well reversible, and, as we will describe later, we concluded that the spectrum I corresponds to the water-containing state of $K^+ \cdot CA^-$ while the spectrum II to the water-free state.

A similar change of infrared spectrum was observed on the $Na^+ \cdot CA^-$ salt. The infrared spectrum of the $Na^+ \cdot CA^-$ powder which had been kept in the atmospheric air, is shown in Fig. 1(b) as the spectrum I.[8] This is very much similar to the spectrum of the water-containing powder of $K^+ \cdot CA^-$ (spectrum I of Fig. 1(a)), exhibiting absorption bands at 3400, 1630, and 1000 cm^{-1}. In this case, however, the above three bands did not disappear even if we kept the powder in a vacuum desiccator for a week with silica gel, although their intensities were reduced to some extent after the above treatment. The spectrum II of Fig. 1(b) is the one obtained of the powder that had been heated to 120 °C in the ordinary atmosphere. The same spectrum was obtained with a sample which had been dried well over phosphorus pentoxide. These spectra are free from the 3400, 1630 and 1000 cm^{-1} bands, and almost the same as the infrared spectrum of the water-free powder of $K^+ \cdot CA^-$.

In Fig. 1(c), we show the spectrum of the $Na^+ \cdot BA^-$ powder which had been kept in the atmospheric air (spectrum I), and that of the powder which had been heated to 120 °C (spectrum II).[9] As we compare these two spectra, we can see that the former exhibits absorption bands at 3400, 1630 and 940 cm^{-1} while these bands can not be found in the latter. We can consider that the former is the spectrum of the water-containing state of $Na^+ \cdot BA^-$. Interestingly, no indication of the formation of the water-containing state was found in the case of $K^+ \cdot BA^-$. The $K^+ \cdot BA^-$ powder always gave a spectrum nearly the same as that of the water-free powder of $Na^+ \cdot BA^-$. The observed spectrum was in good agreement with the spectrum of the $K^+ \cdot BA^-$ salt reported by Iida,[10] who showed that all observed bands are assignable to the vibrational modes of the BA^- ion.

As we have shown above, the infrared spectrum of the water-containing state is characterized by the presence of the three bands, at 3400, 1630 and 1000 cm^{-1} in the case of $K^+ \cdot CA^-$ and $Na^+ \cdot CA^-$ and at 3400, 1630 and 940 cm^{-1} in the case of $Na^+ \cdot BA^-$. Seemingly it is most reasonable to attribute these bands to the water molecules contained in the salt crystals. A free water molecule is known to have three vibrational modes: the symmetric and antisymmetric stretching vibrations, at 3657 and 3756 cm^{-1} respectively, and the H–O–H bending vibration at 1595 cm^{-1}. Naturally, the infrared absorption bands associated with these vibrational modes are broadened and shifted when the water molecule is contained in the crystal lattice of a salt. In effect, it was reported that the crystals of inorganic hydrates usually show a broad infrared absorption band in the 3000—3500 cm^{-1} region, due to the O–H stretching vibration of water, and one in the 1600—1650 cm^{-1} region, due to the H–O–H bending vibration.[11] Therefore we can attribute the 3400

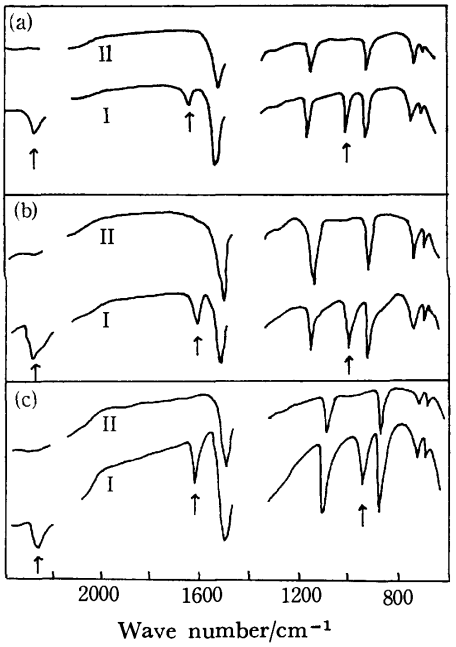

Fig. 1. Infrared spectra of the water-containing states (I) and the water-free states of the salts: (a) $K^+ \cdot CA^-$, (b) $Na^+ \cdot CA^-$ and (c) $Na^+ \cdot BA^-$.
The bands characteristic of the water-containing state are indicated with arrows.

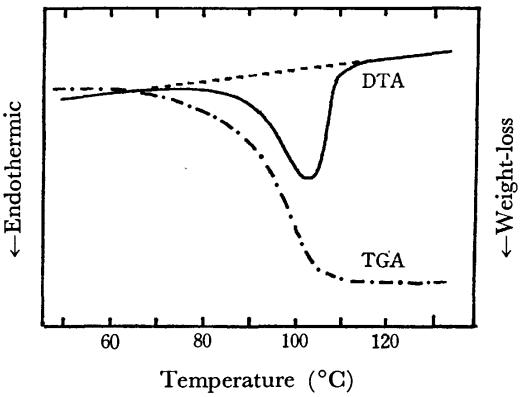

Fig. 2. Differential thermal analysis (DTA) curve and thermogravimetric analysis (TGA) curve of the $Na^+ \cdot BA^-$ powder which has been exposed to the atmospheric air.

and 1630 cm^{-1} bands which are commonly found in the infrared spectra of the water-containing powders of $K^+ \cdot CA^-$, $Na^+ \cdot CA^-$ and $Na^+ \cdot BA^-$, to the O-H stretching and H–O–H bending vibrations of water. There remains a question as regards the origin of the band at about 1000 cm^{-1}. In this connection, it is interesting to see that inorganic hydrates often exhibit infrared absorption bands in the 800—1000 cm^{-1} region, and these bands have been attributed to the librational motion of water molecule in the crystal lattice.[11] Presumably the 1000 cm^{-1} (or 940 cm^{-1}) bands of the present salts can be attributed to the same origin.

We have reproduced in Fig. 2 the DTA and TGA curves obtained of the $Na^+ \cdot BA^-$ powder which had been kept in the atmospheric air. The DTA curve exhibits an endothermic peak in the temperature region, 67—102 °C, where the TGA curve indicates that a weight loss is taking place. By means of the gas chromatography, we examined the chemical species coming out from the powder in the above endothermic process, and were able to confirm that it was entirly composed of water vapor. Similar results were obtained on the air-exposed powders of $K^+ \cdot CA^-$ and $Na^+ \cdot CA^-$, although the height and temperature range of the endothermic peak were different for different salts.

From the DTA-TGA (or DSC-TGA) experiments, we simultaneously determined for each powder sample enthalpy of dehydration and the amount of water per one mol of the salt. These values varied depending on the humidity of the atmosphere in which the powder had been kept and on the time length of keeping the powder in such an atmosphere. The mole ratio of water salt, found for the two typical conditions, are shown in Table 1, where "the normal state" means that the sample powder had been kept for one week in a vacuum desiccator(at about 10^{-3} Torr) containing silica gel, and "the highly-hydrated state" means that the sample powder had been exposed for two days to the air saturated with water vapor at the room temperature. Seemingly the latter corresponds to the state of the maximum water content. It is to be noted that the maximum water mole ratio is more than 6 in the case of $Na^+ \cdot BA^-$ whereas it seems to be about 3 in the cases of $K^+ \cdot CA^-$ and $Na^+ \cdot CA^-$.

In Figures 3(a)—(c), we have plotted the enthalpy of dehydration ΔH per one mol of the salt, against the water mol ratio, n. In the $K^+ \cdot CA^-$ salt, ΔH is proportional to n up to $n=2$, but ceases to increase when $n>2$. This relation between ΔH and n, suggests that there are some changes as regards the state of water molecules in the salt crystals when the water mole ratio exceeds 2. A similar relation between ΔH and n was observed on $Na^+ \cdot CA^-$, in which, although the slope of the ΔH *vs.* n curve changes at about $n=2$, ΔH is still increasing with a further increase of the water content. The enthalpy of dehydration per one mol of water corresponding to the initial linear region of the ΔH *vs.* n plot, was estimated as 11.0 and 14.0 kcal/mol for $K^+ \cdot CA^-$ and $Na^+ \cdot CA^-$ respectively.

The ΔH *vs.* n plot of the $Na^+ \cdot BA^-$ salt is significantly different from the above two salts. In this case, ΔH was found to be proportional to n in a wider range of water content, with the enthalpy of dehydration per one mol of water, 13.3 kcal/mol.

Table 1. Amount of water contained in the powder samples

Salt	Water mole ratio (water/salt)	
	Normal state[a]	Highly-hydrated state[a]
$K^+ \cdot CA^-$	0	2.8
$Na^+ \cdot CA^-$	2.0	3.1
$Na^+ \cdot BA^-$	1.3	6.2

a) see text.

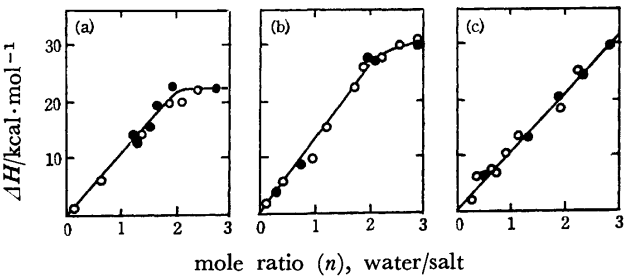

Fig. 3. Relation between the enthalpy of dehydration ΔH (per one mol of salt), and the water mole ratio n; (a) $K^+ \cdot CA^-$, (b) $Na^+ \cdot CA^-$ and (c) $Na^+ \cdot BA^-$. Solid circles are from differential scanning calorimetry and open circles from differential thermal analysis.

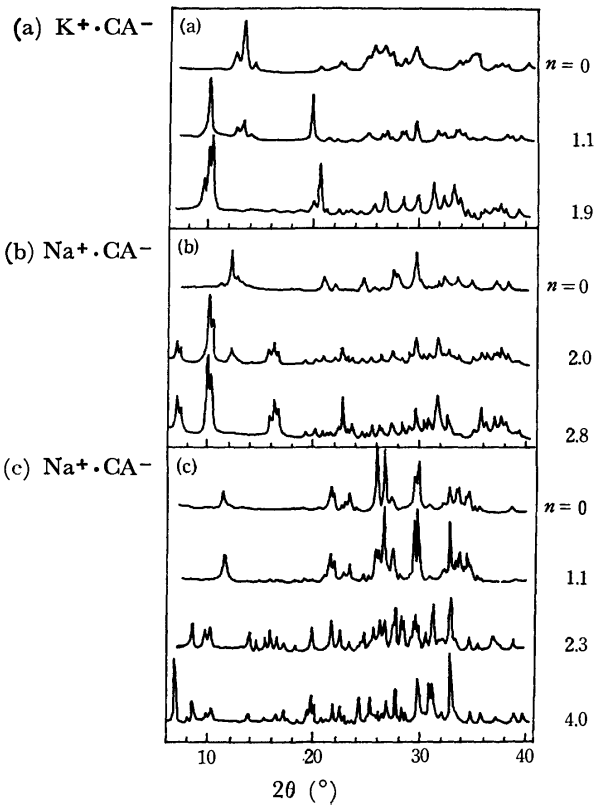

Fig. 4. X-ray diffraction patterns of the salt powders of different water mole ratios; (a) $K^+ \cdot CA^-$, (b) $Na^+ \cdot CA^-$ and (c) $Na^+ \cdot BA^-$.
The value of water mole ratio is indicated at the right of each diffraction pattern.

The X-ray powder diffraction patterns of the three salts at different water contents are reproduced in Fig. 4. Konno *et al.*[12] reported that there are two modifications of the $K^+ \cdot CA^-$ salts, α- and β-form, at the room temperature, and carried out the crystal structure analysis on the α-form crystal. By comparing with the crystal data reported by these authors, we were able to conclude that the X-ray powder diffraction pattern of the water-free sample shown in Fig. 4(a), is the one due to the α-form crystals. According to the reported crystal structure of the α-form crystal, CA^- ions are stacked on each other with equal intervals to form columns parallel to the c axis, and such CA^- columns are mutually held together through K^+ ions without leaving such a space that can accommodate water molecules. Therefore, a considerable change must take place in the crystal structure in order to accommodate water molecules in the crystal lattice to form a hydrate crystal. In effect new peaks were observed in the diffraction patterns of water-containing samples. When the water mole ratio was in the range $0<n<2$, the diffraction pattern was consisting of the peaks due to the hydrate crystals and those due to the water-free crystals, and the relative intensities of the former peaks increased on increasing the water mole ratio. The above change in the powder diffraction pattern implies that the water molecules are not distributed uniformly among the crystals in the powder, but the powder is, in reality, a mixture of the water-free crystals and the hydrate crystals. Thus the observed water mole ratio of a powder sample should be interpreted as the average value over such an heterogeneous system.

When the water mole ratio of the $K^+ \cdot CA^-$ powder is about 2 or higher, the powder diffraction pattern shows peaks different from those of the hydrate crystals mentioned above (see the diffraction pattern of the sample with $n=1.9$ in Fig. 4(a)). These peaks are likely to be due to another type of hydrate with a higher water content. We will tentatively call this as hydrate II and the other as hydrate I. The powder diffraction patterns indicated that the powders of the water mole ratios, $2<n<3$, are composed of the crystals of hydrate I and hydrate II, and the latter content increases with the increase of the water mole ratio of the powder. As we compare the change in the powder diffraction pattern and the relation between ΔH and n shown in Fig. 3, it is most likely that hydrate I has the water mole ratio of approximately 2, and hydrate II a value higher than that, possibly about 3.

The water-containing samples of $Na^+ \cdot CA^-$ showed the X-ray diffraction patterns which consisted of the peaks due to the water-free crystals and those due to the hydrate crystals. With the increase of the water mole ratio of the powder, the former peaks decreased their intensities, but did not disappear until the water mol ratio exceeded 2.5. We noted also that the position of the diffraction peaks of the hydrate crystal little changed throughout the studied region of the water mole ratio, while their intensities relative to each other varied a little depending on the water content. These facts seem to suggest that the hydrate crystal formed in the initial stage of hydration has a composition corresponding to the water mole ratio higher than 2, and its structure has a space to accommodate more water molecules without causing a significant change in the skelton of the crystal structure.

The behavior of the $Na^+ \cdot BA^-$ salt was found to be markedly different from those of the above two salts. The diffraction pattern of the powder sample of which water mole ratio was 1.1, was not very much different from that of the water-free sample (see Fig. 4(c)). This seems to indicate that, in the first stage of hydration, water molecules can enter into the lattice of the water-free crystal of $Na^+ \cdot BA^-$ without any significant change of the crystal structure. The second stage of hydration was found to take place as the water mole ratio of the powder was about 2, where new peaks started to appear in the powder diffraction pattern. Another type of diffraction pattern was observed with the samples of a higher water mole ratio. Thus we can presume that there are three or more different stages of hydration in the case of $Na^+ \cdot BA^-$.

Crystal Spectra of the Hydrates. We studied the effects of hydration on the electronic spectra of the single crystals of the salts using a microspectrophotometer equipped with a cryostat at the sample stage of the microscope system of the spectrometer. We used the cryostat as the sample cell for the purpose to control the ambient atmosphere and temperature of the sample crystal. On each salt, we first measured the absorption

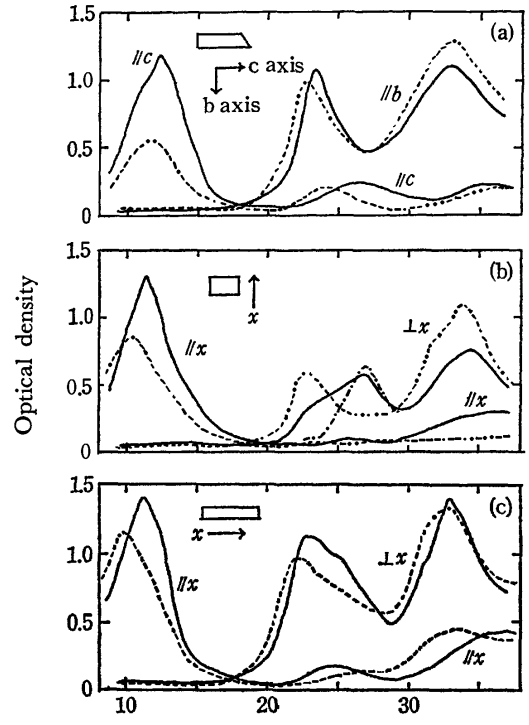

Fig. 5. Polarized absorption spectra of single crystals of $K^+ \cdot CA^-$ (a), $Na^+ \cdot CA^-$ (b) and $Na^+ \cdot BA^-$ (c): —— hydrated state, - - - - water-free state.
(The lowest $^2B_{1u} \leftarrow {}^2B_{2g}$ band observed at a highly-hydrated state of the $Na^+ \cdot CA^-$ crystal is indicated in Fig. 5 (b) with —·—·—)

spectrum of the sample crystal in the atmospheric air, then pumped out the air from the sample cell and, if necessary, heated the crystal to about 100 °C for a short while, and then measured again the absorption spectrum at the room temperature without breaking the vacuum of the sample cell.[13] The results of such experiments are shown in Fig. 5. Unfortunately there was no way to know the water content of the sample crystal at the condition of the spectral measurement, but we can consider that, in each case, the sample crystal was originally in the state of hydrate with the water mole ratio of about 2,[14] and was converted to the water-free state by the treatment given within the sample cell of the spectrometer.

In the case of the $K^+ \cdot CA^-$ salt, the crystal changed to the water-free state without any heat-treatment as soon as the air was pumped out from the sample cell, and the reverse change to the hydrate took place as the atmospheric air was introduced into the sample cell. In our previous paper,[2] we discussed the assignment of each absorption band of the spectrum of the water-free crystal, and attributed the 11.5×10^3 cm^{-1} band of the *c*-axis spectrum to the charge transfer between CA^- ions, the 24.0×10^3 cm^{-1} band of the same spectrum to the lowest $^2A_u \leftarrow {}^2B_{2g}$ transition of the CA^- ion, and the 23.1×10^3 and 32.7×10^3 cm^{-1} bands of the *b*-axis spectrum to the lowest and next $^2B_{1u} \leftarrow {}^2B_{2g}$ transitions of the CA^- ion, respectively.

The most prominent difference between the hydrate form and the water-free form was found in the region of the charge-transfer band, where the intensity decreased as the crystal changed from the hydrate form to the water-free form, and increased in the reverse process. The differences were less prominent in the region of local excitation bands. However, as compared with the spectrum of the water-free form, the first band of the *b*-axis spectrum of the hydrate was shifted to higher energy by about 500 cm^{-1} with a little increase of intensity, while the second band of the same spectrum remained at the same position with a little decrease of intensity, and, in the *c*-axis spectrum, the band due to the $^2A_u \leftarrow {}^2B_{2g}$ transition was shifted to higher energy by about 1200 cm^{-1}.

The above-described features of the spectrum of the hydrate resemble in all respects those of the crystal spectrum of the low-temperature phase of the water-free form. We can derive several conclusions concerning the hydrate crystal from these results. First of all, we can conclude that, like in the water-free crystal, CA^- ions in the hydrate crystal must be closely stacked on each other to form the CA^- columns parallel to the crystal axis corresponding to the c axis of the water-free state. Second, we can conclude that the interaction between the neighboring CA^- ions in such a column, is much stronger in the hydrate than in the high temperature phase of the water-free form. This means either that the intervals of CA^- ions in the column have uniformly decreased from those in the water-free crystal or that the CA^- ions are taking a dimeric arrangement in the CA^- columns of the hydrate crystal. Presumably, in the hydrate crystal, the separation between CA^- columns is larger than in the water-free crystal, so that water molecules are located in the space thus produced between the columns.[15]

The crystal structure analysis has not yet been carried out on the $Na^+ \cdot CA^-$ salt. We observed the spectrum for the two polarizations, parallel and perpendicular, respectively, to the *x axis* that is illustrated in Fig. 5(b). In this case, we needed to heat the sample crystal for a short while to about 100 °C in the vacuum of the sample cell in order to convert the hydrate to the water-free state. The spectra of the water-free state thus obtained resembled the spectra of the water-free crystal of $K^+ \cdot CA^-$. Consequently, the first absorption band, at 10.3×10^3 cm^{-1}, completely polarized in the *x* direction, can be assigned to the charge transfer band, and the 22.7×10^3 and 33.8×10^3 cm^{-1} bands of the $\perp x$ spectrum to the local excitation bands associated with the two $^2B_{1u} \leftarrow {}^2B_{2g}$ transitions of the CA^- ion. However, we noted that the intensity of the charge-transfer band, relative to those of the local excitation bands, is appreciably higher in the water-free $Na^+ \cdot CA^-$ $\parallel$ crystal than in the water-free $K^+ \cdot CA^-$ crystal. Thus we can consider that CA^- ions in the crystal of $Na^+ \cdot CA^-$ are forming columns parallel to the *x* axis, with the interaction between CA^- ions stronger than in the CA^- column of the $K^+ \cdot CA^-$ crystal.

The hydrate crystal exhibits the charge transfer band stronger than that of the water-free form, with a shift of the band maximum by 1300 cm^{-1} to higher energy. Interestingly, the first band of the $\perp x$ spectrum was significantly different from the corresponding band of the water-free form: it showed a maximum at 26.7×10^3 cm^{-1} together with a shoulder at 23×10^3 cm^{-1}, whereas the maximum was located at 22.7×10^3 cm^{-1} in the spectrum of the water-free state. Furthermore, the 23×10^3 cm^{-1} shoulder disappeared when we increased the humidity of the air in the sample cell (see Fig. 5(b)). It has been reported that the CA^- dimer is formed in the solution, and this dimer exhibits the local excitation band associated with the lowest $^2B_{1u} \leftarrow {}^2B_{2g}$ transition, at 26.3×10^3 cm^{-1}, while the corresponding band is located at 23.1×10^3 cm^{-1} in the spectrum of the CA^- monomer.[16] In comparion with the above data the appearance of the 26.7×10^3 cm^{-1} band in the spectrum of the highly-hydrated state is likely to be an indication of the strong interaction between CA^- ions. Possibly, CA^- ions are taking a dimeric arrangement in the CA^- column of the hydrate of $Na^+ \cdot CA^-$.

The spectra of the water-free and hydrate states of $Na^+ \cdot BA^-$ are shown in Fig. 5(c). We observed the spectra for the two polarizations, parallel and perpendicular respectively to the elongated direction of the crystal (the *x* direction in Fig. 5(c)). In this salt, it was necessary to heat the crystal to about 100 °C to convert it to the water-free state.

The solution spectrum of the BA^- ion exhibits absorption bands at 22.2×10^3 and 30.3×10^3 cm^{-1} respectively (see Fig. 6). These two absorption bands correspond to the two $^2B_{1u} \leftarrow {}^2B_{2g}$ bands (at 22.2×10^3 and 31.1×10^3 cm^{-1}) of the solution spectrum of the CA^- ion. Thus we can attribute the two absorption

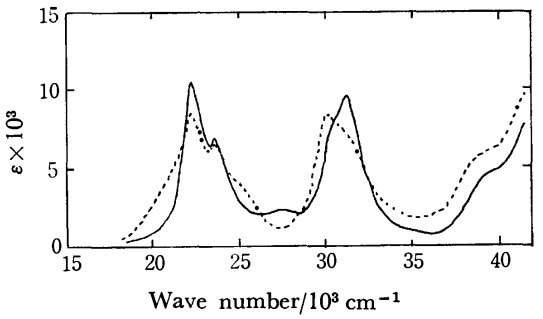

Fig. 6. Absorption spectrum of the CA^- ion (——) and that of the BA^- ion (- - - -) in the acetonitrile solutions of $K^+ \cdot CA^-$ and $K^+ \cdot BA^-$, respectively.

bands in the $\perp x$ spectrum of the $Na^+ \cdot BA^-$ crystal to the local excitations associated with the above two transitions of the BA^- ion, and the near-infrared band in the $\parallel x$ spectrum to the charge-transfer band.

We can consider that, in the crystal of $Na^+ \cdot BA^-$, BA^- ions are stacked along the crystal axis parallel to the *x direction*, with a considerably strong interaction between BA^- ions.

As in the cases of other two salts, the charge-transfer band is shifted to higher energy as a result of the hydration, with a little increase of intensity: the maximum is located at 11.3×10^3 cm^{-1} in the spectrum of the hydrate while it is at 9.6×10^3 cm^{-1} in the spectrum of the water-free state. Interestingly, the intensity of the charge-transfer band decreased for further increase of the degree of hydration, and the charge-transfer band almost disappeared in the highly-hydrated state.

Spin Concentrations of the Hydrates. All salts studied here showed ESR absorptions due to the anion radicals, CA^- or BA^-, but their intensities were found to be markedly affected by hydration. In Table 2, we listed the observed spin concentrations of the powder samples. The spin concentration was generally higher in the water-free state than in the water-containing state. In particular, a marked difference was found in the case of $K^+ \cdot CA^-$: the spin concentration of the water-free powder corresponds to almost 90 percent of the theoretical value that is expected when we assign one free spin to each CA^- ion, whereas that of the water-containing state corresponds to only 5 percent of this theoretical value. The latter is nearly the same as the spin concentration of the low temperature phase of the water-free state. In the cases of $Na^+ \cdot CA^-$ and $Na^+ \cdot BA^-$, the spin concentration was very low even in the water-free state, but it decreased further in the water-containing state. Interestingly, however, the spin concentration of the $Na^+ \cdot BA^-$ powder increased again as the water mol ratio exceeded 4, and reached a value of about 5×10^{23} spin per mol at the state of the highest water mole ratio.

If we compare the results described above with the effects of hydration on the crystal spectra, it is quite evident that there is a close correlation between the spin concentration and the intensity of charge-transfer band. In the case of the $K^+ \cdot CA^-$ salt, the hydration results in an appreciable increase of the intensity of charge-transfer band, which is accompanied by a marked decrease of spin concentration, and, in the cases of other salts also, the spin concentration is always found to be lower when the intensity of charge-transfer band is higher.

Table 2. The spin concentrations of the powder samples (spins per mol of the salt)

Salt	Water-free state	Water-containing state[a)]
$K^+ \cdot CA^-$	5.5×10^{23}	2.2×10^{22} ($n=1.9$)
$Na^+ \cdot CA^-$	3.9×10^{22}	2.7×10^{22} ($n=2.0$)
$Na^+ \cdot BA^-$	6.3×10^{22}	1.0×10^{22} ($n=2.3$)

a) The water mole ratio of the powder sample is given in the parentheses.

In our previous paper,[2)] we have shown that the intensity of charge-transfer band of the water-free $K^+ \cdot CA^-$ crystal increases as the salt changes from the high spin state to the low spin state on lowering the temperature below the transition point, and there is a close correlation between the temperature dependence of spin concentration and that of the intensity of charge-transfer band. We pointed out that the above correlation can be understood in the following way; If we assume a dimeric arrangement of CA^- ions in the CA^- columns of the $K^+ \cdot CA^-$ crystal of the low temperature phase, there will be a singlet state and a triplet state associated with the interaction between CA^- anion radicals, in which the former state will be a little stabilized in respect to the latter state because of the charge-transfer interaction, consequently, the population of such a singlet state will increase while that of the triplet state will decrease on lowering the temperature, and, since the intensity of charge transfer band is governed by the singlet population whereas the spin concentration is governed by the triplet population, the former increases while the latter decreases as the temperature is lowered.

As we have shown in the preceeding section, the crystal spectra indicate that the charge-transfer interaction between the neighboring CA^- ions in the CA^- columns is much stronger in the hydrated state of the $K^+ \cdot CA^-$ crystal than in the water-free state. Therefore, we can presume that the singlet state associated with the interaction between CA^- ions has been much stabilized in the hydrate than in the water-free crystal. This must result in the higher singlet population and lower triplet population in the hydrate crystal as compared with the water-free crystal, hence a higher intensity of the charge-transfer band and a lower spin concentration. These are in accord with the observations. Presumably, the same model can be applied for understanding the effects of hydration on the spin concentrations of other salts.

Solvent-containing Forms of $K^+ \cdot CA^-$. We have confirmed from the infrared spectrum and X-ray powder diffraction pattern that the $K^+ \cdot CA^-$ powder prepared from the acetone solution is usually not containing solvent molecules. This was also the case when methyl ethyl ketone or dichloromethane was used as the solvent. However, we found that the solvent-containing form of $K^+ \cdot CA^-$ can be prepared by exposing the salt powder which has been brought to a

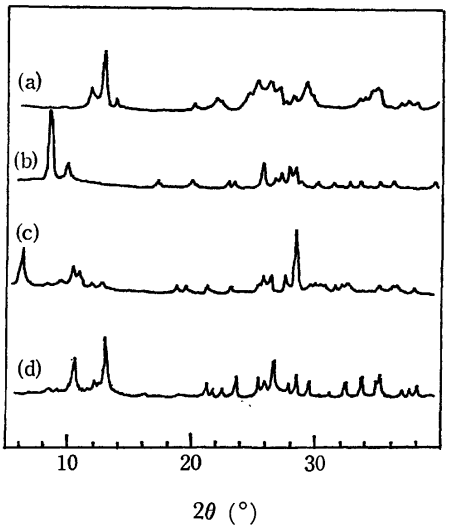

Fig. 7. X-ray diffraction patterns of the solvent-free and solvent-containing powders of $K^+ \cdot CA^-$.
(a): Solvent-free, (b): acetone, (c): methyl ethyl ketone, (d): dichloromethane.

nearly water-free state, to the solvent vapor for a sufficiently long period.

The X-ray powder diffraction patterns of such solvent-containing states are shown in Fig. 7, together with the diffraction pattern of the solvent-free state. We can see that the diffraction patterns of the solvent-containing states are different both from that of the water-free state and from those of the hydrates, of which diffraction patterns have been shown in Fig. 4.

In the infrared spectra of the solvent-containing states, we were able to find the bands due to the included solvent molecules: for instance, the bands at 1710 cm^{-1} (C=O stretching) and 1230 cm^{-1} (C–C=O antisymmetric stretching) in the case of acetone, and at 725 and 700 cm^{-1} (C–Cl stretching) in the case of dichloromethane.

The solvent molecules are liberated when we heat the solvent-containing crystals. By means of the DSC-TGA experiment, we determined the amount of the solvent contained in the salt, and the enthalpy of solvent evolution. The maximum amount of the included solvent and the enthalpy of solvent evolution per one mol of the solvent are shown in Table 3 together with the observed spin concentration of the solvent-containing powder.

Table 3. Properties of the solvent-containing states of $K^+ \cdot CA^-$

Solvent	Maximum amount of solvent[a] (mole ratio, solvent/$K^+ \cdot CA^-$)	Enthalpy of solvent evolution[b] [Kcal/mol of solvent]	Spin concentration [spins/mol of $K^+ \cdot CA^-$]
Acetone	0.90	19	7×10^{21}
Methyl ethyl ketone	0.55	20	3.2×10^{23}
Dichloromethane	0.33	13	2.0×10^{23}

a) The amount of solvent obtained on the powder sample which had been kept for a sufficiently long period in the solvent vapor. b) The value obtained by dividing the value of the enthapy change corresponding to the endothermic peak of DTA curve, due to the solvent evolution, by the amount of the solvent initially contained in the sample.

The results described above prove that the solvent molecules do enter into the crystal lattice of $K^+ \cdot CA^-$ to form the solvent-containing forms. At present, we do not know the reason why we did not obtain the solvent-containing crystal on synthesizing the salt from the acetone solution. We noted that the formation of the solvent-containing form becomes rather difficult if we completely remove water from the powder of $K^+ \cdot CA^-$. This might have bearings on the phenomenon mentioned above.

In the visible absorption spectra of the solvent-containing crystals, the charge-transfer band was observed with the same polarization as that of the spectrum of the solvent-free crystal. Therefore we can consider that CA^- columns of the $K^+ \cdot CA^-$ crystal are not destroyed on forming the solvent-containing crystals, and the solvent molecules are likely to be located in the space between CA^- columns.

References and Notes

1) J. J. Andre and G. Weil, *C. R. Acad. Sci., Paris, Ser. B*, **266**, 1057 (1968); *ibid.*, **269**, 499 (1969); *Chem. Phys. Lett.*, **9**, 27 (1971).
2) S. Hiroma and H. Kuroda, This Bulletin, **46**, 3645 (1973).
3) M. Tsuda, N. Sakai, I. Shirotani, and K. Murano, *Chem. Lett.*, **1973**, 427.
4) H. A. Torrey and W. Hunter, *J. Amer. Chem. Soc.*, **34**, 702 (1912).
5) For the details of the spectrometer and the procedures of the measurement, refer to the following paper; H. Kuroda, S. Hiroma, T. Kunii, and H. Akamatu, *J. Mol. Spectrosc.*, **22**, 60 (1967). The sample crystals used for the spectral measurement were typically of the size, a few micron in width and length and less than one micron in thickness.
6) Y. Iida, This Bulletin, **43**, 345 (1970).
7) A. Girlando, H. Morelli, and C. Pecile, *Chem. Phys. Lett.*, **22**, 553 (1973).
8) A similar result was reported recently by Tsuda *et al.* (Ref. 3), who reported also the X-ray diffraction pattern of a water-containing powder.
9) The powder that had been dried over phosphorus pentoxide showed the same infrared spectrum as the spectrum II.
10) Y. Iida, This Bulletin, **46**, 2955 (1973).
11) R. E. Hester, K. Krishnan, and C. W. J. Scaife, *J. Chem. Phys.*, **49**, 1100 (1968).
12) M. Konno, H. Kobayashi, F. Marumo, and Y. Saito, This Bulletin, **46**, 1987 (1973).
13) The vacuum was in the order of 10^{-5} Torr.
14) This was concluded by examining the average water mol ratio of the crystalline powder from which the sample crystals were selected out.
15) This seems to be consistent with the observed changes of the X-ray powder diffraction pattern.
16) N. Sakai, I. Shirotani, and S. Minomura, This Bulletin, **44**, 675 (1971).

Transition-metal Complexes of Pyrrole Pigments. X.*[1] Divalent and Trivalent Manganese Chelates of Dipyrromethenes

Yukito MURAKAMI, Kazunori SAKATA, Kenji HARADA, and Yoshihisa MATSUDA

Department of Organic Synthesis, Faculty of Engineering, Kyushu University, Hakozaki, Higashi-ku, Fukuoka 812

(Received November 29, 1973)

The solution spectra of two tris(dipyrromethenato)manganese(III) complexes and of one bis(dipyrromethenato)manganese(II) as well as the diffuse reflectance spectrum for the latter were examined. The high spin state was confirmed for all the manganese complexes by magnetic susceptibility measurements. For the tris-complexes, one broad low energy band (~9500 cm^{-1}) is assigned to the $^5A_{1g} \leftarrow {}^5B_{1g}$ transition and one pair of higher energy bands (~14000 cm^{-1}) are attributed to the $^5B_{2g} \leftarrow {}^5B_{1g}$ and $^5E_g \leftarrow {}^5B_{1g}$ transitions for a D_{4h} symmetry as a consequence of Jahn-Teller effect. In the bis-complex, manganese(II) is placed in a tetrahedral ligand field and one group of ligand-field bands lying below 16000 cm^{-1} are assigned to: $^4T_1(^4G) \leftarrow {}^6A_1(^6S)$, $^4T_2(^4G) \leftarrow {}^6A_1(^6S)$, and ^4E, $^4A_1(^4G) \leftarrow {}^6A_1(^6S)$ in an increasing order of energy. The exceedingly high intensity of these bands is ascribed to the covalent nature of coordinate bonds. A strong IR band due to the skeletal stretching mode of the dipyrromethene moiety was observed in the 1600 cm^{-1} range and shifted slightly toward lower energy upon metal-coordination.

Our previous investigations on the structural aspects of the first transition-metal complexes of dipyrromethenes have clarified the three major facts. Firstly, metal ions, which are in the divalent state of favorable stability, form the metal chelates of a 2 : 1 molar ratio of ligand to metal without any other additional ligand. These bis-complexes have a distorted tetrahedral structure, and the extent of this distortion very much depends on the coordination behavior of a central metal and the bulkiness of 5,5'-substituents in a ligand. If the central metals have an electronic configuration favorable for the planar coordination (*e.g.*, Cu(II) and Ni(II)), the yielded complexes come close to the planar geometry to an extent that the steric interaction between 5- and 5'-substituent groups of different ligand molecules in the same complex allows. Consequently, the structure of these complexes depends on the bulkiness of the substituent groups placed at 5- and 5'-positions.[2] On the other hand, when the electronic configuration of the central metals is in favor of the formation of tetrahedral geometry (*e.g.*, Co(II)), the bulkiness of 5,5'-moieties is not significant factor controlling the coordination structure. The covalent nature of coordinate bonds in these cases tends to distort the geometry from regular tetrahedron toward planar.[2]

Secondly, the central metals, which possess the slightly stable trivalent state relative to the divalent, yield tris-complexes with dipyrromethene ligands having no bulky 5,5'-substituents. However, when either or both of these positions are occupied with methyl or bulkier groups, only bis-complexes are obtained. An appropriate example is seen for the iron chelate system.[1]

Thirdly, the reaction of a metal ion, the trivalent state of which is much more stable than the divalent, and a 5,5'-substituted dipyrromethene gives only a complex of the distorted octahedral structure. This type of complex consists of two dipyrromethene molecules and an additional ligand, as observed for chromium(III) by the formation of acetatobis(3,3',5,5'-tetramethyldipyrromethenato)chromium(III).[3]

In the present work, the correlation between the valency state of manganese in a complex and the nature of the 5,5'-substituents placed in the ligands is to be elucidated by employing 3,3',4-trimethyl- (**1**), 3,3',4,4'-tetramethyl- (**2**), and 3,3',5,5'-tetramethyldipyrromethene (**3**) as bidentate ligands.

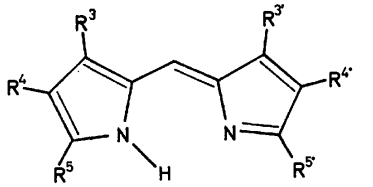

1: $R^3=R^{3'}=R^4=CH_3$, $R^{4'}=R^5=R^{5'}=H$
2: $R^3=R^{3'}=R^4=R^{4'}=CH_3$, $R^5=R^{5'}=H$
3: $R^3=R^{3'}=R^5=R^{5'}=CH_3$, $R^4=R^{4'}=H$

Experimental

Ligands. The synthetic procedures for the present ligands have been described previously.[1,2,4]

Tris(3,3',4-trimethyldipyrromethenato)manganese(III). 3,3',4-Trimethyldipyrromethene hydrochloride (0.4 g) and manganese dichloride tetrahydrate (0.2 g) were suspended in 100 ml of methanol. Crystalline precipitates of green luster developed from the dark reddish reaction mixture upon dropwise addition of dilute aqueous ammonia. The precipitates were recovered by filtration after the mixture being allowed to stand in a freezer for some time. The crystalline solid was extracted with chloroform. After evaporation of the solvent *in vacuo*, the residue was recrystallized from ethanol-chloroform as fine crystals of green luster; yield 0.10 g (36%).

Found: C, 70.11; H, 6.39; N, 13.47%; mol wt (osmometry),[5] 610. Calcd for $C_{36}H_{39}N_6Mn$: C, 70.79; H, 6.45; N, 13.76%; mol wt, 610.7.

Tris(3,3',4,4'-tetramethyldipyrromethenato)manganese(III). Dilute aqueous ammonia was added dropwise into the suspension of 3,3',4,4'-tetramethyldipyrromethene hydrochloride (0.15 g) and manganese dichloride tetrahydrate (0.07 g) in 40 ml of methanol. Reddish orange precipitates developed immediately. After heating on a water-bath (75 °C) for one minute, the reaction mixture was allowed to stand in a freezer for some time. The crystalline solid of green luster was recovered and extracted with chloroform. To the extract was added the same volume of acetone to precipitate fine crystals of green luster; yield 0.06 g (44%).

Found: C, 68.17; H, 6.79; N, 11.80%; mol wt,[5] 590.

* Contribution No. 317 from this Department.

Table 1. Molar magnetic susceptibilities (χ_M) and magnetic moments (μ_{eff}) for dipyrromethene-manganese chelates at room temperature

Chelate	Temp, °K	$10^6 \times \chi_M$, CGS	$10^6 \times \chi_M^{cor}$, CGS	μ_{eff}, BM	$[4S(S+1)]^{1/2}$	No. of unpaired electrons
Tris-complex[a]	293.7	9525	9872	4.82	4.90	4
Bis-complex[b]	297.0	14234	14489	5.87	5.92	5

a) Tris(3,3',4-trimethyldipyrromethenato)manganese(III). b) Bis(3,3',5,5'-tetramethyldipyrromethenato)manganese(II).

Calcd for $C_{39}H_{45}N_6Mn$: C, 71.76; H, 6.95; N, 12.88%; mol wt, 652.3.

Bis(3,3',5,5'-tetramethyldipyrromethenato)manganese(II).[6] Six ml of an aqueous solution of manganese dichloride tetrahydrate (0.12 g) was mixed with an ethanol solution (20 ml) containing 3,3'5,5'-tetramethyldipyrromethene (free base, 0.12 g). Aqueous ammonia (28%, 2 ml) was added dropwise into the solution with stirring. Developed precipitates of green luster was recovered after the reaction mixture being allowed to stand in a freezer for one day. The solid was recrystallized from *n*-hexane as fine crystals of green luster; yield 0.10 g (88%).

Found: C, 68.68; H, 6.68; N, 12.23%; M^+, 453.[7] Calcd for $C_{26}H_{30}N_4Mn$: C, 68.86; H, 6.69; N, 12.12%; mol wt, 453.58.

Physical Measurements. Electronic spectra covering the 7000—30000 cm^{-1} range were recorded on a Hitachi EPS-2 spectrophotometer for chloroform solutions at room temperature. Since bis(3,3',5,5'-tetramethyldipyrromethenato)-manganese(II) gradually decomposed in chloroform for long standing, its spectral measurement was performed immediately after the solution was prepared. Diffuse reflectance spectrum for the bis-complex was measured by a Hitachi EPU-2 spectrophotometer equipped with a R-3 reflectance attachment, MgO being used as a reference sample. Infrared spectra in the range of 200—4000 cm^{-1} were measured with a JASCO DS-403G spectrophotometer by a Nujol mull technique. Magnetic susceptibility measurements of solid samples were carried out by the Faraday method. Calibrations were made by the aid of $Hg[Co(NCS)_4]$, while diamagnetic corrections were performed by using Pascal's constants.

Results and Discussion

The reaction of the manganese(II) salt with 5,5'-unsubstituted dipyrromethenes (**1** and **2**) resulted in the formation of the corresponding manganese(III) complexes having a ligand to metal ratio of 3 : 1 (tris-complex), while the same metal salt reacted with 5,5'-dimethyl-substituted ligand **3** to give the 2 : 1 dipyrromethene-manganese(II) complex (bis-complex). For the dipyrromethene-manganese chelate system, the trivalent manganese state appears to be electronically more stable than the divalent due to the ligand-field stabilization effect brought about by octahedral coordination unless other factors such as steric effects come into play. The introduction of methyl groups at 5,5'-positions gives out a significant steric interaction among these substituents of different ligand molecules in the same complex to such an extent that the formation of a tris-complex is completely inhibited. Similar state of affairs has been observed for the dipyrromethene-iron chelate system.[1]

Magnetic Susceptibilities. The results of magnetic susceptibility measurements are listed in Table 1. It became apparent that the tris-complexes as well as the bis-complex hold a spin-free state. It is quite interesting to note that the present tris-complexes are in a high-spin ground state on the contrary to the low-spin state of the corresponding tris-complex of iron(III).[1]

Electronic Spectra. The electronic absorption

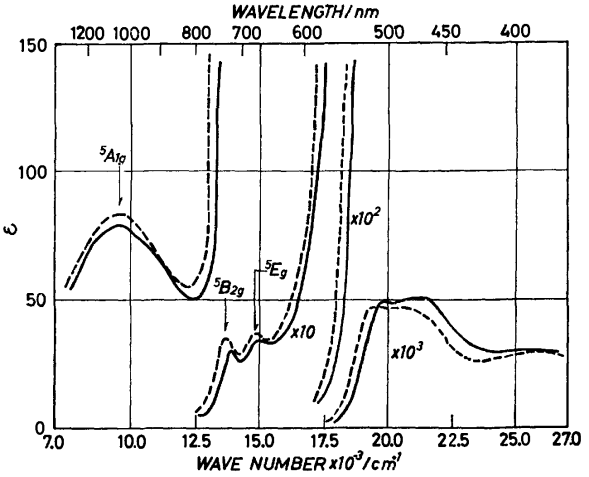

Fig. 1. Electronic absorption spectra of manganese-(III) chelates of dipyrromethenes in chloroform at room temperature: ——, 3,3',4-trimethyldipyrromethene; - - - -, 3,3',4,4'-tetramethyldipyrromethene. Numbers in this figure (10, 10^2, and 10^3) refer to the enlarging factors of the absorption intensity.

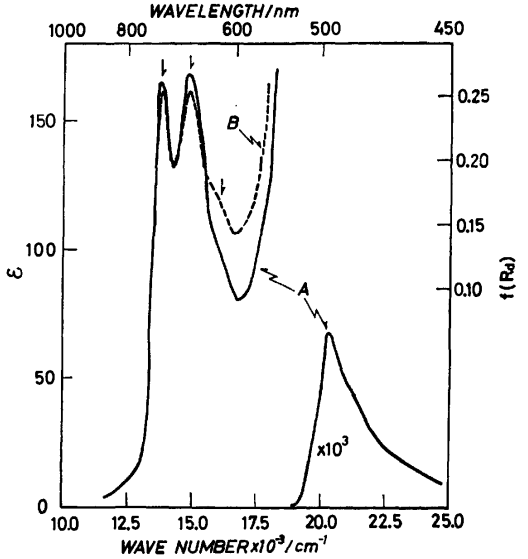

Fig. 2. Electronic spectra of bis(3, 3', 5, 5'-tetramethyldipyrromethenato) manganese(II) at room temperature: A, absorption spectrum in chloroform; B, diffuse reflectance spectrum.

TABLE 2. SPECTROSCOPIC DATA AND LIGAND-FIELD PARAMETERS FOR SOME HIGH-SPIN MANGANESE(III) COMPLEXES AT ROOM TEMPERATURE

Ligand	Complex type	Medium	Ligand-field bands, $cm^{-1}(\varepsilon)$			Ligand-field parameter, cm^{-1}			Ref.
			$^5A_{1g}\leftarrow{}^5B_{1g}$	$^5B_{2g}\leftarrow{}^5B_{1g}$	$^5E_g\leftarrow{}^5B_{1g}$	Dq	Ds	Dt	
1	$Mn(L)_3$	Chloroform	9410(78)	13750(297)	14900(338)	1375	1510	675	This work
2	$Mn(L)_3$	Chloroform	9450(84)	13580(350)	14800(370)	1358	1520	670	This work
Tropolonate	$Mn(L)_3$	Chloroform	9090(89)	15875(248)	17545(318)	1587	1535	590	8
2,4-Pentanedione	$Mn(L)_3$	Cyclohexane	9520(110)	17900(200)	21500	1790	1875	405	a)
Oxalate	$K_3Mn(L)_3$	Reflectance	9100	19050	20400	1905	1495	625	a)
F	K_3MnL_6	Reflectance	9000	17800	19400	1740	1600	520	b)

a) J. P. Fackler, Jr., T. S. Davis, and I. D. Chawla, *Inorg. Chem.*, **4**, 130 (1965). b) G. C. Allen, G. A. M. El-Sharkawy, and K. D. Warren, *ibid.*, **10**, 2538 (1971).

spectra for the tris-complexes are shown in Fig. 1, while the absorption and diffuse reflectance spectra for the bis-complex in Fig. 2. Lower intensity bands lying below 16000 cm^{-1} are apparently due to ligand-field transitions for all the manganese complexes in reference to the ligand-field bands for the other transition metal complexes previously studied.[1,2,4]

Ligand-field spectrum for each tris-complex consists of one broad band at 9500 cm^{-1} and one pair of bands in the 14000 cm^{-1} range. The electronic configuration [core]$3d^4$ (spin-free) produces E_g ground state in fields of octahedral symmetry. This state is susceptible to Jahn-Teller forces which causes the removal of the orbital degeneracy. The existence of a lower energy band at 9500 cm^{-1} and the correlation between this and the coexisting higher energy bands can not be elucidated reasonably in terms of other phenomena, such as spin-orbit coupling, solvent interaction, *etc.*, which may cause the removal of degeneracy. An electronic splitting of this magnitude can occur only if sizable effective distortions of the nuclear geometry from a regular tetrahedron. Jahn-Teller effects of this nature provide distortion to D_{4h} symmetry along with the removal of the E_g degeneracy. Thus, transitions may occur between components of the E_g (under O_h) ground state and from the ground state to the components of T_{2g}, which is less seriously split (Fig. 3). The broadness of the low-energy band ($\sim$9500 cm^{-1}) can also be attributed to the nature of potential energy surfaces for Jahn-Teller split E_g state.[8] Similar spectral behaviors have been observed for some manganese(III) complexes,[8] *e.g.*, tris(tropolonato)manganese(III), tris(2,4-pentanediono)manganese(III), potassium hexafluoromanganate, *etc.* It is not obvious whether the Jahn-Teller effects cause static or dynamic splitting of the E_g ground state for these manganese(III) complexes. Nevertheless, under assumption that the ground state becomes B_{1g} due to the effective D_{4h} field with axial elongation (Fig. 3), the transition energies can be represented as follows.[9]

$$E(^5A_{1g}\leftarrow{}^5B_{1g}) = 4Ds + 5Dt$$

$$E(^5B_{2g}\leftarrow{}^5B_{1g}) = 10Dq$$

$$E(^5E_g\leftarrow{}^5B_{1g}) = 3Ds - 5Dt + 10Dq$$

Spectral assignments and the ligand-field parameters thus evaluated are summarized in Table 2 along with some reference data from literatures.

Ligand-field spectrum for the bis-complex consists of three bands in a region lying below 16000 cm^{-1} as shown in Fig. 2. The tetrahalomanganate(II) complexes have been shown to assume tetrahedral coordination and their spectra analyzed[10] quantitatively by the aid of the secular equations of Tanabe and Sugano.[11] Similar interpretation would be applied to the present bis-complex, since structural require-

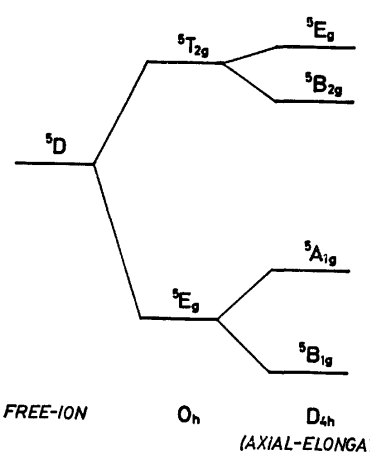

Fig. 3. Energy level diagrams for high-spin d^4 configuration under O_h and D_{4h} symmetries (not to scale).

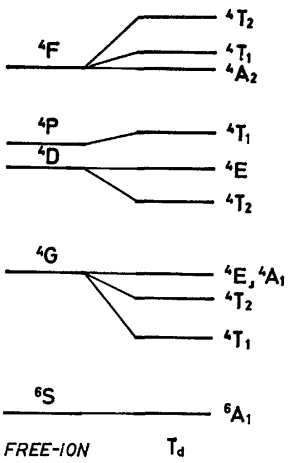

Fig. 4. Energy level diagram for high-spin d^5 configuration under T_d symmetry (not to scale).

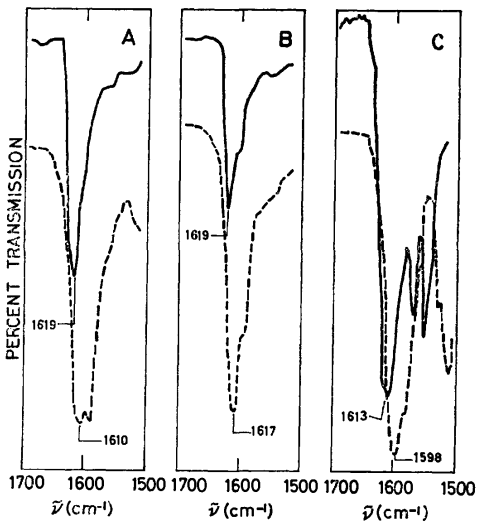

Fig. 5. Infrared spectra of manganese chelates (- - - -) and dipyrromethene free base (——) by a Nujol mull technique: A, 3,3′,4-trimethyldipyrromethene and its manganese(III) chelate; B, 3′3′,4,4′-tetramethyldipyrromethene and its manganese(III) chelate; C, 3,3′,5,5′-tetramethyldipyrromethene and its manganese (II) chelate. Number refers to the skeletal vibrational mode of the dipyrromethene moiety.

ment of the present dipyrromethene ligand forces manganese(II) to occupy a tetrahedral ligand field. The present ligand-field bands are tentatively assigned as follows (refer to Fig. 4).

$^4T_1(^4G) \leftarrow {}^6A_1(^6S)$: 13800 cm^{-1} (ε 165)

$^4T_2(^4G) \leftarrow {}^6A_1(^6S)$: 14900 cm^{-1} (ε 168)

$^4E, {}^4A_1(^4G) \leftarrow {}^6A_1(^6S)$: 16100 cm^{-1} (ε ~97 sh)

Since the higher energy ligand-field bands are hidden in the present case due to the presence of high intensity bands attributable to charge-transfer and ligand $\pi \rightarrow \pi^*$ transitions, the critical spectral analysis, to an extent as performed for the tetrahalomanganate system, was not attempted.

In spite of these interpretation for the bis-complex, absorption intensity of these bands is exceedingly high for the ordinary spin-forbidden transitions. If covalent nature of the coordinate bond increases, the orbital angular momentum for the ground state cannot be referred to pure A_1 state any longer. Thus, this interaction tends to act in favor of transition probability increase.[12] In addition, the covalent interaction may provide any tendency to distort a tetrahedrally coordinated complex toward planar geometry as postulated for other dipyrromethene complexes of divalent first-transition metals.[2,3]

Vibrational Spectra. The IR absorption spectra for manganese chelates, covering the 1500—1700 cm^{-1} region, are shown in Fig. 5. A strong band due to the skeletal stretching mode of the dipyrromethene moiety appears in the 1600 cm^{-1} range. These bands show a slight shift upon metal-coordination.

In the far-infrared region, 700—200 cm^{-1}, the bis-complex shows an absorption peak of medium intensity in the 400—350 cm^{-1} range in a manner similar to the cobalt(II), nickel(II), copper(II), and iron(II) chelates of some dipyrromethenes reported previously.[1,2] This band can be associated with the metal-ligand (M—N) stretching mode: 379 cm^{-1} for bis(3,3′,5,5′-tetramethyldipyrromethenato)manganese(II). On the other hand, we failed to assign such a vibrational mode to the tris-complexes.

The authors wish to acknowledge partial support of this work by the Asahi Glass Foundation for the Contribution to Industrial Technology. Thanks are also due to the Research Institute of Yoshitomi Pharmaceutical Co., Ltd. for mass spectral measurements and to Drs. Shigeo Kida and Hisashi Okawa of our University for magnetic susceptibility measurements.

References

1) Part IX: Y. Murakami, Y. Matsuda, K. Sakata, and K. Harada, This Bulletin, **47**, 458 (1974).

2) Y. Murakami, Y. Matsuda, and K. Sakata, *Inorg. Chem.*, **10**, 1728 (1971).

3) Y. Murakami, Y. Matsuda, and K. Iiyama, *Chem. Lett.*, **1972**, 1069.

4) Y. Murakami and K. Sakata, *Inorg. Chim. Acta*, **2**, 273 (1968).

5) A Hitachi Model 115 vapor pressure osmometer was used to measure the molecular weight of a sample dissolved in chloroform.

6) Preparation of this metal chelate was aided by Mr. Kiyotaka Iiyama of this Laboratory.

7) The mass spectral analysis was carried out on a JEOL JMS-01SG spectrometer.

8) T. S. Davis, J. P. Fackler, and M. J. Weeks, *Inorg. Chem.*, **7**, 1994 (1968).

9) C. J. Ballhausen, "Introduction to Ligand Field Theory," McGraw-Hill Book Co., Inc., New York (1962).

10) F. A. Cotton, D. M. L. Goodgame, and M. Goodgame, *J. Amer. Chem. Soc.*, **84**, 167 (1962).

11) Y. Tanabe and S. Sugano, *J. Phys. Soc. Japan*, **9**, 753 (1954).

12) Since the absorption intensity of these bands is much high for the ordinary spin-forbidden transitions, there exists some opinion against these assignments given above. Our interpretation will be confirmed by means of ESR study in the near future.

Transition-metal Complexes of Pyrrole Pigments. XI. Zinc(II) Chelates of Some Dipyrromethenes*

Yukito MURAKAMI and Kazunori SAKATA

Department of Organic Synthesis, Faculty of Engineering, Kyushu University, Hakozaki, Higashi-ku, Fukuoka 812

(Received March 11, 1974)

The zinc(II) chelates of five dipyrromethenes which have methyl substituents to a various extent, as well as that of 5,5′-diphenyldipyrromethene, have been prepared. The behaviors of methyl resonances upon metal-coordination were classified into three cases: (1) a down-field shift, but not greater than that of the corresponding ligand hydrochloride (3,3′-$C\underline{H}_3$); (2) nearly no change in chemical shift (4,4′-$C\underline{H}_3$); and (3) a profound up-field shift, the methyl resonance of the corresponding ligand hydrochloride showing a down-field shift on the contrary (5,5′-$C\underline{H}_3$). A marked change in chemical shift for the methine proton upon zinc(II)-coordination is related to conjugation in the chelate ring—the presence of aromaticity. As a whole, methyl resonances for the zinc chelates are consistent with the tetrahedral coordination geometry. Electronic absorption peaks for the zinc chelates, which were located in the lowest energy region with the highest intensity, were assigned to the intra-ligand $\pi\rightarrow\pi^*$ transition and the metal→ligand charge-transfer as well. Vibrational absorption bands appearing in the 1600 cm^{-1} range and in the 400—350 cm^{-1} region have been assigned to the skeletal stretching mode of the dipyrromethene moiety and the metal-ligand stretching mode, respectively, for the zinc chelates.

In order to make a further exploration into the coordination ability of various pyrrole pigments, the zinc(II) chelates of six dipyrromethenes (**1**—**6**) have

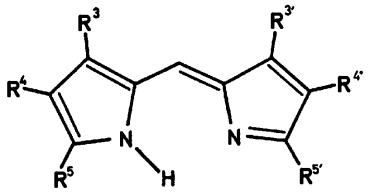

1: $R^3=R^{3'}=R^4=R^{4'}=CH_3$, $R^5=R^{5'}=H$
2: $R^3=R^{3'}=R^5=CH_3$, $R^4=R^{4'}=R^{5'}=H$
3: $R^3=R^4=R^5=CH_3$, $R^{3'}=R^{4'}=R^{5'}=H$
4: $R^3=R^{3'}=R^5=R^{5'}=CH_3$, $R^4=R^{4'}=H$
5: $R^3=R^{3'}=R^4=R^{4'}=R^5=R^{5'}=CH_3$
6: $R^5=R^{5'}=C_6H_5$, $R^3=R^{3'}=R^4=R^{4'}=H$

been prepared in this work. From our structural investigations on various divalent metal chelates of substituted dipyrromethenes, cobalt(II) was found to coordinate tetrahedrally to dipyrromethene molecules.[1-3] In connection with the coordination behavior of cobalt(II) ion, the zinc(II) ion, which has a good tendency of typical tetrahedral coordination, was employed to yield the corresponding dipyrromethene complexes. The structural aspects of the present zinc-(II) complexes as well as dipyrromethene ligands were investigated primarily by means of NMR spectroscopy. An additional information was also obtained by electronic and vibrational spectroscopy. Although Fergusson *et al.* carried out NMR studies on zinc(II), cadmium(II), mercury(II), and palladium(II) complexes of some dipyrromethenes,[4,5] their information is rather limited due to non-systematic utilization of dipyrromethene ligands with respect to substituent groups. The present study provides a thorough information on the proton resonance signals due to methyl groups substituted at all positions of the dipyrromethene skeleton as well as on their correlations.

* Contribution No. 322 from this Department.
Part X: Y. Murakami, K. Sakata, K. Harada, and Y. Matsuda, This Bulletin, **47**, 3021 (1974).

Experimental

Ligands. The synthetic procedures for the present ligands have been described previously.[1,2]

Metal Chelates. Bis(3,3′,4,4′-tetramethyldipyrromethenato)-zinc(II): Zinc chloride (anhydrous, 50 mg) dissolved in 2 ml of water was added with stirring to an ethanol (15 ml) solution of the ligand hydrochloride (0.1 g) at room temperature. After addition of 3% aqueous ammonia (0.5 ml), the mixture was heated at 80 °C for 2 min with stirring and subsequently allowed to cool down to room temperature. Repeated recrystallization from chloroform–ethanol gave olive-green crystals; yield 41 mg (42%).

Found: C, 67.34; H, 6.58; N, 12.03%. Calcd for $C_{26}H_{30}N_4Zn$: C, 67.31; H, 6.52; N, 12.08%.

Bis(3,3′,5-trimethyldipyrromethenato)zinc(II): The reaction of the ligand hydrochloride (0.1 g) and zinc chloride (anhydrous, 80 mg), following the above procedure, gave reddish orange crystals; yield 57 mg (58%).

Found: C, 65.85; H, 5.79; N, 12.88%. Calcd for $C_{24}H_{26}N_4Zn$: C, 66.13; H, 6.01; N, 12.86%.

Bis(3,4,5-trimethyldipyrromethenato)zinc(II): The reaction of the ligand hydrochloride (0.4 g) and zinc chloride (anhydrous, 0.26 g), following the above procedure, gave olive-green crystals; yield 0.25 g (64%).

Found: C, 65.88; H, 5.93; N, 12.99%. Calcd for $C_{24}H_{26}N_4Zn$: C, 66.13; H, 6.01; N, 12.86%.

Bis(3,3′,5,5′-tetramethyldipyrromethenato)zinc(II): The reaction of the ligand hydrochloride (0.1 g) and zinc chloride (anhydrous, 50 mg), following the above procedure, gave orange crystals; yield 63 mg (64%).

Found: C, 67.17; H, 6.57; N, 12.00%. Calcd for $C_{26}H_{30}N_4Zn$: C, 67.31; H, 6.52; N, 12.08%.

Bis(3,3′,4,4′,5,5′-hexamethyldipyrromethenato)zinc(II): A mixture of the ligand hydrochloride (0.1 g), zinc acetate dihydrate (80 mg), and urea (0.8 g) in 15.5 ml ethanol was refluxed for 2 hr and subsequently allowed to cool down to room temperature. Repeated recrystallization from benzene gave orange crystals; yield 68 mg (70%).

Found: C, 69.49; H, 7.25; N, 10.97%. Calcd for $C_{30}H_{38}N_4Zn$: C, 69.29; H, 7.37; N, 10.78%.

Bis(5,5′-diphenyldipyrromethenato)zinc(II): A mixture of the ligand (free base, 0.5 g) and zinc acetate dihydrate (0.26 g) in 45 ml of ethanol was refluxed for 2 hr, and subsequently

Table 1. NMR data for dipyrromethenes and zinc(II) chelates[a)]

Ligand	Form	Assignment (ppm)					Abbreviation
		5,5'-C<u>H</u>$_3$	4,4'-C<u>H</u>$_3$	3,3'-C<u>H</u>$_3$	-C<u>H</u>=	Pyrrole-ring proton	
1	HCl salt		2.06	2.31	7.30	7.63	**1**-HCl
	Zn chelate		1.95	2.23	7.13	7.13	**1**-Zn
2	HCl salt	2.68		2.39	7.21	7.70, 6.30	**2**-HCl
	Free base	2.31		2.26, 2.21	6.76	7.09, 6.08	**2**
	Zn chelate	1.89		2.37, 2.31	7.16	7.23, 6.19, 6.02	**2**-Zn
3	HCl salt	2.67	2.00	2.27	7.16	7.67, 7.06, 6.45	**3**-HCl
	Free base	2.27	1.90	2.05	6.63	7.04, 6.55, 6.23	**3**
	Zn chelate	1.88	1.85	2.20	7.10	7.26, 6.98, 6.31	**3**-Zn
4	HCl salt	2.62		2.35	7.08	6.14	**4**-HCl
	Free base	2.32		2.21	6.71	5.96	**4**
	Zn chelate	1.96		2.31	7.02	5.98	**4**-Zn
5	HCl salt	2.58	1.97	2.24	7.02		**5**-HCl
	Free base	2.27	1.91	2.10	6.62		**5**
	Zn chelate	1.90	1.90	2.21	6.98		**5**-Zn

a) Measured in chloroform-*d* with TMS as an internal reference.

allowed to cool down to room temperature. Repeated recrystallization from chloroform–ethanol gave olive-green crystals; yield 0.39 g (70%).

Found: C, 76.39; H, 4.69; N, 8.33%. Calcd for $C_{42}H_{30}N_4Zn$: C, 76.89; H, 4.61; N, 8.54%.

Spectral Measurements. A Varian A-60 spectrometer was used to obtain NMR spectra in chloroform-*d* at room temperature. Chemical shifts were reported in ppm from internal TMS and calibrated by the use of chloroform signal as the secondary reference. Ultraviolet and visible spectra in chloroform were recorded on a Hitachi Model EPS-2 spectrophotometer at room temperature. Infrared and far-infrared spectra covering the 4000—200 cm^{-1} range were measured with a JASCO Model DS-403G grating spectrophotometer at room temperature, where Nujol mull technique was adopted.

Results and Discussion

NMR Spectra. Methyl Group Resonances: (a) Ligands. The hydrochloride of 3,3',5-trimethyldipyrromethene (**2**–HCl) showed methyl-proton peaks at 2.68 and 2.39 ppm with 1 : 2 ratio of signal intensity. Thus, the former signal was assigned to methyl-protons placed at the 5-position, while the latter to those at the 3- and 3'-positions. On the basis of these assignments, all the methyl resonances have been assigned for dipyrromethene hydrochlorides as listed in Table 1. A positive charge on the hydrochloride forms of dipyrromethenes is apparently delocalized throughout the dipyrromethene skeleton according to these data. The removal of positive charge results in the up-field shift of methyl resonances as shown in Table 1 for the free-base forms.*

* Fergusson *et al.*[4)] assigned the methyl resonances: 3,3'-C<u>H</u>$_3$', δ 2.58 and 5,5'-C<u>H</u>$_3$, 2.45 for 4,4'-diethoxycarbonyl-3,3',5,5'-tetramethyldipyrromethene (free base); 3'-C<u>H</u>$_3$, δ 2.62 and 5'-C<u>H</u>$_3$, 2.46 for 3,4'-diethoxycarbonyl-5-chloro-3',4,5'-trimethyldipyrromethene. Their assignments for 3(3')-C<u>H</u>$_3$ and 5(5')-C<u>H</u>$_3$ should be interchanged in reference to our present study.

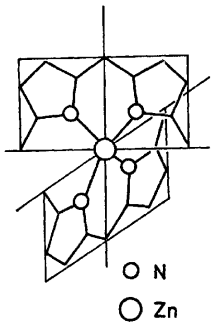

Fig. 1. Plausible spatial arrangement of the ligand molecules around zinc(II).

(b) Zinc Chelates. The metal nucleus in various zinc complexes generally demonstrates the tetrahedral coordination geometry by utilizing its $(4s)(4p)^3$ hybrid orbitals. The coordination geometry for the dipyrromethene chelates is shown schematically in Fig. 1. Consequently, the methyl groups substituted at the 5- and 5'-positions are to be placed in the shielding zone provided by a pyrrole ring as well as a chelate ring of another dipyrromethene moiety in the same chelate molecule. The behaviors of methyl resonances upon metal-coordination can be classified into three cases relative to those of the corresponding ligands (free base): (1) a down-field shift but not greater than the methyl resonance of the corresponding ligand hydrochloride (3,3'-C<u>H</u>$_3$); (2) nearly no change in chemical shift, even though that of the corresponding ligand hydrochloride shows down-field shift (4,4'-C<u>H</u>$_3$); and (3) a profound up-field shift, the methyl resonance of the corresponding ligand hydrochloride showing a down-field shift on the contrary (5,5'-C<u>H</u>$_3$). All the down-field shifts can be attributed to the deshielding effect due to positive charge provided by either proton or zinc(II). The tetrahedral coordination geometry undoubtedly gives out the unique behavior of methyl resonances classified as (3). An apparent non-variation

of methyl resonances classified as (2) seems also due to some structural coordination effect—minor shielding effect.

Methine Group Resonances: A marked change in chemical shift for the methine proton upon zinc(II)-coordination should be directly related to conjugation in the chelate ring. The methine proton is significantly deshielded on protonation as observed for the porphyrin nucleus.[6] This is attributed to delocalization of a positive charge throughout the dipyrromethene molecule, which leaves out a partial positive charge on the methine carbon atom. The proton NMR investigations of acetylacetonate and porphyrin complexes have shown that no deshielding of the methine proton could be detected.[7,8,9] Consequently, the behavior of methine group resonances for the present zinc(II) chelates can be cited as an evidence for the presence of aromaticity in the chelate ring due to coordinate bonds of significant covalent character. In conclusion, the methyl resonances for the zinc chelates are consistent with the tetrahedral geometry as depicted in Fig. 1.

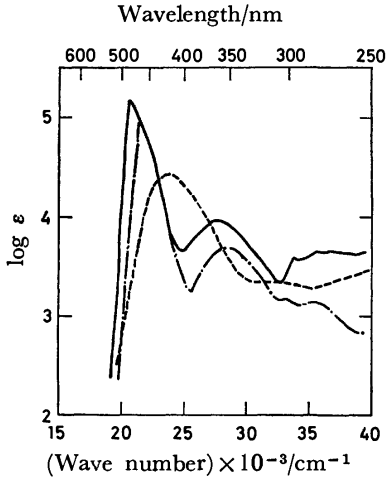

Fig. 2. Electronic absorption spectra for 3,3′,5-trimethyldipyrromethene and the zinc(II) chelate in chloform at room temperature: ——, zinc(II) chelate; —·—, ligand hydrochloride; - - - -, ligand free base.

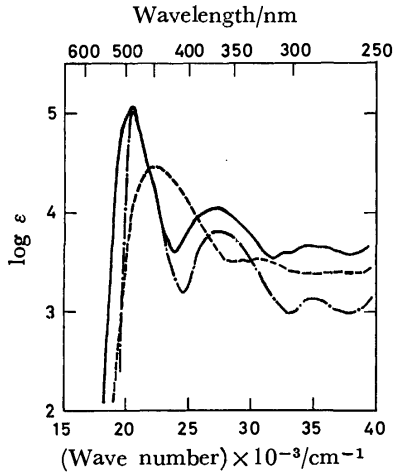

Fig. 3. Electronic absorption spectra for 3,3′,4,4′,5,5′-hexamethyldipyrromethene and the zinc(II) chelate in chloroform at room temperature: ——, zinc(II) chelate; —·—, ligand hydrochloride; - - - -, ligand free base.

Electronic Spectra. Visible and ultraviolet spectra for the ligands in free base and hydrochloride forms as well as for the zinc chelates are shown in Figs. 2 through 4 for the selected cases. The ligands in free base forms show the most intense $\pi\rightarrow\pi^*$ band in the lowest energy range (Table 2). The $\pi\rightarrow\pi^*$ transition energy decreases as a number of methyl groups substituted in the dipyrromethene skeleton increases (Fig. 5). This phenomenon can be attributed to the hyperconjugation effect due to methyl groups. Upon protonation to a pyrrole-nitrogen (hydrochloride species), the $\pi\rightarrow\pi^*$

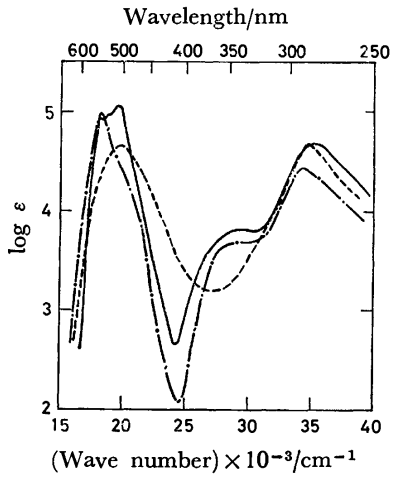

Fig. 4. Electronic absorption spectra for 5,5′-diphenyldipyrromethene and the zinc(II) chelate in chloroform at room temperature: ——, zinc(II) chelate; —·—, ligand hydrochloride; - - - -, ligand free base.

Table 2. Electronic absorption bands appearing in the lowest energy range for dipyrromethene ligands and zinc(II) chelates[a]

Ligand	Form	Transition energy in cm^{-1} (ε)
1	Free base	23300(28000)
	HCl salt	20900(68900)
	Zn chelate	20000(120000), 20700(93800)
2	Free base	23700(26200)
	HCl salt	21500(91900)
	Zn chelate	20700(144000), 22000sh(70600)
3	Free base	25200(23200)
	HCl salt	21400(64500)
	Zn chelate	20600(97300), 21800sh(75900)
4	Free base	22700(32300)
	HCl salt	21200(109000)
	Zn chelate	20500(166000), 21300sh(100000)
5	Free base	22300(29400)
	HCl salt	20500(107000)
	Zn chelate	19800sh(84400), 20500(117000), 21100sh(65300)
6	Free base	19500(44400)
	HCl salt	18100(94700)
	Zn chelate	18100(84700), 18900sh(95200), 19600(114000)

a) Measured in chloroform at room temperature.

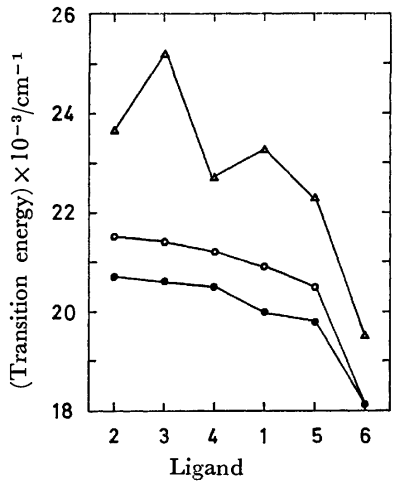

Fig. 5. Correlations between lowest electronic transition energy and nature of substituent groups in the dipyrromethene skeleton for ligand free bases(△), ligand hydrochlorides(○), and zinc(II) chelates(●): a number of methyl group increases from left to right (except **6**).

band further shift to a lower energy region (Figs. 3—5) along with an increase in its intensity. In a manner as pointed out by Corwin and Brunings for di-*N*-methyldipyrromethenes,[10,11] the steric interaction between *N*-protons in di-*N*-protonated dipyrromethenes seems to give out a significant effect on their electronic structure, thus raising the occupied π-energy levels relative to the free-base ligands. The intensity increase may be attributed to the polarity effect provided by the presence of a positive charge in the dipyrromethene skeleton. The effect of methyl-substitution (red-shift) is seen to be similar to that observed for the free-base ligands (Fig. 5). The electronic transition appearing in the lowest energy region for the zinc chelates are accompanied with multi-peaks (Table 2, Figs. 2—4), often along with a slight red-shift relative to that for the corresponding ligand hydrochlorides. The bands may be assigned to the $\pi \rightarrow \pi^*$ transition of similar origin as described for the ligands. On the other hand, the metal→ligand charge-transfer transitions, as generally observed for transition-metal complexes in a similar energy region, may be expected to appear in this region. Thus, we do hold the possibility of co-occurrence of charge-transfer and $\pi \rightarrow \pi^*$ transitions in the same range, although Fergusson *et al.* simply assigned these bands to the intra-ligand $\pi \rightarrow \pi^*$ transition and a band in the 28000 cm^{-1} range to the metal→ligand charge-transfer.

Vibrational Spectra. A strong band due to the skeletal stretching mode of the dipyrromethene moiety appears in the 1600 cm^{-1} range as listed in Table 3 for the free ligands and the corresponding zinc chelates. A slight shift of this band to lower energy is observed for each ligand upon metal-coordination.

Table 3. Infrared absorption band assigned to the skeletal stretching mode of the dipyrromethene moiety for ligands and zinc chelates

Ligand	Form	IR band in cm^{-1}
1	Free base	1619
	Zn chelate	1610
2	Free base	1622
	Zn chelate	1603
3	Free base	1625
	Zn chelate	1605
4	Free base	1613
	Zn chelate	1599
5	Free base	1611
	Zn chelate	1596
6	Free base	1618
	Zn chelate	1612

In the far-infrared region, 700—200 cm^{-1}, there was observed an absorption peak of medium intensity in the 400—350 cm^{-1} range in a manner similar to the cobalt(II), nickel(II), copper(II), iron(II), and manganese(II) chelates of some dipyrromethenes.[1,2,12,13] This band can be associated with the metal-ligand stretching mode: **3**-Zn, 383 cm^{-1}; **4**-Zn, 386 cm^{-1}; **5**-Zn, 363 cm^{-1}. We refrained from assigning a band of this origin for some zinc chelates due to the complexity of absorption spectra caused by ligand-nature.

References

1) Y. Murakami and K. Sakata, *Inorg. Chim. Acta*, **2**, 275 (1968).
2) Y. Murakami, Y. Matsuda, and K. Sakata, *Inorg. Chem.*, **10**, 1728 (1971).
3) Y. Murakami, Y. Matsuda, K. Sakata, and A. E. Martell, *J. Chem. Soc., Dalton*, **1973**, 1729.
4) F. C. March, D. S. Couch, K. Emerson, J. E. Fergusson, and W. T. Robinson, *J. Chem. Soc., A*, **1971**, 440.
5) F. C. March, J. E. Fergusson, and W. T. Robinson, *J. Chem. Soc., Dalton*, **1972**, 2069.
6) R. J. Abraham, *Mol. Phys.*, **4**, 145 (1961).
7) W. S. Caughey and W. S. Koski, *Biochemistry*, **1**, 923 (1961).
8) D. A. Doughty and C. W. Dwiggins, Jr., *J. Phys. Chem.*, **73**, 423 (1968).
9) J. A. S. Smith and E. J. Wilkins, *J. Chem. Soc., A*, **1966**, 749.
10) K. J. Brunings and A. H. Corwin, *J. Amer. Chem. Soc.*, **64**, 593 (1942).
11) K. J. Brunings and A. H. Corwin, *ibid.*, **66**, 337 (1944).
12) Y. Murakami, Y. Matsuda, K. Sakata, and K. Harada, This Bulletin, **47**, 458 (1974).
13) Y. Murakami, K. Sakata, K. Harada, and Y. Matsuda, *ibid.*, **47**, 3021 (1974).

Studies of the Substituent Effect on the Stability Constants of Bis(2-hydroxy-4 or 5-substituted acetophenonato)copper(II)

Masami HARUTA, Zen-ichi YOSHIDA,* and Hisanobu OGOSHI*

Research Laboratory for Chemical Fibers, Nitto Boseki Co., Ltd. Koriyama-shi, Fukushima-ken 963

**Department of Synthetic Chemistry, Faculty of Engineering, Kyoto University, Yoshida, Sakyo-ku, Kyoto 606*

(Received April 9, 1974)

The dissociation constants of eleven 2-hydroxy-4 or 5-substituted acetophenones were determined in a 22.5% water-dioxane-mixed solvent system at 25 and 40 °C by potentiometric titration. They were then discussed in terms of the electronic effect of the substituents and the linear-free-energy relationship. The stability constants bis(2-hydroxy-4 or 5-substituted acetophenonato)copper(II) were also determined under the same experimental conditions; a linear relationship between the dissociation constants and the stability constants was obtained for bis(2-hydroxy-4 or 5-substituted acetophenonato)copper(II). No significant difference has been found in the effects of 4- and 5-substituted groups on the stability constants.

The dissociation constants of eleven 2-hydroxy-4 or 5-substituted acetophenones were determined in 22.5% water-dioxane at 25 and 40 °C by potentiometric titration.

The values obtained were discussed in terms of the electronic effect of the substituents and the linear free-energy relationship. The stability constants of bis-(2-hydroxy-4 or 5-substituted acetophenonato)copper (II) were also determined under the same experimental conditions, and a linear relationship between the dissociation constants and the stability constants was discussed in comparison with those of bis(4- or 5-substituted salicylaldehydato)copper(II).

Although several studies of the stability constants for metal complexes, especially copper complexes, of salicylaldehyde and its derivatives have been reported,[1-4] few studies of copper complexes of *o*-hydroxyacetophenone derivatives have appeared so far.[5] It would be interesting to study the stability constants of the copper complex of *o*-hydroxyacetophenone derivatives which have no steric factors in the course of the complex formation and to compare them with those of the copper complexes of the corresponding salicylaldehyde derivatives.

Since *o*-hydroxyacetophenone derivatives, salicylaldehyde derivatives, and their metal complexes are not very soluble in water, nonaqueous or mixed solvent systems are usually employed for the measurement of the equilibrium constants. The use of such solvents, however, raises the question of the interpretation of the potential obtained from a cell containing a glass electrode and a liquid junction error. Therefore, the calibration of the glass electrode must be made for the solvent system. An empirical calibration for pH-meter reading was made by the method reported by Van Uitert and Haas[6] for the 22.5% water–dioxane system at 25 and 40 °C.

The electronic effect of the substituent on the dissociation constants(pK_a) of 2-hydroxy-4 or 5-substituted acetophenones were interpreted in terms of the linear free-energy relationship.

The stability constants of bis(2-hydroxy-4 or 5-substituted acetophenonato)copper(II) were compared with those of bis(4- or 5-substituted salicylaldehydato)-copper(II). A linear relationship between the pK_a and the stability constant has been predicted by Calvin,[1] assuming that the enthalpy change for the complex formation is predominant over the entropy change to the stability constant. On the contrary, Jones *et al.*[2] have shown a non-linear relationship between the pK_a's and the log K's for salicylaldehyde derivatives and their copper complexes; they explained their result in terms of the interaction of the d_ϵ-electron of the cupric ion. Since it has since been found, though, that the latter work involves some experimental errors together with the use of a ligand determined incorrectly,[7] the determination of the stability constants of bis(4- or 5-substituted salicylaldehydato)-copper(II) should be reexamined in order to elucidate the electronic effect of the substituent on the complex formation.

Experimental

Materials. 2-Hydroxyacetophenone, 4-methyl, 5-methyl, 4-chloro, 5-chloro, 4-bromo, 5-bromo, and 4-nitro derivatives of 2-hydroxyacetophenone were prepared by the usual Fries-rearrangement of the corresponding substituted phenyl acetates. 4-Methoxy and 5-methoxy derivatives were obtained by the Friedel-Crafts reaction of acetyl chloride with resorcinol and hydroquinone dimethyl ether respectively.[8] 2-hydroxy-5-nitroacetophenone was synthesized by the nitration of 2-hydroxyacetophenone. All of these compounds were purified by recrystallization. Dioxane was purified by a previously reported method.[9] Sodium perchlorate was recrystallized twice from water at 50 °C. Potassium chloride was purified by the Pinching and Bates method.[10] Hydrochloric acid was distilled twice, and the middle fraction was used. Deionized water was distilled under a nitrogen atmosphere.

The other reagents employed in this study were commercially available and were used without further purification.

Preparation of Bis(2-hydroxy-4 or 5-substituted acetophenonato)-copper(II). The general procedure was as follows: About 0.5 g of the ligand was dissolved in methanol containing an equivalent amount of potassium hydroxide; then the mixture was diluted with the same volume of water. A one half equivalent of cupric chloride was dissolved in a small amount of water and added to the ligand solution. The copper chelate was collected by filtration, washed with 50% aqueous methanol, and dried at room temperature *in vacuo*. The results of elemental analyses are summarized in Table 4.

Titration. The titration apparatus employed was the same as that reported in a previous paper.[11] Titration was carried out by the method reported by Irving and Rossotti.[12] The ionic strength was maintained at 0.3 with potassium

TABLE 1. DISSOCIATION CONSTANTS OF 2-HYDROXY-4 OR 5-SUBSTITUTED ACETOPHENONES IN 22.5% AQUEOUS DIOXANE AT 25 AND 40 °C

Substituent	$pK_{a25\,°C}$	$pK_{a40\,°C}$	$\Delta\Delta G_i$ (kcal/mol)
4-OCH_3	10.475	10.267	+0.43
5-OCH_3	10.849	10.631	−0.08
4-CH_3	11.127	10.902	−0.46
5-CH_3	11.395	11.162	−0.82
H	10.794	10.578	0.00
4-Cl	9.780	9.591	+1.38
5-Cl	10.148	9.948	+2.26
4-Br	9.680	9.494	+1.52
5-Br	9.959	9.766	+1.14
4-NO_2	8.617	8.460	+2.97
5-NO_2	7.265	7.144	+4.81

nitrate, while the temperatures were 25.0±0.1 °C and 40.0±0.1 °C. The metal solution was standardized by the usual EDTA-titration method.[13]

Correction of pH Meter Reading. An empirical calibration of the glass electrode in 22.5% aqueous dioxane at 25.0 and 40.0 °C (±0.1 °C) was carried out by the method reported by Van Uitert and Haas.[6]

A Hildebrand-type platinum electrode, 3000-10T, of the Hitachi-Horiba Manufacturing Co., was platinized[14] in each measurement and employed as a hydrogen electrode. A silver-silver chloride electrode** was used as the reference electrode.

The standard potential of the reference electrode and the mean activity coefficient of hydrogen chloride were obtained by interpolation from the data of Harned and Owen.[15] The conversion factors(U_H) were obtained by means of the relationship between the pH meter reading(B) and the hydrogen-ion concentration ([H]).

Determination of the Dissociation Constants(pK_a). The dissociation constants of 2-hydroxy-4 or 5-substituted acetophenones were obtained by the usual titration method with a pair of glass and calomel electrodes at 25.0 and 40.0 °C (±0.1 °C) and were calculated by means of Irving and Rossotti's equation.[16] The pK_a's were corrected by the Van Uitert and Haas method.[6b] The values thus obtained are shown in Table 1.

Calculation of the Stability Constants. The stability constants of bis(2-hydroxy-4 or 5-substituted acetophenonato) copper(II) were calculated by the method reported in a previous paper.[11]

Results and Discussion

The conversion factor and the correction factor for the 22.5% aqueous dioxane system were found to be reasonable in comparison with the values obtained by a graphic method.[6]

According to the generalized equation of the linear free-energy relationships,[17] the dissociation constants and the difference in the free energy change can be expressed as follows:

$$\log(K_i/K_0) \equiv X_i \text{ or } \sigma_i\rho_i$$
$$\Delta\Delta G_i = \Delta G_i - \Delta G_0 = -2.303RT\sigma_i\rho_i$$

** Kindly prepared and provided by Toa Electronics, Ltd., Tokyo.

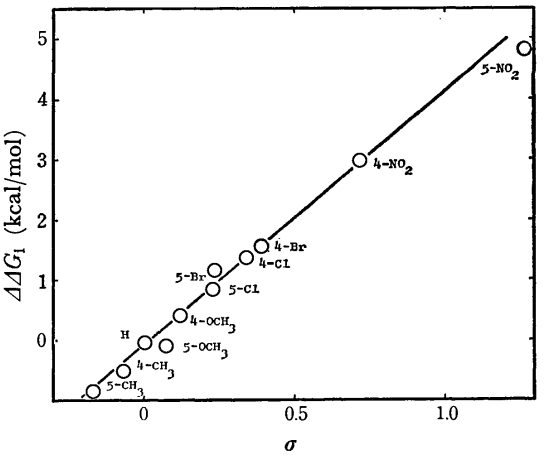

Fig. 1. Correlation of the difference of the free energy change ($\Delta\Delta G_i$) for the dissociation constant of 2-hydroxy-4 or 5-substituted acetophenones with Hammett σ constants.

where the i and 0 subscripts indicate the values for 2-hydroxy-4 or 5-substituted acetophenones and 2-hydroxyacetophenone respectively. Figure 1 shows the relation between the $\Delta\Delta G_i$ values of 2-hydroxy-4 or 5-substituted acetophenones and the Hammett σ constants. Bekkum's σ value(σ=0.076) for the 5-methoxy derivative[18] and the polarizability effect (σ=1.27) for the 5-nitro derivative[19] are used to evaluate the effect of those substituents. Those two plots deviate from the linear relationship.

In the case of the 5-nitro derivative, a remarkable precipitation of the complex was found in the course of titration, whereas no such precipitation was observed for the other ligands. Some experimental error may be involved in the stability constant for bis(2-hydroxy-5-nitroacetophenonato)copper(II) for the 5-nitro de-

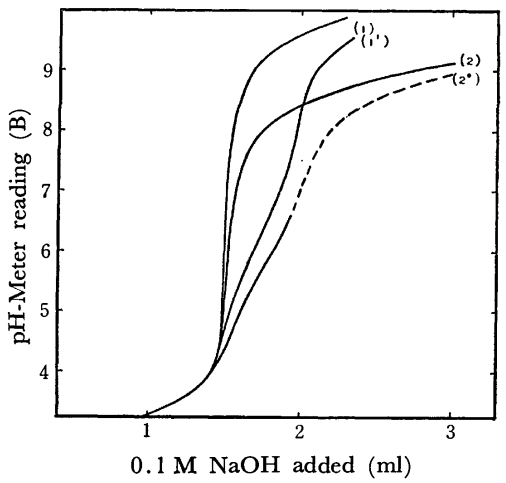

Fig. 2. Typical titration curves of 2-hydroxyacetophenone and their Cu(II) complexes in 22.5% aqueous dioxane at 25 °C.
(1); 5×10^{-3} M 2-hydroxyacetophenone, 1.9413×10^{-3} M HNO_3, 3×10^{-3} M KNO_3, (1'); Chelating agent, acid and salt as (1), 2.5042×10^{-4} M Cu(II), (2); 5×10^{-3} M 2-hydroxy-4-chloroacetophenone, acid and salt as (1), (2'); Chelating agent, acid and salt as (2), Cu(II) as (1').

TABLE 2. STABILITY CONSTANTS OF 2-HYDROXY-4 OR 5-SUBSTITUTED ACETOPHENONES AND Cu(II) IN 22.5% AQUEOUS DIOXANE AT 25 °C AND IONIC STRENGTH 0.3 (KNO_3)

Substituent	pK_a	pA			β	log K_{MA}	log K_{MA_2}
		n=0.5	n=1.0	n=1.5			
4-OCH_3	10.47	7.35	6.72	6.15	2.75×10^{13}	7.27	6.23
5-OCH_3	10.85	7.37	6.76	6.19	3.27×10^{13}	7.29	6.28
4-CH_3	11.13	7.79	7.14	6.57	1.93×10^{14}	7.71	6.66
5-CH_3	11.39	7.74	7.12	6.41	1.72×10^{14}	7.66	6.47
H	10.79	7.58	6.94	6.30	7.48×10^{13}	7.50	6.37
4-Cl	9.78	7.10	6.53	5.98	1.14×10^{13}	6.99	6.06
5-Cl	10.15	7.30	6.93	6.07	1.41×10^{13}	7.21	6.16
4-Br	9.68	6.88	6.28	5.78	3.66×10^{12}	6.79	5.89
5-Br	9.96	7.00	6.39	5.89	6.08×10^{12}	6.91	6.00
4-NO_2	8.62	6.68	6.03	5.62	1.14×10^{12}	6.61	5.73
5-NO_2	7.26	4.54	3.89	3.49	6.08×10^{7}	4.46	3.61

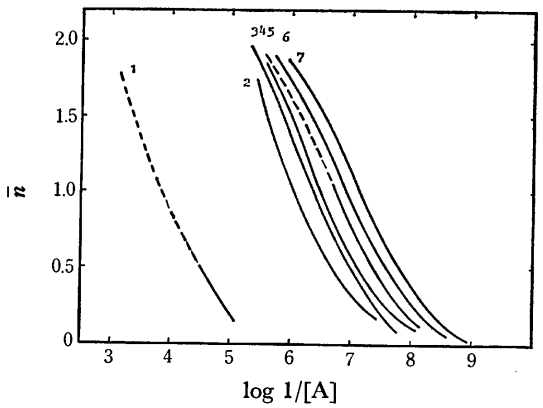

Fig. 3. Typical formation curves of 2-hydroxyacetophenone derivatives and Cu(II) complexes in 22.5% aqueous dioxane at 25 °C, and ionic strength 0.3 (KNO_3).
1; 2-OH-5NO_2-acetophenone, 2; 2-OH-4-NO_2-acetophenone, 3; 2-OH-5-Br-acetophenone, 4; 2-OH-4-Cl-acetophenone, 5; 2-OH-5-OCH_3-acetophenone, 6; 2-OH-acetophenone, 7; 2-OH-4-CH_3-acetophenone.

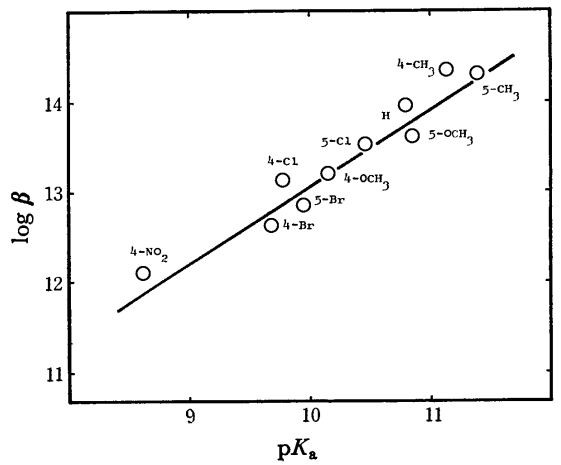

Fig. 4. The relation between the dissociation constants (pK_a) of 2-hydroxy-4 or 5-substituted acetophenones and the over-all stability constants (log β) of their copper(II) complexes.

rivative under the conditions here employed. Typical titration curves for some complex formations are illustrated in Fig. 2, while in Fig. 3 the formation curves for typical complexes are presented, with a dotted line indicating the precipitation of the complex. Among these complexes, the 5-nitro and 4-chloro derivatives showed poor solubility under the present conditions. A comparison of the formation curves indicates that a similar type of complex formation may occur during the titration. The stability constants obtained are summarized in Table 2.

It has been reported that a linear relationship can be established for the dissociation constants of salicylaldehyde derivatives and the stability constants of bis(substituted salicylaldehydato)copper(II).[7] A similar trend was confirmed in the eleven bis(4- or 5-substituted salicylaldehydato)copper(II) complexes. Slightly convex curves were obtained in the cases of 2-hydroxyacetophenone derivatives and pentane-2,4-dione derivatives.[2,6c] These trends have been explained by Jones *et al.*[2] in terms of the σ and π-electronic effects of the substituents. That is, the nitro group acts as a σ and π-electron acceptor, whereas the chloro group acts as a σ-acceptor and π-donor. Therefore, larger stability constants may be expected for the nitro derivatives than the chloro derivatives. The predominant stabilization of the complexes is attributed to the "back donation" of the d_ε-electron of the copper ion. However, the above-mentioned hypothesis, which was proposed for the interpretation of the stability constants salicylaldehyde complexes, has been criticized by Postmus *et al.*,[7] since the structure of 4-chlorosalicylaldehyde was not correctly identified. Some experimental error may indeed be included in the determination of the stability constant of the 5-nitro derivative.

The linear relationship between the stability constants and the dissociation constants, which has been predicted by Calvin[1] in view of the thermodynamic functions for the formation of the complex, is expressed as follows:

$$\log K = a\ \mathrm{p}K_a + b$$

where log K is the stability constant(log K_{MA}, log K_{MA_2}, log β), pK_a is the dissociation constant of the ligand, and a and b are constants. The constants, a and b, obtained from the plot of the stability constant against pK_a are presented in Table 3, along with those of

Table 3. Values of the constants(a, b) in equation $\log K = a\,pK_a + b$, and the correlation coefficients(r) for copper(II) complexes of 4 or 5-substituted salicylaldehydes and 2-hydroxy-4 or 5-substituted acetophenones in 22.5% aqueous dioxane at 25 °C

	$\log K_{MA}$			$\log K_{MA_2}$			$\log \beta$		
	a	b	r	a	b	r	a	b	r
4 or 5-Substituted salicylaldehyde	0.79	−0.79	0.96	0.76	−1.50	0.96	1.51	−2.04	0.96
2-Hydroxy-4 or 5-substituted acetophenone	0.43	2.81	0.95	0.32	2.90	0.94	0.85	4.59	0.96

Table 4. Elemental analyses of bis(2-hydroxy-4 or 5-substituted acetophenonato)copper(II)

Substituent	Formula	Found (%)					Calcd (%)				
		C	H	N	X	Cu[a]	C	H	N	X	Cu
4-OCH_3	$C_{18}H_{18}O_6Cu$	54.84	4.73	—	—	16.11	54.89	4.61	—	—	16.13
5-OCH_3	$C_{18}H_{18}O_6Cu\cdot 0.5H_2O$	53.33	4.60	—	—	16.03	53.66	4.75	—	—	15.77
4-CH_3	$C_{18}H_{18}O_4Cu\cdot H_2O$	56.44	5.09	—	—	17.02	56.91	5.31	—	—	16.73
5-CH_3	$C_{18}H_{18}O_4Cu\cdot H_2O$	57.00	4.98	—	—	17.10	56.91	5.31	—	—	16.73
H	$C_{16}H_{14}O_4Cu\cdot 0.5H_2O$	56.35	4.44	—	—	19.07	56.06	4.41	—	—	18.53
4-Cl	$C_{16}H_{12}O_4Cl_2Cu$	47.54	3.03	—	17.76	14.91	47.72	3.00	—	17.61	15.78
5-Cl	$C_{16}H_{12}O_4Cl_2Cu\cdot 0.5H_2O$	46.98	3.12	—	17.34	15.05	46.68	3.18	—	17.22	15.43
4-Br	$C_{16}H_{12}O_4Br_2Cu$	38.86	2.55	—	32.91	12.25	39.09	2.46	—	32.51	12.93
5-Br	$C_{16}H_{12}O_4Br_2Cu$	39.28	2.63	—	32.51	11.97	39.09	2.46	—	32.51	12.93
4-NO_2	$C_{16}H_{12}O_8N_2Cu$	45.69	3.08	6.47	—	13.84	45.34	2.85	6.61	—	14.99
5-NO_2	$C_{16}H_{12}O_8N_2Cu$	45.62	3.02	6.60	—	13.03	45.34	2.85	6.61	—	14.99

a) Obtained from per cent ash as copper oxide.

bis(4- or 5-substituted salicylaldehydato)copper(II).

The a constants for the salicylaldehyde derivative were found to be larger than those for the 2-hydroxyacetophenone derivative in all cases. This fact indicates that the effect of the substituent of the salicylaldehyde derivatives on the stability constant is more significant than the effect of that of the 2-hydroxyacetophenone derivatives. This finding may be interpreted in terms of the difference in polarizability between the two series of ligands induced by the cation.[20]

The stability constant of a metal complex is strongly dependent on the basicity of its ligand. An electron-donating substituent group increases the electron density on the keto oxygen atom or the phenolic oxygen atom; this, in turn, results in an enhancement of the stability constant of the metal complex. The position of the substituent does not make any essential difference in the stability constants. It seems that the 4-substituent group increases the electron density on the keto oxygen atom, whereas the 5-substituent group enhances the electron density on the phenolic oxygen atom. Therefore, these trends can be explained in terms of classical substituent effects as a whole, such as the Hammett σ values.

References

1) M. Calvin and K. W. Wilson, *J. Amer. Chem. Soc.*, **67**, 2003 (1945).

2) J. G. Jones, J. B. Poole, J. G. Tomkinson, and R. J. P. Williams, *J. Chem. Soc.*, **1958**, 2001.

3) K. Clarke, R. A. Cowen, G. W. Gray, and E. H. Osborne, *ibid.*, **1963**, 245.

4) B. J. James, M. Parris, and R. J. P. Williams, *ibid.*, **1961**, 4630.

5) L. G. Sillén and A. E. Martell, "Stability Constants of Metal Ion Complexes," Special Publication No. 17, The Chem. Soc., London, (1964) p. 566.

6) a) L. G. Van Uitert and C. G. Haas, *J. Amer. Chem. Soc.*, **75**, 451 (1953); b) L. G. Van Uitert and W. C. Fernelius, *ibid.*, **76**, 5887 (1954); c) L. G. Van Uitert, W. C. Fernelius, and B. E. Douglas, *ibid.*, **75**, 457 (1953).

7) C. Postmus, Jr., L. B. Magnusson, and C. A. Craig, *Inorg. Chem.*, **5**, 1154 (1966).

8) W. Baker, N. C. Brown, and J. A. Scott, *J. Chem. Soc.*, **1939**, 1926.

9) C. A. Kraus and R. A. Vingee, *J. Amer. Chem. Soc.*, **56**, 511 (1946).

10) G. D. Pinching and R. G. Bates, *J. Res. Natl. Bur. Std.*, **37**, 311 (1946).

11) M. Haruta and S. Harada, *Makromol. Chem.*, in press.

12) H. Irving and H. S. Rossotti, *J. Chem. Soc.*, **1954**, 2910.

13) G. Schwarzenbach, "Die Komplexometrische Titration," Ferdinand Enke Verlag, Stuttgart, (1955) p. 65.

14) R. G. Bates, "Determination of pH. Theory and Practice," John Wiley & Sons. Inc., New York (1964) p. 242.

15) H. S. Harned and B. B. Owen, "Physical Chemistry of Electrolytic Solutions", 3rd. Ed., Reinhold Pub. Corp., New York (1958) p. 715, 717.

16) H. M. Irving and H. S. Rossotti, *J. Chem. Soc.*, **1954**, 2904.

17) P. R. Wells, *Chem. Revs.*, **63**, 171 (1963).

18) H. van Bekkum, P. E. Verkade, and B. M. Wepster, *Rec. Trav. Chim. Pays-Bas*, **78**, 815 (1959).

19) H. H. Jaffé, *Chem. Revs.*, **53**, 191 (1953).

20) G. Schwarzenbach, G. Anderegg, W. Schneider, and H. Senn, *Helv. Chim. Acta*, **38**, 1147 (1955).

Synthesis of Chelating Agents. X. Chelating Behavior of 1,2-Diamines with Specific Configurations: *cis*- and Diequatorial *trans*-Diamino-*trans*-decalins, *cis*- and *trans*-Diaminotetralins and 3,3-Dimethyl-1,2-diaminobutane*

Tairoku YANO, Hiroshi KOBAYASHI, and Keihei UENO

Department of Organic Synthesis, Faculty of Engineering, Kyushu University, Hakozaki, Higashi-ku, Fukuoka 812

(Received May 14, 1974)

Stability constants were determined at 25 °C for the metal chelates of racemic *cis*- and diequatorial *trans*-2,3-diamino-*trans*-decalins, *cis*- and *trans*-2,3-diaminotetralins and 3,3-dimethyl-1,2-diaminobutane (BEDA), where Cu(II), Ni(II) and Zn(II) are metal ions. Alicyclic *trans*-diamines afforded 1 : 1 complexes more stable than those with *cis*-isomers, regardless of the metal ions. Stability of the metal chelates with BEDA is comparable to that of the *trans*-diamines. The difference in stability of the *trans*- and *cis*-diamine complexes increased in the order Cu-, Zn- and Ni ions. Upon formation of 1 : 2 complexes, it became greater with Ni ion, but practically no difference was observed with the others. An explanation was given on the basis of stereochemistry of the diamines and coordination structures of the divalent metal ions.

Chelating behavior with transition metal ions has been extensively studied for various aliphatic 1,2-diamines capable of internal rotation around the axis of 1,2-carbon atoms, such as ethylenediamine and 2,3-diaminobutane.[1]

In order to elucidate stereochemical effects of the chelating agents on their metal complex formation, we have studied the synthesis of complexanes with certain conformations. This paper deals with the chelating behavior of some precursory 1,2-diamines such as 2(*ax*), 3(*eq*)-dimaino-*trans*-decalin [D(A,E)], 2(*eq*), 3(*eq*)-diamino-*trans*-decalin [D(E,E)], *cis*-2,3-diaminotetralin [T(A,E)], *trans*-2,3-diaminotetralin [T(E,E)] and 3,3-dimethyl-1,2-diaminobutane [BEDA].[2,3] In these diamines, the stereochemical relationship between the two amino groups is considered to be restricted to a certain extent by their less flexible carbon framework or the steric hindrance of bulky substituents.[4]

Experimental

Potentiometric measurements were carried out in a jacketed 100 ml titration vessel, maintained at 25.0±0.1 °C by circulation of thermostated water through the outer jacket. Ionic strength of a solution was adjusted to 0.10 by addition of potassium nitrate for the diaminodecalins D(E,E) and D(A,E) and *cis*-diaminotetralin T(A,E). Potassium chloride was used for *trans*-diaminotetralin T(E,E), since potassium nitrate caused precipitation during the course of titration, particularly for copper(II) ion even in a lower pH region.

A Hitachi-Horiba model P pH-meter fitted with glass(1026)- and calomel(2010) electrodes was calibrated by titration of an acetic acid solution with a 0.1 M potassium hydroxide free from carbonate ion, to give $-\log [H^+]$. After each measurement the acetic acid solution was again titrated in order to reconfirm the variation in pH-meter reading to be within 0.02.

Titration curves for a metal ion were obtained on two solutions (1 : 1 and 1 : 2 metal to ligand ratios). The total concentration of each ligand was kept constant at 1.0×10^{-3} M, while that of a metal ion was varied correspondingly 1.0×10^{-3}—5.0×10^{-4} M. Computations were carried out by use of a FACOM 230-60 of the Computer Center in Kyushu University. Preparation of the ligand materials was described previously.[2,3]

Results and Discussion

Dissociation Constants. The dissociation constants of the conjugate acids of T(E,E) and T(A,E) were calculated as dibasic acids according to Schwarzenbach.[5] The results are summarized in Table 2 along with those of some related diamines.

The pK_{a2} values of diaminotetralins are approximately 1 unit lower than those of the other alicyclic diamines. A similar comparison for aminocyclohexane and 2-aminotetralin, with pK_a values 10.64[6] and 9.80,[7] respectively, showed that the base strengths of tetralin derivatives are much weaker than those expected from Taft's polar effect of a phenethyl group,[8,9] indicating the existence of a direct field effect.

Stability Constants. Titration curves of the diaminodecalins are shown in Figs. 1 and 2. Similar curves were obtained for the diaminotetralins and BEDA.

The equilibria on the chelate formation might be represented as follows.

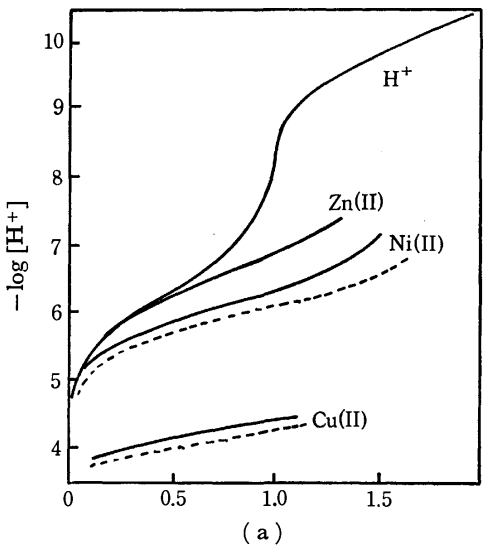

Fig. 1. Potentiometric titration curves of D(A, E) in the presence of various cations, —— 1 : 2 solution, and ---- 1 : 1 solution.

* Contribution No. 334 from the Department of Organic Synthesis, Kyushu University.

TABLE 1. ELEMENTAL ANALYSES OF PRECIPITATES RESULTING FROM TITRATION OF 1 : 2 SOLUTIONS

Compound	Molecular formula	Elemental analysis					
		C%		H%		N%	
		Found	Calcd	Found	Calcd	Found	Calcd
$CuT(E,E)_2(NO_3)_2$	$C_{20}H_{28}N_6O_6Cu$	46.69	46.89	5.53	5.51	16.48	16.42
$CuT(E,E)_2(NO_3)_2$[a]	$C_{20}H_{28}N_6O_6Cu$	46.89	46.89	5.47	5.51	16.29	16.42
$NiT(E,E)_2Cl_2(H_2O)_2$[a]	$C_{20}H_{32}N_4O_2Cl_2Ni$	48.86	49.00	6.54	6.53	11.24	11.44
$ZnT(E,E)_2(NO_3)_2$	$C_{20}H_{28}N_6O_6Zn$	46.54	46.73	5.86	5.49	15.94	16.36
$ZnT(E,E)Cl_2$[a]	$C_{10}H_{14}N_2Cl_2Zn$	40.36	40.21	4.77	4.69	9.40	9.38
$CuT(A,E)_2(NO_3)_2$	$C_{20}H_{28}N_6O_6Cu$	46.80	46.89	5.51	5.51	16.43	16.42
$CuD(E,E)_2(NO_3)_2$	$C_{20}H_{40}N_6O_6Cu$	45.28	45.85	7.64	7.64	16.14	16.05
$NiD(E,E)_2(NO_3)_2$	$C_{20}H_{40}N_6O_6Ni$	46.32	46.27	7.64	7.71	16.13	16.19
$CuD(A,E)_2(NO_3)_2$	$C_{20}H_{40}N_6O_6Cu$	45.21	45.85	7.53	7.64	15.81	16.05
$CuD(A,E)_2(NO_3)_2$[a]	$C_{20}H_{40}N_6O_6Cu$	45.56	45.85	7.60	7.64	15.87	16.05
$NiD(A,E)_2(NO_3)_2$	$C_{20}H_{40}N_6O_6Ni$	46.04	46.27	7.60	7.71	16.01	16.19

a) resulting from a 1 : 1 solution.

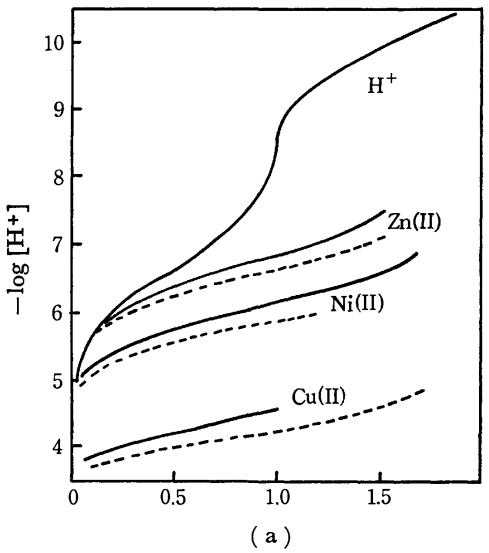

(a)

Fig. 2. Potentiometric titration curves of D(E, E) in the presence of various cations, —— 1 : 2 solution, and ---- 1 : 1 solution.

$$M + L \rightleftarrows ML \qquad K_{ML} = \frac{[ML]}{[M][L]} \qquad (1)$$

$$ML + L \rightleftarrows ML_2 \qquad K_{ML_2} = \frac{[ML_2]}{[ML][L]} \qquad (2)$$

$$ML(OH^-) + H^+ \rightleftarrows ML \qquad K_{MLOH} = \frac{[ML]}{[ML(OH^-)][H^+]} \qquad (3)$$

$$2ML \rightleftarrows ML_2 + M \qquad (4)$$

where M and L stand for a divalent metal cation and a diamine ligand, respectively. Reactions (1) and (3) should play important roles in the 1 : 1 solution, and (1) and (2) in the 1 : 2 solution. If this is the case, a set of K_{ML} and K_{MLOH} and one of K_{ML} and K_{ML_2} might be calculated from the titration data of the 1 : 1 and 1 : 2 solutions, respectively, in combination with mass- and charge balance. The stability constants of the diaminodecalins thus obtained are summarized in Table 2. Titration data from the 1 : 1 solutions of

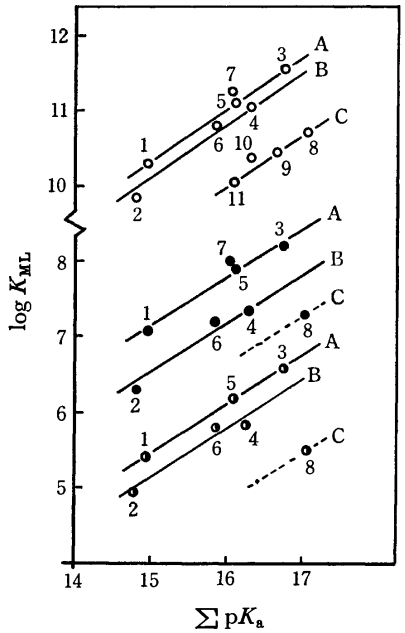

Fig. 3. Relationship of the 1 : 1 chelate stabilities against the total basicities of 1,2-diamines.
1, T(E,E); 2. T(A,E); 3, D(E,E); 4, D(A,E); 5, *t*-CYDA; 6, *c*-CYDA; 7, BEDA; 8, ethylenediamine;[a] 9, 1,2-diaminopropane;[b] 10, 1,2-diaminobutane;[b] and 11, 1,2-diamino-2-methylpropane.[b] ○, Cu chelate; ●, Ni chelate; and ◑, Zn chelate.

a) For chelate stability, T. Davis, S. S. Singer, and L. A. K. Staveley, *J. Chem. Soc.*, **1954**, 2304; measured at 25 °C under μ=0.1, and for acid dissociation, H. K. Powell and N. F. Curtis, *J. Chem. Soc. B*, **1966**, 1205; measured at 25.0 °C under μ =0.1 ($NaClO_4$-$Ba(ClO_4)_2$).

b) For chelate stability, H. K. Powell and N. F. Curtis, *J. Chem. Soc. A*, **1967**, 1441; measured at 25.0 °C under μ=0.1 ($NaClO_4$-$Ba(ClO_4)_2$, and for acid dissociation, the same reference as cited in a).

the diaminotetralins and BEDA, however, could not be analyzed by the above procedure. Precipitates of 1 : 2 composition (metal to ligand) were formed during the course of titration of the 1 : 1 solutions

Table 2. Acid dissociation and chelate stability constants of various diamines measured at 25.0 °C under μ=0.10 with KNO_3

Cation		T(E,E)[b]	T(A,E)	D(E,E)	D(A,E)	*t*-CYDA[c]	*c*-CYDA[c]	BEDA
H^+	pK_{a1}	5.98	5.79	6.68[a]	6.36[a]	6.34	6.04	6.26[d]
	pK_{a2}	8.97	9.00	10.08	9.93	9.77	9.80	9.78
	$\sum pK_a$	14.95	14.79	16.76	16.29	16.11	15.84	16.04
Cu^{2+}	$\log K_{ML}$	10.29	9.86	11.55[e]	11.06[f]	11.09	10.82	11.26
	$\log K_{ML_2}$	8.89	8.71	10.23	10.13	9.64	9.50	9.92
	$\sum \log K$	19.18	18.57	21.78	21.19	20.73	20.37	21.18
Ni^{2+}	$\log K_{ML}$	7.09	6.31	8.22[g]	7.34	7.88	7.20	8.00
	$\log K_{ML_2}$	6.07	5.02	7.09	5.70	6.78	5.87	6.67
	$\sum \log K$	13.16	11.33	15.31	13.04	14.66	13.07	14.67
Zn^{2+}	$\log K_{ML}$	5.39	4.95	6.57	5.86	6.19	5.82	
	$\log K_{ML_2}$	4.82	4.74	5.73	5.23	5.36	5.43	
	$\sum \log K$	10.21	9.69	12.30	11.09	11.55	11.25	

a) Ref. 2, 25.0 °C, μ=0.10 (KNO_3). b) 25.0 °C, μ=0.10 (KCl). c) C. R. Bertsch, W. C. Fernelius, and B. P. Bloch, *J. Phys. Chem.*, **62**, 444 (1958); interporated from the data at 20.0 and 30.0 °C, and converted into μ=zero by Debye-Hückel equation. d) Ref. 3, 25.0 °C, μ=0.10 (KCl). e) Paired $\log K_{MLOH}$=5.01. f) Paired $\log K_{MLOH}$=5.26. g) Paired $\log K_{MLOH}$=6.60.

(Table 1). The results suggest that even in the 1 : 1 solution, the disproportionation reaction (4) takes place, to give a complex ML_2. Stability constants of of the diaminotetralins and BEDA (Table 2) are thus obtained only from the titration data of the 1 : 2 solutions, where those of BEDA complex with zinc(II) could not be obtained because of fluctuation of pH-meter readings probably due to an extremely slow reaction to attain equilibrium.

Stability of the 1 : 1 metal chelate increases in the order T(A,E), T(E,E), *c*-CYDA,** D(A,E), *t*-CYDA,** and D(E,D), in general agreement with the increase in the total basicity of the diamino group, as expressed by ($pK_{a1}+pK_{a2}$), irrespective of metal ion.

Plots of $\log K_{ML}$ against the total basicity of diamines (Fig. 3) indicate that the 1,2-diamines can be classified into three groups: the alicyclic diamines of *trans*-configuration (line A), those of *cis*-configuration (line B) and acyclic diamines capable of rotational isomerism, such as ethylenediamine and propylenediamine (line C). The data for each group fall on straight lines parallel to each other.

According to the conformation theory regarding a cyclohexane ring, it is well-known that a conformation with an *axial* bulky substituent is less stable than one with the same group in the *equatorial* position. If one refers to the conformation of the metal chelates with the ligand of a *trans*-group against those with the ligand of a *cis*-group, either one of amino group must be in the *axial* position of the ligand molecule for the latter chelate group. The coordination of aquo ion to this site might cause considerable steric hindrance. In the case of the former groups, however, both amino groups are in the *equatorial* position, so that the coordination of an aquo ion to these sites causes little steric hindrance.

Thus the vertical difference between the correlation lines of a *trans*-group and a *cis*-group could be regarded as values proportional to the stabilization free energy of the *trans*-group over the *cis*-group upon metal complex formation with respective metal ions. The difference is the highest in the nickel chelates, and ascribable to the octahedral hexacoordination structure of nickel(II) ion, which is the most bulky in comparison with tetrahedral zinc(II) and square planar copper(II). A small separation between the correlation lines of *trans*- and *cis*-diamine copper complexes might be regarded to indicate a loose aquation along the axis perpendicular to the square coordination plane of copper ion, to form a distorted octahedral structure in the 1 : 1 chelates.

Diamines with free internal rotation show a relatively lower chelate stability despite their higher

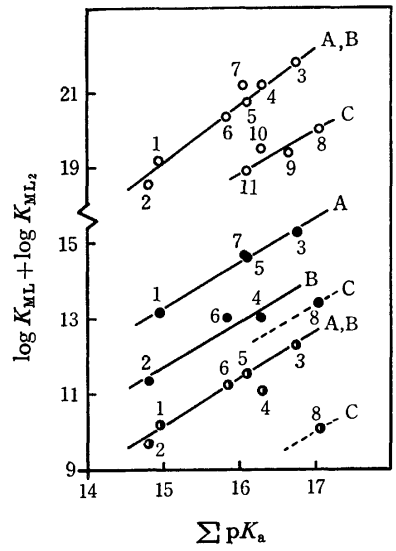

Fig. 4. Relationship of the 1 : 2 chelate stabilities against the total basicities of 1,2-diamines. Notation and references are the same as described in Fig. 3.

** *c*- and *t*-CYDA are abbreviations of *cis*- and *trans*-1,2-diaminocyclohexanes, respectively.

basicities. This can be explained by the loss of freedom in the internal rotation with the chelate ring formation. It should be noted that BEDA is aligned with the *trans*-diamines on a line. A bulky *t*-butyl group hinders the internal rotation in the free ligand molecule to fix the two amino groups in a *gauche* position favorable to form a chelate ring. The entropy loss upon chelation becomes to a certain extent similar to that of alicyclic *trans*-diamines of rigid structures.

Relationships between the stability of 1 : 2 metal-diamine complexes, as expressed by $(\log K_{ML}+\log K_{ML_2})$, and the total basicity (Fig. 4) differ somewhat from those observed (Fig. 3). The data for copper- and zinc complexes of the *trans*- and *cis*-diamines can be correlated with single lines, in contrast to nickel chelates, in which each *trans*-diamine afforded 1 : 2 complexes more stable than those of the *cis*-isomer.

The *dl-trans*- and *dl-cis*-diaminodecalins may possibly afford two and four kinds of diastereomeric 1 : 2 copper complexes, respectively, with respect to the configurations of chelate rings around the central metal atom. Molecular model study suggests that the coordinated diamines would be sterically hindered with a ligand, if present on the *z*-axis, in two of the diastereomeric complexes with the *cis*-diamines. The *dl-trans*- and *cis*-diaminocyclohexanes can also afford two diastereomeric copper complexes, and the coordinated diamines in one diastereomer with the *cis*-diamine is subject to steric hindrance with a ligand on the *z*-axis to a greater extent than in the other.

The situation in the nickel complexes would be similar to the above if the 1 : 2 chelates took configurations in which the four amino groups were arranged in a square plane.

Thus the results seem to suggest that the completion of a square ligand field with four amino-nitrogen atoms on the *x-y* plane in the 1 : 2 copper chelates leads to dissociation of aquo-ligands on the *z*-axis,[10] while in the nickel chelates aquo-ligands on the *z*-axis remain intact even in the 1 : 2 chelates.

The fact that the data on the 1 : 2 zinc chelates of *trans*- and *cis*-diamines fall on a single correlation line can be regarded as an evidence for a very small inter-ligand interaction in the tetrahedral coordination sphere of zinc(II) ion. If this is the case, the separation between correlation lines in the 1 : 1 zinc chelates should be ascribed to penta- or hexacoordination structures[11] of 1 : 1 diamine–zinc complexes in aqueous solutions rather than to the tetrahedral structure. The former structure would be transformed into the latter with completion of a coordination sphere by four amino groups in 1 : 2 complexes.

Refeeences

1) L. G. Sillen and A. E. Martell, "Stability Constants of Metal-Ion Complexes," Special Publication No. 17, The Chemical Society, London, 1964.
2) T. Yano, H. Kobayashi, and K. Ueno, This Bulletin, **46**, 985 (1973).
3) Y. Yanagihara, T. Yano, H. Kobayashi, and K. Ueno, *ibid.*, **45**, 554 (1972).
4) E. L. Eliel, N. L. Allinger, S. J. Angyal, and G. A. Morrison, "Conformational Analysis," John Wiley & Sons, Inc., New York, N. Y., 1965.
5) G. Schwarzenbach, A. Will, and R. O. Bach, *Helv. Chim. Acta*, **30**, 1303 (1947).
6) N. F. Hall and M. R. Splinkle, *J. Amer. Chem. Soc.*, **54**, 3469 (1932).
7) F. Kieffer and P. Rumfp, *C. R. Acad. Sci. Paris*, **230**, 2303 (1950).
8) H. K. Hall, Jr., *J. Amer. Chem. Soc.*, **79**, 5441 (1957).
9) R. W. Taft, Jr., "Steric Effects in Organic Chemistry," M. S. Newman, ed., John Wiley and Sons, Inc., New York, N. Y., 1956.
10) F. A. Cotton and G. Wilkinson, "Advanced Inorganic Chemistry," 2nd Ed., Interscience Publishers, New York, N. Y., 1966, p. 905.
11) Ref. 10, p. 610.

ESR and Optical Absorption Studies of Various Bis(*N*-salicylidenealkylaminato)copper(II) Complexes with Tetrahedrally-distorted Coordination Geometry

Hiroshi YOKOI

Chemical Research Institute of Non-aqueous Solutions, Tohoku University, Katahira, Sendai 980

(Received June 11, 1974)

The ESR and visible absorption spectra of a number of bis(*N*-salicylidenealkylaminato)copper(II) complexes with different kinds of alkyl groups were measured in toluene. The coordinations of these complexes in toluene are distorted towards a tetrahedral geometry to varying extents; the relationship between the degree of the distortion and the ESR and visible absorption parameters was systematically investigated. Especially, the experimental fact that the absolute values of the hyperfine coupling constant with the copper nucleus decrease with an increase in the degree of distortion was discussed. A configurational equilibrium between two species with different degrees of the distortion was found to exist for the complexes with R=isopropyl and cyclohexyl in toluene.

A number of crystal structure determinations of bis(*N*-salicylidenealkylaminato)copper(II) complexes by three dimensional X-ray methods have been carried out,[1-6] and some of the complexes have been revealed to adopt tetrahedrally-distorted configurations in crystals, depending on the nature of the alkyl groups. Many other physicochemical measurements of these complexes in various states have been made in order to obtain some information about the stereochemistry and related properties.[7] There have been a few ESR reports on various copper(II) complexes with tetrahedral-coordination geometry.[8-10] It seems, however, that a satisfactory method for the precise interpretation of the ESR parameters of those complexes has not yet been established. In the present work, therefore, ESR and optical absorption studies of a series of bis(*N*-salicylidenealkylaminato)copper(II) complexes with many different kinds of alkyl groups, which are distorted towards a tetrahedral configuration to varying extents in solutions, have been carried out systematically.

Experimental

Materials. 11 kinds of bis(*N*-salicylidenealkylaminato)-copper(II) complexes were prepared and purified according to the usual method,[11] using commercial reagents; all the complexes are listed in Table 1, and hereafter they will be designated as Cu(*N*-R-sal)$_2$. Commercial toluene was purified by successive shaking with sulfuric acid and sodium hydroxide, followed by drying over sodium, and, finally, fractional distillation.

ESR and Visible Absorption Measurements. The ESR spectra of the above-mentioned complexes in toluene at a concentration of 1.0×10^{-2} mol/l were measured at room temperature and at the temperature of liquid nitrogen by means of a Hitachi 771 X-band ESR spectrometer. The visible absorption spectra of the complexes in toluene were recorded at room temperature on a Cary 14 spectrometer, using 1-cm quartz cells.

Results and Discussion

The crystal structures of the Cu(*N*-R-sal)$_2$ complexes with R=methyl,[1] *n*-propyl,[3] and *n*-butyl[5] are known to adopt normal planar configurations. On the other hand, X-ray analytical studies have revealed that the complexes with R=isopropyl[4] and *t*-butyl[6] in crystals are distorted towards a tetrahedral configuration because the alkyl groups are sufficiently bulky to prevent normal planar complexes from being formed. There is, however, an unexpected observation that Cu(*N*-ethylsal)$_2$ is distorted from planarity.[2] It appears, therefore, that intermolecular forces, *i.e.*, crystal packing forces, play an important and delicate role in determining the distortion. It is now unambiguous that the complexes with bulky alkyl groups in toluene are similarly distorted towards a tetrahedral configuration. The dipole-moment measurements of these complexes in dioxane and benzene suggest that this holds true.[12] This fact has also been supported by optical absorption spectral studies in such inert solvents as benzene and in various solid states.[12]

In this work, the visible absorption spectra were again measured at room temperature for all the present complexes in toluene in order to obtain systematic information about the coordination geometry; all the observed spectra are shown in Fig. 1. This figure indicates that the d-d spectra of the complexes appear

Table 1. ESR parameters[a] for Cu(*N*-R-sal)$_2$ in toluene

R	$g_{//}$	$g_{\perp}$[b]	$\lvert A_{//}\rvert$ $\times10^4$ cm^{-1}	g_0[c]	$\lvert A_0\rvert$[c] $\times10^4$ cm^{-1}
Methyl	2.217	2.055	195	2.109	76
Ethyl	2.221	2.055	186	2.110	74
n-Propyl	2.222	2.056	185	2.111	73
n-Butyl	2.223	2.055	184	2.111	73
n-Amyl	2.224	2.051	183	2.112	74
n-Hexyl	2.224	2.056	182	2.112	74
Isobutyl	2.222	2.057	181	2.112	73
Isopropyl	2.230		180	2.120	63
	2.253		156		
Cyclohexyl	2.230		180	2.117	65
	2.253		156		
s-Butyl	2.253	2.055	156	2.121	63
t-Butyl	2.270	2.068	145	2.135	43

a) Experimental errors in $g_{//}$ factor were ±0.001 and in $\lvert A_{//}\rvert$, ±1 (in the same unit as in the table), but those in g_0 and $\lvert A_0\rvert$ became somewhat large respectively, especially when the $\lvert A_0\rvert$ values were small. b) calculated from $g_0=(g_{//}+2g_{\perp})/3$. c) measured at room temperature.

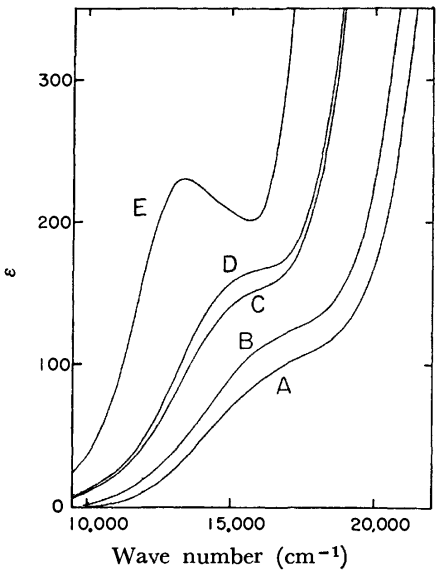

Fig. 1. Visible absorption spectra of the Cu(*N*-R-sal)$_2$ complexes in toluene at room temperature.
A: R=methyl. B: R=ethyl, *n*-propyl, *n*-butyl, isobutyl, *n*-amyl, and *n*-hexyl. C: R=cyclohexyl. D: R=isopropyl and *s*-butyl. E: R=*t*-butyl.

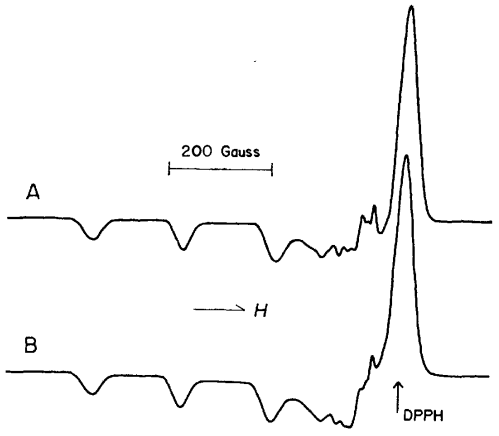

Fig. 2. X-band ESR spectra of the Cu(*N*-R-sal)$_2$ complexes with R=ethyl (A) and *n*-hexyl (B) in toluene at 77 K.

as shoulders on the longer-wavelength side of the near-ultraviolet intense bands, except for Cu(*N*-*t*-butyl-sal)$_2$, whose d-d spectrum appears only as a peak. It is difficult, therefore, to discuss these d-d spectra in detail. Two important observations, however, can be made in Fig. 1. One is the tendency for the intensities of the d-d spectra to increase in the spectral order of I to V, while the d-d spectra shift to longer wavelengths in the same spectral order. This tendency is consistent with the dependence of the spectral change on a distortion of the coordination geometry towards tetrahedron.[13,14] The other is the fact that the Cu(*N*-R-sal)$_2$ complexes with R=ethyl, *n*-propyl, *n*-butyl, isobutyl, *n*-amyl, and *n*-hexyl exhibit almost the same spectra, while the d-d spectra of the complexes with *R*=α-branched alkyl (*s*-alkyl) groups, *i,e.*, isopropyl, *s*-butyl, *t*-butyl, and cyclohexyl, become more intense than those of the R=α-non-branched alkyl groups.

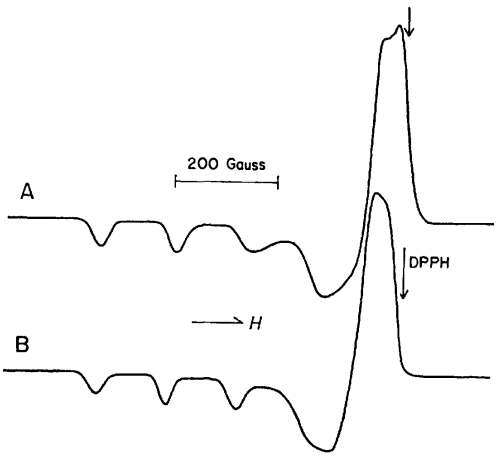

Fig. 3. X-band ESR spectra of the Cu(*N*-R-sal)$_2$ complexes with R=*s*-butyl (A) and *t*-butyl (B) in toluene at 77 K.

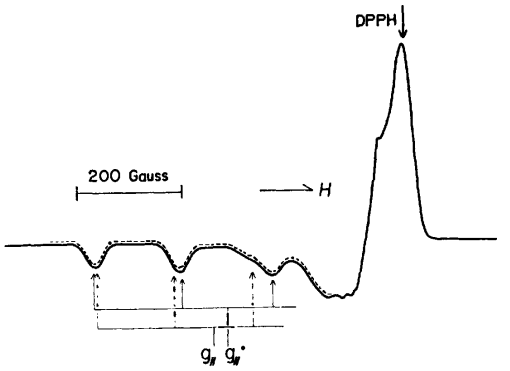

Fig. 4. X-band ESR spectrum of Cu(*N*-isopropyl-sal)$_2$ in toluene at 77 K (see the text as to the dotted line, $g_{\parallel}$, and $g_{\parallel}'$ written in the figure).

A similar classification of the Cu(*N*-R-sal)$_2$ complexes could also be made on the basis of ESR results. The ESR spectra of the complexes with R=ethyl, *n*-propyl, *n*-butyl, isobutyl, *n*-amyl, and *n*-hexyl were similar to one another; two of them are shown in Fig. 2. Cu(*N*-methyl-sal)$_2$, however, was different from the above-mentioned group of complexes in that its ESR spectrum was made up by the superposition of a spectrum due to those mentioned above and of a spectrum due to a triplet-state dimer.[15] On the other hand, the ESR spectra of the complexes with R=*s*-butyl, *t*-butyl, isopropyl, and cyclohexyl, the former three of which are shown in Figs. 3 and 4, were quite different in line shape from those in Fig. 2; the spectrum of the last complex was similar to the one in Fig. 4. The spectra in Fig. 3 are different in both line width and line position from those in Fig. 2. A detailed discussion of Fig. 4 will be given later. All the ESR parameters, which are listed in Table 1, were determined on the assumption that all the *g* and *A* tensors are of an axial or nearly axial symmetry. This assumption is supported by the experimental fact that the ESR spectra in Fig. 3 are of an axial type of line shape.

The expressions for the principal values of *g* and *A* tensors in terms of the coefficients in one-electron LCAO MOs have already been given in detail for the copper-

(II) complexes, whose coordination around the metal ion is a flattened tetrahedron.[8,9] It has been revealed experimentally and theoretically that, for each of the complexes, the $g_{//}$ value increases with an increase in the degree of the distortion towards a tetrahedral coordination geometry, and that there is a slight increase in the $g_{\perp}$ value (or g_x and g_y) up to the limit of a small degree of distortion.[10] It can, furthermore, be reasonably estimated from the equation of $A_{//}$ that the $|A_{//}|$ value also decreases with an increase in the degree of the distortion, since then the increases in both the $g_{//}$ value and the square value of the mixing coefficient of the 4p atomic orbital in the equation effectively contribute to a decrease in the $|A_{//}|$ value.[8,9]

The ESR data listed in Table 1 clearly indicate that the $g_{//}$ values of the Cu(*N*-R-sal)$_2$ complexes with R= methyl, ethyl, *n*-propyl, *n*-butyl, *n*-amyl, and *n*-hexyl increase slightly in this order of complexes, and that the $|A_{//}|$ values also decrease slightly in the same order. It is obvious that Cu(*N*-isobutyl-sal)$_2$ also belongs to this group. In this order of complexes, however, the two neighbors between which the largest differences in the $g_{//}$ and $|A_{//}|$ values were detected are the complexes of R=methyl and ethyl, as may be seen in the table. This fact, combined with the visible absorption spectral results shown in Fig. 1 and the crystal structural result that even Cu(*N*-ethyl-sal)$_2$ can adopt a tetrahedrally-distorted configuration,[2] suggest that all the complexes of this group except Cu(*N*-methyl-sal)$_2$ may have similar structures, with a slight distortion towards tetrahedral coordination geometry in toluene. On the other hand, the $g_{//}$ values of the complexes with R=*s*-butyl and *t*-butyl are remarkably large, and their $|A_{//}|$ values are remarkably small, compared with those of the above-mentioned group of complexes. This fact, combined with the visible absorption spectral results and the crystal structural results for Cu(*N*-*t*-butyl-sal)$_2$, indicates that the coordination geometry of these two complexes in toluene is highly distorted towards tetrahedron.

It is a noteworthy experimental fact that the $|A_0|$ values of the complexes with R=α-branched alkyl groups become considerably smaller than those of the complexes with R=α-non-branched alkyl groups, as is shown in Table 1. For Cu(*N*-*t*-butyl-sal)$_2$, furthermore, the decrease in the $|A_0|$ value was found to be comparable in magnitude to that in the $|A_{//}|$ value. A_0 is written in terms of the Fermi contact term for the free ion, κ, by this relation:[8,9]

$$A_0 = -(P_d a^2 + P_p b^2),$$

where $P_{d,p}=2\gamma\mu_0\mu_N\langle r^{-3}\rangle_{3d,4p}$, μ_N being the nuclear magneton and γ being the nuclear gyromagnetic ratio, and where a and b are the mixing coefficients of the 3d and 4p atomic orbitals in the ground-state unpaired-electron molecular orbital. One has $P_d : P_p = 828.7 : (925\pm40)$[8,9] and $P_d = 0.036\ cm^{-1}$.[16] The equation of A_0 states that A_0 is almost independent of any distortion towards a tetrahedral configuration. The above-mentioned experimental fact, therefore, is clearly in conflict with an estimation derived from this equation. Freeman and Watson have revealed, through an unrestricted Hartree-Fock calculation of the spin-polarization of the 4s electrons by an exchange interaction with the 3d unpaired electron for a copper atom in the $3d^94s^2$ configuration, that the spin-polarization of the 4s electrons contributes to a weakening of the isotropic Fermi contact interaction.[17,18] The small $|A_0|$ values of the complexes with R=*s*-butyl and *t*-butyl, therefore, can be interpreted in terms of an increase in the electron density on the 4s orbital with an increase in the degree of distortion. This interpretation is plausible in view of the fact that the charge neutralization on the metal ion is facilitated by electron donation from the ligand orbitals to the metal 4s orbital, rather than by that to the metal 3d orbital, because the interaction between the ligand and 3d orbitals is weakened by the tetrahedral distortion. On the basis of this interpretation, the degree of decrease in the $|A_0|$ value would give a measure of the electron density on the metal 4s orbital. The possibility that there may be another mechanism of decrease in the $|A_0|$ value, however, can not be excluded, because there has been no information about the spin-polarization of all the s-electrons caused by an exchange interaction with the metal 4p unpaired electron inevitably produced in the unpaired-electron molecular orbital.

The dipole moments of a number of the Cu(*N*-R-sal)$_2$ complexes have been measured in dioxane and benzene.[13,7] The results have revealed that the complexes of R=isopropyl and *t*-butyl do have substantial permanent dipole moments, and that the values increase in this order: *n*-propyl$\sim$*n*-butyl$<$isopropyl$\sim$*s*-butyl$<$*t*-butyl. These data, however, do not distinguish between a configurational equilibrium as is found for many nickel(II) complexes[7] and the existence of a single structural species. The ESR spectrum of Cu(*N*-isopropyl-sal)$_2$ in toluene, which is shown in Fig. 4, is different in line shape from the types of spectra in both Figs. 2 and 3. The dotted line in the low-field part of Fig. 4 is a spectrum simulated according to the superposition of the types of spectra in both Figs. 2 and 3 with $g_{//}'$ and $g_{//}$ at the intensity ratio of 3 to 2; actually, the spectrum of Fig. 3(A) itself was utilized for the spectral simulation. The dotted-line spectrum is in satisfactory agreement with the observed one, especially at the part of the hyperfine absorption lines of $I_z=1/2$, as may be seen in Fig. 4. Thus, we may conclude that a configurational equilibrium between two complex species with different degrees of the tetrahedral distortion exists for this complex in toluene. Such is also the case with Cu(*N*-cyclohexyl-sal)$_2$, since this complex showed an ESR spectrum analogous to that of Cu(*N*-isopropyl-sal)$_2$. On the other hand, the ESR line shapes shown in Fig. 3 suggest that the complexes of R=*t*-butyl and *s*-butyl may be dissolved as a single structural species in toluene.

The author wishes to thank Professor Taro Isobe for his encouragement throughout this work; thanks are also due to Mr. Makoto Chikira for many helpful suggestions relating to this work.

References

1) E. C. Lingafelter, G. L. Simmons, and B. Morosin, *Acta Crystallogr.*, **14**, 1222 (1961).

2) E. N. Baker, G. R. Clark, D. Hall, and T. N. Waters, *J. Chem. Soc. A.*, **1967**, 251.
3) G. Bombieri, C. Panattoni, E. Forsellini, and R. Graziani, *Acta Crystallogr.*, **B25**, 1208 (1969).
4) P. L. Orioli and L. Sacconi, *J. Amer. Chem. Soc.*, **88**, 277 (1966).
5) D. Hall, R. H. Summer, and T. N. Waters, *J. Chem. Soc. A*, **1969**, 420.
6) T. P. Cheeseman, D. Hall, and T. N. Waters, *ibid.*, **1966**, 685.
7) R. H. Holm, G. W. Everett, Jr., and A. Chakravorty, "Progress in Inorganic Chemistry," Vol. 7, ed. by F. A. Cotton, Interscience Publ., New York (1966), p. 83, and the references therein
8) C. A. Bates, W. S. Moore, K. J. Standley, and K. W. H. Stevens, *Proc. Phys. Soc.*, **79**, 73 (1962).
9) M. Sharnoff, *J. Chem. Phys.*, **42**, 3383 (1965).
10) Y. Murakami, Y. Matsuda, and K. Sakata, *Inorg. Chem.*, **10**, 1734 (1971).
11) P. Pfeiffer and H. Glaser, *J. Prakt. Chem.*, **153**, 265 (1939).
12) J. Sacconi and M. Ciampolini, *J. Chem. Soc.*, **1964**, 276.
13) See for example: C. J. Ballhausen, "Introduction to Ligand Field Theory," McGraw-Hill, Inc., New York (1962).
14) Y. Murakami, Y. Matsuda, and K. Sakata, *Inorg. Chem.*, **10**, 1728 (1971).
15) M. Chikira and T. Isobe, This Bulletin, **45**, 3006 (1972).
16) D. Kivelson and R. Neiman, *J. Chem. Phys.*, **35**. 149 (1961).
17) A. J. Freeman and R. E. Watson, "Magnetism," Vol. IIA, ed. by G. T. Rado and H. Shul, Academic Press, Inc., New York (1965), p. 167.
18) B. R. McGarvey, *J. Phys. Chem.*, **71**, 51 (1967).

Binuclear Metal Complexes. XI.[1] Substituent Effect upon Magnetisms of Binuclear Oxovanadium(IV) and Copper(II) Complexes of the Schiff Bases, 2,6-Bis[*N*-(2-hydroxy-5-substituted-phenyl)iminomethyl]-4-methylphenol

Hisashi Okawa, Isao Ando*, and Sigeo Kida

Department of Chemistry, Faculty of Science, Kyushu University, Hakozaki, Higashi-ku, Fukuoka, 812

**Department of Chemistry, Faculty of Science, Fukuoka University, Nanakuma, Nishi-ku, Fukuoka, 814*

(Received June 17, 1974)

Binuclear oxovanadium(IV) and copper(II) complexes, M_2(fsalap-R)(OMe) (R=H, CH_3, Cl, and NO_2) were synthesized and characterized, where H_3fsalap-R denotes 2,6-bis[*N*-(2-hydroxy-5-substituted-phenyl)iminomethyl]-4-methylphenol and the metal ions are connected by the phenolic oxygen and a methanolate ion. The cryomagnetic properties of the complexes except Cu_2(fsalap-NO_2)(OMe) could be interpreted on the basis of the Bleaney-Bowers equation. It was found that the $-2J$ values for the oxovanadium(IV) complexes increase in the order $(VO)_2$(fsalap-CH_3)(OMe) < $(VO)_2$(fsalap-H)(OMe) < (VO_2)(fsalap-Cl)(OMe), while those for the copper(II) complexes decrease in the order Cu_2(fsalap-CH_3)(OMe) > Cu_2(fsalap-H)(OMe) > Cu_2(fsalap-Cl)(OMe). These facts could be reasonably explained in terms of the difference in structures and spin-exchange mechanisms between the oxovanadium(IV) and the copper(II) complexes. $(VO)_2$(fsalap-NO_2)(OMe) showed a very strong antiferromagnetic spin-exchange interaction ($-2J=545$ cm^{-1}) compared with the other complexes (180—280 cm^{-1}). On the other hand, the magnetism of Cu_2(fsalap-NO_2)(OMe) could be interpreted in terms of the Ising model.

Since both oxovanadium(IV) and copper(II) ions have one unpaired electron in each of their 3d-shells, magnetic exchange interactions of binuclear oxovanadium(IV) complexes are to be discussed in relation to those of binuclear copper(II) complexes. Many binuclear copper(II) complexes have been studied extensively.[2] On the other hand, relatively less number of binuclear oxovanadium(IV) complexes have been synthesized.[3-10] It seems interesting to synthesize binuclear oxovanadium(IV) and copper(II) complexes with the same ligand system and to compare their magnetic properties, but only few have been reported concerning such kind of research.[4,11,12] Ginsberg *et al.* synthesized binuclear oxovanadium(IV) and copper(II) complexes of the Schiff bases prepared from 5-R-salicylaldehydes and 4-R′-2-aminophenols.[4] They found that the magnitude of the spin-exchange interaction for the copper(II) complexes increases with the decreasing order of electron-withdrawing abilities of R groups. However, they could not find such regularity for the oxovanadium(IV) complexes.

In the preceeding papers of this series,[13-18] it was shown that 2,6-diformyl-4-methylphenol and its Schiff bases form stable binuclear complexes with copper(II) and nickel(II) ions. In the present study, the Schiff bases, 2,6-bis[*N*-(2-hydroxy-5-substituted-phenyl)-iminomethyl]-4-methylphenol, were used for the preparation of binuclear oxovanadium(IV) and copper(II) complexes. The Schiff bases are abbreviated to H_3-fsalap-R, in which R is H, CH_3, Cl or NO_2, the substituents being attached to 4-position of 2-aminophenol. The complexes obtained were characterized as a binuclear complex bridged by the phenolic oxygen in the 2,6-diformyl-4-methylphenol moiety and methanolate ion (Fig. 1). The complexes are denoted by M_2-(fsalap-R)(OMe). Their magnetic properties were investigated over the temperature range 77.4—300 K and discussed on the basis of the Heisenberg model and/or the Ising model.

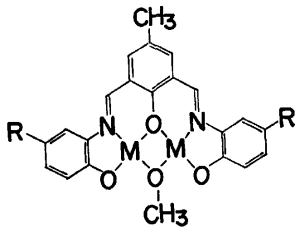

Fig. 1.

Experimental

Syntheses. The synthetic method of 2,6-diformyl-4-methylphenol is described elsewhere.[15]

$(VO)_2$(fsalap-H)(OMe). Vanadium(IV) oxodichloride (500 mg) was dissolved in absolute methanol(30 ml), and the solution was filtered to remove any insoluble materials. To this solution was added a methanolic solution(30 ml) 2,6-diformyl-4-methylphenol(164 mg) and 2-aminophenol (218 mg). Orange crystals immediately separated. After the reaction mixture was stirred at 60 °C for 3 hr, the crystals were collected, thoroughly washed with absolute methanol and dried under vacuum.

Found: C, 51.46; H, 3.60; N, 5.37%. Calcd for $C_{22}H_{18}N_2O_6V_2$: C, 51.99; H, 3.57; N, 5.51%.

$(VO)_2$(fsalap-CH_3)(OMe). This complex was obtained by nearly the same method mentioned above except for using 2-amino-4-methylphenol(264 mg) instead of 2-aminophenol. The mixture was stirred for 3 hr at 60 °C to give orange-brown crystals, which were collected, washed with absolute methanol and dried under vacuum.

Found: C, 53.95; H, 4.03; N, 5.31%. Calcd for $C_{24}H_{22}N_2O_6V_2$: C, 53.75; H, 4.13; N, 5.22%.

$(VO)_2$(fsalap-Cl)(OMe). 2,6-Diformyl-4-methylphenol (164 mg) and 2-amino-4-chlorophenol(288 mg) were dissolved in absolute methanol (40 ml), and the mixture was neutralized with 1M sodium methoxide solution(3 ml). Then this solution was added to a solution of vanadium(IV) oxodichloride (500 mg) in methanol (30 ml). Orange-brown crystals which separated were filtered and dried under vacuum.

Found: C, 45.63; H, 3.04; N, 4.66%. Calcd for C_{22}-

$H_{16}N_2O_6Cl_2V_2$: C, 45.78; H, 2.79; N, 4.85%.

$(VO)_2$(fsalap-NO_2)(OMe). 2,6-Diformyl-4-methylphenol (164 mg) and 2-amino-4-nitrophenol(308 mg) were dissolved in the mixture of absolute methanol (25 ml) and dioxane (25 ml). This solution was then added to a solution of vanadium(IV) oxodichloride(500 mg) in absolute methanol (30 ml), and the whole was stirred at 60 °C for 3 hr to give yellowish brown crystals. They were collected, washed with methanol and dried under vacuum.

Found: C, 43.93; H, 2.78; N, 9.22%. Calcd for $C_{22}H_{16}N_4O_{10}V_2$: C, 44.17; H, 2.70; N, 9.36%.

Cu_2(fsalap-H)(OMe)·CH_3OH. This complex was obtained by the similar method to that for $(VO)_2$(fsalap-H)(OMe) except for using copper(II) acetate monohydrate (440 mg) instead of vanadium oxodichloride. It forms brown crystals, containing one molecule of methanol.

Found: C, 52.42; H, 3.88; N, 5.44%. Calcd for $C_{22}H_{18}N_2O_4Cu_2\cdot CH_3OH$: C, 52.56; H, 4.22; N, 5.33%.

Cu_2(fsalap-CH_3)(OMe). This complex was prepared by the similar method to that for $(VO)_2$(fsalap-CH_3)(OMe), using copper(II) acetate monohydrate(440 mg). It forms orange-brown crystals.

Found: C, 54.51; H, 4.46; N, 5.34%. Calcd for $C_{24}H_{22}N_2O_4Cu_2$: C, 54.44; H, 4.19; N, 5.29%.

Cu_2(fsalap-Cl)(OMe). The synthetic procedure of this complex resembles that for $(VO)_2$(fsalap-Cl)(OMe) except for using copper(II) acetate monohydrate (440 mg) instead of vanadium(IV) oxodichloride. It forms orange-brown crystals.

Found: C, 47.04; H, 2.95; N, 4.88%. Calcd for $C_{22}H_{16}N_2O_4Cl_2Cu_2$: C, 46.33; H, 2.83; N, 4.91%.

Cu_2(fsalap-NO_2)(OMe)·$2H_2O$. This complex was obtained by treating a methanolic solution of copper(II) acetate monohydrate(440 mg) with a solution of 2,6-diformyl-4-methylphenol(164 mg) and 2-amino-4-nitrophenol(308 mg) in methanol–dioxane(1 : 1, 50 ml). Brown crystals which separated were filtered and washed with methanol. It contains two molecules of water.

Found: C, 42.71; H, 2.97; N, 9.11%. Calcd for $C_{22}H_{16}N_4O_8Cu_2\cdot 2H_2O$; C, 42.11; H, 2.89; N, 8.93%.

Measurements. Infrared spectra were measured with a 215 Hitachi Infrared Grating Spectrophotometer in the region 4000—650 cm^{-1}, using KBr-disk and hexachlorobutadiene-mull methods. ESR spectra(X-band) of polycrystalline samples were measured with a JEOL ESR-apparatus model JESME-3X at −100 °C and at room temperature. Magnetic susceptibilities were measured by the Faraday method in the range from liquid nitrogen temperature to room temperature. Pascal's constants[19] were used for diamagnetic correction. Mercuric tetrathiocyanatocobaltate(II) was used as a magnetic standard. The effective magnetic moments at room temperature were calculated from the expression, $\mu_{eff}=2.828\sqrt{(\chi_A-N\alpha)T}$

Results and Discussion

In the IR spectra of the complexes no absorption band due to the formyl group was found in the region 1700—1620 cm^{-1} and a strong band was found around 1600 cm^{-1}. This band may be attributed to the C=N stretching vibration. The V=O stretching vibration of $(VO)_2$(fsalap-R)(OMe) (R=H, CH_3, and Cl) was observed near 990 cm^{-1}. On the other hand, the V=O stretching vibration of $(VO)_2$(fsalap-NO_2)(OMe) shifted to a region of considerably low frequency (900 cm^{-1}). This fact implies that $(VO)_2$(fsalap-NO_2)(OMe) has a different molecular structure from other oxovanadium(IV) complexes. In the spectrum of Cu_2(fsalap-NO_2)(OMe)·$2H_2O$ was observed a broad band around 3200 cm^{-1}, which was assigned to the O–H vibration of water. This complex showed a loss of weight corresponding to two moles of water, when it was heated at 70 °C for several hours under vacuum. It recovered the weight when it was left standing in the atmosphere at room temperature. Therefore, it should be noted that Cu_2(fsalap-NO_2)(OMe) possesses a different structure from other Cu_2(fsalap-R)(OMe) complexes.

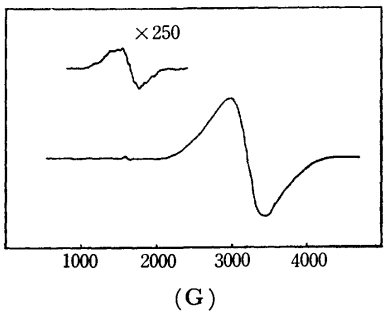

Fig. 2. ESR spectrum of $(VO)_2$(fsalap-H)(OMe) at room temperature.

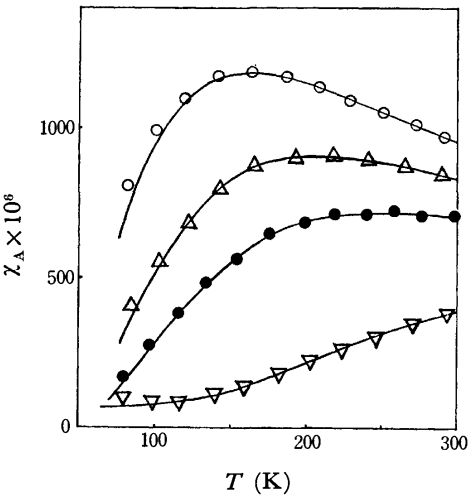

Fig. 3. Temperature dependeuce of magnetic susceptibilities of (○) $(VO)_2$(fsalap-CH_3)(OMe), (△) $(VO)_2$(fsalap-H)(OMe), (●) $(VO)_2$(fsalap-Cl)(OMe), and (▽) $(VO)_2$(fsalap-NO_2)(OMe).

The ligand field bands of the complexes could not be identified because of the intense absorption due to the ligand in visible region.

The ESR spectra of the complexes (polycrystalline sample) were measured. All spectra resemble each other. As an example the spectrum of $(VO)_2$(fsalap-H)(OMe) is shown in Fig. 2. A broad band around 3200 Guass (2000 G width) and a weak band near 1600 G were tentatively assigned to the $\Delta M_s=1$ and $\Delta M_s=2$ transitions respectively. All of these data are consistent with the structure given in Fig. 1.

The effective magnetic moments of the complexes at room temperature are lower than the spin-only value, 1.73 B.M.. The magnetic susceptibilities were measured at various temperatures. As shown in Figs. 3 and 4, the magnetisms of the complexes except Cu_2-

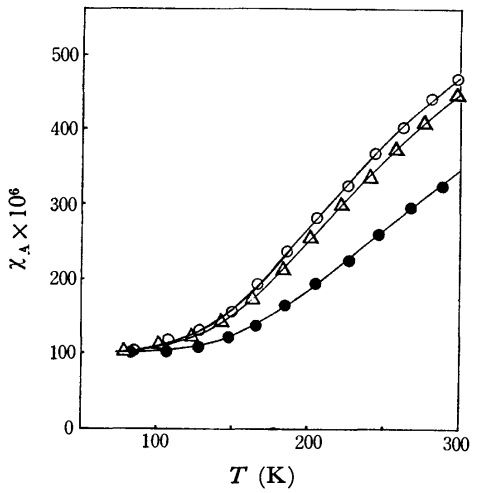

Fig. 4. Temperature dependence of magnetic susceptibilities of (●) Cu_2(fsalap-CH_3)(OMe), (△) Cu_2-(fsalap-H)(OMe), and (○) Cu_2(fsalap-Cl)(OMe).

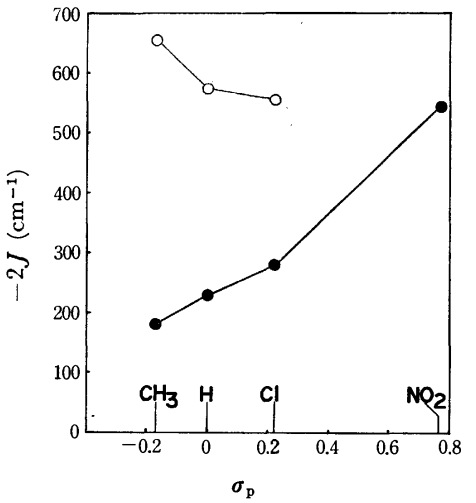

Fig. 5. The relations between the $-2J$ values and Hammett's σ_p values for (●) $(VO)_2$ (fsalap-R)(OMe) and for (○) Cu_2 (fsalap-R) (OMe).

(fsalap-NO_2)(OMe) (anhydrous form) can be interpreted on the basis of the Bleaney-Bowers equation,[20]

$$\chi_A = \frac{Ng^2\beta^2}{3kT}\left[1+\frac{1}{3}\exp(-2J/kT)\right]^{-1} + N\alpha,$$

where J is the exchange integral between a magnetically coupled pair and $N\alpha$ is the temperature independent paramagnetism. The agreements between theoretical and experimental $\chi_A - T$ curves are satisfactory when the parameters, g, J and $N\alpha$, are assumed as listed in Table 1. Slight deviations from the theoretical curves at low temperature may be attributed to a trace of paramagnetic impurities. The effective magnetic moments of the complexes are also given in Table 1.

As seen in Table 1, with the increasing order of electron-withdrawing abilities of the substituents the $-2J$ value (singlet-triplet energy separation) increases in the case of the oxovanadium(IV) complexes, but decreases in the case of the copper(II) complexes, This is more clearly shown by Fig. 5 in which the $-2J$ values are plotted *versus* Hammett's σ_A values.

It is well known that many oxovanadium(IV) complexes have square-pyramidel structures with the oxygen atom at the apex, vanadium atom being slightly lifted from the vasal plane. The electron-donating substituent at the 4-position in 2-aminophenol moiety increase the electron density on the phenolic oxygen atom and *vice versa*. According to an electrostatic model,[12] it is expected that the deviation of vanadium atom from the vasal plane is the largest for $(VO)_2$(fsalap-CH_3)-(OMe) and the smallest for $(VO)_2$(fsalap-Cl)(OMe) among the present complexes. Since the direct coupling between d_{xy}-orbitals is expected to be the dominating factor for the spin-exchange interaction in binuclear oxovanadium(IV) complexes,[12,22,23] the overlapping of d_{xy}-orbitals increases in the order $(VO)_2$-(fsalap-CH_3)(OMe) < $(VO)_2$(fsalap-H)(OMe) < $(VO)_2$-(fsalap-Cl)(OMe), whereby the $-2J$ value increasing in this order.

Table 1. Magnetic parameters and effective magnetic moments of complexes

M_2(fsalap-R)-(OMe) M	R	$-2J$ (cm^{-1})	g	$N\alpha\times10^6$	μ_{eff} (K)
VO	CH_3	180	1.87	60	1.46(291.0)
VO	H	230	1.86	40	1.37(291.2)
VO	Cl	280	1.81	45	1.25(298.0)
VO	NO_2	545	1.95	70	0.85(295.7)
Cu	CH_3	655	2.15	100	0.70(288.5)
Cu	H	570	2.15	100	0.88(298.1)
Cu	Cl	555	2.15	100	1.04(298.1)
Cu	NO_2				1.18(288.3)

On the other hand, the majority of copper(II) complexes have tetragonal structures. It has been revealed[24,25] that the spin-pairing interaction in the binuclear copper(II) complexes increases when the equatorial bonds are strengthened. This can be interpreted in term of a superexchange pathway through p_π(Cu)-p_π(bridging atom)-d_π(Cu) orbitals.[12,26-28] Our finding that the $-2J$ value decreases in the order Cu_2(fsalap-CH_3)(OMe) > Cu_2(fsalap-H)(OMe) > Cu_2-(fsalap-Cl)(OMe) is consistent with the above rule, because the electron density on the 2-aminophenolic oxygen atom decreases in this order and accordingly the Cu–O bond is weakened in the same order.

It is noteworthy that $(VO)_2$(fsalap-NO_2)(OMe) shows a very strong antiferromagnetic spin-exchange interaction and its V=O stretching vibration is observed at 900 cm^{-1}. Since such a shift of the V=O band to the low-frequency region is attributable to the intermolecular ···V=O···V=O··· interaction,[4,29] it is natural to assume the polymeric structure given in Fig. 6 for $(VO)_2$(fsalap-NO_2)(OMe). Hence the configuration around vanadium(IV) ion might not be distorted tetragonal-pyramidal but pseudo-octahedral. In fact the deviation of vanadium(IV) ion from the plane in *N,N'*-1,3-propylenebis(salicylaldiminato)-oxovanadium(IV),[29] whose linear chain structure of ···V=O···V=O··· bonding was demonstrated on the basis of X-ray analysis, is only 0.31 A, which is much

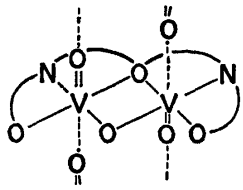

Fig. 6.

smaller than 0.54—0.58 A in the common oxovanadium(IV) complexes.[30,31] Accordingly the equatorial bonding system, 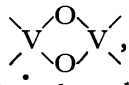 , is made more coplanar, and this will bring about larger overlapping between the vanadium d_{xy}-orbitals. The intermolecular spin-exchange interaction *via* ···V=O···V=O··· bonds is very weak compared with the intramolecular spin-exchange interaction, since the magnetism of $(VO)_2$(fsalap-NO_2)-(OMe) can be interpreted in terms of the Bleaney-Bowers equation. Such anomalous magnetisms have been reported for other binuclear oxovanadium(IV) complexes of the nitro-substituted Schiff bases.[4] It is likely that the strongly electron-withdrawing nitro group attached to the 4-position of 2-aminophenol moiety reduces the electron density on the phenolic oxygen atom, thereby weakening the ligand-field and allowing the axial coordination to the vanadium(IV) ion.

The magnetic property of Cu_2(fsalap-NO_2)(OMe) (anhydrous form), on the other hand, could not be interpreted on the basis of the Bleaney-Bowers equation. Its magnetism can be interpreted in terms of the Ising model. According to this model, the effective magnetic moment is expressed by the equation,[32]

$$\mu_{eff}^2 = \frac{1}{4}[\exp(4K) + (2+K^{-1})\exp(2K) - K^{-1} \times \exp(-2K) + 5][\exp(2K) + \exp(-2K) + 2]^{-1},$$

where K is J/kT. The good agreement of the experimental μ_{eff} values with this equation is shown in Fig. 7. Therefore, it is clear that Cu_2(fsalap-NO_2)(OMe) has a polymeric structure. However, further detailed information about the molecular structure can not be obtained at present. The high electron-withdrawing ability of the nitro group seems to play an important role in the formation of polymeric structure.

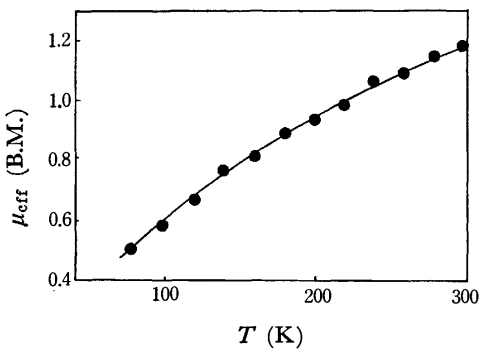

Fig. 7. Temperature dependeuce of the effective magnetic moment of Cu_2(fsalap-NO_2)(OMe). The solid line is theoretically obtained by assuming $g=2.15$ and $J=-225\ cm^{-1}$.

The authors are grateful to the Ministry of Education for a Scientific Research Grant-in-aid.

References

1) Part X. N. Manada, H. Okawa, and S. Kida, Submitted to this Bulletin.
2) M. Kato, H. B. Janossen and J. C. Fanning, *Chem. Rev.*, **64**, 99 (1964).
3) V. V. Zelentsov, *Russ. J. Inorg. Chem.*, **7**, 670 (1962).
4) A. P. Ginsberg, E. Koubek, and H. J. Williams, *Inorg. Chem.*, **5**, 1656 (1966).
5) C. C. Lee, A. Syamal, and L. T. Theriot, *ibid.*, **10**, 1669 (1969).
6) R. L. Belford, N. D. Chasteen, H. So, and R. E. Tapscott, *J. Amer. Chem. Soc.*, **91**, 4675 (1969).
7) V. T. Kalinnikov, V. V. Zelentsov, O. N. Kuzmicheva, and T. G. Aminov, *Russ. J. Inorg. Chem.*, **15**, 341 (1970).
8) Y. Kuge and S. Yamada, This Bulletin, **45**, 799 (1972).
9) G. O. Carlisle and A. Crutchfield, *Inorg. Nucl. Chem. Lett.*, **8**, 443 (1972).
10) A. Syamal, E. F. Carey, and L. J. Theriot, *Inorg. Chim. Acta*, **4**, 203 (1970).
11) A. P. Ginsberg, R. C. Sherwood, and E. Koubek, *J. Inorg. Nucl. Chem.*, **29**, 353 (1967).
12) E. F. Hasty, T. J. Colburn, and D. H. Hendrickson, *Inorg. Chem.*, **12**, 2414 (1973).
13) H. Okawa, This Bulletin, **43**, 3019 (1970).
14) H. Okawa and S. Kida, *ibid.*, **44**, 1172 (1971).
15) H. Okawa and S. Kida, *ibid.*, **45**, 1759 (1972); *Inorg. Nucl. Chem. Lett.*, **7**, 751 (1971).
16) H. Okawa, S. Kida, Y. Muto, and T. Tokii, This Bulletin, **45**, 2480 (1972).
17) H. Okawa, T. Tokii, Y. Nonaka, Y. Muto, and S. Kida, *ibid.*, **46**, 1462 (1973).
18) H. Okawa, T. Tokii, Y. Muto, and S. Kida, *ibid.*, **48**, 2464 (1973).
19) A. Earnshaw, "Introduction to Magnetochemistry," Academic Press, London (1968), pp. 5,6.
20) B. Bleaney and K. D. Bowers, *Proc. Roy. Soc., Ser. A*, **214**, 451 (1952).
21) J. Zemann, *Z. Anorg. Allg. Chem.*, **324**, 241 (1963).
22) J. McCormick, J. L. Featherstone, H. J. Stoklosa, and J. R. Wasson, *Inorg. Chem.*, **12**, 692 (1973).
23) G. M. Larin, Russ. *J. Inorg. Chem.*, **17**, 1394 (1972).
24) Y. Muto, M. Kato, H. B. Jonassen, and L. J. Cusachs, This Bulletin, **42**, 417 (1969).
25) M. Kato, Y. Muto, H. B. Jonassen, K. Imai, K. Katsuki and S. Ikegami, *ibid.*, **42**, 2555 (1969).
26) J. A. Bertrand and J. A. Kelley, *Inorg. Chim. Acta*, **4**, 203 (1970).
27) Y. Ishimura, Y. Nonaka, Y. Nishida, and S. Kida, Bulletin, **46**, 3728 (1973).
28) S. Kida, Y. Nishida, and M. Sakamoto, *ibid.*, **46**, 2428 (1973).
29) M. Mathew, A. J. Carty, and J. Palenik, *J. Amer. Chem. Soc.*, **92**, 3197 (1970).
30) D. Bruins and D. L. Weaver, *Inorg. Chem.*, **9**, 139 (1970).
31) E. From, E. S. Raper, R. E. Oughtred, and H. M. M. Sherer, *Chem. Comm.*, **1972**, 945.
32) A. T. Casey, E. Sinn, and J. R. Thackeray, *Aust. J. Chem.*, **25**, 1195 (1972).

Binuclear Metal Complexes. XIII.[1] Syntheses and Magnetic Properties of Thiocyanato-Bridged Binuclear Copper(II) Complexes

Tomoko ICHINOSE, Yuzo NISHIDA, Hisashi OKAWA,* and Sigeo KIDA

Department of Chemistry, Faculty of Science, Kyushu University, Hakozaki, Higashi-ku, Fukuoka 812

(Received July 26, 1974)

Three binuclear copper(II) complexes, Cu_2(fsal-NMe_2)$(NCS)_3$, Cu_2(fsal-NEt_2)$(NCS)_3$ and Cu_2(fsal-pa)-$(NCS)_3$, have been synthesized and characterized, where Hfsal-NMe_2, Hfsal-ENt_2 and Hfsal-pa denote the Schiff bases prepared by the condensation reaction of 2,6-diformyl-4-methylphenol with *N,N*-dimethylethylenediamine, *N,N*-diethylethylenediamine and 2-pyridylmethylamine, respectively. It was demonstrated that the complexes essentially consist of a binuclear unit of the thiocyanato-bridged skeleton, 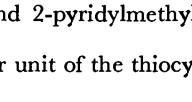 . The cryomagnetic properties could be explained on the basis of the equation for the tetranuclear cluster formed with two binuclear units linked by the out-of-plane bonding. The magnetisms and structures of the complexes were discussed in comparison with those of the Cu_2(fsal-NR_2)X_3 (X=Cl, Br).

It is well known[2-7] that the Schiff bases of 2,6-diformyl-4-methylphenol form binuclear copper(II) complexes, in which copper(II) ions are connected by two different groups, *i.e.*, the phenolic oxygen and an anion, X^-, such as Cl^-, Br^-, OH^-, OR^-, N_3^-, and $C_3H_3N_2^-$ (the conjugate base of pyrazole). However, no binuclear copper(II) complexes possessing thiocyanato-bridging group has been obtained. In the preceeding paper of this series,[5] we reported the syntheses and magnetisms of some binuclear copper(II) complexes of the Schiff bases derived from 2,6-diformyl-4-methylphenol and *N,N*-dialkylethylenediamines (See Fig. 1). Their magnetic properties were well explained in terms of the Bleaney-Bowers equation and it was found that the magnitude of the spin-exchange integral, $-J$, decreased in the order X=OH>Br>Cl.

The object of this study is to synthesize the thiocyanato-bridged binuclear copper(II) complexes and to investigate their magnetic properties in comparison with those of the corresponding hydroxo-, chloro-, or bromo-bridged complexes.

The ligands used in this work are the Schiff bases derived from 2,6-diformyl-4-methylphenol and amines such as *N,N*-dimethylethylenediamine, *N,N*-diethylethylenediamine, and 2-pyridylmethylamine (the ligands are abbreviated to Hfsal-NMe_2, Hfsal-NEt_2, and Hfsal-pa respectively). On treating these ligands and diisothiocyanatodipyridinecopper(II) in acetonitrile, green prisms were obtained. Based on the results of elemental analyses, the complexes are formulated as Cu_2(fsal-NR_2)$(NCS)_3$ (R=Me and Et) and Cu_2(fsal-pa)$(NCS)_3$. The structures of these complexes were investigated on the basis of the infrared spectra, electronic spectra and magnetic measurements. The spin-exchange interactions between copper(II) ions were studied by measuring the temperature variation of magnetic susceptibility.

Experimental

Syntheses. The synthetic method of 2,6-diformyl-4-methylphenol was described elsewhere.[8] *N,N*-Dimethylethylenediamine, *N,N*-diethylethylenediamine and 2-pyridylmethylamine were of commercial origin.

Cu_2(fsal-NMe_2)$(NCS)_3$. 2,6-Diformyl-4-methylphenol (165 mg), and *N,N*-dimethylethylenediamine (176 mg) and diisothiocyanatodipyridinecopper(II) (675 mg) were mixed in acetonitrile (100 ml) and the mixture was stirred at room temperature for 20 hr. The green precipitate which separated was collected, recrystallized from dimethyl sulfoxide-methanol and dried over P_2O_5 under a reduced pressure.

Found: C, 39.62; H, 4.62; N, 16.00; Cu, 20.20%. Calcd. for $C_{22}H_{31}N_7OS_3Cu_2$: C, 39.72; H, 4.50; N, 16.21; Cu, 21.01%.

Cu_2(fsal-NEt_2)$(NCS)_3$. This complex was prepared by a method similar to that for Cu_2(fsal-NMe_2)$(NCS)_3$ except for using *N,N*-diethylethylenediamine (232 mg) instead of *N,N*-dimethylethylenediamine. The green product was recrystallized from acetonitrile and dried over P_2O_5 under a reduced pressure.

Found: C, 43.61; H, 5.24; N, 14.69; Cu, 18.93%. Calcd for $C_{24}H_{35}N_7OS_3Cu_2$: C, 43.62; H, 5.34; N, 14.84; Cu, 19.23%.

Cu_2(fsal-pa)$(NCS)_3$. This complex was synthesized by the reaction of 2,6-diformyl-4-methylphenol (165 mg), 2-pyridylmethylamine (216 mg) and diisothiocyanatodipyridinecopper(II). The green product was recrystallized from acetonitrile and dried over P_2O_5 under a reduced pressure.

Found: C, 44.28; H, 2.90; N, 14.92; Cu, 20.58%. Calcd for $C_{24}H_{19}N_7OS_3Cu_2$: C, 44.71; H, 2.97; N, 15.21; Cu, 19.71%.

Measurements. Infrared spectra were measured with a Hitachi 215 grating spectrophotometer on a KBr disk. Electronic spectra were measured with a Hitachi EPS-3T recording spectrophotometer. Magnetic susceptibilities were measured by the Faraday method over the range from liquid nitrogen temperature to room temperature. Effective magnetic moments were calculated from the equation, $\mu_{eff}=2.828\sqrt{(\chi_A-N\alpha)T}$, where χ_A is the atomic magnetic susceptibility corrected for diamagnetism and $N\alpha$ is the temperature-indepenent paramagnetism. Pascal's constants[9] were used for the correction of diamagnetism.

Results and Discussion

Infrared absorption bands, ligand-field bands (reflectance on solids) and effective magnetic moments at room temperature of the complexes are given in Table 1. The complexes obtained have the composition of L (organic ligand moiety) : Cu : NCS^-=1 ;

* To whom correspondence should be addressed.

Table 1. IR bands, d-d bands, and effective magnetic moments of complexes

	IR (cm^{-1})				Reflectance (kK)	μ_{eff} (K) (B.M.)
	C≡N	C-S	C=N	skeletal		
$Cu_2(fsal\text{-}NMe_2)(NCS)_3$	2080 2070	815 700	1635 1630	1550	15.2	1.57(298.0)
$Cu_2(fsal\text{-}NEt_2)(NCS)_3$	2080 2070	810 730	1640 1627	1550	14.3	1.62(297.0)
$Cu_2(fsal\text{-}pa)(NCS)_3$	2080 2060	820 720	1640	1550	14.3	1.57(296.0)

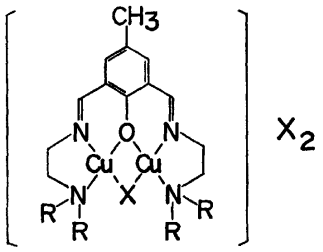

Fig. 1.

2 : 3. Therefore, the structures of the complexes are expected to be similar to those of the previously reported complexes given in Fig. 1. In fact the infrared spectra of $Cu_2(fsal)\text{-}NR_2)(NCS)_3$ are very similar to those of the corresponding $Cu_2(fsal\text{-}NR_2)X_3$[5] (X=Cl or Br, the halogenobridged complexes given in Fig. 1) in the region 4000—650 cm^{-1}, except some additional absorption bands observed for the present complexes. Hoskins *et al.*[7] studied the structure of the binuclear nickel(II) complex of 2,6-bis(thiosemicarbazonomethyl)-4-methylphenol and found that it has a skeleton 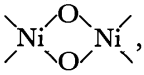 , *i.e.*, nickel(II) ions are connected by the phenolic oxygen and a $C_2H_5O^-$ group. Judging from this fact and from the infrared spectra of $Cu_2(fsal\text{-}NR_2)(NCS)_3$ similar to those of $Cu_2(fsal\text{-}NR_2)X_3$, it is likely that the present complexes have a skeleton 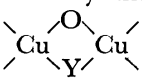 (Y=$^-$SCN or $^-$NCS).

In the infrared spectra of the complexes the band due to a skeletal vibration of the benzene ring is observed at 1550 cm^{-1}. This implies that the phenolic oxygen is concerned with bridging.[10] Two C-N stretching vibrations of thiocyanate group were found in the region 2080—2060 cm^{-1}, suggesting that there are two kinds of thiocyanate group of different bonding modes in the complexes. There are also two bands in the regions 820—810 and 730—700 cm^{-1}, which may be assigned to the C-S stretching vibrations of thiocyanate group. The band at 820—810 cm^{-1} may be due to the Cu-NCS bond, since this band is very close in frequency to the ν_{C-S} band of [Cu(tren)NCS]NCS, whose copper(II)-NCS linkage was demonstrated from the X-ray investigation.[11] The band at 730—700 cm^{-1} is located at lower frequency side compared with the ν_{C-S} band (745—750 cm^{-1}) of non-coordinated thiocyanate ion. In general the C-S stretching vibration of the soft metal complexes such as $(Et_4N)_2[Pd(SCN)_4]$ containing M-SCN bond are found in the region 720—690 cm^{-1}.[12] Therefore it is natural to assign this band to the C-S stretching vibration of the S-bonded thiocyanate group. It is well known that thiocyanate is always coordinated to a copper(II) ion with its N-atom. In addition to this the >S-C≡N bridging mode is known,[13] whereas the >N=C=S bridging have never been demonstrated. Thus it is very likely that two copper(II) ions are connected by the >S-C=N group and the N-bonded thiocyanates coordinate to copper(II) ions in the apical positions. It seems that the steric requirement of the ligands favors the formation of the binuclear copper(II) complex with the 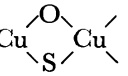 skeleton.

All complexes show effective magnetic moments smaller than the spin-only value at room temperature. The magnetic susceptibilities were measured over a temperature range from liquid nitrogen temperature to room temperature. The magnetic parameters for $Cu_2(fsal\text{-}NMe_2)(NCS)_3$ can be estimated as $g=1.99$, $N\alpha=60\times10^{-6}$ c.g.s., e.m.u. and $-2J=205$ cm^{-1} from the best fit of the χ_A values to the Bleaney-Bowers equation,[14]

$$\chi_A=\frac{Ng^2\beta^2}{3kT}\left[1+\frac{1}{3}\exp\left(-2J/kT\right)\right]^{-1}+N\alpha$$

However, it seems unreasonable to assume the g value smaller than 2.0 for copper(II) complexes. When the $-2J$ value is chosen so as to fit the χ_A value calculated from the Bleaney-Bowers equation to the experimental χ_A value at room temperature, assuming $g=2.15$ and $N\alpha=60\times10^{-6}$ c.g.s., e.m.u. (which are very common values for copper(II) complexes), significant deviation is observed between the experimental and theoretical χ_A-T curves as shown in Fig. 3. $Cu_2(fsal\text{-}NEt_2)(NCS)_3$ and $Cu_2(fsal\text{-}pa)(NCS)_3$ displayed similar magnetic behaviors. The facts mentioned above imply that the present complexes are not binuclear.

Recently Hoskins *et al.*[15] reported that the cobalt(II)-cobalt(III) complex of the Schiff base derived from 2,6-diformyl-4-methylphenol and 2-aminophenol has a tetranuclear structure, in which the planar binuclear units are linked by out-of-plane bonds. Therefore, it is likely that the present complexes also have a similar structure and show a magnetic property of a tetranuclear cluster. Based on the tetranuclear structure given in Fig. 2, the spin Hamiltonian may be described as

$$\mathcal{H}=-2J_{13}S_1S_3-2J_{24}S_2S_4-2J_{12}S_1S_2-2J_{23}S_2S_3-2J_{14}S_1S_4-2J_{34}S_3S_4.$$

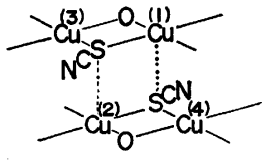

Fig. 2.

On assuming $J_{13}=J_{24}=J$, $J_{12}=J_{23}=J_{14}=J'$ and $J_{34}=0$, the magnetic susceptibility is expressed by the equation,

$$\chi_A = \frac{3g^2}{32T} \times \frac{\begin{array}{l}10\exp[(J+3/2J')/kT]+2\exp[(-J-J'/2)/kT] \\ +2\exp[(-J'/2+\sqrt{2J'^2-2JJ'+J^2})/kT] \\ +2\exp[(-J'/2-\sqrt{2J'^2-2JJ'+J^2})/kT]\end{array}}{\begin{array}{l}4\exp[(J+3/2J')/kT]+2\exp[(-J-J'/2)/kT] \\ +\exp[-Q(11)/kT]+\exp[-Q(22)/kT] \\ +\exp[-Q(33)/kT]+\exp[-Q(44)/kT] \\ +3\exp[(-J'/2+\sqrt{2J'^2-2JJ'+J^2})/kT] \\ +3\exp[(-J'/2-\sqrt{2J'^2-2JJ'+J^2})/kK]\end{array}} + N\alpha,$$

where $Q(11)$, $Q(22)$, $Q(33)$ and $Q(44)$ have the same meaning as was given by Hatfield *et al.*[16] As is shown in Fig. 3, the magnetic properties of the complexes can be well explained on the basis of the equation. The magnetic parameters, $-J$, $-J'$, g and $N\alpha$, obtained from the best fit of experimental χ_A values to the equation are listed in Table 2. Accordingly, it is evident that $Cu_2(fsal\text{-}NR_2)(SCN)_3$ and $Cu_2(fsal\text{-}pa)(NCS)_3$, which are essentially binuclear complexes with 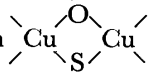 linkage, exhibit the magnetic behavior of a tetranuclear cluster, because of the out-of-plane linkage between two binuclear units. The most probable molecular structures of the complexes are given in Fig. 4.

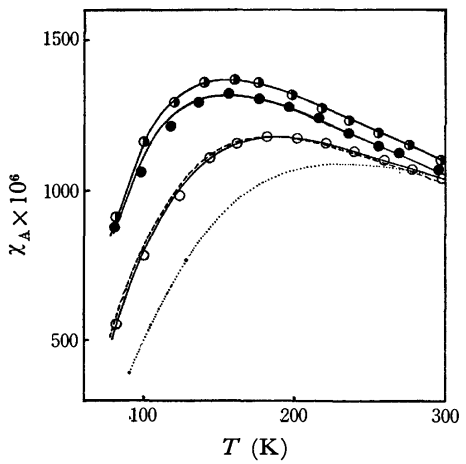

Fig. 3. Variation of molar suceptibilities per copper atom of (○) $Cu_2(fsal\text{-}NMe_2)(NCS)_3$, (◑) $Cu_2(fsal\text{-}NEt_2)(NCS)_3$ and (●) $Cu_2(fsal\text{-}pa)(NCS)_3$ as a function of temperature.
solid lines : theoretical curves based on the tetranuclear cluster using the parameters given in Table 2.
broken line : theoretical curve based on the Bleaney-Bowers equation using the parameters $g=1.99$, $N\alpha=60\times10^{-6}$ c.g.s. e.m.u. and $-2J=-205$ cm^{-1}.
dotted line : theoretical curve based on the Bleaney-Bowers equation assuming $g=2.15$, $N\alpha=60\times10^{-6}$ c.g.s. e.m.u. and $-2J=260$ cm^{-1}.

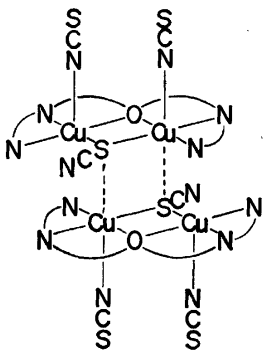

Fig. 4. Most probable structure of the complexes.

Table 2. Magnetic parameters of complexes

	$-J$ (cm^{-1})	$-J'$ (cm^{-1})	g	$N\alpha\times10^6$ (c.g.s.e.m.u.)
$Cu_2(fsal\text{-}NMe_2)(NCS)_3$	105	15	2.18	43
$Cu_2(fsal\text{-}NEt_2)(NCS)_3$	87.5	20	2.17	50
$Cu_2(fsal\text{-}pa)(NCS)_3$	87.5	25	2.15	45

As is seen in Table 2, the $-J'$ values are of the order of 1/7~1/4 of the $-J$ values. It is also seen that the $-J$ value is decreased when the $-J'$ value is increased. It is generally observed that the larger spin-exchange interaction operates between the copper(II) ions, the more coplanar the 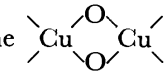 plane becomes.[17,18] It is compartible with this trend that the largest $-J$ value was observed for $Cu_2(fsal\text{-}NMe_2)(NCS)_3$ whose d-d band is highest in energy among those of the presently studied complexes. We were unsuccessful to obtain $Cu_2(fsal\text{-}N\text{-}i\text{-}Pr_2)(NCS)_3$. This fact implies that the bulky substituents attached to the nitrogen sterically hinder the complex formation of this type of structure.

References

1) Part XII: H. Okawa, M. Tanaka, and S. Kida, *Chem. Lett.*, **1974**, 987.
2) H. Okawa, This Bulletin, **43**, 3019 (1970).
3) H. Okawa and S. Kida, *ibid.*, **44**, 1172 (1971).
4) H. Okawa, S. Kida, Y. Muto, and T. Tokii, *ibid.*, **45**, 2480 (1972).
5) H. Okawa, T. Tokii, T. Nonaka, Y. Muto, and S. Kida, *ibid.*, **46**, 1462 (1973).
6) R. Robson, *Inorg. Nucl. Chem. Lett.*, **6**, 125 (1970).
7) B. F. Hoskins, R. Robson, and H. Schaap, *ibid.*, **8**, 21 (1972).
8) H. Okawa and S. Kida, This Bulletin, **45**, 1759 (1972).
9) P. W. Selwood, "Magnetochemistry," Interscience Publishers, New York (1956), pp. 78, 91.
10) S. J. Gruber, C. M. Harris, and E. Sinn, *J. Inorg. Nucl. Chem.*, **30**, 1805 (1968).
11) K. N. Raymond and F. Basolo, *Inorg. Chem.*, **5**, 1632 (1966).

12) K. Nakamoto, "Infrared Spectra of Inorganic and Coordination Compounds," John Wiley & Sons (1970), pp. 188, 189.
13) A. Mawby and G. E. Pringle, *Chem. Commun.*, **1970**, 385.
14) B. Bleaney and K. D. Bowers, *Proc. Roy. Soc., Ser. A*, **214**, 451 (1952).
15) B. F. Hoskins, R. Robson, and D. Vince, *Chem. Commun.*, **1973**, 392.
16) W. E. Hatfield and G. W. Inman, Jr., *Inorg. Chem.*, **8**, 1376 (1969).
17) Y. Muto, M. Kato, H. B. Jonassen, and L. C. Cusachs, This Bulletin, **42**, 417 (1969).
18) M. Kato, Y. Muto, H. B. Jonassen, K. Imai, K. Katsuki, and S. Ikegami, *ibid.*, **42**, 2555 (1969).

Six-coordinate Copper(II) Complexes Derived from the Reactions of Bis(acetylacetonato)- and Bis(ethyl acetoacetato)-copper(II) with Some Bidentate Nitrogen Bases

Takeo KURAUCHI,* Masanori MATSUI, Yukio NAKAMURA,** Shun'ichiro OOI, Shinichi KAWAGUCHI, and Hisao KUROYA

Department of Chemistry, Faculty of Science, Osaka City University, Sumiyoshi-ku, Osaka 558

(Received July 22, 1974)

Green-to-blue six-coordinate mixed complexes, $Cu(acac)_2(en)$ and $Cu(etac)_2(diamine)$(acac=acetylacetonate anion; etac=ethyl acetoacetate anion; diamine=ethylenediamine, trimethylenediamine, 2,2′-bipyridine or 1,10-phenanthroline) have been isolated by the reactions of the respective parent β-diketonate with the corresponding diamine in dry dichloromethane. On the other hand, the reaction of $Cu(acac)_2$ with en in the mole ratio of one-to-two in dichloromethane saturated with water has resulted in purple crystals of $Cu(acac)_2(en)_2\cdot 2H_2O$. This compound has been shown by X-ray analysis to consist of a square-planar copper(II) cation, coordinated by two ethylenediamine molecules, and two planar acetylacetonate anions, the plane of which is not perpendicular to, but slanted against, the CuN_4 plane. One oxygen atom of the anion participates in the N-H···O hydrogen bonding with an NH_2 group of the ethylenediamine molecule, while the other occupies the axial position of $Cu(en)_2^{2+}$ (Cu···O: 2.79(1) Å). Therefore, the compound can be designated by the formula $[Cu(en)_2]\cdot(acac)_2\cdot 2H_2O$. The water hydrogen atoms seem to take part in the hydrogen bonding with the anion oxygen atoms.

It is well-known that the bis(β-diketonato)copper(II) complexes may behave as Lewis acids and react with nitrogen bases to form addition compounds.[1] Several five-coordinate addition compounds of square-planar bis(β-diketonato)copper(II) complexes with heterocyclic nitrogen bases have been isolated.[2-6]

The Lewis acidity of the bis(β-diketonato)copper(II) complexes is affected by the relative electron-withdrawing power of the β-diketonate ligand.[7,8] When, for example, the highly electronegative CF_3-group is introduced in plane of the CH_3-group in acetylacetone, the affinity of the copper atom for the axial ligand is enhanced and the addition of two molecules of a monodentate nitrogen base proceeds quite readily. Thus, many six-coordinate addition compounds of bis(trifluoroacetylacetonato)-,[6,9] bis(hexafluoroacetylacetonato)-[6-8] and bis(thenoyltrifluoroacetonato)-[6,10] copper(II) complexes with monodentate nitrogen bases have been isolated thus far. Similar 1 : 2 adducts of the monodentate nitrogen base are also produced with the copper(II) complexes in which the central methine proton of the parent acetylacetonate ligand is replaced by another electron-withdrawing substituent, such as a nitro- or cyano-group.[11]

On the other hand, there have been only a few reports concerning the reactions of bis(β-diketonato)-copper(II) with bidentate nitrogen bases. A stable 2,2′-bipyridine adduct of bis(hexafluoroacetylacetonato)copper(II) was isolated, as its structure was determined by means of single-crystal X-ray analysis.[12] More recently, another research group has also described the reaction of the same copper(II) complex with some chelating diamines including ethylenediamine.[13,14]

We wish now to report on the reactions of bis(acetylacetonato)copper(II), $Cu(acac)_2$, with ethylenediamine (en), and of bis(ethyl acetoacetato)copper(II), $Cu(etac)_2$, with en, trimethylenediamine (tn), 2,2′-bipyridine (bipy), and 1,10-phenanthroline (phen).

Results and Discussion

Six complexes have been isolated; they are listed in Table 1, together with their analytical and magnetic data. All these complexes have normal magnetic moments as monomeric copper(II) compounds.

The 1 : 1 Complex Yielded by the Reaction of Bis(acetylacetonato)copper(II) with Ethylenediamine in Dry Dichloromethane. The reaction of $Cu(acac)_2$ with equimolar en in dry dichloromethane gave a pale green precipitate, composed of the 1 : 1 adduct of the parent complex with en. The same adduct was also obtained by the reaction of the parent complex suspended in dry ether

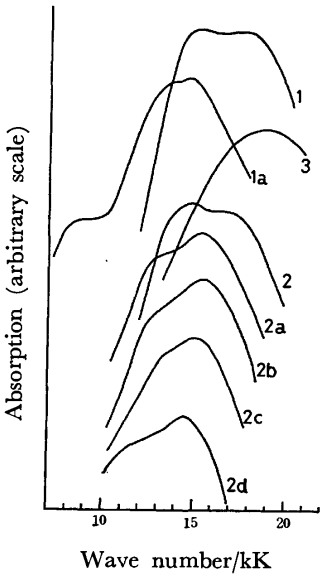

Fig. 1. The diffuse reflectance spectra of: (1), $Cu(acac)_2$; (1a), $Cu(acac)_2(en)$; (2), $Cu(etac)_2$; (2a), $Cu(etac)_2(en)$; (2b), $Cu(etac)_2(tn)$; (2c), $Cu(etac)_2(bipy)$; (2d), $Cu(etac)_2(phen)$ and (3), $[Cu(en)_2](acac)_2\cdot 2H_2O$.

* Present address: Research Department, Nippon Paint Co., Ltd., Neyagawa, Osaka

** To whom correspondences should be addressed.

TABLE 1. COLOR, CHEMICAL ANALYSES, AND MAGNETIC MOMENTS OF THE ISOLATED COMPLEXES

	Color	Found (%)				Calcd (%)				μ_{eff} (B.M.)
		C	H	N	Cu	C	H	N	Cu	
1 : 1 Complexes										
$Cu(acac)_2(en)$	pale green	44.60	6.93	8.78	19.36	44.78	6.89	8.70	19.74	1.84
$Cu(etac)_2(en)$	pale blue	43.07	6.89	7.37	16.83	44.03	6.86	7.33	16.64	1.88
$Cu(etac)_2(tn)$	pale green	45.40	7.32	6.81	15.68	45.50	7.13	7.07	16.05	1.99
$Cu(etac)_2(bipy)$	green	55.60	5.54	5.74	13.32	55.28	5.48	5.86	13.29	1.81
$Cu(etac)_2(phen)$	green	57.25	5.26	5.86	13.16	57.53	5.23	5.59	12.68	1.94
1 : 2 Complex										
$[Cu(en)_2](acac)_2 \cdot 2H_2O$	purple	39.50	8.12	13.27	15.09	40.23	8.20	13.40	15.20	1.84

TABLE 2. FREQUENCIES (kK) OF MAXIMUM ABSORPTIONS IN DIFFUSE REFLECTANCE SPECTRA

Parent complexes				
$Cu(acac)_2$			15.0	18.0
$Cu(etac)_2$			14.9	17.3
1 : 1 Complexes				
$Cu(acac)_2(en)$	8.7	13.6	14.6	
$Cu(etac)_2(en)$	—	12.8	15.4	
$Cu(etac)_2(tn)$	—	12.8	15.6	
$Cu(etac)_2(bipy)$	—	13.4	14.9	
$Cu(etac)_2(phen)$	—	11.9	14.4	
1 : 2 Complex				
$[Cu(en)_2](acac)_2 \cdot 2H_2O$		—	—	18.9

TABLE 3. CHARACTERISTIC IR BANDS OF THE DIAMINE GROUP IN BIS(ACETYLACETONATO)ETHYLENEDIAMINECOPPER(II) AND THE CORRESPONDING ETHYLENEDIAMINE-d_4 COMPLEX

$Cu(acac)_2(en)$	$Cu(acac)_2$-(en-d_4)	ν_{NH_2}/ν_{ND_2}	Assignment
3240 m	2400 w	1.35	NH_2 stretch
3160 m	2335 w	1.35	
~1600[a]	1183 w	1.35	NH_2 scissor
1332 m	1005 m	1.33	NH_2 wag
1159 m	900 m	1.29	
1110 w, sh	885 sh	1.25	NH_2 twist
1021 m	750 w	1.36	
785 m			NH_2 rock

a) This band is obscured by the intense absorption of the acetylacetonate ligand.

with en. The product can hardly be dissolved in usual organic solvents at room temperature without partial dissociation. However, it can be recrystallized from hot benzene. It is decomposed in moist air and turns violet, but it is stable for a long time under dry conditions.

The ligand-field spectrum of $Cu(acac)_2$ shows two indefinite absorption maxima at about 15.0 and 18.0 kK,[1] while that of the mono-pyridine adduct has only one broad absorption maximum at 15.2 kK.[15-17] On the other hand, the diffuse reflectance spectrum of the present 1 : 1 adduct of $Cu(acac)_2$ with en has two definite absorption maxima, one appearing at 14.6 kK, accompanied by an indefinite shoulder at about 13.6 kK, and the other, at 8.7 kK (Fig. 1, 1a and Table 2). These spectral features fit in well with the step-by-step change in the stereochemistry around the copper atom from square-planar $Cu(acac)_2$ through the five-coordinate pyridine adduct to the tetragonally-distorted octahedral environment, as was shown for the bis(acetylacetonato)- or bis(hexafluoroacetylacetonato)-copper(II)-pyridine system by Funch and Ortolano.[7] Recently, very similar spectra have been reported for the bis(pyridine) adducts of the copper(II) γ-nitro- and γ-cyano-acetylacetonates.[11]

The IR spectra of the 1 : 1 adduct of $Cu(acac)_2$ with en in the higher-frequency region, except for 1700—1500 cm^{-1}, can be understood, on the whole, as an overlap of the spectra of the acetylacetonate ligand and coordinated en. By a recent isotopic study[18,19] of the IR spectra of $Cu(acac)_2$, two absorption bands in the carbonyl region were definitely assigned: the band at 1578 cm^{-1} mainly to the C=O stretching vibration, and the second one, at 1527 cm^{-1}, to the antisymmetric vibration of the C—C—C segment of the chelate ring. On the other hand, in the IR spectra of the en adduct, the band assignable to the carbonyl stretching is shifted to the higher-frequency side (1615 cm^{-1}), while the other is shifted to the lower-frequency side (1501 cm^{-1}). These shifts may be caused by a weakening of the copper-ligand bond due to the coordination of diamine. Similar spectral features have also been observed for $Mn(acac)_2(en)$.[20] Characteristic bands attributable to the diamine ligand are listed in Table 3; they were assigned by reference to the literature[21] and also to the deuteration effect. There are no bands due to free diamine in the frequency region higher than 3320 cm^{-1}, indicating that both nitrogen atoms of the diamine are linked to the copper atom.

Figure 2 shows the far-IR spectra of the complex, together with those of $Cu(acac)_2$ and $Cu(etac)_2$ as references. The spectra of $Cu(acac)_2$ (1) have three bands between 600 and 280 cm^{-1}, two of which (455 and 291 cm^{-1}) are assigned to the pure Cu–O stretching modes.[22] In the case of the 1 : 1 en adduct (1a), the band near 450 cm^{-1} disappeared, while three intense bands (572, 545 and 490 cm^{-1}) and one broad band (415 cm^{-1}) appeared. The former bands are assigned to the ring vibrations of the en chelate ring, while the latter is assumed by reference to the literature[23] to be an overlap of the Cu–O (415 cm^{-1}) and the Cu–N (405 cm^{-1}, shoulder) stretching vibrations.

It is obvious from the analytical and spectroscopic results presented above that the 1 : 1 en adduct with

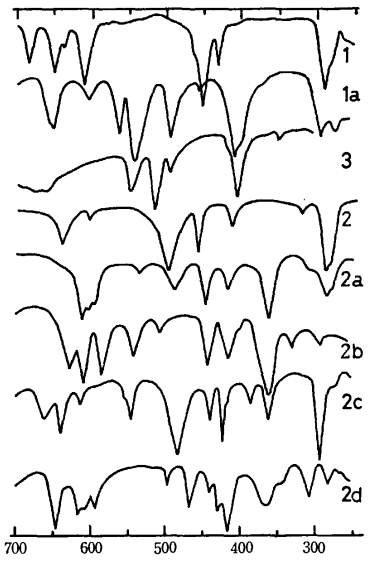

Fig. 2. The far-IR spectra of: (1), $Cu(acac)_2$; (1a), $Cu(acac)_2(en)$; (2), $Cu(etac)_2$; (2a), $Cu(etac)_2(en)$; (2b), $Cu(etac)_2(tn)$; (2c), $Cu(etac)_2(bypy)$; (2d), $Cu(etac)_2(phen)$ and (3), $[Cu(en)_2](acac)_2 \cdot 2H_2O$.

$Cu(acac)_2$ is the first example of an isolated stable adduct which has an octahedral stereochemistry around the copper atom, without any electron-withdrawing substituent in the acetylacetonate ligand. This stability may be attributed to the chelating effect of the diamine ligand. However, its thermal stability is not so high as that of the corresponding manganese complex,[20] which begins to decompose at around 95 °C. The thermogravimetric analysis, as is shown in Fig. 3 (1), indicates that $Cu(acac)_2(en)$ begins to decompose at around 35 °C, thus liberating en, which was identified by a method described previously.[20] The weight loss below 72 °C amounts to 19% just fitting the calculated value of 18.7% for the en content in this adduct. When a sample was heated further, a rapid weight loss occurred because of the sublimation of the residual bis-chelate.

Martell and Calvin[24] pointed out that the formation of a quadridentate imine from acacH and en is catalyzed by Cu(II) ions in aqueous solutions. Candlin, Taylor and Thompson[25] also assumed that the reaction probably involves the attack of en on the coordinated acetylacetone. However, our results have revealed that such a reaction does not occur, at least not in dichloromethane at room temperature. It might occur at higher temperatures, although attempts to cause the primary amine adducts of bis(β-diketonato)nickel(II) to undergo a Schiff-base rearrangement in nonpolar solvents were unsuccessful,[26] as was an attempt to prepare an imine from the bis(haxafluoroacetylacetonato)ethylenediaminecopper(II) complex by a gas-phase template reaction.[13c]

The 1 : 1 Complexes Yielded by the Reactions of Bis(ethyl acetoacetato)copper(II) with Some Diamines in Dichloromethane. Only the en adduct was isolated in several attempts to prepare diamine adducts with $Cu(acac)_2$. On the contrary, the reactions of $Cu(etac)_2$ with en, tn, bipy, and phen gave the corresponding 1 : 1 diamine adducts. This may be due to the Lewis acidity of the parent complex, enhanced by the substitution of the ethoxy group into the acetylacetonate ligand.[3] All these complexes were isolated as green-to-blue crystals. They are stable in air relative to $Cu(acac)_2(en)$, but are unstable in solution and partially dissociate into $Cu(etac)_2$ and the diamine.

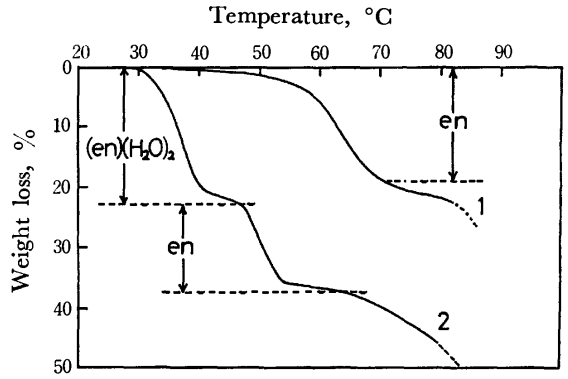

Fig. 3. The thermogravimetric curves of: (1), $Cu(acac)_2(en)$ and (2), $[Cu(en)_2](acac)_2 \cdot 2H_2O$.

The diffuse reflectance spectra of these adducts (Fig. 1, 2a-2d and Table 2) exhibit shifts similar to those observed for $Cu(acac)_2(en)$, but a new maximum does not appear around 8 kK. Thus, a question is raised whether or not these complexes have an octahedral stereochemistry around the copper atom. However, the maximum absorptions of these spectra differ clearly from those of five-coordinate pyridine or the substituted pyridine adducts of $Cu(etac)_2$, in which only one broad absorption maximum is observed, at 14.1 kK.[3,16] Moreover, a discrepancy similar to the one mentioned above in the reflectance spectra is also observed between the two spectra of dihydrate and the bis(pyridine) adduct of copper(II) hexafluoroacetylacetonate.[7] There is no doubt, in light of the spectral similarity with diamine adducts of copper(II) hexafluoroacetylacetonate and the IR spectral evidence to be presented in the next paragraph, that these complexes have a six-coordinate octahedral stereochemistry around the copper atom.

The IR spectra of parent complexes in the higher-frequency region are also composed of those due to the ethyl acetoacetate ligand and those due to the coordinated diamine. However, a significant and diagnostic difference caused by the coordination of a diamine is observed in the $\nu(C{=}O)$ region. These spectra exhibit two or three medium-to-strong bands between 1700 and 1500 cm^{-1}: (a) $Cu(etac)_2(en)$, 1653(s), 1615(m), 1517(s) cm^{-1}; (b) $Cu(etac)_2(tn)$, 1652(s), 1610 (m), 1521(s) cm^{-1}; (c) $Cu(etac)_2(bipy)$, 1660(s), 1613 (s), 1517(s) cm^{-1}; (d) $Cu(etac)_2(phen)$, 1646(s), 1514 (s) cm^{-1}. Of those listed above, one medium band of each aliphatic diamine adduct was assigned to the NH_2 deformation mode on the basis of the deuteration effect, while the strong band at 1613 cm^{-1} of the bipy adduct was assigned to the bipy-ring vibration.[27] The remaining two bands on each adduct around 1650 and 1515 cm^{-1} were assigned mainly to the C=O stretching vibration and the antisymmetric vibration of the C-

C–C segment of the chelate ring, by reference to the assignment of the acetylacetonate complex. The higher-frequency shift of the former band and the lower-frequency shift of the latter band from those (1600 and 1536 cm^{-1}) in the parent complex, $Cu(etac)_2$, are both larger than the corresponding shifts in the case of $Cu(acac)_2(en)$. This may suggest that the weakening of the copper-ligand bond strength by the coordination of diamine is larger than in the case of $Cu(acac)_2(en)$. Relevant shifts were also noticed in the region of ester absorption bands: that is, the "ester C–O–R bands" (1291(s) and 1184(s) cm^{-1}) of the parent $Cu(etac)_2$ shift to 1237(s), 1173(s) (en complex), 1234(s), 1173(s), (tn complex), 1277(s), 1117(s) (bipy complex), and 1226(s), 1165(s) (phen complex) cm^{-1} respectively. Such large shifts of the "ester C–O–R" bands to the lower-frequency side are accompanied by a shift of the carbonyl C=O band to the higher-frequency side, disclosing a significant weakening of the "ester carbonyl" (C=O)-copper bond strength in comparison with that of the parent $Cu(etac)_2$.

The spectra of both en and tn adducts exhibit characteristic bands due to the diamine ligand at 3320, 3260, and 3160 cm^{-1} and at 3320(sh), 3270, and 3160 cm^{-1} respectively. They also have no bands due to free diamine in the frequency region higher than 3320 cm^{-1}. This may indicate coordination by both nitrogen atoms of the diamines. The coordination of phen to the copper atom is evidenced by the splitting of the strong bands at 728 and 850 cm^{-1}.[27] In the spectra of the bipy adduct, the shift and split of the characteristic band (751 cm^{-1}) of the free bipy ligand to 777 and 785 cm^{-1} may also reveal the complexation of bipy to the copper atom.[27,28]

The far-IR spectra of $Cu(etac)_2$ and its 1 : 1 diamine adducts are shown in Fig. 2(2, 2a—2d). The band at 454 cm^{-1} assignable to the ν(Cu–O) in the spectra of parent complex (2) will be shifted to the lower-frequency side by the addition of diamine. Hence, for adducts containing aliphatic diamine the bands at 446 cm^{-1} (en complex, 2a) and 443 cm^{-1} (tn complex, 2b) were assigned to the ν(Cu–O) vibrations, and the new strong bands at 363 cm^{-1} (en complex, 2a) and 360 cm^{-1} (tn complex, 2b), to the ν(Cu–N) vibrations. In the case of adducts containing heterocyclic diamine, their spectra are more complicated because of their many ligand vibrations. The ν(Cu–O) bands of the bipy and phen adducts (2c and 2d) can not be unequivocally assigned, although they are expected to appear in the 400—450 cm^{-1} region. The bands at 296 cm^{-1} (bipy complex, 2c) and 279 cm^{-1} (phen complex, 2d) were also assigned to the ν(Cu–N) vibrations, according to the literature.[29]

From all the above discussion, it may be concluded, with regard to the structure of the 1 : 1 diamine adducts, that the apical positions are occupied by the two carbonyl oxygen (or ester carbonyl oxygen) atoms of the four originally-coordinating oxygen atoms of planar chelate, and that the equatorial plane is composed of the residual two oxygen atoms and two nitrogen atoms of the diamine ligand, as is shown in Fig. 4. Such a

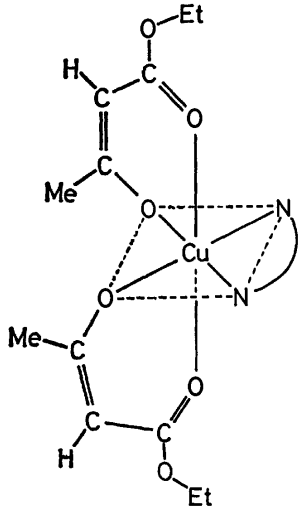

Fig. 4. The suggested structure of $Cu(etac)_2$(diamine).

structure has also been proposed for $Cu(etac)_2$ in pyridine.[30]

Graddon and Watton[3] isolated the bis(pyridine) adduct of $Cu(etac)_2$, but concluded that the second molecule of pyridine was only filling spaces in the crystal lattice and was not coordinated to the copper atom. Therefore, the 1 : 1 diamine adducts of $Cu(etac)_2$ isolated here seem to be the first examples of stable adducts with an octahedral stereochemistry around the copper atom.

The 1 : 2 Complex Yielded by the Reaction of Bis(acetylacetonato)copper(II) with Ethylenediamine in Wet Dichloromethane.[31] The reaction of $Cu(acac)_2$ with en in the mole ratio of one-to-two in wet dichloromethane gave a violet precipitate composed of two en molecules, two acetylacetonate anions, and two water molecules per copper atom. It dissolves in water to give a violet solution, and in methanol to result in a blue solution with some decomposition, but it is insoluble in non-polar organic solvents.

The diffuse reflectance spectrum of the compound is entirely different from that of $Cu(acac)_2$ (Fig. 1 (3) and Table 2). With only one absorption maximum at 18.9 kK, it can be compared with the spectra of the oxyanion salts of the square-planar cations $Cu(en)_2^{2+}$; for the sulphate, nitrate, and perchlorate, the maxima are observed at 17.6, 18.6, and 18.8 kK respectively.[32] The shifts to a higher frequency are attributed to the reduced interaction of the copper atom with the oxygen atoms of the acetylacetonate ligand. This compound may be compared with bis(ethylenediamine)copper(II) perchlorate as to its copper-oxygen bonding character, which may be ionic rather than covalent.

The IR spectrum of the compound differs little from that of $Cu(acac)_2(en)$ except for the additional bands due to the lattice water. It has a broad band assignable to the ν(C=O) vibration at 1607 cm^{-1}, and also a strong band assignable to the antisymmetric vibration of the C–C–C segment of the acetylacetonate ligand at 1508 cm^{-1}. It also has bands due to the coordinated diamine at 3200 (shoulder) and 3100 cm^{-1}. As was pointed out

by George and Robinson,[33] the bands at 1206 and 768 cm^{-1} in the anhydrous sodium acetylacetonate are split, but they are not split in the dihydrate. These bands are assigned to the C–H in-plane and out-of-plane deformations; their splitting suggests that some interactions occur between adjacent ions in the lattice. However, in our compound, only the former band is split. Even if two moles of en are forced to react with one mole of $Cu(acac)_2$ in dry dichloromethane, only the 1 : 1 complex is formed. Water molecules seem to play a very important role in changing the linkage mode of acetylacetonate ligands.

The far-IR spectra of the compound, as is shown in Fig. 2(3), are very simple, and the sharp band at 403 cm^{-1} is easily assigned to the ν(Cu–N) vibration by comparison with those of $Cu(acac)_2(en)$. As is to be expected from the diffuse reflectance spectrum of the compound, no bands due to the ν(Cu–O) vibration appeared in the frequency region measured. This also suggests that the compound has a square-planar cation, $Cu(en)_2^{2+}$, and two acetylacetonate anions.

It seemes interesting to examine the thermal property of the compound because of the anionic character of the acetylacetonate group. As is shown in Fig. 3(2), it decomposed rapidly at temperatures above 30 °C and lost one en and two water molecules below 47 °C, where the curve has a slightly gentle slope. When the temperature of the sample was further raised, the thermogravimetric curve showed the same pattern as that of the 1 : 1 adduct. All this behavior in the thermogravimetric analysis may be represented by the following equation;

$$[Cu(en)_2](acac)_2\cdot 2H_2O \rightarrow Cu(acac)_2(en) \rightarrow Cu(acac)_2$$

It is interesting that the acetylacetonate anions recombine with the copper atom, forming chelate rings by displacing en molecules.

The conductivity of this compound in a 10^{-3} M aqueous solution is 170 $ohm^{-1}\cdot cm^2\cdot mol^{-1}$. This value falls between those of 1 : 1- and 1 : 2-electrolytes, suggesting the occurrence of a dissociation such as the following;

$$[Cu(en)_2](acac)_2\cdot 2H_2O \rightleftarrows [Cu(en)_2]^{2+} + 2acac^- + 2H_2O$$

This dissociation is also evidenced by the visible spectrum of the compound in an aqueous solution.

To ascertain the bonding nature of the acetylacetonate anions and the role of water molecules in this compound, a single crystal X-ray analysis was performed.

A perspective drawing of the complex is shown in Fig. 5. The copper atom lies on a crystallographic center of symmetry and has a square-planar coordination by four N atoms of the two en molecules, which are in a *gauche* conformation. The mean Cu–N bond length is 2.00 Å; this value is comparable with those found in $[Cu(en)_2](BF_4)_2$ (2.02 Å),[34] $[Cu(en)_2](NO_3)_2$ (2.03 Å),[35] and $[Cu(en)_2](NCS)(ClO_4)$ (2.02 Å).[36] The bond lengths and angles are summarized in Table 4.

The acetylacetonate anion is planar; the equation of the plane is given in Table 5. Moreover, the anion has an approximate mirror plane which is perpendicular

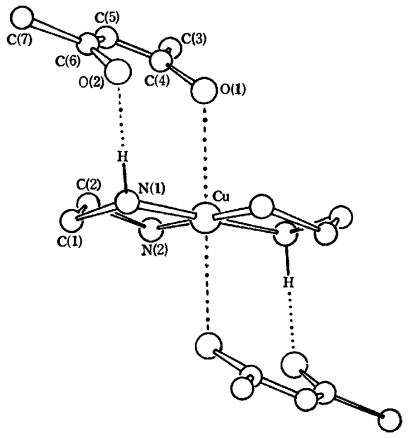

Fig. 5. The structure of $[Cu(en)_2)](acac)_2$.

Table 4. Bond distances and angles

Cu-N(1)	1.98(1) Å	N(1)-Cu-N(2)	85.9(4)°
Cu-N(2)	2.01(1)	N(1)-Cu-O(1)	82.2(3)
Cu-O(1)	2.79(1)	N(2)-Cu-O(1)	91.1(3)
N(1)-C(1)	1.51(2)	Cu-N(1)-C(1)	109.6(7)
N(2)-C(2)	1.49(2)	Cu-N(2)-C(2)	108.5(7)
C(1)-C(2)	1.51(2)	N(1)-C(1)-C(2)	108.4(9)
O(1)-C(4)	1.23(1)	N(2)-C(2)-C(1)	108.4(9)
O(2)-C(6)	1.26(1)	Cu-O(1)-C(4)	125.7(7)
C(4)-C(5)	1.39(2)	O(1)-C(4)-C(5)	125(1)
C(5)-C(6)	1.38(2)	O(1)-C(4)-C(3)	117(1)
C(3)-C(4)	1.50(2)	C(3)-C(4)-C(5)	118(1)
C(6)-C(7)	1.55(2)	C(4)-C(5)-C(6)	127(1)
		C(5)-C(6)-C(7)	118(1)
		C(7)-C(6)-O(2)	115(1)
		C(5)-C(6)-O(2)	126(1)

Table 5. Least-squares planes in terms of orthogonal axes,* and deviations (Å) of relevant atoms from the planes in square brackets

Plane of acetylacetonate anion
$-0.501X-0.176Y-0.848Z=-2.31$
[O(1), 0.02; O(2), −0.00; C(3), −0.01; C(4), 0.01; C(5), −0.02; C(6), −0.02; C(7), 0.03 Å]

Plane defined by Cu, N(1) and N(2)
$0.641X+0.598Y+0.481Z=0$
[C(1), −0.28; C(2), 0.36 Å]

* $X=ax+by\cos\gamma+cz\cos\beta$, $Y=by\sin\gamma-cz\sin\beta\cos\alpha^*$
$Z=z/c^*$

to the plane of the anion and which bisects the C(4)—C(5)—C(6) bond angle. Although this suggests a complete delocalization of π electrons in the anion, the accuracy of the bond length and angle is not great enough to allow a definite conclusion to be reached.

The hexacoordinate copper(II) compounds are well-known to show Jahn-Teller distortions. Thus, the four Cu–O bonds in the equatorial plane of the tris(hexafluoroacetylacetonato)cuprate(II), $Cu(hfac)_3^-$, average 2.015(5) Å, and the two axial bonds 2.176(7) Å.[37] The mixed complexes, $Cu(hfac)_2(py)_2$[38] and $Cu(hfac)_2$-

(bipy),[12] show the *cis* octahedral CuO_4N_2, and the Cu–O distances *trans* to the Cu–N bonds in the equatorial plane are 1.998(4) Å for the pyridine complex and 1.967(4) Å for the bipy complex, while the axial Cu–O distances are 2.283(6) and 2.296(4) Å respectively.

In the present complex, the Cu–O distances are much more longer than the Jahn-Teller elongation. Of the two oxygen atoms in the acetylacetonate anion, O(1) occupies the axial position of $[Cu(en)_2]^{2+}$ and the Cu···O distance is 2.79 Å. This value is comparable with that (2.793 Å) found in bis(hexafluoroacetylacetonato)bis(*N*,*N*-dimethylethylenediamine)copper(II), $Cu(hfac)_2(dmed)_2$[13b] indicating that there exists only a weak interaction between Cu and O(1). In $[Cu(en_2](acac)_2 \cdot 2H_2O$, the tetragonality ratio, $T=R_S/R_L$, defined by Hathaway,[39] where R_S and R_L are the mean equatorial and axial bond lengths, is 0.68.[40] This value is close to those for the Cu(II) complexes with the square-planar structure[41]; hence, the Cu–O(1) bond can be regarded as essentially ionic in character.

On the other hand, O(2) is close to N(1) (O···N, 3.02 Å), the axial N(1)–H bond protruding towards O(2) with the N(1)–H···O(2) angle of 175°. The interatomic distance between the H and O atoms is estimated to be 2.06 Å, which is considerably smaller than the sum of the Van der Waals radii of these atoms. Thus, N–H···O hydrogen bonding seems to exist between N(1) and O(2), though the direction of the N(1)···O(2) bond is nearly perpendicular to the plane of the anion.

The mode of interaction between the cation and the anion in the present complex is similar to that in $Cu(hfac)_2(dmed)_2$,[13b] but the structure of the former is different from that of the latter. In the hfac analogue, the plane of hfac is almost perpendicular to the plane defined by Cu and four N atoms (interplanar angle, 90.7°), while the Cu···O–C angle is 166.7°. In the present complex, however, the plane of the anion is not perpendicular to the CuN_4 plane, but is, rather, slanted against it (interplanar angle, 34°), with the Cu···O–C angle of 126°; the relative orientation of the cation and the anion is much less favorable to the formation of a covalent Cu–O bond.

The crystal structure viewed down the *b* axis is shown in Fig. 6. There are O–H···O and N–H···O hydrogen bonds in the crystal; they are indicated by dashed lines in the figure. Although no hydrogen

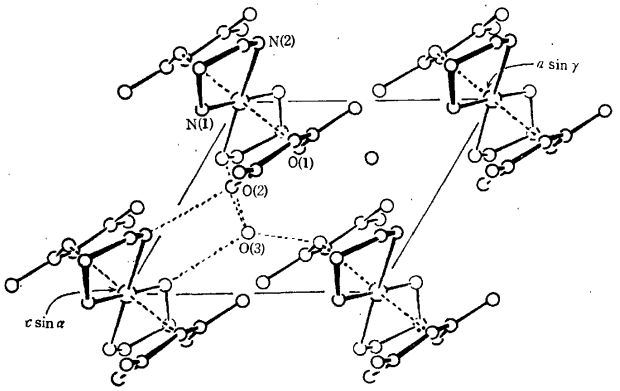

Fig. 6. Crystal structure viewed along *b* axis. The thin dashed lines indicate hydrogen bonds.

Table 6. Interatomic distances and angles related to the hydrogen bonds

A—H···B		A···B	H···B	A-H-B	Positions* of A	B
N(1)	O(3)	2.97(1) Å	2.06 Å	153°	3	1
N(2)	O(2)	2.97(1)	2.12	142	4	1
N(2)	O(3)	3.04(1)	2.07	165	2	1
O(3)	O(1)	2.79(1)			1	5
O(3)	O(2)	2.83(1)			1	1
N(1)	O(2)	3.02(1)	2.02	175	1	1

Atoms A	B	C	A-B-C	Positions* of A	B	C
C(4)	O(1)	O(3)	109.3(7)°	5	5	1
C(6)	O(2)	O(3)	131.7(7)	1	1	1
C(6)	O(2)	N(2)	141.6(7)	1	1	4
N(2)	O(2)	O(3)	81.0(3)	4	1	1
N(1)	O(2)	N(2)	93.6(3)	1	1	4
N(1)	O(2)	O(3)	88.7(3)	1	1	1
N(1)	O(2)	C(6)	105.0(7)	1	1	1
O(1)	O(3)	O(2)	139.1(4)	5	1	1
O(1)	O(3)	N(2)	86.1(3)	5	1	2
O(1)	O(3)	N(1)	120.0(4)	5	1	3
O(2)	O(3)	N(1)	100.9(4)	1	1	3
O(2)	O(3)	N(2)	93.1(3)	1	1	2
N(1)	O(3)	N(2)	93.0(3)	3	1	2

* Numercials refer to the following equivalent positions:
1 x, y, z 2 $-x, -y, -z$ 3 $-x, -y, 1-z$
4 $x, y, 1+z$ 5 $1-x, 1-y, 1-z$

atom could be found in the final difference synthesis, these hydrogen bonds were confirmed by deducing the positions of hydrogen atoms.[42] The data of the hydrogen bonds are summarized in Table 6. All the hydrogen atoms in NH_2 groups participate in the N–H···O hydrogen bonding. The oxygen atom of a water molecule is surrounded tetrahedrally by O(1) $(1-x, 1-y, 1-z)$, O(2) (x, y, z), N(1) $(-x, -y, 1-z)$, and N(2) $(-x, -y, -z)$ at distances of 2.79, 2.83, 2.97, and 3.04 Å respectively; hence, both of the water H atoms seem to take part in hydrogen bonds, in which the O(1) and O(2) atoms act as proton acceptors. It is noteworthy that the O(2) atom participates not only in the "intermolecular" hydrogen bonding, but also in the "intramolecular" N(1)–H···O(2) hydrogen bond as an acceptor.

Experimental

Materials. The $Cu(acac)_2$[43] and $Cu(etac)_2$[44] were synthesized according to the literature and were recrystallized twice from benzene–chloroform and dichloromethane respectively. Commercial en and tn were distilled over metallic sodium just before use. Analytical-grade bipy and phen-monohydrate were used without further purification. The dichloromethane was purified by the usual methods described previously.[45] The diethyl ether was dried with calcium chloride and distilled over sodium. The mercury(II) tetraisothiocyanatocobaltate(II) was prepared according to Figgis and Nyholm[46] and used as a reference substance for

the magnetic measurements (Found: C, 9.73; N, 11.39%).

Measurements. The IR spectra in the 4000—650 cm^{-1} region were measured with a Jasco IR-E Infrared Spectrophotometer, and those in the 700—250 cm^{-1} region, with a Hitachi grating infrared spectrophotometer EPI-L. The diffuse reflectance spectra were recorded with a Hitachi-Perkin Elmer 139 Spectrophotometer or a Hitachi EPU-2 Recording Spectrophotometer. The conductivity was measured by the use of a Yanagimoto Conductivity Outfit, NY-7. The magnetic susceptibilities were measured at room temperature by the Faraday method, with a Shimadzu Magnetic balance and employing mercury(II) tetraisothiocyanatocobaltate(II) as a reference substance. The diamagnetic corrections were calculated from Pascal's constants. The thermogravimetric analyses were performed using a thermo-spring-balance C-282 of Hamada Denki Seisakusho, Ltd., under reduced pressure. The rate of temperature elevation was fixed at 10 °C/hr.

Preparations of Complexes. Bis(acetylacetonato)ethylenediaminecopper(II) $Cu(acac)_2(en)$: To a solution of $Cu(acac)_2$ in dry dichloromethane, we added, drop by drop with magnetical stirring, a solution of equimolar en in dry dichloromethane. The pale-green precipitate thus produced was transferred from the reaction vessel *via* polyethylene tubing to a filtering apparatus set up in a desiccator containing phosphorus pentoxide. It was then recrystallized from dry benzene. Mp 112 °C (decomp.). The same compound was also prepared by the reaction of $Cu(acac)_2$ suspended in dry ether with equimolar en in dry dichloromethane.

The corresponding deuterated en complex was prepared by the following method: ethylenediamine-d_4 was prepared by repeated fractional distillation from heavy water solutions and characterized by means of its NMR spectra. Into a solution of 0.1 g of $Cu(acac)_2$ in 10 ml of dry dichloromethane, we stirred a few drops of en-d_4 until a small amount of pale green precipitate was formed. The precipitate thus produced was filtered rapidly and submitted to the measurement of its IR spectra.

Bis(ethyl acetoacetato)ethylenediaminecopper(II), $Cu(etac)_2(en)$: This complex was prepared in a manner similar to that used for the corresponding acetylacetonate complex and was recrystallized from benzene. Mp 144 °C (decomp.).

Bis(ethyl acetoacetato)trimethylenediaminecopper(II), $Cu(etac)_2(tn)$: To a solution of $Cu(etac)_2$ in dichloromethane, we added an equimolar amount of tn in dichloromethane. After a while a pale green precipitate was produced; this was filtered out and dried *in vacuo*. Mp 130 °C (decomp.).

Bis(ethyl acetoacetato)(2,2'-bipyridine)copper(II), $Cu(etac)_2(bipy)$: About three times as many moles of bipy were added to a solution of $Cu(etac)_2$ in dichloromethane. After refluxing for 3 hr, the solvent was evaporated until a green powder was produced. The mixture was filtered, washed with acetone to exclude any unchanged materials, and dried *in vacuo*. Mp 124 °C (decomp.).

Bis(ethyl acetoacetato)(1,10-phenanthroline)copper(II), $Cu(etac)_2(phen)$: A small excess of phen-monohydrate was added to a solution of $Cu(etac)_2$ in dichloromethane. After heating for about ten minutes, the solution was concentrated by evaporation under reduced pressure; then petroleum ether was added to the concentrate to produce a green precipitate. It was filtered and recrystallized from dichloromethane–petroleum ether. Mp 115 °C (decomp.).

Bis(ethylenediamine)copper(II) acetylacetonate dihydrate, $[Cu(en)_2](acac)_2\cdot 2H_2O$: Into a solution of $Cu(acac)_2$ in wet dichloromethane, we added, drop by drop with vigorous stirring, a solution containing two times as many moles of en in dichloromethane. A violet precipitate thus formed was filtered out and recrystallized from warm (below 50 °C) benzene containing a small amount of en. Mp 62 °C (decomp.).

X-ray-data Measurement. Parallelepiped crystals of $[Cu(en)_2](acac)_2\cdot 2H_2O$ were obtained by recrystallization from a 1 : 1 mixture of benzene and dichloromethane containing a small amount of en. Because of the remarkable air- and moisture-sensitivity, crystals used for the X-ray work were sealed into thin-walled glass capillaries.

Crystal Data: $Cu(C_2H_8N_2)_2(C_5H_7O_2)_2\cdot 2H_2O$, $M=418$, triclinic, $a=7.730(7)$, $b=11.53(1)$, $c=7.007(7)$ Å, $\alpha=72.7(1)°$, $\beta=121.8(1)°$, $\gamma=100.2(1)°$, $V=506.7$ Å^3, $Z=1$, $D_c=1.73$ g·cm^{-3} (D_m not measured, because of the instability of the crystal in air), $\lambda(CuK\alpha)=1.5418$ Å, $\mu(CuK\alpha)=19.6$ cm^{-1}; space group $P\bar{1}$ or $P1$, shown to be the former from the subsequent satisfactory solution and refinement of the structure.

The unit-cell dimensions were determined by a least-squares analysis of the $\sin^2\theta$ values from high-angle reflections on zero-level Weissenberg photographs calibrated with aluminum powder.

The intensity data were measured visually from equi-inclination Weissenberg photographs (layers $hk0$—5) by the multiple-film technique with $CuK\alpha$ radiation. The crystal used for the collection of intensity data had dimensions of $0.7\times0.4\times0.2$ mm. Although preliminary data were recorded about the other axes, photographs suitable for intensity measurements could be obtained only about the c axis. Corrections were applied for the Lorentz and polarization factors and for the absorption. A total of 1550 independent reflections were obtained, of which 115 were too weak to be measured.

Determination and Refinement of the Crystal Structure. The positions of all the non-hydrogen atoms were found from a three-dimensional Patterson synthesis on the assumption that the space group was $P\bar{1}$. The atomic coordinates and thermal parameters were refined by the block-diagonal-matrix least-squares method, the function minimized being $\sum w(|F_o|-|F_c|)^2$. At every termination of several cycles of the least-squares calculation, the layer scales were calculated so that relative $\sum|F_o|=\sum|F_c|$ for each of the layers; the new scales thus obtained were then used in the following calculation.

Table 7. The final atomic coordinates, temperature factors and their e.s.d.s.

Atom	x	y	z	B
Cu	0	0	0	*
N(1)	−0.135(1)	0.112(1)	0.045(1)	3.3(1)
N(2)	−0.059(1)	0.124(1)	−0.298(1)	3.2(1)
C(1)	−0.242(2)	0.209(1)	−0.175(2)	4.0(2)
C(2)	−0.115(2)	0.240(1)	−0.292(1)	3.5(2)
C(3)	0.482(2)	0.282(1)	0.050(2)	5.3(2)
C(4)	0.377(2)	0.246(1)	0.188(1)	3.6(2)
C(5)	0.318(2)	0.337(1)	0.233(2)	3.7(2)
C(6)	0.219(1)	0.322(1)	0.355(1)	3.3(1)
C(7)	0.161(2)	0.439(1)	0.375(2)	5.2(2)
O(1)	0.345(1)	0.133(1)	0.251(1)	4.1(1)
O(2)	0.162(1)	0.224(1)	0.444(1)	4.1(1)
O(3)	0.351(1)	−0.004(1)	0.692(1)	4.4(1)

* B_{11}	B_{22}	B_{33}	B_{12}
0.0263(6)	0.0076(1)	0.0286(5)	0.0073(4)
B_{13}	B_{23}		
0.0349(8)	−0.0014(4)		

The anisotropic thermal parameters for Cu atom is of the form

$$\exp[-(B_{11}h^2+B_{22}k^2+B_{33}l^2+B_{12}hk+B_{13}hl+B_{23}kl)].$$

Continued refinements ($w=1.0$ for all reflections) with isotropic temperature factors reduced R to 0.16. In the subsequent refinements, the following weighting scheme was employed:

$$w = 0.5 \text{ for } |F_0| < |F_{\min}|$$
$$w = 1.0 \text{ for } |F_{\min}| \leq |F_0| \leq |F_{\max}|$$
$$w = |F_{\max}|/|F_0| \text{ for } |F_{\max}| < |F_0|$$

$|F_{\max}|$ and $|F_{\min}|$ were varied as is indicated by the $|F_0|$ and $(\sin\theta/\lambda)$ analyses of $\sum w(|F_0|-|F_c|)^2$. Four further cycles of the calculation were made using anisotropic thermal parameters for the copper atom, and R was improved to 0.13. All the layer scales were almost invariant as compared with the preceding ones, the maximum change being within the range of one per cent. Four reflections, thought to be suffering from extinction errors (010, 111, 121, $\bar{1}11$), were omitted in the final refinement, which led to a convergence at R 0.12 ($|F_{\max}|=7.9$ and $|F_{\min}|=2.6$). In the final cycle of refinement, all the shifts were $<0.3\,\sigma$. The atomic scattering factors for neutral copper, oxygen, nitrogen, and carbon atoms, as well as the correction for the real part of the anomalous dispersion for the copper atom, were taken from Ref. 47. The final list of coordinates and thermal parameters is given in Table 7. A complete list of the observed and calculated structure factors is preserved by the Chemical Society of Japan (Document No. 7425). All the computations were carried out by means of the FACOM 270—30 computer at Osaka City University.[48]

The authors are indebted to Dr. H. Kobayashi of Kyoto University for her help in the magnetic measurements and also to Mr. J. Gohda for the elemental analyses. Financial aid by the Ministry of Education is also acknowledged.

References

1) D. P. Graddon, *Coord. Chem. Rev.*, **4**, 1 (1969).
2) G. T. Morgan and H. W. Moss, *J. Chem. Soc.*, **105**, 189 (1914).
3) D. P. Graddon and E. C. Watton, *J. Inorg. Nucl. Chem.*, **21**, 49 (1961).
4) A. F. Garito and B. B. Wayland, *J. Amer. Chem. Soc.*, **91**, 866 (1969).
5) W. R. Walker, *Aust. J. Chem.*, **4**, 161 (1961).
6) W. R. Walker and N. C. Li, *J. Inorg. Nucl. Chem.*, **27**, 2255 (1965).
7) L. L. Funch and T. R. Ortolano, *Inorg. Chem.*, **7**, 567 (1968).
8) W. Partenheimer and R. S. Drago, *ibid.*, **9**, 47 (1970).
9) R. D. Gillard and G. Wilkinson, *J. Chem. Soc.*, **1963**, 5885.
10) N. C. Li, S. M. Wang, and W. R. Walker, *J. Inorg. Nucl. Chem.*, **27**, 2263 (1965).
11) T. M. Sheperd, *J. Chem. Soc., Dalton*, **1972**, 813.
12) M. V. Veidis, G. H. Schreiber, T. E. Gough, and G. J. Palenik, *J. Amer. Chem. Soc.*, **91**, 1859 (1969).
13) a) M. A. Bush, D. E. Fenton, R. S. Nyholm, and M. R. Truter, *Chem. Commun.*, **1970**, 1335; b) M. A. Bush and D. E. Fenton, *J. Chem. Soc. A*, **1971**, 2446; c) M. F. Richardson and R. E. Sievers, *J. Inorg. Nucl. Chem.*, **32**, 1895 (1970).
14) D. E. Fenton, R. S. Nyholm, and M. R. Truter, *J. Chem. Soc., A*, **1971**, 1577.
15) D. P. Graddon, *Nature*, **183**, 1610 (1959).
16) T. Shigematsu, M. Tabushi, M. Matsui, and M. Munakata, This Bulletin, **41**, 2656 (1968).
17) H. Yokoi, M. Sai, and T. Isobe, *ibid.*, **45**, 1100 (1972).
18) B. Bock, K. Flatau, H. Junge, M. Kuhr, and H. Musso, *Angew. Chem., Intern. Ed. (Engl.)*, **10**, 225 (1971).
19) S. Pinchas, B. L. Silver, and I. Laulicht, *J. Chem. Phys.*, **46**, 1506 (1967).
20) Y. Nishikawa, Y. Nakamura, and S. Kawaguchi, This Bulletin, **45**, 155 (1972).
21) D. B. Powell and N. Sheppard, *Spectrochim. Acta*, **17**, 68 (1961).
22) K. Nakamoto, C. Udovich, and J. Takemoto, *J. Amer. Chem. Soc.*, **92**, 3973 (1970).
23) a) A. B. P. Lever and E. Mantovani, *Inorg. Chem.*, **10**, 817 (1971); b) *Inorg. Chim. Acta*, **5**, 429 (1971); c) G. W. Rayner Canham and A. B. P. Lever, *Can. J. Chem.*, **50**, 3866 (1972).
24) A. E. Martell and M. Calvin, "Chemistry of Metal Chelate Compounds," Prentice-Hall, New York, N. Y. (1952), pp. 389, 424.
25) J. P. Candlin, K. A. Taylor, and D. T. Thompson, "Reactions of Transition-Metal Complexes," Elsevier Publishing Company, New York, N. Y. (1968), p. 88.
26) J. T. Hashagen and J. P. Fackler, Jr., *J. Amer. Chem. Soc.*, **87**, 2821 (1965).
27) A. A. Schilt and R. C. Taylor, *J. Inorg. Nucl. Chem.*, **9**, 211 (1959).
28) S. P. Sinha, *Spectrochim. Acta*, **20**, 879 (1964).
29) R. G. Inskeep, *J. Inorg. Nucl. Chem.*, **24**, 763 (1962); Y. Saito, J. Takemoto, B. Hutchinson, and K. Nakamoto, *Inorg. Chem.*, **11**, 2003 (1972).
30) H. Yokoi, N. Sai, and T. Isobe, This Bulletin, **43**, 1078 (1970).
31) Preliminary communication was presented in M. Matsui, T. Kurauchi, S. Ooi, Y. Nakamura, S. Kawaguchi, and H. Kuroya, *Inorg. Nucl. Chem. Lett.*, **9**, 1041 (1973).
32) I. M. Procter, B. J. Hathaway, and P. Nicholls, *J. Chem. Soc., A*, **1968**, 1678.
33) W. O. George and F. V. Robinson, *ibid.*, **1968**, 1950.
34) D. S. Brown, J. D. Lee, and B. G. A. Melson, *Acta Crystallogr.*, **B24**, 730 (1968).
35) Y. Komiyama and E. C. Lingafelter, *ibid.*, **17**, 1145 (1964).
36) M. Cannas, G. Carta, and G. Marongiu, *J. C. S. Dalton*, **1973**. 251.
37) D. E. Fenton, M. R. Truter, and B. L. Vickery, *Chem. Commun.*, **1971**, 93.
38) J. Pradilla-Sorzano and J. P. Fackler, Jr., *Inorg. Chem.*, **12**, 1174 (1973).
39) A. A. G. Tomlinson, B. J. Hathaway, D. E. Billing, and P. Nicholls, *J. Chem. Soc. A*, **1969**, 65.
40) In the calculation of $R_L=R_L(\text{obs})\times(R_S^N/R_S^O)$, the average value of Cu-O bond distances (1.908 Å) in bis(γ-methylacetylacetonato)copper(II) (I. Robertson and M. R. Truter, *J. Chem. Soc. A*, **1967**, 309) was used for R_S^O.
41) B. J. Hathaway and D. E. Billing, *Coord. Chem. Rev.*, **5**, 143 (1970); B. J. Hathaway, "Structure and Bonding" **14**, 49 (1973); B. J. Hathaway and P. G. Hodgson, *J. Inorg. Nucl. Chem.*, **35**, 4071 (1973).
42) The coordinates of hydrogen atoms were calculated on the assumption that the N-H bond length is 1.0 Å.
43) H. F. Holtzclaw, Jr., A. H. Carlson, and J. P. Collman, *J. Amer. Chem. Soc.*, **78**, 1838 (1956).
44) R. L. Belford, A. E. Martell, and M. Calvin, *J. Inorg. Nucl. Chem.*, **2**, 11 (1956).
45) Y. Nakamura and S. Kawaguchi, This Bulletin, **38**, 954 (1965).
46) B. N. Figgis and R. S. Nyholm, *J. Chem. Soc.*, **1958**, 4190.
47) "International Tables for X-ray Crystallography", Vol. III. Kynoch Press, Birmingham (1962), p. 202.
48) The computer programs used in this work were RSSFR-3 (Fourier synthesis), HBLS-IV (least-squares calculation) and DAPH (interatomic distance and angle, and least-squares plane) which were adapted by Mr. Ken Hirotsu of Osaka City University to FACOM 270-30 computer.

Circular Dichroism Spectra of Cobalt(III) Complexes Containing Amino-Alcohols

Toshikazu NISHIDE, Kazuko OGINO,* Junnosuke FUJITA,** and Kazuo SAITO

Department of Chemistry, Faculty of Science, Tohoku University, Aramaki, Sendai 980

(Received August 5, 1974)

Several cobalt(III) complexes containing amino-alcohol (amOH) chelate rings, $[Co(amOH)(NH_3)_4]X_3$, $[Co(amOH)(en)_2]X_3$ and $[Co(amOH)(R\text{-chxn})_2]X_3$ (en=ethylenediamine, chxn=*trans*-1,2-diaminocyclohexane, $X^-=Cl^-$, Br^- or ClO_4^-, amOH=2-aminoethanol, 2-amino-1-propanol, 1-amino-2-propanol, *etc.*) were synthesized and separated into optical isomers. Their circular dichroism (CD) spectra change remarkably by the change in pH of the solution. The changes were ascribed to the dissociation of the alcoholic proton of coordinated amOH. The complexes containing a deprotonated chiral amO^- chelate ring exhibit strong vicinal CD bands in the first and second absorption band region. The signs and the magnitudes of these CD bands seem to depend mainly on the conformation of the amO^- chelate ring.

Extensive studies have been made on the circular dichroism (CD) spectra of cobalt(III) complexes containing diamine and aminocarboxylate chelate rings.[1] However there has been little work on the optical activity of amino-alcohol complexes.[2,3] In the previous communication,[3] we reported CD spectra of Λ-$[Co(etaH)(en)_2]^{3+}$ (etaH=2-aminoethanol, en=ethylenediamine) and Δ- and Λ-$[Co(S\text{-praH})(en)_2]^{3+}$ (praH=2-amino-1-propanol) complexes. The CD behavior of these complexes was found to be considerably different from that of $[Co(diamine)_3]^{3+}$ or $[Co(am)(en)_2]^{2+}$ (am^-=aminocarboxylate ion); the deprotonated *S*-pra^- chelate ring gives an exceptionally large vicinal contribution to the optical activity. We have extended the work to several other coablt(III) complexes containing an amino-alcohol chelate ring.

Experimental

Ligands.† Amino-alcohols except *S*-leucinol and *S*-2-amino-1-propanol were obtained commercially. *S*-Leucinol was kindly supplied by Mr. K. Ohashi of Ibaragi University. *S*-2-Amino-1-propanol was synthesized by the method of Vogl and Pöln.[4] *trans*-1,2-Diaminocyclohexane(chxn) was resolved into optical isomers by the method of Treptow.[5]

Syntheses of Aminoalcoholtetraammine Complexes, $[Co(amOH)(NH_3)_4]X_3$ (amOH=etaH, *S*-praH, *S*-leuH, *R*-abnH *and R and S*-ispraH). The etaH complex was prepared by the following procedure. $[CoCl(H_2O)(NH_3)_4]SO_4$ (2 g) was added to a mixture of 1 M sodium hydroxide (5 ml), water (1 ml), 2-aminoethanol (0.4 ml) and one drop of 28% aqueous ammonia. The solution was heated at 65—75 °C for 2.5 hr, cooled in an ice bath for 1 hr, and filtered. The filtrate was passed through a column ($\phi 2\times 20$ cm) containing the anion exchanger Dowex 1X4 in the bromide form. The eluate was treated with hydrobromic acid to adjust the pH to 1—2 and evaporated to dryness under reduced pressure at 40—50 °C. The residue was dissolved again in about 40 ml of water and filtered. Addition of a few drops of 40% hydrobromic acid to the filtrate gave orange crystals, which were filtered off, washed with methanol and air-dried. Recrystallization was carried out from water containing hydrobromic acid. Found: C, 5.71; H, 4.65; N, 16.66%. Calcd for $CoC_2H_{19}N_5OBr_3$: C, 5.61; H, 4.48; N, 16.37%.

Other complexes, $(-)_D$-$[Co(S\text{-praH})(NH_3)_4]Cl_3$, $(-)_D$-$[Co(S\text{-leuH})(NH_3)_4]Cl_3\cdot 3H_2O$, $(+)_D$-$[Co(R\text{-abnH})(NH_3)_4]Cl_3\cdot H_2O$ and $[Co(R,S\text{-ispraH})(NH_3)_4](ClO_4)_3$ were synthesized by a method similar to that for the etaH complex. For *S*-praH complex, Found: C, 11.43; H, 7.07; N, 22.77%. Calcd for $CoC_3H_{21}N_5OCl_3$: C, 11.68; H, 6.86; N, 22.70%. For *S*-leuH complex; Found: C, 17.91; H, 7.97; N, 17.74%. Calcd for $CoC_6H_{32}N_5O_4Cl_3$: C, 17.85; H, 7.99; N, 17.35%. For *R*-abnH complex; Found: C, 14.15; H, 7.66; N, 20.32%, Calcd for $CoC_4H_{25}N_5O_2Cl_3$: C, 14.12; H, 7.40; N, 20.57%. For *R,S*-ispraH complex; Found: C, 7.57; H, 4.08; N. 13.99%. Calcd for $CoC_3H_{21}N_5O_{13}$: C, 7.20; H, 4.23; N, 14.00%.

The complex $(-)_D$-$[Co(R\text{-ispraH})(NH_3)_4]Cl_3\cdot 2.5H_2O$ was obtained by the following method. $[Co(R,S\text{-ispraH})(NH_3)_4](ClO_4)_3$ (0.4 g) was adsorbed on an SP-C-25 Sephadex column ($\phi 5\times 95$ cm) and eluted with 0.2 M potassium antimony *d*-tartrate at a rate of 0.6 ml/min. The column gave two separated orange bands. The $(-)_D$-isomer was eluted first and the $(+)_D$-isomer followed. The antimony *d*-tartrate salt of the $(-)_D$-isomer was converted into chloride by passing the first eluate through a column ($\phi 2\times 10$ cm) of SP-C-25 Sephadex, and eluting the adsorbed band with 0.5 M hydrochloric acid. The eluate was evaporated to a small volume under reduced pressure below 35 °C, and filtered. The filtrate was dried up in a vacuum desiccator over diphosphorus pentoxide. The complex was hygroscopic powder. Found: C, 10.41; H, 7.30; N, 19.87%. Calcd for $CoC_3H_{26}N_5O_{3.5}Cl_3$: C, 10.19; H, 7.41; N, 19.81%. $(+)_D$-$[Co(S\text{-ispraH})(NH_3)_4]Br_3\cdot 2.5H_2O$ was obtained similarly from the second eluate described above by use of a column containing anion exchanger Dowex 1X4 in bromide form. Found: C, 7.01; H, 5.48; N, 14.67%. Calcd for $CoC_3H_{26}N_5O_{3.5}Br_3$: C, 7.39; H, 5.38; N, 14.38%.

Syntheses of Aminoalcoholbis(ethylenediamine) Complexes. a) *cis*-$[CoBr(R,S\text{-ispraH})(en)_2]Br_2$. To *trans*-$[CoBr_2(en)_2]Br$ (5 g) in dimethyl sulfoxide (DMSO) (100 ml) was added *R,S*-ispraH (0.9 g) with stirring. The solution was stirred overnight and filtered. Ethanol and ether were added to the solution and then it was kept in a refrigerator for crystallization. Red-violet crystals were collected, washed with ethanol and air-dried. Found: C, 17.30; H, 5.34; N, 13.90 %. Calcd for $CoC_7H_{25}N_5OBr_3$: C, 17.02; H, 5.10; N, 14.18%.

b) $[Co(R,S\text{-ispraH})(en)_2]Br_3\cdot 2.5H_2O$ and $[Co(N\text{-MeetaH})(en)_2]Cl_3\cdot 2H_2O$. These complexes were prepared

* Present address: College of Medical Sciences, Tohoku University, Seiryo-machi, Sendai.

** Present address: Department of Chemistry, Faculty of Science, Nagoya University, Nagoya.

† The following abbreviations are used: etaH=2-aminoethanol, praH=2-amino-1-propanol, ispraH=1-amino-2-propanol, leuH=leucinol, abnH=2-amino-1-butanol, *N*-MeetaH=*N*-methylethanolamine.

TABLE 1. NUMERICAL DATA OF ABSORPTION AND CD SPECTRA OF AMINO-ALCOHOL COMPLEXES

Complex[a]	I band				II band			
	Absorption		CD		Absorption		CD	
	$\bar{\nu}/10^3$ cm^{-1}	log ε	$\bar{\nu}/10^3$ cm^{-1}	$\Delta\varepsilon$	$\bar{\nu}/10^3$ cm^{-1}	log ε	$\bar{\nu}/10^3$ cm^{-1}	$\Delta\varepsilon$
[Co(etaH)$(NH_3)_4$]$^{3+}$	20.12	1.82			29.10	1.89		
[Co(eta)$(NH_3)_4$]$^{2+}$	20.04	1.99			27.60	2.06		
[Co(*S*-praH)$(NH_3)_4$]$^{3+}$	20.12	1.77	18.45	+0.21	29.10	1.84		
			21.01	−0.36				
[Co(*S*-pra)$(NH_3)_4$]$^{2+}$	20.04	1.99	17.86	+0.17	27.60	2.04	24.80	+0.85
			20.20	−1.18				
[Co(*S*-leuH)$(NH_3)_4$]$^{3+}$	20.12	1.81	18.42	+0.21	29.10	1.87		
			21.14	−0.45				
[Co(*S*-leu)$(NH_3)_4$]$^{2+}$	20.04	2.00	17.89	+0.17	27.62	2.08	25.00	+1.04
			20.33	−1.36				
[Co(*R*-isopraH)$(NH_3)_4$]$^{3+}$	20.10	1.78	18.69	−0.44	29.07	1.86	28.57	+0.04
			21.51	+0.33				
[Co(*R*-isopra)$(NH_3)_4$]$^{2+}$	20.04	1.96	17.93	−0.60	27.62	2.05	25.00	−1.25
			20.33	+1.82				
[Co(*R*-abnH)$(NH_3)_4$]$^{3+}$	20.16	1.76	18.52	−0.26	28.74	1.83		
			21.10	+0.51				
[Co(*R*-abn)$(NH_3)_4$]$^{2+}$	20.04	1.99	17.86	−0.20	27.62	2.04	25.00	−1.18
			20.20	+1.58				
Λ-[Co(etaH)$(en)_2$]$^{3+}$	20.40	1.95	19.61	+1.96	28.80	1.99	26.67	+0.14
Λ-[Co(eta)$(en)_2$]$^{2+}$	20.20	2.05	18.87	+1.93	sh. 25.6	2.04	25.97	+0.45
			21.83	−0.68	28.40	2.09	sh. 28.6	+0.18
Λ-[Co(*S*-praH)$(en)_2$]$^{3+}$	20.53	1.94	19.22	+1.74	29.33	2.05	26.52	+0.20
			22.42	−0.12			29.6	+0.11
Λ-[Co(*S*-pra)$(en)_2$]$^{2+}$	20.37	2.06	18.50	+1.72	sh. 25	1.95	25.25	+1.16
			21.22	−1.52	28.82	2.09		
Δ-[Co(*S*-praH)$(en)_2$]$^{3+}$	20.49	1.94	20.41	−2.01	29.07	2.05	28.33	+0.13
Δ-[Co(*S*-pra)$(en)_2$]$^{2+}$	20.37	2.06	20.00	−2.82	sh. 25	1.95	24.88	+1.33
					28.65	2.09		
Λ-[Co(*R*-isopraH)$(en)_2$]$^{3+}$	20.28	1.95	20.58	+1.88	28.90	2.01	28.57	−0.11
Λ-[Co(*R*-isopra)$(en)_2$]$^{2+}$	20.12	2.02	sh. 17.54	+0.37	sh. 25.6	1.99	24.69	−1.55
			20.08	+3.13	28.40	2.12		
Λ-[Co(*S*-isopraH)$(en)_2$]$^{3+}$	20.03	1.95	19.46	+2.44	28.82	1.99	26.67	+0.13
Λ-[Co(*S*-isopra)$(en)_2$]$^{2+}$	20.22	2.04	18.48	+2.68	sh. 25.6	2.05	25.25	+1.55
			21.19	−1.97	29.85	2.09		
[Co(*N*-MeetaH)$(en)_2$]$^{3+}$	20.22	1.99			28.50	2.01		
[Co(*N*-Meeta)$(en)_2$]$^{2+}$	20.04	2.04			sh. 25.2	1.95		
					28.30	2.04		
[Co(*N*-Meeta)$(en)_2$]$^{2+}$ [b]	20.04	2.04			sh. 25.2	1.95		
					28.30	2.04		
Δ-[Co(etaH)(*R*-chxn)$_2$]$^{3+}$	20.24	1.94	19.05	−2.44	28.74	1.99	26.32	−0.09
Δ-[Co(eta)(*R*-chxn)$_2$]$^{2+}$	20.20	2.04	18.45	−2.69	sh. 25.6	2.02	25.32	−1.20
			21.28	+1.73	27.78	2.10		
Δ-[Co(*S*-praH)(*R*-chxn)$_2$]$^{3+}$	20.10	1.92	19.88	−2.40	28.61	1.97	28.01	+0.15
Δ-[Co(*S*-pra)(*R*-chxn)$_2$]$^{2+}$	20.00	2.06	19.65	−3.32	27.93	2.05	24.51	+1.48

a) The spectra of [M(amOH)]$^{3+}$ complexes were obtained by dissolving the salt of [M(amOH)]$^{3+}$ in acidic solutions (pH<2), and those of [M(amO)]$^{2+}$ complexes in solutions whose pH is above 5, unless otherwise stated.
b) Spectral data were obtained in an aqueous solution of [Co(*N*-Meeta)$(en)_2$]$(ClO_4)_2$.

by a method similar to that for [Co(etaH)$(en)_2$]$Br_3\cdot H_2O$ by Buckingham *et al.*[6] Anal. For 1-amino-2-propanol complex; Found: C, 15.21; H, 5.25; N, 13.11%. Calcd for $CoC_7H_{30}N_5O_{3.5}Br_3$: C, 15.60; H, 5.61; N, 13.00%. For *N*-methylethanolamine complex, Found: C, 20.89; H, 7.71; N, 17.80%. Calcd for $CoC_7H_{29}N_5O_3Cl_3$: C, 21.20; H, 7.37; N, 17.66%.

c) [Co(*N*-Meeta)$(en)_2$]$(ClO_4)_2$. This complex was obtained by adding lithium perchlorate to an aqueous solution of [Co(*N*-MeetaH)$(en)_2$]$Cl_3\cdot 2H_2O$ neutralized with sodium hydroxide. Found: C, 18.60; H, 5.66; N, 15.38%. Calcd for $CoC_7H_{24}N_5O_9Cl_2$: C, 18.59; H, 5.35; N, 15.49%.

*Separation of Λ,Δ-[Co(*R,S*-isopraH)$(en)_2$]$^{3+}$ Complexes.* a) *Λ*-(+)$_D$-[Co(*R*-isopraH)$(en)_2$]$Cl_3\cdot 3H_2O$. *Λ,Δ*-[Co(*R,S*-iso-

praH)$(en)_2$]$Br_3 \cdot 2.5H_2O$ was separated into four isomres by means of column chromatography. Two grams of the complex was adsorbed on an SP-C-25 Sephadex column (ϕ 3×90 cm) and the adsorbed orange band was eluted with 0.2M potassium antimony *d*-tartrate at a rate 0.5 ml/min. The eluate was fractionated into 25 ml portions. The CD spectrum of each fraction was checked, and the fractions were grouped into three parts (A,B,C) in the order of elution. The first part (A), about one tenth of the total eluate, was poured on an SP-C-25 Sephadex column (ϕ3×96 cm) again and eluted with 0.2 M potassium antimony tartrate. First several portions of the eluate showed the same CD curves. They were combined, adsorbed on an SP-C-25 Sephadex column (ϕ 1.7×10 cm) and eluted with 0.5 M hydrochloric acid. The eluate was evaporated to a small volume under reduced pressure below 35 °C, filtered and stored in a vacuum desiccator over diphosphorus pentoxide. The hygroscopic powder thus obtained was assigned to Λ-[Co(*R*-isopraH)$(en)_2$]$Cl_3 \cdot 3H_2O$ as shown later. Found: C, 20.50; H, 7.60; N, 16.37%. Calcd for $CoC_7H_{31}N_5O_4Cl_3$: C, 20.58; H, 7.54; N, 16.89%.

b) Λ-$(+)_D$-(*S*-isopraH)$(en)_2$]$(ClO_4)_3$. The last a few fractions of the eluate(A) in the second elution (with 0.2 M potassium antimony tartrate) described above were found to contain only one isomer by measurement of CD. These portions were combined and passed through the anion exchange resin column containing Dowex 1X8 in the perchlorate form to give perchlorate salt. The hygroscopic powder was assigned to Λ-[Co(*S*-isopraH)$(en)_2$]$(ClO_4)_3$ as shown later. Found: C, 15.38; H, 4.72; N, 12.71%. Calcd for $CoC_7H_{25}N_5O_{13}Cl_3$: C, 15.21; H, 4.56; N, 12.68%.

The fractions B and C mentioned in (a) were found to be mixtures of Λ-[Co(*S*-isopraH)$(en)_2$]$^{3+}$ and Δ-[Co(*S*-isopraH)-$(en)_2$]$^{3+}$, and Δ-[Co(*S*-isopraH)$(en)_2$]$^{3+}$ and Λ-[Co(*R*-isopraH)-$(en)_2$]$^{3+}$ isomers respectively. But the latter two isomers were not isolated.

*Syntheses of Aminoalcoholbis(*R-trans-*1,2-diaminocyclohexane)-complexes.* *a)* Λ-$(-)_D$-[Co(etaH)(*R*-chxn)$_2$]$(ClO_4)_3$. A mixture of *trans*-[$CoCl_2$(*R*-chxn)$_2$]Cl[5] (1 g) and 2-aminoethanol (0.2 ml) in DMSO (50 ml) was stirred for two days. The solution was treated with ethanol (150 ml) and ether (700 ml) and kept in an ice bath for 6 hr. The supernatant was decanted and the remaining oily residue was dissolved again in water (50 ml) and hydrolyzed at pH 9 (pH-stat) with 1 N sodium hydroxide. After 2 hr, the pH of the solution was adjusted to 1.5 with 6 M hydrochloric acid. The solution was evaporated to a small volume under reduced pressure at 40 °C and passed through an SP-C-25 Sephadex column (ϕ3×77 cm). Elution with a mixture of 0.15 M sodium *d*-tartrate and 0.09 M hydrochloric acid gave several portions showing the same CD curves, which were combined and concentrated under reduced pressure. After removal of sodium salt by filtration, 60% perchloric acid and sodium perchlorate were added to the filtrate. Orange crystals were filtered off and dried in air. The CD specturm remains unchanged after three times recrystallization from water. The absolute configuration of this complex was assigned to Λ as shown later. Found: C, 26.20; H, 5.72; N, 10.54%. Calcd for $CoC_{14}H_{35}N_5O_{13}Cl_3$: C, 26.00; H, 5.46; N, 10.83%.

b) Λ-$(-)_D$-[Co(*S*-praH)(*R*-chxn)$_2$]$(ClO_4)_3$. This complex was synthesized by a method similar to that for the etaH complex (a) using *S*-praH instead of etaH and purified by recrystallization from water. Found: C, 27.18; H, 5.77; N, 10.33%. Calcd for $CoC_{15}H_{37}N_5O_{13}Cl_3$: C, 27.26; H, 5.64; N, 10.60%.

Measurements. The absorption spectra were recorded with a Hitachi 323 Recording Spectrophotometer. The CD spectra were obtained with a JASCO Model ORD/UV-5 Spectrometer with CD attachment. The pH of the solution was adjusted to appropriate values either with perchloric acid or with sodium hydroxide solution. The acid dissociation constants of the complexes were determined with a Metrohm Combi Titrator 3D at 25 °C.

Results and Discussion

Acid-base Equilibria of Amino-alcohol Complexes. Absorption and CD spectra of the amino-alcohol complexes obtained in this work changed markedly with change in pH of the solution. The spectra of *S*-2-amino-1-propanoltetraammine complex at three pH's are shown in Fig. 1. Several isosbestic points are observed. The spectral changes are instantaneous and reversible, and attributed to an acid-base equilibrium of the alcoholic proton:

$$M(amOH)^{3+} \rightleftharpoons M(amO)^{2+} + H^+$$

where M denotes Co(diamine)$_2$ or Co$(NH_3)_4$ moiety. pH Titration of the complexes gave pK_a values of *ca.* 3.6, 3.2 and 3.2 for [Co(amOH)$(NH_3)_4$]$^{3+}$ (amOH =etaH, *S*-praH, *S*-leuH, *S*-abnH and isopraH), [Co-(amOH)$(en)_2$]$^{3+}$ (amOH=etaH, *S*-praH and isopraH) and [Co(*S*-praH)(*R*-chxn)$_2$]$^{3+}$, respectively at 25 °C and ionic strength *ca.* 0.05. Thus the spectra of these complexes at pH below ~2 should be those of the protonated form, M(amOH)$^{3+}$ and the spectra at pH above~5 those of the deprotonated form, M(amO)$^{2+}$. The absorption spectrum of [Co(*N*-Meeta)$(en)_2$]$(ClO_4)_2$ in an aqueous solution was almost identical with that of [Co(*N*-MeetaH)$(en)_2$]$Cl_3 \cdot H_2O$ in an alkaline solution. This result supports the existence of acid-base equilibria. The reversible change of CD spectra upon pH change implies that the racemization or epimerization of the present amino-alcohol complexes is slow. Low pK_a values of hydroxyl group of coordinated alcohols have been reported for several complexes.[6,7]

Numerical data of the absorption and CD spectra of the complexes are shown in Table 1.

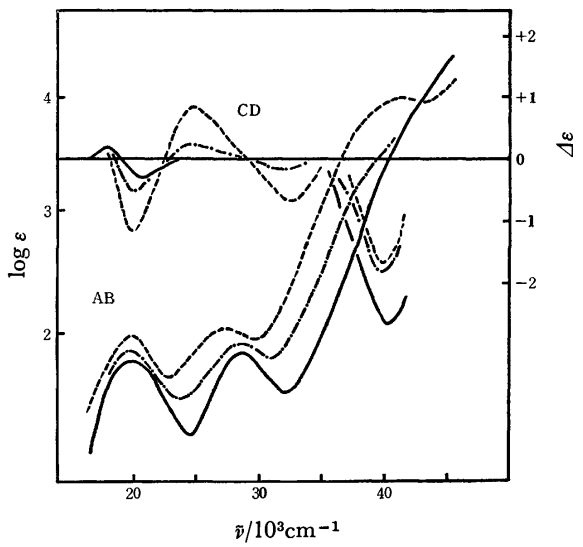

Fig. 1. Absorption and CD spectra of $(-)_D$-[Co(*S*-praH)$(NH_3)_4$]Cl_3 at pH 1.36 (——), at pH 2.75 (—·—) and at pH 9.50 (----).

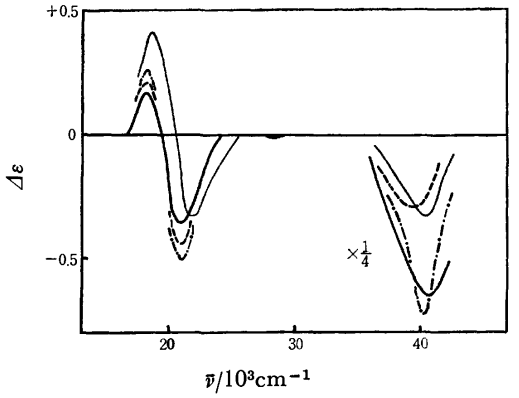

Fig. 2. CD spectra of $[Co(S\text{-amOH})(NH_3)_4]^{3+}$ complexes (protonated form).
——: *S*-praH complex ----: *S*-leuH complex
—·—: *S*-abnH complex : *S*-isopraH complex

CD Spectra of Tetraamminecobalt(III) Complexes. The CD spectra of $[Co(S\text{-amOH})(NH_3)_4]^{3+}$,[8] with protonated hydroxyl group are shown in Fig. 2. The patterns are similar to that of $[Co(NH_3)_4(S\text{-pn})]^{3+}$ (pn=1,2-diaminopropane)[9-11], a positive and a negative CD band are seen from lower to higher wave number in the first absorption band region, while the CD magnitude in the second absorption band region is almost zero except for $[Co(S\text{-isopraH})(NH_3)_4]^{3+}$. A large negative CD band is observed in the charge transfer region. The similarity suggests that both *S*-amOH and *S*-pn chelates in the complexes are in a similar conformational structure, *δ-gauche*.[9-11]

Since the complexes of the type, $[Co(S\text{-amOH})(NH_3)_4]^{3+}$ are approximated to C_{4v} symmetry, the positive and the negative CD band in the first absorption band region may be assigned to the $A_1 \rightarrow E$ and the $A_1 \rightarrow A_2$ component, respectively.[12]

$(+)_D$-$[Co(isopraH)(NH_3)_4]^{3+}$ shows the positive $A_1 \rightarrow E$ and the negative $A_1 \rightarrow A_2$ CD bands in the first absorption band region. Therefore, the isopraH in this isomer will be in *δ-gauche* conformation with an equatorial methyl group, and consequently of *S* absolute configuration. The CD magnitude of the $A_1 \rightarrow E$ band is greater than that of the $A_1 \rightarrow A_2$ band in contrast to the other *S*-amOH complexes. The relative CD magnitudes of the $A_1 \rightarrow E$ and the $A_1 \rightarrow A_2$ components may be related to the difference in the position of substituents on chelate rings. The isopraH has methyl group at α position to the hydroxyl group while the other *S*-amino-alcohols the substituents at β position.

The CD spectra of the deprotonated complexes, $[Co(S\text{-amO})(NH_3)_4]^{2+}$ are reproduced in Fig. 3. All the complexes including the *S*-isopra⁻ complex show a similar pattern; a weak positive and a strong negative CD band in the first absorption band region, a fairly strong positive CD band in the second absorption band region (~25000 cm^{-1}) and two strong negative CD bands in the charge transfer region (~33000 and 37000—40000 cm^{-1}). This result confirms the previous assignment of the absolute configuration for the isopraH in the $(+)_D$-isomer.

The positive and the negative CD bands in the first absorption band region may be also assigned to the

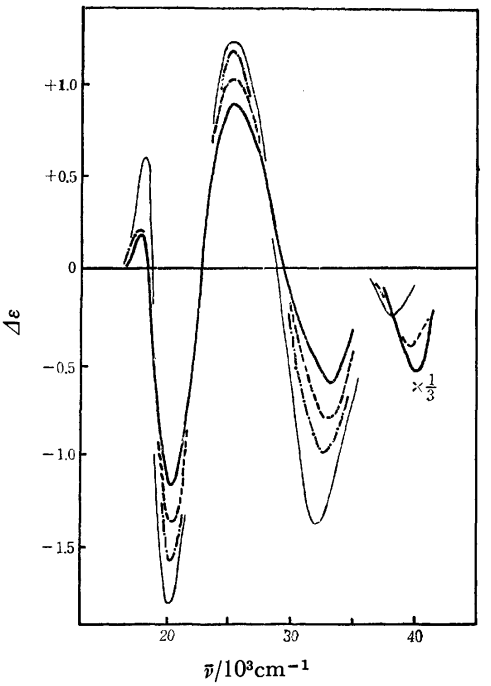

Fig. 3. CD spectra of $[Co(S\text{-amO})(NH_3)_4]^{2+}$ complexes (deprotonated form).
——: *S*-pra⁻ complex ----: *S*-leu⁻ complex
—·—: *S*-abn⁻ complex : *S*-isopra⁻ complex

$A_1 \rightarrow E$ and the $A_1 \rightarrow A_2$ component, respectively. The magnitude of the latter component is markedly enhanced in the deprotonated complexes as compared with that in the protonated complexes. The strong CD band at about 25000 cm^{-1} in the second absorption band region is quite characteristic of the deprotonated complexes. The CD corresponding to the second absorption band of a cobalt(III) complex is generally very weak, since this absorption is intrinsically magnetic dipole forbidden. The CD peak positions at about 25000 cm^{-1} do not coincide with the second absorption maxima at about 27600 cm^{-1}, and there seems to exist a band component at about 25000 cm^{-1} in the absorption spectra (see Fig. 1). The deprotonated isopra⁻ complex which contains an asymmetric carbon atom adjacent to the alcoholic oxygen atom gives the biggest CD peaks among the *S*-amO⁻ complexes in the first and the second absorption band region.

Very recently, Hawkins *et al.*[11] reported the CD of the tetraammine complexes containing *S*-lactic acid, *S*-2-amino-1-propanol, *S*-alanine and *S*-1,2-diaminopropane in 0.1 M perchloric acid, in aqueous solution and in 0.005 M potassium hydroxide solution. The CD spectra of *S*-2-amino-1-propanol complex show a strong pH-dependence as those in our study. A similar pH-dependence is also exhibited in the *S*-lactato complex.

CD Spectra of Bis(ethylenediamine)cobalt(III) Complexes. The absorption and CD spectra of *Λ*-$[Co(etaH)(en)_2]^{3+}$, *Λ*-$[Co(S\text{-praH})(en)_2]^{3+}$ and *Λ*-$[Co(S\text{-praH})(en)_2]^{3+}$ and their conjugate bases were reported in the previous communication.[3] The spectra of two isomeric isopraH complexes and their conjugate bases are shown in Figs. 4 and 5. The CD spectra of the protonated complexes

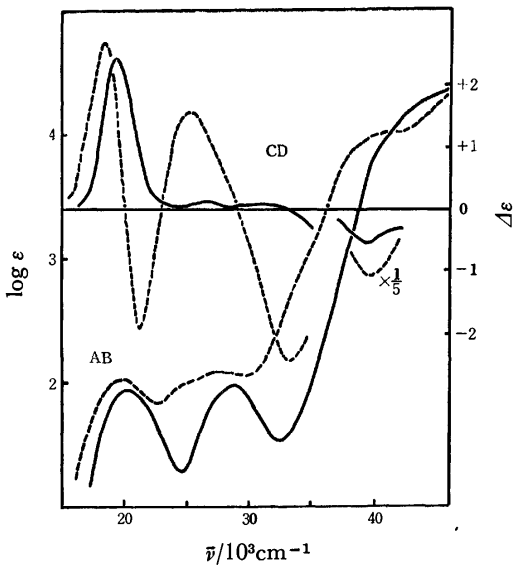

Fig. 4. Absorption and CD spectra of *Λ*-[Co(*S*-isopraH)(en)$_2$]$^{3+}$ (protonated form) (——) and *Λ*-[Co(*S*-isopra)(en)$_2$]$^{2+}$ (deprotonated form) (---).

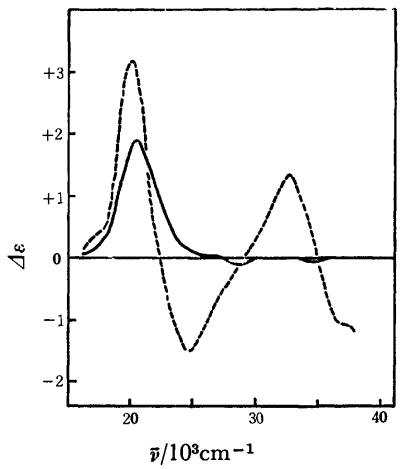

Fig. 5. CD spectra of *Λ*-[Co(*R*-isopraH)(en)$_2$]$^{3+}$ (protonated form) (——), and *Λ*-[Co(*R*-isopra)(en)$_2$]$^{2+}$ (deprotonated form) (----).

[Co(amOH)(en)$_2$]$^{3+}$ resemble those of [Co(diamine)$_3$]$^{3+}$ and [Co(am)(en)$_2$]$^{2+}$. A strong and a weak CD band are observed in the first and the second absorption band region, respectively.

The absolute configurations of the amino-alcohol complexes can be assigned on the basis of the sign of the main CD band at about 20000 cm^{-1}. Thus the complexes shown in Figs. 4 and 5 are assigned to *Λ* configuration. The absolute configuration of 1-amino-2-propanol in these complexes can be assigned from comparison of their CD spectra with those of the ethylenediamine analogs of *S*-praH and *S*-pra$^-$.[3] As the CD curves of the isopraH and isopra$^-$ complexes in Fig. 4 are similar to those of the corresponding *Λ*-[Co(*S*-praH)(en)$_2$]$^{3+}$ and its conjugate base respectively, the absolute configuration of isopraH in this isomer will be assigned to *S*. In an analogous manner, the absolute configuration of isopraH in the other isomer, whose CD curves are given in Fig. 5, was assigned

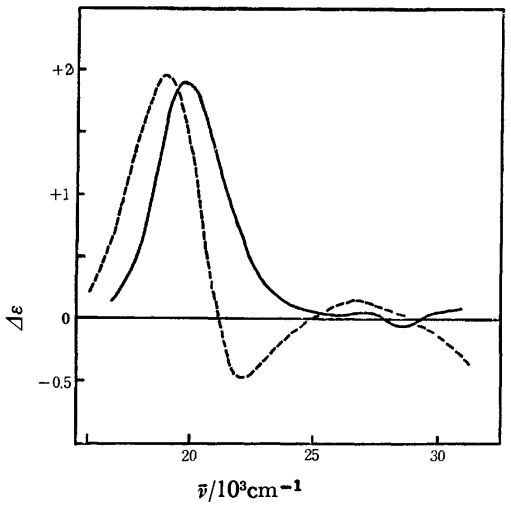

Fig. 6. Configurational effects of [Co(*R*-isopraH)(en)$_2$]$^{3+}$ (protonated form) (——) and [Co(*R*-isopra)(en)$_2$]$^{2+}$ (deprotonated form) (----).

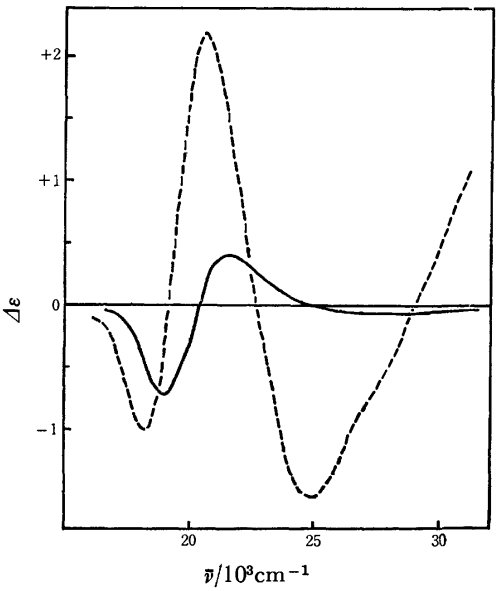

Fig. 7. Vicinal effect curves of [Co(*R*-isopraH)(en)$_2$]$^{3+}$ (——) (protonated form) and [Co(*R*-isopra)(en)$_2$]$^{2+}$ (----) (deprotonated form).

to *R*.

The CD magnitudes of the deprotonated complexes [Co(amO)(en)$_2$]$^{2+}$ are considerably enhanced as compared with those of their conjugate acids. The characteristics of the CD spectra of the deprotonated complexes are the appearance of two strong bands with opposite signs at 20000—21000 cm^{-1} and about 25000 cm^{-1}. In the absorption spectra of these complexes, a shoulder is observed at about 25000 cm^{-1}. These shoulder bands may also be related to the strong CD bands at about 25000 cm^{-1}, as seen in the tetraammine complexes with deprotonated amO$^-$.

It is known that the contributions of the configurational and vicinal effects are additive in the CD spectra of a series of cobalt(III) complexes containing five-membered chelate rings.[10,13] The configurational and the vicinal effects in the CD spectra of two isomeric

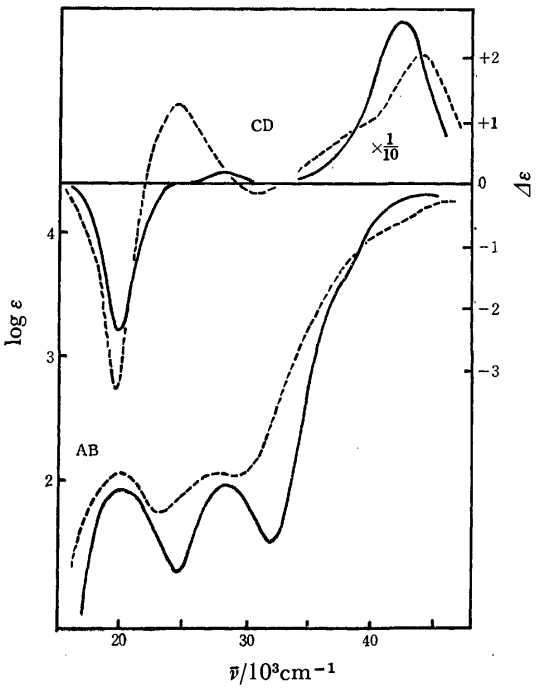

Fig. 8. Absorption and CD spectra of Δ-[Co(*S*-praH)-(*R*-chxn)$_2$]$^{3+}$ (protonated form) (——), Δ-[Co(*S*-pra)-(*R*-chxn)$_2$]$^{2+}$ (deprotonated form) (----).

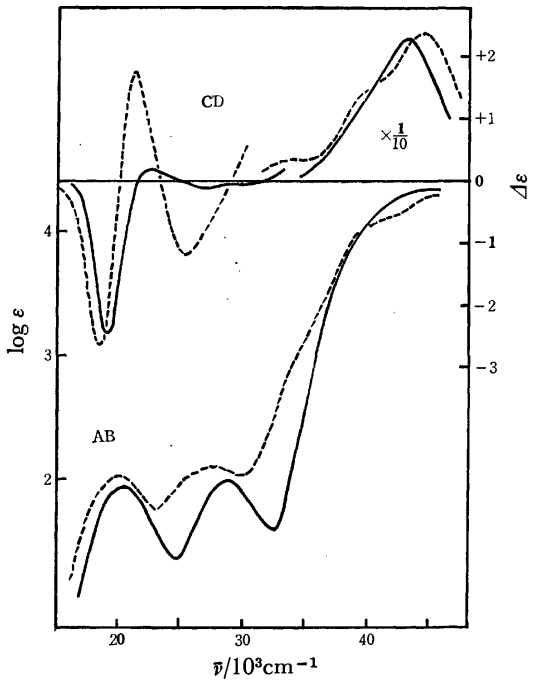

Fig. 9. Absorption and CD spectra of Δ-[Co(etaH)-(*R*-chxn)$_2$]$^{3+}$ (protonated form) (——), Δ-[Co(eta)-(*R*-chxn)$_2$]$^{2+}$ (deprotonated form) (----).

[Co(isopraH)(en)$_2$]$^{3+}$ and their conjugate bases, are estimated as shown in Figs. 6 and 7. The vicinal effect curves in Fig. 7 resemble the CD curves of the corresponding tetraammine complexes, indicating that the additivity of the two effects holds in these complexes. The configurational effect curves are similar between the protonated and the deprotonated complexes, while the vicinal effect curves are considerably different from each other, the CD magnitude of the deprotonated complexes being enhanced considerably. A similar result has been obtained for the CD spectra of Δ- and Λ-[Co(*S*-praH)(en)$_2$]$^{3+}$ and their conjugate bases.[3] Thus the enhanced CD magnitude of the deprotonated complexes may be attributed to the vicinal effect of an amino-alcoholate chelate ring. The similarity of the vicinal effect curves of *S*-pra$^-$ and *S*-isopra$^-$ complexes implies that the conformation of the five-membered chelate ring contributes to the CD more than does the position of substituent on the chelate ring. The CD band at $\sim$25000 cm^{-1} of Δ- or Λ-[Co(amO)(en)$_2$]$^{2+}$ depends only on conformation of amO$^-$ chelate ring because the configurational effect curve has no bands in this region.

The enhanced CD magnitude of the deprotonated amino alcoholato complexes might be related to the coordinated alcoholate oxygen atom with two sets of nonbonding electron pairs. Recently Kipp and Haines[14] reported that [Co(*R*-lac)(diamine)$_2$]$^+$(lac^{2-}= divalent lactate ion) complexes exhibit strong CD. These complexes also possess coordinated alcoholate oxygen atom.

*CD Spectra of Bis(*R-trans-1,2-*diaminocyclohexane)cobalt-(III) Complexes.* The absorption and CD spectra of [Co(amOH)(*R*-chxn)$_2$]$^{3+}$ complexes and their conjugate bases are shown in Figs. 8 and 9. The absolute configurations of the complexes around the cobalt(III) ion were assigned from the sign of the main CD band in the first absorption band region of the protonated complexes. In the present study Λ-isomers were formed too little, and we have isolated only the Δ-isomer for each complex.

The CD spectrum of Δ-[Co(*S*-praH)(*R*-chxn)$_2$]$^{3+}$ would consist of the configurational and the vicinal effects due to *S*-praH and the two *R*-chxn chelate rings. The *R*-chxn chelate ring will take λ-*gauche* conformation and consequently the C–C bond in the chelate ring is *lel*[15] to the pseude-three fold axis of the Δ-complex. The *S*-praH chelate ring will have the C–C bond *ob*[15] to the pseudo-three fold axis.

The CD spectra of Δ-[Co(*S*-praH)(*R*-chxn)$_2$]$^{3+}$ and its conjugate base are similar to those of Δ-[Co(*S*-praH)-(en)$_2$]$^{3+}$ and its conjugate base(see Table 1 and spectra in Ref. 3) respectively. This similarity indicates that these ethylenediamine chelate rings take λ(*lel*) conformation preferentially. The *S*-pra$^-$ chelate ring must give strong vicinal effect similarly to the en and the chxn complex and seems to have given similar patterns to them. The CD spectra of Δ-[Co(etaH)(*R*-chxn)$_2$]$^{3+}$ and its conjugate base are cosiderably different from the corresponding ethylenediamine analogs (see Table 1 and spectra in Ref. 3). The difference might be related to the difference in the conformation of etaH or eta$^-$ in the *R*-chxn and the en complexes. The complex ion Λ-[Co(eta)(en)$_2$]$^{2+}$ shows only small CD bands at 25970 cm^{-1}. The CD band in this region has been shown to depend only on the conformation of the amO$^-$ chelate ring. The conformation of eta$^-$ chelate ring in the en complex is thus considered to be in equilibrium between δ and λ, and the equilibrium to be in favor of the δ only to a small extent.

On the other hand, Δ-[Co(eta)(*R*-chxn)$_2$]$^{2+}$ exhibits fairly strong CD bands at 21280 cm^{-1} and 25320 cm^{-1} and the whole CD curve is almost enantiomeric with that of Λ-[Co(*S*-pra)(en)$_2$]$^{2+}$. Since the *S*-pra$^-$ chelate ring in the ethylenediamine complex will take δ conformation stereoselectively, the eta$^-$ chelate ring in Δ-[Co(eta)(*R*-chxn)$_2$]$^{2+}$ may be mostly in λ conformation. The stereoselectivity of the conformation of eta$^-$ chelate ring in the bis(*R*-chxn) complex seems to be much larger than that in the bis(en) complex. Such a large stereoselectivity might be brought about by the steric interaction between the eta$^-$ and *R*-chxn chelate rings.

It is concluded that an amino-alcoholate chelate ring without asymmetric atoms can give strong vicinal effect when it takes a chiral conformation stereoselectively.

Absorption Spectra. The first absorption bands of all the deprotonated amino-alcoholate complexes are at somewhat lower wave number than those of the corresponding protonated amino-alcohol complexes. However, the wave number differences are small compared with that observed for aqua- and hydroxo-pentaammine complexes which belong to the same [CoN$_5$O] type as the present amino-alcohol complexes.

It the second absorption band region, on the other hand, the spectra of the tetraammine complexes exhibit somewhat different behavior from those of the bisdiamine complexes. The tetraammine complexes with deprotonated amO$^-$ have the second absorption maxima at lower wave numbers than those of the protonated complexes by *ca.* 150 cm^{-1}. However, most of the bisdiamine complexes with deprotonated amO$^-$ give their second absorption bands at only slightly lower wave number than those of the protonated complexes, and exhibit a distinct shoulder band at about 25000 cm^{-1}. Such a shoulder band is the most pronounced in [Co(*N*-Meeta)(en)$_2$]$^{2+}$ among the amino-alcoholate complexes studied here. As stated previously, all the complexes containing deprotonated chiral amino-alcoholate chelate ring show a strong CD band in this region, $\sim$25000 cm^{-1}. Thus, it may be concluded that all the deprotonated complexes have an absorption component at about 25000 cm^{-1}, even though there is no obvious shoulder in the absorption spectra as in the tetraammine complexes. In such complexes the shoulder band might have been masked by the main component of the second absorption band. The apparrent second absorption maximum is thus seen at a relatively lower wave number.

A similar shoulder in the second absorption band region has been reported for several complexes; [Co(OH)(edta)]$^{2-}$,[16] (edta^{4-}=ethylenediaminetetraacetate ion), [Co(OH)(penten)]$^{2+}$ [17] (penten=*N*,*N*,*N*',*N*'-tetrakis(2'-aminoethyl)-1,2-diaminoethane) and *mer*-(*trans*-NH$_3$)-[CoCO$_3$(am)(NH$_3$)$_2$][18] (am$^-$=aminocarboxylate ion). The nature of these shoulder bands is not clear at present. However, all the complexes including the present aminoalcoholate complexes are those containing both chelate rings and coordinated oxygen atom with two sets of nonbonding electron pairs. [Co(guH)(en)$_2$]$^{3+}$ and [Co(gu)(en)$_2$]$^{2+}$ (guH=guanylurea) show also a broad second absorption band but the structures of these complexes remain uncertain.[19]

The authors wish to thank Mr. K. Ohashi of Ibaragi University for supplying *S*-leucinol and also Ministry of Education for Grant in Aid.

References

1) See for example: J. Fujita and Y. Shimura, in "Spectroscopy and Structure of Metal Chelate Compounds" (K. Nakamoto and P. J. McCarthy, S. J., ed.), John Wiley & Sons (1968), p. 156; C. J. Hawkins, "Absolute Configuration of Metal Complexes," John Wiley & Sons (1971), p. 148.
2) K. Ohashi, J. Fujita, B. Shimoyama, and K. Saito, This Bulletin **41**, 2422 (1968).
3) K. Ogino, T. Uchida, T. Nishide, J. Fujita, and K. Saito, *Chem. Lett.*, **1973**, 679.
4) O. Vogl and M. Pöln, *Monatsh.*, **83**, 541 (1952).
5) R. S. Treptow, *Inorg. Chem.*, **5**, 1593 (1966).
6) D. A. Buckingham, C. E. Davis, and A. M. Sargeson, *J. Amer. Chem. Soc.*, **92**, 6159 (1970).
7) R. B. Jordan, A. M. Sargeson, and H. Taube, *Inorg. Chem.*, **5**, 1091 (1966); V. V. Udovenko and L. G. Reitor, *Russ. J. Inorg. Chem.*, **15**, 958 (1970); L. E. Bennett, R. H. Lane, M. Gilroy, F. A. Sedor, and P. Bennett, Jr., *Inorg. Chem.*, **12**, 1200 (1973).
8) CD curves of [Co(*S*-abnH)(NH$_3$)$_4$]$^{3+}$ and its conjugate base in Figs. 2 and 3 are obtained by changing the sign of those of the *R*-abnH complex and its conjugate base.
9) C. J. Hawkins, E. Larsen, and I. Olsen, *Acta Chem. Scand.*, **19**, 1915 (1965).
10) K. Ogino, K. Murano, and J. Fujita, *Inorg. Nucl. Chem., Lett.*, **4**, 351 (1968).
11) C. J. Hawkins and G. A. Lawrence, *ibid.*, **9**, 1183 (1973).
12) H. Yamatera, This Bulletin, **31**, 95 (1958).
13) B. E. Douglas, *Inorg. Chem.*, **4**, 1813 (1965); C. T. Liu and B. E. Douglas, *ibid.*, **3**, 1356 (1964).
14) E. B. Kipp and R. A. Haines, *ibid.*, **11**, 271 (1972); R. A. Haines and A. A. Smith, *ibid.*, **12**, 1426 (1973).
15) E. J. Corey and J. C. Bailar, Jr., *J. Amer. Chem. Soc.*, **81**, 2620 (1959).
16) C. K. Jørgensen, *Acta Chem. Scand.*, **9**, 1362 (1955).
17) E. P. Emmenegger and G. Schwarzenbach, *Helv. Chim. Acta*, **49**, 625 (1966).
18) S. Kanazawa and M. Shibata, This Bulletin, **44**, 2424 (1971); K. Nakai, S. Kanazawa, and M. Shibata., *ibid.*, **45**, 3544 (1972).
19) K. Igi, T. Yasui, J. Hidaka, and Y. Shimura, *ibid.*, **44**, 426 (1971).

A Polarographic Investigation of the Reactions between Nitrate Ions and Chromium(II)–Cyclohexanediaminetetraacetate, Chromium(II)–Trimethylenediaminetetraacetate, and Chromium(II)–*N*-(2-Hydroxyethyl)ethylenediaminetriacetate Complexes

Nobuyuki TANAKA, Taisaku KANO, Hiroshi OGINO, and Akifumi YAMADA

Department of Chemistry, Faculty of Science, Tohoku University, Aoba, Aramaki, Sendai 980

(Received April 1, 1974)

Kinetic studies of the reactions between nitrate ions and Cr(II)-Y complexes, where Y represents cyclohexanediaminetetraacetic acid (CyDTA), trimethylenediaminetetraacetic acid (TRDTA), and *N*-(2-hydroxyethyl) ethylenediaminetriacetic acid (HEDTA), have been carried out. The reaction mechanisms of these complexes at the dropping mercury electrode were found to be expressed by the following equations:

$$\begin{array}{lll} \text{Cr(III)-Y} + \text{e} & \longrightarrow & \text{Cr(II)-Y} \\ \text{Cr(II)-Y} + \text{H}^+ & \overset{K}{\rightleftharpoons} & \text{Cr(II)-HY} \\ \text{Cr(II)-Y} + \text{NO}_3^- & \overset{k_1}{\longrightarrow} & \text{Cr(III)-Y} \\ \text{Cr(II)-HY} + \text{NO}_3^- & \overset{k_2}{\longrightarrow} & \text{Cr(III)-Y} \end{array}$$

The formation constant, K, and the rate constants, k_1 and k_2, were determined in 0.1 M acetate buffer solutions of $\mu=0.5$ by procedures including a curve-fitting method; the results were $K=2.0\times10^4$ M^{-1}, $k_1=0.55$ M^{-1} s^{-1} and $k_2=2.8$ M^{-1} s^{-1} for Cr(II)-CyDTA, $K=2.4\times10^5$ M^{-1}, $k_1=1.0\times10^2$ M^{-1} s^{-1}, and $k_2<3$ M^{-1} s^{-1} for Cr(II)-TRDTA and $k_1\sim2\times10^3$ M^{-1} s^{-1} for Cr(II)-HEDTA.

It was reported in a previous paper[1] that chromium(II)–EDTA complexes which were formed by the electroreduction of ethylenediaminetetraacetatoaquochromate(III) ions were oxidized by nitrate ions at the surface of the electrode; a catalytic reaction took place in solutions containing both chromium(III)–EDTA and nitrate ions. The stoichiometry and the rate constant of the reaction were determined, and the reaction mechanisms were discussed.[1]

In this paper, the polarographic investigation of the reaction between nitrate ions and Cr(II)–Y at the dropping mercury electrode is presented, where Y represents CyDTA, TRDTA, and HEDTA. The stoichiometry and the mechanisms of the reaction are discussed, and the formation constant of the acid complex of Cr(II)-Y, and the second-order rate constants of the reactions between nitrate ions and Cr(II)–Y and Cr(II)–HY are presented.

Experimental

Sodium cyclohexandiaminetetraacetatochromate(III), Na[Crcydta]·4H$_2$O, sodium trimethylenediaminetetraacetatochromate(III), Na[Crtrdta]·4H$_2$O, and *N*-(2-hydroxyethyl)-ethylenediaminetriacetatochromium(III), [Cr(H$_2$O)hedta], were prepared according to Tanaka *et al.*,[2] Ogino *et al.*[3] and Bustin and Early[4] respectively. All the chemicals used were of a guaranteed grade.

Current-potential curves were obtained with a pen-recording polarograph, Yanagimoto Graphrecorder, with an automatic potential scanner. The dropping mercury electrode (DME) used in the measurement of the limiting current of Crcydta$^-$ had a rate of mercury flow (m) of 1.86 mg s^{-1} and a drop time (t_d) of 5.00 s, as measured in an air-free solution containing a 0.1 M acetate buffer (pH 4.9) at -0.5 V *vs.* SCE and at a pressure of 50 cm of mercury. The DME used in the measurement of Crtrdta$^-$ and Cr(H$_2$O)hedta had an m value of 1.34 mg s^{-1} and a t_d value of 4.75 s in an air-free solution containing a 0.1 M acetate buffer (pH 4.9) and 0.4 M sodium perchlorate at -1.34 V *vs.* SCE and at a pressure of 60 cm of mercury.

The potential of DME was referred to the saturated calomel electrode (SCE). The temperature of the electrolytic solution was maintained at 25±0.2 °C by means of a thermostated bath. Dissolved oxygen in the electrolytic solution was removed by bubbling pure nitrogen gas through the solution. Extra pure nitrogen gas (99.999%) was used in determining the stoichiometric ratio of the Cr(II) complexes to the nitrate ion of the reaction. No maximum suppressor was used in the cases of Crcydta$^-$ and Cr(H$_2$O)hedta. As the reduction wave of Crtrydta$^-$ gave a maximum, 2 μM LEO was added in determining the limiting current of Crtrdta$^-$.

The measurements were made in 0.1 M acetate buffer solutions. The ionic strength was adjusted to 0.5 with sodium perchlorate, unless otherwise stated. The stoichiometry of the reactions of the Cr(II) complex with the nitrate ion was determined by the method reported in a previous paper.[1]

The controlled potential electrolysis was carried out with a Yanagimoto Controlled Potential Electrolyser. The working electrode was a mercury pool, while the auxiliary electrode was a platinum wire which was connected to the electrolytic solution through a sodium chloride agar bridge. The potential of the working electrode was referred to the SCE. Nitrogen gas was bubbled through the solution continuously to provide stirring and to remove atmospheric oxygen.

Results

Polarograms of Crcydta$^-$, Crtrdta$^-$, and Cr(H$_2$O)hedta Obtained at Various Concentrations of Nitrate Ions. The polarographic waves of Crcydta$^-$, Crtrdta$^-$, and Cr(H$_2$O)hedta obtained in acetate buffer solutions were of a one-electron diffusion-controlled reduction. Upon the addition of nitrate ions to these solutions, the limiting currents of these waves increased in height. Figure 1 shows as examples the reduction waves of Crcydta$^-$ in the absence and in the presence of nitrate ions. Current $\bar{I}_c$ in Fig. 1 was found to be independent of the

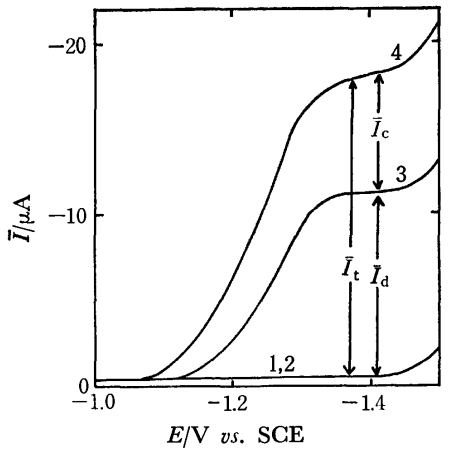

Fig. 1. Polarograms obtained with the solutions containing (1) 0.1M acetate buffer (pH 4.9), (2) (1)+0.25 M $NaNO_3$ (3) (1)+4 mM Crcydta$^-$ and (4) (3)+0.17 M $NaNO_3$.

height of mercury, indicating that $\bar{I}_c$ was kinetic in nature; that is, it was a catalytic current.

Apparent Rate Constants of the Reactions between Nitrate Ions and Cr(II)-CyDTA, Cr(II)-TRDTA, and Cr(II)-HEDTA. Let us consider the electrode processes given by the equations,

$$\begin{array}{l} O + ne \longrightarrow R \\ \uparrow \qquad\qquad \downarrow \\ R + Z \xrightarrow{k} O \end{array} \qquad (1), (2)$$

where O, R, and Z represent, respectively, the oxidant, the reductant, and the substance which is neither reduced nor oxidized at the potential at which O is reduced. The rate constant, k, of the chemical reaction given by Eq. (2) is calculated by means of Eqs. (3) to (7):[5-7]

$$\Psi(\chi_1) = \frac{\bar{I}_t + 2.37\times10^4\, nm^{1/3}t_d^{1/2}DC_o}{\bar{I}_d + 2.37\times10^4\, nm^{1/3}t_d^{1/2}DC_o} \qquad (3)$$

$$= (7/6)\chi_1^{-7/6}\left[2\int_0^{\chi_1}\chi^{2/3}f(\beta)d\chi + \int_0^{\chi_1}\chi^{1/6}\exp(-\chi)d\chi\right] \qquad (4)$$

$$f(\beta) = \int_0^1 \frac{\beta\exp(-\beta^2\chi_1)}{\{1-(1-\beta^2)^{7/3}\}^{1/2}}d\beta \qquad (5)$$

$$\chi_1 = \alpha k C_Z t_d \qquad (6)$$

where D is the diffusion coefficient and where C_O and C_Z are the concentrations of O and Z respectively, Z being present in a large excess of O. α is the stoichiometric ratio of R to Z of Reaction (2). In this study, the Cr(III)–Y, Cr(II)–Y, and nitrate ions correspond to O, R, and Z respectively, and α was determined to be 8 from separate experiments. When $\chi_1 > 10$,

$$\Psi(\chi_1) = 0.812\chi_1^{1/2} + 1.92\chi_1^{-7/6} \qquad (7)$$

The rate constants which were obtained by means of Eq. (7) for the reactions between nitrate ions and Cr(II)–CyDTA, Cr(II)–TRDTA, and Cr(II)–HEDTA under various conditions are given in Tables 1 and 2 and Figs. 2 and 3, in which k_{app} corresponds to k in Eq. (6). The values of k_{app} thus obtained were found to be independent of [Cr(III)–Y] and [NO_3^-].

The catalytic currents of Crcydta$^-$ obtained at the

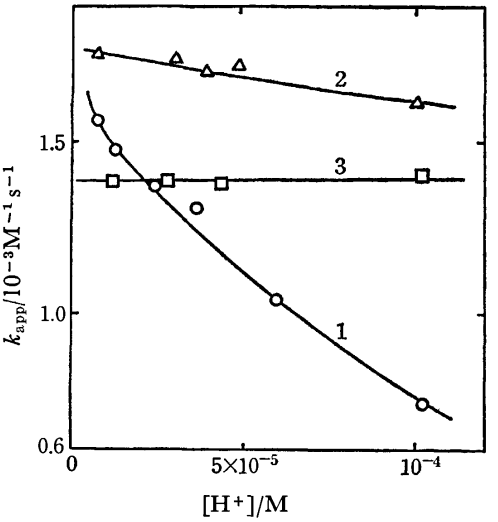

Fig. 2. Apparent rate constants of the reaction between nitrate ions and Cr(II)-HEDTA obtained at various concentrations of hydrogen ions with the solutions containing (1) 0.22 mM $Cr(H_2O)$hedta+1.2 mM $NaNO_3$ (μ=0.5), (2) (1)+1 mM HEDTA and (3) (1)+4 mM HEDTA.

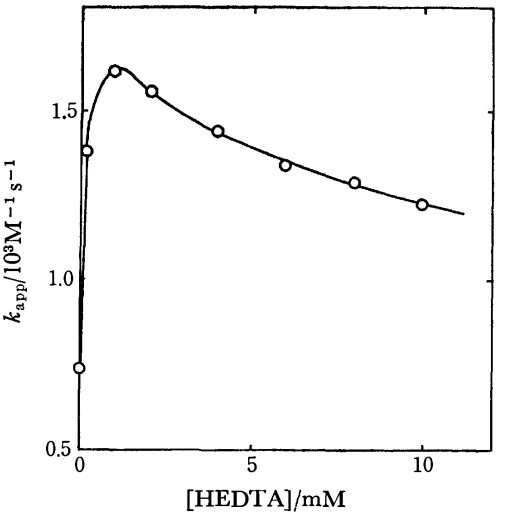

Fig. 3. Apparent rate constants of the reaction between nitrate ions and Cr(II)-HEDTA obtained at various concentrations of HEDTA.

given concentration of nitrate ions and the apparent rate constants calculated thereform increased with the increase in the concentration of hydrogen ions, as is shown in Table 1. However, they did not change upon the addition of the free ligand CyDTA, as long as the other conditions were the same. These results seem to indicate that the acid complex of Cr(II)–CyDTA, Cr(II)–HY, is formed, but not aquochromium(II); the latter reacts with nitrate ions very slowly.[8] In the case of Crtrdta$^-$, the catalytic current and the apparent rate constants calculated therefrom were found to decrease with the increase in the concentration of hydrogen ions, as is shown in Table 2. This tendency is opposite to that obtained with Crcydta$^-$. The height of the catalytic current did not change upon the addition of the free ligand TRDTA, just as in the

Table 1. Total currents of Crcydta$^-$ and apparent rate constants of the reaction between Crcydta$^-$ and nitrate ions measured in the solutions containing 0.8 mM Crcydta$^-$ and 0.16 M $NaNO_3$

$[H^+]/10^{-5}$ M	$-\bar{I}_t/\mu A$	$k_{app}/M^{-1}s^{-1}$
0.166	3.79	0.623
1.26	4.44	0.972
1.90	4.77	1.18
3.31	5.20	1.46
3.62	5.29	1.53
5.50	5.63	1.77
7.25	5.76	1.87

Table 2. Total currents of Crtrdta$^-$ and apparent rate constants of the reaction between Crtrdta$^-$ and nitrate ions measured in the solutions containing 0.32 mM Crtrdta$^-$ and 7.2 mM $NaNO_3$

$[H^+]$ 10^{-5} M	$-I_t$ μA	Potential measured V *vs.* SCE	k_{app} $M^{-1}s^{-1}$
0.151	3.08	−1.46	76.1
0.438	2.70	−1.43	50.5
1.35	1.95	−1.40	24.0
2.04	1.69	−1.39	16.5
3.08	1.34	−1.38	9.97

case of Crcydta$^-$. From the measurements of the half-wave potentials of Crtrdta$^-$ at various concentrations of hydrogen ions, it was found that Cr(II)–TRDTA formed the acid complex, CrHtrdta$^-$.[9] This suggests that no appreciable amount of aquochromium(II) exists in the solution, while the acid complex, CrHtrdta$^-$, does.

The apparent rate constant of the reaction between nitrate ions and Cr(H_2O)hedta$^-$ decreased with the increase in the hydrogen-ion concentration (see Curve 1 in Fig. 2). This pH-dependency of the apparent rate constant became smaller upon the addition of free HEDTA (Curve 2 in Fig. 2). When 4 mM of free HEDTA was present in the solution, the apparent rate constants were found to be almost independent of the hydrogen-ion concentration (Curve 3 in Fig. 2).

The apparent rate constants which were obtained at the same concentration of hydrogen ion increased with an increase in the concentration of free HEDTA, but gave a maximum value at a certain concentration of free HEDTA and then decreased, as is shown in Fig. 3. The increase in the apparent rate constant at lower concentrations of free HEDTA may be explained by considering that aquochromium(II) is formed in the absence of free HEDTA, while the formation of aquochromium(II) is prevented by the addition of HEDTA. On the other hand, the decrease in the apparent rate constant with an increase in the concentration of free HEDTA is not completely understood; it may, however, be due to the reaction between free HEDTA and the reduction intermediates of nitrate ions.

Discussion

It is considered that the mechanisms of the catalytic electrode reactions of Cr(III)–Y taking place in the presence of nitrate ions may be indicated as follows:

$$\text{Cr(III)-Y} + e \longrightarrow \text{Cr(II)-Y} \quad (8)$$

$$\text{Cr(II)-Y} + H^+ \overset{K}{\rightleftharpoons} \text{Cr(II)-HY} \quad (9)$$

$$\text{Cr(II)-Y} + NO_3^- \xrightarrow{k_1} \text{Cr(III)-Y} \quad (10)$$

$$\text{Cr(II)-HY} + NO_3^- \xrightarrow{k_2} \text{Cr(III)-Y} \quad (11)$$

where K is the formation constant of the acid complex and k_1 and k_2 are the second-order rate constants of the reactions given by Eqs. (10) and (11) respectively. When Y is CyDTA or TRDTA, the electrode reactions are considered to proceed by the mechanisms given by Eqs. (8) to (11). When Y is HEDTA, the reaction seems to proceed by the mechanisms given by Eqs. (8) to (10) or by Eqs. (8) to (11), unless free HEDTA exceeds a certain amount. In the latter case, Reaction (10) proceeds as fast as Reaction (11).

If the reaction proceeds according to Eqs. (8) to (11), the apparent rate constant is given by the following equations:

$$-\frac{d[Cr(II)]_t}{dt} = 8k_{app}[Cr(II)]_t[NO_3^-] \quad (12)$$

$$K = \frac{[Cr(II)-HY]}{[Cr(II)-Y][H^+]} \quad (13)$$

$$[Cr(II)]_t = [Cr(II)-Y] + [Cr(II)-HY] \quad (14)$$

$$k_{app} = \frac{k_1 + k_2K[H^+]}{1 + K[H^+]} \quad (15)$$

With the apparent rate constants and the hydrogen-ion concentrations, the formation constant, K, and the rate constants, k_1 and k_2, were obtained by the curve-fitting method; they are given in Table 3.

The value of k_2 is larger than k_1 in the cases of Cr(II)-EDTA and Cr(II)–CyDTA. This seems reasonable,

Table 3. Rate constants of the reaction between Cr(II)Y (Y: CyDTA, TRDTA, and HEDTA) and nitrate ions, and the formation constant of Cr(II)-HY.

	Cr(II)-EDTA	Cr(II)-CyDTA	Cr(II)-TRDTA	Cr(II)-HEDTA
$k_1/M^{-1}s^{-1}$	$(6.2\pm0.1)\times10$	$(5.5\pm0.4)\times10^{-1}$	$(9.8\pm0.8)\times10$	2×10^3
$k_2/M^{-1}s^{-1}$	$(3.0\pm0.1)\times10^3$	2.81 ± 0.08	< 6	—
k_2/k_1	4.8×10	5.1	$< 6\times10^{-2}$	—
K/M^{-1}	$(2.5\pm0.1)\times10^3$	$(2.0\pm0.1)\times10^4$	$(2.4\pm0.3)\times10^5$	—
K/M^{-1}	$10^{3.00}$ [10]	—	10^5 [9]	—

Uncertainties represent standard deviations.

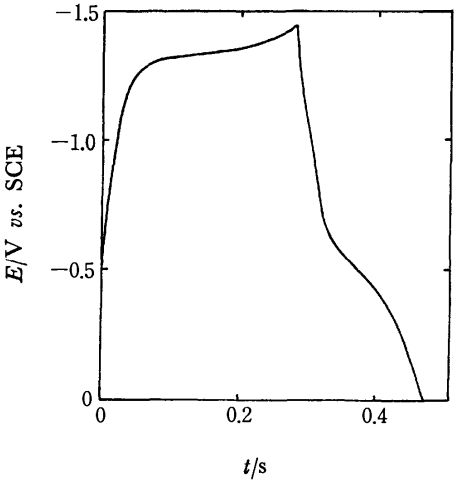

Fig. 4. Chronopotentiogram for the reduction and the subsequent reoxidation of 0.64 mM Crtrdta$^-$ obtained at current density of 5.19×10^{-4} A/cm^2 in the solution containing 0.1 M acetate buffer (pH 4.0) and 0.4 M $NaClO_4$.

because the electrostatic repulsion of acid complexes with nitrate ions is smaller than that of the normal complexes, Cr(II)–EDTA and Cr(II)–CyDTA. The k_2 value of Cr(II)–EDTA is of the same order as the k_1 value of Cr(II)–HEDTA; this is probably because the complexes are similar in both charge and structure. In the case of Cr(II)–TRDTA, on the other hand, k_2 is smaller than k_1. A current-reversal chronopotentiogram of Crtrdta$^-$ indicated an irreversible nature of the electrode reaction; it is shown in Fig. 4. This seems to suggest that the structure of the acid complex of Cr(II)–TRDTA changes rapidly to a structure similar to aquochromium(II), which can react with nitrate ions only slowly.

The magnitudes of the k_1 values of Cr(II)–CyDTA, Cr(II)-TRDTA, and Cr(II)–EDTA are in the following order:

Cr(II)-TRDTA > Cr(II)-EDTA > Cr(II)-CyDTA

The above order may be compared with the standard potentials of these complexes, which are −1.29,[9] −1.220,[11] and −1.198[12] V *vs.* SCE for Cr(III, II)-TRDTA, Cr(III, II)–EDTA, and Cr(III, II)–CyDTA respectively. The correlation between the rate constant and the standard potential is apparent. However, as Cr(III, II)–EDTA and Cr(III, II)–CyDTA have almost the same standard potentials, the difference in the k_1 values of Cr(II)–EDTA and Cr(II)–CyDTA may come from the difference in structure. The standard rate constants of the electrode reactions of $Cr(H_2O)edta^-$ and Crcydta$^-$ show a similar tendency; those of $Cr(H_2O)edta^-$ and Crcydta$^-$ are 0.21 cm s^{-1} [11] and 0.029 cm s^{-1} [12] respectively.

References

1) N. Tanaka and T. Ito, This Bulletin, **39**, 1043 (1966).
2) N. Tanaka, K. Kanno, T. Tomita, and A. Yamada, *Inorg. Nucl. Chem. Letters*, **7**, 953 (1971).
3) H. Ogino, J. J. Chung, and N. Tanaka, *ibid.*, **7**, 125 (1971).
4) D. I. Bustin and J. E. Earley, *J. Amer. Chem. Soc.*, **89**, 1818 (1967).
5) J. Koutecky and J. Ciezek, *Collet. Czech. Chem. Commun.*, **21**, 1063 (1956).
6) K. H. Henke and W. Hans, *Z. Elektrochem.*, **59**, 676 (1955).
7) N. Tanaka, T. Kano, and A. Yamada, the 19th Annual Symposium of Polarography (October 1973, Sapporo).
8) H. Ogino, K. Tsukahara, and N. Tanaka, This Bulletin, **47**, 308 (1974).
9) H. Ogino, J. J. Chung, and N. Tanaka, unpublished result.
10) R. L. Pecsok and W. P. Schaeffer, *Inorg. Chem.*, **2**, 114 (1964).
11) N. Tanaka and A. Yamada, This Buulletin, **42**, 1600 (1969).
12) N. Tanaka, T. Tomita, and A. Yamada, *ibid.*, **45**, 940 (1972).

Nitrosylrhenium(^{14}NO and ^{15}NO) Complexes

Eiichi MIKI, Kunihiko MIZUMACHI, and Tatsujiro ISHIMORI

Department of Chemistry, College of Science, Rikkyo University, 3-Chome, Nishi Ikebukuro, Toshima-ku, Tokyo 171

(Received June 21, 1974)

The ^{15}NO-complexes for $M_2[ReX_5(NO)]$ (M=Rb, Cs, and pyH; X=Cl and Br) were prepared. The ^{15}N-isotopic shift for their N–O stretching vibrations, *ca.* 40 cm^{-1}, supports the view that the oxidation state of the NO group is I, while that of the rhenium atom is II. The Re–(NO) stretching and the Re–(NO) bending vibrations were observed in the 610—620 cm^{-1} region. A new compound, *cis*-(pyH)$[ReCl_4(NO)_2]$, was prepared, the oxidation state of its rhenium atom being considered to be I, and that of the NO group, I.

The isotopic effects of ^{15}N-substitution in the NO group for several transition-metal nitrosyl complexes on the IR spectra have been measured.[1,2] From the comparison of the observed isotopic shifts with the calculated ones, a few rules were established: the isotopic shift of the metal–(NO) stretching vibration is smaller than that of the metal–(NO) bending vibration, independent of the metal–(NO) bond angle; the isotopic shifts of the N–O stretching vibrations observed on NO^+ complexes are almost equal to those calculated by assuming a linear arrangement of a metal–N–O, and are larger than those observed on NO^- complexes; the isotopic shifts of the N–O stretching vibrations decrease with the deviation of the metal–(NO) bond angle from linearity.

On the basis of these facts, the oxidation states of the rhenium atom and the NO group for $M_2[ReX_5(NO)]$ (M=Rb, Cs, and pyH; X=Cl and Br) were investigated. A new compound, *cis*-(pyH)$[ReCl_4(NO_2)]$, was prepared and characterized on the basis of spectroscopic evidence. This compound is the first one formulated containing a O–N–Re–N–O skeleton.

Experimental

Syntheses. $M_2[ReX_5(NO)]$ was prepared by means of a modification of Bandyopadhyay's procedure.[3] The starting materials, $Ag_2[ReCl_6]$ and $K_2[ReBr_6]$, were synthesized from $KReO_4$ by the method of Watt and Thompson.[4] The ^{15}NO-complexes were prepared in a vacuum line by the use of 5—6 mmol of ^{15}NO(^{15}N atom%=95 and 96.8) on the same scale as that used for preparing the ^{14}NO-complexes.

$Cs_2[ReCl_5(NO)]$: A 5-mmol portion of NO gas derived from KNO_3 was trapped in a reaction vessel containing 1.7 mmol of a finely-powdered $Ag_2[ReCl_6]$ by cooling with liquid nitrogen. A green product, $Cs_2[ReCl_5(NO)]$ (*ca.* 100 mg), was then obtained by the procedure shown in Ref. 3. The crude product thus obtained was then washed well with a cold 6 M hydrochloric acid solution to remove any impurities, then it was washed with ethanol and dried under a vacuum. Found: Cs, 39.5; Re, 28.5; N, 2.23; Cl, 26.61%. Calcd for $Cs_2[ReCl_5(NO)]$: Cs, 40.32; Re, 28.24; N, 2.12; Cl, 26.89%. $\mu_{eff.}$ (at 291 K)=1.62 B.M. g(at 296 K)=2.01.

$M_2[ReBr_5(NO)]$ (M=Rb and Cs): A 6-mmol portion of NO gas was trapped in a reaction vessel containing 2 mmol of a finely-powdered $K_2[ReBr_6]$ and then heated at *ca.* 400 °C for 12 hr. A dark brown sublimate which was deposited on the wall of the vessel was dissolved in a hot 90% ethanol solution and then refluxed for 12 hr. The resulting brown filtrate was evaporated to dryness on a boiling-water bath. The solid residue thus obtained was dissolved in 25 ml of a hot 5 M hydrobromic acid solution and refluxed for 6 hr at 90 °C to give a greenish brown solution. An 8-mmol portion of rubidium bromide was added to the filtrate, and the mixture was condensed to *ca.* 10 ml on a boiling-water bath. The brown precipitate thus obtained, $Rb_2[ReBr_5(NO)]$, was filtered out, washed with cold concentrated hydrobromic acid, and dried in a vacuum. Yield, 220—500 mg. Found: Rb, 21.6; Re, 23.7; N, 1.69; Br, 50.61%. Calcd for $Rb_2[ReBr_5(NO)]$: Rb, 21.73; Re, 23.67; N, 1.78; Br, 50.79%. $\mu_{eff.}$ (at 291 K)=1.61 B.M. g(at 87 and 296 K)=2.06. $Cs_2[ReBr_5(NO)]$ was prepared by the same procedure; 5 mmol of NO gas, 1 mmol of $K_2[ReBr_6]$, and 8 mmol of caesium bromide were used. Yield, 250—270 mg. Found: Cs, 29.9; Re, 21.7; N, 1.72; Br, 44.97%. Calcd for $Cs_2[ReBr_5(NO)]$: Cs, 30.15; Re 21.12; N, 1.59; Br, 45.32%. $\mu_{eff.}$ (at 291 K)=1.66 B.M. g(at 296 K)=2.08.

$(pyH)_2[ReCl_5(NO)]$ and cis-*$(pyH)[ReCl_4(NO)_2]$*: A mixture of 5 mmol of NO gas and 1.7 mmol of powdered $Ag_2[ReCl_6]$ was heated at *ca.* 320 °C for 5 hr. The brown sublimate thus obtained was dissolved in 100 ml of 99.5% hot ethanol, and the solution was refluxed for 6 hr. The greenish brown filtrate was evaporated to dryness on a water bath, dissolved in 30 ml of an 8 M hydrochloric acid solution, and refluxed for 21 hr at 95 °C to give a dark green solution. 5 mmol of pyridinium chloride in 5 ml of an 8 M hydrochloric acid solution was added to the filtrate, and the mixture was refluxed at 95 °C for 35 hr. The green solution thus obtained was evaporated on a boiling-water bath. The residue was then boiled with 20 ml of 99.5% ethanol for 1 min. The green extract was condensed in a vacuum line to *ca.* 10 ml with the aid of liquid nitrogen to precipitate olive green needles; (pyH)$[ReCl_4(NO)_2]$. Yield, 100 mg. Found: C, 13.49; H, 1.73; N, 8.87; Cl, 30.04%. Calcd for (pyH)$[ReCl_4(NO)_2]$: C, 12.83; H, 1.29; N, 8.98; Cl, 30.29%. χ_g(at 295 K)$=-0.06\times10^{-6}$(c.g.s.). After the olive green needles had been filtered out, a large excess of ether was added to the filtrate to give a green product, $(pyH)_2[ReCl_5(NO)]$. Yield, 50 mg. Found: C, 21.66; H, 2.28; N, 7.74; Cl, 30.44%. Calcd for $(pyH)_2[ReCl_5(NO)]$: C, 21.69; H, 2.18; N, 7.59; Cl, 32.02%. g(at 296 K)=2.02.

Apparatus. The IR spectra of the compounds as Nujol and hexachlorobutadiene mulls were recorded from 200—4000 cm^{-1} on JASCO DS-402G and JASCO model IR-F spectrophotometers. The wave numbers of the observed bands were calibrated with polystyrene film, 1,2,4-trichlorobenzene, and water vapour. The Raman spectra of the solid-state samples were measured from 100—700 cm^{-1} on a JASCO R-800 spectrometer equipped with an Ar ion laser, and on a Narumi 750Z-1200 double monochromator equipped with a He-Ne laser. The magnetic susceptibility was measured by the Gouy method at room temperature. Electron-spin resonance measurements were carried out in a pure powdered solid at room temperature and at the temperature of liquid nitrogen using a JEOL-ME3X spectrometer. The G-values were measured by shift from an external dilute manganese oxide in a magnesium oxide standard. The nuclear magnetic resonance spectra were measured on a

Table 1. Wave numbers, observed isotopic shifts, and assignments of IR and Raman bands due to the ReNO group

Compound	N–O str ($\Delta\nu_{obsd}$)	Skeletal vibrations between Re and NO ($\Delta\nu_{obsd}$)
$Cs_2[ReCl_5(NO)]$	1720 vs (42)	611 s (7), 610(4)[a]
$(pyH)_2[ReCl_5(NO)]$	1736 vs (44)	608 s (3)[b]
$Rb_2[ReBr_5(NO)]$	1728 vs (38)	617 s (9), 619(4)[a]
$Cs_2[ReBr_5(NO)]$	1720 vs (37)	612 s (9), 615(7)[a]

a) Raman band. b) Overlapped with the absorption band due to the pyridinium ion; $\Delta\nu_{obsd}=\nu^{14}$NO-complex(obsd) $-\nu^{15}$NO-complex(obsd); Abbreviations: str=stretching; vs=very strong; s=strong.

Hitachi Perkin-Elmer R-20A High Resolution NMR spectrometer, using tetramethylsilane as the internal standard.

Results and Discussion

$M_2[ReX_5(NO)]$ (M=Rb, Cs, and pyH; X=Cl and Br). The wave numbers, isotopic shifts, and assignments of the IR and the Raman bands due to the ReNO group for the mononitrosyl complexes are shown in Table 1. The N–O stretching vibrations were observed in the 1720—1740 cm^{-1} region. The isotopic shifts upon ^{15}NO-substitution are 37—44 cm^{-1}, and are almost equal to those for the NO$^+$ complexes which were studied in Ref. 1.

Of the IR and Raman bands in the 100—700 cm^{-1} region, only the strong ones in the 610—620 cm^{-1} region shifted downwards by 3—9 cm^{-1} upon ^{15}NO-substitution for all the compounds. These bands are considered to be due to the skeletal vibrations between the rhenium atom and the NO group. The isotopic shifts observed on the IR spectra were found to be larger than those observed on the Raman spectra.

The ^{15}N-isotopic shifts of the N–O stretching, the Re–(NO) stretching, and the Re–(NO) bending vibrations were calculated from the wave numbers of the ^{14}NO-complexes by assuming a linear arrangement of Re–N–O and using a Valence Force Field. For the NO$^+$ complexes, the calculation of the isotopic shifts by means of the three-body model of the metal and the NO group is useful for assigning distinctly the skeletal vibrations when the metal and the ligands other than the NO group are much heavier than nitrogen and oxygen.[1,2] The calculated isotopic shifts of the N–O stretching, Re–(NO) stretching, and Re–(NO) bending vibrations are 40, 5, and 14 cm^{-1} respectively, while their calculated force constants are 11, 6.9, and 0.4 mdyn/Å respectively. The good agreement of the observed isotopic shift for the N–O stretching vibration with the calculated one is considered to support the theory that the oxidation state of the NO group is I, and that, therefore, that of the rhenium atom is II.

The isotopic shift observed on the 610—620 cm^{-1} band(3—9 cm^{-1}) is smaller than that calculated for the Re–(NO) bending vibration (14 cm^{-1}). The isotopic shift observed on the Raman bands is almost equal to that calculated for the Re–(NO) stretching vibration, while the isotopic shift observed on the IR bands is larger than that calculated for the Re–(NO) stretching vibration. These suggest the possibilities that the band due to the Re–(NO) stretching vibration accidentally overlaps with that due to the Re–(NO) bending one, and that the relative intensity of the Re–(NO) stretching band to the Re–(NO) bending one observed on the IR spectra is smaller than that observed on the Raman ones. However, another possibility, that the intensity of one of the skeletal vibrations is too weak to be observed, can not be excluded.

On the basis of IR and Raman studies of the $[MX_5(NO)]^{n-}$ anion (M=Ru, Os, and Ir; X=Cl, Br, and I),[5] the IR bands at 308(vs, b)[6] with a shoulder at 297 cm^{-1}, and 278 cm^{-1}(m) for $Cs_2[ReCl_5(NO)]$ can be assigned to the Re–Cl stretching E mode, ν_{10}, and the A_1 one, ν_4, respectively, and the IR band at 331 cm^{-1}(m) and the Raman one at 329 cm^{-1}, to the Re–Cl stretching A_1 mode, ν_3. The two Raman bands at 166 and 142 cm^{-1} are assigned to the Re–Cl deformation vibrations. The three IR bands at 330(m), 300(vs, b), and 275 cm^{-1}(m) for $(pyH)_2[ReCl_5(NO)]$ are assigned to the Re–Cl stretching vibrations, ν_3, ν_{10}, and ν_4 respectively, for the Cs-salt, while the IR bands at 250(m) and *ca.* 230 cm^{-1}(w) are considered to be due to the pyridinium ion. The Raman band at 212 cm^{-1} for $Rb_2[ReBr_5(NO)]$ and that at 207 cm^{-1} for $Cs_2[ReBr_5(NO)]$ can be assigned to the Re–Br stretching A_1 mode, ν_3, and the IR band at 221 cm^{-1}(vs) for the Rb-salt and that at 218 cm^{-1}(vs) for the Cs-salt, to the Re–Br stretching E one, ν_{10}.

cis-(pyH)$[ReCl_4(NO)_2]$. The IR bands at 1896 (vs), 1795(vs, b), and 1760 cm^{-1}(m) (the N–O stretching vibrations) shifted to 1859, 1756, and 1726 cm^{-1} respectively. The four IR bands in the 490—610 cm^{-1} region shifted upon ^{15}NO-substitution (from 610(s),

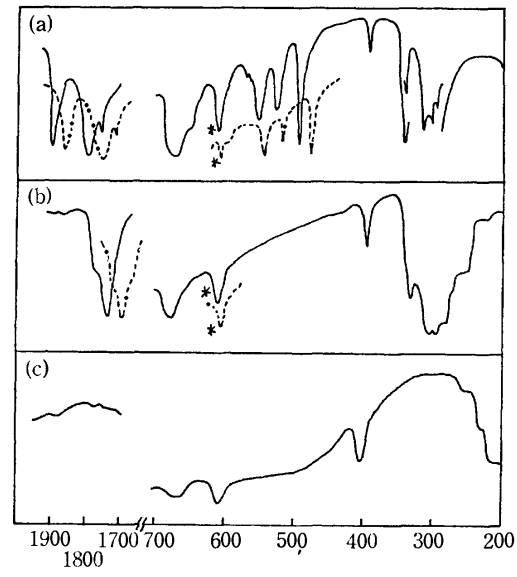

Fig. 1. IR spectra of *cis*-(pyH)$[ReCl_4(NO)_2]$ (a), $(pyH)_2[ReCl_5(NO)]$ (b), and pyHCl (c). ^{14}NO-complex, ——; ^{15}NO-complex(^{15}N atom%=95), ----; in (a) and (b). *; overlapped with the band due to the pyridinium ion.

550(s), 526(s), and 491 cm^{-1}(vs) to 608, 542, 521, and 477 cm^{-1} respectively), as is shown in Fig. 1. The two very strong N–O stretching bands at 1896 and 1795 cm^{-1} suggest the presence of two NO groups in this compound, in a *cis* position to each other. The observed isotopic shifts for the N–O stretching vibrations are about 40 cm^{-1}; hence, the oxidation state of two of the NO groups may be considered to be I.

The ^{15}N-isotopic shifts for the six IR bands in the 490—1900 cm^{-1} region can reasonably be explained on the basis of an O–N–Re–N–O skeleton. If this skeleton belongs to the C_{2v} point group, the number of IR-active bands should be eight. The bands at 1896 and 1795 (and 1760) cm^{-1} can be assigned to the N–O antisymmetric and symmetric stretching vibrations respectively, and the four bands in the 490—610 cm^{-1} region, to the Re–(NO) stretching, its bending, and the N–Re–N bending vibrations. Such a phenomenon was also observed on $[Ir(NO)_2(P(C_6H_5)_3)_2]ClO_4$[1], in which the O–N–Ir–N–O skeleton belongs to the C_{2v} point group.

Two chemical formulae, *cis*-(pyH)$[ReCl_4(NO)_2]$, in which the oxidation state of the rhenium atom is I, and *cis*-$[ReCl_3py(NO)_2]Cl$, in which it is II, are possible, judging from the elementary analyses. However, the latter can be excluded on the basis of the IR spectra. An IR study of pyridine complexes and pyridinium salts has shown that the bands at about 1530—1540 and 1280—1330 cm^{-1} are observed on the pyridinium salts, but not on the pyridine complexes; these are assigned to the N–H deformation vibration and the combination bands involving the N–H deformation.[7] These bands were observed at 1528(s) and 1328(m) for (pyH)$[ReCl_4(NO)_2]$, at 1538(vs) and 1318(m) for pyHCl, and at 1530(s) and 1322 cm^{-1}(m) for $(pyH)_2[ReCl_5(NO)]$. The bands at 393(m) and *ca.* 670 cm^{-1} (vs, b) can be assigned to the ring deformations due to the pyridinium ion, and the other deformation vibration band may overlap with the 610 cm^{-1} band assigned to the skeletal vibrations between the rhenium atom and the NO group.[8] On the basis of the ^{15}N-isotopic shift of the N–O stretching vibrations for *cis*-(pyH)$[ReCl_4(NO)_2]$, the oxidation state of the NO group is considered to be I, —that of the rhenium atom I. The IR spectra for pyHCl, $(pyH)_2[ReCl_5(NO)]$, and *cis*-(pyH)$[ReCl_4(NO)_2]$ are shown in Fig. 1. The bands at 342(s), 311(vs), 300(vs), and 298 cm^{-1}(vs) can be assigned to the Re–Cl stretching vibrations.

The NMR studies of pyHCl and *cis*-(pyH)$[ReCl_4(NO)_2]$ were carried out in $CDCl_3$ and DMSO-d_6, using tetramethylsilane as the internal standard. According to a study of pyHX(X=Cl, Br, and I) by Kotowycz *et al.*,[9] the triplet at δ 8.1—8.3, the triplet at δ 8.6—8.8, and the doublet at δ 8.9—9.1 for (pyH)$[ReCl_4(NO)_2]$ are considered to be due to the C–H protons in the *meta*-, *para*-, and *ortho*-positions respectively. The C–H proton shifts were not so much affected, but the N–H proton shift was sensitive to the counterions, the solvents used, and a trace of water, as is shown in Ref. 9. For pyHCl, the singlet at δ *ca.* 13 in DMSO-d_6 may be assigned to the N–H proton; this peak shifted to a higher magnetic field upon the addition of water to the solvent. The singlet at δ 7.8 for (pyH)$[ReCl_4(NO)_2]$ in DMSO-d_6 may be due to the N–H proton; it shifted to a higher magnetic field upon the addition of water, as was observed on the N–H proton for pyHCl. The integration of the spectra of (pyH)$[ReCl_4(NO)_2]$ and pyHCl in DMSO gives a ratio of the C–H protons to the N–H proton of 5 : 1. The NMR data also suggest the presence of the pyridinium ion in (pyH)$[ReCl_4(NO)_2]$.

The nitrosyl complexes of rhenium so far investigated are not so numerous,[10-12] and the oxidation states of rhenium atoms are 0, I, and II. *cis*-(pyH)$[ReCl_4(NO)_2]$ is the first compound containing an O–N–Re–N–O skeleton in which the oxidation state of the rhenium atom is I.

The authors are indebted to Prof. H. Tadano of Rikkyo University for the measurements of the ESR spectra, and to Mr. H. Saito of Rikkyo University and to Mr. M. Arita of the Japan Spectroscopic Co. Ltd. for the measurements of the Raman spectra. Thanks are also due to Prof. J. Y. Satoh, Dr. C. A. Horiuchi and Miss. K. Suzuki of Rikkyo University for their valuable suggestions and measurements of the NMR spectra.

References

1) E. Miki, K. Mizumachi, T. Ishimori, and H. Okuno, This Bulletin, **46**, 3779 (1973).
2) E. Miki, K. Mizumachi, T. Ishimori, and H. Okuno, *ibid.*, **47**, 656 (1974).
3) D. K. Hait, B. K. Sen, P. Bandyopadhyay, and P. K. Sarkar, *Z. Anorg. Allgem. Chem.*, **387**, 265 (1972); D. K. Hait, B. K. Sen, and P. Bandyopadhyay, *ibid.*, **388**, 184 (1972); Subha Rakshit and P. Bandyopadhyay, *J. Indian Chem. Soc.*, **47**, 1205 (1970).
4) G. W. Watt and R. J. Thompson, "Inorganic Syntheses," Vol. 7, p. 189 (1963).
5) M. J. Cleare, H. P. Fritz, and W. P. Griffith, *Spectrochim. Acta*, **28A**, 2013 (1972).
6) The signs in parentheses indicate the abbreviations of the strength and shape of the absorption band; vs=very strong, s=strong, m=medium, w=weak, b=broad.
7) N. S. Gill, R. H. Nutall, D. E. Scaife, and D. W. A. Sharp, *J. Inorg. Nucl. Chem.*, **18**, 79 (1961).
8) J. R. Durig, B. R. Mitchell, D. W. Sink, J. N. Willis, Jr., and A. S. Wilson, *Spectrochim. Acta*, **23A**, 1121 (1967); R. J. H. Clark and C. S. Williams, *Inorg. Chem.*, **4**, 350 (1965).
9) G. Kotowycz, T. Scheafer, and E. Bock, *Can. J. Chem.*, **42**, 2541 (1964).
10) F. Zingales, A. Trovati, F. Cariati, and P. Uguagliati, *Inorg. Chem.*, **10**, 507 (1971).
11) A. Trovati, P. Uguagliati, and F. Zingales, *ibid.*, **10**, 851 (1971).
12) D. Giusto and G. Cova, *Gazz. Chim. Ital.*, **102**, 265 (1972).

The Gas-chromatographic Behavior of Perhaloalkanes

Ren IWATA, Yoshihiro MAKIDE, and Takeshi TOMINAGA*

Department of Chemistry, Faculty of Science, The University of Tokyo, Bunkyo-ku, Tokyo 113

(Received July 1, 1974)

The retention indices of perhaloalkanes (perbromochlorofluoroalkanes, *etc.*) were measured by using a gas chromatograph with a squalane, Silicone DC 550, or Methoxy polyethylene glycol 350 column, and the correlation of the retention index with various physicochemical parameters was investigated. The retention index was found to correlate linearly with the composition of the halogen atoms in the perhaloalkane molecules; the correlation diagram appears to be of special analytical importance. The relationship between the retention index and the boiling point was also studied. The retention index was correlated linearly with the molar refractivity of the perhaloalkanes, irrespective of the polarity of the columns. The molar refractivity appears to be the inherent parameter which is most adequate for considering the regularity of the retention index. The effect of the polarity of the stationary phase on the retention index was also investigated.

In the course of our study of the recoil and radiolysis reactions in perchlorofluoroalkanes,[1-3] it became necessary to investigate systematically the gas-chromatographic behavior of perhaloalkanes (perbromochlorofluoroalkanes, *etc.*). If the correlation between the retention data and certain physicochemical parameters is established, it may facilitate the identification of unknown products gas-chromatographically without the need to refer to pure standard substances which are not readily available and without the aid of other, complementary means of analyses.

A number of works have been published on the gas-chromatographic behavior of homologous organic compounds. However, perhaloalkanes have received only a little attention,[4,5] and no systematic study of perbromochlorofluoroalkanes had been reported before our preliminary work.[6] The object of the present article is to determine the Kováts retention indices[7] for a number of perhaloalkanes and to study the correlation of those retention indices with various physicochemical parameters.

Experimental

Materials. CBr_3F, $CBrClFCClF_2$, $CBrClFCBrF_2$, and CBr_2FCBrF_2 were synthesized chemically in this laboratory. $CBrClF_2$, $CBrCl_2F$, $CBrF_2CF_3$, and $CBrF_2CClF_2$ were prepared by the γ-irradiation of mixtures of perchlorofluoroalkanes and bromine.[2] The other perhaloalkanes used in this work were obtained commercially from Matheson Gas Products, Inc., PCR, Inc., and the Tokyo Chemical Industry Co.

Determination of Retention Times and Retention Indices. The retention times were measured at a constant temperature between 0 and 100 °C by using a gas chromatograph equipped with a thermal conductivity detector. A water bath was used to keep the column temperature constant over the 0-60 °C range. A stainless steel column (I.D.: 3mm; length: 5m) was packed with squalane, Silicone DC 550, or Methoxy polyethylene glycol 350, 20%-coated on acid-washed Chromosorb W (80-100 mesh). The flow rate of the helium was 15 ml/min. The adjusted retention times obtained at 30 °C were first converted to specific retention volumes,[8] and then these in turn were converted to retention indices according to the following formula:

$$I_x = 100 \cdot \left[z + \frac{\log V_{g(x)} - \log V_{g(z)}}{\log V_{g(z+1)} - \log V_{g(z)}} \right]$$

where I_x denotes the retention index of a compound, x; $V_{g(x)}$, the specific retention volume of x, and $V_{g(z)}$ and $V_{g(z+1)}$, the specific retention volumes of two successive normal alkanes with carbon numbers of z and $z+1$ respectively, which were chosen so that $V_{g(z)} \leq V_{g(x)} < V_{g(z+1)}$.

Results and Discussion

The retention indices obtained for perhaloalkanes indicate an additivity with respect to the number of halogen atoms. Figures 1 and 2 reveal the correlation of the retention index, as measured by means of a Silicone DC 550 column, with the number of halogen atoms in perhalomethane and perhaloethane molecules respectively. The observed values for the γ-radiolysis products (closed circles in Figs. 1 and 2) are plotted nearly at the expected lattice positions of the correlation network. When a halogen atom is replaced by another halogen atom, the increase in the retention index due to the substitution was in the order: Br–for–Cl < Cl–for–F < Br–for–F. Furthermore, the magnitude of the change in the retention index for the same type of halogen substitution remains nearly identical, irrespective of the number of carbon atoms in the perhaloalkane molecules. This fact reveals that the regularity in the retention indices of C_1 and C_2 perhaloalkanes can be ascribed to the property inherent in each halogen atom rather than to that in a perhaloalkane molecule as a whole. We obtained diagrams similar to Figs. 1 and 2 for perhalomethanes and perhaloethanes on squalane and Methoxy polyethylene glycol 350 columns. The correlation was still good, irrespective of the polarity of the stationary phase, whereas the change in the retention index due to halogen substitution was enhanced by increasing the polarity.

While such a correlation appears to be very useful for analytical purposes, it cannot account for the essential nature of the observed regularity.[9] A linear correlation was obtained between the retention index and the boiling point, as is illustrated for perhaloalkanes on a squalane column in Fig. 3. The slope of the correlation curve (straight line) for perhaloethanes is larger than that for perhalomethanes. A similar relationship was obtained with a Silicone DC 550 column. Unlike on such a non-polar or slightly polar column, some plot-points deviate from the linear correlation

* To whom all correspondence should be addressed.

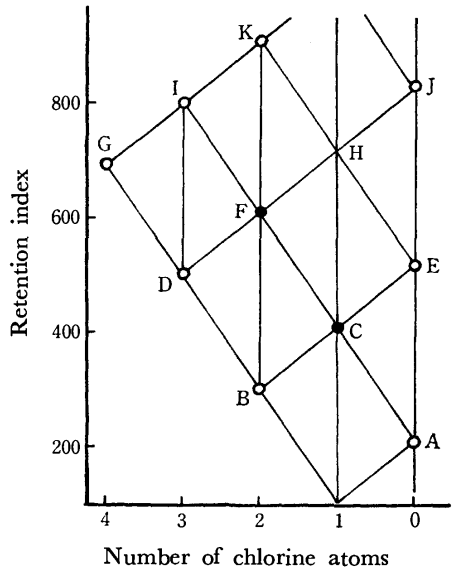

Fig. 1. Correlation between the retention index measured with a Silicone DC 550 column and the halogen composition of perhalomethanes.
In Fig. 1 and Figs. 3-6, (A): $CBrF_3$, (B): CCl_2F_2, (C): $CBrClF_2$, (D): CCl_3F, (E): CBr_2F_2, (F): $CBrCl_2F$, (G): CCl_4, (H): CBr_2ClF, (I): $CBrCl_3$, (J): CBr_3F, (K): CBr_2Cl_2

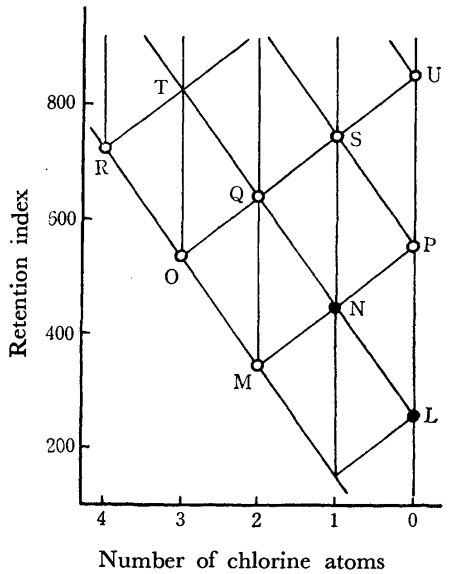

Fig. 2. Correlation between the retention index measured with a Silicone DC 550 column and the halogen compositlon of perhaloethanes.
In Figs. 2-6, (L): C_2BrF_5, (M): $C_2Cl_2F_4$, (N): C_2BrClF_4, (O): $C_2Cl_3F_3$, (P): $C_2Br_2F_4$, (Q): $C_2BrCl_2F_3$, (R): $C_2Cl_4F_2$, (S): $C_2Br_2ClF_3$, (T): $C_2BrCl_3F_2$, (U): $C_2Br_3F_3$

on a strongly polar Methoxy polyethylene glycol 350 column (Fig. 4), since the presence of bromine in the perhaloalkane molecules tends to increase their retention indices systematically (for example, the broken line in Fig. 4).

It is known that molar refractivity is an additive quantity and can be approximated by summing up the refractivities of the atoms composing the molecule.

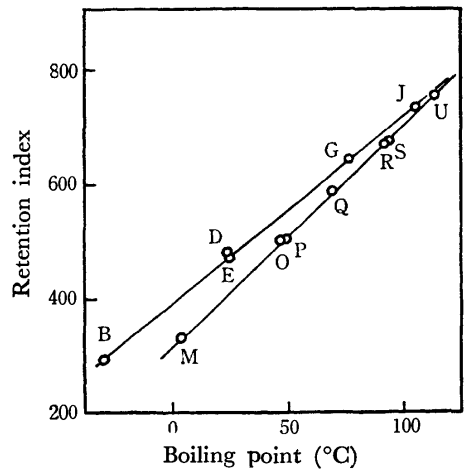

Fig. 3. Correlation between the retention index measured with a squalane column and the boiling point of perhaloalkanes.

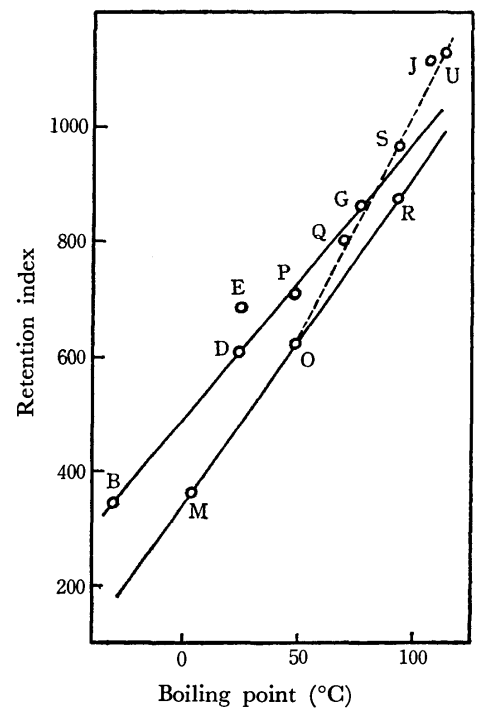

Fig. 4. Correlation between the retention index measured with a Methoxy polyethylene glycol 350 column and the boiling point of perhaloalkanes.

The molar refractivity can be linearly related to the electron polarizability taking part as dispersion and induction energies in the solvent-solute interactions. Hence, the molar refractivity can be taken as the parameter of the interaction between the solute (perhaloalkanes) and the solvent (stationary phase). The relationship between the molar refractivity[10] and the retention index of perhaloalkanes, as measured with a Silicone DC 550 column, is shown in Fig. 5. A linear correlation was observed with perhaloalkanes containing the same number of carbon atoms. Unlike the case of the correlation with the boiling point, the slopes of the correlation curves (straight lines) are nearly identical, irrespective of the number of carbon atoms.

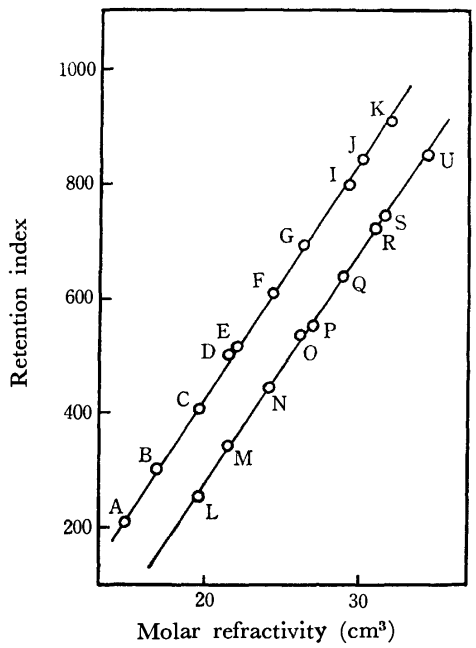

Fig. 5. Correlation between the retention index measured with a Silicone DC 550 column and the molar refractivity of perhaloalkanes.

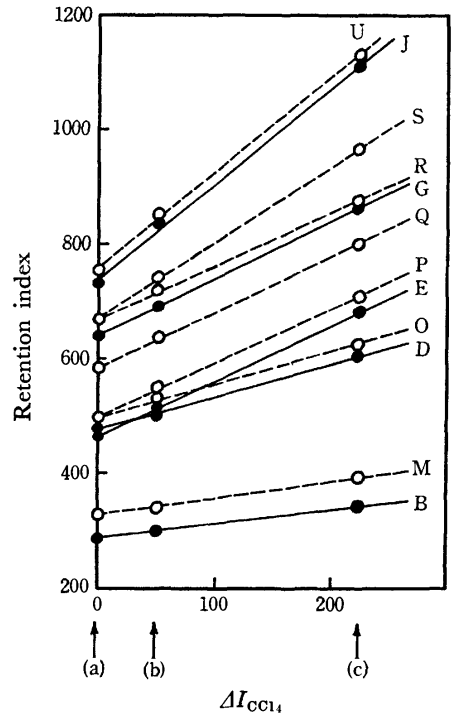

Fig. 6. The relationship of the retention index with the polarity of the stationary phase (in terms of ΔI_{CCl_4}). (a): squalane, (b): Silicone DC 550, (c): Methoxy polyethylene glycol 350.

Almost identical relationships were obtained with squalane and Methoxy polyethylene glycol 350 columns. These observations reveal that, for the perhaloalkanes studied in this work, the molar refractivity may be the inherent parameter, which is most suitable for considering the regularity of the retention index.

As in the case of Rohrschneider's characterization of the stationary phase,[11] we have investigated the influence of the polarity of the stationary phase on the retention indices of the perhaloalkanes. For convenience in comparing the polarity, the increase in the retention index of carbon tetrachloride obtained with an arbitrary polar stationary phase over that obtained with the non-polar stationary phase (squalane) is given as follows:

$$\Delta I_{CCl_4} = I_{CCl_4}(\text{polar}) - I_{CCl_4}(\text{non-polar})$$

Then, the value of ΔI_{CCl_4} obtained with an arbitrary stationary phase is presumed to be a measure for indicating the polarity of the stationary phase. In Fig. 6 are plotted the retention indices of perhaloalkanes against ΔI_{CCl_4}, or the polarity of the stationary phase. It is worth mentioning that the retention indices of all the perhaloalkanes studied in this work are correlated linearly with this measure. Since the retention indices for a new stationary phase can be predicted by measuring the retention index of CCl_4 with that stationary phase, the relationship illustrated in Fig. 6 appears to be very useful for the selection of a new stationary phase.

The present authors wish to express their thanks to Professor Nobufusa Saito, the University of Tokyo, for his encouragement and support.

References

1) T. Tominaga, Y. Makide, S. Okada, Y. Kunimasa, and K. Wada, *Radioisotopes*, **20**, 541 (1971).
2) T. Tominaga, R. Iwata, and Y. Makide, *Chem. Lett.*, **1972**, 871.
3) T. Tominaga, R. Iwata, and Y. Makide, This Bulletin, **46**, 1882 (1973).
4) H. Rotzsche, *Z. Anal. Chem.*, **175**, 338 (1960).
5) A. Foris and J. G. Lehman, *Sep. Sci.*, **4**, 225 (1969).
6) T. Tominaga, R. Iwata, and Y. Makide, *Chem. Lett.*, **1973**, 485.
7) E. Kovâts, *Helv. Chim. Acta*, **41**, 1915 (1958); ASTM, E 355-68 (1968).
8) Since boiling points of perhaloalkanes fall within a wide range, it is difficult to measure all the retention times at one common temperature. Accordingly, the retention times of higher boiling perhaloalkanes measured at higher temperatures were all converted to the values at 30 °C, by extrapolation of the linear correlation between the logarithm of the specific retention volume and the reciprocal of the absolute column temperature.
9) Similar correlation diagrams can be obtained with other additive parameters such as molecular weight. However, they do not represent linear correlations.
10) A. H. Fainberg and W. T. Miller, Jr., *J. Org. Chem.*, **30**, 864 (1965).
11) L. Rohrschneider, *Z. Anal. Chem.*, **236**, 149 (1968); *J. Chromatogr. Sci.*, **11**, 160 (1973).

Oxidation Activity and Acidity of V_2O_5–P_2O_5 Catalyst

Mamoru Ai and Sadao Suzuki

Research Laboratory of Resources Utilization, Tokyo Institute of Technology, Ookayama, Meguro-ku, Tokyo 152

(Received January 9, 1974)

The oxidations of 1-butene, butadiene, and hydrogen in a large excess of air were carried out over various V-P oxide catalysts with different P_2O_5 contents. The oxidation activities were compared with the dehydration activity for isopropyl alcohol, which was used as a measure of the acidity of the catalysts. The surface area and the acidity per unit of surface area sharply decrease with an increase in the P_2O_5 content up to about 20 mol% P_2O_5, while with a further increase in the P_2O_5 they remain almost unchanged. The activity per unit of surface area for the oxidation of butene and butadiene, as well as that for the isomerization of butene, changes in the same direction as the acidity per unit of surface area. The equilibrium constant for the adsorption of olefin changes analogously. The activity per unit of surface area for the oxidation of hydrogen is not affected by the P_2O_5 content. The effects of the P_2O_5 introduced into V_2O_5 on the activity and selectivity are discussed from the viewpoint of the acidic nature of the catalysts.

The oxidation of olefins to carboxylic acids, usually performed at very high conversions using small amounts of olefins in excess air, belongs to the category of the selective oxidations, different from the oxidation to epoxide and those to dienes and aldehydes. The basic requirements for the acid-formation reaction have not yet been satisfactorily defined, since only a few fundamental studies have been made of it, in contrast to the numerous studies of the two above-cited types of oxidations.[1,2] The catalysts used for the acid-formation reactions are generally mixed metal oxides based, in most cases, on V_2O_5, but sometimes on MoO_3, WO_3, SeO_2, As_2O_5, *etc.* It should be noted that all of those substances are typical acidic oxides.

In the oxidation of butadiene to maleic anhydride, most V_2O_5-based catalysts give a relatively high selectivity of 50—60 mol%, while when butene is used as the starting material, the high selectivity of 40—50 mol% is limited to the V_2O_5-based catalysts containing large amounts of P_2O_5. We found in earlier studies[3–5] that the inclusion of P_2O_5 in V_2O_5 increases the selectivity in the first step in the series of consecutive steps from butene to maleic anhydride···that is, in the step of allylic oxidation; $C_4H_8 \rightarrow C_4H_6$.

The present paper is an attempt to make an improvement in the study of the P_2O_5 effect by introducing the idea that the acidic nature of the catalyst governs to a considerable extent the activity and selectivity of the mild oxidations.[6–10]

Experimental

The vapor-phase oxidation of 1-butene, 1,3-butadiene, and hydrogen, the dehydration of *iso*-propyl alcohol (IPA), and the dehydrogenation of ethanol were carried out over a series of vanadium-phosphorus (V_2O_5–P_2O_5) catalysts, while varying the P_2O_5 content from 0 to 67 mol%, in an ordinary continuous-flow-type reaction system, The concentrations of butene, butadiene, hydrogen, IPA, and ethanol were, unless otherwise indicated, about 0.67, 0.67, 3.0, 1.65, and 2.2 mol% in air respectively. The total flow rate (at 25 °C) was kept constant at 1.5 l/min, and the amount of the catalyst used was 2—20 g. The reactor and the experimental and analytical procedures were the same as those employed in previous works.[3–10]

The catalysts used in these experiments were prepared as follows; the required quantities of NH_4VO_3 and H_3PO_4 were dissolved in hot water, together with oxalic acid, if necessary, after which 10—20 mesh pumice was mixed with the solution; then the mixture was evaporated with vigorous stirring. The amount of pumice was 500 ml (about 150 g)/g atom of vanadium and phosphorus. The catalyst was subsequently calcined, under flowing air, at 500 °C for about 4 hr.

Results

Surface Area. The surface area of the catalysts was measured by the BET method using nitrogen at −195 °C (Table 1). It falls markedly with an increase in the P_2O_5 content up to 20 mol% P_2O_5.

Acidity of the Catalyst. Since it is difficult to measure directly the acidity of the V_2O_5–P_2O_5 catalysts, we used the activity for the dehydration of IPA as a measure of the acidity, much as in previous works.[7,8]

A gaseous mixture of IPA and air was passed over 2—10 g of the catalyst at temperatures of 160—220 °C.

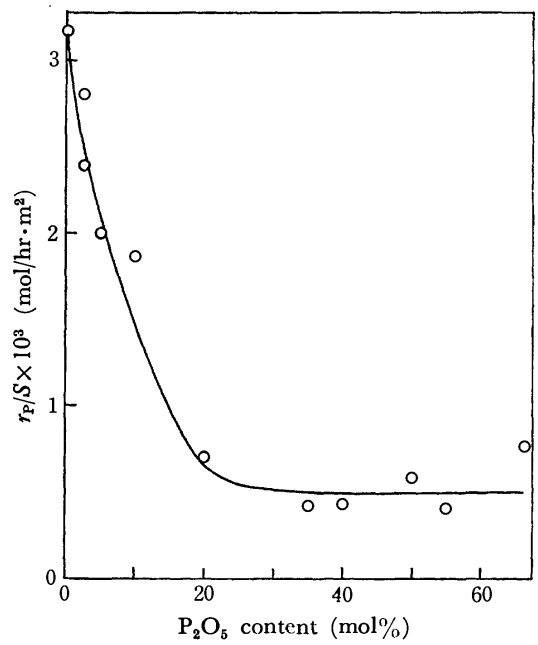

Fig. 1. Rate of IPA dehydration per unit surface area (r_P/S) as a function of the P_2O_5 content. Temp= 185°C, IPA=1.65mol% in air.

Table 1. Properties and activities of V_2O_5-P_2O_5 catalysts

Catalyst compd P/V	Surface area (m^2/g)	Rate of IPA dehydration $r_p \times 10^3$	Dehydrogenation of ethanol: Rate $r_a \times 10^3$	Dehydrogenation of ethanol: $CH_3CHO/CH_2=CH_2$	Isomerization of 1-butene: Rate $I \times 10^2$	Isomerization of 1-butene: $cis\text{-}C_4H_8/trans\text{-}C_4H_8$	Oxidation activities for: Butene $r_B \times 10^4$	Oxidation activities for: Butadiene $r_B' \times 10^4$
0/100	3.5	11.2	19.2	19	3.94	1.1	25	37
2.5/97.5	3.14	7.5	14.1	12	2.62	1.2	10.7	10
2.5/97.5	3.0	8.4						16
5/95	2.6	5.4						
10/90	1.4	2.7	3.3	12	1.01	1.2	5.4	3.5
20/80	0.71	0.5			0.45	1.25	1.0	
35/65	0.69	0.3			0.40	1.3	0.58	1.2
40/60	0.66	0.32			0.2	1.2	0.5	1.5
50/50	0.75	0.30	0.4	1.3	0.3	1.1	2.7	1.5
55/45	1.05	0.4					2.5	0.8
67/33	1.0	0.9			0.45		3.1	0.5

As has been reported in the previous papers,[7-10] propylene was the main product and the rate was almost independent of the IPA concentration at about 185 °C.

The initial rate of the dehydration at 185 °C, r_p (mol/hr·g-cat), was chosen as a measure of the acidity (Table 1). The activity per unit of surface area, r_p/S (mol/hr·m^2), is plotted as a function of the P_2O_5 content in Fig. 1. r_p/S falls sharply with the P_2O_5 content in the P_2O_5<20 mol% region and remains almost unchanged with a further increase in the P_2O_5.

Basicity of the Catalyst. As the basicity of the simple V_2O_5 catalyst is very small (the amount of the adsorption of acetic acid vapor at 150 °C, as measured by means of a chromatographic method,[11] was 1—2 μmol/g-cat, while that of CO_2 at 20 °C, as measured by a conventional static apparatus, was $1—2\times10^{-2}$ ml/g-cat (0.5—1 μmol/g-cat)), it seems hard to get reliable data on the basicity of the V_2O_5–P_2O_5 catalysts by these methods.

It has been reported[12-16] that the dehydrogenation of alcohol is related to the basic properties of the catalyst, although the reaction mechanism has not yet been established firmly. Since, on the V_2O_5–P_2O_5 catalysts, the activity for the dehydrogenation of IPA is very small compared with that for its dehydration, the reaction of ethanol was carried out in a manner similar to that of IPA. The initial rate of the dehydration of ethanol to acetaldehyde at 260 °C, r_a (mol/hr·g-cat), and the ratio of acetaldehyde/ethylene are listed in Table 1. These results suggest that the basic properties of the catalyst also decrease upon the addition of P_2O_5.

Isomerization of Butene. The oxidation of butene over V_2O_5-type catalysts is always accompanied by its isomerization, which is generally said to be attributable to acidic or basic sites of the catalyst. As a measure of the isomerization activity, we adopted for convenience the ratio of (*cis*-2-C_4H_8+*trans*-2-C_4H_8)/(1-C_4H_8+*cis*-2-C_4H_8+*trans*-2-C_4H_8); I under these conditions: temperature of 260 °C, 1-butene of 0.67 mol% in air, a catalyst of 5~20 g. The results are also listed in Table 1. Figure 2 shows the relation between the isomerization activity per unit of area (I/S) and the acidity per unit of area (r_p/S). The *cis*-2-C_4H_8/*trans*-2-C_4H_8 ratio is about 1.2 for every catalyst. These results indicate that the isomerization of olefin is catalyzed by acidic sites of the catalyst.[17]

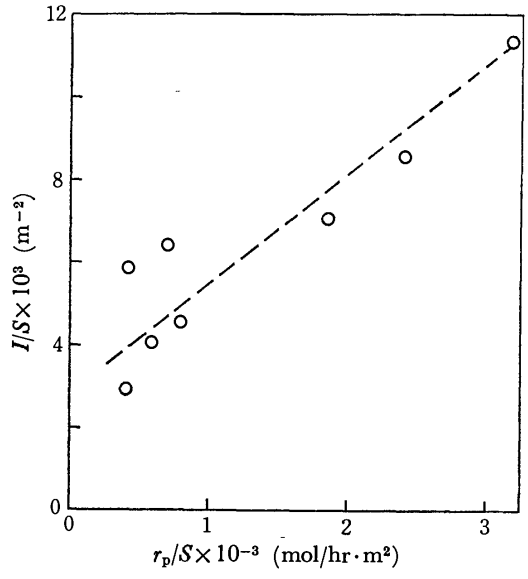

Fig. 2. Relation between I/S and r_p/S.
Isomerization; 260°C, 0.67mol% 1-C_4H_8 in air,
$$I=\frac{(cis\text{-}2\text{-}C_4H_8+trans\text{-}2\text{-}C_4H_8)}{(1\text{-}C_4H_8+cis\text{-}2\text{-}C_4H_8+trans\text{-}2\text{-}C_4H_8)}$$
The variation in these activities has been effected by changing the P_2O_5 content.

Oxidation Activity for Olefins. The effects of the P_2O_5 content on the activity for the oxidation of such olefins as 1-butene and butadiene were examined. The reaction was carried out at 330 °C. The initial rates of the overall consumption of butene and butadiene, r_B and r_B' (mol/hr·g-cat), were also obtained; they are listed in Table 1. The activities for butene and butadiene vary in a similar way and fall sharply with the P_2O_5 content when the P_2O_5 catalyst is less than 20 mol%.

Figure 3 shows the relation between the oxidation activities for olefins per unit of surface area, r_B/S and r_B'/S, and the acidity per unit of surface area. It is found that the oxidation activity for olefins increases with an increase in the acidity of the catalyst.

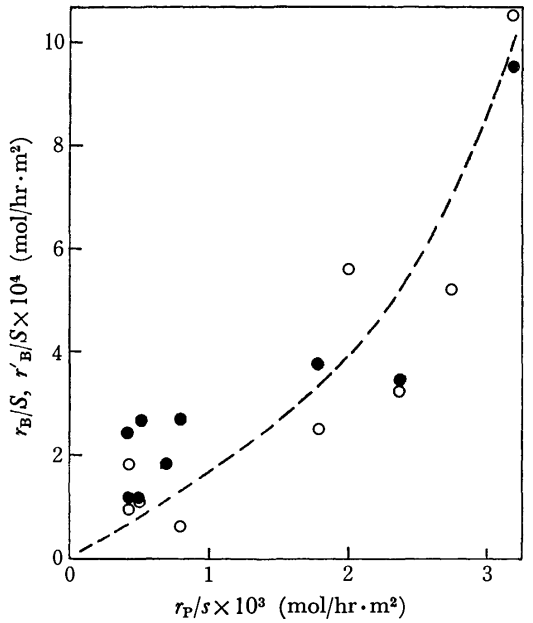

Fig. 3. Oxidation activities for olefins *versus* dehydrantio activity for IPA. The variation in these activities has been effected by changing the P_2O_5 content. ●=butene oxidation (r_B/S), ○=butadiene oxidation (r'_B/S), at 330°C.

Oxidation Activity for Hydrogen. It has been established that hydrogen and parafinic hydrocarbons act upon metal-oxide catalysts as electron donors to some extent. However, this tendency might be so weak that the oxidation activity for these compounds is really governed by the availability of surface oxygen rather than by the activation of the reactant.[18] This leads us to consider that the oxidation activity for hydrogen reflects the availability of oxygen in some measure at least.

Since hydrogen was quite stable compared with olefins and IPA over the V_2O_5–P_2O_5 catalysts, a high temperature of more than 400 °C was required to achieve appreciable conversion. The initial rates of hydrogen consumption at 435 °C, r_H (mol/hr·g-cat) and r_H/S (mol/hr·m²), are plotted as a function of the P_2O_5 content in Fig. 4. It is found that the activity decreases with the P_2O_5 content, but the activity per unit of surface area remains almost unchanged within the range of experimental error.

Adsorption of Olefin. Information on the affinity of olefin for the catalysts may be obtained if the oxidation rates conform to the following Langmuir-Hinshelwood type equation:

$$r = k\cdot N_a\cdot N_0\cdot\left(\frac{KP}{1+KP}\right)\cdot\left(\frac{K_0{}^nP_0{}^n}{1+K_0{}^nP_0{}^n}\right)$$

where r is initial rate of oxidation, k is the rate constant, N_a and N_o are the numbers of sites available for olefin and oxygen, K and K_0 are the equilibrium constants for the adsorption of olefin and oxygen, and P and P_0 are the partial pressures of olefins and oxygen respectively. When oxygen is in a large excess with respect to olefin and P_0 remains constant, $N_0\cdot K_0{}^n\cdot P_0{}^n/(1+K_0{}^nP_0{}^n)$ is a constant value for any one catalyst. Therefore, the above equation can be simplified as:

$$r = k'\cdot\frac{KP}{1+KP},$$

where $k'=k\cdot N_a$.(availability of surface oxygen).

To test this equation, another series of butadiene oxidations was carried out at 330 °C by changing the initial concentration from 0.24 to 1.9 mol% in air (partial pressure=0.24×10^{-2}—1.9×10^{-2} atm). The value of r was obtained at each P for every catalyst. Figure 5 shows a plot of P/r against P.

Good linear relations were obtained between P/r and P for every catalyst; this indicates the validity of the above equation. The values of k' and K were

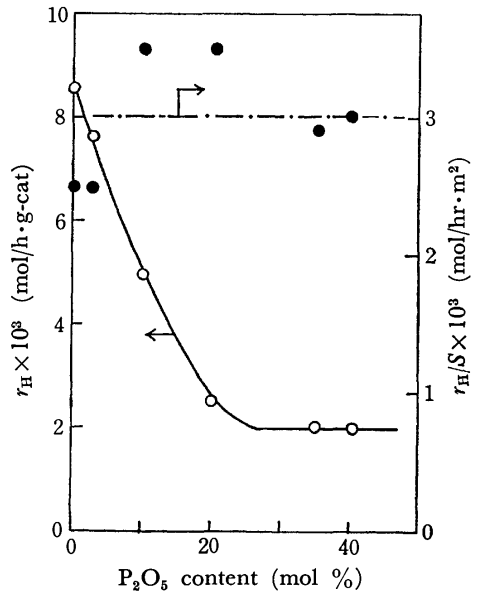

Fig. 4. Oxidation rate of hydrogen (r_H) and the specific rate r_H/S) as a function of the P_2O_5 content. Temp=430°C, hydrogen=3 mol% in air, ○=r_H, ●=r_H/S.

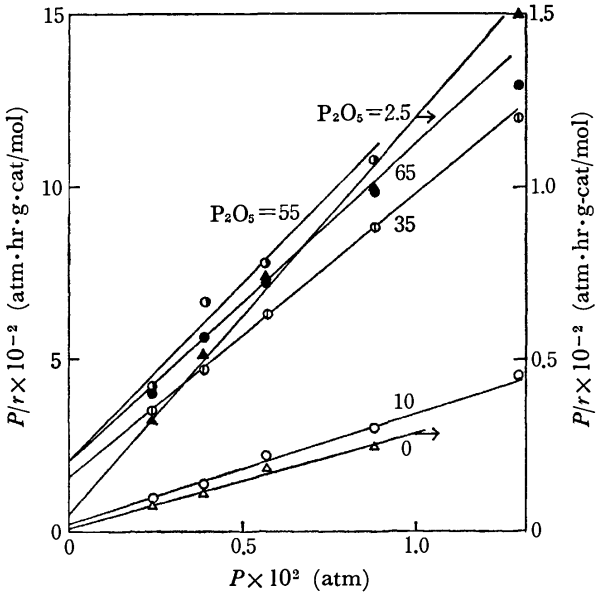

Fig. 5. Test of equation; $r=k'\cdot\frac{KP}{1+KP}$: a plot of P/r *versus* P.

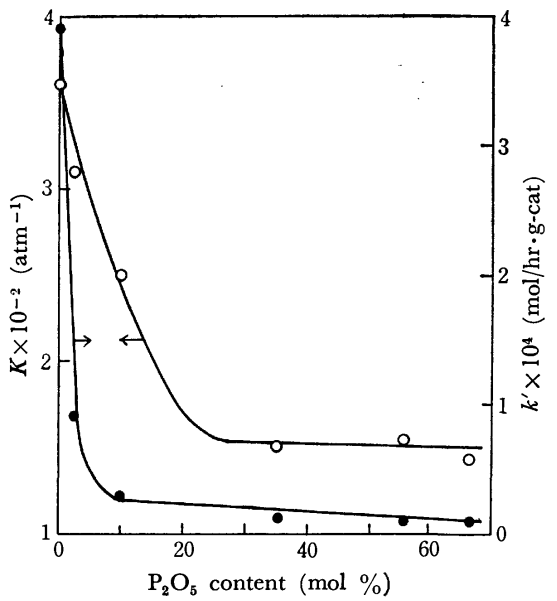

Fig. 6. The values of K and k' *versus* the P_2O_5 content. ○=K, ●=k'.

calculated from the slopes and from the intersections with the ordinate. They are plotted as a function of the P_2O_5 content in Fig. 6. K decreases with the P_2O_5 value up to about 20 mol% P_2O_5, much like the acidity, r_p/S (Fig. 6).

The temperature-dependency of k' and K was also examined (Table 2). The activation energies of the oxidation (E) were in the neighborhood of 20 kcal/mol, and the effect of the P_2O_5 content on the value of E was not clear. The values of K were almost independent of the temperature. It was also found that the amount of butadiene adsorbed on the simple V_2O_5 measured directly by a static apparatus was about 0.1 ml STP/g-cat, almost independent of the temperature in the region of 20—200 °C, and that no adsorption of butadiene was detected by a usual gas-chromatographic technique.[19] These results also suggest that the bond of olefin on the V_2O_5-type catalyst is so loose that the heat of the adsorption cannot be obtained.

Table 2. Values of k' and K

Catalyst P/V	Temp (°C)	$k'\times10^4$ (mol/hr·g)	E (kcal/mol)	$K\times10^{-2}$ (atm^{-1})
0/100	283	1.17	20	4.1
	294	1.63		3.9
	305	2.3		4.2
10/90	294	0.30	18	2.3
	305	0.43		2.3
50/50	317	0.18	25	1.2
	330	0.29		1.0

Discussion

The introduction of P_2O_5 to V_2O_5 causes a decrease in both (1) the surface area and (2) the acid-base properties. The action is remarkable only in the low P_2O_5 range. Probably, the active species of V_2O_5 are gradually modified into other kinds of species with the inclusion of P_2O_5 up to about 20 mol%, while a further increase in the P_2O_5 content causes no substantial change in the nature of the active species.

The decrease in the surface area may be, in part, associated with the fact that a sort of fusion appears at the beginning of the calcination, especially for the catalysts containing relatively high P_2O_5 values.

It should be noted that P_2O_5 is a unique additive which decreases the acidity as well as the basicity of the V_2O_5 catalyst (the additions of all the other oxides, such as Al_2O_3, WO_3, MoO_3, SO_3, and TiO_2, which increase the acidity of the V_2O_5 catalyst decrease the basicity).[20]

By taking into account the fact that the affinity of the catalyst for such basic compounds as olefins reflects the acid strength, the results shown in Fig. 6 suggest that the acid strength of the catalyst also decreases with an increase in the P_2O_5 content and changes in the same direction with the acidity, as has often been observed.[21]

The results shown in Fig. 4 suggest that the availability of surface oxygen (r_H/S) is almost uninfluenced by the P_2O_5 addition. However, this does not accord with the fact that the basicity of the catalyst, which is supposed to be related to the activation of an electron-acceptor-type reactant (oxygen),[20,22] decreases with the P_2O_5 addition. Even if the availability of oxygen decreases with the P_2O_5 addition, it may be considered, from the results of Fig. 3, that the activity for the oxidation of olefins on the acidic-metal oxides is predominantly dependent on the activation of olefins; this phenomenon may be attributed to the acidic sites of the catalyst, as has already been observed by us in the cases of MoO_3–Bi_2O_3–P_2O_5,[6] MoO_3–P_2O_5–X_nO_m,[9] MoO_3–P_2O_5,[10] and V_2O_5–MoO_3.[23] Recently a similar conception has been proposed by Haber *et al.*[24]

Concerning the selectivity to maleic anhydride,[5] the acidic property may be a requirement for satisfactory catalysts for such a type of partial oxidation as basic reactant→acidic product, because the acidic catalysts are active in relation to the basic reactant and inactive in relation to the acidic product. This conception holds well for the oxidation of butadiene.[6,8,20,22] However, in the case of butene oxidation. another factor must also affect the selectivity. When butene is oxidized over V_2O_5-based catalysts not containing P_2O_5, the C–C fission, probably at the double bond,[25] takes place in preference to the allylic C–H fission and the main products are oxygen-containing compounds with a lower number of carbon atoms, such as acetic acid, which are easily oxidized to CO_2 or CO, while in the case of butadiene, the C–C fission is not the main reaction.[20] It is, therefore, conceivable that the selectivity of butene to maleic anhydride is greatly controlled by the C–C fission of butene.[3-5]

The decrease in the activity for the C–C fission of butene due to the P_2O_5 addition is probably attributable either to the acidic or basic properties of the catalyst. The addition of such metal oxides as Al_2O_3, TiO_2, MoO_3, and WO_3 decreases the basicity of the V_2O_5 catalyst. However, it promotes the oxidation of butene to acetic acid.[20] Therefore, it should be considered

that the activity for the C–C fission is related to the acidic property—strictly speaking, the acid strength. That is to say, the catalyst must be acidic in order to get acidic products, but the acidic nature is necessary in an appropriate strength for the maximum selectivity from butene; too high a acid-strength destroys the C–C bond of butene and decreases the selectivity.

We would like to consider that the addition of P_2O_5 to V_2O_5-based catalysts plays a role in lowering the acid strength to a proper extent and, consequently, in suppressing the C–C fission of butene and increasing the selectivity in the step of allylic oxidation: $C_4H_8 \rightarrow C_4H_6$.

References

1) C. F. H. Tipper, "Oxidation and Combustion Reviews," Vol. 1, Elsevier, Amsterdam (1965), p. 271.
2) H. H. Voge and C. R. Adams, "Advances in Catalysis," Vol. 17, Academic Press, New York (1968), p. 151.
3) M. Ai, T. Niikuni, and S. Suzuki, *Kogyo Kagaku Zasshi*, **73**, 165 (1970).
4) M. Ai, K. Harada, and S. Suzuki, *ibid.*, **73**, 524 (1970).
5) M. Ai, This Bulletin, **43**, 3490 (1970).
6) M. Ai and S. Suzuki, *J. Catal.*, **26**, 202 (1972).
7) M. Ai and S. Suzuki, This Bulletin, **46**, 321 (1973).
8) M. Ai and S. Suzuki, *ibid*, **46**, 1208 (1973).
9) M. Ai and S. Suzuki, *Bull. Japan Petro. Inst.*, **15**, 18 (1973).
10) M. Ai and S. Suzuki, *J. Catal.*, **30**, 362 (1973).
11) O. V. Krylov and E. A. Fokina, *Probl. Kinet. Katal., Akad. Nauk. S. S. S. R.*, **8**, 248 (1955).
12) R. Mars, "The Mechanism of Heterogeneous Catalysis" (J. H. de Boer ed.) Elsevier, Amsterdam (1960).
13) K. Tanaka and K. Tamaru, This Bulletin, **37**, 1863 (1962).
14) N. Pernicone, F. Lazzerin, G. Liberti, and G. Lanzavecchia, *J. Catal.*, **14**, 293 (1969).
15) H. Niiyama and E. Echigoya, This Bulletin, **44**, 1739 (1971).
16) C. L. Kibby and W. K. Hall, *J. Catal.*, **31**, 65 (1973).
17) M. Ito, H. Hattori, and K. Tanabe, *Shokubai*, **15**, 88p (1973).
18) W. M. H. Sachtler and N. H. de Boer, 3rd Intern. Congress on Catalysis, Amsterdam, 1964, *I*, 252 (1965).
19) M. Ai, A. Ozaki, and E. Echigoya, *Bull. Japan Petro. Inst.*, **7**, 46 (1965).
20) M. Ai and S. Suzuki, 33rd Shokubai (Catalyst) Meeting Preprint, p. 116 (1973).
21) K. Shibata, T. Kiyoura, J. Kitagawa, T. Sumiyoshi, and K. Tanabe, This Bulletin, **46**, 2985 (1973).
22) M. Ai and S. Suzuki, *Shokubai*, **15**, 159p (1973).
23) M. Ai and S. Suzuki, *Nippon Kagaku Kaishi*, **1973**, 260.
24) J. Haber and B. Crzybowska, *J. Catal.*, **28**, 489 (1973).
25) L. N. Kutseva and L. Ya. Margolis, *J. Gen. Chem. U. S. S. R.* (English Transl.), **32**, 100 (1962).

Abnormal Benzo Substituent Effect on Free Radical Formation Process. A Local Symmetry Effect

Iwao TABUSHI,* Zen-ichi YOSHIDA,** and Yasuhiro AOYAMA**,***

Department of Pharmaceutical Sciences, Kyushu University, Katakasu, Fukuoka 812

***Department of Synthetic Chemistry, Kyoto University, Yoshida, Sakyo-ku, Kyoto 606*

(Received January 30, 1974)

Relative stabilities of 1-bicyclo[2.2.2]octyl (**9**), 1-benzobicyclo[2.2.2]-octenyl (**10**), 1-dibenzobicyclo[2.2.2]octadienyl (**11**), and 1-tribenzobicyclo[2.2.2]octatrienyl(**12**) radicals were obtained by means of the relative rates of the free radical bromine abstraction from the corresponding bridgehead bromides by a silyl radical. It was found that **9** and **12** were more stable than expected. The observed order of stability **9**>**10**>**12**>**11** can not be explained by the usual concepts alone. The extra stabilization of **9** or **12** (or destabilization of **10** or **11**) was interpreted in terms of the local symmetry (or local asymmetry) of these radicals.

In the course of studies on factors influencing radical stability, much attention has been given to the stability of a strained radical in connection with the stable conformation of a free radical.[1] A preferred planar or nearly planar geometry of a simple, unrestricted alkyl radical has been generally accepted from vacuum ultraviolet[2] and electron spin resonance[3] spectroscopy, formation of a racemized product from from an optically active substrate[4] as well as theoretical calculations.[5] The direct kinetic investigation of the decomposition of a series of bridgehead peresters[6] (or azo derivatives[7]) having different bridgehead planarities such as adamantyl, bicyclo[2.2.2]octyl, and bicyclo[2.2.1]heptyl has shown that the decomposition rates were depressed with increasing bridgehead nonplanarity but not so dramatically as in solvolysis reactions. The instability of a strained bridgehead radical was further demonstrated by decarbonylation of a similar series of bridgehead aldehydes[8] and also by unsuccessful bridgehead hydrogen abstraction from strained bicyclo[2.2.1]heptane[9] or bicyclo[2.1.1]hexane[10] in contrast to the ready abstraction of the bridgehead hydrogen of less strained adamantane[11] or bicyclo[2.2.2]octane.[12] All the results seem to suggest that strain, particularly angle strain, is the determining factor of the bridgehead radical stability. It has also been reported[13] that the relative rates of hydrogen abstraction from a series of aliphatic polycyclic hydrocarbons by the trichloromethyl radical were correlated with a computer analysis of the change in strain energy in going from the ground state to the radical. In this connection, a curious observation was reported by Wiberg and coworkers, who were able to show the synthetic utility of the free radical bridgehead substitution on bicyclo[1.1.1]pentane *via* the 1-bicyclo[1.1.1]pentyl radical having the greatest deviation from planarity ever known.[14]

For these highly strained substrates for which no direct kinetic data are available, the bridgehead-to-bridge reactivity ratios in the free radical substitutions (halogenation, chlorocarbonylation, *etc.*) on the parent hydrocarbons (Table I) might be measure of the bridgehead radical stability. As illustrated in the relative reactivities of some polycyclic hydrocarbons toward autoxidation,[15] bridgehead reactivities are generally more sensitive to a structural change than bridge reactivities, presumably because of the ease with which the bridge radical (compared with the bridgehead) takes planarity or near planarity. The variation in the ratios of the bridgehead-to-bridge reactivity (Table 1) is not fully understood from the consideration of the bridgehead angle strain alone but can be interpreted by taking the geometrical symmetry of the bridgehead also into consideration. Of the compounds (Table I) only those which yield symmetrical radicals such as adamantane, bicyclo[2.2.2]octane and bicyclo[1.1.1]-pentane or those which yield radicals of similar symmetry only with respect to the vicinal carbons (this might be called "local symmetry") such as bicyclo-[3.3.0]octane, have appreciable bridgehead reactivities. This might be called local symmetry effect. An experimental evidence of this hypothesis of a local symmetry effect is presented in this paper.

TABLE 1. BRIDGEHEAD-TO-BRIDGE REACTIVITY RATIOS OF SOME POLYCYCLIC HYDROCARBONS IN FREE RADICAL SUBSTITUTIONS[a]

Substrate	Mode of substitution	Reactivity ratio	Ref.
Adamantane	chlorination, bromination	3—5	11a
	clorocarbonylation	3.7	b
Bicyclo[2.2.2]octane	chlorination	6.9	12
Bicyclo[3.3.0]octane	chlorocarbonylation	2.9	c
Bicyclo[2.2.1]heptane	chlorination	0	9
	chlorocarbonylation	0	c
Nortricyclane	chlorination	0	d
Bicyclo[2.1.1]hexane	chlorination	0	10
Tricyclo[3.3.0.$0^{2,6}$]-octane	chlorination	0	e
Bicyclo[3.1.0]hexane	chlorination	0	f
Bicyclo[1.1.1]pentane	chlorination	7	14b
	chlorocarbonylation	17	14b

a) The ratios are statistically corrected for numbers of hydrogens. b) I. Tabushi. J. Hamuro, and R. Oda, *J. Org. Chem.*, **33**, 2108 (1968). c) I. Tabushi, T. Okada, and R. Oda, *Tetrahedron Lett.*, **1969** 1605. d) M. L. Poutsma, *J. Amer. Chem. Soc.*, **87**, 4293 (1965). e) J. Meinwald and B. E. Kaplan, *ibid.*, **89**, 2611 (1967). f) P. K. Freeman, F. A. Raymond, J. C. Sutton, and W. R. Kindley, *J. Org. Chem.*, **33**, 1448 (1968).

* To whom correspondence should be addressed.

*** Present adddress: Department of Organic Synthesis, Faculty of Engineering, Kyushu University, Fukuoka 812.

Results

A series of bridgehead bromides (**1a**, **2a**, **3a**, or **4a**) containing the bicyclo[2.2.2]octane framework was prepared. **1a** was prepared (Scheme 1) by the Hunsdiecker reaction of the corresponding acid (**1c**)[16] obtained by a slight modification of the procedure of Doering *et al.*[17]

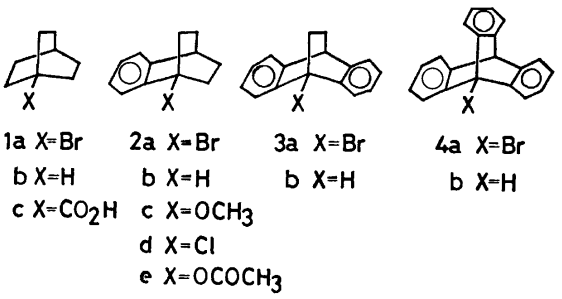

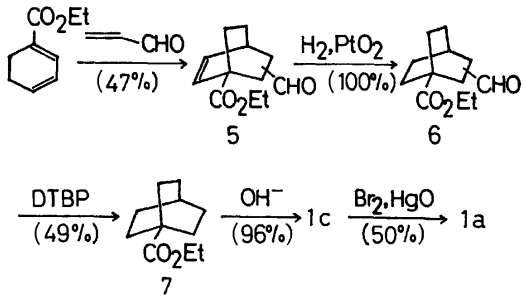

Scheme 1.

The procedure of Suzuki and Morita for converting 1-methoxybicyclo[2.2.2]octanes into 1-halobicyclo[2.2.2]octanes[18] was applied to the synthesis of **2a**. Thus, the 1,4-adduct of benzyne to anisole was, after hydrogenation, converted into **2a** on treatment with acetyl bromide-stannic chloride or stannic bromide (Scheme 2).

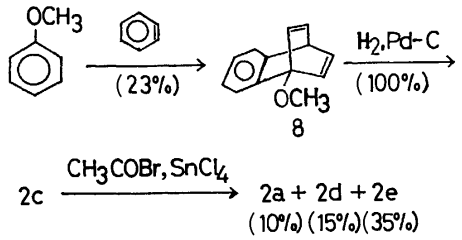

Scheme 2.

The 1,4-addition of 9-bromoanthracene with ethylene[19] or benzyne[20] gave **3a** or **4a**, respectively, in moderate yields.

The reductive debromination of a bromide (**1a**, **2a**, **3a**, or **4a**) with methyldichlorosilane in cyclohexane was carried out in a degassed, sealed tube in the presence of a catalytic amount of di-*tert*-butyl peroxide (DTBP) at 120 °C. The reaction proceeded at an appreciable rate even in the case of **4a**. The only detectable product, besides those from silanes, was the corresponding hydrocarbon (**1b**,[17] **2b**,[21] **3b**,[21] or **4b**[20]).

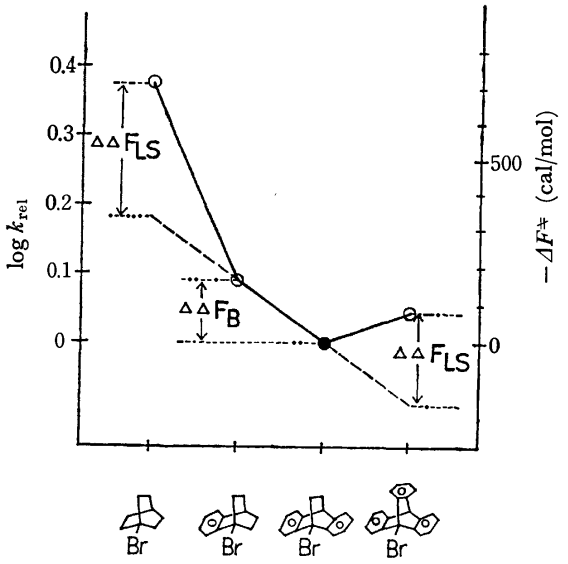

Fig. 1. Logarithmic relative rates of the bromine abstraction from **1a**, **2a**, **3a**, and **4a** by methyldichlorosilyl radical.

That the yield of the reaction was always nearly quantitative indicates that no appreciable side reaction took place.

In order to obtain the relative reactivity of a bromide, a competitive reaction was carried out, in which a bromide (**1a**, **2a**, or **4a**) competed with **3a** (standard) for the attack of the silyl radical. Relative reactivities thus obtained were **1a** (2.36±0.06), **2a** (1.24±0.04), **3a**(1, standard), and **4a** (1.11±0.04). The logarithms of the relative rates (or the relative free energies of activation) are shown in Fig. 1.

Discussion

Ready Formation of Strained Radicals. As already given in many examples,[22] the present reductive debromination can be understood in terms of a radical chain mechanism involving the bromine abstraction from **1a**, **2a**, **3a**, or **4a** by the methyldichlorosilyl radical followed by the hydrogen transfer to the bridgehead radical thus formed (**9**, **10**, **11**, or **12**) from the parent hydrosilane. It is remarkable that the strained radicals **10**, **11**, or **12** can be generated with a rate not much differing from that of **9**, although the triptycyl radical

$$(tert\text{-}C_4H_9O)_2 \rightarrow tert\text{-}C_4H_9O\cdot$$

$$tert\text{-}C_4H_9O\cdot + HSiCl_2CH_3 \rightarrow tert\text{-}C_4H_9OH + \cdot SiCl_2CH_3$$

$$\cdot SiCl_2CH_3 + RBr \rightarrow BrSiCl_2CH_3 + R\cdot$$

$$R\cdot + HSiCl_2CH_3 \rightarrow RH + \cdot SiCl_2CH_3$$

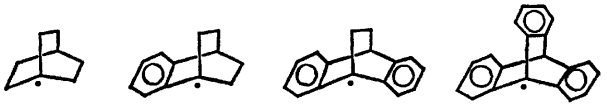

9 **10** **11** **12**

(**12**) is believed to be very unstable in spite of its apparent structural similarity to the stable trityl radical.[23] An attempt to obtain **12** *via* bridgehead hydrogen abstraction of triptycene was unsuccessful.[23a] The instability of **12** was further demonstrated by the observa-

tion that **12** generated by thermolysis of triptoyl peroxide readily abstracted hydrogen even from benzene.[23b] The results show the potentiality of the silyl radical method in ready formation of a strained bridgehead radical which is, otherwise, less accessible. A report was given of a similar ready formation of the strained 1-norbornyl radical from 1-bromonorbornane *via* the bromine abstraction by an organotin radical.[24] A significant exothermicity of the bromine abstraction by a silyl radical[25] might be the principal cause of the reduction in the activation energy, which, in turn, necessarily gives a small structural effect on the rate of abstraction. The electroneutral or weakly nucleophilic character of a silyl radical[26] should also be taken into account. The bridgehead carbon is thus almost electroneutral in the transition state of the bromine abstraction. Destabilization might diminish, which originates from steric (strain) or inductive effect on a carbonium ion-like transition state encountered in a usual hydrogen abstraction[27] or a perester decomposition.[28]

Relative Reactivities. It is noteworthy that the change in the reactivities is not monotonic in going from **1a** to **4a** (Fig. 1). The differences are small but they exceed experimental errors as judged from the reproducibility of the relative rates and accuracy of the glpc analysis. Although the stepwise introduction of a benzo substituent into bicyclo[2.2.2]octane framework lowers the reactivity at first, **4a** has equal or even higher reactivity than **3a**. A benzo substituent would be expected to reduce the bridgehead reactivity because of possible increase in steric crowding around the bridgehead and in the bridgehead strain. On the contrary, an electronegative inductive effect of a benzo substituent might accelerate the reaction by dispersing a possible negative charge developing in the transition state due to the nucleophilic character of a silyl radical,[26] although its nucleophilicity is extremely small. Effects of successive benzo substitution (steric, strain, or inductive) should be additive, and the overall benzo effects cumulative. If no particular effect is caused by a benzo substituent, the reactivity should monotonously decrease or increase in going from **1a** to **4a**. but this is not the case (Fig. 1). Decreasing rates with increasing benzo substituents show that strain and/or steric decelerating effect surpass the inductive accelerating effect. If the reactivity difference between **2a** and **3a**, 170 cal mol^{-1}, is taken to be inherent decelerating benzo effects ($\Delta\Delta F_B$), the present abnormal benzo effects are characterized by the unexpectedly high reactivities of symmetrical **1a** and **4a**. Asymmetrical **2a** or **3a** suffers from abnormal destabilizing effect due to its lack of local symmetry. It should be concluded that an extra stabilization contributes to radicals **9** and **12** (or destabilization to **10** and **11**), which might be correlated with the geometrical symmetry of **9** and **12**. The gap between observed and predicted (from additivity of $\Delta\Delta F_B$, dashed line in Fig. 1) reactivities of **1a** and **4a** ($\Delta\Delta F_{LS}$), *ca.* 300 cal mol^{-1}, is thus ascribed to the local symmetry effect. Introduction of a benzo substituent into symmetrical bicyclo[2.2.2]octane is an appreciable perturbation to the geometry (one bond is shortened and three C–C–C angles at the bridgehead position become nonequivalent) and the local symmetry effect might disappear (or the local asymmetry destabilization appears). Removal of methylene from bicyclo[2.2.2]octane to give bicyclo[2.2.1]heptane would cause a much greater disturbance. The very low reactivity of the bicyclo[2.2.1]heptane bridgehead[9] might, in part, be attributed to the very asymmetrical nature of the 1-bicyclo[2.2.1]heptyl radical; the main reason is the increase in angle strain of this radical.[13] On the other hand, it is highly plausible that the local symmetry makes the bicyclo[1.1.1]pentyl[14] or cubyl[29] radical "stable" for its appreciable angle strain.

Although the theoretical interpretation of a local symmetry effect has not been accomplished* the origin of the effect would be related to the mode of the rehybridization of a radical in such a way that the hybridization energy is sensitive to local symmetry. The present effect should be considered in light of the nonplanarity of some strained secondary (*e.g.* cyclopropyl[30]) radicals with an electronegative α substituent (*e.g.* fluorine[31]). The contributing factors to the geometry of a radical might be: (1) hybridization energies, (2) repulsions of the bonding electrons, and (3) nonbonded interactions between the groups at the ends of the bonds. A planar geometry would be preferable from the viewpoint of minimization of repulsions between bonding electrons and between groups. Since the radical is in the middle of the sp^2 hybridized planar carbonium ion and the sp^3 hybridized tetrahedral carbanion, the hybridization energy of the radical would be less sensitive to planarity[32] than the carbonium ion or carbanion. The energy difference between planar and pyramidal structures should be reduced as is usually the case.[6–8] Factors other than planarity such as symmetry might contribute significantly to the hybridization energy of the radical of a given structure. At the sacrifice of some unfavorable increase in repulsions between bonds the cyclopropyl radical may prefer a nonplanar geometry because of a compensating stabilizing hybridization in a pyramidal or more symmetrical structure with respect to the three angles around the radical center. The enhanced configurational stability of α-fluorocyclopropyl radical[31] may be interpreted on similar grounds. The electron withdrawal by a fluorine substituent reduces the importance of repulsion between bonding electrons, making the hybridization energy the determining factor of the structure. A refined molecular orbital calculation may support the present arguments. It has been shown that the hypothetically strained methyl radical took

* The C_1—C_4 rear-lobe interaction is not important in the present system. The unimportance of the rear-lobe effect has been suggested by the ESR spectrum of the 1-bicyclo[2.2.2]octyl radical see, P. J. Krusic, T. A. Rettig, and P. von R. Schleyer, *J. Amer. Chem. Soc.*, **94**, 995 (1972). An Extended Hückel calculation has also shown that the C_1—C_4 atomic bond population in the 1-bicyclo[2.2.2]octyl cation was negative, showing antibonding, see T. Yonezawa, K. Shimizu, H. Morimoto, and H. Kato, *Nippon Kagaku Zasshi*, **90**, 142 (1969).

a pyramidal structure.[33]

It is anticipated that both the nonplanarity of a strained (nonbridgehead) radical and the local symmetry stabilizing effect on a strained bridgehead radical have the same principle.

Experimental

Materials and Analysis. Melting points were uncorrected. IR spectra were obtained with a Hitachi 215 spectrophotometer. NMR spectra were taken in $CDCl_3$ with TMS as a standard and were recorded with a Varian T-60 spectrometer. Mass spectra were obtained with a Hitachi mass spectrometer. Glpc analyses were performed with a Yanagimoto 550T gas chromatograph using a poly(ethylene glycol) or silicone DC 550 column. Cyclohexane was shaken with concentrated sulfuric acid and distilled over sodium after repeated washing with water. Methyldichlorosilane was distilled prior to use. DTBP was used as received.

*1-Bromobicyclo[2.2.2]octane (**1a**).* A mixture of 30 g of 1-carbethoxy-1,3-cyclohexadiene[34] and 80 g of acrolein was heated at 150 °C under reflux for 90 hr. Distillation at 100—110 °C/1.5 mmHg afforded 19 g (47%) of the Diels-Alder adduct **5**, which was hydrogenated in an equal volume of acetic acid at atmospheric pressure in the presence of platinum oxide. After removal of the catalyst and most of the solvent, 15 g of DTBP was added (in three portions) and the mixture was heated at 130 °C for 20 hr under dry, oxygen free nitrogen. Distillation at 98—100 °C/10 mmHg (lit. 96—98 °C/12 mmHg,[34] 75—76 °C/3 mmHg[35]) afforded 8.1 g 49%) of the decarbonylated ester **7**, which was hydrolyzed[34] to give **1c** in a 96% yield. **1a** was prepared in *ca.* 50% yield by the Hunsdiecker reaction of **1c**[16]; mp 61—62 °C (lit. 58.8—59.5 °C,[16] 66—68 °C[34]); IR(KBr): 1453, 968, and 815 cm^{-1}; NMR: τ 7.53—8.00 (6H, m, methylene vicinal to Br) and 8.00—8.35 (7H, m, other methylene and bridgehead); Mass: *m/e* 190 and 188 (M^+, relative intensity 5.6), 109 (100), and 81 (40).

*1-Bromobenzobicyclo[2.2.2]octene (**2a**).* A mixture of benzenediazonium-2-carboxylate (from 10 g of anthranilic acid and 20 ml of iso-amyl nitrite[36]) and 200 ml of sodium dry anisole was heated at 70 °C for 15 hr. The anisole was expelled and the residue was distilled. A fraction boiling at 104—105 °C/6 mmHg was collected (4.3 g), and was found to be a mixture[37] of the 1,4-adduct **8** and benzobicyclo[2.2.2]-octadien-2-one[38] (approximately 6 : 1[37]). The mixture was hydrogenated in methanol under atmospheric pressure in the presence of palladium charcoal. The catalyst was removed by filtration and a calculated amount of tosylhydrazine was added. The mixture was refluxed for 15 hr to convert the undesired ketone into hydrazone and then passed through a silica gel column. After removal of methanol, the residue was distilled at 107 °C/2.7 mmHg to give 2.9 g of **8**; IR (neat): 1330, 1163, 1123, 1102, 1070, 1060, and 746 cm^{-1}; NMR: τ 2.30—2.95 (4H, m, aromatic), 6.45 (3H, s, methyl), 7.05 (1H, broad s, bridgehead), and 7.80—8.75 (6H, m with peaks at 7.97, 8.13, 8.42, and 8.57, methylene). To an ice-cooled mixture of 500 mg (2.6 mmol) of **8** and 640 mg (5.2 mmol) of acetyl bromide was added ten drops of anhydrous stannic chloride. The mixture was stirred at room temperature for 3 hr and at 80 °C for 15 hr, poured on ice and extracted with methylene chloride. The methylene chloride was distilled off and the residue was chromatographed on a silica gel column. Elution with petroleum ether gave 140 mg (25%) of a mixture of the bromide **2a** and the chloride **2d** (1 : 1.5). Further elution with petroleum ether–methylene chloride (1 : 1) afforded 220 mg (37%) of the acetate **2e**. Pure **2a** was obtained by means of a preparative glpc after the column chromatographic separation of **2e**. When stannic bromide was used instead of stannic chloride, **2a** and **2e** were obtained in a 1 : 3 ratio but in much lower total yield.

2a had mp 83.5—84.5 °C; IR(KBr): 962, 898, 860, 747 cm^{-1}; NMR: τ 2.17—2.47 (1H, m, aromatic (peri)), 2.53—2.97 (3H, m, other aromatic), 6.95 (1H, broad s, bridgehead), and 7.20—8.83 (8H, m with major peaks at 8.02 and 8.22, methylene); Mass: *m/e* 238 and 236 (M^+, 6.0), 210 and 208 (40), 157 (46.7), and 129 (100).

2d had IR(neat): 1035, 970, 913, 872, 755, 737, and 697 cm^{-1}; NMR: τ 2.20—2.60 (1H, m, aromatic (peri)), 2.60—3.00 (3H, m, other aromatic), 7.00 (1H, broad s, bridgehead), and 7.40—8.80 (8H, m, methylene); Mass: m/e 194 (M^+, 26), 192 (M^+, 73), 166 (32), 165 (49), 164 (64), 163 (67), 129 (100), 128 (76), and 127 (53).

2e had IR(neat): 1740, 1248, 1092, 1040, and 750 cm^{-1}; NMR: τ 2.55—3.00 (4H, m, aromatic), 7.02(1H, broad s, bridgehead), 7.78 (3H, s, methyl), and 7.30—8.65 (8H, m with peaks at 7.45, 7.90, 8.06 and 8.28); Mass: m/e 216 (18), 174 (100), 146 (84), and 145 (76).

*1-Bromodibenzobicyclo[2.2.2.]octadiene (**3a**).* To a solution of 5 g of 9-bromoanthracene and 50 mg of 2,5-di-*tert*-butylhydroquinone in 150 ml of chlorobenzene in an autoclave was introduced ethylene to a pressure of 60 atm. The mixture was heated at 150 °C for 40 hr under stirring (maximal pressure was 110 atm). After distillation of most of the chlorobenzene the residue was chromatographed on a silica gel column. **3a** was obtained by elution with petroleum ether. Recrystallization three times from petroleum ether gave *ca.* 2 g of pure **3a** in white powder; mp 137.5—138 °C; IR(KBr): 1457, 1300, 1160, 1140, 1030, 915, 823, 755, and 738 cm^{-1}; NMR: τ 2.10—2.50 (2H, m, aromatic (peri)), 2.57—3.05 (6H, m, other aromatic), 5.67 (1H, broad s, bridgehead), 7.55—7.95 (2H, m, methylene vicinal to Br), and 7.95—8.35 (2H, m, other methylene); Mass: *m/e* 286 and 284 (M^+, 6.1), 258 and 256 (100), 205 (3.8), 204 (7.0), 203 (10), 202 (12), 177 (25), and 176 (32).

*1-Bromotribenzobicyclo[2.2.2]octatriene (1-Bromotriptycene **4a**).* A mixture of 3 g of 9-bromoanthracene and benzenediazonium-2-carboxylate (from 8.2 g of anthranilic acid and 16 ml of iso-amyl nitrite) in 240 ml of ethylene chloride was heated at 70 °C for 15 hr. Evaporation of the solvent gave a tarry material, which was chromatographed on a silica gel column. Crude **4a** eluted with benzene was repeatedly washed with petroleum ether to remove unchanged 9-bromoanthracene. Pure **4a** (1 g) was obtained as white powder by recrystallization from benzene; mp 253—254.7 °C (lit,[39] 246—248 °C); IR(KBr): 1450, 1290, 1155, 1033, 925, 850, 840, 820, and 738 cm^{-1}; NMR: τ 2.10—2.35 (3H, m, aromatic (peri)), 2.45—3.15 (9H, m, other aromatic), and 4.53 (1H, s, bridgehead); Mass: *m/e* 334 and 332 (M^+, 37) and 253 (100).

Reductive Debromination. A solution of *ca.* 30 mg of a bromide (**1a**, **2a**, **3a**, or **4a**), *ca.* 300 mg of methyldichlorosilane and a catalytic amount of DTBP in 3 ml of cyclohexane was degassed and sealed. The mixture was heated at 120 °C for 1—3 hr. The crude reaction mixture was then analyzed by glpc. Identification of the product (**1b**, **2b**, **3b**, or **4b**) was made on the basis of the glpc retention time and IR spectrum. Authentic **1b** was obtained by the procedure of Doering *et al.*[17] All the other authentic hydrocarbons (**2b**, **3b**, and **4b**) were prepared by the addition of benzyne to benzene,[21] naphthalene,[21] and anthracene,[20] respectively, followed by hydrogenation when necessary (in the case of **2b** and **3b**). Controlled experiment showed that the reaction did not

Derivatives of 1,2-Dithiole-3-thiones. VII.[1] Study of Reaction of Thiocarbonyl *S*-Imide with Amines

Seizo TAMAGAKI, Keishi SAKAKI, and Shigeru OAE*

Department of Applied Chemistry, Faculty of Engineering, Osaka City University, Sugimoto-cho, Sumiyoshi-ku, Osaka 558
**Department of Chemistry, Tsukuba University, Sakura-mura, Niihari-gun, Ibaraki-ken 300-31*

(Received February 12, 1974)

Thiocarbonyl *S*-imide of 4,5-benzo-1,2-dithiole-3-thione reacted with primary and secondary amines of various types to give both rearranged and amine-exchanged imines. By kinetical studies a plausible mechanism involving the addition and elimination of amine on the tetravalent sulfur atom was proposed.

Thiocarbonyl *S*-imides (>C=S̈–N̄–) are isoelectronic nitrogen-analogs of sulfines (>C=S̈–Ō) or thiocarbonyl ylides (>C=S̈–C̄<). Thiocarbonyl *S*-imides are thus expected to resemble sulfines or ylides in both chemical and physical properties. However, we have recently initiated the preparation of a stable thiocarbonyl *S*-imide of 1,2-dithiole-3-thione,[2] the characteristics of its chemistry not having been fully explored.

We wish to report detailed mechanistic aspects of the reaction of the thiocarbonyl *S*-imide (I) with various amines, in which a nucleophilic attack of amines on the sulfur atom at the initial step of the reaction is involved. As in the nucleophilic substitution on the divalent sulfur of sulfenyl chloride, the trivalent sulfur of sulfonium, or the tetravalent sulfur of sulfoxide or sulfilimine, the nucleophilic attack on the tetravalent sulfur atom of thiocarbonyl *S*-imide appears to proceed *via* a somewhat similar path.

Results

The reaction of the thiocarbonyl *S*-imide of 4,5-benzo-1,2-dithiole-3-thione (II) with an equimolar amount of a primary aryl or alkyl amine at room temperature in acetonitrile afforded the corresponding rearranged product, (*N*-benzenesulfonyl-4,5-benzo-1,2-dithiole-3-imine (IIIa)), the amine-exchanged product (*N*-aryl- or alkyl-4,5-benzo-1,2-dithiole-3-imine (IVa)), the benzenesulfonamide, elemental sulfur, as well as a small amount of the trithione:

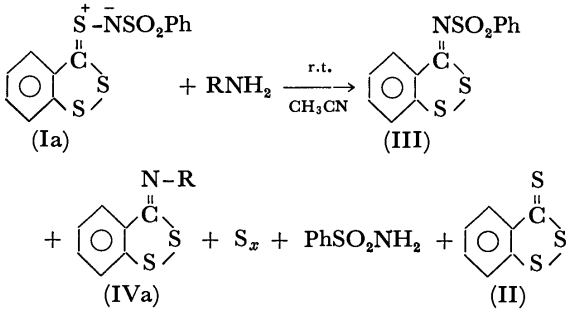

Similarly, treatment of the *S*-imide (Ib) of 4-phenyl-1,2-dithiole-3-thione with aniline gave *N*,4-diphenyl-1,2-dithiole-3-imine (mp 166—167 °C) in a moderate yield.

Results for the reactions of the thiocarbonyl *S*-imide (I) with various amines, including secondary and tertiary amines, are summarized in Table 1.

In order to find the rate-determining step of the

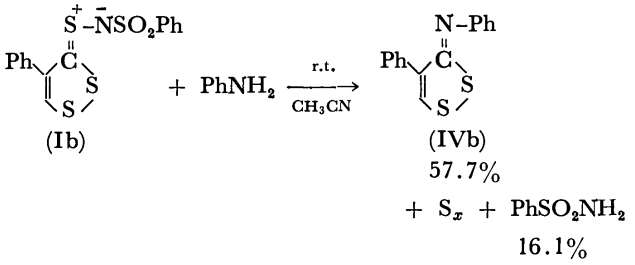

reaction, a kinetic study was undertaken by observing the disappearance of the characteristic UV absorption band due to the thiocarbonyl *S*-imide at nearly 500 nm in acetonitrile, using about 15 mol excess amine, so as to keep the pseudo-first-order condition. The first-order dependence of the rate on the imide concentration was clearly observed. A typical run is given in Table 2.

The first-order dependence of k_{obsd} on the amine concentration is also shown in Fig. 1. The fact that the rate was found exactly proportional to the initial concentration of the amine indicates that at the rate-determining step of the reaction the attack of amine occurs on the sulfur atom without any concomitant base- or acid-catalyzed proton donation and/or removal. Namely, like the addition of primary amines to simple carbonyl compounds[3] the reaction is not the base-catalyzed nucleophilic substitution reaction. The sec-

TABLE 1. REACTION OF THIOCARBONYL *S*-IMIDE (I) WITH VARIOUS AMINES IN CH_3CN AT ROOM TEMPERATURE

Amine	IIIa	IVa	Sulfonamide	II	S_x
$ClC_6H_4NH_2$	13.0	75.5	72.4	6.0	99.6
$PhNH_2$	17.5 (0.0)[e]	60.0 (79.0)	44.6 (a))	13.6 (11.6)	a)
$MeOC_6H_4NH_2$	1.3	66.5	66.0	5.0	a)
t-$BuNH_2$[b]	6.3	95.0	88.1	0.0	a)
$C_6H_{11}NH_2$	3.3	64.3	88.5	7.6	a)
$ClC_6H_4NH_2$[c]	10.1	83.0	a)	a)	a)
$PhNHCH_3$	44.6	0.0	82.8	14.3	a)
Et_2NH	27.7	0.0	57.7	7.5	15.6
$PhN(CH_3)_2$[d]	35.2	0.0	a)	11.4	a)
Et_3N[d]	31.3	0.0	a)	42.4	35.3
$PhNHNH_2$	a)	83.8	98.2	6.7	a)

a) No further determination attempted. b) As solvent. c) Ten fold excess amine used. d) Twenty fold excess amine used. e) In the presence of an equimolar amount of *p*-toluenesulfonamide; this run indicates the absence of the anion-exchange during the formation of (III).

Table 2. Reaction of (Ia) with *p*-toluidine[a] at 24.8 °C in CH_3CN

$\log a/(a-x)$	Time, s	$1/t \cdot \log a/(a-x) = 10^3 k_{obsd}$
0.103	10	10.3
0.208	20	10.4
0.307	30	10.2
0.406	40	10.2
0.503	50	10.1
0.599	60	10.0
0.687	70	9.8

a) Fifteen equivalents.

Table 3. Substituent effect on the reaction rate in CH_3CN

Substituent, X[a]	$10^4 k_2$, $M^{-1} s^{-1}$ [c]
Br	6.87
H	6.47
CH_3	6.05
$\rho_X = +0.13$ (Y=CH_3)	
Substituent, Y[b]	**$10^4 k_2$, $M^{-1} s^{-1}$ [c]**
NO_2	no reaction
Cl	0.27
H	1.56
CH_3	6.73
CH_3O	33.1
$\rho_Y = -3.49$ (X=H)	

a) X: *para*-substituents of aryl groups in compound (Ia). b) Y: *para*-substituents in *para*-substituted anilines. c) reaction temperature 24.8 °C.

ond-order rate constants (k_2) can be easily obtained from the values of k_{obsd}, by dividing them by the concentration of amine. The resulting data are summarized in Tables 3 and 4. The second-order rate constants for the reaction of a few para-substituted thiocarbonyl *N*-benzenesulfonyl imides with *p*-substituted anilines are given in Table 3.

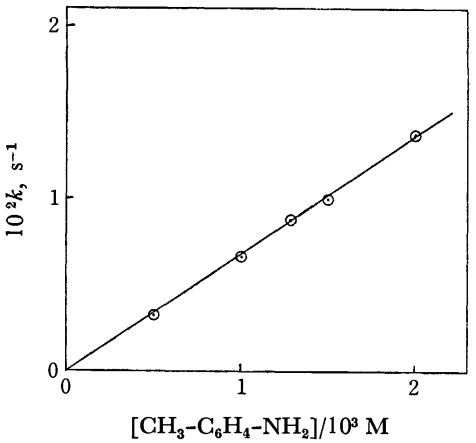

Fig. 1. Dependence of reaction rate on amine concentration in CH_3CN at 24.8°.

Discussion

The products as well as their relative yields thus obtained (Table 1) indicate that the initial attack of amine on the tetravalent sulfur atom of thiocarbonyl *S*-imide moiety yields both the rearranged (III) and the amine-exchanged (IV) products as outlined in Scheme 1.

The initially formed dipolar intermediate (V) could break down through the symmetrical intermediate (VI) eventually to the ion pair (VII). Subsequently there are two competitive reactions: a) attack of a foreign amine molecule on the carbon-3, giving the amine-exchanged imine (IVa) upon elimination of RNHSH, and b) the intramolecular nucleophilic addition of the sulfonamide anion to the carbon-3, eventually leading

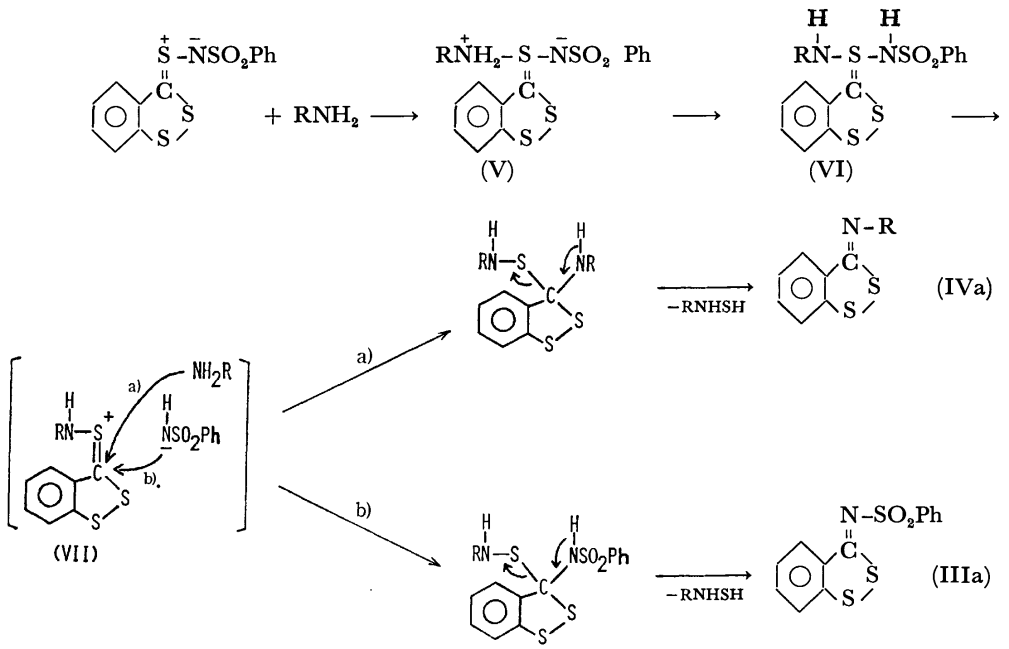

Scheme 1.

to the *N*-benzenesulfonyl imine (IIIa).

The above pathway does not contradict with the following finding that treatment of *N*-monomethylaniline with Ia afforded exclusively IIIa alone, since the second proton-transfer, which is required in the overall reaction sequence to form IVa, would be prohibited for any amine having only one proton on nitrogen atom.

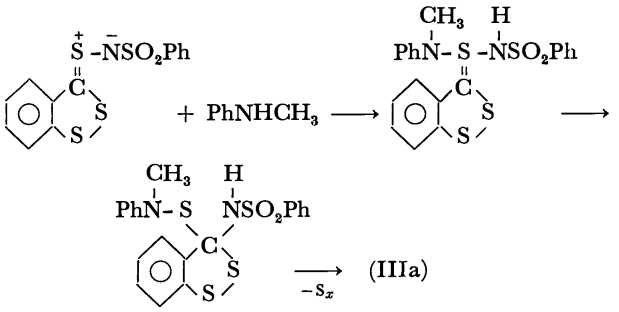

Scheme 2.

As shown in Scheme 2, tertiary amines bearing no protic hydrogen attached to a nitrogen atom cannot be expected to react at all under similar conditions. In fact, a carefully purified tertiary amine, DABCO ($pK_a=8.7$), did not yield the rearranged product (IIIa). Anomalous results (Table 1) where treatment of Ia with 20 mol excess tertiary amines such as *N,N*-dimethylaniline and triethylamine gave the rearranged imine (IIIa) in yields similar to cases for secondary amines can be attributed to the contamination of a considerable amount of the corresponding secondary amines.

As one can see from Table 3 a straight line was obtained by plotting log k_2 values against the Hammett sigma values. The rho values of $\rho_x=+0.13$ and $\rho_y=-3.5$ were obtained for the respective reactions. Evidently, the reaction involves a nucleophilic attack of aniline molecule. The remarkably large and negative ρ_y value due to *p*-substituents on the nucleophile as well as the small ρ_x value due to *p*-substituents on the leaving group seem to suggest that this substitution is not a true S_N2 process. A more plausible mechanism would be one including the intervention of an unsymmetrical addition complex in which both the entering and the leaving groups are bound to the central sulfur atom of the intermediate of either trigonal bipyramid or square pyramid with or without involvement of 3d-orbitals.[4] Such a hypervalent intermediate involving the central sulfur atom has been reported in other substitution reactions[5] and in some cases isolated.[6] For example, the formation of a metastable addition intermediate at divalent sulfur was postulated in the reaction between triphenylmethylsulfenyl chloride and *n*-butylamine.[7] Evidence for the existence of the tetracoordinated sulfur complex as an intermediate has been reported by Givens and Kwart for chlorination of sulfenyl chloride[8] and by Trost *et al.* for the reaction of the sulfonium salts with organometallic compounds.[9]

In our case, the marked solvent effect on the rate, *i.e.*, the faster rate in polar CH_3CN than in nonpolar THF by a factor of 3.6, and the large negative activation entropy (Table 4) indicate the existence of a rigid,

Table 4. Temperature effect on reaction rate in CH_3CN

Reaction temp., °C	$10^4 k_2$, $M^{-1} s^{-1}$ a)
33.75	8.20
29.25	7.47
26.70	7.20
20.40	6.10

a) X=H, Y=CH_3; $E_a=4.0$ kcal/mol, $\Delta S^{\neq}=-59.0$ e.u.

polar, and solvation-susceptible intermediate. Moreover, the activation energy of 4.0 kcal/mol implies that no bond cleavage takes place at the transition state. Thus, the intervention of a stable unsymmetrical intermediate (V) is more likely. The markedly small activation energy would eliminate the direct carbon attack where the activation barrier would be very large since the aromaticity ought to be destroyed. An insignificant increase in the rate of only less than two fold even by adding ten equimolar amounts of protic acid to aniline indicates also that the sulfonamide anion does not leave the reaction center at the transition state. If an S_N2 mechanism were in operation, a prior protonation should be required and the addition of acetic acid would result in a marked acceleration of the rate However, this was not found to be the case.

We may thus conclude that one more likely pathway should involve the initial formation of an unsymmetrical addition complex which, upon a stepwise proton switch from the aniline nitrogen of the charge-separated pentavalent intermediate to the sulfonamide nitrogen carrying the formal negative charge, gives a symmetrical complex that undergoes the subsequent cleavage of the old S–N bond to give the products shown in Scheme 1.

The addition complex could have a structure quite close to a square pyramid (VIII) where the attacking and leaving groups occupy *cis* or *trans* positions to each other, rather than a trigonal bipyramid. In fact, a structurally similar planar compound (IX),[10] isoelectronic around the sulfur atom, has recently been synthesized.

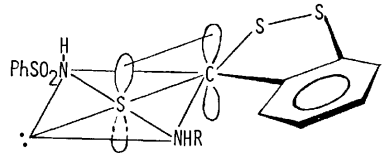

(VIII)

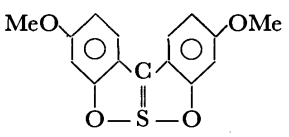

(IX)

It should be emphasized that such a mechanism of the displacement on the sulfur atom is somewhat similar to that of the formation of the thiocarbonyl *S*-imide itself (I) from trithione and chloramine-B, where the reaction involves the initial formation of the chlorosulfonium-like salt followed by the displacement at the sulfur atom,[11] as was already established in detail

in the formation of the sulfilimine.[12]

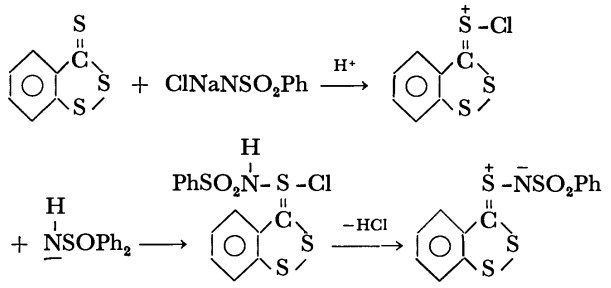

Experimental

Materials. Thiocarbonyl *S*-imides were prepared by the method described previously.[2] To the benzotrithione dissolved in methanol was added a solution containing a slight excess of the *p*-substituted or unsubstituted chloramine with stirring at room temperature. After a few minutes red colored crystalline thiocarbonyl *S*-imide was filtered and washed with pure water and methanol. A typical reaction of thiocarbonyl *S*-imide with aniline is as follows: one equimolar amount of thiocarbonyl *S*-imide (Ia) (339 mg, 1 mmol) and *p*-chloroaniline (127.5 mg, 1 mmol) was mixed with stirring in acetonitrile at room temperature. After ten minutes the solvent was distilled off and residual crystals were dissolved in a small amount of $CHCl_3$. The solution was fractionated with thin layer chromatography on Kieselgel using benzene as an eluant. Each fraction was extracted with $CHCl_3$-EtOH (9 : 1), filtered off and evaporated. The product was purified by recrystallization from benzene or benzene-hexane. Physical properties and spectral data of thiocarbonyl *S*-imides and rearranged products are given in Tables 5 and 6, and analytical values of the rearranged products in Table 7.

Solvent. Commercial acetonitrile was dried over phosphorus pentoxide and distilled just before use.

Kinetics. A typical procedure is as follows: thiocarbonyl *S*-imide (I) (3.39 mg, 0.01 mmol) was dissolved in 50 ml acetonitrile. *p*-Methylaniline (160.5 mg, 1.5 mmol) was also dissolved in 50 ml of the same solvent, the solution being diluted to one tenth of concentration. Both solutions were kept at 25 °C in a thermostat. Each solution (1.5 ml) was then mixed quickly in a UV cell which was also kept at the same temperature. Thus, the concentrations of thiocarbonyl *S*-imide and *p*-methylaniline at the initial reaction stage were 0.1 mmol/l and 1.5 mmol/l, respectively. Determination of the reaction rate was carried out as follows. The UV recorder was set at a certain wave length (490 nm due to thiocarbonyl *S*-imide). As soon as the reaction was initiated by mixing each solution, the recorder pen was started moving. Thus the chart obtained shows the decrease of thiocarbonyl *S*-imide concentration with time. The pseudo-first order rate constants were calculated by the integral form (2) of the differential equation (1), where a signifies the initial concentration of the thiocarbonyl *S*-imide reacted at a given time t from the start, while k is the pseudo-first-order rate constant.

$$\frac{dx}{dt} = k(a-x) \quad (1)$$

$$\ln\frac{a}{a-x} = kt \quad (2)$$

Table 5. Physical properties of thiocarbonyl *S*-imides and products

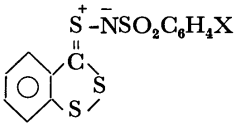

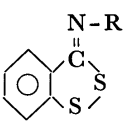

Imide, X	Mp (°C)	Imine, R	Mp (°C)
H	130	Cl-C_6H_4	124.5—125
CH_3	126—127	Ph	78—78.5
m-NO_2	129—130	PhNH	96—97
Br	137—139	*t*-Bu	oil
		C_5H_{11}	189—190

Table 6. IR spectral data of thiocarbonyl *S*-imides and products

Imide, X	cm^{-1}
H	1590, 1278, 1137, 1087, 969, 920, 760, 570
CH_3	1590, 1280, 1138, 1086, 969, 915, 828, 572, 550
m-NO_2	1589, 1540, 1354, 1282, 1152, 1112, 965, 928, 763, 577, 568
Br	1589, 1139, 1082, 968, 917, 758, 600, 568
Imine, R	
Cl-C_6H_4	1614, 1587, 1489, 1445, 1089, 918, 829, 763
Ph	1610, 1590, 1490, 1450, 1305, 1280, 1250, 1195, 1070, 925, 756
PhNH	3260, 1602, 1588, 1508, 1422, 1259, 1113, 952, 757, 740, 694
t-Bu	2980, 1620, 1365, 1210, 1070, 1025, 890, 755, 720
C_6H_{11}	2960, 2880, 1610, 1455, 1310, 1146, 1015, 983, 900, 740
(IVb)	3090, 1592, 1537, 1492, 1343, 1330, 1740, 1148, 890, 767, 700, 569

Table 7. Analytical values of products

Imine, R		%C	%H	%N
Cl-C_6H_4	Found:	56.14	2.90	4.89
	Calcd for $C_{13}H_8NS_2Cl$:	56.22	2.88	5.05
Ph	Found:	64.05	3.62	5.95
	Calcd for $C_{13}H_9NS_2$:	64.20	3.70	5.76
PhNH	Found:	60.57	3.99	10.85
	Calcd for $C_{13}H_{10}N_2S_2$:	60.47	3.88	10.85
t-Bu	Found:	59.58	6.24	5.90
	Calcd for $C_{11}H_{13}NS_2$:	59.11	5.83	6.28
C_6H_{11}	Found:	62.81	6.39	5.65
	Calcd for $C_{13}H_{15}NS_2$:	62.90	6.64	5.64
(IVb)	Found:	66.65	4.11	5.23
	Calcd for $C_{15}H_{11}NS_2$:	66.91	4.09	5.20

The authors wish to thank Professor T. Otsu for helpful discussions.

References

1) For paper VI, see S. Tamagaki, R. Ichihara, and S. Oae, This Bulletin, submitted for publication.

2) S. Tamagaki and S. Oae, *ibid.*, **1159** (1972); S. Tamagaki, K. Sakaki, and S. Oae, This Bulletin, **46**, 2608

(1973).

3) W. P. Jencks, *J. Amer. Chem. Soc.*, **94**, 4731 (1972); *ibid.*, **94**, 3262 (1972).

4) R. Hoffmann, J. M. Howell, and E. L. Muetterties, *ibid.*, **94**, 3047 (1972); I. Ugi, D. Marquarding, H. Klusacek, P. Gillespie, and E. Kamirer, *Accounts Chem. Res.*, **4**, 288 (1971).

5) E. Ciuffarin and G. Guaraldi, *J. Amer. Chem. Soc.*, **91**, 1745 (1969); F. A. Davis, S. Divald, and A. H. Confer, *Chem. Commun.*, **1971**, 294.

6) J. C. Martin and R. J. Arhart, *J. Amer. Chem. Soc.*, **93**, 2339 (1971); J. M. Shreeve, *Accounts Chem. Res.*, **6**, 387 (1973), E. F. Perozzi, J. C. Martin, and I. C. Paul, *J. Amer. Chem. Soc.*, **96**, 578 (1974).

7) O. A. Musher, *Angew. Chem., Int. Ed. Engl.*, **8**, 54 (1969); W. G. Phillips, *Tetrahedron Lett.*, **1961**, 2101; D. C. Owsley, G. K. Helmkamp, and M. F. Rettig, *J. Amer. Chem. Soc.*, **91**, 5239 (1969).

8) E. N. Givens and H. Kwart, *J. Amer. Chem. Soc.*, **90**, 378 (1968).

9) B. M. Trost, R. LaRochell, and R. C. Atkins, *ibid.*, **91**, 2175 (1969).

10) I. Pomerantz, L. Miller, E. Lustig, D. Mastbrook, E. Hausen, R. Barron, N. Oates, and J. Y. Chen, *Tetrahedron Lett.*, 5307 (1969); R. D. Gilardi, and I. L. Karle, *Acta Crystallogr., Sect. B.*, **27**, 1073 (1971).

11) T. Yamamoto, Y. Harigaya, and M. Okawara, *Chem. Lett.*, **1972**, 1009.

12) K. Tsujihara and S. Oae, This Bulletin, **42**, 2631 (1969).

The Photochemical Raction of 2-Alkoxy-1,4-naphthoquinones with Olefins. II. The Formation of Tetrahydropyran-ring Compounds[1)]

Tetsuo OTSUKI

Department of Chemistry, Faculty of Home Economics, Kyoto Women's University, Kyoto 605

(Received April 3, 1974)

The photochemical reaction of 2-alkoxy-1,4-naphthoquinones with numerous types of olefins was investigated. The reaction was found to proceed smoothly in possible combinations of quinones and olefins to give photo-addition compounds in good yields. The structure of the addition compounds was determined to be **10** by their elemental analyses, mass, IR, PMR, and chemical reactions. The photo-addition reaction is characterized by the formation of a tetrahydropyran ring. This type of photo-addition reaction has not been previously known. The scope and limitations of the new photochemical reaction were described.

The photochemistry of quinones is one of the most attractive fields of study because quinones have been found to play an important role in nature. The irradiation of quinones with olefins produces addition compounds which are difficult to be prepared by any another method.[2)] Such a photochemical reaction of quinones has been found to provide a versatile synthetic route to form C–C and/or C–O bonds.[2)] The photochemistry of 1,4-naphthoquinone with olefins has been investigated by several workers,[3–5)] but systematic investigations in the field have been sparse.

1,4-Naphthoquinone gives, in general, 1,4-naphthoquinhydrone in photochemical reactions with olefins which have active hydrogen atoms such as allylic hydrogen atoms. Olefins with no active hydrogen atoms give, on the other hand, addition compounds in photochemical reactions with 1,4-naphthoquinone, though the yields are relatively poor. The photo-addition compounds can be classified into three structural types: **1**, **2**, and **3**. The mechanism of the

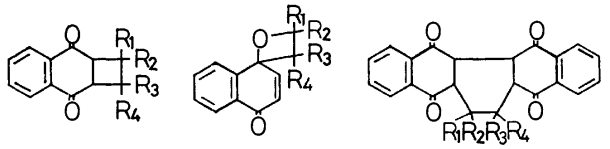

1 **2** **3**

formation of **3** has been investigated in detail.[6)] The low yields of the photo-addition products and the complicated features in the photo-addition reaction of 1,4-naphthoquinone with olefins originate partly from hydrogen-atom abstraction from olefins due to the relatively higher positive oxidation potnetial of 1,4-naphthoquinone.[7,8)]

Since 2-alkoxy-1,4-naphthoquinones have lower positive oxidation potentials compared with that of 1,4-naphthoquinone itself,[7,8)] it seemed that it would be interesting to scrutinize the photochemical reactivities of the former to olefins. Although the photochemical reactions of 2-methoxy-1,4-naphthoquinone with some acetylenic compounds have been reported to yield

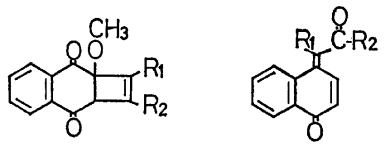

4 **5**

cyclobutene derivatives **4**, as well as their rearranged compounds **5**,[9–12)] no reaction mechanisms have been elucidated thus far.

In this work, the photochemical reactions of 2-alkoxy-1,4-naphthoquinones with olefins were examined, and it was found that the reactions proceed quite smoothly to give a novel type of photo-addition compound.

Results and Discussion

The 2-alkoxy-1,4-naphthoquinones examined here are 2-methoxy-, 2-ethoxy-, 2-isopropoxy-, and 2-allyloxy-1,4-naphthoquinone. The olefins selected in this work are 1-hexene, 1-heptene, 1-octene, cyclohexene, cyclooctene, 1,4-cyclooctadiene, bicyclo[2.2.1]hept-2-ene, bicyclo[2.2.1]hept-2,5-diene, styrene, and indene. A benzene solution of a mixture of a 2-alkoxy-1,4-naphthoquinone and an olefin was subjected to photochemical reaction by irradiation with a high pressure Hg arc lamp at room temperature. Neither the precipitation of 2-alkoxy-1,4-naphthoquinhydrones nor any coloration was observed during the course of the reaction, even when olefins had active hydrogen atoms, such as 1-hexene. The reaction proceeded smoothly; this is one of the extremely different features of 2-alkoxy-1,4-naphthoquinones compared with 1,4-naphthoquinone. Photo-addition compounds were obtained in fairly good yields in every case examined here.

The yields of the photo-addition compounds are tabulated in Table 1.

The structures of the photo-addition compounds were determined by the following procedures. As a typical example, the photochemical reaction of 2-methoxy-1,4-naphthoquinone with styrene will be illustrated. After the usual work-up of the reaction mixture, white needles were obtained as the main reaction product in a 69% yield. Elemental analysis and molecular-weight determination by mass spectrometry revealed that the photo-addition compound was composed of one molecule of the 2-methoxy-1,4-naphthoquinone moiety and one molecule of the styrene moiety. The addition compound contained both a hydroxyl group and a carbonyl group, judging from an inspection of its infrared and electronic spectra. The PMR spectrum (Fig. 1) showed seven characteristic groups of lines. The PMR signals corresponding to H_c disappeared after the treatment of the chloroform solution with D_2O. The nuclear spin-spin interactions among H_a, H_b, H_d, and H_e were confirmed by the spin-decoupling technique.

Table 1. The yields of the photo-additon compounds obtained in the reaction of 2-alkoxy-1,4-naphthoquinones with olefins

2-Alkoxy-1,4-naphthoquinone	Olefin	Photo-addition compound	Yield[a] (%)	Mp (°C)
2-Methoxy-1,4-naphthoquinone	1-Hexene	**10a**	25	—
2-Methoxy-1,4-naphthoquinone	1-Heptene	**10b**	50	80.0—81.0
2-Methoxy-1,4-naphthoquinone	1-Octene	**10c**	67	101.0—101.5
2-Methoxy-1,4-naphthoquinone	Cyclohexene	**10d**	39	—
2-Methoxy-1,4-naphthoquinone	Cycloöctene	**10e**	74	191.0—198.0
2-Methoxy-1,4-naphthoquinone	1,4-Cycloöctadiene	**10f**	29	184.0—186.0
2-Methoxy-1,4-naphthoquinone	Bicyclo[2.2.1]hept-2-ene	**10g**	50	214.0—217.0
2-Methoxy-1,4-naphthoquinone	Bicyclo[2.2.1]hept-2,5-diene	**10h**	35	199.0—201.0
2-Methoxy-1,4-naphthoquinone	Styrene	**10i**	69	164.0—164.5
2-Methoxy-1,4-naphthoquinone	Indene	**10j**	73	225.0—227.0
2-Ethoxy-1,4-naphthoquinone	Styrene	**10k**	60	168.0—169.0
2-Isopropoxy-1,4-naphthoquinone	Styrene	**10l**	7.1	117.0—118.0
2-Allyloxy-1,4-naphthoquinone	Styrene	**10m**	27	139.0—140.0

a) The yields were calculated on the basis of the starting quinones consumed.

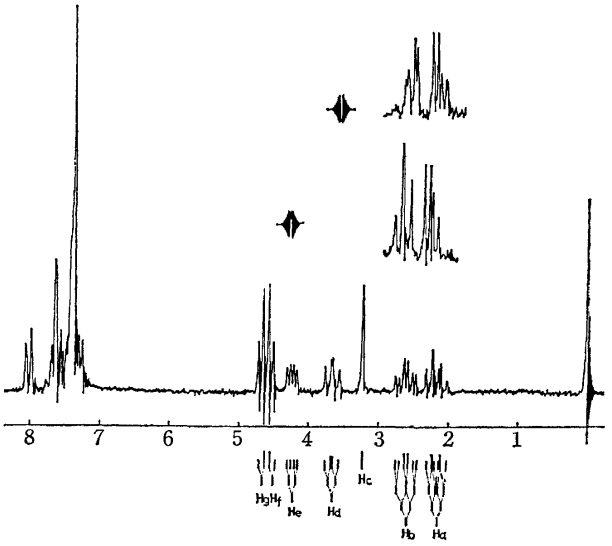

Fig. 1. PMR spectrum of the photo-addition compound.

When 2-deuteriomethoxy-1,4-naphthoquinone was subjected to the same photochemical reaction, the PMR signals corresponding to H_f, and H_g (Fig. 1) of the photo-addition compound disappeared. On the other hand, the PMR signals corresponding to H_d disappeared completely when 2-methoxy-3-deuterio-1,4-naphthoquinone was used in the reaction. These results indicate that the protons, denoted by H_d, H_f, and H_g, of the photo-addition compound originated from the 2-methoxy-1,4-naphthoquinone moiety. From these results, the structure **6** could be proposed as the most probable one for the addition compound. In order to ascertain the structure **6**, the addition compound was submitted to the following chemical reactions. Upon treatment with acetyl chloride, an acetylated product was obtained. This acetylated product was confirmed to be **7** by its IR, PMR, and mass analyses. The Clemmensen reduction of the photo-addition compound gave a mixture of the two compounds. Their structures were assigned to **8** and **9**

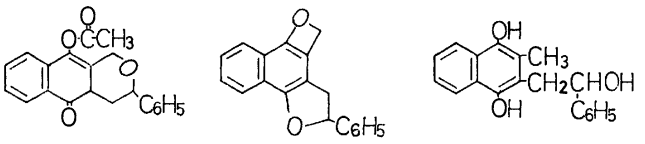

7 **8** **9**

respectively on the basis of an inspection of their IR, PMR, and mass spectra. A similar reaction was reported by the Clemmensen reduction of eleutherins.[13]

Taking these results into account, the structure of the photo-addition compound should be the structure **6**.

The photo-addition compound is characterized by containing a tetrahydropyran ring. A similar type of photochemical reaction was found to proceed in all the 2-alkoxy-1,4-naphthoquinones examined here with a variety of olefins. The structures of the photo-addition compounds obtained here are concluded to have a tetrahydropyran ring and to be **10** on the basis of analyses of their mass, IR, and PMR spectra and their elemental analyses.

The photo-addition reaction could be initiated by the excitation of 2-alkoxy-1,4-naphthoquinones by irradiation, and the addition reaction may proceed *via* radical intermediates to give compounds characterized by containing a tetrahydropyran ring.

To give **10**, the 1,4-naphthoquinone moiety of 2-alkoxy-1,4-naphthoquinones should migrate from the oxygen atom to the α-carbon atom of the alkoxy group during the course of the photochemical reaction; the diradical should then add to olefins to give a final product. Two different routes seem to be plausible

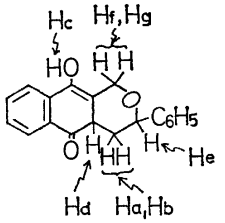

6

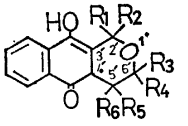

10

	R_1	R_2	R_3	R_4	R_5	R_6
10a	H-	H-	n-C_4H_9-	H-	H-	H-
b	H-	H-	n-C_5H_{11}-	H-	H-	H-
c	H-	H-	n-C_6H_{13}-	H-	H-	H-
d	H-	H-	H-	$-(CH_2)_4-$		H-
e	H-	H-	H-	$-(CH_2)_6-$		H-
f	H-	H-	H-	$-(CH_2)_2CH{=}CH(CH_2)_2-$		H-
g	H-	H-	H-	$-CH<^{CH_2}_{(CH_2)_2}>CH-$		H-
h	H-	H-	H-	$-CH<^{CH_2}_{CH=CH}>CH-$		H-
i	H-	H-	C_6H_5-	H-	H-	H-
j	H-	H-	H-	$-CH_2$ (benzo)		H-
k	H-	CH_3-	C_6H_5-	H-	H-	H-
l	CH_3-	CH_3-	C_6H_5-	H-	H-	H-
m	H-	CH_2=CH-	C_6H_5-	H-	H-	H-

for the migration.

When the migration proceeds *via* Route (i), the scrambling of the hyrdogen atom at Position Three in the starting quinones should be observed. However, this is not the case, as was determined by the reaction of deuterium-labelled quinone derivatives. That is, the PMR signal corresponding to H_d in the photo-addition compound (see **6**) disappeared completely when 2-methoxy-3-deuterio-1,4-naphthoquinone was used as the starting quinone. From this fact only Route (ii) remains as a possible route for the migration of the 1,4-naphthoquinone moiety.

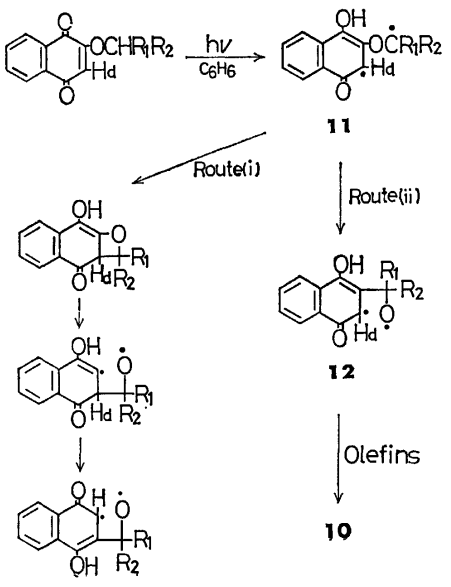

Table 2. Yield dependencies of the photo-addition products on 2-alkoxy groups

R_1, R_2 of the alkoxy groups		Yield of the product **10**[a]	
H	H	**10 i**	69 %
H	CH_3	**10 k**	60 %
CH_3	CH_3	**10 l**	7.1%

a) The yields were calculated on the basis of the starting quinones consumed.

On the other hand, when three quinones with different alkoxy groups were submitted to photochemical reactions with styrene under the same conditions, the yields of similar types of photo-addition compounds vary with the structures of the alkoxy groups. The results obtained are summarized in Table 2. Taking into account the stability of the diradical **11**, the trend of the yields for the photo-addition compounds (**10 i**, **10 k**, and **10 l**) is explicable. The most stable diradical having one of the two radical centers on the tertiary carbon atom (**11**, R_1, R_2=CH_3); an intremediate derived from the reaction of 2-isopropoxy-1,4-naphthoquinone shows the least tendency to yield **10 l**. In this case, another type of photo-addition compound **13** was obtained as the main reaction product; this is the compound produced by the simple addition of **11** to styrene.

In the absence of olefins, compound **14** was isolated as a photochemical reaction product of 2-methoxy-1,4-naphthoquinone. The formation of **14** is feasible *via* the generation of a free radical **11** (R_1,R_2=H), the subsequent 1,2-migration of the 1,4-naphthoquinone

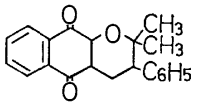

13

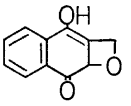

14

moiety to **12**, and the final ring closure. All of the results described above confirm the intermediacy of the free radical **11**, and the subsequent 1,2-migration process.

Tetrasubstituted olefins, such as 2,3-dimethylbut-2-ene and tetraphenylethylene, however, give no photo-addition products, but only compound **14** in the photochemical reaction with 2-methoxy-1,4-naphthoquinone. This is presumably because of their sterical requirements.

Experimental

Starting Materials. *2-Methoxy-1,4-naphthoquinone*:[14] 2-Hydroxy-1,4-naphthoquinone (5.0 g), methanol (80 ml), and concd. sulfuric acid (1.2 ml) were heated under reflux for 5 hr. 2-Methoxy-1,4-naphthoquinone precipitated as yellow needles was isolated by a usual work-up and was recrystallized from ethanol (4.0 g); mp 178.0—180.5 °C. Found: C, 70.48; H, 4.25%. Calcd for $C_{11}H_8O_3$: C, 70.21; H, 4.29%. IR(KBr disk); 1680, 1650 cm^{-1} (C=O). UV max($CHCl_3$); 274 nm (log ε=4.22), 355 nm (log ε=3.54).

PMR(CCl_4); δ: 3.88 (3H, singlet), 6.02 (1H, singlet, 7.56—8.08 ppm (4H, multiplet).

2-Ethoxy-1,4-naphthoquinone:[15] By treating 2-hydroxy-1,4-naphthoquinone (2.5 g) with ethanol (30 ml) in the presence of concd. sulfuric acid (1.0 ml) for 8 hr, 2-ethoxy-1,4-naphthoquinone was obtained as yellow needles (1.5 g); mp 118.0—119.0 °C. IR(KBr disk); 1680, 1640 cm^{-1} (C=O). PMR(CCl_4); δ: 1.56 (3H, triplet, J=7.0 Hz), 4.08 (2H, quartet, J=7.0 Hz), 6.02 (1H, singlet), 7.60—8.10 ppm (4H, multiplet).

2-Isopropoxy-1,4-naphthoquinone:[16] 2-Hydroxy-1,4-naphthoquinone (1.0 g), isopropyl alcohol (20 ml), and the boron trifluoride ether complex (3.0 ml) were heated at 70 °C for 7 hr. After cooling, 2-isopropoxy-1,4-naphthoquinone precipitated was collected by filtration, washed with an aqueous solution of sodium hydrogencarbonate until the filtrate was colorless, and then washed once with isopropyl alcohol (0.7 g); mp 111.5—112.0 °C. IR(KBr disk); 1680, 1660 cm^{-1} (C=O). PMR(CCl_4); δ: 1.44(6H, doublet. J=6.0 Hz), 4.56(1H, septet, J=6.0 Hz), 6.00(1H, singlet), 7.58—8.10 ppm (4H, multiplet).

2-Allyloxy-1,4-naphthoquinone:[16] 2-Hydroxy-1,4-naphthoquinone (1.0 g), allyl alcohol (20 ml), and the boron trifluoride ether complex (3.0 ml) were heated at 70 °C for 5 hr. After cooling, water (80 ml) was added to the reaction mixture. 2-Allyloxy-1,4-naphthoquinone precipitated was collected by filtration, washed with an aqueous solution of sodium hydrogencarbonate until the filtrate was colorless, and then recrystallized from ligroin as yellow needles (0.45 g); mp 98.0—100.0 °C. IR(KBr disk); 1680, 1650 cm^{-1} (C=O). PMR(CCl_4); δ: 4.60(2H, broad doublet, J=4.0 Hz), 5.52 (2H, multiplet), 6.00(1H, multiplet), 6.16(1H, singlet), 7.64—8.20 ppm (4H, multiplet).

Olefins: All the olefins used here were commercially available and were purified by distillation before use.

General Procedures. 2-Alkoxy-1,4-naphthoquinone (1 mmol) and olefin (2 mmol) were dissolved in benzene (20 ml) and irradiated in a glass tube by means of a high pressure Hg arc lamp (300 W) through a 5-cm thick water layer. After the 2-alkoxy-1,4-naphthoquinone had been consumed completely, the benzene was distilled off under reduced pressure. Then the reaction mixture was purified by chromatography on silica gel and then further purified by recrystallization from an appropriate solvent.

Identification of the Photo-addition Compound: *6'-n-Butyltetrahydropyrano*[c-*2,3*]-*1-hydroxy-4-oxo-3,4-dihydronaphthalene* (**10a**); yellow oil (yield, 25%). Mass; m/e=272 (M^+). IR(liq. film); 3480 (OH), 2920, 2840 (CH), 1680 cm^{-1} (C=O). PMR (CCl_4); δ: 0.96 (3H, CH_3, broad triplet), 1.40 (6H, aliphatic protons, broad multiplet), 1.64—1.90(2H, C-5' CH_2, multiplet), 2.84(1H, C-6' CH, multiplet), 3.28(1H, C-4' CH, triplet, J=10.0 Hz), 3.80 (1H, OH, singlet), 4.34, 4.56(2H, C-2' CH_2, AB-quartet, J=6.0 Hz), 7.24—7.92 ppm (4H, aromatic protons, multiplet).

6'-n-Pentyltetrahydropyrano[c-*2,3*]-*1-hydroxy-4-oxo-3,4-dihydronaphthalene* (**10b**); white needles from *n*-hexane (yield, 50%); mp 80.0—81.0 °C. Mass; m/e=286(M^+). Found: C, 75.78; H, 8.05%. Calcd for $C_{18}H_{22}O_3$: C, 75.49; H, 7.74%. IR(KBr disk); 3360 (OH), 2920, 2840 (CH), 1670 cm^{-1} (C=O). PMR(CCl_4); δ: 0.92 (3H, CH_3, broad triplet), 1.36 (8H, aliphatic protons, broad multiplet), 1.64—1.90 (2H, C-5' CH_2, multiplet), 2.92 (1H, C-6' CH, multiplet), 3.28 (1H, C-4' CH, triplet, J=10.0 Hz), 3.92 (1H, OH, singlet), 4.34, 4.56 (2H, C-2' CH_2, AB-quartet, J=6.0 Hz), 7.22—7.96 ppm (4H, aromatic protons, multiplet).

6'-n-Hexyltetrahydropyrano[c-*2,3*]-*1-hydroxy-4-oxo-3,4-dihydronaphthalene* (**10c**); white needles from *n*-hexane (yield, 67%); mp 101.0—101.5 °C. Mass; m/e=300(M^+). Found: C, 76.21; H, 8.32%. Calcd for $C_{19}H_{24}O_3$: C, 75.97; H, 8.05%. IR(KBr disk); 3320 (OH), 2920, 2840 (CH), 1680 cm^{-1} (C=O). PMR(CCl_4); δ: 0.92 (3H, CH_3, broad triplet), 1.36 (10H, aliphatic protons, broad multiplet), 1.64—1.90 (2H, C-5' CH_2, multiplet), 2.92 (1H, C-6' CH, multiplet), 3.30 (1H, C-4' CH, triplet, J=10.0 Hz), 3.50 (1H, OH, singlet), 4.38, 4.58 (2H, C-2' CH_2, AB-quartet, J=6.0 Hz), 7.28—7.96 ppm (4H, aromatic protons, multiplet).

5',6'-Tetramethylenetetrahydropyrano[c-*2,3*]-*1-hydroxy-4-oxo-3,4-dihydronaphthalene* (**10d**); yellow oil (yield, 39%). Mass; m/e=270(M^+). IR(liq. film); 3350 (OH), 2920, 2840 (CH), 1660 cm^{-1} (C=O). PMR($CDCl_3$); δ: 0.80—3.25 (10H, aliphatic protons, multiplet), 3.42 (1H, C-4' CH, doublet, J=8.0 Hz), 4.48, 4.64 (2H, C-2' CH_2, AB-quartet, J=6.0 4.80 (1H, OH, singlet), 7.24—8.10 ppm (4H, aromatic protons, multiplet).

5',6'-Hexamethylenetetrahydropyrano[c-*2,3*]-*1-hydroxy-4-oxo-3,4-dihydronaphthalene* (**10e**); white crystals (yield, 74%); mp 191.0—198.0 °C (decomp.). Mass; m/e=298(M^+). IR(KBr disk); 3360 (OH), 2920, 2840 (CH), 1660 cm^{-1} (C=O). PMR($CDCl_3$); δ: 0.90—3.00 (14H, aliphatic protons, multiplet), 3.04 (1H, C-4' CH, doublet, J=8.0 Hz), 4.52, 4.64 (2H, C-2' CH_2, AB-quartet, J=6.0 Hz), 4.72 (1H, OH, singlet), 7.36—8.12 ppm (4H, aromatic protons, multiplet).

5',6'-3''-Hexenylenetetrahydropyrano[c-*2,3*]-*1-hydroxy-4-oxo-3,4-dihydronaphthalene* (**10f**); white crystals (yield, 29%); mp 184.0—186.0 °C (decomp.). Mass; m/e=296(M^+). IR(KBr disk); 3320 (OH), 3000, 2910, 2840 (CH), 1670 cm^{-1} (C=O). PMR($CDCl_3$); δ: 1.00—2.80 (11H, aliphatic protons and OH, multiplet), 3.16 (1H, C-4' CH, doublet, J=10.0 Hz), 4.68 (2H, C-2' CH_2, broad singlet), 5.52 (2H, C-5'' and C-6'' CH's, broad doublet), 7.28—7.96 ppm (4H, aromatic protons, multiplet).

Bicyclo[*2.2.1*]*heptano*[*2'',3''*-e]*tetrahydropyrano*[c-*2,3*]-*1-hydroxy-4-oxo-3,4-dihydronaphthalene* (**10g**); white crystals from chloroform (yield, 50%); mp 214.0—217.0 °C. Mass; m/e=282 (M^+). Found: C, 76.49; H, 6.63%. Calcd for $C_{18}H_{18}O_3$: C, 75.56; H, 6.44%. IR(KBr disk); 3420 (OH), 2960, 2930, 2880 (CH), 1670 cm^{-1} (C=O). PMR($CDCl_3$); δ: 1.04—2.16 (7H, aliphatic protons, multiplet), 2.42 (2H, aliphatic protons, multiplet), 2.82 (1H, OH, singlet), 2.90 (2H, aliphatic protons, multiplet), 4.56, 4.72 (2H, C-2' CH_2, AB-quartet, J=6.0 Hz), 7.24—7.92 ppm (4H, aromatic protons, multiplet).

Bicyclo[*2.2.1*]*hept-5''-eno*[*2'',3''*-e]*tetrahydropyrano*[c-*2,3*]-*1-hydroxy-4-oxo-3,4-dihydronaphthalene* (**10h**); white crystals from chloroform (yield 35%); mp 199.0—201.0 °C. IR(KBr disk); 3380 (OH), 2960, 2880 (CH), 1665 cm^{-1} (C=O). PMR($CDCl_3$); δ: 1.22—2.00 (3H, aliphatic protons, multiplet), 2.60 (1H, OH, singlet), 2.76 (2H, aliphatic protons, multiplet), 3.06 (2H, aliphatic protons, multiplet), 4.64, 4.78 (2H, C-2' CH_2, AB-quartet, J=6.0 Hz), 6.04 (2H, C-5'' and C-6'' CH's, multiplet), 7.24—7.96 ppm (4H, aromatic protons, multiplet).

6'-Phenyltetrahydropyrano[c-*2,3*]-*1-hydroxy-4-oxo-3,4-dihydronaphthalene* (**10i≡6**); white needles from benzene (yield, 69%); mp 164.0—164.5 °C. Mass; m/e=292(M^+). Found: C, 78.03; H, 5.45%. Calcd for $C_{19}H_{16}O_3$: C, 78.08; H, 5.52%. IR(KBr disk); 3250 (OH), 2940 (CH), 1675 cm^{-1} (C=O). UV max ($CHCl_3$); 290 nm (log ε=3.48). PMR($CDCl_3$); δ: 2.16 (1H, C-5' CH, multiplet), 2.58 (1H, C-5' CH, multiplet), 3.22 (1H, OH, singlet), 3.62 (1H, C-4' CH, double doublet, J=8.0, 12.0 Hz), 4.18 (1H, C-6' CH, double doublet, J=6.0, 10.0 Hz), 4.56, 4.64 (2H, C-2' CH_2, AB-quartet, J=6.0 Hz), 7.24—8.10 ppm (9H, aromatic protons, multiplet).

Indeno[*2″,3″-e*]*tetrahydropyrano*[c-*2,3*]-*hydroxy-4-oxo-3,4-dihydronaphthalene* (**10j**); white needles from benzene-petroleum ether (yield, 73%); mp 225.0—227.0 °C (decomp.). Mass; *m/e*=304 (M^+). Found: C, 79.22; H, 5.28%. Calcd for $C_{20}H_{16}O_3$: C, 78.93; H, 5.30%. IR(KBr disk); 3320 (OH), 2920 (CH), 1675 cm^{-1} (C=O). PMR($CDCl_3$); δ: 2.04 (1H, OH, singlet), 2.64 (1H, C-5′ CH, multiplet), 3.04 (2H, C-1″ CH_2, double doublet, J=6.0, 10.0 Hz), 3.19 (1H, C-2′ CH_2, AB-quartet, J=6.0 Hz), 7.10—8.00 ppm (8H, aromatic protons, multiplet).

2′-Methyl-6′-phenyltetrahydropyrano[c-*2,3*]-1-*hydroxy-4-oxo-3,4-dihydronaphthalene* (**10k**); white needles from benzene (yield, 60%); mp 168.0—169.0 °C. Found: C, 78.73; H, 5.73%, Calcd for $C_{20}H_{18}O_3$: C, 78.41; H, 5.92%. IR(KBr disk); 3280 (OH), 2980 (CH), 1680 cm^{-1} (C=O). PMR($CDCl_3$); δ: 1.16 (3H, CH_3, doublet, J=6.0 Hz), 2.16 (1H, C-5′ CH, multiplet), 2.58 (1H, C-5′ CH, multiplet), 2.94 (1H, OH, singlet), 3.62 (1H, C-4′ CH, double doublet, J=8.0, 12.0 Hz), 4.18 (1H, C-6′ CH, double doublet, J=6.0, 10.0 Hz), 4.70 (1H, C-2′ CH, quartet, J=6.0 Hz), 7.22—8.10 ppm (9H, aromatic protons, multiplet).

2′,2′-Dimethyl-6′-phenyltetrahydropyrano[c-*2,3*]-*1-hydroxy-4-oxo-3,4-dihydronaphthalene* (**10l**); white needles from benzene (yield, 7.1%); mp 117.0—118.0 °C. Mass; *m/e*=320(M^+). Found: C, 78.55; H, 6.22%. Calcd for $C_{21}H_{20}O_3$: C, 78.72; H, 6.29%. IR(KBr disk); 3320 (OH), 2990, 2920 (CH), 1680 cm^{-1} (C=O). PMR($CDCl_3$); δ: 0.92 (3H, CH_3, singlet), 1.46 (3H, CH_3, singlet), 2.16(1H, C-5′ CH, multiplet), 2.58 (1H, C-5′ CH, multiplet), 2.92 (1H, OH, singlet), 3.62 (1H, C-4′ CH, double doublet, J=8.0, 12.0 Hz), 4.18 (1H, C-6′ CH, double doublet, J=6.0, 10.0 Hz), 7.20—8.16 ppm (9H, aromatic protons, multiplet).

6′-Phenyl-2′-vinyltetrahydropyrano[c-*2,3*]-*1-hydroxy-4-oxo-3,4-dihydronaphthalene*(**10m**); white needles from benzene yield, 27%); mp 139.0—140.0 °C. Mass; *m/e*=318(M^+). IR(KBr disk); 3280 (OH), 3060, 3020, 2880 (CH), 1680 cm^{-1} (C=O). PMR($CDCl_3$); δ: 2.16(1H, C-5′ CH, multiplet), 2.58(1H, C-5′ CH, multiplet), 3.00(1H, OH, singlet), 3.80(1H, C-4′ CH, double doublet, J=8.0, 12.0 Hz), 4.12(1H, C-6′, CH, double doublet, J=6.0, 10.0 Hz), 5.04—6.16(4H, vinyl protons and C-2′, CH, multiplet), 7.22—8.18(9H, aromatic protons, multiplet).

6′,6′-Dimethyl-5′-phenyltetrahydropyrano[b-*2,3*]-*1,4-dioxo-1,2,3,4-tetrahydronaphthalene* (**13**); white needles (yield, 41%); mp 91.0—92.0 °C. Mass; *m/e*=320(M^+). Found: C, 79.07; H, 5.85%. Calcd for $C_{21}H_{20}O_3$: C, 78.75; H, 6.25%. IR(KBr disk); 2970(CH), 1690, 1680 cm^{-1}(C=O). PMR (CCl_4); δ: 0.68(3H, CH_3, doublet, J=6.0 Hz), 0.90(3H, CH_3 doublet, J=6.0 Hz), 2.14(1H, C-4′ CH, multiplet), 2.83(1H, C-4′ CH, multiplet), 3.60—4.00(3H, C-2′, C-3′ and C-5′ CH's, multiplet), 7.24 (5H, aromatic protons, singlet), 7.60—8.24 ppm(4H, aromatic protons, multiplet).

Oxetano[b-*3,2*]-*1-hydroxy-4-oxo-3,4-dihydronaphthalene* (**14**); white crystals (yield, 9%); mp 213.0—218.0 °C (decomp.). Mass; *m/e*=188(M^+). IR(KBr disk); 3450(OH), 1685 cm^{-1} (C=O). PMR(CCl_3); δ: 3.20(1H, CH, singlet), 4.80, 5.28 (2H, CH_2, AB-quartet, J=6.0 Hz), 5.30(1H, OH, singlet), 7.40—8.24 ppm (4H, aromatic protons, multiplet).

Acetylation of a Photo-addition Compound. A photo-addition compound (**6**) (50 mg) was treated with acetyl chloride (2.5 ml) in 1,2-dichloroethane (10 ml) at room tempreature. After having been stirred for 8 hr, the solution was poured onto crashed ice and extracted with chloroform. The chloroform layer was then separated and dried on anhydrous sodium sulfate, and then the reaction mixture was purified by thin layer chromatography on silica gel. An acetylated product (**7**) was isolated as yellowish crystals; mp 160.0—164.0 °C. Mass; *m/e*=334(M^+). IR(KBr disk); 2920 (CH), 1735, 1680 cm^{-1} (C=O). PMR($CDCl_3$); δ: 1.96(3H, $COCH_3$, singlet), 2.50—3.10(2H, C-5′ CH_2, multiplet), 3.60—4.40(2H, C-4′ and C-6′ CH's, multiplet), 4.54, 4.78(2H, C-2′ CH_2, AB-quartet, J=10.0 Hz), 6.90—8.24 ppm (9H, aromatic protons, multiplet).

Clemmensen Reduction of Photo-addition Compound. A photo-addition compound (**6**) (500 mg), toluene (5 ml), amalgamated zinc (10 g), and concd. hydrochloric acid (12 ml) were heated for 8 hr. Two reaction products, **8** and **9**, were then isolated from the reaction mixture using thin layer chromatography on silica gel. The physical properties were as follows; product **8**; white needles; mp 137.0—139.0 °C (decomp.). Mass; *m/e*=274 (M^+). Found: C, 83.06; H, 5.35%. Calcd for $C_{19}H_{14}O_2$: C, 83.20; H, 5.15%. IR(KBr disk); no absorption signals due to OH or C=O. PMR ($CDCl_3$); δ: 3.14 (2H, CH_2, multiplet), 4.82 (1H, CH, double doublet, J=4.0, 10.0 Hz), 5.44 (2H, CH_2, AB-quartet, J=15.0 Hz), 7.14—7.90 ppm (9H, aromatic protons, multiplet). product **9**; colorless oil. Mass; *m/e*= 276 (M^+-18 (H_2O)). IR(liq. film); 3580, 3400 cm^{-1} (OH). PMR(CCl_4); δ: 2.56 (3H, CH_3, singlet), 3.18 (2H, CH_2, doublet, J=6.0 Hz), 4.82 (1H, CH, triplet, J=6.0 Hz), 7.10—8.00 (9H, aromatic protons, multiplet).

The author wishes to express his gratitude to Professor Kazuhiro Maruyama, Kyoto University, for his invaluable suggestions and encouragement. He also wishes to thank the Ministry of Education for the financial support granted for this research.

References

1) Part I for this series. K. Maruyama and T. Otsuki, *Chem. Lett.*, **1974**, 129.
2) L. M. Bruce, *Quart. Revs.*, **21**, 405 (1967).
3) C. H. Krauch and S. Farid, *Tetrahedron Lett.*, **1966**, 4783.
4) K. Maruyama, T. Otsuki, and Y. Naruta, *Chem. Lett.*, **1973**, 641.
5) K. Maruyama, T. Otsuki, A. Takuwa, and S. Kako, *Bull. Inst. Chem. Res., Kyoto Univ.*, **50**, 344 (1972).
6) K. Maruyama, T. Otsuki, and Y. Naruta, The 24th Symposium on Organic Reaction Mechanisms, held at Fukuoka in October, 1973.
7) K. Wallenfals and W. Möhle, *Ber.*, **76**, 924 (1943).
8) P. Zuman, *Coll. Czech. Chem. Commun.*, **27**, 2035 (1962).
9) S. P. Pappas and N. A. Portnoy, *J. Org. Chem.*, **33**, 2200 (1968).
10) S. P. Pappas, B. C. Pappas, and N. A. Portnoy, *ibid.*, **34**, 520 (1969).
11) S. P. Pappas and N. A. Portnoy, *Chem. Commun.*, **1969**, 597.
12) S. P. Pappas and N. A. Portnoy, *ibid.*, **1970**, 1126.
13) H. Schmid, A. Ebnöther, and Th. M. Meijer, *Helv. Chim. Acta*, **33**, 1751 (1950).
14) cf. R. B. Woodward, F. Sondheimer, D. Taub, K. Hensler, and W. M. Lamore, *J. Amer. Chem. Soc.*, **74**, 4223 (1952).
15) L. F. Fieser, *ibid.*, **48**, 2922 (1926).
16) L. F. Fieser, *ibid.*, **70**, 3165 (1948).

Spectrophotometric Studies of the Acidities of Dichlorophene and Hexachlorophene

Hiroyasu INOUE and Naomi ASAOKU

Department of Applied Chemistry, Faculty of Technology, Kanagawa University, Kanagawa-ku, Yokohama 221

(Received April 13, 1974)

It has been found that dichlorophene (bis-(2-hydroxy-5-chlorophenyl)methane) and hexachlorophene (bis-(2-hydroxy-3,5,6-trichlorophenyl)methane) have abnormally high acidities as compared with the corresponding reference compounds, *i.e.*, 2-methyl-4-chlorophenol and 2,4,5-trichlorophenol respectively. The values of pK_a for the first and second ionizations of dichlorophene in a mixed solvent of ethanol and water (1 : 1) were determined to be 9.10 and 13.1, and those of hexachlorophene, to be 5.87 and 11.9, at 18 °C. On the basis of the infrared spectra, these observations could be interpreted in terms of the additional stabilization of the resulting mono-anions of these bis-phenolmethanes by means of the intramolecular hydrogen bondings between the OH and O^- groups.

The acidities of organic compounds are more or less influenced by various types of intra- and intermolecular interactions. For many substituted phenols, the effects of intra- and intermolecular hydrogen bondings on their acidities have been widely studied.[1] It is well known that salicylic acid is a stronger acid than *o*-methoxybenzoic acid, and this has been attributed to the additional stabilization of the resulting mono-anion of salicylic acid by the intramolecular hydrogen-bonding between the COO^- and OH groups.[2-6]

In the present investigation, the acidities of two bis-phenolmethanes, dichlorophene (bis-(2-hydroxy-5-chloro phenyl)methane), and hexachlorophene (bis-(2-hydroxy-3,5,6-trichlorophenyl)methane), are compared with those of 2-methyl-4-chlorophenol and 2,4,5-trichlorophenol respectively, which can be regarded as reference compounds for the above bis-phenolmethanes because their ultraviolet spectra resemble well those of the respective bis-phenolmethanes. If, in the bis-phenolmethanes, there take place some intramolecular interactions between the two moieties separated by the methylene group, their acidities may be expected to be different from those of the reference compounds. In fact, when water is added to a solution of hexachlorophene in ethanol, a new absorption band appears at 320 nm, with an intensity depending upon the concentration of the added water; this band disappears when the solution is made acidic, thus suggesting that hexachlorophene ionizes partly even in a neutral aqueous solution. On the other hand, this is not the case for 2,4,5-trichlorophenol. Accordingly, we will deal with the factors accounting for the abnormally high acidities of the bis-phenolmethanes as studied by means of ultraviolet and infrared spectroscopies.

Results and Discussion

Figures 1 and 2 show the spectral changes on the variation in the pH values of solutions of dichlorophene and hexachlorophene respectively in a mixed solvent of ethanol and water (1 : 1 in volume). These spectral changes can safely be attributed to the first and second ionizations of the phenolic hydroxyl groups of these bis-phenolmethanes. In Figs. 1 and 2 the solid and the broken lines represent the spectral changes due to the first and the second ionizations respectively. The absorption intensities of the newly-appearing bands change with a change in the pH value of the solutions, as is shown in Fig. 3. As may be seen from this figure, the second ionization of each compound occurs in a distinctly higher pH region than the first ionization.

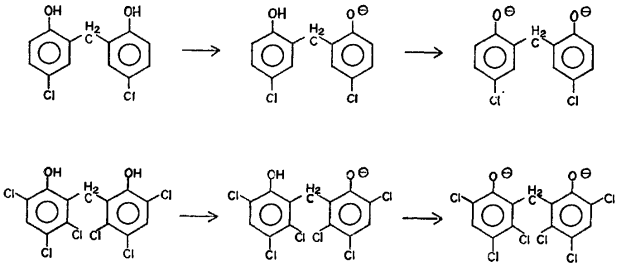

Therefore, the pK_a values for the first and second ionizations of these bis-phenolmethanes can be determined from the absorbances of the newly-appeared bands by the application of the usual equation. The results are summarized in Table 1, in which the results for 2-methyl-4-chlorophenol and 2,4,5-trichlorophenol obtained in the same manner are also presented for the sake of comparison. As may be seen from this table, the pK_a values for the first ionizations of the bis-phenolmethanes are significantly smaller than those of the

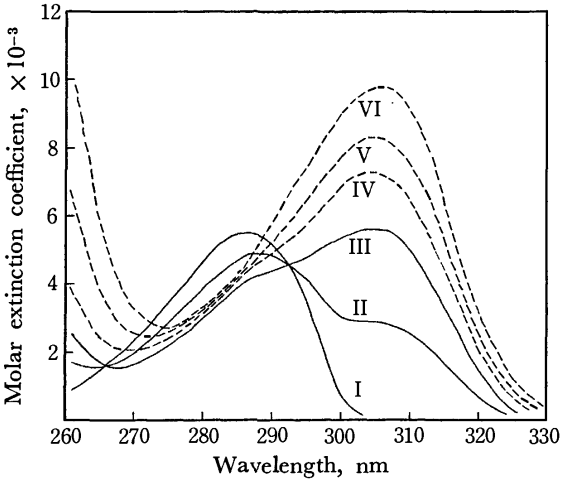

Fig. 1. Spectral change of the solution of dichlorophene in mixed solvent of ethanol and water (1 : 1) on variation of pH.
pH; I: 6.8, II: 8.9, III: 9.9, IV: 12.4, V: 13.1, VI: 13.7

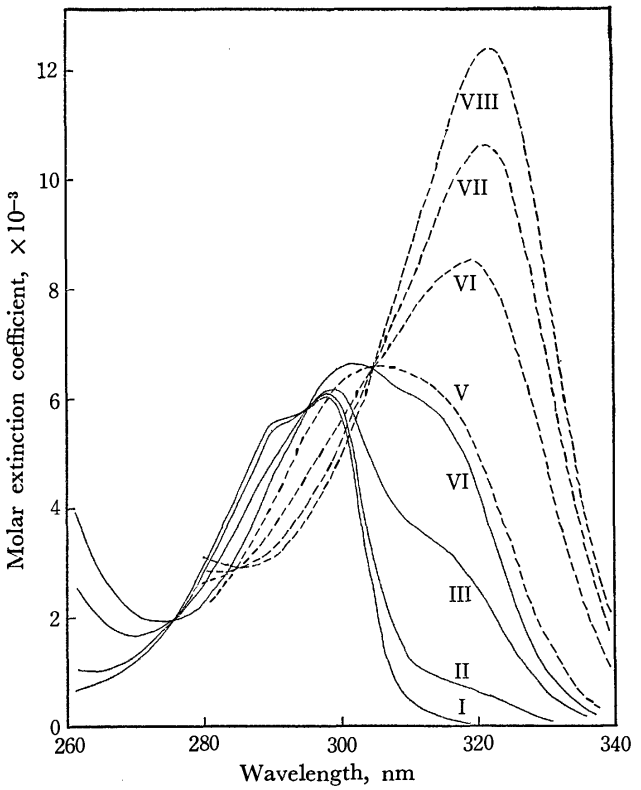

Fig. 2. Spectral change of the solution of hexachlorophene in mixed solvent of ethanol and water (1 : 1) on variation of pH.
pH; I: 3.4, II: 4.6, III: 5.4, IV: 6.7, V: 10.5, VI: 12.0, VII: 12.4, VIII: 12.9

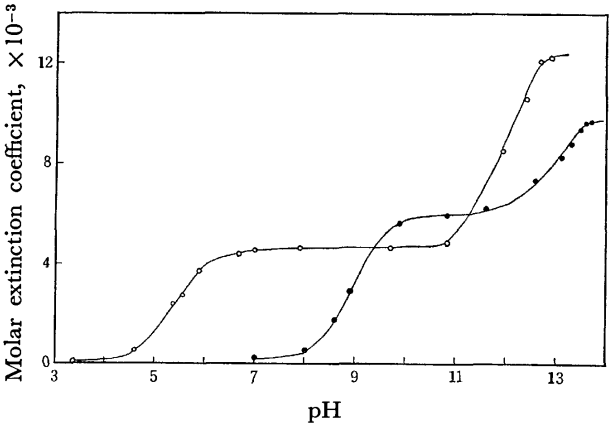

Fig. 3. Plot of absorption intensity of the new band against pH.
●: Dichlorophene, at 304 nm, ○: Hexachlorophene, at 320 nm

respective reference compounds. On the other hand, the pK_a values for the second ionizations are fairly large. These results strongly suggest that an intramolecular interaction takes place for each of the bis-phenolmethanes in the ionized species.

Next, the interaction of the bis-phenolmethanes with triethylamine in *n*-hexane was studied. It has been established that various types of interactions exist between such phenols as *p*-nitrophenol and triethylamine, including the formations of a simple hydrogen bond, a hydrogen-bonded ion pair, a solvent-separated ion pair, and dissociation into individual ions, depending upon the solvent employed.[7,8] The spectral changes on the addition of triethylamine to a *n*-hexane solution of the present bis-phenolmethanes are shown in Fig. 4. As for hexachlorophene, the first ionization into the ions, probably the ion pair, is considered to occur in *n*-hexane on the addition of triethylamine, judging from the spectra shown in Fig. 4. In the case of dichlorophene, however, the ionization does not occur; however, the hydrogen bonding with triethylamine does seem to take place, because the addition of triethylamine causes a small shift of the absorption band (from 286 nm to 293 nm) compared with the case of the ionization. By the application of the method of Rose and Drago,[9] the equilibrium constants for the first ionization of hexachlorophene in *n*-hexane and for the formation of the hydrogen bond between dichlorophene and triethylamine were determined to be 29500 and 5900 at 25 °C respectively. 2,4,5-Trichlorophenol undergoes only the hydrogen-bonding with triethylamine in *n*-hexane. That the difference in the pK_a values determined in aqueous ethanol reflects the different types of interactions for hexachlorophene and 2,4,5-trichlorophenol with triethylamine in *n*-hexane clearly indicates that the abnormally high acidity of hexachlorophene can not be attributed to the effect of the solvation of the ionized species.

It is expected that the presence of two hydroxyl groups

Table 1. The pK_a values for the first and the second ionizations in aqueous ethanol

	pK_a(I)	pK_a(II)
Hexachlorophene	5.87(18°), 5.69(40°)	11.9(18°)
2,4,5-Trichlorophenol	8.44(18°), 8.25(38°)	
Dichlorophene	9.10(18°), 8.83(38°)	13.1(18°)
2-Methyl-4-chlorophenol	10.89(18°), 10.13(38°)	

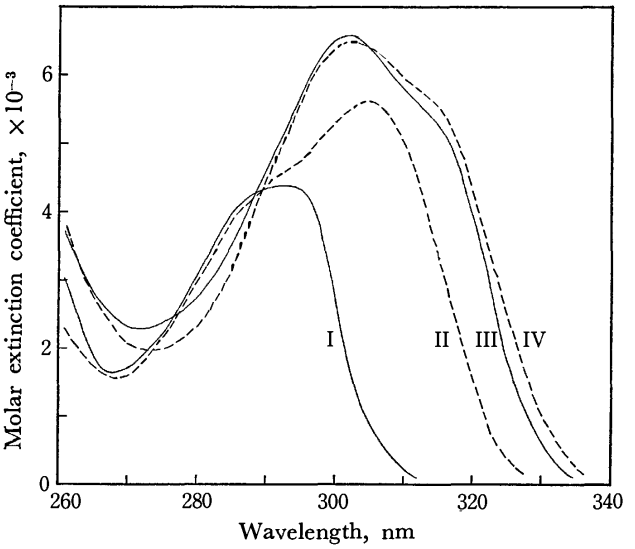

Fig. 4. Absorption spectra.
I: Dichlorophene in *n*-hexane containing triethylamine, II: Dichlorophene in aqueous ethanol, pH: 9.9, III: Hexachlorophene in *n*-hexane containing triethylamine, IV: Hexachlorophene in aqueous ethanol, pH: 6.7

in each of the bis-phenolmethanes is essentially related to the abnormal ease of the first ionizations. In fact, according to Higuchi *et al.*,[10] *o*-methylhexachlorophene has a pK_a value of 8.22 and hexachlorophene monosuccinate has a pK_a value of 8.14 for the ionization of the phenolic group. These values are very close to the pK_a value of 2,4,5-trichlorophenol. Hence, it can be considered that two hydroxyl groups of the bis-phenolmethanes take part in an intramolecular interaction. Although intramolecular hydrogen bonding has been known to be formed in bis-(2-hydroxy-3-*t*-butyl-5-methylphenyl)methane between the two hydroxyl groups judging from the fact that this compound has its infrared absorption at 3500 cm^{-1} as a broad band,[11] such intramolecular hydrogen bonding does not occur in the case of hexachlorophene. This can be deduced from the fact that the OH stretching band is sharp in shape and appears at 3525 cm^{-1}, similarly to that of 2,4,5-trichlorophenol, as is shown in Fig. 5. However, in the case of the resulting mono-anion, an intramolecular hydrogen bond may be expected to be formed between the OH and O^- groups because of the relatively strong electronegativity of the latter. From the spatial point of view, these groups are perhaps brought close together by twisting around the C(methylene)—C(ring) bond axes.

In order to ascertain whether or not such a hydrogen bond was present, the infrared absorption spectrum of the mono-anion of hexachlorophene was measured, using tetrachloroethylene as the solvent and triethylamine as the base.[12] The results are presented in Fig. 5. The sharp band of the OH stretching vibration at 3525 cm^{-1} diminishes on the addition of triethylamine, and a broad band appears around 2100 cm^{-1}. This spectral change is due to the first ionization, and the band at

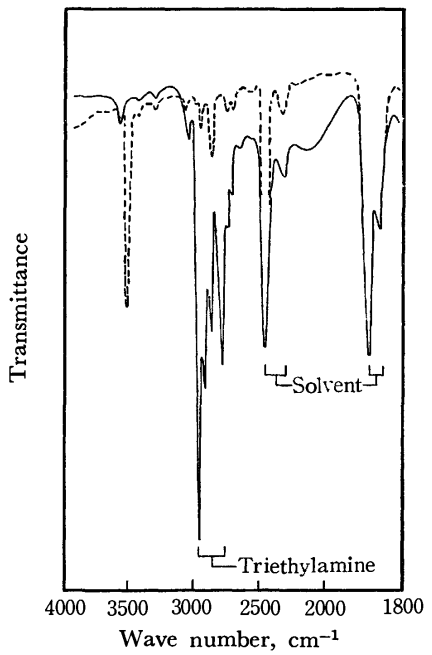

Fig 5. Infrared spectra of hexachlorophene in tetrachloroethylene.
----: Absence of triethylamine, ——: Presence of triethylamine

2100 cm^{-1} can be assigned to the OH stretching vibration of the resulting mono-anion, because no other band appears on the addition of the base in the relatively higher wave number region. The very low wave number and the broadening of this band indicate that the mono-anion has an intramolecular hydrogen bond between the OH and O^- groups. Moreover, judging from the surprisingly low wave number, this hydrogen bond seems to be extraordinarily strong, and the following intramolecular proton transfer may occur in the anion.

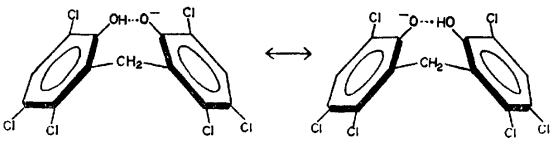

The formation of such an intramolecular hydrogen bond may cause an additional stabilization of the resulting mono-anion. Consequently, the difference in the pK_a values for hexachlorophene and 2,4,5-trichlorophenol may be ascribed to the presence of this intramolecular hydrogen bond in the former. This may also be the case for dichlorophene. Also, the abnormally high acidity of salicylic acid has been interpreted in terms of an intramolecular hydrogen-bonding between the hydroxyl and carboxylic groups. However, in the case of salicylic acid the hydrogen bond is formed even in the neutral species. This is in contrast with the situation with hexachlorophene.

As for hexachlorophene, its high acidity as compared with that of dichlorophene may be attributed to the additional inductive effect of the chlorine atoms at the 3- and 3'-positions.

The stabilization of the mono-anions of the bisphenolmethanes by the intramolecular hydrogen bond should result in higher $pK_a(II)$ values than those of the corresponding reference compounds. This is indeed the case, as is shown in Table 1. However, the high $pK_a(II)$ values may also be attributed to some extent to the repulsion of the charge in the resulting di-anions.

Experimental

Materials. All the materials used here were obtained commercially and were purified by repeated recrystallizations from a suitable solvent for each compound.

Procedures. The values of pK_a were determined spectrophotometrically by the use of the following equations;

$$pK_a(I) = pH + \log \frac{\frac{D}{A} - \varepsilon_m}{\varepsilon_n - \frac{D}{A}}$$

$$pK_a(II) = pH + \log \frac{\frac{D}{A} - \varepsilon_d}{\varepsilon_m - \frac{D}{A}}$$

where A is the initial concentration of acids and where D and ε are, respectively, the absorbance and the molar extinction coefficient. The subscripts, n, m, and d, denote neutral species, the mono-anion, and the di-anion respectively. A

mixture of ethanol and water (1 : 1) was used as the solvent.

The ultraviolet absorption spectra were measured with a Shimadzu Spectrophotometer QV-50, using 1 cm quartz cells. The cell box was maintained at a constant temperature by passing water from a constant-temperature bath through the cell box. The infrared absorption spectra were recorded on a Hitachi Infrared Spectrophotometer EPI-G3, using a 0.5 mm NaCl cell.

References and Notes

1) C. H. Rochester, "The Chemistry of the Hydroxyl Group," Part 1, ed. by S. Patai, Intersci, Pub., London (1971), p. 327.

2) A. O. McDougall and F. A. Long, *J. Phys. Chem.*, **66**, 429 (1962).

3) Z. L. Ernst and J. Menashi, *Trans. Faraday Soc.*, **59**, 230, 1803 (1964).

4) D. Chapman, D. R. Lloyd, and R. H. Prince, *J. Chem. Soc.*, **1964**, 550.

5) G. E. Dunn and F. L. Kung, *Can. J. Chem.*, **44**, 1261 (1966).

6) G. E. Dunn and T. L. Penner, *ibid.*, **45**, 1699 (1967).

7) H. Baba, A. Matsuyama, and H. Kokubun, *Spectrochim. Acta*, **25A**, 1709 (1969).

8) R. A. Hudson, R. M. Scott, and S. N. Vinogradov, *J. Phys. Chem.*, **76**, 1986 (1972).

9) N. J. Rose and R. S. Drago, *J. Amer. Chem. Soc.*, **81**, 6138 (1959).

10) T. Higuchi, H. Takechi, I. H. Pitman, and H. L. Fung, *ibid.*, **93**, 539 (1971).

11) N. D. Coggeshall, *ibid.*, **72**, 2836 (1950).

12) The infrared spectrum of dichlorophene was not measured because of its poor solubility in tetrachloroethylene.

The Synthesis of Coenzyme Q

Seiichi INOUE, Ryohei YAMAGUCHI, Kenji SAITO, and Kikumasa SATO

Department of Applied Chemistry, Faculty of Engineering, Yokohama National University, Ooka, Minami-ku, Yokohama 233

(Received April 17, 1974)

A new, efficient synthesis of coenzyme Q is described. The bromination of 2,3-dimethoxy-5-methyl-*p*-benzoquinone gives 6-bromo-2,3-dimethoxy-5-methyl-*p*-benzoquinone, which is then converted to the corresponding hydroquinone diacetate by the action of zinc dust in acetic anhydride. 6-Bromo-2,3-dimethoxy-5-methylhydroquinone diacetate is reacted with 1,1-dimethyl-π-allylnickel bromide in hexamethylphosphoramide at 60 °C to afford a 70% yield of 2,3-dimethoxy-5-methyl-6-prenylhydroquinone diacetate, which is hydrogenolyzed with lithium aluminum hydride in ether and then oxidized with aqueous ferric chloride to give coenzyme Q_1 in a 76% yield. Similarly, coenzyme Q_2, Q_9, and Q_{10}, and 6′, 10′, 14′-hexahydrocoenzyme Q_4 are synthesized by the reaction of the aryl bromide with π-geranyl-, π-solanesyl-, π-decaprenyl-, and π-phytylnickel bromide respectively and by subsequent treatment with $LiAlH_4$ and $FeCl_3$. The stereochemistry of the products is also described.

A new synthetic method which involves a selective carbon-carbon bond formation between π-allylnickel halide complexes (**1**) and organic halides has recently been reported by Corey and Semmelhack,[1] and the intrinsic value of this coupling reaction for the synthetic chemistry has been shown in the syntheses of various

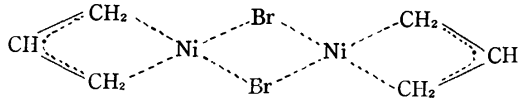

1

natural substances, α-santalene,[1] epi-β-santalene,[1] ethyl geranate,[2] geranyl acetate,[2,3] coenzyme Q_1,[4,5] and vitamin K.[6]

We wish to report here a new synthesis of coenzyme Q (**2**) employing the promising allylation reaction of π-allylnickel bromides.

In a previous work, we utilized 6-bromo-2,3-dimethoxy-5-methylhydroquinone bis(methoxymethyl) ether (**3**) for the construction of the aromatic moiety of coenzyme Q_1.[4] It was found that the regeneration of the hydroquinone in the later stage of synthetic sequences could be achieved conveniently by the acid-catalized solvolysis of the bis(methoxymethyl) ether in methanol. However, **3** is not crystalline and is rather unstable, so it must be purified carefully by column chromatography. Therefore, we investigated another synthetic equivalent of **3**.

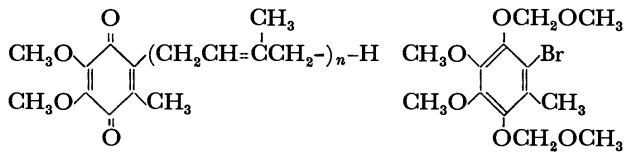

2 **3**

The bromination of 2,3-dimethoxy-5-methyl-*p*-benzoquinone (**4**)[7] afforded 6-bromo-2,3-dimethoxy-5-methyl benzoquinone (**5**),[4] which was then converted to the

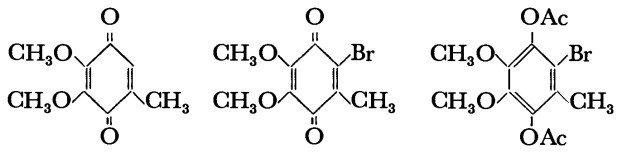

4 **5** **6**

corresponding hydroquinone diacetate **6** by the action of zinc in acetic anhydride.

When **6** reacted to 1,1-dimethyl-π-allylnickel bromide (**7**, $n=1$)[8] in hexamethylphosphoramide (HMPA) at 60 °C for 7 hr, 2,3-dimethoxy-5-methyl-6-prenylhydroquinone diacetate (**8**, $n=1$) was obtained in a 70% yield. By this fact, the diacetate **6** was found to be as sufficiently reactive toward **7** ($n=1$) as the corresponding bis(methoxymethyl) ether **3**, which had afforded the coupling product with **7** ($n=1$) in HMPA at 60 °C in a 57% yield.[4] All earlier attempts at the alkaline hydrolysis or acid-catalyzed hydrolysis of **8** ($n=1$) to the corresponding hydroquinone had failed. Finally, the diacetate **8** ($n=1$) was treated with excess $LiAlH_4$ in ether at reflux for 24 hr and then oxidized with aqueous $FeCl_3$ to afford coenzyme Q_1(**2**, $n=1$) in a 76% yield. The IR and NMR spectra were satisfactory for the structure **2**($n=1$).

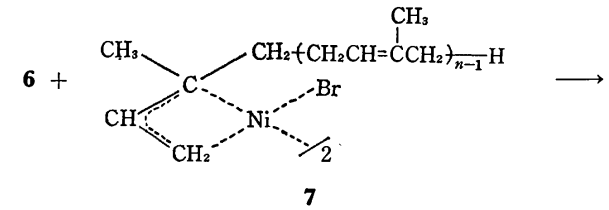

7

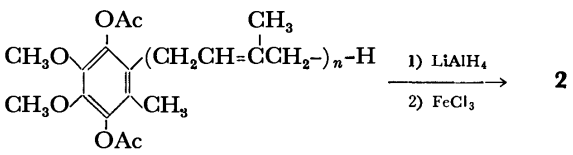

8

Although the nature of π-allylnickel complexes, except for π-geranylnickel bromide,[1] possessing in their own molecule some olefin moieties which may act as stable π-ligands, has not yet been clarified, the above results distinctly suggest the possibility of synthesizing the higher homologues of coenzyme Q. Such an anticipation was successfully realized, as will be indicated below. The bromide **6** reacted to π-geranylnickel bromide (**7**, $n=2$)[8] in HMPA at 60 °C to afford 6-geranyl-2,3-dimethoxy-5-methylhydroquinone diacetate (**8**, $n=2$) (88% yield), which was then converted, by the removal of the acetate groups with $LiAlH_4$

and by subsequent oxidation by aqueous $FeCl_3$, to coenzyme Q_2 (**2**, $n=2$) in a 75% yield.

The procedure was also extended to the synthesis of the higher homologues of coenzyme Q. The bromide **6** reacted to π-solanesylnickel bromide (**7**, $n=9$)[8] in HMPA at 70 °C for 10 hr. After purification with a silica-gel column we obtained 6-solanesyl-2,3-dimethoxy-5-methylhydroquinone diacetate (**8**, $n=9$) (45 % yield), which was then converted to coenzyme Q_9 (**2**, $n=9$) by the above-described procedure (71% yield); this substance melted at 26—28 °C (lit,[10] mp 45 °C for naturally-occurring coenzyme Q_9). The synthesis of coenzyme Q_{10} (**2**, $n=10$) was similarly effected by the reaction of π-decaprenylnickel bromide (**7**, $n=10$)[8] with **6** in HMPA at 75 °C for 7 hr (40% yield), followed by the treatment of **8** ($n=10$) with $LiAlH_4$ and then aqueous $FeCl_3$ to give **2** ($n=10$) in a 69% yield; mp 20—22 °C (lit,[10,11] mp 49 °C for the natural coenzyme Q_{10}).

The low melting points of our products are attributable to the coexistence of the *cis* isomer[12] in regard to the first double bond in the side chain originating in the π-allyl moiety of **7**. This was supported by the 100 MHz NMR spectroscopy measurement; the calculation of the peak areas of olefinic methyl protons revealed that the *trans*-to-*cis* ratio of the product was 55 : 45. For the synthetic utility and isolation of all-*trans*-coenzyme Q, a higher *trans* stereoselectivity is needed. For the investigation of the stereoselectivity of this coupling reaction, the geranyl side chain was not a suitable model, because the NMR spectrum of **2** ($n=2$) showed complicated olefinic methyl signals at δ 1.5—1.7, so the determination of the *trans*-to-*cis* ratio was very difficult.[13] For this purpose, the phytyl side chain or a much higher (*i.e.* solanesyl or decaprenyl) side chain was suitable. We have already found[6] that the conduction of the coupling reaction in lesser coordinative polar solvents, such as *N*,*N*-dimethylacetamide (DMAc) or *N*-methyl-2-pyrrolidone (MPD), and at lower temperature leads to higher *trans*-to-*cis* ratios of the coupling products in the synthesis of vitamin K. A similar solvent effect was also observed in the present work. The reaction of **6** with π-phytylnickel bromide in DMAc or MPD gave the *trans* isomer of the coupling product (6′,10′,14′-hexahydrocoenzyme Q_4) above a 70% stereoselectivity. In the synthesis of coenzyme Q_9 with **6** and **7** ($n=9$) in DMAc at 60 °C, the products **8**($n=9$) (48% yield) and, therefore, **2** ($n=9$) were both 74 : 26 mixtures fo *trans* and *cis* forms.

The isolation of the all-*trans*-coenzyme Q_9 was effected by silica-gel column chromatography, eluting with *n*-hexane–diisopropyl ether (90 : 10). The first several fractions eluted contained only the *cis*-isomer, while the all-*trans* compound (mp 42—4 °C) was eluted in the rather late fractions in a high *trans* recovery.

The efficacy of the synthesis of **2** by the π-allylnickel complex allylation process depends on the unreactivity of σ- or π-allylnickel complexes toward the ester function and the facile reactivity thereof toward the trigonal carbon halides. This procedure avoids the disadvantages of several kinds of side reactions, which render the product isolation much difficult. The sole by-product of the present method, hydrocarbons arising from the thermal decomposition of **7**, can easily be separated, and the unchanged diacetate **6** is recovered quantitatively. This method seems to be highly effective for the synthesis of naturally-occurring isoprenoid quinones and related substances, including coenzyme Q, vitamin K, and tocophenols,[14] for which there exists only a very limited synthetic methodology.

Investigations are continuing from the mechanistic point of view and concerning reaction conditions which would realize a much higher stereoselectivity.

Experimental

The melting points were taken on a hot-stage apparatus and are uncorrected. The spectral measurements were determined with the following instruments; IR, a Hitachi Model 215 spectrophotometer; NMR, a JEOL Model C-60 or PS-100 spectrometer in a carbon tetrachloride or deuteriochloroform solution, with tetramethylsilane as the internal reference; UV, a Hitachi Model EPS-3T spectrophotometer.

6-Bromo-2,3-dimethoxy-5-methyl-*p*-benzoquinone (**5**),[4] geranyl bromide, phytyl bromide, solanesyl bromide,[9] and decaprenyl bromide[9] were obtained by the methods described in the literature, their physical properties agreed with those previously reported. Reactions involving π-allylnickel complexes were carried out under nitrogen or argon.

6-Bromo-2,3-dimethoxy-5-methylhydroquinone Diacetate (6). A solution of 5.0 g of **5** in 20 ml of acetic anhydride containing a few drops of pyridine was warmed to 60—65 °C, and then 7.5 g of zinc dust was added to this solution. The mixture was stirred well until the red color faded and was then kept at 60 °C for a further 30 min. The mixture was filtered, and the residue was washed with acetone. The combined

Table 1. Summary of the yields and stereoselectivity of the coupling reaction

π-Complex	Solvent	Temp.	Time	Product	Yield[a]	*trans* : *cis*[b]
Phytyl	DMAc	50 °C	6 hr	H. H. Q_4[c]	30%	71 : 29
phytyl	MPD	50	20	H. H. Q_4	42	73 : 27
solanesyl	HMPA	70	10	Q_9[d]	45	55 : 45
solanesyl	DMAc	70	5	Q_9	35	67 : 33
solanesyl	DMAc	60	20	Q_9	48	74 : 26
solanesyl	DMAc	50	20	Q_9	41	70 : 30
solanesyl	MPD	50	20	Q_9	25	70 : 30

a) Isolated yield of the cross-coupling product and based on the diacetate **6**. b) These ratios were determined by 100 MHz NMR spectroscopy. c) H. H. Q_4 indicates 6′,10′,14′-hexahydrocoenzyme Q_4 hydroquinone diacetate. d) Q_9 indicates coenzyme Q_9 hydroquinone diacetate **8** ($n=9$).

filtrate was poured into water, after which the separated oily product slowly crystallized. The collected precipitates were recrystallized from petroleum ether to give 5.9 g (83%) of **6** as colorless needles; mp 68—69 °C; IR (KBr) 2940, 1750, 1470, 1420, 1365, 1200, 1080, and 1020 cm^{-1}; NMR ($CDCl_3$) δ 3.75 (6H, s, $2CH_3O$), 2.31, 2.28 (each 3H, 2s, 2AcO), 2.16 (3H, s, $ArCH_3$).

Found: C, 44.93; H, 4.34%. Calcd for $C_{13}H_{15}O_6Br$: C, 44.98; H, 4.36%.

General Preparative Method of π-Allylnickel Bromide (7). To a stirred solution of a 15% benzene solution of nickel carbonyl (*ca.* 1.5-fold excess), a 15% benzene solution of the allylic bromide was added drop by drop over 1—1.5-hr period at 50 °C; the mixture was then stirred for a further 2—3 hr. The resulting solution was cooled to below 10 °C, and the benzene and excess nickel carbonyl were removed under reduced pressure. The red residue was the corresponding π-complex and was used directly in the next reaction.

Coenzyme Q_1 (2, n=1). 1,1-Dimethyl-π-allylnickel bromide (**7**, $n=1$) was prepared from 4.5 g of 1-bromo-3-methyl-2-butene and 8.7 g of nickel carbonyl by means of the above-described procedure. After the removal of the benzene, 36 ml of HMPA and 5.2 g of **6** in 36 ml of HMPA were added to the dark residue at 10 °C. The mixture was heated to 60 °C for 7 hr, and then poured into water and extracted with petroleum ether. The extract was washed with water, dried ($MgSO_4$), and freed of the solvent. The crude product (5.1 g) was found by NMR assay to consist of 70% of **8** ($n=1$) and 30% of **6**, but **8** could not be isolated by silica gel column chromatography.[15] This mixture (1.3 g) was dissolved in 30 ml of dry ether and reduced by the use of 0.8 g of $LiAlH_4$ at reflux for 24 hr. The excess $LiAlH_4$ was decomposed by the addition of a small portion of ethanol and ethyl acetate, neutralized by an aqueous saturated ammonium chloride solution, and extracted with ether. The extract was concentrated to a small volume, oxidized by aqueous $FeCl_3$ at room temperature for 3 hr, and extracted with ether. The extract was washed with water, dried ($MgSO_4$), and evaporated. The crude product was chromatographed on silica gel, using *n*-hexane–diisopropyl ether (80 : 20) for elution, to give 0.5 g of coenzyme Q_1 (**2**, $n=1$). All the spectral data were identical with those previously obtained in our laboratory.[4]

Coenzyme Q_2 (2, n=2). π-Geranylnickel bromide (**7**, $n=2$) was prepared from 8.7 g of geranyl bromide and 10.3 g of nickel carbonyl by means of the above-described method. After changing the solvent to 40 ml of HMPA, 5.3 g of **6** in 35 ml of HMPA were added at 10 °C, and the mixture was treated at 60 °C for 7 hr. When the reaction mixture was worked up in the usual manner, 7.2 g of a crude product was obtained. This was found by NMR assay to be a mixture of **8** ($n=2$) (88%) and **6** (12%), but the removal of the **6** by the use of the silicagel column was very difficult.[16] This mixture (1.5 g) was reduced by the use of 0.7 g (of $LiAlH_4$ in dry ether at reflux for 24 hr, and then worked up in the usual manner. The ether extract was concentrated to a small volume and then oxidized by aqueous $FeCl_3$ at room temperature for 3 hr. The organic layer was washed with water, dried ($MgSO_4$), and freed of the solvent. The crude product was chromatographed on silica gel; subsequent elution with *n*-hexane–diisopropyl ether (80 : 20) gvae 0.7 g of coenzyme Q_2 (**2**, $n=2$). The estimated yield of **2** ($n=2$) from **8** ($n=2$) was 75%. IR (neat) 2930, 1650, 1610, 1450, 1270, 1210, 1160, 1100, 1010, 950, and 740 cm^{-1}; NMR ($CDCl_3$) δ 4.96 (2H, t, 2-CH=), 3.97 (6H, s, $2CH_3O$), 3.16 (2H, d, $ArCH_2$), 1.99 (4H, bs, methylene chain), 1.97 (3H, s, $ArCH_3$), 1.72, 1.67 (3H, 2s, *trans* and *cis* olefinic CH_3), 1.63 1.56 (each 3H, 2s, terminal olefinic CH_3);[13] UV λ_{max} (*n*-hexane) 270 nm (15600).

Found: C, 71.87; H, 8.35%. Calcd for $C_{19}H_{26}O_4$: C, 71.67; H, 8.23%.

6′,10′,14′-Hexahydrocoenzyme Q_4. π-Phytylnickel bromide was prepared from 1.9 g of phytyl bromide and 1.3 g of nickel carbonyl; after the solvent had been changed to 30 ml of DMAc, 1.3 g of **6** was added, and the mixture was treated under the conditions shown in Table 1. The reaction mixture was then worked-up in the usual manner, and silica-gel-column chromatography afforded the corresponding diacetate: IR (neat) 2930, 1770, 1485, 1475, 1370, and 1195 cm^{-1}; NMR ($CDCl_3$) δ 5.00 (1H, t, –CH=), 3.86 (6H, s, $2CH_3O$), 3.25 (2H, d, $ArCH_2$), 2.26, 2.24 (each 3H, 2s, 2AcO), 2.08 (3H, s, $ArCH_3$), 1.72 (3H, bs, olefinic CH_3), 1.20 (21H, bs, methylene chain), 0.88 (12H, d, side-chain CH_3).

Found: C, 72.77; H, 10.16%. Calcd for $C_{33}H_{54}O_6$: C, 72.49; H, 9.95%.

To a suspension of 0.7 g of $LiAlH_4$ in 40 ml of dry ether, 1.00 g of the hydroquinone diacetate in 20 ml of ether was added, and the mixture was treated at reflux for 7 hr. After extraction, the extract was concentrated to a small volume and oxidized by aqueous $FeCl_3$ at room temperature for 3 hr. The crude product, obtained by the usual work-up, was chromatographed on silica gel; subsequent elution with *n*-hexane–diisopropyl ether (70 : 30) gave 0.61 g of 6′,10′,14′-hexahydrocoenzyme Q_4 (72%); IR (neat) 2920, 1645, 1602, 1457, 1375, 1285, 1260, and 1202 cm^{-1}; NMR ($CDCl_3$) δ 4.94 (1H, t, –CH=), 3.97 (6H, s, $2CH_3O$), 3.19 (2H, d, $ArCH_2$), 2.00 (3H, s, $ArCH_3$), 1.78, 1.72 (3H, 2s, *trans* and *cis* olefinic CH_3), 1.20 (21H, bs, methylene chain), 0.88 (12H, d, side-chain CH_3).

Found: C, 75.60; H, 10.60%. Calcd for $C_{29}H_{48}O_4$: C, 75.61; H, 10.50%.

Coenzyme Q_9 (2, n=9). π-Solanesylnickel bromide (**7**, $n=9$) was prepared from 6.0 g of solanesyl bromide and 1.6 g of nickel carbonyl. After the solvent had been changed to 40 ml of DMAc, a 1.6-g portion of **6** was added and the mixture was treated under the conditions shown in Table 1. After a usual work-up, followed by silica gel column chromatography, pure coenzyme Q_9 hydroquinone diacetate **8** ($n=9$) was obtained; IR (neat) 2920, 1770, 1660, 1480, 1450, 1370, 1260, 1200, 1190, and 1100 cm^{-1}; NMR ($CDCl_3$) δ 5.14 (9H, m, 9–CH=), 3.85 (6H, s, $2CH_3O$), 3.22 (2H, d, $ArCH_2$), 2.35, 2.31 (each 3H, 2s, 2AcO), 2.02 (35H, bs, methylene chain and $ArCH_3$), 1.62 (30H, bs, side chain CH_3).

Found: C, 79.29; H, 10.29%. Calcd for $C_{58}H_{88}0_6$: C, 79.09; H, 10.06%.

To a suspension of 0.8 g of $LiAlH_4$ in 20 ml of dry ether, we added 1.4 g of **8** ($n=9$) in 25 ml of ether, after which the mixture was refluxed for 7 hr. The reaction mixture was then worked-up into ether and oxidized by aqueous $FeCl_3$ at room temperature for 3 hr. The crude product, obtained by the usual work-up, was chromatographed on silica gel; subsequent elution with *n*-hexane–diisopropyl ether (75 : 25) gave 0.9 g of coenzyme Q_9(**2**, $n=9$) (71%); mp 26—28 °C; IR (neat) 2920, 1650, 1605, 1450, 1380, 1285, 1265, 1205, 1150, and 1100 cm^{-1}; NMR ($CDCl_3$) δ 5.15 (8H, m, 8–CH=), 4.96 (1H, t, –CH=), 4.00 (6H, s, $2CH_3O$), 3.19(2H, d, $ArCH_2$), 2.00 (35H, bs, methylene chain and $ArCH_3$), 1.72 (s, *trans* olefinic CH_3 on C–3′), 1.68 (s, *cis* olefinic CH_3 on C–3′ and terminal *cis* CH_3), 1.60 (24H, olefinic CH_3); UV λ_{max} (*n*-hexane) 272 nm (ε 4200).

Found: C, 81.59; H, 10.64%. Calcd for $C_{54}H_{82}O_4$: C, 81.54; H, 10.39%.

Isolation of all-trans-Coenzyme Q_9. Silica gel (72 g) was used to fill up a column (20 mm × 450 mm) with *n*-hexane. After the adsorption of 700 mg of the coenzyme Q_9 (mp 31 °C, *trans* : *cis* = 71 : 29), it was eluted with *n*-hexane–diisopropyl ether (90 : 10). The eluted solution was divided into 13 fractions, each 30 ml. The first 3 fractions contained only the *cis* isomer (119 mg), while the 7—13 fractions (total, 369 mg) had a mp of 42—44 °C, showing no melting-point depression upon mixing with the natural coenzyme Q_9. The NMR spectrum also supported the all-*trans* structure. The *trans* recovery amounted to 76%.

Coenzyme Q_{10} (**2**, $n=10$). π-Decaparenylnickel bromide (**7**, $n=10$) was prepared from 10.0 g of decaprenyl bromide and 4.5 g of nickel carbonyl. After the solvent had been changed to 30 ml of HMPA, 2.0 g of **6** in 20 ml of HMPA was added at room temperature and the mixture was treated at 75 °C for 7 hr. After a usual work-up and silica gel column chromatography, eluting with *n*-hexane–diisopropyl ether (75 : 25), 2.2 g (40%) of **8** ($n=10$) were obtained; IR (neat) 2910, 1765, 1440, 1370, 1190, 1100, and 1020 cm^{-1}; NMR (CCl_4) δ 4.92 (10H, m, 10–CH=), 3.70 (6H, s, $2CH_3O$), 3.10 (2H, d, $ArCH_2$), 2.20 2.18 (each 3H, 2s, 2AcO), 1.95 (39H, bs, methylene chain and $ArCH_3$), 1.55 (33H, bs, side-chain CH_3).

Found: C, 79.54; H, 10.50%. Calcd for $C_{63}H_{96}O_6$: C, 79.70; H, 10.19%.

To a suspension of 0.5 g of $LiAlH_4$ in 20 ml of dry ether, we added 0.8 g of **8** ($n=10$) in 15 ml of ether; the mixture was then refluxed for 24 hr. After the decomposition of the excess $LiAlH_4$, the mixture was neutralized and extracted with ether. The extract was concentrated to a small volume and then oxidized by aqueous $FeCl_3$ at room temperature for 3 hr. The crude product, obtained by the usual work-up, was chromatographed on silica gel to give 0.5 g (69%) of coenzyme Q_{10} (**2**, $n=10$): mp 20—22 °C; IR (neat) 2900, 1650,1610, 1450, 1390, 1270, 1210, 1155, 1105, and 750 cm^{-1}; NMR (CCl_4) δ 4.92 (10H, m, 10–CH=), 3.84 (6H, s, $2CH_3O$), 3.05 (2H, d, $ArCH_2$), 1.92 (39H, bs, methylene chain and $ArCH_3$), 1.55 (33H, bs, side-chain CH_3); UV λ_{max} (*n*-hexane) 272 nm (ε 12300).

Found: C, 82.31; H, 10.69%. Calcd for $C_{59}H_{90}O_4$: C, 82.08; H, 10.51%.

The authors are greateful to the Japanese Ministry of Education for its grant-in-aid for scientific research.

References

1) E. J. Corey and M. F. Semmelhack, *J. Amer. Chem. Soc.*, **89**, 2755 (1967).

2) K. Sato, S. Inoue, S. Ota, and Y. Fujita, *J. Org. Chem.*, **37**, 462 (1972).

3) F. Guerrieri and G. P. Chiusoli, *Chim. Ind.* (Milan), **51**, 1252 (1969).

4) K. Sato, S. Inoue, and R. Yamaguchi, *J. Org. Chem.*, **37**, 1889 (1972).

5) L. S. Hugedus, E. L. Waterman, and J. Catline, *J. Amer. Chem. Soc.*, **94**, 7155 (1972), where coenzyme Q_1 was synthesized by the conjugate addition of π-prenylnickel bromide to the quinone **4**.

6) a) K. Sato, S. Inoue, and K. Saito, *Chem. Commun.*, **1972**, 953. b) K. Sato, S. Inoue, and K. Saito, *J. Chem. Soc. Perkin I*, **1973**, 2289.

7) K. Sato, S. Inoue, and H. Sato, This Bulletin, **45**, 3455 (1972), and literatures cited therein.

8) 1,1-Dimethyl-π-allynickel bromide (**7**, $n=1$) was generated by the reaction of 3,3-dimethyl-allyl bromide with excess nickel carbonyl. Other π-allylnickel bromides **7** were similarly prepared from geranyl bromide, phytyl bromide, solanesyl bromide[9] and decaprenyl bromide,[9] and used without further purification. See experimental section.

9) R. Rüegg, U. Gloor, R. N. Goel, G. Ryser, O. Wiss, and O. Isler, *Helv. Chim. Acta*, **42**, 2616 (1959).

10) R. L. Lester, F. L. Crane, and Y. Hatefi, *J. Amer. Chem. Soc.*, **80**, 4751 (1958).

11) R. A. Morton, U. Gloor, O. Schindler, W. M. Wilson, L. H. Chopard-dit-Jean, F. W. Hemming, O. Isler, W. M. F. Leat, J. F. Pennock, R. Rüegg, U. Schwieter, and O. Wiss, *Helv. Chim. Acta*, **41**, 2343 (1958).

12) Although naturally occurring coenzyme Q has all-*trans* configuration, the biochemical activity (restoration of succinoxidase activity of the 2′-*cis* isomer is as high as is *trans*-coenzyme Q. G. Lenaz, L. Szarkowska, K. Folkers, and Moore, *Biochim. Biophys. Res. Commun.*, **23**, 386 (1966).

13) L. M. Jackman, R. Rüegg, G. Ryser, C. von Planta, U. Gloor, H. Mayer, P. Schudel, M. Kofler, and O. Iser, *Helv. Chim. Acta*, **48**, 1332 (1965), where the NMR assignment of the *trans* and *cis* mixture of vitamin K_2 was reported.[10] We determined the NMR assignment of coenzyme Q_2 by this reference.

14) Regiospecific synthesis of three isomeric monomethyltocols was performed in high yields in these laboratories. Details will appear elsewhere.

15) As a result of comparison with the NMR spectrum of **6**, chemical shifts of protons in **8** ($n=1$) are as follows; (CCl_4) δ 4.83 (1H, t, -CH=), 3.68 (6H, s, $2CH_3O$), 3.08 (2H, d, CH_2), 2.21 (6H, s, 2AcO), 1.95 (3H, s, $ArCH_3$), 1.68, 1.65 (each 3H, 2s, side-chain methyls).

16) As a result of comparison with the NMR spectrum of **6**, chemical shifts of protons in **8** ($n=2$) are as follows; (CCl_4) δ 4.80 (2H, br.t, 2-CH=), 3.67 (6H, s, $2CH_3O$), 3.08 (2H, d, $ArCH_2$), 2.18, 2.16 (each 3H, 2s, 2AcO), 2.01—1.90 (7H, m, methylene chain and $ArCH_3$), 1.66—1.53 (9H, m, side-chain methyls).

Synthesis of Dimeric and Trimeric 2-(*p*-Tolyloxy)ethyl Acetate-Formaldehyde Polymer Model Compounds

Akira NINAGAWA, Haruo MATSUDA, and Sumio MATSUDA

Department of Petroleum Chemistry, Faculty of Engineering, Osaka University, Yamadakami, Suita, Osaka 565

(Received April 22, 1974)

The dimeric and trimeric 2-(*p*-tolyloxy)ethyl acetate-formaldehyde polymer model compounds and the halogenated compound of the dimer were synthesized. 2,2'-Methylenebis(5-methyl-1,2-phenyleneoxy)diethyl acetate was synthesized by the reaction of 2-(*p*-tolyloxy)ethyl acetate with formaldehyde in acidic media. 2-[2-(2-Acetoxyethoxy-3-chloro-5-methylbenzyl)-4-methylphenoxy]ethyl acetate was prepared by the reaction of 6-chloro-4,4'-dimethyl-2,2'-methylenediphenol with 2-chloroethanol, followed by treatment with acetic anhydride, and 2-[2,6-bis(2-acetoxyethoxy-5-methylbenzyl)-4-methylphenoxy]ethyl acetate from 2,6-bis(2-hydroxy-5-methylbenzyl)-4-methylphenol.

A high molecular weight polymer was obtained[2] by the reaction of 2-(*p*-tolyloxy)ethyl acetate with formaldehyde in acetic acid solution in the presence of perchloric acid as a catalyst.

We have synthesized the dimeric and trimeric 2-(*p*-tolyloxy)ethyl acetate-formaldehyde polymer model compounds and the halogenated compound of the dimer.

Synthesis of the Dimeric Compounds. The dimer of 2-(*p*-tolyloxy)ethyl acetate-formaldehyde polymer model compounds and the halogenated compound were synthesized as shown in Chart 1. The reaction of 4,4'-dimethyl-2,2'-methylenediphenol(**1**) with 2-chloroethanol and sodium gave 2-[2-(2-hydroxy-5-methylbenzyl)-4-methylphenoxy]ethanol(**5**) in an 83% yield, but not 2,2'-methylenebis(5-methyl-1,2-phenyleneoxy)-diethyl acetate (**8**). 6-Chloro-4,4'-dimethyl-2,2'-methylenediphenol(**2**) gave 2-[2-(2-hydroxyethoxy-3-chloro-5-methylbenzyl)-4-methylphenoxy]ethanol(**6**) in a 75% yield. **6** was acetylated with acetic anhydride to form 2-[2-(2-acetoxyethoxy-3-chloro-5-methylbenzyl)-4-methylphenoxy]ethyl acetate (**7**).

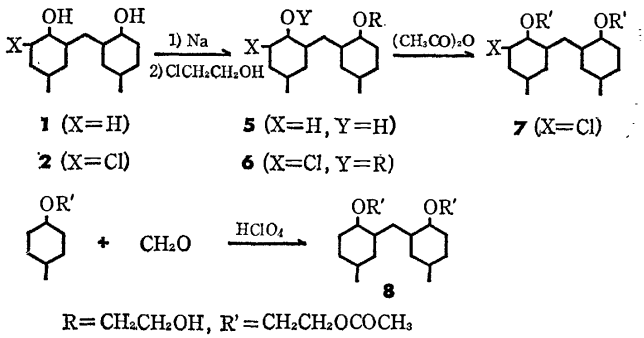

Chart 1.

The reaction of 2-(*p*-tolyloxy)ethyl acetate with formaldehyde in acetic acid solution in the presence of perchloric acid as a catalyst gave **8**.

Synthesis of the Trimeric Compounds. The reaction of 2,6-bis(2-hydroxy-5-methylbenzyl)-4-methylphenol(**3**) with 2-chloroethanol and sodium gave mono, di, and tri ethanol derivatives; 2-(2-hydroxyethoxy-5-methylbenzyl)-6-(2-hydroxy-5-methylbenzyl)-4-methylphenol(**9**), 2,6-bis(2-hydroxyethoxy-5-methylbenzyl)-4-methylphenol(**10**), and 2-[2,6-bis(2-hydroxyethoxy-5-methylbenzyl)-4-methylphenoxy]ethanol(**11**). The tri

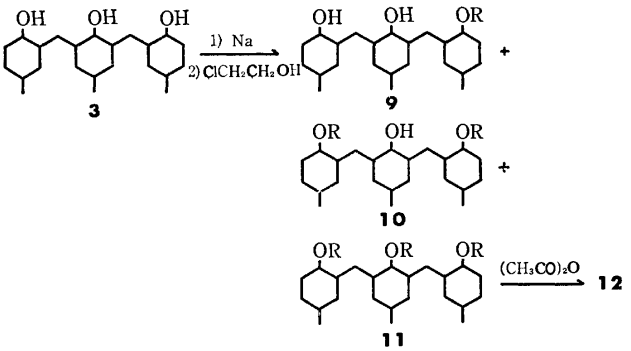

Chart 2.

ethanol derivative(**11**) was acetylated to give the desired compound; 2-[2,6-bis(2-acetoxyethoxy-5-methylbenzyl)-4-methylphenoxy]ethyl acetate(**12**)(see Chart 2).

2-(2-Hydroxyethoxy-3-chloro-5-methylbenzyl)-6-(2-hydroxyethoxy-5-methylbenzyl)-4-methylphenol(**13**) was isolated in a low yield from the reaction product of 2-(2-hydroxy-3-chloro-5-methylbenzyl)-6-(2-hydroxy-5-methylbenzyl)-4-methylphenol(**4**) with 2-chloroethanol and sodium.

Hydrogen Bonds of the Oligomeric Phenols. The presence of hydrogen bonds has been postulated to explain the peculiar behavior of certain phenolic resin intermediates.[3] Infrared spectroscopic,[4-7] potentiometric,[8-10] and kinetic[11] results showed the presence of intramolecular OH···OH-bonds in a number of polyphenols of novolak type. The IR spectral data of the oligomeric phenols are given in Table 1. Compound **1** exhibits three OH absorptions in carbon tetrachloride in line with the previous IR studies.[7] The concentration-independent band at 3553 cm^{-1} has been assigned to an intramolecular OH···OH-bond. The band at 3605 cm^{-1} can be assigned to the stretching vibrations of the free OH group, while the broad concentration-dependent band at 3300 cm^{-1} is assigned to the closed ring of H-bonds resulting from dimeric association. On account of the intramolecular OH··· OH-bond as illustrated in I, the reactivity of the hydrogen-bonded OH group of **1** might be lower than that of the free OH group.

Compound **2** has a more complex spectrum, show-

Table 1. Hydroxy stretching frequencies, ν(OH) of the oligomeric phenols in carbon tetrachloride

Compound	Concn. (mM)	ν (cm^{-1})	ε	Concn. (mM)	ν (cm^{-1})	ε	Assignments
p-Cresol	25	3615	211				Free
		3480	8				Inter
2-Chloro-*p*-cresol	25	3610	12				Free
		3553	108				Intra OH···Cl
1	25	3605	98	2.5	3605	180	Free
		3460	116		3470	132	Intra OH···OH
		3300 br	154				Inter
2	25	3610	63	2.5	3615	68	Free
		3532	151		3532	160	Intra OH···Cl
		3490	121		3495	116	Intra OH···OH
		3375	123				Inter
		3240	85				Inter
3	4.0	3590	32				Free
		3350 sh					Intra OH···OH
		3214 br	241				Inter
4	3.0	3525	152				Intra OH···Cl
		3418 br	206				Intra OH···OH
		3240	152				Inter

All the samples were examined in 1.0 mm. cells. br, broad. sh, shoulder.

ing three concentration-independent bands in the OH region. The band at 3610 cm^{-1} is characteristic of the free OH group. Two bands at 3545 and 3490 cm^{-1} can be assigned to an intramolecular OH···Cl-bond and an intramolecular OH···OH-bond, respectively. Thus, we suggest that two conformers (II-a and II-b) are present in compound **2**.

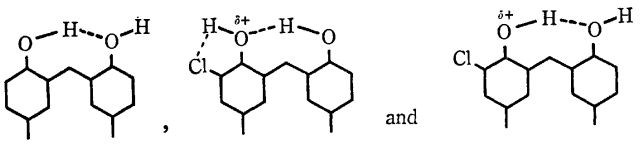

I II-a and II-b

The intramolecular OH···OH-bond of type II-a might be weaker than that of **1** on account of the electron withdrawing of Cl-atom and the fact that the OH···Cl-bond is weaker than the OH···OH-bond, while the H-atom having the H-bond of type II-b might easily be released from phenol nucleus.

Actually, 2-chloro-*p*-cresol, which has mainly a *cis*-form[12] involving an intramolecular OH···Cl-bond (3553 cm^{-1}), gave 2-chloro-4-methylphenoxy-ethanol in a 70% yield.[13] The bonding shift of the intramolecular H-bond of **1** (Δ145 cm^{-1}) is higher than that of **2** (Δ120 cm^{-1}).

This stronger intramolecular H-bond might disturb the addition reaction.

Compound **3** shows the presence of three OH absorptions. From the previous results,[4] we assign two bands at 3590 and 3350 cm^{-1} to an intramolecular OH···OH···OH-bond, two H-atoms being involved in an intramolecular H-bond. Compound **4** shows three OH absorptions. Two bands at 3525 and 3148 cm^{-1} are assigned to an intramolecular OH···OH···OH···Cl-bond. The broad, concentration-dependent, band at 3240 cm^{-1} is assigned to the intermolecular H-bonds.

However, these spectroscopic studies can give no explanation for the present synthetic results.

Experimental

General. Melting points are uncorrected. ^{1}H-NMR spectra were taken on a JEOL Model PS-100 spectrometer in a deuterochloroform or carbon tetrachloride solution, with tetramethylsilane as an internal standard. Chemical shift values are given in terms of τ. IR spectra were obtained on a Hitachi EPI-G2 or a Hitachi Model 225 spectrophotometer. Mass spectra were obtained on a Hitachi RMU-6 mass spectrometer at 70 eV.

Materials. 2-(*p*-Tolyloxy)ethyl acetate; bp 92—94 °C/2 mmHg[2] [lit,[2] 104—110 °C/5 mmHg], 2-chloro-*p*-cresol; bp 82—83 °C/13 mmHg[14] [lit,[14] 195—197 °C], 4,4′-dimethyl-2,2′-methylenediphenol(**1**); mp 123—125 °C[15] [lit,[15] 126 °C], 6-chloro-4,4′-dimethyl-2,2′-methylenediphenol (**2**); mp 168—172 °C[16] [lit,[16] 170 °C], 2,6-bis(2-hydroxy-5-methylbenzyl)-4-methylphenol(**3**); mp 214—217 °C[15] [lit,[15] 215 °C], and 2-(2-hydroxy-3-chloro-5-methylbenzyl)-6-(2-hydroxy-5-methylbenzyl)-4-methylphenol(**4**); mp 188—190 °C[17] [lit,[17] 187 °C] were prepared by the methods in the literature. All other reagents were commercial products.

*2-[2-(2-Hydroxy-5-methylbenzyl)-4-methylphenoxy]ethanol(**5**).* A mixture of **1** (45.6 g) and sodium (11 g) in ethanol (140 ml) was stirred for 16.5 hr at 80 °C. 2-Chloroethanol (41.6 g) was then added to the solution and refluxed for 20.5 hr. After being cooled, the product which separated was recrystallized from ligroin to give colorless plates (**5**); yield, 44 g (83%), mp 99—100 °C. IR(KBr); 3375 and 3240 cm^{-1}. NMR ($CDCl_3$, 5.0%); 2.88—3.48 (6H, m, phenyl), 5.01 (2H, b, OH), 5.76—6.30 (6H, m, CH_2CH_2 and $PhCH_2Ph$), 7.74(3H, s, CH_3), and 7.79 (3H, s, CH_3). MS; *m/e* 272 (M^+). Found: C, 75.18; H, 7.38%. Calcd for $C_{17}H_{20}O_3$: C, 74.97; H, 7.40%.

5 (2.7 g) was refluxed with acetic anhydride (20 ml) for 5 hr to give 2-[2-(2-acetoxy-5-methylbenzyl)-4-methylphenoxy]ethyl acetate; yield, 3.1 g, mp 50—51.8 °C (from ligroin). IR(KBr); 1750 cm^{-1}. Found: C, 70.69; H, 6.66%.

Calcd for $C_{21}H_{24}O_5$: C, 70.77; H, 6.79%.

2-[2-(2-Acetoxyethoxy-3-chloro-5-methylbenzyl)-4-methylphenoxy]-ethyl Acetate (7). **2** (105 g) was added to a solution of sodium (22.1 g) in ethanol (280 ml). After being stirred for 14 hr at refluxing temperature, 2-chloroethanol (80.5 g) was added to the reaction mixture at room temperature and the mixture was refluxed for 17 hr. The precipitated sodium chloride was removed and the filtrate was cooled to 0 °C to give white crystal (105 g); 2-[2-(2-hydroxyethoxy-3-chloro-5-methylbenzyl)-4-methylphenoxy]ethanol (**6**). yield, 85%; mp 114—116 °C (from a mixture of benzene and ligroin). IR(KBr); 3440 and 3390 cm^{-1}. Found: C, 64.52; H, 6.78%. Calcd for $C_{19}H_{23}O_4Cl$: C, 65.05; H, 6.61%.

A mixture of **6** (70 g) and acetic anhydride (204 g) was refluxed for 13 hr. After the solvents had been removed, benzene solution of the residue was washed successively with sodium hydroxide solution and water, dried over anhydrous sodium sulfate, and then distilled to give **7** (70 g) as a colorless viscous liquid; bp 205—210 °C/0.001 mmHg. IR(neat); 1735 cm^{-1}. NMR (CCl_4, 10%); 3.04—3.50 (5H, m, phenyl), 5.58—6.15(8H, m, $C\underline{H}_2C\underline{H}_2$), 6.13(2H, s, $PhC\underline{H}_2$-Ph), 7.72(3H, s, $PhC\underline{H}_3$), 7.82(3H, s, $PhC\underline{H}_3$), 8.02(3H, s, $COC\underline{H}_3$), and 8.06 (3H, s, $COC\underline{H}_3$). MS; *m/e* 434(M^+). Found: C, 63.21; H, 6.19%. Calcd for $C_{23}H_{27}O_6Cl$: C, 63.52; H, 6.26%.

2,2'-Methylenebis(5-methyl-1,2-phenyleneoxy)diethyl Acetate (8). Perchloric acid (10 ml) was added to a solution of 2-(*p*-tolyloxy)ethyl acetate (14.4 g) and paraformaldehyde (0.7 g) in acetic acid (70 ml). The reaction mixture was stirred for 30 hr at 30 °C. After completion of the reaction, the mixture was poured into water and washed with water. Oily product was recrystallized from benzene to give **8** (7.2 g); colorless plates, mp 98—101 °C. IR(KBr); 1730 cm^{-1}. NMR ($CDCl_3$, 15%); 2.98—3.41(6H, m, phenyl), 5.53—6.04(8H, m, $C\underline{H}_2C\underline{H}_2$), 6.01(2H, s, $PhC\underline{H}_2Ph$), 7.78(6H, m, $PhC\underline{H}_3$), and 7.95(6H, s, $COC\underline{H}_3$). MS: *m/e* 400(M^+). Found: C, 68.72; H, 7.21%. Calcd for $C_{23}H_{28}O_6$: C, 68.98; H, 7.05%.

After **8** (2.0 g) was refluxed in methanol (17 ml) containing NaOH (0.5 g) for 2 hr, the reaction mixture was poured into ice water. White precipitate was recrystallized from benzene to give 2,2'-methylenebis(5-methyl-1,2-phenyleneoxy)diethanol (1.5 g); mp 105—107 °C. IR(KBr); 3350 cm^{-1}. Found: C, 72.26; H, 7.68%. Calcd for $C_{19}H_{24}O_4$: C, 72.13; H, 7.65%.

*Reaction of **3** with 2-Chloroethanol.* **3** (52 g) was added to a solution of sodium (12.4 g) in ethanol (250 ml). After being kept at 80 °C for 25 hr, 2-chloroethanol (45 g) was added to the solution and refluxed with stirring for 20 hr. After the reaction, the reaction mixture was concentrated to give a residue which separated three compounds according to the given scheme.

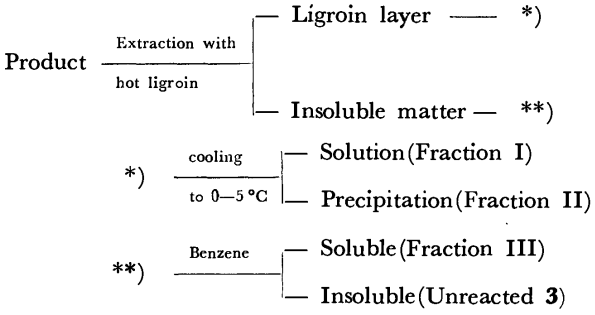

The compound(Fraction I) easily soluble in ligroin was recrystallized from ligroin. Colorless needle crystals were obtained, mp 146—149 °C. Yield, 0.82 g. IR(KBr): 3360 and 3250 cm^{-1}. NMR($CDCl_3$, 14%); 1.98—2.44(2H, b, O$\underline{H}$), 2.90—3.36(8H, m, phenyl), 5.82—6.18 (8H, m, $C\underline{H}_2$-$C\underline{H}_2$), 6.17(2H, s, $PhC\underline{H}_2Ph$), 6.20(2H, s, $PhC\underline{H}_2Ph$), 7.40—7.60(1H, b, O$\underline{H}$), 7.73(3H, s, $C\underline{H}_3$), and 7.77(6H, s, $C\underline{H}_3$). MS; *m/e* 392(M^+). Found: C, 76.14; H, 7.14%. Calcd for $C_{25}H_{28}O_4$: C, 76.50; H, 7.19%. The compound was concluded to be 2-(2-hydroxyethoxy-5-methylbenzyl)-6-(2-hydroxy-5-methylbenzyl)-4-methylphenol (**9**). A solution of **9** (0.2 g) in acetic anhydride (10 ml) was treated by the previous method to give acetylated compound (0.1 g); colorless needle, mp 95—97 °C. IR(KBr); 1750 cm^{-1}. Found: C, 71.73; H, 6.62%. Calcd for $C_{31}H_{34}O_7$: C, 71.80; H, 6.60%.

The hot ligroin soluble compound(Fraction II) was recrystallized from benzene to give 2,6-bis(2-hydroxyethoxy-5-methylbenzyl)-4-methylphenol(**10**); colorless plate, mp 115—120 °C, yield, 3.5 g. IR(KBr); 3400 cm^{-1}. NMR($CDCl_3$, 5.0%); 2.90—3.45(8H, m, phenyl), 4.60—5.50(3H, b, O$\underline{H}$), 5.85—6.30(8H, m, $C\underline{H}_2C\underline{H}_2$), 6.14(2H, s, $PhC\underline{H}_2Ph$), 7.75 (6H, s, $C\underline{H}_3$), and 7.83 (3H, s, $C\underline{H}_3$). MS; *m/e* 436(M^+). Found: C, 74.09; H, 7.46%. Calcd for $C_{27}H_{32}O_5$: C, 74.29; H, 7.39%. The acetylation of **10** gave oily product. IR(neat); 1730 cm^{-1}. Found: C, 70.04; H, 6.87%. Calcd for $C_{33}H_{38}O_8$: C, 70.44; H, 6.81%.

2-[2,6-Bis(2-hydroxyethoxy-5-methylbenzyl)-4-methylphenoxy]ethanol(**11**) was obtained by repeated crystallizations from the fraction III, with benzene as a solvent; mp 118—121 °C, yield, 2.2 g. IR(KBr): 3400 cm^{-1}. NMR ($CDCl_3$, 2.0%); 2.85—3.45(8H, m, phenyl), 5.90—6.40(15H, m, $C\underline{H}_2C\underline{H}_2$ and O$\underline{H}$), 6.60(4H, s, $PhC\underline{H}_2Ph$), 7.72(3H, s, $C\underline{H}_3$), and 7.83(6H, s, $C\underline{H}_3$). MS; *m/e* 480(M^+). Found: C, 72.45; H, 7.48%. Calcd for $C_{29}H_{36}O_6$: C, 72.48; H, 7.55%.

*2-[2,6-Bis(2-acetoxyethoxy-5-methylbenzyl)-4-methylphenoxy]ethyl Acetate(**12**).* A sample of **11** (1 g) was refluxed with acetic anhydride (20 ml) to give **12** (0.8 g); colorless plate, mp 64—65 °C (from ligroin). IR(KBr); 1735 cm^{-1}. NMR ($CDCl_3$, 5.0%); 2.90—3.40(8H, m, phenyl), 5.50—6.00(12H, m, $C\underline{H}_2C\underline{H}_2$), 6.04(4H, s, $PhC\underline{H}_2Ph$), 7.78(6H, s, $PhC\underline{H}_3$), 7.86(3H, s, $PhC\underline{H}_3$), 7.97(3H, s, $COC\underline{H}_3$), and 7.99(6H, s, $COC\underline{H}_3$). MS; *m/e* 606(M^+). Found: C, 69.02; H, 6.93%. Calcd for $C_{35}H_{42}O_9$: C, 69.29; H, 6.98%.

*Reaction of **4** with 2-Chloroethanol.* **4** (46 g) was added to a solution of sodium (9.9 g) in ethanol (150 ml). The resulting solution was stirred at 80 °C for 22 hr, 2-chloroethanol (36 g) then being added. The mixture was refluxed for 22 hr. After being cooled, the residue which separated was recrystallized from a mixture of ligroin and dioxane to give 2-(2-hydroxyethoxy-3-chloro-5-methylbenzyl)-6-(2-hydroxyethoxy-5-methylbenzyl)-4-methylphenol (**13**); colorless plate, mp 143—145 °C, yield, 3 g. IR(KBr): 3400 cm^{-1}. NMR ($CDCl_3$, 7.0%); 2.89—3.45(7H, m, phenyl), 5.26—6.35 (15H, m, $PhC\underline{H}_2Ph$ and $C\underline{H}_2C\underline{H}_2$), 7.25(3H, s, $C\underline{H}_3$), 7.79(3H, s, $C\underline{H}_3$), and 7.84(3H, s, $C\underline{H}_3$). MS; *m/e* 470(M^+). Found: C, 68.90; H, 6.67%. Calcd for $C_{27}H_{31}O_5Cl$: C, 68.85; H, 6.63%. Acetylated compound of **13** was an oily substance. IR (neat); 1750 cm^{-1}. Found: C, 66.52; H, 6.22%. Calcd for $C_{33}H_{37}O_8Cl$: C, 66.38; H, 6.25%.

References

1) Part 15: A. Ninagawa, Y. Katsuya, H. Matsuda, and S. Matsuda, *Makromol. Chem.*, **174**, 225 (1973).

2) T. Sakakibara, H. Maeda, A. Ninagawa, H. Matsuda, and S. Matsuda, *Kogyo Kagaku Zasshi*, **74**, 2190 (1971).

3) K. Hultzsch, *Angew. Chem.*, **61**, 93 (1949).
4) N. D. Coggeschall, *J. Amer. Chem. Soc.*, **72**, 2836 (1950).
5) T. Cairns and G. Eglinton, *Nature*, **196**, 535 (1962).
6) T. Cairns and G. Eglinton, *J. Chem. Soc.*, **1965**, 5906.
7) S. Kovac and G. Eglinton, *Tetrahedron*, **25**, 3599 (1969).
8) G. R. Sprengling, *J. Amer. Chem. Soc.*, **76**, 1190 (1954).
9) S. K. Chatterjee, *Can. J. Chem.*, **12**, 2323 (1969).
10) N. D. Gupta and S. K. Chatterjee, *J. Polym. Sci. Polym. Chem. Ed.*, **12**, 211 (1974).
11) M. Imoto, I. Ijichi, C. Tanaka, and M. Kinoshita, *Makromol. Chem.*, **113**, 117 (1968).
12) O. R. Wulf and U. Liddel, *J. Amer. Chem. Soc.*, **57**, 1464 (1935).
13) A. Ninagawa, H. Matsuda, and S. Matsuda, *Makromol. Chem.*, in press.
14) P. P. T. Sah and H. H. Anderson, *J. Amer. Chem. Soc.*, **63**, 3164 (1941).
15) M. Z. Köbner, *Angew. Chem.*, **46**, 251 (1933).
16) H. Kämmerer and W. Rausch, *Makromol. Chem.*, **18/19**, 9 (1956).
17) H. Kämmerer and W. Rausch, *ibid.*, **24**, 152 (1957).

Nitration of 9,10-Dimethylanthracene and 9,10-Diethylanthracene[1]

Hitomi SUZUKI, Hajime YONEDA, and Terukiyo HANAFUSA

Department of Chemistry, Faculty of Science, Hiroshima University, Higashi-sendamachi, Hiroshima 730

(Received April 23, 1974)

9,10-Dimethylanthracene gave 9-nitromethyl-10-methylanthracene as a major product, when treated with fuming nitric acid in dichloromethane at low temperatures. In contrast, 9,10-diethylanthracene yielded 9-nitro-10-hydroxy-9,10-diethyl-9,10-dihydroanthracene, which in refluxing alcohol was readily converted into 9,10-dialkoxy-9,10-diethyl-9,10-dihydroanthracene. Possible reaction sequences for the side-chain nitration have been discussed.

The mechanistic course of side-chain nitration of polymethylated aromatics proceeds along one of two paths depending on the nature of the substrate involved. Action of nitric acid upon polymethylbenzenes at low temperatures usually leads to the formation of benzyl nitrates.[2] In contrast, a similar treatment of polymethylnaphthalenes results in side-chain nitration, giving 1-naphthylnitromethanes as a major porduct.[3] Formation of these unusual products has been explained in terms of a nitromethylene cyclohexadiene intermediate (I or II), derived from the nitroarenium ion by proton release from the activated alkyl side-chain.[4] Thus, a marked difference in the modes of reaction observed for the benzene and the naphthalene series of compounds would be attributed to the presence of a fused benzene ring in the latter systems. If the dichotomy between the reaction courses taken in the nitration of benzenes on the one hand and of naphthalenes on the other comes from the difference in the relative stabilities of I and II, 9,10-dimethylanthracene (III) is expected to behave in a manner analogous to polymethylnaphthalenes, giving a side-chain nitrated product (VI), since the initial attack of nitronium ion on the hydrocarbon occurs at 9-position to form the arenium ion (IV), from which a nitromethylene cyclohexadiene (V) flanked with fused benzene rings on both sides would be formed (Scheme 1). The relative stability of the intermediate dienes should increase in the order I<II<V with an increase in the number of intact benzene rings. 9,10-Dimethyl- and 9,10-diethylanthracenes (III and IX) were prepared, their behavior towards the nitrating agent being investigated.

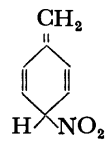

I

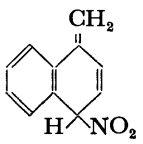

II

A dilute solution of III in purified dichloromethane was treated with two equivalent amounts of nitric acid (d=1.5) at −10—−5 °C in the dark. Chromatography of the crude product on deactivated alumina gave rise to the isolation of a new crystalline compound (VI), mp 197—198 °C, as the main product (82%); molecular formula $C_{16}H_{13}NO_2$, infrared bands (NO_2) at 1546 and 1360 cm^{-1}, and proton resonances at δ 3.20 (s, 3H), 6.51 (s, 2H), 7.50—7.75 (m, 4H), and 8.23—8.55 (m, 4H). The mass spectrum showed the expected peaks at m/e 251 (M^+) and 205 (M^+-NO_2). The results are in line with its formulation as 9-nitromethyl-10-methylanthracene (VI). Its identity was further confirmed by an independent synthesis; 9-methylanthracene was chloromethylated to 9-chloromethyl-10-methylanthracene,[5] which was then treated with silver nitrite in acetonitrile to yield VI.

When III was treated with the nitrating agent in commercial dichloromethane of GR grade and the crude product mixture was passed over a deactivated alumina column, an appreciable amount of another nitro-compound (VII), with a composition fitting $C_{17}H_{17}NO_3$ best, was obtained besides VI. Proton NMR spectrum showed peaks at δ 1.64 (s, 3H), 2.16 (s, 3H), 2.91 (s, 3H), and 7.26—7.91 ppm (m, 8H). A molecular ion peak at m/e 283 is in line with the hypothesis that one more carbon atom is added to anthracene during the reaction. Additional peaks were observed at m/e 268 (M^+-Me), 253 (M^+-2Me), 237 (M^+-Me-MeO or M^+-NO_2), 222 (M^+-Me-NO_2), and 206 (M^+-MeO-NO_2). In the infrared spectrum, there were strong bands at 1535 and 1348 cm^{-1} (NO_2), and 1100 cm^{-1} (C-O-C). Heating of VII in methanol caused facile replacement of the nitro group by the methoxy group, giving a compound (VIII) with composition $C_{18}H_{20}O_2$. Proton NMR spectrum of VIII showed resonance at δ 1.63 (s, 6H), 2.80 (s, 6H), and 7.28—7.79 ppm (m, 8H) with an intensity ratio 3 : 3 : 4. Its mass spectrum showed peaks at 268 (M^+), 253 (M^+—Me), 237 (M^+—MeO), 222 (M^+—Me—MeO), and 206 (M^+—2MeO), its infrared spectrum indicating the presence of ether linkage (1100 cm^{-1}). Chemical and spectral data of VII and VIII are in line with the formulation of the former compound as 9-nitro-10-methoxy-9,10-dimethyl-9,10-dihydroanthracene and the latter as 9,10-dimethoxy-9,10-dimethyl-9,10-dihydroanthracene. *cis*-Configuration can be assigned to VIII by comparison with known spectral data.[6] Discrepancy in the results from the reactions in commercial dichloromethane and purified dichloromethane would be attributed to the presence of a very minor amount of methanol as an impurity or an antioxidant. A possible course for the formation is indicated in Scheme 1.

It is assumed that nitronium ion attacks hydrocarbon III to form arenium ion IV, which will release a proton from the activated methyl group at 10-position to form a methylene cyclohexadiene V, which is then transformed into nitromethyl compound VI. In the presence of methanol, the arenium ion IV would scavenge the nucleophile to form an addition product

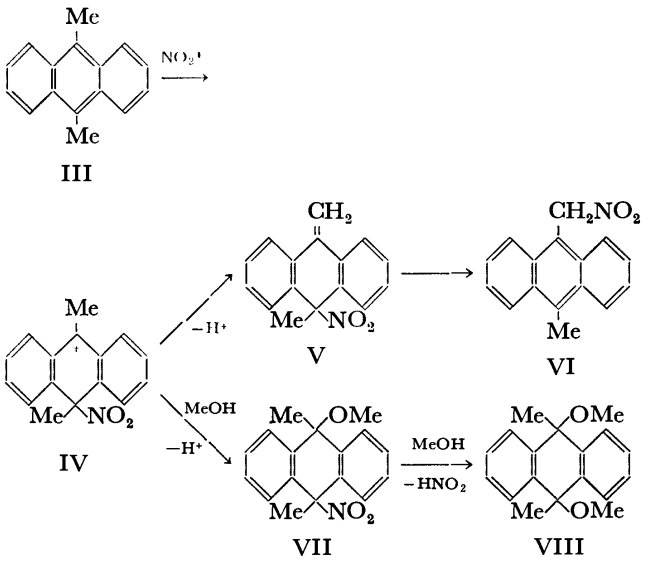

Scheme 1.

VII rather than to release proton from the side-chain to form V.

When 9,10-diethylanthracene (IX) was allowed to react with nitric acid in purified dichloromethane, a single crystalline product with the composition $C_{18}H_{19}NO_3$ was isolated in a 47% yield. It showed infrared bands at 3540 (OH), 1542, and 1358 cm^{-1} (NO_2), and ^1H NMR peaks at δ 0.31 (t, 3H), 0.50 (t, 3H), 2.11 (q, 2H), 2.34 (s, H), 2.89 (q, 2H), and 7.30—8.01 ppm (m, 8H). The results are in line with the structure, 9-nitro-10-hydroxy-9,10-diethyl-9,10-dihydroanthracene (XI). When refluxed in methanol, XI was converted into a mixture of *cis*- and *trans*-9,10-dimethoxy-9,10-diethyl-9,10-dihydroanthracenes (XII), the former being predominant on prolonged heating.[6] A similar treatment of XI in ethanol led to the formation of 9,10-diethoxy-9,10-diethyl-9,10-dihydroanthracene (XIII).

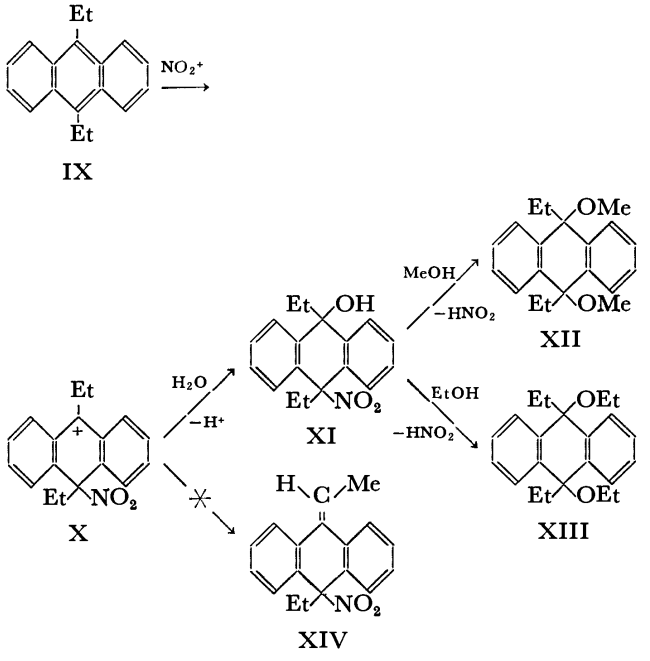

Scheme 2.

Nitration of IX is in contrast to that of pentaethylbenzene, which gave 2,3,4,5-tetraethyl-α-methylbenzyl nitrate as the sole significant product.[7] Failure of IX to undergo reactions on the side-chain might be taken as an evidence for the intermediacy of a nitromethylene cyclohexadiene V in the side-chain substitution. Conversion of the arenium ion (X) into the diene (XIV) forces the ethylidene group to be coplanar with the *peri*-hydrogen atoms subjected to a considerable steric interaction. Thus, X would take up an anion to form an adduct XI rather than to release α-proton to form XIV (Scheme 2).

A sharp change in the modes of reaction towards the nitrating agent on passing from benzenes to naphthalenes and anthracenes would reflect the diminished tendency of the intermediate dienes II and V toward aromatization. With less stable diene I derived from polymethylated benzene, the initial process could involve heterolytic scission of the carbon-nitrogen bond to give a benzyl cation-nitrite ion pair. The benzylic cation carries most of its positive charge on the *exo*-cyclic carbon atom. Thus, it tends to recombine with the ambident nitrite ion at benzylic carbon atom through the more negative oxygen atom, giving benzyl nitrite which will be oxidized to the corresponding nitrate. With the more stable dienes II and V derived from polymethylated naphthalene and anthracene, their tendency to aromatize decreases due to the presence of one or two intact benzene nuclei. This corresponds to the partial formation of a positive charge on the *exo*-cyclic carbon atom, when the fission of the nitrogen-carbon bond takes place.[8] Thus, the combination of 1-naphthylmethylium and 9-anthrylmethylium ions with the ambident nitrite ion would occur preferably through the less negative nitrogen atom rather than oxygen atom, leading to the formation of side-chain nitro compounds.

Alternative explanations can be given for the conversion of nitromethylene cyclohexadienes into side-chain substitution products. The side-chain nitration might proceed via S_E2' mechanism which involves the attack of nitronium ion on the terminal methylene carbon of II or V, redistribution of electrons to regain the aromatic system, and the concomitant departure of the nitro group from the ring. The side-chain nitrooxylation might take place through a formally reversed sequence, S_N2' mechanism, which involves attachment of the nitrate ion to the terminal methylene carbon of I, departure of the nitro group as an anion, and reorganization of the system to aromatic nucleus.

Experimental

All melting points are uncorrected. Infrared spectra were measured in Nujol mulls with a Jasco DS-402G spectrophotometer. Proton NMR spectra were obtained for deuteriochloroform solutions on a Varian T-60 spectrometer with TMS as an internal standard.

9,10-Dimethylanthracene (mp 180—181 °C;[9] ^1H NMR: δ 3.07(s, 6H), 7.36—7.71 (m, 4H), and 8.20—8.55 ppm (m, 4H)) was prepared by the LAH reduction of 9,10-bis(chloromethyl)-anthracene,[10] and 9,10-diethylanthracene (mp 144—145

°C;[11] ^{1}H NMR: δ 1.39 (t, 6H), 3.49 (q, 4H), 7.41—7.78 (m, 4H), and 8.28—8.63 ppm (m, 4H)) was obtained by the reduction of 9,10-diethyl-9,10-dihydroxy-9,10-dihydroanthracene with stannous chloride in methanol.[12]

Purification of Dichloromethane Used as Solvent for Nitration. Commercial dichloromethane (GR grade as well as for spectroscopic use, Tokyo Kasei, Nakarai, Wako, and Katayama) was shaken several times with one-fifth its volume of concentrated sulfuric acid and then thoroughly washed with water. This was then shaken with 5%-aqueous sodium hydroxide, washed thoroughly with water, refluxed over calcium hydride for two hours, and finally distilled through an efficient column; the first and last portions of the distillate were discarded.

9-Nitromethyl-10-methylanthracene (VI). A warm solution of 9-chloromethyl-10-methylanthracene[5] (1.14 g) in acetonitrile (10 ml) was added all at once to a magnetically stirred solution of silver nitrite (1.0 g) in acetonitrile (5 ml). The mixture was stirred overnight and silver chloride was removed by filtration. The residue obtained after removal of the solvent was taken up in hot ethanol, from which VI separated as fine needles. Mp 196—198 °C. Yield, 0.5 g.

Found: C, 76.23; H, 5.25; N, 5.51%. Calcd for $C_{16}H_{13}NO_2$: C, 76.47; H, 5.22; N, 5.57%.

Procedure for the Nitration of 9,10-Dialkylanthracenes. 1) A solution of 9,10-dialkylanthracene (0.002 mol; 0.41 g for III and 0.47 g for IX) in purified dichloromethane (5 ml) was vigorously stirred with external cooling at −12 to −2 °C, and a solution of nitric acid (d=1.5; 0.002 mol, 0.86 ml) in the same solvent (4 ml) was added through a syringe over a period of 30 min. The mixture was kept in the dark at −10 to −5 °C for 3 hr and then quenched by the addition of water. The organic layer was separated, washed with dilute aqueous sodium hydrogen carbonate, and dried over anhydrous magnesium sulfate. The crystalline solid obtained after removal of the solvent was examined by infrared and proton NMR spectroscopy as well as by thin-layer chromatography.

Crude product (0.50 g) from III was crystallized from benzene to give VI as slightly yellow needles, mp 197—198 °C. Yield, 0.41 g (82%).

Found: C, 76.53; H, 5.27; N, 5.25%. Calcd for $C_{16}H_{13}NO_2$: C, 76.48; H, 5.21; N, 5.57%.

Crude product (0.59 g) from IX was recrystallized from a mixture of carbon tetrachloride and light petroleum to give XI as ivory-colored needles, mp 138—139 °C. Yield, 0.27 g (46%).

Found: C, 72.44; H, 6.40; N, 4.42%. Calcd for $C_{18}H_{19}NO_3$: C, 72.71; H, 6.44; N, 4.71%.

2) A solution of III (2.06 g, 0.01 mol) in dichloromethane (GR grade, 100 ml) was treated with nitric acid (d=1.5, 0.43 ml; 0.02 mol) in a similar manner to that for 1). A crude product (2.14 g) obtained after ordinary work-up was found to be a mixture of several compounds, as shown by a complicated feature of its proton NMR spectrum; at least eight prominent peaks were observed in the aromatic and aliphatic methyl proton regions (δ 1.64, 1.69, 1.78, 2.16, 2.36, 2.84, 2.91, and 3.20 ppm). Chromatography of this mixture on alumina gave VII from benzene eluates as needles, mp 152—155 °C. Yield, 0.75 g.

Found: C, 71.73; H, 5.99; N, 4.73%. Calcd for $C_{17}H_{17}NO_3$: C, 72.07; H, 6.05; N, 4.94%.

Alcoholysis of Addition Products. The addition product was dissolved in excess alcohol and heated under reflux for a few minutes. Evaporation of the solution gave the corresponding bis-alkoxy ether in a good yield.

VIII (*cis*): mp 161—166 °C.

Found: C, 80.34; H, 7.51%. Calcd for $C_{18}H_{20}O_2$: C, 80.56; H, 7.51%.

XII (*cis*): mp 147—149 °C. ^{1}H NMR: δ 0.76 (t, 3H), 2.02 (q, 2H), 2.71 (s, 3H), and 7.23—7.78 ppm (m, 8H).[6,13] *trans*-Isomer exhibited absorptions at δ 0.27 (t, 3H), 2.08 (q, 2H), 2.90 (s, 3H), and 7.23—7.78 ppm (m, 8H).

XIII: mp 125—126 °C. ^{1}H NMR: δ 0.26 (t, 3H), 1.10 (t, 3H), 2.11 (q, 2H), 3.02 (q, 2H), and 7.20—7.80 ppm (m, 8H).

Found: C, 81.15; H, 8.75%. Calcd for $C_{22}H_{28}O_2$: C, 81.44; H, 8.70%.

The presence of only one set of signals in the proton NMR spectrum of XIII suggests that the obtained compound is one of the two possible geometrical isomers, probably *cis*, and not their mixture.

Expenses for this work were defrayed by a grant from the Ministry of Education.

References

1) The Reaction of Polysubstituted Aromatics. Part XXXVII; Part XXXVI: H. Suzuki, O. Yagiu, and T. Hanafusa, This Bulletin, **47**, 2260 (1974).

2) H. Suzuki and K. Nakamura, *ibid.*, **43**, 473 (1970); **44**, 227 (1971).

3) R. Robinson and H. Thompson, *J. Chem. Soc.*, **1932**, 2015; H. Suzuki and K. Nakamura, This Bulletin, **44**, 303 (1971); A. Fischer and A. L. Wilkinson, *Can. J. Chem.*, **50**, 3988 (1972).

4) For a possible role of nitromethylene cyclohexadienes as an intermediate in the side-chain substitution, see S.R. Hartshorn and K. Schofield, "Some Aspects of Recent Work on Nitration" in "Progress in Organic Chemistry," Vol. 8, Chap. 7, Butterworths, London (1973), pp 289—293; S. R. Hartshorn, *Chem. Soc. Rev.*, **3**, 167 (1974).

5) J. L. Adelfang and G. H. Daub, *J. Amer. Chem. Soc.*, **80**, 1405 (1958).

6) V. D. Parker, J. P. Dirlam, and L. Eberson, *Acta Chem. Scand.*, **25**, 341 (1971).

7) H. Suzuki and K. Nakamura, This Bulletin, **43**, 473 (1970).

8) R. Ettinger, *Tetrahedron*, **20**, 1579 (1964); R.Zahradnik, A. Kröhn, J. Paínck, and J. Sňobl, *Collect. Czech. Chem. Commun.*, **34**, 2552 (1969).

9) C. S. Gibson and J. D. A. Johnson, *J. Chem. Soc.*, **1931**, 753.

10) N. K. Moshchinskaya and M. S. Ogii, *Khim. i Khim. Tekhnol.*, **4**, 843 (1961).

11) W. G. Bachmann and J. M. Chemerda, *J. Org. Chem.*, **4**, 583 (1939).

12) R. W. Rimmer, R. G. Christiansen, R. K. Brown, and R. B. Sandin, *J. Amer. Chem. Soc.*, **72**, 2298 (1950).

13) V. D. Parker, *Acta Chem. Scand.*, **24**, 3455 (1970).

α,β-Unsaturated Carboxylic Acid Derivatives. VI. New Synthesis of N-Acyl-α-dehydroamino Acid Esters[1]

Chung-gi SHIN, Katsumi NANJO, Eiichi ANDO, and Juji YOSHIMURA*

Laboratory of Organic, Chemistry, Faculty of Technology, Kanagawa University, Rokkakubashi, Kanagawa-ku, Yokohama 221

**Laboratory of Chemistry for Natural Products, Faculty of Science, Tokyo Institute of Technology, Ookayama, Meguro-ku, Tokyo 152*

(Received April 25, 1974)

A new synthetic route to α,β-unsaturated *N*-acyl-α-amino acid esters (*N*-acyl-α-dehydroamino acid esters) is described. The dehydroamino acid esters were prepared by the dehydration of α-(*N*-acylhydroxyamino) acid esters (**10**), derived from the acylation of α-hydroxyamino acid esters (**2** and **6**), and by the elimination of carboxylic acid from α-(*N*-acyl-*O*-acetyl), α-(*N,O*-diacetyl, dipropionyl and diethoxycarbonyl-hydroxyamino) acid esters, obtained by the acylation of **2**, **6** and **10**, in the presence of triethylamine.

It is known that synthetic methods of 2-(2-substituted-acetamino)-2-alkenoic acids,[2] *i.e.*, *N*-acyl-α-dehydroamino acids (**4** and **8**) were derived in the following ways. Greenstein *et al.* and Wieland *et al.* reported the preparation of several *N*-acyl-α-dehydroamino acids (**4**; free acid) by treating a mixture of α-oxocarboxylic acids and acetonitrile[3] or acetamide[4] with dry hydrogen chloride or concentrated sulfuric acid, respectively. However, the yields are low, and isolation and purification of the products is difficult.[3-5] A convenient synthesis of *N*-chloroacetyl-α-dehydroamino acid esters by the condensation of several ethyl α-oxocarboxylates with chloroacetamide in the presence of concentrated sulfuric acid or phosphoryl chloride was recently reported.[6]

Bergmann *et al.*[7] and other workers[8-10] described another preparative method of **4** *via* the corresponding 4-alkylidene and arylidene-2-substituted-oxazolones.

Shin *et al.* reported that compound **4** was obtained by acylation of β-substituted-α-amino-α-alkenoic acid esters obtained by the reduction of the corresponding nitroolefins or β-methoxy-α-nitro compound.[11]

This paper deals with another route for the preparation of *N*-acyl α-dehydroamino acid esters from the α-hydroxyamino acid esters (**2** and **6**) *via* α-(*N*-monoacylhydroxyamino) (**10**) and α-(*N,O*-diacylhydroxyamino) acid esters (**3** and **7**).

Results and Discussion

Preparation of 2 and 6. *t*-Butyl α-hydroxyamino carboxylates (**2**) were obtained by the reaction of *t*-butyl α-bromocarboxylates (**1**),[12] obtained by the esterification of the corresponding acid bromide with hydroxylamine in methanol in the presence of triethylamine in good yields. However, ethyl α-hydroxyamino carboxylates (**2**), which could not be obtained directly by the reaction of ethyl α-bromocarboxylates with hydroxylamine, were prepared by the esterification of the free α-hydroxyamino carboxylic acids (**2**; R^1=H)[13] obtained by the saponification of **2** (R^1=*t*-Bu) with concentrated hydrochloric acid.

By a method reported recently,[11b] ethyl 2-hydroxyamino-3-methoxy-3-phenylpropanoate (**6**) was prepared by the reduction of ethyl 3-methoxy-2-nitro-3-phenylpropanoate (**5**), derived from ethyl 2-nitrocinnamate and methanol in the presence of sodium methoxide, with aluminum-amalgam in ether at room temperature.

The IR spectra of the products (**2**) and (**6**) showed N–OH and N–H bands at 3450—3250 and 3275—3150 cm^{-1} regions. The results are summarized in Table 1.

Acylation of 2 and 6. Acylation of **2** and **6** was performed mainly by the following two routes. When an equimolar mixture of **2** or **6**, pyridine and acyl chloride was stirred in dry benzene at room temperature, the corresponding *N*-acyl derivatives (**10**) were obtained as crystals, together with a reddish syrup, which was confirmed to be the *O*-acyl isomers (**9**).[14]

Further acetylation of **10** with acetic anhydride at 100—110 °C for half an hour gave the corresponding *N,O*-diacyl derivatives (**3** and **7**) in good yields. These compounds were also obtained directly from **2** or **6** under similar conditions by use of more than 2 equimolar amounts of acid anhydride or ethyl chloroformate, respectively. Only the *N*-phthaloylglycyl-*O*-acetyl derivatives (**3** and **7**) were obtained as colorless needles or prisms.

Structures of the monoacyl (**9** and **10**) and diacyl derivatives (**3** and **7**) were characterized by elementary analysis and infrared spectrum. **10** showed deep violet coloration with methanolic ferric chloride. Isomerization of **9** to **10** even in the absence of alkali[14] at room temperature was confirmed by the coloration. The syrup (**9**) could not be isolated in a pure state. It showed a N–H band in the 3300—3100 cm^{-1} region, the absorption shifting towards 3450—3250 cm^{-1} region (OH band) with the progress of isomerization. The results are summarized in Tables 2 and 3.

Synthesis of N-Acyl-α-dehydroamino Acid Esters. Treatment of **3** or **7** with more than 2 equimolar amounts of triethylamine in dry benzene under reflux or at room temperature gave the expected α-dehydroamino acid esters (**4** and **8**) in pure state in good yields. It was found that **10** was directly dehydrated to give **4** in higher yield than in the above experiment, by refluxing in benzene for a longer time in the presence of triethylamine. Structures of these α-dehydroamino acid esters were confirmed by elementary analyses and their infrared absorption spectra which were similar to those of the α-dehydroamino derivatives obtained earlier.[5,6,9,11,15] The results are summarized in Table 4.

TABLE 1. ETHYL AND *t*-BUTYL α-HYDROXYAMINOALKANOATES (**2**) $\left(\begin{matrix}\text{R-CH}_2\text{-CH-COOR}^1\\ \quad\quad\text{|}\\ \quad\text{NHOH}\end{matrix}\right)$

Substituents R	Substituents R^1	Yield (%)	mp °C (bp °C/mmHg)	Formula	Found, % C	Found, % H	Found, % N	Calcd, % C	Calcd, % H	Calcd, % N	IR Spectrum cm^{-1}, in KBr
H	*t*-Bu	98.0	70.5—71.5[a]	$C_7H_{15}NO_3$	52.43	9.42	8.57	52.15	9.38	8.69	3260, 3150, 1750
CH_3	Et	55.6	(80—82/2)[b]	$C_6H_{13}NO_3$	48.96	9.04	9.50	48.96	8.90	9.52	3450, 3275, 1740
CH_3	*t*-Bu	96.7	50—52[a]	$C_8H_{17}NO_3$	54.75	9.74	7.86	54.83	9.78	7.99	3260, 3150, 1740
C_2H_5	Et	74.5	(80—80.5/1)[b]	$C_7H_{15}NO_3$	52.21	9.30	8.63	52.15	9.38	8.69	3430, 3270, 1745
C_2H_5	*t*-Bu	97.4	65.5—69.0[a]	$C_9H_{19}NO_3$	57.33	10.17	7.40	57.11	10.12	7.40	3250, 3150, 1745
C_6H_5	Et	39.0	47.5—48.0[c][d]	$C_{11}H_{15}NO_3$	63.29	7.27	6.66	63.14	7.23	6.69	3250, 3200, 1735

a) Colorless needles from benzene and petroleum ether. b) Colorless viscous oil. c) Colorless needles from di-*n*-butyl ether. d) R^1=H, yield 75.0%, mp 150 °C (mp 156—157 °C).[16]

TABLE 2. ETHYL AND *t*-BUTYL α-(*N*-ACYLHYDROXYAMINO)ALKANOATES (**10**) $\left(\begin{matrix}\text{R-CH}_2\text{-CH-COOR}^1\\ \quad\quad\text{|}\\ \text{N(OH)-CO-X}\end{matrix}\right)$

Substituents R	Substituents R^1	Substituents X	Yield (%)	mp °C[b]	Formula	Found, % C	Found, % H	Found, % N	Calcd, % C	Calcd, % H	Calcd, % N	IR Spectrum cm^{-1}, in KBr
H	*t*-Bu	P. T[a]	61.5	149.5—150.0	$C_{17}H_{20}N_2O_6$	58.89	5.77	8.02	58.61	5.79	8.04	3260, 1740, 1660
CH_3	Et	P. T	81.4	118—119	$C_{16}H_{18}N_2O_6$	57.60	5.27	8.33	57.48	5.43	8.38	3160, 1735, 1645
CH_3	*t*-Bu	P. T	52.3	170.0—171.5	$C_{18}H_{22}N_2O_6$	59.76	6.06	7.73	59.66	6.12	7.73	3380, 1715, 1685
CH_3	*t*-Bu	C_6H_5	37.6	85—86	$C_{15}H_{21}NO_4$	64.73	7.80	4.99	64.49	7.58	5.01	3280, 1720, 1620
C_2H_5	Et	P. T	62.0	134—136	$C_{17}H_{20}N_2O_6$	58.97	5.65	8.06	58.61	5.79	8.04	3400, 1725, 1670
C_2H_5	*t*-Bu	P. T	22.1	149.5—150.5	$C_{19}H_{24}N_2O_6$	61.07	6.43	7.44	60.62	6.43	7.44	3400, 1715, 1685
C_6H_5	Et	P. T	26.4	143—145	$C_{21}H_{20}N_2O_6$	63.85	5.08	7.31	63.63	5.09	7.07	3300, 1725, 1670

a) P. T=Phthalyliminomethyl group. b) Colorless needles from benzene and petroleum ether.

Table 3. Ethyl and *t*-butyl α-(*N*,*O*-diacyl-hydroxyamino)alkanoates (**3**) $\left(\begin{array}{l} R\text{-}CH_2\text{-}CH\text{-}COOR^1 \\ \quad\quad\quad\quad | \\ \quad\quad\quad N\text{-}CO\text{-}X \\ \quad\quad\quad\quad | \\ \quad\quad\quad O\text{-}CO\text{-}Y \end{array}\right)$

Substituents				Yield (%)	mp °C (bp °C/mmHg)	Formula	Found, %			Calcd, %			IR Spectrum cm^{-1}, in KBr
R	R^1	X	Y				C	H	N	C	H	N	
H	*t*-Bu	P. T[a]	CH_3	83.0	111—112[b]	$C_{19}H_{22}N_2O_7$	58.53	5.68	7.09	58.45	5.68	7.18	1800, 1730, 1705
CH_3	Et	P. T	CH_3	97.8	syrup[c]								1800, 1720
CH_3	*t*-Bu	P. T	CH_3	89.9	90.0—91.5[b]	$C_{20}H_{24}N_2O_7$	59.38	6.02	6.92	59.10	5.98	6.93	1805, 1725, 1685
CH_3	Et	P. T	CH_3	98.2	syrup[c]								1800, 1725
C_2H_5	*t*-Bu	P. T	CH_3	90.0	128—129[d]	$C_{21}H_{26}N_2O_7$	60.04	6.27	6.65	60.28	6.26	6.70	1800, 1730, 1700
C_2H_5	*t*-Bu	CH_3	CH_3	76.2	(114—115/1)[e]	$C_{13}H_{23}NO_5$	57.52	8.63	5.41	57.12	8.48	5.13	1800, 1740, 1700
C_2H_5	*t*-Bu	C_2H_5	C_2H_5	71.5	(123—128/3)[e]	$C_{15}H_{27}NO_5$			4.78			4.65	1800, 1740, 1700
C_2H_5	*t*-Bu	OC_2H_5	OC_2H_5	54.5	(123—126/3)[e]	$C_{15}H_{27}NO_7$			4.33			4.20	1800, 1740
C_6H_5	Et	P. T	CH_3	99.0	syrup[c]								1800, 1725

a) P. T=Phthalyliminomethyl group. b) Colorless needles from di-*n*-butyl ether. c) Unstable colorless syrup, structure of which was confirmed by means of IR spectra and conversion into compound **4**. d) Colorless tablets from di-*n*-butyl ether. e) Colorless oil.

Table 4. Ethyl and *t*-butyl *N*-acyl-α-amino-α-alkenoates (**4**) $\left(\begin{array}{l} R\text{-}CH{=}C\text{-}COOR^1 \\ \quad\quad\quad | \\ \quad NH\text{-}CO\text{-}X \end{array}\right)$

Substituents			Yield (%)		mp °C (bp °C/mmHg)	Formula	Found, %			Calcd, %			IR Spectrum cm^{-1}, in KBr
R	R^1	X	A[a]	B[b]			C	H	N	C	H	N	
H	*t*-Bu	P. T[c]	87.5		194—195[d]	$C_{17}H_{18}N_2O_5$	61.59	5.42	8.44	61.81	5.49	8.48	3350, 1720, 1700
CH_3	Et	P. T	97.3		176—179[e]	$C_{16}H_{16}N_2O_5$	60.87	5.11	9.29	60.75	5.10	8.86	3250, 1730, 1680
CH_3	*t*-Bu	P. T	64.8	71.8	152—152.5[e]	$C_{18}H_{20}N_2O_5$	62.92	5.88	8.26	62.78	5.85	8.14	3170, 1740, 1675
C_2H_5	Et	P. T	84.5		173—174.5[e]	$C_{17}H_{18}N_2O_5$	61.71	5.57	8.48	61.81	5.49	8.48	3270, 1740, 1685
C_2H_5	*t*-Bu	CH_3	76.0	80.6	(136—138/3)[f]	$C_{11}H_{19}NO_3$	61.47	9.04	6.85	61.94	8.98	6.57	3260, 1730, 1670
C_2H_5	*t*-Bu	C_2H_5	82.6		(128—131/1)[f]	$C_{12}H_{21}NO_3$	62.77	9.19	5.77	63.11	9.31	6.16	3270, 1730, 1670
C_2H_5	*t*-Bu	OC_2H_5	86.8		(115—117/1)[f]	$C_{12}H_{21}NO_4$			5.68			5.76	3330, 1730, 1670
C_2H_5	*t*-Bu	P. T	93.4		124—126[e]	$C_{19}H_{22}N_2O_5$			7.83			7.82	3260, 1730, 1685
C_6H_5	Et	P. T	92.5		191—193[e]	$C_{21}H_{18}N_2O_5$	66.75	4.89	7.55	66.66	4.80	7.40	3260, 1725, 1690

a) From compound **3**. b) From compound **10**. c) P. T=Phthalyliminomethyl group. d) Colorless prisms from glacial acetic acid. Decomposition. e) Colorless needles from ethanol and water. f) Colorless viscous oil.

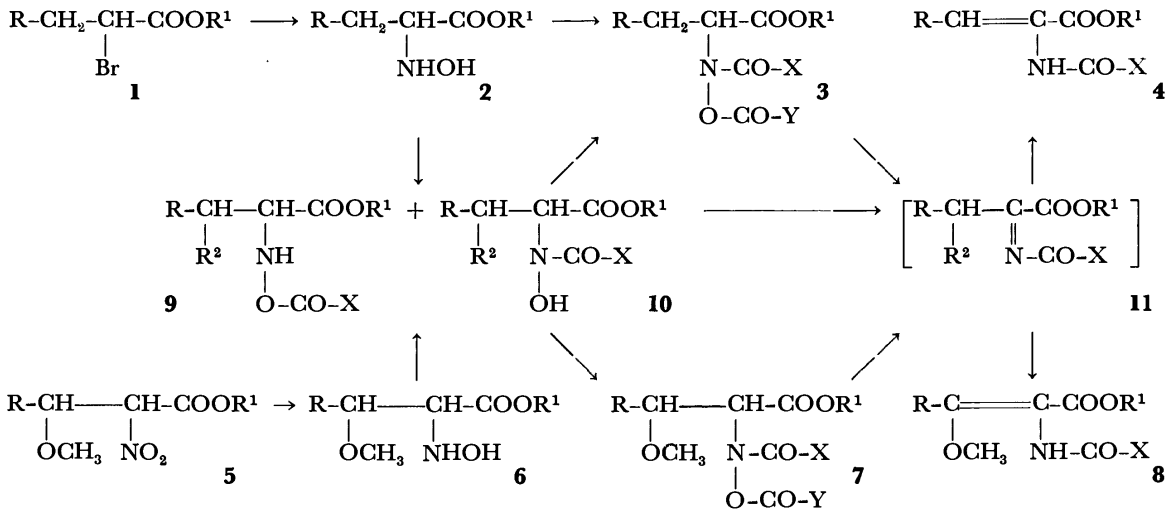

Scheme 1

Conversion of **3**, **7** and **10** into **4**, **8** and **4**, respectively, is deduced to proceed through the corresponding *N*-acyl-α-imino intermediate (**11**), which subsequently isomerizes to a more stable form.[15] This is supported by the fact that ethyl α-(*N*-acyl-hydroxyamino)-β-methoxycarboxylates react with ethanolic ammonia to afford 4-imidazolidone derivatives instead of the expected 2,5-piperazinedione derivatives[14] and that chloroacetylation of ethyl 2-imino-3-methylbutanoate gives the isomerized compound; ethyl 2-(2-chloroacetamido)-3-methyl-2-butanoate.[15]

Experimental

All boiling and melting points are uncorrected. The IR spectra were recorded with a Hitachi EPI-S2 Spectrometer.

Material. Ethyl 3-methoxy-2-nitro-3-phenylpropanoate (**5**) was prepared by the method reported.[11b] Yield 91.6%, colorless prisms from benzene and petroleum ether, mp 81—83 °C. IR(KBr): 1760, 1565, 1380 cm^{-1}. Found: C, 57.01; H, 6.17; N, 5.46%. Calcd for $C_{12}H_{15}NO_5$: C, 56.71; H, 5.97; N, 5.53%.

*t-Butyl α-Bromoalkanoates (**1**).* α-Bromoalkanoic acid bromide (0.443 mol) was added dropwise, with stirring, to a mixture of pyridine (0.447 mol) and *t*-butyl alcohol (120 ml) at a temperature below 30 °C. After being stirred at room temperature for 6 hr, the reaction mixture was allowed to stand overnight at room temperature. After removal of the pyridinium salt separated out, benzene (300 ml) was added to the resulting solution, which was washed successively with water, 3M-hydrochloric acid twice, saturated aqueous solution of sodium hydrogen carbonate and then finally with water. The benzene layer was dried over anhydrous magnesium sulfate and then evaporated. The residual oil was distilled under reduced pressure to give colorless oil. *t*-Butyl 2-bromopropanoate, yield 87.1%, bp 64—65 °C/18 mmHg (bp 62 °C/13 mmHg).[12] *t*-Butyl 2-bromobutanoate, yield 86.7%, bp 71—75 °C/12 mmHg. Found: C, 43.51; H, 6.55%. Calcd for $C_8H_{15}O_2Br$: C, 43.32; H, 6.73%. *t*-Butyl 2-bromopentanoate, yield 84.0%, bp 98—100 °C/19 mmHg. Found: C, 45.77; H, 6.98%. Calcd for $C_9H_{17}O_2Br$: C, 45.57; H, 7.18%.

*t-Butyl α-Hydroxyaminoalkanoates (**2**).* When a solution of **1** (0.37 mol), hydroxylamine (made from hydroxylamine hydrochloride (0.41 mol) and sodium (0.41 mol)) and triethylamine (0.37 mol) in methanol (300 ml) was refluxed for 30 hr and then evaporated, a residual syrup was obtained. After addition of dry ether (300 ml) to the syrup and removal of the triethylamine hydrogen bromide separated out, the ether layer was evaporated to give a residual syrup, which was gradually crystallized or distilled under reduced pressure. The results are summarized in Table 1.

*α-Hydroxyaminoalkanoic Acids (**2**; $R^1=H$).* *t*-Butyl α-hydroxyaminoalkanoate (**2**; 0.246 mol) was dissolved in concentrated hydrochloric acid (350 ml) and then the solution was allowed to stand at room temperature for a day. After evaporation of the reaction solution under reduced pressure, the acidic residual syrup was dissolved in water (30 ml) and maintained within the pH range 6—7 with concentrated aqueous ammonia. After being allowed to stand overnight in a refrigerator, the colorless crystals separated out were collected and then washed with cold water. Recrystallization from water gave colorless prisms. 2-Hydroxyaminobutanoic acid, yield 78.0%, mp 189—191 °C (mp 193—194 °C).[13] 2-Hydroxyaminopentanoic acid, yield 78.3%, mp 192—194 °C (mp 194—195 °C).[13]

*Ethyl α-Hydroxyaminoalkanoates (**2**; $R^1=Et$).* When concentrated sulfuric acid (40 ml) was added dropwise, with stirring, to a suspension of **2** ($R^1=H$, 0.125 mol) in ethanol (100 ml) under cooling, the crystals gradually dissolved. The solution was allowed to stand at room temperature for two days and poured into ice water (200 ml) and then neutralized with solid sodium bicarbonate. After extraction of the reaction solution with ether several times, the ether extracts were washed with water and then dried over anhydrous magnesium sulfate. After concentration of the extracts, the residual syrup was distilled under reduced pressure to give pale yellow oil (See Table 1).

*Ethyl 2-Hydroxyamino-3-methoxy-3-phenylpropanoate (**6**).* This compound was prepared by the reduction of **5** according to the method reported.[11b] Recrystallization from benzene and petroleum ether gave colorless prisms, yield 28.9%, mp 84—85 °C. IR(KBr): 3400, 3250, 1738 cm^{-1}. Found: C, 60.66; H, 7.20; N, 6.03%. Calcd for $C_{12}H_{17}NO_4$: C, 60.24; H, 7.16; N, 5.85%.

*Ethyl and t-Butyl α-(N-Acyl-hydroxyamino)alkanoates (**10**).* To a solution of **2** (0.0272 mol) and pyridine (0.0272 mol) in dry benzene (40 ml) was added with stirring a solution of appropriate acyl chloride (0.0272 mol) in dry benzene (15 ml)

dropwise at room temperature. After stirring for several hours, the resulting benzene layer was washed successively with water, aqueous solution of sodium hydrogen carbonate, 3M-hydrochloric acid and then finally with water. The benzene solution was dried over anhydrous magnesium sulfate and then evaporated. The residual crystals were collected, washed with water and then recrystallized. The results are summarized in Table 2.

Reaction of **6** *with Phthaloylglycyl Chloride.* To a solution of **6** (0.0083 mol) and pyridine (0.0087 mol) in dry benzene (20 ml) was added with stirring a solution of phthaloylglycyl chloride (0.0092 mol) in dry benzene (10 ml) dropwise at room temperature. After stirring for several hours, crystals separated out were collected and washed with water. Recrystallization from ethanol gave colorless needles, which were identified as ethyl 3-methoxy-3-phenyl-2-(*N*-phthaloylglycylhydroxyamino)propanoate (**10**), yield 65.1%, mp 170—172 °C. IR (KBr): 3300, 1700, 1664 cm^{-1}. Found: C, 62.25; H, 5.05; N, 6.76%. Calcd for $C_{22}H_{22}N_2O_7$: C, 61.96; H, 5.20; N, 6.57%.

The benzene filtrate was washed successively with water, 3M-hydrochloric acid and with water, and dried over anhydrous magnesium sulfate and then evaporated. The residual oil was chromatographied on silica-gel column with benzene and the effluent was condensed under reduced pressure to give a pale yellow syrup, which was identified as ethyl 3-methoxy-3-phenyl-2-(*O*-phthaloylglycylhydroxyamino)propanoate (**9**), yield 8.5%. IR(KBr disk): 3250, 1730 cm^{-1}. Found: C, 62.31; H, 5.29; N, 6.38%. Calcd for $C_{22}H_{22}N_2O_7$: C, 61.96; H, 5.20; N, 6.57%.

t-*Butyl 2-(*N,O-*Diacetyl- or Dipropionyl-hydroxyamino)pentanoate (***3***;* R^1*=Et).* A mixture of *t*-butyl 2-hydroxyaminopentanoate (0.053 mol) and appropriate acid anhydride (27 ml) was heated at 100—110 °C for half an hour. After concentration of the reaction solution under reduced pressure, the residual syrup was distilled under reduced pressure to give colorless oil (See Table 3).

t-*Butyl 2-(*N,O-*Diethoxycarbonylhydroxyamino)pentanoate (***3***;* R^1*=Et).* To a solution of *t*-butyl 2-hydroxyaminopentanoate (0.0265 mol) and pyridine (0.053 mol) in dry benzene (40 ml) was added dropwise with stirring a solution of ethyl chloroformate (0.053 mol) in dry benzene (10 ml) at room temperature. After stirring for 3 hr and removal of pyridinium salt separated out, the benzene layer was concentrated to give a syrup. The syrup was distilled under reduced pressure to give colorless oil (See Table 3).

Ethyl and t-*Butyl α-(*O-*Acetyl-*N-*phthaloylglycyl-hydroxyamino)-alkanoates (***3***) and Ethyl 3-Methoxy-3-phenyl-2-(*O-*acetyl-*N-*phthaloylglycylhydroxyamino)-propanoate (***7***).* A mixture of **10** (0.00585 mol) and acetic anhydride (22 ml) was heated at 100—110 °C for half an hour. After concentration of the reaction solution under reduced pressure, a viscous syrup, which was gradually crystallized, or crystals were obtained. The results are summarized in Table 3. Ethyl 3-methoxy-3-phenyl-2-(*O*-acetyl-*N*-phthaloylglycyl-hydroxyamino)propanoate (**7**) was also obtained in 45.5% yield as colorless needles from ethanol, mp 124—126 °C. IR(KBr): 1800, 1720 cm^{-1}. Found: C, 61.34; H, 5.15; N, 6.07%. Calcd for $C_{24}H_{24}N_2O_8$: C, 61.53; H, 5.16; N, 5.98%.

Ethyl and t-*Butyl* N-*Acyl-α-amino-α-alkenoates (***4***).* *a) From 3*: A solution of **3** (0.0011 mol) and triethylamine (0.0026 mol) in dry benzene (10 ml) was stirred at room temperature for 24 hr. After being allowed to stand at room temperature for over a day, the reaction solution was neutralized by 3M-hydrochloric acid and washed with water and then dried over anhydrous magnesium sulfate. Evaporation of the benzene layer under reduced pressure gave colorless crystals or syrup. The results are summarized in Table 4.

b) From ***10***: When a solution of **10** and triethylamine in dry benzene was refluxed for 12 hr in an analogous manner to the case of **3**, compound **4** was obtained in good yield (See Table 4).

*Ethyl 3-Methoxy-3-phenyl-2-(*N*-phthaloylglycylamino)-2-propenoate (***8***).* In an analogous manner to the case of **3**, compound **7** was treated with triethylamine to give compound **8** in 87.5% yield as colorless needles from benzene, mp 178—179 °C. IR(KBr): 3250, 1725, 1660 cm^{-1}. Found: C, 64.76; H, 4.96; N, 6.89%. Calcd for $C_{22}H_{20}N_2O_6$: C, 64.70; H, 4.94; N, 6.86%.

References

1) Part V: C. Shin, Y. Yonezawa, and J. Yoshimura, *Nippon Kagaku Kaishi*, **1974**, 718.

2) a) J. P. Greenstein and M. Winitz, "Chemistry of Amino Acids," Vol. 2, John Wiley & Sons, Inc., New York (1961), pp. 838—860; b) J. P. Greenstein, "Advances in Enzymology," Vol. 8, F. F. Nord, Ed., Interscience Publishers, Inc., New York (1948), pp. 117.

3) a) V. E. Price and J. P. Greenstein, *J. Biol. Chem.*, **171**, 477 (1947); b) A. Meister and J. P. Greenstein, *ibid.*, **195**, 849 (1952); c) L. Levintov, S.-C. J. Fu, V. E. Price, and J. P. Greenstein, *ibid.*, **184**, 633 (1950).

4) T. Wieland, G. Ohnacker, and W. Ziegler, *Chem. Ber.*, **90**, 194 (1957).

5) C. Shin, Y. Chigira, M. Masaki, and M. Ohta, This Bulletin, **42**, 191 (1969).

6) a) C. Shin, M. Fujii, and J. Yoshimura, *Tetrahedron Lett.*, **1971**, 2499. b) C. Shin, K. Sato, A. Ohtsuka, K. Mikami, and J. Yoshimura, This Bulletin, **46**, 3876 (1973).

7) M. Bergmann, V. Schmidt, and A. Miekeley, *Z. Physiol. Chem.*, **187**, 264 (1930).

8) J. C. Scheehan and W. E. Duggins, *J. Amer. Chem. Soc.*, **74**, 2475 (1950).

9) C. Shin, Y. Chigira, M. Masaki, and M. Ohta, *Tetrahedron Lett.*, **1967**, 4610.

10) H. Kurita, Y. Chigira, M. Masaki, and M. Ohta, This Bulletin, **41**, 2758 (1968).

11) a) C. Shin, M. Masaki, and M. Ohta, *J. Org. Chem.*, **32**, 1860 (1967). b) C. Shin, M. Masaki, and M. Ohta, This Bulletin, **43**, 3219 (1970).

12) A. Vollmar and M. S. Dunn, *J. Org. Chem.*, **25**, 387 (1960).

13) L. Neelakantan and W. H. Hartung, *ibid.*, **23**, 964 (1958).

14) C. Shin, K. Nanjo, and J. Yoshimura, *Chem. Lett.*, **1973**, 1039.

15) C. Shin, M. Masaki, and M. Ohta, This Bulletin, **44**, 1657 (1971).

16) E. Buehler and C. B. Brown, *J. Org. Chem.*, **32**, 265 (1967).

Restricted Rotation Involving the Tetrahedral Carbon. XI. Barriers to Rotation and Conformational Preferences of Substituted 9-Isopropyltriptycenes[1]

Fumio SUZUKI, Michinori ŌKI, and Hiroshi NAKANISHI*

Department of Chemistry, Faculty of Science, The University of Tokyo, Hongo, Tokyo 113

**National Chemical Laboratory for Industry, Shibuya-ku, Tokyo 151*

(Received May 14, 1974)

Several 9-isopropyltriptycene derivatives were prepared by addition of benzynes to 9-isopropylanthracenes. Rotation about the C_9-C_{pr} bond of these compounds is found to be frozen at room temperature on the NMR time scale. Those compounds which carry a substituent at 1-position exist as *dl*-isomers, at least overwhelmingly. No sign of existence of *meso*-isomer is found. On the other hand, 9-isopropyl-2,4-dimethyltriptycene exists as a mixture of *d*, *l*, and *meso* isomers, composition of which is almost 1 : 1 : 1. Repulsive nonbonding interaction is a decisive factor to determine the conformational preference. Approximate methods for line shape analysis of two methyl groups in an isopropyl group are discussed. Activation energies for rotation about the C_9-C_{pr} bond increase with the increase in the size of 1-substituent except for the methyl group. The smaller effective size of the methyl group than that expected from the van der Waals radius is attributed to cogwheeling arrangement of methyl and isopropyl groups at the transition state of rotation and/or the higher energy level of the ground state due to the severe interaction between methyl and isopropyl groups.

Considerable efforts have been made to measure the restricted rotation about C_{sp^3}-C_{sp^3} bonds and conformational preferences by means of dynamic nuclear magnetic resonance spectroscopy.[2] Extensive studies on substituted ethanes show that the effects of substituents on conformational equilibria and on rotational barriers are not directly correlated with the size of van der Waals radii of the substituent.[2,3] These data reveal that barrier to rotation and conformational preference can not be explained in terms of simple steric repulsion. Several theoretical investigations suggest that attractive interactions are important in determining the conformational energies of halogenated ethanes[4] and Wolfe proposed the *gauche* effect.[5] Others suggested that there exists an attractive interaction between the C–H group and lone pair of electrons in other cases.[6] We thought it of interest to see whether this kind of interaction is present in cases where steric overcrowding is very severe. We have been able to isolate very stable rotamers of a 9-*t*-butyltriptycene type compound (**1**) at room tempreature.[7] Since the scale model of this compound shows that the substituent at 1-position and the methyl group of *t*-butyl type substituent are located within the sum of van der Waals radii, this type of compound should be suitable for testing the intramolecular interaction in an extreme case.

This paper deals with the intramolecular interaction and the mode of interchange among rotational isomers. It has been shown that dimethyl 9-isopropyl-9,10-dihydro-9,10-ethenoanthracene-11,12-dicarboxylate (**2**) exists as *dl* isomers, almost exclusively, and

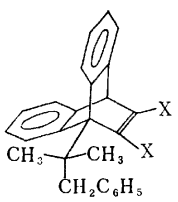

(1)

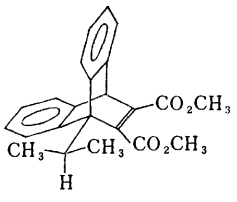

(2)

internal rotation of the isopropyl group is to and fro motion rather than the full rotation.[8] It would be of interest to estimate the generality of the observation of this sort. Several 9-isopropyltriptycene type compounds were prepared and their PMR spectra examined at various temperatures. A method of approximation of line shape analysis of the isopropyl group is also proposed.

Experimental

Syntheses. 9-Isopropyltriptycenes were prepared by treating 9-isopropylanthracenes with benzynes, as illustrated in the following schema. Some new 9-isopropylanthracene derivatives were synthesized by the Grignard reaction of substituted anthrones with isopropylmagnesium bromide followed by dehydration.

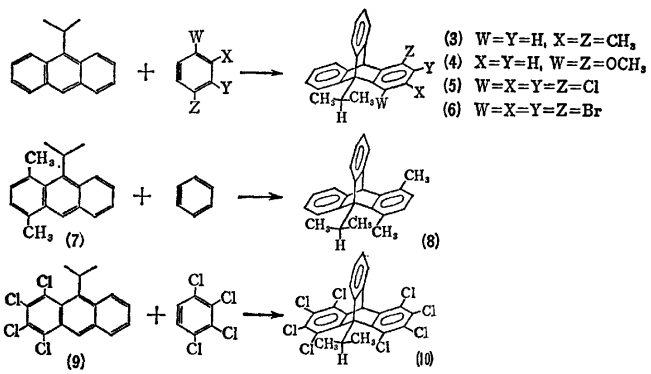

1,4-Dimethyl-9-isopropylanthracene (7). To a solution of isopropylmagnesium bromide, prepared from 3.7 g (0.03 mol) of isopropyl bromide, 0.7 g (0.03 mol) of magnesium and 100 ml of ether, was added 2.2 g (0.01 mol) of 1,4-dimethylanthrone[9] in small portions at room temperature. After stirring for 30 min, 50 ml of benzene was added and the reaction mixture refluxed for 1 hr. After cooling to 0 °C, the mixture was treated with dilute hydrochloric acid. The organic layer was separated, dried and evaporated. The residue dissolved in 150 ml of carbon tetrachloride was warmed on a steam bath with 30 g of phosphorus pentoxide for 2 hr.

Table 1. The NMR data of 9-isopropyltriptycenes in deuteriochloroform at 34 °C (δ ppm)

Compound	Isopropyl methyls	Other methyls	Isopropyl methine	Bridge head proton	Aromatic protons
3	1.86(6H, d, J=6.4 Hz)	2.18(2H, s) 2.40(2H, s) 2.22(1H, s) 2.50(1H, s)	3.52(1H, sept, J=6.4 Hz)	5.48(1H, s)	6.52—7.75(10H, m)
8	1.75(3H, d, J=6.7 Hz) 1.87(3H, d, J=6.7 Hz)	2.43(3H, s) 2.56(3H, s)	3.96(1H, sept, J=6.7 Hz)	5.51(1H, s)	6.60(2H, s) 6.62—7.90(8H, m)
4	1.75(3H, d, J=6.7 Hz) 1.78(3H, d, J=6.7 Hz)	3.16(3H, s) 3.24(3H, s)	3.82(1H, sept, J=6.7 Hz)	5.78(1H, s)	6.43(2H, s) 6.70—7.90(8H, m)
5	1.75(3H, d, J=6.8 Hz) 1.87(3H, d, J=6.8 Hz)		4.35(1H, sept, J=6.8 Hz)	5.92(1H, s)	6.91—8.00(8H, m)
6	1.74(3H, d, J=6.8 Hz) 1.85(3H, d, J=6.8 Hz)		4.57(1H, sept, J=6.8 Hz)	6.01(1H, s)	6.78—7.72(8H, m)
10	1.77(6H, d, J=6.9 Hz)		5.35(1H, sept, J=6.9 Hz)	6.64(1H, s)	7.05—8.30(8H, m)

The supernatant liquid was decanted, washed with water and dried. The solvent was removed and the residue was chromatographed on neutral alumina. Elution with hexane gave the desired compound, mp 110—112 °C, in *ca.* 30% yield (7 g). NMR ($CDCl_3$, δ from TMS): 1.69 (6H, d, J=6.6 Hz), 2.68 (3H, s), 2.84 (3H, s), 4.44 (1H, sept, J=6.6 Hz), 6.98—8.74 (7H, m). The compound was used for the preparation of a triptycene derivative **8**.

*1,2,3,4-Tetrachloro-9-isopropylanthracene (**9**)*, mp 172—173 °C, was similarly prepared from 1,2,3,4-tetrachloroanthrone[10] and isopropylmagnesium bromide. The yield was *ca.* 10%. Found: C, 57.22; H, 3.22; Cl, 39.48%. Calcd for $C_{17}H_{12}Cl_4$: C, 57.02; H, 3.38; 39.60%.

*2,4-Dimethyl-9-isopropyltriptycene (**3**).* To a refluxing mixture of 0.36 g (0.015 mole) of magnesium, 2.04 g (0.01 mol) of 9-isopropylanthracene and 70 ml of dry tetrahydrofuran was added 2.0 g (0.01 mol) of 3,5-dimethyl-2-fluoro-1-bromobenzene[11] in 20 ml of dry ether with stirring. Heating and stirring were continued for 5 hr. The mixture was cooled and treated with water. Organic layer was separated after adding 100 ml of ether, dried over sodium sulfate, and evaporated. The residue was taken up in benzene and chromatographed on alumina. Elution with hexane-benzene gave pure **3**, mp 154.5—156.5 °C, in 0.48 g (*ca.* 15%) yield. Found: C, 92.40; H, 7.15%. Calcd for $C_{25}H_{24}$: C, 92.55; H, 7.45%. The product was a mixture of **3** and 1,3-dimethyl-9-isopropyltriptycene. Isolation of the latter was tedious, but no attempt was made by other means.

Assignments of the structure are based on the PMR spectra. **3** gave signals as shown in Table 1, whereas 1,3-dimethyl-9-isopropyltriptycene at 1.75 (3H, d, J=6.7 Hz), 1.88 (3H, d, J=6.7 Hz), 2.25 (3H, s), 2.52 (3H, s), 3.70 (1H, sept, J=6.7 Hz), 5.10 (1H, s), and 6.72—7.80 (8H, m). The features indicate the chemical shifts of the bridge head protons. **3** gives the signal at 0.38 ppm down field from the corresponding signal of the isomer. This means that the bridge head proton of **3** suffers from the van der Waals shift because of the proximity of a methyl group at 4-position. Nearly the same chemical shift as the bridge head proton of **8** may be taken as another support for the structure. This assignment is also consistent with the presence of two rotamers in **3** and the absence of the *meso* form in the isomer.

*1,4-Dimethyl-9-isopropyltriptycene (**8**).* To a refluxing solution of 1.2 g (0.01 mol) of butyl nitrite and 2.44 g (0.01 mol) of 1,4-dimethyl-9-isopropylanthracene in 20 ml of dichloromethane was added 1.37 g (0.01 mol) of anthranilic acid in 20 ml of ether with stirring. Heating and stirring were discontinued after 0.5 hr and the solvent was evaporated. The residue was taken up in benzene and chromatographed on alumina. Elution with hexane-benzene gave 1.3 g (40% yield) of **8**, mp 199—201 °C. The compound was purified by recrystallization from chloroform-ethanol. Found: C, 92.50; H, 7.67%. Calcd for $C_{25}H_{24}$: C, 92.55; H, 7.45%.

*1,2,3,4-Tetrachloro-9-isopropyltriptycene (**5**)*, mp 267—269 °C, was similarly prepared by treating 9-isopropylanthracene in dichloromethane with a benzyne produced from tetrachloroanthranilic acid[12] in dry acetone; yield 26%. Recrystallization from hexane-benzene afforded a pure sample. Found: C, 63.55; H, 3.69; Cl, 32.52%. Calcd for $C_{23}H_{16}Cl_4$: C, 63.64; H, 3.73; Cl, 32.66%.

*1,2,3,4-Tetrabromo-9-isopropyltriptycene (**6**)*, mp 290—292 °C, was prepared by treating 9-isopropylanthracene with a benzyne produced from tetrabromoanthranilic acid;[13] yield 15%. We failed to obtain satisfactory analytical results probably because of poor combustibility. Purity of the compound was checked by its PMR spectrum. High resolution mass spectrum showed a molecular ion peak at 607.7838, while that of the calculated value is 607.798.

*1,2,3,4,5,6,7,8-Octachloro-9-isopropyltriptycene (**10**)*, mp 303—304 °C, was similarly prepared with the use of tetrachloroanthranilic acid, butyl nitrite and 1,2,3,4-tetrachloro-9-isopropylanthracence; yield *ca.* 5%. This compound also gave unsatisfactory analytical results. Purity was checked by its PMR spectrum. The high resolution mass spectrum showed a molecular ion peak at 567.8287. The calculated value is 567.830.

*1,4-Dimethoxy-9-isopropyltriptycene (**4**).* A suspension of phenylsodium,[14] prepared from 2.25 g (0.02 mol) of chlorobenzene, 0.92 g (0.04 mol) of sodium, and 20 ml of benzene, was added dropwise to a stirred solution of 1.72 g (0.01 mol) of 2-chloro-1,4-dimethoxybenzene[15] and 2.04 g (0.01 mol) of 9-isopropylanthracene in 20 ml of benzene at room temperature under a nitrogen atmosphere. Stirring was discontinued after 3 hr and the mixture was treated with water. The organic layer was separated, dried over sodium sulfate and evaporated. The residue was taken up in benzene and chromatographed on alumina. Elution with benzene followed by recrystallization from chloroform-ethanol gave pure **4** mp 156—158 °C, in 1.1 g (30%) yield. Found: C, 84.03; H, 6.54%. Calcd for $C_{25}H_{24}O_2$: C, 84.21; H, 6.79%.

Spectral Measurement. The PMR spectra were recorded on a Hitachi R-20B spectrometer operating at 60 MHz. The samples were dissolved in appropriate solvents to make up *ca.* 10% (wt/vol) solution. Temperatures were read by the difference in chemical shifts of protons of ethylene glycol and are believed to be accurate within an error of ± 1 °C. T_2 was measured from the line-width of the proton signal of tetrachloroethane added in the sample solution.

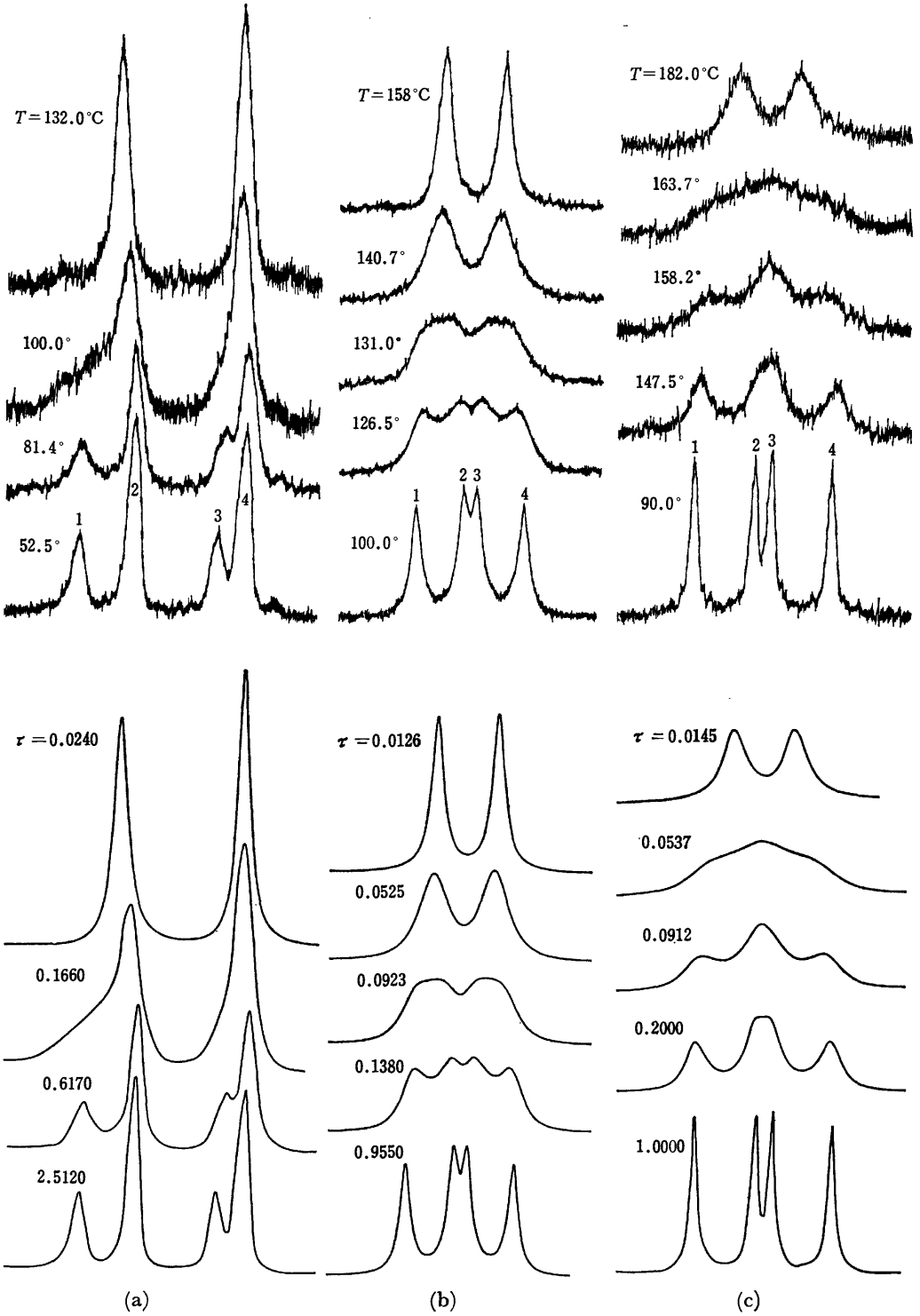

Fig. 1. The observed and calculated spectra of 9-isopropyltriptycenes at various temperatures: a) compound **3**, b) compound **8**, c) compound **5**.

Calculation. Calculation was carried out with a FACOM 270/30 computer. A computer program named EXNMRO[8] was written along lines described in the Line Shape Analysis. Theoretical spectra were calculated to get a best fit with the observed spectra by varying the rate constants. Agreement between the experimental and theoretical spectra was excellent (Fig. 1). Logarithms of the rate constants of rotation obtained at various tempreatures are plotted against $1/T$. A good linear relationship was obtained and the activation energy was calculated. Other kinetic parameters were obtained by putting these data into Eyring's equations. The results are shown in Table 2.

Line Shape Analysis

Since the rotation of an isopropyl group corresponds to the exchange of two methyl groups, six protons which couple with a methine proton should be taken into ac-

Table 2. Activation parameters for rotation (at 25 °C)

Compound	T_c	E_a kcal/mol	$\Delta H^{\ddagger}$ kcal/mol	$\Delta S^{\ddagger}$ eu	$\Delta G^{\ddagger}$ kcal/mol	Solvent
3	100[a)] 85[b)]	17.8±1.4	17.2±1.4	9.1±3.7	19.9±2.5	tetrachloroethylene
8	128	22.0±0.7	21.4±0.7	1.5±1.7	21.8±1.1	hexachlorobutadiene
4	140	25.4±1.1	24.8±1.1	3.9±2.7	23.6±1.9	hexachlorobutadiene
5	164	30.7±1.4	30.1±1.4	15.5±2.3	25.5±2.3	hexachlorobutadiene
6	>200				>26	hexachlorobutadiene

a) Coalescence temperature for the methyl group at 2-position. b) Coalescence temperature for the methyl group at 4-position.

count in the line shape analysis. In terms of spin notation, the process is an exchange of the A_3B_3X spin system since resonance frequency of the methine proton is far apart from those of methyl protons. Strictly speaking, complete line shape analysis of this system should be carried out by the density matrix method,[16,17] which is applied to a spin exchange system having spin-spin couplings. However, the exchanging seven-spin system requires the treatment of two 7×7, two 147×147, two 735×735, and one 1225×1225 dimension matrices in the spin function representation. It is practically impossible to calculate theoretical spectra of this system.

As a means to overcome this difficulty, we might use the composite particle method, in which the spin system of an isopropyl group is regarded as AML, the angular momentum operators I of A, M and L being 1/2, 3/2 and 3/2, respectively. The computation time, however, is still too long for the exchanging system to be analyzed in our laboratory.

Fortunately, the chemical shift of the methine proton of isopropyl group is far apart from the two chemical shifts of methyl protons (Table 1). Mixing transition between the spins of methine and methyl protons might be small. As a good approximation, four peaks of the methyl groups could be analyzed by means of the modified Bloch equation[18] which is applicable to spin systems including no spin couplings instead of the density matrix method. Computation time will be greatly reduced in this approximation. When the modified Bloch equation method is applied to this system, the small effect of mixing transition between the spins of methine and methyl protons of the isopropyl group can be included in the "natural" line width terms of the four peaks of the two doublets due to the methyl groups. Thus, in our calculation, the apparent line width equals the real natural line width plus the line width broadened by the small spin couplings between methine and methyl protons.

The line widths of the four peaks corresponding to methyl protons in the observed spectra differ from each other with compounds **3**, **4**, **5** and **8** at temperatures where the internal rotation about the C_9-C_{pr} bond is frozen. This means that the mixing transition is neither negligibly small nor considerably large, since the line widths of the four peaks should be the same in the former case and the lines should be split further in the latter case. Therefore the above consideration seems to lead to a good approximation.

Since the degree of mixing transition effect remains unchanged for all temperatures, *i.e.*, the off-diagonal elements in the imaginary parts of the density matrices of the spin system of isopropyl group are independent of temperature, the ratios of "natural" line widths of the four peaks of the methyl groups will not vary with temperature. The four "natural" line widths were determined by visual fitting of calculated spectra with the observed. Actually, the ratios described above are almost the same for all the compounds examined at low temperatures.

In the line shape analysis using the modified Bloch equation method, absorption intensity $I(\omega)$ at each frequency is given by

$$I(\omega) = \frac{1}{\pi} Re(-\mathbf{P}\cdot[i(\boldsymbol{\Omega}-\boldsymbol{\omega})+\mathbf{D}]^{-1}\cdot\mathbf{1})$$

where notations of matrices ($\mathbf{P}, \boldsymbol{\Omega}, \boldsymbol{\omega}, \mathbf{D}, \mathbf{1}$) refer to those used in the work of Johnson[17]. Re standing for the real part of the matrices.

The dimension of matrices is four for compounds **4**, **5** and **8**, since two pairs of doublet peaks exchange in rotation of the isopropyl group. In these compounds, the *meso* form does not exist. Thus *d* and *l* isomers give two kinds of methyl signals, the chemical shifts of which are influenced by peri-substituents. Rotation of the isopropyl group is considered to be not a full rotation but a to and fro motion.

In the spectrum of compound **8**, the methyl peaks are denoted by (1, 3) and (2, 4), as in Fig. 1. It is reasonable to assume that peaks 1 and 3 exchange with peaks 2 and 4 and that probabilities of spin transfer of 1→3 or 4, and 2→3 or 4 are zero, since it is not likely that the lower level of one methyl group exchanges with the higher level of the other. Thus a matrix of the probability of spin transfer is as follows:

$$\mathbf{D} \equiv \begin{pmatrix} -1 & 1 & 0 & 0 \\ 1 & -1 & 0 & 0 \\ 0 & 0 & -1 & 1 \\ 0 & 0 & 1 & -1 \end{pmatrix}$$

For compound **4**, the same **D** matrix can be used in calculation of spectra, because the spectra show similar line shapes as with compound **3** at various temperatures.

Compound **5**, however, shows a different pattern. Two pairs of doublet peaks for the methyl groups are shown in Fig. 1. A similar consideration for compound **8** leads to the use of the following **D** matrix for compound **5**:

$$\mathbf{D} \equiv \begin{pmatrix} -1 & 0 & 1 & 0 \\ 0 & -1 & 0 & 1 \\ 1 & 0 & -1 & 0 \\ 0 & 1 & 0 & -1 \end{pmatrix}$$

In the case of compound **3**, the difference in chemical shifts of two methyl groups was so small that the signal appeared as a doublet. This is reasonable since **3** carries no substituent at peri positions and the calculation outlined above is made impossible. However, *meso* form (**11b**) coexists with *dl* forms (**11a** and **11a'**) in this case and the former gives methyl signals at different chemical shifts from those of the latter in the aromatic methyl region. Thus it was possible to perform line shape analysis in this region using the modified Bloch equation method.

Since the chemical shifts of the protons of *d* and *l* forms are the same and the observed signals of both aromatic methyl protons split into two peaks, respectively, in the ratio of 2 : 1 (Fig. 1), the populations of *d*, *l*, and *meso* isomers are considered to be the same. This means that the ground state levels for the respective forms are the same. The rates of exchange, $d \rightleftharpoons l$ and d(or l)$\rightleftharpoons$*meso*, can be assumed to be the same also, since there is no substituent at the peri positions and populations are equal. The transition states can also be considered to be the same. Taking the above into account, matrices are written as follows and calculation can be performed using only one rate constant.

$$\mathbf{P} \equiv \begin{pmatrix} 1 & 2 & 1 & 2 \end{pmatrix}$$

$$\mathbf{D} \equiv \begin{pmatrix} -1 & 1 & 0 & 0 \\ 1 & -1 & 0 & 0 \\ 0 & 0 & -1 & 1 \\ 0 & 0 & 1 & -1 \end{pmatrix}$$

Results and Discussion

Conformational Preferences. PMR data of the triptycenes **3**, **4**, **5**, **6**, **8** and **10** in deuteriochloroform at 34 °C are summarized in Table 1. Compounds **4**, **5**, **6** and **8** show a pair of doublets for the methyl groups of the isopropyl group. The intensities are equal for the pair. Rotation about C_9-C_{pr} bonds should be frozen on the NMR time scale. The appearance of two doublets may be accounted for by assuming either the presence of *dl*-isomers only (absence of *meso* isomer) or an accidental overlap of the chemical shifts of the two kinds of methyls (*cf. e.g.* the Newman type projection **12**). Either way could be chosen for this case, but the former is taken herewith because the feature of the spectra did not change in other solvents and it is unlikely that the chemical shifts of the two methyl groups coincide in compounds **5** and **6**, in which chlorine and bromine atoms give a strong effect on the chemical shifts.[19] One might argue that the chemical shifts of the methyl group in the *meso* form coincide with one of the doublets. However, if this were the case, the intensities of the two doublets should have been different.

Compound **3** shows only a doublet for the methyl groups of the isopropyl group. However, in the aromatic methyl region, four peaks can be seen, the relative intensities being 1 : 2. This indicates that the compound exists as a mixture of *meso* and *dl* forms but the chemical shifts of two methyl groups of the isopropyl group in the *dl* form happens to be the same. The coincidence of chemical shifts is not surprising as this compound carries no substituent at peri-possition and the magnetic environments for the two methyl groups do not differ much. The intensity ratio of 1 : 2 may be interpreted by assuming that *meso* (**11b**), *d*, and *l* (**11a** and **11a'**) isomers are of the same potentials and exist with 1 : 1 : 1 population ratio. Lack of peri-substituent should again be the cause of this phenomenon.

The ratio racemate/*meso* was measured in the temperature range 0—60 °C. The ratio of 2.0 was constant throughout the range. This is a strong support for the idea that the *meso* and the *dl* isomers are of the same energy. Preference of the *dl* isomers is of the statistical origin.

Compound **10** gives only one doublet for the isopropyl methyl groups. Because of the large magnetic effect of chlorine,[19] it is not reasonable to assume that the chemical shifts of the two methyl groups coincided under the conditions examined. Rather, the sole presence of a *meso* form, which gives the same chemical shifts for the methyls, is a more plausible reason for the phenomenon. This assumption is consistent with the idea that an isomer with the least repulsion exists, since a *dl* isomer of this compound would have the severe steric interaction between one of the methyls and two chlorine atoms at peri-positions.

The overwhelming preference of the *dl* isomer in

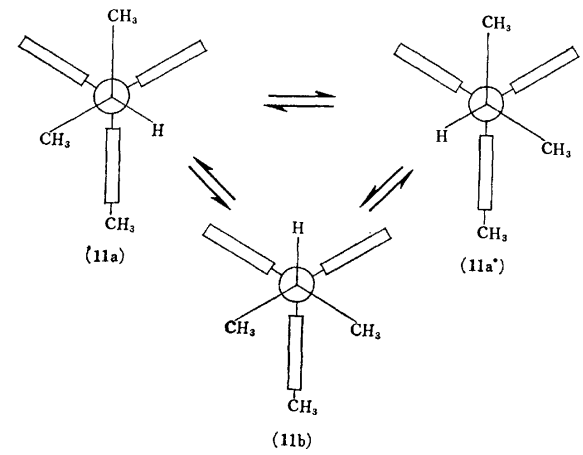

Scheme 1.

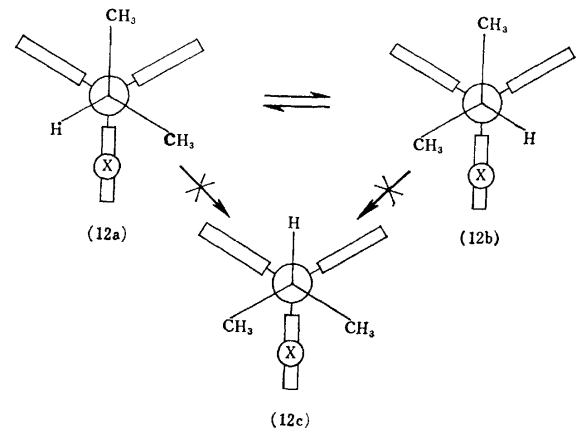

Scheme 2.

Fig. 2. Possible conformations of 9-isopropyltriptycenes.

1-substituted 9-isopropyltriptycenes was rather surprising. It can arise with either thermodynamic control or kinetic control. Thermal equilibration was attempted to shed light on this problem. The PMR spectra, after heating at 200 °C for 24—100 hr, did not show any change from those prior to heating. The possibility that the barrier leading to the *meso* form (**13a** and **13a'**; *vide infra*) is too high to produce any such isomer cannot be ruled out completely, but the long heating could produce at least a small fraction of the *meso* form, if it were thermodynamically feasible. Thermal equilibration was possible with an analogous compound under similar conditions.[20] Thus the population of these conformers seems to be controlled by the thermodynamic effect.

It is concluded that conformational equilibria (Fig. 2) of 9-isopropyltriptycene derivatives are mostly determined by the repulsive term of the van der Waals interaction between the methyl group and the substituent. No piece of evidence for the attractive interaction between the methyl group and lone pair electrons was obtained. The strong conformational preference may be attributed to the extreme closeness between the two groups concerned.

Rotational Barriers. As the temperature was raised, methyl signals of **3**, **4**, **5** and **8** gradually collapsed, whereas those of **6** and **10** remained intact up to 200 °C. From the chemical shift difference between the two methyl groups and temperature independence up to 200 °C, the barrier to rotation about the C_9–C_{pr} bond of **6** is estimated to be at least 26 kcal/mol. Since the bromine at 1-position must eclipse a methyl group at the transition state, this conformation becomes very unstable. If rotation about the C_9–C_{pr} bond should take place in compound **10**, change in chemical shifts should also have been observed, since the rotation should result in formation of *dl*-isomers. The lack of temperature dependence of the spectra indicates that the barrier to rotation about the C_9–V_{pr} bond of this commpound is also very high.

While the mechanism of exchanging process in **3** is the full rotation about the C_9–C_{pr} bond (scheme 1), that for the isopropyl group of compounds **4**, **5**, and **8** seems to be the exchange between two racemic forms for the following reasons (Scheme 2). If significant population of a *meso* isomer should result by rotation about the bond in question, temperature dependence of the chemical shifts of both methine and methyl protons is expected. Particularly since the chemical shift of the methine proton of compound **3** and that of compound **5** differ so much from each other and the former can be taken as a model of the chemical shift of the *meso* form of compound **5**, drift in chemical shift should arise. However, such is not the case. A comparison should be made of the models of transition states. If a methyl group eclipses a substituent at a peri-position, the energy of the conformation (**13a** and **13a'**) should be higher than a conformation (**13b**) in which hydrogen eclipses the substituent. The former is the transition state of *meso*⇌*dl* and the latter that of *dl*⇌*ld*. Thus the racemization process or to and fro motion of the isopropyl group is more likely to occur with greater ease. The to and fro motion seen in the 9-isopropyltriptycene type compound seems to be the general motion for compounds including **2**.

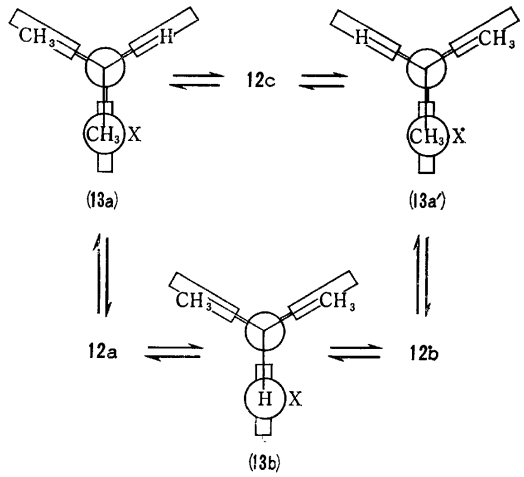

The spectra at various temperatures were simulated by the use of a computer along the lines discussed in Line Shape Analysis. The Arrhenius plots yielded good linear relationships, kinetic parameters being obtained. The results are given in Table 2.

The extreme proximity of interacting groups should be responsible for the extremely high barriers to rotation involving the isopropyl group. Even the barrier of **3** is higher than that of compound **2** ($\Delta G_c^{\ddagger}=17.7$ kcal/mol, $T_c=64$ °C).[8] This means that the triptycene skelton is more effective than 9,10-(dimethoxycarbonyletheno)-9,10-dihydroanthracene skeleton in raising the barrier. Similar phenomena have also been observed.[20]

The barrier to rotation, as judged from either E_a or $\Delta H^{\ddagger}$, increases as the size of substituent at 1-position increases, except for the methyl case. The magnitude of change in barriers due to the substituent size is surprisingly large. This is in striking contrast to the small change in ethane derivatives. The reason for this contrast must be the rigidity of the triptycene skeleton and extreme proximity of the substituent at 1-position. The barriers to rotation seem to be also interpreted by nonbonding repulsions.

The barrier to rotation of compound **8** is rather small. Since the van der Waals radius of a methyl group is 2.0 Å and that of bromine 1.95 Å, these two substituents are often cited to possess nearly the same van der Waals radii. However, in the present case, the methyl group in compound **8** seems to be much smaller than the bromine in a similar situation (compound **6**), and even smaller than the chlorine and methoxyl groups. This is again in sharp contrast to the fact that the methyl group is often considered to be larger than the chlorine and methoxyl groups.[21] A reasonable explanation for this anomaly may be given by considering two factors, rise of ground state because of the larger size of the methyl group which increases the nonbonding repulsion, and the characteristic structure of the methyl group which contains three hydrogens and a carbon atom. In the usual sense, the methyl group is considered to be a symmetrical

top because it rotates almost freely. Halogen atoms behave similarly. However, in a situation where the steric conditions are severe as in the present case, the methyl group may not be considered to be a symmetrical top any longer but a rotating tetrapod. Under these circumstances, the isopropyl group and the methyl group may be considered as a pair of gears. At the transition state, these two gears may take cogwheeling arrangement (**14**) which reduces the effective size of the methyl group. A similar situation was found for 9-methyltriptycene derivatives.[1)]

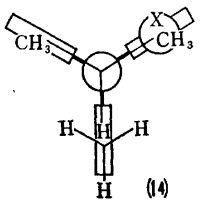

(14)

We wish to thank Dr. O. Yamamoto, National Chemical Laboratory for Industry, for helpful suggestions and discussion on the total line shape analysis.

References

1) Preceding paper: M. Nakamura, M. Ōki, H. Nakanishi, and O. Yamamoto, This Bulletin, **47**, 2415 (1974).

2) J. A. Pople, W. G. Schneider, and H. J. Bernstein, "High-Resolution Nuclear Magnetic Resonance," McGraw-Hill Book Co., New York, 1959, Chap. 13: J. W. Emsley, J. Feeney, and L. H. Sutcliffe, "High Resolution Nuclear Magnetic Resonance Spectroscopy," Vol. 1, Pergamon Press, New York, 1965, Chap. 9: H. Kessler, *Angew. Chem. Int. Ed. Engl.*, **9**, 219 (1970).

3) a) F. J. Weigert, M. B. Winstead, J. I. Garrels, and J. D. Roberts, *J. Amer. Chem. Soc.*, **92**, 7359 (1970): B. L. Hawkins, W. Bremser, S. Borcic, and J. D. Roberts, *ibid.*, **93**, 4472 (1971). b) C. H. Bushweller and W. G. Anderson, *Tetrahedron Lett.*, **1972**, 1811. c) J. E. Anderson and H. Pearson, *J. Chem. Soc. B*, **1971**, 1209: J. E. Anderson and H. Pearson , *Chem. Commun.*, **1971**, 871. d) R. A. Newmark and C. H. Sederholm, *J. Chem. Phys.*, **43**, 602 (1965): H. S. Gutowsky, G. G. Belford, and P. E. McMahon, *ibid.*, **36**, 3353 (1962): T. D. Alder, H. S. Gutowsky, and R. L. Vold, *ibid.*, **47**, 3130 (1967); F. Heatley and G. Allem, *Mol. Phys.*, **16**, 77 (1969).

4) N. Sheppard, *Adv. Spectroscopy*, **1**, 288 (1959): R. J. Abraham and K. Parry, *J. Chem. Soc., B*, **1970**, 539.

5) S. Wolfe, *Accounts Chem. Res.*, **5**, 102 (1972).

6) J. B. Lambert, D. S. Bailey, and C. E. Miran, *J. Org. Chem.*, **37**, 377 (1972): N. D. Epiotis, D. Bjorkquist, L. Bjorkquist, and S. Sarkanen, *J. Amer. Chem. Soc.*, **95**, 7558 (1973): R. J. Abraham and Z. L. Rossetti, *J. Chem. Soc. Perkin II*, **1973**, 582: papers cited therein.

7) M. Ōki and G. Yamamoto, *Chem. Lett.*, **1972**, 45.

8) M. Ōki and M. Suda, This Bulletin, **44**, 1876 (1971).

9) F. Bell and D. H. Waring, *J. Chem. Soc.*, **1949**, 267.

10) M. Goi and K. Konishi, *Osaka Furitsu Kogyo-Shoreikan Hokoku*, No. 24, 51 (1960); P. Kniel, *Helv. Chim. Acta*, **46**, 492 (1963).

11) S. R. Sandler and W. Karo, "Organic Functional Group Preparations," Vol. 1, Academic Press, New York, 1968, p. 138.

12) H. Heaney and J. M. Jablonski, *J. Chem. Soc. C*, **1968**, 1895.

13) H. Heaney, K. G. Mason, and J. M. Sketchley, *ibid.*, **1971**, 567.

14) G. Ehrhart, *Chem. Ber.*, **96**, 2042 (1963): G. Ehrhart and G. Seidl, *ibid.*, **97**, 1994 (1964).

15) G. Catelfranchi and G. Borra, *Ann. Chim.* (Rome), **43**, 293 (1953).

16) O. Yamamoto and H. Nakanishi, *Tetrahedron*, **29**, 781 (1973).

17) C. S. Johnson, Jr., "Advances in Magnetic Resonance," Vol. 1, Academic Press, New York, 1965, p. 33.

18) O. Yamamoto, M. Yanagisawa, K. Hayamizu, and G. Kotowycz, *J. Mag. Resonance*, **9**, 216 (1973).

19) a) Reference 1. b) G. Yamamoto and M. Ōki, *Chem. Lett.*, **1974**, 67.

20) G. Yamamoto and M. Ōki, *Chem. Commun.*, **1974**, 713.

21) R. Adams and J. B. Hale, *J. Amer. Chem. Soc.*, **61**, 2825 (1939): S. L. Chien and R. Adams, *ibid.*, **56**, 1787 (1934): R. W. Stoughton and R. Adams, *ibid.*, **54**, 4426 (1932).

Molybdenum(V) Chloride as a Reagent for *cis* Chlorination of Olefins

Sakae UEMURA,* Akira ONOE, and Masaya OKANO

Institute for Chemical Research, Kyoto University, Uji, Kyoto 611

(Received May 27, 1974)

Treatment of nonconjugated olefins such as *cis*- and *trans*-2-butenes, *cis*-2-octene, and cyclohexene with $MoCl_5$ in CCl_4 gave *vic*-dichloroalkanes whose *cis*-isomer was formed predominantly, the ratio of *cis*- to *trans*-addition being 4.9—12.1, together with monochloroalkanes. Preferential formation of *exo-cis*-dichloride was observed in the case of norbornene and norbornadiene. Bromochlorination and chloroiodination of olefins, and aromatic bromination and iodination were carried out with mixtures of $MoCl_5$ and halogens. The reaction scheme for chlorination is discussed.

Chlorine reacts with olefins *via* both homolytic and heterolytic pathways, stereochemistry of the addition depending on the kind of olefins. Thus, the addition occurs non-stereospecifically with conjugated olefins, *cis* addition usually predominating, while with nonconjugated linear olefins it proceeds with high *trans* stereospecificity.[1] Chlorination of nonconjugated olefins by other chlorinating agents, however, shows a somewhat different stereospecificity from that by chlorine; *i.e.*, *cis*-addition sometimes predominates in the reaction of *cis*- or *trans*-2-butene with $CuCl_2$[2] and in the chlorination of 1-alkylpropene with (dichloroiodo)-benzene.[3] $SbCl_5$ is an effective reagent for the *cis*-chlorination of nonconjugated olefins such as 2-butene, 2-octene and cyclohexene.[4] In the course of further studies on olefin chlorination by other metal or metalloidal chlorides we found that *cis*-chlorination also occurred by $MoCl_5$ with higher *cis* stereospecificity than in the case of $SbCl_5$. Although the chlorinating action of $MoCl_5$ was noted in the chlorination of aromatic hydrocarbons,[5] no report seems to have been given on the direct chlorination of olefins. We describe here the results of the chlorination of olefins by $MoCl_5$ in CCl_4, together with those of the mixed halogenation of olefins and aromatic halogenation with mixtures of $MoCl_5$ and halogens.

Results and Discussion

Chlorination. The reaction was carried out by adding or introducing olefinic hydrocarbons into a pale red-brown homogeneous solution of $MoCl_5$ in CCl_4 or CH_2Cl_2 at appropriate temperature, followed by stirring for 0.25—10 hr under N_2 atmosphere. The products were *vic*-dichloroalkanes(**1**) (*cis* and *trans*) and monochloroalkane(**2**) (Scheme 1).

$$\mathrm{RCH\text{-}CHR' \xrightarrow[CCl_4]{MoCl_5} RCH(Cl)\text{-}CHR'(Cl) + RCH_2CHR'(Cl)} \quad (1)$$

(**1**) (**2**)

Some results are summarized in Table 1. Compared to the chlorination by $SbCl_5$,[4] the yield of **1** was lower, while the selectivity for *cis*-chlorination was much higher. Separate experiments using isomeric dichlorobutanes and dichlorocyclohexanes revealed that no interconversion occurred between *cis*-**1** and *trans*-**1** under the present reaction conditions. We see from Table 1 that elongation of the reaction time does not affect so much the ratio of *cis*- to *trans*-addition in the chlorination of cyclohexene despite the increase in the yield of **1** (Compare Runs 6 and 7). This shows that the observed ratio of *cis*- to *trans*-addition is kinetically controlled.

The reaction in other chlorinated solvents such as chloroform and dichloroethane gave no satisfactory results, *viz.*, none of **1** and **2** was obtained in the former solvent, while the yield of **1** and **2** as well as the *cis*-selectivity was quite low in the latter one. No chlorination occurred in more polar solvents such as acetonitrile, nitromethane, alcohols, DMF, and DMSO, probably because of the reactions of $MoCl_5$ with these solvents forming such salts as $Mo_2Cl_6L_3$, $MoOCl_3$ and/or $MoOCl_3L_2$.[6-8] No reaction occurred with ethyl fumarate and ethyl maleate, but a small amount of **1** (<5% yield) was obtained from the reaction of styrene together with a lot of dimeric compound. When the chlorination of cyclohexene was carried out in the presence of *m*-dinitrobenzene or oxygen, no change in the yield or in the *cis*/*trans* ratio of **1** was observed, suggesting that the reaction is not of a radical nature.

In the case of norbornene and norbornadiene the reaction proceeded in CCl_4 at room temperature to give the various chlorinated compounds as illustrated in schemes 2 and 3, the yields of the dichlorinated compounds being 40—45% and 20—25%, respectively. Although the polymerization of norbornene by using $MoCl_5$ as catalyst is known,[9] only a slight amount of polymerization product was obtained under the present reaction conditions. The kind of product and its distribution differed very much from those in the chlorination by Cl_2 or $SbCl_5$. The characteristic feature of this reaction is a preferable formation of **8** and **13**, *exo-cis*-dichlorocompounds, which were hardly obtained at all in the chlorination by $SbCl_5$. **4**—**7** were the main products in the chlorination of norbornene by $SbCl_5$, while nortricyclyl chloride(**9**) and *exo*-2-*syn*-7-dichloronorbornane were mainly obtained by using Cl_2 gas.[7] In the case of norbornadiene chlorination by Cl_2 gave **10**—**12** as the main products,[10] but we found such a case also in the reaction by $SbCl_5$. Thus, although the dissociation of $MoCl_5$ to $MoCl_4$ and Cl_2 has been reported,[11] possible chlorination with chlorine arising from this dissociation can be excluded.

In order to consider the reaction scheme of chlorination, it is desirable to know the structure of $MoCl_5$

* To whom correspondence should be addressed.

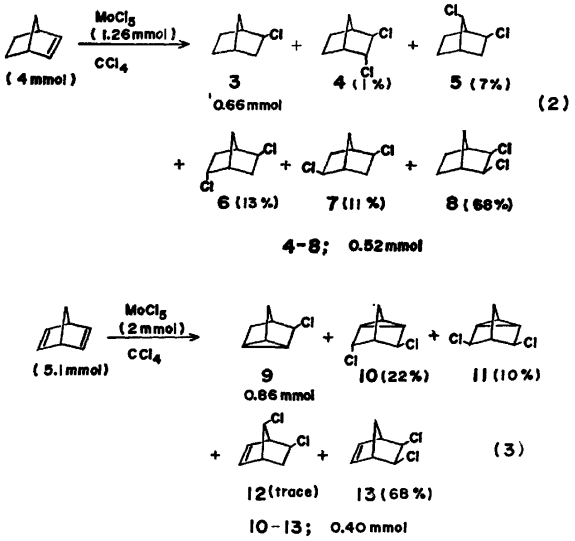

in solution. It is known that the crystal structure of $MoCl_5$ consists of a dimeric molecule with the chlorine atoms forming two distorted octahedra which have a common edge (**15**).[12] However, different views are given on the nature of $MoCl_5$ in solution; it is monomeric in solution (**14**) and solvated;[7] it preserves its dimeric state in CCl_4.[12] Another kind of dimeric species, namely a polarized dimer complex which may be illustrated as **16**, was also considered in the direct aromatic chlorination by $MoCl_5$ where aromatic compound itself was used as a solvent.[5b] Thus it is possible that such an equilibrium (Scheme 4) is present in the solution of $MoCl_5$. Assuming that this equilibrium is involved in CCl_4, the predominant formation of **8**, **13** and other *cis*-dichlorides can be most reasonably explained by a concerted molecular addition of **14** or **15** to olefins, as has been proposed for the *cis*-chlorination by $SbCl_5$.[4]

$$2MoCl_5 \rightleftarrows (MoCl_5)_2 \rightleftarrows MoCl_4^+MoCl_6^- \qquad (4)$$

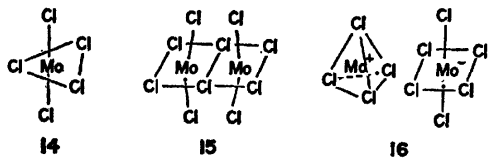

14 **15** **16**

On the other hand, as to the minor formation of *trans*-dichlorides, **16** seems to be the attacking species, reacting with olefin to give carbonium ion intermediate(**17**) followed by the attack of chloride ion (Scheme 5). Formation of the dichlorides, **4**—**7** and **10**—**12**,

$$\underset{\mathbf{16}}{>C{=}C<} \longrightarrow \underset{\mathbf{17}}{[>C(Cl)-C^+<]MoCl_6^-} \rightarrow \mathbf{1}(trans) \qquad (5)$$

could also be explained by this scheme where the intermediate carbonium ions would be nonclassical ones; *i.e.*, **18** for **4**—**7** and **19** for **10**—**12**. By comparison of the results of the chlorination by $MoCl_5$ with those by $SbCl_5$, the two following differences are evident. Selectivity for *cis*-chlorination is higher in the former case; *exo-cis*-dichlorides are formed preferably from norbornene and norbornadiene in the former, but none in the latter where the reaction was carried out at various concentrations of $SbCl_5$. The results might suggest that $MoCl_5$ mainly exists in the form of **14** or **15** in CCl_4, while in the case of $SbCl_5$ the more polarized form of **15** seems to have a rather large contribution in the same solvent. The difference could be attributed to the stronger Lewis acidity (the ability of the chloride ion abstraction from another molecule) of $SbCl_5$ than $MoCl_5$.

18 **19**

As to a source of hydrogen chloride which may add to olefin to give **2**, two possibilities are conceivable; the decomposition of $MoCl_5$ to $MoOCl_3$ and HCl[8] by moisture, and hydride ion abstraction by $MoCl_5$ from olefin to give the molybdenum salt of allylic cation, $MoCl_3$, and hydrogen chloride, as was proposed in the case of the reaction with $SbCl_5$.[4] The former possibility does not seem to be important, since even in a careful experiment under N_2 in a dried condition the formation of **2** was observed, its amount being unaffected. Moreover, if hydrogen chloride arises only by the hydrolysis of $MoCl_5$, the amount of **2** in Run 8 (Table 1) should be larger than that in Run 6, since the time before the addition of olefin is much longer in Run 8 than in Run 6. In order to ascertain the latter possibility, we attempted the reaction of dihydroanthracene with $MoCl_5$ in CCl_4 just as in the case of $SbCl_5$.[13] Formation of anthracene was observed (see Experimental), although it was impossible to isolate hexachloromolybdate salt of 9-anthracenium cation. This shows that the molybdenum salt such as **20** can exist in solution (Scheme 6) by considering the reported observation using $SbCl_5$,[13] and consequently that $MoCl_5$ can abstract the hydride ion from certain organic compounds. In the chlorination of cyclohexene and octenes, resinous products were always obtained, probably because of the formation of dienes by elimination of hydrogen from olefin as described in scheme 6, and their polymerization. The reaction of 1,3-cyclooctadiene with $MoCl_5$ readily gave the polymerized product under the same conditions. We thus propose that the important source of hydrogen chloride is the hydride ion abstraction from allylic position of olefins by $MoCl_5$.

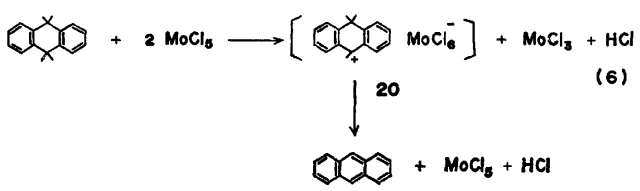

Mixed Halogenation of Olefins and Aromatic Halogenation. Bromochlorination and chloroiodination of olefins[14a] and the aromatic halogenation[14b] were carried out by using mixtures of antimony chlorides and halogens in

TABLE 1. CHLORINATION OF OLEFINS BY MOLYBDENUM(V) CHLORIDE IN CCl_4 (CCl_4 50 ml)

Run	Olefin	mmol	$MoCl_5$ (mmol)	Temp. (°C)	Time (hr)	Products, mmol				Ratio of *cis*- to *trans*- add.
						1			2	
						cis-add.	*trans*-add.	total yield, %[a]		
1	*trans*-2-Butene	75	1.4	20	0.33	0.65[b]	0.06[c]	51	0	10.8
2	*trans*-2-Butene	80	2.3	74	0.33	0.81[b]	0.15[c]	85	0	12.1
3	*cis*-2-Butene	70	1.6	21	0.25	0.51[c]	0.09[b]	38	0	5.7
4	*cis*-2-Butene	50	2.0	74	0.33	1.57[c]	0.27[b]	92	0	5.8
5	*cis*-2-Octene	11	2.4	20	10	0.39[d]	0.08[e]	20	2.2	4.9
6	Cyclohexene	20	1.6	22	2	0.46[f]	0.04[g]	32	1.1	11.5
7	Cyclohexene	26	1.2	22	10	0.64[f]	0.06[g]	58	1.4	10.7
8[h]	Cyclohexene	20	1.0	22	2	0.68[f]	0.16[g]	84	0.6	4.3
9[i]	Cyclohexene	10	1.2	22	2	0.58[f]	0.05[g]	53	1.0	11.6
10	1-Octene	50	1.6	18	10	0.92		57	2.1	—

a) Based on $MoCl_5$ and the stoichiometry shown in Scheme 4. b) *dl*. c) *meso*. d) *erythro*. e) *threo*. f) *cis*. g) *trans*. h) Cyclohexene was added after stirring a solution of $MoCl_5$ for 10 hr. i) Solvent, CH_2Cl_2.

TABLE 2. BROMOCHLORINATION AND CHLOROIODINATION WITH $MoCl_5$ (solvent, CCl_4 50 ml; at 25 °C for 0.5 hr)

Olefiin	mmol	$MoCl_5$ (mmol)	X_2 (mmol)	Product	Yield[a] (%)
Cyclohexene	10	2.0	Br_2 2.0	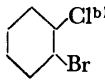	63[c]
Cyclohexene	12	1.7	I_2 8.5	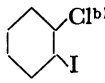	37
trans-2-Butene	32	2.0	I_2 2.2	$CH_3CHClCHICH_3$[d]	33
cis-2-Butene	43	2.0	I_2 2.1	$CH_3CHClCHICH_3$[e]	49

a) Based on $MoCl_5$ and the stoichiometry shown in Scheme 7. b) *trans*. c) Other products; *cis*- and *trans*-1,2-dichlorocyclohexane (16% and 7%), *trans*-1,2-dibromocyclohexane (1%), and chlorocyclohexane (0.34 mmol). d) *erythro*. e) *threo*.

TABLE 3. AROMATIC BROMINATION AND IODINATION BY $MoCl_5$

(ArH 50-70 mmol; $MoCl_5$ 1.7-2 mmol; halogen 2 mmol; solvent, CCl_4 50 ml)

Substituent in ArH	Halogen	Temp. (°C)	Time (hr)	Yield[a] (%)	Isomer distribution of ArX[b] (%)	
					o-	*p*-
H	Br_2	21	1	93	—	—
CH_3	Br_2	25	0.5	92	26	74[c]
Cl	Br_2	76	1	88	12	88[d]
Br	Br_2	76	1	87	12	88[d]
H	I_2	76	3	93	—	—
CH_3	I_2	76	1	77	52	48[c]
Cl	I_2	76	3	73	16	84[d]
Br	I_2	76	3	68	16	84[d]

a) Based on halogen and the stoichiometry shown in Scheme 8. b) *meta*- <1%. c) Determined by NMR. d) Determined by glc.

TABLE 4. COMPETITIVE HALOGENATION

(benzene 100 mmol; toluene 20 mmol; halogen 2 mmol; $MoCl_5$ 2 mmol; solvent 50 ml)

Halogenating agent	Solvent	k_T/k_B	*o*/*p* ratio
(a) Bromination[a]			
Br_2+MoCl_5	CCl_4	349	0.37
Br_2+MoCl_5	$ClCH_2CH_2Cl$	28	0.67
(b) Iodination[b]			
I_2+MoCl_5	CCl_4	111	1.07

a) At 25 °C. b) At 76 °C.

$$2\,\rangle C{=}C\langle + MoCl_5 + X_2 \rightarrow 2\,\rangle C(X)-C\langle(Cl) + MoCl_3 \qquad (7)$$

$$2\,ArH + MoCl_5 + X_2 \rightarrow 2\,ArX + MoCl_3 + 2HCl \qquad (8)$$

CCl_4 or CH_2Cl_2 as solvent.[14a] We found that similar reactions occurred by using $MoCl_5$ instead of $SbCl_5$. The reactions of olefins with a mixture of $MoCl_5$ and Br_2 or I_2 gave *trans*-bromochloro- or chloroiodo-alkanes respectively according to the stoichiometry shown in scheme 7 (Table 2), and the nuclear halogenation of benzene, toluene, halobenzenes occurred under similar conditions by use of aromatic compounds as substrates instead of olefins (Scheme 8 and Table 3). From a synthetic view point, however, the reactions using $MoCl_5$ were inferior to those with $SbCl_5$: The yield in the mixed halogenation was lower, the bromochlorination was accompanied by side reactions, the selectivity in aromatic halogenation was lower, and the aromatic compounds with electron-withdrawing groups such as nitrobenzene and ethyl benzoate could not be halogenated. In the reactions (Schemes 7 and 8),

the mixed halogens such as BrCl and ICl may be formed *in situ*, and the k_T/k_B value and the *o*/*p* ratio in the competitive halogenation (Table 4) suggest that the attacking species is not Br^+ or I^+ but the mixed halogen itself activated by $MoCl_5$, as in the reaction with $SbCl_5$.[14b] The larger k_T/k_B value and smaller *o*/*p* ratio in the $MoCl_5$ case than in the $SbCl_5$ case show that $MoCl_5$ is a weaker Lewis acid than $SbCl_5$ in line with the results of Friedel-Crafts aromatic acylation.[15]

Experimental

Commercial *trans*-2-butene(contains 1% of the *cis*-isomer) and *cis*-2-butene(contains 2.4% of the *trans*-isomer) were used without further purification. All the other organic substrates and solvents were purified by distillation before use. Commercial $MoCl_5$ (99% pure), Br_2, and I_2 were used without purification.

All the reactions were carried out by the method reported previously[4,14] by using $MoCl_5$ in the place of $SbCl_5$ or $SbCl_3$. Identification of the products in Tables 1, 2, and 3 except for 2-chloro-3-iodobutanes was described previously.[4,14]

Reaction of Norbornene with $MoCl_5$. To a solution of $MoCl_5$ (0.345 g, 1.26 mmol) in CCl_4(50 ml) was added norbornene (0.375 g, 3.99 mmol) at 25 °C and the resulting mixture was stirred for 2 hr under N_2. Aqueous NaOH was then added to stop the reaction. After the usual work-up, the organic layer was evaporated to *ca.* 20 ml. Acetone was added to give a small amount of white organic precipitates of norbornene polymer which were filtered off. The filtrate was analyzed by glc and found to contain **3** (0.664 mmol), **4**(0.006 mmol), **5**(0.035 mmol), **6**(0.068 mmol), **7** (0.060 mmol), and **8**(0.352 mmol) as organic products. The yield of the sum of **4**—**8** was 41.5% based on $MoCl_5$ charged. The identification of **4**—**7** was reported in a previous paper.[4] An authentic sample of **3** for glc was prepared by the method using norbornene and hydrogen chloride.[16] **8** was isolated from the combined distillates of several runs by preparative glc, its NMR spectrum being identical with the reported one.[10,17]

Reaction of Norbornadiene with $MoCl_5$. A similar reaction to that described above by using $MoCl_5$ (2.0 mmol) and norbornadiene (5.1 mmol) in CCl_4 (100 ml) gave **9**(0.86 mmol), **10**(0.088 mmol), **11**(0.040 mmol), **12**(trace), **13**(0.273 mmol), and a slight amount of norbornadiene polymer. The yield of the sum of **10**—**13** was 20.1%. Identification of the products was carried out as follows. Authentic samples of **9** and **12** for glc were prepared by the reported methods from the reactions of Cl_2 with norbornene[18] and norbornadiene,[10] respectively. NMR spectrum of **12** which was isolated by preparative glc was identical with the reported one.[19] Each of **10**, **11**, and **13** was isolated from the combined distillates of several runs by preparative glc. Each NMR spectrum was identical with the reported one.[19,20]

Reaction of Dihydroanthracene with $MoCl_5$. To a solution of $MoCl_5$ (0.52 g, 1.88 mmol) in CCl_4 (80 ml) was added dihydroanthracene (0.153 g, 0.86 mmol) dissolved in CCl_4 (20 ml) at 25 °C and the resulting mixture was stirred for 1 hr under N_2. Aqueous $NaHCO_3$ was then added. The organic layer was separated, washed with water, dried over Na_2SO_4, and concentrated to *ca.* 20 ml which was revealed by glc to contain 0.31 mmol of unreacted dihydroanthracene and 0.34 mmol of anthracene. A similar reaction by using $MoCl_5$ (2.03 mmol) and dihydroanthracene (1.02 mmol) for 5 hr gave 0.38 mmol of anthracene.

erythro- *and* threo-*2-Chloro-3-iodobutanes.* *trans*-2-Butene (2.2 g, 39.2 mmol) was bubbled at 25 °C for 30 min under stirring into a solution of CH_3CN(50 ml) containing anhydrous $CuCl_2$(1.46 g, 10.9 mmol) and I_2(2.83 g, 11.1 mmol). Glc analysis of ether extract after the usual work-up of the reaction mixture showed the presence of 15.8 mmol of *erythro*-2-chloro-3-iodobutane(72% yield) as porduct. Distillation gave 2.1 g of pure compound; bp 55.5 °C/18 mmHg(lit,[21] bp 34.8—35.3 °C/5 mmHg). NMR ($CDCl_3$) δ 1.68(d. 3H, J=6.5 Hz), 2.01 (d, 3H, J=6.5 Hz), 3.98 (quintet 1H, J=6.5 Hz), 4.28(quintet 1H, J=6.5 Hz).

A similar reaction of *cis*-2-butene(41 mmol) with $CuCl_2$ (10 mmol) and I_2(10.8 mmol) gave *threo*-isomer in 61% yield. Distillation gave 1.2 g of pure compound; bp 58—58.5 °C/18 mmHg (lit,[21] bp 33.2—33.5 °C/4 mmHg). NMR($CDCl_3$) δ 1.62(d, 3H, J=6.5 Hz), 1.93(d. 3H, J=6.5 Hz), 4.11(m. 1H), 4.49(m. 1H).

Analytical Instruments. The NMR spectra were determined by means of a Varian A-60 spectrometer in $CDCl_3$ and CCl_4 using TMS as an internal standard. Glc analysis was carried out with two Shimadzu apparatuses 5APTF and 4BMPF[EGSS-X(15%)-Chromosorb-W(3m), PEG 6000 (25%)-Chromosorb-W(3m), and Apiezon-L (30%)-Celite (1m) columns; carrier gas, N_2].

References

1) R. C. Fahey, "Topics in Stereochemistry," Vol. 3, ed. by E. L. Eliel and N. L. Allinger, Interscience, New York (1968), p. 265—278.
2) T. Koyano, This Bulletin, **43**, 1439 (1970).
3) M. Devillier and H. Bodot, *Bull. Soc. Chim. Fr.*, **1972**, 227.
4) S. Uemura, A. Onoe, and M. Okano, This Bulletin, **47**, 692 (1974).
5) a) B. Aronheim, *Chem. Ber.*, **8**, 1400 (1875). b) P. Kovacic and R. M. Lange, *J. Org. Chem.*, **30**, 4251 (1965).
6) C. Miniscloux, G. Martino, and L. Sajus, *Bull. Soc. Chim. Fr.*, **1973**, 2179.
7) F. A. Cotton and G. Wilkinson, "Advanced Inorganic Chemistry," 3rd Ed., Interscience, New York (1972), p. 958—959.
8) J. W. Mellor, "A Comprehensive Treatise on Inorganic and Theoretical Chemistry," Vol. 11, Longmans, London (1930), p. 625.
9) T. Oshika and H. Tabuchi, This Bulletin, **41**, 211 (1968).
10) S. Masson and A. Thuillier, *Bull. Soc. Chim. Fr.*, **1969**, 4368.
11) I. M. Pearson and C. G. Garner, *J. Phys. Chem.*, **65**, 690 (1961).
12) M. L. Larson, *J. Amer. Chem. Soc.*, **82**, 1223 (1960).
13) J. Holmes and R. Pettit, *J. Org. Chem.*, **28**, 1695 (1963).
14) a) S. Uemura, A. Onoe, and M. Okano, This Bulletin, **47**, 143 (1974). b) S. Uemura, A. Onoe, and M. Okano, *ibid.*, **47**, 147 (1974).
15) O. C. Dermer and R. A. Billmeier, *J. Amer. Chem. Soc.*, **64**, 464 (1942).
16) H. Kwart and R. K. Miller, *ibid.*, **78**, 5010 (1956).
17) M. L. Poutsma, *ibid.*, **87**, 4300 (1965).
18) J. D. Roberts, F. O. Johnson, and R. A. Carboni, *ibid.*, **76**, 5692 (1954).
19) R. Hüttel, H. Reinheimer, and K. Nowak, *Chem. Ber.*, **101**, 3761 (1968).
20) D. D. Tanner and G. C. Gidley, *J. Org. Chem.*, **33** 43 (1968).
21) H. J. Lucas and H. K. Garner, *J. Amer. Chem. Soc.* **72**, 2145 (1950).

The Thermal Polycondensation of Glycine in the Presence of Urea

Yasuaki KŌZAI, Yoshiyuki IKEDA, and Masakazu YOSHIDA

Department of Chemistry, Faculty of Science, Kōnan University, Okamoto, Higashinada-ku, Kōbe 658

(Received May 29, 1974)

After the discovery of the polycondensation of glycine to form the glycine oligomer by heating in the presence of urea in a sealed tube, we investigated in order to establish the optimum reaction conditions as well as to study the reaction mechanism. The optimum conditions are attained when a mixture of 0.0133 mol (1 g) of glycine and 0.0016 mol (0.1 g) of urea is heated at about 160 °C for 20—30 hr. Under these conditions, an oligomer, composed of glycine units, with a polymerization degree of 17—18 is obtained with a 50—52% yield. The mechanism of oligomer formation is considered to be as follows: first, the urea is melted and part of it is used for converting the glycine to the corresponding amide. The glycinamide thus formed and the glycine dissolve locally in the molten urea, resulting in condensation between them. A repetition of the condensation leads to longer peptide chains.

The thermal polycondensation of glycine has long been investigated. Oligomers of glycine are formed by heating in the presence of glycerine,[1] the hippuric ester,[2] and mineral acids.[3] Recently, Oró and and Guidry[4] obtained the glycine oligomer with a polymerization degree of 12—18 by heating glycine in the presence of aqueous ammonia at 140—160 °C in a sealed tube, and Okamoto and Nakahara[5] reported that polyglycine with a high molecular weight was obtained by heating glycine in phosphoric acid.

The present authors also have investigated the thermal polycondensation of glycine for several years; so far they have obtained glycine oligomers with a polymerization degree of 10—20 by heating glycine in a sealed tube in the presence of water, inorganic acids, salts, and organic bases,[6] and organic acids.[7] We have also reported that the *N*-terminal of the oligomer thus obtained is acylated if organic acids are employed.

The authors chose urea as another possible effective polycondensation agent because it would not only act as a solvent, but would also be thermally decomposed into a biuret to evolve the NH_3 gas and would promote conversion to amide when heated with a carboxylic acid. They examined the thermal polycondensation of glycine in the presence of urea with a considerably high yield of the glycine oligomer. Then, some further examinations were made in order to establish the optimum reaction conditions and in order to clarify the reaction mechanism and the properties of the oligomer obtained. In this paper, the experimental data and results will be reported.

Experimental

Thermal Polycondensation. The sample, placed in a nitrogen-filled sealed tube (I.D., 1 cm; length, about 25 cm) was heated in a temperature-controlled oil bath at various temperatures for various periods of time. After the heating, the content of the tube was taken out and washed well with hot water. Then the residue was dialyzed for 24 hr in water which had been treated by an ion-exchanger and dried in a vacuum dessicator to obtain the glycine oligomer. Although the hot water contained a certain amount of unchanged glycine and a glycine oligomer with a polymerization degree of below 4, no attempt has been made to examine them.

Measurements. The average polymerization degree of the oligomer was determined by the Sōrensen formol titration method (*C*-terminal determination) and the Van Slyke amino-nitrogen determination method (*N*-terminal determination) after the oligomer had been dissolved in 50% aqueous calcium chloride.

The IR spectra were measured by means of the Hitachi EPI-S2 infrared spectrophotometer.

Results and Discussion

Reaction Conditions and Properties of Oligomer. In order to examine the effect of the amount of added urea on the thermal polycondensation of glycine, a a given amount of urea (0—0.01 mol) was added to 0.0133 mol (1 g) of glycine, after which the mixture was heated at a constant temperature (130—170 °C) for 20 hr. Figure 1 shows the results. The optimum amount of urea depends upon the heating temperature. An excess of urea leads to lower yields of the oligomer. In our experiments, the highest yield of the oligomer was obtained when the reaction mixture was heated at about 160 °C in the presence of 0.0016 mol of urea. A pale yellow oligomer was obtained in a yield of about 51%. The relationship between the amount of urea and the polymerization degree of the oligomer is shown in Fig. 2. This shows that, as the amount of urea increases, the polymerization degree of the oligomer grows higher at the *C*- and *N*-terminal determinations, but the difference between them gradually

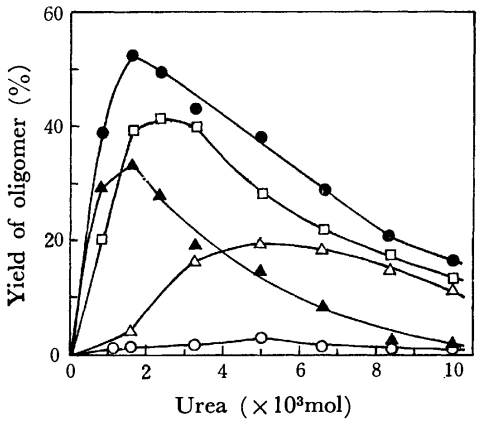

Fig. 1 Effect of the amount of urea on the thermal polycondensation of glycine.
Glycine: 0.0133 mol(1 g), Urea: 0-0.01 mol, Temperature: 130-170°C, Time: 20hr.
○: 130°C, △: 140°C, □: 150°C, ●: 160°C, ▲: 170°C

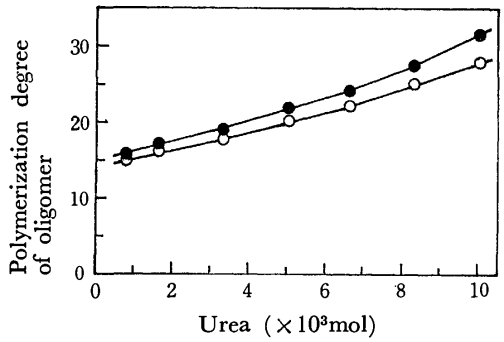

Fig. 2 Relation between polymerization degree of oligomer and the amount of urea on the thermal polycondensation of glycine.
Glycine: 0.0133 mol(1 g), Urea: 0-0.01 mol, Temperature: 160°C, Time: 20 hr.
○: *C*-terminal determination, ●: *N*-terminal determination

becomes greater and the polymerization degree in the latter case indicates a more or less higher value. This seems to be due to an irreversible decomposition of the glycine oligomer, judging from the facts that the reaction product in the sealed tube turned black or brown with urea concentrations higher than 0.005 mol, that the oligomer taken out of the tube was yellowish brown or brown, and that a reduction was observed in the yield of the oligomer.

Next, in order to examine the effects of the heating temperature and heating time, 0.0133 mol (1 g) of glycine and 0.0016 mol (0.1 g) of urea were mixed and heated to 140—180 °C for 0—100 hr. Figure 3

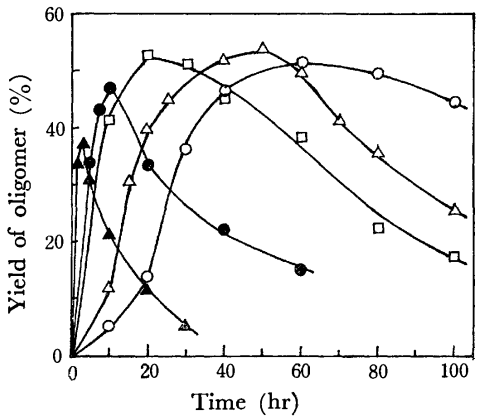

Fig. 3 Effects of heating temperature and heating time on the thermal polycondensation of glycine in the presence of urea.
Glycine: 0.0133 mol(1 g), Urea: 0.0016 mol(0.1 g).
○: 140°C, △:150°C, □: 160°C, ●: 170°C, ▲: 180°C

shows the results. According to the figure, the yield of the oligomer at each heating temperature increases with the heating temperature to reach a maximum. A higher temperature emphasizes this trend, but decreases the maximum yield of the oligomer. The relations between the heating temperature and the heating time for the yields higher than 50% are as follows:

Temperatures	Heating times
140 °C	60—70 hr
150 °C	40—60 hr
160 °C	20—30 hr

The polymerization degree of the oligomer obtained under these conditions and that of the oligomers which provided the maximum yields at 170 °C and 180 °C were measured by means of the *C*- and *N*-terminal determinations. The results are tabulated in Table 1. This table shows that the polymerization degrees increase with the heating temperatures. When the heating temperature reaches 170 °C, however, a gradual deviation between the values obtained by the *C*- and *N*-terminal determinations becomes significant. As is shown in Fig. 4, a similar trend can be observed in the relations between the heating time and the polymerization degree of the oligomer at 160 °C. As elevated heating temperatures and extented heating times decreased the yields of the oligomer, as the mixtures turned dark, as the internal pressure of the sealed tube increased, and as CO_2 gas was detected in the NH_3-rich gas, an irreversible decomposition of the glycine oligomer might occur, as has been mentioned previously.

Table 1. Relation between heating temperature and polymerization degree of glycine oligomer
Glycine: 0.0133 mol (1 g), Urea: 0.0016 mol (0.1 g)

Heating temperature (°C)	Heating time (hr)	Polymerization degree of oligomer	
		C-terminal determination	*N*-terminal determination
140	60	11.0	12.0
150	50	13.2	13.8
160	20	16.5	17.0
170	10	18.1	20.2
180	3	19.4	22.5

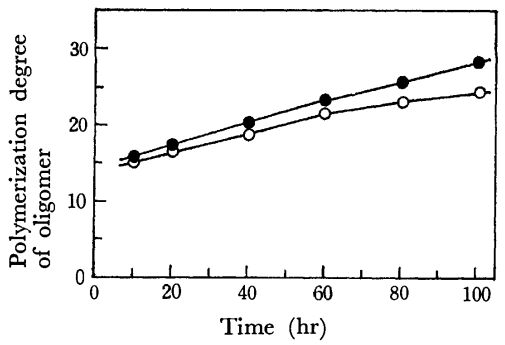

Fig. 4 Relation between polymerization degree of oligomer and heating time.
Glycine: 0.0133 mol (1 g), Urea: 0.0016 mol (0.1 g), Temperature: 160°C.
○: *C*-terminal determination, ●: *N*-terminal determination

From the experimental results so far obtained, it can be concluded that the optimum conditions for the polycondensation of glycine in the presence of urea occur when a mixture of 0.0133 mol (1 g) of glycine and 0.0016 mol (0.1 g) of urea is heated at 160 °C for

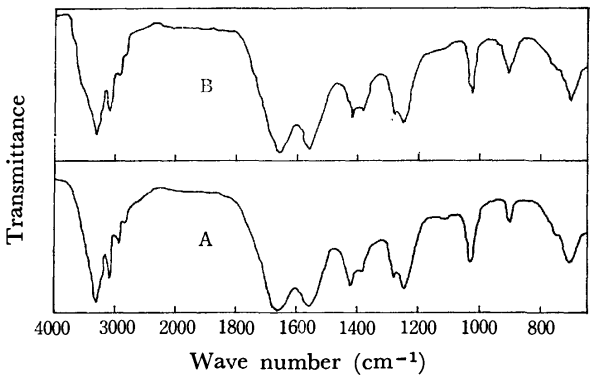

Fig. 5 Infrared absorption spectra (KBr).
A: Glycine oligomer obtained in the presence of urea,
B: Glycine oligomer obtained in the presence of water.

20—30 hr, with the polymerization degree of 17—18 and a yield of 50—52%. The oligomer thus formed is a pale yellow powder. It is soluble in concentrated aqueous solutions of calcium chloride, lithium bromide, or phosphoric acid, as well as in trichloroacetic acid, while it is very slightly soluble or insoluble in ordinary organic solvents and slightly soluble in an alkaline aqueous solution, presenting a distinct color change in a biuret reaction. The substance is influenced by heating in such a way that it begins to discolor at 230 °C, turns brown at 260 °C, and is completely carbonized at 280 °C. Furthermore, as is shown in Fig. 5, the IR spectrum of the oligomer found in the presence of urea coincides with that of the glycine oligomer obtained in the presence of water;[6] it showed typical peptide absorptions at 3300, 3070, 1648, and 1256 cm^{-1}, and a specific absorption at 1030 cm^{-1} based on the -Gly-Gly-connection. From the spectral analysis, it may be considered that the oligomer is composed of a single glycine unit.

Reaction Mechanism. As glycine undergoes polycondensation in the presence of urea with the evolution of CO_2, urea and glycine must first react with each other to form glycinamide. As is shown in Table 2, the polycondensation of glycine and glycinamide does not take place in the absence of glycerine, but the polycondensation of glycinamide alone does. However, a short heating treatment of the two substances in glycerine results in polycondensation between them, and through repeated condensation reactions, the peptide chains become longer with a considerably high yield of the glycine oligomer. Accordingly, urea may be considered to act as a solvent, just like glycerine, as well as converting glycine to glycinamide. Likewise, the use of a biuret instead of urea seems to give almost the same polycondensation results, as is shown in Table 3. Therefore, it may be considered that, as in the the case of urea, the biuret reacts with glycine to form glycinamide and acts as a solvent. Cyanuric acid, however, seems to show no such characteristics.

Table 2. Thermal polycondensation of glycine in the presence of glycinamide

Glycine: 0.0133 mol (1 g), Heating temperature: 160 °C

Reaction conditions			Oligomer		
				Polymerization degree	
Glycinamide (g)	Glycerine (g)	Time (hr)	Yield (g)	*C*-terminal determination	*N*-terminal determination
0.1	0	20	0.05	13.8	10.7
0.2	0	20	0.12	13.7	10.2
0.5	0	20	0.19	13.5	10.9
0.1	0.5	5	0.25	11.5	11.9
0.2	0.5	5	0.32	11.0	10.9
0.3	0.5	5	0.40	10.9	11.1
0	0.5	5	0.02	9.8	10.0

Table 3. Thermal polycondensation of glycine in the presence of biuret

Glycine: 0.0133 mol (1 g), Biuret: 0.97 mmol (0.1 g), Temperature: 160 °C

Heating time (hr)	Oligomer		
	Yield (%)	Polymerization degree	
		C-terminal determination	*N*-terminal determination
5	23.6	15.4	16.1
10	46.0	16.3	17.0
15	50.1	16.9	17.7
20	52.4	17.0	17.8
25	51.1	17.2	18.0
30	47.3	17.5	19.3
35	37.8	17.8	19.5

References

1) L. Balbiano and D. Trasiatti, *Ber.*, **33**, 1501 (1900); *ibid.*, **34**, 2323 (1901); L. C. Maillard, *Ann. Chim.*, **1**, 519 (1914); *ibid.*, **2**, 210 (1914).
2) T. Curtius and A. Benrath, *Ber.*, **37**, 1279 (1904).
3) A. B. Meggy, *J. Chem. Soc.*, **1953**, 851; *ibid.*, **1956**, 1444.
4) J. Oró and C. L. Guidry, *Arch. Biochem. Biophys.*, **93**, 166 (1961).
5) S. Okamoto and A. Nakahara, *Nippon Nogei Kagaku Kaishi*, **38**, 28 (1964).
6) H. Watanabe and Y. Kōzai, *Nippon Kagaku Zasshi*, **84**, 744 (1963).
7) H. Watanabe and Y. Kōzai, *ibid.*, **87**, 613 (1966); *ibid.*, **91**, 581 (1970).

Dopaquinone and Related Compounds. The Reaction with Cyclopentadiene

Yoshimori OMOTE and Toshihiko KOMATSU

Department of Chemistry, University of Tsukuba, Sakura, Niihari, Ibaraki 300-31

(Received June 6, 1974)

The trapping of *o*-quinones produced during the oxidation of 4-substituted catechols(I, R=CH_3, $CH_2CH_2CO_2H$, $CH_2CH_2NH_3Br$, $CH_2CH(NH_3Cl)CO_2CH_3$) in the presence of cyclopentadiene affords adducts, which are changed into 8-substituted 5,6-diacetoxy-1,4-dihydro-1,4-methanonaphthalenes(IV, R=CH_3, $CH_2CH_2CO_2H$, $CH_2CH_2NHCOCH_3$, $CH_2CH(NHCOCH_3)COCH_3$) by treatment with acetic anhydride-pyridine Dopaquinone (IIe) is trapped with cyclopentadiene, followed by acetylation and methylation with acetic anhydride–pyridine–methanol (13 : 2 : 2) to give the *N*-acetyl-2-(5,6-diacetoxy-1,4-dihydro-1,4-methanonaphthyl-8)-L-alanine methyl ester (IVd).

In a previous report we described the synthesis of dopaquinone protected by methylation and benzoylation.[1] However, free dopaquinone was labile to be isolated or trapped by *o*-phenylenediamine. We have continued to inquire into the method of trapping *o*-quinone[2] and have succeeded in proving the presence of free dopaquinone by trapping with cyclopentadiene.

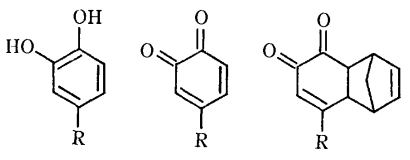

I II III

(a) R: CH_3, (b) R: $CH_2CH_2CO_2H$
(c) R: $CH_2CH_2NH_3Br$, (d) R: $CH_2CHCO_2CH_3$ (NH_3Cl)
(e) R: CH_2CHCO_2H (NH_2)

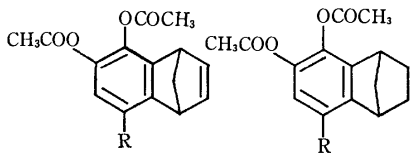

IV V

(a) R: CH_3, (b) R: $CH_2CH_2CO_2H$
(c) R: $CH_2CH_2NHCOCH_3$, (d) R: $CH_2CHCO_2CH_3$ ($NHCOCH_3$)

Results and Discussion

The UV spectrum with time intervals of the equimolar mixture of the *N*-benzoyl-DOPA methyl ester (I, R=$CH_2CH(NHCOC_6H_5)CO_2CH_3$) and *o*-chloranil indicates a decrease in *o*-chloranil absorption at 350 and 410 nm as well as an increase in a new absorption near 380 nm attributable to the formation of a new *o*-quinone (Fig. a). On the contrary, the spectral change of the mixture of dopamine hydrobromide(I, R=$CH_2CH_2NH_3Br$) and *o*-chloranil does not show any formation of the *o*-quinone in spite of the decrease in *o*-chloranil (Fig. b). It is known that DOPA and dopamine are easily oxidized into the corresponding indoline derivatives.[3] Consequently, a similar reaction seems to have occurred in the latter case.

For the purpose of trapping this intermediate, the reaction with cyclopentadiene was examined. Substituted *o*-benzoquinones(II) are known to give adducts(III) with cyclopentadiene.[2] Also, it is known that these adducts can be acetylated in the reaction mixture to give a stable catechol diacetate(IV).[2b,2c] These reactions were applied to the trapping of the *o*-benzoquinone. As a typical model experiment, 4-

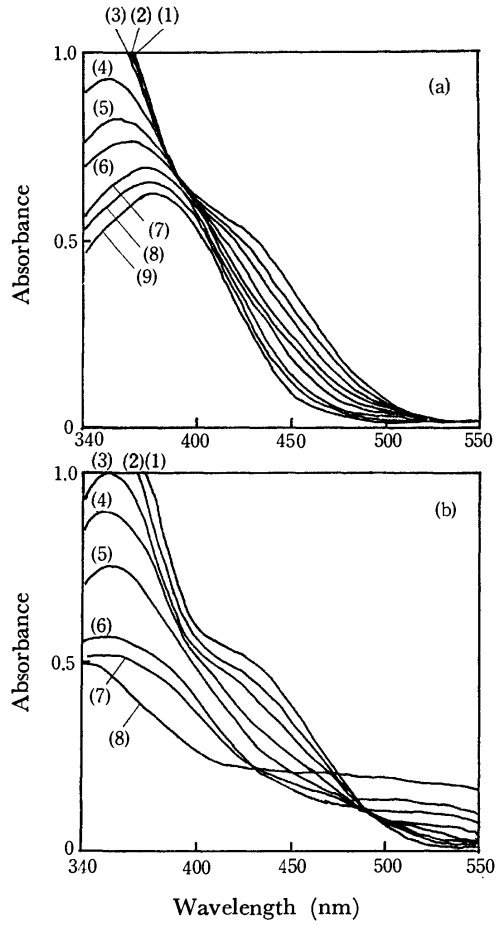

Fig. 1. Time-dependent UV and visible spectrum of the equimolar mixture of
(a) *N*-benzoyl-DOPA methyl ester and *o*-chloranil
(1) 2 min after addition of *o*-chloranil to the substrate; (2) 4 min; (3) 10 min; (4) 20 min; (5) 35 min; (6) 45 min; (7) 120 min; (8) 180 min; (9) 300 min.
(b) dopamine hydrobromide and *o*-chloranil
(1) 2 min after addition of *o*-chloranil to the substrate; (2) 5 min; (3) 30 min; (4) 45 min; (5) 105 min; (6) 200 min; (7) 280 min; (8) 20 hr.
conc. 5.00×10^{-4} mol/l in EtOH.

methylcatechol(Ia) was oxidized with *o*-chloranil in the presence of cyclopentadiene, the reaction mixture being warmed with acetic anhydride–pyridine to afford Compound IVa. The structure of IVa was confirmed by the NMR, IR, and UV spectra and elemental analysis. Furthermore, IVa was quantitatively hydrogenated to give Va.

Cyclopentadiene is known to give an adduct with *o*-chloranil,[4] but under the present experimental conditions it does not react with *o*-chloranil and only reacts selectively with the newly-formed *o*-quinones. The characteristic feature of this trapping method is that the labile adduct of an *o*-benzoquinone with cyclopentadiene is, without isolation, transformed into a stable compound by acetylation.

The trapping transformation is applied to the oxidation of dihydrocaffeic acid (Ib), and the IIb quinone is thus trapped in the form of an acetyl compound, IVb. The cyclic isomer of IIb, a lactone,[5] is not found. Next, the trapping of dopamine hydrobromide (Ic) was examined, Compound IVc was thus obtained. This is chemical proof of the dopaminequinone adduct with cyclopentadiene (IIIc). It is obvious that cyclopentadiene adds to IIc under conditions similar to those described above, without cyclization into an indoline derivative, the free amino group in IIc doing no harm to the trapping.

Finally, the trapping experiment was successful in giving Compound IVd from the DOPA methyl ester (Id) and IVd from DOPA itself. In the case of DOPA, the isolation of IV, R=$CH_2CH(NHCOC_6H_5)CO_2H$, is very difficult. Therefore, the isolation of IVd was carried out after the esterification of the carboxyl group with methanol.

Experimental

1,4-Dihydro-8-methyl-1,4-methanonaphthalene-5,6-diol Diacetate (IVa). *(a)*: An ethereal solution of *o*-chloranil (2.00 g) was slowly added to a solution of 4-methylcatechol (1.00 g) in 20 ml of ether with stirring under nitrogen at −78 °C. After the mixture had been stirred for 1 hr, cyclopentadiene (1 ml) was added, the mixture was then stirred for an additional 4 hr at −78 °C and for 12 hr at room temperature. After the evaporation of the solvent, a mixture of acetic anhydride (35 ml) and pyridine (1 ml) was added to the residue, and the mixture was heated at 80—90 °C for 2 hr. A precipitate of tetrachlorocatechol diacetate was then removed, and the filtrate was evaporated and chromatographed on silica-gel to yield 1.66 g (74%) of IVa; white solid (sublimed); mp 90—91 °C; UV λ_{max}^{EtOH} (ε): 271 (430) and 280(355) nm; NMR ($CDCl_3$): δ 2.20(s, 3H), 2.23(m, 2H), 2.25(s, 6H), 3.82(m, 1H), 3.95(m, 1H), 6.48(s, 1H), and 6.73(m, 2H); IR (KBr): 3000, 2930, and 1770 cm^{-1}. Found: C, 70.58; H, 5.97%. Calcd for $C_{16}H_{16}O_4$: C, 70.57; H, 5.92%.

(b) A solution of *o*-chloranil (400 mg) in THF (10 ml) was added to a mixture of Ia (200 mg) and cyclopentadiene (0.2 ml) in THF (10 ml) at −78 °C. After the evaporation of the solvent, the residue was treated as has been described in *(a)*.

(c) At room temperature, a solution of *o*-chloranil (600 mg) in THF was added to a mixture of Ia (300 mg) and cyclopentadiene (1 ml) in THF. After 5 hr stirring and the removal of the solvent, the residue was treated with acetic anhydride–pyridine to yield 544 mg of IVa (75%).

(d) A solution of cerium(IV) sulfate (1.27 g) in 20% aqueous sulfuric acid (20 ml) was added to a mixture of Ia (200 mg) and cyclopentadiene (1 ml) in THF (20 ml) under nitrogen at −5 °C. After having been stirred overnight at room temperature, the mixture was extracted with ethyl acetate, washed, dried, and treated with acetic anhydride–pyridine to give 179 mg of IVa (37%).

(e) An aqueous solution of hydrochloric acid(2M, 2 ml) was added to a solution of Ia (300 mg) and cyclopentadiene (1 ml) in THF (30 ml), a solution of *o*-chloranil (600 mg) was then dropped into the mixture at room temperature, and the mixture was stirred for 5 hr. The yield was 483 mg (66.5%).

3-(5,6-Diacetoxy-1,4-dihydro-1,4-methanonaphthyl-8-)propionic Acid(IVb). Dihydrocaffeic acid (500 mg) gave 508 mg (56%) of IVb by the method (*b*) described in the preceding section; white needles from benzene; mp 131—132 °C; UV λ_{max}^{EtOH} (ε): 273(800) and 280(760) nm; NMR($CDCl_3$): δ 2.23(s, 3H), 2.25(m, 2H), 2.27(s, 3H), 2.4—3.0(m, 4H), 3.83(m, 1H), 4.02(m, 1H), 6.55(s, 1H), 6.75(m, 2H), and 7.77 (broad s, 1H, D_2O exchangeable); IR (KBr): 3200—3500, 1765, and 1700 cm^{-1}. Found: C, 65.39; H, 5.57%. Calcd for $C_{18}H_{18}O_6$: C, 65.44; H, 5.49%.

N-Acetyl-2-(5,6-diacetoxy-1,4-dihydro-1,4-methanonaphthyl-8-)ethylamine(IVc). Dopamine hydrobromide(Ic, 500 mg) gave 304 mg (42%) of IVc by the (*c*) method except that methanol was used instead of THF; glassy solid; NMR ($CDCl_3$): δ 1.90(s, 3H), 2.25, 2.30(s, 3H×2, and 2H), 2.75 (t, J=7 Hz, 2H), 3.28(t, J=7 Hz, 2H), 3.85(m, 1H), 4.00 (m, 1H), 6.30(broad m, 1H, D_2O exchangeable), 6.50 (s, 1H), and 6.75(m, 2H); IR (KBr): 3400, 3300, 2950, 1770, and 1650 cm^{-1}.

The N-Acetyl-2-(5,6-diacetoxy-1,4-dihydro-1,4-methanonaphthyl-8-)-L-alanine Methyl Ester(IVd) from DOPA methyl Ester. DOPA methyl ester hydrochloride (Id, 1.00 g) gave 668 mg (41%) of IVd by the (*c*) method; glassy solid; NMR ($CDCl_3$): δ 1.77(s, 3H), 2.24 2.29(s, 3H×2, and 2H), 3.10(d, J=7 Hz, 2H), 3.68(s, 3H), 3.83(m, 1H), 3.97(m, 1H), 4.83(q, J=7 Hz, 1H), 6.23(broad d, J=7 Hz, D_2O exchangeable), 6.45(s, 1H), and 6.75(m, 2H).

N-Acetyl-2-(5,6-diacetoxy-1,4-dihydro-1,4-methanonaphthyl-8-)L-alanine Methyl Ester(IVd) from DOPA. DOPA (Ie, 500 mg) was dissolved in hydrochloric acid (2M, 2 ml) and diluted to 30 ml with THF, to this mixture a solution of *o*-chloranil (625 mg) in THF was then added under nitrogen at room temperature, followed by the addition of cyclopentadiene (2 ml). After stirring for 2 hr, the solvent was removed and the residue was placed in a mixture of methanol (20 ml), acetic anhydride (130 ml), and pyridine (20 ml). The mixture was heated with stirring at 90—100 °C for 1 hr. Then the solvent was removed, and precipitates of tetrachlorocatechol diacetate were separated by filtration. Ethyl acetate was added to the filtrate, which was then washed with water, dried over anhydrous sodium sulfate, and evaporated to afford a residue which was subsequently purified by column chromatography on silica-gel, and eluted by ethyl acetate–benzene. The yield was 140 mg (14%) of IVd.

1,2,3,4-Tetrahydro-8-methyl-1,4-methanonaphthalene-5,6-diol Diacetate(Va). The catalytic hydrogenation of IVa with platinum oxide in acetic acid gave Va quantitatively as colorless prisms from cyclohexane; mp 99—100 °C; UV λ_{max}^{EtOH} (ε): 266(290) and 273(250) nm; NMR ($CDCl_3$): δ 1.0—2.0(m, 6H), 2.26(s, 3H), 2.29(s, 6H), 3.32(m, 1H), 3.43(m, 1H), and 6.67(s, 1H); IR(KBr): 2950 and 1765 cm^{-1}. Found: C, 70.11; H, 6.60%. Calcd for $C_{16}H_{18}O_4$: C, 70.05; H, 6.61%.

N-*Acetyl-2-(5,6-diacetoxy-1,2,3,4-tetrahydro-1,4-methanonaphthyl-8-)-ethylamine(Vc)*. Colorless prisms from benzene; mp 140 °C; UV λ_{max}^{EtOH} (ε): 267(460) and 274(420) nm; ($CDCl_3$): δ 1.0—2.0(m, 6H), 1.96(s, 3H), 2.29(s, 3H), 2.31(s, 3H), 2.80(m, 2H), 3.3—3.6(m, 2H×2), 5.85(broad m, 1H, D_2O exchangeable), and 6.71(s, 1H); IR (KBr): 3250, 3070, 2960, 1770, and 1640 cm^{-1}. Found: C, 66.32; H, 6.63; N, 4.13%. Calcd for $C_{19}H_{23}O_5N$: C, 66.07; H, 6.71; N, 4.06%.

The N-*Acetyl-2-(5,6-diacetoxy-1,2,3,4-tetrahydro-1,4-methanonaphthyl-8-)-*L*-alanine Methyl Ester(Vd)*. Glassy solid; UV λ_{max}^{EtOH}: 267 and 274 nm; NMR ($CDCl_3$): δ 1.0—2.0(m, 6H), 1.97(s, 3H), 2.23(s, 3H), 2.28(s, 3H), 3.06(d, J=7 Hz, 2H), 3.46(m, 2H), 3.67(s, 3H), 4.81(broad q, J=7 Hz, 1H), 6.30(broad d, J=7 Hz, 1H, D_2O exchangeable), and 6.60(s, 1H); IR (KBr): 3400, 3300, 2970, 1770, 1750, and 1660 cm^{-1}; MS: *m/e* 403 (M^+).

References

1) Y. Omote, T. Hirama, and T. Komatsu, This Bulletin, **48**, 1957 (1974).

2) a) L. Horner and K. Sturm, *Ann.*, **597**, 1 (1955). b) F. J. Evans, H. S. Wilgus, III, and J. W. Gates, Jr., *J. Org. Chem.*, **30**, 1655 (1965). c) W. M. Horspool, J. M. Tedder, and Zia Ud Din, *Chem. Commun.*, **1966**, 775. d) M. F. Ansell, A. F. Gosden, and V. J. Leslie, *Tetrahedron Lett.*, **1967**, 4537.

3) a) J. D. Bu'Lock and J. Harly-Mason, *J. Chem. Soc.*, **1951**, 2248. b) N. Fischer and A. S. Dreiding, *Helv. Chim. Acta*, **53**, 1937 (1970) c) Y. Omote, Y. Fujinuma, K-T. Kuo, and N. Sugiyama, *Nippon Kagaku Zasshi*, **87**, 760 (1966).

4) L. Horner and W. Spietschka, *Ann.*, **579**, 159 (1953).

5) A. Kaiser, W. Koch, M. Scheer, and U. Wölcke, *Helv. Chim. Acta*, **53**, 1708 (1970).

Reactions of Group IV Organometallic Compounds. XXX.[1] Stepwise Addition of Isocyanates and Isothiocyanates with *N*-Trimethylstannyl(diphenylmethylene)amine

Hiroharu SUZUKI, Kenji ITOH,* Isamu MATSUDA, and Yoshio ISHII

Department of Synthetic Dhemistry, Faculty of Engineering, Nagoya University, Nagoya 464

(Received June 24, 1974)

Stepwise addition of two isocyanates to *N*-trimethylstannyl(diphenylmethylene)amine, $Ph_2C{=}NSnMe_3$, gives 3,4-dihydro-1,3-dialkyl-4,4-diphenyl-6-trimethylstannoxy-1,3,5-triazin-2(1*H*)-one (II) by a polar [4+2] cycloaddition of the 1/1 adduct and the second isocyanate. The isothiocyanate adducts of $Ph_2C{=}NSnMe_3$ react with either isocyanates or isothiocyanates to yield the corresponding consecutive insertion products (IV).

In a previous paper[2] on the insertion reaction of *N*-trimethylsilyl(diphenylmethylene)amine with isocyanates or isothiocyanates, it was reported that the amine with isocyanates in a 1/2 ratio yielded 3,4-dihydro-1,3-dialkyl-4,4-diphenyl-6-trimethylsiloxy-1,3,5-triazin-2(1*H*)-one by a polar [4+2] cycloaddition.

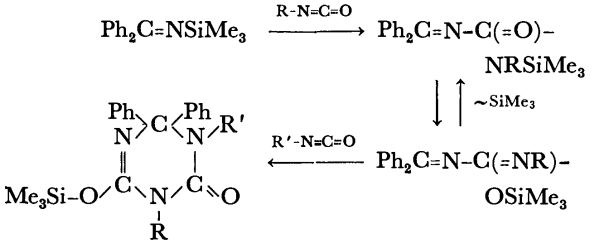

R=R'=Me and Ph

Several reactions of *N*-organostannyl(alkylidene)-amines have been reported. Harrison[3] found many insertion reactions of $Ph_2C{=}NSnBu_3$ with unsaturated bonds including isocyanates and isothiocyanates. We were interested in the fact that the Sn–O bond of aldehyde adducts added to isocyanates or isothiocyanates results in consecutive insertion products.

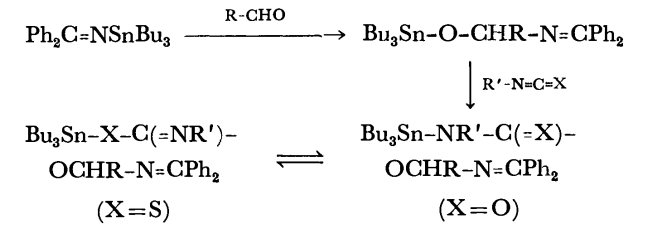

Lappert *et al.*[4] investigated various hydrogen abstraction, and insertion reactions of $R_2C{=}NSnMe_3$. They pointed out two aspects of the insertion reactions; (1) the N–H bond of trace $Ph_2C{=}NH$ showed a catalytic action, (2) the nucleophilic attack of the nitrogen atom was the primary step, resulting in a polar intermediate. This paper deals with the stepwise reactions of *N*-trimethylstannyl(diphenylmethylene)amine; $Ph_2C{=}N{-}SnMe_3$, with R–N=C=X (X=O and S), in order to determine whether the stepwise reaction is a polar [4+2] cycloaddition[2] or a consecutive insertion reaction.[3]

Results and Discussion

Structure of 1/1 Insertion Products. Equimolar reaction of $Ph_2C{=}NSnMe_3$ with R–N=C=X gave the corresponding insertion products, $Ph_2C{=}N{-}C(=X){-}NR{-}SnMe_3$ (1a—1e) in line with results reported.[3,4] Spectroscopic data for 1/1 insertion products are shown in Table 1.

The appearance of satellites of the methylamino proton signals in the case of Ia and Ib (R=Me) suggests that the trimethyltin group is attached to the nitrogen atom. However, the values of $J_{Sn-N-CH}$ (Ia, 24 Hz; Ib, 12 Hz) are much lower than those of $Me_3Sn{-}NMe_2$ (J^{117}=39.2 Hz and J^{119}=41.0 Hz).[5] The depression of the coupling constant is consistent with the weakening of the Sn–N bond by the coordination of the lone pair to tin atom.

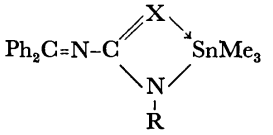

I: R=Me and Ph, X=O and S

This is strongly supported by the low frequency of the carbonyl stretching bands of the isocyanate adducts (Ia and Ic). It is reasonable to conclude that the coordination of the sulfur atom of Ib ($J_{Sn-N-CH_3}$= 12 Hz) is stronger than that of oxygen atom of Ia

TABLE 1. 1/1 ADDUCTS: $Ph_2C{=}N{-}C(=X){-}NR{-}SnMe_3$

Compound	R	X	Yield %	IR (cm^{-1})		NMR	
				$\nu_{C=N}$	$\nu_{C=O}$	τ_{CH_3-Sn} ($J^{117/119}$; Hz)	τ_{CH_3-N} ($J_{Sn-N-C-H}$)
Ia	Me	O	80	1627	1600	9.79 (55.5/57.0)[a]	7.47 (24.0)[d]
Ib	Me	S	80	1622		9.68 (54.8/56.5)[b]	7.38 (12.0)[d]
Ic[c]	Ph	O	97	1621	1589	9.73 (55.0/58.0)[a]	
Id	Ph	S	99	1616		9.60 (56.1/58.5)[b]	
Ie	PhCO	O	95	1626	1673[e] 1603	9.68 (55.5/58.0)[b]	

a) Benzene solution. b) Carbon tetrachloride solution. c) Prepared by Lappert *et al.*[4] d) The splitting of J^{119}Sn and J^{117}Sn was not clear. e) Absorption due to benzoyl group.

($J_{Sn-N-CH_3}$=24 Hz). Diphenylmethylenealkyl-ureas or thioureas, $Ph_2C{=}N{-}C(=X){-}NHR$, were obtained by the destannylation of Ia—Ie with ethanethiol. Their UV spectra showed $\pi\rightarrow\pi^*$ transition bands around 248—258 nm characteristic of the heterodiene linkage ($>C{=}N{-}\overset{|}{C}{=}N$).

Consecutive Reactions of 1/1 Adducts. The subsequent addition of the second heterocumulene to the 1/1 adducts can occur in two ways: a polar [4+2] cycloaddition yielding 3,4-dihydro-1,3-dialkyl-4,4-diphenyl-6-trimethylstannoxy-1,3,5-triazin-2(1*H*)-one(II). The destannylation of II giving hexahydro-1,3-dialkyl-4,4-diphenyl-1,3,5-triazin-2,4-dione (V); a consecutive insertion of the second heterocumulene into the Sn–N bond of the 1/1 adduct giving either of the two possible linear insertion products, III or IV. Both linear adducts III and IV afford the same *N,N'*-dialkylmethylenebiuret (VI) by destannylation.

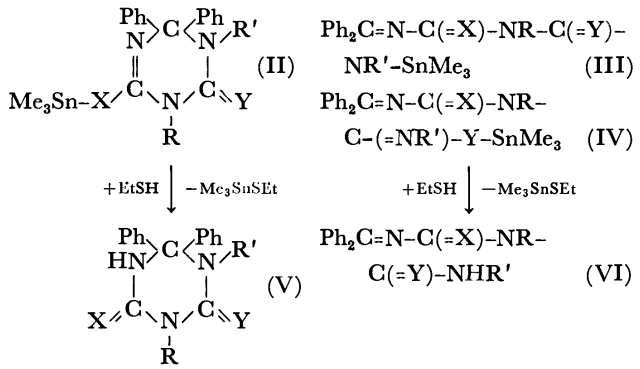

Both the two pathways are actually operating, and the primary heterocumulene component of 1/1 insertion reactions plays the most important role in controlling the subsequent reactions.

(a) Annelation Reactions of Isocyanate 1/1 Adducts: When the isocyanate 1/1 adduct (Ia or Ib) was treated with methyl or phenyl isocyanate, crystalline products were isolated in good yields. They were concluded to be 1/2 adducts by analyses, NMR and IR spectra. The destannylation of isolated 1/2 adducts proceeded quantitatively by means of ethanethiol. None of the destannylation products showed a $\pi\rightarrow\pi^*$ transition due to a heterodiene linkage, $>C{=}N{-}\overset{|}{C}{=}O$. This supports the cyclic structure (V: X=Y=O) and is not consistent with the linear structure (VI: X=Y=O). Much stronger evidence of the cyclic structure (V) was obtained from the mass spectra of the destannylation products. Two destannylation products (runs a and c) showed peaks due to $[Ph_2C{=}N{-}CH_3]^+$ (m/e=195) and $[Ph_2C{=}N{=}CH_2]^+$ (m/e=194). The appearance of these peaks suggests the direct bonding of diphenylmethylene with the alkylamino group (R'–N) introduced by the second isocyanate, and are explained by the cyclic structure (V). The destannylation product of run b (order of addition: methyl then phenyl isocyanate) showed M^+–MeNCO peak (m/e=300). The presence of M^+–MeNCO is fully consistent with structure (V), because fragmentation of the linear structure (VI) should occur from the terminal position (only M^+—PhNCO would appear; direct elimination of the central component M^+—MeNCO, not being detectable). The IR spectrum of run d is also consistent with the cyclic structure (V: R=R'=Ph, X=Y=O); the carbonyl stretching frequencies at 1730 and 1657 cm^{-1} were similar to those of 1,3,5-triazindiones (1720 and 1680 cm^{-1}).[6] Mixed mp analyses, IR, and NMR spectra were the same as those of authentic hexahydro-1,3-dialkyl-6,6-diphenyl-1,3,5-triazin-2,4-dione (V).[2] Thus, the consecutive insertion process, giving III or IV then VI, is excluded, and the annelation products of isocyanate 1/1 adducts with the second isocyanate are concluded to be 3,4-dihydro-1,3-dialkyl-4,4-diphenyl-6-trimethylstannoxy-1,3,5-triazin-2(1*H*)-one (IIa—IIe) by a polar [4+2] cycloaddition.

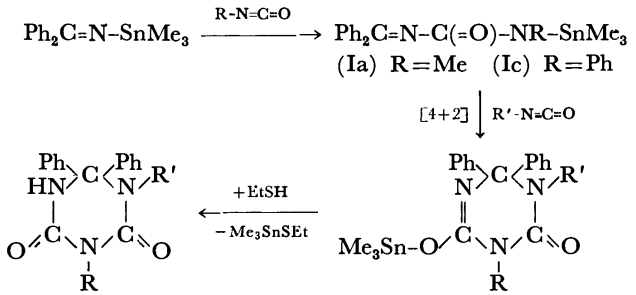

(Va) R=R'=Me
(Vb) R=Me, R'=Ph
(Vc) R=Ph, R'=Me
(Vd) R=R'=Ph

(IIa) R=R'=Me
(IIb) R=Me, R'=Ph
(IIc) R=Ph, R'=Me
(IId) R=R'=Ph

The treatment of IIa and IId with ethanethiol afforded the corresponding hexahydro-1,3-dialkyl-6,6-diphenyl-1,3,5-triazin-2,4-dione (Va—Vd) quantitatively. This method provides a synthetic route for the preparation of triazindiones with three different

Table 2. The [4+2] cycloaddition of isocyanate adducts; 3,4-dihydro-1,3-dialkyl-4,4-diphenyl-6-trimethylstannoxy-1,3,5-triazin-2(1*H*)-one (II) and their demetallation products; hexahydro-1,3-dialkyl-6,6-diphenyl-1,3,5-triazin-2,4-dione (V)

Run	R	R'	II					V[a]		
			Yield (%)	Mp (°C)	ν_{max} (cm^{-1})	τ_{CH_3-Sn}($J^{117/119}$)	τ_{CH_3-N}	Mp (°C)	$\nu_{C=O}$ (cm^{-1})	τ_{CH_3-N}
a	Me	Me	77	149.0—152.0	1688, 1621	9.89(56.0/58.0)	7.41 6.75	238.0—239.0[b]	1723, 1648[b]	7.29 7.03
b	Me	Ph	76	169.0—172.0	1686, 1624	9.83(54.5/57.0)	6.73	240.0—241.0	1720, 1674	6.93
c	Ph	Me	46	179.0—181.0	1692, 1630	9.90(55.5/57.5)	7.38	264.0—265.0	1729, 1663	7.22
d	Ph	Ph	96	166.0—167.0	1731, 1697	9.88(53.0/55.3)	—	215.0—216.0[b]	1730, 1657[b]	—

a) Formation of V by the destannylation of II was quantitative. b) Identical with values in Ref. 2.

substituents on the nitrogen atoms such as Vb and Vc. The yields and properties of these [4+2] cycloaddition products (IIa—IId) and their destannylation products (Va—Vd) are summarized in Table 2.

An atempt to react phenyl isothiocyanate with isocyanate 1/1 adducts (Ia and Ic) was unsuccessful, resulting in the recovery of starting materials. The less reactive phenyl isothiocyanate cannot add to 1/1 isocyanate adducts (Ia and Ic), since the nucleophilicity of the nitrogen atom in Ia or Ic is depressed by the electron-withdrawing group.

(b) Insertion Reactions of Isothiocyanate 1/1 Adducts: Further reactions of Ib or Id (isothiocyanate 1/1 adducts) with other isocyanates or isothiocyanates were found to proceed by a consecutive insertion reaction in a similar manner to those reported by Harrison.[3] The demetallation products of 1/2 adducts were concluded to be *N*-diphenylmethylene-*N'*,*N''*-dialkylthio- or dithiobiuret, which showed apparent $\pi\rightarrow\pi^*$ transitions due to the heterodiene linkage, >C=N–C=S, around 269~292 nm (log $\varepsilon\simeq4$). The fragmentation pattern of the destannylation products from the reaction of Ib with methyl isocyanate is consistent with the linear structure (VI), $[Ph_2C{=}N{-}C{=}S]^+$ (*m/e*=224), $[Ph_2C{=}N]^+$ (*m/e*=180), $[Ph_2C{=}N{-}C(=S){-}NMe]^+$ (*m/e*=253). Thus a further reaction of isothiocyanate adducts (Ib or Id) with either isocyanate or isothiocyanate should give the corresponding linear products(III or IV). No ^{117}Sn, or ^{119}Sn satellite band corresponding to the CH_3–N proton signal were observed in the NMR spectra of the products obtained in the case of runs e and f. Only linear structure (IV) is consistent with these spectroscopic properties.

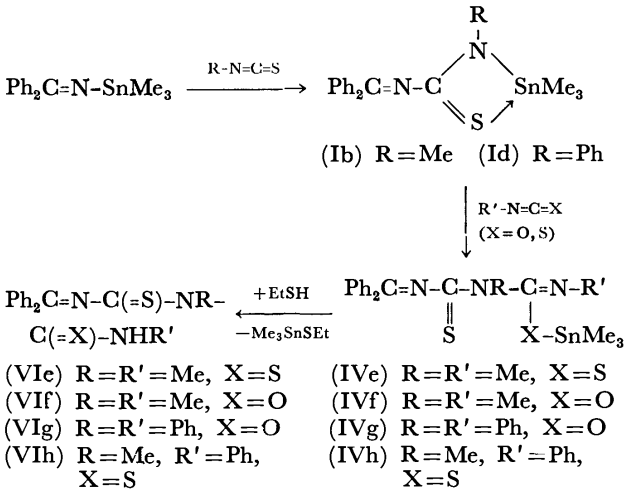

TABLE 3. CONSECUTIVE INSERTION OF ISOCYANATES AND ISOTHIOCYANATES TO ISOTHIOCYANATE 1/1 ADDUCTS

Run	R	R'	X	IV Yield (%)	IV Mp (°C)	IV ν_{max}[a] (cm^{-1})	IV τ_{CH_3-Sn} ($J^{117/119}$)[a]	IV τ_{CH_3-N}[a]	VI[e] Mp °C	VI $\nu_{C=O,\ C=N,\ C=S}$[b] (cm^{-1})	VI λ_{max}[c] (nm)	VI τ_{CH_3-N}[d]
e	Me	Me	S	84	158.0—160.0	1597, 1371	9.72(57.0/59.0)	6.93 6.31	242.0—244.0	1531, 1290	278	6.79 6.36
f	Me	Me	O	67	163.0—166.0	1683, 1603	9.76(55.0/57.0)	7.39 6.66	241.0—242.0	1692, 1533, 1296	269	7.20 6.65
g	Ph	Ph	O	100	165.0—166.0	1698, 1355	9.72(55.5/58.5)	—	252.0—254.0	1703, 1513, 1240	279	—
h	Me	Ph	S	80[f]	not isolated				213.0—215.0	1521, 1287	292	6.36
i	Ph	Me	S		no reaction							

a) Benzene solution. b) KBr disk. c) Ethanol solution. d) Deuterochloroform solution. e) The formation of VI was quantitative. f) Yield of VIh was 80% based on Ib.

TABLE 4. ANALYTICAL DATA[a,b]

Compd.	C (%)	H (%)	N (%)	Calcd for
Ia	54.08 (53.90)	5.63 (5.53)		$C_{18}H_{22}N_2OSn$
Ic	59.85 (59.65)	5.27 (5.22)		$C_{23}H_{24}N_2OSn$
Ie	58.78 (58.69)	5.05 (4.92)		$C_{24}H_{21}N_2O_2Sn$
IIa	58.63 (58.24)	5.80 (5.83)		$C_{20}H_{25}N_3O_2Sn+C_6H_6$
IVe	51.38 (51.18)	5.26 (5.27)		$C_{20}H_{25}N_3S_2Sn+(1/3)C_6H_6$
IVf	53.97 (53.82)	5.45 (5.50)		$C_{20}H_{25}N_3OSSn+(1/2)C_6H_6$
IVg	60.05 (60.22)	4.91 (4.89)		$C_{30}H_{29}N_3OSSn$
Vb	73.40 (73.93)	5.47 (5.36)	11.60 (11.76)	$C_{22}H_{19}N_3O_2$
Vc	74.09 (73.93)	5.50 (5.36)	11.60 (11.76)	$C_{22}H_{19}N_3O_2$
VIe	65.34 (65.54)	5.59 (5.50)	11.34 (11.46)	$C_{17}H_{17}N_3S_2+C_6H_6$
VIf	68.58 (68.54)	5.83 (5.75)	12.25 (11.99)	$C_{17}H_{17}N_3OS+(1/2)C_6H_6$
VIg	76.74 (77.16)	5.59 (5.30)	7.78 (8.18)	$C_{27}H_{21}N_3OS+C_6H_6$
VIh	67.07 (67.83)	5.00 (4.92)	10.56 (10.79)	$C_{22}H_{19}N_{19}N_3S_2$

a) Calculated values in parentheses. b) The demetallated products, Va and Vd, were identified with the authentic samples.

The consecutive insertion products of isothiocyanate 1/1 adducts [IVe—IVh] are summarized in Table 3.

(c) Mechanism of the Subsequent Reaction of the 1/1 Adducts: The drastic variation of the addition depending on the first component of the 1/1 adducts is illustrated by the following scheme.

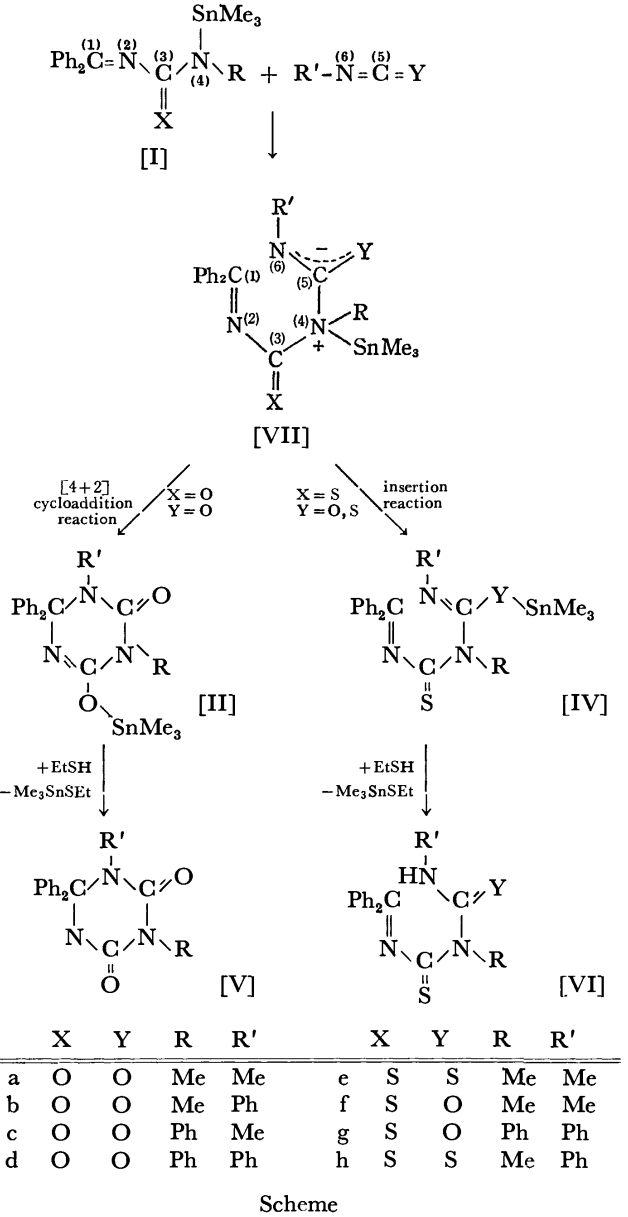

	X	Y	R	R′		X	Y	R	R′
a	O	O	Me	Me	e	S	S	Me	Me
b	O	O	Me	Ph	f	S	O	Me	Me
c	O	O	Ph	Me	g	S	O	Ph	Ph
d	O	O	Ph	Ph	h	S	S	Me	Ph

Scheme

The primary step of addition of the Sn–N bond to the heterocumulene was assumed to occur by the nucleophilic attack of the nitrogen atom[4] giving a zwitterionic intermediate(VII). When X=O (run a∼d) the positive charge on C(1) is enhanced largely by the conjugated carbonyl group and is stabilized by resonance with the two phenyl rings. Thus the nucleophilic ring closure occurs between N(6) and C(1). The following migration of the trimethylstannyl group from the ammonium nitrogen to the oxygen atom yields the 1,3,5-triazin-2(1*H*)-one derivatives [IIa∼IId]. The positive charge on C(1) is small when X=S (run e∼h), since the thiocarbonyl group is weakly electron-withdrawing as compared with the carbonyl group. Consequently, the anionic center(Y) captures the electrophilic trimethylstannyl group giving the corresponding consecutive insertion products [IVe∼IVh]. In Harrison's case,[3] the aldehyde adducts did not have an electron-withdrawing group at C(3), and the formal charge on C(1) is consequently zero. The [4+2] cycloaddition reaction would therefore be impossible.

Experimental

Mps were determined in sealed capillaries filled with argon. Analyses were carried out by Alfred Bernhardt Mikroanalytisches Laboratorium, West Germany. IR spectra were recorded with a Japan Spectroscopic Co., Ltd. IR-S instrument. ^{1}H NMR spectra were measured with a Japan Electron Optics Lab. Co., Ltd. C-60HL instrument. *N*-Trimethylstannyl(diphenylmethylene)amine was prepared according to Chan and Rochow.[7] Isocyanates and isothiocyanates were distilled before use.

Reaction of N-*Trimethylstannyl(diphenylmethylene)amine with one Molar Equivalent of Benzoyl Isocyanate.* A colorless solution was obtained by addition of benzoyl isocyanate (0.692 g, 4.71 mmol) to a solution of *N*-trimethylstannyl(diphenylmethylene)amine (1.77 g, 5.15 mmol) in *ca.* 6 ml of benzene at 0 °C. The reaction was completed instantaneously. The 1/1 adduct (Ie) precipitated as white needles by the addition of *ca.* 4 ml of *n*-hexane was washed with *n*-hexane and dried *in vacuo* (2.19 g, 95%). Mp 52.0—54.0 °C. Found: C, 58.78; H, 5.05%. Calcd for $C_{24}H_{24}N_2O_2Sn$: C, 58.69; H, 4.92%. IR (in C_6H_6): 1673 and 1626 cm^{-1}. ^{1}H NMR (in $CDCl_3$): τ 9.68 (Me_3Sn, $J^{117/119}$ Sn–C–H=55.0/58.0 Hz). Equimolar reactions of *N*-trimethylstannyl(diphenylmethylene)amine with other isocyanates or isothiocyanates were carried out under similar reaction conditions (at 0 °C under an atmosphere of nitrogen). The yields and results of elemental analyses of the 1/1 adducts are summarized in Tables 1 and 4, respectively.

*Reaction of 1/1 Adduct (Ia) with Methyl Isocyanate. Formation of 3,4-Dihydro-1,3-dimethyl-4,4-diphenyl-6-trimethylstannoxy-1,3,5-triazin-2(1*H*)-one (IIa)*: To a solution of 0.81 g (2.02 mmol) of the 1/1 adduct of methyl isocyanate in 2 ml of *n*-hexane was added 0.129 g (2.26 mmol) of methyl isocyanate at 0 °C under nitrogen. White needles which separated out in a few minutes were washed with *n*-hexane and recrystallized from a mixed solvent of *n*-hexane and benzene (1/1). This was identified as 1/2 adduct (IIa) (0.835 g, 77%). Elemental analysis and ^{1}H NMR spectrum identified the crystal as 3,4-dihydro-1,3-dimethyl-4,4-diphenyl-6-trimethylstannoxy-1,3,5-triazin-2(1*H*)-one (IIa) containing 1 equivalent of benzene of crystallization. Mp 149.0—152.0 °C. Found: C, 58.63; H, 5.80%. Calcd for $C_{20}H_{25}N_3O_2Sn+C_6H_6$: C, 58.24; H, 5.83%. IR (in C_6H_6) 1688 and 1621 cm^{-1}. ^{1}H NMR (in $CDCl_3$): τ 9.88(Me_3Sn, $J^{117/119}$ Sn–C–H=54.0/56.0 Hz), 7.43 (Me–N), 6.96 (Me–N). Preparation of other 3,4-dihydro-4,4-diphenyl-1,3,5-triazin-2(1*H*)-ones; IIb (1-methyl-3-phenyl), IIc (1-phenyl-3-methyl), and IId (1,3-diphenyl) was achieved similarly. Yields and spectroscopic results are summarized in Table 2, and analytical data in Table 4.

Treatment of IIa with Ethanethiol. Formation of Hexahydro-1,3-dimethyl-6,6-diphenyl-1,3,5-triazin-2,4-dione (Va): Addition of ethanethiol to a benzene solution of the 1/2 adduct (IIa) afforded the destannylated product (Va) as white prisms. Mp 238.0—239.0 °C. IR (in KBr) 1723 and 1648 cm^{-1}. This compound was identified as the triazindione [Va] which could be prepared independently by the hydrolysis of the 1/2 adduct of *N*-trimethylsilyl(diphenylmethylene)amine with

methyl isocyanate. Preparation of other *s*-triazindiones Vb, Vc, and Vd was achieved similarly. Yields, mp, and IR data are given in Table 2 and elemental analysis data in Table 4.

Reaction of 1/1 Adduct (Id) with One Equivalent of Phenyl Isocyanate. To a solution of 0.910 g (2.65 mmol) of *N*-trimethylstannyl(diphenylmethylene)amine in *ca.* 2 ml of benzene was added 0.350 g (2.59 mmol) of phenyl isothiocyanate at 0 °C under the atmosphere of nitrogen. On addition of phenyl isothiocyanate the color of the reaction mixture turned yellowish brown. The reaction mixture was left overnight at room temperature. Its IR spectrum showed the formation of 1/1 adduct [Id]. A solution of 0.314 g (2.64 mmol) of phenyl isocyanate in *ca.* 4 ml of benzene was then added at 0 °C. The mixture was warmed up to room temperature and allowed to stand for 15 hr. White prisms of the 1/2 adduct (IVg) separated out quantitatively were washed with benzene and recrystallized from a mixed solvent of *n*-hexane and benzene (4/6). Mp 164.5—166.0 °C. Found: C, 60.05; H, 4.91%. Calcd for $C_{30}H_{29}N_3OSSn$: C, 60.22; H, 4.89%. IR (in C_6H_6) 1698 and 1355 cm^{-1}. ^1H NMR (in $CDCl_3$) τ 9.72 (Me_3Sn, $J^{117/119}$ Sn–C–H= 56.0/58.0 Hz).

Destannylation of IV. Addition of ethanethiol to the benzene solution of 1/2 adduct (IVg) gave the destannylated product (VIg) as white prisms. Mp 252.0—254.0 °C. IR (in KBr) 1703 cm^{-1}. λ_{max}^{EtOH} 279 nm (log ε=4.50). Consecutive insertion reactions of the isothiocyanate 1/1 adducts (Ib or Id) with another isocyanate or isothiocyanate were performed under similar reaction conditions. The yields and the results of the elemental analyses are summarized in Tables 3 and 4, respectively.

References

1) (a) Part XXIX, K. Itoh, H. Hayashi, M. Fukui, and Y. Ishii, *J. Organometal. Chem.*, **78**, 339 (1974).
(b) A part of this paper was reported by one of the authors (Y. Ishii) at the VIth Internat. Conf. Organometal. Chem., Amherst, U. S. A., August 1973.
2) I. Matsuda, K. Itoh, and Y. Ishii, *J. Chem. Soc. Perkin I*, **1972**, 1678.
3) P. G. Harrison, *ibid.*, **1972**, 130.
4) M. F. Lappert, J. McMeeking, and D. E. Palmer, *J. Chem. Soc. Dalton*, **1973**, 151.
5) J. Lorberth, *J. Organometal. Chem.*, **16**, 235 (1969).
6) R. Richter and W. P. Trautwein, *Chem. Ber.*, **102**, 931, 938 (1969).
7) L. H. Chan and E. G. Rochow, *J. Organometal. Chem.*, **9**, 231 (1967).

Synthesis of Butirosin B and Its 3′,4′-Dideoxy Derivative[1]

Daishiro IKEDA, Tsutomu TSUCHIYA, Sumio UMEZAWA, and Hamao UMEZAWA*

Department of Applied Chemistry, Faculty of Engineering, Keio University, Hiyoshi, Yokohama 223

**Institute of Microbial Chemistry, Kamiosaki, Shinagawa-ku, Tokyo 141*

(Received June 26, 1974)

The total synthesis of butirosin B (**5**) is described. Its 3′,4′-dideoxy derivative (**11**) has been synthesized, a cyclic carbamate derivative (**2**) being used as the key compound. The dideoxy derivative (**11**) was prepared by hydrogenation of a 3′,4′-unsaturated derivative (**10**) obtained by the reaction of a di-*O*-mesyl derivative (**9**) with sodium iodide and zinc dust. The dideoxy derivative (**11**) was found to have significant activity against resistant bacteria producing phosphotransferase I.

Butirosins[2] and the related antibiotic, ribostamycin[3] show an interesting contrast. Chemically, butirosin B is an acylated derivative of ribostamycin with (*S*)-4-amino-2-hydroxybutyryl side chain attached to the C-1 amino group of the 2-deoxystreptamine moiety. A comparison of the antibacterial spectrum of butirosin B and that of ribostamycin showed that butirosin has a broader spectrum, inhibiting kanamycin-resistant bacteria which produce kanamycin phosphotarnsferase I.[4] The present paper deals with the syntheses of butirosin B and its 3′,4′-dideoxy derivative from ribostamycin. Since ribostamycin has been synthesized,[5] the present synthesis constitutes the total synthesis of butirosin B.

As the starting material we used tetra-*N*-benzyloxycarbonyl-3′,4′;2″,3″-di-*O*-cyclohexylidene-5″-*O*-(1-methoxycyclohexyl)ribostamycin (**1**), an intermediate in the synthesis of 3′,4′-dideoxyribostamycin.[6] The derivative (**1**) has one hydroxyl group adjacent to the 1-*N*-benzyloxycarbonyl group, other hydroxy and amino groups being protected. When sodium hydride was added in a solution of **1** in DMF at room temperatures, smooth reaction occurred to give tri-*N*-benzyloxycarbonyl-3′,4′;2″,3″-di-*O*-cyclohexylidene-5″-*O*-(1-methoxycyclohexyl)ribostamycin 1,6-carbamate (**2**) in 78% yield. The IR spectrum showed a sharp peak at 1770 cm^{-1}, indicating the presence of a cyclic carbamate.[7] The structure of (**2**) was also confirmed by its NMR spectrum. A method was given for simultaneous blocking of adjacent amino and hydroxyl groups in a trans-diequatorial configuration by carbamate-ring formation, the above reaction being used as an alternative method. Formation of cyclic carbamate can be viewed as an anchimeric attack of the C-6 alkoxide-ion on the urethane carbonyl at C-1.

Treatment of the carbamate (**2**) with a limited amount of barium hydroxide in aqueous dioxane selectively cleaved the carbamate ring, to give an aminol (**3**) in 70% yield. The aminol was then condensed with (*S*)-2-hydroxy-4-phthalimidobutyric acid[8] (HPBA) by the active ester method to give the acylated product (**4**), which was treated successively with hydrazine in 80% ethanol to remove the phthaloyl group, with palladium black and hydrogen to remove the benzyloxycarbonyl groups and with 1M hydrochloric acid to remove the cyclohexylidene groups, giving butirosin B (**5**). The R_f values on ppc and tlc, the optical rotation, the IR and NMR spectra and the antibacterial activity[1] were identical with those of the natural specimen of butirosin B.

We undertook to prepare a modification of butirosin B. Butirosin A is active against kanamycin-resistant bacteria producing phosphotransferase I but inactivated by bacteria producing phosphotransferase II[3] (*e.g.*, *E. coli* JR 66/W677) by phosphorylation of the 3′-hydroxyl group. Synthesis of 3′,4′-dideoxybutirosin B was therefore undertaken.

Compound **4** was taken as the starting material and the 5″-protecting group was selectively removed by controlled acid-hydrolysis to give **6**. After acetylation, the tri-*O*-acetyl derivative (**7**) was further treated with acetic acid to give the diol (**8**). Mesylation then gave the 3′,4′-di-*O*-mesyl derivative (**9**). Similar treatment of **9** with sodium iodide and zinc dust in DMF to that for the preparation of 3′,4′-dideoxykanamycin B (under stricter conditions) gave 3′,4′-dideoxy-3′-eno derivative (**10**) in yield of 73%.[9] Hydrogenation of the double bond followed by the removal of the protecting groups gave 3′,4′-dideoxybutirosin B (**11**). In order to confirm the structure, **11** was partially hydrolyzed to give 1-*N*-((*S*)-4-amino-2-hydroxybutyryl)-3′,4′-dideoxyneamine.[1]

3′,4′-Dideoxybutirosin B was found to be active[1] against kanamycin-resistant bacteria producing phosphotransferase II as expected.

Experimental

Thin layer chromatography (tlc) was carried out on silica gel and the spots were visualized with sulfuric acid. Paper chromatography (ppc) was performed on Toyo-Roshi paper No. 50. The spots were detected with 0.5% ninhydrin in pyridine.

3,2′,6′-Tri-N-benzyloxycarbonyl-3′,4′; 2″,3″-di-O-cyclohexylidene-5″-O-(1-methoxycyclohexyl)ribostamycin 1,6-Carbamate (2). 50% Oily sodium hydride (97 mg) was added to an ice-cold solution of **1** (1.30 g) in dry DMF (15 ml), after displacement of the air in the reaction vessel with nitrogen, and the mixture was stirred at room temperature for 2 hr. On tlc with benzene–ethyl acetate (3 : 2), the solution showed a single spot at R_f 0.40 (**1**: 0.87). The pale-yellow solution was neutralized with acetic acid, evaporated, and the residue was poured into a mixture of chloroform and water with stirring. The organic layer separated was washed with water, dried with Na_2SO_4 and evaporated. The resulting syrup was chromatographed on a short column of silica gel with benzene–ethyl acetate–triethylamine (60 : 30 : 0.5) to give a solid, 930 mg (78%), $[\alpha]_D^{25}$ +14.4° (*c* 2, $CHCl_3$); IR(KBr): 1770, 1720, 1530 cm^{-1}.

Found: C, 63.55; H, 7.03; N, 4.68%. Calcd for $C_{61}H_{78}$-

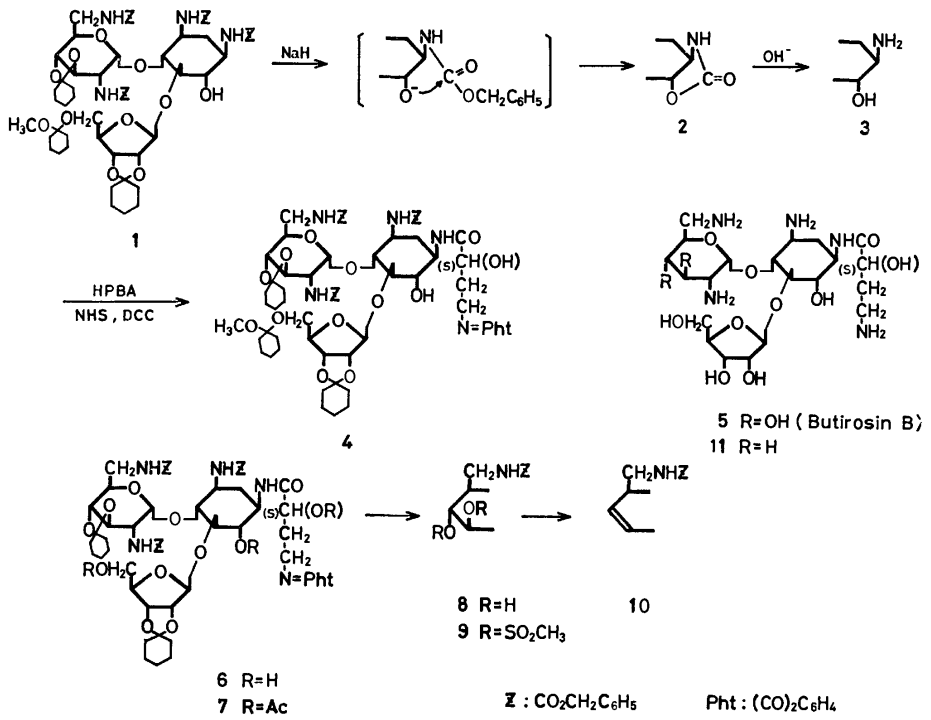

N_4O_{18}: C, 63.42; H, 6.80; N, 4.85%.

NMR (in $CDCl_3$): τ 8.8—8.2 (30H, cyclohexylidene), 6.82 (3H s, OCH_3), ~2.67 (15H, $CH_2C_6H_5$).

3,2',6'-Tri-N-benzyloxycarbonyl-3',4';2'',3''-di-O-cyclohexylidene-5''-O-(1-methoxycyclohexyl)ribostamycin (3). A barium hydroxide solution (2.5 ml, containing 68 mg of barium hydroxide octahydrate) was added to a solution of **2** (500 mg) in dioxane (2 ml), and the mixture was stirred at 98 °C for 40 min. The solution became neutral. On tlc with benzene–methanol (7 : 1), the solution gave two spots of R_f 0.11 (**3**) and R_f 0.75 (**2**) in almost equal strength. Another aliquot (2.5 ml) of barium hydroxide solution was added and the solution was treated as above. The solution became weakly alkaline and, on tlc, gave three spots of R_f 0.11 (major), 0.75 (slight) and 0.87 (slight). After introducing carbon dioxide, the solution was evaporated and the residue was extracted with chroloform. The solution was washed with water, dried with Na_2SO_4 and evaporated. The residue (485 mg) was chromatographed on a column of silica gel with benzene–ethyl acetate (3 : 1) and then with benzene–methanol–triethylamine (70 : 10 : 0.5) to give a solid, 342 mg (70%), $[\alpha]_D^{27}$ +16.7° (*c* 2, $CHCl_3$); weakly ninhydrine positive; IR (KBr): 1720, 1530 cm^{-1}.

Found: C, 63.69; H, 7.28; N, 4.90%. Calcd for $C_{60}H_{80}N_4O_{17}$: C, 63.81; H, 7.41; N, 4.96%.

3,2',6'-Tri-N-benzyloxycarbonyl-3',4';2'',3''-di-O-cyclohexylidene-1-N-((S)-2-hydroxy-4-phthalimidobutyryl)-5''-O-(1-methoxycyclohexyl)ribostamycin (4). To an ice-cold solution of HPBA (62 mg, 1.3 mol eq.) and *N*-hydroxysuccinimide (NG) (27 mg, 1.3 mol eq.) in THF (2 ml) was added dicyclohexylcarbodiimide (54 mg, 1.3 mol eq.) and the mixture was stirred for 1 hr in the cold. A solution of **3** (200 mg, 1 mol eq.) and triethylamine (30 mg) in THF (2 ml) was added to the resulting suspension containing dicyclohexylurea, and the mixture was stirred at room temperature overnight. On tlc with benzene–ethyl acetate (1 : 1), the mixture showed three spots of R_f 0.7, 0.4 (**4**) and 0. After filtration, the solution was evaporated and the residue was chromatographed on a column of silica gel with benzene–ethyl acetate–triethylamine (60 : 40 : 0.5) to give a solid, 161 mg (67%), $[\alpha]_D^{27}$ +9.9° (*c* 2, $CHCl_3$); IR (KBr): 1710, 1655, 1530 cm^{-1}.

Found: C, 63.58; H, 6.56; N, 5.04%. Calcd for $C_{72}H_{89}N_5O_{21}$: C, 63.56; H, 6.59; N, 5.15%.

NMR (in $CDCl_3$): τ 9.0—7.5 (~36H, cyclohexylidene, $(CH_2)_2$, two OH (?)), 6.82 (3H s, OCH_3), 2.73—2.6 (15H, $CH_2C_6H_5$), 2.28 (4H, $(CO)_2C_6H_4$).

1-N-((S-4-Amino-2-hydroxybutyryl)ribostamycin (Butirosin B) (5). 80% Hydrazine hydrate (3 g) was added to a suspension of **4** (198 mg) in 80% aqueous ethanol (4.5 ml), and the mixture was heated at 60 °C for 2 hr. On tlc with ethyl acetate–methanol (1 : 1), the clear solution showed a ninhydrin-positive spot (R_f 0.15). The solution was evaporated and the residue was extracted with chloroform. The solution was evaporated and the residue was extracted with dioxane. The solution was filtered and to the filtrate (2 ml) were added water (1 ml) and a few drops of acetic acid and the mixture was hydrogenated with palladium black at 40—45 °C overnight. The reaction mixture was filtered, evaporated, and the residue was dissolved in 1M hydrochloric acid (1 ml). The solution was heated at 55° C for 1 hr. Addition of acetone gave a solid, which was chromatographed on a column of CM-Sephadex C-25 (NH_4^+ form, 20 ml) with water (100 ml) and aqueous ammonia of 0.05—0.5 M (linear increase). Butirosin B was eluted with *ca.* 0.4 M ammonia. Evaporation of the solution gave a soild, 51 mg (63%), $[\alpha]_D^{30}$ +34° (*c* 2, H_2O) [lit,[2] +33° (*c* 1.5, H_2O)]; ppc, $R_{f\,\text{ribostamycin}}$ 0.53 (1-butanol–pyridine–water–acetic acid (6 : 4 : 3 : 1)], the value being identical with that of natural butirosin B; IR (KBr): 1640, 1560 cm^{-1}.

Found: C, 43.65; H, 7.49; N, 12.08%. Calcd for $C_{21}H_{41}N_5O_{12}\cdot H_2O$: C, 43.97; H, 7.56; N, 12.21%.

NMR (in D_2O): τ 8.3—7.7 (5H), 4.6 (2H m, H-1', 1'').

3,2',6'-Tri-N-benzyloxycarbonyl-3',4';2'',3''-di-O-cyclohexylidene-1-N-((S)-2-hydroxy-4-phthalimidobutyryl)ribostamycin (6). A solution of **4** (440 mg) in 40% acetic acid–acetone (1 : 9, 10 ml) was allowed to stand at room temperature for 2 hr. 40% Acetic acid (0.6 ml) was added and the solution was allowed to stand for 6 hr. On tlc with benzene–ethyl

acetate (1 : 2), the solution showed three spots at R_f 0.72 (**4**, slight), 0.43 (**6**, major) and 0 (slight). The latest one increased with prolonged reaction. The solution was poured into a mixture of chloroform and sodium hydrogen carbonate solution with stirring. The organic layer was washed with water, dried with Na_2SO_4 and evaporated. The residue (410 mg) was chromatographed on a column of silica gel with benzene–ethyl acetate (1 : 2). After complete elution of **4** (100 mg), the eluant was changed to chloroform-methanol (27 : 1, **6** is scarcely soluble in the first solvent system, but soluble in this system). A solid (290 mg, 71%) obtained was reprecipitated from chloroform–*n*-hexane, $[\alpha]_D^{28}$ +16° (*c* 2, $CHCl_3$).

Found: C, 62.34; H, 6.33; N, 5.55%. Calcd for $C_{65}H_{77}N_5O_{20}$: C, 65.54; H, 6.22; N, 5.61%.

NMR (in $CDCl_3$): τ 8.9—7.5 (~26H), 4.9 (6H, $CH_2C_6H_5$), ~2.7 (15H two peaks, $CH_2C_6H_5$), 2.25 (9H incomplete d, $(CO)_2C_6H_4$).

1-N-*((S)-2-Acetoxy-4-phthalimidobutyryl)-6,5″-di*-O-*acetyl-3,2′, 6′-tri*-N-*benzyloxycarbonyl-3′,4′;2″,3″-di*-O-*cyclohexylideneribostamycin (**7**).* A sample (320 mg) of **6** was treated with acetic anhydride and pyridine in the usual manner to give a solid, 311 mg (88%, reprecipitated from benzene–*n*-hexane), $[\alpha]_D^{25}$ +9° (*c* 1.7, $CHCl_3$).

Found: C, 62.22; H, 6.27; N, 4.99%. Calcd for $C_{11}H_{83}N_5O_{23}$: C, 62.04; H, 6.09; N, 5.10%.

NMR (in $CDCl_3$): τ 7.94, 7.85 and 7.78 (each 3H s, Ac).

1-N-*((S)-2-Acetoxy-4-phthalimidobutyryl)-6,5′-di*-O-*acetyl-3,2′, 6′-tri*-N-*benzyloxycarbonyl-2″,3″*-O-*cyclohexylideneribostamycin (**8**).* A solution of **7** (300 mg) in 60% acetic acid–acetone (4 ml+ 5 ml) was allowed to stand at 60 °C for 75 min. On tlc with benzene–ethyl acetate (1 : 3), the solution showed a single spot of R_f 0.42. The solution was evaporated and the residue was shaken with a mixture of chloroform and saturated sodium hydrogen carbonate solution. From the organic layer, a solid of **8** was obtained, 252 mg (90%, reprecipitated from chloroform–*n*-hexane), $[\alpha]_D^{25}$ +1.5° (*c* 1.7, $CHCl_3$).

Found: C, 60.69; H, 6.11; N, 5.15%. Calcd for $C_{65}H_{75}N_5O_{23}$: C, 60.32; H, 5.84; N, 5.41%.

NMR (in $CDCl_3$): τ 8.8—8.3 (10H, cyclohexylidene), 8.2—7.6 (4H), 7.97, 7.87 and 7.82 (each 3H s, Ac), 4.9 (6H, $CH_2C_6H_5$), 2.70 and 2.65 (5H s, 10H s, respectively, $CH_2C_6H_5$), 2.20 (4H incomplete d).

1-N-*((S)-2-Acetoxy-4-phthalimidobutyryl)-6,5″-di*-O-*acetyl-3,2′, 6′-tri*-N-*benzyloxycarbonyl-2″,3″*-O-*cyclohexylidene-3′,4′-di*-O-*mesylribostamycin (**9**).* Mesyl chloride (45 mg) was added to a solution of **8** (240 mg) in pyridine (5 ml), and the solution was allowed to stand for 37 °C overnight. On tlc with benzene–ethyl acetate (1 : 1), the solution showed two spots at R_f 0.18 (monomesyl derivative) and 0.39 (**9**). Mesyl chloride (20 mg) was added and the solution was heated at 60 °C for 2 hr. After addition of a drop of water, the solution was evaporated and the residue was dissolved in chloroform. The solution was washed successively with potassium hydrogen sulfate solution, sodium hydrogen carbonate solution and water, dried over Na_2SO_4, and evaporated to give a syrup, which was reprecipitated from chloroform–*n*-hexane to give a solid of **9**, 258 mg (98%), $[\alpha]_D^{20}$ −9° (*c* 2, $CHCl_3$); IR 1175 cm^{-1}.

Found: C, 55.82; H, 5.63; N, 4.79; S, 4.27%. Calcd for $C_{67}H_{79}N_5O_{27}S_2$: C, 55.84; H, 5.49; N, 4.83; S, 4.42%.

NMR (in $CDCl_3$): τ 7.93, 7.86 and 7.77 (each 3H s, Ac), 7.23 and 6.96 (each 3H s, SO_2CH_3).

1-N-*((S)-2-Acetoxy-4-phthalimidobutyryl)-6,5″-di*-O-*acetyl-3,2′, 6′-tri*-N-*benzyloxycarbonyl-2″,3″*-O-*cyclohexylidene-3′,4′-dideoxy-3′-enoribostamycin (**10**).* Sodium iodide (2.1 g; dried at 110 °C for 2 hr), zinc dust (1.0 g; dried at 110 °C for 2 hr) and molecular sieves (100 mg; Union Carbide Co., Grade 3A, dried at 260 °C for 3 hr) were added to a solution of **9** (200 mg) in DMF (4 ml; dried over CaH_2 and distilled in vacuo just before use), and the mixture was stirred at 89.5—90 °C (oil bath temperature) for 1 hr. The temperature was maintained strictly in the above range with a thermostabilizer. Temperature fluctuation caused a decrease in the tlc with benzene–ethyl acetate (1 : 1), the mixture showed a spot at R_f 0.48 (**10**) and trace spots at R_f 0.56 (**9**) and 0. Chloroform (20 ml) was added and the mixture was filtered with the aid of chloroform (20 ml). The filtrate was washed successively with saturated sodium chloride solution, sodium thiosulfate solution and water, dried over Na_2SO_4 and evaporated. The syrup was chromatographed on a short column of silica gel with benzene–ethyl acetate (1 : 1) to give a solid of **10**, 128 mg (73%), which was reprecipitated from chloroform–*n*-hexane, mp 99—102 °C, $[\alpha]_D^{23}$ −24.5° (*c* 2, $CHCl_3$).

Found: C, 61.77; H, 5.71; N, 5.56%. Calcd for $C_{65}H_{73}N_5O_{21}$: C, 61.94; H, 5.84; N, 5.56%.

NMR (in $CDCl_3$): τ 7.99, 7.90 and 7.83 (each 3H s, Ac), 4.38 (2H slightly broadened s, H-3′,4′).

1-N-*((S)-4-Amino-2-hydroxybutyryl)-3′,4′-dideoxyribostamycin (3′,4′-Dideoxybutirosin B) (**11**).* A sample of **10** was treated as in the preparation of butirosin B from **4**, giving **11**, yield 80%, $[\alpha]_D^{16}$ +25° (*c* 1.8, H_2O), $R_{f\,\text{butirosin B}}$ 1.73 (ppc with 1-butanol-pyridine-water-acetic acid (6:4:3:1)), R_f 0.24 (tlc with chloroform-methanol-17% ammonia (1 : 4 : 3)).

Found: C, 46.74; H, 7.70; N, 13.13%. Calcd for $C_{21}H_{41}N_5O_{10}\cdot H_2O$: C, 46.57; H, 8.00; N, 12.93%.

NMR (in D_2O): τ 9.0—7.5 (~10H), 4.6 (2H m, H-1′,1″).

References

1) Part XL of "Studies on Aminosugars," primarily by S. Umezawa. Presented in part in short communications: a) D. Ikeda, T. Tsuchiya, S. Umezawa, and H. Umezawa, *J. Antibiot.* (Tokyo), **25**, 741 (1972); b) D. Ikeda, T. Tsuchiya, S. Umezawa, H. Umezawa, and M. Hamada, *ibid.*, **26**, 307 (1973).

2) P. W. K. Woo, H. W. Dion, and Q. R. Bartz, *Tetrahedron Lett.* **1971**, 2617; P. W. K. Woo, *ibid.*, **1971**, 2621; P. W. K. Woo, H. W. Dion, and Q. R. Bartz, *ibid*, **1971**, 2628.

3) T. Shomura, N. Ezaki, T. Tsuruoka, T. Niwa, E. Akita, and T. Niida, *J. Antibiot.* (Tokyo), **23**, 155 (1970).

4) M. Yagisawa, H. Yamamoto, H. Naganawa, S. Kondo, T. Takeuchi, and H. Umezawa, *ibid.*, **25**, 748 (1972).

5) T. Ito, E. Akita, T. Tsuruoka, and T. Niida, *Agr. Biol. Chem.*, **34**, 980 (1970).

6) S. Umezawa, T. Tsuchiya, D. Ikeda, and H. Umezawa, *J. Antibiot.* (Tokyo), **25**, 613 (1972); D. Ikeda, T. Suzuki, T. Tsuchiya, S. Umezawa, and H. Umezawa, This Bulletin, **46**, 3210 (1973).

7) S. Umezawa, T. Tsuchiya, and Y. Takagi, This Bulletin, **43**, 1602 (1970); *ibid*, **44**, 1411 (1971).

8) E. Akita, Y. Horiuchi, and T. Ito, Japanese Patent, 49-20166, Feb. 22 (1974).

9) S. Umezawa, H. Umezawa, Y. Okazaki, and T. Tsuchiya, This Bulletin, **45**, 3624 (1972).

Synthesis of 1-*N*-[(*S*)-4-Amino-2-hydroxybutyryl]-3′,4′-dideoxyneamine[1)]

Yasushi TAKAGI, Daishiro IKEDA, Tsutomu TSUCHIYA, Sumio UMEZAWA, and Hamao UMEZAWA*

Department of Applied Chemistry, Faculty of Engineering, Keio University, Hiyoshi, Yokohama 223

**Institute of Microbial Chemistry, Kamiosaki, Shinagawa-ku, Tokyo 141*

(Received June 26, 1974)

The titled compound (**5**) has been prepared from 3′,4′-dideoxyneamine or ribostamycin *via* 1,6-cyclic carbamate intermediates (**2** and **12**). 3′,4′-Dideoxygenation, which is the key step in the synthesis from ribostamycin, was accomplished by the hydrogenation of 3′,4′-unsaturated derivative which was prepared from the corresponding 3′,4′-di-*O*-mesyl derivative by the action of sodium iodide and zinc dust in DMF. The title compound was found to have an improved antibacterial spectrum broader than 3′,4′-dideoxyneamine.

As described in the preceding paper,[2)] 3′,4′-dideoxygenation of butirosin B was found to give a compound having a broader antibacterial spectrum than butirosin B. The recognition of the remarkable effects of combination of 3′,4′-dideoxygenation and N-1 acylation with (*S*)-4-amino-2-hydroxybutyryl group led us to the synthesis of N-1 acylated derivative of 3′,4′-dideoxyneamine. Since neamine forms a large portion of kanamycin B and ribostamycin, and appears to play an essential role in the antibacterial action of these antibiotics, we were interested in studying the above-mentioned modification of neamine. The present paper deals with the synthesis of 1-*N*-[(*S*)-4-amino-2-hydroxybutyryl]-3′,4′-dideoxyneamine (**5**).

The selective acylation of C-1-amino group of 2-deoxystreptamine moiety is generally difficult, however, in the present synthesis, the N-1-acylation has been achieved through a cyclic carbamate intermediate by a method[3)] similar to that described for butirosin synthesis.[2)]

When tetra-*N*-benzyloxycarbonyl-3′,4′-dideoxyneamine (**1**), which has been prepared from 3′,4′-dideoxyneamine,[4)] was treated with sodium hydride in DMF, the cyclic 1,6-carbamate (**2**) was obtained in 62% yield. Selective hydrolysis of the cyclic carbamate group with a limited amount of barium hydroxide in aqueous dioxane yielded 3,2′,6′-tri-*N*-benzyloxycarbonyl 3′,4′-dideoxyneamine (**3**). Acylation of the C-1-amino group with (*S*)-2-hydroxy-4-phthalimidobutyric acid[5)] (HPBA) in the presence of *N*-hydroxysuccinimide (NHS) and dicyclohexylcarbodiimide (DCC) gave the N-1-acyl derivative (**4**), which, on deblocking, led to the title compound (**5**).

An alternative synthesis of the title compound (**5**) has been achieved by a route from ribostamycin. Methanolysis of tetra-*N*-benzyloxycarbonylribostamycin[6)] (**6**) gave tetra-*N*-benzyloxycarbonylneamine (**7**) in high yield. Direct benzyloxycarbonylation of neamine has also been attempted, however, in this case, separation of the product from inorganic material was unusually troublesome.

Selective cyclohexylidenation of **7** has been accomplished in a manner similar to that described in the synthesis of 3′,4′-dideoxyneamine,[4)] affording **8**. Mesylation gave the 3′,4′-di-*O*-mesyl derivative (**9**), which, on treatment with sodium iodide and zinc dust in DMF by the procedure previously reported,[2,7)] furnished the 3′,4′-unsaturated derivative (**10**) in 76% yield.

Decyclohexylidenation of **10** by acid hydrolysis gave **11**, which was then treated with sodium hydride in DMF to give the cyclic carbamate **12**. The carbamate was selectively hydrolyzed by alkaline treatment to give **13**. Finally, N-1-acylation of **13** with HPBA, NHS and DCC followed by hydrogenation and deblocking afforded **5**, which was identical with the specimen prepared by the foregoing method.

Retention of configuration at C-2 of the side chain in **5** was confirmed by acid hydrolysis,[8)] which gave (*S*)-4-amino-2-hydroxybutyric acid.

The N-1-acylated derivative (**5**) of 3′,4′-dideoxyneamine showed enhanced antibacterial activity broader than 3′,4′-dideoxyneamine, exhibiting activity against various strains of sensitive and resistant bacteria[1)] as expected.

Experimental

1,3,2′,6′-Tetra-N-*benzyloxycarbonyl-3′,4′-dideoxyneamine (**1**).* Prepared in the usual manner,[9)] $[\alpha]_D^{15}$ +45° (*c* 2, $CHCl_3$).

3,2′,6′-Tri-N-*benzyloxycarbonyl-3′,4′-dideoxyneamine 1,6-Carbamate (**2**).* A solution of **1** (1.34 g) in DMF was ice-cooled and, after replacement of the atmosphere with nitrogen, 50% oily NaH (235 mg) was added and the mixture was stirred for 30 min. The clear solution was allowed to stand overnight at ~5 °C. On tlc with $CHCl_3$–EtOH (20 : 1), the solution showed a single spot (R_f 0.25) except **1** (R_f 0.33). After neutralizing the solution with AcOH, the solution was poured into a mixture of $CHCl_3$–H_2O with stirring. The organic layer was washed with H_2O, dried (Na_2SO_4), and evaporated to give a yellow syrup. The syrup was chromatographed on a short column of silica gel with $CHCl_3$–EtOH (20 : 1) to give a solid, which was reprecipitated from $CHCl_3$–*n*-hexane, 683 mg (62%), $[\alpha]_D^{25}$ +58° (*c* 1.9, $CHCl_3$); IR (KBr): 1770, 1710, 1535 cm^{-1}.

Found: C, 61.92; H, 5.99; N, 7.67%. Calcd for $C_{37}H_{42}N_4O_{11}$: C, 61.83; H, 5.89; N, 7.80%.

3,2′,6′-Tri-N-*benzyloxycarbonyl-3′,4′-dideoxyneamine (**3**).* To a solution of **2** (620 mg) in dioxane (12 ml), an aqueous $Ba(OH)_2$ solution (5 ml, which contained 150 mg of $Ba(OH)_2 \cdot 8H_2O$) was added and the mixture was stirred at 60 °C for 1 hr. Another aliquot (5 ml) of $Ba(OH)_2$ solution was added and the solution was stirred for further 1 hr. On tlc with C_6H_6–EtOH (10 : 1), the mixture showed spots of R_f 0.06 (**3**, major), 0.16 (slight), 0.25 (slight) and 1 (**2**, slight). Carbon dioxide was introduced and after filtration, the solution was evaporated to give a solid (590 mg). The solid showed no peak near 1760 cm^{-1}. Since purification of the solid was tedious, the crude solid was used for the next step without purification.

3,2′,6′-Tri-N-*benzyloxycarbonyl-3′,4′-dideoxy-1*-N-[(S)-2-hydroxy-

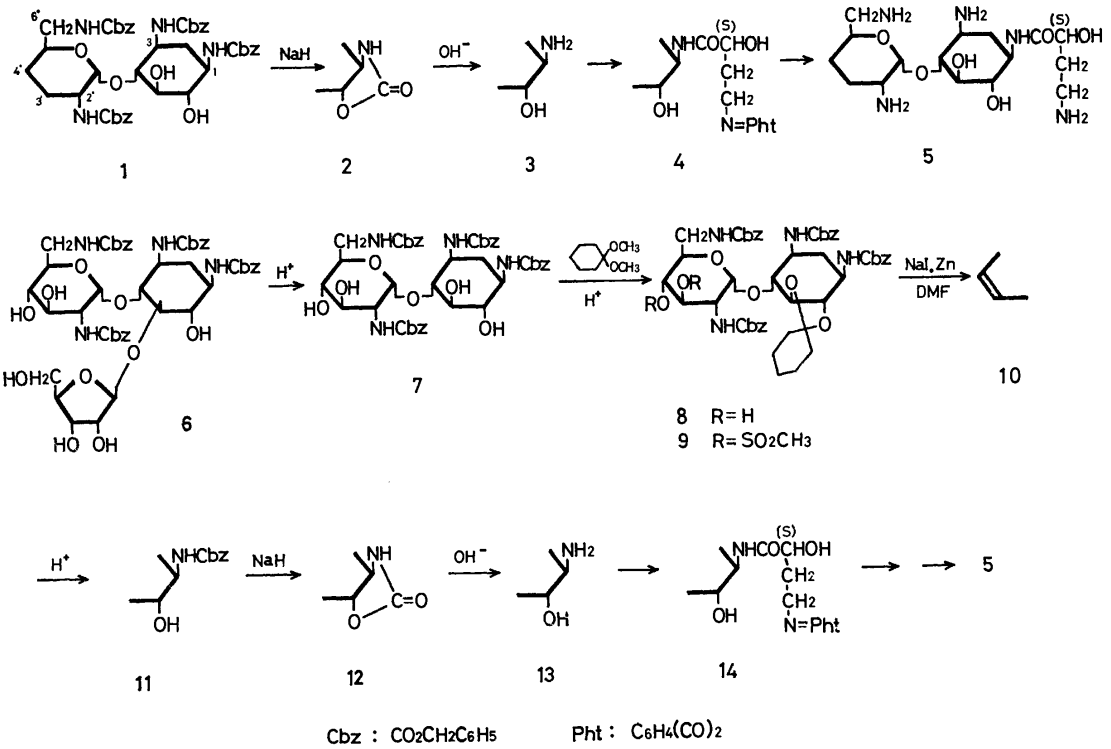

4-phthalimidobutyryl)neamine (4). To an ice-cold solution of HPBA (136 mg) and NHS (69 mg) in THF (4 ml), DCC (120 mg) was added and the mixture was stirred for 1 hr in the cold. A suspension of well dried **3** (crude 290 mg) and triethylamine (30 mg) in dioxane (3 ml) was added and the mixture was stirred at room temperatures overnight. On tlc with $CHCl_3$–EtOH (20 : 1), the mixture showed a spot of **4** at R_f 0.33. After filtration, the solution was evaporated and the residue was chromatographed on a column of silica gel with $CHCl_3$–EtOH (20 : 1) to give a solid, 240 mg (62%), which was recrystallized from MeOH, mp 228—230 °C, $[\alpha]_D^{22}$ +32° (*c* 1.5, $CHCl_3$); IR (KBr): 1705, 1690, 1655, 1535 cm^{-1}.

Found: C, 61.34; H, 5.93; N, 7.39%. Calcd for $C_{48}H_{53}N_5O_{14}\cdot H_2O$: C, 61.20; H, 5.89; N, 7.43%.

1-N-[(S)-4-Amino-2-hydroxybutyryl]-3',4'-dideoxyneamine (5). *a) From 4:* To a solution of **4** (111 mg) in dioxane-80% aqueous EtOH (1 : 1, 2 ml), 80% hydrazine hydrate (80 mg) was added and the mixture was heated at 60 °C for 2 hr. On tlc with EtAc-MeOH (1 : 1), the solution showed a ninhydrin-positive spot (R_f 0.13). The solution was evaporated and the residue was dissolved in 50% aqueous dioxane (2 ml). After addition of a drop of AcOH, the solution was hydrogenated with Pd black at 40—45 °C overnight. The mixture was filtered, evaporated, and the residue was chromatographed on a column of CM-Sephadex C-25 (NH_4 form, 10 ml) with H_2O and then with aqueous ammonia of 0.2—0.5 M. At about 0.4 M ammonia, **5** was eluted; a solid, 25 mg (53%), $[\alpha]_D^{22}$ +38° (*c* 0.85, H_2O); IR (KBr): 1650, 1560 cm^{-1}; R_f 3',4'-dideoxyneamine 0.47 (ppc with 1-BuOH–pyridine–H_2O–AcOH (6 : 4 : 3 : 1)).

Found: C, 46.92; H, 8.52; N, 17.24%. Calcd for $C_{16}H_{33}N_5O_6\cdot H_2O$: C, 46.93; H, 8.62; N, 17.10%.

b) From 14: To a solution of **14** (101 mg) in dioxane-80% aqueous EtOH (1 : 1, 3 ml), 80% hydrazine hydrate (96 mg) was added and the solution was heated at 60 °C for 2 hr. On tlc with $CHCl_3$–MeOH–17% NH_3 (2 : 1 : 1), the solution showed a single spot (R_f 0.2) except **14** (R_f 0.7). The solution was evaporated and the residue was dissolved in 50% aqueous dioxane (3 ml). After addition of a drop of AcOH, the solution was hydrogenated with Pd black and then the product was purified similarly as described above to give a solid, 40 mg (93%), $[\alpha]_D^{20}$ +36° (*c* 1.2, H_2O). The IR and NMR spectra were identical with those of the specimen prepared from **4**.

1,3,2',6'-Tetra-N-benzyloxycarbonylneamine (7). A solution of **6** (28.4 g) in 0.4 M methanolic hydrogen chloride (300 ml) was allowed to stand at room temperature. After 10 min, a solid began to precipitate. After overnight standing, the upper clear layer showed, on tlc with $CHCl_3$–EtOH (10 : 1), a spot of R_f 0.1 (**6** and methyl riboside; both gave the same R_f value) and the precipitate showed a spot of R_f 0.4 (**7**). The mixture was filtered and the solid was washed with hot MeOH to give a solid (19.24 g). From the methanol solution, another crop of the solid (2.43 g) was obtained. Total yield 21.7 g (88%). The solid was reprecipitated from hot dioxane–H_2O, $[\alpha]_D^{20}$ +44° (*c* 0.8, DMF); IR (KBr): 1705, 1695, 1535; 730, 695 cm^{-1}.

Found: C, 61.19; H, 5.87; N, 6.39%. Calcd for $C_{44}H_{50}N_4O_{14}$: C, 61.53; H, 5.87; N, 6.52%.

1,3,2',6'-Tetra-N-benzyloxycarbonyl-5,6-O-cyclohexylideneneamine (8). To a solution of **7** (10 g) in DMF (50 °C, 100 ml), *p*-toluenesulfonic acid (390 mg) and 1,1-dimethoxycyclohexane (12 ml) were added and the solution was heated at 55 °C (bath temperature) under stirring *in vacuo* (25 Torr) for 1 hr. Another aliquots of *p*-toluenesulfonic acid (195 mg) and 1,1-dimethoxycyclohexane (11 ml) were added and the solution was again treated as above for 1.5 hr. After overnight standing at room temperatures, the solution showed, on tlc with $CHCl_3$–EtOH (25 : 1), spots of R_f 0.8 (dicycolhexylidene derivative), 0.3 (**8**, major) and 0.15 (slight, 3',4'-*O*-cyclohexylidene isomer). The solution was poured into $NaHCO_3$ solution to give a precipitate (12.35 g). The solid was then treated with hot benzene to remove the benzene-soluble products (4.98 g; R_f 0.8 and 0.3 (slight)). The benzene-insoluble product (R_f 0.3 and 0.15 (slight)) was reprecipitat-

ed from $CHCl_3$–ether to give a solid, 5.72 g (52%), mp 185.5—187 °C, $[\alpha]_D^{20}$ +5.3° (*c* 0.9, $CHCl_3$); IR (KBr): 1705, 1535 cm^{-1}.

Found: C, 64.22; H, 6.29; N, 5.74%. Calcd for $C_{50}H_{58}N_4O_{14}$: C, 63.95; H, 6.23; N, 5.97%.

NMR (in DMSO-d_6): τ 8.5 (10H, broad, cyclohexylidene), 2.57 (20H s, $CH_2C_6H_5$).

1,3,2',6'-Tetra-N-*benzyloxycarbonyl-5,6*-O-*cyclohexylidene-3',4'-di*-O-*mesylneamine* (**9**). A sample of **8** was treated similarly as described in the preparation of compound **9** in a preceding paper;[2] yield 98%, $[\alpha]_D^{20}$ +11° (*c* 0.9, $CHCl_3$), R_f 0.35 (tlc with $CHCl_3$–EtOH (50 : 1)); IR (KBr): 1350, 1175 cm^{-1} (ν SO_2).

Found: C, 57.34; H, 5.76; N, 4.93; S, 5.89%. Calcd for $C_{52}H_{62}N_4O_{18}S_2$: C, 57.03; H, 5.71; N, 5.12; S, 5.85%.

NMR (in $CDCl_3$): τ 7.20 and 6.92 (each 3H s, SO_2CH_3).

1,3,2',6'-Tetra-N-*benzyloxycarbonyl-5,6*-O-*cyclohexylidene-3',4'-dideoxy-3'-enoneamine* (**10**). To a solution of **9** (1.60 g) in dry DMF (30 ml), sodium iodide (17 g) and zinc dust (7.8 g) were added and the mixture was stirred at 95—96 °C (oil bath temperature) for 1.5 hr. On tlc with $CHCl_3$–EtOH (50 : 1), the mixture showed spots at R_f 0.25 (**10**, major) and 0 (trace). The solution was then treated with $CHCl_3$ as described for compound **10** in the preceding paper[2] and the resulting solid was chromatographed on silica gel and $CHCl_3$–EtOH (50 : 1) to give a solid, 1.00 g (76%), which was recrystallized from EtOH, mp 198—199.5 °C, $[\alpha]_D^{20}$ −23° (*c* 0.8, $CHCl_3$); IR (KBr): 1705, 1525 cm^{-1} (peaks at 1350 and 1175 cm^{-1} in **9** had disappeared).

Found: C, 66.38; H, 6.29; N, 6.14%. Calcd for $C_{50}H_{56}N_4O_{12}$: C, 66.36; H, 6.24; N, 6.19%.

NMR (in $CDCl_3$): τ 4.43 (2H incomplete s, H-3',4').

1,3,2',6'-Tetra-N-*benzyloxycarbonyl-3',4'-dideoxy-3'-enoneamine* (**11**). To a solution of **10** (903 mg) in $CHCl_3$ (15 ml). *p*-toluenesulfonic acid hydrate (21 mg) in MeOH (7 ml) was added and the solution was heated at 50 °C for 1.5 hr. After triethylamine (0.03 ml) was added, the solution was evaporated to give a solid, which was washed throughly with H_2O; yield 810 mg (98%). The solid was recrystallized from EtOH, mp 234—238 °C, $[\alpha]_D^{20}$ −26° (*c* 0.8, dioxane).

Found: C, 64.02; H, 5.92; N, 6.77%. Calcd for $C_{44}H_{48}N_4O_{12}$: C, 64.07; H, 5.87; N, 6.79%.

NMR (in DMSO-d_6): τ 4.31 (2H incomplete s, H-3',4'), 2.5—3.0 (4H, disappeared on deuteration, $NHCO_2$-).

3,2',6'-Tri-N-*benzyloxycarbonyl-3',4'-dideoxy-3'-enoneamine 1,6-Carbamate* (**12**). The solution of **11** (917 mg) in DMF (10 ml) was treated with 50% NaH (167 mg) as described for the preparation of **2**. The reaction completed in 2 hr. The crude product (880 mg) was chromatographed on a column of silica gel with $CHCl_3$–EtOH (15 : 1) to give a solid, 577 mg (73%), which was reprecipitated from $CHCl_3$–*n*-hexane, $[\alpha]_D^{20}$ −19° (*c* 1, dioxane); R_f 0.35 (tlc with $CHCl_3$–EtOH (15 : 1); **11**: R_f 0.40); IR (KBr): 1770, 1700, 1525 cm^{-1}.

Found: C, 62.03; H, 5.82; N, 7.88%. Calcd for $C_{37}H_{40}N_4O_{11}$: C, 62.00; H, 5.63; N, 7.82%.

NMR (in $CDCl_3$): τ 4.43 (2H incomplete s, H-3',4').

3,2',6'-Tri-N-*benzyloxycarbonyl-3',4'-dideoxy-3'-enoneamine* (**13**). To a solution of **12** (361 mg) in aqueous dioxane (12 : 13, 12 ml), anhydrous Na_2CO_3 (447 mg) was added and the mixture was heated at 80 °C for 2 hr. The solution was cooled and then filtered from precipitants. The filtrate was evaporated to give a solid, which was extracted with chloroform. The solution was evaporated to give a solid, 287 mg (83%), which was reprecipitated from $CHCl_3$–*n*-hexane, $[\alpha]_D^{20}$ −19° (*c* 1.1, $CHCl_3$); R_f 0.5 (tlc with $CHCl_3$–MeOH–17% NH_3 (2 : 1 : 1); **12**: R_f 0.65); IR (KBr): 1700, 1535 cm^{-1}.

Found: C, 62.31; H, 6.08; N, 7.65%. Calcd for $C_{36}H_{42}N_4O_{10}$: C, 62.60; H, 6.13; N, 8.11%.

NMR (in $CDCl_3$): τ 4.33 (2H broad s, H-3', 4').

3,2',6'-Tri-N-*benzyloxycarbonyl-3',4'-dideoxy-3'-eno-1*-N-[*(S)-2-hydroxy-4-phthalimidobutyryl*]*neamine* (**14**). The active ester prepared from HPBA (138 mg), NHS (66 mg) and DCC (184 mg) in THF was treated with **13** (227 mg) in dioxane containing triethylamine (38 mg) in a manner as described for the preparation of **4**. The crude product (550 mg) was dissolved in $CHCl_3$ and the solution was washed with water. The product was chromatographed on a column of silica gel with $CHCl_3$–EtOH (15 : 1) to give a solid, 155 mg (51%), which was recrystallized from EtOH, $[\alpha]_D^{20}$ −32° (*c* 1.3, dioxane); R_f 0.25 (tlc with $CHCl_3$–EtOH (15 : 1); **13**: R_f 0); IR (KBr): 1780 (5-membered imide), 1710, 1640, 1540 cm^{-1}.

Found: C, 62.76; H, 5.65; N, 7.33%. Calcd for $C_{48}H_{51}N_5O_{14}$: C, 62.53; H, 5.58; N, 7.60%.

NMR (in DMSO-d_6): τ 4.37 (2H, H-3',4'), 2.08 (4H s, $(CO)_2C_6H_4$).

References

1) Part XLI of "Studies on Aminosugars", primarily by S. Umezawa. Presented in part in a short communication: S. Umezawa, D. Ikeda, T. Tsuchiya and H. Umezawa, *J. Antibiot.* (Tokyo), **26**, 304 (1974).

2) D. Ikeda, T. Tsuchiya, S. Umezawa, and H. Umezawa, This Bulletin, **47**, 3136 (1974).

3) S. Umezawa, Y. Takagi, and T. Tsuchiya, *ibid.*, **44**, 1411 (1971).

4) S. Umezawa, T. Tsuchiya, T. Jikihara, and H. Umezawa, *J. Antibiot.* (Tokyo), **24**, 711 (1971): This Bulletin, **46**, 3507 (1973).

5) E. Akita, Y. Horiuchi and T. Ito, Japanese Patent 49-20166. Feb. 22 (1974).

6) D. Ikeda, T. Suzuki, T. Tsuchiya, S. Umezawa, and H. Umezawa, This Bulletin, **46**, 3210 (1973).

7) S. Umezawa, Y. Okazaki, and T. Tsuchiya, This Bulletin, **45**, 3619 (1972).

8) P. W. K. Woo, H. W. Dion, and Q. R. Bartz, *Tetrahedron Lett.*, **1971**, 2617.

9) See for example, H. Umezawa, T. Tsuchiya, R. Muto and S. Umezawa, This Bulletin, **45**, 2842 (1972) (See the preparation of compound **8** in the article.)

Reactions of Ethylene with Chloroform Initiated by Amine–Ferrous Chloride System

Teruzo ASAHARA, Manabu SENŌ, and Noritaka OHTANI

Institute of Industrial Science, The University of Tokyo, Roppongi, Minato-ku, Tokyo 106

(Received July 2, 1974)

The reactions of ethylene with chloroform initiated by alkylamine–ferrous chloride systems were examined in detail. Two main products, α,α,α-trichloroalkanes (I) and α,α,ω-trichloroalkanes (II), were obtained. Their composition was independent of the kind of amine but dependent upon the total carbon number of alkylamine. When amines having higher alkyl groups were used, the main product was α,α,ω-trichloropropane (II-1). When lower alkylamines were used, the main products were α,α,α-trichloroalkanes which contained considerable amounts of higher telomers. The results support the view that the reactions proceed according to the "caged free radical" process.

A number of reports on the radical reaction of olefins with polyhaloalkanes have been presented and various initiators have been explored for this reaction. The peroxides afforded telomers in most cases, whereas some transition metal complexes gave a 1 : 1 adduct in a good yield.[1] It was previously reported that amine–cupric chloride,[2] triethyl phosphite–iron chloride,[3] *N*-chloroalkylamine–ferrous chloride,[4] and others[5] also give a 1 : 1 adduct of ethylene with carbon tetrachloride as the main product. We suggested that a "caged radical" process would proceed along with the so-called "free radical" propagating process.[6] In order to confirm the above reaction mechanism, the reaction of ethylene with chloroform initiated by amine-ferrous chloride was investigated in detail and the results are given in this paper. A combination of ethylene and chloroform is suitable for this purpose, since "free" trichloromethyl radical adds readily to ethylene as compared with other higher olefins,[1g] and two products, α,α,α-trichloroalkanes (I) and α,α,ω-trichloroalkanes (II), could be derived in the reaction of ethylene with chloroform. The former is the product of the peroxide-initiated reaction and, therefore, considered to be formed *via* a "free radical" propagating process, and the latter is considered to be formed mainly *via* a "caged radical" process.

Experimental

Materials. Ethylene (purity 99.8%), amines and metallic salts of commercial special grade were used without further purification. Commercial chloroform was purified through an activated alumina column and the purity was examined by gas chromatography.

Reactions of Ethylene with Chloroform. The reaction was carried out in a 200 ml stainless steel autoclave with a magnetic stirrer. Chloroform (1 mol) and a certain amount of initiators were placed in the autoclave and the air inside was replaced several times with ethylene. After ethylene was charged to 20 kg/cm² at 30 °C, the autoclave was heated up to 130 °C. After the reaction, the autoclave was chilled to room temperature and the reaction mixture was washed with 1 M hydrochloric acid to remove amine and metallic salts.

Analyses of the Products. The reaction products were analysed by a temperature-programmed gas chromatograph using a 2 m column of Silicone DC 550 at 40—200 °C. *n*-Hexane was used as an internal standard. Authentic samples were prepared by the following method. α,α,α-Trichloroalkanes $CCl_3(C_2H_4)_nH$ (I) (n=1,2,3), α,α,ω-trichloroalkanes $CHCl_2(C_2H_4)_nCl$ (II) (n=1,2), and α,α,α,ω-tetrachloroalkanes $CCl_3(C_2H_4)_nCl$ (IV) (n=1,2) were prepared by the reaction of ethylene with chloroform initiated by di-*t*-butylperoxide (DTBP), by that of ethylene with chloroform initiated by the iron chloride–hexamethylphosphoric triamide (HMPA) system[5] and by that of ethylene with carbon tetrachloride initiated by DTBP, respectively. The products were purified several times by fractional distillation and the purity was confirmed by glc. α,α-Dichloroalkanes $CHCl_2(C_2H_4)_nH$ (III) (n=1,2) and γ,γ-dichloroalkanes $HC_2H_4CCl_2(C_2H_4)_nH$ (VII) (n=1,2) were prepared by the reactions of the corresponding aldehydes or ketones with phosphorus pentachloride and purified by distillation. For quantitative analyses of α,γ,γ-trichloroalkanes $ClC_2H_4CCl_2(C_2H_4)_nH$ (V) (n=1,2) and α,γ,γ,ω-tetrachloroalkanes $ClC_2H_4CCl_2(C_2H_4)_nCl$ (VI) (n=1), type I and IV telomers with the same molecular weights as those of V and VI, respectively, were used.

Results and Discussion

Several initiator systems were examined and the results are summarized in Table 1. In the presence of iron particles, the reaction had an induction period (about 30 min) and proceeded very slowly. Ferrous chloride gave the same products as those in the case of iron particles at a rather slow reaction rate. *n*-Butylamine greatly accelerated the reaction, whereas di-*n*-butylamine was not effective. A combination of ferrous chloride (0.002 mol) with di-*n*-butylamine (0.02 mol), however, induced the reaction without an induction period (the decrease in ethylene pressure, $-\Delta P$= 6 kg/cm² for 90 min). An equimolar mixture of amine with iron particle or ferrous chloride increased the reaction rate. In the case of di-*n*-butylamine–iron particle system, the reaction rate changed considerably in the course of reaction; the reaction proceeded slowly at first 70 min ($-\Delta P$=4 kg/cm²) and then the rate was greatly increased. A similar stepwise change in the reaction rate was seen in the *n*-butylamine-iron particle system though the extent of change was not so large.

In the absence of amine, dichloromethyl radicals which act as initiating radicals are possibly formed:

$$Fe + 2\,CHCl_3 \longrightarrow FeCl_2 + 2\cdot CHCl_2 \quad (1)$$

$$Fe + CHCl_3 \longrightarrow FeCl_3 + \cdot CHCl_2 \quad (2)$$

The possibility of radical formation by the reaction of polyhaloalkane and amine in the absence of metal has been examined.[7] When *n*-butylamine was added

Table 1. Reaction of ethylene with chloroform[a)]

Initiator system	Time min	Conv. of chloroform %	Total yield g	$-\Delta P$ of ethylene kg/cm²	Product mol%[b)] I	II	III	IV	V	VI	VII
None	180	0	0	51—51	—	—	—	—	—	—	—
Fe	120	5	8	51—43	98	—	2	—	—	—	—
$FeCl_2 \cdot 4H_2O$	180	12	20	48—31	97	—	2	tr	—	—	—
n-$BuNH_2$	120	11	18	50—33	93	—	4	2	1	—	—
n-Bu_2NH	120	tr	tr	50—49	98	—	2	tr	—	—	—
n-$BuNH_2/Fe$	60	13	22	47—25	91	1	5	3	—	—	—
n-Bu_2NH/Fe	103	18	29	49—25	42	24	13	7	12	2	tr
n-$BuNH_2/FeCl_2 \cdot 4H_2O$	50	17	29	46—25	87	2	4	4	—	—	3
n-$Bu_2NH/FeCl_2 \cdot 4H_2O$	44	22	33	44—25	6	63	10	6	6	8	1

a) Reaction conditions: charged ethylene pressure, 20 kg/cm² at 30 °C; chloroform, 1 mol; reaction temperature, 130 °C; each initiator component, 0.02 mol. b) In all Tables, the telomers except for those contained in Experimental are omitted since their amounts were very small in all runs.

Table 2. Reaction of ethylene with chloroform using various amine–ferrous chloride systems[a)]

Amine		Time[b)] min	Conv. of chloroform %	Total yield g	Product mol% I	II	III	IV	V	VI	VII
$C_2H_5NH_2$	(**1**)	122	17	29	95	—	2	3	—	—	—
n-$C_3H_7NH_2$	(**2**)	85	17	28	90	—	3	6	—	—	1
n-$C_4H_9NH_2$	(**3**)	50	17	29	87	2	4	4	—	—	3
n-$C_6H_{13}NH_2$	(**4**)	120[c)]	12	20	59	11	9	13	4	—	4
n-$C_8H_{17}NH_2$	(**5**)	120	17	28	17	40	14	8	11	7	3
$(C_2H_5)_2NH$	(**6**)	114	16	27	60	8	9	13	4	—	6
$(n$-$C_3H_7)_2NH$	(**7**)	45	17	27	31	24	15	13	10	2	4
$(n$-$C_4H_9)_2NH$	(**8**)	44	22	33	6	63	10	6	6	8	1
$(C_2H_5)_3N$	(**9**)	46	17	27	27	20	18	13	11	5	6
$(n$-$C_3H_7)_3N$	(**10**)	26	25	39	3	71	8	5	5	8	tr
$(n$-$C_4H_9)_3N$	(**11**)	16	23	35	2	77	7	2	5	7	tr
cyclo-$C_6H_{11}NH_2$	(**12**)	30	16	27	71	9	6	9	2	—	3
$(cyclo$-$C_6H_{11})_2NH$	(**13**)	25	20	31	10	62	8	4	9	6	1
$C_5H_{11}N$	(**14**)[d)]	131	18	29	52	12	11	14	5	tr	6

a) Reaction conditions: charged ethylene pressure, 20 kg/cm² at 30 °C; chloroform, 1 mol; reaction temperature, 130 °C; amine and ferrous chloride, 0.02 mol. b) Reaction was continued until ethylene pressure fell down to 25 kg/cm² at 130 °C. c) The change of ethylene pressure was from 46 to 34 kg/cm² at 130 °C. d) Piperidine.

to ethylene and chloroform in the absence of added metal, a considerable amount of telomers of type I was obtained. Although it is uncertain whether trace of metal is necessary for the reaction or not, it is probable that the surface of the autoclave would effect the reaction. As the reaction is very low in the absence of added metal and the change of the reaction rate in the course of reaction is observed for the amine-iron particle system, it is considered that what induces the initiation reaction is not iron metal, but mainly ferrous ions. The radical formation possibly takes place, for the most part, according to Eq. 3. Through the interaction of chloroform with ferrous chloride activated by amines, dichloromethyl radical is formed.

$$Fe^{2+}L_k + CHCl_3 \rightleftharpoons [Fe^{3+}L_kCl^- \cdot CHCl_2] \quad (3)$$

X

L=amine

Results of reactions using various amine-ferrous chloride systems are shown in Table 2. The reactions were continued until the ethylene pressure fell down to 25 kg/cm² from the initial value of about 50 kg/cm² at 130 °C, and the compositions of the products were compared at the same value of ethylene conversion. It was found that the composition of products was independent of the kind of amine, but dependent upon the total carbon number of alkylamine. The main products are α,α,α-trichloroalkanes (I) when the number of alkyl carbons of amines is less than six. The ratio of α,α,ω-trichloroalkanes (II) to the total products increases as the alkyl group becomes larger, II becoming a main product for alkylamines having more than eight carbons.

The molecular weight distributions of each type product for the triethylamine–ferrous chloride system are shown in Fig. 1. The amount of the n=2 telomer of type I, α,α,α-trichloropentane (I-2), is comparable to that of the 1 : 1 adduct, α,α,α-trichloropropane (I-1), a considerable amount of n=3 telomers being also produced. The molar distribution of $\alpha,\alpha,\alpha,\omega$-tetrachloroalkanes (IV) is similar to that of I. The distribution curves of I and IV remain unchanged when

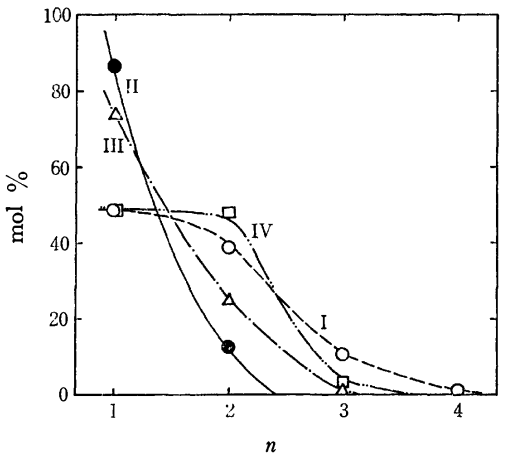

Fig. 1. Product distribution of each type telomer.

amines other than triethylamine are used. For the products of type II, however, the 1 : 1 adduct, α,α,ω-trichloropropane (II-1), is produced almost exclusively. The distribution curve of α,α-dichloroalkane (III) lies between the curve of II and that of I or IV.

The results can be explained by a reaction mechanism in which a "caged radical" process proceeds along with a "free radical" propagating process. When bulky molecules of amine coordinate ferrous ions, most of the dichloromethyl radicals formed according to Eq. 3 are trapped within a cage formed by the coordinating amine and add to ethylene invading into the cage (Eq. 4).

$$X + C_2H_4 \longrightarrow \underset{X_1}{[Fe^{3+}L_kCl^- \cdot C_2H_4CHCl_2]} \quad (4)$$

$$X_1 \longrightarrow Fe^{2+}L_k + \underset{\text{II-1}}{ClC_2H_4CHCl_2} \quad (5)$$

$$X_1 + CHCl_3 \rightarrow Fe^{3+}L_kCl^- + \underset{\text{III-1}}{HC_2H_4CHCl_2} + \cdot CCl_3 \quad (6)$$

$$X_1 + C_2H_4 \longrightarrow \underset{X_2}{[Fe^{3+}L_kCl^- \cdot (C_2H_4)_2CHCl_2]} \quad (7)$$

$$X \longrightarrow Fe^{3+}L_kCl^- + \cdot CHCl_2 \quad (8)$$

$$\cdot CHCl_2 + nC_2H_4 + CHCl_3 \rightarrow \underset{\text{III}}{CHCl_2(C_2H_4)_nH} + \cdot CCl_3 \quad (9)$$

$$\cdot CCl_3 + nC_2H_4 + CHCl_3 \rightarrow \underset{\text{I}}{CCl_3(C_2H_4)_nH} + \cdot CCl_3 \quad (10)$$

$$CHCl_2(C_2H_4)_n \cdot + Fe^{3+}L_kCl^- \rightarrow \underset{\text{II}}{CHCl_2(C_2H_4)_nCl} + Fe^{2+}L_k \quad (11)$$

$$CCl_3(C_2H_4)_n \cdot + Fe^{3+}L_kCl^- \rightarrow \underset{\text{IV}}{CCl_3(C_2H_4)_nCl} + Fe^{2+}L_k \quad (12)$$

The ω,ω-dichloropropyl radical in the cage would take part in three ways in the following steps of the reaction. For the most part, the radical abstracts chlorine atom from ferric chloride to afford II-1 (Eq. 5). The hydrogen abstraction from chloroform around the cage may partly occur and α,α-dichloropropane (III-1) and "free" trichloromethyl radical are formed (Eq. 6). The chain propagating reaction in the cage (Eq. 7) would rarely occur, because other ethylene molecules should be supplied into the cage. When smaller amines are used, the dichloromethyl radical would be relatively mobile and get out of the cage, and then a "free radical" propagating process would take place to form telomers of type III and trichloromethyl radicals (Eqs. 8 and 9).

Trichloromethyl radicals afford telomers I by the chain reaction (Eq. 10). Chloride abstraction reactions of ω,ω-dichlorolakyl radical and ω,ω,ω-trichloroalkyl radical from chloride complex give telomers II and IV, respectively (Eqs. 11 and 12).

ω,ω-Dichloroalkyl free radical is expected not to differ much from ω,ω,ω-trichloroalkyl free radical in reactivity against chloroform, ethylene, or chloride complex. According to the above reaction scheme, the product of type II is formed both in the caged radical process of Eq. 5 (mainly 1 : 1 adduct) and in the free radical process of Eq. 11 (mainly high telomers). It is seen from Fig. 2 that the ratio of II-1 to the total amount of type II products increases as the composition ratio of II to the total products increases. This can be explained by the predominant occurrence of the "caged process". Conversely, as the "free radical" process becomes predominant, the molecular weight distribution of II would gradually resemble that of I or IV with the decrease in the product ratio of II. Figure 2 shows that this is the case. The variation in total yield or the conversion of chloroform at a definite ethylene conversion in Table 2 is explained in the same way.

The effects of reaction time, ethylene pressure, and reaction temperature on the composition ratio of products were examined and the results are shown in Tables 3, 4, and 5, respectively. With the elongation

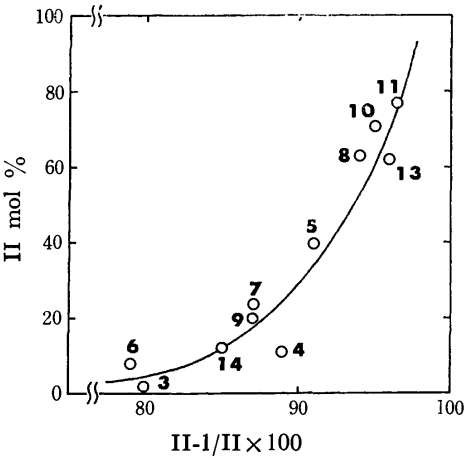

Fig. 2 Ratio of II-1 to Type II products.

TABLE 3. EFFECT OF REACTION TIME ON Et_3N-$FeCl_2 \cdot 4H_2O$ SYSTEM[a]

Time min	Conv. of $CHCl_3$ %	Product mol%						
		I	II	III	IV	V	VI	VII
15	8	40	21	15	15	5	1	3
30	10	30	27	16	14	7	3	3
45	12	25	29	17	13	8	4	4

a) Amount of triethylamine and ferrous chloride is 0.01 mol for both. Other reaction conditions are the same as those given in Table 2.

Table 4. Effect of ethylene pressure for n-Bu_2NH-$FeCl_2 \cdot 4H_2O$ system[a)]

Charged ethylene kg/cm² at 30 °C	Conv. of $CHCl_3$ %	Product mol%						
		I	II	III	IV	V	VI	VII
10	12	8	70	8	7	3	5	—
15	13	10	64	10	6	5	5	—
20	15	5	62	13	7	5	8	tr

a) Reaction was continued until $-\Delta P = 10$ kg/cm² at 130 °C. Other reaction conditions are the same as those given in Table 2.

Table 5. Effect of reaction temperature for Et_3N-$FeCl_2 \cdot 4H_2O$ system[a)]

Temp. °C	Time min	Conv. of $CHCl_3$ %	Product mol%						
			I	II	III	IV	V	VI	VII
110	230	15	31	25	16	11	8	3	6
120	120	15	28	24	19	11	9	3	5
130	46	17	27	20	18	13	11	5	6

a) Reaction conditions except reaction temperature are the same as those given in Table 2.

of reaction time, the composition ratios of products of types I and IV decreased, accompanied by an increase in the ratios of V, VI, and VII for all the amine–ferrous chloride systems examined. The products of types I and IV, having a trichloromethyl group, may react as a telogen in the same manner as for chloroform and give products of types V, VI, and VII.[1f)] The slight increase of II with an increase in reaction time seems to be connected with the change in ethylene pressure. The ratio of II is slightly greater at a low ethylene pressure compared with that at a high pressure as is shown in Table 4. The increase in reaction temperature scarcely affects the composition ratio of products. The ratio of II tends to increase somewhat at lower temperatures.

It should be noted that the amine–cuprous chloride system shows a similar tendency to the amine–ferrous chloride system. The main products in the case of $EtNH_2$–CuCl were of type I, whereas those in the case of $BuNH_2$–CuCl and Bu_2NH–CuCl were of ty peII. The reactions in the amine–cuprous chloride system probably proceed according to a similar mechanism to that in the amine–ferrous chloride system.

The authors would like to express their thanks to Mr. H. Nojiri for assistance in the experiments.

References

1) a) M. Asscher and D. Vofsi, *J. Chem. Soc.*, **1963**, 1887; M. Asscher and D. Vofsi, *ibid.*, **1963**, 3921. b) D. J. Burton and L. J. Kehoe, *J. Org. Chem.*, **35**, 1339 (1970). c) T. Susuki and J. Tsuji, *ibid.*, **35**, 2982 (1970). d) H. Matsumoto, T. Nakano, and Y. Nagai, *Tetrahedron Lett.*, **1973**, 5147. e) T. Asahara, M. Seno, and C. C. Wu, This Bulletin, **43**, 1127 (1970). f) T. Asahara, A. Kurita, and T. Sato, *Kogyo Kagaku Zasshi*, **74**, 1847 (1971). g) T. Sato, M. Seno, and T. Asahara, *Yukagaku*, **22**, 298 (1973). h) T. Sato, M. Senō, and T. Asahara, *Yuki Gosei Kagaku Kyokai Shi*, **32**, 184 (1974).

2) T. Asahara, M. Senō, and C. C. Wu, *Kogyo Kagaku Zasshi*, **72**, 1822 (1969).

3) T. Asahara and T. Sato, *ibid.*, **74**, 703 (1971).

4) T. Asahara, M. Senō, and N. Ohtani, This Bulletin, **46**, 3193 (1973).

5) a) T. Asahara and T. Sato, *Seisan Kenkyu*, **23**, 138 (1971). b) T. Asahara and T. Sato, *Kogyo Kagaku Zasshi*, **74**, 1845 (1971).

6) T. Asahara, M. Senō, and N. Ohtani, This Bulletin. **47**, 2007 (1974).

7) a) M. Imoto, K. Takemoto, T. Iwasaka, and M. Sasabe, *Kogyo Kagaku Zasshi*, **73**, 2473 (1970). b) J. R. L. Smith and Z. A. Malik, *J. Chem. Soc., B*, **1970**, 617; J. R. Smith and Z. A. Malik, *ibid.*, **1970**, 920.

Studies on the Synthesis of Histidine Peptides. I. N^{im}-Tosylhistidine Derivatives as Starting Materials[1,2]

Toshiyuki FUJII* and Shumpei SAKAKIBARA**

Peptide Institute, Protein Research Foundation, Ina 476, Minoh, Osaka 562

(Received July 20, 1974)

N^{α}-Nps-, Z(OMe)-, Z-, Boc-, and Aoc-derivatives of N^{im}-tosylhistidine were synthesized as materials for the syntheses of histidine-containing peptides, and the reactivity of the N^{im}-tosyl group was examined under several conditions commonly used for peptide syntheses. Although the N^{im}-tosyl group was somewhat more unstable than N^{im}-benzyl group, the use of the tosyl derivative was found to be advantageous in several points: the enhancement of the solubility of its peptide derivatives, the suppressive effect of racemization during its coupling reactions, and the high removability of the tosyl group under mild conditions.

Although several different procedures for the incorporation of histidine residues into peptides have been published by many workers, those methods still have several problems.[3] Histidine-peptides can be synthesized without the protection of the imidazole group, but only limited, mild conditions have to be used for their coupling reactions because of the remaining presence of active hydrogens in the side chains. Further, the strict purification of the each intermediate is indispensable to obtain the final product in a reasonable purity. To improve the situation, the following N^{im}-protective groups have been proposed by many workers: benzyl,[4] benzyloxycarbonyl,[5] trityl,[6] adamantyloxycarbonyl,[7] 2,2,2-trifluoro-1-acylaminoethyl,[8] piperidinocarbonyl,[9] dinitrophenyl,[10] diphenylmethyl,[11] trinitrophenyl,[12] and *t*-butyloxycarbonyl.[13] These protective groups are each characteristic and may be useful in specific cases, but we cannot declare that all the problems involved in the synthesis of histidine peptides have been solved. Especially when histidine peptides are synthesized by the solid-phase method, the histidine residue is preferably incorporated into resin as a form of an N^{im}-protected derivative, which is highly soluble in methylene chloride or chloroform. Further, it may be desirable for the N^{im}-protecting group to be stable during successive coupling reactions and readily removable under mild conditions in the final stage. The present study will introduce a new N^{im}-protecting group which is useful for the relief of those problems.[1]

Originally, the tosyl group had been recognized as a stable amino-protecting group, and sodium treatment in liquid ammonia was the only practical procedure to remove the protective group from the peptide derivatives. Recently, however, the same group attached to the guanido group of arginine has been demonstrated to be removable[14] in anhydrous hydrogen fluoride (HF) at 0 °C.[15] Therefore, we checked the stability of the tosyl group attached to the imidazole moiety of histidine, and found that the group is also removable under the same conditions in anhydrous HF.[1] Thus, several derivatives of the N^{im}-tosylhistidine were synthesized in order to examine their applicability to the synthesis of histidine peptides.

Syntheses of Several N^{α}*-protected Derivatives of* N^{im}*-tosylhistidine.* The N^{im}-tosylhistidine derivatives were synthesized *via* two different procedures, shown in Schemes 1 and 2. One route started from the histidine methyl ester[16] (Method A), and the other route, from N^{α}-Z-histidine[5] (Method B). In Method A, the histidine methyl ester was acylated with acyl chlorides or azides, and the remaining unacylated histidine methyl ester was removed as completely as possible at this stage. The mono- and di-acylated histidine methyl esters thus obtained were saponified to obtain N^{α}-acyl-histidine, which was then tosylated using tosyl chloride in the saponification mixture (Scheme 1). If the saponification mixture is contaminated by the unreacted histidine ester, N^{α}, N^{im}-ditosylated histidine should be formed and its removal from the final product must be problem. Generally, the acylation of the

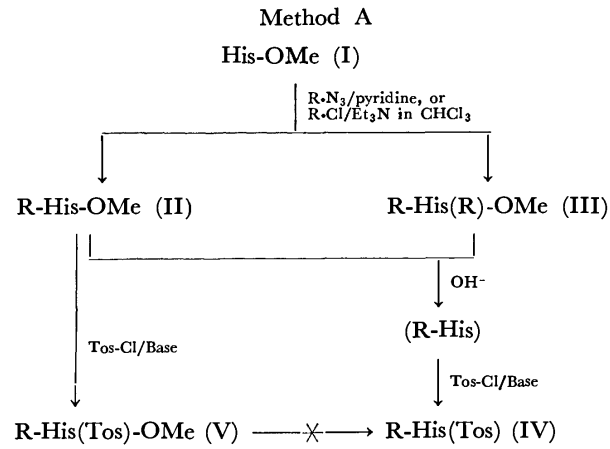

[R: a=Aoc, b=Boc, c=Z(OMe), and d=Nps.]

Scheme 1.

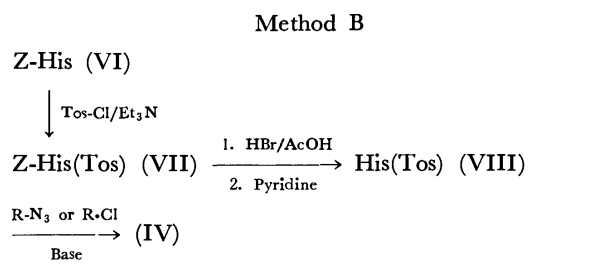

[R: a=Aoc, b=Boc, c=Z(OMe), and d=Nps.]

Scheme 2.

*Present address: Tanabe Seiyaku Co., Ltd., Higashi-Yodogawa-ku, Osaka.

** To whom requests for reprints should be addressed.

histidine methyl ester gives a mixture of mono- and di-acyl esters, depending on the reaction conditions and on the reactivity of the reagents used. When two moles of Aoc- or Boc-chloride were used as the acylating reagent, the histidine methyl ester was acylated to form diacyl esters; in this stage, the unchanged histidine methyl ester was removed completely by simple washing with water, since the diacyl histidine ester is almost insoluble in water. When Aoc- or Boc-azide was used as the reagent, the N^{α}-acyl histidine ester was formed as the major product, even if two moles of the reagent were used; in this case, care must be taken to extract the product from the reaction mixture completely because the mono-acyl esters are somewhat soluble in water. In the present study, mono- and di-Boc-histidine esters were isolated as crystals in order to confirm their properties, as will be shown in the Experimental section.

In the case of the synthesis of the Nps-derivative, the formation of the mono-Nps-histidine methyl ester was predominant.[17] Although the N^{α}-Nps-histidine methyl ester has been reported to be a crystalline material, we could not crystallize it in the present study; thus, it was purified by silica-gel-column chromatography. The histidine benzyl ester[18] was also used as a starting material for the same purpose.

In one experiment, the N^{α}-Nps-histidine methyl ester was converted to the tosyl derivative, and then we attempted to obtain N^{α}-Nps-N^{im}-tosyl-histidine by saponification. However, we were unsuccessful because of the susceptibility of the N^{im}-tosyl group to caustic alkali.

In the case of the synthesis of the Z(OMe)-derivative using the azide method, there was no difficulty in washing out the unreacted histidine ester from the reaction mixture, since both the mono- and di-Z(OMe)-histidine esters were almost insoluble in water; the mixture of the mono- and di-acylated derivatives was directly saponified to obtain N^{α}-Z(OMe)-histidine, which was then further converted to the N^{im}-tosyl derivative, as has been shown before.

In Method B, N^{α}-Z-histidine[5] was tosylated with tosyl chloride; the product was treated with anhydrous hydrogen bromide in acetic acid to obtain N^{im}-tosyl-histidine, which was then treated with the respective acyl chlorides or azides to obtain N^{α}-protected-N^{im}-tosyl-histidines (Scheme 2). This procedure gave products identical with those obtained by Method A, but the yields were generally lower than those obtained by means of Method A. This may be attributed to the partial decomposition of the tosyl group during the HBr treatment and to the acylation reactions. The catalytic hydrogenolysis of the N^{α}-Z-N^{im}-tosyl-histidine with a palladium catalyst was attempted in order to obtain N^{im}-tosylhistidine, but the attempt was unsuccessful; during the reaction, the N^{im}-tosylhistidine formed was precipitated out over the catalyst and further hydrogenolysis was disturbed.

Generally, N^{α}-acylated histidines which are obtained by the direct acylation of histidine are soluble in water, and troublesome procedures are necessary to remove any unchanged histidine from the reaction mixture. Therefore, the direct synthesis of N^{α}-acyl-N^{im}-tosyl-histidine from free histidine was concluded to be impractical.

The physical constants and analytical data of N^{α}-protected-N^{im}-tosylated histidine derivatives synthesized by Methods A and B are listed in Table 1.

Stability of the N^{im}-*Tosyl Group.* N^{α}-Protected-N^{im}-tosyl-histidines, such as N^{α}-Boc-, N^{α}-Z(OMe)-, and N^{α}-Nps-derivatives, were found to decompose gradually during storage at room temperature. This decomposition may be caused by the enhanced acidity of their own carboxyl groups resulting from the presence of the tosyl group in their side chains. Therefore, the storage of these compounds in the form of DCHA salts was considered to be practical.

The stability of the N^{im}-tosyl group was compared with that of other protective groups under various conditions commonly used for peptide synthesis; the data are summarized in Table 2. The tosyl group was removed easily in aqueous 1 N sodium hydroxide at room temperature, but 50% of this group survived in 25% aqueous ammonia at room temperature during

Table 1. Physicochemical properties of N^{α}-protected-N^{im}-Tos-histidine derivatives

		Mp (°C)	$[\alpha]_D$ (c 1)	Formula	Anal. % Calcd/Found			
					C	H	N	S
Aoc-L-His(Tos)-OH	IV-a	109—111 (dec.)	+10.0(f)	$C_{19}H_{25}N_3O_6S$	53.89 54.00	5.95 5.68	9.93 9.98	7.57 7.76
Boc-L-His(Tos)-OH	IV-b	123—115	+15.1(g)	$C_{18}H_{23}N_3O_6S$	52.81 52.83	5.66 5.55	10.27 10.32	7.81 7.58
Z(OMe)-L-His(Tos)-OH[a]	IV-c	179.5—180.5	+20.0(e)	$C_{34}H_{46}N_4O_7S$	62.37 62.11	7.08 7.21	8.56 8.44	4.90 4.85
Z-L-His(Tos)-OH[a]	VII	150—152 (dec.)	+19.1(e)	$C_{33}H_{44}N_4O_6S$	63.44 63.43	7.10 6.96	8.97 9.00	5.12 4.98
Nps-L-His(Tos)-OH	IV-d	141—142 (dec.)	+39.9(e)	$C_{19}H_{18}N_4O_6S_2$	49.35 49.62	3.92 3.74	12.12 12.21	13.84 13.39
Nps-L-His(Tos)-OMe	V-d	101—103	+34.1(e)	$C_{20}H_{20}N_4O_6S_2$	50.42 50.78	4.23 4.20	11.76 11.98	13.45 12.97
Nps-L-His(Tos)-OBzl		102—104	+24.8(e)	$C_{26}H_{24}N_4O_6S_2$	56.52 56.37	4.38 4.18	10.14 10.15	11.58 11.52

a)=DCHA salt (e)=DMF (f)=pyridine (g)=MeOH

Table 2. Behavior of N^{im}-protective groups under various conditions

N^{im}-protective group	H_2/Pd	Na/NH_3	1 M-NaOH[a]	25% aq. NH_3[a]	2 M-HBr in AcOH[a]	4 M-HCl in Dioxane[a]	Anhyd. CF_3CO_2H[b]	Anhyd. HF[c]	HOBT.[a]
Bzl[4]	B	A	S	S	S	S	S	S	S
Z[5]	A	A	A	A	B	B	B	A	B
Tri[6]		A	S		B	B	A		
Boc-TF[8]	S				A	A	A		
Tos	S	A	A	B	C	C	S	A	A

A: Removed. B: Slowly removed. C: Partially removed. S: Stable.
a) At room temp. 1 hr. b) At 15 °C 30 min. c) At 0 °C 1 hr.

one hour's treatment. From these facts, it was concluded that the N^{im}-tosyl group was little more stable than the N^{im}-Z group under alkaline conditions; the N^{im}-Z group is known to be removed not only in caustic alkali, but also in aqueous ammonia.[5] Only about 10% of the tosyl group was removed in 2 M HBr in acetic acid or in 4 M HCl in dioxane during one hour's treatment at roo mtemperature, while the complete removal of the group was observed during further storage overnight at room temperature.

As has been pointed out before, the N^{im}-tosyl group was readily cleaved in anhydrous HF at 0 °C within 30 min. When Nps-containing compounds weret reated by HF, the addition of skatole as a scavenger was effective, as will be shown in the second paper of this series.

One of the characteristics of the N^{im}-tosyl group was that it was almost unaffected by anhydrous trifluoroacetic acid during short treatment at room temperature; thus, Aoc-, Boc-, Z(OMe)-, and Nps-groups can be removed selectively from peptides containing the N^{im}-tosylhistidyl residue. This property was successfully used in the synthesis of Angiotensin II by the solid-phase procedure.[19]

The N^{im}-tosyl group did not interfere with the catalytic hydrogenolysis of other groups; however, a small amount of the tosyl group was found to be cleaved during the removal of *N*-benzyloxycarbonyl groups. This may be explained by a nucleophilic attack of the formed amino group during the hydrogenolysis. Bergmann and Zervas have pointed out that the N^{im}-acetyl group migrates to other amino groups under physiological conditions.[20] Later, Sakiyama *et al.*[4b] reported the same phenomenon with di-Z-histidine, in which the N^{im}-Z-group was observed to transfer to the amino group of the glycine methyl ester in dioxane at 50—60 °C. In the present study, although N^{α}-Boc-N^{im}-tosylhistidine was treated with the glycine methyl ester under the same condition, no migrated product was detectable within one hour in a reaction mixture. After six hours, however, the formation of the tosylglycine methyl ester was observed in a yield of more than 6.5%.

The N^{im}-tosyl group remained unchanged at room temperature for 24 hr. in the presence of two equivalents of triethylamine in dimethylformamide; this property should also be counted as an advantage of this protecting group in peptide synthesis.

Finally, it was noteworthy that the N^{im}-tosyl group was readily removed at room temperature in the presence of excess 1-hydroxybenzotriazole (HOBT), which is widely used as a convenient reagent for peptide synthesis.[21] During the reaction, the formation of 1-(tosyloxy)benzotriazole as the main product was confirmed. Those facts indicate that Geiger's procedure should always result in the formation of imidazole-free peptides, even if an N^{im}-tosyl derivative is used as the starting material. This procedure has also been successfully applied to the synthesis of histidine-peptides, as will be shown in the following report.

On the contrary, the N^{im}-Z group was found to be much more stable against the same reagent.

Experimental

The melting points were measured by the capillary method and were not corrected. Thin-layer chromatography (tlc) was carried out on Merck's Silica Gel G using the following solvent systems: (1) chloroform–methanol–acetic acid (95 : 5 : 3), and (2) *n*-butanol–acetic acid–water (4 : 1 : 1). The IR spectra were determined on a Shimadzu IR-27G Spectrometer, and the UV spectra, on a Hitachi ESP-2U spectrometer.

N^{τ}-Aoc-His–OMe (II-a) and N^{α},N^{im}-di-Aoc-His–OMe (III-a). Aoc-azide (15.7 g, 100 mmol) was added to a solution of His-OMe (I) in dry pyridine (20 ml), which had been isolated from His-OMe·2HCl (12 g, 50 mmol) following the procedure of Wünsch;[22] the mixture was then allowed to react for 3 days at 30 °C under stirring. The pyridine was removed under reduced pressure, the remaining oil was flushed with benzene, the residue was dissolved in ethyl acetate, and a small amount of an insoluble material was removed by filtration. *n*-Hexane was added to the filtrate until a part of the product precipitated out. After the mixture had been kept in a refrigerator for 5 hr, the crystals were collected by filtration and recrystallized from ethyl acetate to afford II-a; wt. 9.8 g (70%); mp 122—124 °C, $[\alpha]_D^{22}$ −13.0° (*c*, 2.2, pyridine). Found: C, 54.89; H, 7.58; N, 14.89%. Calcd for $C_{13}H_{21}O_4N_3$: C, 55.11; H, 7.47; N, 14.83%.

The filtrate of the crude crystals and mother liquor of the recrystallization were combined and concentrated under reduced pressure, and the residual oil was redissolved in ethyl acetate. The solution was washed well with water, dried over anhydrous sodium sulfate, and concentrated again to a residue, which was then used in the following reaction as N^{α}, N^{im}-di-Aoc-His-OMe without further purification.

Aoc–His(Tos) (IV-a via Method A). Compound II-a (9.5 g) and the oily residue obtained above were dissolved together in methanol (30 ml), after which the solution was treated with 1 N aqueous sodium hydroxide (100 ml) at room temperature. The saponification of the ester group and the

deacylation of the N^{im}-Aoc group were monitered by tlc using the (1) solvent. After the completion of the reactions had been confirmed by tlc, an aqueous solution of sodium carbonate (18 g in 300 ml) was added to the mixture and a solution of tosyl chloride (17.6 g, 90 mmol) in dioxane (50 ml) was stirred, drop by drop, into the mixture at room temperature. Stirring was continued for 4 hr; then water (500 ml) was added, and the mixture was washed three times with 100-ml portions of ether to remove the excess tosyl chloride. The aqueous phase was acidified to pH 2 with 0.5 M sulfuric acid, and the separated oily material was extracted with ethyl acetate. The extract was washed well with water, dried over anhydrous sodium sulfate, and concentrated to dryness under reduced pressure. The residue was recrystallized from ethyl acetate–*n*-hexane to obtain needles; wt. 15.8 g (75% from I·2HCl). The melting point, the $[\alpha]_D$ value, and the results of elemental analysis are shown in Table 1.

Z-His(Tos)·DCHA (VII·DCHA). Tosyl chloride (9 g, 47 mmol) was added, portion by portion, to a solution of Z-His (VI) (10 g, 35 mmol)[5b] and sodium carbonate (7 g) in water (100 ml) over a 30-min period under vigorous stirring at 10—15 °C. Stirring was continued for an additional 4 hr at room temperature, and then the reaction mixture was washed twice with 50-ml portions of ether to remove the excess tosyl chloride. The aqueous phase was then acidified to pH 2 with 1 N sulfuric acid. The separated oil was extracted three times with 100-ml portions of ethyl acetate. The extracts were combined, and the combined solution was washed with water, dried over anhydrous sodium sulfate, and concentrated under reduced pressure. The residue was redissolved in ethyl acetate (100 ml), and dicyclohexylamine (5.5 g) was added to the solution; the crystalline materials thus formed were separated by filtration and recrystallized from methanol–ethyl acetate as needles; wt, 15.4 g (70.5%). The melting point, the $[\alpha]_D$ value, and the results of the elemental analysis of this compound are shown in Table 1.

Aoc-His(Tos) (IV-a via Method B). A suspension of VII·DCHA (10 g, 16 mmol) in 1 N sulfuric acid was vigorously shaken with ethyl acetate, and the extract was concentrated under reduced pressure. The residue was treated with 4 N HBr in acetic acid (20 ml) for 1 hr at room temperature. Then, the product was precipitated by the addition of dry ether (200 ml), and the precipitate was washed well by decantation with dry ether. After having been dried in a vacuum desiccator over sodium hydroxide, the solid mass was dissolved in methanol (100 ml), and the solution was neutralized with dry pyridine (6 ml) until precipitation occurred. The precipitates were collected by filtration and washed well with methanol; wt. 3.5 g (51.7%); mp 140—145 °C. This material (3.1 g, 10 mmol), which corresponds to VIII, was then dissolved in 5% aqueous sodium bicarbonate (50 ml). Aoc-azide (1.7 g, 10 mmol) was added to the solution, together with triethylamine (1.6 ml), and the mixture was stirred at room temperature for 2 days. Some insoluble materials thus formed were filtered off, and the filtrate was acidified to pH 2 with 1 N sulfuric acid. The separated oily material was extracted with ethyl acetate, and the extract was washed with water, dried over sodium sulfate, and concentrated to dryness under reduced pressure. The residue was recrystallized from ethyl acetate–*n*-hexane; wt. 2.6 g (63%); mp 109.5—110.5 °C, $[\alpha]_D^{22}$ +10.3° (*c* 1, pyridine). The melting point showed no depression upon mixing with the same compound as synthesized by Method A.

Boc-His(Boc)-OMe (III-b). A solution of Boc-chloride in tetrahydrofuran, which had been prepared from *t*-butylalcohol (148 g) and phosgene (200 g) using an improved procedure described by Sakakibara *et al.*,[23] was stirred vigorously into a suspension of His–OMe·2HCl (I·2HCl) (120 g, 0.5 mol) and triethylamine (280 ml, 2 mol) in chloroform (800 ml) at 0—5 °C. Stirring was continued for an additional 2 hr at room temperature, and then chloroform (500 ml) was added to the reaction mixture. The chloroform solution was washed well with water, 1 N sulfuric acid, and a saturated sodium chloride solution successively, and then dried over anhydrous sodium sulfate. The dried solution was concentrated to dryness. A part of this material was crystallized from ether–*n*-hexane for analysis; mp 95—98 °C, $[\alpha]_D^{22}$ +13.0 °C (*c* 1, THF). Found: C, 54.95; H, 7.39; N, 11.71%. Calcd for $C_{17}H_{27}O_6N_3$: C, 55.27; H, 7.37; N, 11.38%.

Boc–His(Tos) (IV-b). The crude di-Boc-His-OMe obtained above was dissolved in methanol (340 ml), and aqueous 1 N sodium hydroxide (450 ml) was added to the solution at 10—15 °C. After 2 hr, a 10% solution of sodium carbonate (2 l) was added to the reaction mixture, and the whole mixture was washed well with ether. A solution of tosyl chloride (124 g, 0.65 mol) in dioxane (300 ml) was added to the washed solution under vigorous stirring at 10 °C. After the stirring had been continued for 3 hr at room temperature, the reaction mixture was washed well with ether, the aqueous phase was acidified to pH 2 with 1 N sulfuric acid, and the separated oily material was extracted with ethyl acetate. The extract was washed with a saturated sodium chloride solution, dried over anhydrous sodium sulfate, and evaporated to dryness under reduced pressure. The residue was recrystallized from ethyl acetate to afford colorless needles; wt. 107 g (52% yield from I). The melting point, the $[\alpha]_D$ value, and the results of elemental analysis are shown in Table 1. The DCHA salt of Compound IV-b was prepared and then recrystallized from methanol–ethyl acetate; mp 160—162 °C, $[\alpha]_D^{22}$ +26.5° (*c* 1, MeOH). Found: C, 61.25; H, 7.95; N, 9.46; S, 5.38%. Calcd for $C_{30}H_{46}O_6N_4S$: C, 61.01; H, 7.79; N, 9.49; S, 5.13%.

N^{α}-Boc-His-OMe (II-b). This material was obtained much as in the case of N^{α}-Aoc-His-OMe (II-a), using 1.5 equivalents of Boc-azide as the reagent. The yield was 75%; mp 124—125 °C, $[\alpha]_D^{22}$ −13.5° (*c* 1, pyridine). Reported:[22] mp 124—125 °C, $[\alpha]_D$ −13.1° (*c* 2, pyridine).

Z(OMe)–His(Tos) (IV-c). Compound IV-c was synthesized *via* Method A (Scheme 1) in the same manner as IV-a, without any isolation of acylated histidine esters; it was then crystallized as the DCHA salt in an overall yield of 82%. The melting point, the $[\alpha]_D$ value, and the results of elemental analysis are shown in Table 1.

Nps-His-OMe (II-d). Nps-chloride (19 g, 0.1 mol) was added, portion by portion, to a suspension of I·2HCl (12 g, 50 mmol) and triethylamine (28 ml, 0.2 mol) in methanol (150 ml) at 5—10 °C over a 30-min period. The mixture was agitated vigorously during the reaction. After 2 hr, water (500 ml) was added to the reaction mixture, and then it was acidified to pH 2 with 1 N sulfuric acid. The mixture was washed well with three 200-ml portions of ethyl acetate; then excess sodium bicarbonate was added to the mixture, and an oily material thus separated was extracted with ethyl acetate. The extract was washed with water, dried over anhydrous sodium sulfate, and concentrated under reduced pressure in a water bath below 40 °C. The oily residue was charged on the top of a silica-gel column (5×150 cm), using a mixture of $CHCl_3$–MeOH–pyridine (95 : 5 : 3), and the column was eluted with the same solvent system. The main fraction was collected and concentrated under reduced pressure to obtain Compound II-d as an oily material; 13.4 g (83%). Reported:[17] mp 134—136 °C.

Nps–His(Tos) (IV-d via Method A). The oily com-

pound, II-d (13.4 g), obtained above was dissolved in dioxane (125 ml) and then treated with aqueous 2 N sodium hydroxide (45 ml) over a period of 1 hr at 10—15 °C. After triethylamine (11 ml) had been added to the reaction mixture, a solution of tosyl chloride (11 g, 58 mmol) in dioxane (20 ml) was stirred into the mixture at 10 °C over a 45-min period. Stirring was continued for an additional 1 hr at 10—15 °C; then the mixture was neutralized to pH 7 with 1 N sulfuric acid, and the dioxane was removed by distillation under reduced pressure below 40 °C. Water (300 ml) was added to the residual solution, the solution was acidified to pH 2 with 1 N sulfuric acid, and an oil which separated was extracted with ethyl acetate. The ethyl acetate extract was washed with water, dried over anhydrous magnesium sulfate, and concentrated under reduced pressure at below 40 °C. The residual solid was washed with ether and recrystallized from ethyl acetate–*n*-hexane; wt. 14.4 g (75%). The melting point, the $[\alpha]_D$ value, and the results of elemental analysis are shown in Table 1.

Nps-His(Tos)-OMe (V-d). A solution of tosyl chloride (1.4 g, 7.4 mmol) in dioxane (5 ml) was stirred into a mixture of Compound II-d (2 g, 6.2 mmol) and triethylamine (1.4 ml) in dioxane (20 ml) at 5—10 °C over a 15-min period. Then the reaction mixture was diluted with water (50 ml), and the oil which separated was extracted with ethyl acetate. The extract was washed successively with 1 N sulfuric acid, water, aqueous 5% sodium bicarbonate, and water, and dried over anhydrous magnesium sulfate. The dried solution was concentrated to a residue under reduced pressure, and the solid was washed with ether and recrystalliyed from ethyl acetate; wt. 2.37 g (80.0%). The melting point, the $[\alpha]_D$ value, and the results of elemental analysis are shown in Table 1.

Nps-His(Tos)-OBzl. This compound was derived from His-OBzl-2Tos-OH[18] in a 72% yield in the same manner as has been described above. The melting point, the $[\alpha]_D$ value, and the results of elemental analysis are shown in Table 1.

Migration of the Tosyl Group from Boc-His(Tos) (VI-b) to Gly-OMe. Compound IV-b (4.1 g, 10 mmol) was added to a solution of the glycine methyl ester in absolute dioxane (40 ml); the free ester was then isolated from the hydrochloride (2.6 g, 20 mmol) using a procedure involving chloroform-ammonia.[22] The mixture was kept for 6 hr at 50—60 °C; then the solvent was distilled off under reduced pressure and the residue was redissolved in ethyl acetate (30 ml). The solution was shaken well with water (20 ml), washed further successively with 1 N sulfuric acid, aqueous 5% sodium bicarbonate, and water, and dried over anhydrous sodium sulfate. The dried solution was concentrated to an oil under reduced pressure, and the residue was dissolved in methanol. An aqueous 0.1 N sodium hydroxide solution (10 ml) was added to the solution, and the mixture was allowed to react for 1 hr at room temperature. Then, the methanol was removed by evaporation, and the aqueous layer was washed with ethyl acetate and acidified to pH 2 with 6 N sulfuric acid. The acidified solution was extracted well with ethyl acetate, and the extract was dried over anhydrous sodium sulfate and concentrated to a residue under reduced pressure; the residue was then recrystallized from ethyl acetate-petroleum ether; wt. 150 mg, mp 149—150 °C (reported value: 149—150 °C[24]). The IR spectrum of this material was identical with that of an authentic Tos–Gly. The melting point of a mixture of the product and the authentic Tos–Gly showed no depression. The presence of Bos-His in the water-layer was confirmed by tlc using the (2) solvent.

Treatment of Boc–His(Tos)–Gly–OBzl with HOBT. HOBT (0.87 g, 6.4 mmol) was added to a solution of Boc–His(Tos)–Gly–OBzl[25] (1.8 g, 3.2 mmol) in tetrahydrofuran (30 ml), after which the mixture was kept for 1 hr at room temperature. The solution was concentrated to residue under reduced pressure, and the residue was taken in ethyl acetate (70 ml). The ethyl acetate solution was shaken with 1 N sulfuric acid, and the aqueous layer was separated and then neutralized with sodium carbonate to pH 8. The aqueous solution was extracted with two portions of ethyl acetate (100 ml), and the combined extract was washed with a saturated sodium chloride solution and dried over anhydrous sodium sulfate. The dried solution was concentrated to a residue, which was subsequently recrystallized from ethyl acetate; wt. 10 g (78%); mp 138—140 °C, $[\alpha]_D^{22}$ −33° (*c* 1, THF). This material was confirmed to be Boc–His-Gly-OBzl by elemental analysis and by a study of its spectral data. Anal. Found: C, 59.72; H, 6.56; N, 13.66%. Calcd for $C_{20}H_{26}O_5N_4$: C, 59.69; H, 6.51; N, 13.92%. IR ν_{max}^{Nujol}: 3420, 3350, 3230, 1740, 1725, 1600, 1515, 1230, 1212, 1100 cm^{-1}. UV λ_{max}^{EtOH}: absence of 233 nm (ε 10530) [attributable to the N^{im}-tosyl group of Boc–His(Tos)–Gly–OBzl].

The original ethyl acetate layer, which was shaken with 1 N sulfuric acid to extract out the Boc–His-Gly-OBzl, was washed with aqueous sodium carbonate to remove the excess HOBT, after which the organic layer was washed further with water and then dried. The dried solution was concentrated under reduced pressure, and the residue was recrystallized from ethyl acetate; wt. 0.7 g (75.5%); mp 82—84 °C. Elemental analysis showed this material to be 1-(tosyloxy)-benzotriazole. Anal. Found: C, 54.19; H, 4.01; N, 14.46; S, 10.85%. Calcd for $C_{13}H_{11}O_3N_3S$: C, 53.98; H, 3.83; N, 14.53; S, 11.06%. The IR and UV spectra of this material were identical with those of an authentic sample.

1-(Tosyloxy)-benzotriazole. HOBT (2.7 g, 20 mmol) and Tos-chloride (3.8 g, 20 mmol) were dissolved together in tetrahydrofuran (50 ml), and then triethylamine (2.8 ml) was slowly added to the mixture. The materials thus precipitated were filtered off, and the filtrate was concentrated to a residue under reduced pressure. The residue was recrystallized from ethyl acetate; wt. 2.6 g (89.7%); mp 84—85 °C. IR ν_{max}^{Nujol}: 1617, 1592, 1400, 1395, 1200, 1186 cm^{-1}, absence of 3270 cm^{-1} (attributable to the *N–OH* band of HOBT). UV λ_{max}^{THF}: 236.5 nm (ε 17230).

Treatment of Boc–His(Z)–Gly–OBzl with HOBT. When Boc–His(Z)–Gly–OBzl (0.54 g, 1 mmol) was treated with HOBT as has been described above the starting material was recovered in an 89% yield under the same reaction conditions. Mp 107—108 °C, $[\alpha]_D^{22}$ +53° (*c* 1, THF). Found: C, 62.70; H, 6.28; N, 10.43%. Calcd for $C_{28}H_{32}O_7N_4$: C, 62.67; H, 6.01; N, 10.44%.

References

1) Preliminary report: S. Sakakibara and T. Fujii, This Bulletin, **42**, 1466 (1969).

2) Abbreviations used in this report are those recommended by IUPAC-IUB: *J. Biol. Chem.*, **247**, 977 (1972): Aoc, *t*-amyloxycarbonyl; DCC, *N,N'*-dicyclohexylcarbodiimide; DCHA, dicyclohexylamine.

3) E. Schröder and K. Lübke, "The Peptides," Vol. 1 Academic Press, New York (1965) p. 176.

4) V. du Vigneaud and O. K. Behrens, *J. Biol. Chem.*, **117**, 27 (1937).

5) a) A. Patchornik, A. Berger, and E. Katchalski, *J. Amer. Chem. Soc.*, **79**, 6416 (1957). b) S. Akabori, K. Okawa and F. Sakiyama, *Nature*, **181**, 772 (1958); F. Sakiyama, K. Okawa, T. Yamakawa, and S. Aakbori, This Bulletin, **31**,

926 (1958).
6) G. C. Stelakatos, D. M. Theodoropoulos, and L. Zervas, *J. Amer. Chem. Soc.*, **81**, 2884 (1959).
7) W. L. Hass, E. V. Krumkalns, and K. Gerzon, *J. Amer. Chem. Soc.*, **88**, 1988 (1966).
8) F. Weygand, W. Siedel, and P. Pietta, *Chem. Ber.*, **100**, 3841 (1967).
9) G. Jäger, R. Geiger, and W. Siedel, *ibid.*, **101**, 3537 (1968).
10) S. Shaltiel, *Biochem. Biophys. Res. Commun.*, **29**, 178 (1967); F. Chillemi and R. B. Merrifield, *Biochemistry*, **8**, 4344 (1969); S. Shaltiel and M. Fridkin, *ibid.*, **9**, 5122 (1970).
11) G. Losse and U. Krychowski, *J. Prakt. Chem.*, **312**, 1097 (1970).
12) G. Losse and U. Krychowski, *Tetrahedron Lett.*, **1971**, 4121.
13) E. Schnabel, J. Herzog, P. Hoffmann, E. Klauke, and I. Ugi, *Ann. Chem.*, **716**, 175 (1968); M. Fridkin and H. J. Goren, *Can. J. Chem.*, **49**, 1578 (1971).
14) R. H. Mazur and G. Plume, *Experientia*, **24**, 661 (1968).
15) S. Sakakibara, Y. Kishida, R. Nishizawa, and Y. Shimonishi, This Bulletin, **41**, 438 (1968); S. Sakakibara, Y. Shimonishi, Y. Kishida, M. Okada, and H. Sugihara, *ibid.*, **40**, 2164 (1967).
16) B. O. Handford, T. A. Hylton, K. T. Wang, and B. Weinstein, *J. Org. Chem.*, **33**, 4251 (1968).
17) I. Phocas, C. Yovanidis, I. Photaki, and L. Zervas, *J. Chem. Soc.*, **1506** (1967).
18) S. Akabori, S. Sakakibara, and S. Shiina, This Bulletin, **31**, 784 (1958).
19) T. Fujii and S. Sakakibara, *ibid.*, **43**, 3954 (1970).
20) M. Bergmann and L. Zervas, *Z. Physiol. Chem.*, **175**, 145 (1928).
21) W. König and R. Geiger, *Chem. Ber.*, **103**, 788 (1970).
22) E. Wünsch and A. Zwick, *Chem. Ber.*, **97**, 2497 (1964).
23) S. Sakakibara, M. Shin, M. Fujino, Y. Shimonishi, S. Inoue, and N. Inukai, This Bulletin, **38**, 1522 (1965).
24) E. Fisher and M. Bergmann, *Ann. Chem.*, **398**, 96 (1913).
25) T. Fujii, T. Kimura and S. Sakakibara, This Bulletin, in preparation.

Thiocarbonyl Ylides. Attempted Preparation and Related Reactions[1]

Shuichi MITAMURA, Masaaki TAKAKU, and Hitosi NOZAKI*

Department of Industrial Chemistry, Kyôto University, Yoshida, Sakyô-ku, Kyôto 606

(Received July 22, 1974)

The attempted preparation of thiocarbonyl ylides (I) by the proton abstraction of thiouronium salts (III) has disclosed a fast isomerization of I to enethiols (V) (Y=H) and an alternative desulfurization to enediamines (VII) (Y=Ph), the by-products being olefins (VIII) and sulfides (IX). The second route to I examined consists of the reaction of tetramethylthiourea (II) with diazomalonate, which gives rise to enediamine (VII_g). Rotation about the C=C bond of enediamines is discussed on the basis of IR and NMR spectra.

Thiocarbonyl ylides should be resonance hybrides involving 1,3-dipole[2] and tetravalent sulfur.

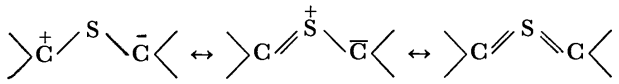

Recently Kellogg[3] reported that the thermally-induced loss of nitrogen from 1,3,4-thiadiazolines afforded transient thiocarbonyl ylides, which then cyclized to thiiranes or alternatively reacted with azo compounds to give $[4_s+2_s]$ cycloadducts. Middleton[4] isolated a stable thiocarbonyl ylide in the reaction of thiourea with dicyanocarbene.

The present authors attempted to obtain thiocarbonyl ylides (I) based on tetramethylthiourea (II) by the deprotonation of the corresponding thiouronium salts (III) and by the reaction of II with carbene IV (Scheme 1). These reactions failed to give the expected ylides (I), but, instead, they afforded four products: enethiols (V),[5] enediamines (VII), olefins (VIII), and sulfides (IX) in the yields listed in Table 1.

Novel thiouronium salts (IIIa—IIIf) were readily prepared in good yields from II and halides, XCHRY (X=halogen: R=H or Ph: Y=COOEt, COOMe, COPh, Ph). The results of analyses are listed in Table 2, while the yields, the melting points, and the IR and NMR spectra are shown in Table 3.

Base Treatment of Thiouronium Salts (III). The

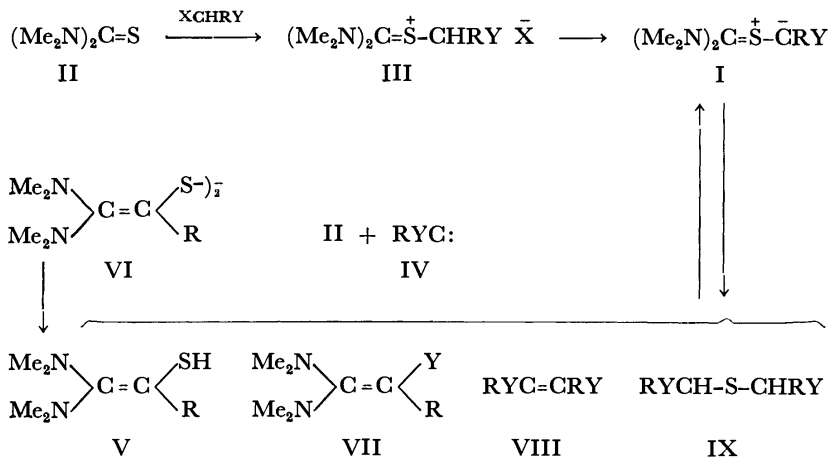

Scheme 1.

TABLE 1. TREATMENT OF III WITH BASES. CONDITIONS AND PRODUCT DISTRIBUTIONS

Compd.	R	Y	X	Base	Solvent	Reaction time hr	Products (%) VI[a]	VII	VIII	IX	II	Others
IIIa	COOEt	H	Br	Et_3N	THF	316	5.5	—	—	34	29	—
				NaH	THF	3	83	—	—	—	tr.	—
IIb	COOMe	H	Br	NaH	THF	3	41	—	—	—	7.4	—
IIIc	COPh	H	Br	Et_3N	THF	24	—	—	—	28	48	—
				NaH	DMSO	0.5	64	—	—	—	tr.	—
IIId	COOEt	Ph	Br	NaH	THF	24	c)	44	b)	—	42	d)
IIIe	COOMe	Ph	Br	NaH	THF	120	c)	31	12	—	34	—
IIIf	Ph	H	I	NaH	THF	120	—	—	—	23	8.5	—

a) Thiols V were isolated as the corresponding disulfides VI. b) There was obtained an oil whose IR suggested an olefinic ester structure. c) No thiol is expected. d) Elemental sulfur was obtained in 22% yield.

* To whom reprint requests should be addressed.

Table 2. Elemental analyses of thiouronium salts III

Compd.	R	Y	X	Formula	Calcd C	Calcd H	Found C	Found H
IIIa	COOEt	H	Br	$C_9H_{19}BrN_2O_2S$	36.1	6.4	36.2	6.5
IIIb	COOMe	H	Br	$C_8H_{17}BrN_2O_2S$	33.7	6.0	33.4	6.2
IIIc	COPh	H	Br	$C_{13}H_{19}BrN_2OS$	47.1	5.8	46.6	5.6
IIId	COOEt	Ph	Br	$C_{15}H_{23}BrN_2O_2S$	48.0	6.2	48.0	6.0
IIIe	COOMe	Ph	Br	$C_{14}H_{21}BrN_2O_2S$	46.5	5.9	46.6	6.0
IIIf	Ph	H	I	$C_{12}H_{19}IN_2S$	41.2	5.5	41.1	5.5

Table 3. Yields, melting points and spectral data of III

Compd.	Yield %	Mp °C	IR (KBr) cm^{-1}	NMR ($CDCl_3$) δ ppm
IIIa	83	131	1733, 1610	1.31(t, 3H), 3.54(s, 12H), 4.05(s, 2H), 4.23(q, 2H)
IIIb	84	117	1735, 1612	3.48(s, 12H), 3.77(s, 3H), 4.08(s, 2H)
IIIc	96	117	1683, 1602	3.44(s, 12H), 5.09(s, 2H), 7.4—8.3(m, 5H)
IIId	87	146	1722, 1604	1.21(t, 3H), 3.51(s, 12H), 4.23(q, 2H), 5.44(s, 1H), 7.3—7.6(m, 5H)
IIIe	99	137	1730, 1610	3.50(s, 12H), 3.80(s, 3H), 5.49(s, 1H), 7.3—7.5(m, 5H)
IIIf	96	151	1601, 703	3.41(s, 12H), 4.43(s, 2H), 7.2—7.5(m, 5H)

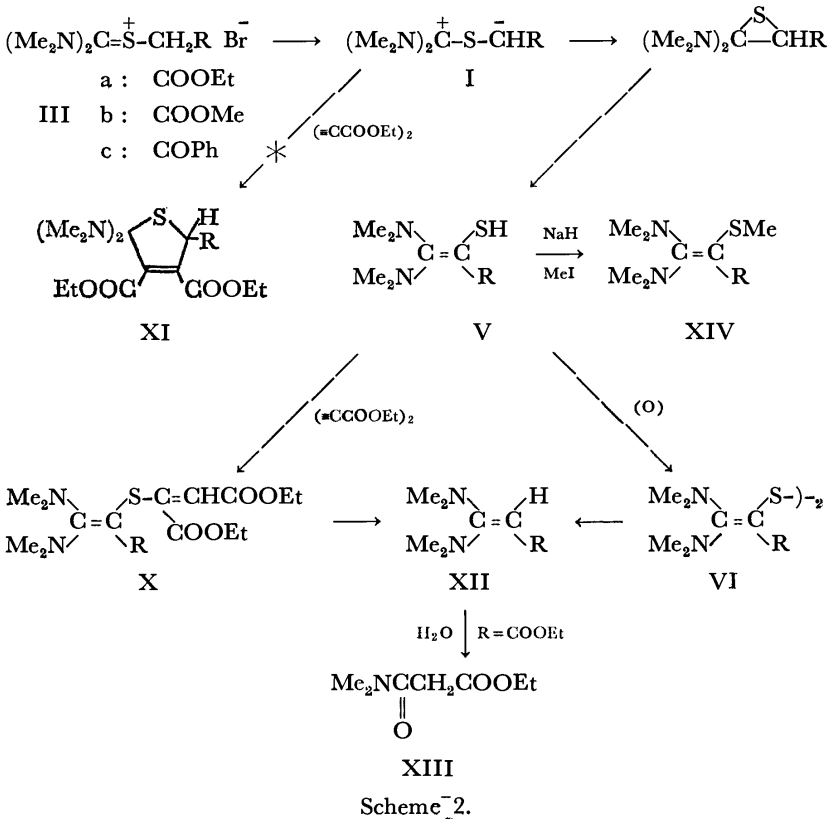

Scheme 2.

deprotonation of III may result in the formation of transient ylides (I). However, they do experience a fast isomerization to enethiols (V), which also are labile compounds; various products arising therefrom have been isolated to prove the intermediacy of these species.

A mixture of IIIa and excess diethyl acetylenedicarboxylate in tetrahydrofuran (THF) was treated with triethylamine to afford an adduct (Xa) in a 73% yield (Scheme 2). Similarly, IIIb gave Xb in a 70% yield. The isomeric structures, XIa and XIb, were excluded as follows. The mass spectra (Fig. 1) exhibited four fragment peaks due to carbon-sulfur bond fission. The desulfurization of Xa with Raney nickel afforded diethyl succinate and ethyl 3,3-bis(dimethylamino)acrylate (XIIa), whereas that of Xb gave diethyl succinate

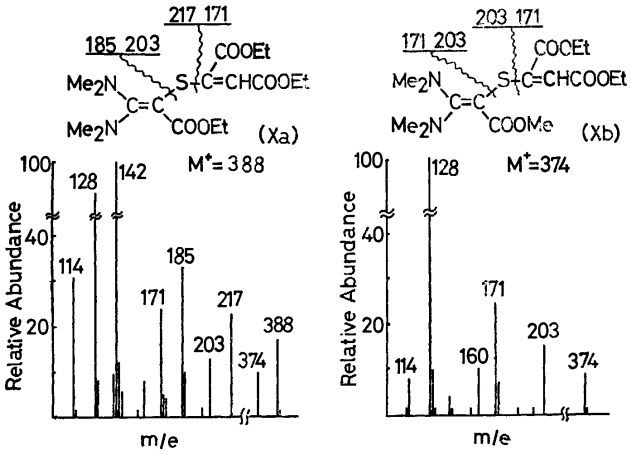

Fig. 1. Mass spectra of Xa and Xb.

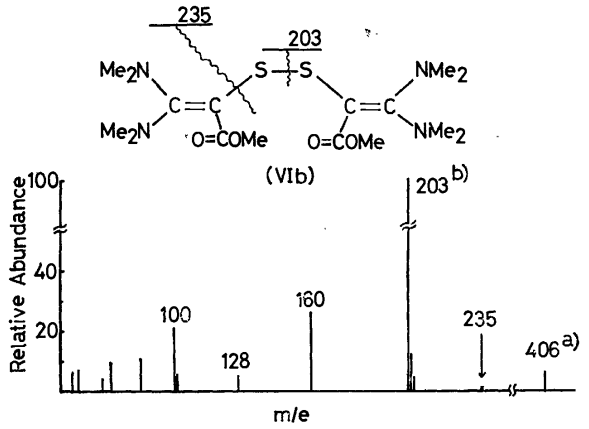

Fig. 2. High resolution mass spectrum of VIb.
a) Exact mass: 406.171, Calcd for $C_{16}H_{30}N_4O_4S_2$: 406.171. b) Exact mass: 203.086, Calcd for $C_8H_{15}N_2O_2S$: 203.085.

and XIIb. The hydrolysis of XIIa yielded ethyl *N,N*-dimethylmalonamidate (XIII), which was alternatively prepared from ethyl chloroformylacetate and dimethylamine.

The treatment of IIIa with equimolar sodium hydride in THF or dimethyl sulfoxide (DMSO), followed by a work-up, afforded VIa, which is the oxidative dimer of Va. Similarly, that of IIIb gave VIb. The spectral data, including the high-resolution mass spectrum of VIb (Fig. 2), were consistent with the structure. The desulfurization of VIa gave XIIa, and that of VIb yielded XIIb. When a solution of IIIa in carefully degassed THF was treated with 2 mol of sodium hydride and then with methyl iodide, there obtained a methylthio compound (XIVa) along with VIa. Applying a similar procedure to IIIb in dimethylformamide (DMF) gave XIVb.

The treatment of IIIc with sodium hydride in DMSO yielded VIc, whereas sulfide (IXc) was the predominant product in THF (Scheme 1, Table 1). DMSO seems to play the role of oxidant. In the presence of diethyl acetylenedicarboxylate, the salt IIIc failed to give the expected adduct (Xc).

The prerequisite for the formation of the enethiols, V, is the presence of a methylene group adjacent to the

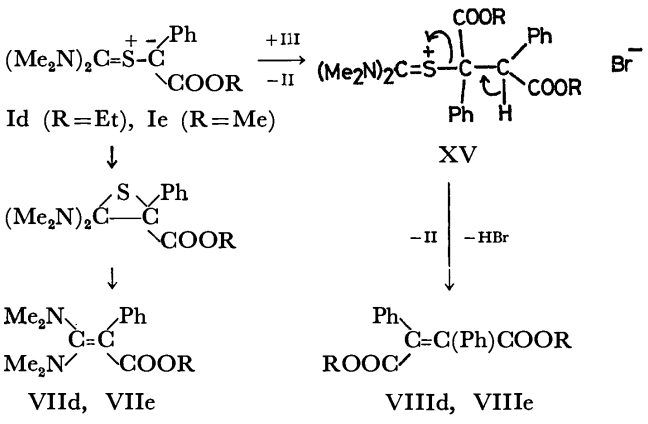

Scheme 3.

sulfur atom in III, or Y=H. The treatment of IIId or IIIe (Y=Ph) must, therefore, take a different course (Scheme 3). When IIId was treated with sodium hydride in THF, an enediamine (VIId) was obtained in a 44% yield, along with elemental sulfur (22%), II(42%), and an oil whose IR suggested the possibility of its being VIIId. Similarly, IIIe gave VIIe (31%), and an olefinic ester (VIIIe) which was a *ca.* 1 : 1 mixture of (*Z*) and (*E*) isomers.

The formation of VIId and VIIe can be explained as is shown in Scheme 3. The ylides, Id and Ie, may be cyclized to thiiranes, which are then decomposed spontaneously to VIId or VIIe and sulfur. In the presence of dimethyl acetylenedicarboxylate, no addition product was obtained and the product distributions were not affected. These results indicate that the decomposition of Id and Ie is a fast process.

A possible account of the formation of VIIIe is given also in Scheme 3. In analogy to the recorded thermal decomposition of methylphenylsulfonium phenacylide to tribenzoylcyclopropane,[6] the nucleophilic ylide (Ie) may attack the salt IIIe to afford XV, whose Hofmann elimination then gives VIIIe. Such an intermolecular reaction of the labile ylide Ie might be possible if Ie is generated close enough to the unchanged IIIe.

Finally, under appropriate conditions, the sulfides, IXa, IXc, and IXf, were obtained from IIIa, IIIc, and IIIf respectively. The S-benzylthiouronium salt, IIIf (R=Ph, Y=H), gave IXf and II upon treatment with sodium hydride, neither VIf nor VIIf and was obtained (see Table 1). The direct precursor of IX is not yet known.

Reaction of II with Diazomalonate. A cyclohexane solution of II and diethyl diazomalonate was heated

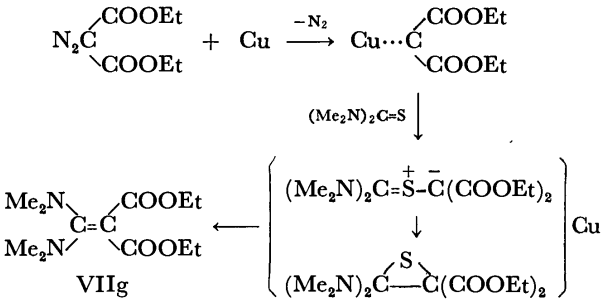

Scheme 4.

Table 4. Spectral features of β,β-bis(dimethylamino)-α,β-unsaturated carbonyl compounds XVI

Compd.	R	R′	IR ($\nu_{C=O}$ cm^{-1})	NMR (δ NMe_2 in $CDCl_3$)[c]
XIIa	OEt	H	1675[a]	2.79 (s, 6H), 2.87 (s, 6H)
XIVb	OMe	SMe	1651[a]	2.88 (s, 12H)
XIVa	OEt	SMe	1645[b]	2.92 (s, 12H)
VIa	OEt	-S-S-	1633[b]	2.96 (s, 12H)
VIId	OEt	Ph	1642[b]	2.94 (s, 12H)
XIIc	Ph	H	1513[b]	2.96 (s, 12H)
VIc	Ph	-S-S-	1510[b]	2.85 (s, 12H)
VIIg	OEt	COOEt	1658, 1625[b]	2.97 (s, 12H)

a) Obtained in neat liquid film. b) Obtained in KBr tablet. c) Measured at 23 °C.

under reflux for 12 hr in the presence of copper powder to afford VIIg in a 25% yield. An attempted photoreaction[7] of the components failed. No nitrogen evolution was observed in the absence of the copper catalyst in the dark, either.

We are tempted to assume the intermediacy of a copper carbenoid[8] (Scheme 4), but the exact nature of catalysis is not yet known. Copper salts or chelates gave much inferior yields of VIIg. Copper powder may effectively facilitate the desulfurization step.

Characteristic Spectra of Enediamines (XVI). Table 4 shows the spectral features of XVI, including the wave numbers of the carbonyl stretching and the NMR signals of the dimethylamino groups measured in deuteriochloroform at room temperature. The implications of these data may be summarized as follows. 1) The CO stretching vibrations occur at lower frequencies than those of regular α,β-unsaturated esters or ketones. 2) The *N*-methyl proton signals appear approximately 0.5—0.7 ppm downfield from ordinary ones.[9] 3) Though the two dimethylamino groups should be nonequivalent on the assumption of a restricted rotation about the C=C bond,[10] the chemical shifts of all the dimethylamino protons coincided except for those of XIIa. Such characteristic data point to the idea that the contribution of a betain form, XVI′, is predominant in contrast to usual α,β-unsaturated carbonyl compounds.

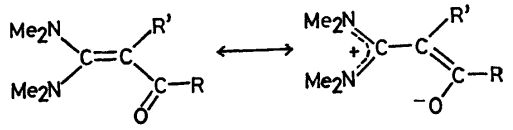

XVI XVI′

Experimental

All the mps and bps are uncorrected. The microanalyses were performed at the Elemental Analyses Center of Kyôto University. The NMR spectra were taken with a JEOL C-60H spectrometer at 60 MHz or a Varian HA 100 spectrometer at 100 MHz. The mass spectra were obtained on a Hitachi RMU-6L spectrometer, a Hitachi RMU-6D spectrometer, or a Hitachi RMS-4 spectrometer. The high-resolution mass spectrum of VIb was obtained on a JMS-OlSG spectrometer.

S-Ethoxycarbonylmethyl-N,N,N′,N′-tetramethylthiouronium Bromide (IIIa). A solution of II (6.7 g, 50 mmol) and ethyl bromoacetate (8.4 g, 50 mmol) in acetone (100 ml) was stirred for 3 hr at room temperature to give white precipitates of IIIa (13.8 g, 92%). The spectral data and the elemental analyses of IIIa are shown in Tables 2 and 3.

The other thiouronium salts (IIIb—IIIf) were prepared in a similar way.

Ethyl 3,3-Bis(dimethylamino)-2-[1,2-bis(ethoxycarbonyl)vinylthio]acrylate (Xa). Into a suspension of IIIa (3.0 g, 20 mmol) and diethyl acetylenedicarboxylate (3.4 g, 20 mmol) in THF (70 ml), triethylamine (3.0 g, 30 mmol) was added, drop by drop, under a nitrogen atmosphere at room temperature. The reaction mixture was then stirred for 12 hr, diluted with water (200 ml), and repeatedly extracted with chloroform. The combined extracts were washed with water, dried (magnesium sulfate), and concentrated *in vacuo*. The residual oil was purified by column chromatography (silica gel, chloroform) to yield an oil which solidified upon trituration with ether. Recrystallization from ethanol-hexane gave Xa (2.8 g, 73%); mp 91—92 °C. IR (KBr): 1733, 1705, 1660, 1590, 1530, 1150, 1069, 770 cm^{-1}. NMR (δ, $CDCl_3$): 1.22 (t, 3H), 1.24 (t, 3H), 1.33 (t, 3H), 2.86 (s, 12H), 4.12 (q, 2H), 4.16 (q, 2H), 4.30 (q, 2H), 5.50 (s, 1H). The mass spectrum of Xa is shown in Fig. 1. Found: C, 52.9; H, 7.3%. Calcd for $C_{17}H_{28}N_2O_6S$: C, 52.6; H, 7.3%.

Similarly, methyl 3,3-bis(dimethylamino)-2-[1,2-bis(ethoxycarbonyl)vinylthio]acrylate (Xb) was obtained in a 70% yield as colorless crystallines; mp 79—80 °C (recrystallized from ethanol-hexane). IR (KBr): 1740, 1705, 1661, 1590, 1529, 1150, 1069, 770 cm^{-1}. NMR (δ, $CDCl_3$): 1.24 (t, 3H) 1.35 (t, 3H), 2.88 (s, 12H), 3.68 (s. 3H), 4.12 (q, 2H), 4.30 (q, 2H), 5.56 (s, 1H). The mass spectrum of Xb is shown in Fig. 1. Found: C, 51.6; H, 7.1%. Calcd for $C_{16}H_{26}N_2O_6S$: C, 51.3; H, 7.0%.

Di[2,2-bis(dimethylamino)-1-(ethoxycarbonyl)vinyl] Disulfide (VIa). To a stirred suspension of IIIa (6.0 g, 20 mmol) in THF (200 ml), sodium hydride (0.90 g of a 52% dispersion in mineral oil, 20 mmol) was added in one portion. The reaction mixture was stirred until the evolution of hydrogen had stopped (*ca.* 3 hr). After it had then been filtered, the filtrate was evaporated to give a yellow solid of VIa, which was subsequently washed with ether. The crude product (3.6 g, 83%) was recrystallized from ethanol; mp 142—143 °C. IR(KBr): 1633, 1510, 1050, 766 cm^{-1}. NMR (δ, $CDCl_3$): 1.23(t, 6H), 2.96 (s, 24H), 4.07 (q, 4H). Found: C, 49.6; H, 8.1; S, 14.8%. Calcd for $C_{18}H_{34}N_4O_4S_2$: C, 49.8; H, 7.9; S, 14.7%.

Similarly, di[2,2-bis(dimethylamino)-1-(methoxycarbonyl)-vinyl] disulfide (VIb) was obtained in a 42% yield as a yellow solid; mp 163—164 °C (from ethanol). IR (KBr): 1640, 1515, 1056, 767 cm^{-1}. NMR (δ, $CDCl_3$): 2.95 (s, 24H), 3.57 (s, 6H). The high-resolution mass spectrum of VIb is shown is Fig. 2. Found: C, 47.3; H, 7.6; S, 15.6%. Calcd for $C_{16}H_{30}N_4O_4S_2$: C, 47.3; H, 7.4; S, 15.7%.

thyl 3,3-Bis(dimethylamino)-2-(methylthio)acrylate (XIVa). THF (100 ml) was completely degassed *in vacuo* (1 mmHg) for

3 hr at −60 °C. To this, sodium hydride (1.0 g of a 51.9% dispersion in mineral oil, 22 mmol) and IIIa (2.3 g, 7.7 mmol) were added successively under a nitrogen atmosphere at room temperature. After stirring for 12 hr, methyl iodide (1.5 g, 106 mmol) was added, drop by drop. The mixture was then stirred for 3 hr and filtered, after which the filtrate was concentrated *in vacuo* to afford an oil. Chromatography on a silica-gel column with benzene, ether, and ethanol as the eluents gave II (84 mg, 8.3%), VIa (200 mg, 12%), and XIVa as a colorless oil which solidified upon trituration with hexane at −50 °C (300 mg, 17%). Recrystallization from hexane gave an analytical sample; mp 31—32 °C. IR (KBr): 1645, 1517, 1210, 1056, 767 cm^{-1}. NMR (δ, CCl_4): 1.27 (t, 3H), 2.03 (s, 3H), 2.78 (s, 6H), 2.88 (s, 6H), 4.07 (q, 2H). Mass spectrum (*m/e*): 232 (M^+). Found: C, 52.4; H, 9.1%. Calcd for $C_{10}H_{20}N_2O_2S$: C, 51.7; H, 8.7%.

Methyl 3,3-Bis(dimethylamino)-2-(methylthio)acrylate (XIVb). Sodium hydride (3.0 g of a 51.9% dispersion in mineral oil, 65 mmol) was washed three times with hexane and then suspended in DMF (100 ml). To this, *S*-methoxycarbonylmethyl-*N,N,N',N'*-tetramethylthiouronium bromide (IIIb) (5.7 g, 20 mmol) was added in small portions under a nitrogen atmosphere at room temperature. After the evolution of hydrogen had ceased (*ca.* 1 hr), methyl iodide (5.0 g, 35 mmol) was added, drop by drop. The mixture was then stirred for 1 hr, diluted with water (200 ml), neutralized by the addition of ammonium chloride, and extracted with chloroform. After drying (magnesium sulfate), the combined extracts were distilled *in vacuo* to yield XIVb as a colorless oil (320 mg, 7.3%); bp 88—90 °C/0.07 mmHg. IR (neat): 1651, 1525, 1210, 1060, 770 cm^{-1}. NMR (δ, CCl_4): 2.03 (s, 3H), 2.81 (s, 6H), 2.89 (s, 6H), 3.61 (s, 3H). Found: C, 49.6; H, 8.6%. Calcd for $C_9H_{18}N_2O_2S$: C, 49.5; H, 8.3%.

Ethyl 3,3-Bis(dimethylamino)acrylate (XIIa). To a solution of VIa (2.2 g, 5 mmol) in ethanol (100 ml), Raney nickel (W-2) (36 g) was added. The mixture was stirred at room temperature for 2 hr and filtered, and the filtrate was distilled *in vacuo* to afford XIIa as a colorless oil (1.4 g, 76%); bp 76.5—77 °C/1 mmHg. IR (neat): 1675, 1555, 1158, 1050, 780 cm^{-1}. NMR (δ, $CDCl_3$): 1.26 (t, 3H), 2.79 (s, 6H), 2.87 (s, 6H), 3.96 (s, 1H), 4.09 (q, 2H). Mass spectrum (*m/e*): 186 (M^+). Found: C, 57.5; H, 10.0%. Calcd for $C_9H_{18}N_2O_2$: C, 58.0; H, 9.7%.

Similarly, the desulfurization of VIb afforded methyl 3,3-bis(dimethylamino)acrylate (XIIb) as a colorless oil in a 68% yield; bp 87—88 °C/4 mmHg. IR (neat): 1675, 1550, 1120, 1054, 779 cm^{-1}. NMR (δ, $CDCl_3$): 2.81 (s, 6H), 2.88 (s, 6H), 3.62 (s, 3H), 3.96 (s, 1H). Mass spectrum (*m/e*): 172 (M^+). Found: C, 55.6; H, 9.6%. Calcd for $C_8H_{16}N_2O_2S$: C, 55.8; H, 9.4%.

Desulfurization of Xa. Raney nickel (W-2) (2 g) was added to a solution of Xa (250 mg, 0.64 mmol) in ethanol (50 ml). After stirring for 15 min at room temperature, the mixture was filtered and the filtrate was concentrated to afford an oil, which consisted of diethyl succinate and XIIa. Identification was made by a comparison of the IR spectra and the retention times of glc (High vacuum silicone grease 30%) with those of authentic samples. The yield of diethyl succinate, as calculated from the peak area in glc, was 80%, while that of XIIa was 56%.

Similarly, the desulfurization of Xb with Raney nickel afforded diethyl succinate (68%) and XIIb (40%).

Ethyl N,N-Dimethylmalonamidate (XIII). Ethyl hydrogen malonate (3.5 g, 26 mmol) was added, drop by drop, to thionyl chloride (20 ml); the solution was heated at 50 °C for 2 hr and then under reflux for 1 hr. After cooling, the solution was concentrated *in vacuo* to yield ethyl chloroformylacetate.[11] An excess of anhydrous dimethylamine gas was passed through a solution of ethyl chloroformylacetate in ether (50 ml) to give white precipitates. The reaction mixture was then filtered, and the filtrate was distilled *in vacuo* to yield XIII as a colorless oil (4.5 g, 94% based on ethyl hydrogen malonate); bp 94—96 °C/1 mmHg. IR (neat): 1735, 1645, 1250, 1170, 1030 cm^{-1}. NMR (δ, CCl_4): 1.30 (t, 3H) 2.91 (s, 3H), 3.02 (s, 3H), 3.32 (s, 2H), 4.16 (q, 2H). Found: C, 52.7; H, 8.2; N, 8.8%. Calcd for $C_7H_{13}NO_3$: C, 52.8; H, 8.2; N, 8.8%.

Hydrolysis of XIIa. A solution of XIIa (0.48 g, 2.6 mmol) and *p*-toluenesulfonic acid (5 mg) in THF-water (1 : 1, 50 ml) was stirred at room temperature for 3 days and then extracted four times with chloroform (70 ml). The extracts were combined, shaked with an aqueous sodium bicarbonate solution, washed with water, dried (magnesium sulfate), and concentrated *in vacuo* to give an oil which consisted of XIIa and XIII. Identification was made by a comparison of the IR spectra and the retention times of glc (Polyethylene glycol-$AgNO_3$ 30%) with those of authentic samples.

Di[2,2-bis(dimethylamino)-1-benzoylvinyl] Disulfide (VIc). Sodium hydride (0.50 g of 51.9% dispersion in mineral oil, 11 mmol) was washed with *n*-hexane and then suspended in DMSO (50 ml). Into this, *S*-phenacyl-*N,N,N',N'*-tetramethylthiouronium bromide (IIIc) (3.3 g, 10 mmol) was stirred in small portions at room temperature. After the evolution of hydrogen had stopped (*ca.* 30 min), the brown-red solution was diluted with water (100 ml), and extracted four times with chloroform (150 ml); the combined extracts were then washed three times with water (100 ml), dried (magnesium sulfate), and concentrated *in vacuo* to give an oil. This oil solidified on trituration with ether to yield a yellow solid of VIc (1.56 g, 64%). Recrystallization from ethanol upon the addition of ether gave an analytical sample; mp 192—195 °C. IR (KBr): 1600, 1590, 1510, 1400, 710, 660 cm^{-1}. NMR (δ, $CDCl_3$): 2.85 (s, 24H), 7.2—7.6 (m, 10H). Found: C, 62.4; H, 7.1%. Calcd for $C_{26}H_{34}N_4O_2S_2$: C, 62.6; H, 6.9%.

Reaction of S-[α-(Methoxycarbonyl)benzyl]-N,N,N',N'-tetramethylthiouronium Bromide (IIIe) with Sodium Hydride. Sodium hydride (0.50 g of a 51.9% disperion in mineral oil, 11 mmol) was suspended in THF (50 ml). To this, IIIe (3.6 g, 10 mmol) was added under a nitrogen atmosphere at room temperature. The mixture was stirred for 5 days and then filtered, after which the filtrate was concentrated *in vacuo* to afford an oil, which was subsequently chromatographed on a silica gel column. From the benzene eluent, we obtained a mixture of dimethyl 2,3-diphenylfumarate and dimethyl 2,3-diphenylmaleate (VIIIe) as a colorless solid (0.17 g, 12%). The (Z) and (E) isomers could not be separated, but the intensities of the methoxy protons in NMR indicated that the ratio of the (Z) to the (E) isomers was *ca.* 1. IR (nujol): 1720, 1500, 1275, 1225, 1210, 1010, 725, 700 cm^{-1}. NMR (δ, CCl_4): 3.46 (s, 3H), 3.77 (s, 3H), 7.0—7.4 (m, 10H). Mass spectrum (*m/e*): 296 (M^+). Recrystallization from ethanol gave an analytical sample; mp 103—107 °C.[12] Found: C, 72.9; H, 5.3%. Calcd for $C_{18}H_{16}O_4$: C, 73.0; H, 5.4%.

The benzene–ether eluent (4 : 1) gave II (0.43 g, 34%), which was identified by a comparison of its IR spectrum with that of authentic sample.

From the ether eluent, we obtained methyl 3,3-bis(dimethylamino)-2-phenylacrylate (VIIe) (0.77 g, 31%) as a colorless solid. Recrystallization from hexane gave an analytical solid. Recrystallization from hexane gave an analytical sample; mp 69 °C. IR (KBr): 1632, 1520, 1180, 1050,

770, 690 cm^{-1}. NMR (δ, CCl_4): 2.75 (broad s, 12H), 3.57 (s, 3H), 6.7—7.2 (m, 5H). Found: C, 67.9; H, 8.4; N, 11.2%. Calcd for $C_{14}H_{20}N_2O_2$: C, 67.7; H, 8.1; N, 11.3%.

Reaction of S-[α-*(Ethoxycarbonyl)benzyl*]-N,N,N′,N′-*tetramethylthiouronium Bromide (IIId) with Sodium Hydride.* To a stirred suspension of sodium hydride (0.50 g of a 51.9% dispersion in mineral oil, 11 mmol) in THF (50 ml), IIId (4.0 g, 11 mmol) was added under a nitrogen atmosphere at room temperature. The mixture was then stirred for 24 hr and filtered, after which the filtrate was concentrated *in vacuo* to afford an oil, which was subsequently chromatographed on a silica gel column. The benzene eluent gave elemental sulfur (74 mg, 22%) and an oil (0.57 g) whose IR (neat, 1725, 1690, 1600, 1450, 1370, 1200, 1010, 720, 680 cm^{-1}) suggested the presence of Ph- and EtOOC- groups. The benzene-ether eluent (4 : 1) gave II (0.59 g, 42%). The ether eluent gave ethyl 3,3-bis(dimethylamino)-2-phenylacrylate (VIId) as a colorless solid (1.23 g, 44%); mp 63 °C (from hexane). IR (KBr): 1642, 1514, 1290, 1170, 1050, 770, 695 cm^{-1}. NMR (δ, CCl_4): 1.22 (t, 3H), 2.74 (s, 12H), 4.05 (q, 2H), 6.7—7.2 (m, 5H). Found: C, 68.9; H, 8.4%. Calcd for $C_{15}H_{22}N_2O_2$: C, 68.8; H, 8.5%.

Treatment of IIIa with Triethylamine. To a suspension of IIIa (6.0 g, 20 mmol) in THF (100 ml), triethylamine (6.0 g, 60 mmol) was added, drop by drop, under a nitrogen atmosphere at room temperature. The mixture was stirred for 2 weeks, diluted with water (300 ml), and extracted with chloroform (200 ml). The combined extracts were dried (magnesium sulfate) and then concentrated *in vacuo* to give an oil. Chromatography on a silica gel column, with benzene, ether, and methanol as eluents, gave predominantly diethyl thiodiglycolate (IXa) as a colorless oil; bp 89 °C/2 mmHg (lit,[13] bp 105 °C/3 mmHg) (0.70 g, 34%). IR (neat): 1730, 1270, 1150, 1025 cm^{-1}. NMR (δ, CCl_4): 1.30 (t, 6H), 3.32 (s, 4H), 4.11 (q, 4H). Found: C, 46.8; H, 7.1; S, 15.8%. Calcd for $C_8H_{14}O_4S$: C, 46.6; H, 6.8; S, 15.5%.

The other products were II (0.87 g, 29%) and VIa (0.24 g, 5.5%), which were identified by a comparison of their IR spectra with those of authentic samples.

Treatment of IIIc with Triethylamine. To a stirred suspension of IIIc (9.9 g, 30 mmol) in THF (100 ml), triethylamine (10 g, 0.10 mol) was added, drop by drop, under a nitrogen atmosphere, after which the mixture was stirred at room temperature for 24 hr. Working up the product, followed by chromatographic separation on a silica gel column with benzene and ether as eluents, yielded diphenacyl sulfide (IXc) (1.12 g, 28%); mp 74—75 °C (from ethanol) (lit,[14] 74 °C). IR (KBr): 1690, 1595, 1450, 985, 750, 685, 645 cm^{-1}. NMR (δ, $CDCl_3$): 4.00 (s, 4H), 7.2—8.1 (m, 10H). Found: C, 71.5; H, 5.2%. Calcd for $C_{16}H_{14}N_2S$: C, 71.1; H, 5.2%.

Another product, II (1.90 g, 48%), was identified by comparison of its spectrum with that of an authentic specimen.

Treatment of S-*Benzyl*-N,N,N′,N′-*tetramethylthiouronium Bromide (IIIf).* Sodium hydride (0.25 g of a 51.9% dispersion in mineral oil, 55 mmol) was washed with *n*-hexane and then suspended in THF (30 ml). To this stirred mixture, IIIf (1.75 g, 50 mmol) was added under nitrogen. After the mixture had been stirred for 5 days at roon temperature and filtered, the filtrate was concentrated *in vacuo* to give an oil. Chromatography on a silica gel column, with benzene and ether as eluents, gave dibenzyl sulfide (IXf) 124 mg, 23%); mp 45—46 °C (lit,[15] mp 49 °C). IR (neat): 1600, 1598, 1455, 755, 683 cm^{-1}. NMR (δ, CCl_4): 3,47 (s, 4H), 7.17 (s, 10H). Mass spectrum (*m/e*): 214 (M^+). The by-product was tetramethylthiourea II (68 mg, 8.5%).

Diethyl Bis(dimethylamino)methylenemalonate (VIIg). To a stirred mixture of II (6.6 g, 50 mmol) and copper powder (1.0 g) in cyclohexane (50 ml), diethyl diazomalonate (1.86 g, 10 mmol) was added at room temperature under nitrogen. The reaction mixture was then heated under reflux for 12 hr and filtered, after which the filtrate was evaporated *in vacuo* to give an oil, which was chromatographed on a silica gel column. After the elution of II with ether, the residue was eluted with chloroform. The combined extracts were dried (magnesium sulfate) and concentrated *in vacuo* to afford an oil, which solidified upon trituration with ether at −30 °C to yield a colorless solid of VII g (0.65 g, 25%); mp 64 °C (from *n*-hexane) (lit,[16] mp 67—68 °C). IR (KBr): 1658, 1625, 1560, 1520, 1275, 1210, 1060, 905, 796 cm^{-1}. NMR (δ, $CDCl_3$): 1.28 (t, 6H), 2.97 (s, 12H), 4.17 (q, 4H). Found: C, 55.9; H, 8.7; N, 10.9%. Calcd for $C_{12}H_{22}N_2O_4$: C, 55.8; H, 8.6; N, 10.7%.

The authors are grateful to the Staff of the Sankyo Co. for determining the high-resolution mass spectra. Financial support from the Ministry of Education, the Japanese Government, and from the Toray Science Foundation is acknowledged with pleasure.

References

1) Part of this paper was published in a preliminary form: M. Takaku, S. Mitamura, and H. Nozaki, *Tetrahedron Lett.*, **1969**, 3651.

2) R. Huisgen, *Angew. Chem.*, **75**, 604 (1963).

3) R. M. Kellogg and S. Wassenaar, *Tetrahedron Lett.*, **1970**, 1987. R. M. Kellogg, S. Wassenaar, and J. Buter, *ibid.*, **1970**, 4689.

4) W. J. Middleton, *J. Org. Chem.*, **31**, 3731 (1966).

5) The enethiols, (V) were not isolated, but there were obtained products arising from them. See following discussion.

6) H. Nozaki, M. Takaku, and K. Kondo, *Tetrahedron*, **22**, 2145 (1966).

7) W. Ando, T. Yagihara, S. Tozune, S. Nakaido, and T. Migita, *Tetrahedron Lett.*, **1969**, 1979. W. Ando, T. Yagihara, S. Tozune, and T. Migita, *J. Amer. Chem. Soc.*, **91**, 2789 (1969).

8) R. Noyori, H. Takaya, Y. Nakanisi, and H. Nozaki, *Can. J. Chem.*, **47**, 1242 (1969) and references cited therein.

9) L. M. Jackmann and S. Sternhell, "Applications of Nuclear Magnetic Resonance Spectroscopy in Organic Chemistry," 2nd Ed., Pargamon Press, Oxford, London, Edinburgh, New York, Toronto, Study, Paris, Brauschweig (1969), p. 161.

10) For the internal rotation in olefins, see Y. Shvo and H. Shanan-Atidi, *J. Amer. Chem. Soc.*, **91**, 6683, 6689 (1969).

11) K. Fleischer, H. Hittel, and P. Wolff, *Ber. Dtsch. Chem. Ges.*, **53**, 1847 (1920).

12) Dimethyl 2,3-diphenylmaleate melted at 110—112° C: W. Methesics and H. Zeiss, *J. Amer. Chem. Soc.*, **81**, 4117 (1959).

13) C. G. Overberger, H. J. Mallon and R. Fine, *J. Amer. Chem. Soc.*, **72**, 4958 (1950).

14) B. Croth, *Arkiv. Kemi. Mineral. Geol.*, **9**, 1 (1924).

15) C. Mäker, *Ann. Chem.*, **136**, 88 (1865).

16) H. Bredereck and K. Bredereck, *Chem. Ber.*, **94**, 2278 (1961).

Synthesis and Photochemical Reaction of 1,5,5,9-Tetramethyl-2-decalone

Tochiro TATEE, Takahiko TSUYUKI, Reiko AOYAGI, and Takeyoshi TAKAHASHI
Department of Chemistry, Faculty of Science, The University of Tokyo, Bunkyo-ku, Tokyo 113
(Received July 31, 1974)

1,5,5,9-Tetramethyl-2-decalone (**6**) was synthesized from 5,5,9-trimethyl-1-decalone (**7**) and irradiated in *n*-hexane under a nitrogen atmosphere using a high pressure mercury lamp. Oxygen was passed through the reaction mixture in the dark to give a seco-nor acid, 1-carboxymethyl-2-ethyl-2,6,6-trimethylcyclohexane (**8a**) and a seco acid, 1-(2-carboxyethyl)-2-ethyl-2,6,6-trimethylcyclohexane (**9a**).

In the photochemical reaction of cycloalkanones, α-cleavage to form a biradical is well known as one of the primary photoreactions.[1] The biradical undergoes elimination of carbon monoxide and/or hydrogen shift to afford an unseturated aldehyde and/or a ketene, depending on the structural requirement.[2] In protic solvents such as alcohols or aqueous solvents, the ketene immediately reacts with the solvents to afford an ester or a carboxylic acid, respectively. However, the ketene formed in aprotic solvents is inert to the (aprotic) solvents.

In the previous papers[3] we reported the photochemical reaction of friedelin (**1a**) in *n*-hexane and isolation of 5α-ethyl-10β-formylmethyl-des-A friedelane (**2**), 10β-carboxymethyl-5α-ethyl-des-A-friedelane (**3**), and 10β-(2-carboxyethyl)-5α-ethyl-des-A-friedelane (**4**). Since a 3,4-seco-friedelin skeleton bears no hydrogen atom on the δ-carbon atoms, the acyl-alkyl biradical produced from **1a** could not afford a δ-unsaturated aldehyde, but could lead to the ketene (**5**).[3] During the subsequent separation work-up, the ketene (**5**) gave the seco acid (**4**) by addition of water, while the seco-nor aldehyde (**2**) was formed by autoxidation of the ketene (**5**); **2** was further oxidized by air to give the seco-nor acid (**3**).[3]

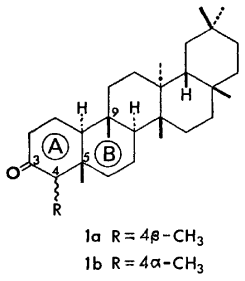

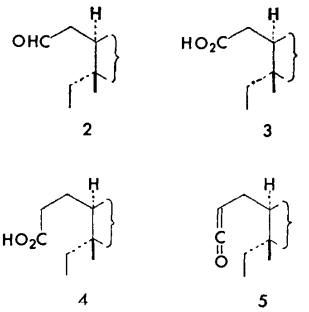

In order to examine the general formation of the seco-nor product in a system such as friedelin (**1a**), photochemical behavior of 1,5,5,9-tetramethyl-2-decalone (**6**), as a simple bicyclic model compound corresponding to the A/B ring of **1a**, was investigated.

In this paper, we wish to describe the synthesis of 1,5,5,9-tetramethyl-2-decalone (**6**) from 5,5,9-trimethyl-1-decalone (**7**) and the formation of 1-carboxymethyl-2-ethyl-2,6,6-trimethylcyclohexane (**8a**), 1-(2-carboxyethyl)-2-ethyl-2,6,6-trimethylcyclohexane (**9a**), and 2-ethyl-1-formylmethyl-2,6,6-trimethylcyclohexane (**10**) in the photochemical reaction of **6** in *n*-hexane followed by oxygen introduction in the dark.

5,5,9-Trimethyl-1-decalone (**7**)[4] was treated with methylmagnesium iodide to give two alcohols (**11**)

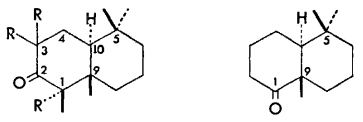

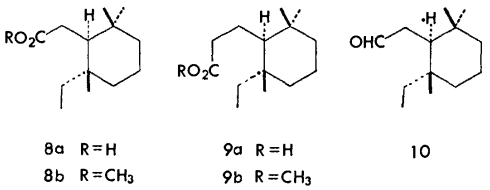

and (**12**) in 63% and 20% yield, respectively, which were separated by silica gel chromatography. Assignment of the hydroxyl group was easily accomplished by PMR measurement using $Eu(dpm)_3$ as a shift reagent (Figs. 1 and 2). The signal due to the methyl group geminal to the hydroxyl group suffered the most significant shift in each alcohol. The shift for the

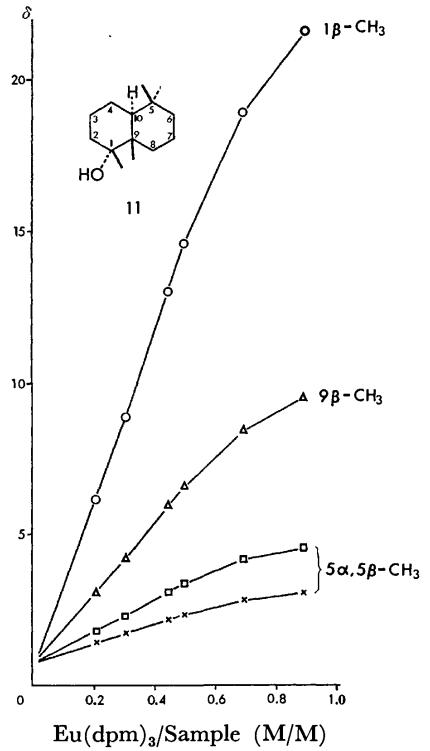

Fig. 1. Induced paramagnetic shifts for the alcohol **11**. [$Eu(dpm)_3$ was added to a 7% (w/v) soln of **11** in CCl_4].

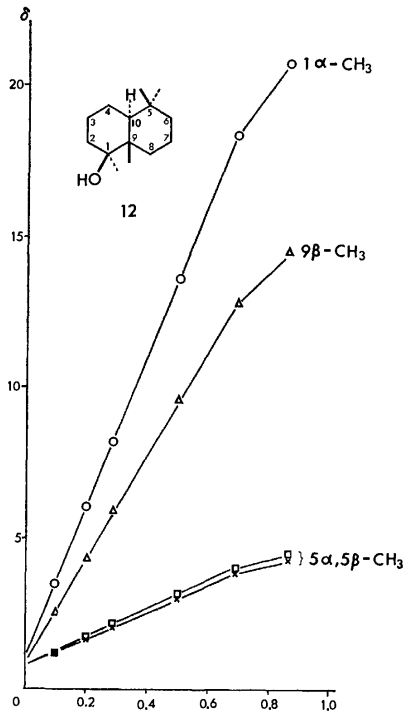

Fig. 2. Induced paramagnetic shifts for the alcohol **12**. [Eu(dpm)$_3$ was added to a 7% (w/v) soln of **12** in CCl_4].

angular methyl group of **11** was smaller than that of **12**. Each alcohol (**11** and **12**) was subjected to dehydration with iodine at 140 °C yielding an olefin mixture (**13**, **14**, and **15**) whose ratio was 61 : 8 : 31 and 6 : 18 : 76, respectively. The olefin mixture was separated by silver nitrate-impregnated silica gel chromatography. The main olefin (**13**) obtained by the dehydration of the alcohol (**11**) showed the presence of an olefinic methyl (δ 1.58, d, J=2 Hz), an olefinic proton (δ 5.18, m), and three tertiary methyls (δ 0.87, 0.89, and 1.02; each s) in the PMR spectrum. The structure of **13** was further supported by the formation of the ketone (**6**) (*vide infra*).

Treatment of the olefin mixture with *p*-toluenesulfonic acid in chloroform gave a mixture of **14** and **15** in a ratio of 1 : 4; **13** was absent in the resulting mixture. The mixture of **14** and **15** was separated by a column of silica gel impregnated with silver nitrate. Each olefin (**14** or **15**) gave the same equilibriating

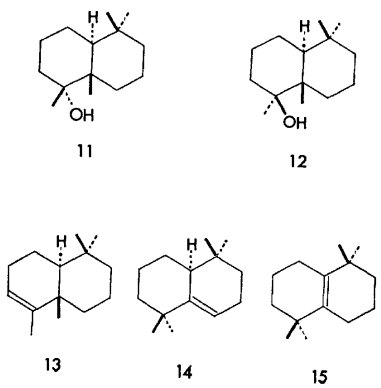

mixture of **14** and **15** in a ratio of 1 : 4 by treatment with *p*-toluenesulfonic acid. The structures of these olefins (**14** and **15**) were also confirmed by their PMR and IR spectral data.

The olefin mixture (**13**, **14** and **15**) derived from the alcohol (**11**), without separation, was subjected to hydroboration and subsequent Jones' oxidation to give 1,5,5,9-tetramethyl-2-decalone (**6**) and several minor oxidation products, which were not further examined. The structure of the main product (**6**) was supported by the PMR and IR spectral data. However, an alternative structure (**16**) might be possible to explain the spectral data for **6**. The ketone (**16**) would be derived from an olefin (**17**) which might be formed by a skeletal rearrangement during dehydration of the alcohol (**11**). In order to confirm that the Jones' oxidation product possesses a decalone skeleton, it was deuterated to give the deuterated ketone (**6**-d_3), which

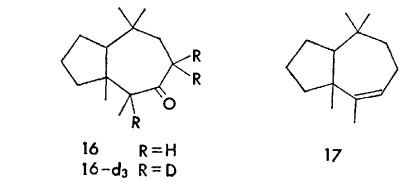

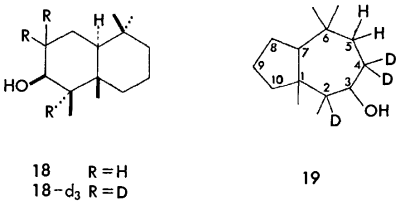

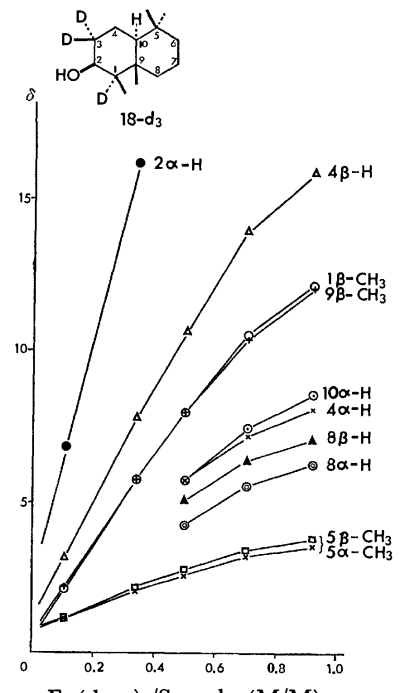

Fig. 3. Induced paramagnetic shifts for the alcohol **18**-d_3. [Eu(dpm)$_3$ was added to a 8% (w/v) soln of **18**-d_3 in CCl_4].

was converted with sodium borohydride into an alcohol (**18**-d_3). The PMR spectral measurement of **18**-d_3 using Eu(dpm)$_3$ as a shift reagent was then effected. The signals due to 4β, 4α, 10α, 8β, and 8α-hydrogens were separated distinctly (Fig. 3). A triplet (J=13 Hz) due to the 4β-hydrogen coupled with the 4α-hydrogen (geminal) and the 10α-hydrogen (trans) was observed (cf. Experimental). These results are in good accordance with those reported for friedelan-3β-ol.[5] If the alcohol had a structure **19**, which might be derived from the olefin (**17**), the signal due to 5α- and 5β-hydrogens must have been observed as an AB quartet. This was not the case in reality. Thus the structure of the decalone, obtained by Jones' oxidation was shown to be **6** except the configuration at C-1.

The induced paramagnetic shift experiments on **6** using Eu(fod)$_3$-d_{27} as a shift reagent showed a large shift for the signals due to a secondary methyl at C-1 (δ 0.89) and a tertiary methyl at C-9 (δ 0.73), while a smaller shift for the signals due to two tertiary methyls at C-5 (δ 0.88 and 0.98)(Fig. 4). These methyl signals suffer a solvent shift when the solvent was replaced from deuteriochloroform to deuteriobenzene (Table 1). A small downfield shift (Δ −0.02 ppm) observed for the C-1 methyl of **6** was parallel to the shift (Δ −0.10 ppm) observed for the 4β(equatorial)-methyl of friedelin (**1a**), while different from an appreciable upfield shift (Δ +0.25 ppm) for 4α(axial)-methyl of 4-epifriedelin (**1b**).[6] The methyl group at C-1 of **6** was thus inferred to be equatorial (1β).

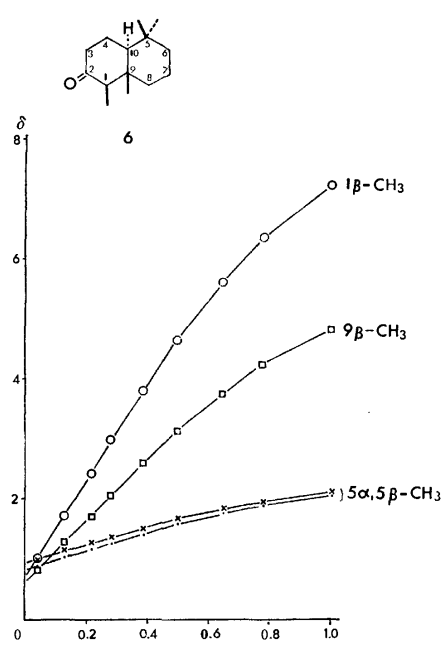

Fig. 4. Induced paramagnetic shifts for the ketone **6**. [Eu(fod)$_3$-d_{27} was added to a 5% (w/v) soln of **6** in CCl_4].

1,5,5,9-Tetramethyl-2-decalone (**6**) was irradiated in *n*-hexane with a high pressure mercury lamp under a nitrogen atmosphere at room temperature and then slow stream of oxygen was introduced into the solution in the dark. The reaction product was subjected to GC-MS examination and the formation of the seco-nor aldehyde, 2-ethyl-1-formylmethyl-2,6,6-trimethylcyclohexane [**10**; *m/e* 196 (M^+ $C_{13}H_{24}O$)] was suggested. However, a further confirmation was not furnished, because of lack of the material.

The reaction product was separated by silica gel chromatography to give an acid fraction. On treatment with diazomethane, the acid fraction was converted into the methyl esters in about 10% yield from **6**, which were found to consist of two components (**8b** and **9b**). The mixture of the esters was separated by preparative glc to give two esters. One methyl ester with lower R_f value on tlc showed a molecular ion peak at *m/e* 240 and was shown to be identical with 2-ethyl-1-(2-methoxycarbonylethyl)-2,6,6-trimethylcyclohexane (**9b**) in respect to IR, mass, glc, and tlc, which was prepared by the photochemical reaction of **6** in methanol.

The other methyl ester gave a molecular ion peak at *m/e* 226. This suggested that the ester would be a methyl ester derived from a seco-nor acid, 1-carboxymethyl-2-ethyl-2,6,6-trimethylcyclohexane (**8a**). This was confirmed by the synthesis of the seco-nor ester, 2-ethyl-1-methoxycarbonylmethyl-2,6,6-trimethylcyclohexane (**8b**) from the seco ester (**9b**) by the Barbier-Wieland degradation *via* a diphenylcarbinol (**20**) and a diphenylethylene derivative (**21**). Therefore, the structure of the original seco-nor acid was shown to be 1-carboxymethyl-2-ethyl-2,6,6-trimethylcyclohexane (**8a**). The formation mechanism of **8a** from 1,5,5,9-tetramethyl-2-decalone (**6**) could be inferred to be the same as that of the seco-nor acid (**3**) from friedelin (**1a**).[3]

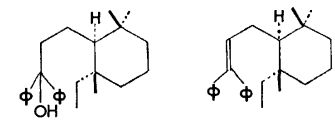

20 21

Table 1. Solvent shifts in the PMR spectra[a]

		δ_{CDCl_3}	$\delta_{C_6D_6}$	Δ		δ_{CDCl_3}	$\delta_{C_6D_6}$	Δ		δ_{CDCl_3}	$\delta_{C_6D_6}$	Δ
1a	4β-CH_3	0.87	0.97	−0.10	5β-CH_3	0.72	0.63	+0.09	9β-CH_3	0.87	0.74	+0.13
1b	4α-CH_3	1.11	0.86	+0.25	5β-CH_3	0.87	0.69	+0.18	9β-CH_3	0.92	0.85	+0.07
6	1β-CH_3	0.89	0.91	−0.02	9β-CH_3	0.73	0.57	+0.16	5β-CH_3 and 5α-CH_3	0.88 0.98	0.67 0.78	+0.21 +0.20

a) $\Delta = \delta_{CDCl_3} - \delta_{C_6D_6}$

Experimental

IR spectra were measured on a Hitachi EPI-G2 spectrometer. Mass spectra were taken on a Hitachi RMU-6-Tokugata mass spectrometer operating at 70 eV with an indirect inlet system unless otherwise stated. High resolution mass spectra were taken using a Hitachi RMH-2 mass spectrometer operating at 70 eV. PMR spectra were measured using a JEOL JNM PS-100 (100 MHz), a Hitachi R-20 (60 MHz) or a Hitachi R-24 (60 MHz) spectrometer. Chemical shifts were expressed in δ downfield from TMS as an internal standard and coupling constants in Hz. Gas chromatography-mass spectrometry (GC-MS) was performed on a Hitachi gas chromatograph model K-53 connected with the mass spectrometer mentioned above. Analytical gas chromatography (glc) was carried on a Shimadzu gas chromatograph model GC-4APF, and preparative gas chromatography was carried on a Hitachi gas chromatograph model K-53. Thin layer chromatography (tlc) was carried out on Kieselgel G (E. Merck) in 0.25 mm thickness. For column chromatography, Wakogel C-200 (Wako Pure Chemical Ind.) was used. All melting points were determined on a hot block and reported uncorrected. Liquid samples for elemental analyses were purified by rechromatography on silica gel.

*1-Hydroxy-1,5,5,9-tetramethyl-*trans*-decalins (**11** and **12**).* To the Grignard reagent prepared from methyl iodide (15 g) and magnesium (1 g) in dry ether (15 ml) at 0 °C was added a solution of 5,5,9-trimethyl-1-decalone (**7**[4]; 1.84 g) in dry ether (30 ml). The reaction mixture was stirred for 1.5 hr at 0 °C, then decomposed with aqueous ammonium chloride solution, and extracted with ether three times. The ethereal layer was washed with brine twice, and dried over magnesium sulfate. Evaporation of the solvent gave a residue (2.16 g), which was chromatographed on a column of silica gel (100 g) using the following solvents as eluents: light petroleum–ether (20 : 1) frs 1—4, each 150 ml; fr 5, 100 ml; frs 6—12, each 50 ml; light petroleum–ether (10 : 1) frs 13—22, each 50 ml; light petroleum–ether (5 : 1) frs 23—30, each 75 ml. Fractions 4—13 gave 1α-hydroxy-1β,5α,5β,9β-tetramethyl-*trans*-decalin (**11**; 1.26 g, 63%) as an oil, IR (liquid) 3480 cm^{-1}; PMR ($CDCl_3$) δ 0.84, 0.88, 0.97, and 1.08 (each 3H, s, t-CH_3); mass *m/e* 210 [M^+ ($C_{14}H_{26}O$); 13%] and *m/e* 81 (100%): Found: C, 79.81; H, 12.40%. Calcd for $C_{14}H_{26}O$: C, 79.93; H, 12.46%. Fractions 16—23 afforded 1β-hydroxy-1α,5α,5β,9β-tetramethyl-*trans*-decalin (**12**; 0.41 g, 20%), mp 52—53 °C (sublimation at 50 °C/1 mmHg), IR (Nujol) 3430 cm^{-1}; PMR ($CDCl_3$) δ 0.86 (6H, s, 2$\times$*t*-CH_3), 1.03, and 1.28 (each 3H, s, t-CH_3); mass *m/e* 210 [M^+ ($C_{14}H_{26}O$); 7%] and *m/e* 81 (100%); Found: C, 79.66; H, 12.23%. Calcd for $C_{14}H_{26}O$: C, 79.93; H, 12.46%.

*1,5,5,9-Tetramethyl-2-decalone (**6**).* The alcohol (**11**; 2.00 g) was heated at 140 °C and iodine (34 mg) was added at 5 min intervals over a period of 20 min. To the reaction mixture, after cooling, ether was added, and the ethereal solution was washed with aqueous sodium thiosulfate and sodium hydrogen carbonate solutions and with brine, and then dried over magnesium sulfate. On evaporation of the solvent, a residue (1.58 g) was obtained, which was shown to be a mixture of three olefins in a ratio of 61 : 8 : 31 for **13**, **14**, and **15**, respectively, by glc analysis (column: C-20M, 150 °C; N_2 65 ml/min; retention time: 10.3, 6.3, and 5.5 min for **13**, **14**, and **15**, respectively). The olefin mixture obtained from the alcohol (**12**; 295 mg) and iodine (6 mg) at 140 °C was shown to consist of **13**, **14**, and **15** in a ratio of 6 : 18 : 76 by glc analysis.

The former olefin mixture (65 mg) obtained from **11** was dissolved in light petroleum and passed through a column of silica gel (7 g) impregnated with 20% silver nitrate. Elution with light petroleum (each 20 ml) gave the olefin (**13**; 30 mg, frs 4 and 5) as an oil; IR (liquid) 1660 and 795 cm^{-1}; PMR ($CDCl_3$) δ 0.87, 0.89, 1.02 (each 3H, s, t-CH_3), 1.58 (3H, d, J=2 Hz, C=C–CH_3), and 5.18 (1H, m, C=CH); MW 192.1858, Calcd for $C_{14}H_{24}$: 192.1876; mass *m/e* 192 (M^+, 9%) and *m/e* 41 (100%).

The latter olefin mixture (280 mg), obtained from the alcohol (**12**), was dissolved in chloroform (5.5 ml). After *p*-toluenesulfonic acid (51 mg) was added, the resulting solution was allowed to stand at 60 °C for 4hr. Extraction with ether and usual treatment gave an oil, which was shown to be a mixture of **14** and **15** in a ratio of 1 : 4 by glc analysis. The mixture was chromatographed on a column of silica gel (22 g) impregnated with 20% silver nitrate. Elution with light petroleum (each 10 ml) afforded the olefin (**15**; 137 mg, from frs 1 and 2) as an oil; IR (liquid) neither absorption band due to C=C–H nor C=C was observed. PMR ($CDCl_3$) δ 0.97 (12H, s, 4$\times$*t*-CH_3); mass *m/e* 192 [M^+($C_{14}H_{24}$); 15%] and *m/e* 177 (100%). From the fractions 4—6, the olefin (**14**, 7 mg) was obtained as an oil; IR (liquid 3050 and 1635 cm^{-1}; PMR ($CDCl_3$) δ 0.81, 0.88, 1.01, and 1.05 (each 3H, s, *t*-CH_3) and 5.45 (1H, m, C=C–H); mass *m/e* 192 [M^+ ($C_{14}H_{24}$), 13%], *m/e* 136 (39%, a peak due to retro-Diels Alder fragmentation), and *m/e* 55 (100%).

Treatment of each olefin (**14** and **15**) in chloroform with *p*-toluenesulfonic acid as described above gave an oil, which was shown to consist of **14** and **15** in a ratio of 1 : 4 by glc analysis.

To the crude olefin mixture (**13**, **14**, and **15**; 1.49 g; obtained by the dehydration reaction of **11**) in tetrahydrofuran (20 ml) was added a tetrahydrofuran solution (20 ml) of diborane prepared from boron trifluoride etherate (15 g) and sodium borohydride (2 g). The mixture was kept at room temperature for 70 min and the excess diborane was decomposed by addition of water (1.8 ml). The organoborane solution, kept at 40 °C, was oxidized with 3M sodium hydroxide (3 ml) and 30% hydrogen peroxide (3 ml). After the reaction mixture was kept at room temperature for 1 hr, potassium carbonate (9 g) and water were added. Extraction with ether and usual work-up afforded a residue (1.77 g).

The crude alcohol, obtained above, was dissolved in acetone (20 ml) and oxidized with Jones' reagent (2 ml) at 0 °C. The reaction mixture was stirred for 40 min and then diluted with brine (40 ml). Extraction with ether and usual work-up gave a residue (1.57 g), which was subjected to column chromatographic separation on silica gel (200 g) and eluted with light petroleum–ether (20 : 1, each 60 ml). On removal of the solvents (frs 6—12), 1,5,5,9-tetramethyl-2-decalone (**6**; 838 mg, one spot on tlc) was obtained in 45% yield from **11**. Mp 55—56 °C (from light petroleum), IR (Nujol) 1715 cm^{-1}; PMR ($CDCl_3$) δ 0.73, 0.88, 0.98 (each 3H, s, *t*-CH_3), and 0.89 (3H, d, J=7 Hz, *s*-CH_3); mass *m/e* 208 [M^+($C_{14}H_{24}O$), 5%] and *m/e* 41 (100%); Found: C, 80.41; H, 11.51%. Calcd for $C_{14}H_{24}O$: C, 80.71; H, 11.61%. 2,4-Dinitrophenylhydrazone (crystallized from ethanol): mp 159—160 °C, Found: C, 61.60; H, 7.26; N, 14.27%. Calcd for $C_{20}H_{28}N_4O_4$: C, 61.84; H, 7.27; N, 14.42%.

*1,3,3-Trideuterio-1,5,5,9-tetramethyl-2-decalone (**6**-d_3).* 1,5,5,9-Tetramethyl-2-decalone (**6**; 46 mg) in tetradeuteriomethanol (1 ml) was allowed to stand with 2 drops of 30% sodium deuterioxide (isotopic purity: 99 atom % D) in deuterioxide. Diluted hydrochloric acid was added and the mixture was extracted with ether three times, washed with aqueous sodium hydrogen carbonate solution and with brine, and dried over magnesium sulfate. After evaporation of the

solvent, a residue (38 mg), without further purification, was subjected to mass spectrometric analysis with a direct inlet system operating at 70 eV. The deuterated decalone (**6**-d_3) was shown to consist of -d_3 (71%), -d_2 (25%), and -d_1 (4%). IR (liquid) 1715 cm^{-1}; PMR (CCl_4) δ 0.71, 0.82, 0.89, and 0.98 (each 3H, s, t-CH_3).

*1,3,3-Trideuterio-2β-hydroxy-1,5,5,9-tetramethyldecalin (**18**-d_3).* The above-obtained decalone-d_3 (**6**-d_3; 26 mg) was dissolved in methanol (0.5 ml), cooled with ice-salt, and reduced with sodium borohydride (10 mg). After the solution was maintained at 0 °C for 30 min, acetic acid (2 drops) was added. The reaction mixture was extracted with ether, washed with aqueous sodium hydrogen carbonate solution and with brine, and dried over magnesium sulfate. Evaporation of the solvent gave a residue (32 mg), which was chromatographed on a column of silica gel (3 g) and eluted with light petroleum–ether (20 : 1) to afford 1,3,3-trideuterio-2β-hydroxy-1,5,5,9-tetramethyldecalin (**18**-d_3; 21 mg), IR (Nujol) 3360 cm^{-1}; PMR spectral data using Eu(dpm)$_3$ was shown in Fig. 3. Signals due to a proton at C-4β appeared at δ 16.00 as a triplet ($J_{4\alpha,4\beta}=13$ and $J_{4\beta,10\alpha}=13$ Hz) [Eu(dpm)$_3$/**18**-d_3 (M/M): 0.92].

*Photochemical Reaction of 1,5,5,9-Tetramethyl-2-decalone (**6**) in n-Hexane Followed by Introduction of Oxygen in the Dark.* A solution of 1,5,5,9-tetramethyl-2-decalone (**6**; 185 mg) in *n*-hexane (650 ml) was irradiated with a high pressure mercury lamp (100 W, Rikosha) under a nitrogen atmosphere for 11 hr at room temperature. After the irradiation, dry oxygen was passed through the solution for 6 hr in the dark. On evaporation of the solvent, a residue (199 mg) was obtained, which was examined by GC-MS and the formation of 2-ethyl-1-formylmethyl-2,6,6-trimethylcyclohexane (**10**) was inferred [column: OV-17, 150 °C, He 0.8 kg/cm^2; retention time 4.2 min; mass *m/e* 196 (M^+($C_{13}H_{24}O$), 6%) and *m/e* 69 (100%)].

The reaction mixture was chromatographed on silica gel (20 g). After the starting ketone (**6**) was eluted with light petroleum–ether (20 : 1), elution with ether afforded an acid fraction (62 mg), which was treated with diazomethane to give a mixture (20 mg) of methyl esters (**8b** and **9b**; 20% silver nitrate-impregnated silica gel tlc showed two spots, R_f 0.42 and 0.38 for **8b** and **9b**, respectively). The mixture was separated by preparative glc (column: OV-17, 140 °C, N_2 1 kg/cm^2, retention time 3.8 min and 7.7 min for **8b** and **9b**, respectively).

The methyl ester (**8b**), an oil, showed IR (liquid) 1745 cm^{-1}; mass *m/e* 226 [M^+($C_{14}H_{26}O_2$), 2%] and *m/e* 69 (100%). IR, tlc, glc, and mass of this substance were identical with those of the authentic specimen prepared from **9b** by the Barbier-Wieland degradation (*vide infra*).

The other methyl ester (**9b**), an oil, showed IR (liquid) 1745 cm^{-1}; mass *m/e* 240 [M^+($C_{15}H_{28}O_2$), 1%] and *m/e* 69 (100%). This substance was identified to be 2-ethyl-1-(2-methoxycarbonylethyl)-2,6,6-trimethylcyclohexane by comparison (IR, tlc, glc, and mass) with the authentic sample prepared by photoreaction of **6** in methanol (*vide infra*).

*2-Ethyl-1-(2-methoxycarbonylethyl)-2,6,6-trimethylcyclohexane (**9b**).* 1,5,5,9-Tetramethyl-2-decalone (**6**; 201 mg) in methanol (750 ml) was irradiated with a high pressure mercury lamp 100 W, Rikosha) under nitrogen for 20 hr. After evaporation of the solvent, the residue (254 mg) was chromatographed on silica gel (20 g). Elution with light petroleum–benzene (100 : 1) and removal of the solvents afforded the methyl ester (**9b**; 179 mg, 77%) as an oil, IR (liquid) 1745 cm^{-1}; PMR ($CDCl_3$) δ 0.82, 0.88, 0.90 (each 3H, s, t-CH_3), 2.20—2.53 (2H, m, $CH_2CO_2CH_3$), and 3.65 (3H, s, CO_2CH_3); mass *m/e* 240 [M^+($C_{15}H_{28}O_2$), 1%] and *m/e* 69 (100%); Found: C, 74.83; H, 11.96%. Calcd for $C_{15}H_{28}O_2$: C, 74.95; H, 11.74%.

*2-Ethyl-1-methoxycarbonylmethyl-2,6,6-trimethylcyclohexane (**8b**).* To the methyl ester (**9b**; 150 mg) dissolved in tetrahydrofuran (20 ml) was added bromobenzene (950 mg) and magnesium (150 mg), and the reaction mixture was heated under reflux for 2.5 hr. After usual treatment, the residue (660 mg) was chromatographed on silica gel (20 g) and elution with light petroleum–ether (50 : 1) gave a diphenylcarbinol (**20**; 222 mg, 98%), as an oil. IR (liquid) 3600, 3550, and 3460 cm^{-1}; PMR ($CDCl_3$) δ 0.70, 0.78, and 0.80 (each 3H, s, t-CH_3); mass *m/e* 346 [$(M-H_2O)^+$; 8%] *m/e* 71 (100%); Found: C, 86.15; H, 9.71%. Calcd for $C_{26}H_{36}O$: C, 85.66; H, 9.95%.

The diphenylcarbinol (**20**; 200 mg) in benzene (3 ml) was refluxed with iodine (9 mg) for 4 hr. To the reaction mixture aqueous sodium thiosulfate solution was added. Extraction with ether and usual work-up afforded a residue (210 mg), which was passed through a column of silica gel (10 g) and eluted with light petroleum. A diphenylethylene derivative (**21**; 170 mg, 90% from **20**), as an oil, was obtained, IR (liquid) 1660 cm^{-1}; PMR ($CDCl_3$) δ 0.68, 0.76, 0.88 (each 3H, s, t-CH_3), 2.00—2.37 (2H, m, -CH_2-CH=C), and 6.07 (1H, t, $J=7$ Hz, CH=C); mass *m/e* 346 [M^+ ($C_{26}H_{34}$), 5%] and *m/e* 71 (100%); Found: C, 90.33; H, 9.99%. Calcd for $C_{26}H_{34}$: C, 90.11; H, 9.89%.

The diphenylethylene derivative (**21**; 138 mg) in acetic acid (10 ml) was oxidized with chromium trioxide (0.4 g) in acetic acid (6 ml) and water (0.3 ml) at room temperature for 69 hr. The excess oxidizing reagent was destroyed by addition of methanol, and usual treatment gave a residue (183 mg), which was dissolved in ether and allowed to stand with diazomethane in ether. After evaporation of the solvent, the residue (196 mg) was subjected to separation by silica gel (20 g) column chromatography. Elution with light petroleum–ether (100 : 1) gave the methyl ester (**8b**; 68 mg, 75% from **21**), an oil, IR (liquid) 1745 cm^{-1}; PMR ($CDZl_3$) δ 0.81, 0.84, 0.90 (each 3H, s, t-CH_3), 2.25 (2H, d, $J=5$ Hz, $CH_2CO_2CH_3$), and 3.64 (3H, s, CO_2CH_3); MW 226.1920, Calcd for $C_{14}H_{26}O_2$: 226.1930; mass *m/e* 226 [M^+($C_{14}H_{26}O_2$), 1%] and *m/e* 69 (100%).

References

1) *Cf.* O. L. Chapman and D. S. Weiss, "Organic Photochemistry," Vol. 3, p. 197, Marcel Dekker, Inc., New York (1973).

2) J. D. Coyle, *J. Chem. Soc., B*, **1971**, 1736.

3) R. Aoyagi, T. Tsuyuki, M. Takai, T. Takahashi, F. Kohen, and R. Stevenson, *Tetrahedron*, **29**, 4331 (1973) and the references cited therein.

4) F. Sondheimer and D. Elad, *J. Amer. Chem. Soc.*, **79**, 5542 (1957).

5) P. V. Demarco, T. K. Elzey, R. B. Lewis, and E. Wenkert, *ibid.*, **92**, 5737 (1970).

6) R. Aoyagi, S. Yamada, T. Tsuyuki, and T. Takahashi, This Bulletin, **46**, 959 (1973). And the references cited therein.

NOTES

BULLETIN OF THE CHEMICAL SOCIETY OF JAPAN, VOL. 47(12), 3163—3164 (1974)

ESR Study on Molecular Motion of CO_2^- Radical Adsorbed on Zeolite

Ove EDLUND,† Junkichi SOHMA, and Kunihisa SOGABE*

College of Engineering, Hokkaido University, Sapporo 060

* *College of Science, Hiroshima University, Hiroshima 730*

(Received December, 17, 1973)

Synopsis. Molecular motion of $^{13}CO_2^-$ radical adsorbed on zeolite was quantitatively analysed from the temperature variation of the separation of hyperfine structure of ESR spectra from $^{13}CO_2^-$ radicals.

CO_2 molecules enriched with ^{13}C were adsorbed on a Linde X-type zeolite, which had been heat-treated at 500 °C for 5 hr. Free radicals were produced from the adsorbed CO_2 by γ irradiation. ESR spectra of these systems were reported by one of the authors (K.S.) and his collaborators.[1] They found that the spectra change with temperature. In the ESR spectra consisting of three bands, the central part is the spectrum originated from the $^{12}CO_2^-$ radical and the wings are the doublet ascribed to the ^{13}C ($I=1/2$) coupling of $^{13}CO_2^-$ radical. The wings of the spectrum observed at 77 K show the so-called amorphous pattern,[2] the characteristic line-shape for an anisotropic hyperfine (hf) coupling of radicals trapped in an amorphous matrix. This pattern can be simulated by the program of Lefebvre and Maruani.[3] The principal value of the hf coupling tensor giving the best fit pattern to the observed one at 77 K were obtained as $A_x=150.0$ G, $A_y=156.0$ G, $A_z=197.5$ G. The principal values of the hf coupling tensors of the spectra observed at temperatures 180, 190, and 200 K were determined in a similar way and are listed with other ESR parameters in Table 1.

TABLE 1. THE PRINCIPAL VALUES OF THE g-TENSOR AND THE A-TENSOR, AND THE LINE WIDTH $\Delta H_{1/2}$, WHICH GIVE THE BEST FIT TO THE OBSERVED LINE-SHAPE, AND THE CORRELATION TIMES τ

Temp.	g-tensor		A-tensor (G)		ΔH (G)	$\tau\times10^8$ (s)
77 K	g_x	1.9975	A_x	150.0	5.5	
	g_y	2.0032	A_y	156.0		
	g_z	2.0015	A_z	197.5		
180 K	g_x	1.99998	A_x	154.1		
	g_y	2.00155	A_y	158.7	7.0	4.29
	g_z	2.00073	A_z	190.7		
190 K	g_x	2.00073	A_x	157.5		
	g_y	2.00073	A_y	161.0	7.0	2.09
	g_z	2.00073	A_z	185.0		
200 K	g_x	2.00073	A_x	160.0		
	g_y	2.00073	A_y	162.6	7.0	1.34
	g_z	2.00073	A_z	180.9		

ESR spectra of free radicals produced from adsorbed CO_2 are shown in Fig. 1. The shapes of the wings of the spectra become more isotropic with increasing temperature. At 77 K the CO_2^- radicals are almost completely frozen, the anisotropy of the coupling tensor being clearly observed. At 200 K no shoulder appears in the wing peaks and the doublet appears nearly symmetrical. The symmetric pattern indicates that the anisotropy of the hf coupling tensor is almost averaged out by the random motion of the adsorbed radicals at such a high temperature. The results indicate that the radicals adsorbed on the zeolite become more mobile at higher temperatures. In the process from the frozen state to the mobile one, *i.e.* in the temperature range 77—200 K, the anisotropy of the coupling tensor is partially averaged due to the gradually activated molecular motion of the radical. We can obtain quantitative information on the molecular motion of the adsorbed radical from the observed partial averaging of the anisotropic hf coupling tensor, based on the theory developed by Moriuchi and Sohma.[4] According to their theory partial averaging of each principal value of the hf coupling tensor is given by

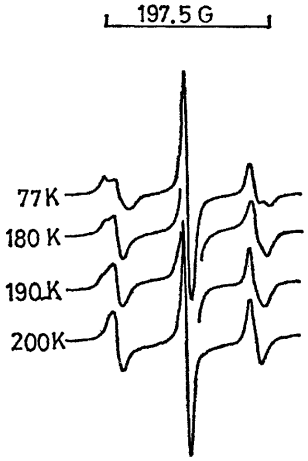

Fig. 1. Temperature variation of observed spectra of the CO_2^- radicals adsorbed on zeolite. The separation of the outermost peaks, 197.5 G, at 77 K, corresponds to the A_z principal values of the hyperfine coupling tensor.

$$\langle A_x\rangle_{Av} = a + A_{xo}\frac{2}{\pi}\tan^{-1}\frac{\tau}{T_2'}$$

$$\langle A_y\rangle_{Av} = a + A_{yo}\frac{2}{\pi}\tan^{-1}\frac{\tau}{T_2}$$

$$\langle A_z\rangle_{Av} = a + A_{zo}\frac{2}{\pi}\tan^{-1}\frac{\tau}{T_2'}$$

where a is the isotropic component of the coupling constant, A_x, A_y and A_z are the principal values of the

† On leave from Swedish Research Council's Laboratory, Studsvik, Nyköping, Sweden.

hf coupling tensor, and A_{xo}, A_{yo} and A_{zo} the anisotropic components of each principal value in the completely frozen state; τ is the correlation time of the molecular motion and T_2' is related to the inverse of the experimentally determined line width, that is $T_2'=1/\pi\cdot\Delta H_{1/2}$ in Lorentzian line-shape, $T_2'=(\ln 2/\pi)^{1/2}\,1/\Delta H_{1/2}$ in the Gaussain one. Experimentally determined principal values of the hf coupling tensor at each temperature result from partial averaging of the anisotropic hf coupling tensor due to the molecular motion of the responsible radical, $^{13}CO_2^-$ in this case, at this temperature. The isotropic coupling constant a was experimentally obtained by the equation $a=1/3(A_x+A_y+A_z)$ and the observed values of each component at 77 K, since one can assume that molecular motion at 77 K is completely frozen. T_2''s are determined from the line widths, experimentally determined by simulation with the observed spectrum at each temperature. The results are listed in Table 1. Since the peak corresponding to A_z appears most clearly in the doublet and changes distinctly with temperature, we used the observed value of the A_z-component at each temperature in order to estimate τ at this temperature. The correlation times are plotted against $1/T$ in Fig. 2. The activation energy for this molecular motion of the adsorbed CO_2^- radical on the zeolite was determined to be 4.1 kcal/mol.

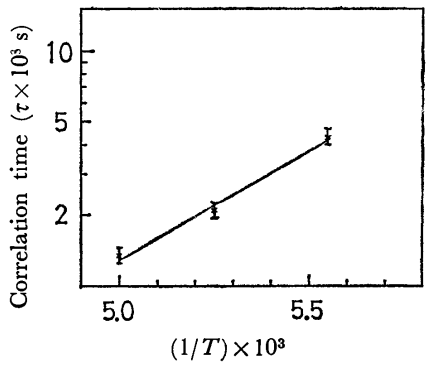

Fig. 2. The Arrhenius plot of the correlation times estimated from the partial averaging of the A_z component.

The observed ESR spectra and their analysis give us quantitative information on the molecular motion of the adsorbed CO_2^- radicals on the zeolite. The molecular motion of the adsorbed CO_2^- is completely hindered at 77 K but liberated gradually from 180 K until free random motion is attained at 200 K.

The authors thank Dr. A. Hasegawa, Hiroshima University, for his valuable discussion. One of the authors (O.E.) wishes to express his sincere thanks to the Japan Society for Promotion of Science for the fellowship which enabled him to work at Hokkaido University.

References

1) K. Sogabe, A. Hasegawa, Y. Yamada, and M. Miura, This Bulletin, **45**, 3362 (1972).
2) For example, F. K. Kneubuhl, *J. Chem. Phys.*, **33**, 1074 (1960).
3) R. Lefebvre and J. Maruani, *ibid.*, **42**, 1480 (1965).
4) S. Moriuchi and J. Sohma, *Mem. Fac. of Eng. Hokkaido Univ.*, **13**, No. 4, 335 (1974).

BULLETIN OF THE CHEMICAL SOCIETY OF JAPAN, VOL. 47(12), 3165—3166 (1974)

Ionic Equilibria in Micellar Solutions

Keishiro SHIRAHAMA

Department of Chemistry, Faculty of Science and Engineering, Saga University, Honjo-machi, Saga 840

(Received March 30, 1974)

Synopsis. Ionic equilibria in micellar solutions are discussed on the basis of micelle-monomer equilibrium, mass-conservation, and electroneutrality. The present treatment gives a larger degree of counterion dissociation from micelles than ever estimated. Another conclusion is a decreasing concentration of monomeric surface-active ion as micellar concentration increases.

Since Botré *et al.* firstly applied the membrane potential measurement to elucidate a degree of dissociation of counterion from micelles,[1] many investigators have followed the same kind of trials by using either ion-exchange membrane or pNa glass electrode.[2-5] As a starting point of discussion, Eq. (1) has been assumed,

$$a = \gamma(C_0 + \alpha n C_m) \quad (1)$$

where a is the activity of counterion, γ activity coefficient, α a degree of counterion dissociation from micelle, n aggregation number of a micelle and C_m a micellar concentration. This expression is based on "*formal separation*"[1] of counterions originated from micelles and those from free surfactant ions. However no one can make this distinguishment *a priori*.

Alternatively, we express, as an approximation, the pseudo-phase model for a 1 : 1 type ionic surfactant forming a micellar solution in the absence of extraneous electrolyte,

$$C_c C_s f_\pm^2 = (C_0 f_0)^2 \quad (2)$$

where f_0 and $f_\pm$ are the activity coefficients of surfactant at cmc and at any arbitrary concentration above cmc, C_c and C_s are the concentrations of, respectively, counterion and surface-active ion in equilibrium with micelles. Eq. (2) is considered to hold to a good approximation, even when a more general mass action law model is taken into account. Furthermore one obtains Eq. (3) as a consequence of mass balance,

$$C = C_s + nC_m \quad (3)$$

where C is the total (analytical) concentration of the surfactant. Electroneutrality also requires the following relation.

$$C_c = C_s + \alpha n C_m \quad (4)$$

Combing Eq. (3) with Eq. (4), one has

$$C_c = C_s + \alpha(C - C_s) \quad (5)$$

or introducing Eq. (2), one obtains

$$C_c = (C_0^2/C_c)(f_0/f_\pm)^2 + \alpha[C - (C_0^2/C_c)(f_0/f_\pm)^2] \quad (6)$$

Note that Eq. (1) can be reproduced only if C_s is replaced by C_0, or at the limit $C \to C_0$.

Rearrangement of Eq. (6) gives

$$C_c - (C_0^2/C_c)(f_0/f_\pm)^2 = \alpha[C - (C_0^2/C_c)(f_0/f_\pm)^2] \quad (7)$$

With the knowledge of C, C_c and the activity coefficients, α can be calculated. In order to do so, the potentiometry of micellar solution is very useful. Such potentiometry is schematically shown in Fig. 1, where an electronic potential, E motivated from the counterion activity is plotted against log C. Tracing $C \to B \to A \to C_c$, one obtains C_c at a total concentration C. It is rather difficult to estimate the ratio of the activity coefficients in micellar solution. In the present treatment as well as any other theories using a parameter α, all the effects arising from micelles are included in the parameter, and the coexisting coions and counterions (unbound) are considered to behave as if they were in a solution of the same concentration. This idea is identical with so-called additivity rule well accepted in the field of polyelectrolyte solutions.[6] Therefore we

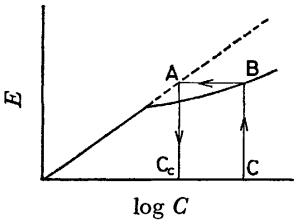

Fig. 1. A schematic representation of potential E *vs.* log C profile.

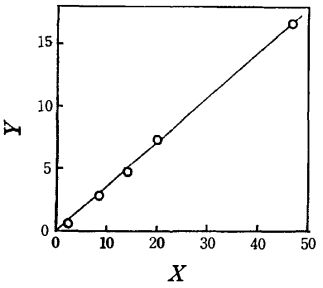

Fig. 2. Y *vs.* X plot. See the text for detail. The original data are already published by us.[5]

TABLE 1. THE DEGREE OF COUNTERION DISSOCIATION OF SODIUM DODECYLSULFATE

Author		Degree of dissociation α previous	Degree of dissociation α present	Ref.
Botré *et al.*	(1959)	0.16		1
Shedlovsky *et al.*	(1963)	0.22	0.32	2
Satake *et al.*	(1969)	0.25	0.40	4
Shirahama	(1972)	0.29	0.36	5
Birch and Clarke	(1972)	0.25	0.30[a]	13

a) They calculated the value of α on the basis of mass-action law, which also predicts a decrease of surface-active ion above cmc, as in the present treatment.

set $(f_0/f_\pm) \fallingdotseq 1$. In Fig. 2 $Y=C_c-(C_0^2/C_c)$ is plotted against $X=C-(C_0^2/C_c)$ for sodium dodecylsulfate. As is seen, a linear relation with the slope α is obtained. The published data are recalculated for sodium dodecylsulfate and shown in Table 1, from which it is clear that, in any case, the value of α is larger than those ever estimated by the assumption of Botre *et al.*, or Eq. (1). Another conclusion obtainable from Eq. (2) and an increasing counterion concentration even above cmc (experimental facts) is that the concentration of monomeric surface-active ion in equilibrium with micelles is decreasing as the total concentration increases. The same results have been derived in a little different manner in the works of Elworthy *et al*,[7] and of Birch and Clarke.[13] It is misleading that the monomer concentration in equilibrium with micelles is constant. Thus, the studies based on the incorrect assumption, such as conductivity,[8] surfactant-polymer interaction,[9] calorimetry,[10] solubilization,[11] and nmr[12] are required to be re-investigated.

The author thanks Prof. M. Tanaka of Fukuoka University and Mr. K. Tsujii of Kao Soap Co., Ltd. for their interest and discussion on the present topics.

References

1) C. Botré, V. L. Crescenzi, and A. Mele, *J. Phys. Chem.*, **63**, 650 (1959).
2) L. Shedlovsky, C. W. Jakob, and M. B. Epstein, *ibid.*, **67**, 2075 (1963).
3) M. E. Feinstein, and H. L. Rosano, *J. Colloid Interface Sci.*, **24**, 73 (1967).
4) I. Satake, T. Tahara, and R. Matuura, This Bulletin, **42**, 319 (1969).
5) K. Shirahama, *Kolloid Z. Z. Polymere*, **250**, 620 (1972).
6) F. Oosawa, "Polyelectrolytes," M. Dekker, (1971), p. 87.
7) P. H. Elworthy, A. T. Florence, and C. B. Macfarlane, "Solubilization by Surface Active Agents," Chapman and Hall, (1968), p. 48.
8) H. Kimizuka, and I. Satake, This Bulletin, **35**, 251 (1962).
9) M. L. Fishman, and F. R. Eirich, *J. Phys. Chem.*, **75**, 3135 (1971).
10) M. N. Jones, and J. Piercy, *Kolloid Z. Z. Polymere*, **251**, 343 (1973).
11) ref. 7, p. 80.
12) T. Drakenberg, and B. Lindman, *J. Colloid Interface Sci.*, **44**, 184 (1973).
13) B. J. Birch, and D. E. Clarke, *Anal. Chim. Acta*, **61**, 159 (1972).

BULLETIN OF THE CHEMICAL SOCIETY OF JAPAN, VOL. 47(12), 3167—3168 (1974)

Dissociative Electron Attachment to (Chloroethyl)benzenes in γ-Irradiated Organic Glassy Matrices

Takayuki SAITO and Hiroshi YOSHIDA
Faculty of Engineering, Hokkaido University, Kita-ku, Sapporo 060

(Received May 17, 1974)

Synopsis. Free radicals formed from (1- and 2-chloroethyl)benzene in γ-irradiated organic matrices were studied with a fluroescence spectrophotometer. The observed spectra suggest the transformation of phenetyl radical primarily formed from (2-chloroethyl)benzene to α-methylbenzyl radical and indicate interaction between the α-methylbenzyl radical, formed from both (1- and 2-chloroethyl)benzene, and chloride anion before complete dissociation.

There is a current interest in radiation chemistry in condensed media in studies of the relaxation process[1] before the formation of thermodynamically stable intermediates such as trapped electrons and anions. Recently, we have studied the formation of benzyl radical from benzyl derivatives and obtained spectroscopic evidence that the benzyl associates temporarily with fragment anion when formed through dissociative electron attachment in organic glassy matrices.[2]
In order to see the generality of this behavior, the study was extended to (1- and 2- chloroethyl)benzene by means of a fluorescence spectrophotometric method. The method has great advantages in studying intermediates formed in γ-irradiated matrices on account of its high sensitivity, applicability to non-transparent specimens and the possibility to distinguish a spectrum from other overlapping ones. Prominent results are: (1) a temporary association is evidenced also between α-methylbenzyl radical and chloride anion and (2) phenetyl radical transforms readily to α-methylbenzyl radical in the matrices at 77 K.

3-Methylhexane was used as non-polar solvent after being purified several times by washing with a sulfuric acid–nitric acid mixture and then with water and drying with anhydrous calcium chloride and calcium hydride. Ethanol of spectro-grade was used without further purification as a polar solvent. Solutes of analytical grade, ethylbenzene, (1-chloroethyl)benzene and (2-chloroethyl)benzene, were used without further purification. The effect of purification was checked once for 2-chloroethylbenzene, no difference in results being found.

Solution of 10^{-1}—10^{-2} M concentration was prepared in a vacuum of about 10^{-6} Torr, for desired combination of solvent and solute, and sealed in tubes of pure quartz (originally for ESR). The samples were frozen into glassy state, irradiated with ^{60}Co γ-rays to a dose of about 3×10^{5} rad or with UV light from a high pressure mercury lamp, and examined with a recording fluorescence spectrophotometer (Hitachi, Model MPS-2A) at 77 K.

Typical examples of emission and excitation spectra of α-methylbenzyl radicals generated in different ways are given in Fig. 1. The emission spectra are observed in visible region with a 0-0 band at about 470 nm. Excitation spectra are observed in visible, near-UV (at about 320 nm) and far-UV (at about 270 nm) regions. However, spectral lines of excitation source (Xe lamp) interfered accurate recording of the weak visible excitation spectra. The emission spectra were recorded by excitation at the peak of the near-UV excitation spectra, though the shape of the emission spectra was not affected by the excitation wavelength. The near-UV and far-UV spectra were recorded by observation at the maximum point of the emission spectra. Characteristics of the recorded spectra are summarized in Table 1.

Ethylbenzene. Free radicals generated from ethylbenzene were studied for comparison. The spectra obtained by photolysis in the non-polar matrix (Fig. 1A) are close to those of photolytically generated benzyl radicals,[2] except that the strong 0-0 band in the emission spectrum indicates a partial removal of the forbidden nature of this band by methyl substitution, and thus they are attributed to the α-methylbenzyl radical. Porter and Starachen reported the absorption spectrum in the near-UV region (maximum at 322.2 nm) of the α-methylbenzyl radical formed by the photolysis of ethylbenzene in ether–isopentane–ethanol mixed glass.[3] The present spectra are consistent with theirs.

The γ-irradiation gives the same spectra as those in Fig. 1A, irrespective of solvent (Table 1). This in-

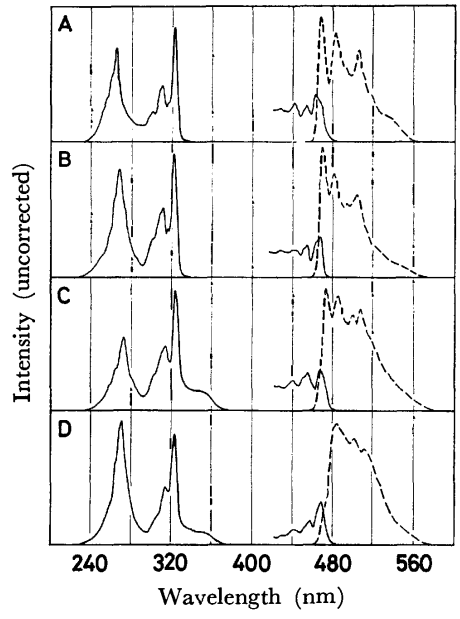

Fig. 1. Emission (——) and excitation (——) spectra of α-methylbenzyl radicals generated (A) from ethylbenzene by photolysis in 3-methylhexane, from (1-chloroethyl)benzene by γ-irradiation (B) in ethanol and (C) in 3-methylhexane, and (D) from (2-chloroethyl)benzene by γ-irradiation in 3-methylhexane.

TABLE 1. EXCITATION AND EMISSION SPECTRA OBSERVED AT 77 K OF α-METHYLBENZYL RADICALS GENERATED PHOTOLYTICALLY OR RADIOLYTICALLY IN ORGANIC GLASSY MATRICES

Parent molecules	Matrices	Generation method	Excitation spectra		Emission spectra
			Near-UV band λ_{max} (nm)	350 nm band	λ_{max} (nm)
$C_6H_5CH_2CH_3$	3MHx[a]	Photolysis	322	—	467.5
	3MHx	Radiolysis	322.5	—	468
	EtOH[b]	Radiolysis	323	—	468
$C_6H_5CHClCH_3$	3MHx	Radiolysis	323.5	Observed	473
	EtOH	Radiolysis	322	—	469
$C_6H_5CH_2CH_2Cl$	3MHx	Photolysis	323.5	—	469
	3MHx	Radiolysis	323.5	Observed	483[c]
	EtOH	Radiolysis	323.5	—	469.5

a) 3-methylhexane. b) Ethanol. c) Does not apparently correspond to the 0—0 band of the spectrum.

dicates the formation of α-methylbenzyl radicals also by radiolysis. Although radiation chemical processes involved are not known in detail, it is unconceivable that the methylbenzyl radical is formed through the electron attachment to ethylbenzene. A hydrogen atom or some other radical might be formed as a counterpart of the methylbenzyl radical by the homolytic C–H bond rapture. Radical formation may be possible by energy transfer from solvent to solute.[4] An alternative may be charge neutralization between ethylbenzene cation and electron to form excited ethylbenzene, as proposed for the formation of benzyl radical from toluene in aqueous solution.[5]

(1-Chloroethyl)benzene. When α-methylbenzyl radicals are generated from (1-chloroethyl)benzene by γ-irradiation, the spectra differ depending on the nature of matrices, polar or non-polar. The spectra in the polar matrix are the same as those of normal methylbenzyl radicals (compare Fig. 1B with Fig. 1A), whereas the spectra in the non-polar matrix (Fig. 1C) differ in the following way. (1) The visible emission and near-UV excitation spectra are more or less red-shifted. Although the band structure in the far-UV spectrum is not resolved, its peak also red-shifts from 267.5 to 272.5 nm. (2) The band width of the spectra becomes broader in the non-polar matrix, as seen clearly in the visible emission spectra. (3) A new broad excitation spectrum is observed around 350 nm. These observations are completely analogous to those for benzyl radicals formed from benzyl chloride.[2] The methylbenzyl radical is generated with chloride anion as a counterpart through dissociative electron attachment to (1-chloroethyl)benzene. The first two observations are qualitatively interpreted to be due to the local Coulombic effect of nearby anion, as in the case of radical cation spectra perturbed by counter anions.[6] The effect of the counter anion is dominant in the non-polar matrix but almost absent in the polar matrix because of the solvent polarization and anion solvation. According to the assignment of electronic transitions given to benzyl-type radicals,[7] the new spectrum may possibly be due to the $2^2B_2 \rightarrow 1^2B_2$ transition, hidden by the intense near-UV spectrum of the $2^2A_2 \rightarrow 1^2B_2$ transition in the absence of the effect of nearby anion.[2] The association between the α-methylbenzyl radical and the anion temporarily occurs after the dissociative electron attachment to (1-chloroethyl)benzene in the glassy matrix. The efficiency of methylbenzyl radical formation by photolysis is too low to record spectra.

(2-Chloroethyl)benzene. The dissociative electron attachment to (2-chloroethyl)benzene results in the formation of phenethyl radical as a primary intermediate. However, the spectra observed after γ-irradiation indicate that α-methylbenzyl radicals are trapped in the irradiated matrices. The phenethyl radical is unstable even in rigid matrices and readily transforms to the methylbenzyl radical, $\dot{C}_6H_5CH_2CH_2 \rightarrow C_6H_5\dot{C}HCH_3$. In this case also, the methylbenzyl radicals formed by γ-irradiation show spectra dependent on the polarity of the matrix. In the polar matrix, the spectra are the same as those of the "free" methylbenzyl radical (Fig. 1B). In the non-polar matrix, the effect of a nearby anion is seen in the excitation spectra (Fig. 1D). Although the 0-0 band of the emission spectrum is not resolved in this case, it is evident that the spectrum is also red-shifted and the band width is extremely large.

When (2-chloroethyl)benzene is photolyzed, the counterpart of the methylbenzyl radical is necessarily a chlorine atom rather than a chloride anion. In fact, photolysis in the non-polar matrix gives spectra typical of the "free" methylbenzyl radical (Table 1). This observation strongly supports the view that the perturbed spectra of the α-methylbenzyl radical formed by dissociative electron attachment are attributed to the temporary radical-anion pair before complete dissociation.

References

1) See for example, T. Higashimura, M. Noda, T. Warashina, and H. Yoshida, *J. Chem. Phys.*, **53**, 1152 (1970); T. Higashimura, A. Namiki, M. Noda, and H. Hase, *ibid.*, **76**, 3744 (1972); L. Kevan, *ibid.*, **56**, 838 (1972) and H. Hoshino, S. Arai, and M. Imamura, *J. Phys. Chem.*, **78**, 1473 (1974).

2) M. Irie, M. Shimizu, and H. Yoshida, *Chem. Phys. Lett.*, **25**, 102 (1974).

3) G. Porter and E. Strachan, *Trans. Faraday Soc.*, **54**, 1595 (1958).

4) M. Kato, Y. Saitake, T. Miyazaki, and Z. Kuri, This Bulletin, **46**, 2004 (1973) and the references cited therein.

5) J. P. Mittal and E. Hayon, *Nature Phys. Sci.*, **240**, 20 (1972).

6) K. Kimura, S. Katsumata, and K. Sawada, *J. Phys. Chem.*, **76**. 639 (1972).

7) See for example, P. M. Johnson, and C. A. Albrecht, *J. Chem. Phys.*, **48**, 851; O. M. Friedrich, and A. C. Alarecht, *ibid.*, **58**, 4766 (1973).

BULLETIN OF THE CHEMICAL SOCIETY OF JAPAN, VOL. 47(12), 3169—3170 (1974)

On the Additivity of π-Bond Energies in Linear Polyenes

Jun-ichi AIHARA

Department of Chemistry, Faculty of Science, Hokkaido University, Sapporo 060

(Received May 24, 1974)

Synopsis. The additivity of π-bond energies in linear polyenes was confirmed by taking nonaromatic [infinity]-annulene and -polyene as reference compounds. The π-bond energies determined by Hess and Schaad were found to be oriented to polyenes of a medium size.

Dewar and his collaborators, using the LCAO–SCF–MO method, have found that the bond energies of acyclic polyenes are additive.[1,2] One can readily calculate the total energy of any acyclic polyene merely by summing the energies of all its bonds. Figeys applied the LCAO–BETA method to the calculation of the total energies of linear polyenes[3] and indicated that linear polyene can be represented in terms of localized single and double C–C bonds, in agreement with their finding.

In 1971, Hess and Schaad found that a similar treatment of the HMO π-energies allows the calculation of π-bond energies in a much simpler way.[4] They classified the single and double C–C bonds further into eight types according to the number of attached hydrogen atoms; they determined the corresponding eight π-bond energies, which are listed in Table 1.

TABLE 1. HMO π-BOND ENERGIES OF CARBON-CARBON BONDS OF ACYCLIC POLYENES CALCULATED BY HESS AND SCHAAD[4]

Designation	Type of bond	Calculated π-bond energy (β)
E_{23}	$H_2C{=}CH$	2.0000
E_{22}	$HC{=}CH$	2.0699
E_{22}'	$H_2C{=}C$	2.0000
E_{21}	$HC{=}C$	2.1083
E_{20}	$C{=}C$	2.1716
E_{12}	HC–CH	0.4660
E_{11}	HC–C	0.4362
E_{10}	C–C	0.4358

The total π-energy of any acyclic polyene was then found to be very accurately calculated with these π-bond energies in an additive manner. This means that the π-bonds in polyene are quite localized at the conventionally-written double bonds. In this connection, we reexamined the additivity of π-bond energies of linear polyenes within the framework of the HMO theory, and without any additional assumptions.

Results and Discussion

The total HMO π-energy (E_{HMO}) of linear polyene is calculated from the following simple expression:[5]

$$E_{\mathrm{HMO}}([\mathrm{N}]\text{-polyene}) = 2\,\mathrm{cosec}\frac{\pi}{2\mathrm{N}+2} - 2. \tag{1}$$

Similarly, the total HMO π-energy of annulene is evaluated using the following expression:[5]

$$E_{\mathrm{HMO}}([\mathrm{N}]\text{-annulene}) = \begin{cases} 4\,\mathrm{cosec}\dfrac{\pi}{\mathrm{N}} & \text{for } [4n+2]\text{-annulene} \\ 4\cot\dfrac{\pi}{\mathrm{N}} & \text{for } [4n]\text{-annulene.} \end{cases} \tag{2}$$

In the above expressions, N is the number of carbon atoms in linear polyene (1) or annulene (2). The energies obtained from the expressions (1) and (2) are given in units of β.

It is generally accepted that, as the ring of annulene becomes very large, the $(4n+2)$ π rule on aromaticity no longer operates, and the annulene is considered to be a nonaromatic cyclic polyene.[6] Assuming that the π-bond energies are additive, [infinity]-annulene can be employed as one of the reference compounds in determining the π-bond energies. When N is large enough, the total π-energy of [N]-annulene can be expressed with the use of Hess and Schaad's notation (See Table 1) as:

$$E_{\mathrm{HMO}}([\mathrm{N}]\text{-annulene}) \sim \frac{\mathrm{N}}{2}(E_{22}+E_{12}). \tag{3}$$

Therefore, the π-bond energy of the unit structure in annulene, which is a combination of CH=CH and CH–CH bonds, is estimated at the nonaromatic limit as:

$$E_{22}+E_{12} = \lim_{\mathrm{N}\to\infty}\frac{E_{\mathrm{HMO}}([\mathrm{N}]\text{-annulene})}{\left(\frac{\mathrm{N}}{2}\right)} = \frac{8}{\pi} = 2.5464791\cdots\cdots . \tag{4}$$

The same quantity can be derived from the following expression concerning linear polyenes:

$$E_{22}+E_{12} = \lim_{\mathrm{N}\to\infty}\{E_{\mathrm{HMO}}([\mathrm{N}+2]\text{-polyene}) - E_{\mathrm{HMO}}([\mathrm{N}]\text{-polyene})\} = \frac{8}{\pi} \tag{5}$$

The coincidence between the above two values supports strongly the absence of aromaticity in large annulene, as was expected.[6] In this sense, Hess and Schaad's estimate of the limiting REPE (resonance energy per π-electron) of annulene at 0.0053β appears to be unlikely.[7]

On the other hand, the difference in the total HMO π-energies between [infinity]-annulene and the corresponding linear polyene is associated with the π-bond energy of the $CH_2{=}CH$ type (E_{23}). That is,

$$2E_{22}+E_{12}-2E_{23} = \lim_{\mathrm{N}\to\infty}\{E_{\mathrm{HMO}}([\mathrm{N}]\text{-annulene}) - E_{\mathrm{HMO}}([\mathrm{N}]\text{-polyene})\} = 2 - \frac{4}{\pi} = 0.7267605\cdots\cdots \tag{6}$$

Table 2. π-Energies in units of β of linear polyenes

N	E_{HMO}	E_A	$E_{HMO}-E_A$	E_{HS}	$E_{HMO}-E_{HS}$
4	4.4721	4.3662	0.1059	4.4660	0.0061
6	6.9879	6.9127	0.0752	7.0019	−0.0140
8	9.5175	9.4592	0.0584	9.5378	−0.0203
10	12.0533	12.0056	0.0477	12.0737	−0.0204
12	14.5925	14.5521	0.0403	14.6095	−0.0171
14	17.1335	17.0986	0.0350	17.1455	−0.0120
16	19.6759	19.6451	0.0308	19.6814	−0.0055
18	22.2191	22.1916	0.0276	22.2173	0.0018
20	24.7630	24.7380	0.0250	24.7532	0.0098
22	27.3073	27.2845	0.0228	27.2891	0.0182
24	29.8519	29.8310	0.0210	29.8250	0.0269
26	32.3969	32.3775	0.0194	32.3609	0.0360
28	34.9420	34.9239	0.0181	34.8968	0.0452
30	37.4873	37.4704	0.0169	37.4327	0.0546
32	40.0328	40.0169	0.0159	39.9686	0.0642
34	42.5783	42.5634	0.0150	42.5045	0.0738
36	45.1240	45.1099	0.0142	45.0404	0.0836
38	47.6698	47.6563	0.0134	47.5763	0.0935
40	50.2156	50.2028	0.0128	50.1122	0.1034
42	52.7615	52.7493	0.0122	52.6481	0.1134
44	55.3074	55.2958	0.0116	55.1840	0.1234
46	57.8534	57.8423	0.0111	57.7199	0.1335
48	60.3994	60.3887	0.0107	60.2558	0.1436
50	62.9455	62.9352	0.0103	62.7917	0.1538

Therefore, as long as the π-bond energies are additive, the total π-energy of linear [N]-polyene can reasonably be estimated by combining Eqs. (4) and (6) as follows:

$$E_A([N]\text{-polyene}) = \frac{N}{2}(E_{22}+E_{12}) - (2E_{22}+E_{12}-2E_{23})$$

$$= \frac{4(N+1)}{\pi} - 2. \qquad (7)$$

Table 2 shows the total π-energies of linear polyenes estimated by using Eq. (7) (E_A), together with those estimated from Table 1 (E_{HS}).

As may easily be seen, the total HMO π-energies are excellently reproduced by the present treatment. It must be noted that E_A was derived simply on the assumption of the additivity of π-bond energies. Since there is no arbitrariness in deriving Eq. (7), E_A is a unique solution for linear polyene. The deviation of E_A from E_{HMO} is generally very small, and at its maximum at N=4, for which E_A is only 2.37 percent less than E_{HMO}. Even though every π-bond energy can not be evaluated by the present consideration, we can safely say that the additivity of π-bond energies was verified in this manner. The small energy difference between E_A and E_{HMO} might be considered as a kind of stabilization energy, though it is not well grounded. This apparent stabilization energy is a result of taking [infinity]- annulene and -polyene as reference compounds; it may be related to the stability of relatively small polyenes.[8] The energy difference diminishes gradually on going to longer polyenes.

In this sense, the total π-energies determined by using Hess and Schaad's π-bond energies (E_{HS}) appear to be influenced by the above effect. Since their intention was to attain the best additivity of π-bond energies for acyclic polyenes of a medium size,[4] the additivity itself is considerably better for polyenes with N-values less than 22. The energy deviation of E_{HS} from E_{HMO} is suppressed at less than 0.22 percent of the total π-energy in that range of N. However, we could not find any meaning in the energy deviation, as it is not systematic with respect to N. It is totally dependent on the choice of π-bond energies. Some parts of the energy deviation are possibly due to the arbitrary assignment of the value to two of the eight π-bond energies made by Hess and Schaad.[4] The energy deviation of E_{HS} from E_{HMO} as well as the percent energy deviation increases monotonously beyond N= 22.

As is indicated in Eq. (4), the π-bond energy of the unit structure of annulene was estimated at 2.5465β, which is quite comparable to the value determined from Table 1 (2.5359β). On the other hand, the quantity defined by Eq. (6) (0.7268β) is somewhat larger than the corresponding value determined from Table 1 (0.6058β). Such a discrepancy is suggestive of the peculiar contribution of the edge double bonds in polyene.

The above discussion has been made on the basis of the simple HMO theory, in which the effect of bond alternation was completely disregarded for the sake of simplicity. As long as the effect of the more striking bond alternation near both edges of the polyene[5] is assigned simply to E_{23} only, it must be slightly larger than was expected by Hess and Schaad.[4] This fact also suggests that, when the additive π-bond energies derived from relatively small polyenes are used to spurious estimate the resonance energies of cyclic systems, spurious results might sometimes be produced.

We are grateful to the Hokkaido University Computing Center for the use of their FACOM 230—60, on which all the calculations were performed.

References

1) M. J. S. Dewar and G. J. Gleicher, *J. Amer. Chem. Soc.*, **87**, 692 (1965).
2) M. J. S. Dewar and C. de Llano, *ibid.*, **91**, 789 (1969).
3) H. P. Figeys, *Tetrahedron*, **26**, 5225 (1970).
4) B. A. Hess, Jr. and L. J. Schaad, *J. Amer. Chem. Soc.*, **93**, 305 (1971).
5) C. A. Coulson and A. Streitwieser, Jr., "Dictionary of π-Electron Calculations," W. H. Freeman, San Francisco, Calif. (1965).
6) G. M. Badger, "Aromatic Character and Aromaticity," Cambridge University Press, London (1969).
7) B. A. Hess, Jr., L. J. Schaad, and C. W. Holyoke, Jr., *Tetrahedron*, **28**, 5299 (1972).
8) See *e.g.*, "The Chemistry of Alkenes," edited by S. Patai, Interscience Publ., London (1964).

BULLETIN OF THE CHEMICAL SOCIETY OF JAPAN, VOL. 47(12), 3171—3172 (1974)

Formation of Erbium and Holmium Mixed Complexes with Complexane and Carbonate Ion

Tomitsugu TAKETATSU

College of General Education, Kyushu University, Fukuoka 810

(Received February 16, 1974)

Synopsis. The formation of erbium and holmium mixed complexes with one species of complexanes and carbonate ion in alkaline solution (pH 10.5—10.7) was investigated spectrophotometrically. The results suggest that carbonate ion additionally combines with the EDTA and CyDTA chelates, while does not with the DTPA chelates.

In a previous paper[1], the mechanism of formation and composition of erbium and holmium chelates with one of complexanes and 5-sulfosalicyclic acid in alkaline solution were investigated. It is well known that tripositive rare earth salts, especially the heavier rare-earth salts are dissolved in a potassium carbonate solution because the carbonate complex forms.[2,3] The formation of the erbium and holmium carbonate complexes causes a remarkable enhancement of the intensity in the hypersensitive bands of the metal ions.[4] Though the rare earth–complexane chelates are very stable, the enhancement of the intensity is not remarkable.[1] In the present paper, the formation of the mixed complexes has been studied by inquiring the enhancement of the intensity of a hypersensitive band with increasing concentration of carbonate ions added to the alkaline solutions of the rare earth-chelates of ethylenediaminetetraacetic acid (EDTA), *trans*-1,2-cyclohexanediamine-*N,N,N',N'*-tetraacetic acid (CyDTA), and diethylenetriamine-*N,N,N',N'',N''*-pentaacetic acid(DTPA).

Experimental

All the absorption spectra were measured with a Hitachi EPS-3T automatic recording spectrophotometer.

The preparation of the reagents and the experimental procedure were carried out by the similar manner described in the previous paper.[1] A potassium hydroxide solution for adjusting pH was stored in a reagent bottle with a soda lime tube.

Results and Discussion

The absorption spectra of the alkaline solution (pH 10.5—10.7) containing various combination of erbium and holmium (Ln), one species of the complexanes and the carbonate ion were recorded between 340 and 650 nm. As references the characteristic spectra in the region of 380 nm for erbium and 450 nm for holmium, obtained from these systems with the corresponding spectra of the rare earth–carbonate complexes (pH 10.5—10.7) and the rare earth chlorides (pH 2.0) are given in Figs. 1 and 2. From the results, the absorption spectra of the Ln-EDTA-CO_3^{2-} and Ln-CyDTA-CO_3^{2-} systems are quite different from that of the Ln–EDTA and Ln–CyDTA systems, respectively,

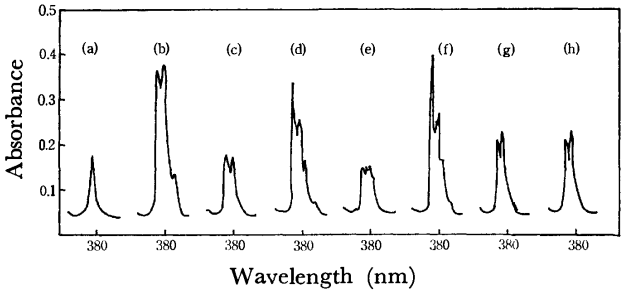

Fig. 1. Absorption spectra of aqueous solutions of erbium-complexane-CO_3^{2-} systems. (a) $ErCl_3$, (b) Er : CO_3^{2-} = 1 : 40.4, (c) Er : EDTA = 1 : 1.1, (d) Er : EDTA : CO_3^{2-} = 1 : 1.1 : 2.1, (e) Er : CyDTA = 1 : 1.3, (f) Er : CyDTA : CO_3^{2-} = 1 : 1.3 : 2.0, (g) Er : DTPA = 1 : 1.3, (h) Er : DTPA : CO_3^{2-} = 1 : 1.3 : 2.0. The ratio represents mole ratio (concentration of Er^{3+} is 0.02276 M).

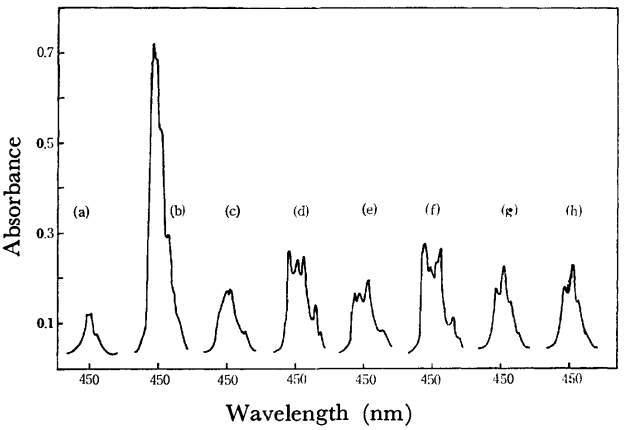

Fig. 2. Absorption spectra of aqueous solution of holmium-complexane-CO_3^{2-} systems. (a) $HoCl_3$, (b) Ho : CO_3^{2-} = 1 : 39.2, (c) Ho : EDTA = 1 : 1.3, (d) Ho : EDTA : CO_3^{2-} = 1 : 1.3 : 2.0, (e) Ho : CyDTA = 1 : 1.3, (f) Ho : CyDTA : CO_3^{2-} = 1 : 1.3 : 2.0, (g) Ho : DTPA = 1 : 1.3, (h) Ho : DTPA : CO_3^{2-} = 1 : 1.3 : 2.0. The ratio represents mole ratio (concentration of Ho^{3+} is 0.02348 M).

and also from that of the Ln–CO_3^{2-} systems.

As Fig. 3 shows, the absorbance at the maximum of the absorption band in the Er-CyDTA system increases with increasing concentration of carbonate ions, and becomes almost constant in the region above one of $[CO_3^{2-}]/[Er^{3+}]$ mole ratio. Similar results were obtained from the Er–EDTA, Ho–EDTA, and Ho-CyDTA systems. Moreover, the continuous variation method was applied to study the mole ratio at which CO_3^{2-} combines with the chelates. The composition

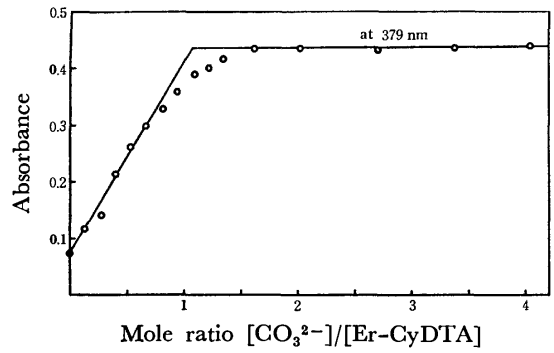

Fig. 3. Variation in absorbance as a function of mole ratio of [CO_3^{2-}]/[Er-CyDTA]. (concentration of Er^{3+} is 0.02276 M)

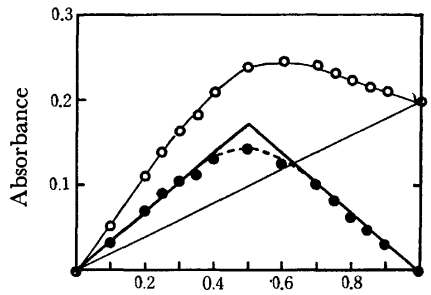

Fig. 4. Continuous variation plots in Er-CyDTA and CO_3^{2-} system. (at 379 nm)

of the rare earth–EDTA and –CyDTA chelates is well known to be 1 : 1 mole ratio.[5,6] The result obtained, for instance, from the Er–CyDTA–CO_3^{2-} system is shown in Fig. 4. The total concentration of Er–CyDTA and CO_3^{2-} ion was maintained at 0.02276 M. The peak (at 379 nm) at mole fraction [Er-CyDTA]/([Er-CyDTA]+[CO_3^{2-}]) of 0.5 indicates combining ratio of 1 : 1. Similar results were obtained from all the other systems. Therefore, the combining ratio of these mixed complexes can be estimated to be Ln : complexane : CO_3^{2-}=1 : 1 : 1. The spectra obtained from the Ln-complexane-CO_3^{2-} systems were affected neither by an addition of excess CO_3^{2-} ion nor by that of excess EDTA and CyDTA. Accordingly, it is deduced that the formation of the mixed complexes is based on an addition reaction of the second ligand CO_3^{2-} ion to the rare earth-complexane chelates. The difference in the absorption spectra between the Ln–DTPA and Ln-DTPA-CO_3^{2-} systems is scarcely recognized as Figs. 1 and 2 show.

From these results, it is considered that the coordination sites of the rare earth ions are not completely occupied by the coordination center of hexadentate EDTA and CyDTA, while completely occupied by that of octadentate DTPA, that is, the preferred coordination number of the metal ions seems to be 8 than 6.

References

1) T. Taketatsu and S. Yoshida, *J. Inorg. Nucl. Chem.*, **35**, 881 (1973).
2) T. Taketatsu, This Bulletin, **37**, 906 (1964).
3) T. Taketatsu, *Anal. Chim. Acta*, **32**, 40 (1965).
4) N. S. Poluektov and L. I. Kononenko, *Russ. J. Inorg. Chem.*, **6**, 938 (1961).
5) G. Schwarzenbach, G. Gut, and H. Anderegg, *Helv. Chim. Acta*, **37**, 937 (1954).
6) T. Moleller and T. M. Hesu, *J. Inorg. Nucl. Chem.*, **24**, 1635 (1962).

BULLETIN OF THE CHEMICAL SOCIETY OF JAPAN, VOL. 47(12), 3173—3174 (1974)

Oxidation of 1-Cyclohex-1-enecarbaldehyde and Related Compounds with Caro's Acid

Masaaki Ito,* Kazuo Abe, Hideo Abe, Keiichi Yamada, and Tadashi Masamune**

Department of Industrial Chemistry, Kitami Institute of Technology, Kitami, 090

*** Department of Chemistry, Faculty of Science, Hokkaido University, Sapporo, 060*

(Received May 1, 1974)

Synopsis. Three cyclic α,β-unsaturated aldehydes (**1**—**3**) were oxidized with an equivalent of Caro's acid in methanol, giving both simple oxidation products and the corresponding norketones in moderate yields.

The Baeyer-Villiger oxidation of α,β-unsaturated ketones has been investigated extensively with various acids.[1] However, only a few reports were given on the reactions of α,β-unsaturated aldehydes[2] with Caro's acid. In connection with the chemical reactivity of thujopsene,[3] we have examined the oxidations of a few cyclic, α,β-unsaturated aldehydes. The results are given in this paper.

Three aldehydes, (−)-*cis*-thujopsenal (**1**), (−)-perillaldehyde (**2**) and 1-cyclohex-1-enecarbaldehyde (**3**), were used as starting materials. Oxidation was carried out in methanol with an equivalent of Caro's acid. The products were separated and purified by gas, thin layer and column chromatography and identified by spectral data (see Experimental). The results are summarized in Table 1.

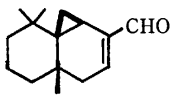

1

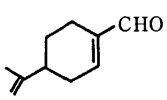

2

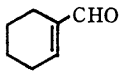

3

Methyl esters (**5**, **7** and **9**), formed by simple oxidation, and the corresponding norketones (**4**, **6** and **8**) were formed with moderate yields, the ratios apparently depending on the steric structures of starting aldehydes. The norketones might be produced *via* cyclohexenyl formates as depicted in the Scheme. In general, the major products of the Baeyer-Villiger oxidation of α,β-unsaturated ketones are the epoxy esters, which are no doubt derived from the enol esters.[1a] Norketones might be formed by the facile methanolysis of enol formates.

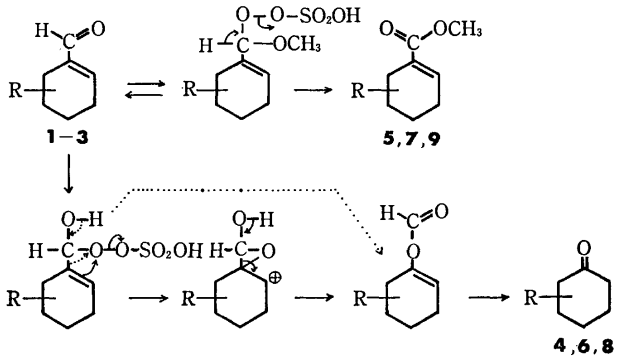

1—3 **5,7,9** **4,6,8**

Table 1. Oxidation of cyclic α,β-unsaturated aldehydes with Caro's acid

Aldehydes	Conversion[a]	Products and yields (%)[b]	
		Methyl esters	Norketones
1	97.2	**5** 10.2 (6.7)	**4** 55.4(39.0)
2	100.0	**7** 42.0(25.0)	**6** 26.5(20.7)
3	88.8	**9** 10.2 (6.3)	**8** 33.5(29.6)

a) Figures denote 100×(moles of aldehydes reacted/moles of aldehydes charged). b) Calculated by glc. Figures in parentheses give yields of isolated products.

* Present address: Chemistry Laboratory, Faculty of Pharmacy, East Japan University, Nakaonbetsu, Onbetsu, 088-02.

Experimental

Melting points were determined with a Büchi melting-point apparatus and are uncorrected. The homogenity of each compound was confirmed by tlc over silica gel (Merck G) and/or by glc (Shimadzu GC-1C) over 15% Silicon OV-17 Uniport (column A) and diethylene glycol succinate on Shimalite (B), using naphthalene as an internal standard. The UV and IR spectra were measured in ethanol and CCl_4, respectively. The NMR spectra were obtained in CCl_4, at 60 and/or 100 MHz, unless otherwise stated, TMS being used as an internal reference. Abbreviations "s" and "m" denote singlet and multiplet, respectively.

Oxidation of (−)-cis-Thujopsenal (1). To a solution of **1**[3] (4.4 g), mp 74—75 °C, prepared by SeO_2 oxidation[4] of thujopsene, in anhydrous methanol kept at 10 °C was added dropwise Caro's acid (10.4 g), prepared from ammonium persulfate (4.6 g) and 85% sulfuric acid (5.8 g), for 30 min. The solution was stirred at 15 °C for 4 hr, then poured into ice-water and extracted with ether. The ether solution was washed with water, dried over anhydrous Na_2SO_4 and evaporated to leave a crude product (4.1 g), which crystallized partially and was found to contain 6 components by glc (column A, 180 °C). The crystalline material was collected by filtration and then recrystallized from ethyl acetate to give pure colorless crystals (1.6 g), mp 108—109 °C, identified as thujopsene anhydrodihydroketone[5] (**4**) by direct comparison with the authentic specimen; Mass, *m/e* 206 (M^+); UV, λ_{max} 207 nm (ε 5500); IR, ν_{max} 3020, 1690 and 1679 cm^{-1}; NMR ($CDCl_3$), δ 0.59, 1.10 and 1.17 (each 3H, s, CH_3) Found: C, 81.34; H, 10.49%; mol wt (Rast, benzene), 205. Calcd for $C_{14}H_{22}O$: C, 81.55; H, 10.68%; mol wt, 206.3.

The mother liquors obtained by filtration and recrystallization were evaporated and purified by preparative tlc with 3 : 97 mixture of ethyl acetate and *n*-hexane to give colorless crystals (0.33 g), mp 105—106 °C, identified as methyl thujopsenate[6] (**5**); IR, ν_{max} 3010, 1718, 1713, 1652, and 1086 cm^{-1}; NMR, δ 0.72 1.11 and 1.17 (each 3H, s, CH_3), 3.65

(3H, s, $COOCH_3$), and 6.41 (1H, m, olefinic H). Found: C, 77.25; H, 9.59%; mol wt (Rast), 246. Calcd for $C_{16}H_{24}O_2$: C, 77.38; H, 9.74; mol wt, 248.4.

Oxidation of (−)-Perillaldehyde (2). Aldehyde **2** (3.0 g), bp 92.5—93.5 °C/5 mmHg (Nippon Terpene Co. Ltd.) purified by treatment with $NaHSO_3$ was oxidized in methanol (24 g) with Caro's acid (10.4 g) in the same manner as **1** afforded an oily product (2.7 g), consisting of 4 components (glc, column B, 145 °C). The product was separated by preparative tlc using a 1 : 9 mixture of ethyl acetate and *m*-hexane to give two compounds, colorless (0.57 g) and pale yellow oil (0.9 g), in pure state. The former was identified as 4-isopropenylcyclohexanone[7] (**6**); UV, λ_{max} 205 nm (ε 1000); IR, ν_{max} 1717, 1645 and 892 cm^{-1}; NMR, δ 1.73 (3H, s, CH_3) and 4.80 (2H, s, exo CH_2). Found: C, 78.10; H, 10.15%. Calcd for $C_9H_{14}O$: C, 78.21; H, 10.21%.

The latter was identified as methyl 1-(4-isopropenylcyclohex-1-ene)carboxylate[8] (**7**); IR, ν_{max} 1712, 1646, 1245, and 887 cm^{-1}; NMR, δ 1.70 (3H, s, CH_3), 3.64 (3H, s, $COOCH_3$), 4.72 (2H, s, exo CH_2), and 6.82 (1H, m, olefinic H). Found: C, 73.20; H, 8.82%; mol wt (Rast), 179. Calcd for $C_{11}H_{16}O_2$: C, 73.30; H, 8.95%; mol wt, 180.3.

Oxidation of 1-Cyclohex-1-enecarbaldehyde (3). The oxidation of **3**[3] (3.3 g), bp 67—68 °C/13 mmHg, in methanol (25 g) was carried out with Caro's acid (15.6 g) in the same way as for **1** and an oily product (2.6 g). The product was found to consist of 6 components by glc (column A, 165 °C), from which two compounds, cyclohexanone (**8**) (0.88 g) methyl 1-cyclohex-1-enecarboxylate[9] (**9**) (0.26 g), were isolated in pure state by preparative glc with a 2 m × 10 mm column of 20% Silicone SE-30 on Chromosorb W. Ester (**9**) gave the following data; IR, ν_{max} 1718, 1712, 1648, and 1083 cm^{-1}; NMR, δ 3.59 (3H, s, $COOCH_3$) and 6.82 (1H, m, olefinic H). Found: C, 68.35; H, 8.48%. Calcd for $C_8H_{12}O_2$: C, 68.55; H, 8.63%.

References

1) a) A. DeBoer and R. E. Ellwanger, *J. Org. Chem.*, **39**, 77 (1974), and refs cited therin. b) H. O. House, "Modern Synthetic Reactions," W. A. Benjamin Inc., New York, N. Y. (1965), p. 123. c) C. H. Hassall, *Org. Reactions*, **9**, 73 (1957).

2) M. N. Prilejaeff, *Bull. Soc. Chim. France*, [4], **42**, 687 (1927).

3) M. Ito, T. Nishimura, and K. Abe, This Bulletin, **45**, 1914 (1972).

4) E. A. Braude and E. A. Evans, *J. Chem. Soc.*, **1955**, 3334.

5) a) T. Nozoe, H. Takeshita, S. Ito, T. Ozeki, and S. Seto, *Chem. Pharm. Bull.*, **8**, 936 (1960). b) W. G. Dauben and A. C. Ashcraft, *J. Amer. Chem. Soc.*, **85**, 3673 (1963).

6) Cf. H. Kobayashi, S. Nagahama, and S. Akiyoshi, This Bulletin, **34**, 1123 (1961).

7) H. Erdman and T. Norin, *Acta Chem. Scand.*, **13**, 1124 (1959).

8) Cf. H. Walbaum and O. Hüthig, *J. Prak. Chem.*, [2], **71**, 469 (1905).

9) Cf. K. Auwers, *Ann. Chem.*, **432**, 97 (1923).

BULLETIN OF THE CHEMICAL SOCIETY OF JAPAN, VOL. 47(12), 3175—3176 (1974)

Absolute Configuration of Some Chiral Cyclopropanes

Kazuyoshi NISHIYAMA, Jun'ichi ODA, and Yuzo INOUYE
Institute for Chemical Research, Kyoto University, Uji, Kyoto 611

(Received June 19, 1974)

Synopsis. The absolute configurations of (1*S* : 2*R*)-(−)-*cis*-, and (1*S* : 2*S*)-(+)-*trans*-1-phenylcyclopropane-1,2-dicarboxylic acids, and (1*S* : 2*R*)-(−)-*cis*-, and (1*S* : 2*S*)-(+)-*trans*-1-phenyl-1,2-bis(acetoxymethyl)cyclopropanes were established by correlation to (*R*)-(−)-2,2-diphenylcyclopropane-1-carboxylic acid.

During the course of studies on asymmetric synthesis, we found that establishment of the absolute configuration of a series of chiral cyclopropanes is necessary.

Absolute assignment of configuration is given to *trans*-, (**3**) and *cis*-1-phenylcyclopropane-1,2-dicarboxylic acids (**4**), and *trans*-, (**5**) and *cis*-1-phenyl-1,2-bis(acetoxymethyl) cyclopropanes (**6**) by chemical transformations. These chiral cyclopropanes are correlated to (−)-2,2-diphenylcyclopropane-1-carboxylic acid (**1**) of the known (*R*)-configuration[1] through the key compound, methyl cyclopropane-1,1,2-tricarboxylate[2] (**2**).

(*R*)-(−)-2,2-Diphenylcyclopropane-1-carboxylic acid, −231°, was ozonized to give, after esterification of the ozonolysis product with diazomethane, methyl cyclopropane-1,1,2-tricarboxylate (**2**) having a rotation of −134.8°. The *R*-configuration is thus assigned to (−)-(**2**).

Methyl (+)-*trans*-1-phenylcyclopropane-1,2-dicarboxylate +134.0°, derived from the partially resolved acid (**3**), +85.8°, was converted in the same manner as described above into (+)-(**2**) with a dextrorotation +124.6°. From the conversion, the *S*-configuration can be assigned to the chiral carbon-2 in the parent (+)-(**3**) and consequently, the *S*-configuration of another chiral carbon-1 in (+)-(**3**) reasonably follows from the *trans*-geometry of carboxyl groups.

The optical purity of (+)-(**2**) derived from (+)-(**3**) is 92.4% based on the maximum rotation +134.8°, so that the value 92.8° is given to (+)-(**3**) as its maximum rotation, which is in good agreement with the value 92.9° attained by optical resolution *via* brucine salt. The agreement not only warrants the fact that neither racemization nor fractionation occurred during ozonolysis and the subsequent work-up in the present transformations, but also provides evidence for stereochemical integrity of compounds involved.

The base-catalyzed isomerization of methyl (−)-*cis*-1-phenylcyclopropane-1,2-dicarboxylate obtained by esterification of the corresponding free acid (−)-(**4**), −185.3°, afforded (+)-*trans*-(**3**)-ester with a dextrorotation of +126.1°, which is evidently epimeric at the ring carbon-2. It follows that (−)-(**4**) is assigned to the (1*S* : 2*R*)-configuration and should possess the maximum rotation −212.0°.

The lithium aluminum hydride reduction of optically pure (+)-(**3**), followed by acetylation of the reduction mixture gave the corresponding diol acetate, (+)-1-phenyl-*trans*-1,2-bis(acetoxymethyl)cyclopropane (+)-(**5**), +5.4°, while the same treatment of (−)-*cis*-(**4**)-ester −178.8° afforded (−)-1-phenyl-*cis*-1,2-bis(acetoxymethyl)cyclopropane −45.5°, (−)-(**6**). The (1*S* : 2*S*)-configuration of (+)-(**5**) and (1*S* : 2*R*)-configuration of (−)-(**6**) are evident, the maximum rotation of the latter being inferred to be −52.1°.

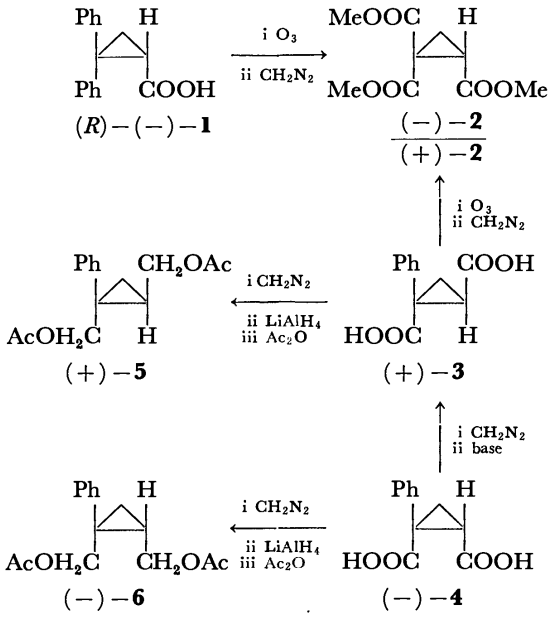

The Brewster calculation of conformational asymmetry[3] predicts the sign and magnitude of molecular rotation in fair agreement with those observed.

	$[M]°_{calcd}$	$[M]°_{obsvd}$
(*R*)−(**2**)	−135	−291
(1*S* : 2*S*)−(**3**)	+135	+191
(1*S* : 2*R*)−(**4**)	−210	−437
(1*S* : 2*S*)−(**5**)	+60	+14
(1*S* : 2*R*)−(**6**)	−90	−137

Experimental

Specific rotations were measured on a Perkin Elmer 241 polarimeter at 25 °C in 1% methanol solution unless otherwise stated.

Ozonolysis. According to the procedure we previously described,[4] (−)-2,2-diphenylcyclopropane-1-carboxylic acid $[\alpha]_D$ −231.1° (chloroform) was ozonized in acetic acid at room temperature and the resulting product was esterified by the standard method with diazomethane to give, after isolation by preparative vpc, methyl cyclopropane-1,1,2-tricarboxylate (−)-(**2**). The IR- and NMR-spectra were identical with those of the authentic specimen.[2] n_D^{30} 1.4477, $[\alpha]_D$ −134.8°.

In the same way, (+)-*trans*-1-phenylcyclopropane-1,2-dicarboxylic acid $[\alpha]_D$ +85.5°, (+)-(**3**), prepared and resolved according to McCoy,[5] gave (+)-(**2**) whose identity was fully substantiated by means of spectroscopy, n_D^{30} 1.4477, $[\alpha]_D$

+124.6°.

Epimerization of methyl (−)-*cis*-1-phenylcyclopropane-1,2-dicarboxylate (50 mg: $[\alpha]_D$ −178.8°; (−)-(**4**)-methyl ester) was effected by treating with methyl phenylacetate (100 mg) and sodium hydride (30 mg) in DMF (1.5 ml) at 40 °C for 1 hr and, after neutralization, the product was subjected to preparative vpc to give pure (+)-(**3**)-methyl ester (28 mg); $[\alpha]_D$ +126.1°.

Resolution of (±)-(**3**), mp 198.5—199 °C,[5] and of (±)-(**4**), mp 152.5—153 °C[5] was performed *via* the brucine salt by fractional crystallizations from methanol eventually to give (+)-(**3**), mp 144 °C, $[\alpha]_D$ +92.9° (methyl ester, n_D^{25} 1.5153, $[\alpha]_D$ +144.3°), and (−)-(**4**), mp 154 °C, $[\alpha]_D$ −185.3°, (methyl ester, n_D^{25} 1.5133, $[\alpha]_D$ −178.8°) respectively.

For the lithium aluminum hydride reductions, the method by Inamasu *et al.*[6] was followed: (+)-(**3**)-methyl ester $[\alpha]_D$ +144.3° gave, after purification by preparative vpc, (+)-1-phenyl-*trans*-1,2-bis(acetoxymethyl)cyclopropane (+)-(**5**), n_D^{25} 1.5004, $[\alpha]_D$ +5.4°, while (−)-(**4**)-methyl ester $[\alpha]_D$ −178.8° yielded the *cis*-counterpart (−)-(**6**), n_D^{25} 1.5018, $[\alpha]_D$ −45.5°. Identification of each was obtained by IR- and NMR- spectroscopies.

Partial support of this work by a grant (966047) in aid from the Ministry of Education is gratefully acknowledged (J. O.).

References

1) H. M. Walborsky and F. M. Hornyak, *J. Amer. Chem. Soc.*, **77**, 6026 (1955); *idem.*, *ibid.*, **83**, 2517 (1961): C. Djerassi, K. Undheim, and A. Weidler, *Acta Chem. Scand.*, **16**, 1147 (1962).
2) E. Buchner and R. von der Heide, *Ber.*, **38**, 3112 (1905).
3) J. H. Brewster, *J. Amer. Chem. Soc.*, **81**, 5483 (1959).
4) K. Nishiyama and Y. Inouye, This Bulletin, **44**, 2795 (1971).
5) L. L. McCoy, *J. Amer. Chem. Soc.*, **84**, 2246 (1962).
6) S. Inamasu, M. Horiike, and Y. Inouye, This Bulletin, **42**, 1393 (1969).

BULLETIN OF THE CHEMICAL SOCIETY OF JAPAN, VOL. 47(12), 3177—3178 (1974)

Olefin Disproportionation by Molybdenum(0) Complexes and Aluminum Halides[1)]

Masanobu HIDAI, Takashi TATSUMI, and Yasuzo UCHIDA

Department of Industrial Chemistry, Faculty of Engineering, The University of Tokyo, Hongo, Tokyo 113

(Received June 21, 1974)

Synopsis. $MoN_2(PPh_3)_2 \cdot PhMe$ and $Mo(CO)(PPh_3)_2$ were activated by aluminum halides to give catalysts effective for the disproportionation of 2-pentene.

Halide complexes of molybdenum or tungsten in combination with organoaluminum have been known to be effective for olefin disproportionation.[2-4)] We wish to report new molybdenum catalyst systems, free of metal alkyls, for the disproportionation of 2-pentene. Metal alkyl-free catalysts comprised of tungsten combounds have been briefly reported before.[5,6)]

Treatment of $MoN_2(PPh_3)_2 \cdot PhMe$[7)] (**1**) with $AlCl_3$ in bromobenzene afforded a brown suspension, which was effective for the disproportionation of 2-pentene to 2-butene and 3-hexene at ambient temperature. The system became active with an increase in the Al/Mo ratio, but the large excess of $AlCl_3$ promoted the alkylation of the solvent (Table 1). In the evaluation of other molybdenum(0) complexes, it was found that $Mo(CO)(PPh_3)_2$ (**2**) also was a satisfactory catalyst precursor. $AlCl_3$ could not produce catalytic systems in combination with other molybdenum(0) compounds, except that some activity was produced with *trans*-$Mo(N_2)_2(Ph_2PCH_2CH_2PPh_2)_2$[7)] (Table 2).

To determine the effectiveness of Lewis acids as cocatalyst with **1**, parallel preparations were made with several aluminum and other metal halides. Among the aluminum halides the order of the activity was $AlCl_3 \gg AlBr_3 > AlEtCl_2$ (Table 3). With **2** the activity decreased in the same order. The system derived from other aluminum compounds such as AlI_3, $AlEt_2Cl$, or $AlEt_3$ was not effective. Other metal halides such as LiCl, $MgCl_2$, $BF_3 \cdot Et_2O$, $TiCl_4$, $MoCl_5$, $FeCl_3$, $ZnCl_2$, or $SnBr_4$ were ineffective, whereas very little activity was produced by $ZrCl_4$. It is likely that traces of moisture provides HCl from $AlCl_3$ and that it is an alternative cocatalyst. Treatment of **2** with HCl in bromobenzene afforded a reddish brown suspension, which exhibited, however, no activity.

TABLE 1. EFFECT OF $AlCl_3$/Mo MOLAR RATIO
1: 0.05 mmol, 2-pentene: 9.4 mmol, PhBr: 4 ml, reaction time: 2 hr.

Al/Mo ratio	Olefin yield, mol%[a)]		
	C_4	C_5	C_6
1	t[b)]	99	t[b)]
3	5.6	81	5.2
6	17	51	17
9	19	43	19
12	16	47	15

a) mol% of each olefin to the amount of 2-pentene used. b) t; trace.

TABLE 2. EFFECT OF MOLYBDENUM(0) COMPLEXES
Complex: 0.05 mmol, 2-pentene: 9.4 mmol, PhCl: 4 ml.

Molybdenum complex	$AlCl_3$/Mo ratio	Reaction time, hr	Olefin yield, mol%		
			C_4	C_5	C_6
$MoN_2(PPh_3)_2 \cdot PhMe$ (**1**)	9	2	6.8	64	6.8
$Mo(CO)(PPh_3)_2$ (**2**)	9	2	12	33	12
trans-$Mo(N_2)_2(dpe)_2$[a)]	20	24	2.2	40	2.2
cis-$Mo(CO)_2(dpe)_2$[a)]	20	72	0.0	43	0.0
trans-$Mo(CO)_4(PPh_3)_2$	9	2	0.1	43	0.1
$Mo(CO)_6$	6	120	0.2	19	0.2
$Mo(Ph_2PCH_2PPh_2)_3$	17	120	0.1	22	0.1
$Mo(CO)_3(PhH)$	9	72	0.0	40	0.0

a) dpe = 1,2-bis(diphenylphosphino)ethane.

TABLE 3. EFFECT OF LEWIS ACIDS
1: 0.05 mmol, 2-pentene: 9.4 mmol, PhCl: 4 ml.

Lewis acid	Acid/Mo ratio	Reaction time, hr	Olefin yield, mol%		
			C_4	C_5	C_6
$AlCl_3$	9	2	6.8	64	6.8
$AlBr_3$	12	20	3.7	39	4.7
$AlEtCl_2$	20	20	1.6	82	1.0
$ZrCl_4$	9	24	0.3	43	0.3

The reaction of **2** with $AlCl_3$ in bromobenzene yielded a reddish brown complex, which had a band at 1900 cm^{-1} assigned to ν(CO) in its IR spectrum. This band is *ca.* 90 cm^{-1} higher than that of **2**. The shift is reasonable because the electron density in the molybdenum atom would be decreased by the interaction of molybdenum(0) base with the Lewis acid, resulting in a decrease in back π-bonding from the molybdenum to the CO ligand. Bencze and Markó have recently reported highly reactive adducts of halocarbonyl complexes of tungsten with $AlCl_3$, which also show higher shifts of ν(CO).[8)] In the reaction of **2** with $AlEtCl_2$ or $AlBr_3$, ν(CO) was similarly shifted to higher frequency by 15 cm^{-1} or 165 cm^{-1}, respectively. Accordingly, the increment of ν(CO) falls in the usually accepted order of Lewis acidity, $AlBr_3 > AlCl_3 > AlEtCl_2$, while the order of effectiveness for the disproportionation was $AlCl_3 \gg AlBr_3 > AlEtCl_2$.

When $AlCl_3$ was added to **1** in bromobenzene, the absorbance at 1905 cm^{-1} attributed to ν(NN) disappeared. Since N_2 is a weaker π-acceptor than CO, a decrease in back donation from the molybdenum must weaken the Mo–N_2 bond so much, resulting in liberation of N_2 from the complex. Other molybdenum(0) complexes such as *cis*-$Mo(CO)_2(Ph_2PCH_2CH_2PPh_2)_2$ and

trans- $Mo(CO)_4(PPh_3)_2$ were also observed to interact with $AlCl_3$; $\nu(CO)$ bands of these complexes were shifted to higher frequencies by *ca.* 70—100 cm^{-1}. As described above, they were, however, not effective as catalyst precursors. The molecular weight of **2** was found to be 1290 by the vapor pressure osmometric method, indicating that **2** has a dimeric structure (Calcd 1296). Since **1** can be easily converted to **2** in the presence of CO and has the empirical formula analogous to **2**, it may also have a dimeric structure. It is to be noted that the 6-coordinate mononuclear molybdenum(0) complexes did not afford active catalyst systems by the addition of aluminum halides, but that the complexes, **1** and **2**, presumed to have unusual dimeric structures showed a remarkable catalytic activity.

Recently Lewandos and Pettit have reported that arene-$W(CO)_3$ complexes can act as catalyst precursors for olefin disproportionation.[9] These systems are, however, not notably effective, and prolonged heating to 98 °C is necessary in order to activate the catalyst systems. We have observed that **2** itself also exhibited very little disproportionation activity at 98 °C, while the addition of $AlCl_3$ markedly stimulated the activity. Although Wang and Menapace suggested a W(IV) (d^2) catalytic intermediate in the WCl_6-*n*-BuLi sistem,[10] Mo(IV) (d^2) complexes such as $MoCl_4(EtCN)_2$ or $MoCl_4(PPh_3)_2$ could neither act as catalysts by themselves nor be activated by $AlCl_3$.

The systems using bromobenzene or chlorobenzene as the solvent were clearly superior to those using benzene or *n*-hexane (Table 4). In the case of the latter solvents the system became almost heterogeneous, suggestive of active species having some ionic character. The complex **1** was recovered quantitatively after being allowed to stand for a long time in bromobenzene or chlorobenzene, ruling out the posibility that the oxidative addition of the solvent occurred. The disproportionation was completely inhibited using iodobenzene, which rapidly reacted with **1**. If the catalyst was prepared in toluene and 2-pentene was added, almost exclusive and rapid alkylation of toluene took place.

Table 4. Solvent effect

1: 0.05 mmol, $AlCl_3$: 0.45 mmol, 2-pentene: 9.4 mmol, solvent: 4 ml, reaction time: 2 hr.

Solvent	Olefin yield, mol%		
	C_4	C_5	C_6
PhMe	0	2.8	0
PhH	0.7	44	0.7
PhCl	6.8	64	6.8
PhBr	19	43	19
PhI	0	100	0

It has been established that in the transition metal-olefin interaction, two factors are operating, *i.e.*, σ-donation from the olefin to the metal and back π-bonding from the metal to the olefin. The magnitude of the contribution of these two factors are partly dependent on the electron density on the metal atom. The fact that $AlCl_3$ is the most effective cocatalyst with the molybdenum complexes may be explained in terms of moderate decrease in the electron density on the molybdenum by adduct formation, as indicated by the increase in $\nu(CO)$. The most active catalyst systems reported for homogeneous olefin disproportionation are composed of halide complexes of either molybdenum or tungsten and organoaluminum compounds. In those systems metal halides are supposed to react with organoaluminum to produce, transiently, molybdenum(0) or tungsten(0) complexes with formation of aluminum halides, leading to catalyst systems similar to our combinations. We may conclude that in the catalyst systems previously reported, organoaluminum functions not only as a reducing agent but also as an electron modifier of the reduced molybdenum or tungsten.

References

1) This work was presented at the 26th Annual Meeting of the Chemical Society of Japan, Hiratsuka, April, 1972.
2) N. Calderon, E. A. Ofstead, J. P. Ward, W. A. Judy, and K. W. Scott, *J. Amer. Chem. Soc.*, **90**, 4133 (1968).
3) E. A. Zuech, W. B. Hughes, D. H. Kubicek, and E. T. Kittleman, *ibid.*, **92**, 528 (1970).
4) L. Bencze and L. Markó, *J. Organometal. Chem.*, **28**, 271 (1971).
5) L. Hérrison, Y. Chauvin, N. H. Phung, and G. Lefebre, *C. R. Acad. Sci. Ser. C.* **269**, 661 (1969).
6) N. Calderon, *Accounts Chem. Res.*, **5**, 127 (1972).
7) M. Hidai, K. Tominari, and Y. Uchida, *J. Amer. Chem. Soc.*, **94**, 110 (1972).
8) L. Bencze and L. Markó, *J. Organometal. Chem.*, **69**, C19 (1974).
9) G. S. Lewandos and R. Pettit, *J. Amer. Chem. Soc.*, **93**, 7087 (1971).
10) J. L. Wang and H. R. Menapace, *J. Org. Chem.*, **33**, 3794 (1968).

BULLETIN OF THE CHEMICAL SOCIETY OF JAPAN, VOL. 47(12), 3179—3180 (1974)

Substituent Effect in the Nucleophilic Attack by the Bromide Ion on the *p*-Tolyl-Substituted Phenyliodonium Ions

Yorinobu YAMADA, Koichi KASHIMA, and Makoto OKAWARA

Research Laboratory of Resources Utilization, Tokyo Institute of Technology, Ookayama, Meguro-ku, Tokyo 152

(Received September 9, 1974)

Synopsis. *p*-Tolyl-substituted phenyliodonium bromides were prepared and their nucleophilic substitution reactions were carried out in the DMF solution and molten state. Their substituent effects were discussed from the reaction products and the spectra of the iodonium salts.

Beringer *et al.* have reported the syntheses of various diaryliodonium salts and their reactions in the solution.[1] In general, the nucleophile tends to attack the more electron-deficient phenyl-1-carbon. We have already reported the influences of the ligand and steric effect on the reaction of various iodonium salts.[2] However, a systematic investigation has not been undertaken to determine the effect of various substituents on the nucleophiles in the reaction of diaryliodonium salts.

In the present paper, we wish to report the syntheses of various *p*-tolyl-substituted phenyliodonium bromides and their reactions in both solution and molten states.

p-Tolyl-substituted phenyliodonium bromides (I) were synthesized from toluene and substituted phenyliodoso acetate. *p*-Tolyl-*p'*-carboxyphenyliodonium bromide was synthesized from *p*-iodobenzoic acid and toluene in the presence of potassium persulfate in concd. sulfuric acid according to the Beringer's method.[3] These results are summarized in Table 1. The thermal decomposition of the iodonium bromides (I) was carried out in both DMF solution (100 °C, 10 hr) and molten state (235 °C, 5 min). The results are shown in Table 2. As can be seen from this Table, the mode-T reaction, in which the bromide ion attacks the tolyl group to give *p*-tolyl bromide and substituted phenyl iodide, and the mode-A reaction, in which the bromide ion attacks the substituted phenyl group to give the substituted phenyl bromide and *p*-tolyl iodide, were found to occur competitively in both DMF solution and molten state.

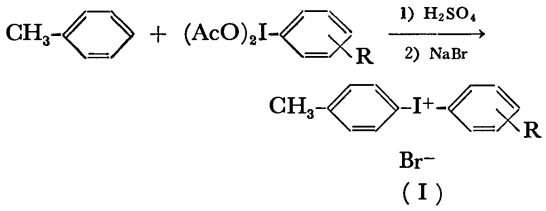

(I)

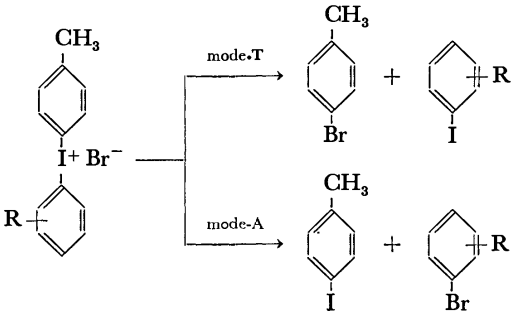

These results show that the mode-A reaction is inclined to occur in the reaction of I with electron-withdrawing substituents such as the nitro group. On the other hand, the mode-T reaction tends to occur in the reaction of I with electron-releasing substituents such as the methoxy group. The product ratios suggest that the reaction proceeds by an aromatic bimolecular nucleophilic substitution mechanism. Furthermore, there is no significant difference between the solution and molten reaction. It is of interest that the mode-A reaction is difficult to occur in the reaction of I with the *p'*-chloro group compared to that of I with the *m'*-chloro group. It can be deduced from the contribution of the resonance structure, in which the bond between iodonium ion and *p'*-chlorophenyl-1-carbon acquires some double bond character owing to the lone pair of *p'*-chloro group, to the reaction tendency. Such a resonance effect has been observed also in the case of *p*-chlorophenyl-2-thienyliodonium bromide.[2c]

TABLE 1. SYNTHESES OF *p*-TOLYL-SUBSTITUTED PHENYLIODONIUM BROMIDE

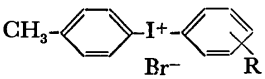

Substituent R-	Yield (%)	Mp (°C)	Elemental analyses (%) Found C	Found H	Found Halogen	Calcd C	Calcd H	Calcd Halogen
p-MeO	68.2	182—184	41.54	3.44	50.31	41.47	3.46	51.05
m-Me	92.6	180—181	42.66	3.66	52.61	43.21	3.63	53.16
H	42.6	183—184	41.66	3.05	55.09	41.63	3.23	55.14
p-Cl	90.4	192—194	38.35	2.68	58.64	38.13	2.71	59.17
m-Cl	78.9	183—184	37.91	2.77	58.97	38.13	2.71	59.17
p-COOH	50.0	193—194	39.77	3.12	50.00	40.13	2.89	49.35
p-NO_2	28.8	154—155	37.30	2.49	48.62	37.17	2.64	49.23

Table 2. Cleavage tendency of *p*-tolyl-substituted phenyliodonium bromides

Substituent R-	Molten state		Solution state	
	mode-T : mode-A		mode-T : mode-A	
p-MeO	80.9	19.1	72.9	27.1
H	38.2	61.8	26.8	73.2
p-Cl	40.0	60.0	30.9	69.1
m-Cl	34.6	65.4	19.4	80.6
p-COOH	13.3	86.7	7.5	92.5
p-NO_2	3.7	96.3	—	—

Table 3. UV spectra of *p*-tolyl-substituted phenyliodonium bromide in methanol

Substituent R-	λ_{max} (nm)	log ε_{max}
p-MeO	247	4.21
m-Me	232	4.47
H	232	4.38
p-Cl	238	4.38
m-Cl	233	4.20
p-COOH	239	4.44
p-NO_2	253	4.32

From the UV spectra of I (Table 3), the increase in λ_{max} in going from unsubstituted or *m'*-chloro substituted to *p'*-chloro substituted iodonium bromide suggests the presence of such a conjugated system. The increase in λ_{max} of the iodonium bromides with the electron-withdrawing substitutents such as the nitro and carboxyl groups at the *p'*-position and their cleavage tendencies suggest the presence of the resonance structure owing to the hyperconjugation effect of *p*-methyl group enhanced by the *p'*-electron-withdrawing substituent. In these cases, the mode-A reaction becomes to be increasingly liable to occur owing to both the inductive and resonance effects.

Experimental

All the melting points are uncorrected. The ultraviolet spectra were measured with a Hitachi EPS-3T-type spectrometer. A Hitachi 023-5051-type gas chromatograph analyzer was used with a column (stainless 1 m) packed with Silicone SE 30 on Celite 545 at 100 °C.

p-Tolyl-Substituted Phenyliodonium Bromide (I). *p*-Tolyl-substituted phenyliodonium bromides were prepared by a procedure like that given for *p*-tolyl-*p'*-methoxyphenyliodonium bromide. To a well-stirred mixture of 5.28 g (15 mmol) of *p*-methoxyphenyliodoso acetate, 2.76 g (30 mmol) of toluene, and 50 ml of acetic anhydride kept below 10 °C there was added 12 ml of concd. sulfuric acid. After having been stirred at room temperature for 3 hr, the reaction mixture was diluted with 200 ml of ice-water, extracted with ether until color was no longer removed and treated with active carbon. The aqueous layer was added to 10.3 g (100 mmol) of sodium bromide dissolved in 50 ml of water, giving 4.0 g *p*-tolyl-*p'*-methoxyphenyliodonium bromide.

p-Tolyl-p'-carboxyphenyliodonium Bromide. To a solution of 2.98 g (12 mmol) of *p*-iodobenzoic acid in 100 ml of concd. sulfuric acid there was added with stirring 6.5 g (42 mmol) of potassium persulfate at −10 °C and then, after 15 min, 16 g (174 mmol) of toluene at −20 °C. The mixture was stirred at −10 °C for 1 hr and at 0 °C for 3 hr and then was processed as in the preceding manner to give 2.5 g of *p*-tolyl-*p'*-carboxyphenyliodonium bromide.

Pyrolysis Reaction of p-Tolyl-Substituted Phenyliodonium Bromide in the Molten State. About 0.2 g of *p*-tolyl-substituted phenyliodonium bromide was enclosed in a Pyrex tube. The ampoule was then placed in an oil bath kept at 235 °C for 5 min. After the end of the pyrolysis reaction the pyrolysate was disolved in a small quantity of ether and the amounts of *p*-iodotoluene and *p*-bromotoluene were determined by a gas chromatograph. Chlorobenzene was used as an internal standard.

Reaction of p-Tolyl-Substituted Phenyliodonium Bromide in DMF Solution. The reaction of iodonium bromide was conducted by a procedure like that given for *p*-tolyl-*p'*-methoxyphenyliodonium bromide. *p*-Tolyl-*p'*-methoxyphenyliodonium bromide (0.214 g, 0.2 mol) dissolved in 50 ml of DMF was held at 100 °C for 10 hr. At the end of the reaction the mixture was poured into cold water, extracted with ether two times and the extract was dried over anhydrous magnesium sulfate. After removing the solvent by distillation, the residue was redissolved in a small quantity of ether and then treated in the same manner as shown above. In every case the concentration was held at 0.25 mol/l.

References

1) F. M. Beringer, M. Drexler, and C. C. Lumpkin, *J. Amer. Chem. Soc.*, **75**, 2705 (1953); F. M. Beringer and R. A. Nathan, *J. Org. Chem.*, **34**, 685 (1969).

2) a) Y. Yamada and M. Okawara, *Makromol. Chem.*, **152**, 153 (1972); Y. Yamada and M. Okawara, *ibid.*, **152**, 163 (1972). b) Y. Yamada and M. Okawara, This Bulletin, **45**, 1860 (1972). c) Y. Yamada and M. Okawara, *ibid.*, **45**, 2515 (1972).

3) F. M. Beringer and I. Lillien, *J. Amer. Chem. Soc.*, **82**, 725 (1960).

BULLETIN OF THE CHEMICAL SOCIETY OF JAPAN, VOL. 47(12), 3181—3182 (1974)

Dye-sensitized Photolysis of Diazonium Compounds in the Presence of Thioacetamide

Eiichi INOUE, Hiroshi KOKADO, Tsuneo IKAWA,* Toshihiro YAMASE,* andYasuo INOUE

Imaging Science and Engineering Laboratory, Tokyo Institute of Technology, Ookayama, Meguro-ku, Tokyo 152

** Research Laboratory of Resources Utilization, Tokyo Institute of Technology, Ookayama, Meguro-ku, Tokyo 152*

(Received August 4, 1973)

Synposis. Effects of solution pH and molecular oxygen on the quantum yields of methylene blue-sensitized photolysis of diazonium salt have been studied in aqueous solutions, using thioacetamide as an activator. The quantum yield increased with an increase in pH when other parameters were kept constant. The presence of oxygen at pH (<7) promoted dye sensitization, but at pH (>7) dominance of the pathway of oxygen quenching of the excited dye triplet caused its suppression. The polymerization of acrylamide in the deaerated solution was readily initiated by dye-sensitized photolysis. A mechanism involving an electron transfer to diazonium cation from unprotonated semimethylene blue formed by a photoredox reaction between excited triplet dye and thioacetamide was in line with these observation.

The methylene blue (MB) sensitized photolysis of 4-diazodiphenylamine sulfate (4DS) solutions containing sodium *p*-toluenesulfinate (STS) or 1,4-diazabicyclo-[2,2,2]octane (DABCO) as an activator was studied by flash photolysis and continuous illumination.[1,2] The mechanism of photolysis was shown to be an electron transfer (see the simplified reaction scheme).

$$MB^{+*} + STS \rightarrow MB\cdot\cdot\cdot STS \xrightarrow{O_2} MB\cdot + STS\text{-}O_2\cdot \quad (1)$$

$$MB^{+*} + DABCO \rightarrow MB\cdot\cdot\cdot DABCO \rightarrow MB\cdot + DABCO\cdot \quad (2)$$

$$MB\cdot + 4DS \rightarrow MB^{+} + \text{diphenylamine radical} + N_2 \quad (3)$$

Here the primary reaction takes place between MB triplet (MB^{+*}) and STS or DABCO (called "activator") with the formation of a complex consisting of a semi-MB ($MB\cdot$) and a half-oxidized activator radical (sulfonyl radical or DABCO cation radical). In the STS system, oxygen was necessary for the dye sensitization at pH below 7. This could be explained in terms of an attack of oxygen on the sulfonyl radical component in a complex, which caused the escape of a semi-MB from the complex (the second step of reaction (1)). The semi-MB was considered to decompose 4DS according to (3). In the absence of oxygen, the complex reverted rapidly to MB and STS in the ground state. The quantum yield markedly decreases if low concentration of STS is chosen for fulfilling the dominance of the pathway of oxygen quenching of triplet MB.[3] The suppression of dye sensitization by oxygen indicates that oxygen quenches triplet MB. In order to understand the operation of dye-sensitized diazo systems, it is important to study a dye-sensitizing system containing other activators such as thioacetamide. Using MB, 4DS and thioacetamide (TAA) which act as an activator, effects of solution pH and oxygen on the quantum yield of MB-sensitized photolysis of 4DS were studied. All the experiments were performed at room temperature 23±1 °C. The solutions were degassed to 10^{-4} mm Hg by the usual freeze-pump-thaw cycle. Experimental procedures were the same as those described previously.[1,2] Oxygen concentrations in aqueous solutions under various partial pressures of oxygen gas were calculated by use of Bunsen's absorption coefficient 0.03 (at 23 °C).[4] Figure 1 shows the absorption spectra of the aerobic solution containing 2.0×10^{-5}M MB, 5.0×10^{-3}M thioacetamide (TAA) and 4.0×10^{-5} M 4DS at pH 6.0 before and after irradiation. Photo-excitation of MB brought about the sensitized photolysis of 4DS as represented by the decrease of an absorption maximum of 4DS at 380 nm. 4DS was stable in the dark at pH lower than 8.4. In the absence of TAA no significant sensitization occurred. The presence of oxygen at pH 6.0 promotes dye sensitization, since quantum yields were about 0.13, and 0.05 for the aerobic and deaerated systems containing 2.0×10^{-5} M MB, 5.0×10^{-3} M TAA, and 4.0×10^{-5} M 4DS at pH 6.0, respectively. Oxygen effect on

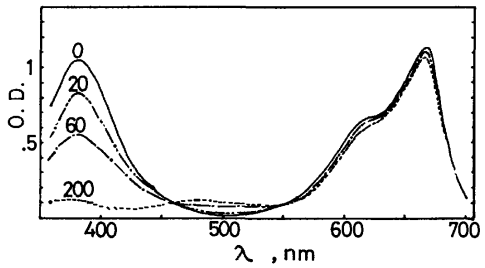

Fig. 1. Absorption spectra of 4DS solutions containing MB and TAA under an aerobic condition.
Numbers indicate the irradiation time (s) of red light (2.1×10^{-6} Einstein absorbed/l·s). Cell thickness is 1 cm. [4DS]=4.0×10^{-5} M, [TAA]=5.0×10^{-3} M, [MB]=2.0×10^{-5} M, pH 6.0.

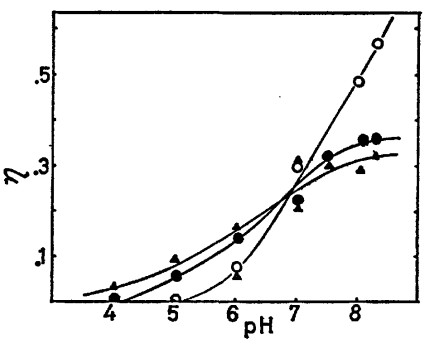

Fig. 2. Dependence of quantum yields (η) on solution pH [4DS]=3.8—4.2×10^{-5} M, [TAA]=5.0×10^{-3} M, [MB]=2.0×10^{-5} M, ○: N_2-bubbled, ●: aerobic, △: deaerated, ▲: O_2-bubbled.

quantum yields of dye-sensitized photolysis of 4DS is shown for the deaerated, N_2-bubbled, aerobic, and O_2-bubbled solutions, together with pH effect in Fig. 2. In the deaerated, N_2-bubbled, aerobic and O_2-bubbled systems, oxygen concentrations were taken to be $\sim 10^{-11}$ M, $\sim 10^{-9}$ M, 3×10^{-4} M, and $1 \sim 2 \times 10^{-3}$ M, respectively. The quantum yield in all systems increased with an increase in pH. It increased with an increase in oxygen concentration at pH below 7, whereas the reverse was the case at pH above 7.

In the deaerated system containing 1M acrylamide, MB excitation efficiently induced the free radical polymerization of acrylamide accompanied by sensitized photolysis of 4DS. The pH dependence of monomer conversion and the amount of MB bleached and 4DS decomposed under the exposure to the red light for 15 s is shown in Fig. 3. The rates of the sensitized photolysis and polymerization increased with an increase in pH. The molecular weights of polymers were of the order of millions. No significant polymerization of acrylamide was observed in the absence of 4DS or TAA. The results suggest that the photopolymerization of acrylamide in the deaerated TAA system is initiated by diphenylamine radical formed *via* an electron transfer from semi-MB to 4DS as reported for STS or DABCO systems.[2] At higher pH where the sensitized photolysis of 4DS was observed, a greater part of the MB triplet should be in an unprotonated form, since pK_a of protonated MB-triplet was 6.7.[5] Thus, little MB bleaching during polymerization can be explained in terms of an electron transfer causing the regeneration of MB^+ (reaction 3).

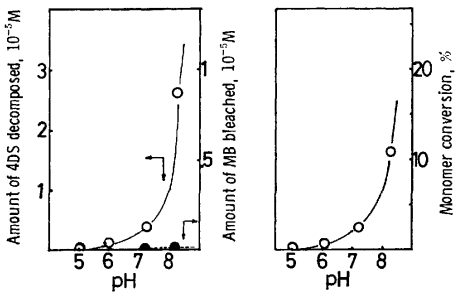

Fig. 3. Effect of solution pH on the sensitized photolysis of 4DS, MB photo-bleaching, and monomer conversion.
Intensity of red light: 2.2×10^{-6} Einstein absorbed/l·s.
$[MB]_{ini} = 2.0 \times 10^{-5}$ M, $[TAA]_{ini} = 5.0 \times 10^{-3}$ M,
$[4DS]_{ini} = 3.8$—4.0×10^{-5} M, $[Acrylamide]_{ini} = 1$ M,
Irradiation time: 15 s.

At pH above 7, oxygen suppression of the dye-sensitized photolysis of 4DS might be related to a quenching mechanism of triplet MB such as singlet oxygen mechanism.[3] If oxygen quenching of triplet MB or semi-MB alone is taken into account, oxygen effect on quantum yield at a pH less than 7 should be similar to that at a pH above 7. However, oxygen at pH (<7) promoted dye sensitization (Fig. 2). When aerobic aqueous solutions containing 2.0×10^{-5} M MB and 5.0×10^{-3} M TAA in the pH region 5~9 were exposed to red light, the dissolved oxygen was consumed by TAA. According to studies of thionine-sensitized photooxygenation of allylthiourea by Kramer and Maute,[6] the primary reaction takes place between thionine triplet and allylthiourea accompanied by the formation of semithionine radical and allylthiourea cation radical. Oxygen is involved only after the radicals have been formed.

The effectiveness of dissolved oxygen at pH (<7) suggests a mechanism in which molecular oxygen reacts with a charge-transfer complex formed between triplet MB and TAA to form semi-MB effective for dye sensitization, and which was disscussed for the STS system.[2] An attempt to check the above possibility by flash photolysis (400 J, 20 μsec) was unsuccessful since the amount of transient MB-bleaching observed in solutions containing MB and TAA was too small to measure the effect of oxygen or 4DS on the transient bleaching. The spectral changes of TAA in more alkaline or acidic solutions are attributed to the reaction:[7]

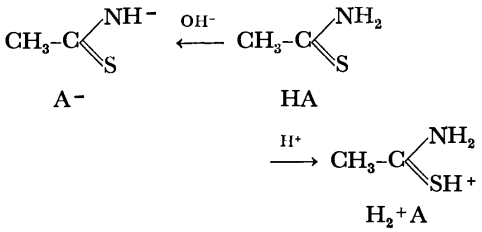

(4)

TAA is neutral in the pH region we worked with, since pK_a's of HA and $H_2{}^+A$ are 13.4 and −1.9, respectively. The pK_a of $H_2{}^+A$ was determined from a relationship ($[HA]/[H_2{}^+A] = K_a/h_+$) between $[HA]/[H_2{}^+A]$ and acidity function ($H_+ = -\log h_+$) in sulfuric acid solutions. Thus, it seems unreasonable that a loss of electron donating power derived from a protonation of TAA brought about a decrease in the quantum yield at lower pH. The space cause of the difference in quantum yield with different pH is unknown.

References

1) T. Yamase, T. Ikawa, H. Kokado and E. Inoue, *Photogr. Sci. Eng.*, **17**, 28 (1973).
2) T. Yamase, T. Ikawa, H. Kokado and E. Inoue, *ibid.*, **17**, 268 (1973).
3) C. S. Foote, *Accounts Chem. Res.*, **1**, 104 (1968).
4) G. Brauer, "Handbuch der präparativen anorganischen Chemie," Stuttgart (1954), p. 352.
5) S. Kato, M. Morita, and M. Koizumi, This Bulletin, **37**, 117 (1964).
6) H. E. A. Kramer and A. Maute, *Photochem. Photobiol.*, **15**, 7, 25 (1972).
7) J. T. Edward and I. C. Wang, *Can. J. Chem.* **40**, 399 (1962).